PETER W. MACFARLANE
ADRIAAN VAN OOSTEROM
OLLE PAHLM
PAUL KLIGFIELD
MICHIEL JANSE
JOHN CAMM *EDITORS*

Comprehensive Electrocardiology

Volume 1 · Second Edition

Springer

Comprehensive Electrocardiology

Peter W. Macfarlane · A. van Oosterom · Olle Pahlm ·
Paul Kligfield · Michiel Janse · John Camm (Eds.)

Comprehensive Electrocardiology

Second Edition

With 698 Figures and 122 Tables

Springer

Editors
Peter W. Macfarlane
University of Glasgow
Glasgow
UK

A. van Oosterom
Radboud University Nijmegen
Nijmegen
The Netherlands

Olle Pahlm
Lund University
Lund
Sweden

Paul Kligfield
Weill Cornell Medical College
New York, NY
USA

Michiel Janse
University of Amsterdam
Amsterdam
The Netherlands

John Camm
St. George's, University of London
London
UK

ISBN 978-1-84882-045-6 e-ISBN 978-1-84882-046-3
Print and electronic bundle ISBN: 978-1-84882-047-0
DOI 10.1007/978-1-84882-046-3

Library of Congress Control Number: 2010937436

Printed on acid-free paper

Springer is part of Springer Science+Business Media (www.springer.com) SPIN: 10981870 2109SPi–543210

Editors-in-Chief

Preface

The first edition of *Comprehensive Electrocardiology* was published in 1989, when e-mail was still in its infancy (!!), and it was never envisaged at that time that a new edition would be prepared. It is probably fair to say that the majority of physicians would have regarded electrocardiography in particular as having reached its maximum usefulness with little additional information to be obtained therefrom. The intervening 20 years have shown how untrue this was.

An update to the book is long overdue. Sadly, some of the former contributors have died since the first edition was published and it is with regret that I note the passing of Philippe Coumel, Rudolph van Dam, David Detweiler, Karel den Dulk, Ramesh Gulrajani, Kenici Harumi, John Milliken, Jos Willems and Christoph Zywietz. Where relevant, their contributions continue to be acknowledged but in some cases, chapters have been completely rewritten by new contributors. On the other hand, eight completely new chapters have been added and the appendices restructured.

In some ways, it is inconceivable what has taken place in the field of electrocardiology since the first edition. New ECG patterns have been recognised and linked with sudden death, new prognostic indices have been developed and evaluated, the ECG has assumed a pivotal role in the treatment of an acute coronary syndrome and among many other things, automated ECG interpretation is now commonplace. Significant advances have been made in the field of mathematical modelling and a solution to the inverse problem is now applied in routine clinical use. Electrophysiological studies have taken giant steps over the past 20 years and biventricular pacing is a relatively recent innovation. Electrocardiology has certainly not stood still in the last 20 years. Of course there have been parallel advances in imaging techniques but the ECG still retains a unique position in the armamentarium of the physician, let alone the cardiologist.

For this edition, my previous co editor, Professor T D Veitch Lawrie, decided to step aside and I wish to congratulate him on reaching his 90th birthday in September 2010. However, I am pleased that other very eminent individuals agreed to assist with the editing of the book, namely Adriaan van Oosterom, Olle Pahlm, Paul Kligfield, Michiel Janse and John Camm. In the nature of things, some of these co-editors undertook much more work than others. I particularly have to acknowledge the support of Adriaan van Oosterom with preparation of volume 1 where he has now authored 4 chapters and edited 4 others. Olle Pahlm read copious numbers of chapters on which he commented while Paul Kligfield similarly helped review and edit many chapters. I am also grateful to Michiel Janse and John Camm for their assistance with relevant chapters in their field. Without the support of all, this edition would not have been possible.

Locally, I am very much indebted to my secretary Pamela Armstrong for a huge contribution in checking and subediting every chapter which went out from my office to the publisher. This was a Herculean task carried out with great aplomb. I would also like to thank Ms. Julie Kennedy for her contribution to a variety of tasks associated with preparing selected chapters, including enhancements to the English presentation on occasions.

I also wish to thank Springer for their considerable support throughout. Grant Weston initially commissioned the book and I am grateful to him for his confidence in supporting the preparation of a new edition. Jennifer Carlson in New York also assisted very significantly, as did the team in Pondicherry, India under the able supervision of Sivakumar Kunchithapatham.

I also must thank my long suffering wife Irene who has had to fight to gain access to our home PC almost every night over these past few years!

This 2nd Edition of *Comprehensive Electrocardiology* aims to bring together truly comprehensive information about the field. A book can never be completely up to date given the speed of publication of research findings over the internet these days but hopefully this publication will continue to be of significant use to readers for many years to come. This is particularly true with the many reference values to be found in the appendices, some of which are published for the first time, particularly data relating to the neonatal ECG collected in my own lab.

Now that this huge effort has been completed and the book is available electronically, it should be much easier to produce the next edition…….!!

Peter Macfarlane
Glasgow
Summer 2010

Table of Contents

Volume 2

Volume 3

List of Contributors

K. Martijn Akkerhuis
Erasmus University Medical Centre
Rotterdam
The Netherlands

Luigi De Ambroggi
University of Milan
Milan
Italy

Frits W. Bär
University of Maastricht
Maastricht
The Netherlands

R.C. Barr
Duke University
Durham, NC
USA

Dana Brooks
Northeastern University
Boston, MA
USA

Martin Buist
National University of Singapore
Singapore
Singapore

John Camm
St. George's, University of London
London
UK

Leo K. Cheng
The University of Auckland
Auckland
New Zealand

Alexandru D. Corlan
University Emergency Hospital of Bucharest
Bucharest
Romania

Alain Coulomb
Hopital Pitie-Salpetriere
Paris
France

Iwona Cygankiewicz
Medical University of Lodz
Lodz
Poland

D. Wyn Davies
Imperial College London
London
UK

David K. Detweiler
University of Pennsylvania
Philadelphia, PA
USA

Parvin C. Dorostkar
University of Minnesota
Minneapolis, MN
USA

Gordon E. Dower
Loma Linda University Medical Centre
Loma Linda, CA
USA

Karel Den Dulk
University of Maastricht
Maastricht
The Netherlands

Thomas Fåhraeus
University Hospital
Lund
Sweden

Guy Fontaine
Hopital Pitie-Salpetriere
Paris
France

Robert Frank
Hopital Pitie-Salpetriere
Paris
France

Alireza Ghodrati
Draeger Medical
Andover, MA
USA

Anton P.M. Gorgels
University of Maastricht
Maastricht
The Netherlands

Helena Hänninen
Helsinki University Central Hospital
Helsinki
Finland

Johan Herlitz
Sahlgrenska University Hospital
Gothenburg
Sweden

Gerard Van Herpen
Erasmus University Medical Centre
Rotterdam
The Netherlands

V. Hombach
University Hospital of Ulm
Ulm
Germany

B. Milan Horáček
Dalhousie University
Halifax, NS
Canada

Michiel J. Janse
University of Amsterdam
Amsterdam
The Netherlands

Julian Jarman
Imperial College London
London
UK

Per Johansson
Sahlgrenska University Hospital
Gothenburg
Sweden

Raija Jurkko
Helsinki University Central Hospital
Helsinki
Finland

Demosthenes G. Katritsis
Athens Euroclinic
Athens
Greece

Paul Khairy
Montreal Heart Institute
Montreal, QC
Canada

Michael Koa-Wing
Imperial College London
London
UK

Petri Korhonen
Helsinki University Central Hospital
Helsinki
Finland

Jan A. Kors
Erasmus University Medical Centre
Rotterdam
The Netherlands

Jèrôme Lacotte
Hopital Pitie-Salpetriere
Paris
France

T.D. Veitch Lawrie
University Of Glasgow
Glasgow
UK

Jerome Liebman
Case Western Reserve University School of Medicine
Cleveland, OH
USA

S.M. Lobodzinski
California State University
Long Beach, CA
USA

Mário G. Lopes
Institute of Preventive Cardiology
Lisbon
Portugal

Robert L. Lux
University of Utah
Salt Lake City, UT
USA

Peter W. Macfarlane
University of Glasgow
Glasgow
UK

Rob MacLeod
University of Utah
Salt Lake City, UT
USA

J.E. Madias
Mount Sinai School of Medicine
New York, NY
USA

Markku Mäkijärvi
Helsinki University Central Hospital
Helsinki
Finland

Ariane J. Marelli
McGill University Health Centre
Montreal, QC
Canada

Vias Markides
Imperial College London
London
UK

Nuno Marques
Institute of Preventive Cardiology
Lisbon
Portugal

Andrew D. Mcgavigan
Royal Melbourne Hospital
Melbourne, VIC
Australia

John A. Milliken
Queens University
Kingston, ON
Canada

N. Sydney Moïse
Cornell University
Ithaca, NY
USA

Martyn P. Nash
The University of Auckland
Auckland
New Zealand

Peter Okin
Weill Cornell Medical College
New York, NY
USA

A. van Oosterom
Radboud University Nijmegen
Nijmegen
The Netherlands

Tobias Opthof
University Medical Centre Utrecht
Utrecht
The Netherlands

Fernando de Pádua
Institute of Preventive Cardiology
Lisbon
Portugal

Olle Pahlm
Lund University
Lund
Sweden

Armando Pereirinha
Institute of Preventive Cardiology
Lisbon
Portugal

Nicholas Peters
Imperial College London
London
UK

R. Plonsey
Duke University
Durham, NC
USA

Andrew J. Pullan
The University of Auckland
Auckland
New Zealand

F. Russell Quinn
Glasgow Royal Infirmary
Glasgow
UK

Alan P. Rae
Royal Infirmary Glasgow
Glasgow
UK

Andrew C. Rankin
University of Glasgow
Glasgow
UK

Pentti M. Rautaharju
Wake Forest University School of Medicine
Winston-Salem, NC
USA

Michael R. Rosen
Columbia University
New York, NY
USA

Oliver R. Segal
University College London
London
UK

Ronald H. Selvester
University of Southern Carolina
Columbia, SC
USA

Pentti Siltanen
Helsinki University Central Hospital
Helsinki
Finland

Maarten L. Simoons
Erasmus University Medical Centre
Rotterdam
The Netherlands

Michael B. Simson
Hospital of the University of Pennsylvania
Philadelphia, PA
USA

Leif Sörnmo
Lund University
Lund
Sweden

Maciej Sosnowski
Medical University of Silesia
Katowski
Poland

David G. Strauss
Lund University
Lund
Sweden

Borys Surawicz
The Care Group at St Vincent Hospital
Indianapolis, IN
USA

Leif Svensson
Stockholm Prehospital Center
Stockholm
Sweden

Elin Trägårdh-Johansson
Lund University
Lund
Sweden

Heikki Väänänen
Aalto University School of Science and Technology
Espoo
Finland

Galen S. Wagner
Duke University
Durham, NC
USA

Hein J.J. Wellens
University of Maastricht
Maastricht
The Netherlands

Ronald Wilders
University of Amsterdam
Amsterdam
The Netherlands

Andrew L. Wit
Columbia University
New York, NY
USA

Wojciech Zareba
University of Rochester Medical Centre
Rochester, NY
USA

Antonio Zaza
Università di Milano-Bicocca
Milano
Italy

Section 1

Introduction

1 The Coming of Age of Electrocardiology

Peter W. Macfarlane

P. W. Macfarlane, A. van Oosterom, O. Pahlm, P. Kligfield, M. Janse, J. Camm (eds.), *Comprehensive Electrocardiology*, DOI 10.1007/978-1-84882-046-3_1,

1.1 Introduction

The history of electrocardiography and vectorcardiography is relatively well established [1, 2]. Indeed, it is now well over one hundred years since the electrocardiogram was first recorded in a human and the 100th anniversary of this event resulted in a number of reviews dealing with the early days of electrocardiography [3–7].

While, in the relatively early days of a new century, it would seem appropriate to look back over developments in the last century, others recently have recently reviewed the present status of the ECG [8] and this author has referred to a renaissance in electrocardiography [9] since the first edition of this book. Electrocardiography has come under increasing pressure in recent years with the advent of new techniques such as echocardiography, which undoubtedly provide information that complements the electrocardiogram. On the other hand, Wellens [10] regretted the fact that younger physicians are increasingly unable to interpret electrocardiograms correctly. He referred to the views of Fisch [11] who had emphasized the fact that the ECG is a noninvasive technique that is inexpensive, simple and reproducible. He might have added that the ECG can be rapidly recorded with extremely portable equipment (the most recent having integral computer facilities as well as wireless or telephone transmission capabilities) and is always able to be derived unlike the echocardiogram, which in some situations cannot be satisfactorily obtained. Of course, the ECG provides unique information that cannot be obtained by any other technique; it is only necessary to think of secondary ST-T changes due to left ventricular hypertrophy and their prognostic importance for proof of this. Furthermore, as Fisch indicated [11], "He who maintains that new knowledge of electrocardiography is no longer possible or contributive, ignores history." This new edition of Comprehensive Electrocardiology proves how prophetic these words were.

Much of the early work in electrocardiography was carried out in Europe, where today there is still considerable development effort being expended, particularly in the field of computer-based electrocardiography (see Chap. 37). There is much work elsewhere mainly based around mathematical modeling. A European physician and physiologist, the late Professor Pierre Rijlant wrote an article in 1980 entitled "The Coming of Age of Electrophysiology and Electrocardiography" [12]. It is from this article that the title for the present chapter is drawn, in memory of the contribution of Rijlant, President of the 1958 World Congress of Cardiology, to the field of electrocardiology.

It is questionable where the term "electrocardiology" arose. In 1959, the first of a series of colloquia on vectorcardiography was organized by Kowarzyk and held in Wroclaw in Poland. For many years thereafter, an International Colloquium Vectorcardiographicum was organized, and Rijlant was the driving force and Honorary President of the Organizing Committee. In 1973, the author attended a meeting of the Organizing Committee in Yerevan, Armenia, USSR, at which it was agreed that, from 1974 onwards, the name of the meeting should be changed to the International Congress on Electrocardiology. The first such meeting was organized in Wiesbaden in 1974 and was attended by many prominent researchers including the late Ernst Simonson, well known for his work on the normal electrocardiogram (see Chap. 13).

Earlier, in 1968, Zao and Lepeschkin founded the *Journal of Electrocardiology,* which grew in strength under the editorship of Startt/Selvester, who has contributed to Chap. 16, and is now being significantly restructured by Wagner, who has also contributed to the same chapter. Lempert [13] in 1976 also commented on the transition from the term "electrocardiography" to "electrocardiology" and pointed out he had used the term "electrocardiology" in his 1961 textbook, written in Latvian, and the 1963 edition written in Russian. (Professor Ruttkay-Nedecky from Bratislava has recently pointed out that J. Martinek used the term "electrocardiology" in 1959 in the title of his paper referring to "electrocardiology in the USA" at a meeting in Wroclaw, Poland, which became the forerunner of the Colloquium Vectorcardiographicum). "Electrocardiography" conjures up a view of 12 leads, perhaps recorded singly on an electrocardiograph. The explosion of technology in recent years and the variety of investigative techniques now available for studying the cardiac electrical activity demands that the relatively newer term of "electrocardiology" be used to encompass the various subject areas associated with the electric and magnetic fields generated by the individual cells of the heart. It is hoped that it will be evident from the contents of this book that the term "electrocardiography" would be inappropriate.

1.2 The Groundwork for Electrocardiography

By the mid-nineteenth century, it was generally agreed that nerves, muscles and so on could be stimulated by artificial electrical generators [11]. The first galvanometer had beeninvented by that time and physiologists were engaged in

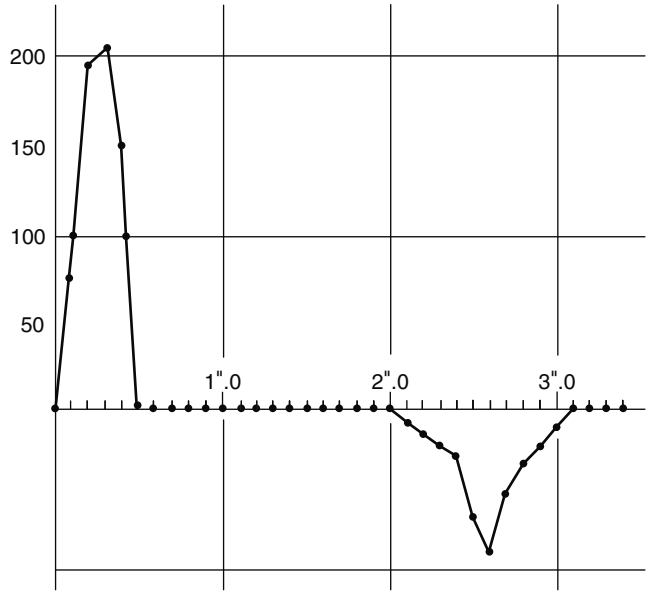

Figure 1.1
The potential variation recorded from a tortoise heart in 1878 by the use of a differential rheotome, which was an instrument that measured current flow at a varying interval following the application of a stimulus. (After Burdon Sanderson and Page [18]. © Royal Society of London, London. Reproduced with permission.)

exploring the discharge from electric eels, the flow of current through frogs and the effects of injury. Such work was probably initiated by Galvani [14]. He was criticized by Volta who argued that electrical current was generated only by different metals making contact-the basic work that ultimately led to the development of batteries. It was du Bois-Reymond who continued much of this work as highlighted by Rijlant [12]; in particular he found that action current in muscle was opposite to the direction of a continuous current, which his pupil Hermann showed later was present only following an injury to the muscle [14]. In 1856, Kölliker and Muller [15] demonstrated bioelectric potentials in the frog's heart. As far as is known, this was the first recording of cardiac electrical activity. These authors described a negative deflection that could be measured by a galvanometer prior to each contraction. This confirmed earlier work of du Bois-Reymond in muscle from a guinea pig and a frog. In 1876, Marey used the capillary electrometer invented by Lippmann and photographically recorded the electrical activity of the frog's heart [16]. Engelmann [17] as well as Burdon Sanderson and Page [18] were also among the earliest to plot the potential variation of electrical activity of the heart (Fig. 1.1). It is fascinating to read that in 1879, Burdon Sanderson and Page stated [19]: "We owe most to the labors of Engelmann whose researches on the propagation of the wave of contraction in the ventricles, on the electromotive properties of the resting heart, and on the electrical charges which immediately follow excitation, leave little more to be done."

It is evident that, as is usually the case, a whole series of developments finally led to a "first" – in this case, the first known recording of the human electrocardiogram (Fig. 1.2) by Waller in 1887 [20]. Waller published further observations in 1889 [21] on his dog Jimmie, which is almost as well known as its owner (Fig. 1.3)! The dog was in fact used in many of Waller's studies involving the capillary electrometer (Fig. 1.4).

Besterman and Creese [22] lamented the fact that the contribution of Waller to the development of electrocardiography is often ignored. At the time of his publication of the human electrocardiogram, Waller was lecturer in physiology at St. Mary's Hospital, Paddington, London. The electrical activity of the exposed heart was already known as discussed above, but Waller decided to investigate the possibility of recording potentials from the limbs of animals and from man. Note, however, that the ECG of Fig. 1.2 was obtained from electrodes on the front and back of the chest. According to Besterman and Creese, the following is attributed to Waller at an informal talk in London in 1915 [22].

Figure 1.2

The first published human electrocardiogram recorded by Waller in 1887. The ECG is represented by the lowest black/white interface (e), which represents the movements of mercury in the Lippmann Electrometer. The tracing denoted (h) records chest-wall movement and essentially is a form of apex cardiogram. The top calibration pulses represent the time (t) in one second intervals between the onset of each pulse. This ECG was recorded with one electrode, which was strapped to the front of the chest, connected to the mercury column in the electrometer, while the other electrode, on the back of the patient's chest was connected to the sulfuric acid which formed the interface at the top of the mercury column in the electrometer. Note that this ECG did not exhibit atrial activity. (After Waller [20]. © Physiological Society, London. Reproduced with permission.)

Figure 1.3

A photograph of Waller with his dog Jimmie. (After Besterman and Creese [22]. © British Medical Association, London. Reproduced with permission.)

▶ "I studied the hearts of all sorts of animals and one fine day after leading off from the exposed heart of a decapitated cat to study the cardiogram by aid of a Lippmann electrometer, it occurred to me that it ought to be possible to use the limbs as electrodes and thus lead off from the heart to the electrometer without exposing the heart, i.e., from the intact and normal organ. Obviously man was the most convenient animal to use so I dipped my right hand and left foot into a couple of basins of salt solution, which were connected with the two poles of the electrometer and at once had the pleasure of seeing the

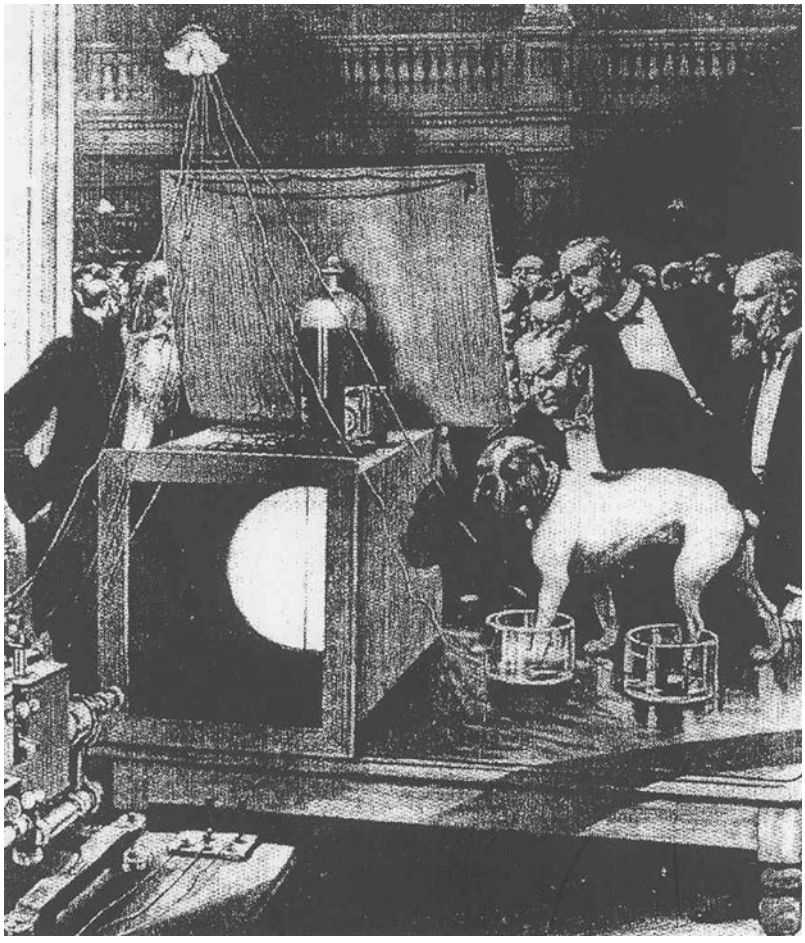

Figure 1.4
Waller's dog, Jimmie, being used to demonstrate the recording of an electrocardiogram to the Royal Society. (Reproduced from Levick JR, An Introduction to Cardiovascular Physiology, 3rd Edition, London, Arnold, 2000.)

> mercury column pulsate with the pulsation of the heart. This first demonstration was made in St. Mary's Laboratory in 1887 and demonstrated there to many physiologists and among others, to my friend Professor Einthoven of Leiden…During the summer of that year, I made a complete summary of all sorts of leads from the hand and feet and mouth (Fig. 1.5)."

There is an anecdotal story that a question was also asked in the House of Commons concerning the use of Jimmie in experiments where the dog's limbs were immersed in the saline solutions (Fig. 1.4). The questioner asked whether such a procedure should not be prohibited under the Cruelty to Animals Act of 1876. The answer given, reputed to be by the Secretary of State at the time, Mr. Gladstone, suggested that if the Honorable Member who had posed the question had ever paddled in the sea, he would have appreciated fully the sensation obtained from this simple pleasurable experience! [22].

Physiological measurement technicians, or cardiac physiologists as they are now known in the UK, would be interested to know that Waller's early electrocardiograms were recorded photographically on a plate which was mounted on a toy railway wagon running on rails (Fig. 1.6) in order to move the plate across a light beam which cast a shadow on the moving mercury meniscus of the electrometer [4]. Indeed, what would now be called the frequency response of the electrometer was so poor that the recorded deflections did not give an accurate recording of the cardiogram, but mathematical techniques were later used to correct this shortcoming [23].

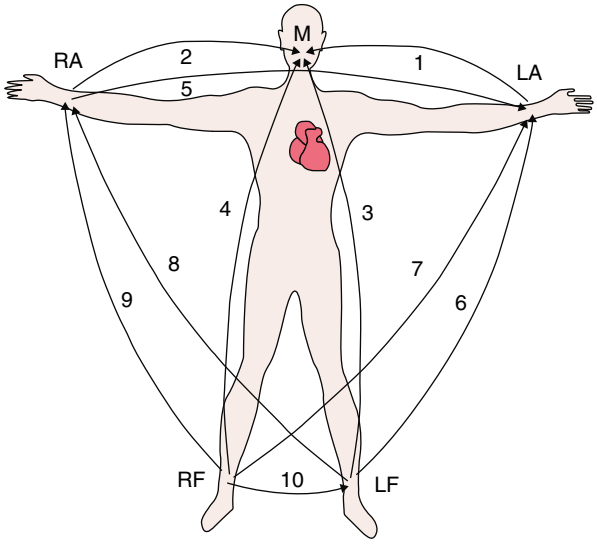

Figure 1.5

A schematic representation of the various electrode combinations used by Waller in his early investigations. Note that, in addition to the four limb electrodes, the mouth was used as a fifth electrode. This allowed the derivation of 10 bipolar leads. (Adapted from Bioelectromagnetism – Principles and Applications of Bioelectric and Biomagnetic Fields, Oxford University Press, New York, 1995 by J. Malmivuo and R. Plonsey. Reproduced with permission from http://www.bem.fi/book/index.htm.)

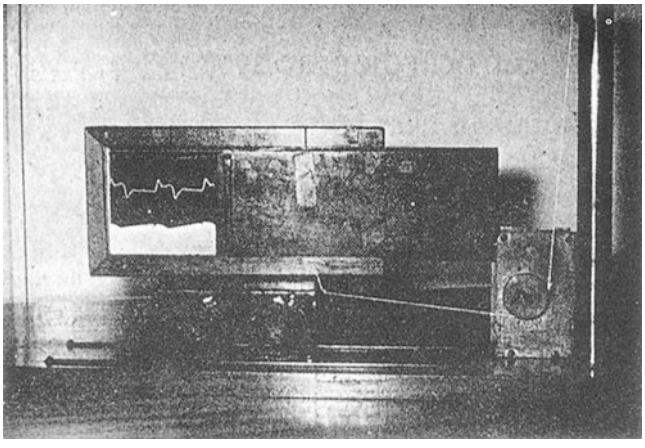

Figure 1.6

The train wagon which was used to transport the photographic plate on which Waller recorded electrocardiograms. (After Besterman and Creese [22]. © British Medical Association, London. Reproduced with permission.)

It is of parochial interest that Waller qualified in medicine at Aberdeen, Scotland in 1878 [4], but he was not Scottish! It is also of historical interest to note that in 1889 in Berlin, he demonstrated the recording of an electrocardiogram on a dog, on a horse linked to equipment inside a building by lengthy recording leads and also on du Bois-Reymond [4].

There would appear to be some controversy as to who was the first to introduce the term "electrocardiogram." Burch and de Pasquale ([1], p. 29) state that it was Einthoven who introduced the term. Snellen ([24], p. l0) states that "the term electrocardiogram was coined by Einthoven."

However, Burchell [6] wrote that in 1912 Einthoven said [25]: "It gives me a special pleasure to bring to remembrance here, that the human EKG was first recorded by a London physiologist, Augustus D. Waller, who also introduced the term 'electrocardiogram' into science." There would therefore seem to be no doubt that Waller first used the term "electrocardiogram."

1.3 The Beginnings of Modern Electrocardiography

It is likely that most cardiologists, if asked about the origins of the electrocardiogram, would state that the Dutch physician Willem Einthoven developed a string galvanometer and thereafter applied it extensively to record the electrical activity of the heart. However, as alluded to in Sect. 1.2, most advances take place by refinement of earlier work, and it is therefore not surprising to find some controversy over the question of who in fact invented the string galvanometer. According to Cooper [3], the French electrical engineer Ader [26] invented a number of items including amplifier systems. He also developed "a highly sensitive, rapidly moving galvanometer that used a small wire instead of a coil to register electricity" [3]. The device was used to study underwater cables that were being laid at that time for transoceanic telegraphy [1].

Cooper [3] and Burch and de Pasquale [1] indicate that Einthoven, having been dissatisfied with the performance of the Lippmann electrometer, used a different instrument called the Deprez-d'Arsonval galvanometer. This galvanometer utilized a light coil of wire suspended between the poles of a permanent magnet, but Einthoven found that an improved sensitivity could be obtained by replacing the coil by a single fiber (a string). Einthoven then described his new galvanometer, and in that publication [27], acknowledged the Ader galvanometer, which also used a fine wire stretched between poles of a magnet. Cooper [3] suggests that Einthoven's wire was 0.002 mm in diameter, approximately one tenth as thick as that used by Ader. Cooper [3] also points out that one of Einthoven's teachers, Bosscha, had thirty years earlier in his own thesis suggested that a "single needle hanging from a silk thread" would form an appropriate moving part of a galvanometer [28].

Burchell [29] reviewed the controversy. His view was basically that the use of the word "invent" in respect of Einthoven's instrument was justified in the sense that Einthoven's device was an instrument specifically designed for recording the cardiac electrical activity. As such, it would have been feasible to patent it because it allowed recordings to be obtained that were not previously possible. He agreed that it was not "a discovery," and as has been suggested in this chapter, there can be very few situations in the history of scientific development where a new instrument is truly unique.

Notwithstanding the above, it is evident that Einthoven did not invent a galvanometer de novo. His major achievement was to design a device that was sensitive enough to record electrical potentials from the surface of the body. He developed a method of moving a photographic plate falling under gravity at a constant rate, and by directing a beam of light on the galvanometric string, its movements were recorded on the falling plate [1]. Einthoven's first electrocardiograph was extremely heavy, weighing around 600 lb, and required five operators. His first results appeared in 1903 [30].

Einthoven's laboratory was approximately one mile from the local hospital and so he had to develop a method for transmitting the ECG over telephone lines. The methods used and the results obtained are described in a classic paper published in 1906 [31]. At that time, leads I, II and III had been introduced and a variety of different electrocardiographic abnormalities demonstrated. This paper was followed by another classic in 1908 [32]. Burch and de Pasquale [1] state that "Einthoven's paper of 1908 may well be the most important single publication dealing with the subject of electrocardiography for it demonstrated to the medical profession that the electrocardiograph was of practical, as well as theoretic importance."

One of the last papers published by Einthoven and colleagues [33] included the now classic Einthoven triangle, whereby the body was represented in electrical terms by an equilateral triangle. From this, the mean QRS axis could be calculated. In addition, the well-known Einthoven's law was put forward around that time and is mentioned in the paper. In this book, the lead systems of electrocardiography are discussed in Chaps. 10 and 11. Axis calculations are highlighted in Chap. 13.

In his early papers, Einthoven used the terminology of PQRST to describe the deflection of the electrocardiogram (Fig. 1.7). It was suggested that the letters were selected to leave room for further discoveries such as the U wave, which Einthoven later detected using his string galvanometer. However, Cooper's view [3] was that the letters were chosen to conform with the terminology of mathematicians of the day, and Burchell [29] also supported this notion quoting Henson

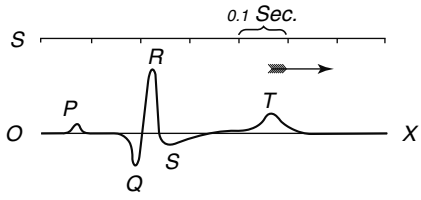

Figure 1.7
The early notation for the electrocardiogram as proposed by Einthoven. The largest deflection, positive or negative, was termed the R wave. (After Einthoven [30]. © Springer, New York. Reproduced with permission.)

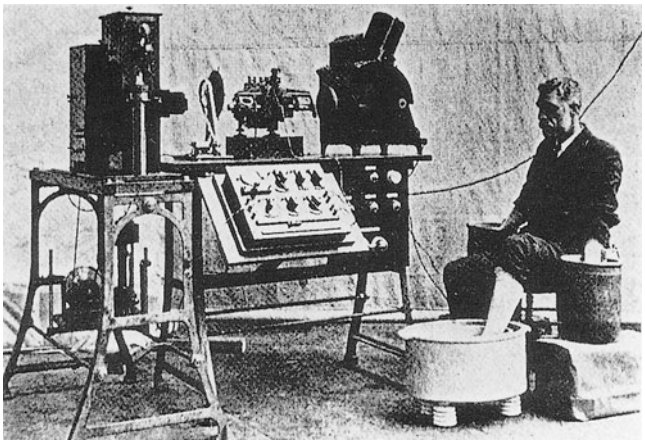

Figure 1.8
An early commercial version of the electrocardiograph manufactured by Cambridge Scientific Instrument Company of London in 1911. On the left is the camera incorporating the plate falling under gravity, the galvanometer is in the center and on the right is the light source required for the recording. (After Br. Med. J. 1950;1: 720. © British Medical Association, London. Reproduced with permission.)

[34] who traced the use of PQRST for mathematical reasons back to Descartes. More recently, Hurst has reviewed the naming of all the components of the ECG including the delta and epsilon waves [35]. Gussak et al. [36] also reviewed the J (Osborn) wave.

It is worth noting that Einthoven's galvanometer was developed commercially by the Cambridge Instrument Company (Fig. 1.8) in the UK. Early models found their way into the laboratory of other distinguished electrocardiographers such as Lewis and Wilson. In 1924, two years after Waller's death, Einthoven was awarded the Nobel Prize in Medicine for his contribution to electrocardiography.

1.4 Analysis of Cardiac Rhythm

It is relevant to diverge briefly in order to consider parallel work on the study of the rhythm of the heart, because much of the early work in electrocardiography was concerned with this topic. Of course, the study of the rhythm of the heart goes back centuries before the development of electrocardiography, since the rhythmic pulsation of arteries provided an external means of assessing the rhythm of the heart – once it was understood that such pulsation was indeed caused by the beating of the heart. In a historical review of the study of arrhythmias, Scherf and Schott [37] stated that approximately 3,500 years ago there was thought to be a connection between the pulse and the heart. These authors also quoted Read [38] who confidently indicated that a more scientific understanding of the pulse seemed to date in ancient China from

about 500 BC. In the same historical review, Hubotter [39] was referenced as indicating that the occurrence of dropped pulse beats was related to prognosis. The more frequent the dropped beat, the higher the number of organs considered to be diseased and therefore the shorter the expected life span.

Not surprisingly, the ancient Greeks and Romans have also been credited with the study of cardiac rhythm. The Greek word *dikrotos* meaning double beating was apparently used by Herophilus (born 300 BC) to describe a dicrotic pulse [40]. Later, in the second century AD, Claudius Galen, a famous medical scholar of that time, introduced the term *eurhythmus* to describe a normal pulse. His original Latin text also used the term *arhythmus* to describe an abnormal pulse, which was further subdivided into three different types. His work remained prominent for over fifteen centuries. A few of his original Latin writings can be found in the review of Scherf and Schott [37].

In order to leap forward in time, it is convenient to link "arrhythmias" with one of the early texts on cardiac rhythm, namely, that by Wenckebach [41] entitled "Arhythmia of the Heart" (Fig. 1.9). The English translation of this Dutch physician's treatise was published in 1904. In his book, Wenckebach acknowledged the contributions of a Scottish physician, Mackenzie, who in 1902 had published his own work on the study of the pulse [42]. At that time he was a general practitioner in the north of England and had spent many years accumulating data on patients with heart disease. What readers may find difficult to imagine is that all of Mackenzie's recordings were made with a polygraph, an instrument which allowed two channels of pressure tracings to be recorded. Mackenzie recorded the arterial and jugular pulsations simultaneously with his homemade instrument. His work at the time was largely ignored, but in 1908 he published a classic paper entitled "Diseases of the Heart" [43] and this brought him much worldwide acclaim.

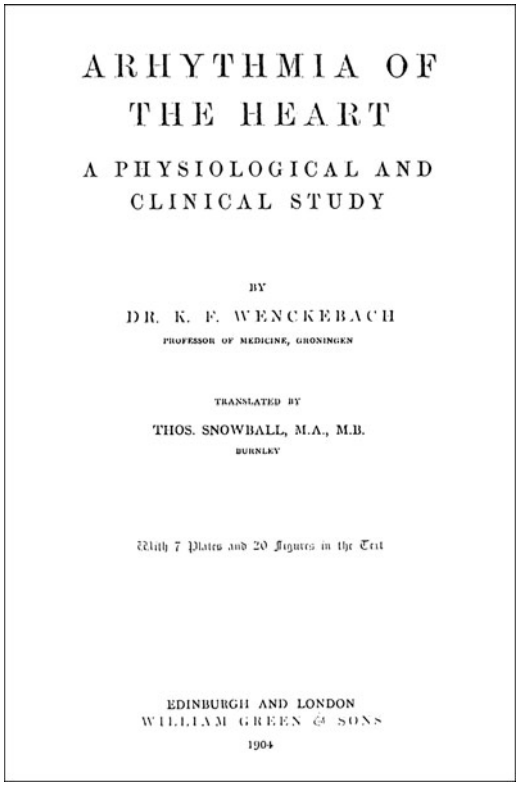

ARHYTHMIA OF THE HEART

A PHYSIOLOGICAL AND CLINICAL STUDY

BY

DR. K. F. WENCKEBACH

PROFESSOR OF MEDICINE, GRONINGEN

TRANSLATED BY

THOS. SNOWBALL, M.A., M.B.

BURNLEY

With 7 Plates and 20 Figures in the Text

EDINBURGH AND LONDON
WILLIAM GREEN & SONS
1904

Figure 1.9

The frontispiece of the English edition of Wenckebach's text on the "Arhythmia of the Heart" published in 1904.

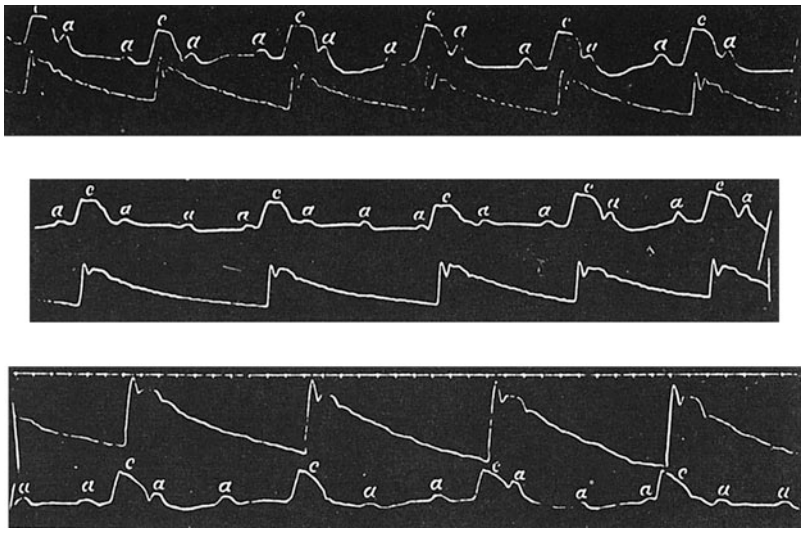

Figure 1.10
Three illustrations of complete heart block recorded from a 66-year-old man: a, atrial contraction; c, carotid pulse. The second trace represents the radial pulse. (After MacKenzie [42]. © Pentland, Edinburgh. Reproduced with permission.)

An illustration of Mackenzie's tracings is provided in Fig. 1.10. These were first published in Mackenzie's 1902 book [42] and were reproduced by Wenckebach [41]. The recordings are from a 66-year-old man in "fair health" who was capable of considerable exertion. There was marked variation in heart rate from 23 per min to 42 per min. In the illustration, the small "a" waves represent atrial contraction, while the c waves are indicative of the carotid pulse. The larger waves on the second tracing denote the radial pulse. These recordings illustrate heart block. Wenckebach acknowledged Mackenzie's genius as follows.

> "So Mackenzie succeeded in recording the action of all the four chambers in man for the first time, and in establishing beyond doubt the complete heart block, the continued action of the two auricles, and the simultaneous cessation of both ventricles. We are under great obligations to this keen and clever observer for showing how this can be accomplished. A clearer proof for the recurrence of heart-block in persons who were certainly not in the throes of death (Hering) cannot be desired."

Wenckebach also discussed the "conductivity or power of conduction" which he denoted *A*. Changes in the rapidity of conduction were studied by examining the interval between auricular and ventricular contraction denoted $A_s - V_s$. In reporting another irregularity of conduction, Wenckebach stated the following.

> "A great diminution of the conduction power and its consequences can be best demonstrated on a dying frog's heart at the interval $A_s - V_s$.
>
> As the conduction gradually grows worse and worse, this interval gets always longer; the conduction may become so bad that the ventricle does not begin to contract until just before the next auricular systole. Anyone that had not followed the way in which this phenomenon slowly developed would think that the auricular systole followed the ventricular; in other words, that there was a reversal of the usual order of contraction. But if *A* continues to grow worse, there finally comes a time when the stimulus is no longer conducted (or not with sufficient strength?), $A_s - V_s = \infty$; in other words, the ventricle does not contract. During the pause that arises through the missing of this systole, however, *A* will have plenty of time to recover again so far that the next stimulus is again conducted to the ventricle, and it contracts; but after a few systoles have occurred, *A* is again so much reduced that another beat is missed. In this way a ventricular contraction may continue to be dropped after the same number of systoles for a considerable time, thus producing a regular intermission of the ventricle. A very beautiful example of this missed ventricular systole is given in Fig. 1.11; the tracing was obtained from a frog's heart and was taken from Engelmann's paper on Conduction of Stimuli [44].

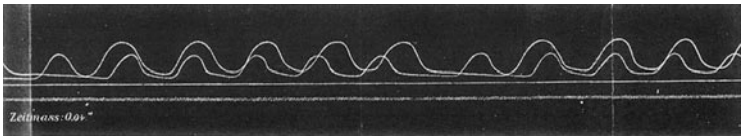

Figure 1.11

The lower amplitude waveform represents atrial contraction, and the larger waveform ventricular contraction, in a frog's heart. Note that the ventricular contraction is missed after the sixth beat. The tracing was first recorded by Engelmann [44]. (After Wenckebach [41]. © Green, Edinburgh. Reproduced with permission.)

> At a later stage of asphyxia, auricular contractions soon drop out in consequence of the defective conduction from the sinus to the auricle. The contractions of the heart are thereby made to appear in groups which may assume a very complicated form from further interference with the conduction power and the other functions. In these cases, we speak of the "periodic" action of the heart and the groups are called after their discoverer "Luciani's periods"."

There is a great temptation to follow the extract with an exclamation, because what nowadays is referred to as the "Wenckebach" phenomenon was acknowledged by Wenckebach to have been described by others, Again, therefore, there is evidence of the interlinking of the work of many in the advancement and understanding of a field of knowledge.

A complete review of the early work on arrhythmias is beyond the scope of this chapter. It is of interest, however, to mention that a Scot called McWilliam first used the term atrial flutter and in 1887 proposed the concept of ventricular fibrillation [45], a topic that was to interest him, particularly its relationship to sudden death, for 40 years. In 1893, His described the AV bundle [46], a finding which he himself said 40 years later [47] was largely ignored at the time. When electrocardiography became possible, there was of course great interest in the study of cardiac rhythm. Einthoven produced records of ventricular extrasystoles, ventricular bigeminy and atrial fibrillation [31] although it was left to others, notably Hering [48] and Lewis [49] to examine the latter in more detail. Today, our understanding of arrhythmic mechanisms has grown immeasurably through the medium of EPS (electrophysiology study) testing via multiple catheters and perhaps basket electrodes inserted into the heart. The techniques are discussed fully in Chaps. 24 and 25 while a variety of arrhythmias is presented in Chaps. 26–30.

1.5 Clinical Development of Electrocardiography

By the middle of the first decade of the twentieth century, the Einthoven galvanometer had been developed, the electrocardiogram was beginning to be investigated more extensively and much work on the irregularity of the heart beat had been undertaken using polygraphic methods, which probably arose from the early work of the French physiologist Marey. The first commercial version of the Einthoven electrocardiograph was produced in 1908 by the Cambridge Instrument Company, and other models soon came into use throughout Europe. Interestingly, the first electrocardiograph to be shipped to the United States was developed by Edelmann, who had originally manufactured Einthoven's machine, but because of disagreements over royalty payments, the two had parted company. The Edelmann machine was taken to the USA by Cohn in 1909 after he had spent some time in London working with Mackenzie and one of his junior staff, Thomas Lewis [1]. In the same year, a Russian physiologist Samojloff wrote a short text in German entitled "Elektrokardiogramme" [50]. He had visited Einthoven in Leiden in 1904 and later bought the sixth electrocardiograph to be manufactured by the Cambridge Scientific Instrument Company [51]. Samojloff was a good friend of a Professor Lepeschkin, whose son Eugene remembered spending summer holidays in close proximity to the Samojloff family, as they each had a summer home near Kazan in Russia. Lepeschkin [52] himself later did much fundamental work on electrocardiography and, indeed, married the daughter of Frank Wilson whose unipolar leads have briefly been referenced already [7] and which will be discussed in more detail later. It is fascinating to tie together the various friendships established in the field of electrocardiography, almost as if there had been one large family tree of fellow electrocardiographers! In turn, this leads to some further detail of the extremely distinguished physician later to become Sir Thomas Lewis, whose first work on the mechanism of the heart beat [53] was dedicated to James Mackenzie and Willem Einthoven – a family tree indeed!

Figure 1.12
Photograph of Einthoven (left) and Lewis probably taken in 1921 during Lewis' last visit to Leiden. (© Museum Boerhaave, Leiden. Reproduced with permission.)

Lewis was born in Wales in 1881, and one hundred years later a series of editorials was published in the *British Heart Journal* to commemorate his birth [54–57]. Lewis' career was not entirely devoted to electrocardiography, but a large portion of his working life from around 1905 to 1925, when he published the third edition of his now famous textbook, retitled "The Mechanism and Graphic Registration of the Heart Beat" [58], was taken up with the subject. Interestingly, in this edition the former dedication to Mackenzie and Einthoven was removed. In the interim, however, Lewis had formed a strong friendship with Einthoven (Fig. 1.12) and they exchanged much correspondence in the intervening years, as was diligently uncovered by Snellen [24]. Lewis' book of 1925 represented a major advance for electrocardiography. It summarized much of the earlier work on cardiac arrhythmias, but this time ECGs were published in support of the various theories of circus movement, and so on. Electrocardiograms representing hypertrophy with preponderance of one or other ventricle were presented but unfortunately, the now well-publicized ECGs from right and left bundle branch block were wrongly described, that is, what Lewis described as a defect of "the right division of the AV bundle" (Fig. 1.13) was in fact a left bundle branch block. Because the recordings were thought to represent activation principally of the left ventricle, they were called the human "levocardiogram." Conversely, as shown in Fig. 1.14, the human dextrocardiogram was thought to represent a defect of the left division of the AV bundle. It should be remembered, however, that at that time Lewis was working only with the three limb leads of Einthoven, and even now it would be difficult, given only the three leads of Fig. 1.14, to say whether the curve truly represented a right bundle branch block or one obtained from a more complex congenital cardiac lesion. Lewis had undertaken much experimental work on dogs in order to prove his conclusions, but it was not until 1929–1931 that the error was corrected by Frank Wilson and colleagues in the USA [59]. In fact, the conclusion that, in left bundle branch block, the principal deflection of the QRS complex would be positive, that is, upwards in lead I, had already been predicted in 1920 by Fahr [60], who had earlier worked with Einthoven.

In the series of editorials [54–57] mentioned above, repeated reference was made to Lewis' book as a classic. That so much of clinical value could have been derived from the available apparatus speaks volumes for the ability and tenacity of those early workers. It is interesting to read the section of Lewis' book [58] on electrodes that were advocated for connecting the patient as shown in Figs. 1.15 and 1.16. "A porous inner vessel is filled with warm water, salt and well-washed cotton wool, to give a mixture of porridge-like consistence." In fact, the porous pot was "surrounded by an outer vessel containing saturated zinc sulphate in which was immersed a sheet of zinc to which the leading off wire was soldered." This technique was still in use in the late 1940s. Modern electrode technology is discussed in Chap. 12.

Lewis was a prolific writer, producing twelve books and over two hundred scientific papers. He was invited by Mackenzie to found the journal *Heart,* which first appeared on 1st July 1909. It is not therefore surprising to find that he had strong views on various matters, and Burchell [54] pointed out Lewis' long campaign "to establish clinical science as a discipline, separate and definable, from both physiology and medical practice." Lewis held the view that

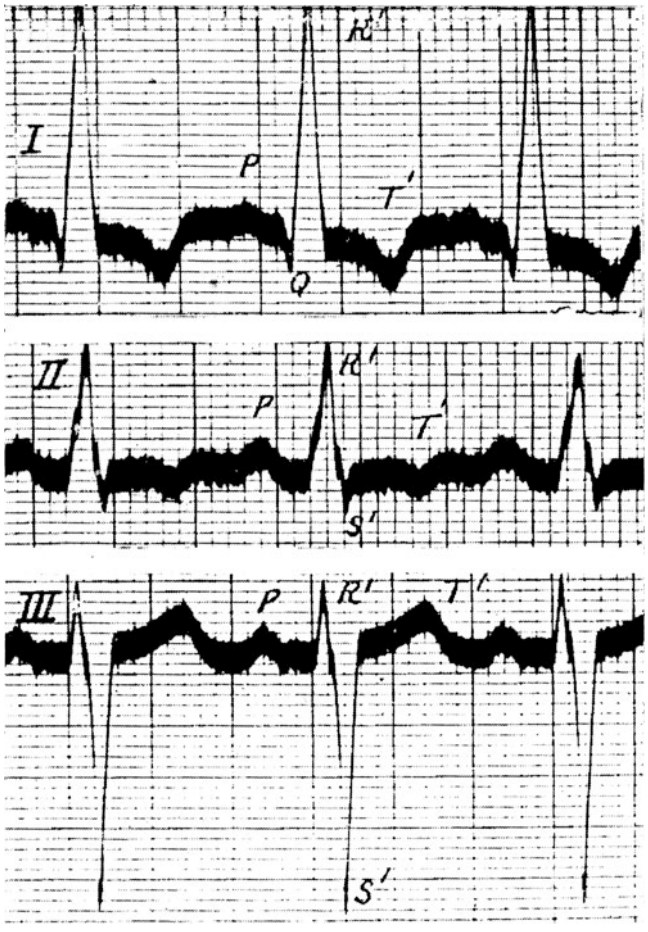

Figure 1.13
Leads I, II and III (not recorded simultaneously) recorded from a patient who was described by Lewis as having a defect "of the right division of the AV bundle." (After Lewis [58]. © Shaw, London. Reproduced with permission.)

"efficient medical practitioners are not scientists" [61]. He discontinued his research into electrocardiography around 1925, perhaps feeling there was not much more of interest, even though the area of myocardial infarction had not been studied.

1.6 The American Connection

As mentioned in Sect. 1.5, one of the early Edelmann galvanometers found its way to the USA in 1909. Five years later, Frank Wilson, working at the University of Michigan, obtained a string galvanometer manufactured by the Cambridge Instrument Company and became deeply involved with electrocardiography, a research field that was to occupy him for the rest of his academic career. By now the reader should no longer be surprised to learn of one further link in the family tree of electrocardiographers. According to Burch and de Pasquale [1], Wilson was stationed in England during World War I in a rehabilitation hospital under the command of none other than Sir Thomas Lewis! Indeed, his first paper appeared in *Heart,* which was edited by Lewis in 1915 [62].

A glance at the contents list of Lewis' book [58] reveals that only one chapter deals with the morphology of the QRS complex in relation to hypertrophy, aberrant contractions and displaced heart. This represents a small proportion in a

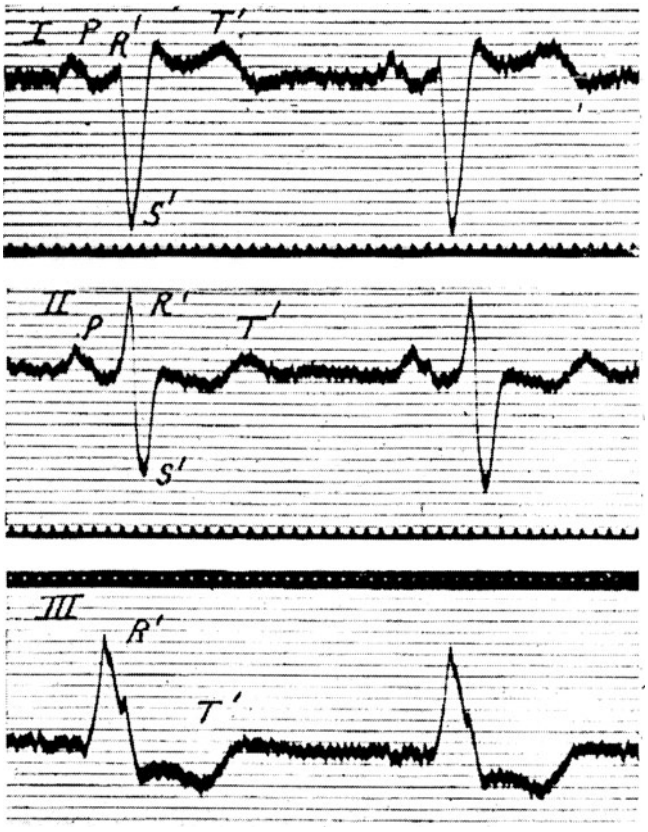

Figure 1.14

Leads I, II and III recorded from a patient who according to Lewis had a defect in the "left division of the bundle." The time marks each represent 1/30 s. (After Lewis [58]. © Shaw, London. Reproduced with permission.)

book of 38 chapters. The significance of the contribution of Wilson can then be seen in the fact that he concentrated his work on the QRS and T morphologies whereas Lewis, often using bipolar chest leads, concentrated heavily on the study of cardiac rhythm.

Although Wilson's initial work appears to have been undertaken in England, Kossmann, in his review of unipolar electrocardiography [7], indicated that Wilson's research in the University of Michigan was based on "a two-string-in-tandem electrocardiograph built by Willem Einthoven and his son." Recordings were at half of normal sensitivity (1 mV = 0.5 cm) in order that two simultaneous recordings could be accommodated on narrow recording film (10 cm wide).

During the 1920s, Wilson and his team undertook a great many studies on correlating the ECG (essentially limb leads I, II and III) with abnormalities such as ventricular hypertrophy and bundle branch block. Some of their work is discussed elsewhere in the book. In particular, the concept of ventricular gradient (› Chaps. 5 and › 17) is still used by many authors today to explain certain phenomena. For example, Abildskov suggests that inequality in the ventricular gradient in different areas of the myocardium may be responsible for ventricular arrhythmias [63]. Nevertheless, it is likely that the major contribution of Wilson will be acknowledged as his "central terminal" with which unipolar chest leads could be recorded. The matter is dealt with fully in › Chaps. 10 and › 11 and will not be reiterated in detail here. In summary, however, the technique allows the potential variation at a single point on the chest to be recorded with respect to a relatively constant reference potential obtained by averaging the potentials of the right and left arms and the left leg.

At this point, it is necessary to consider the confusion that existed around 1930 in terms of the polarity of ECG waveforms. Waller had used a bipolar chest lead in his initial ECG recording of 1887 [20]. However, more extensive

Figure 1.15

An illustration of an early method of recording the Einthoven limb leads. Further details are in the text (After Lewis [58]. © Shaw, London. Reproduced with permission.)

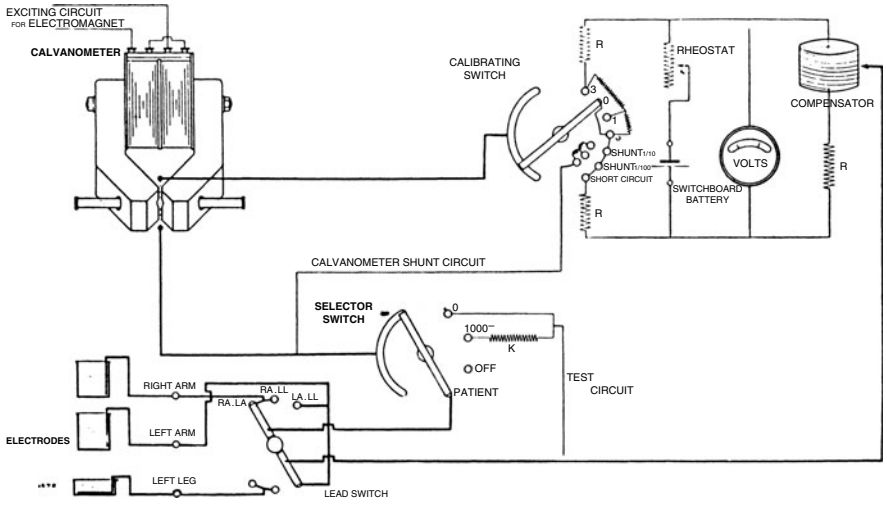

Figure 1.16

A diagram showing the connections from the electrodes of Fig. 1.15 to the galvanometer, as in the Cambridge Electrocardiograph.

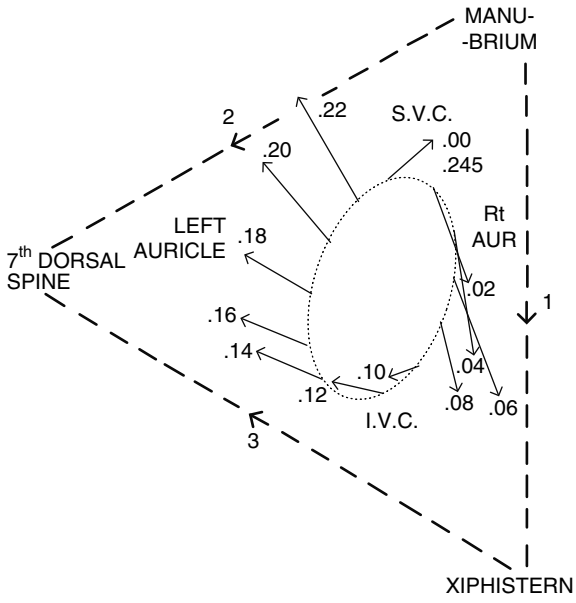

Figure 1.17

A chest electrode system used by Lewis in his studies of atrial flutter. The connection points for the Einthoven electrodes are shown on the diagram (see text for further explanation). Note also that Lewis used these three leads to calculate the axis of the flutter waves shown in Fig. 1.18. The direction of the axis is shown at 20 ms intervals. Lewis indicated that "the flutter in this patient depended upon a circulating wave." He regarded this as strong, if not conclusive, evidence "that circus movement is the basis of clinical auricular flutter." (After Lewis [58]. © Shaw, London. Reproduced with permission.)

use of chest leads was certainly made by Lewis, and Fig. 1.17 shows a lead system which he described for recording three bipolar leads from the chest. The notation 1–3 refers to the bipolar leads of Einthoven, but in this case, the left arm lead is connected to an electrode on the xiphisternum, the right arm lead is connected to the manubrium and the left leg is connected to the seventh dorsal spine. Recordings obtained from these leads in a patient with "clinical flutter" are shown in Fig. 1.18. Einthoven had arranged his galvanometer so that when the left arm connection was relatively positive compared to the right arm connection, an upward deflection was produced by the instrument. In Lewis' system, therefore, the potentials obtained with the connections for lead II and lead III indicate that for the most part the electrode on the spine is relatively positive compared to those on the front of the chest. In fact, in very general terms, the appearances in leads 2 and 3 of Fig. 1.18 would approximately resemble an inverted V2 used nowadays.

In 1931, Wood and colleagues in Pennsylvania recorded a bipolar chest lead on a patient who had a spontaneous attack of chest pain. The bipolar lead was recorded using the Einthoven lead I connections but the left arm electrode was placed on the back and the right arm electrode was on the precordium "at the cardiac level, just to the left of the midline." This lead configuration was described as lead IV since it was an addition to the three leads of Einthoven. During the attack of pain, lead IV showed marked ST depression in a lead that had essentially a dominant R wave. (It should be noted that Einthoven had always called the most prominent deflection, be it positive or negative, the R wave.) This work was subsequently described by Woolferth and Wood in 1932 [64].

In view of the foregoing comments on polarity, what was recorded at that time as ST depression would nowadays be manifested as significant ST elevation in a lead such as V2.

The use of bipolar chest leads proliferated and various combinations were introduced, e.g., the bipolar chest lead CR had the indifferent electrode on the right arm and the exploring electrode on the chest. Such bipolar chest leads are discussed further in Chap. 11. In 1960, in a letter to Burch [1], Wood commented that he still used the CR leads although the hospital ECG department had changed to unipolar precordial leads.

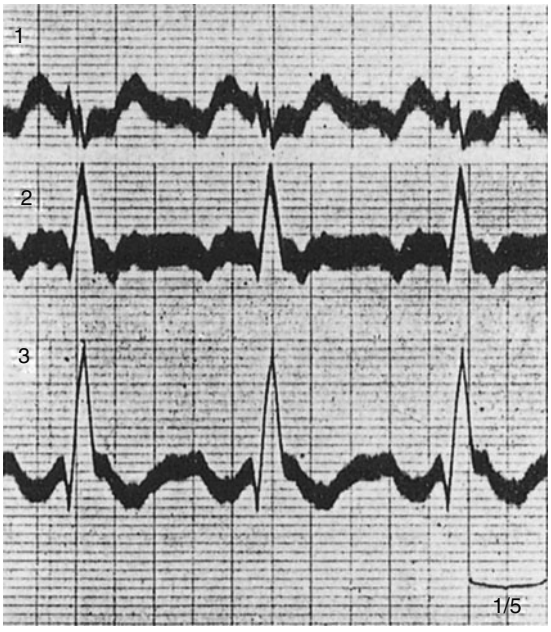

Figure 1.18

The ECGs recorded with the lead system of Fig. 1.17 in a patient with "clinical flutter." Note how appearances in leads denoted 2 and 3, which very approximately resemble V_2 and V_3 used nowadays, have the opposite polarity. (After Lewis [58]. © Shaw, London. Reproduced with permission.)

What was a unipolar precordial lead? As Kossmann has pointed out [7], during all the experimenting with chest leads, a paper of Wilson and colleagues in 1932 [65] largely went unnoticed. By linking the left arm, right arm and left leg through equal resistors to a central terminal, a relatively stable reference potential was obtained with respect to which the potential at an exploring electrode could be measured. The circuit (Fig. 1.19) was also described by Wilson and colleagues in another classic paper in 1934 [66]. Because the potential of the central terminal was essentially constant, the potential difference recorded by the galvanometer reflected the variation at a single point – hence the term "unipolar" lead. Ultimately, these leads became known as "V leads" so that when the exploring electrode was placed on the left arm, the lead was called "VL" (Fig. 1.19). More recently, there has been some discussion [67] on the fact that every ECG lead is bipolar in the sense that the "galvanometer" always measures a potential difference but this author feels that where the potential at one terminal of the galvanometer is essentially constant, the signal generated reflects the potential variation at the other terminal – hence "unipolar" is still an adjective with some meaning even though some would say it was incorrect!

The next stage in the evolution of the unipolar lead was for Wilson's team to specify six precordial positions for the exploring electrode [68]. However, the leads designated V_1 to V_5 covered an area from approximately the fifth rib at the right sternal border to the sixth rib in the left anterior axillary line. The sixth precordial lead was designated VE, where the exploring electrode was placed at the tip of the ensiform process.

In order to try to restore some order from the chaos, a joint group of cardiologists representing the Cardiac Society of Great Britain and Ireland on the one hand and the American Heart Association on the other issued a paper recommending standardization of only one chest electrode position [69]. This paper is very often quoted in error as the definitive recommendation for placement of precordial electrodes. However, it was a second paper, which was published unilaterally later in the same year by the American Heart Association, that did in fact define what are now accepted as the six precordial leads [70]. A further supplementary report was issued by the same committee in 1943 [71].

The story of the American contribution to the development of lead systems (at least for conventional electrocardiography) is completed with the introduction, in 1942, by Goldberger of what became known as the augmented unipolar

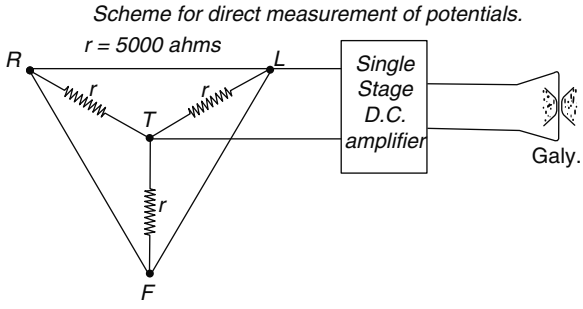

Figure 1.19

A diagram of the Wilson central terminal, denoted T. The limb leads are connected through equal resistors to the central point T. In this case, the circuitry for VL is shown. (After Wilson et al. [66]. © Mosby, St Louis, Missouri. Reproduced with permission.)

limb leads [72]. The modification introduced by Goldberger for recording unipolar limb leads was to remove the Wilson central terminal connection from the limb on which the exploring electrode was placed. In other words, if the exploring electrode were placed on the right arm, the Goldberger terminal, that is, the modified Wilson terminal, would consist only of connections from the left arm and left leg to a central point. It can be shown that the net effect is to augment the potential recorded by VR by 50% exactly (Chap. 11). Thus the term "augmented unipolar limb lead" was introduced. Clearly, there were only three such leads, namely, aVR, aVL and aVF, which could be recorded with this technique.

The development of what is now known as the conventional 12-lead ECG was therefore complete. There were three limb leads I, II and III from Einthoven; three augmented unipolar limb leads aVR, aVL, and aVF from Goldberger's modification of Wilson's central terminal; and six precordial leads V_1–V_6 arising out of the Wilson terminal. The 12-lead ECG is today used everywhere that electrocardiography is practised. Appearances in disease are discussed extensively in Chaps. 14–22. Cardiac arrhythmias are discussed separately in Chaps. 23–30.

As mentioned above, Einthoven had described the maximum deflection of the ventricular complex as the R wave irrespective of whether it was positive or negative [33]. Lewis, on the other hand, had used Q and S for "downward" deflections even when there was a dominant S wave such as in lead I in right axis deviation [58]. This approach prevailed. The standardization of the precordial leads has also helped to ensure that negative deflections in chest leads resulted in downward displacement, and so on. Pardee [73] suggested that if two upward deflections were present, the first should be designated Ra and the second Rb, but although the concept of both upward deflections being called R waves was accepted, it was subsequently the case that the first R wave was called R and the second R′.

1.7 Vectorcardiography

The concept of a vector is introduced in Chap. 2, but for the less mathematically inclined it can be summarized as a device for representing an entity such as a force with which would be associated a magnitude and a direction. Almost from the beginnings of electrocardiography, the concept of a vector force was invoked initially by Waller [21] who had produced an isopotential map (see Sect. Section 1.10) which suggested that the electromotive force of the heart could be represented by a single dipole, a physical entity which is discussed in Chap. 2. Later, Einthoven and colleagues in their classic paper of 1913 [33] introduced the concept of measuring the mean electrical axis of the heart, which was represented by a vector (Fig. 1.20). There are a number of ways of calculating such a mean axis (see Chap. 13) but, in addition, it should be realized that the concept as illustrated in Fig. 1.20 allows what might be called an instantaneous axis to be calculated given a knowledge of the potentials in leads I, II and III at the same instant in time. Lewis was also one of the earliest to exploit this idea and, having recorded leads I, II and III singly from a dog whose right bundle had been cut, he plotted the deflections shown in Fig. 1.21. Thereafter, given the concept of the Einthoven triangle it was feasible to plot a vector for successive instants in the cardiac cycle, and these are also shown in Fig. 1.21. However,

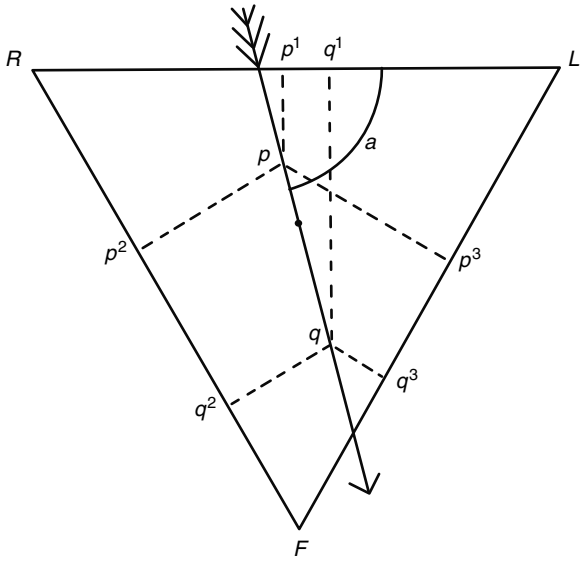

Figure 1.20

An illustration of the resultant cardiac electromotive force represented by a vector *pq* which makes an angle a with the lead I axis. The projection of the vector on the different leads is denoted p^1q^1, p^2q^2 and p^3q^3. (After Einthoven et al. [33]. © Springer, New York. Reproduced with permission.)

although the directions are shown, the magnitude of each vector is apparently constant. Nevertheless, the concept of a vectorcardiogram began to evolve. This work was published by Lewis in his monograph [58] but it had previously appeared in 1916 [74]. It is of interest to note the length of papers published at that time, with this one in particular occupying almost 90 pages.

Burch has reviewed the history of vectorcardiography [2] and he has pointed out that the first publication describing a method for manually deriving "a vectorcardiogram" from standard limb leads was written by Williams and published in 1914 [75]. The methodology is shown in Fig. 1.22. In this case, however, an amplitude is associated with each vector direction, and if the tips of the vectors had been joined in the correct sequence, an approximate figure-of-eight configuration would have been seen. In fact, this was done shortly afterwards by Mann [76], and the loop thus obtained was called a monocardiogram (Fig. 1.23). It should be emphasized that, at that time, all leads were still being recorded singly and therefore, Lewis, Williams and Mann had to align the three complexes as best as possible. Although Mann subsequently invented a monocardiograph, which according to Burch was developed in 1925 though not described until 1938 [77], the advent of the cathode ray oscilloscope radically changed the approach to displaying loops.

The advantage of the oscilloscope was that two separate leads could be applied to opposite pairs of plates in order to deflect the electron beam in proportion to the strength of the signal on each axis (Fig. 1.24). It should be realized that any two different ECG leads applied to an oscilloscope will produce a loop independent of any vector theory. However, in keeping with the concept of a frontal plane loop, Fig. 1.24 shows how lead I could be used to produce a lateral component and VF a vertical component that might give an approximate indication of frontal plane vector forces.

Apparently, Schellong in Germany [78], Wilson's team in the USA [79] and Hollmann and Holmann in Germany [80], independently of each other, developed systems for displaying loops. Of these three groups, Schellong was the first to publish loops recorded with the cathode ray oscilloscope. According to Burch [2], Rijlant also used the cathode ray oscilloscope in 1936 but for the display of the scalar electrocardiogram [81]. It can be imagined how the advent of a new tool was eagerly adopted by many laboratories worldwide with the resultant relatively simultaneous publication of results.

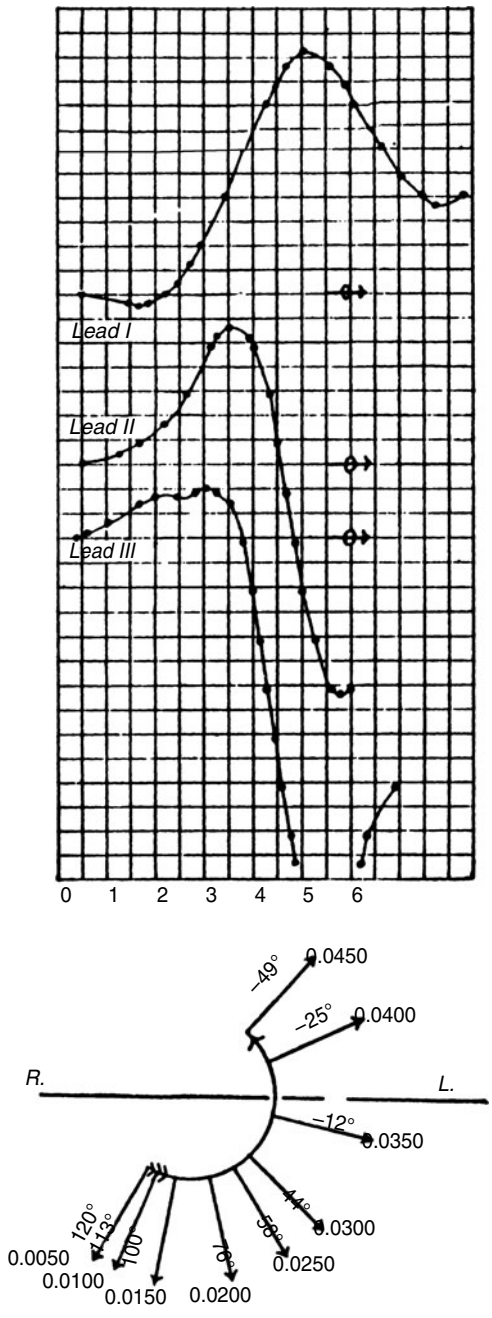

Figure 1.21

Leads I, II and III recorded from a dog in which the right division of the bundle had been destroyed. Lewis, who had recorded the leads singly, aligned them as best as possible in order to calculate the frontal plane QRS axis at 5 ms intervals. It can be seen that the vector moves in a counterclockwise direction during the QRS complex. (After Lewis [58]. © Shaw, London.)

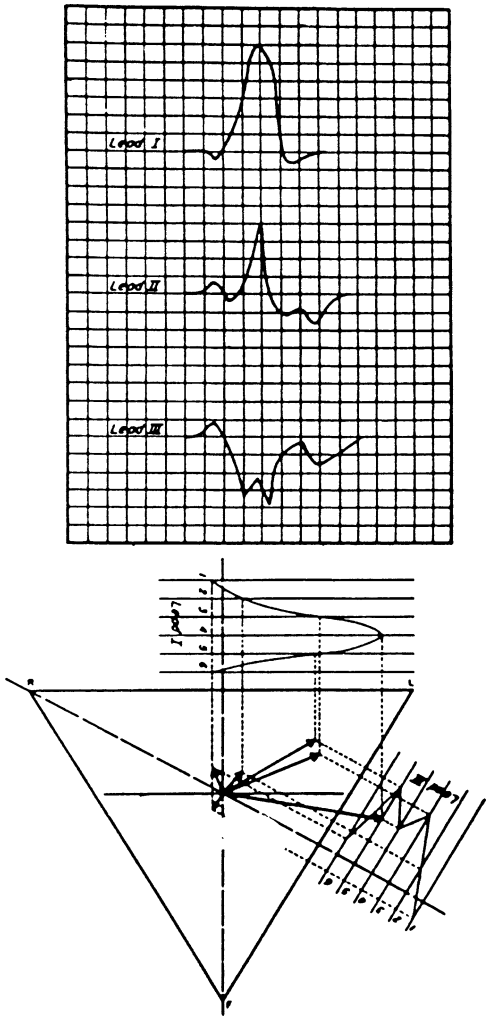

Figure 1.22
Calculation of the resultant cardiac vector in the frontal plane using leads I and III. (After Williams [75]. © American Physiological Society, Bethesda, Maryland. Reproduced with permission.)

Although early efforts at constructing loops were in the frontal plane, the use of the oscilloscope allowed other planes to be viewed with relative ease. The concept of a three-dimensional loop in space gradually grew, and a number of lead systems were introduced to derive the components of the resultant cardiac vector, as discussed in Chapter II.

1.8 Lead Theory

It would be appropriate at this point to diverge briefly in order to review the development of lead theory and its influence on vectorcardiographic lead systems before concluding this section of the history. The theoretical aspects are considered in detail in Chap. 10, but it is of relevance at this point to underline the fact that although electrodes may be placed such that a line joining them is along one of the natural axes of the body, it is not necessarily the case that the potential difference measured by them is a true reflection of the component of the cardiac electromotive forces in that particular direction. The whole concept of vectorcardiography was based on deriving a resultant vector given a knowledge of the

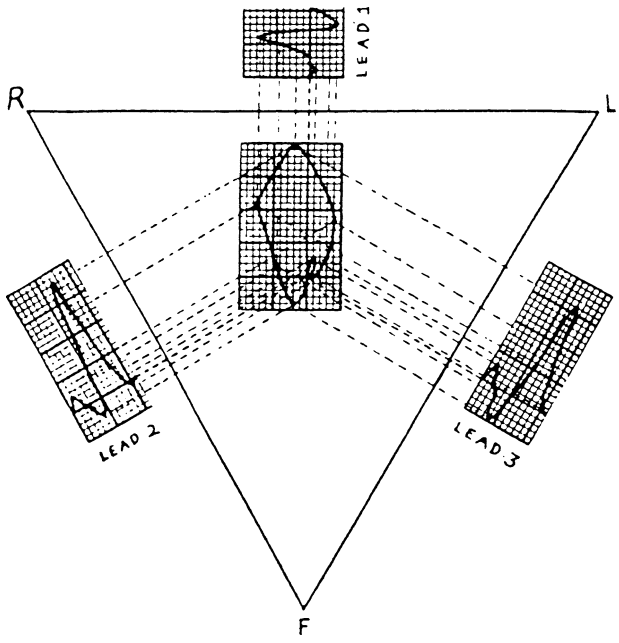

Figure 1.23

Using a procedure similar to that of Fig. 1.22, Mann produced the loop which he called a "monocardiogram." (After Mann [76]. © American Medical Association, Chicago, Illinois. Reproduced with permission.)

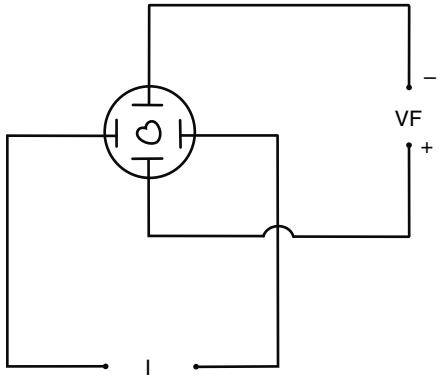

Figure 1.24

A schematic representation showing how two ECG leads applied to opposite pairs of plates of an oscilloscope would deflect the electron beam to produce a loop. The electron beam is deflected in a horizontal direction by an amount in proportion to the amplitude of lead I and is similarly deflected in a vertical direction by VF.

component forces in three mutually perpendicular directions as shown in Fig. 1.25. The aim of lead design was therefore to develop electrode configurations that would faithfully measure components in the desired direction.

If a vector alters its magnitude and direction over a period of time, it is feasible to imagine that its tip traces out a path in three dimensional space, as shown in Fig. 1.26. This illustration also indicates how the loop can be "projected" onto three mutually perpendicular planes to produce 3 two-dimensional loops. In fact, each of these three loops was originally

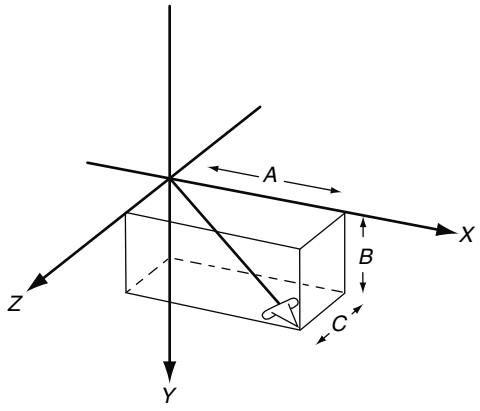

Figure 1.25

The concept of a resultant vector being derived given a knowledge of its components *A*, *B* and *C* in three mutually perpendicular directions *X*, *Y* and *Z*, respectively. A corrected orthogonal-lead system attempts to derive the components *A*, *B* and *C*.

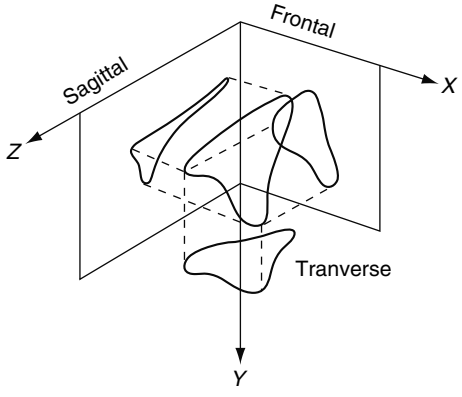

Figure 1.26

The projection of a spatial loop onto three mutually perpendicular planes. The three planar loops are known collectively as the vectorcardiogram.

derived by the methods shown in Fig. 1.24 and detailed in Chap. 11; nowadays, computer-assisted methods are used. Wilson and Johnston [82] introduced the term "vectorcardiogram" to describe the three loops of Fig. 1.26.

A classic series of papers by Burger and van Milaan dealing with lead theory appeared from 1946 to 1948 [83]. These authors showed that in electrical terms, the Einthoven triangle was decidedly not of an equilateral nature (see Fig. 10.3). Other attempts to study lead characteristics were made using two-dimensional media such that current flow and electrical field could be assessed [84, 85]. For example, Fig. 1.27 shows flow lines for lead I obtained from a model where the body was represented by a homogenous conducting medium. The same figure also shows the field map of a normal human subject. Note that the current flow is essentially perpendicular to the lead field. McFee and Johnston, in a classic series of three papers [86], elegantly reviewed the theory of electrocardiographic leads.

Separately, at approximately the same time, Frank made use of a tank model of a human torso in which an artificial generator was situated in order to study the effects of different leads. An important outcome was the creation of an image surface [87], which effectively delineated an imaginary torso where lines joining two points bore a true theoretical relationship to the direction of current flow between the two corresponding points on the actual torso. In other

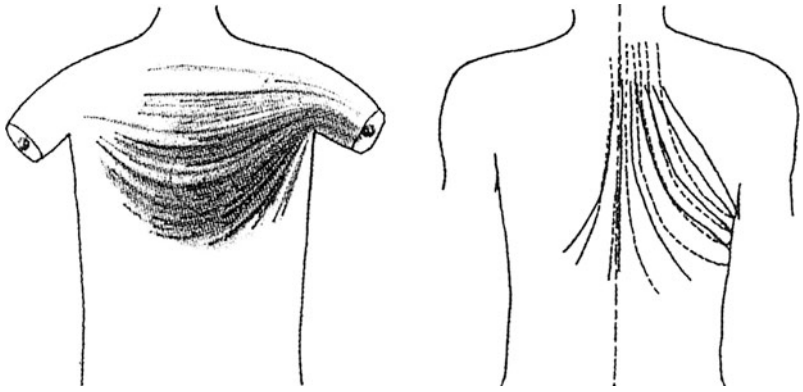

Figure 1.27
Two-dimensional model studies showing on the left, current flow lines from a lead I configuration and on the right, the corresponding electrical field. (After McFee et al. [84]. © American Heart Association, Dallas, Texas. Reproduced with permission.)

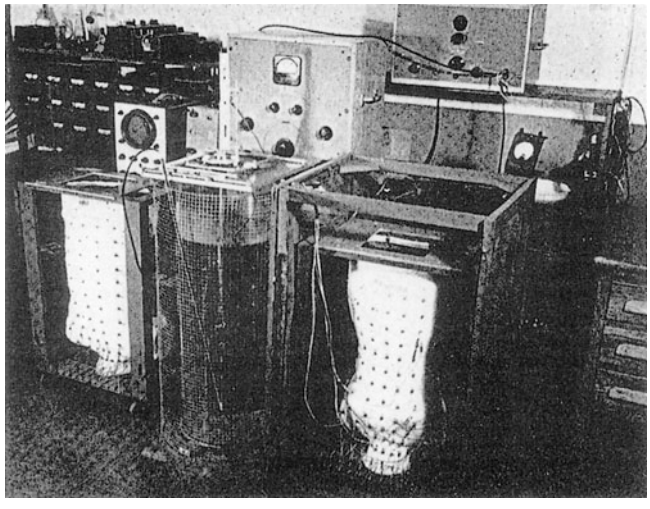

Figure 1.28
A photograph of Frank's laboratory showing a male and female torso model with electrodes attached. The models are mounted upside down to facilitate accurate positioning of the artificial generator. (After Frank E. *Circulation* 1954;9: 723. © American Heart Association, Dallas, Texas. Reproduced with permission.)

words, if a bipolar lead were formed by two electrodes, the line joining the two points in image space corresponding to their positions would indicate the direction associated with that lead, that is, the direction in which the component of the resultant cardiac e.m.f. would be measured. Frank's original model with electrodes attached is shown in Fig. 1.28.

The net result of Frank's studies was the development of a "corrected orthogonal-lead system" which purported to measure the true components of the resultant cardiac vector in three mutually perpendicular directions [88]. This system is probably the most popular lead system for vectorcardiography wherever the technique is still practised. However, it is of interest to note that Burch [2] is somewhat critical of the prominence of the Frank system on account of its susceptibility to repeat variation and the difficulty of applying electrodes properly in all patients, particularly obese women and neonates; he felt that the Equilateral Tetrahedron introduced by Wilson and colleagues [89] was the preferred system.

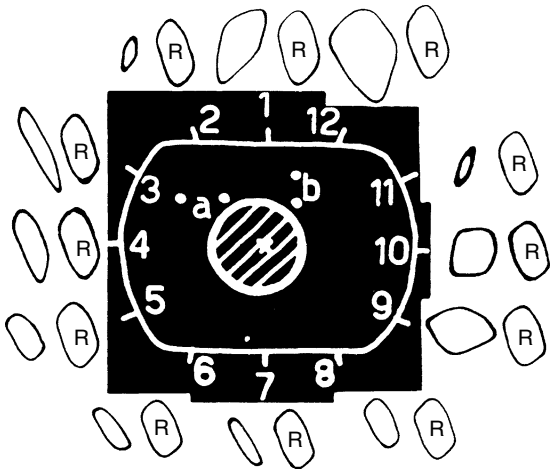

Figure 1.29

A tank model with an elliptical horizontal cross section in which an artificial electrical generator is positioned at a and b. A nonconducting volume is enclosed within the hatched circle. Different electrode positions are denoted 1 to 12. "Vectorgrams" recorded with the network (see text) are denoted R and essentially have the same configuration whichever group of electrodes is used to record the loop. On the other hand, the corresponding vectorgrams derived without being input via the network show marked variation. (After Rijlant [90]. © Academie Royal de Medécine de Belgique, Brussels. Reproduced with permission.)

It would seem that if vectorcardiographic systems do continue in existence, it will not be with this system, for which little data is available.

There have been many other systems of vectorcardiography introduced (see Chap. 11). Rijlant in 1956 proposed the use of a complex electrode array on the body surface consisting of 72 uniformly distributed electrodes. The aim was to link the electrodes together in such a way that they effectively measured potential at an infinite distance from the source assumed to be in a homogenous conducting medium. Such a network minimizes the local or proximity effects. Figure 1.29 shows how "vectorgrams" derived from the network using different combinations maintain an almost uniform shape, while corresponding loops derived simply from the electrode potentials, not fed via the network, show a variety of configurations depending on the combination of electrodes chosen [90]. Schmitt also made many contributions to theoretical and practical studies in electrocardiography; not least, together with Simonson, he introduced the SVEC III (stereo vector electrocardiography) system [91]. In the author's laboratory, despite extensive experience of 3-lead electrocardiography, it was apparent in the mid-1970s that clinicians were reluctant to move from the 12-lead electrocardiogram. For this reason, a hybrid lead system was introduced [92] to combine the 3 and 12-lead ECGs (see Chap. 11). This system is no longer used routinely.

Does vectorcardiography have a future? When the hybrid lead system was first described in 1977 at a private meeting, Rautaharju, author of Chap. 40 of this book, said that it would be the last orthogonal-lead system to be introduced! He was subsequently proved wrong [93, 94], but the substance of his comment is clear. On the other hand, as discussed in Chap. 11, there are other methods for deriving the orthogonal-lead (or X, Y, Z lead) ECG and hence the vectorcardiogram from the conventional 12-lead ECG. Dower, for example, has long been a proponent of polarcardiography (see Chap. 45), which is an alternative form of displaying the orthogonal leads. However, in order to minimize the need for recording both XYZ and 12-lead ECGs, he introduced a method of deriving the 12-lead ECG from the XYZ leads [95]. Essentially, by making use of Frank's image surface, a set of transfer coefficients was derived which allows each of the 12 leads to be expressed as a linear combination of the XYZ leads. Subsequently, there have been several attempts (discussed in Chap. 11) to adopt the inverse procedure, where the XYZ leads are derived from a linear combination of the conventional 12 leads to give the so-called derived XYZ leads [96–98]. The vectorcardiographic loops derived do not compare exactly with the originals but the discrepancies may prove to be of small consequence. The major advantage of

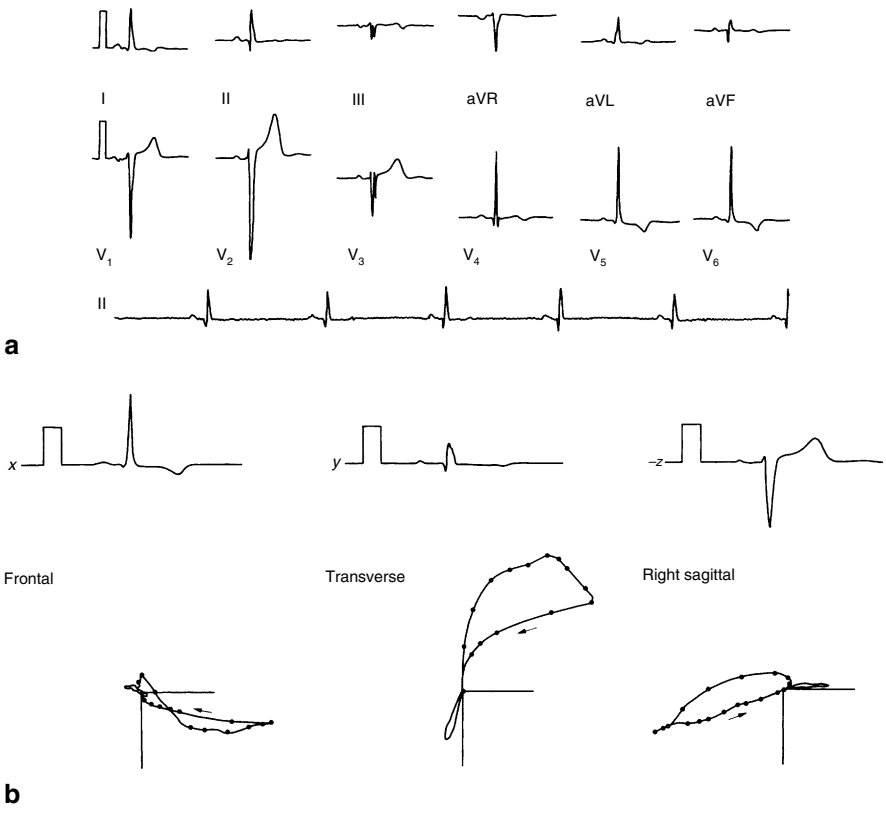

Figure 1.30

12-lead ECG and vectorcardiographic loop derived from the 12-lead ECG (using equations in [96]) in a patient with a history of myocardial infarction. Note that the 12-lead ECG does not show definite evidence of infarction according to classical criteria although $RV_3 < RV_2$, yet the clockwise inscription of the loop in the transverse plane is quite abnormal, being consistent with anteroseptal infarction. The low R waves in V_3 might be considered as caused by LVH. The patient was a 48-year-old male with severe disease of the right coronary artery and the left anterior descending coronary artery. The cardiothoracic ratio was 0.5.

the derived XYZ lead system is that vectorcardiographic loops can be obtained without any additional electrodes compared to the 12-lead ECG requirements, and from these loops, information relating to the phase relationships between the leads can be derived. An example is shown in Fig. 1.30 where the 12-lead ECG does not show clear evidence of myocardial infarction, but where the vectorcardiographic loops with clockwise inscription in the transverse plane are quite abnormal, being consistent with the history of such a clinical abnormality. Dower also developed his EASI lead system [94], so called because of his choice of electrode positions taken from Frank's nomenclature for his own lead system [88]. The EASI lead system is presented in Chap. 11. With only four electrodes plus a neutral electrode, the 12 lead ECG can be derived.

The development of lead systems certainly does not end at this point and the more recent concept of limited lead systems [e.g., 99, 100]. In this approach, a subset of the chest leads, such as V2 and V5 only, is recorded and the other four chest leads are calculated therefrom. This can be done in different ways and the matter is discussed in Chap. 11. The opposite of reduced lead systems is body surface mapping but before looking at this technique, it would be appropriate to consider parallel developments in mathematical modeling of the electrical activity of the heart.

It could be said that the first attempt at modeling the electrical activity of the heart was represented by Waller's illustration of the electrical activity on the surface of the body as being of dipolar configuration [101] – see Fig. 1.31. Einthoven's concept of the mean axis continued the same idea [33] and much work has been done over the intervening years to prove

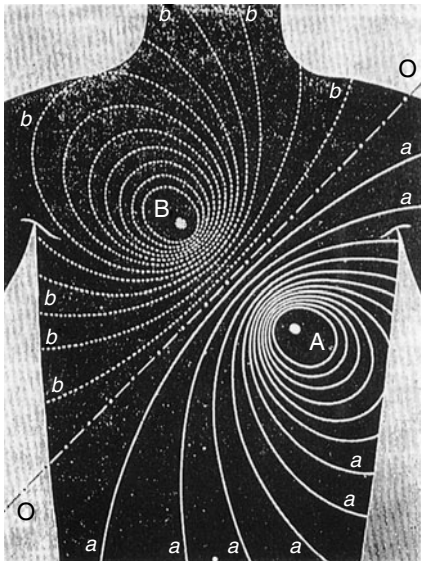

Figure 1.31
The dipolar distribution of the electrical activity of the heart as described by Waller in 1888. The solid isopotential lines indicate positive potentials and the dashed lines indicate negative potentials. (After Waller [101]. © British Medical Association, London. Reproduced with permission.)

whether or not the single-dipole hypothesis was an adequate representation of what became known as the "equivalent cardiac generator." For example, Geselowitz [102] was one of the earliest to discuss the concept of higher-order components such as the quadrupole. Others including Selvester et al. [103] used a multiple-dipole model of the heart to calculate the appearances of vectorcardiographic loops (Fig. 1.32). Although some of this work was first described in the early 1960s, patient research in the interim has resulted in new concepts for the diagnosis of myocardial infarction, as explained fully by Selvester in Chap. 16. The original analogue model of Selvester and colleagues was shortly thereafter transformed into a digital computer model in which simulated myocardial infarction could be studied on the vectorcardiogram [104].

On the other hand, by recording body-surface potentials and using an inverse solution, it is also possible to derive the activities of multiple dipoles as was done for different groups of subjects by Holt and colleagues [105] following on mathematical work undertaken by Lynn and Barnard et al. [106]. Similar work was undertaken in the author's laboratory [107] and Fig. 1.33 shows a ten-dipole model from which the average dipole strengths during ventricular depolarization for a group of 35 normal adult males have been computed. Using the model, the author's group suggested in 1974 that right ventricular infarction could be detected from reduced dipole activity in the right ventricular dipole areas [108]. This paper was greeted with some scepticism when first presented to the British Cardiac Society.

The topic of the forward and inverse problems of electrocardiography is discussed extensively in Chaps. 8 and 9, while other aspects of modeling cardiac cells are discussed in Chap. 6. This area is still one of considerable activity at the present time and particular emphasis is being put on solutions for calculating the epicardial potential distribution from the body-surface potentials, as discussed in Chap. 9. Rudy and his team now based in St. Louis, have demonstrated a very high degree of correlation between calculated and measured isopotential maps using sophisticated modeling techniques allied to a detailed knowledge of anatomy determined from magnetic resonance imaging or computed tomography [109]. The technique which they call ECG imaging, or ECGI, is now being applied to localize the site of cardiac arrhythmias [110]. Boyett and colleagues are also developing a complex model of cardiac activation [111] as part of their goal of producing a "virtual heart" with accurate anatomy and electrophysiology.

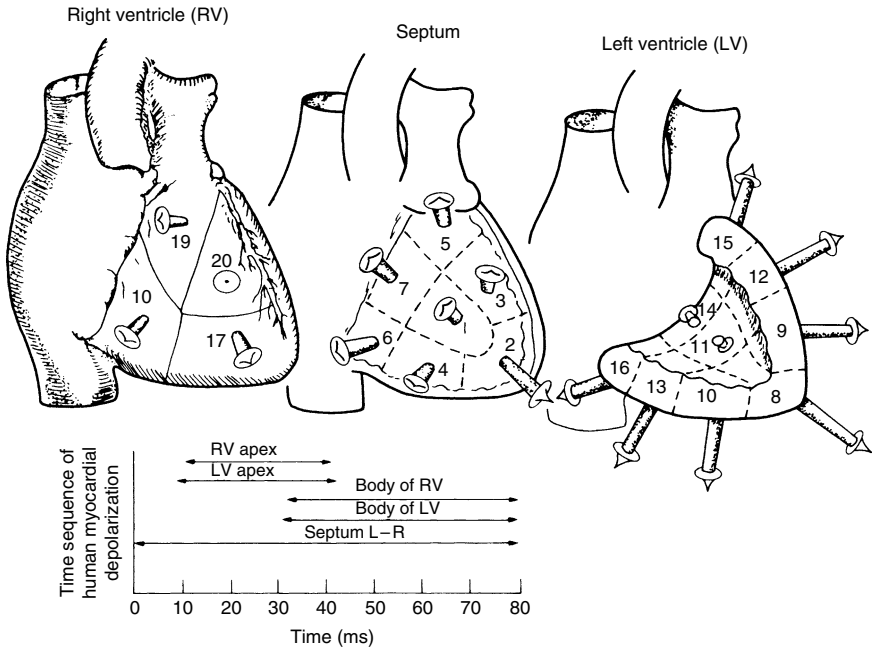

Figure 1.32

A multiple-dipole model of the heart described by Selvester and colleagues in 1965. The dipoles were activated according to the time sequence shown in the lower part of the diagram and the resultant electrical activity was calculated. From this, vectorcardiographic loops were derived. (After Selvester el al. [103]. © American Heart Association, Dallas, Texas. Reproduced with permission.)

1.9 Electrocardiographic Mapping

Although Waller [101] had sketched isopotential maps, it was not really until the 1960s that interest grew in mapping the thorax. Prior to that there had been isolated reports on mapping; and perhaps the first body-surface map (Fig. 1.34) was obtained by Nahum et al. in 1951 [112]. However, there is no doubt that Taccardi has been the pioneer in this field and many references to his work can be found in the appropriate Chap. 32. He is still active and recently published data on the three dimensional sequence of repolarisation and associated potential fields in the ventricles [113].

There are two facets of body-surface mapping. On the one hand, the technique can be regarded as purely empirical in that the spread of excitation can be studied and correlated with other clinical findings in order to derive diagnostic criteria and to obtain a better understanding of the spread of excitation within the heart. On the other hand, recording of potentials, for example, from over 100 points on the thorax allows a mathematical estimation of the total information content on the body surface and from this can be derived subsets of electrodes which can be used to obtain all information of clinical value while retaining the capability of producing the body surface map for visual display. A few brief historical comments are offered on each of these aspects.

In 1971, Barr, who has co-authored Chap. 5 of this book, suggested together with colleagues that 24 electrodes was an adequate number for recovering the total information on the thorax [114]. Later, Korneich [115] suggested that nine leads were required to obtain the clinically important information some of which was missing when only the *XYZ* leads were recorded ([105], see Chap. 11). This result had been obtained after mapping the thorax with a 126-electrode system. A few years later, after extensive mapping of subjects using 192 electrodes, Lux, who has written Chap. 31 of this book, and his colleagues suggested that the order of 30 electrodes was adequate for deriving the total surface information [116]. This allowed the group to design "a limited-lead" system of 32 electrodes which they now use routinely. It is thus evident that body-surface mapping techniques have led to the development of newer lead systems.

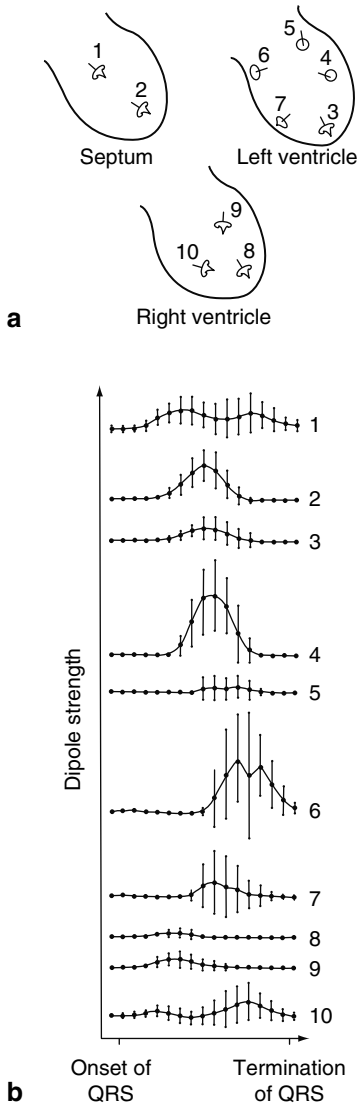

Figure 1.33

In (a), a ten-dipole model of the electrical activity of the heart is shown; (b) shows the average dipole strengths during ventricular depolarization recorded from a group of 35 normal adult males. The standard deviation about the mean values is also shown.

In addition, however, mapping has contributed other findings. In 1965, Taccardi and Marchetti [117] published a hand-drawn isopotential map that showed clearly the nondipolarity of the surface potential distribution at a selected instant during the QRS complex (Fig. 1.35). They indicated that this multipolar situation lasted for 3–10 ms. These findings had been presented at a meeting on the electrophysiology of the heart, which had been chaired by Rijlant in Milan in October 1963. Finally, in connection with mapping, it would be topical to point out that isopotential mapping is claimed to be superior to the 12 lead ECG in the diagnosis of acute myocardial infarction [118].

Various applications of surface mapping are discussed elsewhere in this book. The contribution of body-surface mapping to the field of electrocardiology is ongoing but despite the commercial availability of mapping systems producing attractively colored isopotential maps, it is still true to say, over 20 years after this chapter was first written, that the claimed

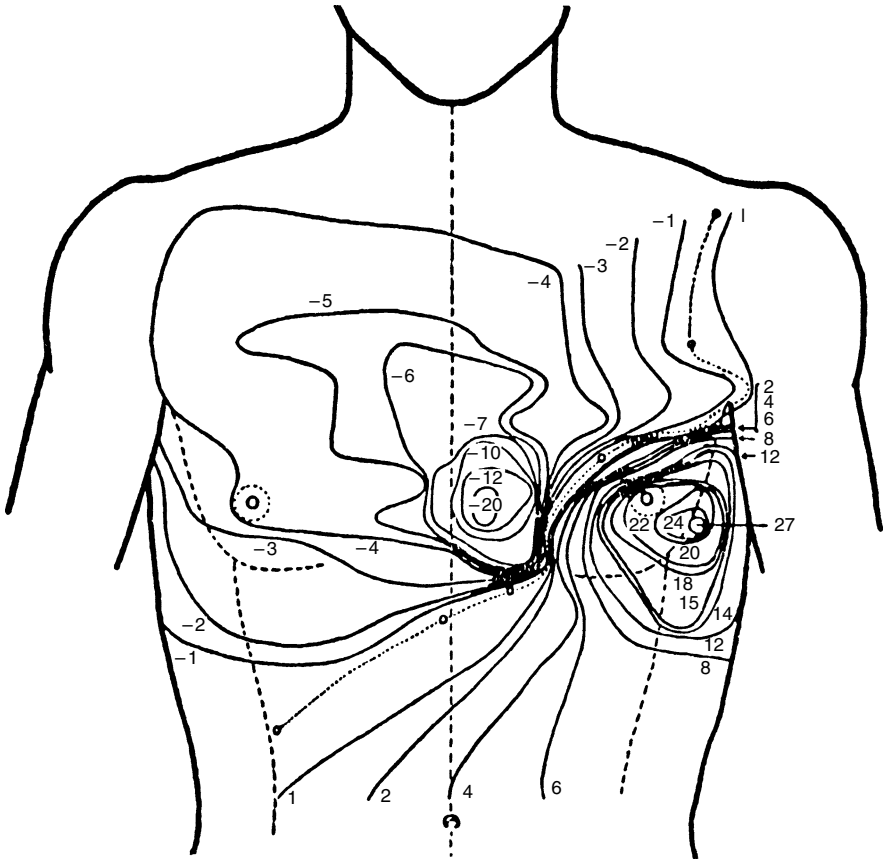

Figure 1.34

An isopotential map at the instant of time defined by the peak of the R wave in lead I in an 18-year-old male patient. The map was plotted by recording a unipolar lead at various points on the precordium simultaneously with lead I which was used as a time reference. This map was published in 1951. (After Nahum et al. [112]. © American Physiological Society, Bethesda, Maryland. Reproduced with permission.)

advantages of mapping per se, as distinct from inverse modeling, have not been readily accepted by the cardiological community at large.

1.10 Activation of the Heart

Studies on the activation of the heart at microscopic and macroscopic level have been in progress from before the start of the twentieth century. The effects of injury had been known at the time of du Bois-Reymond and an article from Burdon Sanderson [119] published in 1900, but possibly displaying data obtained in 1880 according to Burch [1], showed a monophasic action potential recorded from an area of injured myocardium (Fig. 1.36). The first monophasic action potential to be recorded from within a myocardial cell of an intact mammalian heart was reported in 1950 by Woodbury and colleagues [120]. Since then, there has been a dramatic growth in knowledge of the generation of the action potential of individual cells, and in Chap. 3, the current understanding is explained. Of interest in recent times has been the discovery of M cells by Antzelevitch and co-workers [121] in an isolated dog heart preparation. These cells have a longer action potential than endocardial or epicardial cells (Fig. 1.37). An excellent review of the M cell can be found elsewhere [122]. There is currently some controversy as to the role of M cells, which were at one point said to be responsible for the

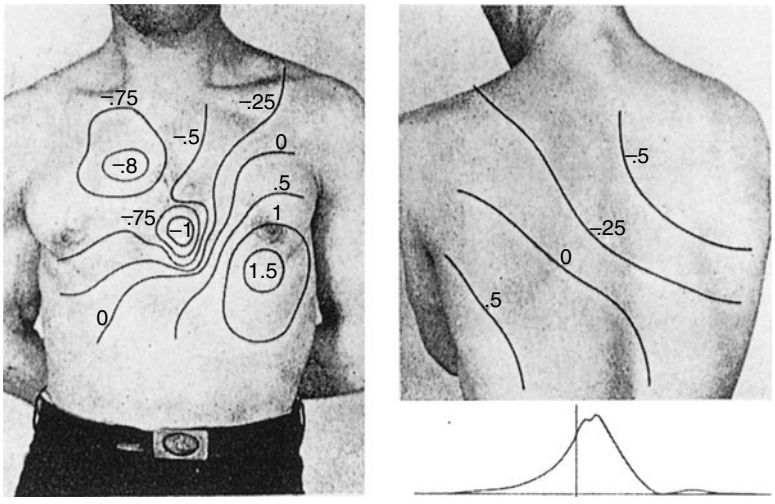

Figure 1.35

A body-surface map drawn at the instant indicated by the vertical line during ventricular activation. Note the multiple minima in the upper right side of the chest indicating a nondipolar potential distribution. (After Taccardi and Marchetti [117]. © Pergamon, Oxford. Reproduced with permission.)

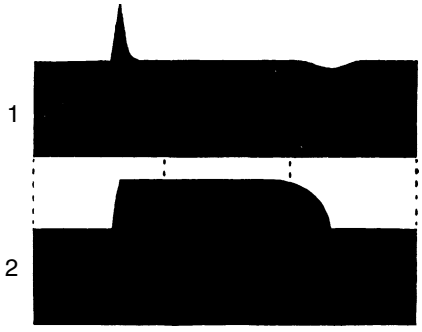

Figure 1.36

Tracing 1 shows a biphasic action potential recorded from an intact heart, while tracing 2 shows a monophasic action potential recorded from an electrode placed on an area of injured myocardium at the apex of the heart. (After Burdon Sanderson [119]. © Pentland, Edinburgh. Reproduced with permission.)

U wave, a theory which is now discounted. The M cell characteristics are well documented in isolated cells but their characteristics may differ in the intact heart. Rudy has pointed out that there is a difference of 90 ms between the action potential durations of simulated M cells and epicardial cells in isolation but that the difference reduces to 18 ms when the cells are well coupled [123].

In Chap. 23, the cellular basis of cardiac arrhythmias is discussed. With the rapid increase of therapeutic preparations for the control of cardiac arrhythmias, there has also been a widespread investigation into the effects of such antiarrhythmic drugs on the action potentials of myocardial cells. An early review of the understanding of action potentials, as well as the role of sodium and calcium ions in the genesis of action potentials, can be found in a symposium on the electrophysiology of the heart [124]. Many well-known European authors contributed to this original work including Grundfest, Girardier, Trautwein, Hecht, Hutter, Corabouf and Wiedmann. This field has also seen an explosion in knowledge in recent years and particularly in the understanding of different ion channels and their role in the generation of cardiac action potentials (see for example [125]). Full details can be found in Chap. 3.

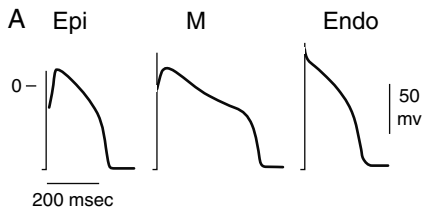

Figure 1.37

An illustration of the different action potential durations of myocytes isolated from the epicardial (Epi), endocardial (Endo) and M regions of the canine left ventricle. Adapted with permission from Antzelevitch C, Zigmunt AC, Dumaine R. Electrophysiology and Pharmacology of Ventricular Repolarization. In Gussak I, Antzelevitch C (eds). Cardiac Repolarization. Humana Press. 2003.

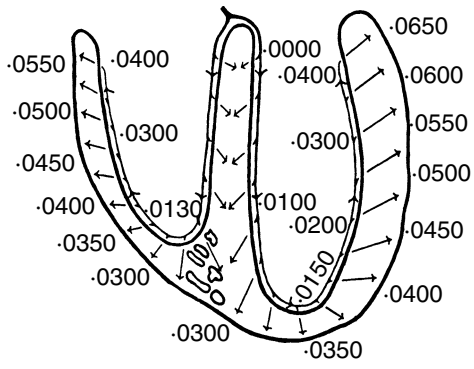

Figure 1.38

Lewis' conception of the spread of excitation in the human heart derived from a study of the human electrocardiogram as well as a knowledge of canine excitation and its relationship to the canine ECG. (After Lewis [58]. © Shaw, London. Reproduced with permission.)

At the macroscopic level, data on the spread of excitation has continued to accumulate through the years. Lewis in his monograph included a number of illustrations of the spread of excitation in the human and dog hearts, the latter in various experimental situations. Fig. 1.38 shows Lewis' attempt to describe the spread of excitation in the human heart "with some pretence to accuracy." In fact, Lewis had carefully studied excitation in the dog heart, and by comparing human ECGs with those of the dog, which in turn were correlated with canine activation, he derived the data of Fig. 1.38. Other notable early contributors to the study of myocardial excitation were Scher and Young [126, 127] as well as the group of Durrer [128] in Amsterdam. The latter group was able to study myocardial activation in the human heart using needle electrodes, and their 1970 paper is an all time classic. One of the authors of that work, namely Janse, has written Chap. 4 outlining current understanding on the activation of the heart. Important early work in this area was also contributed by Boineau [129] and the group of Spach [130].

Although myocardial activation has been well documented, myocardial recovery is still an area requiring further study, although Abildskov and Burgess have spent much time researching this field [131], particularly in the dog heart. Work still continues in the Salt Lake City lab and Taccardi et al. recently published newer data on repolarization in the dog ventricles [113]. Interesting data on recovery in the human heart was reported by Cowan [132] who studied nineteen patients, fourteen of whom with upright T waves were undergoing coronary artery bypass grafting while the remaining five were having surgery for aortic valve replacement, including four with T-wave inversion. He found that in patients with upright T waves there was an inverse relation between the time of activation and the duration of the monophasic action potential, which he also recorded. As a result, activation and repolarization proceeded in opposite directions. The mean sequence of activation was from the septum to the free wall and from the apex to base, whereas during repolarization

the sequence was from base to apex and from the free wall towards the septum. However, in the patients with T-wave inversion, the repolarization sequence resembled that of activation. Thus, it can be seen that there is still much to be explored in the field of cardiac electrophysiology, both at the microscopic and macroscopic levels.

1.11 Arrhythmias, Conduction Defects and Sudden Death

The history of the early work in arrhythmias has been described in Sect. 1.4, when it was made clear that much information on the pulse obtained from the polygraph was used to infer the nature of the "arrhythmia." How different matters are today, when an average of four intracardiac catheters with multiple electrodes or even basket catheters may be used to determine the precise nature of an arrhythmia, as described in Chaps. 24 and 25. Although Krikler [133] suggested that the first clinical intracardiac recording of the electrical activity of the bundle of His was made in Dundee [134], he also acknowledged earlier intracardiac recordings made in France by Lenegre and Maurice [135] during World War II. However, other earlier recordings of the His-bundle activity had also been made in the dog by Alanis et al. [136] and by Giraud et al. [137] in man. Figure 1.39 shows one of the earliest (1958) recordings from the dog. However, it

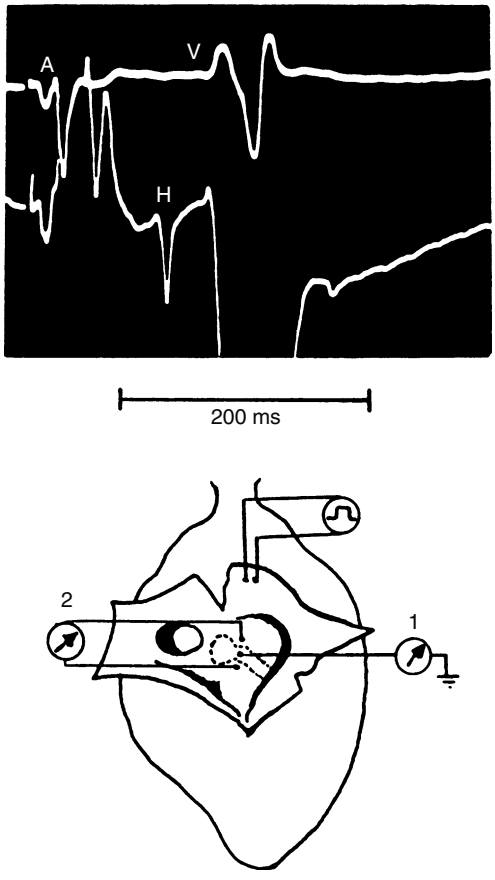

Figure 1.39

A recording made in 1958 of His-bundle activity (H) in a dog. The lower diagram shows the position of the stimulating and recording electrodes. The lower ECG tracing shows the recording from the exploring electrode 1 while the upper tracing shows the bipolar lead 2, when the electrodes were placed 1.5 mm above and below the exploring electrode. (After Alanis et al. [136].

was the work of Scherlag and colleagues [138] that established a standard technique for recording His-bundle activity using an endocardial catheter. About the same time, however, other groups, notably that of Durrer [139] in Amsterdam, had used intracardiac leads for initiating and terminating supraventricular tachycardia and a whole new branch of electrocardiology was opened. The precise mechanisms for arrhythmias could be determined in individual patients and appropriate therapies selected for treatment. Chaps. 25–30 discuss standard surface electrocardiography for the diagnosis of arrhythmias, and wherever necessary, intracardiac electrocardiography for a more detailed analysis of specific arrhythmias. Additional historical details can be found in Chap. 24.

There has been an explosion in clinical electrophysiology in recent years with many cardiologists specialising in this area. With major advances in the use of ablation for treatment of arrhythmias and for disabling accessory pathways, Chap. 25 is devoted to techniques for intracardiac mapping.

At about the same time as a standard technique for His-bundle recording was introduced, Rosenbaum and colleagues in Argentina introduced their concept of a conduction defect in either of the two main fascicles of the left bundle branch-namely, the anterior and posterior fascicles [140]. The concept of divisional block was not totally new [141], but Rosenbaum et al., on the basis of experimental and clinical data, established the various electrocardiographic patterns for what they called left anterior hemiblock and left posterior hemiblock. In view of the trifascicular nature of the left-sided conducting system (see Chap. 4), some authors have preferred to use the term "fascicular block" rather than "hemiblock." In 1981, when writing on the occasion of the 100th anniversary of the birth of Lewis [57], Rosenbaum explained that he used Lewis' illustration of the conduction system of a walrus heart (Fig. 1.40) because it clearly demonstrated what Rosenbaum called the "bifascicular character" of the left bundle branch. This is somewhat contradictory to what was stated immediately above in this section and to what is apparent in Chap. 4. Nevertheless, the point of interest was the reference back to what Rosenbaum called "the gospel." He also went on to recount presenting his ideas in the presence of the late Louis N. Katz who said: "What you have just presented is beautiful; the only problem is that it is not true." Two years later when they met again in San Francisco, Katz told Rosenbaum: "You were right; I was persuaded by having a look at Fig. 1.4 in the Lewis book"! The legend to Fig. 1.4 of Lewis' book, reproduced as the legend to Fig. 1.40, mentions that the further arborization of the two main branches consists of "free strands which cross the cavity." Is this an early demonstration of false tendons that have been suggested as the cause of the wide variation in frontal-plane QRS axis in healthy individuals [142]. Conduction defects are discussed in Chap. 14.

If a good example is required of the earlier reference to the comment of Fisch [10] scorning comments to the effect that further developments in electrocardiography are no longer possible, then the recent "discovery" of the Brugada syndrome [143] linking a right bundle branch block type ECG with sudden death is a perfect case in point (Fig. 1.41). This finding has unleashed a major effort to establish genetic links with the ECG appearances and has already been the topic of two consensus reports [144, 145]. By the same token, the long QT syndrome for many years associated with sudden death (and deafness in some cases) has been the subject of much investigation in relation to various genetic abnormalities in certain chromosomes, while over 10 types of long QT have now been described. Much further detail can be found in Chap. 19. Conversely, the short QT syndrome, first described in 2000 by Gussak et al. [146] is similarly leading to much research in the way of genotyping. Ott and Marcus recently reviewed the various ECG markers linked with sudden death [147].

1.12 Technical Advances

It must be self-evident that the technical advances throughout the twentieth century almost defy description. With them has come a whole host of new investigative techniques of diagnostic and therapeutic value, only a few of which have been discussed here. No history of electrocardiology would be complete without a brief comment on these newer techniques. Because they are relatively recent in inception, the relevant historical details can generally be found in the various chapters in this book that describe their evolution.

Perhaps one of the most widely appreciated developments of the century has been the microelectronic revolution leading to miniaturized computers with a high processing capacity. Electrocardiography has been one field that has not been left behind by such developments. In the late 1950s, the use of computers for ECG interpretation was first evaluated by Pipberger and colleagues [148] using the orthogonal-lead ECG and by Caceres [149] and his team using the 12 lead ECG. At that time, large central computers were used for the analysis and at most, leads were recorded in groups of three simultaneously in analog form. In 1964, the author was introduced to electrocardiography by Professor T.D. Veitch Lawrie

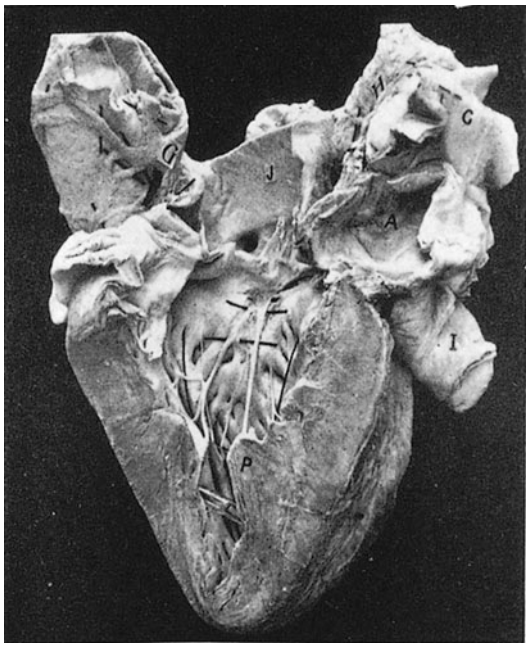

Figure 1.40

A specimen in the Royal College of Surgeons Museum, photographed with the kind permission of Professor Keith. The heart of a walrus dissected from the left side. The greater portions of wall of the left ventricle and left auricle (A) have been removed and the aorta has been divided vertically at its base (J) and the left half taken away. The interventricular septum and the cusps of the aortic valve are exposed. The right anterior cusp of the valve is fully exposed and the mouth of the right coronary artery is seen. Directly beneath the posterior end of this cusp (to the right in the figure), the left division of the auriculoventricular bundle enters the ventricle and immediately splits into two chief branches; these branches lie upon two horizontal bristles, over which there has been a very small amount of dissection. The further course of these branches is perfectly clear, the arborization consisting of free strands which cross the cavity; several large branches enter the papillary muscles, the bases of which are seen (P). Two long bristles are placed behind finer branches of the course network. I lies on the inferior cava; G on the pulmonary artery. Note the large collections of nerve tissue at the base of the heart; bristles are placed behind the thick strands at G, H and C. (After Lewis [58]. © Shaw, London. Reproduced with permission.)

who, with great foresight, anticipated the role of the computer in this field. By the early 1970s, certainly in the Glasgow Royal Infirmary laboratory, the technique had advanced to the stage whereby a small recording unit could be taken to the bedside to make an analog ECG recording which could subsequently be replayed to a laboratory PDP8 minicomputer for interpretation ([150], Fig. 1.42). Nowadays, all 12 leads can be recorded effectively simultaneously in digital form using a microprocessor-based electrocardiograph that can produce an interpretation within seconds of the recording being completed (Fig. 1.43). Full details of computer analysis of ECGs can be found in Chap. 37.

Computer techniques have also helped to enhance exercise testing as discussed in Chap. 30. In particular, the ability of the microprocessor to undertake averaging of the QRST complex in real time represents a significant step forward in improving the quality of data presentation. A word of caution has to be added. Because an average beat represents a collection of beats recorded over a period of time, the trade-off in improved quality possibly has to be set against a small hysteresis in the average beat responding to change in ST-T configuration in particular. Nevertheless, it is now commonplace to use exercise ECG criteria that involve measurement of the ST-T segment 60–80 ms after the end of QRS and this has been greatly facilitated by computer measurement techniques.

Advanced signal processing techniques have also led to a greater interest in the concept of microvolt T wave alternans where small beat to beat variations in T wave amplitude can be measured. David Rosenbaum et al. [150] first used

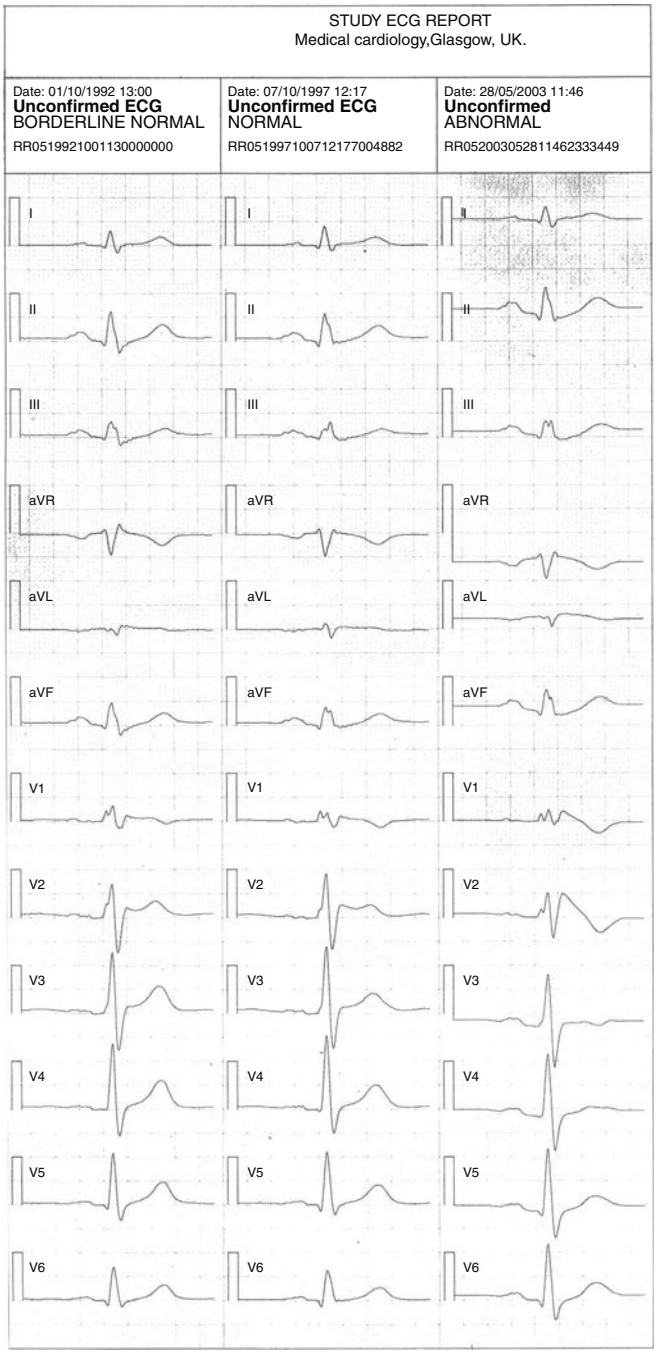

Figure 1.41

An example of the Brugada pattern with the "shark's fin' appearances seen clearly in V_1 and V_2 in the recording made in 2003 in a 71 year old male. It is important to note that earlier recordings as far back as 1992 do not show such obvious changes.

Figure 1.42
A PDP8E minicomputer connected to an analog tape recorder (right-hand side) for analysis of three orthogonal-lead ECGs. This 1971 illustration, taken in Glasgow Royal Infirmary, shows probably the first hospital departmental minicomputer system for routine ECG analysis.

cardiac pacing to increase heart rate and induce microvolt T wave alternans, which they demonstrated to be linked to life threatening ventricular arrhythmias. They paced the heart at around 100 beats per minute prior to making recordings but nowadays, patients may be exercised on a bicycle to achieve a similar heart rate at which point the ECG can be analysed for the presence of T wave alternans. However, Klingenheben recently concluded that the predictive efficacy of the test was highly dependent on the population studied [151].

One of the most significant developments in terms of noninvasive electrocardiographic techniques in the second half of the twentieth century has been the rapid advance of Holter electrocardiography. The technique was named after its inventor, Norman J. Holter, who died in 1983. A brief biographical note was published by Roberts and Silver that year [152]. Holter was a scientist with degrees in physics and chemistry. His early interests were related to radiotelemetry used to stimulate the brain of a rat, essentially by remote control, into which a small radio receiver had been implanted. After World War II, Holter established his own research foundation for "trying to broadcast by radio the more obvious electrophysiological phenomena occurring in humans so that they could be free to do something besides lie quietly on a couch." After working with electroencephalograms (EEGs), his team turned their attention to the ECG. According to Roberts and Silver [153], "the first broadcast of an ECG required 85 lb of equipment, which Holter wore on his back and an accurate electrocardiogram during exercise was recorded." Maclnnis [154] visited Holter in his laboratory in Helena in Montana and was the first to report on the use of the radiotelemetry technique for monitoring the cardiac patient.

Figure 1.43
A microprocessor-based portable electrocardiograph (Burdick Atria 6100) with integral interpretative facilities.

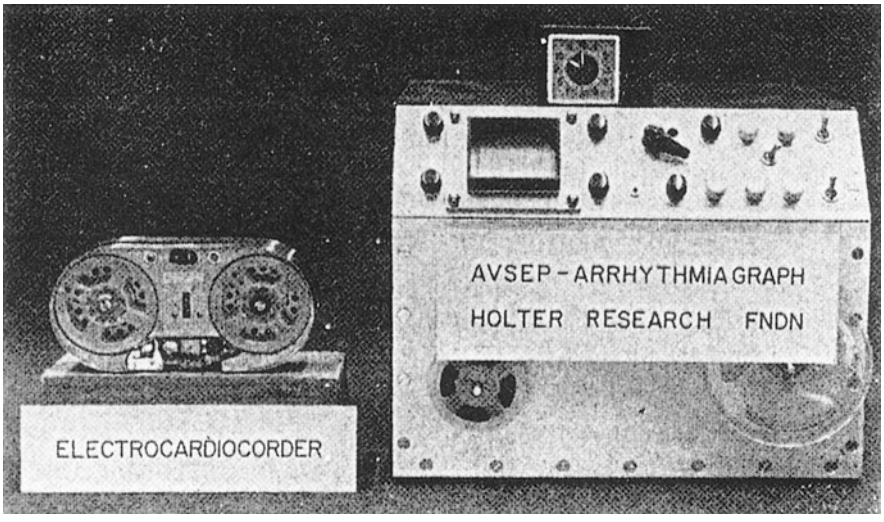

Figure 1.44
The original electrocardiocorder developed by Holter together with the AVSEP analysis unit (see text for further discussion). (After Holter [155]. © American Association for the Advancement of Science. Washington, DC. Reproduced with permission.)

The receiving equipment was situated in Holter's office and the patient was free to walk about in the street outside the building.

The miniaturization of equipment continued and the radio receiver became small enough to place in a briefcase into which a tape-recording device was also incorporated. However, this was still somewhat inconvenient and further development resulted in what Holter termed [155] the electrocardiocorder (Fig. 1.44). This was the forerunner of what is nowadays generally called a Holter recorder. The reel-to-reel tape recorder was small enough to be carried in a man's coat pocket or, as suggested by Holter, in a woman's "strap-type handbag." The first recorder was able to operate for ten hours.

Not only did Holter produce the recorder, he developed an analyzer where initially all beats were superimposed on a cathode ray screen in what was called the AVSEP (audio visual superimposed electrocardiogram presentation) technique.

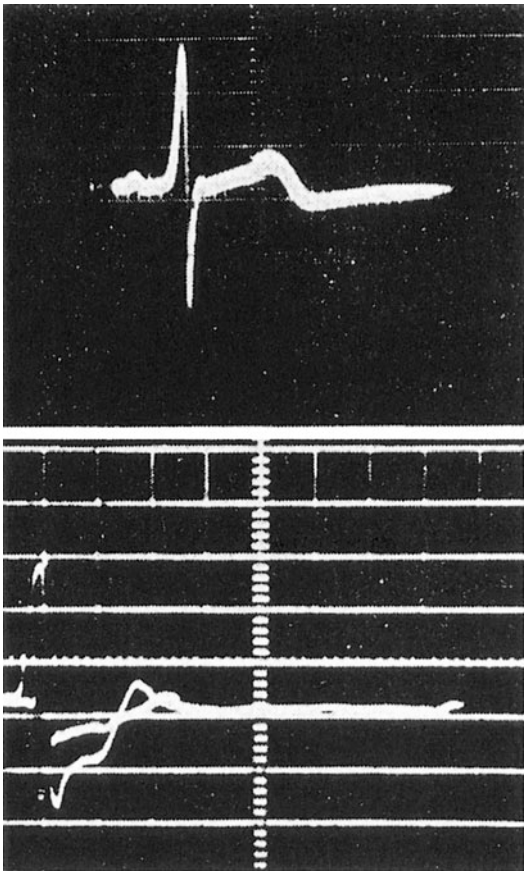

Figure 1.45

The top waveform shows the superimposition of PQRST cycles in sinus rhythm using the AVSEP technique. The lower tracing shows the same approach in a patient with ventricular bigeminy where two different waveforms can be seen. (After Holter [155]. © American Association for the Advancement of Science, Washington, DC. Reproduced with permission.)

Figure 1.45 shows the original presentation of Holter. His early paper also introduced the arrhythmiagram, which was essentially a presentation of R-R intervals as shown in Fig. 1.46. It is also of great interest to note that in his 1961 paper, Holter also presented examples of marked ST depression which he said was evidence of "an attack of angina pectoris in an individual doing forbidden heavy work" (Fig. 1.47). Even allowing for possible shortcomings in the frequency response of the recording system, the ST-T abnormalities do look extremely convincing. Thus from the outset, Holter conceived of his equipment as being of use both for arrhythmia analysis and for the detection of ischemic ST-T changes. This must surely be the first documented Holter ECG evidence of ischemic change.

In their biographical note, Roberts and Silver laid stress on Holter's own belief in serendipity as well as non-goal directed research, that is, the two together could be summarized as discovery by chance. That would seem to be a far cry from today's grant-oriented research teams striving for survival!

The technique of Holter monitoring has opened up a new diagnostic field, while it can also be used to assess the effect of drugs in suppressing arrhythmias. In addition, with modern technology, which mostly involves direct digital recording, accurate ST segment analysis has become possible and this is now of increasing importance in the detection of so-called silent myocardial ischemia and in the evaluation of antianginal drug therapy. Newer concepts such as heart rate turbulence have also evolved from long term ECG recording [156]. Current techniques are discussed in detail in Chap. 33.

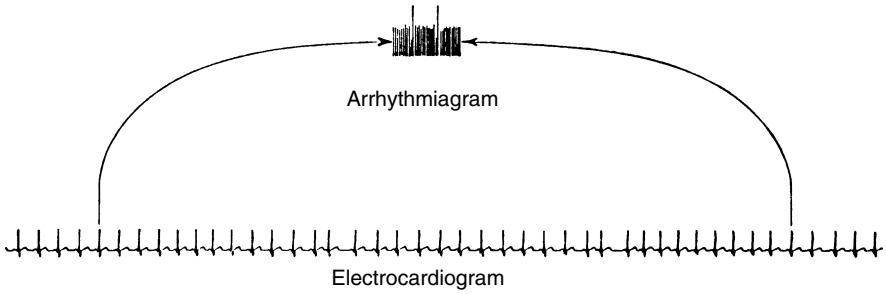

Figure 1.46
Holter's arrhythmiagram, which is essentially a presentation of R-R intervals. When supraventricular extrasystoles are present, as in this case, the long compensatory pause stands out as the tall spike in the arrhythmiagram. (After Holter [155]. © American Association for the Advancement of Science, Washington, DC. Reproduced with permission.)

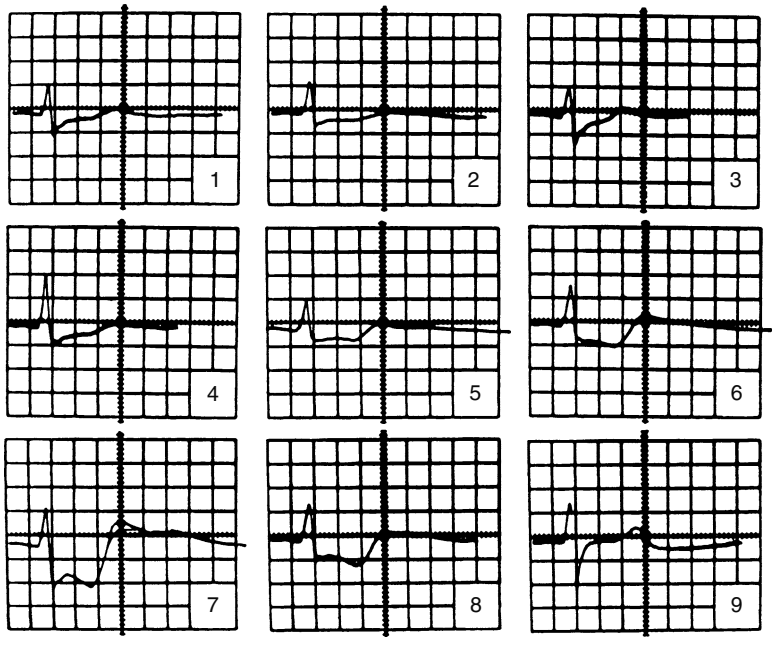

Figure 1.47
A series of AVSEP patterns showing marked ST-T abnormalities. These were recorded with Holter's electrocardiocorder in 1961. (After Holter [155]. © American Association for the Advancement of Science, Washington DC. Reproduced with permission.)

Heart rate variability (HRV) is a technique that has been under investigation for many years though it has not quite broken through into the area of routine clinical application. In part, this may be due to the variety of measures used to quantify HRV. Recently, Sosnowski et al. [157] introduced the heart rate variability fraction which is a much more easily remembered index (cf ejection fraction). This could be one route to greater acceptability (and understanding) of HRV. Further details are to be found in Chap. 35.

The use of microprocessor technology has also led to considerable interest in the study of the high-frequency components of the ECG. In particular, much effort has been spent in assessing the prognostic value of so-called late potentials (see Chap. 39) where low-amplitude high-frequency waves persist at the end of the QRS complex into the early ST segment. These have been associated with ventricular tachycardia in different groups of susceptible patients. Bedside devices now exist for deriving a plot of the high-frequency averaged ECG with a printout of relevant measurements of area and

so on during the last 40 ms of the QRS complex, for example. The high-frequency content of the electrocardiographic signal per se is now enjoying a resurgence of interest almost 50 years after it was first suggested as being of significance in ischemic heart disease [158]. These aspects are also mentioned in Chap. 39, where it is concluded that high frequency electrocardiography will be an area of more intensive research in the coming years.

The first artificial cardiac pacemaker was implanted in Stockholm in 1958 [159]. The device was a simple fixed-rate ventricular pacemaker and from this evolved another aspect of electrocardiology. This was followed by rate-responsive pacemakers (possibly dual chamber) that attempt to detect increased activity on the part of the patient and respond by increasing the rate of stimulation in the most appropriate way for the particular condition of the patient. In turn, this has opened up a new area of pacemaker electrocardiography, which is discussed in Chap. 38. Instead of simply trying, as in the early days, to decide whether a fixed-rate pacemaker was functioning satisfactorily or not, the problem of assessing whether the modern pacemaker is functioning properly according to its true design performance is a complex task requiring considerable skill on the part of the cardiologist. Many implanted pacemakers now incorporate a so-called "Holter" function, by which is meant a memory facility for recording pacemaker activity.

Cardiac resynchronization therapy involving the use of a catheter electrode to pace the left ventricle via the coronary sinus is a recently introduced technique [160]. This presents challenges to electrocardiographers and automated ECG analysis systems in detecting three pacemaker stimuli, though this is only possible if the so called VV interval (between right and left ventricular stimuli) has a measurable duration of a few milliseconds. Initial work in the author's lab is promising.

The use of animals in medical research must not be forgotten. To this end, an extensive review of the dog electrocardiogram is presented in Chap. 41. Interpretation of the canine ECG is an art in itself, requiring a good understanding of the normal appearances in the different breeds. An accompanying Chap. 42 on comparative electrocardiography provides an exceptionally detailed compendium of appearances in various species of mammals, from certain types of whale to the elephant.

For centuries, the relationship between the electric and magnetic fields has been known. However, it was not until 1963 that the magnetic field of the heart was first detected by Baule and McFee [161]. At that time, as explained in Chap. 44, signal averaging had to be used to detect the weak signal from the cardiac magnetic field. In general in the early days, shielded rooms had to be used with equipment which was rather large and immobile. Although the situation has improved in recent years with a reduction in the size of equipment, the technique of magnetocardiography is, as far as is known, still limited to a few research centers in Germany, Italy, Scandinavia and North America. The electric and magnetic vectors of the heart, as of any source, are perpendicular to each other, and as such there has to be a close relationship between the magnetocardiogram and the electrocardiogram. On the other hand, the injury potentials that produce TP depression on the ECG, which is often detected as ST elevation, can be differentiated in the magnetocardiogram. The technique has its proponents, but it still remains to be seen whether any advantages which can be demonstrated outweigh the benefit of the simpler recording equipment required for the electrocardiogram.

The advances in technology have allowed computer databases to contribute to epidemiological investigations as discussed in Chap. 40 and, to a certain extent, in Chap. 13. Although there have been many large-scale studies with electrocardiograms interpreted by conventional means and even coded by hand, it is now the case that computer processing relieves cardiologists and technicians of this chore, though there is a requirement to check the individual results to ensure that technical problems have not interfered with coding. Much can still be gained by diligent, painstaking, methodical collection of ECGs and follow-up of patients over a period of years. Perhaps one of the best known epidemiological studies is that of the population in Framingham in Massachusetts, and many interesting ECG findings have emerged [162, 163]. It was shown that nonspecific ST-T wave changes carried a significantly increased risk of coronary morbidity and mortality and the combination of both seemed most "hazardous." It was concluded that individuals who develop nonspecific ST-T changes without explanation require vigorous preventive management against coronary heart disease. Furthermore, in a separate paper, the same group showed that while ECG data did not contribute to a predictive model for sudden unexpected death, they did improve substantially the predictive model for sudden death in persons with known coronary heart disease. While computer techniques were not used for ECG analysis in these studies, the message is that the use of the ECG in epidemiological studies is invaluable.

Very recently, there has been a rapidly growing interest in utilising ECG measures in genome wide association studies. For example, the long QT interval has been associated with the NOS1AP gene [165]. It can be expected that there will be a growing number of publications in this area in the near future.

1.13 Conclusion

This chapter has presented a necessarily brief review of the history of electrocardiology, and much has had to be omitted. Additional information can be found in many other chapters in the book but it is hoped that if nothing else, the foregoing continues to justify the use of the term "Electrocardiology" rather than "Electrocardiography." Of course, the history of the latter is greater and has received more attention, since most readers will be relatively familiar with the newer aspects of electrocardiology. Perhaps advances over the next few years will be as dramatic as those in the past so that today's techniques will seem so old by comparison that they will merit inclusion in any future historical review.

References

1. Burch, G.E. and N.P. de Pasquale, *A History of Electrocardiography*. Chicago: Year Book Medical, 1964.
2. Burch, G.E., The history of vectorcardiography. *Med. Hist.*, 1985;**5**: 103–131.
3. Cooper, J.K., Electrocardiography 100 years ago. *N. Engl. J. Med.*, 1986;**315**: 461–464.
4. Sykes, A.H., A D Waller and the electrocardiogram, 1887. *Br. Med. J.*, 1987;**294**: 1396–1398.
5. Lamas, G.A., L.R. Koller, E.M. Antman, and T.W. Smith, Electrocardiogram by Einthoven 63 years earlier. *Am. J. Cardiol.*, 1984;**54**: 1163–1165.
6. Burchell, H.B., A centennial note on waller and the first human electrocardiogram. *Am. J. Cardiol.*, 1987;**59**: 979–983.
7. Kossmann, C.E., Unipolar electrocardiography of wilson: A half century later. *Am. Heart J.*, 1985;**110**: 901–904.
8. Barold, S.S., Advanced 12 lead electrocardiography. *Cardiol Clin.*, 2006;**24**: 305–513.
9. Macfarlane, P.W., Renaissance in electrocardiography. *Lancet*, 1999;**353**: 1377–1379.
10. Wellens, H.J.J., The electrocardiogram 80 years after Einthoven. *J. Am. Coll. Cardiol.*, 1986;**7**: 484–491.
11. Fisch, C., The clinical electrocardiogram: A classic. *Circulation*, 1980;**62**(Suppl. III): 1–4.
12. Rijlant, P., The coming of age of electrophysiology and electrocardiography. *NTM-Schriftenr. Gesch. Naturwis,s.Tech.Med.*, 1980;**17**: 108–123.
13. Lempert, G.L., From electrocardiography to electrocardiology. *Adv. Cardiol.*, 1976;**16**: 57–61.
14. Snellen, H.A., A History Of Cardiology. Rotterdam: Donker, 1984.
15. Kölliker, A. and H. Muller, Nachweis der negativen Schwankung des Muskelstroms am naturlich sich contrahirenden Muskel. *Verh. Phys. Med. Ges. Wiirzburg*, 1856;**6**: 528–533.
16. Marey, E.J., Des variations electriques des muscles et du coeur en particulier etudies au moyen de l"electrometer de M Lippmann. *C. R. Acad. Sci.*, 1876;**82**: 975–977.
17. Engelmann, T.W., Ueber das electrische Verhalten des thatigen Herzens. *Pflug. Arch.*, 1878;**17**: 68–99.
18. Burdon Sanderson, J. and F.J.M. Page, Experimental results relating to the rhythmical and excitatory motions of the ventricle of the heart of the frog, and of the electrical phenomena which accompany them. *Proc. R. Soc. London*, 1878;**27**: 410–414.
19. Burdon Sanderson, J. and F.J.M. Page, On the time-relations of the excitatory process in the ventricle of the heart of the frog. *J. Physiol.*, 1879;**2**: 384–435.
20. Waller, A.D., A demonstration on man of electromotive changes accompanying the heart's beat. *J. Physiol.*, 1887;**8**: 229–234.
21. Waller, A.D., On the electromotive changes connected with the beat of the mammalian heart, and of the human heart in particular. *Phil. Trans. R. Soc. London, Ser. B.*, 1889;**180**: 169–194.
22. Besterman, E. and R. Creese, Waller-pioneer of electrocardiography. *Br. Heart J.*, 1979;**42**(1): 61–64.
23. Burch, G.J., On a method of determining the value of rapid variations of a difference of potential by means of the capillary electrometer. *Proc. R. Soc. London (Bioi)*, 1890;**48**: 89–93.
24. Snellen, H.A., *Two Pioneer"s of Electrocardiography. The Correspondence Between Einlhoven and Lewis from* 1908–1926, Rotterdam: Donker, 1983.
25. Einthoven, W., The different forms of the human electrocardiogram and their signification. *Lancet*, 1912;**1**: 853–861.
26. Ader, C., Sur un nouvel appareil enregistreur pour cables sous-marins. *C. R. Acad. Sci. (Paris)*, 1897;**124**: 1440–1442.
27. Einthoven, W., Un nouveau galvanometre. *Arch. Neerl. Sci. Exacles Nal.*, 1901;**6**: 625–633.
28. Bosscha, J., *Dissertatio Physica Inauguralis De Ralvanomelro Differenliali*. Leiden: Menzel, 1854.
29. Burchell, H.B., Did Einthoven invent a string galvanometer? *Br. Heart J.*, 1987;**57**: 190–193.
30. Einthoven, W., Die galvanometrische Registrirung des mensch lichen Elektrokardiogramms, zugleich cine Beurtheilung der Anwendung des Capilar-Elektrometers in der Physiologie. *Plug. Arch.*, 1903;**99**: 472–480.
31. Einthoven, W., Le Telecardiogramme. *Arch. fIll. Physiol.*, 1906;**4**: 132–164 (Translation: Matthewson, F.A.L. and Jack, H. *Am. Heart J.*, 1955;**49**: 77–82. Blackburn H.W. *Am. Heart J.*, 1957;**53**: 602–615.)
32. Einthoven, W., Weiteres uber das Elektrokardiogramm. *Plug. Arch.*, 1908;**122**: 517–584.
33. Einthoven, W., G. Fahr, and A. de Waart, Uber die Richtung und die manifeste Grosse der Potentialschwankungen immensch lichen Herzen und uber den Einfluss der Herzlage auf die Form des Elektrokardiogramms. *Pflug. Arch.*, 1913;**150**: 275–315. (Translation: Hoff, H.E., Sekelj, P. *Am. Heart J.*, 1950;**40**: 163–194.)
34. Henson, J.R., Descartes and the ECG lettering series. *J. Hist. Med. Allied Sci.*, 1971;**26**: 181–186.
35. Hurst, J.W., Naming of the waves in the ECG, with a brief account of their Genesis. *Circulation*, 1998;**98**: 1937–1942.
36. Gussak, I., P. Bjerregaard, T.M. Egan, and B.R. Chaitman, ECG phenomenon called the J wave: History, pathophysiology and clinical significance. *J. Electrocardiol.*, 1995;**28**: 49–58.

37. Scherf, D. and A. Schott, *Extrasystoles and Allied Arrhythmias*, 2nd edn, London: Heinemann Medical, 1973.
38. Read, B.E., Gleanings from old Chinese medicine. *Ann. Med. Hist.*, 1926;**8**: 16–19.
39. Hubotter, F., *Die chinesische medizin zu beginn des XX. jahrhunderts und ihr historischer Entwicklungsgang.* Leipzig: Asia Major (Schindler), 1929.
40. Arcieri, J.P., *The Circulation of the Blood And Andrea Cesalpino of Arezzo*, New York: Vanni, 1945.
41. Wenckebach, K.F., *Arhythmia of the Heart: A Physiological and Clinical Study.* Edinburgh: Green, 1904.
42. Mackenzie, J., *The Study of the Pulse, Arterial, Venous, and Heptic, and of the Movements of the Heart.* Edinburgh: Pentland, 1902.
43. Mackenzie, J., *Diseases of the Heart.* London: Frowde, 1908.
44. Engelmann, T.W., Beobachtungen und Versuche am suspendirten Herzen. 2. Abh. Ueber die Leitung der Bewegungsreize im Herzen. *Pflug. Arch.*, 1894;**56**: 149–202.
45. McWilliam, J.A., Fibrillar contraction of the heart. *J. Physiol.*, 1887;**8**: 296–310.
46. His, W., Ueber die Tiitigkeit des embryonalen Herzens und deren Bedeutung fur die Lehre von der Herzbewegung beim Erwachsenen. *Arb. Med. Klin. Leipzig.*, 1893;**1**: 14–50.
47. His, W., Zur Geschichte des Atrioventrikularbundels nebst Bemerkungen uber die embryonale Herztiitigkeit. *Klin. Wochenschr.*, 1933;**12**: 569–574.
48. Hering, H.E., Ober den Pulsus irregularis perpetuus. *Dtsch. Arch. Klin. Med.*, 1908;**94**: 185–204.
49. Lewis, T., Irregular action of the heart in mitral stenosis: The inception of ventricular rhythm, etc. *Q. J. Med.*, 1909;**2**: 356–367.
50. Samojloff, A., *Eleklrokardiogramme.* Jena: Fischer, 1909.
51. Krikler, D.M., The search for Samojloff: A Russian physiologist in times of change. *Br. Med. J.*, 1987;**295**: 1624–1627.
52. Lepeschkin, E., *Modern Electrocardiography*. Baltimore: Williams and Wilkins, 1951.
53. Lewis, T., *The Mechanism of the Heart Beat,with Special Reference to its Clinical Pathology*, London: Shaw, 1911.
54. Burchell, H., Sir Thomas Lewis: His impact on American cardiology. *Br. Heart J.*, 1981;**46**: 1–4.
55. Snellen, H.A., Thomas Lewis (1881–1945) and cardiology in Europe. *Br. Heart J.*, 1981;**46**: 121–125.
56. Hollman, A., Thomas Lewis the early years. *Br. Heart J.*, 1981;**46**: 233–244.
57. Rosenbaum, M.B., Sir Thomas Lewis: A view from the south. *Br. Heart J.*, 1981;**46**: 349–350.
58. Lewis, T., *The Mechanism and Graphic Registration of the Heart Beat*, 3rd ed. London: Shaw, 1925.
59. Wilson, F.N., A.G. Macleod, and P.S. Barker, The interpretation of the initial deflections of the ventricular complex of the electrocardiogram. *Am. Heart J.*, 1931;**6**: 637–664.
60. Fahr, G., An analysis of the spread of the excitation wave in the human ventricle. *Arch. Intern. Med.*, 1920;**25**: 146–173.
61. Lewis, T., *Research in Medicine and Other Addresses.* London: Lewis, 1939.
62. Wilson, F.N., Report of a case showing premature beats arising in the junctional tissues. *Heart*, 1915;**6**: 17–22.
63. Abildskov, J.A., Prediction of ventricular arrhythmias from ECG waveforms. *J. Electrocardiol.*, 1987;**20**(Suppl.): 97–101.
64. Woolferth, C.C. and F.C. Wood, The Electrocardiographic diagnosis of coronary occlusion by the use of chest leads. *Am. Heart J.*, 1932;**7**: 404 (abstract).
65. Wilson, F.N., A.G. Macleod, and P.S. Barker, Electrocardiographic Leads which record potential variations produced by the heart beat at a single point. *Proc. Soc. Exp. Bioi. Med.*, 1932;**29**: 1011–1012.
66. Wilson, F.N., F.D. Johnston, A.G. Macleod, and P.S. Barker, Electrocardiograms that Represent the potential variations of a single electrode. *Am. Heart J.*, 1934;**9**: 447–471.
67. Kligfield, P., L.S. Gettes, and J.J. Bailley, et al., Recommendations for the standardization and interpretation of the electrocardiogram: Part 1: The electrocardiogram and its technology. *Circulation*, 2007;**115**: 1306–1324.
68. Kossmann, C.E. and F.D. Johnston, The precordial electrocardiogram. I. The potential variations of the precordium and of the extremities in normal subjects. *Am. Heart J.*, 1935;**10**: 925–941.
69. Joint Recommendations of the American Heart Association and the Cardiac Society of Great Britain and Ireland. Standardization of precordial leads. *Am. Heart J.*, 1938;**15**: 107–108.
70. Committee of the American Heart Association for the Standardization of Precordial Leads. Standardization of precordial leads. supplementary report. *Am. Heart J.*, 1938;**15**: 235–239.
71. Committee on Precordial leads of the American Heart Association for the Standardization of Precordial Leads. Standardization of precordial leads. second supplementary report. *J. Am. Med. Assoc.*, 1943;**121**: 1349–1351.
72. Goldberger, E., A simple, indifferent, electrocardiographic electrode of zero potential and a technique of obtaining augmented, unipolar, extremity leads. *Am. Heart J.*, 1942;**23**: 483–492.
73. Pardee, H.E.B., Nomenclature and description of the electrocardiogram. *Am. Heart J.*, 1940;**20**: 655–666.
74. Lewis, T., The spread of the excitatory process in the vertebrate heart. *Phil. Trans. R. Soc. London, Ser. B.*, 1916;**207**: 221–310.
75. Williams, H.B., On the cause of the phase difference frequently observed between homonymous peaks of the electrocardiogram. *Am. J. Physiol.*, 1914;**35**: 292–300.
76. Mann, H., A method of analyzing the electrocardiogram. *Arch. Intern. Med.*, 1920;**25**: 283–294.
77. Mann, H., The monocardiograph. *Am. Heart J.*, 1938;**15**: 681–699.
78. Schellong, F., Elektrographische Diagnostik der Herzmuskelerkrankungen. *Verh. Dtsch. Ges. Inn Med.i* 1936;**48**: 288–310.
79. Wilson, F.N., F.D. Johnston, and P.S. Barker, The use of the cathode-ray oscillograph in the study of the monocardiogram. *J. Clin. Invest.*, 1937;**16**: 664–665.
80. Hollmann, W. and H.E. Hollmann, Neue Elektrokardiographische Untersuchungsmethoden. z. *Kreislaufforsch.*, 1937;**29**: 546–558.
81. Rijlant, P., Introduction a l'"etude de la distribution spatiale des variatiolls de potentiel produites par le coeur chez l'homme. *C. R. Seances Soc. Biol.*, 1936;**121**: 1358–1361.
82. Wilson, F.N. and F.D. Johnston, The vectorcardiogram. *Am. Heart J.*, 1938;**16**: 14–28.
83. Burger, H.C. and J.B. Van Milaan, Heart vector and leads. I, II and III. *Br. Heart J.*, 1946;**8**: 157–161, 1947;**9**: 154–160 and 1948;**10**: 229–233.
84. McFee, R., R.M. Stow, and F.D. Johnston, Graphic representation of electrocardiographic leads by means of fluid mappers. *Circulation*, 1952;**6**: 21–29.
85. Brody, D.A., B.D. Erb, and W.E. Romans, The approximate determination of lead vectors and the burger triangle in normal human subjects. *Am. Heart J.*, 1956;**51**: 211–220.

86. McFee, R. and F.D. Johnston, Electrocardiographic leads. I. Introduction. *Circulation*, 1953;8: 554–68. II. Analysis. *Circulation*, 1954;9: 255–266. III. Synthesis. *Circulation*, 1954;**9**:868–880.
87. Frank, E., The image surface of a homogenous torso. *Am. Heart J.*, 1954;**47**: 757–768.
88. Frank, E., An accurate, clinically practical system for spatial vectorcardiography. *Circulation.*, 1956;**13**: 737–749.
89. Wilson, F.N., F.D. Johnston and C.E. Kossmann, The substitution of a tetrahedron for the Einthoven triangle. *Am. Heart J.*, 1947;**33**: 594–603.
90. Rijlant, P., Principe et methode de la vectorcardiographie. *Bull. Acad R. Med. Belg, Ser.*, 1957;**22**: 156–171.
91. Simonson, E., K. Nakagawa, and O.H. Schmitt, Respiratory changes of the spatial vectorcardiogram recorded with different lead systems. *Am. Heart J.*, 1957;**54**: 919–939.
92. Macfarlane, P.W., A hybrid lead system for routine electrocardiography, in *Progress in Electrocardiography*, P W.Macfarlane, Editor, Tunbridge Wells, Pitman Medical, 1979, pp. 1–5.
93. Castillo, H.T., An anatomical orthogonal four-electrode X-Y-Z Lead system for universal ECG recording. *Eur. J. Cardiol.*, 1979;**10**: 395–404.
94. Dower, G., A. Yakush, S.B. Nazzal, R.V. Jutzy, and C.E. Ruiz, Deriving the 12 lead electrocardiogram from four (EASI) electrodes. *J Electrocardiol.*, 1988;**21**(suppl): 182–187.
95. Dower, G.E., H.B. Machado, and J.A. Osborne, On deriving the electrocardiogram from vectorcardiographic leads. *Clin.Cardiol.*, 1980;**3**: 87–95.
96. Edenbrandt, L. and O. Pahlm, Comparison of various methods for synthesizing frank-like vectorcardiograms from the conventional 12-lead ECG, in *Computers in Cardiology IEE Comp Soc*, Baltimore, Maryland, 1987, pp. 71–74.
97. Uijen, G.J.H., A. van Oosterom, and R.T.H. van Dam, The relationship between the 12-lead standard ECG and the XYZ vector leads, in *Proceedings of the 14th International Congress on Electrocardiology*, E.Schubert, Editor, Berlin, Adakemie Verlag, 1988, pp. 301–307.
98. Willems, J., *Common Standards for Quantitative Electrocardiography. 4th Progress Report.* Leuven: Acco, 1984, pp. 199–200.
99. Nelwan, S.,J.A. Kors, S.H. Meij, J.H. van Bemmel, and M. Simoons, Reconstruction of the 12th lead electrocardiogram from reduced lead sets. *J Electrocardiol.*, 2004;**37**: 11–18.
100. Wei, D., T. Kojima, T. Nakayama, and Y. Sakai, US Patent No. 6,721,591: Method of deriving standard 12-lead Electrocardiogram and electrocardiogram monitoring apparatus. *US Patent Office*, 2004.
101. Waller, A.D., Introductory address on the electromotive properties of the human heart. *Br. Med. J.*, 1888;**2**: 751–754.
102. Geselowitz, D.B., Multipole representation for an equivalent cardiac generator. *Proc IRE.*, 1960;**48**: 75.
103. Selvester, R.H., C.R. Collier, and R.B. Pearson, Analog computer model of the vectorcardiogram. *Circulation*, 1965;**31**:45–53.
104. Selvester, R.H., R. Kalaba, C.R.Collier, R. Bellman, and H. Kagiwada, A digital computer model of the vectorcardiogram with distance and boundary effects: Simulated myocardial infarction. *Am. Heart J.*, 1967;**74**: 792–808.
105. Holt, J.H. Jr., A.C.L. Barnard, M.S. Lynn, P. Svendsen, and J.O. Kramer Jr., A study of the human heart as a multiple dipole electrical source. I. normal adult male subjects. *Circulation*, 1969;**40**: 687–696. II. Diagnosis and quantification of left ventricular hypertrophy. *Circulation*, 1969;**40**: 697–710. III. Diagnosis and quantification of right ventricular hypertrophy. *Circulation*, 1969;**40**: 711–718.
106. Lynn, M.S., A.C.L. Barnard, J.H. Holt, and L.T. Sheffield, A proposed method for the inverse problem in electrocardiography. *Biophys. J.*, 1967;**7**: 925–945.
107. Young, B.D., A Computer Study of the Electrical Activity of the Heart, Ph.D. thesis. Glasgow: University of Glasgow, 1972.
108. Macfarlane, P.W., A.R. Lorimer, R.H. Baxter, and T.D.V. Lawrie, Multiple dipole electrocardiography. *Br. Heart J.*, 1973;**35**:863–864.
109. Intini, A., R.N. Goldstein, P. Jia, et al., Electrocardiographic imaging (ECGI) – A novel diagnostic modality used for mapping of focal ventricular tachycardia in a young athlete. *Heart Rhythm.* 2005;**2**: 1250–1252.
110. Ramanathan, C., R.N. Ghanem, P. Jia, K. Ryu, and Y. Rudy, Noninvasive electrocardiographic imaging for cardiac electrophysiology and arrhythmia. *Nat Med.*, 2004;**10**: 422–428.
111. Boyett, M.R., J. Li, S. Inada, H. Dobrzynski, J.E. Schneider, A.V. Holden, and H. Zhang, Imaging the heart: computer 3-dimensional anatomic models of the heart. *J Electrocardiol.*, 2005;**38**(Suppl): 113–120
112. Nahum, L.H., A. Mauro, H. Chernoff, and R.S. Sikand, Instantaneous equipotential distribution on surface of the human body for various instants in the cardiac cycle. *J. Appl. Physiol.*, 1951;**3**: 454–464.
113. Taccardi, B., B.B. Punske, F. Sachse, X. Tricoche, P. Colli-Franzone, L.F. Pavarino, and C. Zabawa, Intramural activation and repolarization sequences in canine ventricles. Experimental and simulation studies. *J Electrocardiol*, 2005;**38**(Suppl): 131–137.
114. Barr, R.C., M.S. Spach, and G.S. Herman-Giddens, Selection of the number and positions of measuring locations for electrocardiography. *IEEE Trans. Biomed. Eng.*, 1971;**18**: 125–138.
115. Kornreich, F., The missing waveform information in the orthogonal electrocardiogram (Frank leads). I. Where and how can this missing waveform information be retrieved? *Circulation*, 1973;**48**: 984–995.
116. Lux, R.L., M.J. Burgess, R.F. Wyatt, A.K. Evans, G.M. Vincent, and J.A. Abildskov, Clinically practical lead systems for improved electrocardiography: comparison with precordial grids and conventional lead systems. *Circulation*, 1979;**59**: 356–363.
117. Taccardi, B. and Marchetti, G., Distribution of heart potentials on the body surface and in artificial conducting media, in *Int. Symp. Electrophysiology of the Heart*, B. Taccardi, G. Marchetti, Editors. Oxford, Pergamon, 1965, pp. 257–280.
118. Maynard, S.J., I.B.A. Menown, G. Manoharan, J. Allen, J.McC. Anderson, and A.A. J. Adgey, Body surface mapping improves early diagnosis of acute myocardial infarction in patients with chest pain and left bundle branch block. *Heart*, 2003;**89**:998–1002.
119. Burdon Sanderson, J., The mechanical, thermal, and electrical properties of striped muscle, in *Textbook of Physiology*, E.A. Schafer, Editor, Chapter 2, Edinburgh, Pentland, 1900, p. 446.
120. Woodbury, L.A., J.W. Woodbury, and H.H. Hecht, Membrane resting and action potentials of single cardiac muscle fibers. *Circulation*, 1950;**1**: 264–266.
121. Sicouri, S. and C. Antzelevitch, A subpopulation of cells with unique electrophysiological properties in the deep subepicardium of the canine ventricle. The M cell. *Circ. Res*, 1991;**68**: 1729–1741.

122. Antzelevvitch, C., W. Shimuzu, G.X. Yan, S. Sicouri, J. Weissenburger, V.V. Nesterenko, A. Burashnikov, J. Di Diego, J. Saffitz, and G.P. Thomas, The M Cell: its contribution to the ECG and to the normal and abnormal electrical function of the heart. *J Cardiovasc Electrophysiol.*, 1999;**10**: 1124–1152.
123. Rudy, Y., Lessons learned about slow discontinuous conduction from models of impulse propagation. *J Electrocardiol.*, 2005;**38**(Suppl): 52–54.
124. Taccardi, B. and G. Marchetti, Editors, *Int. Symp. Electrophysiology of the Heart*, Oxford, Pergamon, 1965.
125. Hulme, J.T., T. Scheuer, and W.A. Catterall, Regulation of cardiac ion channels by signaling complexes: Role of modified leucine zipper motifs. *J Mol Cell Cardiol.*, 2004;**37**: 625–631.
126. Scher, A.M. and A.C. Young, Ventricular depolarization and the genesis of the QRS. *Ann. N. Y. Acad. Sci.*, 1957;**65**: 768–778.
127. Scher, A.M., Excitation of the heart, in *Handbook of Physiology. Section* 2: *Circulation*, Vol. 1, W.F. Hamilton, Editor, Washington DC, American Physiological Society, 1962, pp. 287–322.
128. Durrer, D., R.T.H. van Dam, G.E. Freud, M.J. Janse, F.L. Meijler, and R.C. Arzbaecher, Total excitation of the isolated human heart. *Circulation*, 1970;**41**: 899–912.
129. Boineau, J.P., C.B. Miller, R.B. Schuessler, L.J. Autry, A.C. Wylds, and W.R. Roeske, Comparison between activation and potential maps during multicentric atrial impulse origin in dogs, in *Computerized Interpretation of The Electrocardiogram*, R.H.Selvester, and B.D. Geselowitz, Editors, New York, New York Engineering Foundation, 1984, pp. 55–62.
130. Spach, M.S. and R.C. Barr, Origin of epicardial ST-T wave potentials in the intact dog. *Circ. Res.*, 1976;39: 475–487.
131. Burgess, M.J., L.S. Green, K. Millar, R. Wyatt, and J.A. Abildskov, The sequence of normal ventricular recovery. *Am. Heart J.*, 1972;**84**: 660–669.
132. Cowan, J.C., Epicardial repolarization sequence and T wave configuration. *Br. Heart J.*, 1988;**59**: 85.
133. Krikler, D.M., Electrocardiography then and now: Where next? *Br Heart J.*, 1987;**57**: 113–117.
134. Watson, H., D. Emslie-Smith, and K.G. Lowe, The intracardiac electrocardiogram of human atrioventricular conducting tissue. *Am. Heart J.*, 1967;**74**: 66–70.
135. Lenegre, J. and P. Maurice, De quelques resultats obtenus par la derivation directe intracavitaire des courants electriques de l'oreillette et du ventricule droits. *Arch. Mal. Coeur Vaiss.*, 1945;**38**: 298–302.
136. Alanis, J., H. Gonzallez, and E. Lopez. The electrical activity of the bundle of his. *J. Physiol.*, 1958;**142**: 127–140.
137. Giraud, G., P. Puech, and H. Latour, Variations de potentiel liees a l'activite du systeme de conduction auriculo ventriculaire chez I'homme (Enregistrement electrocardiographique endocavitaire). *Arch. Mal. Coeur Vaiss.*, 1960;**53**: 757–16.
138. Scherlag, B.J., S.H. Lau, R.H. Helfant, W.D. Berkowitz, E. Stein, and A.H. Damato, Catheter techniques for recording his bundle activity in man. *Circulation*, 1969;**39**: 13–18.
139. Durrer, D., Electrical aspects of human cardiac activity: A clinical-physiological approach to excitation and stimulation. *Cardiovasc. Res.*, 1968;**2**: 1–18.
140. Rosenbaum, M.B., M.V. Elizari, and J.O. Lazzari, *Los Hemibloqueos*. Buenos Aires, Paidos, 1968. (Translation: *The Hemiblocks*. Oldsmar, Florida: Tampa Tracings, 1970.)
141. Grant, R.P., *Clinical Eleclrocardiography: The Spatial Vector Approach*. New York: Blakiston, 1957.
142. Beattie, J.M., F.A. Gaffney, and C.G. Blomqvist, Transcavitary conduction and the mean frontal QRS axis, in Electrocardiology '87, E. Schubert, and D. Romberg, Editors, Berlin, Akademie Verlag, 1988. pp. 71–74.
143. Brugada, P. and J. Brugada, Right bundle branch block, persistent st elevation and sudden cardiac death: a distinct clinical and electrocardiographic syndrome: A multicenter report. *J Am Coll Cardiol.*, 1993;**20**: 1391–1396.
144. Wilde, A.A.M., C. Antzelevitch, M. Borggrefe, et al., Consensus report. proposed diagnostic criteria for the brugada syndrome. *Eur. Heart J.*, 2004;**23**: 1648–1654.
145. Antzelevitch, A., P. Brugada, M. Borggrefe, et al., Brugada syndrome: report of the second consensus conference. *Circulation*, 2005;**111**: 659–670.
146. Gussak, I., P. Brugada, J. Brugada, et al., Idiopathic short QT interval: A new clinical syndrome? *Cardiology*, 2000;**94**: 99–102.
147. Ott, P. and F.I. Marcus, Electrocardiographic markers of sudden death. *Cardiol. Clin.*, 2006;**24**: 453–469.
148. Stallman, F.W. and H.V. Pipberger, Automatic recognition of electrocardiographic waves by digital computer. *Circ. Res.*, 1961;**9**: 1138–1143.
149. Caceres, C.A., C.A. Steinberg, S. Abrahams, et al., Computer extraction of electrocardiographic parameters. *Circulation*, 1962;**25**: 356–362.
150. Macfarlane, P.W., H. Cawood, T.P. Taylor, and T.D.V. Lawrie, Routine automated electrocardiogram interpretation. *Biomed. Eng.*, 1972;**7**: 176–180.
151. Rosenbaum, D., L.E. Jackson, J.M. Smith, J.N. Ruskin, and R.J. Cohen, Electrical alternans and vulnerability to ventricular arrhythmias. *N. Eng. J. Med.*, 1994;**330**: 235–241.
152. Klingenheben, T., Microvolt T wave alternans for arrhythmia risk stratification in left ventricular dysfunction. *J Am Coll Cardiol.*, 2007;**50**: 174–175.
153. Roberts, W.C. and M.A. Silver, Norman jefferies holter and ambulatory ecg monitoring. *Am. J. Cardiol.*, 1983;**52**: 903–906.
154. MacInnis, H.F., The clinical application of radioelectrocardiography. *Can. Med. Assoc. J.*, 1954;**70**: 574–576.
155. Holter, N.J., New method for heart studies. *Science*, 1961;**134**: 1214–1220.
156. Schmidt, G., M. Malik, P. Barthel, et al., Heart-rate turbulence after ventricular premature beats as a predictor of mortality after acute myocardial infarction. *Lancet*, 1999;**353**: 1390–1396.
157. Sosnowski, M., E. Clark, S. Latif, P.W. Macfarlane, and M. Tendera, Heart rate variability fraction – A new reportable measure of 24-hour R-R interval variation. *Ann of Noninvasive Electrocardiol.*, 2005;**10**: 7–15
158. Langner, P.H. Jr., D.B. Geselowitz, and F.T. Mansure, High-frequency components in the electrocardiograms of normal subjects and of patients with coronary heart disease. *Am. Heart J.*, 1961;**62**: 746–755.
159. Schuller, H. and T. Fahraeus, Pacemaker electrocardiograms: An introduction to practical analysis. *Solna. Siemens-Elema.*, 1983;**1**: 1.
160. Barold, S., M.C. Giudici, B. Herweg, and A.B. Curtis, Diagnostic value of the 12-lead electrocardiogram during conventional and biventricular pacing for cardiac resynchronization. *Cardiol Clin.*, 2006;**24**: 471–490.
161. Baule, G.M. and R. McFee, Detection of the magnetic field of the heart. *Am Heart J.*, 1963;**66**: 95–96.

162. Kannel, W.B., K. Anderson, D.L. McGee, L.S. Degatano, and M.J. Stampfer, Non-specific electrocardiographic abnormality as a predictor of coronary heart disease: The framingham study. *Am. Heart J.*, 1987;**113**: 370–376.
163. Kreger, B.E., L.A. Cupples, and W.B. Kannel, The electrocardiogram in prediction of sudden death. Framingham Study experience. *Am. Heart J.*, 1987;**113**: 377–382.
164. Tobin, M.D., M. Kahonen, P. Braund, T. Nieminen, C. Hajat, M. Tomaszewski, J. Viik, R. Lehtinen, R.A. Ng, P.W. Macfarlane, P.R. Burton, T. Lehtimaki, and N.J. Samani, Gender and effects of a common genetic variant in the NOS1 regulator NOS1AP on cardiac repolarization in 3761 individuals from two independent populations. *Int. J. Epidemiology*, 2008;**37**: 1132–1141.

2 Introductory Physics and Mathematics

R. Plonsey · A. van Oosterom

P. W. Macfarlane, A. van Oosterom, O. Pahlm, P. Kligfield, M. Janse, J. Camm (eds.), *Comprehensive Electrocardiology*, DOI 10.1007/978-1-84882-046-3_2,

2.1 Introduction

The goal of this chapter is to project an organized presentation of a central core of mathematics and physics that is related to the topics that are discussed elsewhere in this book. Some of the more specialized (and sophisticated) mathematics and physics are not included but, rather, will be found in the particular associated electrocardiographic topic to which they are applied. The reader should also be aware that the choice of material for this chapter is limited to that required for this text; if greater breadth is desired for another purpose, the corresponding reference at the end of this chapter could be consulted.

2.2 Vector Analysis

Mathematical development and application of a variety of electrocardiographic topics presented in this book are greatly facilitated by the use of vector concepts and vector calculus. Some readers may have knowledge of this material, but need a review; a few may have had no formal study of vector analysis, but require that knowledge presently. Presented here are the concepts of gradient, divergence and Laplacian, which play an important role in describing both the heart as a generator of currents and the torso as a site for the flow of these volume-conductor currents.

2.2.1 Scalars and Vectors

All biophysical problems can be described by the behavior of one or more associated variables. For physical quantities, the variables will be either scalars or vectors. If the variable is defined by a simple (single) value (electric potential, conductivity, temperature, etc., it is designated a scalar. If both magnitude and direction are needed (current density, electric field, force, etc.), then the quantity is described as a *vector.*

In a given preparation, a scalar property might vary as a function of position (the conductivity as a function of position in a body) and this is referred to as a *scalar field.* A vector (blood flow at different points in a major artery) is, similarly, described as a vector field. A scalar is designated by unmodified letters, while vectors in 3D space are denoted with an arrow over the letter. For example, t is used for temperature, $\vec{J}$ for current density, while $\vec{J}(x, y, z)$ denotes a vector field where at each point (x, y, z) a particular vector $\vec{J}$ exists. The magnitude of a vector $\vec{J}$ is written as $|\vec{J}|$, or J.

2.2.2 Vector Addition

The sum (or difference) of two vectors is more complicated than scalar addition (or subtraction) because direction as well as magnitude is involved. If vector $\vec{A}$ is represented by a displacement from 1 to 2 as illustrated in Fig. 2.1 and vector $\vec{B}$ is represented by a further displacement from 2 to 3, then their sum $\vec{C}$ is clearly the displacement from 1 to 3 as shown. Vector $\vec{C}$ may also be obtained by constructing a parallelogram with $\vec{A}$ and $\vec{B}$ as sides, in which case $\vec{C}$ is the diagonal from the common origin for $\vec{A}$ and $\vec{B}$. This law of vector summation is often referred to as the *parallelogram law*. It can easily be verified geometrically either from Fig. 2.1 or from the parallelogram construction, that the order of addition of $\vec{A}$ and $\vec{B}$ is immaterial. Vector addition is said to be *commutative*, *i.e.*

$$\vec{C} = \vec{A} + \vec{B} = \vec{B} + \vec{A} \tag{2.1}$$

The negative of a vector is defined to be a vector of opposite direction but with equal magnitude. The subtraction of vector $\vec{B}$ from $\vec{A}$ can then be expressed as the sum of $\vec{A}$ and $(-\vec{B})$. In Fig. 2.1, it can be confirmed geometrically that $\vec{B} + (-\vec{C}) = -\vec{A}$, which rearranges to Eqn. (2.1).

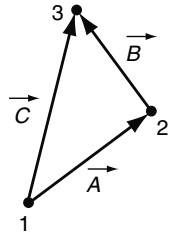

Figure 2.1
Illustration of vector addition.

2.2.3 Unit Vectors

The result of multiplying a vector $\vec{A}$ by a scalar m is a new vector with the same orientation but a magnitude m times great. If this is designated by $\vec{B}$, then

$$\vec{B} = m\vec{A} \tag{2.2}$$

$$|\vec{B}| = |m\vec{A}| \text{ or } B = mA \tag{2.3}$$

A unit vector is one which has a magnitude equal to unity. It is sometimes convenient to describe a vector $\vec{A}$ by the product of its magnitude $A = |\vec{A}|$ and a unit vector $\vec{e}_A$ which specifies its direction. Thus, $\vec{A} = A\vec{e}_A$. Correspondingly, throughout this chapter ($\vec{e}_x$, $\vec{e}_y$, $\vec{e}_z$) denote (dimensionless) unit vectors along the principal coordinate axes x, y, z of a Cartesian coordinate system. If A_x, A_y and A_z are the projections of vector $\vec{A}$ on the x, y and z axes, respectively, then

$$\vec{A} = A_x\vec{e}_x + A_y\vec{e}_y + A_z\vec{e}_z \tag{2.4}$$

as illustrated in Fig. 2.2. The magnitude of $\vec{A}$ is related to its rectangular components by

$$A = \left(A_x^2 + A_y^2 + A_z^2\right)^{1/2} \tag{2.5}$$

as is clear from Fig. 2.2. Equal vectors have the same magnitude and direction and, consequently, equal respective components. For example, (2.1) can be written as

$$\vec{e}_x(A_x + B_x) + \vec{e}_y(A_y + B_y) + \vec{e}_z(A_z + B_z) = \vec{e}_xC_x + \vec{e}_yC_y + \vec{e}_zC_z \tag{2.6}$$

so that

$$A_x + B_x = C_x; \quad A_y + B_y = C_y; \quad A_z + B_z = C_z \tag{2.7}$$

2.2.4 Scalar Product of Two Vectors

The scalar product of two vectors is defined as the scalar representing the product of their magnitudes times the cosine of the angle between them (drawn from a common origin).

From Fig. 2.3, it can be seen that the scalar product of $\vec{A}$ and $\vec{B}$ is the product of the magnitude of one of them (say B) times the projection of the other on the first (*i.e.*, $A\ \cos\ \theta$). For any two vectors that are normal (at right angles) to each other, this means that their scalar product is equal to zero.

The scalar product is denoted as $\vec{A} \bullet \vec{B} = A\,B\ \cos\ \theta$ and correspondingly (usually) referred to as the dot product.

It is clear from the definition that

$$\vec{A} \bullet \vec{B} = \vec{B} \bullet \vec{A} \tag{2.8}$$

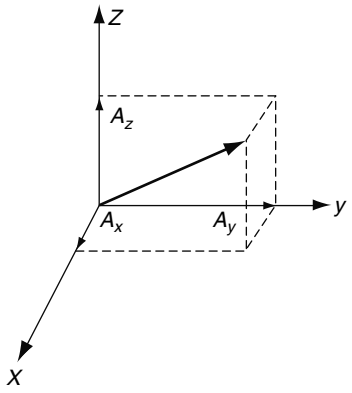

Figure 2.2
Resolution of a vector into its Cartesian components.

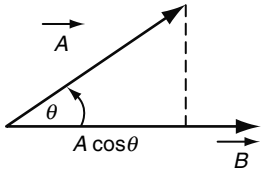

Figure 2.3
Scalar product of two vectors.

so that the *commutative* law of multiplication applies to this type of product. It can also be verified from graphical analysis that

$$(\vec{A} + \vec{B}) \bullet \vec{D} = \vec{A} \bullet \vec{D} + \vec{B} \bullet \vec{D} \tag{2.9}$$

that is, the *distributive* law of multiplication applies to the dot product of two vectors.

Since both the distributive and commutative laws hold, scalar multiplication of vectors follows the familiar rules of algebra. We now apply these rules to the dot product of $\vec{A} = A_x\vec{e}_x + A_y\vec{e}_y + A_z\vec{e}_z$ and $\vec{B} = B_x\vec{e}_x + B_y\vec{e}_y + B_z\vec{e}_z$. The fact that the vectors $\vec{e}_x$, $\vec{e}_y$ and $\vec{e}_z$ have unit lengths and are orthogonal to one another is expressed by the dot products:

$$\vec{e}_x \bullet \vec{e}_x = \vec{e}_y \bullet \vec{e}_y = \vec{e}_z \bullet \vec{e}_z = 1 \text{ and } \vec{e}_x \bullet \vec{e}_y = \vec{e}_y \bullet \vec{e}_z = \vec{e}_z \bullet \vec{e}_x = 0, \tag{2.10}$$

respectively. By using these properties to evaluate $\vec{A} \bullet \vec{B}$ we find that

$$\vec{A} \bullet \vec{B} = A_x B_x + A_y B_y + A_z B_z \tag{2.11}$$

2.2.4.1 Vector Product of Two Vectors

Vector product of two vectors $\vec{A}$ and $\vec{B}$ is defined as vector $\vec{C}$ that is orthogonal to the plane spanned by the two vectors, having as its magnitudes the product of the magnitudes of the two vectors multiplied by sine of the smallest angle needed for rotating $\vec{A}$ to line up with $\vec{B}$ (Fig. 2.3). The vector product is denoted as

$$\vec{C} = \vec{A} \times \vec{B}, \tag{2.12}$$

from which stems the alternative name 'cross-product' for the vector product. For the situation shown in Fig. 2.3, the vector $\vec{A} \times \vec{B}$ points into the plane of the figure and the vector $\vec{B} \times \vec{A}$ points into the opposite direction, and we have

$$\vec{C} = \vec{A} \times \vec{B} = -\vec{B} \times \vec{A} \tag{2.13}$$

2.2.5 Scalar and Vector Fields

If a fluid-filled container is shaken and swirled, the velocity of the fluid at each point will, in general, be different. The velocity vector is a function of position and this function can be expected to be reasonably well behaved. As noted earlier, a vector function of position constitutes a vector field.

To each point on the surface of the earth, an elevation (above sea level) can be ascertained. Only a single quantity (scalar) is involved and a scalar field is defined in this way. It is convenient to describe such a field by connecting (mapping) points of similar elevation. In this manner, lines on which the field has a constant value are identified, where the constants are chosen from a set of discrete scalar values separated by an interval that is sufficiently large enough for adequate resolution of the field, yet do not have excessive detail.

Isofunction lines, or contour lines, provide valuable graphical information on the topographic field. In a similar way, a representation of an electrical potential field through plotting its isopotential contours depicts, graphically, the behavior of the field.

A vector field may be described in terms of its rectangular (scalar) components so that a vector field would be represented by three scalar fields. A more direct representation is in the construction of flow lines, which are space curves that are tangential to the vector field everywhere. Only a finite number of such lines (they are infinite in number) would be drawn; the number chosen is a trade-off between increasing resolution and excessive complexity. For a two-dimensional map, the total flow between adjoining flow lines is usually chosen to be constant and, consequently, flux density is proportional to the density of the flow lines plotted.

While flow lines are easy to be interpreted when the physical entity constitutes an actual flow (*i.e.*, current), such representation is equally possible for a non-flow type vector field. The direction and density of the flow lines is then simply proportional to the direction and magnitude of the vector field.

2.2.6 Gradient

In this book, there is an interest in situations where an electrical potential field Φ (due to electrical generators in the heart) is established in some region that is electrically conducting (e.g., the torso). A consequence of such an occurrence is a resulting flow of current (which can be described by application of Ohm's law). The direction of current will correspond to the direction of the maximum rate of decrease in potential; the magnitude of the current density will be proportional to the magnitude of this rate of change.

In this section is described the gradient operation which is defined in order to extract, from a scalar potential field, a vector field which is precisely in the direction of the maximum rate of change of potential and with a magnitude equal to that rate of change. Its value (among others) is for evaluating a current flow field from a given potential field.

Let $\Phi(x, y, z)$ be a scalar field (scalar function of position) and assumed that it is a single-valued, continuous and differentiable function of position. Physical fields invariably satisfy these requirements. A surface C of constant value c is defined by

$$\Phi(x, y, z) = c \tag{2.14}$$

In applications of interest, Φ is a potential (electrical or chemical), in which case a surface of constant value is referred to as an equipotential or isopotential surface.

If c takes on a succession of, say, increasing values, a family of nonintersecting equivalued surfaces results. A plot of such equipotential surfaces (or plot of the intersections of these surfaces with principal planes) provides a graphical description of the potential field itself.

Consider two closely spaced points P_1 and P_2, where P_1 lies on the surface C_1 defined by $\Phi(x, y, z) = c_1$ and P_2 may or may not lie on this surface (see Fig. 2.4). If the coordinates of P_1 are (x, y, z) then the coordinates of P_2 could be described as $[(x + dx), (y + dy), (z + dz)]$. The displacement (a vector) from P_1 to P_2 is simply the vector sum of its rectangular components, namely,

$$d\vec{l} = \vec{e}_x dx + \vec{e}_y dy + \vec{e}_z dz \tag{2.15}$$

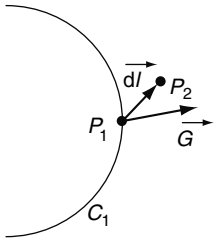

Figure 2.4
Equipotential surface and gradient.

Now, the difference in potential from P_1 to P_2 (the total derivative) is

$$d\Phi = \frac{\partial \Phi}{\partial x}dx + \frac{\partial \Phi}{\partial y}dy + \frac{\partial \Phi}{\partial x}dz \tag{2.16}$$

We now define $\vec{G}$ as the vector in 3D space having the above partial derivatives as its rectangular components:

$$\vec{G} = \frac{\partial \Phi}{\partial x}\vec{e}_x + \frac{\partial \Phi}{\partial y}\vec{e}_y + \frac{\partial \Phi}{\partial z}\vec{e}_z \tag{2.17}$$

In view of the definition of the scalar product of two vectors as expressed by (2.11),

$$d\Phi = \vec{G} \bullet d\vec{l} = G\, d\ell\, \cos\, \theta \tag{2.18}$$

Some of the properties of any nonzero $\vec{G}$ can be deduced from this equation. First, suppose that both P_1 and P_2 lie on C_1 and hence, $d\Phi = 0$. Since P_2 is only an infinitesimal (but nonzero) distance from P_1, $d\vec{l}$ is tangential to C_1 at P_1. Equation (2.18) indicates that in this situation $\cos\theta = 0$ and thus $\vec{G}$ must be normal to C_1. Next, we consider any nonzero $d\vec{l}$ directed from P_1 on C_1 to a field point P_2 on C_2 for which $d\Phi = c_2 - c_1 > 0$. Equation (2.18) also indicates that $d\Phi$ attains a maximum value if $\vec{G}$ and $d\vec{l}$ point in the same direction, and with $d\vec{l}$ directed towards a higher value of Φ, $\vec{G}$ always points toward higher values of Φ.

The magnitude of $\vec{G}$ follows from (2.18). Since

$$d\Phi/dl = G\cos\theta, \tag{2.19}$$

indicating that the derivative of Φ along a line l depends on the local direction, $d\vec{l}$, of the line, the gradient is a *directional derivative*. From (2.19), with $\theta = 0$ and dn a distance directed along the surface normal $\vec{n}$, we have

$$G = d\Phi/dn \tag{2.20}$$

The vector field $\vec{G}$ as defined in (2.17) is called the gradient of a scalar field Φ; if the scalar function is the electric potential, it is called the gradient of the potential.

In summary, a (nonzero) gradient of the potential is a vector field oriented normal to an equipotential surface. It always points towards a region having higher potential values. Its magnitude quantifies the maximum local change in the potential per unit distance.

The gradient of the potential is usually written as $\nabla\Phi$, where

$$\nabla = \vec{e}_x\frac{\partial}{\partial x} + \vec{e}_y\frac{\partial}{\partial y} + \vec{e}_z\frac{\partial}{\partial z} \tag{2.21}$$

is the gradient operator. When applied, each term in (2.21) acts on Φ through the taking of the indicated partial derivatives and appending the corresponding unit vector. It can immediately be verified that this leads, correctly, to the right-hand side of (2.17).

2.2.7 Divergence

A basic vector field required for the analysis of electrophysiology is the electric current density $\vec{J}$ in a volume conductor: the electric current per unit area passing an infinitesimally small area. The structure of the $\vec{J}$ field depends on the presence of sites at which current is either introduced (sources) or withdrawn (sinks). In this respect, the behavior of $\vec{J}(x, y, z)$ is analogous to the vector field that describes fluid flow, which similarly arises from a distribution of sources and sinks. This class of vector field has certain general properties that are exemplified by the current flow field. In the following, the term "sources" is used to include "sinks" (which are, simply, negative sources). It will be shown that a determination of the sources of a field permits that field to be determined everywhere (although, frequently, certain boundary conditions must also be taken into account). For an arbitrary source distribution, $\vec{J}$ will be a complex but well-behaved vector function of position. In particular, for a region that contains no sources, since charge must be conserved the net flow of $\vec{J}$ across the surface bounding any segment of tissue (for example, with inflow taken to be negative while outflow is positive) is required to be zero. This condition is also said to preserve continuity of current. The evaluation of the net flow across a closed surface can then be taken as a measure of the net source (or sink) within the region enclosed by that surface.

For a differential rectangular parallelepiped, an expression that evaluates the net outflow is derived as follows, expressed in rectangular coordinates. Referring to Fig. 2.5 and assuming a field $\vec{J}(x, y, z)$, the outflow through surface (2) is then $dz\, dy\, (J_x + \frac{1}{2}(\partial J_x/\partial x)\, dx)$+ higher terms, where J_x is the value of $J_x(x, y, z)$ at the center of the parallelepiped (which accounts for the factor of $\frac{1}{2}$ in the expression). For the surface (1), the outflow is $-dz\, dy\, (J_x - \frac{1}{2}(\partial J_x/\partial x)\, dx)$– $dzdy$, where the leading minus sign arises because outflow is in the negative x direction. The sum of these contributions is then $dx\, dy\, dz\, \partial J_x/\partial x$. In the same way, the remaining two pairs of faces contribute $dx\, dy\, dz\, \partial Jy/\partial y$ and $dx\, dy\, dz\, \partial J_z/\partial z$. Consequently, their sum is

$$\oint \vec{J} \bullet d\vec{S} = (\partial J_x/\partial x + \partial J_y/\partial y + \partial J_z/\partial z)\, dx\, dy\, dz \tag{2.22}$$

Note that $\vec{J} \bullet d\vec{S}$ is the outflow of $\vec{J}$ across an arbitrary surface element and that the sign $\oint$ indicates that the integral is over a closed surface. In this case, the differential rectangular parallelepiped described in Fig. 2.5 is the designated closed surface, which is evaluated in the right-hand side of (2.22).

If both sides of (2.22) are divided by $(dx\, dy\, dz)$, then the ratio $\oint \vec{J} \bullet d\vec{S}/(dx\, dy\, dz)$ is called the divergence of $\vec{J}$. Note that this is evaluated in the limit that the volume $(dx\, dy\, dz)$ approaches zero (the divergence is a differential quantity).

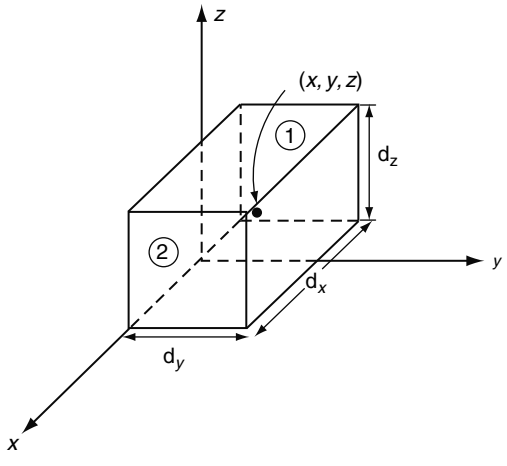

Figure 2.5
Evaluation of divergence.

This limit is designated by

$$\mathrm{div}\vec{J} = \lim_{V\to 0} \frac{\oint \vec{J} \bullet \mathrm{d}\vec{S}}{V} = \frac{\partial J_x}{\partial x} + \frac{\partial J_y}{\partial y} + \frac{\partial J_z}{\partial z} \tag{2.23}$$

This indicates that the divergence of a vector (field) is a scalar (field).

The divergence of $\vec{J}$ equals the net outflow per unit volume of the vector $\vec{J}$ at each point in the space. The definition of the divergence applies to any vector field. The field can be interpreted as a flow and its divergence as a source of the flow field. If the ∇ operator, defined in (2.21), is treated as having vector-like properties, then in view of (2.23) and the properties of the dot product given in (2.11), it follows that

$$\nabla \bullet \vec{J} = \mathrm{div}\vec{J} = \frac{\partial J_x}{\partial x} + \frac{\partial J_y}{\partial y} + \frac{\partial J_z}{\partial z} \tag{2.24}$$

2.2.8 Gauss' Law

In the previous section, it was pointed out that the net outflow of current from a given volume is a quantity of interest since it is a measure of the net source contained in the volume. For a volume V bounded by a closed surface S, the outflow is given by

$$\text{outflow} = \oint \vec{J} \bullet \mathrm{d}\vec{S}, \tag{2.25}$$

where $\mathrm{d}\vec{S}$ is a surface element whose direction is along the outward normal. It has just been established that $\nabla \bullet \vec{J}$ evaluates the net outflow per unit volume for an infinitesimally small volume element, so the outflow evaluated in (2.25) can also be found by integrating $\nabla \bullet \vec{J}$ through the volume bounded by S. In fact,

$$\int \nabla \bullet \vec{J} \mathrm{d}V = \oint \vec{J} \bullet \mathrm{d}\vec{S} \tag{2.26}$$

This relationship holds true for all well-behaved vector fields, such as $\vec{J}$, and is known as Gauss' theorem, or the *divergence theorem*.If the region is source-free, then the net flow across the bounding surface is zero as a consequence. Conversely, if there is a net outflow then within the surface there must be sources with net magnitude equal to the (net) outflow. For a single current dipole (Sect. 2.5.1.2) inside a closed surface, the total current flow passing the surface is zero.

2.2.9 Laplacian

In Sect. 2.2.6, it has been shown that the gradient operation converts a given scalar field Φ into a vector field $\nabla\Phi$. The divergence operation, on the other hand, converts a vector field into a scalar field. If the vector field is itself the gradient of a scalar function, the result can be expressed through the successive application of the ∇ operator, namely

$$\begin{aligned} \nabla \bullet \nabla\Phi &= \nabla \bullet \left(\vec{e}_x \frac{\partial \Phi}{\partial x} + \vec{e}_y \frac{\partial \Phi}{\partial y} + \vec{e}_z \frac{\partial \Phi}{\partial z} \right) \\ &= \frac{\partial^2 \Phi}{\partial x^2} + \frac{\partial^2 \Phi}{\partial y^2} + \frac{\partial^2 \Phi}{\partial z^2} \end{aligned} \tag{2.27}$$

The final result can be interpreted as if the original scalar field is operated on by the differential operator:

$$\nabla^2 = \frac{\partial^2}{\partial x^2} + \frac{\partial^2}{\partial y^2} + \frac{\partial^2}{\partial z^2} \tag{2.28}$$

The operator ∇^2 is called the Laplacian. It converts a scalar potential field into another scalar field (the latter specifying the sources for the first). The properties of the Laplacian are discussed later in this chapter.

2.2.10 Vector Identities

In this section, a short list is presented on the relationships that are known as vector identities. These hold true for all "well-behaved" scalar and vector functions treated in this chapter, with "well-behaved" expressing the fact that taking the various derivatives can be formally justified. Here, and in other chapters, these vector identities will prove useful in deriving biophysical relationships. A proof is included for the first expression; the reader may use this as a model for confirming the others. In the following, Φ and Ψ are taken to be scalar functions, $r = (x^2 + y^2 + z^2)^{1/2}$ and $\vec{A}$ is a vector field.

$$\nabla \bullet (\Phi \vec{A}) = \vec{A} \bullet \nabla\Phi + \Phi \nabla \bullet \vec{A} \tag{2.29}$$

$$\nabla(\Phi\Psi) = \Phi\nabla\Psi + \Psi\nabla\Phi \tag{2.30}$$

$$\nabla \bullet \nabla\Psi = \nabla^2\Psi = \frac{\partial^2\Psi}{\partial x^2} + \frac{\partial^2\Psi}{\partial y^2} + \frac{\partial^2\Psi}{\partial z^2} \tag{2.31}$$

$$\nabla^2 r = 0 \tag{2.32}$$

For $\vec{R} = (x' - x)\,\vec{e}_x + (y' - y)\,\vec{e}_y + (z' - z)\,\vec{e}_z$, with length $R = \{(x' - x)^2 + (y' - y)^2 + (z' - z)^2\}^{1/2}$, we have

$$\nabla(1/R) = \vec{R}/R^3 = -\nabla'(1/R), \tag{2.33}$$

in which ∇' denotes the differentiation with respect to the primed variables.

To verify (2.29), replace $\vec{A}$ by its rectangular components $(A_x\vec{e}_x + A_y\vec{e}_y + A_z\vec{e}_z)$ leading to

$$\nabla \bullet (\Phi \vec{A}) = \nabla \bullet (\Phi A_x \vec{e}_x + \Phi A_y \vec{e}_y + \Phi A_z \vec{e}_z) \tag{2.34}$$

Using the definition of the divergence given in (2.24) results in

$$\nabla \bullet (\Phi \vec{A}) = \frac{\partial}{\partial x}(\Phi A_x) + \frac{\partial}{\partial y}(\Phi A_y) + \frac{\partial}{\partial z}(\Phi A_z) \tag{2.35}$$

By the product rule of differentiation, it follows that

$$\nabla \bullet (\Phi\,\vec{A}) = \Phi\frac{\partial A_x}{\partial x} + A_x\frac{\partial \Phi}{\partial x} + \Phi\frac{\partial A_y}{\partial y} + A_y\frac{\partial \Phi}{\partial y} + \Phi\frac{\partial A_z}{\partial z} + A_z\frac{\partial \Phi}{\partial z} \tag{2.36}$$

Collecting terms gives

$$\nabla \bullet (\Phi\,\vec{A}) = \Phi\left(\frac{\partial A_x}{\partial x} + \frac{\partial A_y}{\partial y} + \frac{\partial A_z}{\partial z}\right) + A_x\frac{\partial \Phi}{\partial x} + A_y\frac{\partial \Phi}{\partial y} + A_z\frac{\partial \Phi}{\partial z} \tag{2.37}$$

In addition,

$$\begin{aligned}\vec{A} \bullet \nabla\Phi &= \vec{A} \bullet \left(\frac{\partial \Phi}{\partial x}\vec{e}_x + \frac{\partial \Phi}{\partial y}\vec{e}_y + \frac{\partial \Phi}{\partial z}\vec{e}_z\right) \\ &= A_x\frac{\partial \Phi}{\partial x} + A_y\frac{\partial \Phi}{\partial y} + A_z\frac{\partial \Phi}{\partial z}\end{aligned} \tag{2.38}$$

so that substituting (2.38) and (2.24) into (2.37) leads to

$$\nabla \bullet (\Phi \vec{A}) = \vec{A} \bullet \nabla\Phi + \Phi \nabla \bullet \vec{A}, \tag{2.39}$$

which confirms (2.29).

2.2.11 Coordinate Systems

Up to this point, vector fields and vector operations have been expressed in rectangular coordinates, and these are, indeed, the easiest to use as well as being the most frequently used. Often, however, cylindrical or spherical (or other) coordinates are more appropriate. The differential operators of gradient, divergence and Laplacian can be expressed in any of the orthogonal coordinate systems and it is useful to have such expressions available. Their derivation follows their basic definition, taking the coordinate system into account. For example, in Fig. 2.6(a) the cylindrical coordinate system is illustrated. In this system, an arbitrary point is described by a distance r to the z-axis, an azimuth angle ϕ from the x axis and a distance z along z-axis. Figure 2.6(b) illustrates the spherical coordinate system. According to the definition and property of $\nabla\Phi$, it is a vector whose component in any direction is the directional derivative of Φ in that direction. Consequently

$$\nabla\Phi = \vec{e}_r \frac{\partial\Phi}{\partial r} + \vec{e}_\phi \frac{\partial\Phi}{\partial\phi} + \vec{e}_z \frac{\partial\Phi}{\partial z} \tag{2.40}$$

Note that in (2.40) the rate of change of Φ per unit length in the ϕ direction requires the limit of $\Delta\Phi/(r\Delta\phi)$ where the denominator is the appropriate element of length and Δ denotes taking of a small difference. The spherical coordinate system is illustrated in Fig. 2.6(b) where r is the radial distance from the origin, θ is the polar angle and ϕ is the azimuth angle. For this system, the gradient is expressed as

$$\nabla\Phi = \vec{e}_r \frac{\partial\Phi}{\partial r} + \vec{e}_\theta \frac{1}{r}\frac{\partial\Phi}{\partial\theta} + \vec{e}_z \frac{1}{r\sin\phi}\frac{\partial\Phi}{\partial\phi} \tag{2.41}$$

The expressions for the divergence and Laplacian in cylindrical and spherical coordinates are listed below. The reader can verify these using the basic definitions, or by recourse to one of the standard references listed at the end of this chapter.

2.2.11.1 Divergence and Laplacian in Cylindrical Coordinates

$$\nabla \bullet \vec{A} = \frac{1}{r}\frac{\partial}{\partial r}(rA_r) + \frac{1}{r}\frac{\partial A_\phi}{\partial\phi} + \frac{\partial A_z}{\partial z} \tag{2.42}$$

$$\nabla^2\Phi = \frac{1}{r}\frac{\partial}{\partial r}\left(r\frac{\partial\Phi}{\partial r}\right) + \frac{\partial^2\Phi}{\partial\phi^2} + \frac{\partial^2\Phi}{\partial z^2} \tag{2.43}$$

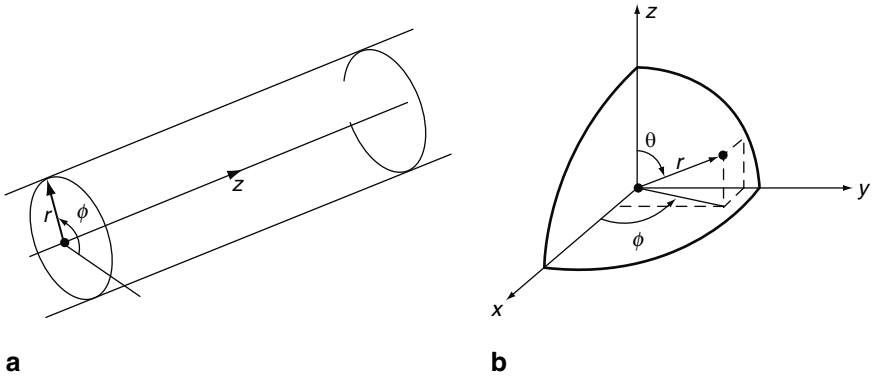

Figure 2.6
Coordinate systems: (a) circular cylindrical; (b) spherical.

2.2.11.2 Divergence and Laplacian in Spherical Coordinates

$$\nabla \bullet \vec{A} = \frac{1}{r^2}\frac{\partial}{\partial r}(r^2 A_r) + \frac{1}{r\sin\theta}\frac{\partial}{\partial\theta}(A_\theta \sin\theta) + \frac{1}{r\sin\theta}\frac{\partial A_\phi}{\partial\phi} \tag{2.44}$$

$$\nabla^2\Phi = \frac{1}{r^2}\frac{\partial}{\partial r}\left(r^2\frac{\partial\Phi}{\partial r}\right) + \frac{1}{r^2\sin\theta}\frac{\partial\Phi}{\partial\theta}\left(\sin\theta\frac{\partial\Phi}{\partial\theta}\right) + \frac{1}{r^2\sin^2\theta}\frac{\partial^2\Phi}{\partial\phi^2} \tag{2.45}$$

2.2.12 Solid Angle: Definition and Theory

Solid angle is an extension to 3D space of the familiar concept of a 'common' angle in 2D space. For an object in 2D space, the angle of view from some location is defined as the fraction of the circumference of a circle with unit radius, centered at the location of the observer, occupied by the intersections with the circle of the lines connecting all the elements of the object to the center of the circle. In 3D, the analogous definition relates to the similar projection of the object onto the surface of a sphere with unit radius. Being a fraction, the solid angle is unitless. However, to stress its special nature, the solid angle is frequently expressed in the 'unit' star-radian. Observed from an arbitrary point inside a closed surface, this definition results in a total solid angle 4π, as is explained below.

In many of the applications of volume conduction theory, the surface S carries a double layer, which requires assigning a direction to its surface normal. In the sequel, for a closed surface this direction is always taken to be (positive) towards the exterior region: the outward normal.

Consider an observation point $\vec{X}'$ in three-dimensional space in which an arbitrary surface S is situated. Let $d\omega$ be the projection of a small element dS on the surface of a sphere having a unit radius (Fig. 2.7).

Then, the solid angle subtended by dS at $\vec{X}'$ is defined as $d\omega$. The solid angle Ω subtended at $\vec{X}'$ by the entire surface S is found by the addition of all projections $d\omega$ of all elements dS. Mathematically this is expressed as

$$\Omega(S) = \int_S d\omega = \int_S \frac{\cos\alpha\, dS}{R^2}, \tag{2.46}$$

in which R is the length of the vector $\vec{R}$ pointing from surface element dS to observation point $\vec{X}'$, and α the angle between the local surface normal $d\vec{S}$ and $\vec{R}$. If the surface S is decomposed into a set of non-overlapping segments, $S1$, $S2$, $S3$, ... The linearity of integration shows that we have

$$\Omega(S) = \Omega(S_1 \cup S_2 \cup S_3 \cdots) = \Omega(S_1) + \Omega(S_2) + \Omega(S_3) + \cdots \tag{2.47}$$

By defining $d\vec{S}$ as the vector of size dS that is oriented along the outward normal of dS and by using the property of the dot product $\vec{R} \bullet d\vec{S} = R\, dS \cos\alpha$, Eqn. (2.46) can be written as

$$\Omega(S) = \int_S d\omega = \int_S \frac{\vec{R} \bullet d\vec{S}}{R^3} \tag{2.48}$$

The sign of Ω depends on the definition of the direction of both $\vec{R}$ and $d\vec{S}$. Note that the term 'outward' normal relates in a natural manner to closed surfaces only. For a non-closed surface it needs to be defined on the basis of the application involved.

For an observation point $\vec{X}'$ placed at the center of a spherical surface S, the solid angle subtended by S at the $\vec{X}'$ is -4π; its magnitude is equal to the surface area of a unit sphere, the negative sign follows from the definition of the directions of $\vec{R}$ and $d\vec{S}$.

For any arbitrary internal point of non-intersecting closed S, the value of Ω is independent of the actual shape the surface and, moreover, also holds true irrespective of the position of the interior observation point. This most fundamental property can be appreciated by inspecting Fig. 2.8. In the left panel, a cross section of a closed three-dimensional surface

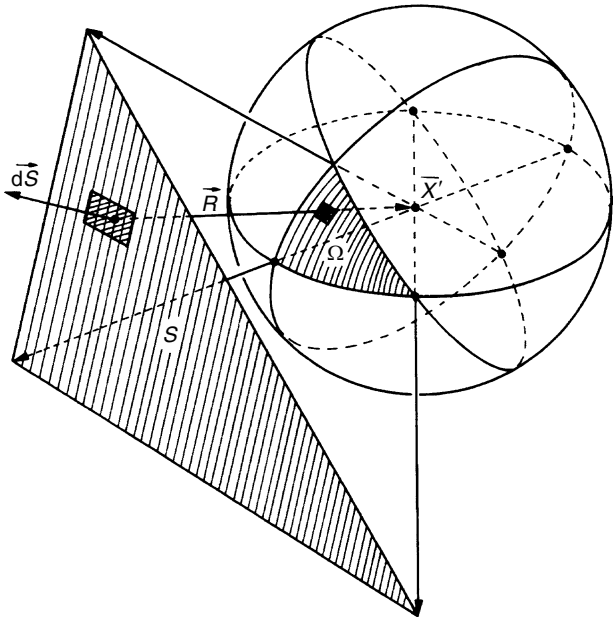

Figure 2.7

Diagram introducing the solid angle Ω. The outline of a small element d*S* of an arbitrary surface *S* is projected on the surface of a sphere with unit radius. The solid angle dω subtended by d*S* at observation point $\vec{X}'$, the center of the sphere, is defined as the area of the projection of d*S* onto the sphere. The solid angle Ω of *S* is the sum of the projections dω of all elements d*S*. The surface *S* may have an arbitrary shape, it is drawn here as triangle for ease of presentation.

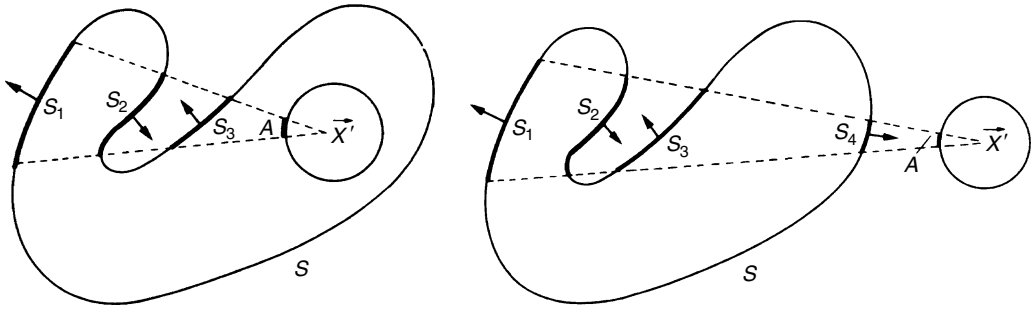

Figure 2.8

Cross-sections of a 3D closed surface *S*. Observer at $\vec{X}'$. *Left*. Apart from their sign, the solid angles subtended by S_1, S_2, and S_3 are equal to *A*, the part of a unit sphere around $\vec{X}'$; their sum equals –*A*. *Right*: the situation for an external observation point. Part *A* of a unit sphere around $\vec{X}'$ has, apart from its sign, the same solid angle as the individual segments S_1, S_2, S_3, and S_4. The sum of the solid angles is zero as a result of the paired sign differences.

S is shown in which three segments S_1, S_2 and S_3 are indicated. The observation point lies inside and a unit circle is drawn around it. The area *A* of the unit sphere represents the solid angle of the segments. Since $\Omega(S_1) = -\Omega(S_2) = \Omega(S_3) = -A$, it follows, by using (2.47), that $\Omega(S_1 \cup S_2 \cup S_3) = \Omega(S_1) + \Omega(S_2) + \Omega(S_3) = -A$. By applying the same type of analysis to the intersections of all possible sectors of the unit sphere with *S*, it is evident that indeed, for any arbitrary location of an internal point

$$\Omega(S) = -\text{total area of the (unit) sphere} = -4\pi \tag{2.49}$$

When $\vec{X}'$ is an exterior point of S, we find, by the same type of reasoning (right panel), that

$$\Omega(S) = 0 \tag{2.50}$$

When $\vec{X}'$ lies *on* surface S, the definition of Ω by means of expression cannot be used since $\vec{R}$ = zero. In that situation, $\vec{X}'$ may be taken as having approached S from either the interior or the exterior. Taking this limit from the inside for a locally planar part of the surface, we have

$$\Omega(S) = -2\pi \tag{2.51}$$

An approach from the outside results in

$$\Omega(S) = +2\pi \tag{2.52}$$

For an arbitrarily shaped part of the surface, the limit depends on the local curvature. Whatever the value of the local curvature, the value of the solid angle jumps by a value of 4π when crossing the surface. The sign of the jump is positive if the surface is crossed towards its exterior.

2.3 Static Electric Fields

Electrical activation and recovery of cardiac muscle gives rise to the flow of electric current in the heart and out into the torso. Associated with these currents is the establishment of electrocardiographic potentials within the torso and at the body surface. While the current and potential fields vary with time, at each instant of time they satisfy mathematical expressions which arise in the study of static fields. Accordingly, this section reviews the physical principles associated with the establishment of static electric fields as well as their mathematical description.

2.3.1 Coulomb's Law

Coulomb's famous experiments led to a quantitative description of the force between two point charges. It was established that this force is directed along a line connecting the two point charges (the force is attractive if the charges are of opposite sign and repulsive if the charges are of the same sign) while the force magnitude is proportional to the product of the charge magnitudes and inversely proportional to the square of the distance separating the charges. This description is expressed in the following equation for the force $\vec{F}_{12}$ exerted on charge q_2 by charge q_1, namely,

$$\vec{F}_{12} = \frac{q_1 q_2}{4\pi\varepsilon r_{12}^2}\vec{e}_{12}, \tag{2.53}$$

where e_{12} is a unit vector directed from 1 to 2, r_{12} is the distance between point charges, and ε is the dielectric permittivity of the medium (assumed to be uniform and essentially infinite in extent). Note that the direction and magnitude of the interactive force evaluated by (2.53) correspond to the word description given above. In (2.53), if q_1 and q_2 are expressed in coulombs, r_{12} in meters and ε in farads per meter, then $\vec{F}$ is in newtons. For free space (vacuum), the permittivity $\varepsilon = 8.8542 \cdot 10^{-12}$ Fm^{-1}. Note that $\vec{F}_{12} = -\vec{F}_{21}$ so that "action" is equal and opposite to the "reaction", as required by Newton's laws of mechanics.

Figure 2.9 shows an arrangement of charges for which the force on charge q_o, owing to the presence of several point charges q_1, q_2 and q_3, is to be evaluated. This can be accomplished by the successive application of Coulomb's law (between q_1 and q_o, q_2, and q_o, q_3 and q_o) leading to the component forces $\vec{F}_1$, $\vec{F}_2$ and $\vec{F}_3$, respectively. These are illustrated in Fig. 2.9 where all the charges are assumed to be of the same sign. The net force exerted on q_o is the vector sum (superposition) of $\vec{F}_1 + \vec{F}_2 + \vec{F}_3 = \vec{F}$. In fact, for any system of point charges, the force exerted on any one of these (designated as q_o) is

$$\vec{F} = \frac{q_o}{4\pi\varepsilon}\sum_i \frac{q_i \vec{e}_{io}}{r_{i0}^2}, \tag{2.54}$$

where r_{i0} is the displacement from the ith charge to the 0th charge.

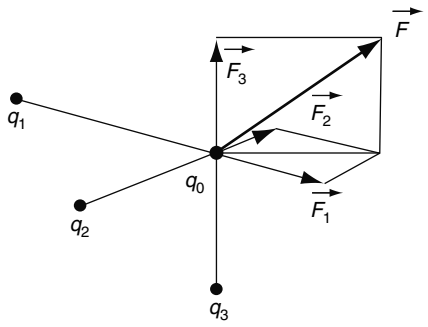

Figure 2.9
Vector sum of electrostatic force components.

2.3.2 Electric Field

Force exerted on one charge by another does so across the intervening space, a phenomenon known as "action at a distance". The force can also be viewed as arising from a two-step process whereby one charge is first assumed to establish an electric field, the field then transmits a force to the other charge. For two point charges q_1 and q_2, the first step introduces the concept of the electric field $\vec{E}$ arising from q_1, defined by

$$\vec{E}(r) = \frac{q_1}{4\pi\varepsilon r^2}\vec{e}_r, \tag{2.55}$$

where r is the radial distance from q_1 and $\vec{e}_r$ is the unit vector directed radially away from q_1. Next, the force exerted on the point charge q_2 by this field is given by

$$\vec{F}(r_2) = q\vec{E}(r_2), \tag{2.56}$$

where r_2 is the radial distance to q_2 from q_1. The force on q_2 because of q_1 found by combining (2.55) and (2.56) is precisely that as stated by Coulomb's law and expressed by (2.53).

A more rigorous definition of the electric field, accounting for required point charge nature of charge, with vanishingly small strength, is

$$\vec{E} = \lim_{\Delta q \to 0}(\vec{F}/\Delta q) \tag{2.57}$$

The advantage of the field concept is that it separates the process in which fields are established (by their sources, such as q_1 in (2.55)) from the actions produced by the field (i.e., the force exerted on q_2 in (2.56)). If a number of point charges are present, as in Fig. 2.9, the electric field at any point in space can be found by superposition, taking into account the contribution from each individual point source and summing vectorially. The net force on a point charge is found from the action of the net field according to (2.56). Where there is a very large number of point charges in a certain region, it is convenient to describe their distribution by means of a charge density function $\rho(x, y, z)$, where

$$\rho = \lim_{\Delta v \to 0}(\Delta q/\Delta v) \tag{2.58}$$

and Δq is the net charge in the volume Δv. The charge density is a function of position. The total charge Q in a volume v is found from (2.58) by integrating through the volume:

$$Q = \int \rho \mathrm{d}v \tag{2.59}$$

Since $\rho \mathrm{d}v$ is an element of charge that is essentially a point source, its electric field $\mathrm{d}\vec{E}$ would be given by (2.55), namely

$$\mathrm{d}\vec{E} = \frac{\rho \mathrm{d}v}{4\pi\varepsilon r^2}\vec{e}_r \tag{2.60}$$

The electric field established by the entire distribution is given by

$$\vec{E}(x',y',z') = \frac{1}{4\pi\varepsilon}\int \frac{\rho(x,y,z)}{r^2}\vec{e}_r \mathrm{d}v, \tag{2.61}$$

where r is the length of the vector $\vec{r}$ from an element of charge located at (x, y, z) to the point at which the field is being evaluated: $r = \{(x'-x)^2 + (y'-y)^2 + (z'-z)^2\}^{1/2}$.

Note that the integration in (2.61) is over the unprimed coordinates ($\mathrm{d}v = \mathrm{d}x\mathrm{d}y\mathrm{d}z$), these being the coordinates in which the source (charge density) is defined. The field point location, given by the primed coordinates, is assumed to be fixed during the integration. In actually performing the integration indicated in (2.61), it must be kept in mind that $\vec{e}_r$ varies according to the location of the source (integration) point and that a vector summation must actually be performed.

2.3.3 Gauss' Flux Theorem

The electric field from a point charge q is given by (2.55). Although $\vec{E}$ does not represent the flow of any substance, it can be treated as if it did; that is, it may be interpreted as an electric flux (flow) density. Then the net flow through an arbitrary, closed surface S surrounding a point charge q can be found from

$$\oint \vec{E} \bullet \mathrm{d}\vec{S} = \frac{q}{4\pi\varepsilon}\oint \frac{\vec{e}_r \bullet \mathrm{d}\vec{S}}{r^2}, \tag{2.62}$$

with $\vec{e}_r$ a unit vector directed along the vector from the point charge to a point on the surface S. The integrand in (2.62), corresponds to the elementary solid angle $\mathrm{d}\omega$ (Sect. 2.2.12) subtended by the elementary surface element $\mathrm{d}S$ as observed from the source location:

$$\frac{\vec{e}_r \bullet \mathrm{d}\vec{S}}{r^2} = \frac{\vec{r} \bullet \mathrm{d}\vec{S}}{r^3} = \mathrm{d}\omega \tag{2.63}$$

Consequently,

$$\oint \vec{E} \bullet \mathrm{d}\vec{S} = \frac{q}{4\pi\varepsilon}\oint \mathrm{d}\omega = \frac{q}{\varepsilon} \tag{2.64}$$

since the total solid angle of any closed surface as viewed from an interior point is 4π. Hence, the total flux emanating from q depends on the magnitude of q. If a number of point charges q_i were enclosed within S, then by superposition the right-hand side of (2.64) becomes, simply, the total charge divided by ε. Thus,

$$\oint \vec{E} \bullet \mathrm{d}\vec{S} = \frac{1}{\varepsilon}\sum_i q_i = \frac{Q}{\varepsilon} \tag{2.65}$$

In a similar fashion, if the sources within S were represented by a charge density ρ, then

$$\oint \vec{E} \bullet \mathrm{d}\vec{S} = \frac{1}{\varepsilon}\int \rho \mathrm{d}v = \int \frac{\rho}{\varepsilon}\mathrm{d}v \tag{2.66}$$

Note that since ε is independent of position, it could be moved about freely from across integration or summation signs.

We now combine Gauss' flux theorem ((2.26)) with (2.66), yielding

$$\oint \vec{E} \bullet \mathrm{d}\vec{S} = \int \nabla \bullet \vec{E}\,\mathrm{d}v = \int \frac{\rho}{\varepsilon}\mathrm{d}v \tag{2.67}$$

which applies to arbitrarily small volume elements and consequently we have

$$\nabla \bullet \vec{E} = \frac{\rho}{\varepsilon} \tag{2.68}$$

2.3.4 Electric Scalar Potential

Equation (2.68) shows that the divergence of the electric field $\vec{E}$ is a scalar function. For all vector fields having this property, it can be shown that they, in turn, are determined uniquely by the negative gradient of another scalar function [1]. In electrostatics, this function is called the electric potential, denoted by Φ, and

$$\vec{E} = -\nabla'\Phi \tag{2.69}$$

Note that (2.69) defines the electric potential up to a constant only.

The potential difference between two points in space is the work required for moving a unit positive charge from any position A to another position B along a path $\vec{\ell}$ connecting these locations. The work required follows from the line integral along the path:

$$V_{BA} \doteq \Phi_B - \Phi_A = -\int_A^B \vec{E}(\vec{\ell}) \bullet d\vec{\ell} = -\int_A^B \nabla\Phi(\vec{\ell}) \bullet d\vec{\ell}$$

If the work required is positive, the potential at B is higher than in A.

The potential function may thus be found by integration of the scalar function $-\nabla \bullet \vec{E}$. Under static conditions, the outcome of the integration is independent of the path taken.

The property described by (2.69) is demonstrated here in the application to the electric field of a point charge as specified by (2.55). On the basis of the definition of the gradient expressed in spherical coordinates ((2.41)), (2.55) can be written as

$$\vec{E} = \frac{q}{4\pi\varepsilon r^2} = -\nabla'\left(\frac{q}{4\pi\varepsilon r}\right), \tag{2.70}$$

where ∇' operates at the field point. By using (2.33), (2.70) can also be written as

$$\vec{E} = \nabla\left(\frac{q}{4\pi\varepsilon r}\right) \tag{2.71}$$

Hence, it is necessary to be particularly careful when designating coordinates.

Examination of (2.70) shows that the electric field $\vec{E}$ is equal to the negative gradient of the scalar function $\Phi = \frac{q}{4\pi\varepsilon r}$. For a collection of point charges, the potential function Φ can be obtained by superposition (in this case, a simple scalar addition) so that

$$\Phi = \frac{1}{4\pi\varepsilon}\sum_i \frac{q_i}{r_i} + c, \tag{2.72}$$

where r_i is the distance from q_i to the field point and c is an arbitrary constant.

A further generalization considers the potential field from a volume charge density ρ. Since ρdv behaves like a point source, it sets up a field according to (2.72). The entire distribution can be taken into account by superposition (summation) leading to

$$\Phi = \frac{1}{4\pi\varepsilon}\int \frac{\rho}{r} dv + c, \tag{2.73}$$

which shows the potential to be a weighted volume integral of the (scalar) charge density, the weighting function being $1/r$. The electric field can be found from (2.71) by the gradient operation indicated in (2.69). Note that the field is independent of the choice of the constant c, the value of which is therefore completely arbitrary. This determination of the electric field from multiple sources may be easier to carry out than that indicated in (2.61), which requires vector summation.

Combining (2.68) and (2.69), while dropping the prime, gives

$$\nabla^2\Phi = -\rho/\varepsilon, \tag{2.74}$$

which is known as Poisson's equation. Dropping the prime is permitted here, in view of the fact that the Laplacian of $1/r$ turns out to be the same for primed and unprimed coordinates (Sect. 2.6.4.1).

Equation (2.73) is an integral form of solution to the partial differential (2.74) as can be verified by direct substitution of (2.74) in (2.73).

2.3.5 Capacitance

Consider two insulated conducting bodies of arbitrary shape. If a voltage V is connected between the two for a period of time, a quantity of charge Q will be transferred from one to the other. The charge will distribute itself on each conducting body in such a way as to result in the electric field tangential to the conductor being reduced to zero (a nonzero tangential field would cause movement and further redistribution of charge). The potential between the two conducting bodies can be found from the steady-state charge distribution by applying (2.72) at each body. If the total charge is doubled, then each charge element ρdv must also double since the system is linear. Consequently, the difference of potential V is proportional to the total charge Q on either body. The constant of proportionality is the capacitance C. That is:

$$C = Q/V, \tag{2.75}$$

where Q is in coulombs, V in volts and C in farads. A conducting pair that holds a greater amount of charge for the same applied voltage will have a higher capacitance.

If the two conducting bodies are parallel, rectangular, conducting plates of area A and separation d (where $d << \sqrt{A}$), then the field between the plates will be uniform and

$$V = Ed \tag{2.76}$$

In view of (2.66) and the fact that the field lies solely between the two plates, $EA = Q/\varepsilon$. Consequently,

$$V = \frac{Qd}{\varepsilon A} \tag{2.77}$$

and

$$C = \frac{\varepsilon A}{d} \tag{2.78}$$

This result is strictly correct only for $d << \sqrt{A}$, which is a condition for minimum fringing of the field (that is, for a predominantly uniform field). If the medium between the plates is anything other than vacuum, the dielectric permittivity $\varepsilon = \varepsilon_r \varepsilon_0$ is effective where ε_r is the relative permittivity (a dimensionless factor scaling $\varepsilon = \varepsilon_0$ as defined previously (approx. $(1/36\pi)10^{-9}\,\mathrm{F\,m^{-1}}$)).

For biological membranes, which have a high lipid content, $\varepsilon_r = 3$ and $d \cong 3$ nm which is roughly the lipid-layer thickness. The capacitance is then calculated as $0.9\,\mu\mathrm{F\,cm^{-2}}$, a value which is usually measured for nerve tissue and is also applied as the value for the membranes of cardiac myocytes.

2.4 Electric Current Flow in Conductive Media

In the previous section, static electric fields arising from electric charges, where the medium is insulating, were considered. The only property of the medium involved was the specification of the dielectric permittivity ε. Any possible flow of electric current inside the medium was ruled out. While electric fields of cardiac origin also behave (instant by instant) as a static field, such fields generally lie in conducting media. As a consequence, associated with that field is a stationary (steady) current. In a dielectric, no energy is required to maintain a charge configuration and its associated (steady) electric field, but in a conducting body any initial arrangement of charges would quickly dissipate as a result of current flow; the maintenance of a source distribution (and associated electric and current flow field) in a conducting medium requires the continual renewal of such sources. Such steady sources (and associated steady currents) can arise in the presence of physical (electrochemical) batteries. Action currents arising from cellular action potentials (such as those that occur in cardiac muscle) are also based on an electrochemical process. Each cardiac cell, while undergoing activation, can be thought of as an electrochemical cell (battery) and (in effect) a steady current is generated by the (biological) cell. The energy required to maintain the current flow comes, ultimately, from the metabolic processes within the cell.

2.4.1 Ohm's Law of Conductivity

A medium is described as conducting if charged particles are present which are free to move. Electrocardiographic preparations comprise biological tissues (volume conductors) which contain electrolytes. Consequently, they are conducting; their conductivity being caused by the presence of positive and negative ions which can move more or less freely. If an electric field is established in such a medium, each charged particle will experience a force (according to (2.56)) and a flow of charge (i.e., a current) results. The magnitude of current is limited by collisions between the charge carriers and the remaining medium. In fact, if λ is the mean free path (mean distance between collisions), then the time-average drift velocity (for particles with a single electronic charge) is

$$\vec{v} = \frac{q_e \lambda \vec{E}}{2mv_0} = u\vec{E}, \tag{2.79}$$

where $\vec{E}$ is the electric field, q_e is the electronic charge, m is the particle mass, v_0 the average thermal velocity (note that $v << v_0$) and u is the mobility. The mobility, mass and mean free path in (2.79) are, of course, specific to the ion species being considered. If the ion concentration is C particles per cubic meter, then the electric current density equals $Cq_e v$ or

$$\vec{J} = \frac{Cq_e^2 \lambda}{2mv_0}\vec{E} \tag{2.80}$$

This expression reflects the convention that positive current is associated with the flow of positive charge.

For an electrolyte, the total current will arise from the movement of several ions, each of which contributes a component given by (2.80). The relative contribution of component ion species to the total current is described by their respective transference numbers. For example, if sodium, potassium and chloride ions constitute the charge carriers and if J is the total current density then

$$J_K = t_K J; \quad J_{CI} = t_{Cl} J; \quad J_{Na} = t_{Na} J, \tag{2.81}$$

where

$$J = J_K + J_{Cl} + J_{Na} \tag{2.82}$$

The transference numbers t_K, t_{Cl} and t_{Na} for potassium, chloride and sodium depend on their relative ionic concentration and mobility since, for example, using (2.79),

$$J_K = C_K q_e v_K = C_K q_e u_K E \tag{2.83}$$

The linear relationship between $\vec{J}$ and $\vec{E}$, expressed in (2.80), has been verified experimentally under a broad variety of conditions. The coefficient linking these two variables is the electrical conductivity σ, defined through

$$\vec{J} = \sigma\vec{E} \tag{2.84}$$

linking $\vec{E}$, the electric field (V m^{-1}) and $\vec{J}$, the current density (A m^2). As a consequence, the conductivity σ has a dimension (S m^{-1}). Introduced in the way shown above, the conductivity is a scalar constant, a tissue-specific parameter that can be related to molecular quantities through (2.80) or obtained experimentally by the application of (2.84). For some types of tissues, the conductivity has been shown to depend on fiber orientation, which is expressed by calling it *anisotropic,* which demands its specification by means of a tensor.

Equation (2.84) is a differential form of Ohm's law; under dc conditions, it relates to a conduction current arising from the presence of the electric field $\vec{E}$ as a driving force. Under conditions of alternating currents, (2.84) can be generalized if $\vec{J}$ and $\vec{E}$ are interpreted as complex phasors, in which case σ will also, in general, be a complex phasor reflecting reactive properties of the medium. Experimental results, which show that under electrocardiographic conditions σ is essentially real, are described later in this chapter.

2.4.2 Tissue Impedance

An important goal in the biophysical study of electrocardiography is a determination of the currents which flow in the torso owing to the presence of cardiac generators. To accomplish this, it is necessary to describe the electrical conductivity of all torso tissues (along with their geometry). Historically, the following tissues have been thought important enough to require specific inclusion in a rigorous treatment of electrocardiographic current flow: heart muscle, intracavitary blood, lungs, surface fat, surface muscle and the pericardium.

The classical approach to the determination of the conductivity of a material is to incorporate a uniform sample of known size in an electric circuit. A known or measured current is then applied and the resulting voltage is measured. If the voltage is measured at the points at which the current is introduced, the method is called the two-electrode method; if separate voltage lead-off points are used, the method is called the four-electrode method. Since the dimensions of the current-carrying preparation is known, the values of current and voltage are sufficient to determine the conductivity. The four-electrode method, since it avoids electrode interface artifact, is the preferred technique; examples are found in references [2] and [3].

Most biological tissues are not strictly homogeneous, but can be satisfactorily treated as such to a good approximation. The value of conductivity obtained using a typical (macroscopic) sample reflects averaged properties that are normally precise as desired for a simplified, gross, model simulation.

Tissue samples invariably contain biological cells (and cell membranes, of course) so that a determination of conductivity at dc or at different ac frequencies may vary because of the effect of variations in the membrane admittance. For example, in Fig. 2.10 the conductivity of a sample (of skeletal muscle) varies with frequency. At a high enough frequency, the membranes become totally "transparent" and no further reduction in conductivity arises. It can also be seen in Fig. 2.10 that at low frequencies the conductivity transverse to the fiber axis is lower than that along the axis, a consequence of the greater number of intervening membranes in the former case. At elevated frequencies, when the membrane admittance is negligible, the conductivity becomes isotropic. This example shows that, in fact, the response of a tissue sample to an electric field may not be described by a single scalar conductivity value, but depends on frequency and field orientation (the field displays anisotropy). For muscle, the frequency dependence can be traced to the fact that the current flows both in the intracellular and interstitial space and the mix depends, among other things, on the admittance of the membrane. Anisotropic conductivity can be expected for cardiac as well as for skeletal muscle. However, the range of tissue anisotropy of various tissues as reported in the literature is quite substantial. Moreover, its influence may also affect the appropriate specification of the equivalent primary sources. As a consequence, too detailed analysis of the effect of anisotropy should be carried out with great caution[4]. The effect of anisotropy is an essential element of the

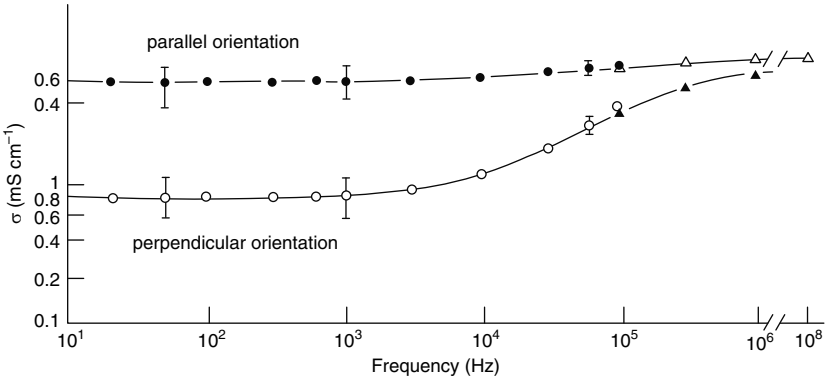

Figure 2.10

Conductivity of canine skeletal muscle at 37°C, in the parallel and perpendicular orientations, measured using a two-electrode (triangles), or four-electrode technique (circles). Each point represents the average of five separate measurements (four-electrode) or two measurements (two-electrode) in each orientation; typical standard errors are shown (adapted from Epstein and Foster [3]).

Table 2.1

Ratio of displacement current to conduction current of tissues at different frequencies [1]

Tissue	Frequency			
	10 Hz	100 Hz	1000 Hz	10,000 Hz
Lung	0.15	0.025	0.05	0.14
Fatty tissue		0.01	0.03	0.15
Liver	0.20	0.035	0.06	0.20
Heart muscle	0.10	0.04	0.15	0.32

Table 2.2

Tissue conductivity (S cm^{-1})

Tissue	Blood	Lung	Liver	Fat	Human trunk
Conductivity	0.67	0.05	0.14	0.04	0.21

bi-domain theory topic addressed in Chaps. 6 and 8. Some other aspects are treated in Chap. 8. The handling of volume conductor effects as presented in this chapter is restricted to the isotropic situations.

Because of the presence of cells and their membranes in tissues, and because the cell membrane has a very high specific capacitance, the macroscopic tissue response to an applied field is both a conduction current and a displacement (capacitive) current. The relative strength of the latter depends on the frequency; for tissue under electrocardiographic conditions, the conductivity (both magnitude and phase) is dispersive (depends on frequency) for this reason.

Measurements on those tissues which are important in electrocardiography show the ratio of displacement to conduction currents to be negligible. Such measurements are summarized in Table 2.1. It can be concluded that torso tissues may be treated as if they are purely resistive. Mean conductivity values of these tissues are given in Table 2.2. Additional data may be found in the review papers [5–7].

The validity of conductivity values in Table 2.2 might possibly be questioned for lung and muscle because for those tissues their cellular structure plays an important role in determining the effective (macroscopic) resistance to current flow. Being complex structures, it may not always be possible or appropriate to describe currents with a simple scalar conductivity parameter. Aside from this proviso, torso tissues are conventionally assumed to be purely resistive, with values of tissue conductivity being essentially those given in Table 2.2.

2.4.3 Quasistatic Conditions

The conduction current in a physiological preparation with conductivity $\sigma(x, y, z)$ is related to the electric field by (2.84). Since the electric field is conservative, this expression cannot be true at every point of the preparation – that would imply a dissipation of energy (associated with current flow in a resistive medium) with no source of energy. To include the presence of active sources, a nonconservative term is added to (2.84) so that

$$\vec{J} = \sigma\vec{E} + \vec{J}^{\,i}, \tag{2.85}$$

where $\vec{J}^{\,i}$ is an impressed (applied) current. In (2.85), $\vec{J}^{\,i}$ is nonzero only at primary source sites; $\vec{J}^{\,i}$ constitutes a nonconservative field. Since the total current in (2.85) is solenoidal (the net flow into or out of any closed region is zero), in order to preserve continuity of current,

$$\nabla \bullet \vec{J} = 0 = \nabla \bullet (\sigma\vec{E}) + \nabla \bullet \vec{J}^{\,i} \tag{2.86}$$

If the medium has a homogeneous isotropic conductivity, that is, $\sigma(x, y, z) = \sigma$, then by using (2.29) and (2.86) reduces to

$$\sigma\nabla \bullet \vec{E} + \nabla \bullet \vec{J}^{\,i} = 0 \tag{2.87}$$

It is obvious from viewing the electrocardiogram that the potential field arising from sources in the heart varies with time. In fact, for a normal subject at rest, the potential and current flow field is periodic at the heart rate. If the ECG is subjected

to a Fourier analysis, it can be determined that the spectral content is from dc to perhaps 100 Hz [8]. The behavior of an ac source in a conducting medium with the size of the human torso and with impedance properties described in Tables 2.1 and 2.2 has been studied using Maxwell's equations, which govern such time-varying phenomena [9]. The outcome is that, to a very good approximation, the electric field may be derived as the gradient of a scalar potential, namely

$$\vec{E} = -\nabla\Phi \tag{2.88}$$

If (2.88) is substituted into (2.87), then we obtain

$$\nabla^2\Phi = \frac{\nabla \bullet \vec{J}^{\mathrm{i}}}{\sigma} \tag{2.89}$$

The integral solution to Poisson's (2.89) for Φ in the infinite homogeneous medium can be found by comparison with the mathematically equivalent (2.74) and (2.73) of electrostatics. This yields

$$\Phi = \frac{1}{4\pi\sigma}\int \frac{-\nabla \bullet \vec{J}^{\mathrm{i}}}{r}\mathrm{d}v, \tag{2.90}$$

where r is the distance from a point of integration to the fixed point at which the field is being evaluated.

A comparison of (2.88) to (2.90) with (2.69), (2.74) and (2.73) shows that the potential and electric field under electrocardiographic conditions obey the same mathematical relationships as for electrostatics. These are described as quasistatic relationships since, at any instant of time, these potentials appear as if they were static for all time, yet changes in value of potential over time do occur.

Many solutions to problems in electric current flow are equivalent to those of comparable problems in electrostatics. The similarity in the respective fundamental relationships has already been noted. Equation (2.69) and (2.73) can be transformed to (2.88) and (2.73) and vice versa if the following replacements are made:

$$\varepsilon \leftrightarrow \sigma \tag{2.91}$$

$$\rho \leftrightarrow -\nabla \bullet J^{\mathrm{i}} \tag{2.92}$$

The similarity may be stressed further by introducing the notation $i_{\mathrm{v}} = -\nabla \bullet J^{\mathrm{i}}$ as an impressed current volume density (A m^{-3}).

2.5 Current Sources

In the previous sections the fundamentals for studying the potential field arising from impressed current sources under quasi-static conditions have been described, as well as the main mathematical tools required for this analysis. We now apply these tools to the description of the main electric current source models that have been found effective.

The analogy between electric current flow in conductive media and electrostatics, the principle of duality, shows up again in the basic expression (2.90), which implies, and permits, the use of the *superposition principle*: the contributions of elementary sources to the potential field simply add up to the (total) potential. The latter is a consequence of the experimentally observed linearity between current strength and resulting potential, which holds true inside the body for natural bioelectric sources.

Bioelectric currents stem from the biochemical processes at the cell membrane. As such, these are not observable. Their presence, nature, and magnitude can only be inferred from the potential field generated; they need to be evaluated from measurements of tissue excitation, with particular reference to the activation of cardiac muscle. The basic expression (2.90) shows that, when interpreting measured potentials, the conductivity of the medium should be included, as well as its distribution throughout the tissue in the case of inhomogeneity.

The discussion begins with a derivation of source–field relationships for the monopole and dipole. It will be seen that these serve as the building blocks of all electrophysiological sources. It should be realized that these source descriptions

are models of the actual current generation. They are physical abstractions that serve to describe the observed potentials at some distance from the actual current generating mechanisms only. As such they are referred to as *equivalent sources*. To facilitate the discussion, the medium is assumed to be of infinite extent and have a homogeneous, isotropic conductivity. The potential field generated is referred to as the infinite medium potential. Although this configuration is clearly unrealistic, it facilitates the appreciation of the nature of the source description in isolation of the complexity caused by inhomogeneities. As will be shown in a subsequent section, these complexities can be treated in an "add-on" fashion.

2.5.1 Point Sources

2.5.1.1 Monopole

Consider that a current I_0, emanating from a vanishingly small volume, is impressed into a uniform conducting medium of conductivity σ and infinite in extent. Let the source position be (x, y, z), as illustrated in Fig. 2.11. This type of current source is analogous to the point charge of electrostatics, and is referred to as a point current source.

The potential field set up inside the medium is evaluated as follows. In view of the symmetry, the current flow is in the radial direction and the current density is uniform on any sphere having the source as its center. Thus if the total current is I_0, then over a concentric spherical surface of radius r the current density $\vec{J}$ is given by

$$\vec{J}(r) = \frac{I_0}{4\pi r^2}\vec{e}_r, \tag{2.93}$$

where $\vec{e}_r$ is a unit vector pointing from the source to the field point (x', y', z') and r denotes their distance: $r = \{(x'-x)^2 + (y'-y)^2 + (z'-z)^2\}^{1/2}$.

Now, according to Ohm's law, the current density $\vec{J}$ and the electric field $\vec{E}$ are related by the conductivity as specified by (2.84). Furthermore, the electric field is obtained as the negative gradient of scalar potential Φ according to (2.88). Consequently,

$$\nabla\Phi = -\frac{I_0}{4\pi\sigma r^2}\vec{e}_r. \tag{2.94}$$

So, using the r component if the gradient operator as listed in (2.41),

$$\mathrm{d}\Phi/\mathrm{d}r = -\frac{I_0}{4\pi\sigma r^2} \tag{2.95}$$

Integration with respect to r gives an expression for the scalar potential associated with a monopole current source, namely

$$\Phi(r) = \frac{I_0}{4\pi\sigma r} + c \tag{2.96}$$

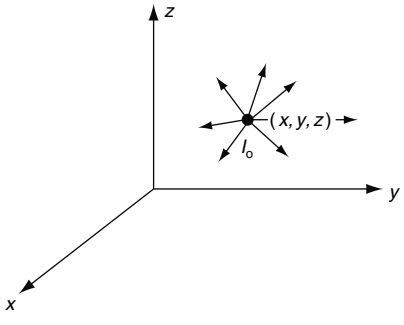

Figure 2.11
Current flow from a point source (monopole).

The result is directly related to (2.72), by applying duality. The integration constant c may be determined by *choosing* the point in space where the potential is taken to be 0. In the infinite medium configuration, this point is conveniently placed at infinity, which yields: $c = 0$.

2.5.1.2 Dipole

The basic current source of biophysics is the (mathematical) current dipole. It can be introduced by first considering the potential distribution generated by a current (point) source of strength I_0 (expressed in amperes (A)) and a current sink of strength $-I_0$, separated by a (small) distance vector $\vec{\delta}$ (Fig. 2.12), with length δ. This generator configuration is called a "bi-pole," or physical dipole. The magnitudes of the strengths of source and sink are equal. Since no net current can be generated by a biophysical source, the current is merely "pumped around."

For infinitesimally small values of δ, the total field under these conditions can be evaluated by

$$\Phi(\vec{r}\,') = \frac{I_0}{4\pi\sigma}\frac{\partial(1/R)}{\partial\delta}\delta \tag{2.97}$$

The partial derivative evaluates the rate of change in the field which results from displacing I_0 in the direction of $\vec{\delta}$, and this is multiplied by δ to obtain the actual change in potential. The partial derivative is with respect to the unprimed, source coordinates while the primed, field coordinates are held constant.

In (2.97), the directional derivative of $1/R$ can be recognized, and hence, it can be written as

$$\Phi(\vec{r}\,') = \frac{I_0}{4\pi\sigma}\nabla(1/R)\bullet\vec{\delta} \tag{2.98}$$

From (2.33) we have

$$\Phi(\vec{r}\,') = \frac{I_0}{4\pi\sigma}\frac{\vec{R}}{R^3}\bullet\vec{\delta} = \frac{1}{4\pi\sigma}\frac{\vec{R}}{R^3}\bullet\vec{D}, \tag{2.99}$$

which introduces $\vec{D} = I\vec{\delta}$ as the (mathematical) dipole, *defined*as the (hypothetical, equivalent) generator that generates its potentials described by (2.99) throughout the medium, i.e., irrespective of the field point's proximity to the generator. The potential reference at infinity is taken to be zero.

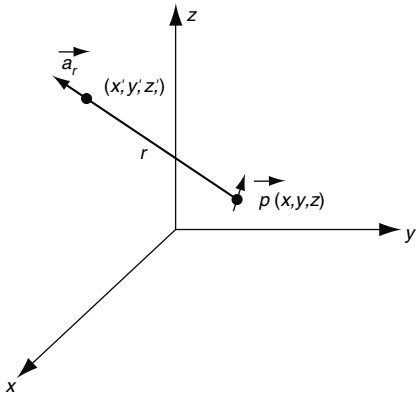

Figure 2.12
Diagram introducing the concept of a current dipole; $\vec{0}$ denotes the origin of the coordinate system.

The dipole is a vector quantity, directed from sink to source. Its physical unit is (A m). As shown, it may be interpreted as the result of a limiting process in which the distance between the two poles of a bi-pole is reduced to zero while keeping the product $I \times \delta$ constant. An alternative expression to (2.99) is

$$\Phi(\vec{r}\,') = \frac{1}{4\pi\sigma}\frac{D\cos\varphi}{R^2}, \tag{2.100}$$

with φ being the angle between $\vec{R}$ and $\vec{\delta}$ (Fig. 2.12).

The current dipole is a useful mathematical concept that may be used to describe (represent, specify) the potential distribution generated by bioelectric sources at a distance. For observation points arbitrarily close to the dipole, the potential prescribed by (2.99) becomes arbitrarily large (infinite), which is clearly physiologically unrealistic. The double layer source model, discussed in Sect. 2.5.2 as well as in Chaps. 6–8, does not suffer from this limitation, and has a direct link to the basis of the bioelectric sources, the biochemical phenomena taking place at the cell membrane (Chap. 7).

2.5.1.3 Evaluation

From the way the monopole and the dipole were introduced above, it is evident that they can indeed be classed as *point sources*: their spatial extent is restricted to a single point. They are physical abstractions, valid for describing the potential field at a distance from the source only, as follows from the fact that at close proximity to their position (x, y, z) the potential field as well as the current density that they generate tend to infinite values. This follows from (2.96) and (2.100) for the monopole and the dipole, respectively. This phenomenon is referred to as a point singularity of the potential field.

The single monopole has an additional unrealistic nature when it is applied to a medium that is bounded, as is the human body. In such a medium a single current monopole would keep charging up the tissue continuously (current is the flow of electric charge per unit of time), which is clearly not the case. So it has a value only if accompanied by a sink of equal strength, as was the case while introducing the dipole. Similarly, inside a bounded medium, a collection of current monopoles may be used provided the sum of their strengths equals zero.

In its application to a medium, be it bounded or not, the dipole does not suffer from this lack of realism: no net charge is introduced into the medium. The dipole may be likened to a circulation pump placed in a swimming pool: it "sucks" water at its inlet valve and ejects it at its outlet valve.

The concept of building a dipole from a pair of monopoles can be extended to the inclusion of a larger number of monopoles. Like the mathematical dipole, the total, more complex configuration remains located at a single point in space. A series of current sources of increasing complexity may be conceived in this manner, called *multipoles*. The monopole and the dipole form the first two terms of this series. Conversely, an arbitrary source distribution may be uniquely specified by a weighted sum of the multipoles of increasing order: a so-called multipole expansion [1, 10, 11].

As follows from (2.96), for the monopole, the multipole of order 0, the potential decreases as $1/r$ when moving away from the source. For the dipole, the first-order multipole, the potential decreases as $1/r^2$. For a multipole of order k, the decrease is as fast as $1/r^{k+1}$. This is a highly significant property: with the monopole being absent in a bounded medium, the potential at increasing distances from the source will invariably be dominated by the dipole contributions, the contributions by the higher order terms decreasing more rapidly with distance. This explains the fact that at a distance, the potential field of an arbitrary current source tends to have a dipolar nature. As a rule of thumb, at a distance of, say, 5 times that of the spatial extent of a source, the contributions of the higher order may already be difficult to establish experimentally.

2.5.2 Surface Source Densities

Current monopoles and current dipoles may be used as building blocks for more complex source configurations. To this end, like in electrostatics, these sources may be specified by density functions, specifying their strength per unit of volume. Alternatively, when restricted to some surface, their strength is specified per unit of surface area. The expressions for determining the source–field relationships (in the infinite medium under quasi-static conditions) are (2.85) to (2.90).

These will now be used to describe the properties of two particular variants of distributed surface source densities: the current monopole layer and the current dipole layer. These two source types are the major players in the various applications of volume conduction theory discussed in this book.

2.5.2.1 Monopole Layer; Monolayer

In the case of the current monopole layer, or monolayer, a monopole surface density of strength $J(x, y, z)$ is assumed to be present at a surface S, with $J\mathrm{d}S$ representing an elementary current source (dimension: A). The dimension of the density function J is A m^{-2}, which is the same as that of the current density $\vec{J}$, but unlike $\vec{J}$ the density is a scalar function.

The potential field for this source is

$$\Phi = \frac{1}{4\pi\sigma}\int \frac{J\mathrm{d}S}{r} \tag{2.101}$$

To illustrate some of the major properties of the monolayer, the potential along the axis of a disk carrying a uniform monopole current density J is derived. The geometry is shown in Fig. 2.13, where a cylindrical coordinate system is set up, with the origin at the center of the disk and polar axis normal to the plane of the disk. The disk radius is a. Based on symmetry the contributions of all source points on an annular ring of radius r and width dr, to the potential at a point along the axis at a distance z from the disk are equal:

$$\mathrm{d}\Phi(z) = \frac{2\pi r\mathrm{d}rJ}{4\pi\sigma(r^2+z^2)^{1/2}}, \tag{2.102}$$

where the numerator of (2.102) is the total current impressed through the annulus, and $(r^2+z^2)^{1/2}$ is the distance between source element and observation point.

By adding up the elementary contributions, through the integration of (2.102), we find

$$\Phi(z) = \frac{J}{2\sigma}\int_0^a \frac{r\mathrm{d}r}{(r^2+z^2)^{1/2}} = \frac{J}{2\sigma}\{(a^2+z^2)^{1/2} - |z|\} + c \tag{2.103}$$

Choosing the potential at infinity to be zero requires setting $c = 0$, which yields

$$\Phi(z) = \frac{J}{2\sigma}\{(a^2+z^2)^{1/2} - |z|\} \tag{2.104}$$

From this expression it follows that the potential along the z-axis is continuous at $z = 0$, i.e., when crossing the monolayer. For the electric field along the z-axis the situation is different. Here we have

$$E_z = -\frac{\mathrm{d}}{\mathrm{d}z}\{\Phi(z)\} = -\frac{J}{2\sigma}\left\{\frac{z}{(a^2+z^2)^{1/2}} - \frac{z}{|z|}\right\}, \tag{2.105}$$

which is discontinuous at $z = 0$. By denoting the current flow along the z-axis that results from this source configuration as $J_z = \sigma E_z$ it follows that while approaching the disk along the negative z-axis a limiting value of $J_z = -J/2$ is reached, whereas on the other side of the disk we have $J_z = J/2$. This corresponds to an outflow of current away from the monolayer.

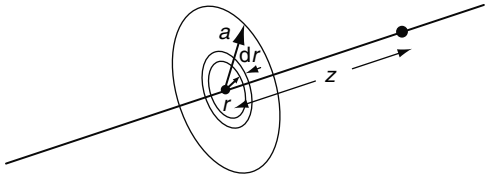

Figure 2.13
Geometrical arrangement for calculating the potential on the axis of a disk carrying a uniform current density.

2.5.2.2 Dipole Layer; Double Layer

The distribution of dipole sources confined to a surface S is referred to as a *double layer*. The elements dS of S are taken to carry an elementary current dipole with strength $\vec{M}_S dS$, $\vec{M}_S$ denoting the dipole moment per unit area (dimension: A m/m^2 = A m^{-1}). By using superposition applied to (2.99), the potential field is

$$\Phi = \frac{1}{4\pi\sigma} \int \frac{\vec{M}_S \bullet \vec{r}}{r^3} dS \tag{2.106}$$

If the orientation of the dipole density $\vec{M}_S$ lines up with the normal of the surface S carrying it, then $\vec{M}_S dS = M_S d\vec{S}$ and (2.106) may be written as

$$\Phi = \frac{1}{4\pi\sigma} \int M_S \frac{\vec{r}}{r^3} \bullet d\vec{S} = \frac{1}{4\pi\sigma} \int M_S d\omega, \tag{2.107}$$

where $d\omega$ is an element of solid angle defined earlier (see (2.63)). If, moreover, the double layer strength M_S is uniform (over S), then (2.107) has a simple form, namely

$$\Phi = \frac{M_S}{4\pi\sigma} \Omega, \tag{2.108}$$

where Ω is the solid angle subtended by the entire double layer at the field point (Sect. 2.2.12).

Equation (2.108) has major significance. If S is a closed surface and the double layer is indeed normal to it and has uniform strength, then for any field point external to S we have $\Omega = 0$. For any interior point of S the total solid angle has a magnitude -4π ((2.49) and (2.50)). From this it follows that while crossing the surface S from outside, the solid angle changes by 4π. As a consequence, the potential is discontinuous across the layer, exhibiting a jump of magnitude

$$\Delta\Phi = V_D = M_S/\sigma \tag{2.109}$$

By defining $V_D = M_S/\sigma$, an alternative characterization of the strength of the double layer is obtained and, when applied to (2.107), this yields

$$\Phi = \frac{1}{4\pi} \int V_D \frac{\vec{r}}{r^3} \bullet d\vec{S} = \frac{1}{4\pi} \int V_D d\omega \tag{2.110}$$

For a nonuniform double layer that is oriented along the surface normal, any potential jump observed experimentally reflects the local double layer strength.

The nature of the current dipole layer may be illustrated by taking S once more to be a circular disk of radius a, and computing the potential along the axis of symmetry. This is the same configuration as depicted in Fig. 2.13, but now the disk carries a uniform dipole density with strength M_S, directed along the z-axis. The potential along the z-axis follows from (2.108). For this axial symmetric configuration the solid angle Ω subtended by the disk at observation point z follows immediately from the definition of the concept *solid angle* as such. For positive values of z the result is

$$\Omega(z) = 2\pi \left\{ \frac{z}{|z|} - \frac{z}{(a^2 + z^2)^{1/2}} \right\} \tag{2.111}$$

The term $z/(a^2+z^2)^{1/2}$ is equal to the cosine of the top angle α of the cone spanning from z to the disk. When approaching the disk along the negative z-axis, the limiting value for the solid angle is -2π. The negative sign corresponds to the fact that the surface normal is taken to be lined up with the dipole direction, whereas for a negative z the source to field vector points in the opposite direction. When approaching the double layer from the other side, the value of Ω tends to 2π. Recall that total 3D space spans a solid angle of 4π, and close to a plane which remains just one half of that. Thus the solid angle jumps by 4π while crossing the double layer. By writing $V_D = M_S/\sigma$ and substituting (2.111) in (2.108) we find

$$\Phi(z) = \frac{1}{2} V_D \left\{ \frac{z}{|z|} - \frac{z}{(a^2 + z^2)^{1/2}} \right\} = \frac{1}{2} V_D \{\pm 1 - \cos\alpha\} \tag{2.112}$$

Because of symmetry, the gradient of the potential along the z-axis is directed along this axis. By differentiating (2.112), we find for the component electric field along the z-axis

$$E_z = -\frac{\mathrm{d}}{\mathrm{d}z}\{\Phi(z)\} = -\frac{1}{2}V_\mathrm{D}\left\{XX - \frac{1}{(a^2+z^2)^{1/2}} + \frac{z^2}{(a^2+z^2)^{3/2}}\right\} = \frac{1}{2}V_\mathrm{D}\left\{-XX + \frac{a^2}{(a^2+z^2)^{3/2}}\right\} \tag{2.113}$$

The function $\Phi(z)$ is discontinuous at $z = 0$. This demands some special care while taking its derivative. The term XX expresses the singularity of the derivative at $z = 0$. This has the dipole-like nature of two so-called delta functions with opposite sign that are infinitesimally close at $z = 0$.

Apart from this singularity, the field strength can be seen to be a positive, even function of z. This corresponds to a current flow in one direction: toward the double layer along the negative z-axis, away from it along the positive z-axis. This is in agreement with the circulation pump analogy. Note that close to $z = 0$, the gradient of the potential is proportional to $1/a$, which tends to zero when increasing a, the radius of the disk.

2.5.2.3 Evaluation; Primary and Secondary Sources

The analyses in the previous two sections show that the monolayer and the double layer have a contrasting behavior of the potential at their boundary: for the monolayer the potential is continuous and its gradient is discontinuous. For the double layer it is just the other way round. Although this is demonstrated here for a relatively simple configuration: assuming a uniform strength and a simple shape of S, this type of behavior can be shown to hold true in general (Panofsky & Phillips; p. 20).

Like the monopole, the uniform monolayer has no place by itself in a bounded medium since it does not conserve charge. The nonuniform variant clearly has a place when adding the constraint that the integral of its density over the surface carrying it be zero. Even so, it is rarely used as a model for the true, primary sources that originate from membrane processes. Its natural place is as one of the equivalent sources that are used for treating the relationship between potentials on the heart surface and body surface potentials (Sect. 2.6.5.4).

The double layer source model has a natural place as a primary, equivalent source, as well as a secondary source for treating the effect of inhomogeneities in the electric conductivity of the medium (Sect. 2.6).

2.5.3 Volume Source Densities

A volume distribution of dipole sources can be described by a density function, just as a volume distribution of point charges in electrostatics could be described by a volume charge density function. If $\vec{M}_\mathrm{v}$ is a dipole moment per unit volume, with dimension $\mathrm{A\,m^{-2}}$, then $\vec{M}_\mathrm{v}\mathrm{d}v$ is an elementary dipole whose potential field, according to (2.99), is

$$\mathrm{d}\Phi = \frac{1}{4\pi\sigma}\frac{\vec{M}_\mathrm{v}\bullet\vec{r}}{r^3}\mathrm{d}v \tag{2.114}$$

The total potential field is found by integrating (2.114), giving

$$\Phi = \frac{1}{4\pi\sigma}\int\frac{\vec{M}_\mathrm{v}\bullet\vec{r}}{r^3}\mathrm{d}v \tag{2.115}$$

The field of the double layer discussed in the previous section may be viewed as a degenerate case of (2.115), with $\vec{M}_v dv = \vec{M}_S dS$.

More generally, if a conducting region contains an arbitrary impressed current source density $\vec{J}^i$, then the potential field is

$$\Phi = \frac{1}{4\pi\sigma} \int \frac{-\nabla \bullet \vec{J}^i}{r} dv \tag{2.116}$$

as was shown in (2.90). The volume of integration expressed in (2.116) relates to any volume that contains all impressed sources; at the surface of such a chosen volume, $\vec{J}^i = 0$ necessarily. As a consequence, if $\vec{J}^i/r$ is integrated over such a bounding surface, the result must also be zero. That is

$$\int (\vec{J}^i/r) \bullet d\vec{S} = 0 \tag{2.117}$$

If the divergence theorem ((2.26)) is applied to (2.117), then

$$\int \nabla \bullet (\vec{J}^i/r)\, dv = \int \frac{\vec{J}^i}{r} \bullet d\vec{S} = 0 \tag{2.118}$$

and by application of the vector identity given by (2.29), (2.118) yields

$$\int \vec{J}^i \bullet \nabla(1/r) dv = -\int (1/r) \nabla \bullet \vec{J}^i dv \tag{2.119}$$

Consequently (2.116) can be replaced by

$$\Phi = 1/(4\pi\sigma) \int \vec{J}^i \bullet \nabla(1/r) dv \tag{2.120}$$

from which it follows that

$$\Phi = 1/(4\pi\sigma) \int \vec{J}^i \bullet \vec{r}/r^3 dv, \tag{2.121}$$

where $\vec{r}$ points from source to field point, as before. A comparison of (2.121) and (2.115) provides an alternative interpretation of the impressed current density $\vec{J}^i$ $(\mathrm{A\,m^{-2}})$ as a dipole moment per unit volume. Note that both interpretations have the same dimensions: $\mathrm{A\,m^{-2}} = \mathrm{A\,m/m^3}$. The potential field can be found from $\vec{J}^i$ using either (2.116), where $-\nabla \bullet \vec{J}^i$ behaves like a current *mono*pole volume density i_v $(\mathrm{Am^{-3}})$, or (2.121), where $\vec{J}^i$ behaves like a *di*pole moment volume density $(\mathrm{A\,m^{-2}})$.

2.6 Potential Fields in Inhomogeneous Media

Up to this point, all expressions for the potential fields discussed in this chapter have assumed that the sources lie in a volume conductor of infinite extent having a uniform isotropic electric conductivity. When inhomogeneities of the electric conductivity are in fact present, as is always the case in bioelectricity, their effect on the observed potential field must be taken into account. This section describes some of the methods that are used for evaluating these effects. The goal in mind is their application to the determination of electrocardiographic potential fields.

The methods discussed assume the inhomogeneities to be restricted to nonintersecting subregions, each having its individual homogeneous, isotropic electric conductivity.

The most prominent inhomogeneity relates to the fact that the electric conductivity of the region outside the body (air) is zero. As a consequence, in the normal situation, no electric current flow takes place across this surface. Other, major differences in conductivity values with respect to those of the surrounding tissues are those of the lungs (lower conductivity) and the blood inside the cavities of atria and ventricles (higher conductivity).

To introduce the problem, consider a dipole source in a conducting medium of infinite extent. Current flow lines, directed along the local electric field, exists as shown in ❯ Fig. 2.14. Where appropriate, and to distinguish it from the

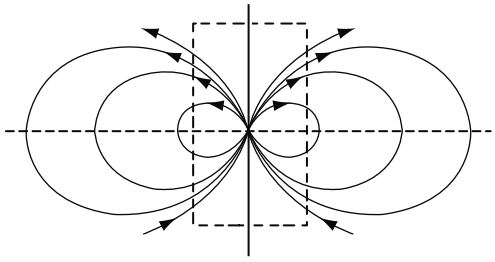

Figure 2.14
Current flow lines generated by a dipole pointing upward, lying in a uniform, unbounded, conducting medium.

inhomogeneous situation, the potential field set up by the electric current generator inside this type of medium will be denoted as the *infinite medium potential* Φ_∞.

Suppose that at some instant the entire region external to the rectangular parallelepiped (shown dotted in Fig. 2.14) is cut away leaving a nonconducting medium. This constitutes a more realistic model of bioelectrical volume conduction, in a medium of finite extent bounded by air. In this case, since the current cannot enter the nonconducting exterior region, the current flow in the interior region will be diverted such that no current will pass the interface between the conducting and the insulating region.

More generally, if at an instant of time the region external to the parallelepiped in Fig. 2.14 were to have a different conductivity (not necessarily zero, as just considered), then boundary conditions at the interface between the two regions of different conductivity (labeled by subscripts 1 and 2) need to be satisfied

$$\Phi_1 = \Phi_2 \tag{2.122}$$

$$\sigma_1 \partial\Phi_1/\partial n = \sigma_2 \partial\Phi_2/\partial n = J_n, \tag{2.123}$$

where ∂n is taken along the local surface normal to the interface.

Equation (2.123) represents the continuity of the normal component of the current density J_n, which must hold true in the steady state (no accumulation of charge at the interface). This continuity condition and that of potential (2.122) form the basis for finding the potential field set up by an electric current generator inside a piece wise inhomogeneous medium.

If a medium, such as the human torso, can be subdivided into a number of subregions each having a uniform conductivity, a dedicated pair of such conditions will apply at each of the respective interfaces. The total set of these conditions can be shown to be sufficient to uniquely find the current flow pattern [12]. The associated potential field is then, as always, uniquely specified up to a constant only. If the medium is in fact bounded, like the thorax normally is, choosing the location of the reference point for the potential at infinity is no longer possible.

2.6.1 Basic Formulation; Uniqueness Theorem

2.6.1.1 Basic Formulation

The determination of electrocardiographic potential fields arising from bioelectric primary sources is referred to as the Forward Problem of Electrocardiography (Chap. 8). The solution methods discussed here are selected in view of their high conceptual relevance. As introduced above, we consider one or more subregions, each having its own electric conductivity. In one more of these subregions, bioelectric current sources may be situated. The problem of finding the resulting potential field anywhere inside the medium or at its boundary may be handled by finding the potential field resulting from

each of these sources separately, followed by adding up their individual contributions (superposition theorem). This is justified by the linearity of the basic source–field relationship:

$$\nabla^2\Phi = \frac{-i_v}{\sigma_k} = \frac{\nabla \bullet \vec{J}^i}{\sigma_k}, \tag{2.89a}$$

being Poisson's equation.

Inside a homogeneous subregion k with conductivity σ_k, the potential field Φ is found by solving the variant of the differential (2.89a), those without primary bioelectric sources by solving Laplace's equation

$$\nabla^2\Phi = 0 \tag{2.124}$$

At the boundaries of the subregions the continuity conditions for the potential and the current density normal to the interfaces, (2.122) and (2.123), need to be satisfied

2.6.1.2 Uniqueness Theorem

Once, by whatever means, a solution Φ has been found that satisfies (2.122), (2.123), and (2.124) it can be shown that it is unique up to a constant only. This property is known as the *uniqueness theorem* [12].

2.6.2 Method of Images

The solution method based on images is well known from electrostatics. Because of the analogy between electrostatics and volume conduction theory, cf. (2.91) and (2.92), the same method may also be applied in bioelectricity. However, the number of configurations for which the method can be applied in bioelectric volume conduction problems is rather limited. Here, a discussion on this topic is included to introduce and illustrate some important basic theoretical concepts.

The problem treated is the situation where volume conduction in the semi-infinite space $z \leq 0$ has a conductivity value σ_1. In the remaining (upper) part of space, the conductivity is σ_2. On the z-axis, an electric dipole with strength $\vec{D}$ is situated at $z = -d$, with dipole elements (D_x, D_y, D_z). The problem addressed here is finding the potential field Φ_1 in the lower space, Φ_2 in the upper space and in particular at the interface $z = 0$. Inspired by the image theory of electrostatics, we consider a virtual *infinite* space having a uniform conductivity σ_1, in which we place a (virtual) image source $\vec{V}_2$ at the z-axis at $z = +d$. In the lower semi-space, the dipole potentials generated by both sources clearly satisfy Poisson's equation, irrespective of the strength of $\vec{V}_2$. The potential field in the upper semi-space, Φ_1, is assumed to be generated by a (virtual) image source $\vec{V}_1$ located on the z-axis at $z = -d$; $d > 0$ (with no virtual sources in the upper semi-space). In this upper semi-space the dipole potential generated by $\vec{V}_1$ satisfies Laplace's equation since the upper region is source free. However, without a proper specification of $\vec{V}_1$ and $\vec{V}_2$, it is not guaranteed that the boundary conditions at the interface $z = 0$, (2.122) and (2.123), are met. Without loss of generality, we may put $D_y = 0$, and correspondingly, because of the symmetry involved, $V_{1,y} = 0$ and $V_{2,y} = 0$. In this virtual, infinite space, the potential at, $z = 0$ is continuous if, using the expression for the dipole potential, (2.99),

$$\Phi_1(x,y,0) = \frac{1}{4\pi\sigma_1}\left(\frac{D_x x + D_z d}{R_1^3} + \frac{V_{2,x}x - V_{2,z}d}{R_2^3}\right) = \Phi_2(x,y,0) = \frac{1}{4\pi\sigma_1}\left(\frac{V_{1,x}x + V_{1,z}d}{R_1^3}\right), \tag{2.125}$$

with R_1 the length of $\vec{R}_1 = (x, y, z + d)$ and R_2 the length of $\vec{R}_2 = (x, y, z - d)$, pointing from the respective dipole sources to the field point at $(x, y, z = 0)$. Since $R_1 = R_2$, and the equality is required to hold true independently of x, (2.125) reduces to the conditions

$$V_{1,x} - V_{2,x} = D_x \text{ and } V_{1,z} + V_{2,z} = D_z \tag{2.126}$$

Next we demand the virtual sources to be such that the continuity equation for the current density in the original, inhomogeneous situation is also satisfied in the virtual, homogeneous space. To evaluate (2.123), the respective contributions

of the dipole sources to the potential in their respective domains are differentiated with respect to z, the z-axis being directed according to the normal of the interface. For $z = 0$, this means that we demand

$$\sigma_1 \frac{\partial \Phi_1}{\partial z}(x,y,0) = \sigma_1 \frac{1}{4\pi\sigma_1}\left(\frac{-3D_x xd + (R_1^2 - 3d^2)D_z}{R_1^5} + \frac{3V_{2,x}xd + (R_2^2 - 3d^2)V_{2,z}}{R_2^5}\right) \tag{2.127}$$

$$\sigma_2 \frac{\partial \Phi_2}{\partial z}(x,y,0) = \sigma_2 \frac{1}{4\pi\sigma_1}\left(\frac{-3V_{1,x}xd + (R_1^2 - 3d^2)V_{1,z}}{R_1^5}\right) \tag{2.128}$$

This equality should hold true, again independently of x, and since $R_1 = R_2$, equating (2.127) to (2.128) yields

$$\kappa V_{1,x} + V_{2,x} = D_x \text{ and } \kappa V_{1,z} - V_{2,z} = D_z, \tag{2.129}$$

with $\kappa = \sigma_2/\sigma_1$. The four equations specified by (2.126) and (2.129) is sufficient to solve the strengths of the components of the virtual sources $\vec{V}_1$ and $\vec{V}_2$. We find

$$\vec{V}_1 = \left(\frac{2}{1+\kappa}D_x, 0, \frac{2}{1+k}D_z\right) \text{ and } \vec{V}_2 = \left(\frac{1-\kappa}{1+\kappa}D_x, 0, -\frac{1-\kappa}{1+\kappa}D_z\right) \tag{2.130}$$

Since the potential fields specified by the combinations of the primary dipole and the virtual dipole sources satisfy the boundary conditions pertaining to the original, inhomogeneous problem formulation, the solutions also apply to the "real world" formulation of the problem. This follows as a direct consequence of the uniqueness theorem, Sect. 2.6.1.2. Note that, although the medium considered is inhomogeneous, it is still of infinite extent and hence the implied location of the potential reference could be, and was in fact taken, at infinity.

2.6.2.1 Inferences

The relatively simple configuration of Sect. 2.6.2 provides a suitable entry to introduce and illustrate some basic concepts related to the effect of inhomogeneity of volume conduction.

In combination with the primary dipole source, the virtual source specification implied in (2.130) permits the computation of the field potential everywhere in the medium.

We first consider the potential field $\Phi(x,y)$ at the plane $z = 0$ for the source–volume conductor configuration introduced in Sect. 2.6.2. By introducing $\vec{V}_2$ as specified by (2.130) in (2.125), we find

$$\Phi(x,y,0) = \frac{1}{4\pi\sigma_1}\frac{D_x x + D_z d}{R^3} + \frac{1}{4\pi\sigma_1}\frac{1-\kappa}{1+\kappa}\frac{D_x x + D_z d}{R^3}, \tag{2.131}$$

with R the length of $\vec{R} = (x,y,\pm d)$. The first term on the right represents the infinite medium potential, the second term the effect of the inhomogeneity. The second term has a source strength that is proportional to that of the primary source term. Correspondingly, $\frac{1-\kappa}{1+\kappa}\vec{V}_2$ constitutes a *secondary* current source; for $\kappa = 1$ (the homogeneous situation), its contribution vanishes. At the plane $z = 0$ we see that (2.131) reduces to

$$\Phi(x,y,0) = \frac{1}{4\pi\sigma_1}\frac{1-\kappa}{1+\kappa}\frac{D_x x + D_z d}{R^3} \tag{2.132}$$

If $\sigma_2 = 0$, corresponding to the medium being nonconductive above $z = 0$, we have $\kappa = 0$ and the potential $\Phi(x,y,0)$ is twice that in the infinite medium:

$$\Phi(x,y,0) = 2\Phi_\infty(x,y,0). \tag{2.133}$$

Next, more generally, we consider the potential field at an arbitrary plane $z = -a\,; a > 0$ in the lower semi-infinite space. Here we have

$$\Phi(x,y,-a) = \frac{1}{4\pi\sigma_1}\frac{D_x x + D_z(-a+d)}{R_1^3} + \frac{1}{4\pi\sigma_1}\frac{1-\kappa}{1+\kappa}\frac{D_x x - D_z(a+d)}{R_2^3}, \tag{2.134}$$

with R_1 the length of $\vec{R}_1 = (x, y, -a + d)$ and R_2 the length of $\vec{R}_2 = (x, y, -a - d)$. Note that $|-a+d|$ is the distance between the location of the primary source and the plane of observation. At this plane R_1 and R_2 are not equal. As a consequence, for $\kappa = 0$ the potential field (2.131) does no longer follow a simple expression of the nature of (2.134).

If the distance d (recall $d > 0$) between primary source and the interface is large compared to $|-a+d|$, the contribution of the secondary source to the potential in (2.134) is small. Consider, for example, the situation where $\kappa = 0$ (bounded medium) and $D_x = 0$ (a primary source dipole pointing toward the interface). By assigning $|-a+d|$ a constant value c, the contribution of the primary source term in (2.134) is proportional to the constant factor $1/c^2$, whereas that of the secondary source is proportional to $1/(2d-c)^2$, which rapidly decreases for increasing values of d.

This indicates that for the interpretation of potential fields observed close to primary sources, the effect of *distal* inhomogeneities may, to a first-order approximation, be neglected.

2.6.2.2 Alternative Secondary Sources

The secondary source description stemming from the method of images is by no means unique. Alternative variants are the introduction of monolayers or double layers at the interfaces between the inhomogeneous subregions. The potential field set up by the virtual sources satisfies Laplace's equation, that of the primary sources (the infinite medium solution) satisfies the associated Poisson's equation. The strength of such virtual sources may be computed such that all boundary conditions are satisfied, and thus (unicity theorem) the sum of both fields in the virtual, infinite space into which the primary and secondary sources are introduced is also the solution for the "real world" problem.

2.6.3 Spherically Shaped Interfaces

Although including inhomogeneity, the volume conductor treated in Sect.2.6.2 is still insufficient for the analysis of the bioelectric potentials, since the semi-space is of infinite extent. The method of images may be applied to treating bounded media, but here the bounding geometry needs to be restricted, e.g., to be box-like.

For some types of geometric alternative, analytical methods are available for solving the involved volume conduction problem. A particular class is formed by spherical interfaces. In this section, the method of handling such interfaces is discussed, and is illustrated with respect to their application to a single bounded sphere, the earliest bounded volume conductor model considered in electrocardiography.

2.6.3.1 General Solution of Laplace's Equation; Spherical Harmonics

As shown in Sect. 2.6.2.2, the potential field generated by the secondary sources should satisfy Laplace's equation, and for treating spherical boundaries the expression of Laplace's equation in spherical coordinates (r, θ, ϕ), (2.45), is the natural starting point. It can be shown that the general *solution* to (2.45) can be formulated as a sum of basic analytical functions, involving, in general, an infinite member of terms [1, 10]. This expression reads

$$\Phi(r,\theta,\phi) = \sum_{n=0}^{\infty} \sum_{m=0}^{n} (a_{n,m} \cos m\phi + b_{n,m} \sin m\phi)(c_{n,m} r^n + d_{n,m} r^{-(n+1)}) P_n^m(\mu), \tag{2.135}$$

with $\mu = \cos\theta$. The function $P_n^m(\mu)$ is the associated Legendre function of degree n and order m [13, p. 332]. In combination with the sine and cosine functions involved, these functions form the set of the so-called spherical harmonics. For $m = 0$ these are referred to as the Legendre polynomials $P_n(\mu) = P_n^0(\mu)$. The factors $a_{n,m}$, $b_{n,m}$, $c_{n,m}$, and $d_{n,m}$ are the expansion coefficients that specify the solution $\Phi(r, \theta, \phi)$. The great significance of the expansion (2.135) stems from the fact that the spherical harmonics form an orthogonal set. This means that the integral over a product of two such functions of the same order and degree is nonzero, whereas it will be zero if any of the two orders or degrees differs. As a

consequence, a unique set of expansion coefficients may be computed for any potential field $\Phi(r,\theta,\phi)$. The derivatives of $P_n(\mu)$ are related to the associated Legendre function, in fact we have:

$$\frac{\mathrm{d}^m}{\mathrm{d}\mu^m}P_n(\mu) = (-1)^m(1-\mu^2)^{-m/2}P_n^m(\mu), \tag{2.136}$$

[13 p. 334]. For $n = 0, 1, 2, 3$ the Legendre polynomials are

$$P_0(\mu) = 1, \quad P_1(\mu) = \mu, \quad P_2(\mu) = \frac{1}{2}(3\mu^2 - 1) \text{ and } P_3(\mu) = \frac{1}{2}(5\mu^3 - 3\mu), \tag{2.137}$$

those for higher degrees follow from the recurrence expression

$$(k+1)P_{k+1}(\mu) = (2k+1)\mu P_k(\mu) - kP_{k-1}(\mu) \tag{2.138}$$

These polynomials are orthogonal over the interval $-1 < \mu < 1$. The integral of $(P_n(\mu))^2$ over this interval, called the squared norm of $P_n(\mu)$, is

$$\int_{-1}^{1}(P_n(\mu))^2\mathrm{d}\mu = \frac{2}{2n+1} \tag{2.139}$$

2.6.3.2 Application: Current Dipole Inside a Bounded Sphere

As an example of the use of spherical harmonics, we compute the potential field generated by a current dipole placed inside a bounded sphere with radius a, centered around the origin. Other applications of this method are worked out in other chapters of this volume.

The internal homogeneous conductivity of the sphere is taken to be σ. Without loss of generality, the dipole is placed on the z-axis at $z = d, 0 \le d < a$, and its strength taken to be $\vec{D} = (D_x, 0, D_z)$. The infinite medium potential, expressed in Cartesian coordinates is

$$\Phi_\infty(x,y,z) = \frac{1}{4\pi\sigma}\frac{D_x x + D_z(z-d)}{R^3} = \frac{1}{4\pi\sigma}\frac{D_x x}{R^3} + \frac{1}{4\pi\sigma}\frac{D_z(z-d)}{R^3} \tag{2.140}$$

The first term on the right represents the contribution to the potential field of the component of the dipole vector that is tangential to the surface of the sphere, the second term that of the radial component. The expression of the same function in spherical coordinates reads

$$\Phi_\infty(r,\theta,\phi) = \frac{1}{4\pi\sigma}\frac{D_x r\sin\theta\cos\phi}{(\sqrt{r^2+d^2-2dr\cos\theta})^3} + \frac{1}{4\pi\sigma}\frac{D_z(r\cos\theta - d)}{(\sqrt{r^2+d^2-2dr\cos\theta})^3} \tag{2.141}$$

After introducing $\mu = \cos\theta$, in the second term on the right the function

$$\frac{r\cos\theta - d}{(\sqrt{r^2+d^2-2dr\mu})^3} = \frac{\partial}{\partial d}\left(\frac{1}{\sqrt{r^2+d^2-2dr\mu}}\right) = \frac{\partial}{\partial d}\left(\frac{1}{R}\right), \tag{2.142}$$

as can be verified by differentiation. Similarly, in the first term on the right of (2.141), the function

$$\frac{r}{(\sqrt{r^2+d^2-2dr\mu})^3} = \frac{1}{d}\frac{\partial}{\partial\mu}\left(\frac{1}{R}\right) \tag{2.143}$$

The function $1/R$ may be expanded in a Taylor series. For $r > d$ the result is

$$\frac{1}{R} = \frac{1}{r}\sum_{\ell=0}^{\infty}\left(\frac{d}{r}\right)^\ell P_\ell(\mu)$$

and for $r < d$ we have

$$\frac{1}{R} = \frac{1}{d}\sum_{\ell=0}^{\infty}\left(\frac{r}{d}\right)^{\ell} P_\ell(\mu) \tag{2.144}$$

The appearance of the Legendre polynomials in this Taylor series expansion is not accidental: in fact the Legendre polynomials have been defined on the basis of this expansion. These properties allow the two terms in the right hand side of (2.141) to be expanded as a series of Legendre polynomials, thus opening the way for solving the bounded medium potential. This is demonstrated here by computing the potential field generated by the radial dipole component. The treatment of the contribution of the tangential dipole component may be carried out in a similar way.

For $r > d$ the infinite medium potential generated by radial dipole is

$$\Phi_\infty(r,\theta,\phi) = \frac{D_z}{4\pi\sigma}\frac{r\mu - d}{(\sqrt{r^2 + d^2 - 2d\mu})^3} = \frac{D_z}{4\pi\sigma}\frac{\partial}{\partial d}\left(\frac{1}{R}\right)$$

and by using (2.144) we find

$$\Phi_\infty(r,\theta,\phi) = \frac{D_z}{4\pi\sigma}\frac{1}{r^2}\sum_{\ell=1}^{\infty}\ell\left(\frac{d}{r}\right)^{\ell-1} P_\ell(\mu) \tag{2.145}$$

Note that the summation starts at $\ell = 1$, as the term for $\ell = 0$ is wiped out by the factor ℓ that results from the applied differentiation. Also note that the expression on the right does not depend on ϕ, in agreement with the axial-symmetric nature of this part of the problem.

To this infinite medium potential we now add the general solution of Laplace's Equation (2.135) and demand that the potential field expressed by the sum satisfies the boundary condition at the surface of the sphere. For a bounded medium this means that the normal derivative of the field is zero. The nature of the problem is such that a relatively simple form of (2.135) is involved. First, because of the axial-symmetric nature of both the infinite medium potential and the volume conductor, no terms involving ϕ should play a role. Second, since the contribution to the potential field at the origin is desired to be finite, all terms involving negative powers of r should be absent. This leaves as the possible contribution satisfying Laplace's equation

$$\Phi(r,\theta,\phi) = \sum_{n=0}^{\infty} c_n r^n P_n(\mu), \tag{2.146}$$

and, for $r > d$ the general nature of the total potential field is

$$\Phi(r,\theta,\phi) = \frac{D_z}{4\pi\sigma}\frac{1}{r^2}\sum_{\ell=1}^{\infty}\ell\left(\frac{d}{r}\right)^{\ell-1} P_\ell(\mu) + \sum_{n=0}^{\infty} c_n r^n P_n(\mu) \tag{2.147}$$

The expansion coefficients c_n remain to be determined from the boundary condition. Because of the radial symmetry of the volume conductor, the normal derivative of the interface is found by differentiation with respect to r and the boundary condition is satisfied if this derivative is zero for $r = a$.

Carrying out the differentiation, followed by substituting $r = a$, leads to the equation

$$-\frac{D_z}{4\pi\sigma}\frac{1}{a^3}\sum_{\ell=1}^{\infty}\ell(\ell+1)\left(\frac{d}{a}\right)^{\ell-1} P_\ell(\mu) + \sum_{n=0}^{\infty}(nc_n a^{n-1})P_n(\mu) = 0 \tag{2.148}$$

The determination of the expansion coefficients from this expression may seem to be difficult. However, as demonstrated in the sequel, it is a straightforward, standard procedure based on the application of the orthogonality properties of the Legendre polynomials (Sect. 2.6.3.1). The procedure is as follows. For all integer values of k, $k \geq 0$, multiply both sides of (2.148) by $P_k(\mu)$ followed by the integration of the result with respect to μ over the interval $-1 < \mu < 1$. Because of the orthogonality properties of the Legendre polynomials, for any given k the terms in the first summation yield nonzero terms only for $\ell = k$, and those of the second summation only for $n = k$. Moreover, by using the expression for the norms of the Legendre polynomials, (2.139), we find

$$-\frac{D_z}{4\pi\sigma}\frac{1}{a^3}k(k+1)\left(\frac{d}{a}\right)^{k-1}\frac{2}{2k+1} - +c_k k a^{k-1}\frac{2}{2k+1} = 0 \tag{2.149}$$

From this expression the expansion coefficients c_k can be computed easily. Note that, for didactic reasons, the norms of the Legendre polynomials are included in (2.149), but in fact drop out of the equation. Moreover, for $k = 0$ the equation does not yield a value for c_k. For other values of k we find

$$c_k = \frac{D_z}{4\pi\sigma}(k+1)\frac{d^{k-1}}{a^{2a+1}}. \tag{2.150}$$

Substitution of this result in (2.147) then yields as the final solution for the potential field for $d < r \leq a$:

$$\Phi(r,\theta) = \frac{D_z}{4\pi\sigma r^2}\sum_{k=1}^{\infty} k\left(\frac{d}{r}\right)^{k-1} P_k(\mu) + \frac{D_z}{4\pi\sigma r^2}\sum_{k=1}^{\infty}(k+1)\left(\frac{d}{r}\right)^{k-1}\left(\frac{r}{a}\right)^{k+2} P_k(\mu) \tag{2.151}$$

2.6.3.3 Discussion

The relatively simple configuration of Sect. 2.6.3.2 provides a suitable means for illustrating some basic consequences of the bounded nature of a volume conductor, as is worked out in the sequel. As indicated, (2.151) holds true in the domain $d < r \leq a$. For the remaining part of the sphere, $r < d$, the potential field may be found using the same procedure as in Sect. 2.6.3.2, but now using the Taylor expansion valid for this region as shown in the second part of (2.144). The computation of the complete potential field generated by the tangential dipole component may be carried out in a similar way.

Notes:

1. In (2.151), the first expression on the right represents the infinite medium potential, while the second represents the effect of the sphere being bounded. This second term may be interpreted as the field arising from a virtual, secondary source placed in an infinite medium. Its magnitude depends linearly on that of the primary source. The nature of the secondary source may be diverse. A potential field inside the sphere having the required nature may be generated by a virtual dipole having an appropriate position and strength, a monolayer at the interface or a double layer at the interface.
2. The contribution of the secondary source tends to zero if the boundary is distal, i.e., if $a >> r$, due to the factor $(r/a)^{k+2}$. As a consequence, the potential field observed at a distance to the source that is small relative to the distance to the boundary tends to the infinite medium potential; for the interpretation of observed potentials at this field point, the boundary effects may be neglected.
3. For observation points on the spherical boundary, $r = a$, (2.151) reduces to

$$\Phi(r,\theta) = \frac{D_z}{4\pi\sigma a^2}\sum_{k=1}^{\infty}(2k+1)\left(\frac{d}{a}\right)^{k-1} P_k(\mu) \tag{2.152}$$

   For a dipole located at the center of the sphere ($d \to 0$), the only remaining term in the summation is the one for $k = 1$. This leaves

$$\Phi(r,\theta) = 3\frac{D_z}{4\pi\sigma a^2}\cos\theta, \tag{2.153}$$

   since, (2.137), $P_1(\mu) = \mu = \cos\theta$. This demonstrates that for a dipolar source placed at the center of a spherical surface, the effect of bounding the sphere produces a potential field on the spherical boundary that is threefold that of the infinite medium potential. For source locations close to the spherical surface, the effect of bounding the medium is less, tending to the factor 2 (2.133) for a planar boundary. For an arbitrary bound, the factor may be expected to lie within these two limits, 2 and 3.
4. While evaluating the expansion coefficients c_k, (2.150) no value could be identified for $k = 0$. The Legendre polynomial for $k = 0$, (2.137), $P_0(\mu) = 1$. This leaves the mean value of the potential field undetermined. The potential field (2.151) has an implicit zero mean of the potential over the boundary, as a consequence of excluding a term for $k = 0$ and the orthogonality of the Legendre polynomials.

5. The mean level of the potential is unrelated to the impressed current density, as was discussed in Sect. 2.5.1.1. For a bounded medium the location in space as a reference for measured potential difference cannot be chosen at infinity, but must be selected somewhere on, or inside, the boundary. The selection of this location may be guided by practical considerations. However, contrary to a frequently encountered belief, no universal, theoretical optimum exists [14, 15].

2.6.4 Realistically Shaped Interfaces; The Boundary Element Method

Although the inclusion of spherical bounds or interfaces, like the basic version treated in Sect. 2.6.3, are more realistic than the one treated in Sect. 2.6.2, they still only poorly resemble the shapes of the interfaces of the most prominent inhomogeneities, such as the torso boundary, the high conductivity of blood, or the low conductivity of lung tissue.

For the treatment of volume conduction effects involving such shapes, analytical methods of the type described in the previous section are not available. Instead, several numerical methods have been developed over the past few decades. The most prominent are the finite difference method (FDM), the finite element method (FEM), the finite volume method (FVM), and the boundary element method (BEM). The BEM lacks the possibility of treating situations involving anisotropic electric conductivity that some of the other methods have but its conceptual relevance is higher. It is for this reason that this topic is treated in this chapter. The other methods (FDM, FEM, and FVM) are discussed in Chap. 8. The BEM is based on formulations described by in 1939 by Smythe [10].

2.6.4.1 Mathematical Preliminaries

The mathematics involved in the theory of the BEM uses some specific results from the field of vector calculus. To make this section self-contained, these results are listed here. As in Sect. 2.2.2, all specific conditions required are assumed to be satisfied. Dedicated proofs can be found in the standard references listed at the end of this chapter. Throughout, in the scalar function 1/R, R denotes the length of the vector $\vec{R} = \vec{r}\,' - \vec{r}$ pointing from (source) point $\vec{r}$ to (field) point $\vec{r}\,'$ (compare Sect. 2.2.10), $\vec{A}$ is a vector field, Ψ and Φ are arbitrary scalar functions.

- For vector field $\vec{A}$ within a volume closed by a boundary S

$$\int_V \nabla \bullet \vec{A}\,\mathrm{d}V = \int_S \vec{A} \bullet \mathrm{d}\vec{S} \quad \text{(Gauss' divergence theorem; (2.26))} \tag{2.154}$$

$$\nabla^2 \frac{1}{R} = -4\pi\delta(\vec{r}\,', \vec{r}) = \nabla'^2 \frac{1}{R} \tag{2.155}$$

This is the result that is most specific for this section. The function $\delta(\vec{r}\,', \vec{r})$ is the 3D Dirac delta function. It is a so-called distribution function, defined through the properties of a volume integral over a volume V of its product with a scalar function $f(\vec{r})$. The defining equations are

$$\int_V \delta(\vec{r}\,', \vec{r}) f(\vec{r})\,\mathrm{d}V = 0 \quad \text{if V does not encompass } \vec{r}\,', \tag{2.156}$$

$$\text{else,} \quad \int_V \delta(\vec{r}\,', \vec{r}) f(\vec{r})\,\mathrm{d}V = f(\vec{r}\,') \tag{2.157}$$

Note that this definition implies that $\int_V \delta(\vec{r}\,', \vec{r})\,\mathrm{d}V = 1$ and, hence, its unit is m^{-3}.

- Application of Gauss' theorem to $\vec{A} = \Psi\nabla\Phi$ yields

$$\int_V \nabla \bullet \Psi\nabla\Phi\,\mathrm{d}V = \int_V \nabla\Psi \bullet \nabla\Phi\,\mathrm{d}V + \int_V \Psi\nabla^2\Phi\,\mathrm{d}V = \int_S \Psi\nabla\Phi \bullet \mathrm{d}\vec{S} \tag{2.158}$$

This result is known as Green's first theorem.

- Correspondingly, by exchanging Ψ and Φ, we have

$$\int_V \nabla \bullet \Phi \nabla \Psi \mathrm{d}V = \int_V \nabla\Phi \bullet \nabla\Psi \mathrm{d}V + \int_V \Phi \nabla^2 \Psi \mathrm{d}V = \int_S \Phi \nabla\Psi \bullet \mathrm{d}\vec{S} \tag{2.159}$$

- Finally, by subtracting second equation in (2.158) from the corresponding part of (2.159), we see that

$$\int_V \Phi \nabla^2 \Psi \mathrm{d}V - \int_V \Psi \nabla^2 \Phi \mathrm{d}V = \int_S \Phi \nabla\Psi \bullet \mathrm{d}\vec{S} - \int_S \Psi \nabla\Phi \bullet \mathrm{d}\vec{S} \tag{2.160}$$

This result is known as Green's second theorem.

2.6.4.2 Equivalent Surface Sources

The BEM is based on the use of equivalent surface sources [10, 16–18]. To introduce this, we first consider the source–volume–conductor configuration shown in Fig. 2.15. It depicts a volume segment bounded by a closed surface S. Its interior has uniform conductivity σ and contains a primary, impressed current source (dotted region). Its exterior is left unspecified: it may or may not contain primary sources and may or may not have the same conductivity.

Starting point for the theory described here is Green's second theorem, (2.160), in which we substitute $\Psi = \frac{1}{R}, \vec{R} = \vec{r}\,' - \vec{r}$ pointing from (source) point $\vec{r}$ to (field) point $\vec{r}\,'$ as before, and take for Φ the potential field inside S, which leads to

$$\int_V \Phi \nabla^2 \frac{1}{R}\,\mathrm{d}V - \int_V \frac{1}{R}\nabla^2\Phi\,\mathrm{d}V = \int_S \Phi\,\nabla\frac{1}{R} \bullet \mathrm{d}\vec{S} - \int_S \frac{1}{R}\,\nabla\Phi \bullet \mathrm{d}\vec{S} \tag{2.161}$$

All integrations are carried out with respect to the unprimed variable $\vec{r}$, and $\mathrm{d}\vec{S}$ is the local outward normal of S. The four integrals shown are worked out as follows.

Based on (2.155) and (2.157), the first one is found to be equal to $-4\pi\,\Phi(\vec{r}\,')$. The second integral equals $-4\pi\,\Phi_\infty(\vec{r}\,')$, the potential field generated by the primary sources inside S when placed in an infinite medium having a conductivity σ. This follows from (2.116). The third integral may be written as $\int_S \Phi(\vec{r})\,\mathrm{d}\omega$, with $\mathrm{d}\omega$ the solid angle subtended by $\mathrm{d}\vec{S}$ at $\vec{r}\,'$ (combine (2.63) and (2.33)). Note that for $\vec{r}$ on S, as is the case for this integral and $\vec{r}\,'$ an interior point of surface S, $\vec{R}$ is pointing inward and consequently the sign of $\mathrm{d}\omega$ is negative. Finally, in the fourth integral $\nabla\Phi \bullet \mathrm{d}\vec{S}$ is equal to $-E_n\mathrm{d}S$, with E_n the normal component of the electric field at $\vec{r}$ on S. For the latter, by using (2.84), we may write $E_n(\vec{r}) = J_n(\vec{r})/\sigma$, with $J_n(\vec{r})$ the normal component of the current density passing the surface S at $\vec{r}$.

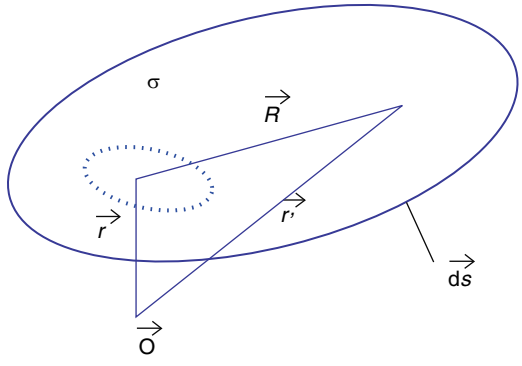

Figure 2.15

A part of space, delineated by a surface S, with uniform conductivity σ. Primary current sources are located in the region surrounding $\vec{r}$. The field point is $\vec{r}\,'$, $\vec{R} = \vec{r}\,' - \vec{r}$.

Substitution of the above expressions for the four integrals of (2.161), followed by a reordering of the terms, results in the following, fundamental expression

$$\Phi(\vec{r}\,') = \Phi_\infty(\vec{r}\,') - \frac{1}{4\pi}\int\limits_S \Phi(\vec{r})\mathrm{d}\omega(\vec{r}\,',\vec{r}) - \frac{1}{4\pi\sigma}\int\limits_S \frac{J_n(\vec{r})}{R(\vec{r}\,',\vec{r})}\mathrm{d}S(\vec{r}) \tag{2.162}$$

It signifies that at any point inside any volume V with homogeneous conductivity σ, bounded by a surface S, the potential field can be expressed as the sum of the local infinite medium potential, a weighted sum (integral) of the potentials $\Phi(\vec{r})$ at S, and a weighted sum (integral) of the normal component of the current density $J_n(\vec{r})$ passing surface S.

The two additions represent the effect of the conditions in the external domain: the effects of any primary sources present in that domain and/or differences of the electric conductivity with respect to the internal, homogeneous value σ. Based on the results from Sect. 2.5.2, the first of these contributions may be interpreted as arising from a virtual double layer source, (2.107), the second one as a virtual mono layer source, (2.101), both located at S.

2.6.4.3 Application to Homogeneous, Bounded Volume Conductors

The results of the previous subsection facilitate the introduction of the BEM for evaluating the effect of bounds on the electric conductivity having an arbitrary shape. To this end, we reconsider the same situation as depicted in Fig. 2.15, now taking the part of space exterior of S to be nonconducting. This being the case, no current will pass S and (2.162) reduces to

$$\Phi(\vec{r}\,') = \Phi_\infty(\vec{r}\,') - \frac{1}{4\pi}\int\limits_S \Phi(\vec{r})\mathrm{d}\omega(\vec{r}\,',\vec{r}) \tag{2.163}$$

In this expression, $\Phi(\vec{r})$ represents the potential field at S in the bounded state, which needs to be known before the potential at an arbitrary internal point can be computed. To find $\Phi(\vec{r})$, the field point $\vec{r}\,'$ is moved toward S. While assuming no primary current sources close to S, the potential field $\Phi(\vec{r}\,')$ is continuous, and in the limit of approaching S we have $\Phi(\vec{r}\,) = \Phi(\vec{r}\,')$. Expression $\mathrm{d}\omega(\vec{r}\,',\vec{r}) = \vec{R}\bullet\mathrm{d}\vec{S}/R^3$ requires special attention, since both numerator and denominator approach zero when $\vec{r}\,'$ approaches $\vec{r}$. Its value may be found by taking an appropriate limit L. For a (locally) planar surface its value is $L = -2\pi$, in which 2π is the solid angle subtended by a planar semi-space and the minus sign stems from the fact that locally, $\vec{R}$ and $\mathrm{d}\vec{S}$ point in opposite directions. In numerical computations based on (2.163), the surface S is approximated by a large number of small triangles. In early applications, the field points $\vec{r}\,'$ were situated at the centers of gravity of these triangles, in which case $L = -2\pi$ for all field points (on S). In this case (2.163) may be formulated as

$$\Phi(\vec{r}\,') = \Phi_\infty(\vec{r}\,') - \frac{1}{4\pi}\oint\limits_S \Phi(\vec{r})\mathrm{d}\omega(\vec{r}\,',\vec{r}) - \frac{-2\pi}{4\pi}\Phi(\vec{r}\,'), \tag{2.164}$$

in which the integration excludes the small region $\mathrm{d}S$ around $\vec{r}\,' = \vec{r}$, yielding

$$\Phi(\vec{r}\,') = 2\Phi_\infty(\vec{r}\,') - \frac{1}{2\pi}\oint\limits_S \Phi(\vec{r})\mathrm{d}\omega(\vec{r}\,',\vec{r}) \tag{2.165}$$

In numerical implementations in which the field points are formed by the triangle vertices, the absolute value of $L = L(\vec{r})$ depends on the local curvature of S. For locally convex surface patches (as seen from the outside) it is less than 2π, while for concave surface patches it is greater than 2π.

Numerical Implementation

For each of N observation points on S, the numerical handling of (2.165) leads to a linear equation in the unknown values $\varphi_n = \Phi(\vec{r}\,'_n)$, $n = 1, 2 \ldots N$. The total set of N equations in the N unknown φ_n values can be solved by computer implementations of the appropriate methods of linear algebra. The solution found is unique only up to a constant, corresponding to the physics of the problem. It requires the specification of a point of the medium acting as a potential reference to

make the solution unique, just like when measuring bioelectric potentials. This point may be chosen at will. The outcome of the entire procedure for determining all elements φ_n of a N-dimensional numerical vector φ may be formulated as a matrix multiplication of the (numerical) vector φ_∞ by a transfer matrix, say **A,** constituting a numerically determined set of weighting coefficients, representing the effect of all volume conductor effects (inhomogeneities and bounds of the volume conductor) [19]

$$\varphi = \mathbf{A}\varphi_\infty \tag{2.166}$$

The matrix **A** is a linear operator acting on the infinite medium potentials.

The computation of the involved elementary solid angles $\mathrm{d}\omega(\vec{r}',\vec{r})$ can be approximated using a discretized representation of the surfaces involved, based on small triangular elements. Analytical expressions for the basic, required computations are available in [20, 21].

Discussion

The method described above constitutes the essence of the BEM. Frequently, the interest lies in determining the potentials on the bounding surface only. The determination of the elements of the transfer matrix constitutes the most elaborate part of the BEM. However, once the potential $\Phi(\vec{r})$ on S has been determined, the potential field at any interior point can be found by means of (2.163).

For several applications, it is of particular significance, and a pronounced advantage of the BEM over some of the other methods such as the FEM, that the transfer matrix **A** depends on the geometry of S only. Hence, when considering a set of different locations of the source points, the most elaborate part of the procedure, the computation of **A**, needs to be carried out only once, which greatly facilitates inverse procedures [22].

As discussed in Sect. 2.6.3.4, based on the results from Sect. 2.5.2, the integral in (2.163) may be interpreted as representing the contribution from a virtual double layer source at S. This is specific for the variant of the BEM described here. An alternative BEM approach has been formulated in which the virtual source of S is a monolayer. This was in fact the case in the very first application of the BEM in electrocardiography [18].

2.6.4.4 Application of the BEM to Inhomogeneous Volume Conductors

The BEM can be extended to the handling of the effect of internal regions of the volume conductor having a different, homogenous conductivity. This is worked out here in some detail for an application to a single inhomogeneous region inside a bounded volume conductor. The generalization for multiple inhomogeneous regions is straightforward.

The starting point for the theory described here is once more Green's second theorem, (2.160).

We apply it separately to the subregions I and II illustrated in Fig. 2.16. Subregion I has conductivity σ_1 and is bounded by surfaces S_1 and S_2. It is assumed to contain primary sources. Subregion II is bounded by S_2, has conductivity σ_2 and is assumed to be source free.

For subregion I, with both the integration variable $\vec{r}$ and the field point lying within subregion I, (2.161),

$$\Phi_I(\vec{r}\,') = \Phi_{I,\infty}(\vec{r}\,') - \frac{1}{4\pi}\int_{S_1}\Phi(\vec{r})\mathrm{d}\omega(\vec{r}\,',\vec{r}) + \frac{1}{4\pi}\int_{S_2}\Phi(\vec{r})\mathrm{d}\omega(\vec{r}\,',\vec{r}) + \frac{1}{4\pi\sigma_1}\int_{S_2}\frac{J_n(\vec{r})}{R(\vec{r}\,',\vec{r})}\mathrm{d}S(\vec{r}) \tag{2.167}$$

The first term on the right represents the potential generated by the primary sources in an infinite medium having the conductivity of the source region, which will be referred to as σ_s. In the case illustrated, this conductivity is $\sigma_s = \sigma_1$. The third term on the right stems from the fact that the subregion is bounded by both S_1 and S_2. The difference in sign compared with the corresponding term for S_1 stems from the fact that the outward normal of region I at S_2 is the reverse of the outward normal of region II at S_2. The latter also explains the sign of the final term involving the current density across S_2. This term is clearly nonzero, since the conductivity of region II is nonzero.

Next, we leave the field point within subregion I, while applying Green's second theorem to region II.

$$\int_{V_{II}}\Phi\nabla^2\frac{1}{R}\mathrm{d}V - \int_{V_{II}}\frac{1}{R}\nabla^2\Phi\mathrm{d}V = \int_{S_2}\Phi\nabla\frac{1}{R}\bullet\mathrm{d}\vec{S} - \int_{S_2}\frac{1}{R}\nabla\Phi\bullet\mathrm{d}\vec{S} \tag{2.168}$$

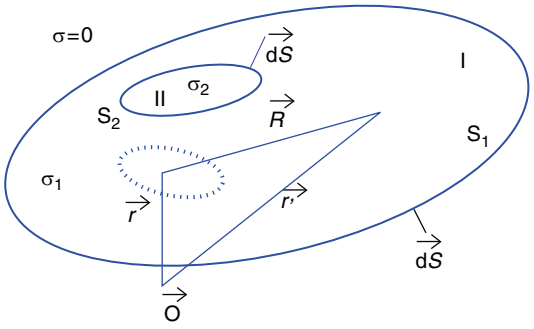

Figure 2.16

Volume conductor. Region I is bounded by surfaces S_1 and S_2, with uniform conductivity σ_1. Internal region II is bounded by S_2, with uniform conductivity σ_2. Primary current sources are located within region I, around arbitrary point $\vec{r}$ of region I. Field point $\vec{r}\,'$ is also shown in region I, with $\vec{R} = \vec{r}\,' - \vec{r}$.

The first integral on the left is zero since $\vec{r}\,'$ is exterior to subregion I ((2.156) and (2.155)). The second integral is also zero since there are no primary sources within subregion II: $\nabla^2\Phi = 0$. Hence, as was the case when deriving (2.162), we now have

$$0 = -\frac{1}{4\pi}\int_{S_2}\Phi(\vec{r})\mathrm{d}\omega(\vec{r}\,',\vec{r}) - \frac{1}{4\pi\sigma_2}\int_{S_2}\frac{J_n(\vec{r})}{R(\vec{r}\,',\vec{r})}\mathrm{d}S(\vec{r}) \tag{2.169}$$

By comparing (2.167) and (2.169) it can be seen that the integrals involving $J_n(\vec{r})$ are identical: both represent the current density across S_2. As a consequence these integrals will be eliminated by multiplying (2.167) by σ_1, and multiplying (2.169) by σ_2, followed by the addition of both equations. After rearranging the terms of this addition and dividing the result by σ_1, the following expression is found for $\Phi_I(\vec{r}\,')$, the potential field inside subregion I.

$$\Phi_I(\vec{r}\,') = \frac{\sigma_s}{\sigma_1}\Phi_{I,\infty}(\vec{r}\,') - \frac{1}{4\pi}\int_{S_1}\Phi(\vec{r})\mathrm{d}\omega(\vec{r}\,',\vec{r}) - \frac{1}{4\pi}\frac{\sigma_2-\sigma_1}{\sigma_1}\int_{S_2}\Phi(\vec{r})\mathrm{d}\omega(\vec{r}\,',\vec{r}) \tag{2.170}$$

Besides the infinite medium contribution of the primary sources, the expression shows two virtual double layer sources, one for each of the surfaces that form the border of subregion I. Note that for $\sigma_1 = \sigma_2$, the contribution of the final term is zero, as required. The factor σ_s/σ_1 in the first term on the right, a factor equal to one in the current example, arises when the primary sources are present in a subregion different to the one where the potential field is evaluated.

When the field point $\vec{r}\,'$ is located in subregion II, the same method as shown above may be used to find the potential field. The result is

$$\Phi_{II}(\vec{r}\,') = \frac{\sigma_s}{\sigma_2}\Phi_{II,\infty}(\vec{r}\,') - \frac{1}{4\pi}\int_{S_1}\Phi(\vec{r})\mathrm{d}\omega(\vec{r}\,',\vec{r}) - \frac{1}{4\pi}\frac{\sigma_2-\sigma_1}{\sigma_2}\int_{S_2}\Phi(\vec{r})\mathrm{d}\omega(\vec{r}\,',\vec{r}), \tag{2.171}$$

which, apart from a different scaling factor, is the same as (2.170). However, note that all solid angle terms, the factors weighting the equivalent double layer strengths, are different because of the different location of field point $\vec{r}\,'$.

If K, possibly nested, subregions are present within the bounded volume conductor, the potential field within any subregion k, a generalization of (2.170) and (2.171) can be formulated as

$$\Phi_k(\vec{r}\,') = \frac{\sigma_s}{\sigma_k^-}\Phi_{k,\infty}(\vec{r}\,') - \frac{1}{4\pi}\sum_{\ell=1}^{K}\frac{\sigma_\ell^- - \sigma_\ell^+}{\sigma_k^-}\int_{S_\ell}\Phi_\ell(\vec{r})\mathrm{d}\omega(\vec{r}\,',\vec{r}), \tag{2.172}$$

in which subregion k is defined by the label of its outermost interface, where σ_ℓ^+ is the conductivity just outside the interface ℓ and σ_ℓ^- is the conductivity just inside. If $k = 1$ is the surface encompassing the entire medium, and if its exterior is nonconducting, then $\sigma_1^+ = 0$.

Discussion

Equation (2.172) constitutes the essence of the BEM. It expresses the potential field in any number of inhomogeneous subregions as the sum of the contributions to the potential inside a virtual infinite medium of (a scaled version of) the impressed primary sources and those of virtual double layer sources at each of the interfaces bounding the subregions. The strength of these secondary sources is small if the differences between conductivity values at both sides of an interface are small.

In a practical application (2.172) can only be used if the potentials $\Phi_\ell(\vec{r})$ at the interfaces are known. These may be computed numerically in the same manner as discussed in the previous subsection for the single interface problem.

2.6.4.5 The BEM Used To Compute Potentials On The Heart Surface

The final demonstration of the use of the BEM discussed here is its application to the computation of the transfer between potentials on the heart surface and the potentials on the body surface. The inverse of this transfer function is the key element for the computation of potentials on the heart surface from observed body surface potentials. This topic is discussed in Chap. 9. The methods are based on the fact that if no primary sources are present within a volume conductor bounded by a surface S_1 and an internal *closed* region S_1 the potential fields on these surfaces are linked in a unique manner. The medium in between may contain different subregions having a different conductivity. The treatment presented here considers just S_1 representing the body surface, and the surface S_2, representing a surface closely encompassing the heart. This surface is usually referred to as the epicardium, but its identification with the pericardium is more appropriate.

The volume conductor of the problem addressed is shown in Fig. 2.17. The transfer can be computed on the basis of (2.167), which describes the field in subregion I. Since there are no primary sources in this subregion, this equation reduces to

$$\Phi(\vec{r}\,') = -\frac{1}{4\pi}\int_{S_1}\Phi_1(\vec{r})\mathrm{d}\omega(\vec{r}\,',\vec{r}) + \frac{1}{4\pi}\int_{S_2}\Phi_2(\vec{r})\mathrm{d}\omega(\vec{r}\,',\vec{r}) + \frac{1}{4\pi\sigma_1}\int_{S_2}\frac{J_\mathrm{n}(\vec{r})}{R(\vec{r}\,',\vec{r})}\mathrm{d}S(\vec{r}) \tag{2.173}$$

In the computation of the forward transfer, the potential field $\Phi_2(\vec{r})$ on S_2 is assumed to be known. This leaves $\Phi_1(\vec{r})$, the potential on S_1, as well as the current density $J_n(\vec{r})$ at S_2, to be determined. As in the preceding subsections the numerical approximation of these functions is carried out by placing field points on S_1 and S_2. For N_1 points placed on S_1 and M_2 points placed on S_2 this results in a system of N_1+M_2 linear equations in the unknown variables φ_n and J_m. The system has a unique solution for any set of assumed values φ_m on S_2. The indeterminacy of the potential that needed to be addressed in the Sect. 2.6.3.3 and 2.6.3.3 is not present here, since the specified φ_m values implicitly define the mean level of the potential [23]. The application of these types of numerical methods is discussed in Chap. 8 (Sect. 8.5.4).

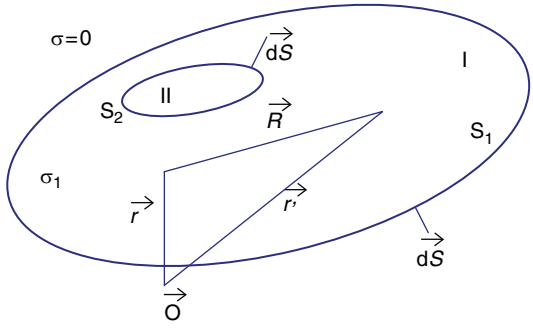

Figure 2.17

Volume conductor. Region I is bounded by surfaces S_1 and S_2, with uniform conductivity σ_1 Internal region II, bounded by S_2, contains primary sources, conductivity unspecified. No primary current sources are present within region I; $\vec{r}$ is an arbitrary point of region I. Field point $\vec{r}\,'$ is restricted to region I, with $\vec{R} = \vec{r}\,' - \vec{r}$.

Appendix A Tools from Linear Algebra and Their Notation

A.1 Introduction

In some chapters of this book, notations and methods are used that are taken from linear algebra. These are the basic tools involved in the numerical computation of potential fields (Chap. 2): the forward problem (Chap. 8) and in particular for solving various variants of the inverse problem (Chap. 9). This appendix introduces some of the basic concepts. For a formal, more complete treatment the reader is referred to the general literature on linear algebra and its numerical implementation. Highly valuable examples are: [24–27]. Specific variants of vectors and matrices, as well as of various definitions and notations used are listed in Sect. A.5.

A.1.1 Vectors

In Sect. 2.2, the vector concept is introduced in its application to 3D space. Any vector $\vec{A}$ can be seen to be characterized by three elements, A_x, A_y, and A_z (Sect. 2.2.3). Addition and multiplication rules are treated in Sects. 2.2.3–2.2.4. In linear algebra these concepts have been generalized by introducing variables that are specified by the values of an arbitrary number of elements. Different types of notations for such "numerical" vectors can be found in the literature. Here introduced are the notations used throughout this book.

In the sequel, the term "vector" will refer to a variable that is specified by a set of numbers being its elements. These elements may either be listed in a single row or in a single column. In the latter situation, a vector is referred to as a column vector, which is denoted by a bold lower case symbol. For vector $\mathbf{a}$ with m elements we have

$$\mathbf{a} = \begin{bmatrix} a_1 \\ a_2 \\ \cdot \\ \cdot \\ a_m \end{bmatrix} \tag{A.1}$$

The listing of the values of the complete set of elements of a column vector may demand much space. A more economical way is to listing the same values in a row. Accordingly, $\mathbf{a}$ may also be defined by its "transpose": $\mathbf{a}^T$, defined as

$$\mathbf{a}^T = [a_1 \;\; a_2 \;\; \cdot \;\; \cdot \;\; a_m], \tag{A.2}$$

which is called a row vector. The notation ^{T}, signifies "transpose", a term that is clarified in A.1.3.

In analogy with vectors in 3D space, a numerical vector having m elements is called an m-dimensional vector. Note that for $m = 1$ the vector reduces to a scalar.

There is a particular role for vectors comprising zero elements only. Such vectors are called zero vectors (Sect. A.5).

A.1.2 Basic Vector Algebra

A.1.2.1 Vector Addition

The familiar rules of addition that apply to "ordinary," i.e., scalar, variables can be extended to vectors by defining that these rules be applied to all corresponding elements. Applied to vectors $\mathbf{a}$ and $\mathbf{b}$ demands that both vectors have the same number of elements, and that the elements s_i, $i = 1, \cdots, m$ of the sum vector $\mathbf{s}$:

$$\mathbf{s} = \mathbf{a} + \mathbf{b} \tag{A.3}$$

be $s_i = a_i + b_i$.

A.1.2.2 Vector Multiplication

The most elementary version of multiplication involving vectors is the one in which a vector is multiplied by a scalar. The elements of vector **a** after multiplication by a scalar c is carried out by multiplying all elements a_i of **a** by the scalar, which implies a uniform scaling of the elements by c. As a consequence we have

$$c\,\mathbf{a} = \mathbf{a}\,c. \tag{A.4}$$

Note that a combination of the definition of vector addition and scalar multiplication with $c = -1$ also defines the subtraction of vectors:

$$\mathbf{v} = \mathbf{a} - \mathbf{b} = \mathbf{a} + (-1)\mathbf{b}. \tag{A.5}$$

All these properties can be seen to be straightforward generalizations of those defined in Sect. 2.2.2 for the vectors in 3D space. In a similar fashion to what is shown in Sect. 2.2.4, the scalar product of two vectors **a** and **b** is the scalar d that is the outcome of the pair-wise multiplication of their elements, followed by the summation of the resulting products:

$$d = \sum_{i=1}^{m} a_i b_i = \mathbf{a}^T\,\mathbf{b} = \mathbf{b}^T\,\mathbf{a}. \tag{A.6}$$

The significance of the notation $\mathbf{a}^T\mathbf{b}$ is explained in the next section.

If the product of two vectors is zero the vectors are said to be orthogonal, analogous to the definition in Sect. 2.2.4.

The generalization of the magnitude of a 3D vector (Sect. 2.2.3) leads to the definition of the "norm" of a vector as:

$$|\mathbf{a}| = \sqrt{\mathbf{a}^T\mathbf{a}}. \tag{A.7}$$

It is interesting to note that even the concept of the angle between two vectors in 3D space (Sect. 2.2.2) can be carried over to two vectors in n-dimensional space, an angle that is computed as

$$\alpha = \mathrm{acos}\left(\frac{\mathbf{a}^T\mathbf{b}}{|\mathbf{a}|\,|\mathbf{b}|}\right). \tag{A.8}$$

A.1.3 Matrices

Many numerical methods lead to a problem formulation involving a collection of several, say n, column vectors of dimension m. This collection is called a matrix. In the sequel, bold face capitals are used to denote matrices. Matrix **A**, with elements $a_{i,j}$, $i = 1, \cdots, m; j = 1, \cdots, n$, can be visualized as

$$\mathbf{A} = \begin{bmatrix} a_{1,1} & a_{1,2} & \cdots & a_{1,j} & \cdots & a_{1,n} \\ \cdot & \cdot & \cdots & \cdot & \cdots & \cdot \\ a_{i,1} & a_{i,2} & \cdots & a_{i,j} & \cdots & a_{i,n} \\ \cdot & \cdots & \cdots & \cdot & \cdots & \cdot \\ a_{m,1} & a_{m,2} & \cdots & a_{m,j} & \cdots & a_{m,n} \end{bmatrix} \tag{A.9}$$

There are $m \times n$ elements in the above matrix; its size is defined as (m, n). If $m = n$ the matrix is called "square."

Next to any matrix **A** of size (m, n) there is a corresponding one, the transposed matrix $\mathbf{A}^T$ of size (n, m). Its elements are the elements $a_{j,i}$ of **A**.

If, in matrix **A**, $n = 1$, the matrix reduces to a single column. Thus, an m-dimensional column vector may be viewed as a matrix of size $(m, 1)$. Similarly, a row vector having n elements may be viewed as a matrix of size $(1, n)$. The notation $\mathbf{a}^T$ introduced for a row vector paves the way for a unified formalism for multiplications involving matrices, vectors, or both.

Definitions of specific matrices and their properties are listed in Sect. A.5.

A.1.3.1 Matrix Addition

As explained for vectors, the familiar rules of addition that apply to "ordinary," i.e., scalar, variables can be extended to matrices by demanding that these rules be applied to all corresponding elements. Applied to vectors **A** and **B** this requires that both matrices be of the same size and that the elements $s_{i,j},\ i = 1, \cdots, m;\ j = 1 \cdots, n$, of the sum **S**:

$$\mathbf{S} = \mathbf{A} + \mathbf{B} \tag{A.10}$$

be $s_{i,j} = a_{i,j} + b_{i,j}$.

A.1.3.2 Multiplication and Matrices

The most elementary version of multiplication involving matrices is the one in which a matrix is multiplied by a scalar. As worked out for the vector, multiplication by a scalar c is carried out by multiplying all elements $a_{i,j}$ of **A** by c. This also defines the difference of two matrices, as shown for the vector.

The most important, basic multiplication of two matrices is defined as follows. Let **A** be a matrix of size (m, n) and **B** a matrix of size (n, p), then their product is defined as the matrix **C** of size(m, p):

$$\mathbf{C} = \mathbf{AB} \tag{A.11}$$

having elements

$$c_{i,\ell} = \sum_{j=1}^{n} a_{i,j} b_{j,\ell}. \tag{A.12}$$

Note that this definition demands that the number of columns of **A** be the same as the number of rows of **B**. It is only if this condition is satisfied that this type of matrix multiplication is meaningful.

Contrary to the multiplication rules for scalars, this matrix multiplication does not have the property of commutativity, i.e., generally,

$$\mathbf{AB} \neq \mathbf{BA}. \tag{A.13}$$

This can be seen most easily by comparing the multiplication of **A** specified by row vector [1 2 3] and **B** a column vector specified by its transpose: [1 0 −2]. By applying the rules of matrix multiplication (A.12) we see that

$$\mathbf{AB} = [1\ \ 2\ \ 3] \begin{bmatrix} 1 \\ 0 \\ -2 \end{bmatrix} = -5. \tag{A.14}$$

In contrast,

$$\mathbf{BA} = \begin{bmatrix} 1 \\ 0 \\ -2 \end{bmatrix} [1\ \ 2\ \ 3] = \begin{bmatrix} 1 & 2 & 3 \\ 0 & 0 & 0 \\ -2 & -4 & -6 \end{bmatrix}. \tag{A.15}$$

Another basic property of matrix multiplication is

$$(\mathbf{AB})^T = \mathbf{B}^T \mathbf{A}^T, \tag{A.16}$$

as can be verified from the definition of "transpose" and the rule of matrix multiplication (A.12).

linearity
By combining the properties of matrix addition and multiplication it follows that

$$\mathbf{A}(\mathbf{B}+\mathbf{C}) = \mathbf{AB}+\mathbf{AC}, \tag{A.17}$$

expressing the associatative law of matrix multiplication. The full set of definitions given identifies matrix multiplication as a so-called linear operation.

The rank of a matrix, denoted as $rank(\mathbf{A}) = r \leq \min(m,n)$, is the maximum number of independent columns or rows it comprises. For the product of two matrices **A** and **B** we have [24]

$$rank(\mathbf{AB}) = \min(rank(\mathbf{A}), rank(\mathbf{B})). \tag{A.18}$$

A.2 Solving Linear Equations: the Problem Definition

The basic problems that require the use of linear algebra for their solution can be formulated as: find **x** that satisfies the matrix equation

$$\mathbf{y} = \mathbf{Ax}+\mathbf{n}. \tag{A.19}$$

The symbols denote
y, a column vector, of size $(m,1)$ representing known or observed variables
A, a matrix, of size (m,n) usually representing a model based transfer
x, a column vector, either directly representing a signal or its parameters
n, a column vector, size$(m,1)$, usually referred to as noise. It represents any uncertainties in the problem formulation or measurement errors.
As a consequence, it is an unknown vector, but its statistical properties may be known.

In some applications, a set of t column Vectors (multiple realizations) **y** and **n** are available and the problem to be solved is: find matrix **X** that satisfies the equation

$$\mathbf{Y} = \mathbf{AX}+\mathbf{N} \tag{A.20}$$

involving matrices with
$size(\mathbf{Y}) = (m,t)$
$size(\mathbf{X}) = (n,t)$
$size(\mathbf{N}) = (m,t)$, and
$size(\mathbf{A}) = (m,n)$ as in (A.19)

In the practice of analyzing observed data there is generally no exact solution to the so-called linear systems (A.19) or (A.20). Instead, the true solutions are replaced by estimates, $\widehat{\mathbf{x}}$ for (A.19), computed such that the difference between both sides of the equation is as small as possible. The next section introduces this approach.

A.3 Solution Types

The problem formulation as outlined in Sect. A.2 leads to two essentially different types of solutions. These are discussed here for the basic variant of the problem formulation (A.19) with $\mathbf{n} = \mathbf{0}$.

A.3.1 True Solutions

The basic variant of the problem formulation (A.19) reads as

$$\mathbf{y} = \mathbf{Ax}, \tag{A.21}$$

with $\mathbf{A}$ a matrix of size (m, n) and rank r. This system of equations may, or may not have a solution. Three different situations can be distinguished.

- There is no solution. This is the case when the vector products of all possible vectors $\mathbf{Ax}$ and $\mathbf{y}$ are nonzero. An equivalent statement of this condition is $rank([\mathbf{y}\ \mathbf{A}]) > rank(\mathbf{A})$.
- There is a single, unique solution. This is the case when $rank([\mathbf{y}\ \mathbf{A}]) = rank(\mathbf{A})$ and $rank(\mathbf{A}) = r = n$.
- A multitude of different solutions exists. This is the case when $rank([\mathbf{y}\ \mathbf{A}]) = rank(\mathbf{A})$ and $r < n$. This follows from the definition of the rank of a matrix: $r < n$ signifies that there exist nonzero vectors $\mathbf{z}$ such that $\mathbf{Az} = \mathbf{0}$. Thus, if $\mathbf{x}$ is a solution to $\mathbf{Ax} = \mathbf{y}$ then $\mathbf{A}(\mathbf{x} + \mathbf{z}) = \mathbf{y}$, which indicates that $\mathbf{x} + \mathbf{z}$ is also a solution. A matrix for which $r < n$ is called a rank-deficient matrix.

If the system has a solution it is called consistent, otherwise it is called inconsistent.

In linear algebra the treatment of (A.21) is usually restricted to square versions of $\mathbf{A}$. If $r = n$, a unique solution exists, but for this situation only, which can be denoted as

$$\mathbf{x} = \mathbf{A}^{-1}\mathbf{y}, \tag{A.22}$$

with $\mathbf{A}^{-1}$ denoting the inverse of matrix $\mathbf{A}$. Note that under these conditions the existence of a unique solution $\mathbf{x}$ depends on the properties of $\mathbf{A}$ only and not on the involved $\mathbf{y}$. With $rank(\mathbf{A}) = n$, matrix $\mathbf{A}$ is called non-singular, otherwise: singular.

This document is directed towards solving (A.21) in the more general situation where $\mathbf{A}$ is not square.

A.3.2 Least Squares Solutions

The linear systems that arise in several applications of numerical analysis are often inconsistent and, or rank deficient. It is for the handling of these situations that the methods used in this chapter have been developed. Such methods are based on the minimization of the squared Euclidean norm of $\mathbf{y} - \mathbf{Ax}$. As such they are called "least squares methods."

If no further information is available on the nature of the problem (A.21) the so-called ordinary least squares (OLS) solution $\widehat{\mathbf{x}}$, [28], can be computed. This is the solution resulting from minimizing with respect to $\mathbf{x}$ of RES^2, the squared (Euclidean) norm of the difference vector $\mathbf{r} = \mathbf{y} - \mathbf{Ax}$, i.e., $\|\mathbf{y} - \mathbf{Ax}\|_2^2$. Accordingly, the solution $\widehat{\mathbf{x}}$ is taken from

$$\min_{\mathbf{x}} \|\mathbf{y} - \mathbf{Ax}\|_2^2. \tag{A.23}$$

The minimization is carried out by equating all partial derivatives of the squared norm in (A.23) with respect to the elements of $\mathbf{x}$ to zero. The result of this procedure leads to the following condition, which needs to be satisfied by any least square solution $\widehat{\mathbf{x}}$,

$$\mathbf{A}^T\mathbf{A}\widehat{\mathbf{x}} = \mathbf{A}^T\mathbf{y}. \tag{A.24}$$

An important property of (A.24) is that it has at least one solution [27], irrespective of whether the system $\mathbf{Ax} = \mathbf{y}$ is consistent. How these are found is treated below.

A.3.2.1 Specific Notations

After minimization, the following variables can be distinguished:

$\widehat{\mathbf{x}}$ ≡ the OLS solution
$\mathbf{y}$ ≈ $\mathbf{A}\widehat{\mathbf{x}}$ $\widehat{\mathbf{x}}$ solves the system in the least squares sense
$\widehat{\mathbf{y}}$ = $\mathbf{A}\widehat{\mathbf{x}}$
$\widehat{\mathbf{r}}$ = $\mathbf{y} - \mathbf{A}\widehat{\mathbf{x}}$, the residual difference (=$\mathbf{y} - \widehat{\mathbf{y}}$)
RES = the norm of $\widehat{\mathbf{r}}$

A.3.2.2 The Over Determined Situation: $m \geq n$

1. *full-rank case*: $r = rank(\mathbf{A}) = n$
   In this situation a unique solution to (A.24)

$$\widehat{\mathbf{x}} = (\mathbf{A}^T\mathbf{A})^{-1}\mathbf{A}^T\mathbf{y} \tag{A.25}$$

   exists, as follows immediately from (A.24). It requires $\mathbf{A}^T\mathbf{A}$ to be non-singular, which is the case in this full-rank situation.
2. *rank-deficient case*: $r < n$
   If $r < n$ matrix $\mathbf{A}^T\mathbf{A}$ is singular and (A.25) cannot be used, and so (A.25) does not have a non-unique solution. The solution can be made unique by imposing additional constraints on the solutions. A frequently used constraint is to demand that the norm of the solution vector $\mathbf{x}$ be minimal. Other types of constraints as well as their implementations are discussed in Chap. 9.

A.3.2.3 The Underdetermined Situation: $m < n$.

1. *full-rank case:* $m = r < n$
   Here a multitude of solutions to (A.21) exist. A unique solution

$$\widehat{\mathbf{x}} = \mathbf{A}^T(\mathbf{A}\mathbf{A}^T)^{-1}\mathbf{y} \tag{A.26}$$

   is found by requiring it to be the one that minimizes the norm of $\mathbf{x}$, subject to the constraint $\mathbf{y} = \mathbf{A}\mathbf{x}$. The fact that $m = r$ guarantees that $\mathbf{A}\mathbf{A}^T$ is non-singular, and thus the solution is indeed unique.
2. *rank-deficient case:* $r < m < n$
   Here, again, a multitude of solutions exist, all having the same value of RES, and can be made unique only by imposing appropriate constraints.

A.3.3 General Methods

Several different methods have been described in the literature for solving the basic equations (A.19) or (A.20). All of these require the inversion of a matrix, either one included in the basic equations, or the one resulting from the least squares approach (A.25). Usually, the solution is made unique by imposing a constraint that minimizes the norm of the solution.

Algorithm HFTI [26] as well as SVD [25] produce LS solutions for all cases, yielding minimum norm solutions in the underdetermined situations.

Algorithm HFTI produces the solution only, algorithm SVD yields a decomposition into three matrices from which the solution $\mathbf{x}$ can be found easily, as is shown below. The SVD is summarized in Sect. A.4. Both algorithms can also be used to find (to estimate) the covariance of the solution (the estimate) for the general situation involving noise.

For the SVD-based approach involving any matrix of rank r, the least squares solution having minimum norm is

$$\widehat{\mathbf{x}} = \mathbf{V}_r\boldsymbol{\Sigma}_r^{-1}\mathbf{U}_r^T\mathbf{y}, \tag{A.27}$$

with $\boldsymbol{\Sigma}_k^{-1}$ a square diagonal matrix having elements $1/\sigma_i$ for $i = 1, r$.
For the notation used, see A.4.1.

A.4 The Singular Value Decomposition

One of the major tools of linear algebra is the singular value decomposition of a matrix. It has a great value in theoretical derivations as well as for practical computations. The treatment in this section is mainly descriptive. Proofs of the various

statements can be found in Refs. [24–26]. However, they also follow directly from the way in which the various matrices are constructed by the SVD algorithm.

A.4.1 The Basic Statement

For any real matrix $\mathbf{A}$ of size (m, n) there exist matrices $\mathbf{U}$ of size (m, m) and $\mathbf{V}$ (n, n), and a matrix $\mathbf{\Sigma}$ of size (m, n) having non-negative elements $\sigma_i = \sigma_{i,i}$ for $1 \le i \le k \le \min(m, n)$, all remaining elements being zero, such that

$$\mathbf{A} = \mathbf{U}\mathbf{\Sigma}\mathbf{V}^T. \tag{A.28}$$

This so-called factorization of $\mathbf{A}$ is referred to as its singular value decomposition (SVD).

The elements σ_i, $i = 1, k$, are called the singular values of $\mathbf{A}$. They are usually ordered such that $\sigma_i \ge \sigma_{i+1}$, accompanied by a reordering of the corresponding columns of $\mathbf{U}$ and $\mathbf{V}$, $\mathbf{u}_i$ and $\mathbf{v}_i$, $i = 1, k$, respectively.

The matrices $\mathbf{U}$ and $\mathbf{V}$ have the following properties:

- $\mathbf{U}$ (size(m, m)) is orthogonal: $\mathbf{U}^T\mathbf{U} = \mathbf{I}$, hence $\mathbf{U}^T = \mathbf{U}^{-1}$.
- $\mathbf{V}$ (size(n, n)) is orthogonal: $\mathbf{V}^T\mathbf{V} = \mathbf{I}$, hence $\mathbf{V}^T = \mathbf{V}^{-1}$.

The integer variable k can be shown to be equal to the rank r of the matrix.

Based on the rank r of $\mathbf{A}$, the ordered variant of the decomposition can be partitioned as

$$\mathbf{A} = \begin{bmatrix} \mathbf{U}_r & \mathbf{U}_{m-r} \end{bmatrix} \begin{bmatrix} \mathbf{\Sigma}_r & \mathbf{0} \\ \mathbf{0} & \mathbf{0} \end{bmatrix} \begin{bmatrix} \mathbf{V}_r^T \\ \mathbf{V}_{n-r}^T \end{bmatrix},$$

where the matrix subscripts denote the number of columns of the respective matrices.

By excluding the entries for $\sigma_i = 0$ this partitioning indicates that a different factorization of $\mathbf{A}$ is

$$\mathbf{A} = \mathbf{U}_r\mathbf{\Sigma}_r\mathbf{V}_r^T, \tag{A.29}$$

the so-called "lean" variant of the decomposition. It expresses the essence of the decomposition in its application to solving the linear system. Some computer codes generate $\mathbf{U}_r$ and $\mathbf{V}_r$ only. It involves the first r columns of matrices $\mathbf{U}$ and $\mathbf{V}$. Matrix $\mathbf{\Sigma}_r$ is a diagonal matrix of size (r, r) comprising positive diagonal elements.

For the submatrices involved one has

- The columns of $\mathbf{U}_r$ are orthogonal: $\mathbf{U}_r^T\mathbf{U}_r = \mathbf{I}_r$.
- The columns of $\mathbf{U}_{m-r}$ are orthogonal: $\mathbf{U}_{m-r}^T\mathbf{U}_{m-r} = \mathbf{I}_{m-r}$.
- The columns of $\mathbf{V}_r$ are orthogonal: $\mathbf{V}_r^T\mathbf{V}_r = \mathbf{I}_r$.
- The columns of $\mathbf{V}_{n-r}$ are orthogonal: $\mathbf{V}_{n-r}^T\mathbf{V}_{n-r} = \mathbf{I}_{n-r}$.

Note that, since $\mathbf{U}_r$ and $\mathbf{V}_r$ need not be square, their transposed versions generally do not represent their inverses.

Yet another form of the basic expression (A.28) is

$$\mathbf{A} = \sum_{i=1}^{r} \sigma_i \mathbf{u}_i \mathbf{v}_i^T, \tag{A.30}$$

expressing $\mathbf{A}$ as a sum of the matrix products of corresponding column vectors $\mathbf{u}_i$ and $\mathbf{v}_i$: $\mathbf{u}_i\mathbf{v}_i^T$, each being a so-called rank-one matrix.

A.4.2 Applications of the Decomposition

For square, non-singular matrices ($m = n = r$) the inverse of matrix $\mathbf{A}$ as required in (A.21) can be computed from the three matrices (factors) resulting from the SVD algorithm: equation (A.28). Since all three factors involved are non-singular and have the same size we immediately find, by applying the properties listed in Sect. A.5, as well as the orthogonality of $\mathbf{U}$ and $\mathbf{V}$,

$$\mathbf{A}^{-1} = (\mathbf{U}\boldsymbol{\Sigma}\mathbf{V}^T)^{-1} = (\mathbf{V}^T)^{-1}\boldsymbol{\Sigma}^{-1}\mathbf{U}^{-1} = \mathbf{V}\boldsymbol{\Sigma}^{-1}\mathbf{U}^T. \tag{A.31}$$

Because of the diagonal nature of $\boldsymbol{\Sigma}$ and the fact that all its elements σ_i are positive, matrix $\boldsymbol{\Sigma}^{-1}$ is also diagonal, having elements $1/\sigma_i$.

If matrix $\mathbf{A}$ is singular or non-square, it does not have an inverse. As discussed in A.3.2, one then reverts to least squares methods. At one stage or another, of these methods require solving expressions like (A.21). Below it is shown that the least squares solution to this problem having a minimal norm is

$$\widehat{\mathbf{x}} = \mathbf{V}_r\boldsymbol{\Sigma}_r^{-1}\mathbf{U}_r^T\mathbf{y}, \tag{A.32}$$

with all matrices shown as defined in (A.29).

We start by demonstrating that this solution is a least squares solution, which requires that it satisfies condition (A.24). To this end, we multiply the left side of (A.32) by $\mathbf{A}^T\mathbf{A}$ and the right side by the same factor, now expressed by in terms of the equivalent variant (A.29). This is permitted since $\mathbf{A}$ and $\mathbf{A}_r$ have the same rank. We then find, by using the properties of the matrices $\mathbf{V}_r$, $\boldsymbol{\Sigma}_r$ and $\mathbf{U}_r$ as specified above, that

$$\begin{aligned}\mathbf{A}^T\mathbf{A}\widehat{\mathbf{x}} &= \mathbf{V}_r\boldsymbol{\Sigma}_r\mathbf{U}_r^T\,\mathbf{U}_r\boldsymbol{\Sigma}_r\mathbf{V}_r^T\mathbf{V}_r\boldsymbol{\Sigma}_r^{-1}\mathbf{U}_r^T\mathbf{y},\\ &= \mathbf{V}_r\boldsymbol{\Sigma}_r\boldsymbol{\Sigma}_r\boldsymbol{\Sigma}_r^{-1}\mathbf{U}_r^T\mathbf{y}\\ &= \mathbf{V}_r\boldsymbol{\Sigma}_r\mathbf{U}_r^T\mathbf{y}\\ &= \mathbf{A}^T\mathbf{y}.\end{aligned} \tag{A.33}$$

Finally, we show that solution $\widehat{\mathbf{x}}$ as found from (A.32) has a minimum norm. Let $\widehat{\mathbf{x}} + \mathbf{z}$ be any other vector resulting in the same (minimal) residual. Equation (A.32) shows that $\widehat{\mathbf{x}}$ is a linear combination of the first r columns of $\mathbf{V}$ appearing in the full SVD of $\mathbf{A}$. The weighting coefficients are the r-dimensional row vector $\boldsymbol{\Sigma}_r^{-1}\mathbf{U}_r^T\mathbf{y}$. Adding an arbitrary linear combination of the $n - r$ columns of matrix $\mathbf{V}_{n-r}$, with weighting coefficients $\mathbf{w}$ to the least squares solution $\widehat{\mathbf{x}}$ will result in the same residual since

$$\mathbf{A}\mathbf{V}_{n-r}\mathbf{w}^T = \begin{bmatrix}\mathbf{U}_r & \mathbf{U}_{m-r}\end{bmatrix}\begin{bmatrix}\boldsymbol{\Sigma}_r & \mathbf{0}\\ \mathbf{0} & \mathbf{0}\end{bmatrix}\begin{bmatrix}\mathbf{V}_r^T\\ \mathbf{V}_{n-r}^T\end{bmatrix}\mathbf{V}_{n-r}\mathbf{w}^T,$$

and so

$$\mathbf{A}\mathbf{V}_{n-r}\mathbf{w}^T = \mathbf{U}_{m-r}\mathbf{0}\mathbf{w}^T = \mathbf{0}. \tag{A.34}$$

This proves that the vector $\widehat{\mathbf{x}} + \mathbf{V}_{n-r}\mathbf{w}^T$ is also a least squares solution. However, its norm is necessarily higher because of the fact that the basis vectors, the columns of $\mathbf{V}_r$ and $\mathbf{V}_{n-r}$, are orthogonal.

The matrix $\mathbf{A}^+ \triangleq \mathbf{V}_r\boldsymbol{\Sigma}_r^{-1}\mathbf{U}_r^T$ is called the natural pseudo-inverse of matrix $\mathbf{A}$.

A.5 Definitions and Notations

The following notations are used throughout.

General

$\triangleq$	is defined as
iff	if and only if
$\approx$	equals in the least squares sense
^{T}	the transpose of a vector or a matrix
$\perp$	is orthogonal to

Vectors

	Column vectors are denoted by bold-face lower-case characters *e.g.*, $\mathbf{x}$, their elements as $x_i,\ i = 1, \cdots, n$
$\mathbf{0}$	a vector having all elements = 0
$\mathbf{x} = \mathbf{0}$	a vector having all elements $x_i = 0$
$\mathbf{x} > \mathbf{0}$	a vector having all elements $x_i \geq 0$ with at least one element $x_i > 0$
$\|\mathbf{x}\|$	norm of a vector (Euclidean norm): $\|\mathbf{x}\| \triangleq (\sum_i x_i^2)^{1/2}$
dependent	k vectors are called dependent if set of numbers $\alpha(i), i = 1, \cdots, k$ exist, not all zero, such that $\mathbf{x}_1\alpha_1 + \mathbf{x}_2\alpha_2 + \cdots + \mathbf{x}_k\alpha_k = \mathbf{0}$, else they are called independent

Matrices

General

	Matrices are denoted by bold-face upper-case characters, e.g., $\mathbf{A}$, Matrix $\mathbf{A}$ of size (m, n) has elements $a_{i,j},\ i = 1, \cdots, m;\ j = 1, \cdots, n$
$r = rank(\mathbf{A})$	rank r, of a matrix is the maximum number of independent columns or rows it contains; $r <= \max(m, n)$
$\mathbf{A}^+$	denotes a pseudo-inverse of matrix $\mathbf{A}$
$\mathbf{A}^\circ$	alternative notation of a pseudo-inverse of matrix $\mathbf{A}$
$\mathbf{0}$	a matrix having zero elements only
$\mathbf{A} \neq \mathbf{0}$	a matrix having at least one element $a_{i,j} \neq 0$
$\mathbf{U}$	is an orthogonal matrix if $\mathbf{U}^T\mathbf{U} = \mathbf{I}$, i.e., if all its columns, treated as vectors, are mutually orthogonal and their scalar products equal one
$\|\mathbf{A}\|_F$	Freebies norm (also Euclidean norm): $\|\mathbf{A}\|_F =\triangleq (\sum_i \sum_j a_{i,j}^2)^{1/2}$

Square matrices

$\mathbf{D}$	a diagonal matrix. All off-diagonal elements are zero
$\mathbf{D}$=$\mathbf{D}^T$	$\mathbf{D}$ diagonal
$\mathbf{I}$	the identity matrix: a diagonal matrix having unit diagonal elements
$\mathbf{A}^{-1}$	denotes the inverse of matrix $\mathbf{A}$: a matrix such that $\mathbf{A}^{-1}\mathbf{A} = \mathbf{A}\mathbf{A}^{-1} = \mathbf{I}$
$(\mathbf{AB})^{-1} = \mathbf{B}^{-1}\mathbf{A}^{-1}$	(non-singular square matrices of the same size)
$\mathbf{AA} = \mathbf{A}^2$	notation valid for square matrices only
$\kappa(\mathbf{A})$	condition number of matrix $\mathbf{A}$ with respect to inversion: $\kappa(\mathbf{A}) \triangleq \|\mathbf{A}\|.\ \|\mathbf{A}^{-1}\|$
$\mathrm{tr}(\mathbf{A})$	the trace of $\mathbf{A}$: $\mathrm{tr}(\mathbf{A}) \triangleq \sum_i a_{i,i}$

Statistics

$E(\mathbf{x})$	the mathematical expectation of $\mathbf{x}$ if its elements are stochastic
i.i.d.	"independent and identically distributed" elements of a stochastic vector
$Cov(\mathbf{x})$	$\triangleq E\{(\mathbf{x}-E(\mathbf{x}))(\mathbf{x}-E(\mathbf{x}))^T\}$, the covariance of $\mathbf{x}$; in matrix notation: $\mathbf{\Gamma_x}$
$Var(\mathbf{x})$	$\triangleq diag(\mathbf{\Gamma_x})$, the variance of $\mathbf{x}$
white noise	independent samples drawn from a zero-mean Gaussian distribution

References

1. Panofski, W.K.H. and M. Phillips, Classical Electricity and Magnetism. 1962. Addison-Wesley: London.
2. Schwan, W.H.K. and C.F. Kay, The conductivity of living tissues. Ann N.Y. Acad Sci., 1957;**65**: p. 1007–1013.
3. Epstein, B.R. and K.R. Foster, Anisotropy in the dielectric properties of skeletal muscle. *Med. Biol. Eng. Comp.*, 1983;**21**: p. 51–56.
4. Plonsey, R. and A. van Oosterom, Implications of Macroscopic Source Strength on Cardiac Cellular Activation Models. *J. Electrocardiol.*, 1991;**24/2**: p. 99–112.
5. Rush, S., J.A. Abildskov, and R.S. McFee, Resistivity of body tissues at low frequencies. *Circulation Res.*, 1963;**7**: p. 262–267.
6. Geddes, L.A. and L.E. Baker, The Specific Resistance of Biological Material, a Compendium of Data for the Biomedical Engineer and Physiologist. *Med. Biol. Eng. Comput.,* 1967;**5**: p. 271–293.
7. Gabriel, C., S. Gabriel, and E. Corthout, The dielectric properties of biological tissues, (I): Literature Survey. *Phys. Med. Biol.*, 1996;**41**: p. 2231–2249.
8. Thomas, C.W., Electrocardiographic measurement system response, in *Pediatric Electrocardiography*, J. Liebman, R. Plonsey, and P.C. Gilette, Editors. Williams and Wilkins: Baltimore. 1982. pp. 40–59.
9. Plonsey, R. and D. Heppner, Considerations of Quasi-stationarity in Electrophysiological Systems. *Bull. Math. Biophys.*, 1967;**29**: 657–664.
10. Smythe, W.R., Static and Dynamic Electricity. 1968. McGraw-Hill: New York.
11. Geselowitz, D.B., Multipole Representation for an Equivalent Cardiac Generator. Proc. IRE, 1960: pp. 75–79.
12. Jackson, J.D., *Classical Electrodynamics*, 2 edn., 1975. New York: John Wiley & Sons.
13. Abramowitz, M. and I.E. Stegun, Handbook of mathematical functions, 1970; New York: Dover.
14. Burger, H.C., The Zero of Potential: A Persistent Error. *Am. Heart J.*, 1955;**49**: 581–586.
15. Geselowitz, D.B., The Zero of Potential. IEEE *Eng. Med. Biol. Mag.*, 1998;**17**(1): 128–132.
16. Geselowitz, D.B., Bioelectric potentials in an inhomogeneous volume conductor, in *QPR*. 1960, MIT, p. 218–226.
17. Plonsey, R., The formulation of bioelectric source-field relationships in terms of surface discontinuities, *J. Franklin Inst.*, 1974; 317–324.
18. Gelernter, H.L. and J.C. Swihart, A Mathematical-physical Model of the Genesis of the Electrocardiogram. *Biophys. J.*, 1964;**4**: p. 285–301.
19. Oostendorp, T.F. and A. van Oosterom, Source parameter estimation in inhomogeneous volume conductors of arbitrary shape. *IEEE Trans. Biomed. Eng.*, 1989;*BME* **36**(3): 382–391.
20. van Oosterom, A. and J. Strackee, The Solid Angle of a Plane Triangle. *IEEE Trans. Biomed. Eng.*, 1983;*BME* **30**: 125–126.
21. Munck, J.C.D., A Linear Discretization of the Volume Conductor Boundary Integral Equation using Analytically Integrated Elements. *IEEE Trans. Biomed. Eng.*, 1992;*BME* **39**: 986–990.
22. Oostendorp, T.F. and A. van Oosterom, Source parameter estimation in inhomogeneous volume conductors of arbitrary shape. *IEEE Trans. Biomed. Eng.*, 1989;*BME* **36**: 382–391.
23. van Oosterom, A. and T.F. Oostendorp, On Computing Pericardial Potentials and Current Densities. *J. Electrocardiol.,* 1992; **25**(Suppl): 102–106.
24. Golub, G.H. and C.F. Van Loan, *Matrix Computations*, The Johns Hopkins University Press, Baltimore, 1996. 3rd edition.
25. Forsythe, G.E., M.A. Malcolm, and C.B. Moler, *Computer Methods for Mathematical Computations*, Prentice-Hall, Englewood Cliffs, N.J., 1977.
26. Lawson, C.L. and R.J. Hanson, *Solving Least Squares Problems*, Prentice-Hall, Englewood Cliffs, N.J., 1974.
27. Steward G.W., *Introduction to Matrix Computations*, Academic Press, New York, 1973.
28. Beck J.V. and K.J. Arnold, *Parameter Estimation in Engineering and Science*, Wiley, New York, 1977.

General References

Smythe, W.R., *Static and Dynamic Electricity*. New York: McGraw-Hill, 1968; first published in 1939.

Stratton, J.A., *Electromagnetic Theory*. New York: McGraw-Hill, 1941.

Jackson J.D. *Classical Electrodynamics*. New York: Wiley, 1962.

Panofsky W.K.H, Phillips M. *Classical Electricity and Magnetism,* 2nd ed. Reading, MA: Addison-Wesley, 1962.

Plonsey R, Collin R. *Principles and Applications of Electromagnetic Fields*. New York: McGraw-Hill, 1961.

Plonsey R. *Bioelectric Phenomena*. New York: McGraw-Hill, 1969.
Gulrajani, R.M. *Bioelectricity and Biomagnetism*. New York: Wiley, 1998.
Plonsey R., Barr R.C., *Bioelectricity: A Quantitative Approach*, third edition. New York: Springer, 2007.

Appendix Bibliography

1. Golub GH and Van Loan CF. *Matrix Computations*. The Johns Hopkins University Press, Baltimore, 1996. 3rd edition.
2. Forsythe GE, Malcolm MA, and Moler CB. *Computer Methods for Mathematical Computations*. Prentice-Hall, Englewood Cliffs, N.J., 1977.
3. Lawson CL and Hanson RJ. *Solving Least Squares Problems*. Prentice-Hall, Englewood Cliffs, N.J., 1974.
4. Steward GW. *Introduction to Matrix Computations*. Academic Press, New York, 1973.
5. Beck JV and Arnold KJ. *Parameter Estimation in Engineering and Science*. Wiley, New York, 1977.

Section 2

Cardiac Electrophysiology

3 Cellular Electrophysiology

A. Zaza · R. Wilders · T. Opthof

P. W. Macfarlane, A. van Oosterom, O. Pahlm, P. Kligfield, M. Janse, J. Camm (eds.), *Comprehensive Electrocardiology*, DOI 10.1007/978-1-84882-046-3_3,

3.1 Introduction

The beginning of the era of cardiac electrophysiology can be attributed to the end of the nineteenth century, when Einthoven discovered the ECG and described its configuration [1], defining it more quantitatively in a later study [2]. While the ECG remains an essential clinical tool and a symbol of cardiac electrophysiology, the discipline has evolved to address the function of single myocytes, or even of specific processes within myocytes.

Myocytes represent the functional unit of the cardiac muscle; nonetheless, the heart behaves more or less like an electrical syncytium, whose global activity depends on low resistance coupling between the myocytes. The phrase "more or less" is used here intentionally to imply that, while the activity intrinsic to individual myocytes is affected by coupling, its features remain recognizable within the context of the whole heart and are important to determine its function.

The ECG signal represents the electrical activity of the whole organ and its relation with the activity of individual myocytes is quite complex. Indeed, the potentials recorded by body surface electrodes are affected by spatial and temporal summation of myocyte activity at different locations in the heart. This results in so many electrical signals being cancelled, especially during the repolarization phase [3], that the same ECG pattern may be compatible with different activation and repolarization sequences. This implies that it would be theoretically possible to construct the ECG from the action potentials of all underlying myocytes, but we cannot deduce individual myocyte behavior from the ECG, a condition recognized by biophysicists as the "inverse problem" [4]. In the same way, analysis of the mechanisms and modulation of the electrical activity of single myocytes provides information relevant to the function of the whole heart, which cannot be obtained from the ECG.

This chapter deals with the basic mechanisms of myocyte functioning such as excitation, repolarization, and automaticity, which are relevant to the initiation and orderly propagation of electrical activity in the whole heart. The aim is to provide a link between phenomena at the molecular level, potential targets of drug therapy or genetic manipulation, and macroscopic electrical behavior. We have focused on issues essential to pursue this aim, sacrificing for the sake of clarity, some of the overwhelming complexity of cardiac cell physiology. Reviews have been quoted to cover settled topics, and references reserved for original papers and more recent or controversial issues.

3.1.1 Annotation Conventions

Knowledge of a few conventions on the annotation of physical parameters is useful for understanding the following discussion.

1. Following commonly used annotation, we have used E to denote electrochemical equilibrium potentials (e.g., E_K for potassium equilibrium potential) and V to denote membrane potential (V_m, V_{rest}). For the sake of clarity, it should be stressed that both E and V denote an electrical potential difference across the cell membrane and thus have identical units (mV).
2. The symbol I_m refers to *net current across the cell membrane*. I_m may reflect the algebraic summation of currents carried by different ion channels, possibly with different signs. Thus, $I_m = 0$ does not necessarily imply that individual currents are also null. Individual currents are appropriately annotated (e.g., I_{Na} for Na^+ current).
3. In defining the sign of potentials and currents, the extracellular electrode is used as reference (i.e., at 0 mV by convention). Thus: (1) $V_m = -80$ mV means that the intracellular side is 80 mV negative to the extracellular one; (2) membrane current has a positive sign whenever positive charges leave the cell (outward current); inward current has a negative sign.
4. The term "mole" refers to a quantity of substance (containing a number of molecules equal to Avogadro's number), whereas the term "molar" (M) refers to a concentration (1 M = 1 mol/L).

3.2 Outline of Structure and Function

3.2.1 Myocyte Structure and Relation to Excitation–Contraction Coupling

Each myocyte is surrounded by a plasma membrane named sarcolemma. Its basic structure is a lipid bilayer, a few nanometers thick, impermeable to ions and with a high dielectric constant. Ions can cross the sarcolemmal membrane only via specialized embedded proteins, named ion channels. The sarcolemma forms multiple invaginations perpendicular to the long cell axis, named T-tubules (Fig. 3.1). They serve as extensions of the cell surface and host a large density of ion channels and transporters important for excitation-contraction coupling. Myocytes contain a specialized cisternal system, the sarcoplasmic reticulum (SR), in which Ca^{2+} is actively accumulated by ATP-driven transport (SR Ca-ATPase or SERCA). The SR is in close vicinity (about 10 nm) to the T-tubule sarcolemma on one side and to the contractile apparatus on the other, but is not in contact with them. This kind of structural arrangement is essential for the coupling between electrical excitation of the sarcolemma and massive release of Ca^{2+} from the SR. Indeed, coupling is mediated by a relatively small influx of Ca^{2+} through voltage-gated sarcolemmal Ca^{2+} channels (L-type channels, carrying I_{CaL}), which open Ca^{2+}-activated Ca^{2+} channels in the SR membrane (ryanodine receptor (RyR) channels), a process named Ca^{2+}-induced Ca^{2+}-release (CICR) [5] (Fig. 3.1c). Each L-type Ca^{2+}-channel on the sarcolemma corresponds to a cluster of RyR channels on the SR membrane, forming a sort of Ca^{2+} release unit. RyR channels within a unit open and close in a "cooperative" fashion, so as to make Ca^{2+} release of the cluster a quantal (all-or-none) process. Such unitary Ca^{2+}

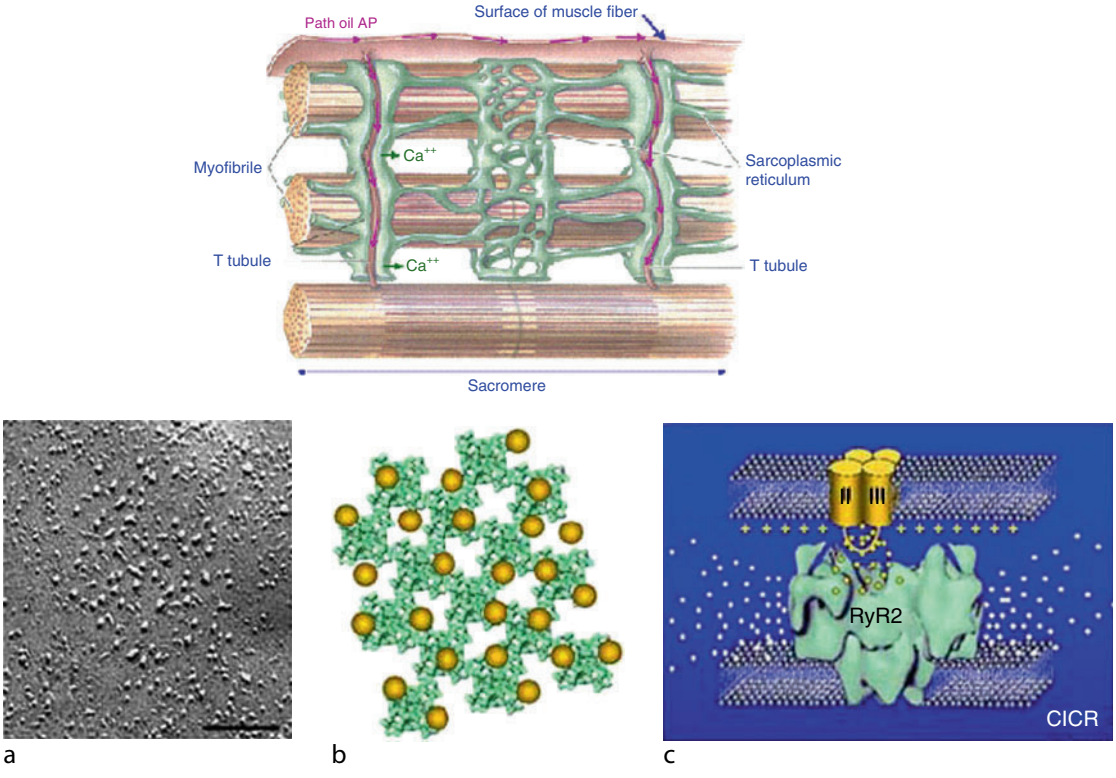

Figure 3.1

Myocyte structure. *Upper panel*: arrangement of T-tubules, sarcoplasmic reticulum (SR) and sarcomeres within a cardiac myocyte. *Bottom panels*: (a) clustering of Ryanodine receptors (RyR) on SR membrane, (b) spatial relationship between dihydropyridine receptor (yellow) in sarcolemma and underlying RyR clusters (green); (c) Ca^{2+} release by RyR, induced by Ca^{2+} entry through dihydropyridine receptor (CICR: Ca^{2+} induced Ca^{2+} release).

releases have been named "Ca^{2+} sparks" [6]; physiological contraction is triggered by the fusion of multiple sparks into a "Ca^{2+} transient," supported by synchronous activation of all release units by Ca^{2+} entry through L-type Ca^{2+}-channels during the action potential.

The transmission of action potentials from cell to cell occurs via non-selective, large-conductance ion channels, closely packed in large arrays named gap junctions. These are primarily located within the intercalated disks connecting myocytes along their longitudinal axis, but are also present on lateral margins, to provide side-to-side connections. Each cardiac gap junction channel is made of 12 connexin molecules. Six of these form a hemichannel (connexon) in one myocyte, which faces another hemichannel in the adjacent myocyte. Together they form a full channel providing electrical continuity between myocytes. There are several isoforms of these connexins, but the most important one, abundantly present in working atrial and ventricular muscle, is connexin43 (Cx43; see for review [7]). Intercalated disks also provide the physical structure where mechanical force can be transmitted.

3.2.2 Tissue Structure and Relation to Global Heart Excitation

There are five functionally and anatomically separate types of heart muscle: sinoatrial (SA) node, atrioventricular (AV) node, His-Purkinje system, atrial muscle and ventricular muscle. To date there is no convincing evidence for the existence of "internodal pathways". Under normal circumstances only the first three are capable of pacemaker function. The SA node generates the cardiac impulse, whereas the AV node and His-Purkinje system have a prominent role in its conduction. The primary function of the remaining atrial and ventricular muscle tissues is force development, as expressed by the comprehensive definition of "working myocardium." The bundle of His and Purkinje fibers were anatomically described in the nineteenth century, and the SA and AV nodes were discovered during the first decade of the twentieth century [8, 9]. Indeed, an impressive, comprehensive review of the origin and conduction of the heartbeat appeared as the opening paper in the very first issue of *Physiological Reviews* in 1921 [10]. At that time the principal structural components of the heart were known, but the study of function had to await a number of important technical breakthroughs. First, in 1949, Ling and Gerard introduced the microelectrode, which permitted the measurement of transmembrane potentials [11]. Thirty years later, two important techniques were developed. Cell isolation techniques permitted the study of the characteristics of single myocytes [12]. The patch clamp technique paved the path for the study of membrane currents at the level of individual membrane channels [13].

The SA node is composed of a heterogeneous population of cells with some common features. The myocytes are small and generally spindle-shaped. They have little contractile material, which is not organized in myofibrils with a clearly periodical structure. Compared to their relatively low myofilament density, they have a remarkably high mitochondrial density. They do not have a significant T-tubular system, but they do possess many caveolae [14]: cholesterol-rich membrane domains containing a high density of receptor and channel proteins. In the SA node, myocytes form clusters and bundles surrounded by abundant collagen. The SA node border is deeply interdigitated with the surrounding atrial myocardium, forming structures in which relatively thin atrial bundles penetrate a larger mass of nodal myocytes.

Whether propagation from the SA node to the AV node occurs through specialized conduction tissue is an unresolved issue. Internodal pathways have not been conclusively demonstrated and the dominating opinion is that the conduction pattern results from the longitudinally oriented tissue architecture of the crista terminalis at the junction between the intercaval area and the right atrium.

AV nodal cells are similar in both shape and function to those of the SA node [14, 15]. In contrast to the SA node with its central origin of the cardiac impulse and radial propagation, the AV node has two functional inputs and one functional output communicating with the bundle of His. Under pathological conditions, this morphological and functional triangular make-up provides the substrate for AV nodal reentrant arrhythmias. Even in structurally normal hearts, isolated echobeats can be provoked by appropriate stimulation protocols, not only in animal studies [15], but also in humans [16].

The specialized conduction system distal to the AV node (His bundle, bundle branches, fascicles and Purkinje network) is composed of Purkinje myocytes, longitudinally oriented in bundles, packed by dense connective tissue. Purkinje myocytes are of similar shape but larger than working myocytes, have less contractile material and contain large amounts of glycogen. Connexins are abundantly expressed, particularly in terminal gap-junctional connections. Myocytes at the transition between Purkinje fibers and working ventricular muscle have an intermediate morphology [17].

Atrial and ventricular myocytes are rod-shaped and about 100 µm long. Ventricular myocytes are about 20 µm wide, atrial ones are slightly thinner. Both cell types contain a large amount of contractile proteins, organized in clearly periodic myofibrils, a large number of mitochondria and glycogen deposits. T-tubules are well developed in ventricular myocytes, but almost missing in atrial myocytes. The latter contain secretory granules, related to their endocrine activity (atrial natriuretic peptide (ANP) secretion).

The morphological and functional differences between cardiac tissues account for orderly impulse propagation, providing the coordinated contraction required for pump efficiency. After the initiation of the cardiac impulse in the sinus node (invisible in the surface ECG) the impulse travels rapidly over the atria, giving rise to the P wave in the ECG, followed by atrial contraction. The impulse conducts through the AV node for a considerable time (between 120 and 200 ms; invisible in the ECG, leading to the PR interval), during which period the ventricles fill passively and are assisted by atrial contraction. Once the impulse has passed the AV node, the His-Purkinje system is activated. Again this system has not enough mass to show up on the ECG. The function of the His-Purkinje system is to warrant rapid ventricular activation (visible in the ECG as the QRS complex with a duration of about 100 ms). Moreover the site of earliest (septal) activation is closer to the apex than to the base (in the human heart, not in the murine heart, for example), which is relevant for hemodynamic reasons. Finally, after a long plateau phase of the ventricular action potentials (invisible in the ECG, leading to the ST segment), the ventricles repolarize, leading to the T wave in the ECG. In the next sections we describe the basic active and passive membrane properties at the cellular and organ level.

3.3 Biological Membranes

3.3.1 Bilayer Structure and Physical Properties

The basic structural component of biological membranes is a phospholipid bilayer, formed by molecules containing a hydrophylic head and a hydrophobic tail (amphiphilic molecules). When put in water, pairs of such molecules turn their tails to each other and their heads to face the water. Many such pairs form a sort of carpet, with a hydrophobic core and hydrophylic shell, whose energy of interaction with water (hydration energy) provides a strong stabilizing mechanism. In spite of its structural stability, the phospholipid bilayer is fluid. Its constituent molecules are in continuous random motion, which occasionally generates small gaps in the hydrophobic core, through which water molecules can pass. Thus, in spite of its lipidic nature, the bilayer is significantly permeable to water by simple diffusion [18]. In biological membranes, additional water permeability can be provided by water channel proteins, named "aquaporins," which are variably expressed in different cell types [19]. While uncharged molecules dissolve in the bilayer and freely permeate it by diffusion, charged molecules, such as ions, do not.

Due to its impermeability to ions and thinness, the phospholipid bilayer is able to separate charges at a very close distance (20–30 nm) and favors their electrostatic interaction (high dielectric constant); thus, the bilayer is an electrical condenser (or capacitor). The *capacity* of a condenser (charge accumulated per unit voltage, $C = \Delta Q/\Delta V$) (Electrical capacity is expressed in farad (F), 1 F = 1 C/V. It should be noted that 1 F is a large capacity, e.g., found in heavy-duty industrial condensers.) is proportional to its surface area. The presence of membrane invaginations (T-tubules, caveolae etc.) increases the ratio between membrane surface and cell volume. Capacity per unit area (specific capacitance) is rather constant among biological membranes and amounts to about 1 µF/cm^2.

3.3.2 Special Routes for Ion Permeation: Ion Channels

To allow ion permeation, a hydrophilic pathway must be created through the phospholipid bilayer. This is provided by "ion channels," protein molecules inserted in the bilayer and connected to the cytoskeleton [20].

Ion channels allow permeation of ions by generating a water-filled pore or, more often, by providing a path of charged amino acidic residues which temporarily bind the ion, freeing it from its hydration shell. Since each permeation path may bind different ions with different affinities, permeation is selective. Selectivity of ion channels is very important functionally and may range among different channels from loose (e.g., cations vs. anions, monovalents vs. divalents) to very strict (e.g., K^+ vs. Na^+, Ca^{2+} vs. Mg^{2+}).

3.3.3 Ion Movements Require Energy: Electrochemical Potentials

Energy is required to move ions along the channel (i.e., to make them jump from one binding site to the next). This energy (also named "driving force") is provided by the electrochemical gradient, generated across the membrane by (1) the presence in the cytosol of non-diffusible anions (mainly negatively charged proteins, to which the membrane is totally impermeable); (2) active redistribution of ions, operated mainly by the Na^+/K^+ pump through consumption of metabolic energy (ATP). The direction of current flow in an ion channel is always along the electrochemical gradient of the ion which permeates the channel. Only active transporters (different from channels) can move ions against their gradient, by using metabolic energy.

The "electrochemical" gradient is a potential energy generated simultaneously by a difference in concentration (generating chemical energy) and in charge (generating electrical energy). When chemical and electrical energies are equal in magnitude and of opposite sign they cancel each other and the net ion flow is null. This condition is named "electrochemical equilibrium" and the membrane potential at which it occurs, is called "equilibrium potential." To exemplify, given the physiological distribution of K^+ ions across the membrane, with a high intracellular concentration ($\approx$ 150 mM) and a low extracellular concentration ($\approx$ 4 mM), the equilibrium potential of K^+ (E_K) is about −94 mV (negative toward the cytosol). This implies that if the membrane potential is equal to −94 mV the net K^+ flow across the membrane is null. When the membrane potential (V_m) differs from E_K, K^+ flows through the membrane, carrying a current proportional to the difference between V_m and E_K, also known as the "driving force" for the ion. The current is outward if V_m is more positive than E_K and vice versa. The V_m value at which the current reverses its direction is also named "reversal potential" of the current. If the channel is selectively permeable to a single ion species (e.g., K^+) the current reversal potential and the ion equilibrium potential coincide. If the channel is permeable to different ions, the current reversal potential is in between the equilibrium potentials of the individual ions, and its precise value is determined by the ratio of the respective permeabilities. For instance, if the channel is permeable to both K^+ ($E_K \approx -94$ mV) and Na^+ ($E_{Na} \approx +70$ mV), the current reversal potential will be positive to −94 mV and will approach +70 mV as the Na^+/K^+ permeability ratio increases.

3.3.4 Changes in Membrane Selective Permeability: Ion Channel Gating

Changes in membrane selective permeability are caused by the opening and closing of selective ion channels. Opening and closing correspond to changes in the conformation of the channel protein (or "state" of the channel). The energy required for such transitions (gating energy) can be of a different kind for different channels. For most cardiac channels, gating energy is provided by the transmembrane electrical potential field (voltage–gated channels), which acts by orienting charged amino acid residues in the channel protein. However, some channels in the heart respond to the binding of a specific molecule (ligand-gated channels), to membrane stretch (stretch-activated channels) etc.

Each specific current (e.g., I_{Na}) is actually carried by a large number of individual channel proteins of the same kind (e.g., single Na^+ channels) which can either be closed or open. The sum of such single channel currents generates an ensemble (or "macroscopic") current, whose magnitude can vary in an apparently "continuous" fashion. The historical interpretation of channel gating (Hodgkin-Huxley model, see Sect. 3.14.1) considers "ensemble" currents, carried by "ensemble" channels. Conductance of the ensemble channel (g) is given by

$$g = x \times g_{max}, \tag{3.1}$$

in which g_{max} is maximal conductance and x (gating variable, ranging from 0 to 1) is the fraction of g_{max} actually expressed in a given condition. Channel "gating" (activation, deactivation etc.) is modeled by varying the value of x.

In the following discussion, we will always refer to *ensemble* "channel," "current," "conductance," etc. Nonetheless, the relation between single channel and ensemble behavior can be easily understood by considering g_{max} as the g value observed when all single channels are open ($x = 1$) and x as the fraction of all single channels which are open in a given condition (also named the "open probability" of the single channel). Channel "gating" corresponds to changes in the open probability.

To summarize, the amount of current flowing through an ion channel is proportional to the product of (1) the driving force for the permeating ion(s) and (2) the channel conductance:

$$I = x \times g_{max} \times (V_m - E_{rev}), \tag{3.2}$$

where g_{max} represents the maximal conductance (all channels open), x the proportion of g_{max} actually available (activation variable) and the term in parenthesis corresponds to the driving force. Notably, in voltage-gated channels, x and the driving force are both affected by V_m. Moreover, in some of them (e.g., I_{Na} and I_{CaL}), the same V_m change (e.g., depolarization) leads to two subsequent transitions: the channel is first activated (x approaches 1) and then "inactivated" (made non-conductive). This is expressed by adding an "inactivation variable" y, with a dependency on V_m opposite to that of x:

$$I = x \times y \times g_{max} \times (V_m - E_{rev}). \tag{3.3}$$

In this case, the current is present when both x and y are not null; thus, upon depolarization, the current flows only for a very short time (a few ms), i.e., when x is already greater than 0 and y is not yet 0. Subsequent return of y to 1 (allowing current to pass) is referred to as "recovery from inactivation" and it is the cause of excitation "refractoriness." For further discussion on modeling of ion channel gating, the reader is referred to Sect. 3.14.1.

By convention (see Sect. 3.1.1), outward current makes V_m more negative (repolarization or hyperpolarization). Similarly, inward current makes V_m more positive (depolarization). For cations (e.g., Na^+, Ca^{2+}, K^+) the direction of ion movement and current coincide. Anions (e.g., Cl^-) leaving the cell cause membrane depolarization and are said to generate an "inward current."

3.4 How Membrane Current Affects Membrane Potential

Thus far, we have addressed the dependency of ionic currents on membrane potential (voltage dependent gating). Now it is time to ask the opposite question: how does membrane current change membrane potential? We will start considering the case of net membrane current (I_m). If the membrane would behave as a simple resistance (R_m), the change in membrane potential (ΔV_m) would be given by Ohm's law ($\Delta V_m = I_m \times R_m$). However, a membrane is also a condenser, which needs to be charged by I_m before V_m develops to the value predicted by Ohm's law; thus, the change in V_m always follows I_m with a lag proportional to membrane capacity (C_m). This can be expressed by the following relation:

$$-\mathrm{d}V_m/\mathrm{d}t = I_m/C_m \tag{3.4}$$

which states that I_m magnitude determines the *velocity* ($-\mathrm{d}V_m/\mathrm{d}t$) by which the V_m change takes place (This relation is valid only if I_m is used entirely to charge C_m, i.e., in the absence of current flow along the cytoplasm (axial current = 0). This is generally true in a single myocyte, but not during propagation between electrically coupled myocytes. In the latter case, part of I_m is used as axial current, thus leading to a smaller $\mathrm{d}V_m/\mathrm{d}t$.) (the minus sign implies that inward I_m moves V_m in the positive direction). A larger C_m makes the relationship between *velocity* and current shallower. C_m is constant in a given cell; thus, in practice it is safe to state that, at least in a single myocyte, the velocity of depolarization (or repolarization) linearly depends on the absolute magnitude of net transmembrane current. Such a simple relation is pivotal to the understanding of action potential complexity.

To predict the effect of a specific ionic current (e.g., I_{Na}) on membrane potential the following should be considered. At each instant V_m tends to a value equal to the reversal potential of I_m (E_m), whose composition changes over time. (Before V_m achieves the reversal potential of I_m, membrane capacity needs to be filled up with charge (saturated). When a channel opens (membrane permeability changes), charge flows through it and charges capacity; the larger the current, the faster the charging process. The reversal potential (at which current is null) is truly achieved only at steady state, i.e., when the capacitor is charged to saturation.) During rest, the prevailing permeability is that for K^+. Accordingly V_m is close to E_K (e.g., −90 mV); during excitation Na^+ permeability prevails (Na^+ channels open and K^+ channels close), thus V_m quickly approaches +70 mV (fast depolarization). Thereafter, K^+ permeability increases again over Na^+ and V_m returns toward E_K (repolarization).

3.5 Maintaining Electrochemical Gradients: Membrane Transports

An alternative path for the movement of molecules through biological membranes is provided by membrane transporters. Similar to ion channels, transporters are protein molecules embedded in the phospholipid bilayer that undergoes conformational changes when exposed to energy. However, they show notable functional differences with respect to channels. These consist mainly of (1) lower and more sharply saturable transport rates, and (2) the capability, at least for "active transporters," of transporting molecules against their electrochemical gradient by using other energy sources.

The lower transport rates and complete saturability depend on the fact that the conformational change corresponds to translocation of one or few bound molecules at a time, rather than to opening of a continuous permeation path. Thus, translocation is slow and, once all the binding sites on the protein are occupied, flow cannot increase further (saturation). Flow through channels may also saturate to some extent and recent observations suggest that, under specific conditions, transporters can actually behave as ion channels. This has led us to question the ground for a sharp distinction between the two types of mechanism; nonetheless, such a distinction remains meaningful for most applications.

Active transporters can (1) directly hydrolyze ATP to ADP and use its energy to propel the transport; (primary active transport, e.g., the Na^+/K^+ pump), or (2) simultaneously transport one substance against its gradient and a different one along its gradient, with the latter providing the propulsion energy (secondary active transport, e.g., the Na^+/Ca^{2+} exchanger). In the case of secondary transport, the propelling gradient must be maintained by another active transport. For instance, by extruding Na^+, the Na^+/K^+ pump generates the inward Na^+ gradient necessary to actively extrude Ca^{2+} through the Na^+/Ca^{2+} exchanger and to actively extrude protons through the Na^+/H^+ exchanger.

If the number of charges carried in the two directions is not the same, the transport will also generate an electrical current and is said to be "electrogenic." If a transport is electrogenic it is also sensitive to V_m; in this case, as for ion channels, an electrochemical "equilibrium potential" of the transport can be measured, at which transport is null and current flow reverses. Under physiological conditions, the Na^+/K^+ pump carries outward current (I_{NaK}) throughout the electrical cycle (i.e., its equilibrium is more negative than physiological values of V_m). The Na^+/Ca^{2+} exchanger current (I_{NaCa}) is inward during diastole (corresponding to Ca^{2+} extrusion) but, due to the attending changes in cytosolic Ca^{2+} concentration, tends to reverse during systole (Ca^{2+} may enter through the exchanger, which then acts in "reverse mode"). More details on membrane transport can be found in [21].

3.6 Resting Membrane Potential

Most nerve and muscle cells and also epithelial cells have a negative resting membrane potential (V_{rest}) between −60 and −90 mV. This potential difference exists over a membrane only 5 nm thick and therefore the electrical field is very strong, in the order of 10^5 V/cm. Such a powerful electrical field will influence the behavior of single ions strongly. A constant and stable V_{rest} is needed in the working atrial and ventricular muscles that are supposed to follow a stimulus generated elsewhere.

As mentioned above, the value of V_{rest} in the working myocardium is mainly determined by the presence of an overwhelming K^+ conductance, based on the membrane current named "inward rectifier" (I_{K1}), which is open at negative potentials. High permeability to K^+ brings V_{rest} close to the K^+ equilibrium potential and effectively prevents its oscillations. Smaller contributions to V_{rest} are also made by currents generated by Na^+/K^+ and Na^+/Ca^{2+} transports. Since V_{rest} is based on the K^+ electrochemical gradient, even small increases in extracellular concentration of this ion may cause membrane depolarization (e.g., in acute ischemia). The effect of a decrease in extracellular K^+ is more complex: while it would tend to make V_{rest} more negative, it also causes a marked decrease in I_{K1} conductance, resulting in loss of polarization. The two effects balance off at a K^+ concentration of about 3 mM and V_{rest} may become very unstable at lower concentrations. This is one of the mechanisms underlying the adverse effect of hypokalemia on cardiac electrical stability and explains why severe hypokalemia (as severe hyperkalemia) is incompatible with life.

3.7 Excitability

Excitability concerns conversion of a small triggering stimulus to a large, stereotypical response (the action potential). Such a conversion implies the existence of a voltage "threshold," below which the triggering stimulus is ineffective (subliminal). Thus, membrane excitation occurs in two phases: (1) achievement of the threshold, in which the membrane passively responds to the triggering current (*electrotonic* phase); (2) autoregenerative excitation, which involves active membrane properties (i.e., voltage dependent channel gating) and becomes independent of the triggering stimulus.

Two autoregenerative processes cooperate to determine the threshold: (1) activation of an inward current (I_{Na}) and (2) removal of the outward current responsible for stabilizing diastolic potential (I_{K1}). The former is due to the positive feed-back interaction between I_{Na} and V_m. The latter depends on the peculiar voltage dependency of I_{K1}, whose conductance is dramatically decreased if V_m is depolarized to a certain extent above its resting value. This I_{K1} property, named "inward rectification," is caused by intracellular cations (polyamines, Mg^{2+} and Ca^{2+}) plugging the channel when attracted into its pore by the favorable potential gradient provided by depolarization [22–24]. I_{Na} activation and I_{K1} depression are simultaneously a cause and consequence of depolarization, as required by an autoregenerative process.

Achievement of the activation threshold (electrotonic phase) depends on both amplitude and duration of the triggering stimulus. We can understand this by realizing that the sarcolemma has both electrical resistance (R_m) and capacity (C_m). A current (I_m) injected into the membrane charges C_m along an exponential time course, to produce a steady-state voltage (V_{mSS}) given by $V_{mSS} = I_m \times R_m$). If V_{mSS} is equal to the activation threshold (liminal stimulus), excitation may require the whole charging time (several ms); on the other hand, if V_{mSS} exceeds the threshold (supraliminal stimulus), excitation may be achieved before V_{mSS} is fully developed, that is in a shorter time.

There is a relationship between the amplitude and the duration of the stimulus required to achieve excitation. This relation is named "strength-duration" curve and its steepness depends on tissue properties. The minimum stimulus amplitude which, irrespective of duration (made very long), is required for excitation is named "rheobase." The term "chronaxy" refers to the minimum effective duration of a stimulus of an amplitude twice the rheobase. Such parameters are also useful in defining the energies required to stimulate the myocardium by external sources (e.g., artificial pacemakers). At the functional level the basic concept of rheobase can be regarded as the diastolic threshold for activation. Refractory periods are normally assessed by short stimuli (e.g. 2 ms) with an amplitude twice the threshold one.

3.8 Action Potential

The ability to generate action potentials (AP) is the distinctive feature of excitable cells, for which conserved propagation of the electrical signal is a functional requirement. The AP is essentially an electrical transient, which can propagate over long distances preserving its amplitude. Such a "constancy" of the AP is achieved by basing its initiation (excitation followed by depolarization) and termination (repolarization) on autoregenerative phenomena which, once initiated, become independent of the triggering stimulus. To initiate the autoregenerative process, the triggering stimulus must achieve a "threshold" of amplitude and duration.

3.8.1 The Cardiac Action Potential Contour

The cardiac electrical cycle has been schematically divided in five "phases," four of them describing the AP contour and one the diastolic interval (Fig. 3.2).

Phase 0 refers to the autoregenerative depolarization, which occurs when the excitation threshold is exceeded. Phase 0 is supported by activation of two inward (depolarizing) currents, I_{Na} and I_{CaL}. Membrane depolarization quickly activates these channels and, with a delay of several milliseconds for I_{Na} and of tens of ms for I_{CaL}, inactivates them. Thus, membrane depolarization provides both the triggering and breaking mechanism for the autoregenerative depolarization. Although short-lived, I_{Na} is large and provides most of the charge influx required for propagation (see below). I_{CaL} has a small component with fast activation/inactivation (I_{CaT}) and a larger one with slower kinetics (I_{CaL}). I_{CaL} mediates most of Ca^{2+} influx required to trigger myocyte contraction and may support propagation under conditions in which I_{Na} is not expressed or functional (e.g., in the nodes). Phase 0 depolarization also activates K^+ currents, which contribute to

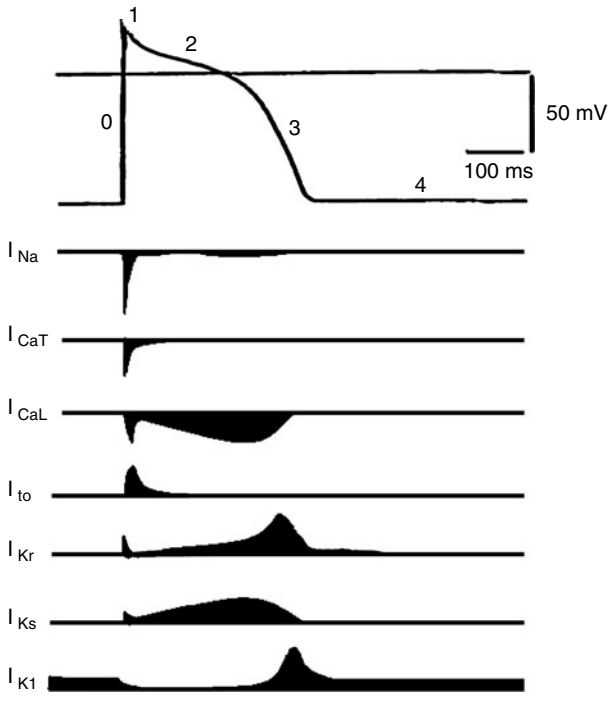

Figure 3.2

Phases of a prototypical ventricular action potential (AP) and underlying currents. The numbers refer to the 5 phases of the action potential. In each current profile the horizontal line represents the zero current level; inward currents are below the line and outward ones are above it. See text for abbreviations of the membrane currents.

its termination and to subsequent repolarization. Among these, the transient outward current (I_{to}) is sufficiently fast to limit depolarization rate during phase 0.

Phase 1 is the initial phase of repolarization, mainly supported by I_{to}. The latter is a K^+ current that, similarly to I_{Na}, is activated and quickly inactivated by depolarization. Thus, I_{to} supports fast repolarization. Recovery of I_{to} from inactivation occurs during the diastole and is slow enough to make this current poorly available at high heart rates. I_{to} is unequally expressed across the ventricular wall (see below), thus phase 1 is more prominent in subepicardial layers than in subendocardial ones [25].

Phase 2, also named AP "plateau," is the slow repolarization phase, which accounts for the peculiar configuration of the cardiac AP. The net transmembrane current flowing during phase 2 is small and it results from the algebraic summation of inward and outward components. The outward one (promoting repolarization) mainly consists of depolarization-activated K^+ currents collectively named "delayed rectifiers" (I_K). I_K is actually the sum of rapid (I_{Kr}) and slow (I_{Ks}) components, carried by separate channels with different properties and pharmacology [26]. The interplay and roles of I_{Kr} and I_{Ks} in determining repolarization rate will be discussed in more detail below. The inward phase 2 currents (opposing repolarization) are mostly carried by "window" components of I_{Na} and I_{CaL}, which flow when V_m is such that the activated state of these channels is not yet completely offset by the inactivation process. Thus, very small proportions of I_{Na} and I_{CaL} can contribute to the whole duration of phase 2 [27, 28]. Small Na^+ currents with slow inactivation gating also exist in Purkinje fibers [29]. The current generated by the operation of the Na^+/Ca^{2+} exchanger (I_{NCX}) can variably contribute to phase 2, according to the magnitude and course of the cytosolic Ca^{2+} transient and to the subsarcolemmal Na^+ levels [30].

Phase 3 is the terminal phase of repolarization, and differs from phase 2 for its faster repolarization rate. Phase 3 is dominated by I_{Kr} and I_{K1}, both characterized by a kinetic property, named "inward rectification" [23, 31, 32], suitable to support autoregenerative processes [33]. Initiation of phase 3 is probably supported by I_{Kr}, with a threshold determined

by the balance between its onset and waning of phase 2 inward currents. I_{K1} takes over during the final part of phase 3 [33, 34] and effectively "clamps" membrane potential back to its diastolic value.

Phase 4 describes membrane potential during diastole. In myocytes expressing a robust I_{K1} (e.g., atrial and ventricular myocytes), V_m is stabilized at a value close to the current reversal and a significant current source is required to re-excite the cell. On the other hand, if I_{K1} is poorly expressed (Purkinje myocytes) or absent (nodal cells) [35, 36], phase 4 becomes more positive and unstable. Under such conditions even small inward currents may cause progressive depolarization, eventually leading to re-excitation (automatic behavior) [37]. Besides the time-dependent currents, specific for each AP phase, time-independent (or "background") currents may also contribute to the whole AP course. These mainly include the Na^+/K^+ pump current (I_{NaK}) and the Na^+/Ca^{2+} exchanger current (I_{NCX}). Direction and magnitude of these currents during the various AP phases will be determined essentially by their electromotive force, which may vary according to the distribution of the transported ions across the cell membrane.

3.8.2 The Repolarization Process

3.8.2.1 Large Hearts have Long APs

Figure 3.3 (from [38]) shows that action potentials are longer at low heart rate and that their duration is somewhat proportional to heart size (short in rat and mouse, longer in rabbit, guinea-pig, dog etc.). This may be dictated by functional needs. In an electrical syncytium, such as myocardium, the direction of propagation is indifferent; thus, any point along a propagation path, unless refractory, can be re-excited by activity occurring distal to it [39]. Thus, extinction of excitation during each cycle requires that cells at any point of the propagation path remain refractory until all cells downstream

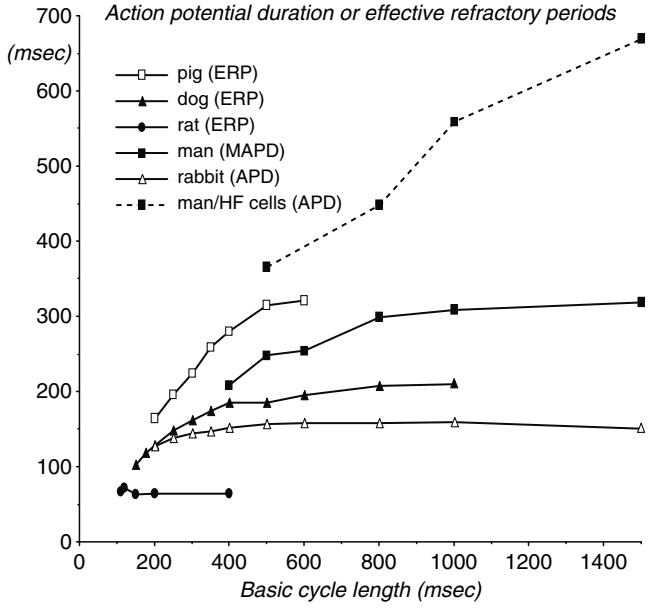

Figure 3.3

Cycle length and action potential duration (APD) or effective refractory period (ERP). Only in the rat, ERP seems independent of cycle length. In man, two relations are shown. The solid line with filled squares represents monophasic action potential duration in the normal human heart (MAPD). The dashed line with filled squares shows APD measured in single myocytes obtained from explanted hearts from patients with heart failure (HF). In heart failure, action potentials are prolonged compared to those in non-failing hearts. This is due to the combined effect of heart failure and to cell isolation which causes per se prolongation of the action potential by loss of electrotonic interaction. (See also [43]) (modified from [38]).

have been activated. In accordance with the seminal theoretical work of Wiener and Rosenblueth [40] and Moe [41], the "leading circle" theory [42] predicts that the minimum length of the propagation path at which re-excitation can occur, named wavelength (WL in cm), equals the product of refractory period (RP in s) and conduction velocity (CV in cm/s)

$$WL = RP \times CV.$$

Thus, in a large heart with a large mass, re-excitation can be prevented only by a large RP × CV product. This requirement is fulfilled in larger animals by prolonged RP, resulting from long AP duration (APD). (Since I_{Na} quickly recovers from inactivation once V_m has repolarized, the refractory period is largely determined by APD under normal conditions.) The same functional requirement justifies the observation that APD is generally longer at proximal than at distal sites along a physiological propagation path. Therefore, it is understandable that preservation of correct temporal and spatial repolarization patterns is essential for maintenance of cardiac electrical stability [43].

In addition to the fact that APD is longer in species with larger hearts, Fig. 3.3 also shows the pivotal effect of electrotonic interaction on APD. Thus, APD in *isolated* human ventricular myocytes is substantially longer than in the *intact* heart. This effect is probably much stronger than the APD prolongation caused by myocardial remodeling during the development of hypertrophy and heart failure (see also [43]).

3.8.2.2 Where Stability and Flexibility Meet

The need for repolarization stability and optimization of its synchrony contrasts with that of adapting APD to changes in heart rate, and with the existence, even during normal functioning, of numerous factors potentially perturbing the repolarization profile. (Notably those linking AP profile to mechanical activity, through Ca^{2+}-sensitivity of many among currents active during repolarization (I_{CaL}, I_{NCX}, I_{Ks}, I_{Kl})) Thus, mechanisms to buffer perturbations and to allow flexible rate-adaptation must coexist in repolarization; understanding these might help us in predicting conditions at risk of cardiac electrical instability. Some clues may be provided by considering how the properties of I_{Kr} and I_{Ks} might be suited to afford repolarization stability at different heart rates.

I_{Ks} is a repolarizing current, which when increased, tends to shorten APD; it has slow systolic activation and slow diastolic deactivation [26]. Only a small proportion of total I_{Ks} is activated during an AP and its deactivation may be incomplete during short diastolic intervals (DI). Thus, an increment in the APD/DI ratio, as the one occurring as rate is increased, allows more I_{Ks} to be activated and less to be deactivated during each cycle. This makes I_{Ks} a good tool for APD rate-adaptation, particularly in the high heart-rate range, when incomplete diastolic deactivation becomes significant [33]. However, recent reports indicate that I_{Ks} deactivation may be distinctly faster in dog [44] and man [45] than in the guinea pig [46]; therefore, the role of I_{Ks} in human rate-dependency of repolarization is controversial. I_{Ks}'s contribution to rate-adaptation is also mediated by the sensitivity of this current to ß-adrenergic stimulation [26, 47] and to increases in cytosolic Ca^{2+} [48], both conditions physiologically associated with tachycardia. APD prolongation allows for more I_{Ks} activation which, in turn, shortens APD again; thus, APD and I_{Ks} are tied in a negative feed-back loop. This points to a potential role of I_{Ks} in stabilizing APD at each cycle length and in limiting its maximal duration at long ones [49]. At the same time, this negative feed-back loop may also set a limit to the maximum amount of shortening of APD at extreme high heart rates, when the reduction of relaxation time (diastole) may exceed that of activation time (systole). Under these circumstances I_{Ks} would tend to become a steady-state current. However, it should be considered that negative feed-back loops are paradoxically prone to oscillate whenever the conditions change quickly as compared to their response time. This may result in specific forms of APD instability, such as APD alternans, facilitated by abrupt changes in heart rate [50].

As shown in recent experiments, I_{Kr} kinetic features and response to heart rate are entirely different from those described above for I_{Ks} [33]; I_{Kr} deficiency also leads to major repolarization instability [51], suggesting a complementary role for the two K^+ currents. At variance with what has initially been hypothesized [52], at high heart rates I_{Kr} conductance may increase similarly to that of I_{Ks} [33]. However, the mechanism underlying the rate-dependent enhancement is fundamentally different between the two currents. Figure 3.4 (modified from [33]) shows that the extent of I_{Kr} activation is in fact independent of the diastolic interval. APs recorded at paced cycle length of 250 ms and 1,000 ms were applied to drive the membrane as I_{Kr} was recorded under voltage clamp conditions (Fig. 3.4). In one case (left panels) APs were applied as originally recorded (i.e., with both AP profile and diastolic interval variable), in the other (right panels)

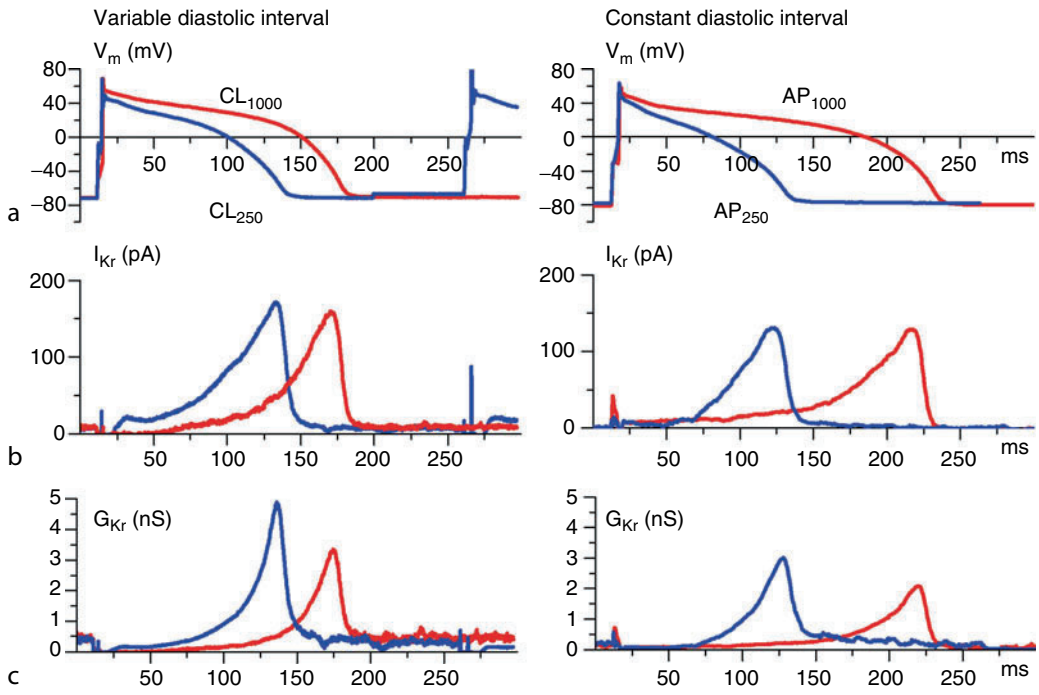

Figure 3.4

Rate-dependency of I_{Kr}. (a) each panel shows action potential waveforms recorded at cycle lengths (CL) of 250 (blue) and 1,000 (red) ms. (b) I_{Kr} recorded during repetitive application, at the appropriate CL, of the action potentials shown in A. (c) I_{Kr} conductance (G_{Kr}), obtained by dividing the traces in B by the K^+ driving force (calculated from the traces in (a)). In the right side panels, the experiment was repeated by applying the waveforms in A after adjusting the CL to keep the diastolic interval constant. A remarkable increase in I_{Kr} amplitude and speed is observed at the shorter CL, irrespective of whether the diastolic interval is changing or not. This indicates that I_{Kr} increase at shorter CL is secondary to the change in action potential shape, rather than depending on CL itself (modified from [33]).

the cycle length was adjusted to keep the diastolic interval constant. In both cases, I_{Kr} conductance (G_{Kr}) was larger and faster at the shorter cycle length. This suggests that AP profile, rather than diastolic interval, determined I_{Kr} magnitude and course. As shown in Fig. 3.5 (modified from [33]), the feature of AP profile responsible for I_{Kr} rate-dependency is actually the repolarization rate. Modeling studies suggest that dependency of I_{Kr} conductance on repolarization rate can be explained by the interplay between the processes of deactivation and recovery from inactivation [33]. Since larger I_{Kr} results in faster repolarization, I_{Kr} and APD may be tied in a positive feed-back loop, acting as an "autoregenerative" repolarization mechanism. On the other hand, as I_{Kr} increase at high rates was the consequence of APD shortening; the latter must have been initiated by other mechanisms, probably including I_{Ks}. These findings suggest complementary roles for I_{Ks} and I_{Kr} and may explain why the effects of their simultaneous inhibition are more than additive [53].

Repolarization results from a balance between outward and inward currents. Thus, the properties of inward current components are equally important in determining repolarization course. Besides their role in sustaining the AP plateau, ion movements through I_{CaL}, I_{Na} and I_{NCX} determine the Ca^{2+} flux balance across the sarcolemma. Thus, unlike outward ones, inward currents are directly involved in contractile function and in its modulation.

The feature of I_{Na} and I_{CaL} most relevant to the course of repolarization is probably the rate and extent of their inactivation during the AP plateau. Normally I_{Na} is quickly inactivated by voltage and only a *small* "window" component persists during repolarization. Since such a component is a minor proportion of activated I_{Na}, even apparently small deviations from normal inactivation properties may lead to significant increments in plateau current [54–56]. I_{CaL} inactivation is partly voltage-dependent and partly induced by subsarcolemmal Ca^{2+}, through a Ca^{2+}- binding protein (Ca-calmodulin)

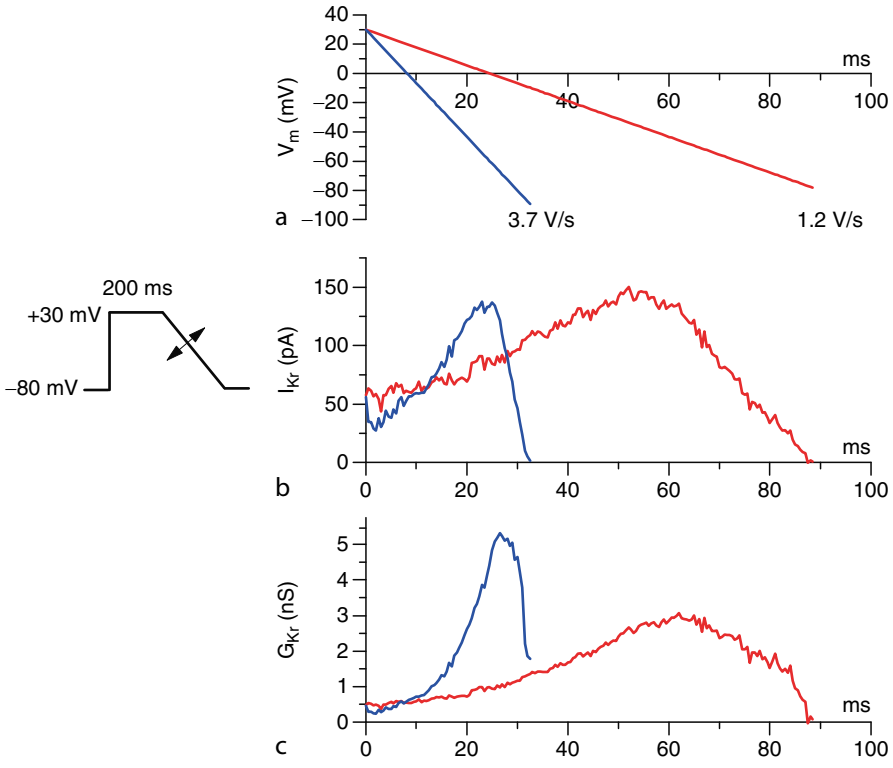

Figure 3.5

I_{Kr} dependency on repolarization rate. (a) I_{Kr} was recorded during repolarizing ramps of different velocity (voltage protocol shown in the inset). (b) I_{Kr} recorded during the two ramps. (c) I_{Kr} conductance (G_{Kr}) obtained by dividing the traces in b by the K^+ driving force (calculated from the traces in (a)) (modified from [33]).

[57, 58]. Ca^{2+}-induced I_{CaL} inactivation provides feedback regulation of Ca^{2+} influx and is part of a set of mechanisms adjusting APD to intracellular Ca^{2+} content. Changes in subsarcolemmal Ca^{2+} profile may cause major APD changes [59]. The availability of I_{CaL} during AP plateau strictly depends on the time course of membrane potential within the "window" range. Plateau prolongation may cause autoregenerative oscillatory depolarization (EADs) based on undue I_{CaL} reactivation [60]. Thus, even if intrinsically normal, I_{CaL} may amplify repolarization abnormality secondary to other causes. Finally, the direction and magnitude of I_{NCX} are sensitive to the Ca^{2+} transient profile, which may be altered in response to the needs of contractility modulation. With this in mind, inward currents seem to serve contractility requirements better than repolarization stability. Thus, for the repolarization process per se, inward currents might be viewed as a source of perturbation which, under normal conditions, is buffered by sufficiently strong outward currents.

3.9 Pacemaker Function

The high right atrium had been recognized as the "primum movens" as well as the "ultimum moriens" for over centuries. Doubt, however, has existed on the question of whether automaticity was an intrinsic property of the heart, or whether, alternatively, the heart depended on the brain for its rhythmic activity. This controversy was still not completely settled when Eyster and Meek published their famous review in the very first issue of *Physiological Reviews* [10]. The discovery of the sinus node [8] in the mole's heart by Martin Flack in the late summer of 1906, as described by Sir Arthur Keith in a historical paper dating back to 1942 [61], provided an anatomical base for the natural pacemaker of the heart. The relation between function and ultrastructure was reported in 1963 by Trautwein and Uchizono [62], although it took until 1978

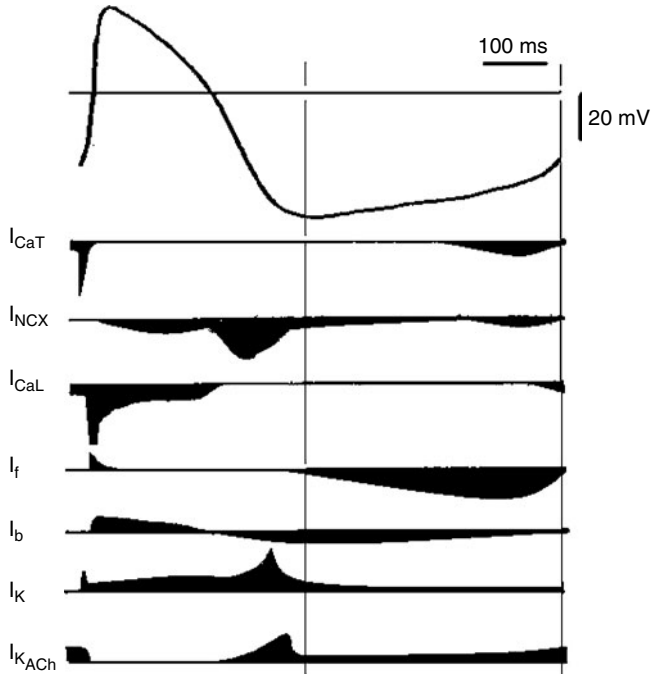

Figure 3.6

Outline of membrane currents of sinus node cells: current profiles (drawn by hand) are time aligned with the action potential. Vertical lines delimit diastolic depolarization. While the time course of currents approximates the real one, their relative magnitude may not be accurate.

before the anatomical location of myocytes, from which sinus node action potentials had been recorded, was identified by tagging through the recording electrode [63].

Cardiac cells express currents of opposite sign and different time courses (e.g., I_{CaL} and I_K), linked by a common dependency on V_m (Fig. 3.6). In such a situation the genesis of spontaneous V_m oscillations is very likely, unless there is a specific mechanism to prevent them (e.g., I_{K1} expression in non-pacemaker cells). Thus, multiple mechanisms may contribute to automaticity, and the absence of this function, rather than its presence, may be viewed as a functional specificity. This view is supported by the observation that, at early stages of maturation, all cardiac cells are spontaneously active and electrophysiological differentiation into working myocytes corresponds to the onset of I_{K1} expression [64]. This provides the theoretical ground for localized I_{K1} knock-out, obtained through genetic manipulation, as a means to artificially generate biological pacemakers in the ventricle [37].

A distinguishing feature of nodal tissues is indeed the lack of I_{K1} expression [35], which is responsible for many of the functional peculiarities of pacemaker cells. These include (1) the presence of diastolic depolarization, and (2) maximum (most negative) diastolic potentials of −60 to −40 mV, i.e., positive to those generated by a constantly high K^+ permeability. Such depolarized potentials would, per se, functionally inactivate I_{Na}; moreover, this current is also transcriptionally downregulated in the nodes, making the upstroke of their action potentials dependent on I_{CaL} (Ca^{2+}-dependent action potentials).

In light of this, it is not surprising that the attempt to identify the mechanism for the initiation of the heartbeat with a specific current has been a matter of scientific controversy in recent years [65, 66]. Nonetheless, in spite of the aspecific nature potentially underlying automaticity, pacemaker tissues (nodal and Purkinje cells) are equipped with a current, named I_f, with properties suitable to support pacemaker function and its modulation by autonomic transmitters [65]. I_f is only scantily expressed in non-pacemaker tissues and has properties which make its functional role negligible under

physiological conditions in those tissues [67, 68]. The specific role of I_f will be discussed below, along with that of other currents contributing to diastolic depolarization.

3.9.1 Currents Underlying Diastolic Depolarization and its Autonomic Modulation

The membrane currents of sinus node cells have been reviewed in detail [14, 66, 69] and are summarized in Fig. 3.6.

Diastolic depolarization occurs at a low rate, thus requiring only a small amount of net inward transmembrane current (several pA in a single SA myocyte). However, such small net inward current results from the balance of larger inward and outward components; the direct effect of an increase in inward components is acceleration of depolarization (increased sinus rate), the opposite is true in case of an increase in outward ones.

Three voltage- and time-dependent currents, I_f and I_{CaL} (inward) and I_K (outward), are active during diastolic depolarization and are modulated by autonomic transmitters. (Other currents of smaller magnitude, or not directly modulated by neurotransmitters (I_{CaT}, I_{NCX}) are present during diastolic depolarization. Their role in pacemaking is discussed in Sect. 3.9.2.) These are superimposed on time-independent (background) currents, including inward (I_b) (Several different inward background currents, potentially contributing to I_b, have been described. Dissection of I_b in its components is not essential to the understanding of pacemaking and will not be discussed further) and outward (I_{KACh}) ones.

I_f is an inward current (carried by Na^+ at diastolic potentials); when increased it accelerates diastolic depolarization. Contrary to most cardiac currents, I_f is activated by membrane hyperpolarization [65]; the more negative the diastolic potential, the larger the I_f activation. Being triggered by the preceding repolarization, I_f may contribute to initiation of diastolic depolarization [70]. Due to its peculiar voltage-dependency and kinetics, I_f may provide an efficient buffer mechanism preventing excessive slowing of sinus rate by other mechanisms (see below). I_f is directly stimulated by binding of cytosolic cAMP [71]; thus, it is reciprocally regulated by membrane receptors increasing adenylate cyclase activity (ß-adrenergic, glucagone) and decreasing it (M2-muscarinic, A1-adenosine etc.) [72, 73]. I_{CaL} plays a role both in diastolic depolarization and in the generation of the upstroke of the SA nodal AP. Thus, its inhibition may cause pacemaker slowing and arrest in central nodal cells. However, I_{CaL} activates only in the terminal portion of diastolic depolarization [70] and it is probably not involved in its initiation (but see [74]). I_{CaL} is stimulated by cAMP-dependent protein kinase (PKA) [75]. Its receptor modulation is slower (channel phosphorylation requires extra time) but is consensual to that of I_f.

At first glance, it may be surprising that I_K (an outward current) is important to support pacemaking. Indeed, its main role is to repolarize the membrane to its maximum diastolic potential. However, I_K-mediated repolarization is essential for I_f activation (see above); this accounts for the apparently paradoxical observation that I_K inhibition leads to pacemaker slowing [76]. I_K deactivation is slow, causing a decay of outward current during the whole diastolic depolarization. If summed to adequately large background inward current (I_b), such a decay would result in a progressive increase of net inward current, which might alone sustain diastolic depolarization. Such a mechanism, although not specific to pacemaker tissues, might serve a backup function in the SA node [77]. I_K is stimulated by PKA and by cytosolic Ca^{2+} [48] therefore it is enhanced by the same receptors stimulating I_{CaL}. I_K stimulation should theoretically slow the rate; however, a larger I_K leads to more I_f activation, and the net effect is hardly predictable.

I_{KACh} is an inward rectifier K^+ current, structurally and functionally similar to I_{K1} [78]. However, different from I_{K1}, I_{KACh} channels are active only in the presence of acetylcholine (or adenosine). I_{KACh} activation adds outward current during diastolic depolarization, brings it to more negative potentials and, if sufficiently large, may cause pacemaker arrest. However, I_{KACh}-induced hyperpolarization activates I_f to a larger extent, which may limit the direct depressant effect [77]. A physiological amount of vagal stimulation is accompanied by an increase in membrane conductance [79]. When a decrease of I_f would be the predominant effect of vagal stimulation, a decrease in membrane conductance, *not an increase* would be expected. This might suggest that $I_{K,Ach}$ activation constitutes the most relevant mediator of cholinergic pacemaker modulation [79]. Nonetheless, acetylcholine concentrations required to activate I_{KACh} in sinoatrial myocytes also inhibit I_f [80]. Therefore, physiological pacemaker regulation may be based on simultaneous modulation of both currents. This view is supported by model simulations. Figure 3.7 suggests that modulation of both currents may provide more efficient rate control than separate modulation of either I_{KACh} or I_f. Functional

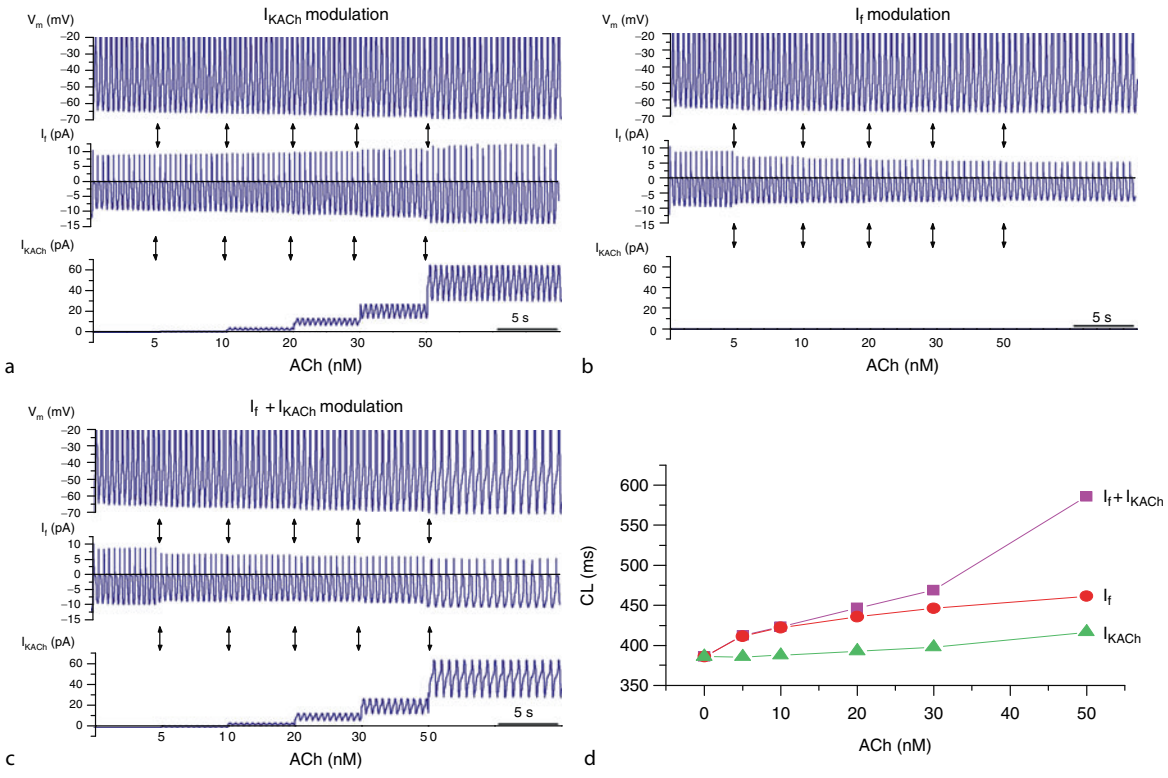

Figure 3.7

Interaction between I_{KACh} and I_f modulation by acetylcholine (ACh) in the control of pacemaker rate. Model simulations of sinoatrial pacemaking (Oxsoft Heart model [Noble D. *Oxsoft Heart 4.8 Program Manual*. Oxford, UK: Oxsoft Ltd. 1997]) considering the action of ACh as I_{KACh} activation only (a), I_f inhibition only (b) and combined I_{KACh} and I_f modulation (c). In each panel the top trace shows membrane potential (shown only negative to −20 mV to illustrate changes in maximum diastolic potential), the middle trace I_f and the bottom trace I_{KACh}. Vertical arrows mark the change in ACh concentration. (d) Pacemaker cycle length is plotted vs. ACh concentration for the three simulations. ACh effect on I_{KACh} and I_f was simulated according to the quantitative data in [80]. The simulation shows that coupled modulation of the two currents is required to modulate CL on a wide range of ACh concentrations. In particular, the effect of I_{KACh} modulation alone is very small because it is offset by the increase in I_f, secondary to membrane hyperpolarization (A. Zaza, unpublished data).

coupling between the two currents is probably instrumental in a wide-range and fail-safe regulation of sinus rate by vagal activation.

Controversy on the role of each of the above currents in SA pacemaking (I_f and I_{CaL}) largely stems from the observation that pharmacological blockade of either of them may fail to suppress diastolic depolarization. This is not only true for I_f [81], but under conditions of Ca^{2+}-independent excitability, true also for I_{CaL} [14]. On the one hand this may reflect the existence, within SA myocytes, of multiple pacemaker mechanisms, possibly taking over when one is abolished. On the other hand, this might also be the consequence of fail-safe mechanisms, determined by the kinetic properties of pacemaker currents. Figure 3.8 shows model simulations in which I_f was deliberately made essential for diastolic depolarization. The model predicts that even after 80% I_f blockade, pacemaker activity and its cholinergic modulation would still be preserved. While the mechanisms underlying this surprising observation are discussed elsewhere [82], this demonstrates that the interpretation of the effects of current blockade on cellular electrical activity may be quite complex.

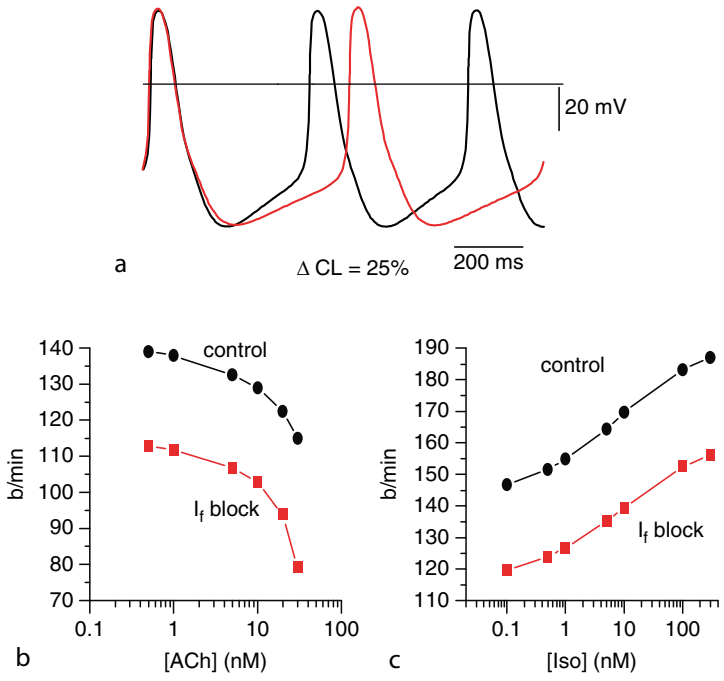

Figure 3.8

Effect of I_f blockade on pacemaker rate and its modulation in an I_f –dependent pacemaker model. Model (Oxsoft Heart [Noble D. *Oxsoft Heart 4.8 Program Manual*. Oxford, UK: Oxsoft Ltd. 1997]) parameters were set to obtain complete pacemaker arrest in the presence of 100% I_f inhibition (I_f-dependent pacemaking). (a) I_f inhibition by 80% (red trace, e.g., by 2 mM Cs^+) caused only 25% prolongation of cycle length (similar to the change experimentally observed with 2 mM Cs^+). (b) Pacemaker rate changes induced by ACh under control conditions and in the presence of 80% I_f blockade. ACh effects simulated by I_f and I_{KACh} modulation as in Fig. 3.7. (c) Pacemaker rate changes induced by ß-receptor stimulation with isoprenaline (Iso) under control conditions and in the presence of 80% I_f blockade. Iso effects simulated by I_f and I_{CaL} modulation according to the quantitative data in [72]. The simulation shows that such a large amount of I_f blockade results in only a moderate decrease in pacemaker rate, and preservation of its autonomic modulation, although full blockade of I_f causes quiescence. (A. Zaza, unpublished data).

3.9.2 Intracellular Ca^{2+}-Dynamics may Contribute to Pacemaking

Pacemaker function of various cardiac tissues, including SA myocytes, is inhibited by ryanodine, an alkaloid which blocks Ca^{2+} release from the sarcoplasmic reticulum. This observation has raised interest in the role of intracellular Ca^{2+} dynamics in the genesis and modulation of SA pacemaking. Earlier reports of ryanodine effects have been followed by confocal microscopy studies establishing temporal and causal relationship between (1) voltage-dependent activation of sarcolemmal I_{CaT} during diastole, (2) a small "pre-systolic" Ca^{2+} release from the sarcoplasmic reticulum, and (3) the genesis of a slow inward current transient, crucially contributing to achievement of the SA activation threshold [83]. As for other Ca^{2+}-dependent membrane potential oscillations, in this case the Na^+/Ca^{2+} exchanger may also be primarily involved in coupling the pre-systolic SR Ca^{2+} release to the genesis of inward current transient [84, 85]. The contribution of the SR to SA pacemaker activity has been further extended by more recent studies suggesting that pre-systolic SR Ca^{2+} release may even occur as part of an oscillatory phenomenon, intrinsic to SR and independent of voltage-gated activation of sarcolemmal Ca^{2+} channels. A direct role of the "SR Ca^{2+} oscillator" in the pacemaker activity is suggested by correlation between the intrinsic frequencies of the two phenomena [86]. While SR-based pacemakers are common in smooth muscle cells, this represents the first example of such a mechanism in cardiac muscle.

Inhibition of SR Ca^{2+} release by ryanodine has also been reported to abolish ß-adrenergic receptor (ß-AR) modulation of pacemaker rate [87]. Although this finding is consistent with the important effect of ß-AR on SR function, it does not imply that adrenergic modulation of pacemaker rate may entirely occur through SR modulation. Indeed, sarcolemmal currents involved in pacemaker control (I_f, I_{CaL}) are altered by the change in cytosolic Ca^{2+} caused by ryanodine by beta AR.

The finding of a role for SR in pacemaking has potentially important pathophysiological implications because SR dysfunction is common in cardiac disease and possibly part of the maladaptive response associated with myocardial hypertrophy/failure. Nonetheless, the emphasis recently put on this novel pacemaker mechanism should not lead to the conclusion that SR-mediated phenomena are the only relevant mechanism in the genesis and modulation of sinoatrial automaticity.

3.9.3 Redundancy and Safety Factor in Pacemaking

As described above, redundancy in pacemaking mechanisms may be intrinsic to each myocyte. Nonetheless, a further factor in pacemaker safety is probably how the sinus node cells communicate with each other and with the surrounding atrium. The interest in the specificity in SA intercellular coupling stems from the apparent disproportion between the small excitation source, provided by the SA node, and the large current sink (electrical load) imposed on it by the surrounding atrial tissue, to which the impulse must propagate. Moreover, in the presence of low resistance coupling, quiescent and more polarized atrial myocytes would tend to "clamp" SA myocyte potential, thus preventing diastolic depolarization. This makes the coexistence of pacemaking and sinoatrial synchronization and conduction towards the atrium an apparent mystery.

As in the whole heart, gap junctions are a prerequisite for conduction in the SA node. Still, it has been argued that the spread of activation within the sinus node should be regarded as synchronization rather than as conduction [88]. Semantics or not, the resistance for intercellular current spread is high in the sinus node centre, mainly due to low density of gap junctions [89]. Moreover, at variance with working myocardium, smaller sinus node cells from the (putative) primary pacemaker area virtually lack connexin43. Their gap junctions are made of connexin40 and connexin45 proteins only [90]. Honjo et al. [90] have found, however, that larger sinoatrial cells from the (putative) more peripheral area – relevant for communication with the surrounding atrial muscle- express connexin45 and connexin43. Connexin45 has a lower unitary conductance than connexin43 [7]. As a consequence the "space constant" in the sinus node is around 300–500 µm, as compared to several mm in Purkinje fibers. This implies that pacemaker cells within the sinus node centre do not "see" much of their surroundings. From the central, primary pacemaker region, towards the periphery, the density of gap junction increases [91], thus establishing the lower resistance connection required for effective sinoatrial propagation. Centrifugal changes in the densities of intrinsic membrane currents [14] and gap junctions [91] predict that the "space constant" might be different according to the direction of propagation (node to atrium vs atrium to node); this prediction awaits experimental confirmation. This special feature is, however, functionally exemplified by the fact that the centre of the sinus node is "blind" to the effects of atrial fibrillation. Indeed, during this arrhythmia, central nodal cells continue their regular spontaneous discharge, unaffected by neighboring chaotic activity occurring at cycle lengths as short as 100 ms [92]. Thus, the delicate requirement to reconcile pacemaking with sinoatrial propagation is solved by a suitable arrangement of intercellular coupling, still adequate for pacemaker synchronization, but limiting the influence of atrial tissue. Nonetheless, coupling of the sinus node to the right atrium does slow pacemaker rate, as demonstrated experimentally [93, 94] and in computer simulations [95]. I_f response to membrane hyperpolarization (see above) contributes to the limiting of such an effect.

3.9.4 Functional Inhomogeneity in the Sinus Node

One of the most intriguing features of the sinus node is that its intrinsic cycle length is remarkably constant, although this is not the case with respect to its individual myocytes. Thus, isolated sinus node cells show substantial beat-to-beat

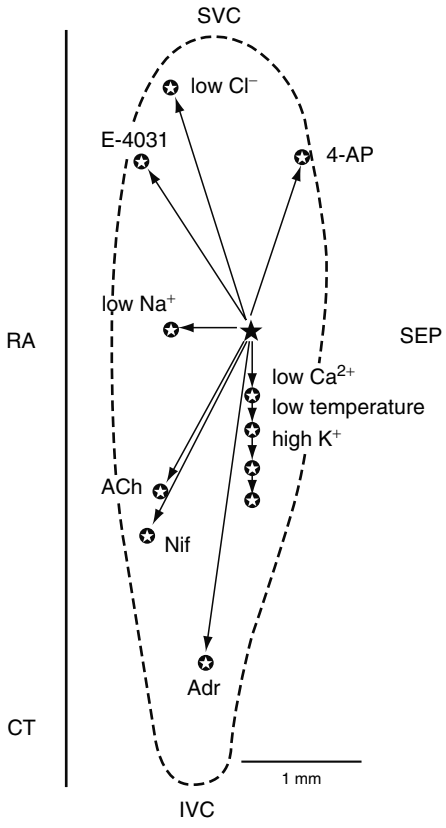

Figure 3.9

Shifts in pacemaker location within the sinus node. Scheme of (rabbit) sinus node with primary pacemaker location (asterisk). Arrows indicate shift of the site of pacemaker dominance under various conditions: SVC: superior vena cava; SEP: interatrial septum; IVC: inferior vena cava; CT: crista terminalis; RA: right atrium; E-4031: blocker of the rapid component of delayed rectifier current (I_{Kr}); 4-AP: 4-aminopyridine (blocker of transient outward current (I_{to})); Adr: adrenaline; Nif: nifedipine (blocker of L-type Ca^{2+} current); Ach: acetylcholine. Based on [14] and [97]. Reproduced from [14] with permission from Elsevier Science.

variability [93, 96] but this irregularity already disappears in clusters of sinus node cells of less than 1 mm × 1 mm [93, 94]. Sinus node cells in small clusters have shorter action potentials than in the intact node [93]. The intact sinus node is in fact an inhomogeneous mixture of cells with different responses to environmental changes. A larger number of sinus nodal myocytes is not only required to obtain beat-to-beat regularity, but also to expand the frequency range of beating. Changes in the ionic composition of the extracellular fluid, drugs and autonomic stimulation induce pacemaker shifts between different areas within the sinus node [14, 97] with different pacemaker rates (Fig. 3.9, from [14]). This probably reflects not only the presence, within the node, of cell populations with different channel expression and receptor density, but also the presence of inhomogeneity in innervation. The functional implication is that, the whole sinus node is capable of producing a larger range of cycle lengths than individual sinus node cell. Also, an intact heterogeneous sinus node may produce a larger cycle length range than an homogeneous one. Positive chronotropy results from myocytes with the highest sensitivity to the applied agent, f.e. noradrenalin. Negative chronotropy by vagal activation results from shift of pacemaking from the area with highest intrinsic rate to another one with lower intrinsic rate, but less sensitive to the depressant effect of acetylcholine [98, 99] (see also Fig. 3.9). The chronotropic response of the intact sinus node cannot be deduced from the chronotropic responses of its constituent cells [97–99].

3.9.5 Abnormal Automaticity

Abnormal automaticity is defined as the occurrence of spontaneous firing in cardiac cells which are normally quiescent (e.g., working atrial and ventricular myocytes). Since such cells lack the mechanisms underlying physiological pacemaker function, abnormal automaticity is based on different mechanisms, put into action by pathological conditions. A common cause of abnormal automaticity is partial membrane depolarization, to a range of potentials at which I_{K1} conductance is reduced. Under such conditions, diastolic potential becomes unstable and is likely to be driven by mechanisms which are normally silenced. Such mechanisms may be based on the interplay between time- and voltage-dependent currents with opposite signs, such as I_{CaL} and I_K and on Ca^{2+} -activated currents. The intrinsic rate of an abnormal focus based on such mechanisms is generally proportional to the degree of membrane depolarization [100]. It has been recently observed that in hypertrophic ventricular myocytes I_f may be expressed at an abnormally high density and with kinetic properties [101] favoring its role in pacemaker activity. Thus it is possible that, under specific pathological conditions, I_f may contribute to abnormal automaticity.

Action potentials resulting from abnormal automaticity generally arise in partially depolarized membranes, in which I_{Na} is partially or completely inactivated. Thus, depending on the extent of I_{Na} inactivation, their upstroke may be partially or completely dependent on I_{CaL} [102]. Accordingly, abnormal automaticity is often suppressed by Ca^{2+} channel inhibition.

If abnormal automaticity occurs at a rate exceeding the sinoatrial one, the automatic focus becomes the dominant pacemaker and its activity may be propagated to the whole heart. If the abnormal automatic rate is lower than the sinoatrial one, its discharge can become manifest only if the automatic focus is protected from resetting by the dominant activity. This may occur through a unidirectional "entry block," which prevents propagation of sinoatrial activity to the abnormal focus, but allows propagation of abnormal activity to the surrounding myocardium. Even if reset by sinoatrial activity (i.e., in the absence of entry block), abnormal foci are less sensitive to overdrive suppression than normal pacemaker tissue [103]. They may therefore become active during slow heart rate and are not easily overdriven when the sinus node resumes its activity. Low rate abnormal automaticity is a common mechanism of "parasystolic" arrhythmias and "escape" ventricular beats. Due to its dependency on Ca^{2+} current, abnormal automaticity is strongly enhanced by ß-adrenergic stimulation.

Subacute and chronic myocardial infarction are probably the conditions in which abnormal automaticity is most common and a frequent cause of arrhythmia [39]. Tissue at the junction between the pulmonary veins and the left atrium is particularly prone to abnormal automaticity [104]. Its role in triggering atrial fibrillation has been recently identified with a major impact on the therapeutic approach to this arrhythmia [105].

3.10 Ionic Homeostasis and Electrical Activity

Bioelectricity constitutes by far the fastest communication system of the body. Action potentials come with a price. They disturb the ionic homeostasis, which has ultimately to be corrected by the Na^+/K^+ pump at the dispense of metabolic energy. The disturbance of the homeostasis is surprisingly small. If we consider a cylindrical myocyte with a length of 100 µm and a diameter of 20 µm, we arrive at a cellular surface of 6,912 μm^2 and a cellular volume of 31, 416 μm^3. The surface is necessary for the calculation of the number of ions that pass the membrane during the action potential upstroke, which can be considered as a depolarizing step of 100 mV. We need the volume in order to calculate the disturbance of the cellular Na^+ concentration under the assumption that all depolarizing current is carried by Na^+ ions. The amount of charge related to an upstroke of the action potential can be calculated with

$$Q = C \times V$$

in which Q is charge in coulomb (C), C is cell capacitance in farad (F) and V is voltage in volt (V). The typical capacitance of cellular membranes is 1 $\mu F/cm^2$. Thus, with the above cellular surface of 6,912 μm^2, the capacitance of one myocyte is 6.9×10^{-11} F. Here we have neglected the effect of caveolae on the cell surface, which might double it. Because the amplitude of the action potential (100 mV) equals 0.1 V, we obtain a total charge (see formula) of 6.9×10^{-12} C. Because the passage of the membrane by 1 mol equals a charge of 96,500 C (Faraday constant), the amount of 6.9×10^{-12} C is carried by 7.2×10^{-17} mol of Na^+ ions. Multiplying by the number of Avogadro (6.022×10^{23}, i.e., the number of ions

or molecules in 1 mol) then yields the number of Na^+ ions that passes the sarcolemma of a myocyte with a length of 100 µm and a width of 20 µm during the upstroke of an action potential with an amplitude of 100 mV. This number amounts to 43 million. The number may seem impressive, but in a cellular volume of 31,416 μm^3 (see above), which equals 3.14×10^{-11} L, these 43 million Na^+ ions only increase the intracellular Na^+ concentration by 2.3 µM. Given the intracellular Na^+ concentration of 10 mM, one action potential results in an increase of 0.02% in the intracellular Na^+ concentration. Thus, assuming for the sake of simplicity that the action potential configuration does not change over time, the intracellular Na^+ concentration would double after 5,000 action potentials, that is, after more than one hour at normal heart rate, if this "extra" Na^+ were not pumped back by the Na^+/K^+ pump.

Although the concentration increase of Na^+ (2.3 µM) per action potential is small compared with the normal Na^+ concentration (10 mM), this concentration step is substantial compared with both the systolic and diastolic intracellular Ca^{2+} concentrations, which are at and below the micromolar level.

3.11 Region-Specific Currents

While the nodes represent the most striking case of functional specificity within the heart, relevant differences in action potential shape and underlying currents also characterize other cardiac tissues. Rather than providing a systematic description of regional variations in electrical activity, the aim of this section is to illustrate some examples of major pathophysiological relevance.

3.11.1 Receptor-Activated Current (I_{KACh}) Replaces I_{K1} in the Nodes and is Highly Expressed in the Atria

As discussed above, I_{K1} is responsible for diastolic membrane potential stability in working myocardium and its absence from nodal tissues is instrumental to pacemaker function. Nonetheless, all atrial tissues (including the nodes) express at high density I_{KACh}, an inward-rectifier current strictly related to I_{K1} in terms of channel structure and function [78]. However, unlike I_{K1} constitutive activation, I_{KACh} is turned on by the binding of acetylcholine or adenosine to M2 and A1 receptors respectively. Activation occurs through direct channel interaction with beta-gamma subunits of receptor coupled G-proteins (G_i or G_o) [106]. I_{KACh} activation leads to substantial hyperpolarization of the diastolic potential and decreased membrane input resistance, both contributing to lower excitability, and APD shortening. This translates into negative chronotropic and dromotropic effects in nodal myocytes and reduced refractoriness in the atria. Recent reports suggest that I_{KACh} channels are also present in ventricular myocytes, but their functional expression is limited by competition with other K^+ currents (e.g., I_{K1}) for a common pool of subsarcolemmal K^+ [107]. I_{KACh} function also depends on PKA-mediated phosphorylation [108] and on the availability of a membrane phospholipid component (PIP2), which is a substrate of phospholipase C (PLC). Accordingly, I_{KACh} availability is limited by PLC activating receptors (endothelin, angiotensin, α-adrenergic, etc.) that consume PIP2 [109].

3.11.2 Different Delayed Rectifier Currents Underlie Repolarization in the Atria

Atrial repolarization, characterized by a prominent phase 1, is distinctly faster than ventricular repolarization. This suggests differences in the expression of repolarizing currents. I_{to} and two components of delayed-rectifier current, with properties similar to I_{Ks} and I_{Kr} in the ventricle, have been described in canine [110] and human atrial myocytes [111]. However, atrial myocytes also express an additional depolarization activated K^+ current characterized by (1) fast activation and deactivation; (2) slow and only partial inactivation; (3) sensitivity to low (µM) 4-aminopyridine concentrations. Currents with such properties have been identified in animal and human atrial myocyte by different groups and named I_{sus} [112], I_{Kur} [113], and I_{so} [114]. Despite slightly different properties, possibly due to different recording conditions, all these currents are probably carried by the same channel protein $K_v1.5$. Due to its kinetic properties I_{Kur} may contribute to the whole repolarization process. Since its amplitude is reduced at high stimulation rates [115], I_{Kur} probably does not play a role in rate-dependent APD shortening. In terms of molecular nature, I_{Kur} is closer to I_{to}, with which it shares

pharmacological properties, than to ventricular delayed rectifiers. This provides the rationale for targeting I_{Kur} as a tool for selective prolongation of atrial repolarization.

3.11.3 Differential Expression of K^+ Currents Generates a Gradient of Electrophysiological Properties Across the Ventricular Wall

In subepicardial layers phase 1 is prominent and results in a "spike and dome" AP morphology, which is at variance with subendocardial layers, in which the repolarization course is more monotonic [25]. As a consequence, a significant gradient of action potential morphologies exists across the ventricular wall [116]. Different phase 1 amplitude is the consequence of a gradient in functional I_{to} expression, resulting from non-uniform distribution of a functionally essential channel subunit [117]. Electrical heterogeneity across the ventricular wall is also contributed by lower expression of I_{Ks} in midmyocardial layers [118], albeit established at non-physiological conditions. Myocytes isolated from these layers (M cells) are characterized by a particularly steep rate-dependency of repolarization, with marked APD prolongation at long CLs [119]. Lack of I_{Ks} also makes isolated M cells susceptible to develop early afterdepolarizations during sympathetic activation. The functional significance of these transmural inhomogeneities has been subject to vigorous debate even in the dog, the species in which M cells have been extensively investigated [120, 121]. Recently, Janse and coworkers, in a study performed with high density recording over and within the wall, showed that transmural repolarization is remarkably synchronous in the canine left ventricle [122]. The role of M cells in the human heart has only been assessed in a very limited number of studies. M cells have been identified in the human wedge preparation [123], but not in whole human hearts [124, 125], and also not in a larger wedge preparation obtained from the human heart [125]. A midmural zenith in action potential duration cannot be demonstrated in the left human ventricle [124], let alone a midmural zenith in repolarization time [125]. Although the electrical peculiarity of M cells may be less apparent within the myocardial syncytium, they may become functionally important in the presence of I_{Kr} blockers, when they have been suggested to lead to repolarization abnormalities [121]. However, even under such challenging conditions the role of M cells has been questioned [126]. While methodological differences might contribute to the discrepancy between these studies, the contribution of M cells to overall cardiac repolarization remains controversial. Overall, intercellular coupling (electrotonic interaction) seems to substantially blunt repolarization heterogeneity within the ventricular wall. This may be particularly true in larger species, including man, with long action potential duration and relatively high membrane resistance during repolarization, which in turn, is likely to increase intercellular communication (see below) [43, 125].

3.12 Cardiac Channel Proteins

The molecular identity of most cardiac ion channels has been identified; the corresponding proteins have been cloned and can be expressed by heterologous transfection in various cell types [127]. Many functional studies are nowadays performed on heterologously expressed channel clones, whose nomenclature is often unrelated to that of the native current. Table 3.1 summarizes the correspondence between each native current and its molecular counterpart (see also [128]).

Each functional channel results from the interaction between several proteins (subunits): an α-subunit, usually including permeation and gating structures, and one or more β-subunits, which confer to the channel specific kinetic and pharmacological properties. Within the cell membrane, α-subunits are generally clustered in tetramers. The latter may be composed by a single (homeotetramers) or different (heterotetramers) isoforms of the protein, often resulting in different functional properties [129]. In many instances, expression of the cloned proteins does not precisely reproduce the functional properties of the native current. This is true even if all the α- and β-subunits known to contribute to the channel are coexpressed. Moreover, function of a channel clone can change according to the cell type in which it is expressed [130], to reflect the multiplicity of factors contributing to the function of the native channel. Nonetheless, functional changes induced by drugs or structural abnormalities (mutations) in cloned channels expressed in mammalian cell lines have been thus far reasonably predictive of those occurring in native ones [131]. Thus, as long as its intrinsic limitations are duly considered, heterologous expression of channel clones is a useful tool for electrophysiological studies.

Table 3.1

Correspondence between cardiac ionic currents and channel proteins

Current	α-subunit(s)	β-subunits	Notes
I_{Na}	$Na_V1.5$ (SC5NA)	$\beta1$, $\beta2$, $\beta3$	TTX-sensitive type
I_{CaT}	$Ca_V3.1$ (α_{1G})	$\gamma6$	Mainly in nodes
I_{CaL}	$Ca_V1.2$ (α_{1C}), $Ca_V1.3$ (α_{1D})	ß, γ, δ	$Ca_V1.3$ in nodes
I_f	HCN1 + HCN4	MiRP1 (KCNE2)	Specific for pacemaker tissues
I_{K1}	$K_{ir}2.1$ (IRK1)	$K_{ir}2.2$	"Inward rectifier"
I_{KATP}	$K_{ir}6.2$	SUR	Inactive at physiological [ATP]
I_{KACh} (I_{Kado})	$K_{ir}3.4$ (GIRK4) + $K_{ir}3.1$ (GIRK1)		Activated by ACh or adenosine; mostly atrial and nodal
I_{to}	$K_V4.2$ + $K_v4.3$	KChIP2	Mainly subepicardial
I_{Kur} (I_{Ksus})	$K_V1.5$	KChAP, $K_V\beta_1$, $K_V\beta_2$	Specific for atrium
I_{Kr}	$K_V11.1$(HERG)	MiRP1 (KCNE2)	Rapid "delayed rectifier"
I_{Ks}	K_V 7.1(KVLQT1)	minK (KCNE1)	Slow "delayed rectifier"
I_{NCX} (I_{TI})	NCX1		Na^+/Ca^{2+} exchanger current
I_{NaK}	NaK α 1,2,3	$\beta1$, $\beta2$	Na^+/K^+ pump current
I_{GJ}	Cx43 (ventricle), Cx40, Cx45 (nodes)		Gap-junctional current

Denomination of α-subunits according to the IUPHAR compendium of voltage-gated ion channels [128]. Other frequently used denominations in parentheses

3.13 Propagation

3.13.1 General Mechanism of Propagation

If considered in detail, propagation of excitation through the heart is very complex, as described in some excellent reviews by Kléber, Janse and Fast [132], and Kléber and Rudy [133]. Nonetheless, a relatively simple description of its basic principles is possible and very useful for the understanding of cardiac pathophysiology.

During propagation there is a difference in membrane potential between the excited myocytes (i.e., the site of an action potential) and the still unexcited neighboring one. This difference defines the "activation front." Let us suppose that an activation front moves from left to right through a strand of myocytes. At the left the inside of the myocytes is positively charged (due to inward current of Na^+ ions from the extracellular space into the intracellular space), whereas the inside of the not yet excited myocytes is still at the resting membrane potential of about −90 mV. This potential difference causes an intracellular current flow along the cell axis and through gap junctions, i.e., the positive charge moves from the excited cell to the unexcited one. At the same time, in the extracellular space a current flows in the opposite direction; this is because the extracellular side of the excitation site is made negative by the movement of Na^+ ions into the cell. To summarize, during propagation, local current moves forward through the intracellular space and backward in the extracellular space, forming a complete "propagation circuit." As a result of intracellular current positive charge accumulates under the membrane of the cell to be excited and depolarizes it to the excitation threshold; this triggers a new autoregenerative I_{Na} activation (action potential). The latter, in turn, serves as the "source" of charge for excitation of the next cell and the process is repeated. In this process, the cell(s) to be excited can be viewed as the electrical "load" to be imposed on the charge "source." The relevant parameter is actually the amount of membrane capacity to be charged, which directly depends on the area of membrane electrically coupled to the source. For propagation to occur, the charge supplied by the source must at least match the charge required by the load. Under physiological conditions, the former largely exceeds the latter; such a redundancy of the system is important in establishing a "safety factor" for propagation, which may prevent the occurrence of conduction block in a wide range of conditions.

Propagation is characterized by its "conduction velocity" (in cm/s) and the "safety factor," which we consider in more detail in the next two subsections.

3.13.2 Conduction Velocity

The speed at which the activation front travels essentially depends on how many cells along the propagation path can be simultaneously excited by the charge supplied by the "source." This, in turn depends on (1) the amount of source charge (I_{Na} density in working myocardium and I_{CaL} density in the nodes), and (2) how far along the cell axis charge can travel without being dissipated to the extracellular space. According to cable theory, the latter can be characterized by the ratio between specific membrane resistance (R_m, in $\Omega \cdot m^2$) and specific axial resistance (R_i, in $\Omega \cdot m$) (R_m and R_i are expressed here with the conventional units of "specific resistance". The term a/2 is omitted if R_m is specific resistance per circumference unit ($\Omega \cdot m$) and R_i is specific resistance per cross-sectional area (Ω/m)) and is defined by a parameter named "space constant" (λ):

$$\lambda \sim \sqrt{\{(R_m/R_i) \times (a/2)\}}$$

where a is the radius of the cable and λ is the distance over which the amplitude of a small voltage deflection has decayed to 37% of its original value. R_m essentially depends on how many membrane ion channels are open, whereas R_i is determined by the sum of cytoplasmic, gap junctional, and extracellular resistances.

In the sinus node, R_m is high due to the absence of I_{K1}; however this is off-set by a high R_i due to the low density and conductance of gap junctions, thus resulting in a small λ ($\leq$0.5 mm). In the Purkinje system, in which I_{K1} is small compared with the working ventricular myocardium, but large compared with the sinus node, and in which the gap junctional density is high, λ can be in the order of several mm, substantially larger than in the working myocardium. It should be noted that, for technical and theoretical reasons, λ is measured only at the resting membrane potential [134], at which R_m is substantially different than during an action potential. For instance, during the upstroke of the action potential R_m is smaller, due to the massive opening of Na^+ channels; during the plateau phase and early repolarization R_m is higher (no I_{K1}, small currents). This predicts that λ may be maximal, thus supporting optimal electrotonic interaction, during the action potential plateau and the early phase of repolarization. The fact that electrotonic interaction may be lower in smaller animals (e.g., rodents) due to their shorter action potential duration, caused by larger repolarizing currents and leading to a smaller R_m during repolarization, is starting to be recognized [43, 135].

An important consequence of the role of gap junctional resistance is that it creates a physiologically relevant difference in velocity between propagation parallel to cell orientation (longitudinal propagation) or perpendicular to it (transverse propagation). This difference is named "electrical anisotropy" and can be explained as follows. Cardiac myocytes are elongated (about 70–100 µm long and 10–20 µm wide); when packed in the tissue they can establish side-to-side and end-to-end connections. Thus axial current will travel in both directions. However, to travel the same tissue distance (e.g., 1 cm), current must cross about fivefold more cell borders (i.e., gap junctions) in the transverse than in the longitudinal direction. Gap junctions are "in series" with respect to axial current flow, which implies that their individual resistances are summed. Thus as far as the contribution of gap junctions in R_i (specific axial resistance; sum of cytoplasmic, gap junctional, and extracellular resistances) is involved, it can be expected that conduction velocity is lower in transversal than in longitudinal direction. Variation in the density of gap junction expression and more complex arrangement of cells (e.g., end-to-side connections) may also contribute to determine the anisotropy ratio. Measured anisotropy ratio is about 2.7 in dog [132], but it might be substantially less in human ventricle, where these simple measurements are surprisingly scarce [136]. An anisotropy ratio even larger than predicted by tissue geometry may reflect propagation "discontinuity" [137], resulting in junctional delays larger than predicted for continuous propagation.

These considerations have an interesting bearing on conduction velocity in hypertrophy and heart failure. Both are in general associated with delayed conduction [138], which is often considered to be the result of decreased conduction velocity. However, hypertrophy per se (increase in cell size), results in a smaller number of junctions per unit length of the propagation path. Thus, as long as no factors other than cellular dimensions change during hypertrophy, an increase and *not* a decrease, in tissue conduction velocity is expected, as was recently confirmed experimentally [139]. Under such circumstances an observed conduction delay is explained by increased cardiac mass, which is insufficiently compensated for by *increased* conduction velocity. On the other hand, at more severe stages of hypertrophy, concomitant interstitial fibrosis and changes in gap junction expression may cause a decrease in conduction velocity itself. Further pathological changes in the density of membrane channels, also known as remodeling, may exacerbate this process.

Besides electrotonic interaction, conduction velocity is also affected by the magnitude of the current source, which is substantially larger for I_{Na} than for I_{CaL}. Thus, differential expression of these currents contributes to the large difference in conduction velocity among cardiac tissues. Longitudinal conduction velocities are in the order of 2 and 5 cm/s in SA and AV nodes respectively, and around 60 cm/s in atrial and ventricular working myocardium. In specialized conducting tissues conduction velocity is higher; values of 100 and 130 cm/s can be measured in crista terminalis and Bachman's bundle respectively and 200–300 cm/s in Purkinje fibers [132].

3.13.3 Safety Factor of Propagation

As introduced above, the propagation safety factor is determined by the ratio between the electrical charge supplied by the "source" and that required by the "load" [132, 133, 140]. The former is primarily determined by the magnitude of depolarizing current (I_{Na} in the working myocardium and Purkinje, I_{CaL} in the nodes) available at a given time. The latter is determined by the electrical capacity to be charged, physically represented by the membrane area electrically coupled to the source. Under physiological conditions, the current size available in a single cell is large enough to charge the membrane capacity of the cell itself plus a number of connected cells.

Source/load mismatch can result from (1) depression of I_{Na} (or I_{CaL} in the nodes), by incomplete recovery from inactivation (partial membrane depolarization, extrasystoles falling in the relative refractory period etc.), drugs or genetic defects with loss of function (e.g., the LQT3 syndrome), and (2) tissue geometry such as to impose a large load on a small source. Illustrative examples of the latter are discrete Purkinje-myocardial junctions, at which a small number of Purkinje cells are coupled to a relatively large mass of underlying myocardium (i.e., a large membrane capacity). Under such circumstances the safety factor is low for orthodromic and high for antidromic propagation, setting the stage for the occurrence of unidirectional conduction block. In the case of the Purkinje-myocardial junction the potential source/load mismatch is compensated by a very high expression of Na^+ channels and long action potential duration in Purkinje cells. However, under pathological conditions, a similar tissue geometry may be generated by patchy fibrosis, producing expanses of myocardium connected by relatively thin bundles of excitable tissue. In this case compensatory mechanisms are absent and arrhythmias resulting from unidirectional block (reentry) are greatly facilitated.

Although safety factor and conduction velocity are affected in the same direction by several factors (e.g., I_{Na} magnitude), their changes are not always consensual. Indeed, an increase in gap junctional resistance decreases conduction velocity (smaller λ), but may simultaneously increase the safety factor [141]. This is because the effective membrane capacity "seen" by the source decreases when coupling resistance increases [142]. This is the mechanism underlying the observation that, although longitudinal propagation is faster, depression of I_{Na} may lead to blocking of longitudinal propagation with persistence of the transverse one [143]. The relation between safety factor, conduction velocity and coupling resistance is illustrated in Fig. 3.10.

Under source/load mismatch conditions, I_{CaL} may become necessary to support propagation even if I_{Na} is intact [144, 145]. This unexpected observation has been interpreted as follows. Due to discrete distribution of axial resistance (at gap junctions), a small delay occurs whenever excitation crosses a cell border. Thus, even if apparently continuous at macroscopic level, propagation is "discontinuous" at the microscopic one [146]. Under source/load mismatch conditions such delays may be increased and outlast the duration of I_{Na} flow. In this case the smaller, but longer lasting I_{CaL} may become pivotal to provide the sustained generator current required for excitation of the downstream cell. Thus, not only the magnitude, but also the duration of the generator current may be important in determining the safety factor of propagation.

3.14 Mathematical Models

Over the past decades patch-clamp experiments have provided us with detailed information on the different types of ion channels that are present in the cardiac cell membrane. The sophisticated cardiac cell models that are available today can help us understand how the different types of ion channels act together to produce the cardiac action potential (cf. Figs. 3.6 and 3.8). Moreover, such models have become essential instruments for the assessment of the functional

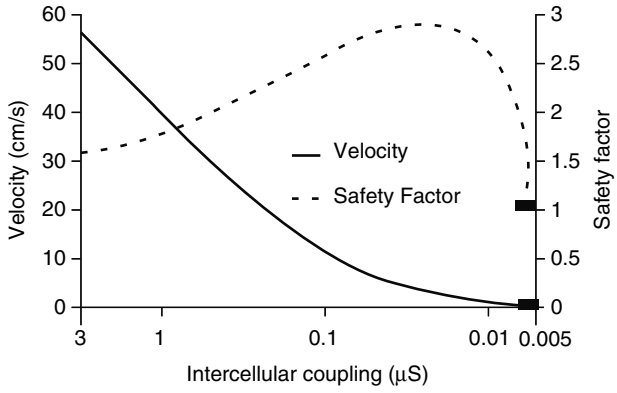

Figure 3.10

Influence of junctional coupling conductance on conduction velocity and safety factor. Conduction velocity (*left* ordinate) and safety factor for conduction (*right* ordinate) as a function of intercellular coupling (abscissa). At first glance, against intuition, a decrease in intercellular coupling leads to a transient increase in safety of conduction, before conduction blocks. Reproduced from [128] with permission from Physiological Reviews. This figure is adapted from Fig. 3.5a in Shaw RM, Rudy Y. Circ Res 1997; 81: 727–741.

implications of changes in density or kinetics of ion channels, e.g., changes due to ion channel mutations underlying the congenital long-QT syndrome.

Back in 1928, van der Pol and van der Mark presented the first mathematical description of the heartbeat, which is in terms of a relaxation oscillator [147]. Their work has given rise to a family of models of nerve and heart "cells" (excitable elements) in terms of their key properties, i.e., excitability, stimulus threshold, and refractoriness. These models are relatively simple with a minimum number of equations and variables [148, 149]. Because they are compact, these models have been widely used in studies of the spread of excitation in tissue models consisting of large numbers of interconnected "cells" (e.g., [149]).

A major drawback of this family of models is the absence of explicit links between the electrical activity and the underlying physiological processes like the openings and closures of specific ion channels. Today's sophisticated cardiac cell models provide such links and are all built on the framework defined by the seminal work of Hodgkin and Huxley [150], for which they received the Nobel Prize in Physiology or Medicine in 1963.

3.14.1 The Seminal Hodgkin-Huxley Model

Hodgkin and Huxley investigated the electrical activity of the squid giant axon, on which they published a series of five (now classical) papers in 1952. In their concluding paper they summarized their experimental findings and presented "a quantitative description of membrane current and its application to conduction and excitation in nerve" [150]. This "quantitative description" included a mathematical model derived from an electrical equivalent of the nerve cell membrane. They identified sodium and potassium currents flowing across the giant axon membrane and represented these in terms of the sum of conductive components that we now identify as ion channels, and membrane capacitance. In the electrical equivalent, the cell membrane was represented by a capacitor (cf. Sect. 3.3.1) in parallel with three resistors representing the sodium conductance, the potassium conductance and a leakage conductance. The associated sodium and potassium currents were described using the mathematical formulation introduced in Sect. 3.3.4.

In their series of papers, Hodgkin and Huxley demonstrated that g_m can be separated into sodium and potassium components (g_{Na} and g_K, respectively), which are both functions of V_m and time. In their analysis they introduced the

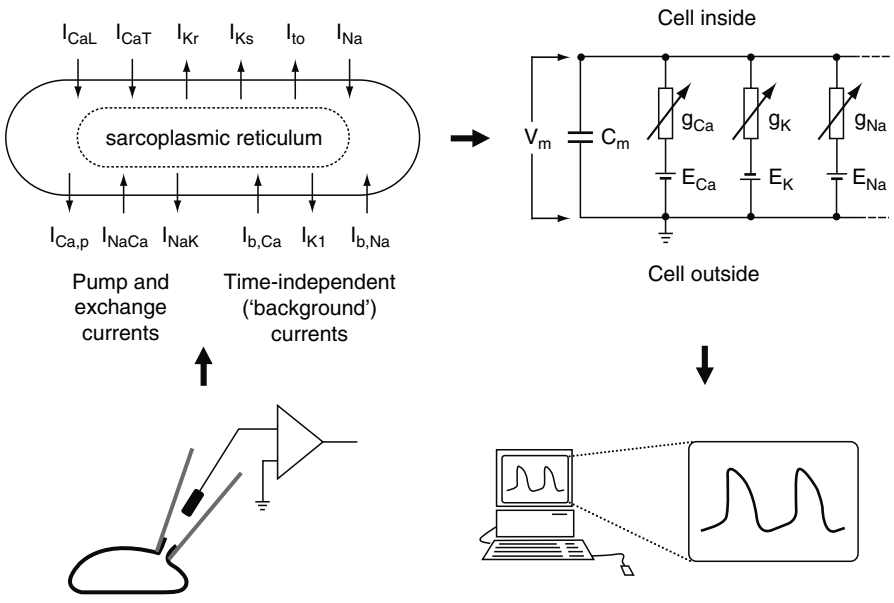

Figure 3.11

Common layout of cardiac cell models. Data from patch-clamp experiments (*bottom left*) provide quantitative information on each of the individual membrane current components (*top left*). This information is turned into an electrical equivalent (*top right*). The resulting equations, together with equations describing intracellular processes, e.g., the calcium uptake and release by the sarcoplasmic reticulum, are then compiled into a computer model of the cardiac cell, e.g., an SA nodal cell model (*bottom right*).

concept of activation and inactivation "gates" and provided equations governing the time and voltage dependence of these gates. Upon a change in V_m, x (the gating variable introduced in Sect. 3.3.4) changes with time as:

$$dx/dt = \alpha \times (1 - x) - \beta \times x, \tag{3.5}$$

where α and β are "rate constants," which are both functions of V_m. In this concept, α is the rate at which x gates change from the closed to the open state, whereas β is the rate at which x gates change from the open to the closed state.

As illustrated in Fig. 3.11, today's ionic cardiac cell models still follow the concept of Hodgkin and Huxley. The ionic currents that have been identified in patch-clamp experiments are described in terms of "activation" and "inactivation" and turned into components of an electrical circuit, which underlies the set of model equations. The only extension to the concept of Hodgkin and Huxley is the inclusion of an additional set of equations governing the changes in intracellular ion concentrations (sodium, potassium, and calcium) and the intracellular calcium uptake and release processes ("second-generation models," see Sect. 3.14.4).

3.14.2 Early Cardiac Cell Models (1960–1989)

The Hodgkin and Huxley concept was first applied to cardiac cells by Noble [151, 152]. His model of cardiac Purkinje fibers was relatively simple and had five variables. With more experimental data becoming available, the model was updated twice, in the seventies by McAllister et al. [153] and in the eighties by DiFrancesco and Noble [154]. The latter two models formed the basis for the development of ventricular, atrial, and sinoatrial cell models (Table 3.2; [151–162]).

Table 3.2
Early ionic models of mammalian cardiac cells (1960–1989)

Model	Parent model
Purkinje fibre models	
Noble [151, 152]	–
McAllister et al. [153]	Noble [151, 152]
DiFrancesco and Noble [154]	McAllister et al. [153]
Ventricular cell models	
Beeler and Reuter [155]	McAllister et al. [153]
Drouhard and Roberge [156]	Beeler and Reuter [155]
Atrial cell models	
Hilgemann and Noble [157]	DiFrancesco and Noble [154]
Sinoatrial cell models (*rabbit*)	
Yanagihara et al. [158]	–
Irisawa and Noma [159]	Yanagihara et al. [158]
Bristow and Clark [160]	McAllister et al. [153]
Noble and Noble [161]	DiFrancesco and Noble [154]
Noble et al. [162]	Noble and Noble [161]

3.14.3 Detailed Cardiac Cell Models (1990–2005)

According to current standards, the models that were developed during the first three decades of cardiac cell modeling (Table 3.2; [151–162]) were simple, with a small number of variables and equations, and of a generic nature, with limited specificity regarding species or location within the tissue. This changed rapidly during the subsequent period. Starting in the early nineties, a large number of cardiac cell models of increasing complexity have been developed, profiting from the immense progress made in cardiac cellular electrophysiology and the powerful computer resources that have become available (Table 3.3; [153, 163–194]). Among these models, the "Luo-Rudy II" ventricular cell model [167], also known as "phase-2 Luo-Rudy" or "LR2" model, has become a classical one. Several more recent ventricular and atrial cell models have been built upon the Luo-Rudy equations. After the Luo-Rudy II model was published in 1994, it has been updated several times, keeping track with experimental data appearing in literature. The source code of the current version of the model ("LRd model"), as well as that of several other models, is available on the Internet (see Sect. 3.14.8).

3.14.4 First-Generation and Second-Generation Models

In the early ionic models of cardiac cells, all the concentrations of the various ionic species were held fixed, so that no provision had to be made for pumps and exchangers to regulate these concentrations. We refer to models that incorporate variable ion concentrations as well as pumps and exchangers as "second-generation" models, in contrast to the earlier "first-generation" models [195]. There are two major problems with the more physiologically realistic second-generation models, in which, besides membrane potential and gating variables, ion concentrations vary in time: (1) drift, with very slow long-term trends in some of the variables, particularly some ionic concentrations, and (2) degeneracy, with non-uniqueness of equilibrium solutions such as steady states and limit cycles (see [195] and primary references cited therein). Drift has been managed in several ways, including stimulus current assignment to a specific ionic species [196]. The other major problem noted with second-generation models is degeneracy. Essentially, second-generation models form a system of $N-1$ equations in N unknowns. As a result, there is a continuum of equilibrium points ("steady-state solutions"), rather than isolated equilibrium points, so that, e.g., the resting potential of a quiescent system depends on the initial conditions.

Table 3.3

Detailed ionic models of mammalian cardiac cells (1990–2005)

Model	Species	Parent model
Ventricular cell models		
Noble et al. [163]	Guinea pig	Earm and Noble [164]
Luo and Rudy [165]	Guinea pig	Beeler and Reuter [155]
Nordin [166]	Guinea pig	–
Luo and Rudy [167]	Guinea pig	Luo and Rudy [165]
Jafri et al. [168]	Guinea pig	Luo and Rudy [167]
Noble et al. [169]	Guinea pig	Noble et al. [163]
Priebe and Beuckelmann [170]	Human	Luo and Rudy [167]
Winslow et al. [171]	Canine	Jafri et al. [168]
Pandit et al. [172]	Rat	Demir et al. [173]
Puglisi and Bers [174]	Rabbit	Luo and Rudy [167]
Bernus et al. [175]	Human	Priebe and Beuckelmann [170]
Matsuoka et al. [176]	Guinea pig	–
Bondarenko et al. [177]	Mouse	–
Shannon et al. [178]	Rabbit	Puglisi and Bers [174]
Ten Tusscher et al. [179]	Human	–
Iyer et al. [180]	Human	–
Hund and Rudy [181]	Canine	Luo and Rudy [167]
Atrial cell models		
Earm and Noble [164]	Rabbit	Hilgemann and Noble [167]
Lindblad et al. [182]	Rabbit	–
Courtemanche et al. [183]	Human	Luo and Rudy [167]
Nygren et al. [184]	Human	Lindblad et al. [182]
Ramirez et al. [185]	Canine	Courtemanche et al. [183]
Sinoatrial cell models		
Wilders et al. [186]	Rabbit	–
Demir et al. [173]	Rabbit	–
Dokos et al. [187]	Rabbit	Wilders et al. [186]
Demir et al. [188]	Rabbit	Demir et al. [173]
Zhang et al. [189]	Rabbit	–
Zhang et al. [190]	Rabbit	Zhang et al. [189]
Zhang et al. [191]	Rabbit	Zhang et al. [189]
Kurata et al. [192]	Rabbit	–
Sarai et al. [193]	Rabbit	–
Lovell et al. [194]	Rabbit	–

*Model has Markov type channel gating

This can be overcome through a "chemical" approach using an explicit formula for the membrane potential of cells in terms of the intracellular and extracellular ionic concentrations [197].

When using cardiac cell models, one should realize that first-generation models tend to reach a steady state within only a few beats, whereas second-generation models should be run for a much longer time to reach steady state. For example, in the canine atrial cell model by Kneller et al. [196] action potential duration reached steady state after approximately 40 min of pacing, which limits its suitability for performing large-scale (whole-heart) simulations, where simulating a single beat may take several hours on a state-of-the-art computer. Furthermore, it should be emphasized that the equations

representing the calcium subsystem of the second-generation models are still evolving and even the latest comprehensive models fail to adequately represent fundamental properties of calcium handling and inactivation of L-type calcium current by intracellular Ca^{2+} (see, e.g., [180, 198] and primary references cited therein).

3.14.5 Deterministic, Stochastic and Markov Models

Until a few years ago, cardiac cell models all employed the traditional Hodgkin-Huxley formulation of ion channel gating. In this concept, the state of an ion channel is defined by one or more independent gates that can each flip between their open and closed state, with the channel being open if and only if all of its gates are in their open position. Accordingly a channel with n different gates, can reside in any of 2^n different states (Fig. 3.12a). It had been noted that many ionic currents can more accurately be described using state diagrams that are not limited to the Hodgkin-Huxley concept of one or a few independent gates. The generic Markov type models, named after the mathematician Andrei Markov (1856–1922), are used instead. Markov models allow for more complex interactions between open, closed or inactivated states, as illustrated in Fig. 3.12b, and thus have the advantage of being more closely related to the underlying structure and conformation of the ion channel proteins. A disadvantage is that Markov models often introduce additional differential equations to the model that must be solved, thus slowing the computation time. In the recent comprehensive model of a rabbit ventricular myocyte by Shannon et al. [178], Markov channel models were therefore generally avoided unless considered necessary.

Markov models should not be confused with stochastic models. Cardiac cell models employing Markov type channel gating are as deterministic as models employing the Hodgkin-Huxley channel gating. The number of ion channels occupying a certain channel state is represented as a fraction (between 0 and 1) that changes with time as a continuous number. The changes with time are described by a set of differential equations governing the *average* behavior of the thousands of individual ion channels. Stochastic models are non-deterministic (probabilistic) models in which the stochastic "random" openings and closures of each individual ion channel are taken into account. The number of ion channels occupying a certain channel state is then represented as a discrete number that changes "randomly" with time: the computation of changes in these numbers with time involves drawing of random numbers instead of solving differential equations. As a consequence, action potential parameters may show beat-to-beat fluctuations, like experimental recordings [199, 200]. Stochastic ionic models of cardiac pacemaker cells have been developed by Wilders et al. [199] and Guevara and Lewis [201]. Recently, Greenstein and Winslow [202] have developed an ionic model of the canine ventricular myocyte incorporating stochastic gating of L-type calcium channels and ryanodine-sensitive calcium release channels.

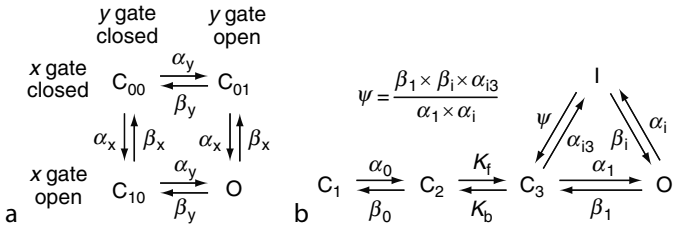

Figure 3.12

Hodgkin-Huxley and Markov type models of I_{Kr} (HERG, *KCNH2*) channel gating. (a) State diagram of classical Hodgkin-Huxley type model. The conductive state of the channel is controlled by two independent activation and inactivation gates (*x* and *y*, respectively), resulting in four different channel states. (b) State diagram of Markov type scheme (after [207]). C_1, C_2, and C_3 are closed states, O is the open state, and I the inactivated state. All transition rates, except K_f and K_b, are a function of membrane potential. Ψ is defined as a function of other transition rates to satisfy the microscopic reversibility condition.

3.14.6 Computational Aspects

The original computations by Hodgkin and Huxley [150] were done by hand. As memorized by Huxley in his Nobel lecture, "this was a laborious business: a membrane action took a matter of days to compute, and a propagated action potential took a matter of weeks." For his initial Purkinje fiber action potential simulations, Noble [151, 152] could make use of the university computer for which he had to write a program in machine code. It took two hours of CPU time to simulate a single action potential of the 5-variable model. In the seventies, Beeler and Reuter used a mainframe computer to solve the differential equations of their 8-variable ventricular cell model. A single action potential could be computed in about 40 s [155]. In subsequent decades, computational power has grown exponentially. Simulating a single Noble or Beeler-Reuter action potential now takes no more than one or a few milliseconds on a moderate personal computer. Nevertheless, computational efficiency is still an important issue when modeling cardiac cells. Models have not only become much more complex, but also require much longer time to reach steady state (see Sect. 3.14.4). Computational efficiency is of course, of particular importance in large-scale tissue or whole-heart simulations.

The ongoing demand for computational power is illustrated by the development of human ventricular cell models. The models by Priebe and Beuckelmann [170] and ten Tusscher et al. [198], with 15 and 16 variables, respectively, are of a similar complexity. Both use Hodgkin and Huxley type equations for the ionic currents and they model intracellular sodium, potassium, and calcium dynamics. The Iyer et al. [180] human ventricular cell model uses Markov type models rather than Hodgkin-Huxley type equations to describe the dynamics of the major ionic currents. As set out above, this allows one to fit single channel experimental data and to incorporate knowledge on ion channel structure, but this comes at the cost of a much higher number of variables; as many as 67 in the case of the Iyer et al. model [180].

Apart from the number of variables, the computational efficiency of a model is also determined by the "stiffness" of its equations: a model with "stiff" equations requires a small integration time step for a stable and precise solution of its differential equations. Ten Tusscher et al. [198] compared the computational efficiency of the above human ventricular cell models under standardized conditions, using simple Euler forward integration, which is the most widely used integration method for large-scale spatial simulations in electrophysiology. They observed that the Priebe & Beuckelmann and the ten Tusscher et al. models allowed for a much larger integration time step (20 μs) than the Iyer et al. model (0.02 μs). Together, the differences in the number of variables and the integration time step cause simulations with the Priebe and Beuckelmann and the tenTusscher et al. models to be approximately equally fast, whereas the Iyer et al. model is almost 1,000 times "slower."

3.14.7 Multicellular Simulations

The "bidomain" model has been widely accepted as the major approach for theoretical and numerical investigation of macroscopic electric phenomena in cardiac tissue. It is based on the representation of the tissue as two interpenetrating extra- and intracellular domains each of them having different conductivities along and across the direction of the fibers [203]. The state variables describing the system are the local intracellular and extracellular potentials (φ_i and φ_e, respectively), with the transmembrane potential defined as $V_m = \varphi_i - \varphi_e$. Although the bidomain model gives the most accurate approximation of heart tissue, it requires considerable computational power for calculations, both in terms of CPU speed and computer memory. The bidomain model of the human heart developed by Potse et al. [204], for example, requires > 20 GB of computer memory and takes 2 days on a 32-processor parallel computer to simulate a complete cardiac cycle. This explains why large-scale simulations are often "monodomain," i.e., φ_e is ignored and set to zero. Differences between monodomain and bidomain simulation results are small enough to permit the use of a monodomain model for propagation studies, even when extracellular potentials are required. However, bidomain models should be used if external currents are applied (pacing, defibrillation) [204].

Ionic models of single cardiac cells are also "monodomain": as in experiments on isolated cardiac cells, the extracellular space is grounded to earth (cf. Fig. 3.11). Given the required computational power, only simple first-generation cardiac cell models, with few variables and equations, can be used in large-scale bidomain simulations. Thus, bidomain simulations do not permit highly detailed studies of the effects of individual ionic currents on cardiac activation. This also holds, to a lesser extent, for monodomain simulations. Cardiac cell models that are typically used in large-scale simulations include the simplified ionic models by Fenton and Karma [205] and Bernus et al. [175].

Table 3.4

Cardiac cell models available on the Internet

Source code
Source code of numerous models in CellML format Web address: http://www.cellml.org/
Source code of cardiac cell models from the Rudy group (C++, Matlab) Web address: http://rudylab.wustl.edu/
Source code of cardiac cell models from the Winslow group (C++, Fortran) Web address: http://www.ccbm.jhu.edu/
Source code of the "Kyoto model" (several formats) Web address: http://www.card.med.kyoto-u.ac.jp/Simulation/
C++ source code of the Bernus et al. [175] human ventricular cell model Web address: http://www.physiol.med.uu.nl/wilders/
C++ source code of the ten Tusscher et al. [179] human ventricular cell model Web address: http://www-binf.bio.uu.nl/khwjtuss/
Fortran source code of the Zhang et al. [189, 190] rabbit sinoatrial cell models Web address: http://personalpages.umist.ac.uk/staff/H.Zhang-3/
Ready-to-use Java applets
Applets of numerous ionic models from the Centre for Arrhythmia Research at Hofstra University Web address: http://arrhythmia.hofstra.edu/
iCell: Java-based interactive cell modeling resource Web address: http://ssd1.bme.memphis.edu/icell/
Ready-to-use Windows program
LabHEART: Windows version of Puglisi & Bers rabbit ventricular cell model [174] Web address: http://www.meddean.luc.edu/templates/ssom/depts/physio/labheart.cfm

See Table 1 of [206] for a comprehensive list of tools for cardiac cell modeling

3.14.8 Cardiac Cell Models on the World Wide Web

The source code of various cardiac cell models is available through the Internet. This code can be compiled into a computer program using the appropriate "compiler," which requires basic computer programming skills. Table 3.4 lists some of the sites at which source code is made available. A few "ready-to-use" programs are also available. These include Java applets of several ionic models as well as a Windows version of the rabbit ventricular cell model by Puglisi and Bers [174].

Several efforts have been made to set a language standard for cardiac cell modeling. One example is the "CellML" language, which is an open standard based on the XML markup language, being developed by the Bioengineering Institute at the University of Auckland and affiliated research groups. The purpose of CellML is to store and exchange computer-based mathematical models. A large number of models are already available on the CellML website (Table 3.4). To run simulations, a simulation environment that imports CellML files is required.

References

1. Einthoven, W., Über die Form des menschlichen Electrocardiogramms. *Pflug. Arch. Ges. Phys.*, 1895;**60**: 101–123.
2. Einthoven, W., The different forms of the human electrocardiogram and their signification. *Lancet*, 1912;**1**: 853–861.
3. Burgess, M.J., K. Millar, and J.A. Abildskov, Cancellation of electrocardiographic effects during ventricular recovery. *J. Electrocardiol.*, 1969;**2**: 101–107.
4. Van Oosterom, A., Genesis of the T wave as based on an equivalent surface source model. *J. Electrocardiol.*, 2001;**34**(Suppl.): 217–226.
5. Fabiato, A. and F. Fabiato, Contractions induced by a calcium-triggered release of calcium from the sarcoplasmic reticulum of single skinned cardiac cells. *J. Physiol.*, 1975;**249**:469–495.

6. Cheng, H., W.J. Lederer, and M.B. Cannell, Calcium sparks: elementary events underlying excitation-contraction coupling in heart muscle. *Science*, 1993;**262**: 740–744.
7. Van Veen, A.A.B., H.V.M. Van Rijen, and T. Opthof, Cardiac gap junction channels: modulation of expression and channel properties. *Cardiovasc. Res.*, 2001;**51**: 217–229.
8. Keith, A. and M. Flack, The form and nature of the muscular connection between the primary divisions of the vertebrate heart. *J. Anat. Physiol.*, 1907;**41**: 172–189.
9. Tawara, S., *Das Reizleitungssystem des Säugetierherzen*. Jena, 1906.
10. Eyster, J.A.E. and W.J. Meek, The origin and conduction of the heart beat. *Physiol. Rev.*, 1921;**1**: 1–43.
11. Ling, G. and R.W. Gerard, The normal membrane potential of frog sartorius muscle. *J. Cell. Compar. Physiol.*, 1949;**34**: 383–396.
12. Powell, T. and V.W. Twist, A rapid technique for the isolation and purification of adult cardiac muscle cells having respiratory control and a tolerance to calcium. *Biochem. Biophys. Res. Commun.*, 1976;**72**: 327–333.
13. Neher, E., B. Sakmann, and J.H. Steinbach, The extracellular patch-clamp: a method for resolving currents through individual open channels in biological membranes. *Pflug. Arch.*, 1978;**375**: 219–228.
14. Boyett, M.R., H. Honjo, and I. Kodama, The sinoatrial node, a heterogeneous pacemaker structure. *Cardiovasc. Res.*, 2000;**47**: 658–687.
15. Meijler, F.L. and M.J. Janse, Morphology and electrophysiology of the mammalian atriventricular node. *Physiol. Rev.*, 1988;**68**: 608–647.
16. Schuilenburg, R.M. and D. Durrer, Atrial echo beats in the human heart elicited by induced atrial premature beats. *Circulation*, 1968;**37**: 680–693.
17. Tranum-Jensen J., A.A.M. Wilde, J.T. Vermeulen, and M.J. Janse, Morphology of electrophysiologically identified junctions between Purkinje fibers and ventricular muscle in rabbit and pig hearts. *Circ. Res.*, 1991;**69**: 429–437.
18. Harris, H.W., Jr., Molecular aspects of water transport. *Pediatr. Nephrol.*, 1992;**6**: 304–310.
19. Benga, G., Birth of water channel proteins-the aquaporins. *Cell. Biol. Int.*, 2003;**27**: 701–709.
20. Calaghan, S.C., J.Y. Le Guennec, and E. White, Cytoskeletal modulation of electrical and mechanical activity in cardiac myocytes. *Prog. Biophys. Mol. Biol.*, 2004;**84**: 29–59.
21. Fozzard, H.A. and R.B. Gunn, Membrane transport, in *The Heart*, 2nd ed., H.A. Fozzard, E. Haber, R.B. Jennings, A.M.J. Katz, and H.E. Morgan, Editors. New York: Raven Press, 1991, pp. 99–110.
22. Matsuda, H. and J.D.S. Cruz, Voltage-dependent block by internal Ca^{++} ions of inwardly rectifying K^+ channels in guinea-pig ventricular cells. *J. Physiol.*, 1993;**470**: 295–311.
23. Lopatin, A.N., E.N. Makhina, and C.G. Nichols, Potassium channel block by cytoplasmic polyamines as the mechanism of intrinsic rectification. *Nature*, 1994;**372**: 366–369.
24. Zaza, A., M. Rocchetti, A. Brioschi, A. Cantadori, and A. Ferroni, Dynamic Ca^{2+}-induced inward rectification of K^+ current during the ventricular action potential. *Circ. Res.*, 1998;**82**: 947–956.
25. Litovsky, S.H. and C. Antzelevitch, Transient outward current prominent in canine ventricular epicardium but not endocardium. *Circ. Res.*, 1988;**62**: 116–126.
26. Sanguinetti, M.C. and N.K. Jurkiewicz, Two components of cardiac delayed rectifier K^+ current. Differential sensitivity to block by class III antiarrhythmic agents. *J. Gen. Physiol.*, 1990;**96**: 195–215.
27. Attwell, D., I.S. Cohen, D.A. Eisner, M. Ohba, and C. Ojeda, The steady state TTX-sensitive ("window") sodium current in cardiac Purkinje fibres. *Pflug. Arch.*, 1979;**379**: 137–142.
28. Hirano, Y., A. Moscucci, and C.T. January, Direct measurement of L-type Ca^{++} window current in heart cells. *Circ. Res.*, 1992;**70**: 445–455.
29. Gintant, G.A., N.B. Datyner, and I.S. Cohen, Slow inactivation of a tetrodotoxin-sensitive current in canine Purkinje fibers. *Biophys. J.*, 1984;**45**: 509–512.
30. Bers, D.M., Sarcolemmal Na/Ca exchange and Ca-pump, in *Excitation-Contraction Coupling and Cardiac Contractile Force*, D.M. Bers, Editor. Boston: Kluwer Academic Publishers, 2002, pp. 133–160.
31. Ishihara, K., T. Mitsuiye, A. Noma, and M. Takano, The Mg^{2+} block and intrinsic gating underlying inward rectification of the K^+ current in guinea-pig cardiac myocytes. *J. Physiol.*, 1989;**419**: 297–320.
32. Smith, P.L., T. Baukrowitz, and G. Yellen, The inward rectification mechanism of the HERG cardiac potassium channel. *Nature*, 1996;**37**: 833–836.
33. Rocchetti, M, A. Besana, G.B. Gurrola, L.D. Possani, and A. Zaza, Rate-dependency of delayed rectifier currents during the guinea-pig ventricular action potential. *J. Physiol.*, 2001;**534**: 721–732.
34. Shimoni, Y., R.B. Clark, and W.R. Giles, Role of inwardly rectifying potassium current in rabbit ventricular action potential. *J. Physiol.*, 1992;**448**: 709–727.
35. Noma, A., T. Nakayama, Y. Kurachi, and H. Irisawa, Resting K conductances in pacemaker and non-pacemaker heart cells of the rabbit. *Jpn. J. Physiol.*, 1984;**34**: 245–254.
36. Cordeiro, J.M., K.W. Spitzer, and W.R. Giles, Repolarizing K^+ currents in rabbit heart Purkinje cells. *J. Physiol.*, 1998;**508**: 811–823.
37. Miake, J., E. Marbán, and H.B. Nuss, Biological pacemaker created by gene transfer. *Nature*, 2002;**419**: 132–133.
38. Janse, M.J., T. Opthof, and A.G. Kléber, Animal models of cardiac arrhythmias. *Cardiovasc. Res.*, 1998;**39**: 165–177.
39. Janse, M.J. and A.L. Wit, Electrophysiological mechanisms of ventricular arrhythmias resulting from myocardial ischemia and infarction. *Physiol. Rev.*, 1989;**69**: 1049–1169.
40. Wiener, N. and A. Rosenblueth, The mathematical formulation of the problem of conduction of impulses in a network of connected excitable elements, specifically in cardiac muscle. *Arch. Inst. Cardiol. Mex.*, 1946;**16**: 205–265.
41. Moe, G.K. and C. Mendez, Basis of pharmacotherapy of cardiac arrhythmias. *Mod. Conc. Cardiov. Dis.*, 1962;**31**:739–744.
42. Allessie, M.A., F.I.M. Bonke, and F.J.G. Schopman, Circus movement in rabbit atrial muscle as a mechanism of tachycardia. The "leading circle" concept: a new model of circus movement in cardiac tissue without the involvement of an anatomical obstacle. *Circ. Res.*, 1977;**41**: 9–18.
43. Conrath, C.E. and T. Opthof, Ventricular repolarization. An overview of (patho)physiology, sympathetic effects, and

genetic aspects. *Prog. Biophys. Mol. Biol.*, 2005;**92**(3): 269–307. doi:10.1016/jpbiomolbio.2005.05.009.

44. Stengl, M., P.G. Volders, M.B. Thomsen, R.L. Spätjens, K.R. Sipido, and M.A. Vos, Accumulation of slowly activating delayed rectifier potassium current (I_{Ks}) in canine ventricular myocytes. *J. Physiol.*, 2003;**551**: 777–786.
45. Virág, L., N. Iost, M. Opincariu, J. Szolnoky, J. Szécsi, G. Bogáts, P. Szenohradszky, A. Varró, and J.G. Papp, The slow component of the delayed rectifier potassium current in undiseased human ventricular myocytes. *Cardiovasc. Res.*, 2001;**49**: 790–797.
46. Lu, Z., K. Kamiya, T. Opthof, K. Yasui, and I. Kodama, Density and kinetics of I_{Kr} and I_{Ks} in guinea pi45d r rabbit ventricular myocytes explain different efficacy of I_{Ks} blockade at high heart rate in guinea pig and rabbit. *Circulation*, 2001;**104**:951–956.
47. Volders, P.G., M. Stengl, J.M. van Opstal, U. Gerlach, R.L. Spätjens, J.D. Beekman, K.R. Sipido, and M.A. Vos, Probing the contribution of I_{Ks} to canine ventricular repolarization: key role for ß-adrenergic receptor stimulation. *Circulation*, 2003;**107**: 2753–2760.
48. Nitta, J.-I., T. Furukawa, F. Marumo, T. Sawanobori, and M. Hiraoka, Subcellular mechanism for Ca^{2+} -dependent enhancement of delayed rectifier K^+ current in isolated membrane patches of guinea pig ventricular myocytes. *Circ. Res.*, 1994;**74**: 96–104.
49. Jost, N., L. Virág, M. Bitay, J. Takács, C. Lengyel, P. Biliczki, Z. Nagy, G. Bogáts, D.A. Lathrop, J.G. Papp, and A. Varró, Restricting excessive cardiac action potential and QT prolongation: a vital role for I_{Ks} in human ventricular muscle. *Circulation*, 2005;**112**: 1392–1399.
50. Saitoh, H, J.C. Bailey, and B. Surawicz, Alternans of action potential duration after abrupt shortening of cycle length: differences between dog Purkinje and ventricular muscle fibers. *Circ. Res.*, 1988;**62**: 1027–1040.
51. Curran, M.E., I. Splawski, K.W. Timothy, M.G. Vincent, E.D. Green, and M.T. Keating, A molecular basis for cardiac arrhythmia: HERG mutations cause long QT syndrome. *Cell*, 1995;**80**: 795–803.
52. Jurkiewicz, N.K. and M.C. Sanguinetti, Rate-dependent prolongation of cardiac action potentials by a methanesulfonanilide class III antiarrhythmic agent. Specific block of rapidly activating delayed rectifier current by dofetilide. *Circ. Res.*, 1993;**72**:75–83.
53. Biliczki, P., L. Virág, N. Iost, J.G. Papp, and A. Varró, Interaction of different potassium channels in cardiac repolarization in dog ventricular preparations: role of repolarization reserve. *Br. J. Pharmacol.*, 2002;**137**: 361–368.
54. Bennett, P.B., K. Yazawa, N. Makita, and A.L. George, Jr., Molecular mechanism for an inherited cardiac arrhythmia. *Nature*, 1995;**376**: 683–685.
55. Clancy, C.E., M. Tateyama, H. Liu, X.H. Wehrens, and R.S. Kass, Non-equilibrium gating in cardiac Na^+ channels: an original mechanism of arrhythmia. *Circulation*, 2003;**107**: 2233–2237.
56. Berecki, N.G., J.G. Zegers, Z.A. Bhuiyan, A.O. Verkerk, R. Wilders, and A.C.G. van Ginneken, Long-QT syndrome related sodium channel mutations probed ny dynamic action potential clamp technique. *J. Physiol.*, 2006;**570**: 237–250.
57. Lee, K.S., E. Marbán, and R.W. Tsien, Inactivation of calcium channels in mammalian heart cells: joint dependence on membrane potential and intracellular calcium. *J. Physiol.*, 1985;**364**: 395–411.
58. Zuhlke, R.D., G.S. Pitt, K. Deisseroth, R.W. Tsien, and H. Reuter, Calmodulin supports both inactivation and facilitation of L-type calcium channels. *Nature*, 1999;**399**: 159–162.
59. Goldhaber, J.I., L.H. Xie, T. Duong, C. Motter, K. Khuu, and J.N. Weiss, Action potential duration restitution and alternans in rabbit ventricular myocytes: the key role of intracellular calcium cycling. *Circ. Res.*, 2005;**96**: 459–466.
60. January, C.T. and J.M. Riddle, Early after depolarizations: mechanism of induction and block A role for L-type Ca^{2+} current. *Circ. Res.*, 1989;**64**: 977–990.
61. Keith, A., The sino-auricular node: a historical note. *Br. Heart J.*, 1942;**4**: 77–79.
62. Trautwein, W. and K. Uchizono, Electron microscopic and electrophysiologic study of the pacemaker in the sinoatrial node of the rabbit heart. *Z. Zellforsch. Mikrosk. Anat.*, 1963;**61**: 96–109.
63. Taylor, J.J., L.S. d'Agrosa, and E.M. Berns, The pacemaker cell of the sinoatrial node of the rabbit. *Am. J. Physiol.*, 1978;**235**: H407–H412.
64. Maltsev, V.A., A.M. Wobus, J. Rohwedel, M. Bader, and J. Hescheler, Cardiomyocytes differentiated in vitro from embryonic stem cells developmentally express cardiac-specific genes and ionic currents. *Circ. Res.*, 1994;**75**: 233–244.
65. DiFrancesco, D., Pacemaker mechanisms in cardiac tissue. *Annu. Rev. Physiol.*, 1993;**55**: 451–467.
66. Irisawa, H., H.F. Brown, and W. Giles, Cardiac pacemaking in the sinoatrial node. *Physiol. Rev.*, 1993;**73**: 197–227.
67. Yu, H., F. Chang, and I.S. Cohen, Pacemaker current i_f in adult canine cardiac ventricular myocytes. *J. Physiol.*, 1995;**485**: 469–483.
68. Robinson, R.B., H. Yu, F. Chang, and I.S. Cohen, Developmental change in the voltage-dependence of the pacemaker current, i_f, in rat ventricle cells. *Pflug. Arch.*, 1997;**433**: 533–535.
69. DiFrancesco, D., The cardiac hyperpolarizing-activated current I_f. *Prog. Biophys. Mol. Biol.*, 1985;**46**: 163–183.
70. Zaza, A., M. Micheletti, A. Brioschi, and M. Rocchetti, Ionic currents during sustained pacemaker activity in rabbit sino-atrial myocytes. *J. Physiol.*, 1997;**505**: 677–688.
71. DiFrancesco, D. and M. Mangoni, Modulation of single hyperpolarization-activated channels (I_f) by cAMP in the rabbit sino-atrial node. *J. Physiol.*, 1994;**474**: 473–482.
72. Zaza, A., R.B. Robinson, and D. DiFrancesco, Basal responses of the L-type Ca^{2+} and hyperpolarization-activated currents to autonomic agonists in the rabbit sinoatrial node. *J. Physiol.*, 1996;**491**: 347–355.
73. Zaza, A., M. Rocchetti, and D. DiFrancesco, Modulation of the hyperpolarization activated current (I_f) by adenosine in rabbit sinoatrial myocytes. *Circulation*, 1996;**94**: 734–741.
74. Verheijck, E.E., A.C.G. van Ginneken, R. Wilders, and L.N. Bouman, Contribution of L-type Ca^{2+} current to electrical activity in sinoatrial nodal myocytes of rabbits. *Am. J. Physiol.*, 1999;**276**: H1064–H1077.
75. Reuter, H., Calcium channel modulation by neurotransmitters, enzymes and drugs. *Nature*, 1983;**301**: 569–574.
76. Verheijck, E.E., A.C.G. van Ginneken, J. Bourier, and L.N. Bouman, Effects of delayed rectifier current blockade by E-4031 on impulse generation in single sinoatrial nodal myocytes of the rabbit. *Circ. Res.*, 1995;**76**: 607–615.
77. Noble, D., J.C. Denyer, H.F. Brown, and D. DiFrancesco, Reciprocal role of the inward currents $I_{b,Na}$ and I_f in controlling and stabilizing pacemaker frequency of rabbit sino-atrial node cells. *Proc. R. Soc. Lond. B Biol. Sci.*, 1992;**250**:199–207.

78. Nishida, M. and R. MacKinnon, Structural basis of inward rectification: cytoplasmic pore of the G protein-gated inward rectifier GIRK1 at 1.8 Å resolution. *Cell*, 2002;**111**:957–965.
79. Duivenvoorden, J.J., L.N. Bouman, T. Opthof, F.F. Bukauskas, and H.J. Jongsma, Effect of transmural vagal stimulation on electrotonic current spread in the rabbit sinoatrial node. *Cardiovasc. Res.*, 1992;**26**: 678–686.
80. DiFrancesco, D., P. Ducouret, and R.B. Robinson, Muscarinic modulation of cardiac rate at low acetylcholine concentrations. *Science*, 1989;**243**: 669–671.
81. Boyett, M.R., I. Kodama, H. Honjo, A. Arai, R. Suzuki, and J. Toyama, Ionic basis of the chronotropic effect of acetylcholine on the rabbit sinoatrial node. *Cardiovasc. Res.*, 1995;**29**:867–878.
82. Zaza, A. and M. Rocchetti, Regulation of the sinoatrial pacemaker: selective I_f inhibition by ivaradine, in *Heart Rate Management in Stable Angina*, K. Fox and R. Ferrari, Editors. London: Taylor & Francis, 2005, pp. 51–67.
83. Huser, J., L.A. Blatter, and S.L. Lipsius, Intracellular Ca^{2+} release contributes to automaticity in cat atrial pacemaker cells. *J. Physiol.*, 2000;**524**: 415–422.
84. Bogdanov, K.Y., T.M. Vinogradova, and E.G. Lakatta, Sinoatrial nodal cell ryanodine receptor and Na^+-Ca^{2+} exchanger: molecular partners in pacemaker regulation. *Circ. Res.*, 2001;**88**: 1254–1258.
85. Lakatta, E.G., V.A. Maltsev, K.Y. Bogdanov, M.D. Stern, and T.M. Vinogradova, Cyclic variation of intracellular calcium: a critical factor for cardiac pacemaker cell dominance. *Circ. Res.*, 2003;**92**: e45–e50.
86. Vinogradova, T.M., Y.Y. Zhou, V. Maltsev, A. Lyashkov, M. Stern, and E.G. Lakatta, Rhythmic ryanodine receptor Ca^{2+} releases during diastolic depolarization of sinoatrial pacemaker cells do not require membrane depolarization. *Circ. Res.*, 2004;**94**: 802–809.
87. Vinogradova, T.M., K.Y. Bogdanov, and E.G. Lakatta, Beta-adrenergic stimulation modulates ryanodine receptor Ca^{2+} release during diastolic depolarization to accelerate pacemaker activity in rabbit sinoatrial nodal cells. *Circ. Res.*, 2002;**90**: 73–79.
88. Michaels, D.C., E.P. Matyas, and J. Jalife, Mechanisms of sinoatrial pacemaker synchronization: a new hypothesis. *Circ. Res.*, 1987;**61**: 704–714.
89. Masson-Pévet, M.A., W.K. Bleeker, and D. Gros, The plasma membrane of leading pacemaker cells in the rabbit sinus node. A quantitative structural analysis. *Circ. Res.*, 1979;**45**: 621–629.
90. Honjo, H., M.R. Boyett, S.R. Coppen, Y. Takagishi, T. Opthof, N.J. Severs, and I. Kodama, Heterogeneous expression of connexins in rabbit sinoatrial node cells: correlation between connexin isoform and cell size. *Cardiovasc. Res.*, 2002;**53**: 89–96.
91. Masson-Pévet, M.A., W.K. Bleeker, E. Besselsen, B.W. Treytel, H.J. Jongsma, and L.N. Bouman, Pacemaker cell types in the rabbit sinus node: a correlative ultrastructural and electrophysiological study. *J. Mol. Cell. Cardiol.*, 1984;**16**: 53–63.
92. Kirchhof, C.J. and M.A. Allessie, Sinus node automaticity during atrial fibrillation in isolated rabbit hearts. *Circulation*, 1992;**86**: 263–271.
93. Opthof, T., A.C.G. VanGinneken, L.N. Bouman, and H.J. Jongsma, The intrinsic cycle length in small pieces isolated from the rabbit sinoatrial node. *J. Mol. Cell. Cardiol.*, 1987;**19**: 923–934.
94. Kodama, I. and M.R. Boyett, Regional differences in the electrical activity of the rabbit sinus node. *Pflug. Arch.*, 1985;**404**: 214–226.
95. Joyner, R.W. and F.J.L. van Capelle, Propagation through electrically coupled cells: how a small SA node drives a large atrium. *Biophys. J.*, 1986;**50**: 1157–1164.
96. Wilders, R. and H.J. Jongsma, Beating irregularity of single pacemaker cells isolated from the rabbit sinoatrial node. *Biophys. J.*, 1993;**65**: 2601–2613.
97. Opthof, T., The mammalian sinoatrial node. *Cardiovasc. Drugs Ther.*, 1988;**1**: 573–597.
98. Mackaay, A.J.C., T. Opthof, W.K. Bleeker, H.J. Jongsma, and L.N. Bouman, Interaction of adrenaline and acetylcholine on cardiac pacemaker function. *J. Pharmacol. Exp. Ther.*, 1980;**214**: 417–422.
99. Mackaay, A.J.C., T. Opthof, W.K. Bleeker, H.J. Jongsma, and L.N. Bouman, Interaction of adrenaline and acetylcholine on sinus node function, in *Cardiac Rate and Rhythm*, L.N. Bouman and H.J. Jongsma, Editors. The Hague: Nijhoff, 1982, pp. 507–523.
100. Katzung, G.B. and H.A. Morgenstern, Effects of extracellular potassium on ventricular automaticity and evidence of a pacemaker current in mammalian ventricular myocardium. *Circ. Res.*, 1977;**40**: 105–111.
101. Cerbai, E, R. Pino, F. Porciatti, G. Sani, M. Toscano, M. Maccherini, G. Giunti, and A. Mugelli, Characterization of the hyperpolarization-activated current, I_f, in ventricular myocytes from human failing heart. *Circulation*, 1997;**95**: 568–571.
102. Imanishi, S., Calcium-sensitive discharges in canine Purkinje fibers. *Jpn. J. Physiol.*, 1971;**21**: 443–463.
103. Dangman, K.H. and B.F. Hoffman, Studies on overdrive stimulation of canine cardiac Purkinje fibers: maximal diastolic potential as a determinant of the response. *J. Am. Coll. Cardiol.*, 1983;**2**: 1183–1190.
104. Cheung, D.W., Electrical activity of the pulmonary vein and its interaction with the right atrium in the guinea-pig. *J. Physiol.*, 1981;**314**: 445–456.
105. Haissaguerre, M., P. Jais, D.C. Shah, A. Takahashi, M. Hocini, G. Quiniou, S. Garrigue, A. Le Mouroux, P. Le Metayer, and J. Clementy, Spontaneous initiation of atrial fibrillation by ectopic beats originating in the pulmonary veins. *New Engl. J. Med.*, 1998;**339**: 659–666.
106. Logothetis, D.E., Y. Kurachi, J. Galper, E.J. Neer, and D.E. Clapham, The beta-gamma subunits of GTP-binding proteins activate the muscarinic K^+ channel in heart. *Nature*, 1987;**325**: 321–326.
107. Bender, K., M.C. Wellner-Kienitz, L.I. Bosche, A. Rinne, C. Beckmann, and L. Pott, Acute desensitization of GIRK current in rat atrial myocytes is related to K^+ current flow. *J. Physiol.*, 2004;**561**: 471–483.
108. Müllner, C., D. Vorobiov, A.K. Bera, Y. Uezono, D. Yakubovich, B. Frohnwieser-Steinecker, N. Dascal, and W. Schreibmayer, Heterologous facilitation of G protein-activated K^+ channels by beta-adrenergic stimulation via cAMP-dependent protein kinase. *J. Gen. Physiol.*, 2000;**115**: 547–558.
109. Cho, H., D. Lee, S.H. Lee, and W.K. Ho, Receptor-induced depletion of phosphatidylinositol 4,5-bisphosphate inhibits inwardly rectifying K^+ channels in a receptor-specific manner. *Proc. Natl. Acad. Sci. USA*, 2005;**102**: 4643–4648.
110. Gintant, G.A., Two components of delayed rectifier current in canine atrium and ventricle. Does I_{Ks} play a role in the reverse rate dependence of class III agents? *Circ. Res.*, 1996;**78**: 26–37.

111. Wang, Z., B. Fermini, and S. Nattel, Rapid and slow components of delayed rectifier current in human atrial myocytes. *Cardiovasc. Res.*, 1994;**28**: 1540–1546.
112. Wang, Z., B. Fermini, and S. Nattel, Sustained depolarization-induced outward current in human atrial myocytes. Evidence for a novel delayed rectifier K^+ current similar to Kv1.5 cloned channel currents. *Circ. Res.*, 1993;**73**: 1061–1076.
113. Crumb, W.J., Jr., B. Wible, D.J. Arnold, J.P. Payne, and A.M. Brown, Blockade of multiple human cardiac potassium currents by the antihistamine terfenadine: possible mechanism for terfenadine-associated cardiotoxicity. *Mol. Pharmacol.*, 1995;**47**: 181–190.
114. Amos, G.J., E. Wettwer, F. Metzger, Q. Li, H.M. Himmel, and U. Ravens, Differences between outward currents of human atrial and subepicardial ventricular myocytes. *J. Physiol.*, 1996;**491**: 31–50.
115. Koidl, B., P. Flaschberger, P. Schaffer, B. Pelzmann, E. Bernhart, H. Machler, and B. Rigler, Effects of the class III antiarrhythmic drug ambasilide on outward currents in human atrial myocytes. *Naunyn Schmiedebergs Arch. Pharmacol.*, 1996;**353**: 226–232.
116. Antzelevitch, C., S. Sicouri, S.H. Litovsky, A. Lukas, S.C. Krishnan, J.M. Di Diego, G.A. Gintant, and D.W. Liu. Heterogeneity within the ventricular wall. Electrophysiology and pharmacology of epicardial, endocardial, and M cells. *Circ. Res.*, 1991;**69**: 1427–1449.
117. Rosati, B., F. Grau, S. Rodriguez, H. Li, J.M. Nerbonne, and D. McKinnon, Concordant expression of KChIP2 mRNA, protein and transient outward current throughout the canine ventricle. *J. Physiol.*, 2003;**548**: 815–822.
118. Liu, D.W. and C. Antzelevitch, Characteristics of the delayed rectifier current (I_{Kr} and I_{Ks}) in canine ventricular epicardial, midmyocardial, and endocardial myocytes. A weaker I_{Ks} contributes to the longer action potential in the M cell. *Circ. Res.*, 1995;**76**: 351–365.
119. Sicouri, S. and C. Antzelevitch, A subpopulation of cells with unique electrophysiological properties in the deep subepicardium of the canine ventricle. The M cell. *Circ. Res.*, 1991;**68**: 1729–1741.
120. Anyukhovsky, E.P., E.A. Sosunov, R.Z. Gainullin, and M.R. Rosen, The controversial M cell. *J. Cardiovasc. Electrophysiol.*, 1999;**10**: 244–260.
121. Antzelevitch, C., W. Shimuzu, G.-X. Yan, S. Sicouri, J. Weissenburger, V.V. Nesterenko, A. Burashnikov, J. Di Diego, J. Saffitz, and G.P. Thomas, The M cell: its contribution to the ECG and to normal and abnormal electrical function of the heart. *J. Cardiovasc. Electrophysiol.*, 1999;**10**: 1124–1152.
122. Janse, M.J., E.A. Sosunov, R. Coronel, T. Opthof, E.P. Anyukhovsky, J.M.T. de Bakker, A.N. Plotnikov, I.N. Shlapakova, P. Danilo, Jr., J.G.P. Tijssen, and M.R. Rosen, Repolarization gradients in the canine left ventricle before and after induction of short-term cardiac memory. *Circulation*, 2005;**112**: 1711–1718.
123. Drouin, E., F. Charpentier, C. Gauthier, K. Laurent, and H. Le Marec, Electrophysiological characteristics of cells spanning the left ventricular wall of human heart: evidence for the presence of M cells. *J. Am. Coll. Cardiol.*, 1995;**26**: 185–192.
124. Taggart, P., P.M.I. Sutton, T. Optof, R. Coronel, R. Trimlett, W. Pugsley, and P. Kallis, Transmural repolarisation in the left ventricle in humans during normoxia and ischaemia. *Cardiovasc. Res.*, 2001;**50**: 454–462.
125. Conrath, C.E., R. Wilders, R. Coronel, J.M.T. De Bakker, P. Taggart, J.R. De Groot, and T. Opthof, Intercellular coupling through gap junctions masks M cells in the human heart. *Cardiovasc. Res.*, 2004;**62**: 407–414.
126. Bauer, A., R. Becker, K.D. Freigang, J.C. Senges, F. Voss, A. Hansen, M. Müller, H.J. Lang, U. Gerlach, A. Busch, P. Kraft, W. Kubler, and W. Schols, Rate- and site-dependent effects of Propafenone, Dofetilide and the new I_{Ks}-blocking agent Chromanol 293b on individual muscle layers of the intact canine heart. *Circulation*, 1999;**100**: 2184–2190.
127. Roden, D.M., J.R. Balser, A.L. George, Jr., and M.E. Anderson, Cardiac ion channels. *Annu. Rev. Physiol.*, 2002;**64**: 431–475.
128. Catterall, W.A. and G. Gutman, Introduction to the IUPHAR compendium of voltage-gated ion channels. *Pharmacol. Rev.*, 2005;**57**: 385.
129. Hanlon, M.R. and B.A. Wallace, Structure and function of voltage-dependent ion channel regulatory β subunits. *Biochemistry*, 2002;**41**: 2886–2894.
130. Qu, J., C. Altomare, A. Bucchi, D. DiFrancesco, and R.B. Robinson, Functional comparison of HCN isoforms expressed in ventricular and HEK 293 cells. *Pflug. Arch.*, 2002;**444**: 597–601.
131. Yang, T., D. Snyders, and D.M. Roden, Drug block of I_{Kr}: model systems and relevance to human arrhythmias. *J. Cardiovasc. Pharm.*, 2001;**38**: 737–744.
132. Kléber, A.G., M.J. Janse, and V.G. Fast, Normal and abnormal conduction in the heart, in *Handbook of Physiology. Section 2 The Cardiovascular System, vol. 1 The Heart*. Oxford: Oxford University Press, 2001, pp. 455–530.
133. Kléber, A.G. and Y. Rudy, Basic mechanisms of cardiac impulse propagation and associated arrhythmias. *Physiol. Rev.*, 2004;**84**: 431–488.
134. Weidmann, S., Electrical constants of trabecular muscle from mammalian heart. *J. Physiol.*, 1952;**118**: 348–360.
135. Sampson, K.J. and C.S. Henriquez, Electrotonic influences on action potential duration dispersion in small hearts: a simulation study. *Am. J. Physiol. Heart Circ. Physiol.*, 2005;**289**: H350–H360.
136. Taggart, P., P.M.I. Sutton, T. Opthof, R. Coronel, R. Trimlett, W. Pugsley, and P. Kallis, Inhomogeneous transmural conduction during early ischaemia in patients with coronary artery disease. *J. Mol. Cell. Cardiol.*, 2000;**32**: 621–630.
137. Spach, M.S., Transition from continuous to discontinuous understanding of cardiac conduction. *Circ. Res.*, 2003;**92**:125–126.
138. Winterton, S.J., M.A. Turner, D.J. O'Gorman, N.A. Flores, and D.J. Sheridan. Hypertrophy causes delayed conduction in human and guinea pig myocardium: accentuation during ischaemic perfusion. *Cardiovasc. Res.*, 1994;**28**: 47–54.
139. Wiegerinck, R.F., A.O. Verkerk, C.N. Belterman, T.A.B. van Veen, A. Baartscheer, T. Opthof, R. Wilders, J. de Bakker, and R. Coronel, Larger cell size in rabbits with heart failure increases myocardial conduction velocity and QRS duration. *Circulation*, 2006;**113**: 806–813.
140. Wang, Y. and Y. Rudy, Action potential propagation in inhomogeneous cardiac tissue: safety factor considerations and ionic mechanism. *Am. J. Physiol. Heart Circ. Physiol.*, 2000;**278**: H1019–H1029.
141. Shaw, R.M. and Y. Rudy, Ionic mechanisms of propagation in cardiac tissue. Roles of the sodium and L-type calcium currents during reducted excitability and decreased gap junction coupling. *Circ. Res.*, 1997;**81**: 727–741.

142. Spach, M.S., W.T. Miller, III, D.B. Geselowitz, R.C. Barr, J.M. Kootsey, and E.A. Johnson, The discontinuous nature of propagation in normal canine cardiac muscle. Evidence for recurrent discontinuities of intracellular resistance that affect the membrane currents. *Circ. Res.*, 1981;**48**: 39–54.
143. Spach, M.S., P.C. Dolber, and J.F. Heidlage, Influence of the passive anisotropic properties on directional differences in propagation following modification of the sodium conductance in human atrial muscle. A model of reentry based on anisotropic discontinuous propagation. *Circ. Res.*, 1988;**62**: 811–832.
144. Sugiura, H. and R.W. Joyner, Action potential conduction between guinea pig ventricular cells can be modulated by calcium current. *Am. J. Physiol.*, 1992;**263**: H1591–H1604.
145. Rohr, S. and J.P. Kucera, Involvement of the calcium inward current in cardiac impulse propagation: induction of unidirectional conduction block by nifedipine and reversal by Bay K 8644. *Biophys. J.*, 1997;**72**: 754–766.
146. Spach, M.S., Transition from a continuous to discontinuous understanding of cardiac conduction. *Circ. Res.*, 2003;**92**:125–126.
147. van der Pol, B. and J. van der Mark, The heartbeat considered as a relaxation oscillation and an electrical model of the heart. *Philos. Mag.*, 1928;**6**: 763–775.
148. FitzHugh, R., Impulses and physiological states in theoretical models of nerve membrane. *Biophys. J.*, 1961;**1**: 445–466.
149. van Capelle, F.J.L. and D. Durrer, Computer simulation of arrhythmias in a network of coupled excitable elements. *Circ. Res.*, 1980;**47**: 454–466.
150. Hodgkin, A.L. and A.F. Huxley, A quantitative description of membrane current and its application to conduction and excitation in nerve. *J. Physiol.*, 1952;**117**: 500–544.
151. Noble, D., Cardiac action and pacemaker potentials based on the Hodgkin-Huxley equations. *Nature*, 1960;**188**: 495–497.
152. Noble, D., A modification of the Hodgkin-Huxley equations applicable to Purkinje fibre action and pace-maker potentials. *J. Physiol.*, 1962;**160**: 317–352.
153. McAllister, R.E., D. Noble, and R.W. Tsien, Reconstruction of the electrical activity of cardiac Purkinje fibres. *J. Physiol.*, 1975;**251**: 1–59.
154. DiFrancesco, D. and D. Noble, A model of cardiac electrical activity incorporating ionic pumps and concentration changes. *Philos. Trans. R. Soc. Lond. B Biol. Sci.*, 1985;**307**: 353–398.
155. Beeler, G.W. and H. Reuter, Reconstruction of the action potential of ventricular myocardial fibres. *J. Physiol.*, 1977;**268**:177–210.
156. Drouhard, J.P. and F.A. Roberge, Revised formulation of the Hodgkin-Huxley representation of the sodium current in cardiac cells. *Comput. Biomed. Res.*, 1987;**20**: 333–350.
157. Hilgemann, D.W. and D. Noble, Excitation-contraction coupling and extracellular calcium transients in rabbit atrium: reconstruction of the basic cellular mechanisms. *Proc. R. Soc. Lond. B Biol. Sci.*, 1987;**230**: 163–205.
158. Yanagihara, K., A. Noma, and H. Irisawa, Reconstruction of sino-atrial node pacemaker potential based on the voltage clamp experiments. *Jpn. J. Physiol.*, 1980;**30**: 841–857.
159. Irisawa, H. and A. Noma, Pacemaker mechanisms of rabbit sinoatrial node cells, in *Cardiac Rate and Rhythm*, L.N. Bouman and H.J. Jongsma, Editors. The Hague: Nijhoff, 1982, pp. 35–51.
160. Bristow, D.G. and J.W. Clark, A mathematical model of primary pacemaking cell in SA node of the heart. *Am. J. Physiol.*, 1982;**243**: H207–H218.
161. Noble, D. and S.J. Noble, A model of sino-atrial node electrical activity based on a modification of the DiFrancesco-Noble (1984) equations. *Proc. R. Soc. Lond. B Biol. Sci.*, 1984;**222**: 295–304.
162. Noble, D., D. DiFrancesco, and J.C. Denyer, Ionic mechanisms in normal and abnormal cardiac pacemaker activity, in *Neuronal and Cellular Oscillators*, J.W. Jacklet, Editor. New York: Marcel Dekker, 1989, pp. 59–85.
163. Noble, D., S.J. Noble, G.C. Bett, Y.E. Earm, W.K. Ho, and I.K. So, The role of sodium-calcium exchange during the cardiac action potential. *Ann. NY Acad. Sci.*, 1991;**639**: 334–353.
164. Earm, Y.E. and D. Noble, A model of the single atrial cell: relation between calcium current and calcium release. *Proc. R. Soc. Lond. B Biol. Sci.*, 1990;**240**: 83–96.
165. Luo, C.-H. and Y. Rudy, A model of the ventricular cardiac action potential: depolarization, repolarization and their interaction. *Circ. Res.*, 1991;**68**: 1501–1526.
166. Nordin, C., Computer model of membrane current and intracellular Ca^{2+} flux in the isolated guinea pig ventricular myocyte. *Am. J. Physiol.*, 1993;**265**: H2117–H2136.
167. Luo, C.-H. and Y. Rudy, A dynamic model of the cardiac ventricular action potential, I: simulations of ionic currents and concentration changes. *Circ. Res.*, 1994;**74**: 1071–1096.
168. Jafri, S., J.R. Rice, and R.L. Winslow, Cardiac Ca^{2+} dynamics: the roles of ryanodine receptor adaptation and sarcoplasmic reticulum load. *Biophys. J.*, 1998;**74**: 1149–1168.
169. Noble, D., A. Varghese, P. Kohl, and P. Noble, Improved guinea-pig ventricular cell model incorporating a diadic space, i_{Kr} and i_{Ks}, and length- and tension-dependent processes. *Can. J. Cardiol.*, 1998;**14**: 123–134.
170. Priebe, L. and D.J. Beuckelmann, Simulation study of cellular electric properties in heart failure. *Circ. Res.*, 1998;**82**: 1206–1223.
171. Winslow, R.L., J. Rice, S. Jafri, E. Marbán, and B. O'Rourke, Mechanisms of altered excitation-contraction coupling in canine tachycardia-induced heart failure, II: model studies. *Circ. Res.*, 1999;**84**: 571–586.
172. Pandit, S.V., R.B. Clark, W.R. Giles, and S.S. Demir, A mathematical model of action potential heterogeneity in adult rat left ventricular myocytes. *Biophys. J.*, 2001;**81**: 3029–3051.
173. Demir, S.S., J.W. Clark, C.R. Murphey, and W.R. Giles, A mathematical model of a rabbit sinoatrial node cell. *Am. J. Physiol.*, 1994;**266**: C832–C852.
174. Puglisi, J.L. and D.M. Bers, LabHEART: an interactive computer model of rabbit ventricular myocyte ion channels and Ca transport. *Am. J. Physiol. Cell Physiol.* 2001;**281**: C2049–C2060.
175. Bernus, O., R. Wilders, C.W. Zemlin, H. Verschelde, and A.V. Panfilov, A computationally efficient electrophysiological model of human ventricular cells. *Am. J. Physiol. Heart Circ. Physiol.*, 2002;**282**: H2296–H2308.
176. Matsuoka, S., N. Sarai, S. Kuratomi, K. Ono, and A. Noma, Role of individual ionic current systems in ventricular cells hypothesized by a model study. *Jpn. J. Physiol.*, 2003;**53**:105–123.
177. Bondarenko, V.E., G.P. Szigeti, G.C. Bett, S.J. Kim, and R.L. Rasmusson, Computer model of action potential of mouse ventricular myocytes. *Am. J. Physiol. Heart Circ. Physiol.*, 2004;**287**: H1378–H1403.

178. Shannon, T.R., F. Wang, J. Puglisi, C. Weber, and D.M. Bers, A mathematical treatment of integrated Ca dynamics within the ventricular myocyte. *Biophys. J.*, 2004;**87**: 3351–3371.

179. ten Tusscher, K.H., D. Noble, P.J. Noble, and A.V. Panfilov, A model for human ventricular tissue. *Am. J. Physiol. Heart Circ. Physiol.*, 2004;**286**: H1573–H1589.

180. Iyer, V., R. Mazhari, and R.L. Winslow, A computational model of the human left-ventricular epicardial myocyte. *Biophys. J.*, 2004;**87**: 1507–1525.

181. Hund, T.J. and Y. Rudy, Rate dependence and regulation of action potential and calcium transient in a canine cardiac ventricular cell model. *Circulation*, 2004;**110**: 3168–3174.

182. Lindblad, D.S., C.R. Murphey, J.W. Clark, and W.R. Giles, A model of the action potential and underlying membrane currents in a rabbit atrial cell. *Am. J. Physiol.*, 1996;**271**: H1666–H1691.

183. Courtemanche, M., R.J. Ramirez, and S. Nattel, Ionic mechanisms underlying human atrial action potential properties: insights from a mathematical model. *Am. J. Physiol.*, 1998;**275**: H301–H321.

184. Nygren, A., C. Fiset, L. Firek, J.W. Clark, D.S. Lindblad, R.B. Clark, and W.R. Giles, Mathematical model of an adult human atrial cell: the role of K^+ currents in repolarization. *Circ. Res.*, 1998;**82**: 63–81.

185. Ramirez, R.J., S. Nattel, and M. Courtemanche, Mathematical analysis of canine atrial action potentials: rate, regional factors, and electrical remodeling. *Am. J. Physiol. Heart Circ. Physiol.*, 2000;**279**: H1767–H1785.

186. Wilders, R., H.J. Jongsma, and A.C.G. van Ginneken, Pacemaker activity of the rabbit sinoatrial node: a comparison of mathematical models. *Biophys. J.*, 1991;**60**: 1202–1216.

187. Dokos, S., B. Celler, and N. Lovell, Ion currents underlying sinoatrial node pacemaker activity: a new single cell mathematical model. *J. Theor. Biol.*, 1996;**181**: 245–272.

188. Demir, S.S., J.W. Clark, and W.R. Giles, Parasympathetic modulation of sinoatrial node pacemaker activity in rabbit heart: a unifying model. *Am. J. Physiol.*, 1999;**276**: H2221–H2244.

189. Zhang, H., A.V. Holden, I. Kodama, H. Honjo, M. Lei, T. Varghese, and M.R. Boyett, Mathematical models of action potentials in the periphery and center of the rabbit sinoatrial node. *Am. J. Physiol. Heart Circ. Physiol.*, 2000;**279**: H397–H421.

190. Zhang, H., A.V. Holden, D. Noble, and M.R. Boyett, Analysis of the chronotropic effect of acetylcholine on sinoatrial node cells. *J. Cardiovasc. Electrophysiol.*, 2002;**13**: 465–474.

191. Zhang, H., A.V. Holden, and M.R. Boyett, Sustained inward current and pacemaker activity of mammalian sinoatrial node. *J. Cardiovasc. Electrophysiol.*, 2002;**13**: 809–812.

192. Kurata, Y., I. Hisatome, S. Imanishi, and T. Shibamoto, Dynamical description of sinoatrial node pacemaking: improved mathematical model for primary pacemaker cell. *Am. J. Physiol. Heart Circ. Physiol.*, 2002;**283**: H2074–H2101.

193. Sarai, N., S. Matsuoka, S. Kuratomi, K. Ono, and A. Noma, Role of individual ionic current systems in the SA node hypothesized by a model study. *Jpn. J. Physiol.*, 2003;**53**:125–134.

194. Lovell, N.H., S.L. Cloherty, B.G. Celler, and S. Dokos, A gradient model of cardiac pacemaker myocytes. *Prog. Biophys. Mol. Biol.*, 2004;**85**: 301–323.

195. Krogh-Madsen, T., P. Schaffer, A.D. Skriver, L.K. Taylor, B. Pelzmann, B. Koidl, and M.R. Guevara, An ionic model for rhythmic activity in small clusters of embryonic chick ventricular cells. *Am. J. Physiol. Heart Circ. Physiol.*, 2005;**289**: H398–H413.

196. Kneller, J., R.J. Ramirez, D. Chartier, M. Courtemanche, and S. Nattel, Time-dependent transients in an ionically based mathematical model of the canine atrial action potential. *Am. J. Physiol. Heart Circ. Physiol.*, 2002;**282**: H1437–H1451.

197. Endresen, L.P., K. Hall, J.S. Hoye, and J. Myrheim, A theory for the membrane potential of living cells. *Eur. Biophys. J.*, 2000;**29**: 90–103.

198. ten Tusscher, K.H., O. Bernus, R. Hren, and A.V. Panfilov, Comparison of electrophysiological models for human ventricular cells and tissues. *Prog. Biophys. Mol. Biol.*, 2006;**90**: 326–345.

199. Wilders, R. and H.J. Jongsma, Beating irregularity of single pacemaker cells isolated from the rabbit sinoatrial node. *Biophys. J.*, 1993;**65**: 2601–2613.

200. Zaniboni, M., A.E. Pollard, L. Yang, and K.W. Spitzer, Beat-to-beat repolarization variability in ventricular myocytes and its suppression by electrical coupling. *Am. J. Physiol. Heart Circ. Physiol.*, 2000;**278**: H677–H687.

201. Guevara, M.R. and T.J. Lewis, A minimal single-channel model for the regularity of beating in the sinoatrial node. *Chaos*, 1995;**5**: 174–83.

202. Greenstein, J.L. and R.L. Winslow, An integrative model of the cardiac ventricular myocyte incorporating local control of Ca^{2+} release. *Biophys. J.*, 2002;**83**: 2918–2945.

203. Henriquez, C.S., Simulating the electrical behavior of cardiac tissue using the bidomain model. *Crit. Rev. Biomed. Eng.*, 1993;**21**: 1–77.

204. Potse, M., B. Dubé, J. Richer, A. Vinet, and R.M. Gulrajani, A comparison of monodomain and bidomain reaction-diffusion models for action potential propagation in the human heart. *IEEE Trans. Biomed. Eng.*, 2006;**53**(12): 2425–2435.

205. Fenton, F. and A. Karma, Vortex dynamics in three-dimensional continuous myocardium with fiber rotation: filament instability and fibrillation. *Chaos*, 1998;**8**: 20–47.

206. Sarai, N., S. Matsuoka, and A. Noma, SimBio: a Java package for the development of detailed cell models. *Prog. Biophys. Mol. Biol.*, 2006;**90**: 360–377.

207. Mazhari, R., J.L. Greenstein, R.L. Winslow, E. Marbán, and H.B. Nuss, Molecular interactions between two long-QT syndrome gene products, HERG and KCNE2, rationalized by in vitro and in silico analysis. *Circ. Res.*, 2001;**89**: 33–38.

4 Activation of the Heart

M.J. Janse

P. W. Macfarlane, A. van Oosterom, O. Pahlm, P. Kligfield, M. Janse, J. Camm (eds.), *Comprehensive Electrocardiology*, DOI 10.1007/978-1-84882-046-3_4,

4.1 Introduction

The cardiac electrical impulse is initiated in the sinoatrial node and spreads rapidly over the atria, slowly through the atrioventricular node, and rapidly over the specific ventricular conduction system and myocardium of both ventricles. These excitable tissues are able to generate an action potential in response to a suprathreshold current stimulus. The voltage difference between excited and resting tissue drives local current circuits that excite the resting tissue thereby causing spread of excitation in a wave-like manner. The main factors that determine propagation are (1) the properties of the ionic channels in the cell membrane, (2) the passive electrical properties of the tissue, and (3) in two- or three-dimensional media the curvature of the excitation wave. In atrial and ventricular myocardium, and in the specific ventricular conduction system, the current responsible for the action potential upstroke and for delivering local current for propagation is carried by Na^+ ions. In the cells of the sinoatrial node and the atrioventricular node a major contribution is made by the Ca^{2+} current. In tissue with a high degree of electrical cell-to-cell uncoupling and in tissue with geometrical discontinuity, flow of inward Ca^{2+} current becomes necessary to maintain propagation [2, 3]. The various regions of the heart differ with respect to distribution of ionic channels, and with respect to passive electrical properties, which depend on cell morphology, type and distribution of gap junctions, and the arrangement of cells in strands and layers. Therefore values of conduction velocity vary from about 0.05 m/s, the lowest value found in the atrioventricular node, to about 3.5 m/s, the highest value in the His-Purkinje system [4].

4.2 The Sinoatrial Node

The morphological sinoatrial, or sinus node, first described by Keith and Flack in 1907 [5], lies at the junction of the superior vena cava and the right atrium close to the crest of the atrial appendage. Its boundaries are not sharply defined in all species [6, 7]. The node consists of two types of myocytes [6–9]. The central nodal cells are arranged in a complex interdigitating manner interspersed with connective tissue. They contain very few myofilaments. The intracellular organized structures (myofilaments, mitochondria, nuclei and sarcoplasmic reticulum tubules) occupy only 50% of the cell volume, whereas in atrial cells these structures comprise 90% of cell volume. The second type of myocytes is transitional in that it changes gradually from the typical central nodal cell to an ordinary atrial cell. In some species, such as the rabbit, the zone of transitional cells is large, in others, such as the dog or the pig, it is narrow. The boundary between transitional and atrial cells is morphologically often poorly defined. Studies using immunohistochemical staining techniques did show a sharp boundary between nodal and atrial cells [10]. Nodal cells reacted with a monoclonal antibody against bovine Purkinje fibers and did not react to an antibody against connexion 43. Atrial cells on the other hand did not react to the antibody against Purkinje fibers but did react with the connexion 43 antibody. Since no electrophysiologic measurements were made, and no morphological studies were performed to quantify the number of intracellular organelles and filaments, no certainty exists whether some cells defined as atrial by immunohistochemical criteria might not be transitional according to other criteria. In a study combining immunohistochemistry, electrophysiology and electronmicroscopy [11], it was found, in contrast to previous studies, that atrial cells could be found in the very center of the node. Furthermore, the sinus node comprised three morphologically distinct cells that had the same electrophysiological characteristics. In contrast to the traditional concept of a transitional zone in which the transition from nodal cells to atrial cells occurred gradually, the situation in human, feline, and canine nodes is such that typical nodal cells are intermingled with atrial cells, and the transition is formed by a zone in which the density of atrial cells gradually increases from the central node to the crista terminalis [7, 11, 12].

A striking feature of the sinus node, including that in the human, is the presence of abundant connective tissue surrounding the nodal cells [13–17]. There are marked species differences regarding the amount of collagen. In cats 75–95% of the volume of the sinus node may consist of collagen; in pigs 75%, and in guinea-pigs 50% [14–16]. Attempts to correlate the amount of connective tissue with age yielded variable results. Thus, in humans approximately 50% of the sinus node in young individuals has been reported to be occupied by myocytes, while at the age of 70 years the proportion of the node occupied by myocytes may be as low as 10% [17]. In another study, the relative volume of collagen in the sinus node was found to remain constant once adulthood was reached in both cats and humans. No consistent relationship between the amount of collagen and sino-atrial conduction time could be established [18]. An increase in the amount of adipose tissue between the transitional cells has been reported to be age related [19].

The first combined electrophysiological and morphological studies on the pacemaker of the heart were performed in 1910 [20, 21]. The site of origin of the heartbeat was determined by searching for the site of primary extracellular negativity, which was found on the epicardial surface of the canine right atrium in the sulcus terminalis near the vena cava superior. This site of "primary negativity" coincided with the site of the histological sinus node. Transmembrane potentials from pacemaker cells were first recorded from the sinus venosus of the frog heart in 1952 [22] and in 1955 from the sinus node of mammalian hearts [23]. These studies revealed the most characteristic electrophysiological feature of pacemaking cells: spontaneous diastolic depolarization of the membrane potential. A number of ionic currents are involved in normal pacemaking in the sinus node: a decay in outward current carried by potassium ions following repolarization, an inward current carried by sodium ions, called If, which is activated after repolarization, and finally the slow inward current carried by calcium ions, which is activated as the membrane depolarizes [24–28].

In 1963 Trautwein and Uchizono [29] determined the ultrastructure of cells very close to cells from which typical pacemaker potentials were recorded, and in 1978 direct identification of the cell from which the pacemaker potential had been recorded was made [30]. Not unexpectedly, pacemaker potentials originated from nodal cells. Microelectrode recording in isolated, superfused rabbit heart preparations [8, 9, 31–34] resulted in maps depicting the spread of excitation during spontaneous sinus beats (see Fig. 4.1). Dominant pacemaker cells, i.e., those with the earliest action potential upstrokes, the fastest rate of diastolic depolarization, the slowest rate of rise of the action potential, and a gradual transition from diastolic to systolic depolarization, comprise a small area of about 0.3 mm square, containing about 5,000 cells that fire synchronously. Gap junctions, although less frequent than in transitional or atrial cells, were found in every cell contour in ultrathin sections. It was estimated that every cell in the pacemaker center was coupled to other cells via at least 100 gap junctions [8]. This is far in excess of what is needed to ensure synchronisation of diastolic depolarization [35, 36].

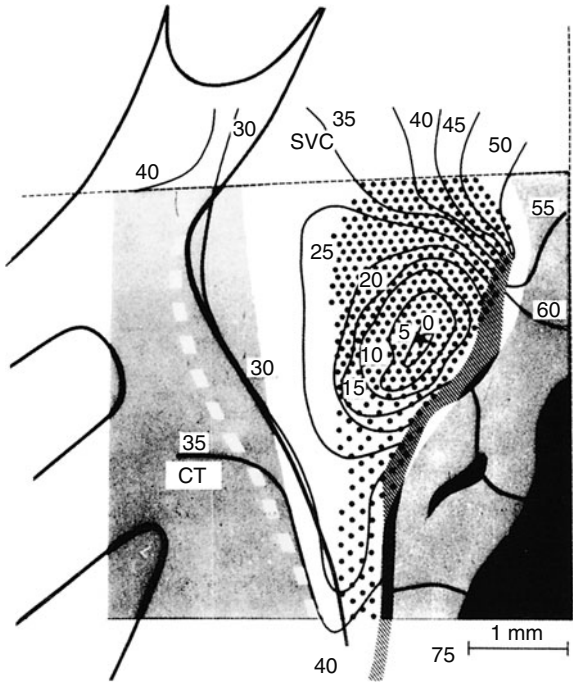

Figure 4.1

Isochronal map of spread of excitation from the sinus node of an isolated rabbit heart preparation. Numbers correspond to activation times in ms. Configuration of action potentials is shown along the pathway of conduction from central node towards the atrium. The dashed line indicates the beginning of the atrial electrogram used as a time reference. Towards the periphery the action potentials show an increase in amplitude and dV/dtmax and a decrease in the rate of diastolic depolarization. The hatched area is an area of conduction block (© reproduced with permission from Bleeker et al. [9]).

This is in apparent contrast with a study in which the sinus node failed to react with antibodies against connexion 43 [10], although in another study nodal cells did show a reaction [37].

Electrotonic interaction between atrial and nodal cells plays a crucial role in the functioning of the sinus node. Pacemaker activity in the peripheral transitional cells is suppressed because they are coupled to atrial cells, which do not have the capacity for spontaneous diastolic depolarization. Because the constant resting potential of atrial cells is more negative than the maximum diastolic potential of transitional cells, an electrotonic current flows from atrial to transitional cells, hyperpolarizing the latter and thus suppressing diastolic depolarization. When transitional cells are isolated from the surrounding atrium, their intrinsic pacemaking rate is actually higher than that from the centrally located "dominant" pacemaker [16, 38, 39]. Computer simulations have shown that a critical degree of coupling between atrial and transitional cells, as well as a gradual decrease in coupling resistance from central nodal cells towards the atrium, are necessary for the small group of nodal cells to activate the atrium. When coupling resistance is too low, electrotonic current from the large mass of surrounding atrial tissue will suppress diastolic depolarization. When coupling resistance is too high, the current provided by the small group of dominant pacemaker cells will not be sufficient to depolarize atrial cells to threshold [40].

As shown in Fig. 4.1 conduction from the central node towards the crista terminalis in the isolated rabbit heart preparation occurs preferentially in an oblique cranial direction. This can be explained by the tissue architecture, conduction being faster in areas where fibers are arranged in parallel. Conduction block occurs towards the interatrial septum, due to a reduced excitability of cells in this region [41]. In intact hearts, the excitation process is more complicated. First of all, alterations in the activity of the autonomic nervous system not only cause changes in sinus rate, they also produce pacemaker shifts. Under the influence of acetylcholine, the dominant pacemaker shifts away from the central area of the node towards transitional cells in the cauda; adrenalin induces a pacemaker shift towards a more inferior site [42–44]. Extracellular recordings form intact canine and human hearts [45, 46] showed that in the area of the sinus node two deflections of low amplitude and frequency precede the large high-frequency deflection caused by activity of atrial tissue: a "diastolic slope" corresponding to diastolic depolarization and an "upstroke slope" corresponding to systolic depolarization. Asynchronous activity of several pacemaking groups was recorded, suggesting that, despite strong coupling within one group of pacemaking cells, intergroup coupling may not be strong. Earliest right atrial activation could result from impulses arising from more than one automatic group within the sinus node. Studies by Boineau and coworkers in the canine heart showed that impulses were simultaneously initiated from up to three atrial sites separated by more than 1 cm [47–49]. Multiple depolarization waves originating from these sites, merged into a common wavefront after 10–15 ms. Changes in heart rate were associated with changes in the sites of origin. It was argued that these findings should be explained by a multicenter pacemaker model, and that the system of atrial pacemakers is much larger than the sinus node, extending both craniocaudally and mediolaterally. At extreme heart rates, extranodal pacemakers could dominate the pacemakers in the sinus node. Thus, whereas in isolated preparations the site of the dominant pacemaker is constant, in the heart in vivo, considerable pacemaker shifts may occur and the earliest activated atrial areas may shift as well. Fig. 4.2 shows that in the human heart, simultaneous atrial activation may occur at multiple sites [50]. To quote Cosio et al.: "The expression 'sinus node area' is commonly used as a reference for the diagnosis of ectopic atrial tachycardia; however, our data show that the origin of activation can be so wide as to make this expression almost meaningless" [50].

4.3 Subsidiary Pacemakers with Normal Automaticity

Cells with the capacity of spontaneous diastolic depolarization can be found in other areas of the heart besides the sinus node, particularly along the crista terminalis and in the inter-atrial septum, in the atrioventricular junction and in the specialized ventricular conduction system [51–53]. The intrinsic rate of impulse formation is highest in the sinus node and decreases progressively in pacemakers in the atrium, atrioventricular junction and His-Purkinje system. Normally, the sinus node is the dominant pacemaker over a wide range of heart rates because diastolic depolarization of latent pacemakers is inhibited by repeated excitation by impulses from the sinus node. This inhibition is called overdrive suppression [54]. Overdrive suppression is mediated by enhanced activity of the Na^+/K^+ pump. This pump, depending on energy derived from a membrane-bound ATPase, is responsible for maintaining ionic homeostase by pumping Na^+ ions

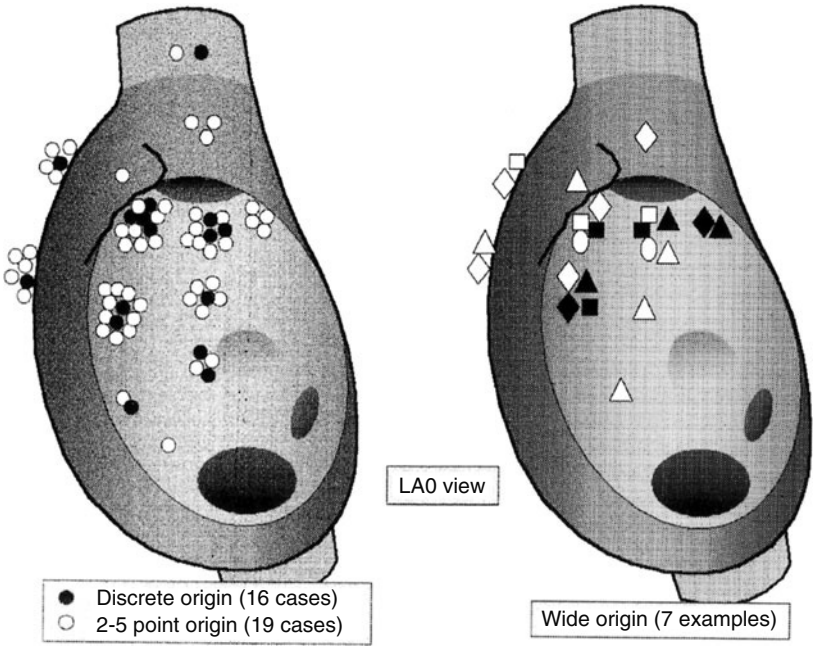

Figure 4.2

Schematic representation of the right human atrium in a left anterior oblique view displaying points of earliest activation. The orifices of the superior vena cava, inferior vena cava, coronary sinus, and the ring of the oval fossa are shown for orientation. *Left*: Points of onset of activation in all patients are represented in black for cases with single endocardial zero points and in white for cases with multiple points of onset. *Right*: Seven examples of onset of activation simultaneously in multiple points are represented. Each shape and tone (black or white) identifies multiple sites in each patient (© reproduced with permission from Cosio et al. [50]).

that entered the cell during the action potential upstroke out of the cell, and pumping K^+ ions that left the cell during repolarization back into the cell. When a latent pacemaker is driven by the sinus node at a faster rate than its normal intrinsic rate more Na^+ ions enter the cell than would have been the case if the pacemaker were firing at its own intrinsic rate. The activity of the Na^+/K^+ pump is largely determined by the level of intracellular Na^+ concentration [55], so that pump activity is enhanced during high rates of stimulation. Since the pump drives three Na^+ ions out of the cell against two K^+ ions into the cell, it generates a net outward current that hyperpolarizes the cell membrane and counteracts inward currents responsible for spontaneous diastolic depolarization. If the dominant pacemaker is stopped, for example by strong vagal stimulation, the overdrive suppression is responsible for a period of quiescence which lasts until the intracellular Na^+ concentration, and hence pump current, becomes small enough to allow subsidiary pacemakers to depolarize spontaneously to threshold. Impulse generation by latent pacemakers begins at a low rate and gradually speeds up to a final steady state. When sudden atrioventricular block occurs and pacemaker cells in the distal atrioventricular node or His-Purkinje cells need a long time to recover from overdrive suppression, the period of cardiac standstill may be long enough to cause loss of consciousness (Adams-Stokes attack).

Another mechanism that may suppress subsidiary pacemakers is electrotonic interaction between pacemaker cell and non-pacemaker cells. This mechanism is particularly important in preventing overt pacemaker activity in the central part of the atrioventricular node. In these cells the action potential upstroke is, like that of the central sinus node, largely dependent on the slow inward calcium current. Therefore, in those cells far less Na^+ ions enter the cell than in cells of the atrium and His-Purkinje system. As a result there is far less stimulation of the Na^+/K^+ pump during overdrive and less overdrive suppression. Isolated small preparations of atrioventricular nodal cells have intrinsic pacemaker activity that is as rapid as that in the sinus node and is not easily overdrive suppressed [53]. Because of electrotonic inhibition, ectopic

pacemaker activity seldom occurs in the central atrioventricular node. Normally, the atrioventricular nodal pacemakers that drive the heart during complete atrioventricular block are located in the distal node [51]. These cells are overdrive suppressible.

4.4 Atrial Activation

Lewis, who was the first to map the spread of excitation in the atria, described this process as follows: "the excitation wave in the auricle may be likened to the spread of fluid poured upon a flat surface, its edges advancing as an ever widening circle, until the whole surface is covered; such variation as exists in the rate of travel along various lines in the auricle is fully accounted for by the simple anatomical arrangement of the tissue" [56]. In the accompanying figure the isochrones deviate over the crista terminalis, indicating preferential conduction over that bundle. The right atrium is a "bag full of holes." The orifices of the superior and inferior vena cava, the ostium of the coronary sinus, and the fossa ovalis divide the atrial myocardium into various muscular bands. Owing to this architecture, there are only a limited number of routes available for conduction of the impulse from sinus node to atrioventricular node. From the many studies in which atrial activation was mapped [31, 58–66], it emerged that internodal conduction follows routes indicated by gross anatomical landmarks. The crista terminalis and the anterior limb of the fossa ovalis are the main routes for preferential conduction between the sinus node and the atrioventricular node, and these prominent muscle bands provide a dual input to the atrioventricular node. A similar activation sequence as that found in isolated rabbit heart was found in the human heart during surgery [66]. Here also, the AV node received a dual input. In most patients, the anterior septum was activated some 10 ms prior to the posterior input via the crista terminalis. In patients with a low crista terminalis pacemaker the AV node was activated via the crista terminalis 15–20 ms before activation of the anterior input (NB: in the older literature the terms anterior and posterior are used. Given the position of the heart in the body, it is better to use "superior" instead of "anterior," and "inferior" instead of "posterior").

There are two main routes for the sinus impulse towards the left atrium: an anterior one corresponding to Bachmann's bundle, and a posterior one via interatrial posteromedial connections inserting around the orifices of the right pulmonary veins [67, 68]. Some authors consider Bachmann's bundle as the most important connection [67], others find the posterior interatrial connection as important as Bachmann's bundle for activation from right to left, whereas activation from left to right occurs predominantly via Bachmann's bundle [68].

Irrespective of the site of earliest breakthrough, the pattern of left atrial activation is determined by a line of conduction block related to an abrupt change in left atrial endocardial fiber orientation and wall thickness at the lateral margin of the septal pulmonary bundle as this traverses the posterior left atrium between the pulmonary veins towards the septal mitral annulus [69]. A third interatrial connection exists through the coronary sinus [70–74]. This muscular connection has a variable anatomy in the human heart [74], and is particularly important during pacing from the coronary sinus [68].

A typical feature of left atrial activation is that different wavefronts simultaneously proceed in different directions and that wavefronts frequently collide [50, 61]. In a study on atrial activation of the horse, it was said that the explanation for the "chaotic pattern of left atrial activation may be that the two great pulmonary veins break the left atrial surface into discontinuous islets in which no general front of depolarization can develop" [62]. The major portion of the left atrium depolarizes after right atrial activation has been completed. In the canine heart, atrial activation is completed in approximately 60 ms, in the isolated human heart after 90–100 ms [59, 61, 63].

During retrograde atrial activation, studied while pacing the ventricles at a rate higher than the sinus rate, the pattern of left atrial activation is similar to that during sinus rhythm [63, 64, 75–77]. The retrograde wavefront quickly spreads up the interatrial septum to emerge very early at Bachmann's bundle. Activation then proceeds over this bundle to activate the left atrium in much the same way as during sinus rhythm. When the atrium is paced from the posteroinferior left atrium or from a site just posterior (or rather inferior) to the ostium of the coronary sinus, Bachmann's bundle is activated late, and P waves in leads I, III, and avF are negative. When Bachmann's bundle was activated early, as during ventricular pacing or from an atrial site anterior (superior) to the coronary sinus, P waves are positive [75, 77]. The time of arrival of a retrograde wavefront at Bachmann's bundle is therefore critical in determining the polarity of a "retrograde" P wave.

4.5 Specialized Internodal Pathways?

Controversy regarding the spread of activation of the sinus impulse has existed since the discovery of the sinus node and the atrioventricular node. In 1909 Thorel [78] claimed to have demonstrated continuity between both nodes via a tract of "Purkinje-like" cells. This possibility was debated during a meeting of the Deutschen pathologischen Gesellschaft in 1910 [79] and the consensus of this meeting was that both nodes were connected by simple atrial myocardium. In the 1960s and 1970s, the concept of specialized internodal tracts was again promoted, notably by James [70]. This promotion was so successful that the tracts are denoted in the well-known atlas of Netter [80] in a fashion analogous to that used to delineate the ventricular specialized conduction system. In the 1960s and 1970s pediatric cardiac surgeons took care not to damage these tracts. The specialized tracts were considered to play a role in the genesis of atrial flutter [81]. A review of the early literature, together with own experimental and histological data was presented by Janse and Anderson in 1974 [82]. It was concluded that there was no well-defined specialized conduction system connecting the sinus node to the atrioventricular node. The definitive proof that specialized internodal tracts do not exist was given by Spach and co-workers [83]. They argued that preferential conduction in atrial bundles could either be due to the anisotropic properties of the tissue or to the presence of a specialized tract. If the point of stimulation would be shifted to various sites of the bundle, isochrones of similar shape would result from stimulating multiple sites if the anisotropic properties primarily influenced local conduction velocities. On the other hand, isochrones of different shapes would be obtained if there was a fixed position specialized tract in the bundle. Their experimental results clearly provided evidence that preferential conduction in the atria is due to the anisotropic properties of cardiac muscle.

4.6 The Atrioventricular Junction

The atrial part of the atrioventricular (AV) junction is contained within the triangle of Koch, as depicted for the human heart in ❯ Fig. 4.3. The triangle is delineated by the tendon of Todaro, the attachment of the septal leaflet of the tricuspid valve, and by the ostium of the coronary sinus. In 1906, Tawara [85] described a spindle-shaped compact network of small cells in the superior part of Koch's triangle. These cells were connected via *Knotenpunkte* in which four or five fibers were joined together. It was this characteristic that prompted him "for simplicity's sake" to call this compact network *Knoten* (node). Nowadays, this part of the AV junction is usually called the compact node. The compact node is surrounded by transitional cells. Although Tawara did not use the term transitional cells, he wrote that between the compact node and the atrial musculature "the cells are very small. They do not form a complicated network, but course more or less parallel. They are joined into several small bundles, separated by strands of connective tissue, which in this area is abundant" (p. 136). "These bundles are connected to atrial muscle. . .these connections are so gradual that no sharp boundary can be detected. . . . Either single cells become gradually larger and change inconspicuously into atrial fibers, or several small bundles gradually join into a broader bundle which then merges with atrial muscle" (p. 137). There is room for confusion when speaking of the atrioventricular (AV) node, because some authors mean by this the compact node only, others the whole area occupied by compact node and transitional cells. Tawara was unable to determine precisely where the atrium ended and the specialized AV nodal region begins, because of the gradual change from atrial to transitional cells, as were subsequent investigators [86–88]. When traced superiorly, the compact node, without any perceptible change in cellular configuration, enters the central fibrous body. This point marks the transition from compact node to the penetrating atrioventricular bundle, or bundle of His. Tawara noted that at the point of entry in the central fibrous body, typical nodal cells were interspersed with larger His bundle cells. Again, on a histological basis, he could not tell where the AV node ended and the His bundle began. "I set the boundary at the site where this system penetrates into the membranous septum" (p. 127; all quotations from Tawara are in my translation).

4.7 Activation of the Atrioventricular Nodal Area

In 1960, Paes de Carvalho and de Almeida studied the activation pattern of the AV node in isolated rabbit heart preparations [87]. Based on activation times and transmembrane action potential characteristics, they described three cell

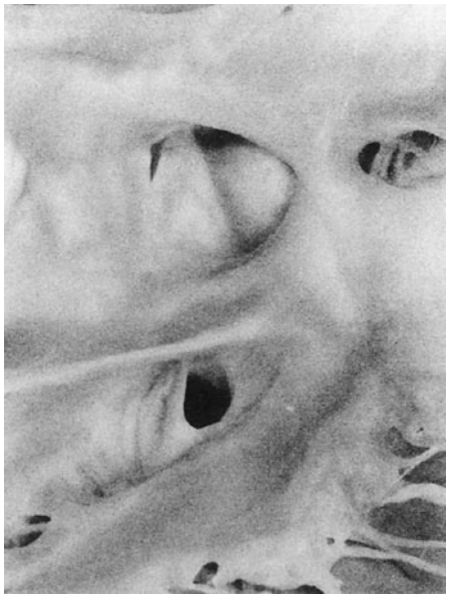

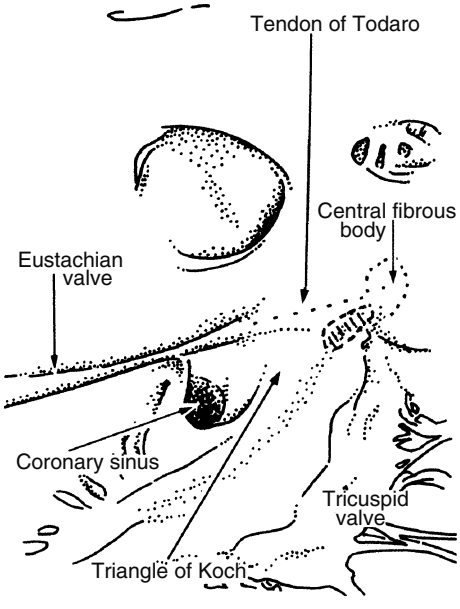

Figure 4.3

Anatomy of the AV junction. Photograph and sketch of a normal human heart showing the anatomical landmarks of the triangle of Koch. The approximate site of the compact AV node is indicated by the stippled area adjacent to the central fibrous body (© reproduced with permission from Janse et al. [84]).

types arranged in different layers and classified them into atrionodal (AN), nodal (N), and nodo-His (NH). N cells had action potentials with low amplitudes and upstroke velocities, the AN zone was a transitional zone between fast conducting atrial tissue and the slowly conducting N zone, and the NH zone was a transitional zone between the N zone and the His bundle, where conduction became rapid and action potential upstroke velocity became high. AN potentials were found to be generated by transitional cells, N potentials by the compact node, and NH potentials by the distal AV node [89]. However, N potentials could also be recorded from transitional cells and from cells in the tract of lower nodal cells in continuity with the His bundle. This raises the question whether there is a strict correlation between cellular electrophysiology and histology. In a study on isolated, arterially perfused canine and porcine hearts, it was found that cells with N type action potentials were not confined to the triangle of Koch, but extended along both AV orifices. These cells had low resting membrane potentials between −55 and −65 mV, a maximum upstroke velocity lower than 5 V/s, a low action potential amplitude between 45 and 65 mV, and they responded to the administration of adenosine by a further reduction of action potential amplitude and upstroke velocity. Histologically, these cells were similar to atrial cells, but they lacked the gap-junctional protein connexin 43 (Cx43) [90]. It is possible that immunohistochemistry is a more discriminating tool than light microscopy in delineating various cell types in the AV junction. Thus, Petrecca and co-workers [91] showed a paucity of sodium channel immunofluorescence in the central compact node. A gradual increase of expression was detected when moving to the peripherally located circumferential transitional cells. In the transitional zone, and in the lower nodal cell tract, levels of sodium channel immunoreactivity were comparable to that found in atrial and ventricular myocardium. The pattern of distribution of Cx43 was similar to that of the sodium channel, with a paucity of Cx43 immunoreactivity central mid-nodal cells. Both factors contribute to the slow conduction in the N zone.

There are only two studies in which mapping of Koch's triangle have been performed by both extra- and intracellular electrodes simultaneously [92, 93]. Mapping with extracellular electrodes is difficult because the rate of change in extracellular deflections may be very slow, because extracellular potentials may have multiple deflections, and because activation of the central node is a three-dimensional event where slow, low-amplitude action potentials in deep layers may not generate extracellular potentials of sufficient amplitude to be recorded by surface electrodes. The two studies mentioned above differ with respect to the cause of extracellular potentials with double components. In a study on superfused rabbit and canine preparations [92], where extracellular waveforms with multiple deflections were found at the posterior (inferior) approach to the node, the initial rapid deflection corresponded to the action potential upstroke of superficial atrial cells, the second, usually slower deflection originated from underlying nodal cells. In a study on arterially, blood-perfused canine and porcine hearts, the initial rapid deflection originated from deep atrial cells, the second slow deflection from more superficial nodal cells [93].

In shows an activation map of the superfused rabbit heart preparation, where sites transmembrane potential were recorded, the activation sequence is depicted in 20 ms intervals, with time zero being the activation time of a site close to the sinus node. The main features of the activation sequence are (1) there is a dual input into the AV nodal region, a posterior (inferior) one via the crista terminalis and an anterior (superior) one in front of the ostium of the coronary sinus; (2) in the central part of Koch's triangle, the activation pattern is complex and isochronal lines cannot be drawn. This is so in part because at one location superficial cells may be excited up to 40 ms earlier than deeper cells. The speed of propagation is very slow; it takes some 60 ms to cover a distance of about 1 mm, which corresponds to a conduction velocity in the order of 1.7 cm/s; (3) in the last part to be activated (at 90–110 ms), activation is rapid and synchronous. There is a sharp demarcation between cells activated early and cells activated late. The anterior (superior) input does not bypass the central node but curves posteriorly (inferiorly) to merge with the posterior (inferior) input. One feature is not apparent is this case is the existence of "dead-end pathways." These consist of cells that do not participate in transmitting the impulse from atrium to His bundle and vice versa. They can be identified by expressing their moment of excitation as a percent of the atrium-His bundle and His bundle-atrium conduction time during anterograde and retrograde conduction, respectively. The sum of these times for cells in the mainstream is around 100%. For dead end pathway cells, this sum far exceeds 100%, indicating that they activated too late in both modes of conduction. One dead-end pathway consists of atrial overlay fibers terminating in the base of the septal leaflet of the tricuspid valve, another one branches off the central node and extends posteriorly (inferiorly) along the tricuspid orifice [89, 95].

4.8 Dual Atrioventricular Nodal Pathways and Reentry

The two atrial inputs into the AV nodal area have different properties. When pacing the atria at a relatively fast rate, stimulation on the crista terminalis (inferior input) still results in 1:1 conduction to the His bundle, while pacing at the same rate on the superior input causes 2:1 block [96]. It is now customary to call these inputs "slow" and "fast" pathways, which are thought to underlie AV nodal reentry.

As early as 1913, Mines [97] described what he called a reciprocating rhythm after electrical stimulation of the auricle-ventricle preparation of the electric ray, a species which does not have a real atrioventricular node as described by Tawara. He reasoned that the atrioventricular connection had two divisions with a slight difference in the rate of recovery. A premature stimulus delivered to the ventricle "should spread up to the auricle by that part of the A-V connection having the quicker recovery process and not by the other part. In such a case, when the auricle would be excited by this impulse. The other portion of the A-V connection would be ready to take up transmission again back to the ventricle. Provided the transmission in each direction was slow, the chamber at either end would be ready to respond (its refractory phase being short) and thus the condition once established would tend to continue, unless upset by the interpolation of a premature systole" [97]. A similar explanation was given two years later by White, who described a clinical case where, during AV dissociation, idioventricular beats were sometimes conducted back to the atria, and the retrograde inverted P wave was followed by a narrow QRS complex [98]. In 1926, Scherf and Shookhoff studied reciprocating rhythms in dogs and introduced the term "longitudinal dissociation" [99], Moe et al. in 1956 suggested "dual AV transmission" [100], and Rosenblueth in 1958 coined the phrase "ventricular echoes" [101]. Reciprocation in the other direction, where an atrial premature impulse turns back in the AV node to reexcite the atria as an echo was also described [102].

When catheters were used for intracardiac recording and stimulation in patients, many studies reported on the induction of both atrial and ventricular echoes in hearts without apparent conduction abnormalities and without arrhythmias, so that functional longitudinal dissociation was considered to be a property of the normal AV node [102–106]. Animal studies supported this conclusion [100, 107, 108]. In some animal studies, it was possible, if only occasionally, to induce repetitive reciprocation leading to sustained AV nodal reentrant tachycardia [109–112], but in humans with normal AV nodal function this was not observed. In patients with spontaneous AV nodal reentrant tachycardias, this arrhythmia could easily be induced by premature stimulation [103, 106, 113].

A key factor thought to indicate the presence of dual AV pathways is the so-called discontinuity in the AV conduction curve during premature stimulation, which can be demonstrated both in individuals with and without spontaneous tachycardia [103, 106]. During atrial premature stimulation the interval between the premature atrial response and the subsequent His bundle deflection (the A2–H2 interval) gradually prolongs with increasing prematurity until at certain coupling interval it abruptly increases ("jumps") and then continues to increase gradually. The explanation is that with moderate prematurity AV conduction proceeds over a fast pathway that has a long refractory period. When at a certain coupling interval the fast pathway is refractory, conduction now occurs over the slow pathway having a shorter refractory period. During ventricular premature stimulation, the exits of slow and fast pathways correspond the posterior (inferior) and anterior (superior) inputs found in animal experiments [96, 114, 115]. These findings form the basis for successful surgical or catheter ablation of either fast or slow pathway to cure AV nodal reentrant tachycardia [116, 117]. No anatomical abnormalities have been detected in the AV nodal region in patients with proven dual AV nodal pathways [118], but it has been shown that fast and slow pathways are formed by connexin 43-expressing bundles, surrounded by tissue without connexin 43 [119].

There is a long standing debate on the precise location of the reentrant circuit, and on the question whether atrial tissue forms a substantial part of the circuit. Josephson and Miller [120] introduced premature atrial stimuli during the tachycardia prior to the time the atria would have been retrogradely activated by the reentrant wave. Even when perinodal atrial myocardium was depolarized 10–130 ms before the expected arrival of the retrograde wavefront, the tachycardia was not interrupted, nor was its cycle length changed. Mignone and Wallace [108] came to the same conclusion by showing that perinodal atrial tissue could be made refractory by pre-excitation without abolishing ventricular echoes. However, other investigators [121–123] suggested that atrial tissue, including the sinus septum above the ostium of the coronary sinus, is involved in the circuit. The fact that AV nodal reentrant tachycardia can successfully be terminated by catheter ablation of sites far from the compact node was also seen as evidence that atrial tissue is involved in the circuit. However, in isolated, blood-perfused canine hearts, it was demonstrated that the reentrant pathway during ventricular and atrial echo beats was confined to the compact node [124, 125]. Interestingly, in these hearts there was no "jump" in the AV or VA

conduction curve during premature stimulation of atria or right bundle branch. It is of course possible that in sustained AV nodal reentrant tachycardia, the circuit is different from that during single echo beats.

4.9 Factors That Cause AV Nodal Delay

There is no single factor responsible for the slowing of the impulse as it traverses the AV nodal area. Various geometrical factors, such as the small size of AV nodal cells, the paucity of intercellular connections, and the complex network of small bundles separated by connective tissue where summation and collision of impulses occur, play a role in addition to the role of the slow calcium inward current, which is the dominant current depolarizing AV nodal cells.

Conduction velocity in a linear cable is proportional to the square root of the fiber diameter. Given a diameter of Purkinje fibers of 50 μm, and of 7 μ for AV nodal cells, the ratio of conduction velocity of both tissues would be 2.7, if fiber diameter would be the only factor. In fact, the ratio is much higher, conduction velocity in the Purkinje system being in the order of meters per second, that in the N zone being less than 5 cm/s.

Several studies have measured space constants in the AV node [126–129]. The reported values are much lower than those for other cardiac tissue, with the lowest value in the N zone in the order of 170 μm. All measurements were made in superfused tissue, where the large volume of extracellular fluid acts as an extracellular shunt resistance. In densely packed tissue, extracellular resistance has a value similar to the intracellular resistance, and the space constant of arterially perfused papillary muscle is 357 μm, as compared to 528 μm in superfused tissue [130]. Thus, in the intact heart, the space constant of the densely packed compact node may be much smaller than that of isolated, superfused tissue. Assuming that the extracellular resistance would be the same as in an arterially perfused papillary muscle, and that intracellular resistance is a higher by a factor ten, conduction velocity in the node would be about three times less than in ventricular tissue, in the order of 20 cm/s, which still is about ten times that of the lowest values found in the N zone.

Summation of impulses, arriving more or less simultaneously over converging pathways, appears to play an important role in AV conduction [96, 131–133]. As already mentioned, AV nodal conduction is much less effective when the site of initial activation is switched from crista terminalis to the interatrial septum [96]. Zipes et al. [133] separated both nodal inputs by making a cut through the roof and floor of the coronary sinus. Premature stimulation of each input separately gave rise to a local response in an n cell, while simultaneous stimulation of both inputs resulted in a fully developed action potential that was propagated to the His bundle.

There is no doubt that the calcium current plays a dominant role in depolarizing nodal cells. However, the question whether central AV nodal cells have no sodium channels at all, or are merely inactivated by the low resting potential, has not been settled.

Recovery from inactivation of the slow calcium current is slow, and may lag behind completion of repolarization [134]. This may be an important factor in causing cycle length-dependent conduction delay. Figure 4.4 shows selected action potentials from the AV nodal area during application of five successive atrial premature stimuli at progressively shorter coupling intervals. The key feature is that with prolongation of the atrium-His bundle conduction time, the action potential upstroke of cells in the N region separate into two components. The first component coincides with the upstroke of the last activated AN cells, the second component with the upstroke of the earliest activated NH cells. No action potential were recorded with upstrokes occurring in between these two components. The cycle length-dependent conduction delay appears to be caused by a local discontinuity of conduction, rather than by a progressive slowing of continuous propagation. One may also speak of "saltatory" conduction. The explanation given by Billette et al. [135] is that the excitability of the N cells progressively diminished at short cycle lengths, so that at very short cycles the N cells acted as a purely passive barrier between late AN cells and early NH cells, capable only of transmitting electrotonic currents that would slowly bring NH cells to threshold.

4.10 Ventricular Activation

In the mammalian heart, the impulse that has passed through the AV node reaches the ventricular myocardium by way of the specialized conduction system, consisting of the His bundle, the main right and left bundle branches, and the peripheral Purkinje network, which at discrete sites – the Purkinje-ventricular muscle junctions – is in contact with

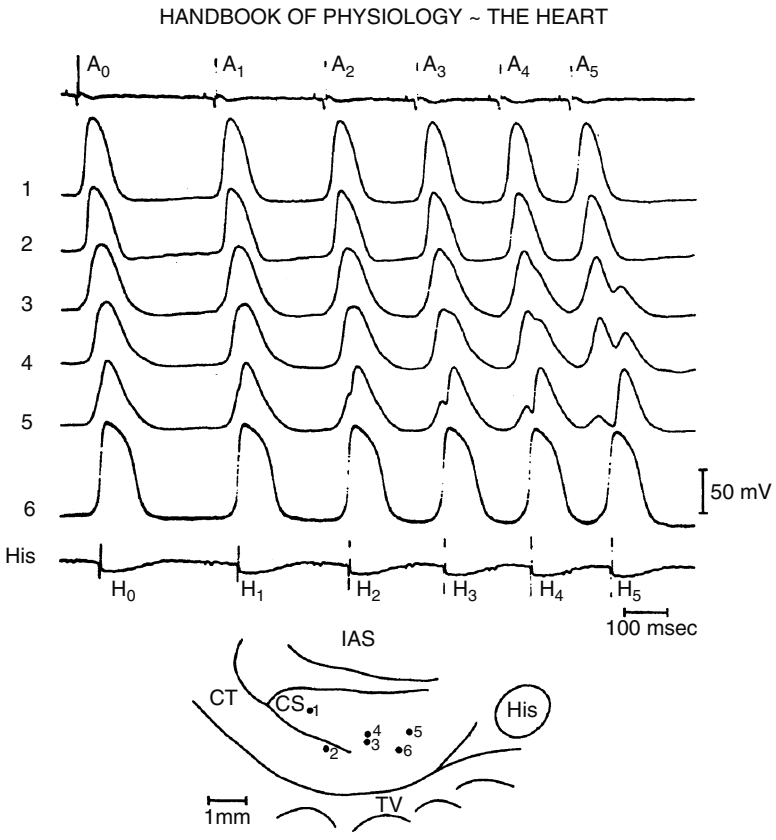

Figure 4.4

Cycle length-dependence of AV nodal conduction. Action potentials show dependency of first and second component of the upstroke of N cells on late AN cells and early NH cells. Signals 1 and 2 were recorded from AN cells, signals 3, 4 and 5 from N cells, and signal 6 from an NH cell. *Inset* shows position of cells. First component is largest in N cells close to AN cells, second component is largest in cells close to NH cells (© reproduced with permission from Billette et al. [135]).

ventricular myocardium. Proximal to the Purkinje-muscle junctions the specialized conduction system has no functional contact with the myocardium because it is isolated from it by a thin collagenous sheet [136]. Conduction velocity in the bundle branches is high, in the order of 2 m/s [4].

It is often assumed that the main left bundle in its course below the membranous part of the interventricular septum splits into two divisions: the anterior and posterior fascicles. As shown in Fig. 4.5, in a number of hearts there is a more or less separate middle fascicle occupying the left midseptal area [137]. This was already described by Tawara in 1906 [85]. In isolated, Langendorff-perfused human hearts, three distinct areas of initial myocardial activation have been found that correspond to the transition of these three fascicles into the peripheral Purkinje network (6, see Fig. 4.6).

Because of the many connections between the main branches of the left sided conduction system, only extensive lesions result in complete block in the left bundle branch system. In clinical electrocardiography, a distinction is made between incomplete bundle branch block, anterior and posterior fascicular block, and complete bundle branch block [138].

After activation of the subendocardial myocardium by the specialized conduction system, at anterior, midseptal and posterior sites on the septum, excitation of the left ventricular wall in the human and canine heart occurs by myocardial conduction in an endocardial to epicardial direction with a more or less concentric arrangement of the isochrones [63, 139]. Epicardial breakthrough in the human left ventricle occurs almost simultaneously in anterior and posterior paraseptal areas located halfway between apex and base, after about 30 ms following onset of ventricular activation.

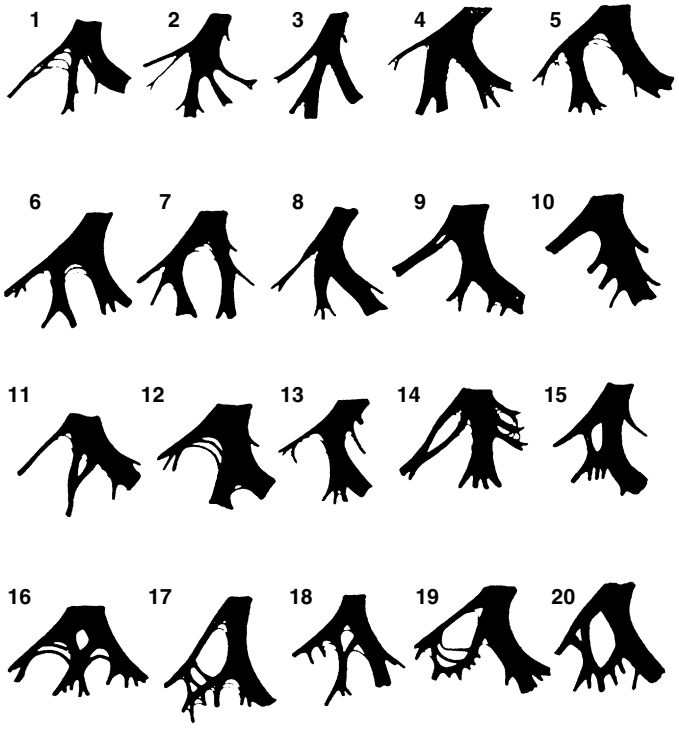

Figure 4.5

Division of the left bundle branch. An illustration of the variation of the structure of the divisions of the left bundle in 20 different human hearts (© reproduced with permission from Demoulin and Kulbertus [137]).

The septum is largely activated in a left-to-right direction, although a small part of this structure is activated in the opposite direction by a wavefront originating in the lower right septal surface. The basal portions of the septum, particularly the posterior parts, are devoid of Purkinje fibers and are the last to be depolarized.

The papillary muscles are activated via false tendons, consisting mainly of Purkinje fibers, that run through the ventricular cavity from the septal surface to the apex of the anterior and posterior papillary muscles. From there, activation proceeds over the sheet of Purkinje fibers to excite the muscles via the Purkinje-muscle junctions (see later) at their base, nearly synchronously with the onset of depolarization of the initially activated left septal areas.

The myocardium of the left ventricular wall consists of discrete muscle layers that follow a curving radial path from the subendocardium to the subepicardium [140]. To which extent the laminar organization of the ventricular wall affects propagation is unclear. Intramural recordings, utilizing needles with multiple electrodes at 1 mm distance have not revealed discontinuities in the spread of excitation from endocardium to epicardium [63]. On a microscopic scale, one might suppose that the pathway of activation is convoluted, if the muscle layers are electrically insulated and make contact only via direct muscle branches. It is possible that the structural anisotropy may lead to irregular pattern of activation when coupling between muscle layers becomes impaired, but direct evidence for this is lacking.

The right bundle branch in its course over the right endocardial surface of the septum ends at the base of the anterior papillary muscle, where it gives off branches to the lower right anterior surface of the septum, to the free right ventricular wall at the pretrabecular area, and to the subendocardial Purkinje network of the right ventricular free wall [140, 141]. Initial right ventricular activation occurs near the base of the papillary muscle and the overlying free wall (see Fig. 4.6). From there, activation proceeds in a right-to-left direction in the septum, and tangentially towards the epicardium of the right ventricular free wall. Right ventricular epicardial breakthrough occurs about 25 ms after onset of left septal activation. The last parts of the right ventricle to be activated are the outer layers of the outflow tract and the crista supraventricularis.

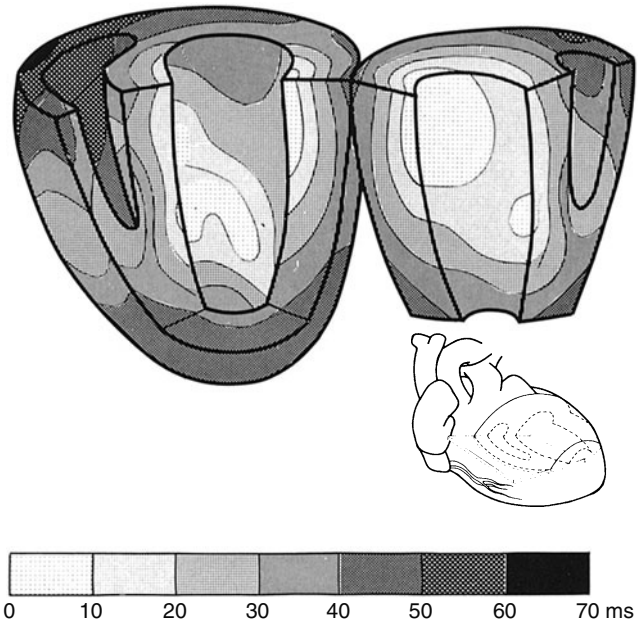

Figure 4.6

Activation sequence of ventricular myocardium in an isolated, Langendorff-perfused normal human heart, as determined from intramural electrodes. The ventricles are shown opened, according to the *inset* in the *lower right*. Note initial activation at three sites of the inside of the left ventricle and terminal activation in the right ventricular conus. Activation of the interventricular septum begins at the left endocardial surface and meets between 30 and 40 ms with an excitation front that has started at 20–25 ms in the right ventricle. Activation times are in milliseconds after the onset of left ventricular activation (© reproduced with permission from Durrer et al. [63]).

4.11 The Purkinje-Muscle Junction

The junctions between the terminal Purkinje fiber and ventricular muscle are electrophysiologically defined as sites where unipolar electrograms show a completely negative muscle deflection that is preceded by 2–5 ms by a Purkinje spike [142]. At non junctional sites where both Purkinje and muscle deflections are found, the muscle deflection is characterized by initial positivity ("R wave"). Unidirectional block has been shown to occur at Purkinje-muscle junctions, where conduction is maintained in a muscle-Purkinje direction but fails in the opposite direction [143, 144]. Mendez et al. proposed the "funnel" hypothesis in which "the narrow portion would correspond to a terminal Purkinje fiber whose conical part would be composed of a progressively increasing number of interconnected muscle fibers" [144]. In this view, the Purkinje network is seen as a branching cable, and at the Purkinje-muscle junction the "terminal" Purkinje fiber has to provide excitatory current to a three-dimensional mass of ventricular muscle. Joyner and co-workers suggested that the Purkinje network is better represented by a two-dimensional sheet that is coupled at discrete sites to the deeper muscle mass [142, 145, 146]. If coupling resistance at these sites is too low, the load that the large muscle mass imposes on the Purkinje network would prevent activation of the Purkinje sheet. If coupling resistance is too high, the Purkinje network could not deliver sufficient excitatory current to activate the muscle layers. A certain resistive barrier between the two tissues allows rapid propagation of the Purkinje layer over the endocardial surface to synchronize ventricular activation, facilitates ventricular activation, and maintains a longer action potential duration in the Purkinje layer as compared to ventricular muscle [145, 147]. Microelectrode recordings by Alanis and co-workers suggested that the delay between the Purkinje fiber and ventricular muscle was not due to slow conduction but to a "stop of the impulse in this region" [148]. Action potentials from junctional sites can be typical for Purkinje cells or ventricular muscle cells, or they can show upstrokes with multiple components. These latter action potentials were thought to arise from "transitional

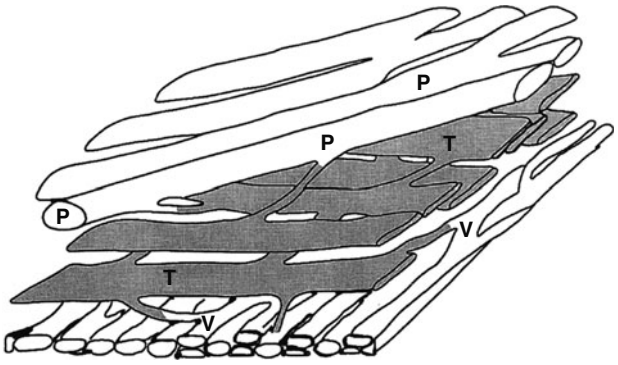

Figure 4.7

Schematic representation of the structure of a rabbit Purkinje-muscle junction. *P* Purkinje fibers, *T* transitional cells, *V* ventricular muscle (© reproduced with permission from Tranum Jensen et al. [149]).

cells" [148–150]. They show a slow foot and a dissociation of the upstroke into two or more components. This feature is consistent with the view that conduction at the junction is discontinuous and is compatible with the existence of one or several resistive barriers between Purkinje and muscle. Transitional cells in the rabbit heart are thin, broad, band-like cells (30–35 μm by 3–5 μm) arranged in one or two sheets in the subendocardium between Purkinje and muscle. Transitional cells are coupled via short, thin strands to both Purkinje and muscle fibers. Distances between Purkinje-transitional cell coupling sites and transitional cell-ventricular muscle coupling sites varied between 100 and 1, 000 μm. This arrangement is schematically depicted in Fig. 4.7 [149]. In this structure there are two high resistance barriers: the thin connections between Purkinje fibers and transitional cells and those between the sheet of transitional cells and ventricular muscle. In the pig, another type of Purkinje-muscle junction was frequently observed, but only rarely in the rabbit. Here, a short linear segment of small transitional cells connected large-diameter Purkinje cells to ventricular muscle. This arrangement would be compatible with the "funnel" hypothesis.

4.12 The M Cell

Besides the cells of the specialized conduction system there appear to be other specialized cells in the ventricle. There is one report on the existence of a bundle of slowly conducting cells on the left septal surface of the normal human heart [151]. This report awaits confirmation by other studies, and the functional significance is unclear.

Another specialized cell is the midmural M cell [152–155]. Its most conspicuous feature is that its action potential duration is significantly longer than that of epicardial or endocardial cells, especially at (very) long cycle lengths. In addition, their maximal upstroke velocity is considerably greater than that of epicardial and endocardial cells. The slowly activating component of the delayed rectifier, IKs, is smaller in M cells than in epicardial and endocardial cells, and this may account for the longer action potential duration of M cells [156]. Most attention has been given to the role of M cells in ventricular repolarization, but the latter feature suggests that M cells may conduct the impulse faster than other ventricular myocardial cells. As already mentioned, on a macroscopic scale (i.e., electrodes 1 mm apart) no discontinuities in propagation from endocardium to epicardium have been found [63].

The existence of M cells in isolated cells and isolated in vitro preparations is well documented, although they could not be found in myocytes form the pig heart [157]. However, their role in the intact heart is uncertain. Electrotonic interaction between cells with intrinsically different action potential durations will shorten the long action potentials and prolong the short ones. As summarized by Tan and Joyner "the isolated rabbit ventricular cell is extremely sensitive to even a very small electrical load, with shortening of the action potential by 50% with electrical coupling to a model cell (of similar input resistance and capacitance to the ventricular cell) as high as 1,000 MΩ, even though the action potential amplitude and current threshold are very insensitive to the electrical load" [158]. In a review by Anyukhovsky et al. [159], literature data

are summarized in their Fig. 4.9. The difference between longest and shortest action potential, or Activation-Recovery-Interval, are in the order of 20 ms for intact hearts, 40 ms for ventricular wedge preparations, 80 ms for thick myocardial slices, 120 ms for thin slices, and 90 ms for isolated cells. Most studies in intact hearts have failed to provide evidence for a midmyocardial layer with longer repolarization times. This was the case for studies in which refractory periods were measured at various depths in the left ventricular wall [160–164], and for studies in which Activation-Recovery-Intervals or repolarization times were measured at intramural sites in intact canine or human hearts [159, 165–168]. It therefore appears that in the intact heart, M cells have no functional significance.

References

1. Janse, M.J. and M.J. Davies, Generation and conduction of the heart beat and their disturbances, in *Diseases of the Heart*, 2nd ed., D.G. Julian, A.J. Camm, K.M. Fox, R.J.C. Hall, and P.A. Poole-Wilson, Editors. London, WB Saunders Company Ltd, 1996, pp. 88–114.
2. Kucera, J.P., A.G. Kléber, and S. Rohr, Slow conduction in cardiac tissue: II. Effects of branching tissue geometry. *Circ. Res.*, 1998;**83**: 795–805.
3. Shaw, R.M. and Y. Rudy, Ionic mechanisms of propagation in cardiac tissue. Roles of sodium and L-type calcium currents during reduced excitability and decreased gap junction coupling. *Circ. Res.*, 1997;**81**: 727–741.
4. Kléber, A.G., M.J. Janse, and V.G. Fast, Normal and abnormal conduction in the heart, in *Handbook of Physiology, section 2 The Cardiovascular System. Volume 1: The Heart*. New York, Oxford University Press, 2001, pp. 455–530.
5. Keith, A. and M. Flack, The form and nature of the muscular connections between the primary divisions of the vertebrate heart. *J. Anat. Physiol.*, 1907;**41**: 172–189.
6. Tranum-Jensen, J., The fine structure of the sinus node: a survey, in *The Sinus Node*, F.I.M. Bonke, Editor. The Hague, Nijhoff, 1978, pp. 149–165.
7. Opthof, T., The mammalian sinoatrial node. *Cardiovasc. Drugs Ther.*, 1988;**1**: 573–597.
8. Masson-Pévet, M., W.K. Bleeker, A.J.C. Mackaay, L.N. Bouman, and J.M. Houtkooper, Sinus node and atrial cells from the rabbit heart: a quantitative electron microscopic description after electrophysiological localization. *J. Mol. Cell. Cardiol.*, 1979;**11**: 555–568.
9. Bleeker, W.K., A.J.C. Mackaay, M. Masson-Pévet, L.N. Bouman, and A.E. Becker, Functional and morphological organization of the rabbit sinus node. *Circ. Res.*, 1980;**46**: 11–22.
10. Oosthoek, P.W., S. Viragh, A.E.M. Mayen, M.J.A. van Kempen, W.H. Lamers, and A.F.M. Moorman, Immunohistochemical delineation of the conduction system: I. The sinoatrial node. *Circ. Res.*, 1993;**73**: 473–481.
11. Verheijck, E.E., A. Wessels, A.C.G. van Ginneken, J. Bourier, M.W.M. Markman, J.L.M. Vermeulen, J.M.T. de Bakker, W.H. Lamers, T. Opthof, and L.N. Bouman, Distribution of atrial and nodal cells within the rabbit sinoatrial node. Models of sinoatrial transition. *Circulation*, 1998;**97**: 1623–1631.
12. Opthof, T., B. de Jonge, H.J. Jongsma, and L.N. Bouman, Functional morphology of the mammalian sinuatrial node. *Eur. Heart J.*, 1987;**8**: 1249–1259.
13. James, T.N., The sinus node. *Am. J. Cardiol.*, 1977;**40**: 965–986.
14. Opthof, T., B. de Jonge, A.J. Mackaay, W.K. Bleeker, M. Masson-Pévet, H.J. Jongsma, and L.N. Bouman, Functional and morphological organization of the guinea-pig sinoatrial node compared with the rabbit sinoatrial node. *J. Mol. Cell. Cardiol.*, 1985;**17**: 549–564.
15. Opthof, T., B. de Jonge, M. Masson-Pévet, H.J. Jongsma, and L.N. Bouman, Functional and morphological organization of the cat sinoatrial node. *J. Mol. Cell. Cardiol.*, 1986;**18**: 1015–1031.
16. Opthof, T., B. de Jonge, H.J. Jongsma, and L.N. Bouman, Functional morphology of the pig sinoatrial node. *J. Mol. Cell. Cardiol.*, 1987;**19**: 1221–1236.
17. Davies, M.J., Pathology of atrial arrhythmias, in *The Conduction System of the Heart*, M.J. Davies, R.H. Anderson, and A.E. Becker, Editors. London: Butterworths, 1983, pp. 203–215.
18. Alings, A.M.W., The aging sino-atrial node, Ph.D. thesis. University of Amsterdam, 1993.
19. Shiraishi, I., T. Takamatsu, T. Minamikawa, Z. Onouchi, and S. Fujita, Quantitative histological analysis of the human sinoatrial node during growth and aging. *Circulation*, 1992;**85**: 2176–2183.
20. Wybauw, R., Sur le point d'origine de la systole cardiaque dans l'oreillette droite. *Arch. Int. Physiol.*, 1910;**10**: 78–89.
21. Lewis, T., B.S. Oppenheimer, and A. Oppenheimer, The site of origin of the mammalian heart beat: the pacemaker in the dog heart. *Heart*, 1910;**2**: 147–169.
22. Trautwein, W. and K. Zink, Über Membran-und Aktionspotentiale einzelner Muskulfasern des Kalt-und Warmblüterherzens. *Pflug. Arch.*, 1952;**256**: 68–84.
23. West, T.C., Ultramicroelectrode recording from the cardiac pacemakers. *J. Pharmacol. Exp. Ther.*, 1955;**115**: 282–290.
24. Yanagihara, D. and H. Irisawa, Inward current activated during hyperpolarization in the rabbit sinoatrial node. *Pflüg. Arch.*, 1980;**385**: 11–19.
25. DiFrancesco, D. and C. Ojeda, Properties of the current if in the sino-atrial node of the rabbit compared with those of the current iK, in Purkinje fibers. *J. Physiol. (London)*, 1980;**308**: 353–367.
26. Reuter, H., Ion channels in cardiac cell membranes. *Annu. Rev. Physiol.*, 1984;**46**: 473–484.
27. DiFrancesco, D., A. Ferroni, M. Mazzanti, and C. Tromba, Properties of the hyperpolarizing-activated current (if) in cells isolated from the rabbit sino-atrial node. *J. Physiol. (London)*, 1986;**377**: 61–88.
28. Irisawa, H., H.F. Brown, and W. Giles, Cardiac pacemaking in the sinoatrial node. *Physiol. Rev.*, 1993;**73**: 197–227.

29. Trautwein, W. and K. Uchizono, Electrophysiologic study of the pacemaker in the sino-atrial node of the rabbit heart. *Z. Zellforsch*., 1963;**61**: 96–109.
30. Janse, M.J., J. Tranum-Jensen, A.G. Kléber, and F.J.L. van Capelle, Techniques and problems in correlating cellular electrophysiology and morphology in cardiac nodal tissue, in *The Sinus Node*, F.I.M. Bonke, Editor. The Hague: Nijhoff, 1978, pp. 183–194.
31. Sano, T. and S. Yamagishi, Spread of excitation from the sinus node. *Circ. Res*., 1965;**16**: 423–431.
32. Steinbeck, G., M.A. Allessie, F.I.M. Bonke, and W.E.J.P. Lammers, The response of the sinus node to premature stimulation of the atrium studied with microelectrodes in isolated preparations of the rabbit heart, in *The Sinus Node*, F.I.M. Bonke, Editor. The Hague: Nijhoff, 1978, pp. 245–257.
33. Bouman, L.N., A.J.C. Mackaay, W.K. Bleeker, and A.E. Becker, Pacemaker shifts in the sinus node. Effects of vagal stimulation, temperature, and reduction of extracellular calcium, in *The Sinus Node*, F.I.M. Bonke, Editor. The Hague: Nijhoff, 1978, pp. 245–257.
34. Bouman, L.N. and H.J. Jongsma, Structure and function of the SA node: a review. *Eur. Heart J*., 1986;**7**: 94–104.
35. de Haan, R.L., Discussion on models of entrainment of cardiac cells, in *Cardiac Rate and Rhythm*, L.N. Boumans and H.J. Jongsma, Editors. The Hague: Nijhoff, 1982, pp. 359–361.
36. Rook, M.B., B. de Jonge, and H.J. Jongsma, Gap junction formation and functional interaction between neonatal rat cardiocytes in culture. *J. Membr. Biol*., 1990;**118**: 179–192.
37. Trabka, J.E., W. Coombs, M. Lemanski, M. Delmar, and J. Jalife, Immunohistochemical localization of gap junctional channels in adult mammalian sinus nodal cells- immunolocalization and electrophysiology. *J. Cardiovasc. Electrophysiol*., 1994;**5**: 125–137.
38. Kodama, I. and M.R. Boyett, Regional differences in the electrical activity of the rabbit sinus node. *Pflug. Arch*., 1985;**404**: 214–226.
39. Kirchhof, C.J., F.I.M. Bonke, M.A. Allessie, and W.E.J.P. Lammers, The influence of the atrial myocardium on impulse formation in the rabbit sinus node. *Pflug. Arch*., 1987;**410**: 198–203.
40. Joyner, R.W. and F.J.L. van Capelle, Propagation through electrically coupled cells. How a small SA node drives a large atrium. *Biophys. J*., 1986;**50**: 1157–1164.
41. Opthof, T., W.K. Bleeker, M. Masson-Pévet, H.J. Jongsma, and L.N. Bouman, Little-excitable transitional cells in the rabbit sinoatrial node: a statistical, morphological and electrophysiological study. *Experientia*, 1983;**39**: 1099–1101.
42. Meek, W.J. and J.A.E. Eyster, Experiments on the origin and propagation of the impulse in the heart. IV. The effect of vagal stimulation and cooling on the location of the pacemaker within the sino-atrial node. *Am. J. Physiol*., 1914;**34**: 368–383.
43. Bouman, L.N., E.D. Gerlings, P.A. Biersteker, and F.I.M. Bonke, Pacemaker shift in the sino-atrial node during vagal stimulation. *Pflug. Arch*., 1968;**302**: 255–267.
44. Mackaay, A.J.C., T. Opthof, W.K. Bleeker, H.J. Jongsma, and L.N. Bouman, Interaction of adrenaline and acetylcholine on sinus node function, in *Cardiac Rate and Rhythm*, L.N. Bouman and H.J. Jongsma, Editors. The Hague: Nijhoff, 1982, pp. 507–523.
45. Hariman, R.J., B.F. Hoffman, and R.E. Naylor, Electrical activity from the sinus node region in conscious dogs. *Circ. Res*., 1980;**47**: 775–791.
46. Hariman, R.J., E. Krongrad, R.A. Boxer, F.O. Bowman, J.R. Malm, and B.F. Hoffman, Methods for recording electrograms from the sino-atrial node during cardiac surgery in man. *Circulation*, 1980;**61**: 1024–1029.
47. Boineau, J.P., R.B. Schuessler, C.R. Mooney, A.C. Wylds, C.B. Miller, R.D. Hudson, J.M. Borremans, and C.W. Brockus, Multicentric origin of the atrial depolarization wave: the pacemaker complex. Relation to dynamics of atrial conduction, P-wave changes and heart rate control. *Circulation*, 1978;**58**: 1036–1048.
48. Boineau, J.P., C.B. Miller, R.B. Schuessler, W.R. Roeske, L.J. Autry, A.C. Wylds, and D.A. Hill, Activation sequence and potential distribution maps demonstrating multicentric atrial impulse origin in dogs. *Circ. Res*., 1984;**54**: 332–347.
49. Schuessler, R.B., J.P. Boineau, and B.I. Bromberg, Origin of the sinus impulse. *J. Cardiovasc. Electrophysiol*., 1996;**7**: 263–274.
50. Cosio, F., A. Martín-Peñato, A. Pastor, A. Nuñez, M.A. Montero, C.P. Cantale, and S. Schames, Atrial activation mapping in sinus rhythm in the clinical electrophysiology laboratory: observations during Bachmann's bundle block. *J. Cardiovasc. Electrophysiol*., 2004;**15**: 524–531.
51. Hoffman, B.F. and P.F. Cranefield, *Electrophysiology of the Heart*. New York: McGraw-Hill, 1960.
52. Rozanski, G.J. and S.L. Lipsius, Electrophysiology of functional subsidiary pacemakers in the canine right atrium. *Am. J. Physiol*., 1985;**249**: H594–H601.
53. Kokobun, S., N. Nishimura, A. Noma, and H. Irisawa, The spontaneous action potential of rabbit atrioventricular node. *Jpn. J. Physiol*., 1980;**30**: 529–539.
54. Vassalle, M., Electrogenic suppression of automaticity in sheep and dog Purkinje fibers. *Circ. Res*., 1970;**27**: 361–377.
55. Glitsch, H.G., Electrophysiology of the sodium-potassium-ATPase in cardiac cells. *Physiol. Rev*., 2001;**81**: 1791–1826.
56. Lewis, T., *Lectures on the Heart*. New York, Shaw and sons, 1915.
57. Tranum-Jensen, J., The fine structure of the atrial and atrioventricular (AV) junctional specialized tissues of the rabbit heart, in *The Conduction System of the Heart*, H.J.J. Wellens, K.I. Lie, and M.J. Janse, Editors. Leiden: Stenfert-Kroese, 1976, pp. 55–99.
58. Janse, M.J. and R.H. Anderson, Specialized internodal pathways: fact or fiction? *Eur. J. Cardiol*., 1974;**2**: 117–136.
59. Puech, P., M. Esclavissat, D. Sodi-Pallares, and F. Cineros, Normal auricular activation in the dog's heart. *Am. Heart J*., 1954;**47**: 174–191.
60. Yamada, K., M. Horiba, Y. Sakaida, M. Okajima, H. Horibe, H. Muraki, T. Kobayashi, A. Miyauchi, H. Oishi, A. Nonogawa, K. Ishikawa, and J. Toyama, Origination and transmission of impulse in right atrium. *Jpn. Heart J*., 1965;**6**: 71–97.
61. Spach, M.S., T.D. King, R.C. Barr, D.E. Boaz, M.N. Morrow, and S. Herman-Giddens, Electrical potential distribution surrounding the atria during depolarization and repolarization in the dog. *Circ. Res*., 1969;**24**: 857–873.
62. Hamlin, R.L., D.L. Smetzer, T. Senta, and C.R. Smith, Atrial activation paths and P waves in horses. *Am. J. Physiol*., 1970;**219**: 306–313.
63. Durrer, D., R.Th. van Dam, G.E. Freud, M.J. Janse, F.L. Meijler, and R.C. Arzbaecher, Total excitation of the isolated human heart. *Circulation*, 1970;**41**: 895–912.
64. Goodman, D., A.B.M. van der Steen, and R.T.H. van Dam, Endocardial and epicardial activation pathways of the canine right atrium. *Am. J. Physiol*., 1971;**220**: 1–11.

65. Spach, M.S., M. Lieberman, J.G. Scott, R.C. Barr, E.A. Johnson, and J.M. Kootsey, Excitation sequences of the atrial septum and the AV node in isolated hearts of dog and rabbit. *Circ. Res.*, 1971;**29**: 156–172.
66. Wittig, J.H., M.R. de Leval, and G. Stark, Intraoperative mapping of atrial activation before, during and after the mustard operation. *J. Thorac. Cardiovasc. Surg.*, 1977;**73**: 1–13.
67. De Ponti, R., S.Y. Ho, J.A. Salerno-Uriarte, M. Tritto, and G. Spadacini, Electroanatomic analysis of sinus impulse propagation in normal human atria. *J. Cardiovasc. Electrophysiol.*, 2002;**13**: 1–10.
68. Markides, V., R.J. Schilling, S.Y. Ho, A.W.C. Chow, D.W. Davies, and N.S. Peters, Characterization of left atrial activation in the intact human heart. *Circulation*, 2003;**107**: 733–739.
69. Betts, T.R., P.R. Roberts, and J.M. Morgan, High-density mapping of left atrial endocardial activation during sinus rhythm and coronary sinus pacing in patients with paroxysmal atrial fibrillation. *J. Cardiovasc. Electrophysiol.*, 2004;**15**: 1111–1117.
70. James, T.N., The connecting pathways between the sinus node and the A–V node and between the right and left atrium of the human heart. *Am. Heart J.*, 1963;**66**: 498–508.
71. Rossi, L., Interatrial, internodal, and dual reentrant atrioventricular nodal pathways: an anatomical update of arrhythmogenic substrates. *Cardiologia*, 1996;**41**: 129–134.
72. Sanchez-Quintana, D., D.W. Davies, S. Yen Ho, P. Oslizlok, and R.H. Anderson , Architecture of the atrial musculature in and around the triangle of Koch: its potential relevance to atrioventricular nodal reentry. *J. Cardiovasc. Electrophysiol.*, 1997;**8**: 1396–1407.
73. Inoue, S. and A.E. Becker, Posterior extensions of the human compact atrioventricular node: a neglected anatomical feature of potential clinical significance. *Circulation*, 1998;**97**: 188–193.
74. Chauvin, M., D.C. Shah, M. Haïssaguerre, L. Marcellin, and C. Brechenmacher, The anatomic basis of connections between the coronary sinus musculature and the left atrium in humans. *Circulation*, 2001;**101**: 647–652.
75. Moore, E.N., S.L. Jomain, J.H. Stuckey, J.W. Buchanan, and B.F. Hoffman, Studies on ectopic atrial rhythms in dogs. *Am. J. Cardiol.*, 1967;**19**: 676–685.
76. Moore, E.N., J. Melbin, J.F. Spear, and J.D. Hill, Sequence of atrial excitation in the dog during antegrade and retrograde activation. *J. Electrocardiol.*, 1971;**4**: 283–290.
77. Waldo, A.L., K.J. Vittikainen, and B.F. Hoffman, The sequence of retrograde atrial activation in the canine heart: correlation with positive and negative retrograde P waves. *Circ. Res.*, 1975;**37**: 156–163.
78. Thorel, C., Vorläufige Mitteilung über eine besondere Muskelverbindung zwischen dem Cava superior und die Hissischen Bundel. *Münch med Wschr* 1908;**56**: 2159–2164.
79. Bericht über die Verhandlungen der XIV Tagung der Deutschen pathologischen Gesellschaft in Erlangen vom 4–6 April 1910. *Z allg Path path Anat* 1910;**21**: 433–496.
80. Netter, F.H., *The Heart. The Ciba Collection of Medical Illustrations*, vol. 5, 1969, p. 13.
81. Pastelin, G., R. Mendez, and G.K. Moe, Participation of atrial specialized conduction pathways in atrial flutter. *Circ. Res.*, 1978;**42**: 386–393.
82. Janse, M.J. and R.H. Anderson, Specialized internodal atrial pathways. Fact or fiction? *Eur. J. Cardiol.*, 1974;**2**: 117–136.
83. Spach, M.S., W.T. Miller, R.C. Barr, and D.B. Geselowitz, Electrophysiology of the internodal pathways: determining the difference between anisotropic cardiac muscle and a specialized tract system, in *Physiology of Atrial Pacemakers and Conductive Tissues*, R.C. Little, Editor. Mount Kisco, New York: Futura Publishing Company, 1980, pp. 367–380.
84. Janse, M.J., R.H. Anderson, M.A. McGuire, and S.Y. Ho, "AV nodal" reentry: Part I: "AV nodal" reentry revisited. *J. Cardiovasc. Electrophysiol.*, 1993;**4**: 561–572.
85. Tawara, S., *Das Reizleitungssystem des Säugetierherzens. Eine anatomisch-histologische Studie über das Atrioventrikularbündel und die Purkinjeschen Fäden*. Jena: Fischer, 1906.
86. Anderson, R.H., Histologic and histochemical evidence concerning the presence of morphologically distinct cellular zones within the rabbit atrioventricular node. *Anat. Rec.*, 1972;**173**: 7–23.
87. Paes de Carvalho, A. and D.F. de Almeida, Spread of activity through the atrioventricular node. *Circ. Res.*, 1960;**8**: 801–809.
88. Becker, A.E. and R.H. Anderson, Morphology of the human atrioventricular junctional area, in *The Conduction System of the Heart: Structure, Function and Clinical Implication*, H.J.J. Wellens, K.I. Lie, and M.J. Janse, Editors. Philadelphia, PA: Lea and Febiger, 1976, pp. 263–286.
89. Anderson, R.H., M.J. Janse, F.J.L. van Capelle, J. Billete, A.E. Becker, and D. Durrer, A combined morphological and electrophysiological study of the atrioventricular node of the rabbit heart. *Circ. Res.*, 1974;**35**: 909–922.
90. McGuire, M.A., J.M.T. de Bakker, J.T. Vermeulen, A.F. Moorman, P. Loh, B. Thibault, J.L.M. Vermeulen, A.E. Becker, and M.J. Janse, Atrioventricular junctional tissue. Discrepancy between histological and electrophysiological characteristics. *Circulation*, 1996;**94**: 571–577.
91. Petrecca, K., F. Amellal, D.W. Laird, S.A. Cohen, and A. Shrier, Sodium channel distribution within the rabbit atrioventricular node and surrounding myocardium as analyzed with confocal microscopy. *J. Physiol.*, 1997;**501**: 263–274.
92. Spach, M.S., M. Lieberman, J.G. Scott, R.C. Barr, E.A. Johnson, and J.M. Kootsey, Excitation sequences of the atrial septum and the AV node in isolated hearts of the dog and rabbit. *Circ. Res.*, 1971;**29**: 156–172.
93. McGuire, M.A., J.M.T. de Bakker, J.T. Vermeulen, T. Opthof, A.E. Becker, and M.J. Janse, Origin and significance of double potentials near the atrioventricular node. Correlation of extracellular potentials, intracellular potentials, and histology. *Circulation*, 1994;**89**: 2351–2360.
94. Janse, M.J., F.J.L. van Capelle, R.H. Anderson, P. Touboul, and J. Billette, Electrophysiology and structure of the atrioventricular node of the rabbit heart, in *The Conduction System of the Heart*, H.J.J. Wellens, K.I. Lie, and M.J. Janse, Editors. Leiden: Stenfert Kroese, 1976, pp. 296–315.
95. Van Capelle, F.J.L., M.J. Janse, P.J. Varghese, G.E. Freud, C. Mater, and D. Durrer, Spread of excitation in the atrioventricular node of isolated rabbit hearts studied by multiple microelectrode recording. *Circ. Res.*, 1972;**31**: 602–616.
96. Janse, M.J., Influence of the direction of the atrial wave front on A–V nodal transmission in isolated hearts of rabbits. *Circ. Res.*, 1969;**25**: 439–449.

97. Mines, G.R., On dynamic equilibrium in the heart. *J. Physiol.*, 1913;**46**: 349–382.
98. White, P.D., A study of atrioventricular rhythm following auricular flutter. *Arch. Intern. Med.*, 1915;**16**: 517–535.
99. Scherf, D. and C. Shookhoff, Experimentelle Untersuchungen über die "Umkehr-Extrasystole" (reciprocating beats). *Wien Arch Inn Med* 1926;**12**: 501–529.
100. Moe, G.K., J.B. Preston, and H.J. Burlington, Physiologic evidence for a dual A–V transmission system. *Circ. Res.*, 1956;**4**: 357–375.
101. Rosenblueth, A., Ventricular "echoes." *Am. J. Physiol.*, 1958; **195**: 53–60.
102. Kistin, A.D., Atrial reciprocating rhythm. *Circulation*, 1965;**32**: 697–707.
103. Puech, P., La conduction réciproque par le noeud de Tawara. Bases expérimentales et aspects cliniques. *Ann. Cardiol. Angeiol.*, 1970;**19**: 21–40.
104. Schuilenburg, R.M. and D. Durrer, Atrial echo beats in the human heart elicited by induced atrial premature beats. *Circulation*, 1968;**37**: 680–693.
105. Schuilenburg, R.M. and D. Durrer, Ventricular echo beats in the human heart elicited by induced ventricular premature beats. *Circulation*, 1968;**40**: 337–347.
106. Bigger, J.T., Jr. and B.N. Goldreyer, The mechanism of supraventricular tachycardia. *Circulation*, 1970;**42**: 673–688.
107. Mendez, C., J. Han, P.D. Garcia de Jalon, and G.K. Moe, Demonstration of a dual AV conduction system in the isolated rabbit heart. *Circ. Res.*, 1965;**19**: 562–581.
108. Mignone, R.J. and A.G. Wallace, Ventricular echoes. Evidence for dissociation and reentry within the A–V node. *Circ. Res.*, 1966;**19**: 638–649.
109. Mendez, C. and G.K. Moe, Demonstration of a dual AV nodal conduction system in the isolated rabbit heart. *Circ. Res.*, 1966;**19**: 378–393.
110. Moe, G.K., W. Cohen, and R.L. Vick, Experimentally induced paroxysmal A-V nodal tachycardia in the dog. *Am. Heart J.*, 1963;**65**: 87–92.
111. Janse, M.J., F.J.L. van Capelle, G.E. Freud, and D. Durrer, Circus movement within the AV node as a basis for supraventricular tachycardia as shown by multiple microelectrode recordings in the isolated rabbit heart. *Circ. Res.*, 1971;**28**: 403–414.
112. Wit, A.L., B.N. Goldreyer, and A.N. Damato, An in vitro model of paroxysmal supraventricular tachycardia. *Circulation*, 1971;**43**: 862–875.
113. Coumel, P., C. Cabrol, A. Fabiato, R. Gourgon, and R. Slama, Tachycardie permanente par rythme réciproque. *Arch. Mal. Coeur Vaiss.*, 1967;**60**: 1830–1864.
114. McGuire, M.A., J.P. Bourke, M.C. Robotin, I.C. Johnson, W. Meldrum-Hanna, G.R. Nunn, J.B. Uther, and D.L. Ross, High resolution mapping in Koch's triangle using sixty electrodes in humans with atrioventricular nodal (AV nodal) reentrant tachycardia. *Circulation*, 1993;**88**: 2315–2328.
115. Sung, R.J., H.L. Waxman, S. Saksena, and Z. Juma, Sequence of retrograde atrial activation in patients with dual atrioventricular nodal pathways. *Circulation*, 1981;**64**: 1059–1067.
116. Ross, D.L., D.C. Johnson, A.R. Denniss, M.J. Cooper, D.A. Richards, and J.B. Uther, Curative surgery for atrioventricular junctional ("AV nodal") reentrant tachycardia. *J. Am. Coll. Cardiol.*, 1985;**6**: 1383–1392.
117. Haissaguerre, M., F. Gaita, B. Fischer, D. Commenges, P. Montserrat, P. d'Ivernois, P. Lemetayer, and J. Warin, Elimination of atrioventricular nodal reentrant tachycardia using discrete slow potentials to guide application of radiofrequency energy. *Circulation*, 1992;**85**: 2162–2175.
118. Ho, S.Y., J.M. McComb, C.D. Scott, and R.H. Anderson, Morphology of the cardiac conduction system in patients with electrophysiologically proven dual atrioventricular pathways. *J. Cardiovasc. Electrophysiol.*, 1993;**4**: 504–512.
119. Nikolski, V.P., S.A. Jones, M.K. Lancaster, M.R. Boyett, and I.R. Efimov, Cx43 and dual-pathway electrophysiology of the atrioventricular node and atrioventricular nodal reentry. *Circ. Res.*, 2003;**92**: 469–475.
120. Josephson, M.E. and J.M. Miller, Atrioventricular nodal reentry: evidence supporting an intranodal location. *Pacing Clin. Electrophysiol.*, 1993;**16**: 599–614.
121. Mendez, C., J. Han, P.D. Garcia de Jalon, and G.K. Moe, Some characteristics of ventricular echoes. *Circ. Res.*, 1965;**16**: 562–581.
122. Iinuma, H., L.S. Dreifus, T. Mazgalev, R. Price, and E.L. Michelson, Role of the perinodal region in atrioventricular nodal reentry: evidence in an isolated rabbit heart preparation. *J. Am. Coll. Cardiol.*, 1983;**2**: 465–473.
123. Mazgalev, T., L.S. Dreifus, J. Bianchi, and E.L. Michelson, The mechanism of AV junctional reentry: role of the atrionodal junction. *Anat. Rec.*, 1981;**202**: 179–188.
124. Loh, P., J.M.T. de Bakker, M. Hocini, B. Thibault, R.N.W. Hauer, and M.J. Janse, Reentrant pathway during ventricular echoes is confined to the atrioventricular node. *Circulation*, 1999;**100**: 1346–1353.
125. Loh, P., S.Y. Ho, T. Kawara, R.N.W. Hauer, M.J. Janse, G. Breithardt, and J.M.T. de Bakker, Reentrant circuits in the canine AV node during atrial and ventricular echoes: electrophysiologic and histologic correlation. *Circulation*, 2003;**108**: 231–238.
126. Bukauskas, F.F. and R.P. Veteikis, Passive electrical properties of the atrioventricular region of the rabbit heart. *Biofizika*, 1977;**22**: 499–504.
127. De Mello, W.C., Passive electrical properties of the atrioventricular node. *Pflug. Arch.*, 1977;**371**: 135–139.
128. Ikeda, N., J. Toyama, T. Shimizu, I. Kodama, and K. Yamada, The role of electrical uncoupling in the genesis of atrioventricular conduction disturbance. *J. Mol. Cell. Cardiol.*, 1980;**12**: 809–826.
129. Kokobun, S., M. Nishimura, A. Noma, and H. Irisawa, Membrane currents in the atrioventricular node. *Pflug. Arch.*, 1982;**393**: 15–22.
130. Kléber, A.G. and C.B. Riegger, Electrical constants of arterially perfused rabbit papillary muscle. *J. Physiol.*, 1987;**385**: 307–324.
131. Cranefield, P.F., B.F. Hoffman, and A. Paes de Carvalho, Effects of acetylcholine on single fibers of the atrio-ventricular node. *Circ. Res.*, 1959;**7**: 19–23.
132. Mazgalev, T., L.S. Dreifus, H. Iinuma, and E.L. Michelson, Effects of the site and timing of atrio-ventricular input on atrioventricular conduction in the isolated perfused rabbit heart. *Circulation*, 1984;**70**: 748–759.
133. Zipes, D.P., C. Mendez, and G.K. Moe, Evidence for summation and voltage dependency in rabbit atrioventricular nodal fibers. *Circ. Res.*, 1973;**32**: 170–177.

134. Gettes, L.S. and H. Reuter, Slow recovery from inactivation of inward currents in mammalian myocardial fibres. *J. Physiol.*, 1974;**240**: 703–724.
135. Billette, J., M.J. Janse, F.J.L. van Capelle, R.H. Anderson, P. Touboul, and D. Durrer, Cycle-length-dependent properties of AV nodal activation in rabbit hearts. *Am. J. Physiol.*, 1976;**231**: 1129–1139.
136. Truex, R.C., Comparative anatomy and functional considerations of the cardiac conduction system, in *The Specialized Tissues of the Heart*, A. Paes de Carvalho, W.C. De Mello, and B.F. Hoffman, Editors. Amsterdam: Elsevier, 1961, pp. 22–43.
137. Demoulin, G.C. and H.E. Kulbertus, Histopathological examination of concept of left hemiblock. *Brit. Heart J.*, 1972;**34**: 807–814.
138. Rosenbaum, M.B., M.V. Elizari, and J.G. Lazzari, *The Hemiblocks:New Concepts of Intraventricular Conduction Based on Human Anatomical, Physiological and Clinical Studies*. Oldsmar: Tampa Tracings, 1970.
139. Scher, A. and A.C. Young, Ventricular depolarization and the genesis of the QRS. *Ann. NY Acad. Sci.*, 1957;**65**: 766–778.
140. Le Grice, I.J., B.H. Smaill, L.Z. Chai, S.G. Edgar, J.B. Gavin, and P.J. Hunter, Laminar structure of the heart: ventricular myocyte arrangement and connective tissue architecture in the dog. *Am. J. Physiol.*, 1995;**269**: H571–H582.
141. Nagao, K., J. Toyama, I. Kodama, and K. Yamada, Role of the conducting system in the endocardial excitation spread in the right ventricle. *Am. J. Cardiol.*, 1981;**48**: 864–870.
142. Veenstra, R.D., R.W. Joyner, and D.A. Rawling, Purkinje and ventricular activation sequences of canine papillary muscle. Effects of quinidine and calcium on the Purkinje-muscle delay. *Circ. Res.*, 1984;**54**: 500–515.
143. Overholt, E.D., R.W. Joyner, R.D. Veenstra, D.A. Rawling, and R. Wiedmann, Unidirectional block between Purkinje and ventricular muscle layers of papillary muscle. *Am. J. Physiol.*, 1984;**247**: H584–H595.
144. Mendez, C., W.J. Mueller, and X. Urguiaga, Propagation of impulses across the Purkinje fiber-muscle junctions in the dog. *Circ. Res.*, 1970;**36**: 135–150.
145. Joyner, R.W., R.D.E. Veenstra, D.A. Rawling, and A. Chorro, Propagation through electrically coupled cells. Effects of a resistive barrier. *Biophys. J.*, 1984;**45**: 1017–1025.
146. Rawling, D.A., R.W. Joyner, and E.D. Overholt, Variations in the functional electrical coupling between the subendocardial Purkinje and ventricular layers of the canine left ventricle. *Circ. Res.*, 1985;**57**: 252–261.
147. Joyner, R.W., Effects of the discrete pattern of electrical coupling on propagation through an electrical syncytium. *Circ. Res.*, 1982;**50**: 192–200.
148. Alanis, J., D. Benitez, and G. Pilar, A functional discontinuity between the Purkinje and ventricular muscle cells. *Acta Physiol. Lat. Am.*, 1961;**11**: 171–183.
149. Tranum Jensen, J., A.A.M. Wilde, J.T. Vermeulen, and M.J. Janse, Morphology of electrophysiologically identified junctions between Purkinje fibers and ventricular muscle in rabbit and pig hearts. *Circ. Res.*, 1991;**69**: 429–437.
150. Martinez-Palomo, A., J. Alanis, and D. Benitez, Transitional cardiac cells of the conductive system of the dog heart. Distinguishing morphological and electrophysiological features. *J. Cell Biol.*, 1970;**47**: 1–17.
151. Kaneko, Y., Y. Taniguchi, T. Nakajima, M. Manita, T. Ito, M. Akiyama, and M. Kurabayahi, Myocardial bundles with slow conduction properties are present on the left interventricular septal surface of normal human hearts. *J. Cardiovasc. Electrophysiol.*, 2004;**15**: 1010–1018.
152. Sicouri, S. and C. Antzelevitch, A subpopulation of cells with unique electrophysiological properties in the deep subepicardium of the canine ventricle. The M cell. *Circ. Res.*, 1991;**68**: 1729–1741.
153. Sicouri, S., J. Fish, and C. Antzelevitch, Distribution of M cells in the canine ventricle. *J. Cardiovasc. Electrophysiol.*, 1994;**5**: 824–837.
154. Sicouri, S. and C. Antzelevitch, Electrophysiologic characteristics of M cells in the canine left ventricular free wall. *J. Cardiovasc. Electrophysiol.*, 1995;**6**: 591–603.
155. Anyukhovsky, E.P., E.A. Sosunov, and M.R. Rosen, Regional differences in electrophysiological properties of epicardium, midmyocardium, and endocardium: in vitro and in vivo correlations. *Circulation*, 1996;**94**: 1981–1988.
156. Liu, D.-W. and C. Antzelevitch, Characteristics of the delayed rectifier current (IKr and IKs) in canine ventricular epicardial, midmyocardial, and endocardial myocytes. *Circ. Res.*, 1995;**76**: 351–365.
157. Rodriguez-Sinovas, A., J. Cinca, A. Tapias, L. Armadans, M. Tresanchez, and J. Soler-Soler, Lack of evidence of m cells in porcine lefty ventricular myocardium. *Cardiovasc. Res.*, 1997;**33**: 307–313.
158. Tan, R.C. and R.W. Joyner, Electrotonic influences on action potentials from isolated cells. *Circ. Res.*, 1990;**67**: 1071–1081.
159. Anyukhovsky, E.P., E.A. Sosunov, R.Z. Gainullin, and M.R. Rosen, The controversial M cell. *J. Cardiovasc. Electrophysiol.*, 1999;**10**: 244–260.
160. Van Dam, R.Th. and D. Durrer, Experimental study on the intramural distribution of the excitability cycle and on the form of the epicardial T wave in the dog heart in situ. *Am. Heart J.*, 1961;**61**: 537–542.
161. Burgess, M.J., L.S. Green, K. Millar, R. Wyatt, and J.A. Abildskov, The sequence of normal ventricular recovery. *Am. Heart J.*, 1972;**84**: 660–669.
162. Janse, M.J., The effect of changes in heart rate on the refractory period of the heart, Ph.D. thesis. University of Amsterdam, Amsterdam, The Netherlands: Mondeel Offset Drukkerij, 1971.
163. Janse, M.J., A. Capucci, R. Coronel, and M.A. Fabius, Variability of recovery of excitability in the normal canine and ischemic porcine heart. *Eur. Heart J.*, 1985;**6**(Suppl. D): 41–52.
164. Bauer, A., R. Becker, K.D. Freigang, J.C. Senges, F. Voss, A. Hansen, M. Müller, H.J. Lang, U. Gerlach, A. Busch, J. Kraft, and W. Schöls, Rate-and site-dependent effects of propafenone, dofetilide, and the new IKs blocking agent chromanolol 293b on individual muscle layers of the intact heart. *Circulation*, 1999;**100**: 2184–2190.
165. Chinushi, M., M. Tagawa, H. Karai, T. Washizuka, A. Abe, H. Furushima, and Y. Aizawa, Correlation between the effective refractory period and activation-recovery-interval calculated from the intracardiac unipolar electrograms of humans with an without dl-sotalol treatment. *Jpn. Circ. J.*, 2001;**65**: 702–706.
166. Taggart, P., P.M. Sutton, T. Opthof, R. Coronel, R. Trimlett, W. Pugsley, and P. Kallis, Transmural repolarisation in the left

ventricle in humans during normoxia an ischaemia. *Cardiovasc. Res.*, 2001;**50**: 454–462.

167. Conrath, C., R. Wilders, R. Coronel, J.M.T. de Bakker, P. Taggart, J. de Groot, and T. Opthof, Intercellular coupling through gap junctions masks M cells in the human heart. *Cardiovasc. Res.*, 2004;**62**: 407–414.
168. Janse, M.J., E.A. Sosunov, R. Coronel, T. Opthof, E.P. Anyukhovsky, J.M.T. de Bakker, A.N. Plotnikov, I.N. Shlapakova, P. Danilo, J.G.P. Tijssen, and M.R. Rosen, Repolarization gradients in the canine left ventricle before and after induction of short-term cardiac memory. *Circulation*, 2005;**112**: 1711–1718.

5 Genesis of the Electrocardiogram

R.C. Barr · A. van Oosterom

P. W. Macfarlane, A. van Oosterom, O. Pahlm, P. Kligfield, M. Janse, J. Camm (eds.), *Comprehensive Electrocardiology*, DOI 10.1007/978-1-84882-046-3_5,

5.1 Introduction

In the beginning, Waller [1] measured voltage differences between two electrodes placed on the body surface and found that they changed in rhythm with the heartbeat. That was more than 100 years ago [2].

It is now known that electrocardiograms (ECGs) are possible because active tissues within the heart generate electrical currents that flow intensively within the heart muscle itself, and with lesser intensity throughout the entire body. The flow of current creates voltage differences between sites on the body surface where electrodes may be placed. These voltage differences, measured as a function of time, are called ECGs.

Since access to the body surface is much easier than access to the heart, it is not surprising that ECGs were measured extensively before an explanation of their origin, in terms of electrical events within the heart, could be obtained. What is more surprising is how productively ECGs were used before most of what are now considered the fundamental underlying principles were known. In fact, quantitative explanations for some significant electrocardiographic phenomena remain unavailable even today.

A consequence is that an understanding of the genesis of the ECG requires two frames of reference. The first derives from the colorful history of electrocardiography, which is the frame of reference from which most of the conventions of notation and practice, as well as a tremendous base of empirical knowledge, originated. Accordingly, a few salient points are presented in the section that follows. A more extensive history has been given in Chap. 1.

The second frame of reference is the base of knowledge available from studies of cardiac electrophysiology. Especially significant is the knowledge about the way currents flow in and around the cells of the heart as a whole. As with electrocardiography, important progress in cardiac electrophysiology has been accumulating for more than a century. However, only within the last 50 years have many central experimental methods been invented and used for the study of transmembrane potentials and currents within and throughout larger cardiac structures. A theoretical framework has been developed to assimilate and organize the experimental findings describing transmembrane and intracellular potentials, and how their associated currents flow and change with time. Many electrophysiological developments have come about largely independently of electrocardiographic viewpoints and conventions. The same applies to the insights stemming from the more recent biophysical studies in the field of electrocardiography. Much of the current electrocardiographic practice seems to be anchored more on the first 50 years than on the period thereafter.

This chapter aims at providing a link between the treatment of the fundamental aspects of electrocardiography found in clinical text books and the more advanced treatment of the same material discussed in detail in the other chapters of this volume.

5.2 Historical Summary

5.2.1 Electrocardiography

The curious history of electrocardiography was said by Burch and DePasquale [3] to be a history of errors and misconceptions, and by Johnson and Flowers [4] to be a "chronicle of wonder and discovery."

An immediate problem for the first electrocardiographers was that the capillary electrometer used by Waller gave tracings of poor quality. Electrocardiography advanced greatly when Einthoven invented the string galvanometer [5, 6] around 1900. Although heavy and bulky, the string galvanometer produced ECG waveforms (measurements of voltage versus time) that had a quality comparable to modern recordings. An electrocardiographic waveform as a whole was seen to consist of a series of deflections. For purposes of identification, Einthoven marked the peaks of the successive major deflections with the labels P, Q, R, S and T (Fig. 5.1).

While the string galvanometer provided a means for recording ECGs, it did not provide an explanation of their genesis. There were substantial differences of opinion about the origin of the deflections, or even whether they had clinical significance. Einthoven demonstrated their clinical significance by showing differences between waveforms recorded from normal subjects and patients suffering from arrhythmias. For this work Einthoven received the Nobel prize in 1924.

There remained many questions and controversies about how electrocardiographic deflections originated within the heart. Thomas Lewis [7, 8] recognized that the temporal sequence of the deflections of the ECG occurred because there

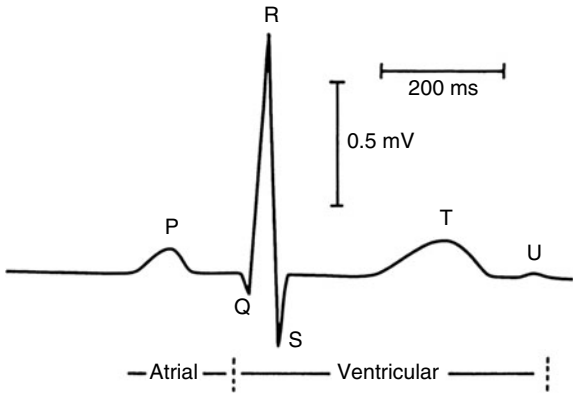

Figure 5.1

P-Q-R-S-T-U peaks on a lead II waveform. While Einthoven's nomenclature implicitly emphasized the waveform's peaks, the durations of the intervals such as P-R and Q-T often are also carefully examined. The point where S rises to the baseline and abruptly changes slope is often identified as the J ("junctional") point.

was a temporal sequence in which different cardiac structures became electrically active. To prove this thesis, Lewis measured the sequence of electrical excitation directly from the atria and ventricles of dogs, while simultaneously measuring ECGs from the body surface.

Because of the limited sensitivity of the original recording devices, early ECGs sometimes were measured from subjects whose hands or feet were placed in buckets of saline solution. The buckets of saline were "electrodes," which had a large contact area with the skin. As time went by, a system of "standard leads" evolved. The standard leads used measurements between specific limbs (Fig. 5.2). For example, lead II uses the left leg as the positive input and the right arm as the negative input and so the signal observed by lead II represents the time course of the potential at the left leg minus that at the right arm.

Frank Wilson and others recognized the limitations in a system where all the electrodes were distant from the heart. They demonstrated the value of the precordial leads, which use electrodes placed on the chest. Voltages from the precordial leads are measured with respect to "Wilson's central terminal" (WCT), which is the average potential of the three limbs, right arm (RA), left arm (LA), and left leg (LL) [9]. This average was originally found by connecting the electrodes to the three limbs with 5,000 Ohm resistors. Under most circumstances, potentials ahead of an advancing excitation wave are more positive than the potential at Wilson's central terminal, and potentials behind the excitation wave are more negative. Combinations of standard leads and precordial leads measured with respect to Wilson's central terminal form the basis for the measurements of most ECGs even today. Lead theory and lead systems are discussed more extensively in Chaps. 10 and 11 respectively.

5.2.2 Electrophysiology

In 1949 Ling and Gerard introduced the glass microelectrode [10], a tool suitable for measuring potential differences across the membranes of individual cells, thereby greatly advancing the study of transmembrane potentials. This tool was rapidly adapted to cardiac studies. For example, in 1951 Woodbury, Hecht and Christopherson [11] reported on measurements from cardiac cells. In time, such methods allowed an extensive description of cardiac action potentials. Examples of their variation from structure to structure (nodes, atria, conduction system, ventricles) became available through sources such as Hoffman and Cranefield [12]. Figure 5.3 is a drawing of action potential wave forms of different cardiac structures [13].

The value of the transmembrane potential recordings was magnified by the mathematical descriptions put forward by Hodgkin and Huxley [14] to describe membrane currents in nerves. The Hodgkin-Huxley formulation provided a framework for the development of related mathematical descriptions for the cardiac muscle. An early example of this is the Beeler and Reuter model [15] and its later modifications, such as the one proposed in [16]; it assumes that only

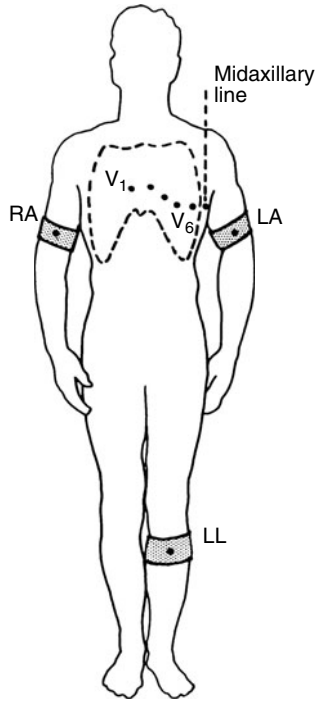

Figure 5.2
Electrode placement. Electrodes attached to the limbs are used for the "standard leads" I, II and III. For example, lead II measures the potential at electrode LL (connected to the positive input of the recorder) with reference to the potential on the electrode RA. "Unipolar" lead V_1 is measured with electrode V_1 located as shown on the chest, with reference to the average potential at electrodes RA, LA and LL. This configuration is called "Wilson's central terminal," WCT. The locations of the electrodes V_1-V_6 are indicated by dots on the chest. Potentials measured at these *electrodes* with reference to WCT are referred to as *leads* V_1-V_6.

capacitative displacement current and sodium-channel current contribute during the time period of the action-potential upstroke. The model provides a quantitative description of the upstroke of the cardiac action potential using voltage-clamp data obtained from small spherical clusters of tissue-cultured heart cells. In a marked contrast are the much more comprehensive models of DiFrancesco-Noble [17] or Luo and Rudy [18] for ventricular myocardium, or those like that of Courtemanche et al. for the atria [19]. These include other channel currents and provide a much more comprehensive picture of the contribution of different ionic currents to the total membrane current.

A picture of the flow of currents within and around cells during the course of an action potential has emerged from these measurements and models. On the one hand, this picture can be used to examine in detail potentials and currents in the vicinity of active fibers and relate them to ionic movements through the membrane, as done, for example, by Spach and Kootsey [20]. The same picture can be used as a building block for models of larger segments of cardiac muscle, whether quantitatively, as with the bidomain model [21] (see also Chap. 7), or only qualitatively. Such models form the basis for much of the modern understanding of the genesis of the ECG. Cardiac electrophysiology is discussed more fully in Chap. 3.

5.2.3 Synthesis

Recent years have seen a renewed emphasis on unifying the electrocardiographic and electrophysiological frames of reference, a goal held from the beginnings of electrocardiography. The objective is to provide an explanation of the genesis of

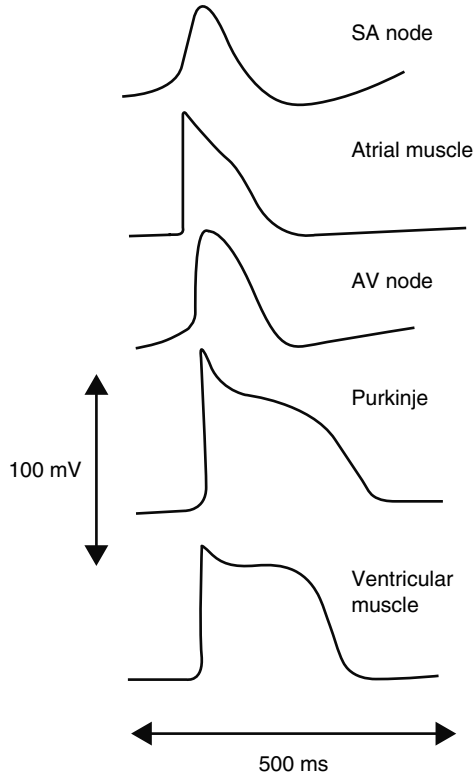

Figure 5.3
Characteristic action potentials drawn for different cardiac structures. Among the evident differences are the sloping baselines for the SA and AV nodal traces, and the flat baselines elsewhere; the differences in duration; and the differences in rate of rise during depolarization, a characteristic associated with the velocity of propagating wave fronts, showing some of their characteristic differences. Striking color drawings of cardiac structures and their action potentials have been presented by Netter [13].

ECGs that is consistent with the underlying electrophysiology, quantitatively as well as qualitatively. For quantitative consistency, it is necessary to have mechanisms that are presented mathematically and then verified through measurements of sufficient precision; this ambitious goal remains to be accomplished in many important respects. More qualitatively, it is from the perspective of attempting to explain the genesis of the ECG in terms of the underlying cardiac events that the remainder of this chapter is presented.

5.3 Electric Current Sources and Their Potential Fields

How can the potentials and currents from individual fibers be related to those potentials observed some distance away? Such questions have been analyzed extensively elsewhere (as in [22]) and are examined in detail in Chaps. 6 and 7. Some central elements that relate to the genesis of the ECG are summarized here.

5.3.1 Source Character of a Single Fiber

The most basic building block for describing the cardiac electric generator is the single cardiac cell. Its properties are described in Sect. 6.3.1. Here we take it to be a single cardiac fiber along which, after being activated at one end, a process

of local depolarization followed by repolarization propagates. Its properties as an equivalent electric source (Sect. 2.5) are discussed from a different perspective in Sect. 6.3.1. The transmembrane potential V_m, is the difference between the potentials Φ_i and Φ_e at two points just inside and outside the membrane of cardiac cells or fibers, defined by convention as $V_m = \Phi_i - \Phi_e$. Figure 5.4 illustrates the potentials and currents generated during the propagation of an excitation along the fiber. This figure is drawn to illustrate the main concepts involved.

If the fiber is immersed in an extensive conducting medium the transmembrane current per unit length, i_m, (unit: A m^{-1}) acting as an equivalent line current source density for the extracellular compartment, may be approximated as

$$i_m(x,t) = \pi a^2 \sigma_i \frac{\partial^2 V_m(x,t)}{\partial x^2}, \tag{5.1}$$

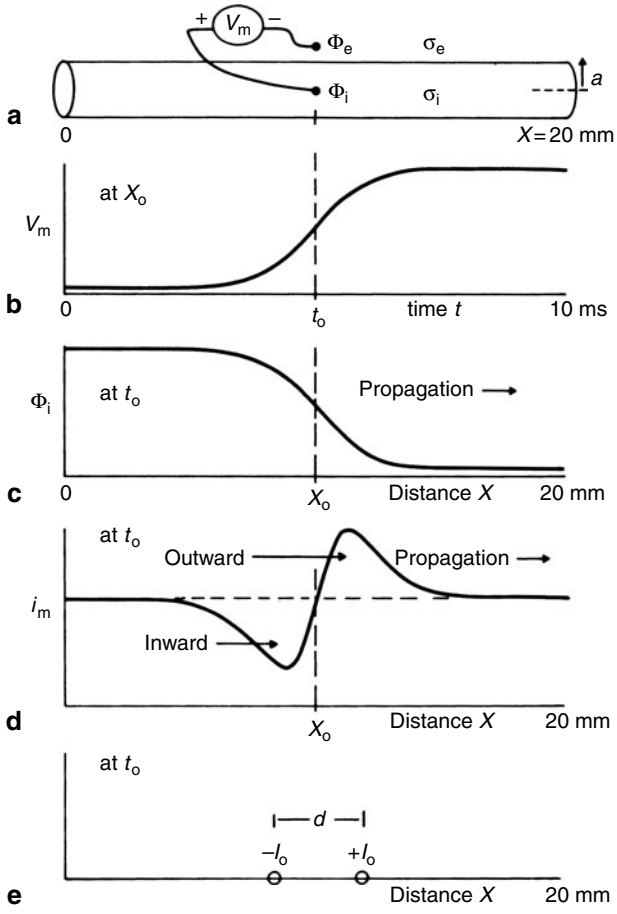

Figure 5.4

Potentials and currents of an action potential propagating to the right along a fiber. Part (a) identifies a site for measuring intracellular potential Φ_i and extracellular potential Φ_e with respect to a reference electrode located at an arbitrary point in the surrounding medium. V_m is the local transmembrane potential. The cylinder has radius *a* and intracellular and extracellular conductivities σ_i and σ_e. Part (b) shows a hypothetical tracing of V_m as a function of *time* at position x_o on the cylinder. Such a waveform might result from a previous excitation on the left. Because of the time scale used, only the depolarization phase is shown. Time t_o is taken to be near the middle of the upstroke of this waveform. Part (c) shows the value of Φ_i as a function of *distance* along the fiber at time t_o for the same fiber. Note that the potential declines to the resting value to the right. Part (d) shows the spatial distribution of the corresponding transmembrane current i_m along the fiber, defined as positive for outward flowing current and negative for inward flowing current.

with σ_i the intracellular conductivity and a the fiber radius. This expression is derived from the linear core-conductor model of the membrane processes along a single linear fiber [22]. It holds true quite generally, i.e., for the segments that locally depolarize, as well as for those that are repolarizing. Applying the potential profile along the fiber at time instant t requires taking the second spatial derivative of the function shown in Fig. 5.4c. This results in the distribution of the source strength i_m along the fiber at that same time instant t shown in Fig. 5.4d.

5.3.2 Extracellular Current Flow

In a segment of local depolarization, from the viewpoint of the extracellular space, the presence of an action potential in the fiber produces two major effects. First, there is a large current entering the extracellular space just ahead of the advancing excitation wave. Second, there is a large current sink just behind it. This is illustrated in Fig. 5.5. The potential field set up in the external medium is positive ahead of the wave front and negative behind it, both with reference to the potential at some remote reference point.

Inside the fiber, there is an axial gradient of the potential set up by the *active* processes at the cell membrane (Fig. 5.4c). The intracellular current I_i flows "down" this gradient and is directed from the location of the (extracellular) sink to the (extracellular) source. Outside the strand, the *passive* return current flows from source to sink near the strand (along path A). It also flows, but less intensively, along pathways further away, such as path B. As a result, a potential field Φ_e is generated throughout the external volume by the current flow.

This current flow pattern can be understood intuitively in the following way. An approaching excitation wave drives large currents of magnitude I_0 out of the membrane, in effect, by discharging the membrane capacitance. (The ionic charge accumulation across the membrane is high because the membrane is thin and the polarizing voltages, at rest, are substantial.) Once the approaching excitation wave has depolarized the membrane past a threshold level, the membrane has a large sodium conductance, so large inward currents I_0 flow through the membrane. The inward currents are driven in part by the concentration gradient of sodium ions between the inside and the outside. The inward currents are also driven by the potential difference driving positive ions inward. Large intracellular potential differences exist along the fiber between the partially depolarized region where the current is entering, and the fully polarized regions ahead of the advancing excitation wave. These axial intracellular potential differences cause large intracellular axial currents, I_i. The intracellular currents then begin the process of discharge at the next portion of the membrane capacitance.

These processes occur within the membrane because of its ability to change conductivities in an ion-selective manner. They create relatively positive voltages on the outer surface of the membrane at the (extracellular) current source and a relatively negative voltage on the outer membrane near the sink. In contrast, the current flow through the intracellular and extracellular volumes (all the way out to the body surface) is essentially a passive current flow in the surrounding conducting medium.

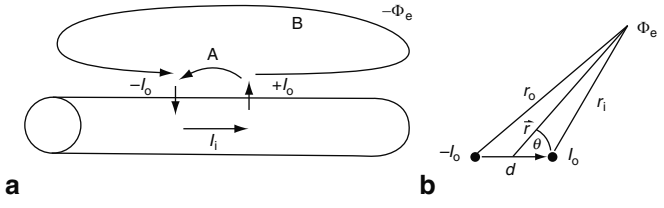

Figure 5.5

Current flow patterns in and around the fiber during depolarization. Intracellular longitudinal current I_i, transmembrane currents I_0, and extracellular current flowpaths A and B are shown. The flow of current throughout the extracellular volume creates the potential field Φ_e.

5.3.3 Potential Field arising from Lumped Sources; Current Dipoles

For observation points in the external medium with electric conductivity σ_e, at some distance from the fiber the (infinite medium) potential field is indistinguishable from the one that results by lumping the inward currents together into a single current monopole $-I_0$ (sink) and all outward currents into a single current monopole I_0 (source) (Sect. 2.5.1.1.), separated by a distance d.

At distances from the monopole pair that are much greater than d, the potential field in the external medium approaches the one generated by a current dipole $\vec{D} = I_0\vec{d}$, Sect. 2.5.1.2. Vector $\vec{D}$ is called the dipole moment; its strength is proportional to the gradient of the transmembrane potential along the fiber. The potential field (generated in an infinite medium) at a field point $\vec{r}'$ with reference to the position of the dipole is,

$$\Phi_e(\vec{r}') = \frac{1}{4\pi\sigma_e}\frac{\vec{D}\bullet\vec{R}}{R^3}, \tag{5.2}$$

or, equivalently, as

$$\Phi_e(\vec{r}') = \frac{1}{4\pi\sigma_e}\frac{D\,\cos\varphi}{R^2} \tag{5.3}$$

This expression shows that the potential produced by the dipole depends on several factors. One is the dipole's magnitude D (unit: A m). Another is the cosine of the angle φ between the dipole direction (from sink to source) and a line from dipole location to the field point. A third is the reciprocal of the square of the distance R from the dipole location to the field point. See also Sect. 2.5.1.3.

5.3.4 Potential Field Around a Single Fiber

A more general expression for the external potential generated by the membrane processes of a fiber follows from the addition (superposition) of the contributions to the potential at field point (x', ρ') arising from elementary current monopoles $i_m(x,t)\,\Delta x$, with $i_m(x,t)$ as specified in (5.1) and Δx a small segment along the fiber. Based on (2.96) we have

$$\Phi_e(x',\rho';t) = \frac{\pi a^2\sigma_i}{4\pi\sigma_e}\int_{-\infty}^{\infty}\frac{1}{\sqrt{(x'-x)^2+\rho'^2}}\frac{\partial^2 V_m(x;t)}{\partial x^2}\mathrm{d}x, \tag{5.4}$$

in which ρ' denotes the distance from the external observation point to the fiber axis.

An alternative, equivalent expression, found by means of partial integration, is as follows

$$\Phi_e(x',\rho';t) = \frac{-a^2\sigma_i}{4\sigma_e}\int_{-\infty}^{\infty}\frac{x'-x}{\left((x'-x)^2+\rho'^2\right)^3}\frac{\partial\, V_m(x;t)}{\partial x}\mathrm{d}x \tag{5.5}$$

By introducing $\vec{S}(x) = \pi a^2\vec{e}_x$ in (5.5), and since $\partial V_m(x,t)/\partial x$ has components along the fiber only, we may write

$$\Phi_e(x',\rho';t) = \frac{-\sigma_i}{4\pi\,\sigma_e}\int_{-\infty}^{\infty}\frac{\partial V_m(x;t)}{\partial x}\frac{\vec{R}}{R^3}\bullet\vec{S}(x)\mathrm{d}x, \tag{5.6}$$

with $\vec{R}$ the vector from source point $(x,0)$ to field point (x',ρ'). By using (2.110) we find

$$\Phi_e(x',\rho';t) = \frac{-\sigma_i}{4\pi\,\sigma_e}\int_{-\infty}^{\infty}\frac{\partial V_m(x,t)}{\partial x}\Omega(x,\vec{r}')\mathrm{d}x, \tag{5.7}$$

with $\Omega(x,\vec{r}')$ the solid angle of the cross-section of the fiber at location x along the fiber subtended at field point (x',ρ') (Sect. 2.2.12). This expresses the external potential field as the sum of the contributions from elementary double layers

with strength $\Delta M_S = -\sigma_i(\partial V_m/\partial x)\,dx$, stacked up along the fiber and pointing in the direction of propagation at locations that are depolarizing.

Equation (5.7) has great significance for the description of the potential field generated by bioelectric sources. A more complete treatment of this topic is presented in Chaps. 6 and 7. In this chapter it is used mainly for source descriptions during the depolarization phase, for which the source strength (dipole density) is assumed to be uniform over the depolarization wave front.

Equations (5.4) and (5.5) involve the so-called convolution integrals. The first one is the convolution of a monopole source function derived from the second spatial derivative of the transmembrane potential along the fiber and the function $1/R$, and as can be seen from (5.7), the second that of a double layer with its strength proportional to the first spatial derivative and the function expressing the solid angle subtended by the wave front.

5.3.5 Source Description at Depolarization Wave Fronts; Uniform Double Layer Theory

What if there are many fibers rather than just one, as in some extensive part of the myocardium?

A first approximation is to compute the potential when many fibers are active, as the sum of the potentials generated by each one (superposition). At the depolarization wave front this can be viewed as a collection of elementary dipoles distributed over the surface $S(t)$ of the wave front at time t, as illustrated in Fig. 5.6.

The expression for the potential then reads

$$\Phi_e(\vec{r}\,';t) = \frac{1}{4\pi\,\sigma_e}\int_{S(t)} \frac{\vec{M}_S(\vec{r};t)\bullet\vec{R}}{R^3}\,dS(\vec{r}), \tag{5.8}$$

with $\vec{R} = \vec{r}\,' - \vec{r}$ the vector from source location $\vec{r}$ on S to field point $\vec{r}\,'$, with length R (Sect. 2.5.2.2). Note that, as a consequence of the propagation, the integration at different time instants t is taken over different surfaces $S(t)$.

Next, we assume the direction of the dipole density $M_S(\vec{r}\,';t)$ to be lined up with the direction of local propagation of the wave front. Then (5.8) becomes

$$\Phi_e(\vec{r}\,';t) = \frac{1}{4\pi\,\sigma_e}\int_{S(t)} M_S(\vec{r};t)\,d\omega(\vec{r}), \tag{5.9}$$

compare (5.7). If, moreover, M_S is a constant over the wave front $S(t)$, then (5.9) takes on a particularly simple form:

$$\Phi_e(\vec{r}\,';t) = \frac{M_S}{4\pi\sigma_e}\Omega(\vec{r}\,';t), \tag{5.10}$$

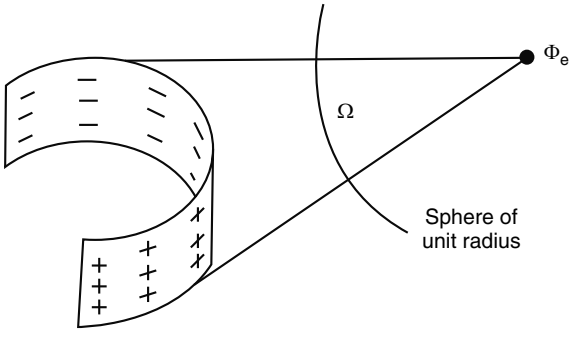

Figure 5.6

Depolarization wave front propagating towards an observer. The potential Φ_e generated by the distributed sources and sinks is proportional to the solid angle of the excitation wave as seen from the field point.

where $\Omega(\vec{r}';t)$ is the solid angle subtended by the entire wave front $S(t)$ as seen from the field point, as illustrated in Fig. 5.6.

The source model based on the two assumptions of elementary dipoles lined up with the direction of the wave front propagation and having uniform strength is known as the uniform double layer (UDL). Based on (5.10), the theory of its application is referred to as the solid angle theory. It is a classic source model, originating from the work of Wilson et al. [23]. It is used in most basic texts on the relationship between electric cardiac sources and resulting potentials, as in the sequel. A particularly thorough demonstration of its usefulness has been published by Holland and Arnsdorf [24]. Note that this model is restricted to describing the major sources during depolarization only; its validity is discussed in Chap. 6.

5.3.6 The Effects of the Geometry of Torso Boundary and Inhomogeneous Tissue Conductivity

The expressions for the potentials Φ_e above assume implicitly that a uniform medium of infinite extent surrounds the active fibers. In reality, cardiac sources are immersed in a volume conductor containing regions of different conductivity. These include the blood within the heart, the lungs and skeletal muscle. Rather than having infinite extent, the volume conductor is sharply delimited at the body surface by the torso-air boundary. A cross-sectional drawing of the human torso identifying the locations of the heart and lungs within the torso is given in Fig. 5.7. The level corresponds to the fourth intercostal space, the level of electrodes V_1 and V_2. The position of the remaining four electrode placements, as projected into the plane of the figure are those proposed by Goldman [25]. The drawing shows the asymmetric placement of the ventricular muscle within the thorax. Note how closely the right ventricular (RV) free wall approaches the chest near V_1, and how much further V_6 is from the left ventricular (LV) free wall. In the preceding section, it was established that the distances between the cardiac sources and the sites of electrodes on the body surface was highly significant, in that potentials from the dipole sources declined as $1/R^2$. Gross inspection of Fig. 5.7 shows that moving around the thorax circumference, starting from the position of V_1, the length of R may vary by as much as a factor of 10, depending on the particular membrane that is active. That implies that the potentials may vary in magnitude by a factor of 100 because of distance effects alone. As a consequence, large deviations from normality may remain unnoticed in clinical recordings.

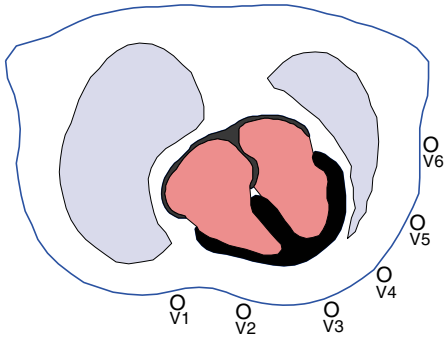

Figure 5.7

Superior view of a cross-sectional drawing of a human torso; derived from magnetic resonance images, showing, in increasingly darker shades, the lungs, the blood filled cavities, the atrial and ventricular myocardium. Circumferential locations of the six precordial electrodes as described by Goldman [25]. The transverse level is that of the fourth intercostal space, the level of electrodes V_1 and V_2; the remaining four are placed more inferiorly (Fig. 5.2).

One way of mathematically taking into account the presence of boundaries and inhomogeneities is by the use of Green's theorem, as discussed in Sect. 2.6.4. An example of its use is the following equation for the potential on the body surface:

$$\Phi_B(\vec{r}') = \frac{\sigma_s}{\sigma_B}\Phi_{B,\infty}(\vec{r}') - \frac{1}{4\pi}\frac{\sigma_L - \sigma_B}{\sigma_B}\int_{S_L}\Phi_L d\omega_L - \frac{1}{4\pi}\int_{S_B}\Phi_B d\omega_B \tag{5.11}$$

This expression is a specific form of (2.172), dedicated to its application to field points positioned at the body surface S_B. It describes the computation of the effect of the low conductivity of the lungs relative to that of other body tissues. It is assumed that bounding surfaces S_L can be drawn around "lungs" separating uniform regions of different conductivity inside and outside the boundaries (Fig. 5.7). Potentials on the lung and body surfaces are designated by Φ_L and Φ_B respectively. Within the lung, and on the remaining parts of the body, the conductivities are given by σ_L and σ_B respectively.

The first term of (5.11) expresses the infinite medium potential of the source at field points on the torso surface, e.g., as in (5.9) placed in a medium with conductivity σ_s. In addition, (5.11) contains two integrals expressing the contributions of the secondary sources representing the effect of different conductivity values across the lung and torso interfaces. Note that if the conductivity values at both sides of the lung interface were taken as equal, then the contribution of the associated secondary sources would vanish.

The single, most dominating factor on the magnitude of the potentials on the body surface is the distance between source location and observation point (Sect. 2.5.1.3 and 5.3.6). Next in rank is the effect of the torso boundary. To a first approximation, potential magnitudes are increased by a factor of 2 to 3 as a consequence (Sect. 2.6.3.3).

As can be seen from an inspection of (5.11), the specific effects of the torso boundary or internal inhomogeneities are not described by a simple rule. Accordingly, extensive variations from these first approximations occur. Qualitative relationships between cardiac and body-surface events can often be accomplished satisfactorily even when volume-conductor effects are ignored, but the quantitative effects are quite substantial. Note that (5.11) as shown ignores other significant aspects of the volume conductor. These aspects include the inhomogeneity consisting of the highly conductive blood within the chambers, and the anisotropic nature of the conductivity of skeletal muscle. A more detailed treatment of this topic is presented in Chap. 8.

5.3.7 Depolarization Summary

Depolarization consists of a complex of excitation waves moving through the active tissue. Excitation waves correspond to the upstroke of the transmembrane action potential, moving by means of active propagation. From an extracellular viewpoint, excitation waves frequently consist of a source-sink pair, having a spacing of about one millimeter, traveling at a speed of the order of $0.4\,\mathrm{m\,s^{-1}}$ across the fiber measured in situ in the canine ventricle [26] and up to $1\,\mathrm{m\,s^{-1}}$ measured in vitro along the fibers of the strips of the cardiac muscle [27]. Using the mathematical equations above, it can be seen that during depolarization the magnitude of the extracellular potential Φ_e depends on the following:

(a) The intensity of the line density expressing the membrane current $i_{m(x,t)}$, discussed in Sect. 5.3.1 (unit: $\mathrm{A\,m^{-1}}$). This affects I_0 of Sect. 5.3.3 (unit: A) as well as M_S, the dipole layer strength (unit: $\mathrm{A\,m^{-1}}$). This intensity depends on the second spatial derivate of the intracellular potentials and, correspondingly on the magnitude of the action potentials (5.1).
(b) The distance R from the source of membrane current to the field point, i.e., the point where the extracellular potential, Φ_e, is being determined (5.3).
(c) The orientation of the source-sink pair with respect to the point where the extracellular potential, Φ_e, is being determined. The potential Φ_e is positive when the field point is on the source side of the pair.
(d) The number of fibers involved, i.e., the extent of the source region (5.9). Both the extent of the source region and the distance to it are taken into account in the solid angle Ω.
(e) The torso boundaries and inhomogeneities in conductivity within the volume conductor.

A more extensive treatment of linking the electrophysiology of the depolarization wave front with its expression in terms of an equivalent source description is contained in Chap. 6.

5.3.8 Repolarization Summary

Repolarization occurs when the action potential returns to its resting level. Current flow during repolarization can be analyzed in a fashion similar to that provided above for depolarization. However, significant differences between depolarization and repolarization include the following.

(a) Repolarization currents across the membrane and associated changes in the voltage of the membrane occur after a time delay following depolarization. Hence repolarization is not propagated in the same sense that depolarization is, although membrane currents at one site continue to be affected by events at neighboring sites.
(b) The time required for the membrane to repolarize is fifty or more times the length of the time required for depolarization. Hence the source distribution of the membrane current is much more widely dispersed in space than during depolarization. As a consequence the distribution cannot simply by represented in terms of the propagation of dipoles.
(c) As the sources and sinks are so much more widely separated, describing, specifically, the transition from (5.6) to (5.7) is no longer possible with good accuracy. For single fibers, the analysis requires a return to Eqns. (5.1–5.4), as was done, e.g., by Spach et al. [28].
(d) The intensity of the current emerging from (or entering) the membrane at any one site is much less during repolarization than during depolarization. Conversely, the current emerges (or enters) over a much wider region. These effects offset each other differently at varying distances from a strand of myocardial tissue. Near the tissue, deflections in electrograms taken at close distance from the myocardium during repolarization are small relative to those during depolarization. On the body surface, the T waves have magnitudes much more comparable to those of the QRS complexes.

The modeling of the electric sources for representing body surface potentials during repolarization has long been restricted to a single dipole. This type of source cannot easily be given an electrophysiological basis. A recent development has yielded the source description of the equivalent double layer, which has a clear link with electrophysiology, both during depolarization and repolarization. This topic is discussed in Chap. 7.

5.4 Attributes of the Deflections

The principles enumerated in the previous section provide a basis for understanding the attributes of each of the phases of the ECG, which are considered in turn. In each section, brief comments are included about the excitation of the underlying cardiac structures and about the resulting electrocardiographic deflections. Most topics presented here are analyzed in greater detail in other chapters of this volume. In this chapter, the main objective is to discuss linkages between what is happening within the heart and how this is expressed in the signals observed on the body surface.

5.4.1 Cautions

The mathematical relationships established above have served as a basis for many reports relating to body-surface potentials to currents and to potentials within the heart. In sequel, they are used as a guide to the qualitative relationships. Even so, it is important to realize that they ignore many aspects of the real tissue, including the anisotropy of the tissue, the different access of deep and superficial fibers to the extracellular volume, the blood within the cardiac chambers, and the anisotropy of the skeletal muscle.

Another concern is the fact that the electric potential as such does not relate in any way to the electric current sources expressing the electric activity of the heart (Sect. 2.5). It is only the potential *differences* observed by at least two electrodes placed at some distance on the thorax that are related to such activity. In any recorded signal, if one of the electrodes involved is taken to be the reference, the potential at the reference is often tacitly assumed to be zero. Within a bounded

volume conductor, this assumption is unjustified [29, 30], and is in fact incorrect. This also applies to the Wilson Central Terminal, the potential reference most frequently used in ECG recordings. In the documentation of any ECG signal the involved reference should be specified.

The qualitative explanations of QRS amplitudes and wave forms based on the solid angle theory, usually address the potential generated at the sensing electrode only. This implicitly assumes the solid angle of the wave fronts as seen by the reference electrode to be zero. For the correct application of the solid angle theory to the interpretation of the potential difference between two electrodes, the different solid angles subtended by the wave front as seen from the locations of the two electrodes should be subtracted [31].

The potential difference between any two different electrode locations reflects the integral of the component of the electric field along the path traveled from one electrode to the other. As a potential difference is a scalar, the route taken does not affect the outcome (Sect. 2.5). The discussion on what is "seen" by either of the two electrodes, or which of the two electrodes acts at the reference [32] is meaningless and does not reflect basic physical principles [33]. The term reference electrode should be reserved for situations in which multiple signals are studied, all referred to a single location. Such signals are commonly referred to as unipolar leads, a complete misnomer that should preferably be replaced by "common reference signals."

5.5 P Wave

In a normal sinus rhythm, excitation begins at the "sinoatrial (SA) node and spreads in a pattern similar to that produced by dropping a stone into still water" (Scher [34]). James [35] has emphasized the different histological appearances of different atrial cells and suggested that different specialized pathways may exist in the atrium, in some fashion analogous to the conduction system of the ventricles (see Chap. 4 for further discussion of this point). However, measurements of the spread of the excitation, from the time of Peuch [36] to the measurements of Spach [37], differ. The measurements show that different velocities of excitation arise primarily from differences in the propagation velocity along and across atrial fibers. A review of this question was given by Sano [38].

From an electrocardiographic viewpoint (Fig. 5.8), during the generation of the P wave, the active membrane is relatively distant from the electrodes on the torso surface. The extent of the sources will be small, since the atrial wall is

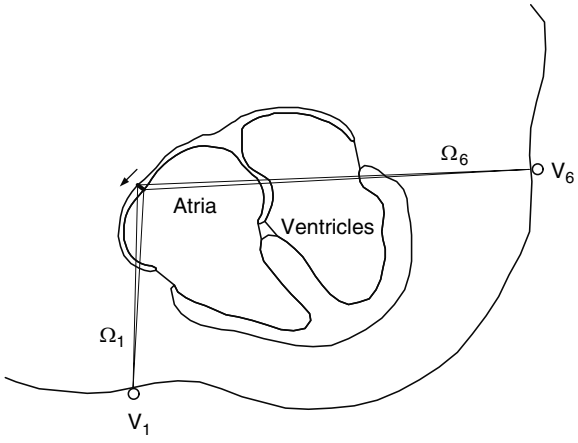

Figure 5.8

Solid angles during atrial excitation. A small region of atrial muscle is hypothesized to be active and identified by a bold line. Propagation is in the direction of the arrow. Solid angles from V_1 and V_6 are indicated by the straight lines drawn. Note that the solid angle concept in fact relates to 3D space. The drawing indicates that the area of the active surface is small and the distances from either body surface site relatively long. Both these effects will lead to a small solid angle and thereby small potentials during the P wave.

thin, and the muscle is excited by propagation proceeding tangentially to the wall. The dominant active electric sources are few during depolarization. The consequence is that the corresponding manifestation of atrial activity on the body surface, the P wave, normally has a low magnitude (in the range of 60–120 μV).

As excitation proceeds from the SA node, the leading (positive) side of the excitation wave front will be leftward and downward. The contribution of the small front shown in Fig. 5.8 produces a negative deflection in lead V_6 and positive deflection in lead V_1. The total excitation process usually produces positive apex P wave values in lead VF, and negative ones in lead VR. The duration of atrial excitation, and therefore the duration of the P wave, is about 100 ms.

In the past, the fact that the magnitude of the P wave was often frequently not much higher than the noise level of ECG recorders, has introduced considerable imprecision into P-wave standards as documented in the literature. These were restricted mainly to P wave amplitudes and durations. As a consequence the P wave has been mainly used to provide the relative timing between atrial and ventricular events. With the advances in recording technology (lower noise levels), and the current interest in atrial electric activity during atrial flutter or atrial fibrillation, efforts are directed towards extracting more information about atrial electric activity from the ECG.

5.6 PQ Segment

On an ECG recorded with standard methods, the P wave is followed by an interval of about 70 ms leading on to the onset of depolarization of the ventricles: the PQ segment. Because of the small magnitudes of potential differences on the thorax generated during this interval, this period is usually considered to be electrically silent. However, early applications of the body surface mapping technique have identified clear, non-zero patterns of potential differences on the thorax during this period, with magnitudes that are about one third of those during depolarization of the atria [39, 40]. The time course of these patterns is almost the reverse of those during depolarization, suggesting that these potentials relate to the repolarization of the atria, with a very small dispersion of the durations of the action potentials of atrial myocytes [41, 42]. At the moment of onset of ventricular depolarization, these potential differences may have magnitudes up to 30 μV. The locations showing maximal potential differences are not included in the electrodes of the standard 12-lead ECG [41].

In a normal heart, atrial excitation initiates excitation of the atrioventricular (AV) node, which in turn initiates excitation of the ventricular conduction system. As the diameter of the fibers of the AV node is small, the conduction velocity through them is low (about 0.05 m s^{-1}). Conversely, the fibers of the ventricular conduction system are large, so conduction is much faster (about 2 m s^{-1}).

Though excitation is progressing through the AV node and conduction system, excitation includes a small number of fibers, distant from the surface. The potentials observed during the PQ segment have also been attributed to this process. On the body surface these are in the range of 1–10 μV peak-to-peak. In 1973 and 1974, Berbari et al. [43], Flowers et al. [44] and others began publishing a series of papers that indicated that recordings could be obtained from the body surface, during the PR interval. In 1983, Flowers et al. [45] presented an analysis of PR intervals in normal subjects and patients with abnormalities of the conduction system. Their recordings showed a biphasic deflection during the PQ segment, having a magnitude of about 2.5 μV. Earlier studies in animals, as well as recordings from humans with normal and abnormal AV conduction, support the hypothesis that these signals arise from the His-Purkinje system, primarily through the temporal linkages between the His-Purkinje waveforms and those known to arise from the ventricles.

5.7 QRS Complex

The QRS deflections arise from the excitation of the ventricular muscle. In normal excitation, the conduction system causes excitation of the muscle to begin more or less simultaneously at a number of right and left ventricular endocardial sites. (Detailed maps are presented in Chap. 4.) One consequence is that excitation has a substantial radial as well as tangential direction throughout the excitation of much of the ventricular wall.

There are a number of general characteristics about the electrocardiographic effects of ventricular excitation that arise from the overall geometric relationships between ventricular and body-surface points as they interact with the gross

features of ventricular excitation. Several of these are illustrated in Fig. 5.9, in which the two heavy lines represent excitation waves, one in the right ventricle (Fig. 5.9a) and one in the left (Fig. 5.9b). Both advance toward the epicardium. Electrode sites are identified on the body surface at V_1 and V_6. Suppose the potential at V_1 and V_6 are measured with respect to Wilson's central terminal the following should be noted.

(a) An electrode at point V_1 or V_6 on the body surface "sees" a solid angle Ω_1 associated with the excitation wave in the right ventricle (left panel) or from the excitation wave in the left ventricle (right panel). The solid angle reflects the entire excitation surface in three dimensions that results from the excitation wave extending above and below the plane of the figure, not simply the cross-sectional line drawn there. The solid angles at V_1 and V_6 are different, because the distance and orientation of V_1 from either excitation wave differs from that of V_6. Moreover, for the wave fronts shown, their signs differ.

(b) If both activation fronts are present, the potential at V_1 or V_6 is the algebraic sum of the potentials produced by each of the excitation waves separately. In Fig. 5.9, a positive voltage is produced at V_1 by the RV excitation wave, and a negative voltage by the LV excitation wave. The sum is probably slightly positive. The fact that the sum is algebraic means that the sum is lower in magnitude than would be the case if either excitation wave were present separately. This phenomenon is called *cancellation* [46] in the electrocardiographic literature. One consequence is that if only one excitation wave is present, the magnitude of the body surface deflection is higher than if two are present. A similar effect is seen at V_6.

(c) As the right ventricle is closer to an electrode on the anterior chest, such as V_1, than to the left ventricle, a right ventricular excitation wave will have a greater solid angle, and therefore produce a greater voltage at V_1, than an excitation wave of the same extent and orientation in the left ventricle.

(d) Excitation waves in either ventricle extend over greater distances when excitation is predominantly in the endocardial to epicardial direction than when excitation proceeds in a direction tangential to the surface of the walls.

(e) The right ventricular excitation wave generally starts somewhat later than the one initiated at the left ventricular aspect of the septum. Moreover, the right ventricle is relatively thin and, once activated, its excitation is for the greater part directed along the right ventricular wall and ends later than that of the left ventricle. The consequence is that the earliest part of the QRS deflection normally reflects septal activation, the middle part a combination of left and right ventricular activity, while the final part reflects predominantly the excitation of the basal part of the right ventricle.

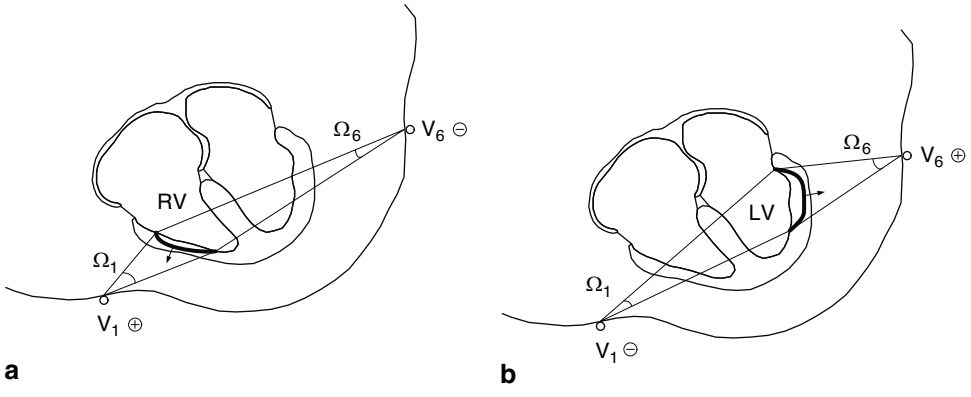

Figure 5.9

Solid angles during ventricular excitation. An excitation wave is drawn in (left panel) the right ventricle and (right panel) the left ventricle. Comparison with Fig. 5.8 shows the solid angles to be much larger during QRS than during P, so that larger potentials are to be expected. The larger solid angles occur mostly because of the greater extent of either excitation wave, since excitation proceeds radially as well as tangentially in a normal sequence. Conversely, note that the orientation of the RV and LV excitation waves shown produces potentials of opposite sign at either V_1 or V_6. If both excitation waves are present simultaneously their effects will tend to cancel.

(f) The conduction system "programs" normal excitation of the ventricles in such a way that excitation is completed relatively rapidly. RV and LV excitation overlap extensively (with electrical cancellation). Many cardiac abnormalities (e.g., conduction system defects) tend to produce body-surface waveforms that are longer and of greater magnitude, because the normal "program" is lost. In later chapters the specific electrocardiographic changes arise from the presence of conduction defects, infarction, hypertrophy and other clinical conditions.

5.8 ST Segment

Following the QRS deflections, the ECG has a relatively quiescent period before the large deflection of the T wave occurs. A simple qualitative explanation of this phenomenon is as follows

(A model based interpretation of the ST-T signals is given in Chap. 7). Consider Fig. 5.10. Suppose there are two electrodes located on the endocardial and epicardial surfaces of the ventricular wall (electrodes 1 and 2, Fig. 5.10a). Suppose further that the wave forms of the transmembrane potentials (TMPs) at the endocardial and epicardial sites are identical (as illustrated by the stylized shape of Fig. 5.10b). A difference of excitation between the endocardial and epicardial sites results in the situation shown in Fig. 5.10c.

There are periods during which the overlapping tracings have the same potential value. One is the baseline phase (identified as b on Fig. 5.10c). Another is the plateau phase, denoted as p, of the action potentials. During period p there is no intracellular potential difference between sites 1 and 2. Therefore, no intracellular current flows between these sites during interval p. Consequently, no extracellular (or electrocardiographic) potential differences are generated in the case of the stylized TMPs.

Similarly, if the TMPs throughout the entire ventricle have the same baseline and plateau voltages, and if there is a period of time following excitation (QRS) during which the plateau voltages throughout the ventricles overlap, then during this period of time (the ST segment) the observed electrocardiographic voltages return to the baseline, i.e., are zero.

Available evidence indicates that neither condition is precisely satisfied in normal human hearts, though both exist, more or less. Measurement of body-surface potential distributions [47] during the ST segment in chimpanzees and in normal human subjects show that there is no period of time following excitation when either epicardial or body-surface potentials return uniformly to the baseline. Instead, there is a period of overlap between the potentials that arise from the last portions of muscle to be excited and repolarization potentials from other regions. This period may last for 10 ms or more. However, in a normal sequence, both the potentials at the end of depolarization and the beginning of repolarization are small, so the ECG does return to a voltage near the baseline.

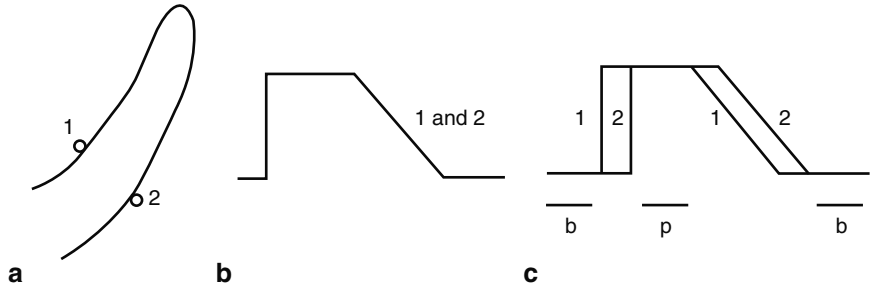

Figure 5.10

ST segment with identical transmembrane potential waveforms. Part (a) identifies two electrodes across a portion of the ventricular wall. Part (b) shows a single TMP shape hypothesized to be present at all ventricular sites. Part (c) shows the TMPS if excitation at site 2 occurs later than at site 1. Nonetheless, there are periods of time, identified b (baseline) as p (plateau phase), when both action potentials at endocardium and epicardium are the same. During this time there are no intracellular potential differences among sites and therefore no intracellular or extracellular currents.

The J point of the ECG is identified as the time when a tracing changes slope abruptly at the end of the S wave. The J point is sometimes used as a marker for the end of excitation. Comparison of the electrocardiographic waveform with the complete body-surface potential distribution or, when available, epicardial electrograms, shows that the J point marks the end of excitation only approximately. Again the approximation occurs because of the overlap of potentials at the ending of depolarization and the beginning of repolarization [47].

Changes in the cardiac excitation sequence or changes in the action-potential wave shape can be expected to change the amplitude and wave form of the electrocardiogram during the ST time period.

If the amplitude or the wave form of the TMP changes in a region of muscle, then the situation portrayed in Fig. 5.11 arises. Electrodes 1 and 2 are again sites on the endocardium and epicardium respectively. Suppose the TMP from site 1 differs in its time course, as well as at its time of onset, as compared to that at site 2. In Fig. 5.11a, it is assumed that the TMP at site 1 has half the magnitude of that at site 2, but otherwise is the same.

As the TMPs differ, there is no longer a period of time during the plateau when no potential difference exists between sites 1 and 2. Consequently, a current will flow intracellularly from site 2 to site 1 at time t_p, as shown diagrammatically in Fig. 5.11b. (Whether the current will flow all the way from the epicardium to the endocardium, or only across a much narrower region, will depend on the potential distribution between sites 1 and 2.) As there now exists an intracellular current, currents will flow extracellularly as well, as indicated by the flow I_e in Fig. 5.11b.

In the example shown, the current flow pattern will cause the extracellular potential to be relatively positive on the endocardium near site 1, and relatively negative on the epicardium near site 2 (Fig. 5.11c). Consequently, ECGs recorded from a region overlying site 2 will be seen to have "ST-segment depression." Interpretations based on this kind of analysis are often used to explain ECGs recorded in patients with ischemic muscle regions and in those with recent infarctions. A widely examined analysis of ST potentials in relation to infarct size was developed by Maroko et al. [48].

It is worth noting that in Fig. 5.11a the action potentials also differ in potential during the baseline segments. Elevations or depressions of the "baseline" during the T-P interval with opposite polarity to those during the ST segment therefore occur [49]. However, most electrocardiographic recording systems use ac-coupled amplifiers. (Such amplifiers filter out dc voltages of tens of millivolts that are created at the electrochemical interface between the skin and body-surface electrodes.) Consequently, electrocardiographic records do not indicate whether voltages between surface electrodes are present during the "baseline" period. Analysis of ECGs is often based on conventions that assume that no currents or potentials exist prior to the P wave. Assuming that such potentials are not present when they are has the effect of increasing the magnitude of the change said to be present during the ST segment. An exaggerated change during ST comes about because individual tracings show correctly the difference between the baseline voltage and that during the ST segment (Sect. 12.4.4.4.)

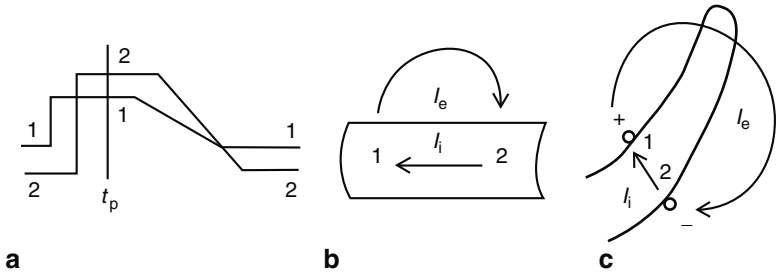

Figure 5.11

ST segment with non-uniform action potentials. (a) shows that site 2 has the same action-potential waveform as used in Fig. 5.10. In contrast, site 1 has an action potential that is reduced in magnitude, but otherwise the same. Now there is no time during the plateau when all intracellular sites have the same voltage. Consequently (b) shows an intracellular longitudinal current I_i; and extracellular current I_e flow at time t_p. If action potentials with reduced amplitude are present throughout an endocardial region near electrode 1, then (c) negative potentials will occur over the epicardial region and positive potentials over the endocardial one.

5.9 T Wave

5.9.1 T Wave in the Case of Uniform Action Potential Duration

Repolarization of ventricular muscle fibers from active to resting transmembrane voltages produces the T wave. Since the voltage changes of repolarization traverse the same range as those of depolarization, except in the reverse direction, it is tempting to think of the T wave as depolarization in reverse. However, if this were true, all ECG wave forms observed during repolarization should have a reversed polarity compared to those during depolarization, with a lower amplitude and slower time course due to the much slower rate of repolarization (Chap. 7). As this is not in agreement with experimental observations, this simple hypothesis must be rejected.

5.9.2 Normal T Waves

Because the signs of the T waves in the ECG do not all have the reversed polarity of the corresponding QRS complexes, the hypothesis of a uniform duration for all TMP wave forms must be wrong. What would be an alternative? Clearly this must be related to non-uniformity and/or local differences in TMP wave forms throughout the myocardium. The weight of available measurements from intact animals indicates that the duration of the action potential varies from endocardium to epicardium. More specifically, it appears that action potentials nearer the endocardium are longer. Moreover, Burgess et al. [50], using refractory period measurements in dogs, found that repolarization normally occurs later at the apex than toward the base. Somehow, based on such data, the notion has emerged that the timing of repolarization at the epicardium precedes that on the endocardium. However, the correct statement is that, generally, epicardial action-potential durations (APD) are shorter than those of the endocardium. The differences involved are not uniform for different parts of the ventricular myocardium, as it depends on the timing of depolarization and are different between LV and RV. More recently, different experimental studies have shown regression lines of APD as a function of local activation time having a slope of about −0.4 [51, 52]. The full consequence of this complexity in a full 3D model of the ventricular myocardium can only be worked out by using an advanced model of the sources during repolarization. An example of such a model-based analysis of T wave properties [53] is described in Chap. 7.

5.9.3 Intrinsic, Primary and Secondary T Waves

As described above, the excitation sequence interacts with the variation in action-potential duration from place to place.

What if there were no such interaction? In concept, the "intrinsic" T wave is the T wave that results if all cells in the ventricle depolarize simultaneously. An intrinsic T wave can be created experimentally by applying a large stimulus to the entire muscle simultaneously. The intrinsic T wave thereby occurs because of differences in action-potential duration from site to site.

Conversely, the "secondary" T wave was defined by Abildskov et al. [54] as the one necessary to make the ventricular gradient (see below) equal to zero, a condition that will be fulfilled if all myocytes have the same APD. Thereby, the secondary T wave occurs because of differences in action-potential onset. The secondary T wave, not a naturally occurring waveform, can be constructed numerically.

The "primary" T wave was defined by Abildskov et al. [54] as the difference between the actual T wave and the secondary T wave. Like the secondary T wave, it can be constructed numerically. If the actual T waves occur because of a mixture of the effects of the depolarization sequence and the effects of variations in action-potential duration, and if subtracting the secondary T wave is equivalent to subtracting the effects from the depolarization sequence, then it seems intuitively reasonable that the "primary T wave" is the same as the "intrinsic T wave." Horan et al. [55] examined the question of whether they were identical and found that the primary T wave approached identity with the intrinsic T wave. Failure of absolute congruence was attributed to the lack of a precise marker to provide precise time alignment between all waveforms.

At the present time, the intrinsic, primary, and secondary T waves are used mostly as concepts and constructions made in the course of better understanding the source of the actual T waves, rather than as waveforms routinely constructed for physiological or clinical interpretation.

5.9.4 Ventricular Gradient

Closely related to the different T waves discussed in the preceding section is the concept of the ventricular gradient. In 1934, Wilson et al. [56] introduced the idea that the area under the ventricular deflections of the ECG had a significance beyond that provided from a moment-by-moment evaluation. They determined the area under electrocardiographic curves during QRST, the ventricular deflections. In determining the area, "due care" was used to construct a baseline, as doing so was "a matter of greatest importance." Then the net area between the waveform and the baseline was found. Those portions of the area that lay below the baseline were considered negative and subtracted, while those that lay above the baseline were considered positive and added.

Wilson et al. concluded that if all action potentials had the same shape, magnitude and duration, the net area under each electrocardiographic deflection was zero. However, many waveforms showed net areas that were nonzero. In analyzing these waveforms, Wilson et al. looked principally at excitation sequences where action potentials from region to region varied at the onset and duration, but not otherwise. They concluded that any net area was a "measure of the effects produced by local variations in the excitatory process, and particularly by local variations in the duration of the excited state."

To analyze the differences in areas, Wilson et al. made use of Einthoven's triangle. In concept, ECGs were obtained from electrodes at the apices of an equilateral triangle, centered on the heart. (Actual electrodes were on the limbs.) Wilson et al. considered the vector formed by replacing the waveform at each apex with the waveform's net area. The vector was the one whose projection onto each side of the triangle gave the observed difference between apices. They considered, for example, the vector produced by a uniform gradient in the duration of the excited state. They concluded that the vector that "represents the effects produced by this gradient will point from the end of the fiber where the systole is longer to the end where it is shorter, and will have a length proportional to the difference in the length of systole at the two ends." Further, the vector remained unchanged for any excitation sequence if the duration of the excited systole at each site remained unchanged.

The idea that the differences in action-potential duration can be determined from body-surface waveforms has proved an intriguing object of theoretical study, as in the work of Burger [57] and Geselowitz [58]. Experimentally, QRST areas have been determined from many body-surface leads [59], aimed at relating these areas to arrhythmias. Over the years these investigations have refined the ventricular gradient concept, often presenting the refinements more unambiguously than the text descriptions of Wilson et al.

A mathematically precise presentation of the concepts of the ventricular gradient is as follows [60]. It is based on the well-founded notions on the genesis of bioelectric potentials listed below. These are referred to here as "properties."

- The generation of the potential differences outside a cell stems from biochemical processes at the cell membranes.
- The nature of these sources is that of a current generator [61].
- The volume conduction properties of tissues, however complex, are linear: the superposition principle applies.
- At any moment in time, any field generated in the extra-cellular domain stems from the spatial gradients of the TMPs, denoted as $V_m\ (\vec{r}, t)$, at source locations $\vec{r}$ [23].
- If all cells are completely polarized (at a constant value) the electric field set up by the sources in the surrounding medium is zero [23].

Taking the gradient of any scalar function involves computing spatial differences of the TMPs of individual cells, which is a linear operation. The application of the superposition principle is, again, a linear operation. Hence, the potential differences in the extra-cellular domain stem from a linear operator (superposition) acting on a linear operator (taking the gradient) acting on the TMPs. The cascade of two linear operations is also linear, hence: all external fields arise from a linear (spatial) operator acting on the TMPs of all myocytes. Expressing the strengths of all myocytes by matrix $\mathbf{V}_m$, with

its rows representing the time courses of all individual TMPs, and its columns their instantaneous strengths, the linear operation involved, conveniently denoted by a matrix multiplication (Sect. 2.A.1.3), is

$$\mathbf{\Phi} = \mathbf{A}\mathbf{V}_{\mathrm{m}} \tag{5.12}$$

This equation expresses the potentials in the extra-cellular domain, $\mathbf{\Phi}$, as the (matrix) multiplication of the TMPs $\mathbf{V}_{\mathrm{m}}$ by the transfer matrix $\mathbf{A}$. Matrix $\mathbf{A}$ expresses all volume conduction effects, be it inhomogeneous or homogenous, isotropic or anisotropic. In words: the potential in any observation point ℓ (c.q. lead position), $\phi_{\mathrm{l}}(t)$, is found to be a linear combination of the TMPs at that same instant of time. The weighting factors are the element of row ℓ of matrix $\mathbf{A}$.

From Prop.5 it follows that the sum of all elements of any row ℓ of this matrix is zero. Hence, when "feeding" the transfer matrix $\mathbf{A}$ with any constant column vector $\mathbf{c}$, a vector having identical elements c, the resulting potential is zero for all observation points, expressed in matrix terms:

$$\mathbf{A}\mathbf{c} = 0 \tag{5.13}$$

We now consider the integration over time (QRST interval) applied to the TMPs of all myocytes. The integral over time, the area under the curve, of the TMP of myocyte n is denoted as v_n, and the entire set of these integrals of all myocytes as the column vector $\mathbf{v}$. The effect of the corresponding integration over time of the potentials observed in lead ℓ, row ℓ of matrix $\mathbf{\Phi}$, (5.12), is denoted as $IQRST_{\ell}$. The set of all integrals constitutes a column vector $\mathbf{i}_{\mathrm{QRST}}$. The result of the integration over time applied to both sides of (5.12) can thus be expressed as

$$\mathbf{i}_{\mathrm{QRST}} = \mathbf{A}\mathbf{v} \tag{5.14}$$

Each myocytes n is assumed to be activated at depolarization time δ_n and, by taking the time of its maximal downward slope as a marker, to repolarize at time instant ρ_n. The corresponding activation recovery interval, ARI [62], is denoted as $\alpha_n = \rho_n - \delta_n$. For each myocyte, integral v_n depends on the value of its resting potential r_n, the magnitude of the upstroke of its action potential, u_n and its ARI value $\alpha_n = \rho_n - \delta_n$.

By considering action potentials having approximately the same shape (Assumption.1) it follows that for the integral of the TMP curve we may write $v_n = \alpha_n\,(r_n + u_n)$. In situations where both the upstroke (Assumption 2) and the resting potentials (Assumption 3) may be taken to have uniform values, each with integral c, it follows that for the complete set of QRST integrals at the field points we have

$$\mathbf{i}_{\mathrm{QRST}} = c\mathbf{A}\boldsymbol{\alpha}, \tag{5.15}$$

which shows that, within the validity of the assumptions of uniform general shape, uniform upstroke and uniform resting potential, integrals over time of lead potentials are a linear combination of the individual ARI values of all myocytes.

The previous formulation can be refined. To this end we write the ARIs' column vector, $\boldsymbol{\alpha} = \bar{\boldsymbol{\alpha}} + \Delta\boldsymbol{\alpha}$ in which $\bar{\boldsymbol{\alpha}}$ denotes a column vector having all elements equal to the mean, $\bar{\alpha}$, of the individual values α_n, and $\Delta\boldsymbol{\alpha}$ denotes the column vector of all individual deviations α_n from their mean. Substitution of $\boldsymbol{\alpha} = \bar{\boldsymbol{\alpha}} + \Delta\boldsymbol{\alpha}$ into (5.15) then yields

$$\mathbf{i}_{\mathrm{QRST}} = c\mathbf{A}\left(\bar{\boldsymbol{\alpha}} + \Delta\boldsymbol{\alpha}\right) = c\mathbf{A}\Delta\boldsymbol{\alpha} \tag{5.16}$$

Note that $\mathbf{A}\bar{\boldsymbol{\alpha}} = 0$ because of (5.13).

This analysis, (5.16), identifies the QRST integral of each lead signal as a linear combination of the elements of $\Delta\boldsymbol{\alpha}$. The weights are lead specific. The vector $\Delta\boldsymbol{\alpha}$ is the full representation of the total dispersion of APDs of all myocytes, and so the refinement of the statement following (5.15) is that the QRST integral of a lead signal is a linear combination of the elements of the dispersion of the action potential durations of all myocytes. The weights are lead specific.

In the case of the ventricular gradient introduced by Wilson, the "areas under the curve," $\mathbf{i}_{\mathrm{QRST}}$ were derived from three signals only. The result was expressed as the ventricular gradient, a vector in 3D space. Equation (5.16) is a generalization of this concept, constituting a vector in L dimensional space. The concept of the ventricular gradient is seen to be meaningful only within the assumptions used in this analysis. The analysis may be extended to the interpretation of the QRS and STT integrals separately [60].

The magnitudes of the vectors representing the (QRS)(T)-integrals, are influenced by the transfer of the volume conductor: (differences in) heart position and orientation, as well as by thorax geometry. Since both vectors have passed through one and the same filter (matrix $\boldsymbol{A}$), the angles involved are less sensitive to inter-individual differences in geometry. The angle β between any two L-dimensional vectors $\boldsymbol{a}$ and $\boldsymbol{b}$ in the plane they share follows from

$$\cos(\beta) = (\boldsymbol{a} \cdot \boldsymbol{b}) / (a \cdot b), \tag{5.17}$$

in which the dot indicates the sum of the product of all corresponding elements of vectors $\boldsymbol{a}$ and $\boldsymbol{b}$, and a and b their lengths. If vectors $\boldsymbol{a}$ and $\boldsymbol{b}$ are referred to zero mean, the right hand side of (5.17) is the linear correlation coefficient between the elements of $\boldsymbol{a}$ and $\boldsymbol{b}$. Both the angle β [63] and its cosine [64] have been tested as markers of repolarization abnormality.

5.10 U Wave

The U wave is a low amplitude, usually mono-phasic, ECG deflection directly following, and partly merged with, the T wave. Until recently, it has not received much attention in electrocardiographic literature. Many considered it a rarity, but in fact, by applying proper baseline correction procedures, it can be observed in almost all healthy subjects. Reasons for it having escaped notice are its low magnitude and a baseline correction performed at a premature timing.

Surawicz [65]described the U wave as a separate deflection of relatively low amplitude, usually detectable at slow or moderate heart rates, with an apex occurring about 100 ms following the end of the T wave. The U wave coincides with isovolumic relaxation. The presence, genesis and significance of the U wave have been a source of controversy. In part, the controversy has arisen because it is often hard to see U waves in experimental recordings in the presence of noise, as there is no clear demarcation between the end of T and the beginning of U or the onset of the P wave in the waveform of a given lead. The experimental difficulties are great, once causing Lepeschkin [66], who studied the U wave extensively, to remark jovially that the main question about the U wave is whether it exists or not.

In addition, differences of opinion have existed about the genesis of the U wave because various diastolic deflections recorded in local electrograms do not necessarily have the same timing as the U wave in human surface ECGs [66]. Such discrepancies are significant because the genesis of most other electrocardiographic deflections has been determined by comparing the timing of deflections on electrograms with those on the surface ECG.

There are two classic theories of U-wave genesis. Kishida et al. [67] describe these as follows. One theory attributes U-wave genesis to the repolarization of Purkinje fibers. The other theory attributes the U wave to potentials generated during relaxation of the ventricular myocardium.

Hoffman and Cranefield [12] argued in favor of the former-theory, saying "the action-potential of Purkinje fibers is considerably longer than that of ventricular muscle, and the phase of rapid repolarization of Purkinje fibers is coincident in time with the U wave."

Lepeschkin [66] discussed both theories extensively, but favored the latter, as did Surawicz [65]. Surawicz said that mechano-electrical coupling was the most likely cause of the U wave, because "it has been shown that stretch prolongs terminal repolarization in single fibers" [68], and "therefore may be expected to produce an ECG deflection after the T wave." Changes from a more stressed apex to a less stressed base, the "stretch gradient theory," are thought to result in different potentials between those regions, and thereby the U wave.

More recently, explanations based on the expression of mid-cardial myocytes [69], after-potentials [70] and late repolarization [71] have appeared in the literature.

Whatever its origin, Kishida et al. [67] described a negative U wave as highly specific for the presence of heart disease, most commonly systemic hypertension, aortic and mitral regurgitation, and ischemic heart disease.

5.11 Vectorial and Other Interpretations of the ECG

Analysis of the generation of ECGs has been accomplished within a number of frameworks having substantial conceptual differences. Most have focused on QRS. Many investigators from the time of the early electrocardiographers until the present day have analyzed ventricular excitation from the viewpoint of thinking of the electrical activity of the heart

as coming from a single "equivalent" dipole. This is a hypothetical current source that, when placed inside a homogeneous volume conductor, would generate the potential field on the surface of the thorax that most closely resembles the measured field. To this end its position, strength and orientation are tuned.

That the field generated by a complex current generator such as the heart can be approximated by that of a single dipole stems from the theory of multipoles [72]. That theory shows that an "equivalent dipole" will closely approximate the infinite medium potentials at distances like that of the body surface as the heart itself. However, because some of the cardiac surface comes close to the chest, the theory can be applied only as a first approximation. It appears that many early investigators considered the errors involved in approximating real cardiac potentials with those from a single equivalent dipole to be small [73]. For the full time course of the potential field during the QRS complex, the relative difference *RD*, defined as the RMS difference between the potentials generated by the equivalent dipole and the measured ones relative to the RMS value of the measured ones, is of the order of $RD = 0.2$. For more obese subjects the error tends to be lower, for lean subjects it is higher.

In more recent years, experimental evidence, particularly from body-surface maps [74], has demonstrated unequivocally that no single dipole can be "equivalent" in the sense of accurately reproducing the body-surface observations. As a result, multiple-dipole models of cardiac excitation were proposed, particularly by Barber and Fischman [75] and Selvester et al. [76]. Multiple-dipole models conceptually divide the ventricular muscle into several regions. Such models envisage each imaginary dipole as functioning "equivalently," in an electrical sense, to one region. Such models have been used very effectively, as by Ritsema van Eck [77] and, later, Miller and Geselowitz [78]. In this way it was shown how electrocardiographic changes observed on the body surface result from plausible alterations in cardiac action potentials and their timing. An interactive simulation package for studying such effects, including a demonstration of vector properties, has been made available from the internet [79].

A major weakness of both single- and multiple-dipole models springs from their being imaginary "equivalent" entities. The equivalence is, even in concept, an equivalence at a distance from the source only. This follows directly from (5.3), which shows that close to the dipole the potential may be infinite. Consequently, the currents and potentials near the active muscle may behave quite differently from those of an equivalent dipole, even if there may be a fair "equivalence" on the body surface. For a full discussion on this point, see Chaps. 8 and 9.

5.12 Evaluation

The fact that electrocardiography has been in use for more than a century leads one to think that most aspects of the relationships between the electrocardiographic waveforms and the underlying cardiac events would have been fully established by now. However, that is not the case. One of the main reasons is that acquiring accurate measurements of what is taking place electrically within the heart remains very difficult. This is particularly so when the volume conductor is intact. Recent years have seen marked changes in the recognition of the importance of anisotropies within the cardiac muscle, the quality of the quantitative descriptions of volume conductor behavior and the ability to link together such knowledge by means of numerical models. As the full weight of an improved understanding of the genesis of ECGs comes to bear fruit, further significant improvements in the quality and value of electrocardiographic interpretation are to be expected.

References

1. Waller, A., A demonstration on man of the electromotive changes accompanying the heart's beat. *J. Physiol.*, 1887;**8**: 229–234.
2. Einthoven; 100 Yeart of Electrocardiography, in M.J. Schalij, M.J. Janse, A. van Oosterom, V.D.W.E.E. and H.J.J. Wellens, Editors. Leiden: The Einthoven Foundation, 2002, pp. 616.
3. Burch, G.E. and N.P. DePasquale, *A History of Electrocardiography*, Chicago: Illinois, 1964.
4. Johnson, J.C. and N.C. Flowers, History of electrocardiography and vectorcardiography, in *The Theoretical Basis of Electrocardiology*, C.V. Nelson, and D.B. Geselowitz, Editors. Oxford, Clarendon Press, 1976.
5. Einthoven, W., Un nouveau galvanometer. *Arch. Neerl. Sci. Exactes Nat.*, 1901;**6**: 625–633.
6. Einthoven, W. and K. de Lint, Ueber das normale menschliche Elektrokardiogram und Uber die capillar-elektrometrische

Untersuchung einiger Herzkranken. *Pflugers Arch. Ges. Physiol.*, 1900;**80**: 139–160.
7. Lewis, T., J. Meakins, and P.D. White, The excitatory process in the dog's heart. Part I-The auricles. *Phil. Trans. R. Soc. London Ser. B.*, 1914;**205**: 375–420.
8. Lewis, T. and M.A. Rothschild, The excitatory process in the dog's heart. Part II. *Phil. Trans. R. Soc. London Ser. B.*, 1915;**206**: 181–226.
9. Wilson, F.N., F.D. Johnston, A.G. MacLeod, and P.S. Barker. Electrocardiograms that represent the potential variations of a single electrode. *Am. Heart. J.*, 1934;**9**: 447–458.
10. Ling, G. and R.W. Gerard, The normal membrane potential of frog sartorius fibers. *J. Cellular Comp. Physiol.*, 1949;**34**: 383–396.
11. Woodbury, L.A., H.H. Hecht, and A.R. Christopherson, Membrane resting and action potentials of single cardiac muscle fibers of the frog ventricle. *Am. J. Physiol.*, 1951;**164**: 307–318.
12. Hoffman, B.F. and P.F. Cranefield, *Electrophysiology of the Heart*. New York: McGraw-Hil, 1960.
13. Netter, F.H., *Heart*, vol **5**. New York: CIBA, 1969.
14. Hodgkin, A.L. and A.F. Huxley, A quantitative description of the membrane current and its application to conduction and excitation in nerve. *J. Physiol.*, 1952;**117**: 500–544.
15. Beeler, G.W. and H. Reuter, Reconstruction of the action potential of ventricular myocardial fibers. *J. Physiol. (London)*, 1977;**268**: 177–210.
16. Ebihara, L. and E.A. Johnson, Fast sodium current in cardiac muscle. A quantitative description, *Biophysical Journal*, 1980;**32**: 779–790.
17. DiFrancesco, D. and D. Noble, A model of cardiac electrical activity incorporating ionic pumps and concentration changes. *Phil. Trans. R. Soc. London Ser. B.*, 1985;**307**: 353–398.
18. Luo, C. and Y. Rudy, A dynamic model of the cardiac ventricular action potential. I. Simulation of ionic currents and concentration changes. *Circ. Res.*, 1994;**74**: 1071–1096.
19. Courtemanche, M., R.J. Ramirez, and S. Nattel, Ionic mechanisms underlying human atrial action potential properties: Insights from a mathematical model. *Am. J. Physiol.*, 1998;**275**: 301–321.
20. Spach, M.S. and M.J. Kootsey, Relating the sodium current and conductance to the shape of transmembrane and extracellular potentials by simulation: Effects of propagation boundaries. *IEEE Trans. Biomed. Eng.*, 1985;**BME-32**: 743–755.
21. Plonsey, R. and R.C. Barr, Mathematical modeling of electrical activity of the heart. *J. Electrocardiol.*, 1987;**20**: 219–226.
22. Plonsey, R. and R.C. Barr, *Bioelectricity: A Quantitative Approach*. New York: Springer, 2007.
23. Wilson, F.N., A.G. Macleod, and P.S. Barker, The distribution of action currents produced by the heart muscle and other excitable tissues immersed in conducting media. *J. Gen. Physiol.*, 1933;**16**: 423–456.
24. Holland, R.P. and M.F. Arnsdorf, Solid angle theory and the electrocardiogram: physiologic and quantitative interpretations. *Prog. Cardiovasc. Dis.*, 1977;**19**: 431–457.
25. Goldman, M.J., *Principles of Clinical Electrocardiography*, 10 ed. Los Altos: Lange, 1979.
26. Scher, A.M., A.C. Young, A.L. Malmgren, and R.R. Paton, Spread of electrical activity through the wall of the ventricle. *Cardiovasc. Res.*, 1953;**1**: 539–547.
27. Sano, T., N. Takayama, and T. Shimamoto, Directional differences of conduction velocity in the cardiac ventricular syncytium studied by microelectrodes. *Circ. Res.*, 1959; **VII**: 262–267.
28. Spach, M.S. and R.C. Barr, Origin of epicardial ST-T wave potentials in the intact dog. *Circ. Res.*, 1976;**39**(4): 475–487, (1978).
29. Burger, H.C., The zero of potential: A persistent error. *Am. Heart J.*, 1955;**49**: 581–586.
30. Geselowitz, D.B., The zero of potential. *IEEE Engineering in Medicine and Biology Magazine*, 1998;**17**: 128–132.
31. van Oosterom, A., Solidifying the solid angle. *J. Electrocardiol.*, 2002;**35S**: 181–192.
32. Kondo, M., V. Nesterenko, and C. Antzelevitch, Cellular basis for the monophasic action potential. Which electrode is the recording electrode? *Cardiovasc. Res.*, 2004;**62**: 635–644.
33. Vigmond, E.J., The electrophysiological basis of MAP recordings. *Cardiovasc. Res.*, 2005;**68**: 502–503.
34. Scher, A.M., and Excitation of the heart, in *The theoretical basis of electrocardiology*, C.V. Nelson, and D.B. Geselowitz, Editors. Oxford: Clarendon Press, 1976: 44–69
35. James, T.N., The connecting pathways between the sinus node and A-V node and between the right and the left atrium in the human heart. *Am. Heart J.*, 1963;**66**: 498–508.
36. Puech, P., *L'activite electrique auriculaire normale et pathologique*, Paris: Masson et Cie, 1956.
37. Spach, M.S., M. Lieberman, J.G. Scott, R.C. Barr, E.A. Johnson, and J.M. Kootsey, Excitation sequences of the atrial septum and the AV node in isolated hearts of the dog and rabbit. *Circ. Res*, 1971;**29**: 156–172.
38. Sano, T., Conduction in the heart, in *The theoretical basis of electrocardiology*, C.V. Nelson and D.B. Geselowitz, Editors. Oxford: Clarendon Press, 1976.
39. Spach, M.S., R.C. Barr, R.B. Warren, D.W. Benson, A. Walston, and S.B. Edwards, Isopotential body surface mapping in subjects of all ages: emphasis on low-level potentials with analysis of the method. *Circulation*, 1979;**59**: 805–821.
40. Mirvis, D.M., Body surface distribution of electrical potential during atrial depolarization and repolarization. *Circulation*, 1980;**62**: 167–173.
41. Ihara, Z., A. van Oosterom, and R. Hoekema, Atrial repolarization as observable during the PQ interval. *J. Electrocardiol.*, 2006;**39**(3): 290–297.
42. van Oosterom, A. and V. Jacquemet, Genesis of the P wave: Atrial signals as generated by the equivalent double layer source model. *Europace*, 2005;**7**: S21–S29.
43. Berbari, E.J., R. Lazzara, P. Samet, and B.J. Scherlag, Noninvasive technique for detection of electrical activity during the PR segment. *Circulation*, 1973;**48**: 1005–1013.
44. Flowers, N.C., R.C. Hand, P.C. Orander, C.B. Miller, M. Walden, and L.G. Horan, Surface recording of electrical activity from the region of the bundle of His. *Am. J. Cardiol.*, 1974;**33**: 384–389.
45. Flowers, N.C., V. Shvartsman, H.L.G.P. Palakurthy, G. S. Som, and M. R. Sridharan, Analysis of PR subintervals in normal subjects and early studies in patients with abnormalities of the conduction system using surface His bundle recordings. *J. Am. Coll. Cardiol.*, 1983;**2**: 939–946.
46. Helm, R.A., Electrocardiographic cancellation. Mathematical basis. *Am. Heart J.*, 1960;**60**: 251–265.
47. Spach, M.S., R.C. Barr, D.W. Benson, Walston, and S.B. Edwards, Body surface low-level potentials during repolarization with analysis of the ST segment. *Circulation*, 1979; **59/4**: 822–836.

48. Maroko, P.R., P. Libby, J.W. Covell, B.E. Sobel, J.J. Ross, and E. Braunwald, Precordial S-T segment elevation mapping: An atraumatic method for assessing alterations in the extent of myocardial ischemic injury. *Am. J. Cardiol.*, 1972;**29**: 223–230.
49. Janse, M.J., F.J.L.V. Capelle, H. Morsink, A.G. Kléber, F. Wilms-Schopman, C.N. d'Alnoncourt, and D.D. Durrer, Flow of injury current and patterns of excitation during ventricular arhythmias in acute regional myocardial ischemia in isolated porcine and canine hearts. *Circ. Res.*, 1980;**47**: 151–165.
50. Burgess, M.J., L.S. Green, K. Millar, R. Wyatt, and J.A. Abildskov, The sequence of normal ventricular recovery. *Am. Heart J.*, 1972;**84**(5): 660–669.
51. Franz, M.R., K. Bargheer, W. Rafflenbeul, A. Haverich, and P.R. Lichtlen, Monophasic action potential mapping in a human subject with normal electrograms: Direct evidence for the genesis of the T wave, *Circulation*, 1987;**75/2**: 379–386.
52. Cowan, J.C., C.J. Hilton, C.J. Griffiths, S. Tansuphaswadikul, J.P. Bourke, A. Murray, and R.W.F. Campbell, Sequence of epicardial repolarization and configuration of the T wave. *Br. Heart J.*, 1988;**60**: 424–433.
53. van Oosterom, A., Genesis of the T-wave as based on an equivalent surface source model. *J. Electrocardiol.*, 2001;**34S**: 217–227.
54. Abildskov, J.A., M.J. Burgess, M.J. Millar, R. Wyatt, and R. Baule, The primary T wave- a new electrocardiographic waveform. *Am. Heart J.*, 1971;**81/2**: 242–249.
55. Horan, L.G., R.C. Hand, J.C. Johnson, M.R. Sridharan, T.B. Rankin, and N.C. Flowers, A theoretical examination of ventricular repolarization and the secondary T wave. *Circ. Res.*, 1978;**42/6**: 750–757.
56. Wilson, F.N., A.G. Macleod, P.S. Barker, and F.D. Johnston, The determination and significance of the areas of the ventricular deflections of the electrocardiogram. *Am. Heart J.*, 1934;**10**: 46–61.
57. Burger, H.C., A theoretical elucidation of the notion: Ventricular gradient. *Am. Heart J.*, 1957;**53/2**: 240–246.
58. Geselowitz, D.B., The ventricular gradient revisited: Relation to the area under the action potentials. *IEEE Trans. Biomed. Eng.*, 1983;BME-**30/1**: 76–77.
59. Abildskov, J.A., P. Urie, R. Lux, M.J. Burgess, and R. Wyatt, Body surface distribution of QRST area. *Adv. Cardiol.*, 1978;**21**: 59–64.
60. van Oosterom, A., Reflections on T waves, in *Advances in Electrocardiology*, M. Hiraoka, S. Ogawa, I. Kodama, I. Hiroshi, H. Kasnuki, and T. Katoh, Editors. New Jersey, World Scientific, 2005, pp. 807–815.
61. Plonsey, R., An extension of the solid angle formulation for an active cell. *Biophysical J.*, 1965;**5**: 663–666.
62. Haws, C.W., and R.L. Lux, Correlation between in vivo transmambrane action potential durations and activation-recovery intervals from electrograms. *Circulation*, 1990;**81/1**: 281–288.
63. Kardys, I., J.A. Kors, I.M. van der Meer, A. Hofman, D.A.M. van der Kuip, and J.C.M. Witteman, Spatial QRS-T angle predicts cardiac death in a general polulation. *Eur. Heart J.*, 2003;**24**: 1357–1364.
64. Zabel, M., B. Acar, T. Klingenheber, M.A. Franz, S.H. Holenlozer, and M. Malik, Analysis of 12-lead T-wave morphology for risk stratification after myocardial infarction. *Circulation*, 2000;**102**: 1252–1257.
65. Surawicz, B., U wave - the controversial genesis and the clinical significance. *Jpn. Heart J.*, 1982;**23**(suppl.I): 17–22.
66. Lepeschkin, E., Physiologic basis of the U wave, in *Advances in Electrocardiography*, R.C. Schlant and J.W. Hurst, Editors. New York, Grune and Stratton, 1972.
67. Kishida, H., J.S. Cole, and B. Surawicz, Negative U wave: A highly specific but poorly understood sign of heart d disease. *Am. J. Cardiol.*, 1982;**49**: 2030–2036.
68. Lab, M.J., Mechanically dependent changes in action potentials recorded from the intact frog ventricle. *Circ. Res.*, 1978;**42**: 519–528.
69. Antzelevitch, C., and S. Sicouri, Clinical relevance of cardiac arrhythmias generated by after-depolarsations: Role of M-cells in the generation of U-waves, triggered activity and torsade de pointes. *J. Am. Coll. Cardiol.*, 1994;**23**: 259–277.
70. di Bernardo, D., and A. Murray, Origin on the electrocardiogram of U-waves and abnormal U-wave inversion. *Cardiovasc. Res.*, 2002;**53**: 202–208.
71. Ritsema van Eck, H., J.A. Kors, and G. van Herpen, The U wave in the electrocardiogram: A solution for a 100-year-old riddle. *Cardiovasc. Res.*, 2005;**67**: 256–262.
72. Geselowitz, D.B., Multipole representation for an equivalent cardiac generator. *Proc. IRE*, 1960, pp. 75–79.
73. Frank, E., Absolute quantitative comparison of instantaneous QRS equipotentials on a normal subject with dipole potentials on a homogeneous torso model. *Circ. Res.*, 1955;**3**: 243–251.
74. Taccardi, B., Distribution of heart potentials on the thoracic surface of normal human subjects. *Circ. Res.*, 1963;**12**: 341–352.
75. Barber, M.R., and E.J. Fischmann, Heart dipole regions and the measurement of dipole moment. *Nature*, 1961;**192**: 141–142.
76. Selvester, R.H., J.C. Solomon, and T.L. Gillespie, Digital computer model of a total body electrocardiographic surface map. An adult male-torso stimulation with lungs. *Circulation*, 1968;**38**: 684–690.
77. Ritsema van Eck, H.J., *Digital Simulation of Cardiac Excitation and Depolarization*, PhD. thesis. Halifax, NS, Canada, Dalhousie University, 1972.
78. Miller, W.T., and D.B. Geselowitz, Simulation studies of the electrocardiogram. I. The normal heart. *Circ. Res.*, 1978;**43**: 301–315.
79. van Oosterom, A., and T.F. Oostendorp, ECGSIM: An interactive tool for studying the genesis of QRST waveforms. *Heart*, 2004;**90**: 165–168.

Section 3

Mathematical Modeling

6 Macroscopic Source Descriptions

A. van Oosterom

P. W. Macfarlane, A. van Oosterom, O. Pahlm, P. Kligfield, M. Janse, J. Camm (eds.), *Comprehensive Electrocardiology*, DOI 10.1007/978-1-84882-046-3_6,

6.1 Introduction

Throughout the cardiac cycle, the cells of the heart deliver varying amounts of electric current to the surrounding tissues. The effect of these currents at the body's surface is the production of potentials which change continuously during the course of a heartbeat. In attempting to understand the nature of these body-surface potentials, various models have been postulated. These models describe the electrical sources and the volume conductor in which these sources are embedded, i.e., the human torso.

The computation of the potential distribution at the body surface based on such modeling assumptions is called the "forward problem of electrocardiography" (Chap. 8). Its solution is a prerequisite for the solution of a problem of more direct clinical interest, the so-called "inverse problem of electrocardiography." By this is meant the study of the electrical state of the heart through analysis of the potentials at the body surface (Chap. 9). Since this problem has no unique solution, it is imperative that constraints be imposed on the description of the source, i.e., the electrical generators of the heart.

Two different classes of source descriptions can be distinguished. The first class is that of the equivalent generators of physics (Chaps. 2 and 8) in which sources like the single dipole (vectorcardiography), the single moving dipole, multiple dipoles or multipoles are used. Theoretically, these generator models allow a unique determination of their strength from observed body-surface potentials but the link with cellular electrophysiology is not straightforward (Sect. 5.11).

The second class is that of macroscopic source descriptions. These form an *intermediate* step between the cellular activity and the electric field within the heart muscle at a scale of, say, 1 cm, which is small in comparison with heart size but large in comparison with cell size. The justification for this approach is that the total number of cells involved in the genesis of the ECG is so large (10^{10}) that it prohibits the consideration of the contribution by each individual cell. Formulations of macroscopic equivalent generators aim at representing as much as is feasible (and known) of cellular morphology in a source description of the potential field at a distance that is, say, ten times that of the length of a single myocyte.

This class of macroscopic source descriptions is the subject of this chapter. A major part of the chapter is devoted to the discussion of the classic model for the description of the electric sources during ventricular depolarization: the uniform double layer (UDL). The expression of the potential field is worked out by using the solid angle theory. The objective of the detailed analysis of this classic source model is to illustrate the potential fields and associated signals that are generated by this source. This forms the essential background for a discussion on its validity and usefulness.

A generalization of the UDL source model that permits the modeling of the sources during repolarization, is discussed in Chap. 7.

The formulations are mainly cast in terms of homogeneous, isotropic configurations. The effect of anisotropy is discussed only briefly. More complete models, in which the anisotropy of the ventricular wall is incorporated, are treated in Chap. 8.

6.2 Estimation of Macroscopic Cardiac Sources

The true cellular electrical generators are the biochemical processes that are active at the level of the cell membrane (Chap. 3). A macroscopic equivalent source model is a description of the cellular electrical generator which results in a potential field in the exterior of the cell which, on a macroscopic scale, is indistinguishable from the observed potential field. From a known description of the electric sources, the potentials at some distance from the sources can be determined by applying the laws of electric current flow. The implied so-called forward problem of finding the potentials has a unique solution that can be computed for all types of source complexity.

The current sources actually generating the observed potentials are in general not amenable to direct observation, they need to be *derived* from observed potential differences.

The slow progress that has been made in the application of source models can be linked to the fact that the corresponding inverse computation, the determination of sources from the observed potentials, generally does *not* have a unique solution. This doom that lies over the inverse problem is fundamental and cannot be solved, as was pointed out as early as 1853 by von Helmholtz [1], even long before electrocardiology was "invented." The only way out of this problem is to postulate *in advance* a source description, a source *model*, and to merely be content with establishing the parameters

(specifications) of this source on the basis of the observed potentials. The inverse problem subsequently constitutes a parameter estimation problem.

The transfer between the sources and the potentials is dominated by the geometry of the source-observation point configuration and by the entire spatial distribution of the electric conductivities of the body tissues. The doom on the inverse problem [1] now crops up again: the spreading out of electric currents diminishes the potentials in the medium and diffuses the image of the sources the further one moves away from the sources. This doom not only lies on the interpretation of potentials observed on the body surface but also on those observed inside the heart (myocardium; cavities).

For a diagnostic application, the source description should preferably have a direct physiological significance and, hence, one would like to include as much as is possible of the complexity of the relevant physiological details that have become available through invasive studies. However, the further one moves away from the source, the more sober the a priori source specification has to be, demanding a parsimonious use of source parameters. If a more abundant source specification is postulated, the correspondence – in forward computations – between observed data and computed potentials may improve, but in the related inverse problem the confidence intervals of the estimated parameters become unacceptably large. Although one may wish to include the reality of rotating, non-uniform, anisotropic myocardial conductivity in the analysis, in the ultimate, clinical application of the models the accuracy of the relevant parameters values is usually insufficient.

The analysis presented in this chapter relates to sober source descriptions, with parameters derived from sober models of the conducting medium surrounding the source while computing the potential field.

6.3 Equivalent Sources of the Membrane

6.3.1 The Single Cell

We first consider a model for the potential field generated by a single cell situated in an infinite medium of homogeneous, isotropic electrical conductivity σ_e (unit: S m^{-1}), Fig. 6.1, and we take the potential at infinity to be zero (Sect. 2.5).

The interior of the cell (the axoplasma) is assumed to be a passive conductor having a homogeneous, isotropic electrical conductivity σ_i. The interior and exterior of the cell are separated by the membrane, which is bounded by two surfaces: S_i and S_e. All active (biochemical) electric sources are considered to be lying between these two surfaces. Using standard results from potential theory and realistic estimates of the membrane properties, it can be shown [2–4] that the potential $\Phi(\vec{r}')$ at a field point $\vec{r}'$ (observation point, with reference to the origin at $\vec{O}$) in the exterior medium is

$$\Phi(\vec{r}') = -\frac{1}{4\pi\sigma_e}\int_S (\sigma_i\Phi_i - \sigma_e\Phi_e)\mathrm{d}\omega \tag{6.1}$$

The surface S lies just between the surfaces S_i and S_e. It specifies the entire configuration since, at a macroscopic scale, the membrane can be considered to be infinitesimally thin. The potentials Φ_i and Φ_e denote the potentials just inside

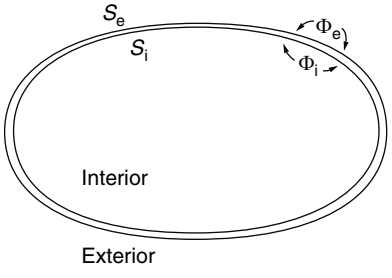

Figure 6.1
Configuration of a single cell, used for evaluating the external potential field.

and outside this surface, respectively. The term $d\omega$ of (6.1) is the solid angle of element dS of the membrane surface S subtended at $\vec{r}'$, $\frac{\vec{R} \bullet d\vec{S}}{R^3}$, with $d\vec{S}$ pointing outward and $\vec{R} = \vec{r}' - \vec{r}$ directed from the source locations $\vec{r}$ on the membrane to field point $\vec{r}'$ (Sect. 2.5.2.2).

The expression $\sigma_i\Phi_i - \sigma_e\Phi_e$ in (6.1) is a generalization of the concepts introduced by Wilson et al. [5], which formed the basis for the solid angle theory as used in theoretical electrocardiography. The expression can be identified as the strength of an (equivalent) double layer. It expresses a current dipole density per unit area M_S; with unit: A m^{-1}, as discussed in Sect. 2.5.2.2. This shows that the basic cardiac electric generator must be viewed as a *current* source [3], which justifies the use of the superposition principle when computing the potential field generated by multiple sources. When placed in an infinite medium, this virtual, equivalent double layer determines the potential field external to the cell. The double layer is directed normal to the membrane surface and has a strength that depends on transmembrane potential differences *as well as* on differences in the electric conductivities at either side of the membrane.

When an isolated cell is completely polarized, the transmembrane voltage $V_m = \Phi_i - \Phi_e$ is constant ($V_m \sim -80$ mV) over the entire closed surface of the membrane and the double-layer strength is uniform over this surface. Hence, in the exterior region the potential field is zero. This follows from

$$\Phi(\vec{r}') = \frac{-1}{4\pi\sigma_e}(\sigma_i\Phi_i - \sigma_e\Phi_e)\int_S d\omega = 0 \tag{6.2}$$

since $\int_S d\omega = 0$ for any observation point $\vec{r}'$ exterior to any closed surface S, as is discussed in Sect. 2.5.1.2.

Similarly, when the cell is completely depolarized, V_m is uniform over the closed surface of the membrane ($V_m \sim 5$ mV), and the potential in the exterior region is, again, zero.

When the cell is partly depolarized, the potential in the exterior region can only be determined through integration as in (6.1). An instructive approximation of this case is to consider the field due to an elongated membrane, with an idealized transmembrane potential that is constant over both the depolarized section and over the section which is still at rest, i.e., polarized, with potential values of $V_d \sim +5$ mV and $V_p \sim -80$ mV, respectively (Fig. 5.5 and Fig. 6.2).

In this case, the potential in the region exterior to the cell is approximately equal to that generated (in the homogeneous medium) by a double-layer source of strength $(V_d - V_p)\sigma_i$ placed at cross-section A. The exterior potential at $\vec{r}'$ generated by this equivalent source is

$$\Phi(\vec{r}') = \frac{1}{4\pi\sigma_e}\sigma_i(V_d - V_p)\,\Omega\,(\vec{r}'), \tag{6.3}$$

with $\Omega(\vec{r}')$ the solid angle subtended by cross-section A, with area A, at observation point $\vec{r}'$ (Fig. 6.3). The membrane is shown by dashed lines, as a reminder that the equivalent source at cross-section A is active in the infinite medium. Since V_p is negative, $V_d - V_p$ is positive and the equivalent dipole has the same direction as the propagation.

The approximation involved assumes $\sigma_i\Phi_i \gg \sigma_e\Phi_e$. For this situation (6.3) can be explained as follows. We first place virtual double layers of equal strength V_d, but having opposite orientations, at cross-section A. One of these two has the same strength as that of the membrane to the left of A. Together these form a closed surface, which produces a zero external potential field. Next we repeat the same process for the region to the right of A, now with virtual double-layer

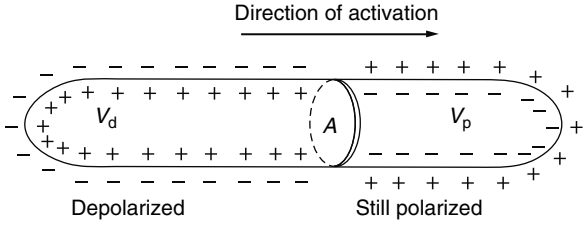

Figure 6.2

Simplified diagram of an elongated cell which is activated from left to right. The cross-section A closes the depolarized zone (*left*) and the region still at rest (*right*).

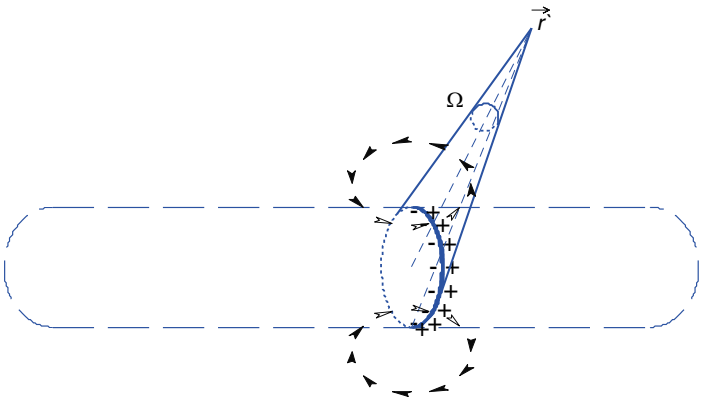

Figure 6.3
Equivalent source for the partly depolarized cell shown in Fig. 6.2. The arrowheads indicate the direction of local current flow.

strengths of V_p. Here again, one of these virtual layers forms a closed surface, now to the right of A, having a uniform strength and, hence, producing a zero external field. The remaining two virtual double layers form the double layer as shown in Fig. 6.3, having the effective source strength implied in (6.3).

For distal observation points this expression (6.3), may be simplified further by using the approximation

$$\Omega\,(\vec{r}\,') \sim \frac{\vec{A} \bullet \vec{R}}{R^3},$$

with $\vec{R}$ a vector of magnitude R pointing from the center of the disk A to observation point $\vec{r}\,'$, and $\vec{A}$ a vector of magnitude A directed towards the region of the cell that is still polarized. In this case,

$$\Phi(\vec{r}\,') = \frac{1}{4\pi\sigma_e} \frac{\sigma_i(V_d - V_p)\vec{A} \bullet \vec{R}}{R^3} \tag{6.4}$$

The term $\sigma_i(V_d - V_p)\vec{A}$ can be identified as a current dipole $\vec{D}$ (Sect. 2.5.1.2), pointing towards the zone that is still at rest; thus

$$\Phi(\vec{r}\,') = \frac{1}{4\pi\sigma_e} \frac{\vec{D} \bullet \vec{R}}{R^3} \tag{6.5}$$

The plus and minus signs in Figs. 6.2 and 6.3 serve to indicate the sign of local potential differences across the membrane and the virtual double layer, respectively. In some text books on this subject the associated membrane charge is erroneously used to explain the external field in terms of electrostatics, rather than in the required terms of equivalent current generators demanded by electrical volume conduction theory (Chap. 2).

6.3.2 The Single Fiber

The conditions for the application of (6.3) are not usually met in practice. For long fibers, the situation is never such as depicted in Fig. 6.2, but much more like that indicated in Fig. 6.4 for propagated activation along a fiber, where the transmembrane potential is different along the length of the fiber. At the time instant shown the segment on the left is in different stages of recovery of polarization, in the middle part various, successive stages of depolarization are present; the segment on the right is still at rest, i.e., polarized.

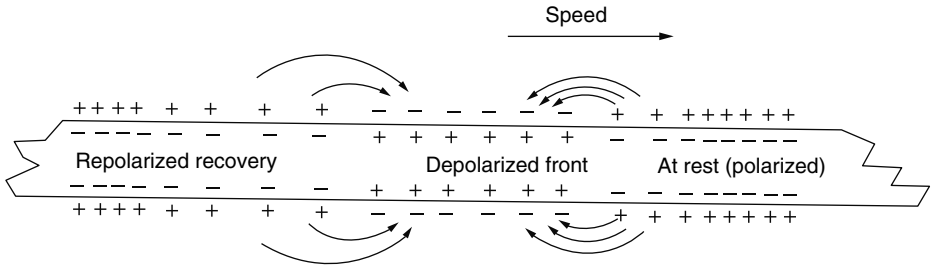

Figure 6.4
Schematized, propagating depolarization and repolarization along an elongated fiber.

To find the potential at $\vec{r}'$ in this situation we return to the general expression (6.1), while assuming the transmembrane potential difference to be a function of the distance ℓ along the fiber only (axial symmetric distribution). Moreover, we define $M_S(\ell)$ as

$$M_S(\ell) = -(\sigma_i \Phi_i(\ell) - \sigma_e \Phi_e(\ell)) \tag{6.6}$$

The term $d\omega$ of (6.1) relates to the membrane element $\vec{R} \bullet d\vec{S}/R^3$, with $d\vec{S}$ an element of the membrane defined as pointing outward, and $\vec{R}$ directed from the source locations on the membrane to field point $\vec{r}'$, so we need to evaluate

$$\Phi(\vec{r}') = \frac{1}{4\pi\sigma_e} \int_S M_S(\ell) \frac{\vec{R}}{R^3} \bullet d\vec{S} \tag{6.7}$$

To this end we apply Gauss' divergence theorem (2.26), to the integral in (6.7), which yields

$$\int_S M_S(\ell) \frac{\vec{R}}{R^3} \bullet d\vec{S} = \int_V \nabla \bullet \left(M_S(\ell) \frac{\vec{R}}{R^3} \right) dv = \int_V \nabla M_S(\ell) \bullet \frac{\vec{R}}{R^3} dv + \int_V M_S(\ell) \nabla \bullet \frac{\vec{R}}{R^3} dv \tag{6.8}$$

(using (2.29)). The second integral on the right is zero since

$$\nabla \bullet \frac{\vec{R}}{R^3} = \nabla \bullet \nabla \frac{1}{R} = \nabla^2 \frac{1}{R},$$

and any integral including the latter is zero for non-zero values of R, which is the case for external observation points (Sect. 2.6.4.1), and so we find

$$\Phi(\vec{r}') = \frac{1}{4\pi\sigma_e} \int_V \frac{\partial M_S(\ell)}{\partial \ell} \frac{\ell' - \ell}{R^3} dv = \frac{1}{4\pi\sigma_e} \int_L \int_{S_\ell} \frac{\partial M_S(\ell)}{\partial \ell} \frac{\ell' - \ell}{R^3} dS \, d\ell \tag{6.9}$$

where ℓ' is the coordinate of the external field point $\vec{r}'$ along an axis parallel to the fiber. The first integral is taken over length L of the fiber, the second one over the cross-section of the fiber at location ℓ.

We now take the gradient of the function $M_S(\ell)$ to be uniform over the cross-section S_ℓ and, hence, the integration over this surface yields $\Omega(\ell; \vec{r}')$, the solid angle subtended at an external field point $\vec{r}'$ by S_ℓ, a disk with an area of πa^2, with a the radius of the fiber (Sect. 5.3.4), and so (6.9) reduces to

$$\Phi(\vec{r}') = \frac{1}{4\pi\sigma_e} \int_L \frac{\partial M_S(\ell)}{\partial \ell} \Omega(\ell; \vec{r}') \, d\ell \tag{6.10}$$

Equation (6.10) generally holds true, and may also be used if the fiber is curved. In these circumstances the variable ℓ must be taken to be the length traveled along the fiber.

For remote field points and a straight fiber, the solid angle $\Omega(\ell;\vec{r}')$ may be approximated by

$$\Omega(\ell;\vec{r}') \approx \pi a^2 \frac{\ell' - \ell}{R^3}, \tag{6.11}$$

in which $R = \sqrt{(\ell' - \ell)^2 + y'^2 + z'^2}$, with the fiber coordinate ℓ taken to be lined up along the x-axis.

The result expressed by (6.10), which was derived from general membrane properties (6.1), is identical to the result expressed by (5.7), derived from the linear core-conductor model expressed by (5.1).

6.3.3 Electrograms Generated by a Single Fiber

Equation (6.1) may be used to describe the electrograms recorded by electrodes placed near a fiber along which electric activity is propagating. However, the computation of the integral involved demands the full spatio-temporal specification of the intra and extracellular potentials at the membrane of the full length of fiber. Such data is generally not available. One of the more interesting applications of simplified fiber models is as follows. We assume:

1. Fiber length to be much greater than the electrode to fiber distance;
2. The approximation $\sigma_i\Phi_i \gg \sigma_e\Phi_e$ to be justified, and hence $M_S(\ell) = -(\sigma_i\Phi_i(\ell) - \sigma_e\Phi_e(\ell)) \approx -\sigma_i V_m(\ell)$;
3. A transmembrane potential that propagates along the fiber at constant velocity v.

The assumption of constant velocity implies that the time course of the transmembrane potential is identical for all points along the fiber, although exhibiting its upstroke at increasingly later time instances for locations more to the right. At location ℓ along the fiber, this function is denoted as $V_m(\ell, t)$. At time instant t during propagation, the corresponding expression for the transmembrane potential as a function of space (along the fiber) then reads

$$V_m(\ell;t) = \widetilde{V}_m(t - \ell/v), \tag{6.12}$$

substitution of $M_S(\ell, t) = -\sigma_i\, \widetilde{V}_m(t - \ell/v)$ in (6.10) yields

$$\Phi(\ell';t) = \frac{-\sigma_i}{4\pi\sigma_e} \int_{-\infty}^{\infty} \frac{\partial \widetilde{V}_m(t - \ell/v)}{\partial \ell} \Omega(\ell' - \ell)\, \mathrm{d}\ell \tag{6.13}$$

Finally, by introducing τ as $\tau = \frac{\ell}{v}$, which invokes a change of variables, we find

$$\Phi(\ell';t) = \frac{\sigma_i}{4\pi\sigma_e} \int_{-\infty}^{\infty} \frac{\partial \widetilde{V}_m(t - \tau)}{\partial \tau} \Omega(\ell' - v\tau)\, \mathrm{d}\tau \tag{6.14}$$

For fixed observation points, ℓ', the integral in (6.14) can be recognized as the convolution, in the temporal domain, of the *first* derivative of $\widetilde{V}_m(t - \tau)$ representing the source and a weighting function $\Omega(\ell' - v\,\tau)$ representing the volume conduction effects in the temporal domain. As is discussed in Sect. 5.3.4, an equivalent expression can be formulated in terms of the convolution of the *second* derivative of $\widetilde{V}_m(t - \tau)$ and the function $1/R(\ell' - v\,\tau)$. An early paper on this topic claimed just the second type of source description to be the correct one [6]. However, both can be justified.

A graphical illustration of the result expressed by (6.14) is shown in Fig. 6.5. Panel A depicts the time course of a stylized transmembrane potential (TMP), the function $\widetilde{V}_m(t)$. The activation propagates along a fiber with radius a = 0.5 mm at velocity v = 0.1 m/s. For the duration of the action potential shown (APD), about 150 ms, the instantaneous, spatial extent of the TMP is 15 mm. The TMP function shown is the product of two logistic functions, one representing the fast depolarization phase and the other the repolarization phase [7]. The maximum slopes of the logistic functions were set at 100 and −2 mV/ms, respectively. The corresponding duration of the upstroke of the TMP is about 3 ms. The solid line depicts the derivative of $\widetilde{V}_m(t)$. The right panel shows the function $\Omega(\tau)$ for observation point $(\ell' = 0, \rho' = a)$ on the

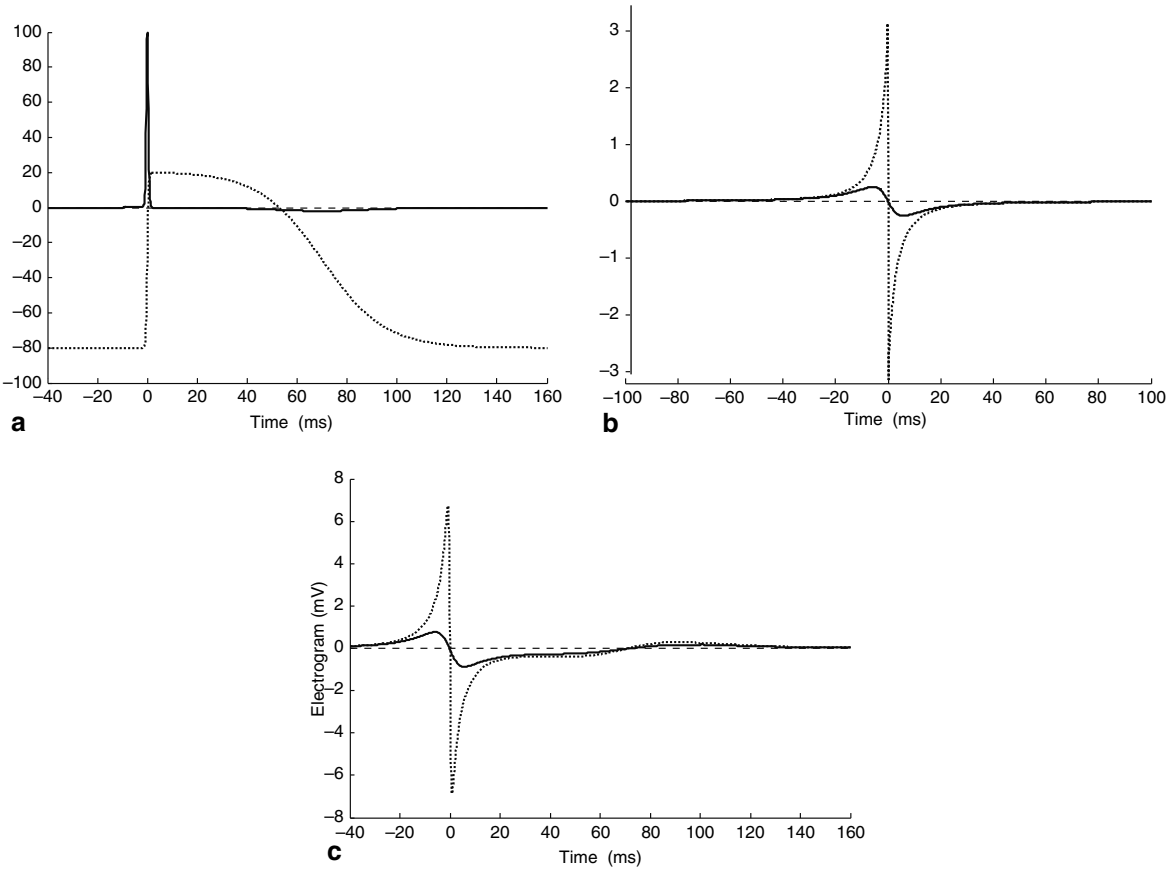

Figure 6.5

Simulated electrograms based on (6.14). Panel A: dotted line: stylized transmembrane potential $\widetilde{V}_m(t)$, vertical scale in mV; solid line: its derivative; panel B: dotted line: solid angle function $\Omega(\tau - \tau')$ for field point on the fiber, $\rho' = a = 0.5$ mm (dotted line) and at distance $\rho' = 2\,a = 1$ mm (solid line); note its extreme values of $\pm\pi$; panel C: corresponding electrograms; dotted line: at field point $\rho' = a$, solid line: at $\rho' = 2\,a$; vertical scale in mV.

outside of the membrane, as well as for $(\ell' = 0, \rho' = 2\,a)$. The lower panel shows the electrograms at $\ell = 0$ resulting from the convolution of $\frac{\partial \widetilde{V}_m(t-\tau)}{\partial \tau}$ with the two functions shown in Panel B. The ratio σ_i/σ_e, the parameter scaling the magnitude of the electrograms, was set at 0.4. All parameter settings were aimed at endowing the illustration in Fig. 6.5 of some general aspects of the genesis of electrograms. Note that for an APD of 400 ms of a TMP traveling at a transmural velocity of 0.5 m/s (ventricular myocardium) the spatial extent of the TMP would be 20 cm.

Inspection of (6.14) and the resulting wave forms (Fig. 6.5) leads to the following conclusions, all valid within the limitations of the assumptions listed in the first part of this section.

1. The equivalent source strength of a propagatitng TMP is proportional to the derivative of the TMP. As a consequence, the mean level of the TMP does not influence the electrograms.
2. For field points with $\rho' = a$ (on the outside of the membrane) the solid angle function (SA) exhibits a jump of 2 π, independent of the fiber radius. As a consequence, the magnitude of the electrogram at that location is independent of the radius of the fiber.
3. The duration (e.g., its half-width w) of the SA curve for $\rho' = a$ (dotted line in Fig. 6.5, Panel B), is proportional to a/v.

4. If the upstroke of the TMP takes far less time than the half-width w of the SA curve, as is the case in Fig. 6.5, the shape of the solid angle curve dominates the wave form of the fast deflection in the electrogram.
5. For distal field points the amplitude of the SA curve is proportional to a^2/ρ'^2.
6. For field points (ℓ', ρ') on the line parallel to the fiber for which $\ell' \gg \rho'$, the solid angle subtended by a cross-section of the fiber at $\ell = 0$ is approximately equal to $\frac{1}{4}a^2/(\ell'^2 + \rho'^2) \approx \pi\, a^2/\ell'^2$. Since this value is independent of ρ' the two curves shown in Panel B merge beyond, say, $|t| = 25$ ms. As a consequence, the magnitudes as well as wave forms of the two signals shown in Panel C are very similar during repolarization. See also point (d) of Sect. 5.3.8.

6.3.4 Estimating Sources from Electrogramsyh

The model of the genesis of an electrogram discussed in Sect. 6.3.2 assumes a uniform potential profile that propagates at a uniform velocity along an infinite fiber placed in an infinite medium. The fiber is taken to have a uniform diameter.

The validation of this model requires a documentation of all relevant parameters such as: (1) fiber diameter, (2) propagation velocity along the fiber, (3) the transmembrane potential at all points along the fiber, (4) values for the intra and extracellular conductivity of the fiber, assumed to be uniform along the fiber. Moreover, the fact that the fiber (necessarily) is of finite length and that the medium in which it is situated is finite needs to be accounted for. The latter necessitates the use of a well-defined potential reference (Sect. 5.4.1).

If all modeling assumptions do not strictly hold true, the more general expression of (6.1) should be used as the source term, supported by the handling of the volume conduction effects by methods like the ones discussed in Chap. 2.

6.4 Macroscopic Source Descriptions During Depolarization

Equation (6.14) may be applied to the description of potentials arising from the fibers of the conduction system. The application of (6.12) and its consequence (6.14), for describing the potential distribution arising from the electrical activity of the muscle cells of the myocardium is not possible: the cells are too short to justify the assumptions used in deriving these equations. Moreover, the external medium in the direct vicinity of the cell is not homogeneous, but is formed by all neighboring cells, some of which are in direct contact with the cell considered (Chap. 3). Any attempt to account for all details of the possible interactions between these cells in terms of their intrinsic generator characteristics and of the volume conduction configuration is not feasible.

To circumvent this problem, a source description can be used which is derived from the observed macroscopic potential distribution within the ventricular myocardium, the sole object of which is to serve as a source description for the genesis of the potentials at the body surface (the ECG). Over the years, several such source descriptions have been put forward. The best known of these is that of the uniform double layer (UDL), first implied in the work of Wilson et al. [5].

Following a local stimulus in the myocardium, the cells in the direct vicinity of the stimulus are activated. The interiors of these cells are coupled through several low-resistive connections to neighboring cells. As a result, these cells are activated as well and in turn activate their (previously passive) direct neighbors. At a macroscopic level, this can be described in terms of an activation boundary which propagates like a wavefront through the myocardium.

As discussed in Sect. 5.3.5, the UDL theory postulates a double-layer current of uniform strength at the surface separating myocytes that are depolarized and those that still at rest, i.e., polarized: the activation wavefront. Following an initiation of the activation at one or more sites, one or more wavefronts propagate throughout the myocardium and, barring early repolarization, the UDL sources form the major generator of the currents during this period, which ends when all myocytes have been activated.

For many years, the UDL model has served to explain in a qualitative way the shapes of the various ECG waveforms during the depolarization phase of the ventricles [8, 9]. In later years its validity has been questioned, as is discussed in Sect. 6.4.4.1. This has triggered off the search for alternative source descriptions in which the anisotropy of the generator characteristics and of the conductivity of the medium in which these generators are situated is incorporated at different levels of complexity. As a result of the difficulty in the analysis of these problems, some of the attempts have been restricted to the analysis of monolayers of cardiac cells [10]. There have been some attempts at deriving a description for the full

three-dimensional source configuration which might serve to replace, or improve on, the uniform double layer. Three such alternative source descriptions are described in Sect. Section 6.6. But first, to appreciate to what extent these predictions differ from those based on the UDL, the properties of the UDL are discussed in detail. As it is the most simple source description, this also makes it suitable for introducing the concepts involved.

The analysis of the potentials generated by the UDL source is based on a series of models of source extent and volume conductors with step-wise increasing complexity.

6.4.1 Potentials Generated by Basic Wavefront Geometries Carrying a UDL Source

In this classic UDL source description, the sources are assumed to be of a (current) dipolar nature: each surface element ΔS of the activation wave front is assumed to carry an elementary dipole of strength $\Delta\vec{D} = M_S\Delta\vec{S}$, which is directed towards the myocytes still at rest. The strength M_S of this dipole layer is assumed to be uniform over the entire activation boundary. We start by considering the situation with the source placed inside an infinite medium, and taking the reference potential at infinity to be zero. As shown in Sect. 5.3.5 the source yields a potential field

$$\Phi(\vec{r}') = \frac{M_S}{\sigma}\frac{\Omega}{4\pi},$$

for which we now write

$$\Phi(\vec{r}') = \frac{M_S}{\sigma}\frac{\Omega}{4\pi} = V_D\frac{\Omega}{4\pi} \tag{6.15}$$

The variable V_D is the potential difference across the double layer (compare (6.3)) and Ω is the solid angle subtended by the wave front at the observation point (compare (6.3)). Throughout this section the value $V_D = 40\,\text{mV}$ is used, a value that was based on intramural recordings of the canine ventricle, as is discussed in Sect. 6.4.3.2.

The simplicity of (6.15) is partly the reason for its popularity as a source description. The potentials predicted by this source description will now be shown in some illustrative cases, which differ only with respect to the shape and extent of the double layer.

6.4.1.1 A Circular Disk

We first consider the potential field of a double layer that has the shape of a flat circular disk of radius R (Fig. 6.6(a)). This configuration was introduced for studying basic membrane properties as early as 1933 by Wilson et al. [5], who also described the solution.

The solid angle subtended by the disk at a field point on the x-axis is given by (2.112). Inserting this expression into (6.15) yields as the potential distribution (potential profile) along the x-axis

$$\Phi(x) = \frac{1}{2}V_D\left(\frac{x}{|x|} - \frac{x}{\sqrt{x^2+R^2}}\right) = 20\,(\pm 1 - \cos\alpha) \quad (\text{mV}) \tag{6.16}$$

with α the top angle of the cone specified by the observation point $(x, 0, 0)$ as its top and the passing through the rim of the disk. A plot of this potential profile, expressed in units V_D, for $R = 1$ is shown in Fig. 6.6 (right panel). Note the potential jump of magnitude V_D when crossing the disk at $x = 0$.

6.4.1.2 A Hemisphere

Next we consider a double layer having the shape of a hemispherical shell of radius R (Fig. 6.7 (left panel)). This is the simplest possible equivalent model for the source strength of a wavefront inside a myocardial layer (bounded by the

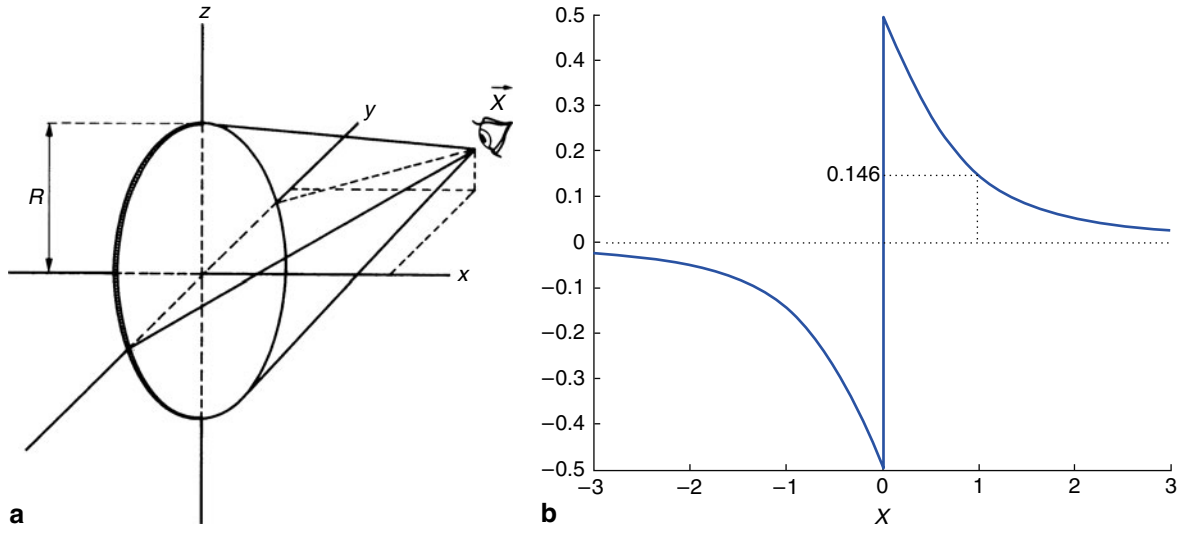

Figure 6.6

***Left*: Double layer having the shape of a disk of radius *R* viewed by the eye drawn at field point $\vec{x}$; *right*: resulting potential profile along the *x*-axis according to (6.16), expressed in units $V_D = 40$ mV; R = 1, *x* and *R* in the same arbitrary unit.**

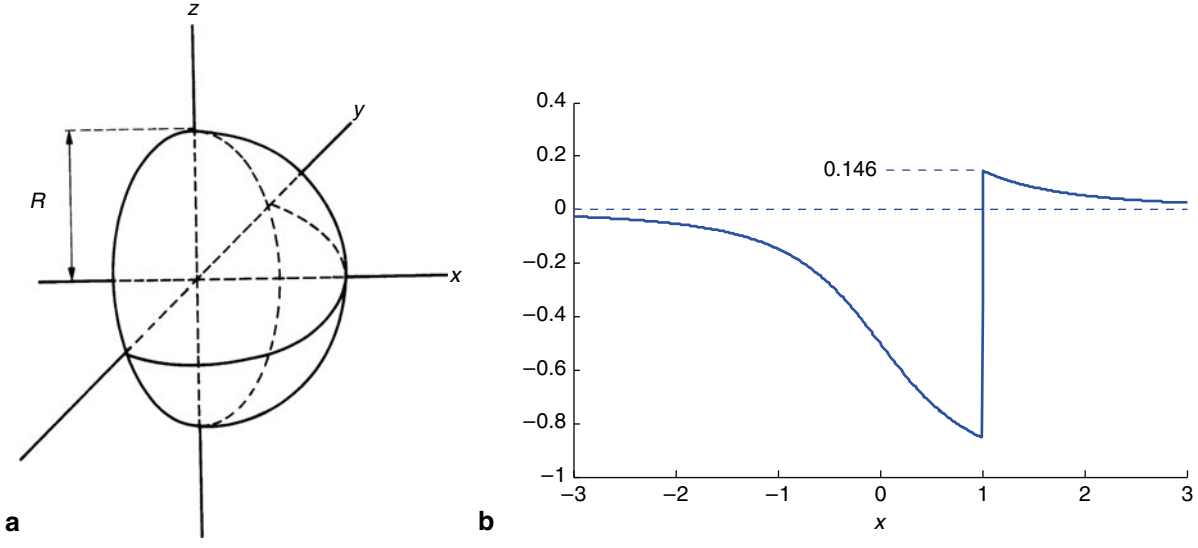

Figure 6.7

***Left*: Double layer having the shape of a hemispherical shell of radius $R = 1$; *right*: resulting potential profile along the *x*-axis according to (6.17), expressed in units $V_D = 40$ mV; *x* and *R* are expressed in the same, arbitrary unit.**

plane $x = 0$) that has progressed in radial fashion following a stimulus at $x = 0$. The potential field follows, again, from the solid angle subtended by the hemisphere. To this end, we consider two disks with radius *R* that close the hemisphere, carrying the same strengths as that of the hemisphere, but with opposite polarity. One of these disks combined with the sources on the hemisphere form a closed double layer, which has a zero external field (Sect. 2.2.12). The potential exterior to the closed source configuration is, hence, identical to the field of the remaining disk. For interior field points

this also holds true, but here the solid angle of the closed hemispherical shell is $-4\,\pi$ (Sect. 2.2.12). As a consequence, we now have

$$\Phi(x) = \frac{1}{2}\,V_D\left(\frac{x-R}{|x-R|} - \frac{x}{\sqrt{x^2+R^2}}\right), \tag{6.17}$$

this potential profile is depicted in Fig. 6.7 (right panel).

A comparison of (6.16) and (6.17) leads to an interesting interpretation. The first terms, $\frac{1}{2}\,V_D\,\frac{x}{|x|}$ in (6.16) and $\frac{1}{2}\,V_D\,\frac{x-R}{|x-R|}$ in (6.17), describe the potential jump while crossing the double layer, reflecting its *local* strength. The second term, $-\frac{1}{2}\,V_D\,\frac{x}{\sqrt{x^2+R^2}}$, describes the *global* properties of the double layer, i.e., its spatial extent, which is completely specified by the surface closing the hemisphere. For the hemisphere the jump in the potentials by V_D now occurs at $x = R$, starting from the level of $-\frac{1}{2}\,V_D\left(1+1/\sqrt{2}\right)$. An initial oversight in the need for inclusion of the first term in (6.17), as can be observed in [11], initiated a discussion on the validity of this type of equivalent source description.

No simple expression is available for evaluating the potential field off-axis. However, numerical methods are available. A particularly effective method is the one in which the surface involved is tessellated by triangular elements. The solid angle is found by adding up the solid angles of these elements, each computed by means of an analytical expression [12]. This method can be used for double layers having an arbitrary shape. It was used to draw Fig. 6.8, which depicts the potential field for the source configuration shown in the left panel of Fig. 6.7 in the plane $y = 0$.

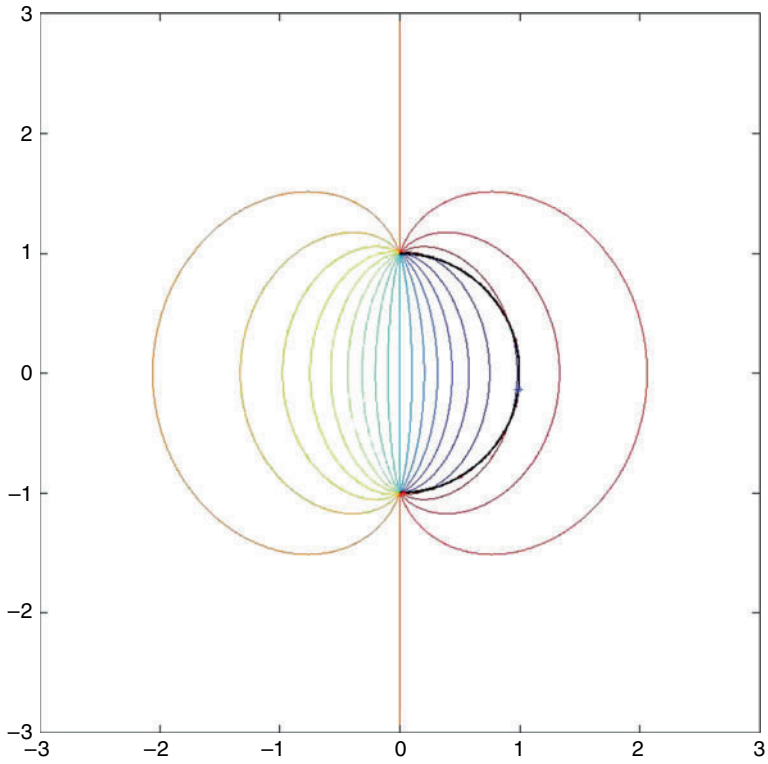

Figure 6.8

Potential field in the plane $y = 0$ generated by the hemispherical double layer shown in Fig. 6.7. Isopotential lines drawn at $V_D/10 = 4$ mV intervals; the heavy solid line is the cross-section of the plane with the double layer. Potentials to the right of the double layer are positive, elsewhere they are negative. The potential profile along *x*-axis is shown in the *right* panel of Fig. 6.7. Position of absolute minimum of −34.12 mV indicated by an asterisk; maxima of 9.08 mV near the edge of the hemisphere.

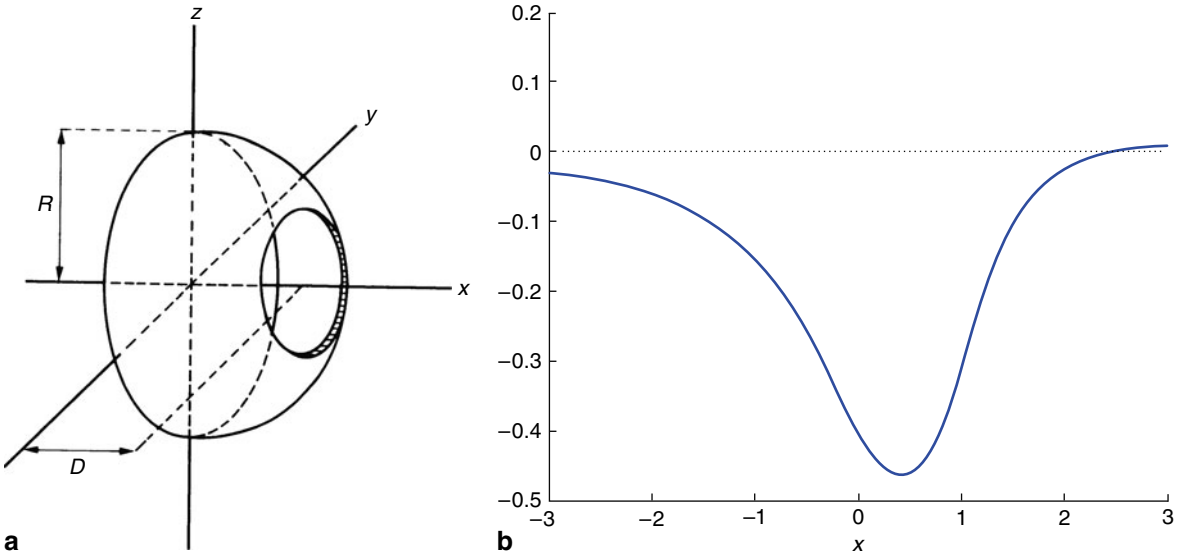

Figure 6.9

***Left*: Double layer having the shape of a de-capped hemisphere of radius *R*; *right*: the resulting potential profile along the *x*-axis according to (6.18), expressed in units V_D = 40 mV; R = 1.25; D = 1; *x*, *R* and *D* expressed in the same arbitrary unit.**

6.4.1.3 A De-Capped Hemisphere

Here the sources are again on a hemisphere of radius R but now the top has been lifted, leaving a layer of width D (6.9 (left panel)). This models a similar situation to the one described in the previous subsection, but now at the – later – stage where the wavefront has broken up at a boundary of the myocardium. The potential distribution in this case is easily found (using the superposition principle) by subtracting the potentials arising from the cap from those described for Case 2. The potentials from the cap are identical to those of hypothetical double layer sources on a disk with a radius $R_c = \sqrt{R^2 + D^2}$ closing the cap. For points on the x-axis the potential thus reads

$$\Phi(x) = \frac{1}{2} V_D \left(\frac{x - D}{\sqrt{(x - D)^2 + R_c^2}} - \frac{x}{\sqrt{x^2 + R^2}} \right) \tag{6.18}$$

This potential profile is shown in the right panel of Fig. 6.9. Note that the x-axis here does *not* cross the actual double layer, and so no potential jump of magnitude V_D comes into view along this axis.

6.4.1.4 A Dispersed Double Layer

The equivalent source double associated with ventricular depolarization is not a double layer in the mathematical sense described in Sect. 6.3.1. When crossing the wavefront the successive myocytes passed are at different stages of depolarization. As a consequence, the equivalent sources and sinks of electric current are spread out along the normal of the activation boundary and extend over a distance of the order of 1 mm, the length of about ten myocytes. The potential profile across the activation boundary shows a smooth, S-shaped curve rather than the jump that is seen in Fig. 6.7. For the purpose of modeling this local property of the potential profile different functions may be used. Here we will use the simple expression

$$S(x) = \frac{x}{\sqrt{x^2 + w^2}},$$

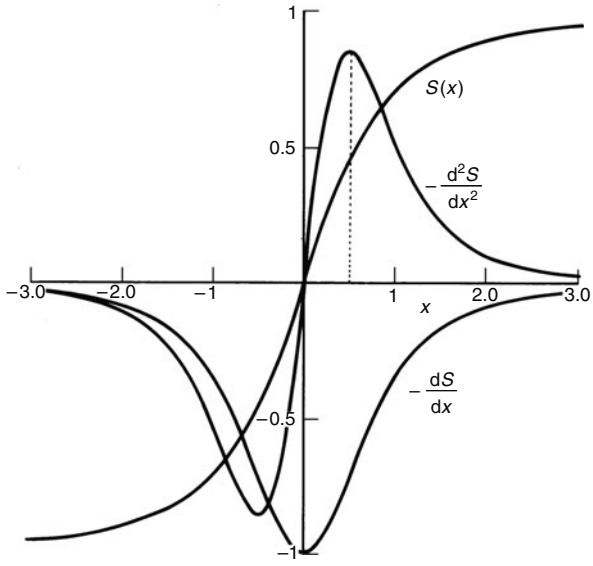

Figure 6.10
Plot of $S(x)$, as well as its first derivative and its second derivative (shown negative); w = 1 mm.

with w (of the order of 1 mm) specifying the distance of the current source distribution along the normal of the activation boundary. This function is merely an empirical function, chosen to represent the dispersed nature of the sources; it will now be taken to represent the local properties of the double layer and so it can replace the term $\frac{x}{|x|}$ in (6.16). This function is depicted in Fig. 6.10, $S(x)$, as well as the plots of its first and second derivative with respect to x.

In those cases where the local curvature of the activation surface is small, or zero in the case of a planar wavefront, the second derivative can be interpreted as representing the current-source volume density along the normal to the wavefront. In that case, but in that case only, Poisson's equation (Sect. 2.6.1.1),

$$\nabla^2\Phi = \frac{-i_v}{\sigma},$$

with i_v the current source volume density (units: A m^3) impressed by the biochemical processes at the membranes and

$$\nabla^2\Phi = \frac{\partial^2\Phi}{\partial x^2} + \frac{\partial^2\Phi}{\partial y^2} + \frac{\partial^2\Phi}{\partial z^2},$$

can be approximated as

$$\nabla^2\Phi \approx \frac{d^2\Phi}{dx^2} = \frac{-i_v}{\sigma},$$

the distance between the maximum (current source) and the minimum (current sink) of d^2S/dx^2 for this $S(x)$ is w. The expression for the potential profile of the hemispherical dispersed UDL along the x-axis, replacing (6.17), now reads

$$\Phi(x) = 20\left(\frac{x-R}{\sqrt{(x-R)^2+w^2}} - \frac{x}{\sqrt{x^2+R^2}}\right)\ (\text{mV}), \tag{6.19}$$

the shape of this profile is plotted in Fig. 6.11 (solid line) in which the corresponding potential profile of the mathematical double layer (Fig. 6.7 (right panel)) is also drawn (dashed line). Note that the distal profile is not affected by the

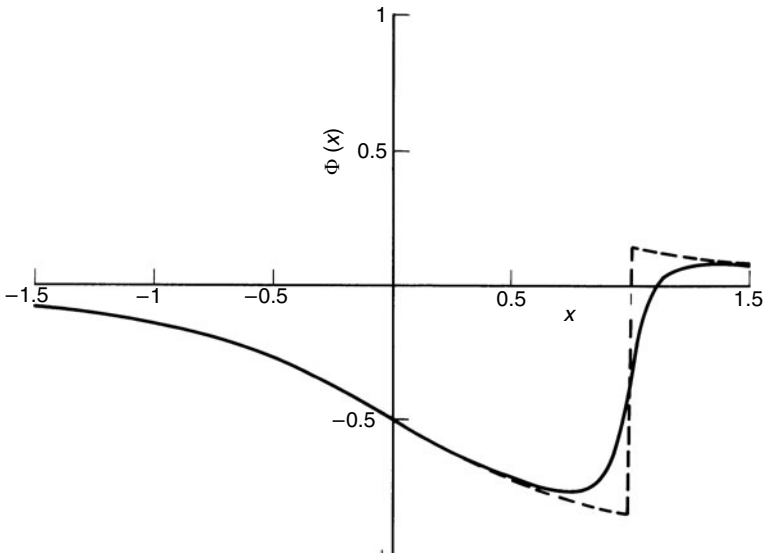

Figure 6.11

Potential (in units: V_D = 40 mV) along the *x*-axis (units: cm) of a hemisphere, like in Fig. 6.7, but now carrying a dispersed double layer (solid line); w = 1 mm, R = 1 cm. The dashed line replicates the potential generated by the mathematical double layer (Fig. 6.7 (*right* panel)).

distributed nature of the sources. The difference between the maximum and minimum of the potential profile is reduced. This means that if this difference were taken as an estimate of V_D (as has been done), it would be an underestimation; the wider the sources are spread out, that is the larger w, the greater the underestimation will be.

6.4.2 Potentials Generated by the UDL at a Propagating Wavefront

The setting of the UDL source used in the previous section implies planar boundaries of the myocardium at the endocardium and the epicardium. We now consider the more realistic configuration of uniform myocardial tissue contained in a thick-walled spherical shell. Based on this model, electrograms and potential profiles generated by the UDL source are illustrated, resulting from the propagation of wavefronts initiated at either an endocardial or an epicardial site. The velocity of the propagation is put at a uniform value of 1 m/s. The wavefronts shown correspond to the traveling time from stimulus point while propagating through the myocardium (Huygens principle). The sequences of the resulting wavefronts are shown in Fig. 6.12. Note that in the right panel the direction of the total wavefront reverses after about 22 ms; the terminal wave fronts resulting from the endocardial and the epicardial stimulus site are highly similar.

We now consider a selection of potentials generated by the sequence of activation wavefronts shown in Fig. 6.12. The double-layer strength V_D is put at 40 mV. The stimulus is at time t = 5 ms. The field points involved are documented in Fig. 6.13. Owing to the axial symmetry of the problem, the field points situated in the plane of Fig. 6.13 suffice. The field points chosen are A(1)–A(13) on the endocardium; B(1)–B(13) on the epicardium and a series of 12 points along straight lines from the center of the sphere passing through the wall. Such field points are similar to those at intramural electrode arrays used in electrophysiological studies, also known as "plunge" electrodes [13].

6.4.2.1 Infinite Medium Potentials

We start by examining the infinite medium potentials generated by the sequence of activation wavefronts shown in Fig. 6.12, i.e., the potentials are generated assuming the electric conductivity of the entire, infinite medium to be uniform.

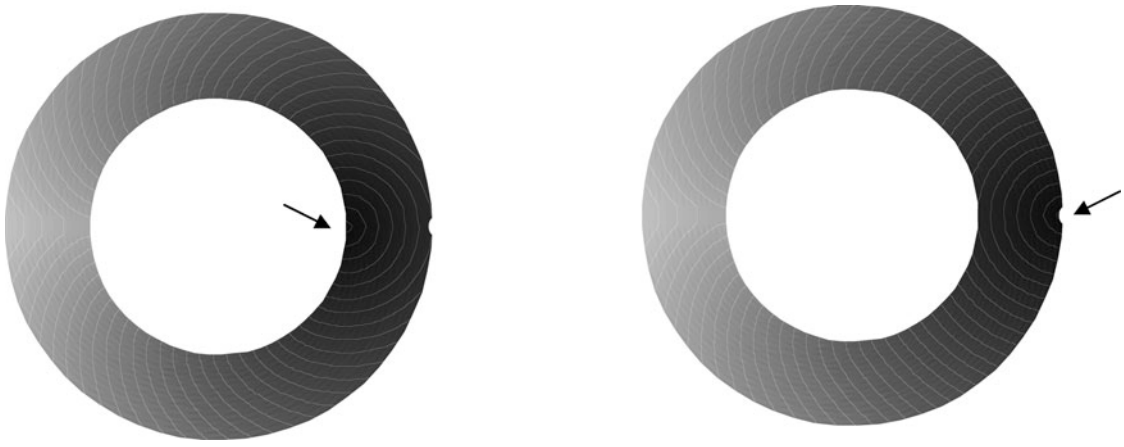

Figure 6.12

Activation wavefronts inside a thick-walled spherical shell *model* of myocardial tissue, drawn in the plane symmetry, resulting from a single, local stimulus. *Left* panel: endocardial stimulus; *right* panel: epicardial stimulus. *Arrows* indicate stimulus sites. Isochrones drawn at 2.5 ms intervals. Assumed uniform propagation velocity of 1 m/s. Radius of outer sphere (epicardium) 4 cm; radius of inner sphere (endocardium) 2.4 cm. Total duration of the propagation 83.5 and 93.5 ms for endocardial and epicardial stimulus sites, respectively.

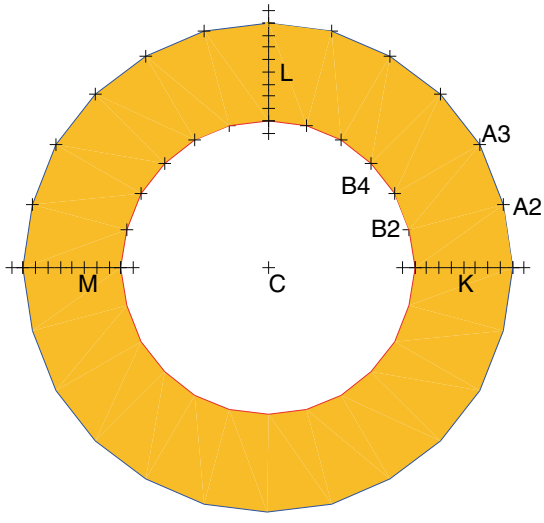

Figure 6.13

Locations of epicardial field points (a), endocardial field points (b), field points at needle electrodes (K,L,M) and one at the center of the spherical shell (c). Note that the needle electrodes include field points external to the wall, one just inside the cavity and another one just outside the wall. 13 epicardial and 13 endocardial field points are labeled anti-clockwise; 11 points along the needle electrodes are labeled inside outward. Stimulus sites as used in Fig. 6.12 are along needle K.

In Fig. 6.14 a sequence of the potential profiles along the line from center C to the line K (Fig. 6.13). Time instants shown, at 4 ms intervals, correspond to the initial stages of the propagating UDL front. The dotted lines represent the infinite medium potentials. The left panel relates to an endocardial stimulus, in the right panel to a stimulus at the epicardium. Note that, in both situations, the potential jump at the wavefront remains constant right up to the moment

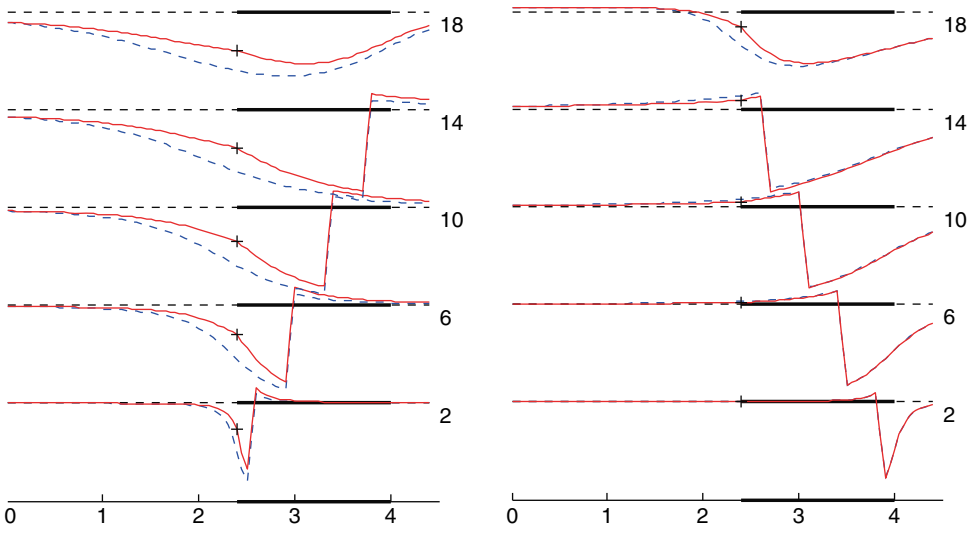

Figure 6.14

Sequence of potential profiles along a line from center C passing through line K shown in Fig. 6.13. Time instants shown, at 4 ms intervals, are selected during the initial stages of the propagating UDL front. Dotted lines: infinite homogeneous medium; solid lines: potentials in the presence of higher conductivity inside the cavity. *Left*: stimulus at endocardial electrode of needle K; *right*: stimulus at epicardial electrode of needle K. Distance along horizontal axis in cm. The heavy lines along the horizontal axes mark the location of electrode K, as well as the zero level of individual potential profiles. Potential reference is at infinity. Vertical spacing of the profiles corresponds to 40 mV, thus calibrating the potential. Figures next to the profiles denote the time from stimulus in ms.

of breakthrough of the wavefront. Following that moment, the sharp jump in the potential is no longer present, and the profiles (not shown) become increasingly flat with time. Note that these potential profiles imply a common reference for the potential specified at all field points considered. Here, in the infinite medium model used, the zero reference was set at infinity.

Traditionally, intramural electrograms have been recorded and studied rather than the transmural potential profiles shown in Fig. 6.14. To facilitate a direct comparison between predicted and recorded potentials, the results of the same computations are now shown as electrograms at the field points specified in Fig. 6.13. The electrograms simulated at the 11 terminals of the intramural electrode K shown in Fig. 6.13, are presented by the dotted lines in Fig. 6.15. The electrograms at the 13 endocardial field points B and 13 epicardial field points A are shown in Figs. 6.16 and 6.17, respectively. Note, by comparing Fig. 6.15 with Figs. 6.16 and 6.17, that the magnitude of potential jump at field points at the boundary of the myocardium is 20 mV, i.e., one half that of the value $V_D (= 40\,\text{mV})$ at intramural field points. Interestingly, the progression of electrogram wave forms along the epicardium in the right panel of Fig. 6.16 is from the rS to the Rs configuration of standard electrocardiographic terminology.

6.4.2.2 The Effect of Inhomogeneous Conductivity; the Brody Effect

The electric conductivity of blood is higher than that of the isotropic representation of myocardial tissue. The effect of this on the potential field is generally known as the Brody effect [14]. To evaluate its significance for the UDL source model, all potentials arising from the propagating wavefronts shown in Fig. 6.12 were also computed for the situation that the conductivity of the inner sphere, representing a blood-filled cavity, is threefold that of the (infinite) medium around it. The results are presented by the solid lines in Figs. 6.14–6.17, alongside those pertaining to the homogeneous situation, the dotted lines. The computations involved were carried out by means of the boundary element method (BEM), Sect. 2.6.4.

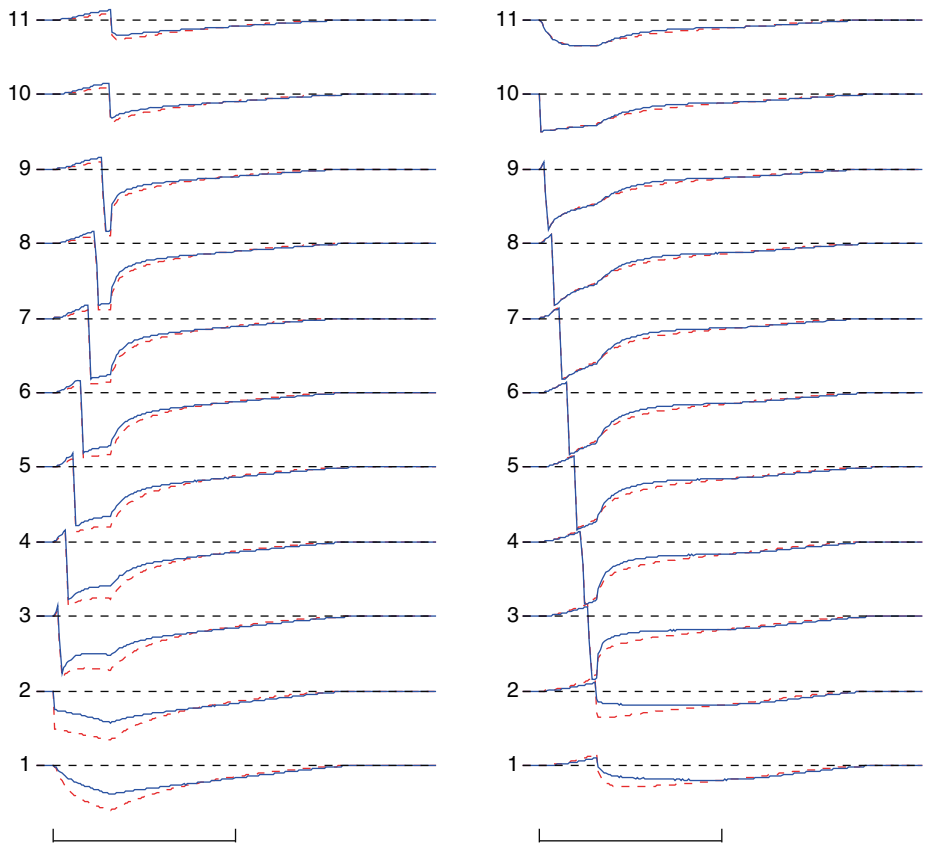

Figure 6.15

Electrograms at electrodes 1–11 of intra-mural electrode K indicated in Fig. 6.13. Potential reference at infinity. Dotted lines: infinite homogeneous medium; solid lines: potentials in the presence of higher conductivity inside the cavity. *Left*: stimulus at endocardial electrode of needle K; *right*: stimulus at epicardial electrode of needle K. Time bar 50 ms. Vertical spacing of the profiles corresponds to 40 mV, and calibrates the potential.

In Fig. 6.14 the effect can be seen most clearly at the endocardial field point. In the potential profile a discontinuity in its slope can be observed at this location. The value of this slope multiplied by the local conductivity is equal to the current density $J_n(\mathrm{A\,m^{-2}})$ normal to the boundary. This density is continuous across any boundary (2.128), so where the conductivity is large the slope should be small, as is indeed observed. On the profiles, the discontinuity is marked by the + sign. On the endocardium the higher conductivity reduces the potential jump of 20 mV over the wavefront as found for the homogeneous situation by a factor of 2, as expected on the basis of the conductivity ratio at the interface (Sect. 2.6). This leaves 10 mV as the theoretical maximum jump that can be expected for V_D = 40 mV. Inside the myocardium, the potential jump at the wavefront is unaffected by the inhomogeneity, as can be expected from the UDL model. The inhomogeneity does affect the level at which the jump takes place. On the epicardium the reduction factor for the passing (but not crossing) wavefront is less than 2, which can be explained by a larger distance from the inhomogeneous region. For the more realistic situation of dispersed sources at the wavefront, as discussed in Sect. 6.4.1.4, the potential gradients at the wavefront set up by the global distribution of the sources interact with the local gradients.

In Sect. 2.6 it is shown that the effect of local discontinuities in the conductivity may be described by virtual sources at the interfaces where the conductivity occurs. For field points that are relatively far away from such interfaces, the effect of the local gradient of the potential field is mainly limited to the setting of the overall level of the local potential. This explains the relatively minor effect of the inhomogeneous cavity on the early profiles shown in the right panel of

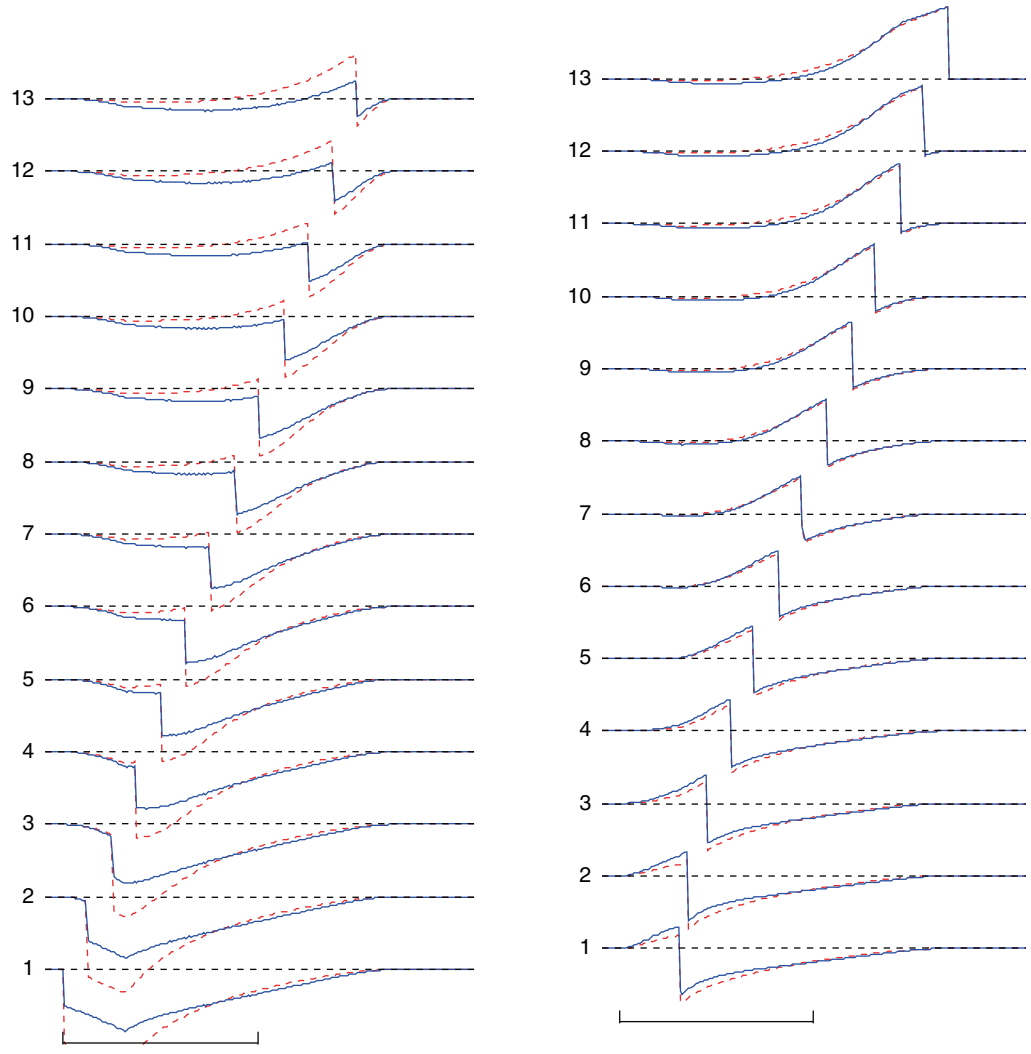

Figure 6.16

Electrograms along endocardium; field points B1–B13 indicated in Fig. 6.13. Potential reference at infinity. Dotted lines: infinite homogeneous medium; solid lines: potentials in the presence of higher conductivity inside the cavity. *Left*: stimulus at endocardial electrode of needle K; *right*: stimulus at epicardial electrode of needle K. Time bar 50 ms. Vertical spacing of the profiles corresponds to 20 mV, and calibrates the potential. *Note that scaling differs* by a factor 2 from what is used in Fig. 6.15.

Fig. 6.14, as well as on the electrograms shown in Figs. 6.16 and 6.17. An overall evaluation of the Brody effect on the potential field confirms its significance, but also that it can not be represented by a single scaling factor [15].

6.4.2.3 Bounding the Medium; the Influence of the Reference

The expression of the cardiac electric activity is invariably observed in a bounded medium, be it the thorax or some fluid-filled container used during in vitro experiments.

In both circumstances the effect of these bounds may be limited, mainly restricted to setting the overall level of the potential field, similar to what is described in the previous section with regard to the Brody effect.

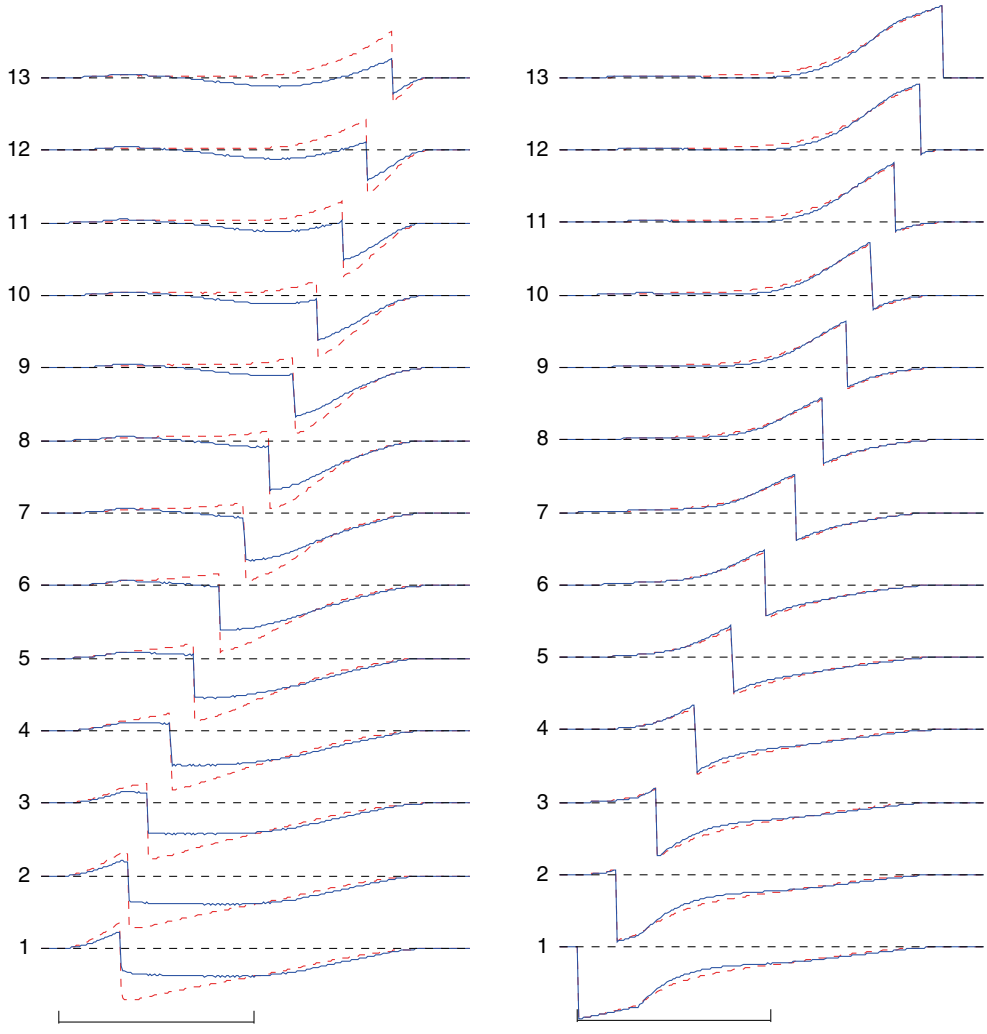

Figure 6.17

Electrograms along epicardium; field points A1–A13 indicated in Fig. 6.13. Potential reference at infinity. Dotted lines: infinite homogeneous medium; solid lines: potentials in the presence of higher conductivity inside the cavity. *Left*: stimulus at endocardial electrode of needle K; *right*: stimulus at epicardial electrode of needle K. Time bar 50 ms. Vertical spacing of the profiles corresponds to 20 mV, and calibrates the potential. *Note that scaling differs* by a factor 2 from plots in Fig. 6.15. The epicardium in the *right* panel of Fig. 6.16 is from the rS to the Rs configuration of standard electrocardiographic terminology.

Of greater significance is the fact that one of the two the electrodes essential for measuring potential differences, commonly called the reference electrode, can no longer be set at infinity (Sect. 5.4.1). If the dimension of the myocardial tissue is small compared to that of the volume conductor (thorax, container) holding it, the potential gradients set up at the boundary by the electric sources will be small relative to those close to the tissue, the ones as picked up by the sensing electrode. This will cause the observed potential differences between sensing electrode and reference electrode to be largely independent of the location of the reference on the boundary. However, the dimensions of the heart relative to its distance from the torso boundary cannot taken to be small, and so the selection of any reference will influence the observed ECG wave forms. The same applies to potential differences observed between a micro electrode placed inside a cell and a reference electrode placed nearby. The location of the latter may greatly influence the magnitudes and wave forms of the observed potential differences.

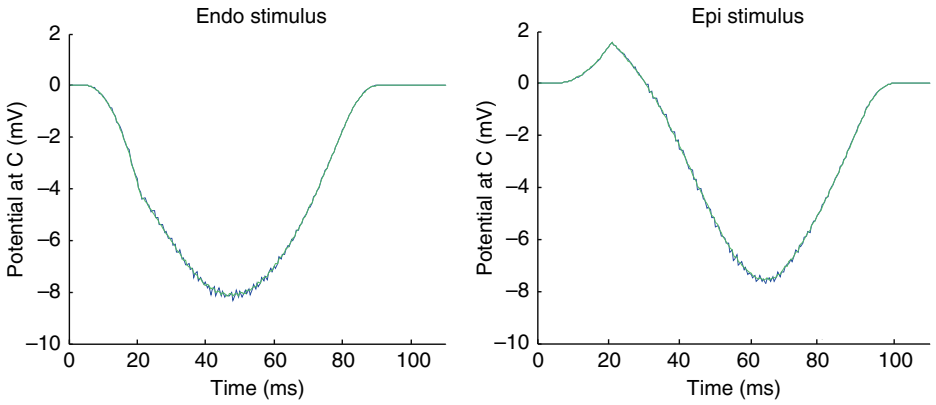

Figure 6.18

Electrograms at field point C, the center of the spheres indicated in Fig. 6.13. Superposition of infinite medium potentials and potential including Brody effect. *Left*: stimulus at endocardial electrode of needle K; *right*: stimulus at epicardial electrode of needle K.

To illustrate this point, first, in Fig. 6.18, electrograms at field point C of Fig. 6.13 are shown. This location is similar to the cavity reference used in some of the early mapping of cardiac electric activity. The electrograms shown are those inside the infinite homogeneous medium, and superimposed those including the Brody effect at this field point. The timing of the wavefronts is shown in Fig. 6.12. Note that for the source configuration considered, the magnitude of the electrograms is about one fifth of the assumed double-layer strength $V_D (= 40\,\mathrm{mV})$, and that the effect of the higher conductivity of blood at the center of the sphere is very small. The initial positivity following the epicardial stimulus reflects the initial orientation of the total wavefront in 3D space toward C (right panel Fig. 6.12) having, correspondingly, the total solid angle of the wavefront is positive. After about 25 ms point C views the rear of the wavefront only (negative total solid angle). Following the endocardial stimulus, field point C views the rear exclusively. This indicates that the predominant negativity as observed experimentally may be explained by the solid angle theory, in combination with the predominantly convex geometry of the myocardium.

Next, in Fig. 6.19, the effect for the inhomogeneous situation (Brody effect) is illustrated that result if the potential at field point C is used as the reference. The comparison is documented for the endocardial stimulus, for which the electrograms based on the infinite medium reference are shown by the solid lines in the left panels of Figs. 6.16 and 6.17. In Fig. 6.19 these results are reproduced, with superimposed (dashed lines) the corresponding electrograms based on taking the potential at field point C as the reference. Since the infinite medium potentials at the endocardium have magnitudes that are similar, the effect of using the reference at C can be seen more clearly in the endocardial signals.

6.4.2.4 Discussion

The model study presented in the previous sub-sections permits the analysis of the fields generated by the UDL model in isolation of a multitude of unknown, or poorly specifiable factors affecting the data observed during electrophysiological measurements.

All potential profiles and electrograms shown in the previous sub-sections are based on the simple model of UDL source, isotropic electric conductivity, and a Huygens type of propagation assuming uniform velocity. In spite of this, a wide variety of wave forms can be observed. The qualitative nature of the signals corresponds well to experimental observations. Being based on the UDL source at propagating wavefronts, all effects of ongoing repolarization effects were excluded, which resulted in a return to baseline at the termination of propagation for all signals. Any decay towards the baseline, hence, relate to depolarization currents only, with details of the decay being related to the time course of the total solid angle of the wavefront subtended at the field point; sharp deflections signify a passing wavefront.

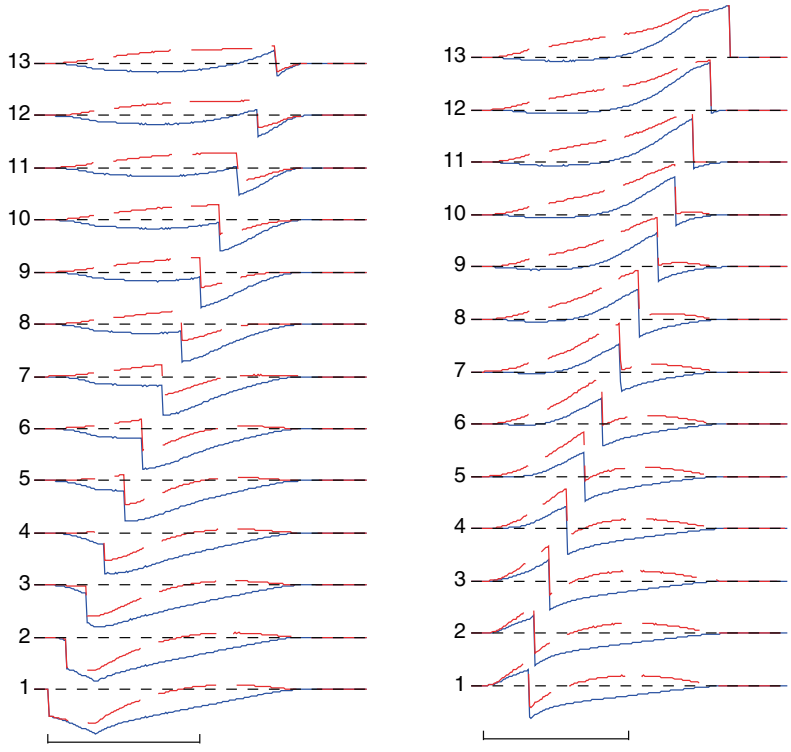

Figure 6.19

Electrograms in the presence of the Brody effect, following an endocardial stimulus. Solid lines: potential reference at infinity; dashed lines: reference at the center of the spheres (field point C). *Left*: endocardial field points B1–B13; *right*: epicardial field points A1–B13. Time bar 50 ms; vertical spacing of the profiles corresponds to 20 mV, and calibrates the potential.

The simulated signals at the needles L and M demonstrated a regular, gradual progression of the wave forms along the needles between those documented for the endocardial side and the epicardial side. For needle L, all fast down slopes occurred almost simultaneously, in agreement with the isochrones shown in Fig. 6.12. Without the full knowledge of the position of these wavefronts, any interpretation of the observed data may easily lead to incorrect interpretations of such data.

The relevance of the potential at the reference electrode can be seen to be quite significant. A different location of the reference than that of C shown in Fig. 6.13 yields different effects than those visible in, e.g., Fig. 6.19.

Initially, electrophysiological studies relied on data presented in the form of electrograms. The study discussed in Sect. 6.4.3.1 introduced the method of studying potential profiles along the intra mural electrodes. More recently, mapping the potentials transmural potential field or potential fields on the heart surface have been used, as shown, e.g., in [11, 16]. These methods are complementary, and form essential tools in the understanding of the complex spatio-temporal nature of the electric activity of the heart.

6.4.3 Electrophysiology Based UDL Parameters

The validation of any source model entails a comparison of the potentials (potential differences) generated by the model and those observed experimentally. As is discussed in Sect. 6.3.4 for the single fiber, this demands the matching of the complexity of the experimental setup and those used in the computations. In the case of the source modeling of the entire heart, this requirement cannot easily be fulfilled. Below, experimentally observed potentials are interpreted in terms of the UDL model.

6.4.3.1 Potentials Recorded Inside the Canine Myocardium

The potentials along a linear multi-terminal intramural electrode array (IME; plunge electrode), following an endocardial stimulus, have been recorded in the free part of the canine left ventricular wall [17]. The electric properties of the canine myocardium have been shown to be comparable to that of the human myocardium. The animals were anesthesized using 20 mg Nembutal per kg body mass. Respiration was maintained artificially through tracheal intubation. The thorax was opened by median sternotomy. Following the insertion of the IMEs, different series of recordings were made. In some of these, the part of the ventricular myocardium studied was exposed to air, in other ones the thorax was closed as tightly as possible, while filling up any remaining gaps with a fluid having approximately the same electric conductivity as the mean conductivity of body tissues [18]. The results shown in this section pertain to the latter configuration. The diameter of the IME was 1 mm, as was the inter-electrode distance. The IME was surrounded by four other IMEs, inserted into the wall at distances of about 1 cm from the central one. The simultaneously recorded potentials at these flanking IMEs served as a check on the nature of the propagation along the central IME. In particular, the possible involvement of activity initiated by the Purkinje fibres needed to be ruled out. The potentials along the central IME are shown in Fig. 6.20. In the left column electrograms are shown that were recorded with respect to a common reference at the aortic root. Such signals with a common reference are commonly, but incorrectly, referred to as unipolar leads, one of the many unfortunate misnomers in the field of electrocardiography.

Evaluation

The electrograms can be compared with the simulations as depicted in the left panel of Fig. 6.15. However, note that, inevitably, the simulated potentials have a different common reference. The middle column depicts the corresponding bipolar signals: the potential differences observed between pairs of successive electrodes along the IME: the potential at any electrode minus that of its neighbor situated closer to the cavity. The right column depicts the corresponding sequence of recorded transmural potential profiles at successive time instants; time increases from top to bottom. These can be compared to the simulated profiles shown in the left panel of Fig. 6.14. The discontinuity of the slope at the endocardial electrode, resulting from the Brody effect, can be clearly seen, in particular for time instances between 22 and 44 ms.

The electrograms measured inside the ventricular wall following the stimulus artifact, shown in the left column of Fig. 6.20, display the progression of a negative deflection, which passes along at uniform velocity, consistent with conditions used in generating model signals (Fig. 6.15). The magnitude of the down slope of the experimental data is uniform along the IME. The same conclusion can be drawn from the bipolar signals and potential profiles shown in Fig. 6.20.

In the full report on this study [18] it was reported that the same qualitative correspondence between potentials observed experimentally and those based on the UDL source was observed for potentials during spontaneous activity sinus beat in the free wall of the left ventricle. In that situation, the potentials observed at the flanking IMEs revealed a more planar nature of the wavefront, traveling transmurally from endocardium to epicardium. No significantly different details were observed in the profile for mid-myocardial locations of the wavefront compared to locations close to either endocardium or epicardium. Other observed signals and profiles, such as following an epicardial stimulus, transmural data in the septum and in the right ventricular free wall, could be described well on the basis of the UDL source. This was taken as a justification of the use of this source model.

The exampled shown in Figs. 6.6–6.19 all relate to an axial symmetric distribution of the sources, the axis being, e.g., the line through needles K and M in Fig. 6.13. If anisotropic propagation is involved any of the circular configuration, like the one shown in Fig. 6.6 the on an elliptical shape. The potential profiles along the axis, like the one shown in Fig. 6.7, are different, but only in a minor way, even if the ratio of the longest and the shortest axes of the ellipse is a high as 8.

6.4.3.2 Parameters of the UDL Source Estimated from Measured Potentials

Based on the experimentally observed transmural potential profiles described in Sect. 6.4.3.1, the parameters V_D and w of the UDL have been estimated. These were found to be of the order $V_D = 40$ mV and $w = 0.7$ mm.

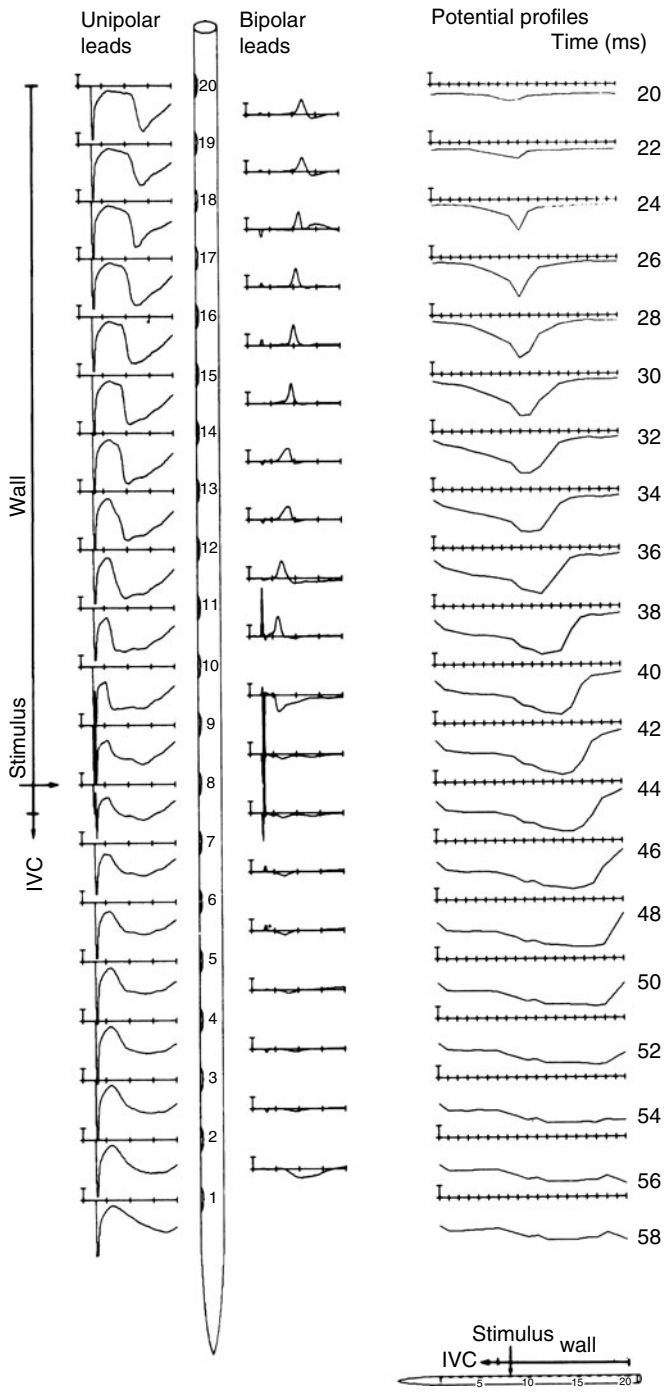

Figure 6.20

Potentials measured inside canine ventricular myocardium following endocardial stimulation. The *left* column shows common reference electrograms and bipolar electrograms, respectively. The *right* column depicts the corresponding potential profiles along 1 mm spaced electrodes along an IME at the time instants indicated on the *right*. The stimulus site on the electrode is indicated; the stimulus is delivered at $t = 10$ ms. The *abscissae* of the *left* and middle columns are marked at 20 ms/div; those in the *right* column are marked at 1 mm/div. IVC denotes intra ventricular cavity.

The observed value of w indicates (using the observed transmural propagation velocity of 0.4 m s^{-1}) that the duration of the passage of the depolarization phase of the dispersed sources across the wavefront is of the order of

$$t \cong \frac{2w}{v} = \frac{1.4 \times 10^{-3}}{0.4} = 3.5 \text{ ms},$$

the associated dipole surface density (6.15) was computed by taking some realistic value for the overall macroscopic conductivity of the cardiac tissue. Taking $\sigma = 0.16\,\mathrm{Sm}^{-1}$, it follows that $M_S = \sigma V_D = 6.4 \times 10^{-3}\,\mathrm{Am}^{-1}$.

The electric field strength, $E = -\mathrm{d}\Phi/\mathrm{d}x$, along the profile can be derived from (6.19) as

$$E(x) = -\frac{1}{2} V_D \left(\frac{w^2}{((x-R)^2 + w^2)^{3/2}} - \frac{R^2}{(x^2 + R^2)^{3/2}} \right),$$

at the activation boundary $x = R$ the field strength has a maximum value of

$$E_{\max} = -\frac{1}{2} V_D \left(\frac{1}{w} - \frac{1}{R} \right),$$

if $R >> w$ this results in $E_{\max} = 28\,\mathrm{V\,m}^{-1}$. The condition stated, $R >> w$, illustrates the interaction of the local and the global properties of the source. Only for a planar front were $(R = \infty)$ does the second derivative along the axis of the potential profile exclusively represent the local macroscopic source properties. For wave fronts set up just following a stimulus, its apparent strength is smaller than its actual strength.

For the associated impressed current density, $J = \sigma E$, its maximum value can now be estimated as

$$J_{\max} \cong -4.5\,\mathrm{Am}^{-2},$$

the impressed macroscopic current source volume density i_v can be estimated in the approximation $(R >> w)$

$$\nabla^2 \Phi \cong \frac{d^2\Phi}{dx^2} = \frac{-i_v}{\sigma},$$

the maximum value of i_v occurs at $x = {}^1\!/_2 w$ (Fig. 6.10), for which

$$i_{v;\max} = \frac{0.43\,\sigma\,V_D}{w^2} \cong 5.8 \times 10^3\,\mathrm{Am}^{-3},$$

the above are gross overall estimates of the various ways in which the macroscopic cardiac sources can be specified by physical parameters. They are interrelated by the assumed potential distribution of the dispersed uniform double layers (6.19). They characterize the in situ situation of intact, healthy cardiac tissue during an activation sequence which is predominantly transmural. During spontaneous ventricular activation, the main activation sequence at the free wall of the left ventricle is from endocardium to epicardium (Chap. 4). The UDL source during such an activation sequence can be quantified by the parameter values described in this sub-section.

6.4.4 Validity of the UDL Source Model

The validation (i.e., non-falsification) of any source model entails a comparison of the potentials (potential differences) generated by the model and those observed experimentally. This demands the matching of the complexity of the experimental setup and that used in the computations. Even for the single fiber, as is discussed in Sect. 6.3.4, this requirement cannot easily be fulfilled, and even less for the source modeling of the entire heart, this.

For many years the uniform double-layer model has served to explain in a qualitative fashion the potentials recorded at the body surface. The most thorough presentation of its potential for this qualitative description was given by Holland and Arnsdorf [9].

In several quantitative studies, involving approaches to the "forward problem of electrocardiography" (Chap. 8), the implied cellular model for healthy cardiac tissue is that of the uniform double layer [19, 20]. The results described in Sects. 6.3.3 and 6.3.4 also suggest that the uniform double layer describes the macroscopic potentials inside the ventricular wall during a transmural activation sequence in healthy myocardium quite well. However, several other studies have led to severe criticisms about the validity of the uniform double layer [21], in particular in view of the well-established anisotropic nature of the electric properties of myocardial tissue. These studies gave rise to the formulation of several alternative models, which are necessarily more complex in nature. A discussion on the use of the UDL model was described in [22]. The main arguments exposed in that paper are as described in Sect. 6.4.4.1. Throughout, the essentially anisotropic nature of myocardial tissue [23, 24] needs to be kept in mind.

6.4.4.1 The UDL Model Criticized

The critique on the UDL was initiated by a group that had previously been advocating its use [8]. In a report published in 1976 [25] it was shown forward computations based on the UDL and on the observed activation data failed to produce potentials comparable to those observed on the surface of a cylinder containing a conducting fluid into which a canine heart was submerged. The possibility that this might be due to an insufficient accuracy of a) the recorded geometry, b) the depolarization sequence as estimated from the spatial sampling implied in the use of the intramural electrodes, or c) the calculations performed, was not discussed. Hence, their doubt about the validity of the UDL source model remained. As an alternative, the axial model, described in Sect. 6.5, was postulated.

However, more recent studies have demonstrated a close correspondence between UDL-based forward simulations and observations made under similar conditions [26]. A significant, all be it indirect, support of the UDL source model came from a study, in which the UDL was used to estimate (inverse problem) the individual depolarization sequences of three human subjects. These inverse computations used, separately for each subject, MRI data that specified the relevant interfaces of regions with different conductivity. Next, the estimated depolarization sequence was used (forward problem, Chap. 8) in a straight forward procedure, to compute the magnetocardiograms (MCG). This was done prior to the recording of the magnetic data. Without applying any tuning or fitting procedure, the subsequently recorded MCGs showed a great similarity with the simulated data, regarding both gross wave form morphology and their magnitude.

In 1976, in an attempt to explain the poor simulation results, potentials inside the canine myocardium recorded by means of a (limited) number of intramural "plunge" electrodes were processed to represent instantaneous potential distributions throughout the ventricular wall [11]. The UDL "predictions" were computed in the infinite medium approximation (Fig. 7a of [11]) and were found to be essentially different from the observed data. The observed field showed a gradient across the wavefront, which the simulation did not. In a more recent publication on this point (Fig. 6a of [21]), the correct field produced by the hemispherical UDL is shown, similar to the one originally like the one shown in [18], and drawn here as Fig. 6.8.

An analysis (Sect. 6.5.1) of the alternative axial model that was proposed by the group demonstrates that this source model also fails to produce the potential wavefronts across the wavefronts.

Additional experimental data fuelling the dispute came from the Scher group. Based on potential readings on a restricted area of the epicardium as well as within the myocardium directly below, their data initially [27, 28] stressed anisotropy. However, from a later paper [29] support for the UDL can be distilled.

A major impetus for the concern regarding validity of the UDL came from an increasing insight into the anisotropic nature of the myocardium. In a much quoted study by Clerc [30] the work of Weidmann on propagation and conductivities along fibers was extended to the transverse fiber situation. For the interpretation of his data Clerc used the one-dimensional (cable) model applied to a configuration of closely packed cylinders.

His results on various conductivity values reported in the along fiber direction are in agreement with those of Weidmann [31]. For the transverse fiber direction Clerc's interpretation of the experimental data led him to state conductivity values, which gave rise to high values for the anisotropy ratios, the ratios of intra and extracellular conductivity.

In [32], Clerc's interpretations of his transverse fiber experimental data were criticized, as were the resulting estimates of the various anisotropy ratios. Up until now, no complete, and completely validated set of values for the (anisotropic) conductivities has become available [33]. Compare the data listed in Tables 1 and 2 of [32].

After studying the potentials recorded by Taccardi and his group at small distances from the epicardium of a dog heart submerged in a cylindrical bath, the importance of anisotropy was stressed by Colli-Franzone et al. [34]. Here in the observed epicardial potential distribution, in the region exterior to the approximately ellipsoidal depolarized region following an epicardial stimulus, a small region of positive values were found ahead of the wavefront. The observation was accentuated by drawing about as many isopotential lines around the small positive peak as were used for the large negativity overlying the depolarized area. Here the effect of the conductivity of the bath, which was much lower than that of the myocardium, creating secondary sources, may have played a part in exaggerating the apparent anisotropy.

The same phenomenon was stressed in later publications by the group [16]. Following an epicardial stimulus, local maxima of about 5 mV were observed ahead of the wavefront, whereas the depolarized region exhibited values of up to 33 mV. The observations were made on the epicardium in a region exposed to air. In the presence of this type of boundary the UDL source in an otherwise homogeneous medium does not create local maxima on the boundary ahead of the wavefront.

The results shown in Fig. 6.19 stress the significance of the position of the reference electrode [35].

6.4.4.2 The Strength of the UDL Source Model

The above examples demonstrate the difficulty in evaluating simplified source models from observed potentials. For a correct evaluation the full spatial extent of the source distribution and a full account of the passive conduction properties is required. Anisotropy is an inherent property of fiber structure. It dominates the propagation of activity as well as electric conductivity and, hence, current spread. In spite of this, the UDL source model has been shown to be a useful concept [36]. A simplified argument as to why this may work is as follows. In the macroscopic approach, the local double-layer source, with strength V_D, is taken to feed currents generated at the membranes of the myocytes into the tissue. As shown in Sect. 6.3.2, $M_S = -(\sigma_i \Phi_i - \sigma_e \Phi_e) \approx -\sigma_i V_m$. The isotropic, homogeneous medium with conductivity σ_e, and combined with $V_D = M_S/\sigma_e$, this yields an extra-cellular potential field,

$$\Phi(\vec{r}') = V_D \frac{\Omega}{4\pi} \sim \frac{\sigma_i V_m}{\sigma_e} \frac{\Omega}{4\pi} \tag{6.20}$$

Anisotropy will affect all of the 3 factors of the first fraction shown in this expression. The scalar conductivities become tensors and the membrane potential V_m has to be replaced by a variable having directional properties. When the bi-domain approach [37] is applied (Chap. 8) to the problem of finding the potential field reduces to a mono-domain formulation if an equal anisotropy ratios for intracellular and extracellular domain is assumed. Considerations with regards to cell coupling and cell geometry support this assumption; insufficient experimental evidence has been put forward to reject it [32]. The experimental values of $V_D = 40$ mV for the transverse fiber source strength [17] and $V_D = 51$ mV for along fiber source strength [38] are the ones most closely corroborating the equal anisotropy ratio assumption and, indirectly, the UDL source model.

A further explanation as to why the UDL works is the following. For the entire heart, anisotropy is not uniform, because of the complex lining up of overlaying muscle layers of the myocardium. This tends to fudge the overall effect of anisotropy, in particular when the potentials observed are those on the body surface.

Based on the experimental data discussed in Sect. 6.4.3.1, the value for the strength of the UDL was taken to be 40 mV [17, 18]. It is in agreement with the order of magnitude found for the fast deflection of the down slope of intramural electrograms found in early electrophysiological studies [13, 39]. The analysis presented Sect. 6.4.2 shows that this would result in a maximum value of 20 mV, the down slope of an electrogram generated by a wavefront passing along the epicardium in contact with a conductive medium with conductive properties similar to that of the myocardium. This is similar to values observed experimentally (Fig. 2 of [16]). In the latter study the shape of the wavefront was elliptical rather than circular as is implied in Sect. 6.4.2. On the epicardium exposed to air the potential difference across the wavefront following from an epicardial stimulus can be expected to be of the order of 40 mV, provided the wavefront has not yet broken through the endocardium. On the other hand, if the myocardium is in direct contact with a medium that has a conductivity that is higher than that of the myocardium, the potential differences are smaller. Assuming the conductivity of blood to be threefold that of myocardial tissue, a twofold reduction can be expected, leaving about 10 mV

as the expected maximum amplitude of an electrogram recorded on the endocardium. This value is in agreement with experimental observations in the ventricles as well as in the atria.

6.5 Anisotropic/Non-Uniform Models

In the uniform double-layer model, both the strength of the double layer and the conductivity of the medium in which this equivalent source is located are assumed to be independent of the direction in which the cardiac fibers are aligned within the myocardium. In reality, the elementary sources may be expected to depend, with regard to strength and in direction, on fiber orientation. The conductivity of the medium is known to be dependent on fiber orientation; the electrical current in passive myocardium is conducted more easily in the fiber direction than in a direction across the fibers. As a consequence, at a macroscopic local level the conductivity is a tensor rather than a scalar. This means that the conductivity should be specified by the components:

1. longitudinal conductivity σ_ℓ, the conductivity along fibers;
2. transverse conductivity σ_{t1}, the conductivity across fibers, in a direction perpendicular to fiber orientation, tangent to the ventricular wall; and
3. transverse conductivity σ_{t2}, the conductivity in a direction perpendicular to fiber orientation as well as to the ventricular wall.

The latter two transverse conductivities are usually assumed to be equal: $\sigma_{t1} = \sigma_{t2} = \sigma_t$.

As a consequence of fiber orientation, the elementary dipole strengths of a depolarization wavefront, the conductivity of the medium, or both may be assumed to be anisotropic and the inclusion of this aspect necessarily leads to an anisotropic, possibly non-uniform, source model.

6.5.1 The Axial Model

The first attempt to replace the uniform double layer was described by Corbin and Scher in 1977 [28]. The assumptions of their model are as follows.

A large section of myocardium is considered in which all fibers are aligned in parallel (Fig. 6.21). Let $\vec{\ell}$ be a (dimensionless) unit vector in the fiber direction. All surface elements $d\vec{S}$ of a depolarization wavefront within this tissue are assumed:

a. To carry a current dipole having a strength proportional to $\vec{\ell} \bullet d\vec{S}$
b. To point in the local fiber direction, toward the tissue still at rest
c. To be situated within a homogeneous tissue of isotropic conductivity

The elementary dipoles $\vec{D}$ involved can be expressed as $\vec{D} = p(\vec{\ell} \bullet d\vec{S})\,\vec{\ell}$, with p the dipole surface density, which is assumed to be uniform. Since the conductivity of the medium was taken to be homogeneous and isotropic, the potential $\Phi(\vec{r}')$ generated by an elementary dipole $p\,d\vec{S}$ at some observation point $\vec{r}'$ is

$$\Phi(\vec{r}') = \frac{1}{4\pi\sigma} \frac{p\,\vec{\ell} \bullet d\vec{S}\;\;\vec{\ell} \bullet \vec{R}}{R^3} \tag{6.21}$$

with $\vec{R}$ the vector pointing from the dipole location to the observation point, and R its length. The potential at $\vec{r}'$ generated by all sources on the depolarization boundary S can be found by using the superposition principle, as the sum (integral) of the contributions of all elementary dipoles:

$$\Phi(\vec{r}') = \frac{p}{4\pi\sigma} \int_S \frac{\vec{\ell} \bullet \vec{R}\;\;\vec{\ell} \bullet d\vec{S}}{R^3} \tag{6.22}$$

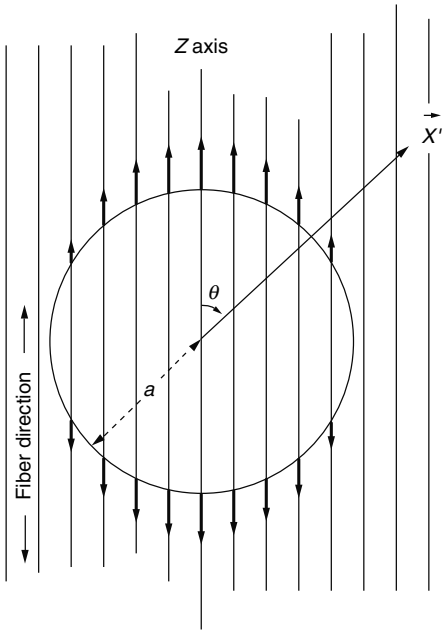

Figure 6.21

Spherical depolarized region inside the myocardium. Axial source strength is lined up exclusively with the fiber direction (*z*-axis). Elementary source strength at the spherical surface proportional to the cosine of the angle between fiber direction and the vector pointing from the center of the sphere and the observation point.

The corresponding expression for the UDL source model is (5.8) (see also Sect. 2.5.2.2).

The axial model prescribes all elementary dipoles to point in the fiber direction. Their strength is maximal for a wavefront propagating in the fiber direction, is zero for propagation across fibers and, in general, is proportional to the cosine of the angle between the direction of propagation of the wavefront and local fiber direction. Note, once more, that the conductivity of the tissue itself was taken to be the scalar, which implies an isotropic conductivity.

6.5.1.1 Potentials Generated by the Axial Model

The potentials generated by an arbitrarily-shaped depolarization wavefront based on the axial model can be found from (6.22), taking into account the particular shape of the wavefront *S*. In general this integral can only be solved numerically but there is one interesting exception. When the wavefront is assumed to be a closed sphere, the integral can be solved analytically. The resulting potential distribution can be used to assess the character of the axial model.

In [40] it is shown that the potential at an observation point $\vec{r}'$ that lies at a distance R from the center of a sphere of radius a carrying a source distribution corresponding to the axial model is

$$\Phi(R,\theta) = -\frac{p}{3\sigma}, \quad 0 \le R < a, \tag{6.23}$$

$$\Phi(R,\theta) = \frac{p}{3\sigma}\left(\frac{a}{R}\right)^3 \left(2\cos^2\theta - 1\right), \quad R > a, \tag{6.24}$$

with θ the angle between R and the fiber direction. When crossing the activation boundary at an angle θ with respect to the fiber direction, the potential jumps by $\Delta V = (p\,\cos^2\theta)/\sigma$, which is zero for across-fiber propagation.

These analytical results can be compared with the corresponding results for a uniform double layer with the same geometry, which are

$$\Phi(R) = -V_D, \quad 0 \le R < a, \tag{6.25}$$

$$\Phi(R) = 0, \quad R > a, \tag{6.26}$$

independent of θ.

The assumed source configuration can be studied experimentally by delivering an epicardial stimulus under the conditions of an epicardium exposed to air. The volume conduction effects of this exposure on the potentials set up inside the myocardium can, in the planar wall approximation, be treated by introducing a virtual source distribution that is the mirror image of the actual, hemispherical or hemi-ellipsoidal wavefront. This mirror image, combined with the actual source, forms a closed surface to which the preceding result ((6.23) and (6.24)) may be applied. Note that this is a valid description only as long as the wavefront has not yet broken through at the endocardium.

As shown by (6.24) the axial model predicts that ahead of the wavefront in a direction close to that of the fibers (small values of θ), small positive potentials are expected. These have been observed experimentally. The (mathematical) uniform double-layer model is incapable of explaining these. When looking at the transmural, transverse (across fiber) part of the activation wavefront, matters are entirely different. Here, the axial model predicts the absence of a potential jump across the wavefront, which is incorrect since major, nonzero potential jumps are clearly present for transmural, transverse propagation (Fig. 6.20).

6.5.2 The Oblique Dipole Model

The discussions about which model is preferable have led to the formulation of a new model, the "oblique dipole model" [34], which can be considered as a synthesis of the classical uniform double-layer model and the axial model. As in the previously discussed models, the medium in which this source description is situated is assumed to be a homogeneous, isotropic, infinite medium. The anisotropy of the fibers is exclusively assigned to the source description. In the oblique dipole model, in addition to the axially oriented sources of the axial model, dipole sources are postulated, which are oriented exclusively in the transverse direction. It is therefore necessary to distinguish between the surface tissue dipole densities p_ℓ for the longitudinal or fiber directions and p_t for the transverse direction. The contributions to the potential generated by the transverse sources alone now can be expressed as

$$\Phi(\vec{X}) = \frac{p_t}{4\pi\sigma} \int_S \frac{\vec{t} \bullet \vec{R} \quad \vec{t} \bullet d\vec{S}}{R^3} \tag{6.27}$$

where $\vec{t}$ is a (dimensionless) unit vector in the plane defined by $\vec{R}$ and fiber direction $\vec{\ell}$, pointing across fibers, towards the tissue still at rest (compare (6.21)).

In general, the combination of the axial and the transverse components is not perpendicular, i.e., oblique, to the surface elements dS of the depolarization wavefront S, from which property the name of this model was derived.

The combined axial and transverse dipolar sources yield the potential distribution

$$\Phi(\vec{X}) = \frac{1}{4\pi\sigma} \int_S \frac{[p_t(\vec{t} \bullet \vec{R})\,\vec{t} + p_l(\vec{l} \bullet \vec{R})\,\vec{\ell}\,] \bullet d\vec{S}}{R^3} \tag{6.28}$$

When $p_\ell = p_t = p$ this equation reduces to

$$\Phi(\vec{X}) = \frac{p}{4\pi\sigma} \int_S \frac{\vec{R} \bullet d\vec{S}}{R^3}, \tag{6.29}$$

The expression for the UDL, since in that case, p can be moved in front of the integral and $(\vec{t} \bullet \vec{R})\vec{t} + (\vec{\ell} \bullet \vec{R})\vec{\ell}$ represents $\vec{R}$ as the vector sum of its projections on $\vec{t}$ and $\vec{\ell}$. For this situation, the oblique model reduces to the classic uniform double-layer model. When $p_t = 0$ the oblique model reduces to the axial model.

An alternative way of expressing the potential due to the oblique dipole model results by substituting $p_t = p_u$ and $p_\ell = p_a + p_u$ in (6.28). By using

$$p_t(\vec{t} \bullet \vec{R})\vec{t} + p_\ell(\vec{\ell} \bullet \vec{R})\vec{\ell} = p_u(\vec{t} \bullet \vec{R})\vec{t} + (p_a + p_u)(\vec{\ell} \bullet \vec{R})\vec{\ell} = p_u\vec{R} + p_a(\vec{\ell} \bullet \vec{R})\vec{\ell}$$

this shows that the potential generated by the oblique dipole model can be viewed as the sum of

$$\Phi_u(\vec{X}) = \frac{p_u}{4\pi\sigma}\int_S \frac{R \bullet d\vec{S}}{R^3},$$

contributed by a purely uniform source, and

$$\Phi_a(\vec{X}) = \frac{p_a}{4\pi\sigma}\int_S \frac{(\vec{\ell} \bullet R)\vec{\ell} \bullet d\vec{S}}{R^3},$$

the contribution of a purely axial source [34].

The application of the oblique dipole model to the interpretation of recorded potentials generated by myocardial tissue now demands a potential jump at the activation boundary of $\Delta V_\ell = (p_u + p_a)/\sigma$ for propagation in the longitudinal direction, and of $\Delta V_t = p_t/\sigma$ in the transverse direction.

In some experimental studies, values of $\Delta V_\ell = 74$ mV and $\Delta V_t = 43$ mV were reported. In terms of the oblique dipole model, this indicates that the contribution of purely axial sources, required to supplement those of the uniform double layer, are quite substantial, i.e., roughly of the same magnitude. However, in experiments carried out by the authors of the oblique dipole model [34] in which the potential distribution generated by a perfused heart contained in a large container was accurately measured, the ratio p_ℓ/p_t required for an optimal fit of the computed to the observed potentials was found to be even much larger (> 15). This discrepancy is probably caused by the experimental conditions of the latter experiments. In particular, the fact that the conductivity of the fluid in the bath containing the heart was much larger than that of the myocardial tissue may have influenced these results.

6.5.3 Fully Anisotropic Models

All source models described in the previous paragraphs, modeling the potential distribution in the myocardium and the surrounding medium, are macroscopic source models, which have in common that they are taken to feed the current that they generate into a medium of isotropic conductivity. All of these fail, in one way or another, to account completely for the potentials observed experimentally. The anisotropy of the sources as expressed in the axial model and in the oblique dipole model solved by no means all problems: anisotropy is reflected in source strength only. To derive any further improvement, the obvious next step is not only to consider the source anisotropy but also the anisotropy in the conductivity of the myocardial tissue, caused by the same fiber structure. There have been several studies aimed at achieving this goal [11, 28, 29, 34, 36, 41]. In particular, the study by Roberts and Scher [29] should be consulted to see how far this approach can lead. One of their conclusions is that the full treatment of anisotropy is definitely needed to account for the potential distribution inside the ventricular wall. It is, however, complicated by the complex architecture of cardiac fibers which are not all neatly lined up in parallel [23, 24]. The more complete handling of this problem is based on the so-called bi-domain theory [4, 37, 41, 42]. This topic is treated in Chap. 8 (Sect. 8.3.2) and in Chap. 7, "Appendix: The EDL and Bidomain Theory".

6.6 Evaluation

When describing the potential in the region outside the heart, for some applications of the uniform double layer, being the simplest of all models, may still be used. This applies certainly to qualitative description of QRS waveforms [9] and also to some quantitative approaches to the genesis of the electrocardiogram [19, 20, 43, 44]. It has been mainly applied to the modeling of ventricular activity. It has been found to serve well as an entry to the inverse computation of the timing

of ventricular activation sequence [43, 45–49]. The latter problem is currently referred to as activation time imaging. At present the accuracy of parameters specifying anisotropy is insufficient for the inclusion of the complexity of the fiber structure in inverse procedures.

This chapter is restricted to the modeling of the sources during depolarization, and in particular to the properties and usefulness of the UDL model. In the next chapter a generalization of this source model is described that provides a means for modeling the sources during repolarization. It may also be used for the modeling of the electric sources of the atria.

References

1. von Helmholtz, H., Ueber einige Gezetze der Verteilung elektrischer Ströme in körperliche Leitern mit Anwendung auf die thierisch-elektrischen Versuche. Pogg. *Ann. Physik und Chemie*, 1853;**89**: 211–233; 353–377.
2. Plonsey, R., *Bioelectric Phenomena*. New York: McGraw-Hill, 1969.
3. Plonsey, R., An extension of the solid angle formulation for an active cell. *Biophys. J.*, 1965;**5**: 663–666.
4. Plonsey, R., and R.C. Barr, *Bioelectricity: A Quantitative Approach*. New York: Kluwer Academic/Plenum Press, 2000.
5. Wilson, F.N., A.G. Macleod, and P.S. Barker, The distribution of action currents produced by the heart muscle and other excitable tissues immersed in conducting media. *J. Gen. Physiol.*, 1933;**16**: 423–456.
6. Spach, M.S., et al., Extracellular potentials related to intracellular action potentials in the dog Purkinje system. *Am. Heart J.*, 1972;**30**: 505–519.
7. van Oosterom, A. and V. Jacquemet, A parameterized description of transmembrane potentials used in forward and inverse procedures, in *International Conference on Electrocardiology*. Gdansk, Poland: Folia Cardiologica, 2005.
8. Scher, A.M. and A.C. Young, Ventricular depolarization and the genesis of the QRS. *Ann. NY Acad. Sci.*, 1957;**65**: 768–778.
9. Holland, R.P. and M.F. Arnsdorf, Solid angle theory and the electrocardiogram: physiologic and quantitative interpretations. *Prog. Cardiovasc. Dis.*, 1977;**19**: 431–457.
10. Spach, M.S., et al., Extracellular potentials related to intracellular action potentials during impulse conduction in anisotropic canine cardiac muscle. *Circulation. Res.*, 1979;**45**: 188–204.
11. Scher, A.M., L.V. Corbin, and A.C. Young, *Cardiac cell-to-cell conduction in electrocardiographic modelling*, in *Measuring and Modelling of the Cardiac Electric Field*. Slowak Acc. Science; Bratislava: VEDA, 1980.
12. van Oosterom, A. and J. Strackee, The Solid Angle of a Plane Triangle. *IEEE Trans. Biomed. Eng.*, 1983;**BME-30**(2): 125–126.
13. Durrer, D. and L.H. van der Tweel, Spread of activation in the left ventricular wall of the dog. *Am. Heart J.*, 1953;**46**: 683–691.
14. Brody, D.A., A theoretical analysis of intracavitary blood mass influence on the heart-lead relationship. *Circ. Res.*, 1956;**IV**: 731–738.
15. van Oosterom, A. and R. Plonsey, The Brody effect revisited. *J. Electrocardiol.*, 1991;**24**: 339–348.
16. Taccardi, B., et al., Effect of myocardial fiber direction on epicardial potentials. *Circulation*, 1994;**90–96**: 3076–3090.
17. van Oosterom, A. and R.T. van Dam, Potential distribution in the left ventricular wall during depolarization. *Adv. Cardiol.*, 1976;**16**: 27–31.
18. van Oosterom, A., Cardiac Potential Distributions. Department of Medical Physics,University of Amsterdam: Amsterdam, The Netherlands, 1978.
19. Ritsema van Eck, H.J., Digital Simulation of Cardiac Excitation and Depolarization. Dalhousie University: Halifax, NS, 1972.
20. Miller, W.T. and D.B. Geselowitz, Simulation studies of the electrocardiogram. I. The normal heart. *Circ. Research.*, 1978;**43**: 301–315.
21. Scher, A.M., Validity of the uniform double layer in the solution of the ECG forward problem. *J. Electrocardiol.*, 1995;**27**(Suppl.): 163–169.
22. van Oosterom, A., Solidifying the solid angle. *J. Electrocardiol.*, 2002;**35S**: 181–192.
23. Greenbaum, R.A., et al., Left ventricular fibre architecture in man. *Br. Heart J.*, 1981;**45**: 248–263.
24. Streeter, D.D.J., et al., Fiber orientation in the canine left ventricle during diastole and systole. *Circ. Res.*, 1969;**24**: 339–347.
25. Scher, A.M., Excitation of the heart, in *The Theoretical Basis of Electrocardiology*, C.V. Nelson and D.B. Geselowitz, Editors. Oxford: Clarendon Press, 1976, pp. 44–69.
26. Oostendorp, T.F., R. MacLeod, and A. van Oosterom, Non-invasive determination of the activation sequence of the heart validation with invasive data. Proc. 19-th IEEE/EMBS Conf, 1997, IEEE-Engineering in Medicine Society. CDROM: pp 335–338.
27. Ramirez, I.F., et al., Effects of cardiac configuration, paddle placement and paddle size on defibrillation current distribution: a finite element model. *Med. Biol. Eng. Comput.*, 1989;**27**: 587–594.
28. Corbin, L.V. and A.M. Scher, The canine heart as an electrocardiographic generator. *Circ. Res.*, 1977;**41/1**: 58–67.
29. Roberts, D.E. and A.M. Scher, Effect of tissue anisotropy on extracellular potential fields in canine myocardium in situ. *Circ. Res.*, 1982;**50**: 342–351.
30. Clerc, L., Directional differences of impulse spread in trabecular muscle from mammalian heart. *J. Physiol.*, 1976;**255**: 335–346.
31. Weidmann, S., Electrical constants of trabecular muscle from mammalian heart. *J. Physiol.*, 1970;**210**: 1041–1054.
32. Plonsey, R. and A. van Oosterom, Implications of macroscopic source strength on cardiac cellular activation models. *J. Electrocardiol.*, 1991;**24/2**: 99–112.
33. Roth, B.J., Electrical conductivity values used with the bidomain model of cardiac tissue. *IEEE Trans. Biomed. Eng.*, 1997;**BME-44**: 326–328.
34. Colli-Franzone, P., et al., Potential fields generated by oblique dipole layers modeling excitation wavefronts in the anisotropic myocardium: comparison with potential fields elicited by

paced dog hearts in a volume conductor. *Circ. Res.*, 1982;**51**: 330–346.
35. Taccardi, B., et al., ECG waveforms and cardiac electric sources. *J. Electrocardiol.*, 1996;**29S**: 98–100.
36. van Oosterom, A., Anisotropy and the double layer concept, in *Progress in Electrocardiology*, P.W. Macfarlane, Editor. Tunbridge Wells: Pitman Medical, 1979, pp. 91–97.
37. Henriquez, C.S., Simulating the electrical behavior of cardiac tissue using the bidomain model. *Crit. Rev. Biomed. Eng.*, 1993;**21**(1): 1–77.
38. Kléber, A.G. and C.B. Riegger, Electrical constants of arterially perfused rabbit papillary muscle. *J. Physiol.*, 1987;**385**: 307–324.
39. Scher, A.M., et al., Spread *of electrical activity through the wall of the ventricle*. *Cardiovasc. Res.*, 1953;**1**: 539–547.
40. van Oosterom, A., Cell models – macroscopic source descriptions, in *Comprehensive Electrocardiology*, P.W. Macfarlane and T.T.V. Lawrie, Editors. Oxford: Pergamon Press, 1989, pp. 155–179.
41. Muler, A.L. and V.S. Markin, Electrical properties of anisotropic nerve-muscle syncytia-II, spread of flat front of excitation. *Biophysics*, 1977;**22**: 536–541.
42. Gulrajani, R.M., *Bioelectricity and Biomagnetism*. New York: Wiley, 1998.
43. Cuppen, J.J.M. and A. van Oosterom, Model studies with the inversely calculated isochrones of ventricular depolarization. *IEEE Trans. Biomed. Eng.*, 1984;**BME-31**: 652–659.
44. van Oosterom, A. and T.F. Oostendorp, ECGSIM: an interactive tool for studying the genesis of QRST waveforms. *Heart*, 2004;**90**(2): 165–168.
45. Greensite, F., Y.J. Qian, and G.J.M. Huiskamp, Myocardial activation imaging: a new theorem and its implications, in Basic and Applied Biomedical Engineering, Building blocks for health care. *Proceedings of the 17th Annual International Conference of the IEEE Engineering in Medicine and Biology Society*, 1995.
46. Huiskamp, G.J.M. and A.V. Oosterom, Forward electrocardiography based on measured data, in Images of the Twenty-First Century. *Proceedings of the Annual International Conference of the IEEE Engineering in Medicine and Biology Society*, Y.K.A.F.A. Spelman, Editor. New York: IEEE Publishing Services, 1989, pp. 189–190.
47. Huiskamp, G.J.M., et al., Invasive confirmation of the human ventricular activation sequence as computed from body surface potentials. in *Computers in Cardiology '92*. Los Alamitos, CA: IEEE Computer Society Press, 1993.
48. Huiskamp, G.J.M., et al., The depolarization sequence of the human heart surface computed from measured body surface potentials: confrontation with invasive measurements. in *Electrocardiology'88*. Wiesbaden: Elsevier, 1989.
49. Modre, R., et al., Atrial noninvasive activation mapping of paced rhythm data. *J. Cardiovasc. Electrophysiol.*, 2003;**13**: 712–719.

7 The Equivalent Double Layer: Source Models for Repolarization

A. van Oosterom

P. W. Macfarlane, A. van Oosterom, O. Pahlm, P. Kligfield, M. Janse, J. Camm (eds.), *Comprehensive Electrocardiology*, DOI 10.1007/978-1-84882-046-3_7,

7.1 Introduction

The modeling of the electric current sources during depolarization by means of the uniform double layer (UDL) is described in general terms in Chap. 5, and in greater detail in Chap. 6. It is linked to the electrophysiology of wave fronts propagating through the myocardium. Some decades ago [1, 2], studies appeared that exploited the equivalence between the actual double layer at the wave fronts and a source description on the heart surface, the surface bounding the myocardium. This source description has been found to be very effective in the inverse determination of the timing of depolarization on the basis of observed body surface potentials (Chap. 9), a method now commonly referred to as activation time imaging.

Around the same period [3], the development of a source model started in which the equivalent cardiac electric generator is expressed in terms of the electric potentials on a surface encompassing the myocardium, similar to the pericardium. In most related studies the surface involved is referred to as the epicardium. Such voltage sources are based on the theoretical unique one-to-one relationship between the voltage on the surface bounding a volume conductor and those on some interior surface, on condition that the surface is *closed* and that no primary sources are present in between. All active sources are assumed to lie within the inner surface. Inverse methods based on this relationship aim at obtaining a "closer look" at the sources without assuming any a priori knowledge about the nature of these sources (Chap. 9).

Both source models can be classed as being equivalent surface source models (ESS). In the case of the extended UDL variant the current sources are of the double layer type, in the second approach the electric current sources stem from a specification of the potential distribution on the epicardium.

This chapter describes the properties of the first source model: the equivalent current double layer surface source, which will be referred to here as the EDL model. This model has the potential of describing the cardiac electric generator during the depolarization phase (QRS segment) as well as during the repolarization phase of the cardiac cycle (STT segment), both in a manner that is related to the underlying electrophysiology. As such, it has been claimed to be promising in serving to explain STT wave morphology [4].

There is a direct link between the UDL and the EDL source model, which is based on the solid angle formulation, as is explained in Sect. 7.2. Next, in Sect. 7.3 a recent development of the theory is described, which justifies the handling of the sources during repolarization by means of the EDL. The development is based on a theoretical formulation derived by Geselowitz [5, 6]. The section describes only the most essential parts of this development. A more complete recapitulation of the theory is presented in Appendix. In Sect. 7.4 some types of STT wave morphology are shown based on the EDL source. Sect. 7.5 lists and discusses some of the major inferences on the STT wave forms as generated on the basis of the model. Finally, Sect. 7.6 discusses some potentials and limitations of the EDL source model.

7.2 Linking the UDL to the EDL

The direct link between the UDL source for modeling the sources at the wave fronts to the equivalent representation on the surface S_h stems directly from the properties of the solid angle $\boldsymbol{\Omega}$ appearing in the fundamental expression that links wave front shape and extent to the resulting potential field $\Phi(\vec{r}')$ in the infinite medium,

$$\Phi(t;\vec{r}') = V_D \frac{\Omega(t)}{4\pi} \tag{7.1}$$

This is the expression discussed in Sect. 6.3.1 (6.15), here with the temporal behavior of the solid angle wave front shown explicitly. In the EDL formulation, the surface S_h considered is the closed surface encompassing the entire myocardium; for the ventricles: the epicardium and endocardium, as well as their connection at the base. The essence is explained by using the diagrams shown in Fig. 7.1.

We first consider panel A. It depicts the situation where, following a stimulus at the endocardium, the shaded region has been depolarized. The wave front carrying the UDL source is indicated by the heavy solid line. In 3D space its shape is as depicted in Fig. 6.7. The front is denoted by S_{UDL}. The field points are taken to lie outside the myocardium. For such field points the potential field generated by UDL sources on S_{UDL} is exactly the same as that generated by an equivalent UDL source, having the same strength as the one at the wave front, placed on the segment of the endocardial surface,

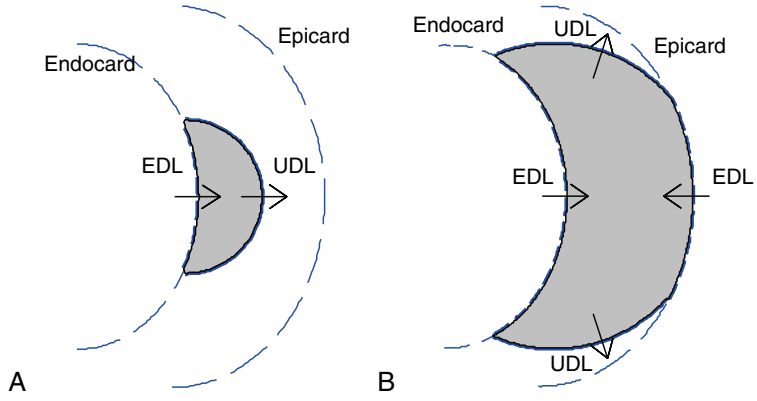

Figure 7.1

Schematic diagram illustrating the link between UDL and EDL. Shaded region represents depolarized myocardium; arrows denote polarity of UDL and EDL double strength. Heavy solid lines and dotted lines represent UDL and EDL locations, respectively. *Panel A*: Early stage of depolarization following an endocardial stimulus. *Panel B*: later stage of depolarization; wave front previously broken through at the epicardium.

S_{endo}, bounding the depolarized region (heavy, dashed line). This follows from the fact that for an exterior observation point both surfaces subtend the same solid angle. The same holds true for all other wave fronts lying entirely within the myocardium that have a different shape, while having an identical intersection with the endocardium: the border of the wavefront at S_{endo}. Hence, for the external field points, the UDL source at the wave front may be replaced by an equivalent (UDL type) source at S_{endo}. In Fig. 7.1A, this source is marked by the arrow EDL. Note that it points into the depolarized region, whereas the UDL source at the wave front points away from that region.

Next, the situation depicted in Panel B is treated. A break-through of the wave front has occurred and its shape may be similar to that depicted in Fig. 6.9: the de-capped hemisphere. In Fig. 7.1B the direction of the UDL sources at the wave front is identified by the two arrows labeled UDL, as always, pointing away from the depolarized region. Let the closed surface bounding the depolarized region be S_{D}. The latter is the union of the surface S_{UDL} of the wave front, its intersection with the endocardium S_{endo}, and its intersection with the epicardium, S_{epi}:

$$S_{\text{D}} = S_{\text{UDL}} \cup S_{\text{endo}} \cup S_{\text{epi}}$$

As an entry to the introduction of the EDL, we consider the effect of the placing on S_{D} of an extra, virtual double layer with strength V_{Dvir}. Being a closed surface, this does not generate an external field, and for external field points we find, based on (2.47) of Sect. 2.2.12 and on (7.1),

$$4\pi\,\Phi(\vec{r}\,') = V_{\text{D}}\Omega(S_{\text{UDL}}) + V_{\text{Dvirt}}\left(\Omega(S_{\text{UDL}}) + \Omega(S_{\text{endo}}) + \Omega(S_{\text{endo}})\right),$$

an expression that holds true for any value of V_{Dvir} In particular, by choosing $V_{\text{Dvirt}} = -V_{\text{D}}$, the two terms involving $\Omega(S_{\text{UDL}})$ cancel, and so is found that

$$\Phi(\vec{r}\,') = \frac{1}{4\pi}V_D\Omega(S_{\text{UDL}}) = \frac{-1}{4\pi}V_D\left(\Omega(S_{\text{endo}}) + \Omega(S_{\text{epi}})\right) \tag{7.2}$$

By once more using (2.47) and defining $S_{\text{dep}}(t)$ as $S_{\text{endo}}(t) \cup S_{\text{epi}}(t)$, representing the segment of the total heart surface S_{h} overlaying tissue that has been depolarized prior to the time t considered in Fig. 7.1b, it can be seen that a straightforward generalization of (7.2) reads

$$\Phi(t,\vec{r}\,') = \frac{-1}{4\pi}V_D\Omega(S_{\text{dep}}(t)) \tag{7.3}$$

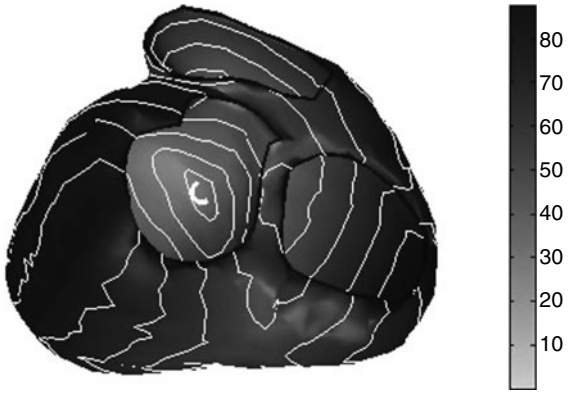

Figure 7.2

Activation sequence spreading over the S_h of a human ventricle is shown by means of the isochrones of the local activation time τ. The heart is depicted in a superior-right-posterial view. The activation is initiated in the middle of the left ventricular aspect of the septum (small circle). The sequence shown propagates at a constant velocity of 1.1 m/s through the myocardial tissue. The isochrones are drawn at 10 ms intervals.

The minus sign relates to the convention of using the outward normal of S_h in the definition of the solid angle (Sect. 2.2.12), as well as to the change in the direction of the virtual double, as expressed by the arrows labeled EDL shown in Fig. 7.1b. Equation (7.3) can be seen to cover likewise the situation depicted in Fig. 7.1a.

An expression that is mathematically equivalent to (7.3) reads

$$\Phi(t,\vec{r}\,') = \frac{-1}{4\pi} V_D \int_{S_h} H\left(t - \tau(\vec{r})\right)\, \mathrm{d}\omega(\vec{r}), \tag{7.4}$$

in which the function H denotes the Heaviside step function expressed on S_h, which is zero if $t < \tau(\vec{r})$, the time of local depolarization, and equal to one otherwise. It describes the successive switching on of the contribution of elementary double layer source elements on S_h at location $\vec{r}$ at time instants $\tau(\vec{r})$. During normal propagation, all parts of S_h are successively depolarized: depolarization spreads over S_h like an oil-slick over water. Correspondingly, at the end of depolarization we have $H = 1$ over the entire closed surface S_h. At this time the integral represents the solid angle of a closed surface for an exterior field point, which is zero (2.50), as is the external field. An example of the propagation over the ventricles following a single stimulus in the middle part of the septum facing the left ventricular cavity is presented in Fig. 7.2. The isochrones shown are drawn at equal distances from the stimulus site while traveling through the myocardium [7]. At any moment in time $t = \tau(\vec{r})$ the source strength H in the region ahead of any isochrone τ is zero; at that same moment it is equal to one in the area previously depolarized, i.e., having lower values τ.

7.2.1 Discussion

If the transmural spread of the depolarizarion wave is known, the UDL source present at the wave front and its representation by the UDL source on the heart surface S_h generate exactly the same exterior potential fields, as is shown in the preceding section. For the evaluation of the forward problem there can, hence, be no advantage in using either expression (7.1) or its equivalent, variant (7.4). However, for the inverse problem of estimating the timing of depolarization from observed field potentials the situation is different. As discussed in Sect. 7.1, within the context of the UDL source, the potential fields generated by different wave fronts that have the same intersection with the surface S_h are identical. As a consequence, the actual location of the wave front inside the myocardium can not be estimated on the basis of observed potential fields.

In contrast, by using the boundary S_h as the location of the UDL sources as in (7.4), a unique inverse exists [8]. The uniqueness holds true provided that the surface S_h is known. It forms the most essential prior information required for solving the associated inverse problem (Chap. 11). From the introduction of (7.4) onward, magnetic resonance imaging has been used as the technique for documenting S_h [1].

Equation (7.4) expresses the most basic variant of the equivalent double layer source EDL: a double layer distribution over the surface S_h that has zero strength until the local region depolarizes, after which the local strength is one. An alternative formulation reads

$$\Phi(t,\vec{r}\,') = \int_{S_h} A(\vec{r}\,',\vec{r})\, S(t,\vec{r})\, \mathrm{d}S(\vec{r}), \tag{7.5}$$

where $S(t;\vec{r}) = H\,(t - \tau(\vec{r}))$, and the double layer strength V_D as well as the remaining variables of (7.4) are represented by the transfer from sources at location $\vec{r}$ to the potential at the field point $\vec{r}\,'$: $A(\vec{r}\,',\vec{r})\ \mathrm{d}S(\vec{r})$. The function $S(t,\vec{r})$ is dimensionless, expressing the spatio-temporal character of the EDL source. An overall scaling factor, specifying its nature (elementary current dipole density) and overall strength, is incorporated in the transfer function $A(\vec{r}\,',\vec{r})$.

7.3 Generalization of the EDL

The EDL source as described in the previous section is an equivalent expression for the UDL sources at the propagation wave fronts during depolarization. The effect of repolarization, which starts right from the moment of the first local depolarization, is disregarded. As a consequence, as is described above, after depolarization is complete, no external potential field remains. In the ECG this is taken to be the moment at the end of the QRS complex, the J point. However, although in the normal ECG the potential differences observed on the thorax around the J point are small, they are invariably non-zero. A more complete model of the sources of the ECG would therefore require the inclusion of the repolarization phenomena. This holds all the more true since the time interval following the J point, the STT segment, has been long recognized as yielding highly relevant diagnostic information. The generalization of the EDL source described in the next section provides a valuable model for describing (modeling) the current sources of the ECG throughout the entire cardiac cycle.

7.3.1 Linking EDL Source Strength to Transmembrane Potentials

In this section the generalization of the EDL is described in its most basic form, using the general character of impressed current density of individual cells and the various notations introduced in Chap. 2. The derivation shown here is an alternative to the one presented by Geselowitz [5, 6]. A more complete treatment is included in the appendix to this chapter.

We start from the field of an individual cell as discussed in Sect. 6.3.1, in particular from (6.1), which is recapitulated here as

$$\Phi(\vec{r}\,') = \frac{1}{4\pi\sigma_e} \int_S -\left(\sigma_i\Phi_i - \sigma_e\Phi_e\right) \mathrm{d}\omega \tag{7.6}$$

The surface S is the cell membrane (Fig. 6.1). By reintroducing the notation $M_S = -\left(\sigma_i\Phi_i - \sigma_e\Phi_e\right)$ for the strength of the equivalent dipole surface density directed along the outward normal of S (6.6), and using

$$\mathrm{d}\omega = \frac{\vec{R}}{R^3} \bullet \mathrm{d}\vec{S} = \nabla\frac{1}{R} \bullet \mathrm{d}\vec{S}$$

(2.48 and 2.33), we see that

$$\Phi(\vec{r}\,') = \frac{1}{4\pi\sigma_e} \int_S M_S \nabla\frac{1}{R} \bullet \mathrm{d}\vec{S} \tag{7.7}$$

Next, we apply Gauss' law (2.26) to the integral on the right. For the (virtual) vector field

$$M_S(\vec{r})\nabla\frac{1}{R(\vec{r})}$$

this yields

$$\int_S M_S \nabla \frac{1}{R} \bullet \mathrm{d}\vec{S} = \int_V \nabla \bullet \left(M_S(\vec{r}) \, \nabla \frac{1}{R(\vec{r})} \right) \mathrm{d}V = \int_V \nabla \bullet M_S(\vec{r}) \, \nabla \frac{1}{R(\vec{r})} \, dV + \int_V M_S(\vec{r}) \, \nabla^2 \frac{1}{R(\vec{r})} \, \mathrm{d}V \tag{7.8}$$

The second integral on the right is zero, because R is non-zero for exterior field points $\vec{r}'$.

Equation (2.161); the integration is over the internal source locations within the cell volume V. With the remaining first integral applied to (7.7) we see that

$$\Phi(\vec{r}') = \frac{1}{4\pi\sigma_e} \int_S M_S \, \nabla \frac{1}{R} \bullet \mathrm{d}\vec{S} = \frac{1}{4\pi\sigma_e} \int_V \nabla \bullet M_S(\vec{r}) \, \nabla \frac{1}{R(\vec{r})} \, dV, \tag{7.9}$$

which identifies $\nabla \bullet M_S(\vec{r})$ as a (virtual) volume source density throughout cell volume V (Sect. 2.5.3).

With the potential field generated by a single cell now being expressed by (7.9), we may compute the potential for field points outside the myocardium by taking the volume V to represent the entire myocardial tissue. However, this volume also includes the interstitial space. This may be accounted for by introducing a local volume fraction $0 \le f_v(\vec{r}) \le 1$, the fraction of space occupied locally by the cell volume. For densely packed myocardial cells this fraction is of the order of 0.8.

Inserting this (scalar) factor in (7.9) and reversing the derivation along (7.7)–(7.9) leads to the interpretation of surface S in (7.7) as representing the surface bounding the myocardium. The expression for the external potential field then reads

$$\Phi(\vec{r}') = \frac{1}{4\pi\sigma_e} \int_{S_h} f_v(\vec{r}) M_S(\vec{r}) \, \mathrm{d}\omega(\vec{r}', \vec{r}) \tag{7.10}$$

Note that both the volume fraction and the virtual double layer source density in this expression relate to their values at S_h (only). In the applications of this expression shown in the next section, the approximation $M_S = -(\sigma_i \Phi_i - \sigma_e \Phi_e) \approx -\sigma_i V_m$ is used, leading to

$$\Phi(\vec{r}') = \frac{-1}{4\pi\sigma_e} \int_{S_h} f_v \sigma_i V_m \mathrm{d}\omega \tag{7.11}$$

Finally, if σ_i and f_v are assumed to be uniform over S_h, and by reintroduction of the temporal nature of the transmembrane potential, we have

$$\Phi(t, \vec{r}') = \frac{-f_v \sigma_i}{4\pi\sigma_e} \int_{S_h} V_m(t, \vec{r}) \, \mathrm{d}\omega(\vec{r}', \vec{r}), \tag{7.12}$$

which may be cast in the same form as in (7.5) by writing

$$\Phi(t, \vec{r}') = \int_{S_h} A(\vec{r}', \vec{r}) V_m(t, \vec{r}) \, dS(\vec{r}), \tag{7.13}$$

with all scaling factors, including the negative sign, now absorbed in the (solid angle) transfer function A. The overall scaling factor used in the sequel is taken such that, by assigning a shape to V_m that is identical to that of the function S used in Sect. 2.1 in (7.5) during depolarization, the potential field resulting from using (7.13) is the same as the one based on (7.5). The value of the scaling factor used in the sequel corresponds to taking the effective double layer strength inside a medium of unit conductivity to be 40 mV, an overall value previously deduced from experimental studies [9–11].

7.3.2 Discussion

Equation (7.13) defines the spatio-temporal potentials in the infinite medium. For a bounded medium, the same basic formulation can be used. In this situation the potential field can be found by applying the spatial linear filter expressing

all volume conductor effects, as is explained in Sect. 2.6.4.3. This yields as the final, most direct expression for the potential field of the EDL

$$\Phi(t,\vec{r}\,') = \int_{S_h} B(\vec{r}\,',\vec{r})\, V_m(t,\vec{r})\, dS(\vec{r}), \tag{7.14}$$

with $B(\vec{r}\,',\vec{r})$ the linear function expressing the full transfer between EDL source elements around $\vec{r}$ on S_h to the potential at field points $\vec{r}\,'$ inside the bounded medium external to S_h. Note that this also handles the situation where the conductivity outside S_h has a conductivity $\sigma_o \neq \sigma_e$.

If either f_v or σ_i are non-uniform over S_h, (7.11) needs to be used instead of (7.12), which requires a full specification of these variables.

Interestingly, within the various assumptions implied in deriving (7.14), the EDL source model indicated that any sources *within* S_h do not directly influence the external potential field. However, the activity of such internal sources does affect the propagation of all depolarization waves that may be simultaneously propagating within the myocardium and thus the wave form and timing of the sources at S_h. The same applies to the subsequent repolarization process.

The effectiveness of the EDL source model in describing ECGs as well as electrograms, both during depolarization and repolarization, is illustrated in the next section.

7.4 ECG Signals Generated by the EDL

The properties of the EDL source model are illustrated here in an application to simulating ECG wave forms on the thorax and electrograms on the heart surface S_h. As discussed in Sect. 7.3.2 (7.14), this requires the computation of the transfer function $B(\vec{r}\,',\vec{r})$ describing the volume conduction properties, the surface S_h carrying the EDL and the spatio-temporal transmembrane potential over S_h. Simulations of this type have been described in the literature both for the ventricles [12, 13] and for the atria [14]. Here, an application to ventricular activity is shown. The evaluation of (7.14) was carried out numerically, in which the field potentials transfer $\Phi(t,\vec{r}\,')$, the transfer matrix $B(\vec{r}\,',\vec{r})$ and the $V_m\ (t,\vec{r})$ were represented by matrices $\mathbf{\Phi}$, $\mathbf{B}$ and $\mathbf{V}_m$, respectively. The numerical variant of (7.14) then reads

$$\mathbf{\Phi} = \mathbf{B}\mathbf{V}_m, \tag{7.15}$$

an expression similar to (5.12) in Sect. 5.9.4. As discussed in that same section, the sum of all elements of any row of matrix $\mathbf{B}$ equals zero.

7.4.1 Source Specification

The shape of S_h is shown in Fig. 7.2. It was obtained from magnetic resonance images (MRI) taken from a healthy male subject. The image shown is that of a triangulated version of S_h, specified by N = 1,500 evenly distributed nodes. Realistic transmembrane potentials were assigned to each node n. Their wave forms are based on an analytical function involving logistic curves [15]. The parameters of this function were fixed, apart from a parameter δ_n specifying, for each individual node n, the local timing of the maximum upslope during depolarization, and a parameter ρ_n specifying the timing of the maximal downslope during repolarization. The difference $\alpha_n = \rho_n - \delta_n$ represents the local duration of the transmembrane potential, a measure similar to the activation recovery interval (ARI) introduced in the work of Haws and Lux [16]. The variety of wave forms of the assigned TMPs is illustrated in Fig. 7.3, by showing the TMPs of the nodes having maximum δ_n, ρ_n and α_n values, as well as of those having minimum δ_n, ρ_n and α_n values. Maps of local depolarization times δ_n and repolarization times ρ_n on the heart surface S_h used for the demonstration of the properties of the EDL source model are shown in Fig. 7.4. The numerical expression of the entire source configuration is that of a matrix $\mathbf{V}_m$. Its N = 1,500 rows represent the individual TMPs at all nodes on S_h. Each row expresses a TMP sampled at 1 ms intervals, comprising T = 500 samples. The descriptive statistics of the basic parameters of all 1,500 nodes are as shown in Table 7.1.

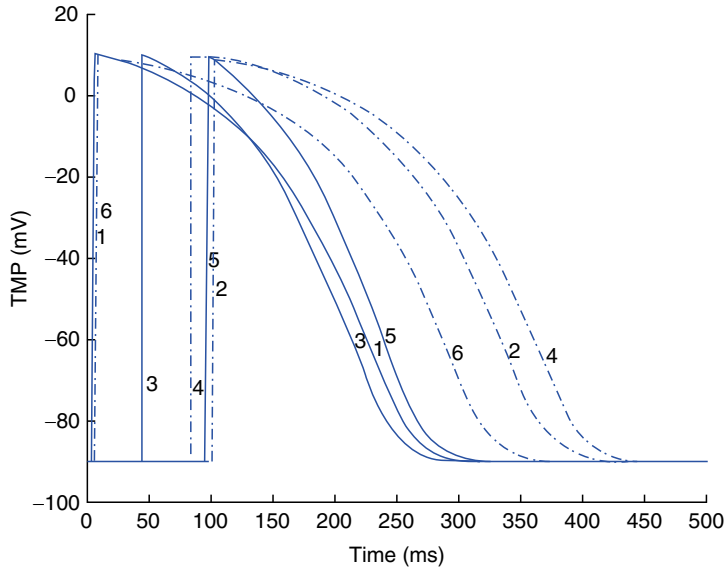

Figure 7.3

Stylized transmembrane potentials of six nodes on S_h. Labels shown to the right of the traces near maximum upslope (timing δ_n), maximal downslope (timing ρ_n) of the TMPs. Labels refer to the TMPs with (1) earliest δ_n, (2) latest δ_n, (3) earliest ρ_n, (4) latest ρ_n, (5) shortest α_n, and (6) longest α_n.

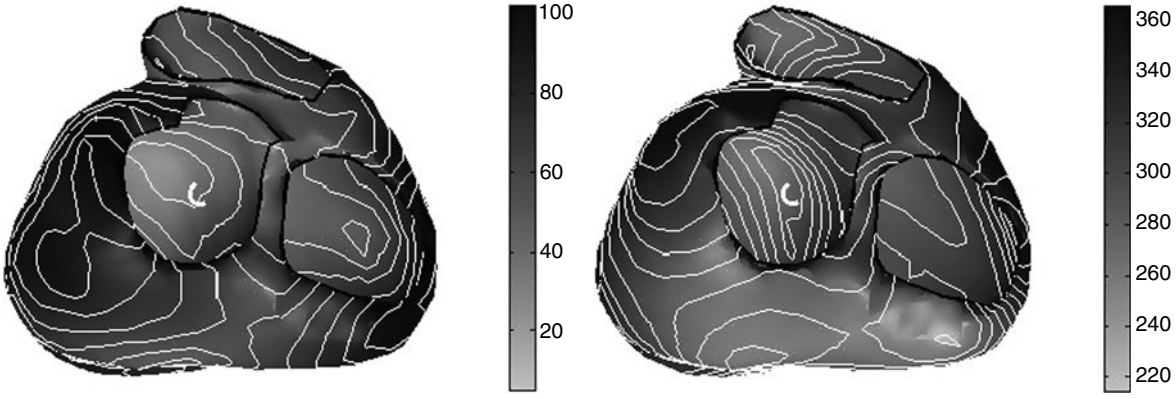

Figure 7.4

***Left*: Timing of depolarization times δ_n of 1,500 nodes on S_h of a human ventricle, used in EDL based simulation of QRST wave forms. *Right*: corresponding values for the local repolarization times ρ_n. The isochrones are drawn at 10 ms intervals. The heart is depicted in a superior-right-posterial view. The small semicircle marks the site on the septum where depolarization was earliest.**

7.4.2 The Transfer Function B

The numerical expression of $B(\vec{r}', \vec{r})$ (7.14), the linear function expressing the full transfer related to the volume conduction effects inside the thorax, can be represented by a matrix **B**. Each of its elements expresses the transfer between an individual EDL source element at node n of S_h to the potential at any of L locations (field points) of interest. These

Table 7.1

TMP parameters of all 500 nodes on S_h

	Mean	SD	Min	Max	Range (max–min)
dep δ (ms)	52.2	19.7	4.95	102	97
rep ρ (ms)	276	21.7	214	367	152
ARI α (ms)	225	24.4	142	285	143

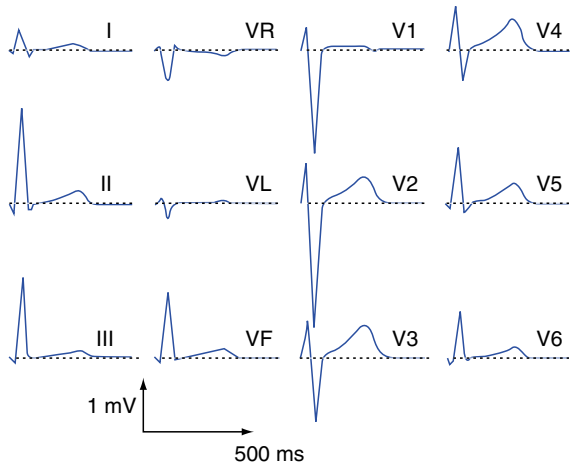

Figure 7.5

Superposition of measured standard 12-lead ECG (dash-dot line) and the EDL based simulations (solid lines). The high quality of the simulated signals causes the traces in the two line styles to be almost indistinguishable. Note that the signals at the extremity electrodes, VL, VR and VF, are shown in an unaugmented scaling, which emphasizes their equal footing with the precordial signals V1–V6, all nine being referred to the same reference (WCT).

matrix elements were computed by using the boundary element method (Sect. 2.6.4.3) applied to an MRI documentation of the geometry of thorax, lungs and the blood filled cavities of the subject for whom the EDL properties are discussed in this chapter. These compartments constitute the inhomogeneous representation of the most relevant, significant inhomogeneities inside the thorax.

For any desired set of L locations (field points) the EDL based wave forms of potentials on the thorax or any other set of field points outside the myocardium, such as electrograms on endocardium or epicardium, can be computed from (7.15).

The matrix $\mathbf{\Phi}$ representing the simulated potentials has L rows (L wave forms), specified at T subsequent time instances. Dedicated versions of the transfer matrix $\mathbf{B}$ may be computed for the field points of interest, lying, e.g., on the thorax surface or on the surface S_h. In the following two sections examples are shown for ECGs and electrograms.

7.4.3 Standard 12-Lead ECG

The matrix $\mathbf{\Phi}$ of the EDL based simulated potentials at the electrode positions of the standard 12-lead ECG is shown in Fig. 7.5. The simulated signals are superimposed on the signals measured on the subject studied.

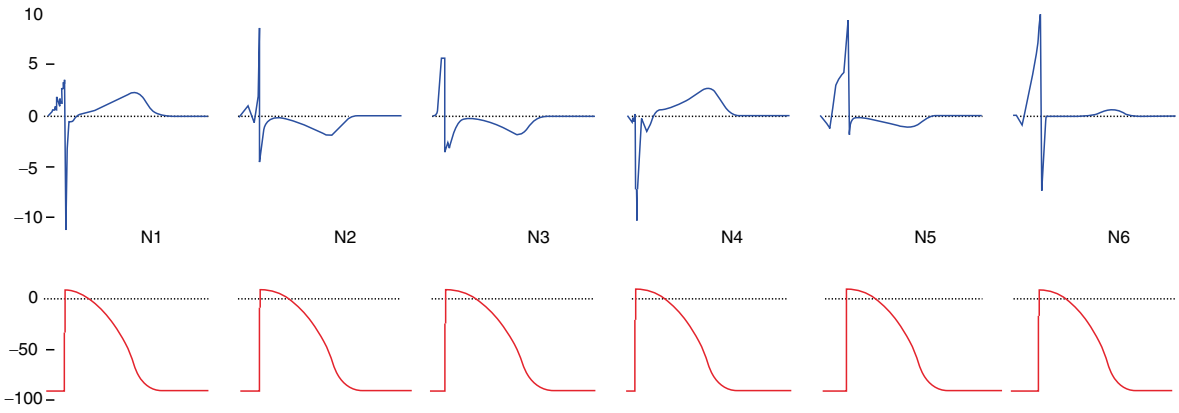

Figure 7.6

***Upper traces*: EDL based electrograms at six nodes of S_h. *Lower traces*: TMPs (local EDL source strength) at these nodes. Note the fast downward deflection in the electrograms, with their timing coinciding with the fast upstroke of the TMPs. Time interval: 500 ms; vertical scale in mV.**

Table 7.2

TMP parameters and electrogram features of 6 of the 1,500 nodes on S_h shown in Fig. 7.6

	node					
	N1	N2	N3	N4	N5	N6
Location	epi RV	endo RV	septal RV	septal LV	endo LV	epi RV
δ_n (ms)	59	60	34	25	86	82
ρ_n (ms)	268	287	273	240	294	284
α_n (ms)	208	227	239	215	208	202
Amplitude fast negative deflection electrograms (mV)	14.7	13.2	9.22	10.7	11.2	18.4
Apex T wave electrogram (mV)	2.24	–1.89	–1.83	2.71	–1.16	0.576

7.4.4 Endocardial and Epicardial Electrograms

EDL based electrograms simulated at six of the 1,500 nodes on S_h are illustrated in Fig. 7.6. The nodes were selected along the intersection of a straight line, crossing the myocardium, from N1 (epicardial node at the free wall of the right ventricle) to N6 (epicardial node on the free wall of the left ventricle). The remaining four nodes are: node N2: the RV endocardial node closest to node N1, node N3: the node at the intersection of the line and RV aspect of the septum, node N4: the node at the intersection of the line and the LV aspect of the septum, node N5: the node on the endocardium of the LV closest to N6. The potential reference was the mean of the potentials at all nodes. The TMP parameters of the six nodes and some of the features of the electrograms are listed in Table 7.2.

7.4.5 Discussion

The realism of the signal wave forms shown in Figs. 7.5 and 7.6 demonstrates the power of the EDL source model for modeling electrocardiographic signals. Being based on apparently minor differences in the TMP wave forms, the morphology of the signals arises from the geometry of the myocardium (S_h), the timing of depolarization and repolarization at S_h and the transfer expressing volume conduction effects.

The high correlation between the simulated and the measured potentials is no guarantee that the source model as such is valid. A proper validation would also require the various model components to be realistic. The major emphasis here lies on the realism of the timing of depolarization δ_n and repolarization ρ_n. The timing used in the simulations, shown in Fig. 7.4, are based on an inverse procedure, similar to the one described in [17]. The realism of the resulting depolarization times has been established by comparing them with those found in invasive studies, notably the study by Durrer et al. published in 1970 [18]. The timing of repolarization has, similarly, been derived from a dedicated adaptation of the inverse procedure [13]. Here no complete set of reference data derived from invasive measurements is available, but the sparse data that is available seems to agree with the global nature of the isochrones shown in the right panel of Fig. 7.4 [19, 20]. For a more complete discussion of this topic, see [4].

The wave forms of electrograms on the epicardium, with the heart placed inside an infinite homogeneous medium, were simulated by Simms and Geselowitz. The surface source model implied is the EDL. The global morphology and magnitudes of their results, documented during depolarization only, are in full agreement with those described for the spherical shell discussed in Chap. 6. In the study by di Bernardo and Murray of the genesis of the T wave [21], the implied source model was also the EDL. The examples shown here relate to ventricular activity only. However, the application of this source model to the electric activity of the atria has also proved to be effective [14].

7.4.6 T Waves as Explained in Standard Text Books

Most ECG textbooks include some notions related to the genesis of the T wave. Correct as these may be in a general sense, they do not do justice to the complexity of the problem. In this chapter the full spatio-temporal character of the sources is represented by an equivalent surface source situated at the boundary of ventricular tissue. The local source strength is assigned the characteristic wave form of the transmembrane potentials of ventricular muscle cells. The simulated potentials shown in Figs. 7.5 and 7.6 were derived from a linear combination of a large number of assigned transmembrane potentials.

In contrast, in ECG textbooks the morphology of the T wave is explained by subtracting just two typical transmembrane wave forms. Differences in timing in agreement with the general concepts of electrophysiology are assigned to it [22]. An example of this approach is shown in Fig. 7.7. In the upper traces, paired TMP potential wave forms of the type shown in Fig. 7.6 are depicted. The solid lines were assigned all upstrokes at $\delta = 30$ ms; the timing of the maximal downslope is at $\rho = 290$ ms. The dash-dot lines all have their upstroke at $\delta = 40$ ms, and ρ values, from left to right: 250, 270, 290, 310 and 330 ms.

The lower traces depict the differences between the paired electrograms shown above them (solid traces minus dash-dot traces). These may be likened to the wave forms of either electrograms or basic ECGs. Here we will refer to these wave forms as electrograms.

1. As a consequence of the applied subtraction, the amplitude of their "QRS" complexes would be 100 mV, a value that is clearly unrealistic. In practice the involved scaling depends on the volume conductor configuration, in particular the distance between source and field points.
2. For the TMPs shown, the baseline of the electrograms is zero: a common resting potential of the TMPs does not become expressed.
3. The sign of the T wave reflects the sign of the difference between the repolarization times of the two TMPs: $\Delta\rho = \rho_{solid} - \rho_{dash\text{-}dot}$. Similarly, $\Delta\delta = \delta_{solid} - \delta_{dash\text{-}dot}$ corresponds to the sign of the "QRS." This results in QRS and T waves having the same polarity (concordant signs) if the signs of $\Delta\rho$ and $\Delta\delta$ as defined above, are the same. Non-concordant signs result if the order of the sequence of depolarization is the same as that of repolarization.
4. The timing of the apex of the T wave shown is [268 280 X 299 307], which is approximately equal to the mean of the repolarization times ρ_{solid} and $\rho_{dash\text{-}dot}$. The X corresponds to the situation of the third pair: since both TMP repolarize simultaneously, no T wave is generated.
5. The absolute value of apex T is proportional to $\Delta\rho$. In particular, if $\Delta\rho = 0$ the amplitude of the T wave is zero.

In basic textbooks on electrocardiography the justification for the approach of subtracting two slightly different TMPs and taking the difference to represent ECG morphology is usually not discussed. The EDL theory can be used for this purpose, while also pinpointing the limitations of the simple approach, as is shown below.

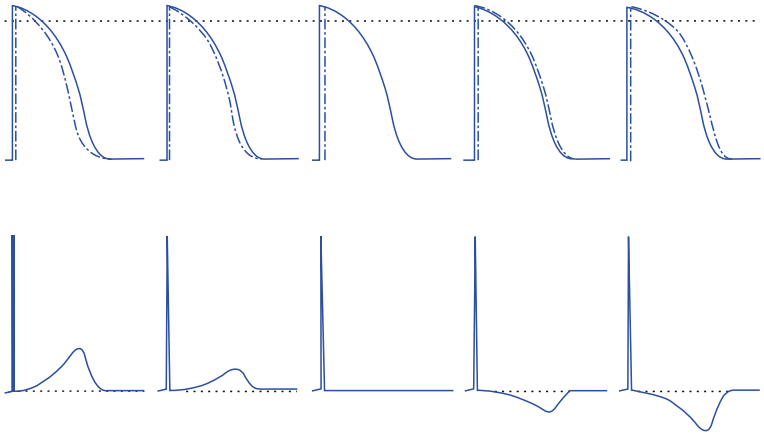

Figure 7.7

***Upper traces*: TMP wave forms similar to the ones shown in Fig. 7.6; solid lines: timing upstroke: 30 ms for all five traces from left to right; timing maximal downslope 290 ms for all traces. Dash-dot lines timing upstroke: 40 ms for all five traces; timing maximal downslope (from left to right) 250, 270, 290, 310 and 330 ms. *Lower traces*: subtraction of the respective two TMPs (solid traces – dash-dot traces) shown above. Time interval: 500 ms; Upstroke TMP's from −90 to +10 mV; Vertical scale of lower traces in arbitrary units. Dotted lines drawn at zero level.**

The subtraction method, resulting in an electrogram $\phi_\ell(t)$ can be formulated as

$$\phi_\ell(t) = 1 \times V_{\mathrm{m},1}(t) + (-1) \times V_{\mathrm{m},2}(t), \tag{7.16}$$

which expresses the electrogram as a linear combination of two transmembrane potentials. The weights of the linear combination are 1 and −1, respectively. This, in turn, can be written as

$$\mathbf{\Phi} = \mathbf{B}\mathbf{V}_{\mathrm{m}}, \tag{=(7.15)}$$

with the matrix **B** here being the row vector [1 −1]. The motivation for highlighting this parallel is that, as is evident, the sum of the elements of the row is zero, similar to that which holds true for volume conduction effects acting on transmembrane potentials derived sources (Sect. 5.9.4), as is the EDL.

In some studies, electrograms were considered in their relationship to two subtracted transmembrane potentials [23, 24]. The signals were observed on a small part of myocardial tissue (referred to as a wedge) placed in a small perfusion chamber (bath). The potential difference was recorded between two electrodes in the bath, each placed at some distance from two opposing sides of the tissue, the endocardial side and the epicardial side. This signal was referred to as the ECG. In addition, two intracellular traces were shown, one recorded at the endocardial and one at the epicardial aspect of the tissue. The question here is: what type of source model can be proposed to justify this procedure? How could a local transmembrane potential act as the source for an external electrogram?

This question can be answered on the basis of by the EDL. In the study, the sources were assumed to lie on the endocardial aspect, S_1, and on the epicardial aspect, S_2, of the surface S bounding the tissue. Any sources on the remaining part of S were ignored. Moreover, all "sources" on the endocardium were implicitly assumed to have the same strength (TMP): $V_{m,1}(\mathrm{t})$, those on the epicardium $V_{\mathrm{m};2}(\mathrm{t})$. Under these conditions, let $\phi_1(t)$ denote the potential at the electrode in the bath facing S_1 and $\phi_2(t)$ the potential at the electrode facing S_2 based on (7.12). By writing

$$c = \frac{f_{\mathrm{v}}\sigma_{\mathrm{i}}}{4\pi\,\sigma_{\mathrm{e}}}$$

we see that

$$\phi_1(t) = -c\,(V_{\mathrm{m},1}(t)\,\Omega_{1,1} + V_{\mathrm{m},2}(t)\,\Omega_{1,2}) \tag{7.17}$$

Similarly, the potential at field point 2 reads

$$\phi_2(t) = -c\,(V_{\mathrm{m},1}(t)\,\Omega_{2,1} + V_{\mathrm{m},2}(t)\,\Omega_{2,2}) \tag{7.18}$$

Note that $\Omega_{i,j}$ is the solid angle subtended by the entire surface S_j at field point i, $(i,j = 1, 2)$. If the thickness of the preparation is discarded we have, in fair approximation, $\Omega_{1,1} = -\Omega_{1,2} \triangleq \Omega_1$ and $\Omega_{2,1} = -\Omega_{2,2} \triangleq \Omega_2$ and, hence the potential difference between the field points, taken to be the electrogram $E(t)$ follows, by subtracting (7.18) from (7.17), as

$$E(t) = \phi_1(t) - \phi_2(t) = -c\,(\Omega_1 + \Omega_2)(V_{\mathrm{m},1}(t) - V_{\mathrm{m},2}(t)) \tag{7.19}$$

Within the assumed validity of the ELD source, this indeed justifies taking the electrogram to be the (scaled) difference between two transmembrane potentials, but only if the rim of the wedge may be assumed to be very thin, which allows the contribution to the potential of any "activity" on the rim to be ignored. Moreover, both faces (epicardial and endocardial) need to be activated uniformly. In all other circumstances, like that of the intact heart, (7.12) needs to be evaluated in full detail, involving multiple sub-segments of the surface, each having their individual transmembrane potential.

The scaling factor depends on the conductivities and solid angles involved: $-c\,(\Omega_1 + \Omega_2)$. The individual solid angles are larger for observation points closer to the surface of the tissue, with 2π being their maximum magnitude for a planar surface (2.52).

This analysis also emphasizes that, when applying the solid angle theory to electrocardiography, at least two solid angles need to be considered. The first one is the solid angle subtended by the EDL source at the observation point. The second one is its solid angle subtended at the reference point. Any observed electrogram or body surface potential relates to the *difference* between these two solid angles. The analysis remains valid when the effect of the finiteness and/or inhomogeneity of the volume conductor is included, since this effect can be viewed a linear operator acting on the infinite medium potentials (Sect. 2.6.4.3).

7.5 EDL Based Inferences for Basic STT Parameters

A discussion of T wave features derived from completely general physical and physiological principles is presented in Sect. 5.9.4. The resulting fundamental, basic expressions, (5.12) and (5.13) are the same as shown in this chapter for the EDL. In Sect. 5.9.4, the matrix $\mathbf{V}_\mathrm{m}$ represents the transmembrane potentials of all myocytes, acting as the source. In this chapter the matrix $\mathbf{V}_\mathrm{m}$ represents the transmembrane potentials at the surface bounding the myocardium. Within the limitations of this approximation, the inferences drawn from (5.12) and (5.13) may be carried over to the T waves as generated by the EDL. Some additional inferences of T wave morphology as derived from the EDL based signals, as previously published [13, 25], are as follows.

The first three points apply in general:

1. Rather than being a weighted sum (the difference) of two TMPs, the ECG is a weighted sum of numerous transmembrane potentials. The weighting coefficients relate to the positions of the field points relative to the heart as well as to volume conduction effects. For any field point, the sum of the weighting coefficients is zero, as is the case for the two weights $(+1, -1)$ expressing a subtraction.
2. Both depolarization (QRS) and repolarization (STT) morphology will generally not be monophasic if resulting from the subtraction of two TMPs as shown Fig. 7.7, but rather biphasic or triphasic as shown in Fig. 7.5, involving numerous, slightly different TMPs.
3. The notion that the timing of local epicardial repolarization precedes that of local endocardial repolarization may be true in the statistical sense (Table 7.2) but is not necessarily valid at all transmural locations (Table 7.1 and Fig. 7.4).

The remaining remarks apply to the situation discussed in Sect. 5.9.4: the TMPs acting as the source for the EDL are assumed to have a similar shape, differing mainly in the timing of local depolarization δ_n and repolarization ρ_n only. Moreover, the individual deviations from the mean repolarization time, $\Delta\rho_\mathrm{n} = \rho_\mathrm{n} - \bar{\rho}$, being the full expression of dispersion of the timing of repolarization, are assumed to be small relative to the duration of the downslope of the

TMPs [13, 25, 26]. These assumptions apply to the healthy myocardium of subjects at rest. Deviations from it show up as differences in the features listed below. All weights mentioned below are lead specific and depend on the volume conductor properties of the thorax.

1. The individual T wave morphologies of any lead is a weighted sum of the derivative of a mean transmembrane potential, $\bar{V}_m(t)$. The function $-\bar{V}_m(t)$ has been named the Dominant T wave [25]. The negative sign was included to bring its polarity in line with that of the T wave polarity observed in most of the precordial standard leads.
2. The timing of the Dominant T wave is equal to the mean repolarization time $\bar{\rho}$ [16, 25]. Note that this is a generalization of what is found when subtracting just two TMPs (Sect. 7.4.6).
3. The integral over time of any lead potential reflects a weighted sum of the individual $\Delta\rho_n$ values.
4. The magnitude of the apex value of an individual T wave is a weighted sum of the $\Delta\rho_n$ values. Note that this is a generalization of what is found when subtracting just two TMPs (Sect. 7.4.6).
5. The width of individual T waves reflects the duration of the downslope of the mean TMP.

7.6 Discussion

The most general expression of the use of the EDL source model discussed in this chapter is (7.13) or, in its discretized form, (7.15). The way in which the EDL is introduced in Sects. Section 7.2 and 7.3 is through its link with the classic UDL source model. However, a far more general variant, expressed in its numerical form, is

$$\mathbf{\Phi} = \mathbf{BS}, \tag{7.20}$$

in which matrix $\mathbf{S}$ specifies the strength of an equivalent double layer (current dipole layer) on any surface S bounding all active, primary sources (Chap. 2). Based on the general laws of volume conduction theory (Chap. 2) it can be shown that such a source description provides a unique specification of the potential field in the region exterior to S [8].

The EDL variant discussed in this chapter takes S to coincide with S_h, the surface bounding all myocytes. Moreover, its strength is taken to be proportional to the local transmembrane potential $\mathbf{V}_m(t)$ at S_h. In view of the realism of the wave forms based on this source model, Fig. 7.5 for ECG wave forms and Fig. 7.6 for electrograms, it can be concluded that the source model appears to be appropriate for describing the genesis of ECG during the repolarization phase of the cardiac myocytes. The wave forms shown relate to healthy myocardium of a subject at rest. The dispersion of the timing of repolarization was small, ischemia was absent and individual TMP wave forms were assumed to have a similar shape.

Other simulations based on the EDL have been reported in the literature, e.g., [12, 27–29]. The interactive simulation package ECGSIM [30] in fact uses the EDL as the source model. Such simulations reveal that by reducing local transmembrane potentials on S_h the effect of acute ischemia on STT wave forms can be studied in individual leads.

It may seem to be puzzling that only the myocytes close to S_h are involved as elements of the EDL, thus discarding any contributions of mid-myocardial myocytes. The main explanation for this is that the effective source strength derived from local mid-myocardial myocytes is proportional to local differences (the divergence, Sect. 2.2.7) of the gradients of their TMPs. These tend to cancel for mid-myocardial myocites, but not for myocytes at S_h. Even so, the EDL source model must be considered as an effective first order approximation. This topic is treated in greater detail in the Appendix. The treatment is relevant only for circumstances in which the EDL source $\mathbf{S}$, as in (7.20), can be taken to be the local transmembrane potential $\mathbf{V}_m(t)$ at S, as in (7.15), with S coinciding with the heart surface S_h. In all other situations the general expression for the EDL source strength $\mathbf{S}$, as in (7.20), may still be used in a forward simulation. This requires $\mathbf{S}$ to be known.

Appendix: The EDL and Bidomain Theory

The equivalent double layer source on the closed surface S_h bounding the myocardium can be used to represent the potential field outside S_h as generated by all myocytes within S_h. The derivation of the EDL presented in Sect. 3.1 uses the approximation $-(\sigma_i\mathbf{\Phi}_i - \sigma_e\mathbf{\Phi}_e) \approx -\sigma_i V_m$, which expresses the double layer strength generating the field of a single

cell placed inside a large container [31, 32]. The approximate nature of this step is clear when computing the contribution to the potential field of an individual myocyte surrounded by closely packed neighbors: the presence of such neighbors will affect the external potential field.

General Formulation

An alternative derivation may be based on the bidomain theory [33–38] (Sect. 8.3.2), which is a macroscopic description of the potential field based on the concept of two interpenetrating domains: one representing the intercellular space, the other the extracellular space [38]. Both are treated as being homogenized, having effective conductivities $\mathbf{G_i}$ and $\mathbf{G_e}$, respectively. The latter differs from the "normal" conductivity in that the geometry of the cellular compartment and the interstitial space is taken into account. The notation using bold capitals stresses the fact that most biological tissues exhibit anisotropic conductivity as a consequence of their fiber structure. This needs to be expressed by a tensor rather than by a scalar. The tensor involved can be expressed by a symmetric 3×3 matrix.

Although the membranes as such are not represented explicitly, the electric sources at the membranes are accounted for by impressed currents. The derivation of the EDL source as based on the bidomain theory, and explained by using lead field concepts (Chap. 10) was formulated by Geselowitz [5, 6]. Below, the essential steps are presented in a condensed form, exclusively derived from the bidomain theory.

The full bidomain based expression (compare (8.10)) for computing the extracellular potential from $\nabla V_\mathrm{m}(\vec{r})$ reads

$$\nabla \bullet \left(\left(\mathbf{G}_\mathrm{i}(\vec{r}) + \mathbf{G}_\mathrm{e}(\vec{r}) \right) \nabla \phi_\mathrm{e}(\vec{r}) \right) = -\nabla \bullet \left(\mathbf{G}_\mathrm{i}(\vec{r}) \nabla V_\mathrm{m}(\vec{r}) \right) \tag{7.21}$$

Recall that the nabla operator,∇, acting on a scalar function produces a gradient field, the vector consisting of the three spatial partial derivatives. The divergence operator, $\nabla\bullet$ acting on a vector, sums the spatial derivatives of its (vector) argument, thus producing a scalar field (Sects. 2.2.6 and 2.2.7).

The solving of (7.21) needs to be carried out numerically. Its complexity hampers the drawing of inferences from the formulation as such. In order to proceed, some simplifying assumptions are made, the realism and validity of which are discussed at the end of this appendix.

Equal Anisotropy Ratio Assumption

We first assume the ratio of the extracellular and intracellular conductivity tensors to be a constant κ, independent of position:

$$\mathbf{G}_\mathrm{e}(\vec{r}) = \kappa\, \mathbf{G}_\mathrm{i}(\vec{r}) \tag{7.22}$$

For elements of the conductivity tensors along (L) fiber direction or transverse to it (T) this corresponds to assuming $g_{\mathrm{eL}} = \kappa\, g_{\mathrm{iL}}$, $g_{\mathrm{eT}} = \kappa g_{\mathrm{iT}}$ and, hence, $g_{\mathrm{eL}}/g_{\mathrm{eT}} = g_{\mathrm{iL}}/g_{\mathrm{iT}}$. Based on this, the assumption is referred to as the "equal anisotropy ratio assumption."

Inserting (7.22) in (7.21), leads to

$$\nabla \bullet \left(\mathbf{G}_\mathrm{e}(\vec{r}) \nabla \phi_\mathrm{e}(\vec{r}) \right) = -\nabla \bullet \left(\frac{\kappa}{1+\kappa} \mathbf{G}_\mathrm{i}(\vec{r}) \nabla V_\mathrm{m}(\vec{r}) \right) = -\nabla \bullet \left(\mathbf{G}_\kappa(\vec{r}) \nabla V_\mathrm{m}(\vec{r}) \right), \tag{7.23}$$

with

$$\mathbf{G}_\kappa \triangleq \frac{\kappa}{1+\kappa} \mathbf{G}_\mathrm{i}$$

Equation (7.23) applies to the medium inside S_h, the myocardium. Outside S_h we want to find the potential field ϕ_0, while assuming a local conductivity $\mathbf{G}_0$. Since no primary sources are present outside S_h we have

$$\nabla \bullet \left(\mathbf{G}_0 \nabla \phi_0 \right) = 0 \tag{7.24}$$

With no primary sources present on S_h, the standard continuity conditions of current flow (2.127) and (2.128) apply at S_h, and so we have for field points on S_h:

$$\phi_0 = \phi_e \quad \text{and} \quad \vec{e}_n \bullet (\mathbf{G}_0 \nabla \phi_0) = \vec{e}_n \bullet (\mathbf{G}_e \nabla \phi_e) \tag{7.25}$$

We now introduce potential field ϕ, and define it to be equal to ϕ_0 outside S_h and equal to ϕ_e inside S_h. The potential field is taken to be present in a medium with conductivity $\mathbf{G}(\vec{r}) = \mathbf{G}_0(\vec{r})$ in the region outside S_h, and $\mathbf{G}(\vec{r}) = \mathbf{G}_e(\vec{r})$ inside S_h. Correspondingly, we have $\mathbf{G}_\kappa(\vec{r}) = \mathbf{G}(\vec{r})/(1+\kappa)$. It can be seen that a function ϕ that is a solution to

$$\nabla \bullet (\mathbf{G}(\vec{r}) \nabla \phi(\vec{r})) = \nabla \bullet \vec{J}^i \tag{7.26}$$

in which

$$\vec{J}^i = -\mathbf{G}_\kappa(\vec{r}) \nabla V_m(\vec{r}) \tag{7.27}$$

satisfies the continuity equations (7.25) as well as (7.23) and (7.24).

The solution to (7.26) links the impressed volume conduction density $i_v = -\nabla \bullet \vec{J}^i$, a scalar function (unit: A m^{-3}), to the desired potential field $\phi(\vec{r}')$, which is also a scalar function (unit: V) (Sect. 2.5.3). Based on the linearity of the conductive medium, the superposition principle may be applied, with the integral adding up the contributions of the elementary sources. This may be expressed as

$$\phi(\vec{r}') = \int_{vol} Z(\vec{r}', \vec{r})\, i_v(\vec{r})\, \mathrm{d}V = -\int_{vol} Z(\vec{r}', \vec{r})\, \nabla \bullet \vec{J}^i(\vec{r})\, \mathrm{d}V \tag{7.28}$$

The scalar function $Z(\vec{r}', \vec{r})$ represents the transfer between individual point sources $i_v(\vec{r})\, \mathrm{d}V$ (unit: A) and the potential. Through Ohm's law, it has as its unit: Ohm. It is the solution to the variant of the basic problem to be solved, (7.26),

$$\nabla \bullet (\mathbf{G}(\vec{r}) \nabla Z(\vec{r}', \vec{r})) = -\delta(\vec{r}', \vec{r}), \tag{7.29}$$

with $\delta(\vec{r}', \vec{r})$ the 3D Dirac delta function (Sect. 2.6.4.1) expressing the source density of a point source at $\vec{r}$.

Equation (7.28) applies completely generally, irrespective of any inhomogeneity or anisotropy. In complex volume conductor configurations the function $Z(\vec{r}', \vec{r})$ may not easily be computed. The derivation of the EDL shown utilizes the general nature of (7.28).

The application of the divergence theorem (2.26) to the vector field $Z(\vec{r}', \vec{r})\vec{J}^i(\vec{r})$ shows that

$$\int_{vol} \nabla \bullet (Z(\vec{r}', \vec{r})\, \vec{J}^i(\vec{r}))\, \mathrm{d}V = \int_{S_h} Z(\vec{r}', \vec{r})\, \vec{J}^i(\vec{r}) \bullet \mathrm{d}\vec{S} = 0$$

The integral on the right is zero since the boundary condition used for the internal domain is $\vec{J}^i(\vec{r}) \bullet \mathrm{d}\vec{S} = 0$ at S_h. From the above, we have

$$\int_{vol} \nabla \bullet (Z(\vec{r}', \vec{r})\, \vec{J}^i(\vec{r}))\, \mathrm{d}V = \int_{vol} \nabla Z(\vec{r}', \vec{r}) \bullet \vec{J}^i(\vec{r})\, \mathrm{d}V + \int_{vol} Z(\vec{r}', \vec{r})\, \nabla \bullet \vec{J}^i(\vec{r})\, \mathrm{d}V = 0$$

and (7.28) is seen to be equivalent to

$$\phi(\vec{r}') = -\int_{vol} \vec{J}^i(\vec{r}) \bullet \nabla Z(\vec{r}', \vec{r})\, \mathrm{d}V = -\int_{vol} \mathbf{G}_\kappa(\vec{r}) \nabla V_m(\vec{r}) \bullet \nabla Z(\vec{r}', \vec{r})\, \mathrm{d}V \tag{7.30}$$

Since, like all conductivity tensors, $\mathbf{G}_\kappa$ is symmetric equation (7.30) may be written as

$$\phi(\vec{r}') = -\int_{vol} \nabla V_m(\vec{r}) \bullet (\mathbf{G}_\kappa(\vec{r}) \nabla Z(\vec{r}', \vec{r}))\, dV, \tag{7.31}$$

Next, we consider the following identity

$$\begin{aligned}\nabla \bullet (V_m(\vec{r})\, \mathbf{G}_\kappa(\vec{r}) \nabla Z(\vec{r}', \vec{r})) = {} & \nabla V_m(\vec{r}) \bullet (\mathbf{G}_\kappa(\vec{r}) \nabla Z(\vec{r}', \vec{r})) \\ & + V_m(\vec{r}) \nabla \bullet (\mathbf{G}_\kappa(\vec{r})\, \nabla Z(\vec{r}', \vec{r}))\end{aligned}$$

which is used to replace the integrand in (7.31). This results in

$$\phi(\vec{r}') = -\int_{vol} \nabla \bullet (V_m(\vec{r})\, \mathbf{G}_\kappa(\vec{r}) \nabla Z(\vec{r}', \vec{r}))\, dV + \int_{vol} V_m(\vec{r}) \nabla \bullet (\mathbf{G}_\kappa(\vec{r}) \nabla Z(\vec{r}', \vec{r}))\, dV$$

The first volume integral can be converted to an integral over the bounding surface S_h by applying the divergence theorem. In the second integral we substitute $\mathbf{G}_\kappa(\vec{r}) = \mathbf{G}(\vec{r})/(1+\kappa)$, and use the delta function properties of $\nabla \bullet (\mathbf{G}(\vec{r}) \nabla Z(\vec{r}', \vec{r}))$ resulting from the equation defining $\nabla Z(\vec{r}', \vec{r})$, (7.29). The resulting final expression for the potential reads

$$\phi(\vec{r}') = -\frac{1}{1+\kappa} \int_{S_h} V_m(\vec{r}) (\mathbf{G}(\vec{r}) \nabla Z(\vec{r}', \vec{r})) \bullet d\vec{S} - \frac{1}{1+\kappa} V_m(\vec{r}') \chi(\vec{r}'), \tag{7.32}$$

with $\chi(\vec{r}') = 1$ for field points within S_h and $\chi(\vec{r}') = 0$ otherwise.

Equation (7.32) mainly replicates (11) shown in [6]. Its notation is more general in that it stresses the anisotropy as well as the dependency on the source location of all variables involved. For field points outside S_h the second term on the right of (7.32) is zero. The remaining part of this appendix relates to external field points only.

By using the symmetric nature of $\mathbf{G}$ we now have

$$\phi(\vec{r}') = -\frac{1}{1+\kappa} \int_{S_h} V_m(\vec{r})\, \nabla Z(\vec{r}', \vec{r}) \bullet \mathbf{G}(\vec{r})\, d\vec{S} \tag{7.33}$$

The conductivity tensor expresses the effect of the fibrous structure of the myocardium. Within this context two different constituents may be identified: the one along the local fiber direction, g_ℓ, and one in the direction normal to the fibers, the transverse conductivity, g_t. Note that the distinction between intra- and extra-cellular values is not required as a consequence of the assumed equal anisotropy ratio. By introducing the local fiber direction in 3D space by the unit vector $\vec{a} = \vec{a}(\vec{r})$ it can be shown [39] that

$$\mathbf{G} = g_t \mathbf{I} + (g_\ell - g_t)\mathbf{A}, \tag{7.34}$$

with $\mathbf{A}$ denoting the tensor derived from the fiber direction $\vec{a}$ (the rank one matrix $\vec{a}\vec{a}^T$, with $\vec{a}$ interpreted as a column vector and $\vec{a}^T$ as a row vector), and $\mathbf{I}$ the 3×3 identity matrix. Since fiber direction $\vec{a}$ and surface normal $d\vec{S}$ are orthogonal at S_h the substitution of (7.34) in (7.33) yields

$$\phi(\vec{r}') = -\frac{1}{1+\kappa} \int_{S_h} g_t(\vec{r})\, V_m(\vec{r})\, \nabla Z(\vec{r}', \vec{r}) \bullet d\vec{S} \tag{7.35}$$

Equation (7.35) indicates that, in the case of a uniform, equal anisotropy ratio, all variables determining the external potential field are expressed by their values at S_h only and are permitted to be inhomogeneous throughout the myocardium. This pertains both to the "active" variable $V_m(\vec{r})$ and to the remaining ones that describe the passive electric volume conduction properties of the medium.

The Final Step

The application of (7.35) requires the function $\nabla Z(\vec{r}', \vec{r})$ to be known. As indicated while introducing the function $Z(\vec{r}', \vec{r})$ (7.28), this function is the solution to (7.29) and expresses the infinite medium potential at field point $\vec{r}'$ generated by a point source at $\vec{r}$, now restricted to a position *on* S_h, but still inside a medium in which an inhomogeneous, anisotropic medium (the region within S_h) is present. In this final step of the discussion we use the approximation

$$Z(\vec{r}', \vec{r}) = \frac{c}{4\pi\sigma_0}\frac{1}{R}, \tag{7.36}$$

with R the length of the vector $\vec{R} = \vec{r}' - \vec{r}$. As shown in Sect. 2.5.1, the spatial behavior of this function is that of the potential field generated by a current monopole with unit strength placed inside an infinite medium with homogeneous isotropic conductivity σ_0. The constant c is included to express the presence of the passive electrical properties of the medium inside S_h. Inserting this approximation in (7.35) gives

$$\begin{aligned}\phi(\vec{r}') &= -\frac{c}{4\pi\sigma_0(1+\kappa)}\int_{S_h} g_t(\vec{r})\, V_m(\vec{r})\, \nabla\frac{1}{R} \bullet \mathrm{d}\vec{S} \\ &= -\frac{c}{4\pi\sigma_0(1+\kappa)}\int_{S_h} g_t(\vec{r})\, V_m(\vec{r})\, \mathrm{d}\omega\end{aligned} \tag{7.37}$$

Finally, if $g_t(\vec{r})$ is taken to be uniform at S_h we see that the external field potential is

$$\phi(\vec{r}) = -\frac{c\, g_t}{4\pi\sigma_0(1+\kappa)}\int_{S_h} V_m(\vec{r})\, \mathrm{d}\omega, \tag{7.38}$$

which is a weighted sum of the local transmembrane potential at S_h, with weights that are proportional to the elementary solid angles $\mathrm{d}\omega = \mathrm{d}\omega(\vec{r}; \vec{r}')$. As discussed in Sect. 7.4.2, the effect of the bounded nature of the volume conduction inside the thorax, as well as that of any inhomogeneities present may be accounted for by a dedicated transfer function acting on the infinite medium potentials (7.14).

Evaluation

The ECG signals as generated by the EDL source as described in Sect. 7.4 are based on (7.12), which has the same structure as that of (7.38). The derivation of (7.12) uses the approximation $-(\sigma_i\mathbf{\Phi}_i - \sigma_e\mathbf{\Phi}_e) \approx -\sigma_i V_m$ for the impressed current dipole surface density ($\mathrm{A\ m^{-1}}$) assumes the medium inside S_h to be homogeneous and isotropic. In contrast, the derivation of (7.38) is based on the bidomain theory, with $\vec{J}^i = -\mathbf{G}_\kappa(\vec{r})\nabla V_m(\vec{r})$ expressing an impressed current density ($\mathrm{A\ m^{-2}}$). If the full anisotropic nature of both domains representing the passive medium inside S_h is taken into account the computation of the potential field must be found by solving (7.21).

By assuming a constant anisotropy ratio for both domains the potential field in the external medium can be found from (7.35). This, interestingly, allows the active sources to be inhomogenous throughout the myocardium (interior of S_h), and demands its value to be known at S_h only. The same holds true for the term $g_t(\vec{r})\ \nabla Z(\vec{r}', \vec{r})$ that describes the passive conductive tissue properties. The final expression (7.38) assumes a uniform value of the transverse conductivity at S_h and approximates the conductivity of the medium inside takes the tissue inside S_h to be homogeneous and isotropic, but only for computing $Z(\vec{r}', \vec{r})$. Note that in the case of a completely isotropic passive medium we have

$$\phi(\vec{r}) \doteq \int_{S_h} g_t(\vec{r})\, V_m(\vec{r})\, \mathrm{d}\omega \tag{7.39}$$

and if, moreover, the transverse conductivity is taken to be uniform at S_h

$$\phi(\vec{r}, t) \doteq \int_{S_h} V_m(\vec{r}, t)\, \mathrm{d}\omega, \tag{7.40}$$

which expresses the basic aspects of the classic UDL source model (solid angle theory) as well as its generalization in the form of the EDL (the inclusion of a source description during repolarization).

The equal anisotropy assumption used in this appendix serves as an essential step in the derivations shown. Direct validation of the assumption is difficult because of the wide range of the values of g_{eL}, g_{iL}, g_{eT} and g_{iT} reported in the literature [10]. More recent publications on this point have not led to a clarification on this point [40, 41]. Indirect support for using the equal anisotropy assumptions came from the experimentally observed values of the potential difference across wave fronts propagating either purely transverse or along fibers. For the correct interpretation of such data the local shape of the wave front needs to be planar. Experimental studies in which this condition was satisfied yielded values of about 40 mV for both the propagation in the transverse direction and along fibers [9, 10, 42]. Recent large scale simulation experiments revealed only minor differences between the results obtained using the bi-domain formulation and those of the monodomain formulation based on the equal anisotropy assumption [35].

If the full complexity of the distribution of the inhomogenous anisotropy of the conductivity tensor is desired to be taken into account, this demand should be confronted with the limited accuracy with which such data would be available, as well as with the reality of the complete complex morphology of the myocardial tissue. The inclusion of such data in the interpretation of the ECG of individual subjects does not seem to be feasible.

References

1. Cuppen, J.J.M. and A. van Oosterom, Model studies with the inversely calculated isochrones of ventricular depolarization. *IEEE Trans. Biomed. Eng.*, 1984;**BME-31**: 652–659.
2. Salu, Y., Relating the multipole moments of the heart to activated parts of the epicardium and endocardium. *Ann. Biomed. Eng.*, 1978;**6**: 492–505.
3. Martin, R.O., *Inverse Electrocardiography*. Duke, NC: Duke University, 1970.
4. van Oosterom, A., The equivalent surface source model in its application to the T wave, in *Electrocardiology'01*. University Press São Paolo, 2002.
5. Geselowitz, D.B., On the theory of the electrocardiogram. *Proc. IEEE*, 1989;**77/6**: 857–876.
6. Geselowitz, D.B., Description of cardiac sources in anisotropic cardiac muscle. Application of bidomain model. *J. Electrocardiol.*, 1992;**25**(Suppl.): 65–67.
7. van Oosterom, A. and P. van Dam, The intra-myocardial distance function as used in the inverse computation ot the timing of depolarization and repolarization, in *Computers in Cardiology*. France: Lyon, 2005.
8. Cuppen, J.J.M., Calculating the isochrones of ventricular depolarization. *SIAM J. Sci. Stat. Comput.*, 1984;**5**: 105–120.
9. van Oosterom, A. and R.T. van Dam, Potential distribution in the left ventricular wall during depolarization, in *Adv. Cardiol.*, 1976;27–31.
10. Plonsey, R. and A. van Oosterom, Implications of macroscopic source strength on cardiac cellular activation models. *J. Electrocardiol.*, 1991;**24/2**: 99–112.
11. Roberts, D.E. and A.M. Scher, Effect of tissue anisotropy on extracellular potential fields in canine myocardium in situ. *Circ. Res.*, 1982;**50**: 342–351.
12. Simms, H.D. and D.B. Geselowitz, Computation of heart surface potentials using the surface source model. *J. Cardiovasc. Electrophysiol.*, 1995;**6**: 522–531.
13. van Oosterom, A., Genesis of the T-wave as based on an equivalent surface source model. *J. Electrocardiol.*, 2001;**34S**: 217–227.
14. van Oosterom, A. and V. Jacquemet, Genesis of the P wave: atrial signals as generated by the equivalent double layer source model. *Eurospace*, 2005;**7**(Suppl. 2): S21–S29.
15. van Oosterom, A. and V. Jacquemet, A parameterized description of transmembrane potentials used in forward and inverse procedures, in *International Conference on Electrocardiology*. Gdansk; Poland: Folia Cardiologica, 2005.
16. Haws, C.W. and R.L. Lux, Correlation between in vivo transmembrane action potential durations and activation-recovery intervals from electrograms. *Circulation*, 1990;**81/1**: 281–288.
17. Huiskamp, G. and A. Van Oosterom, The depolarization sequence of the human heart surface computed from measured body surface potentials. *IEEE Trans. Biomed. Eng.*, 1989;**35**(12): 1047–1058.
18. Durrer, D., et al., Total excitation of the isolated human heart. *Circulation*, 1970;**41**: 899–912.
19. Franz, M.R., et al., Monophasic action potential mapping in a human subject with normal electrograms: direct evidence for the genesis of the T wave. *Circulation*, 1987;**75/2**: 379–386.
20. Cowan, J.C., et al., Sequence of epicardial repolarization and configuration of the T wave. *Br. Heart J.*, 1988;**60**: 424–433.
21. di Bernardo, D. and A. Murray, Explaining the T-wave shape in the ECG. *Nature*, 2000;**403**: 40.
22. Harumi, K., M.J. Burgess, and J.A. Abildskov, A theoretic model of the T wave. *Circulation*, 1966;**XXIV**: 657–668.
23. Yan, G.X., W. Shimizu, and C. Antzelevitch, Characteristics and distribution of M cells in arterially perfused canine left ventricular wedge preparation. *Circulation*, 1998;**98**: 1921–7.
24. Antzelevitch, C., et al., The M-cell: its contribution to the ECG and to normal and abnormal electrical function of the heart. *J. Cardiovasc. Electrophysiol.*, 1999;**10**: 1124–52.
25. van Oosterom, A., The dominant T wave and its significance. *J. Cardiovasc. Electrophysiol.*, 2003;**14**(Suppl. 10): S180–S187.
26. van Oosterom, J., The singular value decomposition of the T wave: its link with a biophysical model of repolarization. *Int. J. Bioelectromagnetism*, 2002;**4**: 59–60.

27. Hooft van Huysduynen, B., et al., Dispersion of repolarization in cardiac resynchronization therapy. *Heart Rhythm*, 2005;**2**: 1286–1293.
28. Huiskamp, G.J.M., Simulation of depolarization and repolarization in a membrane equations based model of the anisotropic ventricle. *IEEE Trans. Biomed. Eng.*, 1998;**BME-45/7**: 847–855.
29. Hooft van Huysduynen, B., et al., Validation of ECG indices of ventricular repolarization heterogeneity. *J. Cardiovasc. Electrophysiol.*, 2005;**16**: 1097–1103.
30. van Oosterom, A. and T.F. Oostendorp, ECGSIM: an interactive tool for studying the genesis of QRST waveforms. *Heart*, 2004;**90**(2): 165–168.
31. Wilson, F.N., A.G. Macleod, and P.S. Barker, The distribution of action currents produced by the heart muscle and other excitable tissues immersed in conducting media. *J. Gen. Physiol.*, 1933;**16**: 423–456.
32. Plonsey, R., An extension of the solid angle formulation for an active cell. *Biophys. J.*, 1965;**5**: 663–666.
33. Muler, A.L. and V.S. Markin, Electrical properties of anisotropic nerve-muscle syncytia-II, Spread of flat front of excitation. *Biophysics*, 1977;**22**: 536–541.
34. Geselowitz, D.B. and W.T.I. Miller, A bi-domain model for anisotropic cardiac muscle. *Ann. Biomed. Eng.*, 1983;**11**: 191–206.
35. Potse, M., et al., A comparison of monodomain and bidomain reaction-diffusion models for action potential propagation in the human heart. *IEEE Trans. Biomed. Eng.*, 2006;**53**(12): 2425–2435.
36. Gulrajani, R.M., *Bioelectricity and Biomagnetism*. New York: Wiley, 1998.
37. Henriquez, C.S., Simulating the electrical behavior of cardiac tissue using the bidomain model. *Crit. Rev. Biomed. Eng.*, 1993;**21**: 1–77.
38. Schmitt, O., Biological information processing using the concept of interpenetrating domains, in *Information Processing in the Nervous System*, K.N. Leibovic, Editor. New York: Springer, 1969.
39. Panfilov, A.V., Modelling of re-entrant patterns in an anatomical model of the heart, in *Computational Biology of the Heart*, A.V. Panfilov and A.V. Holden, Editors. Chistester, UK: Wiley, 1997.
40. Gabriel, R.W. and L. Gabriel, The dielectric properties of biological tissues. (II) Measurements in the range of 10 Hz to 20 GHz, Phys. Med. Biol., 1996;**41**: 2251–2269.
41. Roth, B.J., Electrical conductivity values used with the bidomain model of cardiac tissue. *IEEE Trans. Biomed. Eng.*, 1997;**BME-44**: 326–328.
42. Kléber, A.G. and C.B. Riegger, Electrical constants of arterially perfused rabbit papillary muscle. *J. Physiol.*, 1987;**385**: 307–324.

8 The Forward Problem of Electrocardiography

Rob MacLeod · Martin Buist

P. W. Macfarlane, A. van Oosterom, O. Pahlm, P. Kligfield, M. Janse, J. Camm (eds.), *Comprehensive Electrocardiology*, DOI 10.1007/978-1-84882-046-3_8,

8.1 Introduction

In this chapter we describe a class of problems known collectively as the "forward problem of electrocardiography," which all share the goal of describing cardiac and torso electrical potentials starting from some description of electrical sources within the heart. To solve this forward problem, these electrical sources must be known beforehand, which may suggest a certain degree of artificiality, or at least impracticality, when viewed from the clinical context. The goal of clinical electrocardiography is to use the body-surface potentials from a patient to extract relevant parameters of the cardiac sources, which is the essence of the inverse problem of electrocardiography discussed in the following chapter. The forward problem, in contrast, has a more fundamental role in that it must capture the entire relationships between some description of the sources and the remote manifestations of cardiac bioelectricity.

In its full scope, the forward problem begins with the membranes of the cardiac myocytes and goes to the body-surface potentials; more limited formulations can start, for example, with potentials or activation times on the epicardial and endocardial surfaces, while others can start with descriptions of extracellular tissue potentials and predict epicardial electrograms. In all cases, a practical forward solution must first describe the sources, ideally in some way that strikes a compromise between spatial/temporal fidelity and tractability, i.e., it should be possible to measure or compute the values of interest. The forward solution must also capture in adequate detail the effect of the volume in which the sources are located, the "volume conductor," as its shape and electrical conductivity will determine the currents and potentials that form the solution of the forward problem.

In this chapter, we present a rather broad view of the forward problem, one that includes all four components of a "versatile, present-day heart model" that Gulrajani outlined [1] and are reflected in the goals of the Physiome and Cardiome projects [2]. These components include the anatomical and physical substrate of the heart, the transmembrane action potential as the elemental bioelectric source of activation, the spread or propagation of this activation from cell to cell or element to element within the heart, and, finally, a volume conductor (typically the thorax) through which bioelectric currents pass from the heart to the outer surface, where they generate the electrocardiogram (ECG). One can examine each component of the complete problem with a range of approaches that include experiments with living tissues or mathematical and computational simulations, and complete coverage of all these options is well beyond the scope of this chapter. In this regard, our emphasis will be on mathematical and numerical approaches, although there will be some description of relevant findings from experiments.

A notable challenge of a forward problem is its multiscale nature, i.e., a complete forward solution encompasses information from the scale of the ion-channel protein to the complete human thorax and from the nanosecond to minutes or even hours of time. One can measure or simulate transmembrane potentials from a cardiac cell (myocyte) or even unitary currents through single channels of a cell membrane; however, both these approaches are intractable when the goal is to capture the behavior of the whole heart – there are thousands of ionic channels in a myocyte and billions of myocytes in a heart. Although mathematical models can include larger numbers of points to represent the heart than is possible with direct measurements, the density and complexity of representation are also limited by computer memory and computational capacity. Hence, one must accept simplifications and approximations that lead to workable formulations at the cost of detail and accuracy. Thus, for example, direct electrical measurements of the heart can come from extracellular potentials, sometimes only from the accessible surface(s), and at spacings in the range of millimeters to centimeters. At millimeter spatial resolution, the measurements can cover only small portions of the complete organ; to achieve more complete coverage results in a spatial resolution in the range of centimeters even with the most advanced measurement systems. Mathematical formulations of the forward problem are somewhat less restricted in the number of spatial locations that they can include but are also constrained in this case by computational resources.

It is a general observation common to most biological system that the extreme complexity of the physiology of the heart at each scale requires simplification. It is not feasible to use the same detailed model of membrane behavior suitable for a simulation of a single cell when the goal is to study cardiac arrhythmias in a heart that contains billions of such cells. As a result, the choice of specific source representation and volume conductor resolution derive from the type of behavior one wishes to simulate and the questions such simulations might answer. In this chapter, we describe, for example, formulations that predict potentials on the body surface from those on the epicardial surface and that solve the resulting equations using a boundary element approach. There is simplification in that the problem includes only

potentials on these two surfaces, which, in turn, has the advantage that we can represent each of these surfaces with a large number of points (high spatial resolution) before exceeding the memory capacity of the computer. On the other hand, such a formulation forfeits direct information about cells or ionic channels or even the effects of the blood in the chambers of the heart.

Although one pictures the forward solution as a physically or anatomically outwardly directed process, this is not necessarily the case. It is possible to formulate an inwardly directed forward problem in which the sources are located in the heart tissues and the goal is to compute the electric potentials in the blood volume. This formulation is perhaps especially notable because it leads to a tractable inverse formulation that is the basis for a device that is the most widely used clinical application of the cardiac inverse problem [3].

The development of the forward problem has relied on both experimental and mathematical results and each approach has its respective strengths and limitations. The advantages of experimental approaches include the preservation, without simplification, of heart geometry and physiology, e.g., action potentials and spread of activation, and the ability to impose changes in this physiology through the use of drugs, artificial stimulation, temperature, mechanical load, or reduced coronary blood flow. Although experimental models contain the full complexity of the living tissues, measuring the parameters of interest is limited by physical access and the maximum number – and thus spatial resolution and coverage – of simultaneous measurement channels. For example, it is not possible to capture a truly complete image of the time-dependent potentials or currents within a whole heart. Even measurements limited to, for example, the epicardial potentials can only occur invasively, thus disrupting the integrity of the physiologic volume conductor and the resulting body-surface ECG.

Mathematical approaches remove the limitations of access and, to a certain extent, the number of parameters that one can monitor. The main challenge then becomes how to represent the true physiology in a realistic manner. Analytical approaches to mathematical solutions to the forward problem calculate the remote potentials from closed-form expressions for the cardiac sources. They offer great numerical precision, complete access at any desired resolution, and continuous variation of parameters. However, they are only possible under the most simplified geometric assumptions, e.g., that the heart and body are perfectly spherical or that lungs completely surround the heart in a concentrically spherical shape. They also implement an often highly simplified representation of the action potentials or spread of activation and sometimes compute body surface potentials not as time signals (ECG's) but rather as sparse snapshots in time under specific conditions during which simple sources adequately capture cardiac fields.

Numerical approximations of forward problems are certainly the most flexible and potentially powerful of all the options because they can, at least in principle, represent any sort of geometry in the form of discrete polygonal models and also any conceivable representation of bioelectric sources and spread of activation. Numerical forward problems in electrocardiography are generally unique in the sense that a specific set of source conditions leads to one and only one set of body-surface or epicardial potentials. As we describe in the following chapter, the same is not generally true of the inverse solution, e.g., multiple sets of cardiac source conditions can lead to the same set of body-surface potentials so that it may be impossible to determine which of the source conditions is correct. The presence of uniqueness should not, however, suggest that solving forward problems is trivial; there are considerable technical challenge and effort required to create the necessary geometric models, biophysical formulations, and numerical approximations. The geometry of the body is complex and contains regions of varying and even anisotropic electrical conductivity and there are many nonlinear relationships among relevant parameters. The complexity of simulations is also limited by computer capacity so that even relatively simplified simulations may take hours or even days to generate. Thus the main areas of research in numerical forward problems involve the creation of realistic geometric models, the choice of appropriate simplifications of complex electrophysiology, and the search for more efficient means of implementing them.

Although all three of these approaches – experimental, analytical, and numerical – have contributed to the knowledge of the forward problem, the dominant form in contemporary research is clearly the numerical simulation approaches with experimental results serving the essential role of validation. As we shall describe, this research has led to many recent findings and also encouraged the development of publicly available software and experimental data sets to allow non-experts to carry out forward solutions using modest computational resources and time.

The content of the rest of this chapter will address in more detail all the aspects of the problem outlined above and will seek to capture the current state of understanding and research in the area of forward problems in electrocardiography. We begin with a discussion of each of the three main approaches to solving the forward problem in electrocardiography, including at least brief overviews of the generation of action potentials and propagation simulations. We then continue with a section on the computational aspects of capturing the geometry and solving the forward problem using numerical

approaches. The chapter ends with a list of the major research challenges that we have identified. We have chosen to emphasize contemporary themes at the expense of the rich history in the field and refer to the previous edition of this chapter for readers interested in more detailed coverage of this history [4]. In choosing the topics and literature to include in the chapter, we have tried to be comprehensive and balanced, however, we extend apologies for inevitable omissions.

To describe the choice of physical formulation, especially in mathematical terms, we will draw heavily on the concepts of Chaps. 2, 6, and 7, which cover the underlying physics of bioelectricity and cardiac sources, respectively. Chap. 5 provides a valuable overview of bioelectric sources and their links to the body-surface ECG and therefore contains information required to appreciate fully this chapter. This chapter, in turn, should serve as source of background information for the chapter that follows, which is dedicated to the electrocardiographic inverse problem.

8.2 Experimental Approaches

There is a close link in the field of electrocardiography – and electrophysiology in general – between breakthroughs in measurement technology and new insights into the structure and mechanisms of the underlying behavior. This link exists at all levels of scale and has influenced the development of diverse forward problems in electrocardiography. The first ECG recordings were from Waller in the late nineteenth century [5], but the real breakthroughs in ECG analysis and interpretation came, more than 20 years later, at least in part, because of Einthoven's improvements to the string galvanometer that allowed rapid recordings from patients located remotely from the equipment [6]. Near the other end of the size spectrum, the understanding of ion-channel function was first suggested by Hodgkin and Huxley based on their implementation of voltage clamp methods [7] and then later expanded greatly because of the information that came from patch-clamp methods developed by Neher and Sakmann [8]. The importance of such experimental techniques is further underscored by the fact that each of these breakthroughs resulted in a Nobel Prize for its innovators.

From the enormous richness of experimental approaches and findings that have advanced electrocardiography and forward problems, we highlight here just a tiny sample of findings and information that is most relevant. Because of the large scope of the modern view of forward problems, such coverage must include cellular, tissue, whole heart, and thorax components. As we shall see, each of these fields of experimentation has a naturally synergistic counterpart in the domain of simulation and modeling and one cannot imagine contemporary research without close coupling between these domains.

8.2.1 Cellular Electrophysiology

The broad goals of electrophysiological measurements at the cellular level are to determine the resting and dynamic electric potentials across the cell membrane and to measure the associated currents that flow through the membrane. This current flow occurs through hundreds to thousands of ion channels, each of which belongs to one of tens of channel types. Each channel is composed of an opening or pore, surrounded by complex amino-acid helices that form several separate proteins of largely known composition. It is the characteristics of these proteins and the changes in structure that they undergo that ultimately give rise to ionic currents, changes in membrane voltage, and the driving forces for bioelectricity in the heart and thorax. These channel types differ in terms of their selectivity for particular ions, their electrical conductivity, and their time and voltage-dependent activity. The characterization of these features in normal and diseased channels forms the central theme of a great deal of experimental studies.

Measurements of transmembrane potential generally occur by means of electrodes placed inside individual cells, much as one measures potential difference between two locations in a circuit. Because cells in the myocardium are relatively small (roughly brick shaped with 100 μm length and 10–20 μm sides), electrodes are created from small pieces of glass tubing pulled under heat to a diameter of under 1 mm [9]. Measurements of individual ion currents typically occur by means of slightly larger glass microelectrodes that attach to the membrane and isolate small numbers and even single channels. The measurements in this case are of the currents that flow through the small patch of membrane under the electrode tip [8].

For use in forward problems, the most important variation on this basic theme is the voltage-clamp configuration, which uses either two separate electrodes or one that switches between functions at a frequency high enough for it to

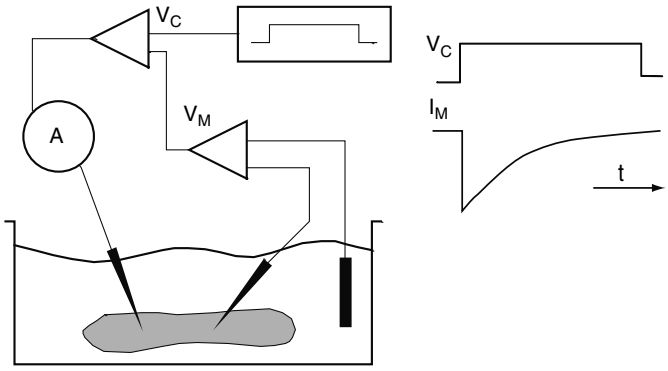

Figure 8.1

Schematic diagram of the voltage clamp procedure. Two electrodes impaled in the cell provide membrane potentials measurement and current injection. Comparison of the membrane voltage V_m and the command potential V_c creates a difference signal that injects measured current into the cell in order to maintain $V_c = V_m$. Time signals indicate the response of time- and voltage-dependent current to a step pulse of the control potential.

carry out the roles of both separate electrodes [10]. As shown in Fig. 8.1, the purpose of the voltage clamp paradigm is to hold, or clamp, the transmembrane voltage at a chosen value and then measure the ionic current required to maintain this potential. Because the voltage is held constant across the membrane, i.e., the voltage-dependent behaviors are fixed, the resulting current measurements reveal the temporal behavior of the channels.

Another essential tool for studying cellular electrophysiology is a set of drugs that selectively block individual ion-selective currents. Hodgkin and Huxley made use of TTX, a toxin derived from the puffer fish that very selectively blocks Na^+ channels (and still causes many deaths each year among puffer-fish gourmands) and TEA, a blocker of some types of potassium channels [11]. With selective channel blockers, it is possible to isolate individual currents and use voltage clamp to determine their unique voltage and time dependence. Thus, it was that Hodgkin and Huxley were able to determine the time- and voltage-dependent characteristics of sodium and potassium channels in the squid giant axon and both formulate and test their Nobel-prize winning approaches to mathematically modeling the behavior of ion channels [12].

The widespread availability of techniques from molecular biology and knowledge of the protein sequence of ion channels continues to shape the contemporary approach to cellular electrophysiology. It is now possible to alter in very controlled ways the sequence of amino acids that make up ion channels and to them embed these modified channels into selected cell types and then study their behavior. In this way, it is possible to address questions in basic cellular electrophysiology and also to create experimental models of a wide range of disease states. Such changes in structure are possible through direct cloning of ion channels, but also by manipulating the genetic code of (usually) mice to create viable transgenic species lines that exhibit specific disease states. As just one example of this powerful approach, researchers altered the structure of the sarcolemmal ATP-sensitive potassium (KATP) channels and compared them with normal (wild type) channels in cells and intact transgenic mice [13]. These studies showed that the KATP channel is primarily responsible for the changes in action potential morphology during myocardial ischemia that lead to the shifts in body-surface ST-segment potentials that are the most common diagnostic feature for myocardial ischemia and infarction.

8.2.2 Tissue and Whole Organ Experiments

The science and technology of experimental approaches for myocardial tissue and the whole hearts is enormous and includes applications in both basic research and day-to-day clinical practice (see, for example, Lux et al. for one recent review [14]). Here we outline the general conceptual framework for such measurements as they relate to the description of bioelectric sources and to some specific approaches that are relevant to any discussion of the electrocardiographic forward problem.

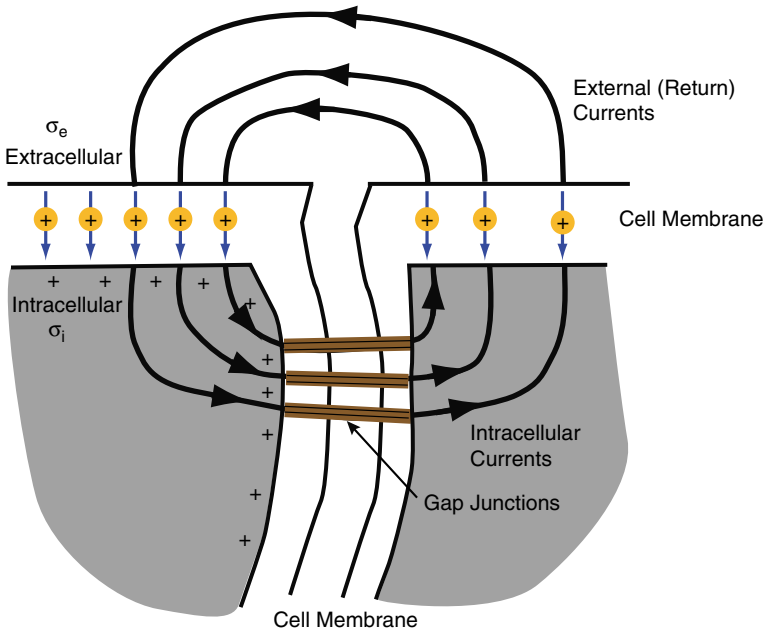

Figure 8.2

Schematic diagram of currents flowing between cells. The figure shows the interface between two cells with cell membrane and gap junctions linking the ends of cells. The left-hand cell is depolarized so that its intracellular space becomes positive with respect to the right-hand cell; hence, current flows directly from one intracellular space to the other through the gap junctions. Extracellular currents form the necessary return path for these currents. Conductivities σ_i and σ_e characterize the intracellular and extracellular space, respectively.

The main goal of experimental approaches at the tissue and whole-organ level is to measure features of cell-to-cell coupling and observe behaviors that arise from the integration of many cells into the complex, three-dimensional structure of the heart. The measured quantity is almost invariably voltage coming from the extracellular current, i.e., the return current that flows between cells through the extracellular space. In fact, it is the qualitative appreciation of the difference between intracellular and extracellular measurements and currents that is perhaps most relevant to any discussion of the electrocardiographic forward problem. This conceptual framework provides the bridge between ionic currents and the macroscopic bioelectric fields that is central to any discussion of cardiac sources, which we describe in Sect. 8.3.

Figure 8.2 shows schematically the relationship between ionic currents and the passive currents that flow between cells and into the extracellular space. In the figure, the left-hand cell is depolarized while the right-hand cell is at rest, thus producing the potential difference that is *always* necessary for current to flow from cell to cell, and by extension, from one part of the heart to another. Current is able to flow easily between neighboring cells because of the presence of gap junctions so that the downstream cell then also begins to accumulate charge. This initial charge accumulation, in turn, provides capacitive current that appears to flow (as all capacitive currents *appear* to flow – there is no ion flow across the membrane but rather a movement of ions on both sides that is the current) into the extracellular (interstitial) space. This extracellular, or return, current flows through the interstitium, which has a discrete conductivity, σ_e, and thus generates local voltage differences that one can measure.

8.2.2.1 Lead Systems and Electrode Arrays

There are two basic approaches to measuring cardiac activity: *unipolar* and *bipolar* leads. Both have physical implementations in the form of contact electrodes. A *lead* is the potential-difference time-signal recorded between two locations in

or around the heart or body; signals from the body surface are *electrocardiograms* (ECG's) and signals from the heart are *electrograms* (EG's). Unipolar leads in measurements of cardiac bioelectricity represent the potential difference between one site on or near the heart and a reference, or *indifferent* electrode typically located remotely from the heart. The actual electrodes can be a small metal pellets, disks, or uninsulated lengths of wire, placed in direct contact with myocardium (see Fig. 8.4). The electrode is connected to the noninverting input of an electronic differential amplifier, while the inverting (negative) inputs of all the amplifiers are connected to the indifferent electrode. Thus, the potential measured by each amplifier represents the difference of voltage between an individual electrode recording site and the reference site. The main advantages of unipolar leads is that they share a common reference and thus provide the necessary information for comparing values over different leads and hence over space. The recording of voltage over space is known as *cardiac potential mapping*. A disadvantage of unipolar leads is that the signals contain both local information, attenuated fields from remote events, and measurement noise, and one often wishes to separate local from remote events. The signals in Panels A and B in Fig. 8.3 are examples of unipolar electrograms.

Bipolar leads consist of two, closely spaced electrodes, with one connected to the inverting and the other to the noninverting input of an amplifier and have the advantage of increased sensitivity to local activity while reducing the effects from distant activity and noise. The bipolar signal represents the algebraic difference between the unipolar signals that would have been recorded from the separate electrodes. This subtraction removes common information or similarities in the two unipolar signals, leaving only those aspects of the unipolar signals that are different. Such differences, in turn, are the result of local events so that bipolar leads emphasize the passage of the activation wavefront and may improve

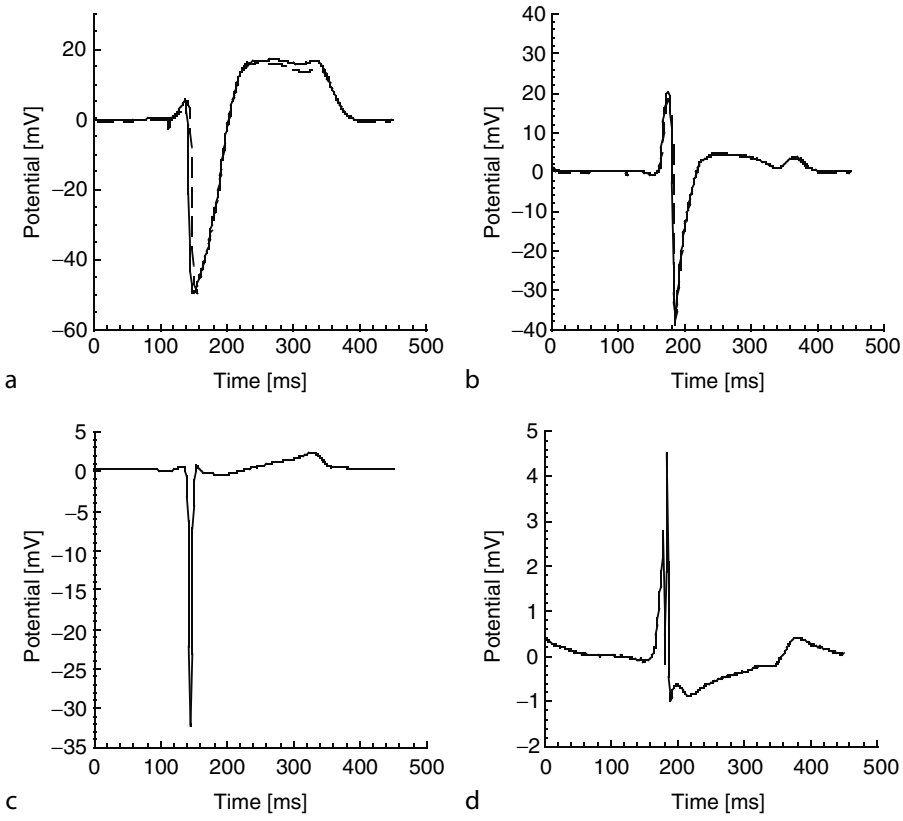

Figure 8.3

A sample of unipolar electrograms and the bipolar leads derived from their difference. (a and b) each contain two very similar unipolar electrogram from neighboring sites in a 1,200-lead epicardial array. (c and d) contain the bipolar leads derived from the two unipolar signals in (a and b) respectively. Note the different vertical scales in each plot. (From [14] with permission)

detection of activation. One weakness of bipolar leads is that they do not share a common reference and thus cannot be compared with other leads in any sort of mapping based on amplitude or time course of the signals. Figure 8.3 shows two pairs of unipolar EGs recorded from closely spaced electrodes (Panels A and B) as well as their differences – the bipolar signals that would have been recorded from them (Panels C and D).

From the perspective of the electrocardiographic forward problem, another salient features of lead type is that unipolar and bipolar leads sense different information and each type provides data for a different formulation of the forward problem, as we shall see in Sect. 8.3.2. Unipolar leads recorded from the epicardial surface(s) of the heart provide direct information for the form of the forward problem based on surface potentials sources. Bipolar leads, on the other hand, provide direct source information for forward models based on activation times. It is imperative to note that one can fairly easily derive activation times from unipolar electrograms [15–19], but that it is impossible to derive potential maps from bipolar leads.

A fundamental question in any mapping and forward or inverse modeling application is the number and location of electrodes required. From a purely experimental perspective, the best number/location configuration of electrodes is based on a combination of features such as the desired biomedical goal, the accessibility of the heart to measurements, the types of electrodes available, and the capabilities of the acquisition system. The question of the minimum required spatial resolution has not been resolved completely, but current consensus indicates that a spacing of ≈ 2.5 mm is required to capture the details of cardiac activation [20]. This resolution assumes simple linear interpolation between measurement sites, either through explicit interpolation or implicitly in the visualization or signal processing required to identify features of interest. There are, however, more sophisticated forms of interpolation that allow, for example, lower density measurements (≈ 10–15 mm) on the epicardial surface and are still capable of reconstructing activation wavefronts [21, 22]. In an even more extreme case, if a set of high-resolution training data is available, it is possible using statistical estimation techniques to reconstruct activation maps on the entire ventricular surface from a very unevenly spaced set of only 10–40 electrodes restricted to the coronary veins [23, 24].

A selection of typical electrode configurations of unipolar and bipolar lead configurations used in contemporary electrophysiology, a subset of which is shown schematically in Fig. 8.4, includes the following:

1. Epicardial arrays sewn into nylon socks that cover some or all of the ventricles;
2. Rigid plaque arrays with regular electrode spacing that cover 1–10 cm^2 areas of the ventricles or atria;
3. Sets of transmural plunge needles with 3–12 electrodes in each needle;
4. Catheters with 1–16 electrodes that are placed in the ventricles, atria, or coronary veins;
5. Basket catheters consisting of 4–6 strands, each containing 4–8 electrodes for insertion into the right or left atrium; and
6. An inflatable, multielectrode balloon or large bore catheter with 10–80 electrodes that can be introduced into the ventricles through an incision or through the coronary vessels.

8.2.3 Physical Models and Phantoms of the Thorax

Physical models of cardiac sources and volume conductors have existed almost as long as the field of electrocardiography and much of the original understanding of the electrocardiographic field came from studies with such models. One can argue whether the ultimate goal of such models has been to solve the forward problem or the inverse problem of electrocardiography; investigators simply set out to understand the relationship between some form of cardiac source and the resulting potentials and currents on and in the torso volume conductor. Chapter 9 also includes coverage of this topic, and here, we introduce the topic with some results and interpretation. We also refer to other recent reviews of the topic [25, 26].

One of the earliest and certainly most thorough evaluations of a physical model based on a single bipolar source in a realistically shaped three-dimensional torso model was that of Burger and Van Milaan [27, 28]. The physical model of the torso was an electrolytic tank made out of a michaplast shell molded on a statue of a supine human. The tank split horizontally to provide access to the interior, which was filled with copper sulfate solution and equipped with copper foil electrodes fixed to the inner surface (see Fig. 8.5). The heart source model was a set of copper disks oriented along one of the body axes and adjustable from outside the tank by means of a rod. The first model used only the electrolyte as the

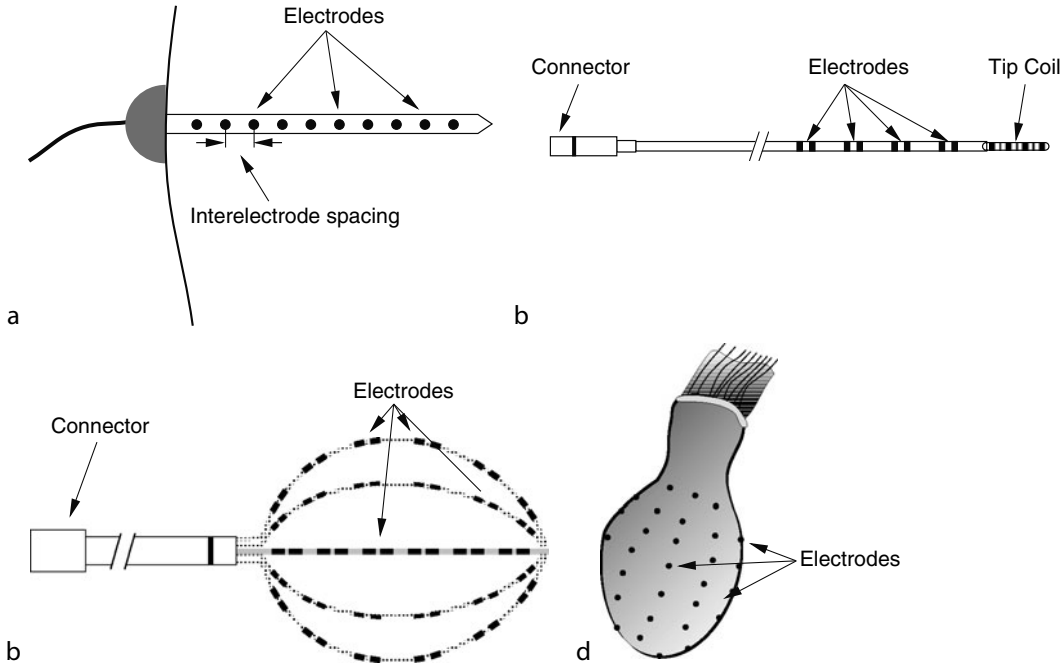

Figure 8.4

A sample of electrode arrays commonly used in cardiac mapping. (a) plunge needle with ten individual electrodes; (b) multi-electrode catheter arranged in four bipolar pairs; (c) basket catheter with six wands, each containing six bipolar pairs; and (d) inflatable sock array for surgical insertion into the left ventricle. (From [14] with permission)

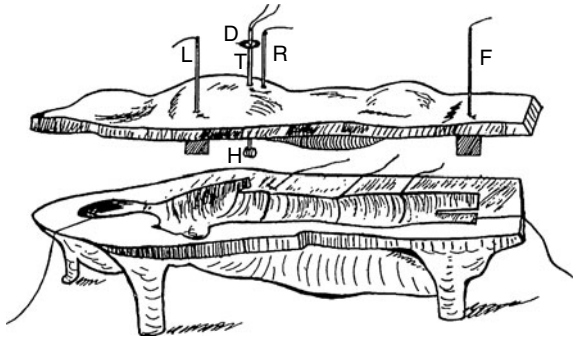

Figure 8.5

Electrolytic tank from Burger and van Milaan (from *British Heart Journal*, 9: 154–160, with permission).

homogeneous volume conductor [27], but subsequent versions incorporated inhomogeneous regions constructed from cork and sand bags for spine and lungs respectively [28].

It is relevant at this point to note that the source of the forward problem in these and many subsequent studies was the single dipole, described in Chap. 2. The dipole is also the basis for the lead field concept described in detail in Chap. 10. Burger and van Milaan were able to derive both algebraic and geometric forms of this relationship for each of the standard limb leads by fitting their measurements of limb lead potentials for known heart vector positions to a simple linear equation,

$$\phi_i = \vec{p} \cdot \vec{L}_i, \tag{8.1}$$

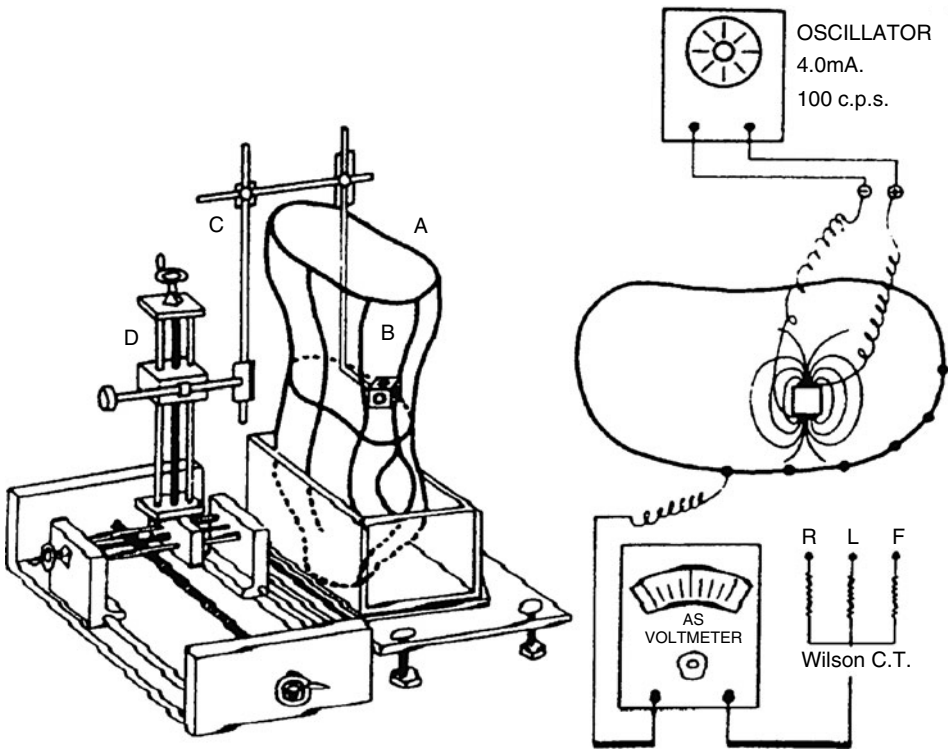

Figure 8.6
Electrolytic tank from Nagata (from *Japanese Heart Journal*, 11(2): 183–194, with permission).

where ϕ_i is the potential for a particular lead i, $\vec{p}$ represents the dipole moment vector, and $\vec{L}_i$ is the lead vector corresponding to the specific lead (Sect. 10.3). To explore the effects of the volume conductor, they repeated the derivation after including various inhomogeneities in the tank and observing the effect on the weighting coefficients of the algebraic expressions. Theirs and subsequent studies by Grayzel and Lizzi, who used conductive paper (Teledeltos) to create two-dimensional inhomogeneous models of the human thorax [29, 30], were among the first to recognize the importance to the ECG not only of volume-conductor shape but also of the role of inhomogeneities in the volume conductor.

Another major breakthrough in the sophistication of physical models came from Nagata, who described several further refinements of artificial source and volume conductor models and subsequently introduced the use of biological sources rather than dipoles [31, 32]. In a preliminary study, Nagata placed a bipolar source in 27 different locations and measured the torso tank surface potentials at electrode sites equivalent to eight different lead systems in common usage at that time [31]. Like Burger and van Milaan, Nagata used a torso geometry based on a three-dimensional human thorax (see Fig. 8.6) and made measurements both in the homogeneously conducting tank as well as (in a subsequent study) with inflated dog lungs and agar gel models of human lungs inserted into the tank [32]. The goal of the studies was to derive the lead vector – expressed here as the "impedance transform vector" – from measurements over a wide variety of bipole source locations and lead systems. A second goal was to evaluate the effects of torso boundaries and inhomogeneities on the shape of the lead vector field. The limitations of this study lay in the lead field approach, which represents the heart as a single dipole rather than a distributed source of bioelectric current.

The later study by Nagata was notable also because he introduced a significant improvement over all previous studies by replacing the synthetic bipolar source with a perfused dog heart, thus achieving a much higher degree of realism than available with simple current bipoles [32]. Nagata did not measure cardiac potentials directly and therefore had no means of describing the real heart quantitatively. Instead, his study focused on the relationship between ECG signal parameters such as R-wave amplitude and signal morphology and the presence or absence of torso inhomogeneities.

There followed then several studies with the goal of evaluating the suitability of the single dipole as a representative source model. De Ambroggi and Taccardi carried out very careful studies of the electrocardiographic field from two bipoles in a two-dimensional electrolytic bath [33]. Their aim was to establish whether it was possible to characterize sources composed of two eccentrically placed bipoles based on potentials measured at sites distributed throughout the bath. Hence, it was not a validation of a quantitative forward solution but more a qualitative evaluation of the relationship between cardiac sources and body surface potentials. Subsequent studies by Mirvis et al. set out to address this same question with rabbit hearts placed inside spherical electrolytic tanks [34–36]. They found that a single moving dipole was not an adequate representation of the heart's electrical activity but that any of three different higher order discrete sources they tested did virtually equally well at reproducing the potentials on the surface of the tank in which the hearts were suspended. The important result of this study was to demonstrate from an experimental model that the single heart dipole model of electrocardiography was incomplete. A new source description was necessary.

It was Barr et al. who provided the new source description when they proposed representing the heart in terms of its epicardial potentials [37, 38]. This also led to a new series of validation studies based on this formulation, the first of which Barr et al. carried out not using an electrolytic tank, but instead an instrumented complete animal model [39]. This preparation included surgical implantation of 75 epicardial electrodes, re-closure of the chest wall in order to restore the integrity of the thoracic volume conductor, and, after a 2-week recovery period, measurement of both epicardial and 150 body-surface potentials with a 24-channel acquisition system. To record geometric information, the thorax of the animal was later sliced and photographed to create a model consisting of the electrode locations on the epicardial and torso surfaces. This landmark study provided data that have been used by several other investigators to validate their forward and inverse solutions [40, 41]. The major limitation of this validation model was that the spatial resolution of the geometric model was modest (the geometric model consisted of only the electrical measurement sites). Furthermore, because of the limited number of recording channels available (20), the potential measurements were performed in sequence and then time aligned, increasing the risk that changes occurring on a beat-to-beat basis or over the time of the measurements would be captured in only a subset of the recordings. Chap. 9 describes the most modern version of this form of physical studies by Nash et al. using an intact pig with instrumented epicardial surface and (re-)closed chest [25, 42].

Most of the experimental phantom studies performed since those of Barr et al. have been of the hybrid type pioneered by Nagata using an isolated heart either with an electrolytic tank [43–63] or with endocardial and catheter measurements for the endocardial inverse solution [64–66]. The main advantages of this type of preparation over instrumented whole animal experiments are the relative ease of carrying out the experiments and the increased level of control they provide. The isolated heart is more directly accessible when suspended in an electrolytic tank, which permits manipulations of its position, pacing site, coronary flow, temperature, etc. as well as the injection of drugs. The simplified geometry of the (usually homogeneous) tank also makes constructing customized geometric models simpler and faster than when a complete medical imaging scan is required for a whole animal.

A contemporary example of the isolated dog heart and human-shaped electrolytic tank preparation is shown in Fig. 8.7 (see also Chap. 9). This preparation uses a second dog to provide circulatory support for the isolated heart, which achieves very stable physiologic conditions over many hours. With the isolated heart, it is also possible to cannulate individual arteries and then regulate the coronary flow rate, blood temperature, and the infusion of cardioactive drugs in order to examine the effects of physiologic change on forward and inverse solutions [55, 59, 61–63, 67–69].

The advantages of physical models include the extreme level of control and intervention that is possible with such preparations. One has excellent access to the source and the volume conductor and can induce changes in either, in some cases within seconds, and can then measure the resulting changes in bioelectric potentials. The source especially can be very realistic with live, perfused, beating hearts available, albeit in most cases with compromised (through anesthesia and surgery) or even absent autonomic nervous systems. In the closed chest animal preparations, there is even a certain degree of realism to the volume conductor, although again with caveats of surgery and anesthesia. One of the challenges of these models is measuring and controlling for geometric details, at least for parts of the preparation. A rigid torso-shaped tank has a very precisely known geometry but the same is not true, for example, in the case of a re-closed chest cavity in a pig. Even with the rigid torso tank, the location and shape of the heart can be challenging to determine with high precision. As we shall see in the following section, obtaining precise geometry is one of the emerging themes of the forward problem and contemporary research in this area. One final challenge, common to all animal experiments and especially with artificial sources of cardiac bioelectricity, is that although the results may be useful to develop and evaluate problem formulations, one must use great care in extrapolating the physiological findings to humans.

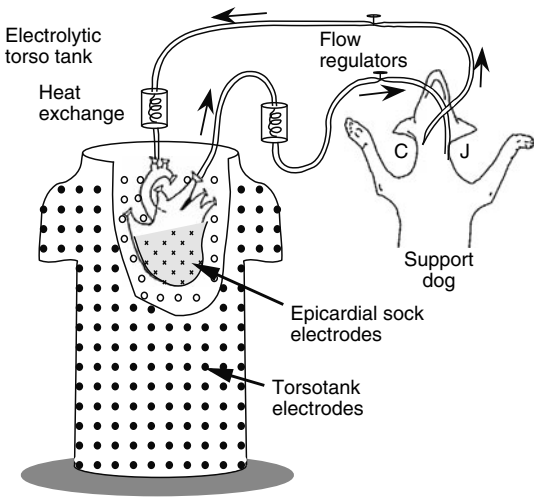

Figure 8.7

Physical model of forward problem originally devised by Taccardi et al. with an isolated, perfused dog heart suspended in the electrolytic tank. Recording electrodes consist of 192–384 tank surface electrodes and a 64–490 lead epicardial sock array.

8.3 Modeling Cardiac Bioelectricity

Creating and using simulations of cardiac bioelectricity has a long and rich history and also covers an enormous range of scale and mathematical sophistication. In this chapter, we provide only a brief overview of this material and focus on the methods that are most relevant in the contemporary research and that drive the forward problem in electrocardiography. As we have defined it, the scope of the forward problem is also very large, and therefore, we include at least some coverage over the complete spectrum from ionic channels to whole hearts.

The unifying goal of simulating cardiac sources is to represent in some compact and mathematically defined way the currents and electric potentials that the heart produces. These representations may be based on explicit anatomical information and even require geometric models of cells, tissue, or the whole heart. Source models may, however, also bear little resemblance to realistic anatomy, but be abstractions of real biophysical sources that are useful only when the distances from the source are large compared with the extent of the source. One can view such a range of representations as similar to describing a source of light either in terms of the actual filament shape of the bulb or, simplified, as a point source radiating equally in all directions; both representations are useful at some scale but not usually across the full range of possible scales. Similarly, representations of cardiac bioelectricity even at the same scale may differ in degree of accuracy or sophistication and they may also vary in terms of the range of situations they can simulate. For example, a source model may create highly realistic potentials for a normal heart beat but be completely inadequate for pathological states. In all cases, source representations are approximations and hence reflect some degree of compromise, usually in order to be mathematically or computationally tractable.

8.3.1 Models of Cardiac Myocytes

The requirement of a model of cardiac cells is that they simulate with acceptable fidelity both the resting and dynamic behavior of the cell. Resting potentials depend on the concentrations of ions on both sides of the cell membrane and on the resting conductivity of ion channels, and a complete model of the cell will reflect these dependencies and even allow for variations in these parameters that reflect pathophysiology, e.g., a cell model should allow the resting potential to rise (depolarize) with elevation in extracellular potassium ($[K_e^+]$), as a real cell does during acute ischemia. Accurate representation of the action potential of the cell is a much more challenging requirement, especially given that, again, this

behavior must reflect a wide range of variations in all the relevant ion channels and their time and voltage dependence. The action potential of a myocyte is the sum of tens of different types of channels arranged in densities that vary with the cell type, species, and even location in the same heart. Each ion channel, in turn, opens and closes in a stochastic manner and thus allows current to flow in a complex time, voltage, and ligand dependent manner, described ultimately by the set of proteins that make up the channel structure. An ideal model of the cell would allow predictions of ionic currents and action potential shape on the basis of variation in the underlying protein structure, i.e., the sequence of amino acids that make up the proteins, determined by the DNA of the cell nucleus.

Such a complete model does not yet exist but there do exist frameworks in which to approach the required (or desired) sophistication. Moreover, there are formalisms that are based on at least reasonable simplifications and ensemble averages of the individual ion channel characteristics that seek to predict the behavior of pieces of cell membrane and whole cells. Even more simplified models also exist that approximate the essential parameters of action potential behavior and are driven by empirical mathematical formulations. Here, we describe briefly these first category of cell models as they represent the far dominant form in forward solution formulations.

8.3.1.1 Biophysically Based Models

There are two levels of biophysically based modeling approaches in common use today: one that describes the opening and closing of individual ion channels and the other that computes currents and voltages for the entire cell. Both of them share the characteristic that they appeared before there was clear experimental proof of the behavior and especially the structure that they attempt to simulate. In this sense they illustrate one of the most powerful applications of simulations, that is to start with a concept of the underlying mechanism and then create a quantitative model that reflects this concept as a means of testing it against measured data.

The Hodgkin–Huxley formalism was the result of breakthroughs in both measurement and theory that occurred in the period of rapid progress that followed World War II. Hodgkin and Huxley made use of the electronic circuitry and devices developed during the war to implement and then apply the voltage-clamp technique described in Sect. 8.2.1 to the squid giant axons [7]. In order to describe first conceptually and then quantitatively the results of these experiments, they proposed the idea of ion channels, that is, openings in the axon membrane that were selective to specific ions and that had time and voltage dependencies that voltage clamp allowed them to investigate. Starting from first-order kinetic equations common in physical chemistry and ordinary differential equations frequently used to describe simple rate dependencies, they adjusted parameters in order to fit the measured data and presented calculations to support these concepts [11, 12, 70]. Subsequent experiments, requiring numerous technological breakthroughs and performed by their successors, proved that the concept of ion channels was sound and led to a Nobel Prize for Hodgkin and Huxley. This simulation formalism is still central to most modern membrane and cell models and there are excellent descriptions in many review articles and even text books [71–73].

Figure 8.8 is a schematic circuit diagram that shows the essentials of the Hodgkin–Huxley formalism applied to the cardiac myocyte. Components include an expression for membrane potential expressed as the product of ionic currents and the capacitance of the lipid bilayer that makes up cellular membranes. The original models of Hodgkin and Huxley applied only to nerve axon and included single Na^+ and K^+ currents; to represent cardiac action potentials substantial modifications are necessary.

The basic equation from the circuit in Fig. 8.8 that drives all models based on the formalism of Hodgkin and Huxley is

$$\frac{\partial V_m}{\partial t} = -\frac{1}{C_m}(I_{ion} + I_{stim}), \tag{8.2}$$

where V_m is the membrane potential, C_m is the membrane capacitance, I_{ion} is the sum of the active ion currents, and I_{stim} is a stimulus current (usually) required to depolarize the cell to reach threshold.

The ionic current is the sum of individual currents that flow through ion-selective channels driven by an equilibrium potential and regulated by a time- and voltage-dependent conductance, expressed as

$$I_{ion} = I_{Na} + I_K + I_{Ca} \ldots, \tag{8.3}$$

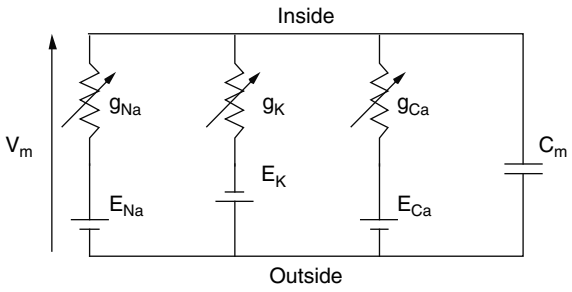

Figure 8.8

Circuit diagram for the Hodgkin–Huxley formalism applied to cardiac myocytes. The parallel circuit of membrane capacitive current and individual ion currents passing through variable resistors captures the essence of the electrical behavior of the cell.

where ... indicates that the list of individual currents is variable and may include different subspecies of currents for the same ion, each having a different time and voltage dependence. Each individual current, in turn, can be expressed according to the circuit diagram as the product of a voltage difference and a conductivity

$$i_X(V,t) = (V_m - E_X)g_X(V,t), \tag{8.4}$$

where I_X is the current for ion X, which flows whenever membrane voltage V_m diverges from the equilibrium potential for the particular ion, E_X, and the conductivity for that ion, g_X, is non-zero. The equilibrium potential, E_X, is a function of the relative concentrations of the particular ion on both sides of the semipermeable membrane and is predicted by the Nernst equation:

$$E_X = \frac{RT}{Z_X F}\ln\left(\frac{[X]_e}{[X]_i}\right), \tag{8.5}$$

where R is the gas constant constant, T is temperature, Z_X is the valance of ion species X, F is the Faraday constant, and $[X]_e$ and $[X]_i$ are the extracellular and intracellular concentrations respectively, of ion species X. Conceptually, the Nernst potential is the membrane potential difference at which there is no incentive for net movement of a particular ion, i.e., the voltage at which, at least for a particular ion, there is equilibrium between inward and outward currents. At any other membrane potential, each ion will experience a net *driving force* equal to $V_m - E_X$ that will move ions across the membrane if the membrane has adequate permeability to that ion.

With this formulation, the descriptions of individual ion currents reside essentially in the time and voltage dependence of the conductivities. As part of their original formulation, Hodgkin and Huxley developed simple expressions for these conductivities based on first-order rate equations that in some way capture their idea of the underlying channel behavior. They fitted the parameters of these equations in order to agree with experimental voltage-clamp results. The resulting formalism remains the most commonly used in modern simulation of electrically active membranes.

The first model of cardiac membranes was by Noble et al. in 1962 and there are at least 30 different variations on this theme known in the literature today [73]. Each model varies in terms of the number and type of individual ion channels included and the animal species for which individual parameters are known from experimental studies. Perhaps, most commonly used are the models from Luo and Rudy [74, 75], which include not only ion channels but (in the 1994 edition) also support for intracellular buffering of calcium. Sachse has recently summarized very well the state of membrane simulation models, including both electrical and mechanical models [73].

From the perspective of the electrocardiographic forward problem, the choice of membrane simulation model is always sharply constrained by the limits of computation. We describe in Sect. 8.3.2 models of cardiac tissue, some of which include individual membrane models as the primary drivers. Because of the desire to simulate pieces of myocardium up to the size of whole heart, it is necessary to discretize the tissue into hundreds of thousands, even millions, of tiny elements, each of which contains its own membrane model. In order to then be able to compute electrical activity

for even a reasonable part of a single heart beat, it is necessary to find efficient, simplified ion-channel models. This simplification in model comes at a cost of accuracy but is an acceptable compromise, in part, because the very existence of tissues reduces the impact of individual cells or small groups of cells on the overall behavior of the simulation.

8.3.2 Models of Cardiac Tissue

In this section, we step from the cellular level to the tissue and whole heart and describe models that capture aspects of their electrical behavior that are relevant to the forward problem. As with the cell, some models of myocardium represent a biophysical approach and are based on accurate anatomical features of the heart. Others are parametric in that they use abstractions of some sort to capture the essential features of the electric fields from myocardium, often requiring a certain distance between the source and the observation location. In general, such parametric representations are less accurate but much simpler to compute; their other major weakness is that it is rarely possible to measure them directly or even to uniquely associate their parameters to anatomical or physiological characteristics of the real heart.

8.3.2.1 Discrete Source Models

The simplest and best known means of representing the electrical activity from the heart is the heart dipole, first described and applied to the heart by Einthoven [6, 76] and still the description with the largest impact on clinical education and the interpretation of the ECG [77]. While simple to grasp physically and to compute numerically, the single dipole is only a barely adequate description of the electrical activity of the heart and even at the body surface cannot explain certain features of potential distributions and the ECG [78]. If anything, it is remarkable that a representation encapsulated by only six parameters can do as well as it does and this fact is perhaps the best evidence of the attenuation, smoothing, and smearing effects of the volume conductor that we explore in more depth in Sect. 8.5. However, for the purpose of quantitative simulation and the detailed study of almost any aspect of normal or abnormal cardiac electrophysiology, the dipole is an inadequate model and hence is rarely considered in contemporary research studies.

There are other forms of discrete sources, based on combinations of dipoles or other higher order forms of this basic current source. Some have proved useful in very special circumstances, such as representing the earliest phase of an ectopic beat, when it resembles a pair of waves moving in opposite directions and hence as a pair of dipoles or a quadrapole [79]. The occurrence of an accessory pathway connecting the atria and ventricles as it arises in the Wolff–Parkinson–White (WPW) syndrome has also been modeled as a discrete dipole that is active only for a few milliseconds [80–86]. This accessory pathway is a tissue band that links the atria with the ventricles and thus forms a connection secondary to that via the atrio-ventricular (AV) node. This connection can create a circular pathway of excitation that goes from atria to ventricles back to atria and thus a reentrant circuit that can be the substrate for ventricular arrhythmias and even death [86, 87]. During the instant in which the excitation travels through the accessory pathway, this bioelectric source is very focal and discrete, and the electric field from this source resembles that of a single current dipole. There have also been many reported studies in which a set of distributed dipoles, each with unique orientation and activation times has represented the potentials from the heart – as we will see, this is still a representation that allows models of propagation to generate extracardiac fields (Sect. 8.4). One such model was even the source for a complex inverse solution expressed in terms of on time and off times for a multiple dipole source [88].

In the contemporary context, there are more accurate and sophisticated formulations that are both more accurate, and through modern computers, tractable sources of cardiac bioelectricity. The rest of this section focuses on these, but for more detail on discrete models, the review by Gulrajani is an excellent resource [1].

8.3.2.2 Bidomain Method

One of the most successful and perhaps initially confusing approaches to representing the electrical activity of the myocardium is the bidomain technique, first conceived by Schmitt [89], proposed by Miller and Geselowitz [90] and

Tung [91] for the heart, and later expanded and used by others to examine all facets of cardiac excitation and stimulation [92–97]. We present here only a brief overview of the method and refer to an excellent review by Henriquez for more details [98].

The main goal of the bidomain approach is to simplify through a process of "homogenization" the features of an aggregate of individual myocytes so as to enable feasible computations of pieces of heart tissue and ultimately the entire heart. Computation that did not employ such a simplification but instead included every cell of the heart would require approximately 10 billion sets of parameters for each time instant, where each set of parameters could include as many as 30 variables, clearly beyond the scope of any computer. The bidomain approach makes explicit use of the fact that the heart is essentially a syncytium, that is, every cell connects via its immediate neighbors to all other cells. This means that, in principle, stimulating a single cell will eventually lead to all cells firing an action potential (and contracting) in a sequence. The bidomain then describes the heart as composed of two domains, one for all intracellular space and the other for all extracellular space, both coexisting in the same physical space (the myocardium). Thus, what is actually a discrete syncytium of many individual cells, each with their its transmembrane voltage, becomes two continuous domains. Intracellular potential and extracellular potential then become continuous functions of space, as does their difference, the transmembrane voltage. Similarly, other parameters of the tissue, most notably electrical resistance, become continuous functions in the intracellular and extracellular spaces. Joining the two domains of the bidomain is the membrane, which in the classic bidomain has no volume but is likewise distributed everywhere throughout the tissue. Most importantly, the membrane contains the ionic channels represented by voltage- and time-dependent currents that generate action potentials within the cells. Figure 8.9 shows schematically the organization of intracellular and extracellular spaces with a membrane linking the two. Also visible in the figure is the current that leaves the extracellular space and travels into the extramyocardial volume conductor; it is this current that is ultimately responsible for the torso and body-surface potentials (ECG).

As with other aspects of the forward problem, *analytical* expressions in terms of continuous functions are rarely available so that *numerical* approaches or discrete approximations of myocardial geometry are necessary. Thus, somewhat paradoxically, what starts as a discrete arrangement of myocytes eventually becomes a discrete organization of small pieces of tissue, each small enough to be treated as uniform with regard to potentials and ionic currents. We describe this process of homogenization and subsequent discretization in the following section.

The derivation of the governing equations of bidomain techniques begins with the statement of Ohm's Law in terms of conductivities for the intracellular and extracellular spaces as

$$\begin{aligned} \vec{J}_{\mathrm{i}} &= -\sigma_{\mathrm{i}} \nabla \phi_i \\ \vec{J}_{\mathrm{e}} &= -\sigma_{\mathrm{e}} \nabla \phi_{\mathrm{e}}, \end{aligned} \tag{8.6}$$

where the subscripts i and e on each of $\vec{J}$, σ, and ϕ indicate intracellular or extracellular spaces respectively.

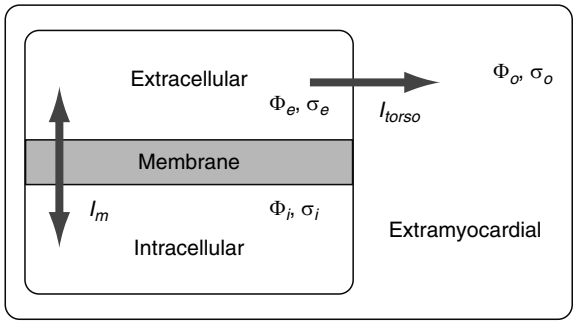

Figure 8.9

Schematic view of the bidomain method of describing myocardium. The heart contains intracellular and extracellular spaces that are linked by a membrane. Currents from the extracellular space (I_{torso}) flow into the extramyocardial volume conductor to produce body-surface potentials.

Conservation of current requires that whatever current leaving the intracellular domain must enter the extracellular: a condition that is possible because both domains are assumed to exist at the same point in space. This allows one to write

$$\nabla \cdot \vec{J}_{\mathrm{i}} = -\nabla \cdot \vec{J}_{\mathrm{e}} \tag{8.7}$$

Substituting (8.6) into (8.7) provides a conservation equation in terms of the intracellular and extracellular potential fields as

$$\nabla \cdot (\sigma_{\mathrm{i}} \nabla \phi_i) = -\nabla \cdot (\sigma_{\mathrm{e}} \nabla \phi_{\mathrm{e}}) \tag{8.8}$$

We can now make use of the definition of the transmembrane potential

$$V_{\mathrm{m}} = \phi_i - \phi_{\mathrm{e}} \tag{8.9}$$

to express (8.8) in terms of V_{m} and ϕ_{e} by subtracting $\nabla \cdot (\sigma_{\mathrm{i}} \nabla \phi_{\mathrm{e}})$ from both sides to obtain

$$\nabla \cdot ((\sigma_{\mathrm{i}} + \sigma_{\mathrm{e}}) \nabla \phi_{\mathrm{e}}) = -\nabla \cdot (\sigma_{\mathrm{i}} \nabla V_{\mathrm{m}}) \tag{8.10}$$

This equation is the first of the two bidomain equations and calculates the extracellular potential field, given a transmembrane potential distribution. Note that this is essentially a form of Poisson's equation with a source term based on the current density associated with the transmembrane potential field. In fact, the extracellular domain of the bidomain is contiguous with the passive regions outside the heart so that one could consider the whole torso to be a bidomain in which the contributions from V_{m} are only non-zero in the heart region.

As shown in Fig. 8.9, any transfer of current between the intracellular and extracellular domains must pass through the intervening membrane so that

$$\nabla \cdot \vec{J}_{\mathrm{i}} = -\nabla \cdot \vec{J}_{\mathrm{e}} = A_{\mathrm{m}} I_{\mathrm{m}} \tag{8.11}$$

Here A_{m} is known as the surface-to-volume ratio of the bidomain membrane and essentially describes how much membrane surface area is present per volume of tissue. The function I_{m} describes the current flow across the membrane per unit of membrane area. It is the sum of a time-dependent capacitive current and a second current, I_{ion}, representing the flow of ions through selectively permeable channels in the membrane as described in Sect. 8.3.1:

$$I_{\mathrm{m}} = C_{\mathrm{m}} \frac{\partial V_{\mathrm{m}}}{\partial t} + I_{\mathrm{ion}}, \tag{8.12}$$

where C_{m} now denotes the membrane capacitance per unit area.

Combining (8.11) and (8.12) gives

$$\nabla \cdot (\sigma_{\mathrm{i}} \nabla \phi_i) = A_{\mathrm{m}} \left(C_{\mathrm{m}} \frac{\partial V_{\mathrm{m}}}{\partial t} + I_{\mathrm{ion}} \right), \tag{8.13}$$

in which I_{ion} is a function of V_{m}, and therefore, it is common (but not universal) practice to re-state the left hand side of (8.13) in terms of V_{m} by adding and subtracting $\nabla \cdot (\sigma_{\mathrm{i}} \nabla \phi_{\mathrm{e}})$ and again imposing the definition of V_{m} to write

$$\nabla \cdot (\sigma_{\mathrm{i}} \nabla V_{\mathrm{m}}) + \nabla \cdot (\sigma_{\mathrm{i}} \nabla \phi_{\mathrm{e}}) = A_{\mathrm{m}} \left(C_{\mathrm{m}} \frac{\partial V_{\mathrm{m}}}{\partial t} + I_{\mathrm{ion}} \right) \tag{8.14}$$

Equation (8.14) is the second bidomain equation and from it, one can calculate the transmembrane potential.

It is possible for an external stimulus current to be applied to either domain (I_{s1} and I_{s2}); this allows the two bidomain equations to be written as

$$\nabla \cdot ((\sigma_{\mathrm{i}} + \sigma_{\mathrm{e}}) \nabla \phi_{\mathrm{e}}) = -\nabla \cdot (\sigma_{\mathrm{i}} \nabla V_{\mathrm{m}}) + I_{\mathrm{s1}}, \tag{8.15}$$

$$\nabla \cdot (\sigma_{\mathrm{i}} \nabla V_{\mathrm{m}}) + \nabla \cdot (\sigma_{\mathrm{i}} \nabla \phi_{\mathrm{e}}) = A_{\mathrm{m}} \left(C_{\mathrm{m}} \frac{\partial V_{\mathrm{m}}}{\partial t} + I_{\mathrm{ion}} \right) - I_{\mathrm{s2}}, \tag{8.16}$$

where I_{s1} and I_{s2} are the stimulus currents.

These two equations are highly coupled and indeed solutions can prove to be computationally prohibitive over large domains and/or on high resolution meshes. If either the extracellular domain is assumed to be highly conducting ($\sigma_e \sim \infty$) or the domains are assumed to be equally anisotropic ($\sigma_i = k\sigma_e$), it is possible to reduce the bidomain system to a single equation with a significant reduction in computational complexity. The result is known as the monodomain equation,

$$\nabla \cdot (\sigma \nabla V_m) = A_m \left(C_m \frac{\partial V_m}{\partial t} + I_{ion} \right) - I_s, \tag{8.17}$$

in which σ is defined by $\sigma^{-1} = \sigma_e^{-1} + \sigma_i^{-1}$. This expression is essentially a nonlinear cable equation when reduced to its one-dimensional form. Thus one can think of the bidomain approach as a multidimensional generalization of the nonlinear cable equation.

8.4 Simulating Propagation

To simulate a full heart beat, it is necessary to have bioelectric sources that vary with time, ideally over more than one beat if the goal is to study arrhythmias or other effects related to heart rate. The most realistic way to generate time-varying sources is to simulate the spread of excitation within tissue, and there are many approaches to describing such propagation in the heart. As with all simulation components, there exists a range of levels of sophistication and degrees of realism and flexibility that such a model can simulate.

There are two stages to this type of simulation and multiple approaches to both. The first step is to predict the sequence in which different regions of the tissue depolarize, the actual spread of excitation. The result is a set of activation and/or repolarization times, parameters which are immediately useful to address some highly relevant questions. The second step is to use the timing values of the excitation and repolarization to generation potentials either within the tissue, or more often, on the epicardium and endocardium. In the context of the forward problem, one usually wishes to generate such potentials at the body surface (although we leave this last step to the section on volume conductors). As described in ❯ Sect. 8.3.2, a common approach to calculating potentials is to represent different regions of the heart as dipole sources and use the activation wavefronts to provide their orientation and active/repolarization times and thus determine their timing. Another approach, described in detail in ❯ Chaps. 6 and ❯ 7, is to represent the sources as moving double layers, with timing and path determined from the propagation parameters. Rather than explicitly computing the spread of excitation, it is also possible to assume knowledge of this sequence, e.g., to acquire it from experiments, and then generate extracardiac potentials from this information.

We use this approximate taxonomy of stages to describe and categorize specific models and begin with simulation approaches that generate the *sequence of activation* or *spread of excitation*, which we take as equivalent expressions. Here, again, we emphasize the intuition of each approach over its mathematical description and solution and refer readers to other sources for more detail.

8.4.1 Physiology Background

We begin with a qualitative description of the process by which excitation travel through the heart. Like all organs, the heart comprises a large number of cells, each of which must be stimulated (partially depolarized) in order to generate an action potential. At the tissue level, the question arises as to how the impetus to depolarize passes from one cell to the next. The answer is via Ohm's Law and gap junctions. Ohm's Law ($I = V/R$) states that current will flow when a potential difference arises and the resistance between regions at different potentials is low enough. Thus, if one cell depolarizes, it will become more positive than its neighbors so that current will flow, providing there is a conductive pathway. The conductive pathway is provided by what are known as "gap junctions". Gap junctions are a form of protein channel embedded in the cell membrane that form direct connections between the interior of one cell and the interior of a neighboring cell through which charged ions may flow – each one represents a resistor with relatively low resistance compared with surrounding tissue. While return currents do flow in the extracellular space, the gap junction connections are the primary means of transferring electrical information between cardiac cells. ❯ Figure 8.2 in ❯ Sect. 8.2.2 shows schematically the

relationship between two cells coupled by gap junctions, the primary current pathway through the gap junctions, and the return current through the extracellular space.

There are some characteristic features of propagation in myocardium that follow from these mechanisms and any attempt at simulating propagation must also take them into account. In fact, appreciation of these features can lead to simplified formulations of propagation, as we will show. The first notable feature is syncytial nature of the heart described in Sect. 8.3.2, by which each cell is connected to all other cells by means of a series of neighbors – a single depolarized cell will eventually cause all cells to depolarize as long as there is a path to each cell. Similarly, all paths from one cell to a nonneighboring cell must go through intermediary cells, i.e., there are generally no short cuts or direct connections between remote regions of the heart. The exception to this rule is a set of special cells, superimposed and only partially connected to the rest of the heart, that are typically noncontractile and preferentially carry extrication more rapidly than surrounding tissues. This *conduction system* is responsible for the coordination and timing of the spread of excitation, ensuring, for example, through a branching network of fibers that most of the subendocardial regions of the ventricular septum are stimulated almost simultaneously. Not all elements of the conduction system accelerate the spread of excitation. In fact, the atrio-ventricular (AV) node is the only electrical link between atria and ventricles – in a normal heart, at least – and it exhibits especially slow conduction speed because of weak intercellular coupling and smaller, rather slowly rising action potentials of the cells. A complete propagation model of the heart must incorporate all these behaviors, or at least must be able to mimic them in some form.

We will now describe some of the more common forms of simulating propagation in physical and mathematical terms and also direct the reader to Chap. 6 of this volume for a discussion of the specific example of double layer sources.

8.4.2 Cellular Automata

The concept of cellular automata dates back to the 1940s and two scientists, Stanislas Ulam and John von Neumann, but by far the most widely recognized use is John Conway's *Game of Life* [99]. Moe et al. adopted this approach in the early 1960s [100] and the methods still find great popularity today due to its computational efficiency [101–107]. A cellular automata approach divides the electrical wave propagation problem into two components. First, the domain of interest is divided up into a regular grid. Each point on the grid has a set of neighboring points, the number of which depends on the dimension of the problem and the topology of the grid. The second component is the automaton that is used to represent the behavior of a single cell and is so named because its actions are solely determined by a set of internal rules. Note that because of computational constraints, an element or cell of the grid in this context is usually substantially larger than a physical cardiac cell.

In its simplest form, a cell in a cellular automata model would have two states, resting and excited (essentially on and off) plus a set of rules to describe the transition from one state to the other and back again. This system mimics a piecewise approximation of an action potential. To then replicate the behavior necessary for propagation, there are rules that determine how the state of one cell affects those of its neighbors. Typically, a cell may transition to the excited state a fixed time after it senses that one or more of its neighbors have been excited. The same cell would then have a rule whereby it returns to the resting state after some further period of time has elapsed, thus encapsulating the ordered cell-by-cell coordination prescribed by the underlying physiology.

More complex – and realistic – cellular automata incorporate additional states in order to capture, for example, refractory properties. One example of such a model from Bailie et al. [108] includes three states: quiescent (Q), excited (E), or refractory (R). In addition there are a total of six rules that govern the transition into and out of each state, summarized in Table Table 8.1.

Starting from a quiescent state, a cell makes the transition to the excited state if it detects that one or more of its neighbors are in an excited state. Next, after a prescribed time period, the cell transitions to the refractory state, and then after another period of time, returns to the initial quiescent state. Figure 8.10 shows the initial stages of propagation using this simple automaton.

We present here a few examples of the many modern applications of cellular automata models, each of which has added notable features in order to better replicate real spread of excitation (and in some cases repolarization) in normal and diseased tissue. A summary of earlier examples can be found in the review of Saxberg [109].

Table 8.1

Rules governing a simple three state cellular automata model

State(t)	Count(t)	Neighbor(t)	State(t+1)	Count(t+1)
Q	(any)	0	Q	0
Q	(any)	≥ 1	E	1
E	$< E_T$	(any)	E	Count(t)+1
E	E_T	(any)	R	1
R	$< R_T$	(any)	R	Count(t)+1
R	R_T	(any)	Q	1

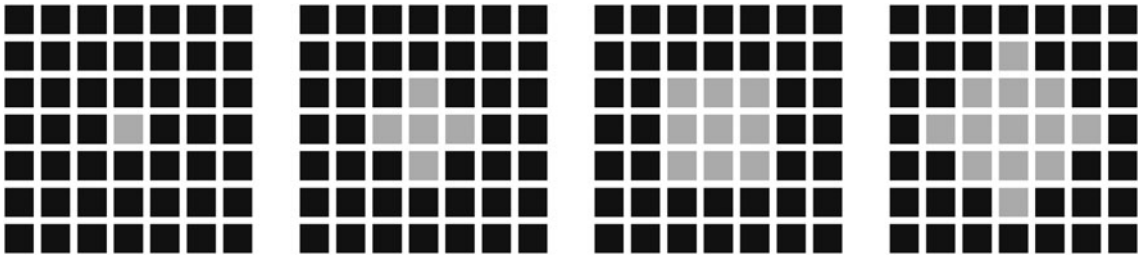

Figure 8.10

Propagation from a point source using a cellular automata approach. Initially, one cell is set to be in an excited state (*light*) while the remainder are quiescent (*dark*). Subsequent images show neighboring cells making the transition to the excited state.

Leon et al. described in a series of studies a cellular automata model that incorporated anisotropic propagation in a human ventricle model by altering the rules of interaction among cells [103, 110, 111]. In order to change from resting to activated state, each target cell received inputs from all neighboring cells, each with its contribution weighted by the direction between the target cell and each neighbor relative to the local fiber direction. In this way, neighboring cells that lie along the local fiber direction have more influence on a target cell than neighbors that lie in the cross-fiber direction. They then used this model to simulate reentrant propagation and to illustrate some of the effects of rotational anisotropy on conduction in a very realistic heart model with 1 mm resolution.

Wei et al. constructed an anatomically based heart mesh that included descriptions of the atria and ventricles, using approximately 50,000 connected elements [112]. The structure was such that each element was connected to 12 adjacent neighbors. The authors divided the heart into 16 cell types with different properties and simulated a normal cardiac excitation pattern. At each time step 54 dipolar sources were constructed from the transmembrane potential distribution and these were used to simulate the ECG and also the vectorcardiogram. WeiXue et al. used CT images to construct a 65,000 element heart model at a resolution of 1.5 mm [113]. The hexahedral elements were arranged in a cubic close-packed structure meaning that each was connected to 26 neighbors. Again a cellular automata approach was used to model propagation and in this case the primary interest was in the epicardial and body surface potential distributions associated with Wolff–Parkinson–White syndrome. Hren et al. developed even more finely resolved cellular automata models with 0.5 mm cell size and used it to simulate various forms of arrhythmia and determine a functional limit of the resolving power of body surface potentials, and to investigate their use in guiding radio-frequency ablation procedures [114, 115].

Following the success of the Visible Human Project [116], there has been much interest in using this high-resolution data source in biomedical computations. Sachse et al. segmented the cardiac geometry from the Visible Man [117], and like Weixue et al. [113], used the pixelated structure as a template for a cellular automata solution. In their study, the transmembrane potential distribution at each time point was used to construct ECG signals from both normal sinus rhythm and also a number of conduction pathologies. Freudenberg et al. also constructed a heart model but in this case

using the Visible Female data set [118]. The resolution of the original images was scaled down by a factor of two in each direction to limit the number of variables that the computation had to encompass.

The main advantage of the cellular automata approach over more biophysically detailed models is the computational speed; whole heart simulations are possible without the need for expensive supercomputing facilities. There are, however, drawbacks to this approach. For most implementations, the shape of the resulting wavefront is dependent on the topology of the grid – a mesh tiled with squares produces a topologically square wavefront [109]). Although it is possible to generate curved wavefronts [118], these are restricted by the need for a characteristic dimension for the curvature. The cellular automata approach is also unsuitable for simulations in which dynamic cellular activity is important, such as the onset of ischemia, as they do not include realistic cellular electrophysiology and hence cannot respond to most external stimuli.

Huygens' Principle Models

From a macroscopic perspective, one can consider the spreading electrical excitation passing through the heart as a wave and therefore look toward other wave representations to model the phenomena. Huygens' principle, also known as Huygens' wavefront method, originated in the 1600s with the Dutch physicist Christian Huygens and his studies of the wave theory of light. The idea is conceptually simple and based on an assumption of constant wave speed. From a given time point and knowing the wave speed, one can construct the location of the wavefront at the next time point by simply drawing circles (or spheres in three dimensions) of an appropriate size along the existing wavefront as shown in Fig. 8.11. From a point source, the Huygens' principle is essentially like dropping a pebble into a pond and observing the path of the first wave.

Numerically for a Huygens' wave simulation, the heart tissue is usually divided into regular pieces, each on a scale much larger than a single myocyte. The activation sequence is best described with reference to Fig. 8.11, in which the dark grey cells behind the wavefront have been previously activated. As the wave moves from its initial position (solid line) to its final position (dashed line), it moves over the centers of the light grey squares and these are then added to the list of active cells. Ahead of the wavefront the white cells indicate that the tissue is yet to be activated.

Early examples of this idea in the cardiac field date back to the 1960s, for example, Okajima et al. [119], who constructed a model of the ventricles using 27,000 cubes and solved it under the assumption of isotropic conduction within this geometry. Resolutions quickly increased with Solomon and Selvester publishing a ventricular model with 750,000 points giving a spatial resolution of 1 mm [120].

Huygens' principle simulations can also incorporate anisotropy by assuming that the wave speed differs depending on local fiber orientation. Lorange et al. developed such a model but did not align wave speeds with realistic fiber orientation so that the resulting elliptical wavefronts did not match experiments [121]. Later models did include this alignment and incorporated fiber rotations in two and three dimensions, including an anatomically based ventricular geometry [122]. More details on this form of propagation model are available in an excellent review by Plonsey and Barr [123].

In general, the Huygens' approach describes only the location of the activation wavefront and cannot describe repolarization. This limitation can be circumvented by a cellular automata-like set of rules to return each cell to its original state after a predetermined period of time has elapsed since the initial activation. Besides the lack of a biophysical basis

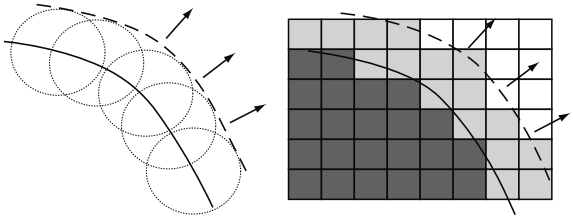

Figure 8.11

Huygens' wavefront method uses a constant wave speed approach. The new position of the wavefront can be found by placing circles of an appropriate diameter on the existing wavefront (*left*). With previously excited cells drawn dark grey and quiescent cells white, the cells which will become active as the wavefront moves forward are shown in light grey (*right*).

for this approach, the main limitation of this model is that propagation is restricted to occur in a finite number of directions (perpendicular to the wavefront) – in other words, the curvature of the wavefront has no effect on the speed of propagation.

8.4.3 Eikonal Curvature

An eikonal equation will generate the position of the wavefront in a manner that does allow the wavefront curvature to influence the speed of propagation. Essentially, a concave wavefront creates a current density that is higher than that of a plane wave, because the wave is propagating into a smaller area (see Fig. 8.12) and this causes the wave to accelerate. The opposite is true for a convex wavefront in which the wave moves into a larger area of resting tissue, which causes the wave to decelerate.

Mathematically a general eikonal equation has the form

$$|\nabla u(\boldsymbol{x})| = F(u(\boldsymbol{x})), \tag{8.18}$$

where $u(\boldsymbol{x})$ is the travel time, or eikonal, from the source to the point $\boldsymbol{x}$. The equation governing the propagation of a Huygens' wavefront is actually a simplification of (8.18) where $F(u(\boldsymbol{x})) = 1$. To correct for the dependence of the wave speed on the wavefront curvature, (8.18) can be written as

$$|\nabla u(\boldsymbol{x})| = 1 + \nabla^2 u(\boldsymbol{x}) \tag{8.19}$$

This is an elliptic equation, and therefore, the wavefront position at all times can be calculated in a single step. There are a small number of variations on this equation in the literature, including some based on parabolic representations; however, the essential feature is the inclusion of the Laplacian term, which allows wavefront curvature to influence the wave speed.

There are two classes of Eikonal equation based studies of cardiac propagation: those for which the position of the wavefront is the desired outcome and those for which it is an intermediate step. As an example of the former class, Keener developed a parabolic eikonal model that he solved using a finite difference approach and applied it to investigate microstructural effects [124]. More recently Hooks et al. used a finite element method to solve an eikonal equation over an orthotropic canine ventricular geometry [125]. The final model required only 180 tricubic Hermite elements to describe the wavefront position. For examples of the second class of models, Colli-Franzone and his colleagues have made many

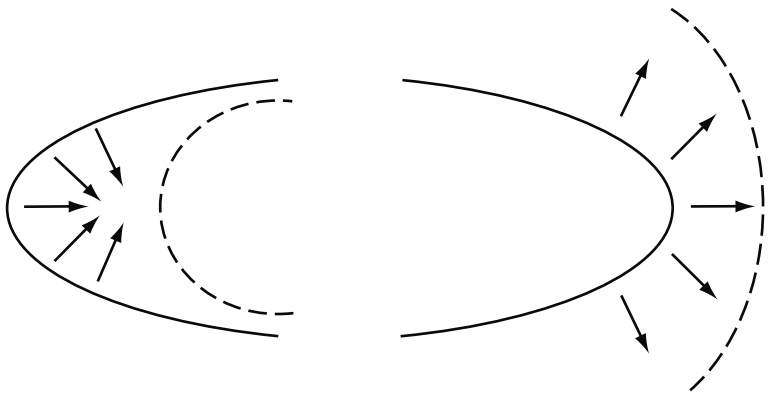

Figure 8.12

A concave wavefront creates a high local current density that causes the wavefront to accelerate and flatten out as it propagates (*left*). A convex wavefront creates a low local current density that causes the wavefront to decelerate and flatten out (*right*).

outstanding contributions and have developed what is probably the current state of the art in eikonal models [126–131]. Their studies include models of the spread of activation under a wide variety of conditions and the most recent examples also include simulations of repolarization wave fronts and potentials [130].

8.4.4 FitzHugh and Nagumo

The FitzHugh–Nagumo model is a popular method of describing not only cardiac propagation but also other reaction-diffusion systems such as other excitable organs [132], calcium waves, and chemical reactions. Unlike many of the cardiac models that bear the name of their authors, FitzHugh and Nagumo developed their ideas independently and largely concurrently [133, 134].

Given a dimensionless activation variable u and a dimensionless recovery variable v, the FitzHugh–Nagumo model can be written as

$$\frac{du}{dt} = c_1 u\,(u-\alpha)\,(1-u) - c_2 v + \nabla\cdot \boldsymbol{D}\nabla u, \tag{8.20}$$

$$\frac{dv}{dt} = b\,(u - dv) \tag{8.21}$$

with the boundary condition

$$\frac{du}{d\boldsymbol{n}} = 0 \tag{8.22}$$

Here $\boldsymbol{D}$ is the diffusion tensor, c_1 is an excitation rate constant, c_2 is an excitation decay constant, b is a recovery rate constant, d is a recovery decay constant, α is the dimensionless threshold potential and $\boldsymbol{n}$ is a unit outward normal vector. This system defines a cubic polynomial activation profile while the inclusion of a recovery variable allows the system to return to its initial resting state, thus enabling the simulation of phenomena that depend on repeated activations.

This type of model can be thought of as an oscillator and a careful selection of parameters can form an excitable model with the model equilibrium below α (as is needed for ventricular cells) or a self-exciting oscillator with the model equilibrium above α (as is appropriate for sinoatrial node pacemaker cells). The presence of the Laplacian term means that in most cases, an appropriate numerical solution technique is required, e.g., finite element or finite difference. An omission of the Laplacian term from (8.20) removes the propagation aspect and leaves a single-cell model that can be adjusted to return I_{ion}, which can then feed into the monodomain or bidomain equations. One could also easily think of this model as a nondimensionalized monodomain equation with a simple two-variable cell model. Given a resting membrane potential V_{r}, a peak membrane potential V_{p}, and a threshold of V_{th}, the following relationships can be used to convert between the dimensional monodomain equation and the nondimensional form.

$$u = \frac{V_{\text{m}} - V_{\text{r}}}{V_{\text{p}} - V_{\text{r}}}, \tag{8.23}$$

$$\alpha = \frac{V_{\text{th}} - V_{\text{r}}}{V_{\text{p}} - V_{\text{r}}}, \tag{8.24}$$

$$I_{\text{ion}} = C_{\text{m}}\,(V_{\text{p}} - V_{\text{r}})\,\frac{du}{dt} \tag{8.25}$$

Rogers and McCulloch made a slight modification to (8.20) in order to provide a more cardiac-like waveform, multiplying the recovery variable by the activation variable [135].

$$\frac{du}{dt} = c_1 u\,(u-\alpha)\,(1-u) - c_2 uv + \nabla\cdot \boldsymbol{D}\nabla u \tag{8.26}$$

Their recommended parameter values were $\alpha = 0.13$, $b = 0.013$, $c_1 = 0.26$, $c_2 = 0.1$, and $d = 1.0$. In isotropic simulations, D had the value 1.0 and in anisotropic simulations $\boldsymbol{D}$ was 4.0 in the direction of the muscle fibers and 1.0 in the transverse direction. Among other results, this parameter set was used to provide a demonstration of the influence wavefront curvature has on propagation velocity.

Although the FitzHugh–Nagumo approach has been used to investigate a number of different phenomena, it is in the simulation of reentrant waves (representing arrhythmias) in which it has proved to be most useful. The popularity of this formalism arises in large part because it is computationally efficient for simulating activation and recovery; modeling reentrant waves requires considerably longer simulations (several to tens of beats) than for a single heart beat. Examples of this type of model appeared in the early 1970s and subsequently focused primarily on two-dimensional tissue blocks [136, 137] but as computational power increased, three-dimensional models appeared, including some based on anatomically realistic geometries [138–140].

8.4.5 Computing Extracardiac Potentials

With a propagation sequence available, either from measurements or from one of the propagation models already described, the second stage of bioelectric source modeling is converting information that is essentially timing into the electric sources – typically currents – that would then generate the potentials measured from the heart or the body surface. The typical approach is to use the activation time and some assumptions about the resulting potential gradients that arise at the spreading wavefront to create some reasonable number of current sources. Because current and current density have direction, it is also necessary to determine the orientation of discrete current sources, which in turn requires knowledge of the spatial orientation of the spreading activation wavefront. The final component required is the amplitude of the current sources, which one can derive naturally from the spatial gradient of the potential in the myocardium.

The typical assumption during the activation phase is that the most significant potential gradients are localized in the region of the spreading wave of excitation so that it is necessary to evaluate only those regions of the heart. One particular simplifying assumption is to assign a fixed potential difference across all regions of the activation wavefront, which assumes that both the extracellular and intracellular potentials are identical for every cell. A more realistic version of this scheme assigns an action potential to each region of the heart, based either on a local implementation of one of the cell simulation models described in Sect. 8.3.1 or on measurements and taking into account the natural variations in action potential characteristics over the heart.

Mathematically, one can express this approach as computing a current density from Ohm's Law

$$\mathbf{J}_i = -\sigma_i \nabla \Phi_i, \tag{8.27}$$

where $\mathbf{J}_i$ is the current density in some region i, σ_i is the effective intracellular conductivity (which may be a tensor quantity), and $\nabla \Phi_i$ is the potential gradient over the same region. Depending on the model geometry and structure, there is a discrete form of this equation that applies at some appropriate resolution either throughout the heart or in regions of appreciable gradients (defined, for example, by the location of the activation wavefront at any given time).

In some formulations of the extracardiac potential, this expression for current density is enough, while in others, a more discrete form is necessary and one computes a dipole moment by integrating the current density over some region in space,

$$\mathbf{P}_{l,m,n} = -\int \sigma_i \nabla \Phi_i \, dl \, dm \, dn, \tag{8.28}$$

where $dl\, dm\, anddn$ describe some region in the (usually discrete) representation of the region collapsed into a single dipole with moment $\mathbf{P}_{l,m,n}$.

8.4.6 Applications

The applications of the bidomain approach and propagation modeling are very numerous and include a wide range of problems. One of the earliest applications of this approach to cardiac propagation was by Henriquez et al., who constructed detailed models of bundles of cardiac tissue and examined the critical values for spread of excitation [93, 94].

A more modern version of this approach has recently appeared in simulations by Stinstra et al., first of the passive electrical characteristics of cardiac tissue [141, 142], and then using those parameters to simulate at unparalleled spatial resolution the effects of cell shape and size on propagation [143]. Henriquez and his various colleagues have published a series of report of applying bidomain approaches to ever more complex slabs of tissue to investigate the role of structure, coupling and especially anisotropy on cardiac excitation in the ventricles [144–148].

Bidomain models have also become tractable enough to simulate some behaviors in whole heart models. For example Fischer et al. used a bidomain model of the heart together with a propagation model to simulate cardiac potentials under realistic conditions of anisotropy [95]. Other studies by Weinstein and Henriquez et al. have described the first computations of cardiac potentials in mice using bidomain models [149, 150]. Hopenfeld et al. also used a realistic, anisotropic dog heart model and the bidomain approach to simulate cardiac potentials from acute ischemia under varying conditions of ischemic zone location and depth [97, 151]. The fact that they simulated an essentially static condition from potentials during the plateau phase of the action potential made these simulations very tractable compared with models with propagation. For that, the model allowed unprecedented examination of the relationship between ischemic border zone shape and alignment with local myocardial fiber structure.

There are some less obvious applications of the bidomain for problems of tissue stimulation that make use of the unique ability of this formulation to capture spatially variable anisotropy. In one such application, Frazier et al. used a bidomain model of heart tissue to investigate the fields that arise during extracellular stimulation of tissue and thus to investigate the role of tissue structure, electrode location, and stimulus strength on stimulation [152]. Using even stronger extracellular fields, Trayanova and her colleagues have published many studies on defibrillation using the bidomain approach [153–157]. Recent studies by Jolley and Triedman et al. have illustrated the feasibility of carrying out simulations of cardiac defibrillation using realistic electrode placements inside the human child thorax [158]. Successful studies such as these will make it possible to simulate intracardiac defibrillator placement in subject-specific models and thus optimize lead placement and defibrillation protocols for each patient.

8.5 Models of Volume Conductor Potentials

In this section we describe the mathematical models and numerical methods required to compute body surface potentials from cardiac bioelectric sources. This is the last of the four components of the complete forward solution introduced in Sect. 8.1, which, in essence, describes the biophysical characteristics of the volume conductor, a passive medium with heterogeneous electrical conductivity. In practice, however, it is necessary to match the model of the volume conductor to the specific representation of the source and the desired outcome of the forward problem. For example, if one represents the heart as Einthoven did as a single current dipole [6] and seeks to compute the body-surface ECG, the volume conductor model and the associated mathematical formulation will differ from the case of the source described in terms of activation times on the epicardial and endocardial surfaces. Thus any discussion of the volume conductor potentials is closely tied to the source formulation, a fact that we reflect in the organization of this section.

The choice of numerical method is also a product of the type of source model and desired outcome of the simulation, as well as assumptions about the volume conductor itself. For example, a forward problem based on epicardial and endocardial surface activation times and under assumptions of heterogeneous but isotropic torso volume conductor leads naturally to a numerical implementation based on the boundary element method (BEM). By contrast, a solution based, for example, on bidomain computations of cardiac currents embedded in an anisotropic model of the heart and heterogeneous (and possibly anisotropic) torso is better served by an implementation using the finite element method (FEM). Wherever possible, we will indicate the numerical approach best suited for a particular problem formulation and direct the reader to Sect. 8.6 for details of the associated numerical methods.

This section describes the biophysics and mathematics of volume conductors required to form the bridge between the descriptions of bioelectric sources in the previous sections to the numerical methods that are necessary to implement working solutions to electrocardiographic forward problems. It is impossible in a single chapter to provide comprehensive coverage of all combinations of source models and volume conductors so that we focus here on some of the more frequently studied scenarios and describe at least the main numerical methods in contemporary use.

8.5.1 Biophysical Background

The physics of potential fields describes this component of the forward problem and is also the topic of Sect. 2.6 of this volume. Here we avoid some of the simplifications of Sect. 2.6 and arrive at a more general framework, specifically one that supports a wider range of realistic tissue characteristics.

The basic formulation of all such problems leads either to Poisson's or Laplace's equation, i.e.,

$$\nabla \cdot (\sigma \nabla \Phi) = -i_v = \nabla \cdot \vec{J}^i, \tag{8.29}$$

as in (2.87), the general expression that applies to inhomogeneous, anisotropic conductivity. In case the conductivity is anisotropic, σ denotes the tensor character (Chap. 7, "Appendix: The EDL and Bidomain Theory").

Similarly, we can write a Laplace's equation

$$\nabla \cdot (\sigma \nabla \Phi) = 0 \tag{8.30}$$

for any region in which there are no active sources, i.e., $i_v = 0$. To make use of Laplace's equation, the solution domain cannot include the sources, which then appear as imposed boundary conditions of the resulting solution, an approach outlined in Sect. 2.6.4. These boundary conditions include electric potentials that are known at some subset of the problem domain, typically on or within the heart, and this is known as the "Dirichlet" boundary condition.

The solutions of (8.29) and (8.30) also depend on boundary conditions that arise from the physics of the problem. At the boundary of the outer surface of the torso and air, for example, no current flow leaves the body so that

$$(\sigma \nabla \Phi) \cdot \mathbf{n} = 0, \tag{8.31}$$

where $\mathbf{n}$ is a unit vector pointing in normal direction to the surface. This is known as the "Neumann" boundary condition on the flux through the surface. At the boundaries within the volume conductor there are also boundary conditions dictated by the fact that potentials must be equal on both sides of a shared boundary and normal current flow must therefore also be the same, i.e., for a boundary between compartments p and q

$$\Phi_p = \Phi_q, \tag{8.32}$$

$$(\sigma_p \nabla \Phi_p) \cdot \mathbf{n}_p = (\sigma_q \nabla \Phi_q) \cdot \mathbf{n}_q \tag{8.33}$$

8.5.2 Analytical Models

Under highly simplified conditions, it is possible to formulate closed form or analytical solutions to (8.29) and (8.30) and there is a rich history of applying this approach to the forward problem in electrocardiography. The simplified conditions typically include a source described in terms of a modest number of discrete current dipoles and a volume conductor with a mathematically simple shape, for example a circle, sphere, or cylinder. Examples of this approach include studies from Wilson and Bayley [159] and then Frank [160], who computed body-surface potentials from a single current dipole source located in a spherical surface model of the torso. Burger et al. [161] and Okada [162] carried out similar studies using cylindrical model of the torso and concentric and eccentric dipole sources, which led eventually to the extensive studies based on a model of eccentric spheres developed by Bayley and Berry [163–165]. Rudy et al. later further developed this approach extensively [166–168], and it is still in use, largely as a means of validating solution techniques based on numerical approximations of the sources and volume conductors [43, 169–173] (as we describe in the following sections). It is rare to use analytical models for any realistic solutions to forward (or inverse) problems in electrocardiography, simply because the resulting accuracy is inadequate when compared with measured values in a real subject/patient.

8.5.3 Discrete Source Models

There is a rich history of forward problem formulations based on discrete source models of the heart, the background of which is covered in Sect. 8.3.2 and Chaps. 2, 5, and 6 of this volume. The underlying notion of all these

approaches is that a very simple current source can adequately represent the electrical activity of the heart, at least when viewed from some distance from the heart, e.g., the body surface. The huge advantage of these approaches is the small number of parameters required to describe the sources and the resulting simplicity of the associated forward (and inverse) problems. The most notable disadvantage is that there are no clear physical or physiological links between discrete sources and either the true sources they represent or any directly measurable quantities; there is no way to directly measure dipole locations or amplitudes nor to unambiguously link their parameters to action potentials or spread of activation. Discrete source models nevertheless play important roles in both the analytical approaches already outlined and the numerical approaches described in the following section.

The descriptions of bioelectric fields from discrete sources begin with the expression for the potential from a single dipole in an infinite space, (2.99), rewritten as

$$\Phi(\vec{r}') = \frac{1}{4\pi\sigma}\frac{\vec{R}}{R^3}\cdot\vec{P}(\vec{r}), \tag{8.34}$$

where $\vec{R}$ is the vector from the location of the dipole to the location $\vec{r}'$ in space where Φ is calculated and $\vec{P}(\vec{r})$ is the srength (dipole moment) of the dipole at location $\vec{r}$, specifying both the direction and the magnitude of the current dipole source.

To compute the potentials from a current dipole located within a finite medium, even one with several regions having different conductivities (σ) is also possible using the equation (derived in Sect. 2.6.4.4 resulting in (2.17))

$$\Phi(\vec{r}') = \frac{1}{4\pi\sigma}\frac{\vec{R}}{R^3}\cdot\vec{P}(\vec{r}) - \frac{1}{4\pi}\sum_{l=0}^{N_S}\int_{S_l}(\sigma_l^+ - \sigma_l^-)\Phi(\vec{r})\, d\Omega_{rr\prime}, \tag{8.35}$$

where σ_l^+ and σ_l^- are the conductivities on either side of the boundary l and $d\Omega_{rr\prime}$ is the solid angle described in Sect. 2.2.12 of Chap. 2. With a numerical implementation of this equation (usually via the boundary element method described in Sect. 2.6.4 and in the following section) it is then possible to compute the potential at any point provided the dipole location, orientation, and strength and the spatial locations of all boundaries and the conductivities around them are known. It is also possible to extend this approach to other discrete sources, i.e., quadropoles or octopoles, which are capable of representing more complex versions of the cardiac sources at the cost of more parameters but still without a clear link to measurements or physiological sources [1].

8.5.4 Cardiac Surface Potential Models

This form of the forward problem is one of the two dominant approaches in modern applications and is based on a source description of epicardial potentials. More precisely, the potentials on any closed surface that encompasses all active cardiac sources forms a completely equivalent representation of the true cardiac sources. Out of convenience – because it permits direct measurement of the source parameters – one usually selects the enclosing surface to be the epicardium (or pericardium) and the challenge then becomes to derive a mathematical formulation that predicts the potentials throughout the thorax (include the body surface) from this source. Barr and his colleagues solved this problem in the mid-1970s in a way that also provides a natural numerical solution by means of the boundary element method [37, 38, 174].

Figure 8.13 describes schematically the configuration and the associated variables involved in linking the potentials the heart surface S_H and the body surface S_B. In this figure, the region between the heart surface and the body surface is taken to have a uniform conductivity. The derivation of this link as derived from the BEM is described in Sect. 2.6.4.5. Equation (2.173) implies that inhomogeneities in the region between S_H and S_B, like those of the lungs, can also be treated by means of the BEM.

In its numerical form, the transfer can be described by a matrix A. Any element a_{BH} of this matrix represents the effect of the potential at location P_{H} on the heart surface S_{H} to points P_{B} on the body surface S_{B}.

The transfer coefficients relate to the specification of the geometry and conductivities of the problem, i.e., it depends only on the volume conductor and not on the time-varying source potentials.

Although the formalities of all the terms of the transfer (2.173) are crucial when carrying out the calculations, it is their qualitative meanings that are fundamental to understanding this entire approach. The equations (and diagrams)

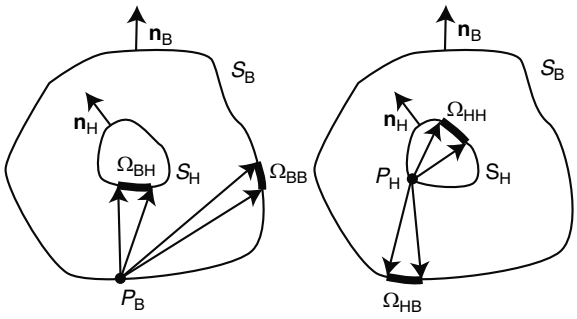

Figure 8.13

Schematic diagram of the forward problem in terms of surface potentials. (a and b) represent the approach to calculating the potentials on each of the heart (P_B on S_B) and body (P_H on S_H) surfaces respectively. Both surfaces have outward normals (n_H and n_B) and all active sources are contained within S_H. The heavy line segments between the tips of the arrows represent the contribution of a surface element to the potential at the common origin of the arrows and the Ω symbols represent the solid angle that weights each of these contributions.

reveal that the potential at any point on the surface of, for example, the body surface is the sum of contributions from the potentials (and perhaps potential gradients) at the other surfaces in the problem.

The full expression of the forward transfer reads

$$\mathbf{\Phi}_B = \boldsymbol{A}_{BH}\mathbf{\Phi}_H \tag{8.36}$$

The computation of potentials on the heart surface from body surface potentials is based on evaluationg the inverse of the transfer matrix involved,a topic treated in Sect. 9.3 of Chap. 9.

One of the essential aspects of this approach to the forward problem is that it is based on epicardial (or pericardial) surface potentials, which are, in principle, measurable quantities. In fact, as we outlined in Sect. 8.2.2, these quantities are measured in experiments and in clinical practice, because they convey directly information about the electrical state of the heart. This form of the forward solution is also unique in the sense that for any given set of source potentials there is one and only one set of associated body surface potentials (as we shall see in the next chapter, the reverse is also true, at least under assumptions of perfect numerical calculations and noise-free measurements). The information necessary to solve this problem consists of a description of the heart and body surfaces and of any other surfaces that separate regions of differing conductivity along with the tissue conductivities of each of these regions.

8.5.5 Equivalent Double Layer Based Models

A final formulation of the forward problem is based on a representation of the spread of activation and repolarization in the heart and this represents the sources not as variable potential amplitudes but on the timing of activation and repolarization on the epicardial and endocardial surfaces of the heart. Chapters 6 and 7 contain descriptions of these sources (the uniform and equivalent double layers) and the resulting forward problem respectively. The ECGSIM software described in Sect. 8.6.6, is a very user-friendly and powerful implementation of this forward model.

8.6 Numerical Approaches and Computational Aspects

8.6.1 Introduction

This section describes a family of numerical methods that are common to many different types of electrocardiographic forward problems and in some cases, several of them may solve the same problem. Hence they are combined here into

one section rather than organized within the previous sections describing the types of problems to which one might apply them. These methods are common not only to forward problems but also to many other applications across the broadest spectrum of engineering and science, which has the considerable advantage that they are well supported with robust theory and easily available implementations as computer programs and libraries. Here we provide only outlines of these methods with emphasis on the intuition that motivates each and the specific applications to the forward problem. We refer the interested reader to other sources through this section.

Please note that in this section the symbol Ω denotes a region in space, rather than a solid angle as used at several other places in this volume, and that Γ denotes its boundary.

To provide a common framework for all these methods, we begin with Laplace's equation (8.30) and note that it is a differential form, also known as a strong form

$$\nabla \cdot (\sigma \nabla \Phi) = 0 \tag{8.37}$$

Numerical solutions to differential equations always involve some degree of approximation and uncertainty. Thus, any numerical solution for (8.37) will also be to some extent approximate. If we use the notation $\hat{\phi}$ to represent the numerical solution, then the substitution of $\hat{\phi}$ into the left hand side of (8.37) will not yield identically 0; there will be some error, or residual, remaining that one would like to minimize, thereby yielding an accurate answer. Different numerical techniques seek to minimize this residual in different ways, typically by trying to force the average (or weighted) error to be zero. The general expression for this is the *weighted residual expression* or "weak form" given by

$$\int_{\Omega} \nabla \cdot (\sigma \nabla \phi)\, \omega \, d\Omega = 0, \tag{8.38}$$

where Ω represents the solution domain whose boundary is denoted Γ and ω is an as-yet-unspecified weighting function. The presence of this weighting function leads to the term weighted residual for this approach. It should be noted that there is nothing inferior or inadequate about the weak form of the equation when compared with the strong form.

In terms of the numerical techniques outlined in the subsequent sections, the finite element method (FEM) and the boundary element method (BEM) both solve the weak form while the finite difference method (FDM) solves the strong form. Consequently the FEM and BEM enforce the governing equation in an integral sense, i.e., the governing equation will be satisfied over each element but not necessarily at any given point. Finite differences, on the other hand, do satisfy the governing equation at the difference points but not necessarily within the space between these points.

The choice of numerical approach is closely tied to the specific forward problem and there is no single best method for all applications [4]. The finite difference method (FDM) is intuitively the most straightforward, because it directly estimates the derivatives explicit in the strong form of the equation (Poisson's or Laplace's). However, the FDM usually requires a regularly sampled, orthogonal grid for the solution domain, which is rarely the most efficient way to describe complex geometries as they arise in the body. The FDM method requires this grid to encompass the entire volume and can represent anisotropic characteristics of this domain. As a result, the FDM approach has seen widespread use in models of regular slabs of myocardium [175, 176] and also to represent the whole torso [117, 177–180]. Recent studies have even suggested a generalized FDM approach suitable for irregular grids applied to the bidomain method [181].

The boundary element method (BEM) is based on a grid of the boundaries of a region, e.g., the surfaces that surround the heart, torso, and internal organs of differing electrical conductivity. The BEM is well suited to inhomogeneous tissues but not to regions with anisotropy. Its major advantage lies in the requirement only for surface descriptions, which is often the first step in creating volume grids and is more flexible and easily adjustable than finite element (or finite volume) methods. A related advantage comes from the fact that the number of nodes – the degrees of freedom – involved in the computation is smaller for BEM than FEM (surface rather than volume). As a result, the matrices involved in solving the forward problem by the BEM are generally much smaller than in the other methods, although, the latter involve sparse matrices so that the overall size of the computation may ultimately be comparable.

Applications of the boundary element method to forward problems in electrocardiography abound and virtually all the early simulation studies (as well as many contemporary studies) have made use of this technique [38, 40, 41, 44, 64, 88, 182–186].

The finite element method (FEM) and the related finite volume method (FVM) have gained broad support in the past decade, in large part for their general utility, their ability to include all forms of tissue conductivity, and the advanced

support available in the form of efficient computational implementations. The chief disadvantage of the FEM is the requirement for carefully constructed volumetric meshes of nodes and polygons: a task that is still arguably the largest barrier to practical use of all forms of numerical methods for partial differential equations. Any changes in geometry of the heart or torso also require a reorganization of the mesh, often best achieved by starting again from the beginning (or at least from the adjusted surfaces). Perhaps the first widely published use of the FEM was from Colli-Franzone et al. [187] but many others have also adopted this technique for all types of electrocardiographic field problems [48, 50, 97, 152, 188–197]. A particularly novel approach has been to combine techniques, taking advantage of their relative strengths in appropriate portions of the solution domain [198, 199].

We now provide brief descriptions of the major numerical methods used for electrocardiographic forward problems and refer the reader to more detailed descriptions.

8.6.2 The Finite Difference Method (FDM)

The finite difference method represents arguably the simplest approach to solving the generalized Laplace equation governing the potential fields and current flows within the torso volume conductor. The inherent simplicity of the FDM relies on an underlying mesh that is a grid of evenly spaced solution points distributed along orthogonal axes across the solution domain. Meshes for the FDM are relatively easy to construct, at least for pieces of tissue that represent rectilinear slabs or in cases for which image data with equal sampling in all directions are available. The resulting system of equations has some advantageous structure that can facilitate computational solution approaches.

The FDM solves the strong or differential form of the generalized Laplace equation shown in (8.37) and thus depends on estimates of first and second spatial derivatives of the potential field variable, ϕ, and the conductivity tensor, σ. The method is illustrated here over a two-dimensional domain but easily extends to three dimension. Expanding (8.37) gives

$$\begin{aligned}\nabla \cdot (\sigma \nabla \phi) = {} & \frac{\partial \sigma_{11}}{\partial x}\frac{\partial \phi}{\partial x} + \sigma_{11}\frac{\partial^2 \phi}{\partial x^2} + \frac{\partial \sigma_{12}}{\partial x}\frac{\partial \phi}{\partial y} + \sigma_{12}\frac{\partial^2 \phi}{\partial x \partial y} \\ & + \frac{\partial \sigma_{21}}{\partial y}\frac{\partial \phi}{\partial x} + \sigma_{21}\frac{\partial^2 \phi}{\partial x \partial y} + \frac{\partial \sigma_{22}}{\partial y}\frac{\partial \phi}{\partial y} + \sigma_{22}\frac{\partial^2 \phi}{\partial y^2},\end{aligned} \tag{8.39}$$

where the two subscripts on σ indicate the value from the appropriate row and column of the conductivity tensor.

Several simplifications may be possible at this stage. If the principle axes of the conductivity tensor are aligned with the coordinate axes then the terms involving σ_{12} and σ_{21} can be omitted. A further simplification is possible if the conductivity tensor is homogeneous throughout the solution domain, in which case the four terms involving derivatives of σ can be omitted. Here, however, we proceed without a loss of generality.

Each continuous partial derivative in (8.39) may be approximated by a discrete finite difference that is usually formed from a truncated Taylor's series expansion of the dependent variable in terms of values at neighboring points. Given a regular mesh with a constant spacing in the x (i) direction of Δx and a constant y (j) spacing of Δy, it is possible to describe, for example, the point one step away in the negative x direction as $(i-1)\,(j)$. Similarly, the point located at $(+\Delta x, +\Delta y)$ from the point of interest can be denoted $(i+1)\,(j+1)$. While a number of formulations are possible using differing numbers of surrounding points to control the accuracy of the approximation, the most common approximation is a second-order, central finite differencing scheme. Using this approach, the second-order partial derivatives from (8.39) can be approximated from a Taylor's series expansion as

$$\frac{\partial^2 \phi}{\partial x^2} = \frac{\phi_{(i-1)(j)} - 2\phi_{(i)(j)} + \phi_{(i+1)(j)}}{\Delta x^2}, \tag{8.40}$$

$$\frac{\partial^2 \phi}{\partial y^2} = \frac{\phi_{(i)(j-1)} - 2\phi_{(i)(j)} + \phi_{(i)(j+1)}}{\Delta y^2}, \tag{8.41}$$

$$\frac{\partial^2 \phi}{\partial x \partial y} = \frac{\phi_{(i-1)(j-1)} - \phi_{(i-1)(j+1)} - \phi_{(i+1)(j-1)} + \phi_{(i+1)(j+1)}}{\Delta x \Delta y} \tag{8.42}$$

The first-derivatives from (8.39) for a generic variable u can be approximated as

$$\frac{\partial u}{\partial x} = \frac{u_{(i+1)(j)} - u_{(i-1)(j)}}{2\Delta x}, \tag{8.43}$$

$$\frac{\partial u}{\partial y} = \frac{u_{(i)(j+1)} - u_{(i)(j-1)}}{2\Delta y}, \tag{8.44}$$

where u can be substituted for either the potential field, ϕ, or any of the σ_{ij} components as necessary.

The discrete derivative approximations given in Eqs. (8.40)–(8.44) can then be substituted into (8.39) in place of the continuous derivatives. Following this, (8.39) can be rearranged to uncover the weighting coefficients for ϕ at each referenced point resulting in an expression of the form

$$\begin{aligned} &k_1\phi_{(i-1)(j-1)} + k_2\phi_{(i)(j-1)} + k_3\phi_{(i+1)(j-1)} + k_4\phi_{(i-1)(j)} + k_5\phi_{(i)(j)} \\ &\quad + k_6\phi_{(i+1)(j)} + k_7\phi_{(i-1)(j+1)} + k_8\phi_{(i)(j+1)} + k_9\phi_{(i+1)(j+1)} = 0 \end{aligned} \tag{8.45}$$

One such equation will be generated for each finite difference point that does not lie on the boundary of the domain and the resulting equations then assembled into a matrix system of the form

$$\boldsymbol{K}\boldsymbol{\phi} = \boldsymbol{f}, \tag{8.46}$$

where the right-hand side vector, $\boldsymbol{f}$, will be zero at all internal points.

On the boundary of the solution domain, either a potential (Dirichlet) or a flux (Neumann) boundary condition must be set at every point. Dirichlet boundary conditions are set by directly specifying the value of potential at a given point. In order to preserve the matrix structure, this is often achieved by placing a "1" on the diagonal of the appropriate row and the desired value of the boundary potential in the same row of $\boldsymbol{f}$. For Neumann boundary conditions, a simple one-sided difference is often adequate, e.g.,

$$c = \sigma\frac{\partial\phi}{\partial n} = \sigma\frac{\phi_{(i+1)} - \phi_i}{\Delta x}, \tag{8.47}$$

where c is the magnitude of the flux condition (zero on the surface of the torso). The coefficients of the ϕ terms are assembled into $\boldsymbol{K}$ and c is placed into $\boldsymbol{f}$. Selecting this form of flux boundary condition preserves the symmetry of $\boldsymbol{K}$, which is also highly sparse for large meshes, and the final system can be readily solved by either direct or iterative means.

8.6.3 The Finite Element Method (FEM)

The finite element method has become increasingly pervasive in traditional engineering disciplines and is also becoming a popular solution methodology for problems in cardiac bioelectricity. The starting equation for the finite element method is the weighted residual form of the generalized Laplace equation given in (8.38), to which we apply Green's first formula, which can be thought of as a multidimensional version of integration by parts.

Given scalar fields f and g with a tensor k, Green's first formula can be written as

$$\int_\Omega \left(f\nabla\cdot(k\nabla g) + \nabla f\cdot(k\nabla g)\right)\, d\Omega = \int_\Gamma fk\nabla g\cdot\boldsymbol{n}\, d\Gamma \tag{8.48}$$

This is also known as the Green–Gauss theorem because the scalar fields must obey the divergence theorem of Gauss. Applying (8.48) to (8.38) yields

$$\int_\Omega \nabla\cdot(\sigma\nabla\phi)\,\omega d\Omega = \int_\Omega (\sigma\nabla\phi)\cdot\nabla\omega d\Omega - \int_\Gamma (\sigma\nabla\phi)\cdot\boldsymbol{n}\omega d\Gamma = 0, \tag{8.49}$$

and from (8.38) we obtain

$$\int_{\Omega} (\sigma \nabla \phi) \cdot \nabla \omega d\Omega = \int_{\Gamma} (\sigma \nabla \phi) \cdot \boldsymbol{n} \omega d\Gamma \tag{8.50}$$

To solve (8.50) using finite elements, as the name suggests, the solution domain is first subdivided into L smaller domains or elements. These elements are nonoverlapping and in combination completely cover Ω. This can be written mathematically as

$$\Omega = \bigcup_{l=1}^{L} \Omega_l \tag{8.51}$$

Typically the geometry of these elements is defined by a set of nodes which, in the simplest cases, correspond to the vertices of the elements. The set of nodes associated with a particular element are known as *local element nodes*.

Field variables can be interpolated between the local element nodes and hence over an element by what are known as *basis functions*. Instead of performing the interpolation in global space, it is preferable to introduce a local element-based coordinate system referred to here as local element or ξ space. In this space, the axes are orthogonal and the ξ directions are normalized to lie between 0 and 1 in each direction. This approach has the advantage that regardless of their physical geometry, each element in the mesh appears identical in ξ space and thus evaluating (8.50) over one element easily extends to the remaining elements. The relationship between global and local element space is illustrated in Fig. 8.14.

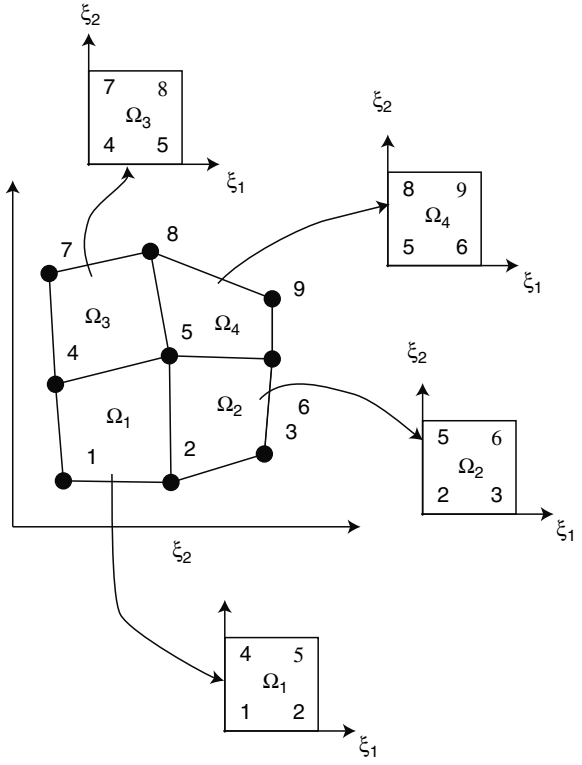

Figure 8.14

A two-dimensional example of the mapping between the solution domain Ω and local finite element space. The solution domain is divided into four finite elements, Ω_1, Ω_2, Ω_3 and Ω_4 with nine global nodes. Each of these elements is then mapped to the normalized local ξ space with four local nodes and the geometric basis functions are used to interpolate nodal quantities over these elements.

The details of the basis functions required to interpolate among the local element nodes in ξ space largely depend on the shape of each element and the number of nodes it contains (e.g., a triangular element will have three nodes while a hexahedral element will have eight). As an example, the bilinear interpolation of a variable u between the four nodes of a quadrilateral element can be described by

$$u(\xi_1, \xi_2) = \Psi_1(\xi_1, \xi_2) u_1 + \Psi_2(\xi_1, \xi_2) u_2 + \Psi_3(\xi_1, \xi_2) u_3 + \Psi_4(\xi_1, \xi_2) u_4, \tag{8.52}$$

where ξ_1 and ξ_2 represent the coordinate axes in local element space and both lie between 0 and 1 inclusive. The terms u_1, u_2, u_3 and u_4 refer to the value of u at each of the four local nodes, and the four basis functions from (8.52) can be written in terms of ξ_1 and ξ_2 as

$$\begin{aligned} \Psi_1(\xi_1, \xi_2) &= (1 - \xi_1)(1 - \xi_2) \\ \Psi_2(\xi_1, \xi_2) &= \xi_1(1 - \xi_2) \\ \Psi_3(\xi_1, \xi_2) &= (1 - \xi_1)\xi_2 \\ \Psi_4(\xi_1, \xi_2) &= \xi_1\xi_2 \end{aligned} \tag{8.53}$$

In general the interpolation of a variable over an element can be written as

$$u(\boldsymbol{\xi}) = \Psi_n(\boldsymbol{\xi}) u_n, \tag{8.54}$$

where n represents the appropriate number of local element nodes and noting the vector form of $\boldsymbol{\xi}$ indicating the presence of an appropriate number of ξ coordinates.

Using these ideas we can rewrite the volume integral from (8.50) in terms of individual elements and their local ξ coordinates as

$$\sum_{l=1}^{L} \int_{\Omega_l} (\sigma \nabla \phi) \cdot \nabla \omega \, d\Omega_l = \sum_{l=1}^{L} \int_{\mathbf{0}}^{\mathbf{1}} (\sigma \nabla \phi) \cdot \nabla \omega \, |J(\boldsymbol{\xi})| \, d\boldsymbol{\xi}, \tag{8.55}$$

where J is the Jacobian for the transformation from global to local element coordinates and all of the terms inside the resulting integral are expressed in terms of local element space. The emboldened integral notation is used to represent the presence of the appropriate number of integrals – three for a volume integral over a three-dimensional element.

To simplify the expressions in the following step, we make use of the Einstein summation convention, which states that the letter used for an index is arbitrary, a repeated index indicates a summation, and no index may be repeated more than twice. An example of such a summation is as follows.

$$x_i y_i = \sum_{i=1}^{3} x_i y_i = x_1 y_1 + x_2 y_2 + x_3 y_3 \tag{8.56}$$

Within the integral the two gradient terms may be expressed as

$$\nabla \phi = \frac{\partial \phi}{\partial \xi_k} \frac{\partial \xi_k}{\partial x_j}, \tag{8.57}$$

$$\nabla \omega = \frac{\partial \omega}{\partial \xi_h} \frac{\partial \xi_h}{\partial x_j}, \tag{8.58}$$

which is essentially just applying the chain rule for partial derivatives. For a scalar conductivity value the integrand then becomes

$$(\sigma \nabla \phi) \cdot \nabla \omega = \sigma \frac{\partial \phi}{\partial \xi_k} \frac{\partial \xi_k}{\partial x_j} \frac{\partial \omega}{\partial \xi_h} \frac{\partial \xi_h}{\partial x_j}, \tag{8.59}$$

noting the summations over h, j, and k. For information on the extension of this formula to a general conductivity tensor, please see Pullan et al. [200].

Within each element, the dependent variable to be evaluated (in this case ϕ) can be described via interpolation using basis functions and (8.54), i.e., $\phi = \Psi_n(\boldsymbol{\xi})\,\phi_n$. It is now necessary to also choose a set of weighting functions ω and a common choice are the dependent variable basis functions, i.e., $\omega = \Psi_{\mathrm{m}}(\boldsymbol{\xi})$, yielding what is known as a Galerkin finite element formulation. Equation (8.59) then becomes

$$(\sigma\nabla\phi)\cdot\nabla\omega = \phi_n\,\sigma\frac{\partial\Psi_n(\boldsymbol{\xi})}{\partial\xi_k}\frac{\partial\xi_k}{\partial x_j}\frac{\partial\Psi_m(\boldsymbol{\xi})}{\partial\xi_h}\frac{\partial\xi_h}{\partial x_j} \tag{8.60}$$

The ϕ_n terms are now no longer functions of space but instead refer specifically to the value of ϕ at the n local element nodes. Thus, they can be moved outside the integral expression, resulting in

$$\sum_{l=1}^{L}\int_{\Omega_l}(\sigma\nabla\phi)\cdot\nabla\omega\,d\Omega_l = \sum_{l=1}^{L}\phi_n\int_{\mathbf{0}}^{\mathbf{1}}\sigma\frac{\partial\Psi_n(\boldsymbol{\xi})}{\partial\xi_k}\frac{\partial\xi_k}{\partial x_j}\frac{\partial\Psi_m(\boldsymbol{\xi})}{\partial\xi_h}\frac{\partial\xi_h}{\partial x_j}\left|J(\boldsymbol{\xi})\right|d\boldsymbol{\xi}_l \tag{8.61}$$

There is seldom an analytical means of evaluating these integrals so that the numerical integration technique known as quadrature is required. The most efficient quadrature scheme for this integral is Gauss–Legendre quadrature, sometimes referred to as Gaussian quadrature [201]. For a single element, (8.61) describes a total of $m \times n$ integrals as there is no implied summation over either of these indices. In a Galerkin formulation $m = n$ and the evaluated integrals can be assembled into an element stiffness matrix, E_{mn}, that is both square and symmetric, resulting in a set of element equations of the form

$$E_{mn}\phi_n = f_m \tag{8.62}$$

Performing the required summation over all of the elements in the solution domain results in a global system of equations that is sparse and also symmetric.

$$\boldsymbol{K}\boldsymbol{\phi} = \boldsymbol{f} \tag{8.63}$$

A zero entry in $\boldsymbol{f}$ is prescribed for all nodes internal to the mesh, representing a conservation of flux at these points. Unlike the FDM, no special treatment of the boundary nodes is needed in order to construct $\boldsymbol{K}$. On the domain boundary, the same weighting function, ω, can be used to transform the boundary integral from the right-hand side of (8.50) where the dependent variable is a flux of the form $(q = (\sigma\nabla\phi)\cdot\boldsymbol{n})$.

$$\boldsymbol{f} = \sum_{l=1}^{L} q_n\int_{\mathbf{0}}^{\mathbf{1}}\Psi_n(\boldsymbol{\xi})\,\Psi_m(\boldsymbol{\xi})\left|J(\boldsymbol{\xi})\right|d\boldsymbol{\xi} \tag{8.64}$$

This gives rise to a matrix system of the form

$$\boldsymbol{K}\boldsymbol{\phi} = \boldsymbol{f} = \boldsymbol{N}\boldsymbol{q} \tag{8.65}$$

After the application of either potential (Dirichlet) or flux (Neumann) boundary conditions at each boundary node, this system can be solved for $\boldsymbol{\phi}$. In practice, the $\boldsymbol{N}$ matrix is rarely constructed and integrated flux values are inserted directly into $\boldsymbol{f}$.

8.6.4 The Boundary Element Method (BEM)

Like the FEM, the derivation of the boundary element method can begin with the weighted residual form of Laplace's equation, a highly relevant conceptual framework that is given a separate theoretical treatment in Sect. 2.6.4. Also, like the other numerical approximation methods, the endpoint of the derivation can be cast in the form of a matrix as follows.

After discretization of its integrals, Eqn. (2.172) can be expressed as

$$\phi = g - \mathbf{A}\boldsymbol{\phi}, \tag{8.66}$$

where ϕ represents the potentials at the nodes of the triangulated boundary surfaces, g are the scaled versions of the same potentials in the virtual, infinite homogeneous medium, and $\mathbf{A}$ is the expression of the inhomogeneities. Recall (Sect. 2.6.4) that in an infinite homogeneous medium the secondary sources vanish ($\sigma^- = \sigma^+$ at all interfaces), and hence, only the first term on the right remains.

Formaly, we may write

$$(\mathbf{I} - \mathbf{A})\boldsymbol{\phi} = g, \tag{8.67}$$

from which the desired potential $\boldsymbol{\phi}$ can be found as

$$\boldsymbol{\phi} = (\mathbf{I} - \mathbf{A})^{-1} g \tag{8.68}$$

By writing $(\mathbf{I} - \mathbf{A})^{-1} = \mathbf{B}$ we may write

$$\boldsymbol{\phi} = \mathbf{B}\mathbf{g} \tag{8.69}$$

and thus express the solution as a simple matrix multiplication. This expression is particularly useful in situations in which the same geometry (and conductivity) apply to a number of sets of potentials, which requires only a change in $\mathbf{g}$ as the coefficient matrix, $\mathbf{B}$, remains the same [202].

Until the 1990s, the BEM approach was the dominant method in bioelectric field problems and it still dominates the literature in problems in which current-dipole sources adequately capture the phenomena of interest, most typically in representing discrete sources of bioelectricity in the brain. As we have already seen, in the electrocardiographic forward problem the sources are usually more elaborate, which has led to a wider range of numerical approaches so that today there is a balance between BEM and FEM applications. As already described, the choice of method is multifaceted and depends on both the source formulation and the shape and nature of the volume conductor, and the ultimate goal of the study. Of particular note in the use of the BEM approach are the breakthroughs of Barr et al. in a series of seminal studies leading to the epicardial potential based electrocardiographic forward (and inverse) problem [37, 38, 182, 203]. Solutions using the BEM approach are typically best suited to conditions in which torso conductivities are at least piecewise constant and isotropic.

Of the three numerical approaches, the BEM has the longest history in the field of cardiac bioelectricity.

8.6.5 Geometric Modeling

The three numerical methods already described all assume some form of discrete representation of the geometry of the problem; the creation of these discrete descriptions is what we refer to as geometric modeling. The broader field of geometric modeling contains many additional aspects of computational geometry and computer aided geometry design that seek to capture shape and structure in analytical or statistical form so that its use in the forward problem is just one limited application. In the description to follow, we take a very pragmatic approach and outline the essential requirements for our problem.

Geometric modeling is required whenever a simulation problem has a specific geometric context, i.e., it uses neither a schematic representation of actual shape nor a geometrically simplified model made from simple shapes such as lines (planes), circles (spheres), rectangles (cylinders) in two (and three) dimensions. Instead, the geometric models of interest here describe real anatomy derived from some form of images or otherwise digitized reference points and represented as a set of points joined into polygonal elements. Thus a typical geometric modeling pipeline begins with (1) raw geometric data, often a set of medical image data from magnetic resonance (MR) or computed X-ray tomography (CT) from a particular subject or patient. These images sometimes contain specific markers or anatomical fiducial points that provide a reference frame for additional geometry information either from other discrete sources or other image modalities. The next step in the pipeline is (2) to extract from the image data the points (pixels or voxels) that define surfaces between regions of different conductivity. Obviously, the surfaces of interest include the outer boundary of the torso, the surfaces on or inside the heart, and surfaces that surround any other region whose conductivity is considered relevant to the simulation – a determination that is still the topic of research. From these surface boundaries, the next step in geometric model is usually to (3) define a set of suitable points on these boundaries and then connect them into surface polygons (lines in two dimensions and triangles or quadrilaterals in three dimensions). For methods like the BEM, the geometric

model is essentially complete at this point but for FDM and FEM, there is an additional step that (4) adds more points and links them into polygons (typically hexahedra or tetrahedra) to describe the volume of the problem domain, e.g., the heart and/or thorax.

1. **Raw geometric data**
   There are two typical sources of raw information for geometric models: medical imaging data from MR or CT and perhaps ultrasound, and sets of discrete points from some form of digitization, e.g., mechanical or electromagnetic digitizer devices, or with growing frequency, location-sensing systems incorporated into catheter-based electrophysiological mapping systems [3, 204–206]. Image data are sampled at very regular intervals, and assuming the field of view is adequate, covers the entire problem domain, even regions inside the otherwise inaccessible interior of organs and tissues.

   Each imaging modality has its own strengths and weaknesses, especially with regard to the types of tissue that appear visible in the images, e.g., CT is an X-ray based system and therefore is especially useful for revealing bone whereas MRI performs much better in differentiating soft tissues. Modern, multiscanner CT systems are very fast whereas MRI is generally slower, a concern of special impact for imaging the heart because it moves and motion artifacts can blur or distort the images and the resulting geometric model. CT, however, presents potential risk to subjects because of its use of ionizing radiation whereas MR imaging has no known risks to subjects–unless they have implanted metal devices, in which case the large magnetic fields of MR devices make this form of imaging impossible. Ultrasound is a widely used modality for medical imaging, especially in cardiac evaluations and presents no known risks to any patients; however, it is a challenging modality for geometric modeling; that quality of individual images is very poor compared with CT or MR, and perhaps more daunting, ultrasound images normally have no fixed reference frame. Instead, the region of view in ultrasound is a wedge-shaped, two-dimensional slice whose orientation depends completely on the location and orientation of a handheld probe. Intracardiac echocardiography (ICE) is a modern version of cardiac ultrasound that addresses both these limitations and has proved suitable for geometric model construction of the ventricular chamber of the heart [207, 208]. Fluoroscopy from a limited set of orientation presents a similar challenge but is constrained enough to be the source of several approaches to creating geometric models of the heart and thorax [209].

   Another challenge of using imaging data for geometric models is the sheer volume of data. Image resolution is glowing rapidly so that data sets with 512^3, or over 130 million voxels, are not unusual. Even more modest data sets of $256 \times 256 \times 100$ still represent over 6 million data values to store and manipulate. A further challenge to using imaging data for quantitative geometric models lies in the distortions and errors that are inevitable in three-dimensional modalities. Such distortions are not so relevant in the clinical use of images, much of which is based on qualitative evaluation or uses quantitative measurements only in rather small regions of the field of view, where distortions are limited. Geometric models are based on quantitative information from throughout the field of view so that corrective measures are often required. In MR imaging, for example, variations in the magnetic field strength that are present (and different) in every device require correction before they are suitable to providing accurate geometric information [210–212].

   Digitizing devices that provide another source of geometric information for models have certain advantages and disadvantages compared with imaging data. A digitizing device, either as a free standing device or as part of a catheter based mapping system, can allow a great deal of user control of the location and density of sample points. When carefully controlled, direct digitization can generate directly the set of points that are used in the polygonal model, thus omitting the segmentation step already described for image data. At a minimum, some form of resampling of points can replace segmentation at considerable savings in time and technical complexity. Of course, with high levels of user control comes a high cost in user time so that acquiring the digitized points typically takes considerably longer than an imaging scan. As we describe in Sect. 8.6.6, there are also few standard software tools for acquiring and especially manipulating digitized point sets, compared with software for at least some parts of the image acquisition and processing phase of creating geometric models. However, the single largest disadvantage of acquired geometry by means of a digitizing device is the lack of access to necessary regions of the problem domain. Digitizers can only reach surfaces adjacent to some form of air or liquid spaces as these spaces provide the physical means of access, e.g., the body surface or the inner walls of the heart chambers. Of most relevance to the electrocardiographic forward problem is the lack of access to the epicardial surface of the heart, which is crucial for many forms of the forward problem.

In cases of life-threatening arrhythmias that justify the invasive nature of the measurement, there are now methods of inserting catheters through the thoracic wall and the pericardium to reach the epicardium [213–215] so that this information is at least potentially available.

Not surprisingly, combining image and digitizer systems for generating raw model data has many advantages. One may, for example, take a CT or MR scan from a patient and then augment this with digitized locations of electrodes or sites of functional or clinical interest such as pacing, ablation, or coronary artery lesions. Because such mixed data sets come from separate scans based on their own, local, coordinate systems, it is necessary to carry out alignment or registration in order to merge them. Such registration, in turn, requires that the same points be in some form visible in all data sets. With such common points measured in each coordinate systems, it is possible to apply robust fitting methods to align these systems [216, 217] and thus create a complete data set.

2. **Segmentation**

Segmentation is a process by which, through either manual or automatic means, one extracts from image data the boundaries between regions of interest. In the context of the electrocardiographic forward problem, this step in geometric modeling typically includes identification of body and heart surfaces along with any regions of inhomogeneous electrical conductivity that should be explicitly incorporated into the model. The topic of segmentation is huge and has a substantial place within the field of computer science. Fortunately, in recent years some of the research in biomedical segmentation has resulted in software (see Sect. 8.6.6) that is useful for electrocardiographic geometry modeling; previously, many geometric models were the product of largely manual tracing of boundaries from individual images [39, 218–220]. While hardly trivial and still not completely automatic, modern segmentation algorithms are capable of identifying most of the bounding surface from which to create geometric models [117, 221–224].

3. **Surface descriptions**

From either a segmented volume or a set of digitized points, it is necessary to next identify a new set of points and polygons linking them that efficiently define the surfaces of the geometric model. The need for identifying a (possible new) set of points may not be altogether clear, especially for the case in which a set of digitized points already exists, but the quality of the resulting model depends on certain features of this point set that are rarely achieved through manual digitization. First, the distance between adjacent points will ultimately determine the size of the surface polygons that one must construct from them. The characteristic size metric for the mesh is a parameter one often wishes to adjust or control at the time of surface model generation and for numerical reasons, this parameter may even vary over the problem domain. Moreover, the selection of high quality point locations and spacing is a function of the underlying surface shape. For example, regions of sharp edges or rapid changes in surface orientation are often captured better when there are points that lie along the edges or at least with relatively higher density than over regions of relatively flat or smooth surface shape.

One common approach to defining surface boundary points is to create from each image (or in each plane in which digitized points lie) parametric descriptions of contours, e.g., B-splines or Bezier curves [225, 226]. To such contours one can then apply variable degrees of smoothing and then compute a new set of points to represent the curves with whatever density is desired. To create surfaces from the contours, one can employ a fairly simple algorithm that will "lace" adjacent sets of nodes into triangular surface elements [227–229]. Figure 8.15 shows schematically the basic configuration (Panel A) and two conditions that may confound algorithms that do not anticipate and recognize such situations (Panels B and C). The goal of the algorithm is to link points from the upper and lower layers of a pair of contours in a way that minimizes the length of the diagonal connection between opposite nodes in each quadrilateral (Segment 2–11 vs. Segment 1–12 in Panel A).

For a segmented volume data set, the need to create a smoothed boundary surface between regions is more obvious because of the tessellation that is inherent in any set of regularly spaced points. One elegant solution to this problem is the "scanline surfacing" algorithm from Weinstein et al., which even deals with abutting and interpenetrating surfaces and has found application in a variety of biomedical geometric modeling applications [230]. This approach identifies the voxels at boundaries between regions of different extracts and then smoothes not the contours, but entire surfaces. This treatment of the problem in its full three-dimensional extent allows more sophisticated recognition of surfaces and reduces the incidence of many problems (like those in Panels B and C of Figs. 8.15) that arise in contour-based methods.

Another class of approaches to the problem of creating surfaces from point sets is to fit them to piecewise analytical functions. Such fitting is part of the scanline surface algorithm [230] and others have used, for example, surface

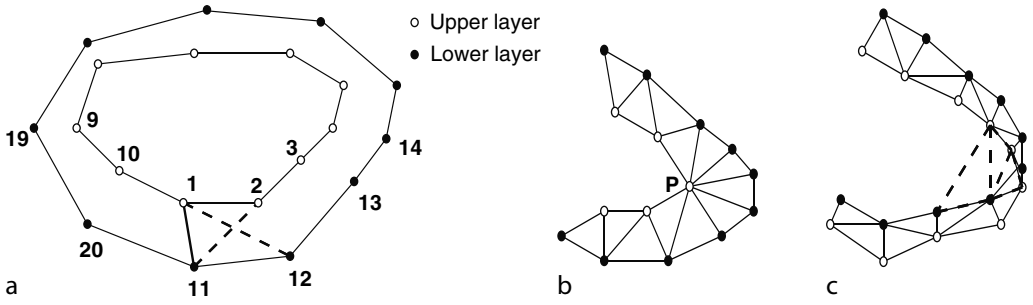

Figure 8.15

Lacing algorithm to create surfaces from surface contours. (a) shows the basic algorithm for linking nodes in surface contours from adjacent layers of a geometric model derived from segmented image data. (b and c) show two different potentially troublesome conditions that arise in such applications and for which the algorithm has to have robust solutions.

harmonics [197, 231] and Hermite polynomials [192, 232] to describe body and or heart surface geometry. Van Oosterom was one of the first to apply such an approach by using Fourier transform to represent the surface shape and then create triangulated surface meshes that are not only smooth but also optimally adjusted to aspects of the boundary element (BEM) solution he then applied to the forward problem [202]. Another approach by Gumhold et al. was to identify local surface features from an existing set of points and then refine the point locations to better represent those features without adding more points (and complexity) to the description [233]. The main advantages of any such representations is the ability from them to create models that have better characteristics in terms of, for example, smoothness, conformity to the original surfaces, and spatial resolution.

4. **Volume mesh generation**

The final step in geometric model construction, required specifically for numerical techniques like the finite difference (FDM) and finite element (FEM) methods already described. This step is known as "mesh generation" in the technical literature and usually starts with a surface representation based on triangles or quadrilaterals and produces a mesh based on tetrahedra and hexahedra respectively [234]. The main challenge of generating such a volume mesh is to introduce additional points within the volume that preserve the quality of the individual mesh elements and also respect the internal boundaries that separate regions of differing characteristics (e.g., electric conductivity). The first, and still challenging, step is to define a metric of quality that an algorithm can apply to evaluate candidate point locations. The most common choice for such a metric is the "Delaunay" criterion, which seeks to maximize the smallest internal angle of a tetrahedron and has led to many useful algorithms [234–239]. Unfortunately, a completely flat tetrahedron can meet Delaunay criteria and yet still be highly unsuitable for numerical calculations so that modifications or additions to the Delaunay criterion are necessary, a recent example of which is from Alliez et al. [240].

In many cases, the mesh that comes from a single application of any set of criteria is not optimal when it forms the basis for a computation of a particular forward problem or when exposed to different boundary conditions. In this case, some sort of adaptive approaches are necessary or at least useful. Adaptive methods seek either to increase the local resolution of a mesh or to otherwise alter it slightly in order to achieve some improvement in simulation efficiency or accuracy. For example, it is easy to imagine that in regions of high amplitude or spatial gradient of the quantity of interest, a higher resolution of the mesh could improve the simulation results. Similarly, in regions of low amplitude or low spatial gradients, it is intuitively apparent that one requires fewer points and larger elements to maintain the same levels of accuracy with reduced numbers of degrees of freedom and hence computational cost. Because full forward problems that go from cells or tissues to the body surface are always computationally daunting, any approaches that reduces degrees of freedom without meaningful loss in accuracy are of interest.

The challenges of all adaptive approaches include defining a good metric by which to determine if adaptation is actually useful and then creating robust and efficient schemes for making appropriate changes to the mesh.

This is an area of research in electrocardiographic problems and there is as yet no single approach that is effective in all cases [196, 237, 238, 241–244].

8.6.6 Software for Electrocardiographic Forward Problems

From a practical perspective, mathematical, and numerical modeling and simulation approaches are only as good as the software that implements them and that is available for scientists to apply to their own problems. As in almost all research environments, most software created in the laboratories of even the most sophisticated and experienced electrocardiographic researchers is used exclusively in those laboratories and is rarely available for other researchers to use or evaluate. Fortunately, in the area of forward simulations, this situation is better than in many other areas, perhaps a reflection of the relative maturity of at least some segments of this research domain.

Software for Cellular Simulations

Software for the simulation of membrane kinetics using the Hodgkin–Huxley formalism described in Sect. 8.3.1 is relatively widely available, although not always in the flexible, efficient, and simple-to-use form that most serious researchers seek. The simulation approach that is most widely used for cardiac myocytes is probably one of the models from Luo and Rudy [74, 75] and the authors provide a version of the software written in C/C++ at their web site (http://www.case.edu/med/CBRTC/LRdOnline/content.htm). The following is a partial list of software available for download that includes support for cardiac myocyte models.

1. *Cell electrophysiology simulation environment (CESE)*: One of the most flexible, portable, and powerful software systems for membrane modeling is a recent projects of Sergey Missan at Dalhousie University, who has created a comprehensive framework that includes implementations for all the leading forms of membrane model [245]. The software is open source and freely available at http://sourceforge.net/projects/cese/.
2. *E-Cell Project*: is an international, multicenter research project aiming at developing necessary theoretical supports, technologies, and software platforms to allow precise whole cell simulation that has recently added support for the Luo–Rudy model [246].
3. *iCell*: is a web-based program from Semahat Demir et al. at the University of Memphis for carrying out simple simulations of nerve or heart cells. It is very simple to use but there is no access to the source code nor can the application become part of another system, thus it is not useful for research (http://ssd1.bme.memphis.edu/icell/).
4. *LabHEART*: is a model of the myocyte developed by Don Bers and investigators at the Loyola University Physiology Department that includes standard electrophysiological parameters as well as a simulation of calcium concentration in the cell. The application is originally written in LabView but the authors have recently created a new version in MATLAB (http://www.luhs.org/depts/physio/personal_pages/bers_d/index.html).

Software for Tissue Simulations

The availability of software for simulation of cardiac tissue is much more limited than for cardiac myocytes, a reflection of the research state of the field and the technical complexity of especially the bidomain forms of simulation. Perhaps the only generally available software for simulation of propagation in cardiac tissue using the bidomain is Cardiowave from Henriquez et al. at Duke University. Cardiowave is capable of creating high-performance simulation programs for a range of platforms, even some that make use of vectorized and parallel computing (http://cardiowave.duke.edu/pmwiki.php). Programming cellular automata is relatively straightforward so that most researchers have developed their own code. There are numerous sources of general purpose cellular automata software, although most of these feature the Game of Life as the driving application (http://cafaq.com/other_software/index.php).

Software for Volume Conductor Problems

There are many public domain and commercial software packages for the solution of BEM, FEM, and FDM problems but only a small number of dedicated systems have been developed for use in electrocardiographic forward problems. Fortunately, these are some of the best developed and well-supported programs in this application area, providing useful entry points for a range of different types of users.

1. *CMISS*: CMISS stands for *C*ontinuum *M*echanics, *I*mage analysis, *S*ignal processing and *S*ystem Identification and is a massive software system developed by investigators at Auckland University for a broad range of problems, including the electrocardiographic forward problem. The system supports membrane models using the *XML* markup language known as *CellML*, bidomain simulations, and volume conductor simulations using both BEM and FEM techniques. (http://www.cmiss.org)
2. *ECGSIM*: ECGSIM is an interactive program that is very specifically directed at the electrocardiographic forward problem based on the uniform double layer formulation described in Sect. 8.5.5 and Chaps. 6 and 7 of this volume [247]. The user can adjust many parameters of the action potentials and immediately see the resulting changes in all relevant whole heart and body surface parameters (depolarization times, repolarization times, action potential durations and amplitudes, transmembrane potentials, and surface potentials). Figure 8.16 shows an example of creating a simulation with ECGSIM.
3. *SCIRun/BioPSE*: SCIRun is a large-scale interactive problem-solving environment developed at the University of Utah, Scientific Computing and Imaging (SCI) Institute [248, 249]. Similar to CMISS, the application domain of SCIRun is very broad, although there has always been a special emphasis on bioelectric field problems of the brain and heart [230, 250–252]. SCIRun software has several different forms of user interface including an interactive network editor for data-flow visual programming (as shown in Fig. 8.17) that allows users to create and modify networks

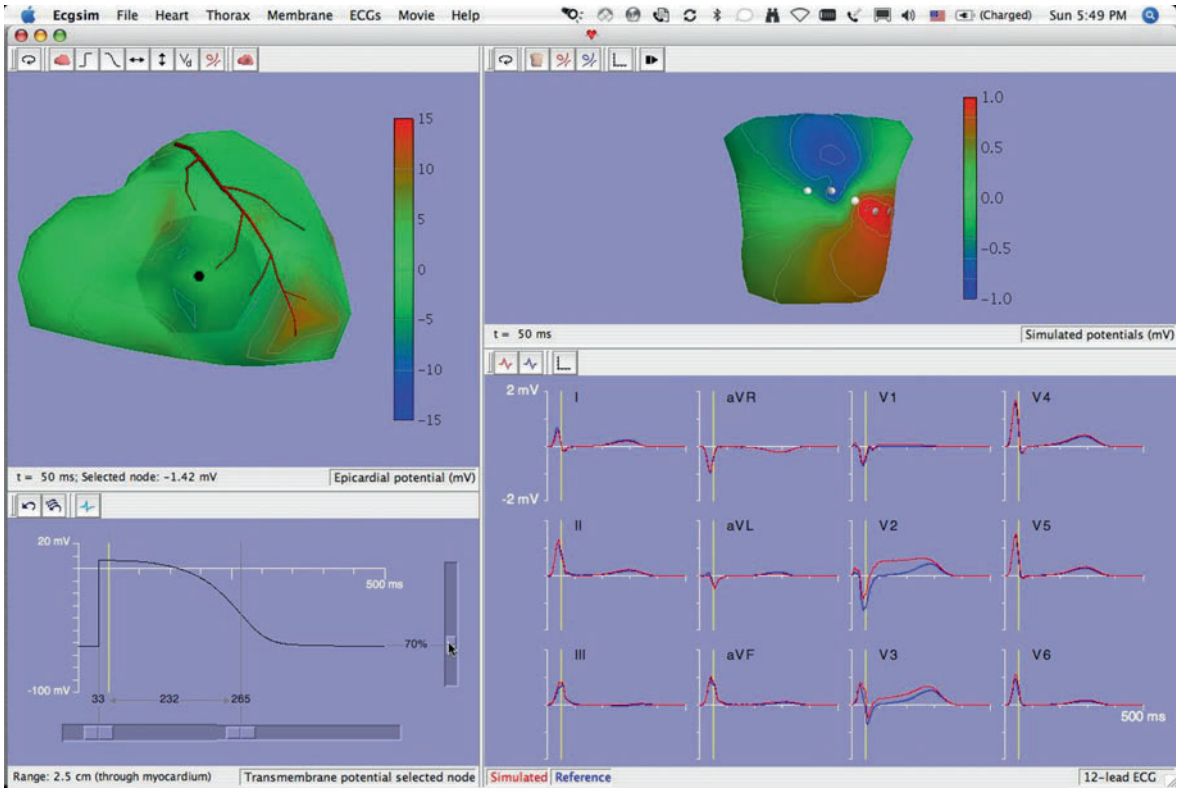

Figure 8.16

User screen for ECGSIM. The user can interact with all panels of the screen to adjust display features, select specific time instants, and adjust action potential parameters. The specific example here shows the effect of elevating the resting potential of action potentials in the anterior right ventricle similar to a local transmural ischemic region. Standard ECG signals show the standard shape (in blue) and simulated for this intervention (in red). Yellow vertical lines in the time signals show the time instant displayed in the spatial distributions of potential on epicardium and body surface.

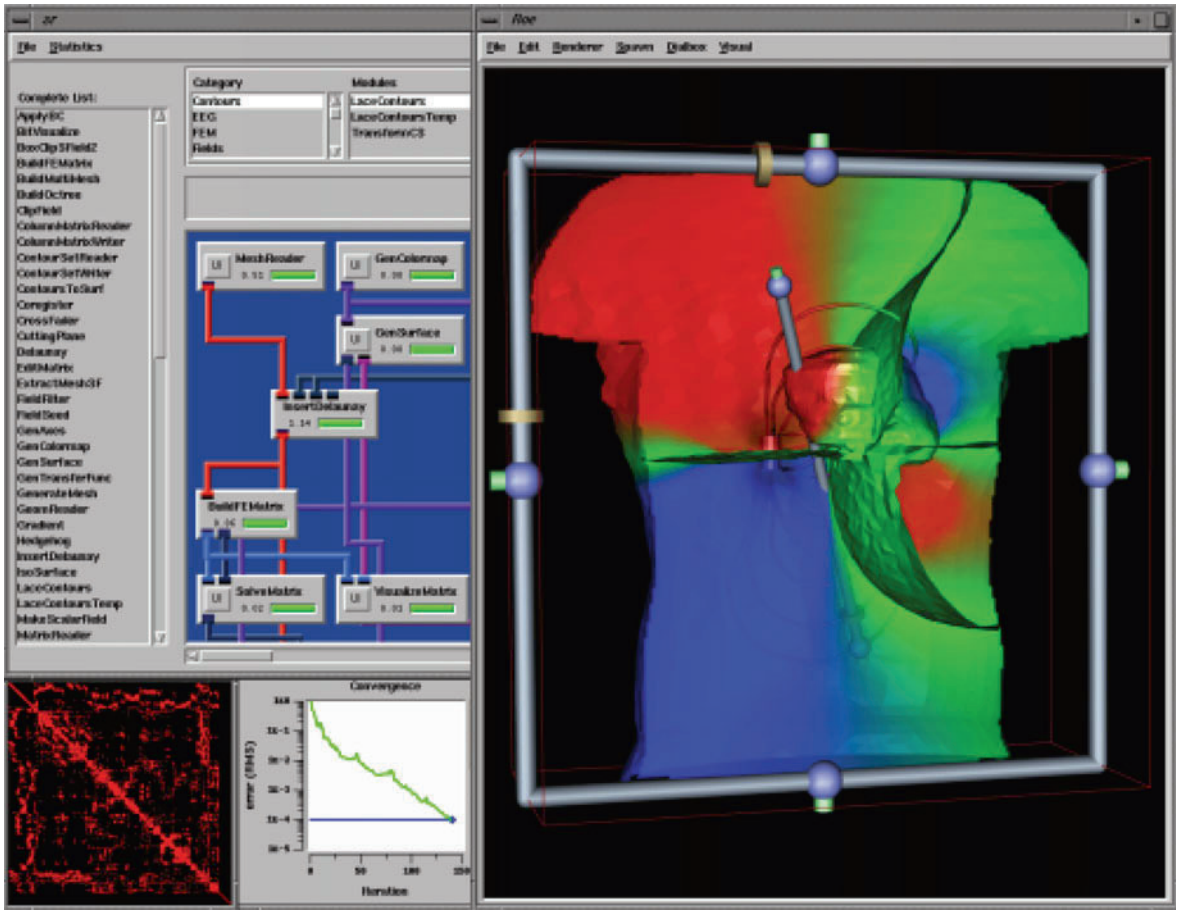

Figure 8.17

SCIRun problem-solving environment for a cardiac defibrillation forward problem. The middle pane shows the network diagram that illustrates the visual programming interface for the program while the right hand panel shows the results of a simulation of internal cardiac defibrillation. The small panels in the lower, left-hand corner show the structure of the resulting solution matrix along with a graph showing the convergence of the linear system solver over time. The user can interact with the visualization of the results and each of the blocks in the network diagram has its own user interface for control of the simulation. Moreover, the user can interactively add new blocks to the network and thus tailor the simulation to specific needs of the application.

from functional modules connected with data pipes. Less flexible but simpler for the user to learn are various forms of "PowerApps," which appear to the user as dedicated applications with a focused set of options and functionality but are actually built on underlying self-modifying networks. The SCIRun/BioPSE suite also includes a dedicated application for segmentation of volume data called Seg3D, which uses core functionality from SCIRun libraries but does not have the data-flow structure of other previous SCIRun software. Finally, the SCI Institute also supports a program called *map3d*, which provides visualization capabilities for the type of surface-based mapping data that is common to many applications of the forward problem and the experimental techniques described in Sect. 8.2 [253]. All these applications are well documented, under constant development, and freely available for download in open-source form (http://software.sci.utah.edu/scirun.html).

8.7 Outstanding Challenges of the Forward Problem

8.7.1 The Multiscale Challenge

Evidence is emerging that one day forward modeling will begin at the subcellular level and extend to predicting the clinical ECG. Such simulations are already being performed at the single and multiple cell levels, and it seems a natural progression to migrate this further up the size continuum. For example, Clancy et al. placed a Markovian model of the cardiac sodium channel within a cardiac cellular model to predict the mechanisms of early depolarization and the effects of mutations in this channel on action potential behavior [254]. The particular behavior under examination was the inactivation and subsequent reactivation of the L-type calcium channel. The same paper reported findings using a larger spatial scale in which slow conduction in a string of cardiac cells was examined. Here the conduction was slowed by reducing the conductivity of the gap junctions between the cells and not through a loss of cellular excitability. This model provided a quantitative measure of the stability of propagation and produced insights into the mechanisms behind very slow conduction that can be observed under certain conditions experimentally. For example, because of the long time taken before a neighboring cell depolarizes, Clancy et al. showed that it was actually the L-type calcium channel that provided the charge gradient for propagation to continue long after the inward sodium current has ceased. It seems a natural path for these types of simulations to consider increasingly larger tissue blocks, leading ultimately to simulations involving the whole heart and torso. Thus, a gene defect may result in a malfunctioning channel, and then, through the forward modeling, gives rise to macroscopic phenomena such as long QT syndrome.

Forward simulation of cardiac electrophysiology may be poised for a revolution driven by rapid developments in biomedicine, imaging, and computing. The completion of the first draft of the human genome sequence [255] provides fundamental information on the structure of the proteins that determine ion-channel function and transmembrane currents. This landmark event signifies the beginning of comprehensive studies of the relationship between genetic code and channel, cell, tissue, and whole-heart function, developments suggested by the authors of the genome project when they stated "In principle, the string of genetic bits holds long-sought secrets of human development, physiology, and medicine. In practice, our ability to transform such information into understanding remains woefully inadequate." Only through sophisticated use of imaging, modeling, and simulations strategies, based on enhanced computational capabilities, will it be possible to overcome these inadequacies.

The challenge therefore is clear – to integrate this incredible wealth of information to allow the determination of structure and function at all levels of biological organization. One has very little choice but to use computation simulation to help to cope with this explosion in complexity: a fact which has led to the development of the Physiome project (see http://www.physiome.org.nz/, [2, 256, 257]). The International Union of Physiological Sciences has adopted the Physiome as a major focus, with the aim of developing mathematical and computer models to integrate the observations from many laboratories into quantitative, self-consistent, and comprehensive descriptions. The models not only will provide new insights into basic science and biological mechanisms but will also fuel breakthroughs in human health. The forward problem in electrocardiography will feed into and benefit from these developments and the relatively mature simulation approaches that exist for this problem make it a natural candidate for further advances based on novel information and computational capabilities.

8.7.2 Computability

One implicit aspect of the challenge of computing the forward problem over multiple scales is the computational burden of such complexity. Computers – and the software that controls them – have always placed limits on the level of detail that a numerical simulation could feasibly incorporate so that simplification has always been required. In fact, the art of numerical simulation lies mainly in selecting the appropriate simplifications and implementing the essential components in the most efficient way possible. Similarly, computer simulations tend to require more or less fixed amounts of time; when the computers become faster or the numerical methods more efficient, the model simply becomes more detailed or enlarged in scope to incorporate more realism so that the time required is once again set at whatever a researcher considers acceptable.

The electrocardiographic forward problem has just under a century of history [6] and thus has seen many changes in the nature and form of simulations. The first simulations were based on single dipoles and required the solution to simple systems of linear equations expressed in terms of measured body-surface potentials and dipole location and/or strength [27, 161, 258]. As computers became first available to scientists and then ever more powerful, so too did the the source models, to the point where we are now able to carry out simulations of both small animal [149, 150] and human ECGs [247]. Some groups have even begun to compute some form of the full forward problem, i.e., from cellular to body-surface ECG [244, 259]. However, it is not currently possible to apply the same level of spatial or temporal detail or level of representation in all these simulations. For example to apply the bidomain equations with a biophysically realistic membrane model, which many consider the minimal acceptable approach for addressing relevant questions in electrophysiology, to a human heart model embedded within a torso model is at or beyond the limit of current computational resources [260]. As a result of this perpetual need for increased complexity, some investigators of the forward model spend significant effort focusing on techniques to improve the efficiency of the calculations [261–263]. Even with such tools, it is necessary to address many of the questions that arise in the electrocardiographic forward problem using lower resolution (and potentially incomplete) models.

8.7.3 Selection of Models/Parameters

There are many sources of variability in the solution methods and parameters for the forward problem, and selecting those most appropriate for a given set of research or clinical goals remains an open challenge. There is a wide range of cell models available for use in the bidomain equations (see, for example, www.cellml.org or ssd1.bme.memphis.edu/icell), all of which give rise to slightly different action potentials. Simulated EG's or ECG's computed using these different cell models generate quantitatively (and possibly qualitatively) different results. Similarly, as described in Sect. 8.5, there are different numerical approaches to solving the volume conductor equations that relate cardiac sources to body-surface potentials, each of which will give different results.

Even after the choice of numerical method and simulation software, however, there are many decisions related to the parameters settings required to make a working simulation. At the membrane/cellular level, one must first determine the appropriate, species-specific parameters that control the dynamics of the ion channels. To further complicate matters, there are a variety of different cell types within any heart, each of which reflects a different balance of ion-channel densities and thus has different action potential features. It is well known that there is a transition of cellular properties from the ventricular endocardium to the mid-myocardial M-cells and then to the epicardium. The affects of these variations in cell characteristics on the ECG are still under debate but may have potentially profound affects on arrhythmia generation and maintenance. The torso also consists of many tissue types, each of which could play a role in shaping the electric current in the thorax and thus the body-surface potentials. It is not yet clear what level of accuracy or fidelity in the electrical conductivity parameters is required to carry out useful forward simulations – the answer will surely depend on the particular goals of the simulation. And across all scales there are variability and uncertainty in the geometry of the problem that can have consequences on solution accuracy. Although the effects of each of these sources of variability are largely unknown as this point, the efficacy of using detailed forward simulation in the clinical arena over the longer term may depend on our ability to include these small-scale features and to understand the multiple interactions among these parameters that are associated with specific pathologies.

8.7.4 Mechanical and Chemical Interactions

The electrical activity of the heart does not occur in isolation. Many factors can significantly influence cardiac electrical activity, including cardiac mechanics, coronary blood flow, cellular metabolism, and the autonomic nervous system. Mathematical models of many of these factors are being developed, but integrating these within a forward modeling framework is extremely challenging. Such combinations will ultimately help to provide the foundations for models that link cardiac excitation to myocardial mechanics, perfusion, and regulation. This form of comprehensive simulation will

ultimately be necessary for in silico study of pathologies such as myocardial ischemia, in which reduced coronary blood flow adversely affects cell and heart function, or heart failure, in which reduced mechanical performance leads to electrical instability.

8.8 Summary

The forward problem in electrocardiography has become very broad and deep in scope in the last decades as mathematical and computational capabilities allow an unparalleled integration of behaviors in the form of simulations. Progress continues at all levels of the problem as researchers uncover the relationships between the genetic code and ion channel structure and function, examine in more and more detail the linking of cells into myocardium, and use advanced imaging and signal acquisition and processing approaches to capture the shape, structure, and bioelectric (and biomagnetic) fields from the body. At every level of this problem, computational and simulation techniques are essential, not just to gather, analyze, and visualize the experimental data but also to begin to test hypotheses about the roles and interactions of all the elements of this problem. Computers are essential to describe and evaluate possible protein structures and to predict the impact of subtle local changes in action potential shape and duration on the resulting body surface ECGs.

The role of the forward problem in cardiac electrocardiography is thus very secure and will provide an intellectual playground for basic questions at all levels of electrophysiology as well as the essential starting point for the inverse problems that we describe in the following chapter.

Acknowledgements

The authors thank their colleagues Drs. Dana Brooks and Andrew Pullan for valuable comments and suggestions for this chapter. We also gratefully acknowledge the support of the Nora Eccles Treadwell Foundation and the National Center for Research Resources (NCRR) at the NIH.

References

1. Gulrajani R.M., Models of the electrical activity of the heart and the computer simulation of the electrocardiogram. *Crit. Rev. Biomed. Eng.*, 1988;**16**: 1–66.
2. Hunter P., P. Robbins, and D. Noble, The iups human physiome project. *Pflugers Arch.*, 2002;**445**(1): 1–9.
3. Beatty G.E., S.C. Remole, M.K. Johnston, J.E. Holte, and D.G. Benditt, Non-contact electrical extrapolation technique to reconstruct endocardial potentials. *PACE*, 1994;**17**(4): 765.
4. Gulrajani R.M., F.A. Roberge, and G.E. Mailloux, The forward problem of electrocardiography, in *Comprehensive Electrocardiology*, P.W. Macfarlane and T.D. Veitch Lawrie, Editors. Pergamon Press, Oxford, England, 1989, pp. 197–236.
5. Waller A.D., A demonstration on man of electromotive changes accompanying the heart's beat. *J. Physiol.*, 1887;**8**: 229–234.
6. Einthoven W., G. Fahr, and A. de Waart, Über die Richting und manifest Grösse der Potentialschwankungen im menschlichen Herzen und über den Einfluss der Herzlage auf die Form des Elektrokardiograms. *Pflügers Arch. ges. Physiol.*, 1913;**150**:275–315.
7. Hodgkin A.L. and A.F. Huxley, Resting and action potentials in single nerve fibres. *J. Physiol.*, 1945;**10**: 176–195.
8. Neher E., B. Sakmann, and J.H. Steinbach, The extracellular patch clamp: A method for resolving currents through individual open channels in biological membranes. *Pflügers Arch. ges. Physiol.*, 1978;**37**: 219–228.
9. Ling G. and R.W. Gerard, The normal membrane potential of frog sartorius fibers. *J. Cell Physiol.*, 1949;**34**: 383–396.
10. Smith T.G., J.L. Barker, B.M. Smith, and T.R. Colburn, Voltage clamping with microelectrodes. *J. Neurosci. Methods*, 1980;**3**: 105–128.
11. Hodgkin A.L. and A.F. Huxley, A quantatative decription of membrane current and its application to conduction and excitation in nerve. *J. Physiol.*, 1952;**11**: 500–544.
12. Hodgkin A.L. and A.F. Huxley, The components of membrane conductance in the giant axon of loligo. *J. Physiol.*, 1952;**11**: 473–496.
13. Li R.A., M. Leppo, T. Miki, S. Seino, and E. Marban, Molecular basis of electrocardiographic ST-segment elevation. *Circ. Res.*, 2000;**87**(10): 837–909.
14. Lux R.L., M. Akhtar, and R.S. MacLeod, Mapping and invasive analysis, in *Foundations of Cardiac Arrhythmias: Basic Concepts and Clinical Approaches*, chapter 15, P.M. Spooner and M.R. Rosen, Editors. Marcel Dekker, New York, 2001, pp. 393–424.
15. Lux P.R. and P.R. Ershler, Reducing uncertainty in the measures of cardiac activation and recovery. in *Proceedings of the IEEE Engineering in Medicine and Biology Society 9th Annual International Conference*. IEEE Press, New York, 1987, pp. 1871–1872.
16. Ndrepepa G., E.B. Caref, H Yin, N. El-Sherif, and M. Restivo, Activation time determination by high-resolution unipolar and bipolar extracellulcar electrograms. *J. Cardiovasc. Electrophysiol.*, 1995;**6**(3): 174–188.

17. Macleod R.S., R.O. Kuenzler, B. Taccardi, and R.L. Lux, Estimation of epicardial activation maps from multielectrode venous catheter measurements. *PACE*, 1998;**21**(4): 595.
18. Ni Q., R.S. MacLeod, and R.L. Lux, Three-dimensional activation mapping in canine ventricles: Interpolation and approximation of activation times. *Ann. Biomed. Eng.*, 1999;**27**(5): 617–626.
19. Punske B.P., Q. Ni, R.L. Lux, R.S. MacLeod, P.R. Ershler, T.J. Dustman, Y. Vyhmeister, and B. Taccardi, Alternative methods of excitation time determination on the epicardial surface. In *Proceedings of the IEEE Engineering in Medicine and Biology Society 22nd Annual International Conference*, 2000.
20. Pieper C.F. and A. Pacifico, The epicardial field potential in dog: Implications for recording site density during epicardial mapping. *PACE*, 1993;**16**: 1263–1274.
21. Ni Q., R.S. MacLeod, R.L. Lux, and B. Taccardi, Interpolation of cardiac electric potentials. *Ann. Biomed. Eng.*, **1997**, 25(Suppl): 61. Biomed. Eng. Soc. Annual Fall Meeting.
22. Ni Q., R.S. MacLeod, R.L. Lux, and B. Taccardi, A novel interpolation method for electric potential fields in the heart during excitation. *Ann. Biomed. Eng.*, 1998;**26**(4): 597–607.
23. Yılmaz B., R.S. MacLeod, B.B. Punske, B. Taccardi, and D.H. Brooks, Training set selection for statistical estimation of epicardial activation mapping from intravenous multielectrode catheters. *IEEE Trans. Biomed. Eng.*, 2005;**52**(11): 1823–1831.
24. Yılmaz B., R.S. MacLeod, B.B. Punske, B. Taccardi, and D.H. Brooks, Venous catheter mapping of epicardial ectopic activation: Leadset analysis for statistical estimation. *Comp. in Biol. & Med.*, (in press), 2006.
25. Pullan A.J. and M.P. Nash, Challenges facing validation of noninvasive electrical imaging of the heart. *Ann. Noninvasive Electrocardiol.*, 2005;**10**(1): 73–82.
26. MacLeod R.S. and D.H. Brooks, Validation approaches for electrocardiographic inverse problems, in *Computational Inverse Problems in Electrocardiography* Peter Johnston, Editor. WIT Press, Ashurst, UK, 2001, pp. 229–268.
27. Burger H.C. and J.B. van Milaan, Heart-vector and leads. Part II. *Br. Heart J.*, 1947;**9**: 154–160.
28. Burger H.C. and J.B. van Milaan, Heart-vector and leads. Part III: Geometrical representation. *Br. Heart J.*, 1948;**10**: 229–333.
29. Grayzel J. and F. Lizzi, The combined influence of inhomogeneities and dipole location. *Am. Heart J.*, 1967;**74**: 503–512.
30. Grayzel J. and F. Lizzi, The performance of VCG leads in homogenous and heterogenous torsos. *J. Electrocardiol.*, 1969;**2**(1): 17–26.
31. Nagata Y., The electrocardiographic leads for telemetering as evaluated from the view point of the transfer impedance vector. *Jap. Heart J.*, 1970;**11**(2): 183–194.
32. Nagata Y., The influence of the inhomogeneities of electrical conductance within the torso on the electrocardiogram as evaluated from the view point of the transfer impedance vector. *Jap. Heart J.*, 1970;**11**(5): 489–505.
33. De Ambroggi L. and B. Taccardi, Current and potential fields generated by two dipoles. *Circ. Res.*, 1970;**27**: 910–911.
34. Mirvis D.M., F.W. Keller, R.E. Ideker, J.W. Cox, R.F. Dowdie, and D.G. Zettergren, Detection and localization of a multple epicardial electrical generator by a two dipole ranging technique. *Circ. Res.*, 1977;**41**: 551.
35. Mirvis D.M., F.W. Keller, R.E. Ideker, D.G. Zettergren, and R.F. Dowdie, Equivalent generator properties of acute ischemic lesions in the isolated rabbit heart. *Circ. Res.*, 1978;**42**: 676–685.
36. Mirvis D.M., Electrocardiographic QRS changes induced by acute coronary ligation in the isolated rabbit heart. *J. Electrocardiol.*, 1979;**12**: 141–150.
37. Barr R.C. and M.S. Spach, Inverse solutions directly in terms of potentials, in *The Theoretical Basis of Electrocardiography*, C.V. Nelson and D.B. Geselowitz, Editors.. Clarendon Press, Oxford, 1976, pp. 294–304.
38. Barr R.C., M. Ramsey, and M.S. Spach, Relating epicardial to body surface potential distributions by means of transfer coefficients based on geometry measurements. *IEEE Trans. Biomed. Eng.*, 1977;**24**: 1–11.
39. Barr R.C. and M.S. Spach, A comparison of measured epicardial potentials with epicardial potentials computed from body surface measurements in the intact dog. *Adv. Cardiol.*, 1978;**21**: 19–22.
40. Pilkington T.C., M.N. Morrow, and P.C. Stanley, A comparison of finite element and integral equation formulations for the calculation of electrocardiographic potentials. *IEEE Trans. Biomed. Eng.*, 1985;**32**: 166–173.
41. Pilkington T.C., M.N. Morrow, and P.C. Stanley, A comparison of finite element and integral equation formulations for the calculation of electrocardiographic potentials – II. *IEEE Trans. Biomed. Eng.*, 1987;**34**: 258–260.
42. Bradley C.P., M.P. Nash and D.J. Paterson, Imaging electrocardiographic dispersion of depolarization and repolarization during ischemia: simultaneous body surface and epicardial mapping. *Circ.*, 2003.
43. Oster H.S., B. Taccardi, R.L. Lux, P.R. Ershler, and Y. Rudy, Noninvasive electrocardiographic imaging: Reconstruction of epicardial potentials, electrograms, and isochrones and localization of single and multiple electrocardiac events. *Circ.*, 1997;**96**(3): 1012–1024.
44. Messinger-Rapport B.J. and Y. Rudy, Noninvasive recovery of epicardial potentials in a realistic heart-torso geometry. *Circ. Res.*, 1990;**66**(4): 1023–1039.
45. Ahmad G.F., D. H Brooks, and R.S. MacLeod, An admissible solution approach to inverse electrocardiography. *Ann. Biomed. Eng.*, 1998;**26**: 278–292.
46. Brooks D.H., G.F. Ahmad, R.S. MacLeod, and G.M. Maratos,. Inverse electrocardiography by simultaneous imposition of multiple constraints. *IEEE Trans. Biomed. Eng.*, 1999;**46**(1):3–18.
47. Burns J.E., B. Taccardi, R.S. MacLeod, and Y. Rudy, Noninvasive electrocardiographic imaging of electrophysiologically abnormal substrates in infarcted hearts: A model study. *Circ.*, 2000;**101**: 533–540.
48. Colli Franzone P., L. Guerri, B. Taccardi, and C. Viganotti, The direct and inverse problems in electrocardiology. Numerical aspects of some regularization methods and applications to data collected in isolated dog heart experiments. *Lab. Anal. Numerica C.N.R.*, Pub. N:222, 1979.
49. Colli Franzone P., G. Gassaniga, L. Guerri, B. Taccardi, and C. Viganotti, Accuracy evaluation in direct and inverse electrocardiology, In *Progress in Electrocardiography*, P.W. Macfarlane, Editor. Pitman Medical, 1979, pp. 83–87.
50. Colli Franzone P., L. Guerri, B. Taccardi, and C. Viganotti, Finite element approximation of regularized solution of the inverse potential problem of electrocardiography and application to experimental data. *Calcolo*, 1985;**22**: 91.
51. Colli Franzone P., L. Guerri, S. Tentonia, C. Viganotti, S. Spaggiari, and B. Taccardi, A numerical procedure for solving the inverse problem of electrocardiography. Analysis of the

time-space accuracy from *in vitro* experimental data. *Math. Biosci.*, 1985;**77**: 353–396.
52. Soucy B., R.M. Gulrajani, and R. Cardinal, Inverse epicardial potential solutions with an isolated heart preparation, in *Proceedings of the IEEE Engineering in Medicine and Biology Society 11th Annual International Conference*. IEEE Press, New York, 1989, pp. 193–194.
53. Oster H. and Y. Rudy, The use of temporal information in the regularization of the inverse problem of electrocardiography, in *Proceedings of the IEEE Engineering in Medicine and Biology Society 12th Annual International Conference*. IEEE Press, New York, 1990, pp. 599–600.
54. Rudy Y. and Oster H. The electrocardiographic inverse problem. *Crit. Rev. Biomed. Eng.*, 1992;**20**: 22–45.
55. MacLeod R.S., B. Taccardi, and R.L. Lux, The influence of torso inhomogeneities on epicardial potentials, in *IEEE Comput. Cardiol.*. IEEE Computer Society, 1994, pp. 793–796.
56. Brooks D.H. and R.S. MacLeod, Imaging the electrical activity of the heart: Direct and inverse approaches, in *IEEE International Conference on Image Processing*. IEEE Computer Society, 1994, pp. 548–552.
57. Brooks D.H., H. On, and R.S. MacLeod, Multidimensional multiresolution analysis of array ECG signals during PTCA procedures, in *IEEE Symposium on Time-Frequency and Time-Scale*. IEEE Computer Society, 1994, pp. 552–555.
58. Brooks D.H., G. Ahmad, and R.S. MacLeod, Multiply constrained inverse electrocardiology: Combining temporal, multiple spatial, and iterative regularization, in *Proceedings of the IEEE Engineering in Medicine and Biology Society 16th Annual International Conference*. IEEE Computer Society, 1994, pp. 137–138.
59. MacLeod R.S., B. Taccardi, and R.L. Lux, Electrocardiographic mapping in a realistic torso tank preparation, in *Proceedings of the IEEE Engineering in Medicine and Biology Society 17th Annual International Conference*. IEEE Press, New York, 1995, pp. 245–246.
60. Oster H.S., B. Taccardi, R.L. Lux, P.R. Ershler, and Y. Rudy, Electrocardiographic imaging: Noninvasive characterization of intramural myocardial activation from inverse-reconstructed epicardial potentials and electrograms. *Circ.*, 1997;**96**:1496–1507.
61. MacLeod R.S., Q. Ni, B. Punske, P.R. Ershler, B. Yilmaz, and B. Taccardi, Effects of heart position on the body-surface ECG. *J. Electrocardiol.*, 2000, **33**(Suppl): 229–238.
62. MacLeod R.S., B. Punske, S. Shome, B. Yilmaz, and B. Taccardi, The role of heart rate and coronary flow during myocardial ischemia. *J. Electrocardiol.*, 2001: 43–51.
63. MacLeod R.S., S. Shome, J.G. Stinstra, B.B. Punske, and B. Hopenfeld, Mechanisms of ischemia-induced ST-segment changes. *J. Electrocardiol.*, 2005;**38**(Suppl): 8–13.
64. Khoury D.S. and Y. Rudy, A model study of volume conductor effects on endocardial and intracavitary potentials. *Circ. Res.*, 1992;**71**(3): 511–525.
65. Khoury D.S. and Y. Rudy, Reconstruction of endocardial potentials from intracavitary probe potentials: a model study. *IEEE Comput. Cardiol.*, 1992: 9–12.
66. Lui Z.W., P.R. Ershler, B. Taccardi, R.L. Lux, D.S. Khoury, and Y. Rudy, Noncontact endocardial mapping: Reconstruction of electrocardiograms and isochrones from intracavitary probe potentials. *J. Cardiovasc. Electrophysiol.*, 1997;**8**:415–431.
67. MacLeod R.S., B. Taccardi, and R.L. Lux, Mapping of cardiac ischemia in a realistic torso tank preparation. In *Building Bridges: International Congress on Electrocardiology International Meeting*, 1995, pp. 76–77.
68. MacLeod R.S., R.L. Lux, M.S. Fuller, and B. Taccardi, Evaluation of novel measurement methods for detecting heterogeneous repolarization. *J. Electrocardiol.*, 1996;**29**(Suppl): 145–153.
69. MacLeod R.S., R.L. Lux, and B. Taccardi, A possible mechanism for electrocardiographically silent changes in cardiac repolarization. *J. Electrocardiol.*, 1997;**30**(Suppl): 114–121.
70. Hodgkin A.L. and A.F. Huxley, The dual effect of membrane potential on sodium conductance in the giant axon of loligo. *J. Physiol.*, 1952;**11**: 497–506.
71. Plonsey R. and R.C. Barr, *Bioelectricity: A Quantitative Approach*. Plenum Publishing, New York, London, 1988.
72. Keener J. and J. Sneyd, *Mathematical Physiology*. Spinger, Berlin, 1998.
73. Sachse F.B., *Computational Cardiology: Modeling of anatomy, electrophysiology, and mechanics*. Springer, Berlin, 2004.
74. Luo C.H. and Y. Rudy, A model of the ventricular cardiac action potential. *Circ. Res.*, 1991;**68**(6): 1501–1526.
75. Luo C.H. and Y. Rudy, A dynamic model of the cardiac ventricular action potential: I. Simulations of ionic currents and concentration changes. *Circ. Res.*, 1994;**74**(6): 1071–1096.
76. Einthoven W., Le telecardiogramme. *Arch. Int. de Physiol.*, 1906;**4**: 132–164.
77. Goldberger A.L. and E. Goldberger, *Clinical Electrocardiography*. C.V. Mosby, 1986.
78. Taccardi B., Distribution of heart potentials on the thoracic surface of normal human subjects. *Circ. Res.*, 1963;**1**: 341–351.
79. Macchi E., G. Arisi, and B. Taccardi, Identification of ectopic ventricular foci by means of intracavity potential mapping: A proposed method. *Acta Cardiol.*, 1992;**XLVII**(5): 421–433.
80. Cobb F.R., S.D. Blumenschein, and W.C. Sealy, Successful surgical interruption of the bundle of Kent in a patient with Wolff–Parkinson–White syndrome. *Circ.*, 1968;**38**: 1016.
81. De Ambroggi L., B. Taccardi, and E. Macchi, Body surface maps of heart potential: Tentative localization of preexcited area of forty-two Wolff–Parkinson–White patients. *Circ.*, 1976;**54**: 251.
82. Lux R.L., P.R. Ershler, K.P. Anderson, and J.W. Mason, Rapid localization of accessory pathways in WPW syndrome using unipolar potential mapping, in *Proceedings of the IEEE Engineering in Medicine and Biology Society 11th Annual International Conference*. IEEE Press, New York, 1989, pp. 195–196.
83. Shenasa M., R. Cardinal, P. Savard, M. Dubac, P. Page, and R. Nadeau, Cardiac mapping. part I: Wolff-Parkison-White syndrome. *PACE*, 1990;**13**: 223–230.
84. Shahidi A.V., P. Savard, and R. Nadeau, Forward and inverse problems of electrocardiography: Modeling and recovery of epicardial potentials in humans. *IEEE Trans. Biomed. Eng.*, 1994;**41**(3): 249–256.
85. Penney C.J., J.C. Clements, M.J. Gardner, L. Sterns, and B.M. Horáček, The inverse problem of electrocardiography: Application to localization of Wolff-Parkinson-White pre-excitation sites, in *Proceedings of the IEEE Engineering in Medicine and Biology Society 17th Annual International Conference*. IEEE Press, New York, 1995, pp. 215–216.
86. Yee R., G.J. Klein, and G.M. Guiraudon, The Wolff–Parkinson–White syndrome, in *Cardiac Electrophysiology, From Cell to Bedside*, D.P. Zipes and J. Jalife, Editors. W.B. Saunders Co., London, 1995, pp. 1199–1214.

87. Gallagher J.J., M. Gilbert, R.H. Svenson, W.C. Sealy, J. Kasell, and A.G. Wallace, Wolff–Parkinson–White syndrome: The problem, evaluation, and surgical correction. *Circ.*, 1975;**5**: 767–785.
88. Barr R.C. and T.C. Pilkington, Computing inverse solutions for an on-off heart model. *IEEE Trans. Biomed. Eng.*, 1969;**16**: 205–214.
89. Schmitt O.H., Biological information processing using the concept of interpenetrating domains, in *Information Processing in the Nervous System*, K.N. Leibovic, Editor. Springer, New York, 1969.
90. Miller W.T. and D.B. Geselowitz, Simulation studies of the electrocardiogram: I The normal heart and II Ischemia and infarction. *Circ. Res.*, 1978;**4**: 301–323.
91. Tung L., *A Bidomain Model for describing ischemic myocardial DC potentials*. PhD thesis, M.I.T., 1978.
92. Roth B.J. and J.P. Wikswo, A bidomain model for the extracellular potential and magnetic field of the cardiac tissue. *IEEE Trans. Biomed. Eng.*, 1986;**33**: 467–469.
93. Henriquez C.S. and R. Plonsey, Simulation of propagation along a cylindrical bundle of cardiac tissue–I: Mathematical formulation. *IEEE Trans. Biomed. Eng.*, 1990;**37**: 850–860.
94. Henriquez C.S. and R. Plonsey, Simulation of propagation along a cylindrical bundle of cardiac tissue–II: Results of simulation. *IEEE Trans. Biomed. Eng.*, 1990;**37**: 861–875.
95. Fischer G., B. Tilg, R. Moore, G.J.M. Huiskamp, J. Fetzer, W. Rucker, and P. Wach, A bidomain model based BEM-FEM coupling formulation for anisotropic cardiac tissue. *Ann. Biomed. Eng.*, 2000;**28**: 1228–1243.
96. Lines G., J. Sundnes, and A. Tveito, A domain embedding strategy for solving the bidomain equations on complicated geometries. *Int. J. Bioelectromagn.*, 2002;**4**(2): 53–54.
97. Hopenfeld B., Stinstra J.G., and MacLeod R.S., Mechanism for ST depression associated with contiguous subendocardial ischemia. *J. Cardiovasc. Electrophysiol.*, 2004;**15**(10):1200–1206.
98. Henriquez C.S., Simulating the electrical behavior of cardiac tissue using the bidomain model. *Crit. Rev. Biomed. Eng.*, 1993;**21**(1): 1–77.
99. Gardner M., Mathematical games. *Scient. Amer.*, October 1970: 120–123.
100. Moe G.K., W.C. Rheinboldt, and J.A. Abildskov, A computer model of fibrillation. *Am. Heart J.*, 1964;**67**: 200–220.
101. Abildskov J.A., Mechanism of the vulnerable period in a model of cardiac fibrillation. *J. Cardiovasc. Electrophysiol.*, 1990;**1**:303–308.
102. Restivo M., W. Craelius, W.B. Gough, and N. El-Sherif, A logical state model of reentrant ventricular activation. *IEEE Trans. Biomed. Eng.*, 1990;**37**: 344–353.
103. Leon L.J. and B.M. Horáček, Computer model of excitation and recovery in the anisotropic myocardium: I Rectangular and cubic arrays of excitable elements. *J. Electrocardiol.*, 1991;**24**: 1–15.
104. Grogin H.R., M.L. Stanley, S. Eisenberg, B.M. Horáček, and M.D. Lesh, Body surface mapping for localization of accessory pathways in WPW syndrome, in *IEEE Comput. Cardiol.*. IEEE Computer Society, 1992, p. 255.
105. Gharpure P.B. and C.R. Johnson, A 3-dimensional cellular automation model of the heart, in *Proceedings of the IEEE Engineering in Medicine and Biology Society 15th Annual International Conference*. IEEE Press, New York, 1993, pp. 752–753.
106. Hren R. and Punske B.B., A comparison of simulated QRS isointegral maps resulting from pacing at adjacent sites: Implications for the spatial resolution of pace mapping using body surface potentials. *J. Electrocardiol.*, 1998;**31**(Suppl): 135.
107. Hren R., J. Nenonen, and B.M. Horacek, Simulated epicardial potential maps during paced activation reflect myocardial fibrous structure. *Ann. Biomed. Eng.* 1998;**26**(6): 1022.
108. Bailie A.H., R.H. Mithchell, and J. McCAnderson, A computer model of re-entry in cardiac tissue. *Comp. in Biol. & Med.* 1990, **20**: 47–54.
109. Saxberg B.E. and R.J. Cohen, Cellular automata models for reentrant arrhythmias. *J. Electrocardiol.*, 1990**23**(Suppl): 95.
110. Leon L.J. and Horáček B.M., Computer model of excitation and recovery in the anisotropic myocardium: II Excitation in the simplified left ventricle. *J. Electrocardiol.*, 1991;**24**: 17–31.
111. Leon L.J. and B.M. Horáček, Computer model of excitation and recovery in the anisotropic myocardium: III Arrhythmogenic conditions in the simplified left ventricle. *J. Electrocardiol.*, 1991;**24**: 33–41.
112. Wei D., O. Okazaki, K. Harumi, E. Harasawa, and H. Hosaka, Comparative simulation of excitation and body surface electrocardiogram with isotropic and anisotropic computer heart models. *IEEE Trans. Biomed. Eng.*, 1995;**42**(4): 343–357.
113. Weixue L. and X. Ling, Computer simulation of epicardial potentials using a heart-torso model with realistic geometry. *IEEE Trans. Biomed. Eng.*, 1996;**43**(2): 211–217.
114. Hren R., R.S. MacLeod, G. Stroink, and B.M. Horáček, Assessment of spatial resolution of body surface potentials maps in localizing ventricular tachycardia foci. *Biomed. Technik*, 1997;**42**(Suppl): 41–44.
115. Hren R. and B.M. Horacek, Value of simulated body surface potential maps as templates in localizing sites of ectopic activation for radiofrequency ablation. *Physiol. Measur.*, 1997;**18**(4): 373.
116. Spitzer V., M.J. Ackerman, A.L. Scherzinger, and D. Whitlock, The visible human male: a technical report. *J Am Med Inform Assoc*, 1996;**3**(2): 118–130.
117. Sachse F.B., C.D. Werner, K. Meyer-Waarden, and O. Dossel, Development of a human body model for numerical calculation of electrical fields. *Comput Med Imaging Graph*, 2000;**24**(3): 165–171.
118. Freudenberg J., T. Schiemann, U. Tiede, and K.H. Hohne, Simulation of cardiac excitation patterns in a three-dimensional anatomical heart atlas. *Comput Biol Med*, 2000;**30**(4): 191–205.
119. Okajima M., T. Fujino, T. Kobayashi, and K. Yamada, Computer simulation of the propagation process in excitation of the ventricles. *Circ. Res.*, 1968;**23**(2): 203–211.
120. Solomon J.C. and R.H. Selvester, Simulation of measured activation sequence in the human heart. *Am Heart J*, 1973;**85**(4): 518–524.
121. Lorange M. and Gulrajani R.M., Computer simulation of the Wolff–Parkinson–White preexcitation syndrome with a modified miller-geselowitz heart model. *IEEE Trans. Biomed. Eng.*, 1986;**33**: 862–873.
122. Saxberg B.E., M.P. Grumbach, and R.J. Cohen, A time dependent anatomically detailed model of cardiac conduction. *Comput Cardiol*, 1985;**12**: 401–404.
123. Plonsey R. and R.C. Barr, Mathematical modeling of electrical activity of the heart. *J. Electrocardiol.*, 1987;**20**: 219–226.
124. Keener J.P., An eikonal-curvature equation for action potential propagation in myocardium. *J Math Biol*, 1991;**29**(7): 629–651.

125. Hooks D.A., K.A. Tomlinson, S.G. Marsden, I.J. LeGrice, B.H. Smaill, A.J. Pullan, and P.J. Hunter, Cardiac microstructure: implications for electrical propagation and defibrillation in the heart. *Circ. Res.*, 2002;**91**(4): 331–338.
126. Colli Franzone P., L. Guerri, and B. Taccardi, Potential distributions generated by point stimulation in a myocardial volume: Simulation studies in a model of anisotropic ventricular muscle. *J. Cardiovasc. Electrophysiol.*, 1993;**4**: 438–458.
127. Colli Franzone P., L. Guerri, and B. Taccardi, Spread of excitation in a myocardial volume: Simulation studies in a model of anisotropic ventricula muscle activated by point stimulation. *J. Cardiovasc. Electrophysiol.*, 1993;**4**: 144–160.
128. Colli Franzone P., L. Guerri, M. Pennacchio, and B. Taccardi, Spread of excitation in 3-d models of the anisotropic cardiac tissue. iii. effects of ventricular geometry and fiber structure on the potential distribution. *Math Biosci*, 1998;**151**(1): 51–98.
129. Colli-Franzone P., L. Guerri, and B. Taccardi, Modeling ventricular excitation: axial and orthotropic anisotropy effects on wavefronts and potentials. *Math Biosci*, 2004;**188**: 191–205.
130. Colli Franzone P., L.F. Pavarino, and B. Taccardi, Simulating patterns of excitation, repolarization and action potential duration with cardiac bidomain and monodomain models. *Math Biosci*, 2005;**197**(1): 35–66.
131. Taccardi B., B.B. Punske, F. Sachse, X. Tricoche, P. Colli-Franzone, L.F. Pavarino, and C. Zabawa, Intramural activation and repolarization sequences in canine ventricles. experimental and simulation studies. *J. Electrocardiol.*, Oct 2005;**38**(4 Suppl): 131–137.
132. Pullan A., L. Cheng, R. Yassi, and M. Buist, Modelling gastrointestinal bioelectric activity. *Prog. Biophys. Mol. Biol.*, 2004;**85**(2–3): 523–550.
133. Fitzhugh R., Impulses and physiological states in theoretical models of nerve membranes. *Biophys. J.*, 1961;**1**: 445–466.
134. Nagumo J., S. Arimoto, and S. Yoshizawa, An active pulse transmission line simulating nerve axons. *Proc. IRL*, 1960;**50**: 2061–2070.
135. Rogers J.M. and A.D. McCulloch, A collocation–galerkin finite element model of cardiac action potential propagation. *IEEE Trans. Biomed. Eng.*, 1994;**41**(8): 743–757.
136. Pertsov A.M., J.M. Davidenko, R. Salomonsz, W.T. Baxter, and J. Jalife, Spiral waves of excitation underlie reentrant activity in isolated cardiac muscle. *Circ. Res.*, 1993;**72**(3): 631–650.
137. Starmer C.F., D.N. Romashko, R.S. Reddy, Y.I. Zilberter, J. Starobin, A.O. Grant, and V.I. Krinsky, Proarrhythmic response to potassium channel blockade. numerical studies of polymorphic tachyarrhythmias. *Circ.*, 1995;**92**(3): 595–605.
138. Karma A., Electrical alternans and spiral wave breakup in cardiac tissue. *CHAOS*, 1994;**4**(3): 461–472.
139. Aliev R.R. and A.V. Panfilov, Modeling of heart excitation patterns caused by a local inhomogeneity. *J Theor Biol*, 1996;**181**(1): 33–40.
140. Fenton F. and A. Karma, Vortex dynamics in three-dimensional continuous myocardium with fiber rotation: Filament instability and fibrillation. *Chaos*, 1998;**8**(1): 20–47.
141. Stinstra J.G., B. Hopenfeld, and R.S. MacLeod, On the passive cardiac conductivity. *Ann. Biomed. Eng.*, 2005;**33**: 1743–1751.
142. Stinstra J.G. , S. Shome, B. Hopenfeld, C.S. Henriquez, and R.S. MacLeod, Modeling the passive cardiac conductivity during ischemia. *Comp. in Biol. & Med.*, 2005;**43**(6): 776–782.
143. Shome S., J.G. Stinstra, B. Hopenfeld, B.B. Punske, and R.S. MacLeod, A study of the dynamics of cardiac ischemia using experimental and modeling approaches, in *Proceedings of the IEEE Engineering in Medicine and Biology Society 26th Annual International Conference*. IEEE EMBS, IEEE Press, New York, 2004.
144. Muzikant A.L. and C.S. Henriquez, Paced activation mapping reveals organization of myocardial fibers: A simulation study. *J. Cardiovasc. Electrophysiol.*, 1997;**8**: 281–294.
145. Muzikant A.L. and C.S. Henriquez, Bipolar stimulation of a three-dimensional bidomain incorporating rotational anisotropy. *IEEE Trans. Biomed. Eng.*, 1998;**45**(4): 449–462.
146. Harrild D.M., R.C. Penland, and C.S. Henriquez, A flexible method for simulating cardiac conduction in three-dimensional complex geometries. *J. Electrocardiol.*, 2000;**33**(3): 241–251.
147. Tranquillo J.V., M.R. Franz, B.C. Knollmann, A.P. Henriquez, D.A. Taylor, and C.S. Henriquez, Genesis of the monophasic action potential: role of interstitial resistance and boundary gradients. *Am. J. Physiol.*, Apr 2004;**286**(4): H1370–H1381.
148. Tranquillo J.V., D.O. Burwell, and C.S. Henriquez, Analytical model of extracellular potentials in a tissue slab with a finite bath. *IEEE Trans. Biomed. Eng.*, Feb 2005;**52**(2): 334–338.
149. Weinstein D.M., C.R. Johnson, J. Tranquillo, C. Henriquez, R.S. MacLeod, and C.R. Johnson, BioPSE case study: Modeling, simulation, and visualization of three dimensional mouse heart propagation. *Int. J. Bioelectromagnet.*, 2003;**5**(1):(in press).
150. Sampson K.J. and C.S. Henriquez, Electrotonic influences on action potential duration dispersion in small hearts: a simulation study. *Am. J. Physiol.*, 2005;**289**(1): H350–H360.
151. Hopenfeld B., J.G. Stinstra, and R.S. MacLeod, The effect of conductivity on ST segment epicardial potentials arising from subendocardial ischemia. *Ann. Biomed. Eng.*, 2005;**33**(6): 751–763.
152. Frazier D.W., W. Krassowska, P.S. Chen, P.D. Wolf, E.G. Dixon, W.M. Smith, and R.E. Ideker, Extracellular field required for excitation in three-dimensional anisotropic canine myocardium. *Circ. Res.*, 1988;**63**: 147–164.
153. Trayanova N., K. Skouibine, and F. Aguel, The role of cardiac tissue structure in defibrillation. *Chaos*, 1998;**8**(1): 221–233.
154. Trayanova N. and J. Eason, Shock-induced arrhythmogenesis in the myocardium. *Chaos*, 2002;**12**(3): 962–972.
155. Trayanova N.A., R.A. Gray, D.W. Bourn, and J.C. Eason, Virtual electrode-induced positive and negative graded responses: new insights into fibrillation induction and defibrillation. *J. Cardiovasc. Electrophysiol.*, Jul 2003;**14**(7): 756–763.
156. Rodriguez B., L. Li, J.C. Eason, I.R. Efimov, and N.A. Trayanova, Differences between left and right ventricular chamber geometry affect cardiac vulnerability to electric shocks. *Circ. Res.*, Jul 2005;**97**(2): 168–175.
157. Trayanova N., Defibrillation of the heart: insights into mechanisms from modelling studies. *Exp Physiol*, 2006;**91**(2): 323–337.
158. Jolley M., J. Triedman, C.F. Westin, D.M. Weinstein, R.S. Macleod, and D.H. Brooks, Image based modeling of defibrillation in children, in *Proceedings of the IEEE Engineering in Medicine and Biology Society 28th Annual International Conference*. IEEE, IEEE Press, New York, 2006, pp. 2564–2567.
159. Wilson F.N. and R.H. Bayley, The electric field of an eccentric dipole in a homogeneous spherical conducting medium. *Circ.*, 1950;**1**: 84–92.
160. Frank E., Electric potential produiced by two point current sources in homogeneous coducting sphere. *J. Appl. Phys.*, 1952;**23**: 1225–1228.

161. Burger H.C., H.A. Tolhoek, and F.G. Backbier, The potential distribition on the body surface caused by a heart vector. calculations on some simple models. *Am. Heart J.*, 1954;**48**: 249–263.
162. Okada R.H., Potentials produced by an eccentric current dipole in a finite-length circular conducting cylinder. *IRE Trans. Med. Electron.*, 1956;**7**: 14–19.
163. Bayley R.H. and P.M. Berry, The electrical field produced by the eccentric current dipole in the nonhomogeneous conductor. *Am. Heart J.*, 1962;**63**: 808–820.
164. Bayley R.H. and P.M. Berry, The arbitrary electromotive double layer in the eccentric "heart" of the nonhomogeneous circular lamina. *IEEE Trans. Biomed. Eng.*, 1964;**11**.
165. Bayley R.H., J.M. Kalbfleisch, and P.M. Berry, Changes in the body's QRS surface potentials produced by alterations in certain compartments of the nonhomogeneous conducting model. *Am. Heart J.*, 1969;**77**.
166. Rudy Y. and R. Plonsey, The eccentric spheres model as the basis for a study of the role of geometry and inhomogeneities in electrocardiography. *IEEE Trans. Biomed. Eng.*, 1979;**26**:392–399.
167. Rudy Y. and R. Plonsey, The effects of variations in conductivity and geometrical parameters on the electrocardiogram, using an eccentric spheres model. *Circ. Res.*, 1979;**44**(1):104–111.
168. Rudy Y. and R. Plonsey, A comparison of volume conductor and source geometry effects on body surface and epicardial potentials. *Circ. Res.*, 1980;**46**: 283–291.
169. Throne R.D., L.G. Olson, T.J. Hrabik, and J.R. Windle, Generalized eigensystem techniques for the inverse problem of electrocardiography applied to a realistic heart-torso geometry. *IEEE Trans. Biomed. Eng.*, 1997;**44**(6): 447.
170. Iakovidis I. and R.M. Gulrajani, Regularization of the inverse epicardial solution using linearly constrained optimization, in *Proceedings of the IEEE Engineering in Medicine and Biology Society 13th Annual International Conference*. IEEE Press, New York, 1991, pp. 698–699.
171. Throne R. and L. Olsen, A generalized eigensystem aproach to the inverse problem of electrocardiography. *IEEE Trans. Biomed. Eng.*, 1994;**41**: 592–600.
172. Throne R. and L. Olsen, The effect of errors in assumed conductivities and geometry on numerical solutions to the inverse problem of electrocardiography. *IEEE Trans. Biomed. Eng.*, 1995;**42**: 1192–1200.
173. He S., Frequency series expansion of an explicit solution for a dipole inside a conducting sphere at low frequencies. *IEEE Trans. Biomed. Eng.*, 1998;**45**(10): 1249–1258.
174. Barr R.C. and M.S. Spachm Inverse calculation of QRS-T epicardial potentials from body surface potential distributions for normal and ectopic beats in the intact dog. *Circ. Res.*, 1978;**42**: 661–675.
175. Pollard A. and Barr R.C. Computer simulations in an anatomically based model of the human ventricular conduction system. *IEEE Trans. Biomed. Eng.*, 1991;**38**: 982.
176. Pollard A.E., M.J. Burgess, and K.W. Spitzer, Computer simulations of three-dimensional propagation in ventricular myocardium. Effects of intramural fiber rotation and inhomogeneous conductivity on epicardial activation. *Circ. Res.*, 1993;**72**(4): 744–756.
177. Budgett D.M., D.M. Monro, S.W. Edwards, and R.D. Stanbridge, Comparison of measured and computed epicardial potentials from a patient-specific inverse model. *J. Electrocardiol.*, 1993;**26**(Suppl): 165–173.
178. Sachse F.B., C. Werner, K. Meyer-Waarden, and O. Dössel, Comparison of solution to the forward problem in electrophysiology with homogeneous, heterogeneous and anisotropic impedance models. *Biomed. Technik*, 1997;**42**(Suppl): 277–280.
179. Geselowitz D.B. and J.E. Ferrara, Is accurate recording of the ECG surface laplacian feasible? *IEEE Trans. Biomed. Eng.*, April 1999**46**(4): 377–381.
180. Wu D., H.C. Tsai, and B. He, On the estimation of the laplacian electrocardiogram during ventricular activation. *Ann. Biomed. Eng.*, 1999;**27**(6): 731–745.
181. Trew M., I. Le Grice, B. Smaill, and A. Pullan, A finite volume method for modeling discontinuous electrical activation in cardiac tissue. *Ann. Biomed. Eng.*, 2005;**33**(5):590–602.
182. Barr R.C., T.C. Pilkington, J.P. Boineau, and M.S. Spach, Determining surface potentials from current dipoles, with application to electrocardiography. *IEEE Trans. Biomed. Eng.*, 1966;**13**: 88–92.
183. Messinger-Rapport B.J. and Y. Rudy, The inverse problem in electrocardiography: A model study of the effects of geometry and conductivity parameters on the reconstruction of epicardial potentials. *IEEE Trans. Biomed. Eng.*, 1986;**33**: 667–676.
184. Rudy Y. and B.J. Messinger-Rapport, The inverse solution in electrocardiography: Solutions in terms of epicardial potentials. *Crit. Rev. Biomed. Eng.*, 1988;**16**: 215–268.
185. Derfus D.L., T.C. Pilkington, and R.E. Ideker, Calculating intracavitary potentials from measured endocardial potentials, in *Proceedings of the IEEE Engineering in Medicine and Biology Society 12th Annual International Conference*. IEEE Press, New York. 1990, p. 635.
186. Charulatha R. and Y. Rudy, Electrocardiographic imaging:I. effect of torso inhomgeneities on body surface electrocardiographic potentials. *J. Cardiovasc. Electrophysiol.*, 2001;**12**: 229–240.
187. Colli Franzone P., B. Taccardi, and C. Viganotti, An approach to inverse calculation of epicardial potentials from body surface maps. *Adv. Cardiol.*, 1978;**21**: 50–54.
188. Colli Franzone P., L. Guerri, C. Viganotti, E. Macchi, S. Baruffi, S. Spaggiari, and B. Taccardi, Potential fields generated by oblique layers modeling excitation wavefronts in the anisotropic myocardium. *Circ. Res.*, 1982;**51**: 330–346.
189. Yamashita Y. and T. Takahashi, Use of the finite element method to determine epicardial from body surface potentials under a realistic torso model. *IEEE Trans. Biomed. Eng.*, 1984;**31**: 611–621.
190. Hunter P.J., A.D. McCulloch, P.M.F. Nielsen, and B.H. Smaill, A finite element model of passive ventricular mechanics. *ASME BED*, 1988;**9**: 387–397.
191. Sepulveda N.G., J.P. Wikswo, and D.S. Echt, Finite element analysis of cardiac defibrillation current distributions. *IEEE Trans. Biomed. Eng.*, 1990;**37**: 354–365.
192. Nielsen P.M.F., I.J. Le Grice, B.H. Smaill, and P.J. Hunter, Mathematical model of geometry and fibrous structure of the heart. *Am. J. Physiol.*, 1991;**260**: H1365–H1378.
193. Panfilov A.V. and J.P. Keener, Modelling re-entry in a finite element model of the heart. *J. Physiol.*, 1993;**467**: 152.
194. Hunter P.J., P.M.F. Nielsen, B.H. Smaill, and I.J. LeGrice, An anatomical heart model with application in myocardial activation and ventricular mechanics, in *High Performance Computing in Biomedical Research*, chapter 1, T.C. Pilkington, B. Loftis, J. F. Thompson, S. L-Y Woo, T.C. Palmer, and T.F. Budinger, Editors. CRC Press, Boca Raton, 1993, pp. 3–26.

195. Klepfer R.N., C.R. Johnson, and R.S. MacLeod, The effects of inhomogeneities and anisotropies on electrocardiographic fields: A three-dimensional finite element study. *IEEE Trans. Biomed. Eng.*, 1997;**44**(8): 706–719.
196. Ramon C., Y. Wang, J. Haueisen, P. Schimpf, S. Jaruvatanadilok, and A. Ishimaru, Effect of myocardial anisotropy on the torso current flow patterns, potentials and magnetic fields. *Phys Med Biol*, 2000;**45**(5): 1141–1150.
197. Hopenfeld B., Spherical harmonic-based finite element meshing scheme for modelling current flow within the heart. *Med. & Biol. Eng. & Comp.*, 2004;**42**(6): 847–851.
198. Stanley P.C. and T.C. Pilkington, The combination method: A numerical technique for electrocardiographic calculations. *IEEE Trans. Biomed. Eng.*, 1989;**36**: 456–461.
199. Pullan A., A high-order coupled finite/boundary element torso model. *IEEE Trans. Biomed. Eng.*, 1996;**43**(3):292–298.
200. Pullan A., M.L. Buist, and L.K. Cheng, *Mathematically Modeling the electrical activity of the heart*. World Scientific Co, Singapore, 2005.
201. Phillips G.M., Numerical integration in two and three dimensions. *Comput. J.*, 1967;**10**(2): 202–204.
202. Oostendorp T.F. and A. van Oosterom, Source parameter estimation in inhomogeneous volume conductors of arbitrary shape. *IEEE Trans. Biomed. Eng.*, 1989;**36**: 382–391.
203. Barr R.C., T.C. Pilkington, J.P. Boineau, and C.L. Rogers, An inverse electrocardiographic solution with an on-off model. *IEEE Trans. Biomed. Eng.*, 1970;**17**: 49–57.
204. Zickler P., Cardiac mapping. *Biomed Instrum Technol (BTI)*, 1997;**31**(2): 173–175.
205. Smeets J., S. Ben Haim, L. Rodriguez, C. Timmermans, and H. Wellens, New method for nonfluoroscopic endocardial mapping in humans. *Circ.*, 1998;**97**: 2426–2432
206. Callans D.J., J.F. Ren, J. Michele, F.E. Marchlinski, and S.M. Dillon, Electroanatomic left ventricular mapping in the porcine model of healed anterior myocardial infarction. correlation with intracardiac echocardiography and pathological analysis. *Circ.*, 1999;**100**: 1744–1750.
207. Rao L., C. Ding, and D.S. Khoury, Nonfluoroscopic localization of intracardiac electrode-catheters combined with noncontact electrical-anatomical imaging. *Ann. Biomed. Eng.*, 2004;**32**(12): 1654–1661.
208. Ding C., L. Rao, S.F. Nagueh, and D.S. Khoury, Dynamic three-dimensional visualization of the left ventricle by intracardiac echocardiography. *Ultrasound Med. Biol.*, 2005;**31**(1): 15–21.
209. Ghanem R.N., C. Ramanathan, P. Jia, and Y. Rudy, Heart-surface reconstruction and ECG electrodes localization using fluoroscopy, epipolar geometry and stereovision: application to noninvasive imaging of cardiac electrical activity. *IEEE Trans. Med. Imaging*, 2003;**22**(10): 1307–1318.
210. Jezzard P. and R.S. Balaban, Correction for geometric distortion in echo planar images from B0 field variations. *Mag. Res. Med.*, 1995;**34**(1): 65–73.
211. Ernst T., O. Speck, L. Ittl, and L. Chang, Simultaneous correction for interdscan patient motion and geometric distortion in echoplanar imaging. *Mag. Res. Med.*, 1999;**42**: 201–205.
212. Studholme C., T. Constable, and J.S. Duncan, A phantom based investigation of non-rigid registration constraints in mapping fMRI to anatomical MRI, in *Medical Imaging 2000: Image Processing, 2000*, 2000.
213. Sosa E., M. Scanavacca, A. D'avila, and F. Pilleggi, A new technique to perform epicardial mapping in the electrophysiology laboratory. *J. Cardiovasc. Electrophysiol.*, 1996;**7**: 531–536.
214. Sosa E., M. Scanavacca, A. D'avila, J. Piccioni, O. Sanchez, J.L. Velarde, M. Silva, and B. Reolao, Endocardial and epicardial ablation guided by nonsurgical transthoracic epicardial mapping to treat recurrent of ventricular tachycardia. *J. Cardiovasc. Electrophysiol.*, 1998;**9**: 229–239.
215. Sosa E., M. Scanavacca, A. D'Avila, F. Oliviera, and J.A.F Ramires, Nonsurgical transthoracic epicardial ablation to treat recurrent of ventricular tachycardia. *J. Am. Coll. Cardiol.*, 2000;**35**(1): 1442–1449.
216. Spoor C.W. and F.E. Veldpaus, Rigid body motion calculated from spatial co-ordinates of markers. *J. Biomech.*, 1980;**13**:391–393.
217. Challis J.H., A procedure for determining rigid body transformation parameters. *J. Biomechanics*, 1995;**28**(6): 733–737.
218. Horáček B.M., *The Effect on Electrocardiographic Lead Vectors of Conductivity Inhomogeneities in the Human Torso*. PhD thesis, Dalhousie University, Halifax, N.S., Canada, 1971.
219. MacLeod R.S., C.R. Johnson, and P.R. Ershler, Construction of an inhomogeneous model of the human torso for use in computational electrocardiography, in *Proceedings of the IEEE Engineering in Medicine and Biology Society 13th Annual International Conference*. IEEE Press, New York, 1991, pp. 688–689.
220. MacLeod R.S., R.M. Miller, M.J. Gardner, and B.M. Horáček, Application of an electrocardiographic inverse solution to localize myocardial ischemia during percutaneous transluminal coronary angioplasty. *J. Cardiovasc. Electrophysiol.*, 1995;**6**: 2–18.
221. Modre R., B. Tilg, G. Fischer, F. Hanser, B. Messnarz, F.X. Roithinger, and F. Hintringer, A clinical pilot study on the accessory pathway localization accuracy applying ECG mapping, in *Proceedings of the IEEE Engineering in Medicine and Biology Society 24th Annual International Conference*, vol. 2, 2002, pp. 1381–1382.
222. Fischer G., B. Pfeifer, M. Seger, C. Hintermuller, F. Hanser, R. Modre, B. Tilg, T. Trieb, C. Kremser, F.X. Roithinger, and F. Hintringer, Computationally efficient noninvasive cardiac activation time imaging. *Methods Inf. Med.*, 2005;**44**(5): 674–686.
223. Fischer G., F. Hanser, B. Pfeifer, M. Seger, C. Hintermuller, R. Modre, B. Tilg, T. Trieb, T. Berger, F.X. Roithinger, and F. Hintringer, A signal processing pipeline for noninvasive imaging of ventricular preexcitation. *Methods Inf. Med.*, 2005;**44**(4): 508–515.
224. Pfeifer B., G. Fischer, F. Hanser, M. Seger, C. Hintermuller, R. Modre-Osprian, T. Trieb, and B. Tilg, Atrial and ventricular myocardium extraction using model-based techniques. *Methods Inf. Med.*, 2006;**45**(1): 19–26.
225. Patterson R.R., Projective transformations os the parameter of a Bernstein-Bézier curve. *ACM Trans. Graph.*, 1985;**4**(4): 276–290.
226. Robeson S.M., Spherical methods for spatial interpolation: Review and evaluation. *Cartog. Geog. Inf. Sys.*, 1997;**24**(1): 3–20.
227. Mercer R.R., G.M. McCauley, and S. Anjilvel, Approximation of surfaces in a quantitative 3-D reconstruction system. *IEEE Trans. Biomed. Eng.*, 1990;**37**: 1136–1146.
228. Vesely I., B. Eickmeier, and G. Campbell, Automated 3-D reconstruction of vascular structures from high definition casts. *IEEE Trans. Biomed. Eng.*, 1991;**38**: 1123–1129.

229. MacLeod R.S., C.R. Johnson, and M.A. Matheson, Visualization tools for computational electrocardiography. In *Visualization in Biomedical Computing*, Bellingham, Wash., 1992. Proceedings of the SPIE #1808, pp. 433–444.
230. Weinstein D., Scanline surfacing: Building separating surfaces from planar contours, in *Proceeding of IEEE Visualization 2000*, 2000, pp. 283–289.
231. Hren R. and G. Stroink, Application of the surface harmonic expansions for modeling the human torso. *IEEE Trans. Biomed. Eng.*, 1995;**42**(5): 521.
232. Bradley C.P., A.J. Pullan, and P.J. Hunter, Geometric modeling of the human torso using cubic hermite elements. *Ann. Biomed. Eng.*, 1997;**25**: 96–111.
233. Gumhold S., X. Wang, and R.S. MacLeod, Feature extraction from point clouds, in *Proceedings, 10th International Meshing Roundtable*. Sandia National Laboratories, 2001, pp. 293–305.
234. Bern M. and D. Eppstein, Mesh generation and optimal triangulation, in *Computing in Euclidean Geomtry*, F.K. Hwang and D.Z. Du, Editors. World Scientific, Singapore, 1992.
235. Lee D.T. and B.J. Schachter, Two algorithms for constructing a Delaunay triangulation. *Int. J. Comp. Inf. Sci.*, 1980;**9**: 219–242.
236. Schumaker L.L., Triangularization methods, in *Topics in Multivariate Analysis*. Academic Press, London, 1987, pp. 219–232.
237. Schmidt J.A., C.R. Johnson, J.A. Eason, and R.S. MacLeod, Applications of automatic mesh generation and adaptive methods in computational medicine, in *Modeling, Mesh Generation, and Adaptive Methods for Partial Differential Equations*, J. Flaherty and I. Babuska, Editors. Springer, Berlin, 1994, pp. 367–394.
238. Schimpf P.H., D.R. Haynor, and Y. Kim, Object-free adaptive meshing in highly heterogeneous 3-D domains. *Int. J. Biomed. Comput.*, 1996;**40**(3): 209–225.
239. Peraire J. and K. Morgan, Unstructured mesh generation including directional refinement for aerodynamic flow simulation. *Finite Elements Anal. Design*, 1997;**25**: 343.
240. Alliez P., D. Cohen-Steiner, M. Yvinec, and M. Desbrun, Variational tetrahedral meshing, in *International Conference on Computer Graphics and Interactive Techniques*. ACM Press, New York, NY, USA, 2005, pp. 617–625.
241. Yu F. and C. R. Johnson, An automatic adaptive refinement and derefinement method, in *Proceedings of the 14th IMACS World Congress*, 1944, pp. 1555–1557.
242. Livnat Y. and Johnson C.R., The effects of adaptive refinement on ill-posed inverse problems. Personal communication, 1997.
243. Schimpf P.H., Y. Wang, D.R. Haynor, and Y. Kim, Sensitivity of transvenous defibrillation models to adaptive mesh density and resolution: the potential for interactive solution times. *Int. J. Med. Inf.*, 1997;**45**(3): 193–207.
244. Lines G., P. Grottum, and A. Tveito, Modeling the electrical activity of the heart –A bidomain model of the ventricles embedded in a torso. *Comput. & Vis. Sci.*, 2003;**5**(4): 195–213.
245. Missan S. and T. F. McDonald, CESE: Cell Electrophysiology Simulation Environment. *Appl. Bioinformat.*, 2005;**4**(2): 155–156.
246. Tomita M., K. Hashimoto, K. Takahashi, T.S. Shimizu, Y. Matsuzaki, F. Miyoshi, K. Saito, S. Tanida, K. Yugi, J.C. Venter, and C.A. Hutchison. E-CELL: software environment for whole-cell simulation. *Bioinformatics*, 1999;**15**(1): 72–84.
247. van Oosterom A. and T.F. Oostendorp, ECGSIM: an interactive tool for studying the genesis of QRST waveforms. *Heart*, 2004;**90**(2): 165–168.
248. SCIRun: A Scientific Computing Problem Solving Environment, Scientific Computing and Imaging Institute (SCI), 2006.
249. BioPSE: Problem Solving Environment for modeling, simulation, image processing, and visualization for biomedical computing applications. Scientific Computing and Imaging Institute (SCI), 2006.
250. Weinstein D.M., S.G. Parker, and C.R. Johnson, A physically based mesh generation algorithm: Applications in computational medicine, in *IEEE Engineering in Medicine and Biology Society 16th Annual International Conference*. IEEE Press, New York,1994, pp. 718–719.
251. Weinstein D.M., L. Zhukov, and C.R. Johnson, Lead-field bases for EEG source imaging. *Ann. Biomed. Eng.*, 2000;**28**(9): 1059–1065.
252. Weinstein D.M., L. Zhukov, and C.R. Johnson, An inverse EEG problem solving environment and its applications to EEG source localization. *NeuroImage (suppl.)*, 2000: 921.
253. MacLeod R.S. and C.R. Johnson, Map3d: Interactive scientific visualization for bioengineering data, in *Proceedings of the IEEE Engineering in Medicine and Biology Society 15th Annual International Conference*. IEEE Press, New York, 1993, pp. 30–31. http://software.sci.utah.edu/map3d.html.
254. Clancy C.E. and Y. Rudy, Linking a genetic defect to its cellular phenotype in a cardiac arrhythmia. *Nature*, 1999**400**(6744): 566–509.
255. Venter J.C., M.D. Adams, E.W. Myers, and P.W. Li, The sequence of the human genome. *Science*, 2001**291**(5507): 1304–1351.
256. Hunter P.J. and T.K. Borg, Integration from proteins to organs: the physiome project. *Nat. Rev. Mol. Cell. Biol.*, 2003;**4**(3): 237–243.
257. Hunter P.J., The iups physiome project: a framework for computational physiology. *Prog. Biophys. Mol. Biol.*, 2004;**85**(2–3): 551–569.
258. H.C. Burger and van Milaan J.B., Heart-vector and leads. Part I. *Br. Heart J.*, 1946;**8**: 157–61.
259. Sundnes J., G.T. Lines, X. Cai, B.F. Nielsen, K.A. Mardal, and A. Tveito, *Computing the Electrical Activity in the Heart*. Spinger, Berlin, 2006.
260. Potse M., B. Dube, J. Richer, A. Vinet, and R.M. Gulrajani, A comparison of monodomain and bidomain reaction-diffusion models for action potential propagation in the human heart. *IEEE Trans. Biomed. Eng.*, 2006;**53**(12): 2425–2435.
261. Austin T.M., M.L. Trew, and A.J. Pullan, Solving the cardiac bidomain equations for discontinuous conductivities. *IEEE Trans. Biomed. Eng.*, 2006;**53**(7): 1265–1272.
262. Austin T., D. Hooks, P. Hunter, D. Nickerson, A.J. Pullan, G. Sands, B. Maaill, and M. Trew, Modelling cardiac electrical activity at the cell and tissue levels, in *Interactive and Integrative Cardiology*, vol. 1080, S. Sideman, R. Beyar, and A. Landesberg, Editors. Annals of NY Academy of Sciences, 2006;**1080**: 334–347.
263. Trew M.L., B.J. Caldwell, G.B. Sands, D.A. Hooks, D.C. Tai, T.M. Austin, I.J. LeGrice, A.J. Pullan, and B.H. Smaill, Cardiac electrophysiology and tissue structure: bridging the scale gap with a joint measurement and modelling paradigm. *Exp Physiol*, 2006;**91**(2): 355–370.

9 The Inverse Problem of Electrocardiography

Andrew J. Pullan · Leo K. Cheng · Martyn P. Nash · Alireza Ghodrati · Rob MacLeod · Dana H. Brooks

P. W. Macfarlane, A. van Oosterom, O. Pahlm, P. Kligfield, M. Janse, J. Camm (eds.), *Comprehensive Electrocardiology*, DOI 10.1007/978-1-84882-046-3_9,

9.1 Introduction

In very broad terms, the inverse problem of electrocardiography may be defined as the determination of the electrical function of the heart from a number of remote recordings of potentials on some noninvasive or minimally invasive surface. In this sense, even clinical electrocardiographic or vectorcardiographic diagnosis is an inverse problem solved on an empirical basis by using previously cataloged information. In this chapter, the phrase "inverse problem of electrocardiography" is used in its more formal sense to mean the deduction of electrical information about the heart by mathematical manipulation of the measured potentials on the body surface (or from inside the cavities of the heart). The description of this inverse problem and various forms of its solution forms the principal subject matter of this chapter. We consider the clinical interpretation of the calculated electrical information only briefly, since clinical deduction may be viewed as subsequent to the solution of the mathematical inverse problem.

In contrast to the forward problem, which can be solved uniquely to within a constant for the zero of potential, the inverse problem does not possess a complete solution that is mathematically unique. By this we mean that it is not possible to identify unique cardiac sources within the heart as long as the active region is inaccessible, because the electric field that they generate outside any closed surface enclosing them may be duplicated by equivalent single- or double-layer sources on the closed surface itself [1]. This difficulty is usually circumvented by using simplified models for the cardiac sources; in this case, the parameters of these models may be uniquely determined from the surface potentials with additional assumptions regarding the intervening volume conductor. (We note that if one takes into account the physiological constraints of cardiac bioelectricity, most notably the electrical anisotropy of cardiac tissue and the wavefront behavior of activation (or the quasi-wavefront behavior of recovery), and one considers measurements at multiple time instants, it is less clear to what extent intramural activity may indeed be imaged. This may seem contradictory to the previous statement; certainly, at any single time instant the "internal" sources are not unique. However, by considering multiple temporal measurements *as a whole*, many solutions which might well be mathematically valid on a time-instant-by-time-instant basis will now be invalid, because they represent source behavior that is nonphysiological. Thus, the spatio-temporal behavior of reasonable solutions, that is, of cardiac sources, can be used to make the space of feasible solutions smaller (in the mathematical sense) and thus make the solution closer to being unique. In summary, it is not yet clear what the limits are on the degree to which one can image intramural activity from body surface or intracavitary measurements, nor how reliable such imaging may be. We discuss in some detail in the following section how to use temporal behavior to improve inverse solutions for surface models, as well as some recent, initial attempts to reconstruct intramural activity.)

A simple description of a parametric model for the inverse problem is the vectorcardiogram (VCG), which assumes that the heart's electrical activity may be approximated by a fixed-location, variable-amplitude, variable-orientation current dipole within a finite homogeneous torso. More sophisticated inverse solutions upgrade the heart source model by using a more realistic description of cardiac depolarization/repolarization. Along with these upgraded heart models, most contemporary simulations include a realistically shaped and often patient-specific geometric model of the torso, as illustrated in Chap. 8. We note that the inverse solution cannot, in general, be obtained unless the corresponding forward problem, using the assumed heart and torso models, is solved first.

Early formulations of the inverse problem in electrocardiography treated it as a kind of extension of the traditional electrocardiogram (ECG), based on measurements made on the body surface. With the advent of intracavitary catheter-based probes for clinical electrophysiology (EP) procedures, researchers also began to use measurements from multielectrode noncontact probes, located inside one of the heart chambers, in an inverse solution to reconstruct the electric potential on the inner wall of the chamber. In the literature, this has been called the "endocardial inverse problem." However, a number of inverse solutions using body surface measurements can reconstruct parameters of electrical activity on the endocardium, and indeed, as we discuss a little later in this section, the surface upon which the measurements are made is not uniquely tied to the location of the sources to be reconstructed. Thus, it is perhaps more accurate to distinguish between measurement surface (body surface or intracavitary) and source locations (discussed in the next paragraph).

The first edition of this chapter dealt almost exclusively with inverse solutions in terms of discrete, equivalent bioelectric sources, i.e., simple-dipole, moving-dipole, multipole-series, or multiple-dipole heart models, and there is no need to repeat that excellent treatment. Here, we have chosen to describe the progression to solutions based on more

realistic sources. Thus, we concentrate on source models that capture electrophysiological parameters that one can physically measure, specifically surface potentials (epicardial and/or endocardial), transmembrane potentials on the epicardial and/or endocardial surfaces or even in the myocardium itself (Transmembrane potentials can be measured as monophasic action potentials, using floating glass microelectrodes, or optically using voltage sensitive dyes; we note, however, that these technologies are not yet suitable for the verification of inverse solutions), or that directly represent fiducial-time parameters such as activation or repolarization times (usually derived from measurements of potentials). The fact that these formulations are based on measurable quantities has opened the possibility of direct validation of the solution, a facet of all approaches that is of fundamental importance. With any discrete source approach (dipole or multipole), such direct validation is not possible because of the difficulty of relating measured activation times or potentials to equivalent dipoles. We note that the term "equivalent sources" can be somewhat ambiguous, since in some sense any source model that does not start with the true cardiac sources at the microscopic scale must use equivalent sources. Indeed, the term appears at times in the literature to mean source models such as the epicardial potential distribution. However, we use it here in the same sense as in the first edition of this book, to mean a small set of discrete dipole or multipole sources that do not attempt to closely mimic any physiological phenomenon.

As described in some detail in Chap. 8, the surface upon which these potential or temporal parameters are reconstructed is somewhat independent of the source model itself. Traditionally, potential-type sources have used a *single-surface* model (the epicardium for body-surface measurements, the endocardium for intracavitary measurements), while fiducial-time based approaches have by necessity used a combined endocardial/epicardial surface. However, as mentioned earlier, since any surface which encloses all the sources is a valid surface on which to model the sources, potential-based methods can also use a combined surface, and indeed at least one recent report [2] described such an approach. Here, to keep an appropriate level of generality, we adopt at times the convention of Messnarz et al. in [2] and use the term "heart surface potentials" (HSP) to include any relevant surface model; when needed, we will use specific variants such as epicardial, endocardial, and combined epi/endocardial potentials.

As in the first edition, any coverage of this vast topic will be incomplete and we apologize in advance for any omissions or oversights. The references cited here are representative and by no means comprehensive. An additional technical note is that we will use the terms "electrocardiology" and "electrocardiography" interchangeably in the context of this inverse problem despite possible differentiations [3].

A final introductory note before addressing the details is the importance of understanding and appreciating from the outset the difficult nature of the inverse problem. Keener and Sneyd summarized the forward/inverse problem relationship well in a recent book [4]:

- "... If the exact location and strength of this dipole surface and the conductivity tensor for the entire body were known, then we could in principle solve the Poisson equation to find the body surface potential at all times during the cardiac cycle."

- This problem is known as the forward problem of electrocardiography.
  "Even more useful ... one could determine the sources by inverting the forward problem. This problem, known as the inverse problem of electrocardiography, is even harder to solve than the forward problem ..."

Despite the conceptual simplicity of this so-called forward problem, as Keener and Sneyd point out, its solution is far from trivial. The major utility of a forward solution is that it provides a means of probing the fundamental relationships between bioelectrical sources and electrocardiographic potentials; it serves as a tool for both learning and experimenting with those relationships. This tool has clinically oriented uses (for instance, design of defibrillators [5] or mapping systems) and forward models are also needed for inverse solutions. By contrast, the most common goal of inverse solutions is to evaluate the state of the heart from remote measurements, and thus it has an explicitly clinical context. We note, however, that results of a forward solution describe *possible* pathways for source-measurement relationships, but by themselves they do not show *causality* – one can easily imagine different parameters in forward models, or even different models, leading to similar predictions of measurements. To establish causality one wants to also show *uniqueness*, or perhaps to quantify the uncertainty in the forward predictions, and this requires an inverse solution.

To appreciate the source of difficulty in the inverse problem, one must examine the extent to which it allows a unique solution, and even when it is unique, whether the problem is sufficiently constrained to actually solve in practice. Simply put, in the inverse problem one would like to *invert* the forward model, or equivalently solve for the source parameters

which, together with the forward model, explain or predict the measurements. However, a naive attempt at this is doomed to failure. As already noted, it is impossible to recreate the electrical state of each cell in the heart (or even each small cluster of cells) from surface or intracavitary electrical recordings, no matter how many recordings are available. Some of the reasons for this are described in previous chapters or will become apparent in the following sections. However, the impossibility of this reconstruction is a mathematical certainty – perhaps most simply explained by the fact that multiple configurations of cellular activity can give rise to the same measurements (that is to say, the problem is not unique). If, however, attention is restricted to finding some alternative parameters to represent the electrical activity of the heart (for instance the epicardial potential distribution), then it is possible to construct an inverse problem with a mathematically unique solution. Unfortunately, unless this problem is appropriately constrained, in all likelihood it will be ill-posed in the sense of Hadamard [6] – the solution will not depend continuously on the data, meaning that small perturbations in the input data will result in disproportionately large changes in the computed solution. This is illustrated in Fig. 9.1c, which shows computed epicardial potentials that best match the measured body surface potentials in a least-squares sense; with no constraints the results are completely erroneous. An important consequence of nonuniqueness and ill-posedness is that the level of detail that one can reconstruct from body surface electrical recordings is significantly lower than that which can be simulated with a similarly resolved forward solution.

Why does ill-posedness arise? We can consider the difficulty and the effects of ill-posedness in an electrocardiographic inverse problem as an imaging problem. The goal in this case is to reconstruct the electrical state of the heart

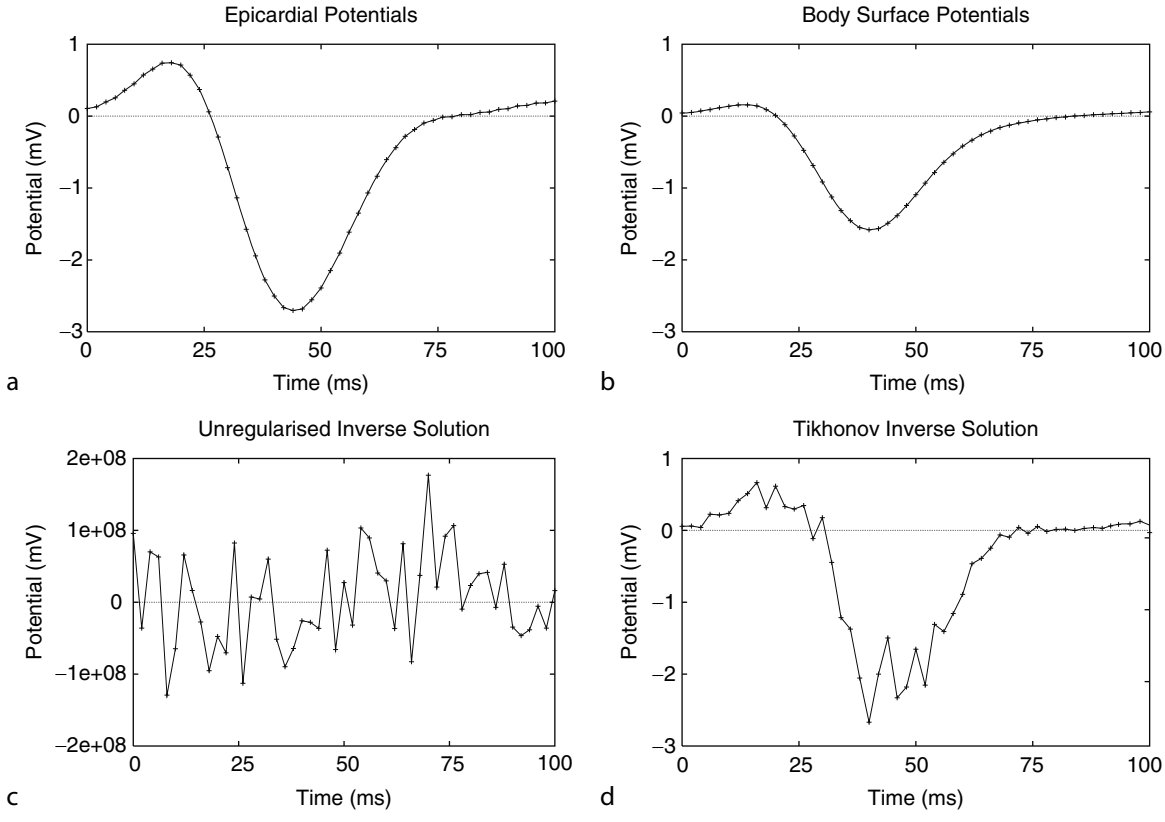

Figure 9.1

An illustration of ill-posedness. Shown are (a) epicardial and (b) body surface signals generated in a forward simulation. Also shown are resultant inverse solutions for (c) an unconstrained inverse solution taken from the data in (b); and (d) a Tikhonov regularized inverse also using data in (b) (see Sect. 9.3.1). The unconstrained epicardial signals are clearly erroneous, highlighting the ill-posedness of such an inverse problem.

just as anatomy is reconstructed using an inverse solution in the more widely known imaging modalities of magnetic resonance imaging (MRI) or computed tomography (CT). In MRI, the forward model is a (discrete) Fourier transform, and thus, there is no difficulty inverting it reliably to create an image. However, for the inverse ECG problem, the forward solution includes attenuation that is of different degrees for different spatial scales (technically, at different spatial frequencies). In particular, higher spatial frequencies (smaller-scale phenomena) are attenuated more than those with lower frequencies. As a consequence, trying to invert the forward solution directly (or solve for the "best-fit-to-data" solution) leads to the amplification of high-frequency components. Of course, any noise in the measurements and any error in the forward model will contain such high-frequency components which will then dominate unconstrained solutions, as seen in Fig. 9.1; the effects of these components on the solution must be constrained if the result is to be useful.

Put more formally, the source/data relationship is subject to the inverse square law inherent in Laplace's and Poisson's equations, while the superposition of currents that takes place in the torso volume means that each measurement is a combination of the entire set of sources – thus the measured body surface potentials are, at best, a highly blurred and attenuated version of the intracardiac sources. Deblurring (inverting) is a tractable mathematical problem only after the application of auxiliary constraints. In the absence of such constraints, the effective nonuniqueness means that there is no unique *deblurred* solution. In other words, there are many equally valid candidates for the electrical image and no way to determine which one actually represents reality. This nonuniqueness implies that one can be completely misled if the wrong solution is chosen, is clearly unacceptable for scientific or clinical applications.

Thus, the great difficulty in solving the inverse ECG problem is the identification and application of appropriate physiological and mathematically tractable constraints so that the nonuniqueness is resolved in a clinically appropriate manner, yielding a physically and physiologically meaningful image of cardiac electrical activity. Indeed, it is the design and application of such constraints as will occupy most of the rest of this chapter.

In the appendix to Chap. 2 a brief introduction is given to the matrix and vector notations used, as well as to some of the basic concepts taken from the field of linear algebra.

9.2 Inverse Problem Formulation

In this section we describe in general terms a formulation of the inverse problem that encompasses all the variants we will then describe in more detail. We will then discuss, again in general terms, solution strategies that address the ill-posedness explained in the previous section.

Two requirements for solving an electrocardiographic inverse problem are: (1) a mathematical (geometric) description of the region through which the electrical currents generated within the heart flow to the recording sensors, whether they are on the torso surface or in the intracavitary blood volume and (2) recordings of those electrical signals themselves, sampled at tens to perhaps two hundred known locations, at typically between 500 and 2,000 samples per second, using lead systems described elsewhere in this book.

Figure 9.2 illustrates the various types of inverse solutions we consider here. As the figure shows, measurements of body surface potentials can be used in one of two ways depending on the source and forward model to which they are applied: either to reconstruct potentials (surface or transmembrane) or to reconstruct fiducial times such as timing of wavefront arrivals on the epicardial and endocardial surfaces (activation times). Measurements of intracavitary potentials can be used to reconstruct surface or even transmembrane potentials as well, although to date this technique has usually been applied to reconstruct endocardial potentials.

To formalize this setting, we first summarize in a general form the results of a solution to the forward problem (note that we use general notation here, leaving more specific notation as appropriate for specific classes of formulations):

$$b = A(x) + n, \tag{9.1}$$

where A is a (possibly nonlinear) forward operator which incorporates a parameterized model of the cardiac sources and produces a prediction of the measured potentials, x holds the solution of interest (e.g., epicardial potentials or activation isochrones), b holds the measurements (whether body-surface or intracavitary), and n represents the measurement noise. For linear forward operators, A becomes a matrix $\boldsymbol{A}$ and measurements, solution and noise can be denoted as column vectors: $\boldsymbol{b}$, $\boldsymbol{x}$, and $\boldsymbol{n}$ respectively. In this situation the forward model becomes

$$\boldsymbol{b} = \boldsymbol{A}\boldsymbol{x} + \boldsymbol{n} \tag{9.2}$$

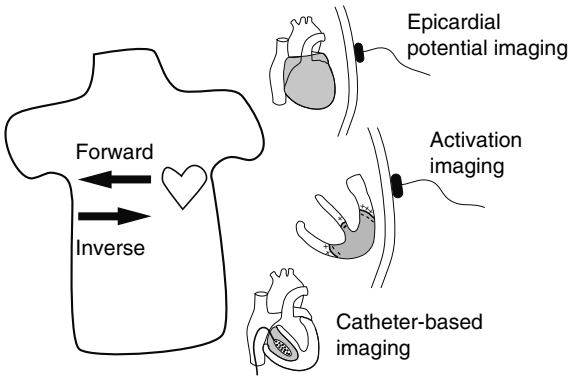

Figure 9.2

There are three basic types of inverse problems treated in this chapter, as illustrated here: in two of them, body surface measurements are used to reconstruct potentials (surface or transmembrane) or activation wavefront locations (isochrones), and in the third intracavitary potentials are used to reconstruct surface potentials.

Although we have written the forward operator A above as free of error, it is important to recognize that generaly none of the components of (9.1) or (9.2) are exact – in addition to measurement noise the forward operator is corrupted to some degree by the geometric noise arising from many sources: inaccuracies in developing the geometric model, errors associated with the numerical solution of the forward problem, errors in conductivities, etc. Moreover, the measured signals have errors in the recording of the positions of the electrodes. Errors may be considered small (e.g., signal noise below 10 microvolts, submillimeter MRI or CT image accuracy) but such errors can and do become greatly amplified in an inverse calculation, especially without careful treatment, due to the ill-posed nature of the problem.

9.2.1 Including Time in the Formulation

There are a number of ways that temporal aspects of the inverse problem can be formulated. We can consider $\boldsymbol{x}$, $\boldsymbol{b}$, and $\boldsymbol{n}$ as representing an entire temporal sequence of the relevant parameters in the case of potential sources. Alternatively, $\boldsymbol{b}$ and $\boldsymbol{n}$ could contain temporal sequences, while $\boldsymbol{x}$ could be the relevant fiducial timings for activation or recovery time source models. An alternative formulation for potential models could be to consider $\boldsymbol{x}$, $\boldsymbol{b}$, and $\boldsymbol{n}$ as spatial samples at a given time instant, and then write a temporal sequence of equations of the form of (9.1), one for each sample instant.

In the context of a linear model, $\boldsymbol{x}$, $\boldsymbol{b}$, and $\boldsymbol{n}$ in (9.2) would be block vectors formed by concatenations of the different time instants, and the matrix $\boldsymbol{A}$ would then be a large block diagonal matrix, with the forward matrix repeated in each of the diagonal blocks. Written explicitly, then, the vector $\boldsymbol{x}$ becomes

$$\boldsymbol{x} = \left[\boldsymbol{x}(t_0)^{\mathrm{T}}\, \boldsymbol{x}(t_0+1)^{\mathrm{T}} \cdots \boldsymbol{x}(t_n)^{\mathrm{T}}\right]^{\mathrm{T}}, \tag{9.3}$$

where $\boldsymbol{x}(t_i)$ is the vector formed by stacking the potentials over the solution surface at time t_i and the time instants taken into consideration range from t_0 to t_n. The block vectors for $\boldsymbol{b}$ and $\boldsymbol{n}$ would be written similarly, and then $\boldsymbol{A}$ would have the form (where here we use $\widetilde{\boldsymbol{A}}$ to represent the single time-instant forward matrix):

$$\boldsymbol{A} = \begin{bmatrix} \widetilde{\boldsymbol{A}} & \boldsymbol{0} & \cdots & \boldsymbol{0} \\ \boldsymbol{0} & \widetilde{\boldsymbol{A}} & \cdots & \boldsymbol{0} \\ \vdots & \ddots & \ddots & \vdots \\ \boldsymbol{0} & \cdots & \boldsymbol{0} & \widetilde{\boldsymbol{A}} \end{bmatrix} \tag{9.4}$$

Another useful formulation is to simply stack each time sample as one column of a matrix and then re-write the forward solution over the entire time sequence as

$$\boldsymbol{B} = \boldsymbol{A}\boldsymbol{X} + \boldsymbol{N}, \tag{9.5}$$

where the matrices $\boldsymbol{B}$, $\boldsymbol{X}$, and $\boldsymbol{N}$ have columns $\boldsymbol{b}$, $\boldsymbol{x}$, and $\boldsymbol{n}$, which are spatial vectors at discrete locations, and each row is a time series at a given spatial position. We note that the block vector/matrix formulation and the matrix/matrix formulations can be formally equated with the use of vectorization and Kronecker product operators.

We point out that there is no explicit time dependence in the forward operator A in any of the above equations. Indeed, in the inverse problem, $\boldsymbol{A}$ is generally taken to be temporally invariant, defined using the geometry of the heart in diastasis without consideration of the dynamic variation of that geometry. One could certainly argue that ignoring the dynamic nature of $\boldsymbol{A}$ (which arises as a result of heart motion, among other sources of physiological motion) is a possibly meaningful source of error. However, there are a number of justifications that support this static assumption. First, because of the delay between excitation and contraction in cardiac myocytes, significant contraction does not occur until after the QRS complex. As a result, ignoring contraction should be a reasonable approximation for imaging the depolarization of the heart. This argument is, of course, not valid for imaging repolarization, and the importance of this additional error source in repolarization imaging has yet to be determined. However, perhaps the strongest reasons for treating $\boldsymbol{A}$ as a static matrix are pragmatic ones. It is already difficult enough to obtain and use image data (e.g., MRI or CT) to create a mesh of the heart and surrounding torso volume of a specific patient at one time instance; repeating this process to construct multiple transfer operators would be prohibitive, given the present state of model-creation technology. One recent attempt to mitigate this problem has been the suggestion to use electrical impedance tomography, which may allow one to image changes in the geometry in a time-resolved fashion [7, 8]. Perhaps most important, to date, no evidence has been presented that indicates that the error incurred by assuming a fixed ventricular geometry during depolarization is as large as that arising from the many other approximations and error sources common to inverse problems.

9.2.2 The Inverse Problem

With the notation mentioned in the previous section, the inverse problem can be stated very succinctly as finding a solution x which (1) matches the measurements that the model A would predict for that particular solution to the actual measurements b and (2) also is indeed a reasonable solution for parameters of cardiac electrical activity. One can think of this as "inverting" the operator in (9.1) (although, as discussed in the following section, there are iterative approaches to finding x that do not explicitly compute an inverse, for either algorithmic or computational reasons). As we have already stated, even with a linear forward matrix and $\boldsymbol{x}$ representing a vector of epicardial potentials $\boldsymbol{\phi}$, the inverse problem is ill-posed. This ill-posedness manifests itself in the severe ill-conditioning of the matrix $\boldsymbol{A}$. There is no reason to expect $\boldsymbol{A}$ to be square, and therefore, it is typically not invertible. The usual solution in such cases, at least if the number of measurements is greater than the number of potentials to be solved for on the solution surface (so that $\boldsymbol{A}$ is over-determined, that is, it has more rows than columns), is to solve for the least-squares solution. This is the solution which minimizes the (Euclidean) magnitude of the residual error $||\boldsymbol{A}\boldsymbol{\phi} - \boldsymbol{\phi}_B||_2$ (where $\boldsymbol{\phi}$ represents the solution $\boldsymbol{x}$ for the specific case of heart surface potentials, and $\boldsymbol{\phi}_B$ represents $\boldsymbol{b}$ for the specific case of body surface measurements). The resulting solution solves the square matrix equation

$$\boldsymbol{\phi} = (\boldsymbol{A}^{\mathrm{T}}\boldsymbol{A})^{-1}\boldsymbol{A}^{\mathrm{T}}\boldsymbol{\phi}_B \tag{9.6}$$

This equation, in theory, has a unique solution if the columns of $\boldsymbol{A}$ are linearly independent (in effect, if the vectors which describe how each source location is related to all the measurement locations are not redundant). However, even in this case, $\boldsymbol{A}^{\mathrm{T}}\boldsymbol{A}$ is even more poorly conditioned than $\boldsymbol{A}$, meaning that its inverse is even more challenging to obtain reliably. In the case that the number of measurements is less than the number of cardiac locations at which one desires to estimate the relevant parameters, (i.e., the matrix $\boldsymbol{A}$ is under-determined) there can be no unique solution. The most common strategy in this case is to find a solution that minimizes the Euclidean magnitude of the residual and is itself the shortest (in Euclidean length) of the infinite number of vectors that will achieve this minimum error. The "formula"

for finding the solution is similar in spirit to (9.6). It too requires solving a very badly conditioned system of equations, which leads to the same problem as discussed in the framework of (9.6).

Thus, since the forward operator is ill-posed, a simple data fit by the minimization of the residual norm $||A(x) - b||_2^2$, for any of these formulations, leads to a (almost certainly) wildly erroneous inverse solution, with unrealistically large magnitudes, as illustrated in Fig. 9.1. To obtain a reasonable inverse solution, prior knowledge about the solution needs to be added to the problem formulation as a constraint or set of constraints. The difficulties in accomplishing this goal include identification of physiologically useful descriptions of such prior knowledge, of mathematically tractable ways of including them into the inverse problem, and of practical algorithmic approaches to solving the resulting constrained optimization problem.

The problem of determining $\boldsymbol{x}$ in (9.2) is an example of a rather general type of "inverse problem" that arises frequently in science and engineering. (For a more general treatment of inverse problems see one of the many good textbooks on the subject, for instance, Hansen [9] or Kaipio and Somersalo [10].) In inverse electrocardiography, as in other such inverse problems, common formulations fall into two categories. One is a deterministic framework, generally referred to as "regularization," in which an objective function to be minimized or a constraint function to be satisfied is composed of a combination of the norm of the residual error and some norm of a constraint function (or multiple constraint functions). The other category of formulation is a statistical framework, in which the solution is treated as random with an appropriate probability model, and a probabilistic error measure is minimized to find a likely solution.

Conceptually, deterministic regularization approaches can be summarized by two different ideas:

1. *Approximate the best-fit-to-data solution.* One or more spatial penalty functions acting on a candidate solution are defined, and then a weighted sum of these functions plus the residual norm is minimized. This approach is generally called Tikhonov regularization [9, 11, 12]. The penalty functions generally used constrain the magnitude of the inverse solution or its high spatial frequency content (often formulated via a first or second order spatial derivative). One can summarize the resulting formulation as:

$$\widehat{x}_\lambda = \text{argmin}\{||A(x) - b||_2^2 + \lambda^2 ||R(x)||\}, \tag{9.7}$$

   where R represents a "regularization operator" and λ is the regularization parameter whose value controls the level of regularization (i.e., the balance between the data fit and the amount of regularization). For a nonlinear operator A or nonlinear regularization operator R, nonlinear optimization methods are used to obtain the solution. For the linear cases, A and R become matrices and the Tikhonov solution simplifies to:

$$\widehat{\boldsymbol{x}}_\lambda = (\boldsymbol{A}^{\mathrm{T}}\boldsymbol{A} + \lambda^2 \boldsymbol{R}^{\mathrm{T}}\boldsymbol{R})^{-1}\boldsymbol{A}^{\mathrm{T}}\boldsymbol{b} \tag{9.8}$$

   (or equivalently solving $(\boldsymbol{A}^{\mathrm{T}}\boldsymbol{A} + \lambda^2 \boldsymbol{R}^{\mathrm{T}}\boldsymbol{R})\boldsymbol{x}_\lambda = \boldsymbol{A}^{\mathrm{T}}\boldsymbol{b}$ by any appropriate algorithm).
2. *Approximate the forward operator.* In this approach, the forward operator A is approximated with an operator A_{r} that is "similar" to A in some well-defined sense, but much better conditioned. Formally, given A_{r} as some well-behaved approximation of A, one solves

$$\widehat{x}_r = \text{argmin}\{||A_r(x) - b||_2^2\} \tag{9.9}$$

   In the discrete linear case, the most common version of this approach is called the Truncated Singular Value Decomposition (TSVD) [9] (see the Appendix to Chap. 2 for a discussion of the Singular Value Decomposition)), and A_{r} is $\boldsymbol{A}_{\mathrm{r}}$, a well-conditioned low-rank least squares approximation to $\boldsymbol{A}$.

We note that under quite general conditions the linear versions of these two approaches can be shown to be closely related, somewhat surprising given the difference in their conceptual underpinnings. We discuss this in more detail in what follows.

In statistical approaches $\boldsymbol{x}$ and $\boldsymbol{n}$ are considered as random vectors with given probability models. In particular, the probability model for $\boldsymbol{x}$ encodes our belief about how a reasonable, or physiological, solution should behave. The optimum Bayesian solution is the posterior mean of $\boldsymbol{x}$ [13], meaning that it is the statistical average, or expected value, of the random

solution given the data and the probability models. Applications of this approach to inverse electrocardiography to date have tended to use a simplified version of this general model with the following assumptions:

1. A linear forward matrix $\boldsymbol{A}$
2. Gaussian statistical models for both $\boldsymbol{x}$ and $\boldsymbol{n}$

Under these assumptions, the Bayesian solution becomes identical to the maximum of the posterior probability distribution of $\boldsymbol{x}$, given the measurements $\boldsymbol{b}$, and this solution is commonly called the Maximum a Posteriori (MAP) solution. With non-Gaussian models, the MAP solution is the best linear mean square error solution for $\boldsymbol{x}$, but not necessarily the optimum Bayesian solution [13].

Independent of the assumption of probability models, there are a number of ways one can treat the temporal variation of $\boldsymbol{x}$ statistically. For simplicity, we discuss the possibilities in the context of Gaussian distributions for both the unknowns and the noise, which means that we need only specify the mean and the covariance. The simplest and most widely used model assumes that each time instant is a vector drawn from a (second-order) stationary distribution; in the case of a Gaussian model, this means that a constant mean (almost always taken to be zero) and a fixed covariance matrix determine the model. One can also assume the covariance matrix to be fixed over time but let the mean be time-varying, or one can assume a constant mean but a general spatio-temporal covariance matrix, or one can let the mean vary in time and have a spatial-temporal covariance matrix as well. In any of the zero-mean cases, the MAP solution can be written as:

$$\widehat{\boldsymbol{x}}_{\mathrm{MAP}} = (\boldsymbol{A}^{\mathrm{T}}\boldsymbol{C}_n^{-1}\boldsymbol{A} + \boldsymbol{C}_x^{-1})^{-1}\boldsymbol{A}^{\mathrm{T}}\boldsymbol{C}_n^{-1}\boldsymbol{b}, \tag{9.10}$$

where $\boldsymbol{C}_x$ and $\boldsymbol{C}_n$ are appropriate solution and noise covariance matrices, respectively.

If $\boldsymbol{n}$ is assumed to be white noise ($\boldsymbol{C}_n = \sigma_n^2\boldsymbol{I}$), the solution becomes:

$$\widehat{\boldsymbol{x}}_{\mathrm{MAP}} = (\boldsymbol{A}^{\mathrm{T}}\boldsymbol{A} + \sigma_n^2\boldsymbol{C}_x^{-1})^{-1}\boldsymbol{A}^{\mathrm{T}}\boldsymbol{b} \tag{9.11}$$

Comparing this result with (9.8), we note a parallel structure; the inverse of the solution covariance matrix plays the role of the regularization term $\boldsymbol{R}^{\mathrm{T}}\boldsymbol{R}$ in the Tikhonov solution and the noise variance plays the role of the regularization parameter.

The relative strengths of the deterministic and statistical formulations lie in the ability to specify constraint functions R or statistical priors as determined by the covariance matrix $\boldsymbol{C}_x$. We will see examples of how each has been used to capture and formulate relevant assumptions about realistic solutions and to then solve the resulting version of the inverse problem.

In the following sections we explicitly deal with the various types of inverse methods that arise from different measurement locations and source assumptions. We note that several acronyms have been presented in the contemporary literature to describe some of these methods, including NICE (Noninvasive functional source imaging [14, 15]), ECGI (electrocardiographic imaging [16, 17]) and 3DEIT (three-dimensional electrocardiography imaging technique [18]).

We also note that the previous edition of this chapter [19] described in excellent detail inverse approaches based on equivalent source models, and therefore we omit coverage of these methods. They are of limited relevance to current practical applications in the heart, although they remain the topic of great attention in the localization of focal electrical activity in the brain [20].

9.3 Potential-Based Inverse Solutions from Body Surface Measurements

In this section, we describe the conceptually most straightforward version of the inverse ECG problem – reconstructing potentials on the heart surface (denoted HSP in what follows) from measurements on the body surface. As is shown in Sect. 8.54, the forward transfer between these potenials can be expressed by a matrix equation (8.36). As already discussed, the nature of the matrix involved demands a more elaborate treatment than just an inversion.

We begin with the most common variant – reconstruction of epicardial potentials – and explain in more detail the two standard deterministic approaches outlined earlier: Tikhonov regularization and TSVD. We then describe some recent efforts to achieve more reliable and accurate solutions by incorporating more prior information through use of truncation

of iterative matrix equation solutions, more complicated statistical models, multiple spatial regularization constraints, and constraints on temporal behavior. We then discuss two other potential-based source models to which inverse solutions have recently been applied: transmembrane potentials and then transmural potentials. From here on, we will use $\boldsymbol{\phi}_H(\boldsymbol{x}, t)$ to represent HSPs at positions $\boldsymbol{x}$ on the heart surface at time t, and similarly, $\boldsymbol{\phi}_B(\boldsymbol{y}, t)$ to represent the potential at positions $\boldsymbol{y}$ on the body surface.

By posing the inverse problem in terms of reconstructing heart surface potentials, the problem is linear and the resulting solution is theoretically unique [21]. However, as already noted, because the inverse problem is ill-posed, such a formulation is inherently unstable; even extremely low levels of signal noise or very small geometric errors can result in an unbounded solution. Hence, in order to stabilize the problem and to obtain a reasonable solution, it is necessary to incorporate further constraints before attempting to solve the equations. The need for constraints in epicardial solutions, graphically illustrated in Fig. 9.1, was first demonstrated by Martin and Pilkington [22] and later via singular-value decompositions of $\boldsymbol{A}$ [23, 24]. As discussed above, the most common and straightforward approach to this problem is via regularization of the inverse problem. A successful regularization procedure will yield a feasible solution that has useful properties in common with the exact solution of the underlying unperturbed problem. The main challenges in applying this approach are to determine both the type and the amount of regularization required to produce the desired solution. Regularization can be viewed as a procedure that imposes constraints on the solution, typically on its magnitude or smoothness. The goal is that these constraints relate to the underlying physiology or other known information about the solution.

Treating every individual column of the system in (9.5) independently and solving for each column, $\boldsymbol{\phi}_B$, to obtain the regularized solution, $\boldsymbol{\phi}$ of (9.6), i.e., the heart potential $\boldsymbol{\phi}_H(t)$

$$\boldsymbol{\phi}_H = \boldsymbol{A}_{\lambda_t}^{\dagger} \boldsymbol{\phi}_B, \tag{9.12}$$

where $\boldsymbol{A}_{\lambda_t}^{\dagger}$ is the regularized inverse matrix at time t (although the matrix $\boldsymbol{A}$ itself is time-invariant, its regularized inverse need not be). Next we describe in detail two of the most common specific approaches to generating the pseudo-inverse, both of which are widely used in cardiac applications.

9.3.1 Tikhonov Regularization

As stated earlier, the Tikhonov regularized solution is obtained by minimizing an appropriate objective function, i.e.,

$$\boldsymbol{\phi}_H = \min \left[\|\boldsymbol{A}\boldsymbol{\phi}_H - \boldsymbol{\phi}_B\|_2^2 + \lambda_t^2 \|\boldsymbol{R}\boldsymbol{\phi}_H\|_2^2 \right], \tag{9.13}$$

where $\boldsymbol{R}$ is an $N \times N$ constraint matrix and $\| \cdot \|_2$ is the Euclidean norm. The $\boldsymbol{R}$ term in (9.13) helps to constrain (or regularize) the inverse solution.

The first term in (9.13) represents the least-squares solution to each column of (9.5), while the second term constrains, in the spatial domain, the amplitude of the solution according to the choice of the particular constraint matrix $\boldsymbol{R}$ [25]. The constant λ_t is the *regularization parameter* at each time, t, which controls the weight given to the residual and solution norm and hence controls the degree of smoothing. The full solution is then a balance between the unconstrained least-squares solution and a set of constraints that in some way encapsulates a priori knowledge of a physiologically realistic solution.

There are three Tikhonov regularization constraints typically used in inverse electrocardiography, known in that literature as zero-order, first-order, and second-order Tikhonov regularization. Zero-order Tikhonov regularization uses $\boldsymbol{R} = \boldsymbol{I}$, the identity matrix, which effectively limits the total magnitude of the solution; first-order Tikhonov regularization uses $\boldsymbol{R} = \boldsymbol{G}$, a discrete approximation to the surface gradient operator, and limits the steepness of the solution; and the second-order Tikhonov method uses $\boldsymbol{R} = \boldsymbol{L}$, a discrete approximation to the surface Laplacian operator, to restrict the rate of change of the steepness, i.e., the overall nonsmoothness of the solution.

With the Tikhonov approach we can write a closed form solution for (9.13) that leads to an expression for the pseudo-inverse [26]

$$\boldsymbol{A}_{\lambda_t}^{\dagger} = (\boldsymbol{A}^{\mathrm{T}}\boldsymbol{A} + \lambda_t^2 \boldsymbol{R}^{\mathrm{T}}\boldsymbol{R})^{-1}\boldsymbol{A}^{\mathrm{T}} \tag{9.14}$$

Messinger-Rapportand Rudy [27] studied regularizations of different orders by comparing analytic solutions in a spherical model [27]. Their results suggested that zero-order Tikhonov regularization performed as well as the higher-order schemes. Others have carried out similar studies comparing regularization on realistic geometries with dipole sources and found that second order Tikhonov performed best [28, 29]. It may be that the choice of the best Tikhonov regularizing function depends on the particular case and conditions.

Substituting (9.14) into (9.12), the solution for zero-order Tikhonov regularization becomes

$$\boldsymbol{\phi}_H = (\boldsymbol{A}^{\mathrm{T}}\boldsymbol{A} + \lambda_t^2\boldsymbol{I})^{-1}\boldsymbol{A}^{\mathrm{T}}\boldsymbol{\phi}_B \tag{9.15}$$

9.3.2 Truncated SVD (TSVD)

As already described, another method of treating the ill-conditioned nature of the transfer matrix $\boldsymbol{A}$ is to derive a new problem with a well-conditioned *rank deficient* transfer matrix [26]. A common approach is to use the singular value decomposition (SVD) [30], a matrix factorization technique that is introduced in the Appendix of Chap. 2. From a singular value decomposition, one can determine the *principal components* of the information contained within a matrix [31]. If an SVD is applied to a transfer matrix $\boldsymbol{A}$, then the transfer matrix can be written in the form

$$\begin{aligned}\boldsymbol{A} &= \boldsymbol{U}_A\boldsymbol{\Sigma}_A\boldsymbol{V}_A^{\mathrm{T}} \\ &= \sum_{i=1}^{N}\sigma_i\boldsymbol{u}_i\boldsymbol{v}_i^{\mathrm{T}},\end{aligned} \tag{9.16}$$

where $\boldsymbol{U}_A$ and $\boldsymbol{V}_A$ are orthogonal matrices (their columns are orthonormal) and diagonal matrix $\boldsymbol{\Sigma}_A$ contains as its diagonal entries the *singular values*, while $\boldsymbol{u}_i$ and $\boldsymbol{v}_i$ are the column vectors forming these orthogonal matrices and σ_i are the singular values for $i = 1, \ldots, N$. We assume in this case that the number of measurements, or the row-size of $\boldsymbol{A}$, M is larger than the number of HSP reconstruction sites, or the column size of $\boldsymbol{A}$, N. If $M < N$ some details change but the results are substantially the same. The singular values are greater than or equal to zero and are typically sorted in order of decreasing size. For a matrix representing an ill-posed process (as is the case here) the range of nonzero singular values covers many orders of magnitude. This large range of singular values is directly related to the noise amplification properties of the direct least squares solution.

The smaller singular values, the reciprocals of which are used in the least-squares inverse, will tend to magnify components in the data which lie in the subspace of their corresponding left singular vectors, while data components in the subspace of the singular vectors corresponding to the larger singular values are not amplified that dramatically. Thus, these "low singular value" components dominate the solution. Moreover, for forward solutions that smooth high frequencies, as in electrocardiography, those same singular vectors will also represent high frequencies and thus contain only highly attenuated information about the sources. As a consequence, the *relative* contribution of the noise to those components will be very large. The result is extreme noise amplification, as seen in our original example in Fig. 9.1.

To overcome this problem, the truncated SVD (TSVD) solution proposes to substitute for $\boldsymbol{A}$ a low rank approximation, which simply leaves out the modes with unstably small singular values, i.e., we replace $\boldsymbol{A}$ with

$$\boldsymbol{A}_{\lambda_t} = \sum_{n=1}^{\lambda_t}\sigma_{A(n)}\boldsymbol{u}_{A(n)}^{\mathrm{T}}\boldsymbol{v}_{A(n)} \qquad \lambda_t \le N, \tag{9.17}$$

where $\boldsymbol{u}_{A(n)}$ and $\boldsymbol{v}_{A(n)}$ are the nth vectors from the SVD of $\boldsymbol{A}$, $\sigma_{A(n)}$ are their corresponding singular values, and N is the full rank of the matrix. The size of λ_t determines the level of regularization for time t (where λ_t is a positive integer). In the notation of (9.17), we wish to emphasize that the right singular vectors have the dimension of, and indeed are a basis for, the "data space," while the left singular vaectors have the dimension of, and indeed are a basis for, the "solution space." Thus below we denote the former as functions of $\boldsymbol{y}$ and the latter as functions of $\boldsymbol{x}$.

The TSVD solution is obtained by minimizing the objective function

$$\boldsymbol{\phi}_H = \min \left\| \boldsymbol{A}_{\lambda_t}\boldsymbol{\phi}_H - \boldsymbol{\phi}_B \right\| \tag{9.18}$$

The solution to this can be computed by means of the pseudo-inverse [26]

$$\boldsymbol{A}_{\lambda_t}^{\dagger} = \left(\boldsymbol{A}_{\lambda_t}^{\mathrm{T}}\boldsymbol{A}_{\lambda_t}\right)^{-1}\boldsymbol{A}_{\lambda_t}^{\mathrm{T}} \tag{9.19}$$

The pseudo-inverse can be found easily from the SVD of $\boldsymbol{A}$ as

$$\boldsymbol{A}_{\lambda_t}^{\dagger} = \tilde{\boldsymbol{V}}_A \tilde{\boldsymbol{\Sigma}}_A^{-1} \tilde{\boldsymbol{U}}_A^{\mathrm{T}}, \tag{9.20}$$

where $\tilde{\boldsymbol{U}}_A$ and $\tilde{\boldsymbol{V}}_A$ contain the first λ_t columns of $\boldsymbol{U}_A$ and $\boldsymbol{V}_A$ respectively, and $\tilde{\boldsymbol{\Sigma}}_A$ is a $\lambda_t \times \lambda_t$ diagonal submatrix of $\boldsymbol{\Sigma}_A$.

Substituting (9.20) into (9.12), the TSVD solution is

$$\begin{aligned}\boldsymbol{\phi}_H &= \tilde{\boldsymbol{V}}_A \tilde{\boldsymbol{\Sigma}}_A^{-1} \tilde{\boldsymbol{U}}_A^{\mathrm{T}}\, \boldsymbol{\phi}_B \\ &= \sum_{n=1}^{\lambda_t} \frac{\boldsymbol{u}_{A(n)}^{\mathrm{T}}\, \boldsymbol{\phi}_B}{\sigma_{A(n)}} \boldsymbol{v}_{A(n)}(x)\end{aligned} \tag{9.21}$$

It is useful to compare this TSVD solution with the zero-order Tikhonov solution given in (9.15). Expressing (9.15) in terms of the $\boldsymbol{u}$ and $\boldsymbol{v}$ components from the SVD of $\boldsymbol{A}$ we can write

$$\begin{aligned}\boldsymbol{\phi}_H &= \left(\boldsymbol{A}^{\mathrm{T}}\boldsymbol{A} + \lambda_t^2 \boldsymbol{I}\right)^{-1}\boldsymbol{A}^{\mathrm{T}}\boldsymbol{\phi}_B \\ &= \sum_{n=1}^{N} f_n(t) \frac{\boldsymbol{u}_{A(n)}^{\mathrm{T}}\, \boldsymbol{\phi}_B}{\sigma_{A(n)}} \boldsymbol{v}_{A(n)}(t),\end{aligned} \tag{9.22}$$

where $f_n(t)$ are the Tikhonov *filter factors* given by

$$f_n(t) = \frac{\sigma_{A(n)}^2}{\sigma_{A(n)}^2 + \lambda_t^2} \begin{cases} 1 & \sigma_{A(n)} \gg \lambda_t \\ \sigma_{A(n)}^2/\lambda_t^2 & \sigma_{A(n)} \ll \lambda_t \end{cases} \tag{9.23}$$

These filter factors have the effect of filtering out contributions to the reconstructed $\boldsymbol{\phi}_H$ that correspond to the small singular values while leaving the SVD components corresponding to large singular values almost unaffected. Equation (9.21) is identical to (9.22) with the corresponding filter factors being equal to zero or one; the terms up to and including λ_t are included in the summation and have a filter factor of one while the remaining terms are zero. In other words, we use an effective λ which is zero for the singular vectors we retain and infinity for those we reject. In practice, the performance of TSVD regularization is often indistinguishable from that of zeroth-order Tikhonov regularization [32]. Thus, as mentioned above, despite the different conceptual basis for the two approaches, the resulting equations are closely connected. For higher-order Tikhonov regularization, and indeed for general regularization matrices, a similar analysis can be made via what is known as the Generalized SVD (GSVD); details can be found in Hansen [9].

9.3.3 Truncated Iterative Approaches

Truncated iterative methods are another deterministic approach to solving the inverse problem. In these methods, a sequence of candidate solutions is produced and each one is evaluated according to a "goodness" criterion: if the solution meets some threshold of accuracy, the iterations stop and otherwise they continue with additional candidate solutions. These approaches draw on the standard techniques for solving large linear systems of equations [30]. However, because such methods, like the unconstrained least-squares methods already described, will converge to unreliable solutions, the regularization approach is to truncate the iterations *before* convergence [9]. In this case, the number of iterations plays the role of a regularization parameter.

Iterative methods are especially favorable for large-scale problems for which direct regularization methods are computationally expensive, and in problems in which a matrix representation of the forward operator or an explicit

representation of the inverse solution are not available. However, their use is not limited to these cases; they can be used as an alternative approach to direct regularization approaches. Most iterative methods can be represented in terms of filter factors such as those already discussed for Tikhonov and TSVD approaches [9], which demonstrates the similarity between iterative methods and direct methods in their filtering of the small singular values of the forward matrix. In regularized iterative methods, the solution converges to the lower frequency modes of the right singular vectors of $\boldsymbol{A}$ in the earlier iterations, and thus stopping the iteration filters out the effect of the otherwise amplified higher frequency modes.

The most commonly used iterative methods in this context are in the class of Krylov subspace methods, for which the connection between iteration number and modes of $\boldsymbol{A}$ is most clear. Brooks et al. [33] reported an early attempt to use this approach, in which the Conjugate Gradient (CG) iterative method was combined with regularization constraints. More recently, Ramanathan et al. [34] have reported using another Krylov subspace method, the Generalized Minimum Residual (GMRes) method, with significant success.

Reports suggest that the inverse solution reconstructed by the GMRes method was more accurate than the Tikhonov solution in terms of the pattern and localization of epicardial potentials [34]. No comparison was reported between the GMRes and CG methods. Also it was reported that in some cases the *L*-curve criterion, based on the condition number of a particular matrix, reflected a clear location at which to specify the regularization parameter, while the appropriate point on the *L*-curve for the Tikhonov approach was difficult to determine [34]. However, despite the strong empirical evidence supporting the GMRes approach, as well as the success of other initial results [33], as yet there is no theoretical justification to explain why this method reconstructs a localized solution better than Tikhonov regularization. We note that in both approaches, Tikhonov-type regularization was *combined* with the iterative regularization, either by iterating on a regularized (albeit under-regularized) set of equations [33] or by using the Tikhonov solution as the starting point for the iterative regularization [34].

9.3.4 Statistical Approaches

Although some of the original reports on inverse electrocardiography for epicardial potentials [35] were based on the statistical model in (9.10), the main challenge of this approach remains specifying the model (i.e., determining appropriate parameters of the mean and covariance of the desired solution and the noise). The simplest technique, which was adopted by these early investigators, is to assume that not only is the noise white and uncorrelated, as in (9.11), but that the *solution* has the same structure, with zero mean and variance σ_x^2. In this case the relevant equation becomes

$$\widehat{\boldsymbol{x}}_{\mathrm{MAP}} = \left(\boldsymbol{A}^{\mathrm{T}}\boldsymbol{A} + \frac{\sigma_n^2}{\sigma_x^2}\boldsymbol{I}\right)^{-1}\boldsymbol{A}^{\mathrm{T}}\boldsymbol{b} \tag{9.24}$$

This is the same as Tikhonov regularization with an identity matrix as the regularizer (i.e., Tikhonov zero-order) and with a statistical model for picking the regularization parameter. Since a good model for the variance of the unknown solution is hard to specify a priori, most of the research that followed these early reports concentrated on the deterministic regularization approaches described above.

However, in the late 1990s, van Oosterom, in a series of publications [36–38], re-introduced the idea of using this model with a more complicated and realistic covariance matrix. He showed that if one can in fact obtain even a reasonable approximation of the true covariance matrix (and assuming the time-invariant, statistically stationary, zero-mean model is valid), one can recover detail about the surface potentials more reliably and one is less sensitive to errors introduced by internal inhomogeneities such as the lungs. The key problem, of course, is how to obtain a useful, valid, and reasonably accurate statistical model of the cardiac sources. One approach, introduced in the context of estimation of activation times all over the heart from sparse catheter-based measurements [39], and then extended to the inverse problem [40–42], is to use previously recorded data to determine such a model. One version of this idea uses a "training database" of prior recordings of the sources, where available, to estimate a covariance matrix to be applied in the inverse solution. An additional enhancement is to use sparse catheter measurements to "tailor" this statistically derived result to an individual subject. The results, based on simulations using canine epicardial recordings, indicated that improvements in the inverse solutions are indeed possible using such an approach, if the necessary prior and catheter measurements can be acquired.

9.3.5 Multiple Spatial Regularization Operators

All of the traditional methods – Tikhonov regularization, TSVD, and the Tikhonov-equivalent "white Gaussian source" statistical model – have produced results that showed that it is indeed possible to recover meaningful information about cardiac surface potentials from body surface measurements. However, these results were neither precise nor reliable enough to be really attractive for potential clinical or even scientific use. An example of these limitations can be seen in Fig. 9.1; the Tikhonov solution shown there, although certainly orders of magnitude improved over the unconstrained solution, is both rather noisy and overly smooth, in the sense that it cannot match the rapid downward deflection of activation in the original electrogram. The next few subsections discuss various ideas introduced to try to improve the accuracy and reliability of inverse reconstructions. One approach that has shown some success is to combine two distinct types of regularization. For instance, TSVD and Tikhonov regularization were used together in Shahidi et al. [43], and we have already mentioned two approaches which combined Tikhonov-type regularization with truncated iterative regularization.

Another approach starts from the observation that if the problem is that we need constraints to improve inverse solutions because the measurements contain insufficient information in themselves, one can consider the possibility of using more than one constraint at the same time. This approach, in the context of simply extending the Tikhonov formalism to more than one constraint, has been applied to inverse electrocardiography using both Tikhonov zero-order and Tikhonov second-order regularizers [44]. The results were reported to be somewhat improved, and in particular were more robust to the exact choice of regularization parameters. (Here, with multiple constraints, one needs multiple regularization parameters as well.) This approach had its difficulties, however, in particular in picking a good set of regularization parameters without undue computational burden, and this problem gets dramatically worse if the number of constraints increases beyond two. At the same time, it was not clear that any particular pair of constraints contained the most useful information for reconstructions.

Ahmad et al. [45] proposed a method that flexibly allows the inclusion of more than two constraints, as well as constraints that do not lend themselves mathematically to easy treatment in the Tikhonov framework. This approach, which had seen significant use in the formally related problem of image restoration, consists in considering the desired solution as a single "point" in some space of possible inverse solutions. Then each constraint, including the constraint that the solution must correspond reasonably well to the measurement data after application of the forward model, can be treated as a constraint set in this solution space. Reasonable – technically, feasible or admissible – solutions would lie inside each constraint set, and only infeasible solutions lie outside it. For example, if we believe that a good solution should have a residual error below some reasonable value, then the corresponding "constraint set" is all solutions that indeed have a residual error less than that value. If the constraint is that the 2-norm of the solution, or its gradient, is below some value, then the constraint set is all solutions for which this is true.

One can easily devise constraints that are somewhat less mathematically simple, for instance bounds on the maximum, or minimum, or some norm other than 2, of the solution or of some spatial derivative of the solution, or even any such constraint applied only to one or several subregions. Moreover, given any number of such constraints, all admissible solutions will lie in the *intersection* of all the constraint sets. It turns out that, if the constraints can all be described by convex functions (a class that includes all the examples given above), one can apply any of a large number of convex optimization algorithms to find a feasible solution. Note that in this approach, the optimization algorithm is stopped as soon as one finds a solution that matches all the constraints, before converging to an "optimal" solution – similar in spirit to the way in which the iterative Krylov-subspace linear system solvers like CG or GMRes are truncated when dealing with ill-posed problems. The application of this approach to inverse electrocardiography, using one such convex optimization algorithm called the ellipsoid algorithm, has shown encouraging results [45]. However, again there was no clear set of constraints on the potentials that emerged as giving the level of accuracy and reliability required.

9.3.6 Spatio-Temporal Approaches

As mentioned in the introduction to this chapter, the temporal behavior of cardiac electrical signals is known to have a strong deterministic, hence at least partially predictable, component. It would make sense to make use of this strong prior knowledge to constrain solutions over multiple time instants. One approach along these lines involves parameterizing the

sources by means of fiducial time parameters, and we discuss such approaches at some length in the following section. With potential-based methods, the temporal behavior of the source, if it can be effectively captured in a constraint, would also seem to be a powerful tool in the inverse solution toolbox.

In fact, from a statistical standpoint, it is commonplace in the fields of statistical signal processing and estimation theory that, if the quantities in (9.10) are taken as potentials at single time instants, the solution is optimal only if the desired heart surface potentials are temporally uncorrelated [46]; otherwise their temporal correlation must be included in the estimation equation. In fact, algorithms commonly used in devices such as modems and cell phones make use of the so-called Viterbi algorithm for Maximum-Likelihood Sequence Estimation that exploits exactly this fact. It should be clear from the earlier chapters in this book that any reasonable model for cardiac sources will be far from temporally uncorrelated, and thus it is not surprising that inverse electrocardiography algorithms have been introduced to take advantage of models of expected temporal behavior.

We first treat extensions of the heart surface potential (HSP) inverse solution formulation described earlier to include temporal or spatio-temporal constraints. We then discuss a relatively new approach that replaces the heart surface model with a transmembrane potential (TMP) model. Based on this model, temporal constraints that are a reasonable approximation of TMP temporal behavior can be applied; the hoped-for advantage is that TMP temporal behavior may lend itself to simpler, more effective and useful, constraints.

9.3.6.1 Spatio-Temporal Constraints with Heart Surface Potential Models

Some of the earliest work in this field used a simple On–Off model to incorporate temporal information [47], but this was not pursued as the importance of various factors such as regularization constraints and parameters and the development of appropriate validation models took precedence. In the late 1980s researchers began to consider again the use of temporal behavior, first in the sense of temporal correlation via a frequency-domain approach [48], and then, in research that had significant historical impact on the field, in a direct regularization framework, by simply adding a temporal constraint after an initial Tikhonov solution [49]. This latter method penalized subsequent time instants for changing too dramatically from the preceding one, by constraining the Euclidean norm of the difference between them as a regularization (generally referred to in the inverse electrocardiography literature as Twomey regularization). Formally, (9.8), with a linear model and linear regularization constraint, becomes:

$$\widehat{\boldsymbol{x}}_\lambda = \text{argmin}\{||\boldsymbol{A}\boldsymbol{x} - \boldsymbol{b}||_2^2 + \lambda^2||\boldsymbol{R}(\boldsymbol{x} - \boldsymbol{x}_0||\}, \tag{9.25}$$

where $\boldsymbol{x}_0$ represents an initial estimate of the solution, as for instance the estimated value of $\boldsymbol{x}$ at a previous time instant. Thus this approach requires an initial estimate of the solution; the quality of the resulting inverse solution was shown to depend on the quality of this estimate, and the final solution is therefore biased towards it [49].

Starting from this approach, several alternative methods were introduced that attempted to *combine* spatial and temporal constraints into a true spatio-temporal regularization method. The three methods that had the most success were:

1. A method that added a temporal constraint to one (or more) spatial constraint(s) [44],
2. A method that added an equation containing an explicit model of temporal evolution of the potentials to the standard forward problem equation (which models the spatial relation between potentials on two different surfaces), with the pair of equations formulated as a state-space model and solved via a Kalman filter or smoother [50, 51], and
3. A method introduced and developed primarily by Greensite and Huiskamp which attempted to simultaneously regularize in time and space by finding a temporal whitening transform according to a statistically informed assumption [52, 53].

The initial version of the method was presented in a specific variant with a heuristic justification that Greensite has since developed into a more general and theoretically based formulation using an assumption he called "isotropy"; here we start with the latter and then include a detailed description of the specific earlier implementation, which has seen the most use in practice. Indeed this earlier method has become perhaps the most widely accepted for reconstruction of

potentials by inverse electrocardiography, used, for example, by groups such as those in Innsbruck and Auckland, who have reported significant success with it [54–56].

Initially, it appeared that these were three distinct methods with no clear connection or comparison among them except in terms of exemplary results. We note that the paper describing the first method did show that the method in Oster and Rudy [49] was a one-step simplified version of an iterative solution to the full multiple regularization method. However, recently it has been shown that in fact all the three of these methods can be cast into the same statistical framework [57]. We outline this framework here, leaving the details to the literature, and then proceed to describe in some detail the popular implementation of Greensite's method. The key to unifying these approaches is to consider (9.11) with the quantities defined as in (9.3) and (9.4); the vectors are all block vectors concatenating the spatial distribution of the potentials across all time instants, and $\boldsymbol{A}$ is a block diagonal matrix with the forward solution matrix repeated on the diagonal blocks. We employ the statistical model described earlier in which both the noise and the unknown signals are assumed to be zero-mean, and the noise is assumed to be white as noted, here in both space and time. In this case the key quantity that governs the solution is the spatio-temporal covariance matrix $\boldsymbol{C}_x$, or equivalently, its inverse:

$$\boldsymbol{C}_x = E\{\boldsymbol{x}\boldsymbol{x}^{\mathrm{T}}\} = E\left\{\begin{bmatrix} \boldsymbol{x}(t_0) \\ \boldsymbol{x}(t_0+1) \\ \vdots \\ \boldsymbol{x}(t_n) \end{bmatrix}\left[\boldsymbol{x}(t_0)^{\mathrm{T}}\ \boldsymbol{x}(t_0+1)^{\mathrm{T}} \cdots \boldsymbol{x}(t_n^{\mathrm{T}})\right]\right\}, \tag{9.26}$$

where $E\{\cdot\}$ represents statistical expectation. Thus, in the spatio-temporal formulation, $\boldsymbol{C}_x$ is a *spatio-temporal* covariance matrix which can be divided into blocks of the form $E\{\boldsymbol{x}(t_i)\boldsymbol{x}(t_j)^{\mathrm{T}}\}$; the dimension of each block is the number of nodes used on the heart surface; the number of blocks (in both directions) is equal to the number of time instants; and each block is a spatial cross-covariance matrix at different time instants (except for the diagonal blocks which are spatial covariances at the same time instant). The temporal covariance is embedded in the variation from block to block across the matrix, as indexed by the difference (or time lag) between t_i and t_j.

Considering this formulation, two significant problems arise:

1. How can one derive or estimate the parameters required to populate this matrix (or its inverse, since the inverse covariance plays the role of regularization constraint matrix)?
2. How can one handle the dramatic increase in computational requirements stemming from the fact that the matrices now have dimensions on each side that are equal to the number of spatial nodes on the relevant surface multiplied by the number of time instants considered?

Each of the three methods introduced separately – multiple regularization, Kalman filtering, and isotropy – solves exactly this same pair of problems, but in different ways, based on different assumptions. Each assumption, and its resulting formulation, turns out to impose a particular structure on $\boldsymbol{C}_x$ or its inverse, which then leads to a specific algorithm or set of algorithms. Here we briefly describe the simplest form of the approach taken in each method; for details see Zhang et al. [57].

1. *Multiple regularization.* In this approach one assumes that we can build separate constraints for the spatial behavior (typically a standard constraint on the norm of the solution or its derivative, effectively a spatial high-pass filter) and for the temporal behavior (again typically a high-pass temporal filter, based on the idea that potentials do not change dramatically from one sample time instant to the next). When formulated in terms of statistical regularization, such assumptions impose a particular structure on the inverse of the spatio-temporal covariance matrix, as the sum of two block matrices; one is a block diagonal matrix, which contains the spatial regularization constraints, and the other is a block matrix that has all its blocks restricted to be themselves diagonal matrices, and that enforces the temporal regularization constraint. A consequence of this structure is that fast algorithms can be developed which reduce the computational complexity down to the order of the number of nodes in the heart surface model [44].
2. *State-space model.* In this approach, the spatial distribution of potentials at each time instant is modeled by a prediction or temporal evolution equation, in which the potentials from each time instant evolve from the previous time by applying a known prediction matrix plus a random perturbation. For example, imposing an identity prediction matrix assumes that the potentials do not change rapidly from one time sample to the next (a random walk model). More general models, which take into account, for instance, the behavior of neighboring nodes, can easily be employed.

One consequence of these assumptions is that the resulting structure of the spatio-temporal covariance matrix shows a kind of block exponential decay (for a stable model) across the blocks. More importantly, the *inverse* covariance matrix has a block tri-diagonal structure; in other words, regularization is applied only between adjacent time instants in this model. The computational consequence of this simple structure is in fact the Kalman filter/smoother algorithm, and thus, a reduction in computational complexity is achieved.

3. *Isotropy model.* One consequence of the assumption of isotropy, which Greensite frames as a kind of invariance to unknown prior information for the case in which one has no useful model of the temporal behavior, is what in statistical terms is known as *separability* between the spatial and temporal correlation. The effect on the structure of the inverse covariance matrix is that all blocks (that is, the spatial cross-covariance matrices) are exactly the same except for a scalar multiplication; the set of scalars needed to relate all the blocks contains the information about the temporal covariance. Mathematically, this assumption means that the spatio-temporal covariance matrix can be factored as the Kronecker product of a single spatial covariance matrix by a single temporal covariance matrix. As a further consequence of this assumption, the temporal covariance of the *heart* surface potentials is identical to within a scalar to that of the *body* surface potentials. This assumption suggests the following algorithm:

   (a) Estimate the temporal covariance matrix of the body surface potentials directly from the data.
   (b) Find the SVD of this matrix; its right singular vectors can be used to decorrelate, or whiten, the entire problem, by a simple matrix multiplication.
   (c) Once the problem has been so whitened, it is optimal to solve it column by column (in effect, "time-instant" by "time-instant" in the new "temporal" coordinate system induced by the decorrelation). Spatial regularization is still required and can be done by any relevant method, including Tikhonov regularization or TSVD. We discuss this last point in more detail in the following section.
   (d) Once the column-by-column solutions are complete, "re-correlate" by multiplying by the transpose of the decorrelating matrix. Since this matrix comes from the SVD and is therefore orthogonal, the optimality of the solution is preserved.

   As should be clear, this algorithm, since it does its primary work on a column-by-column basis, again reduces the computational complexity to the order of the spatial dimension.

As discussed in Zhang et al. [57], each of these methods has its advantages and limitations. The multiple regularization approach gives the designer great freedom in choosing regularizers, but requires considerable prior knowledge to make good choices. Moreover, one cannot consider nearby (or, in fact, any other) spatial nodes when regularizing in time without incurring a dramatic increase in computational complexity. The state-space model gives even more flexibility in the design of the temporal model, and indeed, this model has a very direct physical or physiological interpretation as the expected temporal progression of the solution. Moreover it opens access to a truly vast literature of modeling and solution methods – the literature on Kalman estimation algorithms [e.g. 46, 58, 59]. However, it does depend on an effective prior knowledge of this evolution, and most applications of this method to inverse electrocardiography have simply used the random walk approach. In addition, it does not allow one to directly consider more than one previous time instant in predicting the next time instant, again unless one is willing to increase the computational order and the modeling complexity.

The isotropy/separability method has the significant attraction that one does not need to model or make any further explicit assumptions on the temporal behavior; the required parameters are in the temporal correlation matrix of the body surface potentials, which can be directly estimated out of the measurements. However, the underlying assumption of isotropy, or separability, is difficult to interpret in physical or physiological terms, and it is not yet clear how one can verify or test its accuracy. Moreover, the assumption rests on the idea that one knows nothing about the expected temporal behavior of the solution. If, in fact, one has some prior knowledge, it is not clear if or how one might incorporate that knowledge into this approach. Nonetheless, as already noted, not only the original authors of this method but also independent groups have reported success with it in several settings.

There is one key aspect of the isotropy method, which is critical to its performance, and which indeed was incorporated explicitly in the original, less general, version of the method in Greensite [60]. After the decorrelating transform achieved by multiplication of the data by the right singular vectors of the data matrix, one has exchanged the original set of L equations, where L is the number of time instants used, for a new set of L equations. As mentioned earlier, each of

these equations still involves the badly conditioned forward matrix $\boldsymbol{A}$ and thus still needs to be (spatially) regularized. If one uses a standard method to find an appropriate regularization parameter for each equation, as for instance the L-curve method described in the following section, and then solves all L equations, the results are dominated by noise and are not useful. This is true because the new set of equations has its own set of "singular values" in the transformed domain, which are unknown even under the isotropy assumption (in effect, they are known for the data matrix but not for the "solution matrix," and these two sets of singular values differ). Therefore, one must find a way to "truncate" this process, only solving the set of equations that contain reliable information, because they correspond to the relatively large singular values of the unknown solution matrix. As we describe in the following section, the original version of this spatio-temporal approach, as introduced by Greensite [60] before the isotropy theory was developed, included an ad hoc method for exactly this truncation, via a kind of "double TSVD," which uses an SVD of the data matrix to determine which equations to solve, and an SVD of $\boldsymbol{A}$ to regularize each of those solutions.

We now proceed to a detailed description of the version of the isotropy method generally used in practice. One starts by performing an SVD of the torso surface signal data matrix $\boldsymbol{\Phi}_B$, where $\boldsymbol{\Phi}_B$ is a specific variant of the matrix $\boldsymbol{B}$ in (9.5) which stores the signal information in its rows and the potentials at each time instant in its columns, to determine its principal components. The result of this process is a factorization of $\boldsymbol{\Phi}_B$ into a matrix of spatial singular vectors ($\boldsymbol{U}_B$) and temporal singular vectors ($\boldsymbol{V}_B$). The idea that will be exploited here is that, because of the spatial smoothing and attenuation, only a relatively small number of time signals can represent almost all the information in this data matrix; the rest of these components are dominated by noise.

Indeed, one could, "filter" the data matrix to remove the noise-dominated components before attempting an inversion – even if one ignored any other spatio-temporal constraints, this might improve the results. We note that this relatively low-dimensionality of the torso data has been known, and used, for a long time – in the early 1980s Lux et al. published a series of papers on the use of the principal component method, or Karhunen-Loeve transform, for compression and data reduction of body surface potential maps [61, 62], which indeed used exactly the same principle for temporal compression as the one described here.

Specifically, the columns of $\boldsymbol{U}_B$ and $\boldsymbol{V}_B$ corresponding to small singular values are assumed to correspond to noise-dominated signals and are typically removed [63]. A determination of which singular values correspond to this "noise subspace" can be estimated in a somewhat ad hoc fashion by plotting the log of the ordered singular values against the rank of the matrix obtained from the appropriate subsets of these singular values [64]. This typically results in a characteristic 'L' shaped curve as shown in Fig. 9.3. It has been postulated that the singular values below the point at which the curve

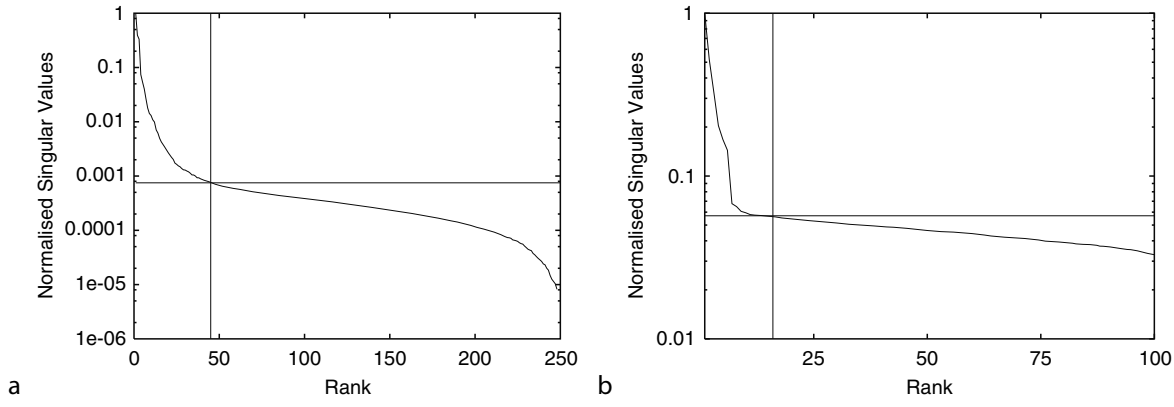

Figure 9.3

Singular value spectra of two different torso surface signal matrices. In panel (a) are the singular values from a signal matrix recorded from a normal male volunteer and in (b) signals from a simulated cardiac source. The singular values have been normalized and plotted on a log scale to emphasize the curvature in their values. The lower right quadrant (as defined by the vertical and horizontal lines) corresponds to the ranks and singular values which have been considered to correspond to noise, and the upper left quadrant those which have been considered as "signal."

levels off correspond to the noise subspace [63]. A number of different methods have been used for determining the best place to locate this leveling off point, including the Akaike Information Criterion [65] and the point of steepest curvature. However, none of these has been found to be truly reliable in practice [66].

The key idea of this version of the isotropy method is not to simply filter the data, as shown, but rather to combine this filtering with regularization. To start, we write the SVD expansion of the matrix of torso potentials matrix as

$$\boldsymbol{\Phi}_B = \boldsymbol{U}_B \boldsymbol{\Sigma}_B \boldsymbol{V}_B^{\mathrm{T}}, \tag{9.27}$$

where $\boldsymbol{U}_B$ is an $M \times N_e$ matrix that represents the spatial basis, $\boldsymbol{\Sigma}_B$ is an $N_e \times N_e$ matrix with the singular values stored on the diagonal, $\boldsymbol{V}_B$ is an $N_e \times N_e$ matrix that represents the temporal basis, and $N_e = \min(M, L)$ where M is the number of recording electrodes on the body surface and L is the number of time samples recorded. We assume once more that the number of measurement locations is greater than the number of nodes on the HSP model, that is, that $M \geq N$. If this is not the case, once again minor changes are required but the procedure is essentially the same. Inserting (9.27) into (9.12) leads to

$$\begin{aligned} \boldsymbol{\Phi}_H &= \boldsymbol{A}_{\lambda_t}^{\dagger} \boldsymbol{\Phi}_B \\ &= \boldsymbol{A}_{\lambda_t}^{\dagger} \boldsymbol{U}_B \boldsymbol{\Sigma}_B \boldsymbol{V}_B^{\mathrm{T}} \end{aligned} \tag{9.28}$$

Multiplying on the right by $\boldsymbol{V}_B$, which is what the isotropy assumption would lead to as the optimal decorrelating transform, leads to

$$\begin{aligned} \boldsymbol{\Phi}_H \boldsymbol{V}_B &= \boldsymbol{A}_{\lambda_t}^{\dagger} \boldsymbol{\Phi}_B \boldsymbol{V}_B \\ &= \boldsymbol{A}_{\lambda_t}^{\dagger} \boldsymbol{U}_B \boldsymbol{\Sigma}_B \boldsymbol{V}_B^{\mathrm{T}} \boldsymbol{V}_B = \boldsymbol{A}_{\lambda_t}^{\dagger} \boldsymbol{U}_B \boldsymbol{\Sigma}_B \end{aligned} \tag{9.29}$$

because of the orthogonality of the matrix $\boldsymbol{V}_B$.

Next, we define

$$\boldsymbol{\Gamma} = \boldsymbol{\Phi}_H \boldsymbol{V}_B \tag{9.30}$$

and proceed by solving $\boldsymbol{\Gamma}$ from

$$\boldsymbol{\Gamma} = \boldsymbol{A}_{\lambda_t}^{\dagger} \boldsymbol{U}_B \boldsymbol{\Sigma}_B \tag{9.31}$$

This problem is tackled for each column vector $\boldsymbol{\gamma}_i$ of $\boldsymbol{\Gamma}$, paired to each column vector i of matrix $[\boldsymbol{U}_B \boldsymbol{\Sigma}_B]$, with $i = 1, \cdots, N_e$.

We use the "noise subspace" method already described, which permits the selection of regularization parameters for each value of i in any type of pseudo-inverse (e.g., Tikhonov of TSVD) selected. The amount of regularization used for each of the paired columns can be determined using the methods described in Sect. 9.6.

The solution to (9.27) is then found from

$$\boldsymbol{\Phi}_H = \boldsymbol{\Gamma} \boldsymbol{V}_B^{\mathrm{T}} \tag{9.32}$$

Note that only the columns of $\boldsymbol{\Gamma}$ deemed significant by testing the singular values of the data matrix are used.

Two recent attempts to incorporate spatio-temporal constraints in the context of wavefront propagation were reported in Ghodrati [67]. The first used the Kalman state-estimation formalism in the context of a constraint based on wavefront propagation. This work, which in principle is like the activation-based methods in that it considers the arrival time of the wavefront at each point on the surface as the unknown values to reconstruct, uses a nonlinear state evolution model built on phenomenological study of canine epicardial data, along with fiber directions drawn from the Auckland heart, to propagate the wavefront on the epicardial surface. A second model, also built from a study of canine epicardial data [189], maps the wavefront location to a potential distribution; the latter is then used with a standard forward matrix to relate the wavefront location at any time instant to the body surface potential measurements. The second approach uses a regularization constraint based on a nonlinear mapping of the previous time instant solution to a wavefront-based

model; this constraint is then used in a standard Tikhonov solution to calculate the solution at the current time instant. Both methods were reported to show a significantly improved localization and extent of reconstructed wavefronts in simulations with cardiac data.

9.3.6.2 Spatio-Temporal Constraints with Surface Transmembrane Potential Models

As described in Chap. 7, transmembrane potentials can also be used as the source strength of a double layer (EDL) upon which an appropriate forward model, and thus a corresponding inverse model, can be formulated. As discussed there, the tractability of this model is greatly improved if one makes simplifying assumptions about homogeneity and isotropy of cardiac conduction. These assumptions are the basis for most activation-based inverse solutions, as described below in Sect. 9.4, which have been under development since the 1980s. However, more recently there has been interest in the development of *potential-based* TMP models. In these models, the forward solution employed is one that maps the TMPs directly to the body surface potentials. TMPs have some conceptual and practical disadvantages compared with HSPs; for example, they require additional isotropy and homogeneity assumptions, and are only guaranteed to be unique (even in theory) if these assumptions hold. In addition, TMPs are more difficult to measure directly in experimental settings, especially for purposes of validation of inverse solutions. In the context of activation-based solutions, as we will see, they have the very important advantage of directly imposing the dominating spatio-temporal constraint, and of the propagating nature of the activation wavefront for QRS reconstructions. These advantages also apply to the reconstruction of repolarization activity.

One effect of the constraints used in activation-based methods is that the height of the jump and the shape of the profile across the wavefront must be constant across the surface, which translates to constant height and constant shape of the action potential, and in particular, of the "phase 0" transition. In an attempt to relax this restriction, Messnarz et al. [54] recently introduced a TMP-based inverse solution. The goal was to achieve some of the flexibility of HSP-based solutions while imposing a physiologically-based constraint based on expected TMP behavior. The specific formulation they employed constrained the TMPs to become progressively more positive over time – i.e., be monotonically nondecreasing, or equivalently have a nonnegative temporal derivative – during the activation (QRS) interval. From a potential-based inverse problem point of view, the idea is that the shape of the TMP is generally much simpler than that of an electrogram and thus lends itself to a simple yet powerful (and physiologically meaningful) constraint such as the one just described.

The formulation of the inverse problem in Messnarz et al. [54] was quite similar to that for the other spatio-temporal models described earlier; the time samples of interest were concatenated into block vectors and the forward matrix became a block diagonal matrix with $\boldsymbol{A}$ on all its blocks (as per (9.4) and (9.5)). A spatial regularization term was used with a Laplacian regularizer, the same way that spatial regularization was accomplished by Brooks et al. [44] in the multiple regularization context, which fits perfectly into the block structure. Imposing the temporal constraint, however, required a matrix inequality constraint, in which the temporal derivative of the solution was approximated via a simple difference operator written as a large, sparse matrix (again similar to the way Brooks et al. [44] applied a high-pass temporal filter). However, instead of simply adding this as a second regularization constraint, it was necessary to enforce the condition that all elements of the vector of temporal derivatives, over all time instants, were nonnegative. Thus, the problem became one of minimizing the spatially regularized residual error, subject to the constraint that the side term, the temporal derivative vector, had all nonnegative elements. This problem falls into the class of convex optimization problems, in which the *forward problem* is linear and the constraint imposed in the inverse problem is nonlinear but convex. Given the relatively simple form of this convex optimization, Messnarz et al. were able to employ a standard version of the interior point optimization approach, an algorithm known as MOSEK [68], rather than the more general ellipsoid algorithm used previously in the truncated convex optimization approach [45] described above. To validate their approach, Messnarz et al. [54] used simulations of normal and abnormal hearts and compared results with standard Tikhonov spatial regularization of the single time instant TMP problem. No attempt was made to use spatiotemporal regularization of any kind with the Tikhonov method, although the authors did impose minimum and maximum amplitude constraints (−90 and +10 mV) on the reconstructed potentials. Results indicated that the method was able to recover important aspects of propagation for both the normal and abnormal hearts more accurately than single-time instant reconstruction of the TMPs.

In a second report, Messnarz et al. [2] explored from both a mathematical and (numerical) experimental viewpoint a direct comparison between the HSP model (using a combined epi/endocardial surface) and their TMP model. The mathematical approach involved examining the numerical null-spaces of the forward problems for the two

methods. The numerical null-space is the space of possible source behaviors that are seen so weakly in the body surface potentials that they are below the measurement noise level. There is a nontrivial null-space of this sort for all complete inverse electrocardiography formulations because of the attenuation and smoothing that makes the problem ill-posed. Messnarz et al. [2] compared the null-spaces and their complements, and the signal-spaces (technically the row spaces), of their implementation of the two (HSP and TMP) forward problems. They showed that the information present in the measurements was insufficient to reconstruct the HSPs or TMPs accurately, confirming the need, widely accepted in the field, to find regularization methods that can "restore" the null-space components. Note that Tikhonov methods do reconstruct some null-space components, while TSVD methods do not. Interestingly, the HSP forward model was somewhat better conditioned than the TMP forward model. The authors suggested that this was due to differences in the uniqueness properties of the HSPs compared with the TMPs. An alternative explanation might be that the HSPs are simply smoother than the TMPs; thus the forward problem from HSP to body surface involves less (additional) smoothing than the forward problem from TMPs to body surface, and hence may be better conditioned. Numerical experiments carried out using the same simulated measurement data for both methods showed that the TMP model produced more accurate reconstructions of activation times, especially on the endocardium. The HSP reconstruction method used was the "truncated isotropy" spatio-temporal regularization method introduced by Greensite and Huiskamp described in detail earlier. The authors attribute the superiority of the TMP reconstructions to what they hypothesize is the ability of the TMP non-decreasing-in-time constraint to better add physiologically correct null-space components to the reconstruction, compared with the isotropy/separability assumption used in the HSP reconstruction. No results were included on the actual null-space components of the HSPs or TMPs themselves, and thus no direct evaluation and analysis of the presumed better reconstruction of these null-space components were reported.

9.3.7 Imaging Transmural Potentials

The inverse methods described earlier attempt to reconstruct electrical activity on the epi- and/or endocardial surfaces of the heart. There have also been a few recent attempts to noninvasively image cardiac electrical activity *within* the myocardial wall [55, 69]. This problem is even more difficult than that of imaging surface electrical activity, as it is less constrained and hence more likely to yield nonunique solutions.

The basic approach used in this type of inverse problem starts with a forward model that incorporates a description of the three-dimensional myocardium. These forward models are designed to simulate surface electrograms that originate from within the myocardium. As discussed earlier, on a time-instant by time-instant basis such models are clearly not unique, and even with temporal constraints included a reasonable question to ask is whether such source models result in a unique inverse solutions for the myocardium. To our knowledge, this question has not been addressed in the literature.

In one approach, He et al. [69] proposed a cellular automata solution procedure based on predefined transmembrane potential descriptions (Sect. 8.4.2). This model required only an initial site (or sites) of activity to be specified to generate a full potential description on the torso surface. The inverse problem was then formulated as an optimization problem in which one minimizes the average correlation covariance between the measured and simulated body surface potentials by altering the initial site (or sites) of myocardial electrical activity used in the forward model. The solution must also satisfy two heuristically designed constraints based on the position of the minima of the body surface potentials and the number of body recording leads whose potentials are less than a certain negative threshold. These extra constraints are justified by the presumed relation of the position of the minima on the body surface with the origin of the activation in the heart (in recent work from the same group [70], these two constraints were replaced by the averaged relative error between the measured and simulated body surface potentials). For this procedure to be computationally feasible, the size of the initial activation sites are generally taken to be significantly larger than the elements of the computational mesh. Once the optimization process has converged, one obtains a representation of the transmembrane potentials everywhere within and on the myocardium. However, we note that these transmembrane potentials are obtained by using a model with predetermined parameters and might not present a good estimate of the true transmembrane potentials; thus, this approach in some senses is more similar to a fiducial-time based imaging method than to a potential-based one.

We also note that this approach applies a very strict spatial-temporal constraint on the solution behavior, since the cellular automata model parameters depend on the physiological properties of the heart. However, these parameters may

vary from one heart to another, and from a normal heart to a diseased one. Therefore, these predefined parameters of the cellular automata model may produce a model error whose effect has not yet been addressed in the literature. A possible solution to this problem might be to reconstruct more parameters of the cellular automata model from the body surface measurements rather than just reconstructing the site of origin of activation.

Skipa et al. [55] reported on another approach to reconstructing the transmural activity of the heart, in which they described the electrical sources in the heart by three-dimensional patches of transmembrane voltage. A linear forward model, obtained by using FEM, related the transmembrane voltages in the heart volume to the body surface potentials, taking into consideration the anisotropic properties of the myocardium. For the inverse problem, Tikhonov zero and second order regularization were used while temporal information was incorporated using the Greensite method. However, the simulation results obtained by this approach did not deliver a meaningful solution for the nodes inside the cardiac wall, while the transmembrane voltages on the epicardial surface were comparable to reconstructions obtained using an epicardial potential source model [71]. We emphasize again that to our knowledge, no discussion about the uniqueness of the myocardial inverse solution has been offered for this approach.

9.4 Fiducial-Time Based Inverse Algorithms

In HSP and TMP methods, the potentials at each point in space and time are essentially free variables in the reconstruction; thus, strong explicit constraints are required to achieve useful solutions, and as we have seen, it is not a trivial matter to find constraints that both capture relevant physiology (and thus produce physiologically accurate, meaningful, and reliable solutions) and are mathematically tractable. Another general approach to the inverse electrocardiography problem starts from almost the other extreme; it imposes very strong physiologically based constraints in the source model itself and reduces the number of free parameters. The basic idea is to focus on reconstructing the time of activation at each point in space on the epicardial and endocardial surfaces (a complementary formulation also exists for finding recovery time). A separate benefit of this approach is that from a physiological standpoint, activation times are the most clinically relevant aspect of cardiac electrical activity; although they can be derived from a potential-based reconstruction (e.g., by finding extrema of temporal derivatives), it is simpler to reconstruct them directly. But perhaps more importantly, from an inverse problems perspective, this formulation becomes much better constrained; instead of needing to reconstruct an entire time series at each surface location, we only need to reconstruct one number at each location to capture the entire heartbeat. Of course, if there is relevant information in other aspects of electrical activity (for example, variation in the height of the wavefront or the location and behavior of the maxima that typically precede it early in activation and that are related to depth in the wall of an ectopic focus [72]), we cannot reconstruct it with such a restricted source model. But the advantage of greatly reduced complexity on the source model, especially when achieved with such a physiologically motivated parameterization, holds great promise for a more robust, accurate, and meaningful solution. One particular advantage that one could hope for from such an approach is greater robustness to errors in the geometry of the forward model; put simply, because the space of the solution is so much smaller, the effects of ill-conditioning are lessened and we can consequently expect to be less sensitive to model error in particular. In addition, from a physiological perspective, the potentials are sensitive to loading effects of the torso volume conductivities, while the activation sequence is not; this adds even greater robustness to this approach.

The main drawback of the activation time imaging formulation is that the forward problem, which now maps activation times to body surface potentials, is nonlinear. For example, adding two vectors of activation times together (for example simply delaying activation in time by making one of the vectors have identical elements) will not produce the sum of the body surface potentials due to each of these sets of activation times. Hence, nonlinear optimization algorithms must be used to solve the inverse problem for the set of activation times that best fits the body surface data. Although somewhat more robust to errors in the input, the problem is still ill-posed and requires regularization. Nonlinear, ill-posed problems are notoriously difficult to solve in general and the same has proved true in this case. In particular, experience has shown that results can be very sensitive to the starting point for these nonlinear optimizations; presumably there are multiple minima in the objective function, even with a regularization term added.

The original papers in this area came from a group in Nijmegen, The Netherlands, in the 1980s [73–76]. In these papers, the starting point for the nonlinear search was found by integrating in time over the entire QRS interval, then using a

Newton-type nonlinear optimization to find an improved estimate. However, this approach was somewhat heuristic and without any particular physiological motivation.

More recently a powerful algorithm by Huiskamp and Greensite [63] based on this activation imaging approach has re-invigorated this area of investigation. This activation-based inverse algorithm is centered around the identification of what are known as "critical points" and associated times in the surface activation function (i.e., epi- and endocardial breakthrough/termination points and times), which are found using a modified MUltiple SIgnal Classification (MUSIC) algorithm [77]. Closely related approaches have been used for the EEG and MEG inverse problems since the early 1990s, presented primarily in a series of papers from Richard Leahy and coworkers, starting from Mosher et al. [78]. Examples of critical points in a cardiac excitation wavefront are shown in Fig. 9.4. The key idea behind this critical-point approach stems from the observation that when an evolving cardiac excitation wavefront intersects the epicardial surface, a *hole* develops in the wavefront. This is a significant change to the topology of the wavefront, which generates a sudden alteration in the surface potential recordings. If $\tau(\boldsymbol{x})$ is defined to be the activation time on the surface of the heart (note that in this formulation, $\boldsymbol{x}$ is a location parameter on the heart surface, and $\tau(\cdot)$ has units of time, measured with respect to some arbitrary $t = 0$), then these breakthrough points are critical points of $\tau(\boldsymbol{x})$; that is, $\nabla\tau(\boldsymbol{x}') = 0$, where $\boldsymbol{x}'$ is the location of the breakthrough point (note that if we use $\boldsymbol{V}_m$ to represent the TMPs, the nonlinearity is in the transfer from $\tau(\boldsymbol{x})$ to $\boldsymbol{V}_m$; given $\boldsymbol{V}_m$ we can define a forward matrix $\boldsymbol{A}$ that predicts the body surface potentials just as in TMP potential-based formulations):

This critical point observation leads, after much mathematical derivation [81], to the two following important results:

1. $\boldsymbol{x}'$ is a critical point of $\tau(\boldsymbol{x})$ with critical time $\tau(\boldsymbol{x}') \Longleftrightarrow \boldsymbol{a}$ is in the space spanned by the spatial singular functions of $\boldsymbol{\Phi}_B$, where $\boldsymbol{a}$ is the column of the $\boldsymbol{V}_m$ to $\boldsymbol{\phi}_B$ transfer matrix $\boldsymbol{A}$ corresponding to $\boldsymbol{x}'$, and
2. with all critical points of $\tau(\boldsymbol{x})$ determined, the computation of $\tau(\boldsymbol{x})$ (on both the epicardial and endocardial surfaces) is a well-posed problem.

The key assumption required to prove the first point is that $\boldsymbol{V}_m$ is modeled as a uniform step jump across the wavefront; i.e.,

$$\boldsymbol{V}_m = a + bH(t - \tau(\boldsymbol{x})), \tag{9.33}$$

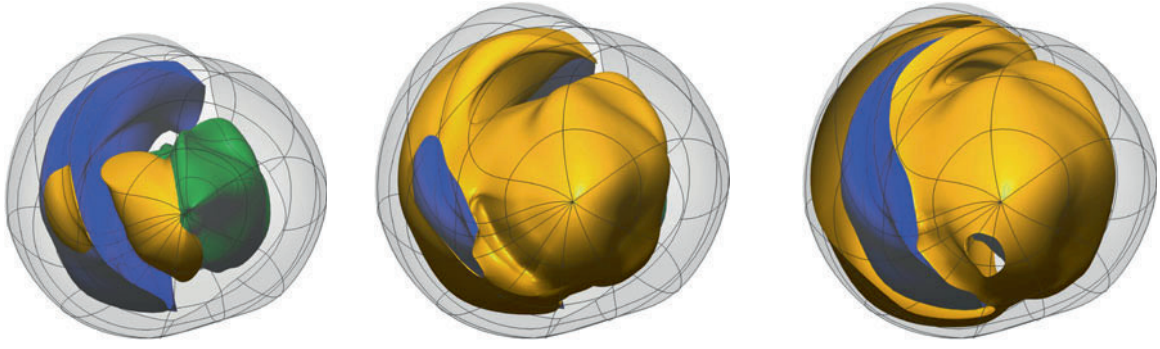

Figure 9.4

The formation of critical points and their associated critical times as an excitation wavefront (*gold surfaces*), derived from a simulation based on an eikonal model, collides with the heart walls [79]. Panel (a) shows the initial excitation sites near the endocardial surfaces. Panels (b) and (c) show critical points as the excitation wavefront (*gold surface*) collides with the epicardial surface and a hole is formed in the wavefront. The heart is viewed from the apex with the epicardium shown as a transparent surface, the left ventricular surface in *green* and the right ventricular surface in *blue*. Figure reproduced from Pullan et al. [80] with permission.

where a is a constant offset value, b controls the height of the step jump of the action potential, H is the Heaviside step function, and $t \in [0, T]$.

The Heaviside step function models an elementary source at a point on the heart surface $\boldsymbol{x}$, excited at time $\tau(\boldsymbol{x})$, which remains excited until the entire domain has been excited. Equation (9.33) represents only phase 0 of the action potential and hence the inverse algorithm derived from the two results just shown is specific to the intervals occupied by the P wave (atrial depolarization) and the QRS complex (ventricular depolarization) of the ECG. If, instead of (9.33), one assumed

$$\boldsymbol{V}_m = a + b - bH(t - \tau(\boldsymbol{x})), \tag{9.34}$$

(i.e., a step jump down) and we now considered $\tau(\boldsymbol{x})$ to be a time corresponding to the phase 3 (repolarization) of the action potential, then results similar to the two listed earlier could be obtained. Thus, any inverse algorithm derived from those two results for imaging depolarization could, in theory, be used to image repolarization, and thus this approach is a means of complete fiducial-time based imaging. However, imaging repolarization is complicated by a number of its unique features. As shown in Fig. 5.3, repolarization occurs over a relatively long time period, and therefore, it is difficult to define a distinct recovery time (compared with the activation time), which means that (9.34) is a more severe approximation than (9.33). Moreover, since it is the change in time of the TMP that produces the "source" in this model, the effective signal-to-noise ratio is considerably reduced. Also, repolarization occurs during the mechanical motion of the heart, meaning that the transfer matrix may contain substantially more geometric error in the repolarization phase compared with the depolarization phase.

The use of the critical-point method to locate breakthroughs suggests a two-step approach for fiducial-time based imaging:

1. Find the critical points and times using the theory above, using, for example, the algorithm described in some detail below, and then
2. Obtain the entire activation sequence by solving a non-linear minimization problem in which the objective is to minimize the difference between the calculated torso potentials $\hat{\boldsymbol{\phi}}_B$, and the measured potentials, $\boldsymbol{\phi}_B$ (where $\hat{\boldsymbol{\phi}}_B$ is calculated using $\boldsymbol{A}(\boldsymbol{x}, \boldsymbol{y})$ and any estimate of $\tau(\boldsymbol{x})$), starting from an initial estimate found $\boldsymbol{n}$ the first step.

During this optimization process, the critical points and times that have been identified can either be fixed or be constrained to remain local extrema of $\tau(\boldsymbol{x})$. Additional constraints on the optimization process can be imposed, such as the surface Laplacian of $\tau(\boldsymbol{x})$ [82],

$$E(\tau(\boldsymbol{x})) = \min\left\{\left\|\boldsymbol{\phi}_B - \hat{\boldsymbol{\phi}}_B\right\|_2 + \lambda \cdot \boldsymbol{L}\tau(\boldsymbol{x})\right\}, \tag{9.35}$$

where E is the objective function being minimized with respect to the activation times on the heart ($\tau(\boldsymbol{x})$), λ is a parameter controlling the degree of regularization imposed on the objective function and $\boldsymbol{L}$ is a discrete approximation of the Laplacian of the excitation field. We return to a discussion of this second optimization step in the following section, but first we describe how the "critical times" can be found computationally.

The following algorithm computes the critical points and times. First, the signal matrix, $\boldsymbol{\Phi}_H$, recorded from surface electrodes, and $\boldsymbol{A}(\boldsymbol{x}, \boldsymbol{y})$ mapping from $\boldsymbol{V}_m$ to $\boldsymbol{\phi}_B$, are required. The spatial singular functions of $\boldsymbol{\Phi}_B(\boldsymbol{y}, t)$ are computed using the singular value decomposition

$$\boldsymbol{\Phi}_B = \boldsymbol{U}_B \boldsymbol{\Sigma}_B \boldsymbol{V}_B^{\mathrm{T}} \quad \text{with an effective rank } R \tag{9.36}$$

As already described, singular vectors corresponding to small singular values are discarded. Noting that each column of $\boldsymbol{A}$ corresponds to the map from a particular node $\boldsymbol{x}$ on the heart surface to all the body surface nodes, the following function can be defined for each $\boldsymbol{x}$ for all values of $t \in [t_0, t_1]$,

$$\boldsymbol{M}_{t_0}^{t_1}(\boldsymbol{x}) = \left(1 - \sum_{r=1}^{R} \left[\tilde{\boldsymbol{a}}(\boldsymbol{y}) \cdot \boldsymbol{u}_r(\boldsymbol{x})\right]^2\right)^{-1}, \tag{9.37}$$

where $\tilde{\boldsymbol{a}}(\boldsymbol{y}) = \dfrac{\boldsymbol{a}(\boldsymbol{y})}{\|\boldsymbol{a}(\boldsymbol{y})\|}$ is the unit (Euclidean) normalized column of the transfer matrix $\boldsymbol{A}(\boldsymbol{x},\boldsymbol{y})$ which corresponds to $\boldsymbol{x}$, and $\boldsymbol{u}_r(\boldsymbol{x})$ is the rth column of the spatial (left) singular matrix $\boldsymbol{U}$ and R is the number of singular values retained, as just described. The summation term in (9.37) is the projection of the normalized vector $\tilde{\boldsymbol{a}}(\boldsymbol{y})$ onto the vector space spanned by the spatial singular vectors $\boldsymbol{u}_r(\boldsymbol{x})$. With the normalization in $\tilde{\boldsymbol{a}}$ and the fact that the singular vectors are also unit norms, if $\tilde{\boldsymbol{a}}(\boldsymbol{y})$ is contained in this space then the summation will yield 1 (and hence $\boldsymbol{M}_{t_0}^{t_1}(\boldsymbol{x})$ will be infinite), while if no component of $\tilde{\boldsymbol{a}}(\boldsymbol{y})$ is contained in this space, the summation will yield 0. This is the principle behind the well-known MUSIC method for spectral estimation and array processing [83]. Hence, (9.37) can be thought of as a measure of the distance of $\tilde{\boldsymbol{a}}(\boldsymbol{y})$ from the space spanned by the set $\boldsymbol{u}_r(\boldsymbol{x})$, which we can think of as the "signal space." This distance measure greatly exaggerates points $\boldsymbol{x}$ that are close to this space. In theory, $\boldsymbol{M}_{t_0}^{t_1}(\boldsymbol{x})$ is singular at critical points $\in [t_0, t_1]$, although, in practice, there are no singularities, due to noise and other errors associated with $\boldsymbol{\Phi}$ and $\boldsymbol{A}$.

To find the activation times corresponding to these critical points, the following matrices are constructed,

$$\boldsymbol{M}_{xt}^{\oplus} = \boldsymbol{M}_0^t(\boldsymbol{x}), \tag{9.38}$$

$$\boldsymbol{M}_{xt}^{\ominus} = \boldsymbol{M}_t^{\mathrm{T}}(\boldsymbol{x}) \tag{9.39}$$

Each row of both matrices corresponds to a particular node $\boldsymbol{x}$, while each element of that row is the value of the function defined in (9.37) for the appropriate interval at a time t in the measurement time series which corresponds to its column index. Thus, these two functions describe the distance from signal space, where the two signal spaces are restricted to $[0, t]$ and $[t, T]$ respectively. From these matrices, a zero-crossing matrix is created, defined by

$$\boldsymbol{Z}_{xt} = \boldsymbol{M}_{xt}^{\oplus} - \boldsymbol{M}_{xt}^{\ominus}, \tag{9.40}$$

which enhances the difference in behavior between $\boldsymbol{M}_{xt}^{\oplus}$ and $\boldsymbol{M}_{xt}^{\ominus}$ at each time t. Each row of this zero-crossing matrix corresponds to the distance from signal space at a particular location on the heart as a function of time.

In Fig. 9.5, we show sample functions defined by the rows of $\boldsymbol{Z}_{xt}$ (called the critical point functions); one observes that they are similar to step functions in the sense that they have high gradients at the point at which the horizontal axis is crossed. Theoretically, the critical point function corresponding to a critical point crosses zero at the critical time. In practice, the distinction between critical points on the one hand, and activation times that occur in regions where the activation surface is continuous, on the other, is not as clear, due to noise and errors. Thus, there are several alternative ways to use the rows of $\boldsymbol{Z}_{xt}$. One could, for instance, define a threshold on the height of the jumps (which can differ dramatically, as seen in the right-hand column of Fig. 9.5), consider those jumps that are above the threshold as detected critical points, and run the optimization algorithm initializing it by fixing or restricting its ability to change the detected critical times. Another alternative is to use the zero-crossing of each critical point function to obtain an initial estimate of the activation time at each location. With critical points and times, or activation times, thus identified, the process of determining $\tau(\boldsymbol{x})$ everywhere is, theoretically, a well-posed problem and in practice can be solved via the optimization process described next.

Once the critical points or initial activation times, or other results of the application of the critical point theorem, are found, we are left with a nonlinear optimization problem such as the one in (9.35), with the critical points serving either simply as a starting point for the optimization or also as an additional constraint throughout the procedure. We note again that this problem is nonlinear because $\hat{\boldsymbol{\phi}}_B$ depends on the fiducial times in a highly nonlinear manner, in contrast to its dependence on the HSP or TMP values. We also note that many optimization algorithms run better if one can compute the appropriate Jacobians. However, if the sources are simply switched on at discrete locations on the heart surface (i.e., the nodal positions) according to (9.33), the resultant simulated potentials $\hat{\boldsymbol{\phi}}_B$ are discontinuous, which in fact gives rise to body surface potentials that are not continuous with respect to the activation times. For use in the optimization phase of the activation inverse procedure, it is more desirable to deal with functions that are continuous; moreover, the speed of convergence is greatly aided by having continuous derivatives [82].

Thus, alternatives to (9.33) have been used by various investigators. The purpose of these alternatives it to generate values of V_m that are smooth and continuous but still contain the general features of the activation phase of a ventricular action potential. One such alternative is the sigmoid function $S(t-\tau)$, as shown in Fig. 9.6 and described in the following section in (9.41), and another is the arctangent function, as used by Tilg et al. [84]. Like the Heaviside step transition,

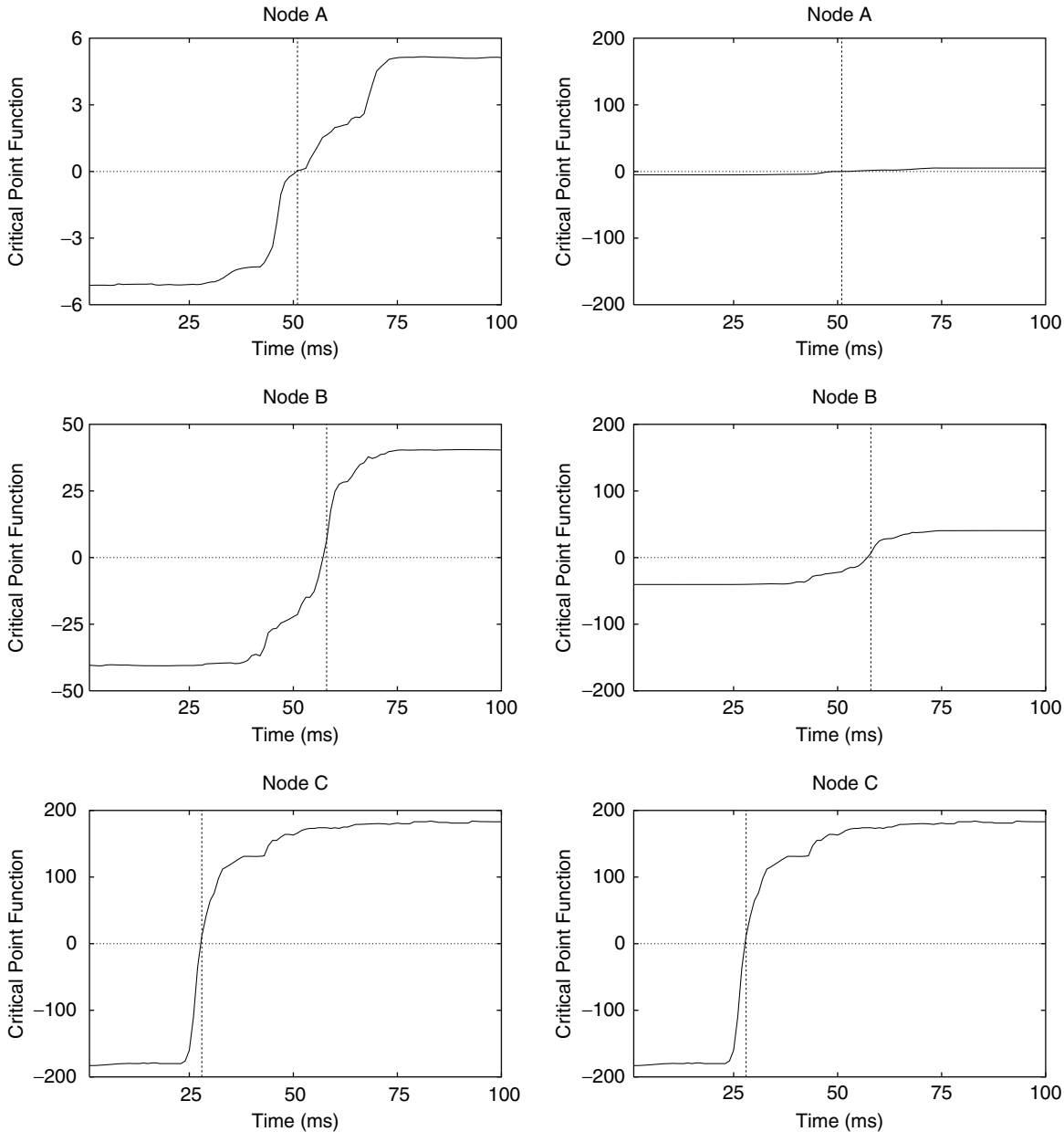

Figure 9.5

Comparison of critical point functions between critical and noncritical points. The *left column* shows the three functions and their corresponding ranges. The *right column* re-plots all the functions scaled to the same range. The larger jump in the critical point function for node C indicates that it corresponds to a critical point. The *vertical line* marks the points at which the functions cross the *horizontal axis* (critical times) and provides an estimate of the activation time at each location.

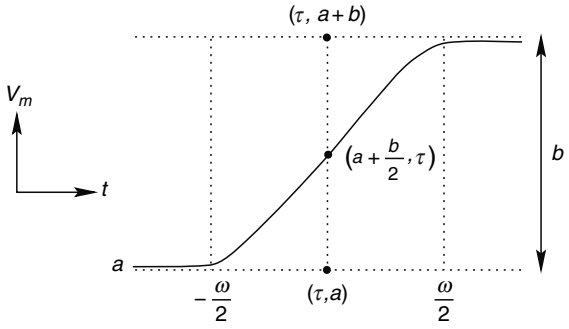

Figure 9.6

Approximation of the Heaviside step function by a sigmoidal function. This function contains the parameters ω and b to determine its shape. The ω parameter controls the width or window of the activation upstroke (i.e., the duration of the depolarization), while the b parameter controls the height of the transmembrane jump, i.e., the difference between the resting potential (a) and the peak of the action potential upstroke. Time is shown on the horizontal axis and the transmembrane potential on the vertical axis.

all these functions rely on assumptions about the shape of the action potential that are likely not a practical restriction for normal hearts, but do provide a measure of the expected spatial resolution of this activation-inverse approach. Moreover, abnormal hearts may provide a more serious problem, a fact that, as noted earlier, motivated the introduction of the surface TMP imaging method described in Sect. 9.3.6.2.

When specifying the sigmoid function as follows, the a and b parameters again represent the transmembrane resting potential and the transmembrane jump respectively. The smooth function is created by gradually activating the sources over a time-span of ω. If u is defined as $t - \tau(\boldsymbol{x})$, the smooth activation function can be represented mathematically by the function

$$S(u) = \begin{cases} a & u \le -\frac{\omega}{2} \\ a + \frac{b}{2}\left(\frac{2}{\omega}u + 1\right)^2 & -\frac{\omega}{2} < u \le 0 \\ b - \frac{b}{2}\left(\frac{2}{\omega}u - 1\right)^2 & 0 < u < \frac{\omega}{2} \\ a + b & u \ge \frac{\omega}{2} \end{cases} \tag{9.41}$$

The derivatives of the torso surface potential with respect to the activation times for use in the optimization phase are then given by

$$\frac{\partial \hat{\phi}_B}{\partial \tau} = \boldsymbol{A} \cdot (-1) \begin{cases} 0 & u \le -\frac{\omega}{2} \\ b\left(\frac{2}{\omega}u + 1\right)\frac{2}{w} & -\frac{\omega}{2} < u \le 0 \\ -b\left(\frac{2}{\omega}u - 1\right)\frac{2}{\omega} & 0 < u < \frac{\omega}{2} \\ 0 & u \ge \frac{\omega}{2} \end{cases} \tag{9.42}$$

A recent addition to the literature on activation-time imaging has suggested an alternative way to solve the nonlinear regularized optimization [85]. This approach, based on a method suggested for general nonlinear inverse problems [86], replaces the iterative gradient descent approach used in Newton methods with iterations using a sequence of linearizations around the current solution. The key benefit claimed for this method is that, for the case of regularized ill-posed problems, it allows one to use a standard regularization parameter determination method (such as the L-curve) on the *linear* update

optimization that needs to be solved on each iteration. Thus, one solves a sequence of linear regularizations, each with its own regularization parameter. Results indicate that this method leads to *L*-curves that are much better defined than the single *L*-curve obtained using a standard Gauss–Newton technique [85], especially when applied to clinical data.

An alternative method for both initializing and regularizing the activation (and recovery) time algorithms has recently been introduced by van Oosterom and coworkers, who report improved results with it over standard initializations and Laplacian-based regularization [87]. The basic idea is to compute a set of simplified propagation patterns, initialized in turn from all of the nodes on the HSP geometry. This pattern is computed by finding the lengths of shortest paths from each node to all other nodes, the paths following straight line segments that lie entirely inside the myocardium. The shortest route is found by using an optimization method called the "shortest path algorithm." Applying an assumed constant propagation velocity to the resulting distances leads to an activation pattern for each node on the surface. The body surface potentials predicted by the forward model based on each of these activation patterns are compared with the measured potentials and the best fit pattern is chosen to initialize the nonlinear optimization as described earlier. The same distance function has also been used to regularize the nonlinear optimization. It is interesting to note that the underlying principle seems to have something in common with the wavefront-based methods for curve and potential reconstruction of Ghodrati et al. [67] described earlier, in that the idea is to impose a propagating wavefront behavior on the reconstruction, although the specifics of both the formulation and the method are quite different.

9.5 Inverse Solutions from Intracavitary Measurements

Another method of inverse electrocardiography is to measure the potentials within a chamber of the heart by means of a noncontact, multielectrode catheter array and then to estimate the endocardial surface potentials from them. The forward model of this approach has a similar form to other potential-based approaches and relates the potentials on the endocardial surface to the measurement leads inside the cavity. Since the measurements are recorded relatively close to the endocardial surface, the corresponding forward matrix is generally less ill-conditioned than the epicardial potential forward matrix. On the other hand, obtaining accurate geometrical data from which to construct the transfer matrix is challenging, because it requires medical imaging [88–90] and because the probe moves due to blood flow in the chamber. Overcoming this challenge is critical, because the accuracy of the computed inverse solutions is highly sensitive to errors in the geometry [91]. The only currently available commercial device based on inverse electrocardiography, the Ensite system produced by St. Jude Medical [90], obtains the geometry of the endocardial surface point by point using a catheter navigating on the endocardial surface. The sampled points are then fitted to a bicubic spline surface to improve the estimate of the actual chamber.

Due to the similarity of the forward model of this approach to the potential-based approach, all inverse methods mentioned in Sect. 9.3 apply to this problem as well. Khoury et al. have tested and reported several inverse methods for the endocardial inverse problem [88, 92, 93] and here we describe briefly two approaches that are slightly different from those covered in Sect. 9.3. While initially developed for the endocardial problem, there is no reason why these approaches could not be used for other potential-based formulations.

1. The first approach, developed by Khoury [92], uses the first order Tikhonov regularization method and the BEM method to define the regularization matrix as the derivative of the endocardial potentials in the normal direction to the surface rather than tangential to the surface. This means that the regularization term constrains the magnitude of the normal current density on the endocardial surface, a strategy that lacks a solid theoretical justification, but nonetheless appears to work. Khoury et al. reported improved accuracy with this approach compared with simple zero-order Tikhonov regularization.
2. The second approach, also from Khoury and his colleagues, is again in the framework of Tikhonov regularization, but tries to define a regularization matrix that will satisfy the discrete Picard condition [93]. The regularization matrix in this approach has the same right and left singular vectors as the forward matrix, but its singular values are determined from the energy spectrum of the data. Therefore, the singular values of the regularization matrix and the particular measured data directly affect the filter factors of the inverse solution. The inverse solution obtained by this method produces superior results than the zero order Tikhonov solution [93].

9.6 Determining the Regularization Parameters

There are many a posteriori methods for determining the appropriate levels of regularization required for virtually all forms of inverse problem. (By a posteriori here we mean that these methods try many regularization parameters, test the results of each trial, and pick one of these based on some criterion. This is in contrast to a priori methods, which rely on the knowledge of noise statistics or other prior knowledge.) Each of these regularization parameter estimation methods attempts to provide a balance between the solution and regularization norm. Commonly accepted methods, which we discuss briefly here, include: the *L*-curve [94], the CRESO criterion [95], the zero-crossing criterion [96], and generalized cross-validation [97]. We briefly explain these methods here with reference to the HSP inverses given in Sect. 9.3. In addition, we first describe the *optimal criterion method*, by which we mean picking the regularization parameter using the knowledge of the true solution – clearly not a practical approach, but useful for simulation studies and in exploring the best case behavior of various inverse methods. For the optimal method, we illustrate the procedure using both the Greensite potential-based inverse and the Tikhonov and TSVD inverses. We explain the other methods described in the following section with reference only to the Tikhonov and TSVD inverses.

9.6.1 Optimal Criterion

The optimal criterion solution, although clinically not feasible because it requires a priori the knowledge of the epicardial potential distribution, places a lower bound on the accuracy of a given regularization scheme and thus leads to a valid comparison measure between relative regularization inverse approaches.

The optimal solution for Tikhonov and TSVD regularization schemes can be obtained by choosing the value of the regularization parameter λ_t at each time t that leads to the best solution to (9.12), i.e., that minimizes

$$\|\hat{\boldsymbol{\phi}}_{H(i)} - \boldsymbol{\phi}_{H(i)}\|_2, \tag{9.43}$$

where $\hat{\boldsymbol{\phi}}_{H(i)}$ is the ith regularized solution and $\boldsymbol{\phi}_{H(i)}$ is the exact solution on the heart. Note that, of course, one could define a different measure of optimality instead of the Euclidean norm of the reconstruction error, but to the best of our knowledge, this one has enjoyed universal support in the field. The optimally regularized solution to Greensite's epicardial potential method can be obtained via regularizing every ith equation individually if the isotropy condition truly holds; since the columns of $\boldsymbol{U}_B$ are orthogonal, they are linearly independent. Thus, for every solution $\boldsymbol{\gamma}_i(\boldsymbol{x})$ to (9.31), the optimal regularization parameter is the value which minimizes

$$\|\sigma_{B(i)}\boldsymbol{\gamma}_i(\boldsymbol{x})\boldsymbol{v}_{B(i)} - \boldsymbol{\Phi}_H\|_F, \tag{9.44}$$

where $\|\cdot\|_F$ denotes the *Frobenius* norm. We note that in practice one does not usually find a true optimal point, but rather tests over a dense grid of regularization parameters to locate the best value.

9.6.2 *L*-Curve Criterion

The *L*-curve method uses a parametric plot of the regularization objective function $||\boldsymbol{R}\hat{\boldsymbol{\phi}}_H||_2$ against the corresponding residual objective function $||\boldsymbol{A}\hat{\boldsymbol{\phi}}_H - \boldsymbol{\phi}_B||_2$ for a wide range of regularization parameters (λ). For discrete ill-posed problems, this curve, when plotted on a log-log scale, often has a characteristic L-shaped appearance with a corner separating the vertical and horizontal components of the curve, as shown in Fig. 9.7. The regularization parameter increases as the curve moves from the upper left to the lower right portions of the graph. The "corner" identifies a value of λ that provides an ideal (in some sense) balance between the two components that are minimized in (9.13). Regularization parameters that correspond to the upper left part of the curve produce results dominated by high regularization error and tend to be overly responsive to the noise and error (under-regularized). Regularization parameters that correspond to the lower right part of the curve produce results dominated by high residual error and tend to be overly insensitive to the measurements (over-regularized). The point for which any change in regularization parameter causes a large increase in one of the two

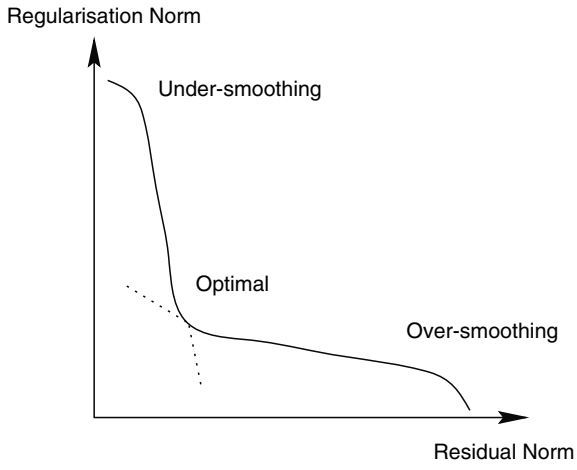

Figure 9.7

The *L*-curve is a log–log plot of the residual norm, $\|A\hat{\phi}_H - \phi_B\|_2$, against the regularization norm, $\|R\hat{\phi}_H\|_2$. This plot is typically of the form of an "L." The corner of the "L" strikes a balance between the residual of the solution and the regularization norm.

terms with little decrease in the other is considered to be a good choice; this occurs at the corner. The corner of the L-curve is also the point of maximum curvature, which provides the basis of a number of automatic methods that can detect this point, either through careful search techniques or using interpolants such as splines.

9.6.3 CRESO Criterion

The Composite REsidual and Smoothing Operator (CRESO) criterion chooses the regularization parameter for which the difference between the derivative of the residual term and the derivative of the smoothing term is maximized [95]. The CRESO regularization parameter is chosen to be the smallest value of λ_t^2 that results in a local maximum of the function

$$C(\lambda_t) = \|\phi_H(\boldsymbol{x}, \lambda_t)\|_2^2 + 2\lambda_t^2 \frac{\mathrm{d}}{\mathrm{d}\lambda_t} \|\phi_H(\boldsymbol{x}, \lambda_t)\|_2^2, \tag{9.45}$$

where $\phi_H(\boldsymbol{x}, \lambda_t)$ are the potentials on the heart regularized by the parameter λ_t. The function $C(\lambda_t)$ is the derivative of the function $B(\lambda_t)$, where

$$B(\lambda_t) = \lambda_t^2 \|\phi_H(\boldsymbol{x}, \lambda_t)\|_2^2 - \|\boldsymbol{A}\phi_H(\boldsymbol{x}, \lambda_t) - \phi_B(\boldsymbol{y}, t)\|_2^2 \tag{9.46}$$

Strictly, the CRESO function is defined only for a continuous regularization parameter and hence cannot be used for the discrete TSVD approximation [98].

9.6.4 Zero-Crossing Criterion

The zero-crossing criterion aims to find the regularization parameter by solving the function $B(\lambda_t) = 0$ in (9.46). If more than one value of λ_t satisfies this condition, then the smallest value is chosen. Thus is essentially the minimum-product criterion proposed by Lian et al. [98] as another approach to locating the corner from the L-curve [99].

9.6.5 Generalized Cross Validation (GCV)

The generalized Cross Validation (GCV) method [97], like the *L*-curve, estimates a regularization parameter as a result of a trade off between minimization of the residual norm (data misfit) and the level of regularization. For this purpose the GCV function is defined as follows:

$$G = \frac{||\boldsymbol{A}\boldsymbol{\phi}_H - \boldsymbol{\phi}_B||_2^2}{\text{trace}(\boldsymbol{I} - \boldsymbol{A}\overset{\circ}{\boldsymbol{A}}_\lambda)}, \tag{9.47}$$

where $\boldsymbol{I}$ is the identity matrix and $\overset{\circ}{\boldsymbol{A}}_\lambda$ is the regularized inverse matrix for regularization parameter, λ. The numerator of the GCV function represents the data misfit and the denominator the level of regularization. The minimum of the GCV function for a range of regularization parameters determines the GCV regularization parameter; therefore, this method chooses a regularization parameter that results in a minimum misfit while regularizing sufficiently. The denominator of the GCV function can be shown to be related to the filter factors, for details see Hansen [9].

9.7 Validation and the Effect of Error

An essential component of any simulation approach is thorough validation of its results; in the case of a technique that aims to provide diagnostic information, validation must also include a careful evaluation of the relationship between error and uncertainty in the model and its ultimate diagnostic accuracy. Hence, it is necessary not only to show that electrocardiographic inverse solutions can provide credible images of cardiac electrical activity but also to establish the limits on the accuracy of the results and determine how errors in all components of the model effect the overall accuracy of the inverse solution. There are two basic approaches that are common to this type of validation, one based on computing the inverse solutions from the results of computed forward solutions (simulation studies) and one based on comparing measured results from experiments or clinical measurements with expectations from simulations of the same conditions (experimental studies). We describe both approaches below and then discuss some of the still unresolved questions about the effects of model components on accuracy.

9.7.1 Simulation Studies

The goal of simulation studies is to generate both source and remote data with a high degree of accuracy and then let the inverse method(s) under examination use only the remote data and seek to predict the sources. Ideally, the method used to generate the simulated test data should be independent of the inverse solution, i.e., use different geometric models and mathematical formulations. Otherwise, the inverse solution is likely to be overly optimistic, since solutions to ill-posed problems tend to magnify all error sources, including modeling error. This type of error is inevitable in practice but in such a validation model will be suppressed. For example, a forward transfer coefficient matrix, $\boldsymbol{A}$, used to generate test data is not the ideal basis of an associated inverse solution because that inverse was specifically created to match the effect of $\boldsymbol{A}$ on the sources. Validation may then indicate how various parameters affect the inverse solution, and perhaps even how different inverse algorithms compare with each other, but not necessarily how well any particular method will work at finding sources from measured remote potentials. One can mitigate the inherent bias of this approach by adding known quantities of random noise to the forward-computed potentials; however, it is generally advisable to maintain independence between the forward solutions used to generate simulated test data and the inverse solutions under evaluation.

Another essential feature of a robust validation scheme is that it includes a wide range of test data. An inverse solution that is very accurate with one type of data or in one specific case (e.g., for a particular geometric model) may perform poorly for a different set of conditions. There is no known comprehensive approach to determining robustness; hence, there is no substitute for testing over a wide range of parameter space.

9.7.1.1 Analytical Solutions

The most straightforward form of simulation to use for validation is one that employs an analytical expression to generate the test data, which then forms the input to a numerical (discrete) inverse solution. This tests all aspects of the inverse solution, including the mathematical formulation and the numerical and computational implementation. Such solutions also allow for a great deal of variation of at least some parameters so that it is possible to compute test data under a wide range of conditions. Unfortunately, for electrocardiographic inverse problems there are relatively few geometries that contain sufficient symmetry and simplicity that an analytical expression is possible.

The best-known analytically tractable validation models in electrocardiology are those based on concentric and eccentric spheres proposed by Bayley and Berry [100–102] developed extensively by Rudy et al. [103–105] and still in use today [106–108]. Rudy et al. used these models not only for validating their numerical solution; by varying source types and locations and geometric model eccentricity, error, and conductivity, as well as regularization functionals used for the inverse solutions, they developed several fundamental hypotheses about the effect of each of these factors on inverse solution accuracy. One of these ideas that has subsequently been validated by physical models and human clinical studies is the relative insensitivity of the inverse solution to variations in thorax conductivity. These studies did indicate, in contrast, a strong sensitivity of the solution accuracy on knowledge of the true heart position; unaccounted shifts of only a few centimeters could result in substantial errors in recovered epicardial potentials [105]. However, the intrinsic limitation of analytical models based on simple geometries is their inability to capture the influence of realistic anatomical structures, which are both complex and asymmetric. This, in turn, means that conclusions drawn from such studies cannot readily be applied to physiologic situations.

Throne et al. also used the layered inhomogeneous eccentric spheres system to evaluate the effect of errors in geometry and conductivity on solutions to the inverse problem of electrocardiology [106]. They compared the abilities of four different numerical methods to solve the inverse problem, two of which used regularization, and found that, although the regularized methods performed better in the presence of geometric errors, small errors in heart size and position still had a significant effect on the resulting solution. Such results are evidence that analytical validation approaches, even under highly simplified conditions, can reveal fundamental insights into the important aspects of the behavior of inverse solutions.

9.7.1.2 Numerical Solutions

An implicit assumption of most simulation-based validation schemes is that the inverse solution is inherently much less accurate than the associated forward solution. This discrepancy comes from the ill-posed nature of the problem; one consequence is that it may be acceptable to treat a numerically computed forward solution as being almost as accurate as one calculated from an analytical solution, at least compared with the associated inverse solution. This observation provides justification for the use of numerical forward solutions to generate test data for the associated inverse problem. The motivation for such an approach is the much broader range of variation that is possible, compared with analytical models, when the constraint of simplified geometry is removed. Thus numerical solutions have become the dominant approach in simulation-based validation schemes.

In order to address the problem of testing an inverse solution using test data from the same forward solution, one can use different simulation methods to create test data. For example, it is possible to use dipole sources to calculate both epicardial and torso surface potentials directly based on a realistic geometry, which are then available to test an explicit torso-to-epicardial-surface inverse solution [28, 109]. Because the two formulations are different, the dipole source forward model does not match exactly the surface-to-surface model. This is one example of cross validation, in which one compares the directly computed epicardial potentials against those inversely computed from the torso potentials.

Hren et al. proposed a valuable extension of this approach by means of a more realistic cross-validation approach, in which the source was not a dipole, but a cellular automata model of cardiac propagation [110–112]. Cellular automata models represent cardiac tissue as a regular mesh of "cells," each representing a region of approximately 0.5–1 mm^3 and use simplified cell-to-cell coupling and state transition rules to determine the activation sequence. Although not as detailed as the monodomain and bidomain models that are based on descriptions of membrane kinetics, cellular automata models have a long history in simulations of normal and abnormal cardiac activation [113–116] (Sect. 8.4.2). In order to apply

cellular automata models to the validation of electrocardiographic inverse solutions, Hren et al. developed a method by which they assigned electrical source strength to the activation wavefront, and were thus able to compute epicardial and torso potentials from the cellular automata model for realistic geometric models of the human torso [110, 117]. They used this technique both to validate inverse solutions [111] and to examine the spatial resolution of body surface mapping [118, 119]. The major weaknesses of this form of validation is inherent to the underlying assumptions of the cellular automata approach, i.e., the limited ability to mimic myocardial sources, especially for pathological conditions such as ischemia or complex ion channel disorders.

Messnarz et al. have reported perhaps the most elaborate example of this approach by using a realistic, anisotropic, finite element model of the heart as the basis for a cellular automata simulation of the activation sequence [2]. The anatomical model also contained lungs and thorax and the simulation assumed unequal anisotropy ratios in the cardiac intracellular and extracellular spaces. From the resulting activation time simulations, they assigned an action potential shape and from these time signals then computed both heart surface and torso potentials.

The most common contemporary approach to validation of inverse problems is to compute remote (e.g., torso surface) potentials from known sources (e.g., epicardial potentials or activation sequences) and then add noise to the results before computing the source using the inverse solution under evaluation. Most often, the scientific focus of these studies is to determine the sensitivity of the inverse solution to variations in model parameters, some of which may be unaccounted for in the inverse formulation. One example would be to study the sensitivity of epicardial potential reconstruction to (unaccounted) shifts or errors in the heart location or to the number of body-surface measurement electrodes.

For example, Modre [120] conducted investigations to determine the effect of varying both the number of torso residuals in the activation inverse and the complexity of the torso model. In that study, the investigators varied the number of body-surface electrodes from 21 to 41 to 62 and used models with and without lungs, and that included unaccounted alterations in geometry. Little variation was seen with the electrode arrangements containing 41 and 62 electrodes, whereas results were significantly poorer when using 21 electrodes and either correct or incorrect geometry.

In a study reminiscent of earlier reports from Rudy et al. using analytical solutions, Ramanathan and Rudy [121] studied the effects of inhomogeneities in tissue conductivity on the reconstruction of epicardial potentials using zero-order Tikhonov regularization. By solving the inverse problem with different torso configurations, they found that spatial variations in conductivity had a minimal effect on the inverse solutions. The resulting assumption that a homogeneous geometric model can perform adequately received further support when they added Gaussian signal noise and electrode location error to the input data and found even less dependence on tissue conductivity.

Cheng et al. reported a comprehensive and systematic simulation-based validation studies [66, 122] that used a framework established by Pullan et al. [123]. These studies compared both epicardial potential- and activation-based inverse procedures, using different cardiac sources, with regularization parameters calculated according to the different methods described in Sect. 9.6 under a variety of both Gaussian and correlated noise conditions. Their results illustrated that the activation-based inverse method produced the most stable solutions in the presence of geometric uncertainty. However, when no geometric error was present in the system (something not achievable in practice), the potential-based approaches performed marginally better. As an example of another parameter important in implementing an inverse solution, their studies also included a comparison of different methods of determining regularization parameters (see Sect. 9.6 for a discussion).

Using the optimal criterion already described for setting regularization levels, all of the potential-based methods in the study by [122] provided similar results. However, this method of selecting the regularization parameter is not usually feasible. Of all the potential-based inverse methods considered in that study, the most favorable results come from using the Greensite potential-based inverse method with the rank of each equation determined by the maximum curvature of the singular values, and using Tikhonov with CRESO or *L*-curve regularization for each equation. This was the case whether the solutions were compared with the original epicardial potential solutions or with the original activation times.

9.7.2 Experimental Validation

By far the oldest approaches to validating both forward and inverse solutions in electrocardiography have been based on experiments with physical analogs of the torso and cardiac sources. For example, the studies by Burger and Van Milaan [124, 125] employed a shell molded on a statue of a supine human into which they inserted a set of copper disks oriented

along one of the body axes and adjustable from outside the tank by means of a rod. More modern variation of this scheme employ more elaborate electrolytic tanks and measuring systems and some have used anesthetized, instrumented animals to record both source and remote data simultaneously. We present here a few examples of the current state of the art and refer to other sources for more detail (e.g., MacLeod and Brooks [126] and Nash and Pullan [127]).

Spach and Barr carried out the earliest studies that included simultaneously recordings from dense arrays of torso and heart electrodes from experimental chimpanzees [128] and dogs [129]. The relative lack of spatiotemporal resolution and the fact that these studies were published prior to the major theoretical developments in ECG inverse techniques have resulted in a somewhat limited interpretation of the results. Neither of these data sets is currently available in electronic form, and this further limits their use in contemporary validation studies. These landmark studies, did, however, allow the first detailed qualitative comparison of heart and body-surface potentials and showed that spatial information is maintained on the body surface. These findings also provided great motivation for the subsequent growth in the field of electrocardiographic imaging.

Simultaneous recording of epicardial and body surface potentials in the closed chest of animals have been attempted by at least two other research groups. At Oxford University, pigs were the animal of choice [130], while Zhang et al. [131] used rabbits. The protocal of the Oxford experiments (shown in Fig. 9.8) involved placing multiple electrodes on the heart and torso of the animal and simultaneously recording the potentials at all electrode locations during normal and abnormal rhythms, as well as recording the geometrical locations of the recording sites [132]. To position the heart

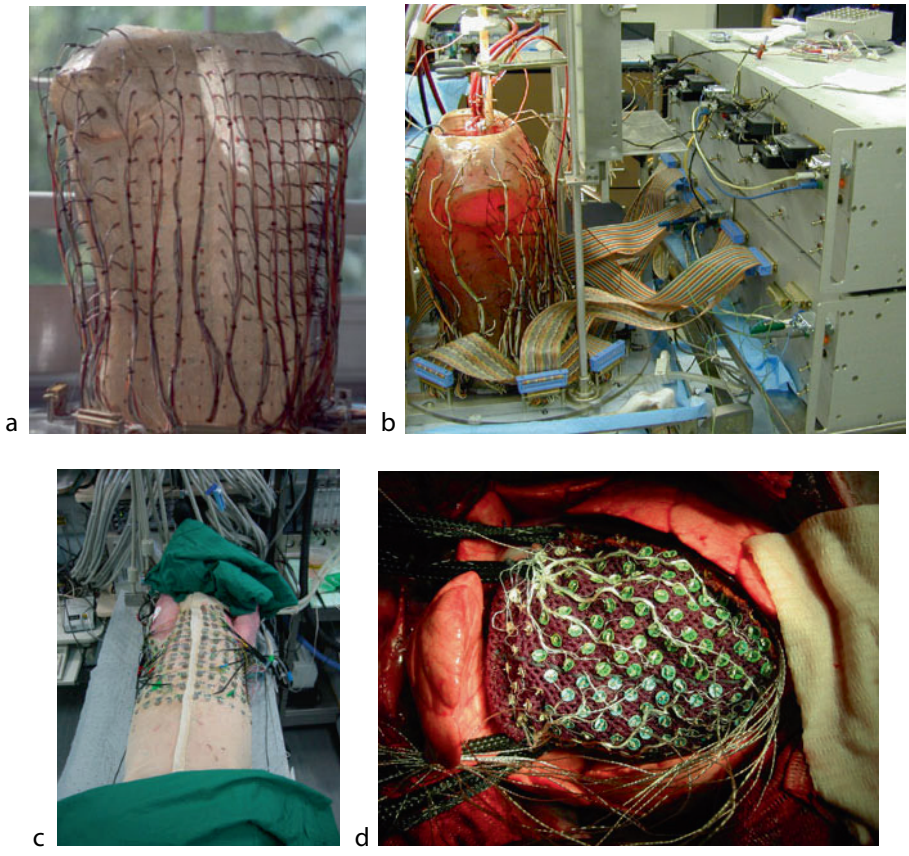

Figure 9.8

Panel (a) shows the torso tank of the Cardiovascular and Research Training Institute, University of Utah, used to collect simultaneous epicardial and body surface electrocardiograms. In panel (b) a perfused heart is suspended within the torso tank which is filled with a saline solution. Panels (c) and (d) show the experimental setup at Oxford University. In panel (c) is the vest of electrodes on the body surface and in (d) the sock of electrodes around the heart.

electrodes, the pigs were thoracotomised and an epicardial electrode sock (containing 256 electrodes) was placed inside the pericardium. Upon successful placement of the sock (as verified by successful recordings from the electrodes) the chest was reclosed, leaving in place a suction line to drain any excess air and fluid to re-establish intrathoracic pressure. A body surface suit, consisting of 256 unipolar electrodes was then placed around the pig, and simultaneous recordings commenced. A variety of abnormal beats were initiated, either by pacing down any of the epicardial electrodes, via the injection of various drugs, or by the closing and opening of ligatures around the left anterior descending coronary artery. Geometrical information was obtained using a mechanical digitiser. These data have proved useful for a variety of studies (e.g., [130, 132, 133]), but unfortunately the lack of a complete accurate geometrical data set has limited the use of these data for quantitative inverse validation work.

In the recent work of Zhang et al. [131] body surface potential maps were used together with their previously described inverse procedure [69] to reconstruct the cardiac activation sequence in rabbits. To validate these results, experimental studies were performed on rabbits. First, the animals were subjected to an ultrafast CT scan to obtain the necessary geometrical data. Three-dimensional intracardiac recordings (up to 200 intramural sites) using specially designed plunge needle electrodes in the (eventually) closed-chested rabbit were made. These data are the first of their kind ever reported in the literature. Estimated activation times were found to be in good agreement with those measured experimentally during left and right ventricular pacing.

In a parallel development over the past 40 years, Taccardi and his colleagues have developed a series of realistically shaped electrolytic tanks and the experimental techniques to suspend isolated, instrumented animal hearts into these tanks. The first studies used a cylindrical tank and a frog heart to study the shape of the bioelectric field from a beating heart [134] and then an isolated, perfused, dog heart in which they occluded a coronary artery to study the effects of injury current [135]. The first studies that generated quantitative validation data for inverse solutions were from Colli-Franzone and Taccardi et al. using the first of a series of human-shaped torso tanks with hearts suspended in an instrumented cage [136, 137]. Data from these experiments have been the subject of subsequent validation studies [25, 138–140] that have greatly advanced the field of electrocardiographic imaging. Subsequent generations of the torso-tank model (as shown in Fig. 9.8) have continued to provide insights and support the advancement of the field through improved instrumentation and a wider variety of interventions and experiments. Data from these preparations have validated not only inverse solutions [34, 141, 142] but also novel interpolation [143, 144] and estimation techniques [39, 145]. They have also supported the study of qualitative and quantitative features of electrocardiology, such as myocardial ischemia [146, 147] and repolarization abnormalities [148, 149].

This experimental model is very well suited to quantitative analysis, because it provides relatively tight control of the size, shape, and orientations of the heart within a known torso geometry, together with locations of the concurrent epicardial and tank surface potential recordings. The weaknesses of this preparation includes the typically homogeneous volume and the unphysiological condition of the heart perfused by retrograde flow through the aorta. For example, the isolated heart does not perform mechanical work and hence presumably responds somewhat differently to stresses that lead to contraction failure, such as ischemia or infarction. Similarly, the autonomic nervous system is absent in this preparation, making it difficult to study, for example, the role of sympathetic stimulation on the genesis and maintenance of arrhythmias. Finally, although it would, in principle, be possible to study human hearts in such a preparation (as Durrer et al. [150] did for their landmark study published in 1970), the lack of availability of human hearts has precluded such studies.

9.7.3 Clinical Validation

9.7.3.1 Inverse Solutions Computed from Body Surface Potentials

The target application of electrocardiographic imaging is, of course, diagnostics and monitoring in humans, so that ultimately, clinical validation is essential. For any inverse algorithm to be accepted as a standard procedure when diagnosing a patient with a cardiac condition, its merit must be justified in the mind of the clinician. It is necessary to prove beyond all reasonable doubt that the inverse results are accurate and robustly reproducible. Because direct, controlled experiments are often ethically unacceptable in humans, investigators have found numerous ways to carry out studies in humans both to validate inverse solutions and to determine their parameter sensitivity. Such approaches are often based on indirect

evidence or make use of information available through invasive procedures or other imaging modalities that are clinically justified.

An excellent early example of a clinical validation strategy is the series of studies that Huiskamp et al. performed to evaluate the role of torso geometry on inversely computed activation times [75, 76]. As an absolute indicator of accuracy, they compared their solutions with the human activation data available from the classic experiments of Durrer et al. [150] under the assumption that key features of the order of activation would be preserved across individual subjects. To determine the role of error in the geometric model, they compared solutions using a standard realistic torso geometry with those from the actual geometry of the subjects and even exchanged geometric models among the subjects while keeping the same body-surface data. The results of these tests suggested that a fixed standard torso model gave unreliable results when used to solve the inverse problem; thus, it was necessary to create a specific model for each subject incorporating at least an accurate torso shape and heart orientation and position with respect to the ECG lead positions. Johnston et al. reported similar findings from a comparable study using 16 realistic torsos with varying sizes and positions of the heart [151].

Although clinical validations seldom offer complete source data, there are a number of investigators who have used indirect methods or methods based on other modalities to identify features that can become the basis for the validation of an electrocardiographic inverse solution. One example from MacLeod et al. [29] used fluoroscopic data from patients undergoing coronary angioplasty (PTCA) to identify the region likely to be at risk from acute ischemia during the angioplasty balloon inflation. They then compared the locations of these regions with those predicted from the inverse solutions on the basis of elevated ST-segment potentials, a typical marker of ischemia.

A clinical modality that provides very useful validation information is catheter-based mapping of endocardial activation by means of one of several available systems [152–154]. These systems allow for electro-anatomical mapping of the heart, often through fusion of measurements from many individual beats and for at least the endocardium, one can compare their results with those from almost simultaneous body surface recordings and activation time based inverse solutions. Tilg and his colleagues have carried out one of the most quantitative clinical ECG inverse validation studies to date using this approach [84, 155, 156]. They created patient specific geometric models based on MR images from each case and then localized an inverse-computed focal site of activation that they compared directly with catheter-based measurements from the patients. Localization of initial activation sites showed good agreement with data measured using the catheter based CARTO system for paced hearts, for patients with Wolff–Parkinson–White syndrome, and in patients with atrial arrhythmias. These are some of the first clinical ECG imaging studies to validate the ECG inverse techniques using concurrent in vivo cardiac and body surface ECGs from humans.

An example of the type of results obtained using such data is shown in Fig. 9.9. The torso model constructed from one particular set of MR images in shown in panel (a) of that figure. The model contains surfaces representing the skin, lungs, epicardium, and left and right endocardial boundaries. Using electrocardiograms recorded at the 51 sites shown on the torso model, an activation time-based inverse method was used to construct the image shown in panel (b). The initial site of excitation is shown in red together with the site of the pacing tip of the catheter.

A recent breakthrough study by Ramanathan et al. [157] used a much expanded form of this approach by evaluating data from patients showing a range of clinical conditions, including right bundle branch block, left and right ventricular pacing from known sites, and chronic atrial flutter. They based their inverse solution on patient-specific geometric models from CT imaging, generating both epicardial potentials and activation and recovery times (extracted from the potential time signals). Evaluation of their results was qualitative, as they were able to show in each case the presence of the abnormality; for the case of single-site pacing they could compare known and predicted sites of earliest activation and found at least qualitative agreement. Further work on validating the inverse results using human data from this group has recently appeared [158, 159]. More directly than any previous studies, research from the Rudy lab provides strong evidence for the clinical potential of inverse cardiac bioelectric imaging.

9.7.3.2 Validation of Endocardial Solutions

The most frequent forms of validation for the endocardial inverse solution are either to measure intracavitary and endocardial potentials from animal preparations or to evaluate somewhat indirectly the accuracy of derived information in human studies. Khoury et al. have reported several studies on validation of the endocardial inverse solution using animal

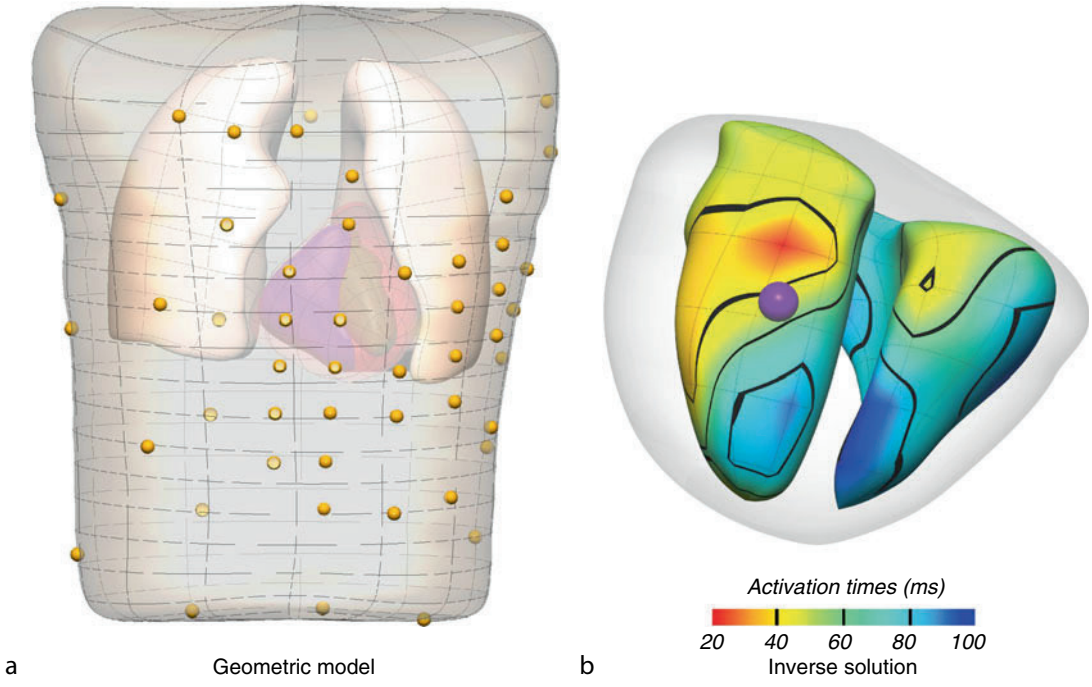

Figure 9.9

Results from clinical inverse solutions. Panel (a) shows the geometric torso model comprised of skin, lungs, epicardium and left and right endocardial surfaces constructed from MRI images. The *gold spheres* represent the 51 body surface potential recording sites. In panel (b) is an anterior view of the heart with inversely computed activation times displayed on the endocardial surfaces. The *purple sphere* (10 mm in diameter) indicates the site of pacing from the catheter tip. This correlates well with the site of initial excitation (colored *red*) on the anterior left ventricular surface. The model and inverse result were computed by the first two authors of this chapter using data supplied by Tilg and coworkers. Figure reproduced from Pullan et al. [80] with permission.

models with simultaneously recorded chamber and endocardial surface potentials. In their earlier approach [93], they used a multielectrode basket-catheter in which expanding the basket inside the heart provided direct contact with the endocardium. However, the most challenging part of this approach was to obtain an accurate geometrical description of the basket (or the endocardium) [91, 160]. In more recent studies [161], they have reported using a recording electrode catheter that navigates the endocardial surface while a low-current locator signal is emitted from the tip electrode to determine its position. To generate accurate endocardial data, they have also used intracardiac echocardiography. Jia et al. also carried out validation studies from a spiral shaped endocardial probe introduced into the left ventricle of an isolated canine heart, which they compared with measurements from transmural needles [162].

The St Jude Medical Ensite catheter mapping system [163] has also been the subject of many validation studies in phantom, canine, and human experiments. As an example, Gornick et al. localized electrodes within an electrolytic tank, compared computed with measured canine endocardial potentials, and marked predicted sites of endocardial pacing all based on the Ensite technology [164]. Kadish et al. applied the same technology to mapping the right atrium in dogs, again comparing computed with directly measured endocardial potentials [165]. Clinical validation of endocardial inverse solutions is challenging because of limited access to complete measured potentials and has often been more qualitative in nature than animal studies. A study by Peters et al. is typical in which the authors documented reentrant endocardial potential patterns characteristic of fascicular tachycardia in a patient known to have this condition [166]. Other studies have validated the accuracy of the endocardial potential solutions according to the clinically relevant criteria of localizing sites of focal activity and treating them with catheter ablation [167]. One recent study applied the Ensite system for

the first time to the determination of repolarization characteristics of the endocardium and compared computed results with directly measured monophasic action potentials [168]. They concluded that computed endocardial potentials could accurately determine activation recovery intervals in humans.

A recent study by Thiagalingam et al. [169] has provided unique quantitative information about the accuracy of the Ensite system and suggested some limitations on its ability to localize myocardial activity. Their results come from extensive comparison of over 32,000 electrograms computed using the Ensite system and measured from sheep hearts in which they located endocardial, midmyocardial, and epicardial myocardial needle electrodes. They found good accuracy of reconstruction of electrograms for sites located within 40 mm of the Ensite catheter but a sharp reduction in accuracy beyond this distance. They also suggested that computed potentials represent a summation of transmural activity, i.e., not simply endocardial or subendocardial activity. Ultimately, the fact that this system has found widespread – though not universal – acceptance in clinical practice, the only device based on an electrocardiographic inverse solution to date, is perhaps the most compelling form of validation.

9.8 Current Status and Futures Direction

The solution to the electrocardiographic inverse problems is motivated largely by the potential for clinical applications, specifically for methods that can determine the state of the heart from painless, noninvasive, ideally cheap, external measurements. Thus, to evaluate the present state of the art, there are a set of questions one must address. First, is there actually a clinical need for such a system? What are the shortcomings of other imaging modalities and what additional information might we expect to gain from electrocardiographic inverse imaging? Second, how close is the field to addressing some of the needs? We have discussed the approaches to validation of inverse problems, and hence, how good are the best systems? Finally, what are the most important remaining hurdles that prohibit successful deployment of inverse technologies and what must occur to overcome them? And is the result (a limited resolution image of the electrical activity of the heart) worth all the extra work compared with a standard 12-lead ECG?

The basis for clinical need lies primarily in the fact the inverse electrocardiographic imaging is a *functional* modality. That is, it generates not anatomical images but images of the spatial distribution of electrical information, clearly very relevant and valuable in the evaluation of the electrophysiological state of the heart. The standard ECG is also a functional measurement, but it lacks the spatial coverage and resolution to be considered an imaging modality. However, although many studies have described the additional information that body surface potential mapping provides [170–175] (see also Chaps. 31 and 32 (Volume III)), there are few such systems in clinical use today because there has not yet been enough value in that additional information to warrant the additional expense of carrying out the measurements. One reason why physicians are willing to forego this additional source of information is that other modalities, most notably echocardiography, provide complementary functional images of the beating heart – in real time and at a reasonable expense. Another reason to avoid this additional complexity is that the standard ECG already provides a cheap, painless, real-time way to monitor at least some aspects of cardiac activity.

The prime clinical application of electrocardiographic mapping is likely to lie in diseases that are essentially electrical in nature and that may not have an anatomical, mechanical, or biochemical counterpart, at least not one that is easily monitored in real time. Moreover, the motivation for applying mapping techniques, i.e., employing enough electrodes to gather spatial as well as temporal information, is strongest in diseases that reflect spatial inhomogeneity or in which distributions over the heart are meaningful. These have, not coincidently, also been the areas of primary interest and success in inverse electrocardiography.

The most common and potentially useful target application domain for inverse electrocardiography has been the study of cardiac arrhythmias, currently carried out by means of multiple catheter-based electrodes introduced into the heart chambers. As already noted, the most successful application of this approach has been by means of the endocardial surface inverse problem [176] and through the use of the Ensite system [163]. Detection of arrhythmias has also been the application in which several contemporary inverse solutions based on body-surface potentials have also shown promising success [155–157, 177]. There are also examples of using inverse solutions to guide interventions, for example, catheter ablation or drug therapy [178, 179]. In ablation procedures, noninvasive determination of the arrhythmogenic focus from body surface ECG recordings would certainly be advantageous; however, achieving this goal may be very challenging in situations of deeply placed focus, e.g., within the ventricular septum. Another potential application is to localize and

document electrophysiological changes that arise during cardiac stress tests with more precision than is currently available with the 12-lead ECG.

And thus, one comes to the second question of how effective current inverse solution technology has become. As we have already described, there are a number of recent reports that suggest promising accuracy in the electrocardiographic inverse problem. The success of the Ensite system [163] and that of Khoury et al. [176] in the endocardial inverse are the most advanced, perhaps because of the inherently better conditions of this inverse problem formulation. The notable success of Rudy and coworkers [157] and Tilg and coworkers [84, 155, 156] also indicate that with enough attention to the details of the geometric model and appropriate application of constraints, it is possible to generate clinically relevant maps of heart surface activation and epicardial potentials. However, it is clear that quantitative clinical validation of inverse ECG methods remains an elusive challenge [127].

This discussion of requirements for an accurate inverse solution leads naturally to the hurdles before this imaging approach can become a useful and ubiquitous technique. The first step in an inverse solution is to create the associated forward solution; many aspects of computing the transfer matrices or the predictive function for the forward problem are very straightforward. However, a substantial and only partially resolved component of this task is creating an accurate, well-structured geometric model. Although modern imaging based on computed tomography or MRI provides excellent raw data for making models, the task of determining boundaries between tissues (segmentation) and creating a computational mesh from these data still involves considerable human guidance and hence time and expertise. For a recent exposition of one of the most current approaches see Pfeifer et al. [180]. Open questions related to this phase of the problem include the relationship between simulation accuracy and the level of model resolution, the set of included inhomogeneous regions, and the level of geometric fidelity, especially the size, shape, and the location of the heart. Most inverse solutions also assume a static geometry, even though the contraction of the heart will affect at least the repolarization phase of the cardiac electric cycle; at present, it is not clear how large the effect of this discrepancy might be nor how to deal with it in practical terms. One technology that may, at least partially, address this concern is electrical impedance tomography (EIT), which may have the potential to allow direct measurement of the actual conductivity profile, in the same sessions as the electrical mapping, and with relatively good temporal resolution [181, 182].

There are several other unresolved practical hurdles to a practical electrocardiographic inverse solution that deserve mention. One open question that is related to the body surface mapping, which is the input of many inverse solutions, is the determination of how many electrodes are required and where they might best be located. A related question is how to resolve the often-dramatic difference between the number of measurement electrodes and the number of nodes on the surface of the geometric model; is it best to interpolate the potential or remove the associated rows or columns from the forward or inverse solutions [183]? It is also necessary to determine where the electrodes lie in space relative to the nodes of the geometric model.

An additional set of open questions involves the choice of the problem formulation and the method of regularization. Some experimental studies suggest that the pattern of cardiac excitation is a more stable parameter than the epicardial potentials in the face of variations of geometric factors or torso conductivities [184, 185], implying that activation-based imaging may be more stable than potential-based imaging. (A relatively recent addition to this set of questions is the possibility of direct imaging of model TMPs [2, 54]). At least some modeling studies have confirmed this suggestion [66, 186]. However, fiducial time formulations of the problem have their own limitations. Implicit in fiducial formulations are assumptions about the electrical anisotropy of the heart; the influence of any weaknesses in these assumptions is still unknown. Also, although the same approaches can predict both activation and recovery times, they cannot at this stage deal appropriately with re-entrant phenomena. They will also fail in the case of myocardial infarction unless the location and the extent of the infarcted region are known a priori [187]. More generally, fiducial time approaches will be unsatisfactory for any pathology or condition that alters potentials without a concomitant change in the timing of fiducials, most notably alterations in ST-segment potentials that are the well-known hallmarks of acute ischemia. The two approaches also differ in their computational complexity; however, with the constant improvements in performance, the additional computing time required for fiducial-based approaches is of ever diminishing importance [188].

Perhaps the most active area of research and controversy in electrocardiographic inverse problems lies in the approaches and tuning of regularization. As we have already discussed, there are a substantial number of different approaches, each of which performs better or worse under different conditions. Moreover, within each approach, there are different ways to determine optimal regularization parameters. The resulting complexity and confusion provide a daunting hurdle to a practical clinical implementation of any of these approaches.

Will electrocardiographic inverse technology eventually take an equal place among the imaging modalities available for diagnosing and treating cardiac abnormalities? As we have discussed, there is clearly a need for imaging the electrical activity of the heart for which there is simply no other direct measurement modality; functional diseases that affect only or primarily cardiac electrophysiology will appear only indirectly in any images that are not electrical (or magnetic) in origin. Other compelling advantages of electrical vs. other forms of imaging include the reduced cost of a system and the relatively small size of the equipment, which enable long-term monitoring of patients and thus capture dynamic aspects of their disease. Compared with ultrasound, the technical skill required to acquire data is also minimal. There are no size constraints or problems with existing implantible devices such as those that arise with MRI. Measuring body-surface potentials has absolutely no risk and includes virtually no discomfort to the subject so that, unlike with, for example, CT, serial scanning and even routine screening are very feasible. Recent results suggest that with enough care and attention to detail, it is already possible to resolve many features of normal and abnormal cardiac activity; one type of inverse solution is already implemented in a clinical device and is in widespread use. Thus the major problem yet to be resolved is creating the necessary tools (some of which require additional research) in order to achieve the required efficiency and ease of use for clinical practice. There is some irony also in the fact that improvements in anatomical imaging of heart will also enhance the usability of electrocardiographic imaging, nominally a competing – but more sensibly a complementary – technology.

In summary, although there are still several hurdles to jump before quantitative noninvasive electrical imaging of the heart becomes a routine tool in cardiovascular research or clinical practice, the benefits of the technology remain extremely compelling and its successful implementation is within reach.

References

1. Yamashita Y., Theoretical studies on the inverse problem in electrocardiography and the uniqueness of the solution. *IEEE Trans. Biomed. Eng.*, November 1982;**29**(11): 719–725.
2. Messnarz B., M. Seger, R. Modre, G. Fischer, F. Hanser, and B. Tilg, A comparison of noninvasive reconstruction of epicardial versus transmembrane potentials in consideration of the null space. *IEEE Trans Biomed. Eng.*, Sept. 2004;**51**(9): 1609–1618.
3. Titomir L.I., The remote past and near future of electrocardiology – view point of a biomedical engineer. *Bratisl Lek Listy*, 2000;**101**(5): 272–279.
4. Keener and Sneyd, *Mathematical Physiology*, volume 8 of *Interdisciplinary Applied Mathematics*, 1st ed. Springer, Berlin, 1998.
5. Schmidt J., C. Johnson, and R. MacLeod, An interactive computer model for defibrillation device design, in *Building Bridges: International Congress on Electrocardiology International Meeting*, T. Oostendorp and G. Oiju, Editors, 1995, pp. 160–161.
6. Hadamard J., *Lectures on Cauchy's Problems in Linear Partial Differential Equations*. Yale University Press, New Haven, CT, 1923.
7. Babaeizadeh S., D.H. Brooks, D. Isaacson, and J. Newell, Electrode boundary conditions and experimental validation for BEM-based EIT forward and inverse solutions. *IEEE Trans. Med. Imag.*, September 2006;**25**(9): 1180–1188.
8. Babaeizadeh S., D.H. Brooks, and D. Isaacson, 3-D Electrical Impedance Tomography for piecewise constant domains with known internal boundaries. *IEEE Trans. Biomed. Eng.*, January 2007;**54**(1): 2–10.
9. Hansen P., *Rank-Deficient and Discrete Ill-Posed Problems: Numerical Aspects of Linear Inversion*. SIAM, Philadelphia, 1998.
10. Kaipio J. and E. Somersalo, *Statistical and Computational Inverse Problems*. Applied Mathematical Sciences, vol. 160. Springer, Berlin, 2005.
11. Tikhonov A. and V. Arsenin, *Solution of Ill-posed Problems*. Winston, Washington, DC, 1977.
12. Hansen P., *Rank-Deficient and Discrete Ill-Posed Problems: Numerical aspects of linear inversion*. PhD thesis, Technical University of Denmark, 1996.
13. Berger J., *Statistical Decision Theory and Bayesian Analysis*. Springer, Berlin, 1988.
14. Greensite F., Cardiac electromagnetic imaging as an inverse problem. *Electromagnetics*, September 2001;**21**(7–8): 559–577.
15. Pullan A.J., Paterson, and Greensite, Noninvasive imaging of cardiac electrophysiology. *Phil. Trans. R. Soc. Lond. A*, June 2001;**359**(1783): 1277–1286.
16. Greensite F., Well-posed formulation of the inverse problem of electrodiography. *Ann. Biomed. Eng.*, 1994;**22**: 172–183.
17. Oster H., B. Taccardi, R. Lux, P. Ershler, and Y. Rudy, Noninvasive electrocardiographic imaging: Reconstruction of epicardial potentials, electrograms, and isochrones and localization of single and multiple electrocardiac events. *Circulation*, 1997;**96**: 1012–1024.
18. Li G. and B. He, Localization of sites of origins of cardiac activation by means of a new heart-model-based electrocardiographic imaging approach. *IEEE Trans. Biomed. Eng.*, June 2001;**48**(6): 660–669.
19. Gulrajani R.M., F.A. Roberge, and G.E. Mailloux, The forward problem of electrocardiography/The inverse problem of electrocardiography, in *Comprehensive Electrocardiography*, P. Macfarlane and T.V. Lawrie, Editors. Pergamon Press, New York, 1989, pp. 197–288.
20. da Silva F.L., Functional localization of brain sources using EEG and/or MEG data: Volume conductor and source models. *Magn. Reson. Imaging*, December 2004;**22**(10): 1533–1538.

21. Yamashita Y., Theoretical studies on the inverse problem in electrocardiography and the uniqueness of the solution. *IEEE Trans, Biomed. Eng.*, 1982;**29**: 719–725.
22. Martin R.O. and T.C. Pilkington, Unconstrained inverse electrocardiography: Epicardial potentials. *IEEE Trans. Biomed. Eng.*, July 1972;**19**(4): 276–285.
23. Damen A.A. and J. van der Kam, The use of the Singular Value Decomposition in electrocardiographs. *Med. Biol. Eng. Comput.*, July 1982;**20**(4): 473–482.
24. Okamoto Y., Y. Teramachi, and T. Musha, Limitation of the inverse problem in body surface potential mapping. *IEEE Trans. Biomed. Eng.*, November 1983;**30**(11): 749–754.
25. Rudy Y. and B. Messinger-Rapport, The inverse solution in electrocardiography: Solutions in terms of epicardial potentials. *Crit. Rev. Biomed. Eng.*, 1988;**16**: 215–268.
26. Hansen P.C., *Rank-Defficient and Discrete Ill-Posed Problems: Numerical Aspects of Linear Inversion*. Society for Industrial and Applied Mathematics, Philadelphia, 1998.
27. Messinger-Rapport B.J. and Y. Rudy, Regularization of the inverse problem of electrocardiology: A model study. *Math. Biosci.*, 1988;**89**: 79–118.
28. MacLeod R., *Percutaneous Transluminal Coronary Angioplasty as a Model of Cardiac Ischemia: Clinical and Modelling Studies*. PhD thesis, Dalhousie University, Halifax, N.S., Canada, 1990.
29. MacLeod R., R. Miller, M. Gardner, and B. Horacek, Application of an electrocardiographic inverse solution to localize myocardial ischemia during percutaneous transluminal coronary angioplasty. *J. Cardiovasc. Electrophysiol.*, 1995;**6**: 2–18.
30. Golub G. and C.V. Loan, *Matrix Computations*. Johns Hopkins, Baltimore, 1989.
31. Press W.H., S.A. Teukolsky, W.T. Vetterling, and B.P. Flannery, *Numerical recipies in FORTRAN, the art of scientific computing*, 2nd ed. Cambridge University Press, Cambridge, 1992.
32. Hansen P.C., Analysis of discrete ill-posed problems by means of the L-curve. *SIAM Review*, December 1992;**34**(4): 561–580.
33. Brooks D., G. Ahmad, and R. MacLeod, Multiply constrained inverse electrocardiology: Combining temporal, multiple spatial, and iterative regularization, in *Proceedings of the IEEE Engineering in Medicine and Biology Society 16th Annual International Conference*. IEEE Computer Society, 1994, pp. 137–138.
34. Ramanathan C., P. Jia, R. Ghanem, D. Calvetti, and Y. Rudy, Noninvasive electrocardiographic imaging (ECGI): application of the generalized minimal residual (GMRes) method. *Ann. Biomed. Eng.*, September 2003;**31**(8): 981–994.
35. Barr R. and M. Spach, A comparison of measured epicardial potentials with epicardial potentials computed from body surface measurements in the intact dog. *Adv. Cardiol.*, 1978;**21**: 19–22.
36. van Oosterom A., Incorporation of the spatial covariance in the inverse problem. *Biomed. Technik*, 1997;**42**(Suppl): 43–52.
37. van Oosterom A., The use of spatial covariance in computing pericardial potentials. *IEEE Trans Biomed. Eng.*, 1999;**46**(7): 778–787.
38. van Oosterom A., The spatial covariance used in computing the pericardial potential distribution, in *Computational Inverse Problems in Electrocardiography*, P.R. Johnston, Editor. WIT Press, Southampton, UK, 2001, pp. 1–50.
39. Yılmaz B., R. MacLeod, B. Punske, B. Taccardi, and D. Brooks, Training set selection for statistical estimation of epicardial activation mapping from intravenous multielectrode catheters. *IEEE Trans Biomed. Eng.*, November 2005;**52**(11): 1823–1831.
40. Serinagaoglu Y., R. MacLeod, and D. Brooks, A Bayesian approach to inclusion and performance analysis of using extra information in bioelectric inverse problems, in *International Conference on Image Processing*. IEEE Press, New York, 2003.
41. Serinagaoglu Y., D. Brooks, and R. MacLeod, Bayesian solutions and performance analysis in bioelectric inverse problems. *IEEE Trans. Biomed. Eng.*, 2005;**52**(6): 1009–1020.
42. Serinagaoglu Y., D.H. Brooks, and R.S. MacLeod, Improved performance of Bayesian solutions for inverse electrocardiography using multiple information sources. *IEEE Trans. Biomed. Eng.*, October 2006;**53**(10): 2024–2034.
43. Shahidi A., P. Savard, and R. Nadeau, Forward and inverse problems of electrocardiography: Modeling and recovery of epicardial potentials in humans. *IEEE Trans Biomed. Eng.*, 1994;**41**(3): 249–256.
44. Brooks D., G. Ahmad, R. MacLeod, and G. Maratos, Inverse electrocardiography by simultaneous imposition of multiple constraints. *IEEE Trans. Biomed. Eng.*, 1999;**46**(1): 3–18.
45. Ahmad G., D.H. Brooks, and R. MacLeod, An admissible solution approach to inverse electrocardiography. *Ann. Biomed. Eng.*, 1998;**26**: 278–292.
46. Kay S.M., *Fundamentals Of Statistical Signal Processing: Estimation Theory*. Prentice-Hall, Englewood Cliffs, NJ, 1993.
47. Barr R. and T. Pilkington, Computing inverse solutions for an on-off heart model. *IEEE Trans Biomed. Eng.*, 1969;**16**: 205–214.
48. Brooks D., C.L. Nikias, and J. Siegel, An inverse solution in electrocardiography in the frequency domain, in *Proceedings of the IEEE Engineering in Medicine and Biology Society 10th Annual International Conference*, 1988, pp. 970–971.
49. Oster H. and Y. Rudy, The use of temporal information in the regularization of the inverse problem of electrocardiography. *IEEE Trans. Biomed. Eng.*, 1992;**39**(1): 65–75.
50. Joly D., Y. Goussard, and P. Savard, Time-recursive solution to the inverse problem of electrocardiography: A model-based approach. In *Proc. 15th Annual IEEE-EMBS Conf.*, 1993, pp. 767–768.
51. El-Jakl J., F. Champagnat, and Y. Goussard, Time-space regularization of the inverse problem of electrocardiography. In *Proc. 17th Annual IEEE-EMBS Conf.*, 1995, pp. 213–214.
52. Greensite F., A new treatment of the inverse problem of multivariate analysis. *Inverse Problems*, 2002;**18**: 363–379.
53. Greensite F., The temporal prior in bioelectromagnetic source imaging problems. *IEEE Trans. Biomed. Eng.*, 2003;**50**: 1152–1159.
54. Messnarz B., B. Tilg, R. Modre, G. Fischer, and F. Hanser, A new spatiotemporal regularization approach for reconstruction of cardiac transmembrane potential patterns. *IEEE Trans. Biomed. Eng.*, Feb. 2004;**51**(2): 273–281.
55. Skipa O., M. Nalbach, F. Sachse, C. Werner, and O. Dossel, Transmembrane potential reconstruction in anisotropic heart model. *Intl. J. Bioelectromagnet.*, 2002;**4**(2): 17–18.
56. Cheng L.K., G.B. Sands, R.A. French, S.J. Withy, S.P. Wong, M.E. Legget, W.M. Smith, and A.J. Pullan, Rapid construction of a patient specific torso model from 3D ultrasound for noninvasive imaging of cardiac electrophysiology. *Med. Biol. Eng. Comput.*, 2005;**43**(3): 325–330.

57. Zhang Y., A. Ghodrati, and D.H. Brooks, An analytical comparison of three spatio-temporal regularization methods for dynamic linear inverse problems in a common statistical framework. *Inverse Problems*, 2005;**21**: 357–382.
58. Anderson B. and J. Moore, *Optimal Filtering*. Prentice-Hall, Englewood Cliffs, NJ, 1979.
59. Kailath T., A.H. Sayed, and B. Hassibi, *Linear Estimation*. Prentice-Hall, Englewood Cliffs, NJ, 2000.
60. Greensite F., Second-order approximation of the pseudoinverse for operator deconvolutions and families of ill-posed problems. *SIAM J. Appl. Math.*, 1998;**59**(1): 1–16.
61. Lux R., K. Evans, M. Burgess, R. Wyatt, and J. Abildskov, Redundancy reduction for improved display and analysis of body surface potential maps: I. Spatial compression. *Circ. Res.*, 1981;**49**: 186–196.
62. Evans K., R. Lux, M. Burgess, R. Wyatt, and J. Abildskov, Redundancy reduction for improved display and analysis of body surface potential maps: II. Temporal compression. *Circ. Res.*, 1981;**49**: 197–203.
63. Huiskamp G. and F. Greensite, A new method for myocardial activation imaging. *IEEE Trans. Biomed. Eng.*, 1997;**44**: 433–446.
64. Hansen P., Analysis of discrete ill-posed problems by means of the L-curve. *SIAM Rev.*, 1992;**34**(4): 561–580.
65. Akaike H., A new look at the statistical model identification. *IEEE Trans. Automat. Contr.*, December 1974;**19**(6): 716–723.
66. Cheng L.K., J.M. Bodley, and A.J. Pullan, Comparison of potential and activation based formulations for the inverse problem of electrocardiology. *IEEE Trans. Biomed. Eng.*, January 2003;**50**(1): 11–22.
67. Ghodrati A., D. Brooks, G. Tadmor, and R. MacLeod, Wavefront-based models for inverse electrocardiography, September 2006; **53**(9): 1821–1831.
68. Andersen E. and K. Andersen, *High Performance Optimization*, chapter The MOSEK interior point optimizer for linear programming: an implementation of the homogeneous algorithm. Kluwer, Dordrecht, the Netherlands, 2000.
69. He B., G. Li, and X. Zhang, Noninvasive imaging of cardiac transmembrane potentials within three-dimensional myocardium by means of a realistic geometry anisotropic heart model. *IEEE Trans. Biomed. Eng.*, October 2003;**50**(10): 1190–1202.
70. Liu C., G. Li, and B. He, Localization of the site of origin of reentrant arrhythmia from body surface potential maps: a model study. *Phys. Med. Biol.*, 2005;**50**(7): 1421–1432.
71. Skipa O., *Linear inverse problem of electrocardiography: Epicardial potentials and Transmembrane voltages*. PhD thesis, University Karlsruhe, 2004.
72. Taccardi B., E. Macchi, R. Lux, P. Ershler, S. Spaggiari, S. Baruffi, and Y. Vyhmeister, Effect of myocardial fiber direction on epicardial potentials. *Circ.*, 1994;**90**: 3076–3090.
73. Cuppen J. and A. van Oosterom, Model studies with the inversely calculated isochrones of ventricular depolarization. *IEEE Trans. Biomed. Eng.*, 1984;**31**: 652–659.
74. Cuppen J., Calculating the isochrones of ventricular depolarization. *SIAM J. Sci. Statist. Comp.*, 1984;**5**: 105–120.
75. Huiskamp G. and A. van Oosterom, The depolarization sequence of the human heart surface computed from measured body surface potentials. *IEEE Trans. Biomed. Eng.*, 1989;**35**: 1047–1059.
76. Huiskamp G. and A. van Oosterom, Tailored versus standard geometry in the inverse problem of electrocardiography. *IEEE Trans. Biomed. Eng.*, 1989;**36**: 827–835.
77. Schmidt R.O., Multiple emitter location and signal parameter estimation. *IEEE Trans. Antennas Propagat.*, March 1986;**34**(3): 276–280.
78. Mosher J.C., P.S. Lewis, and R.M. Leahy, Multiple dipole modeling and localization from spatio-temporal MEG data. *IEEE Trans. Biomed. Eng.*, 1992;**39**(6): 541–557.
79. Tomlinson K.A., *Finite Element Solution of an Eikonal Equation For Excitation Wavefront Propagation in Ventricular Myocardium*. PhD thesis, The University of Auckland, New Zealand, 2000.
80. Pullan A.J., M.L. Buist, and L.K. Cheng, *Mathematically Modelling the Electrical Activity of the Heart: From Cell to Body Surface and Back Again*. World Scientific Publishing Company, Singapore, 2005.
81. Greensite F., Remote reconstruction of confined wavefront propagation. *Inverse Problems*, 1995;**11**: 361–370.
82. Huiskamp G. and A. van Oosterom, The depolarization sequence of the human heart surface computed from measured body surface potentials. *IEEE Trans. Biomed. Eng.*, December 1988;**35**(12): 1047–1059.
83. Stoica P. and R. Moses, *Spectral Analysis of Signals*. Prentice-Hall, Englewood Cliffs, NJ, 2005.
84. Tilg B., G. Fischer, R. Modre, F. Hanser, B. Messnarz, M. Schocke, C. Kremser, T. Berger, F. Hintringer, and F.X. Roithinger, Model-based imaging of cardiac electrical excitation in humans. *IEEE Trans. Med. Imag.*, September 2002;**21**(9): 1031–1039.
85. Modre R., B. Tilg, G. Fischer, and P. Wach, Noninvasive myocardial activation time imaging: a novel inverse algorithm applied to clinical ECG mapping data. *IEEE Trans. Biomed. Eng.*, October 2002;**49**(10): 1153–1161.
86. Tautenhahn U., On a general regularization scheme for nonlinear illposed problems: Ii. regularization in hilbert scales. *Inverse Problems*, 1998;**14**: 1607–1616.
87. van Oosterom A. and P. van Dam, The intra-myocardial distance function used in inverse computations of the timing of depolarization and repolarization, in *Computers in Cardiology '05*, vol. 32, Murray A, Editor. IEEE Computer Society Press, Piscataway, 2005, pp. 567–570.
88. Berrier K.L., D.C. Sorensen, and D.S. Khoury, Solving the inverse problem of electrocardiography using a Duncan and Horn formulation of the Kalman filter. *IEEE Trans. Biomed. Eng.*, 2004;**51**(3): 507–515.
89. Rao L., C. Ding, and D.S., Nonfluoroscopic localization of intracardiac electrode-catheters combined with noncontact electrical-anatomical imaging. *Ann. Biomed. Eng.*, 2004;**32**: 1654–1661.
90. Voth E., The inverse problem of electrocardiography: industrial solutions and simulations. *Int. J. Bioelectromag.*, 2005;**7**(2): 191–194.
91. Khoury D., Importance of geometry in reconstructing endocardial electrograms from noncontact multielectrode cavitary probe data, in *Proceedings of the IEEE Engineering in Medicine and Biology Society 19th Annual International Conference*, vol. 1, 1997, pp. 188–190.
92. Khoury D., Use of current density in the regularization of the inverse problem of electrocardiography, in *Proceedings of the IEEE Engineering in Medicine and Biology Society 16th*

Annual International Conference. IEEE Press, New York, 1994, pp. 133–134.
93. Velipasaoglu E., H. Sun, F. Zhang, K. Berrier, and D. Khoury, Spatial regularization of the electrocardiographic inverse problem and its application to endocardial mapping. *IEEE Trans. Biomed. Eng.*, March 2000;**47**(3): 327–337.
94. Hansen P.C. and D.P. O'Leary, The use of the L-curve in the regularisation of discrete ill-posed problems. *SIAM J. Sci. Comput.*, November 1993;**14**(6): 1487–1503.
95. Colli Franzone P., L. Guerri, B. Taccardi, and C. Viganotti, Finite element approximation of regularised solutions of the inverse potential problem of electrocardiography and applications to experimental data. *Calcolo*, 1985;**22**(1): 91–186.
96. Johnston P.R. and R.M. Gulrajani, A new method for regularization parameter determination in the inverse problem of electrocardiography. *IEEE Trans. Biomed. Eng.*, January 1997;**44**(1): 19–39.
97. Golub G.H., M.T. Heath, and G. Wahba, Generalized cross-validation as a method for choosing a good ridge parameter. *Technometrics*, 1979;**21**: 215–223.
98. Lian J., D. Yao, and B. He, A new method for implementation of regularization in cortical potential imaging, in *Proceedings of the 20th Annual International Conference of the IEEE Engineering in Medicine and Biology Society*, vol. 20, Hong Kong, China, 1998. IEEE Computer Society Press, 1988, pp. 2155–2158.
99. Johnston P.R. and R.M. Gulrajani, Selecting the corner of the L-curve approach to Tikhonov regularisation. *IEEE Trans. Biomed. Eng.*, September 2000;**47**(2): 1293–1296.
100. Bayley R. and P. Berry, The electrical field produced by the eccentric current dipole in the nonhomogeneous conductor. *Am. Heart J.*, 1962;**63**: 808–820.
101. Bayley R. and P. Berry, The arbitrary electromotive double layer in the eccentric "heart" of the nonhomogeneous circular lamina. *IEEE Trans. Biomed. Eng.*, 1964;**11**(4): 137–147.
102. Bayley R., J. Kalbfleisch, and P. Berry, Changes in the body's QRS surface potentials produced by alterations in certain compartments of the nonhomogeneous conducting model. *Am. Heart J.*, 1969;**77**(4): 517–528.
103. Rudy Y. and R. Plonsey, The eccentric spheres model as the basis for a study of the role of geometry and inhomogeneities in electrocardiography. *IEEE Trans. Biomed. Eng.*, 1979;**26**: 392–399.
104. Rudy Y. and R. Plonsey, The effects of variations in conductivity and geometrical parameters on the electrocardiogram, using an eccentric spheres model. *Circ. Res.*, 1979;**44**(1): 104–111.
105. Rudy Y. and R. Plonsey, A comparison of volume conductor and source geometry effects on body surface and epicardial potentials. *Circ. Res.*, 1980;**46**: 283–291.
106. Throne R. and L. Olson, The effect of errors in assumed conductivities and geometry on numerical solutions to the inverse problem of electrocardiography. *IEEE Trans. Biomed. Eng.*, 1995;**42**: 1192–1200.
107. Oster H., B. Taccardi, R. Lux, P. Ershler, and Y. Rudy, Noninvasive electrocardiographic imaging: Reconstruction of epicardial potentials, electrograms, and isochrones and localization of single and multiple electrocardiac events. *Circ.*, 1997;**96**(3): 1012–1024.
108. He S., Frequency series expansion of an explicit solution for a dipole inside a conducting sphere at low frequencies. *IEEE Trans. Biomed. Eng.*, 1998;**45**(10): 1249–1258.
109. Brooks D. and R. MacLeod, Electrical imaging of the heart: Electrophysical underpinnings and signal processing opportunities. *IEEE Sign. Proc. Mag.*, 1997;**14**(1): 24–42.
110. Hren R., *A Realistic Model of the Human Ventricular Myocardium: Application to the Study of Ectopic Activation*. PhD thesis, Dalhousie University, Halifax, Nova Scotia, 1996.
111. Hren R., X. Zhang, and G. Stroink, Comparison between electrocardiographic and magnetocardiographic inverse solutions using the boundary element method. *Med. & Biol. Eng. & Comp.*, 1996;**34**(2): 110.
112. Hren R., R. MacLeod, G. Stroink, and B. Horacek, Assessment of spatial resolution of body surface potentials maps in localizing ventricular tachycardia foci. *Biomed. Technik*, 1997;**42**(Suppl): 41–44.
113. Moe G., W. Rheinboldt, and J. Abildskov, A computer model of fibrillation. *Am. Heart J.*, 1964;**67**: 200–220.
114. Okajima M., T. Fujinaa, T. Kobayashi, and K. Yamada, Computer simulation of the propagation process in excitation of the ventricles. *Circ. Res.*, 1968;**23**: 203–211.
115. Abildskov J., Mechanism of the vulnerable period in a model of cardiac fibrillation. *J. Cardiovasc. Electrophysiol.*, 1990;**1**: 303–308.
116. Gharpure P. and C. Johnson, A 3-dimensional cellular automation model of the heart, in *Proceedings of the IEEE Engineering in Medicine and Biology Society 15th Annual International Conference*. IEEE Press, New York, 1993, pp. 752–753.
117. Hren R., J. Nenonen, and B. Horacek, Simulated epicardial potential maps during paced activation reflect myocardial fibrous structure. *Ann. Biomed. Eng.*, 1998;**26**(6): 1022.
118. Hren R. and B. Punske, A comparison of simulated QRS isointegral maps resulting from pacing at adjacent sites: Implications for the spatial resolution of pace mapping using body surface potentials. *J. Electrocardiol.*, 1998;**31**(Suppl): 135.
119. Hren R., B. Punske, and G. Stroink, Assessment of spatial resolution of cardiac pace mapping when using body surface potentials. *Med. & Biol. Eng. & Comp.*, 1999;**37**(4): 477.
120. Modre R., *A Regularization Technique for Nonlinear Ill-Posed Problems Applied to Myocardial Activation Time Imaging*. PhD thesis, Department of Biophysics, Institute of Biomedical Engineering, Technical University Graz, Austria, February 2000.
121. Ramanathan C. and Y. Rudy, Electrocardiographic imaging: II. Effects of torso inhomogeneities on noninvasive reconstruction of epicardial potentials, electrograms, and isochrones. *J. Cardiovasc. Electrophysiol.*, February 2001;**12**(2): 241–252.
122. Cheng L.K., J.M. Bodley, and A.J. Pullan, Effects of experimental and modeling errors on electrocardiographic inverse problems. *IEEE Trans. Biomed. Eng.*, January 2003;**50**(1): 23–32.
123. Pullan A.J., L.K. Cheng, M.P. Nash, C.P. Bradley, and D.J. Paterson, Noninvasive electrical imaging of the heart: Theory and model development. *Ann. Biomed. Eng.*, October 2001;**29**(10): 817–836.
124. Burger H. and J. van Milaan, Heart-vector and leads. Part II. *Br. Heart J.*, 1947;**9**: 154–160.
125. Burger H. and J. van Milaan, Heart-vector and leads. Part III: Geometrical representation. *Br. Heart J.*, 1948;**10**: 229–233.
126. MacLeod R. and D. Brooks, Validation approaches for electrocardiographic inverse problems, in *Computational Inverse Problems in Electrocardiography*, P. Johnston, Editor. WIT Press, Ashurst, UK, 2001, pp. 229–268.

127. Nash M.P. and A.J. Pullan, Challenges facing validation of noninvasive electrical imaging of the heart. *Ann. Noninvasive Electrocardiol.*, January 2005;**10**(1): 73–82.
128. Spach M.S., R.C. Barr, C.F. Lanning, and P.C. Tucek, Origin of body surface QTS and the T wave potentials from epicardial potential distributions in the intact chimpanzee. *Circulation*, February 1977;**55**(2): 268–288.
129. Barr R.C. and M.S. Spach, Inverse calculation of QRS-T epicardial potentials from body surface potential distributions for normal and ectopic beats in the intact dog. *Circ. Res.*, 1978;**42**: 661–675.
130. Nash M.P., C.P. Bradley, and D.J. Paterson, Imaging electrocardiographic dispersion of depolarization and repolarization during ischemia: Simultaneous body surface and epicardial mapping. *Circulation*, April 2003;**107**(17): 2257–2263.
131. Zhang X., I. Ramachandra, Z. Liu, B. Muneer, S.M. Pogwizd, and B. He, Noninvasive three-dimensional electrocardiographic imaging of ventricular activation sequence. *Am. J. Physiol. Heart Circ. Phyiol.*, 2005;**289**(6): H2724–H2732.
132. Nash M.P., C.P. Bradley, A. Kardos, A.J. Pullan, and D.J. Paterson, An experimental model to correlate simultaneous body surface and epicardial electropotential recordings *in-vivo*. *Chaos, Solitons & Fractals*, 2002;**13**(8): 1735–1742.
133. Nash M.P., C.P. Bradley, L.K. Cheng, A.J. Pullan, and D.J. Paterson, Electrocardiographic inverse validation study: *in-vivo* mapping and analysis. *FASEB J.*, April 2000;**14**(4): A442.
134. Taccardi B. and G. Marchetti, Distribution of heart potentials on the body surface and in artificial conducting media, in *International symposium on the electrophysiology of the heart*, B. Taccardi and G. Marchetti, Editors. Pergamon Press, New York, 1965, pp. 257–280.
135. Taccardi B., Changes in cardiac electrogenesis following coronary occlusion, in *Coronary Circulation and Energetics of the Myocardium*. S. Karger, Basel/New York, 1966, pp. 259–267.
136. Franzone P.C., L. Guerri, B. Taccardi, and C. Viganotti, The direct and inverse problems in electrocardiology. Numerical aspects of some regularization methods and applications to data collected in isolated dog heart experiments. *Lab. Anal. Numerica C.N.R.*, 1979, Pub. N:222.
137. Franzone P.C., G. Gassaniga, L. Guerri, B. Taccardi, and C. Viganotti, Accuracy evaluation in direct and inverse electrocardiology, in *Progress in Electrocardiography*, P. Macfarlane, Editor. Pitman Medical, London, 1979, pp. 83–87.
138. Messinger-Rapport B. and Y. Rudy, The inverse problem in electrocardiography: A model study of the effects of geometry and conductivity parameters on the reconstruction of epicardial potentials. *IEEE Trans. Biomed. Eng.*, 1986;**33**: 667–676.
139. Rudy Y. and H. Oster, The electrocardiographic inverse problem. *Crit. Rev. Biomed. Eng.*, 1992;**20**: 22–45.
140. Throne R., L. Olson, T. Hrabik, and J. Windle, Generalized eigensystem techniques for the inverse problem of electrocardiography applied to a realistic heart-torso geometry. *IEEE Trans. Biomed. Eng.*, 1997;**44**(6): 447.
141. Brooks D. and R. MacLeod, Imaging the electrical activity of the heart: Direct and inverse approaches, in *IEEE International Conference on Image Processing*. IEEE Computer Society, 1994, pp. 548–552.
142. MacLeod R., B. Yilmaz, B. Taccardi, B. Punske, Y. Serinagaoglu, and D. Brooks, Direct and inverse methods for cardiac mapping using multielectrode catheter measurements. *Biomed. Technik*, 2001;**46**(Suppl): 207–209.
143. Ni Q., R. MacLeod, R. Lux, and B. Taccardi, Interpolation of cardiac electric potentials. *Ann. Biomed. Eng.*, 1997;**25**(Suppl): 61. Biomed. Eng. Soc. Annual Fall Meeting.
144. Burnes J., D. Kaelber, B. Taccardi, R. Lux, P. Ershler, and Y. Rudy, A field-compatible method for interpolating biopotentials. *Ann. Biomed. Eng.*, 1998;**26**(1): 37–47.
145. Yilmaz B., R. MacLeod, S. Shome, B. Punkse, and B. Taccardi, Minimally invasive epicardial activation mapping from multielectrode catheters, in *Proceedings of the IEEE Engineering in Medicine and Biology Society 23rd Annual International Conference*. IEEE EMBS, IEEE Press, New York, 2001.
146. MacLeod R., B. Taccardi, and R. Lux, Mapping of cardiac ischemia in a realistic torso tank preparation, in *Building Bridges: International Congress on Electrocardioloegy International Meeting*, 1995, pp. 76–77.
147. MacLeod R., S. Shome, J. Stinstra, B. Punske, and B. Hopenfeld, Mechanisms of ischemia-induced ST-segment changes. *J. Electrocardiol.*, 2005, vol 38, pp. 8–13.
148. MacLeod R., R. Lux, M. Fuller, and B. Taccardi, Evaluation of novel measurement methods for detecting heterogeneous repolarization. *J. Electrocardiol.*, 1996;**29**(Suppl): 145–153.
149. Punske B., R. Lux, R. MacLeod, M. Fuller, P. Ershler, T. Dustman, Y. Vyhmeister, and B. Taccardi, Mechanisms of the spatial distribution of QT intervals on the epicardial and body surfaces. *J. Cardiovasc. Electrophysiol.*, 1999;**10**(12): 1605–1618.
150. Durrer D., R. van Dam, G. Freud, M. Janse, F. Meijler, and R. Arzbaecher, Total excitation of the isolated human heart. *Circ.*, 1970;**41**: 899–912.
151. Johnston P.R. and D. Kilpatrick, The inverse problem of electrocardiology: The performance of inversion techniques as a function of patient anatomy. *Math. Biosci.*, April 1995;**126**(2): 125–146.
152. Jenkins K., E. Walsh, S. Colan, D. Bergau, P. Saul, and J. Lock, Multipolar endocardial mapping of the right atrium during cardiac catheterization: Description of a new technique. *J. Am. Coll. Cardiol.*, 1993;**22**: 1105–1110.
153. Fitzpatrick A., M. Chin, C. Stillson, and M. Lesh, Successful percutaneous deployment, pacing and recording from a 64-polar, multi-strut "basket" catheter in the swine left ventricle. *PACE*, 1994;**17**:482.
154. Smeets J., S.B. Haim, L. Rodriguez, C. Timmermans, and H. Wellens, New method for nonfluoroscopic endocardial mapping in humans. *Circ.*, 1998;**97**: 2426–2432.
155. Modre R., B. Tilg, G. Fischer, F. Hanser, B. Messnarz, M. Seger, M.F. Schocke, T. Berger, F. Hintringer, and F.X. Roithinger, Atrial noninvasive activation mapping of paced rhythm data. *J. Cardiovasc. Electrophysiol.*, 2003;**14**(7): 712–719.
156. Fischer G., F. Hanser, C. Hintermuller, M. Seger, B. Pfeifer, R. Modre, L. Wieser, B. Tilg, S. Egger, T. Berger, F. Roithinger, and F. Hinteringer, A signal processing pipeline for noninvasive imaging of ventricular preexcitation. *Meth. Inf. Med.*, 2005;**44**(4).

157. Ramanathan C., R. Ghanem, P. Jia, K. Ryu, and Y. Rudy, Noninvasive electrocardiographic imaging for cardiac electrophysiology and arrhythmia. *Nat Med*, April 2004;**10**(4): 422–428.
158. Intini A., R.N. Goldstein, P. Jia, C. Ramanathan, K. Ryu, B. Giannattasio, R. Gilkeson, B.S. Stambler, P. Brugada, W.G. Stevenson, Y. Rudy, and A.L. Waldo, Electrocardiographic imaging (ECGI), a novel diagnostic modality used for mapping of focal left ventricular tachycardia in a young athlete. *Hear. Res.*, 2005;**2**(11): 1250–1252.
159. Jia P., C. Ramanathan, R.N. Ghanem, K. Ryu, N. Varma, and Y. Rudy, Electrocardiographic imaging of cardiac resynchronization therapy in heart failure: Observation of variable electrophysiologic responses. *Hear. Res.*, 2006;**3**(3): 296–310.
160. Velipasaoglu E., H. Sun, L. Rao, and D. Khoury, Role of geometry in the endocardial electrocardiographic inverse problem, in *Proceedings of the IEEE Engineering in Medicine and Biology Society 22nd Annual International Conference*, vol. 2, 2000, pp. 902–903.
161. Rao L., R. He, C. Ding, and D.S. Khoury, Novel noncontact catheter system for endocardial electrical and anatomical imaging. *Ann. Biomed. Eng.*, 2004;**32**: 573–584.
162. Jia P., B. Punske, B. Taccardi, and Y. Rudy, Electrophysiologic endocardial mapping from a noncontact nonexpandable catheter: a validation study of a geometry-based concept. *J Cardiovasc Electrophysiol*, Nov 2000;**11**(11): 1238–1251.
163. Beatty G., S. Remole, M. Johnston, J. Holte, and D. Benditt, Non-contact electrical extrapolation technique to reconstruct endocardial potentials. *PACE*, 1994;**17**(4): 765.
164. Gornick C., S. Adler, B. Pederson, J. Hauck, J. Budd, and J. Schweitzer, Validation of a new noncontact catheter system for electroanatomic mapping of left ventricular endocardium. *Circ.*, Feb 1999;**99**(6): 829–835.
165. Kadish A., J. Hauck, B. Pederson, G. Beatty, and C. Gornick, Mapping of atrial activation with a noncontact, multielectrode catheter in dogs. *Circ.*, Apr 1999;**99**(14): 1906–1913.
166. Peters N., W. Jackman, R. Schilling, and D. Divies, Human left ventricular endocardial activation mapping using a novel noncontact catheter. *Circ.*, 1998;**9**: 887–898.
167. Paul T., B. Windhagen-Mahnert, T. Kriebel, H. Bertram, R. Kaulitz, T. Korte, M. Niehaus, and J. Tebbenjohanns, Atrial reentrant tachycardia after surgery for congenital heart disease: endocardial mapping and radiofrequency catheter ablation using a novel, noncontact mapping system. *Circ.*, May 2001;**103**(18): 2266–2271.
168. Yue A., J. Paisey, S. Robinson, T. Betts, P. Roberts, and J. Morgan, Determination of human ventricular repolarization by noncontact mapping: validation with monophasic action potential recordings. *Circ.*, Sep 2004;**110**(11): 1343–1350.
169. Thiagalingam A., E. Wallace, A. Boyd, V. Eipper, C. Campbell, K. Byth, D. Ross, and P. Kovoor, Noncontact mapping of the left ventricle: insights from validation with transmural contact mapping. *Pacing Clin. Electrophysiol.*, May 2004;**27**(5): 570–578.
170. Ambroggi L.D., B. Taccardi, and E. Macchi, Body surface maps of heart potential: Tentative localization of preexcited area of forty-two Wolff–Parkinson–White patients. *Circ.*, 1976;**54**: 251.
171. Essen R.V., R. Hinsen, R. Louis, W. Merx, J. Silny, G. Rau, and S. Effert, On-line monitoring of multiple precordial leads in high risk patients with coronary artery disease – a pilot study. *Eur. Heart J.*, 1985;**5**: 203–209.
172. Green L., R. Lux, and C. Haws, Detection and localization of coronary artery disease with body surface mapping in patients with normal electrocardiograms. *Circ.*, 1987;**76**: 1290–1297.
173. Ambroggi L.D., T. Bertoni, M. Breghi, M. Marconi, and M. Mosca, Diagnostic value of body surface potential mapping in old anterior non-Q myocardial infarction. *J. Electrocardiol.*, 1988;**21**(4): 321–329.
174. Bell A., M. Loughhead, S. Walker, and D. Kilpatrick, Prognostic significance of ST potentials determined by body surface mapping in inferior wall acute myocardial infarction. *Am. J. Cardiol.*, 1989;**64**: 319–323.
175. Anderson J., G. Dempsey, G. Wright, C. Cullen, M. Crawley, E. McAdams, J. McLaughlin, G. MacKenzie, and A. Adgey, Portable cardiac mapping assessment of acute ischaemic injury. *Methods Inf. Med. (MVI)*, 1994;**33**(1): 72–75.
176. Khoury D., K. Berrier, S. Badruddin, and W. Zoghbi, Three-dimensional electrophysiological imaging of the intact canine left ventricle using a noncontact multielectrode cavitary probe: study of sinus, paced, and spontaneous premature beats. *Circ.*, 1998;**97**(4): 399–409.
177. Tilg B., P. Wach, A. Sippensgroenewegen, G. Fischer, R. Modre, F. Roithinger, M. Mlynash, G. Reddy, T. Roberts, M. Lesh, and P. Steiner, Closed chest validation of source imaging from human ECG and MCG mapping, in *Proceedings of The First Joint BMES/EMBS Conference*. IEEE Press, New York, 1999, p. 275.
178. Potse M., R. Hoekema, A.C. Linnenbank, A. Sippens-Groenewegen, J. Strackee, J.M.T. de Bakker, and C.A. Grimbergen, Conversion of left ventricular endocardial positions from patient-independent co-ordinates into biplane fluoroscopic projections. *Med. Biol. Eng. Comput.*, January 2002;**40**(1): 41–46.
179. Tilg B., G. Fischer, R. Modre, F. FH, B. Messnarz, and F.X. Roithinger, Electrocardiographic imaging of atrial and ventricular electrical activation. *Med. Image Anal.*, September 2003;**7**(3): 391–398.
180. Pfeifer B., F. Hanser, and C.H. Modre-Osprian, G. Fischer, M. Seger, H. Mühlthaler, T. TT, and B. Tilg, Cardiac modeling using active appearance models and morphological operators. medical imaging: Visualization, image-guided procedures, and display, in *Proceedings of the SPIE*, 2005.
181. Cheney M., D. Isaacson, and J. Newell, Electrical Impedance Tomography. *SIAM Rev.*, 1999;**41**(1): 85–101.
182. Saulnier G.J., R.S. Blue, J.C. Newell, D. Isaacson, and P.M. Edic, Electrical Impedance Tomography. *IEEE Signal Process. Mag.*, 2001;**18**(6): 31–43.
183. A. Ghodrati, D. Brooks, and R. MacLeod, Methods of solving reduced lead systems for inverse electrocardiography. *IEEE Trans. Biomed. Eng.*, Feb 2007;**54**(2): 339–343.
184. Green L.S., B. Taccardi, P.R. Ershler, and R.L. Lux, Effects of conducting media on isopotential and isochrone distributions. *Circulation*, 1991;**84**(6): 2513–2521.
185. Bradley C.P., M.P. Nash, L.K. Cheng, A.J. Pullan, and D.J. Paterson, Electrocardiographic inverse validation study: Model development and methodology. *FASEB J.*, April 2000;**14**(4): A442.

186. Messnarz B., M. Seger, R. Modre, G. Fischer, F. Hanser, and B. Tilg, A comparison of noninvasive reconstruction of epicardial versus transmembrane potentials in consideration of the null space. *IEEE Trans. Biomed. Eng.*, September 2004;**51**(9): 1609–1618.
187. Oostendorp T., J. Nenonen, and P. Korhonen, Noninvasive determination of the activation sequence of the heart: application to patients with previous myocardial infarctions. *J. Electrocardiol.*, 2002;**35**(Suppl): 75–80.
188. Fischer G., B. Pfeifer, M. Seger, C. Hintermuller, F. Hanser, R. Modre, B. Tilg, T. Trieb, C. Kremser, F. Roithinger, and F. Hintringer, Computationally efficient noninvasive cardiac activation time imaging. *Methods Inf Med*, 2005;**44**(5): 674–686.
189. Nielsen P.M., I.J. LeGrice, B.H. Smaill, and P.J. Hunter, Mathematical model of geometry and fibrous structure of the heart. *Am. J. Physiol.*, 1991;**260**(4 Pt 2): H1365–H1378.

Section 4

Electrocardiographic Lead Systems and Recording Techniques

10 Lead Theory

B. Milan Horáček

P. W. Macfarlane, A. van Oosterom, O. Pahlm, P. Kligfield, M. Janse, J. Camm (eds.), *Comprehensive Electrocardiology*, DOI 10.1007/978-1-84882-046-3_10,

10.1 Introduction

The bioelectric sources arising during the heart's electrical excitation process produce a flow of electric current in the surrounding tissues. It is therefore possible to detect, with a pair of electrodes external to the heart, time-varying potential differences known as electrocardiograms. The pair of electrodes constitutes an electrocardiographic lead in its simplest form.

Lead theory deals with the relationship between cardiac electric sources and the potential differences they generate in electrocardiographic leads. Two components can be considered separately in studying this relationship: the active cardiac electric sources (Chaps. 6 and 7), which are distributed in and restricted to the heart region, and the passive aggregate of electrically conductive extracardiac tissues of the body (the volume conductor), which provides an electric load for cardiac sources and makes the external measurement of cardiac electric activity possible. Lead theory provides a method for visualizing the relationship between cardiac sources and voltages in electrocardiographic leads. This relationship can be studied by performing specific solutions to the volume conductor problem, which consists of evaluating an electric field produced in the bounded volume conductor by a given electric source (Chaps. 2 and 8).

10.1.1 Classical Theory of Electrocardiographic Leads

Classical lead theory – introduced by Einthoven and coworkers and described in every textbook of electrocardiography – assumes that the human body is part of an infinite, homogeneous conductor in which the heart's electric sources are represented by a single, time-varying current dipole (depicted as a two-dimensional heart vector) at a fixed location. Einthoven's leads (designated lead I, lead II, and lead III) use electrodes at three extremities (Chap. 11). Since such electrodes are relatively remote from the cardiac source, Einthoven felt he could define the relationship between the heart vector and the electrocardiographic potentials observed in these leads in very simple terms: he postulated that the potentials at the three extremities as generated by the heart vector were the same as those generated at the vertices of an equilateral triangle in an infinite, homogeneous, two-dimensional conductor with the dipole source located at the triangle's centroid.

The Wilson central terminal with unipolar limb leads, and augmented leads, were later readily incorporated into Einthoven's theory. However, for interpreting potentials in unipolar precordial leads, a more general solid-angle theory (Chaps. 2, 5 and 6) was introduced into electrocardiography by Wilson and coworkers. This theory introduces a double-layer source instead of a single, fixed-location dipole.

10.1.2 Volume Conductor Theory of Electrocardiographic Leads

A more appropriate lead theory, often referred to as the volume-conductor theory, evolved in the 1940s and 1950s. First, Burger and van Milaan took into consideration the fact that the human body is a three-dimensional, bounded, irregularly shaped and inhomogeneous volume conductor. Second, McFee and Johnston, and independently Schmitt, considered the distributed character of cardiac sources. Although Burger's theory is quite general with regard to volume-conductor characteristics, it rests on the fixed-dipole hypothesis; that is, it assumes that at a given instant the potentials anywhere on the body surface can be derived from the projection of a heart vector in 3D space (thought to account for all cardiac sources) into an appropriate spatial lead vector (characterizing lead properties under the assumption that the location of the heart vector is fixed).

The fixed-dipole hypothesis is no longer acceptable, as body-surface potential mapping studies have established (Chap. 27) that the electrocardiographic body-surface potential distributions exhibit features that cannot be accounted for by a single, fixed-location dipole source. McFee and Johnston's lead theory, by taking into account the distributed nature of cardiac electric sources, overcomes the limitations of the fixed-dipole hypothesis; it generalizes the lead vector into the lead-field concept and defines the source-lead relationship for every element of the distributed cardiac source. Schmitt coined the appropriate term "transfer impedance" for the vector field representing the lead field.

The aim of this chapter is to provide an elementary introduction to modern lead theory. The cornerstones of this theory are the superposition and reciprocity theorems of Helmholz, upon which rest, respectively, the lead-vector concept

of Burger and van Milaan and the lead-field concept of McFee and Johnston. The classical concepts of Einthoven and Wilson fit into this lead theory as a special case.

10.1.3 Bibliographic Notes

The equilateral triangle diagram for interpreting limb-lead electrocardiograms was introduced by Einthoven and coworkers [1, 2]. This diagram is described in every text of electrocardiography (Chap. 11), as are the conventions of the Wilson central terminal with the unipolar limb leads [3], augmented leads [4], and unipolar precordial leads [5–7]. Solid-angle theory was introduced into electrocardiography by Wilson et al. [8]; this theory is described in texts, such as Plonsey [9], Plonsey and Barr [10], Malmivuo and Plonsey [11], and in articles [12]. Burger and van Milaan [13–15] took into consideration the fact that the human body is a three-dimensional, inhomogeneous volume conductor. McFee and Johnston [16–18], and Schmitt [19], considered the distributed character of cardiac sources. Reviews of lead theory have been written by Burger [20], Frank [21], McFee and Johnston [16], Schmitt [19], Schaefer and Haas [22], Geselowitz and Schmitt [23], McFee and Baule [24], Geselowitz [25], and Malmivuo and Plonsey [11].

10.2 Prerequisites

The assumptions that underlie electrocardiographic lead theory (as presented in this chapter) are not very restrictive; they allow the theory to be formulated for distributed cardiac sources, for a body of irregular shape and inhomogeneous composition, and for any conceivable electrocardiographic lead. The lead-vector concept requires that only one dipolar source be considered at a time; however, this restriction can be relaxed when the lead vector is interpreted more generally as a local value of the lead field.

10.2.1 Assumptions Concerning Cardiac Bioelectric Sources

Bioelectric sources arising during cardiac activation and repolarization are distributed throughout the heart and are proportional everywhere to the spatial gradient of the transmembrane potential ((7.21) and (8.8)). Such sources can be described as a volume distribution of impressed current density $\vec{J}^{\mathrm{i}}$ (current dipole moment per unit volume, i.e., current per unit area), and $\vec{J}^{\mathrm{i}}\,\mathrm{d}v$ (current dipole moment) may be thought of as an elemental current dipole in a small region of the heart.

Multiple Dipoles

A rigorous but impractical description of cardiac electric sources by a continuous distribution of impressed current density $\vec{J}^{\mathrm{i}}$ can be approximated to any desired degree of accuracy by a finite number of appropriately placed current dipoles; such a source is called a multiple-dipole source. Constituent dipoles of the multiple-dipole source can be obtained by dividing the myocardium into subregions and assigning a local, lumped current dipole to the centroid of each region, i.e.,

$$\vec{p}_k = \int_{\Delta V_k} \vec{J}^{\mathrm{i}}\,\mathrm{d}v, \tag{10.1}$$

where the integration is over the volume ΔV_k of the kth region. The dimension of the vector quantity $\vec{p}_k$ is current times length; thus $\vec{p}_k$ can be approximated by a current dipole (Sect. 2.5.1.2).

Heart Vector

The region for which a lumped current dipole is determined can be chosen arbitrarily; as a special case, it can encompass an entire heart. A dipole so obtained is referred to as a heart vector $\vec{H}$. Thus

$$\vec{H} = \int_{V_H} \vec{J}^i \, dv, \tag{10.2}$$

where the integration is over the entire heart volume V_H. The heart vector thus represents the vectorial sum of all elemental current dipoles and is usually placed at the centroid of the heart region. (The position of $\vec{H}$ can be chosen rigorously so that it satisfies certain criteria of optimality, e.g., minimal content of the quadrupolar component [26].)

The concept of the heart vector can be developed from the analysis of the electric field produced in an infinite homogeneous medium at a sufficient distance from the cluster of dipolar sources. In the immediate vicinity of such a cluster, a complete specification of all constituent dipoles, consisting of the location and moment $\vec{p}_k$ for each, is necessary to determine the field potential accurately. However, at a large distance from the source, the field potential converges to that produced by a single equivalent dipole located at the centroid of the cluster. In physics, this equivalent dipole is known as the dipole moment of the cluster.

Potential Field of a Single Dipole

As shown in Sect. 2.5.1.2 (2.99), the electric field $\Phi(\vec{r}')$ at field point $\vec{r}'$, produced by a single current dipole with moment $\vec{p}$ and location $\vec{r}$ in an infinite homogeneous medium of conductivity σ, is

$$\Phi(\vec{r}') = \frac{1}{4\pi\sigma} \frac{\vec{p}(\vec{r}) \cdot \vec{R}}{R^3} + c \tag{10.3}$$

R is the length of the vector $\vec{R} = \vec{r}' - \vec{r}$ pointing from dipole source location to field point, and c is the arbitrary integration constant. By defining the potential at infinity as zero, we have $c = 0$.

An equivalent variant of (10.3) is

$$\Phi(\vec{r}') = \frac{1}{4\pi\sigma} \frac{p \cos\theta}{R^2} + c, \tag{10.4}$$

with p the magnitude (strength) of the dipole vector and θ the angle beween vectors $\vec{p}$ and $\vec{R}$ (2.100).

Potential Field of a Double Layer

A dipolar double layer is an arbitrary surface with which are associated sources of electric current on one (positive) side and sinks of current on the other (negative) side; it is an excellent approximation of electric primary sources at the activation wave front in the heart (Chap. 6). A double layer can be thought of as a set of dipoles, each representing an element (patch) of double-layer surface (Chap. 2). For field points at a large distance from a double layer the potential field can be approximated by field generated by the dipole that is the vectorial sum of these elemental dipoles representing the source strength of the individual patches.

10.2.2 Assumptions Concerning the Human Torso

The volume-conductor problem in electrocardiology involves the determination of an extracardiac electric field produced in the body and on its surface by the distributed and time-varying electric sources of the heart. To solve this problem it is necessary to apply appropriately electromagnetic theory. The problem has two important features that make it amenable to solution: it is quasistatic and linear.

The term "quasistatic" implies that the extracardiac electric field throughout the body is at every instant in equilibrium with the sources in the heart, and thus, for a given distribution of sources at a given instant a corresponding extracardiac field can be determined without any regard to the source distribution at previous instants.

Another important feature of the volume-conductor problem in electrocardiology is that, at the low current densities that are involved, the body can be considered to be a linear physical system. Capacitive and inductive effects can be neglected, and thus, the term linearity refers to the resistive properties (Sect. 2.4). Consequently, as discussed in Sect. 2.4.3, the relationship between heart-produced current flow and the electric field can be expressed by a vector form of Ohm's law: $\vec{J} = \sigma\vec{E}$, where $\vec{J}$ is a vector of current density, $\vec{E}$ is a vector of electric field intensity and σ, is the conductivity of the extracardiac medium. Associated with the electric field is the electric potential Φ, a scalar function defined from the expression $\vec{E} = -\nabla\Phi$. Since Φ is defined indirectly, i.e., through its gradient (Sect. 2.4), the potential field is always specified from its sources up to an arbitrary constant. However, by considering the difference of the potential between any two points in space, this common constant drops out of the equation and the resulting potential difference has a unique interpretation: it is a scalar quantity defined as the work required to move a unit positive charge from one of the field points to the other (Sect. 2.4.3). When denoting the two field points as A and B, we have

$$V_{AB} = \Phi_A - \Phi_B = -\int_B^A \vec{E} \cdot d\vec{l} \tag{10.5}$$

In the following Sect. 10.3 the notation Φ is used for the potential field, and V denotes potential diferences between two field points and/or two artificially constructed terminals.

Helmholtz stated the three fundamental principles that govern linear physical systems:

1. The principle of superposition
2. The principle of reciprocity
3. The principle of the equivalent double layer

All three principles have a fundamental importance for the theoretical basis of electrocardiography; the first two constitute a foundation of lead theory. The principle of superposition states that an electric field arising from several sources is the sum of the fields that would be present for each source acting separately. Burger and van Milaan made this principle the basis of the lead-vector concept (Sect. 10.3). The reciprocity theorem was applied to electrocardiography by McFee and Johnston, who introduced the lead-field concept (Sect. 10.5).

Finally, a few words about another prerequisite of the electrocardiographic lead theory – Kirchhoff's laws. In electrical network theory, a current and voltage are associated with each branch of the network. Since energy is neither stored nor dissipated in any junction of the network, the electric current must obey a local conservation law. This is expressed by Kirchhoff's current law, which states that the total current leaving any junction must equal the current entering the junction. Since energy is conserved, a series of elements in a closed-loop has a single flow of current, and hence, the sum of voltage differences around the loop equals zero because the potential must be unique at each node of the network; this is Kirchhoff's voltage law.

10.2.3 Definition of Electrocardiographic Lead

Originally, the term "electrocardiographic lead" referred strictly to the configuration (location on the thorax) of two electrodes attached directly to the body for the purposes of recording electrocardiographic signal. This notion had to be later extended to accommodate other recording practices in electrocardiography that produced potential differences between two terminals as weighted sums (linear combinations) of the potentials at multiple electrode sites. The weighting of the surface potentials at the electrode sites was originally performed by using resistive networks (Fig. 10.1). Modern circuitry with operational amplifiers allows the addition/subtraction of voltages from as many recording sites as are deemed necessary. Therefore, the following definition will be adopted:

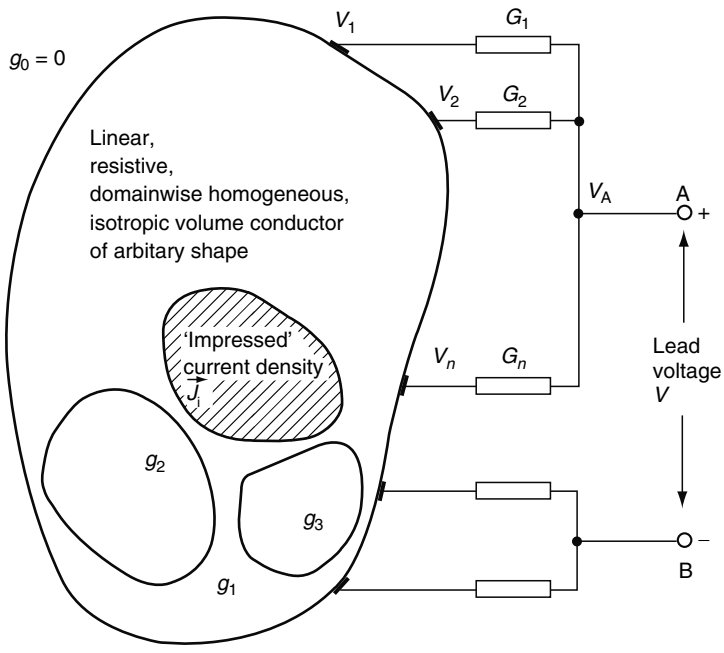

Figure 10.1

Cardiac sources in the abstracted torso and an electrocardiographic lead. A good approximation of the human torso is a bounded, linear, resistive, domainwise homogeneous and isotropic volume conductor, with electric sources in the heart region represented by a volume distribution of "impressed" current density $\vec{J}^i$, which can be in turn approximated to any desired degree of accuracy by a finite number of elemental current dipoles distributed throughout the heart region. Real constants g_0, g_1, g_2, …, g_n denote conductivities of different regions. The electrocardiogram is a time-dependent voltage between two terminals A and B of an electrocardiographic lead; each terminal can be connected either to a single electrode or, via weighting resistors, to several electrodes. Variables V_1 to V_n are potentials at the electrode sites; V_A is a potential at terminal A; G_1 to G_n are conductances of weighting resistors R_1 to R_n ($G_i = 1/R_i$); the lead voltage can be considered an "open-circuit voltage" because the input impedance of modern ECG amplifiers is very high.

The electrocardiographic lead is a pair of terminals with designated polarity, each connected either directly or via a passive/active network to recording electrodes sampling the cardiac potential field on the thorax; the observed potential difference between the two terminals is called the lead voltage.

A lead specification consists of electrode-placement and polarity conventions, and of the diagram of the network; this diagram can be translated into numerical weights for the potentials at all constituent electrodes. The term "composite lead" is sometimes used in this chapter for those leads that include passive/active networks weighting the potentials at one or both lead terminals (Fig. 10.1); the word "composite" emphasizes that the lead is made up of a number of constituent voltages. A well-known composite terminal is Wilson central terminal (WCT), which is formed by taking the mean of the potentials at left arm, right arm, and left foot. WCT was proposed as "indifferent" lead terminal, which approximates for arbitrary cardiac sources the potential that would exist at large distance from these sources (see, however, Sect. 5.4.1).

Note that, somewhat confusingly, the term "lead" is frequently used as a shorthand for time-varying "lead voltage" recorded by means of the physical lead arrangement. A few additional comments on lead/electrode nomenclature are needed:

1. The term "unipolar lead" is a misnomer: measuring potential differences always requires two terminals.
2. The term "bipolar lead" refers to the situation where measured potential differences are derived directly from two electrodes serving as the lead terminals.

3. The term "sensing electrode" for one of the terminals of a bipolar lead only makes sense if the other electrode/terminal can be considered as "indifferent" (see Sect. 5.4.1).

10.2.4 Bibliographic Notes

Any text on electromagnetic theory (e.g., [27, 28]) will cover the material on the field of the dipole and the double layer, as well as on the dipole moment of a cluster of sources. Courant and Hilbert [29] deal with the derivation of basic theorems concerning potential of the dipole and double stratum/layer in two and three dimensions (see also Guillemin [30]). Plonsey [9] and Geselowitz and Schmitt [23] justify the quasistatic assumption. Plonsey and Heppner [31] document the absence of capacitive and inductive effects. In 1853, Hermann von Helmholtz [32] was the first to realize that the correct interpretation of bioelectric measurements requires an understanding of the electric field in a volume conductor; he stated the three fundamental principles that govern linear physical systems. Geselowitz and Schmitt [23] and Geselowitz [25] cover Helmholtz' theorems, including derivations. Oster et al. [33] show the fundamental significance of Kirchhoff's laws in biological systems. One of many texts dealing with electric circuit theory is Desoer and Kuh [34].

The experimental evidence needed to support the assumptions stated in this section was gathered over a long period. The first tissue measurements made specifically with electrocardiographic effects in mind were carried out by Kaufman and Johnston [35]; they showed that substantial differences in resistivity existed between different tissues of the body. Schwan and Kay [36] showed that the phase shift can be ignored for the electrocardiographic frequencies. Accurate resistivity measurements were made by Burger and van Dongen [37], Rush et al. [38] and others. Studies of tissue resistivity have been reviewed by Geddes and Baker [39].

10.3 Lead Vector

Provided the assumptions stated in Sect. 10.2 are satisfied, the relationship between dipolar sources and lead voltages is conceptually very simple. This was first shown by Burger and van Milaan.

10.3.1 Definition

A current dipole with moment $\vec{p}$ can be resolved into three orthogonal components

$$\vec{p} = \vec{e}_x p_x + \vec{e}_y p_y + \vec{e}_z p_z, \tag{10.6}$$

where p_x, p_y, and p_z are the magnitudes of the components and $\vec{e}_x$, $\vec{e}_y$, and $\vec{e}_z$ are unit vectors along the axes of the Cartesian coordinate system (Sect. 2.2.3). The vector $\vec{p}$ represents the lumped cardiac electric sources of a chosen cardiac region (10.1); when an entire heart region is chosen, $\vec{p}$ becomes the heart vector $\vec{H}$ (10.2). In electrocardiography, it is customary to choose a right-handed coordinate system with x, y, and z axes as shown in Fig. 10.9; the x axis is directed from the right to the left of the torso, the y axis from head to feet, and the z axis from front to back.

If the dipole is embedded in an arbitrary volume conductor, bounded or unbounded, the amount that each component of vector $\vec{p}$ contributes to any lead voltage V is directly proportional (as a consequence of the linearity assumption) to that component's magnitude, and all three contributions can be added by virtue of the superposition theorem, i.e.,

$$V = c_x p_x + c_y p_y + c_z p_z, \tag{10.7}$$

where c_x, c_y and c_z are scalar constants. This is Burger's equation, a cornerstone of lead theory.

Based on (2.11), Burger"s equation can be interpreted as the scalar product of two vectors

$$V = \vec{c} \cdot \vec{p}, \tag{10.8}$$

where $\vec{c} = \vec{e}_x c_x + \vec{e}_y c_y + \vec{e}_z c_z$ is a vector that specifies the relationship between the dipolar source at a given location $\vec{r}$ and the voltage V in a given lead. The vector $\vec{c}$ is called the lead vector of a given electrocardiographic lead. It depends on the location $\vec{r}$ of the source, the locations of lead electrodes, and – for a bounded volume conductor – on the shape of the torso and the inhomogeneities of the electric conductivities of the torso as a volume conductor.

The units of the lead vector are ohms per meter, since the units of $\vec{p}$ are ampere × meter and voltage V is measured in volts. If a volume conductor's shape and electric properties do not change, the components of the lead vector will stay constant; since the medium is assumed to be resistive, these constants are real numbers.

Although the relationship between cardiac sources and lead voltages as defined by Burger's equation (10.8) is conceptually simple, the scalar coefficients c_x, c_y, and c_z are not easy to determine except in very simplified cases. To estimate lead vectors of the limb leads, Burger constructed a body-shaped tank, filled it with an electrolyte, and inserted a cork "spine" and sand-bag "lungs." His results indicated that the classical lead theory, embodied in the Einthoven triangle diagram, required revision.

10.3.2 Scalar Product and its Geometrical Interpretation

The scalar product (inner product, dot product) of two vectors $\vec{c}$ and $\vec{p}$ is a scalar quantity

$$\vec{c} \cdot \vec{p} = cp \cos\theta,$$

where θ is the angle between the vectors when they are placed with a common origin (Sect. 2.2.4). As seen in Fig. 10.2, the scalar product has a simple geometrical interpretation: it is the length of one vector multiplied by the length of the projection of the other onto it. Thus, from Burger's equation (10.8), the contribution of a current dipole $\vec{p}$ to the voltage V in any particular lead equals the length of the projection of $\vec{p}$ on the appropriate lead vector $\vec{c}$ times the length of $\vec{c}$. If $\vec{p}$ is orthogonal to $\vec{c}$, $\vec{p} \cdot \vec{c} = 0$; if $\vec{p}$ is parallel/antiparallel to $\vec{c}$, $\vec{p} \cdot \vec{c} = \pm\, p\, c$.

The scalar product is commutative and distributive:

$$\vec{p} \cdot \vec{c} = \vec{c} \cdot \vec{p},$$

and

$$(\vec{c}_1 + \vec{c}_2) \cdot \vec{p} = \vec{c}_1 \cdot \vec{p} + \vec{c}_2 \cdot \vec{p}$$

These as well as other basic properties of the scalar product are discussed in Chap. 2.

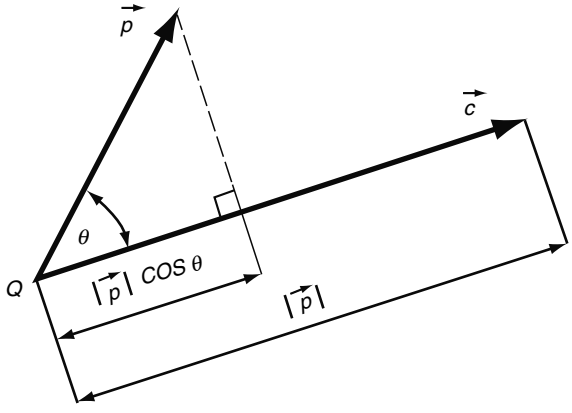

Figure 10.2
Lead-vector projection. According to Burger's equation (10.8), a current dipole $\vec{p}$ produces the voltage $V = \vec{p} \cdot \vec{c}$ in an electrocardiographic lead, where $\vec{c}$ is a lead vector characterizing the lead. This scalar product of two vectors has a simple geometrical interpretation: it is the length of the projection of $\vec{p}$ on the lead vector $\vec{c}$ multiplied by the lead vector's length $|\vec{c}|$.

10.3.3 Lead Vectors and Limb Leads

We consider first the lead vectors associated with the limb leads. There are six limb leads in the set of 12 standard leads; these limb leads are derived from only three independent extremity potentials, and thus only two independent potential differences can be obtained. Even though some limb leads are redundant, they were adopted in the set of 12 standard leads to facilitate the visual interpretation of electrocardiograms.

According to Burger's equation (10.8), any current dipole $\vec{p}$ embedded in any volume conductor of arbitrary shape and extent will produce the following three potential differences at the limb-electrode sites *against any arbitrary reference*.

$$V_R = \vec{c}_R \cdot \vec{p}, \tag{10.9}$$

$$V_L = \vec{c}_L \cdot \vec{p}, \tag{10.10}$$

$$V_F = \vec{c}_F \cdot \vec{p}, \tag{10.11}$$

where $\vec{c}$ denotes a lead vector and the subscripts R, L, and F refer to the right arm, left arm, and the left leg respectively. In the human torso, which is irregularly shaped, the lead vectors $\vec{c}_R$, $\vec{c}_L$, and $\vec{c}_F$ are independent and thus the sum of $V_R + V_L + V_F$ will not necessarily be zero. (However, if WCT is the reference used then $V_R + V_L + V_F = 0$.)

10.3.4 Bipolar Limb Leads

Einthoven introduced bipolar limb leads denoted I, II, and III that yield potential differences V_I, V_{II}, and V_{III} between three limbs:

$$V_I = V_L - V_R, \tag{10.12}$$

$$V_{II} = V_F - V_R, \tag{10.13}$$

$$V_{III} = V_F - V_L, \tag{10.14}$$

Expressed in terms of Burger's equation (10.8), and using (10.9)–(10.14)

$$V_I = \vec{c}_I \cdot \vec{p} = \vec{c}_L \cdot \vec{p} - \vec{c}_R \cdot \vec{p}, \tag{10.15}$$

$$V_{II} = \vec{c}_{II} \cdot \vec{p} = \vec{c}_F \cdot \vec{p} - \vec{c}_R \cdot \vec{p}, \tag{10.16}$$

$$V_{III} = \vec{c}_{III} \cdot \vec{p} = \vec{c}_F \cdot \vec{p} - \vec{c}_L \cdot \vec{p} \tag{10.17}$$

Since scalar multiplication is distributive, the lead vectors of bipolar limb leads can be defined in terms of lead vectors for unipolar limb leads:

$$\vec{c}_I = \vec{c}_L - \vec{c}_R, \tag{10.18}$$

$$\vec{c}_{II} = \vec{c}_F - \vec{c}_R, \tag{10.19}$$

$$\vec{c}_{III} = \vec{c}_F - \vec{c}_L \tag{10.20}$$

10.3.5 Burger Triangle

From the definitions of the bipolar limb-lead voltages (and their designated polarity) it follows that

$$V_I + V_{III} = V_{II}, \tag{10.21}$$

that is, the sum of the lead voltages if leads I and III at any time instant equals the lead voltage of lead II. In electrocardiography this property is known as Einthoven's law; it is a specific application of Kirchhoff's voltage law for a closed circuit. By substituting the expressions shown in the previous subsection it is found that

$$\vec{c}_I + \vec{c}_{III} = \vec{c}_{II} \tag{10.22}$$

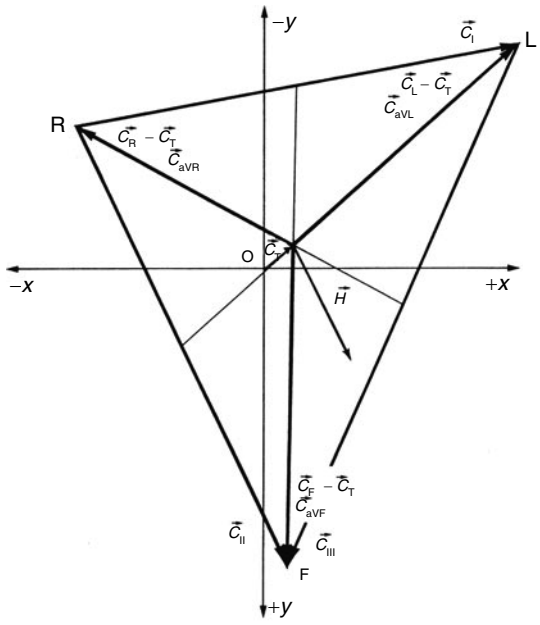

Figure 10.3

Burger triangle: frontal plane projection. Lead vectors of bipolar limb leads I, II and III satisfy the constraint $\vec{c}_I + \vec{c}_{III} = \vec{c}_{II}$, and thus they form a triangle (the Burger triangle), which does not necessarily lie in the frontal plane. Lead vectors $\vec{c}_R - \vec{c}_T$, $\vec{c}_L - \vec{c}_T$, $\vec{c}_F - \vec{c}_T$ of unipolar extremity leads originate at the median point of this triangle, as can be seen from the definition of the Wilson central terminal (Sect. 10.3.4). Lead vectors $\vec{c}_{aVR}$, $\vec{c}_{aVL}$ and $\vec{c}_{aVF}$ of augmented leads start, respectively, at the midpoints of $\vec{c}_{III}$, $\vec{c}_{II}$ and $\vec{c}_I$, and terminate at the opposite vertex of the Burger triangle; therefore, these lead vectors are concurrent at the median point and are 3/2 of the length of the lead vectors of the corresponding unipolar extremity leads. A heart vector $\vec{H}$ can be placed at the median point, and, in accordance with Burger's equation, its projection on the appropriate lead vector multiplied by that lead vector's length defines the lead voltage. The points R, L, F depicted here are denoted R', L', F' in image space (Fig. 10.8).

This shows that Einthoven's law for the bipolar limb lead potentials has a similar formulation in the corresponding lead vectors. It holds true for an arbitrary cardiac source in any volume conductor that satisfies the linearity assumption. In Fig. 10.3 the lead vectors of leads I, II, and II are depicted as the edges of a scalene triangle: Burger's triangle. This geometrical interpretation is justified by (10.22). The triangle does not necessarily lie in the frontal plane. In the next subsection it is shown that the Einthoven equilateral triangle is a special case of Burger's scalene triangle.

10.3.6 Einthoven's Triangle

In contrast to Burger's triangle, classical Einthoven's triangle diagram is based on a much more simplified representation of cardiac sources and of extracardiac volume conductor.

1. Three field points R, L, and F, corresponding to right arm, left arm, and left leg are located in the frontal plane; they are the vertices of an equilateral triangle (Fig. 10.4).
2. The position of the source dipole $\vec{p}$ is at the centroid of the triangle and its direction is confined to the triangle's plane.
3. The volume conductor involved may be considered to be either two- or three-dimensional; it may be taken to be of infinite extent, or bounded by a circle (2D space) or a sphere (3D space).

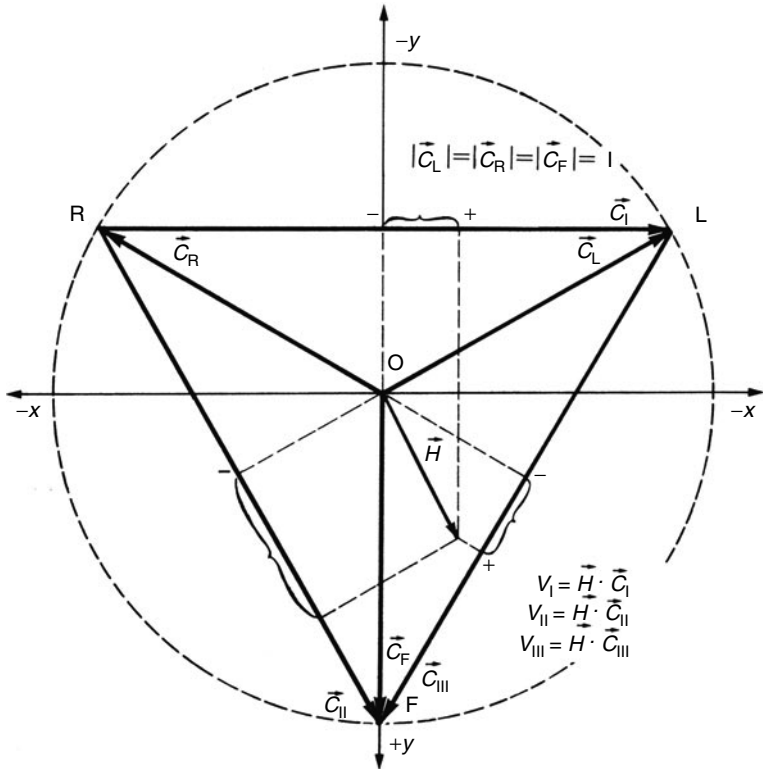

Figure 10.4

Einthoven triangle in terms of lead vectors. The lead vectors implicitly assumed by Einthoven for limb leads I, II and III lie in the frontal plane and are of equal length, thus forming an equilateral triangle. The projection of the heart vector $\vec{H}$ on sides I, II and III of the Einthoven triangle is equivalent to the scaled scalar product of the heart vector $\vec{H}$ with lead vectors $\vec{c}_I$, $\vec{c}_{II}$ and $\vec{c}_{III}$, respectively; this is Burger's equation.

For all volume conductor configurations already mentioned the potentials at field points R, L, and F can be shown to be

$$\Phi = \alpha\, \vec{e} \cdot \vec{p} + c, \tag{10.23}$$

where $\vec{e}$ represents the unit vector directed from the dipole location to the respective field point (R, L, or F). The factor α is a proportionality constant depending on the particular volume conductor configuration. For a bounded sphere with unit radius its value is $3/(4\pi\sigma)$ (2.153). The constant C specifies the potential at an arbitrary common reference. It drops out of the equation when considering lead voltages, since the term is common for both terminals of any lead considered.

By choosing the WCT as the common reference, for which $V_R + V_L + V_F = 0$, we find for any of the lead potentials V_R, V_L, and V_F,

$$V(\vec{e}) = \alpha\, \vec{e} \cdot \vec{p} \tag{10.24}$$

A comparison of (10.24) with Burger's equation (10.8) identifies the vectors $\alpha\, \vec{e}$ as lead vectors. Thus, after normalization by taking $\alpha = 1$, the radius vectors of R, L, and F are the lead vectors $\vec{c}_R$, $\vec{c}_L$, and $\vec{c}_F$ respectively. Because of the symmetry of the assumed source-volume conductor configuration we have $\vec{c}_R + \vec{c}_L + \vec{c}_F = 0$, which now – in contrast to the more general situation of Burger's triangle – is as in $V_R + V_L + V_F = 0$. Recall that the latter property always holds true when using Wilson's central terminal.

10.3.7 Composite Leads with Passive Networks

We now consider a lead terminal, e.g., terminal A in Fig. 10.1, joining n electrodes via conductances $G_1, G_2, \ldots, G_n$. In the past, networks of resistors in electrocardiographic leads had to be designed so that their resistances, $R_i = 1/G_i$, were larger than the impedance of the skin-electrode interface, yet smaller than the input impedance of an amplifier; this problem is now largely irrelevant with the use of operational amplifiers in the lead networks.

Let V_A designate a potential difference *against an arbitrary reference* at junction A and $V_1, V_2, \ldots, V_n$ the potential differences (against the same reference) at the electrode sites connected to terminal A. According to Kirchhoff's current law,

$$(V_A - V_1)G_1 + \ldots + (V_A - V_n)G_n = 0, \tag{10.25}$$

and a potential at terminal A under open-circuit conditions is

$$V_A = \frac{\Sigma G_i V_i}{\Sigma G_i} \tag{10.26}$$

From (10.26) and from Burger's equation (10.8), the potential difference V_A at terminal A is

$$V_A = \frac{\Sigma G_i \vec{c}_i \cdot \vec{p}}{\Sigma G_i}, \tag{10.27}$$

and therefore, because the scalar product is distributive, the following lead vector can be associated with terminal A:

$$\vec{c}_A = \frac{\Sigma G_i \vec{c}_i}{\Sigma G_i} \tag{10.28}$$

This means that the lead vector $\vec{c}_A$ is a linear combination of lead vectors corresponding to all constituent electrode sites.

The Wilson central terminal is defined as the junction of three equal resistors connected to the electrodes with potential differences V_R, V_L, and V_F at the three limbs. It follows from ((10.9)–(10.11), (10.26), and (10.28)) that the potential V_T at the Wilson central terminal (relative to the arbitrary common reference) is

$$V_T = \frac{V_R + V_L + V_F}{3}, \tag{10.29}$$

and

$$\vec{c}_T = \frac{\vec{c}_R + \vec{c}_L + \vec{c}_F}{3}, \tag{10.30}$$

Since the final points of lead vectors $\vec{c}_R$, $\vec{c}_L$, and $\vec{c}_F$ may be viewed as lying at the vertices of the Burger triangle, it follows from (10.30) that the final point of lead vector $\vec{c}_T$ is at the median point of the Burger triangle (Fig. 10.3). The potential of the Wilson central terminal can be zero for an arbitrary source only if the vectorial sum of the three lead vectors $\vec{c}_R$, $\vec{c}_L$, and $\vec{c}_F$ (based on the arbitrary common reference) is zero. Since these vectors are independent, this is not necessarily the case.

By using (10.30), it can be seen that for potentials recorded against an arbitrary reference we have

$$V_R - V_T = \frac{2V_R - V_L - V_F}{3}, \tag{10.31}$$

$$V_L - V_T = \frac{2V_L - V_R - V_F}{3}, \tag{10.32}$$

and

$$V_F - V_T = \frac{2V_F - V_L - V_R}{3} \tag{10.33}$$

In this application, the lead vectors to be used are $\vec{c}_R$, $\vec{c}_L$, $\vec{c}_F$, and $\vec{c}_T$, also with respect to the arbitrary common reference. Note from (10.29), (10.31), (10.32), and (10.33) that the sum of such unipolar limb-lead voltages is zero as is the sum of corresponding lead vectors. If the arbitrary common reference is in fact WCT, the term V_T in the three equations is zero.

The set of three limb leads, known as augmented unipolar limb leads (designated aVR, aVL, and aVF) produces 50% higher voltages than unipolar limb leads. Each augmented lead is defined by two terminals; the positive terminal is at one of the three limbs (left arm, right arm, left leg) and the negative terminal is at the junction of two equal resistors connected to the remaining two limbs. Consider the lead vectors associated with these leads. It follows from (10.28) that when lead terminal A is connected via resistors to just two constituent electrode sites, the final point A of the terminal's lead vector $\vec{c}_A$ lies on the line joining the final points of lead vectors corresponding to the constituent electrode sites, dividing this line into segments whose lengths are in the same ratio as the resistances between A and the electrodes; for augmented leads these resistances are equal, and therefore their corresponding segments are of equal length. This lead arrangement produces the following voltages:

$$V_{aVR} = \frac{2V_R - V_L - V_F}{2} = \frac{3(V_R - V_T)}{2}, \tag{10.34}$$

$$V_{aVL} = \frac{2V_L - V_R - V_F}{2} = \frac{3(V_L - V_T)}{2} \tag{10.35}$$

and

$$V_{aVF} = \frac{2V_F - V_L - V_R}{2} = \frac{3(V_F - V_T)}{2}, \tag{10.36}$$

Since these are merely scaled up versions of the extemity lead potentials their lead vectors are similarly scaled and $V_{aVR} + V_{aVL} + V_{aVF} = 0$ as well as $\vec{c}_{aVR} + \vec{c}_{aVL} + \vec{c}_{aVF} = 0$.

10.3.8 Composite Leads with Active Networks

The specification of the potential at a terminal of a composite lead depicted in Fig. 10.1, given by the (10.28), involves a weighted sum of the potentials at the electrodes connected to the terminal by means of conductances. The individual values of these conductances are positive, and as a consequence, all weights $G_i/\Sigma G_i$ are nonnegative and not greater than one.

The application of active networks with operational amplifiers permits the construction of arbitraty weights, with unsrestricted sign and magnitude. As an example, consider the following summation/subtraction of voltages of Einthoven's bipolar limb leads that produces three new voltages V_{SR}, V_{SL}, and V_{SF}:

$$V_{SR} = V_I + V_{II}, \tag{10.37}$$

$$V_{SL} = V_I - V_{III}, \tag{10.38}$$

and

$$V_{SF} = V_{II} + V_{III}, \tag{10.39}$$

These voltages can be again expressed in the form of Burger's equation (10.8), and because the scalar multiplication is distributive, the lead vectors of the leads SR, SL, and SF (which are created by summation of bipolar limb leads and therefore may be called "sigma leads" [40]) can be defined in terms of lead vectors for unipolar limb leads:

$$-\vec{c}_{SR} = 2\vec{c}_R - \vec{c}_L - \vec{c}_F = 3(\vec{c}_R - \vec{c}_T), \tag{10.40}$$

$$\vec{c}_{SL} = 2\vec{c}_L - \vec{c}_R - \vec{c}_F = 3(\vec{c}_L - \vec{c}_T), \tag{10.41}$$

and

$$\vec{c}_{SF} = 2\vec{c}_F - \vec{c}_L - \vec{c}_R = 3(\vec{c}_F - \vec{c}_T) \tag{10.42}$$

For this particular lead system, it follows from (10.40) to (10.42) that its lead vectors are collinear with the respective lead vectors of unipolar extremity leads and augmented leads; their magnitude is three times as large as the magnitude of lead vectors of unipolar extremity leads and twice as large as the magnitude of the lead vectors of augmented leads, as can be seen from the Burger triangle (Fig. 10.3).

10.3.9 Bibliographic Notes

The reader will find most of the references pertinent to this section in Sect. 10.1.3. The article by Schaefer and Haas in the Handbook of Physiology [22] reviews the properties of the electrocardiogram and gives an account of elementary electrocardiographic theory. Geselowitz and Schmitt [23], Plonsey [9], and Plonsey and Barr [10] provide a comprehensive review of modern electrocardiographic theory, including the derivation of formulae for lead vectors of composite leads. The text by Malmivuo and Plonsey [11] is richly illustrated and is accessible via Internet.

10.4 Image Surface

The Einthoven triangle and the Burger triangle provide heart-vector projection diagrams for interpreting voltages in the leads that use extremities for electrode sites. This geometric approach can be generalized so that it applies to any electrocardiographic lead. This section will introduce an experimental method of lead-vector construction applicable in an arbitrarily shaped linear volume conductor, and develop a notion of the three-dimensional image surface as a set of lead vectors for all possible body-surface leads. With no loss in generality, the method will be first illustrated in the two-dimensional case, where the image contour will assume the place of the image surface.

10.4.1 Image Surface of Bounded Two-Dimensional Conductor

Imagine a conductive sheet with a body-shaped boundary (Fig. 10.5) and at point Q, somewhere in the "heart region" on this sheet, a dipolar source with moment $\vec{p}$.

The potential difference between any point k on the boundary and an arbitrarily selected point of reference potential (e.g., point 0 on the boundary) is related to the dipole $\vec{p}$ through Burger's equation (10.7):

$$V_k = c_{kx}p_x + c_{ky}p_y \tag{10.43}$$

If the source dipole $\vec{p}$ becomes a unit dipole oriented along the x axis, then $p_x = 1$, $p_y = 0$, and (10.43) becomes

$$V_k = c_{kx} \tag{10.44}$$

Similarly, if $\vec{p}$ is oriented along the y axis, $V_k = c_{ky}$. Having determined c_{kx} and c_{ky} from voltage responses to unit dipoles oriented along the x and y axes, it is possible to construct the lead vector $\vec{c} = \vec{e}_x c_{kx} + \vec{e}_y c_{ky}$ (as defined by (10.8)). For this, a system of coordinates can be assumed where the potential at the reference point maps into the origin (Fig. 10.5). The same procedure can be repeated for as many points on the boundary as necessary; when the final points of the resulting lead vectors are connected, a contour is formed that will be termed the image contour (Fig. 10.5).

Several investigators who attempted to estimate the properties of electrocardiographic leads under realistic boundary conditions constructed two-dimensional scaled models of the torso from semiconducting (Teledeltos) paper. Grayzel and Lizzi determined image contours for both homogeneous and inhomogeneous two-dimensional torso models, and for several dipole-source locations. They cut torso forms from Teledeltos paper and simulated conductivity inhomogeneities caused by lungs and intracavitary blood masses by punching holes or painting silver disks to decrease or increase the conductivity. Unit dipoles along the x and y axes were approximated by a pair of closely spaced pinpoint probes, one of which fed current and the other of which withdrew current, and the voltage V_k at boundary points was measured with respect to the model's right "leg." Image contours obtained by means of a numerical replica of Grayzel and Lizzi's torso (Fig. 10.6) closely resemble those obtained using the Teledeltos paper model (Fig. 10.7). The computational method was analogous to that introduced by Barnard et al. [41] for the three-dimensional inhomogeneous torso; the differences were only in the formulae for the field potential of a dipole and a dipolar double layer (Sect. 10.2.1). The image contours are shown, with inscribed Burger triangle, for four selected locations of the dipole source and three different compositions of the torso. Even a casual examination of these

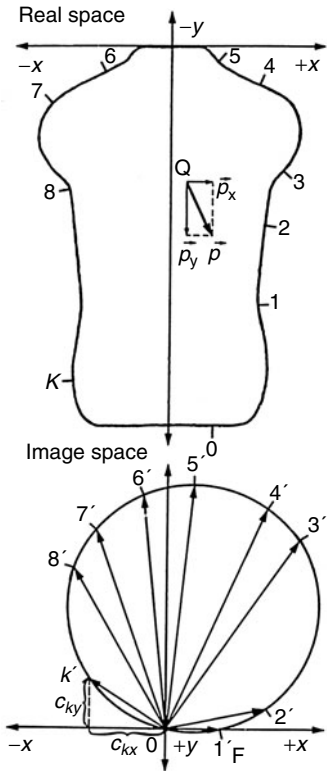

Figure 10.5

Two-dimensional image contour construction. For a conductive sheet with an arbitrary boundary and a dipolar source $\vec{p}$, the potential difference between any point k on the boundary and an arbitrarily selected point of reference potential (e.g. point 0 on the boundary) is related to the dipole $\vec{p}$ through Burger's equation $V_k = c_{kx}p_x + c_{ky}p_y$. If the unit dipole is oriented along the x axis, $V_k = c_{kx}$. Similarly, by setting $p_x = 0$ and $p_y = 1$, it is possible to obtain a value of c_{ky}. With both components determined, the lead vector can be constructed; for this a system of coordinates is assumed where potential at the reference point maps into the origin. This procedure can be repeated for as many points on the boundary as necessary; when the terminal points of their lead vectors are connected, a contour (termed the "image contour") is formed.

image contours reveals a striking effect of dipole-source location and boundaries. This two-dimensional modeling gives valuable insight into lead-vector determination in the arbitrarily shaped inhomogeneous conductor; however, it is not quite sufficient for assessing the effect of torso shape and inhomogeneities in the real, three-dimensional setting.

10.4.2 Image Surface of Bounded Volume Conductor

To extend the method of lead-vector determination into three dimensions, let us consider an experimental study performed by Frank, in which the torso-shaped electrolytic tank was used as a substitute for the human torso and the bipolar electrodes located in the model's heart region provided "dipolar" current sources. Frank's method of lead-vector determination was in principle identical to that already described for the two-dimensional case. Frank determined, for an array of pick-up electrodes on the surface of the torso model, the three components of the lead vector $\vec{c}$ by energizing, in turn, bipoles oriented along the x, y, and z axes and measuring for each bipole potential differences between torso-surface electrodes and a reference terminal.

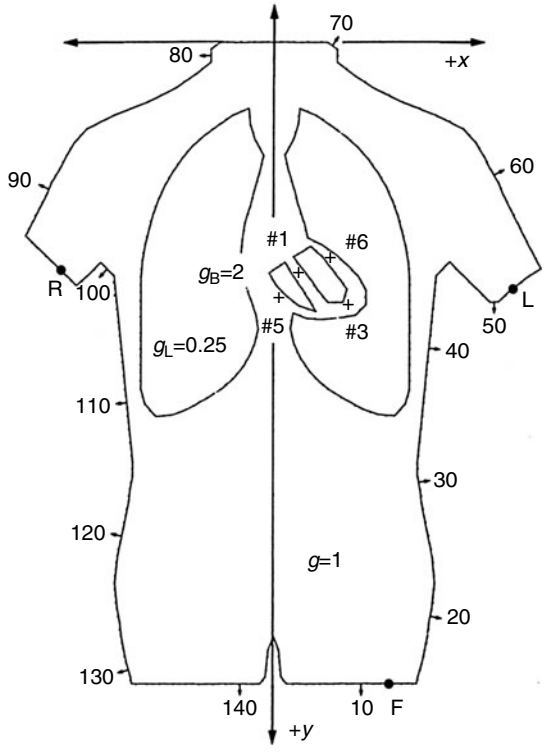

Figure 10.6

Two-dimensional numerical replica of an inhomogeneous model of a torso constructed from conductive Teledeltos paper by Grayzel and Lizzi [55]. The "lungs" were assigned conductivity $g_L = 0.25$, "blood masses" had conductivity $g_B = 2.0$ (in accordance with Grayzel and Lizzi), and the rest of "body tissues" had conductivity $g = 1.0$. Unit dipoles along the *x* and *y* axes were approximated by bipoles. These sources were placed at dipole-source locations marked by numbers.

By using this experimental technique (or its numerical alternative), the Burger triangle diagram can be extended as follows. Consider the three-dimensional torso model with three electrodes R, L, and F attached to it at the two "arms" and the left "leg"; in addition, let there be an electrode B attached, for instance, on the back. Thus, beside Einthoven's bipolar limb leads I, II, and III, three new leads can be formed, each obtained by pairing one limb electrode with B; these leads will each be characterized by a lead vector originating at some common image point B′ (determined by Frank's method) and terminating on one of the vertices of the Burger triangle (Fig. 10.8). The six lead vectors connecting image points R′, L′, F′, and B′ will form a tetrahedron the four faces of which will be lead triangles; it is called the Wilson tetrahedron (Sect. 10.4.4). In the Wilson tetrahedron as in the Burger triangle, the potential difference in a lead is determined by multiplying the length of the appropriate lead vector, which forms one of the six connecting sides, by the projection of the dipole-source vector on that side.

The Wilson tetrahedron is a three-dimensional counterpart of the limb-lead triangle. Using the tetrahedron, from any three independent lead voltages that exist between four electrode sites, it is possible to determine all the three components of an arbitrary spatial dipole source (the Einthoven triangle and the Burger triangle, by contrast, permit determination of only two components of a planar dipole source, since only two independent voltages are provided by the set of three electrodes).

Note that in the Wilson tetrahedron, the real space, in which the relationship between points R, L, F, and B is given by vectors of directed distance $\vec{r}$, is replaced by the space in which the relationship between image points R′, L′, F′, and B′ (that correspond to real points R, L, F and B) is given by lead vectors $\vec{c}$.

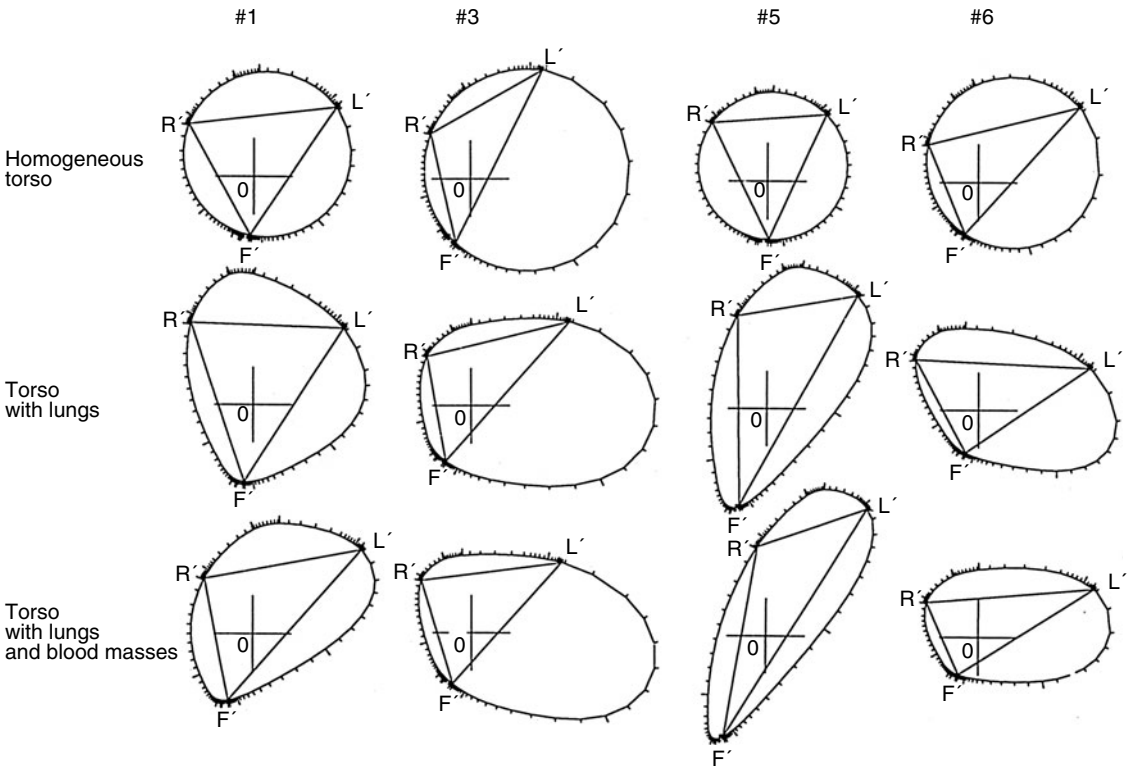

Figure 10.7

Image contours of the two-dimensional torso with inscribed Burger triangle for the torso model shown in Fig. 10.6, for four different locations of the source dipole (*columns*) and three different configurations (*rows*): the homogeneous model (*top*); the inhomogeneous model with lungs (*middle*) and the inhomogeneous model with lungs and intracavitary blood masses (*bottom*). Boundary points are marked in accordance with Fig. 10.6.

It is possible to continue this generalization of Burger triangle by considering the fifth, sixth, . . . , *n*th electrode sites on the surface of Frank's torso model (these sites should preferably form a regular grid that completely covers the torso surface) and determining the lead vector for each. The final points of these lead vectors (image points) define the image surface in the image space (Fig. 10.8). For every point P in the real space there is a point P′ in the image space whose vector from the origin (the origin of the image space corresponds to the reference terminal in the real space) is a lead vector of an electrocardiographic lead formed by an electrode at P and the reference terminal. The same image space is applicable to any dipole at the same dipole-source location Q for which this image space was derived; this follows from the principle of superposition. The lead vector associated with any pair of points on the body may be found by connecting corresponding points on the image surface; this is how the Burger triangle and the Wilson tetrahedron are constructed (Fig. 10.8). Image points corresponding to the lead terminals with passive networks are all enclosed by the image surface; conversely, image points of the lead terminals with active networks and image points of measurement sites that are inside the torso are all outside the image surface.

Numerical models of the human torso currently provide the most convenient method for determining image surfaces; such models can be three-dimensional, realistically shaped, and inhomogeneous. Consider the features of the computed image surface for the dipole-source location Q at the centroid of the heart region; the image surface is displayed in projections into three principal planes in Fig. 10.9. This image surface can be compared with Frank's image surface which was drawn from data obtained in the electrolytic tank. Care was taken to make the dipole-source location Q similar to that of Frank; also, the coordinate system and labeling of grid- points are compatible.

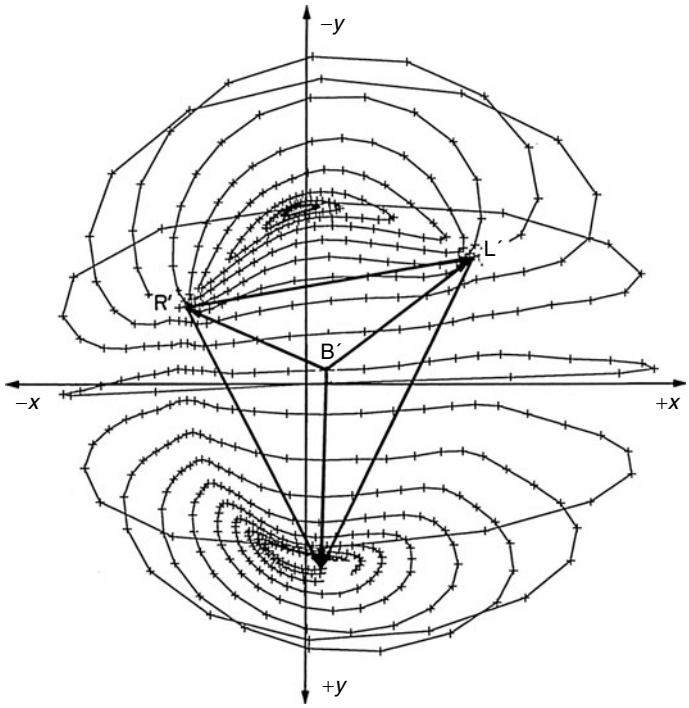

Figure 10.8

Wilson tetrahedron: frontal plane projection. The figure illustrates the construction of an image surface, where R′, L′, F′ and B′ are image points corresponding to R, L, F, B, respectively. In addition to limb leads three new leads can be obtained by pairing each of the three limb electrodes R, L and F with a fourth electrode B, attached, for instance, on the back. (B is placed in the left midscapular region [52].) These leads are each characterized by a lead vector originating at B′ and terminating on one of the vertices of the Burger triangle R′, L′, F′. The six lead vectors connecting points R′, L′, F′ and B′ form a tetrahedron in which, as in the Burger triangle, the potential difference in a lead is determined by multiplying the length of the appropriate lead vector by the projection of the source-dipole vector on that lead vector. If the reference point is fixed while point B is allowed to sweep over the entire surface of the torso, then the final points of all corresponding lead vectors will sweep out a surface in the three-dimensional image space.

Protruding parts of the torso, such as the neck and shoulders, map into areas the relative size of which is diminished on the image surface because the potential gradient in these remote areas is small. In short, the protruding parts of the body "shrink" in the image space. This justifies the use of the human torso (i.e., a body without extremities and head) as a volume-conductor model of the human body. Conversely, the image surface bulges where the torso-surface points P are proximal to the dipole-source location Q. For the source location Q used to compute the image surface in Fig. 10.9, any area on the left anterior chest maps into an area the relative size of which is increased on the image surface. In short, the regions proximal to the source location are "blown up" in the image space. The parallels on the image surface (corresponding to the transverse sections of the torso surface) do not lie in parallel planes; they form spatial loops. Similarly, meridians on the image surface (corresponding to the sections of the torso surface with equiangular planes through the cranio-caudal axis of the torso) do not lie in planes; the spacing between them is magnified for points proximal to the source location Q and diminished for points remote from it.

The image surfaces for the same outer surface of the torso and the same dipole-source location, but with the torso's internal composition altered by conductivity inhomogeneities, change their shape as is evident in Fig. 10.10, which depicts an image surface of the homogeneous torso side-by-side with image surfaces of the torso with inhomogeneities.

For this particular (septal) dipole-source location, the lungs increase the y and z components of many lead vectors and attenuate their x component, while intracavitary blood masses tend to counteract the effect of the lungs. Changes of

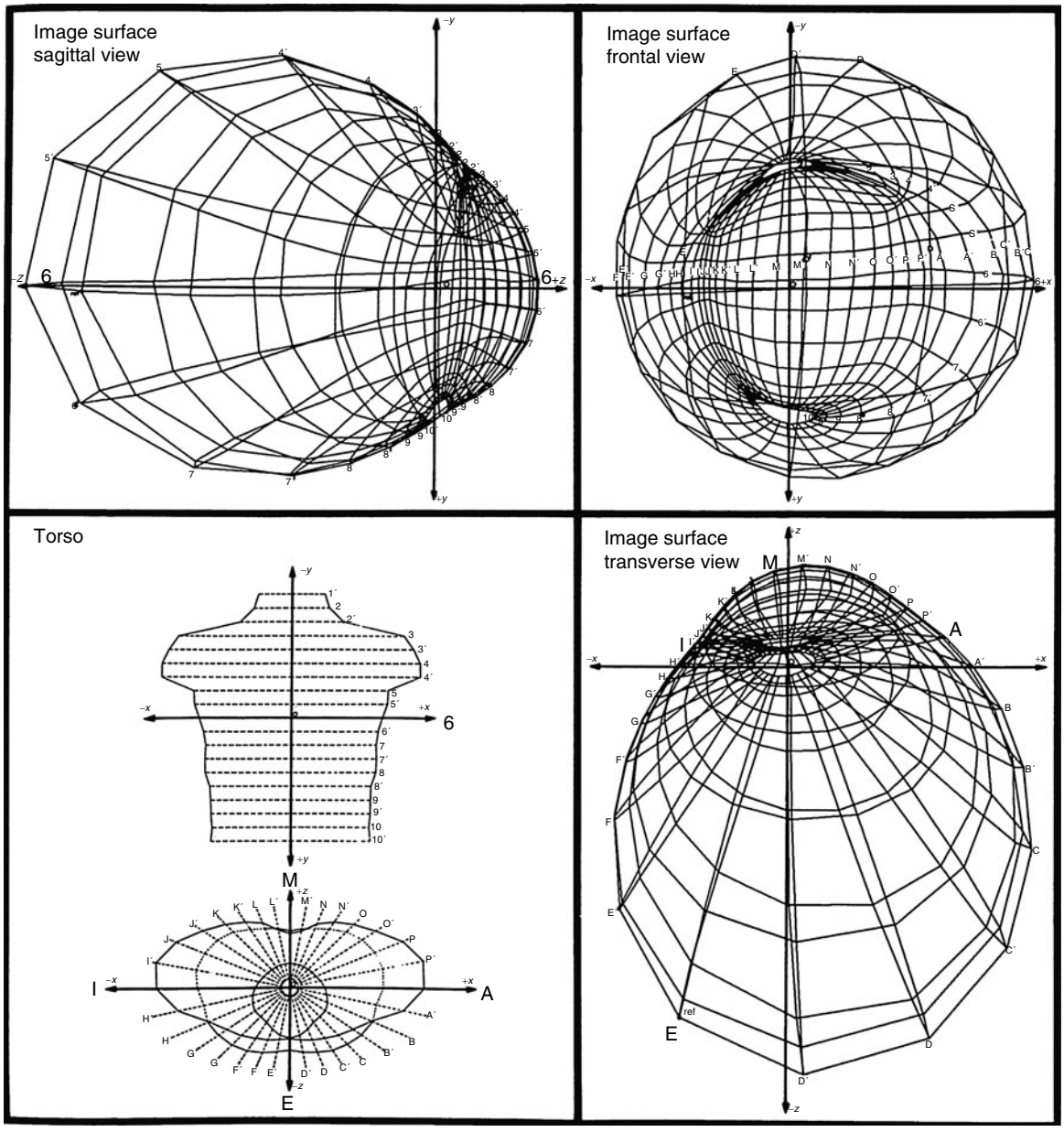

Figure 10.9

Image surface of a homogeneous torso with a coordinate system and a grid. The grid is established by body-surface points at the intersection between transverse planes and equiangular half-planes. The *x* axis runs from the right to left of the torso, the *y* axis from head to foot, and the *z* axis from front to back. The *xy* plane is the frontal plane, the *yz* plane is the sagittal plane and the *xz* plane is the transverse plane. The image surface was computed for the dipole-source location at the centroid of the heart region (level 6, 2.5 cm from the sagittal plane and −4 cm from the frontal plane). Computed lead vectors for all grid points are displayed as three projections of the image surface. Image points corresponding to levels 2–10 on the torso surface form parallels; image points corresponding to torso-surface points in the angular half-planes form meridians. (Horáček and Ritsema van Eck [72]. © Presses Académiques Européennes, Brussels. Reproduced with permission.)

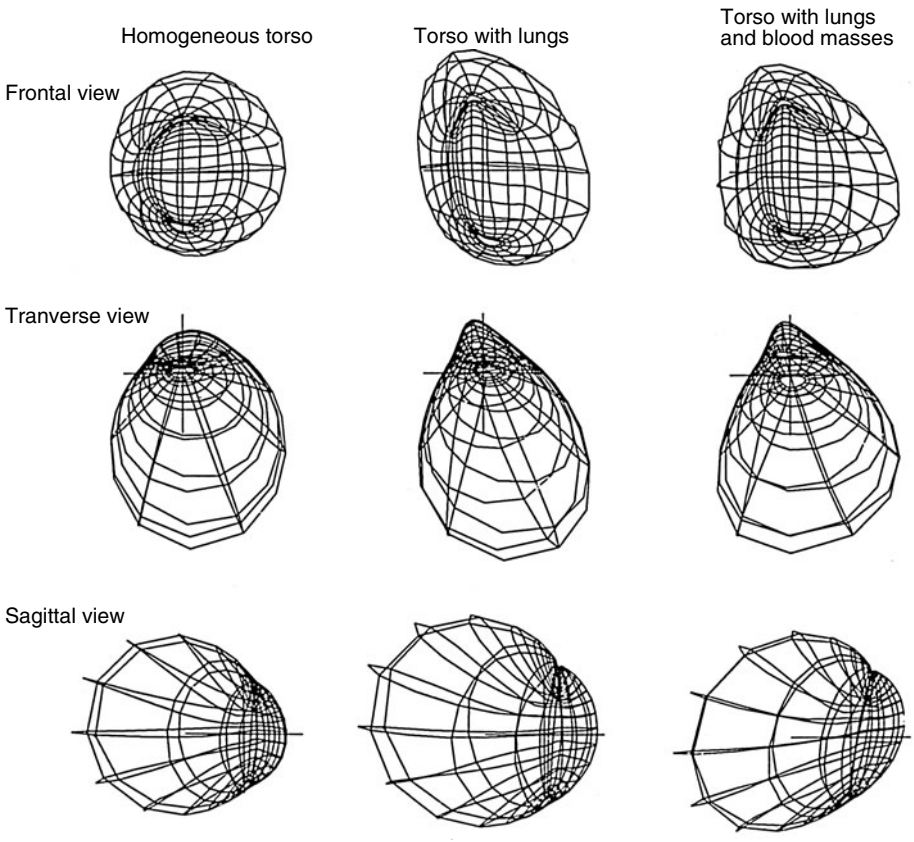

Figure 10.10

The effect of torso inhomogeneities is seen in three image surfaces computed for the dipole-source location at the centroid of the heart region. The projections of the image surface in the first column correspond to the homogeneous torso (conductivity $g = 1$; this image surface is identical to the one in Fig. 10.9 except only 16 of 32 meridians are plotted); the second column shows an image surface of the torso with lungs of low conductivity ($g_L = 0.25$); the third column shows an image surface of the torso with lungs and highly conductive intracavitary blood masses ($g_B = 3.$). (Horáček [67]. © Karger, Basel. Reproduced with permission.)

shape in the image surface owing to intracavitary blood masses can be attributed to the Brody effect (Sect. 6.4.2.2): the x component of an arbitrarily oriented dipole is enhanced, because it is approximately normal to the surfaces of both intraventricular blood masses, while the y and z components are attenuated because they are approximately tangential to these surfaces. The effect of the lungs on lead vectors for the same dipole-source location can be described as a "channelling" effect: the z and y components of lead vectors are increased because the dipoles oriented in the z and y directions are approximately tangential to the surface of the poorly conducting lungs. Shifting the dipole-source location considerably changes the resultant image surfaces.

10.4.3 Image-Surface Definitions

The relationship between an arbitrary dipole source at a fixed location Q and electric potentials on the surface of the torso the shape and composition of which are specified can be displayed by means of the image surface; this geometric concept was introduced by Burger and van Milaan.

The concept of the image space and of the image surface can be formalized as follows. Consider a certain bounded linear volume conductor in which one internal point, to be called Q, is designated as a dipole-source location; let the field point P (at a finite distance from Q) be either inside the volume conductor, or on its outer boundary or at the node of a resistor network that extends beyond this boundary. For this volume conductor with the designated Q there is a corresponding image space with the following properties.

1. Every field point P can be mapped into the image space so that there is a unique corresponding image point P′; this mapping defines the electric potential produced at P by a fixed-location dipole of arbitrary moment embedded in the volume conductor.
2. The origin of the image space corresponds to the arbitrary reference point; with a different choice of reference, all points of the image space undergo translation, but their mutual relationship remains unaffected. The ideal reference is a zero potential at a terminal infinitely remote from Q (or at source dipole's midpoint).
3. In the image space, the vector pointing from one image point B′ to another image point A′ is a lead vector of the lead the positive terminal of which is A and negative (reference) terminal is B. Thus, the Burger triangle, for instance, is constructed in the image space by connecting points R′, L′, and F′.
4. The set of points on the outer boundary of the volume conductor maps into the image surface.
5. The set of points that is inside the volume conductor maps into image points that are outside the image surface.
6. The nodes of the resistor network connected at discrete points to the outer surface of the volume-conductor map into image points inside the image surface; the latter image points are defined by their lead vectors as in (10.28).

The properties of any conceivable lead can be assessed from the image surface. It should be reiterated, however, that each image surface pertains only to one particular torso and one particular dipole-source location.

10.4.4 Bibliographic Notes

Analytical calculations have been performed with various mathematical models. Wilson and Bayley [42], Frank [43], and Geselowitz and Ishiwatari [44] studied the effect of the eccentric location of the heart in the torso by analyzing the case of a dipole in a sphere. Okada [45, 46] and more recently Cornelis and Nyssen [47] have extended this analysis to a cylinder. Plonsey [48] used the method of images to show the effect of the planar insulating boundary near sources. Brody [49] studied the effect of highly conductive intraventricular blood masses and concluded that blood masses emphasize the radial component of source dipoles in the heart (perpendicular to the ventricular wall) and attenuate the tangential component. Mathematical studies of Bayley et al. [50] on the field of a double layer in a system of nested spheres (later redone by Rudy and Plonsey [51]) have yielded the same results.

Wilson et al. [52] suggested substituting a regular tetrahedron for the Einthoven triangle; Burger and van Milaan [15] thought of this tetrahedron as composed of lead vectors obtained in a realistic model of the torso.

An experimental approach to the investigation of the effect of the body shape and conductivity inhomogeneities on lead vectors was employed in numerous studies. Two-dimensional models included fluid mappers used by McFee et al. [53], and Teledeltos mannequins used by Brody and Romans [54], Grayzel and Lizzi [55], and others. Electrolytic-tank models were used by Burger and van Milaan [13], Frank [56], Schmitt [19], Nagata [57], Rush [58] (the latter article contains a review of experimental studies) and others. The idea of an image surface was conceived by Burger and van Milaan [13]; the first experimental determination of the image surface was performed by Frank [56]. The concept of an image surface was used to design the well-known Frank's lead system [59].

Numerical models of the torso were pioneered by Gelernter and Swihart [60], Barr et al. [61], and Barnard et al. [41]. The mathematical methodology of dealing with general inhomogeneous volume conductors was outlined by Geselowitz [62]. An article by Swihart [63] provides an overview of numerical methods for solving the forward problem of electrocardiography (Chap. 8). Pilkington et al. [64] compared the merits of the integral equation approach and the finite-element approach to the solution of the volume-conductor problem. Many important papers on biophysical basis of electrocardiography were assembled in one volume by Pilkington and Plonsey [65]. Horáček [66, 67] used a numerical model

of a three-dimensional, realistically shaped and inhomogeneous human torso to compute image surfaces for various dipole-source locations, and performed as well the analogous computations in a two-dimensional model (Figs. 10.6 and 10.7).

10.5 Lead Field

The simplicity of Burger's lead-vector concept fades when allowance is made for dipolar sources that are distributed over the entire heart region. Clearly, the size of the heart region relative to its distance from most ECG recording sites on the torso is not negligible, and hence the typical lead vector $\vec{L}$ varies when the dipole-source location shifts; for each given lead, there is a family of lead vectors that takes on a complete set of values $\vec{L}$ for various dipole-source locations. Each such family should be viewed as a vector field $\vec{L}(x,y,z)$, that is, a vector quantity the value of which depends on the coordinates. With this concept in mind, Burger's equation (10.8) can be interpreted more generally; it can be rewritten as

$$V = \vec{L}(x,y,z) \cdot \vec{p} \tag{10.45}$$

allowing a given local current-dipole source to act anywhere in the heart region. According to this interpretation of Burger's equation, the voltage that a local current dipole located at (x_0, y_0, z_0) produces in a lead is the scalar product of the moment of the dipole $\vec{p}$ and the vector field $\vec{L}$ evaluated at (x_0, y_0, z_0). Using the superposition principle, the total contribution of distributed cardiac sources to the lead voltage can be defined as

$$V = \int \vec{L}(x,y,z) \cdot \vec{J}^{\mathrm{i}}(x,y,z)\ \mathrm{d}v, \tag{10.46}$$

where $\vec{J}^{\mathrm{i}}(x,y,z)$ is a function defining a distributed impressed current density in the heart region in terms of the current dipole moment per unit volume; the units of $\vec{J}^{\mathrm{i}}$ are $\mathrm{Am/m^3}$, $\vec{L}$ is in $\Omega\,\mathrm{m}^{-1}$, and hence, the units of the volume integral are volts. Equation (10.46) is the most general form of Burger's definition of the relationship between cardiac electric sources and the voltage in an electrocardiographic lead.

10.5.1 Lead-Field Derivation

McFee and Johnston provided a physical basis for this operational definition of the lead vector by invoking Helmholtz's reciprocity theorem as follows. Consider a torso-shaped linear volume conductor (Fig. 10.11) with two pairs of electrode sites. The first pair, A and B, which can be located anywhere except in the heart region, can be thought of as the positive terminal (A) and the negative terminal (B) of an electrocardiographic lead. The remaining pair, C and D, separated by a small vector distance $\vec{l}$ directed from D to C, can be arbitrarily located within the heart region; this pair corresponds to the site of the local cardiac electric source.

The reciprocity theorem asserts that the potential difference V_{AB} produced between open-circuited terminals A and B by a current I injected at point C and removed at point D (the condition of normal energization depicted in Fig. 10.11a) must equal the potential difference V'_{CD} that would be found between points C and D if the same current were injected at point A and removed at point B (the condition of reciprocal energization illustrated in Fig. 10.11b); this reciprocal current is designated I'. In this case $I' = I$, but in general, it does not have to be so, and the reciprocity theorem is formulated as follows: $V_{\mathrm{AB}}/I = V'_{\mathrm{CD}}/I'$.

Consider more closely the conditions under reciprocal energization. A source of current I' placed between terminals A and B gives rise to an electric field in the volume conductor that can be characterized at every point by a vector of electric field intensity $\vec{E}'$. By definition, the potential difference between points C and D is given by a line integral along an arbitrary path from D to C (10.5):

$$V'_{\mathrm{CD}} = -\int_D^C \vec{E}' \cdot \mathrm{d}\vec{l} \tag{10.47}$$

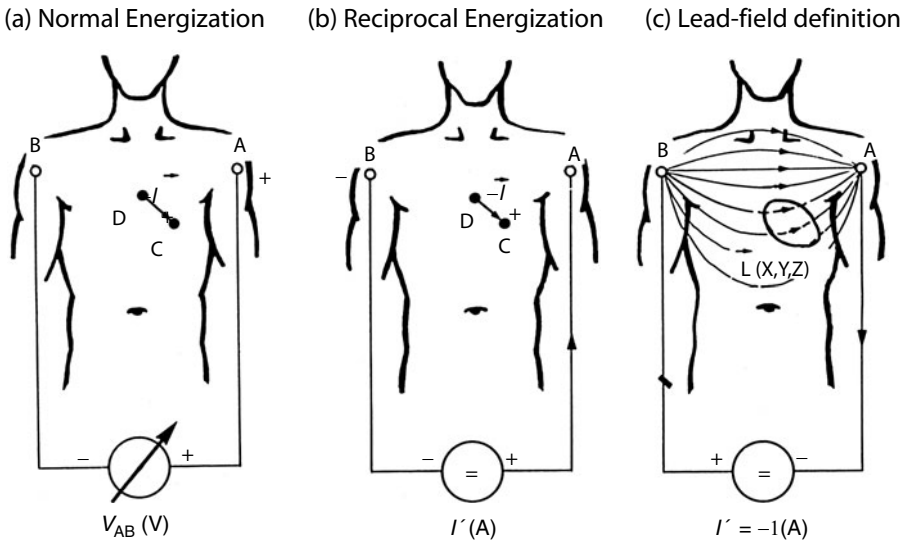

Figure 10.11

Lead-field derivation from the reciprocity theorem. The potential difference V_{AB}, produced between open-circuited terminals of an electrocardiographic lead by a current bipole $I\vec{l}$ in the heart region (part (a)), equals the potential difference V'_{CD} produced between the source and sink of the bipole C and D by a reciprocal current $I' = I$ injected into the lead (part (b)). The electric field intensity in the heart region during the lead's reciproca1 energization defines the lead field (part (c)).

For the small distance between C and D, the field can be considered constant so that the integral becomes simply

$$V'_{CD} = -\vec{E}' \cdot \vec{l}, \tag{10.48}$$

where $\vec{l}$ is the directed distance from D to C.

If the electric field intensity is normalized to a unit reciprocal current the scalar value I' of which is equal to I, and V'_{CD} is replaced with V_{AB} (applying the reciprocity theorem), then

$$V_{AB} = -\left(\frac{\vec{E}'}{I'}\right) \cdot (I\vec{l}) \tag{10.49}$$

This is the desired result; a comparison with the generalized Burger's equation (10.45) clearly shows that the first factor corresponds to the lead vector (measured in $\Omega\,m^{-1}$) and the second factor is the current dipole moment (units A m). The generalized lead vector can be designated as the lead field

$$\vec{L}(x,y,z) = \frac{\vec{E}'}{-I'} \tag{10.50}$$

Note that the lead field has units $\Omega\,m^{-1}$; this is a revision of the original definition by McFee and Johnston.

10.5.2 Lead-Field Definition

At any point in the heart region the lead field of a given electrocardiographic lead is defined as a vector field of electric intensity produced by a source of unit current connected to the lead's terminals in the reverse manner (i.e., with current being injected at the negative terminal and removed at the positive terminal as shown in Fig. 10.11c). Since the electric

Table 10.1

Mean lead field with standard deviations as determined at 1,239 ventricular sites for selected electrocardiographic leads

Lead	$\bar{c}_x$	$\bar{c}_y$	$\bar{c}_z$	$\lvert\bar{c}\rvert$
Homogeneous torso				
I	0.95±0.16	−0.27±0.16	0.07±0.04	**1.00**±0.16
II	0.58±0.10	1.16±0.11	−0.04±0.05	1.31±0.11
III	−0.37±0.16	1.44±0.21	−0.11±0.05	1.50±0.20
aVR	−0.76±0.10	−0.45±0.09	−0.01±0.04	0.89±0.10
aVL	0.66±0.15	−0.85±0.17	0.09±0.04	1.09±0.17
aVF	0.11±0.11	1.30±0.15	−0.08±0.05	1.31±0.14
CT	0.07±0.03	−0.03±0.03	0.21±0.06	0.23±0.05
V_1	−1.07±0.59	−0.22±0.52	−1.21±0.71	1.69±0.95
V_2	−0.13±0.72	−0.55±0.91	−2.26±1.26	2.50±1.44
V_3	0.88±0.88	−0.26±0.79	−2.21±1.15	2.58±1.36
V_4	1.37±0.70	0.07±0.47	−1.44±0.75	2.08±0.95
V_5	1.30±0.50	0.07±0.28	−0.46±0.24	1.41±0.53
V_6	0.85±0.23	0.03±0.16	0.13±0.11	0.88±0.25
V_7	0.56±0.12	0.03±0.12	0.29±0.14	0.64±0.17
V_8	0.33±0.10	0.05±0.11	0.40±0.18	0.54±0.19
V_9	0.08±0.08	0.06±0.11	0.45±0.22	0.48±0.22
V_3 R	−0.98±0.39	0.05±0.20	−0.66±0.26	1.20±0.45
V_4 R	−0.84±0.21	0.09±0.12	−0.36±0.09	0.93±0.22
V_5 R	−0.68±0.10	0.07±0.08	−0.12±0.02	0.70±0.10
X	1.18±0.11	−0.17±0.16	−0.15±0.05	1.21±0.12
Y	0.12±0.04	1.11±0.06	0.07±0.06	1.12±0.05
Z	0.12±0.11	0.17±0.35	1.30±0.34	1.35±0.39
Torso with lungs				
I	0.87±0.10	−0.14±0.11	−0.03±0.04	0.89±0.10
II	0.70±0.08	1.40±0.09	−0.02±0.11	1.57±0.10
III	−0.17±0.10	1.54±0.14	0.01±0.10	1.56±0.14
aVR	−0.79±0.07	−0.63±0.06	0.02±0.07	1.01±0.08
aVL	0.52±0.09	−0.84±0.12	−0.02±0.05	1.00±0.11
aVF	0.26±0.08	1.47±0.11	0.00±0.10	1.50±0.11
WCT	0.07±0.03	−0.01±0.04	0.21±0.07	0.23±0.06
V_1	−1.03±0.64	−0.40±0.52	−1.32±0.81	1.80±1.04
V_2	−0.09±0.73	−0.75±0.97	−2.37±1.31	2.67±1.50
V_3	0.94±0.92	−0.32±0.88	−2.35±1.25	2.75±1.47
V_4	1.45±0.72	0.15±0.54	−1.54±0.79	2.23±1.00
V_5	1.32±0.53	0.21±0.30	−0.56±0.26	1.49±0.56
V_6	0.83±0.24	0.16±0.16	0.05±0.10	0.86±0.24
V_7	0.51±0.12	0.14±0.11	0.23±0.10	0.59±0.14
V_8	0.26±0.05	0.13±0.10	0.36±0.13	0.47±0.13
V_9	−0.01±0.08	0.10±0.09	0.47±0.20	0.49±0.20
V_3R	−0.93±0.44	−0.04±0.21	−0.73±0.34	1.22±0.52
V_4R	−0.79±0.24	0.07±0.13	−0.39±0.14	0.90±0.26
V_5R	−0.64±0.10	0.06±0.08	−0.11±0.04	0.66±0.10

Table 10.1 (Continued)

Lead	$\bar{c}_x$	$\bar{c}_y$	$\bar{c}_z$	$\lvert\bar{\mathbf{c}}\rvert$
X	1.12±0.13	−0.07±0.15	−0.26±0.29	1.16±0.15
Y	0.27±0.07	1.34±0.12	0.12±0.09	1.38±0.12
Z	0.03±0.17	0.22±0.38	1.42±0.40	1.48±0.44
Torso with lungs and blood masses				
I	0.80±0.16	−0.12±0.11	0.00±0.12	0.82±0.18
II	0.66±0.15	1.30±0.28	0.04±0.21	1.48±0.28
III	−0.14±0.20	1.42±0.29	0.04±0.21	1.46±0.30
aVR	−0.73±0.12	−0.59±0.15	−0.02±0.13	0.96±0.13
aVL	0.47±0.16	−0.77±0.18	−0.02±0.14	0.92±0.19
aVF	0.26±0.15	1.36±0.28	0.04±0.20	1.41±0.29
WCT	0.07±0.04	0.00±0.05	0.21±0.08	0.23±0.07
V_1	−0.98±0.60	−0.44±0.49	−1.33±0.98	1.80±1.10
V_2	−0.17±0.64	−0.76±0.86	−2.30±1.53	2.61±1.62
V_3	0.77±0.87	−0.35±0.73	−2.22±1.34	2.54±1.50
V_4	1.29±0.81	0.12±0.43	−1.43±0.83	2.02±1.09
V_5	1.21±0.63	0.20±0.25	−0.50±0.29	1.36±0.66
V_6	0.77±0.30	0.16±0.13	0.08±0.13	0.80±0.30
V_7	0.48±0.15	0.14±0.10	0.24±0.13	0.57±0.19
V_8	0.25±0.07	0.13±0.09	0.36±0.15	0.47±0.16
V_9	0.00±0.08	0.10±0.10	0.46±0.22	0.49±0.22
V_3 R	−0.87±0.40	−0.09±0.26	−0.75±0.44	1.21±0.54
V_4 R	−0.73±0.21	0.02±0.18	−0.40±0.21	0.87±0.25
V_5 R	−0.58±0.09	0.03±0.13	−0.13±0.09	0.62±0.10
X	1.02±0.23	−0.05±0.12	−0.21±0.17	1.06±0.25
Y	0.27±0.12	1.23±0.24	0.15±0.20	1.29±0.25
Z	0.06±0.19	0.24±0.34	1.38±0.55	1.45±0.58

Values of the lead-field components $\bar{c}_x$, $\bar{c}_y$, and $\bar{c}_z$ are in relative units, scaled by $|\bar{\mathbf{c}}_i|$; absolute units can be restored [68]

intensity vector of the reciprocal field $\vec{E}'$ is by definition the negative of the gradient of the scalar potential, the generalized lead vector can be expressed as

$$\vec{L}(x,y,z) = \frac{\nabla V'}{I'}, \tag{10.51}$$

and an alternative definition of the lead field can be put forward as follows. At any point in the heart region the lead field of a given electrocardiographic lead is defined as a gradient of the potential distribution V' produced by the source of unit current connected to the terminals of the lead. (Note that the reciprocal current is injected "properly" at the positive terminal and removed at the negative terminal.)

The lead field is an electric field per unit current, or impedance per unit distance ($\Omega\,\mathrm{m}^{-1}$), and hence, Schmitt introduced this concept into electrocardiography as a vectorial transfer impedance $\vec{Z} = \nabla Z$

$$\vec{L}(x,y,z) = \vec{Z}(x,y,z) = \nabla Z \tag{10.52}$$

Any lead can be described in terms of its lead field or transfer impedance. The lead-field concept can be applied even when the lead terminals are connected to a number of electrodes via a network of resistors. This facilitates synthesis of leads with desired properties; for example, ideal heart-vector leads have uniform lead fields, while lead fields of ideal unipolar leads (with the reference electrode infinitely remote) radiate outwards in straight lines from the exploring electrode with an intensity diminishing inversely with distance squared.

10.5.3 Computed Lead-Field Values

Recently, Horáček et al. [68] used a computer model of a realistic three-dimensional human torso containing lungs and intracavitary blood masses of different conductivities to calculate the lead field for some commonly used electrocardiographic leads. Their torso model is a modification of one described previously [66], with the outer surface modified to simplify the identification of commonly used ECG electrode sites on the model's surface. Three orthogonal components of the lead field were determined at 1,239 ventricular sites for 352 unipolar body-surface leads in the homogeneous torso, in the torso with lungs, and in the torso with lungs and intracavitary blood masses. Mean lead-field values with standard deviations were calculated for commonly used ECG leads from these 1,239 vectors for all three configuration of the torso (Table 10.1). The components of the lead field were calculated in absolute units for unit-dipole sources in the torso of unit conductivity and then normalized by the length of lead vector for lead I and tabulated in relative units. The lead field in absolute units of $\Omega\,m^{-1}$ for unit current dipoles in absolute units of A×m can be restored by multiplying the values listed in Table 10.1 by an appropriate factor [68]. The mean lead-field vectors for leads I, II, and III form a characteristic Burger's triangle, with the length of the vectors for leads II and III exceeding that for lead I. The Wilson central terminal has the shortest length of the mean lead-field vector, with only the z-component having a value that is not negligible. The unipolar precordial leads V_2–V_4 have the largest magnitude of the mean lead field. The lead field for Frank's orthogonal leads X, Y, and Z shows excellent orthogonality and reasonably uniform sensitivity for all three leads. These findings are similar in all three configurations of the torso model; however, closer examination reveals that both lungs and intracavitary blood masses exert a noticeable effect on the lead field in specific leads.

10.5.4 Bibliographic Notes

In the early 1950s, several investigators perceived lead properties operationally. Lepeschkin [69] characterized leads in terms of "tubes of influence" and Brody and Romans [54] performed model experiments aimed at finding lead properties through reciprocal energization; a hydrodynamic analogue of reciprocal energization was constructed by McFee et al. [53]. Schmitt [19] introduced the transfer impedance as a vector field characterizing lead properties and McFee and Johnston [16] were the proponents of the lead-field concept based on the reciprocity theorem. Interestingly, the reciprocity theorem, which became a cornerstone of lead-field theory, can be applied to electrocardiography virtually without changing Helmholtz's original wording which was as follows. (The quote is from the article by Helmholtz published in 1853 [32]; translation from German by Frank N. Wilson [16].)

> Every single element of an electromotive surface will produce a flow of the same quantity of electricity through the galvanometer as would flow through that element itself if its electromotive force were impressed on the galvanometer wire. If one adds the effects of all the electromotive surface elements, the effects of each of which are found in the manner described, he will have the value of the total current through the galvanometer.

In present-day electrocardiography, galvanometers have been replaced by amplifiers that measure open-circuit voltage rather than short-circuit current. Further, cardiac electric sources are, to the best of our knowledge, near-ideal current generators. Under such circumstances, the principle of superposition can be applied to sum both input currents and output voltages, and the reciprocity theorem can be restated for double-layer current sources and the lead voltage.

Applications of the lead field to electrocardiography have been discussed in articles by Plonsey [70], Schmitt [71], and others. See also texts by Plonsey [9], Plonsey and Barr [10], and Malmivuo and Plonsey [11].

References

1. Einthoven, W., The different forms of the human electrocardiogram and their signification. *Lancet*, 1912;**1**: 853–861. (Translation: *Am. Heart J.*, 1950;**40**: 195–211).
2. Einthoven, W., G. Fahr, and A. deWaart, Ueber die Richtung und manifeste Groesse der Potentialschwankungen im menschlichen Herzen und ueber den Einfluss der Herzlage auf die Form

des Electrokardiogramms. *Pfluegers Arch. ges. Physiol.*, 1913;**150**: 275–315. (Translation: *Am. Heart J.*, 1950;**40**: 163–211).
3. Wilson, F.N., F.D. Johnston, A.G. Macleod, and P.S. Barker, Electrocardiograms that represent the potential variations of a single electrode. *Am. Heart J.*, 1933;**9**: 447–471.
4. Goldberger E., A simple, indifferent, electrocardiographic electrode of zero potential and a technique of obtaining augmented, unipolar, extremity leads. *Am. Heart J.*, 1942;**23**: 483–492.
5. Wolferth Ch.C. and F.C. Wood, The electrocardiographic diagnosis of coronary occlusion by the use of chest leads. *Am. J. Med. Sci.*, 1932;**183**: 30–35.
6. Wilson F.N., F.D. Johnston, F.F. Rosenbaum, H. Erlanger, Ch.E. Kossmann, H. Hecht, N. Cotrim, R. Menezes de Oliveira, R. Scarsi, and P.S. Barker, The precordial electrocardiogram. *Am. Heart J.*, 1944;**27**: 19–85.
7. Wilson, F.N., F.D. Johnston, F.F. Rosenbaum, and P.S. Barker, On Einthoven's triangle, the theory of unipolar electrocardiographic leads, and the interpretation of the precordial electrocardiogram. *Am. Heart J.*, 1946;**32**: 277–310.
8. Wilson, F.N., A.G. Macleod, and P.S. Barker, *The distribution of the currents of action and of injury displayed by heart muscle and other excitable tissues*. Univ. Mich. Press, Ann Arbor, Mich., 1933.
9. Plonsey R., *Bioelectric Phenomena*. McGraw-Hill, New York, 1969.
10. R. Plonsey and R.C. Barr, *Bioelectricity: A Quantitative Approach*. Plenum Press, New York, 1988.
11. J. Malmivuo and R. Plonsey, *Bioelectromagnetism: Principles and Applications of Bioelectric and Biomagnetic Fields*. Oxford University Press, New York, 1995. see http://butler.cc.tut.fi/ malmivuo/bem/bembook/15/15.htm.
12. R.P. Holland and H. Brooks, TQ-ST segment mapping: Critical review and analysis of current concepts. *Am. J. Cardiol.*, 1977;**40**: 110–129.
13. Burger H.C. and J.B. van Milaan, Heart-vector and leads. Part I. *Br. Heart J.*, 1946;**8**: 157–161.
14. Burger H.C. and J.B. van Milaan, Heart-vector and leads. Part II. *Br. Heart J.*, 1947;**9**: 154.
15. Burger H.C. and J.B. van Milaan, Heart-vector and leads: Part III, Geometrical interpretation. *Br. Heart J.*, 1948;**10**: 229.
16. McFee R. and F.D. Johnstone, Electrocardiographic leads: I. Introduction. *Circulation*, 1953;**8**: 554–568.
17. McFee R. and F.D. Johnston, Electrocardiographic leads. II. Analysis. *Circulation*, 1954;**9**: 255–266.
18. McFee R. and F.D. Johnston, Electrocardiographic leads. III. Synthesis. *Circulation*, 1954;**9**: 868–880.
19. Schmitt O.H., Lead vectors and transfer impedance. *Ann. N.Y. Acad. Sci.*, 1957;**65**: 1092–1109.
20. Burger H.C., *Heart and Vector: Physical Basis of Electrocardiography*. Philips Technical Library, Eindhoven, The Netherlands, 1968.
21. Frank E., General theory of heart-vector projection. *Circ. Res.*, 1954;**2**: 258–270.
22. Schaefer H. and H.G. Haas, Electrocardiography, in *Handbook of Physiology*, vol. 1. Am. Physiol. Soc., Washington, DC, 1962, pp. 323–415. Vol. 1, Sect. 2 (Circulation).
23. Geselowitz D.B. and O.H. Schmitt, Electrocardiography, in *Biological Engineering*, H.P. Schwan, Editor. McGraw Hill, New York, 1969, pp. 333–390.
24. McFee R. and G.M. Baule, Research in electrocardiography and magnetocardiography. *Proc. IEEE*, 1972;**60**: 290–321.
25. Geselowitz D.B., Electric and magnetic field of the heart. *Annu. Rev. Biophys. Bioeng.*, 1973;**2**: 37–63.
26. Arthur R.M. and D.B. Geselowitz, Effect of inhomogeneities on the apparent location and magnitude of a cardiac current dipole source. *IEEE Trans. Biomed. Eng.*, 1970;**BME-17**: 141–146.
27. Purcell E.M., *Electricity and Magnetism*. McGraw-Hill, New York, 1965. Berkeley physics course – Volume 2.
28. Panofsky W.K.H. and M. Phillips, *Classical Electricity and Magnetism*. Addison-Wesley, Reading, MA, 1962.
29. Courant R. and D. Hilbert, *Methods of Mathematical Physics*. Wiley, New York, 1962. Volume II.
30. Guillemin E.A., *Theory of Linear Physical Systems*. Wiley, New York, 1963.
31. Plonsey R. and Heppner D. Considerations of quasistationarity in electrophysiological systems. *Bull. Math. Biophys.*, 1967;**29**: 657–664.
32. von Helmholtz H.L.F., Ueber einige Gesetze der Verteilung elektrischer Stroeme in korperlischen Leitern mit Anwendung auf die thierisch elektrischen Versuche. *Pogg. Ann. Physiol. Chem.*, 1853;**89**: 222.
33. Oster G.F., A.S. Perelson, and A. Katchalsky, Network thermodynamics: dynamic modelling of biophysical systems. *Quart. Rev. Biophys.*, 1973;**6**: 1–134.
34. Desoer Ch.A. and E.S. Kuh, *Basic Circuit Theory*. McGraw-Hill, New York, 1969.
35. Kaufman W. and F.D. Johnston, The electrical conductivity of the tissues near the heart and its bearing on the distribution of the cardiac action currents. *Am. Heart J.*, 1943;**26**: 42–54.
36. Schwan H.P. and C.F. Kay, Specific resistance of body tissues. *Circ. Res.*, 1956;**4**: 664–670.
37. Burger H.C. and R. van Dongen, Specific electric resistance of body tissues. *Phys. Med. Biol.*, 1961;**5**: 431–437.
38. Rush S., J.A. Abildskov, and R. McFee, Resistivity of body tissues at low frequencies. *Circ. Res.*, 1963;**12**: 40–50.
39. Geddes L.A. and L.E. Baker, The specific resistance of biological material: A compendium of data for the biomedical engineer and physiologist. *Med. Biol. Eng.*, 1967;**5**: 271–293.
40. Rautaharju P.M., The inappropriateness of the commonly used augmentation and lead-recording sequence for ECG analysis. *Pract. Cardiol.*, 1982;**8**: 120–139.
41. Barnard A.C.L., I.M. Duck, M.S. Lynn, and W.P. Timlake, The application of electromagnetic theory to electrocardiology. II. numerical solution of the integral equations. *Biophys. J.*, 1967;**7**: 463–491.
42. Wilson F.N. and R.H. Bayley, The electric field of an eccentric dipole in a homogeneous spherical conducting medium. *Circulation* 1950;**1**: 84–92.
43. Frank E., Electric potential produced by two point current sources in a homogeneous conducting sphere. *J. Appl. Phys.*, 1952;**23**: 1225–1228.
44. Geselowitz D.B. and Ishiwatari H., A theoretical study of the effect of the intracavitary blood mass on the dipolarity of an equivalent heart generator, in *Vectorcardiography, 1965*. North Holland, Amsterdam, 1966, pp. 393–402.
45. Okada R.H., Potentials produced by eccentric current dipole in a finite length circular conducting cylinder. *IRE Trans. Med. Electron.*, PGME, 1956;**7**: 14–19.
46. Okada R.H., The image surface of a circular cylinder. *Am. Heart J.*, 1956;**51**: 489–500.

47. Cornelis J.P.H. and E.H.G. Nyssen, Potentials produced by arbitrary current sources in an infinite- and finite-length circular conducting cylinder. *IEEE Trans. Biomed. Eng.*, 1985;**BME-32**: 993–1000.
48. Plonsey R., Current dipole images and reference potentials. *IEEE Trans. Bio-Med. Electron.*, 1963;**BME-10**: 3–8.
49. Brody D.A., A theoretical analysis of intracavitary blood mass influence on the heart-lead relationship. *Circ. Res.*, 1956;**4**: 731–738.
50. Bayley R.H., J.M. Kalbfleisch, and P.M. Berry, Changes in the body's QRS surface potentials produced by alterations in certain compartments of the nonhomogeneous conducting model. *Am. Heart J.*, 1969;**77**: 517–528.
51. Rudy Y. and R. Plonsey, The eccentric spheres model as the basis for a study of the role of geometry and inhomogeneities in electrocardiography. *IEEE Trans. Biomed. Eng.*, 1979;**BME-26**: 392–399.
52. Wilson F.N., F.D. Johnston, and C.E. Kossmann, The substitution of a tetrahedron for the Einthoven triangle. *Am. Heart J.*, 1947;**33**: 594–603.
53. McFee R., R.M. Stow, and F.D. Johnston, Graphic representation of electrocardiographic leads by means of fluid mappers. *Circulation*, 1952;**4**: 21–29.
54. Brody D.A. and W.E. Romans, A model which demonstrates the quantitative relationship between the electromotive forces of the heart and the extremity leads. *Am. Heart J.*, 1953;**45**: 263–276.
55. Grayzel J. and F. Lizzi, The combined influence of inhomogeneities and dipole location: bipolar ECG leads in the frontal plane. *Am. Heart J.*, 1967;**74**: 503–512.
56. Frank E., Spread of current in volume conductors of finite extent. *Ann. N.Y. Acad. Sci.*, 1957;**65**: 980–1002.
57. Nagata Y., The influence of the inhomogeneities of electrical conductivity within the torso on the electrocardiogram as evaluated from the view point of the transfer impedance vector. *Jap. Heart J.*, 1970;**11**: 489–505.
58. Rush S., An inhomogeneous anisotropic model of the human torso for electrocardiographic study. *Med. Biol. Eng.*, 1971;**9**: 201–211.
59. Frank E., An accurate clinically practical system for spatial vectorcardiography. *Circulation*, 1956;**13**: 737–749.
60. Gelernter H.L. and J.C. Swihart, A mathematical-physical model of the genesis of the electrocardiogram. *Biophys. J.*, 1964;**4**: 285–301.
61. Barr R.C., T.C. Pilkington, J.P. Boineau, and M.S. Spach, Determining surface potentials from current dipoles, with application to electrocardiography. *IEEE Trans. Biomed. Eng.*, 1966;**BME-13**: 88–92.
62. Geselowitz D.B., On bioelectric potentials in an inhomogeneous volume conductor. *Biophys. J.*, 1967;**7**: 1–11.
63. Swihart J.C., Numerical methods for solving the forward problem of electrocardiography, in *The Theoretical Basis of Electrocardiology*, chapter 11, C.V. Nelson and D.B. Geselowitz, Editors. Clarendon Press, Oxford, 1976, pp. 257–293.
64. Pilkington T.C., M.N. Morrow, and P.C. Stanley, A comparison of finite element and integral equation formulations for the calculation of electrocardiographic potentials. *IEEE Trans. Biomed. Eng.*, 1985;**BME-32**: 166–173.
65. Pilkington T.C. and R. Plonsey, *Engineering Contributions to Biophysical Electrocardiography*. Wiley, New York, 1982.
66. Horáček B.M., *The effect on electrocardiographic lead vectors of conductivity inhomogeneities in the human torso*. PhD thesis, Dalhousie University, 1971.
67. Horáček B.M., Numerical model of an inhomogeneous human torso. *Adv. Cardiol.*, 1974;**10**: 51–57.
68. Horáček B.M., J.W. Warren, D.Q. Feild, and C.L. Feldman. Statistical and deterministic approaches to the design of electrocardiographic lead systems. *J Electrocardiol*, 2002; **35**(Suppl): 41–52.
69. Lepeschkin E., *Modern Electrocardiography*, volume 1: The P-Q-R-S-T-U Complex. Williams & Wilkins, Baltimore, 1951.
70. Plonsey R., Reciprocity applied to volume conductors and the ECG. *IEEE Trans. Bio-Med. Electron.*, 1963;**BME-10**: 9–12.
71. Schmitt O.H., The biophysical basis of electrocardiography, in *Proceedings of the 1st National Biophysics Conference*, H. Quastler and H.J. Morowitz, Editors. Yale University Press, New Haven, Connecticut, 1959, p. 510.
72. Horáček B.M. and H.J. Ritsema van Eck, The forward problem of electrocardiography, in *The Electrical Field of the Heart*, P. Rijlant, Editor. Presses Academiques Europeennes, Brussels, 1972, p. 228–238.

11 Lead Systems

Peter W. Macfarlane

P. W. Macfarlane, A. van Oosterom, O. Pahlm, P. Kligfield, M. Janse, J. Camm (eds.), *Comprehensive Electrocardiology*, DOI 10.1007/978-1-84882-046-3_11,

11.1 Introduction

The extensive theory behind the development of electrocardiographic leads has been dealt with in Chap. 10. An understanding of some of the concepts embodied in that chapter will be helpful, though not essential, in following the material presented in this chapter. There is no doubt that an experienced cardiologist can make an excellent interpretation of an ECG without a full understanding of the theory of electrocardiographic lead systems, but on the other hand, such an empirical approach to interpretation through pattern recognition could be enhanced with some understanding of lead systems and the relationship between the various leads.

The aim of this chapter is to describe the lead systems commonly used in different areas of electrocardiography and, wherever possible, to indicate comparisons between different types of leads. This can be of important clinical relevance. For example, a bipolar chest lead consisting of one electrode in the V_5 position and the other in the right infraclavicular fossa is often used for exercise testing or ambulatory electrocardiography. However, it is quite wrong to assume that there is a one-to-one correspondence between such a lead and the unipolar lead V_5. In other words, 0.1 mV of ST depression in V5 does not correspond to the same amount of ST depression in the bipolar lead described. This point will be discussed more extensively later in the chapter but has been used here as an illustration of the importance of understanding lead systems and lead theory.

11.2 The 12-Lead ECG

11.2.1 Bipolar Limb Leads

A bipolar lead measures the potential difference between two points-hence the term bipolar. The most commonly used bipolar leads are the bipolar limb leads introduced by Einthoven [1]. Figure 11.1 shows the circuitry associated with recording these leads. It should be noted that the illustration is didactic and that modern electrocardiographs would incorporate carefully designed electronic circuitry in order to derive these leads (see Chap. 12), but for the purposes of understanding basic electrocardiography, the illustration is of importance. As explained from a more theoretical standpoint in Chap. 10, the three bipolar limb leads illustrated which are denoted I, II and III can be represented mathematically as follows:

$$\mathrm{I} = E_L - E_R$$
$$\mathrm{II} = E_F - E_R$$
$$\mathrm{III} = E_F - E_L$$

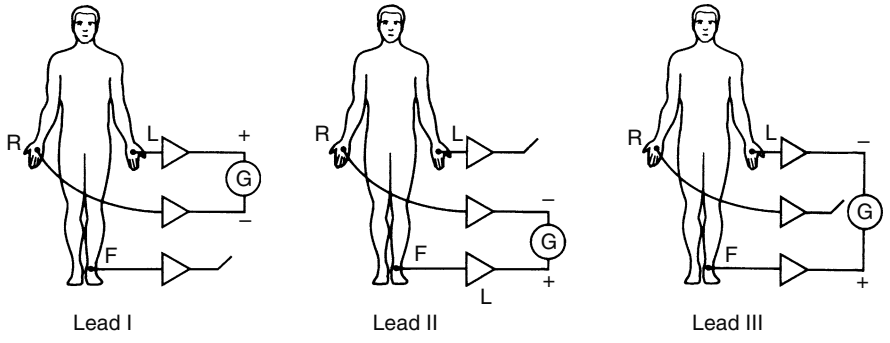

Figure 11.1
A simplified illustration of the circuitry required to record the three standard limb leads I, II and III. Note the polarity of the connections.

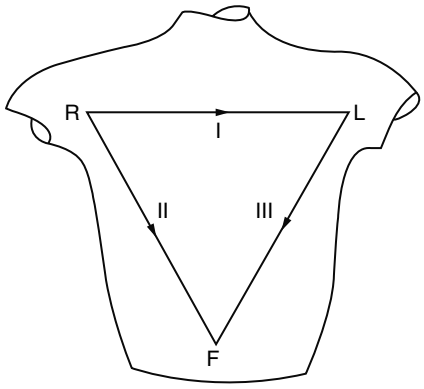

Figure 11.2

The interrelationship of the standard limb leads as depicted by the Einthoven triangle in which the body is assumed to have a triangular configuration from the point of view of its electrical characteristics.

where E_L, E_R and E_F denote the potential at the left and right arms and left leg, respectively. In other words, lead I measures the potential difference between the left and right arms, and so on.

Simple combination of the above equations shows that, at any instant in the cardiac cycle, the following relationship holds:

$$\text{I} + \text{III} = \text{II}$$

This is known as Einthoven's law.

It is important to appreciate that with each of these leads is associated a certain direction corresponding to the lead vector (see Chap. 10). Figure 11.2 shows the directions associated with leads I, II and III based on the notion of the thorax being a homogeneous conductor, which of course is not the case. The three directions form the Einthoven triangle.

The direction of the lead is of relevance in that, by convention, if the net movement of excitation within the heart is similar to the lead direction, then a positive deflection will be recorded by that lead. Thus, if excitation moves from the right towards the left, lead I would be expected to produce an upward deflection while lead III would produce a negative deflection of lower amplitude based on the concepts illustrated in Chap. 10 (Fig. 10.3).

It is also of relevance at this juncture to point out that although electrodes may be positioned on the body such that a line joining them is perhaps parallel to lead I, that does not mean to say that they accurately measure the spread of excitation in that direction. This anomaly arises from the inhomogeneities within the thorax. This problem was investigated by Burger and van Milaan [2] who subsequently modified the shape of the Einthoven triangle as shown in Fig. 10.4. Nevertheless, the idealized shape of the Einthoven triangle as shown in Fig. 11.2 continues to be used for teaching purposes and for illustrating the approximate relationships between the directions associated with the standard limb leads I, II and III.

11.2.1.1 Limb Electrode Positions

Surprisingly, there is still a debate over the positioning of limb electrodes. For example, in a small study of British hospitals, Turner [3] found that 70% of technicians and nurses used the wrists and ankles for limb electrodes while 16% placed these electrodes on the trunk. The 1975 AHA recommendations [4] stated that the arm electrodes could be on any part of the arm below the shoulders while the left leg electrode should be below the inguinal fold anteriorly and the gluteal fold posteriorly. The "right leg" electrode is required for technical reasons and can in fact be placed anywhere on the body. For convenience, it is usually placed, as the name suggests, on the right leg!!

Later, in 1977, the American College of Cardiology Task Force II which formed part of the 10th Bethesda Conference on Optimal Electrocardiography recommended [5] that the arm electrodes be placed on the wrists and the leg electrodes on the ankles.

The most recent 2007 recommendations for the standardization and interpretation of the ECG [6] drew attention to the 1975 recommendations but also to the paper by Pahlm et al. [7] pointing out that variation in the placement of the arm electrodes can alter ECG morphology and influence computer interpretations of the ECG. Kligfield and Macfarlane showed independently [8] and hence in pooled results that, paradoxically, the potential on the forearm of the left arm was very slightly higher than on the left wrist. Historically, limb potentials were recorded at the wrists and ankles as is evident from Figure 1.8 while for many years, plate electrodes were attached to wrists and ankles using straps. This author suggests that many of today's normal limits of ECG measurements were obtained with electrodes limb electrodes on the extremities, i.e., wrists and ankles, and that these positions should continue to be used. Certainly, in the monitoring situation where cardiac rhythm is of concern, electrodes can be shifted to more proximal positions for convenience but it should be appreciated that the ECG morphology will also change. Hence, if ST trending is the reason for monitoring, it should be relative rather than absolute change versus any relevant criterion that is monitored.

11.2.2 Unipolar Limb Leads

A milestone in the development of electrocardiographic leads was the introduction in 1934 of unipolar leads, which are so called because they represent the potential variation at a single point. In order to derive such a lead, Wilson et al. [9] introduced their "central terminal." The circuitry associated with this terminal is shown in Fig. 11.3 from which it can be seen that potentials at the right and left arms and left leg are summed to form a single potential which, in practice, is relatively constant throughout the cardiac cycle. If *Ewct* denotes the potential at the Wilson central terminal, then $Ewct = 1/3\ (E_R + E_L + E_F)$. The potential *Ewct* is often misnamed the "zero potential" but it should be understood that this is incorrect. Figure 11.3 shows how the central terminal is used in practice by being connected to one side of a galvanometer with the other side being linked to an exploring electrode P, here shown on the chest. If the potential of the exploring electrode is denoted by *Ep*, then the potential Vp measured by a unipolar lead is

$$\begin{aligned} \mathrm{Vp} &= Ep - E_{wct} \\ &= Ep - 1/3(E_R + E_L + E_F) \end{aligned}$$

It is clear that if *Ewct* provides a relatively constant potential then the unipolar lead basically records the potential variation at the exploring electrode P. The actual level of potential obtained from the central terminal becomes irrelevant since in broad terms it will essentially influence only the baseline level of the unipolar lead. Because the baseline will be adjusted either by the technician during recording or automatically by the currently available electronic techniques, the varying baseline offset potential difference between the central terminal and the exploring electrode in various positions will be unnoticed. The variation of the central terminal potential was investigated by Frank in 1955 [10].

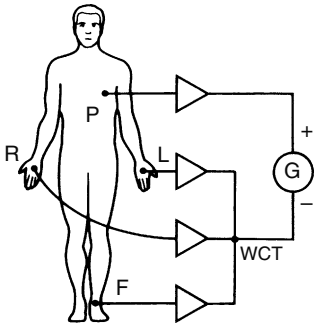

Figure 11.3
The circuitry used to record a unipolar lead in which it can be seen that the potential difference between a single point on the chest and the Wilson central terminal (WCT) is obtained. Note that the illustration is somewhat didactic in that modern electrocardiographs would employ a different technique to achieve the same end.

It should be noted that although a unipolar lead reflects the potential variation at a single point, it is technically a bipolar lead as it measures a potential difference between two terminals, one of which has a relatively constant potential.

If the exploring electrode P is connected to the right arm, then a unipolar limb lead known as VR is obtained. The equation for this lead is as follows:

$$\mathrm{VR} = E_R - Ewct$$

Similarly:

$$\mathrm{VL} = E_L - Ewct$$
$$\mathrm{VF} = E_F - Ewct$$

From the equations presented above, it follows that

$$\mathrm{VR} + \mathrm{VL} + \mathrm{VF} = 0$$

These unipolar limb leads are no longer used but have been replaced by the augmented unipolar limb leads discussed below.

11.2.3 Augmented Unipolar Limb Leads

In 1942, Goldberger [11] modified the Wilson central terminal in order to increase the voltages measured by the unipolar limb leads. The circuitry for one of these leads is shown in Fig. 11.4. Consider the situation in the case of the unipolar lead VR being modified with the removal of the right arm connection from the Wilson central terminal. In this case, the new central terminal consists of the average of the potentials at the left arm and the left leg. Mathematically, if the potential at the modified terminal is denoted E_{GT}, then it follows that:

$$\begin{aligned}\text{modified } \mathrm{V_R} &= E_R - E_{GT}\\ &= E_R - 1/2\,(E_L + E_F)\\ &= 3/2E_R - 1/2(E_R + E_L + E_F)\\ &= 3/2\,\{\mathrm{E}_R - 1/3\,(E_R + E_L + E_F)\}\\ &= 3/2\mathrm{VR}\end{aligned}$$

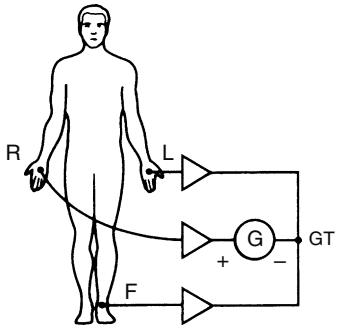

Figure 11.4

Circuitry used to derive the augmented unipolar limb lead aVR. GT denotes the Goldberger terminal for this particular lead. Note that the right arm electrode, which is effectively the exploring electrode in this particular lead, is connected to the positive terminal of the galvanometer. Again, the illustration is didactic.

The modified lead VR became known as an augmented lead because it increased the potential of VR by 50%, and hence the lead was denoted aVR where "a" represented "augmented." Similar considerations apply to the other augmented limb leads denoted aVL and aVF. In summary,

$$\begin{aligned} \text{aVL} &= E_L - 1/2(E_F + E_R) \\ &= 3/2\text{VL} \\ \text{aVF} &= E_F - 1/2(E_L + E_R) \\ &= 3/2\text{VF} \end{aligned}$$

From this it follows that

$$\text{aVR} + \text{aVL} + \text{aVF} = 0$$

at any instant in the cardiac cycle.

11.2.4 Unipolar Chest Leads

With the use of the Wilson central terminal as shown in Fig. 11.3, it became possible to measure potentials at varying points on the chest. A committee of the American Heart Association [12] selected six positions on the precordium in order to standardize recordings. The positions of these electrodes, denoted V_1–V_6, are described in Table 11.1 and are shown in Fig. 11.5. V_1 and V_2 are at the level of the fourth intercostal space at the sternal borders, V_4 is in the midclavicular line one interspace lower, V_6 is in the left mid-axilla at the same horizontal level as V_4 while V_3 is intermediate to V_2 and V_4, and V_5 is intermediate to V_4 and V_6. These six unipolar chest leads are called V_1–V_6. The AHA recommendations of 1975 stated [4] that V_5 was to be placed at the junction of the left anterior axillary line and the level of V_4. The 1977 ACC 10th Bethesda Report [5] gave a similar position. However, the 2007 recommendations [6] added that if the anterior axillary line is ambiguous, then V_5 should be placed midway between V_4 and V_6.

The directions associated with these leads are shown in Fig. 11.6. In Fig. 11.6a the idealized lead directions are shown while in Fig. 11.6b the theoretically derived directions associated with each lead based on a more realistic model of the torso are indicated [13]. In each case, the vectors can be assumed to lie approximately in the transverse plane.

Some clinicians may wish to record leads an interspace higher or lower than those recommended. There are no specific recommendations in terms of denoting such leads, but occasionally in the literature authors have used 1H to denote a lead

Table 11.1

Lead nomenclature (after Sheffield et al. [5])

Electrode	Location of attachment
Right arm (R)	Right wrist
Left arm (L)	Left wrist
Left foot (F)	Left ankle
Right foot (G)	Right ankle
V_1	Right sternal margin, fourth intercostal space
V_2	Left sternal margin, fourth intercostal space
V_3	Midway between V_2 and V_4
V_4	Left midclavicular line, fifth intercostal space
V_5	Left anterior axillary line, V_4 level
V_6	Left midaxillary line, V_4 and V_5 level
V_7 and V_8[a]	Left posterior axillary line and left midscapular line, V_6 level
Leads[a] recorded on right side of thorax, such as V_4R	Right midclavicular line, fifth intercostal space

[a]Optional leads

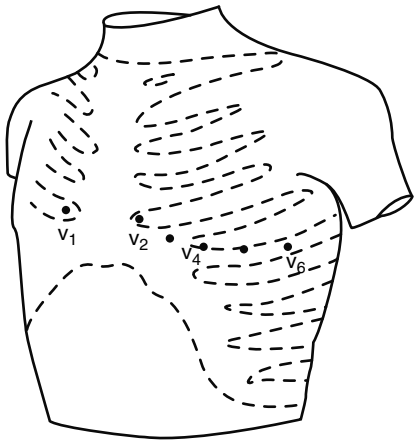

Figure 11.5

The six positions recommended for the exploring electrode in order to record unipolar chest leads (see Table 11.1 for further details). By convention, the leads and hence the positions, are denoted V_1–V_6.

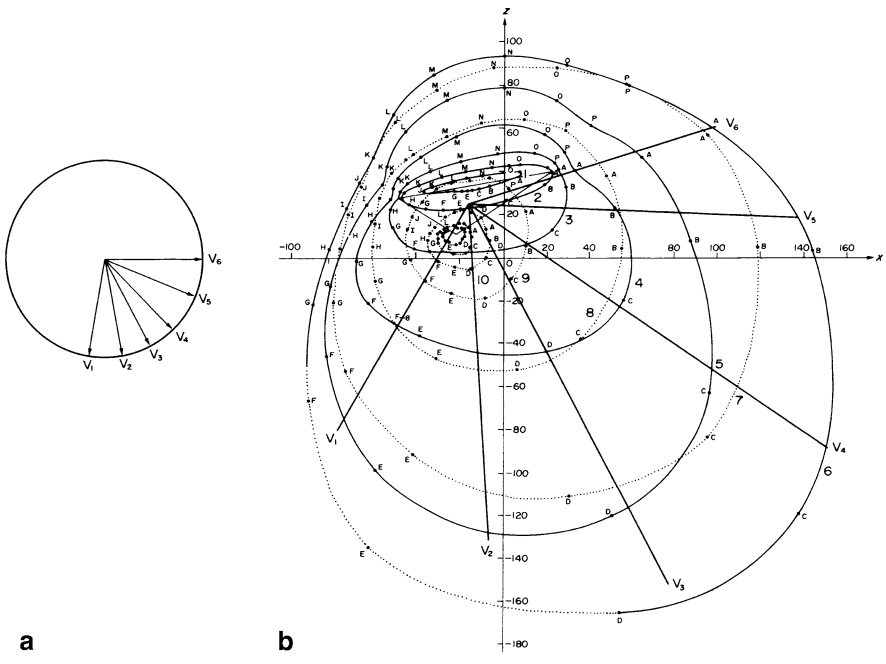

Figure 11.6

In (a), an idealized description of the directions associated with each of the six precordial leads (that is, the direction in which the component of the resultant cardiac electrical force is measured) is shown. In (b), the lead directions of V1 to V6 as derived from Frank's image surface are shown. In this case, the origin of the axes represents the electrical centre of the heart with respect to which the Wilson central terminal is displaced in electrical terms. All lead vectors are drawn from this terminal (at the centroid of the triangle) to the points on the image surface corresponding to the positions of the electrodes on the precordium. The loops 5 and 6 represent different levels of the surface of the thorax separated by two inches approximately at the level of V1 and V4, respectively. Note that leads V1–V6 have different strengths indicated by the length of each lead vector. (After Frank [13]. © Mosby, St Louis, Missouri. Reproduced with permission).

recorded one interspace higher, e.g., $V_2$1H would denote a lead recorded at the left sternal border in the third intercostal space. Similarly, 1L is sometimes used to denote a lead recorded one interspace lower than that recommended.

11.2.5 Additional Chest Leads

In addition to the internationally accepted six precordial-lead positions, it is not uncommon for additional leads to be recorded on the right side of the chest. For example, routinely in children and in adults with acute inferior myocardial infarction, leads on the right side of the chest which reflect lead positions on the left side of the chest may be recorded. These positions are shown schematically in Fig. 11.7 a. For example, a lead in the midclavicular line at the fifth intercostal space on the right side of the chest (i.e., a reflection of V_4) would be denoted V_4R. The lead intermediate between V_1 and V_4R is denoted V_3R. V_3R and V_4R are perhaps the two most commonly used additional leads. However, on rare occasions V_5R and V_6R may also be recorded.

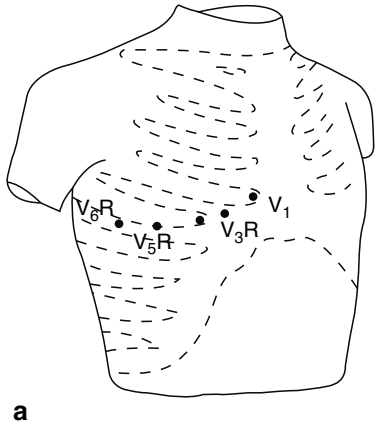

Figure 11.7 a
Right-sided chest lead positions as used mainly in children and occasionally in the detection of right ventricular involvement in myocardial infarction.

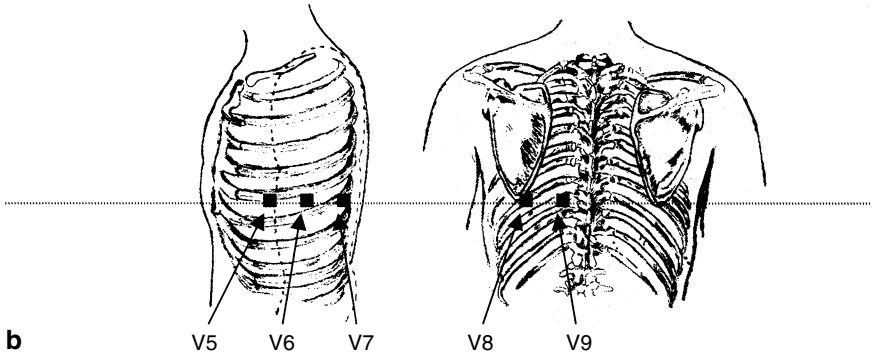

Figure 11.7 b
Additional left sided chest leads V7–V9. See text for further discussion (Reproduced by kind permission of Ian Bolton, Essex Cardiac Services, England).

To assist in the diagnosis of acute ST elevation myocardial infarction, additional leads are sometimes recorded on the posterior chest. V_7, for example, records the potential at the left posterior axillary line [4, 5], V_8 records the potential in the left midscapular line [4, 5], while V_9 records the potential at the left paravertebral border of the spine [6], with all of these electrode positions being at the level of lead V_6 (Fig. 11.7 b).

11.2.6 12-Lead ECG Relationships

The combination of the bipolar limb leads I, II and III, the augmented unipolar limb leads aVR, aVL and aVF, and the six unipolar precordial leads V_1–V_6 is known as the 12-lead ECG. Almost all ECGs recorded worldwide make use of these 12 leads. Additional precordial leads may be recorded as described above, particularly in children, where the six precordial leads are often selected as V_4R, V_1, V_2, V_4, V_5 and V_6.

The limb leads in particular, both bipolar and unipolar, are closely related. In fact, if any two of the six limb leads are recorded simultaneously, the other four can be derived from them. As an example, consider that leads I and II have been recorded. Lead aVF could be calculated from them as follows:

$$\begin{aligned}\text{aVF} &= E_F - 1/2\,(E_L + E_R)\\ &= 1/2\,(E_F - E_L) + 1/2\,(E_F - E_R)\\ &= 1/2\text{III} + 1/2\text{II}\\ &= 1/2\,(\text{II} - \text{I}) + 1/2\text{II}\\ &= \text{II} - 1/2\text{I}\end{aligned}$$

The other limb leads can be expressed in terms of leads I and II as follows:

$$\begin{aligned}\text{III} &= \text{II} - \text{I}\\ \text{aVR} &= -1/2\,(\text{I} + \text{II})\\ \text{aVL} &= \text{I} - 1/2\text{II}\end{aligned}$$

If an alternative strategy had been adopted whereby leads I and a VF were available, then it can be shown that the following relationships hold:

$$\begin{aligned}\text{II} &= \text{aVF} + 1/2\,\text{I}\\ \text{III} &= \text{aVF} - 1/2\,\text{I}\\ \text{aVR} &= -\,(3/4\,\text{I} + 1/2\,\text{aVF})\\ \text{aVL} &= 3/4\,\text{I} - 1/2\text{aVF}\end{aligned}$$

Part of the importance in these relationships is that in computer-based electrocardiography, it is only necessary to record or store two of the limb leads, since the remaining four can be calculated and displayed whenever desired. This has important repercussions in terms of long-term storage on a database where a saving of 33% of data can be achieved by using only the eight independent leads of the 12-lead ECG with the remainder being calculated whenever necessary. In the author's experience, this strategy sometimes creates considerable misunderstanding. The equations described above are totally independent of body habitus. Although the Einthoven triangle is an idealized concept and the Burger triangle represents perhaps a theoretically more exact description of the electrical equivalent of the body, the equations described have been derived from a purely empirical standpoint and are thus independent of body size and internal structure.

The concept of a direction associated with a lead was introduced earlier and the Einthoven triangle (Fig. 11.2) illustrated the directions for the bipolar limb leads. The augmented unipolar limb leads can also be incorporated into the Einthoven triangle as shown in Fig. 11.8. For example, because the Goldberger terminal for aVF is half of the potential at the right and left arms, it can be regarded as the midpoint on the line joining R and L. The direction associated with aVF is therefore from this midpoint to F, that is, a vertical line in the triangle as shown in Fig. 11.8.

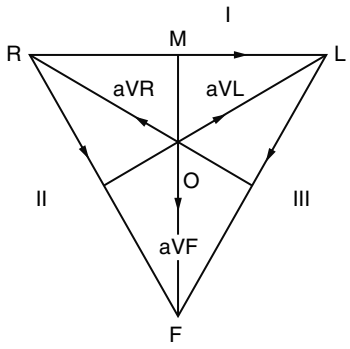

Figure 11.8

A diagram indicating the approximate directions and strengths associated with the six limb leads. Leads I, II and III have the same strength while leads aVR, aVL and aVF have an equal but different lead strength according to the concept of the equilateral Einthoven triangle; for example, the ratio of the strength of I to aVF is RL/MF. In practice, the six leads have different lead strengths as discussed in the text.

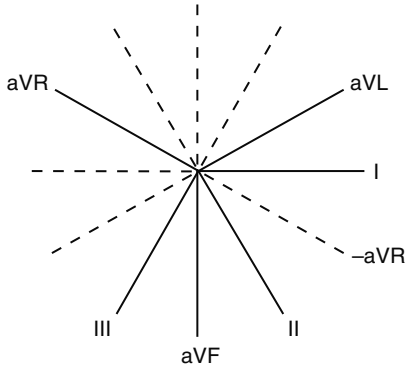

Figure 11.9

The lead directions of the six limb leads presented in an alternative fashion which incorporates –aVR. This lead is sometimes used in the alternative presentation of leads in the sequence of aVL to III in keeping with the clockwise sequence of the leads shown in the illustration. The dotted lines represent the negatively directed axes.

Similar considerations apply to the directions associated with aVL and aVR, and these can be combined into a single diagram showing all six lead directions (Fig. 11.9). Note that this diagram shows the approximate direction and strengths associated with each of these leads. The concept of lead strength is discussed in Chap. 10. It essentially reflects the potential recorded by the lead when a source of unit strength is placed within the thorax and, as such, is used as a relative estimate of the lead capabilities. For example, if there is a potential source within the thorax such that VR measures 1 mV, then aVR would measure 1.5 mV. Theoretically, the relative strengths of aVF and lead I are given by the lengths of the lines MF and RL as shown in Fig. 11.8. In practice, the actual ratio will be different in view of the shortcomings of the equivalent (equilateral) triangle hypothesis (Fig. 11.2). Langner pointed out some time ago [14] that if a particular source of potential was aligned to produce a maximum potential of one unit in lead III, then the same potential source would produce at most one half of that potential in lead I when similarly reoriented to produce a maximum. In turn, this reflects the ratio of the lengths of the sides RL and FL of the Burger triangle (Fig. 10.3).

Figure 11.9 also shows how the lead directions can be translated to another display known as the hexaxial reference frame. This shows more clearly the relative directions of the different limb leads. It also supports the presentation of the limb leads in a sequence aVL, I, -aVR, II, aVF, III, a practice which is universally adopted in most Scandinavian countries.

This sequence is known as the Cabrera (panoramic) presentation [15, 16]. An illustration can be seen in Fig. 13.38. While this is a logical sequence for displaying the leads, most cardiologists in other countries have been taught to view the leads in the more conventional sequence I, II, III, aVR, aVL, aVF and an adjustment to the alternative form of display would be likely to prove most difficult. Nevertheless, with the flexibility of microprocessor-based technology incorporated into currently available electrocardiographs, such alternative displays are easily obtainable at the touch of a button.

11.3 Other Bipolar Leads

11.3.1 Bipolar Chest Leads

Another form of lead which is rarely used nowadays is the bipolar chest lead formed by placing one electrode on one of the limbs with the other on any of the precordial positions shown in Fig. 11.5. If the right arm is used, then a bipolar chest lead derived with the other electrode in the V_1 position would be denoted as CR_1. Similarly, if the limb electrode were on the left leg and the other electrode were applied in the V_6 position, the resulting lead would be denoted CF_6.

Of more interest are bipolar chest leads used for exercise testing or ambulatory monitoring. Most commonly, the positive electrode is placed in the V5 position and the negative electrode is placed at a variety of sites as shown in Fig. 11.10. Those commonly used include the manubrium (giving lead CM) or the right infraclavicular fossa (giving lead CS5). Table 11.2 lists the electrode positions, with additional comments on their use in exercise testing.

As mentioned in the introduction, there is, in the author's opinion, considerable misunderstanding over the difference between the unipolar lead V_5 and a bipolar chest lead such as CM_5. The idea of lead strength and direction has now been introduced, and in order to explain the difference between the leads CC_5, CM_5 and V_5, Fig. 11.11 depicts the lead strength and direction associated with the corresponding lead vectors which have been derived from Frank's image surface [13], a concept described fully in Chap. 10. It can be seen in the transverse and frontal view that the leads CC_5 and CM_5 both have a longer lead vector than V_5. Thus, the potential measured by CM_5 will be approximately 1.2 times that of V_5 for the same size of electrical force parallel to these axes because the potential measured is directly proportional to lead strength (see Fig. 10.8). Similarly, CC_5/V_5 is approximately 1.4. The potential measured is also proportional to the component of the electrical force along the direction of the axes (Fig. 10.2) and in this respect Fig. 11.11 shows that vertically directed electrical forces will have virtually no effect on V_5 and CC_5 while they will influence CM_5. The

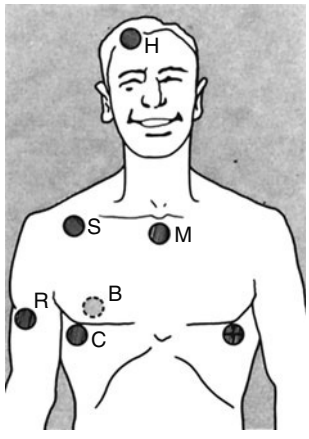

Figure 11.10

The various electrode positions for recording bipolar chest leads where the positive lead is in the V5 position and the negative lead is in one of a number of other positions shown on the diagram. The code for the electrode positions is explained in Table 11.2. (After Froelicher et al. [55]. © American College of Chest Physicians, Park Ridge, Illinois. Reproduced with permission).

Table 11.2

Some bipolar leads used in conjunction with stress testing (after Surawicz et al. [50])

Lead	Positive electrode location	Negative electrode location	Comments
CM_5[a]	V_5 position	Manubrium	One of the most sensitive bipolar leads for detecting ST changes
CH_5	V_5 position	Forehead	favored in Sweden, especially bicycle tests
CS_5	V_5 position	right infraclavicular fossa	Detects somewhat more muscle artefact than lead CM_5
CC_5	V_5 position	V_5R position	Bears a closer resemblance to lead V_5 than most bipolar leads
CB_5	V_5 position	low right scapula	Closely resembles lead V_5 but has more muscle artifact than most other bipolar leads
CR_5	V_5 position	right arm	Used in northern Europe and USSR for pre- and postexercise records, usually with 4 to 6 chest lead positions. High muscle artifact level during exercise

[a]The number 5 refers to the position on the chest of a corresponding V lead such as V_5. Thus the positive electrode could be located in any numbered V lead position

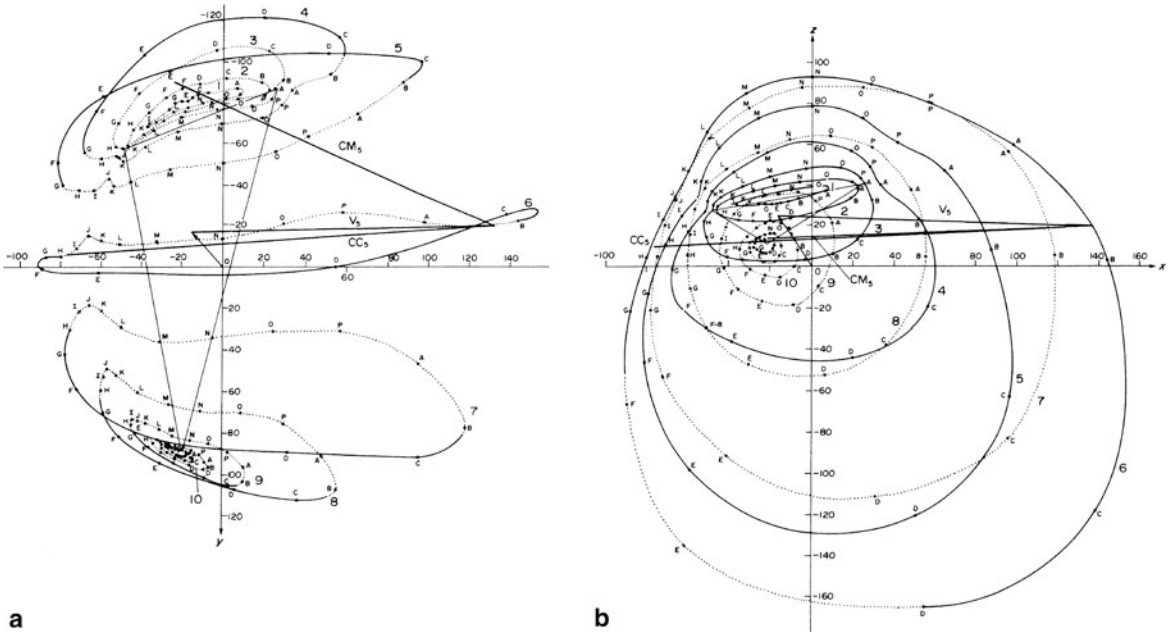

Figure 11.11

The projection of the lead vectors for V5, CM5 and CC5 onto (a) the frontal plane; and (b) the transverse plane. The vectors have been derived from Frank's image surface described in Chap. 10. Note in particular how the frontal view shows quite a divergence in the orientation of the vectors. Since V5 and CC5 are essentially at right angles to the head-to-foot axis, they will not measure any component of an electrical force which is directed along such an axis. The two views summarize a three-dimensional picture from which it can be calculated that the ratio of the lead-vector magnitudes is approximately 1.2: 1 for CM5: V5 and 1.4: 1 for CC5: V5. The tip of the arrow on each view represents the position of the Wilson central terminal in image space (After Frank [13]. © Mosby, St Louis, Missouri. Reproduced with permission).

amplitude of CM_5 will be further enhanced by the fact that its lead-vector direction is essentially parallel to the normal mean QRS axis, so that the QRS component will be greater along CM_5 than along the V_5 lead vector. Similarly, lateral ST abnormalities should be larger in CM_5 than V_5.

From the foregoing, it follows that a criterion of, say, 0.1 mV ST depression may lead to a higher percentage of positive findings in CM_5 in any particular comparison with V_5 and the sensitivity and specificity of the test might be completely misinterpreted. Thus, different criteria should be applied to these different leads.

11.3.2 Nehb Leads

In a few countries in Europe (particularly Germany) there are still some cardiologists who make use of the Nehb leads [17]. Essentially, these consist of three bipolar chest leads. The three electrodes are placed on the thorax as shown in Fig. 11.12. In practice, to record these leads with a single-channel electrocardiograph, the electrode connections used for recording the standard limb leads can be utilized. With this approach, the right arm electrode is placed at the junction of the second rib with the sternum on the right side, the left arm electrode is placed level with the scapular apex on the posterior axillary line, while the left leg electrode is placed on the front of the chest opposite the scapular apex (in proximity to the apex of the heart). The leads recorded are denoted O for dorsal, A for anterior and I for inferior. By using the limb-lead connections, the leads O, A and I would be recorded with the electrocardiograph set up as for leads I, II and III, respectively. Alternatively, the leads are sometimes prefixed with the letter N (after Nehb) giving leads NO, NA and NI. Figure 11.12 should not be misconstrued as representing three electrodes at the same cross-sectional level of the thorax.

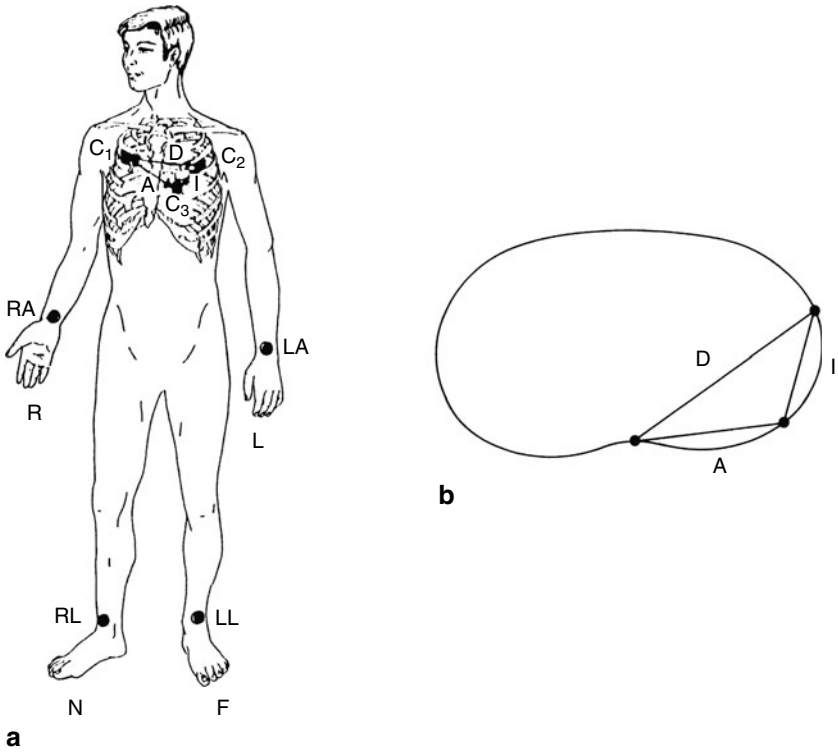

Figure 11.12

The Nehb-lead system comprising the dorsal lead D, the inferior lead I and the anterior lead A. Note that the three electrodes are not placed at the same level on the thorax as suggested in (b) but are at different levels as seen in (a). (© Siemens-Elema. Reproduced with permission).

With a multichannel electrocardiograph it is customary to use the $V_1(C_1)$, $V_2(C_2)$ and $V_3(C_3)$ electrode connections to record the Nehb leads. According to the scheme above, V1 replaces the right arm electrode, V2 the left arm electrode and V3 the left leg electrode. For example, lead D records the potential difference between C1 and C2 (see Fig. 11.12). These leads are also used in experimental work in animals as discussed in the Chap. 11, Sect. 11.17.

11.4 Orthogonal-Lead Systems

In earlier chapters, reference has been made to equivalent cardiac generators, and there has been reference to the equivalent cardiac dipole first suggested by Einthoven [1]. As discussed in Chap. 2, a dipole can be represented mathematically by a vector; that is, an entity having a specific magnitude and direction. In turn, a vector requires three measurements for its definition. In the simplest approach, three such components could be obtained by deriving the projections of the vector onto three mutually perpendicular (orthogonal) axes. Chap. 2 describes fully how given three components *Hx, Hy, Hz* in such directions conventionally denoted as X, *Y* and Z (Fig. 11.13), the resultant vector can be obtained having a magnitude *H* where

$$H = \left(H_x^{\,2} + H_y^{\,2} + H_z^{\,2}\right)^{1/2}$$

and a direction which can be calculated from these three components. By convention, the X component of the vector detects the lateral forces. An electrode array measuring this component is called lead X and by convention produces a positive deflection (similar to lead I) when current flows from right to left within the thorax. Similarly, an electrode array detecting the inferior component is called lead *Y* and, like aVF, by convention, has a positive deflection when current flows towards the feet. An electrode array detecting current flow in an anteroposterior direction is called lead Z. Most authors

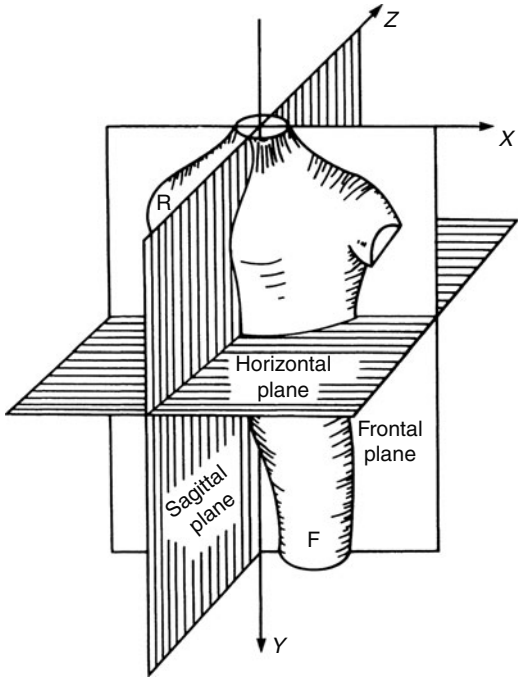

Figure 11.13

The relationship between the various planes and the *X, Y* and *Z* axes. (*Circ. Res* 1954; 2: 257. © American Heart Association, Dallas, Texas. Reproduced with permission).

direct lead Z positively to the back, that is, it shows a pattern like an inverted V2. However, this author prefers to direct lead Z positively to the anterior in order to maintain the similarity with V2 and a meaningful discussion in terms of Q waves, and so on.

11.4.1 Uncorrected Orthogonal-Lead Systems

In the 1940s and early 1950s, a number of investigators had the idea of designing lead systems that would measure the three components of the cardiac dipole. These early attempts essentially produced lead systems such that lines joining the electrode positions were mutually perpendicular (see Fig. 11.14). Examples are the Grishman cube [18], the double cube system of Duchosal [19] and the Wilson tetrahedron system [20]. These systems are essentially no longer in routine use.

The cube system (Fig. 11.14) was a simple arrangement of electrodes such that lines joining the electrode positions lay along the edges of a cube; that is, the three pairs of (bipolar) leads that were formed appeared geometrically orthogonal. The cube system is not used routinely today but still features in research work such as described by Selvester et al. in Chap. 16, where VCGs derived from the cube system are illustrated.

The tetrahedron system (Fig. 11.14b) is easy to apply with three limb electrodes and one centrally located on the back. The X component was taken as lead I while aVF provided the vertical component Y. The anteroposterior component Z was obtained from the unipolar lead VB. This system is not used nowadays except in animal research. Examples can be found in Chaps. 41 and 42.

Around 1945–55, the theory of electrocardiographic leads was much more intensively investigated as described in Chap. 10. From such research came an understanding that while electrode systems might appear to be geometrically orthogonal, the equivalent lead-vector orientations were far from orthogonal. Such systems then became known as "uncorrected" orthogonal-lead systems. What was required was a system of electrodes which, in combination, measured as accurately as possible the components of a dipole in three mutually perpendicular directions. In particular, Frank [13] introduced the concept of image space (see Chap. 10), which allowed assessment of electrocardiographic leads with more precision than had previously been the case.

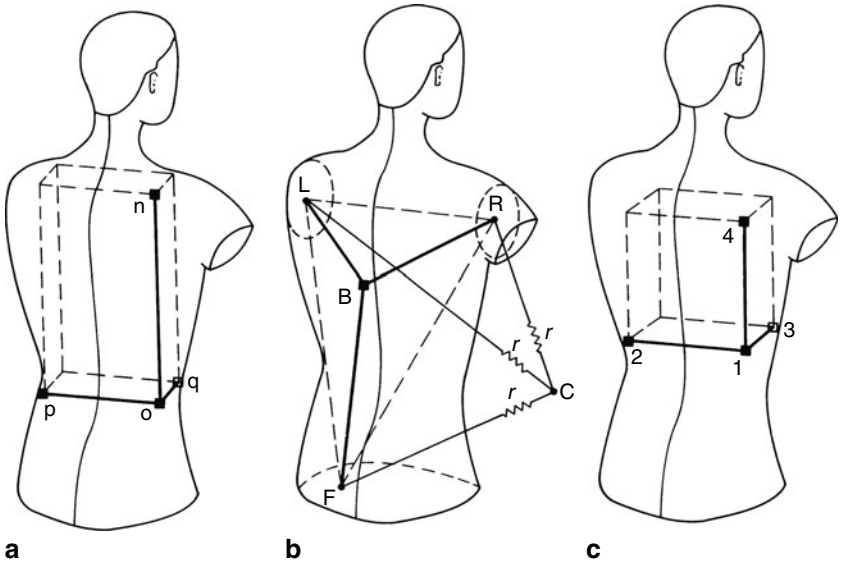

Figure 11.14

The electrode positions of (a) the Duchosal double cube system; (b) the Wilson tetrahedron; and (c) the Grishman cube (After Frank E, *Circulation* 1954; 10: 101. © American Heart Association, Dallas, Texas. Reproduced with permission).

11.4.2 Corrected Orthogonal-Lead Systems

The concept behind a corrected lead system was to produce an electrode network that resulted in lead vectors that were of equal magnitude and were mutually perpendicular – at least according to theoretical and modeling studies. It is shown in Chap. 10 that the potential V measured by a lead is given by the scalar product of two vectors, namely, the cardiac vector H and the lead vector L. Thus,

$$V_{lead} = H\, L_{lead}$$

If L is parallel to the X axis, say, then L has components $(x, 0,0)$ and so

$$Vx = HxLx$$

Thus,

$$Hx = Vx/Lx$$

Similarly,

$$Hy = Vy/Ly$$

and

$$Hz = Vz/Lz$$

The vector magnitude H is calculated from

$$H = \left\{(Vx/Lx)^2 + (Vy/Ly)^2 + (Vz/Lz)^2\right\}^{1/2}$$

In order to avoid distortion, it is necessary for $Lx = Ly = Lz = L$. Then,

$$H = \frac{1}{L}\left\{(V_x)^2 + (V_y)^2 + (V_z)^2\right\}^{1/2}$$

where L is the common lead strength. A lead system with these characteristics is called a corrected orthogonal-lead system.

11.4.2.1 Frank System

In 1956, Frank [21] published details of what was effectively the first truly corrected orthogonallead system. The term "corrected" implies that the lead vectors associated with the system were indeed orthogonal and, on the basis of tank torso model studies, accurately measured components of "cardiac" electrical activity in mutually perpendicular directions. The electrode positions and the resistor network required to derive the three leads are shown in Fig. 11.15.

The electrodes A, C, E, I and M should be placed at a level corresponding to the electrical center of the heart. This point is discussed further below. A and I are positioned in the left and right midaxillary lines, respectively. E and M are positioned on the sternum and spine, respectively. C is positioned such that an angle of 45° is produced with respect to the center of the thorax as shown in Fig. 11.15. This electrode position may need some adjustment in females. Electrode H is usually placed on the back of the neck, although its position is not particularly critical.

It is of passing interest that Frank's electrode position nomenclature was derived very simply from the concept of labeling points around the chest at intervals of 22.5°. Thus, starting from A in the left mid axilla and moving anteriorly, B is 22.5° from A, C is 45° from A. Progressing clockwise in this way, E is 90° from A, I is 180° from A and M is 270° from A.

It can be seen from Fig. 11.16 that the lead vectors for leads X, Y and Z are essentially mutually perpendicular as required. The length of each lead vector is not the same, with the Y lead vector being the smallest. Frank used shunt resistors of 7.15 R and 13.3 R to reduce the gains of the X and Z leads respectively (see Fig. 11.15) so that each equaled 136 units. This lead system is therefore "corrected" with respect to both the lead direction and magnitude. The latter is important if the components of the cardiac vector are not to be distorted by an imbalance in the measurement system.

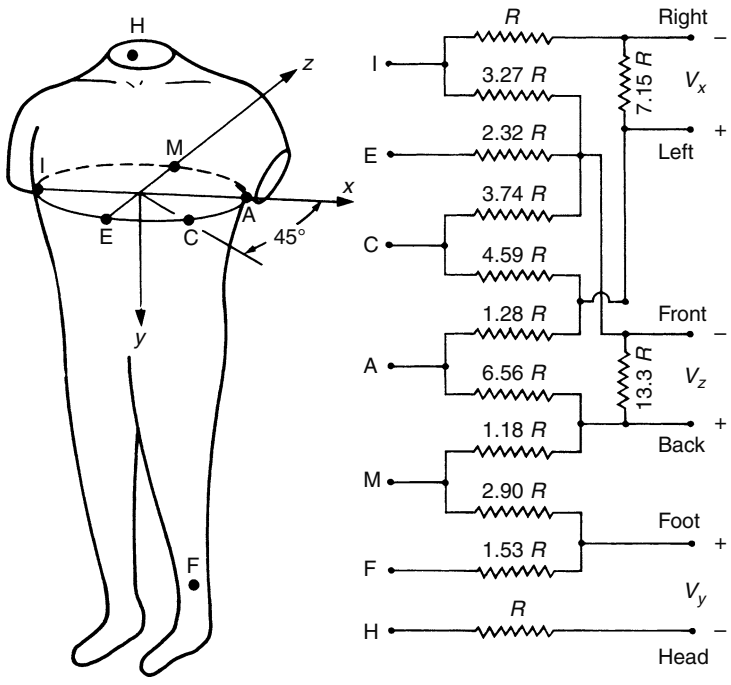

Figure 11.15

Electrodes and circuitry of the Frank-lead system (After Frank [21]. © American Heart Association, Dallas Texas. Reproduced with permission).

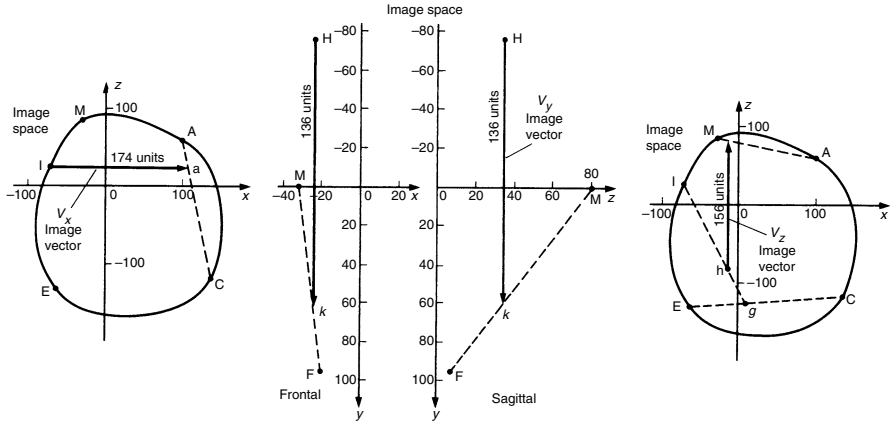

Figure 11.16

The three lead vectors corresponding to leads *X*, *Y* and *Z* of the Frank system as projected onto the transverse, frontal/sagittal and transverse planes, respectively. It can be seen that the lead vectors are parallel to the desired lead directions although they do not intersect at a single point (After Frank [21]. © American Heart Association, Dallas, Texas. Reproduced with permission).

An analysis of the resistor network in Fig. 11.15 leads to the following equations, which show the contribution of each electrode to the potential measured in each lead:

$$Vx = 0.61V_A + 0.171V_C - 0.781V_I$$
$$V_y = 0.655V_F + 0.345V_M - 1.0V_H$$
$$V_z = 0.133V_A + 0.736V_M - 0.264V_I - 0.374V_E - 0.231Vc$$

The Frank system has retained its original popularity wherever vectorcardiography is practised although there are very few medical practitioners nowadays who understand the technique. The only area of controversy in its application has surrounded the use of the fourth or the fifth intercostal space as the reference for siting the precordial electrodes. Frank initially indicated that the electrodes should be placed at a level corresponding to the electrical center of the heart, and described a mechanism for finding such a position [21]. In most early studies the fourth intercostal space was used, and one of the most significant publications on the derivation of normal limits for the Frank *XYZ* leads [22] arose from the use of the system at the fourth intercostal space. Subsequently the tendency has been for the electrodes to be placed in the fifth intercostal space [23]. Part of this stems from an attempt to combine recording of the 12-lead ECG with the Frank leads. In this case, the C and A electrodes of the Frank system (see Fig. 11.15) can also be used to record V_4 and V_6, respectively. Thus, compared to recording the 12-lead ECG alone it is necessary to add four electrodes, namely, E, I, M and H if this approach is adopted [24].

11.4.2.2 Axial-Lead System

In 1955, McFee and Parungao [25] introduced what they termed an axial-lead system for orthogonal-lead electrocardiography. This is illustrated in Fig. 11.17. The *X*+ electrodes in the left anterior axilla are situated approximately 5.5 cm above and below the fifth intercostal space in adults. The *X*− electrode is situated in the right mid axilla at the level of the fifth intercostal space. The *Y* lead is a straightforward bipolar lead recorded between the left leg and the neck. The Z lead consists of three electrodes, arranged in the shape of a triangle, with a distance of 6 cm from the centroid, situated approximately at V2, to each of the apices. This measurement is reduced in children. The Z + electrode was positioned behind the triangle on the back at a point corresponding to the centroid as shown in the illustration. In a study of the lead vectors, Brody and Arzbaecher [26] showed that the axial-lead system had the best orthogonality of all corrected orthogonal-lead systems although the strengths of the leads were unequal. Since this is undesirable, Macfarlane introduced a modification [27] in 1969 which equalized the lead strengths. The correction was based on the relative strengths of the *X*, *Y* and Z leads as published by Brody and Arzbaecher. As a result, the following equations therefore apply:

$$X\,(\text{modified axial}) = 0.92\text{X}\,(\text{axial})$$
$$Y\,(\text{modified axial}) = \text{Y}\,(\text{axial})$$
$$\text{Z}\,(\text{modified axial}) = 0.66\text{Z}\,(\text{axial})$$

The modified axial-lead system was used by Macfarlane in early comparative studies on 12-lead and 3-lead electrocardiography. These showed that there was no significant difference from the diagnostic point of view between 3-lead and 12-lead electrocardiography [28]. For use with children, the system was adapted by reducing the spacing between the triangle of electrodes and the pair of electrodes in the left axilla [29]. A set of templates was constructed for easy application of electrodes.

11.4.2.3 Hybrid-Lead System

Although there were many studies undertaken using orthogonal-lead electrocardiography, it was apparent by the mid-1970s at least that clinicians were reluctant to move towards 3-orthogonal lead systems to the exclusion of the 12-lead ECG.

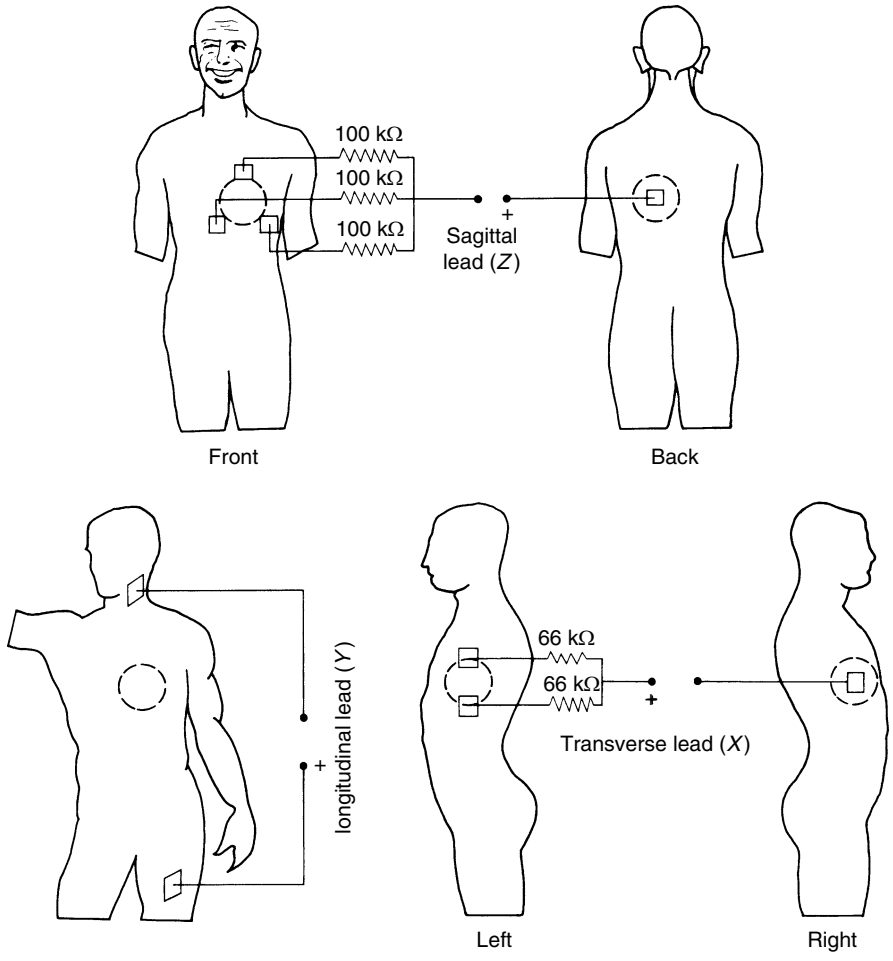

Figure 11.17

The McFee and Parungao axial-lead system. The derivation of the leads is clear from the illustration. Note that each electrode contributes to one lead only (After McFee and Parungao [25]. © Mosby, St Louis, Missouri. Reproduced with permission).

For this reason, Macfarlane designed a new lead system that was aimed at combining the 12-lead and the 3-orthogonal-lead ECG with the minimum number of additional electrodes. The intention was to retain the advantages of the phase relationships of the 3-orthogonal-lead ECG and add them to the information obtained from the 12-lead ECG. The system [30, 31] was also designed by making use of Frank's image space and was intended to produce *XYZ* leads which had a similar orientation and lead strength to those of the modified axial-lead system previously designed by Macfarlane. The electrode positions of this system are shown in Fig. 11.18 where it can be seen that there are only two additional electrodes compared to the use of the 12-lead system alone. These electrodes are placed in the V6R position and on the neck:

With the hybrid system, the 12-lead ECG is recorded in the usual fashion. Lead *X* of the orthogonal-lead ECG is a bipolar lead between V_5 and V_6R. Lead *Y* is similar to the original axial-lead system and the modified axial-lead system, being a potential difference between the neck and the left leg. Lead Z is obtained by averaging the V_1, V_2 and V_3 potentials and from this subtracting the potential at the neck. The relevant gains are controlled by the use of the resistors as shown in Fig. 11.18. In this way, the use of a back electrode is obviated while the three potentials $V_1 - V_3$ replace the triangle of electrodes in the axial system. Figure 11.19 shows how the *XYZ* lead vectors of the hybrid system relate to those of the original axial system. It can be seen that lead Z is displaced superiorly but still remains parallel to the desired Z direction.

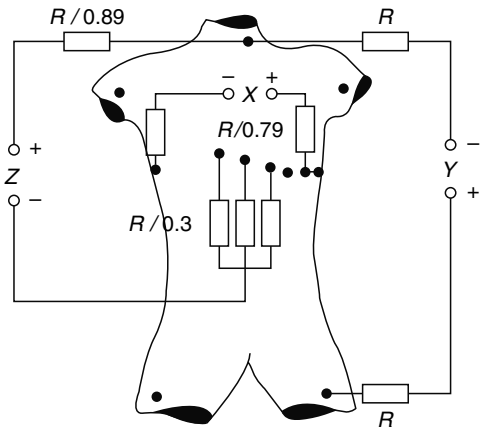

Figure 11.18

The electrode positions and resistor network of the hybrid-lead system. The 12-lead ECG is derived in the usual way while the corrected orthogonal leads *X, Y* and *Z* are derived using the network shown. Note that only two additional electrodes are required compared to the use of the 12-lead ECG alone.

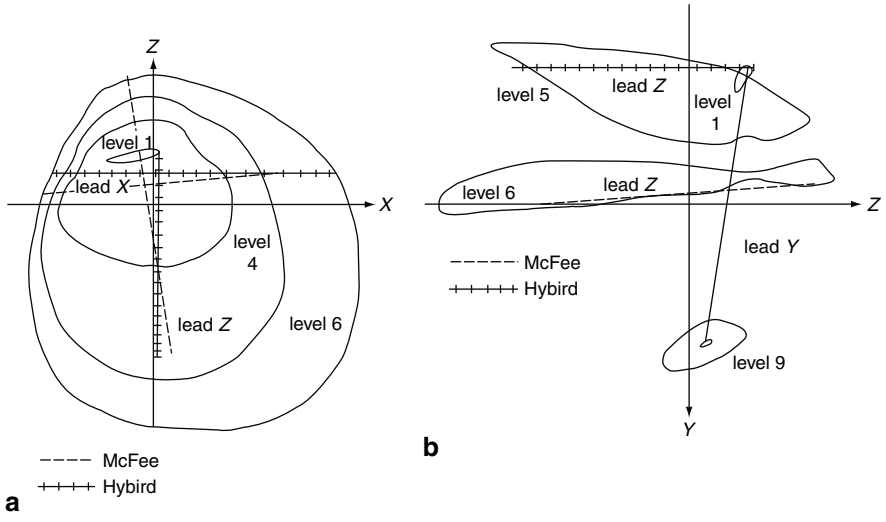

Figure 11.19

The lead vectors of the hybrid-lead system and the original axial-lead system as seen in (a) the transverse view; and (b) the sagittal view. It can be seen that the hybrid leads are more corrected, i.e. parallel to the *X, Y* and *Z* axes, than are the original axial leads. The lead vectors were obtained from analysis of Frank's image surface. The continuous line denotes both the hybrid and axial *Y* lead vector which is identical in each case.

Indeed, it is more corrected than the original axial system at least based on studies using Frank's image space. Likewise, lead *X* is also parallel to the *X* axis and is more corrected than the original axial lead. Since lead *Y* is identical in both cases, only one lead vector can be shown. This is not parallel to the *Y* axis as would be desired in a perfect orthogonal-lead system.

The hybrid system is no longer used routinely by the author but some normal limits of orthogonal-lead measurements discussed in Chap. 13 are based on studies with this system.

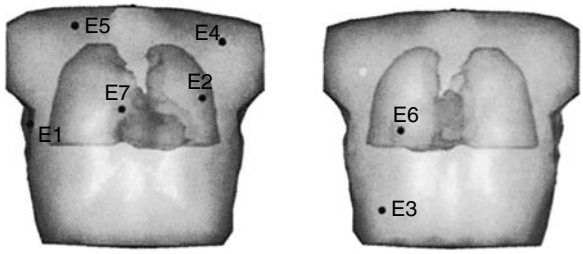

Figure 11.20
Optimized electrode positioning for the detection of atrial fibrillation using a vectorcardiographic lead system incorporating the electrodes shown (After van Oosterom et al. [32]. © Elsevier. Reproduced with permission).

The lead strengths of the *X Y* Z leads derived from the hybrid system were equalized via resistors (Fig. 11.18) calculated from modeling studies. The equations for deriving the orthogonal leads are as follows:

$$X = 0.79\,(V_5 - V_6R)$$
$$Y = V_F - V_{neck}$$
$$Z = 0.89\,\{(V_1 + V_2 + V_3) - V_{neck}\}$$

With the use of this system it is necessary to acquire only ten leads I, II, V_1–V_6, V_6R and V_{neck} from which the remaining five can be derived in order to obtain the full 12-lead plus *X*, *Y* and Z lead presentation. These ten leads have to be recorded simultaneously for this purpose.

11.4.2.4 Lead Systems for the Characterization of Atrial Fibrillation

van Oosterom and colleagues have recently published details [32] of a vectorcardiographic lead system which they say was dedicated to the analysis of atrial fibrillation. The positions of seven electrodes are shown in Fig. 11.20. These electrode positions were chosen after extensive mathematical modeling to find leads that best represent atrial activation. The authors were firmly of the opinion that the best lead systems must include at least one electrode on the back. They also presented a series of transformations that allow the standard 12-lead ECG to be derived from the vectorcardiographic leads.

11.5 Derived 12-Lead ECG Systems

11.5.1 The Derived 12 Lead ECG

The reluctance of cardiologists to move from the use of the 12-lead ECG has already been mentioned. In the mid-1970s, the concept of using only three leads for computer analysis of the ECG was attractive in view of the saving in time for measurement and storage requirements. This led Dower and colleagues to introduce the derived 12-lead ECG [33]. By making use of the image space discussed in Chap. 10, they were able to produce a set of coefficients which allowed the 12-lead ECG to be derived from the *XYZ* leads.

In mathematical terms, the concept of the derived leads is to express each of the 12 leads as a linear combination of the *XYZ* orthogonal leads. Mathematically,

$$\text{derived lead} = aX + bY + cZ$$

where *X*, *Y* and *Z* represent the potentials measured by each of these leads respectively, and *a*, *b*, c represent coefficients which are fixed from a study of Frank's image space. The values of these coefficients for deriving each of the 12 leads are

Table 11.3

Transfer coefficients for deriving the 12-lead ECG from the XYZ leads, as obtained by Dower et al. [33]. Note that Z in this case is directed positively towards the back. For convenience, this table is presented in a 3 × 12 format, although it is used as a 12 × 3 matrix in Sect. 11.6

	I	II	III	aVR	aVL	aVF	V_1	V_2	V_3	V_4	V_5	V_6
X	0.632	0.235	−0.397	−0.434	0.515	−0.081	−0.515	0.044	0.882	1.213	1.125	0.831
Y	−0.235	1.066	1.301	−0.415	−0.768	1.184	0.157	0.164	0.098	0.127	0.127	0.076
Z	0.059	−0.132	−0.191	0.037	0.125	−0.162	−0.917	−1.387	−1.277	−0.601	−0.086	0.230

shown in Table 11.3. These have been slightly modified compared to an earlier publication [34] and appear in a 3 × 12 format for convenience. As an example, lead I would be derived as follows:

$$\text{lead I} = 0.632\,X - 0.235\,Y + 0.059\,Z$$

Note that this calculation has to be carried out at each sampling instant, that is, the *XYZ* values represent simultaneous measurements at one particular instant from each of the *XYZ* leads, and normally, when using computer methods, such measurements are made at least 250 times per second. Thus, the calculation would have to be repeated at this frequency. Note also that if the input from the *XYZ* leads is in mV, then the resultant calculation also produces mV output values.

An alternative approach is to construct an analog equivalent of the transformation coefficients so that if the *XYZ* leads are fed as input to electronic circuitry, then there will be a continuous output for each of the leads [35]. Uijen et al. [36], however, suggested that there was an inconsistency between the coefficients of Table 11.3 and the published hardware implementation [35].

There can be obvious differences between the derived 12-lead ECG and the conventional 12-lead ECG although Dower and colleagues undertook one study [35] which claimed to show that the derived ECG (ECGD) correlated better with the clinical findings than did the actual 12-lead ECG. This is equivalent to saying that in that particular study, the *XYZ* leads were superior to the conventional 12-lead ECG. An example of the similarity and differences is shown in Fig. 11.21.

A report by Uijen et al. [36] claimed that the use of a statistically derived transfer matrix gave better agreement between the 12 derived leads and actual data than did either of the Dower transfer matrices. However, the calculation was based on an evaluation of the training set used to develop the transfer matrix and it was noted that there could be wide variations, particularly in V_3 and V_4, between derived and actual leads. The transfer matrix from this group is shown in Table 11.4.

The value of the derived 12-lead ECG is limited, whatever the method of derivation. No single transfer matrix can be accurate for every patient, and hence the derived 12-lead ECG would require a complete appraisal in terms of normal limits, and so on, before being of more obvious value. Of more interest is the inverse approach described in Chap. 11, Sect. 11.6.

11.5.2 The EASI Lead System

Perhaps the most frequently used derived 12 lead system at present is based on the EASI lead system of Dower and colleagues [37]. In this system, only four electrodes are required. These are placed at the Frank positions A, E, and I as well as at the top of the sternum, denoted S. Rearrangement of the electrode nomenclature leads to the descriptor EASI. Figure 11.22 illustrates this lead system. With the use of these electrodes the three orthogonal leads were derived as follows:

$$X = V_A - V_I$$
$$Y = V_E - V_S$$
$$Z = V_A - V_S$$

The 12 lead ECG was then derived in the usual way described above as a combination of the three "orthogonal" leads. However, Dower did not publish explicit coefficients. Later, Feild et al. published [38] various sets of coefficients derived in

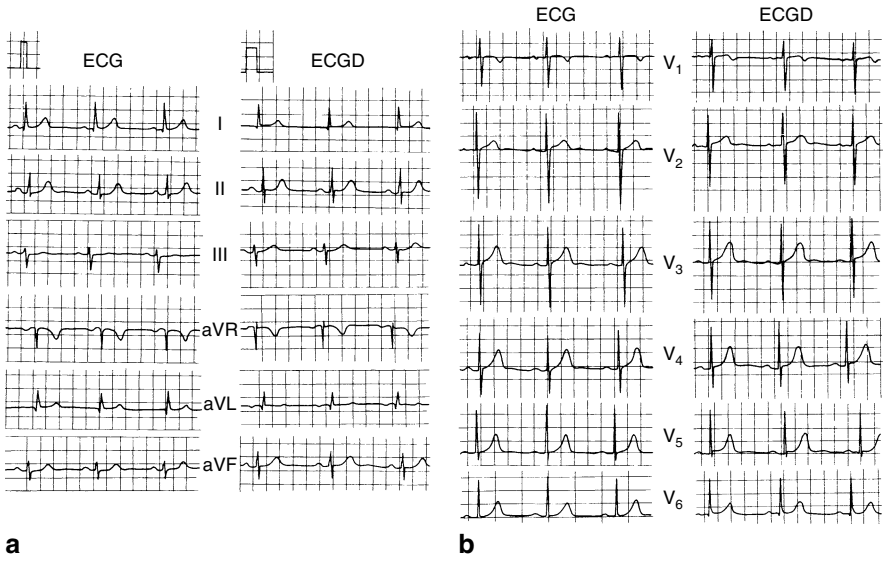

Figure 11.21

A comparison of the 12-lead ECG recorded in the usual fashion with the derived 12-lead ECG (ECGD). In this example, there is generally good agreement in morphology but differences are apparent on closer inspection; for example, there is more obvious ST elevation in the derived ECG than in the original while there are amplitude differences, e.g. the R wave in aVF in the derived ECG is over 50% larger than in the conventional recording (Reproduced with permission of Dr G Dower).

Table 11.4

Transfer coefficients for deriving the 12-lead ECG from the *XYZ* leads. These values were obtained by Uijen et al. [36]. Note that Z is directed positively to the back

	I	II	III	aVR	aVL	aVF	V_1	V_2	V_3	V_4	V_5	V_6
X	0.79	0.24	−0.56	−0.51	0.67	−0.16	−0.52	−0.15	0.69	1.34	1.09	0.65
Y	−0.24	1.05	1.29	−0.41	−0.77	1.17	−0.06	−0.35	0.38	0.68	0.64	0.52
Z	0.08	−0.01	−0.09	−0.03	0.08	−0.05	−1.04	−1.76	−1.16	−0.49	0.01	0.23

different ways, including a statistical approach based on several thousand actual 12 lead ECGs compared to corresponding 12 lead ECGs derived from the same individuals using the EASI lead system (Table 11.5).

There have been a number of studies that have looked at the accuracy of interpretation of ECGs derived from the EASI lead system and suggested that it is perfectly adequate for several types of applications, e.g. diagnosing acute myocardial infarction [39]. Our own work suggested a propensity for the system to exhibit inferior Q waves when none was present in the true 12 lead ECG [40].

11.5.3 Reduced Lead Sets

An alternative approach to reducing the number of electrodes required particularly for the monitoring situation is to use a reduced number of precordial leads from which the remaining leads can be calculated. Nelwan et al. [41–43] have studied this problem extensively. Essentially there are two approaches to the problem.

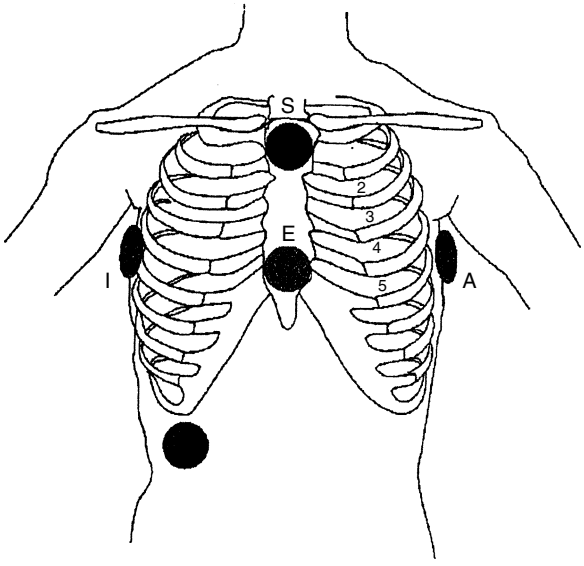

Figure 11.22

The EASI lead system. The electrodes A, E, I relate to the Frank electrode positions while S denotes an electrode at the upper end of the sternum (After Dower [37]. © Elsevier. Reproduced with permission).

Table 11.5

Coefficients for deriving the standard 12 leads from orthogonal leads X, Y, Z obtained using the EASI lead system (Reprinted from [38] with permission)

Lead	AI (X)	ES (Y)	AS (Z)
I	0.701	0.026	−0.174
II	−0.763	−0.002	1.098
III	−1.464	−0.028	1.272
aVR	0.031	−0.012	−0.462
aVL	1.082	0.027	−0.723
aVF	−1.114	−0.015	1.185
V_1	0.080	0.641	−0.391
V_2	1.021	1.229	−1.050
V_3	0.987	0.947	−0.539
V_4	0.841	0.525	0.004
V_5	0.630	0.179	0.278
V_6	0.213	−0.043	0.431

The first is to record a complete 12-lead ECG on an individual. If it is required to monitor the patient using leads V2 and V5 for example (as well as having limb leads available), the missing leads V1, V3, V4 and V6 can each be derived from the remaining leads recorded on that particular patient, namely I, II, V2 and V5. If, for example,

$$V1 = a\,I + b\,II + c\,V2 + d\,V5$$

then a, b, c, d are unique for that individual patient, and the reconstruction is said to be based on a patient specific transformation.

The other approach is to take a group of patients from which a generalized transformation can be developed to enable missing precordial leads to be calculated from a subset such as V2 and V5 plus limb leads as above. The approach to deriving the coefficients a, b, c, d is based on a gathering a training population where all 12 leads are recorded. The optimum values of a, b, c, d are then calculated so that, when applied to all ECGs in the set to produce reconstructed leads, the best correlation is obtained with the original leads. The procedure is repeated for other missing leads. The actual performance accuracy was reported in a separate test set.

Nelwan et al. [42] showed that reconstruction accuracy was high using the generalized approach where the correlation between original and reconstructed leads was approximately 0.93 whereas using a patient specific reconstruction, with up to 4 precordial leads being removed, the correlation increased to 0.97. Thus, as expected, patient specific reconstruction was better than the use of the general transformation.

Figure 11.23 gives an example of general and patient specific reconstruction of leads in an acute situation where recordings have been made at baseline and 24 hours later.

It is clear that the patient specific reconstruction is more labor intensive and can only be used effectively in hospital where there is time to make an initial recording, calculate the transformation values and have appropriate equipment that is then able to use the specific transformation for the patient being monitored. In the acute situation, such as recording in an ambulance, the time constraints are such that it would be simpler to use a generalized transformation if a reduced number of leads is to be used, as this is a much faster process. In any event, the full 12-leads must be positioned to derive a patient specific transform so that the main benefit of reduced leads is likely to be in long term monitoring. Nevertheless, the technique does offer an effective approach to reducing the number of leads required to give accurate 12-lead reconstruction and allow ECG interpretation to be made with a high degree of accuracy.

11.6 Derived Orthogonal-Lead ECG

The inverse of the derived 12-lead ECG is the derived orthogonal-lead ECG. Another way of expressing the equation for deriving the ECGD is as follows:

$$D = CL$$

where C is a 12 × 3 matrix of transformation coefficients (Table 11.3) and L is the 3 × 1 lead array (the values of *XYZ* at a particular instant). Multiplication of C and L produces a 12 × 1 array D containing the derived values of the 12 leads at a particular instant. On the other hand, if it is required to derive the *XYZ* leads, i.e., L given a knowledge of C and D, then the following equations describe the procedure involved [44].

Let

$$M = C^T C$$

and

$$M^{-1}M = I$$

where I is the identity matrix. Then

$$\begin{aligned} L = IL &= M^{-1}ML \\ &= M^{-1}C^T CL \\ &= \left(M^{-1}C^T\right) D \end{aligned}$$

The matrix $M^{-1}C^T$ represents an "inverse Dower" transformation and is shown in Table 11.6. Note that this table shows a 3 × 8 matrix which was all that was published by Edenbrandt and Pahlm [44]. It indicates that the input D is an 8 × 1 matrix consisting of the data from the eight independent leads V_1–V_6, I and II. In this implementation, C therefore is an 8 × 3 matrix where only the 8 independent leads of the 12-lead ECG are used. These authors used V_1–V_6, I and II. Thus, from Table 11.6,

$$\text{lead } X = -0.172V_1 - 0.074V_2 + 0.122V_3 + 0.231V_4 + 0.239V_5 + 0.194V_6 + 0.156I - 0.010II$$

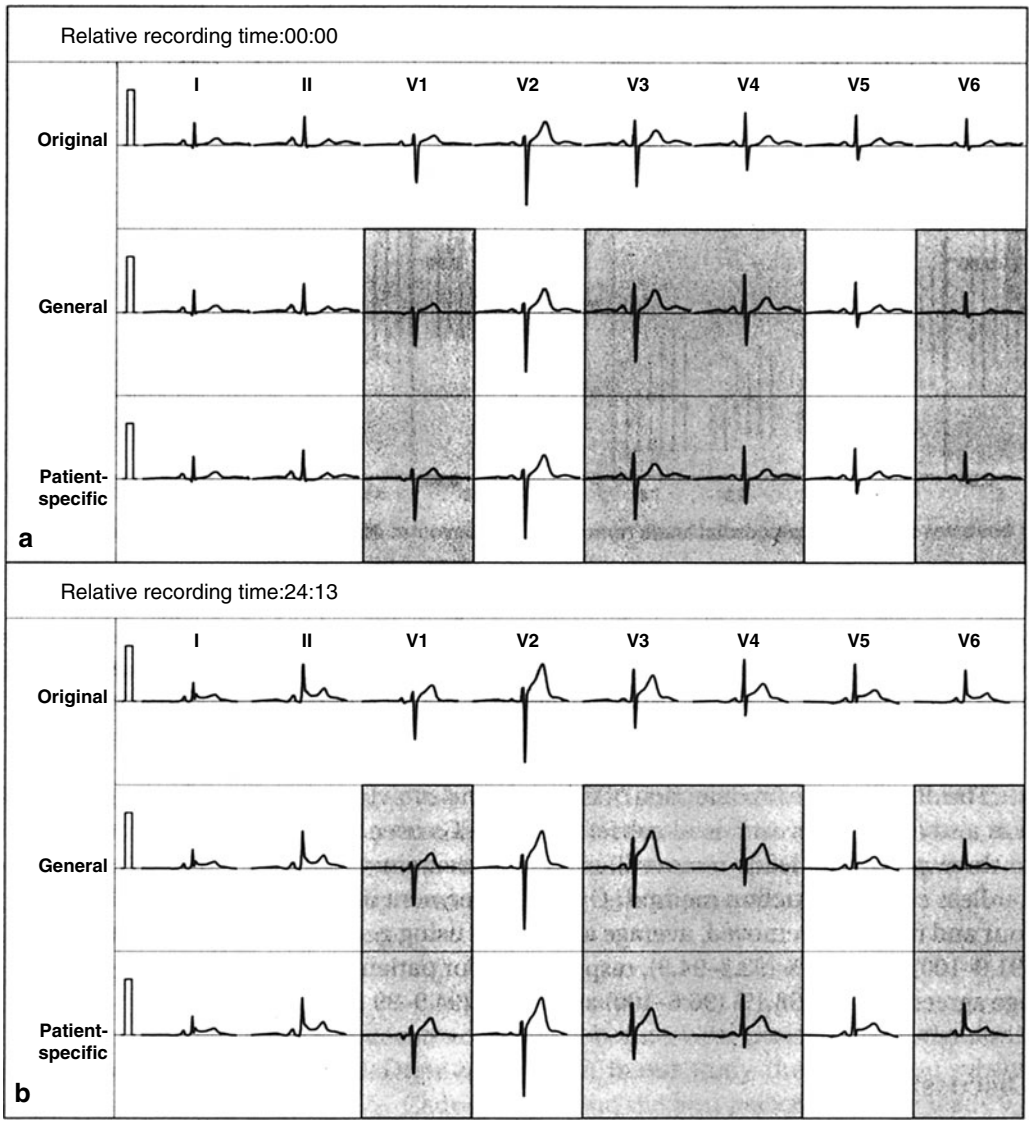

Figure 11.23

The reconstruction of precordial leads V1, V3, V4 and V6 from 4 other leads, namely I, II, V2 and V5. Two time instants are shown with 11.23a being a baseline recording while 11.23b was recorded approximately 24 hours later. ST elevation is apparent in b (After Nelwan et al. [42]. © Elsevier. Reproduced with permission).

Note in the table that the columns represent the coefficients for V_1–V_6, I and II, respectively.

In an essentially identical manner, Uijen and colleagues [36] derived an inverse matrix, but on this occasion they used their own transfer matrix (Table 11.4) as input to the inverse calculation, with a resulting matrix shown in Table 11.7. Note in this matrix that leads VR and VL are specified rather than I and II.

A similar approach was adopted by the group of Van Bemmel and the results were published in the 4th progress report of the study sponsored by the European Community on common standards in electrocardiography (CSE) [45]. Table 11.8 gives the required transfer coefficients. It should be noted that these have been scaled to give the optimum comparison between actual *XYZ* leads and derived *XYZ* leads which were available in the CSE study being directed by Willems [46]. The scaling coefficients are also indicated in the table.

Table 11.6

The transfer coefficients for deriving the *ZYZ* leads from the 12-lead ECG according to Edenbrandt and Pahlm [44]. The resulting *Z* lead will be directed positively to the back

	V_1	V_2	V_3	V_4	V_5	V_6	I	II
X	−0.172	−0.074	0.122	0.231	0.239	0.194	0.156	−0.010
Y	0.057	−0.019	−0.106	−0.022	0.041	0.048	−0.227	0.887
Z	−0.229	−0.310	−0.246	0.063	0.055	0.108	0.022	0.102

Table 11.7

The transfer coefficients for deriving the *XYZ* leads from the 12-lead ECG according to Uijen et al. [36]. The resulting *Z* lead will be directed positively to the back

	VR	VL	V_1	V_2	V_3	V_4	V_5	V_6
X	−0.52	0.82	−0.01	0.04	0.04	0.05	0.07	0.37
Y	−1.53	−1.09	0.03	−0.02	−0.02	0.03	−0.07	0.08
Z	0.43	−0.01	−0.26	−0.28	−0.14	0.04	−0.15	0.34

Table 11.8

The transfer coefficients for deriving the *XYZ* leads from the 12-lead ECG according to the group of Van Bemmel [45][a]

	II	III	V_1	V_2	V_3	V_4	V_5	V_6
X	0.58	−0.82	−1.27	−0.55	0.72	1.86	1.92	1.53
Y	2.58	3.04	−0.71	−0.71	0.10	0.35	0.12	−0.15
Z	−0.80	−1.62	−1.71	−2.26	−2.02	−0.80	0.31	0.97

[a] Scaling: *X* (measured) = 0.134 × *X* (calculated), *Y* (measured) = 0.1565 × *Y* (calculated), and *Z* (measured) = 0.122 × *Z* (calculated)

Table 11.9

The transfer coefficients for deriving the *XYZ* leads from the paediatric 12-lead ECG where V4R is used to the exclusion of V3 [from 47]

	I	II	V4R	V1	V2	V4	V5	V6
X	+0.160	−0.013	−0.128	−0.122	+0.009	+0.275	+0.251	+0.185
Y	−0.235	+0.891	+0.073	+0.019	−0.087	−0.065	+0.025	+0.051
Z	−0.023	+0.128	−0.072	−0.278	−0.439	−0.189	−0.016	+0.084

Edenbrandt and Macfarlane published a set of coefficients for deriving the X, Y and Z leads in children [47]. In this age group, $V4_R$ is normally used in preference to V3 as discussed above. Hence the transfer coefficients of Table 11.3 for example cannot be used. From the image surface data of Frank [13], the coefficients for $V4_R$ were obtained (−0.537, 0.096, −0.272) and these replaced the V3 coefficients in the Dower 12 lead ECG derivation of Table 11.3. The inverse matrix was then calculated using the method described above. The resulting coefficients are shown in Table 11.9.

It is unlikely that there will be more intensive investigation of this approach in view of the continued reluctance of cardiologists to study *XYZ* leads or vectorcardiograms. Nonetheless, the approach is inherently attractive in that with the recording of only the eight independent leads of the 12-lead ECG, it then becomes possible to produce all 15 leads of the 12 plus *XYZ* leads. In other words, there is almost a 50% reduction in the storage space required to retain all 15 leads when recorded by standard methods. Although 15 leads can be derived by this approach, there can, of course, be no additional information compared to that contained in the eight independent leads I, II and V_1–V_6.

It should be realized that although from a theoretical standpoint the derived orthogonal leads should resemble the actual *XYZ* leads if they were recorded, they may on occasion be markedly different on account of the use of a single transfer matrix (set of coefficients) being used for subjects of varying build. Proponents of the technique acknowledge this and advocate its use for various reasons. First, no extra electrodes are required to derive the additional XYZ leads. Second, the value of such an approach is likely to lie in examining the phase relationships between the different leads as

exemplified and studied in vectorcardiography. A simple example is shown later in Fig. 11.27 where two pairs of leads of similar appearance are shown. However, when these leads are plotted to form a vectorcardiographic loop, two entirely different configurations are seen. This is due to the different timing relationships between the leads, as will be evident from careful study of the data in the illustration.

11.7 The Vectorcardiogram

With the availability of three simultaneously recorded corrected orthogonal leads *XYZ*, it becomes possible to display the recording in different ways. Clearly, the conventional scalar presentation of the leads is a basic option. On the other hand, the theory of the resultant cardiac vector (dipole) indicates that the magnitude and movement of the vector during the cardiac cycle could be displayed. If it is imagined that the resultant vector increases from zero magnitude and then alters in magnitude and direction throughout the cardiac cycle, the tip of the vector with coordinates (X, Y, Z) (see Chap. 2) should trace out a loop in space. Conventionally, the projections of this path onto three mutually perpendicular planes have been obtained for study as shown in Fig. 11.24. The projection on the frontal plane (Fig. 11.13) effectively represents the variation in (X, Y) values throughout the cardiac cycle. Similarly, the sagittal and transverse (horizontal) planes represent changes in the (Z, Y) and (X, Z) coordinates, respectively. Thus, with the use of a graph plotter or equivalent device, for example, it is a simple matter to plot the *XY* coordinates during the cardiac cycle and obtain the frontal plane loop. Similar procedures can be used to obtain the sagittal and transverse loops as shown in Fig. 11.25. These loops are known as the vectorcardiogram (VCG). The terminology used to describe vectorcardiographic loops is displayed in Fig. 11.26. The direction of inscription of the loop can be determined in different ways. For example, if a multicolored plotter is available, the efferent limb can be plotted in a different color compared to the afferent limb. Arrowheads can also be used. Older methods of plotting the loops on an oscilloscope are now largely obsolete, while newer technology, such as the laser printer, will be of increasing value.

The separation of the dots on the plotted loops is arbitrary. Nowadays, however, this may depend on the sampling rate of the computer system used, with dots being typically at 2 or 4 ms intervals. The usefulness lies not only in outlining the direction of inscription but in noting where conduction defects may occur, at which time the separation of the dots becomes reduced. The various aspects of vectorcardiographic interpretation are discussed in the respective clinical chapters.

As an aside, it should be noted that quite independent of any theory of vectorcardiography, it is possible to plot pairs of leads to produce loops. Ideally, however, such leads should have directions which are well separated, otherwise the loop

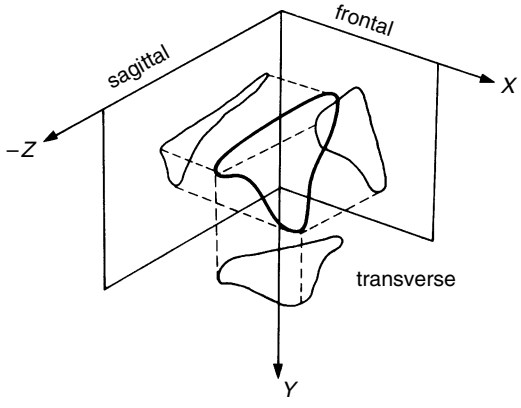

Figure 11.24

The concept of the projection of a loop in space onto three mutually perpendicular planes. For convenience, the −*Z* axis is illustrated.

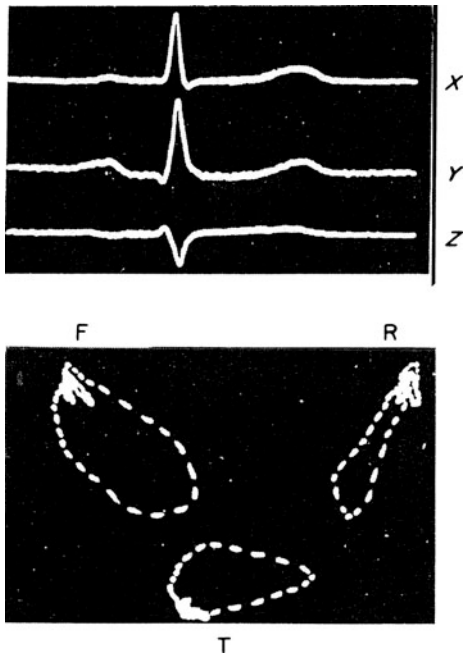

Figure 11.25

An illustration of a VCG obtained in the conventional manner by inputting pairs of leads to opposite points of the oscilloscope. The dashes are separated by 2 ms intervals and inscription is from the thin to the thick end of the dash; for example, there is counterclockwise inscription in the transverse (T) plane (F, frontal; R, right sagittal). The corresponding scalar *XYZ* leads are shown with *Z* directed positively to the anterior (= V_2).

would tend to a straight line as would be the case with plotting two essentially similar leads. Thereafter, a study of the patterns produced could be undertaken on a purely empirical basis. An understanding of the concept of vectorcardiography and the use of leads with approximately orthogonal directions is still recommended.

To see in a simple way how a vectorcardiographic loop is constructed, the reader should carefully study the example of Fig. 11.27. The scalar amplitudes of one pair of leads (*X*, Z) are provided for a small number of instants during the QRS complex for two different cases. For teaching purposes, lead *X* is identical in the two while appearances in each lead Z are similar but bear a different timing relationship to lead *X*. The amplitudes of leads *X* and Z are indicated at corresponding instants in time so that pairs of points (*X*, Z) can be plotted. In this example, Z is directed positively to the anterior, to resemble V_1 or V_2. In Fig. 11.27(a), the direction of inscription of the loop is counterclockwise, which is normal in the transverse plane. In Fig. 11.27(b), the direction of inscription is clockwise, which is abnormal and would suggest the possibility of right ventricular hypertrophy for various reasons (see Chap. 15). Thus, the vectorcardiographic presentation is providing additional information that is not readily seen in the scalar display. The complete VCG would be constructed using the other pairs of leads (*X*, *Y*) and (*Y*, Z) in a similar fashion.

11.8 Derived Vectorcardiogram –12 Lead Vectorcardiography

In Chap. 11, Sect. 11.6, the derived orthogonal-lead ECG was introduced. It follows that the derived VCG is simply another form of displaying the derived *XYZ* leads. In Fig. 11.28, vectorcardiograms are shown which were obtained using the hybrid-lead system and the derived *XYZ* leads based on two forms of inverse Dower transformation [36, 44]. The general similarities can be seen.

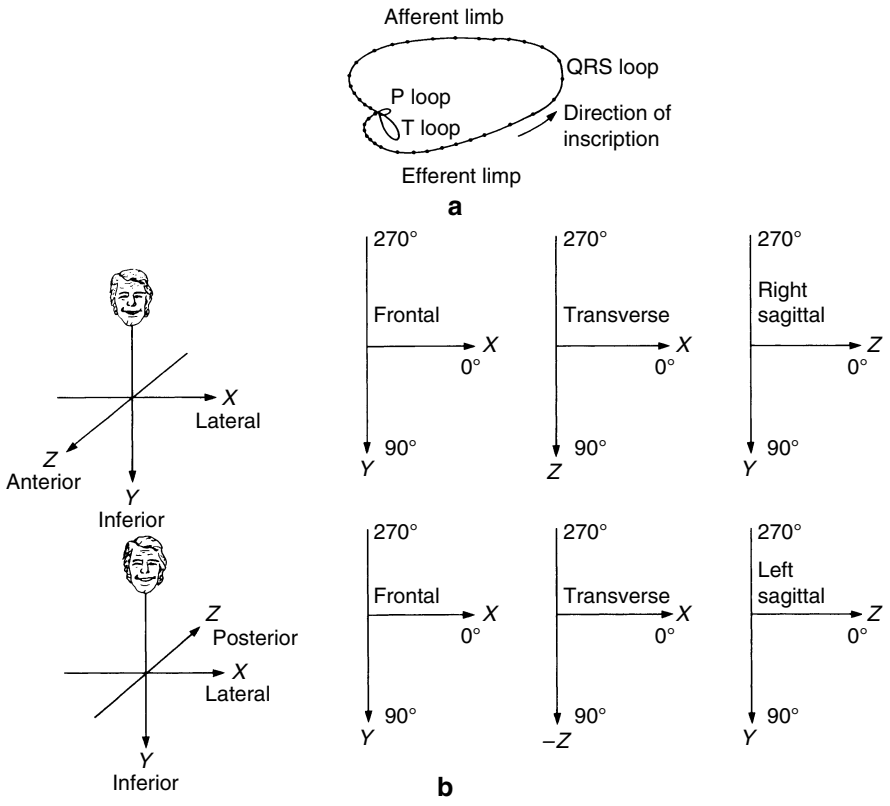

Figure 11.26

In (a), the terminology used to describe a vectorcardiographic loop is shown. In (b), alternative reference frames for measurement and display of VCGs are displayed. The author prefers lead *Z* directed positively to the anterior so that appearances resemble V1 and V2, as shown at the top of Fig. 11.23b. In addition, by choosing the right sagittal view, all reference frames are similar. An alternative scheme, with *Z* directed positively to the back and with the left sagittal view being used, is shown in the lower part of Fig. 11.23b. In practice, the transverse view is similar to the other scheme, but the VCG as seen in the left sagittal view is a mirror image of that in the right sagittal view.

The availability of the derived VCG leads to the possibility of what has been termed "12 lead vectorcardiography" [48]. This topic is discussed more fully in Chap. 43. In short, the advantages of vectorcardiography can be utilized by appropriate processing of the 12 lead ECG. While there can be no additional information, the phase relationships between the leads can be utilized to assist with diagnosis as previously illustrated in Fig. 11.27.

11.9 Interrelationship of the 12-Lead and *XYZ* Lead Electrocardiograms

In schematic form, Fig. 11.29 shows the relationships between the various leads of the 12 and 3-orthogonal-lead ECGs. As shown above, it is quite possible to derive mathematically one lead set from another. However, on a simpler level it is possible to construct a vector loop manually from a knowledge of the 12-lead ECG and vice versa. The advantage of this lies only in a further understanding of the underlying electrical activity. It goes without saying that estimation of the QRS axis from the 12-lead ECG in the frontal plane is implicitly involved in such a procedure. Indeed, Fig. 11.27 provides an

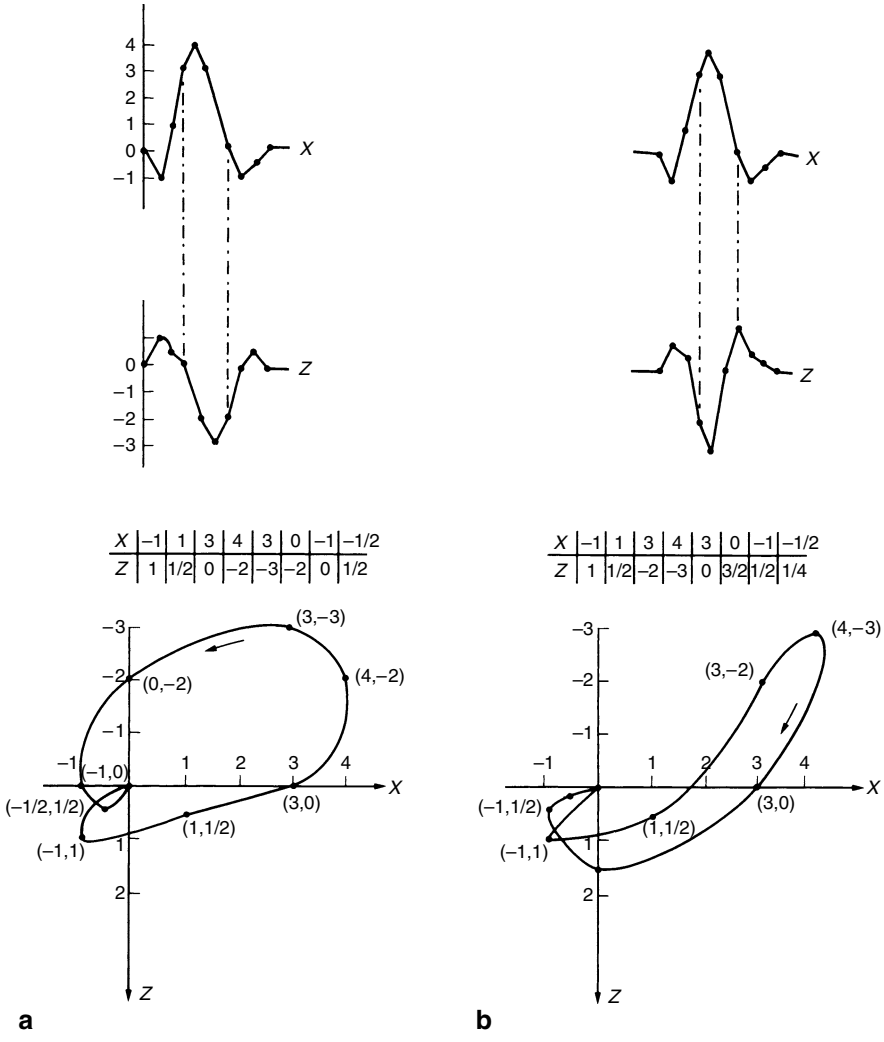

Figure 11.27

The construction of the transverse plane of the vector loop given simultaneous measurements from leads *X* and *Z*. In (a), the loop is inscribed counterclockwise; in (b), the bulk of the loop is inscribed clockwise. It should be noted that lead *X* is identical in each example but that the different timing relationships leads *X* and *Z* in each case lead to the different loop configurations. Lead *Z* is directed positively to the anterior in this example so that the rSr′ pattern resembles that often found in V1 or V2. The value of a VCG in such a case should be understood from this example.

example of a derivation of a transverse loop given leads *X* and Z, although these equally well could have been called V_5 and V_1, respectively.

Suppose that leads I and aVF are recorded simultaneously and that a set of amplitudes at corresponding instants in time are obtained as in Fig. 11.30a. It is then possible to construct a vector loop in the knowledge that this is only an approximation in view of the fact that I and a VF are not electrically orthogonal and have different lead strengths. Nevertheless, using simple graph plotting techniques, a loop can be derived as shown in Fig. 11.30a. The converse is clearly true in that if the loop represented an actual frontal plane VCG, then the reverse procedure would have produced the scalar leads which in reality would have been *X* and *Y*.

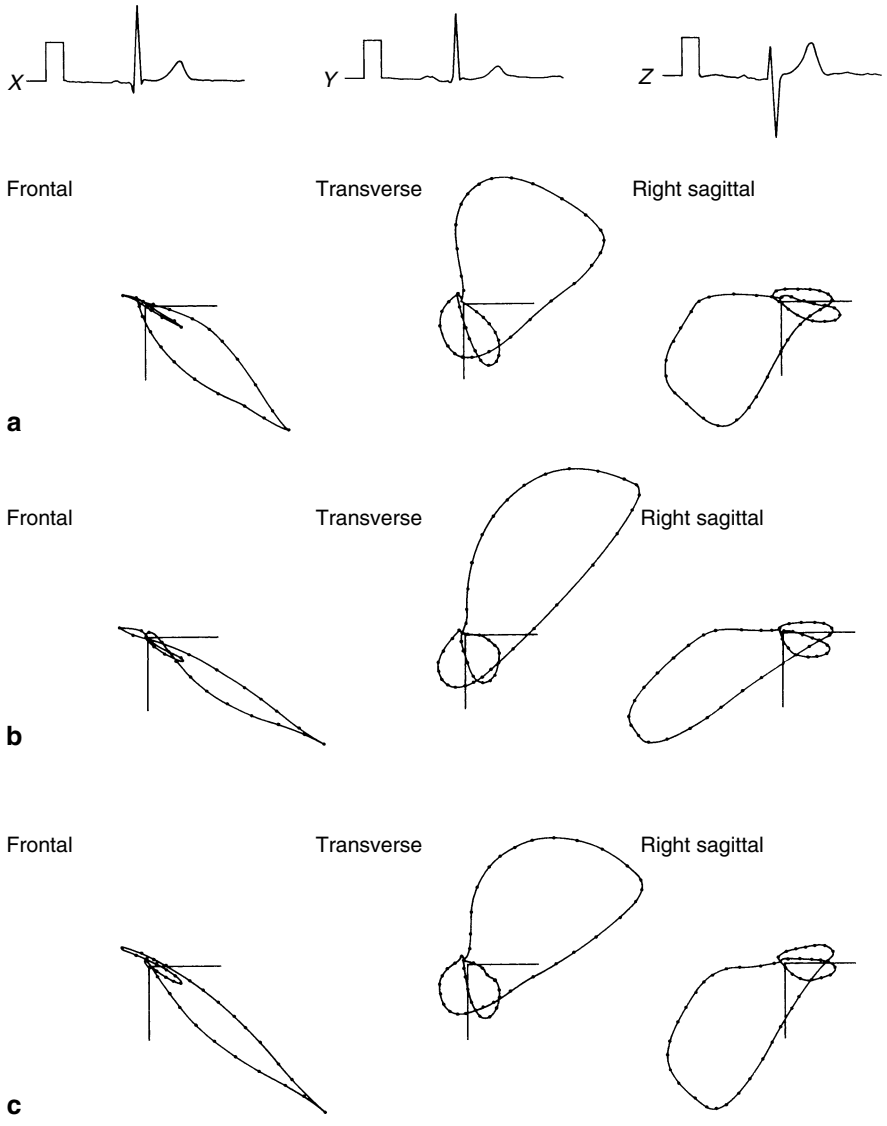

Figure 11.28

The three vectorcardiographic loops: (a), the VCG derived from the hybrid system; (b), the VCG on the same patient derived from the inverse Dower technique using the coefficients described in [44] (c), the VCG from the same patient using the inverse Dower technique described in [45]. There are some differences in shape but the loops are substantially similar. Lead *Z* is directed positively to the anterior.

The important point to note in this particular illustration is how the crossing of the different axes relates to inscription of the VCG. In general terms, if there is clockwise inscription of the loop as in Fig. 11.30a, then the lead I axis is crossed at a point when the Q wave terminates in aVF and generally prior to the peak value of the R wave in lead I. On the other hand, in a situation where there is counterclockwise inscription (Fig. 11.30b), the crossing of the aVF axis corresponds to the end of the Q wave in lead I. Warner and colleagues [49] used this type of information, but from leads II and III, in order to improve the diagnosis of inferior myocardial infarction. A point of note here is the value of using multichannel electrocardiographs that permit I and aVF to be displayed simultaneously.

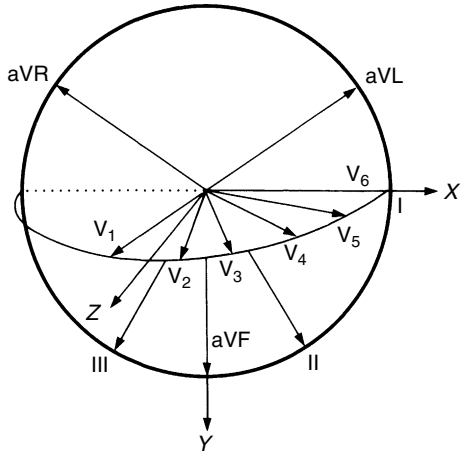

Figure 11.29
The interrelationship between the lead vectors of the 12-lead ECG and the orthogonal-lead ECG. These are shown in an idealized form, that is, no allowance is made for torso inhomogeneties, and so on. Lead *Z* is directed positively to the anterior.

11.10 Nomenclature

There is considerable variation in the nomenclature of leads, particularly V_1–V_6. The American College of Cardiology in its report [50] on optimal electrocardiography suggested the following guidelines (Fig. 11.31).

I, aVL	lateral leads
II, III, aVF	inferior leads
V_1, V_2	septal leads
V_2–V_4	anteroseptal leads
V_3, V_4	anterior leads
V_5, V_6	anterolateral leads

In Chap. 16 on myocardial infarction, Selvester et al. argue strongly for terminology based on recommendations of a working group of which he was a member. Their recommendations (corresponding to Fig. 16.1 which, for convenience, is shown here as Fig. 11.32) are based on the anatomical orientation of the heart in the thorax and concern the nomenclature of myocardial regions. However, the electrocardiographer invokes the inverse process by relating changes in various leads to myocardial abnormalities. This being so, the following can be inferred from Fig. 11.32:

I, aVL, V_5, V_6	posterolateral (apical) leads
II, III, a VF	inferior leads
V_2–V_4	anterior leads

This terminology has evolved from a consideration of coronary arterial distribution and is recommended by Selvester et al. for use in describing myocardial infarction.

Recently, the combination of the ECG and MRI scans has led Bayes de Luna et al. [51] to advocate revised terminology for the location of a myocardial infarction involving the left ventricle. In particular, these authors suggested that the terms "posterior" and "high lateral" should not be used when describing a myocardial infarct and should be replaced by "lateral" and "mid-anterior" respectively (see Fig. 11.33). It has to be noted that these authors are referring to the position of an infarct and are not necessarily ascribing these names to electrocardiographic leads, but historically, lead descriptors and locations of an infarct are often interchanged.

On the other hand, a writing group of the American Heart Association [52] has recently declined to recommend adoption of the proposed changes until additional data is gathered.

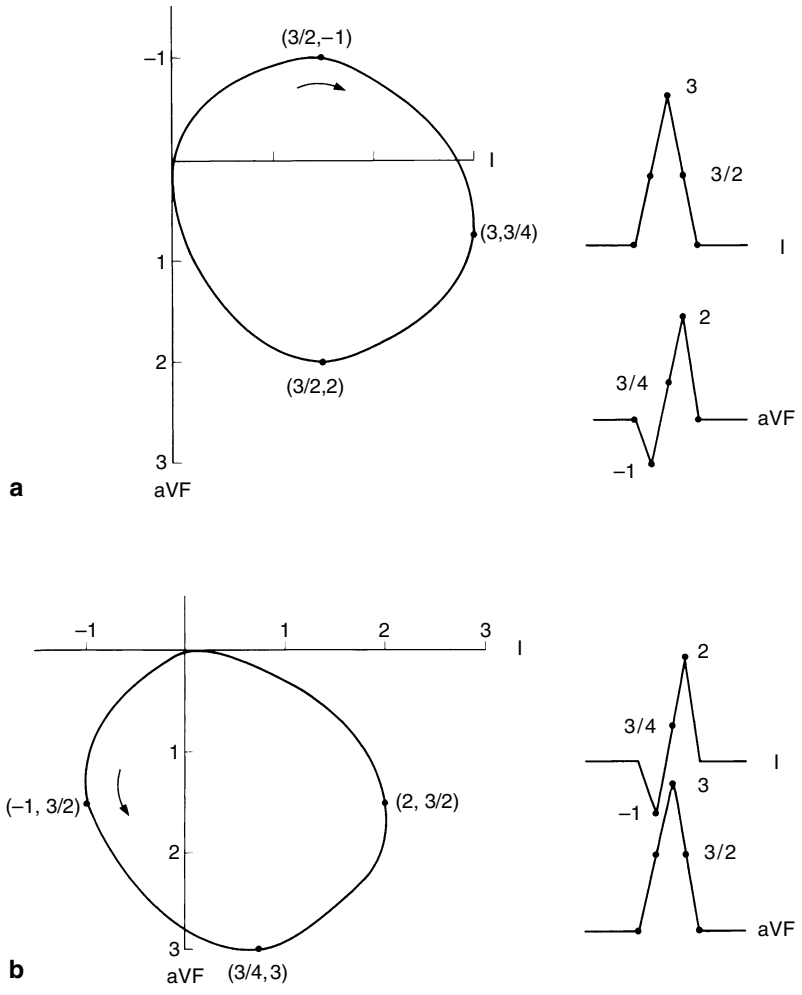

Figure 11.30

Part (a): the construction of a vectorcardiographic loop from leads I and aVF. In this instance, there is clockwise inscription of the vector loop and it can be seen that the termination of the Q wave in aVF is prior to the peak of the R wave in lead I. Part (b): in this example, the relationship of leads I and aVF is such that the derived vectorcardiographic loop has counterclockwise inscription in the frontal plane and, in this case, the end of the Q wave in lead I occurs prior to the peak of the R wave in aVF.

The recent series on recommendations for interpretation of the ECG, in paper II [53], lists the following descriptors for the location of a myocardial infarction:

Anterior
Inferior
Posterior
Lateral
Anteroseptal
Extensive anterior
MI in the presence of LBBB
Right ventricular MI

The publication does not define the leads associated with each descriptor.

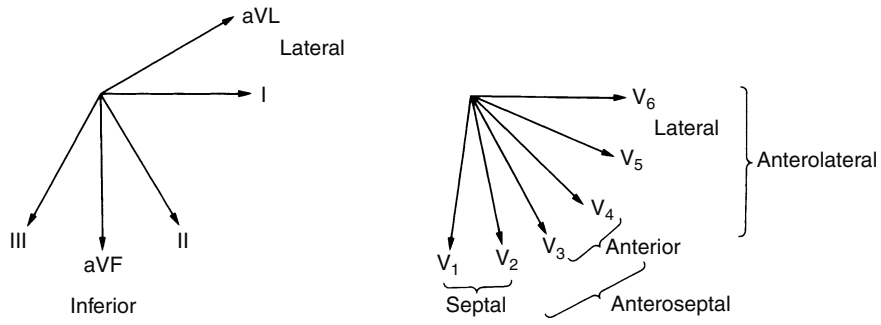

Figure 11.31
Nomenclature used in the description of various leads.

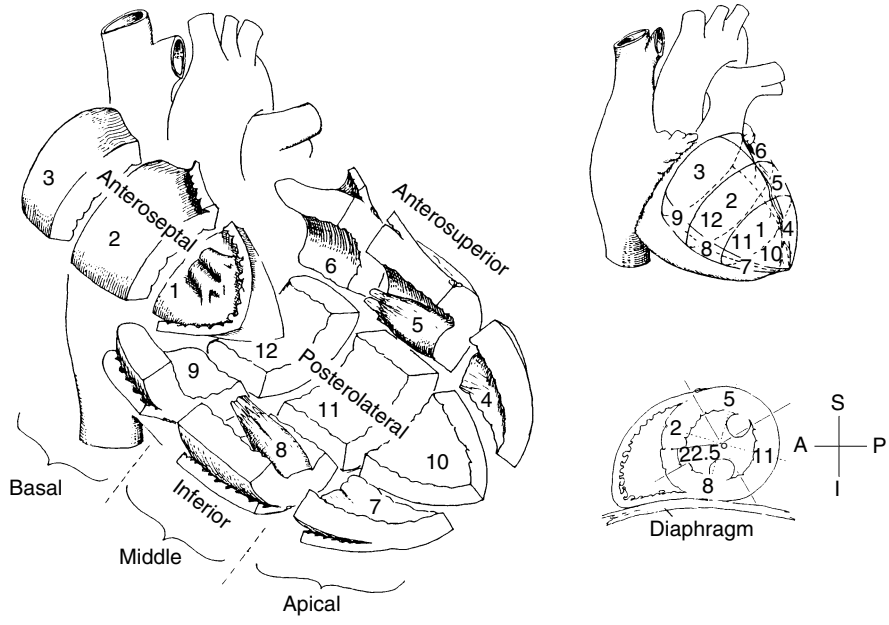

Figure 11.32
The division of the heart into various regions after Selvester et al. (Chap. 16) in which their recommendations for terminology can be found.

11.11 Exercise ECG Lead Systems

A variety of bipolar chest leads has been used for exercise testing in the past. In the main, these have been a reflection on the use of single-channel equipment and the aim of simplifying the procedure as much as possible. Nowadays, with increased availability of computer-based exercise ECG analysis methods, it is common to utilize the conventional 12-lead ECG for exercise testing.

NAME	ECG PATTERN	INFARCTION AREA (CMR)
SEPTAL	Q in V1-V2	
MID ANTERIOR	Q (qs or qr) in aVL and sometimes in I and / or V2-V3	
APICAL-ANTERIOR	Q in V1-V2 to V3-V6	
EXTENSIVE ANTERIOR	Q in V1-V2 to V4-V6. aVL and sometimes I	
LATERAL	RS in V1-V2 and/or Q wave in leads I. aVL, V6 and/or diminished R wave in V6.	
INFERIOR	Q in II, III aVF	

Figure 11.33

Proposed terminology for describing the location of a myocardial infarction from the 12 lead ECG (After Bayes de Luna et al. [51]. © AHA. Reproduced with permission).

In 1966, Mason and Likar published their recommendations for moving the limb electrodes used to record the 12-lead ECG from the limbs to the thorax [54] for exercise electrocardiography. Their repositioned electrodes are shown in Fig. 11.34. They compared ECG recordings where the right and left arm electrodes were positioned in the conventional areas of the arm to those obtained from gradually moving the electrodes to progressively proximal positions up the arms and then over the upper anterior chest. Finally, it was recommended that the right arm electrode be moved to a point in the infraclavicular fossa medial to the border of the deltoid muscle and 2 cm below the lower border of the clavicle. The corresponding position was recommended for the left arm electrode as shown in Fig. 11.34. Further experimentation led to a recommendation that the left leg electrode (denoted LL) be placed in the anterior axillary line halfway between the costal margin and the iliac crest. They suggested that the location of this electrode was not critical; that is, it could be varied by a few centimeters in any direction to avoid skin folds, and so on. Some authors simply regard this reference point as being the left iliac crest [55]. Mason and Likar initially illustrated the right leg electrode as being on the right thigh, but for convenience it is now a matter of routine to place this electrode in the region of the right iliac fossa as recommended by the American College of Cardiology [56].

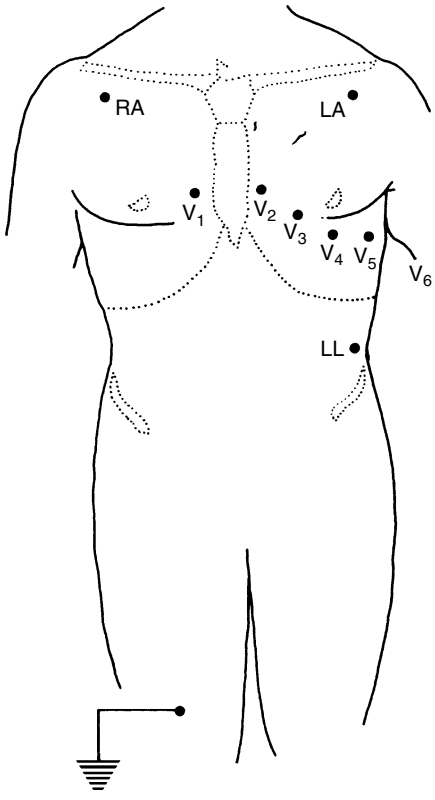

Figure 11.34

The modified electrode positions for the limbs according to Mason and Likar [54]. See text for further discussion. Note that the right leg (ground) electrode is usually nowadays positioned in the right iliac fossa (After Mason and Likar [54]. © Mosby, St Louis, Missouri. Reproduced with permission).

For a number of years, many investigators used a simple combination of chest electrodes to record a bipolar chest lead during exercise testing. Almost always, the positive electrode was placed in the V_5 position while the negative electrode was placed in a variety of positions that are illustrated in Fig. 11.10. If the negative electrode were placed on the manubrium, then the lead was denoted CM_5. The full range of positions that have been adopted in the past for the negative electrode is shown in Fig. 11.10 and listed in Table 11.2. In Chap. 36, there is a discussion of the leads now thought most suited to exercise testing, but for didactic purposes it is instructive to consider further the bipolar leads introduced above.

The configuration of the leads recorded during exercise can vary markedly depending on the position of the negative electrode. This can be seen clearly from scrutiny of Fig. 11.35. In this illustration, three bipolar leads have been recorded simultaneously and marked differences can be seen in the ST segment. Note here that lead CL is a bipolar lead with the positive electrode on the left leg and the negative electrode on the manubrium. Leads CC_5 and CM_5, which at one stage were commonly used, show entirely different ST changes; in the case of the former, the ST segment is upward sloping whereas in the latter it is flat or slightly downward sloping. Chaitman and colleagues [57], who obtained this illustration, suggested that multiple-lead ECG recording improved the sensitivity and efficiency of maximal treadmill exercise testing. This point is discussed further in Chap. 36.

In a separate study, Froelicher et al. [55] assessed CC_5 and CM_5 against the standard lead V_5. They showed that when using visual interpretation, the same criteria could be used for CC_5 and V_5 but different criteria were necessary for interpreting CM_5. Figure 11.36 shows the different mean slopes before and after exercise in both normal and abnormal responders. Clear differences can be seen between the three leads, with CM_5 showing the most ST deviation.

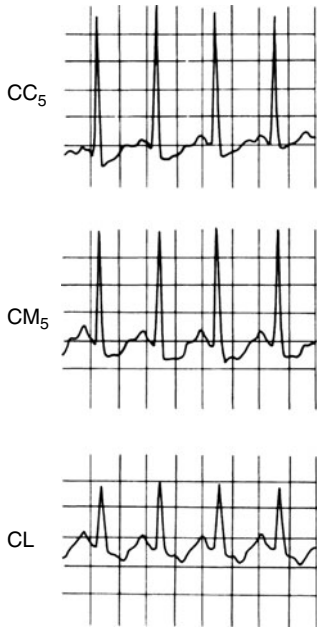

Figure 11.35

An example of three simultaneously recorded leads obtained during exercise. Note the different ST-T configuration in each lead. (After Chaitman et al. [57]. © American Heart Association, Dallas, Texas. Reproduced with permission).

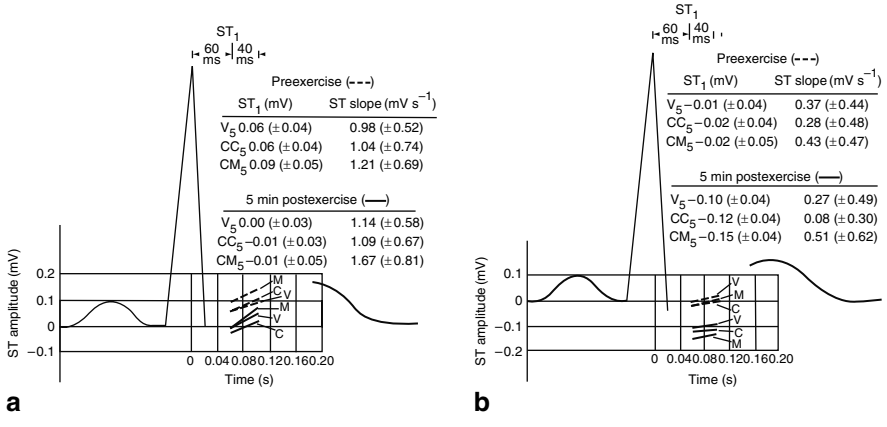

Figure 11.36

The different mean ST amplitudes and slopes before and after exercise for (a), a group of 26 normal responders; and (b), a separate group of 21 abnormal responders who had three leads simultaneously recorded. M denotes CM5, C denotes CC5 and V denotes V5. (Froelicher et al. [55]. © American College of Chest Physicians, Mark Ridge, Illinois. Reproduced with permission).

On the other hand, CM_5 showed the greatest upward slope of the ST segment. These findings reflect the different strengths and orientations of the lead vectors as discussed in Sect. 11.3 and indicate that different criteria must be used when interpreting different leads. This becomes more feasible in the era of computer averaging of exercise ECG leads where more accurate measurement of ST T changes is now possible.

From Fig. 11.11 it can be seen that the lead strength of CM_5 is greater than V_5 and some additional ST -segment depression would be expected in this lead as confirmed by the data of Froelicher [55]. The lead direction for CM_5, as

also would be expected, is quite different to that of CC_5 and V_5, and hence a different ST depression and slope would be expected compared to the other leads which have relatively similar lead-vector directions.

Nowadays, most exercise electrocardiography is 12 lead based with automated analysis of the waveforms. Users should be aware that the averaging techniques used in exercise ECG are of necessity different from those used in a 10 s recording of a resting ECG with some hysteresis involved. Noise can have an effect on the averaging process and scrutiny of the actual recording is recommended in addition to review of the averaged cycles. Furthermore, use of the Mason Likar positions for 12 lead exercise (or resting) electrocardiography results in significant differences in the ECG compared to the standard lead positions and this must always be remembered [7, 58].

11.12 ECG Monitoring in Hospital

It goes without saying that the ECG is used universally for patient monitoring in hospitals. A recent guideline paper set out best practices for hospital monitoring as well as indications for ischemia and QT monitoring among other things [59]. Of relevance to this chapter are the comments on choice of leads for patient monitoring.

The first point to make is that the practice standards acknowledge that for patient monitoring, wrist and ankle electrodes are placed on the torso essentially in the Mason Likar positions [54] described above in 11.11. With 4 electrodes in these positions, a modified version of the six frontal plane leads could be recorded. However, for monitoring purposes, a unipolar chest lead is usually required to assist with rhythm analysis. In this case, conventional circuitry as discussed in 11.2.4 can be used with one to six chest electrodes as desired.

A very simple 3-electrode bipolar system was also included in the hospital monitoring standards [59]. Essentially this used the MCL lead with the third electrode employed as a ground as illustrated in Fig. 11.37. Many other lead systems that can be used in the monitoring situation such as reduced leads, orthogonal leads and derived 12 leads, have all been discussed at an earlier point in this chapter.

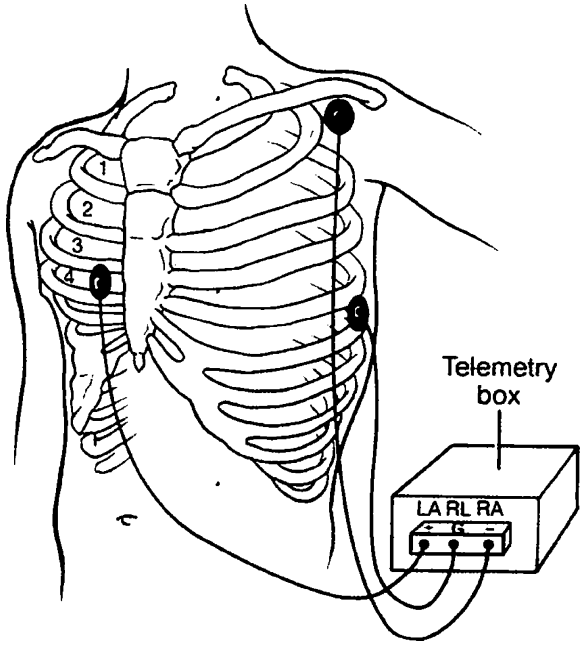

Figure 11.37

A basic 3 electrode bipolar lead system for recording lead CL_1 i.e. positive electrode placed in V_1 and the negative electrode in the left infraclavicular fossa. The reference electrode, here shown in the V_6 position, could be located anywhere. LA = left arm, RA = right arm, RL = right leg. (Reproduced from Circulation 2004; 110: 2721, with permission.)

11.13 Body-Surface Mapping Lead Systems

Body-surface mapping was introduced for two reasons. The first reason was to permit a study of the spread of excitation over the thorax. This allowed the normal patterns to be studied and inferences drawn on the time of epicardial "breakthrough" of activation at the right and left ventricles. In addition, empirical study of abnormal patterns together with clinical correlation allowed methods for interpretation of maps to be developed, as discussed in Chap. 32. Some investigators use between 16 and 240 electrodes to map the thorax using computer techniques for plotting.

The second reason for mapping is to assess in a mathematical way the total electrical information available, and perhaps relate this via an inverse model to epicardial excitation, etc. (see Chap. 9). Barr suggested [60] that 24 surface leads would allow the thorax to be mapped so that with the use of a transformation, the ECG data at other points could be estimated. The aim behind this particular study was to derive information on the equivalent cardiac generator and so attack the inverse problem (see Chap. 9). Kornreich used a 126-lead system to map the body surface and from this concluded that nine independent leads would be adequate to retrieve all of the clinically useful information on the body surface [61, 62]. His array used 18 columns of electrodes with 84 on the anterior chest and 42 electrodes on the back (Fig. 11.38). The group of Taccardi used a 219 irregularly spaced electrode array. Lux et al. [63], as described in Chap. 31, also utilized complex mathematical techniques to reduce the number of electrodes required for mapping to a more limited number on which they were able to calculate normal ranges and assess the results of exercise testing.

Mapping systems used for clinical purposes, such as outlining areas of ST elevation following acute myocardial infarction, generally consist of a small array of unipolar chest leads. The differences between the systems essentially relate only to the number of electrodes and hence to their relative spacing on the chest. Maroko et al. in 1972 [64] suggested the use of a 5 × 7 electrode array for ST mapping following myocardial infarction. In 1979, Fox et al. [65] utilized a 4 × 4 array of electrodes for mapping infarcts and also for exercise testing. It was subsequently suggested that this be reduced to a

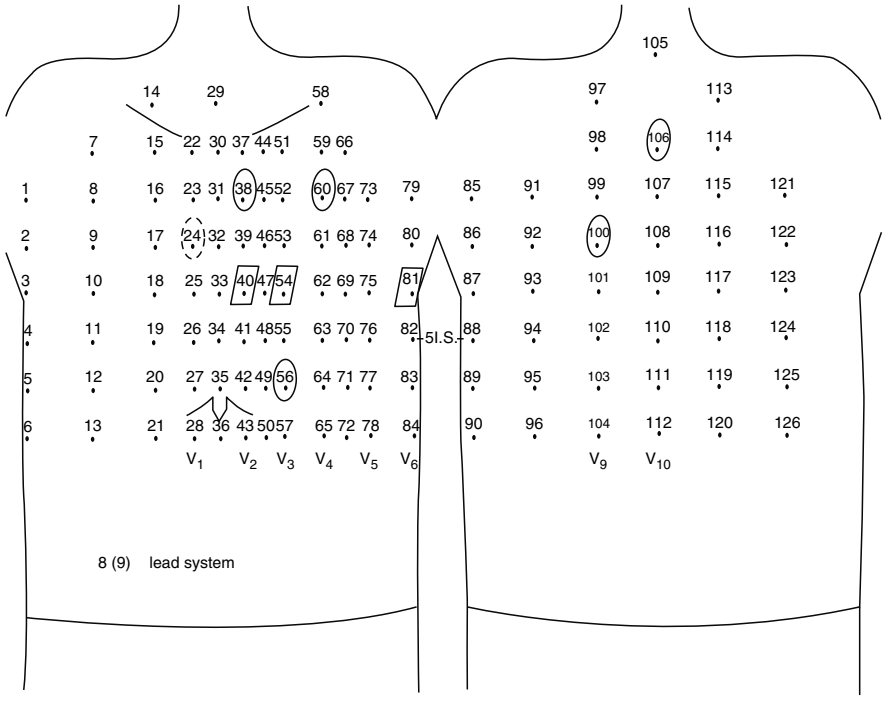

Figure 11.38

The 126 electrodes used by Kornreich for mapping. The nine independent leads, which were claimed to contain all of the information for clinical use on the body surface, are also indicated by circles and rectangles.

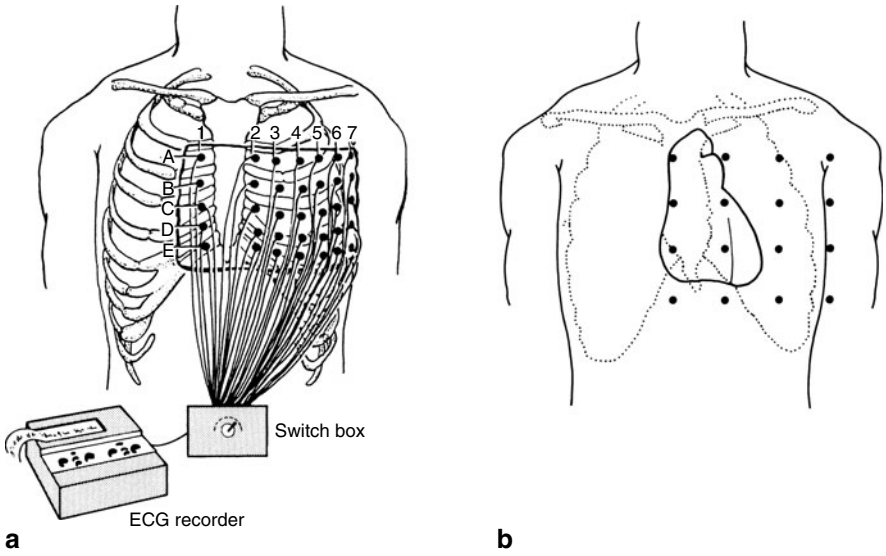

Figure 11.39

In (a), the 35 lead mapping system used by Maroko et al. is shown. (After Maroko et al. [64]. © American College of Cardiology, New York. Reproduced with permission). In (b), the 16-lead array of electrodes used by Fox et al., who subsequently recommended that the rightmost column of electrodes be removed to leave a 12-lead array, is shown. (Fox et al., [65]. © British Medical Association, London. Reproduced with permission).

4 × 3 array [66]. An illustration of these lead systems is shown in Fig. 11.39. Monro et al. [67] utilized a 24-electrode array that explored both the anterior and posterior chest walls, but in addition, with the use of sophisticated mathematical interpolation techniques, the potentials at any other point on the thorax could be calculated [68, 69]. More recently, the group of Adgey have used 64 anterior (including limb) and 16 posterior electrodes in their work on acute myocardial infarction [70].

The topic of body-surface mapping is under active study in a number of centers. Color displays are now used to present maps (see Chap. 21) while commercial mapping systems are becoming increasingly available. Further discussion on mapping can be found in Chaps. 31 and 32, while some early work is summarised in conference proceedings [71, 72].

11.14 Epicardial and Intracardiac Mapping

Cardiac mapping is a term used to describe the recording and display of multiple potentials recorded from the endocardium, the epicardium or transmural sites.

11.14.1 Transmural and Epicardial Mapping

Either for basic research or for clinical purposes, mapping of the spread of cardiac excitation is of value (see Chaps. 4 and 32). Taccardi and colleagues recently described [73] an elegant system for intramural mapping of the dog heart. A form of multi-electrode needle is used with 10 electrodes spaced at 1.6 mm. Up to 56 such needle electrodes together with a sock electrode carrying 242 epicardial electrodes were used. The system allowed recording from up to 1,024 electrodes simultaneously at a sampling rate of 1 KHz. Data were acquired in digital form and processed to produce color coded three dimensional activation maps. An automated system for transmural cardiac mapping has also been described by

Witkowski and Corr [74]. For human cardiac mapping, each needle has eight electrodes from which four bipolar signals are recorded. Data are converted into digital form at 2,000 samples s^{-1} and stored on a computer for further processing, e.g., the construction of isochrones of activation or epicardial isopotential maps.

11.14.2 Endocardial Mapping

Another technique for the study of arrhythmias is endocardial mapping. In this case, different intracardiac catheters, e.g., bipolar, quadrupolar or hexapolar, record ventricular electrograms from which relative timings can be obtained. In a ventricular tachycardia (VT), the earliest electrogram is regarded as the site of origin. Bipolar or unipolar electrograms can be recorded in the usual way (see Chap. 24). This area has seen an explosion of interest in recent years in relation to the treatment of cardiac arrhythmias. It is discussed fully in Chap. 25.

11.14.3 Pace Mapping

Pace mapping has been used to determine the site of origin of a VT [75]. In this case, the tachycardia is maintained by pacing from a particular site. The 12 lead surface ECG recorded during the pacing can be compared with that recorded during spontaneous VT. By changing the site of pacing, the paced ECG which most closely resembles that during spontaneous VT indicates the most likely source of the tachycardia, i.e., the point on the endocardium at which pacing is being undertaken. Epicardial versus endocardial pace mapping has recently been investigated [76] in localizing the site of a VT arising in the right ventricle.

11.14.4 Intracoronary ECG

Although not strictly mapping, a method for recording the intracoronary ECG has recently been described [77, 78]. In practice, the technique can be used to monitor myocardial ischemia during percutaneous transluminal coronary angioplasty. The intracoronary ECG can be obtained by connecting the proximal end of the catheter guidewire as it exits from the balloon catheter to a precordial lead of a surface ECG cable. The Wilson central terminal is used as a reference in the usual way. Friedman et al. [77] filtered the ECG from 0.1 to 100 or 500 Hz, as appropriate. They obtained best results when a short segment of the guidewire protruded beyond the distal lumen of the balloon catheter. DeMarchi et al. [78] recently used the technique in a study which showed that, in patients with chronic stable angina pectoris, after all known determinants of infarct size were taken into account, susceptibility to ischemia is greater in the left than in the right coronary artery region.

11.15 Ambulatory Monitoring Leads

Ambulatory monitoring may be carried out for different purposes, and to a certain extent, the leads selected may reflect the purpose of the test. Perhaps the most common requirement for undertaking ambulatory recording is to investigate cardiac rhythm. For many years, single channel recordings were made on account of cost and availability of equipment. In such cases, a bipolar lead such as CS_5 was, and still is, often employed. More recently, multichannel recording equipment has now become readily available, as have replay facilities that display the recorded leads simultaneously. The use of this approach assists in discriminating artifact from genuine ectopic beats and pauses. The recording of multiple leads also

provides an additional safety factor in the event of malfunction of one channel or perhaps detachment of one electrode, which is a common occurrence.

The American Heart Association (AHA) established a task force of the Committee on Electrocardiography to report on the practice of ambulatory electrocardiography. The recommendations [79] included suggestions for electrode placement for two-channel recording. It is clear that the subcommittee did not wish to be dogmatic about recommended positions since they acknowledged that different positions would be required based on the varying need for undertaking a 24-hour recording. The recommendation for two-channel recording was based on a five-electrode system, one of which is a ground electrode with the other two pairs each forming a bipolar lead. The recommended electrode positions are as follows.

(a) *V_1 type lead*. The positive electrode should be in the fourth right intercostal space, 25 mm from the sternal margin while the negative electrode should be in the lateral third of the left infraclavicular fossa.
(b) *V_5 type lead*. The positive electrode should be in the fifth left intercostal space at the anterior axillary line and the negative electrode should be 25 mm below the inferior angle of the right scapula on the posterior torso. The fifth electrode, the ground. electrode, should be placed in the lateral third of the right infraclavicular fossa.

The subcommittee pointed out that the use of individual negative or reference electrodes contributes to the redundancy of the two-lead recording system in that if a common reference electrode were to fail, both channels would be of no use. The electrode positions are illustrated in Fig. 11.41. With the appropriate circuitry, unipolar precordial leads and limb leads could be recorded using the Mason-Likar electrode positions (Fig. 11.34). Indeed, there are now commercially available ambulatory monitors that record a full 12 lead ECG in digital form for 24 hours.

A second reason for undertaking ambulatory electrocardiography may be to evaluate symptoms that are possibly related to myocardial ischemia. In this case, assuming that equipment with the appropriate characteristics is available (see Chaps. 12 and 33) the recording is aimed at assessing ST-segment changes. The AHA committee noted previous suggestions that a pair of leads approximating V_3 and aVF may detect more ST-segment shifts in patients with unstable angina [80]. In another study [81], Quyyumi et al. utilized two bipolar leads to assess ST changes in patients with varying severity of coronary artery disease. In this case a CM_5 lead and an inferior lead said to resemble aVF were used.

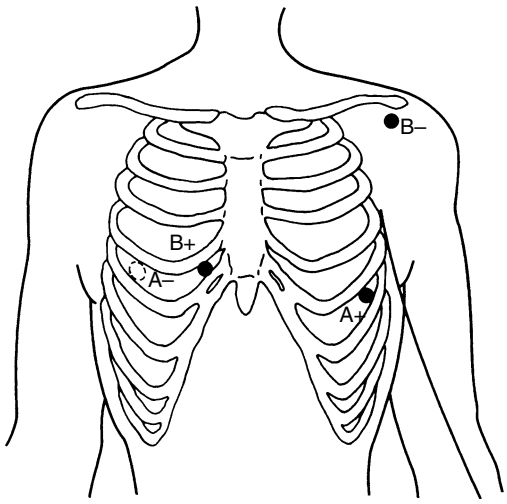

Figure 11.40
The recommended electrode positions for two-channel ambulatory ECG recording according to the subcommittee of the American Heart Association [79], A+ and A– are the positive and negative electrodes for the V5 type lead (not the same as V5) and B+ and B– are the electrodes for the V1 type lead)not the same as V1). The open circle denotes an electrode on the back. See text for a full description of electrode positions.

The latter was obtained with one electrode positioned at the xiphisternum and the other at the left sternoclavicular joint. Further discussion on ambulatory monitoring can be found in Chap. 33.

A more recent set of ACC/AHA guidelines [82] on ambulatory electrocardiography concentrated more on the indications for ambulatory ECG than the technique itself.

11.16 Esophageal Leads

The use of an esophageal lead, for detection of atrial electrical activity in particular, is well established, having been introduced in the 1930s [83]. A more recent development in this area has been the availability of a pill electrode designed by Arzbaecher [84]. This device resembles an ordinary pharmaceutical capsule and is connected to a thin wire claimed to be "threadlike." The pill is swallowed by the patient with water and is allowed to descend into the esophagus. If sufficient length of the wire is used by the technician undertaking the procedure, the electrode will be positioned below the level of the atrium. The other end of the electrode is connected to a small amplifier unit which in turn is linked to lead I cables of an ordinary electrocardiograph.

The technician can then monitor the signal recorded by the pill electrode and withdraw the electrode gradually, i.e., raise the level of the electrode until it is behind the atria. This is recognized by the high-amplitude atrial signal which can be seen in the lead I position of the electrocardiograph. With the use of a multichannel machine, it is possible to record another lead simultaneously for timing purposes even though this additional lead may not be a perfect derivation in view of the fact that the left and right arm connections are linked to the pill electrode. It should be noted that the capsule containing the electrode actually dissolves so that the electrode is then exposed for the ECG recording. Figure 11.41 shows an esophageal ECG recording together with one other lead (lead II).

One report [83] suggested that the esophageal ECG may be diagnostic in 86% of cases where the surface ECG is inconclusive for rhythm determination. Furthermore, the esophageal ECG was used during 24-hour ambulatory monitoring and proved valuable in 41% of patients.

Although the esophageal ECG is normally used for clarification of arrhythmias, it has been used for ischemia detection. Machler et al. [85] in their study concluded that the clinical relevance of the esophageal ECG is that it provides a convenient technique with high sensitivity, for monitoring intraoperative myocardial ischemia and detecting atrial activity during cardioplegia. The technique is not commonly used nowadays though research reports occasionally appear, e.g., for diagnosing paroxysmal supraventricular tachycardia [86].

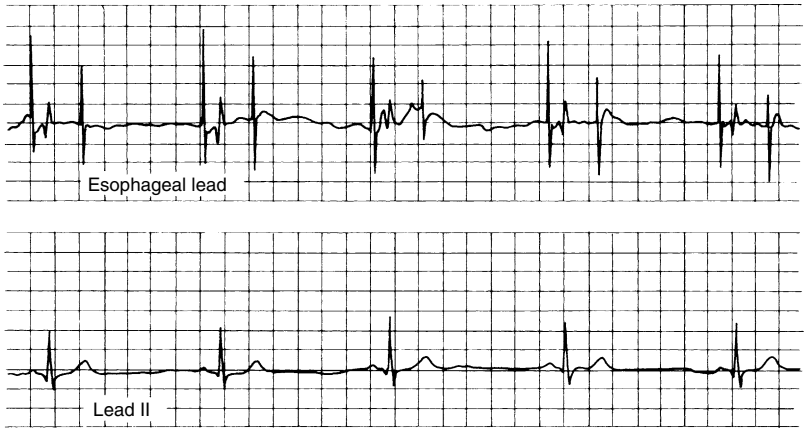

Figure 11.41

A two-channel recording showing an esophageal lead and lead II. In these simultaneously recorded leads, the atrial activation can be seen clearly (the large deflection) in the esophageal lead, where atrial bigeminy can be detected. In lead II, i.e., the surface ECG, the second P wave is essentially hidden in the T wave. (Reproduced with permission of Dr. Arzbaecher).

11.17 Fetal ECG Lead Systems

Fetal ECG recording has been practised for many years to assess the status of the unborn child, principally by heart-rate analysis during labor. In earlier times, it was also used to assess whether the fetus was still alive and occasionally to confirm the presence of twins. The advent of noninvasive ultrasound Doppler telemetry has perhaps diminished the usefulness of the fetal ECG (FECG), but on account of reservations over the safety of ultrasound in fetal monitoring, and in view of the possibility of analyzing the morphology of the FECG, there has been continued interest in fetal electrocardiography.

There are two approaches to recording the fetal ECG. The first is to utilize surface electrodes placed on the abdomen of the mother. Most commonly, a bipolar lead in a vertical direction is used, with the electrodes being placed near the umbilicus and above the mons pubis. Electrodes can be connected to lead I of an ordinary electrocardiograph with the other limb electrodes also being connected to the mother. With a high gain setting, it is normally possible to record the fetal ECG together with the maternal ECG signal. However, the amplitude of the FECG is relatively small compared to the maternal ECG and may on occasion be difficult to separate from background noise. Signal-processing techniques are required, as discussed in Chap. 20.

The second approach to FECG recording during labor is to attach an electrode directly to the fetal scalp. Another electrode, forming the second part of the bipolar lead, can be clipped to the perineum or placed in cervical/vaginal secretions. An indifferent electrode can be attached to a maternal limb. A higher quality FECG signal is obtained with this technique, but computer-based signal processing techniques are still required to facilitate analysis [87].

A different type of abdominal-lead system has also been described by Oostendorp et al. [88]. The 32 electrodes are arranged on the maternal abdomen and back in order to display, after appropriate signal processing, the potential distribution generated by the fetal heart; that is, a "fetal body-surface map" can be produced.

The European Community supported research into this topic, some aspects of which were presented in a series of articles [89]. A much more recent Cochrane review [90] noted that hypoxaemia during labor can alter the morphology of the fetal ECG, notably the relation of the PR to RR intervals, and elevation or depression of the ST segment. Techniques have therefore been developed to monitor the fetal ECG during labor as an adjunct to continuous electronic fetal heart rate monitoring with the aim of improving fetal outcome and minimizing unnecessary obstetric interference. The review concluded that there was some justification for the use of fetal ST analysis when a decision has been made to undertake continuous electronic fetal heart rate monitoring during labor. However, the advantages need to be considered along with the disadvantages of needing to use an internal scalp electrode, after membrane rupture, for ECG waveform recordings.

11.18 Comparative Electrocardiography

Because the ECG is of interest in many investigations assessing the efficacy of new therapeutic agents, the use of lead systems in various animals is introduced. First of all, the reader is referred to Chap. 41 where the dog ECG is discussed extensively. For this reason, no further reference to ECG lead systems in dogs is given here. Chap. 42 also discusses the ECG lead systems in mammals, but it is worth considering the ECG in rats in this chapter in view of the use of the rat as an experimental model. The Nehb leads have been introduced above in Sect. 11.3 and for rats and guinea pigs a modification introduced by Sporri [91] is commonly used. In this case the electrode placements are as follows:

(a) on the right scapula,
(b) over the apex of the heart, and
(c) over the lumbar vertebra

Using a conventional electrocardiograph, these leads would be connected, respectively, to the right arm, left leg and the left arm electrodes. This would allow leads D, A and I (alternatively called J) to be recorded. This modification of the Nehb leads is now referred to as the Nehb-Sporri lead system.

It is also possible to record a form of VCG in the rat using an uncorrected lead system. In this case, the X component would be measured by lead I with the positive electrode being on the left foreleg and the negative electrode on the right foreleg, the *Y* component would be recorded using aVF, i.e., the left and right leg electrodes would be used as with the 12-lead ECG, while the Z component would be obtained using a bipolar lead with electrodes placed on the sternum and

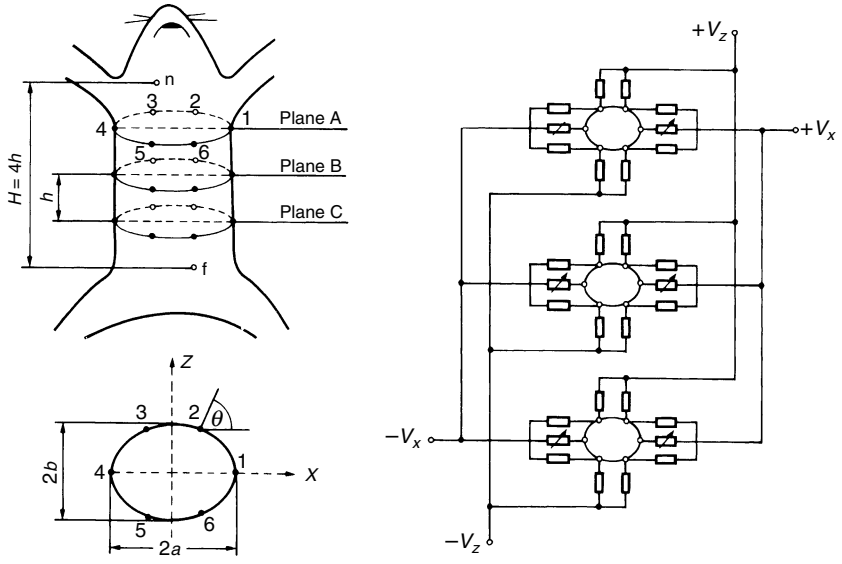

Figure 11.42

The modified form of the Nelson-lead system used by Schwartze and Thoss [93] for recording the VCG in rats. A total of 20 electrodes is used, from which the three vector components can be derived.

the thoracic vertebrae. This system is uncorrected in that the lead strengths would be unequal and therefore considerable distortion of the VCG would ensue.

Yamori et al. [92] have utilized the Takayasu-lead system in order to record the ECG from rats. The X lead is a straightforward bipolar lead with large electrodes on each side of the thorax, the *Y* lead is a bipolar lead between the base of the tail and the bridge of the nose, and the Z lead is also a bipolar lead with a large electrode on the sternum and another over the thoracic vertebrae.

The Frank system [21] has been used in rats by Schwartze and Thoss [93]. These authors also make use of a modified form of the Nelson-lead system [94]. This is illustrated in Fig. 11.42. The theory is based on earlier work of Gabor and Nelson [95], which theorized that the components of the resultant cardiac dipole M could be determined as follows:

$$M_x = \sigma \iint V\, dy\, dz$$

$$M_y = \sigma \iint V\, dx\, dz$$

$$M_z = \sigma \iint V\, dx\, dy$$

where σ is the electrical conductivity of the body and the integrations are over the body surface. Since surface integration is not feasible, discrete approximations are required. Eifrig et al. [96] used three planes with six surface electrodes on each (Fig. 11.42) together with a foot and neck electrode. Then,

$$M_x = \frac{\sigma HP}{24} \sum_{\alpha=A,B,C} \left(V_1^\alpha - V_4^\alpha + \left(V_2^\alpha + V_6^\alpha - V_3^\alpha - V_5^\alpha\right) \cos\theta\right)$$

$$M_y = \sigma D\left(V_f - V_n\right)$$

$$M_z = \frac{\sigma HP}{24} \sum_{\alpha=A,B,C} \left(V_2^\alpha + V_3^\alpha - V_5^\alpha - V_6^\alpha\right) \sin\ \theta$$

where V_i^α is the potential at point i on plane α, V_f and V_n are the foot and neck potentials and H, P and D are the body length, circumference and cross-sectional area, respectively; θ is the angle between the X axis and the normal to the

boundary (Fig. 11.42). Angle θ depends on b/a, the semimajor and minor axes of the thorax cross section, assumed to be elliptical. In practice, the summations are achieved by the resistor network shown in Fig. 11.42, where adjustable potentiometers allow the index b/a to be incorporated. The net effect is that V_x, Y_y and V_z are recorded via the resistor network to give

$$M_x = \sigma K_x V_x, \quad K_x = \frac{3HP}{24}(1 + 2\cos\theta)$$

$$M_y = \sigma K_y V_y, \quad K_y = D(V_y = V_f - V_n)$$

$$M_z = \sigma K_z V_z, \quad K_z = \frac{3HP}{24}\sin\theta$$

The use of such a technique allowed Eifrig et al. [96] to study the relationship between the development of body weight and the dipole moment.

Driscoll [97] reviewed the normal rat ECG and pointed out that the appearances of the rat ECG among other things depended on the form of restraint being used to position the rat during recording. Some authors record the ECG with the rat lying on its back normally under anesthesia; alternatively, others restrain the rat perhaps in a cylindrical device. The important point to realize is the difference in ECG appearances depending on the approach adopted.

Electrocardiograms can be recorded from baboons using the conventional 12-lead or 3-orthogonal-lead ECG. Hermann and Herrmann [98] utilized the 12-lead ECG in their studies. Ruttkay-Nedecky and Cherkovich [99] used the axial-lead system described in Sect. 11.4.2.2 in their studies of baboons.

References

1. Einthoven, W., G.E. Fahr, and A. De Waart, Uber die Richtung und die manifeste Grosse der Potentialschwankungen im menschlichen Herzen und iiber den Einfluss der Herzlage auf die Form des Elektrokardiogramms. *Pflug. Arch.*, 1913;**150**: 275–315. (Translation: Hoff H E. Sekelj P. On the direction and manifest size of the heart on the form of the electrocardiogram. *Am. Heart J.* 1950;**40**: 163–211.)
2. Burger, H.C and J.B. van Milaan, Heart vector and leads. I, II and III. *Br. Heart J.* 1946;**8**: 157–161, 1947;**9**: 154–160, 1948;**10**: 229–233.
3. Turner AM, 12 Lead recordings: Implications of an inconsistent approach. *Cardiology News* 2006;**9**: 10–12.
4. Pipberger, H V., R.C. Arzbaecher, A. Berson et al., Recommendations for standardization of leads and of specifications of instruments in electrocardiography and vectorcardiography. A report of the committee on electrocardiography of the AHA. *Circulation*, 1975;**52**(August Suppl): 11–31.
5. Sheffield, L.T., R. Prineas, H.C. Cohen, A. Schoenberg, and V. Froelicher, Optimal electrocardiography-1977. Task force II: Quality of electrocardiographic records. *Am J. Cardiol.*, 1978;**41**: 146–157.
6. Kligfield, P., L.Gettes, J.J. Bailey et al., Guidelines for the standardization and interpretation of the electrocardiogram, Part 1. The electrocardiogram and its technology. *Circulation*, 2007;**115**: 1306–1324.
7. Pahlm, O., W.K. Haisty, L. Edenbrandt et al., Evaluation of changes in standard electrocardiographic QRS waveforms recorded from activity compatible proximal lead positions. *Am. J. Cardiol.*, 1992;**69**: 253–257.
8. Kligfield, P. and P. Macfarlane, Non equivalence of proximal and distal arm electrode placement in routine electrocardiography. *J. Electrocardiol.*, 2005;**38**(Suppl): 36 (Abs).
9. Wilson, F.N., F.D. Johnston, A.G. MacLeod, and P.S. Barker, Electrocardiograms that represent the potential variations of a single electrode. *Am. Heart J.*, 1934;**9**: 447–458.
10. Frank, E., Determination of the electrical center of ventricular depolarization in the human heart. *Am. Heart J.*, 1955;**9**: 670–692.
11. Goldberger, E., A simple, indifferent, electrocardiographic electrode of zero potential and a technique of obtaining augmented, unipolar, extremity leads. *Am. Heart J.*, 1942;**23**: 483–492.
12. Committee of the American Heart Association for the Standardization of Precordial Leads. Standardization of precordial leads. (a) Supplementary report. *Am. Heart J.*, 1938;**15**: 235–239. (b) Second supplementary report. *J. Am. Med. Assoc.*, 1943;**121**: 1349–1351.
13. Frank, E., The image surface of a homogeneous torso. *Am. Heart J.*, 1954;**47**: 757–768.
14. Langner, P.H., Jr., An octaxial reference system derived from a nonequilateral triangle for frontal plane vectorcardiography. *Am. Heart J.*, 1955;**49**: 696–704.
15. Anderson, S, O. Pahlm, R. Selvester et al., Panoramic display of the orderly sequenced 12-lead ECG. *J. Electrocardiol.*, 1994;**7**: 47–352.
16. Cabrera, E., *Electrocardiographie clinique. Theorie et pratique*. Paris: Masson, 1959.
17. Nehb, W., Zur Standardisierung der Brustwandableitungen des Elektrokardiogramms. Mit Bemerkungen zum Friihbild des Hinterwandinfarkts und des Infarktnachschubs in der Vorderwand. *Klin. Wochenschr.*, 1938;**17**: 1807–1811.
18. Grishman, A. and L. Scherlis, *Spatial Vectorcardiography*. Philadelphia, Pennsylvania: Saunders, 1952.
19. Duchosal, P.W. and R. Sulzer, *La vectocardiographie*. Basel: Karger, 1949.

20. Wilson, F.N., F.D. Johnston, and C.E. Kossmann, The substitution of a tetrahedron for the Einthoven triangle. *Am. Heart J.*, 1947;**33**: 594–603.
21. Frank, E., An accurate, clinically practical system for spatial vectorcardiography. *Circulation*. 1956;**13**: 737–749.
22. Draper, H.W., C.J. Peffer, F.W. Stallmann, D. Littmann, and H.V. Pipberger, The corrected orthogonal electrocardiogram and vectorcardiogram in 510 normal men (Frank lead system). *Circulation*. 1964;**30**: 853–864.
23. Nemati, M., J.T. Doyle, D. McCaughan, R.A. Dunn, and H.V. Pipberger, The orthogonal electrocardiogram in normal women. Implications of sex differences in diagnostic electrocardiography. *Am. Heart J.*, 1978;**95**: 12–21.
24. Teppner, U., S. Lobodzinski, D. Neubert, and M.M. Laks, A technique to evaluate the performance of computerized ECG analysis systems. *J. Electrocardiol.*, 1987;**20** (Suppl.): 68–72.
25. McFee, R. and A. Parungao. An orthogonal lead system for clinical electrocardiography. *Am. Heart J.*, 1961;**62**: 93–100.
26. Brody, D.A. and R.C. Arzbaecher. A comparative analysis of several corrected vectorcardiographic leads. *Circulation*. 1964;**29**: 533–545.
27. Macfarlane, P.W., A modified axial lead system for orthogonal lead electrocardiography. *Cardiovasc. Res.*, 1969;**3**: 510–515.
28. Macfarlane, P.W., A.R. Lorimer, and T.D.V. Lawrie, 3 and 12 lead electrocardiogram interpretation by computer. A comparison of 1093 patients. *Br. Heart J.*, 1971;**33**: 266–274.
29. Macfarlane, P.W., E.N. Coleman, and A. Simpson, Modified axial lead system in children. *Br. Heart J.*, 1977;**39**: 1102–1108.
30. Macfarlane, P.W., A hybrid lead system for routine electrocardiography, in *Progress in Electrocardiology*, P.W. Macfarlane, Editor. Tunbridge Wells, Pitman Medical, 1979, pp. 1–5.
31. Macfarlane, P.W., M.P. Watts, and T.D.V. Lawrie, Hybrid electrocardiography, in *Optimization of Computer ECG Processing*, H.K. Wolf, and P.W. Macfarlane, Editors. Amsterdam, North-Holland, 1980, pp. 57–61.
32. van Oosterom, A., Z. Ihara, V. Jacquemet, and R. Heokema, Vectorcardiographic lead systems for the characterization of atrial fibrillation. *J. Electrocardiol.*, 2007;**40**: 343.e1–343.e11.
33. Dower, G.E., H. Bastos Machado, and J.A. Osborne, On deriving the electrocardiogram from vectorcardiographic leads. *Clin. Cardiol.*, 1980;**3**: 87–95.
34. Dower, G.E., A lead synthesizer for the Frank system to simulate the standard 12-lead electrocardiogram. *J. Electrocardiol.*, 1968;**I**: 101–16,252.
35. Dower, G.E. and H. Bastos Machado, Progress report on the ECGD, in *Progress in Electrocardiology*, P.W. Macfarlane, Editor. Tunbridge Wells, Pitman Medical, 1979, pp. 264–271.
36. Uijen, G.J.H., A. van Oosterom, and R.T.H van Dam, The relationship between the 12-lead standard ECG and the *XYZ* vector leads, in *Proc. 14th Int. Congr. Electrocardiology*, E. Schubert, Editor. Berlin, Academy of Sciences of the DDR, 1988, pp. 301–307.
37. Dower, G.E., A. Yakush, S.B. Nazzal, R.V. Jutzy, and C.E. Ruiz, Deriving the 12-lead electrocardiogram from four (EASI) electrodes. *J. Electrocardiol.*, 1998;**21**(Suppl): 182–187.
38. Field, D.Q., C.L. Feldman, and B.M. Horacek, Improved EASI coefficients: Their values, derivation and performance. *J. Electrocardiol.*, 2002;**35**(Suppl): 23–33.
39. Sejersten, M., G.S. Wagner, O. Pahlm, J.W. Warren, C.L. Feldman, and B.M. Horacek, Detection of acute ischemia from the EASI-derived 12 lead electrocardiogram and from the 12–lead electrocardiogram acquired in clinical practice. *J. Electrocardiol.*, 2007;**40**: 120–126.
40. Suraweera, J., E. Clark, and P.W. Macfarlane, EASI derived 12 Lead ECG v. Conventional 12 Lead ECG, in Computer Applications in Electrical Engineering, Recent Advances, India, IITR, Roorkee, 2005, pp. 1–4.
41. Nelwan, S.P., J.A. Kors, and S.H. Meij, Minimal lead sets for reconstruction of 12-lead electrocardiograms. *J. Electrocardiol.*, 2000;**33**: 163–166.
42. Nelwan, S.P., J.A. Kors, S.H. Meij, J.H. van Bemmel, and M.L. Simoons, Reconstruction of the 12-lead electrocardiogram from reduced lead sets. *J. Electrocardiol.*, 2004;**37**: 11–18
43. Nelwan, S.P., S.W. Crater, and S.H. Meij et al., Assessment of derived 12-lead ECGs using general and patient-specific reconstruction strategies at rest and during transient myocardial ischemia. *Am. J. Cardiol.*, 2004;**94**: 1529–1533.
44. Edenbrandt, L. and O. Pahlm, Vectorcardiogram synthesized from a 12 lead ECG: Superiority of the Inverse Dower Matrix. *J. Electrocardiol.*, 1988;**21**: 361–367.
45. Willems, J.L., *Common Standards for Quantitative Electrocardiography. 4th Progress Report*. Leuven: Aceo, 1984, 199–200.
46. Willems, J.L., P. Arnaud, J.H. Van Bemmel et al., Assessment of the performance of electrocardiographic computer programs with the use of a reference data base. *Circulation*. 1985;**71**: 523–534.
47. Edenbrandt, L., A. Houston, and P.W. Macfarlane, Vectorcardiograms synthesized from 12 lead ECGs: a new method applied in 1792 healthy children. *Pediatr. Cardiol.*, 1994;**15**: 21–26.
48. Macfarlane, P.W., L. Edenbrandt, and O. Pahlm, *12 Lead Vectorcardiography*. Oxford: Butterworth-Heinemann, 1995.
49. Warner, R., N.E. Hill, P.R. Sheehe, S. Mookherjee, C.T. Fruehan, and H. Smulyan, Improved electrocardiographic criteria for the diagnosis of inferior myocardial infarction. *Circulation*. 1982;**66**: 422–428.
50. Surawicz, B., H. Uhley, R. Borun et al., Task force I: Standardization of terminology and interpretation. *Am. J. Cardiol.*, 1978;**41**: 130–145.
51. Bayes de Luna, A., G. Wagner, Y. Birnbaum et al., A new terminology for left ventricular walls and location of myocardial infarcts that present Q waves based on the standard of cardiac magnetic resonance imaging. *Circulation*. 2006;**114**: 1755–1760.
52. Wagner, G., P.W. Macfarlane, H. Wellens et al., Recommendations for the standardization and interpretation of the electrocardiogram. Part VI. Acute ischemia/infarction. *J. Am. Cell. Cardiol.*, 2009;**53**: 1003–1011.
53. Mason, J.W., E.W. Hancock, and L.S. Gettes, Recommendations for the standardization and interpretation of the electrocardiogram: II: Electrocardiography diagnostic statement list. *Circulation*. 2007;**115**: 1325–1332.
54. Mason, R.E. and I. Likar. A new system of multiple-lead exercise electrocardiography. *Am. Heart J.*, 1966;**71**: 196–205.
55. Froelicher, V.F., Jr., R. Wolthius, N. Keiser et al., A comparison of two bipolar exercise electrocardiographic leads to lead V_5. *Chest*. 1976;**70**: 611–616.

56. Sheffield, L.T., R. Prineas, H.C. Cohen, A. Schoenberg, and V. Froelicher, Task force II: Quality of electrocardiographic records. *Am. J. Cardiol*., 1978;**41**: 146–157.
57. Chaitman, B.R., M.G. Bourassa, P. Wagniart, F. Corbara, and R.J. Ferguson, Improved efficiency of treadmill exercise testing using a multiple lead ECG system and basic hemodynamic exercise response. *Circulation*. 1978;**57**: 71–79.
58. Papouchado, M., P.R. Walker, M.A. James, and L.M. Clarke, Fundamental differences between the standard 12-lead electrocardiograph and the modified (Mason-Likar) exercise system. *Eur. Heart J*., 1987;**8**: 725–733.
59. Drew, B.J., R.M. Califf, M. Funk et al., Practice Standards for electrocardiographic monitoring in hospital settings. *Circulation*. 2004;**110**: 2721–2746.
60. Barr, R.C., M.S. Spach, and G.S. Herman-Giddens, Selection of the number and positions of measuring locations for electrocardiography. *IEEE Trans. Biomed. Eng*., 1971;**18**: 125–138.
61. Kornreich, F, The missing waveform information in the orthogonal electrocardiogram (Frank leads). I. Where and how can this missing waveform information be retrieved? *Circulation*. 1973;**48**: 984–995.
62. Kornreich, F. and D. Brismee, The missing waveform information in the orthogonal electrocardiogram (Frank leads). II. Diagnosis of left ventricular hypertrophy and myocardial infarction from "total" surface waveform information. *Circulation*. 1973;**48**: 996–1004.
63. Lux, R.L., C.R. Smith, R.F. Wyatt, and J.A. Abildskov, Limited lead selection for estimation of body surface potential maps in electrocardiography. *IEEE Trans. Biomed. Eng*., 1978;**25**: 270–276.
64. Maroko, P.R., P. Libby, J.W. Covell, B.E. Sobel, J. Ross, Jr., and E. Braunwald, Precordial S T segment elevation mapping: An atraumatic method for assessing alterations in the extent of myocardial ischemic injury. *Am. J. Cardiol*., 1972;**29**: 223–230.
65. Fox, K.M., A.P. Selwyn, and J.P. Shillingford, Projection of electrocardiographic signs in praecordial maps after exercise in patients with ischaemic heart disease. *Br. Heart J*., 1979;**42**: 416–421.
66. Fox, K.M., J. Deanfield, P. Ribero, D. England, and C. Wright, Projection of ST segment changes on to the front of the chest. Practical implications for exercise testing and ambulatory monitoring. *Br. Heart J*., 1982;**48**: 555–559.
67. Monro, D.M., R.A.L. Guardo, P.J. Bourdillon, and J. Tinker, A Fourier technique for simultaneous electrocardiographic surface mapping. *Cardiovasc. Res*., 1974;**8**: 688–700.
68. Monro, D.M., Interpolation by fast Fourier and Chebyshev transforms. *Int. J. Numer. Meth. Eng*., 1979;**14**: 1679–1692.
69. Monro, D.M., Interpolation methods for surface mapping. *Comput. Programs Biomed*., 1980;**2**: 145–157.
70. Menown, I.B.A., J. Allen, J.M. Anderson, and A.A.J. Adgey, Early diagnosis of right ventricular or posterior infarction associated with inferior wall left ventricular acute myocardial infarction. *Am. J. Cardiol*., 2000;**85**: 934–938.
71. Yamada, K., K. Harumi, and T. Musha, Editors. Advances in Body Surface Potential Mapping, *Proc. Int. Symp. Body Surface Mapping*. Nagoya: University of Nagoya Press, 1983.
72. van Dam, R.T.H. and A. van Oosterom, Editors. *Electrocardiographic Body Surface Mapping*. Dordrecht: Nijhoff, 1986.
73. Taccardi, B., B.P. Punske, F. Sachse, F. Tricoche, P. Colli-Franzone, L.F. Pavarino, and C. Zabawa, Intramural activation and reploarization sequences in canine ventricles. Experimental and simulation studies. *J. Electrocardiol*., 2005;**38**(Suppl): 131–137.
74. Witkowski, F.X. and P.B. Corr, An automated simultaneous transmural cardiac mapping system. *Am. J. Physiol*., 1984;**247**: H661–668.
75. Holt, P., P.V.L. Curry, P.B. Deverall, C. Smallpiece, and A.K. Yates, Ventricular arrhythmias-An accurate guide to their localisation. *Br. Heart J*., 1981;**45**: 615–616.
76. Bazan, V., R. Bala, F.C. Garcia, et al., 12 lead ECG features to identify ventricular tachycardia arising from the epicardial right ventricle. *Heart Rhythm*., 2006;**10**: 1132–1139.
77. Friedman, P.L., T.L. Shook, J.M. Kirshenbaum, A.P. Selwyn, and P. Ganz, Value of the intracoronary electrocardiogram to monitor myocardial ischemia during percutaneous trans luminal coronary angioplasty. *Circulation*, 1986;**74**: 330–339.
78. DeMarchi, S.F., P. Meier, P. Oswald, and C. Seiler, Variable signs of ischemia during controlled occlusion of the left and right coronary artery in humans. *Am. J. Physiol*., 2006;**291**: H351–H356.
79. Sheffield, L.T., A. Berson, Bragg-Remschel, et al., Recommendations for standards of instrumentation and practice in the use of ambulatory electrocardiography. *Circulation*, 1985;**71**: 626A–636A.
80. MacAlpin, R.N., Correlation of the location of coronary arterial spasm with the lead distribution of ST segment elevation during variant angina. *Am. Heart J*., 1980;**99**: 555–564.
81. Quyyumi, A.A., L. Mockus, C. Wright, and K.M. Fox, Morphology of ambulatory ST segment changes in patients with varying severity of coronary artery disease. Investigation of the frequency of nocturnal ischaemia and coronary spasm. *Br. Heart J*., 1985;**53**: 186–193.
82. Crawford, M.H., S.J. Bernstein, P.C. Deedwania, J.P. DiMarco, K.J. Ferrick, A. Garson Jr., L.A. Green, H.L. Greene, M.J. Silka, P.H. Stone, and C.M. Tracy, ACC/AHA guidelines for ambulatory electrocardiography: executive summary and recommendations: A report of the American College of Cardiology/American Heart Association Task Force on Practice Guidelines (Committee to Revise the Guidelines for Ambulatory Electrocardiography). *Circulation*, 1999;100:886–893.
83. Schnittger, I., I.M. Rodriguez, and R.A. Winkle, Esophageal electrocardiography: A new technology revives an old technique. *Am. J. Cardiol*., 1986;**57**: 604–607.
84. Arzbaecher, R., A pill electrode for the study of cardiac arrhythmia. *Med. Instrum*., 1973;**12**: 277–281.
85. Mächler, H., A. Lueger, S. Huber, P. Bergmann, P. Rehak, and G. Stark, The Esophageal-ECG: New applications with a new technique. *Internet J. Thoracic Cardiovasc. Surgery*, 1997;**2**(2).

86. Li, Y., L. Rao, S.G. Baidya, Y. Feng, J. Zhang, and J. Yang, The combined use of esophageal electrocardiogram and multiple right parasternal chest leads in the diagnosis of PSVT and determination of accessory pathways involved: A new simple noninvasive approach. *Int. J. Cardiol*., 2006;**113**: 311–319.
87. Jenkins, H.M.L., Technical progress in fetal electrocardiography-A review. *J. Perinat. Med*., 1986;**14**: 365–370.
88. Oostendorp, T.F., A. van Oosterom, H.W. Jongsma, and P.W.J. van Dongen, The potential distribution generated by the fetal heart at the maternal abdomen. *J. Perinat. Med*., 1986;**14**: 435–444.
89. Advances in fetal electrocardiography (Symposium). *J. Perinat. Med*., 1986;**14**: 345–452.
90. Neilson, J.P., Fetal electrocardiogram (ECG) for fetal monitoring during labor, Cochrane Database of Systematic Reviews 2006, Issue 3. Art. No.: CD000116. DOI: 10.1002/14651858.CD000116.pub2
91. Sporri, H., Der Einfluss der Tuberkulose auf das Elektrokardiogramm. (Untersuchungen an Meerschweinchen und Rindern.) *Arch. Wiss. Prakt. Tierheilkd*., 1944;**79**: 1–57.
92. Yamori, Y., M. Ohtaka, and Y. Nara, Vectorcardiographic study on left ventricular hypertrophy in spontaneously hypertensive rats. *Jpn. Circ. J*., 1976;**40**: 1315–1329.
93. Schwartze, H. and F. Thoss, Applicability of two different lead systems in studies of the electrical activity of the hearts in newborn guinea pigs. *J. Electrocardiol*., 1981;**14**: 9–12.
94. Nelson, C.V., P.R. Gastonguay, A.F. Wilkinson, and P.C. Voukydis, A lead system for direction and magnitude of the heart vector, in *Vectorcardiography* 2, I. Hoffman, R.I. Hamby, E. Glassman, Editors. Amsterdam, North-Holland, 1971, pp. 85–97.
95. Gabor, D. and C.V. Nelson, Determination of the resultant dipolt: of the heart from measurements on the body surface. *J. Appl. Phys*., 1954;**25**: 413–416.
96. Eifrig, T., H. Schwartze, and A. Joel. Experiences with the Nelson lead system in physiological animal experiments, in *Electrocardiology* '81, Z. Antaloczy, I. Preda, Editors. Amsterdam, Excerpta Medica, 1982, pp. 461–464.
97. Driscoll, P., The normal rat electrocardiogram (ECG), in *The Rat Electrocardiogram in Pharmacology and Toxicology*, R. Budden, D.K. Detweiler, G. Zbinden, Editors. Oxford, Pergamon, 1981, pp. 1–14.
98. Hermann, G.R. and A.H.W. Herrmann. The electrocardiographic patterns in 170 baboons in the domestic and African colonies at the primate center of the Southwest Foundation for Research and Education, in *The Baboon in Medical Research* H. Vagtborg, Editor. Austin, Texas, University of Texas Press, 1965, pp. 251–264.
99. Ruttkay-Nedecky, I. and G.M. Cherkovich, *The Orthogonal Electrocardiogram and Vectorcardiogram of Baboons and Macaques*. Bratislava: VEDA, 1977.

12 ECG Instrumentation: Application and Design

S.M. Lobodzinski

P. W. Macfarlane, A. van Oosterom, O. Pahlm, P. Kligfield, M. Janse, J. Camm (eds.), *Comprehensive Electrocardiology*, DOI 10.1007/978-1-84882-046-3_12,

12.1 Introduction

This chapter addresses the theory and practice of ECG recording and processing. The current state of the art and latest technical developments in the field of electrocardiography are discussed with respect to:

1. Formation and characterization of ECG signals
2. Biopotential ECG sensors
3. ECG signal recording
4. ECG recording standards
5. Patient safety standards
6. ECG signal processing

The emphasis lies on the treatment of biopotential sensors (electrodes) and in particular on recent developments in this domain. Other topics like instrumentation and signal processing are treated at an introductory level, mainly defining concepts and terminology, with numerous references to the available high quality textbooks and publications in the literature. The brief section on the formation and characterization of basic ECG features includes ample references to the other chapters in this Volume, which describe this topic in greater detail (Chaps. 5–8). In Appendix Section entitled "Basic Digital ECG Signal Processing" some signal processing methods are described by A. van Oosterom, restricted to topics that are highly specific to the ECG.

For additional reading on the material discussed, the reader is referred to the related chapter by the late Christoph Zywietz in the first edition of this book [1], as well as to an overview by E. McAdams in the Encyclopedia of Medical Devices and Instrumentation [2].

12.2 Formation and Characterization of the ECG Signal

The electrical activity of the heart generates an electrical potential field on the body surface. Given the anatomy of the heart and the chest, the potentials at locations on the body surface represent composite electrical activity from the entire heart. A body surface electrocardiogram (ECG) is the manifestation of this electrical activity. It provides a measure of the potential difference between two points on the body surface as a continuous function of time, or between the two terminal points of a network sensing the potential field (Chaps. 10 and 11). The ECG is routinely measured using standard ECG electrodes. Commonly, ten such electrodes are used, four of which are placed on or near the limbs and six of which span the chest, primarily on the left side. As discussed in Chaps. 10 and 11, only nine of these electrodes are involved in documenting the potential field generated by the heart, the tenth electrode (usually attached to the right leg) serving as a means for reducing the interference from external electric fields. From the nine electrodes, at most eight independent signals can be extracted. Hence, those forming the standard set of 12 ECG leads contain some redundancy.

12.2.1 Formation of the ECG

A brief summary of the sequence of events involved in electrical activation of the atria and the ventricles that give rise to the ECG is presented below. A more complete handling of this topic, with increased detail, is given in Chaps. 4–7.

As the heart undergoes depolarization and repolarization, electrical currents spread throughout the body that acts as an electric volume conductor (Chap. 2). If a piece of living myocardium is placed in a bath containing a saline solution, which conducts electric currents, and if the terminals of a voltmeter are placed in the bath on either side of the muscle segment, no potential difference is observed between the sensors when the muscle is in its polarized, resting state (Fig. 12.1a). The reason for this is discussed in Sect. 6.2.1. If the left side of the muscle is stimulated electrically a self-propagating transmembrane potential gradient is produced. A wave of depolarization will sweep through the tissue from left to right (Fig. 12.1b). Midway through this depolarization process, cells on the left part of the tissue (depolarized cells) are negative *on the outside* relative to their inside, whereas the cells ahead of the front, the right, are still polarized (positive on the outside), thus creating a potential difference between the two terminals of the voltmeter. Through the labeling of these two terminals by the signs as shown, the recorded voltage is, by convention, assigned a positive value (upward

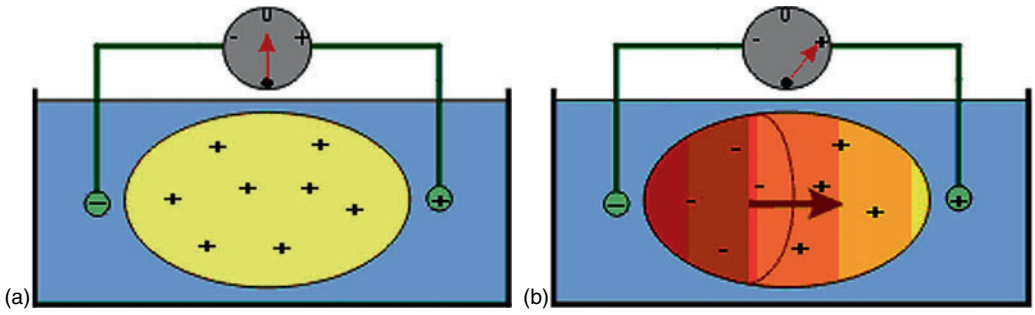

Figure 12.1

Schematic diagram of an elliptically shaped section of myocardial tissue placed inside a saline-filled container. The signs drawn inside the ellipses indicate the potential difference on the outside of the surface bounding the tissue with reference to the intracellular potential. (a) Equilibrium of the potential; all myocytes in their fully polarized state: potential difference observed in the external medium is zero. (b) Situation during a propagated activation. The potential in the external medium is positive ahead of the wave front with respect to that behind it. The small circles denote the two electrodes mentioned in the text. The one carrying the "+" label may be interpreted as the sensing electrode, the other one as the reference electrode (see Chap. 10). Voltage differences between these electrodes result in an upward deflection if the polarity of the difference is concomitant with the signs labeling the electrodes.

deflection in the recording). After the wave of depolarization has swept across the entire muscle mass, the outsides of all cells are negative with respect to their interior, and once again, no potential difference exists between the two sensors. This formulation ignores the field produced by currents originating from the repolarization processes that have already started in the part of the tissue that depolarized first.

12.2.2 Formation of ECG Wave Forms

The entire process of depolarization and repolarization of the myocardium is illustrated in the Fig. 12.2, which is a crude representation of the electrical events that occur in the atria. A more comprehensive treatment of the subject is given in Chap. 5.

During the resting, polarized state, no potential difference is measured between the sensing electrode (labeled as positive) and the reference electrode (labeled as negative). When the sino-atrial node fires, a wave of depolarization spreads out over the atria. During this period, some of the muscle mass overlaying the polarized myocytes temporarily remain positive on the outside, while the part overlaying the depolarized myocytes is negative. This potential gradient in the external medium is sensed as a potential difference between the two electrodes. Once the entire myocardium is depolarized completely, there is once again no potential difference, and the voltage difference sensed by the electrodes is zero just as it was in the polarized state. During repolarization, again starting in the SA-nodal region and then moving across the atria, there will be a potential gradient, but this time the polarity is reversed, causing a downward deflection. Finally, when all of the cells are repolarized, the measured voltage difference will once again be zero until a subsequent activation is initiated.

The cardiac activation creates an electric potential field throughout the body as well as on its surface (Fig. 12.3). The human body may be considered as a resistive, piecewise homogeneous and linear volume conductor (Chap. 2). The electric potential differences measured between specific points on the outer surface of the volume conductor, i.e., on the body surface, are referred to as electrocardiograms, or "the" ECG.

The entire electric activity of the heart may be represented by equivalent electric current generators. Several models of such generators have been formulated, each differing in their complexity and their direct link with the underlying electrophysiology.

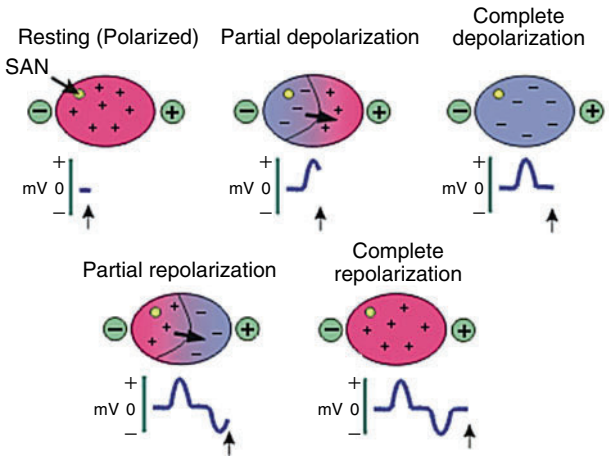

Figure 12.2

The entire process of depolarization and repolarization that is representative of the electrical events that occur in the atria. The ± signs drawn inside the ellipses denote the polarity of the voltage just outside the myocardium with respect to the intra-cellular potential of the myocytes.

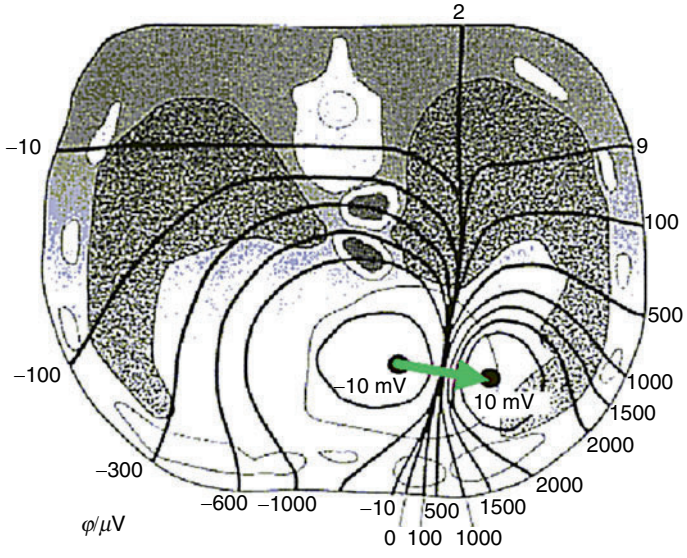

Figure 12.3

Transverse cross section of the thorax showing regions having different electric conductivity (bone, lung, muscle) (from R. Hinz [3]). Isopotential lines illustrate the type of potential field generated by a single dipole.

A classic example of this is the single current dipole, generally placed at the center of gravity of ventricular mass (Fig. 12.3). Other major source descriptions are discussed in Chaps. 2 and 5–8.

Several basic rules emerge from the modeling of potential fields for interpreting observed potential differences in terms of the sources of cardiac electric activity:

1. A wave of depolarization traveling toward the sensing electrode results in a positive deflection in the ECG trace.
2. A wave of repolarization traveling away from the sensing electrode results in a positive deflection.

Table 12.1
Sources of electric signals observable on the body surface [6]

Source	Signal amplitude range	Signal frequency range (Hz)
Heart, electrocardiogram, ECG	0.5–4 mV	0.01–250
Brain, electroencephalogram, EEG	10–5,000 μV	0–150
Gastrointestinal tract, Electrogastrogram, EGG	10–1,000 μV	0–1
Nerve potentials, electroneurogram, ENG	0.01–3 mV	0–10,000
Skeletal muscles, electromyogram, EMG	0.1–5 mV	0–10,000

3. A wave of depolarization or repolarization traveling perpendicular to the axis of an electrode pair results in a biphasic deflection of equal positive or negative voltages at each electrode, and, hence, no deflection.
4. The instantaneous amplitude of the measured potentials depends upon the orientation of the lead relative to the mean electric vector.
5. The voltage amplitude is directly related to the mass of tissue undergoing depolarization or repolarization.

Rules 1–3 are derived from the volume conductor model described above. Rule 4 takes into consideration that, at any given point in time during depolarization in the atria or ventricles, there can be many separate waves of depolarization traveling in different directions relative to the electrode locations. The ECG reflects the time course of the average, instantaneous direction and magnitude (i.e., a mean electrical vector) of all depolarization waves present. Rule 5 simply states that the amplitude of the wave recorded by the ECG is directly related to the mass of the muscle undergoing depolarization or repolarization. For example, when the mass of the left ventricle is increased by hypertrophy, the amplitude of the QRS complex is increased in certain leads, provided that the local source strength (impressed current per unit volume of tissue) remains the same (Chap. 2). Note however, that such simple rules apply strictly only if the observation point is located close to the source of the electric activity.

12.2.3 Other Sources of Electric Signals Inside the Body

In addition to the heart, there are other sources of electric activity present inside the body. The major ones are included in Table 12.1. These generators produce electric signals at various locations within the volume conductor that add to the electrocardiogram. It is important to note that the EEG, EGG and EMG signal amplitudes and the range of their frequency spectra overlap with that of the ECG signal [6].

12.2.4 Characteristics of Composite ECG Signals

The amplitudes of the ECG signal components as measured on the body surface vary with time and range from 0.1 to 5 mV. Significant components in their frequency spectra lie in the range between 0.05 and 250 Hz. The ECG waveforms generally exhibit small but distinct beat to beat variations. In patients with implanted pacemakers, narrow voltage pulses appear superimposed on the ECG signal. These must be identified to differentiate them from the ECG signals in order to prevent an incorrect heart rate evaluation.

The bandwidth of the ECG is defined as the frequency range between low and high frequency cutoffs (−3 dB) of the magnitudes of their Fourier amplitude spectrum [6]. For accurate recording of ECGs, the dynamic input range and the bandwidth of the recording system are of major importance and should at least extend to the highest peak-to-peak amplitude and the highest frequency component in the ECG signal, respectively.

12.3 Biopotential Sensors

A biopotential sensor is a device that responds to the presence of electric charges in living tissues by producing an analog electrical input signal to the instrumentation amplifier. Biopotential sensors carry out a complex transducer function, in which the charge of the ions carrying the current inside the body is transferred to that of the electrons constituting the sensor output current. A common, time-sanctioned practice is to refer to all biopotential sensors as "electrodes."

The word "electrode" was coined by Michael Faraday in 1834 from a combination of the Greek words *elektron* (meaning amber, and from which the word electricity is similarly derived) and *hodos*, a way [4]. It signifies a conductor used to make contact with a non-metallic part of a circuit such as an electrolyte. As an example, we consider a "wet" biopotential sensor, commonly referred to as a "disposable ECG electrode," shown in Fig. 12.4. It comprises an electrochemically active gel in contact with the skin, an electrode connecting clip that is coated with a layer of Ag/AgCl on the inside, mounting flexible foam pad with adhesive and many other electro-mechanical parts not directly involved in conversion of a flux of ions into an electric current carried by electrons. Together, the layer of the gel and the metal electrode perform the transducer function. Since electrochemical sensors also utilize metallic electrodes, we shall use the terms biopotential sensors and electrodes interchangeably where appropriate.

Modern biopotential sensors include electrochemical, capacitive, optical and impedance transducers capable of sensing changes in the immediate electric field caused by the electrical activity of the heart.

There are many types of biopotential sensors in use today that are used for recording electrocardiograms. Those discussed in this chapter are used in clinical and research based electrocardiology. Special devices, such as needle electrodes and microelectrodes used for measurement of intracellular and extracellular electrical activity, are not treated here.

Electrochemical biopotential sensors share two major components:

1. an electrochemical electrode, which may be metallic, carbon, composite electro-conductive film, etc.
2. the electrolyte, which may be an electrolytic medium or gel such as is used with surface electrodes, or it may be the body fluids that come into contact with an electrode such as the perspiration that accumulates under a dry electrode applied to skin containing sweat glands.

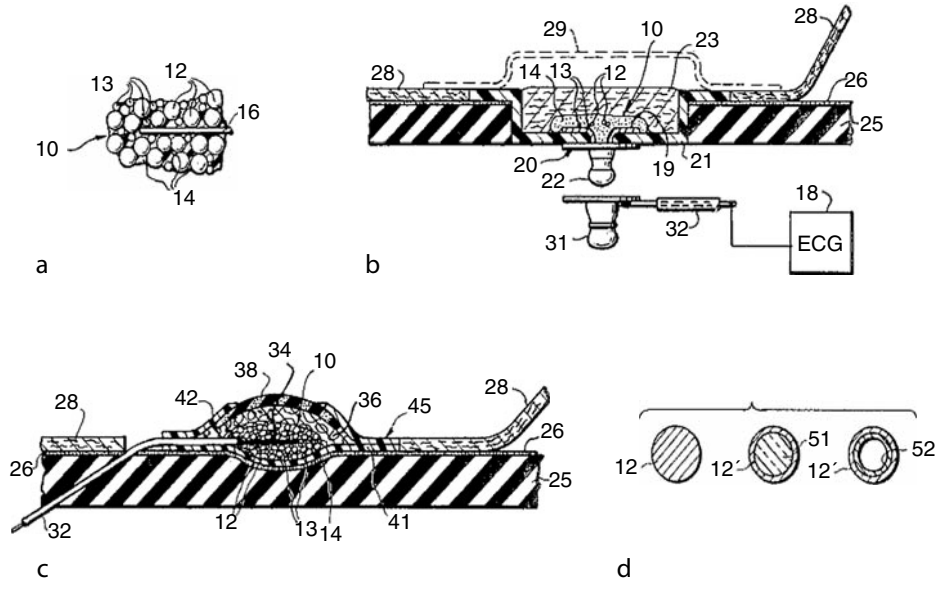

Figure 12.4

The original patent drawing (Sato, US Patent 3,834,373) of a disposable ECG electrode (Biopotential Sensor).

The biopotential sensors that require a direct contact with the skin are referred to as Galvanic Sensors, i.e., they are involved in an electrochemical reaction with electrolytes inside the body. In order to achieve a better understanding of the working principles of galvanic biopotential sensors, some details about the electrode–electrolyte interface are discussed first. This is followed by a discussion of the sensor–skin interface.

12.3.1 The Sensor–Electrolyte Interface

12.3.1.1 Electrochemical Reactions

The electrodes used in biopotential sensors comprise metallic atoms M. They are in contact with an electrolyte, a solution comprising cations of the electrode metal M^+ and anions A^-. When an electrode comes into contact with an electrolyte, an electrochemical reaction is initiated; it can be described as:

$$M \leftrightarrow M^{n+1} + n^{e-} \tag{12.1}$$

$$A^{m-} \leftrightarrow A + m^{e-} \tag{12.2}$$

where n is the valence of M and m is the valence of A. Equation (12.1) tells us that the metal in the electrode at the interface oxidizes to form a cation and one or more free electrons. The cation is then discharged into the electrolyte and the electron remains as a charge carrier in the electrode. Equation (12.2) describes the anion reaction. The anion in contact with the electrode–electrolyte interface can be oxidized to a neutral atom, giving off one or more free electrons to the electrode. The reactions described by (12.1) and (12.2) are reversible. Since the electrolyte contains cations discharged from the electrode, the charge distribution is not neutral. The potential set up by the electrolyte in a direct contact with the electrode is known as the half-cell potential (Fig. 12.5).

When two aqueous ionic solutions of a different concentration are separated by an ion-selective semi-permeable membrane, an electric potential exists across the membrane. Its value follows from the Nernst equation as

$$E_{cell} = E^0_{cell} - \frac{RT}{nF} \ln Q$$

R – gas constant
T – temperature in Kelvin
Q – thermodynamic reaction quotient
F – Faraday's constant
n – number of electrons transferred

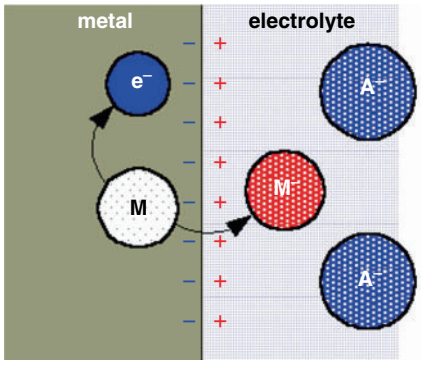

Figure 12.5
Charges at a metal–electrolyte interface.

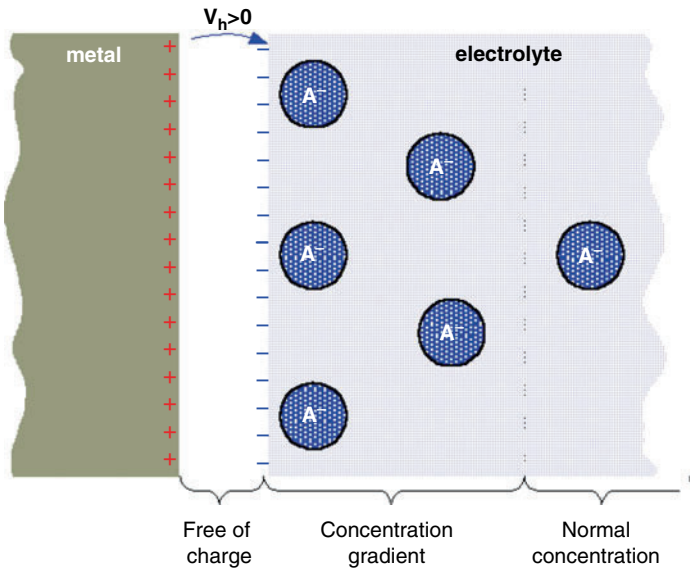

Figure 12.6
A double layer potential at the electrode surface for a metal with a positive half-cell potential. Courtesy of Prof. R. Hinz [3].

The quantity Q, the thermodynamic reaction constant, is like a dynamic version of the equilibrium constant in which the concentrations and gas pressures are the instantaneous values in the reaction mixture [5].

For the general oxidation–reduction reaction we have

$$\alpha A + \beta B \leftrightarrow \gamma D + ne^{-1} \tag{12.3}$$

Each ion has an equilibrium potential associated with it whereby the diffusive forces and the electrical forces balance. The Nernst equation for the so-called half-cell potential set up at the interface is

$$E = E^0 + \frac{RT}{nF} \ln \left[\frac{a_C^{\gamma} a_D^{\delta}}{a_A^{\alpha} a_B^{\beta}} \right] \tag{12.4}$$

E^0 – Standard half-cell potential
E – Half-cell potential
a – Ionic activity (generally same as concentration)
n – Number of valence electrons involved

When a pair of the biopotential sensors is connected to the instrumentation amplifier, a small current may flow through the sensor–electrolyte interface. Any such net transient current crossing the interface interferes with the static equilibrium of the half-cell potential. If the current flow is from electrode to electrolyte, the oxidation reactions dominate, whereas if it is in the opposite direction, the reduction reactions dominate (Fig. 12.6).

Different metals exhibit different half-cell potentials when in contact with an electrolyte, as illustrated in Fig. 12.7.

12.3.1.2 Impedance of the Interface

The electrode–electrolyte interface is highly complex and non-linear in nature and strongly depends on the electrode metal, its contact area, the makeup of an electrolyte, surrounding temperature, and the density and the frequency of the current passing through the interface.

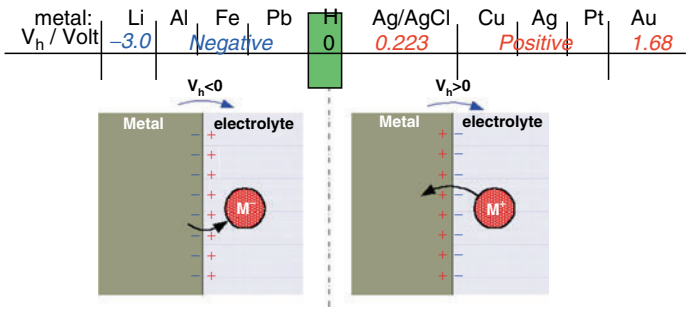

Figure 12.7

Half-cell potentials of various metals in contact with the electrolyte.

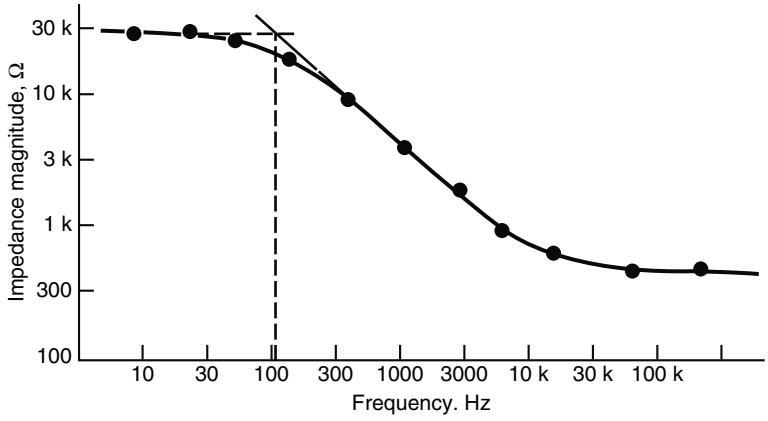

Figure 12.8

Experimentally determined magnitude of the electrode–electrolyte interface impedance as a function of frequency (from [6]).

Electrode impedances can be difficult to measure with high accuracy on living subjects. The term electrode impedance really refers to the impedance at each electrode interface and does not include the impedance of the biological material between the electrodes. Frequently, however, the term is used to describe the total impedance of the circuit between the electrode terminals. An example of the frequency dependency of an experimentally observed electrode impedance is shown in Fig. 12.8.

A simple, linearized equivalent circuit of the interface, including a voltage source in series with an impedance of the interface, is depicted in Fig. 12.9.

Capacitance

The presence of a charge distribution at an electrode–electrolyte interface produces not only an electrode potential but also a capacitance. Conceptually, two layers of charge of opposite sign as shown in Fig. 12.5, separated by a distance, form a capacitance. The distance between the layers of charge is molecular in dimension; therefore the capacitance per unit area is quite large [6]. In combination with R_d the capacitance C_d shown in Fig. 12.9 is usually taken to approximate the experimentally observed frequency dependency of the interface. In fact this dependency is slightly more complex [7]. The resistance Rd in the series-equivalent circuit models the ability of an electrode–electrolyte interface to conduct direct current (DC).

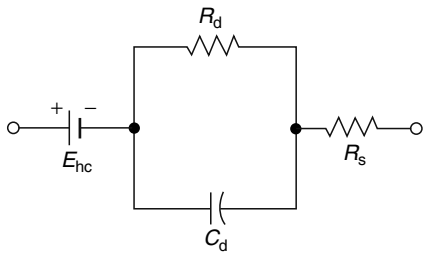

Figure 12.9

A linearized equivalent circuit of the electrode–electrolyte interface. E_{hc} is the half-cell potential, R_d and C_d make up the impedance associated with the electrode–electrolyte interface, and R_s is the series resistance associated with the resistivity of the electrolyte (from [6]).

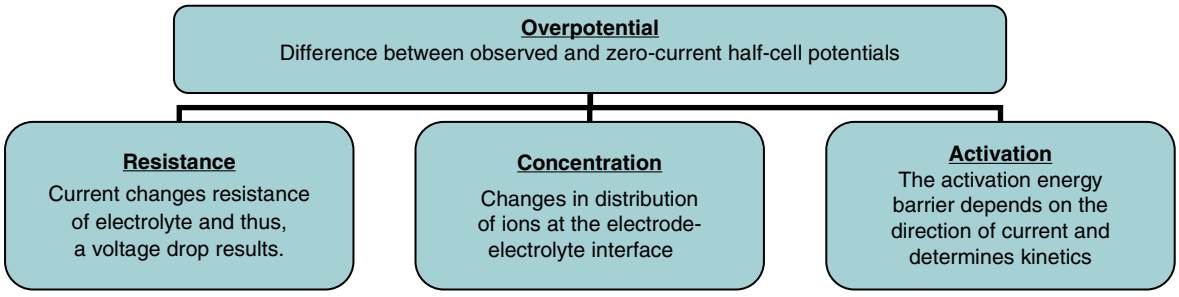

Figure 12.10

Sources of the overpotential in electrochemical electrodes.

Series Resistance

The series resistance R_s shown in Fig. 12.9 is associated with the resistivity of the electrolyte. Its magnitude is (approximately) inversely proportional to the square root of the surface area of the electrode, and also inversely proportional to the conductivity of the electrolyte (or body tissues in the application to the ECG).

12.3.1.3 Electrode Polarization

As discussed above, when two biopotential sensors placed in direct contact with the tissue are connected to the instrumentation amplifier, a very small current will flow through both electrodes and the input impedance of the amplifier. Any current flowing between a pair of biopotential sensors will alter the half-cell potential, effecting the polarization of the electrodes. The difference between the half-cell potential in the presence of current passing the interface and the equilibrium zero-current potential is known as the overpotential [8]. The contributing terms, as identified in Fig. 12.10, are

$$V_P = V_R + V_C + V_A \tag{12.5}$$

12.3.2 Polarizable and Non-polarizable Biopotential Sensors

We distinguish between two types of electrochemical sensors: polarizable and non-polarizable. This classification is based on what happens to a sensor electrode when a current passes it into the electrolyte. The theoretical polarizable electrodes

are those in which no actual charge crosses the electrode–electrolyte interface when a current is applied. In reality, due to the capacitance present at the interface, the displacement current will be present at the interface. The theoretical non-polarizable electrodes are those in which current passes freely across the interface, requiring no energy to make the transition. The overpotentials are not present on non-polarizable electrodes. In practice neither truly non-polarizable nor polarizable sensors can be produced, and hence most practical biopotential sensors may only approximate either of the two types.

12.3.2.1 Polarizable Electrodes

Electrodes made of inert metals such as platinum or stainless steel have difficulty in oxidizing and dissolving. Their characteristics therefore closely approximate those of theoretically polarizable electrodes but only within an electrode potential range called the "double-layer range." In these electrodes, the current passing between the electrode and the electrolyte primarily changes the concentration of ions at the interface, so the major part of the overpotential observed in this type of electrode is the result of the concentration type of overpotential (Fig. 12.10). Figure 12.11 shows a stainless steel electrode (Fe) in contact with an electrolyte. The electrochemical reaction at the electrode–electrolyte interface is described as:

$$Fe \leftrightarrow Fe^{+} + e^{-} \tag{12.6}$$

We note that there is no charge crossing the stainless steel–electrode interface. Stainless steel is subject only to the displacement current, and therefore the electrode behaves like a capacitor. The behavior of polarized electrodes can be modeled by an RC network, also shown in Fig. 12.11.

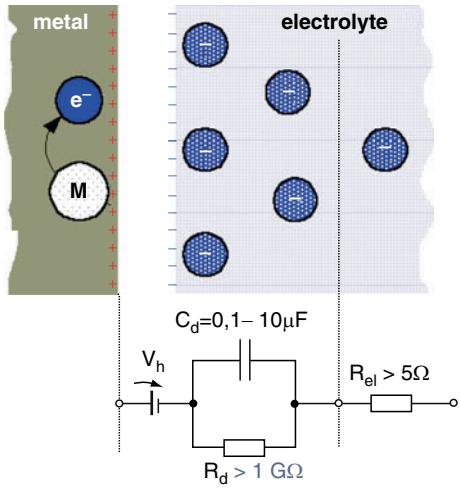

Figure 12.11

A polarizable, metal electrode such as made of stainless steel or iridium in contact with electrolyte. A metal electrode is subject to the displacement current only and therefore the electrode behaves like a capacitor (the very high resistance of R_d effectively blocks ion exchange between the electrode and the electrolyte). V_h is the half-cell potential, C_d is the make up the impedance associated with the electrode–electrolyte interface, and R_{el} is the resistance associated with the resistivity of the electrolyte.

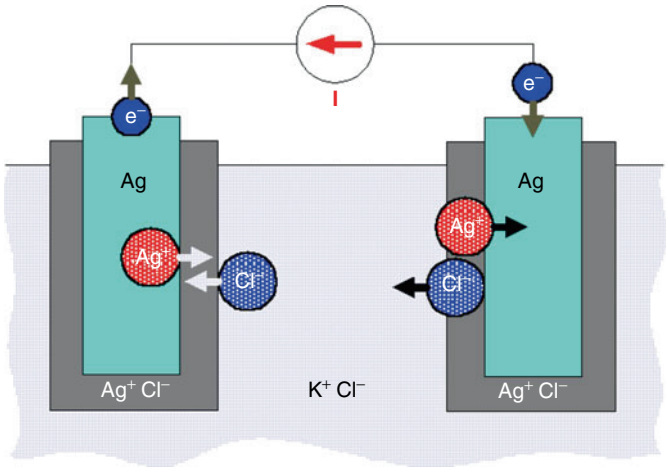

Figure 12.12

Ag/AgCl electrodes submerged in an electrolyte. A current *I* flows through the electrolyte containing ions of Cl^- and K^+. The electrons from electrode (a) flow to the electrode (b), the electrode (a) discharges a silver cation into the electrolyte (oxidation reaction) and the electrode (b) absorbs the silver cation from the electrolyte (reduction reaction).

12.3.2.2 Non-Polarizable Electrodes

Perfectly non-polarizable electrodes allow a free passage of current across the electrode–electrolyte interface, and hence exhibit no accumulation of overpotential. The examples of electrodes closely approximating the characteristics of a theoretically non-polarizable electrode include Ag/AgCl and mercury/mercurous chloride (Hg/Hg_2Cl_2). These electrodes comprise the metal surface coated by a slightly soluble metal chloride layer. The behavior of Ag/AgCl is governed by two chemical reactions, described by (12.7) and (12.8) and illustrated in Fig. 12.12. The first involves the oxidation of silver atoms on the electrode surface to silver ions in the electrolyte solution at the interface. The second reaction occurs immediately after the formation of silver ions. These ions combine with chloride cations already in the solution and form the ionic compound – silver chloride [6]. Since silver chloride is only slightly soluble in water, most of it precipitates from the solution on to the silver electrode, where it forms a silver chloride deposit [9].

$$Ag \leftrightarrow Ag^+ + e^- \,(\text{oxidation}) \tag{12.7}$$

$$Ag^+ + Cl^- \leftrightarrow AgCl \,(\text{reduction}) \tag{12.8}$$

In summary, both the polarizable and non-polarizable electrodes are non-linear, exhibit a reactive behavior, alter the half-cell potential, cause resistive loss and are frequency dependent. A single sensor electrode–electrolyte interface can be modeled by a half-cell potential in series with a resistor–capacitor network; the magnitudes of both depend on the type of metal, its surface area, surface condition, any electric current density passing through the electrode and the type of electrolyte involved as well as its concentration.

12.3.3 The Sensor–Skin Interface

The ECG can be regarded as the potential difference between a pair of biopotential sensors placed on the surface of the body. Therefore the current flowing between two biopotential sensors applied to the skin must also pass the layers of the skin and the underlying tissues. The sensor–skin interface is critical for the sensing of biopotentials, since the electrically charged ions from the body volume conductor must pass through the skin to the body surface to engage in oxidation and reduction reactions at the electrode interface. In this section we shall discuss skin anatomy and its electrical properties [10].

12.3.3.1 Anatomical Details of the Skin

Figure 12.13 shows the main features of the skin. The most superficial layer is called the epidermis and consists of the stratum corneum (SC), the stratum lucidum (seen only on "frictional surfaces"), the granular layer, the prickle cell layer, and the basal or germinating layer. The surface of the corneum (i.e., surface of the skin) is composed of dead cells, while at its base, healthy living cells are to be found. Between these two sites there are transitional cells. This layer is also called the horny layer. Blood vessels are present in the dermis whereas eccrine sweat gland secretory cells are located at the boundary between the dermis and the panniculus adiposus, also referred to as the hypodermis and the superficial fascia. The excretory duct of the eccrine sweat glands consists of a simple tube made up of a single or double layer of epithelial cells; this ascends to and opens out on to the surface of the skin. It is undulating in the dermis but then follows a spiral and inverted conical path through the epidermis to terminate in a pore on the skin's surface. Cholinergic stimulation via fibers from the sympathetic nervous system constitutes the major influence on the production of sweat by these eccrine glands.

From an examination of Fig. 12.14, it can be appreciated that the epidermis ordinarily has a high electrical resistance due to the thick layer of dead cells with thickened keratin membranes. This aspect is not surprising, since the function of the skin is to provide a barrier and protection against abrasion, mechanical assaults, and so on. The entire epidermis (with the exception of the desquamating cells) constitutes the barrier layer, a permeability barrier to flow. Experiments show its behavior to be that of a passive membrane.

The corneum is penetrated by the aforementioned sweat ducts from underlying cells. As these ducts fill, a relatively good conductor (sweat can be considered the equivalent of a 0.3% NaCl salt solution and, hence, a weak electrolyte) emerges, and many low-resistance parallel pathways result. A further increase in conductance results from the hydration of the corneum due to the flow of sweat across the duct walls, a process that is facilitated by the corkscrew duct pathway

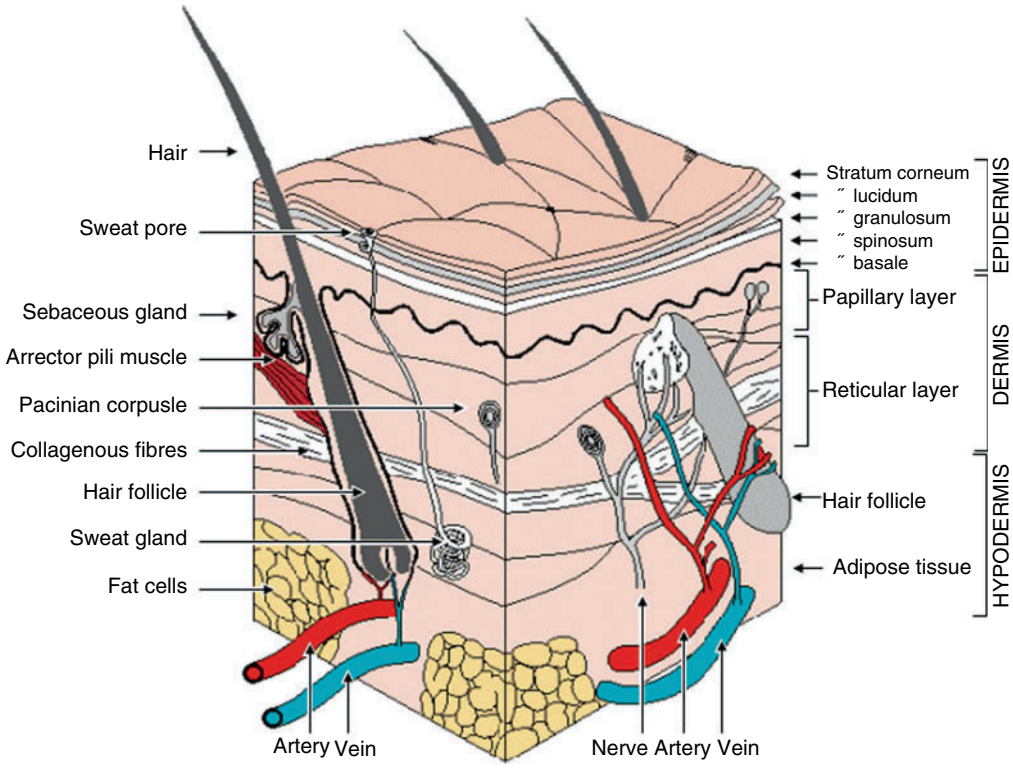

Figure 12.13

Main features of the skin. Section of smooth skin taken from the sole of the foot. Blood vessels have been injected (redrawn from [11]).

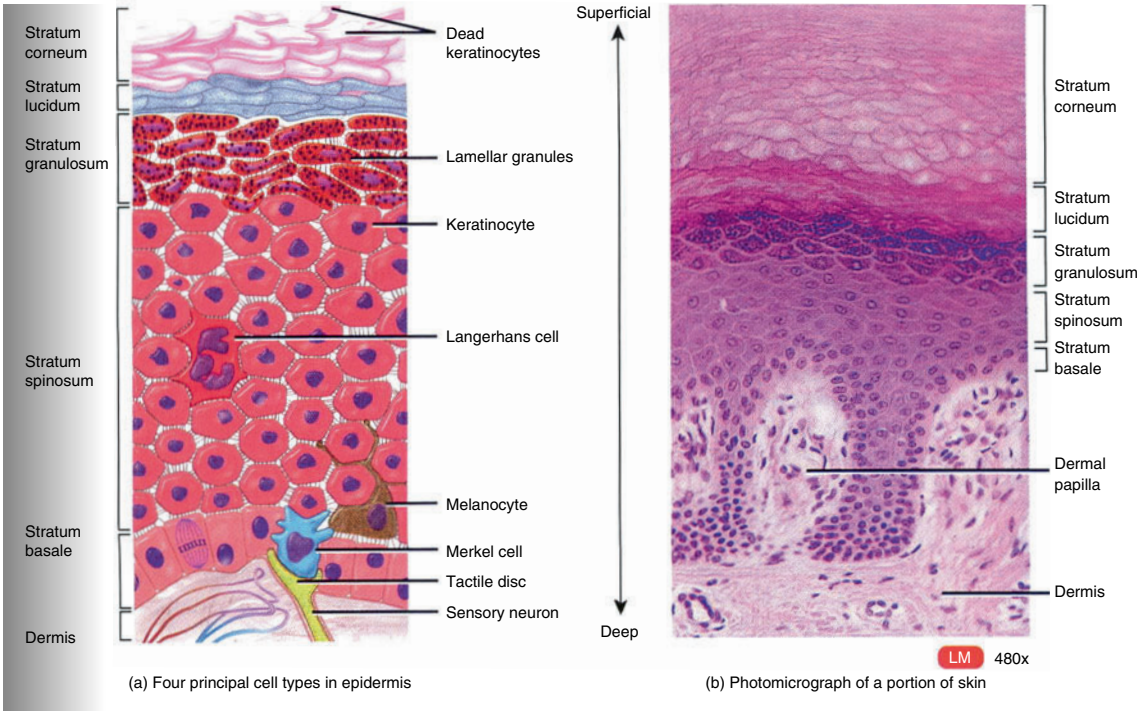

Figure 12.14
Skin layers involved in the passage of the ions.

and the extremely hydrophilic nature of the corneum. As a consequence the effective skin conductance can vary greatly, depending on present and past eccrine activity. It should be noted that the loading of ducts with sweat can already be taking place before any (observable) release of sweat from the skin's surface and/or noticeable diffusion into the corneum. The exertion of sweat modifies the electric properties of the skin. These changes produce transient and non-linear changes in the skin impedance.

Just like the electrode interface, the electric properties of the skin can be modeled by equivalent capacitor and resistor networks. Their properties are based on measurements of the electric current flowing across the skin resulting from a rectangular voltage pulse applied between two electrodes on either side of the skin. It is believed that there are two parallel current pathways, one crossing the lipid-corneocyte matrix (m) of the SC, and the other going through the appendages (a). An equivalent electrical model of this system is shown in Fig. 12.15. The elements in the model are as follows.

Lipid-Corneocyte Matrix Pathway

From an electrostatic point of view, the m-subsystem of the SC can be considered as a dielectric with a resistance (R_m) of 105 Ωcm^2 and a capacitance (C_m) of 0.03 $\mu F/cm^2$ [12, 13].

The Corneocytes

The corneocytes (Fig. 12.14) contain water and small ions resulting in an equipotential domain within these compartments. Thus, the potential drop across the SC occurs predominantly across the lipid domains between the corneocytes [13]. Such lipid domains can be described by parallel resistors and capacitors placed in a series, passing through the SC. There are on average 15–20 corneocyte layers in the SC, each separated by lipid domains of 0.05 mm thickness [14, 15].

The effective thickness of this non-conducting layer is 1 mm, yielding an effective dielectric constant of 15–20. This value is intermediate between that for lipids (2–3) and water (80) and is reasonable for hydrated lipid bilayers. This estimate suggests that the voltage drop is concentrated across lipid bilayers that are oriented "normal" to the electric field.

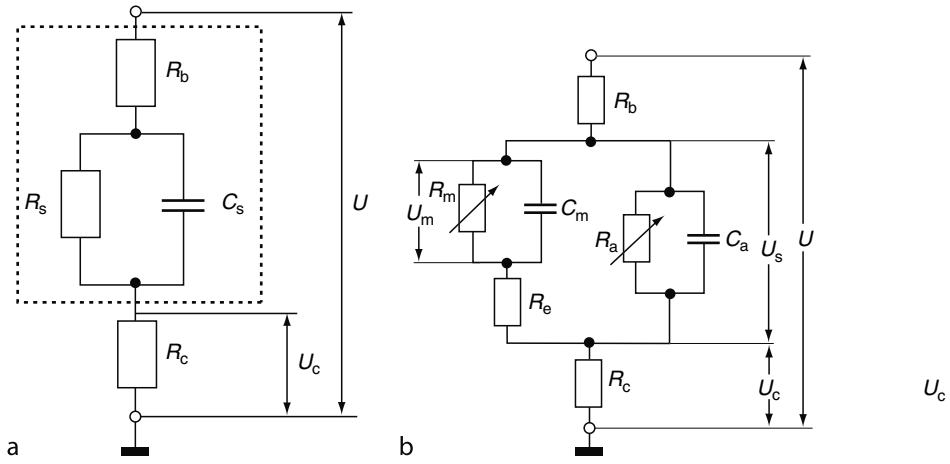

Figure 12.15

The equivalent electrical circuit of an outermost layer of skin. (a) An integral model where R_b, R_s, and R_c are the resistances of bulk solution, skin, and measuring resistor, correspondingly; C_s is skin capacitance. (b) A more detailed version, including two parallel pathways. R_m and C_m refer to the lipid-corneocyte matrix, and R_a and C_a refer to the appendages.

The SC matrix resistance (R_m) and capacitance (C_m) introduced in this way are frequency independent. If the time constant $(\tau_m = R_m C_m)$ of the network is small compared with that of the fluctuations of the processes involved, the equivalent scheme of the SC can be reduced to a simple voltage divider that includes four resistors in sequence, the bulk (R_b), epidermal (R_e), measuring (R_c), and matrix (R_m) resistances (Fig. 12.15b).

12.3.3.2 Equivalent Circuits for the Interface

It is possible to create dedicated versions for polarizing and non-polarizing sensor–skin interfaces, similar to the simplified equivalent circuits for an electrode–electrolyte interface shown in Fig. 12.15. The version shown in Fig. 12.16 represents an example of the polarizing interface (steel-skin), and Fig. 12.17 that of a non-polarizing interface (Ag/AgCl). An inspection of Figs. 12.16 and 12.17 reveals that in addition to the resistive and capacitive components, and previously discussed half-cell potential E_{hc}, there are two other sources of potentials present in the model: one at the electrolyte gel/electrolyte–skin interface E_{se} and the other at the gel/electrolyte–sweat duct/follicle channels' interface E_p.

12.3.3.3 Practical Considerations

The physical size of the components and the properties of the electrolyte will govern their impedances; for this reason it is difficult to specify the magnitudes of the electromotive forces, reactances, and resistances. Nonetheless, a few general statements can be made regarding the characteristics of impedance–frequency measured between the electrode terminals. In the previous discussion, it was shown that the impedance of an electrode–electrolyte interface decreases with increasing frequency (Figs. 12.8 and 12.9). Similarly, the capacitive nature of the electrical model for living tissue also indicates that its impedance decreases with increasing frequency. Therefore the impedance measured between the terminals of a pair of sensors applied to living tissue is high in the lower frequency region, decreases with increasing frequency, and approaches a relatively constant value when the reactances in the circuit become small with respect to their associated resistances. In general, with electrodes having a small surface area, the zero-frequency (i.e., direct current: DC) impedance is largely dependent on the electrode area.

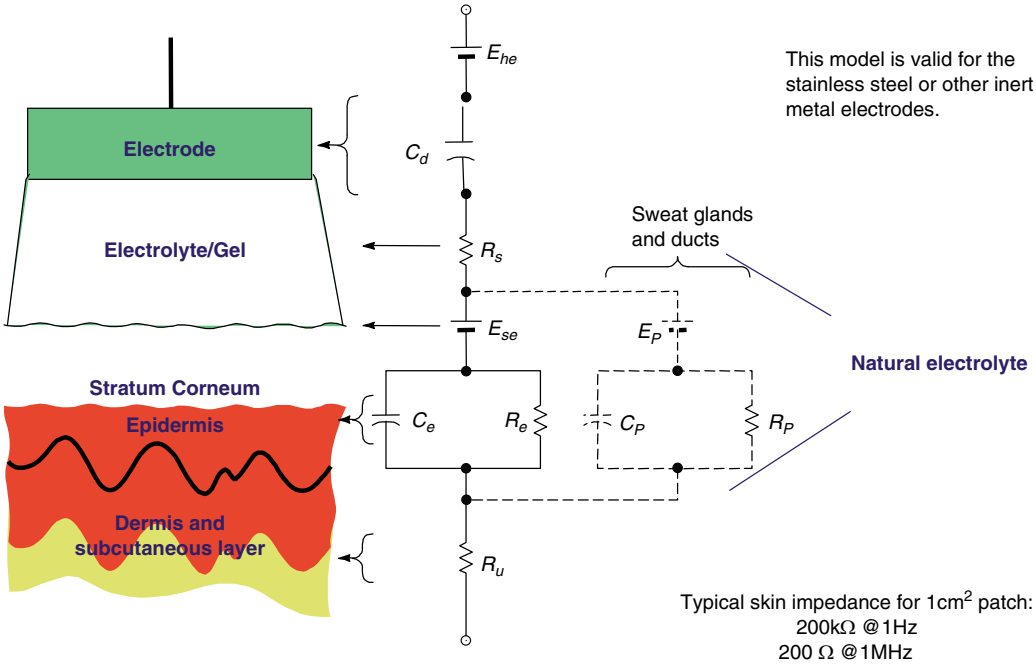

Figure 12.16

The electrical model of a polarizing sensor in contact with the surface of the skin.

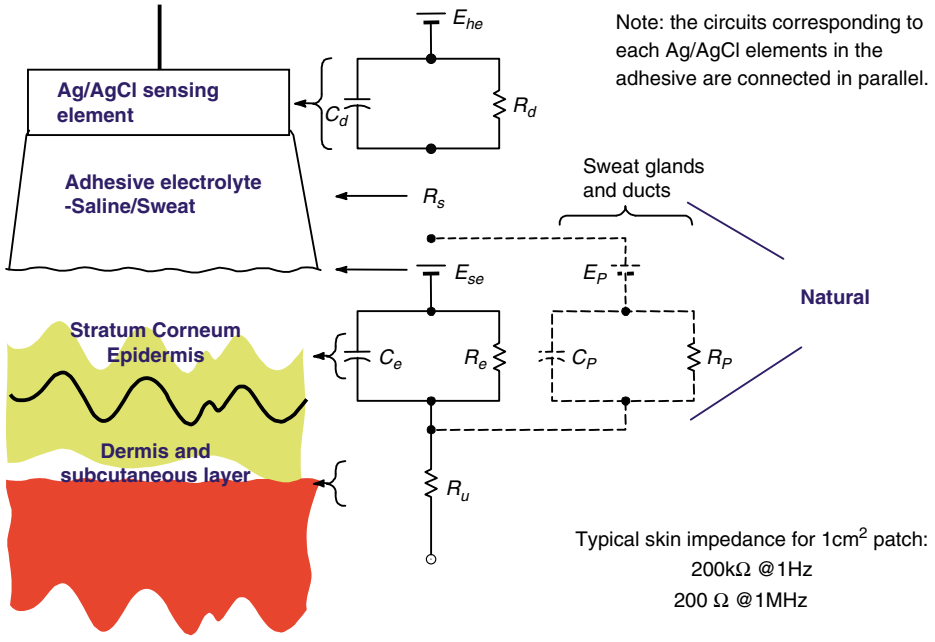

Figure 12.17

The electrical model of a non-polarizing sensor in contact with the surface of the skin.

As mentioned previously, there may be a DC potential appearing across the electrode terminals in the absence of a bioelectric event. For example, if the two half-cell potentials of the electrodes are unequal, a constant potential will be present whose magnitude and polarity depend on the relative magnitudes of the two half-cell potentials. This offset potential is of considerable importance when direct-coupled recording techniques are employed.

12.3.3.4 Measurement Artifacts at the Galvanic Sensor–Skin Interface

As discussed in Sect. 12.3.1, when a polarizing electrode is in contact with an electrolyte, a double layer of charge forms at the interface [6, 16]. If the electrode is moved with respect to the electrolyte, this mechanically disturbs the distribution of the charge at the interface and results in a momentary change of the half-cell potentials until equilibrium can be re-established. If a pair of electrodes is placed in an electrolyte and one of these is shifted while the other remains stationary, a potential difference appears between the terminals of the two electrode cables. This potential is known as a motion artifact and can be a serious cause of interference in the measurement of biopotentials. The major components of this noise lie in the lower frequency range.

The electrode–electrolyte interface is not the only source of motion artifacts. The equivalent electric models in Figs. 12.16 and 12.17 show that E_{hc}, E_{se} and E_p can also cause motion artifacts due to movement of the sensor electrode.

The sensor itself is also a source of measurement noise, which depends on the electrode material (thermal noise), electrode impedance, electrode area, electrolytic gel, the patient, and the placement site. In the frequency band from 0.5 to 500 Hz, root-mean-square electrode noise is usually less than 1 μV for sensors placed face-to-face and ranges from 1 to 15 μV for sensors on the body surface. The spectral density of the noise is highest at low frequencies and it is always higher than the thermal noise from the real part of the electrode impedance. There is a high correlation between electrode offset voltage and electrode noise [17].

12.3.4 Survey of Biopotential ECG Sensors

The need for handy, easy-to-apply sensors with low offset voltage and low impedance, low artifact pickup, high stability of electrical properties and minimal skin irritation has resulted in the design of a number of different electrode types with varying modes of operation. Some typical examples and their advantages and disadvantages are as follows. A more comprehensive description of the theory and design of biopotential sensors can be found in [18, 19].

Most widely used present day ECG sensors utilize the electrolytic gel as a layer between the metallic electrode and the skin. These are commonly referred to as "wet-gel electrodes." Some variations of these sensors for applications in CCU monitoring are made of carbon, to render them X-ray transparent.

Due to the low cost of disposable wet-gel ECG sensors, reusable metal electrodes are less frequently used.

In specific applications dry ECG sensors with built-in amplifiers have been integrated into the sensor housings. Such sensors are referred to as "active electrodes."

Of late, major progress has been made in the development of new materials such as hydrogels, conductive polymers, spike electrodes, capacitive electric field pickups, impedance and optical probes for use in biopotential sensor design.

Offset voltage, low noise, low impedance, short-term stability (during the measurement) and sensor longevity on the body surface remain the design goals. Other important design parameters include considerations of possible biotoxicity of the sensor materials in direct contact with the body, skin irritation and shelf life.

12.3.4.1 Metal Electrodes

Metal electrodes are traditionally made of German silver (a nickel-silver alloy) or stainless steel [6]. Before being attached to the body, their surface is covered with an electrolytic paste or gel. These electrodes are of the "wet" type. They involve the use of an electrolytic paste or gel forming a conductive medium between the skin and the electrode.

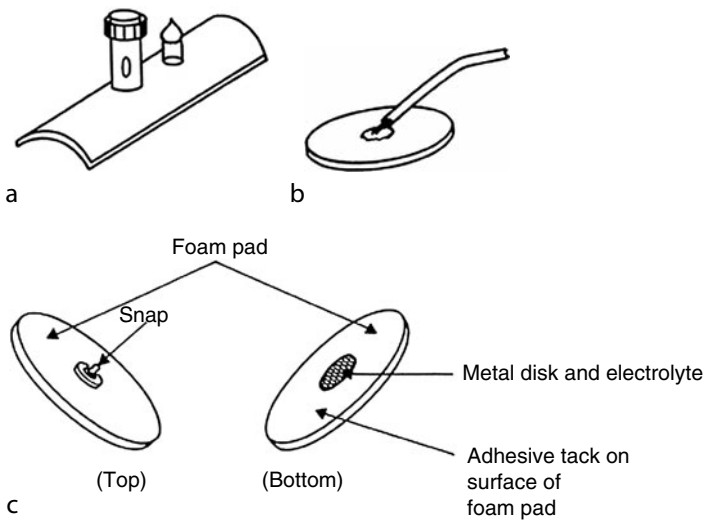

Figure 12.18

(a) Metal-plate electrode used for application to limbs. (b) Metal-disk electrode applied with surgical tape. (c) Disposable foam-pad electrodes, often used with electrocardiograph monitoring apparatus (from [6]).

A typical stainless steel ECG electrode is made of stainless steel grade 304 or 316. Low half-cell potentials can be achieved in stainless steel electrodes if potassium citrate EDTA or sodium sulfate is used in the liquid gel. The electrochemical reactions that govern the operation of a stainless steel electrode include O_2 reduction and H_2 production at the cathode, coupled with O_2 production and formation of metal oxides at the anode, which cause much larger polarization effects than in the Ag/AgCl electrodes. Typical parameters: offset (mV) = 1–50, impedance 800–2,200 Ω and polarization 400–1,200 mV [20].

The large plate electrodes (3–5 cm), which were introduced in 1917 [21], are made of stainless steel, German silver (an alloy of nickel, copper and zinc), nickel or nickel-plated steel. To obtain a stable offset voltage and allow electrode-skin impedance, the metal electrode should be separated from the skin by a film of electrolyte paste.

Metal electrodes of the type shown in Fig. 12.18(a) are usually fixed by rubber straps. These electrodes are well suited for the limb leads, but not for the pre-cordial leads. For the latter, the accuracy of localization is poor and the unstable skin–electrode interface produces motion artifacts in the ECG signal.

The smaller metal disk electrodes of the type shown in Fig. 12.18(b) are made of nickel, a silver alloy sometimes coated with silver chloride or sintered material containing Ag/AgCl. In ECG recording these electrodes have diameters of 1–2 cm. A self-adhesive variation of the metal electrode for monitoring applications is shown in Fig. 12.18(c).

Metal electrodes are rarely used in clinical applications today due to their poor noise immunity and high cost, and due to concerns of cross-infection. The use of electrode paste or gel in routine clinical electrocardiography is a cumbersome procedure. Skin preparation of, and gel application to, each patient for each electrode is time consuming, and the multiple-use electrodes need to be cleaned regularly to maintain low noise and low electrode skin impedance. In long-term applications, gel or paste tends to dry out or may irritate the skin (Table 12.2).

12.3.4.2 Pre-Gelled Galvanic Electrochemical ECG Sensors

A serious source of motion artifacts in solid metal reusable electrodes is caused by variations in a double layer of charge at the electrode–electrolyte interface. To minimize the measurement artifacts common in metallic electrodes, Ag/AgCl electrodes have been developed. Furthermore, in an effort to stabilize the skin–electrode interface, floating ECG sensors

Table 12.2

Summary of the metal electrodes properties

Advantages	Disadvantages
Reusable	Poor noise immunity
Infinite shelf life	Not suitable for long-term applications
	Require liquid gel
	Possibility of cross infection
	Require sterilization
	Require cleaning
	Variable electrode–skin contact area
	Leaking gel causing excessive baseline drift
	High cost

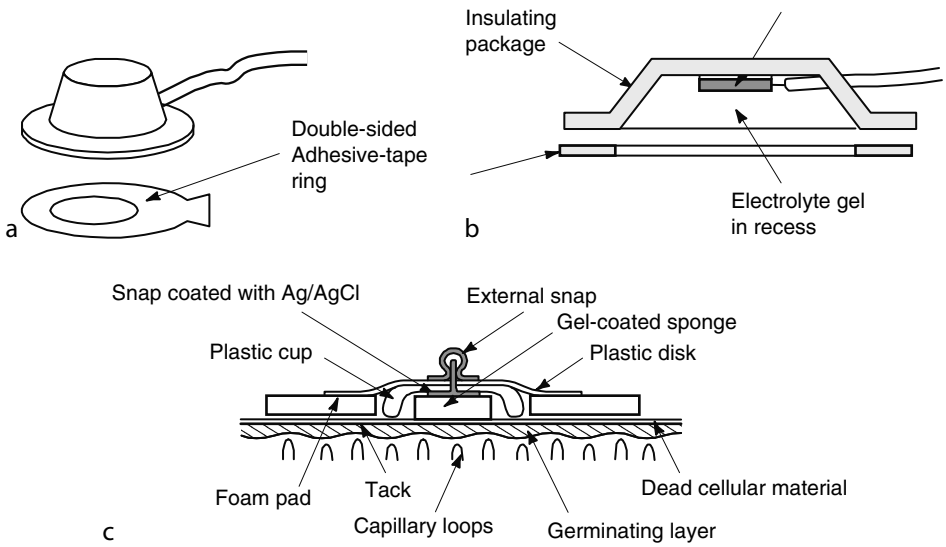

Figure 12.19

Pre-gelled ECG sensor assembly. The sensor comprises a metal snap coated with Ag/AgCl, which is embedded in an electrolytic gel filled cavity (from [6]).

have been devised. Their advantage is high artifact immunity, due to the absence of a direct contact of the sensor metallic electrode with the skin. The single use foam-pad floating sensors are routinely used in rest, stress and monitoring ECG applications. There are many designs of floating sensors, which include metal electrodes and carbon electrodes with Ag/AgCl coated surfaces.

Another type of a pre-gelled ECG sensor comprises of a mesh woven from fine silver-coated wire, with a flexible lead wire attached (Fig. 12.19) [22]. Adhesive electrolytic gel is applied to the mesh. Other models employ a carbon-filled silicone-rubber compound in the form of a thin film strip or disk, which is used as the contact element of the sensor. The lead wire is attached to the surface of the film strip. Such sensors are particularly suitable for the monitoring of newly born infants since the flexible sensors adapt very well to the curvature of a small chest. The thin silver film is X-ray translucent, so that these electrodes do not need to be removed for radiography.

A number of ultra flexible electrodes that use silver-coated nylon gauze and elastomeric materials, such as carbon-filled rubber and vinyls, silver-filled silicone rubber and silver-plated particle-filled elastomers have also been described in [23].

Table 12.3
Summary of the pre-gelled ECG sensor properties

Advantages	Disadvantages
Reasonable noise immunity	Limited shelf life
Single use application	Poor longevity on the body surface
Commonly available from multiple sources	Require skin preparation
Low cost	Not suitable for long-term applications
	Prone to motion artifacts
	Skin irritation
	Poor skin adhesion, especially in hair and sweat

A flexible electrode system where conductive elastomers were used as the electrode element was described in [24]. The electrodes were developed for arrhythmia monitoring of high-risk patients in a field study involving telephone transmission of the ECG [25].

Patten [26] and Roman [27] described "spray-on" electrodes, which were applied directly to the skin. First, the electrode gel was rubbed into the skin with a toothbrush and the skin was then wiped dry with gauze. Subsequently, a film of conductive adhesive was painted or sprayed on the skin, forming a conducting spot of about 20 mm in diameter. A silver-plated copper wire was attached to the skin by conductive adhesive glue. After drying, a coat of insulating cement was applied, to cover the electrode. ECGs from spray-on sensors have been recorded successfully during 100 h in flight and on the ground for air force personnel, indicating that a sufficiently long-term stability of the skin–electrode contact can be obtained (Table 12.3) [18].

12.3.4.3 ECG Sensors for Long-Term Monitoring and Stress Testing

Hospital applications require around the clock ECG monitoring patients during a typical 5-day hospital stay in post acute myocardial infarction (AMI) and coronary artery bypass grafting (CABG). A complete set of 12-lead ECG signals is required for an accurate assessment of acute and old coronary events. An onset of an acute myocardial ischemia usually manifests itself by the development of ST-segment and T-wave changes. ST-segment depression measured by an electrode overlying the injured area is believed to indicate subendocardial involvement, with less extensive myocardial injury. ST-segment elevation reflects transmural involvement, with greater extent of myocardial injury. Clinical decisions concerning treatment are based on ST-segment shifts in the body surface electrocardiogram. It is therefore very important to provide high fidelity ECG signals, since the detection of ST elevation myocardial infarction (STEMI) affects the choice of drug therapy and any accompanying procedures such as percutaneous coronary intervention [28].

Ambulatory applications are predominantly 24 h ECG Holter recordings, interpreted by computer-aided interpretation systems and read over by physicians. There is a growing need for longer term monitoring. Recently, Hindricks et al. [29] have demonstrated that 7 day Holter monitoring of patients after ablation for AF showed intermittent recurrence of AF not detectable by a 24-h procedure. In all ECG applications, signal morphology and rhythm analysis reveal the presence of acute and chronic heart disease.

12.3.4.4 Challenges Encountered in the Current Practice of ECG Monitoring

The traditional electrochemical ECG sensors described above suffer from the potential disadvantages inherent in wet systems, such as skin irritation, loss of electrical contact due to the drying of the paste or lead wires falling off, poor shelf life, etc. Success and failure of these gel- or paste-based electrodes is largely dependent on the hydration level of the skin. Long-term monitoring requires that the sensors and patient cables stay on the body surface for prolonged periods of time. The electrode-wire management imposes a significant burden on patients and caregivers.

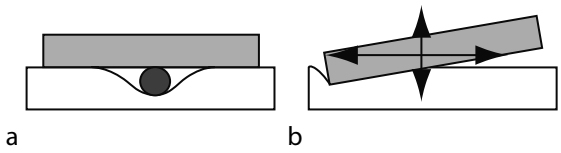

Figure 12.20

(a) Loss of contact area and increase of contact impedance due to hair. (b) Loss of contact and increase of artifacts due to charging effects caused by motion of electrode relative to skin (adopted from Anna Karilainen, Stefan Hansen, and Jörg Müller, Dry and capacitive electrodes for long-term ECG-monitoring. *8th Annual Workshop on Semiconductor Advances for Future Electronics and Sensors*, 1995).

Such wires need to be temporarily detached and then reattached each time a patient is bathed, leaves the bed, or is transported to another department, because current wired ECG monitoring requires a patient to be attached to a monitor by wires. Electrodes are frequently disposed of with each detachment, and new electrodes are applied with the reattachment. In addition to the demand on staff time and materials costs associated with these attachments and detachments, the current wired ECG systems also frequently generate false alarms due to movement of the lead wires and to artifacts due to inconsistent placement of the electrodes. These false alarms require a nurse to attend to the patient, and frequently involve detachment and reattachment of wires. Owing to significant difficulties in obtaining clean signals from wired ECGs in ICE/CCU and ambulatory (Holter) settings, at the present time 12-lead ECG monitoring is rarely used [30].

There is an increasing need for more reliable ECG monitoring technology and new methodology for long-term ECG monitoring.

In ambulatory monitoring, the shaving of a patient before application of the electrodes is often necessary. In long-term monitoring applications, even shaving does not produce stable results because of hair re-growth within a few days. A slightly invasive mechanical abrasion of the skin routinely performed in ambulatory care does not solve the problem because skin regenerates within about 24 h. A shift of the rigid electrodes relative to the skin caused by unavoidable movement of the patient (Fig. 12.20) during long-term monitoring results in random variations of electrode contact area, which may cause severe motion artifacts.

A recent study suggests that reusable ECG electrodes may provide a reservoir for multidrug-resistant bacteria [31]. The author studied 100 selected ECG electrodes that had been reprocessed and were ready for use in new patients. He found one or more antibiotic-resistant pathogens on 77% of the electrodes. In a different study, in the burns ICU at a university medical center, contaminated ECG electrodes were found to have renewed vancomycin-resistant enterococcal (VRE) infections. It was found that in 18% of the cases studied, the ECG electrode cultures tested positive for VRE. In one case, rekindled VRE infection due to electrodes contaminated by a former burns patient were tracked. The present day standards of the Joint Commission on Accreditation of Healthcare Organizations (JCAHO) call for at least one activity in the infection control process to be aimed at preventing the transmission of infections.

12.3.5 Biopotential Fiber Sensors

A newly-developed biopotential fiber sensor (BFS) technology [32] aims at significantly reducing the size of the ECG sensors, eliminates the pastes and gels by the introduction of new sensor materials and does away with patient cables. A typical BFS sensor assembly combines the functions of the sensor itself, a lead wire and a patient cable.

12.3.5.1 Principle of Operation

An equivalent circuit of a galvanic biosensor, shown in Fig. 12.16, suggests that in order to minimize the impedance of the skin–sensor interface, the resistive contributions from electrolyte/gel and the skin itself must be minimized. A key issue in sensor design is the identification of transport pathways that allow body electrolyte molecules to pass through the

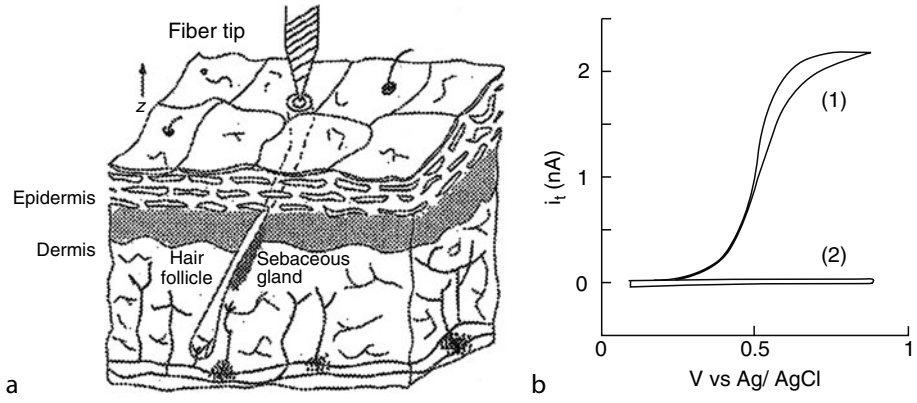

Figure 12.21

(a) Schematic drawing illustrating the fiber tip positioned directly above the opening of a hair follicle. (b) Voltammetric response of a 20 µm-radius fiber tip positioned directly above a hair follicle opening in hairless mouse skin (curve 1) and 150 µm away from the opening (curve 2) (from [34]).

skin. This can be accomplished by increasing the permeability of the skin and reduction of the gel/electrolyte resistance. Recent studies of the dependence of skin permeability on the contact area show that an array of smaller reservoirs is more effective in increasing transdermal electrolyte transport than a large single reservoir of the same total area. Karande [33] showed that Mannitol transport per unit area into and across the skin increased with a decrease in the area in contact with the skin. Mannitol permeability increased approximately sixfold with a decrease in the reservoir size from 16 to 3 mm in the presence of 0.5% SLS in PBS (phosphate buffered saline) as a permeability enhancer. Similar results were obtained when oleic acid was used as an enhancer. The molecular transport across the skin is also affected by hair follicles, which offer low resistance pathways for transport across the stratum corneum.

White [34] reported on studies of molecular transport in skin using scanning electrochemical microscopy (SECM) to investigate and quantify transport in artificial and biological skin and other membranes. Figure 12.21 shows the steady-state voltammetric response of the fiber tip when it is positioned directly above a hair follicle opening (curve 1) and at a lateral distance of ~ 150 µm from the opening (curve 2). In this experiment, the redox-active molecule is transported across skin by diffusion alone and is detected by oxidation at the fiber tip. The sigmoidal-shaped voltammetric curve recorded above the hair follicle (curve 1) corresponds to the oxidation of molecules that have diffused across the skin sample through the hair follicle. The magnitude of the tip voltammetric current is proportional to the local rate at which the molecule permeates the skin. The fiber tip current decreases to background levels (curve 2) when the tip is moved away from the pore opening, demonstrating that the diffusive flux of the molecules is localized to the hair follicle. The sites of highly diffusive flux are independently identified as hair follicles using a dye staining technique in which colloidal Prussian blue is precipitated at the opening of the follicle. Similar experiments using small organic and inorganic redox species, with different charges ($z = +1, 0$, and -1) indicate that hair follicles in skin act as the primary route for transdermal transport. The BFS takes advantage of both the follicular transdermal transport mechanism and enhancing arrays, which lower the skin permeability without the need for mechanical skin preparation.

12.3.5.2 Technology

The sensing fibers were developed by chemically impregnating the surface of synthetic acrylic fibers by metal molecules. The outer conductive layer of the fiber completely surrounded the inner part of the host fibers.

The fiber characteristics are: diameter: 20 µm; thickness of the electrically conductive layer: 30–100 nm; electrical resistance: 10^{-2} Ω cm.

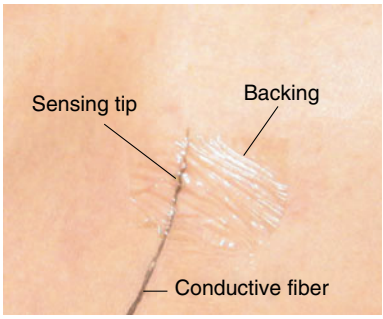

Figure 12.22
BFS applied to the body surface.

The biopotential fiber sensors were made up of the conductive bundle comprising about 100 individual fiber strands coated with an Ag/AgCl ink. The Ag was deposited electrochemically on the exposed sections of the fibers. The Ag surface was chlorinated to AgCl. The chlorination process was performed in a solution of $KCl/AgNO_3$ (1 M, pH 1) at a constant current of 0.2 mA. For the realization of the thin-film sensor a rapid dipping technique was used. As a result, the Ag/AgCl ink was deposited on the outer layer of the fibers. The resulting sensors were treated for 2 h at 120°C. The Ag/AgCl layer of the sensor tip was further coated with a 5 µm layer of the conductive adhesive mixed with skin permeability enhancers (Parker Laboratories, Fairfield, NJ). The non-sensing surface areas of the fibers were coated with a 2.5 µm thick Parylene C layer. The uncoated ends of the conductive fibers were bonded by conductive epoxy (Creative Materials) to gold-plated contact pins of a standard DB-15 connector. The sensing areas of the fibers were applied directly to the unprepared skin and covered by thin transparent dressing (3 M, Tegaderm) as shown in Fig. 12.22.

12.3.5.3 Electric Performance

The following tests on the electric performance of BFSs were carried out; the results were compared with the ANSI/AAMI EC 12:2,000 standard for disposable ECG electrodes.

Environment: All tests were performed at 23 ± 5°C, relative humidity less than 10%.

- Average value of AC Impedance (kΩ) at 10 Hz. Test Conditions: The impedance of a pair of sensors connected surface-to-surface was determined by applying 20 µA p-p sinusoidal current and observing the amplitude of the resulting voltage across the sensors.
- DC offset voltage [mV]. Test Conditions: BFS's sensor pair connected surface-to-surface, continuous 200 nA DC current applied.
- Offset Voltage [mV]. Test Conditions: BFS sensor pair connected surface-to-surface, after 1-min stabilization.
- Combined offset instability and internal noise [µV]. Test Conditions: Sensor pair connected surface-to-surface, after 1-min stabilization, in the band of 0.15–100 Hz, for 5 min.

The results of the test are shown in Table 12.4. All measured parameters were comparable to wet-gel electrodes and well below the limits specified by the AAMI EC:12 standard [37] (Table 12.5).

12.3.5.4 Clinical Testing

Due to their very small mass and excellent flexibility, biopotential fiber sensors can be attached directly to the skin, as shown in Fig. 12.23. An example of an exercise ECG recorded from BFS in a subject running up the stairs is shown in Fig. 12.24.

Table 12.4

Electric characteristics of BFS as compared to wet-gel electrodes and ANSI/AAMI EC12:2,000 limits

	Lead-lok wet-gel	BFS typical	ANSI/AAMI EC 12 Limits
DC offset voltage (mV)	0.15	0.11	Not more than 100
AC impedance @ 10 Hz (Ω)	51	22	Not more than 2,000
DC offset @ 5 s cap dis (mV)	0.7	0.4	Not more than 100
Recovery slope @ 30 s interval (mV/s)	0.0	0.0	Not more than 1.0
AC impedance after defibrillation (Ω)	49	18	Not more than 3,000

Table 12.5

Summary of the BFS sensor properties

Advantages	Disadvantages
Excellent noise immunity	May require more time to apply
Single use application	
Suitable for long-term applications	
No skin preparation required	
Excellent adhesion to the skin, especially in hairy chests	
Suitable for pediatric applications	
Long shelf life	
Low cost	

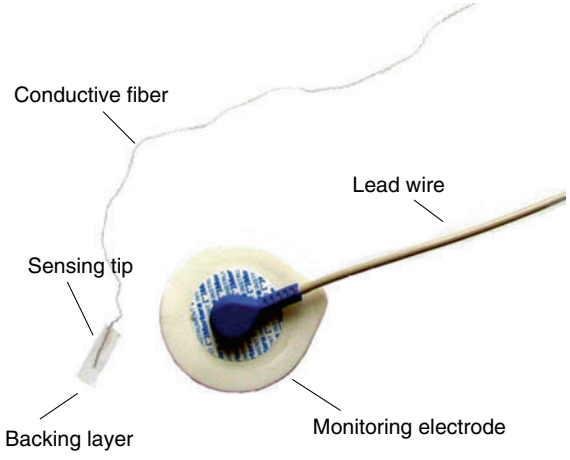

Figure 12.23

BFS compared to a standard wet-gel monitoring electrode with an attached lead wire.

12.3.6 Active ECG Sensors

A considerable research effort went into the development of "active sensors" that incorporate a high impedance amplifier into the sensor itself and required no wet gel or paste as a medium between the sensor electrode and the skin [35]. The placement of an electronic amplifier on the sensor itself is based on the idea that a high impedance amplifier is able to detect a signal from a high impedance source with a minimum of signal distortion, and then drive the signal through a long cable with a minimum of interference by virtue of the low output impedance of the amplifier [36].

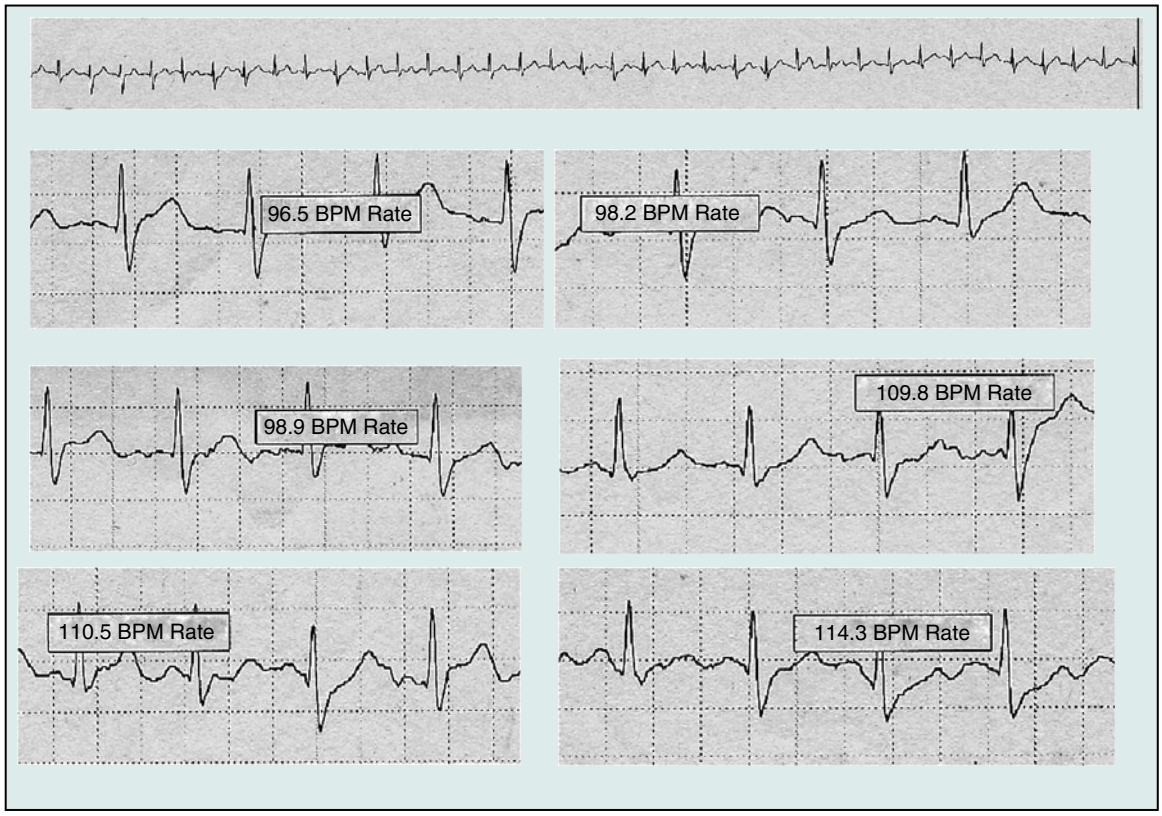

Figure 12.24

***Upper trace*: A full disclosure strip of a subject walking vigorously. *Below*: Exercise ECGs recorded at 40 s intervals from a subject running up the stairs. King of Hearts ECG Monitor (Instromedix). Speed: 25 mm/s, Gain: 10 mm/mV, Highpass Filter: OFF, Lowpass Filter: 100 Hz.**

The idea of having the first amplifier stage integrated with the electrode probably goes back as far in time as the introduction of the transistor. Over the past years, researchers have described the realization of several prototypes, and in most cases these indeed offered the advantages in signal quality that were promised originally by the interference theory [37].

Advances in solid-state electronic technology have made it possible to record surface biopotentials utilizing electrodes that can be applied directly to the skin without abrading the skin or requiring the use of an electrolytic gel. These electrodes are not based on an electrochemical electrode–electrolyte interface. Rather, these electrodes are active and contain a very high impedance-converting amplifier [38]. In this way, biopotentials can be detected with minimal or no distortion. Burke [39] described an active biopotential sensor that utilizes a very low-power preamplifier, intended for use in the pasteless-electrode recording of the ECG. The input signal range of the amplifier was reported to be 100 μV to 10 mV. The amplifier provides a gain of 43 dB in a 3-dB bandwidth of 0.05 Hz to 2 kHz with a defined high input impedance of 75 MΩ. It uses a driven common electrode to enhance the rejection of common-mode interfering signals, including low-frequency motion artifacts, achieving a common-mode rejection ratio (CMRR) of greater than 80 dB over its entire bandwidth (Sect. 12.4.1.2). The amplifier has a power consumption of 30 μW operating from a 3.3 V battery.

Valchinov [40] described an active sensor assembly developed for the measurement of small biopotentials on the body surface (Fig. 12.25). This active sensor features an adjustable anchoring system designed to reduce the electrode-skin contact impedance, its variation and motion artifacts. This is achieved by increasing the electrode-skin tension and

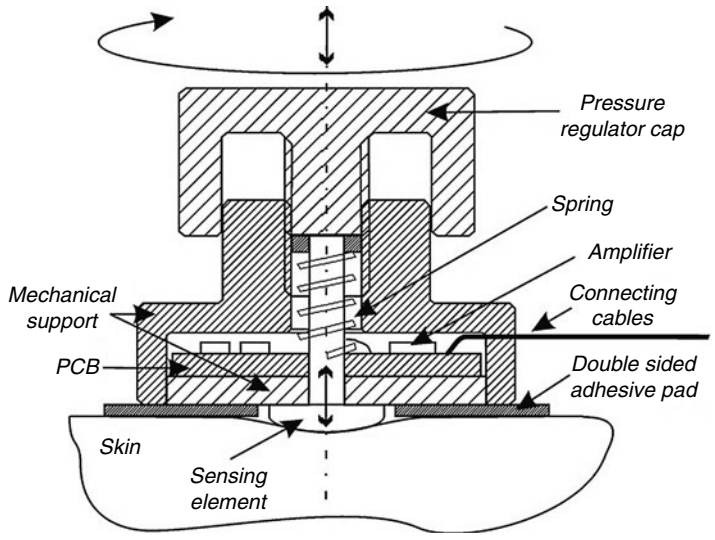

Figure 12.25
An active sensor assembly with an anchoring system.

decreasing its relative movement. Additionally the sensing element provides local constant skin stretching thus eliminating the contribution of the skin potential artifact. The electrode is attached to the skin by a double-sided adhesive pad, where the sensor is a stainless steel element, 4 mm in diameter. The front-end operational amplifiers (op-amps, Sect. 12.4.1.1) of the biopotential amplifier is incorporated in the sensors, thus avoiding the use of extra buffers. The biopotential amplifier features two selectable modes of operation: semi-AC mode with a −3 dB bandwidth of 0.32–1,000 Hz and AC-mode with a bandwidth of 0.16–1,000 Hz. The average measured DC electrode-skin contact impedance of the proposed electrode was 450 kΩ, with electrode tension of 0.3 kg/cm^2 on an unprepared skin of the inner forearm. The peak-to-peak noise voltage, with the input terminals connected to a common mode, was 2 μVp-p referred to the input.

The common-mode rejection ratio of the amplifier was 96 dB at 50 Hz, measured with imbalanced electrode impedances.

Although active electrodes offer the advantage of not requiring some of the preparation needed with conventional electrodes, they have certain inherent disadvantages. One problem is that many previously described designs, including DC biased transistor amplifiers, differential amplifiers, and amplifiers with gains above unity are not compatible with commonly-used ECG equipment unless some adjustment or modifications are made to the front-end of the electrocardiograph. Even with unity-gain, DC-biased transistor amplifiers that are capacitively coupled at the output cannot be conveniently used with different types of electrocardiographs without the risk of linear distortion caused by an impedance mismatch with the different electrocardiograph inputs, and without large transient DC offsets arising when switching leads (Table 12.6).

Defibrillation voltages, static charge accumulation on the skin and clothes, and other medical equipment may cause potentials up to 25,000 V in contact with the input of the electrode amplifier, resulting in permanent failure of the device if not protected. Some designs made use of input resistors or unspecified current limiters for device and patient protection, but failed to show a means for compensating for the degradation of input impedance to the device as a result of parasitic capacitance coupling to ground through the resistor or current limiter. However, a means for adequately protecting the electronic circuitry from repeated exposure to high voltages, without compromising the essential electrical characteristics of the amplifier input, has not yet been devised.

Most active sensors are bulky in size due to the additional electronics and power sources required and they are typically more expensive to produce owing to the electronic assembly required. As of today, there has not yet been a breakthrough in the application of an active sensor to commercially available ECG recorders.

Table 12.6

Summary of the active ECG sensor properties

Advantages	Disadvantages
Reasonable noise immunity	Limited shelf life
Single use application	Poor longevity on the body surface
Commonly available from multiple sources	Require skin preparation
Low cost	Not suitable for long-term applications
	Prone to motion artifacts
	Skin irritation
	Poor skin adhesion, especially in hair and sweat

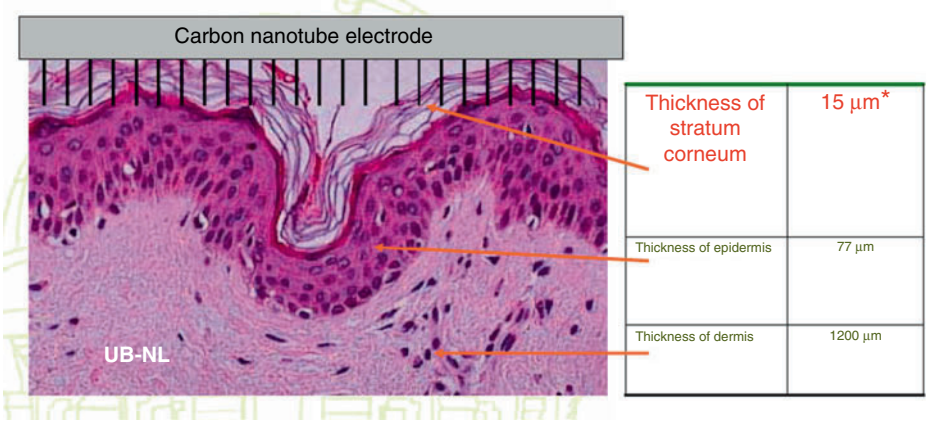

Figure 12.26

The principle of operation of the CNT biopotential sensor.

12.3.6.1 Carbon Nanotube Active Biopotential Sensor

The experimental carbon nanotube (CNT) biopotential sensors [41] utilize a penetrating brush-like structure to provide an electrical contact with the skin (Fig. 12.26). The nanostructure is designed to limit penetration of the stratum corneum of the skin in order to avoid direct contact with the dermis and prevent the risk of infection.

The principle of operation of the CNT biosensor named ENOBIO is similar to the spike electrodes described before. The sensor is shown in Fig. 12.27. The carbon nanotubes, which form a brush-like structure, are coated with silver and then treated with chloride to form an Ag/AgCl type of electrode interface. ENOBIO also features a high impedance amplifier built into the sensor assembly. The amplitude spectral density of the noise signal from the sensor was found to be 1.4 µV RMS in the range of 0.1–100 Hz (Table 12.7).

12.3.7 Paste-Less Electrodes

The other "dry electrodes" reported in the literature comprise either metallic, ceramic or carbon-filled rubber assemblies, which are firmly attached to the body surface [42–44].

Direct skin contact dry ECG sensors for long-term monitoring have been devised. The sensors were embedded in a chest belt. The sensors, which are made of carbon-loaded rubber, are placed into a garment using a thermal molding process [24]. The ECG signal is passed from the body surface to the module PCB by means of a very thin and flexible shielded cable, anchored in the rubber of each sensor (Table 12.8).

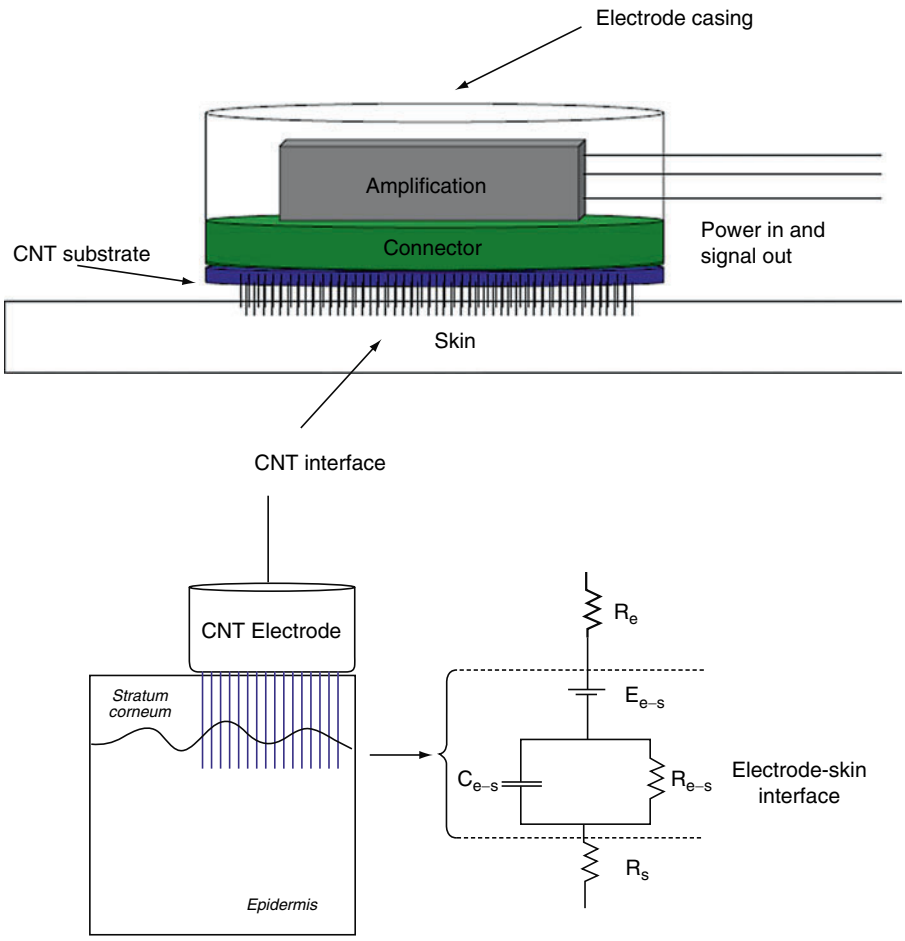

Figure 12.27

CNT ENOBIO active biopotential sensor.

Table 12.7

Summary of the ENOBIO sensor properties

Advantages	Disadvantages
Potentially better noise immunity	Experimental device
	May mechanically abrade the skin
	Nanotubes are potentially toxic
	Not compatible with existing ECG instruments
	Very costly
	Skin irritation
	Poor skin adhesion, especially in hair and sweat

Table 12.8

Summary of the properties of the "dry" sensors

Advantages	Disadvantages
Reasonable noise immunity	Higher noise levels than wet sensors
Longer shelf life	Relatively high cost
Suitable for long-term applications	Not widely avilable
No skin irritation	

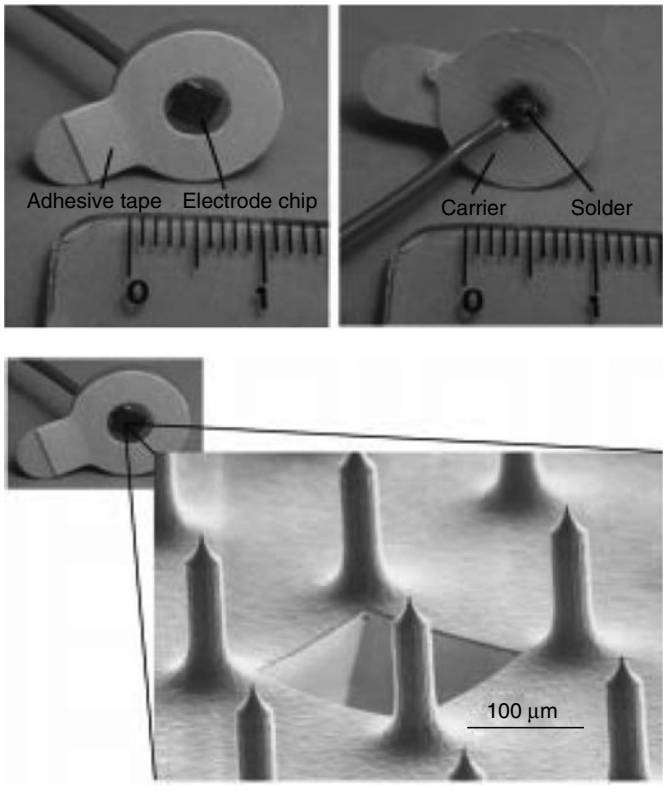

Figure 12.28

Micromachined spiked electrode for measurement of biopotentials. The spikes are placed in the center of the adhesive foam collar, which affixes the assembly to the surface of the skin.

12.3.7.1 Biopotential Sensors with Spiked Electrodes

In 2001, the Microsystem Technology Group of the Royal Institute of Technology (Stockholm,Sweden), in collaboration with the Datex-Ohmeda Division of Instrumentarium Corporation (Helsinki, Finland), presented the concept and fabrication of a micro-machined biopotential electrode, which requires neither electrolytic gel, nor skin preparation, nor an on-chip pre-amplification [45]. The principle of this electrode is based on the penetration of the living epidermis (LE) by micro-scaled spikes (i.e., micro needles). The skin penetrating system reduces the isolating influence of the stratum corneum (SC) on the electrode–skin impedance and brings the electrode into direct contact with the electrically conductive LE (Fig. 12.28). The thickness of the SC, e.g., on the forehead or the forearm, is 10–20 µm. The thickness of the LE varies greatly locally but is approximately 150 µm.

Figure 12.29
Commercial Spiked Electrode Biosensor [46].

The biopotential sensors with spiked electrodes were evaluated for their potential in long-term monitoring applications [45]. The authors of the paper observed a significant dependency of the electrode–skin–electrode impedance (ESEI) on the electrode size (i.e., the number of spikes) and the coating material of the spikes.

Electrodes larger than $3 \times 3\,mm^2$ coated with Ag/AgCl have sufficiently low ESEI to be well suited for recording of the biopotentials. The maximum measured ESEI was 4.24 kΩ and 87 kΩ, at 1 kHz and 0.6 Hz, respectively. The minimum ESEI was 0.65 kΩ and 16 kΩ at the same frequencies. The ESEI of spiked electrodes was stable over an extended period of time.

The arithmetic mean of the generated offset voltage was 11.8 mV immediately after application of the ESEI to the skin and 9.8 mV after 20–30 min. A spectral study of the generated potential difference revealed that the AC part was unstable at frequencies below approximately 0.8 Hz, thus making them unsuitable for some diagnostic ECG applications. The spiked electrodes have found applications in EEG monitoring, where a low frequency response is not required.

A commercial version of the spike electrode for ECG monitoring applications as shown in Fig. 12.29 has been marketed by the Orbital Research Corporation.

12.3.8 Electrical Performance Testing for Disposable Electrochemical Biopotential Sensors

Regulatory agencies such as FDA in the US, EMEA in Europe and PMDA in Japan have adopted performance standards for disposable ECG electrodes exemplified by ANSI/AAMI EC12:2,000. They focus specifically on test methods and establish the minimum performance standards (ST) as discussed below.

12.3.8.1 AC Impedance

Human skin impedance varies from a few hundred to hundreds of thousands of ohms. Electrode impedance is important, because the higher the impedance, the more impedance imbalance is likely to occur between electrodes, thereby lowering the common-mode-rejection ratio (CMRR; Sect. 12.4.1.2) of the ECG amplifier and leading to increased AC interference. The 2 kΩ level specified in the standard represents a compromise, assuring the user of a low probability of interference problems caused by the electrode, while at the same time providing a generous flexibility in electrode design. In the monitoring applications, skin impedances are reduced to 1 kΩ or less by vigorous skin preparation (for example, ambulatory monitoring and stress testing).

Although ECG monitors incorporate protective devices to absorb overloads caused by defibrillation or electrosurgery currents, if the electrode's impedance is high, a substantial amount of heat may be generated at the skin–electrode interface, raising the probability of electrode failure as well as patient injury. The AC impedance requirement for purposes of quality assurance is specified by both a mean value and a permissible upper limit.

The measurement of impedance at 10 Hz, as currently specified in ST, has become an industry standard. The fact that currently marketed electrodes provide adequate performance, supports the adequacy of the 10-Hz measurement as a bench-mark for electrode performance. However, the AC impedance may not be a direct indicator of the sensor performance, since tests carried out by the Utah Biomedical Testing Laboratory (UBTL) indicated that the effective impedance

of an electrode type, when tested on unprepared human skin, did not correlate well with the bench-test measurements of impedances for electrodes joined gel-to-gel. However, a 99% correlation was established between the results of tests on prepared (abraded) skin and those obtained using the bench test.

12.3.8.2 DC Offset Voltage

Because the input buffer amplifiers of cardiac monitors saturate under conditions of excessive DC offset voltage, a reasonable limit must be established regarding the offset voltage contributed by the electrodes.

The maximum allowable DC offset voltage was originally specified at 300 mV, based on the data gathered during the UBTL study [47]. The American National Standard on Cardiac monitors, heart rate meters, and alarms requires that cardiac monitors be capable of tolerating up to 300 mV offsets (AAMI, 1992). A 100 mV offset voltage limit for disposable ECG electrodes would provide reasonable assurance that electrodes conforming to this limit would be acceptable for use with most cardiac monitors. The 100 mV limit for ECG electrodes provides a sufficient operating margin to accommodate increases in electrode offset voltages caused by unequal potentials at the skin–electrode interface, defibrillation overloads, pacemaker currents, and/or ECG amplifier bias current.

The 100 mV offset voltage limit is adequate for accommodating the offset tolerance capabilities of currently available cardiac monitors, most of which can tolerate offsets of at least 200 mV. A DC offset voltage well below 100 mV would be beneficial, since emerging evidence links high offset voltages with motion artifact and other types of interference [48].

12.3.8.3 Combined Offset Instability and Internal Noise

At a 1977 conference on "Optimal Electrocardiography" convened in Bethesda, Md., by the American College of Cardiology, the Task Force on Quality of Electrocardiographic Records reserved its highest rating for baseline drift to those records exhibiting drifts of less than 0.1 mV/s [49]. Recordings exhibiting baseline drifts of 0.1–0.4 mV/s, while judged to be less desirable by the task force, were not considered unacceptable. Although electrocardiographic recording devices generally filter the signals to reduce or eliminate baseline drift, a contribution to the drift rate from the electrode–electrolyte interface of less than 150 V/s is desirable to ensure a minimal contribution by the electrode to the baseline wander.

12.3.8.4 Defibrillation Overload Recovery

After a defibrillation attempt, the ECG is important to the clinician in determining whether the heart has been returned to normal sinus rhythm. For this reason, the ECG trace must return within 5–10 s to an input offset voltage within the range that can be tolerated by cardiac monitors so that the condition of the patient can be assessed as rapidly as possible. During the next 30 s, the offset drift with time should not vary by more than 1 mV/s in order to display a clinically useful ECG. The prolongation of recovery time may also occur, due to the very high input impedance of the monitoring devices.

As many as 20–25 defibrillation attempts for an individual patient have been reported, suggesting the maximum number of consecutive defibrillation overloads that the electrode must absorb. However, this high number of attempts is unusual. An overload of 2 millicoulomb represents a worst-case condition that would be encountered only if the defibrillator paddles are placed in immediate contact with the ECG electrodes. Even if the electrodes are 10 cm (4 inches) away from the paddles, the overloads are likely to be reduced by only 50%. In most clinical situations, where skin preparation is sub-optimal, the circuit impedance will probably be much higher than the average of 1.5 kΩ encountered in UBTL animal testing [47]. On this basis, four consecutive discharges, delivered at 15–30 s intervals, should provide an adequate criterion for judging the performance of the electrode.

12.3.8.5 Bias Current Tolerance

When subjected to DC bias currents, the reactants involved in the chemical reactions occurring at the electrode–electrolyte interface can become depleted, which causes significant variations in the electrode half-cell potential. The ST demands that the compatibility of electrodes with the 200 nA bias current allowed for cardiac monitors must be demonstrated. Older monitors can have higher bias currents, so that a higher bias current tolerance for electrodes might be desirable.

12.3.9 Safety Requirements for Electrodes

12.3.9.1 Biological Response

Certain materials, if used in the fabrication of ECG electrodes, could cause skin sensitivity or skin irritation problems, especially if skin abrasion prior to electrode application is used to enhance the transfer of the ECG signal. The biocompatibility is defined in industry-wide standards such as ANSI/AAMI/ISO 10993:1997. Presently, no universal system exists to grade biocompatibility. Current practice relies on the expert who evaluates the test results and determines whether or not the material is biocompatible in the intended application. The determination of biocompatibility does not necessarily require testing in each new design. The expert, using his/her professional judgment, may decide that, based on the availability of biocompatibility data for the components, in conjunction with an evaluation of the intended application of the new design, additional testing is not required [50].

12.3.9.2 Preattached Lead Wire Safety

Historically, many electrodes with preattached lead wires were connected to the patient cable by means of male pins. There have been incidents where these pins were inserted into detachable power cords, thus applying full-line voltage to the patient. To ensure patient safety, the leadwire/patient-cable connector must not be permitted to make contact with a possibly hazardous potential, or a conductive surface that may be at ground potential, thereby compromising patient isolation.

12.3.9.3 Electrode Adhesiveness

The ability of an electrode to adhere satisfactorily to the skin over the expected period of use is an important feature of its performance. During the development of the initial 1984 standard, a study of the adhesiveness characteristics of disposable ECG electrodes, by the UBTL, did not yield a suitable bench test for evaluating adhesion performance; that is, a bench test that would correlate well with adhesiveness as observed clinically [47].

Over the last 10 years, progress has been made in identifying adhesive tests that can indicate how well certain adhesive systems will perform in ECG electrode applications [50].

12.3.9.4 ECG Cables and Lead Wire Standards

In 1995, the AAMI standard (ANSI/AAMI EC53:1995) on ECG cables and lead wires was published, addressing specific design requirements. It covers cables and patient lead wires used for surface electrocardiographic (ECG) monitoring in cardiac monitors as defined in the ANSI/AAMI EC13-1992 standard: Cardiac monitors, heart rate meters, and alarms. It covers both disposable and reusable lead wires, with certain sections applicable to both types, and certain sections applicable to one only.

This standard defines a safe common interface at the cable yoke and lead wire connector (no exposed metal pins). Specified are standards for: cable labeling, manufacturing, cleaning, disinfection, chemical resistance and sterilization

exposure. Performance requirements (trunk cable and patient lead wires) include the following: dielectric voltage withstand, sink current, defibrillation withstand, cable and lead wire noise, flex life of instrument connector, cable yoke, patient lead wire connector, patient end termination flex relief, tensile strength of cable connections, number of connector mate/unmate cycles, contact resistance, connector retention force and patient lead wire resistance.

This standard also incorporates by reference the DIN 42–802 standard (Connector, touch proof, for electromedical application, 1990). Devices that comply with this standard also meet the FDA mandatory standard 21 CFR Part 898, "Medical Devices; Establishment of a Performance Standard for Electrode Lead Wires and Patient Cables."

The scope of EC53 excludes ECG cables and lead wires that are used in applications that may require special characteristics, such as ambulatory ECG devices, telemetry units, the operating room and the cardiac catheterization lab. The cables and patient lead wires included in the scope of EC53 also relate to other applications than ECG monitoring, such as respiration monitoring by impedance pneumography. The cable and patient lead wires should meet all of the requirements of this standard, unless a requirement is specifically excluded for that device by the standard.

12.3.10 Non-Contact Biopotential Sensors

A desire to replace wet ECG sensors prompted the research toward the development of the non-contact sensors that work on the principle of the displacement current in the body. These are referred to in the literature as insulated, capacitive or impedance probes. Richardson [51] and Lopez used an anodized aluminum disk as the electrode, though in a patent application they claim the use of any conductive material such as "copper, aluminum, or stainless steel having an insulation on its outer or skin contacting surface." In this particular case, the insulating coating was produced using an anodizing process. They maintained that the aluminum oxide can be used so that the film will be "free from pores or grain structure." To produce the film, they immersed the electrode in a standard sulfuric acid anodizing bath for 1.1 h. The process was finalized by dying the oxide, and immersing the electrode in hot water for oxide sealing.

To obtain the dimensions of the insulating layer, they measured the capacitance on the basis of which they calculated the thickness. For the said electrode, the resistance was greater than 4 GΩ and the capacitance was 5,000 pF.

Richardson et al. [51] concluded that "the production of motion artifacts caused by change in coupling capacity limits the use of this type of electrode." This is a major problem with a capacitive electrode-skin junction. With any kind of movement, the capacitance will change because the contact area will change. Despite many years of research, the capacitive insulated sensors have not yet exhibited the same consistency and signal to noise ratio (SNR) as the pre-gelled wet biopotential sensors.

The efforts to realize active insulated electrodes have been prompted by significant research and development in the area of sensor dielectrics. A number of materials have been investigated regarding thin-film capacitor fabrication in sensors of active hybrid electrodes. Some of the materials typically considered for use include silicon monoxide (SiO), silicon dioxide (SiO_2), silicon nitride (Si_3N_4), diamond-like carbon (DLC), and tantalum pentoxide (Ta_2O_5). In practice, deposited dielectric films thinner than 500–700 angstrom (Å) have a fairly high pinhole density and the yields are poor. Pinholes lead to resistive shorts between the electrodes placed in the vicinity of each other and increase the leakage current. Thick dielectric films, or films with a thickness greater than 20,000 Å, also may exhibit problems because of the high internal stress levels found in these films. High compressive forces cause the films to peel off; however, large tensile forces can be relieved by crazing, i.e., the production of fine cracks in the film. These factors thus have limited the thickness of the dielectric material to between 800 and 10,000 Å.

The progress in development of low noise Giga Ohm impedance probes [52] has further enabled research activities in the field of non-contact biopotential sensors.

12.3.10.1 Low Invasive Measurement of Electrocardiogram for Newborns and Infants

In 2003, a group of Japanese researchers reported on the development of a non-contact biopotential sensor for ECG applications in neonatal monitoring [53]. Here, thin silk fabric is used as an insulator between the skin and the sensor. The authors demonstrated that it is feasible to measure the ECG signal through silk with a capacitive sensor if the impedance of the capacitive probe is of the order of 10^{12} Ω at 10 Hz. Consequently, the input impedance of the measurement system

Figure 12.30
This photo shows through-clothing biosignal recording.

has to be higher or at least equal to 10^{12} Ω to detect stable ECG signal. Although the capacitive sensors produced stable ECG signals, they were attenuated at the high frequency range and could not be used for diagnostic purposes.

12.3.11 Recent Developments and Trends

Recent breakthroughs have been made in the form of miniature insulated biopotential sensors [53]. They can measure the electric potential on the skin without resistive electrical contact and with very low capacitive coupling. This has been made possible by a combination of circuit design and the use of a new, low-dielectric material. These sensors enable through-clothing measurements, and results from 40 subjects have shown them to be capable of a higher than 99% correlation with gold standard conventional electrodes. The capacitively coupled non-contact sensor (CCNS) utilizes high impedance, low noise probe technology that measures low frequency electric potentials in free space, i.e., without physical contact to any object. The process of biopotential recording through the clothing is shown in Fig. 12.30.

The CCNS produced signals that are morphologically very similar to the electrocardiogram recorded from the standard Ag/AgCl electrodes as shown in Fig. 12.31.

The first version of the CCNS biopotential sensor, including all amplification electronics, resulted in an approximately 1 inch square and 0.35 inch thick module (Fig. 12.32).

12.3.11.1 A Prototype Biopotential Sensor Shirt

A non-invasive, zero prep time biopotential shirt system utilizing CCNS was developed for use with firemen. The shirt offers the first non-contact system of its kind, allowing an instantaneous biosignal collection (Fig. 12.33).

In another development, common cotton was used as an insulator in between a capacitive sensor and the body. A sheet of conductive fabric was substituted for the conventional metal plate to realize a deformable coupling surface corresponding to the contour of the body [53] as shown in Fig. 12.34.

The measurement system involved is as shown in Fig. 12.35 (see also Sect. 12.4). It comprised of two buffer circuits, a differential highpass filter, an instrumentation amplifier, a lowpass filter, a highpass filter, a band elimination filter, an inverting amplifier, an A/D converter, and a personal computer. Two buffer circuits with high input impedance of 1000GΩ were employed for matching of the high impedance at the coupling involving cloth and the low impedance required by the subsequent circuitry. The differential highpass filter circuit (cutoff frequency: 0.05 Hz) was inserted in front of an instrumentation amplifier to reduce the low frequency component in the detected signal effectively prior to amplification. The cutoff frequency of the lowpass filter was set to 100 Hz. The notch filter was used in order to reduce 50 Hz interference. The total gain of the device was 60 dB.

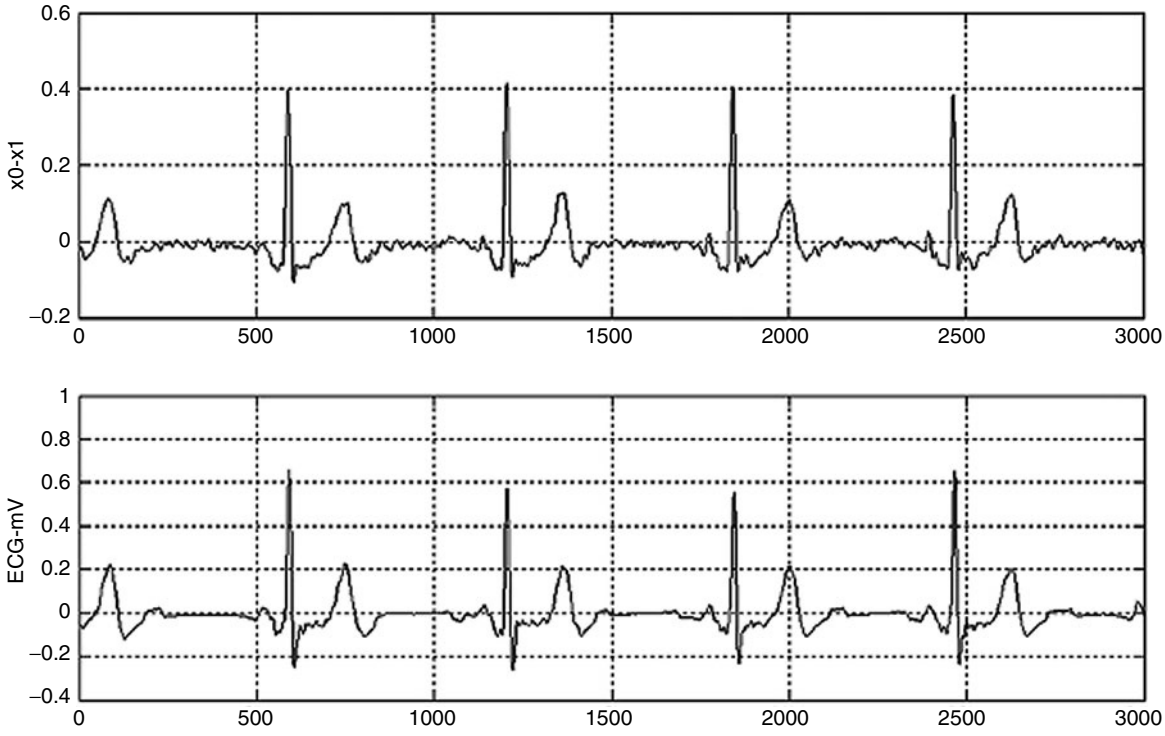

Figure 12.31
CCNS produced biopotential signals compared to ECGs obtained from the Ag/AgCl electrodes in frontal plane.

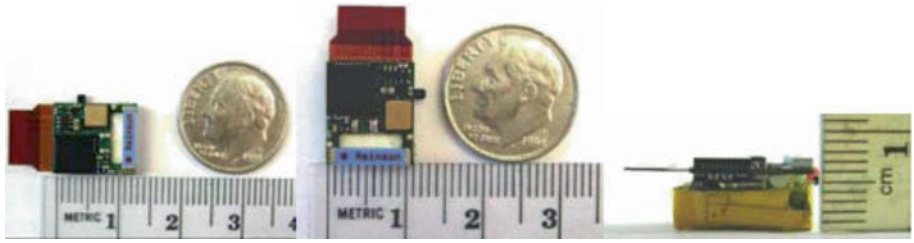

Figure 12.32
The CCNS sensor assembly (13 mm × 11 mm × 7 mm).

12.3.11.2 High Impedance Biopotential Optical Sensor

In 2003, Kingsley [54] reported on the development of a new non-contact ultra high input impedance biopotential sensor, which he named Photrode (Fig. 12.36). The resistive part of its impedance can be as high as 10^{14} Ω, while the capacitive component is commonly a few picofarads. This allows the system to make non-contact capacitively-coupled measurements of ECG signals through clothing. The sensor requires no surface preparation or conductive gel. The Photrode is an optical modulator that employs an electro-optic material, in this case lithium niobate, to modulate the intensity of the light transmitted by the device. Unmodulated light from a laser or super-luminescent light emitting diode (SLD) enters the sensor and intensity-modulated light exits the device. The Photrode is a "Plug-N-GO" component that uses commercial fiber optic connectors at its pigtailed interfaces. A special type of single-mode fiber called a polarization-maintaining fiber

Figure 12.33
A prototype biopotential sensor shirt for real time measurement of the electrocardiogram.

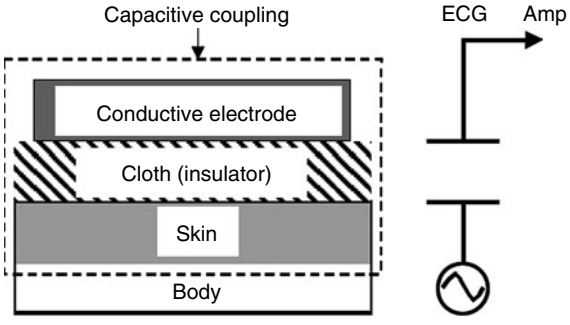

Figure 12.34
A model of a capacitive biopotential sensor coupled to the body surface through cloth.

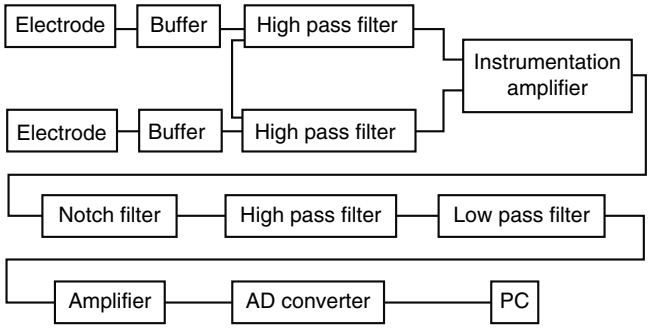

Figure 12.35
Block diagram of the ECG measurement system for capacitive biopotential sensors.

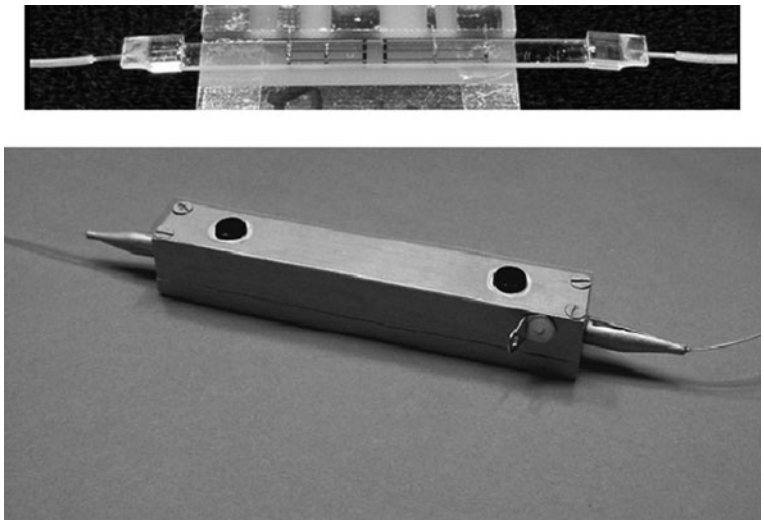

Figure 12.36
Photograph showing a prototype packaged PhotrodeTM designed for ECG and EEG signal monitoring. The upper picture shows the bare optical chip, about 5 cm in length.

Table 12.9
Summary of the non-contact displacement current biopotential sensors

Advantages	Disadvantages
Reasonable noise immunity	Non-standard ECG signal
Multiple use application	Not compatible with standard ECG instrumentation
Excellent longevity on the body surface	High cost
Requires no skin preparation	
Suitable for long-term applications	

connects the device to the light source. A second, single mode fiber conveys the modulated light to an optical receiver, where the signal is converted back to the electronic circuitry, where the ECG signal is processed in a similar fashion to the small voltages that would normally be obtained from a conventional electrode (Table 12.9).

12.3.11.3 Electroactive Fabrics and Wearable ECG Devices

Promising recent developments in material processing, device design and system configuration have enabled the scientific and industrial community to focus their efforts on the realization of smart textiles. All components of a wearable ECG system (sensors, electronics and power sources) can be made from polymeric materials, to be woven directly into textile structures (sensing micro-fibers) or printed or applied onto fabrics (flexible electronics). In particular, intrinsic sensing, dielectric or conductive properties, lightness, flexibility and the relative low cost of many electroactive polymers makes them potentially suitable materials for the realization of such systems.

The use of "intelligent materials" enables the design and production of a new generation of garments incorporating distributed sensors and electrodes [55, 56]. Wearable non- obtrusive systems will permit the user to perform everyday activities with minimal training and discomfort.

A shirt was functionalized with CLR piezo-resistive fabric sensors used to monitor respire trace (RT), and conductive fabrics used as electrodes to detect the ECG [57].

To record the ECG signals, two different square-shaped fabrics (1 × 1 cm) were used: the first was made with steel threads wound round acrylic yarns, the second with a layer of acrylic/cotton fabric coupled with a layer containing stainless steel threads. In order to assess their performances, the signal originating from an Ag/AgCl electrode (Red Dot by 3 M) was recorded simultaneously with the signal detected by the fabric electrode.

12.3.11.4 Trends

The recent advances in miniaturization of ECG devices, as well as mobile computing, have fostered a dramatic growth of interest in wearable sensor technology.

The interest in wearable ECG systems stems from the need to monitor patients over extensive periods of time and reinforces the "doctor is always with you" paradigm since the usual clinical or hospital monitoring of the electrocardiogram provides only a brief window on the status of the patient. Practical wearable ECG systems require to be quite non-obtrusive devices that allow physicians to overcome the limitations of ambulatory technology and provide a response to the need for monitoring individuals over weeks or even months. They will rely on wireless, miniature sensors enclosed in patches or bandages, or in items that can be worn, such as personal jewellery or underwear.

Wearable ECG sensors and systems have evolved to the point that they can be considered ready for clinical application. This is due not only to the tremendous increase in research efforts devoted to this area in the past few years but also to the large number of companies that have recently started investing in the development of wearable products for clinical applications. The current upward trend in the use of this technology suggests that soon wearable ECG systems will be part of routine clinical evaluations. Wearable devices that can intermittently or continuously monitor and record good quality ECG signals will offer an important solution to the limits imposed by traditional monitoring schemes [58, 59].

12.4 ECG Signal Recording and Basic Processing

As discussed in Chap. 10, ECG leads are the signals that represent the time course of the electric potential differences that are observed between any two terminals of a configuration of electrodes attached to the body surface. In its most simple form, a lead represents the potential difference between the ends of the two electric wires connected to the two sensors attached to the body surface (Fig. 12.37).

For most lead configurations the potential difference generated by the heart is typically of the order of 1 mV and, for subsequent display and interpretation of the signal, amplification is needed. Connecting the two wires to a modern electronic amplifier will generally not affect the voltage difference present.

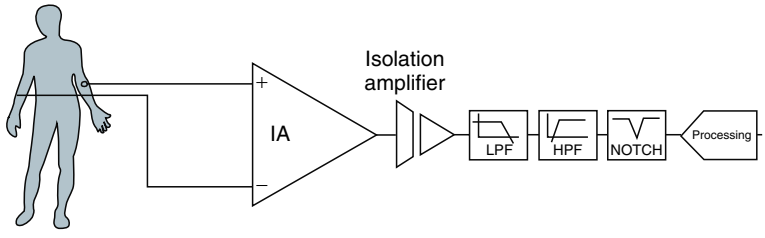

Figure 12.37

ECG Signal processing chain. The biopotentals measured by the sensors are applied to the front-end of an instrumentation amplifier (IA). For safety reasons the front-end is often isolated from other processing circuits by an isolation amplifier that limits current flow from the recording equipment to the patient. The ECG signal is band limited by a combination of a low-pass filter (LP) and a highpass (HP) filter that minimize signal aliasing (Appendix Section "Sampling Theorem and Analog Filters") and cut off the DC voltage, respectively. A notch filter of 50–60 Hz is frequently used to minimize the power line interference.

Next to amplification, ECG measurement and recording systems perform some basic signal pre-processing steps. These may be carried out in analog and/or digital signal processing modules. The need for such signal processing steps and the way in which these are implemented are discussed in the next sub-sections as well as in Appendix Section entitled "Basic Digital Signal Processing." This section treats the most basic notions and principles only. For a more comprehensive treatment of signal analytical methods the reader is referred to the textbooks dedicated to this topic, in particular to Chap. 7 of: Bioelectrical Signal Processing in Cardiac and Neurological Applications by L. Sörnmo and P. Laguna [60].

12.4.1 Amplification and Analog Signal Processing

The potential difference between the two input terminals of the amplifier shown in Fig. 12.37 does not signal just the potential field generated by the heart's electric activity. It also includes contributions of several other sources, the most important ones being: the sum of the two half-cell DC voltages (hundreds of mV) at the sensors (Sect. 12.3.3), the contributions of other bioelectric sources within the patient (muscular activation) and the interference from electromagnetic fields surrounding the patient, e.g., generated by the power line, RF or radio frequencies, electro-surgery devices etc.

The electric part of the electromagnetic field is passed to the body by currents flowing through the (small) capacitance between the power lines and body surface, returning to the "earth" or "ground" of the power line via similar such capacitances. This sets up a potential difference with respect to earth that is common to both electrodes.

12.4.1.1 Front-End of the Amplifier

The first stage of the instrumentation amplifier (IA in Fig. 12.37), its front-end, serves to raise the signal amplitudes to some desired level and also to reduce the representation of any potential that both sensors may have in common relative to the ground of the power supply of the recording equipment. Its basic design is shown in Fig. 12.38.

The triangles shown represent standard operational amplifiers. These have a very high amplification factor; the resistors shown set the actual, overall amplification of the configuration. Ideally, the potential at the output of the second stage shown should be proportional to $V_{ab} = V_a - V_b$ and be completely independent of the mean value of V_a and V_b, the

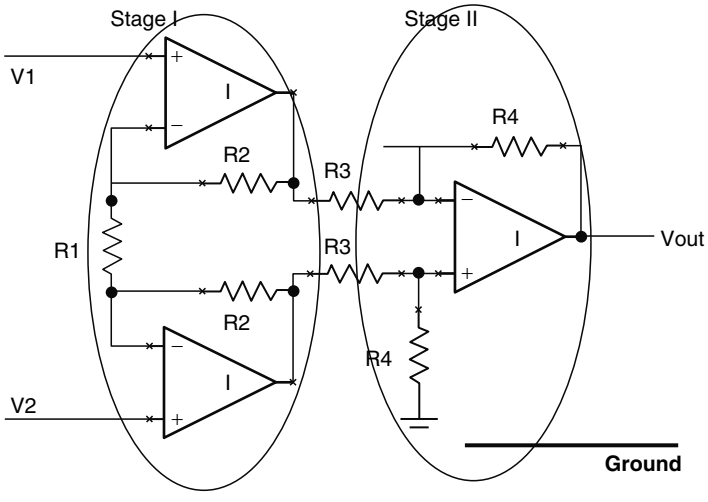

Figure 12.38
First two stages of an ECG instrumentation amplifier.

value the sensing electrodes a and b have in common. By using highly accurate, identical values for the resistors having a common label, a high rejection of the common, mean potential can be achieved.

12.4.1.2 Common Mode Rejection

An outline of the complexity of power line (50/60 Hz) interference, as well as of methods for minimizing its contribution to the ECG signal, is shown in Fig. 12.39.

The capacitances C_{pw}, C_{ca}, C_{ab} couple the body, lead wires and the power supply to other sources of the electromagnetic interference such as 50/60 Hz power lines.

The potential differences at the ECG sensors with reference to "ground" that arise from the capacitive coupling to the mains are almost identical. This creates a common component that, ideally, would not be present between the two terminals of the ECG lead. However, the recording equipment is generally also coupled to the ground of the power line, be it capacitively or galvanically. The provision shown in Fig. 12.38, referred to as the right leg drive, aims at minimizing any incomplete rejection of the common mode interference achieved by the front-end discussed in Sect. 12.4.1.1.

The right leg drive demands the incorporation of an additional electrode (sensor). Its position may influence the quality of the common mode rejection. However it does not, or at least should not, affect the observed wave forms related to the electric activity of the heart. Ten electrodes (wires) are attached to the patient when recording the standard 12-lead system. Besides the right leg electrode, three of the remaining nine electrodes, viz. the three electrodes placed on the other extremities are involved in the definition of Wilson's Central Terminal serving as the reference for the cardiac potential fields. As discussed elsewhere, e.g., Chap. 11, the maximum number of independent signals contained in the standard 12-leads is eight.

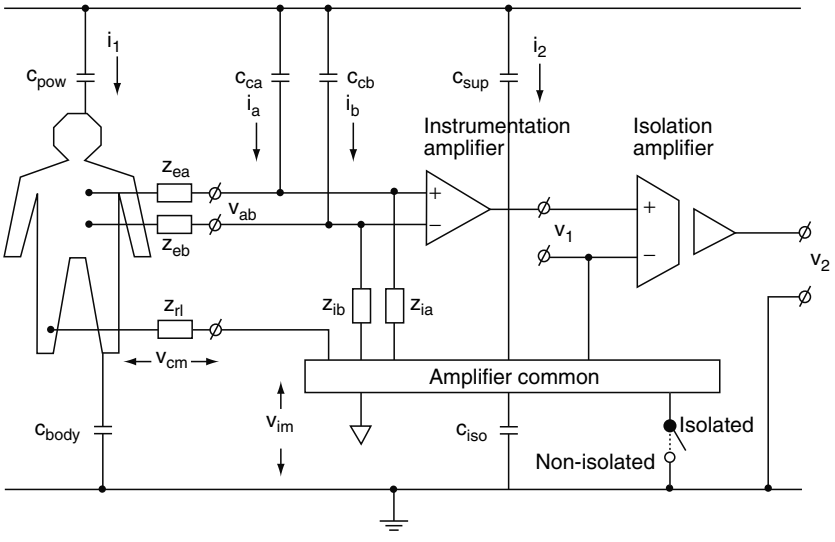

Figure 12.39

A simplified diagram illustrates the environmental sources of interference in ECG measurement. C_{pw}, C_{ca}, C_{ab}, and C_{sup} capacitances couple the sources of electromagnetic energy to the body, lead wires, and power supply respectively. C_{body} and C_{iso} capacitors provide a path to ground for AC leakage currents. V_{im} is the potential between the ECG amplifier common and ground, V_{cm} is a common mode potential on the body surface. I_1, i_a, i_b and i_2 are the AC interference currents. Z_{ea} and Z_{eb} are the equivalent skin–sensor impedances, Z_{rl} is the impedance of the ECG common, the right leg. The Z_{ib} and Z_{ia} are the input impedances of the instrumentation amplifier. V_1 and V_2 denote the non-isolated and the isolated ECG signals respectively (from [61]).

12.4.1.3 The Isolation Amplifier

The isolation amplifier indicated in Fig. 12.37 is included for safety reasons. It isolates the patient from other processing circuits by limiting current flow from the recording equipment to the patient. It demands a galvanically isolated, battery powered front-end. The coupling to the main recording equipment may be achieved by using fiber glass transmission or, RF transmission.

12.4.1.4 The Highpass Filter

The most common disturbance encountered in the ECG signal is the one caused by changes in the half-cell potentials at the sensor–skin interface, which also affect the electrode impedance (Fig. 12.40). This may be due to motion artifacts, temperature changes, changes in skin moisture (perspiration) and leaking gel or paste [55, 56]. This is particularly important in stress testing, respiration and monitoring applications, since the sensors tend to peel off and the skin contact under the sensors change when patients move. The resting ECG signals often show the artifacts caused by respiration or by muscle tremor at low temperatures. Additionally, poor skin preparation on subjects with hairy chests may create noise due to poor sensor adhesion and high skin–sensor impedance interface.

Even during the resting state, the changes at the sensors may give rise to potential fluctuations in the ECG that are larger than the ECG itself. Fortunately, under these conditions the changes have a low frequency spectrum, with frequencies lower than those present in the ECG. The observed effect on the ECG is that of a slowly wandering baseline. This permits the reduction of the so-called baseline wander by means of highpass filtering in the frequency domain of the signal (Appendix Section "Sampling Rate"), a procedure generally carried out in the front-end of the amplifier. Its most simple form of implementation is that of including capacitors in the wires connecting the sensors to the amplifier. The cutoff frequency used depends on the particular application involved.

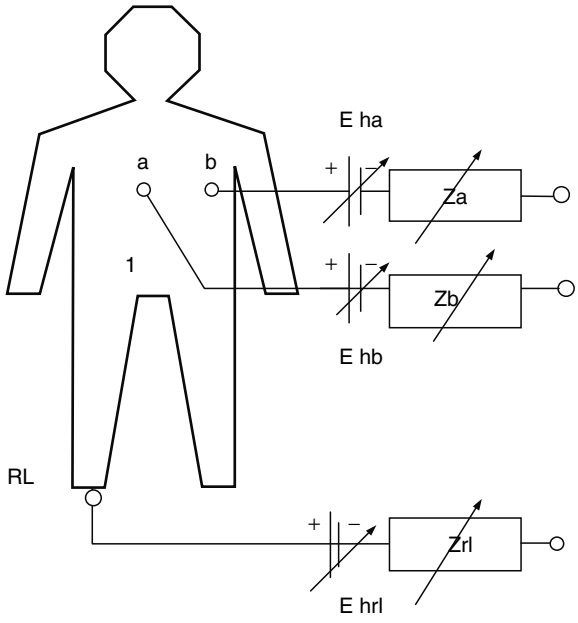

Figure 12.40

Sources of measurement artifacts in ECG signal acquisition. Eha, Ehb and Ehrl denote the variable sensor half-cell potentials, Za, Zb and Zrl the skin–sensor impedances.

Even during the resting state, the changes at the sensors may give rise to potential fluctuations in the ECG that are larger than the ECG itself. Fortunately, under these conditions the changes have a low frequency spectrum, with frequencies lower than those present in the ECG. The observed effect on the ECG is that of a slowly wandering baseline. This permits the reduction of the so-called baseline wander by means of highpass filtering in the frequency domain of the signal (Appendix Section "Sampling Rate"), a procedure generally carried out in the front-end of the amplifier. Its most simple form of implementation is that of including capacitors in the wires connecting the sensors to the amplifier. The cutoff frequency used depends on the particular application involved.

12.4.1.5 The Lowpass Filter

An additional undesirable component in the ECG is the one generated by the electric activity of skeletal muscles. This interference hinders in particular the interpretation of the ECG during exercise-stress testing, or long-term (holter) monitoring. Here, major parts of the frequency spectrum lie above those of the ECG signals, and a lowpass filter can be used to reduce their effect (Fig. 12.37).

Another application of this lowpass filter is that of reducing the influence of the aliasing effect (Appendix Section "Sampling Filters and Analog Filters) that crops up when digitally processing the signals originating from the analog amplifier.

12.4.1.6 Strategies for Ensuring a High Signal Quality ECG Acquisition

Great care must be exercised in the selection of the instrumentation amplifier and in particular of the components at its front-end. Here, very high input impedance, low noise instrumentation amplifiers, involving precision laser trimmed resistors are used for obtaining a high common-mode rejection ratio (CMRR). In addition, most modern front-end designs utilize active elimination of the common mode interference [56, 61, 62] by applying common mode noise signals in the opposite phase to the right leg drive (ECG common), as shown in Fig. 12.39 and, a more basic variant, in Fig. 12.41 [63].

Interfering electric signals from muscles and the internal organs form a composite signal with the ECG and cannot be easily filtered out without affecting the bandwidth of the ECG. Good skin preparation and the relaxation of subjects usually results in lower muscle tremor and baseline shifts.

The power line frequency 50/60 Hz and its harmonics, RF and radio frequency interference are usually eliminated by careful shielding of the lead wires, patient cables and signal filtering [64].

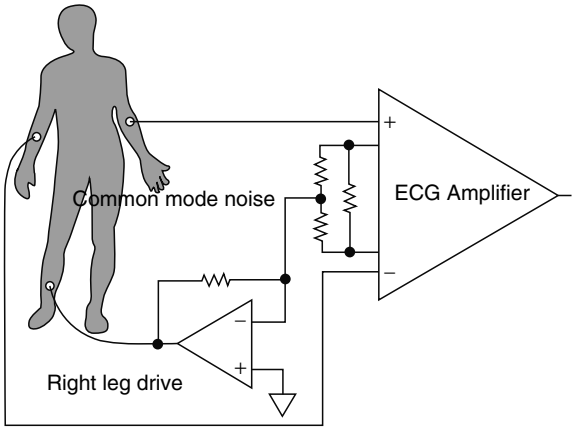

Figure 12.41

Right-leg drive circuit used in ECG front-end designs that minimize common mode "noise."

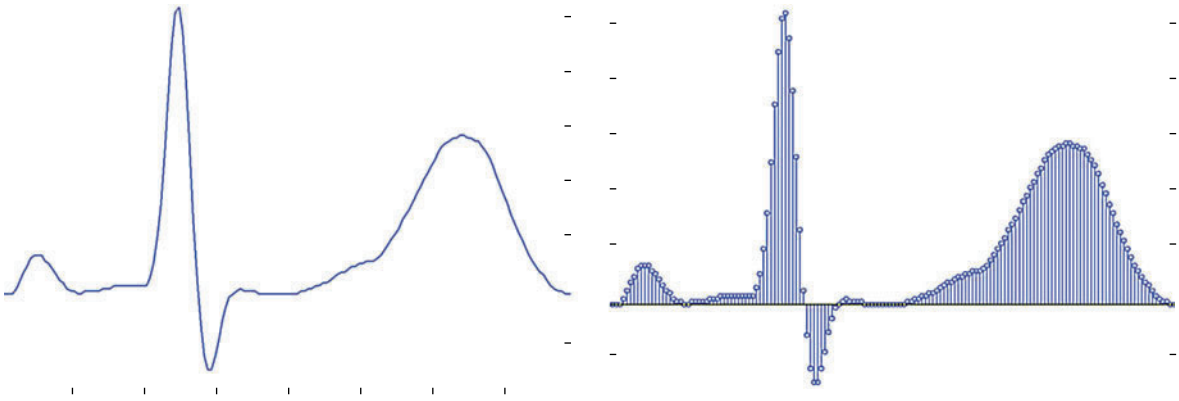

Figure 12.42
***Left*: original analog ECG; *right*: a digitized variant. Time interval shown: 640 ms.**

APPENDIX: Basic Digital ECG Signal Processing

A. van Oosterom

Department of Cardiomet, University of Lausanne, Lausanne, Switzerland

Conversion to Digital Data

Modern ECG systems utilize microcomputers or dedicated digital signal processors (DSP) for ECG signal display, storage, analysis and transmission. This requires that all analog lead voltages must be converted to numbers, i.e., their digital equivalents.

Analog to Digital ECG Signal Conversion

The values of continuous time-domain ECG signals at discrete time intervals can be extracted by means of an electronic device: the analog-to-digital converter (ADC). An example of the result of this procedure is shown in Fig. 12.42. The ECG signal on the left depicts the continuous, analog signal, the one on the right its digitized variant.

The individual, documented numbers representing the instantaneous signal values are referred to as the samples of the signal, the intervals between the subsequent samples being at the sampling interval T_s, which is 4 ms for the example shown in Fig. 12.42 (right panel). An alternative, equivalent specification is the sampling rate $f_s = 1/T_s$, the number of samples taken per second. Its unit is sps, s^{-1}, or less accurately, Hz.

The display of the result of the AD conversion used in Fig. 12.42 has been chosen to emphasize the fact that the result of the digital signal conversion does not specify signal values in between the subsequent samples. The display used in practice usually does not show the vertical lines that mark the individual samples. Instead, the subsequent values of the samples are connected by continuous line segments found by means of an interpolation procedure based on neighboring sample values. Note, however, that the actual information stored is that specified by the sample values only.

Sampling Rate

The amount of detail present in the analog signal that is retained in the digitized signal depends critically on the length of the sampling interval or, equivalently, on the sampling rate. The sampling interval dominates the accuracy with which

derived signal features like peak amplitudes and their timing in the analog version of the signal can be recovered from the digital data.

For any duration P of a signal segment to be stored, the number of samples N_s is

$$N_s = P/T_s = D \times f_s \tag{12.9}$$

The use of higher sampling rates imposes not only a greater demand on the quality of the AD converter but also on the storage capacity of the digital device. This number is multiplied by the number of signals that one may wish to record simultaneously. This poses the question of which sampling rate should be used.

The required sampling rate is linked to the amount of detail that might be contained *within* a sampling interval: the higher this information is expected to be, the higher the sampling rate should be. The "amount of information" is a notion that requires to be specified before the required sampling rate can be selected. The commonly-used specification makes use of the representation of the signal in the so-called frequency domain, a domain based on the theory of the Fourier series. A brief description of this theory is as follows.

Any biological signal recorded over a restricted period of time P can be represented by a constant A_0 to which is added a weighed sum of sinusoidal wave forms having frequencies that are integer multiples of the basic frequency $f_b = 1/P$. The sinusoids having frequencies $f_k = k \times f_b$ $(k = 1, 2, 3, \ldots)$ are called the harmonics of the basic frequency. For $k = 1$, this identifies the sinusoid at the basic frequency as the first harmonic of the signal.

The constant A_0 is the mean value of the signal over the period P. This constant component can be interpreted as having zero frequency, and is referred to as the DC component of the signal. The mean value of the sum of the sinusoids is zero, since, for each harmonic, integer numbers of complete sinusoids are contained within the segment P, and the mean value over time of a complete sinusoid is zero.

By specifying A_0 and the amplitudes A_k for each of the harmonics, as well as a set of individual phase shifts φ_k the entire wave form can be represented at any desired precision, provided that the number of harmonics included is sufficiently large. This shifts the question of specifying the amount of information to: what is the number of harmonics needed? The answer to this question evolves from performing a Fourier analysis of the signal. Applied to sampled signals, this analysis can be carried out by means of the discrete Fourier transform (DFT), from which the amplitudes A_k are computed. The plot of the amplitudes A_k as a function of the frequency $f_k = k \times f_b$ results in the so-called amplitude spectrum. The squared amplitudes form the basis of the so-called power spectrum.

For biological signals, invariably the spectra tend to zero for high values of f_k. Performing a reconstruction of the signal (Fourier synthesis) on the basis of the first K harmonics results in a signal that is almost a replica of the original signal, provided that a sufficiently high value of K is used. If this is possible for a finite number of K, the signal is said to be band limited to frequency f_K.

For progressively lower values of K, the reconstruction results in increasingly larger deviations between the original and the resynthesized signal. Based on this type of analysis the maximum frequency content of the signal is defined as f_K. The final step in the procedure follows from a result stemming from communication theory. It states that for a signal that is band limited at frequency f_K, the number of samples needed for a perfect, i.e., error free, resynthesis should be at least $2 \times K + 1$. This result relates to the fact that the synthesis of the signal requires the specification of the values of K amplitudes, K phases and the DC component. This puts the minimal required sampling rate at

$$f_s \geq \frac{2K+1}{P};\ 2K\frac{1}{P} = 2K f_b = 2f_K, \tag{12.10}$$

expressed in words, the minimal required sampling rate f_s of a signal having harmonics up to the frequency f_K should be at least twice f_K. The variable f_s is known as the Nyquist rate [65]. Correspondingly, the highest frequency possible in a DFT spectrum is $f_K = f_s/2$.

Sampling Theorem and Analog Filters

No ECG signal is truly and perfectly band limited. Signal component at frequencies above f_K may be judged to be unrelated to the heart's electric activity, but rather to the activity of, for example, skeletal muscles. This would allow the suppression

of such signal components by means of analog lowpass filters (Fig. 12.37) prior to the AD conversion step, with their cutoff frequency set at f_K. It prevents the influence of such high frequency components on the sampled signal. Without the inclusion of the filter, the Fourier spectrum, of the signal sampled at the then too low sampling rate, will include contributions of the signal components above f_K. This effect is known as aliasing; it is reduced by the inclusion of the analog lowpass filter.

In practice the signals are often sampled at frequencies that are much higher (up to 5 times) than the minimum value required by the sampling theorem (12.2). This facilitates the subsequent display of the data as well as their analysis.

Basic Digital Signal Processing

After AD conversion, the analog signal $x(t)$ is replaced by a series of numbers

$$x(t) \Rightarrow [x_1, x_2 \ldots x_i \ldots x_N] \tag{12.11}$$

with x_i the value of the sample of the analog signal taken at time $t = t_i$ and N the total number of samples taken. Subsequent digital signal processing procedures are applied to this series. These include:

1. filtering, now by digital filters,
2. identification of timing of onsets and endpoints of signal wavelets,
3. timing of extreme values (peak amplitudes of the signal, like R wave, etc.,
4. extraction of extreme values and slopes,
5. suppression of any power line interference that may remain after the analog filtering,
6. the specification and/or correction of the baseline of the signal.

Some of these procedures affect the wave form of the signal. When inspecting any ECG signal presented on a monitoring device one should be aware of the fact that what is seen may not be the same as what is sensed by the electrodes. Below, a few examples of this are demonstrated. The wave forms shown relate to the signal of lead V3 from a healthy subject, sampled at 1 ms intervals. In their display the subsequent samples are connected by straight line segments. The input signal is shown in Fig. 12.43. It depicts the output of the AD converter. The setting of the analog filters (Fig. 12.37) were lowpass at 500 Hz, and highpass at 0.2 Hz. With the healthy subject at rest in the supine position, the baseline wander, although clearly present, was small.

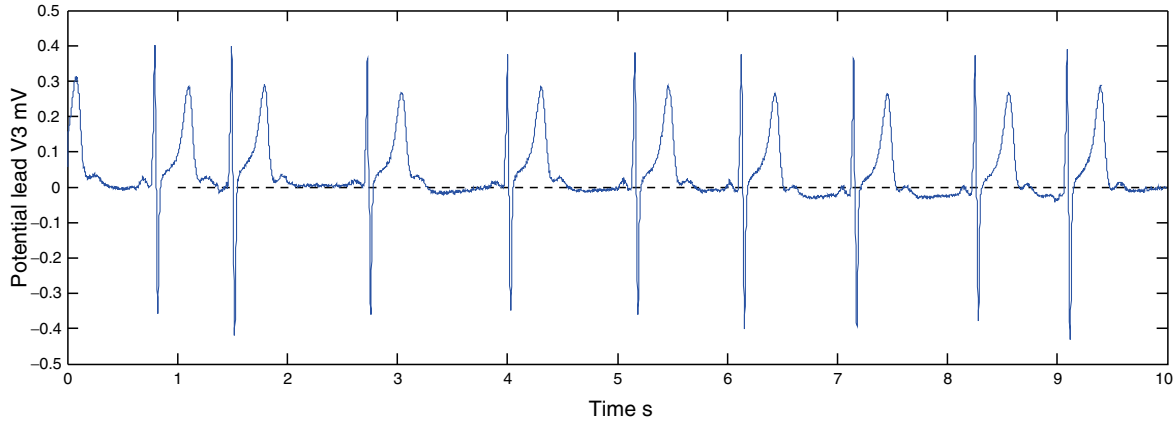

Figure 12.43

Output of an AD converter; 10 s episode from a recording of lead V3.

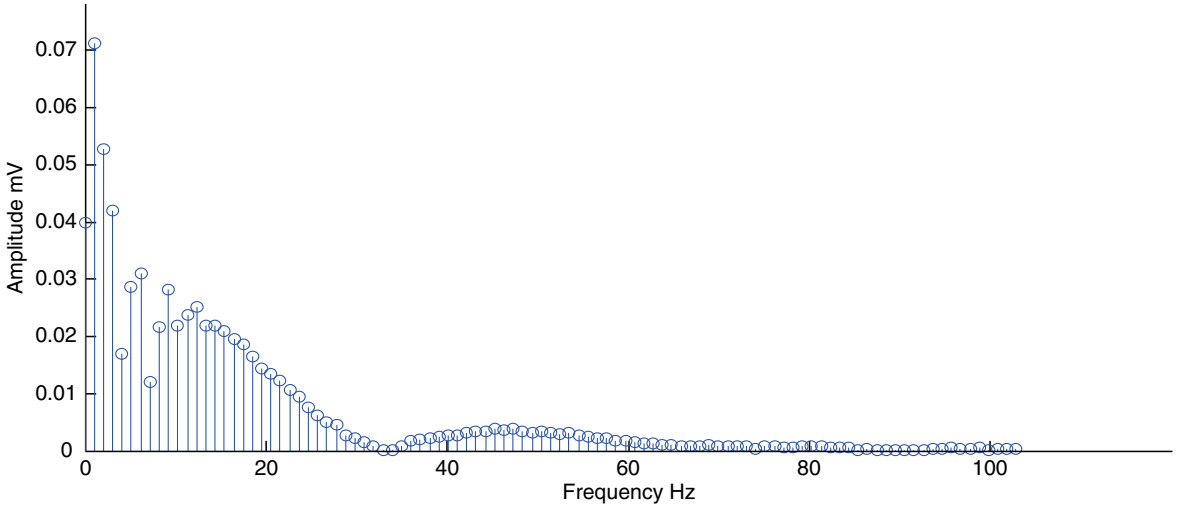

Figure 12.44
Amplitude spectrum of a single beat (beat five of lead V3, shown in Fig. 12.43. Note its discrete character).

Amplitude Spectrum

The amplitude spectrum of the signal during the full duration of a single beat (beat five in Fig. 12.43), determined by means of the discrete Fourier transform (DFT), is shown in Fig. 12.44.

Although the output of the DFT computed over the P = 972 ms duration of the beat, taken from samples at 1 ms intervals, contains frequencies up to $f_K = f_s/2 = 0.5^*1{,}000 = 500$ Hz, only the lower-frequency part of the spectrum is shown here, the amplitudes of the higher frequencies are much smaller than those below 100 Hz. This indicates that the sampling rate used for this signal is more than adequate. As discussed in the previous subsection, the frequency resolution is $f_b = 1/P = 1.029$ Hz.

For intra-cardiac signals, the fast down-stroke of the observed electrograms may demand higher sampling rates. A correct representation in the frequency domain of fast signal segments demands the inclusion of spectral components of high frequencies.

The display method chosen for Fig. 12.44 emphasizes the nature of spectra obtained by using the DFT. In that method, the implied signal representation beyond the period analyzed is that of an infinite periodic repetition of the segment analyzed, thus typifying the method as computing a Fourier series representation rather than a Fourier transform. In most ECG spectra figuring in the literature, this aspect is hidden as a result of the method employed of connecting the individual spectral values by means of continuous line segments.

As discussed in Sect. 12.4.1, the output of the analog amplifier usually includes a highpass filter, which blocks any DC component present in the sensor output. When computed over an infinitely long period, the mean value of the output of the amplifier will therefore be zero. However, this does not apply to a much smaller signal period, even if this period contains a full beat. In Fig. 12.44 this can be seen in the non-zero component of the spectrum at zero frequency.

Additional Filtering

In their digital form, AD-converted analog signals may be processed by numerical methods that resemble those of analog filters. Such filtering may be required for completing an incomplete job performed in the analog amplifier, or to extract, or emphasize some signal features. Since digital signals may be stored easily in digital memory, the filtering procedure for a digital signal value x_i may incorporate preceding signal values x_{i-1}, x_{i-2}, ... as well as later ones x_{i+1}, x_{i+2}, ...

In online applications, the length of the sample string x_{i+1}, x_{i+2}, ... depends on the delay between the occurrence of the event and the time of observation on a monitor. The sharpness of the cutoff of the various filters needs to be tuned to the particular type of application. For a full discussion of the design of such filters the reader is referred to the general literature on this topic [60].

Here, some simple filters are discussed and their effect is illustrated when they are applied to the signal shown in Fig. 12.43. In the notation used, x_i refers to the data used as input of the filter, y_i to its output. The filter parameters used may not correspond to desirable practical settings, but are chosen to clearly illustrate the nature of the effect of the filter. The values shown relate to a sampling rate of 1,000 sps.

Recursive LP Filter

The most simple form of a digital lowpass (LP) filter is defined by the recipe: take $y_0 = 0$, followed by computing for $i = 1, \ldots, N$,

$$y_i = \alpha x_i + (1 - \alpha) y_{i-1} \tag{12.12}$$

As can be seen, the output of the filter depends on the instantaneous input value (x_i) as well as on the value of the preceding output value (y_{i-1}). The latter property classes the recipe as an example of a recursive filter. On-line implementation demands just the storing of this preceding output value. The value of α sets the cutoff frequency, the frequency where the amplitude of a sinusoidal signal applied to the filter is reduced by a factor of $1/\sqrt{2}$ (the −3dB point).

The application of this filter to beat 5 of the reference signal (Fig. 12.43) is shown in Fig. 12.45. The output signal is drawn by a solid line, the dashed line represents the input signal. The value of α was set at 0.2073, resulting in −3B point at 33 Hz, the frequency corresponding to the local minimum in the amplitude spectrum around 33 Hz (Fig. 12.44).

The typical effect of the application of a LP filter can be seen to be:

1. reduction of noise,
2. reduction of the amplitude at sharply peaked signal segments,

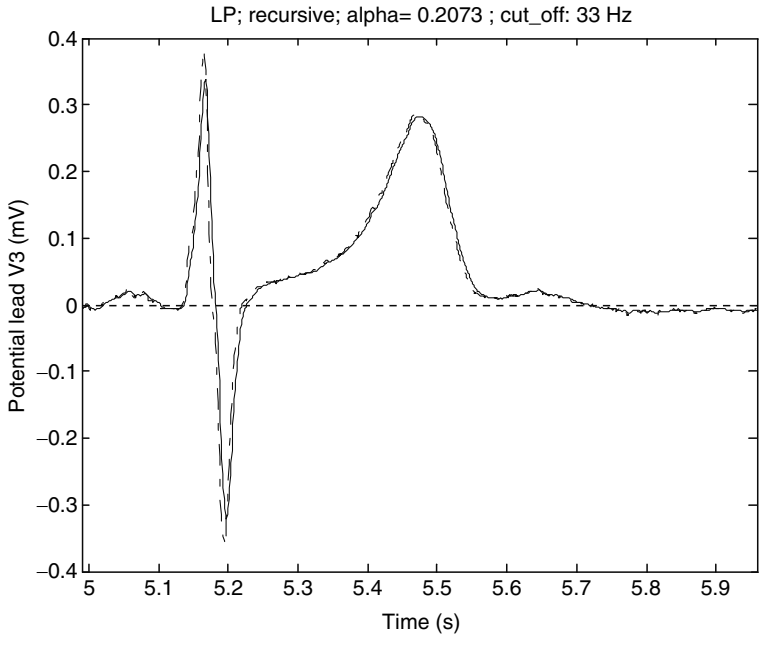

Figure 12.45

***Dash-dot line*: beat 5 of Fig. 12.43. *Solid line*: output of the recursive LP filter having its −3B point at 33 Hz.**

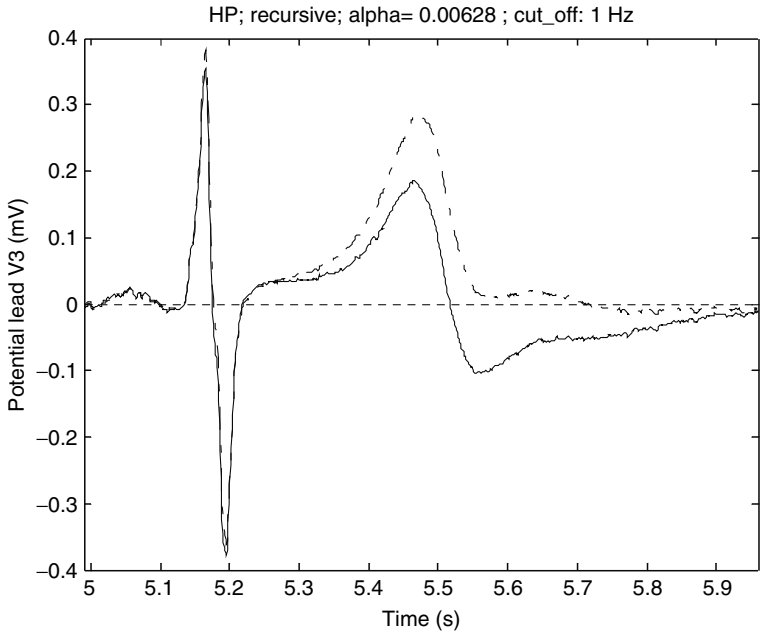

Figure 12.46

***Dash-dot line*: beat 5 of Fig. 12.43. *Solid line*: output of the HP filter.**

3. a reduction of the slope of the fast deflection (R-S segment)
4. a delay in the timing of the signal, as is always the case for recursive filters.

All these effects are more pronounced if the cutoff frequency is set at a lower value.

Recursive HP Filter

The output of a simple form of a digital highpass (HP) filter is found by, after initializing: $v_0 = 0$, $y_0 = 0$, followed by iterating for $i = 1, \ldots, N$,

$$\begin{aligned} y_i &= x_i + v_{i-1} \\ v_i &= \alpha x_i + (1-\alpha) v_{i-1} \end{aligned} \tag{12.13}$$

This may be viewed as the subtraction of a lowpass-filtered version of the input signal (12.4) from the input itself.

The LP filter can be seen to leave the fast signal segments (QRS) relatively unaffected, but the pronounced effect on the slower parts (the STT segment) should be well noted. The filter forces the mean value of the output to be zero.

The application of this filter to beat 5 of the reference signal (Fig. 12.43) is shown in Fig. 12.46. As in Fig. 12.45, the output signal is drawn by a solid line, the dash-dot line represents the input signal. The value of α was set at 0.00628 (sampling interval 1 ms), resulting in −3B point at 1 Hz. This value is close to the basic frequency of the signal segment (1.029 Hz).

Lowpass Moving Average Filter

The final example of simple digital filters is the lowpass moving average filter. Its recipe is

$$y_i = \frac{1}{W} \sum_{k=-W/2}^{W/2} x_{i+k} \tag{12.14}$$

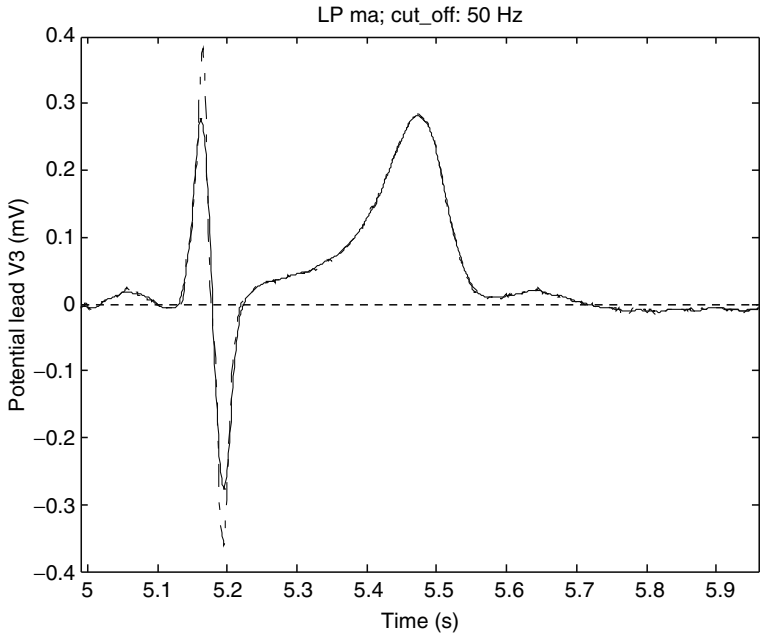

Figure 12.47
***Dash-dot line*: beat 5 of Fig. 12.43. *Solid line*: output of the LP moving average filter; $W = 20$.**

It represents the moving average (sliding average) of W input values (an integer number). Since this does not involve previous output values (like y_{i-1}), it is a called a non-recursive filter. In contrast to the previous examples, this filter demands not just a single stored value, but rather: W values within the sliding window. The value of W determines the filter properties, in particular its cutoff frequency.

In the formulation given here the input includes samples related to later sampling moments and so it cannot be implemented in real time. A major, more general and highly valuable feature of the filter is that it does not produce phase-shift distortion. When using a sampling rate of 1,000 sps, and $W = 20$ the filter has a complete suppression of signal components at frequencies that are integer multiples of 50 Hz. This implies that, in addition to its lowpass character, the filter also suppresses completely any 50 Hz power line interference. The performance of this filter to beat 5 of the signals shown in Fig. 12.43 is presented in Fig. 12.47. The value of 50 Hz lowpass may high enough for some applications (compare Fig. 12.45). Note that, like the recursive filter, it produces some attenuation at the sharp peaks of the signal, but no delay, clearly: the off-line application.

Baseline Correction/Definition

As discussed in Sect. 12.4.1.5, bioelectric potentials observed by means of electrodes are contaminated by the half-cell potentials. The magnitudes of these potentials are much larger than those of the ECG, are unknown, and may change slowly in time: the so-called baseline "wander" or "drift." The common way of treating this problem is by including a highpass filter in the first stage of the amplifier (Fig. 12.37). The resulting signal is referred to as an AC-recording (AC = alternating current). This produces an output signal that, when computed over a very long time, has zero mean value, i.e., the DC component of the signal is zero. If more rapid perturbations of the contact potential occur, the baseline of the signal, i.e., the values in the observed signal that should be assigned a zero value, must be specified on a beat-to-beat basis. Even if the dynamic range of the input stage would be wide enough to encompass the full range of sensor potentials (allowing a DC recording in spite of the presence of the half-cell potentials) the subseqent shift to a zero level remains to be defined.

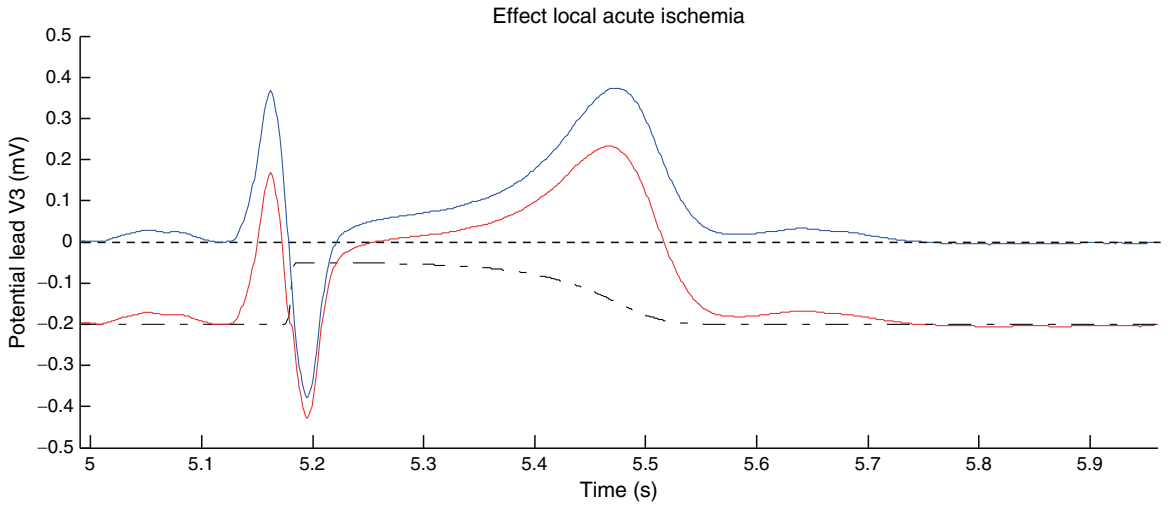

Figure 12.48

***Upper trace*: lead V3, beat 5 of Fig. 12.43. *Dash-dot trace*: expression of the contribution to lead V3 due resulting from acute ischemia in the myocardium close to electrode V3. *Lower*, continuous trace: sum of the previous two traces: the DC representation of lead V3 during the ischemic period.**

The treatment of the problem is generally referred to as baseline correction. However, this is a somewhat misleading term since it assumes that the signal level that should be specified as zero is self evident, which is, in fact, not the case. The problem involved is illustrated by the following examples.

The ECG records differences in the potential field generated at different locations on the thorax. This potential field is uniform over the thorax (thus resulting in zero ECG potential differences) if all myocytes have the same transmembrane potential (Sect. 12.2.1). In healthy myocardial tissue, the time instant at which this situation is most closely approximated is just before the beginning of atrial depolarization: the onset of the P wave. The signal of lead V3 shown in Fig. 12.43 is the (unprocessed) output of an AC-coupled amplifier. Beat 5 of this signal is shown as the upper trace of Fig. 12.48. For this healthy subject and this particular beat, the onsets of the P waves were close to zero, and so only a minor shift would be required to refer this signal to zero baseline.

For the entire segment shown in Fig. 12.43 an optimal baseline definition can be carried out by fitting a continuous function (e.g., a cubic spline) to the signal values at the onsets of the P waves of all beats. Subtraction of this function from the trace of Fig. 12.43 then produces the optimal baseline, provided that baseline wander or other recording artifacts are not too extreme.

The problem of baseline definition is more pressing for recordings taken during periods of acute ischemia. During ischemia, the transmembrane potential (TMP) of the myocytes within the region change: the resting potential decreases (tends to zero), the upstroke of the TMP is reduced. The size of these changes varies during the various stages of ischemia [66]. The coupling of the intra-cellular domains of neighbouring myocytes I in the ischemic region and myocytes H in the healthy region and differences in the TMPs of these myocytes result in a current flow. For the ventricular myocardium, there is a intracellular current flow from cells I to H during the time interval between the end of the T wave and the onset QRS interval. In the extracellular domain there is a return flow of current, flowing in the opposite direction, since charge is conserved. Hence, in the extracellular domain, this can be expressed by an equivalent current sink at the borders of the ischemic zone, which lowers the value of the nearby extracellular potential field [66].

In Fig. 12.48 the effect of this current sink on the potential of lead V3 is simulated by a downward DCshift of 0.2 mV. During the activation of the tissue surrounding the ischemic zone the potential difference between the regions is smaller and as a consequence the loading effect is smaller. In this simulation, Fig. 12.48, the contribution to the potential of lead V3 was set to −0.05 mV. During repolarization the contribution of the sink slowly returns to −0.2 mV. The time course of the contribution of the current sink is shown by the dash-dot line shown in Fig. 12.48. The addition this contribution

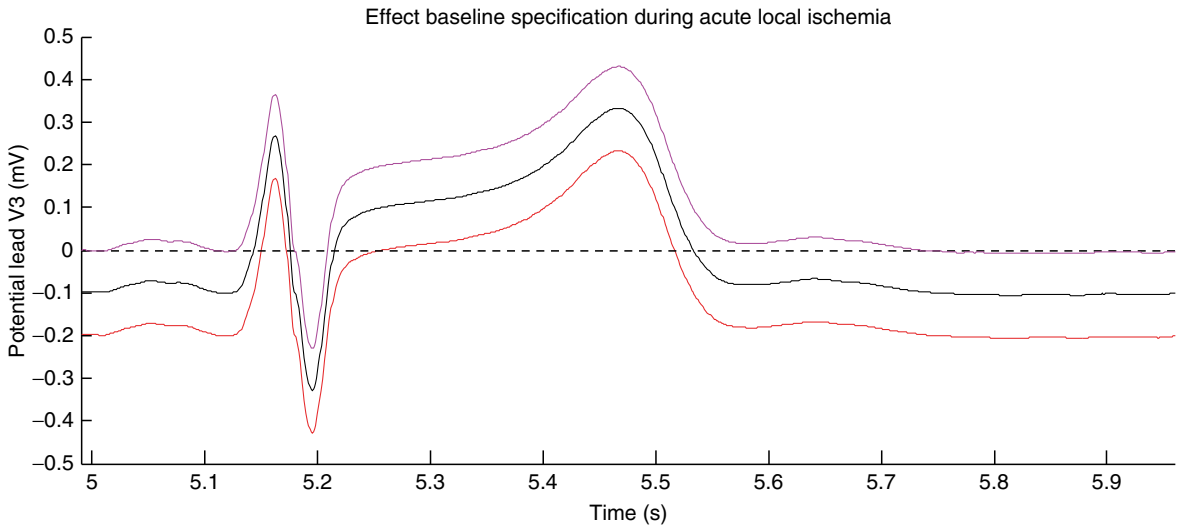

Figure 12.49

***Lower trace*: DC variant of lead V3, beat 5 of Fig. 12.43 during ischemia (*lower* continuous trace of Fig. 12.48). *Middle trace*: zero mean variant of the *lower trace*, as would result from AC coupling. *Upper trace*: a variant of the *lower* trace in which zero baseline is defined at the beginning and the end of the entire beat.**

to the signal of the non-ischemic situation (the upper trace) results in the type of wave form for the V3 signal that can be expected during the ischemic period (the lower solid trace in Fig. 12.48). Note that between the end of the T wave and the moment of depolarization around the ischemic-zone (R-S segment) the signal is lowered by 0.2 mV and the remaining part by 0.05 mV, followed by a slow return to the (depression) of −0.2 mV at the perceivable end of the repolarizing phase.

Standard ECG recordings do not reveal the baseline depression shown in the lower solid trace in Fig. 12.48. The presence of the highpass filter results in a signal that has a zero mean value over the interval indicated (middle trace in Fig. 12.49). A (subsequent) baseline "correction" to the onset of the P wave then results in the upper trace of the same figure. Note that as a result of the current sink formed by the ischemic source, the actual baseline depression is seen to be expressed as an elavation of the ST-segment, merely as a result of the definition of the baseline. This phenomenon cleary hinders a direct intrepetation of the ECG features in terms of the underlying source-sink configurations associated with electrophysiology.

References

1. Zywietz, C., Technical Aspects of Electrogram Recording, in *Comprehensive Electrocardiology; Theory and Practice in Health and Disease*, P.W. Macfarlane and T.D. Veitch-Lawrie, Editors. New York, Pergamon Press, 1989, pp. 353–404.
2. McAdams, E., Bioelectrodes, in *Encyclopedia of Medical Devices and Instrumentation*, J.G. Webster, Editor. New York, Wiley, 2006, pp. 120–166.
3. Hinz, R., *Private Communication*. 2007.
4. Faraday, M., *On Electrical Decomposition*. Philosophical Transactions of the Royal Society, London, 1834.
5. Hill, J.W. and D.K. Kolb, *Chemistry for Changing Times*, 9th ed. New Jersey: Prentice-Hall, 2001.
6. Webster, J., ed. *Medical Instrumentation, Application and Design*, 3rd ed. New York: John Wiley and Son, 1998.
7. de Boer, R.W. and A. van Oosterom, Electrical properties of platinum electrodes: impedance measurements and time-domain analysis. *Med. Biol. Eng. Comput.*, 1978;**16**: 1–10.
8. Fisher, C., Electrode Dynamics, *Oxford Chemistry Primers*, Vol. 34. Oxford: Oxford University Press, 1998.
9. Liebman, J.F., *Structural Chemistry*. New York: Springer, 2004.
10. Scott, E.R., et al., Transport of ionic species in skin: contribution of pores to the overall skin conductance. *Pharm. Res.*, 1993;**10**(12): 1699–1709.
11. Ebling, F., R. Eady, and I.M. Leigh, Anatomy and organization of human skin, in *Textbook of Dermatology*, R.H. Champion and J.L. Burton, Editors. Oxford, Blackwell, 1992.
12. Grimnes, S., Psychogalvanic reflex and changes in electrical parameters of dry skin. *Med. Biol. Eng. Comput.*, 1982;**20**(6): 734–740.

13. Edelberg, R., Electrical properties of skin, in *Biophysical Properties of the Skin*, H.R. Elden, Editor. New York, Wiley, 1992.
14. Holbrook, K.A. and G.F. Odland, Regional differences in the thickness (cell layers) of the human stratum corneum: an ultrastructural analysis. *J. Invest. Dermatol.*, 1974;**62**: 415–422.
15. Swartzendruber, D.C., et al., Organization of the intercellular spaces of porcine epidermal and palatal stratum corneum: a quantitative study employing ruthenium tetroxide. *J Cell Tissue Res.*, 1995;**279**(2): 271–276.
16. Harrison, S.A.B. and D.F. Lovely, Identification of noise sources in surface recording of spinal somatosensory evoked potentials. *Med. Biol. Eng. Comput.*, 1995;**33**(3): 299–305.
17. Fernandez, M. and R. Pallas-Areny, Ag–AgCl electrode noise in high-resolution ECG measurements. *Biomed. Instrum. Technol.*, 2000;**34**(2): 125–130.
18. Geddes, L.A., *Electrodes and the Measurement of Bioelectric Events*. New York: Wiley-Interscience, 1972.
19. Swanson, D.K., et al., *Biomedical Electrode Technology*. New York: Academic Press, 1974.
20. Godin, D.T., P.A. Parker, and R.N. Scott, Noise characteristics of stainless-steel surface electrodes. *Med. Biol. Eng. Comput.*, 1991;**29**: 585–590.
21. Pardee, H.E.B., Concerning the eletrodes used in electrocardiography. *Am. J. Physiol.*, 1917;**44**: 80–83.
22. Way, T.J., *Non-invalsive*, *Radiolucent Electrode*. US Patent 5356428, 1994.
23. Rositano, X., Ultra-soft dry electrodes for electrocardiography. *Med. Instrum.*, 1973;**7**(1): 76.
24. Ryu, C.Y., S.H. Nam, and S. Kim, Conductive rubber electrode for wearable health monitoring, in *IEEE Annual International Conference*. Engineering in Medicine and Biology 27th Annual Conference, Shanghai, China, 2005.
25. Trank, J., R. Fetter, and R.M. Lauer, A spray-on electrode for recording the electrocardiogram during exercise. *J. Appl. Physiol.*, 1968;**24**(2): 267–268.
26. Patten, C.W., F.B. Ramme, and J. Roman, *Dry Electrodes for Physiological Monitoring*. Washington, DC: National Aeronautics and Space Administration, 1966.
27. Roman, J., *Flight Research Program III – High-Impedance Electrode Techniques*, *Nasa Technical Note D-3414 Supplement*. Washington, DC: National Aeronautics and Space Administration, 1966.
28. Wehr, G., et al., A vector-based, 5-electrode, 12-lead monitoring ECG (EASI) is equivalent to conventional 12-lead ECG for diagnosis of acute coronary syndromes? *J. Electrocardiol.*, 2006;**39**(1): 22–28.
29. Hindricks, G., et al., Perception of atrial fibrillation before and after radiofrequency catheter ablation. Relevance of asymptomatic arrhythmia recurrence. *Circulation*, 2005;**112**: II63–II68.
30. Jernberg, T., B. Lindahl, and L. Wallentin, ST-segment monitoring with continuous 12-lead ECG improves early risk stratification in patients with chest pain and ECG nondiagnostic of acute myocardial infarction. *J. Am. Coll. Cardiol.*, 1999;**34**: 1413–1419.
31. Jancin, B., Cell Phones ECG Leads Are Nosocomial Pathways. *Obst. Gyn. News.*, 2003.
32. Lobodzinski, S.M. and M.M. Laks, Biopotential fiber sensor. *J. Electrocardiol.*, 2006;**39**(4 suppl): S41–S46.
33. Karande, P., A. Jain, and S. Mitragotri, Relationships between skin's electrical impedance and permeability in the presence of chemical enhancers. *J. Control. Release.*, 2006;**110**(2): 307–313.
34. White, H., Electrochemical imaging of molecular transport in skin. *The Electrochemical Society Interface*, 2003;12: 29–33.
35. MettingVanRijn, A.C., et al., Low cost active electrode improves the resolution in biopotential recordings, in Proceedings of 18th *Annual International Conference of IEEE Engineering in Medicine Biology*. Amsterdam, IEEE Engineering and Medicine Biology, 1996.
36. Hagemann, B., G. Luhede, and H. Luczak, Improved active electrode for recording bioelectric signals in work physiology. *Eur. J. Appl. Physiol. Occup. Physiol.*, 1985;**54**: 95–98.
37. Padmadinata, F.Z., et al., Microelectronic skin electrode. Sens. actuators, 1990;**B1**: 491–494.
38. MettingVanRijn, A.C., A. Peper, and A.C. Grimbergen, Amplifiers for bioelectric events: a design with a minimal number of parts. *Med. Biol. Eng. Comput.*, 1994;**32**: 305–310.
39. Burke, M.J. and V.D.T. Gleeson, Biomedical Engineering, Issue Page(s): A micropower dry-electrode ECG preamplifier. *IEEE Trans. Biomed. Eng.*, 2000;**47**(2): 155–162.
40. Valchinov, E.S. and N.E. Pallikarakis, An active electrode for biopotential recording from small localized bio-sources. *BioMed. Eng. Online*, 2004;**3**(25): 1.
41. Ruffini, G., et al., *ENOBIO – First tests of a dry electrophysiology electrode using carbon nanotubes*, in *IEEE EMBS Annual International Conference*. New York City, USA, 2006.
42. Bergey, G.E., R.D. Squires, and W.C. Sipple, Electrocardiogram recording with pasteless electrodes. *IEEE Trans. Biomed. Eng.*, 1971;**18**: 206–211.
43. Gondron, C., et al., Nonpolarisable dry electrode based on NASICON ceramic. *Med. Biol. Eng. Comput.*, 1995;**33**: 452–457.
44. Ko, W.H. and J. Hynecek, Dry electrodes and electrode amplifiers, in *Biomed Electrode Technol*, A.C. Miller and D.C. Harrison, Editors. London, U.K, Academic Press, 1974, pp. 169–181.
45. Griss, P., et al., Characterization of micrimachined spiked biopotential electrodes. *IEEE. Trans. Biomed. Eng.*, 2002;**49**(6): 597–604.
46. www.orbitalresearch.com/PDFs/dry-electrode-technology_v.DF.pdf.
47. Schoenberg A.G., Klingler D.R., Baker C.D., Worth N.P., Booth H.E., Lyon P.C. Final report: *Development of test methods for disposable ECG Electrodes*. UBTL Technical Report No. 1605—005, Salt Lake City, UT, 1979.
48. Huigen, E., A. Peper, and C.A. Grimbergen, Investigation into the origin of the noise of surface electrodes. *Med. Biol. Eng. Comput.*, 2002;**40**: 332–338.
49. Sheffield, L.T., et al., Optimal electrocardiographic: task force II – quality of electrocardiographic records. *Am. J. Cardiol.*, 1978;**4**(1): 146–157.
50. *Pressure Sensitive Tape Councel*. 1979, UBTL: Salt Lake City (Utah).
51. Richardson P.C., The insulated electrode: A pasteless electrocardiographic technique, 20th *Proc. Annu. Conf. Eng. Med. Biol.*, Boston, Mass., 1968.
52. Prance, R.J., An ultra-low-noise electrical-potential probe for human-body scanning. *Meas. Sci. Technol.*, 2000;**11**: 1–7.
53. Lee, J.M., et al., Evaluating a capacitively coupled, noncontact electrode for ECG monitoring, in *NATO Research and Technology Organisation (Human Factors and Medicine Panel) meeting*

in cooperation with the Advanced Technology Applications for Combat Casualty Care conference. St. Petersburg, FL, 2004.

54. Kingsley, S.A., et al., Photrode optical sensor for electrophysiological monitoring. *Aviat. Space. Environ. Med.*, 2003;**74**(11): 1215–1216.
55. Pallás-Areny, R., Interference-rejection characteristics of biopotential amplifiers: A comparative analysis. *IEEE Trans. Biomed. Eng.*, 1988;**35**: 953–959.
56. Winter, B.B. and J.G. Webster, Reduction of interference due to common mode voltage in biopotential amplifiers. *IEEE Trans. Biomed. Eng.*, 1983;**30**: 58–62.
57. McAdams, E.T., J. McLaughlin, and J.M. Anderson, Wearable and implantable monitoring systems: 10 years experience at University of Ulster. *Stud. Health. Technol. Inform.*, 2004;**108**: 203–208.
58. Led, S., J. Fernandez, and L. Serrano, Design of a wearable device for ECG continuous monitoring using wireless technology, in *26th Annual international Conference of IEEE Engineering in Medicine and Biological Society*, San Francisco, 2004.
59. Chun, H., et al., IT-based diagnostic instrumentation systems for personalized healthcare services. *Stud. Health. Technol. Inform.*, 2005;**117**: 180–190.
60. Sörnmo, L. and P. Laguna, *Bioelectrical Signal Processing in Cardiac and Neurological Applications*. Amsterdam: Elsevier Academic Press, 2005.
61. MettingVanRijn, A.C., A. Peper, and C.A. Grimbergen, High quality recording of bioelectric events. Part 1: Interference reduction, theory and practice. *Med. Biol. Eng. Comput.*, 1990;**28**: 389–397.
62. Thakor, N.V. and J.G. Webster, Ground-free ECG recording with two electrodes. *IEEE Trans. Biomed. Eng.*, 1980;**BME-27**: 699–704.
63. Winter, X., et al., Driven-right-leg circuit design. *IEEE Trans. Biomedical. Eng.*, 1983;**30**(1): 62–66.
64. Huhta, J.C. and J.G. Webster, 60-Hz Interference in electrocardiography. *IEEE Trans. Biomed. Eng.*, 1973;**20**: 91–101.
65. Nyquist, H., Certain topics in telegraph transmission theory. *Trans. AIEE*, 1928;**47**: 617–644.
66. Janse, M.J., et al., Flow of injury current and patterns of excitation during early ventricular arrhythmias in acute regional myocardial ischemia in isolated porcine and canaine hearts; evidence for two different arrhythmogenic mechanisms. *Circ. Res.*, 1980;**47**: 151–165.

Section 5

Clinical Electrocardiography

13 The Normal Electrocardiogram and Vectorcardiogram

Peter W. Macfarlane · T.D. Veitch Lawrie

P. W. Macfarlane, A. van Oosterom, O. Pahlm, P. Kligfield, M. Janse, J. Camm (eds.), *Comprehensive Electrocardiology*, DOI 10.1007/978-1-84882-046-3_13,

13.1 Introduction

As with all biological phenomena, there can be no clear-cut distinction between normal and abnormal, yet some attempt has to be made to define the limits of normality of the ECG. The only sound basis for the interpretation of the ECG is a thorough understanding of the way in which the ECG pattern in normal, healthy individuals varies from infancy to old age, between male and female, from one racial group to another, and so on. A knowledge of intraindividual variation is also necessary in order to avoid false-positive interpretations and to look for subtle changes in the ECG, even within the normal range of measurements.

In recent years, other noninvasive investigations, such as echocardiography and magnetic resonance imaging, have been added to the diagnostic armamentarium of the physician. Yet, electrocardiography still remains one of the most basic cardiological investigations beyond physical examination and can provide information that is not obtainable by any other means. Even now, it is unlikely that the full potential of the ECG has been realised because of the failure to establish well-defined limits of normality, which vary according to the different factors mentioned above. Furthermore, with the increasing application of computer technology to the interpretation of the ECG, the potential for setting up comprehensive cooperative studies of normal individuals to establish large databases for refining the limits of normality exists, in order to improve the diagnostic capability of the ECG. The alternative of taking ECGs from apparently healthy individuals enrolled in clinical trials, though not fully medically examined, has recently been adopted, enabling large numbers of individuals to be studied [1].

Technology has advanced rapidly, and it is perfectly conceivable that every electrocardiograph could contain facilities for some form of computer-based ECG interpretation (see Chap. 37). However, not all healthcare systems can afford such technology, and simple ECG recorders with no interpretation or measurement facility will survive for years to come. This gives added impetus to the need for a careful appraisal, if not further development, of methods for defining the normal variation of the ECG.

The classic treatise on the normal ECG is that of Simonson [2] who elegantly summarized all the material available at that time, *c.*1960. He himself contributed greatly to the understanding of the variability of the normal ECG, and much of his own thinking still influences present-day electrocardiographers. Nonetheless, technology has advanced dramatically since then, and the availability of computer techniques for the measurement of the ECG and vectorcardiogram (VCG) component amplitudes has greatly facilitated further study of normal limits.

In an assessment of the normal scalar ECG recorded from a few hundred healthy volunteers, Lundh [3] pointed out that if the order of 100 measurements are made on the ECG with each varying independently (which is unlikely to be the case), then only 1% of the ECGs could be expected to fall within normal limits on the basis of utilizing 95% confidence intervals for defining the normal range of each measurement. This, of course, is carrying matters to an extreme, but it does point to the need for a careful development of diagnostic criteria even given well-defined normal ranges. In other words, it has to be made clear from the outset that the availability of normal ranges does not mean that once a single measurement exceeds an upper limit by a small amount, the ECG has to be regarded as abnormal. This point cannot be emphasized too strongly.

13.2 The Establishment of Normal Limits

13.2.1 Sampling Methods

There are a number of different approaches to tackling the problem of establishing normal limits through large-scale population studies. One of the first questions to be resolved is whether the population should be based on apparently healthy individuals in the community or whether it should be derived from persons under investigation in hospitals for problems unrelated to cardiovascular disease. There can be no doubt that the latter offers the convenience of subjects being available close at hand to the recording center, but it is clearly open to question as to whether such individuals can be regarded as healthy. It could be argued that patients in an orthopedic ward who have been admitted for the treatment of a recent injury are no different from an apparently healthy individual in the community, always assuming that the relevant medical history is uneventful. Alternatively, such a source of volunteers is unlikely to yield an adequate distribution of subjects with respect to age and sex.

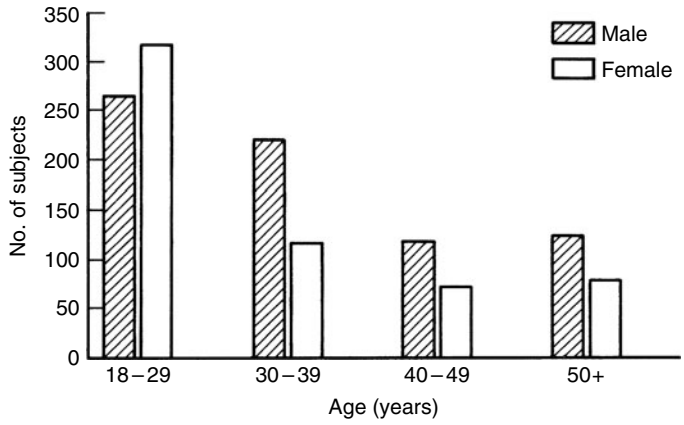

Figure 13.1

The distribution of the 1,338 subjects in the Glasgow study of apparently healthy individuals. A very small number of individuals aged 17 years were included, but are not shown on this graph.

The most satisfactory solution is to obtain apparently healthy subjects from the community at large. Different approaches to population sampling can be adopted. Some investigators favor the use of sampling a population register. For example, Lundh [3] selected every 50th man and woman born between 1915 and 1953 from the local civil registry. Although an even distribution of subjects by age and sex was not obtained, there being a predominance of younger individuals, it was claimed that this reflected the population distribution in the catchment area – a town that had expanded in recent years.

The approach of Macfarlane et al. [4] was to seek volunteers from a variety of departments in the local government within the city of Glasgow and the region of Strathclyde. In this way, a spread of occupations was covered from sedentary office work, such as in finance and library administration, to outdoor occupations, such as in parks and recreation departments. The distribution of the volunteers obtained in this study is shown in Fig. 13.1, where again it can be seen that there is a predominance of younger persons. In this case, there is a different reason for such a distribution. It is evident that younger persons who feel healthy are quite willing to volunteer for such a study, whereas older individuals appear to be more reluctant to come forward in case some hitherto unsuspected abnormality is detected that might result in further medical investigation that would be regarded as inconvenient and potentially job threatening. In addition, because many married women cease employment with the arrival of a family and then only return to work perhaps 10 or 15 years later, there is a lack of female volunteers in the 25–40 age-group. This can be compensated for by concentrating on selecting volunteers from the appropriate age and sex group when, after some time, it becomes apparent that a shortfall is present in a particular category.

A third approach that has been used in a number of studies is simply to investigate a group of employees in a particular industry or government department. Normally, such an approach is associated with screening (see Chap. 40), but it could be regarded as an alternative to the determination of normal limits, always assuming that there was a reasonable distribution of employees by age and sex.

13.2.2 Cardiovascular Screening

When the population sampling method has been chosen, it must then be decided what investigations are necessary in order to establish that an individual is healthy. In studies undertaken in the authors' laboratory and reported later in this chapter, it was decided to undertake a simple clinical examination of volunteers in order to exclude those with any evidence of an illness known to affect the cardiovascular system. In addition, blood-pressure measurements were obtained.

The list of illnesses known to have some influence on the ECG is lengthy, but of major importance are endocrine, respiratory, renal, neurological, alimentary, and hematological disorders, as well as the various cardiovascular diseases, either congenital or acquired. In the authors' study, subjects were asked to volunteer if they were apparently healthy, but, nevertheless, it was clear that a few individuals used the opportunity of participating in such a study as a means of having a checkup on earlier illnesses, which in fact precluded them from entry.

The value of a chest x-ray is questionable. In the first 500 patients in the above study in whom chest x-rays were routinely recorded, there was no single instance in which an apparently healthy volunteer had to be excluded from the study on the basis of an abnormal chest x-ray being the only positive factor. It was therefore decided that in view of the expense and inconvenience involved in arranging chest x-rays, this would not be a necessary requirement for determining that an individual was apparently healthy.

From the outset in this study, it was also decided that the need for routine blood tests was negligible. Again the expense and expected yield of abnormalities did not appear to justify the workload of such an additional test. Thus, the cohort consisted of volunteers regarded as healthy on the basis of history, blood pressure, and physical examination.

It is of interest to note that a group of electrocardiographers in North America [5] reached a similar conclusion. In other words, subjects "not actively seeking medical care" can be accepted as apparently healthy on the basis of physical examination and history, without the need for either a chest x-ray or blood tests to be available.

It can be seen that volunteers are initially regarded as healthy without recourse to ECG findings. On the other hand, it is well known that a right bundle branch block (RBBB) occurs in a small percentage of healthy persons [6] and that an ECG is sometimes the only indicator of myocardial infarction (MI) [7]. In at least two studies – one in Framingham, Massachusetts [8] and the other in Israel [9] – it was found that the ECG provided the only evidence of myocardial infarction in up to 50% of patients in whom it was agreed that a definite infarct had occurred. Notwithstanding these examples, it has to be accepted that individuals must be regarded as apparently healthy on the basis of a clinical examination, history, and other test results excluding the ECG. Thereafter, it is for the statistical techniques to deal with the question of normal ranges.

13.2.3 Statistical Considerations

13.2.3.1 Sample Size

From a statistical point of view, the larger the population studied, the more soundly based will be the results that are derived therefrom. However, consider a simple example and assume that it is desired to study the adult population in the age range of 20–70 years. (The question of variation in infancy and childhood is discussed separately below.) One approach would be to divide the population sample into decades of age so that, for the proposed sample, there would be five age-groups, namely, 20–29, 30–39, 40–49, 50–59, and 60 years and over. Likewise, the population would be split in two on the basis of sex, thereby giving ten subgroups. It is known that the ECG can be influenced by race, and hence if the population is further stratified into black and white (which is a major simplification) the number of subgroups increases to 20. From a practical point of view, if 200 entries could be obtained for each of the groups, then 4,000 individuals are required to constitute a basic population survey. Selvester and colleagues in North America, in proposing the establishment of a normal database, have indicated that up to 30,000 individuals would be required from a statistical point of view [5]. While this may be scientifically desirable, it raises many practical problems, since it entails the need for a multicenter approach. Such a method would cause difficulties in the standardization of methods, not to mention a need for the transfer of data to a central coordinating department that has the ability to analyze the massive amounts of data obtained. Nevertheless, such numbers have been obtained in a more indirect way, as already mentioned [1].

An approximate estimate of numbers required for a particular test can be obtained from the consideration of a simplified example. In a discussion of clinical trials, Schwartz et al. [10] quoted the following equation that is useful, for example, in estimating the number of people, n, required in each group when it is wished to show a significant difference, say of 0.4 mV, in the mean R amplitude between males and females of the same age-group:

$$n = (e_\alpha + e_\beta)^2 B^2 / A^2$$

where A is the difference being assessed (here, 0.4 mV), B is the standard deviation of R amplitude distribution (perhaps derived from a pilot study), e_α denotes the percentage point from the standard normal distribution corresponding to the chosen significance level α of the test, and e_β is the percentage point from the standard normal distribution corresponding to the chosen power β of the test, where β is the maximum probability of failing to detect a difference. It can be shown that 49 people would be required in each group depending on the chosen e_α, e_β, and A. If the difference being assessed is expected to be 0.2 mV, then the number increases to 195 in each group.

13.2.3.2 Normal Ranges

If a set of amplitudes, for example, the R-wave amplitude in V_5, is obtained from a group of apparently healthy individuals within a well-defined age range, there will clearly be a spread of measurements obtained with a predominance of values in the middle of the group and a smaller number at either side. In a classical situation, where there is an even spread of measurements around a central value with the distribution as shown in Fig. 13.2, there is said to be a normal distribution. A point on the bell-shaped curve simply indicates the number of people in the group who have an amplitude of a certain value. Clearly, when the distribution is symmetrical, the mean of the values will be in the middle of the range. Given the set of values, it becomes possible to calculate a mean and standard deviation for the parameter of interest. The standard deviation, SD, is calculated from the formula

$$\mathrm{SD} = \left[\frac{\sum_{i=1}^{n}(x_i - \bar{x})^2}{n-1}\right]^{1/2}$$

where $\bar{x}$ is the mean value, x_i represents the individual values, and n is the number of values in the sample. With a classical normal distribution, the mean plus or minus twice the standard deviation delineates approximately 95% of the range of values, as shown in Fig. 13.2. Hence, if it could be shown that a set of values possessed a normal distribution, then one method of defining the normal range would simply be to calculate the mean and standard deviation and proceed to derive the upper and lower limits of the normal 95 percentile range. By taking such limits, where 2.5% of the values are excluded at either end of the distribution, so-called outliers can be excluded.

With respect to ECG measurements, however, it was pointed out by Simonson [2] many years ago that the range of measurements for most ECG parameters is not normal, that is, it tends to have a skewed distribution, as shown in

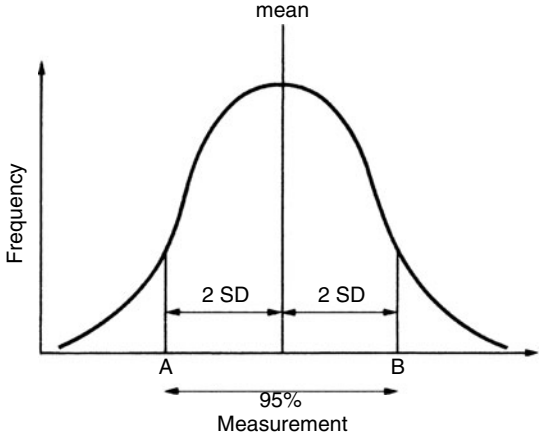

Figure 13.2

An illustration of a normal distribution of a set of measurements. The mean value in this case is in the center of the distribution with two standard deviations, 2SD, being shown on each side of the mean; the distance AB includes approximately 95% of the measurements.

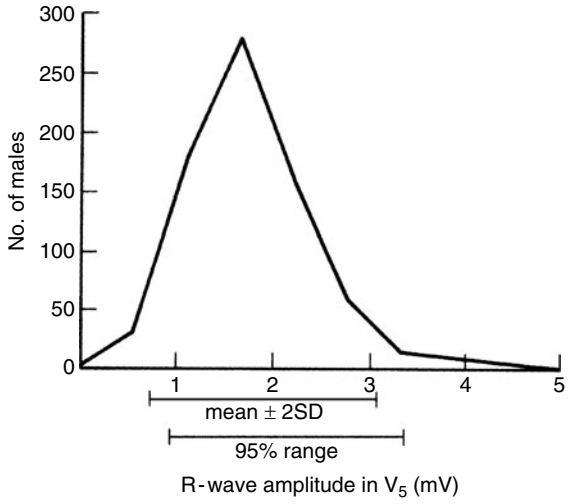

Figure 13.3

The distribution of the R-wave amplitude in V_5 in 738 males in the Glasgow study. It can be seen that the distribution is skewed to the right, that is, toward the larger measurements. The mean ± 2SD has a different range compared to the 95 percentile range obtained by excluding 2.5% at either extreme of the distribution. Note that in many ECG studies, a 96 percentile range is used (see text).

Fig. 13.3 for the R-wave amplitude in V_5. The longer tail of the distribution is toward the higher values with the shorter tail being toward the lower values. Thus, if the 95 percentile range based on the mean ± 2SD is used, a large percentage of values at the upper end of the range are likely to be excluded.

To avoid this difficulty, an alternative approach for deriving the 95 percentile limits can be adopted; namely, 2.5% of values at the upper end of the range are excluded as are 2.5% of values at the lower end. The difference between the two ranges calculated using the alternative techniques is shown in Fig. 13.3.

In many electrocardiographic studies, the 96 percentile range has been adopted, whereby 2% of values at either extreme were removed in calculating what then became known as the "normal range." There are no scientific reasons for choosing 96% rather than 95% other than that in a study of 100 or 200 individuals, it is simpler to remove 2% as opposed to 2.5% of values, since in the latter, interpolation methods would have to be used. The different approaches to the latter were outlined by Simonson [2], but in the context of samples of adequate size, this would appear to be an unnecessary refinement.

Much of the data presented later in this chapter in respect of normal ranges and elsewhere in the Appendices is based on the above concept of the normal range. Mean values and standard deviations are also provided for completeness, wherever possible.

The use of 96% ranges means that an unusually long QRS duration as obtained from a healthy volunteer with RBBB would be excluded from the normal range, as such an abnormality occurs in less than 0.5% of a mixed community [6]. Similar conditions would apply to broad Q waves encountered in persons with silent myocardial infarction.

Another approach to defining a normal limit, particularly where there is a need to consider a continuous limit over a range of ages, is to calculate an upper 95% confidence level for the distribution. This can be done by first obtaining a set of values such as the R-wave amplitude in V_5 for a group of persons, perhaps males aged 18–65 years, as shown in Fig. 13.3. With the use of statistical methods, it is then possible to assess the effect of age and body mass, for example, with respect to their contributions to the amplitude distribution. If it can be shown that the major component contributing to the variation is age, then it is appropriate to calculate the mean amplitude values for various age ranges.Given this data and

knowledge of the appropriate standard deviation, it then becomes feasible to calculate the 95% confidence interval for the mean from the following equation:

$$\text{Mean} \pm K \times \frac{\text{SD}}{(\text{group\_size})^{1/2}}$$

where K is approximately 2 for a group that is normally distributed.

Alternatively, the upper and lower 95% limits of the range of values (i.e., 2.5% of values are excluded at each extreme of an assumed normal distribution) are given by

$$\text{Mean} \pm 2 \times \text{SD}\left(1 + \frac{1}{n}\right)^{1/2}$$

where n is the number of subjects in the group.

The above applies where a single age-group, for example, is being assessed, but the process can, of course, be repeated for the different age ranges. Of interest is the possibility of deriving a continuous equation for predicting the upper limit of normal for a given age. Consider that all R-wave amplitudes in V_5 are known for a group of males aged 18–65 years. The mean and standard deviation of R in V_5 can then be calculated. If the distribution is reasonably normal and it has to be accepted that there will be some error in this assumption, these two values can be used as shown below. Similar considerations apply to age, and again the assumption of a normal distribution would be open to question. The fifth value required is the correlation coefficient. In summary, if $\bar{x}$ denotes the mean of age, S_x is the standard deviation of age, $\bar{y}$ denotes the mean of the R-wave amplitude, S_y is the standard deviation of amplitude, and r is the correlation coefficient between age and amplitude, then the expression depicting the upper 97.5% limit is

$$\left\{\bar{y} + \beta(x - \bar{x}) + 25\left[1 + \frac{1}{n} + \frac{(x - \bar{x})^2}{(n-1)S_x^2}\right]^{1/2}\right\}^2$$

where n is the number of subjects in the study, $\beta = rS_y/S_x$, x denotes age, and $S = S_y(1 - r^2)^{1/2}$. From the authors' own data for males, this equation reduces to

$$\left\{46.8 - 0.01(\text{age}) + 1.96 \times 6.702\left[1 + \frac{1}{736} + \frac{(\text{age} - 435.67)^2}{(144.52)^2 \times 735}\right]^{1/2}\right\}^2$$

where age is in months and amplitude is in microvolts. This line is plotted in Fig. 13.4 together with discrete limits of normality for different age ranges.

This expression can, without any real loss of accuracy (given the assumptions under which it was derived), be reduced to

$$[46.8 - 0.123(\text{age}) + 13.13]^2 \mu\text{V}$$

where age is in years, and clearly further to

$$\text{Upper normal limit} = (59.93 - 0.123\,\text{age})^2 \mu\text{V}$$

Thus, the upper limit of normal is 3.04 mV at age 39 and 3.026 mV at age 40. This compares with a change of 0.5 mV between these two particular ages when discrete limits are used (see Fig. 13.4).

The use of 95 percentile confidence limits where a continuous value can be derived from the equation is at first sight attractive. Clearly, the upper limit of normal for an individual should not change overnight as he changes from one age-group to another as discussed above. Jain and Rautaharju [11] have investigated the use of continuous variables with respect to diagnostic classification capabilities and have suggested that these are possibly of greater significance

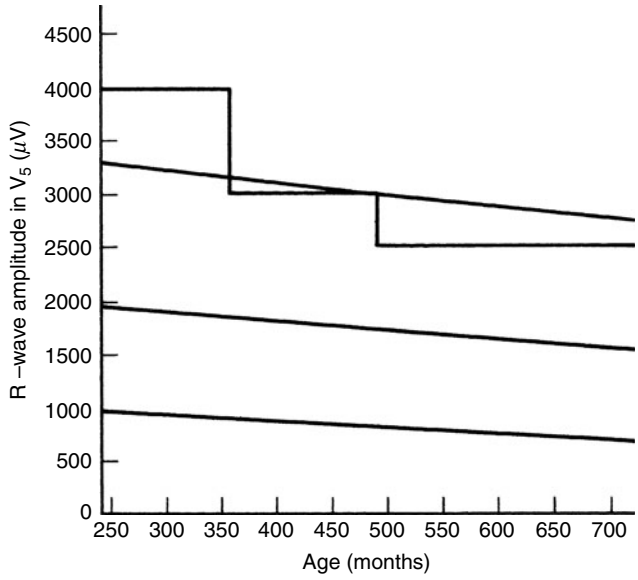

Figure 13.4

A plot of normal limits of the R-wave amplitude in V_5 (in microvolts) against age (in months). The topmost curve or step function illustrates the upper limit of normal for this parameter for three discrete age-groups, 18–29, 30–39, and 40+. Note that within each group the level is fixed, but there is marked discontinuity at 29–30 and 39–40. The three continuous curves show, respectively, the upper 97.5 percentile distribution, the mean, and the lower 2.5 percentile limit, as derived from the equations presented in the text. In this case, the change between ages 29–30 and 39–40 is of the order of approximately 15 μV.

than the use of discrete variables where limits change from one age range to another. This is an area that has not been explored intensively and is one where further study would appear to be merited if the year-to-year variation of the ECG interpretation is to be minimized. This could be important in the context of an annual company medical, for example, where a computer-based interpretation might be employed with discontinuous limits of normality being used for different age-groups. Undoubtedly, this approach would be facilitated with the availability of large databases of normal ECGs.

Indeed, in the Glasgow ECG analysis program for automated analysis of ECGs [12, 13], continuous limits of normality are extensively used. Furthermore, smoothed criteria have been introduced so that thresholds between normal and abnormal can also be blurred [14, 15]. Figure 13.5 illustrates this concept.

13.2.3.3 Angular Data

The treatment of angular data can be difficult. For example, if three vectors are oriented at 0° (360°), 120°, and 240°, what is the mean value? Fortunately, in many situations, the angular data tend to cluster around a prevalent direction and a normal range can be estimated in the manner discussed in Sect. 13.2.3.2. In more difficult situations, an alternative strategy has to be considered. Liebman (see Appendix 1) discusses the matter fully, but a summary is given here.

If a group of vectors is imagined to lie in space, a sphere of suitably small radius, R, could intercept all such vectors. The coordinates of each intercept would then be $(xR/L, yR/L, zR/L)$, where x, y, z are the components of the original vector of length L. The mean value $(\bar{x}, \bar{y}, \bar{z})$ of all such intercepts can then be found; for example,

$$\bar{x} = \sum \frac{(xR/L)}{N}$$

where N is the number of vectors. The prevalent direction can then be calculated.

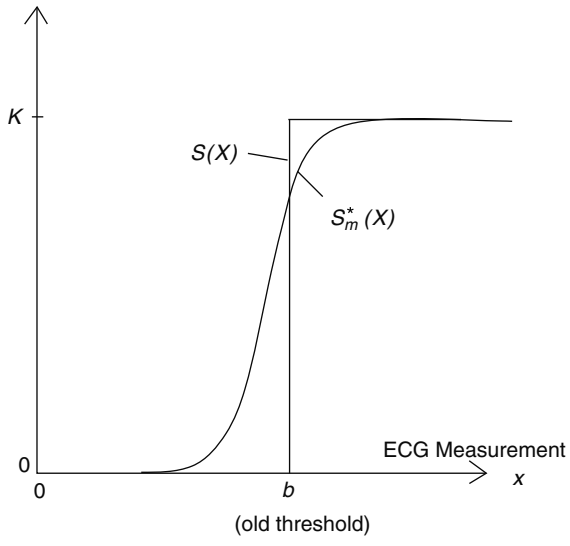

Figure 13.5

A comparison of two scoring methods, namely, a fixed threshold and a continuous function. With the use of a fixed threshold at *b*, *K* points are scored when the threshold is exceeded. Only two values of the score are possible, namely, 0 and *K*. With the continuous function, an infinite number of values of the score between 0 and *K* are possible as the measurement increases and then exceeds *b*. (Reproduced from J Electrocardiol 1993; 26(Suppl): 101–7 by kind permission of Elsevier.)

13.2.3.4 Sensitivity and Specificity

The importance of normal ranges lies in the assessment of specificity of diagnostic criteria. It would therefore seem relevant to introduce the concept of sensitivity and specificity, to which reference is made in other chapters.

Consider that a group of apparently healthy individuals have ECGs recorded, while a separate group of patients with cardiac diseases known to predispose to left ventricular hypertrophy (LVH) also have an ECG recorded. It is conceivable that the distribution of S-wave amplitude in V_2 for each of the groups would appear as in Fig. 13.6. The development of criteria should be such as to obtain the optimum separation between the two groups. It can be seen from this hypothetical example that there is a considerable overlap between the two sets of measurements, which in practice is usually the case. In selecting a borderline value for a simple test to discriminate between the two groups, the investigator must first decide the level of specificity desired. This is the percentage of normal patients that will be correctly reported as normal by the test. Each of these normals is regarded as a true-negative (TN) result. The remainder of the normals wrongly reported as abnormal because their S-wave amplitude lay above the borderline value selected would be classed as false positives (FP). Thus,

$$\text{TN} + \text{FP} = \text{total number of normals}$$

With respect to the abnormal group, those patients with ventricular hypertrophy (VH) who are correctly reported as having the abnormality because their S-wave amplitude values exceed the borderline criterion, would be regarded as true positives (TP). The remainder of this group of patients would then fail to have been reported as having hypertrophy. They would thus falsely have been regarded as normal and are said to constitute the false-normal or false-negative (FN) group. Clearly,

$$\text{TN} + \text{FN} = \text{Total number of patients}$$

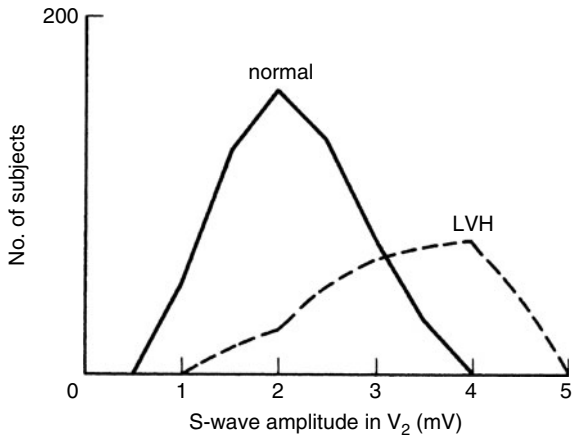

Figure 13.6

A hypothetical example of the distribution of the S-wave amplitude in V_2 in a group of normal subjects and a group with proven left ventricular hypertrophy (LVH). If a value of 4 mV is selected to differentiate between normal and abnormal, over 50% of the cases of LVH would not be detected. The reverse would be true if 2 mV were to be selected; over 50% of the normals would be reported as having LVH.

The following definitions can therefore be given.

$$\text{Specificity} = \frac{\text{Number of normals correctly reported as normal}}{\text{Total number of normals}} \times 100\%$$

$$= \frac{\text{TN}}{\text{TN} + \text{FP}} \times 100\%$$

$$\text{Sensitivity} = \frac{\text{Number of abnormals correctly reported as abnormal}}{\text{Total number of abnormals}} \times 100\%$$

$$= \frac{\text{TP}}{\text{TP} + \text{FN}} \times 100$$

When commenting on the accuracy of diagnostic criteria, in addition to sensitivity and specificity, the following measurements are also often used.

$$\text{Predictive value of an abnormal result} = \frac{\text{TP}}{\text{TP} + \text{FP}} \times 100\%$$

$$\text{Predictive value of a normal result} = \frac{\text{TN}}{\text{TN} + \text{FN}} \times 100\%$$

$$\text{Association index} = \text{sensitivity} + \text{specificity} - 100$$

In the authors' view, specificity should be selected at a high level with the desired aim of maintaining a very low rate of occurrence of false positives. The exact relationship between specificity and sensitivity can be seen more closely in Fig. 13.7. In this illustration, two situations are described [16]. In each case, the distribution of a set of normal values of a particular parameter is shown under the left-hand curve, while the distribution of the corresponding parameter from a set of patients with a particular abnormality is shown under the right-hand shaded curve. The normal group and the set of patients is the same in each case, but the parameter used in II shows a clearer separation between the two groups. If the dividing line between normal and abnormal is chosen at different points, here labelled 1–7 or 1–9

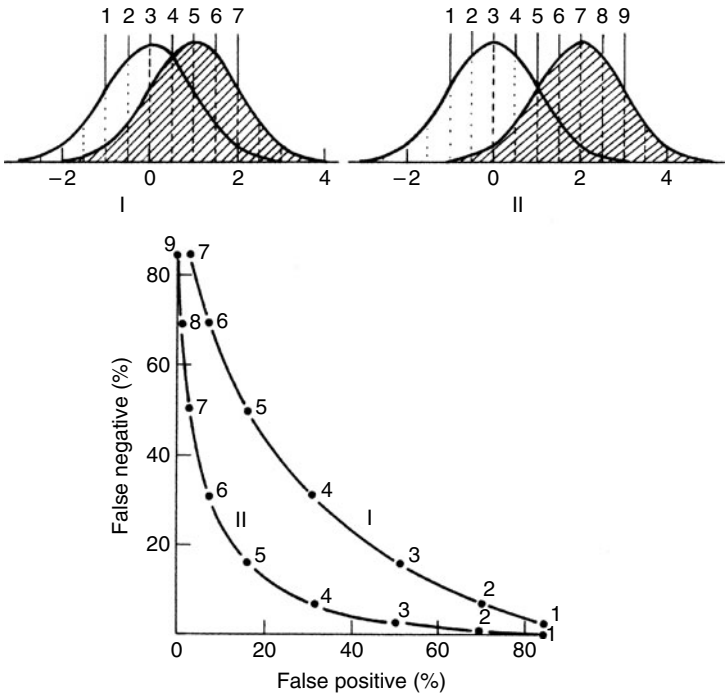

Figure 13.7

The top curves compare the distributions of two parameters (I and II) in two groups of patients. One is a normal group and the other is an abnormal group (shaded distributions). Parameter II clearly provides a better separation between the two groups. Although this is seen visually in the top right set of curves, the findings can be presented as a set of receiver operating characteristic (ROC) curves. The numbers 1–7 represent points at which the separation between normal and abnormal can be taken so that with 1, for example, there would be a high diagnostic sensitivity and very many false-positive interpretations, whereas with 7 there would be very few false-positive interpretations but a poor diagnostic sensitivity. The curve that most closely approaches the origin is superior, and, in this case, parameter II is the better. (After Dudeck and Michaelis [16]. © North-Holland, Amsterdam. Reproduced with permission.)

as the case may be, then the corresponding number of false-positive and false-negative cases for each discriminating value can be plotted. The curves arising from such plots are known as "receiver operating curves" or "receiver operating characteristics" (ROC curves). For particular distributions, they allow the user to select a level of specificity (100% false positive), and from this, the corresponding sensitivity (100% false negative) can be determined from the curve. It can be argued that the value closest to the origin produces the best results, whereby false-positive and false-negative values are minimized. For example, in this case (Fig. 13.7), the lower curve denoted II indicates that this parameter is better than that of I for separating normal and abnormal. This can be a useful way of assessing the best discriminating values for use in the development of diagnostic criteria as evidenced by a recent study of different criteria [17].

The above discussion for illustrative purposes has concentrated on a two-group classification of normal and abnormal. Rautaharju et al. [18] agreed that this approach enhances sensitivity and specificity estimates, and that the relative numbers in the two groups can distort the true picture. They suggested that the comparison should not be between normal and abnormal (i.e., a particular abnormality), but between patients with such an abnormality and all others. In other words, in assessing the specificity of criteria for LVH for example, all normals and other patients known not to have LVH but who might perhaps have a myocardial infarction should be included in the "non-LVH" group, and not simply the normals alone. The alternative definitions that follow from this are summarized in Table 13.1.

Table 13.1

Definition of sensitivity (SE), specificity (SP), mean performance (MP), association index (AI), accuracy of positive test (AP), accuracy of negative test (AN), fraction of subjects with a positive test (F), and overall diagnostic accuracy (D). See text for a discussion on the meaning of negative test

Definitions	
SE = TP/(TP + FN)	AP = TP/(TP + FP)
SP = TN/(FP + TN)	AN = TN/(FN + TN)
MP = (SE + SP)/2	F = (TP + FP)/(TP + FP + FN + TN)
AI = SE + SP − 1	D = F.AP + (1 − F)AN

TP, true positive; FP, false positive; FN, false negative; TN, true negative

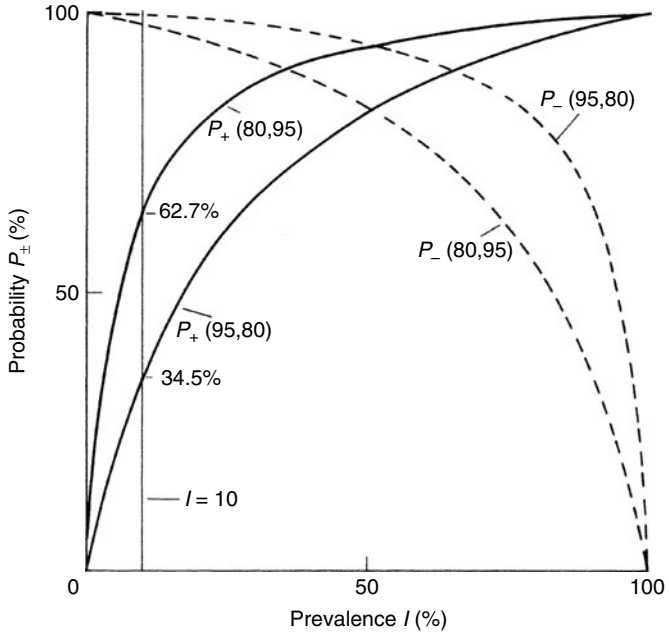

Figure 13.8

The relationship between the probability of an ECG interpretation being correct with respect to a particular diagnosis and the prevalence of that abnormality in the population. The two curves on the left show the probability of a true-positive result, and the two curves on the right show the probability of a true-negative result. Each curve corresponds to a different set of criteria with different sensitivity and specificity. For example, with a sensitivity of 80% and a specificity of 95%, the probability that an ECG interpretation stating a particular abnormality true-positive result, given that the prevalence of the abnormality is 10%, is 62.7%. Likewise, the probability that the omission of such a diagnosis is a true negative is approximately 97%. (After Bailey [19]. © Engineering Foundation, New York. Reproduced with permission.)

A final point to bear in mind is that positive and negative predictive value depend on the prevalence of a particular disease in the population being studied. In other words, in assessing criteria for myocardial ischemia, it would be quite possible to produce a set of criteria that proved to have a high positive predictive value when evaluated in a population where the prevalence of ischemic heart disease is known to be high. Conversely, it is likely that the same criteria applied to a population where ischemic heart disease is known to be low would result in many false-positive diagnoses and a low positive predictive value. The two curves on the left of Fig. 13.8 show the probability of an ECG interpretation of a

particular abnormality being correct (true positive) given the varying prevalence of such an abnormality in the population and a knowledge of the sensitivity and specificity of two sets of criteria [19]. In many ways, these are ROC curves for given populations where the prevalence of the abnormality is known. Conversely, the probability of a negative interpretation being correct (true negative) is also shown for the same two sets of criteria. Note that the sensitivity and specificity of the two sets of criteria are fixed, while the prevalence varies from 0 to 100%. It can be seen that, for a prevalence of disease of 10%, the criteria that are 95% specific produce a higher probability of a true-positive interpretation compared to those that are 80% specific. The equations for calculating the probabilities are as follows [19].

The probability of a correct positive result, P_+, is

$$P_+(Se, Sp) = \frac{SeI}{SeI + (1 - Sp)(1 - I)}$$

where Se is the sensitivity of the criteria, Sp is the specificity of the criteria, and I denotes the prevalence of that abnormality or disease in the patient population.

The probability of a correct negative result, P_-, is

$$P_-(Se, Sp) = \frac{Sp(1 - I)}{Sp(1 - I) + (1 - Se)I}$$

13.2.4 Methods of Measurement

In early studies on normal limits, the quality of the ECG-recording equipment was such that recommendations [20, 21] referred to measuring from the top of the baseline at a particular reference point. At that time, all measurements were made manually in some studies, and later, further suggestions for reference points were published [22, 23]. It was recommended by the American Heart Association [21] that the ST segment, the T wave, and the P wave should all be measured with respect to the isoelectric part of the tracing before the P wave. This recommendation was based on the avoidance of the atrial repolarization potentials, which can produce "depression" of the baseline prior to the QRS onset.

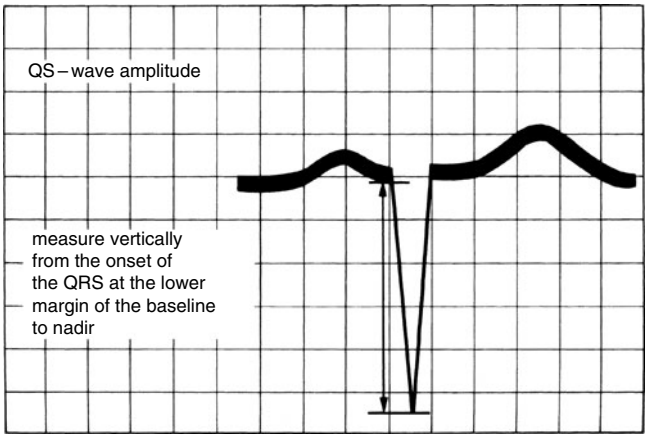

Figure 13.9
Recommendations from the Minnesota code manual on how to measure the depth of the QS wave. (After Prineas et al. [22]. © Springer, London. Reproduced with permission.)

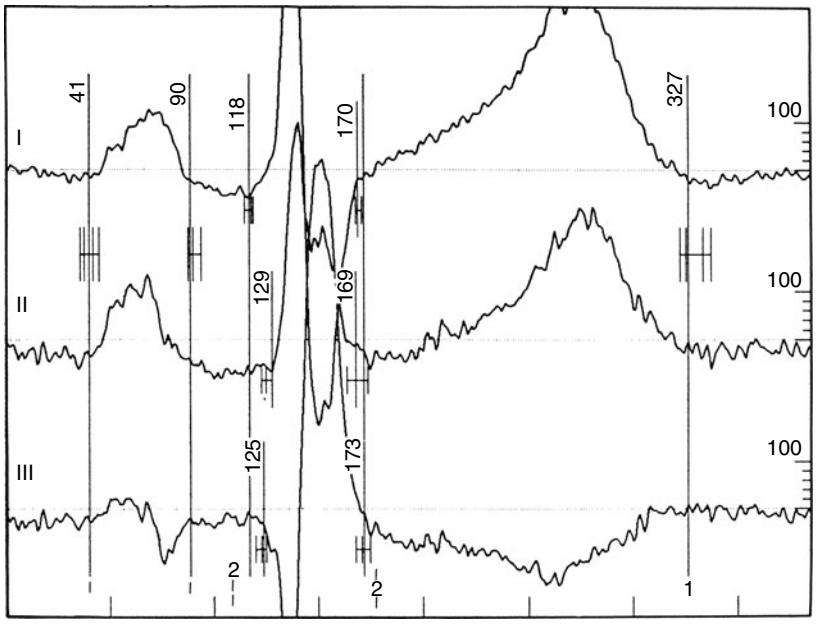

Figure 13.10

Three simultaneously recorded leads, I, II, and III, shown expanded in time and gain. The vertical bars indicate estimates of wave onsets and offsets made by five cardiologists. The agreed onset for lead I differed from that of lead II by 11 sample points in the digitized data, that is, 22 ms. (From Willems JL ed. CSE Atlas of ECGs. 1983 ACCO Leuven. Reproduced with permission.)

Nowadays, with the use of computer technology, recommendations relating to the baseline "thickness" are a little less meaningful, although for manual coding, such rules [22] still apply (Fig. 13.9). The general approach to a measurement involves one form of averaging or another. Normally, a set of beats of similar configuration is grouped together, and from this, an average beat is formed. Measurements are then made on this average beat. Alternative approaches do exist whereby a set of measurements (e.g., six R-wave amplitudes) is obtained and these are then averaged. A further approach is simply to select one single beat that appears to be most representative of the recording. Further details are available in Chap. 37. The use of averaging, however, theoretically leads to an improved signal-to-noise ratio and, hence, more accurate amplitude measurements. The accuracy of computer-derived durations is still under discussion (see below), but it should be noted that if a reference point is wrongly determined (the QRS onset, for example), then any amplitude measured with respect to such a point is open to error. To minimize such errors, most programs find a reference level by averaging in the vicinity of, say, the QRS onset or else fit a smooth curve from which the reference can be taken. In general terms, with respect to ECGs recorded from normal individuals, such small errors in amplitude are not of great significance and have to be set against normal day-to-day variation of measurements, which can be significantly larger [24].

While the above discussion has concentrated on amplitudes, it should also be noted that the possibility of different approaches to measuring durations of ECG components now arises from using technology, whereby all leads are recorded simultaneously. Figure 13.10 shows an actual example from three simultaneously recorded leads of a 12-lead ECG where the QRS complex in lead I appears to commence earlier than in lead II. This is perfectly feasible given an understanding of the concept of projections of electrical activity onto different cardiac axes, as discussed in Chap. 11.

However, with respect to Fig. 13.10, the question then arises as to whether the duration of the wave in lead II should be measured from the earliest QRS onset in any of the leads, or whether it should be measured from the apparent onset of the R wave in that particular lead. The difference could be over 20 ms as in this case. Again, the reader must therefore be aware of another possible source of discrepancy when considering published values for normal limits of wave-component durations.

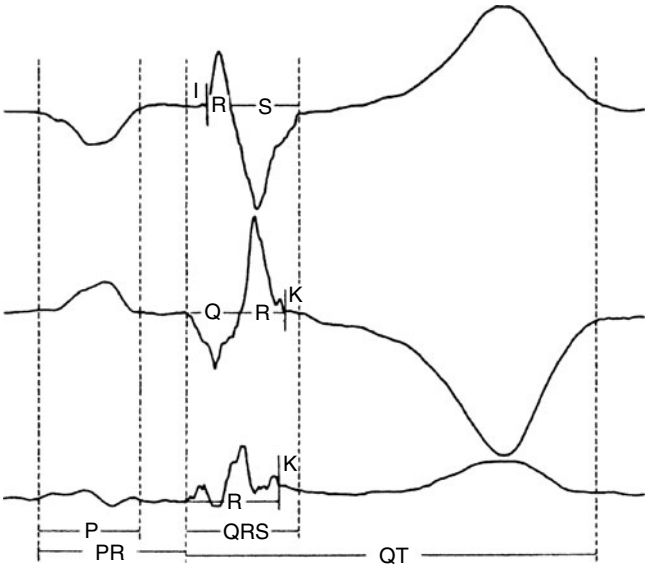

Figure 13.11
An illustration of the definitions of isoelectric segments at the onset (I) and termination (K) of the QRS complex. (After CSE Working Party [25]. © Academic Press, London. Reproduced with permission)

The availability of simultaneously recorded leads and the possibility of detecting "isoelectric" segments in some leads either at the beginning or end of waves have led the EEC working party on Common Standards in Electrocardiography (CSE) to recommend that such segments, denoted I and K for the QRS complex (see Fig. 13.11), be separately measured when detected [25].

A final point that can be made with respect to methods of measurement relates to the determination of QRS axis. Where the VCG is available and all leads have been recorded simultaneously, it is quite feasible to derive any required axis (see Chap. 11). Where the 12-lead ECG is involved, possibly with leads not recorded simultaneously, a different approach has to be utilized. There have been many suggested methods for measuring QRS axis [26–29]. However, the ad hoc Task Force of the World Health Organization (WHO) and the International Society and Federation for Cardiology (ISFC) [30] have recommended that the QRS axis should be measured on the basis of utilizing the areas under the QRS complex in leads I, II, and III. Since two pairs of leads can be selected from the three leads in three different ways, the recommendation is that the QRS axis be calculated using three different pairs of leads with an average value ultimately being derived. This recommendation has clearly been made with computer technology in mind.

An alternative approach is to utilize the sum of the signed Q (negative), R (positive) wave, and S (negative) wave amplitudes in these leads and to calculate similarly a QRS axis. In either case, a function $f(\mathrm{I})$, for example, can be used to represent the measurement (area or component sum) derived in this case from lead I. The following calculation shows how the use of the three standard limb leads I, II, and III, from which three measurements $f(\mathrm{I}), f(\mathrm{II})$, and $f(\mathrm{III})$ are obtained, allows an estimate of a frontal plane axis and avoids the need for repeated calculation and averaging as suggested by the WHO Task Force [30].

Consider that leads I, II, and III with lead directions as conceived in the Einthoven triangle (see Fig. 13.2) are superimposed on a Cartesian coordinate system, as shown in Fig. 13.12. Then, $OL = f(\mathrm{I})$, $OM = f(\mathrm{II})$, and $ON = f(\mathrm{III})$ represent the amplitude of the projection of the desired axis (or vector $\overrightarrow{OA}$) onto the lead axes I, II, and III, as shown in Fig. 13.12.

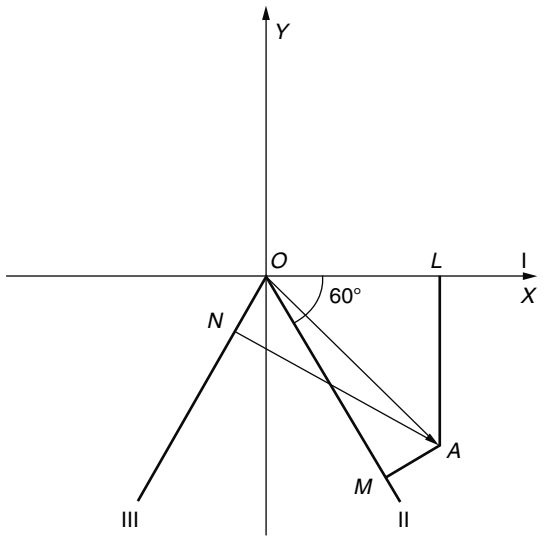

Figure 13.12

An illustration relating to the calculation of the mean QRS vector given measurements from leads I, II, and III. The resultant vector is depicted as OA and has been calculated from a knowledge of its projection onto the three different leads I, II, and III, namely, OL, OM, and ON, respectively. (See text for detailed discussion.)

Thus, the Cartesian coordinates of these projections, that is, the coordinates of L, M, and N are as follows:

axis projection on lead I: $L = (f(\mathrm{I}),\ 0)$
axis projection on lead II: $M = (f(\mathrm{II})\ \cos\ 60^\circ,\ f(\mathrm{II})\ \sin\ 60^\circ)$
axis projection on lead III: $N = (-f(\mathrm{III})\ \cos\ 60^\circ,\ f(\mathrm{III})\ \sin\ 60^\circ)$

It should be noted that the functions $f(\mathrm{I})$, $f(\mathrm{II})$, and $f(\mathrm{III})$ are signed values.

It follows from the above and from the preceding section on angular data (Sect. 13.2.3.3) that the coordinates of the desired mean axis, that is, OA, on a circle of suitably small radius, R, intercepting all vectors, are given by the average component values:

$$\frac{R}{3\cdot \mathrm{OA}}\{[f(\mathrm{I})+f(\mathrm{II})\cos 60^\circ - f(\mathrm{III})\cos 60^\circ],[f(\mathrm{II})\sin 60^\circ + f(\mathrm{III})\sin 60^\circ]\}$$
$$= \frac{R}{3\cdot \mathrm{OA}}\left\{f(\mathrm{I})+\frac{1}{2}[f(\mathrm{II})-f(\mathrm{III})],\frac{\sqrt{3}}{2}[f(\mathrm{II})+f(\mathrm{III})]\right\}$$

The required angle is therefore obtained from the arc tangent of the ratio of the two components:

$$\tan^{-1}\left\{\frac{\frac{\sqrt{3}}{2}[f(\mathrm{II})+f(\mathrm{III})]}{f(\mathrm{I})+\frac{1}{2}[f(\mathrm{II})-f(\mathrm{III})}\right\} = \tan^{-1}\left\{\frac{\sqrt{3}[f(\mathrm{II})+f(\mathrm{III})]}{2f(\mathrm{I})+f(\mathrm{II})-f(\mathrm{III})}\right\}$$

This equation is based on the assumption that leads I, II, and III are related according to the equilateral Einthoven triangle (see Fig. 11.2). It can be used to calculate the P, QRS, or T axis provided the relevant measurement (e.g., P, QRS, or T area in leads I, II, and III) is substituted appropriately.

The experience of the authors' laboratory is contrary to that of the recent recommendations [30] in that the use of the area proved slightly less acceptable than the use of signed amplitudes when compared with angles derived from the VCG [31]. In a number of pathological situations (e.g., RBBB), a broad S wave can distort the measurement of the QRS axis using the area method.

13.2.5 Use of Computers

Computers first began to be utilized for analysis of the ECG in the early 1960s (see Chap. 37). Probably, the first use of the technique in the assessment of the normal limits of the ECG was that of Draper [32] from Pipberger's laboratory. In this study of 510 normal men, computer techniques were used for deriving the amplitude and duration of the P, QRS, and T components of the orthogonal leads *X*, *Y*, and *Z* as well as for calculating selected vector magnitudes and orientations. From this, 96 percentile ranges were derived.

It should not be assumed that because a computer is used for measurement, the ECG component amplitudes and durations are perfectly "correct." Several studies (see Chap. 37) indicate that there is variation between different programs with respect to computer measurement of amplitude, duration, and so on. It should also be noted that different authors measure wave components in different manners. While many workers have taken the QRS onset as a reference point with respect to which all other amplitudes have been measured, there are different recommendations available. For example, the American Heart Association [23] specifies that the T-wave amplitude should be measured with respect to the end of the T wave. The CSE Working Party indicated that the P-wave amplitude should be measured with respect to P-wave onset [25]. This is an approach that has not been adopted in all centers. Figure 13.13 shows three different approaches to the measurement of the P-wave amplitude, namely, with respect to the P-wave onset [23, 25], with respect to the QRS onset [33], and finally with respect to a straight line fitted between the P onset and termination [34].

Although in the vast majority of cases, and particularly when dealing with normal subjects in sinus rhythm, there will be very little difference between measurements. Nevertheless, there are obvious sources of discrepancy in the presence of a sinus tachycardia above 130 bpm and in pathological situations. The reader is therefore urged to look carefully at the different recommendations.

On the other hand, it is known that cardiologists also initially vary when defining wave onsets and terminations, as demonstrated in one of the CSE studies [35]. Furthermore, it would be extremely difficult for a physician to measure hundreds of amplitudes and durations and to calculate vector magnitudes and orientations on a multitude of ECGs. Thus, while the possibility of computer error, like human error, has to be acknowledged, automated methods provide a major step forward in defining normal ranges.

The introduction of computers and the ability to exchange data between different collaborating centers, as demonstrated by the CSE study [25, 35, 36], does support the possibility of developing more extensive databases including those from apparently healthy individuals. As already mentioned, the databases gathered from clinical trials involving one commercial company have been used to assess the limits of normality on 46,219 individuals with a very low probability of having any disease that would affect the ECG [1]. Such a task would simply be impossible without automated assistance. Although the skill of the experienced physician may still be required in reviewing a computer-based ECG interpretation, the capacity of computer systems to remember various normal limits stratified by parameters such as age, sex, and race is far beyond that of the individual. A valid second opinion is therefore provided in such cases by the automated interpretation, which supplements the experience of the physician.

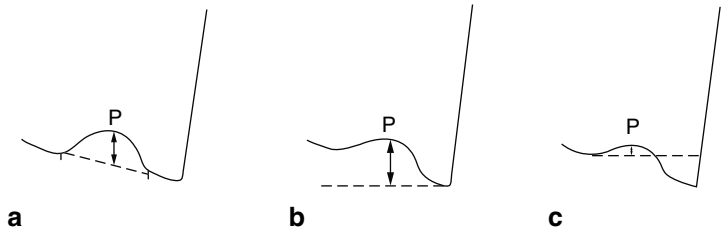

Figure 13.13

An illustration of three methods of measuring the P-wave amplitude. They are with respect to (a) a straight line fitted between P onset and P termination, (b) QRS onset, and (c) P onset. Clearly the amplitude will differ under the various situations depicted here.

13.3 Sources of Error

13.3.1 Technical Sources

Improvements in technology, as discussed in Chap. 12, mean that nowadays the accuracy of ECG recording is high. Digital recording with direct analog-to-digital conversion of the ECG within the modern computer-based electrocardiograph removes a number of sources of potential error in the recording technique.

The approach to population surveying can vary from a straightforward recording of the ECG on paper with manual measurement through to fully automated ECG recording and measurement of amplitudes, and so forth. In the former, a significant problem may arise with manual calibration of the ECG recorder. A 5% error in the setting of the 1 mV calibration signal might be difficult to avoid. Thereafter, the measurement of wave amplitudes and durations would be subject to various sources of error, not the least of which would be human error owing to fatigue. With the use of magnifying glasses for ECG measurement, the baseline written on to the chart recorder naturally appears thick, and measurement rules [37] suggest that amplitudes should be obtained by measuring from the top of the baseline to the top of the R wave, or from the bottom of the baseline to the tip of the Q wave, for example (Fig. 13.9). The S-wave amplitude should be derived by measuring from the foot of the baseline to the bottom of the S wave. Such recommendations are still relevant when applying the Minnesota code, for example [22], to paper-based copies of the ECG. Likewise, the determination of the onset and offset of various components is extremely difficult using manual techniques, particularly if only a single-channel recording is available. Calibration errors can be minimized by the use of a correction factor (CF). For example, if the normal calibration of 1 mV = 10 mm is used, then the correction factor (CF) to be used would be

$$\mathrm{CF} = 10/X$$

where X = actual calibration amplitude (mm). All measured amplitudes would have to be multiplied by this correction factor.

The use of computers for the measurement of ECG parameters is also not without error. While many of the above problems, such as thickness of baseline, are avoided, the computer is still more prone to error in defining reference points, such as P onset and T termination. However, the definition of such reference points can prove troublesome even to experienced ECG reviewers, as evidenced by data from the CSE study [36, 38]. For example, given five referees' estimates of T termination, the standard deviation of the different estimates about each referee's individual mean value in a sample of 250 ECGs ranged from 12.6 to 17.8 ms. Similarly, the standard deviation of nine X, Y, and Z computer program estimates versus the mean of the computer programs ranged from 13.2 to 25.6 ms. In general terms, it is probably true to say that the measurement of amplitude by a computer will be more reliable than the measurement of durations. Some computer programs can measure small Q or R waves of the order of 8 ms duration. This is now the recommended minimum wave duration [25].

If a computer measures an extremely small primary r wave, perhaps of the order of 10 ms duration and 24 μV amplitude, care has to be taken that any larger following r′ wave is correctly utilized. Figure 13.14 illustrates this concept.

It could be argued that these difficulties are of minor significance compared with the actual repeat and day-to-day variation in the ECG itself. Each of these points will now be discussed.

13.3.2 Repeat Variation

If an ECG is recorded on the same individual twice within a short period of time and if the electrode positions are not marked on the chest, there can be marked variation in PQRST amplitudes from one recording to another. The source of this variation can be a result of a number of causes.

A principal source is undoubtedly simply that of the accuracy of placement of electrodes. In population surveys, where there is only one opportunity of recording the ECG, it is therefore of importance that an experienced technician records the ECG, paying meticulous attention to electrode placement.

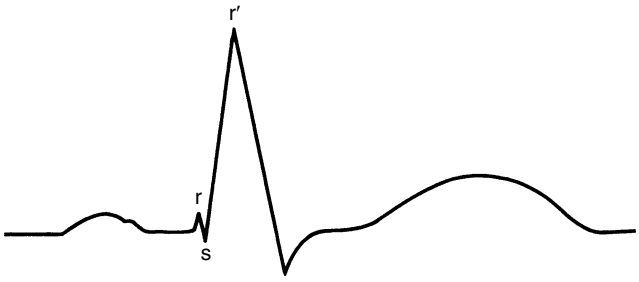

Figure 13.14

In this ECG, a small primary r wave leads to the principal deflection being termed an r′ wave. This could lead to an error in computer diagnoses if criteria for an abnormally high amplitude R wave check only r amplitude and not r′ amplitude in addition.

Table 13.2

Day-to-day, beat-to-beat, and percentage variation of QRS amplitude measurements: only upper limit of 96% variation is presented. R_x denotes the R-wave amplitude in lead *X*, and so on

Measurement	Increased amplitude (mV)				Decreased amplitude (mV)			Ranges (mV)		
	Variation (%)	Mean	SD[a]	96% day-to-day variation	Variation (%)	Mean	SD[a]	96% day-to-day variation	96% beat-to-beat variation	Maximal variation
R_X	13	0.16	0.14	0.41	17	0.22	0.17	0.52	0.377	0.52
R_Y	18	0.16	0.097	0.36	20	0.17	0.13	0.35	0.257	0.36
R_Z	17	0.099	0.082	0.24	14	0.10	0.07	0.23	0.13	0.24
Maximum spatial QRS vector	12	0.19	0.16	0.46	22	0.25	0.17	0.54	0.26	0.54

[a]Standard deviation

Where it has been possible to mark the correct electrode positions on the chest, perhaps with intracutaneous dye injection, repeat variation is minimized [39, 40] but by no means eliminated. Using the orthogonal-lead ECG, Willems et al. [39] showed that the day-to-day variation could be reduced by 25% by using marked electrode positions compared to using unmarked positions. In another study from which the data in Table 13.2 were taken [41], the electrode positions were unmarked. Table 13.2 shows the repeat variation of R-wave amplitudes in the orthogonal leads when ECGs were repeated twice, ECGs being recorded on three different days. It can be seen that the 96 percentile day-to-day variation in component amplitude ranged up to 0.52 mV, a sizable change. In a corresponding fashion, the maximum change in the spatial QRS vector was 0.54 mV.

It was pointed out by Simonson [42] that patients with coronary heart disease exhibit much more variability in repeat ECGs taken at six-week intervals compared to a similar group of apparently healthy individuals. For example, the variation in the frontal plane T-wave axis in patients with coronary artery disease and an abnormal ECG was of the order of 64°, whereas it was only 27° for those with proven coronary artery disease and a normal ECG, while only approximately 10° for normal individuals.

Other factors influencing the repeat variation of the ECG include the phase of respiration in which the ECG is recorded, cigarette smoking [43], drinking of iced water [44], proximity to meals [45], anxiety [46], and so on. While all of these factors can influence ECG appearances in the one-off situation, by implication they must therefore affect repeat and day-to-day variation in the ECG. The experienced electrocardiographer will often have a subjective impression that suspicious appearances in an ECG may be "technical" in origin and will ask for a repeat ECG to be undertaken to make certain that an abnormality can be confirmed. The term "electrocardiographogenic disease" has been applied by

Marriott to the situation where a healthy individual may be categorized as having heart disease on account of an "abnormal" ECG [47]. A knowledge of the causes of day-to-day and repeat variation therefore assists in avoiding heart disease of electrocardiographic origin.

13.4 Factors Influencing Variability

13.4.1 Age

The factor that most influences the variation in ECG appearances is age. While other factors also have a role to play as discussed below, the effects of age are apparent from birth to death. On the other hand, influences due to the sex of an individual, for example, tend to be important in young adulthood but have a much less important role to play at either extremes of age.

As is well known, the ECG varies considerably over the first few days of life as the cardiovascular system adapts to its new role. In general, QRS voltage tends to increase toward adolescence and then begins to decrease thereafter. This can be seen in the composite illustration of Fig. 13.15 based on two different studies, one involving children and the other, adults. While this trend is demonstrated from different age-groups and different samples, the same conclusion has been demonstrated in a longitudinal study of persons in the Framingham study. ECGs recorded 40 years apart from the same individuals show a decrease in QRS amplitude in the second recording compared to the first. This is shown in Fig. 13.16. While it has always been assumed by electrocardiographers that the implication of the results of serial studies in different populations could be applied to the same individual in a longitudinal study, it is thought that this is the first time that such a finding has been demonstrated (Levy, D., personal communication, 1987).

As well as influencing ECG amplitudes, age affects intervals on the ECG. It has been shown that the PR interval increases slightly with increasing age [2], and in our study of adults, this finding has been reproduced as shown in Table 13.3. Likewise, QRS duration is shorter in older subjects compared to young persons (see Table 13.3).

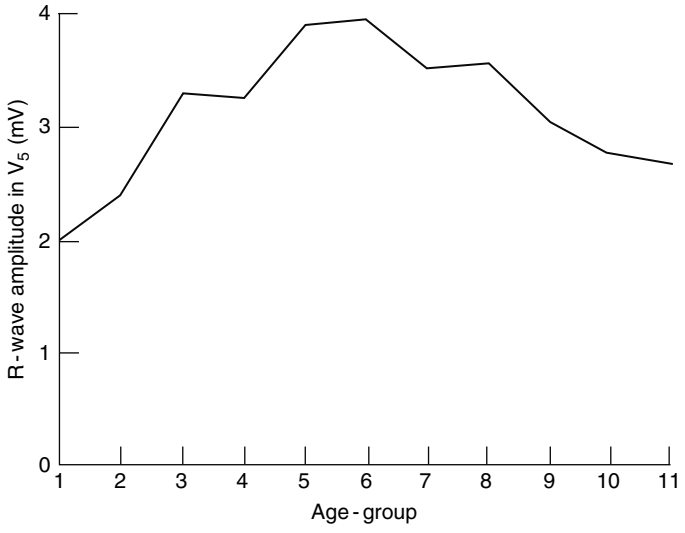

Figure 13.15

A composite illustration of the upper limit of normal R-wave amplitude in V_5 from birth to 50 years and over in males. The peak occurs at age 8–12 years. The age-groups are as follows: (1) 0–1 day, (2) 3–7 days, (3) 1–3 months, (4) 6–12 months, (5) 3–5 years, (6) 8–12 years, (7) 12–16 years, (8) 18–29 years, (9) 30–39 years, (10) 40–49 years, and (11) over 50 years.

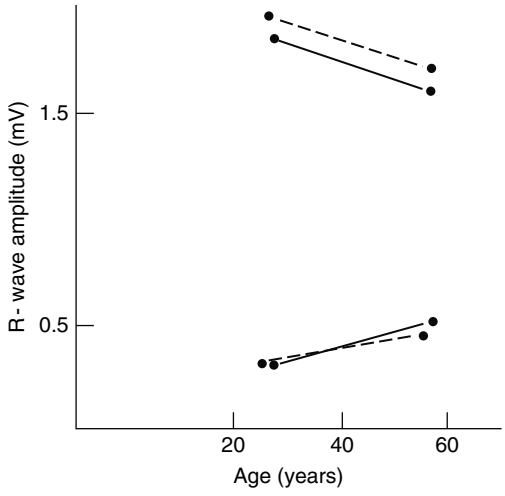

Figure 13.16

Change in the mean R-wave amplitude in V_5 (upper two curves) and in aVL (lower two curves) over a 40-year period. Solid curves are from data kindly provided by Dr. D Levy of the Framingham heart study, while the dashed curves are from the Glasgow database. Framingham data are from the same individuals recorded 40 years ago; Glasgow data are from different individuals.

Table 13.3

Means ± standard deviations and 96% ranges of PR, QRS, QT, and QT_c

Age-group	Sex	No. of subjects (*n*)	PR interval (ms)	QRS duration (ms)	QT interval (ms)	QT_c interval[a] (ms)	QT_c interval[b] (ms)
18–29	Male	265	152.5 ± 23.0	96.4 ± 8.6	385.5 ± 28.9	403.6 ± 19.0	413.9 ± 23.1
			112–208	80–114	336–442	368–444	370–463
	Female	317	145.9 ± 19.7	87.7 ± 7.8	380.0 ± 27.8	411.6 ± 18.0	429.7 ± 22.9
			114–194	72–104	332–440	378–451	386–477
30–39	Male	218	155.7 ± 21.4	95.4 ± 9.8	385.5 ± 29.5	404.8 ± 19.4	416.0 ± 22.9
			116–206	78–114	326–448	366–448	375–468
	Female	115	145.7 ± 18.6	88.6 ± 7.3	386.6 ± 27.7	415.2 ± 16.9	432.6 ± 20.9
			114–184	76–106	330–438	384–445	395–473
40–49	Male	119	157.2 ± 21.8	94.4 ± 9.9	390.8 ± 29.3	409.2 ± 17.9	420.0 ± 21.9
			116–210	78–114	340–450	377–450	377–464
	Female	72	154.9 ± 20.4	89.4 ± 7.9	386.1 ± 27.0	415.2 ± 22.5	433.7 ± 28.4
			108–200	74–108	328–434	347–457	350–483
50	Male	123	161.5 ± 18.9	92.7 ± 9.3	385.5 ± 26.0	407.4 ± 17.5	420.9 ± 22.7
			120–196	74–112	320–434	374–444	380–475
	Female	79	155.6 ± 16.9	87.1 ± 8.7	390.7 ± 31.5	419.5 ± 22.7	438.2 ± 24.8
			122–196	68–104	336–488	376–486	392–506

[a] QT_C corrected according to Hodges et al. [106]
[b] QT_C corrected according to Bazett [105]

13.4.2 Sex

The second important factor affecting appearances in the ECG is that of sex. Sex differences in the ECG are most apparent in young adulthood and tend to diminish to a certain extent thereafter. As an example, Fig. 13.17 shows the mean S-wave amplitude in V_2 for males and females in the authors' own study. Significant differences exist in the age-group 18–30 years, while by the age of 50, there tends to be little difference between S-wave amplitudes recorded from males and females.

It is possible that to some extent this difference in the younger age-group is a reflection of the level of physical activity undertaken by individuals. To investigate this effect, a subgroup of 483 persons aged 18–29 years from the population of the authors' study was subdivided into those who undertook regular exercise and those who did not. It was found that mean amplitudes of S waves in V_2 were lower in the group who did not undertake exercise, but, nevertheless, there were still significant differences between males and females who engaged in regular training activities and also between males and females who did not (Table 13.4).

Another cause of lower ECG amplitudes in women is thought to be a higher fat content [2] and the influence of breast tissue. LaMonte and Freiman [48] assessed the effects of mastectomy and noted an increased QRS amplitude in women following this operation. On the other hand, Rautaharju et al. studied the effect of breast tissue on ECG amplitudes in women and concluded that there was no significant effect [49].

T-wave amplitudes in women also tend to be lower than in men, particularly in the precordial leads, where, apart from V_1, the lower limit of the normal T-wave amplitude is positive in both men and women. In the Appendices, data on T-wave amplitudes show that in V_1, T-wave inversion is much more prevalent in women than men. Indeed, T-wave inversion in V_2 and very occasionally in V_3 can be found in healthy women. On the other hand, in the limb leads, it is well known that apparently healthy young women, and sometimes men, may on occasions exhibit ST-T "changes" (slight ST depression and/or minimal T-wave inversion), particularly in the inferior leads. Since the T wave in III may often be inverted in normal persons, it is aVF that assumes more significance in this case. The exact mechanism for such T-wave changes has never been satisfactorily demonstrated. However, this applies in cases where the QRS complex is mainly upright. A leftward QRS axis shift may be accompanied by a leftward T axis shift so that an inverted T wave may appear in aVF in the presence of a dominant S wave but be of little significance. In such cases, the frontal plane QRS-T angle is small. Increasing the QRS-T angle is associated with increasing degrees of coronary artery calcification in older adults aged 66 or over [50].

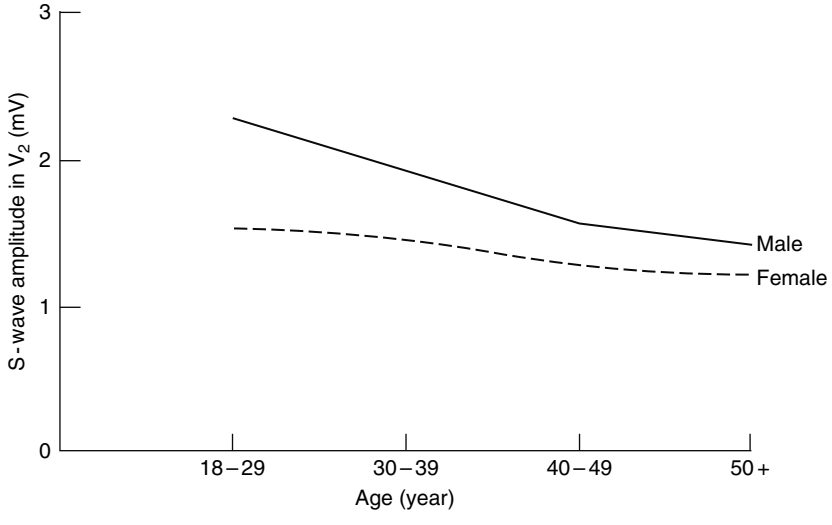

Figure 13.17

The mean S-wave amplitude in V_2 stratified by age. Data were derived from the subjects in the Glasgow study.

Table 13.4

Mean values and 96% ranges of the S-wave amplitude in V_2 for young men and women aged 18–29 years, inclusive, divided into two groups: those taking exercise and those who did not

	Sex	No. of subjects (*n*)	Mean value of wave amplitude (mV)	96% range of S-wave amplitude (mV)
Regular exercise	Male	96	2.43	0.80–4.5
	Female	95	1.53	0.59–3.04
No regular exercise	Male	128	2.18	0.77–3.76
	Female	164	1.53	0.39–2.81

Sex differences can also influence the various intervals in the ECG (Table 13.3). The authors' study group showed a shorter PR interval in women (96 upper percentile = 0.196 s compared to men whose corresponding upper limit was 0.21 s). This might logically be explained on the basis of the average male heart being somewhat larger than that of the average female, necessitating a slightly longer conduction time between the sinus node and the ventricles. It was also found that women had a shorter QRS duration (88 ms, as compared to 95 ms for men) and a longer corrected QT interval (Table 13.3). For some unknown reason, these basic facts are not used in ECG interpretation where most cardiologists will slavishly adhere to 120 ms as the upper limit of normal QRS for males and females and use such a value in clinical decisions on the use of cardiac resynchronization therapy, for example, irrespective of the patient's sex and of the accuracy of QRS measurement [51].

13.4.3 Race

The influence of race on the ECG has been known for some time but, despite the recent availability of computer techniques, has not been used to any significant extent in the interpretation of the ECG.

As early as 1946, Littmann [52] reported on the "persistence of the juvenile pattern in the precordial leads of healthy adult blacks." His study did not involve the use of precordial leads referred to the Wilson central terminal but utilized bipolar chest leads with the indifferent electrode being on the left leg. Since then, there has been controversy over whether or not such T-wave findings are truly representative of the black population: For example, Keller and Johnston [53], using precordial leads based on the Wilson central terminal, were unable to confirm the findings of Littman. On the other hand, Walker and Walker [54] demonstrated that T-wave inversion was found in young South African Bantu subjects. Recent work involving over 1,200 ECGs recorded from healthy adults living in Nigeria using a digital electrocardiograph, and analyzed in Glasgow, paradoxically showed more precordial T-wave inversion (Fig. 13.18) in healthy black females than in healthy black males [55].

In a comparison between Japanese and North American men and women, Simonson [2] showed significant differences in most electrocardiographic parameters. In general terms, the Japanese group showed higher voltages in the precordial leads compared to the American group. The reverse appeared to be true for the limb leads.

In contrast, in a large computer-assisted study involving the authors [56], it was found that precordial voltages of young Chinese men and women were significantly lower than their Western counterparts. This difference diminished with increasing age (Fig. 13.19). In general terms, there was little difference between the two populations with respect to intervals and durations. It should be stressed that the same computer program [57] was used for the analysis of all ECGs in this study. P-wave amplitudes were higher in Caucasians than Chinese, while almost 10% of Chinese women aged between 40 and 49 years had a negative T-wave component in V_3. These comparisons were derived from a study of over 500 apparently healthy Chinese undertaken in Taipei by Chen et al. [58] and from the authors' own normal data. More recently, Wu et al. found very similar normal ranges in a large Chinese cohort [59].

In the Washington code developed by Pipberger et al. [60], different limits of normal are used for white and black subjects and for males and females. The code was developed partly from a study of 518 normal men including 186 black subjects [61] and, probably, a separate study on women, which appeared much later from the same laboratory [62] although racial differences were not considered (despite a significant percentage of black women being included).

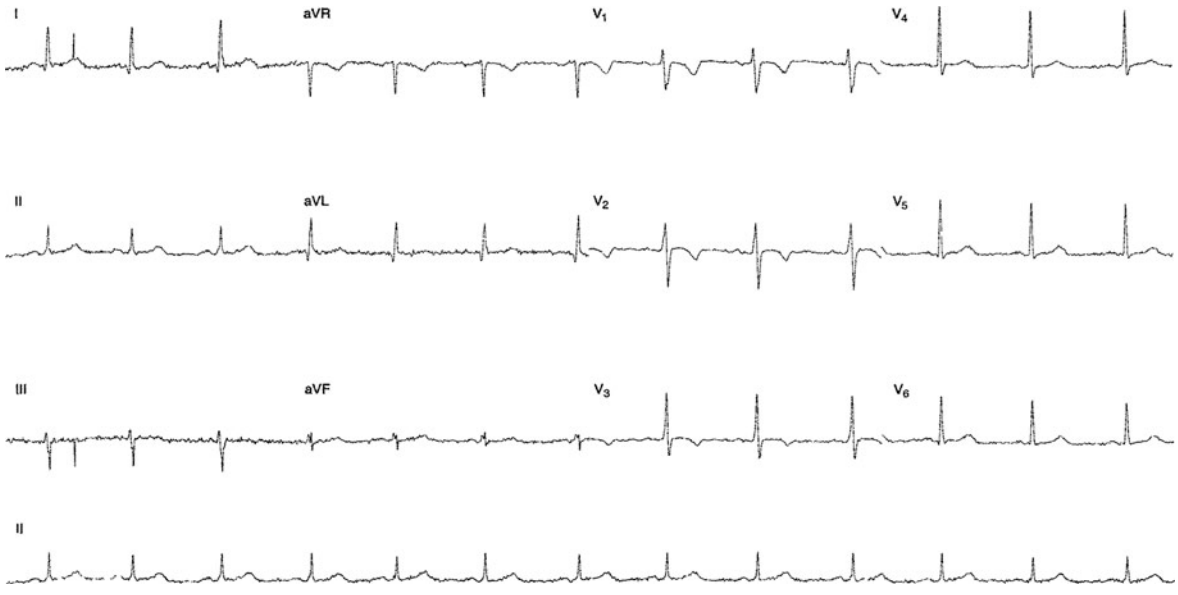

Figure 13.18

An ECG recorded from a 31-year-old healthy Nigerian lady. Note the T-wave inversion in V_2 and V_3. This illustration is reproduced with permission of Dr. I.A. Katibi, University of Ilorin, Nigeria.

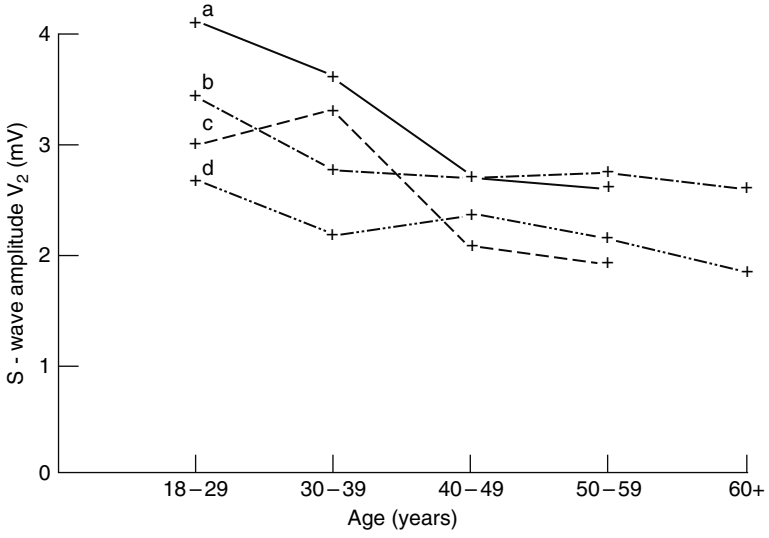

Figure 13.19

Variation in the upper limit of normal of the S-wave amplitude in V_2 in white and Chinese populations. The white subjects were from the Glasgow study, while the Chinese data were obtained from 503 apparently healthy Chinese [56]: (a) white males, (b) Chinese males, (c) white females, and (d) Chinese females.

However, a closer inspection of the published data reveals that with respect to scalar QRS amplitude data from males, the upper limit of normal voltage differed only in RZ (R amplitude in lead Z equivalent to SV_2) where the black limit was almost 30% higher than the white limit. Many other differences, while of statistical significance, were not of practical value. The exception to this is the much smaller Q/R ratio found in the lateral (X) and inferior (Y) leads in black subjects.

This is one area in particular where the continued development of large databases will lead to further enlightenment with regard to the effect of race on ECG wave amplitudes and durations.

13.4.4 Other Constitutional Variables

Other variables that might influence the ECG are those of height and weight. To a certain extent, these can be related by the use of various indices, such as weight/height^2 (Quetelet index, [63], more commonly known as body mass index) and so on. While certain variations and correlations in the ECG can be demonstrated between measurements and such indices (e.g., weight and amplitude [61]), these have never been used to any significant extent in ECG interpretation. Their use is complex in that they add an extra complication to the involvement of age and sex in diagnostic criteria. Likewise, because of the lack of availability of large databases where significant numbers in different groups can be obtained, a full study of the effect of such variables is still awaited. Matthes and coworkers [64] pointed out that some of the variation in the QRS amplitude could in fact be accounted for by an inverse relationship between body mass index and increasing age. They used

$$\frac{W \times 100}{H - 100}\%$$

as an index (where W is the weight in kilograms and H is the height in centimeters). Data from the authors' own study show the relation between the S-wave amplitude in V_2 and the Quetelet index both for males and females (Fig. 13.20b). The results are a little confusing. If data for males alone are considered, then there is a significant correlation between the S amplitude in V_2 and age ($r = 0.466$), which accounts for almost 22% of the variation. There was no correlation of amplitude with height as would be expected, but limited correlation with weight ($r = 0.199$), which therefore accounts for only 4% of the variation: The Quetelet index showed an intermediate relationship to the S amplitude ($r = 0.282$), and therefore accounts for 8% of the variation. Of the two (constitutional) variables, height and weight, the latter is clearly of more significance within the male group as a whole. A similar pattern was found for females although the correlation was less in each case, being 0.216 for age and 0.148 for weight with respect to the S amplitude in V_2, which was treated as a negative number.

If males and females are treated as a single group, then the correlation of the S amplitude in V_2 with age changes to 0.307 and not surprisingly height then shows a negative correlation with the S amplitude ($r = -0.227$). Conversely, the correlation of the S amplitude with weight becomes almost zero.

These results strengthen the existing generalized approach of considering only age and sex when interpreting the ECG. This is also in agreement with the view of Simonson [2] who indicated that "over-all, the effect of age on the ECG is more pronounced and consistent than the effect of relative body weight," overweight, underweight, and so on.

13.4.5 Physical Fitness

The question of fitness affecting the ECG was alluded to above when dealing with the limits of normal voltage in younger persons. With the continued interest in marathon running and the need for individuals to increase the amount of exercise taken in order to reduce cardiovascular risk factors, there have been a number of studies dealing with the effects of physical training on the heart. A review by Oakley and Oakley [65] specifically dealt with the ECG in athletes. As might be expected, an increase in precordial voltage was noted in highly trained athletes together with T-wave abnormalities. It is known from echocardiographic studies [66, 67] that there is an increase in internal left ventricular (LV) diameter together with an increase in posterior LV wall thickness and septal thickness in athletes involved in a variety of sports. It is therefore not surprising that some increase in ECG voltage is obtained. Figure 15.9 shows the ECG from a marathon runner whose echocardiogram indicated that his LV mass was at the upper limit of normal. T-wave changes can be seen in several leads.

Figure 13.21 shows the ECG from a 22-year-old healthy athlete who had a normal echocardiogram and a normal cardiac magnetic resonance image scan. Marked T-wave inversion can be seen in I, aVL, V_2, and V_3. A recent publication suggested that such individuals are at increased risk of cardiomyopathy in later life [68].

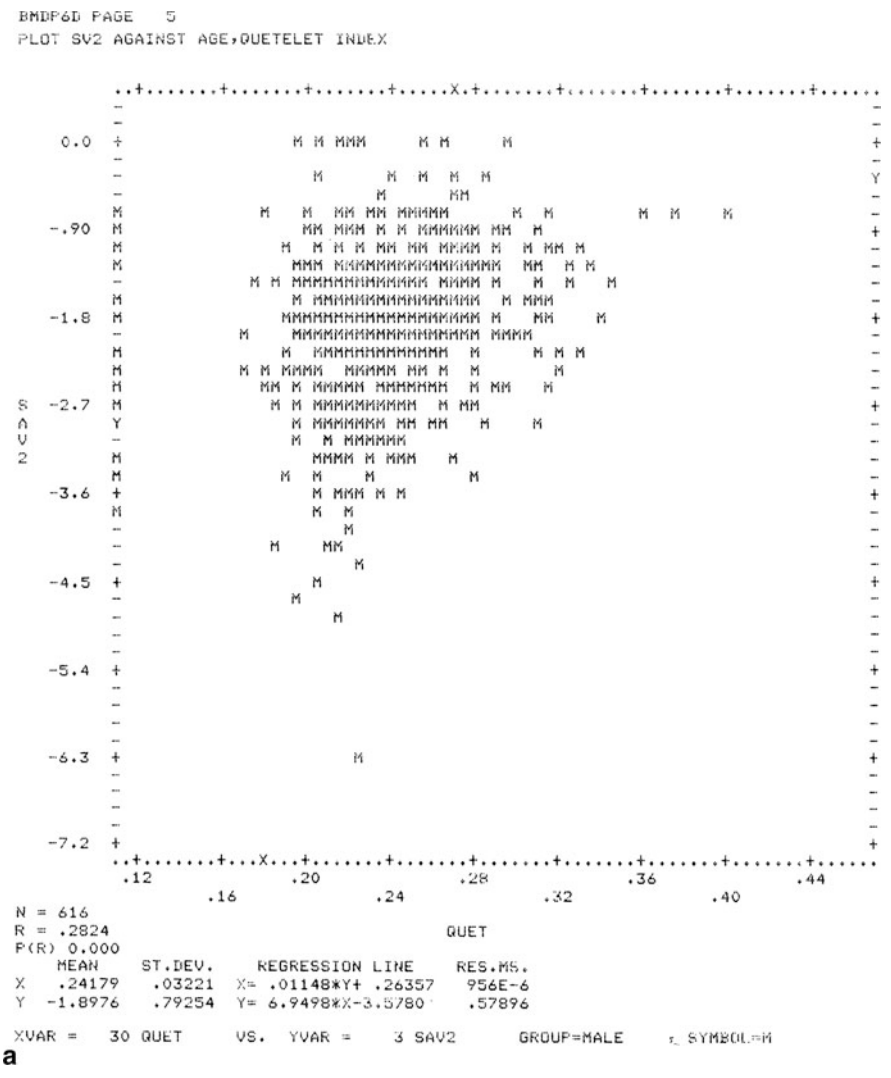

a

Figure 13.20a

Scattergram of S amplitude in V_2 versus the Quetelet index, shown for 616 males. Note that the S amplitude is plotted as a negative number.

In a balanced sample from an apparently healthy population, the occasional abnormality, such as isolated T-wave inversion as shown in Fig. 13.21, would be excluded by the use of the 96 percentile ranges of normal. Alternatively, in developing normal ranges, it might be reasonable to exclude highly trained athletes from a sample of healthy persons. On the other hand, when interpreting an ECG, it is necessary to be aware of the different ECG patterns that can be encountered in the so-called athlete's heart. In an editorial on the subject, Oakley [69] stated that "there is at present no published evidence to suggest that training-induced hypertrophy of whatever type represents anything other than cardiovascular fitness. If a positive diagnosis of cardiomyopathy cannot be made, the patient must be vigorously reassured that he has no abnormality." Indeed, Oakley's patients, many of whom had initially been advised to give up training prior to referral, were subsequently advised to restart training following a detailed investigation including cardiac catheterization.

Unusual, rather than abnormal, ECG findings in sportsmen have been well documented, for example, [68, 70]. On the other hand, some countries, particularly Italy, have been very keen to promote guidelines relating to screening of

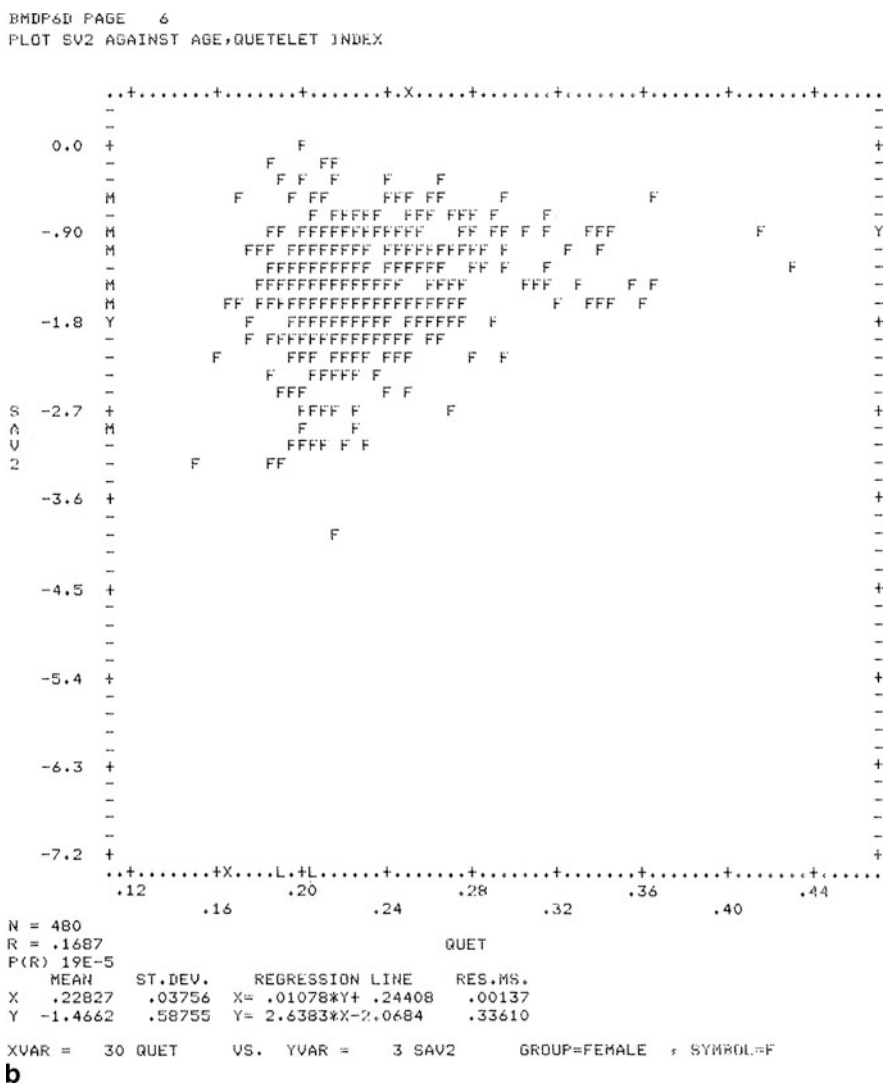

b

Figure 13.20b

Scattergram of S amplitude in V_2 versus the Quetelet index, shown for 480 females. Note that S amplitude is plotted as a negative number.

apparently healthy individuals prior to participation in sport. These have led to internationally approved guidelines [71] that involve ECG recording to exclude the presence of left ventricular hypertrophy as well as other adverse signs, such as the Brugada pattern (see Chap. 14) and long QT (see Chap. 19).

13.4.6 Heart Position

For many years, it was fashionable to describe an ECG as belonging to a particular category based on the orientation of the QRS axis which, in turn, was supposed to be related to the position of the heart. Wilson et al. in 1943 [72] described five positions of the heart on the basis of ECG appearances. These were horizontal, semihorizontal, intermediate, semivertical, and vertical. (They also mentioned a sixth indeterminate position.) An illustration of different positions is indicated in

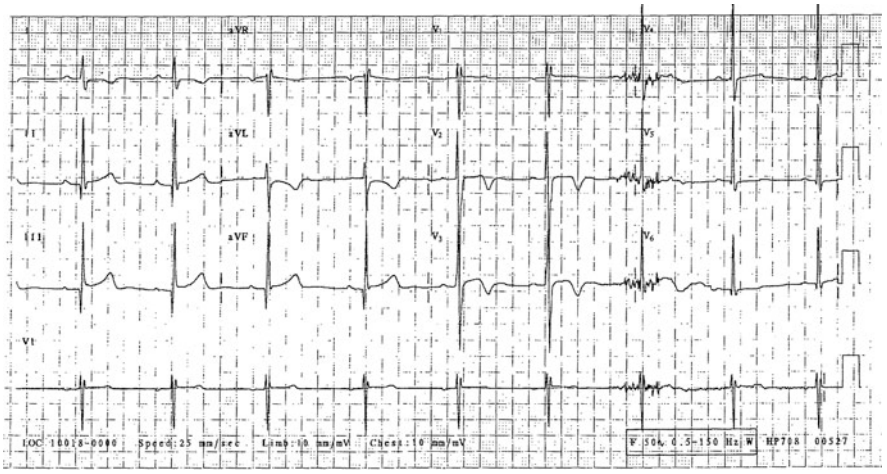

Figure 13.21

The 12-lead ECG from a 22-year-old healthy male athlete. Note the T-wave inversion in I, aVL, V_2, and V_3. There are also deep but narrow Q waves in the inferior leads. Both the echocardiogram and cardiac MRI scan were normal in this individual.

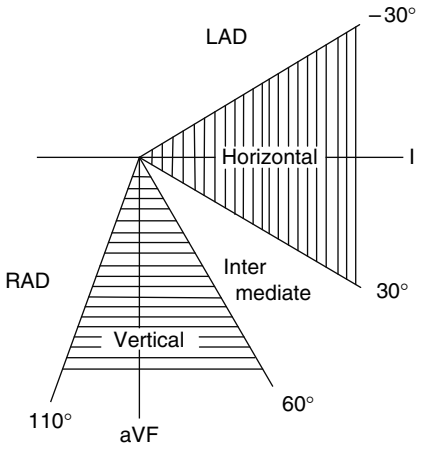

Figure 13.22

The division of the frontal plane into different regions depending on the orientation of the mean QRS vector. LAD, left axis deviation; RAD, right axis deviation.

Fig. 13.22. Later, Simonson [2] modified these by suggesting that the semihorizontal and semivertical positions could be omitted, hence leaving three categories. In essence, if the frontal plane QRS axis were oriented at 60° or more, the heart was said to be in the vertical position, whereas if it were superior to 30°, it was in the horizontal position. ECGs with a QRS axis between 30° and 60° were said to lie in an intermediate position. Such a definition relates to the QRS axis in the different leads although when the description was introduced at first, the definitions essentially related to QRS morphology. Thus, the horizontal heart had a dominant R wave in aVL similar to appearances in V_5 and V_6, while the QRS morphology in aVF resembled V_1 and V_2. On the other hand, in the vertical heart, there is a dominant R wave in aVF similar to V_5 and V_6, while the QRS morphology in aVL resembles that in V_1 and V_2.

A moment's reflection will show that there are bound to be statistically significant differences between R-wave amplitudes in aVF in patients with a vertical heart compared to those with a horizontal heart. However, these are of limited practical significance. What is probably of more value is the relation between the QRS and T axes in these groups.

Table 13.5

Labels of the three positional groups according to the direction of the frontal Q axis and characteristic features in the ECG

Label of positional group	Mean frontal Q axis	Number of Q waves in extremity leads	Q wave in aVL	Q wave in III
Q left	<0°	1–4	+	–
Q intermediate	0–90 °	5–6	±	±
Q right	>90°	1–4	–	+

For example, a T-wave axis around 0° is not uncommon in subjects with a horizontal heart, whereas in a patient with a vertical heart, such a T-wave axis is often regarded with much more suspicion. In other words, the QRS-T angle is larger in this latter situation. Lundh proposed a new classification system [3] for the normal ECG that included a knowledge of the heart position. His positional classification was based on the appearance of small Q waves in the limb leads, leading to the calculation of the so-called Q axis. The classification is based on the Q axes, as outlined in Table 13.5. Note that the presence of a small Q wave in aVL would correspond to a Q axis around −30° (opposite to conventional calculation).

He used this classification to determine different limits of normality for certain electrocardiographic parameters although the conclusion ultimately drawn was that further clinical work was required to prove that the system could be of diagnostic value.

13.5 The Normal Electrocardiogram

13.5.1 Evolutionary Development of the Electrocardiogram

Almost from birth onward, the ECG changes with time as the heart adapts to its new working environment. A number of significant changes occur over the first few days of life before the ECG settles for approximately the first year of life. Thereafter, as the individual continues to grow, the ECG also continues to change likewise until early adulthood when a period of regression of voltages sets in.

A number of authors (see Sect. 13.10) have been responsible for assessing normal limits of the pediatric ECG, and their results are presented in Appendix 2. In particular, Liebman [73] has contributed much to the field of pediatric electrocardiography and deals with this topic elsewhere in the book (Chap. 21). His data, particularly from orthogonal-lead ECGs in healthy children, have been incorporated into the Appendix 2 in this book and are gratefully acknowledged. Together with others, he has also published on ECGs in premature infants [74, 75].

Davignon et al. [76] have published data on the normal 12-lead ECG standards for infants and children. They have chosen to represent their data as a series of charts showing the percentile distributions of various amplitudes and durations versus age. All of these are presented in Appendix 2. With respect to the evolution of the ECG, it is helpful to study the R-wave amplitude in V_1, as shown in Fig. 13.23. Here, it can be seen that the upper 98% limit of normal is maximal during the first 3 days of life and, thereafter, steadily decreases over the first month until by the age of 1–3 months, its value is approximately 70% of that at birth. Over the next 12–16 years, this R-wave amplitude decreases to approximately 55% of its value at 1–3 months. Thus, the change in the upper limit of normal over the first month or two of life is almost as much as the change over the following 15 years.

Conversely, in keeping with a clockwise rotation of the cardiac axis in the horizontal plane over the first years of life, the R-wave amplitudes in the lateral leads increase over the first month and continue to increase more slowly thereafter.

The frontal QRS axis lies between 92° and 185° in 90% of newborn children [76], but by the age of 1–3 months, the corresponding range has altered considerably to 47°–105° (see Appendix 2). Similar findings have been reported by others [77].

Another important parameter is the T-wave amplitude in V_1. In newborns, this can either be positive or negative, although, by the end of 7 days, it is always negative according to the data of Davignon et al. [76]. By the age of 5 years, a small percentage of children exhibit negative T waves in V_1. In Davignon's study, the T-wave amplitude was always positive in V_2 in the 12–16 years age-group. However, it is known from other studies [78] that some adolescents have inverted T waves in V_1 and V_2, these appearances sometimes being known as the juvenile T-wave pattern.

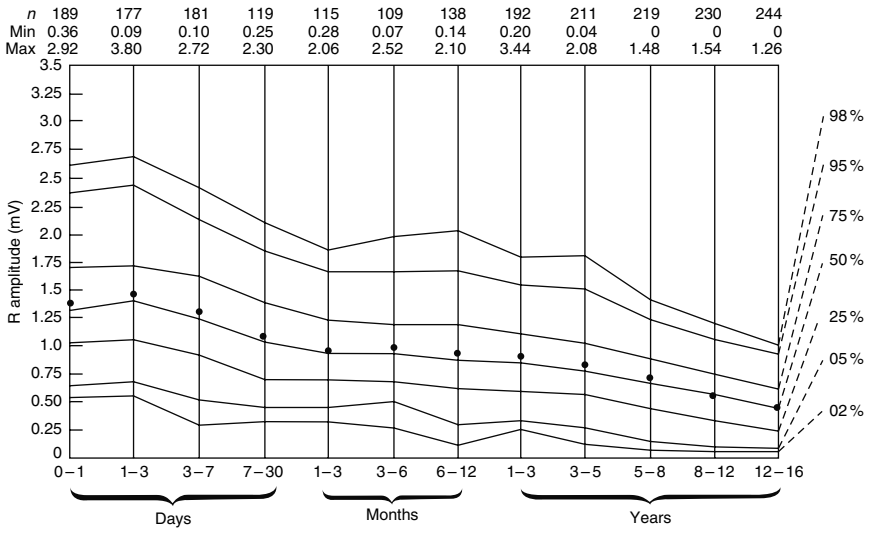

Figure 13.23

A distribution of the R-wave amplitude in V_1 from birth to 16 years of age. The various curves denote the different percentiles of the distribution, while the dots represent the mean values. (After Davignon et al. [76], © Springer, New York. Reproduced with permission.)

Our own study [79] of over 1,500 neonates, infants, and children found similar data, which are presented in detail for the first time in the Appendix 2. The group included 500 neonates whose ECGs were sampled at 500 samples/s compared to the 333 samples/s of Davignon [76]. These showed some very interesting findings, e.g., the variation in the S-wave amplitude in V_2 over the first 3 months of life (Fig. 13.24) and even a differing QRS duration between boys and girls from an early age (Fig. 13.25).

Other significant collections of ECGs from children are those of Rijnbeek et al. [80], where 1,912 ECGs from children aged from 11 days to 15 years were studied to provide normal ranges, and of Sun et al. [81], who recorded 1,166 ECGs in Chinese children. The normal ranges from Rijnbeek et al. tended to show similar trends to those from Glasgow [79], e.g., the QRS duration was slightly longer in boys compared to girls from about 1 year of age onward. Sun et al. [81] also compared ECG appearances in healthy Chinese infants to North American counterparts [81]. R amplitude in V_5 tended to be higher in North American children compared to Chinese children, but surprisingly, R amplitude in V_2 demonstrated the reverse.

The same evolutionary changes can also be seen in the VCG. In the frontal plane, the vast majority of all newborns show a QRS axis oriented vertically or to the right [82], and over the first month or two, it shifts counterclockwise so that the frontal axis is in the range 20°–120°, the prevalent direction being 80° [73]. Similarly, in the transverse plane, there is clockwise rotation of the main QRS vector over the first few months of life. The T vector in the newborn child in the transverse plane is tightly distributed between 130° and 168°, but by 3 days this range has expanded, being 90°–302° [82]. This corresponds to the development of T-wave inversion in V_1. Note, however, that the normal *XYZ*-lead ECG does not always have an upright T in *Z* (*Z* being directed positively to the back).

13.5.2 Examples of the Normal Electrocardiogram

This chapter has already stressed the variety of factors that affect the appearances of the ECG and by implication, the range of normality of ECG patterns. It should therefore be apparent that there is no one ECG or VCG that can be displayed as an example of normality. To this end, a series of ECGs recorded from apparently healthy individuals, including a newborn, is shown in Figs. 13.26–13.29. These ECGs have been selected to show the range of normality and to illustrate the influence of age and sex on ECG appearances.

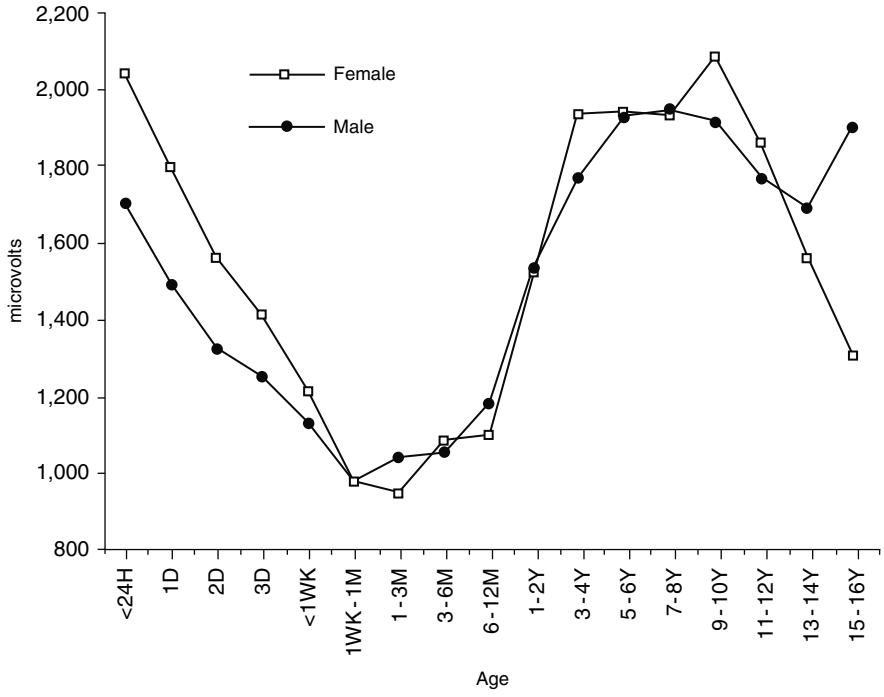

Figure 13.24

The mean S-wave amplitude in V_2 in 1,780 healthy neonates, infants, and children. Note that the scale is nonlinear. There is a remarkable loss of amplitude over the first few days of life followed by a recovery over the first decade. The amplitude then tails off in females around puberty. Reproduced from [79] with permission.

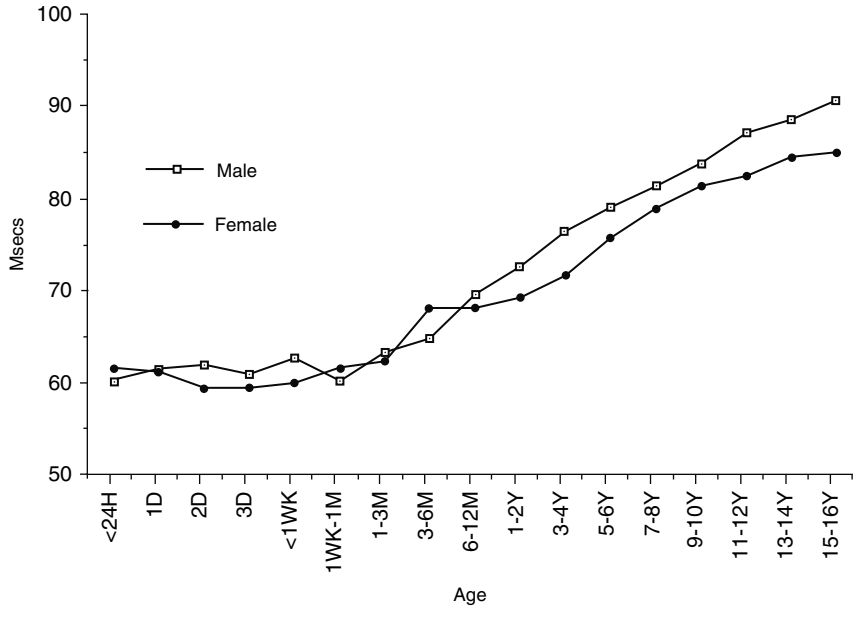

Figure 13.25

Mean QRS duration versus age in 1,780 healthy neonates, infants, and children. Note that the scale is nonlinear. There is a clear separation between males and females from around 1 year of age. Reproduced from [79] with permission.

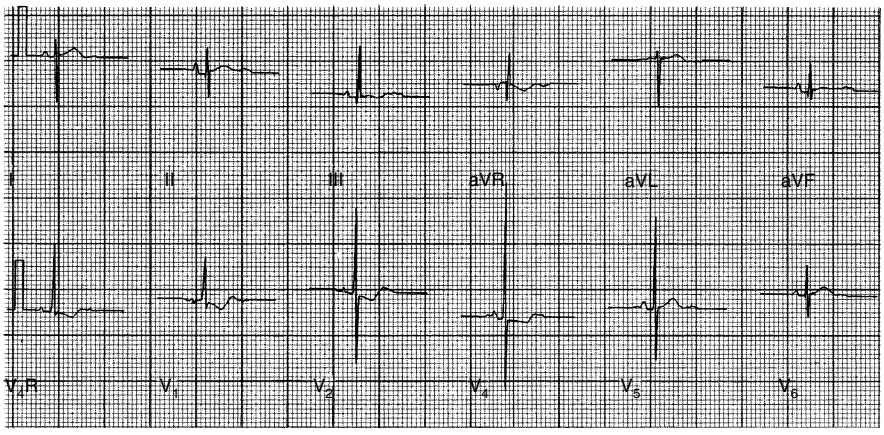

Figure 13.26

ECG from a 4-day-old baby girl. Note the dominant R wave in V_4 R and V_1 typical of the right ventricular preponderance pattern found in the healthy newborn. Average beats are presented.

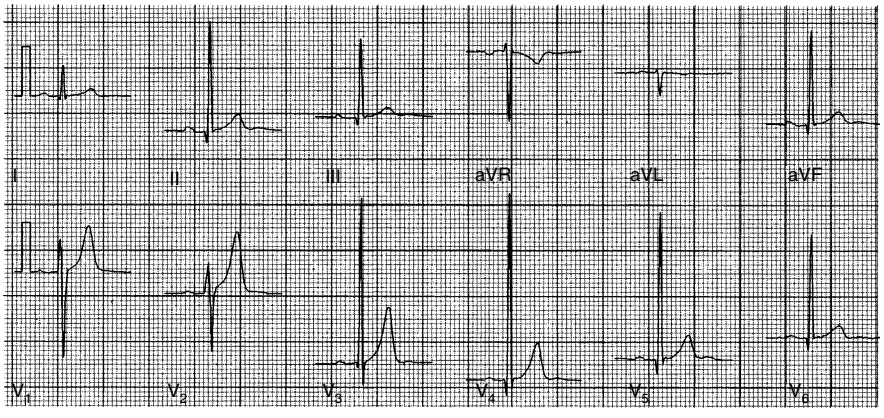

Figure 13.27

ECG recorded from a 35-year-old apparently healthy male. Note the marked change in appearances between V_2 and V_3, which, in this case, delineates the so-called transitional zone, which is the point where the rS complex changes to the Rs configuration. The QRS axis is 74°, and there is a vertical heart. Note how aVL essentially resembles the configuration in V_1 although there are gross amplitude differences. Likewise, aVF resembles V5 typically as in a vertical heart. Average beats are displayed.

For those readers who are relatively inexperienced in electrocardiography, it is sometimes of help to consider that there are only two basic QRST configurations that need to be remembered in the 12-lead ECG in order to differentiate between normal and abnormal. These two patterns and the leads in which they appear are shown in Fig. 13.30. As there is a certain amount of redundancy in the 12-lead ECG (see Chaps. 10 and 11), it is often helpful for the inexperienced electrocardiographer to consider analyzing only leads I, aVF, V_1, V_2, V_4, and V_5. Even the experienced electrocardiosgrapher will be surprised by the amount of information that can be obtained from only these six leads. With respect to this scheme, leads I, aVF, V_4, and V_5 tend to have the same pattern, whereas V_1 and V_2 have the other morphology, as shown in Fig. 13.29. The only exception to this simplified approach is in V_1 where the T wave may often be inverted.

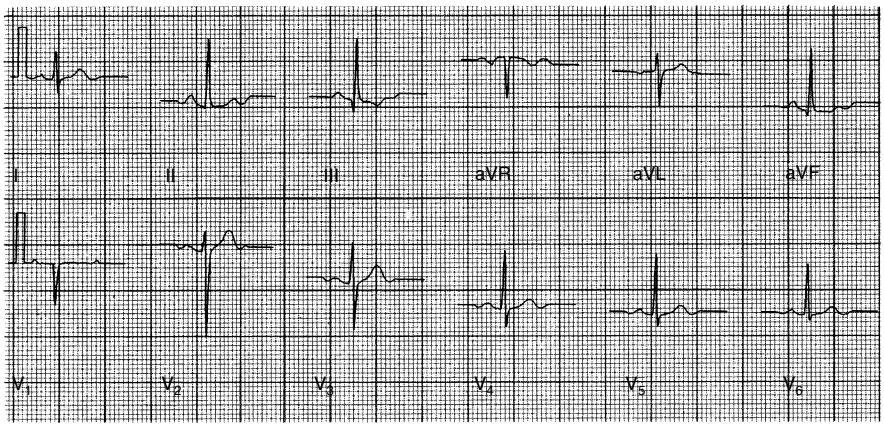

Figure 13.28
ECG recorded from a 34-year-old healthy female. Note the slight ST depression in several leads.

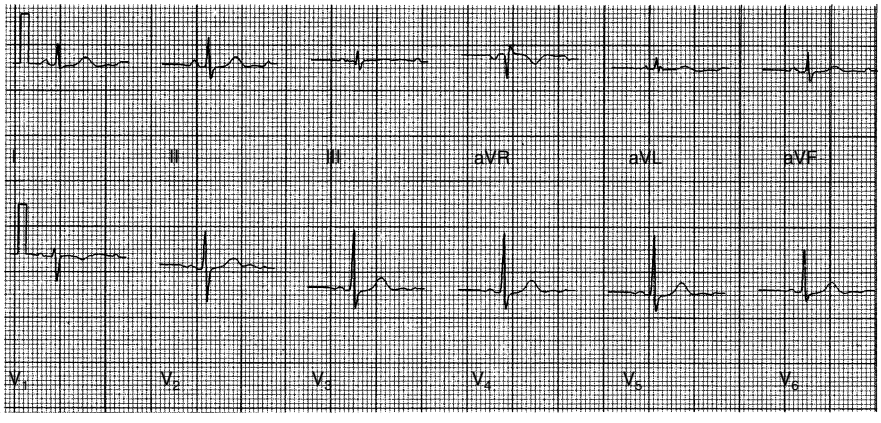

Figure 13.29
ECG recorded from a healthy 60-year-old female. Note the normal T-wave inversion in VI. The QRS axis is 25°, which suggests a horizontal heart. aVF approximately resembles V_1, while there is a small dominant R in aVL.

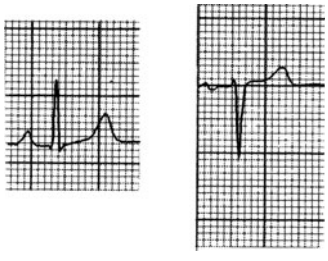

Figure 13.30
Two complexes typifying the principal types of morphology obtained in the normal ECG. The waveform shown on the left is typically found in I, aVF, V_4, and V_5, and the waveform on the right is generally seen in V_1 and V_2. They may, of course, be found in other leads, but the use of six leads for the beginner may be helpful. (See text for further discussion.)

13.6 The Normal Vectorcardiogram

13.6.1 Examples of the Normal Vectorcardiogram

The normal VCG also has a wide range of appearances. Some examples are shown in Figs. 13.31–13.33. In general, however, its appearance in the three different planes (see Chap. 11) can be summarized as follows.

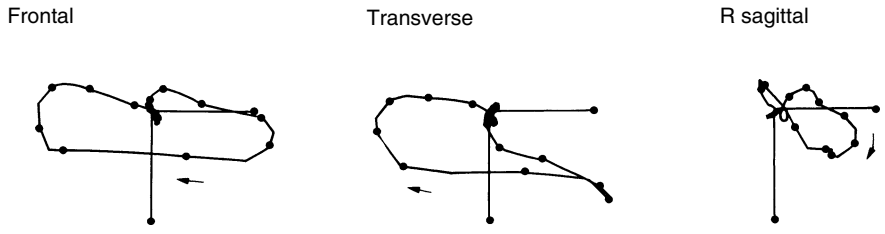

Figure 13.31
The VCG from the newborn whose 12-lead ECG is shown in Fig. 13.26. In this case, the VCG loops have been derived from the 12-lead ECG using the inverse Dower technique (see Chap. 11 for further details). All three loops show clockwise inscription of the (normal) QRS loop. The transverse loop indicates the almost total anterior displacement of the loop owing to normal right ventricular preponderance at this age. Dots are printed on the QRS loop at 4 ms intervals. (R sagittal denotes right sagittal plane.)

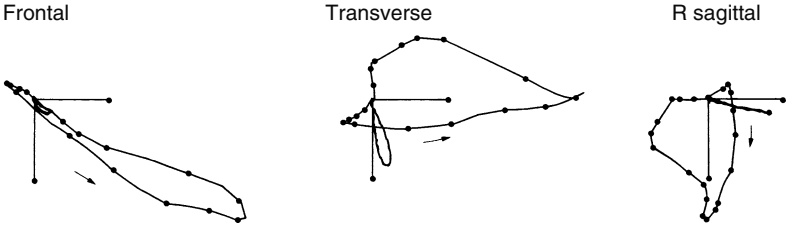

Figure 13.32
VCG corresponding to the 12-lead ECG of Fig. 13.27. The loops were derived using the inverse Dower technique. There is counterclockwise inscription of the QRS loop in the frontal and transverse planes and clockwise inscription of the R sagittal plane. The T-wave loop is prominent in the transverse plane being at one extreme of the normal range. Dots are printed at 4 ms intervals.

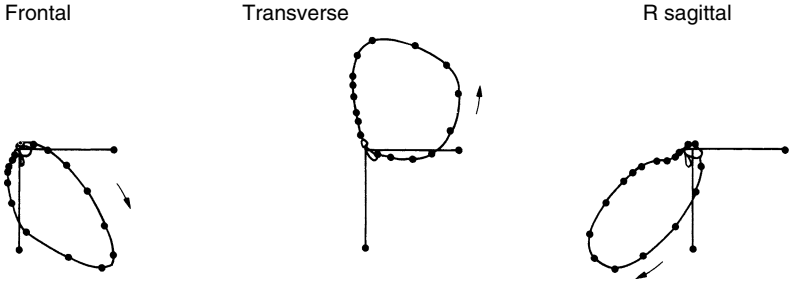

Figure 13.33
VCG corresponding to the 12-lead ECG of Fig. 13.28. The loops were derived using the inverse Dower technique. Note the openness of this type of normal VCG loop. Dots are printed at 4 ms intervals. In the frontal and R sagittal planes, the QRS loop shows clockwise inscription, and in the transverse plane, it shows counterclockwise inscription.

13.6.1.1 Frontal Plane

In the frontal plane, the P loop tends to be inscribed counterclockwise. On the other hand, the QRS loop can be inscribed either in a clockwise or counterclockwise direction. Chou and Helm [83] have suggested that about 65% of individuals have a loop that is inscribed in a clockwise direction. On average, the initial QRS vectors in the frontal plane are directed superiorly to the right, corresponding to small Q waves in *X* and *Y*. However, the absence of such small Q waves will alter the orientation of the initial vectors (the two are intimately related). For example, a Q wave in lead *X* *per se* means that the initial QRS vector is directed to the right, whereas a Q wave in lead *Y* means that the initial QRS vector is directed superiorly. There are therefore four possible combinations all of which can occur in the normal VCG.

The T loop in the frontal plane can be inscribed in either direction that need not necessarily be the same as that of the QRS loop. The maximum T vector is generally directed inferiorly to the left with a mean of around 35°.

13.6.1.2 Transverse Plane

The initial portion of the P loop in the transverse plane is always described in a counterclockwise direction. The whole loop may be similarly directed although there is often a figure-of-eight appearance. The maximum T vector can lie to either side of the *X* axis giving a wide range of normal values. The QRS loop is almost always inscribed in a counterclockwise direction in this plane. In a very small percentage of subjects, there may be a narrow figure-of-eight configuration where the initial part of the loop is inscribed in a counterclockwise direction with the early QRS vectors being oriented anteriorly. Likewise, the T loop is more often than not inscribed in a clockwise direction. Occasionally, however, the loop may be narrow, there being difficulty in determining an exact direction of inscription at least in one particular plane. In this case, the explanation is that the loop itself is essentially perpendicular to the transverse plane so that its projection produces a thin elongated loop.

13.6.1.3 Right Sagittal Plane

It is probably true to say that the right sagittal plane is utilized least of all by vectorcardiographers. The reason is that if appearances in the frontal and transverse planes are available, then the total information is already on display. However, the redundancy of information is often helpful in confirming impressions gained from other projections. In this plane, the P loop tends to be oriented vertically with the inscription always being clockwise. The QRS loop also has a generally inferior displacement and is usually inscribed in a clockwise direction. As with the transverse plane, the initial forces are directed anteriorly and either superiorly or inferiorly depending on the presence or absence, respectively, of a Q wave in lead *Y*. The T loop in this plane is also inscribed in a clockwise direction in most cases.

13.7 Normal Limits

13.7.1 Electrocardiographic Parameters

The methods of measuring ECG variables have already been discussed in Sect. 13.2.4. Before presenting and discussing the normal limits, it remains to describe in more detail the actual measurements to be tabulated. The principal measurements of the ECG waveform are outlined in Fig. 13.34. Note that these amplitudes and durations are referred to well-defined onsets and terminations of the component waves. In practice, as shown earlier in Fig. 13.10, the onset of the first wave in one lead need not necessarily coincide with the apparent onset in other leads. This leads to the concept of introducing isoelectric segments within the QRS complex, as shown in Fig. 13.11. The diagnostic significance of these segments has not yet been evaluated, but they have a relationship to vector orientations in a certain sense.

When computer analysis is available for the measurement of wave amplitudes and durations, it becomes feasible to make a number of additional measurements to assist in the characterization of a waveform. While the human eye at a glance may be able to say whether or not an ST segment is concave or convex upward, it requires several measurements

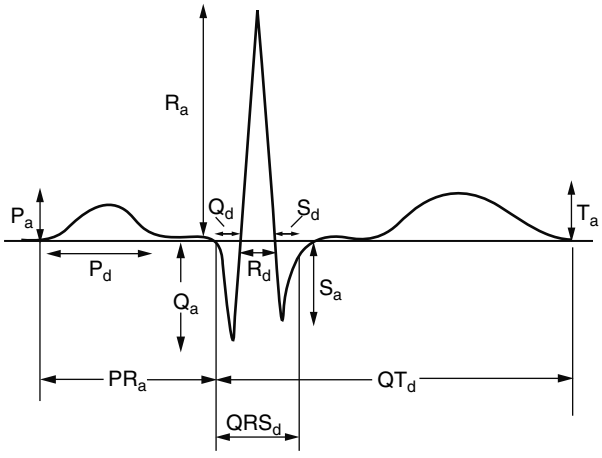

Figure 13.34

Various component amplitudes (subscript a) and durations (subscript d) normally measured by a computer program. Note that here the reference level for all amplitude measurements is the QRS onset.

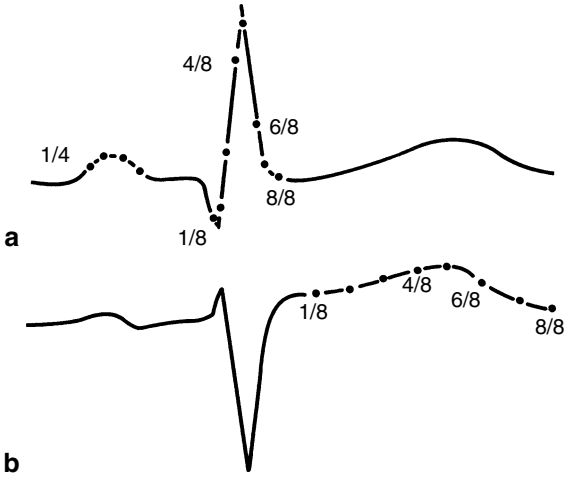

Figure 13.35

An illustration of time normalization of (a) the P wave, which is divided into four, and the QRS complex, which is divided into eight, and (b) the ST-T segment, which is divided into eight equally spaced intervals.

to establish this when using a computer program. For this reason, Pipberger and coworkers [32] introduced the concept of time normalization. With this approach, a component of the ECG such as the QRS complex can be divided into eight equal time intervals and the measurement made at the end of each of these. The ST-T segment can be dealt with in the same way. It was also subsequently suggested [84] that the P wave be divided into four equal time-normalized segments (Fig. 13.35). This approach has certain advantages, but it can suffer from errors in determining the onset and termination of the components.

Another approach for categorizing the P and ST-T segments is to use a simple classification dealing with the number of components – up to two – together with a sign indicating whether the first component is positive or negative. As shown in Fig. 13.36, the P or T waves can be negative–positive or positive–negative in configuration, giving a categorization −2 or +2, respectively. An upright T wave would be classed as +1, and an inverted T wave as −1. This simple approach can also be very helpful in automated interpretation.

Figure 13.36

A simplistic approach to classification of P waves or T waves depending on the number of components present and whether the first is positive or negative.

Table 13.6

Expressions for estimation of the magnitude and orientation of the projection of the maximum spatial vector onto the frontal, sagittal, and transverse planes. *X, Y*, and *Z* are the amplitude values of leads *X, Y*, and *Z* at the instant the maximum spatial vector occurs

Plane	Magnitude	Orientation
Frontal	$(X^2 + Y^2)^{1/2}$	$\tan^{-1}(Y/X)$
Right sagittal	$(Y^2 + Z^2)^{1/2}$	$\tan^{-1}(-Y/Z)$
Left sagittal	$(Y^2 + Z^2)^{1/2}$	$\tan^{-1}(Y/Z)$
Transverse	$(X^2 + Z^2)^{1/2}$	$\tan^{-1}(-Z/X)$

The use of the VCG leads to many new parameters. While time normalization has been introduced for the measurement of scalar amplitudes, it can, of course, be carried over to vectorcardiography on a one-to-one basis so that vector magnitudes and orientations at 1/8, 2/8, QRS, and so on can be determined. In vectorcardiography, it has also been a custom to measure vector amplitudes and orientations at 10 ms intervals following QRS onset and prior to QRS termination. Such parameters are known as the 0.01 s QRS vector, the −0.01 s QRS vector, and so on.

The various vector amplitudes can be described in a number of ways. The amplitude of a vector is calculated simply from the following equation:

$$(X^2 + Y^2 + Z^2)^{1/2}$$

where *X, Y*, and *Z* represent the amplitude of each of the leads *X, Y*, and *Z* at a particular instant in time (see Chap. 2). It is clear that the leads must be recorded simultaneously to ensure perfect time alignment. While this expression can be used to calculate the maximum spatial vector, there are a number of other possibilities that arise. For example, with the use of the three planes described previously, it becomes possible to estimate the magnitude and orientation of the projection of the maximum spatial vector onto each of these three planes. This can be obtained from the expressions in Table 13.6.

Other parameters sometimes utilized are those such as the half area vector, that is, the vector that divides the spatial loop into two equal areas. The direction of inscription of the loop can be calculated mathematically from the cross product of two vectors:

$$\vec{C} = \vec{A} \times \vec{B}$$

where $\vec{C}$ is a vector pointing either upward or downward, depending on whether the rotation of the vector between *A* to *B* is clockwise or counterclockwise, respectively. One final parameter of interest in dealing with the VCG is known as spatial velocity [85].

In some ways, this term is a misnomer in that it is supposed to represent the rate of movement of the tip of the cardiac vector through space, whereas the following equation for spatial velocity, SV, demonstrates that this is not actually the case.

$$\mathrm{SV} = \frac{1}{\Delta t}[(\Delta X)^2 + (\Delta Y)^2 + (\Delta Z)^2]^{1/2}$$

where ΔX is the change in amplitude of X in time Δt, etc.

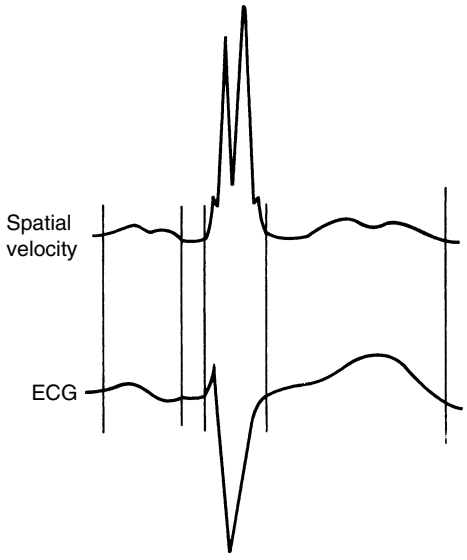

Figure 13.37
A typical curve of spatial velocity and its time relationship to the ECG.

A simplified estimate [86] of this measurement is given by the following equation, which is much more suited to rapid execution on a computer:

$$SV = \left|\frac{\Delta X}{\Delta t}\right| + \left|\frac{\Delta Y}{\Delta t}\right| + \left|\frac{\Delta Z}{\Delta t}\right|$$

Whichever equation is used, the appearance of the spatial velocity is as shown in Fig. 13.37. Through the years, there have been various publications [87, 88] that have suggested that the spatial velocity is of some help in discriminating between the different diagnostic classifications. In the main, however, it has tended to be used recently within computer programs in order to define the onset and termination of various ECG wave components. It has undoubted value in identifying parts of a vector loop where inscription slows. This would be found, for example, in the latter part of the QRS complex in an RBBB, where descriptive terms such as terminal slowing of the QRS inscription would be utilized.

13.7.2 P Wave

The normal limits of the P-wave amplitudes in various leads are as shown in Appendix 1. There are no statistically significant differences between mean P-wave amplitudes in men and women. In general, there is little tendency for the upper limits of the P-wave amplitude to decrease with increasing age in adults, as illustrated for lead II in Fig. 13.38. Of some interest may be the P terminal force in V_1, sometimes known as the Morris index [89], which is used in some diagnostic criteria such as the Romhilt-Estes criteria for LVH (see Chap. 15). Table 13.7 shows the normal limits for this estimate which does have a higher upper limit of normal in men compared to women.

It can also be seen from Appendix 2 that the P-wave amplitude in children in lead II, for example, varies very little between birth and 16 years of age and the upper limit of normal remains essentially static at 0.25 mV during this period.

The duration of the P wave is sometimes used in determining whether there is an abnormality of the left atrium. The normal P wave may often have two components, i.e. it may exhibit an M-shaped complex, and in general terms it has a duration that is less than 0.12 s (Table 13.7). A duration beyond this may possibly arise from the left atrial enlargement, causing a delay in the depolarization of the left atrium, or else from an intra-atrial conduction abnormality (see Chap. 14). Thus, in the presence of broad P waves, there is a tendency to diagnose a left atrial abnormality, that

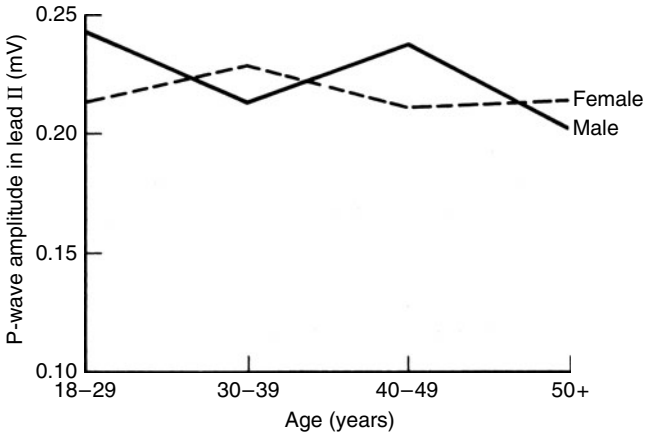

Figure 13.38

The normal upper limit of the P-wave amplitude in lead II. Clearly, there is no age or sex dependence.

Table 13.7

Mean ± standard deviations and 96% range of P terminal force in V_1 and P-wave durations

		P terminal force (mV ms)			P-wave duration (ms)		
Age-group	Sex	No of subjects (*n*)	Mean ± SD	96% range	No. of subjects (*n*)	Mean ± SD	96% range
18–29	Male	265	1.09 ± 1.33	0.00–4.62	266	103.0 ± 14.2	72 – 128
	Female	316	0.75 ± 1.03	0.00–3.54	318	99.0 ± 12.7	70 – 122
30–39	Male	219	1.61 ± 1.21	0.00–3.94	221	105.0 ± 12.3	78 – 130
	Female	118	1.02 ± 1.25	0.00–4.29	118	99.0 ± 11.6	72 – 122
40–49	Male	117	1.49 ± 1.44	0.00–4.42	119	106.0 ± 11.2	84 – 128
	Female	73	1.57 ± 1.40	0.00–5.50	73	104.0 ± 12.9	78 – 128
50+	Male	125	1.47 ± 1.44	0.00–5.45	125	110.0 ± 10.5	86 – 134
	Female	79	1.42 ± 1.37	0.00–4.05	80	106.0 ± 9.5	88 – 126

is, a nonspecific interpretation is made. There is a small increase in the P-wave duration with increasing age both in men and women (Table 13.7), but this is of limited practical significance.

13.7.3 P Vector

The normal limits of the P-vector amplitude are shown in Appendix 1. In general terms, the P-vector loop is small and difficult to analyze, so there is not much additional benefit to be gained from the VCG in terms of the diagnostic value of the P wave.

13.7.4 QRS Complex

The means, standard deviations, and upper and lower limits of normal are set out in the various tables and illustrations in the Appendices. The scalar data relating to children have been taken from the work of Liebman [73] and Davignon et al. [76] as well as from the authors' lab. By way of explanation, a further illustration (Fig. 13.39) dealing with the Q-wave amplitude in V_5 is reproduced for illustrative purposes. The graphs depict the percentile ranges of the Q-wave

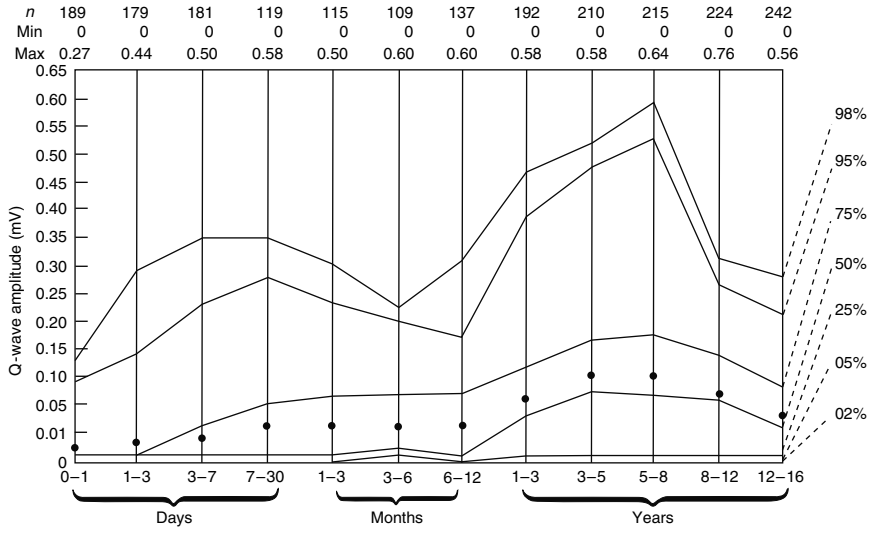

Figure 13.39

The distribution of the Q-wave amplitude in V_5 in normal infants and children from birth to 16 years of age. In broad terms, the Q-wave amplitude increases to a maximum at 5–8 years before decreasing again. Note the scale is nonlinear. (After Davignon et al. [76]. © Springer, New York. Reproduced with permission.)

amplitude from birth to 16 years of age. The upper 98 percentile graph indicates the values within which 98% of the population studied had their Q-wave amplitude; for example, in the age-group 5–8 years, 98% of the 215 children studied had a Q wave in V_5 that was less than 0.60 mV. On the other hand, the lower 2 percentile curve indicates the value above which 98% of the groups studied had a Q-wave amplitude. Thus, in the same age-group of 5–8 years, there were 75% of the children who had a Q wave that was discernible. Within the meaning of 96 percentile ranges as discussed above, the 2 percentile and 98 percentile lines contain the 96% range of the amplitudes. Thus, these values can be regarded as the lower and upper normal limits of the range. The actual maximum value recorded in the study from which the graph was drawn was 0.65 mV for the age-group of 5–8 years. It should be noted that the mean value for the same group was 0.1 mV, which emphasizes the point previously made that the distribution of ECG measurements tends to be skewed, that is, it is not symmetrical about the mean. It is of importance to note that a Q wave in V_5 in excess of 0.5 mV is found in 5% of apparently healthy children in the above age range. In general terms, R-wave amplitudes tend to decrease with increasing age in children in the right precordial leads, whereas, as would be expected, they tend to increase in the left precordial leads.

Table 13.8 summarizes some of the sex differences in R-wave amplitudes found by Davignon et al. in the age-group of 12–16 years. These data would tend to confirm findings of the authors' study, for example, where highly significant differences between men and women were found in the precordial leads.

From about the end of the first month of life, the R/S ratio in V_1 begins to decrease from an upper limit of approximately seven toward the adult value of approximately one. By the age of 5 years, the upper limit of normal has reduced quite considerably to a value of two. It is, of course, still very relevant to bear this in mind when interpreting ECGs from children. The data of Liebman and colleagues are also reproduced in Appendix 2. These show in numerical form the various limits of normality as determined manually from different groups of children. The same general trends can be seen both from the numerical and the graphical representation of results: scalar and vector data are presented.

The normal ranges of the adult ECG will be discussed mainly with respect to the authors' own data gathered from a study of apparently healthy individuals in Glasgow, as described in Sect. 13.2.1. The results presented mainly in Appendix 1 in numerical form have been derived from computer analysis of the ECG, where all leads were recorded simultaneously. Means, standard deviations, and 96 percentile normal ranges are presented for different age-groups that are also stratified according to sex. In order to compress some of the findings for the purposes of discussion, the upper

Table 13.8

Sex differences in R-wave amplitudes in the age-group 12–16 years. Mean values (mV), standard deviations (SD), and percentile limits are listed separately for 105 boys and 142 girls. D denotes the amplitude difference between the sexes

Lead	Sex	Mean	Standard Deviation	Percentile limit				
				02%	05%	50%	95%	98%
aVR	female	0.11	0.11	0.00	0.01	0.09	0.35	0.40
	Male	0.13	0.12	0.00	0.01	0.12	0.37	0.42
	D	0.02 NS[a]						
aVL	Female	0.23	0.18	0.01	0.03	0.18	0.62	0.70
	Male	0.23	0.20	0.01	0.02	0.19	0.60	0.86
	D	0.00 NS						
aVF	Female	0.96	0.33	0.27	0.35	0.95	1.53	1.66
	Male	1.05	0.41	0.17	0.33	1.06	1.73	2.04
	D	0.09 NS						
V_1	Female	0.37	0.23	0.01	0.04	0.35	0.85	0.96
	Male	0.44	0.25	0.02	0.05	0.42	0.94	1.03
	D	0.07[b]						
V_2	Female	0.92	0.36	0.28	0.36	0.87	1.63	1.72
	Male	1.11	0.40	0.23	0.44	1.11	1.79	1.94
	D	0.19[c]						
V_4	Female	1.76	0.57	0.61	0.76	1.74	2.79	3.32
	Male	2.58	0.72	1.11	1.36	2.55	3.81	3.94
	D	0.82[c]						
V_5	Female	1.66	0.50	0.63	0.83	1.63	2.73	2.99
	Male	2.40	0.60	1.09	1.29	2.41	3.39	3.47
	D	0.74[c]						
V_6	Female	1.23	0.30	0.59	0.72	1.22	1.78	1.91
	Male	1.58	0.40	0.80	1.01	1.59	2.23	2.41
	D	0.35[c]						

[a] Nonsignificant difference
[b] $p < 0.05$
[c] $p < 0.0001$

limits of normal for various measurements and different age-groups have been amalgamated into graphs following the style of Simonson [2]. In addition, the limb leads have been, on occasion, treated similarly, and the continuity of sequence in the limb-lead axes, namely aVL, I, −aVR, II, aVF, and III is maintained as shown in Figs. 13.40–13.42. The presentation of scalar leads in this sequence was suggested by Cabrera [90] and is favored by many Europeans, particularly in Scandinavia. This presentation was also used by Lundh in his illustrations [3].

The upper limits of normal voltage for the QRS complex in the precordial leads decrease with increasing age. This is more evident for males than it is for females. Conversely, in the limb leads, the upper limit of normal in the lateral leads I and aVL remains stable although the mean value increases with age, which is in keeping with the rotation of the mean QRS axis superiorly in the frontal plane. This corresponds to the upper limit of normal of the frontal plane QRS axis shifting from −10° to −30° as age changes from young adulthood to middle age. A corollary of this is that the R-wave amplitude in aVF decreases with increasing age.

The sum of the S-wave amplitude in V_1 plus the R-wave amplitude in V_5 (one of the Sokolow and Lyon criteria [91] for LVH) is often used by electrocardiographers. The illustration of Fig. 13.43 shows that in apparently healthy young males, the index can have an upper limit of 5.0 mV. Thus, the commonly used threshold of 3.5 mV for LVH would be somewhat nonspecific if applied to younger individuals.

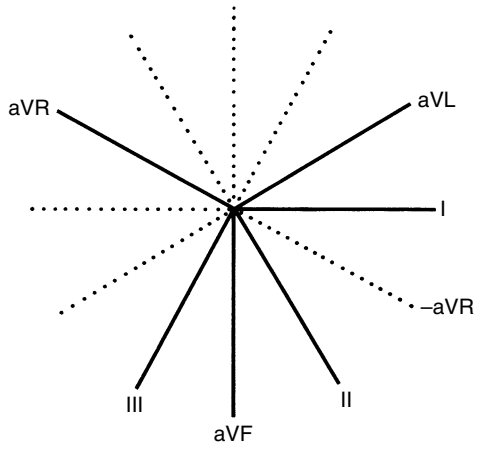

Figure 13.40
The hexaxial lead system showing the relationship of aVR, that is, an inverted aVR to the other limb leads.

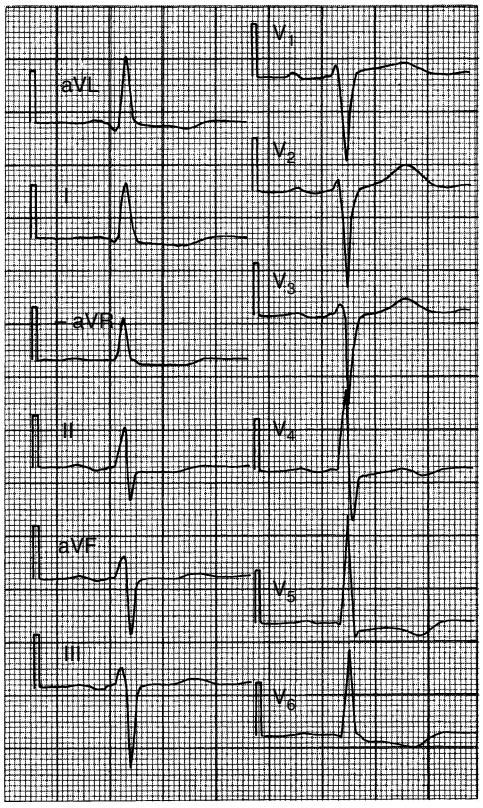

Figure 13.41
A 12-lead ECG displayed using the format suggested by Cabrera. All 12 leads were recorded simultaneously. Note the presence of aVR and the sequence of the limb leads in keeping with the order of the lead axes, as shown in Fig. 13.40.

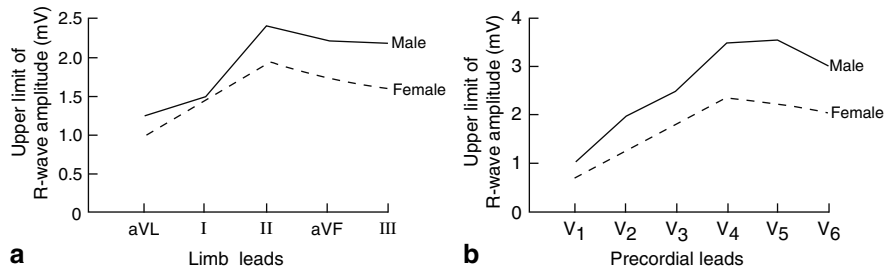

Figure 13.42

The upper limit of the R-wave amplitude in (a) limb leads and (b) precordial leads derived from apparently healthy individuals aged 18–29 years inclusive. Note the large differences between upper limits for males and females.

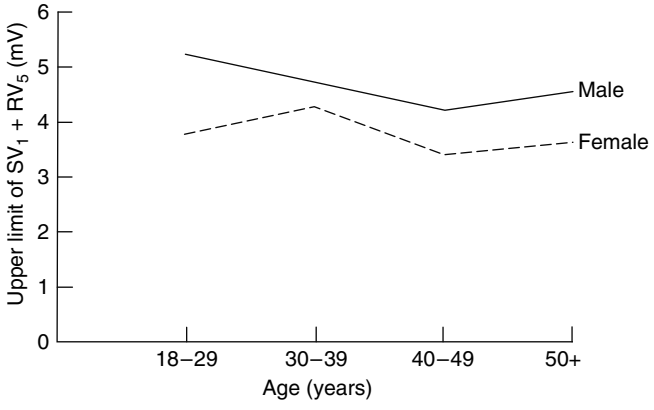

Figure 13.43

The upper limit of normal of the Sokolow and Lyon index [91], that is, $SV_1 + RV_5$, for males and females, as derived from the Glasgow data. Note in particular how this exceeds the classically used limit of 3.5 mV, particularly in males.

13.7.5 Additional Chest Leads

The use of right-sided chest leads (V_4R, for example) in adults has been confined to diagnosing right ventricular hypertrophy (RVH) and, more recently, right ventricular involvement in inferior myocardial infarction. Data on normal limits of such leads are sparse, but Andersen et al. [92] studied 109 subjects without evidence of heart disease in order to derive data on leads V_3R–V_7R. The R-wave amplitude and ST junctional deviation are presented in Table 13.9.

Additional data can be found in the Appendices. Reddy et al. also published a short note on the normal limits of V_7–V_9 [93]. More recently, in our own lab, normal limits of additional chest leads V_7–V_9 as well as V_3R–V_6R were derived from 200 adults [94]. In broad terms, an upper limit of 0.05 mV for the ST_j amplitude is applicable in all such leads except for males in V_3R and V_4R where 0.1 mV is a more specific limit to apply. This work led to such recommendations in a recent guidelines paper [95]. A typical set of waveforms from six simultaneously recorded right-sided chest leads is shown in Fig. 13.44. In children, V_4R is used widely even up to adolescence, while some centers also use V_3R.

The availability of computer methods for the estimation of durations has probably not been capitalized on to any great extent so far. Figure 13.45 shows the normal range of Q-wave durations in aVF for 1,334 adults in our series. From this, it can be seen that the 96 percentile upper limit of normal is approximately 25 ms for males and a little less for females. Conventional criteria [96] for interpreting Q-wave durations normally utilize 30 ms or even 40 ms Q waves. This, of course, is a reflection on manual methods of measurement, and our new data would suggest that, together with other signs of myocardial injury, such as ST- or T-wave change, a Q-wave duration in excess of 25 ms would provide reasonable

Table 13.9

Mean and 95% ranges of r, S, and r′ amplitudes in right precordial leads

	Median	95% fractile values	Mean $\bar{x}$	Range	Number n
r-wave amplitude (mm)	V_3R 1.5	0.4–3.9	1.7	0.1–4.3	107
	V_4R 1.0	0.3–3.3	1.2	0.2–4.2	101
	V_5R 1.0	0.3–2.4	1.0	0.2–5.0	79
	V_6R 0.7	0.2–2.6	0.9	0.2–5.1	59
	V_7R 0.5	0.3–3.6	1.0	0.3–5.6	37
S-wave amplitude (mm)	V_3R 5.1	1.7–11.4	5.7	0.9–13.5	108
	V_4R 3.6	1.1–8.0	3.9	0.9–9.7	104
	V_5R 3.6	1.0–7.7	3.5	0.5–8.8	89
	V_6R 2.5	0.7–6.4	2.9	0.4–7.3	70
	V_7R 2.7	0.8–5.4	2.8	0.7–6.8	45
Secondary r-wave (qr, rSr′) amplitudes (mm)	V_3R 0.8	0.5–1.5	0.9	0.4–1.5	6
	V_4R 0.7	0.2–1.8	0.8	0.2–1.8	11
	V_5R 0.8	0.3–2.5	1.0	0.2–2.5	36
	V_6R 0.9	0.3–3.6	1.3	0.2–4.2	50
	V_7R 0.9	0.3–3.6	1.2	0.1–4.8	71

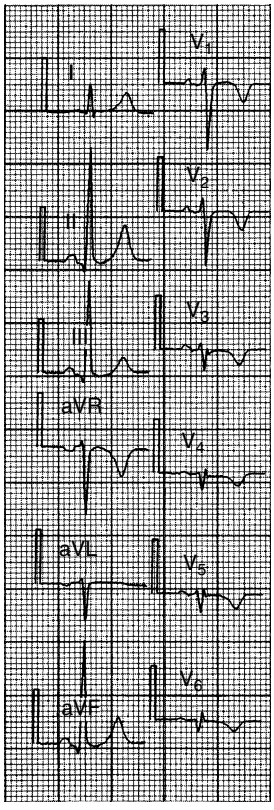

Figure 13.44

Six simultaneously recorded right-sided chest leads are shown together with the limb leads. These were recorded from a healthy 45-year-old male. Note that the labels V_1–V_6 are equivalent to V_2, V_1, V_3R–V_6R.

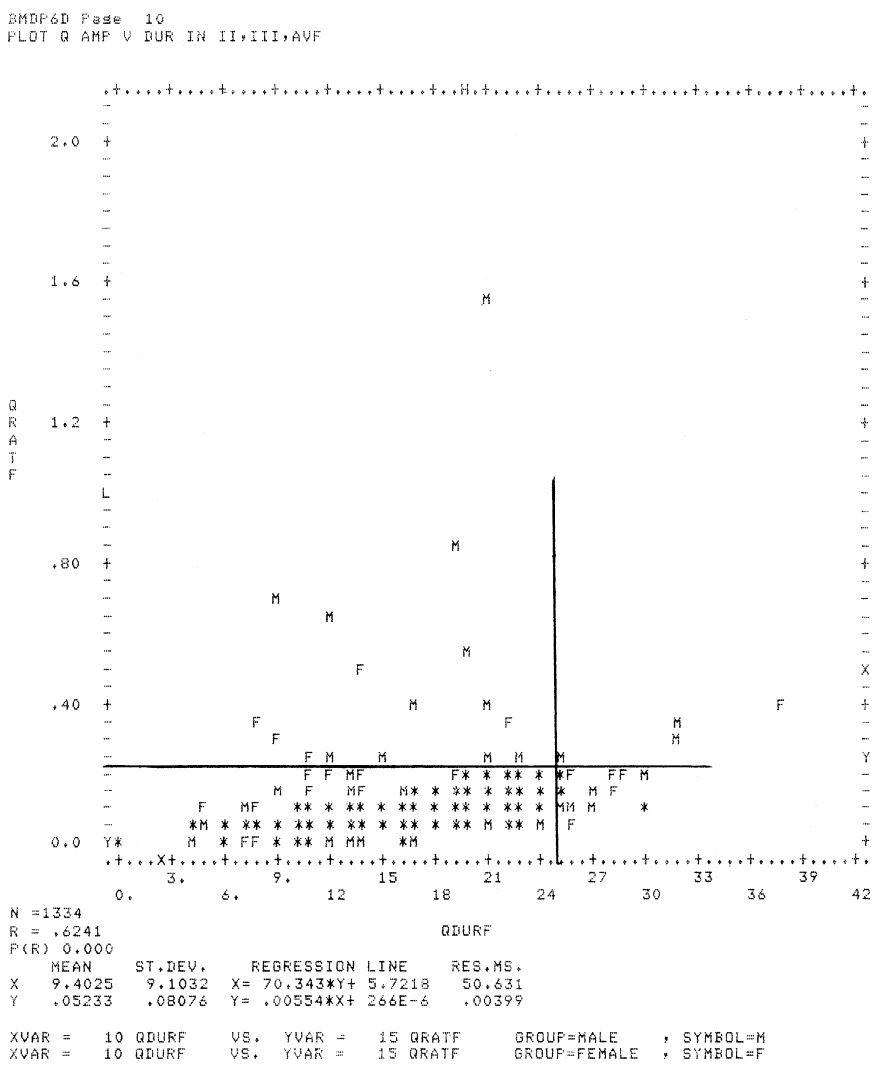

Figure 13.45

Scattergram of Q duration in aVF against the Q/R ratio in aVF for 1,334 adults in the Glasgow study. The 96 percentile limits for each are shown, that is, the bottom left-hand square contains the normal values. M, male; F, female; *, more than one value at the same point on the plot.

grounds for suggesting that myocardial infarction was present. The same figure shows that the upper limit of normal Q:R in aVF is almost exactly 1:4.

The significance of a Q wave in V_1 has been the matter of some controversy. The authors' data show that many apparently healthy individuals (1.42%) have a Q wave in V_1, while 0.67% have a Q wave in both V_1 and V_2. On the other hand, Lundh [3] raised the question of whether the Q wave in V_1 might be related to the presence or absence of a Q wave in V_6. He suggested that a Q wave in V_1 in the absence of such a wave in V_6 was abnormal. The authors' own normal data suggests that this finding has a specificity of 100%.

The effect of race on QRS amplitudes has already been mentioned in Sect. 13.4.3. In this respect, there has been a dearth of large-scale studies on which to confirm the findings. Data available from studies on 1,329 Japanese [97] are presented in Appendix 1. In this study, published in 1963, data were measured by hand and 100% ranges were quoted. A search of the literature has revealed no substantial publications dealing with studies on South Asians, while other studies

on Chinese individuals [56, 59, 98, 99] have suggested that there may be a modest difference between such populations and Caucasians with respect to QRS amplitudes and some other measures. This would tend to be at variance with the larger studies on Japanese individuals.

13.7.6 QRS Loop

The various limits of normal for the QRS vectors are detailed in the Appendices. These include many of the measurements that have been discussed above, but it should be noted that the tables are, on occasion, taken from studies where different lead systems have been used. In each case, the description of the lead system has been clearly indicated, and details of the different lead systems can be found in Chap. 11. The evolution and normal appearances of the VCG have been discussed in Sect. 13.6. It must be obvious that the comments relating to age and sex differences of the ECG also apply to the VCG. The variation of the normal limits of the T-vector magnitude with age and sex are shown in Fig. 13.46. Again, it can be seen that the vector magnitude decreases with increasing age and, in general, is lower for women than men. The maximum T vector in the transverse plane also shifts anteriorly with increasing age, whereas the mean T-vector projection onto the frontal plane tends to be stable around 40° once the adult pattern develops.

The normal limits of maximum spatial velocity are shown in Fig. 13.47 where a typical normal curve is also contrasted with the curves of spatial velocity in patients with different clinical abnormalities. Sano [87] in particular laid great stress on the value of spatial velocity, although this was never confirmed by others. The work of Macfarlane et al. [88] suggested that although there was undoubtedly variation in spatial-velocity curves between one group of patients and another, these did not lead to improved diagnoses. In other words, since the spatial velocity is a derivative of other leads, the information contained therein should also be available in the original waveforms.

13.7.7 ST-T Wave

The interpretation of the ST-T wave is one of the most difficult aspects of electrocardiography, and it should therefore be based on a thorough knowledge of the normal limits of this component of the ECG. The ST amplitude is normally measured at the end of the QRS complex, although, in certain instances, such as for exercise testing, a point 60 or 80 ms after the end of the QRS is now commonly used. For the purposes of this chapter, however, the ST junction will be regarded as the end of the QRS complex.

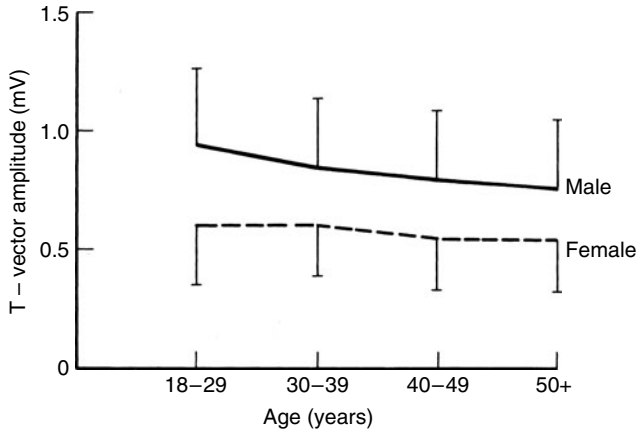

Figure 13.46
Mean and standard deviation of the T-vector amplitude in males and females in the Glasgow study. There is little variation with age but significant differences with respect to sex.

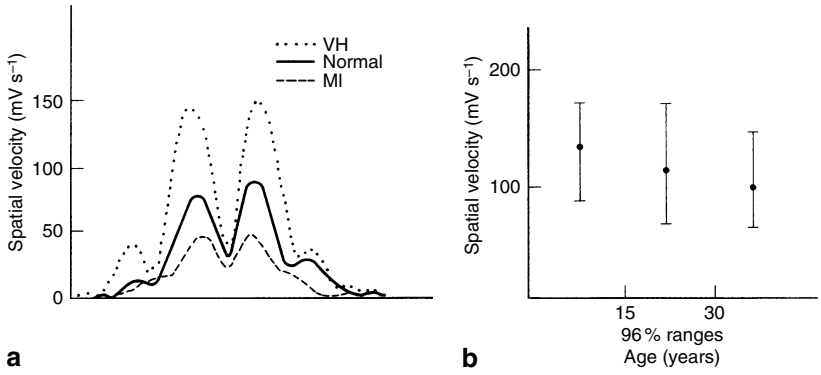

Figure 13.47

(a) Representative curves of spatial velocity from a patient with ventricular hypertrophy (VH), another with myocardial infarction (MI) contrasted with a normal curve. (b) Means and 96 percentile ranges of spatial velocity from 265 healthy individuals, including 18 under 15 years of age, 94 under 29 years of age, and 153 aged 30 and over. (See [88] for further details.)

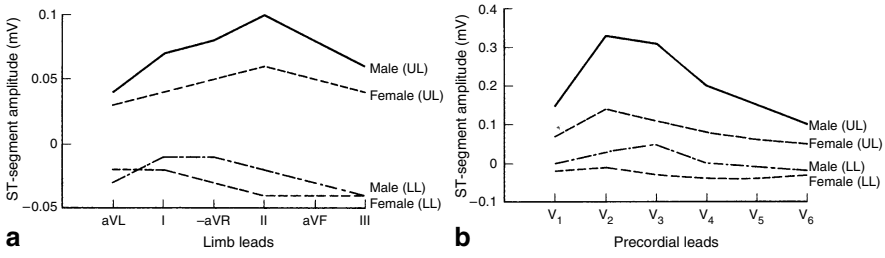

Figure 13.48

The upper and lower limits of ST amplitude for apparently healthy males and females: (a) limb leads and (b) precordial leads. Note the considerable sex differences in the upper limits (UL) and the more negative lower limit (LL) of ST depression in females, particularly in the limb leads.

Data on ST amplitude variation in children is sparse, though our own data in Appendix 2 present tables of normal limits of ST amplitude in this age-group. As expected, the upper normal limit of ST amplitude is generally under 0.1 mV in most leads, though it is higher in some precordial leads.

In general terms, in adults, with the exception of aVR, the ST segment amplitude would be expected to be in excess of −0.05 mV when the heart rate is less than 100 bpm. In the limb leads, there is a small difference of the order of 30 μV in the upper limit of normal ST amplitude between men and women (Fig. 13.48) and a small difference with respect to age (Fig. 13.49a). On the other hand, in the precordial leads, there are highly significant differences between men and women and there is a tendency for the ST amplitude to decrease with increasing age particularly for males in the anteroseptal leads V_2–V_4. Some of these changes can be seen in Fig. 13.49b. The increased ST amplitude in young men in particular is sometimes related to increased vagal tone (vagotonia) and is of no particular significance. It is always associated with a normally shaped ST-T complex in healthy young individuals. There are significant differences between males and females in ST amplitudes in the precordial leads, and also there are significant differences between leads, for example, the upper limit of normal ST amplitude in males in V_1 is twice the upper limit in V_2 both in males (Fig. 13.49c) and females (Fig. 13.49d). This implies that criteria for acute myocardial injury should not be the same in V_1 and V_2.

ST amplitudes of up to 0.1 mV can be found in apparently healthy individuals in the inferior and lateral leads. Sometimes this pattern is referred to as early repolarization. This is often accompanied by a small notch at the end of the QRS complex, particularly in the precordial leads [100]. On occasion, it may be difficult to ascertain whether the ST elevation in a young person is a result of some other abnormality, such as pericarditis, as opposed to being a normal variant.

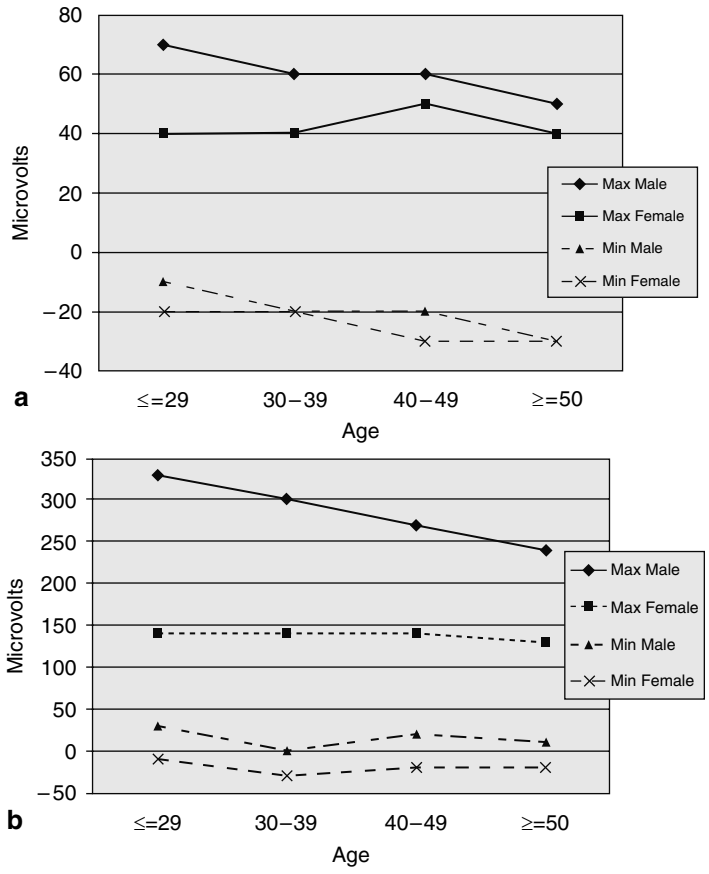

Figure 13.49a, b

(a) Upper and lower limits of normal ST amplitude in lead I in Caucasian men and women. (b) Upper and lower limits of normal ST amplitude in V_2 in Caucasian men and women. Note the very significant difference in the upper limit of normal between males and females, particularly in the younger age-groups. (Reproduced with permission from J Electrocardiol 2001; 34(Suppl): 235–41.)

In such situations, the extent of the ST elevation has to be considered, it being generally more widespread when associated with an abnormality such as pericarditis [101].

It should also be noted that race can influence ST amplitude. Our own data on Chinese and Caucasian normals [56, 58] showed minor differences only, but our most recent work together with Dr. Ibraheem Katibi from the University of Ilorin in Nigeria [55] shows that black males have higher mean and maximum STj values than Caucasians particularly in precordial leads such as V_2, while there is a similar but much less marked trend in females (Fig. 13.50). The ST amplitude in lateral leads shows greater similarity.

The normal ranges of ST-segment slope in Caucasians were evaluated for some of the limb and precordial leads and are presented in the Appendices. Of major interest is the fact that on average, ST slope is always higher in males than females in the leads studied (I, aVF, V_2, V_5, and V_6). It also decreases with increasing age. It was highest in V_2 and lowest in aVF though virtually always positive.

The various T-wave amplitudes, normal ranges, and so on are tabulated in the Appendices. The upper and lower limits of T-wave amplitudes in summary form are illustrated in Fig. 13.51. T-wave amplitudes vary considerably with age and sex, as mentioned in Sect. 13.4. Particularly over the early weeks of life, the T-wave amplitudes in the right precordial leads vary considerably. While the T-wave amplitude can remain inverted in V_1 throughout life, the T wave in V_2 becomes

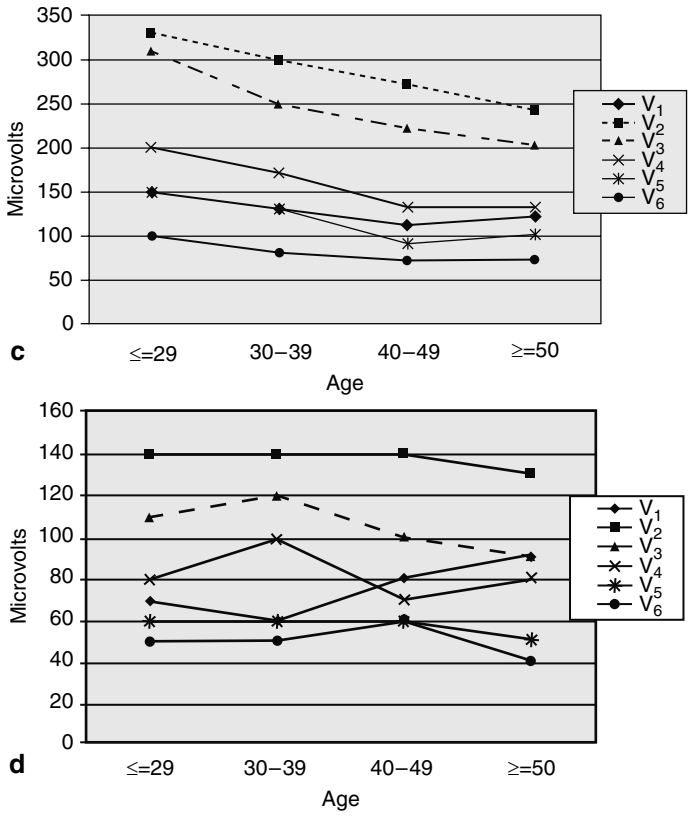

Figure 13.49c, d

(c) Upper limits of normality for the ST amplitude in the precordial leads for males aged over 18 years. (d) Upper limits of normality for the ST amplitude in the precordial leads for females aged over 18 years. (Reproduced with permission from J Electrocardiol 2001; 34(Suppl): 235–41.)

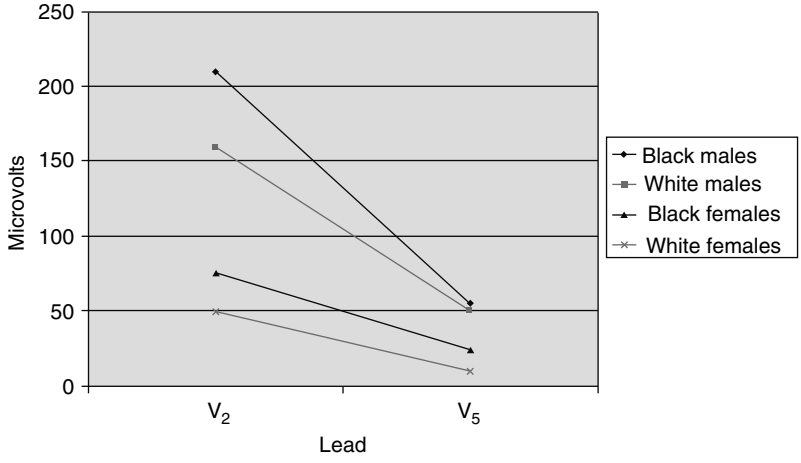

Figure 13.50

A comparison of the mean ST amplitude for V_2 and V_5 in 123 healthy black males and 97 females aged 18–29 years living in Nigeria versus data from 266 healthy Caucasian males and 317 healthy Caucasian females in the same age range.

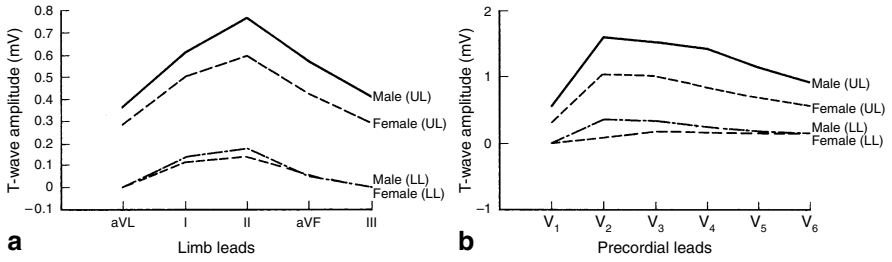

Figure 13.51

The upper and lower limits (UL and LL, respectively) of normal T-wave amplitude in apparently healthy individuals in the Glasgow study: (a) limb leads and (b) precordial leads. The most obvious difference is in the upper limits of normal that are sex dependent.

upright in most people by the age of 12. Nevertheless, T-wave inversion in V_2 particularly in women can often present a diagnostic problem.

In general terms as for the ST segment, the T-wave amplitude in men is much higher than in women, particularly in the precordial leads. Again, however, this difference tends to diminish with increasing age.

From the authors' own data on 601 females, it was found that T-wave inversion in V_2 is indeed an isolated finding and that the lower limit of the normal range for women in this lead is positive. An isolated T-wave abnormality in V_2 in the absence of any other clinical findings should be regarded as equivocal. The range of T-wave amplitudes in V_3 in women shows a similar distribution in that in apparently healthy individuals, the T wave is always positive in this lead. On the other hand, T in V_2 was always positive in men. Similarly, T-wave inversion in the inferior leads, particularly aVF, often presents a diagnostic problem in apparently healthy young men and women.

Our own data in this respect are shown in Fig. 13.52. From this, it can be seen that T-wave inversion up to 0.065 mV occurs in about 4% of healthy women of all ages. This is slightly at variance with the findings of others [3], but may simply be owing to the composition of the different samples. They are, however, in keeping with the data of Simonson [2].

The normal ranges of the T loop are presented in the Appendices. The various comments made for the scalar amplitude also apply to the T-vector loop. In other words, in the frontal plane in women, the T vector may occasionally be superior to 0°, in keeping with shallow inverted T waves in lead Y.

13.7.8 Time Intervals

The advent of simultaneous recording of all 12 leads means that it is possible to compare the apparent onset of the QRS complex in V_6, for example, with the onset in V_1. There can, of course, be only one true QRS onset relating to the start of ventricular activation, but because of the projection of the corresponding electrical activity onto the different lead axes, there can be time delays in the detection of electrical activity in the various leads. Figure 13.53 shows the time intervals measured between the apparent onsets of QRS in V_6 and V_1. It would be expected perhaps that the onset in V_1 would be earlier than in V_6, since septal activation tends to occur from the left to the right of the septum (though anteriorly), thereby giving maximum electrical projection on the V_1 axis and almost zero electrical projection in the direction of V_6. This indeed was found to be the case in the vast majority of ECGs, but nevertheless, there was a sizable group in our normals where electrical activity apparently started earlier in V_6 than in V_1. This, of course, could be a result of measurement error or of a septal activation vector that was essentially directed to the right, that is, oppositely to V_6, producing a small Q wave in V_6 and virtually zero electrical activity in V_1. As yet, few diagnostic criteria have evolved from such simultaneous 12-lead ECG recordings: this is one area of possible development in the future.

The PR interval has diagnostic relevance in relation to the evolution of conduction problems in the heart. In general terms, the PR interval decreases with the increasing heart rate as can be seen particularly in children (see Fig. 13.54). However, at increasingly high rates, it becomes more difficult to determine the precise onset of the P wave, and therefore a degree of uncertainty then enters into the PR-interval estimation. In general terms, PR interval is less than 0.18 ms

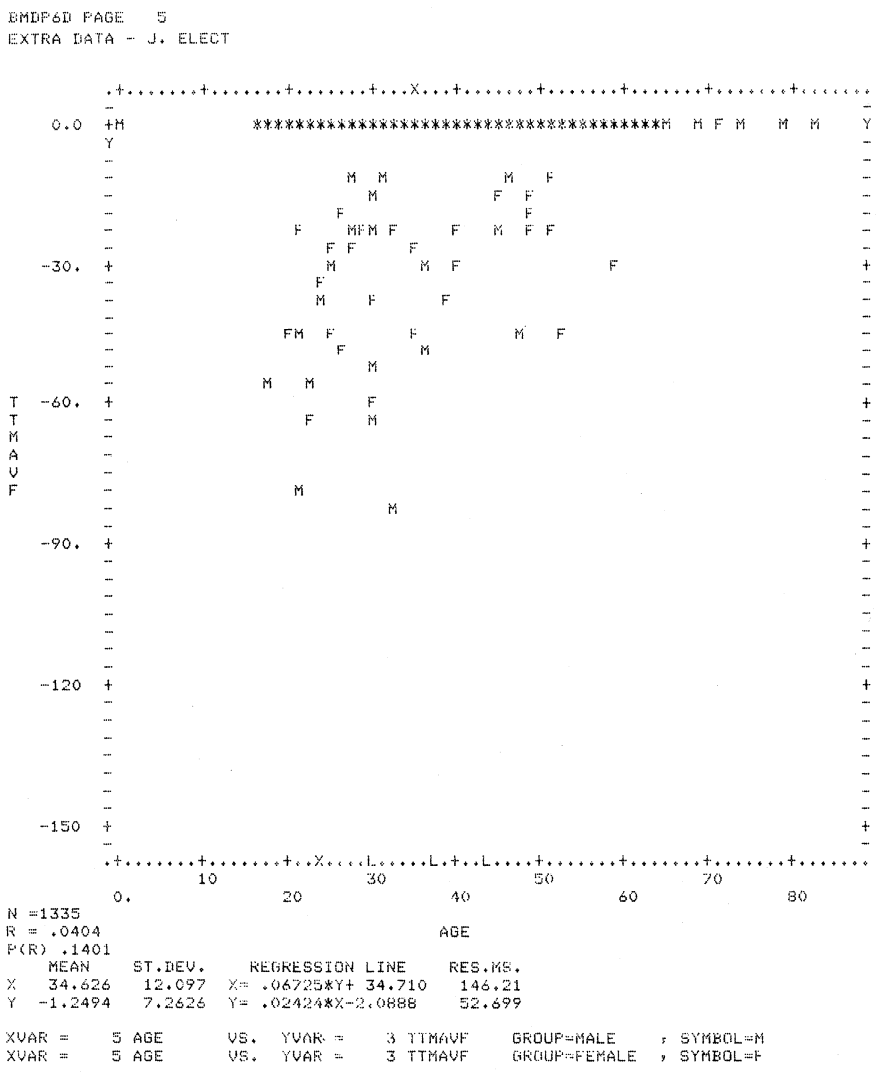

Figure 13.52

Scattergram of negative T-wave components in a VF with respect to age: M, male; F, female. Note that the larger values of negative T amplitude (microvolts) are more often present in young men than young women.

in children and young adults. However, the upper limit of normal gradually increases from 150 up to 175 ms as the age increases from 1 to 16 years. On the other hand, considering the variation in the heart rate for a fixed PR interval, it can also be seen from Fig. 13.54 that the 96 percentile range for the heart rate, when the PR duration is 150 ms, varies from approximately 75 up to 135 bpm. Conversely, at a rate of 140 bpm, the PR varies up to approximately 150 ms. In the adult (Table 13.3), the authors' own data suggests that there is a small but significant difference between the upper limits of normal for males and females, particularly at rates below 80 bpm. The upper limit of normal for males is 210 ms, while for females it is 196 ms. No doubt these very small differences result from the smaller heart size in women.

The QRS duration decreases with increasing age and is shorter in women compared to men. The values are shown in Table 13.3. Because the upper limit of normal in men is a little higher than in women, some diagnostic criteria for conduction defects take limited cognizance of this finding [64]. The authors' data show 7 ms difference between males

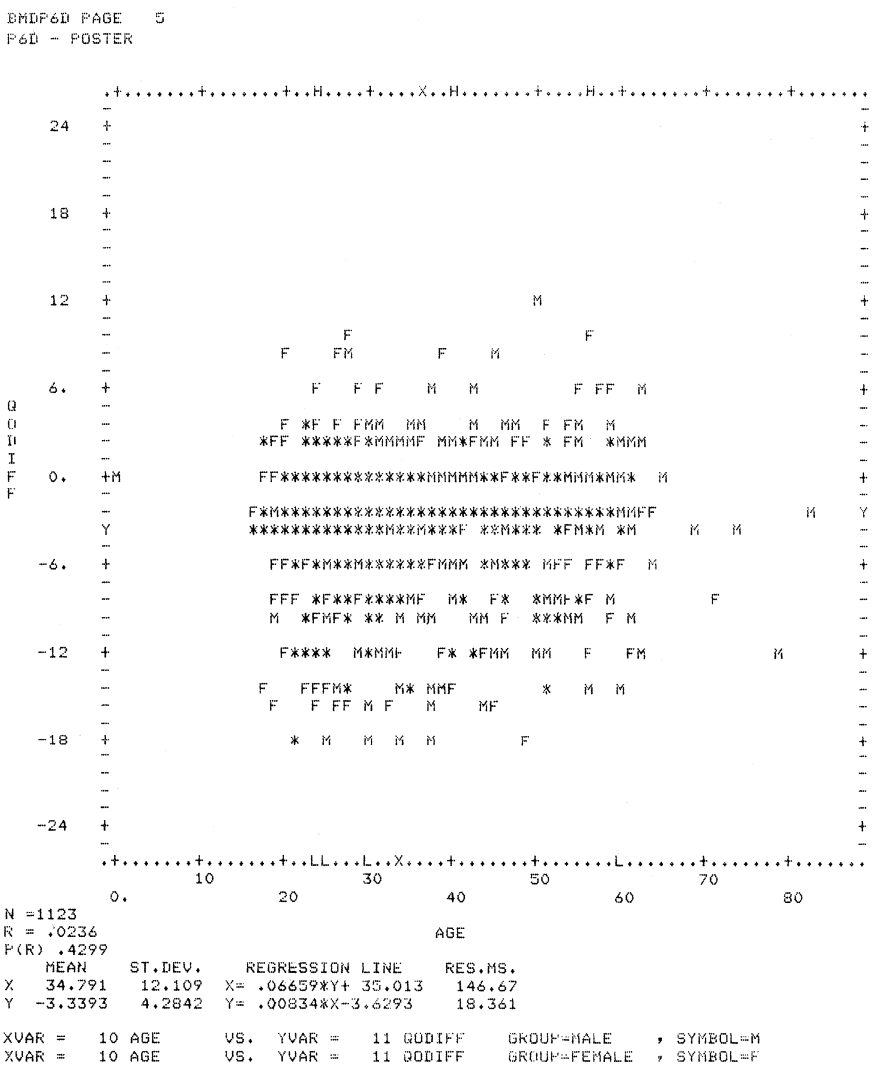

Figure 13.53

Scattergram of the difference in time between the QRS onset in V_1 and V_6. A negative value denotes a later onset in V_6. The 96 percentile range is from −16 to +4 ms. The vast majority of individuals clearly demonstrate a later onset in V_6 than in VI.

and females with respect to the mean normal QRS duration. The data for children are shown in the Appendices where it can be seen that the upper limit of normal QRS duration tends to 0.90 s.

In a comparison of white and black subjects, Pipberger et al. [60] found that on average the QRS duration was 7 ms shorter in black men. In the authors' own comparison of Chinese and Western subjects, no significant difference in QRS durations could be detected. Unless identical methods are used, it is probably not meaningful to compare measurements from different studies. One other QRS interval of some interest is the intrinsicoid deflection or ventricular activation time (VAT). This is the time from the onset of the QRS complex to the peak of the R wave (see Fig. 13.55). This time can be interpreted in a precordial lead as the interval from the onset of ventricular depolarization to the instant that the activation wavefront reaches the area under the electrode. The term more accurately applies to an epicardial electrode. A prolonged intrinsicoid deflection (> 50 ms in V_5) is sometimes used as one of the criteria for LVH.

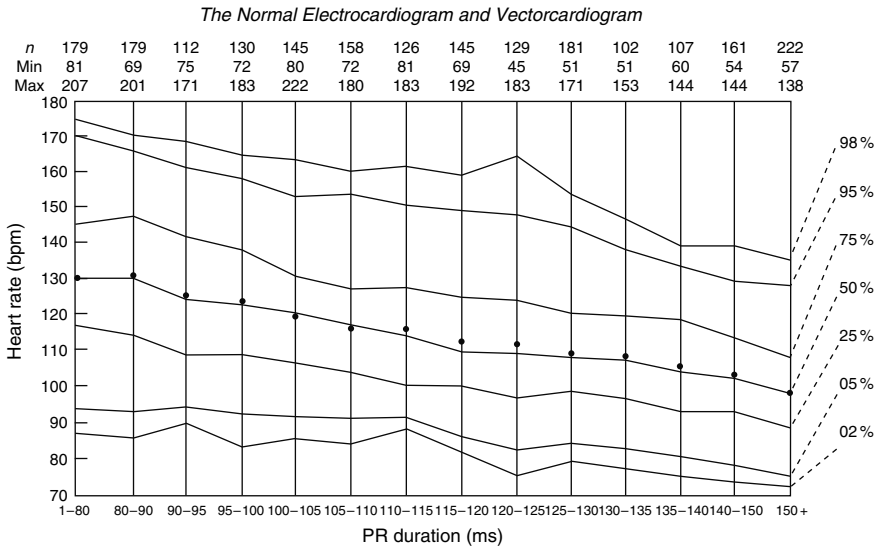

Figure 13.54

The relationship between PR interval and heart rate. The PR interval decreases with increasing heart rate, from 150 ms and over, to 80 ms as the mean rate increases from approximately 100 to 130 bpm. (After Davignon et al. [76]. Springer, New York. Reproduced with permission.)

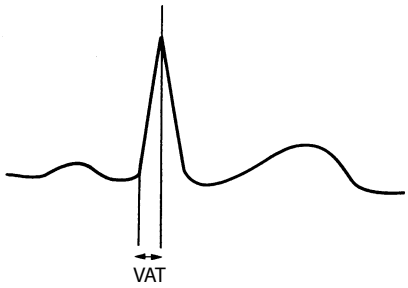

Figure 13.55

An illustration of the definition of ventricular activation time (VAT), which is the time from the onset of QRS to the peak of the maximum wave.

13.7.9 QT Interval

The QT interval has enjoyed something of a renaissance in recent times on account of its susceptibility to change following drug administration and, in certain clinical conditions, for example, following myocardial infarction. Change in the QT interval is also thought to be a precursor of certain arrhythmias, and this too has stimulated considerable research on this variable [102, 103]. The clinical implications associated with the QT interval have been reviewed by Al-Khatib [104] and others. This area of study has grown to such an extent that a separate chapter, Chap. 19, has been devoted to this topic.

Accurate determination of the QT interval, whether it be by computer methods or by manual methods, is difficult. For example, the variation between cardiologists estimating P, QRS, and T reference points in the CSE study [35] was the greatest when they manually estimated the end of the T wave. Likewise, computer programs in the same study also showed the greatest variation when finding the T-wave termination. Furthermore, many researchers wish to monitor QT-interval changes over a period of time by making use of ambulatory monitoring equipment (see Chap. 33). Older recorders are susceptible to variations in speed over a period of 24 h, although the best have time tracks recorded on the tape.

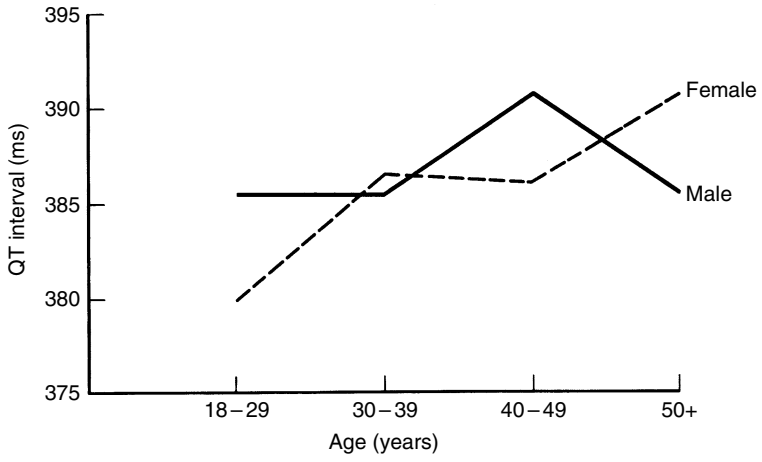

Figure 13.56
Variation in mean QT interval with age and sex, as derived from the Glasgow data.

Modern recorders employ digital technology but with varying sampling rates form 128 to 1000 samples/sec which can cause variation in QT measurement, for example.

Notwithstanding these various limitations, the mean QT-interval variation with age and sex is shown with respect to the authors' data in Fig. 13.56. From this it can be seen that, in general, there are no significant differences between men and women, but there is a small increase in the QT interval with age in women.

It is well known that the QT interval varies significantly with the heart rate and a number of formulae have been derived for correcting the QT interval. The most commonly used is that of Bazett [105], where the corrected interval, QT_c, is given by the formula

$$QT_c = QT\left(\frac{\text{rate}}{60}\right)^{1/2}$$

This is a nonlinear correction of the QT interval. Hodges et al. [106] suggested a linear correction, namely,

$$QT_c = QT + 1.75(\text{rate} - 60)$$

The distribution of the corrected QT using these formulae is shown in Fig. 13.57a, b. Hodges et al. showed that the Bazett formula undercorrects the QT interval at heart rates below 60 bpm and overcorrects the QT interval at rates above 60 bpm. Their own formula was said to "reliably" correct the QT interval over the range of heart rates. Furthermore, with the use of this formula, there was no correlation between the linearly corrected QT interval and the heart rate, whereas with the Bazett formula, there was a highly significant correlation between the corrected QT interval and heart rate (see Fig. 13.57a), defeating the purpose of correcting the QT interval. The authors recommend the formula of Hodges et al. in preference to that of Bazett. Although there are no differences between men and women with respect to the QT interval (see Table 13.3), there is a definite increase in the QT_c of women over the whole age range (see Fig. 13.58). This is of the order of 9 ms for QT_c (Hodges) and 16 ms for QT_c (Bazett).

Another formula that has gained increasing popularity recently is that of Fridericia [107]. It has the form

$$QT_c = QT\left(\frac{\text{rate}}{60}\right)^{1/3}$$

Luo et al. [108] compared this with other formulae including those of Bazett and Hodges and concluded that the Bazett formula was most out of line with the others. Bourdillon [109] reviewed several formulae for correcting the QT interval

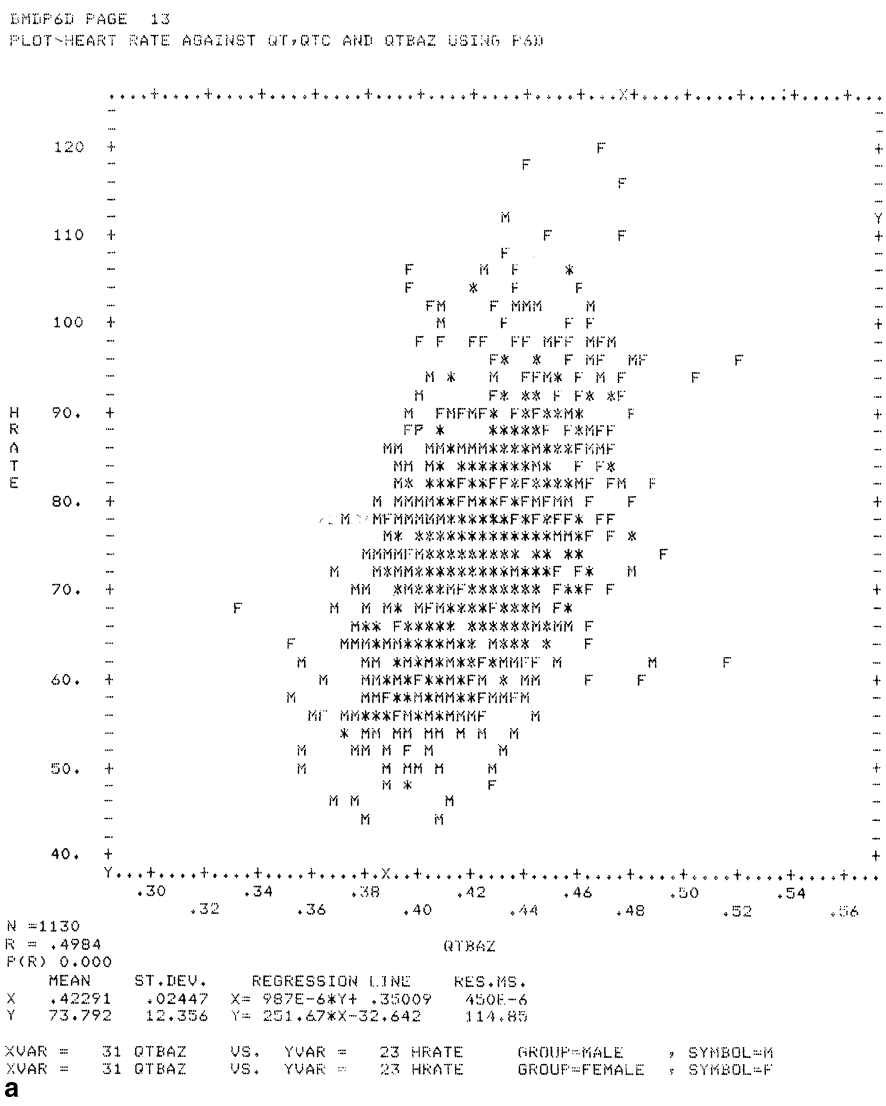

Figure 13.57a

Scattergram of corrected QT interval versus heart rate. The QT is corrected with respect to the Bazett formula, and the correlation with rate is 0.498, that is, the QT is essentially uncorrected. (M, male; F, female; *, more than one value at the same point on the plot.).

in a study of ECGs incorporated in the CSE project. From this, he showed that the QT interval correlated with the QRS duration so that for a particular rate and QRS duration, the QT interval could be predicted. Hence, a prolonged QT could be detected when the measured QT exceeded the predicted QT by a specified amount. The combination of the R-R interval and QRS duration accounted for 52% of the variance in predicting the QT interval. In some ways, this may in fact be related to Wilson's concept of the ventricular gradient [110] discussed in Chaps. 5 and 17.

In view of the various factors that impinge on accurate estimation of the QT interval, it is customary for computer programs to utilize a value of at least 460 ms as the upper limit of normal for the corrected QT interval. Some will extend this limit to 470 ms for females. This maintains a high specificity, as is evident from Fig. 13.57b.

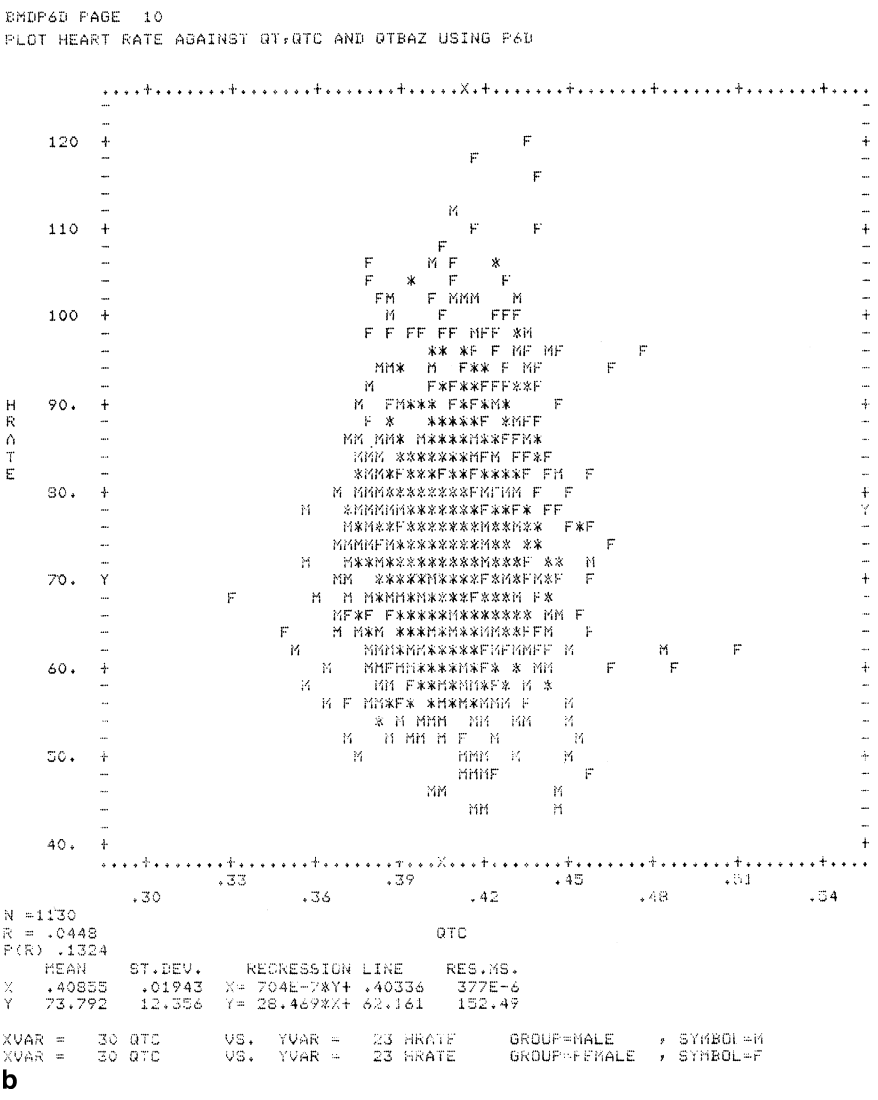

b

Figure 13.57b

Scattergram of corrected QT interval versus heart rate. The QT is corrected with respect to the formula of Hodges et al., and there is essentially no correlation with rate, that is, the QT is highly corrected (M, male; F, female; *, more than one value at the same point on the plot).

13.8 Coding Schemes

13.8.1 Minnesota Code

It is well known that ECG interpretation may vary from one observer to another (and from one computer program to another). Essentially, for the former reason, a coding scheme was developed in 1960 in the University of Minnesota by Blackburn et al. [20], which ultimately became known as the Minnesota code. This set out to describe various ECG appearances, to which a code number could be ascribed. The first point that must therefore be emphasized with respect to the Minnesota code is that it is, *per se*, not a set of diagnostic criteria but rather a set of descriptors. This code has been

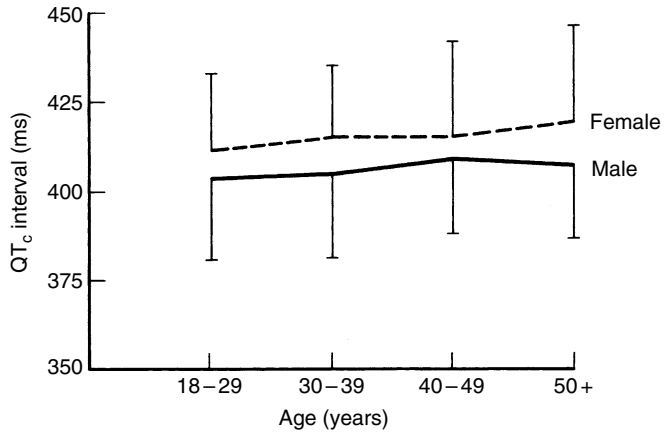

Figure 13.58

Mean and standard deviation of the QT_c interval (corrected with respect to the formula of Hodges et al. [106]). Note the definite increase in QT_c in women compared to men.

used in many studies since 1960, as discussed in detail in Chap. 40. More recently, the section on serial changes has been revised and expanded, while a new manual of procedures for measurement and classification has been published [22].

The Minnesota code is published in full in the Appendices. From this, it can be seen that no actual diagnoses are included with the possible exception of conduction defects and arrhythmias, where the ECG itself provides the objective evidence upon which the classification can be based (corresponding to type B diagnoses of the American College recommendations [111] on optimal electrocardiography – see Appendix). Thus, code 1-1-1 in relation to an anterolateral site involving leads I, aVL, and V_6 specifies a Q/R amplitude greater than 1/3, together with a Q duration greater than 0.03 s in I or V_6. On the other hand, a 1-1-1 classification in a posterior (inferior) site follows from a corresponding set of criteria applied to lead II. Finally, a positive 1-1-1 code in an anterior lead results from similar criteria being applied to any of V_2–V_5. An ECG exhibiting any of these features would be coded as 1-1-1 and not necessarily as a myocardial infarction although that is the implication.

The code certainly has some shortcomings particularly with respect to the lack of use of age and sex in the various criteria, but nevertheless it has stood the test of time as being one of the few methods available where some standardization of the ECG classification, if not interpretation, can be achieved. A number of computer programs have been developed for automatically coding the ECG [112–114] including one in the authors' own laboratory that also incorporates serial comparison according to the Minnesota code rules [115]. From these studies, it has been shown that the accuracy of programs is similar to that of human coders when compared with an agreed set of codes resulting from a group of experienced Minnesota coders amalgamating their opinions on a set of ECGs [116]. Nevertheless, in the authors' laboratory, for example, in an analysis of over 10,000 ECGs from a cooperative study with London University, both the Minnesota code and conventional 12-lead ECG interpretations are provided, since in some ways they are complementary. The former is required for purposes of international acceptance, while the latter is thought to give a more meaningful interpretation of the ECG that can be returned to the subject's general practitioner.

13.8.2 Washington Code

Pipberger et al. [60] published a classification system relating to the orthogonal-lead ECG. This code honored the late Ernst Simonson who had initiated this particular work shortly before his death in 1974. Use was made of data on black and white subjects gathered by Pipberger and coworkers over a number of years [61, 62]. This code was aimed at producing a simple classification scheme that made use essentially of the scalar amplitudes and durations as well as amplitude ratios of the *X*, *Y*, and *Z* leads. Apart from the unique feature of having different criteria for men and women, black and white, this

code also had the novel feature that two different levels of criteria could be established depending on the desired specificity (see Tables 15.7 and 15.11, for example). Furthermore, the codes had a definite electrocardiographic diagnosis assigned. Whereas the Minnesota code classification was designated Q and QS patterns, the corresponding Washington code 2 was designated "myocardial infarction."

Pipberger and colleagues carried out an evaluation of this code in comparison with the Minnesota code and showed that, in general terms, the Washington code [50] was more sensitive than the Minnesota code. This would be expected on the basis of greater use of race and sex in the former.

13.8.3 Punsar Code

A less-well-known code is that of Punsar et al. [117] that was used for categorizing the ST-T segment in an attempt to diagnose ischemic heart disease. Punsar was one of the authors of the original 1960 Minnesota code publication. From the various ST-T classifications of the Punsar code as shown in Fig. 13.59, it can be seen that there are essentially three abnormal categories of ST segment according to this code. In the type labeled ischemic, the ST segment is horizontal or downward-sloping and can be further subdivided into five different grades depending on the degree of ST depression. Grade 1 shows the most depression in excess of 0.2 mV, while Grade 5 shows the least ST depression being less than 0.05 mV. The second category relates to upsloping ST segments where the degree of upslope is somewhat vaguely described as "slowly ascending." Again, further four subdivisions are utilized. The third category relates to upsloping ST segments where there is a more steep slope than in the second category. This group is described as "rapidly ascending" and contains three subdivisions. The fourth and final group of normal ST segments are those where the ST-junction depression is less than 0.05 mV and where the slope is such that the apparent onset of the T wave is above the baseline, that is, it is positive.

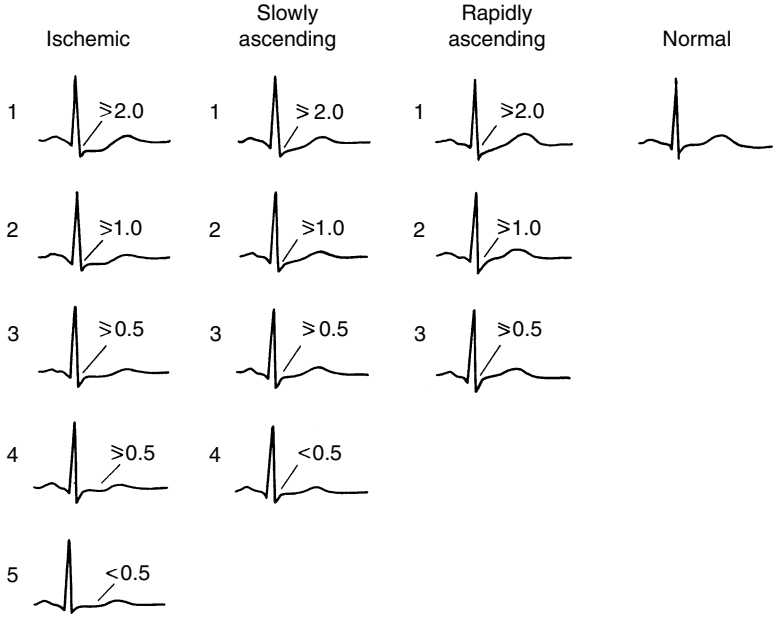

Figure 13.59

The definitions of the Punsar code for the classification of the ST segment. See text for further discussion. (After Punsar et al. [117]. © Finnish Medical Society, Helsinki. Reproduced with permission.)

13.8.4 Novacode

Perhaps one of the most complex coding schemes ever to be developed is the Novacode from the lab of Rautaharju [118]. This code is extremely detailed covering all aspects of the ECG and interpretation including progression and regression of ECG changes. Criteria for hypertrophy are in the traditional voltage-based style with some sex dependence but no age dependence. However, the scheme is designed to be applied in clinical trials and in population studies where most individuals would be middle-aged or older. Criteria for pathological Q waves and ST-T abnormalities are based on scoring techniques. The code is structured in a hierarchical way with the aim of identifying a specific abnormality, which can then be further refined if required. For example, code 3.1 defines LBBB, whereas code 3.1.0 defines LBBB without myocardial infarction, and code 3.1.1 defines LBBB with myocardial infarction. The definitions of 3.1.0 and 3.1.1 each require, not surprisingly, that code 3.1 is present. The code has not been used widely in population studies as yet, perhaps due to a perceived complexity and maybe a need for epidemiologists to cling to Minnesota codes from earlier studies to facilitate comparisons.

13.9 The Electrocardiogram and Employment

The normal limits of the ECG have been discussed in detail, and their bearing on the development of diagnostic criteria is clear. A few points remain to be made, however, in relation to employment.

A normal resting ECG does not always imply a normal heart. It is well known to every cardiologist that many patients with ischemic heart disease may have a normal ECG. A normal ECG cannot therefore be used as evidence of cardiovascular fitness in supporting an application for a license to carry out a particular occupation when there may be other clinical signs and symptoms of abnormality.

Conversely, changes in the ECG should not mitigate against the licence when other investigations, including clinical examination, are normal. Various recommendations have been made which would allow an individual with minor ECG abnormalities to continue in employment. For example, for airline pilots, a number of recommendations have been produced [119, 120]. More recently, an excellent review of matters relating to occupational aspects of heart disease has been published [121].

In conclusion, ECG changes must be assessed in the overall context of other investigations before reaching a conclusion on fitness for employment. There are many other techniques for investigating cardiac status which are complementary to the ECG. Nevertheless, the ECG still contains unique information which mandates that it remains a vital rest in many situations relating to fitness for employment.

13.10 Acknowledgement

The authors gratefully acknowledge the statistical advice provided by Mr. Tom Aitcheson, former senior lecturer in Statistics at the University of Glasgow.

References

1. Mason, J.W., D.J. Ramseth, D.O. Chanter, T.E. Moon, D.B. Goodman, and B. Mendzelevski, Electrocardiographic reference ranges derived from 79,743 subjects. *J. Electrocardiol.*, 2007;**40**: 228–234.
2. Simonson, E., *Differentiation Between Normal and Abnormal in Electrocardiography*. St. Louis, MI: Mosby, 1961.
3. Lundh, B., On the normal scalar ECG. A new classification system considering age, sex and heart position, PhD thesis. Lund: University of Lund. *Acta Med. Scand.*, 1984; Suppl. 691.
4. Macfarlane, P.W., J.A. MacLean, M. Low, et al., Revised limits of the normal ECG, in *Advances in Electrocardiology*, P. D'Alché, Editor. Caen: Centre de Publications de l'Université de Caen, 1985, pp. 160–163.
5. Startt/Selvester, R.H., Comprehensive multilead normal ECG data base for the next few decades, in *Computer ECG Analysis: Towards Standardization*, J.L. Willems, J.H. van Bemmel, and C. Zywietz, Editors. Amsterdam: North-Holland, 1986, pp. 221–226.

6. Ostrander, L.D. Jr., Bundle-branch block. An epidemiologic study. *Circulation*, 1964;**30**: 872–871.
7. Anonymous, Unrecognised myocardial infarction. *Lancet*, 1976;**2**: 449–450.
8. Margolis, J.R., W.B. Kannel, M. Feinleib, T.R. Dawber, and P.M. McNamara, Clinical features of unrecognized myocardial infarction-Silent and symptomatic. Eighteen year follow-up: the Framingham study. *Am. J. Cardiol.*, 1973;**32**:1–7.
9. Medalie, J.H. and U. Goldbourt, Unrecognized myocardial infarction: Five year incidence, mortality and risk factors. *Ann. Intern. Med.*, 1976;**84**: 526–531.
10. Schwartz, D., R. Flamant, and J. Lellouch, *Clinical Trials*. New York: Academic Press, 1980.
11. Jain, U. and P.M. Rautaharju, The use of discretized features for classification of electrocardiograms, in *Optimization of Computer ECG Processing*, H.K. Wolf and P.W. Macfarlane, Editors. Amsterdam: North-Holland, 1980 pp. 117–120.
12. Macfarlane, P.W., B. Devine, S. Latif, S. McLaughlin, D.B. Shoat, and M.P. Watts, Methodology of ECG interpretation in the Glasgow program. *Meth. Inform. Med.*, 1990;**29**: 354–361.
13. Macfarlane, P.W., B. Devine, and E. Clark, The University of Glasgow (Uni-G) ECG analysis program. *Comput. Cardiol.*, 2005;**32**: 451–454.
14. McLaughlin, S., T.C. Aitchison, T.-F. Yang, and P.W. Macfarlane, Smoothing techniques for improving the repeatability of the automated diagnosis of inferior myocardial infarction. *J. Electrocardiol.*, 1994;**27**(Suppl): 182–187.
15. McLaughlin, S., T.C. Aitchison, and P.W. Macfarlane, Methods for improving the repeatability of automated ECG analysis. *Meth. Inform. Med.*, 1995;**34**: 272–282.
16. Dudeck, J. and J. Michaelis, Problems in the diagnostic process in electrocardiography, in *Computer Application on ECG and VCG Analysis*, C. Zywietz and B. Schneider, Editors. Amsterdam: North-Holland, 1973, pp. 283–295.
17. Abreu-Lima, C., D.M. Correia, J. Almeida, M. Antunes-Lopes, and M. Cerqueira-Gomes, A new ECG classification system for myocardial infarction based on receiver operating characteristic curve analysis and information theory. *Circulation*, 1983;**67**: 1252–1257.
18. Rautaharju, P.M., H.W. Blackburn, and J.W. Warren, The concepts of sensitivity, specificity and accuracy in the evaluation of electrocardiographic, vectorcardiographic and polarcardiographic criteria. *J. Electrocardiol.*, 1976;**9**: 275–281.
19. Bailey, J.J., Evaluation methodologies, in *Computerized Interpretation of the Electrocardiogram VI*, R. Bonner, Editor. New York: Engineering Foundation, 1982.
20. Blackburn, H., A. Keys, E. Simonson, P. Rautaharju, and S. Punsar, The electrocardiogram in population studies. A classification system. *Circulation*, 1960;**21**: 1160–1175.
21. Kossmann, C.E., D.A. Brody, G.E. Burch, et al., Report of Committee on Electrocardiography, American Heart Association. Recommendations for standardization of leads and of specifications for instruments in electrocardiography and vectorcardiography. *Circulation*, 1967;**35**: 583–602.
22. Prineas, R.J., R.S. Crow, and H. Balckburn, *The Minnesota Code Manual of Electrocardiographic Findings*, 2nd edn., London: Springer, 2010.
23. Pipberger, H.V., R.C. Arzbaecher, A.S. Berson, et al., Report of the Committee on Electrocardiography, American Heart Association. Recommendations for standardization of leads and of specifications for instruments in electrocardiography and vectorcardiography. *Circulation*, 1975;**52**(AHA Suppl): 11–31.
24. Farb, A., R.B. Devereux, and P. Kligfield, Day-to-day variability of voltage measurements used in electrocardiographic criteria for left ventricular hypertrophy. *J. Am. Coll. Cardiol.*, 1990;**15**: 618–623.
25. CSE Working Party, Recommendations for measurement standards in quantitative electrocardiography. *Eur. Heart J.*, 1985;**6**: 815–825.
26. Chung, E.K., *Electrocardiography: Practical Applications with Vectorial Principles*, 2nd edn. Hagerstown, MD: Harper and Row, 1980, pp. 22–25.
27. Chou, T.-C., *Electrocardiography in Clinical Practice*, 2nd edn. Orlando, FL: Grune and Stratton, 1986, pp. 7–10.
28. Holzmann, M., *Klinische Electrokardiographie*, 3rd edn. Stuttgart: Thieme, 1955.
29. Rowlands, D.J., The normal ECG, Section I, *Understanding the Electrocardiogram: A New Approach*. Macclesfield: ICI, 1980, pp. 46–50.
30. Willems, J.L,, E.O. Robles de Medina, R. Bernard, et al., WHO/ISFC Task Force. Criteria for intraventricular conduction disturbances and pre-excitation. *J. Am. Coll. Cardiol.*, 1985;**5**: 1261–1275.
31. Macfarlane, P.W., M. Marriott, M.J. Podolski, D. MacFarlane, and T.D.V. Lawrie, Simultaneous 3-orthogonal and 12-lead hybrid electrocardiogram, in *Computerized Interpretation of Electrocardiograms VIII*, R.H. Selvester and D. Geselowitz, Editors. New York: Engineering Foundation, 1984, pp. 159–169.
32. Draper, H.W., C.J. Peffer, F.W. Stallmann, D. Littmann, and H.V. Pipberger, The corrected orthogonal electrocardiogram and vectorcardiogram in 510 normal men (Frank lead system). *Circulation*, 1964;**30**: 853–864.
33. Willems, J.L., Common Standards for Quantitative Electrocardiography (EEC Concerted Action Project II.2.2). 2nd Progress Report. CSE Ref. 82-11-20. Leuven: ACCO, 1982, pp. 127–227.
34. Macfarlane, P.W., D.K. MacFarlane, M. Podolski, and T.D.V. Lawrie, The ECG analysis program for the MINGOCARE system. *Electromedica*, 1984;**52**: 126–136.
35. Willems, J.L., P. Arnaud, J.H. van Bemmel, et al., Assessment of the performance of electrocardiographic computer programs with the use of a reference data base. *Circulation*, 1985;**71**: 523–534.
36. Willems, J.L., P. Arnaud, J.H. van Bemmel, et al., Establishment of a reference library for evaluating computer ECG measurement programs. *Comput. Biomed. Res.*, 1985;**18**: 439–457.
37. Rose, G.A. and H. Blackburn, *Cardiovascular Survey Methods*. Geneva: WHO, 1968, Monograph Series No.56.
38. Willems, J.L., Common Standards for Quantitative Electrocardiography (EEC Concerted Action Project II.2.2). 4th Progress Report. CSE Ref. 84-11-15. Leuven: ACCO, 1984, pp. 73–152.
39. Willems, J.L., P.F. Poblete, and H.V. Pipberger, Day-to-day variation of the normal orthogonal electrocardiogram and vectorcardiogram. *Circulation*, 1972;**45**: 1057–1064.
40. Simonson, E., J. Brozek, and A. Keys, Variability of the electrocardiogram in normal young men. *Am. Heart J.*, 1949;**38**: 407–422.
41. Cawood, H.T., P.W. Macfarlane, S. Hillis, and T.D.V. Lawrie, Day to day and beat to beat variation in normal 3 orthogonal lead electrocardiograms. *Br. Heart J.*, 1974;**36**: 1225–1230.

42. Simonson, E., The electrocardiogram in coronary heart disease. *Minn. Med.*, 1955;38:871–873.
43. Graybiel, A., Starr, R.S., and P.D. White, Electrocardiographic changes following the inhalation of tobacco smoke. *Am. Heart J.*, 1938;**15**: 89–99.
44. Wilson, F.N. and R. Finch, The effect of drinking iced-water upon the form of the T detection of the electrocardiogram. *Heart*, 1923;**10**. 275–278.
45. Sears, G.A. and G.W. Manning, Routine electrocardiography: postprandial T wave changes. *Am. Heart J.*, 1958;**56**: 591–597.
46. Magendantz, H. and J. Shortsleeve, Electrocardiographic abnormalities in patients exhibiting anxiety. *Am. Heart J.*, 1951;**42**: 849–857.
47. Marriott, H.J.L., *Practical Electrocardiography*, 6th edn. Baltimore, MD: Williams and Wilkins, 1977, pp. 266–269.
48. LaMonte, C.S. and A.H. Freiman, The electrocardiogram after mastectomy. *Circulation*, 1965;**32**: 746–754.
49. Rautaharju, P., L. Park, F.S. Rautaharju, and R. Crow, A standardizes procedure for locating and documenting ECG chest electrode positions. *J. Electrocardiol.*, 1998;**31**: 17–29.
50. Scherer, M.L., T. Aspelund, S. Sigurdsson, R. Detrano, M. Garcia, G.F. Mitchell, L.J. Launer, G. Thorgeirsson, V. Gudnason, and T.B. Harris, Abnormal T-wave axis is associated with coronary artery calcification in older adults. *Scan. Cardiovasc. J.*, 2008;1–9:iFirst Article URL: http://dx.doi.org/10.1080/14017430802471483
51. Tomlinson, D.R., Y. Bashir, T.R. Betts, and K. Rajappan, Accuracy of manual QRS duration assessment: its importance in patient selection for cardiac resynchronization and implantable cardioverter defibrillator therapy. *Europace*, 2009;**11**: 638–642.
52. Littmann, D., Persistence of the juvenile pattern in the precordial leads of healthy adult Negroes, with report of electrocardiographic survey on three hundred Negro and two hundred white subjects. *Am. Heart J.*, 1946;**32**: 370–382.
53. Keller, D.H. and J.B. Johnston, The T wave of the unipolar precordial electrocardiogram in normal adult Negro subjects. *Am. Heart J.*, 1952;**44**: 494–498.
54. Walker, A.R.P. and B.F. Walker, The bearing of race, sex, age, and nutritional state on the precordial electrocardiograms of young South African Bantu and Caucasian subjects. *Am. Heart J.*, 1969;**77**: 441–459.
55. Katibi, I.A., Normal limits of the 12 lead ECG in a healthy Nigerian cohort, MD Thesis. University of Glasgow. In preparation.
56. Macfarlane, P.W., C.Y. Chen, and B.N. Chiang, Comparison of the ECG in apparently healthy Chinese and Caucasians, in *Computers in Cardiology*, K. Ripley, Editor. 1987. Baltimore, MD: IEEE Computer Society Press, 1988.
57. Macfarlane, P.W., M.P. Watts, M. Podolski, D. Shoat, and T.D.V. Lawrie, The new Glasgow system, in *Computer ECG Analysis: Towards Standardization*, J.L. Willems, J.H. van Bemmel, and C. Zywietz, Editors. Amsterdam: North-Holland, 1986, pp. 31–36.
58. Chen, C.Y., B.N. Chiang, and P.W. Macfarlane, Normal limits of the electrocardiogram in a Chinese population. *J. Electrocardiol.*, 1989;**22**: 1–15.
59. Wu, J., J.A. Kors, P.R. Rijnbeek, G. van Herpen, Z. Lu, and C. Xu, Normal limits of the electrocardiogram in Chinese subjects. *Int. J. Cardiol.*, 2003;**87**: 37–51.
60. Pipberger, H.V., E. Simonson, E.A. Lopez Jr., M.A. Araoye, and H.A. Pipberger, The electrocardiogram in epidemiologic investigations. A new classification system. *Circulation*, 1982;**65**: 1456–1464.
61. Pipberger, H.V., M.J. Goldman, D. Littmann, G.P. Murphy, J. Cosma, and J.R. Snyder, Correlations of the orthogonal electrocardiogram and vectorcardiogram with constitutional variables in 518 normal men. *Circulation*, 1967;**35**: 536–551.
62. Nemati, M., J.T. Doyle, D. McCaughan, R.A. Dunn, and H.V. Pipberger, The orthogonal electrocardiogram in normal women. Implications of sex differences in diagnostic electrocardiography. *Am. Heart J.*, 1978;**95**: 12–21.
63. Keys, A., F. Fidanza, M.J. Karvonen, N. Kimura, and H.L. Taylor, Indices of relative weight and obesity. *J. Chronic Dis.*, 1972;**25**: 329–343.
64. Matthes, T., G. Gottsch, and C. Zywietz, Interactive analysis of statistical ECG, diagnosis on an intelligent electrocardiograph—an expert system approach, in *Computer ECG Analysis: Towards Standardization*, J.L. Willems, J.H. van Bemmel, and C. Zywietz, Editors. Amsterdam: North-Holland, 1986, pp. 215–220.
65. Oakley, D.G. and C.M. Oakley, Significance of abnormal electrocardiograms in highly trained athletes. *Am. J. Cardiol.*, 1982;**50**: 985–989.
66. Fagard, R., A. Aubert, J. Staessen, E. van den Eynde, L. Vanhees, and A. Amery, Cardiac structure and function in cyclists and runners. Comparative echocardiographic study. *Br. Heart J.*, 1984;**52**: 124–129.
67. Shapiro, L.M., Physiological left ventricular hypertrophy. *Br. Heart J.*, 1984;**52**: 130–135.
68. Pellicacia, A., F.M. Di Paolo, F.M. Quattrini, C. Basso, F. Culasso, G. Popoli, R. De Luca, A. Spataro, A. Biffi, G. Thiene, and B.J. Marron, Outcomes in athletes with marked ECG repolarization abnormalities. *N. Eng. J. Med.*, 2008;**358**(2): 152–161.
69. Oakley, D., Cardiac hypertrophy in athletes. *Br. Heart J.*, 1984;**52**: 121–123.
70. Lawless, C.E. and T. Best, Electrocardiograms in athletes: interpretation and diagnostic accuracy. *Med. Sci. Sports Exer.*, 2008;**40**: 787–798.
71. Corrado, D., A. Pelliccia, H.H. Bjornstad, L. Vanhees, A. Biffi, M. Borjesson, N. Panhuyzen-Goedkoop, et al., Cardiovascular pre-participation screening of young competitive athletes for prevention of sudden death: proposal for a common European protocol. Consensus statement of the Study Group of Sport Cardiology of the Working Group of Cardiac Rehabilitation and Exercise Physiology and the Working Group of Myocardial and Pericardial Diseases of the European Society of Cardiology. *Eur. Heart J.*, 2005;**26**: 516–524.
72. Wilson, F.N., F.D. Johnston, F.F. Rosenbaum, et al., The precordial electrocardiogram. *Am. Heart J.*, 1944;**27**:19–85.
73. Liebman, J., R. Plonsey, and P.C. Gillette, eds. *Pediatric Electrocardiography*. Baltimore, MD: Williams and Wilkins, 1982.
74. Sreenivasan, V.V., B.J. Fisher, J. Liebman, and T.D. Downs, Longitudinal study of the standard electrocardiogram in the healthy premature infant during the first year of life. *Am. J. Cardiol.*, 1973;**31**: 57–63.
75. Liebman, J., H.C. Romberg, T. Downs, and R. Agusti, The Frank QRS vectorcardiogram in the premature infant, in *Vectorcardiography*, I. Hoffman and R.C. Taylor, Editors. 1965. Amsterdam: North-Holland, 1966, pp. 256–271.
76. Davignon, A., P. Rautaharju, E. Boiselle, F. Soumis, M. Megelas, and A. Choquette, Normal ECG standards for infants and children. *Pediatr. Cardiol.*, 1979;**1**: 123–152.
77. Ziegler, R.F., *Electrocardiographic Studies in Normal Infants and Children*. Springfield, IL: Thomas, 1951.

78. Strong, W.B., T.D. Downs, J. Liebman, and R. Liebowitz, The normal adolescent electrocardiogram. *Am. Heart J.*, 1972;**83**: 115–128.
79. Macfarlane, P.W., E.N. Coleman, E.O. Pomphrey, S. McLaughlin, A. Houston, and T. Aitchisonn, Normal limits of the high-fidelity pediatric ECG: Preliminary observations. *J. Electrocardiol.*, 1990;**22**(Suppl. 1): 162–168.
80. Rijnbeek, P.R., M. Witsenburg, E. Schrama, J. Hess, and J.A. Kors, New normal limits for the paediatric electrocardiogram. *Eur. Heart J.*, 2001;**22**(8): 702–711.
81. Sun, K., F. Li, Y. Zhou, A.M. Dubin, P.M. Rautaharju, J. Liebman, R.E. Gregg, E.D. Helfenbein, J.M. Lindauer, and S.H. Zhou, Normal ECG limits for Asian infants and children. *Comput. Cardiol.*, 2005;**32**: 455–458.
82. Guller, B., F.Y.K. Lau, R.A. Dunn, H.A. Pipberger, and H.V. Pipberger, Computer analysis of changes in Frank vectorcardiograms of 666 normal infants in the first 72 hours of life. *J. Electrocardiol.*, 1977;**10**: 19–26.
83. Chou, T.-C. and R.A. Helm, *Clinical Vectorcardiography*. New York: Grune and Stratton, 1967, pp. 50–63.
84. Cornfield, J., R.A. Dunn, C.D. Batchlor, and H.V. Pipberger, Multigroup diagnosis of electrocardiograms. *Comput. Biomed. Res.*, 1973;**6**: 97–120.
85. Stallmann, F.W. and H.V. Pipberger, Automatic recognition of electrocardiographic waves by digital computer. *Circ. Res.*, 1961;**9**: 1138–1143.
86. van Bemmel, J.H., J.S. Duisterhout, G. van Herpen, L.G. Bierwolf, S.J. Hengeveld, and B. Versteeg, Statistical processing methods for recognition and classification of vectorcardiograms, in *Vectorcardiography*, vol. 2, I. Hoffman, R.I. Hamby, and E. Glassman, Editors. Amsterdam: North-Holland, 1971, pp. 207–215.
87. Sano, T., F. Suzuki, T. Hiroki, and T. Sawanobori, On the spatial velocity electrocardiogram. II. Clinical application. *Jpn. Heart J.*, 1968;**9**: 64–75.
88. Macfarlane, P.W., J. Mitchell, and T.D.V. Lawrle, Spatial velocity of the heart vector, in *Proceedings of the XIIth International Colloquium on Vectorcardiographicum*, P. Rijlant, Editor. Brussels: Presses Academiques Européennes, 1972, pp. 343–346.
89. Morris, J.J. Jr., E.H. Estes Jr., R.E. Whalen, H.K. Thompson Jr., and H.D. McIntosh, P wave analysis in valvular heart disease. *Circulation*, 1964;**29**: 242–252.
90. Cabrera, E., *Électrocardiographie Clinique: Théorie et Pratique*. Paris: Masson, 1959.
91. Sokolow, M. and T.P. Lyon, The ventricular complex in left ventricular hypertrophy is obtained by unipolar precordial and limb leads. *Am. Heart J.*, 1949;**37**: 161–186.
92. Andersen, H.R., D. Nielsen, and L.G. Hansen, The normal right chest electrocardiogram. *J. Electrocardiol.*, 1987;**20**: 27–32.
93. Taha, B., S. Reddy, M.D. Agarwal, and K. Khaw, Normal limits of ST segment measurements in posterior ECG leads. *J. Electrocardiol.*, 1998;**31**(Suppl. 1): 178–179.
94. Macfarlane, P., J. Petryka, and E. Kaczmarska, Influence of age and sex on normal limits of ST-T amplitudes in right-sided and posterior chest leads. *J. Electrocardiol.*, 2006;**39**(Suppl. 1), S129–S130.
95. Wagner, G.S., P. Macfarlane, H. Wellens, et al., AHA/ACCF/HRS recommendations for the standardization and interpretation of the electrocardiogram: Part VI. Acute ischemia/infarction. *JACC*, 2009;**53**: 1003–1011.
96. Grant, R.P. and R.H. Murray, The QRS complex deformity of myocardial infarction in the human subject. *Am. J. Med.*, 1954;**17**: 587–609.
97. Ueda, H., I. Donomae, E. Kimura, et al., The normal value of electrocardiogram in the Japanese. The Report of the Committee on the Criteria of the Heart Disease and Electrocardiogram. *Jpn. Heart J.*, 1963;**4**: 141–172.
98. Hsu, T.S., C.W. Chiang, and Y.S. Lee, A vectorcardiographic study of normal Chinese adults with some relevant echocardiographic and electrocardiographic observation. *Taiwan I Hsueh Hui Tsa Chih*, 1983;**82**: 410–418.
99. Burns-Cox, C.J., L.C. Lau, and B.H. Toh, The electrocardiogram of healthy young Chinese and Malay men. *J. Electrocardiol.*, 1971;**4**: 211–219.
100. Wang, K., R.W. Asinger, and H.J.L. Marriott, ST-T segment elevation in conditions other than acute myocardial infarction. *N. Eng. J. Med.*, 2003;**349**: 22.
101. Ginzton, L.E. and M.M. Laks, The differential diagnosis of acute pericarditis from the normal variant: new electrocardiographic criteria. *Circulation*, 1982;**65**: 1004–1009.
102. Ahnve, S., E. Gilpin, E.B. Madsen, V. Froelicher, H. Henning, and J. Ross Jr., Prognostic importance of QT_c interval at discharge after acute myocardial infarction: a multicenter study of 865 patients. *Am. Heart J.*, 1984;**108**: 395–400.
103. Krapf, R. and M. Gertsch, Torsade de pointes induced by sotalol despite therapeutic plasma sotalol concentrations. *Br. Med. J.*, 1985;**290**: 1784–1785.
104. Al-Khatib SM, LaPointe NM, Kramer JM, Califf RM. What clinicians should know about the QT interval. *J.A.M.A.*, 2003;**289**: 2120–2127.
105. Bazett, H.C., An analysis of the time relations of electrocardiograms. *Heart*, 1920;**7**: 353–370.
106. Hodges, M., D. Salerno, and D. Erlien, Bazett's QT correction reviewed. Evidence that a linear QT correction for heart is better. *J. Am. Coll. Cardiol.*, 1983;**1**: 694. [Abstract.]
107. Fridericia, L.S., Die Systolendauer im Elektrokardiogramm bei normalen Menschen und bei Herzkranken. *Acta. Med. Scan.*, 1920;**53**: 469–486.
108. Luo, S., P. Johnson, K. Michler, and P.W. Macfarlane, A comparison of commonly used Qt correction formulae: the effect of heart rate on the QTc of normal ECGs. *J. Electrocardiol.*, 2004;**37**(Suppl.): 81–90.
109. Bourdillon, P.J. and J.P. Mulrow, QRS duration is an independent predictor of QT duration. Abstracts. *Computer ECG Analysis: Towards Standardization*. Leuven: CSE Working Conference, 1985: 23.
110. Wilson, F.N., A.G. Macleod, P.S. Barker, and F.D. Johnston, The determination and the significance of the areas of the ventricular deflections of the electrocardiogram. *Am. Heart J.*, 1934;**10**: 46–61.
111. Rautaharju, P.M., M. Ariet, T.A. Pryor, et al., Task Force III. Computers in diagnostic electrocardiography. *Am. J. Cardiol.*, 1978;**41**: 158–170.
112. Wolf, H.K., P.J. Maclnnis, S. Stock, R.K. Helppi, and P.M. Rautaharju, The Dalhousie program: a comprehensive analysis program for rest and exercise electrocardiograms, in *Computer Application on ECG and VCG Analysis*, C. Zywietz and B. Schneider, Editors. Amsterdam: North-Holland, 1973, pp. 231–240.
113. Duisterhout, J.S., J.F. May, and G. van Herpen, A computer program for classification of ECGs according to the Minnesota Code, in *Trends in Computer-Processed Electrocardiograms*, J.H.

van Bemmel and J.L. Willems, Editors. Amsterdam: North-Holland, 1977, pp. 345–352.
114. Tuinstra, C.L. and F.H. Bonjer, Validation of a Minnesota Code program, in *Trends in Computer-Processed Electrocardiograms*, J.H. van Bemmel and J.L. Willems, Editors. Amsterdam: North-Holland, 1977, pp. 353–355.
115. Macfarlane, P.W. and S. Latif, Automated serial comparison based on the Minnesota Code. *J. Electrocardiol*., 1996;**29**(Suppl. 1): 29–34.
116. Tuinstra, C.L., P.M. Rautaharju, R.J. Prineas, and J.S. Duisterhout, Comparison of the operational value of six systems to assess the Minnesota Code, in *New Frontiers of Electrocardiology*, F. de Padua and P.W. Macfarlane, Editors. Chichester: Research Studies Press, 1981, pp. 487–492.
117. Punsar, S., K. Pyoriila, and P. Siltanen, Classification of electrocardiographic S-T segment changes in epidemiological studies of coronary heart disease. *Ann. Med. Intern. Fenn*., 1968;**57**: 53–63.
118. Rautaharju, P.M., L.P. Park, B.R. Chaitman, F. Rautaharju, and Z.-M. Zhang, The Novacode criteria for classification of ECG abnormalities and their clinically significant progression and regression. *J. Electrocardiol*., 1998;**31**: 157–187.
119. Joy, M., (ed) The First European Workshop in Aviation Cardiology. *Eur. Heart J*., 1992;**13**(Suppl. H): 1–175.
120. Joy, M., (ed) The Second European Workshop in Aviation Cardiology. *Eur. Heart J*., 1999;**20**(Suppl. D): D1–D136.
121. Katritsis, D.G. and M.M. Webb-People, Occupational and regulatory aspects of heart disease. *ESC Textbook of Cardiovascular Medicine,* 2nd edn. Chapter 38, Oxford: Oxford University Press, 2009.

14 Conduction Defects

Fernando de Pádua · Armando Pereirinha · Nuno Marques · Mário G. Lopes · Peter W. Macfarlane

P. W. Macfarlane, A. van Oosterom, O. Pahlm, P. Kligfield, M. Janse, J. Camm (eds.), *Comprehensive Electrocardiology*, DOI 10.1007/978-1-84882-046-3_14,

14.1 Introduction

The normal conduction system and the normal electrocardiogram (ECG) (the resultant of normal conduction of the electrical impulse through a normal conduction system) have been previously described in Chaps. 5 and 13.

This chapter deals with conduction defects occurring at the atrial level (intra-atrial or interatrial conduction defects) and at the ventricular level (intraventricular conduction defects). A more particular type of conduction abnormalities – ventricular preexcitation and Brugada syndrome – is dealt with in Sects. 14.4 and 14.5. The description of atrioventricular blocks is presented in Chap. 28.

For each type of conduction defect, two main sets of problems are analyzed: (1) the correct identification of the ECG pattern and the precise localization of the abnormality within the conduction system and (2) the clinical importance of the conduction defect. With regard to the latter, the following questions must be answered:

(a) Is it a "lone electrical abnormality" or an electrical presentation of a more important anatomic (and/or functional) disease of the heart?
(b) Are there any expected complications (either "electrical," e.g., brady and tachydysrhythmias; or functional, e.g., impairment of the pump performance of the heart)?
(c) Does its presence, by itself, change the prognosis of the patient?

14.2 Intra-Atrial Conduction Defects

Detailed data concerning the sequence of the atrial activation in the human heart are scarce. Three specialized tracts containing Purkinje fibers have been described connecting the sinus node to the atrioventricular (AV) node (anterior, middle, and posterior internodal pathways) (Fig. 14.1a). An interatrial pathway (Bachmann bundle) has also been described between the right and the left atrium. The true role of these specialized pathways (even their existence), in normal atrial activation and conduction, has not been clearly demonstrated. On the contrary, different techniques suggest a radial sequence of activation (Fig. 14.1b) [1–3], similar to that shown in the dog [4, 5]. Although zones with thicker atrial fibers (muscle bands) may have different conduction velocities, this does not imply conduction through individualized special pathways [1, 3, 5, 6].

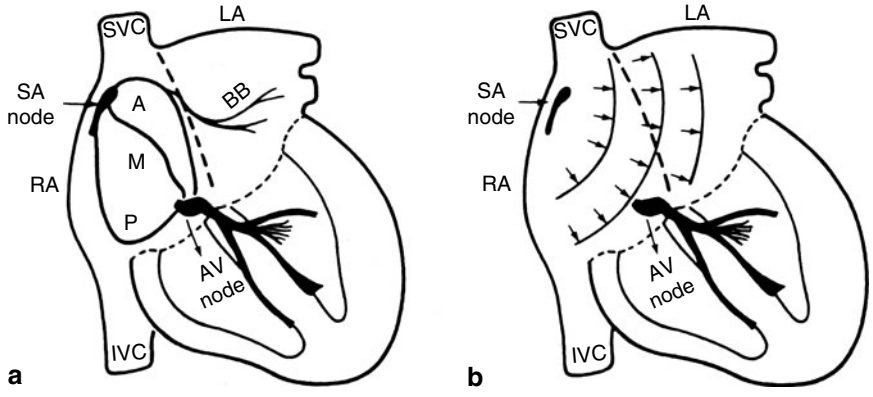

Figure 14.1
Part (a) is a schematic of the specialized internodal pathways (A, anterior; M, middle; P, posterior) and interatrial Bachmann bundle (BB). Part (b) is a schematic of radial activation of the atria as opposed to conduction through the individualized pathways shown in (a) (IVC, inferior vena cava; SVC, superior vena cava; LA, left atrium; RA, right atrium).

14.2.1 Electrical Physiopathology and ECG/VCG Patterns

In the normal sinus rhythm, excitation proceeds from the sinus node, localized in the posterior surface of the high right atrium, to the low right and to the high left atrium, and finally to the low left atrium.

While initially only the right atrium is depolarized, the cardiac impulse travels rapidly across the atria. Since the right atrium is anatomically anterior to the left atrium, and the sinus node is located at the right upper portion of the right atrium, the electrical impulse will spread first inferiorly, then leftward, with resultant vectors that rotate progressively more leftward and posteriorly, when the activation wave invades the left atrium.

The normal P-wave pattern (contour, duration, and polarity) is determined by the time course and sequence of the depolarization of the atrial tissue. An increased duration of the P-wave is expected to be present whenever delayed intra-atrial or interatrial activation (intra-atrial or interatrial conduction defect) occurs.

With either left or combined atrial enlargement, a P-wave of longer duration is observed (Fig. 14.2). In the presence of atrial enlargement, stretching or fibrosis of the atrial muscle may justify the intra-atrial conduction defect pattern.

Right atrial enlargement gives rise to peak but not broadened P-waves. The greater duration of right atrial activation in right atrial enlargement does not surpass the time required for left atrial depolarization.

The pattern of left atrial enlargement (wide P-waves, >0.11 s, with terminal negative forces in lead V_1 > 0.04 s, and with amplitude ≥0.1 mV) has been shown to correspond to delayed activation of the lower left atrium [2].

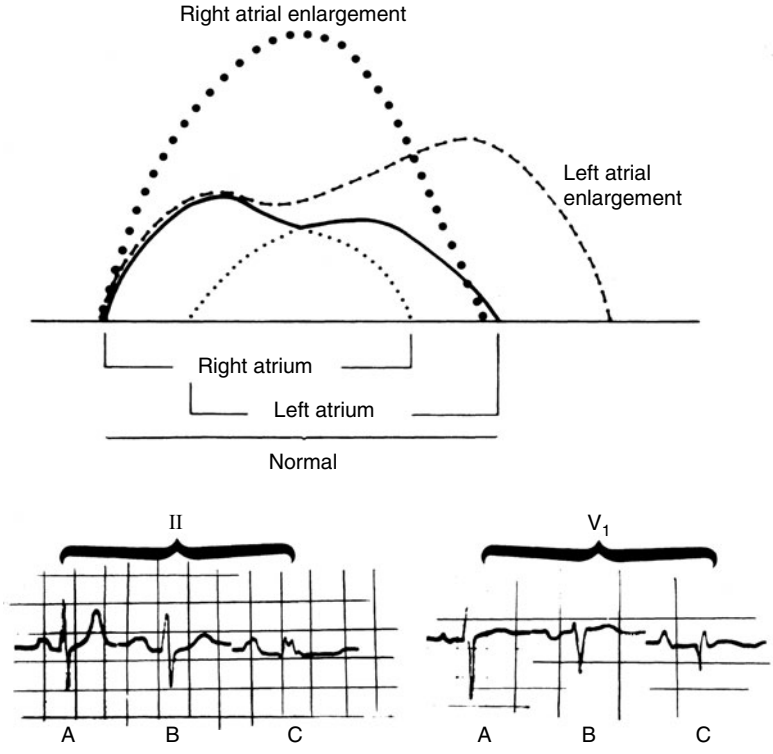

Figure 14.2

Diagram illustrating left and right atrial contribution to the recorded P-wave, explaining the small notch present in P-waves from some normal individuals. Because right atrial activation is completed before that of the left atrium, right atrial enlargement will cause higher voltage of the P-wave with a normal duration. (Although the right atrial component may become enlarged, it will not surpass the normal left atrial component). With left atrial enlargement, the notching will be accentuated with increased duration of the P-wave. Typical examples of these P-wave patterns in leads II and V_1.

It remains uncertain whether local delay (or block) of the atrial activation can result in notching of the P-wave without an increase in its duration. On the other hand, some normal subjects, with no evidence of heart disease, do have a small notch at the peak of the P-wave, which is probably related to the normal asynchronism of activation between both atria. The question remains whether or not by itself notching of the P-wave should be considered evidence of intra-atrial or interatrial conduction defect (usually an interpeak ≥0.04 s is recommended as a criterion for such a conduction defect; however, this usually occurs in cases that also have an abnormal duration of the P-wave).

Another difficult problem is to define the upper limit for normal duration of the P-wave. Several studies of normal populations have been published suggesting an upper limit of 0.10 s [7, 8], 0.11 s [9–11], and 0.12 s [10–12]. It must be remembered, however, that P-wave duration, like other biological values, represents a continuum and consequently, any dividing line will have some normals on the "abnormal" side, as well as some abnormals on the "normal" side. The best cutoff point for the upper limit of normal seems to be 0.11 s.

Besides prolongation of intra-atrial conduction time (first-degree intra-atrial or interatrial block), more advanced degrees of block (second and third degree) have been demonstrated by electrophysiological studies [13–15]. This is also the case for Wenckenbach phenomenon and for dissociated rhythms of the left and right atria or even of a region of one of the atria.

The case of the transplanted heart is a most interesting example, where activation of the remnant auricular tissue can be independent of the activation of the transplanted auricular chambers (Fig. 14.3).

Some cases of apparent first-degree AV block may actually be a result of intra-atrial or interatrial conduction delay with normal conduction through the AV node.

Although the more advanced degrees of interatrial block can be important in the genesis of supraventricular arrhythmias, their identification is not easy using the surface ECG and can only be demonstrated by intracardiac electrophysiological studies.

The Criteria Committee of the New York Heart Association and the World Health Organization/International Society and Federation of Cardiology (WHO/ISFC) Task Force have proposed the following ECG criteria for the diagnosis of intra-atrial (interatrial) conduction defects [8, 16]:

(a) P-wave duration >0.11 s
(b) Notching of the P-wave

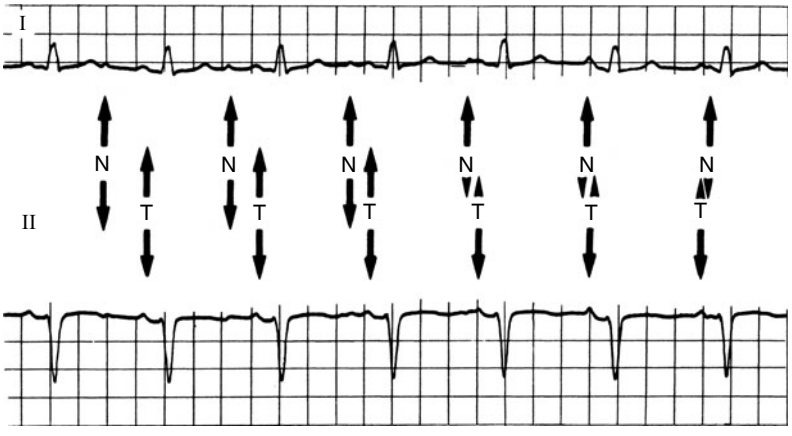

Figure 14.3
Simultaneous leads (I and II) in a patient with a transplanted heart. Two independent and dissociated atrial rhythms are well identified, one without ventricular conduction (remnant native atrial tissue – N) and the other with normal AV conduction and constant PR interval (transplanted heart-T). (Courtesy of Dr. Queiroz e Melo).

14.2.2 Diagnostic Difficulties

The major diagnostic problem is the identification of left atrial enlargement and distinguishing its ECG from intra-atrial conduction delay alone (without atrial enlargement).

Some of the authors studied 83 hypertensive patients by ECG and echocardiography, correlating the pattern of ECG atrial activity with left atrial dimension by echo [17]. Of 74 patients in normal sinus rhythm, 13 (18%) showed increased terminal negative P-wave forces in V_1 (≥0.04 s and ≥0.1 mV) and 20 (27%) had increased duration of the P-wave in lead II (>0.11 s), without increased terminal forces in V_1. The other 41 had normal P-waves.

The former group (increased terminal negative forces in V_1) had a much greater prevalence of left atrial enlargement by echocardiography (62%) than patients with normal P-waves (20%). In our cases, no statistically significant difference was found between patients with enlarged P-waves in lead II and patients with normal P-waves in the same lead, as far as left atrial enlargement prevalence (30% as opposed to 20%) or mean left atrium dimension (38 mm as opposed to 36 mm) were concerned. In our experience, terminal negative P-wave forces in V_1 can be used to identify left atrial enlargement, while P-waves of greater duration, in the absence of increased terminal forces in V_1, do not necessarily imply left atrial enlargement, and more probably correspond to intra-atrial or interatrial conduction defect.

It is suggested that echocardiography should be used to evaluate left atrial dimension in order to decide whether left atrial enlargement is or is not the cause of the abnormal ECG pattern (Fig. 14.2).

14.2.3 Clinical Overview

Intra-atrial and interatrial conduction defects are probably more frequent than is usually recognized. In the presence of an enlarged P-wave, left atrial enlargement should be ruled out (by echocardiography) before the diagnosis of conduction defect is made.

Much is still to be learned about higher degrees of intra-atrial and interatrial block, which need electrophysiological studies to be clearly understood. However, they may play an important role in some cases of supraventricular dysrhythmias [13, 14, 18].

14.3 Intraventricular Conduction Defects

The normal cardiac specialized conduction system has been described in detail in Chap. 5. Normal ventricular activation is summarized here for convenience and to emphasize those aspects of particular relevance to the topic under consideration.

The specialized conduction system consists of the sinoatrial (SA) node, the atrial conduction pathways (whatever their real importance may be), the AV node, the His bundle, the right and left bundle branches (the latter with two main subdivisions – anterosuperior and posteroinferior), and the Purkinje fibers. Occasionally, a third septal subdivision of the left bundle (median or centroseptal) may also be identified [19–21], and in still other cases the branching pattern of the left bundle is not clearly defined (see Sect. 14.3.1) (Fig. 14.4).

The initial electrical stimulus of the cardiac muscle activity is generated at the SA node. From there, it spreads across the atria and reaches the AV node. Within the AV node, it is physiologically delayed before being propagated rapidly along the His bundle and its right and left divisions and subdivisions, to the Purkinje network. When the wave of activation reaches the myocardial cells, it causes their depolarization and subsequent contraction.

Durrer et al. [1] have investigated the initial ventricular activation in the isolated human heart and found that, normally, three endocardial areas are synchronously excited at the beginning of left ventricular activation:

(a) An area located high on the anterior paraseptal wall, below the attachment of the mitral valve, extending inferiorly to the region of the anterior papillary muscle
(b) A central area in the left surface of the interventricular septum
(c) A posterior paraseptal area at about one-third the distance from the apex to the base

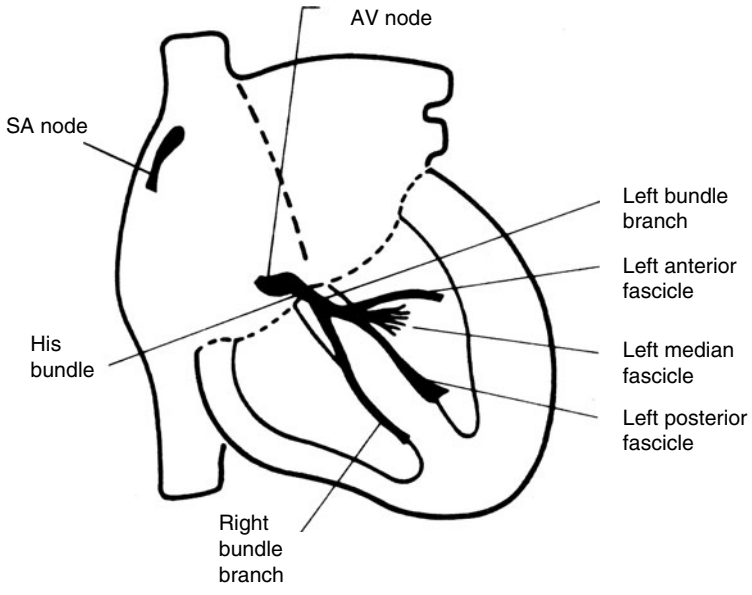

Figure 14.4

Schematic of the normal IV conduction system. A well-individualized median (or centroseptal) fascicle is represented.

Activation of the anterior paraseptal and central areas is mediated by the anterior division of the left bundle branch. The posterior division provides conduction to the posterior paraseptal area (sometimes a less-well-defined subdivision is described providing conduction to the central septum). Since anterior and posterior paraseptal areas are opposite to each other, the direction of the resultant vectors of excitation, during this phase, will be dominated by the potentials of the central area.

After the excitation of the septal areas, the electrical stimulus spreads to the myocardium of the apical and the free wall of both ventricles, which are then activated. As a result of the much larger mass of the left ventricle, the electrical forces produced by its depolarization largely predominate over the right ventricular potentials.

The basal portion of the septum and the posterobasal portion of the free wall of the left ventricle are the latest regions to be depolarized, partly because there is a relative rarity of terminal Purkinje fibers in these areas.

This sequence of ventricular activation can be represented by three basic dominant vectors, as below, occurring sequentially, with their positive extremities inscribing the vectorcardiographic spatial QRS loop.

(a) The initial vector corresponds to the early septal and paraseptal electromotive forces (emfs). The right interventricular septal surface anatomically faces the anterior and right side, either slightly upward or slightly downward (according to the horizontal or vertical positioning of the heart). Since the septum is depolarized from left to right, the initial phase of ventricular depolarization and the subsequent spread of activation across the septum cause the initial vector to be oriented mainly to the right and anteriorly, either upward or slightly downward.
(b) The second vector is the maximal resultant vector related to the activation of the free wall of the ventricles. Left ventricular emfs dominate and give rise to the leftward, inferior and posterior orientation of this vector.
(c) The terminal vector is related to the activation of the basal portions of the ventricles, which results in electrical forces oriented posteriorly, and somewhat superiorly, either slightly to the right or slightly to the left.

These three vectors, when projected upon the axis of the limb and precordial leads, produce, respectively:

(a) A small r in V_1 and a small q in leads I, aVL, and V_6;
(b) A dominant R-wave in I and II as well as V_5 and V_6 with a counterpart in the S-waves of aVR and V_1;
(c) A small s in V_6 and leads I and II, sometimes an r' in V_1.

The remaining leads will present intermediate patterns, which can be derived from the projection of the QRS spatial loop upon their own axis of derivation. Leads III and aVF on one side, and aVL on the other, will be predominantly positive or negative, in normal subjects, according to their body shape (vertical axis in slim individuals and horizontal in the obese).

Anatomic or functional lesions occur at any point of the very sensitive specialized ventricular conduction system, and may result in delay or interruption of the conduction of the electrical stimulus to the areas forward to the lesion. Since the several divisions and subdivisions of the bundle branches are largely interconnected, conduction will follow across the intact divisions and will result in the activation of the whole ventricular mass. However, the sequence of activation will be different, in each case, from that previously described. Different sequences of activation mean different spatial QRS loops and different ECG patterns.

It must be emphasized from the very beginning that although the electrical patterns will facilitate an approach to the identification of the anatomic location of the conduction defect, different locations and different types of conduction defects may result in similar ECG patterns. For example, a complete left bundle branch block can be caused by a functional lesion within the His bundle, before the bifurcation; by a complete interruption of the main left bundle branch (either anatomic or functional); or by lesions located more distally, either in both the left anterior and the left posterior fascicles, or as a diffuse disease of the more distal ramifications of the left bundle (parietal block). On the other hand, the same pattern can coexist with multiple and diffuse lesions along the conduction system. In pure pathological terms, it can sometimes be very difficult to decide which the most important lesions are. Even the determination of the percentage of injured fibers, in each division or subdivision, by microscopy, has been used to study this problem, although not very conclusively [19, 22]. As a matter of fact, such studies are highly demanding and poorly rewarding.

The understanding of intraventricular conduction-defect patterns has evolved through the years. For instance, during the first decades of electrocardiology, right and left bundle branch block (RBBB and LBBB, respectively) were inversely diagnosed, on the basis of dog experiments. Much was learned, but even today much controversy still exists around some of the criteria used in ECG/VCG classification of conduction disturbances.

Great advances were made owing to the concept of fascicular blocks and its correlation with the anatomic and electrophysiological data, mainly those obtained by endocardial and epicardial mapping, as well as His-bundle electrocardiography. Intermittent or iatrogenic (surgical) conduction disturbances have also been of great help in the understanding of some ECG patterns.

An important effort was made by a WHO/ISFC Task Force [16] who attempted to establish a consensus on international criteria for the diagnosis of intraventricular conduction defects. In this chapter, those criteria will be followed and will occasionally be presented along with other more controversial points of view.

14.3.1 Fascicular Blocks

The correlation of the anatomy of the cardiac conduction system with electrocardiographic and electrophysiological data, leading to the concept of fascicular blocks (so-called "hemiblocks"), has added much to our understanding of the mechanisms of electrical activation and of heart block. Despite some arguments as to its validity, the concept of fascicular blocks has provided a most useful theoretical framework for viewing abnormalities of auriculoventricular and intraventricular conduction.

As previously stated, the left-sided intraventricular conduction system is usually described as a multiple strand of fibers emerging from the His bundle itself, at the septal surface (Fig. 14.4), with two main subdivisions or fascicles: one directed anteriorly and superiorly toward the base of the anterior papillary muscle (the left anterior fascicle) and the other directed inferiorly and posteriorly toward the base of the posterior papillary muscle (the left posterior fascicle). The two main subdivisions have extensive interconnecting anastomoses between them. Occasionally, a group of the left median fibers is more clearly identified, constituting a third septal (median or centroseptal) fascicle [19–21, 23] (Fig. 14.4). This led to a debate around the concept of a bifascicular or trifascicular left-sided conduction system (and trifascicular against a tetrafascicular or quadrifascicular system, for the whole conduction apparatus) [20, 21]. Most probably, the anatomic network of the left-sided conduction system has a variable distribution within the population as happens with other anatomic structures (such as the coronary arterial system). Eventually there exists, for the left main bundle, a continuum from either two or three subdivisions to a nondefined branching type (fanning out as a pencil-like division) of the main left bundle branch.

Indeed, a few cases have also been described where false tendons were found running across the ventricle. These tendons contain conduction tissue, which can therefore alter the activation sequence and contribute to the variation of the normal pattern and hence of electrical axis [24].

In fact, all the above-mentioned structures may be involved, organically or functionally, in the aberrations observed in atrial premature beats, mimicking successively all types of intraventricular conduction disturbances: slight axis deviation, fascicular blocks of any type, complete bundle branch blocks, and trifascicular or tetrafascicular blocks [20, 25].

The concept of a conduction disturbance occurring in one of the two left bundle branch subdivisions has been introduced by Rosenbaum, who used the term hemiblock [26, 27]. For those who accept a trifascicular left-sided conduction system, hemiblock became a misnomer, since there exists three different types of "hemi" blocks – left anterior, left posterior, and left median [20, 21, 28].

"Left fascicular blocks" is probably the best way to refer to these localized conduction disturbances and has become the internationally accepted terminology. Nevertheless, the term hemiblock has stood the test of time and sometimes is used even for the third left subdivision – left median hemiblock (for left median fascicular block) [20, 21, 29, 30].

14.3.1.1 Left Anterior Fascicular Block

(a) ECG/VCG pattern

The hallmark of left anterior fascicular block (LAFB) is marked left axis deviation in the limb leads (Fig. 14.5).

Owing to the organic or functional interruption of the conduction through the left anterior division of the left bundle branch, the electrical impulse must travel through the left posterior division to activate the free wall of the left ventricle. The inferior and posterior portions of the left ventricular free wall are depolarized in the normal way (via the intact left posterior subdivision). The activation of the anterior and lateral regions is delayed (by ≈ 0.02 s) because the stimulus cannot be conducted through the interrupted left anterior division. Consequently, the wave of activation will travel in a retrograde fashion, through the network of the Purkinje system, in order to reach the anterolateral wall. The initial electrical forces (0.02 s) do not have the component of the anterior paraseptal area, thus resulting in the dominance of the forces directed inferiorly and to the right. Subsequently, the inferior wall and the apex are activated (forces directed inferiorly) and only afterward in the anterolateral wall depolarized with a leftward, posterior and superior spread of excitation. The latter QRS forces become more prominent because, being delayed, they are unopposed.

The VCG spatial QRS loop will be of normal magnitude (if there are no associated abnormalities) although with slightly prolonged duration of the QRS (not greater than 0.11 s). The initial vectors point inferiorly and to the right while the body of the spatial QRS loop is superiorly and posteriorly displaced, being located in the left superior and posterior octant.

Typically, in the frontal plane projection, the initial QRS deflection points inferiorly and slight to the right, while the efferent limb is leftward and is inscribed counterclockwise, invading the left superior quadrant. The maximal QRS vector and afferent limb of the spatial QRS loop are oriented superiorly and to the left (the maximal QRS vector can rarely point superiorly and to the right).

As the greater portion of the QRS loop is directed leftward and superiorly, a prominent R-wave is detected in leads I and aVL, while deep S-waves are registered in II, III, and aVF. The initial deflection, pointing inferiorly and slightly rightward, projects itself as a small q-wave in leads I and aVL (qR complexes); if they point anteriorly or slightly leftward, an isolated monophasic R-wave will result in lead I. A small r-wave is always present in leads II, III, and aVF since the initial deflection is always inferior. The superior displacement of the main portion of the loop explains the abnormal axis deviation, between −30° and −90°. Usually ST- and T-waves remain within the normal range, pointing downward and to the left. However, the prominent R-wave in aVL may be accompanied by a slightly negative T-wave.

Criteria for left anterior fascicular block are still debatable [31–40]. Rosenbaum's original criteria [26, 27] were the following:

(a) Frontal plane QRS left axis deviation −45° to −80°
(b) QRS duration ≤0.11 s
(c) Small Q-wave ≤0.02 s in leads I and aVL

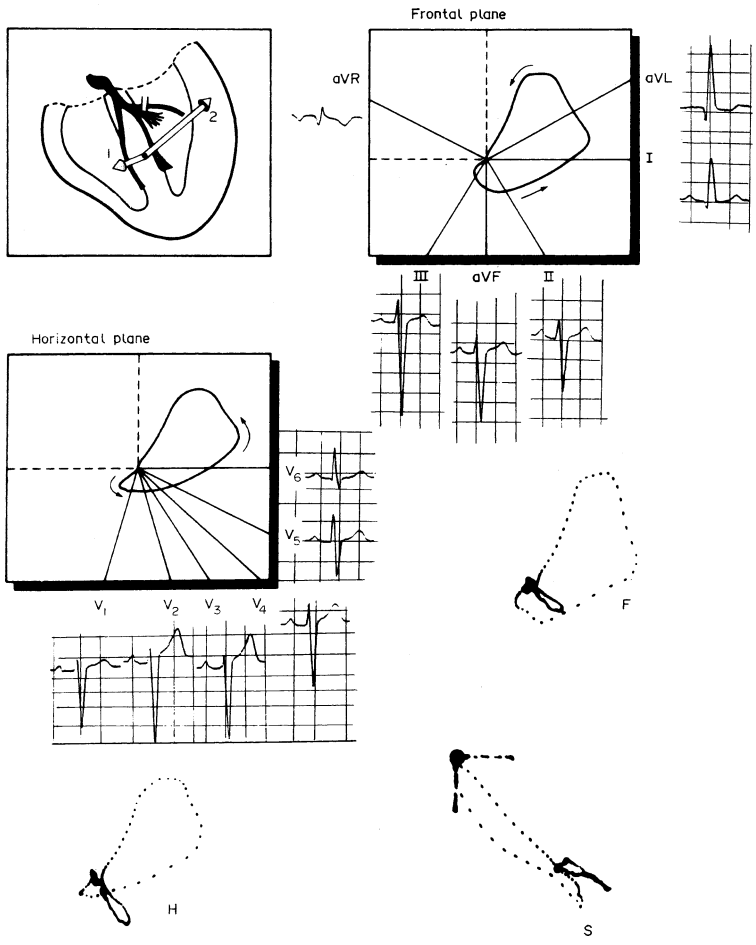

Figure 14.5

Left anterior fascicular block: schematic of the spatial main vectors of ventricular activation resulting from the interruption of the left anterior fascicle (*top left corner*) and a diagram of the projections of the QRS loop on the frontal and horizontal planes and ECG leads and VCG loops of a typical example (F, frontal; H, horizontal; S, sagittal).

As far as left axis deviation is concerned, there is enough agreement [31, 38, 39] in that left axis deviation alone should not be synonymous with LAFB because this shift of electrical forces to the left and superiorly can be observed with other causes such as extreme obesity, chronic pulmonary disease, thoracic malformations, and inferior and inferolateral myocardial infarction. The limit of −45°, as pointed out by Rosenbaum [26, 27], mostly eliminates those other causes but it also eliminates LAFB of lesser degree (as demonstrated in cases of transient LAFB). Thus the limit of −30° has been used by most groups of investigators [32, 40, 41] although some prefer −40°, unless transient shift is observed. It is possible to demonstrate that the axis deviation occurs during the first 60 ms of the QRS complex (especially in cases with QRS duration beyond 0.11 s, owing to other associated intraventricular conduction disturbances – for instance, RBBB or LBBB).

The small Q-waves in leads I and aVL have also caused some controversy [36, 38, 42–44]. Kulbertus et al. [36] found that the initial 10 ms QRS vectors are almost always directed inferiorly. However, while in 55% they were directed to the right, in 45% they pointed to the left, which in some cases may provoke a QS pattern in V_1. Jacobson et al. [35] and Burchell and Tuna [31] also concluded that a Q-wave in leads I and aVL is not an absolute requirement for LAFB. However, they have been found in most cases of transient or paroxysmal LAFB.

Medrano et al. [45] consider that there should be either slurring of the downstroke of the R-wave with delayed R peak time of at least 45 ms in aVL, or a late slurred terminal R-wave in aVR, or else a slurred S-wave in leads V_5 and V_6.

In fact, although the QRS duration is normal in isolated LAFB, there may be a slight widening of the QRS complex of up to 0.02 s compared to appearances prior to the development of LAFB.

The WHO/ISFC Task Force has proposed the following ECG criteria for diagnosis of LAFB [16]:

(a) Left axis deviation of −45° to 90°
(b) qR pattern in aVL
(c) R peak time in aVL ≥45 ms
(d) QRS duration <0.12 s

When these criteria are present with QRS axis deviation of −30° to −45°, the diagnosis of a "possible" LAFB should be made.

Note that the QRS loop in the frontal plane is inscribed counterclockwise – a feature which may be useful in the presence of inferior wall myocardial infarction (the peak of the R-wave in lead III occurs before the peak of the R-wave in lead II).

Lopes [46] has proposed VCG criteria for the diagnosis of LAFB as below:

(a) The QRS duration should be <0.12 s
(b) The frontal plane QRS loop should have the following characteristics:
    (i) Initial vectors directed inferiorly and rightward
    (ii) Counterclockwise inscription
    (iii) QRS axis more superior than −30°

    If the major axis of the QRS loop is not directed upward, but the late part of the loop invades the left superior quadrant, "possible LAFB" may be diagnosed.
(c) The horizontal plane QRS loop should have the following features:
    (i) Initial vectors oriented rightward and anteriorly
    (ii) Counterclockwise inscription in general, but about 20–30% may show a predominant anterior loop with clockwise inscription, which can represent associated median or centroseptal fascicular block [29, 30, 47, 48]
    (iii) Terminal vectors may be normal or located predominantly in the right posterior quadrant

(b) Clinical implications

LAFB has been associated with conduction disturbances in the His bundle, anterior ischemia, anterior myocardial infarction, Chagas disease, sclerodegenerative disease, cardiomyopathy [49], hyperkalemia [50], myocarditis, infiltrative and degenerative diseases, and trauma (its association with incomplete RBBB in ostium primum defect is discussed in Sect. 14.3.2.1). It is usually associated with fibrosis in the anterior fibers, although fibrosis is usually widely distributed over the anterior, mild, and posterior fibers [22].

LAFB unassociated with block in other fascicles is usually considered a benign intraventricular conduction disturbance. Nevertheless, in one angiographic study [51], LAFB was associated with a 50% chance of having 95% or greater occlusion in the left anterior descending artery. However, this was a selected population in which the prevalence of coronary heart disease was high enough to justify a coronary angiographic study. In the Framingham study, the incidence of progression to bifascicular block was 7% and to complete AV block, 3% [52]. In the ambulatory patient, the prognosis of LAFB is exceedingly benign [29, 53, 54]. As will be seen with other types of conduction defects, prognosis depends primarily on the severity of the associated heart disease [55]. In the absence of other cardiovascular abnormalities, LAFB seems not to affect the prognosis, even in old age.

(c) Diagnostic difficulties

LAFB may mimic anteroseptal myocardial infarction (QS in V_1 and/or V_2 and sometimes QR with a negative T-wave in aVL). Sometimes, inferior infarction may also be erroneously diagnosed owing to low voltage of initial R-waves in inferior leads (distinction can be more easily made by the rotation of the frontal plane QRS loop, which is inscribed clockwise in inferior myocardial infarction and counterclockwise in LAFB). The appearance of new initial R-waves in the inferior leads owing to LAFB may hide preexisting inferior myocardial infarction. On the other hand, a recent inferior wall myocardial infarction may abolish the initial R of LAFB in leads II, III, and aVF, so that QS complexes are recorded. All these aspects have been well identified in cases of paroxysmal LAFB. Occasionally, secondary ST–T-wave abnormalities (slight ST depression and negativity of the T-wave in aVL) may also make it difficult to exclude anteroseptal ischemia (Fig. 14.6). R-waves tend to be taller in lead I and aVL when LAFB supervenes; this may occasionally render voltage criteria invalid for left ventricular hypertrophy (false positives).

14.3.1.2 Left Posterior Fascicular Block

(a) ECG/VCG pattern

The hallmark of left posterior fascicular block (LPFB) is the right axis deviation in the limb leads (Fig. 14.7). In fact, in cases of LPFB, either organic or functional, the opposite of LAFB occurs, that is to say, ventricular excitation proceeds through the left anterior division to the anterior paraseptal region and midseptum, and from there to the anterior and anterolateral wall. Activation of the posteroinferior regions of the left ventricle is delayed (proceeding in a retrograde fashion from the anterior fascicle).

Initial QRS forces (10–20 ms) are directed superiorly and leftward (around −45°), with the spatial QRS loop being inscribed clockwise, invading the inferior octants, first the left then the right, either posteriorly or slightly anteriorly.

The main characteristic of LPFB is the inferior and rightward displacement of the spatial QRS loop with an abnormally large portion located in the right inferior and posterior octant. Although there may be slight widening, the duration of the QRS does not exceed 0.11 s. The maximal spatial QRS vector is oriented inferiorly and posteriorly and most of the time to the right.

Initial forces, being leftward, give rise to an initial R-wave in lead I and aVL. Then the rightward displacement of the QRS loop causes deep S-waves in I and aVL while a qR pattern is obtained in II, III, and aVF. The rightward displacement of the loop accounts for the right axis deviation of the QRS.

Rosenbaum [26, 27] first described a QRS deviation ≥ + 120°; later, he accepted +90° as a criterion. Serial observation of the transition to right axis deviation would better support the diagnosis in an individual, more so in cases of intermittent LPFB.

In the horizontal plane, RS complexes in the left precordial leads cause further difficulty in distinguishing LPFB from right ventricular hypertrophy.

In practice, the diagnosis of "pure" LPFB is difficult and needs the clinical exclusion of several conditions which may produce a similar pattern, owing to predominant right ventricular forces, instead of the redistribution of forces within the electrically dominant left ventricle. Examples are right ventricular hypertrophy, chronic obstructive as well as acute pulmonary disease, emphysema, extremely vertical heart (habitus asthenicus), and extensive lateral-wall myocardial infarction. Besides clinical examination, chest x-ray and echocardiography are mandatory. As a result in part of those difficulties, LPFB is rarely recognized [27, 56–58] unless associated with RBBB.

The WHO/ISFC Task Force has proposed the following ECG criteria for the diagnosis of LPFB [16]:

(a) Frontal QRS axis of +90° to +180° (in the absence of other causes of right axis deviation)
(b) rS configuration in leads I and aVL associated with qR pattern in inferior leads (Q-wave is obligatory in leads III and aVF), Q-wave in inferior leads should be ≤0.04 s
(c) QRS duration <0.12 s

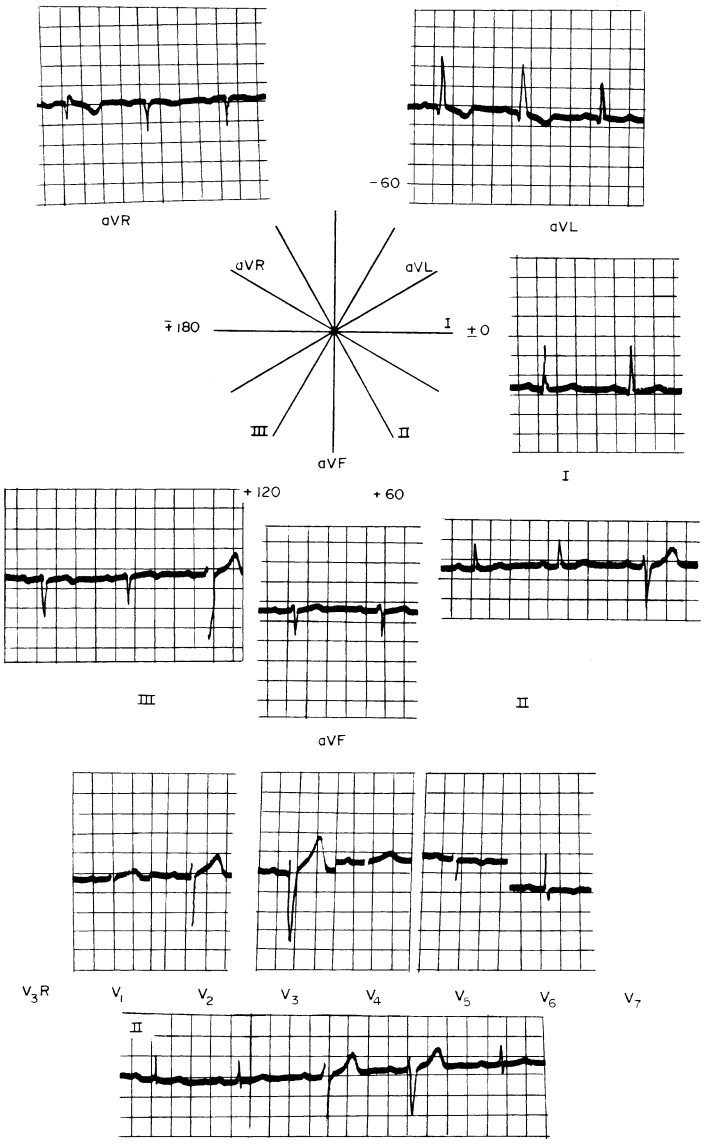

Figure 14.6

Vectorial display of the 12-lead ECG in a case of paroxysmal LAFB. In aVL, first and second QRS complexes show conduction during LAFB followed by normal IV conduction in the third QRS complex. Note negative T-waves during LAFB become positive during normal conduction. Appearance and disappearance of LAFB is not related to significant R–R interval variation (lead II at the bottom).

Lopes [46] has proposed VCG criteria for the diagnosis of LPFB as below:

(a) The QRS duration should be <0.12 s.
(b) The frontal plane QRS loop should have the following characteristics:
  (i) Initial vectors inscribed superiorly and leftward
  (ii) Clockwise inscription
  (iii) QRS axis more rightward than +90°

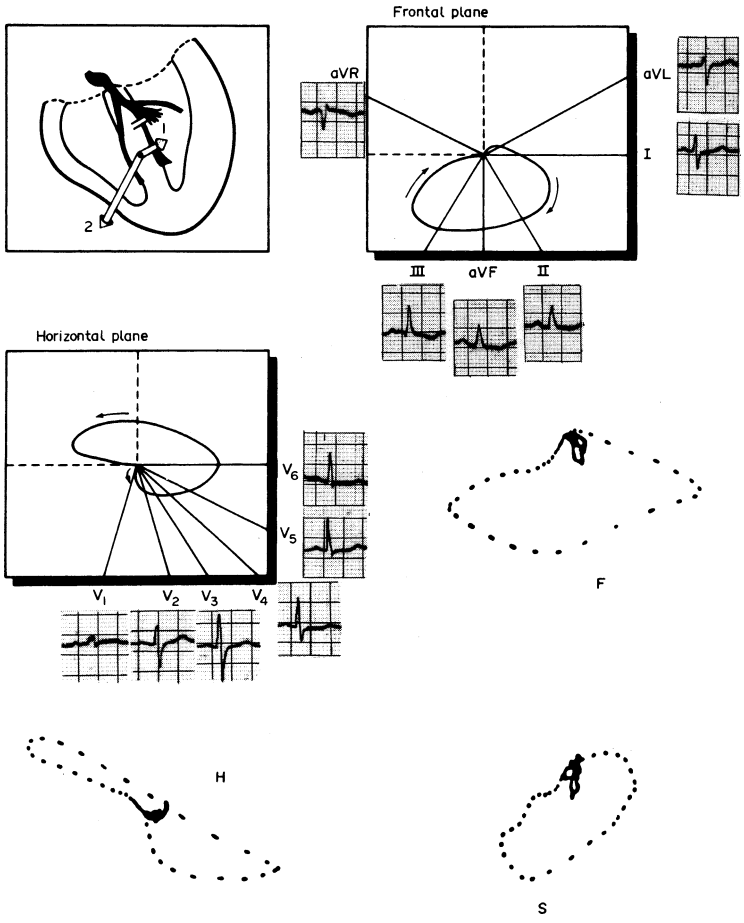

Figure 14.7

Left posterior fascicular block: schematic of the spatial main vectors of ventricular activation resulting from interruption of the left posterior fascicle together with a diagram of the projections of the QRS loop on the frontal and horizontal planes and ECG leads and VCG loops of a typical case of LPFB (F, frontal; H, horizontal; S, sagittal) (see also Figs. 14.18 and 14.19).

(c) The horizontal plane QRS loop should have the following features:
- (i) Initial vector anterior and leftward
- (ii) Counterclockwise or figure-of-eight inscription generally
- (iii) Rightward and either posterior or anterior maximum QRS vector

(b) Clinical implications

LPFB is much rarer than block of the left anterior fascicle, because the left posterior fascicle is substantially larger and apparently better perfused, and therefore less susceptible to damage. Chronic degenerative or fibrotic processes, ischemic processes affecting this fascicle or the Purkinje system (or the myocardium activated by the fascicle), hyperkalemia, myocarditis, Chagas disease, infiltrative disease, and acute cor pulmonale [59] have been described as associated with LPFB.

(c) Diagnostic difficulties

Isolated LPFB may be difficult to recognize. Obviously, it will be most accurately diagnosed when it occurs as an intermittent pattern. LPFB may mimic an inferior myocardial infarction (inferior q-waves). Abnormal Q-waves (>0.04 s)

support the diagnosis of myocardial infarction; history, echocardiography, and radionuclides may help in the differential diagnosis. LPFB may also hide lateral infarction (small r-waves and deep S-waves in lead I and aVL).

When LPFB is associated with positive QRS in V_1 (possibly indicating associated left median fascicular block – see Sect. 14.3.1.3), right ventricular hypertrophy or even hidden Wolff–Parkinson–White syndrome must be ruled out as a cause of the ECG pattern. In young people, the diagnosis is often difficult owing to the vertical axis, and more so if there is constitutional abnormal anatomical position of the heart (extremely vertical).

The tendency for upright T-waves in leads I and aVL may conceal small or slightly inverted ischemic T-wave changes in these leads. T-waves may become inverted in inferior leads thus mimicking an active ischemic process. Anterolateral myocardial infarction (counterclockwise rotation in the frontal plane) must be ruled out for the identification of LPFB. Acute cor pulmonale, as mentioned above, should also be excluded in clinical terms. The $S_I Q_{III}$ pattern suggestive of pulmonary embolism – the McGinn and White pattern – has been interpreted as representing "functional" LPFB [59].

14.3.1.3 Left Median (Centroseptal) Fascicular Block

As mentioned in Sect. 14.3.1, left median fascicular fibers do exist and a left median (centroseptal) fascicular block (LMFB) has been produced experimentally [23]. Indeed, in cases of intermittent fascicular or bundle branch blocks, an anterior displacement of the QRS loop, independent of the axis deviation, can be observed and may be a result of the involvement of centroseptal fibers.

(a) ECG/VCG pattern

The ECG pattern is supposed to show prominent R-waves in the right precordial leads ($V_1 - V_2$), similar to those found in "true" posterior myocardial infarction, concomitant with no abnormal axis deviation in the frontal plane (Fig. 14.8). Left median block is rarely identified as an isolated finding (except when paroxysmal – Fig. 14.9) being confounded with "normal variation." It may explain the anterior displacement of the QRS loop (more prominent R-waves in the right precordial leads) and even the clockwise rotation in the horizontal plane, in cases of left fascicular blocks, RBBB or RBBB associated with either LAFB or LPFB. In relatives of patients with anteriorly displaced loops accompanying more conventional blocks, isolated anterior displacement of the QRS loop has been found. It is uncertain whether this represents normal variation or left median "hemi" block [29, 30, 47, 48].

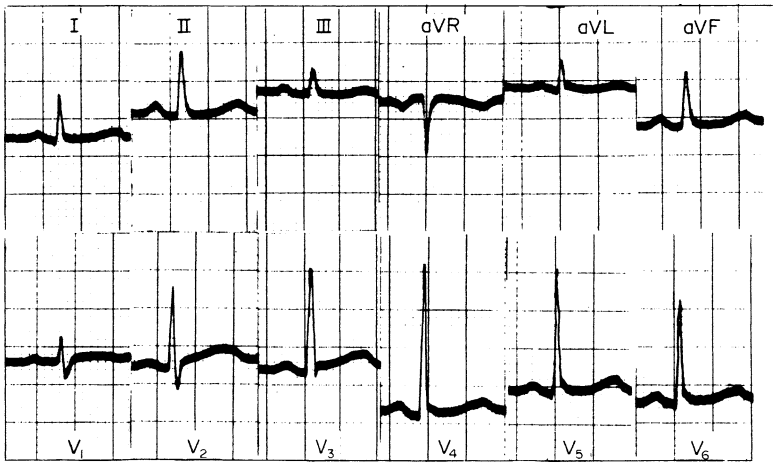

Figure 14.8

ECG with dominant R-waves in "right" precordial leads (V_1 and V_2) with no other ECG abnormalities. Left median fascicular block would be postulated.

Figure 14.9
Paroxysmal left median fascicular block: continuous recording of lead V_1 showing the appearance and disappearance of dominant R-waves without increase in QRS duration.

(b) Clinical implications

LMFB has been described in patients with ischemic heart disease. It is associated with fibrosis of the corresponding fibers, as well as sclerodegenerative changes of the conduction tissue, although similar lesions can be found simultaneously in the other fascicles [19, 23, 60].

Other etiologies include diabetes mellitus and hypertrophic cardiomyopathy.

(c) Diagnostic difficulties

On the basis of interpreting a single ECG, it is essentially impossible to differentiate LMFB from posterior myocardial infarction, some types of right ventricular hypertrophy or variants of normal.

14.3.2 Incomplete Bundle Branch Block

14.3.2.1 Incomplete Right Bundle Branch Block

(a) ECG/VCG pattern

In incomplete RBBB, the transmission through the right bundle is not totally interrupted but only delayed. ECG/VCG patterns may be similar to complete RBBB (see Sect. 14.3.3.1) but of lesser duration (<0.12 s). Only after the left ventricular septum and free-wall activation is initiated are the right interventricular septum and right ventricular free wall depolarized by impulses which are conducted both through the right and the left bundle branches.

Similar to what will be seen in complete RBBB, only the late part of the activation process is disturbed, on the surface ECG and on the special VCG, with orientation of the terminal electrical vectors rightward, anteriorly and either superiorly or inferiorly. The more the conduction through the right bundle is disturbed (three subdivisions have been described [61] and can be gradually involved in the individual patient), the more prominent these late forces become and the more similar the spatial QRS loop lock to complete RBBB with a more-or-less prominent terminal "fingerlike" appendage. The afferent limb and the terminal deflection of the spatial QRS loop become deviated in the anterior and rightward direction. The T loop is directed leftward and posteriorly.

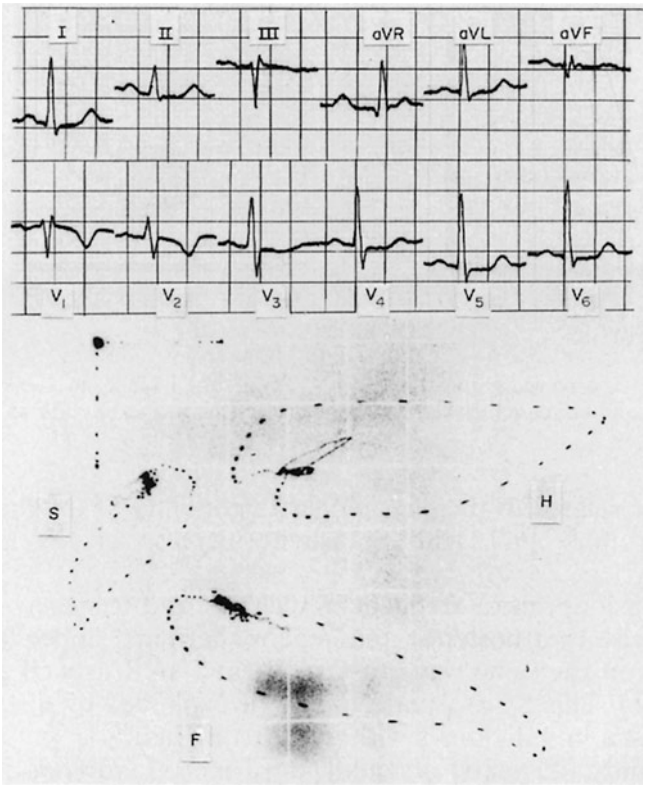

Figure 14.10

ECG leads and VCG loops of a case of typical incomplete RBBB (compare with terminal appendage in horizontal projection of complete RBBB in Fig. 14.13): F, frontal; H, horizontal; S, saggital.

The ECG shows typically an R' wave in lead V_1 and a wider S-wave in lead I and V_6 corresponding to the abnormal anterior and rightward terminal appendage. The amplitude and width of the R′ in V_1 and of the S-wave in leads I and V_6 increase with the degree of conduction delay (Fig. 14.10). By definition, the QRS duration is <0.12 s. T-wave changes arise from the posterior displacement of the spatial T loop. Consequently, the T-wave becomes isoelectric or eventually inverted in the right precordial leads (usually no significant ST–T-wave abnormalities can be identified in the limb and left precordial leads).

The WHO/ISFC Task Force has proposed the following ECG criteria for the diagnosis of incomplete RBBB [16]:

(a) QRS duration <0.12 s
(b) Right precordial pattern rsr′, rsR′, or rSR′ or M-shaped with R′ usually greater than initial R-wave; and
(c) Wide S-wave in leads I and V_5–V_6

The diagnosis is more evident if the condition occurs intermittently.

The VCG criteria for the diagnosis of incomplete RBBB have been recommended as below.

(a) The QRS duration should be <0.12 s.
(b) The spatial QRS loop should have normal overall amplitude but be typically deformed by a small terminal fingerlike appendage, which is oriented to the right.
(c) The transverse plane should have the following characteristics:
    (i) Counterclockwise inscription of the major part of the loop (sometimes figure-of-eight configuration)
    (ii) Initial vector anterior and rightward, with maximal QRS vector leftward and either anterior or posterior

(iii) Small terminal appendage directed rightward and somewhat anteriorly, and slowly inscribed
(iv) Maximal QRS voltage usually less than normal

(d) The frontal plane should have the following features:

(i) The loop generally long and narrow
(ii) Usually clockwise inscription
(iii) Small terminal appendage directed rightward and either superiorly or inferiorly.

(b) Clinical implications and diagnostic difficulties

An incomplete RBBB pattern in the 12-lead ECG can be observed as a "normal variant." Hiss and Lamb [62] reported a prevalence of 2.4% in normal young subjects. Raunio et al. [63] found an rSr′ pattern in V_1 in 2.9% of children, 1.4% of young adults and 0.65% of middle-aged and elderly subjects without evidence of cardiopulmonary disease. Sometimes, these patterns are no longer evident if V_1 in recorded one intercostal space lower [64].

The r′ pattern has been related to the physiological variability of the thickness and distribution of the right ventricular mass [65], with the slight increase of the normal terminal vector described in Sect. 14.3.

A normal variant QRS loop, more frequent in children and teenagers – with more prominent terminal vectors, giving rise to a posterior and superior terminal appendage, slightly directed to the right – may produce, in the same way, an r′ in V_1 and aVR as well as a terminal S-wave in leads I, II, III, and V_6 [66]. This $S_I S_{II} S_{III}$ pattern may be explained by distal delayed activation of the crista supraventricularis in individuals without heart disease.

In a long follow-up study (20 years) of middle-aged men, Liao et al. [67] found no increased risk of death from coronary heart disease and cardiovascular diseases for those patients with incomplete RBBB pattern. Nevertheless, they observed a higher incidence of development of complete RBBB in such cases, which further supports the concept that in middle-aged men, incomplete RBBB can be a manifestation of a primary abnormality of the cardiac conduction system.

It must be emphasized that the majority of cases diagnosed as incomplete RBBB by ECG alone are not actual examples of a conduction defect. Some of them represent the normal variant just described, while many others correspond to moderate right ventricular hypertrophy. One of the first achievements of vectorcardiography (in the early 1950s) was the demonstration that the so-called "incomplete RBBB pattern" could be caused by right ventricular hypertrophy (in mitral stenosis, for example), with quite different QRS loops in the horizontal plane, although projecting themselves in V_1 and V_6 in a manner similar to RBBB [66, 68] (Fig. 14.11). In fact, subsequently, incomplete RBBB became almost synonymous with moderate right ventricular hypertrophy [66, 68].

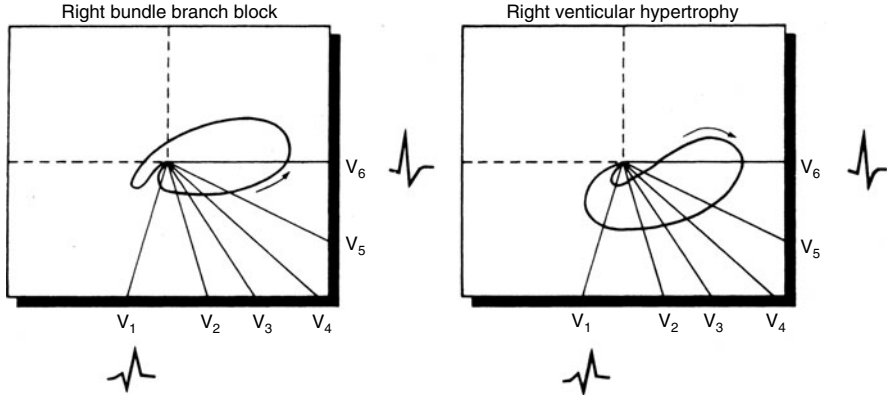

Figure 14.11
Schematic of the vectorcardiographic loops in the horizontal plane, in cases of RBBB and RVH. Quite different loops, with clockwise and counterclockwise rotation, project themselves as rSR′ in V_1 and qRS in V_6 (see also Fig. 11.24).

Actually, right ventricular hypertrophy, owing to either acquired or congenital heart disease, or even chronic lung disease, may cause the typical ECG pattern of incomplete RBBB. However, the morphology and sense of rotation of the spatial QRS loop, mainly its horizontal planar projection, permit an easy differentiation (see the detailed description in Sect. 14.3.3.1). In congenital heart diseases, this pattern may be observed in malformations involving hypertrophy of the crista supraventricularis.

Incomplete RBBB can indeed occur as an isolated congenital electrical abnormality. It is associated with the ostium secundum type of atrial septal defect and/or anomalous pulmonary venous drainage. When incomplete RBBB occurs with the ostium primum type of atrial septal defect, especially with endocardial cushion and interventricular septum defects, there is usually an associated left anterior fascicular block (see Sect. 14.3.4) [69].

Echocardiography [70], as well as radionuclides and angiography, if needed, may help to make the correct diagnosis if the incomplete RBBB pattern is found in a patient with suspected myocardial infarction.

Other clinical factors that may induce an incomplete RBBB pattern are skeletal deformities and LAFB. In the former case, pectus excavatum or straight back syndrome may produce such a pattern. With respect to the latter, sometimes higher degrees of left axis deviation give rise to an r′ in aVR and in V_1–V_2 mainly if registered slightly above the recommended position. On the other hand, leads V_5 and V_6, if recorded lower in the axilla, will exhibit an RS complex instead of R or Rs, recorded slightly above. Both the r′ in V_1–V_2 and/or the S-wave in V_5–V_6, in cases of LAFB, can be erroneously attributed to incomplete RBBB (or right ventricular hypertrophy).

14.3.2.2 Incomplete Left Bundle Branch Block

(a) ECG/VCG pattern

In incomplete LBBB, the conduction of the electrical stimulus through the left bundle branch is not interrupted. However, progression of the wave of excitation should occur at a slower rate and, for this reason (somewhat similarly to complete LBBB – Sect. 14.3.3.2), the initial activation process will enter through the right bundle. The first area to be depolarized will be located in the right septal surface; from there the activation process spreads across the septum and activates the left septal mass from right to left, at a varying degree, because the impulse traveling through the left branch also arrives. Depolarization of the remaining left ventricular free wall then proceeds in a normal fashion. The spatial QRS loop, somewhat elongated, is oriented posteriorly, to the left and either inferiorly or superiorly. The time of occurrence of the maximal QRS vector may be slight delayed (Fig. 14.12).

Therefore, in incomplete LBBB, the initial QRS pattern may be similar to complete LBBB with absence of normal "septal" Q-waves in the left precordial leads and lead I, and sometimes absence of initial r-wave in V_1–V_2. The conduction during the late activation period is less affected, as is the remainder of the QRS (Fig. 14.12).

The more disturbed the conduction through the left bundle branch, the more the ECG/VCG pattern becomes similar to complete LBBB (with progressive prolongation of QRS and delayed R peak time) in the left precordial leads. ST and

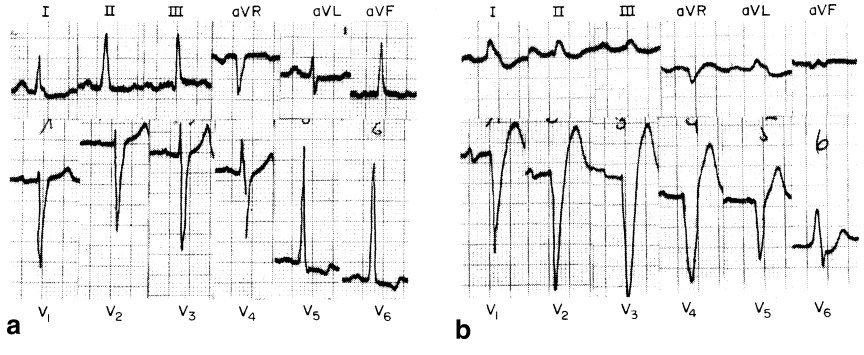

Figure 14.12
Appearance of complete LBBB (part (b)) in a patient with previous LVH with strain (part (a)).

T vectors are usually opposite to the spatial QRS loop thus producing, in the surface ECG, ST-, and T-wave polarities opposite to the main direction of the QRS maximal vector. Surprisingly enough, incomplete LBBB is much more rarely observed than complete LBBB, either as a permanent or as a transient pattern.

A pattern similar to that described for incomplete LBBB can be observed in patients with recognized left ventricular hypertrophy. The question about it being a real conduction defect has been debated [66, 71–74]. Transition within a short time from normal conduction to serial degrees of incomplete and subsequently complete LBBB has been occasionally observed and supports the real existence of incomplete LBBB as a conduction abnormality. Although this evolution would permit a firm diagnosis of conduction defect for the pattern of incomplete LBBB [73], this is only rarely observed and cannot be used for clinical purposes.

The WHO/ISFC Task Force has proposed the following ECG criteria for the diagnosis of incomplete LBBB [16]:

(a) QRS duration >0.10 s but less than the lower limit for complete LBBB (0.12 s);
(b) Prolongation of the R peak time to ≥0.06 s in the left precordial leads
(c) Absence of normal "septal" Q-waves in leads I, V_5, and V_6
(d) Presence of notching, slurring, or both in the ascending limb of the R-wave in the left precordial leads (this is a criteria for increasing the likelihood of the diagnosis of incomplete LBBB).

The VCG criteria for diagnosis of incomplete LBBB have been recommended as follows:

(a) The spatial QRS loop should have the following characteristics:
  (i) Elongated and narrow QRS loop that may be slowly inscribed in the middle and late portion, with a duration <0.12 s
  (ii) Practically, the entire loop oriented posteriorly and to the left
  (iii) Initial vector anterior and leftward
  (iv) Afferent limb superior to the efferent limb
(b) The transverse plane should have the following features:
  (i) Long and narrow loop
  (ii) Clockwise inscription of the majority of the loop
  (iii) Initial vector directed anterior and leftward
  (iv) Afferent limb to the left of the efferent limb
  (v) Slowing on the VCG that may become evident by 40 ms and continues for the entire loop.
(c) The left sagittal plane is characterized by
  (i) A long narrow loop
  (ii) Counterclockwise inscription of the majority of the loop
  (iii) Afferent limb superior to efferent limb
(d) Frontal plane with the following features:
  (i) Small and irregular loop if the spatial QRS loop is almost perpendicular to the frontal plane
  (ii) Counterclockwise inscription of the loop with the afferent limb superior to the efferent limb almost the entire loop on the left

(b) Clinical implications

Incomplete LBBB is associated with the same cardiovascular abnormalities as are usually related to complete LBBB (see Sect. 14.3.3.2). Actually, it represents an intermediate step, occasionally observed, from normal intraventricular conduction to complete LBBB. Incomplete LBBB is frequently associated with left ventricular hypertrophy [75], and has been used by some authors as a criterion for its presence. Its prognosis is related to the underlying heart disease and to its severity, as in the other types of intraventricular conduction defects.

(c) Diagnostic difficulties

Difficulties with diagnosing incomplete LBBB are greater than those found with complete LBBB because the QRS abnormalities are less specific. The following should be considered:

(a) The pattern in right precordial leads may mimic anteroseptal myocardial infarction.
(b) Inverted T-waves in the left-sided leads may mimic anteroseptal ischemia in the same way that positive T-waves in the right precordial leads may conceal ECG signs of anteroseptal ischemia.

14.3.2.3 Complete Bundle Branch Block

The earliest awareness of importance of the specialized conduction system seems to have been related to the identification of the ECG pattern of complete bundle branch block (BBB) resulting from damage caused in the region of the interventricular septum of the canine heart (Eppinger and Rothberger 1909–1910) [76].

Unfortunately, confusion has resulted from the extrapolation of the patterns identified in the vertical heart of the dog to the more horizontally positioned human heart. Consequently, the pattern of complete LBBB was incorrectly diagnosed as complete RBBB and vice versa. This confusion delayed the correct identification of the conduction defect patterns for at least 25 years.

Bundle branch blocks occur in approximately 0.6% of the population and 1–2% of the population over 60 years of age. Up to 80% of patients with BBB do have organic heart disease (coronary heart disease in 50%) [77]. Bundle branch blocks are associated frequently with pathological conditions in the suspected location [78] and with a higher mortality if significant cardiac disease is present [79, 80].

14.3.2.4 Complete Right Bundle Branch Block

(a) ECG/VCG pattern

The hallmark of RBBB is the appearance of an R′ in V_1 with QRS duration ≥0.12 s (Fig. 14.13). When there is complete interruption of the impulse conduction in the right bundle branch, the activation of the right ventricle is delayed. Left ventricular activation will follow the intact left bundle, as in the normal activation sequence.

During the initial phase of the ventricular depolarization process, the early septal and paraseptal activation takes place, as in the normal activation process, spreading from left to right (and somewhat anteriorly and superiorly according to the usual anatomic position of the interventricular septum). No electrical forces are generated at this time in the right septal surface. The activation front then proceeds to the rest of the left septum, and involves the free wall of the left ventricle. The free-wall electromotive forces dominate, with spatial resultant vectors that are oriented leftward and inferiorly, either slightly anteriorly or slightly posteriorly.

Thus, in RBBB, in spite of the lack of right septal activation, the initial phases of ventricular depolarization give rise to potentials and vectors that are rather similar to the normal activation process.

Only after most of the left ventricular free-wall depolarization has already occurred are the right septum and the right ventricular free wall activated, in a delayed and abnormal fashion (slow fiber to fiber conduction across the septum). The resultant late spatial vectors are then directed to the right and anteriorly and either superiorly or inferiorly. At this time, they are dominant because they are no longer concealed by left ventricular potentials.

According to this sequence of events, the spatial QRS loop can be divided into two distinct major portions – initial and terminal. The initial portions remain essentially similar to the normal and consist of the initial deflection, the efferent limb of the loop, and part of its afferent limb which may, in some cases, be displayed somewhat anteriorly, probably owing to centroseptal fascicular lesions. The terminal portion, which is more slowly inscribed, corresponds to the delayed activation of the right septum and right ventricular free wall. This last portion of the loop takes the configuration of a "fingerlike" appendage, pointing anteriorly and to the right. In fact, this late portion represents the most characteristic feature of complete RBBB.

The duration of the QRS loop is ≥0.12 s, with the terminal appendage slowly inscribed (≥0.03 s).

The abnormal activation sequence is followed by an abnormal repolarization course with ST and T vectors directed leftward and posteriorly, opposite to the terminal QRS forces.

The anterior and rightward initial deflection of the QRS loop, when projected in the horizontal plane, is recorded as a small r-wave in lead V_1 and a small q-wave in I, V_5, and V_6 as in the normal individual. If the initial forces are directed either straight anteriorly or slightly leftward, no Q-wave is recorded in these leads. The body of the loop projects itself as an S-wave in V_1, which will be more evident and deeper when the QRS is posteriorly oriented, and may disappear, giving

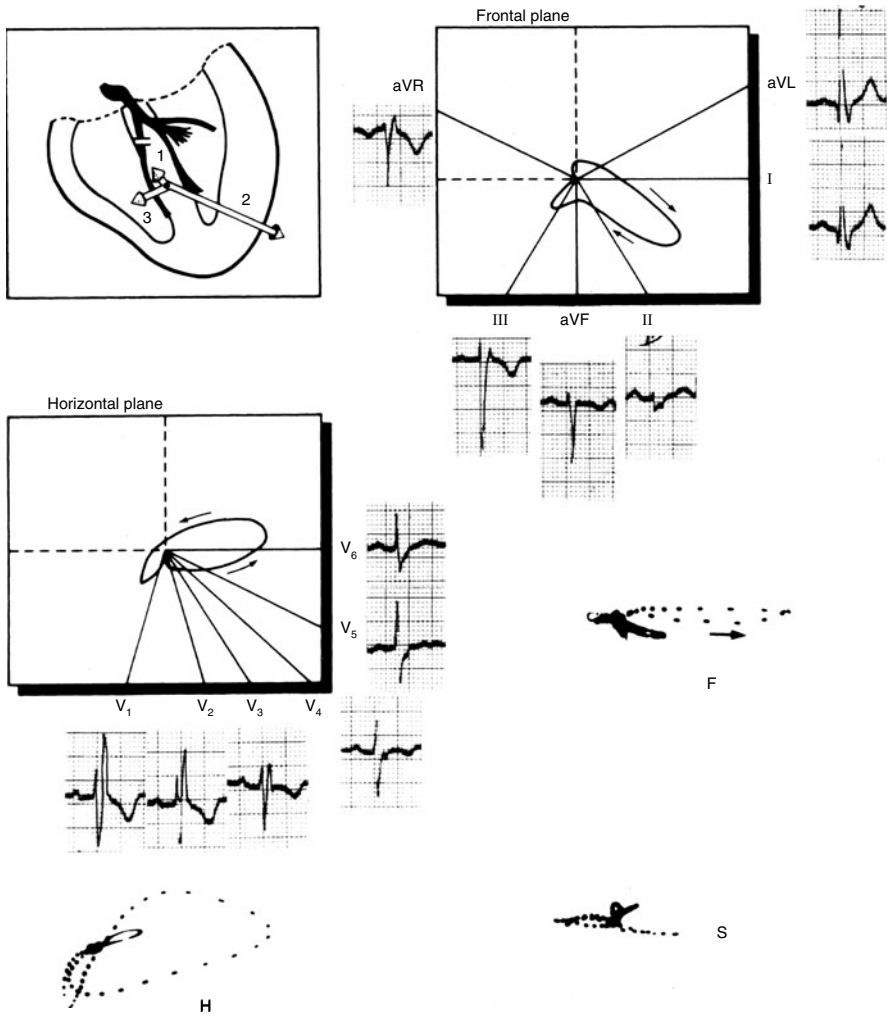

Figure 14.13

Complete right bundle branch block: schematic of the spatial main vectors of ventricular activation resulting from interruption of the right bundle branch together with a diagram of the projections of the QRS loop on the frontal and horizontal planes and ECG leads and VCG loops of a typical case of complete RBBB (F, frontal; H, horizontal; S, sagittal).

rise to a single broad bifid deflection if it points leftward (see Sect. 14.3.1). The delayed terminal appendage, which points anteriorly and to the right, is inscribed as a wide and slurred R' wave in V_1 and an enlarged S-wave in leads I and V_5–V_6.

ST–T patterns are not used as criteria for RBBB diagnosis. The abnormal repolarization pattern appears in the 12-lead ECG as ST-segment depression, as T-wave inversion (or biphasic − +) in V_1 and V_2, and as upright T-waves in leads I, V_5, and V_6.

Since the delayed activation produces alterations only of the terminal, but not of the initial, ventricular depolarization, the electrical QRS axis keeps its normal orientation provided that it was normal before the appearance of the conduction disturbance. In fact, the coexistence of abnormal left or right axis deviation suggests the coexistence of left anterior or left posterior fascicular block (see Sect. 14.3.4).

The WHO/ISFC Task Force has proposed the following criteria for the diagnosis of complete RBBB [16]:

(a) QRS prolongation to ≥0.12 s
(b) Right precordial patterns should be rsr', rsR', or rSR' or M-shaped with R′ usually greater than initial R-wave (occasionally a wide and notched isolated R pattern may be seen)
(c) Leads I and V_5–V_6 pattern must have a wide S-wave (S duration greater than R-wave or >40 ms in adults)
(d) R peak time >0.05 s in V_1 with normal time in V_5 and V_6 (when a notched dominant R pattern is present in V_1).

Lopes has proposed VCG criteria for the diagnosis of complete RBBB as below [46]:

(a) The spatial QRS loop should have normal overall amplitude but is typically deformed by a terminal fingerlike appendage, which is oriented anteriorly and to the right, and loop duration should be ≥0.12 s.
(b) The transverse plane should show the following characteristics:
  (i) Counterclockwise inscription of the major part of the loop, occasionally figure-of-eight or even clockwise (suspect left median fascicular block – see below)
  (ii) Initial vector anterior and rightward, with maximal QRS vector leftward and either anterior or posterior
  (iii) Terminal appendage directed anteriorly and rightward with duration of slowing from 30 to 85 ms
  (iv) Maximal QRS voltage usually less than normal.
(c) The frontal plane should have the following features:
  (i) In general a long and narrow loop
  (ii) Usually clockwise inscription
  (iii) Terminal appendage directed rightward and either superiorly or inferiorly

(b) Clinical implications

Complete RBBB, like complete LBBB, is most frequently identified in adulthood. However, it has been said that it has a higher prevalence in younger subjects than has LBBB [81]. This has not been confirmed in other series [82].

Besides lesions in the right bundle branch, complete RBBB (once more like LBBB) can also occur as a result of anatomic or functional lesions within the His bundle. RBBB can be part of the presenting features of congenital heart disease or be a consequence of corrective surgery [83–85], particularly for pulmonary stenosis, tetralogy of Fallot or large ventricular septal defect [86]. The surgically induced form of RBBB may regress [87] and has been related to prognosis [88]. In adulthood, complete RBBB frequently coexists with hypertension and/or coronary heart disease (either with or without myocardial infarction) [89, 90]. It may appear transiently after primary coronary angioplasty in acute myocardial infarction [91].

Complete RBBB can also represent a secondary manifestation of several cardiomyopathies, including the hypertrophic obstructive type [92]. In fact, an angiographic study [93] performed in 37 predominantly asymptomatic pilots with newly acquired RBBB showed that some of those without evidence of significant coronary artery disease had hemodynamic evidence of a mild diffuse cardiomyopathy. However, the number of cases of "isolated" intraventricular conduction defect which does represent a mild and "insignificant" cardiomyopathy, including ill-defined processes such as bundle branch fibrosis, remains a matter for speculation.

Fibrosis of the right ventricular conduction system with or without the involvement of the left-sided heart skeleton of conduction tissue (respectively, Lev's and Lenegre's disease) [94, 95] may also be the cause of RBBB either associated with ischemia or not. Complete RBBB pattern may also be associated with hyperkalemia [49] and chest trauma [96–99]. Obstructive pulmonary disease [100] and acute pulmonary embolism [101] often appear with RBBB. In the presence of pulmonary disease, complete RBBB may suggest increased systolic and mean pulmonary pressures, thus indicating significant right ventricular overload. The prevalence of associated relevant heart disease, as well as the prognostic implications of complete RBBB pattern, differs according to the type of population studied.

In military studies, a very low prevalence of the heart disease and a very good prognosis have usually been found [81, 93, 102–105]. In a study of 237,000 airmen, Rotman and Triebwasser [81] identified 394 cases of complete RBBB. One hundred cases were younger than 30 years of age: most of them were asymptomatic (97%) and had an otherwise normal cardiovascular examination (94%), 3% had evidence of coronary heart disease, and 2% were hypertensive (these percentages are significantly lower than the prevalences reported in the same study for cases with LBBB; see Sect. 14.3.3.2). During the follow-up (mean 10 years), only one case needed pacemaker implantation.

In hospital-based populations [106–109], a high prevalence of cardiovascular abnormalities is found, although in all series, subjects with "lone" RBBB are described [108, 109]. The presence of associated left fascicular block (see Sect. 14.3.4) has been described as concomitant with a higher prevalence of heart disease and a worse prognosis, including greater progression to advanced AV block [103, 106–112].

In the Framingham study [52] during a follow-up period of 18 years, 70 new cases of complete RBBB were identified. Hypertension was significantly more common in these cases. In 70%, the identification of the RBBB pattern was preceded by at least one cardiovascular abnormality – hypertension in 60%, cardiac enlargement in 25%, and coronary heart disease in 20%. In patients with RBBB, the development of manifestations of coronary heart disease was twice as frequent and that of congestive heart failure almost four times that in control group. After identification of RBBB, four of the 70 cases (6%) developed high-degree AV block. No prior evidence of cardiovascular abnormalities was found in 20 cases: 75% of them remained free of cardiovascular manifestations while 25% developed coronary heart disease, 5% with evidence of congestive heart failure. Although RBBB were as prone as controls to remain completely free of cardiovascular abnormalities, when heart disease was present there was a higher prevalence of advanced stages of disease (cardiac enlargement, clinical coronary heart disease, and congestive heart failure). The more prolonged the QRS duration, the greater the association with cardiovascular abnormalities as well as cardiovascular mortality.

At each 2-year interval after onset of RBBB, cumulative mortality was three times greater than in the control group. Almost one-third of the patients died within 10 years of onset of RBBB (only 11% for an age-matched population, free from RBBB). As in other studies [110], cardiovascular disease mortality appeared to be highly dependent on whether associated cardiovascular abnormalities were present [113].

In conclusion, it may be stated that in young subjects with otherwise normal change their prognosis. The same cannot be said of other subjects. In the presence of underlying heart disease, the prognosis is mostly related to the severity of the cardiovascular abnormality. Consequently, the identification of an intraventricular conduction defect – RBBB in this case – should be considered a sign of high priority for a complete M-mode and two-dimensional echocardiographic evaluation [30], the most important noninvasive tool for anatomic and functional analysis of the left ventricle as well as prognostic evaluation of the conduction disturbance.

(c) Diagnostic difficulties

There are usually no problems in the identification of the Q-waves of transmural myocardial infarction because initial depolarization is not significantly affected by RBBB. On the other hand, RBBB associated with cor polmunale may exhibit Q-waves in the right precordial leads (perhaps suggesting right ventricular hypertrophy), or Q-waves in the inferior leads that may mimic myocardial infarction.

Voltage criteria for left ventricular hypertrophy have a very low sensitivity in the presence of RBBB. The authors have studied 30 patients with complete RBBB by echocardiography [114]. Contrary to what was found in LBBB with left ventricular hypertrophy (see Sect. 14.3.3.2(c)), the ECG/VCG (Sokolow–Lyon/Pipberger) criteria were not able to identify any of the 21 patients that were found to have left ventricular hypertrophy and/or enlargement by echocardiography. The Sokolow–Lyon index also showed no correlation with left ventricular mass calculated by echocardiography.

Thus, it appears that in the presence of complete RBBB, left ventricular hypertrophy cannot be identified either by 12 leads ECG or by VCG, at least on the basis of the criteria quoted above.

Right ventricular hypertrophy can be a cause of complete RBBB. Actually RBBB can also be observed in acute overload of the right ventricle (pulmonary embolism), possibly owing to the distention of the right bundle.

14.3.2.5 Complete Left Bundle Branch Block

(a) ECG/VCG pattern

When the conduction of the electrical impulse through the main left bundle branch (or through its two or three subdivisions) is interrupted or severely delayed by any type of disease process, the ventricular excitation wave is conducted through the right bundle branch (Fig. 14.14). Activation will then begin low on the right septal surface, in the region corresponding, on the left side, to the base of the anterior papillary muscle. From there, the wave of excitation spreads

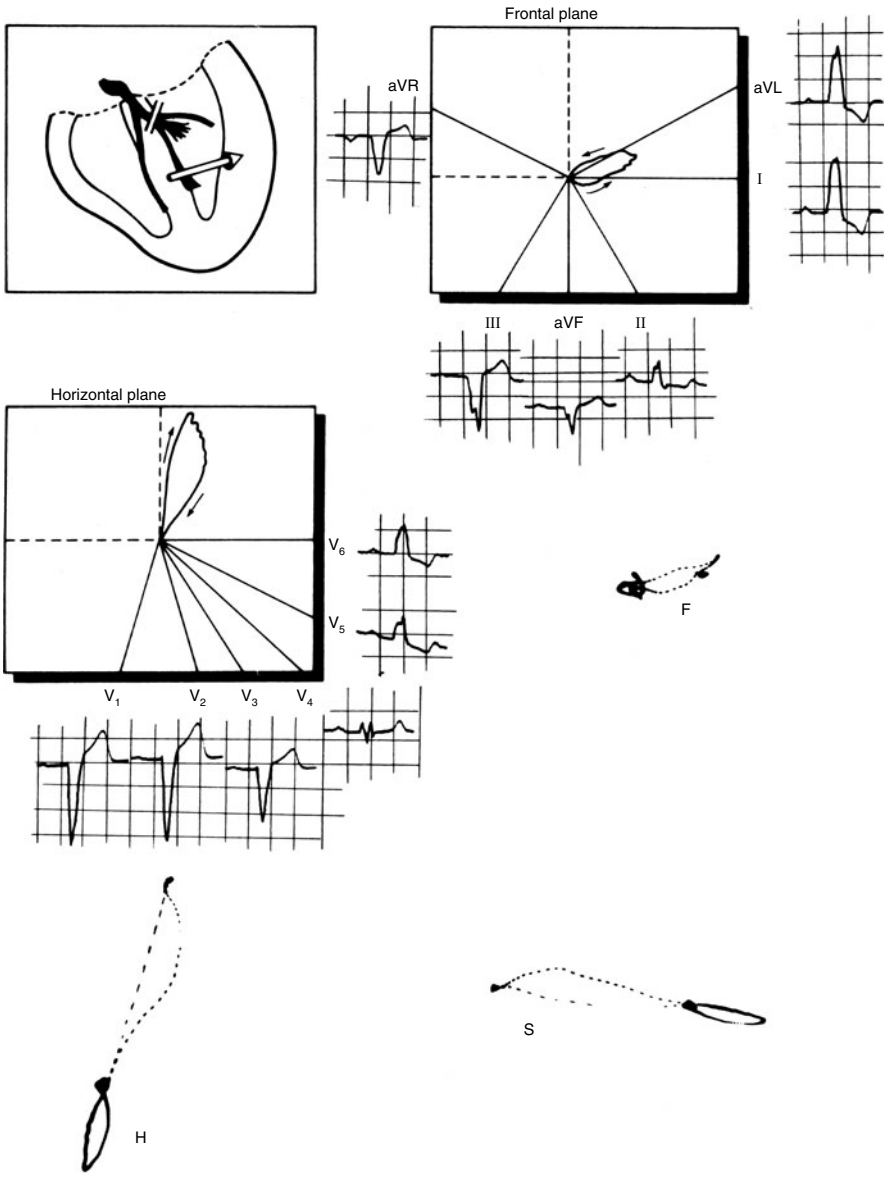

Figure 14.14

Complete left bundle branch block: schematic of the spatial main vectors of ventricular activation resulting from interruption of the left bundle branch and a diagram of the projections of the QRS loop on the frontal and horizontal planes, and ECG leads and VCG loops of a typical case of complete LBBB (F, frontal; H, horizontal; S, sagittal).

to the right ventricle and transeptally to the left ventricle, which is reached from right to left, at a much lower speed, by conduction from one muscular fiber to another. In this situation, the initial vectors of ventricular activation have their origin on the right side of the septum and are directed mainly to the left, and most often anteriorly and inferiorly, in agreement with the way the activation wave spreads, from right to left, to depolarize the left septal mass. Only afterward does the myocardium of the free wall of the left ventricle begin to be depolarized, either from cell to cell or reutilizing the peripheral fascicles of the subdivisions of the left bundle branch. This late activation of the left ventricular mass generates electrical forces directed toward the left, posteriorly, and inferiorly. The leftward orientation remains until the end of the depolarization process, the last vector being directed, as is usual, posteriorly and somewhat superiorly.

According to the spatial orientation of the electromotive forces of ventricular activation, in LBBB, the major portion of the QRS loop is located posteriorly and to the left, pointing either inferiorly or somewhat superiorly (Fig. 14.14).

The leftward orientation of the initial forces accounts for the absence of the normal "septal" Q-waves in lead I and left precordial leads. The initial forces, being slightly anterior, may or may not inscribe a small r-wave in lead V_1 (posterior orientation of the initial forces is rarely seen). The body of the QRS loop is elongated and oriented mainly posteriorly and so produces increased amplitude of the S-wave in V_1 and somewhat decreased amplitude of the R-wave in V_6.

The slower velocity of left ventricular activation (fiber to fiber) results in a greater duration of the QRS loop being slowly inscribed in the middle portion and in the terminal portion, with broader QRS complexes in all ECG leads, along with slurring and notching which are more evident in the R-waves of the left-sided leads (M-shaped RR′ complexes). The time required to complete the ventricular activation process is obviously greater than usual, the QRS duration being by definition ≥0.12 s.

The altered ventricular depolarization accounts for secondary abnormal repolarization forces, with ST and T vectors directed opposite to the main QRS vector.

In the surface leads, the ST-segment is usually depressed and T-waves are negative in the left-sided leads (V_5, V_6, I, and aVL), in the opposite direction to the widened R-waves. On the contrary, in leads V_1 and V_2, deep S-waves coexist with ST-segment elevation and positive T-waves.

The WHO/ISFC Task Force has proposed the following ECG criteria for the diagnosis of complete LBBB [16]:

(a) QRS duration prolonged to ≥0.12 s;
(b) Left-sided leads (V_5, V_6, I, and aVL) with slurred and broad R-waves
(c) Absence of Q-waves in left-sided leads (possible exception of aVL)
(d) R peak time prolonged to more than 0.06 s in V_5 and V_6 (normal in V_1 and V_2, when it can be determined)
(e) Right precordial leads with very small r-waves followed by deep and broad S-waves (occasionally broad QS complexes in V_1 and V_2, rarely in V_3) and the transition zone in the precordial leads displaced to the left.

Lopes has proposed VCG criteria for the diagnosis of complete LBBB [46] as below:

(a) The spatial QRS loop should have the following characteristics:
  (i) Elongated and narrow QRS loop that is generally larger than without block (slowly inscribed in middle and late portions), duration of the loop ≥0.12 s;
  (ii) Practically the entire loop oriented posteriorly and to the left
  (iii) Initial vector anterior and leftward
  (iv) Afferent limb superior to the efferent limb
(b) The transverse plane should have the following features:
  (i) Long and narrow loop
  (ii) Clockwise inscription of the majority of the loop
  (iii) Initial vector anterior and leftward
  (iv) Afferent limb to the left of the efferent limb
  (v) Slowing on the VCG, usually evident by 40 ms and which continues for the entire loop, being most marked in the midportion
(c) The left sagittal plane is characterized by
  (i) Long narrow loop
  (ii) Counterclockwise inscription of the majority of the loop
  (iii) Afferent limb superior to efferent limb
(d) The frontal plane should show
  (i) A small and irregular loop owing to the spatial QRS loop being almost perpendicular to the frontal plane
  (ii) Counterclockwise inscription of the loop with the afferent limb superior to the efferent limb with almost the entire loop on the left

(b) Clinical implications

Complete LBBB is most frequently identified in adulthood. Its occurrence in "normal" healthy infants may be anecdotal owing to isolated congenital malformation of the conduction system. Besides lesions (either anatomic

or functional) of the left bundle branch itself, LBBB can be a result of lesions within the His bundle or of more peripheral lesions (affecting simultaneously the two or three left bundle subdivisions). LBBB has been predominantly associated with hypertensive heart disease, particularly with left ventricular hypertrophy, and with coronary heart disease [115–119] (with or without myocardial infarction). It frequently occurs as a "lone" abnormality as well. It has also been identified in the setting of myocarditis [120, 121], valvular heart disease (particularly aortic valvular disease) and cardiomyopathies, including the obstructive type [92]. Rarely, LBBB can be associated with other conditions such as hyperkalemia [50], bacterial endocarditis [122], and digitalis toxicity [123].

Similar to other types of intraventricular conduction defects, the published prevalence of associated cardiovascular abnormalities, as well as the prognosis, vary largely according to the characteristics of the population under evaluation; for example, hospital populations, asymptomatic ambulatory patients or large community studies. Rotman and Triebwasser [81] published a revision of over 237,000 mostly asymptomatic subjects. Complete LBBB was identified in 125 cases, with a mean age of 40 years; only 12 subjects were younger than 30 years. In their group of 125 LBBB subjects, a low prevalence of coronary heart disease (9%) and hypertension (8%) was found (although greater than that for the subjects with RBBB). Most patients were asymptomatic (95%) and had an otherwise normal cardiovascular examination (89%).

In a study on 67,375 asymptomatic USAF cadets, Lamb [124] found 13 cases with complete LBBB (mean age 35 years) all of them with no demonstrable evidence of cardiovascular disease.

Important information has been published by the Framingham study group [125] concerning the clinical significance of the appearance of LBBB pattern not previously found. During 18 years of follow-up, 55 subjects developed new LBBB; the mean age of appearance of LBBB was 62 years. These patients had a high prevalence of previous hypertension (62%), cardiomegaly by chest roentgenogram (44%), and significant excess of antecedent coronary heart disease.

During the follow-up period, patients who developed LBBB had twice the incidence of coronary heart disease and seven times the incidence of congestive heart failure found in the general population. There was also a highly significant excess of cardiac enlargement by chest x-ray. One-third of the patients free of cardiovascular abnormalities prior to LBBB appearance developed coronary heart disease (more than three times the observed incidence in the control group). Their data suggest that the appearance of new LBBB is usually associated with advanced organic heart disease (and not asymptomatic or milder symptomatic stages of the disease). One-half of those with new LBBB died of cardiovascular disease within 10 years of the onset of LBBB (compared to only 11.6% in an age-matched population free from LBBB). Only 11% of the LBBB subjects remained free of cardiovascular abnormalities for the whole follow-up period (48% in the control group).

These results contrast with those obtained in follow-up studies of newly acquired LBBB in young military populations, which have suggested a relatively benign clinical prognosis [81, 126, 127]. As previously stated, these differences can probably be explained by the high predominance of young men without risk factors found in the military studies (even hypertensive and diabetics were usually excluded).

LBBB in a younger subject with an otherwise normal cardiovascular observation may thus carry a very good prognosis [128, 129]. In older patients with acquired LBBB, careful evaluation and follow-up seems justified because the development of other cardiovascular abnormalities is strongly expected [125]. In the presence of associated organic heart disease, the prognosis is related to the severity of the underlying process [130].

Besides clinical and x-ray evaluation, the identification of LBBB should be considered a high priority for complete M-mode and two-dimensional echocardiography [30].

LBBB and its duration was recently acquired a new clinical importance, particularly in patients with heart failure [131]. In these patients, the duration of LBBB is an important determinant for resynchronization therapy, which consists of the implantation of a bi-ventricular pacemaker which allows improving ventricular performance [132]. This device altered prognosis in patients with advanced heart failure [133].

(c) Diagnostic difficulties

As previously described in Sect. 14.3.2.2(c), LBBB may mimic or conceal other ECG patterns, namely, myocardial infarction [134–136]. A QS pattern in V_1 (and sometimes V_2 and V_3) is occasionally registered in the presence of LBBB without anteroseptal myocardial infarction (cases of intermittent LBBB are occasionally seen which show a QS pattern

in V_1–V_3 with reappearance of normal R-waves when they return to normal conduction). The same may be observed in inferior leads [137] although it may occasionally represent true loss of inferior forces. Havelda et al. [138] indicated that inferior Q-waves in the presence of LBBB were highly specific for myocardial infarction, though not sensitive. On the other hand, anteroseptal or inferior Q- or QS-waves [139] may no longer be seen when LBBB develops [139, 140].

Noninvasive techniques, in particular echocardiography, and isotopic studies can be of great help in identifying localized hypokinesia related to old myocardial necrosis [30, 119, 121]. Single photon emission computed tomography (SPECT) can also be used for differential diagnosis [141, 142].

LBBB by itself has an abnormal repolarization pattern which usually does not enable easy identification of superimposed primary ischemic abnormalities. Nevertheless, serial changing patterns of ST–T, correlated with clinical signs and symptoms, may give important clues concerning myocardial ischemia in the presence of LBBB (sometimes evolving myocardial infarction) [143, 144].

Depending mainly upon leads, the appearance of LBBB may cause a decrease [145] or an increase [146] in voltage, thus making the voltage criteria less accurate for left ventricular hypertrophy.

It is generally recognized that the ECG pattern of LBBB does not allow the differentiation between the presence or absence of left ventricular hypertrophy. However, the authors have found [114], with the help of echocardiography, that voltage criteria may in fact maintain similar accuracy, with similar predictive value, because the negative voltage of the S-wave in V_1 increases, while the positive voltage of the R-wave in V_5 and V_6 correspondingly decreases [114]. Of the patients with left ventricular hypertrophy and/or enlargement detected by echocardiography among 30 patients with LBBB diagnosed by ECG/VCG, the Sokolow–Lyon criteria correctly identified 82% (19/23) with a false-positive rate of 28% (2/7). These percentages are similar to those achieved in a population of hypertensive patients without LBBB [114]. In five cases with transient LBBB the described variation was observed; that is to say, the appearance of LBBB was accompanied by deeper S-waves in V_1 while the amplitude of the R-wave in V_5–V_6 decreases – thus maintaining similar diagnostic accuracy for the Sokolow–Lyon index (Fig. 14.15).

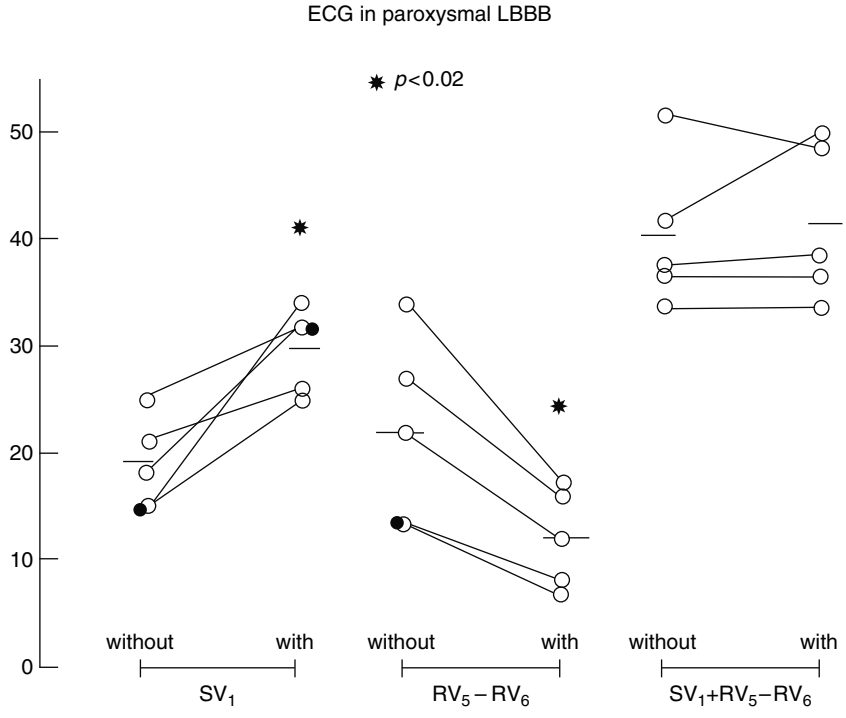

Figure 14.15

Five cases of paroxysmal LBBB. Graphic representation of the observed increase in S-wave amplitude in lead V_1 and corresponding decrease in R-wave amplitude in leads V_5–V_6, maintaining comparable values for the Sokolow–Lyon index.

14.3.3 Bundle Branch Block Associated with Fascicular Block (Bifascicular Block)

According to the fascicular division concept, conduction abnormalities in two of the described fascicles would result in so-called bifascicular block. If LAFB and LPFB occur together, a complete LBBB pattern should result. Some of the cases of complete LBBB may in fact be a result of this type of bifascicular block although, as previously said, the same pattern can also be obtained with other locations of the lesions that cause the block. The combination of RBBB with either left anterior or left posterior block is usually given the designation of bifascicular block. The most common pattern of bifascicular pattern of bifascicular block I that of RBBB with LAFB.

A word must be said about left centroseptal fibers. In some cases of RBBB together with left anterior or posterior fascicular block, the spatial QRS loop is dislocated anteriorly, either counterclockwise or even clockwise in the horizontal plane (Fig. 14.16). In chronic cases, right ventricular hypertrophy or old posterior myocardial infarction may be considered as being the cause of the positive R-waves in the right precordial leads. However, in intermittent blocks (as in the first example that attracted the attention of Rosenbaum, who did not notice this phenomenon) besides the axis deviation in the frontal plane, there can be seen the same anterior displacement that made the authors refer to a third type of "hemi" block, namely, left median fascicular block (see Sect. 14.3.1.3). Trifascicular block (in a tetrafascicular system) should presumptively be considered in such cases [29, 30, 47, 48].

It is still debatable whether, electrocardiographically, LBBB can coexist with LAFB. However, it is conceivable that, in cases of complete LBBB, when the wavefront reaches the left side of the septum, it may find either the left posterior or the left anterior fascicle accessible. If the activation follows one of these high-speed paths of excitation, the pattern of block in the other, i.e., LAFB or LPFB, can be mimicked. This can be one explanation for the cases with marked, either right or left, axis deviation [147–149].

14.3.3.1 Right Bundle Branch Block and Left Anterior Fascicular Block

(a) ECG/VCG pattern

The ventricular activation in RBBB together with LAFB reflects the combination of the two conduction abnormalities giving rise to the pattern of LAFB, with marked left axis deviation, associated with the characteristic rightward and terminal delay of complete RBBB, with no change of the initial QRS vector, or of the maximal QRS vector and direction of inscription of the QRS loop in the frontal plane (Fig. 14.17).

Owing to the double block (RBBB + LAFB), activation must pass through the noninvolved division (in this case the left posterior fascicle). Initial activation will begin in the posterior paraseptal area of the ventricle (and part of the mild-left septum) with initial forces directed inferiorly, anteriorly, and to the right. The impulse then spreads through the inferior wall and apex with electromotive forces directed inferiorly, leftward and somewhat anteriorly. Subsequently, the activation wave proceeds to depolarize the anterolateral and the posterobasal regions with vectors pointing posteriorly, leftward and superiorly, similar to isolated LAFB. Lastly, the activation of the right septum follows, with late activation of the right ventricle caused by RBBB, with slowly inscribed forces directed anteriorly and to the right.

Thus, there are two distinct portions of the spatial QRS loop (Fig. 14.17):

(a) The main portion is located mostly to the left, superiorly and somewhat anteriorly, with the initial deflection and the efferent limb reflecting the LAFB. However, the afferent limb may be slightly displaced by the associated right bundle branch abnormality (or else by associated lesions on the left middle septum – LMFB) [20, 21, 29, 30].
(b) There is also a slowly inscribed terminal appendage similar to that described for isolated RBBB.

The maximal QRS vector is directed leftward, and superiorly (and somewhat anteriorly) with total QRS duration ≥0.12 s.

ECG leads I and aVL usually have a qRS or RS pattern. The small q-wave is caused by the initial rightward activation while the tall R-wave reflects the superior displacement of the spatial loop owing to the LAFB. The broad and slurred S-wave is related to the terminal delay caused by the RBBB (Fig. 14.17).

ST–T-waves are similar to those observed in isolated RBBB.

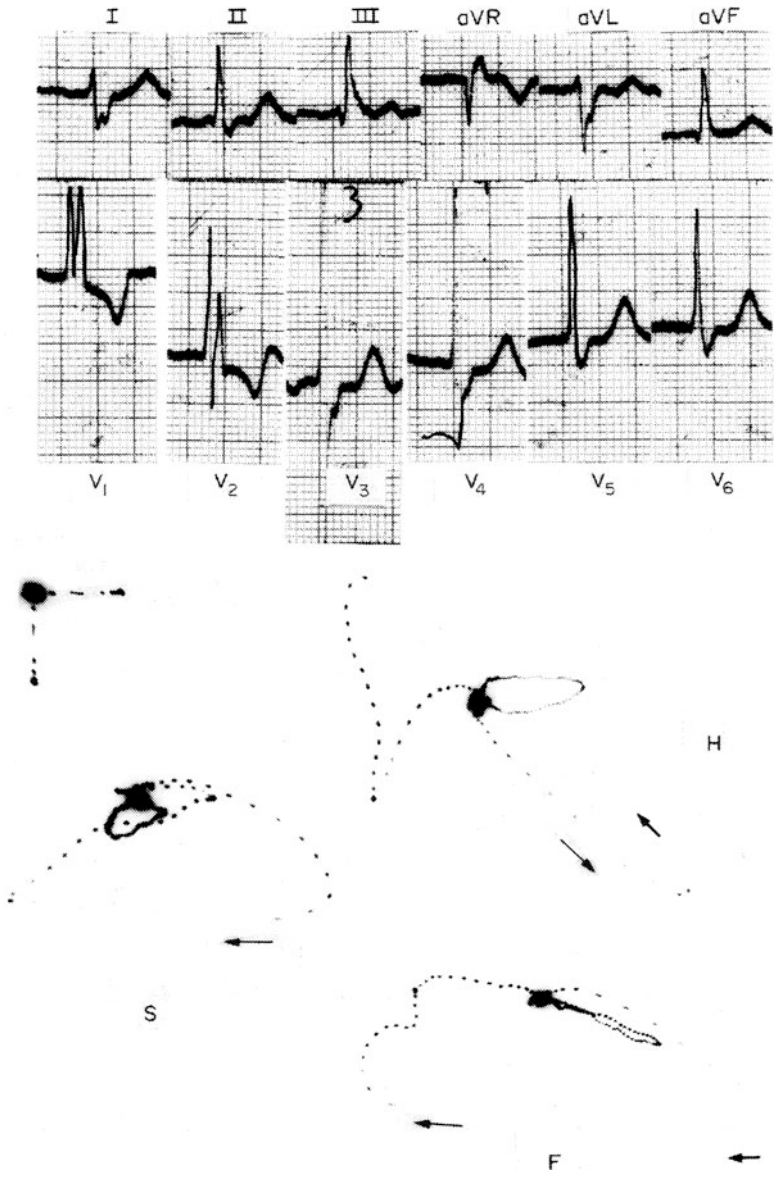

Figure 14.16

ECG leads and VCG loops of a patient with bifascicular block (RBBB + LPFB). Left median fascicular block (prominent anterior forces) may be postulated.

The WHO/ISFC Task Force has proposed the following ECG criteria for the diagnosis of RBBB + LAFB [16]:

(a) QRS prolongation to ≥0.12 s;
(b) Left axis deviation of −45° to −90° (when QRS axis is −30° to −45°, the diagnosis of "possible" associated LAFB should be made)
(c) qR pattern in aVL
(d) rsr′, rsR′, or rSR′ M-shaped right precordial lead pattern with R′ usually greater than initial R-wave (occasionally a wide and notched isolated R pattern may be seen)
(e) Wide S-wave in leads I and V_5–V_6 (S-wave duration greater than R-wave or >40 ms in adults).

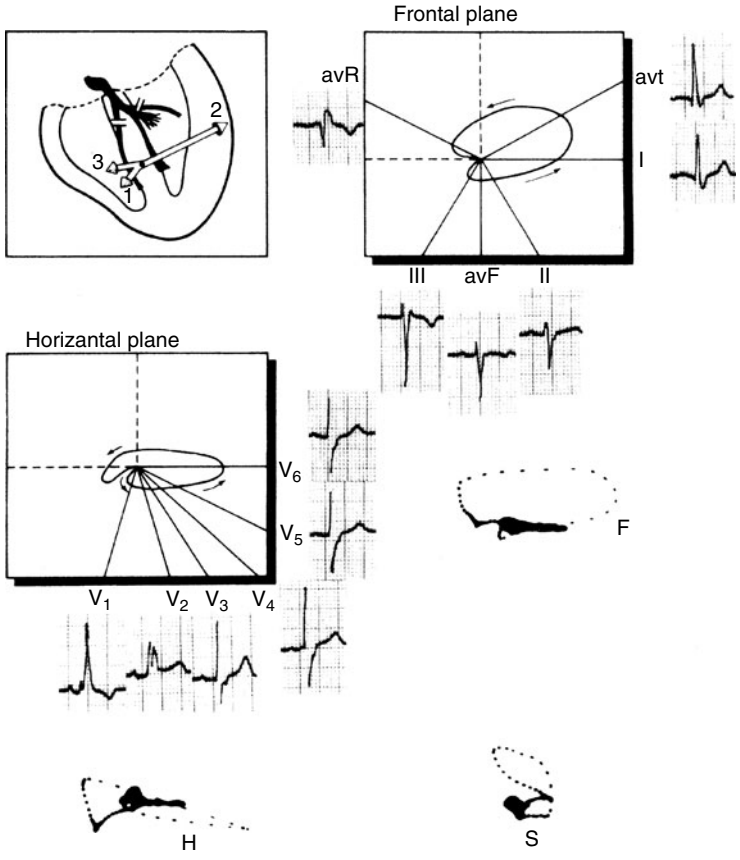

Figure 14.17

Bifascicular block-RBBB + LAFB: schematic of the spatial main vectors of ventricular activation resulting from interruption of the left anterior fascicle as well as the right bundle branch, together with a diagram of the projections of the QRS loop on the frontal and horizontal planes, and ECG leads and VCG loops of a typical case of RBBB + LAFB (F, frontal; H, horizontal; S, sagittal).

Lopes has proposed VCG criteria for the diagnosis of RBBB + LAFB as below [46]:

(a) The frontal plane should have the following characteristics:
  (i) Initial vectors rightward and inferior
  (ii) Counterclockwise inscription
  (iii) QRS axis more superior than −30°
  (iv) Terminal conduction delay oriented rightward and usually superiorly
(b) The horizontal plane is characterized by
  (i) The initial vector being oriented anterior and rightward
  (ii) Counterclockwise or figure-of-eight inscription
  (iii) The maximal QRS vector being oriented leftward
  (iv) The terminal slowing defect being rightward and anterior

If the body of the QRS loop is anteriorly displaced, the centroseptal fascicle may be involved (associated left main "hemi" block) [21, 28]. Note that accepting three subdivisions of the left bundle branch (tetrafascicular or quadrifascicular conduction system) means that this type of block would actually be trifascicular.

(b) Clinical implications

Most often RBBB + LAFB is associated with sclerodegenerative involvement of the specialized conduction system, mainly in the elderly [26], with or without accompanying hypertension [150] or ischemic heart disease, including myocardial infarction [150, 151]. Pathologically, fibrosis and degenerative changes are usually identified within several zones of the cardiac conduction system [152, 153], including bundle branches and fascicular subdivisions.

RBBB + LAFB may also be a result of a congenital abnormality, either isolated [154, 155] or associated with progressive ophthalmoplegia [156], sometimes being part of a familial disorder associated with syncope and high incidence of sudden death [157–159]. It is routinely part of the electrocardiographic picture of congenital defects in the area of the auriculoventricular canal, namely, ostium primum or cushion defects. Other etiologies include Chagas disease, chest trauma [160, 161], hyperkalemia [50], miocarditis, aortic valvular disease, cardiomyopathy, sarcoidosis [162], and other granulomatous diseases.

RBBB + LAFB may be caused by surgical repair of congenital malformations (namely tetralogy of Fallot or ventricular septal defect). In these cases, LAFB would be related to damage to the conduction system, while isolated RBBB may be produced by involvement of the peripheral Purkinje system [163]. Surgically induced RBBB + LAFB may be a poor risk indicator requiring an artificial pacemaker [164] but may have a long survival if there is no evidence of trifascicular block [165].

As in other fascicular conduction disturbances, the prognosis differs significantly between hospitalized and asymptomatic patients. Asymptomatic patients have a good prognosis [166] but hospitalized patients have a significant risk of sudden death and/or development of complete AV block [85, 151, 167] especially if the His-ventricular (HV) interval is markedly prolonged [168].

In the Framingham study [52], a QRS duration ≥130 ms associated with a QRS axis between −45° and −90° identified those patients most likely to have associated cardiovascular abnormalities.

Studies of young military populations [92, 124] showed a lower prevalence of RBBB with marked left axis deviation than of RBBB with normal QRS axis. In other studies, no difference in the prevalence of associated cardiovascular abnormalities was found. However, in the study of Whinnery et al. [105], a higher prevalence of coronary heart disease was found in patients in whom RBBB was associated with left axis deviation.

(c) Diagnostic difficulties

The diagnostic difficulties are the same as described for each of the two isolated conduction defects (see Sects. 14.3.1.1 and 14.3.3.1).

14.3.3.2 Right Bundle Block and Left Posterior Fascicular Block

(a) ECG/VCG pattern

RBBB together with LPFB is manifested as RBBB with otherwise unexplained marked right axis deviation (Figs. 14.18 and 14.19).

As in isolated LPFB, initial activation of the left ventricle involves the anterior paraseptal area with a vector directed anteriorly, superiorly and leftward, and thereafter progresses to the anterior and anterolateral wall. Then the activation proceeds in a retrograde fashion to the area of the posterior fascicle, that is to say, the inferior and posterobasal areas of the left ventricle, with forces that are inferiorly oriented and to the right. Late terminal forces will be directed anteriorly and to the right, reflecting the delayed activation of the right septum and right ventricular free wall.

Similar to RBBB + LAFB, two main portions of the spatial QRS can be identified (Fig. 14.18).

(a) The main body is located in the inferior left and inferior right octants, with the initial deflection and the efferent limb reflecting the LPFB. The afferent limb is modified by the combined effect of the RBBB (and possibly LMFB).
(b) The terminal appendage is similar to that described for isolated RBBB.

The maximal QRS vector is directed inferiorly, either leftward or rightward, as well as either slightly anteriorly or slightly posteriorly. The total duration of the QRS loop in increased to ≥0.12 s.

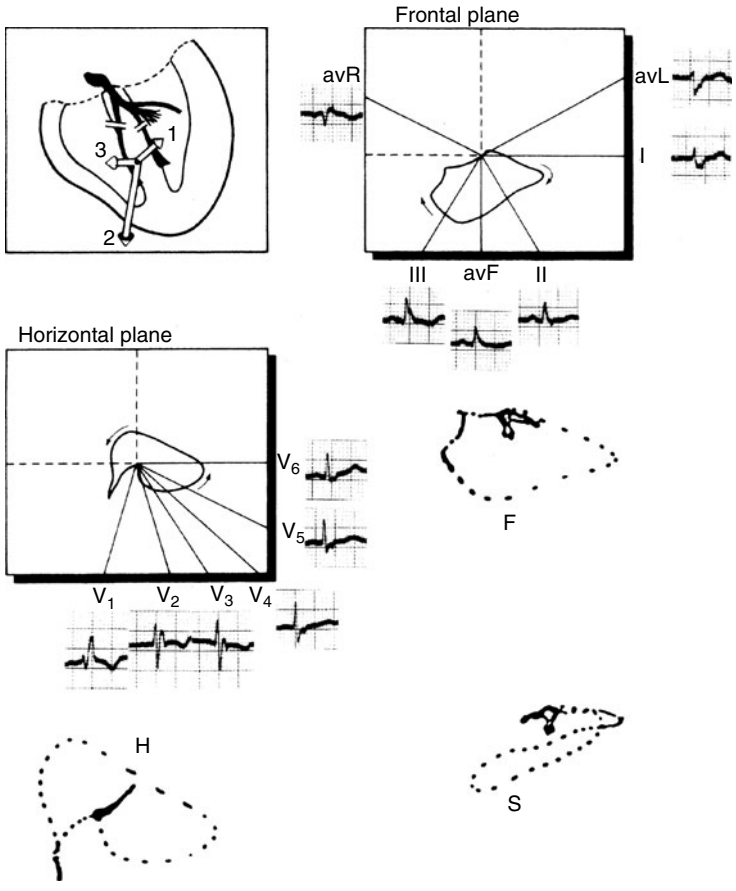

Figure 14.18

Bifascicular block – RBBB + LPFB: schematic of the spatial main vectors of ventricular activation resulting from interruption of the left posterior fascicle as well as the right bundle branch, together with a diagram of the projections of the QRS loop on the frontal and horizontal planes, and ECG leads and VCG loops of a typical case of RBBB + LPFB (F, frontal; H, horizontal; S, sagittal; same patient as in Figs. 14.7 and 14.19).

ECG leads I and aVL have a small r-wave followed by a deep S-wave which is abnormally broad, with delayed inscription of the late part of the S-wave. In inferior leads, III and aVF, a qR or qRS pattern is present with slurring of the last portion of the R or the S-wave. Abnormal right axis deviation (determined from the first part of the QRS, before the slurring wave) is present. Right precordial leads have an RsR′ pattern (small or absent S-wave). In the left precordial leads, R-wave amplitude is reduced and the S-wave is slurred in its late part (Fig. 14.18).

The WHO/ISFC Task Force has proposed the following ECG criteria for the diagnosis of RBBB + LPFB [16]:

(a) QRS prolongation to ≥0.12 s;
(b) Frontal QRS axis of +90° to +180° (in the absence of other causes of right axis deviation)
(c) rS configuration in leads I and aVL associated with qR pattern in inferior leads (Q-wave obligatory in leads III and aVF) in which Q-wave should be ≤0.04 s
(d) rsr′, rsR′, or rSR′ M-shaped right precordial pattern with R′ usually greater than initial R-wave (occasionally a wide and notched isolated R pattern may be seen)
(e) Wide S-wave in leads I and V_5–V_6 (S-wave duration greater than R-wave or >40 ms in adults)
(f) R peak time >0.05 s in V_1 with normal time in V_5 and V_6 (when a notched dominant R pattern is present in V_1).

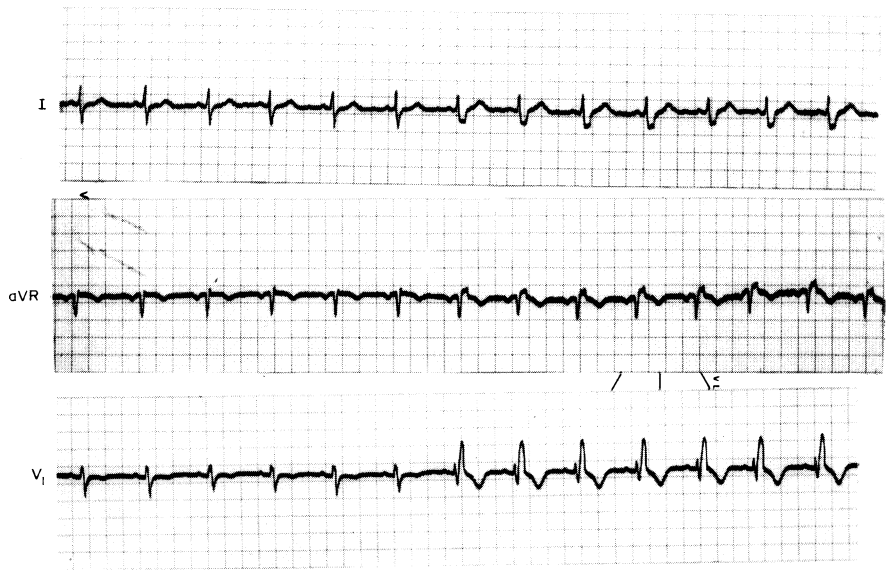

Figure 14.19
Transition from isolated LPFB to LPFB + RBBB (nonsimultaneous leads). No significant R–R interval variation is observed (same patient as in Figs. 14.7 and 14.18).

Lopes has proposed VCG criteria for the diagnosis of RBBB + LPFB as below [46]:

(a) The frontal plane should have the following characteristics:
  (i) Initial vectors that are leftward
  (ii) Clockwise inscription
  (iii) QRS axis > + 110° (others admit +90°)
  (iv) Terminal slowing directed rightward
(b) The horizontal plane should show the following:
  (i) Initial vectors anterior and leftward
  (ii) Figure-of-eight or clockwise inscription (possible associated LMFB) [30]
  (iii) Maximal QRS vector oriented rightward
  (iv) Terminal slowing oriented rightward and anteriorly

(b) Clinical implications

RBBB + LPFB is usually related to sclerosis of the conduction system most often in the presence of coronary artery disease and/or hypertension. This type of bifascicular block is only about 5% as frequent as the combination of RBBB with LAFB.

It has been said that this association is found more rarely because the left posterior fascicle is broader and so is more resistant. On the other hand, it would have a more ominous prognosis with progression to complete AV block than if the more fragile left anterior fascicle were involved.

(c) Diagnostic difficulties

Difficulties are the same as described for each of the isolated conduction defects (see Sects. 14.3.1.2 and 14.3.3.1).

14.3.3.3 Left Bundle Branch Block with Left Fascicular Blocks

When LBBB is associated with either marked left axis deviation or marked right axis deviation, the suspicion may be raised of associated left fascicular block. The abnormal sequence of septal depolarization owing to the LBBB makes it

difficult to identify any type of initial vector alteration. As previously mentioned, the depolarization of the left ventricular free wall may proceed reutilizing the peripheral subdivisions. In this way, it is understandable that block in one of them will alter the sequence of activation in a way similar to isolated fascicular blocks. Some series seem to reflect poorer prognosis when left or right axis deviation is observed in LBBB (corresponding to more extensive lesions either in the conduction system (associated fascicular block) or in the parietal muscle (mural or "distal" block)) [147–149]. Others did not confirm this finding.

14.3.3.4 Progression of Bifascicular Blocks (and Other Intraventricular Conduction Defects) to Advanced AV Block

One particular clinical problem, because of its implications, deserves separate consideration: the possible progression of intraventricular (IV) conduction defects to complete AV block. As a result of the high prevalence of bifascicular blocks, it seems appropriate to include this discussion in this section. However, the conclusions to be reached are relevant to trifascicular blocks as well.

Two different clinical settings must be considered: first, chronic IV conduction defects, and second, IV conduction defects in the setting of acute myocardial infarction.

(a) Chronic IV conduction defects

IV conduction defects are considered to be a risk factor for the development of advanced AV block and eventually prophylactic implantation of a pacemaker is considered. The more advanced the conduction defect (unifascicular block, bifascicular block, or trifascicular block), the larger is the risk of occurrence of complete AV block.

Several studies have demonstrated that a significant number of patients with complete AV block had had prior ECG with patterns of bifascicular block [85, 94, 169–171]. However, quite different risks of progression to advanced AV block have been published – between 10% and 16% for RBBB with LAFB [85, 167, 171–173], but much higher (21–75%) for RBBB + LPFB [85].

In a long-term follow-up study by McAnulty et al. [174], 554 patients with various types of bifascicular or trifascicular blocked were included. The incidence of progression to complete heart block over 5 years was only approximately 1% per year. Most patients with bifascicular block who died suffered ventricular fibrillation rather than complete AV block. An artificial pacemaker was recommended only if symptomatic bradyarrhythmias could be demonstrated.

In the follow up of asymptomatic subjects [81], a very low incidence of advanced AV block was also observed. Other prospective data [52, 125] confirm the low ratios of progression of bundle branch block to complete AV block even for cases with bifascicular block.

Attention has been drawn to the PR interval. Prolongation of the PR interval in the presence of bifascicular block was pointed out as evidence of delay in the other nonblocked fascicle, and thus would represent an indication for pacemaker implantation [175]. Rosen et al. [176] described PR prolongation correlating with His-ventricular prolongation in patients with bifascicular block. However, subsequently, Levites and Haft [177] have shown it to be a poor predictor of trifascicular disease. Denes et al. and Dhingra et al. [178, 179] have also agreed that surface electrocardiographic patterns do not predict high-risk groups.

Scheinman et al. [180] noted that a marked prolongation (≥80 ms) of the HV interval in patients with transient neurological symptoms was a risk indicator of sudden death. However, they later [181] suggested that only patients with moderate or severe congestive heart failure and HV > 70ms were at higher risk of sudden death. It must be remembered that many of their patients had suffered a significant bradyarrhythmia within 3 weeks of admission into the study and thus represent a special subset of patients with transient neurological symptoms.

Dhingra et al. [182] found that an HV ≥ 80 ms did not predict high risk of sudden death. McAnulty et al. [174] observed only a trend suggesting that patients with HV > 75 ms were at greater risk of sudden death. Nevertheless, most deaths in this study were not a result of AV block.

A high prevalence of HV prolongation is found in patients with bifascicular block. Although HV prolongation usually indicates more severe heart disease and increase risk of mortality, it has not been proved to be a good predictive sign for complete heart block. Accordingly, in asymptomatic patients with bifascicular block, it cannot be used to decide whether or not prophylactic pacemaker implantation should be undertaken.

Thus, the incidence of advanced AV block in patients with bundle branch block or bifascicular block is relatively small, and BBB or bifascicular block *per se*, without other symptoms (syncope) or signs (dynamic ECG) does not warrant consideration for prophylactic pacemaker implantation [175].

(b) Acute myocardial infarction

In a study by Hindman et al., the prognosis of patients with acute myocardial infarction associated with BBB correlated with the degree of heart failure. The prognosis of anterior and indeterminate myocardial infarction was worse than that for inferior or posterior infarction. RBBB + LAFB [183] developing in the setting of acute anteroseptal myocardial infarction significantly changes the prognosis for surviving the acute episode (especially if the HV interval is prolonged) [184]. It usually corresponds to a large mass of infarcted tissue.

Although AV block may develop, death is usually caused by pump failure and cardiogenic shock. However, in spite of the fact that a prophylactic pacemaker may not change the prognosis, its implication is considered advisable, since it may benefit some individual patients [185]. This strategy has been suggested even in cases in which RBBB existed prior to the myocardial infarction [186]. The same recommendation is also valid for RBBB + LPFB and may be extended for isolated RBBB or LBBB.

The occurrence of isolated fascicular block *per se*, in the setting of acute myocardial infarction, is not an indication for pacemaker implantation [91, 185, 187, 188]. However, if the conduction defect persists and especially if transient second- or third-degree AV block is observed [187, 189, 190] permanent pacing may prolong life [189, 191, 192] and is indicated [175].

14.3.4 Other Associated Intraventricular Conduction Defects

14.3.4.1 Trifascicular Block

Trifascicular block is the term used for the possible combination of complete or incomplete block in the right bundle branch associated with conduction disturbances either in the two main divisions of the left bundle branch or one of them plus a Hisian delay. Usually, this result in one of the bifascicular blocks previously described, associated with first- or second-degree AV block. In order to avoid semantic errors, it has been recommended that each of the individual conduction defects should be listed separately. The existence of three fascicular subdivisions of the left bundle branch only adds to the confusion if this type of designation is to be maintained without clarification of the real defects present.

Simultaneous complete RBBB and block in the main left fascicles will result in complete AV block.

14.3.4.2 Bilateral Bundle Branch Block

The combination of complete BBB on one side (either right or left) with first- or second-degree AV block has been frequently designated "bilateral bundle branch block," assuming that there is incomplete block in the other bundle. However, this is a diagnostic abuse as the block can be located either in the AV node or in the His bundle and not necessary in the contralateral bundle branch. Electrophysiological studies are mandatory for its identification. The designation bilateral BBB should probably be reserved for cases where alternating conduction impairment is observed, with sequential evidence of RBBB and LBBB (Fig. 14.20).

Simultaneous complete RBBB and LBBB would cause complete AV block.

14.3.4.3 Nonspecific IV Block

When the QRS duration is prolonged to ≥0.11 s, without any of the criteria previously described for right or left incomplete or complete bundle branch block, it should be referred to as nonspecific (or unspecified) IV block (or IV conduction delay). Arborization blocks or peri-infarction blocks [66] may fall into this category and the same applies to mural (parietal) blocks.

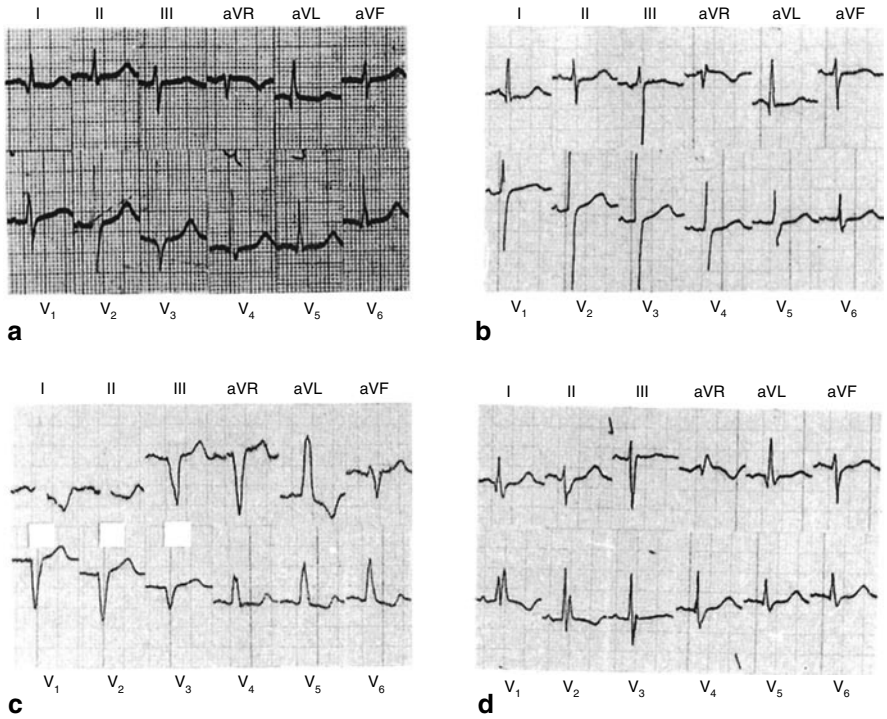

Figure 14.20

Bilateral bundle branch block: evolution from a normal ECG ((a), 1978) to LAFB ((b), 1985), then to LBBB with normal QRS axis ((c), 1986) and finally to LAFB + RBBB ((d), 1987).

Arborization blocks refer to focal lesions located distally in the conduction system, sometimes related to myocardial necrosis. Castellanos and coworkers, using intracavitary electrograms [61, 193, 194] were able to recognize either further enlargement of "central" RBBB owing to associated peripheral block, or the pattern of complete RBBB without delay in right ventricular apical depolarization. In the latter case, they assumed that the conduction disturbance occurs "distally" after the impulse has emerged from the trunk of the right bundle branch.

Mural or parietal blocks, either left or right sided, correspond to delays either in the more peripheral Purkinje ramifications or in the myocardial fibers. They have been experimentally induced by chemical necrosis [195] and may be a result of, in clinical cases, areas of myocardial necrosis and fibrosis (peri-infarction block), infiltrative granulomatous diseases (such as amyloidosis, Chagas disease or sarcoidosis), myocarditis or cardiomyopathies, hyperkalemia, antiarrhythmic drugs toxicity, and even surgical right ventriculotomy [196].

14.3.5 Clinical Overview of Intraventricular Conduction Defects

Intraventricular conductions defects are among the most frequent ECG abnormalities found in clinical practice. This designation encompasses very different types of abnormalities – anatomic and functional lesions either located in the His bundle or in its main divisions (RBBB and LBBB) or in the subdivisions of the left bundle branch (fascicular blocks – anterior, median, and posterior) or even more peripherally in the Purkinje system or the myocardial cells (arborization blocks, parietal blocks, peri-infarction block). Different degrees of conduction delay in such different locations account for very different paths of electrical activation of the ventricles as well as very different ECG patterns. Although the major types of IV conduction defects are well recognized, many points of controversy still remain to be completely understood.

In spite of representing such a heterogeneous group of abnormalities, all of them can appear either isolated or associated with other cardiac abnormalities (with different prevalence for each type of conduction defect and each type of population studied). Although there are anticipated differences in the prognosis of each conduction defect, they all seem more dependent on the presence and severity of any associated heart disease than on the particular type of conduction defect *per se*. For example, isolated fascicular blocks (LAFB being the most prevalent) have an exceedingly benign prognosis unless associated with an otherwise severe heart disease. Therefore, in the presence of any type of conduction defect, a complete cardiac evaluation must be done and should include, as a priority, a complete echocardiographic study, in order to ascertain accurately and noninvasively the presence and severity of any coexisting cardiac abnormalities as well as their functional significance.

On the other hand, conduction defects frequently make it difficult or impossible to identify other ECG abnormalities, namely, those related to coronary heart disease or hypertrophy of the cardiac chambers. In such cases, once again, a complete cardiac evaluation is mandatory, including a complete echocardiographic study (M-mode, two-dimensional, and Doppler) as well as radionuclide evaluation in order to obtain the correct diagnosis hidden by the ECG pattern of the conduction defect.

For certain IV conduction defects, namely, the so-called bifascicular blocks, an ominous prognosis related with the development of advanced AV block has been described. However, even for bifascicular blocks, the incidence of such a complication (advanced AV block) is very low and does not warrant prophylactic pacemaker implantation or electrophysiological study (unless for the evaluation of the specific symptoms such as syncope or hemodynamically distressing arrhythmias).

On the other hand, in the setting of acute myocardial infarction, the identification of a bundle branch block is a poor risk and warrants pacemaker implantation, although the majority of such patients will die in pump failure.

Much has been learned about IV conduction defects and the cardiac conductions system since the 1950s. However, much is still under debate, mainly concerning the underlying abnormalities that are the basis of many paroxysmal and intermittent conduction defects (some of them rate related) or the more peripheral conduction disturbances at the Purkinje–muscular fiber level, most of them only accessible to electrophysiological studies as well as epicardial and endocardial mapping.

14.4 Ventricular Preexcitation

Preexcitation syndromes – conditions in which the conduction disturbance is characterized by earlier activation of the whole or part of the ventricular myocardium – have been the subject of a huge amount of literature (more dictated by its electrophysiological interest and the multitude of allied tachydysrhythmias than for its known prevalence in the general population). Their study has largely contributed to the elucidation of the pathophysiology of reentrant arrhythmias as well as to the present understanding of the whole conduction system and IV conduction disturbances. Electrophysiological studies as well as endocardial mapping of these conditions are described in other sections of this book.

The Wolff–Parkinson–White (WPW) pattern – short PR interval preceding a wide QRS complex – is by far the most typical and well-known preexcitation ECG pattern. Lately, the term has been extended to include other entities where AV conduction has occurred through other types of anomalous AV connections.

Reference will be made to some cases that have similar anatomic connections (with related arrhythmias) in spite of a normal ECG.

14.4.1 Definition

Ventricular preexcitation can be defined [197] as a condition in which, in relation to atrial excitation, all or some portion of the ventricles are activated by the impulse originating from the atria earlier than would be expected if the impulses were to reach the ventricles by way of the normal conduction pathway.

This "earlier activation" (preexcitation) can only be possible because the electrical stimulus travels through an anomalous "short circuit" that directly conducts it from the atria to an ectopic ventricular site (or that, at least, bypasses the area of normal conduction delay). It appears that a few instances are caused by accelerated conduction within the AV node

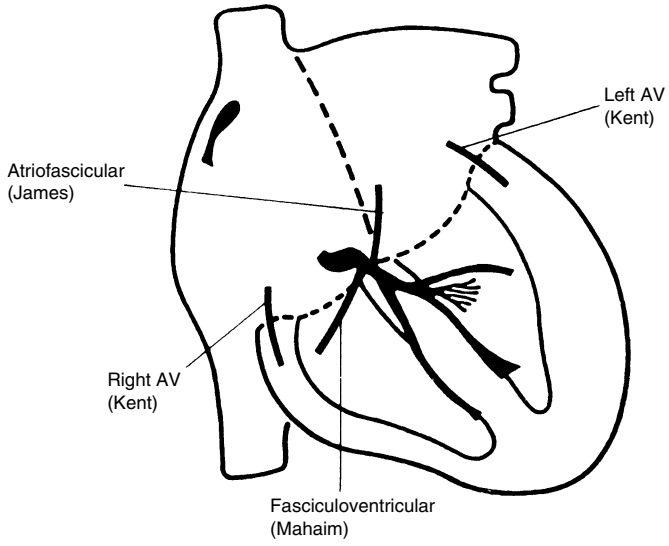

Figure 14.21
Schematic of the more frequent types of anomalous connections in cases of ventricular preexcitation.

itself, without the presence of anomalous conduction pathways (Sect. 14.4.2). Several types of anomalous pathways have been described. The major accessory bypass connections are Kent bundles, James fibers, and Mahaim fibers (Fig. 14.21).

From a histopathological point of view, a distinction between "tract" and "connection" should be made [198]. "Connection" should be used as a general term to describe anomalous conduction pathways that insert into working myocardium while "tract" should be applied to anomalous conduction pathways that insert into specialized conduction tissue. However, the two designations are normally used synonymously.

Preexcitation can be either constant or intermittent, and occasionally can be found on alternate beats. Some patients (particularly those with left-sided accessory pathways) may never show preexcitation in sinus rhythm (be it explained either by enhanced AV conduction or by atrial conduction delay) and only during tachydysrhythmic episodes is the preexcitation pattern observed.

14.4.2 Anatomic Basis

As previously stated, three major types of connection pathways can be described in the human heart [197, 199–204] (Fig. 14.21):

(a) Bundles of Kent are electrically active muscular fibers which directly bridge the atria and the ventricles. Although several locations have been identified for these pathways (actually they can be located almost at any point where the atria and the ventricles are contiguous), they are most frequently identified in a posterior position, connecting the left atrium with the left ventricle [205].
(b) James fibers are presumably continuations of the internodal pathways (connecting the sinus node with the AV node) and connect the atria with the His bundle (atriofascicular accessory pathways) [206]. In this way, they completely bypass the AV node. There is, however, still some dispute on the existence of internodal pathways (see Chap. 4).
(c) Mahaim fibers are accessory pathways between the ventricular muscle on one side and the AV node (nodoventricular) or the His bundle or either of the bundle branches (fasciculoventricular) on the other side. They deviate the electrical impulse from its normal course activating the septal muscle prematurely.

Longitudinal dissociation of the AV node and dual AV nodal pathways have also been described and can present with similar ECG patterns as well as clinical dysrhythmias. Only electrophysiological studies permit the correct diagnosis.

Instead of the above eponyms (Kent, James, Mahaim), which allow some confusion, it is preferable to refer to the several types of connections according to their anatomic location; that is, atrioventricular, nodoventricular, fasciculoventricular, atriofascicular, and intranodal. This is nowadays the accepted classification.

For some cases of preexcitation, an "acquired" theory has been claimed because these syndromes are more frequently identified in adulthood. Nevertheless, it is well known that some accessory pathways remain concealed in sinus rhythm until a precipitating event occurs.

A truly acquired etiology has never been unequivocally demonstrated. However, a case was published by one of the authors [207] in which intermittent WPW, with "concertina" effect (variable shortness of PQ interval as well as a parallel variable enlargement of the QRS [208]) was registered throughout 1 day, in the setting of acute rheumatic fever, to be followed the next day by first-degree AV block (prolonged PR) which later returned to normal.

14.4.3 Wolff–Parkinson–White Syndrome

14.4.3.1 Classification

The classic WPW electrocardiographic pattern was described by Wolff, Parkinson, and White as early as 1930 [204]. It is associated with an AV connection (bundle of Kent) and is estimated to occur in the general population in 0.1–3% depending on the population studied [209]. This estimate is probably low because some pathways do not conduct in the anterograde way and others only have intermittent conduction (see below) and may not be diagnosed [210–214].

Classically, WPW pattern refers to the ECG originally described as consisting of [204]:

(a) Short PR interval <0.12 s during sinus rhythm
(b) The presence of an initial slurring of the QRS ("delta wave") that represents early ventricular activation
(c) An abnormally wide QRS complex ≥0.12 s
(d) Secondary ST-segment and T-wave changes "in healthy young people prone to tachycardia."

Care should be taken to distinguish the WPW pattern and the WPW syndrome [215]. WPW syndrome implies that the patient with the WPW pattern also suffers episodes of tachydysrhytmia.

The QRS pattern will be different according to the specific location of the AV bypass tract, as well as the amount of muscle activated through the accessory pathway. The QRS complexes in preexcitation syndromes can be considered special types of "fusion beats" in which a portion of the activated ventricle is depolarized through the accessory pathways and another portion is activated by the normal pathway. However, if significant delay occurs through the normal pathway, the whole ventricle may be depolarized through the accessory pathway. Some accessory pathways do not conduct anterogradely, either transiently or not, and the whole ventricular activation will always follow the normal pathway. When the "concertina" effect is observed, different types of "fusion beats" will be registered (e.g., nine in the case referred to above [207]) depending upon the gradual increase or decrease of the areas depolarized either normally or through the anomalous pathway. Multiple accessory pathways can coexist in the same patient and give rise to a more complex activation pattern or patterns.

Rosenbaum et al. [216] separated WPW into type A and type B. Type A (Fig. 14.22) was related to a bypass tract between the atria and the posterior left ventricular free wall (left-sided bundle of Kent), which causes an initial anteriorly and rightward delta wave, with an ECG pattern showing predominant or exclusive R-waves in leads V_1 and V_2, in a way similar to RBBB. Conversely, when an anterior bundle of Kent is present, the electrical impulse will pass from the atrium to the anterior right ventricular free wall. In this case (type B WPW) (Fig. 14.23), the delta wave will point posteriorly and to the left and an ECG pattern similar to LBBB (with a dominant S-wave in V_1) will be registered. Other accessory pathways locations (e.g., left septal) were not considered in this classification and were progressively identified. For example, cases with positive delta wave in V_1 trough V_4 but negative in V_5 and V_6 were called type C WPW (related to an abnormal connection on the lateral wall of the left ventricle [217, 218]).

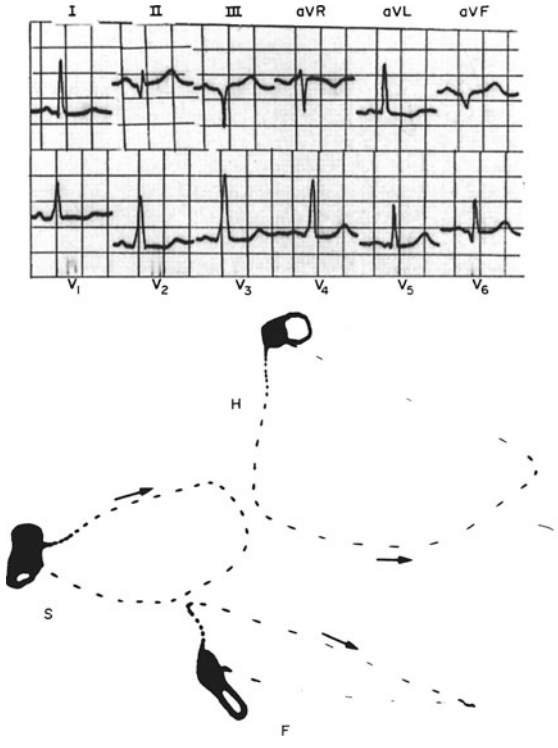

Figure 14.22

ECG leads and VCG loops of a typical example of the classic WPW pattern type A (H, horizontal; S, sagittal; F, frontal). See text for description.

In fact, limb leads contain important data as well. In type A, the delta wave is positive in leads II, III, and aVF and negative in I and aVL. On the contrary, in type B, the delta wave is positive in I and aVL and negative in II, III, and aVF. Using the information contained in the limb leads together with the precordial leads, it is possible to verify that the spatial direction of the initial forces is highly variable.

Fitzpatrick et al. propose an algorithm for accessory atrioventricular pathway localization using a 12-lead ECG (Fig. 14.24) [219]. In this algorithm, if the precordial QRS transition was at or before lead V_1, the pathway had been ablated on the left side. If it was after lead V_2, the pathway had been ablated on the right side. If the QRS transition was between leads V_1 and V_2 or at lead V_2, then if the R-wave amplitude in lead I was greater than the S-wave by ≥1.0 mV, it was right sided; otherwise, it was left-sided (sensitivity 100%, specificity 97%).

The right-sided pathways can be subdivided according to (sensitivity 97%, specificity 95%) the following:

1. If the QRS transition was between leads V_2 and V_3, the pathway was right septal.
2. If after lead V_4, it was right lateral.
3. If it was between leads V_3 and V_4:
   (a) If the delta wave amplitude in lead II was ≥1.0 mV, it was right septal.
   (b) Otherwise, it was right lateral.

Right-sided pathways can be further subdivided (see Fig. 14.24).

The left-sided pathways can be subdivided according to (sensitivity 100%, specificity 100%):

1. Two or more positive delta waves in the inferior leads or the presence of an S-wave amplitude in lead aVL greater than the R-wave, or both, discriminated left anterolateral pathways.

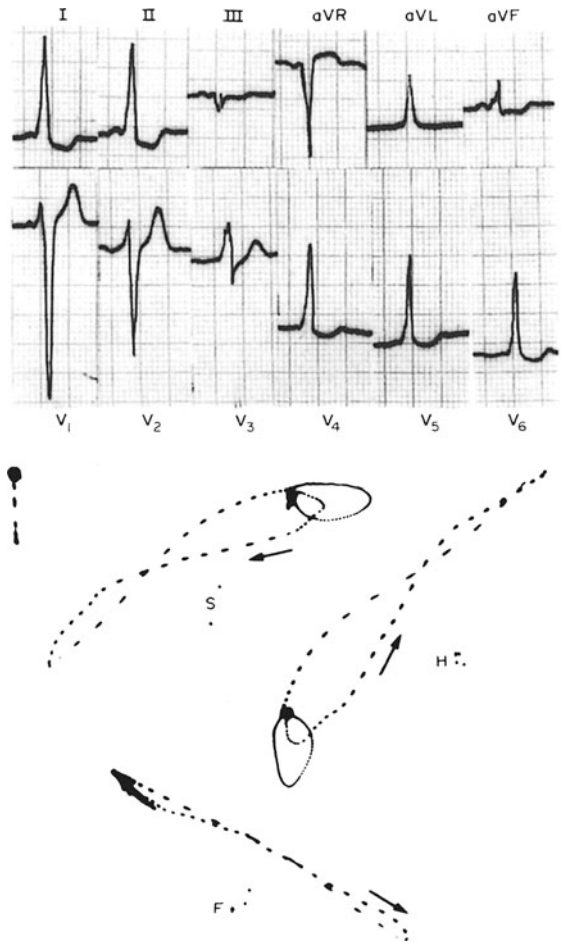

Figure 14.23

ECG leads and VCG loops of a typical example of the classic WPW pattern type B (S, sagittal; H, horizontal; F, frontal). See text for description.

2. If the R-wave in lead I was greater than the S-wave by ≥0.8 mV, and the sum of inferior delta wave polarities was negative, the location was posteroseptal.
3. Otherwise, it was postero-lateral.

However, it must be stressed that any classification of preexcitation pathways based exclusively on standard ECG has important limitations [201] and should be used only as a presumptive clinical approach. The causes of misclassification include [201]:

(a) Coexisting alterations in the QRS complex related to associated congenital or acquired heart abnormalities
(b) The occasional presence of multiple accessory pathways
(c) Variable degrees of "fusion" between normal and accessory conduction
(d) Superimposition of the terminal P-wave with the initial delta wave
(e) Endocardial versus epicardial location of the pathway

With recent advances in the radiofrequency catheter ablation or surgical methods of treatment of refractory dysrhythmias in patients with preexcitation, precise location of the accessory pathways was sought and obtained with special

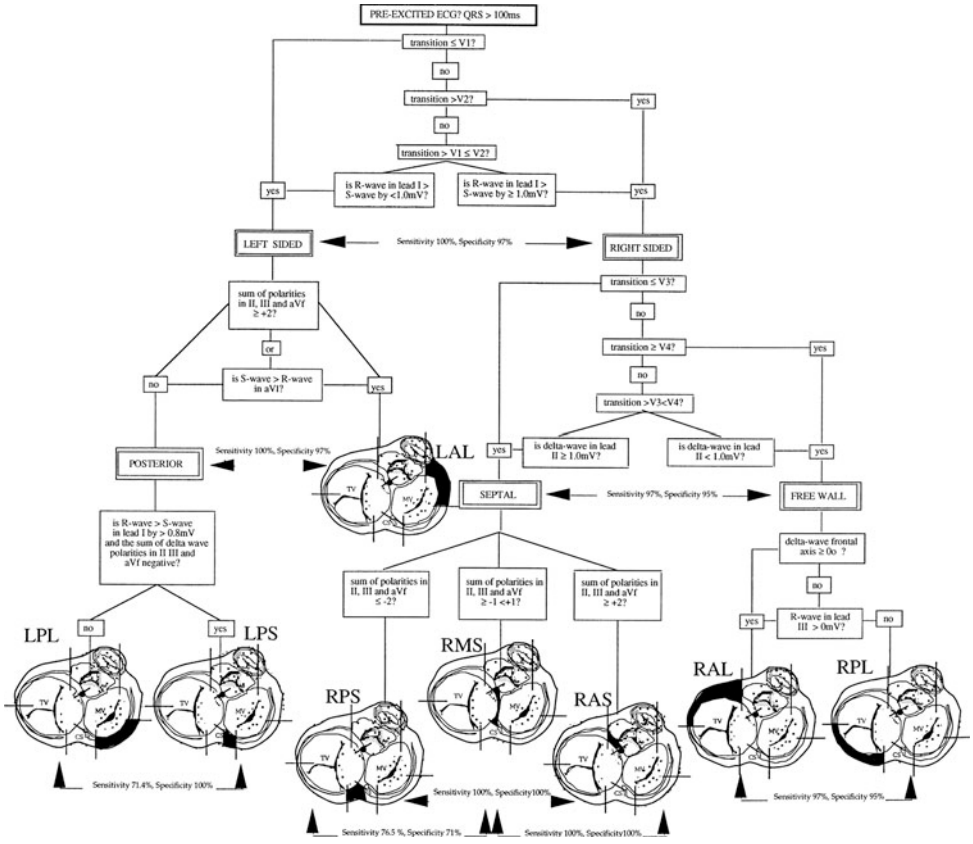

Figure 14.24

Algorithm for defining location of accessory pathways causing preexcitation of the baseline 12-lead electrocardiogram (ECG). Pathways are initially separated into left and right sided. Right-sided pathways may then be separated into five septal or right lateral locations around the tricuspid valve annulus and left-sided pathways into three septal and lateral locations (reproduced from Fitzpatrick et al. [219]).

electrophysiological techniques. These studies have shown a wider variation than expected in the location and functional features of the accessory pathways.

Further discussion on the classification of the WPW pattern using body-surface mapping is given in Chap. 32.

14.4.3.2 Associated Arrhythmias

The prevalence of tachyarrhythmias described in patients with WPW is related to the selection of the population studied and recent studies indicated that his frequency augments with age [220]. Values from 4% to 13% have been published [221]. The most typical and frequent arrhythmia in the setting of WPW syndrome is reciprocating (reentrant) tachycardia with anterograde conduction over the AV node and His bundle, and retrograde conduction through the accessory pathway (Fig. 14.25).

As previously stated, during sinus rhythm, conduction spreading normally as well as through the accessory pathway produces two wavefronts which merge to form a ventricular "fusion beat." Most frequently the refractory period of the accessory pathway, during sinus rhythm, is greater than that of the normal conduction system, although conduction time is usually shorter for the anomalous pathway. With the appearance of a premature atrial beat – the usual precipitating factor – the conduction may be blocked anterogradely through the accessory pathway, but be propagated to the ventricle

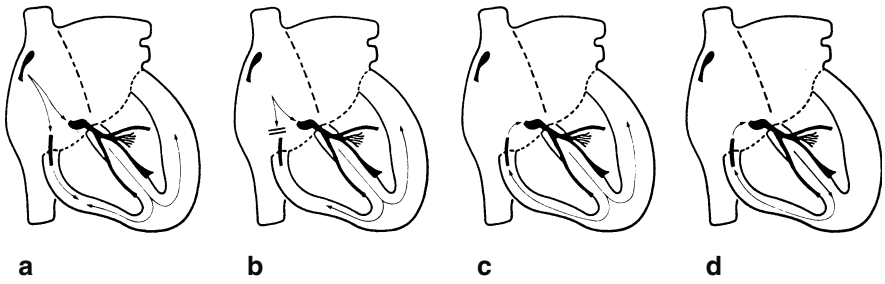

Figure 14.25

Schematic of initiation of orthodromic tachycardia in patients with WPW. A right-side AV (Kent) pathway is represented. During normal sinus rhythm (a), conduction spreads through the accessory pathway as well as through the normal conduction system, producing a "fusion beat" with the classic WPW pattern. With a premature atrial beat (b), the stimulus may find anterograde conduction through the accessory pathway blocked but is conducted through the normal conduction system. Then, retrograde conduction through the accessory pathway (c) may allow the establishment of a reentry circus rhythm (d) (narrow QRS tachycardia).

as usual, through the normal conduction system (thus resulting in a normal QRS complex). This dissociation between the refractory period of the normal and the accessory pathways (precipitated by the occurrence of a premature beat) allow reentry to ensue. Conduction through the ventricle will find the accessory pathway excitable in the retrograde direction, allowing the impulse to go back to the atria, thus establishing a circus rhythm: anterograde conduction through the normal conduction system (normal QRS) and retrograde conduction through the accessory pathway (orthodromic AV tachycardia). The precipitating factor is usually a premature beat which arises in the atrium but which can also be generated in the AV junction or in the ventricles.

Some accessory pathways are only capable of retrograde conduction [210–214, 227]. Such pathways are usually classified as concealed pathways. Patients with this abnormality may experience paroxysmal supraventricular tachycardia but have no delta wave on their standard ECG. The tachycardias are usually attributed to reentry within the AV node but they are actually a result of the accessory pathway [211, 214, 223–225]. Only complete electrophysiological studies can disclose the correct cause of tachydysrhythmia in these patients. If such a connection is identified, they should be managed like any other patients with WPW and tachyarrhythmias. Interestingly enough, they are "protected" against life-threatening rapid ventricular response rates in the setting of atrial fibrillation.

The occasional patient with an accessory pathway that conducts only in the anterograde direction [214, 226–228] will not have the classic form of recurrent AV tachycardia with narrow QRS.

In some WPW patients, the reciprocating rhythm can also occur in the reverse direction, termed "antidromic reciprocating tachycardia" [229]. Anterograde conduction is through the accessory pathway (wide QRS, mimicking ventricular tachycardia) and retrograde conduction over the normal conduction system. This appears to be a rare finding but poses special diagnostic problems (see below) [201] (Fig. 14.26).

Atrial fibrillation (although not atrial flutter), in the setting of WPW, is common, occurring in up to 39% of the patients [201, 230, 231] (obviously depending on the selection of the population). The high prevalence of atrial fibrillation in WPW is probably related to the series of predisposing factors given below:

(a) The rate of reciprocating tachycardia in WPW is usually higher than that owing to reentry through the AV node.
(b) There is a possibility that a retrograde impulse arrives at the atria in the vulnerable phase of atrial recovery.
(c) There is nonuniform depolarization of the atria with multiple impulses being conducted at the same time (either from the sinus node or retrogradely from the ventricle). Actually, transition from reciprocating tachycardia to atrial fibrillation has been observed.

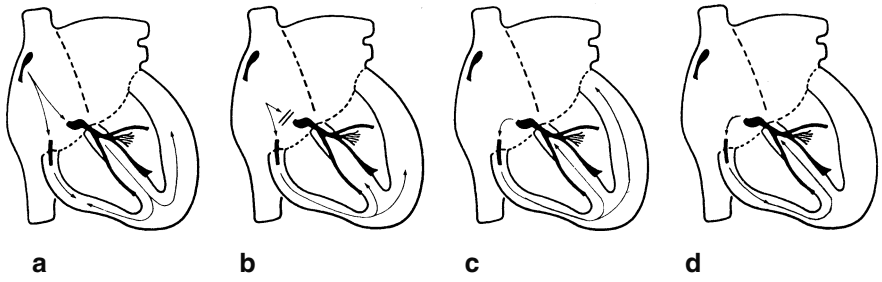

Figure 14.26

Schematic of the mechanism for initiation of antidromic tachycardia in patients with WPW. A right-side AV (Kent) pathway is represented. During normal sinus rhythm (a), conduction spreads both through the accessory pathway and through the normal conduction system, producing a "fusion beat" with the classic WPW pattern. With a premature atrial beat (b), the stimulus may find anterograde conduction through the AV node blocked but is conducted through the accessory pathway. Then, retrograde conduction through the normal conduction system may ensure (c) and allow the establishment of a reentry circus rhythm (d) (wide QRS tachycardia).

The most important problem concerning atrial fibrillation or flutter associated with WPW is the risk of progression to ventricular fibrillation. Owing to the presence of an accessory pathway with short refractory period, a very rapid ventricular rate of response may be observed. Its degeneration to ventricular fibrillation and sudden death has been described [232–240].

It is important to remember that digitalis will not slow AV conduction in cases of atrial fibrillation in which there is anterograde conduction through the anomalous pathway. In fact, cardiac glycosides may shorten its anterograde refractory period, thereby accelerating ventricular response. For practical purposes, digitalis should be contraindicated in WPW patients with either atrial fibrillation or flutter.

14.4.3.3 Associated Congenital Abnormalities

The association of WPW pattern with congenital heart disease has been frequently reported. The most frequent associations are with Ebstein's anomaly and mitral valve prolapse [201, 241, 242]. It is still debatable whether these associations have an embryological basis [243] or not.

Association has been reported with other congenital and acquired heart diseases as well [201], namely, corrected transposition of the great vessels. A familial form of WPW has been reported and may be associated with congestive or hypertrophic cardiomyopathies [244].

14.4.3.4 Diagnostic Difficulties

Besides the incidence of tachyarrhythmias, preexcitation has interested investigators for a long time because it is a frequent cause for difficult ECG differential diagnosis. First, classic type A WPW (left-sided bundle) has been misdiagnosed as RBBB, true posterior myocardial infarction and right ventricular hypertrophy, while type B WPW pattern (right-sided bundle) may resemble LBBB, anterior myocardial infarction or left ventricular hypertrophy. Second, a PR at the lower limit of normal coexisting with either right or left complete bundle branch block may mimic WPW. Third, preexcitation of the diaphragmatic surface of the heart results in superiorly oriented activation forces thus mimicking inferior myocardial infarction [245]. Fourth, following the abnormal depolarization sequence, the repolarization is also modified. Thus an abnormal ST–T-wave pattern may be falsely diagnosed as ischemic. Fifth, WPW is one of the reported causes of a false positive exercise test [246], even in cases in which the conduction abnormality may disappear with exercise, and finally, as previously stated, the tachydysrhythmias associated with WPW are also a cause of difficult diagnosis.

14.4.3.5 Electrophysiological Evaluation

Electrophysiological examination with intracardiac recording and pacing as well as epicardial mapping, and its full indications and usefulness, is dealt with in Chaps. 24 and 25. Intracardiac recordings provide the only possibilities of diagnosing, for example, concealed WPW as well as most cases of WPW associated with either RBBB or LBBB.

Electrophysiological studies are clearly indicated in WPW patients with distressing symptoms or syncope owing to recurrent attacks of tachycardia, or rapid anomalous pathway conduction during episodes of atrial fibrillation or flutter, and in the evaluation of the acute response to drugs in medically refractory paroxysmal tachycardias, and in the last years the electrophysiological laboratory also makes possible ablation of the anomalous pathway, with great success (>90%) and is now the first line of therapy for WPW syndrome [220]. In patients in whom the surgical therapy is contemplated, electrophysiological study will permit not only the confirmation of the presence of the preexcitation and its functional behavior in the clinically observed tachyarrhythmias, but also the location with certainly of the accessory pathway (and sometimes the identification of multiple accessory pathways).

Asymptomatic or mildly symptomatic patients, as well as those with good clinical response to medical management, will not require an electrophysiological study. Fortunately, they form the majority.

14.4.4 Other Forms of Preexcitation

14.4.4.1 Short PR Syndromes

In cases of atriofascicular accessory pathways (James fibers), the AV node zone of physiological delay is bypassed and the ventricular activation follows its normal path. Thus a short PR interval with normal narrow QRS pattern will be registered [197, 200] (Fig. 14.27).

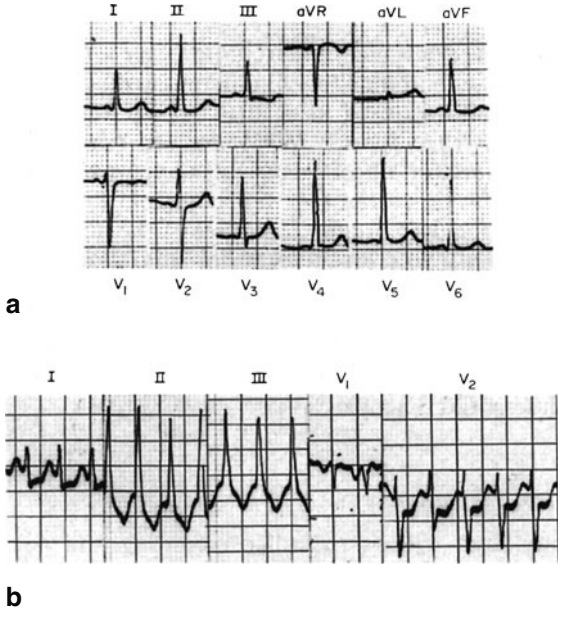

Figure 14.27

Typical case of LGL syndrome. Part (a) shows an ECG pattern with short PR interval and normal QRS. Part (b) is an ECG during an episode of supraventricular tachycardia.

This ECG pattern was first described by Clerc et al. [247] in 1938, but its association with paroxysmal tachyarrhythmias was identified only in 1952 by Lown et al. [248]. The designation of this syndrome (LGL syndrome or short PR syndrome) should be reserved for those cases with tachyarrhytmias associated with the corresponding basal ECG pattern.

Although Lown et al. [248] reported a 9.5% prevalence of paroxysmal tachycardia in patients with short PR interval and normal QRS complex, the actual incidence of supraventricular tachycardia in unselected patients with this ECG pattern remains unknown. Ventricular tachycardia can occur [17, 249]. Actually, two of the patients originally described by Lown et al. with atrial fibrillation died suddenly.

Accelerated conduction through the AV node will give a similar pattern and may represent the electrophysiological substrate of most cases of LGL syndrome. This concept of enhanced AV nodal conduction (EAVN) was proposed for patients found in electrophysiological studies to have little or no prolongation of AV nodal conduction in response to right atrial pacing [201, 250]. EAVN could be explained either by partial bypass of the AV node, or by an underdeveloped or anatomically small AV node, or else by an anatomically normal AV node with rapid conduction properties (functionally or as a consequence of autonomic tone).

14.4.4.2 Nodoventricular Connections

As previously stated, a nodoventricular connection is one of the Mahaim fibers connecting the AV node with the ventricular muscle [198]. The basal PR interval and degree of preexcitation will depend on the relative location of the point where the fiber leaves the AV node to the area (and degree) of AV nodal physiological conduction delay. These fibers can be demonstrated by electrophysiological study. Typically [17], at faster heart rates or with close coupled atrial extrastimuli, the QRS widens and assumes greater degrees of LBBB morphology.

There may be no evidence of ventricular preexcitation in sinus rhythm, becoming manifest only during atrial pacing (because prolonged AV nodal conduction time is produced).

The mechanism of tachycardia involving nodoventricular pathways is not completely understood. Prystowsky et al. [17] suggest that most likely it involves either macroreentry following the nodoventricular fiber, His–Purkinje system and AV node, or AV nodal microreentry with associated anterograde conduction over the nodoventricular connection (Fig. 14.28).

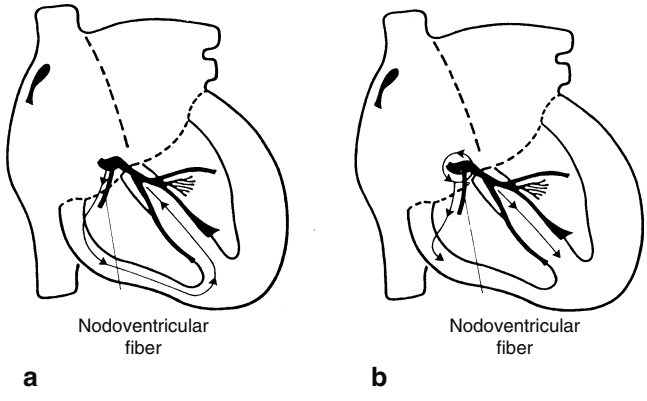

Figure 14.28

Schematic of the suggested mechanisms for tachycardia initiation in patients with a nodoventricular fiber. Part (a) shows macroreentry using the nodoventricular fiber, His–Purkinje system and AV node. Part (b) shows AV nodal microreentry with associated anterograde conduction through the nodoventricular connection.

14.4.4.3 Fasciculoventricular Connections

A fasciculoventricular connection is a type of the Mahaim fibers that arise from the His bundle (or bundle branches) and enters into the ventricle [198].

The PR interval is normal (unless it coexists with EAVN) and usually only minor slurring of the initial QRS forces occurs (because His–Purkinje conduction velocity is rapid with little opportunity for more evident ventricular preexcitation).

In electrophysiological studies, the HV interval is short and during rapid atrial pacing or premature atrial stimulation, the atrial–His (AH) interval lengthens with no change in the HV interval or QRS width [251]. No specific arrhythmias have been causally related to the presence of fasciculoventricular fibers [251].

To conclude the electrical curiosities related to preexcitation, it can be quoted that it is theoretically possible to have an impulse conducted from the atria to the His bundle through James fibers and then to the ventricles by way of Mahaim fibers, thus producing the classic WPW pattern: a short PR interval with a wide QRS complex with delta wave [221].

All the ECG patterns arising from conduction through Mahaim fibers cannot be correctly diagnosed without performing invasive electrophysiological studies.

14.5 The Brugada Syndrome

14.5.1 Classification

In 1992, Pedro and Josep Brugada described a syndrome with an ECG pattern of repolarization and depolarization abnormalities in the right precordial leads that was associated with sudden death in individuals with a structurally normal heart [252]. Brugada Syndrome is suspected to be responsible for 40–60% of what had previously been referred to as "idiopathic ventricular fibrillation" [253]. The criteria for the Brugada Syndrome were presented in a consensus paper [254] which was subsequently followed by a second consensus paper [255] that made some adjustments to the definitions.

The Brugada pattern appears in the ECG as repolarization and depolarization abnormalities in the right precordial leads; three types of repolarization patterns were initially recognized according to the study group of the European Society of Cardiology (Fig. 14.29) [254] but only the first was confirmed as definitively being the Brugada pattern [255]:

- Type 1 prominent coved ST-segment elevation, displaying a J-wave amplitude or an elevated ST-segment ≥2 mm (or 0.2 mV) at its peak, followed by a negative T-wave, with little or no isoelectric separation.
- Type 2 high takeoff ST-segment elevation: in this case the J-wave amplitude ≥2 mm gives rise to a gradually descending ST-segment elevation, remaining ≥1 mm above baseline, followed by a positive or biphasic T-wave, resulting in a saddle back configuration.
- Type 3 ST-segment elevation compromising a <1 mm saddle back or coved configuration (or both).

The PR interval usually is increased and presumably reflects the presence of HV-conduction delay. The QT-interval is either within normal limits or slightly prolonged.

Conduction defects may be specific or nonspecific for any part of the conduction system. Sometimes pronounced broad S in leads I, II, and III, giving rise to an extreme left axis deviation, are encountered. A left axis deviation may indicate left anterior fascicular block. A true RBBB may also be seen. The repolarization pattern type 2 may mimic a RBBB pattern, but the absence of S-waves in the left-lateral leads precludes the true presence of a RBBB.

In Brugada pattern, the ST-segment is dynamic; different patterns may be observed in the same patient sequentially or following the introduction of specific drugs. In the first few hours after DC shock, ECG patterns characteristic of Brugada Syndrome cannot be taken as diagnostic.

This disorder is inherited with an autosomal dominant mode of transmission with incomplete penetrance and an incidence ranging between 5 and 58 per 10,000 [255]. An incidence of 12 per 10,000 was quoted for the Type 1 pattern in Japanese individuals but it was the Type 2 and Type 3 patterns with an incidence of 58 per 10,000 that were much more

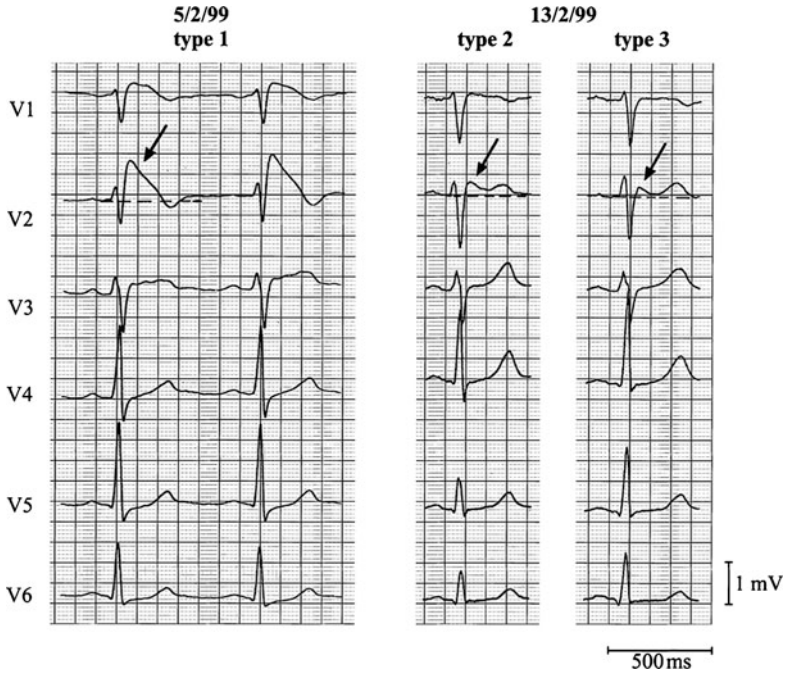

Figure 14.29

Precordial leads of a resuscitated patient with Brugada syndrome. Note the dynamic course of a couple of days. All three patterns are shown. Arrows denote the J-wave (reproduced from Horan et al. [253]. © American College of Chest Physicians, Northbrook, IL).

common in this population [256]. The only mutations linked to the syndrome appear in the gene that encodes for the sodium channel SCN5A [257].

The second consensus conference revised the initial definition. Brugada syndrome is said to be definitively present when the patient has the Type 1 ECG pattern in the presence or absence of a sodium channel blocking agent and at least one of the following clinical characteristics [255]: documented ventricular fibrillation, polymorphic ventricular tachycardia, a family history of SCD before age 45, coved-type ECGs in family members, electrophysiological inducibility of a ventricular tachycardia, syncope, or nocturnal agonal respiration. The appearance of the ECG features, without these clinical features, is sometimes referred to as an idiopathic Brugada ECG pattern. The second consensus paper stated that Type 2 and Type 3 patterns are not diagnostic of the Brugada pattern.

A diagnosis of Brugada syndrome can also be made if a Type 2 or Type 3 pattern is found in more than one right precordial lead but which changes to a Type 1 pattern after sodium channel blocker administration [255].

14.5.2 Molecular Genetics

Brugada syndrome is often inherited with an autosomal dominant mode of transmission [258].

About 20–25% of Brugada patients have documented SCN5A mutations [258]. Genetic studies have demonstrated that some cases of Brugada syndrome and chromosome 3-linked long-QT syndrome are allelic disorders of the cardiac sodium channel gene (SCN5A, 3p21).

Three types of SCN5A mutations have been identified in the Brugada syndrome: splice-donor, frame-shift, and missense [259]. All of these mutations lead to a reduction in the fast sodium channel current.

14.5.3 Associated Arrhythmias

Brugada syndrome has been associated with sudden death related to arrhythmias like VT or VF. Ventricular tachycardia usually starts with a short coupling interval, and rapid polymorphic VTs are responsible for syncope and sudden cardiac death in a majority.

It has been suggested that there is a higher than normal incidence of supraventricular tachyarrhythmias, including atrial and AV reentrant tachycardias in the Brugada population. Monomorphic VT is rare [260].

14.5.4 Diagnostic Difficulties

There are many conditions that can lead to ST-segment elevation in the right precordial leads. In order to establish a diagnosis of Brugada syndrome, it is necessary to exclude all these conditions, namely, arrythmogenic right ventricular cardiomiopathy (ARVC) and the early repolarization syndrome [257].

ARVC may mimic Brugada syndrome and, in some cases, structural abnormalities may only be found at autopsy. Drug challenge with sodium channel blockers (flecainide, ajmaline, or procainamide) may be useful in discriminating between these two entities.

The early repolarization syndrome may mimic a type 2 or type 3 Brugada ECG pattern. Once again, a drug challenge might provide the clue for a proper diagnosis.

Other causes of ST-segment elevation must be ruled out including epicardial injury, pericarditis, or electrolyte abnormalities.

14.5.5 Drug Challenge

Intravenous administration of certain drugs, like sodium channel blockers (ajmaline, flecainide, or procainamide), unmask or exaggerate the ST-segment elevation. Some discussion exists about the sensitivity and specificity of this test. Procainamide has a very low sensitivity. Reproducibility of the test according to recent studies might be near 100% but is not well established [261].

The patient should be monitored while the drug challenge is performed and a defibrillator should be nearby. Drug administration should be stopped when the test is positive (J-wave amplitude >2 mm in lead V_1 and/or V_2 or V_3 with or without RBBB) and/or when ventricular arrhythmias, including ventricular premature complexes, are evident or QRS widening ≥30%.

Drug challenge is indicated in patients with Brugada syndrome pattern Type 2 or 3 in order to clarify the diagnosis (conversion to Type 1 is considered positive as indicated previously).

The more that sodium channel blockade is needed to elicit Brugada syndrome, the less the patient is at risk under baseline conditions.

14.5.6 Electrophysiological Evaluation

Electrophysiological studies (EPS) may be useful in risk stratification and in establishing the diagnosis [262].

Brugada [263] suggested that an EP study is not required in individuals with the Brugada pattern and syncope or aborted sudden death, i.e., an implanted cardioverter defibrillator (ICD) is required. An ICD is also required for patients with a Brugada ECG and an inducible arrhythmia at EPS, e.g., VF. Asymptomatic individuals (a) without an inducible arrhythmia or (b) with a Brugada ECG which appears only after drug challenge are at low risk and only require follow-up.

EPS is recommended in all symptomatic patients as well in asymptomatic patients when there exists a positive family history for sudden cardiac death. The necessity for EPS is questionable in patients displaying the Brugada ECG pattern, but who are asymptomatic and have a negative family history.

References

1. Durrer, D., R.Th. van Dam, G.E. Freud, M.J. Janse, F.L. Meijler, and R.C. Arzbaecher, Total excitation of the isolated human heart. *Circulation*, 1970;**41**: 899–912.
2. Josephson, M.E., D.L. Scharf, J.A. Kastor, and J.G. Kitchen, Atrial endocardial activation in man. Electrode catheter technique for endocardial mapping. *Am. J. Cardiol.*, 1977;**39**: 972–981.
3. Witting, J.H., M.R. de Leval, and J. Stark, Intraoperative mapping of atrial activation before, during, and after the Mustard operation. *J. Thorac. Cardiovasc. Surg.*, 1977;**73**: 1–13.
4. Puech, P.M., M. Esclavissat, D. Sodi-Pallares, and F. Cisneros, Normal auricular activation in the dog's Herat. *Am. Heart J.*, 1954;**47**: 174–191.
5. Vagueiro, M.C., *Electrocardiografia Hisiana e Estimulação Eléctrica Artificial no Estudo das Alterações da Condução e Ritmo Cardíaco*. Lisboa: Tese de Doutoramento, 1975.
6. Janse, M.J. and R.H. Anderson, Specialized internodal atrial pathways – Fact or fiction? *Eur. J. Cardiol.*, 1974;**2**: 117–136.
7. Sorsky, E. and P. Wood, The use of chest leads in clinical electrocardiography. *Am. Heart J.*, 1937;**13**: 183–196.
8. New York Heart Association Criteria Committee, *Nomenclature and Criteria for Diagnosis of Diseases of the Heart and Great Vessels*, 8th edn., Boston, MA: Little Brown, 1979.
9. Ashman, R. and E. Hull, *Essentials of Electrocardiography*, 2nd edn., New York: Macmillan, 1945.
10. Stewart, C.B. and G.W. Manning, A detailed analysis of the electrocardiograms of 500 R.C.A.F. aircrew. *Am. Heart J.*, 1944;**27**: 502–523.
11. White, B.V., R.C. Parker Jr., and A.M. Master, Disease of the mitral valve: Its effects on the pattern of the electrocardiogram. *Arch. Intern. Med.*, 1944;**74**: 94–99.
12. Shipley, R.A. and W.R. Hallaran, The four-lead electrocardiogram in two hundred normal men and women. *Am. Heart J.*, 1936;**11**: 325–345.
13. Castellanos, A. Jr., R. Iyengar, A.S. Agha, and C.A. Castillo, Wenckenbach phenomenon within the atria. *Br. Heart J.*, 1972;**34**: 1121–1126.
14. Castellanos, A., R.J. Sung, J.L. Aldrich, I.J. Mendoza, and R.J. Myerburg, Alternating Wenckenbach periods occurring in the atria, His-Purkinje system, ventricles and Kent bundle. *Am. J. Cardiol.*, 1977;**40**: 853–859.
15. Castellanos, A., R.J. Sung, S.M. Mallon, M.G. Bloom, and R.J. Myerburg, Effects of proximal intra-atrial Wenckenbach on distal atrioventricular nodal, and His-Purkinje, block. *Am. Heart J.*, 1978;**95**: 228–234.
16. Willems, J.L., E.O. Demedina, R. Bernard, et al., World Health Organization/International Society and Federation of Cardiology Task Force. Criteria for intraventricular-conduction disturbances and preexcitation. *J. Am. Coll. Cardiol.*, 1985;**5**: 1261–1275.
17. Prystowsky, E.N., W.M. Miles, J.J. Heger, and D.P. Ziper, Preexcitation syndromes. Mechanisms and management. *Med. Clin. North Am.*, 1984;**68**: 831–893.
18. Narula, O.S., M. Runge, and P. Samet, Second degree Wenckenbach AV block due to block within the atrium. *Br. Heart J.*, 1972;**34**: 1127–1136.
19. Demoulin, J.C. and H.E. Kulbertus, Histopathological examination of the concept of left hemiblock. *Br. Heart J.*, 1972;**34**: 807–814.
20. de Pádua, F., V.M. Lopes, D.D. Dos Reis, M.G. Lopes, and J.P. Miguel, Hemiblocks. *Adv. Cardiol.*, 1977;**19**: 105–114.
21. de Pádua, F., D.D. Reis, V.M. Lopes, et al., Left median hemiblock – A chimera? in *3rd International Congress on Electrocardiography*, (*17th International Symposium on Vectorcardiography*), P. Rijlant and F. Kornreich, Editors. Brussels, 1976.
22. Demoulin, J.-C., L.J. Simar, and H.E. Kulbertus, Quantitative study of left bundle branch fibrosis in left anterior hemiblock: A stereological approach. *Am. J. Cardiol.*, 1975;**36**: 751–756.
23. Uhley, H.N. and L.M. Rivkin, Electrocardiographic patterns following interruption of the main and peripheral branches of the canine left bundle of His. *Am. J. Cardiol.*, 1964;**13**: 41–47.
24. Beattie, J.M., F.A. Gaffney, and C.G. Blomqvist, Transcavitary conduction and the mean frontal QRS axis (abstract), in *14th International Congress on Electrocardiology*, (*28th International Symposium on Vectorcardiography*), R.Th. van Dam, Editor. Berlin, 1987, p. 7.
25. Duchosal, P.W. and J.R. Grosgurin, *Atlas D'electrocardiographie et de Vectocardiographie. Étude du Ventriculogramme dans les Conditions Normales et Pathologiques*. Basel: Karger, 1959.
26. Rosenbaum, M.B., The hemiblocks: Diagnostic criteria and clinical significance. *Mod. Concepts Cardiovasc. Dis.*, 1970;**39**: 141–146.
27. Rosenbaum, M.B., M.V. Elizari, and J.O. Lazzari, *The Hemiblocks*. Oldsmar, FL: Tampa Tracings, 1970.
28. de Pádua, F., V.M. Lopes, D.D. Reis, J.M.P. Miguel, and M.G. Lopes, O hemibloqueio esquerdo mediano – Uma entidade discutível. *Bol. Soc. Port. Cardiol.*, 1976.
29. de Pádua, F., Bloqueios fasciculares – Os hemibloqueios em questão. *Rev. Port. Clin. Terapêutica*, 1977;**3**: 199.
30. de Pádua, F., Intraventricular conduction defects – What future? In *New Frontiers of Electrocardiology*, F. de Pádua and P.W. Macfarlane, Editors. Chichester: Research Studies Press, 1981, pp. 181–185.
31. Burchell, H.B. and N. Tuna, The interpretation of gross left axis deviation in the electrocardiogram. *Eur. J. Cardiol.*, 1979;**10**: 259–277.
32. Corne, R.A., R.E. Beamish, and R.L. Rollwagen, Significance of left anterior hemiblock. *Br. Heart J.*, 1978;**40**: 522–527.
33. Das, G., Left axis deviation: A spectrum of intraventricular condition block. *Circulation*, 1976;**53**: 917–919.
34. Horwitz, S., E. Lupi, J. Hayes, W. Frishman, M. Cardenas, and T. Killip, Electrocardiographic criteria for the diagnosis of left anterior fascicular block. Left axis deviation and delay intraventricular conduction. *Chest*, 1975;**68**: 317–320.
35. Jacobson, L.B., L. LaFollete, and K. Cohn, An appraisal of initial QRS forces in left anterior fascicular block. *Am. Heart J.*, 1977;**94**: 407–413.
36. Kulbertus, H.E., P. Collignon, and L. Humblet, Vectorcardiographic study of the QRS loop in patients with left anterior focal block. *Am. Heart J.*, 1970;**79**: 293–304.
37. McHenry, P.L., J.F. Phillips, C. Fish, and B.R. Corya, Right precordial QRS pattern due to left anterior hemiblock. *Am. Heart J.*, 1971;**81**: 498–502.
38. Milliken, J.A., Isolated and complicated left anterior fascicular block: A review of suggested electrocardiographic criteria. *J. Electrocardiol.*, 1983;**16**: 199–211.

39. Perloff, J.K., N.K. Roberts, and W.R. Cabeen Jr., Left axis deviation: A reassessment. *Circulation*, 1979;**60**: 12–21.
40. Rabkin, S.W., F.A.L. Mathewson, and R.B. Tate, Natural history of marked left axis deviation (left anterior hemiblock). *Am. J. Cardiol*., 1979;**43**: 606–611.
41. Friedman, H.H., *Diagnostic Electrocardiography and Vectorcardiography*. 2nd edn., New York: McGraw-Hill, 1977, pp. 80–55.
42. Cerqueira Gomes, M., F. de Pádua, C. Ribeiro, et al., in *Symposium and Colloquium on the Electrical Field of the Heart*, P. Rijilant, Editor. Brussels: Presses Academiques, 1972.
43. Cerqueira Gomes, M., F. de Pádua, C. Ribeiro, et al., Estudos sobre o desvio esquerdo do eixo médio do QRS (estudo cooperativo). I. Bases experimentais e clínicas. *J. Médico*, 1973;**81**: 345–353.
44. Cerqueira Gomes, M., F. de Pádua, C. Ribeiro, et al., Estudos sobre o desvio esquerdo do eixo médio do QRS (estudo cooperativo). II. Resultados preliminares. *J. Médico*, 1973;**81**: 726–732.
45. Medrano, G.A., C. Brenes, A. DeMicheli, and D. Sodi Pallares, Clinical electrocardiographic and vectorcardiographic diagnosis of the left anterior subdivision block isolated or associated with RBBB. *Am. Heart J*., 1972;**83**: 447–458.
46. Lopes, M.G., *Seminar in Vectorcardiography*. Stanford University Medical School, Stanford, CA: Stanford University Press, 1974.
47. Miguel, J.M.P., D.D. dos Reis, V.M.M. Lopes, B.B. da Costa, and F. de Pádua, O bloqueio de ramo direito nas suas relações com os hemibloqueios esquerdos. *Livro Resumo Congresso Luso-Espanhol de Cardiologia, Valência*, 1973.
48. Miguel, J.P., D.D. dos Reis, V.M. Lopes, C.M. Pereira, and F. de Pádua, Vectorcardiographic study of right bundle branch block and its associations with the left hemiblocks. *Adv. Cardiol*., 1976;**16**: 451–464.
49. Lee, S.J., C. McCulloch, I. Mangat, E. Foster, T. DeMarco, and L.A. Saxon, Isolated bundle branch block and left ventricular dysfunction. *J. Card. Fail*., 2003;**9**(2): 87–92.
50. Cohen, H.C., K.M. Rosen, and A. Pick, Disorders of impulse conduction and impulse formation caused by hyperkalemia in man. *Am. Heart J*., 1975;**89**: 501–509.
51. Kenedi, P., M.V. O'Reilly, and E. Goldberg, Association between intraventricular conduction defects, coronary artery disease and left ventricular function. *Adv. Cardiol*., 1976;**16**: 504–506.
52. Schneider, J.F., H.E. Thomas Jr., B.E. Kreger, P.M. McNamara, P. Sorlie, and W.B. Kannel, Newly acquired right bundle branch block. The Framingham study. *Ann. Intern. Med*., 1980;**92**: 37–44.
53. Lopes, M.G., E. Rocha, V.M. Lopes, D.D. dos Reis, and F. de Pádua, Long-term prognosis of the left anterior hemiblock. *Adv. Cardiol*., 1977;**19**: 115–119.
54. Lopes, V.M., M. Carrageta, and F. de Pádua, 24-hour continuous electrocardiogram in the diagnosis and the prognosis of the so-called left hemiblock. *Adv. Cardiol*., 1976;**16**: 469–478.
55. Biagini, E., A. Elhendy, A.F.L Schinkel, et al., Prognostic significance of left anterior hemiblock in patients with suspected coronary artery disease. *J. Am. Coll. Cardiol*., 2005;**46**: 858–863.
56. Lopes, V.M., J.M.P. Miguel, D.D. dos Reis, B.C.B da Costa, and F. de Pádua, Left-posterior hemiblock. Clinical and vectorcardiographic study of twenty cases. *J. Electrocardiol*., 1974;**7**: 197–214.
57. Lopes, V.M., D.D. Reis, J.M.P. Miguel, B.B. Costa, and F. de Pádua, Left posterior hemiblock. *Neue Ergeb. Elektrokardiol*., 1974;**2**: 189.
58. de Pádua, F., V.M. Lopes, and J.M. Pereira-Miguel, Left posterior hemiblock. Good prognosis? *Adv. Cardiol*., 1975;**14**: 157–175.
59. Scott, R.C., The S_1Q_3 (McGinn-White) pattern in acute cor pulmonale: A form of transient left posterior hemiblock? *Am. Heart J*., 1971;**82**: 135–137.
60. Nakaya, Y., Y. Hiasa, Y. Murayama, et al., Prominent anterior QRS force as a manifestation of septal fascicular block. *J. Electrocardiol*., 1978;**11**: 39–46.
61. Castellanos, A. and R.J. Myerburg, *The Hemiblocks in Myocardial Infarction*. East Norwalk, CT: Appleton-Century-Crofts, 1976, p. 4.
62. Hiss, R.G. and L.E. Lamb, Electrocardiographic findings in 122043 individuals. *Circulation*, 1962;**25**: 947–961.
63. Raunio, H., V. Rissanen, C. Jokinen, and O. Penttilä, Significance of a terminal R wave in lead V_1 of the electrocardiogram. *Am. Heart J*., 1978;**95**: 702–706.
64. Tapia, F.A. and W.L. Proudfit, Secondary R waves in right precordial leads in normal persons and in patients with cardiac disease. *Circulation*, 1960;**21**: 28–37.
65. Moore, E.N., J.P. Boineau, and D.F. Patterson, Incomplete right bundle-branch block: An electrocardiographic enigma and possible misnomer. *Circulation*, 1971;**44**: 678–687.
66. de Pádua, F., *Contribuição Vectocardiográfica para o Estudo das Hipertrofias Ventriculares*, PhD dissertation. Lisbon: Faculty of Medicine, University of Lisbon, 1959.
67. Liao, Y.L., L.A. Emidy, A. Dyer, et al., Characteristics and prognosis of incomplete right bundle branch block: An epidemiologic study. *J. Am. Coll. Cardiol*., 1986;**7**: 492–499.
68. Grishman, A. and L. Schleris, *Spatial Vectorcardiography*. Philadelphia, PA: Saunders, 1952.
69. Dick, M., D.M. Behrendt, K.E. Jochim, and A.R. Castaneda, Electrophysiologic delineation of the intraventricular His bundle in two patients with endocardial cushion type of ventricular septal defect. *Circulation*, 1981;**63**: 225–229.
70. de Pádua, F., M.G. Lopes, D.D. Reis, A. Pereirinha, V.M. Lopes, and R. Nunes, Deslocamento anterior do complexo QRS – Tentativa de esclarecimento etiológico a partir do estudo ecocardiográfico, in Sociedad Cardiologia de Levante. *Bloqueo Cardíaco*. Barcelona: Cientifico Médica, 1980, pp. 248–252.
71. Barold, S.S., J.W. Linhart, F.J. Hildner, O.S. Narula, and P. Samet, Incomplete left brunche-branch block: A definite electrocardiographic entity. *Circulation*, 1968;**38**: 702–710.
72. Sanchez, C., T.J. Walsh, and E. Massie, The vectorcardiogram in incomplete left bundle branch block. *Am. J. Cardiol*., 1961;**7**: 629–637.
73. Schamroth, L. and B.A. Bradlow, Incomplete left bundle-branch block. *Br. Heart J*., 1964;**26**: 285–288.
74. Unger, P.N., M. Greenblatt, and M. Lev, The anatomic basis of the electrocardiographic abnormality in incomplete left bundle branch block. *Am. Heart J*., 1968;**76**: 486–497.
75. Terasawa, F., M. Kuramochi, Y. Yazaki, et al., Clinical and pathological studies on incomplete left bundle Branco block in the aged. *Isr. J. Med. Sci*., 1969;**5**: 732–735.
76. Eppinger, H. and C.J. Rothberger, Zur Analyses des Elektrokardiogramms. *Wien. Klin. Wochenschr*., 1909;**22**: 1091–1098.
77. McAnulty, J. and S. Rahimtoola, Prognosis in bundle branch block. *Annu. Rev. Med*., 1981;**32**: 499–507.
78. Bharati, S., M. Lev, R. Dhingra, et al., Pathologic correlations in three cases of bilateral bundle branch disease with unusual electrophysiologic manifestations in two cases. *Am. J. Cardiol*., 1976;**38**: 508–518.

79. Lister, J.W., R.S. Kline, and M.E. Lesser, Chronic bilateral bundle branch block. Long-term observations in ambulatory patients. *Br. Heart J.*, 1977;**39**: 203–207.
80. Singer, R.B., Mortality in 966 life insurance applicants with bundle branch block or wide QRS. *Trans. Assoc. Life Insur. Med. Dir. Am.*, 1968;**52**: 94–114.
81. Rotman, M. and J.H. Triebwasser, A clinical and follow-up study of right and left bundle branch block. *Circulation*, 1975;**51**: 477–484.
82. Ostrander, L.D. Jr., Bundle-branch block: An epidemiological study. *Circulation*, 1964;**30**: 872–881.
83. Gelband, H., A.L. Waldo, G.A. Kaiser, F.O. Bowman Jr., J.R. Malm, and B.F. Hoffman, Etiology of right bundle-branch block in patients undergoing total correction of Tetralogy of Fallot. *Circulation*, 1971;**44**: 1022–1033.
84. Krongrad, E., S.E. Hefler, F.O. Bowman Jr., J.R. Malm, and B.F. Hoffman, Further observations on the etiology of the right bundle branch block pattern following right ventriculotomy. *Circulation*, 1974;**50**: 1105–1113.
85. Scanlon, P.J., R. Pryor, and S.G. Blount Jr., Right bundle-branch block associated with left superior or inferior intraventricular block. Clinical setting, prognosis, and relation to complete heart block. *Circulation*, 1970;**42**: 1123–1133.
86. AbdEIRahman, M.Y., W. Hui, M. Yigitbasi, et al., Detection of left ventricular asynchrony in patients with right bundle branch block after repair of tetralogy of Fallot using tissue-Doppler imaging-derived strain. *J. Am. Coll. Cardiol.*, 2005;**45**: 915–921.
87. Mehran-Pour, M., G. Borkat, J. Liebman, and J. Ankeney, Resolution of surgically induced right-bundle branch block. *Ann. Thorac. Surg.*, 1977;**23**: 139–144.
88. Yasui, H., Y. Takeda, S. Yamauchi, et al., The deleterious effects of surgically induced complete right bundle branch block on long-term follow-up results of closure of ventricular septal defect. *J. Thorac. Cardiovasc. Surg.*, 1977;**74**: 210–217.
89. Guerrero, M., K. Harjai, G.W. Stone, et al., Comparison of the prognostic effect of left versus right versus no bundle branch block on presenting electrocardiogram in acute myocardial infarction patients treated with primary angioplasty in the primary angioplasty in myocardial infarction trials. *Am. J. Cardiol.*, 2005;**96**: 482–488.
90. Tomoda, H. and N. Aoki, Right bundle branch block in acute myocardial infarction treated by primary coronary angioplasty and stenting. *Angiology*, 2005;**56**: 131–136.
91. Alfonso, F., Immediate resolution of new right bundle branch block in acute myocardial infarction following primary coronary angioplasty. *Int. J. Cardiol.*, 2005;**105**: 117–118.
92. Chen, C.-H., T. Sakurai, M. Fujita, M. Nobuyoshi, and C. Kawai, Transient intraventricular conduction disturbances in hypertrophic obstructive cardiomyopathy. *Am. Heart J.*, 1981;**101**: 672–674.
93. Lancaster, M.C., E. Schechter, and G.K. Massing, Acquired complete right bundle branch block without overt cardiac disease. Clinical and hemodynamic study of 37 patients. *Am. J. Cardiol.*, 1972;**30**: 32–36.
94. Lenegre, J., Etiology and pathology of bilateral bundle branch block in relation to complete heart block. *Prog. Cardiovasc. Dis.*, 1964;**6**: 409–444.
95. Lev, M., Anatomic basis for atrioventricular block. *Am. J. Med.*, 1964;**37**: 742–748.
96. Harris, L.K., Transient right bundle branch block following blunt chest trauma. *Am. J. Cardiol.*, 1969;**23**: 884–887.
97. Jackson, D.H., Transient post-traumatic right bundle branch block: Report of two cases. *Am. J. Cardiol.*, 1969;**23**: 877–883.
98. Kumpuris, A.G., T.B. Casale, D.M. Mokotoff, R.R. Miller, and R.J. Luchi, Right bundle-branch block. Occurrence following nonpenetrating chest trauma without evidence of cardiac contusion. *J. Am. Med. Assoc.*, 1979;**242**: 172–173.
99. Zinsser, H.F. and G.S. Thind, Right bundle branch block after nonpenetrating injury to the chest wall. *J. Am. Med. Assoc.*, 1969;**207**: 1913–1915.
100. Fedor, J.M., A. Walston, G.S. Wagner, and J. Starr, The vectorcardiogram in right bundle branch block. Correlation with cardiac failure and pulmonary disease. *Circulation*, 1976;**53**: 926–930.
101. Stein, P.D., J.E. Dalen, K.M. McIntyre, A.A. Sasahara, N.K. Wenger, P.W. Willis III, The electrocardiogram in acute pulmonary embolism. *Prog. Cardiovasc. Dis.*, 1975;**17**: 247–257.
102. Froelicher, V.F. Jr., A.J. Thompson, R. Wolthuis, et al., Angiographic findings in asymptomatic aircrewmen with electrocardiographic abnormalities. *Am. J. Cardiol.*, 1977;**39**: 32–38.
103. Johnson, R.L., K.H. Averill, and L.E. Lamb, Electrocardiographic findings in 67375 asymptomatic subjects: VI. Right bundle branch block. *Am. J. Cardiol.*, 1960;**6**: 143–152.
104. Massing, G.K. and M.C. Lancaster, Clinical significance of acquired complete right bundle branch block in 59 patients without overt cardiac disease. *Aerosp. Med.*, 1969;**40**: 967–971.
105. Whinnery, J.E., V.F. Froelicher Jr., A.J. Stewart, M.R. Longo Jr., and J.H. Triebwasser, The electrocardiographic response to maximal treadmill exercise of asymptomatic men with right bundle branch block. *Chest*, 1977;**71**: 335–340.
106. Messer, A.L. and R.P. Johnson, Shreenivas, White P D. Prognosis in bundle branch block: III. A comparison of right and left bundle branch block with a note on the relative incidence of each. *Am. Heart J.*, 1951;**41**: 239–245.
107. Perera, G.A., S.A. Levine, and H. Erlanger, Prognosis of right bundle branch block: A study of 104 cases. *Br. Heart J.*, 1942:**4**: 35–42.
108. Reuch, C.S. and J.R. Vivas, Clinical analysis of right bundle branch block. *Am. Heart J.*, 1959;**58**: 543–546.
109. Shreenivas, M.A.L., R.P. Johnson, and P.D. White, Prognosis in bundle branch block: I. Factors influencing the survival period in right bundle branch block. *Am. Heart J.*, 1950;**40**: 891–902.
110. Bauer, G.E., Development of bundle branch block. *Am. J. Cardiol.*, 1964;**14**: 346–351.
111. Mullins, C.B. and J.M. Atkins, Prognosis and management of ventricular conduction blocks in acute myocardial infarction. *Mod. Concepts Cardiovasc. Dis.* 1976;**45**: 129–133.
112. The Coronary Drug Project Research Group. The prognostic importance of the electrocardiogram after myocardial infarction. Experience in the Coronary Drug Project. *Ann. Intern. Med.*, 1972;**77**: 677–689.
113. Madias, J.E., R. Ashtiani, H. Agarwal, V.K. Narayan, M. Win, and A. Sinha, Stability of the ECG features of complete right bundle branch block over time: A methodological study for implementation in research and clinical practice. *Cardiology*, 2005;**103**: 84–88.
114. Lopes, M.G., A. Pereirinha, and F. de Pádua, The diagnosis of left ventricular hypertrophy in the presence of bundle branch block – An ECG/VCG and echocardiographic correlation, in *Modern Electrocardiology*, Z. Antalóczy, Editor. Amsterdam: Excerpta Medica, 1978, pp. 423–427.
115. Herbert, W.H., Left bundle branch block and coronary artery disease. *J. Electrocardiol.*, 1975;**8**: 317–324.

116. Lev, M., P.N. Unger, K.M. Rosen, and S. Bharati, The anatomic base of the electrocardiographic abnormality left bundle branch block. *Adv. Cardiol.*, 1975;**14**: 16–24.
117. Sugiura, M., R. Okada, S. Ohkawa, and H. Shimada, Pathohistological studies on the conduction system in 8 cases of complete left bundle branch block. *Jpn. Heart J.*, 1970;**11**: 5–16.
118. Li, Z.B., K. Wachtell, P.M. Okin, et al., Association of left bundle branch block with left ventricular structure and function in hypertensive patients with left ventricular hypertrophy: The LIFE study. *J. Hum. Hypertension*, 2004;**18**; 397–402.
119. Jain, A.C. and M.C. Mehta, Etiologies of left bundle branch block and correlations with hemodynamic and angiographic findings. *Am. J. Cardiol.*, 2003;**91**: 1375–1378.
120. Brake, C.M., Complete left bundle branch in asymptomatic airmen. *Aerosp. Med.*, 1969;**40**: 781–782.
121. DeMartino, G., M. Santamaria, Q. Parisi, L. Messano, and F. Crea, Myocarditis as a cause of alternating left bundle branch block. *J. Interv. Card. Electrophysiol.*, 2004;**11**; 19–20.
122. Fenichel, N.M. and F.A. Jimenez, Polachek A A. 2:1 left bundle branch block in acute bacterial endocarditis with septal abscess. *J. Electrocardiol.*, 1977;**10**: 287–290.
123. Singh, R.B., B.V. Agrawal, and P.N. Somani, Left bundle branch block: A rare manifestation of digitalis intoxication. *Acta Cardiol.*, 1976;**31**: 175–179.
124. Lamb, L.E., K.D. Kable, and K.H. Averill, Electrocardiographic findings in 67375 asymptomatic subjects. V. Left bundle branch block. *Am. J. Cardiol.*, 1960;**6**: 130–142.
125. Schneider, J.F., H.E. Thomas Jr., B.E. Kreger, P.M. McNamara, and W.B. Kannel, Newly acquired left bundle-branch block: The Framingham study. *Ann. Intern. Med.*, 1979;**90**: 303–310.
126. Smith, R.F., D.H. Jackson, J.W. Harthorne, and C.A. Sanders, Acquired bundle branch block in a healthy population. *Am. Heart J.*, 1970;**80**: 746–751.
127. Frisella, M.E. and D.H. Spodick, Confirmation of the prevalence and importance of a 12-lead investigation for diagnosis. *Am. J. Cardiol.*, 2005;**96**: 696–697.
128. Dillon, J.C., S. Chang, and H. Feigenbaum, Echocardiographic manifestations of left bundle branch block. *Circulation*, 1974;**49**: 876–880.
129. Wong, B., R. Rinkenberger, M. Dunn, and A. Goodyer, Effect of intermittent left bundle branch block on left ventricular performance in the normal heart. *Am. J. Cardiol.*, 1977;**39**: 459–463.
130. vanHemel, N.M., Left is worse than right: The outcome of bundle branch block in middle-aged men. *Eur. Heart J.*, 2005;**26**: 2222–2223.
131. Ozdemir, K., B.B. Altunkeser, B. Korkut, M. Tokac, and H. Gok, Effect of left bundle branch block on systolic and diastolic function of left ventricle in heart failure. *Angiology*, 2004;**55**: 63–71.
132. Turner, M.S., R.A. Bleasdale, D. Vinereanu, et al., Electrical and mechanical components of dyssynchrony in heart failure patients with normal QRS duration and left bundle-branch block – Impact of left and biventricular pacing. *Circulation*, 2004;**109**: 2544–2549.
133. Abraham, W.T., et al., Cardiac resynchronization in chronic heart failure. *N. Engl. J. Med.*, 2002; **346**: 1845.
134. Goldman, M.J. and H.V. Pipberger, Analysis of the orthogonal electrocardiogram and vectorcardiogram in ventricular conduction defects with and without myocardial infarction. *Circulation*, 1969;**39**: 243–250.
135. Pryor, R., Recognition of myocardial infarction in the presence of bundle branch block, in *Complex Electrocardiography*, vol. 2, Philadelphia, PA: Davis, 1974, pp. 255–271, (*Cardiovasc. Clin.* **6**(1)).
136. Brady, W.J., B. Lentz, K. Barlotta, R.A. Harrigan, and T. Chan, ECG patterns confounding the ECG diagnosis of acute coronary syndrome: Left bundle branch block, right ventricular paced rhythms, and left ventricular hypertrophy. *Emerg. Med. Clin. N. Am.*, 2005;**23**: 999.
137. Timmis, G.C., V. Gangadharan, R.G. Ramos, and S. Gordon, Reassessment of Q waves in left bundle branch block. *J. Electrocardiol.*, 1976;**9**: 109–114.
138. Havelda, C.J., G.S. Sohi, N.C. Flowers, and L.G. Horan, The pathologic correlates of the electrocardiogram: Complete left bundle branch block. *Circulation*, 1982;**65**: 445–451.
139. De Kock, J. and L. Schamroth, Left bundle branch block associated with acute inferior wall myocardial infarction. *S. Afr. Med. J.*, 1975;**49**: 397–398.
140. Nguyen, K., J.E. Cigarroa, R.A. Lange, L.D. Hillis, and E.C. Keeley, Presence and extent of angiographic coronary narrowing in patients with left bundle branch block. *Am. J. Cardiol.*, 2004;**93**: 1426–1427.
141. Demir, H., G. Erbay, K.M. Kir, K. Omurlu, F. Berk, and C. Aktolun, Clinical validation of technetium-99m MEBI-gated single-photon emission computed tomography (SPECT) for avoiding false positive results in patients with left bundle-branch block: Comparison with stress-rest nongated SPECT. *Clin. Cardiol.*, 2003;**26**: 182–187.
142. CandellRiera, J., G. OllerMartinez, O. PereztolValdes, et al., Usefulness of myocardial perfusion SPECT in patients with left bundle branch block and previous myocardial infarction. *Heart*, 2003;**89**: 169–174.
143. Reuben, A.D. and C.J. Mann, Simplifying thrombolysis decisions in patients with left bundle branch block. *Emerg. Med. J.*, 2005;**22**: 617–620.
144. Duncan, A.M., D.P. Francis, D.G. Gibson, and M.Y. Henein, Limitation of exercise tolerance in chronic heart failure: Distinct effects of left bundle-branch block and coronary artery disease. *J. Am. Coll. Cardiol.*, 2004;**43**: 1524–1531.
145. Petersen, G.V. and G. Tikoff, Left bundle branch block and left ventricular hypertrophy: Electrocardiographic-pathologic correlations. *Chest*, 1971;**59**: 174–177.
146. Chung, D.-K., N.M. Panitch, and E.K. Chung, A comparison of the conventional criteria for left ventricular hypertrophy before and after the development of complete left bundle branch block. *Jpn. Circ. J.*, 1969;**33**: 19–24.
147. Blondeau, M., Complete left bundle branch block with marked left axis deviation of QRS. Clinical and anatomical study. *Adv. Cardiol.*, 1975;**14**: 25–38.
148. Flowers, N.C., Left bundle branch block: A continuously evolving concept. *J. Am. Coll. Cardiol.*, 1987;**9**: 684–697.
149. Pereirinha, A., J. Correia, F. de Pádua, and M.G. Lopes, Identificacion de los condicionantes del prognostico en pacientes con bloqueo de rama a partir de la repercusion anatomo funcional valorada por Ecocardiografia (abstract). *Rev. Esp. Cardiol.*, 1982;**35**(Suppl. I): 42.
150. Wei-Min, H. and T. Cheng-Lang, Bilateral bundle branch block. Right bundle branch block associated with left anterior fascicular block. *Cardiology*, 1977;**62**: 35–43.
151. Watt, T.B. Jr. and R.D. Pruitt, Character, cause, and consequence of combined left axis deviation and right bundle branch block in human electrocardiograms. *Am. Heart J.*, 1969;**77**: 460–465.

152. Ohmae, M., Correlative studies on the electrocardiogram and histopathology of the conduction system. I. Right bundle branch block with left axis deviation and prolonged P-R interval. *Jpn. Circ. J.*, 1977;**41**: 677–686.
153. Sugiura, M., R. Okada, K. Hiraoka, and S. Ohkawa, Histological studies on the conduction system in 14 cases of right bundle branch block associated with left axis deviation. *Jpn. Heart J.*, 1969;**10**: 121–132.
154. Husson, G.S., M.C. Blackman, M.S. Rogers, S. Bharati, and M. Lev, Familial congenital bundle branch system disease. *Am. J. Cardiol.*, 1973;**32**: 365–369.
155. Schaal, S.F., J. Seidensticker, R. Goodman, and C.F. Wooley, Familial right bundle-branch block, left axis deviation, complete heart block, and early death. A heritable disorder of cardiac conduction. *Ann. Intern. Med.*, 1973;**79**: 63–66.
156. Morriss, J.H., G.S. Eugster, J.J. Nora, and R. Pryor, His bundle recording in progressive external ophthalmoplegia. *J. Pediatr.*, 1972;**81**: 1167–1170.
157. Brink, A.J. and M. Torrington, Progressive familial heart block – Two types. *S. Afr. Med. J.*, 1977; **52**: 53–59.
158. Evans, W., Familial cardiomegaly. *Br. Heart J.*, 1949;**11**: 68–82.
159. Stéphan, E., Hereditary bundle branch system defect. A new genetic entity? *Am. Heart J.*, 1979;**97**: 708–718.
160. Chuquimia, R., T.S. Ramadurai, W. Towne, and K. Rosen, Bifascicular block due to penetrating wound of the heart: Electrophysiology studies. *Chest*, 1974;**66**: 195–197.
161. Gozo, E.G. Jr., H.C. Cohen, and A. Pick, Traumatic bifascicular intraventricular block. *Chest*, 1972;**61**: 294–296.
162. Gozo, E.G. Jr., I. Cosnow, H.C. Cohen, and L. Okun, The heart in sarcoidosis. *Chest*, 1971;**60**: 379–388.
163. Sung, R.J., D.M. Tamer, O.L. Garcia, A. Castellanos, R.J. Myerburg, and H. Gelband, Analysis of surgically-induced right bundle branch block pattern using intracardial recording techniques. *Circulation*, 1976;**54**: 442–446.
164. Wolff, G.S., T.W. Rowland, and R.C. Ellison, Surgically induced right bundle-branch block with left anterior hemiblock. An ominous sign in postoperative Tetralogy of Fallot. *Circulation*, 1972;**46**: 587–594.
165. Yabek, S.M., J.M. Jermakani, and N. Roberts, Postoperative trifascicular block complicating Tetralogy of Fallot repair. *Pediatrics*, 1976;**58**: 236–242.
166. Kulbertus, H.E., Reevaluation of the prognosis of patients with LAD-RBBB. *Am. Heart J.*, 1976;**92**: 665–667.
167. Lasser, R.P., J.I. Haft, and C.K. Friedberg, Relationship of right bundle-branch block and marked left axis deviation (with left parietal or peri-infarction block) to complete heart block and syncope. *Circulation*, 1968;**37**: 429–437.
168. Gupta, P.K., E. Lichstein, K.D. Chadda, Follow-up studies in patients with right bundle branch block and left anterior hemiblock: Significance of H-V interval. *J. Electrocardiol.*, 1977;**10**: 221–224.
169. Blondeau, M. and J. Lenegre, Bloc de branche et bloc auriculo-ventriculaire complet. *Arch. Mal. Cœur Vaiss.*, 1964;**57**: 1–19.
170. Castellanos, A. Jr., O. Maytin, A.G. Arcebal, and L. Lemberg, Significance of complete right bundle-branch block with right axis deviation in absence of right ventricular hypertrophy. *Br. Heart J.*, 1970;**32**: 85–92.
171. Ranganathan, N., R. Dhurandhar, J.H. Phillips, and E.D. Wigle, His bundle electrogram in bundle branch block. *Circulation*, 1972;**45**: 282–294.
172. Barrett, P.A.,C.T. Peter, H.J. Swan, B.N. Singh, and W.J. Mandel, The frequency and prognostic significance of electrocardiographic abnormalities in clinically normal individuals. *Prog. Cardiovasc. Dis.*, 1981;**23**: 299–319.
173. Kulbertus, H. and P. Collignon, Association of right bundle-branch block with left superior or inferior intraventricular block. Its relation to complete heart block and Adam-Stokes syndrome. *Br. Heart J.*, 1969;**31**: 435–440.
174. McAnulty, J.H., S.H. Rahimtoola, E. Murphy, et al., Natural history of "high risk" bundle-branch block: Final report of a prospective study. *N. Engl. J. Med.*, 1982;**307**: 137–143.
175. American College of Cardiology/American Heart Association – Guidelines for Permanent Pacing. *Circulation*, 2002;**106**: 2145.
176. Rosen, K.M., S.H. Rahimtoola, R. Chuquimia, H.S. Loeb, R.M. Gumar, Electrophysiological significance of first degree atrioventricular block with intraventricular conduction disturbance. *Circulation*, 1971;**43**: 491–502.
177. Levites, R. and J.I. Haft, Significance of first degree heart block (prolonged P-R interval) in bifascicular block. *Am. J. Cardiol.*, 1974;**34**: 259–264.
178. Denes, P., R.C. Dhingra, D. Wu, et al., H-V interval in patients with bifascicular block (right bundle branch block and left anterior hemiblock): Clinical, electrocardiographic and electrophysiologic correlations. *Am. J. Cardiol.*, 1975;**35**: 23–29.
179. Dhingra, R.C., P. Denes, D. Wu, et al., Chronic right bundle branch block and left posterior hemiblock: Clinical, electrophysiologic and prognostic observations. *Am. J. Cardiol.*, 1975;**36**: 867–872.
180. Scheinman, M., A. Weiss, and F. Kunkel, His bundle recordings in patients with bundle branch block and transient neurologic symptoms. *Circulation*, 1973;**48**: 322–330.
181. Scheinman, M.M., R.W. Peters, G. Modin, M. Brennan, C. Mies, and J. O'Young, Prognostic value of infranodal conduction time in patients with chronic bundle branch block. *Circulation* 1977;**56**: 240–244.
182. Dhingra, R.C., P. Denes, D. Wu, et al., Prospective observations in patients with chronic bundle branch block and marked H-V prolongation. *Circulation*, 1976;**53**: 600–604.
183. Gould, L., K. Venkataraman, N. Mohammad, and R.F. Gomprecht, Prognosis of right bundle-branch block in acute myocardial infarction. *J. Am. Med. Assoc.*, 1972;**219**: 502–503.
184. Lie, K.I., H.J. Wellens, R.M. Schuilenburg, A.E. Becker, and D. Durrer, Factors influencing prognosis of bundle branch block complicating acute antero-septal infarction. The value of His bundle recordings. *Circulation*, 1974;**50**: 935–941.
185. Aranda, J.M., B. Beferer, and A. Castellanos Jr., His bundle recordings, bundle branch block, and myocardial infarction. *Ann. Intern. Med.*, 1977;**86**: 106–108.
186. Gann, D., P.K. Balachandran, N.E. Sherif, P. Samet, and J.R. Malm, Prognostic significance of chronic versus acute bundle-branch block in acute myocardial infarction. *Chest*, 1975;**67**: 298–303.
187. Atkins, J.M., S.J. Leshin, G. Blomqvist, and C.B. Mullins, Prognosis of right bundle branch block and left anterior hemiblock: A new indication for permanent pacing (abstract). *Am. J. Cardiol.*, 1970;**26**: 624.
188. Lichstein, E., P.K. Gupta, K.D. Chadda, H.-M. Liu, and M. Sayeed, Findings of prognostic value in patients with incomplete bilateral bundle branch block complicating acute myocardial infarction. *Am. J. Cardiol.*, 1973;**32**: 913–918.

189. Atkins, J.M., S.J. Leshin, G. Blomqvist, and C.B. Mullins, Ventricular conduction blocks and sudden death in acute myocardial infarction. Potential indications for pacing. *N. Engl. J. Med.*, 1973;**288**: 281–284.
190. Godman, M.J., B.W. Lassers, and D.G. Julian, Complete bundle branch block complicating acute myocardial infarction. *N. Engl. J. Med.*, 1970;**282**: 237–240.
191. Resnekov, L., Pacemaking and acute myocardial infarction. *Impulse*, 1978;**11**: 1.
192. Ritter, W.S., J.M. Atkins, C.G. Blomqvist, and C.B. Mullins, Permanent pacing in patients with transient trifascicular block during acute myocardial infarction: Long-term prognosis. *Am. J. Cardiol.*, 1976;**38**: 205–208.
193. Castellanos, A., A.V. Ramirez, A. Mayorga-Cortes, et al., Left fascicular blocks during right-heart catheterization using the SwanGanz catheter. *Circulation*, 1981;**64**: 1271–1276.
194. Mayorga-Cortes, A., J.J. Rozánski, R.J. Sung, A. Castellanos, and R.J. Myerburg, Right ventricular apical activation times in patients with conduction disturbances occurring during acute transmural myocardial infarction. *Am. J. Cardiol.*, 1979;**43**: 913–919.
195. Ribeiro, C.S., *Estudo da activação ventricular nos bloqueios intraventriculares esquerdos (contribuição experimental para o seu diagnóstico clínico)*, PhD dissertation. Lisbon: Faculty of Medicine, University of Lisbon, 1967.
196. Hassan, Z.U., R.A. Mendoza, W.E. Steinke, and D.B. Propert, Multiple conduction defects with markedly prolonged ventricular depolarization in cardiomyopathy. *J. Electrocardiol.*, 1977;**10**: 275–278.
197. Durrer, D., R.M. Schuilenburg, and H.J.J. Wellens, Pre-excitation revisited. *Am. J. Cardiol.*, 1970;**25**: 690–697.
198. Anderson, R.H., A.E. Becker, C. Brechenmacher, M.J. Davies, and L. Rossi, Ventricular preexcitation: A proposed nomenclature for its substrates. *Eur. J. Cardiol.*, 1975;**3**: 27–35.
199. Boineau, J.P., E.N. Moore, J.F. Spear, and W.C. Sealy, Basis of static and dynamic electrocardiographic variations in Wolff-Parkinson-White syndrome. Anatomic and electrophysiologic observations in right and left ventricular preexcitation. *Am. J. Cardiol.*, 1973;**32**: 32–45.
200. Ferrer, M.I., *Pre-Excitation, Including the Wolff-Parkinson-White and Other Related Syndromes*. Mount Kisco, New York: Futura, 1976, pp. 1–274.
201. Gallagher, J.J., E.L.C. Pritchett, W.C. Sealy, J. Kasell, and A.G. Wallace, The preexcitation syndromes. *Prog. Cardiovasc. Dis.*, 1978;**20**: 285–327.
202. Gallagher, J.J., W.C. Sealy, J. Kasell, and A.G. Wallace, Multiple accessory pathways in patients with the pre-excitation syndrome. *Circulation*, 1976;**56**: 571–591.
203. Wellens, H.J.J., Wolff-Parkinson-White syndrome. *Mod. Concepts Cardiovasc. Dis.*, 1983;**52**: 53–74.
204. Wolff, L., J. Parkinson, and P.D. White, Bundle branch block with short P-R interval in healthy young people prone to paroxysmal tachycardia. *Am. Heart J.*, 1930;**5**: 685–704.
205. Boineau, J.P. and E.N. Moore, Evidence for propagation of activation across an accessory atrioventricular connection in types A and B pre-excitation. *Circulation*, 1970;**41**: 375–397.
206. James, T.N., Morphology of the human atrioventricular node, with remarks pertinent to its electrophysiology. *Am. Heart J.*, 1961;**62**: 756–771.
207. de Pádua, F., Interpretação vectocardiográfica das arritmias. *Imprensa Médica*, 1957;**21**: 573.
208. Nakagawa, S., K. Maeda, T. Imamura, H. Kondoh, Y. Koiwaya, and K. Tanaka, Increasing pre-excitation ("concertina effect") during vasospastic angina. *J. Electrocardiol.*, 1986;**19**: 299–302.
209. Rosner, M.H., Electrocardiography in the patient with Wolff-Parkinson White syndrome: Diagnostic and therapeutic issues. *Am. J. Emerg. Med.*, 1999;**17**: 705–714.
210. Neuss, H., M. Schlepper, and J. Thorman, Analysis of re-entry mechanisms in three patients with concealed Wolff-Parkinson-White syndrome. *Circulation*, 1975;**51**: 75–81.
211. Pritchett, E.L.C., J.J. Gallagher, W.C. Sealy, et al., Supraventricular tachycardia dependent upon accessory pathways in the absence of ventricular preexcitation. *Am. J. Med.*, 1978;**64**: 214–220.
212. Sung, R.J., A. Castellanos, H. Gelband, and R.J. Myerburg, Mechanism of reciprocating tachycardia initiated during sinus rhythm in concealed Wolff-Parkinson-White syndrome. Report of a case. *Circulation*, 1976;**54**: 338–344.
213. Tonkin, A.M., J.J. Gallagher, R.H. Svenson, A.G. Wallace, and W.C. Sealy, Anterograde block in accessory pathways with retrograde conduction in reciprocating tachycardia. *Eur. J. Cardiol.*, 1975;**3**: 143–152.
214. Zipes, D.P., R.L. DeJoseph, and D.A. Rothbaum, Unusual properties of accessory pathways. *Circulation*, 1974;**49**: 1200–1211.
215. WHO/ISFC Task Force. Definition of terms related to cardiac rhythm. *Am. Heart J.*, 1978;**95**: 796–806.
216. Rosenbaum, F.F., H.H. Hecht, F.N. Wilson, and F.D. Johnston, The potential variations of the thorax and the esophagus in anomalous atrioventricular excitation (Wolff-Parkinson-White syndrome). *Am. Heart J.*, 1945;**29**: 281–326.
217. Tonkin, A.M., G.S. Wagner, J.J. Gallagher, G.D. Cope, J. Kasel, and A.G. Wallace, Initial forces of ventricular depolarization in the Wolff-Parkinson-White syndrome. Analysis based upon localization of the accessory pathway by epicardial mapping. *Circulation*, 1975;**52**: 1030–1036.
218. Wallace, A.G., W.C. Sealy, J.J. Gallagher, and L.J. Kasel, Ventricular excitation in the Wolff-Parkinson-White syndrome, in *The Conduction System of the Heart: Structure, Function, and Clinical Implications*, H.J.J. Wellens, K.I. Lie, M.J. Janse, Editors. Leiden: Stenfert Kroese, 1976, p. 613.
219. Fitzpatrik, A.P., R.P. Gonzales, M.D. Lesh, G.W. Modin, R.J. Lee, and N.M. Scheinman, New algorithm for the localization of accessory atrioventricular connections using a baseline electrocardiogram. *J. Am. Coll. Cardiol.*, 1994;**23**: 107–116.
220. Zipes, D.P., Specif arrhythmias: Diagnosis and treatment, in *Braunwald's Heart Disease: A Textbook of Cardiocascular Medicine*, 7th edn., D.P. Zipes et al., Editor. Philadelphia, PA: Saunders, 2005.
221. Desanctis, R.W. and J. Ruskin, Disturbances of the cardiac rhythm and conduction, in *Scientific American Medicine*, E. Rubenstein and D. Sederman, Editors. 1987: 1–43.
222. Chung, K.-Y., T.J. Walsh, and E. Massie, Wolff-Parkinson-White syndrome. *Am. Heart J.*, 1965;**69**: 116–133.
223. Barold, S.S. and P. Coumel, Mechanisms of atrioventricular junctional tachycardia: Role of reentry and concealed accessory bypass tracts. *Am. J. Cardiol.*, 1977;**39**: 97–106.
224. Coumel, P. and P. Attuel, Reciprocating tachycardia in overt and latent preexcitation: Influence of functional bundle branch block on the rate of the tachycardia. *Eur. J. Cardiol.*, 1974;**1**: 423–436.

225. Coumel, P., P. Attuel, and D. Flammang, The role of the conduction system in supraventricular tachycardias, in *The Conduction System of the Heart*, H.J.J. Wellens, K.I. Lie, M.J. Janse, Editors. Leiden: Kroese, 1976, pp. 424–452.
226. Hammill, S.C., E.L.C. Pritchett, G.J. Klien, W.M. Smith, and J.J. Gallagher, Accessory atrioventricular pathways that conduct only in the antegrade direction. *Circulation*, 1980;**62**: 1335–1340.
227. Lloyd, E.A., R.N. Hauer, D.P. Zipes, J.J. Heger, and E.N. Prystowsky, Syncope and ventricular tachycardia in patients with ventricular preexcitation. *Am. J. Cardiol*., 1983;**52**: 79–82.
228. Wellens, H.J. and D. Durrer, Patterns of ventriculo-atrial conduction in the Wolff-Parkinson-White syndrome. *Circulation*, 1974;**49**: 22–31.
229. Fontaine, G., R. Frank, R. Coutte, et al., Rhythme reciproque antidromique dans un syndrome de Wolff-Parkinson-white de type A. *Am. Cardiol. Angeiol*., 1975;**24**: 59–66.
230. Campbell, R.W.F., R.A. Smith, J.J. Gallagher, E.L.C. Pritchett, and A.G. Wallace, Atrial fibrillation in the preexcitation syndrome. *Am. J. Cardiol*., 1977;**40**: 514–520.
231. Wellens, H.J. and D. Durrer, Wolff-Parkinson-White syndrome and atrial fibrillation: Relation between refractory period of the accessory pathway and ventricular rate during atrial fibrillation. *Am. J. Cardiol*., 1974;**34**: 777–782.
232. Ahlinder, S., A. Granath, S. Holmer, et al., The Wolff-Parkinson-White syndrome with paroxysmal atrial fibrillation changing into ventricular fibrillation, successfully treated with external heart massage. *Nord. Med*., 1963;**70**: 1336–1339.
233. Bashore, T.M., T.D. Sellers, J.J. Gallagher, and A.G. Wallace, Ventricular fibrillation in the Wolff-Parkinson-White syndrome (abstract). *Circulation*, 1976;**54**(Suppl. 2): 187.
234. Castillo-Fenoy, A., A. Goupil, G. Offenstadt, and G.K. Nguyen, Síndrome de Wolf-parkinson-White et mort subite. *Ann. Med. Interne*., 1973;**124**: 871–875.
235. Dreifus, L.S., H.J. Wellens, Y. Watanabe, D. Kimbins, and R. Truex, Sinus bradycardia and atrial fibrillation associated with the Wolff-Parkinson-White syndrome. *Am. J. Cardiol*., 1976;**38**: 149–156.
236. Fox, T.T., J. Weaver, and H.W. March, On the mechanism of the arrhythmias in aberrant atrioventricular conduction (Woff Parkinson White). *Am. Heart J*., 1952;**43**: 507–520.
237. Kaplan, M.A. and K.L. Cohen, Ventricular fibrillation in the Wolff-Parkinson-White Syndrome. *Am. J. Cardiol*., 1969;**24**: 259–264.
238. Lim, C.H., C.C.S. Toh, and B.L. Chia, Ventricular fibrillation in type B Wolff-Parkinson-White syndrome. *Aust. NZ J. Med*., 1974;**4**: 515–517.
239. Martin-Noel, P., B. Denis, and D. Grundwald, Buisson Mme. Deux cas mortels de syndrome de Wolff Parkinson White. *Arch. Mal. Cœur Vaiss*., 1970;**63**: 1647–1656.
240. Okell, B.B., The Wolff-Parkinson-White syndrome: Report of a fatal arrhythmia and autopsy findings of myocarditis, interatrial lipomatous hypertrophy, and prominent right moderator band. *Am. Heart J*., 1968;**41**: 673–678.
241. Antonelli, G., M. Di Biase, G. Biasco, et al., Prolasso della mitrale e síndrome di pre-eccitazione ventricolare. *G. Ital. Cardiol*., 1976;**6**: 1365–1377.
242. Devereux, R.B., J.K. Perloff, N. Reichek, and M.E. Josephson, Mitral valve prolapse. *Circulation*, 1976;**54**: 3–14.
243. Lunel, A.A.V., Significance of annulus fibrosis of heart in relation to AV conduction and ventricular activation in cases of Wolff-Parkinson-White syndrome. *Br. Heart J*., 1972;**34**: 1263–1271.
244. Massumi, R.A., Familial Wolff-Parkinson-White syndrome with cardiomyopathy. *Am. J. Med*., 1967;**43**: 951–955.
245. Ruskin, J.N., M. Akhtar, A.N. Damato, A.R. Ticzon, S.H. Lau, A.R. Caracta, Abnormal Q waves in Wolff-Parkinson-White syndrome: Incidence and clinical significance. *J. Am. Med. Assoc*., 1976;**235**: 2727–2730.
246. Chung, E.K., *Electrocardiography. Practical Applications with Vectorial Principles*. Hagerstown, MD: Harper and Row, 1974.
247. Clerc, A., R. Lévy, and C. Cristesco, A propos du raccourcissement permanent de l'espace P-R de l'électrocardiogramme sans déformation do complexe ventriculaire. *Arch. Mal. Cœur Vaiss*., 1938;**31**: 569–582.
248. Lown, B., W.T. Ganong, and S.A. Levine, The syndrome of short P R interval, normal QRS complex and paroxysmal rapid heart action. *Circulation*, 1952;**5**: 693–706.
249. Benditt, D.G., E.L.C. Pritchett, W.M. Smith, A.G. Wallace, and J.J. Gallagher, Characteristics of atrioventricular conduction and the spectrum of arrhythmias in Lown-Ganong-Levine syndrome. *Circulation*, 1978;**57**: 454–465.
250. Bisset, J.K., N. de Soyza, J.J. Kane, and M.L. Murphy, Altered refractory periods in patients with short P-R intervals and normal QRS complex. *Am. J. Cardiol*., 1975;**35**: 487–491.
251. Gallagher, J.J., W.M. Smith, J. Kasell, D.W. Benson Jr., R. Sterba, and A.O. Grant, Role of Mahaim fibers in cardiac arrhythmias in man. *Circulation*, 1981;**64**: 176–189.
252. Brugada, P. and J. Brugada, Right bundle branch block, persistent ST segment elevation and sudden cardiac death: A distinct clinical and electrocardiographic syndrome. A multicenter report. *J. Am. Coll. Cardiol*., 1992;20: 1391–1396.
253. Mattu, A., R.L. Rogers, K. Hyung, A.D. Perron, and W.J. Brady, The Brugada Syndrome. *Am. J. Emerg. Med*., 2003;**21**(2): 146–151.
254. Wilde, A.A.M., C. Antzelevitch, M. Borggrefe, F. Brugada, R. Brugada, P. Brugada, D. Corrado, R.N.W. Hauer, R.S. Kass, K. Nademanee, S.G. Priori, and J.A. Towbin, Proposed diagnostic criteria for the Brugada Syndrome – Study Group on the molecular basis of Arrhythmias of the European Society of Cardiology. *Eur. Heart J*., 2002;**23**: 1648–1654.
255. Antzelivitch, C., P. Brugada, M. Borggreffe, J. Brugada, R. Brugada, D. Corrado, et al., Brugada Syndrome: Report of the Second Consensus Conference. *Circulation*, 2005;111: 659–670.
256. Miyasaka, Y., H. Tsuji, K. Yamada, S. Tokunaga, D. Saito, Y. Imuro, N. Matsumoto, and T. Iwasaka, Prevalence and mortality of the Brugada-type electrocardiogram in one city in Japan. *J. Am. Coll. Cardiol*., 2001;38: 771–774.
257. Naccarelli, G.V., C. Antzelevitch, D.L. Wolbrette, and J.C. Luck, The Brugada syndrome. *Curr. Opin. Cardiol*., 2002;**17**: 19–23.
258. Rook, M.B., C.B. Alshinawi, W.A. Groenewegen, et al., Human SCN5A gene mutations alter cardiac sodium channel kinetics and are associated with the Brugada syndrome. *Cardiovasc. Res*., 1999;**44**: 507–517.
259. Antzelevitch, C., J.M. Fish, and J.M. Di Diego, *Cellular Mechanisms Underlying the Brugada Syndrome*. Elmsford, U.K.: Blackwell Publishing, 2005, pp. 52–77.
260. Mills, A.T.D., S. Dasan, and A. Whan, Brugada syndrome: Syncope in the younger patient and the risk of sudden cardiac death. *Emerg Med J*., 2005;**22**: 604–606.
261. Brugada, R., J. Brugada, C. Antzelevitch, et al., Sodium channel blockers identify risk for sudden death in patients

with ST-segment elevation and right bundle branch block but structurally normal hearts. *Circulation*, 2000;**101**: 510–515.
262. Giustetto, C., S. Drago, P.G. DeMarchi, P. Dalmasso, F. Bianchi, A.S. Masi, et al., Risk stratification of the patients with Brugada type electrocardiogram: A community based prospective study. *Europace*, 2009;11: 507–513.
263. Brugada, P., Amid the fourth lustrum after the description of Brugada syndrome: Controversies over? *Europace*, 2009;11: 412–413.

15 Enlargement and Hypertrophy

Peter W. Macfarlane · Peter M. Okin · T.D. Veitch Lawrie · John A. Milliken[†]

[†]Deceased.

P. W. Macfarlane, A. van Oosterom, O. Pahlm, P. Kligfield, M. Janse, J. Camm (eds.), *Comprehensive Electrocardiology*, DOI 10.1007/978-1-84882-046-3_15,

15.1 Introduction

Cardiac hypertrophy is an increase in the mass of the heart owing to the enlargement of existing muscle fibers. It may be localized to the apex or septum, for example, or may be diffuse with the latter form being further subdivided into concentric and eccentric hypertrophy depending on whether the chamber size is normal or dilated. Chronic pressure overload as in aortic stenosis or hypertension often results in concentric, diffuse, or global left ventricular hypertrophy (LVH). In contrast, eccentric or dilated hypertrophy is more frequently associated with volume overload, for example, aortic or mitral regurgitation. The terms systolic overload LVH and diastolic overload LVH also have been used as alternatives to pressure and volume overload, respectively [1, 2]. The different types are summarized in Fig. 15.1.

No single set of electrocardiographic criteria can identify such variable types of hypertrophy. Since electrocardiography relies on electrical phenomena to make inferences about anatomy, it is not surprising that any ECG changes which might occur, such as an increase in QRS voltage, have only a moderate relationship with LV mass [3]. The two most commonly used techniques for defining LV hypertrophy or mass have been assessment of mass at postmortem and echocardiographic determination *in vivo* of cavity and wall dimensions from which mass can be calculated. Each method

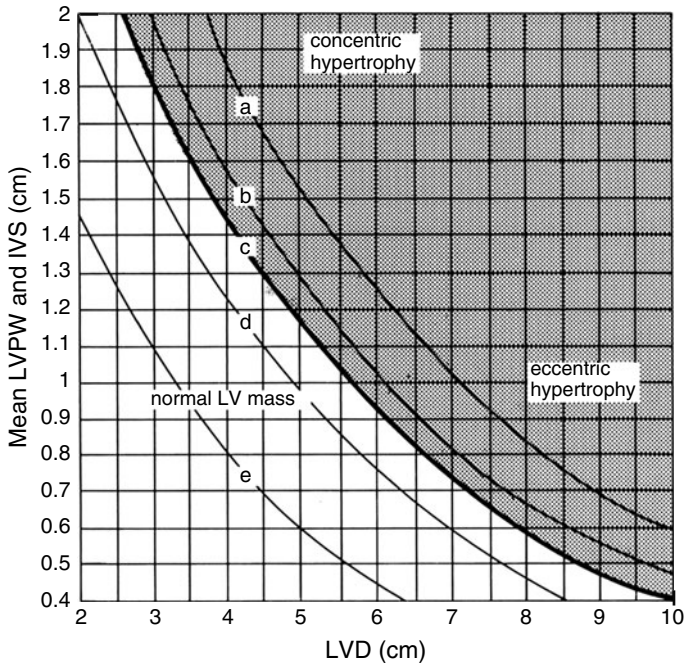

Figure 15.1

The relationship between concentric and eccentric hypertrophy as illustrated on a nomogram for the determination of LV mass from M-mode echocardiographic (ECHO) measurements. The vertical axis is the mean of LV posterior wall thickness (LVPW) and the interventricular septal thickness (IVS). The horizontal axis is the LV chamber diameter (LVD). The curves represent various LV masses: (a) 400 g, (b) 300 g, (c) 265 g, (d) 200 g, and (e) 100 g. The shaded area above curve c (bold) reflects an abnormally increased ECHO LV mass according to criteria of Woythaler et al. [11]. This value was related by regression analysis to a mass of 225 g at postmortem. At the upper extreme in the shaded area are measurements that suggest concentric LVH, where there is increased thickening of the chamber walls without dilation. Toward the middle and lower portions of the shaded area, there is dilation of the LV chamber in proportion to the thickening of the ventricular walls. These echocardiographic measurements were obtained using the recommendations of the American Society of Echocardiographers rather than the Penn convention. (After Woythaler et al. [11]. © American College of Cardiology, Bethesda, MD. Reproduced with permission.)

is discussed in turn in view of its relevance to the establishment of ECG criteria for hypertrophy. Although magnetic resonance imaging (MRI) of the heart has also been utilized for this determination of LV mass and hypertrophy [4], it has not as yet played a significant role in the development and/or validation of ECG criteria for LVH.

15.1.1 Anatomic Standards for Hypertrophy

The chamber-partitioning technique of assessing cardiac ventricular weights, which was first introduced in 1888 and reviewed by Bove et al. [5], has been of limited use. Nevertheless, a number of important criteria have been developed and assessed using this approach, which will be outlined briefly.

At postmortem, the heart is first of all stripped of any surface fatty deposits and the atria are then removed. Next, the valve rings and leaflets are dissected out. The remaining ventricular mass is then sectioned serially in a transverse direction with each slice having the appearance shown in Fig. 15.2. The free right ventricular (RV) wall is dissected away from the septum and the LV wall, as indicated by the dashed line in Fig. 15.2; in this way, the RV muscle can be weighed separately. The septum is somewhat arbitrarily dissected from the remaining muscle by taking a line at right angles to the septum at its junction with the RV free wall (at both sides). In this way, the septal mass and the LV free wall mass can also be determined separately. This allows the total LV mass to be obtained and various ratios of component masses to be assessed. Table 15.1 summarizes anatomical criteria for ventricular hypertrophy derived from this technique.

From their study of 100 hearts, Bove et al. recommended several modifications in attempting to classify mild degrees of cardiac hypertrophy not readily recognized at autopsy. Subsequently, Murphy et al. [6, 7] suggested slightly different definitions of right and left ventricular hypertrophy (see Table 15.1 and Fig. 15.2). The upper limit of normal was defined by a mean plus two standard deviations or as exceeding the 98 percentile range of normal. Unfortunately, adequate numbers of hearts from normal women were not available. Although an attempt was made to base anatomic criteria on the height of the patient (see Table 15.1), there remained a poorly defined region between normal and definitely abnormal, leading to descriptions such as "possible LVH" or "mild LVH" even when anatomical details were known. Subsequent study of this area has resulted in anatomic LV mass being indexed to body size using body surface area or height to the 2.7 power, which more accurately reflects the allometric relations of LV mass to body size and obesity [8]. In view of the above, the reader should be aware of the limitations of anatomic standards especially when the specificity and sensitivity of ECG criteria are reported.

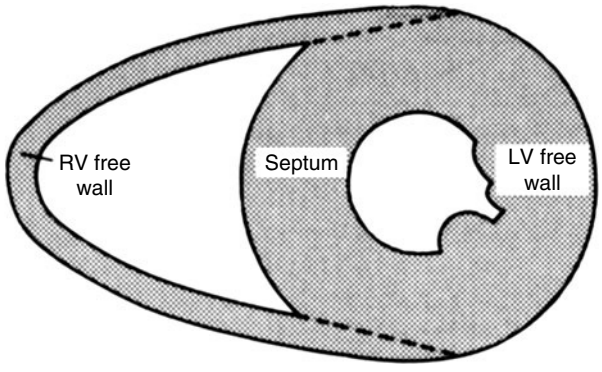

Figure 15.2

A cross section of the heart showing the method of dissecting the RV free wall from the left ventricle and septum. The septum can be somewhat arbitrarily separated from the LV mass by dissecting it at right angles to the septal surface at its junction with the RV free wall. (After Bove et al. [5]. © American Heart Association, Dallas, TX. Reproduced with permission.)

Table 15.1

Anatomical cardiac hypertrophy at autopsy[a]

Classification	Bove [4]	Murphy [5]
Normal	Subject < 1.78 m tall	LV + S < 171 g
	LV + S < 176 g	RV < 62 g
	RV < 65 g	
	(LV + S)/RV ratio 2.1–3.6	
	Subject > 1.78 m tall	
	LV < 200 g	
	RV < 75 g	
Left ventricular hypertrophy	LV + S > 200 g RV < 75 g	LV + S > 171 g
	LV/RV ratio > 3.6	Normal RV
Possible LVH or LV preponderance in small hearts	(LV + S)/RV ratio > 3.6	(LV + S)/RV ratio > 3.9
	Weights normal	Weights normal
Right ventricular hyper trophy	RV > 75 g	RV > 62 g
	LV/RV ratio < 2.1	Normal LV
Possible RVH or RV preponderance in small hearts	LV/RV ratio < 2.1	LV/RV ratio < 2.3
	Weights normal	Weights normal
Biventricular hyperrophy	LV + S > 220 g	LV + S > 171 g
	RV > 75 g	RV > 62 g
Mild BVH	LV + S = 175–220 g	
	RV > 60 g	
	Biatrial hypertrophy	

[a] LV, weight of left ventricle; RV, weight of right ventricle; S, weight of septum; all as defined in Fig. 15.2

15.1.2 Echocardiographic Standards for Hypertrophy

Echocardiography (ECHO) is now regarded as the most accurate noninvasive method for estimating LV mass or LVH, correlating well with autopsy measurements, but the aforementioned difficulty of defining standards is now becoming apparent. Two-dimensional echocardiography may be the preferred technique [9, 10], especially in patients with abnormal LV geometry or segmental disease. However, technically adequate M-mode echocardiograms are more easily recorded and may remain the standard for some time. Indeed, Woythaler et al. [11], in a study of 50 hearts examined at post-mortem where both M-mode and two-dimensional echocardiograms had been recorded within 6 months of death, found a much higher correlation between M-mode estimates of LV mass and those at autopsy than between two-dimensional and autopsy values.

There are several different equations used for the estimation of LV mass given either the M-mode echocardiogram or the two-dimensional sector scan. One approach that utilizes the M-mode echocardiogram is to obtain the short-axis internal diameter D of the left ventricle and to assume that the ventricle is a prolate ellipsoid [12] where the major axis is twice the length of each minor axis. It then follows that the semiminor axes each have the same length $D/2$, i.e. half that of the semimajor axis. The volume V is then

$$V = (4/3)\pi\,(D/2)(D/2)D = (\pi/3)/D^3 = 1.047D^3 \sim D^3$$

If the epicardial and endocardial echoes are obtained from the M-mode display, it is possible to calculate a left ventricular mass (LVM) where

$$\text{LVM} = (D_O^3 - D_I^3) \times \text{muscle density}$$

where D_O is the diameter of the outer ventricular shell and D is the internal ventricular diameter. Density is usually given a value of 1.05 g cm^{-3}.

Using a modification of this approach, Devereux and Reichek [13] have validated the method with an anatomic comparison. They found that the optimum equation for LVM was

$$\text{LVM} = 1.04\{(\text{LVID} + \text{PWT} + \text{IVST})^3 - \text{LVID}^3\} - 13.6\,\text{g}$$

where LVID is the LV internal diameter, PWT is the posterior wall thickness, and IVST is the interventricular septal wall thickness. In these measurements, the thickness of the endocardial echo lines was excluded from wall thickness estimates, but the LVID estimate included the thickness of left septal and posterior wall echo lines (the so-called Penn convention). Where a two-dimensional sector scan is available, then a more complex equation can be utilized as follows:

$$\text{LVM} = \left(\frac{4}{3}\right)\pi\left\{\frac{A+2T}{2}\times\frac{B+2T}{2}\times\frac{B+2T}{2} - \frac{A}{2}\times\frac{B}{2}\times\frac{B}{2}\right\}\times\text{density}$$

where T is the thickness of the LV free wall, and A and B are the lengths of the major and minor axes, respectively. Frequently, however, this is simplified to

$$\text{LVM} = (\text{epicardial enclosed volume} - \text{endocardial enclosed volume}) \times 1.05$$

with the result being indexed to body-surface area.

It should be noted that when assessing ECG-echo studies of cardiac hypertrophy, there is some interobserver variation [14] in measuring the echocardiogram, although this has been minimized with the use of two-dimensional methods.

There is little doubt that the estimation of LV mass is a more sensitive indicator of LVH than is the thickness of the posterior wall or septum. Irrespective of body size, an M-mode mass of 215 g [3] or 265 g (LV + septum) [11] has been used to define LVH.

Several investigators have demonstrated that sex differences for increased LV mass (or LVH) are diminished but not eliminated when LV mass is indexed by body-surface area [9, 15, 16]. It has been further suggested that lean body mass be used to eliminate the sex differences [15]. Devereux et al. have defined the indexed M-mode LV mass for LVH as greater than 134 g/m^2 in men and greater than 110 g/m^2 in women or a single limit of 120 g/m^2 [15], and, subsequently, as LVM > 116 g/m^2 in men and 104 g/m^2 in women, based on the ability of these criteria to predict adverse prognosis [17]. Before accepting the sensitivity and specificity of any suggested ECG criteria, the reader should always check the standard used to define an increased ventricular mass. A single cutoff value may underdiagnose LVH in women and overdiagnose it in large athletic men, particularly when unindexed LV mass is being used to define LVH.

The accuracy of the M-mode echocardiogram in assessing RV mass [18] is questionable. Prakash and Matsukubo [19] used RV wall thickness measurements to diagnose RVH. Diastolic thickness had a sensitivity of 90% and a specificity of 94%, while systolic thickness, with a specificity of 100%, had a sensitivity of only 34%. Baker et al. [18] found that an RV internal dimension in diastole greater than 26 mm identified only 36% of those with anatomic RVH, while an RV wall thickness greater than 5 mm correctly identified 67%. They concluded that neither M-mode measurement is accurate enough to use as a standard for increased RV mass. Since anatomic RV wall thickness and anatomic RV mass have a correlation coefficient r of only 0.29, other measurements are required.

In an enlarged right ventricle, the increase in size is more extensive in the direction of the short axis than in the direction of the long axis [20]. Calculation of the RV volume should, therefore, prove a more useful measurement of enlargement than wall thickness alone, there being a good correlation of angiographic and echocardiographic RV volumes: $r = 0.94$ at end diastole and $r = 0.84$ at end systole [20]. Perhaps RV volume derived using a sector scan will prove a better tool for assessing RV mass [21].

While ventricular enlargement includes both dilatation and hypertrophy, the calculation of total mass and surface area are more objective and verifiable than is cavity size or wall thickness [22]. More accurate methods are necessary.

15.2 Factors Affecting ECG Criteria for Ventricular Hypertrophy

Many factors may be related to the presence of high or increased voltage, e.g., sex, obesity, hypertrophy, enlargement, and sympathetic drive and associated disease such as obstructive coronary atherosclerosis.

15.2.1 Age and Sex

Age is one of the principal factors that affect the criteria for LVH. Since ECG voltages decrease with increasing age (see Chap. 13), the limits of normal voltage should be stratified by age. Although other factors such as body-surface area can be considered, the height and weight of a patient may not be readily available to a cardiologist reporting ECGs. In addition, detailed statistical analysis of over 1,330 normal individuals in the Glasgow database has indicated that age is the most significant factor in explaining voltage variation both in males and females (Chap. 13). The simplest, yet theoretically sound, approach therefore is to utilize age. Likewise, since there are considerable differences between male and female in the limits of normality of ECG measurements, particularly in young adults, criteria should also be sex dependent. This point is discussed further in the Romhilt and Estes scoring technique (Sect. 15.3.1.4) and in the section on Cornell voltage and voltage-duration product (Sect. 15.3.1.6).

15.2.2 Hypertrophy and Dilatation

Antman et al. [23] used LV wall thickness h plotted against the semi-minor radius of the left ventricle R to produce a product hR. A value of this product in excess of 2.6 cm^2 identified all those with LVH by ECG. These authors found that LVH resulting from an enlarged chamber (aortic regurgitation) plays a greater role in augmenting potentials than does a thickened myocardium (aortic stenosis) [23]. In contrast, Devereux et al. concluded that for a given LV mass, ECG voltage criteria of LVH are independent of LV chamber dilatation or other geometric variables. Instead they depend on age, weight, and LV depth in the chest. They suggested that stratification of subjects by these clinical variables might improve the electrocardiographic recognition of LVH [24].

15.2.3 Distance of Heart from Electrodes

Horton et al. [25] found that precordial voltage was strongly influenced by the distance of the left ventricle from the electrodes. They attempted to correct for this by the multiplication of precordial voltage by the square of the distance from the chest wall to the mid-left ventricle. This improved the correlation coefficient of $SV_1 + RV_5$ with LV mass from 0.686 to 0.846.

During an echocardiographic study of ten normal subjects before and after exercise, Feldman et al. [26] noted that there is a direct relationship between R-wave voltage in the left chest leads and LV size. This is true, whether it is measured as LV volume or LV internal dimension. Both LV size and the distance of the heart from V_5 or V_6 seem to interact as determinants of R-wave voltage.

15.2.4 Associated Diseases

The presence of obstructive coronary artery disease may be linked with the development of LVH. Pech et al. [27] showed an increase in LV mass in patients with coronary artery disease compared to those without coronary artery disease. Some muscle fibers became fibrosed with loss of contractility, leading to hypertrophy of the remaining muscle fibers.

15.2.5 Miscellaneous Factors

Other factors influencing voltage in the ECG include the conducting properties of intervening structures and delayed activation in portions of the myocardium. High voltages may commonly occur in young people under the age of 30 (see Chap. 13), thin elderly women, and emaciated individuals [28]. The influence of race should also be acknowledged. Black individuals have a higher precordial voltage on the ECG than white individuals, while the latter have a higher voltage in the ECG than oriental individuals (see Chap. 13). The higher precordial voltages in blacks can lead to the overestimation of LVH prevalence due to lower specificity of these criteria [29]. However, amplitudes and performance of Cornell voltage and Cornell product criteria appear to be relatively independent of race [29]. The modest increase in LV mass seen in athletes also produces a high voltage but, unlike pathologic hypertrophy, is not accompanied by slowed LV diastolic filling [30]. Finally, increasing body mass index is strongly and inversely associated with precordial voltage amplitude, leading to higher specificity and lower sensitivity of precordial voltage criteria in overweight and obese individuals [31], with subsequent underestimation of the prevalence of anatomic LVH in the presence of obesity [32]. In contrast, sensitivity and specificity of Cornell voltage and product criteria vary less with body mass index [31] and provide a more accurate measure of the prevalence and severity of LVH in obese and overweight patients [32]. The authors would contend that criteria should take these factors into account in order to minimize false-positive and false-negative ECG interpretations.

15.2.6 Theoretical Considerations

Elsewhere in this book (e.g., Chaps. 1 and 5), some theoretical considerations on the effect of thoracic inhomogeneities on the electrocardiogram are discussed. It would seem relevant at this point to provide a nonmathematical description of some of these effects and their relationship to the presence or absence of ECG changes in patients with increased LV end diastolic volume or with increased LV wall thickness.

In Chap. 2, the so-called Brody effect is discussed [33]. Essentially, this principle suggests that when there is an increase in blood volume in either ventricle, surface potentials owing to a radial spread of excitation in that ventricle are enlarged and those arising from a more tangential or lateral spread of excitation through the wall muscle are attenuated. This would imply that in patients with aortic regurgitation, for example, there should be an increased voltage in the precordial leads on account of the increased blood volume, even though there may be no increase in muscle thickness. Some quite dramatic changes in voltage can be seen in patients with aortic regurgitation before and after valve replacement (Fig. 15.3), on account of the reduction in blood volume. There have been some apparently contradictory results obtained when low voltages have been found in patients with congestive heart failure [34]. This apparent paradox can be explained on the basis of there being an increase in the conductivity of the lungs owing to the presence of pulmonary edema secondary to heart failure, which then results in an attenuation of surface potentials. Nonetheless, clinical findings with respect to the Brody effect remain conflicting.

Another consideration in the case of a dilated heart is the effect of variation in the generator properties of the muscle. It could be argued that by stretching the myocardium, the electrical sources are more widely available and, therefore, increased. In such a case, Rudy [35] has shown that the voltage increase (82%) is more than double that (35%) in an equally dilated heart where the generator strength remains the same as before dilation.

Other factors that affect the surface voltages have also been discussed fully by Rudy [35] in a theoretical review of the topic. These include the lungs, which tend to reduce the surface voltage as emphasized in patients with chronic obstructive airways disease. The pericardium can also affect surface voltages on account of an increased compression of the heart by an excessive amount of pericardial fluid. The surface muscle layer also contributes to an attenuation of the body-surface potentials on account of a high conductivity so that in any conditions where there is a low muscle conductivity, e.g., Pompe's disease, voltages would be increased.

The final and perhaps most interesting situation is to consider the theoretical effects of increased muscle thickness with a normal ventricular cavity size in comparison to a reduced cavity size. Where the cavity size is normal, but there is an increase in muscle thickness, it can be shown, theoretically, that the surface voltage is increased by 13.6% [35]. The voltage increase, however, is often much greater than this, suggesting that other factors play an important part. On the other hand, an increased muscle thickness with a reduced cavity size is theoretically associated with a decrease of the

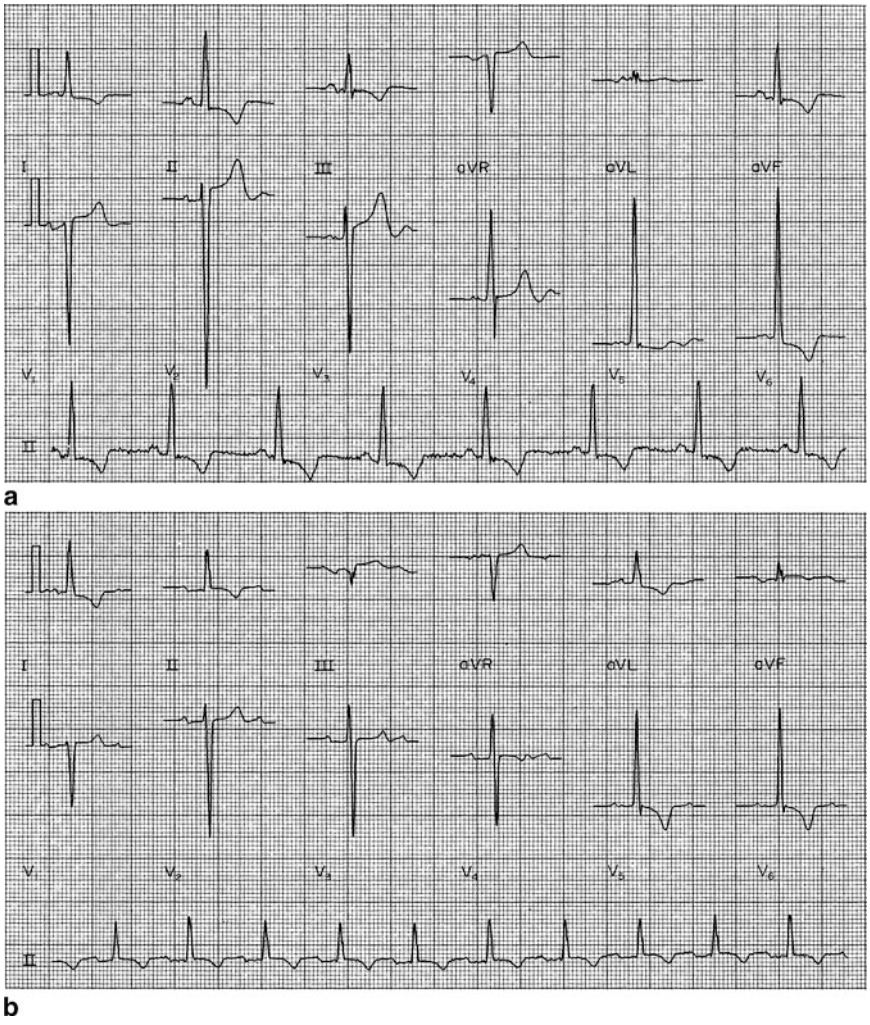

Figure 15.3

Part (a) shows the ECG from a 49-year-old female with aortic stenosis and incompetence. Part (b) shows the ECG taken 11 days later and following aortic valve replacement. Note the dramatic reduction in the voltage; for example, $SV_2 + RV_6$ has decreased from 7.9 to 5.0 mV. The voltage reduction was most likely related to a reduction in LV volume.

same order of magnitude in surface potentials compared to normal. This could explain the not uncommon situation of a grossly thickened heart, such as is found in cardiomyopathy with normal ECG voltages.

15.3 Left Ventricular Hypertrophy (LVH)

15.3.1 ECG Criteria

There are many different criteria for LVH, most of which are presented in Table 15.2 along with sensitivity and specificity from different studies [36–38]. Some of these criteria are discussed in detail.

Table 15.2

Sensitivity and specificity of commonly used criteria for left ventricular hypertrophy

Criteria/parameters	98% upper limits[a] (mV)	Autopsy study[b]		ECHO-LBBB[c]	
		Sensitivity (%)	Specificity (%)	Sensitivity (%)	Specificity (%)
Limb leads					
RI > 1.3 mV	1.3	11	100	7	94
RI + SIII > 2.5 mV	1.9	11	100	12	100
RaVL > 0.7 mV	0.8	23	96		
RaVL > 1.1	0.8	11	100	24	97
RaVL > 1.3	0.8	8	100	8	100
SaVR > 1.4	1.2	7	100	0	100
RaVF > 1.9	1.4	1.3	99	0	100
Lewis index $\geqslant$ 1.7[d]		18	98	37	78
Left-axis deviation of −30° or more		25	87	32	78
Left-axis deviation of −40° or more				26	94
Chest leads					
$SV_1 \geqslant 3.0$ mV				26	91
$SV_1 \geqslant 2.4$	1.6	19	100	47	56
$SV_2 \geqslant 3.0$ and $SV_3 \geqslant 2.5$				49	90
$SV_3 \geqslant 2.5$				57	88
RV_5 or $RV_6 > 2.6$	2.0	25	98	3	100
$RV_6 > 2.0$	1.5	22	88		
$RV_6 > RV_5$		23	89	74	9
VAT V_5 or V_6 = 0.05+ seconds [4]		29	99		
SV_1 or $SV_2 + RV_5$ or $RV_6 > 3.5$	3.8	56	88	81	41
$SV_1 + RV_5$ or $RV_6 > 3.5$	3.3	43	95	50	72
$SV_1 + RV_5 > 3.3$ females		40	93	45	67
$SV_1 + RV_5 > 3.6$ males	3.3	40	93	56	73
$SV_2 + RV_5$ or $RV_6 > 4.5$	4.4	35	97	44	84
R + S > 4.5 (largest R + largest S)		45	93	54	81
Point score system[e]		54	97	35	84

[a] After Murphy et al. [6]

[b] After Romhilt et al. [36] (160 patients with LVH and 200 without LVH were studied)

[c] After Kafka et al. [9, 38] (68 patients with LVH and 32 without LVH were studied). Revised using an indexed LV mass for males $\geqslant$ 132 g cm^{-2} and females $\geqslant$ 110 g cm^{-2}

[d] Lewis index = (RI-RIII) + (SIII – SI)

[e] Romhilt and Estes [43]

15.3.1.1 Lewis Index

The index introduced by Lewis [39] in 1914 is still favored by a number of cardiologists in continental Europe. This index is defined as

$$(\mathrm{RI} + \mathrm{SIII}) - (\mathrm{RIII} + \mathrm{SI})$$

A value of 1.7 mV was suggested as a borderline criterion producing a very high specificity of 98% but a low sensitivity of 18%, as shown in Table 15.2. An illustration of a high Lewis index is presented in Fig. 15.4, where it can be seen that precordial voltages may well be normal.

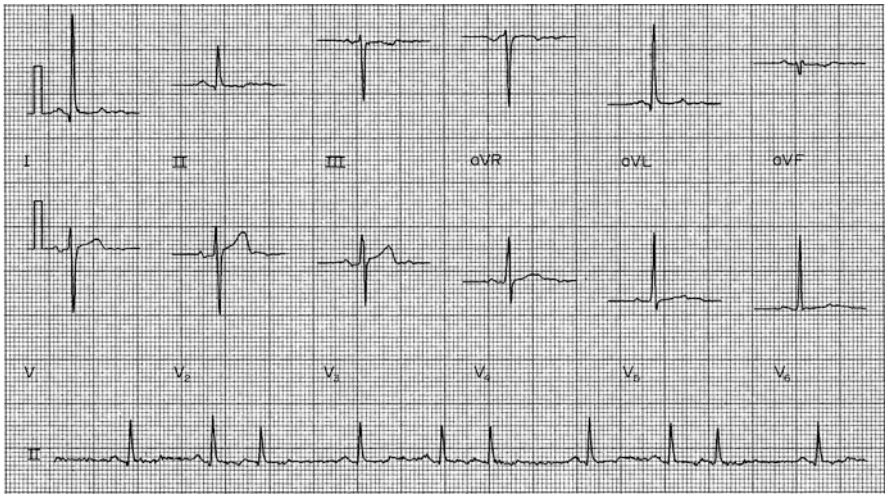

Figure 15.4
ECG showing voltage evidence of LVH in the limb leads, recorded from a 62-year-old male undergoing surgery for aortic valve replacement. The Lewis index is approximately 3.2 mV, which is well above the upper limit of normal, while it can be seen that the precordial voltages are within normal limits.

15.3.1.2 Sokolow and Lyon Index

The voltage criteria of Sokolow and Lyon [40] introduced in 1949 are still used extensively by many cardiologists. These are

(a) $SV_1 + (RV_5 \text{ or } RV_6) \geqslant 3.5$ mV
(b) RV_5 or $RV_6 \geqslant 2.6$ mV
(c) R in aVL $\geqslant 1.1$ mV
(d) R in aVF $\geqslant 2$ mV

Perhaps the most widely used criterion for LVH is $SV_1 + RV_5/V_6 \geqslant 3.5$ mV, sometimes known as the Sokolow–Lyon index, although it was present in only 33% of their 147 patients (Fig. 15.5). Less well known are their ST-T criteria, namely, a depressed ST segment and asymmetric T-wave inversion. In 92% of their cases, ST-T abnormalities were present. Certainly, criterion (a) is too nonspecific for young adults, and the limits should be different for males and females, as demonstrated by Macfarlane and Lawrie (Chap. 13) from their study of 1,330 healthy volunteers (see Fig. 15.6). In addition, Sokolow–Lyon voltages are significantly greater in blacks than in Caucasians [29], leading to lower specificity and higher sensitivity in blacks if these criteria are not adjusted for race as well as sex [29]. As Table 15.2 shows, the sensitivity of (a) at 43% and (b) at 22% was less than that of the point score at 54%. The remaining criteria (c) and (d) were highly specific but very insensitive (11% and 1.3%, respectively).

15.3.1.3 McPhie Criterion

McPhie, in 1958, suggested that the tallest R-wave amplitude be added to the deepest S-wave amplitude in any precordial lead [41]. If this total exceeded 4.5 mV, then LVH was present. While this criterion was of little additional value, it did

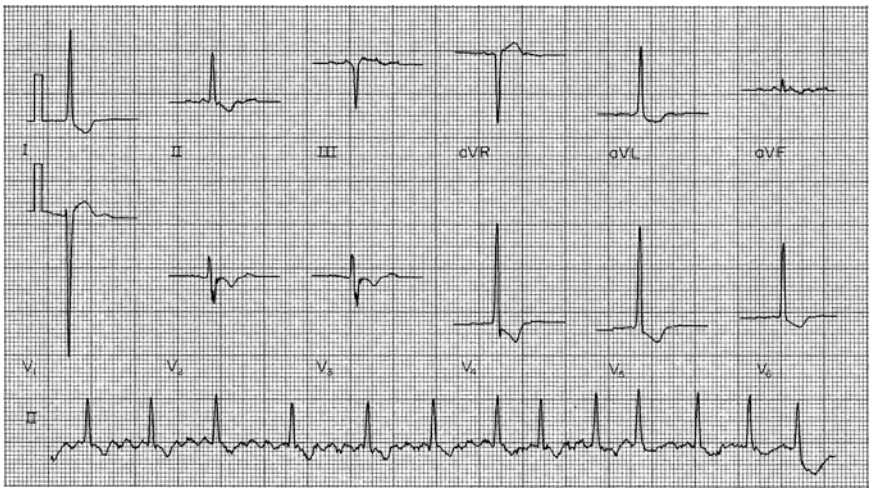

Figure 15.5

ECG of a 75-year-old lady undergoing aortic valve replacement. The Sokolow and Lyon index is approximately 5.6 mV, which is well beyond the upper limit of normal. Limb-lead measurements are also abnormally high, with the R in aVL exceeding 1.1 mV.

recognize that deep S waves in leads V_2 and V_3 may contribute significantly to a diagnosis of LVH. This preoccupation with voltage criteria caused Simonson [42] in 1961 to modify the borderline limit of $SV_1 + RV_5$ slightly to $\geqslant 3.3$ mV for females and $\geqslant 3.6$ mV for males. As can be seen from Table 15.2, there was little change in the sensitivity or specificity. Many precordial-lead voltage criteria have subsequently been recommended, with variable results.

15.3.1.4 Romhilt–Estes Point Score System

In 1968, Romhilt and Estes [43] introduced a point-scoring system for the ECG diagnoses of LVH. Although this approach is cumbersome with respect to conventional ECG interpretation, it has been found useful by a number of authors of computer programs for ECG analysis. The scoring system is detailed in Table 15.3. Essentially it gives a high score for an abnormal amplitude of QRS components in either the limb leads or the precordial leads. A single value of 2 mV is used for the limb leads and 3 mV for the precordial leads. A similar high score is obtained for the appearance of the so-called LV strain pattern (Fig. 15.7) although the number of points is reduced if the patient is taking a digitalis preparation. The other items included are left-axis deviation, an increased QRS duration, and a delayed intrinsicoid deflection in V_5 or V_6. An abnormal P terminal force (PTF) in V_1 (see Fig. 15.23) also contributes significantly to the score. The authors obtained a modest sensitivity of about 60% with a high specificity in excess of 95%.

Murphy et al. [7, 44] have modified the point score slightly and also assessed various combinations. The result was a sensitivity value that varied from 57% to 66% and a specificity that ranged from 85% to 93% depending on the cause of the hypertrophy. Their standard for LVH in their 91 subjects was an LV mass greater than 171 g or, if chamber weights were normal, then LV/RV ratio greater than 3.9.

Table 15.4 shows the age-dependent and sex-dependent upper limits of normal for some measurements of the QRS complex that are used by the Glasgow program for computer interpretation of the ECG as part of a modified Romhilt–Estes scoring system. The values in Table 15.4 replace the single precordial-voltage limit of Romhilt and Estes when assessing the number of points to be awarded for high voltage in the precordial leads. Similar considerations apply in the limb leads. In general, sensitivity should be increased in older subjects by the use of lower upper

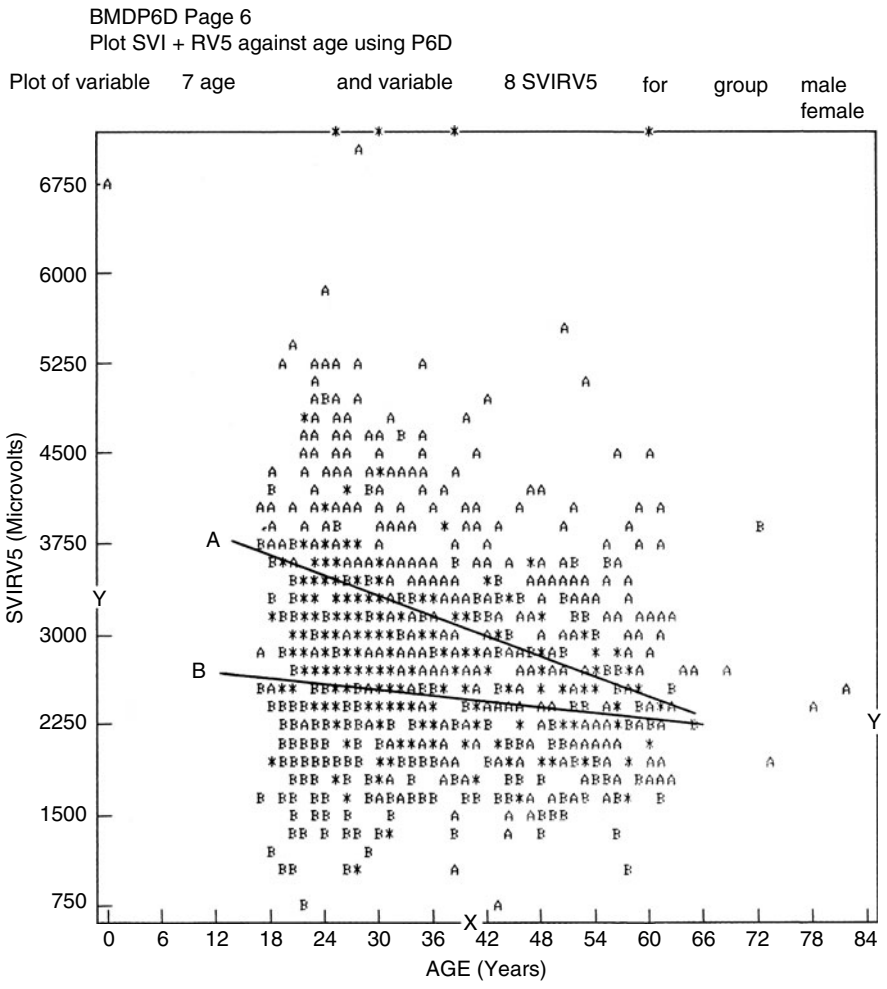

N = 1124
COR = −0.179

	Mean	ST. DEV.	Regression	line	RES. MS.
X	34.811	12.122	X = −0.00257	Y + 42.103	142.37
Y	2837.2	842.46	Y = −12.414	X + 3269.4	687704

Figure 15.6

Scattergram of $SV_1 + RV_5$ from a subgroup of 1,124 apparently healthy individuals in the Glasgow study (see Chap. 13): A, male; B, female; *, more than one individual. The *y* axis is marked in microvolts. Note the high percentage of individuals who have a Sokolow and Lyon index well in excess of the conventional criterion of 3.5 mV. The regression of voltage with age is also shown where it can be seen that sex differences are most marked at younger age levels.

limits of normal, each of which is chosen to be highly specific. Specificity is increased in younger persons by the use of higher limits of normal. Furthermore, the Glasgow scoring system allows an additional point to be scored for each additional 0.5 mV of voltage in excess of the stated values for precordial leads and for each additional 0.3 mV in the limb leads. Note, therefore, that borderline high voltage alone does not constitute ECG evidence of LVH in this system.

Table 15.3

Romhilt–Estes point score system for ECG diagnosis of left ventricular hypertrophy [43][a]

Criteria	Points
Any limb-lead R or S $\geqslant$ 2.0 mV	3
or SV_1 or $SV_2 \geqslant$ 3.0 mV	
or RV_5 or $RV_6 \geqslant$ 3.0 mV	
ST-T is typical of LVH[b]	
No digitalis	3
With digitalis	1
Left atrial involvement[c]	3
P terminal force V_1 > 4 mV ms	
LAD $\geqslant -30°$	2
QRS duration $\geqslant$ 90 ms	1
Intrinsicoid deflection V_5 or $V_6 \geqslant$ 50 ms	1

[a] 5 points indicate definite LVH, 58% of LVH with 2% false positives. 4 points indicate probable LVH, 62% of LVH with 2% false positives
[b] See Fig. 15.7
[c] See Fig. 15.24

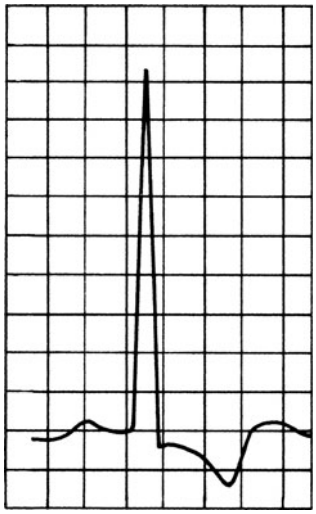

Figure 15.7

Classic appearances of ST-T changes that are secondary to LVH. These changes are often known as the LV strain pattern that is typified by ST depression and a gently downward sloping ST segment that is convex upward, evolving into an inverted T wave.

15.3.1.5 Kansal Criteria

Kansal et al. [45] used a multivariate approach and concluded that the most important ECG variables predictive of LVH are

(a) QRS duration (relative strength F = 27.95)
(b) SV_1 to SV_3 voltage (F = 27.25)
(c) strain in T wave (F = 22.02)
(d) RV_4 to RV_6 voltage (F = 4.03)

Table 15.4

Values used in the Glasgow ECG analysis program as the upper limits of normal voltage for use in the Romhilt–Estes point score system (these values replace those of the first criterion in Table 15.3)

Age (years)	Sex	Lead voltage (mV)				Lewis index
		RI	RaVL	SV_1/V_2	SV_5/V_6	
17–29	Male	1.5	1.1	4.0	4.0	2.5
	Female	1.5	0.9	3.5	2.5	2.0
30–39	Male	1.6	1.2	3.5	3.0	2.5
	Female	1.4	1.0	3.0	2.2	1.8
40–49	Male	1.6	1.3	2.5	2.5	2.0
	Female	1.4	1.2	2.5	2.2	1.8
⩾ 50	Male	1.6	1.3	2.0	2.5	2.0
	Female	1.4	1.2	2.0	2.2	1.8

Table 15.5

Criteria for LVH developed by Casale et al. [46, 49]. Criteria B were published later [49] than criteria A and represent a simplification that makes application easier

Male	Female
Criteria A	
(a) $RaVL + SV_3 > 3.5$ mV or (b) age < 40 years (i) $RaVL + SV_3 > 2.2$ mV (ii) $TV_1 \geqslant 0.0$ mV or (c) age ⩾ 40 years (i) $RaVL + SV_3 > 2.2$ mV (ii) $TV_1 \geqslant 0.2$ mV	(a) $RaVL + SV_3 > 2.5$ mV or (b) age < 40 years (i) $RaVL + SV_3 > 1.2$ mV (ii) $TV_1 \geqslant 0.0$ mV or (c) age ⩾ 40 years (i) $RaVL + SV_3 > 1.2$ mV (ii) $TV_1 \geqslant 0.2$ mV
Criteria B	
$RaVL + SV_3 > 2.8$ mV	$RaVL + SV_3 > 2.0$ mV

They suggest that rescoring these variables in accordance with their correlation with LV mass may improve the ECG sensitivity for LVH.

15.3.1.6 Cornell Multivariate Score and Voltage

Casale et al. have carefully defined LVH using a sex-specific echocardiographic index of LV mass: in men greater than 134 g/m^2 and in women greater than 110 g/m^2 [46]. These values represent approximately the 98th percentile of LV mass index for each sex in two independent normal populations. They demonstrated that the best separation between patients with normal versus increased LV mass at postmortem was obtained using sex-specific LV mass index criteria [47, 48]. The overall accuracy of 83% was better than that for ECHO cross-sectional area (67%) or for indexes of LV wall thickness (39–51%) [48]. They developed new electrocardiographic criteria for the diagnosis of LVH that stratified QRS-voltage and repolarization findings in sex and age subsets (see Table 15.5).

Table 15.6

Multiple logistic regression exponents for detection of left ventricular hypertrophy[a] (After Casale et al. [49])

For patients in normal sinus rhythm
Exponent = $4.558 - 0.092 \times (RaVL + SV_3) - 0.306 \times TV_1 - 0.212 \times QRS - 0.278 \times PTFV_1 - 0.559 \times sex$
For patients in atrial fibrillation
Exponent = $5.045 - 0.093 \times (RaVL + SV_3) - 0.312 \times TV_1 - 0.325 \times QRS - 0.602 \times sex$
Partition values of exponent for detection of LVH
In sinus rhythm: LVH < −1.55
In atrial fibrillation: LVH < −1.20

[a]Units of measurement: voltages of RaVL, SV3, and TV1 in millimeters (1 mm = 0.1 Mv); duration in seconds × 100; P terminal force in lead V1 (PTFV1) in millimeter seconds based on area; sex entered as 1.0 for men and 2.0 for women.

They subsequently applied their criteria prospectively to 135 patients at autopsy, achieving a sensitivity of 42% and a specificity of 96%. By means of logistic regression models based on electrocardiographic and demographic variables with independent predictive values for LVH (and separate equations for those in sinus rhythm and atrial fibrillation), they demonstrated a sensitivity of 62% and a specificity of 92% while having an overall test accuracy of 77% [49]. Their new regression criteria (see Table 15.6) are suitable for computer-based analysis of the electrocardiogram. The Cornell voltage criteria (Table 15.5, criteria B) represent a simplification of the multivariate score, with test specificity and sensitivity that are relatively independent of body habitus [31, 32] and race [20].

15.3.1.7 Perugia Score

Schillaci and Verdecchia and their colleagues from Perugia developed an ECG score based on the presence of ECG LVH by Cornell voltage using modified criteria (> 2.4 mV in men), or a Romhilt–Estes point score ⩾ 4, or the presence of the ECG strain pattern [50, 51]. These criteria improved sensitivity of the ECG for the detection of echocardiographic LVH [50] and improved the prognostic value compared with other ECG LVH criteria [51].

15.3.1.8 Voltage-Duration Product and Time-Voltage Area Criteria

Theoretic modeling [52] and observations that the time-voltage integral of the orthogonal-lead vectorcardiographic QRS complex and the time-strength LV dipole derived from the 126-lead multiple dipole ECG can improve ECG correlation with indexed LV mass [53–55], suggest that an ECG representation of the time-voltage integral of ventricular activation should more accurately reflect the presence and severity of LVH than scores that sum QRS voltage and duration. Subsequent study using the orthogonal-lead signal-averaged ECG demonstrated that the time-voltage integral of the horizontal-plane vector complex significantly improved sensitivity of the ECG for detecting echocardiographic LVH [56]. Using sex-specific partitions with 98% specificity, the 81% sensitivity in women and 71% sensitivity in men was significantly greater than the 27–58% sensitivities of sex-specific 12-lead ECG criteria at matched specificity of 98% [56]. Parallel analyses employing time-voltage area criteria derived from the standard 12-lead ECG [57] found the 76% sensitivity of the 12-lead sum of area and 65% sensitivity of Sokolow–Lyon area to be significantly greater than the 46% and 43% sensitivities of the respective simple voltage criteria and than the 54% sensitivity of voltage-duration product criteria (see below) at matched specificity of 98%. Further study and validation of the time-voltage area approach will be required before these criteria can be adapted for use in computerized electrocardiography.

Because time-voltage area criteria are dependent on computerized ECG analyses that are not readily available to all clinicians and have not been well validated, the simple product of QRS duration and voltage, as an approximation of the area under the QRS complex, has been developed and tested [58, 59]. Calculated by simple multiplication of QRS duration in millisecond by the respective ECG voltage criteria, Cornell voltage-duration product criteria in particular have been demonstrated to significantly improve sensitivity for the detection of LVH compared with simple voltage criteria

and with the Romhilt–Estes point score [58, 59]. These criteria are gender specific, relatively race insensitive [29], not significantly impacted by increasing body mass index [31, 32], and, as further noted below, can be used to track changes in echocardiographic LV mass [60] and to more accurately assess prognosis [61].

15.3.2 ST-T-Wave Changes

ST-contour changes may be seen in LV leads (I, aVL, V_5, and V_6): the ST segment is depressed, convex upward, and slopes into an inverted T wave (Fig. 15.7). Even in the absence of a significant increase in QRS voltage, such ST-T changes are associated with more marked modifications of echocardiographic parameters. Patients with ST abnormalities arising from LVH (secondary abnormalities – see also Chap. 17) have a prolonged interval from minimum cavity dimension to mitral valve opening and a reduced rate of early diastolic wall thinning and dimension increase [62]. These ST-T abnormalities, sometimes called LV strain, may be related to impaired early relaxation that is dissociated from cavity dimension, or to the presence of increased mass alone. They are important, however, because their presence worsens the prognosis[51, 63, 64]. Indeed, the strain pattern has been implicated as the strongest standard ECG marker of increased risk when ECG LVH criteria have been utilized for risk stratification [51, 63], and adds significantly to the Cornell product and Sokolow–Lyon voltage for the prediction of cardiovascular mortality and myocardial infarction (MI) in hypertensive patients [64]. They have a sensitivity of 52% and a specificity of 95% according to Devereux and Reichek [65], and are associated with nearly a threefold higher prevalence of echocardiographic LVH in hypertensive patients after controlling for other risk factors for LVH [66]. More recently, continuous computer measurements of ST depression in leads V_5 and V_6 have been shown to be strong independent predictors of increased LV mass and LVH [67].

More prominent larger U waves or even inverted U waves may be found in V_5 and V_6 (see Chap. 17). When present, other ECG evidence for LVH is usually obvious. LV activation time (the time from QRS onset to R peak) may increase to over 50 ms, but is seen in only a very small percentage of LVH. Finally, LV conduction delay, however, may progress to incomplete left bundle branch block (LBBB) or complete left bundle branch block. In addition, the prolongation of action potential duration and increased inhomogeneity of ventricular repolarization associated with LVH can be manifest as prolongation of the rate-corrected QT interval [68], with increasing QT interval duration seen across quartiles of increasing LV mass and with both concentric and eccentric geometric patterns of LVH [68].

15.3.3 ECG Criteria Summary

Certain 12-lead ECG criteria that may be useful in the diagnosis of LVH in a hospital population where conventional reporting methods are used, may be summarized as follows (where the figures in parentheses under (a) are the upper 98 percentile limits from Murphy et al. [6]).

(a) High voltage as seen in either
  (i) limb-lead voltage (more specific but less sensitive):
    RaVL $\geqslant$ 1.1 mV (0.8 mV) or if axis < −30° then $\geqslant$ 1.3 and SIII $\geqslant$ 1.5 mV,
    RI + SIII > 2.5 mV (1.9 mV),
    RaVF > 1.9 mV (1.4 mV),
    Lewis index $\geqslant$ 1.7 mV; or
  (ii) chest-lead voltage:
    SV_1 + RV_5 or RV_6 > 3.5 mV (3.3 mV) in men and > 3.3 mV in women,
    SV_1 $\geqslant$ 2.5 mV (1.6 mV),
    RV_5 or RV_6 $\geqslant$ 2.5 mV (2.0 mV);
    maximum R + maximum S > 4.5 mV; or
  (iii) combined voltage:
    RaVL + SV_3 > 2.8 mV in men and >2.0 mV in women.

(b) ST contour depressed but convex upward into inverted T waves in LV leads I, aVL, V_5, and V_6 [45].
(c) Left atrial abnormality (LAA, i.e., P terminal force in V1, as defined in Fig. 15.23) is useful but much less specific for LVH.
(d) Left ventricular conduction delay whether incomplete LBBB (usually meets high voltage criteria) or complete LBBB (see Sect. 15.4.4).

The use of multiple criteria to detect LVH is essential when diverse cardiac diseases are considered. A single criterion may have high sensitivity for one disease state only [44]. When more than one criterion is met, the diagnosis becomes more certain ("probable" or "definite") and, in the above criteria, ranges down to "possible" when borderline high voltage in the chest leads is the only abnormality present.

A variety of other miscellaneous criteria for LVH are also included in Table 15.2. While many of them have a low sensitivity, particularly for limb-lead criteria, it should be noted that specificity is high. Therefore, with the use of computer methods, where a number of criteria can be easily checked, different criteria in combination can be very useful.

15.3.4 Orthogonal-Lead and VCG Criteria

As discussed in Chap. 11, the orthogonal-lead ECG can be displayed in two ways, namely, a conventional scalar presentation of the *XYZ* leads and the vectorcardiographic presentation of the frontal, sagittal, and transverse planes of the VCG. Diagnostic criteria for LV hypertrophy can be based on a combination of both scalar and vector parameters.

Since there is a certain, though not exact, correspondence between the *XYZ* and the 12-lead ECG, it would be expected that some of the abnormalities found in the 12-lead ECG would similarly occur in the orthogonal-lead ECG. Thus, increased R-wave amplitude in the lateral lead *X* and in the transverse lead *Z* (directed positively to the back) could occur, as might the classical ST-T abnormality pattern in the lateral lead (Fig. 15.7).

The VCG [69, 70] changes are best seen in the transverse-plane QRS loop, which is displaced to the left and posteriorly. It is increased in magnitude, elongated, and inscribed counterclockwise, but occasionally has a figure-of-eight pattern when hypertrophy is severe. The T loop is usually oriented opposite to the QRS, and so is displaced to the right anteriorly (Fig. 15.8). As a result of LVH, there may be a loss of anterior forces, which may simulate an anterior myocardial infarction. The more R*X* exceeds 1.2 mV or R*X* + R*Z* exceeds 2.5 mV, the more likely the diagnosis of LVH [71].

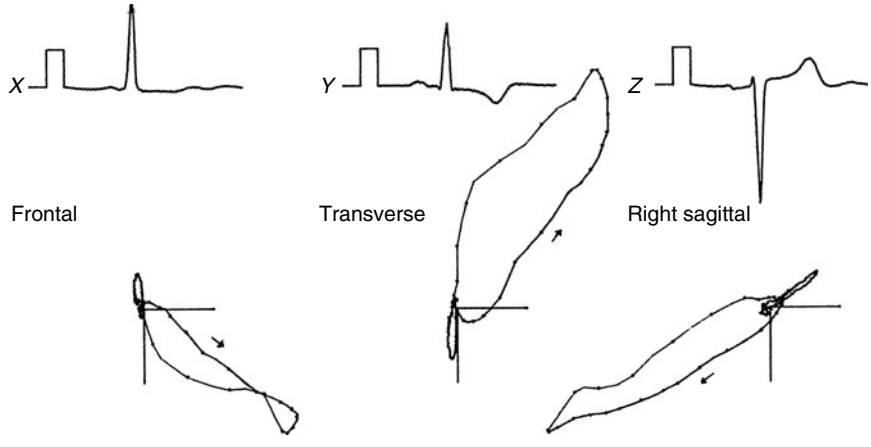

Figure 15.8
Vectorcardiographic appearances in LVH. Note that the T loop is oppositely directed to the QRS loop, which has the normal direction of inscription in the various planes. The dots are printed at 2 ms intervals. Lead *Z* is directed positively anteriorly.

Table 15.7

Frank orthogonal-lead criteria for left ventricular hypertrophy [71] (in the absence of ventricular conduction defects)

		White		Black	
		Males	Females	Males	Females
R*X* amplitude (mV)	A[a]	> 1.9	> 1.4	> 20	> 2.0
	B[b]	> 1.7	> 1.3	> 1.9	> 1.7
R*X* + R*Z* amplitude (mV)	A	> 2.9	> 2.3	> 3.4	> 2.6
	B	> 2.7	> 2.1	> 3.1	> 2.4
R*Z* duration (ms)	A	> 70	> 70	> 60	> 70
	B	> 60	> 70	> 60	> 60

[a]Limits in rows labeled A indicate specificity ⩾ 90% associated with relatively low sensitivity
[b]Limits in rows labeled B indicate a specificity of 80–90% associated with higher sensitivity

Several studies have demonstrated that computer analysis of Frank orthogonal leads (see Chap. 11) improves the detection of LVH [72]. Brohet and Richman [73] found a 26% difference favoring the computer over two physicians (69% versus 43%). Pipberger et al. [74] had earlier demonstrated an even greater advantage, with a difference of 40%. In both of these studies, the greater sensitivity was achieved by means of a Bayesian approach, utilizing prior probabilities and multivariate analysis (see Chap. 37).

Using the modified orthogonal-axial-lead system, Macfarlane et al. [75] devised another point score system for diagnosing LVH. Their sensitivity was 65% and their specificity was 91%. Such scoring systems lend themselves to computer applications rather than regular use in the busy heart station.

As can be seen from Table 15.7, adopted from the Washington code of Pipberger [71] (see Chap. 13), Frank orthogonal-lead criteria can be relatively simple to use. By combining them with the 12-lead ECG criteria, the diagnosis might be enhanced, as suggested in an earlier study [76]. Others have reported that orthogonal criteria are superior to the 12-lead ECG in detecting LVH [77]. As previously noted in Sect. 15.3.1.8, the measurement of the time-voltage area of the horizontal-plane vector integral of the signal-averaged VCG can also significantly improve sensitivity of the VCG for detecting LVH [56].

15.4 Miscellaneous LVH Topics

15.4.1 Apical Hypertrophy

When hypertrophic cardiomyopathy is localized to the apex and lower midanterior septum, it can result in a characteristic ECG pattern, namely, giant negative T waves and ST depression in II, III, aVF, and V_4–V_6, as well as negative U waves and a prolonged QT_c. The depth of the negative T wave and ST-segment depression varies from hour to hour or day to day. Coronary angiography is always normal in these patients. This form of hypertrophy is discussed in Chap. 20 (see Sect. 20.24.3.2).

15.4.2 Athlete's Heart

As a group, trained athletes will have an increased LV mass with a larger diastolic cavity dimension and/or increased thickness of the posterior wall and septum [78]. Strenuous activity of any kind will produce such physiological hypertrophy appropriate to the body size of the athlete and the degree of activity. For example, the LV wall thickness-to-LV dimension ratio will be increased in weight lifters but remains normal in swimmers. Both will have higher peak rates of LV dimension increase than normals, but when adjusted for larger size, all are within normal limits. In contrast, LV volume or pressure overload with pathologic hypertrophy results in abnormalities of diastolic function or even altered systolic function.

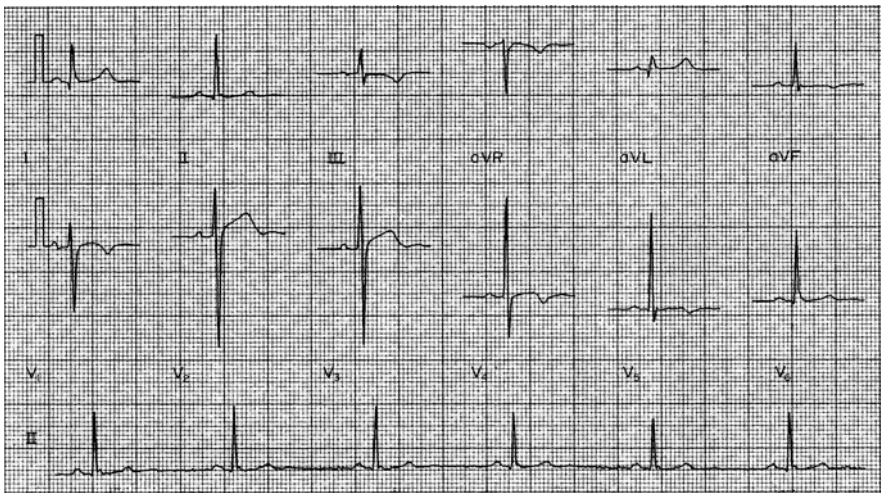

Figure 15.9
ECG recorded from a 46-year-old runner who was apparently healthy. The LV mass on echocardiography was at the upper end of the normal range. Note the T-wave changes in V_4 and V_5 as well as the interior leads.

Highly trained athletes may have ECG criteria for LVH, or have isolated T-wave changes (Fig. 15.9), or other abnormalities [79, 80]. The more extreme changes will cause diagnostic confusion so that exercise electrocardiography and echocardiography may be needed to exclude organic disease. Even left-heart catheterization is justified when doubt still exists. If a positive diagnosis of cardiomyopathy cannot be made and there is no family history of premature sudden death or cardiomyopathy, then such patients should be vigorously reassured that no abnormality is present [81].

15.4.3 Complicating ECG Features

The R waves in V_1 and V_2 may be reduced in amplitude in the presence of LVH with poor R-wave progression, commonly in the right and midprecordial leads. Occasionally, the R is even absent in V_1–V_3 (Fig. 15.10). The resulting QRS complex mimics an anteroseptal infarction. The deeper the S wave in V_1 and V_2, the less likely is anteroseptal infarction and the more likely is LVH.

The absence of septal Q waves in V_5 and V_6 may result from septal fibrosis or incomplete LBBB. On the other hand, Q waves may be produced in the inferior leads in cardiomyopathy.

Some notching of the QRS in midchest leads and an increased QRS duration to 110 ms often accompany increasing degrees of hypertrophy. On the other hand, chronic lung disease, pericardial infusion, or myocardial infarction may all result in reduced R waves masking the voltage criteria for LVH.

15.4.4 Bundle Branch Block and LVH

The diagnosis of LVH is usually considered to be very difficult in the presence of LBBB. However, the occurrence of intermittent LBBB may allow its effects on voltage and axis to be noted, namely, lower voltage in lead I together with a more leftward axis, deeper S waves in V_1 and V_2, and lower R waves in V_5 and V_6 [82]. These changes led Kafka et al. [37, 38] to recommend any one of three criteria for the diagnosis of LVH in the presence of LBBB, namely,

(a) RaVL > 1.1 mV
(b) QRS axis < −40° (RII < SII)
(c) SV_3 > 2.5 mV

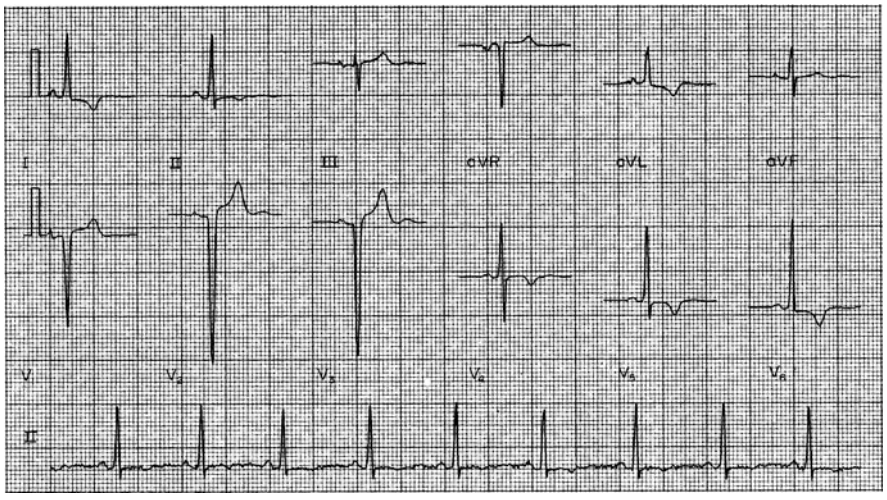

Figure 15.10

ECG recorded from a 17-year-old girl with a hypertrophic obstructive cardiomyopathy. Note the QS complexes in V_1–V_3 resulting from the severe LVH.

From a study of 100 examples of LBBB, Kafka et al. detected 71% with LVH when an indexed LV mass (defined as the M-mode-derived LV mass divided by the body-surface area) exceeded 115g/m^2. Their criteria had a specificity of 90%. Others have also suggested that LVH can be diagnosed in the presence of LBBB [83, 84] (see also Chap. 14).

It should be noted that the incidence of LV enlargement in the presence of LBBB is usually very high. In one series of 1,410 hearts examined at postmortem [85], Havelda et al. found 93% of 70 hearts with ECG LBBB to have LVH. In other words, the diagnosis of LVH in the presence of LBBB can essentially be made by inference alone with a relatively high accuracy.

Since right bundle branch block (RBBB) alters ventricular depolarization markedly, most of the usual criteria for LVH are no longer applicable, but the diagnosis of LVH can still be made (Fig. 15.11). Murphy et al. [86] studied 23 cases of RBBB that at autopsy had LVH by the chamber partition technique (LV mass $\geqslant$ 171 g). They concluded that the use of ECG criteria for left atrial abnormality allows the identification of LVH to rise from 67% to 78% with a false-positive rate of 14–21% depending on the observer.

An echocardiographic study of 47 patients with RBBB revealed 60% with an LV mass greater than 215 g. Vandenberg et al. [87] concluded that limb-lead voltage criteria and the P terminal force in V_1 (see below) are the best detectors of LVH with an "acceptable" specificity of 90%. An R in lead I greater than 1 mV, for example, had a sensitivity of 39% and a specificity of 89%. The specificity might have been higher if they had used the LV mass index as the criterion for LVH.

15.4.5 Regression

Since the introduction of echocardiography (ECHO) for the diagnosis of LVH, measured by LV mass or wall thickness, there have been few properly conducted studies evaluating the correlation between ECG and ECHO markers of LVH. Casale et al. [46] have compared various ECG markers for LVH with M-mode ECHO diagnosis of LVH. The best correlation between ECHO-determined LVH and ECG LVH involved S in V_3 and R in aVL. Hill et al. [88] compared wall thickness to ECG voltages at baseline in an LV regression study in hypertensive patients treated with beta-blockers, but did not find any significant correlation. Wollam et al. [89] assessed the correlation between LV mass and ECG findings in hypertensive patients, treated with a variety of antihypertensive agents, namely, hydrochlorothiazide, methyldopa, and combination therapy. They demonstrated a significant correlation between R-wave amplitude in aVL and LV mass after

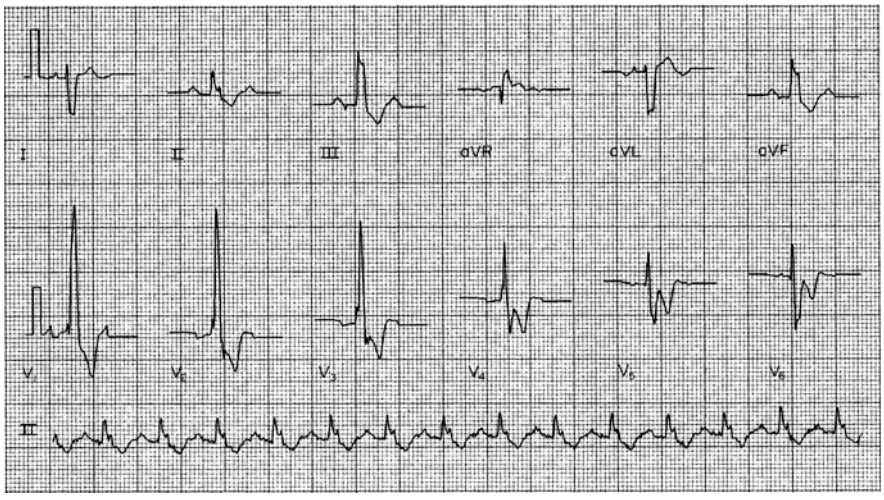

Figure 15.11

RBBB in a patient with echocardiographic evidence of LVH who underwent aortic valve replacement. The indexed LV mass was 196.9 g/m^2 (using the Penn convention). Note the right-axis deviation (QRS axis = 120°), which might be thought to suggest RVH even in the presence of RBBB. However, there was no evidence of RVH on ECHO, or at operation so that the left posterior fascicular block may be the cause of the right-axis deviation. The ST-T changes in the lateral leads in this case are, most probably, caused by LVH. There is also evidence of left atrial overload in view of the increased P terminal force in V_1 (see Sect. 15.8.1). The QT interval is short because of the heart rate of approximately 120 beats min^{-1} in this patient.

6 and 18 months therapy, but no correlation between changes in the Romhilt–Estes score and changes in posterior wall thickness or LV mass index at 6 months. Three other studies [90, 92] demonstrated a decrease in LV wall mass as well as precordial QRS voltage, but did not report a correlation between ECHO and ECG. More recently, Okin et al. [60] demonstrated that regression of Cornell product LVH after 1 year of antihypertensive therapy was strongly associated with decreases in LV mass and identified patients who had a greater likelihood of regression of echocardiographic LVH, independent of treatment modality and of changes in systolic and diastolic blood pressure.

These findings might suggest that LV wall mass changes may be reflected in changes in the R-wave amplitude in aVL. Whether computer assessment of the ECG for determining LV mass may yield more information remains to be seen. To this end, Savage et al. and Rautaharju et al. [93, 94] have studied the correlation between ECHO estimates of LV mass and those derived from an ECG model [95].

In valvular disease, Carroll et al. measured the changes in voltage (SV_1 and RV_5–RV_6) after aortic valve replacement and compared these changes to those in LV mass, diagnosed by ECHO [96]. They concluded that after surgical correction of chronic aortic regurgitation, regression of LVH can be assessed by serial ECG data (see Fig. 15.3), which can identify patients with complete, incomplete, or no regression of LVH.

15.4.6 Prognosis of ECG LVH

From a clinical point of view, ECG evidence of LVH with ST-T changes (ECG LVH) indicates a prognosis as serious as ECG evidence of myocardial infarction (ECG MI), at least in asymptomatic persons [97]. In the Framingham study, 1.5% of the original cohort had definite ECG LVH and 45% of all cardiovascular deaths were preceded by its appearance [98].

The 5-year mortality for men with ECG LVH was 35% compared with 15% without ECG LVH. Possible ECG LVH also carried an increased but lower risk of death. Even cardiovascular morbidity, that is, stroke, heart failure, coronary disease,

and peripheral vascular disease is increased severalfold in subjects with ECG LVH, while ventricular dysrhythmias are more frequent [99–101].

The diagnosis of ECG LVH with repolarization abnormalities doubles the cardiovascular risk compared to voltage evidence only of LVH [99]. In the British Regional Heart study, it was found that middle-aged men with LVH and secondary repolarization changes had over five times the risk of suffering a fatal or nonfatal myocardial infarction in a 5-year follow-up period compared to men with a normal ECG [102]. Among hypertensive men and women in the LIFE Study [64], the presence of the typical strain pattern was associated with a 1.5-fold greater risk of myocardial infarction or cardiovascular death over a 5-year follow-up period, even after adjusting for baseline severity of ECG LVH and for the substantial decreases in blood pressure during treatment.

More recent data suggest that regression of ECG LVH and prevention of progression of ECG LVH are associated with reduced cardiovascular risk [61, 103, 104]. In an observational study of 524 participants in the Framingham Heart Study with ECG LVH by various criteria at a qualifying exam [103], Levy et al. found that a significant decline in Cornell voltage was associated with a lower risk of cardiovascular disease, whereas a significant increase in Cornell voltage identified individuals at increased risk. In the Heart Outcomes Prevention Evaluation (HOPE) trial [104], the combined endpoint of either regression of ECG LVH or prevention of progression to ECG LVH by Sokolow–Lyon voltage criteria in response to ramipril-based therapy was associated with reduced risk of death, myocardial infarction, stroke, and congestive heart failure. Finally, serial ECG evaluation in the LIFE study [61] found that lower in-treatment measurements of both Cornell voltage-duration product and Sokolow–Lyon voltage were associated with significant reductions in the incidence of major cardiovascular morbidity and mortality, independent of treatment-modality-employed baseline Framingham risk score and of both baseline and in-treatment levels of blood pressure. Taken together, these findings suggest that antihypertensive therapy targeted at regression or prevention of ECG LVH may become an additional goal of therapy beyond that of lowering blood pressure, in order to further decrease the risk of cardiovascular morbidity and mortality [61, 105].

15.4.7 Prevalence

The prevalence of LVH in various population studies has been estimated from the ECG (see Chap. 40). On the other hand, as this chapter has pointed out, the sensitivity of ECG criteria is at best around 65% so that there will be considerable underestimation of the true prevalence of LVH using the ECG. Data from the Framingham study have suggested that the prevalence of electrocardiographic LVH increases as the severity of ECHO LV mass index increases [106]. The actual prevalence of LVH as determined by ECHO ranged from 6.6% of younger women to 33% of older females. Corresponding figures for men were 8.6–23.7%. Concentric LVH was most prevalent in the older age-group, and eccentric non-dilated LVH was most common in the younger persons (Table 15.8).

Table 15.8

Prevalence of various forms of electrocardiographic left ventricular hypertrophy in Framingham subjects [106]

Original cohort	Eccentric dilated	Eccentric nondilated	Concentric	Disproportionate septal thickness
Original cohort				
Males (121/510, 23.7%)	24 (20)	38 (31)	54 (45)	5 (4)
Females (282/855, 33.0%)	38 (13.5)	92 (33.5)	136 (48)	16 (6)
Offspring-spouse				
Males (148/1718, 8.6%)	13 (9)	73 (49)	59 (40)	3 (2)
Females (125/1892, 6.6%)	8 (6)	80 (64)	34 (27)	3 (3)

[a] Data expressed as a number, with percent of subjects with ECHO LVH in parentheses.

15.5 Right Ventricular Hypertrophy (RVH)

15.5.1 ECG Criteria

The right ventricular forces are normally masked by the dominant left ventricle. In mild cases of RVH, no apparent change may be noted, whereas when RVH is severe, the precordial leads may show a taller R wave in V_1 than in V_6 (Fig. 15.12).

Since V_1 is closest to the RV mass, it is the lead most sensitive to changes induced by RVH, namely, taller R waves, smaller S waves, and a change in the R:S ratio plus delayed onset of the intrinsicoid deflection (Fig. 15.13). Leads V_3R and V_4R may also be helpful in diagnosing RVH. These leads may show the typical changes usually sought in V_1. Deep S waves in I, V_5, and V_6 also often accompany RVH (Fig. 15.14).

The type of heart disease involved plays a prominent role in the usefulness of various criteria for the detection of RVH. In congenital heart disease for example, the sensitivity of such criteria is generally over 90%. In mitral stenosis, it is approximately 65%, while in chronic cor pulmonale it may be near 30%.

A very extensive study of the sensitivity of the commonly used ECG criteria for RVH is that of Flowers and Horan [107] (see Table 15.9). They examined 819 hearts using the chamber dissection technique and found 178 with RVH. Criteria based on abnormalities in V_1 are the most specific (>90%) but the least sensitive (2–18%); for example, a QR complex in V_1 (Fig. 15.15) is 8% sensitive but almost 100% specific. The inclusion of criteria involving the left precordial leads decreased the specificity to below 90% but improved the sensitivity to about 30%. The "correctness" of a sign was obtained by dividing the true positives and true negatives by the total group studied. Most of the 18 parameters listed in Table 15.9 had a "correctness" of 80–89%. The best combination of sensitivity, specificity, and correctness occurs with the constraint that requires the presence of two signs. Adding more only increases specificity at the expense of sensitivity.

Murphy et al. [7] confirmed the relative ineffectiveness of ECG criteria in the diagnosis of RVH. Using any of the four criteria (the first four in Table 15.10), their sensitivity ranged from 18% to 43% and specificity from 83% to 95%, dependent on patient selection. RVH in the presence of chronic obstructive lung disease proved the most difficult to diagnose, and congenital heart disease with RVH was the easiest to identify. Most of the criteria listed in Table 15.9 have a much higher sensitivity (24–92%) when primary pulmonary hypertension is present [108]; for example, 79% have an R/S ratio in $V_1 > 1.0$ and 76% have an $SV_5 > 0.7$ mV.

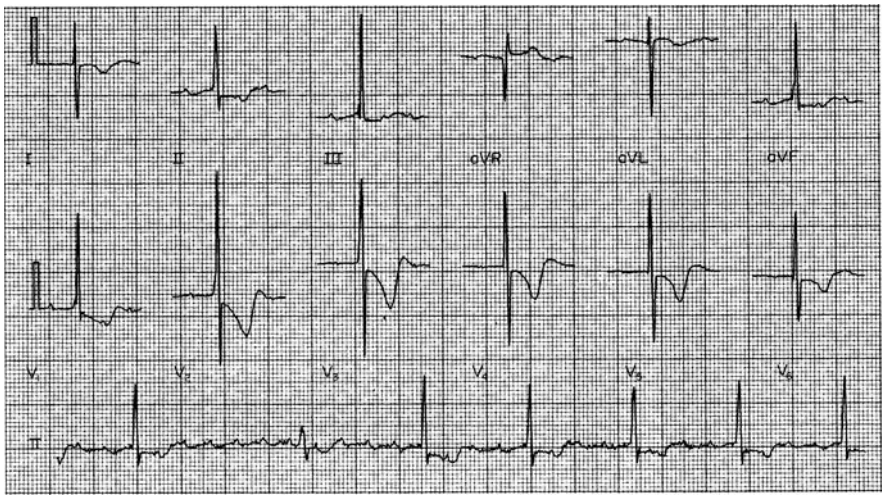

Figure 15.12

Case of severe RVH in a 57-year-old male with rheumatic heart disease and two previous mitral valvotomies. The R wave in V_1 is taller than in V_6, and widespread secondary ST-T changes are in evidence. The pulmonary artery pressure was 110/50, suggesting severe RVH. There is also atrial flutter.

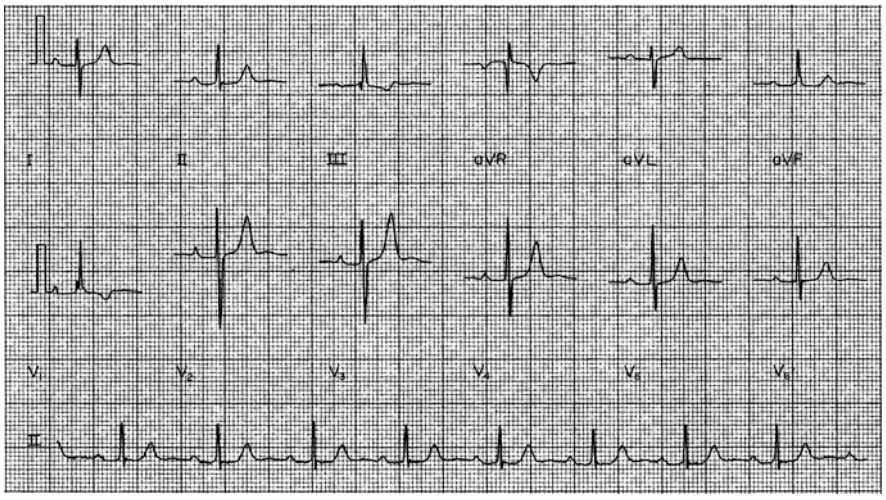

Figure 15.13

Typical changes of RVH as evidenced by the tall R wave in V_1, with T-wave inversion as well as a deep S wave in lead I giving a QRS axis of 97°. The PR interval was measured as 0.214 s. The ECG was recorded from a 39-year-old female with pulmonary stenosis.

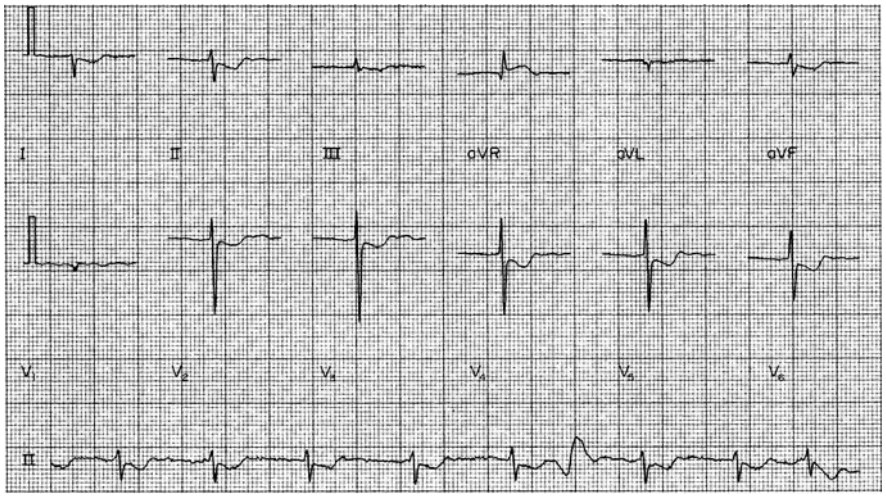

Figure 15.14

ECG from a 67-year-old female with mitral stenosis and atrial fibrillation. Note the deep S wave in leads I, V_5, and V_6. Widespread ST-T changes are also in evidence.

The most useful ECG criteria for RVH are the following. If the QRS duration is less than 0.12 s, then RVH is likely if one or more of the criteria below are present.

(a) Any one of the following:
  (i) Right-axis deviation > 90° (in the presence of disease predisposing to RVH)
  (ii) RaVR ⩾ 0.5 mV
  (iii) RaVR > QaVR

Table 15.9

Sensitivity and specificity of various ECG parameters for the diagnosis of right ventricular hypertrophy (RVH) or enlargement and chronic obstructive pulmonary disease (COPD) with RVH

Parameters	RVH[a]		COPD with RVH[b]	
	Sensitivity (%)	Specificity (%)	Sensitivity (%)	Specificity (%)
Limb leads				
$S_1S_2S_3$	41	88	36	60
S_1Q_3	31	86	48	90
Right-axis deviation > 110° (> 90°)	19	96	(42)	(95)
R aVR > 0.5 mV	0		6	100
P pulmonale	NS		21	65
Lead V_1				
35 ms ⩽ VAT ⩽ 70 ms	13	94	24	85
R/S ratio > 1.0 and T negative	9	98	9	95
qR pattern	8	99	24	100
S < 0.2 mV (and RV_5 ⩽ 0.4 mV)	6	97	(27)	(85)
R > 0.7 mV	3	99	12	95
R′ < 80 ms	4	98	12	95
rSR′ with R′ > 1.0 mV	0		3	100
Other chest leads				
S in V_5 and V_6	78	55		
RV_5 or RV_6 < 0.5 mV	22	88	27	85
R/S ratio V_5 or V_6 ⩽ 1.0	19	93	30	90
SV_5 or SV_6 > 0.7 mV	18	87	15	100
$RV_1 + SV_5$ or SV_6 > 1.0 mV	13	92	0	
R/S ratio V_5 over R/S ratio V_1 ⩽ 0.4	10	99	0	

[a] Modified from Flowers and Horan [107]. RVH defined as RV weight > 71 g or as relative right ventricular enlargement when RV is > 30% of the total ventricular mass.

[b] After Murphy and Hutcheson [110], using 33 RVH patients and 20 normals. RVH is defined as RV weight > 65 g or ratio (LV + S)/RV < 2.1, or probable RVH if RV weight > 0.34 g cm^{-1} body height and RV weight < 65 g.

(b) Any one of the following in V_1:
  (i) R/S ratio > 1.0 and T negative
  (ii) qR pattern
  (iii) 35 ms ⩽ ventricular activation time < 55 ms
  (iv) R ⩾ 0.7 mV
  (v) S < 0.2 mV
  (vi) rSR′ with R′ > 1.0 mV

(c) In other chest leads, any one of the following:
  (i) $RV_1 + SV_5$ (or SV_6) > 1.0 mV
  (ii) R/S ratio V_5 or V_6 ⩽ 1.0
  (iii) RV_5 or RV_6 < 0.5 mV
  (iv) SV_5 or SV_6 > 0.7 mV
  (v) R/S ratio V_5 over R/S ratio V_1 ⩽ 0.4

(d) ST depression and T inversion in right precordial leads – usually seen in severe RVH, for example, in pulmonary stenosis

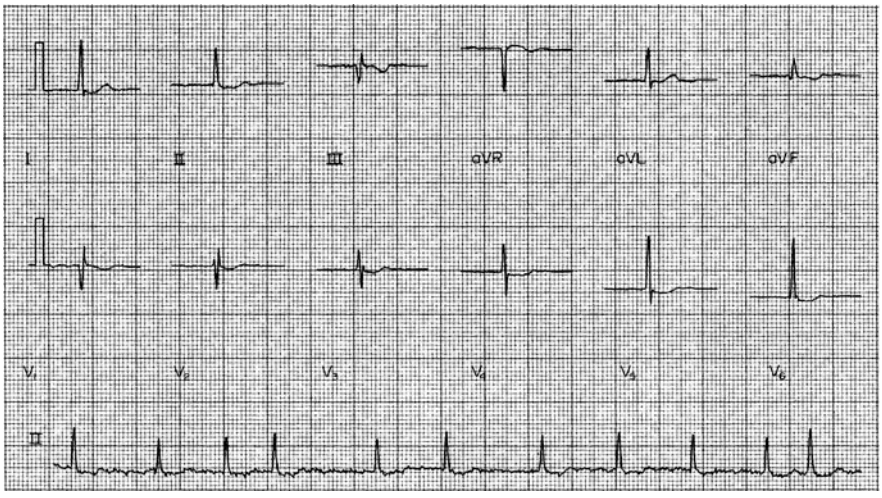

Figure 15.15

QR complex in V_1 from a 53-year-old female with mitral stenosis and atrial fibrillation. Appearances are strongly suggestive of RVH. Note the absence of other QRS changes of hypertrophy, but the ST-T changes in the inferior leads are often supportive of the diagnosis, although in this case they are also caused by digitalis effect.

Table 15.10

Selected ECG criteria for the diagnosis of right ventricular hypertrophy [7]

	Sensitivity[a] (%)	Specificity (%)
R/S ratio V_5 or $V_6 \leqslant 1.0$	44	92
SV_5 or $SV_6 \geqslant 0.7$ mV	26	95
Right-axis deviation > 90°	30	99
P pulmonale or right atrial overload	21	98
Any one of the above criteria	59	86
Any two of first four criteria	40	97
S_1Q_3 pattern	15	92
All others < 10%)		

[a]If BVH is included, then sensitivity falls by ~ 50% for each criterion although specificity is generally similar.

15.5.2 ST-T-Wave Changes

As in LVH, secondary ST-T changes can be found in the right precordial leads in cases of pressure overload of the right ventricle, such as in pulmonary stenosis. The classic appearance is ST depression with a convex upward ST segment merging into a deeply inverted T wave (Fig. 15.16). Since these changes are a direct consequence of the RV hypertrophy, they are often called secondary repolarization abnormalities (or sometimes RV strain).

15.5.3 $S_1S_2S_3$ Syndrome

Although frequently used as a descriptive term by interpreters of electrocardiograms, this type of QRS complex may be seen in normal individuals as well as those with RVH. As a rule, the S waves of smaller amplitude are seen in normals and the deeper S waves are seen in those with RVH. In the latter case, the S wave in lead II is usually larger than the S wave

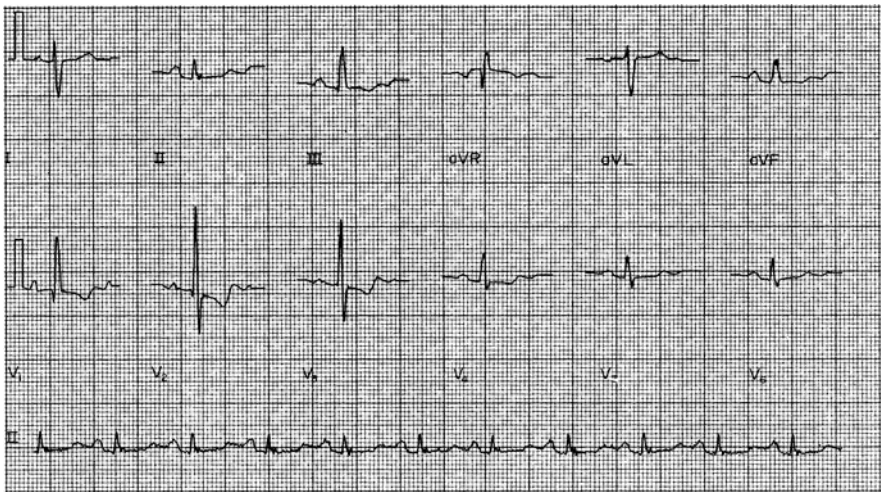

Figure 15.16

ECG recorded from a 46-year-old male with recurrent thromboembolic disease, gross pulmonary hypertension, and RV failure. The chest x-ray showed cardiomegaly and an enlarged pulmonary artery. Note the QR complex in V_1 with secondary ST-T changes in V_1–V_4 indicating RVH. These ST-T changes constitute the classical RV strain pattern. The P waves suggest right atrial enlargement in addition.

in lead III. No definite quantitative definition of the syndrome exists although Chou [109] has suggested the following: an R/S ratio equal to or less than one in each of leads I, II, and III or the S wave exceeds the upper limit of normal for the various age-groups, as defined by Simonson [42] (e.g., in those over 30 years, 0.4 mV in leads I and II and 0.8 mV in lead III).

15.5.4 Chronic Obstructive Pulmonary Disease

The typical ECG changes in patients with chronic obstructive pulmonary disease (COPD) include low voltage P-QRS-T complexes, right-axis deviation, a QS complex in V_1 (Fig. 15.17), and deep S waves in V_5 or V_6, especially when prominent P waves in II, III, and aVF are present. Cor pulmonale should at least be suspected if a subject with known COPD develops any of the following ECG changes:

(a) Rightward shift of the QRS axis by 30° or more
(b) T-wave abnormalities in right precordial leads
(c) ST depression in II, III, and aVF
(d) Transitory RBBB

In general, the diagnosis of RVH (defined as an increased RV mass) superimposed on COPD is difficult. Four suggested criteria [110] for the diagnosis of RVH in the presence of COPD are (a) S_1Q_3 pattern, (b) RAD > 110°, (c) $S_1S_2S_3$ pattern, and (d) an R/S ratio in V_6 < 1.0. When any of these four criteria were used, the sensitivity reached 79% but the specificity fell below 60%. The diagnosis of LVH complicating COPD was unreliable since only 30% of 18 such patients had the required ECG criteria.

The vertical position of the heart relative to the chest electrodes in patients with COPD may result in QS complexes in V_1 to V_4, suggesting an anteroseptal infarction. However, the vertical heart, prominent P waves, low voltage, and so on should help identify COPD as the cause. Occasionally, Q waves appear in the inferior leads suggesting an inferior infarction, but the T waves are not inverted.

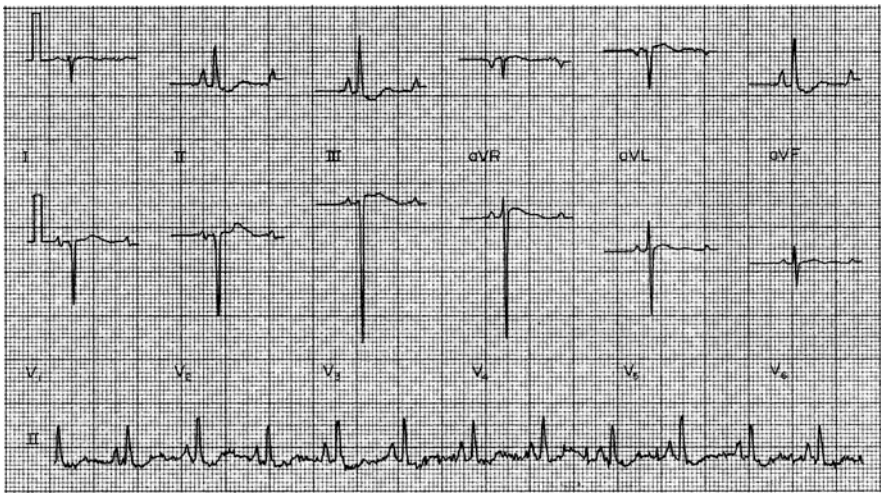

Figure 15.17

ECG recorded from a 58-year-old male with chronic obstructive airways disease. There is evidence of RVH as exemplified by the deep S waves in the lateral leads I and V_5 together with right atrial enlargement as demonstrated by the tall P waves in the inferior leads.

Left-axis deviation may be seen in about 10% of COPD perhaps related to the "axis illusion phenomenon" described by Spodick [111] or even the presence of LVH.

15.5.5 Orthogonal-Lead and VCG Criteria

As with LVH, the orthogonal-lead ECG can contribute to the diagnosis of RVH, using both scalar- and vectorcardiographic measurements. It has been claimed that orthogonal leads can enhance the diagnosis of RVH [77, 112, 113], for instance, in children. Brohet [114] attained a sensitivity of 86% by means of multivariate computer analysis. Scalar criteria, as might be expected, relate to a reduction in the R-wave amplitude in the lateral lead X with a correspondingly low R/S ratio in that lead. In addition, the corresponding scalar orthogonal criterion is an increased Q/R ratio in lead Z (directed positively to the back), analogous to the increased R/S ratio in V_1. In setting out criteria for screening, Pipberger et al. [71] selected the scalar criteria for RVH as illustrated in Table 15.11. The two levels A and B of criteria relate to different specificities. Note that the criteria are dependent on the race of the subject. Since these criteria were chosen for screening, they are not age dependent in order to make them as simple as possible.

The characteristic VCG changes of RVH may produce three different QRS loops (Fig. 15.18) in the transverse plane, but not all cases of RVH can be classified in this way. The three different loops are as follows:

(a) Type A is a clockwise-inscribed QRS loop located in the right and left anterior quadrants (right anterior area > 30%) or, rarely, a figure-of-eight loop, for instance, as in severe RVH in pulmonary stenosis or severe mitral stenosis. The specificity of this pattern is almost 100%.
(b) Type B is a counterclockwise-inscribed QRS loop, located mainly in the left anterior quadrant, but possibly extending posteriorly to the left and right as in atrial septal defect.
(c) Type C is a counterclockwise-inscribed QRS loop located mainly posteriorly, with over 20% in the right posterior quadrant; for example, it occurs in chronic obstructive lung disease or mitral stenosis and is very specific for pulmonary hypertension (> 90% specificity).

A common occurrence in some of these cases is a frontal-plane QRS axis in excess of +90° (Fig. 15.19) despite an 8% false-positive rate in normals and a 10% false-negative rate in severe pulmonary hypertension [113]. Not all authors

Table 15.11

Frank orthogonal-lead criteria for right ventricular hypertrophy [71] (in the absence of ventricular conduction defects)

		White		Black	
		Males	Females	Males	Females
R*X* amplitude (mV)	A[a]	< 4.0	< 3.0	< 5.0	< 5.0
	B[b]	< 5.0	< 4.0	< 5.0	< 6.0
(R/S) *X* amplitude ratio	A	< 1.1	< 0.9	< 1.0	< 1.8
	B	< 1.2	< 1.5	< 1.5	< 2.0
(Q/R) *Z* amplitude ratio	A	> 1.5	> 1.6	> 1.5	> 2.1
	B	> 1.3	> 1.5	> 1.3	> 1.5
R*Z* amplitude (mV)	A	< 3.0	< 2.0	< 4.0	< 2.0
	B	< 4.0	< 4.0	< 4.0	< 3.0

[a]Limits in rows labeled A indicate specificity ⩾ 90% associated with relatively low sensitivity
[b]Limits in rows labeled B have a specificity of 80–90% and are associated with a higher sensitivity than those in A

feel the above classification of types A, B, and C is helpful (see Chap. 21). Cowdery et al. [115] have suggested a specific modification of previous vectorcardiographic criteria for detecting RVH in mitral stenosis. They obtained a sensitivity of 60% and a specificity of 96%.

15.6 Miscellaneous RVH Topics

15.6.1 Complicating ECG Features

Pathological states such as COPD, lateral MI, or left posterior fascicular block, which also cause right-axis deviation, may be suggested by other clinical features.

The differential diagnosis of high posterior MI or other causes of prominent anterior forces (e.g., normal variation, Wolff-Parkinson-White syndrome, IHSS, displaced heart, left median fascicular block, or RBBB) can be difficult. When RVH is severe, it may result in Q waves in the right precordial leads, but with other changes that point to RVH rather than MI. Tall R waves in V_1 and V_2 should not mask a posterior MI since secondary ST changes, namely, negative ST-T waves, usually occur in the presence of RVH while peaked T waves, as are found in posterior infarction, do not occur. Pipberger [71] suggests that if the Q/R amplitude ratio in lead *Y* is greater than 0.25, then posterior MI is likely, especially when the T amplitude in lead *Z* is less than 0.0 (lead *Z* being directed positively to the back). Inferior or lateral MI may also produce an increased R/S ratio in V_1 (Fig. 15.19).

15.6.2 Right Bundle Branch Block and RVH

The diagnosis of RVH in the presence of RBBB (Fig. 15.20) remains a problem despite various criteria for an increased amplitude of $R'V_1$. None of these is reliable, since such amplitudes occur frequently when RVH is absent [116], that is, there are too many false positives and too few true positives. This is particularly true when biventricular hypertrophy (BVH) is present. In 1959, Del Rio et al. [117] reported that the horizontal loop was directed anteriorly, clockwise, and to the right when RBBB occurred with RVH. In 1978, Brohet [118] quantified these findings as an R/S ratio in lead $X < 2.0$, and a maximum horizontal-plane QRS vector 90° to 270°. These criteria help diagnose RVH, particularly in young subjects. An echocardiographic study of RVH in the presence of RBBB may help to develop new ECG and VCG criteria.

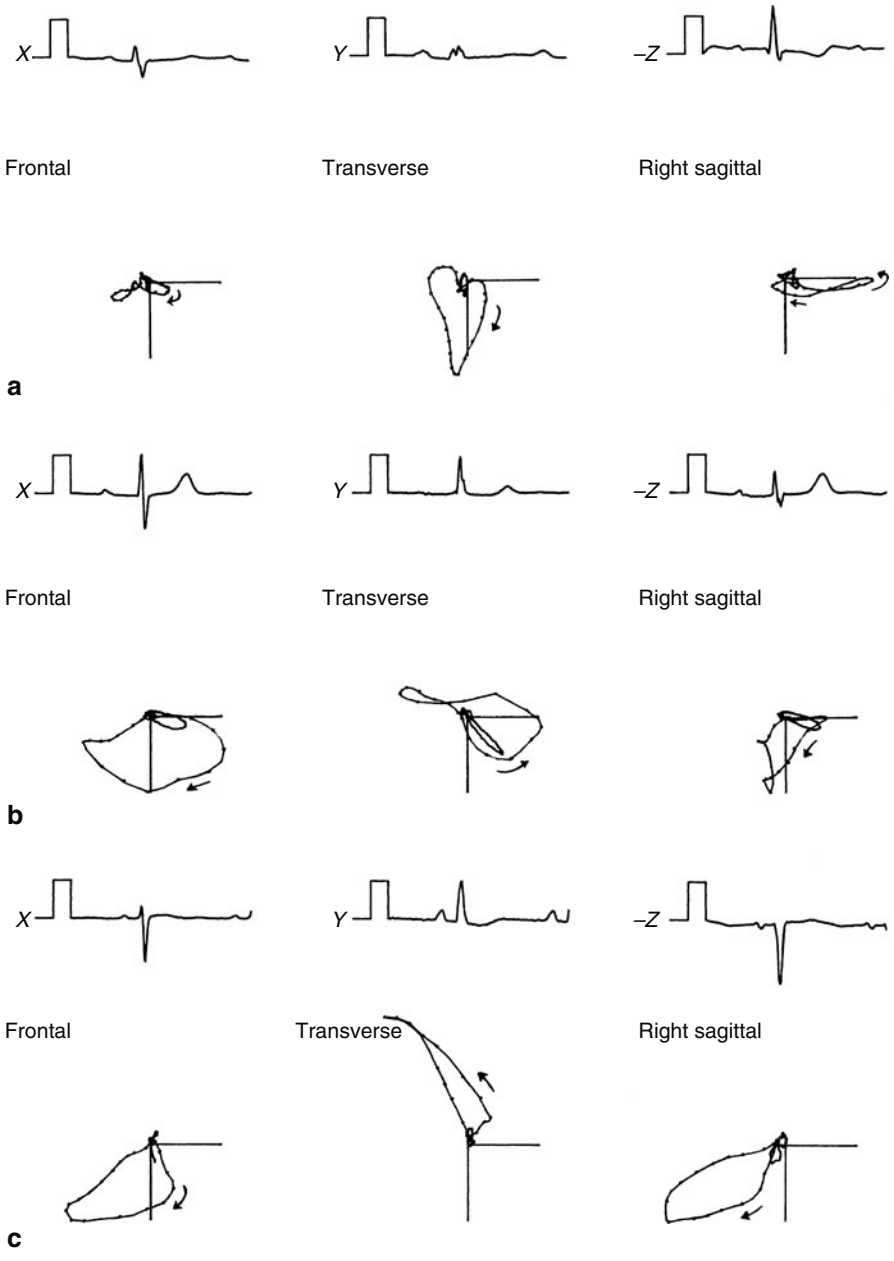

Figure 15.18

Three types of VCG loops suggestive of RVH: (a) the so-called type A RVH, where there is clockwise inscription of the loop in the transverse plane (see Fig. 15.16 for corresponding 12-1ead ECG); (b) type B RVH, where there is increased anterior force with counterclockwise inscription of the loop in the transverse plane (see Fig. 15.13 for corresponding 12-lead ECG); and (c) type C RVH, which has counterclockwise rotation in the transverse plane with a rightward posterior displacement of the maximum QRS vector (see Fig. 15.17 for corresponding 12-lead ECG). Note that lead Z, shown in scalar form, is directed positively anteriorly, that is, appearances resemble V_1 and V_2.

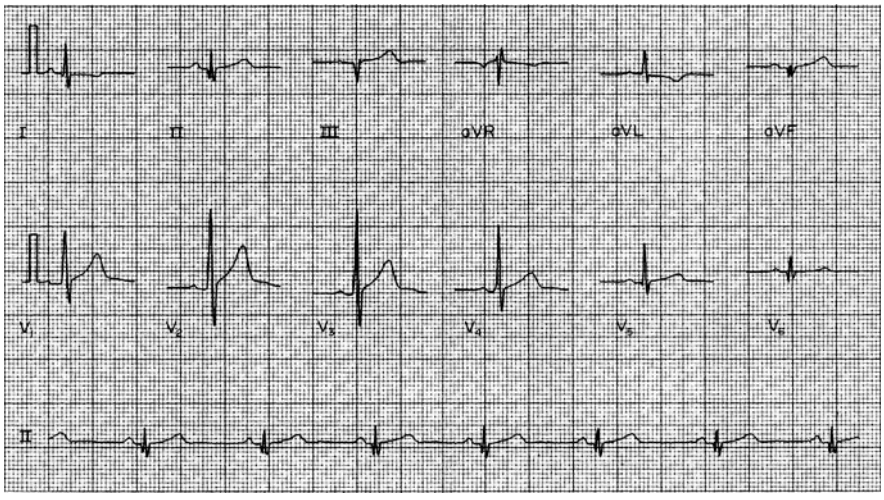

Figure 15.19
ECG recorded from a 36-year-old male with an infarction involving the inferior/posterolateral wall of the left ventricle. Note the resulting increase in the R-wave amplitude in V_1 and V_2.

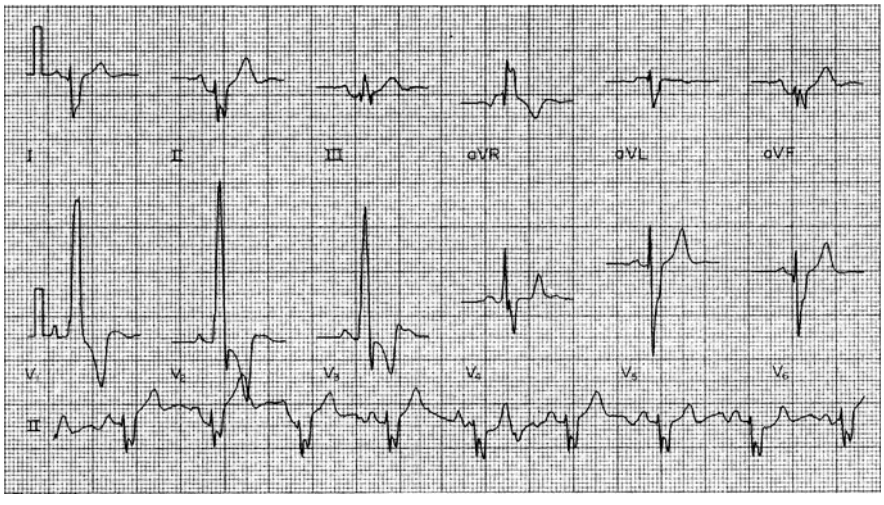

Figure 15.20
RBBB in a 49-year-old male patient with tetralogy of Fallot. The extreme frontal-plane QRS axis (−172°) together with the tall R wave in V_1 is strongly suggestive of RVH.

15.7 Biventricular Hypertrophy (BVH)

15.7.1 ECG Criteria

Combined ventricular hypertrophy or biventricular hypertrophy (BVH) is frequently impossible to identify by means of the electrocardiogram, as marked hypertrophy of one ventricle may mask the hypertrophy of its neighbor. Figure 15.21 shows complementary examples. In Fig. 15.21a, the right ventricular forces in a patient with Eisenmenger's syndrome are dominant, but R in V_5 is 30% above the normal limit suggesting LVH in addition. On the other hand, in Fig. 15.21b,

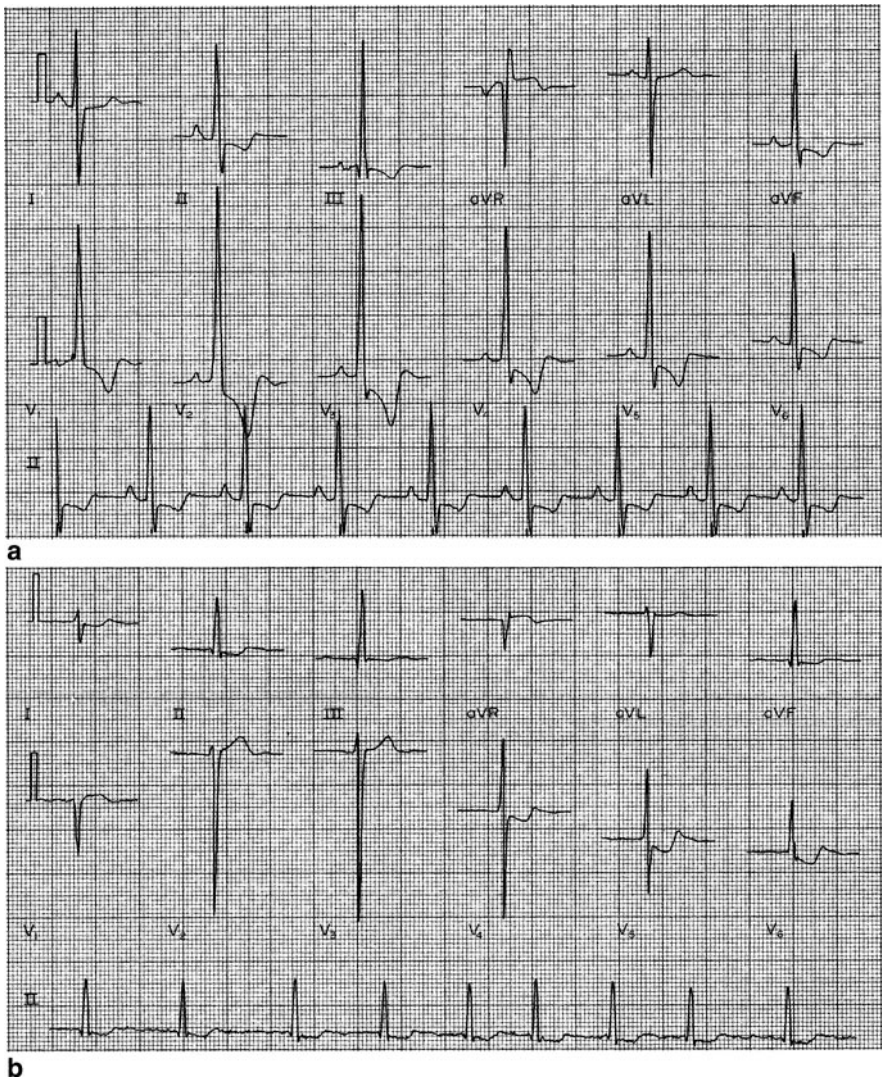

Figure 15.21

Part (a) is the ECG from a 39-year-old female with Eisenmenger's syndrome. The RV enlargement tends to dominate the pattern, but the tall R wave in V_5, together with the secondary ST-T changes in the lateral leads V_5 and V_6, is suggestive of LVH in addition. Part (b) is the ECG from a 66-year-old female with mitral stenosis and incompetence, as well as aortic incompetence. Aside from the obvious ECG changes of LVH, there is a rightward QRS axis (= 102°), suggesting RV enlargement in addition.

from a patient with valvular heart disease, the LVH produces a very deep S in V_2, but there is a rightward QRS axis (102°) suggesting RVH in addition.

Secondary RVH in patients with LVH is frequently masked by the dominant left ventricle, while patients with chronic cor pulmonale may have anatomic LVH that is not detectable on an ECG. If criteria for isolated ventricular hypertrophy are present, signs suggestive of hypertrophy of the other ventricle should be sought since it too is often enlarged. Cancellation of forces can make some ECGs appear entirely normal (pseudonormalization) except perhaps for atrial fibrillation and nonspecific ST abnormalities.

Further support for the concept of overload hypertrophy of one ventricle leading to hypertrophy of the nonstressed ventricle was offered by Gottdiener et al. [119] from an echocardiographic study of 98 patients. Increased RV wall thickness was present in 80% of 49 patients with hypertension and 63% of 16 patients with aortic stenosis. The magnitude of the increase in RV wall thickness was linearly correlated ($r = 0.75$) with LV wall thickness, but was not associated with pulmonary hypertension. The cause of the associated RVH therefore remains elusive.

In the presence of acquired valvular disease producing BVH, the electrocardiographic recognition of LV enlargement is particularly poor. Fortunately, the R/S ratio in $V_1 > 1.0$ remains a sensitive predictor of RV enlargement or severe pulmonary hypertension [120].

Many attempts have been made to develop criteria for the diagnosis of BVH [121–124]. The most reliable criteria are those determined by anatomical standards. By means of a chamber partition technique in an autopsy study of 75 patients, Murphy et al. [7] found that BVH was best diagnosed using left atrial abnormality (indicated by a negative $PV_1 > 0.1$ mV and of a duration > 40 ms) as the sole criterion for LVH, and, in addition, any one of the following three criteria for RVH:

(a) R/S ratio in leads V_5 or $V_6 \leqslant 1$
(b) SV_5 or $SV_6 \geqslant 0.7$ mV
(c) Right-axis deviation > +90°

Even so, the resulting sensitivity was only 20% although the specificity was 94%.

In contrast, Macfarlane et al. [75] studied 26 patients with BVH using the chamber partition technique. Criteria for BVH were developed from the first 14 and tested on the remaining 12 of these patients. Their point score from the modified axial orthogonal-lead system (see Chap. 11) had a specificity of 100% and a sensitivity of 64%, which fell to 42% in the test group, while the specificity remained high at 93%.

In 1969, Gamboa et al. [125] described the usefulness of the Frank orthogonal-lead system in diagnosing BVH. They defined anatomic BVH as

(a) Heart weight exceeding 400 g
(b) LV wall thickness > 13 mm and
(c) RV wall thickness > 4 mm

When BVH cases were differentiated stepwise from normals, LVH and RVH and those misclassified eliminated with each step, only 12% remained correctly classified as BVH. However, if the separation were against normal and LVH, or normal and RVH, the percentages of correctly classified cases rose to 43% and 42%, respectively. Using linear discriminant function analysis for separation of BVH and one covariance matrix for the combination of normal LVH and RVH, they correctly classified 69% with 18% false positives. It may be assumed that BVH is present whenever marked hypertrophy of either ventricle occurs. Since no ECG criteria are satisfactory at present [120], the combination of 12-lead ECG and the *XYZ* leads derived therefrom may be more helpful (see Chap. 11). In any case, computer assistance is likely to be needed as shown by Brohet [114] who diagnosed 62% of 203 examples of BVH by means of statistical methods applied to Frank orthogonal-lead recordings.

15.7.2 Vectorcardiogram

The vectorcardiograms (Fig. 15.22) of about two thirds of those with BVH have characteristic horizontal-plane loops [126]. In Fig. 15.22a, the transverse loop is inscribed clockwise and lies anteriorly indicating RVH, but has over 50% in the left anterior quadrant, suggesting LVH in addition. In contrast, in Fig. 15.22b, the transverse loop has its maximum QRS vector in the posterior right quadrant, suggesting RVH in addition to the LVH producing the high voltages.

The so-called "pie plate" pattern of the horizontal loop is equivalent to the Katz–Wachtel phenomenon of the standard ECG, namely, large diphasic deflections in the midprecordial leads as in large ventricular septal defects (see Fig. 21.54). In the horizontal plane, the counterclockwise loop has large or equivalent anterior and posterior portions, which are greater than the leftward extension.

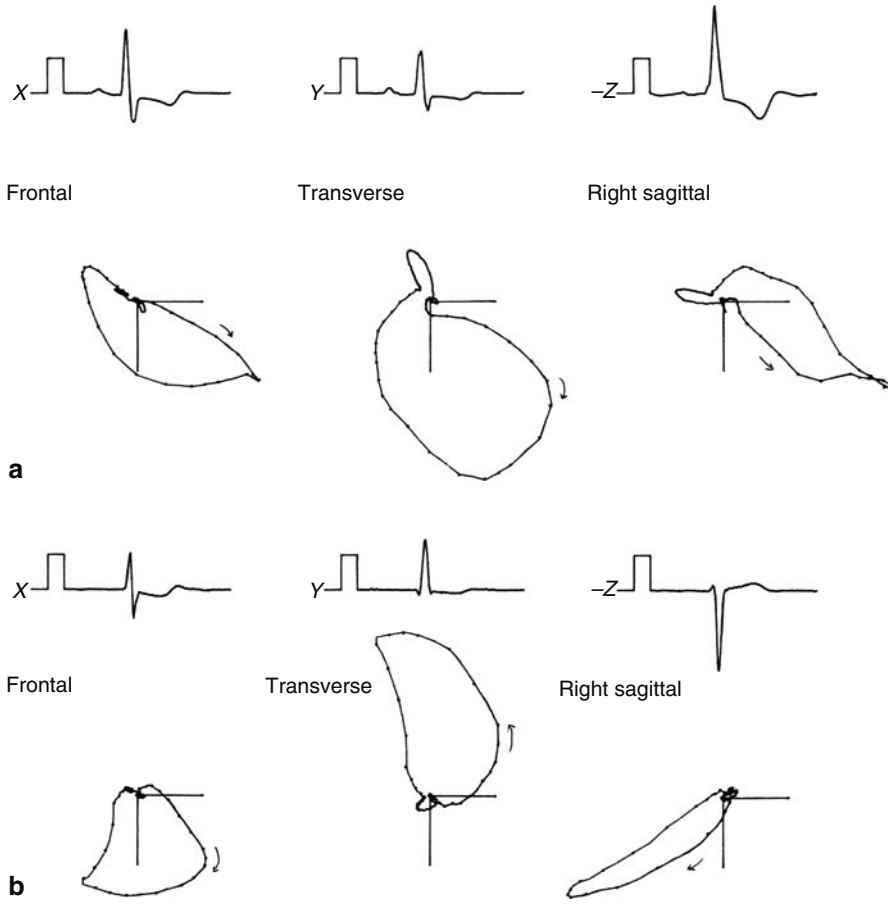

Figure 15.22
Part (a) shows the vectorcardiogram corresponding to the electrocardiogram of Fig. 15.21a. Note the abnormal inscription of the loop in the transverse plane suggesting RV dominance in this particular patient. Lead *Z* is directed positively anteriorly. Part (b) shows the vectorcardiogram corresponding to the electrocardiogram of Fig. 15.21b.

15.7.3 Left Bundle Branch Block and BVH

Right-axis deviation in complete LBBB is a rare occurrence. Tranchesi et al. [127] reported nine patients all of whom had severe congestive failure with marked cardiac enlargement. Usually enlargement of both ventricles was present.

A review by Nikolic and Marriott [128] of the 51 cases reported in the literature indicates it is a rare, insensitive but very specific marker of diffuse myocardial disease, especially idiopathic cardiomyopathy.

15.8 Atrial Enlargement or Overload

The P wave is a neglected area of electrocardiography. Perhaps this is because it is of low amplitude and often has only minor alterations in one or two leads despite a major change in the atrial vector. Furthermore, atrial abnormalities seem to be relatively unimportant as solitary defects because the QRS complexes are frequently obviously abnormal at the same time.

Various terms have been used to describe atrial enlargement or overload. Since an abnormality in atrial conduction may be responsible for a broad notched P wave, it has been suggested that the term left atrial abnormality (LAA) replace left atrial enlargement (LAE) or overload [129–132].

Obviously, better standards for diagnosing atrial enlargement need to be developed. Echocardiography may eventually lead to the development of a standard that includes sex and body-surface area utilizing a 98 percentile normal range as a cutoff rather than a mean plus two standard deviations [133, 134]. Perhaps several-fold amplification of the P wave would enhance its usefulness. Although this was suggested in 1966 [135], there has been little impetus to introduce such a modification in the commercially available computerized ECG systems. Even the simplified bedside method of recording high-gain P waves described by Cristal and Freidberg [136] in 1974 has evoked little enthusiasm.

The early portion of the P wave reflects right atrial depolarization, and the late component largely reflects left atrial depolarization [137]. These components are better visualized in the ECG by increasing the gain fivefold to tenfold [134, 136]. A timed vectorcardiogram was claimed to be over three times as sensitive as the standard ECG [137] in detecting atrial abnormality, while the ordinary VCG was claimed to be more than twice as sensitive [138].

15.8.1 Left Atrial Abnormality

The ECG pattern of left atrial enlargement (LAE) may arise from atrial dilatation, pressure overload [129], atrial pacing, or abnormal intra-atrial conduction [139]. The term left atrial abnormality is therefore preferable although the two terms are used interchangeably. Intra-atrial conduction abnormalities are discussed in Chap. 14.

Echocardiography provides a simple means of assessing left atrial size, and has now replaced radiographic methods in the detection of LAE [129, 133, 140–144]. The suggested M-mode ECHO criteria for LAE consist of

(a) Left atrial dimension > 40 mm [145]
(b) Left atrial dimension/body surface area > 2.2 cm m^{-2} [145]
(c) Ratio of left atrial (LA) dimension to aortic-root diameter > 1.17 [145, 146]

Waggoner et al. [144] studied 307 normals and patients with varying cardiac abnormalities (see Table 15.12), all of whom were in sinus rhythm; of these, 108 or 35% had LAE by M-mode echocardiography defined by (a) or (c) as listed above. Only two of 39%, or 5% of the false-positive ECG diagnoses of LAA, were free of organic heart disease. The authors concluded that the usual ECG criteria detect LAA rather than LAE.

Munuswamy et al. [147] used all three of the above criteria as a definition of LAE when reporting the sensitivity and specificity of various ECG parameters in 49 patients (see Table 15.13). They also tried various combinations of these six parameters with the gain in sensitivity to 90% offset by a loss in specificity to 71%. Since they required all three ECHO

Table 15.12

Sensitivity of commonly used ECG criteria for left atrial enlargement (LAE) of various causes [144] [a]. The total number of patients is 307

	Number of patients	ECHO LAE (%)	Sensitivity (%)	False positive (%)
Normal	55			7
Mitral valve disease	55	67	65	22
Aortic-root disease	52	23	54	31
Left ventricular disease	105	45	58	66
Miscellaneous	40	30	67	11
Left atrial diameter > 40 mm			67	20
Left atrial/aortic-root ratio | > 1.17			59	20

[a] Criteria used: P duration in lead II $\geqslant$ 120 ms, (negative P duration in V_1)/(PR-segment duration) $\geqslant$ 1.0, and terminal force P in V_1 > 3 mV ms. One or more of the criteria are satisfied

Table 15.13

ECG parameters of left atrial enlargement [147]

Criteria	Sensitivity (%)	Specificity (%)
Limb leads		
Notched P with interpeak duration > 40 ms	15	100
P duration > 110 ms	33	88
P duration/PR segment > 1.6[a]	31	64
Lead V_1		
Negative PV_1 duration > 40 ms	83	80
Negative $PV_1 \geqslant 0.1$ mV	60	93
P terminal force > 4 mV ms in V_1	69	93

[a] Macruz index [148]. PR segment is defined as the interval from the end of the P wave to the onset of the QRS complex.

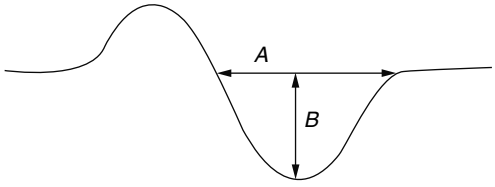

Figure 15.23

Schematic illustration of the P terminal force (PTF) in V_1. It is obtained by multiplying the width (*A*) of the terminal (inverted) portion of the P wave by the depth (*B*) of this component. If *A* is measured in milliseconds and *B* is in millivolts, then the PTF is *AB* mV ms.

measurements to diagnose LAE, indexing left atrial size to body-surface area would, perhaps, have only improved the specificity.

Macruz et al. [148] introduced an index, namely, P duration/PR segment, which was found to vary between 1 and 1.6 in normal individuals. Note that the PR segment is the interval from the end of P to the QRS onset. A value of the index in excess of 1.6 was said to indicate LAE, but it is a somewhat nonspecific criterion.

Only about 50–65% of patients have the LAE pattern on the ECG when the LA dimension is increased [129, 149]. Nevertheless, the usefulness of a P terminal force (PTF) in V_1 in excess of 4 mV ms has been documented [145, 150]. The PTF was introduced by Morris et al. [151] and is sometimes known as the Morris index. It is defined as the product of the amplitude and duration of the terminal component of the P wave in V_1 (see Fig. 15.23). In the case of LAE, the terminal component may have a negative amplitude (biphasic P wave), and hence the PTF would be negative. An example is shown in Fig. 15.24. It correlates moderately with the pulmonary capillary wedge pressure ($r = 0.67$) and only slightly better with the left atrial tension ($r = 0.72$) [141]. However, a normal PTF excludes a pulmonary capillary wedge pressure of 24 mm or over, while an abnormal PTF excludes one less than 10 mm. For general routine use, Miller et al. [150] found a PTF > 6 mV ms to be superior. Perosio et al. [152] have suggested a new index (duration/voltage of P wave in lead II), which has an excellent correlation with the left atrial size ($p < 0.001$). While the PTF in V_1 is the most frequently observed criterion, it is important to look for other parameters, since any one may be the sole indicator of LAE [153].

In children studied by Maok and Krongrad, a notched terminal P wave in the limb leads with a large negative terminal deflection in lead V_1 had only 40% sensitivity but a predictive value of 85%, although among those with mitral regurgitation, the sensitivity for LAE was 77% [149]. The ECG and echocardiogram frequently disagreed.

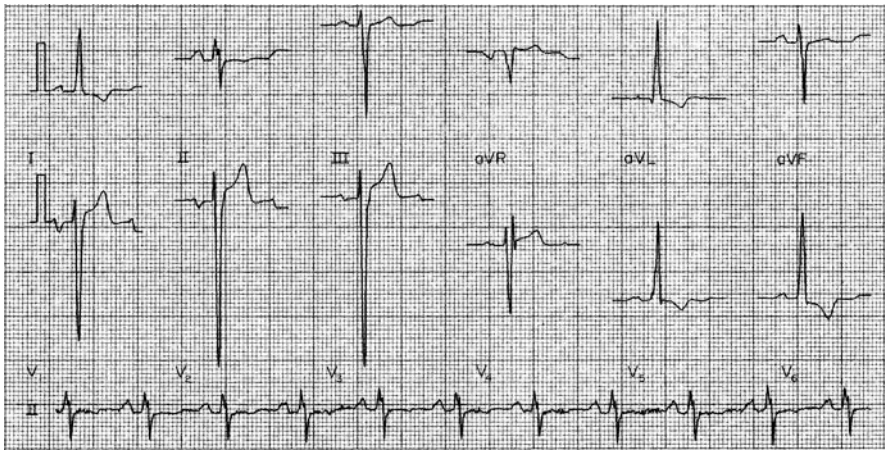

Figure 15.24
Example of LAE in a 76-year-old male with a history of hypertension and myocardial infarction who was admitted for a suspected recent MI. Note the broad and deeply inverted P waves in V_1.

15.8.2 Orthogonal-Lead Criteria for Left Atrial Enlargement

The diagnosis of left atrial enlargement by orthogonal-lead criteria [154, 155] is unlikely to improve the sensitivity obtained using the 12-lead ECG [154–156]. Two possible criteria have been suggested, namely, the sum of the positive amplitudes of P*X* and P*Z* > 0.15 mV, where *Z* is directed positively to the back, that is, the P+ in *Z* compares with the P- in V_1, and P + *Z* > 0.1 mV and P duration > 100 ms. Even so, the best sensitivity obtained was about 30% and the specificity was 92% compared to a PTF V_1 sensitivity of 50% and a specificity of 85% [140].

The time interval between the beginning of the P wave and the second P peak in lead *Y* in excess of 76 ms was the most useful parameter in identifying LAE in mitral valve disease in one study [155]. It identified only 21% of all cases of LAE, but was correct in 52% of those due to mitral valve disease. Unfortunately, it mislabeled 2% of normals and 7% of right atrial enlargement. Therefore, even a twin-peaked P wave is nonspecific unless qualified carefully.

In a fashion corresponding to the abnormal P terminal force in V_1, the P vector loop in the transverse plane can be displaced mainly posteriorly, with the maximum P vector being at approximately 270°, as shown in Fig. 15.25.

15.8.3 Right Atrial Abnormality

The electrocardiographic diagnosis of right atrial abnormality (RAA) is often difficult, even in patients with known right atrial overload or enlargement. It is influenced by various factors, such as age, heart rate, adrenergic stimulation, exercise, hypoxia, and RV compliance. Reynolds [157] noted that the positive portion of the P wave in V_1 is largely caused by right atrial depolarization and suggested a P index for V_1 to aid the diagnosis of RAA in children. He found the occasional patient with RAA who had a prominent terminal negative component in V_1. Unlike LAA, the negative P wave is pointed and is less than 40 ms in duration in RAA, while in LAA the terminal component is rounded and is greater than 40 ms in duration. An example of ECG evidence of RAA in a patient with chronic obstructive airways disease is shown in Fig. 15.17. The criteria for detecting RAA by ECG have been studied many times by radiographic, hemodynamic, or autopsy data to validate right atrial dimensions.

Two-dimensional echocardiography has been used to measure the right atrial size more accurately and test electrocardiographic criteria [7, 158, 159]. Reeves et al. [160] defined RAA as an area greater than 25 cm^2. It was determined after slow-motion, frame-by-frame viewing for maximal right atrial area. P-amplitude criteria alone had little predictive value. RAA was found only in two of 11 with a prominent P in II, and one of five with a prominent P + V_1. In contrast, eight out

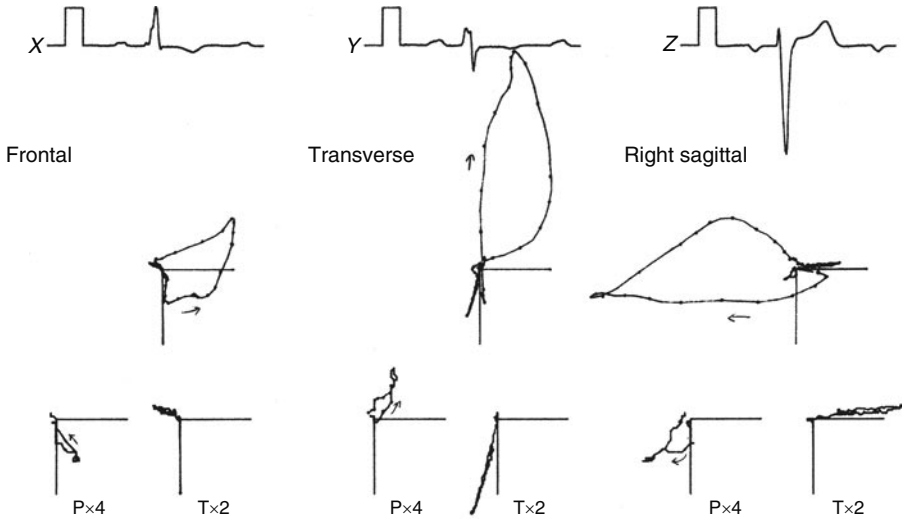

Figure 15.25

Amplified P vector loop in the transverse plane from a patient whose ECG is shown in Fig. 15.24. The P loop is oriented almost totally posteriorly. Note that in this particular ECG, there is clockwise inscription of the vector loop in the transverse plane, suggesting myocardial infarction in addition, even though there is a prominent R in *Z* (directed similarly to V_2).

Table 15.14

Criteria for right atrial enlargement

Diagnosis	Criteria
Probable RAE	0.25 mV < P amplitude < 0.3 mV in any lead P in $V_1 \geqslant 0.5$ mV (but less specific if heart rate >100)
Definite RAE	P amplitude > 0.30 mV in any lead qR in V_1 with coronary disease clinically absent

Table 15.15

Frank orthogonal-lead criteria for right atrial enlargement [71]

	White		Black	
	Males	Females	Males	Females
Positive P*Y* amplitude (mV)	> 0.15	> 0.15	> 0.20	> 0.20
Negative P*Z* amplitude (mV)	< −0.05	< −0.05	< −0.05	< −0.1

of eight with a qR in V_1 and no coronary disease had RAA, as did 13 out of 28 whose total QRS amplitude in V_1 was less than 0.6 mV with a ratio of total QRS amplitude in V_2 to total QRS amplitude in V_1 greater than 3.0. No allowance was made for changing the definition of RAA depending on sex or body-surface area (see Tables 15.14 and 15.15). Cacho et al. [158] used a right atrial area greater than 5.0 cm m^{-2} as a criterion for detecting RVH with 100% sensitivity in their 15 test cases. Obviously, echocardiography may offer a new challenge to the development of superior ECG criteria for the diagnosis of RAE.

The term "pseudo P pulmonale" has been used when prominent P waves are found in the absence of RAA. If left-heart disease is present with pseudo P pulmonale, it is suggested that it reflects an increase in the left atrial component [161].

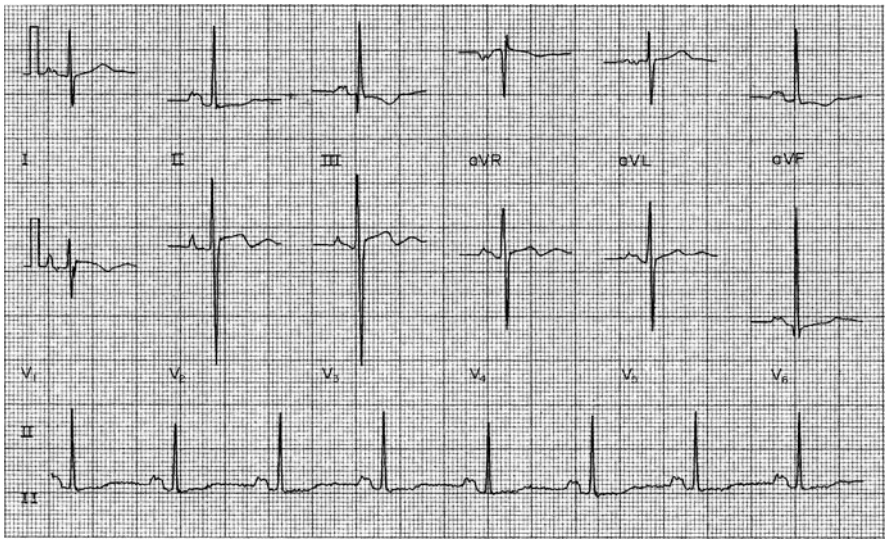

Figure 15.26

Example of biatrial enlargement in a 30-year-old female with tricuspid and mitral valve disease. The tall P waves in V_1 and V_2 indicate RAE, while the broad bifid P waves seen in leads I, II, and III suggest LAE in addition. There is also a broad, though not excessively deep, terminal component of the P wave in V_1.

15.8.4 Orthogonal-Lead Criteria for Right Atrial Abnormality

The orthogonal-lead criteria essentially mirror those of the 12-lead ECG, that is, an increase in P amplitude may be found in lead *Y* as well as in P– in lead *Z* (equivalent to P+ in V_1). P loops are directed inferiorly and anteriorly.

15.8.5 Biatrial Enlargement

The ECG may show features consistent with both RAA (increased P amplitude) and LAA (broad notched P and/or increased PTF V_1), in which case the term biatrial enlargement is appropriate (Fig. 15.26). Usually, however, atrial fibrillation supervenes to prevent its detection. Large fibrillatory waves (>0.2 mV, peak to peak) have been suggested as being indicative of atrial enlargement [162].

References

1. Cabrera, E. and A. Gaxiola, A critical re-evaluation of systolic and diastolic overloading patterns. *Prog. Cardiovasc. Dis.*, 1959;**2**: 219–236.
2. Cabrera, E. and J.R. Monroy, Systolic and diastolic loading of the heart. II. Electrocardiographic data. *Am. Heart J.*, 1952;**43**: 669–686.
3. Reichek, N. and R.B. Devereux, Left ventricular hypertrophy: relationship of anatomic, echocardiographic and electrocardiographic findings. *Circulation*, 1981;**63**: 1391–1398.
4. Grothues, F., G. Smith, J.C.C. Moon, et al., Comparison of interstudy reproducibility of cardiovascular magnetic resonance with two-dimensional echocardiography in normal subjects and in patients with heart failure or left ventricular hypertrophy. *Am. J. Cardiol.*, 2002;**90**: 29–34.
5. Bove, K.E., D.T. Rowlands, and R.C. Scott, Observations on the assessment of cardiac hypertrophy utilizing a chamber partition technique. *Circulation*, 1966;**33**: 558–568.
6. Murphy, M.L., P.N. Thenabadu, L.R. Blue, et al., Descriptive characteristics of the electrocardiogram from autopsied men free of cardiopulmonary disease—a basis for evaluating criteria for ventricular hypertrophy. *Am. J. Cardiol.*, 1983;**52**: 1275–1280.

7. Murphy, M.L., P.N. Thenabadu, N. de Soyza, et al., Reevaluation of electrocardiographic criteria for left, right and combined cardiac ventricular hypertrophy. *Am. J Cardiol.*, 1984;**53**: 1140–1147.
8. de Simone, G., S.R. Daniels, R.B. Devereux, et al., Left ventricular mass and body size in normotensive children and adults: assessment of allometric relations and impact of overweight. *J. Am. Coll. Cardiol.*, 1992;**20**: 1251–1260.
9. Kafka, H., S. Ford, and G. Burggraf, In vitro validation of a two-dimensional echocardiographic method of left ventricular mass estimation using intact postmortem hearts (abstract). *Clin. Invest. Med.*, 1983;**6**(Suppl. I): 44.
10. Reichek, N., J. Helak, T. Plappert, M. St John-Sutton, and K.T. Weber, Anatomic validation of left ventricular mass estimates from clinical two-dimensional echocardiography. Initial results. *Circulation*, 1983;**67**: 348–352.
11. Woythaler, J.N., S.L. Singer, O.L. Kwan, et al., Accuracy of echocardiography versus electrocardiography in detecting left ventricular hypertrophy: comparison with postmortem mass measurements. *J. Am. Coll. Cardiol.*, 1983;**2**: 305–311.
12. Pombo, J.F., B.L. Troy, and R.O. Russell Jr., Left ventricular volumes and ejection fraction by echocardiography. *Circulation*, 1971;**43**: 480–490.
13. Devereux, R.B. and N. Reichek, Echocardiographic determination of left ventricular mass in man. Anatomic validation of the method. *Circulation*, 1977;**55**: 613–618.
14. Ladipo, G.O.A., F.G. Dunn, T.H. Pringle, B. Bastian, and T.D.V. Lawrie, Serial measurements of left ventricular dimension by echocardiography. *Br. Heart J.*, 1980;**44**: 284–289.
15. Devereux, R.B., E.M. Lutas, P.N. Casale, et al., Standardization of M-mode echocardiographic left ventricular anatomic measurements. *J. Am. Coll. Cardiol.*, 1984;**4**: 1222–1230.
16. Wahr, D., Y.-S. Wang, C. Skioldebrand, E. Sehiller, M. Lipton, and N.B. Schiller, Clinical quantitative echocardiography III. Left ventricular mass in a normal adult population. *Clin. Res.*, 1982;**30**: 23A.
17. Koren, M.J., R.B. Devereux, P.N. Casale, D.D. Savage, and J.H. Laragh, Relation to left ventricular mass and geometry to morbidity and mortality in uncomplicated essential hypertension. *Ann. Intern. Med.*, 1991;**114**: 345–352.
18. Baker, B.J., J.A. Scovil, J.J. Kane, and M.L. Murphy, Echocardiographic detection of right ventricular hypertrophy. *Am. Heart J.*, 1983;**105**: 611–614.
19. Prakash, R. and H. Matsukubo, Usefulness of echocardiographic right ventricular measurements in estimating right ventricular hypertrophy and right ventricular systolic pressure. *Am. J. Cardiol.*, 1983;**51**: 1036–1040.
20. Watanabe, T., H. Katsume, H. Matsukubo, K. Furukawa, and H. Ijichi, Estimation of right ventricular volume with two dimensional echocardiography. *Am. J. Cardiol.*, 1982;**49**: 1946–1953.
21. Gibson, T.C., S.W. Miller, T. Aretz, N.J. Hardin, and A.E. Weyman, Method for estimating right ventricular volume by planes applicable to cross-sectional echocardiography: correlation with angiographic formulas. *Am. J. Cardiol.*, 1985;**55**: 1584–1588.
22. Horan, L., N.C. Flowers, and C.J. Havelda, Relation between right ventricular mass and cavity size: an analysis of 1500 human hearts. *Circulation*, 1981;**64**: 135–138.
23. Antman, E.M., L.H. Green, and W. Grossman, Physiologic determinants of the electrocardiographic diagnosis of left ventricular hypertrophy. *Circulation*, 1979;**60**: 386–396.
24. Devereux, R.B., M.C. Phillips, P.N. Casale, R.R. Eisenberg, and P. Kligfield, Geometric determinants of electrocardiographic left ventricular hypertrophy. *Circulation*, 1983;**67**: 907–911.
25. Horton, J.D., H.S. Sherber, and E.G. Lakatta, Distance correction for precordial electrocardiographic voltage in estimating left ventricular mass. An echocardiographic study. *Circulation*, 1977;**55**: 509–512.
26. Feldman, T., R.W. Childers, K.M. Borow, A. Neumann, and R.M. Lang, Relation of ECG R wave amplitude to changes in left ventricular size. *Circulation*, 1984;**70**(Suppl. II): 434.
27. Pech, H.J., J. Witte, R. Romaniuk, R.A. Parsi, and W. Porstmann, Left ventricular mass in coronary artery disease without hypertension. Haemodynamic and angiocardiographic study. *Br. Heart J.*, 1974;**36**: 362–367.
28. Scott, R.C., The correlation between the electrocardiographic patterns of ventricular hypertrophy and the anatomic findings. *Circulation*, 1960;**21**: 256–291.
29. Okin, P.M., J.T. Wright, M.S. Niemienen, et al., Ethnic differences in electrocardiographic criteria for left ventricular hypertrophy: the LIFE Study. *Am. J. Hypertens.*, 2002;**15**: 663–671.
30. Granger, C.B., M.K. Karimeddini, V.E. Smith, H.R. Shapiro, A.M. Katz, and R.L. Riba, Rapid ventricular filling in left ventricular hypertrophy: I. Physiologic hypertrophy. *J. Am. Coll. Cardiol.*, 1985;**5**: 862–868.
31. Okin, P.M., M.J. Roman, R.B. Devereux, and P. Kligfield, Electrocardiographic identification of left ventricular hypertrophy: test performance in relation to definition of hypertrophy and presence of obesity. *J. Am. Coll. Cardiol.*, 1996;**27**: 124–131.
32. Okin, P.M., S. Jern, R.B. Devereux, S.E. Kjeldsen, and F.B. Dahl, for the LIFE Study Group. Effect of obesity on electrocardiographic left ventricular hypertrophy in hypertensive patients: the Losartan Intervention for Endpoint (LIFE) reduction in hypertension study. *Hypertension*, 2000;**35**: 13–18.
33. Brody, D.A., A theoretical analysis of intracavitary blood mass influence on the heart-lead relationship. *Circ. Res.*, 1956;**4**: 731–738.
34. Ishikawa, K., A.S. Berson, and H.V. Pipberger, Electrocardiographic changes due to cardiac enlargement. *Am. Heart J.*, 1971;**81**: 635–643.
35. Rudy, Y., The effects of the thoracic volume conductor (inhomogeneities) on the electrocardiogram, in *Pediatric and Fundamental Electrocardiography*, J. Liebman, R. Plonsey, and Y. Rudy, Editors. Boston, MA: Nijhoff, 1987, pp. 49–73.
36. Romhilt, D.W., K.E. Bove, R.J. Norris, et al., A critical appraisal of the electrocardiographic criteria for the diagnosis of left ventricular hypertrophy. *Circulation*, 1969;**40**: 185–195.
37. Kafka, H., J.A. Milliken, G.W. Burggraf, Improved electrocardiographic diagnosis of left ventricular hypertrophy in left bundle branch block (abstract). *Circulation*, 1984;**70**(Suppl. II): 434.
38. Kafka, H., G.W. Burggraf, and J.A. Milliken, Electrocardiographic diagnosis of left ventricular hypertrophy in the presence of left bundle branch block. An echocardiographic study. *Am. J. Cardiol.*, 1985;**55**: 103–106.
39. Lewis, T., Observations upon ventricular hypertrophy with especial reference to preponderance of one or other chamber. *Heart*, 1914;**5**: 367–402.
40. Sokolow, M. and T.P. Lyon, The ventricular complex in left ventricular hypertrophy as obtained by unipolar precordial and limb leads. *Am. Heart J.*, 1949;**37**: 161–186.
41. McPhie, J., Left ventricular hypertrophy: electrocardiographic diagnosis. *Australas. Ann. Med.*, 1958;**7**: 317–327.

42. Simonson, E., *Differentiation Between Normal and Abnormal in Electrocardiography.* St Louis, MO: Mosby, 1961, pp. 99–101.
43. Romhilt, D.W. and E.H. Estes Jr., A point-score system for the ECG diagnosis of left ventricular hypertrophy. *Am. Heart J.*, 1968;**75**: 752–758.
44. Murphy, M.L., P.N. Thenabadu, N. de Soyza, J. Meade, J.E. Doherty, and B.J. Baker, Sensitivity of electrocardiographic criteria for left ventricular hypertrophy according to type of cardiac disease. *Am. J. Cardiol.*, 1985;**55**: 545–549.
45. Kansal, S., D.I. Roitman, and L.T. Sheffield, A quantitative relationship of electrocardiographic criteria of left ventricular hypertrophy with echocardiographic left ventricular mass: a multivariate approach. *Clin. Cardiol.*, 1983;**6**: 456–463.
46. Casale, P.N., R.B. Devereux, P. Kligfield, et al., Electrocardiographic detection of left ventricular hypertrophy: development and prospective validation of improved criteria. *J. Am. Coll. Cardiol.*, 1985;**6**: 572–580.
47. Devereux, R.B., D.R. Alonso, E.M. Lutas, et al., Echocardiographic assessment of left ventricular hypertrophy: comparison to necropsy findings. *Am. J. Cardiol.*, 1986;**57**: 450–458.
48. Devereux, R.B., P.N. Casale, P. Kligfield, et al., Performance of primary and derived M-mode echocardiographic measurements for detection of left ventricular hypertrophy in necropsied subjects and in patients with systemic hypertension, mitral regurgitation and dilated cardiomyopathy. *Am. J. Cardiol.*, 1986;**57**: 1388–1393.
49. Casale, P.N., R.B. Devereux, D.R. Alonso, E. Campo, and P. Kligfield, Improved sex-specific criteria of left ventricular hypertrophy for clinical and computer interpretation of electrocardiograms: validation with autopsy findings. *Circulation*, 1987;**75**: 565–572.
50. Schillaci, G., P. Verdecchia, C. Borgioni, et al., Improved electrocardiographic diagnosis of left ventricular hypertrophy. *Am. J. Cardiol.*, 1005;**74**: 714–719.
51. Verdecchia, P., G. Schillaci, C. Borgioni, et al., Prognostic value of a new electrocardiographic method for diagnosis of left ventricular hypertrophy. *J. Am. Coll. Cardiol.*, 1998;**31**(2): 383–390.
52. Thiry, P.S., R.G. Rosenberg, and J.A. Abbott, A mechanism for the electrocardiogram response to left ventricular hypertrophy and acute ischemia. *Circ. Res.*, 1975;**6**: 92–104.
53. Uhley, H.N., Study of transmembrane action potential, electrogram, electrocardiogram and vectorcardiogram of rats with left ventricular hypertrophy. *Am. J. Cardiol.*, 1961;**7**: 211–217.
54. Holt, J.H. Jr., A.C.L. Barnard, and M.S. Lynn, A study of the human heart as a multiple dipole electrical source. II. Diagnosis and quantitation of left ventricular hypertrophy. *Circulation*, 1969;**40**: 697–710.
55. Dunn, R.A., H.V. Pipberger, J.H. Holt Jr., A.C.L. Barnard, and H.A. Pipberger, Performance of conventional orthogonal and multiple-dipole electrocardiograms in estimating left ventricular muscle mass. *Circulation*, 1979;**60**: 1350–1353.
56. Okin, P.M., M.J. Roman, R.B. Devereux, and P. Kligfield, Time-voltage area of the QRS for the identification of left ventricular hypertrophy. *Hypertension*, 1996;**27**: 251–258.
57. Okin, P.M., M.J. Roman, R.B. Devereux, T.G. Pickering, J.S. Borer, and P. Kligfield, Time-voltage area of the 12-lead electrocardiogram: detection of left ventricular hypertrophy. *Hypertension*, 1998;**31**: 937–942.
58. Molloy, T.J., P.M. Okin, R.B. Devereux, and P. Kligfield, Electrocardiographic detection of left ventricular hypertrophy by the simple QRS voltage-duration product. *J. Am. Coll. Cardiol.*, 1992;**20**: 1180–1186.
59. Okin, P.M., M.J. Roman, R.B. Devereux, and P. Kligfield, Electrocardiographic identification of increased left ventricular mass by simple voltage-duration products. *J. Am. Coll. Cardiol.*, 1995;**25**: 417–423.
60. Okin, P.M., R.B. Devereux, J.E. Liu, et al., Regression of electrocardiographic left ventricular hypertrophy predicts regression of echocardiographic left ventricular mass: the LIFE study. *J. Hum. Hypertens.*, 2004;**18**: 403–409.
61. Okin, P.M., R.B. Devereux, S. Jern, et al., Regression of electrocardiographic left ventricular hypertrophy during antihypertensive treatment and prediction of major cardiovascular events: the LIFE study. *J.A.M.A.*, 2004;**292**: 2343–2349.
62. Moore, R.B., L.M. Shapiro, and D.G. Gibson, Relation between electrocardiographic repolarisation changes and mechanical events in left ventricular hypertrophy. *Br. Heart J.*, 1984;**52**: 516–23.
63. Kannel, W.B., T. Gordon, and D. Offut, Left ventricular hypertrophy by electrocardiogram: prevalence, incidence, and mortality in the Framingham Study. *Ann. Intern. Med.*, 1969;**71**: 89–105.
64. Okin, P.M., R.B. Devereux, M.S. Nieminen, et al., Electrocardiographic strain pattern and prediction of cardiovascular morbidity and mortality in hypertensive patients. *Hypertension*, 2004;**44**: 48–54.
65. Devereux, R.B. and N. Reichek, Repolarization abnormalities of left ventricular hypertrophy. Clinical, echocardiographic and hemodynamic correlates. *J. Electrocardiol.*, 1982;**15**: 47–53.
66. Okin, P.M., R.B. Devereux, M.S. Nieminen, et al., Relationship of electrocardiographic strain pattern to left ventricular structure and function in hypertensive patients: the LIFE study. *J. Am. Coll. Cardiol.*, 2001;**38**: 514–520.
67. Okin, P.M., R.B. Devereux, R.R. Fabsitz, E.T. Lee, J.M. Galloway, and B.V. Howard, Quantitative assessment of electrocardiographic strain predicts increased left ventricular mass: the strong heart study. *J. Am. Coll. Cardiol.*, 2002;**40**: 1395–1400.
68. Oikarinen, L., M.S. Nieminen, M. Viitasalo, et al., Relation of QT interval and QT dispersion to echocardiographic left ventricular hypertrophy and geometric pattern in hypertensive patients: the LIFE study. *J. Hypertens.*, 2001;**19**: 1883–1891.
69. Abbott-Smith, C.W. and T.-C. Chou, Vectorcardiographic criteria for the diagnosis of left ventricular hypertrophy. *Am. Heart J.*, 1970;**79**: 361–369.
70. Romhilt, D.W. and J.C. Greenfield Jr., Vectorcardiography diagnosis of left ventricular hypertrophy. *Circulation*, 1968;**37**: 15–19.
71. Pipberger, H.V., E. Simonson, E.A. Lopez Jr., M.A. Araoye, and H.A. Pipberger, The electrocardiogram in epidemiologic investigations: a new classification system. *Circulation*, 1982;**65**: 1456–1464.
72. Yankopoulos, N.A., W.K. Haisty, and H.V. Pipberger, Computer analysis of the orthogonal electrocardiogram and vectorcardiogram in 257 patients with aortic valve disease *Am. J. Cardiol.*, 1977;**40**: 707–715.
73. Brohet, C.R. and H.G. Richman, Clinical evaluation of automated processing of electrocardiograms by the Veterans Administration program (AVA 3.4). *Am. J. Cardiol.*, 1979;**43**: 1167–1174.
74. Pipberger, H.V., D. McCaughan, D. Littmann, et al., Clinical application of a second generation electrocardiographic computer program. *Am. J. Cardiol.*, 1975;**35**: 597–608.
75. Macfarlane, P.W., C.Y. Chen, B. Boyce, and R.S. Fraser, Scoring technique for diagnosis of ventricular hypertrophy from

three orthogonal lead electrocardiogram. *Br. Heart J.*, 1981;**45**: 402–410.
76. Macfarlane, P.W., C.Y. Chen, and J.J. Bailey, A comparison of point scoring techniques for the diagnosis of left ventricular hypertrophy, in *New Frontiers of Electrocardiology*, F. de Pádua and P.W. Macfarlane, Editors. Chichester: Research Studies Press, 1981, pp. 353–654.
77. De Backer, G.G., R. Zenner, M. Kornitzer, D.L. Clement, and M.M. Drama, Prevalence of left ventricular hypertrophy in middle-aged men according to various ECG-VCG techniques. *J. Electrocardiol.*, 1983;**16**: 307–311.
78. Shapiro, L.M., Physiological left ventricular hypertrophy. *Br. Heart J.*, 1984;**52**: 130–135.
79. Oakley, D.G. and C.M. Oakley, Significance of abnormal electrocardiograms in highly trained athletes. *Am. J. Cardiol.*, 1982;**50**: 985–989.
80. Magalski, A., B.J. Maron, M.L. Main, M. McCoy, A. Florez, K.J. Reid, H.W. Epps, J. Bates, and J.E. Browne, Relation of race to electrocardiographic patterns in Elite American Football players. *J. Am. Coll. Cardiol.*, 2008;**51**: 2250–2255.
81. Oakley, D., Cardiac hypertrophy in athletes. *Br. Heart J.*, 1984;**52**: 121–123.
82. Cokkinos, D.V., J.N. Demopoulos, E.T. Heimonas, C. Mallios, N. Papazoglou, and E.M. Vorides, Electrocardiographic criteria of left ventricular hypertrophy in left bundle-branch block. *Br. Heart J.*, 1978;**40**: 320–324.
83. Klein, R.C., Z. Vera, A.N. De Maria, and D.T. Mason, Electrocardiographic diagnosis of left ventricular hypertrophy in the presence of left bundle branch block. *Am. Heart J.*, 1984;**108**: 502–506.
84. Noble, L.M., S.B. Humphrey, and G.B. Monaghan, Left ventricular hypertrophy in left bundle branch block. *J. Electrocardiol.*, 1984;**17**: 157–160.
85. Havelda, C.J., G.S. Sohi, N.C. Flowers, and L.G. Horan, The pathologic correlates of the electrocardiogram: complete left bundle branch block. *Circulation*, 1982;**65**: 445–451.
86. Murphy, M.L., P.N. Thenabadu, N. de Soyza, J.E. Doherty, and B.J. Baker, Left atrial abnormality as an electrocardiographic criterion for the diagnosis of left ventricular hypertrophy in the presence of right bundle branch block. *Am. J. Cardiol.*, 1983;**52**: 381–383.
87. Vandenberg, B., K. Sagar, and D. Romhilt, Electrocardiographic criteria for the diagnosis of left ventricular hypertrophy in the presence of complete right bundle branch block. *J. Am. Coll. Cardiol.*, 1985;**5**: 511.
88. Hill, L.S., M. Monaghan, and P.J. Richardson, Regression of left ventricular hypertrophy during treatment with antihypertensive agents. *Br. J. Clin. Pharmacol.*, 1979;**7**(Suppl. 2): 2555–2605.
89. Wollam, G.L., W.D. Hall, V.D. Porter, et al., Time course of regression of left ventricular hypertrophy in treated hypertensive patients. *Am. J. Med.*, 1983;**75**(Suppl. 3A): 100–110.
90. Sonotani, N., S. Kubo, A. Nishioka, and T. Takatsu, Electrocardiographic and echocardiographic changes after one to two years treatment of hypertension. *Jpn. Heart J.*, 1981;**22**: 325–333.
91. Corea, L., M. Bentivoglio, P. Verdecchia, M. Provvidenza, and M. Motolese, Left ventricular hypertrophy regression in hypertensive patients treated with Metoprolol. *Int. J. Clin. Pharm. Ther. Toxicol.*, 1984;**22**: 365–370.
92. Russell, G.I., J.E.F. Pohl, J. Baldwin, et al., Treatment of essential hypertension: changes in blood pressure, echocardiography and electrocardiography on three therapeutic regimes. *Eur. J. Clin. Pharmacol.*, 1985;**28**: 119–124.
93. Savage, D.D., P.M. Rautaharju, J.J. Bailey, et al., The emerging prominence of computer electrocardiography in large population based surveys. *J. Electrocardiol.*, 1987;**20**(Suppl.): 48–52.
94. Rautaharju, P.M., A.Z. laCroix, D.D. Savage, et al., Electrocardiographic estimate of left ventricular mass versus radiographic cardiac size and the risk of cardiovascular disease mortality in the epidemiologic follow-up of the First National Health and Nutrition Examination Survey. *Am. J. Cardiol.*, 1988;**62**: 59–66.
95. Wolf, H., J.W. Warren, P.M. Rautaharju, et al., An electrocardiographic model for prediction of left ventricular mass. *13th Int Congr Electrocardiology* Washington. 1986: 4. [Abstracts.]
96. Carroll, J.D., W.H. Gaasch, S. Naimi, and H.J. Levine, Regression of myocardial hypertrophy: electrocardiographic-echocardiographic correlations after aortic valve replacement in patients with chronic aortic regurgitation. *Circulation*, 1982;**65**: 980–987.
97. Kannel, W.B. and R.D. Abbott, Comparison of ECG-LVH and unrecognized myocardial infarction as predictors of overt cardiovascular events: the Framingham study (abstract). *Circulation*, 1984;**70**(Suppl. II): 434.
98. Savage, D.D., R.D. Abbott, S. Padgett, S.J. Anderson, and R.J. Garrison, Epidemiologic features of left ventricular hypertrophy in normotensive and hypertensive subjects, in *Cardiac Left Ventricular Hypertrophy*, H.E.D.J. Ter Keurs and J.J. Schipperheyn, Editors. Boston, MA: Nijhoff, 1983, pp. 2–3.
99. Kannel, W.B., Prevalence and natural history of electrocardiographic left ventricular hypertrophy. *Am. J. Med.*, 1983;**75**(Suppl. 3A): 4–11.
100. Hamby, R.I., M.N. Prakash, U.A. Wyne, and I. Hoffman, Electrocardiographic left ventricular hypertrophy and coronary artery disease: clinical, hemodynamic, and angiographic correlates. *Am. Heart J.*, 1980;**100**: 794–801.
101. Levy, D., K.M. Anderson, D.D. Savage, S.A. Balkus, W.B. Kannel, and W.P. Castelli, Risk of ventricular arrhythmias in left ventricular hypertrophy; The Framingham heart study. *Am. J. Cardiol.*, 1987;**60**: 560–565.
102. Macfarlane, P.W., British Regional Heart Study; The electrocardiogram and risk of myocardial infarction on follow up. *J. Electrocardiol.*, 1987;**20**(Suppl.): 53–56.
103. Levy, D., M. Salomon, R.B. D'Agostino, A.J. Belanger, and W.B. Kannel, Prognostic significance of baseline electrocardiographic features and their serial changes in subjects with left ventricular hypertrophy. *Circulation*, 1994;**90**: 1786–1793.
104. Matthew, J., P. Sleight, E. Lonn, et al., Reduction of cardiovascular risk by regression of electrocardiographic markers of left ventricular hypertrophy by the angiotensin-converting enzyme inhibitor ramipril. *Circulation*, 2001;**104**: 1615–1621.
105. Gardin, J.M. and M.S. Lauer, Left ventricular hypertrophy: the next treatable, silent killer? *J.A.M.A.*, 2004;**292**: 2396–2398.
106. Savage, D.D., R.J. Garrison, W.B. Kannel, et al., The spectrum of left ventricular hypertrophy in a general population sample: the Framingham Study. *Circulation*, 1987;**75**(Suppl. I): 26–33.
107. Flowers, N.C. and L.G. Horan, Subtle signs of right ventricular enlargement and their relative importance, in *Advances in Electrocardiography*, R.C. Schlant and J.W. Hurst, Editors. New York: Grune and Stratton, 1972, pp. 297–308.

108. Kanemoto, N., Electrocardiogram in primary pulmonary hypertension. *Eur. J. Cardiol.*, 1980;**12**: 181–193.
109. Chou, T.-C., *Electrocardiography in Clinical Practice*. New York: Grune and Stratton, 1979, pp. 22, 23, 77.
110. Murphy, M.L. and F. Hutcheson, The electrocardiographic diagnosis of right ventricular hypertrophy in chronic obstructive pulmonary disease. *Chest*, 1974;**65**: 622–627.
111. Spodick, D.H., Electrocardiographic studies in pulmonary disease. I. Electrocardiographic abnormalities in diffuse lung disease. *Circulation*, 1959;**20**: 1067–1072.
112. Gamboa, R., P.G. Hugenholtz, and A.S. Nadas, Corrected (Frank), uncorrected (Cube) and standard electrocardiographic lead systems in recording augmented right ventricular forces in right ventricular hypertension. *Br. Heart J.*, 1966;**28**: 62–74.
113. Villa, J.G., J. Urbina, J. Sanchez-Dominguez, F. Largo, and A. Menendez, Vectorcardiographic patterns of right ventricular pressure overload, in *New Frontiers of Electrocardiology*, F. de Pádua and P.W. Macfarlane, Editors. Chichester: Research Studies Press, 1981, pp. 357–359.
114. Brohet, C.R., A. Robert, C. Derwael, et al., Computer interpretation of pediatric orthogonal electrocardiograms: statistical and deterministic classification methods. *Circulation*, 1984;**70**: 255–263.
115. Cowdery, C.D., G.S. Wagner, J.W. Starr, G. Rogers, and J.C. Greenfield Jr., New vectorcardiographic criteria for diagnosing right ventricular hypertrophy in mitral stenosis: comparison with electrocardiographic criteria. *Circulation*, 1980;**62**: 1026–1032.
116. Chou, T.-C., *Electrocardiography in Clinical Practice*. New York: Grune and Stratton, 1979, p. 119.
117. Del Rio, R., G. Medrano, V. Rubio, J.P. Olea, J. Soin, and D. Sodi-Pallares, Right bundle branch block with right ventricular hypertrophy. *Am. J. Cardiol.*, 1959;**4**: 294–301.
118. Brohet, C.R., M. Styns, P. Arnaud, and L.A. Brasseur, Vectorcardiographic diagnosis of right ventricular hypertrophy in the presence of right bundle branch block in young subjects. *Am. J. Cardiol.*, 1978;**42**: 602–612.
119. Gottdiener, J.S., J.A. Gay, B.J. Maron, and R.D. Fletcher, Increased right ventricular wall thickness in left ventricular pressure overload: echocardiographic determination of hypertrophic response of the 'non-stressed' ventricle. *J. Am. Coll. Cardiol.*, 1985;**6**: 550–555.
120. Loperfido, F., A. Digaetano, and P. Santarelli, The evaluation of left and right ventricular hypertrophy in combined ventricular overload by electrocardiography: relationship with the echocardiographic data. *J. Electrocardiol.*, 1982;**15**: 327–334.
121. Hiroki, T., Vectorcardiographic diagnosis of combined ventricular hypertrophy in adult patients. *Jpn. Heart J.*, 1974;**15**: 323–336.
122. Lipsett, M.B. and W.J. Zinn, Anatomic and electrocardiographic correlation in combined ventricular hypertrophy. *Am. Heart J.*, 1953;**45**: 86–94.
123. Pagnoni, A. and J.F. Goodwin, The cardiographic diagnosis of combined ventricular hypertrophy. *Br. Heart J.*, 1952;**14**: 451–461.
124. Scoulié, P., J. Laham, I. Papanicolis, and G. Voci, Les Principaux types electrocardiographiques de surcharge ventriculaire combinée. *Arc. Mal. Coeur Vaiss.*, 1949;**42**: 791–810.
125. Gamboa, R., J.D. Klingeman, and H.V. Pipberger, Computer diagnosis of biventricular hypertrophy from the orthogonal electrocardiogram. *Circulation*, 1969;**39**: 72–82.
126. Varriale, P., R.J. Kennedy, and J.C. Alfenito, Vectorcardiogram of combined ventricular hypertrophy: posterior counterclockwise loop (Frank System). *Br. Heart J.*, 1969;**31**: 457–461.
127. Tranchesi, J., P. Moffa, and M. Ebaid, Right axis deviation in left bundle branch block: an electro-vectorcardiographic study, in *Proceedings of the 11th International Symposium on Vectorcardiography 2*, I. Hoffman, R.L. Hamby, and E. Glassman, Editors. Amsterdam: North-Holland, 1971, pp. 283–288.
128. Nikolic, A. and H.J.L. Marriott, Left bundle branch block with right axis deviation: a marker of congestive cardiomyopathy. *J. Electrocardiol.*, 1985;**18**: 395–404.
129. Josephson, M.E., J.A. Kastor, and J. Morganroth, Electrocardiographic left atrial enlargement. Electrophysiologic, echocardiographic and hemodynamic correlates. *Am. J. Cardiol.*, 1977;**39**: 967–971.
130. Saunders, J.L., J.H. Calatayud, K.J. Schulz, V. Maranhao, A.S. Gooch, and H. Goldberg, Evaluation of ECG criteria for P-wave abnormalities. *Am. Heart J.*, 1967;**74**: 757–765.
131. Zoneraich, O. and S. Zoneraich, Intraatrial conduction disturbances: vectorcardiographic patterns. *Am. J. Cardiol.*, 1976;**37**: 736–742.
132. Zoneraich, O. and S. Zoneraich, Electrocardiographic left atrial enlargement versus interatrial conduction defect. *Am. J. Cardiol.*, 1978;**41**: 618–619.
133. Chirife, R., G.S. Feitosa, and W.S. Frankl, Electrocardiographic detection of left atrial enlargement. Correlation of P wave with left atrial dimension by echocardiography. *Br. Heart J.*, 1975;**37**: 1281–1285.
134. Wang, Y.-S., D. Heilbron, J. Outman, D. Wahr, and N.H. Schiller, Clinical quantitative echocardiography. I. End systolic atrial volume in a normal adult population. *Clin. Res.*, 1982;**30**: 23A.
135. Haywood, L.J. and R.H. Selvester, Analysis of right and left atrial vectorcardiograms. Timed records of 100 normal persons. *Circulation*, 1966;**33**: 577–587.
136. Cristal, N. and L. Freidberg, The atriogram. A bedside method for recording high gain P waves. *Chest*, 1974;**65**: 554–555.
137. Selvester, R.H. and L.J. Haywood, High gain, high frequency atrial vectorcardiograms in normal subjects and in patients with atrial enlargement. *Am. J. Cardiol.*, 1969;**24**: 8–17.
138. Benchimol, A., F. Reich, and K.H. Desser, Comparison of the electrocardiogram and vectorcardiogram for the diagnosis of left atrial enlargement. *J. Electrocardiol.*, 1976;**9**: 215–218.
139. Chandraratna, P.A.N. and E. Langevin, On the significance of an abnormal P-terminal force in lead VI. *Am. Heart J.*, 1978;**95**: 267–268.
140. Bosch, X., A. Hayes, J. Doxandabaratz, et al., The value of electrocardiogram and vectorcardiogram in diagnosis of left atrial enlargement. *Adv. Cardiol.*, 1981; **28**: 238–241.
141. Di Bianco, R., J.S. Gottdiener, R.D. Fletcher, and H.V. Pipberger, Left atrial overload: a hemodynamic, echocardiographic, electrocardiographic and vectorcardiographic study. *Am. Heart J.*, 1979;**98**: 478–489.
142. Gutman, J., Y.S. Wang, D. Wahr, and N.B. Schiller, Normal left atrial function determined by 2-dimensional echocardiography. *Am. J. Cardiol.*, 1983;**51**: 336–340.
143. Termini, H.A. and Y.-C. Lee, Echocardiographic and electrocardiographic criteria for diagnosing left atrial enlargement. *South Med. J.*, 1975;**68**: 161–165.

144. Waggoner, A.D., A.V. Adyanthaya, M.A. Quinones, and J.K. Alexander, Left atrial enlargement. Echocardiographic assessment of electrocardiographic criteria. *Circulation*, 1976;**54**: 553–557.
145. Hirata, T., S.H. Wolfe, R.L. Popp, C.H. Helmen, and H. Feigenbaum, Estimation of left atrial size using ultrasound. *Am. Heart J.*, 1969;**78**: 43–52.
146. ten Cate, F.J., F.E. Kloster, W.A. van Dorp, A.T. Meester, and J. Roelandt, Dimensions and volumes of left atrium and ventricle determined by single beam echocardiography. *Br. Heart J.*, 1974;**36**: 737–746.
147. Munuswamy, K., M.A. Alpert, R.H. Martin, R.H. Whiting, and N.J. Mechlin, Sensitivity and specificity of commonly used electrocardiographic criteria for left atrial enlargement determined by M-mode echocardiography. *Am. J. Cardiol.*, 1984;**53**: 829–832.
148. Macruz, R., J.K. Perloff, and R.B. Case, A method for the electrocardiographic recognition of atrial enlargement. *Circulation*, 1958;**17**: 882–889.
149. Maok, J. and E. Krongrad, Assessment of electrocardiographic criteria for left atrial enlargement in childhood. *Am. J. Cardiol.*, 1984;**53**: 215–217.
150. Miller, D.H., R.R. Eisenberg, P.D. Kligfield, R.H. Devereux, P.N. Casale, and M.C. Phillips, Electrocardiographic recognition of left atrial enlargement. *J. Electrocardiol.*, 1983;**16**: 15–21.
151. Morris, J.J. Jr., E.H. Estes Jr., R.E. Whalen, H.K. Thompson Jr., and H.D. McIntosh, P-wave analysis in valvular heart disease. *Circulation*, 1964;**24**: 242–252.
152. Perosio, A.M., L.D. Suarez, A. Torino, J.J. Llera, A. Hallester, and J.M. Roisinblit, Reassessment of electrovectorcardiographic signs of left atrial enlargement. *Clin. Cardiol.*, 1982;**5**: 640–646.
153. Monteiro, A.A., A.C. de Aguiar, and R. Lopes, Mitral stenosis in sinus rhythm: electrocardiographic diagnostic criteria of left atrial enlargement, in *New Frontiers of Electrocardiology*, F. de Pádua and P.W. Macfarlane, Editors. Chichester. *Research Studies Press*, 1981, pp. 360–362.
154. Ishikawa, K., P.M. Kini, and H.V. Pipberger, P wave analysis in 2464 orthogonal electrocardiograms from normal subjects and patients with atrial overload. *Circulation*, 1973;**48**: 565–574.
155. Ishikawa, P. and H.V. Pipberger, Critical evaluation of the twin peaked P wave ("pseudo-P mitrale") in orthogonal electrocardiograms. *J. Electrocardiol.*, 1980;**13**: 181–184.
156. Brohet, C.R., C.-E. Liedtke, and N. Tuna, P wave abnormalities in the orthogonal electrocardiogram: correlation with ventricular overload in pulmonic and aortic valvular heart disease. *J. Electrocardiol.*, 1975;**8**: 103–112.
157. Reynolds, J.L., The electrocardiographic recognition of right atrial abnormality in children. *Am. Heart J.*, 1971;**81**: 748–759.
158. Cacho, A., R. Prakash, R. Sarma, and V.S. Kaushik, Usefulness of two-dimensional echocardiography in diagnosing right ventricular hypertrophy. *Chest*, 1983;**84**: 154–157.
159. Kushner, F.G., W. Lam, and J. Morganroth, Apex sector echocardiography in evaluation of the right atrium in patients with mitral stenosis and atrial septal defect. *Am. J. Cardiol.*, 1978;**42**: 733–737.
160. Reeves, W.C., W. Hallahan, E.J. Schwiter, T.J. Ciotola, E. Buonocore, and W. Davidson, Two-dimensional echocardiographic assessment of electrocardiographic criteria for right atrial enlargement. *Circulation*, 1981;**64**: 387–391.
161. Chou, T.-C. and R.A. Helm, The pseudo P pulmonale. *Circulation*, 1965;**32**: 96–105.
162. Morganroth, J., L.N. Horowitz, M.E. Josephson, and J.A. Kastor, Relationship of atrial fibrillatory wave amplitude to left atrial size and etiology of heart disease: an old generalization re-examined. *Am. Heart J.*, 1979;**97**: 184–186.

16 Myocardial Infarction

Ronald H. Selvester · David G. Strauss · Galen S. Wagner

P. W. Macfarlane, A. van Oosterom, O. Pahlm, P. Kligfield, M. Janse, J. Camm (eds.), *Comprehensive Electrocardiology*, DOI 10.1007/978-1-84882-046-3_16,

16.1 General Angiographic and Pathoanatomic Considerations

16.1.1 Essential Principles

Myocardial infarction (MI) by definition *is the process of the death of heart muscle from loss of its blood supply due to occlusion of the nutrient-supplying coronary artery*. Three important points must be taken into account in the functional/angiographic and pathoanatomic consideration of myocardial infarction. First, the location and potential maximum size of the infarct *resulting from this process* is related to the location and extent of the perfusion bed of the occluded coronary artery. Second, the acute electrocardiographic (ECG) changes of ischemia/injury, the ST displacement vectors, are directed outward away from the center of the epicardium in the region of the involved myocardium. The magnitude of this displacement vector is related to both the extent and severity of regional coronary non-perfusion. The direction of this vector in 3D space is a marker for the specific coronary artery or branch occluded when there is typical coronary artery distribution to the myocardium. Third, the death of myocardial cells and the loss of local electric current dipoles from the myocardial excitation wave surface is the *sine qua non* of a completed myocardial infarct. This is seen as loss of ventricular forces (QRS voltage) over time on the electrocardiogram (ECG), that is, loss of local QRS spatial vectors (see Chap. 2). The extent of the spatial magnitude and duration (the voltage time integral) of the lost pre-existing local QRS vectors (reflected in loss of localized 12-lead ECG forces), is quantitatively related to the size of the resultant infarct.

The atrioventricular (AV) node sends, via the bundle of His and the branching His-Purkinje conduction system, excitation impulses from the sinus node through the upper chambers of the heart to both the right and left ventricles. Bundle branch fascicles insert into the fine ventricular endocardial peripheral network of this conduction system. This starts the wave of ventricular excitation from endocardium to epicardium in the contractile myocardial cells. Even major myocardial infarction occurs without significant damage to this fine inner endocardial peripheral Purkinje network since it receives its blood supply directly from the cavity blood. However, infarction may produce block of all or part of the thicker proximal left or right bundle branches since these receive their blood supply from intramural septal arteries. Thus proximal coronary artery occlusion can result in a complete right bundle branch block (RBBB), left anterior-superior fascicular block (LAFB), left inferior-posterior fascicular block (LIFB), or complete left bundle branch block (LBBB). Infarction is also seen in the presence of ventricular hypertrophy or dilatation, and with repolarization changes of acute or chronic ischemia. The spatial vector change in the finally recorded ECG is a variable combination of all these effects. The complexity of these interactions precludes the memorization of ECG patterns. A thorough understanding of the three-dimensional (3D) spatial aspects of normal excitation and recovery (Chaps. 4 and 5), and that of the conduction defects just described, along with the QRS and ST-T changes tightly linked to them are prerequisites for the rational understanding and interpretation of the ECG. To quote J. Willis Hurst in his 2003 paper [1] on . . . "Suggestions for the Improvement of the Interpretive Process" of clinical ECG, "*The best way to interpret tracings is to learn the basic principles of electrocardiography, including vector concepts, and apply them to each tracing that is being interpreted. Without such an approach, people who memorize are helpless when they see tracings that they have not seen before*."

This chapter is dedicated to bridging this gap. The local spatial vector changes of acute myocardial infarction lend themselves to quantitative analysis relating to the time from the initial incident into the acute phase, the area at risk, and the potential for myocardial salvage. The loss of local QRS forces from the resultant infarct, in normal and abnormal conduction, can be related quantitatively to the resulting infarct size, functional reserve, and life expectancy.

16.1.2 Historical and Future Perspective

In 1963, Hodgkin and Huxley received the Nobel Prize in medicine for "their discoveries concerning the ionic mechanisms involved in excitation and inhibition in the peripheral and central portions of the nerve cell membrane" [2]. They performed key experiments in 1939 and provided an explanation in 1945 of how the nerve conducts its impulse. Their explanation was that the membrane becomes momentarily very permeable to sodium ions which are positively charged and are much more concentrated outside cells than inside. Later, they came across a paper by Overton, who in 1902, made the same observation in muscle [3]. Overton then repeated the experiment on nerve where he put it in salt-free solution,

but the nerve continued to work. He concluded that the nerve is surrounded by a sheath that holds sodium around the fibers.

In 1918, Smith recorded the electrocardiogram in dogs after ligating coronary arteries [4] and, in 1920, Pardee recorded an electrocardiogram of a patient with an acute coronary occlusion [5]. Pardee described the appearance of ST elevation in leads II and III and correctly observed that the ST segment electrical forces were pointing down toward leads II and III. However, at this time it was not understood that the ST vector from transmural ischemia would point away from the heart rather than toward its center.

A number of experiments in the following years showed that electrode location, as well as the size of the ischemic region, affected the magnitude and direction of ST-segment change [6, 7]. In 1933, Frank Wilson applied many of the recently developed electric field theories to the electrocardiogram [8]. Specifically, he developed his central terminal and used the solid angle theorem to evaluate proximity effects [9, 10].

16.1.2.1 The Electrocardiogram to Index the Extent and Severity of Ischemia

In the early 1970s, Braunwald and Maroko proposed that altering myocardial energy supply and demand following coronary occlusion might influence the extent and severity of ischemic injury [11]. They looked to ST-segment elevation on the electrocardiogram as a simple and reproducible means of indexing ischemia. Studies utilizing epicardial electrodes in animals reported that the severity and extent of myocardial ischemia-infarction could be reduced by different therapies including propanolol, nitroglycerin, norepinephrine, mannitol, hypertonic glucose, hyaluronidase, hydrocortisone, cobra venom factor, and others. However, these investigators did not consider the physiologic and theoretical basis of the ST-elevation which had been described decades before by previous investigators. In response, Holland and Brooks performed a series of experiments where they theoretically and experimentally tested the effects of spatial and non-spatial factors on changes in the ST segment in the pig heart [12, 13]. They demonstrated that epicardial ST-segment measurements were not reliable markers of the extent of ischemia, and that increasing size of ischemia could lead to a decrease in the amount of ST-elevation when the electrode was located on the center of the ischemic area. They explained this finding by using solid angle theory.

Following the publications by Holland and Brooks, Braunwald and Maroko published an editorial: "ST-segment mapping: Realistic and unrealistic expectations" [14]. Indeed, direct histological methods to determine infarct size later showed that infarct size expressed as a percentage of the perfusion area was not significantly altered by any of these proposed early therapies [15]. However, this initial work helped stimulate two key fields of research: (1) detailed characterization of the electrophysiology of ischemia and (2) a search for interventions that could limit infarct size.

16.1.2.2 Current and Future Perspective

In the same way as investigators turned to the electrocardiogram when investigations to limit infarct size developed in the 1970s, physicians have recently turned to the electrocardiogram to identify heart failure patients with suspected LV dyssynchrony who might benefit from cardiac resynchronization therapy (CRT) with biventricular pacemakers. This is logical if the patient has a left bundle branch block type electrical activation with considerable delay between contraction of the septum and LV free wall. However, investigators have not used identification of the morphology of LBBB as a criterion for CRT, but rather a QRS duration >120 ms. Not surprisingly, one-third of patients do not respond to CRT. As will be described in this chapter, there are a number of other pathologies that can affect QRS duration which do not have significant asynchrony between the septum and the LV free wall, namely left and right ventricular hypertrophy, left anterior-superior fascicular block, left inferior-posterior fascicular block, right bundle branch block, intra/peri-infarction block, fibrosis, and any combination of these pathologies. Grant and Dodge [16] studied patients with ECGs before and after new onset LBBB and observed that all patients had a QRS duration ≥140 ms with LBBB. Furthermore, as described in this chapter, combinations of fascicular blocks and LVH can cause QRS durations >140 ms that can only be differentiated by QRS morphology. In this chapter, we will make a conscious effort to relate three-dimensional anatomy, electrophysiology, and vector concepts to interpreting ECGs and vectorcardiograms.

16.1.3 Nomenclature and Definitions

The extent of a completed myocardial infarct (MI), defined as the death of myocardial cells from loss of their blood supply, can vary from a few dozen cells replaced by scar, i.e., a microinfarct, to a very large scar from one or more infarcts replacing 50% or more of the heart. Commonly, the term myocardial infarct is used for focal lesions of 1 cm^3 (50–60 million cells) or more caused by major atheromatous and clot occlusion in one or more coronary arteries. *Throughout this chapter, we will use the term* ***acute myocardial infarction*** *for the early process of creating these very large clusters of dead and dying cells and* ***myocardial infarct*** *when the process has been completed, with dead and necrotic cells being, or having been, replaced by a collagen scar***.** Microscopic scars that have replaced a few hundred to a few thousand cells can pathologically and etiologically properly be called micro-infarcts, and larger clusters of scar replacing a few hundred thousand cells can properly be called macro-infarcts. However, in order to separate these minute scars that generally occur with peripheral small vessel disease from the larger ones of 1 cm^3 or more, described above, *it is conventional to refer to clusters of small* (*micro or macro*) *scars as* ***local, multifocal, or diffuse myocardial fibrosis.***

16.1.3.1 Myocardial Subdivisions

As far as nomenclature of the various myocardial regions is concerned considerable inconsistency and ambiguity exist in the pathology literature, the ECG literature, and in the literature of the various disciplines concerned with imaging the heart. In 1984, the Committee on Nomenclature of Myocardial Wall Segments of the International Society of Computerized Electrocardiography [17] recommended the adoption of a 12-segment left ventricular (LV) subdivision (Fig. 16.1) based on the Ideker 24 LV segment [18] and the Horan et al. 12 LV segment subdivision [19]. The earlier Ideker subdivision was made up of eight circumferential (octant) subdivisions starting with the center of the septum in serial bread-loaf cross sections of the heart as shown in the mid LV cross section, lower right of Fig. 16.1. Each two adjacent octants were

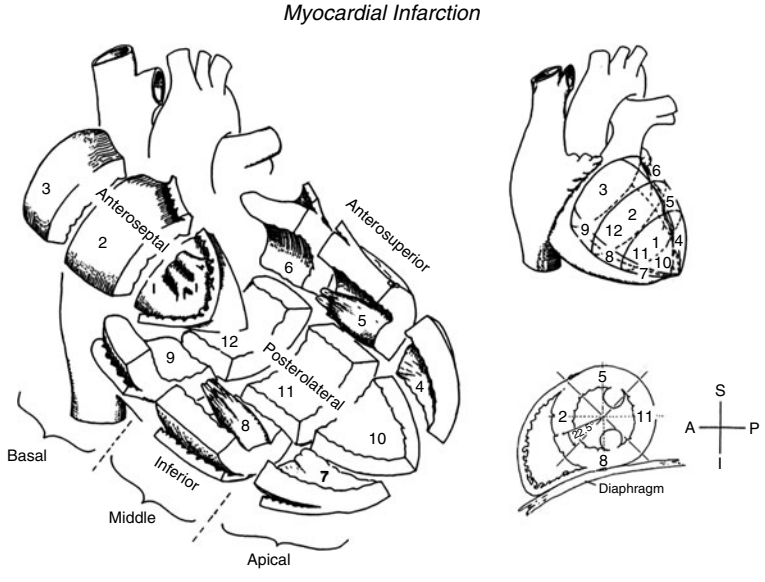

Figure 16.1

12–segment LV subdivision recommended by the Committee on Nomenclature of Myocardial Wall Segments of the International Society of Computerized Electrocardiography. It is derived from the circumferential octant subdivision of Ideker with 24 LV segments merged to a quadrant subdivision of 12 segments as described in the text. The original octant boundaries are indicated by the *dotted lined* in the *lower right portion* of the figure (A. anterior: P. posterior: S superior: I. inferior).

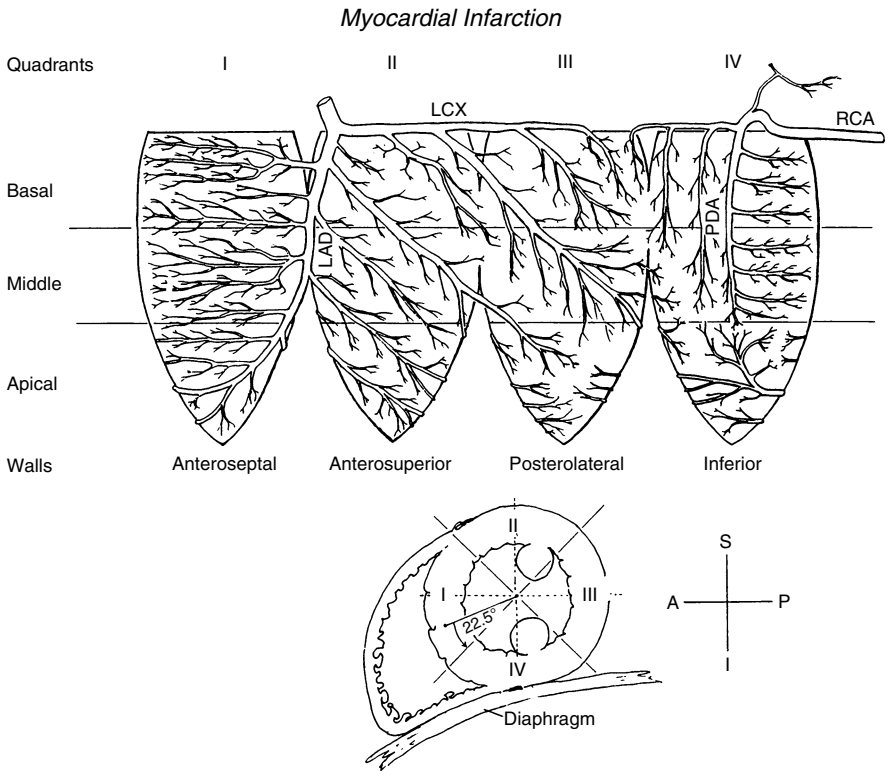

Figure 16.2

A Mercator projection of the epicardial surface of the left ventricle with a typical distribution of the three major coronary arteries. This specific circumferential quadrant subdivision has the advantage of dividing the left ventricle along the lines of the perfusion beds of the three main arteries. As indicated in the cross section of the heart below, the superior 75–80% of the anteroseptal wall is perfused by septal perforator branches of the left anterior descending (LAD). The inferior 20–25% of the septum is perfused by the shorter septal branches of the posterior (inferior) descending artery (PDA), one of the two distal branches of the right coronary artery (RCA) and is included in the inferior wall. The other distal posterolateral branch of the RCA perfuses the other half of the inferior quadrant via 2–4 marginal branches. As indicated in this diagram, the LAD typically supplies all of the three apical (anteroseptal, anterosuperior, inferior) segments and the distal half of the apical posterolateral segment. It also supplies the remaining anteroseptal and anterosuperior walls. The basal segment of the anterosuperior wall has a dual blood supply. Except for the distal half of the apical segment, the posterolateral wall is supplied by the left circumflex (LCX) coronary artery.

combined to provide a quadrant subdivision of four walls: Octant 1 and 2, as anteroseptal, 3 and 4 as anterosuperior, 5 and 6 as posterolateral and 7 and 8 as inferior. Octant 1 was set in the mid septum with the lower anteroseptal boundary dividing the septum, 3/4th for the longer septal arteries from the left anterior descending, and 1/4th for the shorter septals from the posterior descending. The LV was further subdivided from apex to base into three regions (apical, middle, and basal) by passing three planes at right angles to the **internal** long axis of the LV. This internal long axis is divided into three equal parts, thereby producing the final 12 segments of approximately equal volume as shown in Fig. 16.1. This quadrant subdivision of 4 walls of 3 segments each has the advantage, as shown in Fig. 16.2, that the boundaries of the perfusion beds of each of the three main coronary arteries usually overlay segmental boundaries. An analogous recommendation appeared at about the same time from the Committee on Nomenclature and Standards of the American Society of Echocardiography [20]. The anatomic landmarks, definition and nomenclature of the 12 LV segments, which are shown in Fig. 16.1, will be used throughout this chapter.

16.1.3.2 Extent and Sites of Myocardial Infarction and Related Coronary Artery Occlusions

Considerable inconsistency and ambiguity also exists with respect to the labeling of the extent, transmurality, and location of infarcts. The evolution of the labeling of extent/transmurality is as follows: Myocardial infarcts (MIs) with abnormal Q waves have been called transmural and those without were labeled as subendocardial. In later years, a number of investigations [21–23] documented that many of the "transmural" MIs were limited to the subendocardium at autopsy and the absence of abnormal Q waves was noted in a significant number of pathoanatomically large transmural MIs. Thus, in the earlier era of non-reperfusion, descriptive labels "Q-wave MI" and "non-Q MI" gained common usage. In the current early reperfusion era, patients with persistent or unstable resting chest pain and major ST elevation (so called ST elevation MI – or STEMI) have been labeled "acute injury/infarction" with the expectation that a (transmural) Q-wave MI would evolve; those with such chest pain and 1) sub threshold localizing ST elevation or 2) significant ST depression (Non STEMI ECGs) were labeled probable subendocardial infarction. Again, a number of patients with STEMI failed to develop abnormal Q waves and a number with NSTEMI did. The labeling of location and extent of evolving myocardial infarcts has also undergone a similar evolution. The 2007 ACC/AHA guidelines [24] for the management of NSTEMI/UA (Unstable Angina), a subset of Acute Coronary Syndrome, has defined the two major subgroups, (1) and (2) above, of NSTEMI as "High Risk NSTEMI." These groups had a higher in hospital, 30 day and 1 year mortality than acutely revascularized STEMI. These are STEMI equivalents and should be considered for emergency coronary angiography with the intention of performing PCI (percutaneous coronary intervention) or referral to emergency bypass surgery.

The structures and regions in question are all in the human thorax, where the anatomic conventions of the upright human have become widely used: superior, toward the head (cephalad); inferior, toward the feet (caudad); anterior, toward the front of the subject (ventral); and posterior, toward the back (dorsal). The ambiguity in terminology and the plethora of terms, including many hyphenated terms for location (and extent) of MI and cardiac anatomy that have evolved through the last two centuries have arisen from two main sources: (1) the lack of strict adherence to the anatomic conventions of the upright human described above and (2) the fact that the long axis of the heart (and the apex of the LV) is angled forward at about 30° from the frontal plane and downward from the horizontal plane at about the same angle. Three well-defined groups of localized myocardial infarcts can be identified anatomically and angiographically, each being associated with occlusion of one of the three major coronary arteries and/or their branches. Infarcts in each of these arterial distributions range in size from being very small to very large.

Of the ambiguous and at times contradictory terms used to designate location and extent of infarcts, the most contradictory and confusing is "lateral." For infarcts involving the distal LAD and the LV apex with ST elevation and or abnormal Qs in one or more of I, V5, V6, electrocardiographers commonly report "lateral infarct"; if V4 is involved they report "anterolateral" infarct, and when aVL is involved, "high lateral." Early pathoanatomists called the wall between the papillary muscles "lateral," as seen in the LCX distribution in Fig. 16.2. This wall is still being so labeled by some who are currently imaging the heart. Electrophysiologists dealing with accessory pathways from the atrium to the ventricles tend to call tracts to the base of the right ventricle "anterolateral bypass tracts," and those to the mid basal left ventricle "posterolateral bypass tracts." The inferior wall was labeled posterior by early pathoanatomists, cardiologists and electrocardiographers. It has evolved through diaphragmatic to inferior over the past 60 years. Thanks to earlier AHA guidelines, the most inconsistent of this set is often the basal segment of the inferior wall still being called posterobasal in some recent reports. But this appears to be on the wane. The branch of the RCA supplying the inferior wall is in general called the posterior descending artery (PDA), while there is still reference to the posterior papillary muscle which originates from the inferior wall.

To be simple, brief, and anatomically consistent, the anatomic conventions of the upright human will be used throughout this chapter. For the sake of clear interchange between electrocardiographers, vectorcardiographers and those engaged in the various disciplines that image the heart and thorax, the following nomenclature is strongly recommended.

(a) *Anterior myocardial infarct* (with size modifiers in [f] below) is used for all infarcts resulting from occlusion of the left anterior descending (LAD) coronary artery. This involves both the anteroseptal and anterosuperior walls and usually the inferior apical segment, (see Fig. 16.2). Anterosuperior myocardial infarct (with size modifiers in [f] below) is used for occlusion of the major diagonal branch of the LAD.

(b) *Posterolateral myocardial infarct* (with modifiers in (f) below) refers to all infarcts resulting from occlusion of the posterior left circumflex (LCX) coronary artery or its branches. This involves mainly the posterolateral wall (see Fig. 16.2).

(c) *Inferior myocardial infarct* (with modifiers in (f) below) includes all infarcts resulting from occlusion of the usually dominant right coronary artery (RCA) which supplies the posterior (inferior) descending coronary artery (PDA) and its posterolateral branches (as shown in Fig. 16.2). This usually involves mainly the middle and basal segments of the inferior wall.

(d) *Note*: The term "*posterolateral-inferior myocardial infarct*" (with modifiers in (f) below) will be used in the special case where a combination of (b) and (c) occurs with significant infarction of both the posterolateral wall and the inferior wall of the LV. This commonly occurs from occlusion of a dominant LCX artery, which also has the PDA as its most distal branch. It may also occur from occlusion of a rare dominant RCA with a very large posterolateral branch and a diminutive LCX.

(e) *Apical extension*, with ECG and spatial vector changes in right to left apically oriented leads I, aVR, V4, V5, V6, and X, most commonly occurs with an anterior infarct, in which case the size modifiers below indicate apical extension. A specific notation of "with apical extension" or "anteroapical infarct." while quite appropriate, is redundant. Significant apical extension can occur as a part of local posterolateral or inferior infarct, in which case it is appropriate not only to use the probability and size modifiers but to specify "posteroapical," "inferoapical" or "with apical extension." Because of the ambiguous and variable, often contradictory usage of "lateral" by the many disciplines that describe regional cardiac anatomy [25], the term will be used here only in combination with posterior for the posterolateral wall of the LV.

(f) *Probability modifiers such as* **consider, possible**, **probable and none** and *Size modifiers such as* **small, moderate, large** and **very large** will be used with each infarct diagnostic category in order to indicate both the ECG reader's confidence in the interpretation and the extent of the infarct. The quantification of extent or size of the infarct linked to size modifiers and the statistical basis for their combination with the probability modifiers are dealt with in more detail in Sect. 16.3, and Table 16.3.

16.1.3.3 Myocardial Fibrosis (Multifocal Infarct): Etiology and Common Terms

By definition, infarction is the death of any tissue as a result of disruption of its nutrient blood supply. The resultant myocardial infarct may be a consequence of major atheromatous and clot occlusion in the proximal coronary arteries, or arteriolar micro vascular disease such as in diabetes and hypersensitivity vasculitis, rheumatic disease, collagen disease and so on. In this case, the resultant infarct is very small and multifocal owing to small-vessel occlusion, and may be irregularly scattered throughout the heart or may be uniformly distributed. A similar mechanism can be seen in viral and bacterial vasculitis with intramural and perivascular infiltrate, leading to multifocal local arteriolar occlusion and multifocal infarct. Diffuse fibrosis, by this mechanism, causes excessive fragmentation of the QRS complex as seen on a high-gain high-frequency (1000 samples/s and signal averaged) ECG. In many patients of this group, there is a mixed inflammatory and hypersensitivity response, but the myocardial consequence is similar, that is, many small-vessel occlusions leading to multifocal infarcts. The changes as a result of myocarditis are discussed in more detail in Chap. 20 along with the infiltrative diseases of the heart.

The ECG changes produced by these multifocal infarcts depend upon the extent or size of each focal area of necrosis. If these are minute (<0.5 mm across), and diffuse the main consequence will be an overall loss in myocardial substance. The lesions are so small that except for decreased voltage, they produce little discernible local change even in high-gain high-fidelity ECG records. When individual local macro-infarcts are both larger (2–3 mm across) and multifocal, extensive high-frequency notching and fragmentation of the entire QRS in the 150–300 Hz range may occur. While the term "multifocal myocardial infarct" for both micro- and macro- lesions is pathologically and etiologically appropriate, common medical usage has linked the term "myocardial infarct" to larger, more discrete infarcts associated with major coronary artery occlusion. The term "myocardial fibrosis" has gained common usage for these minute infarcts. We will use the term myocardial fibrosis for the usual appropriate modifiers to indicate the severity and extent of the process, and to describe the ECG changes associated with these lesions. They may be either "localized" or "diffuse."

16.1.3.4 High Frequency Signal Averaged ECG Recording

The term "high frequency ECG" has come to be associated with signal averaging and 1000 samples per second (sps) digitizing rate. This sampling rate covers the upper frequency range of 400 Hz. To make maximal use of these higher frequencies, ECG preamplifiers are adapted to be 2.5–3x the usual upper response rate of 150 Hz of conventional ECG recorders. For the signal averaging process, a typical P QRS T waveform for a specific ECG is chosen as the template for the complete cycle. Each following beat or cycle is compared to the template. Those with a high correlation with the template are time aligned with it to the nearest ms (millisecond) and averaged together. Waveforms that are ectopic, aberrant, or very noisy are excluded by this process. Muscle artifact, electromagnetic noise, and baseline wander that is not systematically related to the ECG waveform are suppressed by the averaging of the time aligned ECG signals. The number of beats that must be averaged together depends on the resolution desired for any application, and the severity of the baseline artifact or noise that needs to be suppressed. This methodology is also used for low amplitude high frequency QRS late potentials and for detailed high resolution digital P wave studies. (see Chap. 36).

16.1.4 Regional Distribution of Myocardial Infarcts and Coronary Anatomy

Atherosclerotic occlusive coronary artery disease generally occurs in the proximal third of the coronary tree and involves major branches of this system, often near bifurcations. The posterior descending artery, usually a distal branch of the right coronary artery is the major exception to this rule. The extent of evolving infarction from proximal coronary occlusion in any artery perfusion bed is a function of the size of the area at risk [26]. It is also inversely related to the amount of effective forward collateral circulation that developed around the obstructive lesion and into the area at risk beyond and/or retrograde to collaterals, from well perfused neighboring coronary vascular areas [27]. The size of the associated infarct may vary from none visible angiographically (as in 15–20% of all total occlusions) to all or nearly all of the area at risk in a given perfusion bed (8–10% of all total occlusions). Even though the coronary occlusion is in the proximal few centimeters, in most occlusions smaller infarcts tend to localize to the distal distribution of the involved artery. They are mostly subendocardial consistent with Reimer and Jennings' "wave model of infarction" [28].

16.1.4.1 Left Anterior Descending (LAD) Coronary Artery Occlusion

The resulting infarcts from LAD occlusions, when small, tend to localize at the anterior apex (Fig. 16.3). Moderate-sized infarcts involve the apex and more of the middle segments of the anteroseptal and anterosuperior wall. Large infarcts involve the apex circumferentially and most, or all, of the middle anteroseptal and anterosuperior walls. Very large infarcts involve the same regions and usually extend into the basal segments of the anteroseptal and anterosuperior walls. However, complete involvement of these basal segments even with very large infarcts is uncommon. Four main locations of the LAD coronary artery produce four smaller subsets of these various-sized anterior infarcts as follows:

(a) The mid to distal LAD in most patients, with its "wrap around" onto the distal third of the inferior wall, perfuses the two anteroapical segments of Fig. 16.2, the inferoapical segment and a variable portion of the posteroapical segment. The size of any infarct from distal LAD occlusion thus may vary from small to moderate. In the occasional patient with a very dominant LAD and extension of the "wrap around" well into the inferior middle segment, the infarct may be large. Mid LAD occlusion distal to the first large diagonal may also result in large infarcts.
(b) The proximal main diagonal branch of the LAD perfuses the basal and middle segments of the anterosuperior wall with variable extension to the apical posterolateral segment (see Fig. 16.2). Any infarct from proximal occlusion of this diagonal branch is usually small, occasionally moderate in size, following the diagonal perfusion bed across the anterosuperior wall.
(c) The proximal first septal perforator branch of the LAD perfuses the basal segment of the anteroseptal wall. Isolated occlusion of this branch is uncommon, and the associated infarct is generally small.

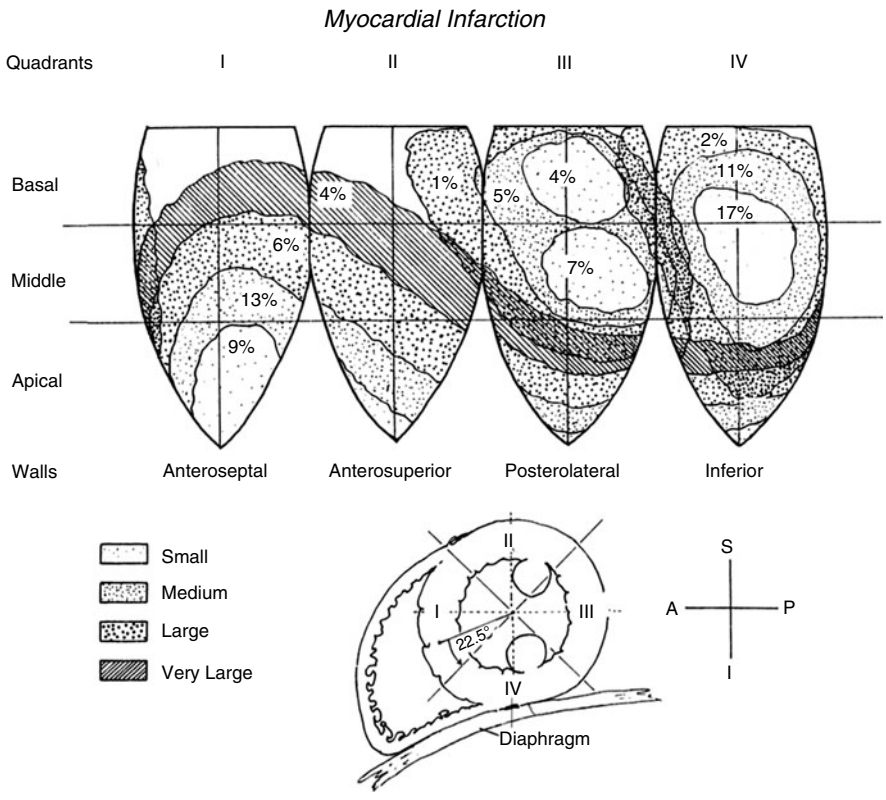

Figure 16.3

The same mercator projection of the epicardial surface of the left ventricle as shown in Fig. 16.2. Shown here is the regional distribution of the single infarcts seen on biplane ventriculograms (79% of visible infarcts from the Rancho/USC database*). Not included in this figure are the 21% of patients with multiple infarcts. Note that the majority of these single infarcts involve less than half of the potential risk area, and when small tend to localize in the distal distribution of the particular vascular bed. As a result of the smaller areas potentially at risk, posterolateral and inferior infarcts tend to be small to moderate in size. Large to very large anterior infarcts involving more than 25% of the left ventricle, with the concomitant severe dysfunction and ejection fraction below 40% occur in 10% of all of these single infarcts but occurs in only 1% for posterolateral infarcts and 2% for inferior infarcts. By contrast, well over half of the 21% of patients with multiple infarcts have the sum of infarcts as large to very large, severe LV dysfunction and ejection fractions usually well below 40%. * Footnote: Beginning in 1967 the Rancho Los Amigos Medical Center campus of the University of Southern California (Rancho/USC) instituted a post-infarction and chronic angina cardiac rehabilitation program. The coronary angiographic database referred to in this figure, and throughout this chapter, consisted of 701 patients from this program. Biplane ventriculograms of 603 revealed local wall motion abnormalities in the distribution of an occluded coronary artery consistent with myocardial infarct. A single infarct was present in 476/603 (79%). Multiple infarcts were noted in 127/603 (21%). An additional 74 patients had one or more totally occluded coronary arteries and no visible infarct. Another 24 had severe multi-vessel coronary disease and diffuse wall motion abnormality (hypokinesis) with no localization, and a low ejection fraction consistent with severe ischemic myopathy.

(d) The LAD perfuses more than 50% of the LV. Occlusion of this artery proximal to the first diagonal and the first septal perforator, produces a sum of all the effects a, b, and c, above. Depending on how late in life this occurred and how aggressive was the formation of collaterals around the obstruction and from the other two major coronary arteries, the infarct size can vary from non existent (15–20% of such occlusions) to very large and lethal.

16.1.4.2 Non-Dominant Left Circumflex (LCX) Occlusion

Three locations of occlusion are found, usually in the proximal third of the LCX distribution. The resultant infarct size varies from none to all of the specific area at risk. The three cases are as follows:

(a) Left obtuse (main) marginal circumflex occlusion usually occurs at or near its origin. The region of perfusion for this artery is mainly the middle segment of the posterolateral wall with variable extension into adjacent regions (Fig. 16.2). Small infarcts are usually localized in the middle posterolateral segment near its junction with the apical posterolateral, middle inferior and apical inferior segments (see Fig. 16.3). Moderately sized posterolateral infarcts involve most or all of the posterolateral mid-region with extension to the aforementioned adjacent regions as well. Large infarcts are uncommon with occlusion of this branch of the LCX.
(b) Local occlusions also occur in the distal circumflex beyond the branch point of the proximal LCX into the main marginal and distal branch. Total occlusion of the distal non-dominant LCX usually produces small basal posterolateral infarcts (Figs. 16.2 and 16.3).
(c) Total occlusion of the proximal non-dominant LCX produces a combination of the effects of (a) and (b). Subsequent infarcts may range in size from virtually nothing (15–20% of such occlusions) to moderate or large posterolateral infarction involving most of the posterolateral wall, usually with extension onto some of the inferior wall.

16.1.4.3 Dominant Left Circumflex (LCX) Occlusion

Only 10–15% of subjects have a dominant LCX in which the posterior descending artery is a branch of the circumflex. Under these circumstances, the circumflex perfuses about half of the left ventricle while the LAD perfuses the other half. Very large infarcts occur with total occlusion of such an LCX artery in about the same percentage of patients as with total LAD occlusion. The low incidence of left dominant anatomy, however, accounts for the very low incidence of single-vessel LCX occlusion with very large posterior-inferior infarcts (0.4% of angiographically demonstrable single infarcts) as compared to single-vessel LAD occlusion and very large anterior infarcts of 4%. In 15–20% of cases with proximal total occlusion of a dominant LCX with good collaterals, like other major coronary arteries, there will be no angiographically demonstrable infarct. Small infarcts usually involve the middle posterolateral and inferior regions (Fig. 16.3). Moderately sized infarcts extend into the inferior posterior base and usually somewhat toward the apex. Large infarcts involve most or all of the inferior and posterolateral mid-region and base, and extend into the apex and the inferior anteroseptal wall.

16.1.4.4 Right Coronary Artery (RCA) Occlusion

Most occlusions of the right coronary artery occur in the proximal third, although a significant number of patients have occlusion of this artery in the middle third, or where the posterior descending artery branches off. The proximal occlusions have a significant incidence of right ventricular involvement whereas the distal occlusions do not. The ECG criteria for the diagnosis of this variable right ventricular infarct are presented in Sect. 16.4.5. The effect on the left ventricle of all three locations of total occlusion of the right coronary artery is similar. One fourth of these occlusions occur with little or no infarction. When present, small infarcts are usually in the inferior mid-region (Fig. 16.3). Moderately sized inferior infarcts will have extended into the basal segments of the inferior and posterolateral walls. Larger inferior infarcts are uncommon and, when present, may extend into the inferior apex, into the lower third of the middle and basal segments of the septum, and into the lower third or more of the entire posterolateral wall. These RCA lesions are associated with a very right dominant coronary artery with a large posterolateral branch and a minimal circumflex. They would be indistinguishable, both anatomically and by ECG, from a mid total occlusion of a dominant LCX artery except in acute infarctions, for the absence of ECG and clinical signs of acute right ventricular infarct in the latter.

In summary, the relationships of size and location of angiographically demonstrable first or single infarct and the percentage distributions of each in the major coronary perfusion beds are shown in Fig. 16.3. Single local infarcts that

are a result of RCA or LCX occlusion are usually small (28% of all infarcts), are occasionally moderate in size (12%) and are only rarely large to very large (3%). On the other hand, anterior infarcts from LAD occlusion are approximately equally distributed between small (10% of all infarcts), moderate (7%), and large to very large (10%). It is prudent to take these prior probabilities as to size and location into account, looking for subtle mid and late (non Q) loss of QRS forces when interpreting ECGs.

16.1.4.5 Multiple-Vessel Occlusion

Multiple lesions from multiple-vessel occlusions account for 21% of all patients with coronary disease and myocardial infarct in the Rancho Los Amigos Hospital, University of Southern California (Rancho/USC) database. While total occlusion of two or three vessels does occur without visible infarct or demonstrable ventricular dysfunction, it is uncommon. In the Rancho/USC series of 45–65 year olds, patients with documented coronary disease, 14% have total occlusion of 1 vessel, 5% have total occlusion of two vessels, and 2% have total occlusion of three vessels without visible infarct on biplane ventriculograms. Not unexpectedly, it is much more usual for multiple-vessel occlusion to be associated with significant infarcts. Three fourths have significant or severe ventricular dysfunction. This is generally because the total extent of infarcts exceeds 30–40% of the LV. The distribution of the extent of damage from multiple occlusions in this dysfunctional subset is as follows: 10% of this group have two small discrete local infarcts that together involve <15%LV; 15% have multiple infarcts with the total extent of damage involving 15–24% LV; 30% of multiple lesions are localized larger infarcts totaling 25–35% LV; and 45% have extensive damage overall of more than 35% of the LV, severe LV dysfunction, and a very poor prognosis. One third of these multiple lesions will not show the "classic changes" of myocardial infarct, but will in general show the extensive QRS slurring and/or notching/splintering, attenuation of R or S, and abnormal R/Q or R/S ratios that will be covered in detail in Sect. 16.3. In 2–3% of all clinical infarcts, severe diffuse ischemic myopathy occurs without obvious localized or regional wall dysfunction. These patients have diffuse and extensive scarring (ischemic cardiomyopathy) at pathological examination that is often unrelated to the overlying specific coronary occlusive lesions.

16.2 Infarct Anatomy and Related Electrophysiology

16.2.1 Geometry and Anatomy of Typical Myocardial Infarcts

Although occlusion of a proximal coronary artery produces a spectrum of changes, from no pathological change to very large infarcts, there is a rather typical anatomy of these lesions related to their size. Generally, infarcts of increasing size develop along the "wavefront" model of Reimer et al. [28] in any coronary distribution. Small infarcts 2–3 cm in diameter are in general limited to the subendocardial half of the myocardial wall. Moderate 4–6 cm lesions generally extend into the subepicardial half of the wall in their central one third, while their peripheral two thirds are subendocardial. The largest infarcts have a similar geometry, most extending to the epicardium in their central third. The shaggy outer border zone of the moderate healed infarct in Fig. 16.4 is an example of the typical admixture of interdigitating islands of collagenous scar and viable electrically active myocardium that is the determinant of the local electric field generated from an infarcted region. An understanding of this complex geometry is the prerequisite to the rational interpretation of surface ECG changes. Infarcts of the size shown in the figure usually are not truly "transmural," because they have significant viable subepicardial myocardium surviving over their central region. While not shown here, in infarcts with substantial replacement of necrotic myocardial cells by collagen scar, the scar shrinks with time, producing considerable thinning of the wall of the heart. In section AA in Fig. 16.4, the effect of the complex border zone where activation fronts must thread their way through and around large pseudopods and islands of scar is clearly evident. The active area of the local electromotive surface changes rapidly, and varies considerably as it moves around the infarct through the viable subepicardium. Since these fronts approach each other as they progress toward the epicardial center over the infarct, they tend to cancel out much of the current fields coming from the "shrinking doughnut" of the excitation wave as it extinguishes itself. This local disruption of the usual continuity of the activation fronts accounts for the remarkable

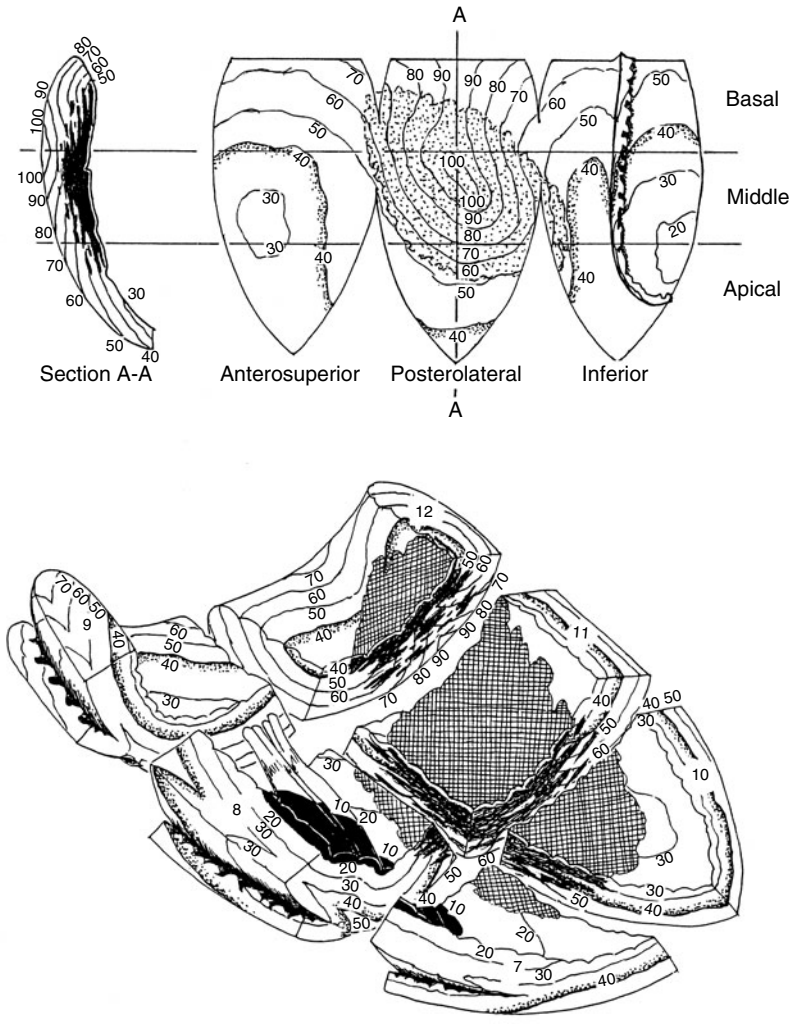

Figure 16.4

Diagrammatic representation of a small posterolateral infarct in the distribution of the main marginal branch of the LCX, as seen in Fig. 16.2. It involves mainly the middle segment of the posterolateral wall. Isochrones of activation at 10 ms intervals are indicated beginning, as shown in black, at the base of the inferior papillary muscle. The mercator projection of the same unrolled LV, except for the anteroseptal wall, is shown in the upper portion of the figure. The infarct shown is confluent in the subendocardium, extends midway through the wall in a small central portion of the middle segment. As is typical of such lesions it has extensive islands and pseudopods of inactive scar interdigitating with electrically and histologically normal myocardium throughout the border zone of the infarct. As the result of the dense scar, activation can only reach the viable epicardial layers of the LV wall from around the border of the infarct, delaying activation of this part of the heart. In the border zones, the activation fronts encounter many small local scars, producing a significant increase in high frequency components of the signal arising from the region. The main surface ECG changes from this lesion will be noted at 30–100 ms into the QRS. There will be significant loss of posterior forces, notching, slurring of the mid-to-late QRS. The attenuation of these posterior vectors leads to an imbalance in the anterior-posterior forces seen in leads V1, V2, V3, and *Z* as smaller S (post.) and larger R (ant.) waves and increased R/S (ant/post) ratios.

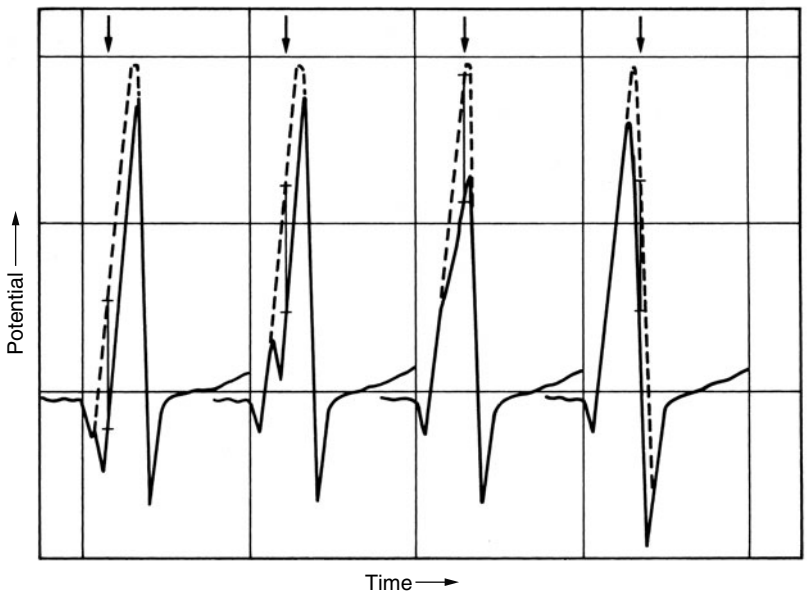

Figure 16.5

The four panels represent V6 with a small infarct (15 × 7 mm) placed at various levels in the junction of the inferior and posteroapical segment of the propagation model of the heart. The dotted line in each case represents the normal activation without infarct as seen in V6. In the first panel the lesion is placed in the endocardium. In each of the following panels, the center of the lesion is moved outward by 2.5 mm. The arrows represent the time when the activation front passed the center of the small lesion in each instance. In the first case abnormal Q waves were produced only by a very strategically placed lesion. Notched R ("bite out"), attenuated peak R or a change in R/S ratio are equally valid markers of infarction in the wall of the left ventricle. In basal segments in general, and in middle posterolateral segments activated in the mid to later portions of the QRS, only mid to late QRS changes will result from even extensive infarction.

increase in high frequency splintering and notching of the QRS complex. These changes are readily seen in properly recorded high frequency, high gain unipolar epicardial electrograms and surface ECGs. Changes are most evident in leads perpendicular to the advancing wavefront in the myocardium, and occur, of course, at that time in the QRS when the local region is being activated. Large infarcts (30–35% LV) usually extend to the epicardium in a circular area a few cm across, but in many a 2–3 mm "peel" of normal electrically active myocardium is still present. This phenomenon can account for low amplitude high frequency "after potentials" occurring well beyond the end of the QRS (as usually measured), and into the ST segment (see Chap. 33).

It is worth noting that commercially available digital ECG recording systems that digitize at a 4 ms (250 Hz) interval, will significantly attenuate the high frequency signal from the border zones of the infarct as described above. Most current ECG recorders now digitize at 2 ms (500 Hz). A 1 ms or less sampling interval (1,000 Hz) is needed to record accurately this potentially important electrical signal information.

16.2.2 Sensitivity of Conventional ECG Criteria for Infarcts

Well controlled pathology studies noted earlier [21–23] have demonstrated the low sensitivity of conventional ECG criteria for infarct. These data have shown that between 40% and 50% of all confluent healed infarcts 2 cm or larger are not associated with "classic" QRS changes of infarction. The data summarized in Figs. 16.3 and 16.5 pinpoint the reason for the poor showing of these criteria. These are as follows:

(a) 15% of all infarcts are limited to the base of the LV and posterolateral wall which is activated during the latter half of the QRS, and thus does not produce initial QRS changes.
(b) 20% of infarcts are small (2–3 cm in diameter) involving less than 10% LV and have only notching, "bite outs," slurring (see Fig. 16.5 panel 2), and attenuation of R waves, or other non-classic QRS changes (panels 3 and 4).
(c) 7% are multiple and the sum larger in size, with neutralizing (cancellation) effects. For example, a typical anterior infarct is masked by a second inferior posterolateral infarct, or vice versa.
(d) 5% of all infarcts will have had preexisting or new LBBB, or ventricular pacing, and an infarct that would not be diagnosable by classic criteria in the presence of these conduction abnormalities.
(e) 3% are patients with diffuse ischemic myopathy without classic QRS changes of infarct.

The vast majority of these patients will have high frequency notching, mid to late attenuation of QRS vectors, abnormal R/S or R/Q ratios, or other major changes described below in the section on quantification of myocardial infarcts. When prior ECGs are in fact available for comparison, the absence of serial changes is predictive of an unchanged ventriculogram with a remarkable 98% reliability [29]. Furthermore, the magnitude and duration of a change, if present, correlates well (r = 0.92) with the size of the new lesion or the change in LV ejection fraction (LVEF) seen on the ventriculogram (see Figs. 16.13 and 16.14 part a, with more detail later in the chapter). The classic criteria must then be expanded to include lesser changes such as abnormal notching, slurring or "bite out," abnormal R/S, R/Q ratios, and related changes, in order to diagnose the smaller 2–3 cm infarcts. They must also be expanded to include mid and terminal QRS abnormalities in order to diagnose posterolateral and basal infarction, or to quantify basal extension of infarcts of the mid-region and/or apex. Such expanded criteria have been developed using the computer simulations mentioned above and validated in a series of specificity, nuclear angiographic, and autopsy studies [30–34]. The criteria are described in detail in the Sect. 16.3 to follow, on quantification of infarcts. Both sensitivity and specificity are significantly improved by incorporating these expanded criteria into the review of serial ECGs, especially using high-gain, high-fidelity recordings.

16.2.3 His-Purkinje Relationship to Coronary Occlusion and Myocardial Infarction

Daniels, Boineau, and Cox made the important observation that because the peripheral Purkinje network is perfused by cavity blood, even with extensive transmural myocardial infarction active Purkinje potentials can be recorded from this network [35, 36]. The timing of the Purkinje excitation is changed very little by the presence of even major transmural infarction over the Purkinje recording site. While the peripheral network is usually not disrupted by infarction, proximal His Purkinje damage does occur in the major fascicles of the left bundle or in the proximal left or right bundle, producing the typical conduction defects described in (Chap. 14). It is estimated that proximal conduction defects of one sort or another occur in about one half of all patients with myocardial infarct. In the remainder, the Purkinje programming of excitation to the endocardium is normal. In this case, very large myocardial infarcts can occur involving the apex or mid region of the left ventricle and produce no prolongation of ventricular activation, i.e. a normal total QRS duration. The QRS duration may in fact be slightly shortened by a septal infarct which removes the part of the heart that produces the first 10 or 15 ms of ventricular activation..

Recent onset left and right bundle branch block in the context of acute myocardial infarction has been reported in a large clinical series by Lie et al., [37]. It was observed that the incidence of recent onset RBBB was 6.6% of all acute myocardial infarcts. In this context, it was associated 20:1 with an evolving acute anterior infarct. In this series, the incidence of recent onset LBBB was 3% and was associated 3:1 with an acute inferior infarct. Persistent left anterior-superior fascicular block occurs in a number of series [38–40] in about 10% of all anterior infarcts, and we present arguments below for our support of the Grant hypothesis [41] that inferior-posterior fascicular (peri-infarction) block occurs in over 85% of all acute inferior infarcts from right coronary occlusion. The ECG changes associated with the various combinations of myocardial infarcts and these conduction abnormalities are delineated in Sect. 16.5.

16.2.4 Ventricular Activation-Recovery and Myocardial Infarction

As summarized in Chap. 4 van Dam and Durrer [42–44] have shown that in revitalized human hearts using multipoint intramural plunge electrodes mapping, ventricular activation is consistent from endocardium to epicardium. The activation sequence of the ventricles, as relates to the specific 12-segment LV subdivision of Fig. 16.1, is initiated by insertion of the middle fascicles of the proximal His Purkinje into the peripheral network on the left septal surface of the middle anteroseptal region near its junction with the apical segment. The adjacent anterior and inferior fascicles insert into their respective papillary muscles and adjacent mural myocardium. This activation sequence has been confirmed by one of the authors, RHS and associates, in a small number of patients at the time of surgery for ventricular pre-excitation, by detailed epicardial mapping and limited intramural plunge electrode recording of the normally conducted beats post-transection of the accessory pathway. An entirely normal surface ECG and body surface potential map was confirmed postoperatively in these patients. Similar data was recorded in more detail in the baboon [45] and chimpanzee. The latter was confirmed by Spach and associates [46]. This normal activation was incorporated into this group's propagation simulation in a 1 mm grid digitized normal human heart from an accident victim, and the 12-segment left ventricular subdivision was used in the development of an ECG infarct-size scoring system which will be considered in detail later (and shown in Fig. 16.16). This normal heart geometry of the 12-segment left ventricle together with the activation sequences were used to develop a teaching diagram relating this cardiac anatomy and electrophysiology to the ECG (see Fig. 16.6a). Colored isochrones for each 10 ms are those defined by the expanded color code at the lower right of this figure. Both the propagating active electromotive surface of excitation and the slower broader surface of the sequence of recovery, show effects of the local electrically dead zone of a local myocardial infarct. The details of these effects on the surface ECG will be covered in following sections.

Figure 16.6b depicts the sequence of ventricular recovery in the same 12-segment LV subdivision. It is adapted from the functional refractory period data of Burgess and coworkers [47–52] and from the detailed intramural data of this phase of the cardiac cycle in the chronic closed-chest dog and chimpanzee preparations by Spach, Barr and associates [46, 53]. Recovery occurs more slowly than excitation from epicardium to endocardium as indicated by the action potentials shown at the lower right. The color coding indicates the timing of the peak of the slope of the rapid recovery phase in each region. According to Spach, Barr and associates, as shown here, the earliest recovery potentials appear on the right side of the septum which behaves electrophysiologically like the epicardium of the left ventricle. Recovery proceeds more rapidly at the base as shown in this figure and from the epicardium (B) to endocardium (A) throughout. The latest recovery potentials are seen in the endocardium in the mid regions near the apex, as shown.

16.2.4.1 Computer Simulation of Ventricular Excitation

Excitation velocities in the wall are rather uniform and the electric field is directed outward from the ventricular cavities. All portions of the electromotive surface of excitation from endocardium to epicardium contribute about equally. The wave fronts in the subendocardium are less well organized and thus somewhat less strong than in the mid-wall or subepicardium, but are by no means silent (Fig. 16.7). A model of this propagating electromotive surface was developed by Solomon [45] from multipoint plunge electrode intramural bipolar electrograms of the baboon, chimpanzee, and the limited human data mentioned above. The simulation of this electromotive surface model propagating in myocardium, developed an electric field that generated intramural bipolar electrograms that matched electrograms observed in humans/primates mentioned above. The specific anatomy for the normal human heart used in the simulations was taken from cross sections of the heart of a 25-year-old accident victim digitized at a 1 cubic mm level. The specific activation sequence generated is entirely determined by the geometry of the heart, the Purkinje distribution, the insertion sites of the proximal to peripheral Purkinje network, and the propagation velocities in each. The simulation includes this heart in an inhomogeneous adult male torso, with lungs and intracardiac blood mass. It can generate body surface potential distributions that can be shown as isopotential maps, perspective plots of potential distributions, 12-lead ECGs, or VCGs for any specified lead system. Fig. 16.8 illustrates the graphic output of this propagating excitation wave in this fine grid heart simulation of normal and fascicular blocks. Part (a) of this figure shows cross sections of the apical, middle and basal myocardial subdivisions defined in Fig. 16.1. In part (b), left anterior (superior) and left inferior (posterior) fascicular blocks (LAFB, LIFB), are simulated by removing the start points for the fan of the left bundle to

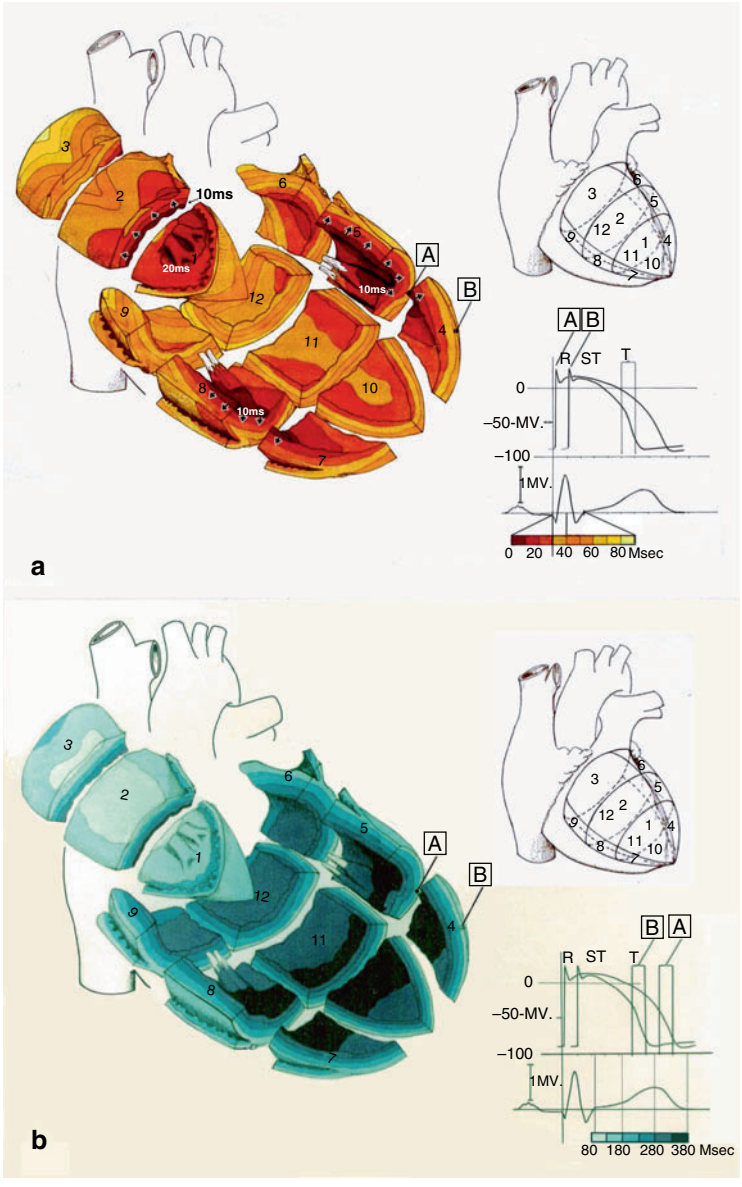

Figure 16.6
A activation, B repolarization sequences of the left ventricle (see Sect. 16.2.4 for details).

the distal Purkinje fiber network. The start points for either the anterior (superior) or inferior subdivisions are removed while leaving the start points for the other, and for the middle fascicles. The separation of the initial and terminal 30 ms vectors described by Grant as "peri-infarction block"... "probably due to a block of the superior or inferior fascicles" [16, 41] is produced by the early activation of one wall and late activation of the other. The late and unopposed activation on the side of the blocked fascicle accounts for the shift of the frontal QRS axis toward the blocked fascicle; that is, leftward and superior in LAFB, rightward and inferior in LIFB. The 1 mm grid resolution of the simulation allows for the inclusion of the fine detail of scar interdigitating with normal viable myocardium typical of the border zone of infarcts as shown in Fig. 16.4. The complex interactions of infarcts, conduction abnormalities, including LAFB, LIFB, RBBB,

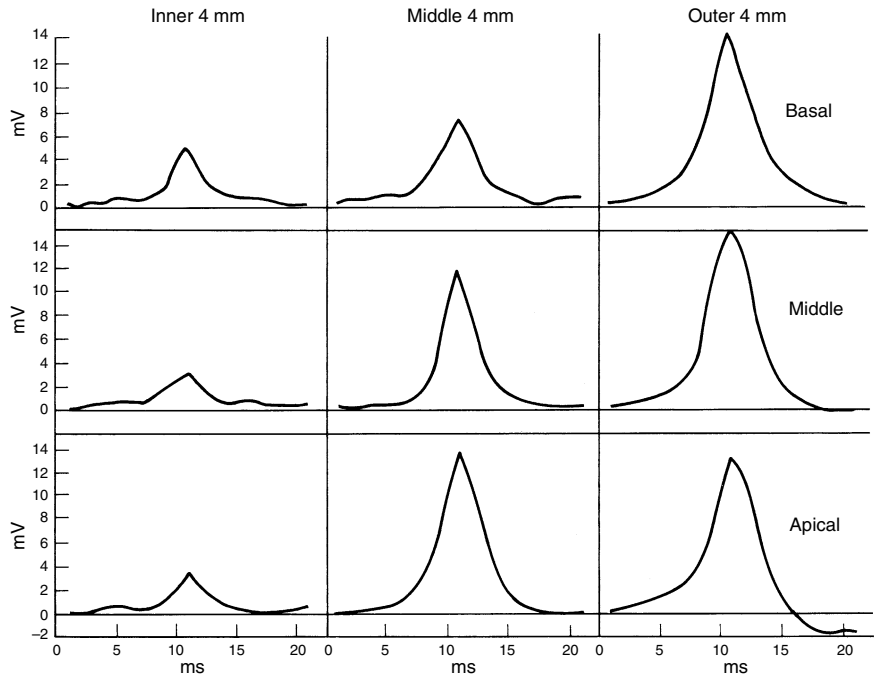

Figure 16.7

Waveforms recorded in a series of dogs with intramural bipolar plunge electrodes with a 1 mm separation, are shown for the inner, middle and outer 4 mm of the same apical, and basal subdivisions shown in Fig. 16.1. Polarity of the recording system was set so that a wavefront moving from endocardium to epicardium and passing a bipolar pair would record a positive potential. The peak amplitude of the bipolar recording would be proportional to the electric field strength of the local electromotive surface of excitation. Each waveform represents the average of 65 observations in each of the nine regions specified after being digitized at a 1 ms interval and time aligned around the peak voltage in each bipolar pair before averaging. The peak of all the waveforms was set at 11 ms. Time in milliseconds represents the duration of the averaged waveforms and has no relationship to the activation sequence. The averaged waveforms are positive throughout, indicating the propagation is from the endocardium to epicardium in all regions of the heart in these animals. In primates including man, the propagation velocity and local field strength from endocardium to epicardium are more uniform than in dog. In man, therefore, each region contributes about equally to the surface ECG and there are no electrically "silent" regions.

LBBB, and ventricular hypertrophies are evaluated in a straightforward manner by this fine-grid computer simulation of the propagating wave of ventricular of excitation and recovery.

For infarcts that localize to the subendocardium, the total extent is usually small. The simulation of such small infarcts introduced into our fine grid (1 cubic mm) model of this ventricular propagating wave in a realistic cardiac geometry and inhomogeneous torso [54–58] was very informative in evaluating the effect on the body surface ECG of these lesions. Small infarcts 20–25 mm across and 3–4 mm thick produce small changes in QRS, i.e., notches, slurs or "bite outs," etc. Only occasionally do such small infarcts produce "classic Q wave" criteria of 30–40 ms for an infarct. They must be strategically placed in that part of the heart activated in the first 15–30 ms of the QRS. These are usually small anterior lesions where proximity effects to the anterior precordial leads are strong. It is also informative to consider a pathological Q wave as loss of normal R wave early in the QRS, as in the first waveform in Fig. 16.5. The same loss of R wave from an area activated a few ms later in the QRS, as shown in the second waveform of this figure, and representing the same size infarct may produce a notch or slur in the upstroke of the R and no abnormal Q waves anywhere in the ECG. An equivalent infarct placed further out in the wall of the left ventricle or in a subendocardial region activated in the mid QRS will

produce loss of mid QRS vectors. and may be seen mainly as attenuation of R waves or an increase in S waves or both. In general, it takes infarcts 3 cm or more in diameter and 5–7 mm thick involving 40% or more of the transmural thickness of a local region of the anterior and inferior left ventricle to produce the 30–40 ms "classic Q wave" abnormalities. These infarcts are located in that part of the heart activated in the initial 40 ms of the QRS needed to produce abnormal Q waves.

Not addressed by these "classic" criteria are those infarcts that occur in the base of all four walls of the heart and the mid posterolateral wall. These regions in general depolarize after 40 ms. Infarcts here produce abnormalities mainly in the terminal half of the QRS. On the other hand, review of Fig. 16.3 indicates that only about 15% of single first infarcts are limited to these regions. The remaining 85% have significant involvement in mid and/or apical portions of the LV anterior and inferior walls. Thus a definite majority of infarcts have early to mid QRS deformities or loss of spatial vectors. If they are 4 cm or larger in the greatest diameter (12% LV or more), they do in general produce classic initial QRS changes. Nearly one-half of all single infarcts, however, are 3 cm or smaller (9% LV) and many of these fail to develop abnormal Q waves. However, they do have slurred and/or notched or attenuated R or S waves, or abnormal R/S or R/Q ratios. Most large or very large infarcts in any of the three major artery distributions have significant involvement of the base of the heart as well. In order to quantify the total extent of these lesions (see section on sizing of infarct below), mid and late QRS changes must be considered in developing criteria for infarct size.

16.2.4.2 Simulation of Ventricular Excitation and the ECG Infarct Scoring System

Typical examples of the simulation of the propagation wave of normal ventricular excitation, and for left anterior (superior) and left inferior (posterior) fascicular block are shown in Fig. 16.8. This simulation produced ECGs typical of normal conduction and of fascicular blocks. The location and detailed anatomy of various sized myocardial infarcts

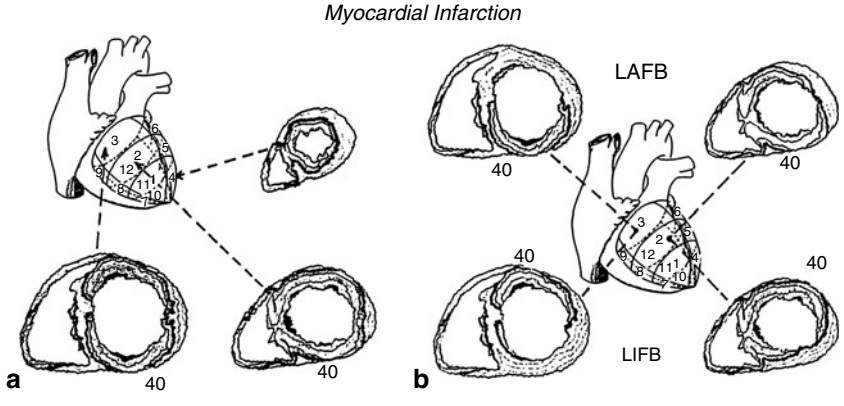

Figure 16.8

Part (a) Ten millisecond isochrones of the simulated normal ventricular activation sequence is shown in cross sections through the mid regions of the apical, middle, and basal myocardial subdivisions defined in Fig. 16.1. The darkened regions on the left ventricular endocardial surface represent the initial 10 ms isochrone. The computer propagation program generates each time step of the activation as it spreads out from these starting regions. Each line on the diagram represents a 10 ms isochrone. The fourth heavy shaded line is the 40 ms isochrone about midway in the activation. In part 2 (b), left anterior (superior) and inferior (posterior) fascicular blocks (LAFB, LIFB) are simulated by removing the starting points fed by the fan of Purkinje fascicles of the left bundle from one outside subdivision while the starting points of the other remains active as does those fed by the middle fascicles. The early activation of one wall and the late unapposed activation on the side of the blocked fascicle accounts for the significant shift of the frontal QRS axis toward the blocked fascicle, i.e. left anterior superior shift in LAFB and right inferior in LIFB.

documented by both ventriculographic and postmortem anatomic studies in each of the three major coronary artery distributions were simulated; i.e., anterior infarcts (left anterior descending artery); posterolateral infarcts (non-dominant left posterior circumflex artery); and inferior infarcts (right coronary artery's posterolateral and posterior descending branches). Simulated moderate to large infarcts in these classic locations produced not only the expected abnormal Q waves (or "Q equivalents") in all the expected ECG leads, but mid and late QRS changes as well. Small infarcts in these same locations often failed to produce classic Q wave changes; but instead produced attenuation of R or S waves, notching in the QRS, decreased R/S ratio and mid to late QRS changes, i.e., notched or attenuated S or late R waves in V1, V2, etc., as described earlier in this section.

It became apparent early in these experiments that in any given lead, at right angles to the excitation surface propagating around the local infarct, the amount of QRS change was proportional to the amount of infarct introduced into the simulations. This formed the basis for the Selvester QRS MI Size Scoring System where each point scored was constructed to represent 3% of the left ventricle infarcted (3% LVI). Change in the score was proportional to the volume of the infarct introduced into the simulations. Criteria were devised for all regions of the myocardium. Infarcts in basal regions of the heart, which activate late in the QRS, could be appropriately scored by the criteria for late QRS changes. See Sect. 16.3.5 below for details of the score and its implementation for normal conduction, and Sect. 16.5 for conduction defects.

16.2.5 Ventricular Repolarization and Myocardial Injury, Ischemia, and Infarction

Most, if not all, of the extant models of recovery are indebted to some extent to the 1934 ventricular gradient model of Wilson [59] and to a number of studies refining it [60–62]. Schafer and associates in 1943 [63], described the monophasic action potential from the intact heart using suction electrodes, and the intracellular equivalent of this was first recorded by Ling and Gerard in 1949 [64]. Seminal work relating the transmembrane action potential duration and wave shapes to the refractory period of these cells, and to the T wave of the ECG, was done in the 1950s by Hoffman, Kao, Suckling, Cranfield, Brady, and Woodbury [65–68]. Working with Lepeschkin, Surawicz, and Herrlich [69], they demonstrated close correspondence to the intracellular transmembrane action potentials and those recorded from the surface of the heart with suction electrodes. Authenreith et al. [70] demonstrated with suction electrodes that in the intact dog heart, the action potential durations were longer at the apex, intermediate in the mid region and shortest at the base. They also noted that, in mapping action potential durations on the surface, the surface potentials ended well before the end of the T wave indicating that areas not accessible to the surface electrodes depolarized later. From 1952–1955 Allan Scher published a series of classic papers [71–73] showing the ventricular excitation in the mammalian ventricle in great detail using multipoint plunge electrodes. This work was also reported at about the same time by Durrer and associates [74], who, with van Dam [75] in the early 1960s, mapped functional refractory periods with intramural electrodes in the open chest dog and showed that the endocardium, while depolarizing first, repolarized last.

In studies noted above, Burgess, Abildskov, Millar, and associates [47–52] reported methodical investigations of functional refractory period in the dog and concluded that there is normally a rather uniform gradient in ventricular recovery times from epicardium to endocardium. The endocardium recovery is longest, the base of the heart has significantly shorter recovery times than the apex, and the right septal side of the interventricular septum behaves like the epicardium of the left ventricle. Finally, Spach and coworkers [46, 53] had recorded bipolar and unipolar electrograms from 300 chronic implanted intramural and epicardial electrodes in dogs and a chimpanzee allowed to recover for several days before measurements were made. The preparations had the advantage that both intramural and epicardial depolarization and repolarization could be mapped in detail in animals that had regained their normal body surface map potential distributions for both QRS and ST-T following chronic electrode implantation. These workers confirmed in this chronic preparation the ventricular activation sequence (depolarization) recorded earlier by Scher, Durrer and van Dam and associates, and by themselves. They also observed that the epicardium at the base of the left ventricle was last to depolarize but first to recover. There was a uniform sequence of recovery from epicardium to endocardium, and that the endocardium in the area at the junction of the mid regions of the left ventricle with the apex was the last to show significant recovery potentials. These data for both normal excitation and recovery in the 12 LV segments of the human heart are shown in Fig. 16.6a, b. A comprehensive review of "The Origin of the T-wave" by Kootsey and Johnson was published in 1980 [76]. This was expanded in considerable detail in the compilation, "Cardiac Repolarization Bridging Basic Science," by Gussak and Antzelevitch [77]. The reader is encouraged to consult these monographs for details not covered in Chaps. 3, 5,

and 16 of this synopsis. These will form the specific background for interpreting the repolarization (ST-T) changes associated with acute and chronic "injury," ischemia, and infarction along with the depolarization (QRS) changes with which they are so inextricably bound.

In relating ventricular excitation and recovery sequences to myocardial "injury," ischemia, and necrosis or infarction, it has traditionally been depicted that, as the result of a decrease or interruption of the blood supply to the myocardium from progressive coronary stenosis, an area of cardiac necrosis is produced. This central area is seen as surrounded by concentric zones of injury and ischemia. Classically, it has been assumed that the QRS changes result from the central area of necrosis, that injury causes the change in the TQ-ST segment, and ischemia the change in T waves. This concept implies that loss of functional heart muscle is greatest in the central area of necrosis, intermediate in the adjacent zone of injury where "leaky" membranes cause systolic and diastolic currents to flow, and least in the peripheral zone of ischemia where alterations in repolarization produce the "ischemic T wave." Loss of myocardium is considered irreversible in the zone of central necrosis, and potentially reversible in the outer regions of injury and ischemia.

In a well documented critique of the subject, Arnsdorf and Louie [78] conclude that there is little or no direct electrophysiologic or ultrastructural evidence to support the notion that these local regions contribute specific information in a unique way to the three components of the ECG. Indeed, as they point out, Janse et al. [79], by recording transmembrane action potentials with floating microelectrodes from cells within the border zone of myocardial ischemia in the isolated perfused pig heart, found cells with very low intracellular action potentials in close proximity to cells with nearly normal action potentials. In addition, nicotinamide adenine dinucleotide fluorescent staining techniques used by Harken and coworkers [80, 81] suggest that the line between normal and abnormal tissue may be very sharp. Pathoanatomic studies by Ideker in our correlative reports, referred to earlier, demonstrated in general a very complex interdigitation of islands and pseudopods of normal and abnormal tissue at the border of an infarct. This geometric detail is shown graphically in Fig. 16.4. Cox et al. [82], using dehydrogenase staining techniques to delineate the changing geometry of the infarct border from 18 h to 1 week after infarct, observed that this complex interdigitation of normal and infarcted tissue was generally evident by 24 h.

16.2.5.1 Computer Simulation of Repolarization

While recognizing a conceptual debt to the ventricular gradient model of Wilson [59], Harumi et al. in 1966 [83] were the first to propose relating action potential durations, and functional refractory periods in a quantitative 2-dimensional model of the T wave. The transmural gradient of action potential durations, their amplitudes, and the sequence of recovery shown in Fig. 16.6b were incorporated into a ventricular cross section, and adjusted so that T vector loops computed by the solid angle theorem conformed to those recorded experimentally. Thiry and Rosenberg [84] were the first to attempt a 3-dimensional multiple dipole model in the form of the cardiac geometry. Miller and Geselowitz in 1978 [85, 86], developed a more realistic simulation that included an external torso boundary still in a homogenous medium and a 4 cubic mm grid to represent the heart. Each 4 cubic mm "cell" was manually assigned action potential wave shapes to conform to those observed experimentally in normal, ischemic, hypoxic, irreversibly injured and dead cells. Both of these latter simplified models, in spite of not taking into account complex internal human torso inhomogeneities, did produce 12 lead ECGs that were quite consistent with normal ECGs. By manipulating regional generator outputs to simulate subendocardial, intramural, subepicardial, and transmural ischemia, and infarction (as shown in a summary form in Fig. 16.9), ECGs were produced that were entirely consistent with clinically observed changes. ECGs produced by these simulations, read by experienced electrocardiographers who were blinded to the simulation, were interpreted as representing the processes simulated (see Chap. 7 for more details). The solid experimental base of a large number of workers of which the foregoing is a very cryptic review, is covered in detail in the Kootsy-Johnson monograph [76]. This review and Chaps. 6–9 of this book and this Chap. 16 provide the basis for a rational interpretation of the body surface ECG of acute myocardial infarction "injury," ischemia, and chronic healed infarct.

In the mid to late 1980s, the author (RHS) and associates incorporated the complex geometry of regional ischemia and/or infarcts into his validated 1 cubic mm grid propagation model, automating the manually entered local cardiac generator changes reported in the Thiry and Rosenberg [84], and the Miller and Geselowitz [85, 86] models. In addition, this simulation also included all the torso and internal boundary effects and inhomogeneities known to influence the surface ECG recordings, and generated as output the total body surface map of which the 12/16 lead ECG is a subset. This allowed

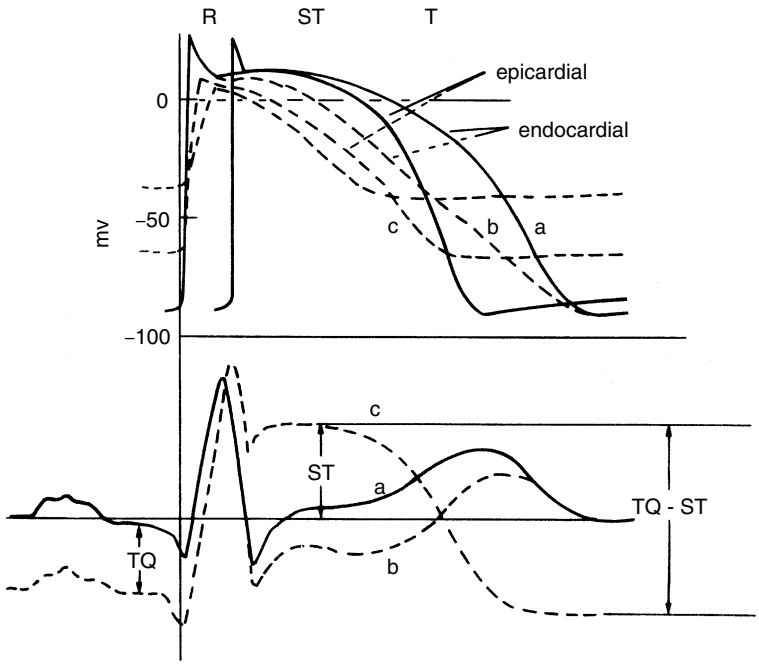

Figure 16.9

Typical myocardial-cell action potentials (*upper curves*), and body surface ECGs (*lower curves*) that represent various degrees of ischemia (b), injury (c), and cell death (necrosis). Curves (a) represent the normal pattern. These individual action potential waveforms will be used to represent the 1 cubic mm "cell" in the fine-grid propagation model (see Fig. 16.8). This will allow for the simulation of regional subendocardial intramural or transmural ischemia, injury or necrosis. Simulation of the fine detail of infarct anatomy/geometry shown in Fig. 16.4 is incorporated into an interactive system, in an anatomically and electrophysiologically realistic and comprehensive model of the heart and inhomogeneous human torso.

us to study in detail the geometrically complex border regions of acute and healed myocardial infarcts for the entire cycle of depolarization and repolarization in subjects with normal conduction (see Fig. 16.10a, b) and those with conduction defects.

The electrophysiologic changes over time of the geometrically complex regions of evolving infarction were included in the simulation. The resulting body surface map, 12 lead ECG, and VCG records integrated the complex boundary effects described above, and the more central loss of QRS forces or vectors from the irreversibly damaged myocardium. Simulations of the local areas of acute ischemia/injury of acute infarction and of chronic subendocardial ischemia [87] produced a major shift in the ST segment that was vectorially related to the local perfusion bed of the coronary artery simulated. The ST field (and vector) for acute ischemia/injury was displaced anteriorly, superiorly and leftward for proximal LAD occlusion, as well as outward from the epicardium via the centroid of the LAD perfusion bed. Similarly there was an inferior, and somewhat rightward and posteriorly directed ST field (and vector) for proximal RCA occlusion, and a posteriorly directed ST for LCX occlusion. There are conflicting data in the clinical literature [88–90], but work by Sederholm et al. [91] using continuous orthogonal lead monitoring suggests that the peak ST elevation of acute injury may occur over a very short time. Both they and Aldrich et al. [92] have demonstrated significant correlation between both the location and extent of the initial ST "injury" currents and the size of the acute infarct that evolved over the next few days, as measured by enzyme methods, the ECG QRS score and radionuclide angiography. The clinical correlates with the simulated acute and evolving infarcts are dealt with in detail later, in Sect. 16.4 of this chapter. These studies confirmed that the simulation projections would be specifically related to the local coronary artery distributions described earlier. In the healed infarct, the direction of the mean T vector away from the local area is a significant predictor of the local area of the infarct [93–95]. The "secondary" ST-T changes of the conduction abnormalities, RBBB, LBBB, ventricular pacing

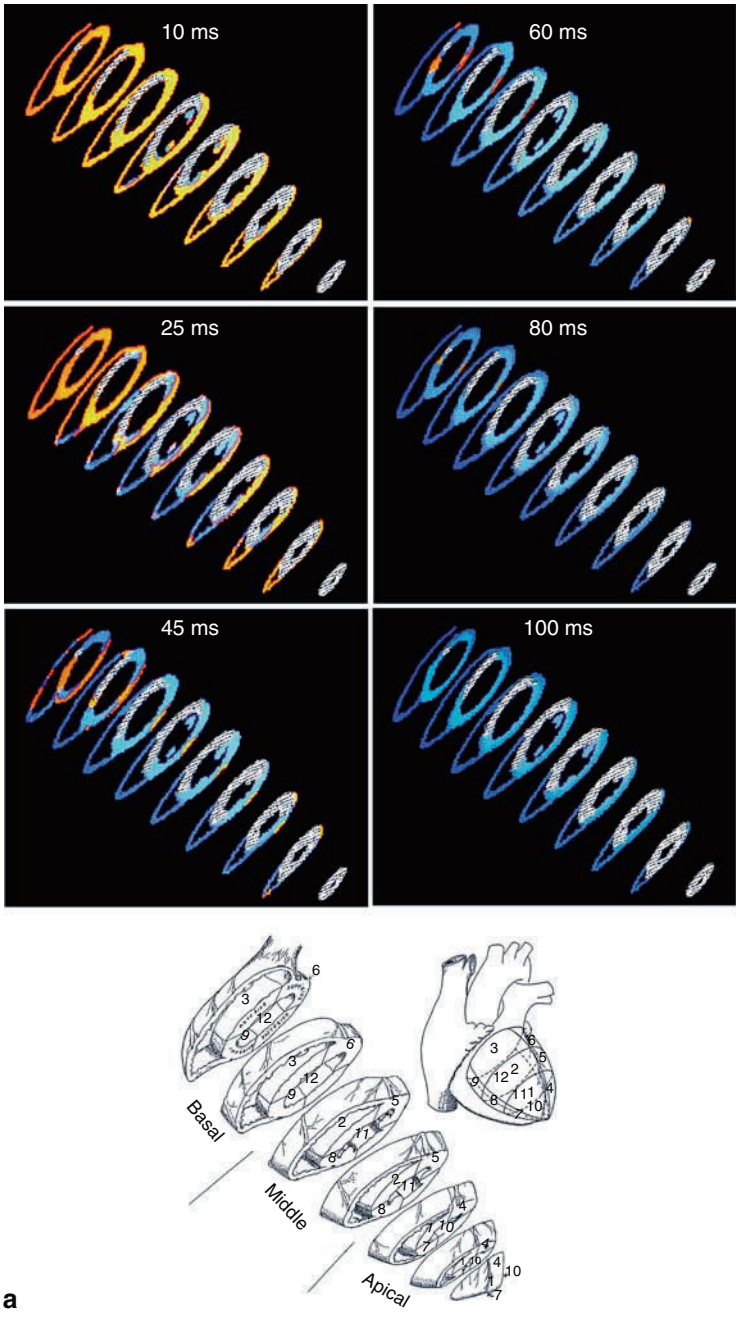

Figure 16.10 **(Continued)**

or pre-excitation, and hypertrophy of either ventricle confound these ST-T changes of acute and chronic infarct. Details of dealing with these confounders are also covered in Sects. 16.4 and 16.5 of this chapter.

The simulated local subendocardial ischemia with localizing ECG ST deviation away (inward) from each major coronary artery perfusion bed described above led to the following hypothesis: Subjects with local resting (or exercise induced) ST deviation away (inward) from the centroid of any of the major coronary artery perfusion beds would have high-grade

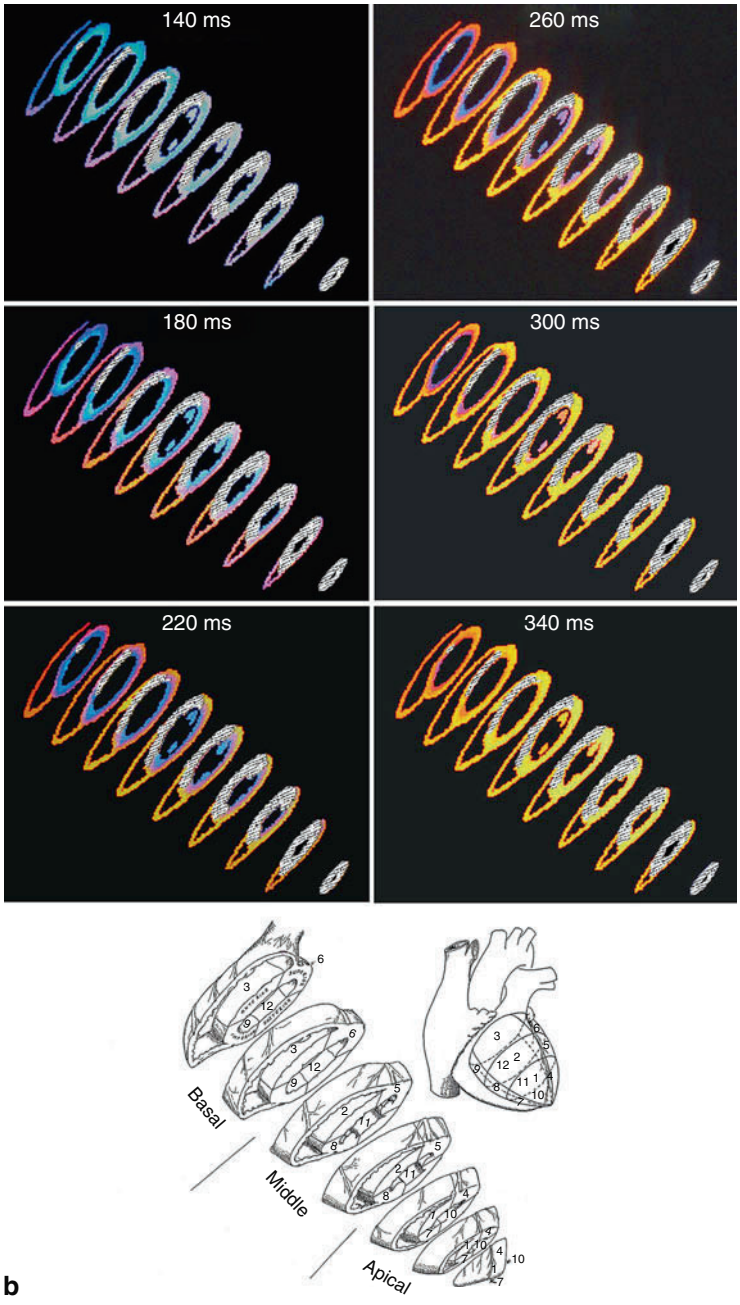

Figure 16.10

(a) Anterior view of serial apex-to-base cross-sections of a human heart showing the under-surface of each section as illustrated in the diagram below. Simulated 20–100 ms. excitation sequences (yellow/orange/red to blue) around a large anterior infarct (striated white). (b) Anterior view of serial apex-to-base cross-sections of a human heart showing the under-surface of each section as illustrated in the diagram below. Simulated 140–340 ms repolarization sequences (reversing blue to red/orange/yellow), as with the excitation sequences, outlining the large anterior infarct.

single vessel occlusion of that specific artery. Consider an ancillary hypothesis: Resting (or exercise induced) ST deviation away from the apex (toward the base) would have high-grade distal LAD (left anterior descending), left main or three vessel occlusion. To test this hypothesis, we recorded 16 lead ECGs at rest and with exercise in a preliminary report of some 48 subjects who also had coronary angiograms/angioplasties (96). In no incidence of high-grade single vessel disease was localizing ST deviation maximal away (inward) from the centroid of the perfusion bed of that specific vessel, including distal LAD disease. Likewise, in a 10-year survey of some 3,000 acute myocardial infarctions seen at this large community teaching hospital, 900 of whom had emergent coronary intervention, there was no incident of single vessel occlusive disease with local ST deviation away (inward) from the involved arterial perfusion bed. Noted in this cohort with early intervention was the following: ST depression in anterior-posterior leads V1–V3 was associated with acute occlusive disease of the left circumflex and, ST depression in inferior-superior leads III, aVF, II, and maximal in aVF (a superior ST deviation vector) was seen with acute occlusion of a ramus or a prominent first diagonal. Apically localized ST depression in apex-base oriented leads V4, V5, V6, I, -aVR was associated with high-grade left main and/or proximal multi-vessel disease. These observations strongly support the Ellestad hypothesis (97) that, resting (or exercise induced) subendocardial ischemic ST change is global.

16.3 Quantification of Infarct Size Using ECG and VCG Criteria

16.3.1 Essential Principles

1. Myocardial infarcts develop, of course, in 3-dimensional space; and therefore understanding of their quantitative alteration of ventricular activation and its body surface representation, the QRS complex, requires consideration of a "3-dimensional ECG." Recording of three orthogonal leads (*X*, *Y*, and *Z*) provides the basis for generating this ECG display, termed a "vectorcardiogram" (VCG). The sequential instantaneous points of summation of the propagating ventricular activation (vectors) in the *X* (direction) lead plotted against those in the *Y* (direction) lead create the "frontal plane VCG loop"; in the *X* and *Z* leads the "transverse plane VCG loop," and in the *Y* and *Z* leads the "sagittal plane VCG loop." See Chap. 43 for a more detailed explanation of the VCG.
2. The QRS deformities between a pre-infarct ECG/VCG and a post-infarct record are a function of infarct size and any change in intraventricular conduction. In patients who maintain normal conduction post-infarct, the degree of QRS deformity, both magnitude and duration, is proportional to the amount of myocardium lost and inversely related to the loss of ventricular function, i.e., to LV ejection fraction (LVEF).
3. Intraventricular conduction defects, when produced, are generally related to a specific coronary artery and a specific local infarct.
4. Once the basic activation sequence (conduction abnormality) is taken into account, the extent of the added QRS change is also proportional to the infarct size and decrease in LVEF.

16.3.2 Infarct Size, Left Ventricular Function, and Prognosis

In recent decades, it has become established that patient prognosis after a myocardial infarct, as well as functional reserve capacity, is related to the amount of the left ventricle (LV) infarcted. Thus, reliable clinical methods, which are able to estimate the extent of both acute and remote myocardial necrosis are needed. The recent interest in the limitation of acute infarct size by therapeutic interventions (clot lysis, coronary atheroma removal, balloon angioplasty, etc.) has prompted the evaluation of many clinical methods aimed at estimating the size of an acute myocardial infarct. In autopsy correlations, Ideker has shown [18] that infarct size and LV ejection fraction (LVEF) are inversely related, with a high correlation (r = 0.88). Patients with extensive myocardial losses from one or more infarcts with total extent of infarction approaching 40% LV, and LVEF less than 30%, have an annual mortality rate of more than 20% and major impairment of their functional reserve [98, 99].

For almost a century the ECG has been used to determine the presence and location of myocardial infarcts. Because it is universally available, noninvasive, inexpensive, and easily repeatable, it is important to make optimal use of recent findings regarding the ability to estimate infarct size from ECG/VCG data. The quantitative QRS infarct size scoring system, which was designed from our computer simulations described earlier [54–58], utilizes information in the ECG and VCG to estimate infarct size. It is the purpose of this section to provide enough background information to make the rationale of the method apparent to the reader. We will describe both the 12-lead ECG scoring method and the VCG method in sufficient detail so that the reader can apply the method directly to routinely recorded ECGs and VCGs.

16.3.3 Infarct Size and Left Atrial Overload

LV infarction decreases the diastolic compliance of the LV – in the acute stages by edema and in the chronic stages by scar. Even small infarcts are associated with some stiffening of the wall and increased ventricular filling pressure. Thus ECG/VCG changes of left atrial overload are common in most infarcts. The larger the infarct, the higher the ventricular end-diastolic filling pressure and the more marked is the left atrial overload change. Thus, acute ST, evolving QRS and left atrial P changes are each related to infarct size. Since the left atrium depolarizes during the latter two-thirds of the P-wave with activation fronts directed mainly to the left and posteriorly, four main criteria can be identified where the degree of change relates to the degree of left atrial overload:

(a) Increase in total P duration (> 110ms),
(b) Increased duration of left atrial intrinsicoid deflection (time from peak anterior to peak posterior in V1, V2, or $Z > 30$ ms),
(c) Increased duration posterior (negative P duration) in V1, V2, and Z (>45ms).
(d) Increased magnitude of late component posterior (negative P amplitude) in V1, V2, and Z (>0.05mV) and/or leftward in V5, V6, and X (>0.1 mV).

These relationships, i.e., the extent of these changes as relates to the severity of the left atrial overload, and degree of LV diastolic dysfunction, are defined in Tables 16.1 and 16.2. They are more related to left atrial and LV end diastolic pressure than to angiographic or echo left atrial size. This was documented in a well-controlled coronary care unit study by Heikkila et al. [100].

Table 16.1

Score for atrial overload. Criteria and the points given for each for quantifying the degree right and left atrial overload. Those criteria on the top row in each case exceed the 98% upper bounds of normal.

Right atrial overload			Left atrial overload					
P amplitude (mV)			P amplitude (mV)			P duration (ms)		
Anterior	Inferior	Points	Leftward	Posterior	Intr. Def.*	Posterior		Points
V1 (V2, Z)	AVF (Y)	Ea Crit◇	V5 (X)	V1 (V2, Z)	V1 (V2, Z)	V1 (V2, Z)	Total	Ea Crit◇
0.100	0.175	4	0.100	0.075	35	45	120	2
0.125	0.200	8	0.125	0.100	40	50	130	4
0.150	0.225	12	0.150	0.150	45	60	140	6
0.200	0.250	16	0.175	0.200	50	70	150	8
0.250	0.300	24	0.200	0.250	60	80	160	12
0.300	0.350	32	0.225	0.300	70	90	170	16
≥0.400	≥0.400	48	≥0.250	≥0.400	≥80	≥100	≥180	24

*Intr. Def: Intrinsicoid deflection; the duration from peak positive P amplitude to the peak negative.
◇ Ea Crit: (Points for) Each criterion met.

Table 16.2

Diagnostic statements relating to total points accrued in Table 16.1

Total points	Diagnostic statement[a]
4–6	Possible mild RAO/LAO
8–10	Probable mild RAO/LAO
12–18	Moderate RAO/LAO
32–46	Severe RAO/LAO
≥48	Very severe RAO/LAO

[a]RAO, right atrial overload; LAO, left atrial overload

16.3.4 Infarct Size and Right Atrial Overload

Patients with right ventricular infarction (see Sect. 16.4.5.1) have right atrial overload, the severity of which is related to the severity of the right ventricular failure. Also, patients with large to very large infarcts or with diffuse ischemic myopathy may have very high left ventricular end diastolic filling pressures and recurrent congestive heart failure. Such patients will have a passive increase in pulmonary pressure to maintain a flow gradient and consequent chronic increase in right ventricular pressure. Such chronic right ventricular overload routinely decreases right ventricular diastolic compliance, producing right atrial overload. The right atrial depolarization from the sinus node region produces activation fronts directed anteriorly and inferiorly. These excitation fronts occur unopposed during the first third of the P-wave at which time leftward and posterior fronts begin to develop in the left atrium. In the adult, a P amplitude >0.1 mV in V1, V2, and *Z* and >0.175 mV inferior in aVF and *Y* exceeds the 98% upper bounds of normal, and are indicative of right atrial overload. The degree of increased anterior and inferior voltage is proportional to the overload of the right atrium as summarized in Tables 16.1 and 16.2. It is a well established clinical axiom that in patients over 50 years of age, the commonest cause of pulmonary hypertension, right ventricular and right atrial overload, is chronic left ventricular failure. It follows from the above that, large to very large infarcts with significant diastolic dysfunction that have not produced chronic left ventricular failure will have moderate to severe left atrial overload but generally normal or minimal right atrial changes. When in addition the ECG/VCG changes of right atrial overload become mild to moderate, associated congestive failure is most likely.

16.3.5 Computer Simulations and QRS Infarct Size Scoring Systems for ECG and VCG

The simulation of ventricular excitation of the human heart formed the basis for an ECG infarct scoring system developed by Selvester, Solomon and co-workers to consider all of the major variables known to influence the surface ECG. These included (1) high resolution (1 cubic mm grid) anatomy of the human myocardium, Purkinje conduction system, and very small to very large infarcts in each of the three major coronary perfusion beds, (2) a simulation of ventricular propagation of excitation at this same resolution, and (3) a simulation of the inhomogeneous volume conductor; including intracardiac blood mass, myocardium, lungs, and an adult torso [55]. It became apparent in the simulation experiments noted earlier in Sect. 16.2.4.2 that in any given lead, at right angles to the propagating excitation surface, the degree of QRS change was proportional to the amount of infarct introduced into the simulations. This led to the ECG scoring system where each point scored was set up to represent infarction of 3% of the left ventricle (LV). Criteria could be devised for all regions of the myocardium, and infarcts in basal regions of the heart which activate late in the QRS could be appropriately scored by the same scoring system, provided late QRS changes were included in the criteria.

A 53-Criteria/32-Point scoring system (representing a total of 96% of the LV) was developed, tested and reported using a learning set of 100 biplane ventriculograms from patients with angiographically proven coronary artery disease [29, 57, 58]. Using the same simulations (Fig. 16.11) and rationale, a nomogram (Fig. 16.12) relating VCG changes (duration and magnitude of a QRS deformity as in Fig. 16.13) was also developed to predict infarct size [29].

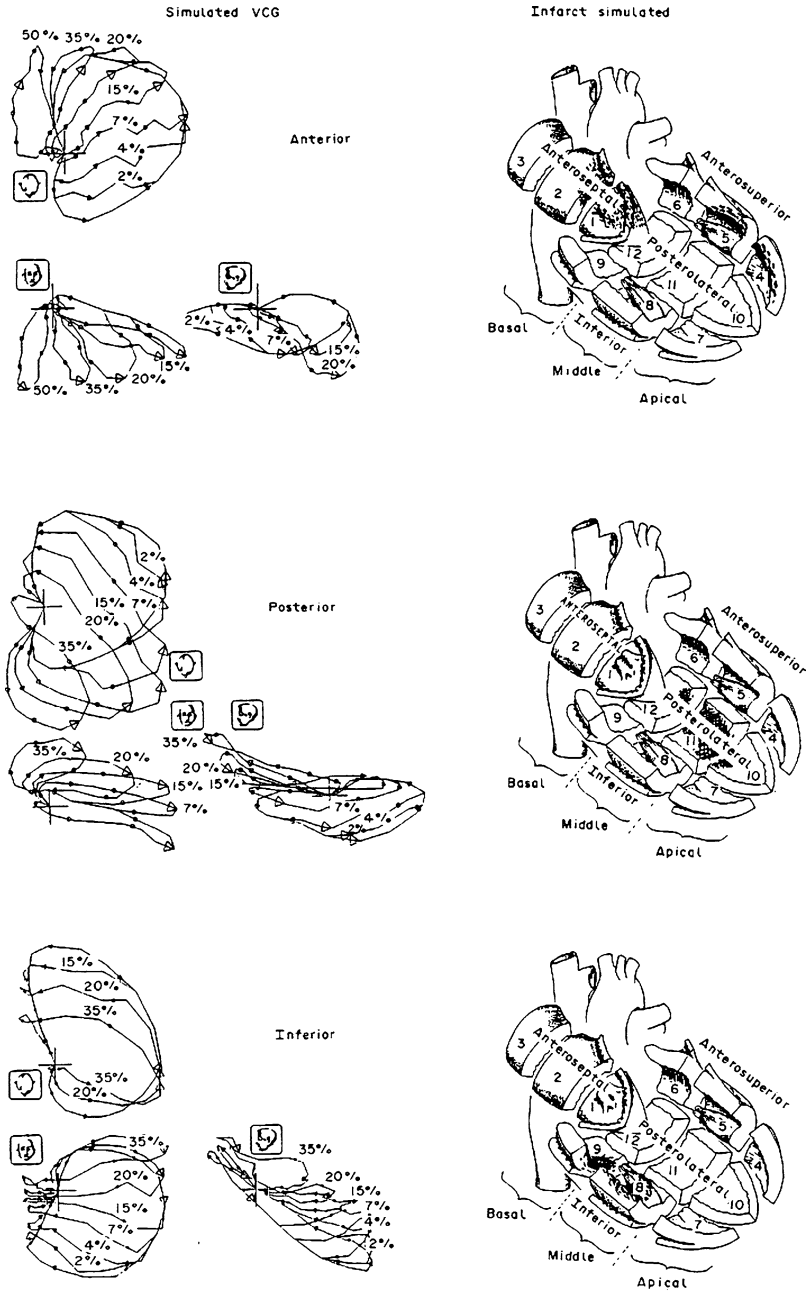

Figure 16.11

Typical examples of moderately sized infarcts (15% of the LV) in each of the main coronary distributions are shown in the 12-segment LV diagrams at the right of the illustration. The program was directed to plot superimposed vector loops in horizontal, frontal and left sagittal projections when various sizes of infarcts had been simulated in each of these typical locations. The number at each VCG loop represents the percentage LV infarct simulated and ranged from 2% LV to 50% LV. Not shown are body-surface maps and 12-lead ECGs that can be plotted routinely for each run of the simulation program. Normal conduction was simulated for the anterior and posterior infarcts shown, while inferior (posterior) fascicular block was needed in the simulation to produce ECGs and VCGs typical of inferior infarct of various sizes associated with RCA occlusion. Multiple infarcts with various combinations of sizes and locations are readily simulated with this model.

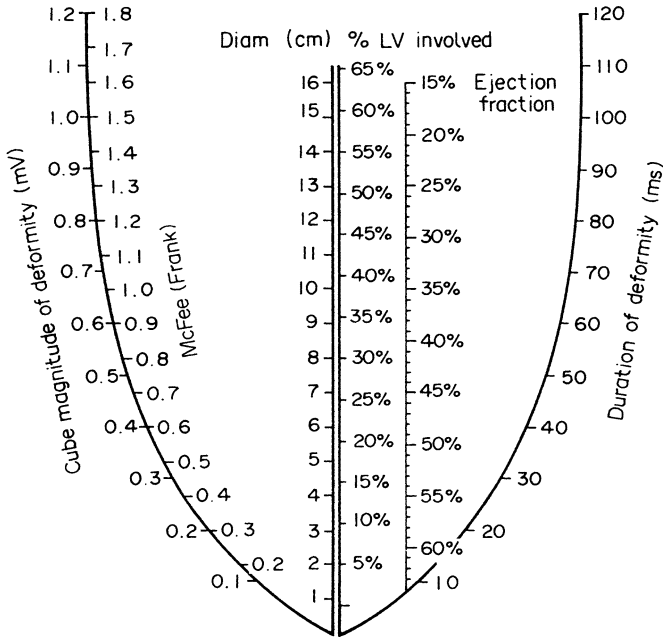

Figure 16.12

Nomogram for predicting infarct size from VCG deformities. When preinfarct records are available, as shown in Fig. 16.13, the peak amplitude of the change (local loop deformity) in records before and after infarct is identified. The amplitude chosen for each lead system is the projection of the loop where the change is greatest. The peak amplitude change for the specific lead system is transferred to the left side of this nomogram, and the duration of that change is transferred to the right side. A line is then constructed through these two points and the point where it crosses the double line in the center of the nomogram is used to determine angiographic infarct size. The latter may be represented by (a) diameter in centimeters (i.e., the longest curvilinear dimensions of akinesis in either projection of the biplane ventriculogram); (b) angiographic percentage LV involved (i.e., the percentage of the circumference of either projection that is akinetic); and (c) ejection fraction as computed by the area length method of Dodge, Sandler and Sanmarco. It should be noted that the percentage LV (circumference) involved here is an angiographic determination, and while clearly related to percentage LV infracted at quantitative planometric pathology, it is a quite different measurement. When a preinfarct record is not available and a small local deformity that is outside normal limits for QRS loop is identified (indicating an infarct), a loop is constructed that would be within the limits of normal using the normal portions of the loop for a guide. The magnitude and duration of the deformity is measured from the reconstructed normal and transferred to the nomogram for the estimation of infarct size. When the deformity is large, the mean normal loop for that particular lead system is used to identify the magnitude and duration of the deformity for transfer to the nomogram. Figure 16.13 is an example of such VCG changes.

16.3.5.1 Validation Studies

In a series of 74 patients with serial biplane ventriculograms and serial ECGs and VCGs [29], an unchanged ECG and VCG was predictive of an unchanged ventriculogram with a remarkable 98% reliability. New change in the ECG/VCG (QRS deformity as in Fig. 16.13) was associated with a change in ventriculogram in 12 out of 14 subjects (Panel a, Fig. 16.14). The size or extent of new infarction, which in each instance was associated with a proximal coronary occlusion, was correlated with ECG/VCG magnitude-duration criteria for infarct size with a correlation coefficient of 0.90. The major ambiguity was in one patient who had sustained right coronary occlusion and had developed changes of inferior fascicular block in addition to new infarction. When infarct size was recomputed by the criteria discussed below for infarct plus inferior fascicular block, the overall correlation improved to 0.92. The two patients with new ECG/VCG deformities and

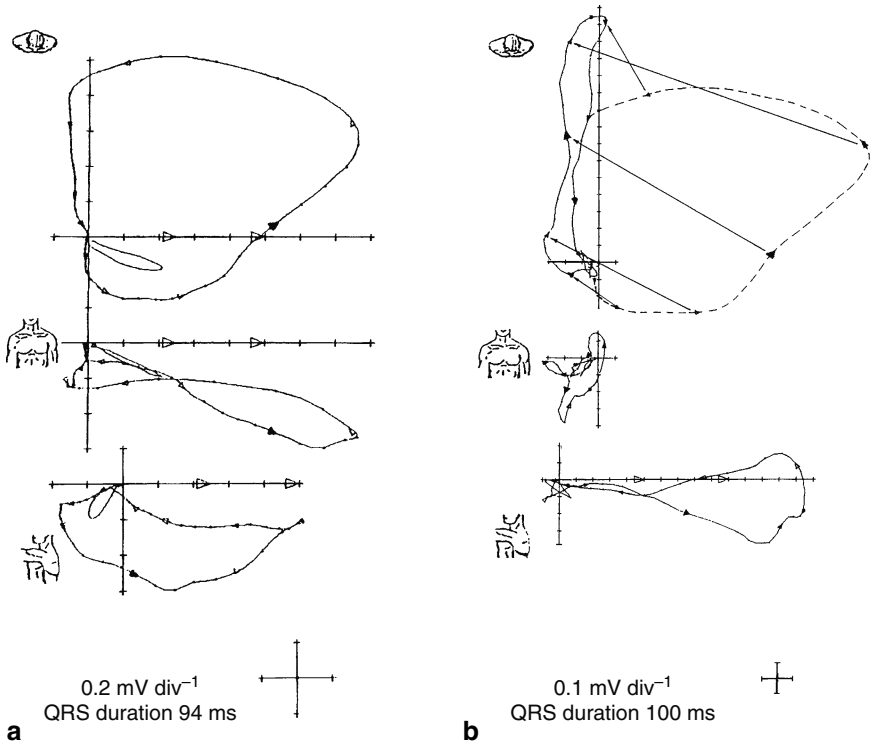

Figure 16.13

Part (a) shows the McFee lead-system VCG of a 51-year-old white male patient with angina pectoris and single-vessel LAD disease which is entirely normal. Part (b) shows the VCG of the same man at 53, recorded a few weeks after an acute anterior myocardial infarction as a result of total occlusion of the proximal LAD lesion and prior to repeat coronary angiography and ventriculography. A major deformity from 10 to 70 ms was produced with major loss of leftward vectors as shown on the *right*, and a maximal magnitude of 1.5 mV at the 50 ms vector. When the 1.5 mV for 60 ms was transferred to the nomogram (Fig. 16.12), a line constructed between the two values for the McFee VCG crossed the double center line at 12 cm and 45% angiographic LV involvement. It predicted an ejection fraction of 30%. At angiography, a very large akinetic anteroseptal anterosuperior and apical segment was seen as the result of the proximal LAD occlusion and an ejection fraction of 26% was recorded.

an unchanged ventriculogram had the ECG/VCG changes of possible small new infarcts (involving 5–10% LV). This suggests that small lesions of this size may produce no discernable wall motion abnormality in the ventriculogram.

Wickline and McNamara [101] reported excellent correlation between infarct size at autopsy in a small number of experimental infarcts in the baboon, and the integral of the change in the vector spatial magnitude compared to the control VCG spatial magnitude in the same animal. Cowan et al. [102] have reported on the integral of the spatial magnitude of initial abnormal depolarization in human subjects in whom control records were not available. She found excellent correlation with quantitative planometric pathoanatomic measurement of infarct size. The correlation was best in anterior infarcts and the correlations with inferior infarcts improved when the integral also included terminal abnormal depolarization [103].

From the authors' data presented above, it follows that carefully recorded high quality multi-lead serial ECGs/VCGs are a simple, inexpensive and effective method to predict the presence or absence of new myocardial damage (98% reliable), and to quantify the degree of damage with more than 90% reliability. WE RECOMMEND, THEREFORE, THAT EVERY YOUNG ADULT ACQUIRE SUCH A HIGH QUALITY BASELINE ECG RECORDING BEFORE AGE 30. A wallet sized photographic and electronic copy could be carried on their person thereafter.

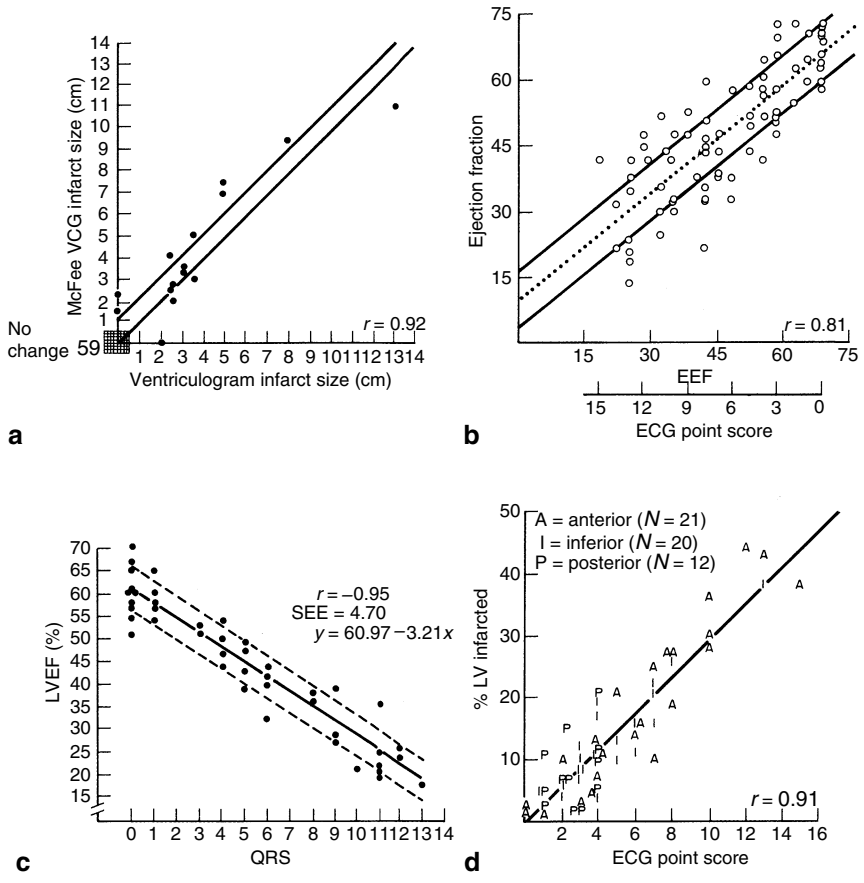

Figure 16.14

Part (a) plots new infarct size (second study) on serial comparison of VCG change and contrast ventriculograms in 74 consecutive serial coronary angiographic studies [29]. The lower line is the line of unity. The $r = 0.92$ is computed for the 14 subjects where significant VCG change was found. Part (b) shows the correlation between the ECG point score for infarct size, discussed in the text (EEF = estimated ejection fraction), and ejection fraction in a series of 74 consecutive patients with 100% LAD occlusion and less than 75% in the other two coronary arteries [58]. All cases were included regardless of the presence or absence of ECG changes of hypertrophy or conduction abnormality. No case of LBBB was observed in this group. Part (c) compares QRS scores for infarct size and nuclear LV ejection fraction (LVEF) in 43 patients 3 weeks after suffering an acute myocardial infarct [31]. Patients with ECG evidence of conduction abnormalities or ventricular hypertrophy were excluded, but those with history of prior infarct were not. SEE denotes the standard error of the estimate. Part (d) relates the ECG point score to the pathological infarct size at quantitative planometric pathology in the first 53 patients with single infarcts reported by Ideker et al. [18, 32, 33]. Twenty-one of these patients have anterior infarcts, 20 have inferior infarcts and 12 have posterior infarcts.

Hindman and associates [108] next evaluated the specificity and intra- and inter-observer agreement of a simplified version of the ECG scoring system proposed by Wagner. The effectiveness of this simplified QRS scoring system for estimating myocardial infarct size was then tested in post-mortem studies involving single infarcts in the anterior [18], inferior [32], and posterolateral [33] quadrants of the left ventricle. Additionally, the simplified scoring system has been found to be of clinical value (see Fig. 16.14 Panel C) in the assessment of left ventricular function after acute myocardial infarction [31, 104, 105].

The simplified system has several potential limitations. Its 29 points are accumulated from 37 criteria which can only indicate infarction in 87% of the LV. There is relative under-representation of the posterior (posterolateral) and basal regions, and it performed suboptimally with infarcts in these locations. Also, minor changes in amplitude and deformities in the QRS (notching) that were apparent in the simulations and in clinical infarcts were not included. The complete quantitative scoring system which includes 20 additional criteria of R and S amplitudes and the presence of notched and late R waves was then evaluated [106, 107]. Fourteen criteria met the 95% specificity standard in normals, three achieved the standard only after modification, and three were excluded. The control population considered at this time was larger and better distributed by age and sex than the original normal population [30]. This study population was composed of 500 consecutively selected Caucasian subjects of both sexes in the five decades between the ages of 20 and 69; there were 50 females and 50 males in each of the decades [107]. Of the 500 subjects, there were 160 healthy volunteers and 340 catheterized patients. The latter underwent diagnostic heart catheterization for the evaluation of chest pain and had totally normal studies including hemodynamics. The resultant 53-criteria/32-point system is presented in Fig. 16.16.

Age and gender adjustments for the QRS amplitude and duration criteria noted lower left of the scoring worksheet are the result of a review of this normal database and the Macfarlane Western Scotland database of 1339 normals (see Vol. 3), with a similar age and gender distribution.

Studies using this complete scoring system in the first 54 patients of the same postmortem subjects reported above [58], demonstrated that it predicted extent of infarct in each of the three major coronary distributions with good correlation (r = 0.91, see Fig. 16.14, Panel d) when compared to quantitative planometric pathoanatomic findings. It was also demonstrated that, on average, the complete scoring system predicted a distribution of damage in the 12 LV segments that correlated well with the average of the planometric pathology found in those same 12 subdivisions, i.e.: anterior infarcts r = 0.93, inferior r = 0.97 and posterolateral r = 0.83 [34].

16.3.5.2 Comparison of QRS Score to MRI Infarct Quantification

Gadolinium delayed-enhancement magnetic resonance imaging (DE-MRI) has recently emerged as the gold standard to quantify infarction in-vivo. Engblom et al. performed two studies comparing the simplified scoring system to infarct size quantified by DE-MRI [108, 109]. The first study included 25 patients with chronic anterior infarction and found only a moderate correlation of r = 0.40 ($P < 0.05$) between ECG and MRI scar size [108]. The reason for this relatively poor correlation is not entirely clear. Of note, the population consisted of chronic ischemic heart disease patients who had significant remodeling and wall thinning that was not taken into account when quantifying infarct size (amount of myocardium lost by necrosis) as had been done in the necropsy studies by Ideker and colleagues [18]. Finally, the accuracy of infarct quantification by MRI in-vivo is confounded by partial volume affects and image quality.

The second study by Engblom et al. in 29 patients with first-time reperfused infarction found a stronger correlation of r = 0.79 between ECG and MRI infarct size [108]. They found the best correlation between local QRS score and infarct size in the middle third of the LV. These small ECG-MRI studies will have to be followed by studies in larger populations before definitive conclusions can be drawn.

16.3.6 Methods for the 12 Lead ECG QRS MI Size Scoring System, Manual

In all the studies reported, either 3- or 8-channel recorders were used to obtain standard 12 lead ECGs. The duration and amplitude of each deflection in the QRS complex were measured with hand held micro-adjustable calipers for 10 of the standard 12 leads (I, II, aVL, aVF, and V1–V6). QRS duration measurements (ms) were made horizontally along the PR segment baseline. Amplitude measurements (mV) were made vertically from this baseline even when the ST segment was shifted. From these measurements, a point score was determined from weighted criteria for each ECG. However, when major ST segment shifts are present (1.0 mV or more beyond the 98% normal confidence limits), scoring is less reliable because the injury current usually distorts the appearance of the QRS complex.

Clinical observations of durations and amplitudes of Q, R and S waves on the standard 12 lead ECG are performed routinely by physicians and paramedical personnel. When these observations are required for identifying specific criteria for a quantitative QRS scoring system for estimating infarct size, precise observations of the waveforms are required.

There are several aspects to this precision: (a) adequate ECG recording, (b) rigorous definition of waveforms, (c) accurate waveform measurement, (d) use of simple guidelines for considering relationships among criteria, and (e) a logical format for presenting the scoring system.

16.3.6.1 Adequate ECG Recording

The performance of the ECG recording equipment should be tested at regular intervals to assure proper writing, alignment between channels, amplitude calibration of 10 mm/mV, and appropriate (0.05–150 Hz) frequency response. A minimum of three channel recording with perfect alignment between channels is required for adequate definition of the times of waveform onsets and offsets. This precision is particularly important for the identification of the initial isoelectric portion of a waveform as in (Fig. 16.15). Several commercially available ECG recorders have the ability to display the ECG at double gain and effectively double speed. Such recordings increase the resolution and decrease the variability of measurements for the manual scoring process.

16.3.6.2 Rigorous Waveform Definitions

If the initial deflection of the QRS complex is negative, a Q wave is present. Prior to returning to the baseline, this negative deflection may be either smooth or notched. A "smooth Q" is present (Fig. 16.15) when the initial negative deflection has no reversal in direction equal to or greater than (≥)0.05 mV ("notch"), preceding a positive (R) deflection. The duration of such a Q is measured as the width of the entire initial negative deflection. When the entire complex is a smooth negative deflection, no S wave is present. Therefore the amplitude of the Q wave should also be considered as the "S wave"

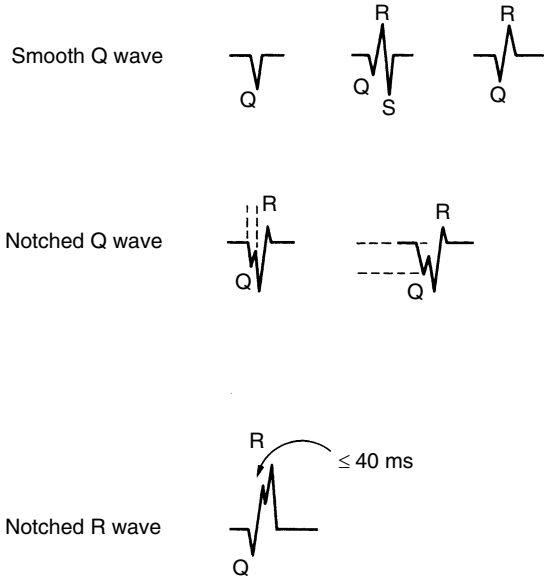

Figure 16.15

A "smooth Q" is present, if there is no reversal in direction ≥0.05 mV in the first negative deflection (preceding the R wave). A "notched Q" is present when there is a reversal in direction ≥0.05 mV within the initial negative deflection. The duration of the Q, as indicated by the vertical dashed line, is taken from the baseline to the point directly above the peak of the notch. The amplitude of the Q, as indicated by the horizontal dashed lines, is measured from the nadir of the negative deflection preceding the notch to the PQ-segment baseline. As indicated by the arrow, a "notched R" for the purpose of ECG scoring of infarct size is defined as a reversal ≥0.05 mV starting within the first 40 ms of the QRS.

amplitude. A "notched Q" is present (Fig. 16.15) if there is any reversal in direction ≥0.05 mV within the initial negative deflection. In this instance, the duration of the Q wave extends along the PR baseline only to the point directly above the peak of the "notch." The amplitude of the Q extends to the nadir of the depression preceding the notch, and when the entire complex is a negative deflection (QS), the amplitude of the S extends to the nadir of the negative deflection following the "notch." When an initial wave is positive an R wave is present. A positive deflection which follows a Q wave is also considered an R wave. For the purpose of the QRS scoring, an "R wave" is considered to be the first positive deflection that appears. It extends until it reaches the baseline to become either an S wave or to complete the QRS complex. A "notched" initial R occurs when there is a reversal in direction ≥0.05 mV beginning within the first 40 ms of the QRS.

Strict and consistent application of the waveform definitions described in detail in this methods section is required to obtain consistent performance of the infarct size criteria. Failure to observe this definition will result in falsely awarding points. For example, an rS complex might be present in lead aVF prior to an infarct. The r wave would then be lost as a result of the infarct, producing an entirely negative deflection. A notch might appear with a peak at 30 ms after the onset. Only three points would be awarded using the above definitions while five points would be awarded if the entire negative deflection were considered a Q wave. A graphic of the waveform definitions of Fig. 16.15 is present in the lower right of the 53-Criteria/32-Point QRS infarct size scoring worksheet, Fig. 16.16.

16.3.6.3 Accurate Waveform Measurement

Careful manual measurements of both amplitudes and durations should be made with micro-adjustable calipers using the center of the trace of the inscribed wave form. ECG recorders with double gain, double speed options (some have recording speeds of 250–500 mm/s) would increase the resolution and decrease the variability of measurements for scoring purposes. Only 3-channel, 12-lead ECG tracings recorded at 10 mm/mV and at 25 mm/s paper speed were available on the majority of the tracings used in the validation studies reported. In the presence of major acute ST elevation in any lead, the amplitude measurements will be influenced by the "injury currents." To minimize these effects, the R amplitude should be measured from the PQ segment baseline and the S amplitude from the J point of the ST.

16.3.6.4 Guidelines for QRS Scoring

Two aspects of individual criteria must be considered (Fig. 16.16): weighting and selecting. Weighting refers to the number of points awarded for criteria satisfied (in brackets in Fig. 16.16). Of the 53 criteria, 37 have a weight of 1, 15 a weight of 2, and 1 a weight of 3. The additional points are awarded when there is increasing magnitude (either amplitude or duration) of the same waveform abnormality. Selecting refers to the process of choosing a single criterion from a group (inside the brackets, Fig. 16.16). When criteria with multiple weights are included within a bracket, they are ordered by decreasing weights. Therefore, proceeding from the top down within a bracket, one should select only the first criterion satisfied. The total point score for each ECG is the sum of the points accumulated from the criteria satisfied. The significance and appropriate diagnostic statements and probabilities for any given total QRS point score is shown in Table 16.3. The six steps to be taken to apply the score in general for infarct size are as follows:

(a) Is normal LV conduction present without ECG changes of emphysema, RVH or LVH? *Score ECG for infarct size and location using age and gender criteria adjustments and attach diagnostic statements with modifiers as tabulated in* Table 16.3.

(b) Are criteria for LVH or conduction defects LAFB, RBBB, LBBB present? If so, they can be QRS scored, with confidence, for infarct size and location using the revised criteria in Appendix and B: Figs. 16.31a, b, LVH+Anterior MI, Fig. 16.37a, b RBBB + Posterolateral MI, Fig. 16.41a, b LBBB + Apical MI and an Inferobasal MI. Figs. 16.30a, b through 16.36a, b are examples of typical healed infarcts in each of the three arterial distributions that illustrate the points made above regarding the scoring methodology.

Myocardial Infarction

INFARCT SIZE - ECG SCORE - "HOW TO" WORKSHEET
COMPLETE 53-CRITERIA/32-POINT QRS SCORING SYSTEM

PANEL A — ECG POINTS (3% LV each)

Lead	Criteria	Pts. each cri.	Lead max. pts.
I	Q>=30 MS	1	
	R/Q<=1	1	2
	R<=0.2 MV		
II	Q>=40 MS	2	2
	Q>=30 MS	1	
aVL	Q>=30 MS	1	2
	R/Q<=1	1	
aVF	Q>=50 MS	3	
	Q>=40 MS	2	
	Q>=30 MS	1	5
	R/Q<=1	2	
	R/Q<=2	1	
V_1 Ant.	any Q	1	1
Post.	R/S>=1	1	
	R>=50 ms	2	
	R>=1.0 mV		
	R>=40 ms	1	4
	R>0.7 mV		
	Q/S<=0.2 mV	1	
V_2 Ant.	any Q		
	R<=10 ms	1	1
	R<=0.1 mV		
Post.	R/S>=1.5	1	
	R>=60 ms	2	
	R>=2.0 mV		
	R>=50 ms	1	4
	R>=1.5 mV		
	Q/S<=0.3 mV		
V_3	Q>=30 ms	2	
	R<=10 mS		2
	R<=0.2 mv	1	
	Q>=20 mS		
V_4	Q>=20 ms	1	
	R/Q<=0.5	2	
	R/S<=0.5		
	R/Q<=1		3
	R/S<=1	1	
	R<=0.5 mV		
	.04Rnotch		
V_5	Q>=30 ms	1	
	R/Q<=1	2	
	R/S<=1		
	R/Q<=2		3
	R/S<=2	1	
	R<=0.6 mV		
	.04Rnotch		
V_6	Q>=30 ms	1	
	R/Q<=1	2	
	R/S<=1		
	R/Q<=3		3
	R/S<=3	1	
	R<=0.6 mV		
	.04Rnotch		
TOTALS:	Points		32 %LVI→

PANEL B — % LV INFARCT IN 12 LV SEGMENTS

Lead	LAD ant. 1 2 3	LAD sup. 4 5 6	RCA inf. 7 8 9	CX post 10 11 12
I		1 1 1 1 1		1
II			2 2 2 2 1	
aVL		2 1 1 2		
aVF			3 2 2 2 2 2 2 1	1 1
			2 3 1 2	1
V_1 Ant. any Q	1 2			
Post. R/S>=1				1 1 1
R>=50 ms R>=1.0 mV		1	1 1	1 1 1
R>=40 ms R>0.7 mV			1	1 1
Q/S<=0.2 mV			1	1 1
V_2 Ant. any Q R<=10 ms R<=0.1 mV	1 2			
Post. R/S>=1.5			1	1 1
R>=60 ms R>=2.0 mV			1 1	1 2 1
R>=50 ms R>=1.5 mV			1	1 1
Q/S<=0.3 mV			1	1 1
V_3 Q>=30 ms R<=10 mS	2 2 1	1		
R<=0.2 mv Q>=20 mS	1 1	1		
V_4 Q>=20 ms	1 1	1		
R/Q<=0.5 R/S<=0.5	2 1	1 1	1	
R/Q<=1 R/S<=1	1 1	1		
R<=0.5 mV .04Rnotch				
V_5 Q>=30 ms	1 1	1		
R/Q<=1 R/S<=1	2 1	1 1	1	
R/Q<=2 R/S<=2	1	1 1		
R<=0.6 mV .04Rnotch				
V_6 Q>=30 ms			1	2
R/Q<=1 R/S<=1		1	1	2 2
R/Q<=3 R/S<=3			1	1 1
R<=0.6 mV .04Rnotch				

If >1 criterion in bracket met, select one with most points.
If >1 criterion in bracket has the same point, score only once.
Age normalize all amplitude criteria to age 55 by increasing them 1%yr age 20–54 and decreasing them 1%/yr for > 55yrs.
For Females further decrease by 10% all QRSdur and QRSamp Criteria.

>= denotes greater than or equal to
<= denoter less than or equal to

INFARCT SIZE - ECG SCORE - HOW TO --

1. CIRCLE EACH ECG CRITERIA MET FROM...PANEL A (If more than one criterion in bracket met, circle one with most points only)
2. CIRCLE POINTS SCORED EACH CRITERIA.. PANEL A (If more than one criterion in bracket has the same point, score only once)
3. CIRCLE %LV INFARCT IN EACH SEGMENT} FOR EACH QRS CRITERIA MET..... PANEL B
4. PLACE ⊗ (FOR EACH 1% LVI) FROM..... PANEL B IN PROPER SEGMENT IN DIAGRAM BELOW

SEGMENT SUBDIVISION

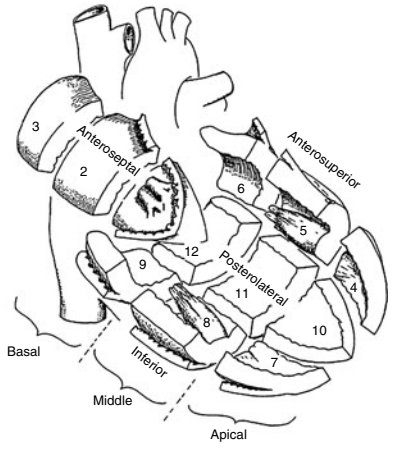

INFARCT SIZE: EJECTION FRACTION:

TOTAL ECG POINTS____x3=% LV INFARCTED (%LVI) _____

65–%LVI = ESTIMATED EJECTION FRACTION (EEF) _____

INFARCT LOCATION: (IN 12 LV SEGMENTS)

EACH ⊗ = 1% OF LV INFARCTED,
8 ⊗ IN A SEGMENT = 100% OF SEGMENT

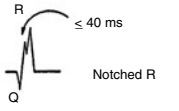

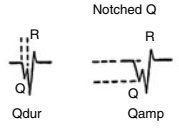

Figure 16.16

Worksheet that can be copied and used for the routine scoring of an ECG for infarct size. Instructions for scoring are given on the lower left and for wave-form definitions of notched R and Q on the lower right. Adjustments to the criteria thresholds for age and female gender are defined lower left. Upper right are instructions for distributing each 1% of LV infarct in panel B (for each criterion met in panel A) into the 12 segment subdivision on the middle right. Also see Sect. 16.3.6.4 for the stepwise use of the score in the presence of hypertrophies or conduction defects.

Table 16.3

Diagnostic statements and significance for ECG infarct-size score

ECG points	Diagnostic statement (fill in location ())	Pathology E% LVI[a] (%)	Angiography EEF (%)[b]	Probability (%)	
				CAD[c]	Normal
I[d]	consider small () infarct	3	62	10–24	10–24
2	possible small () infarct	6	59	25–49	5–9
3	probable small: () infarct	9	56	50–94	3–4
4	small () infarct	12	53	95–97	<2
5–7	moderate () infarct	15–21	50–44	98	<1
8–10	large () infarct	24–30	41–35	>99	<1
≥11	very large () infarct	≥33	<33	>99	<1

[a]E% LVI, estimated % left ventricle infarcted
[b]EEF(%), estimated ejection fraction (%)
[c]CAD, coronary artery disease
[d]Diagnostic statement warranted for 1 point from the following highly specific criteria only: Q ≥ 30 ms, I, aVF, V4, V5, V6; R ≥ 40 ms, V1; R ≥ 50 ms, V2. If screening apparently healthy populations where the incidence of CAD is low, accumulate ≥3 points before a diagnostic statement "consider small…" is made, and ≥4 points for "possible small. . ."

16.3.6.5 Format of Scoring Criteria

The complexity of the criteria characteristics mentioned above requires an innovative format of presentation of the scoring system. The current format (Fig. 16.16) represents a 20-year evolution of attempts to present a simple, logical, and unambiguous approach. As its labeling "INFARCT SIZE – ECG SCORE – 'HOW TO' WORKSHEET" indicates, this worksheet can be readily copied, with enlargement to fill a standard letter copy paper which is the form we have used to good effect for the last several years. The updated worksheets with adjustments for the confounders LVH and conduction defects are in appendices A and B.

16.3.7 Automated ECG Analysis Programs and QRS Score for Infarct Size

The manual method of using the QRS scoring system just described in detail in the preceding section is readily adaptable to automated ECG analysis programs. An automated version of the QRS score that included the distribution of damage into the 12 LV segments as defined in Fig. 16.16 was originally written by Schussler, adapted by Sharp and Laks, and reported in 1983 at the Engineering Foundation Conference by Madrid et al. [110]. A microprocessor based ECG analysis program in a portable bedside cart system of 12 simultaneous leads with the ECG score incorporated into the cart system was assessed by Madrid et al. in 1984 [106]. It was found, not unexpectedly, that both of these automated measurement and analysis systems were more reproducible than even experienced manual readers. The automated measurement programs were, in general, more accurate in making measurements of both amplitude and duration than manual readers. The bedside cart system of 12 simultaneous leads was also consistently more accurate in measuring QRS onset and offset and in identifying those criteria that depended on these measurements. Programs for the application of the QRS score for infarct size by computer are available as special "research tools" options, or by contact with the individual investigators who developed them.

The well known age, race, and sex differences in QRS amplitudes and durations have an effect on every criterion in the QRS scoring system. In the specificity studies reported by Hindman et al. [107], using only normal Caucasian subjects stratified by age in decades, and by gender, it was observed that the QRS scoring system performed best in the decade of 40–50 for which the original criteria were established. The number of false positives increased in the younger age groups, especially males, due to increased voltages commonly seen in this age group, and in older age groups, particularly the older females due to the lower voltages common in these older subjects. The measurement of a large array of amplitude, duration and wave shape descriptors of each wave of each lead on the ECG for large populations of normals stratified

by age, race, and gender, is a near heroic task for the manual reader, but grist for the mill of a modern computer. An important normal database of ECGs from 1,339 ambulatory normal subjects living in Western Scotland recorded using a simultaneous multilead system has been reported by Macfarlane and Lawrie (Vol. 3 of the 1st edition). This database has become widely available for each decades of 1920s–1950s and older, subdivided by gender. A smaller cohort of 503 (255 males, 248 females) normal Chinese was also presented along with a larger cohort of 1,329 Japanese with ECGs recorded earlier on paper and with measurements made by hand. A similar cohort of ambulatory black subjects is not present. Another limitation of this important normal database is the absence of similar data for the older decades, now being seen in chest pain centers with major increased frequency. As comprehensive age, gender and race specific databases become available, the sensitivity and specificity of the ECG diagnosis of the presence, size and location of acute and healed myocardial infarcts in the younger and older decades can be expected to improve significantly. Criteria for the quantification of infarct size can be "fine tuned" to be gender, age, and race specific. Some commercial vendors are now supporting "gender smart" ECG interpretation algorithms and the others appear to be coming online. Enhancements for gender and age are included in our current edition of the QRS MI Size Scoring System presented in Fig. 16.16.

Based on the presence of important high frequency components as a result of disruption of the activation fronts by the complex geometry at the infarct boundary, and by small multifocal infarcts, the optimal normal digital databases will need to be sampled at rates of at least 1,000 samples per second. This will be necessary in order to identify the limits of these high frequency components in normals before they can be applied with statistical confidence to patient populations suspected of having a myocardial infarction.

Automated ECG/VCG analysis systems with their large database storage capability are also ideally suited to the archiving of digitized ECG/VCGs for later comparison to newly acquired tracings. Detailed wave by wave, lead by lead comparison is a simple task for comparative programs. Automatic gain adjustments are routine to correct for individual ECG preamplifier drift in amplitude. Serial comparison using large high resolution ECG databases of normal controls can readily show when newly measured waveforms are outside the 96% or 98% age-race-sex matched normal ranges, and when similar confidence limits for normal variability of serial comparison records have been exceeded. This kind of detailed comparison to large well validated normal databases is possible by manual means but is so labor intensive that this discourages it being done routinely. Such high resolution and comprehensive comparisons are trivial for a modern computer when validated measurement algorithms are installed and the proper digital data is archived in their electronic files. *We again stoutly reaffirm our earlier recommendation*: **THAT EVERY YOUNG ADULT ACQUIRE SUCH A HIGH RESOLUTION BASELINE ECG RECORD BEFORE AGE 30. A wallet sized photographic and electronic copy can be carried personally thereafter**.

16.4 Principal Areas of Infarction and Typical ECG/VCG Changes

16.4.1 Acute Myocardial Infarction, Evolving Changes of Injury, Ischemia and Necrosis

The evolutionary changes that occur after an acute coronary occlusion and subsequent infarction, when viewed from the vectorial perspective, are the same for each of the arterial perfusion beds. In order to maintain the relationship with part or all of these three main coronary artery perfusion beds, it is important to maintain the separation in nomenclature of the regions, anterior for LAD, posterolateral for LCX and inferior for RCA/PDA as indicated earlier in Sect. 16.2.3. The direction and amplitude of local electrical field changes over time (mean vector or axis changes) from injury, ischemia and necrosis or infarct, have major reflections in individual leads of a 12-lead ECG (including the 24-view ECG; to be discussed shortly) or the orthogonal *X*, *Y*, and *Z* leads. This corresponds to the orientation of the specific lead to the mean direction of the electric field from the local arterial perfusion bed distal to the obstruction. As discussed in more detail in Chaps. 2 and 11, if the lead is at right angles to the average direction of the electrical event, that is, on the "null plane" as defined by Grant [41] and others, the particular change, whether it be regional depolarization or repolarization, will be poorly represented in that lead. Likewise, the event will be maximally represented in leads in three-dimensional space that are oriented parallel to the mean axis or vector of the event and perpendicular to the null plane. The orderly sequence (Cabrera) of limb leads used throughout this chapter, including the 24-view 12-lead ECG illustrations, enhance the determination of various axes, i.e., mean P, initial 30 ms, terminal 30 ms and mean QRS, and mean STj and T axes or vectors.

The serial ECG changes of evolving acute myocardial infarction associated with injury/ischemia, necrosis and healing of the infarct can in general be classified into four phases: hyperacute, acute, subacute and completed (chronic healing) (Fig. 16.17). In general, the acute injury/ischemia process is potentially reversible in the hyperacute and early acute phases with progressive infarction occurring throughout the acute phase. The healing phase begins in the subacute and continues with remodeling in the completed or chronic phase. The time course of these phases can vary between individuals. They may be quite rapid as in first infarction occurring early in life with little or no time to have developed collaterals from adjacent normally perfused regions. They may be delayed during gradual or intermittent coronary occlusion in subjects who have developed collaterals. They may be aborted by prompt and sustained reperfusion.

(a) *Hyperacute Phase*: Within seconds after acute coronary occlusion, there is typically a significant increase in amplitude and peaking of the T wave, directed outward from the epicardium of the centroid of the acutely ischemic region. This is commonly called "hyperacute T." Experimental work by Kleber et al. [111] and computer simulation work by Miller and Geselowitz [86] showed that shortening of the action potential is what produces the hyperactue T. Furthermore, more recent work by Shaw and Rudy has suggested that opening of K-ATP channels is what causes the most significant shortening of the ischemic action potential and likely results from shift of excess potassium into the extracellular space [112]. Although this change may persist for some time in a slowly developing process, typically in some seconds to a minute later the ST segment begins to join the hyperacute T as a "current of injury" vector directed outward perpendicular to the epicardium of the centroid of the injured/ischemic region. When these currents of injury/ischemia are large, indicating a large area of severe ischemia, the DC level of the entire baseline (see Fig. 16.9) becomes negative. The middle and late QRS forces are drawn, with the ST-T, outward from the epicardium of the region at risk.

(b) *Acute Phase*: In the early part of this phase, the terminal portion of the T wave and early QRS forces begin to decrease in amplitude along the axis of the acute injury/ischemia vector that is perpendicular to the epicardium of the risk region. During the early half of this phase, the ischemic process is potentially reversible with consequent salvage of the injured myocardium. The specific QRS changes of the evolving local infarct begin to appear and progress,

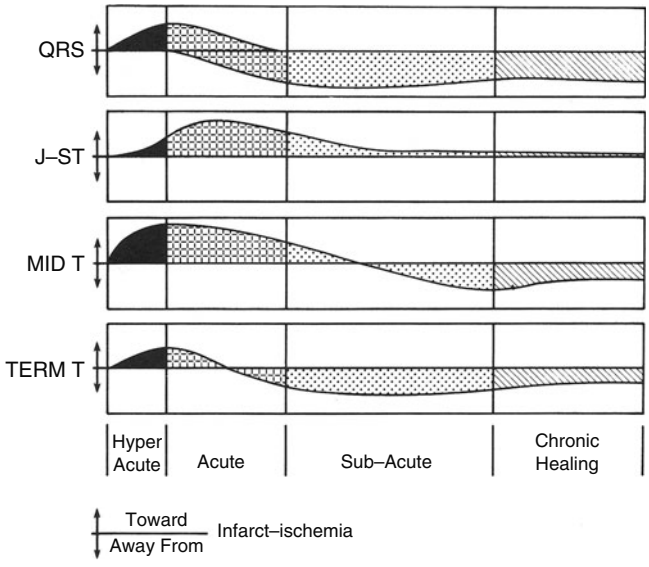

Figure 16.17

Diagram shows the four ECG phases of acute coronary occlusion. Panels showing the evolution of the acute infarction to its chronic stable phase are indicated at the bottom. Each panel illustrates the typical change in direction and amplitude of the QRS complex, J point and ST segment, and mid and terminal T wave. A shift outward toward the ischemic/infarcted area is indicated by an upward-pointing arrow; a shift inward away from this area is indicated by a downward-pointing arrow.

reaching their full extent at the end of the acute phase. As the QRS emerges from the current of injury it shifts away from the region at risk, revealing abnormal Q waves, notched or attenuated R waves, and altered terminal forces. The precise changes depend on the size and location of the infarct. They can be remarkably accelerated following successful early revascularization interventions. In the absence of such interventions, the acute phase typically lasts 6–8 h from the onset of symptoms.

(c) *Subacute (Evolving) Phase*: Over the next day or two, as the infarct evolves through the sub-acute to completed or chronic healing stage, the QRS changes of infarct are fully developed and stable. The ST segments subside toward their normal location, while the mid and terminal T-wave becomes fused with major displacement inward from the infarcted region. The ischemic myocardium has become, in general, irreversibly damaged and healing has begun. T waves are now usually deeply inverted in leads whose positive pole faces the epicardium over the centroid of the infarct. In the 24-lead ECGs of Figs. 16.22–16.26, this relationship is to be noted for either the positive or negative pole.

(d) *Completed phase*: During the completed or chronic healing phase, the changes on the ECG caused by the infarction have stabilized (see Fig. 16.17). If there is no recurrence of ischemia, these changes will gradually move toward resolution. The T wave will remain directed inward away from the infarcted region and will gradually decrease in size unless influenced by ischemia elsewhere, or by ventricular hypertrophy, or bundle branch block.

The reader is encouraged to review the serial changes in Figs. 16.18–16.21 illustrating those changes seen with acute anterior, posterolateral, and inferior infarctions in patients who did not receive revascularization interventions. Scores for

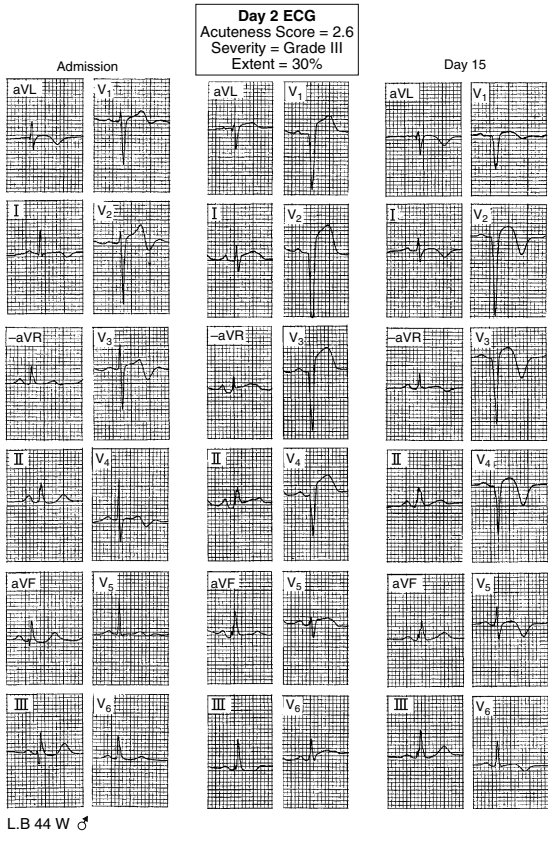

Figure 16.18 (Continued)

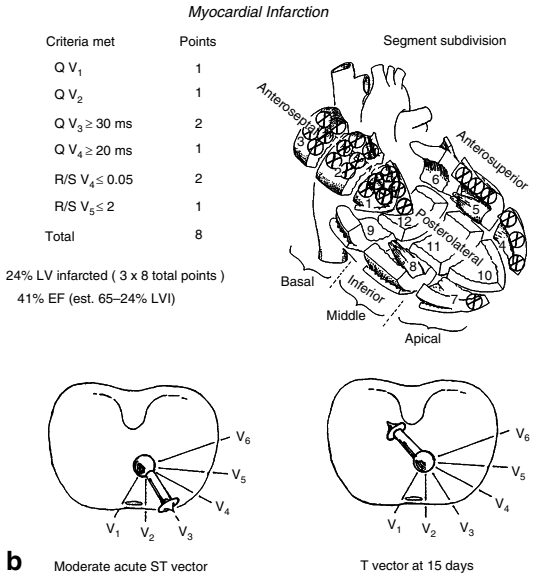

Figure 16.18

(a) Note limb leads are in the orderly (Cabrera) sequence from the top down, aVL, I, -aVR, II, aVF, III. These serial ECGs are of a 44-year-old man with chest pain who was admitted to the hospital with possible acute myocardial infarction. The slight ST elevation with coving and T inversion in aVL, I, and V1–V5, indicating at most a moderate ischemic risk area (see Sect. 16.4.1 for details). By the next morning he has acute ST elevation changes of acute anterior myocardial infarction and had evolved QRS changes of a moderate sized infarct, see (b). By day 15, the typical evolution of the STT with deeply inverted T waves as noted and the QRS changes of a moderate sized anterior infarct show no further evolution. (b) For the case of (a), the moderate peak acute ST vector was plotted by the method of Grant from the day 2 tracing, as was the T vector at day 15. The scoring criteria met in the day 15 record, the points scored for each, and the total of 8 points are tabulated. As indicated each point represents 3% of the left ventricle infarcted (LVI), the 8 points predict 24% LVI and an estimated ejection (EF) of 41%. The distribution into the 12 LV segments on the *upper right* is derived from panel B of the ECG scoring work sheet, shown in more detail for this specific patient in Fig. 16.16. Angiographic data is not available.

the extent, severity and acuteness of ischemia are shown in each of these figures. Detailed descriptions of these acuteness and severity scores are in Sect. 16.4.2.

It follows that major injury, ST-T vectors of acute myocardial infarction or evolving infarct, QRS and T vectors from the anterior or posterolateral wall of the heart, will be seen optimally in anterior-posterolateral oriented leads V1, V2, V3, V4 and *Z*. These changes are usually maximal for either anterior or posterolateral AMI in V2 or V3. Electric field vectors originating in the opposing anterior and posterolateral walls will produce opposite (mirror-image) effects to each other in these same leads. Likewise, anterosuperior or inferior wall injury, ischemia or infarct will produce their main changes in superior-inferior oriented leads aVL, III, aVF, II and Y. As a result of the orientation of the positive end of the leads, III and aVF will generally show mirror-image acute injury/ischemia effects to aVL for acute anterosuperior injury and vice-versa for acute inferior injury. If the lesions also extend toward or localize to the apex (left and 30° inferior) or the left side of the heart, leads with a left-right (base-apex) orientation, i.e., I, -aVR, II, V4, V5, V6, and *X*, will also reflect these changes.

The term "reciprocal changes" which occurs in much of the ECG literature to describe these "mirror image" changes is mainly descriptive. When considered from a vectorial perspective, this term may be misleading and its use should be avoided. It is more anatomically and electrophysiologically correct to assign a direction to these acute ST-T changes, along with a location in the heart, together with size or extent modifiers that denote their significance. When anterior-posterior leads V1–V4 show a prominent anterior ST-T change of acute anterior infarction, the term "with reciprocal changes in

Myocardial Infarction

INFARCT SIZE - ECG SCORE - "HOW TO" WORKSHEET
COMPLETE 53-CRITERIA/32-POINT QRS SCORING SYSTEM

PANEL A — ECG POINTS (3% LV each)

Lead	Criteria	Pts. each cri.	Lead max. pts.
I	Q>=30 MS	1	2
	R/Q<=1	1	
	R<=0.2 MV		
II	Q>=40 MS	2	2
	Q>=30 MS	1	
aVL	Q>=30 MS	1	2
	R/Q<=1	1	
aVF	Q>=50 MS	3	5
	Q>=40 MS	2	
	Q>=30 MS	1	
	R/Q<=1	2	
	R/Q<=2	1	
V_1 Ant.	any Q	1	1
Post.	R/S>=1	1	
	R>=50 ms	2	
	R>=1.0 mV		
	R>=40 ms	1	4
	R>0.7 mV		
	Q/S<=0.2 mV	1	
V_2 Ant.	any Q	1	1
	R<=10 ms		
	R<=0.1 mV		
Post.	R/S>=1.5	1	
	R>=60 ms	2	
	R>=2.0 mV		
	R>=50 ms	1	4
	R>=1.5 mV		
	Q/S<=0.3 mV		
V_3	Q>=30 ms	2	2
	R<=10 ms		
	R<=0.2 mV	1	
	Q>=20 ms		
V_4	Q>=20 ms	1	3
	R/Q<=0.5	2	
	R/S<=0.5		
	R/Q<=1		
	R/S<=1	1	
	R<=0.5 mV		
	.04Rnotch		
V_5	Q>=30 ms	1	3
	R/Q<=1	2	
	R/S<=1		
	R/Q<=2		
	R/S<=2	1	
	R<=0.6 mV		
	.04Rnotch		
V_6	Q>=30 ms	1	3
	R/Q<=1	2	
	R/S<=1		
	R/Q<=3		
	R/S<=3	1	
	R<=0.6 mV		
	.04Rnotch		
TOTALS:		Points 8	32

PANEL B — % LV INFARCT IN 12 LV SEGMENTS

Lead	LAD ant. 1 2 3	LAD sup. 4 5 6	RCA inf. 7 8 9	CX post. 10 11 12
I		1 1 1 1 1		1
II			2 2 2 2 1	
aVL		2 1 1 2		
aVF			3 2 2 2 2 2 2 1	1 1
			2 3 1 2	1
V_1 Ant.	1 2			
Post.		1	1 1 1	1 1 1 1 1 1 1 1
			1	1 1
V_2 Ant.	1 2			
Post.			1 1 1 1	1 1 1 2 1 1 1
			1	1 1
V_3	2 2 1 1 1	1 1		
V_4	1 1 2 1 1 1	1 0 1 1	1 1	
V_5	1 1 2 1 1	1 1 1 1 1	1	
V_6		1	1 1 1	2 2 2 1 1
TOTALS:	6	6 5 3 3	1	

If >1 criterion in bracket met, select one with most points.
If >1 criterion in bracket has the same point, score only once.

Age normalize all amplitude criteria to age 55 by increasing them 1%yr age 20–54 and decreasing them 1%/yr for > 55yrs.

For Females further decrease by 10% all QRSdur and QRSamp Criteria.

>= denotes greater than or equal to
<= denoter less than or equal to

INFARCT SIZE - ECG SCORE - HOW TO --

1. CIRCLE EACH ECG CRITERIA MET FROM...PANEL A (If more than one criterion in bracket met, circle one with most points only)
2. CIRCLE POINTS SCORED EACH CRITERIA.. PANEL A (If more than one criterion in bracket has the same point, score only once)
3. CIRCLE %LV INFARCT IN EACH SEGMENT} FOR EACH QRS CRITERIA MET..... PANEL B
4. PLACE ⊗ (FOR EACH 1% LVI) FROM..... PANEL B IN PROPER SEGMENT IN DIAGRAM BELOW

SEGMENT SUBDIVISION

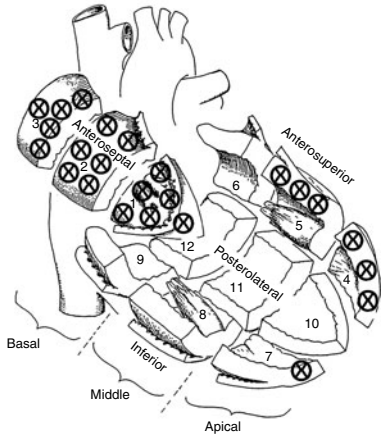

L.B. 44 W. ♂

INFARCT SIZE: EJECTION FRACTION:

TOTAL ECG POINTS 8 x3=% LV INFARCTED (%LVI) **24%**

65–%LVI = ESTIMATED EJECTION FRACTION (EEF) **41%**

INFARCT LOCATION: IN 12 LV SEGMENTS

EACH ⊗ = 1% OF LV INFARCTED,
8 ⊗ IN A SEGMENT = 100% OF SEGMENT

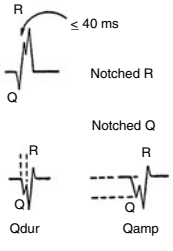

Figure 16.19

The specific criteria met in the day 15 ECG of the patient in Fig. 16.18; the distribution into the 12 LV segments for each criterion is indicated in panel A and B. The totals are depicted in each segment in the diagram to the *right*. This is the method of scoring which is used throughout this chapter.

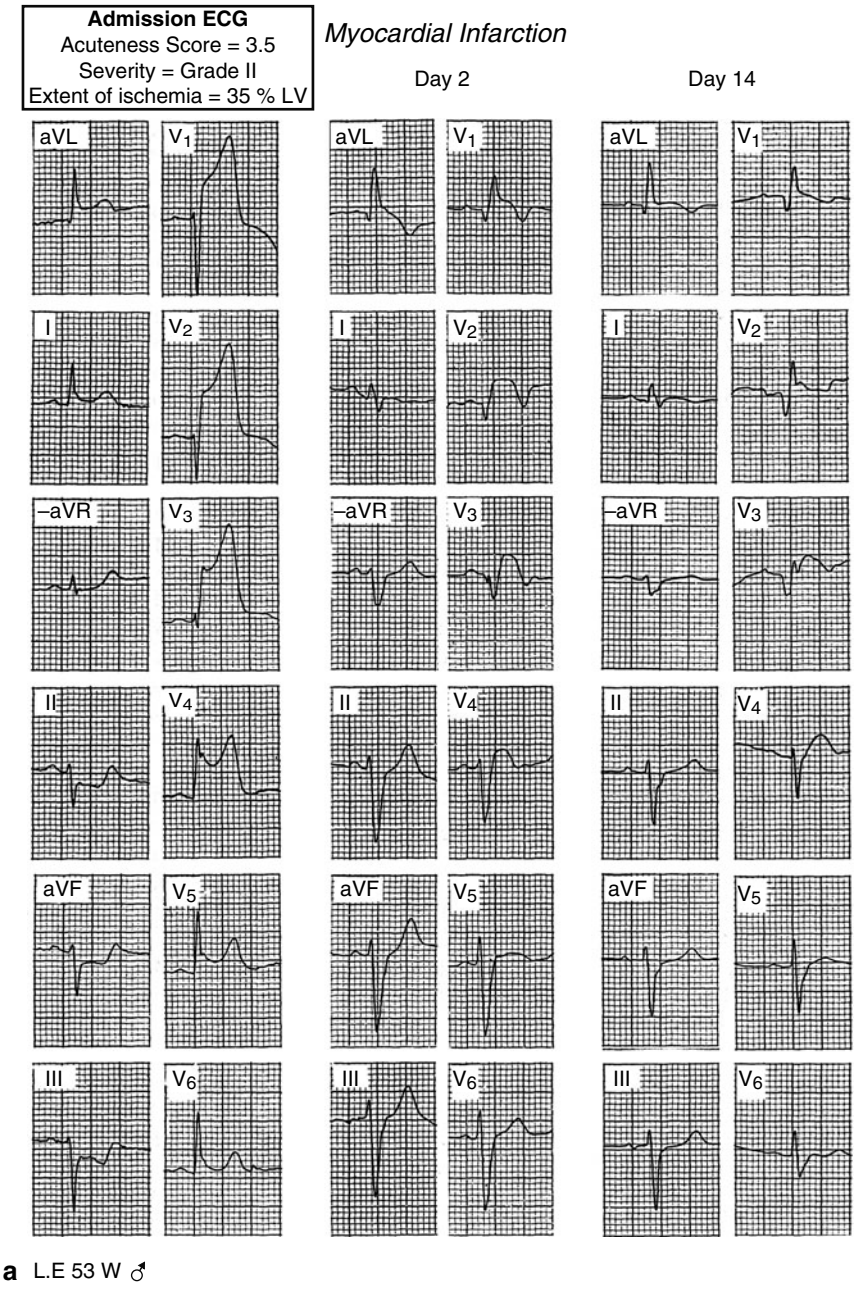

Figure 16.20 **(Continued)**

inferior leads" is ambiguous. When an associated superior ST displacement vector is indicated in superior-inferior leads aVL, III, aVF and II, we prefer to use the phrase "with significant anterosuperior involvement" to flag this evidence for a very large area at risk from LAD occlusion proximal to a large first diagonal branch. When the major acute ST changes occur in V1, V2, V3, and V4, and are directed posteriorly, while additionally a lesser degree of acute ST change is directed inferiorly in II and aVF, the label "acute posterolateral infarction with probable inferior extension" is more anatomically and physiologically appropriate. Conversely when major ST-T changes of acute inferior injury and ischemia are present

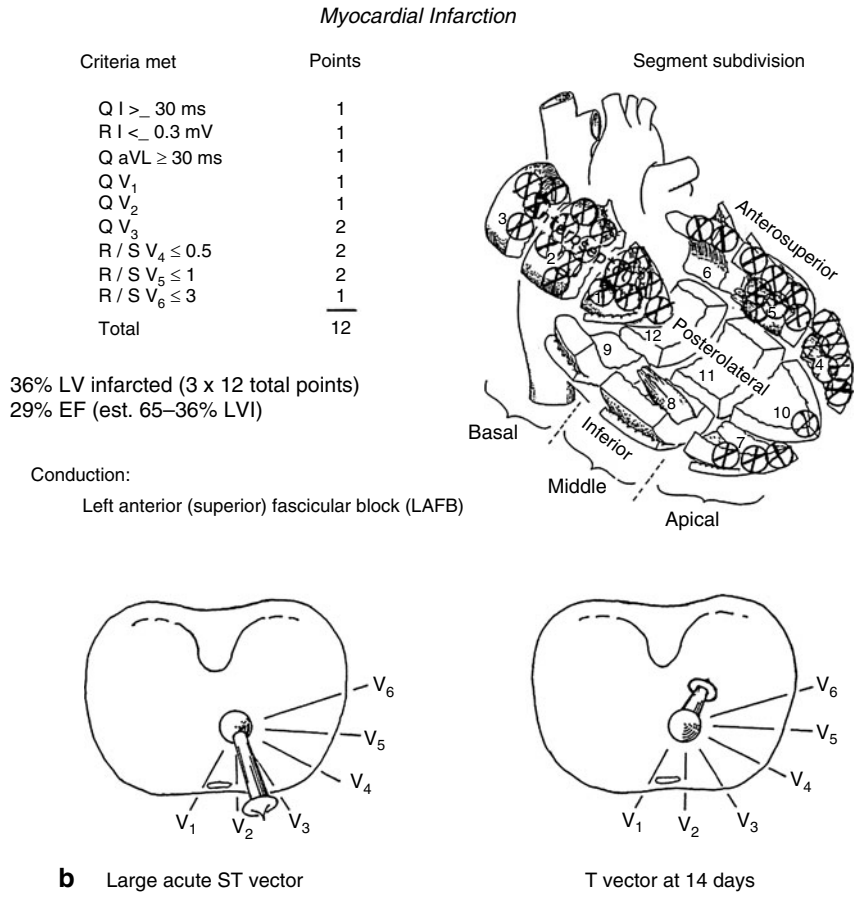

Figure 16.20

(a) Note limb leads are in the orderly (Cabrera) sequence from the top down, aVL, I, -aVR, II, aVF, III. The admission ECG of a 53-year-old man with severe chest pain shows a large ST-T deviation which is anterior and significantly superior and leftward. This is indicative of a large area at risk in the proximal LAD distribution. The new onset right bundle branch block that appears on day 2 does not influence the QRS infarct size score for anterior infarct as shown in (b). For the case of (a) the large anterior and significantly superior and leftward ST vector on admission is consistent with a large LAD area at risk. The presence of a probable left anterior (superior) fascicular block (LAFB) on admission, and of RBBB by day 2 confirms the large area at risk, as does the QRS MI size score 12 points (estimated %LV I (infarct), 36% and an estimated LV ejection fraction of 29%). The predicted distribution of the infarct in the 12 LV segments is shown on the *right*. Angiographic data was not obtained for this patient.

in II, aVF, and III, and posterior changes of a lesser degree are present in V1, V2, and V3, it is more appropriate to diagnose acute inferior myocardial infarction with posterolateral extension, than ascribing the latter to "reciprocal changes." If these local changes extend toward the apex or left border of the heart producing changes in the left-right (apex-base) leads, a notation so indicating would also be consistent, that is, "acute inferior myocardial infarction with probable posterolateral and apical extension." Table 16.4 provides a summary of the anterior, posterolateral, inferior and apical ST-T changes and the culprit artery responsible for them as well as the probable location in that artery. Details for each of these are provided in the following Sects. 16.4.3–16.4.9. We have found that these same local primary acute ST-T changes are seen as add-ons to the secondary ST-T changes of ventricular hypertrophies, bundle branch blocks, ventricular pacing and pre-excitation. These are dealt with in detail in Sect. 16.5.

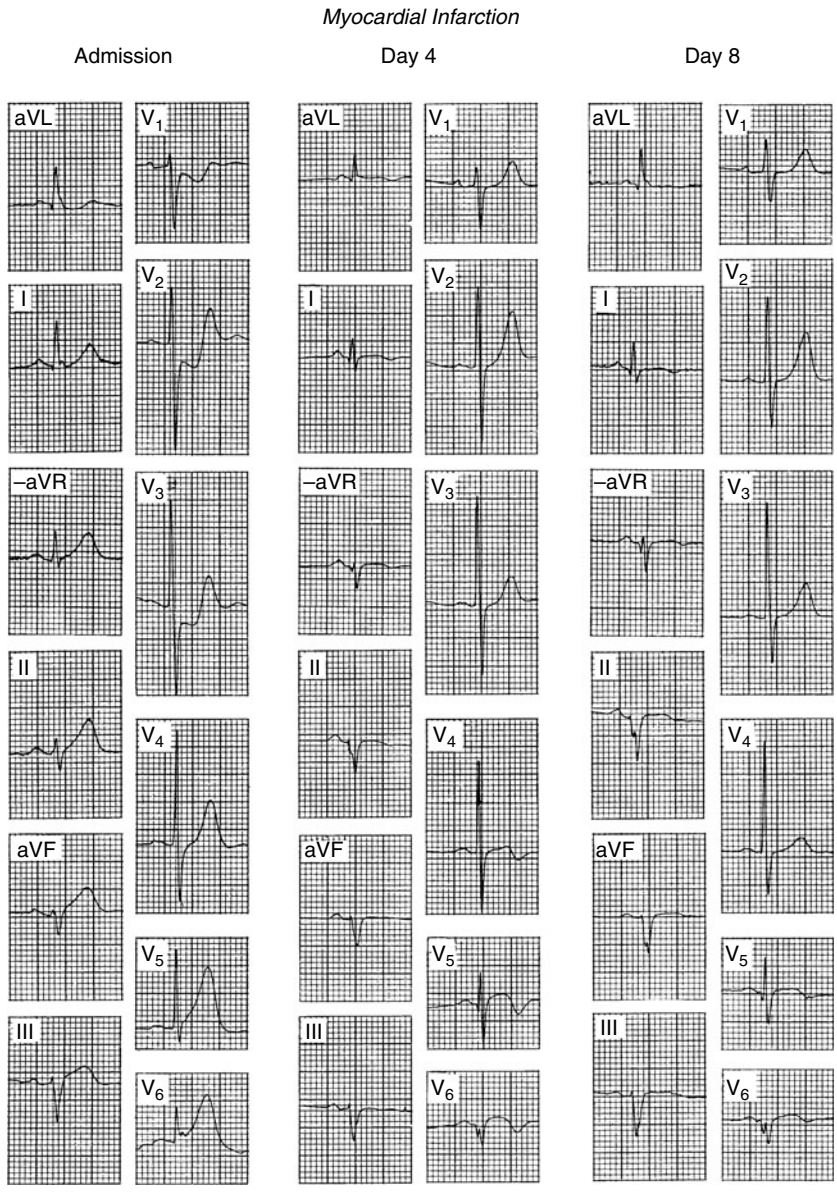

a

Figure 16.21 **(Continued)**

16.4.2 Acuteness, Severity and Extent of Ischemia

Important additions to the ECG evaluation of patients who have acute myocardial ischemia/infarction would be provided by formal indices of the three key aspects of this pathologic process, namely: acuteness, severity and extent. Animal models that incorporated these three variables were able to account for 80% of variability in final infarct size [113], while human studies using the nuclear perfusion agent ^{9}9mTc-Sestamibi were able to account for 70% of the variability in final infarct size [27]. Indeed algorithms for each of these aspects have been developed, and literature regarding their validation has been accumulating for many years. Detailed instructions on how to calculate each of these scores is contained in the text

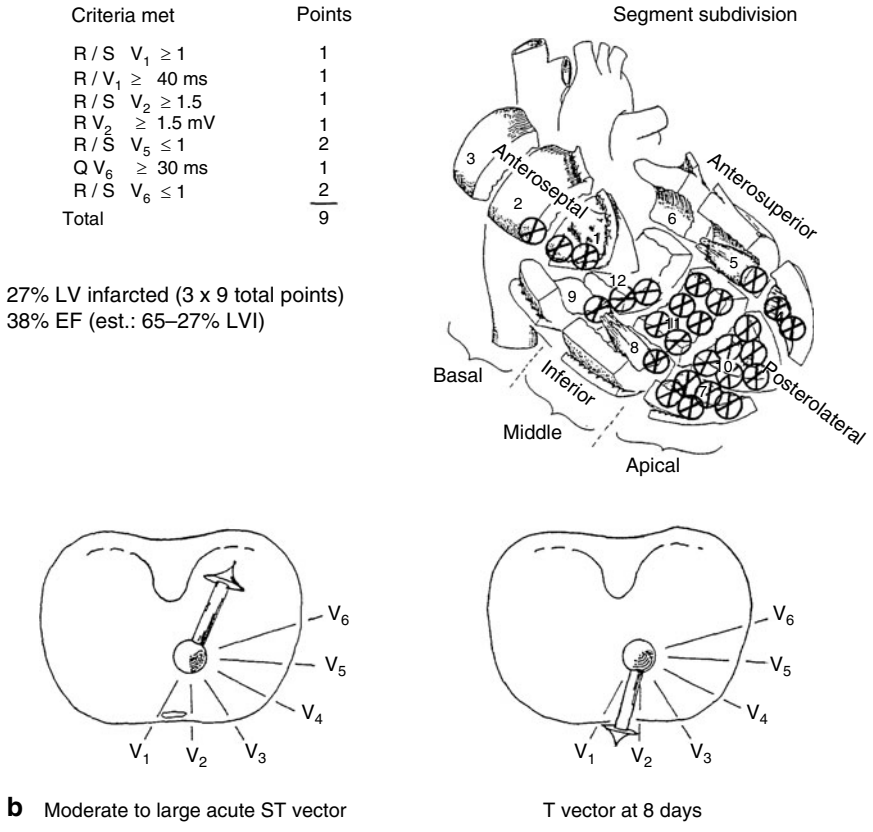

Figure 16.21

(a) Note limb leads are in the orderly (Cabrera) sequence from the top down, aVL, I, –aVR, II, aVF, III. The admission ECG of this 64-year-old man presenting with signs and symptoms of probable acute myocardial infarction had a major acute ST vector directed posterior, and less but significantly leftward. This is diagnostic of a moderate to large area at risk in the LCX distribution. Over the next few days QRS changes of a large posteroapical infarct with inferoapical extension evolved, see (b). (b) The acute ST vector and the evolved T vector at day 8, for the patient of (a), are consistent with a significant posteroapical area of potential infarction. The QRS changes and ECG criteria summarized in the *upper left* and *right* show a large infarct estimated to involve 27% of the left ventricle (estimated EF = 38%). The *upper right* of the figure shows an infarct localized to the distribution of a dominant obtuse marginal branch of the LCX that has significant extension to the inferoapical region. Angiographic data was not available for this patient.

to follow. Examples of the scoring systems are shown in Figs. 16.18–16.20, and 16.25 for anterior MI, Figs. 16.22, 16.28, and 16.29 for inferior MI, and Figs. 16.21 and 16.27 for posterolateral MI.

16.4.2.1 Acuteness of Ischemia

The Anderson-Wilkins score for application on the presenting ECG for estimation of the acuteness of the ischemia/infarction process was introduced in 1995 [114, 115]. It was based on the concept described in Sect. 16.4.1 of the serial hyperacute, acute, and subacute phases of the ischemia/infarction process (Fig. 16.17). The Anderson-Wilkins score is provided as a continuous scale from 4.0 (hyperacute) to 1.0 (subacute) based on the comparative hyperacute T waves versus abnormal Q waves in each of the leads with ST-segment elevation. Table 16.4 shows the abnormal

Table 16.4

Limits for abnormal Q waves and tall T waves in different ECG leads, as used for calculating the AW acuteness score. Reproduced from Heden et al. [116]

Leads	Old abnormal Q-wave criterion	New abnormal Q-wave criterion	Tall T-wave criterion
I	≥30 ms	≥20 ms	≥0.50 mV
II	≥30 ms	≥20 ms	≥0.50 mV
III	≥30 ms and abnormal Q in aVF	≥20 ms and abnormal Q in aVF	≥0.25 mV
aVR	–	–	–
aVL	≥30 ms	≥20 ms	≥0.25 mV
aVF	≥30 ms	≥20 ms	≥0.50 mV
V1	Any Q	Any Q	≥0.50 mV
V2	Any Q	Any Q	≥1.0 mV
V3	Any Q	Any Q	≥1.0 mV
V4	≥20 ms	≥20 ms	≥1.0 mV
V5	≥30 ms	≥20 ms	≥0.75 mV
V6	≥30 ms	≥20 ms	≥0.50 mV

Q-duration and T-amplitude criteria. The Q-duration criteria were modified by Heden and colleagues in 2003 to achieve a better distribution of acuteness scores in anterior and inferior MIs [116].

The Anderson-Wilkins ECG timing method considers each standard lead (except aVR) with either 0.1 mV or greater ST elevation or abnormally tall T waves. Acuteness phase is designated for each of these leads on the basis of the presence or absence of a tall T wave or an abnormal Q wave as defined in Table 16.4:

Phase 1A, tall T wave and no abnormal Q wave;
Phase 1B, positive T wave and no abnormal Q wave;
Phase 2A, tall T wave and abnormal Q wave;
Phase 2B, positive T wave and abnormal Q wave.
The Anderson-Wilkins (AW) acuteness score was calculated from the following formula:

$$\frac{4(\#\,\text{leads 1A}) \pm 3(\#\,\text{leads 1B}) \pm 2(\#\,\text{leads 2A}) \pm 1(\#\,\text{leads 2B})}{\text{Total}\,\#\,\text{leads with 1A, 1B, 2A or 2B}}$$

The anterior MI acuteness score is derived from all precordial leads (V1–V6), and limb leads aVL, and I. The inferior AMI acuteness score is derived from limb leads II, III, and aVF, and from the following instances in some of the precordial leads: For V1 and V2 to be considered, the ST elevation must be greater in V1 than in V2, indicating right ventricular, rather than anterior left ventricular (left anterior descending artery) involvement. For V4–V6 to be included, the ST elevation must be greater in V6 than in V5 and V4, which would also exclude LAD artery occlusion induced anterior wall involvement [117]. To date, the AW-acuteness score has not been developed for patients with posterolateral MI from LCX occlusion. Future work will look at the relation between ST-depression, T wave inversion and large R waves in V1–V3 to calculate the acuteness.

The Anderson-Wilkins acuteness score is an ECG estimate of the time course of the myocardial infarction that has been shown to be superior to time from symptom onset in predicting myocardial salvage in patients receiving angioplasty for acute MI [118–120]. This is shown in Fig. 16.24 from Sejersten et al. [119] where the Aldrich ECG score was used to estimate the extent of ischemia and Selvester QRS score was used to estimate the final infarct size. This study showed a statistically significant relationship between the AW-acuteness score and 1-year mortality, although the event rate was small. A separate study by Engblom et al. showed a stronger relationship between the AW-acuteness score and myocardial

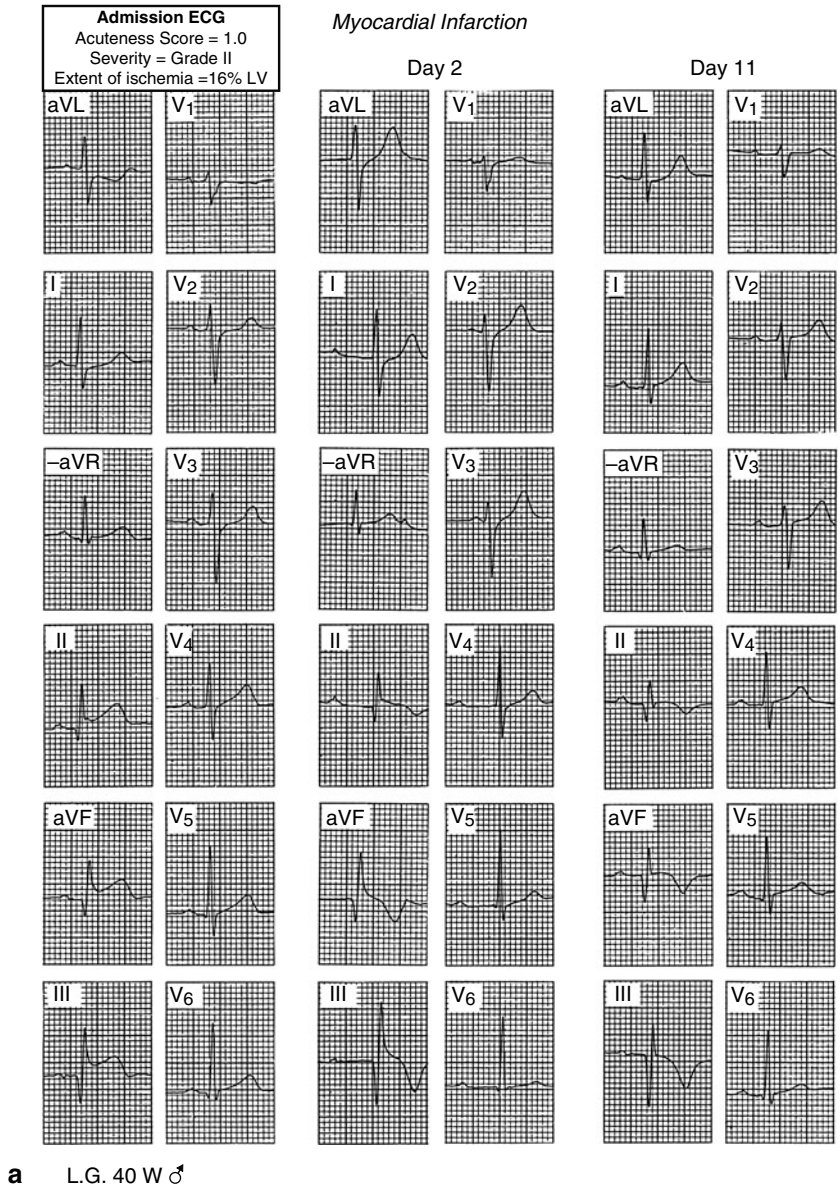

Figure 16.22 **(Continued)**

salvage than time from symptom onset [120]. This study used single photon emission computed tomography (SPECT) to measure the extent of ischemia and MRI to measure final infarct size.

16.4.2.2 The 24-Lead ECG and Acute Myocardial Infarction

The visualization of the spatial 3D ST-T vector and mirror image ("reciprocal") changes associated with acute occlusion of each of the three major coronary arteries or their major branches is facilitated by the use of the 24-lead ECG (which

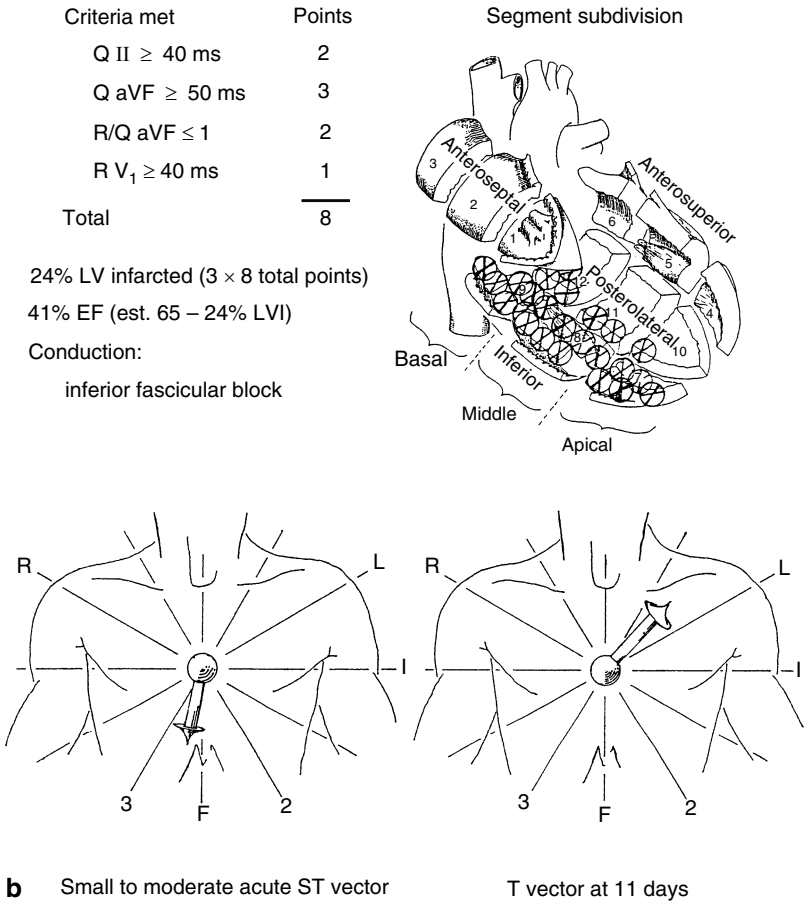

Figure 16.22

(a) Note limb leads are in the orderly (Cabrera) sequence from the *top down*, aVL, I, –aVR, II, aVF, III. The case of a 40-year-old man seen in the emergency room with indigestion and a possible acute infarct. He had significant inferior Q waves, slightly prolonged QRS (120 ms) with wide separation of initial and terminal 30 ms vectors typical of inferior fascicular (peri-infarction) block as described in the text. Only modest ST elevation is seen with minimal terminal inferior T inversion suggesting (with the Q waves above) that at this time the ST-segment changes are already receding. No evidence of RV infarct (see text) is seen but transient second-degree AV block is present on day 2 that has cleared by day 11. (b) For the patient of (a), by day 11 evidence for minor posterior extension of this inferior infarct has evolved. The infarct is somewhat larger (8 points, 24% LV) than the typical inferior infarct, extending more toward the apex than usual. The acute ST vector and the T vector evolution at 11 days are quite typical. The admission ST vector in this case underestimated the area at risk and the large infarct that, in fact, evolved. The patient had been suffering symptoms for several hours before coming to the emergency room and may have been past his peak ST.

includes both poles of the standard 12 leads). This concept was introduced by Pahlm-Webb and colleagues in 2002 [126] to aid in the visual diagnosis of acute occlusion, especially LCX occlusions with ST-segment depression in V1 and V2 but ST elevation in −V1 and −V2 (Fig. 16.29). Cardiac magnetic resonance imaging (MRI) with gadolinium enhancement of the acute ischemic injured area, or the resultant scar when adjusted for wall thinning, provides the basis for a quantitative measure of myocardial infarct. This allows for direct measure of LV and infarct volume, mass, and the percent LV infarcted (%LVI). In the five Figs. 16.25–16.29, the standard 12-lead electrocardiogram was recorded at 50 mm/s, gain

A. Consider only ECGs with (1) no complete RBBB or LBBB, (2) no LVH, (3) no WPW, (4) no ventricular paced or ventricular rhythm, (5) supraventricular QRS morphology, (6) total peak-to-peak QRS amplitude ≥ 0.4 mV, (7) ST elevation (rounded up to ≥ 0.1 mV) and (8) entirely positive T waves and/or tall positive T waves by Gambill criteria (III and aVL ≥ 0.25 mV; I,II, aVF, V1 and V6 ≥ 0.5 mV; V5 ≥ 0.75 mV; and V2, V3 and V4 ≥ 1.0 mV)

B. Measure from PR baseline. If there is PR depression consider TP baseline.

C. Assign Grades I,II, or III, to all leads meeting the stated criteria.

For leads I, II, III, aVL, aVF, V4 V5 and V6:

1. Leads with a QR configuration (i.e. R only or QR):
   Grade I tall positive T wave, no ST elevation
   Grade II positive T wave, J point/R wave amplitude ratio <0.5
   Grade III positive T wave, J point/Rwave amplitude ratio =>20 ms

2. Leads with RS or RSR' configuration (i.e. RSR' or QSR'): In leads with terminal S configuration and ST elev; assign grade II because of the presence of S waves.

Leads V4 and V5 in presence of left axis deviation:

- In cases with QRS axis ≤–30° and with S waves in lead V5: If there is ST elevation with out an S wave present in V4, assume that the pre-event ECG had S waves in V4; therefore assign the lead as Grade III.

- In cases with QRS axis ≤–30° and S waves in V6: If there is ST elevation without an S wave in V5, assume that the pre-event ECG had S waves in V5; therefore assign the lead as Grade III.

For leads V1, V2 and V3 regardless QRS configuration

- Grade I tall, positive T wave, no ST elevation.
- Grade II tall, positive T wave, ST elevation with an S wave below the isoelectric line.
- Grade III tall, positive T wave, ST elevation without an S wave below the iso electric line.

Figure 16.23

Scoring rules for the refined Sclarovsky-Birnbaum [121] Ischemia Severity Grading System. Figure and text reproduced and modified from Billgren et al. [123].

10 mm/mV and displayed as a "24-lead ECG" with 12 views in each of the frontal (above) and transverse (below) planes. The orientation of the x, y, and z axes of each plane is indicated by the perpendicular arrows. The 12 leads in each plane are arrayed as on a clock face around an MRI of the heart within the thorax; as viewed from the front in the frontal plane and from below in the transverse plane. The three dimensional "box" that appears around the heart in situ is expanded on the right of each figure to display the 8 "bread loafed" base to apex slices as viewed from these vantage points. The four quadrants/walls of the LV, (anteroseptal, anterosuperior, posterolateral, and inferior) are defined by the dashed lines on each slice.

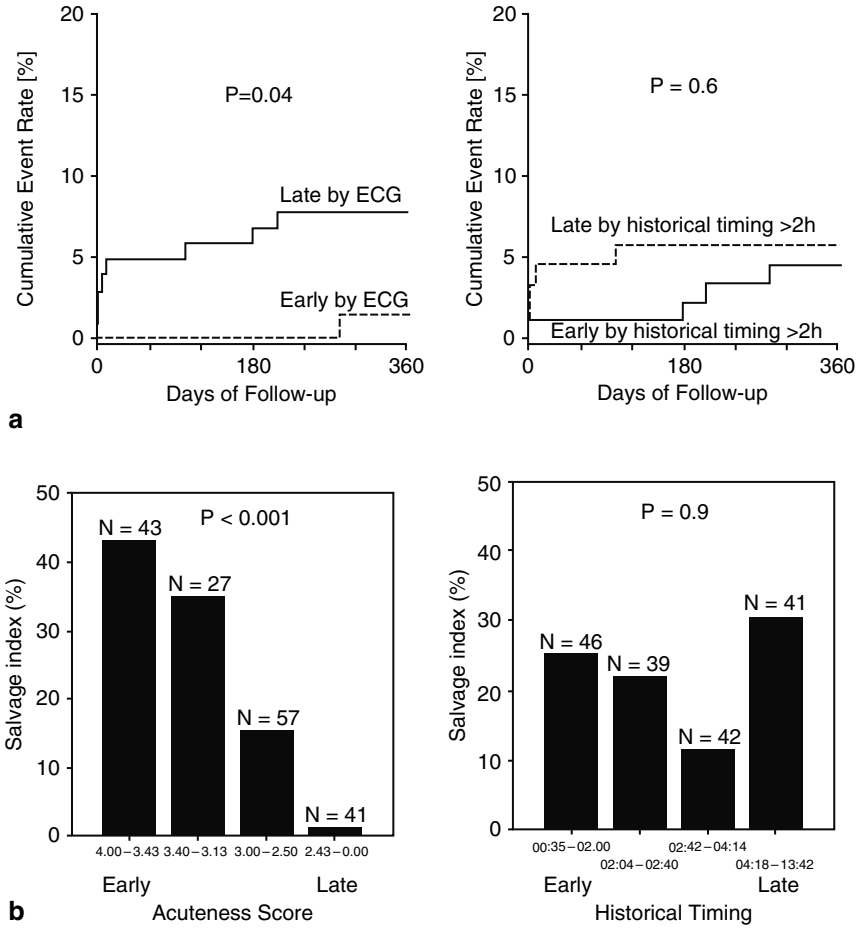

Figure 16.24
Relation of the Anderson-Wilkens acuteness score versus historical timing with myocardial salvage (*top graphs*) and mortality. Reproduced from Sejersten et al. [124].

16.4.2.3 Severity of Ischemia

The Sclarovsky-Birnbaum ischemia grading system was introduced in 1990 as a clinical tool to estimate severity of first time acute MI [121]. The grading system is based on qualitative assessment of changes occurring in the ST segment and the terminal portion of the QRS complex during the early stages ofischemia-infarction. The ischemia grading system consists of three grades representing increasing severity:

Grade 1 = tall upright T waves without ST segment elevation,
Grade 2 = ST segment elevation in ≥2 adjacent leads without terminal QRS distortion, and
Grade 3 = ST segment elevation in ≥2 adjacent leads with terminal QRS distortion.

Note that different criteria are used for identifying grade 3 of ischemia depending on the presumed baseline QRS morphology (Fig. 16.23). The scoring system is based on the concept that the severity of the ischemia/infarction process

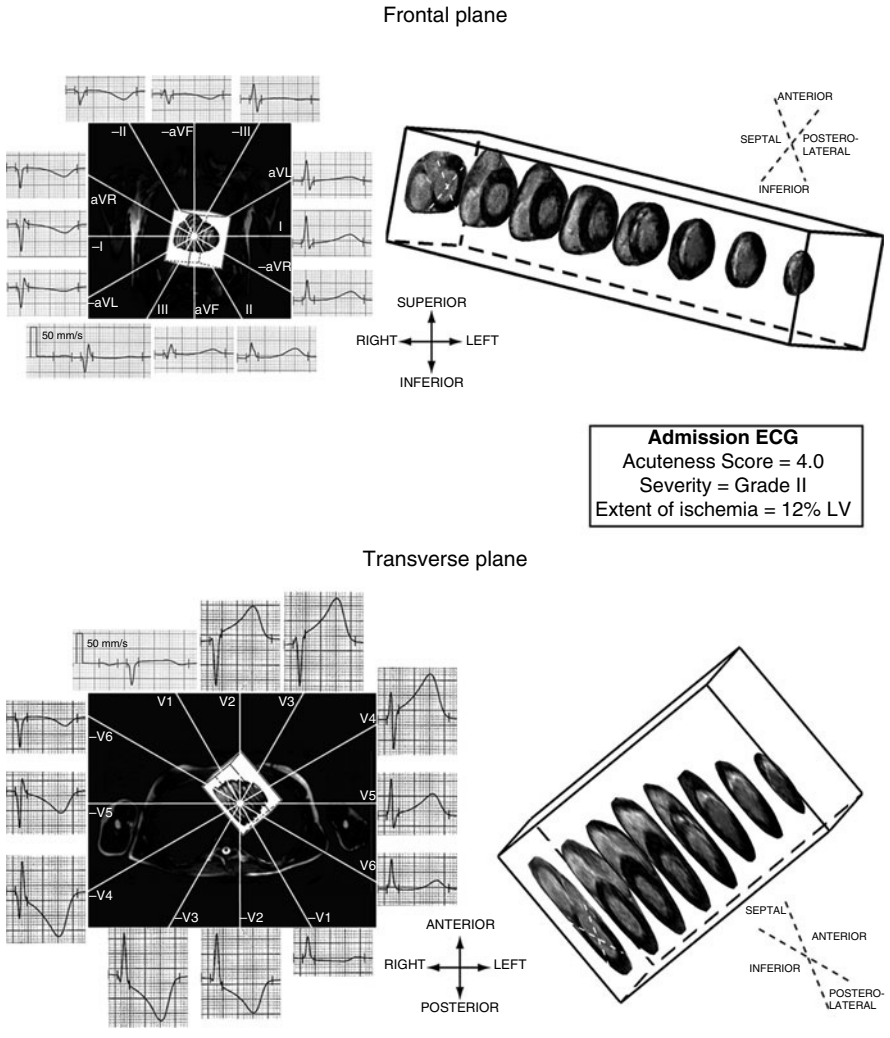

Figure 16.25

Cardiac MRI and 24-lead ECG (50 mm/s, 10 mm/mV) of a patient with a small to moderate acute MI primarily in the anteroseptal LV wall with some involvement of the anterosuperior LV wall caused by occlusion distal to the major diagonal branch of the left anterior descending coronary artery. The infarct is more extensive at the apex. It involves primarily the apical segment with some extension into the middle segment of the anteroseptal wall, and extends into mid and apical segments of the anterosuperior wall. The ECG manifestation of the acute phase of this MI is anterior ST segment deviation in the chest leads of the transverse plane (*below*) maximal toward leads V3 and V4. There is no apparent ST deviation in the frontal plane limb leads (*above*) because the anteriorly directed ST segment deviation is perpendicular to that plane.

is determined by the degree of myocardial protection provided by the combination of collateral vessels and ischemic preconditioning. Studies have shown that patients with grade 3 ischemia have a worse prognosis, larger infarct size, less benefit from reperfusion therapy and less viability in the infarcted zone as compared to patients with grade 2 ischemia [122–124]. Detailed rules for calculation of the score are outlined in Fig. 16.23.

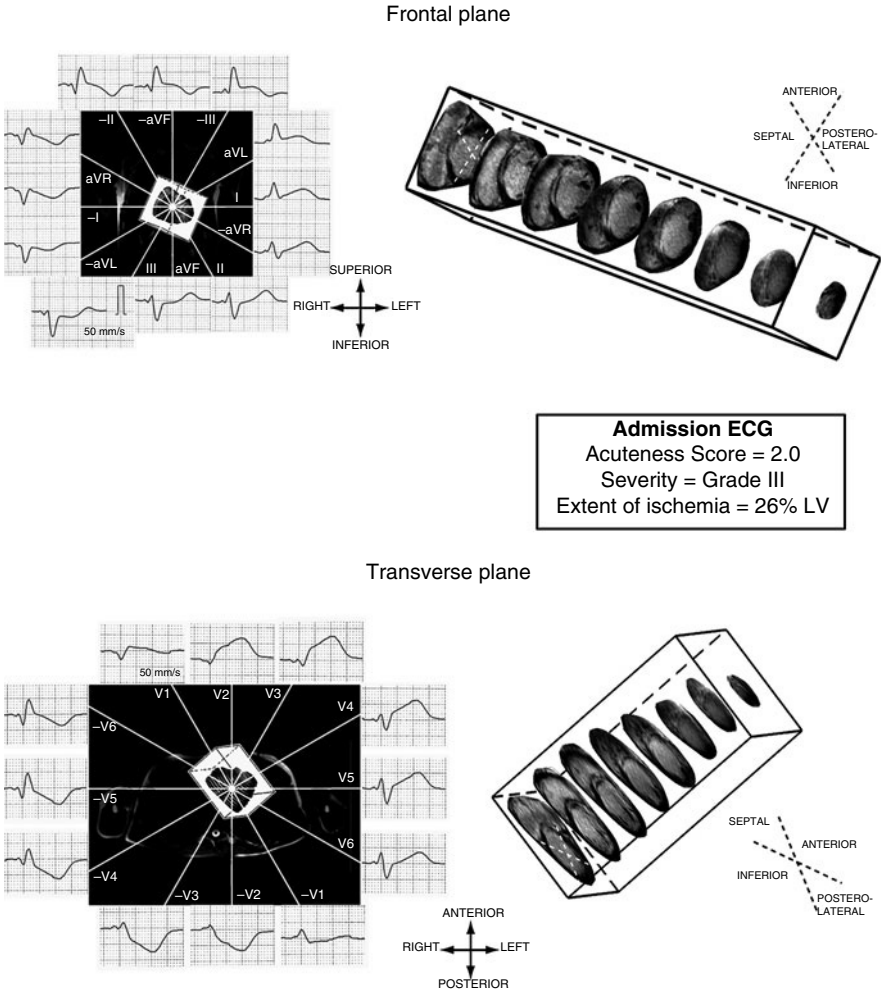

Figure 16.26

Cardiac MRI and 24-lead ECG (50 mm/s, 10 mm/mV) of a patient with large evolving acute MI in the anteroseptal and anterosuperior LV walls caused by occlusion proximal to the major diagonal branch of the left anterior descending coronary artery. The infarct is circumferential at the apex with extensive involvement of the middle and basal segments of both the anteroseptal wall and the anterosuperior wall. The ECG manifestation of the acute phase of this MI is major anterior ST segment deviation in the transverse plane chest leads (*below*) maximally toward lead V3, and superior deviation in the frontal plane limb leads (*above*) maximally away from lead III (toward lead-III). The QRS changes of a large evolving anterior infarction are already present.

16.4.2.4 Extent of Ischemia (Myocardium at Risk)

The Aldrich score for application on the presenting ECG, for estimation of the extent of myocardium at risk of infarction in the absence of successful reperfusion therapy was introduced in 1988 for anterior and inferior MI [93] and in 2005 by Ripa and colleagues for posterolateral MI [125]. It is based on the slope of the relationship between the amount in millimeters of ST segment deviation on the presenting ECG and the QRS score described in this chapter on the predischarge ECG and is expressed as percent LV at risk of infarction.

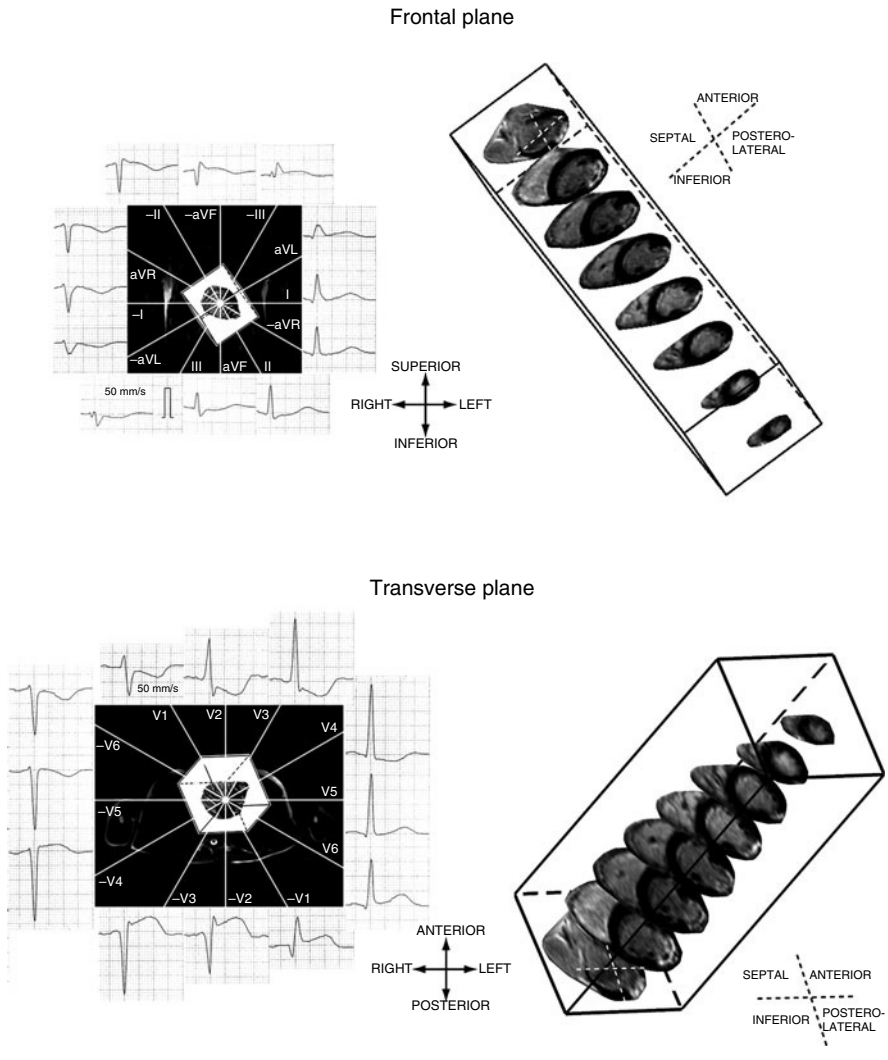

Figure 16.27

Cardiac MRI and 24-lead ECG (50 mm/s, 10 mm/mV) of a patient with a large acute MI primarily in the posterolateral LV wall caused by left circumflex (LCX) coronary occlusion proximal to the first marginal branch. The infarct is more extensive at the base extending slightly into the anterosuperior segment and tapers toward the apex. It involves the basal and middle segments of the posterolateral LV wall extensively, and extends to about 25% of the apical segment. The ECG manifestation of the acute phase of this MI is posterior ST segment deviation in the transverse plane chest leads (*below*) maximally away from lead V2 (toward lead -V2). There is borderline ST deviation superior in the frontal plane limb leads -aVF, -111, aVL (*above*) indicating a minor extension of the risk area into the basal anterosuperior segment.

The formula in anterior ischemia/infarction is

Extent of ischemia (%LV) = 3[1.5(# of leads with ST elevation)−0.4].

The formula in inferior ischemia/infarction is

Extent of ischemia (%LV) = 3[0.6(sum ST elevation in II, III, aVF)+2].

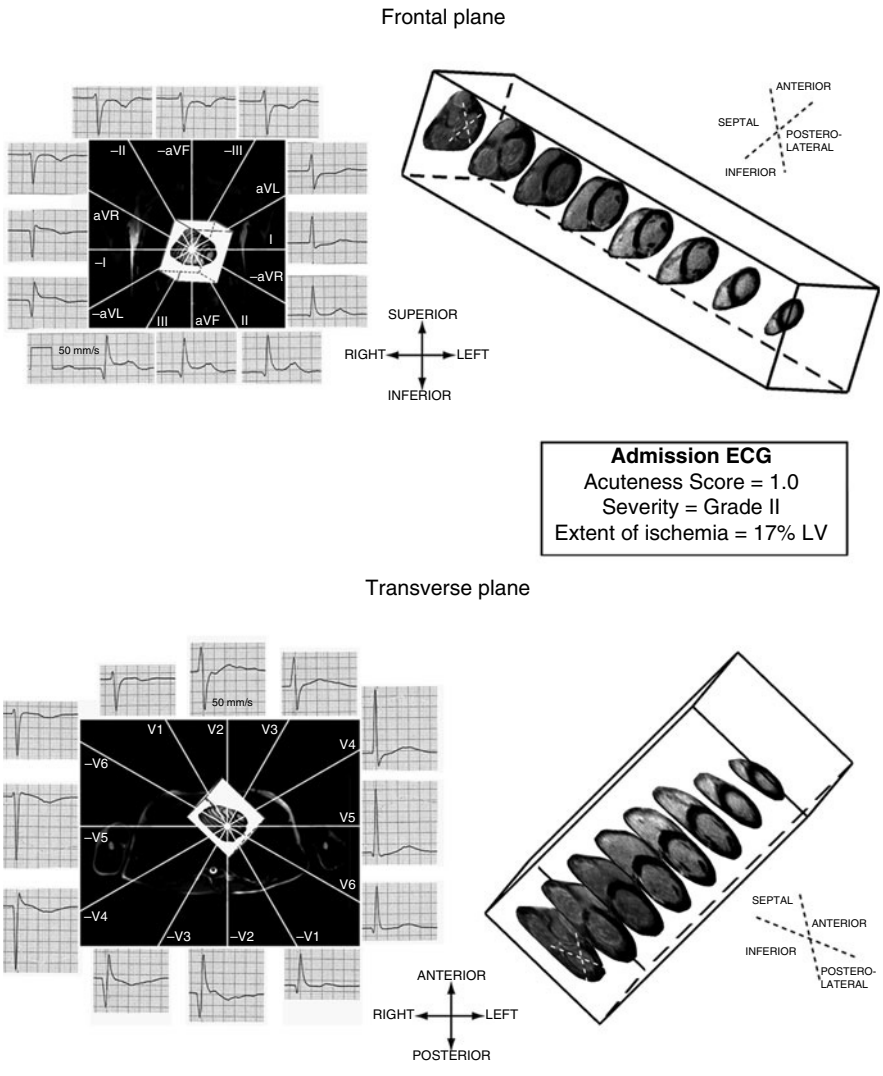

Figure 16.28

Cardiac MRI and 24-lead ECG (50 mm/s, 10 mm/mV) of a patient with a small acute MI involving primarily the middle segment of the inferior wall with minimal extension into the inferobasal and inferoapical segments. This was caused by occlusion of the PDA proximal to its branching from the distal RCA. The ECG manifestation of the acute phase of this MI is minimal with abnormal inferior ST deviation in the frontal plane leads (*above*) maximally toward lead III.

The formula in posterolateral ischemia/infarction is

Extent of ischemia (%LV) = 3[0.22(sum ST elev and ST, dep, all leads)−0.02].

Future work will need to be done to prospectively evaluate the use of all three of these ischemia scoring systems to risk-stratify patients and provide decision support for physicians caring for patients with acute myocardial infarction.

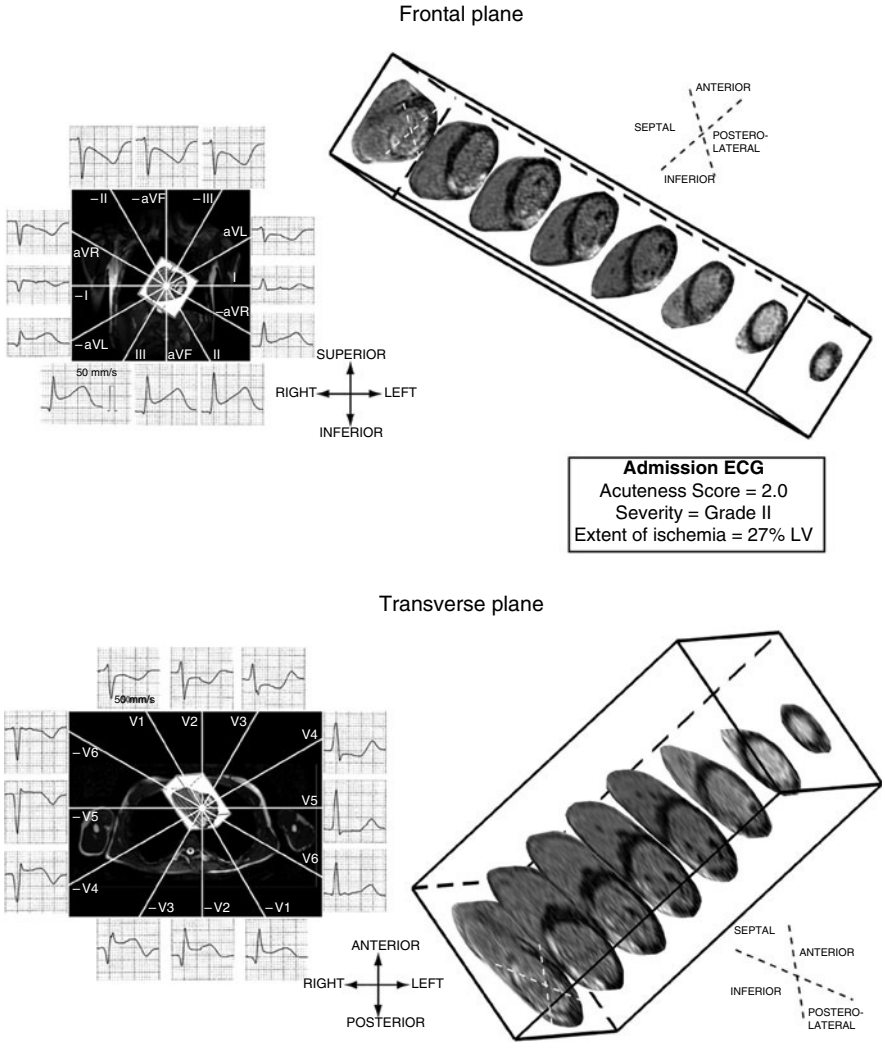

Figure 16.29

Cardiac MRI and 24-lead ECG (50 mm/s, 10 mm/mV) of a patient with a moderate sized acute MI in the inferior and posterolateral LV walls, caused by occlusion distal to the major right ventricular branch of a dominant right coronary artery. The infarct is extensive at the base and tapers toward the apex. It involves primarily the middle and basal segments of the inferior wall, extends into middle and basal segments of the posterolateral wall, and also minimally into the basal inferior septum. The ECG manifestation of the acute phase of this MI is inferior ST segment deviation in the frontal plane limb leads (*above*) about equally toward leads III and aVF, and posterior in the transverse plane chest leads (*below*) maximally away from lead V2 (toward lead -V2). The apical involvement is indicated by the inferior directed ST deviation in the frontal plane extending to lead -aVR.

16.4.3 Left Anterior Descending Occlusion and Typical Anterior Infarcts

16.4.3.1 Spectrum of ECG/VCG Changes from Acute LAD Occlusion

In most patients, the "wrap-around" of the LAD at the apex onto the inferior apex is quite prominent [127]. Thus ***acute occlusion of the distal LAD*** with acute anteroapical infarction will be associated with ST elevation both in anterior apical

directed leads V4, V5, V6, and in apical inferior directed leads –aVR, II, and aVF. The evolving infarct may produce abnormal Q-waves or attenuated/notched R-wave changes in any or all of these leads depending on its size. The differential diagnosis of such changes is covered in more detail in Sect. 16.4.7.

Infarcts associated with local acute occlusion of a ***major first diagonal branch*** of the LAD system may be limited to the anterosuperior wall or extend into the upper part of the middle and apical segments of the posterolateral wall. These are so-called high lateral, lateral or superior infarctions with abnormal anterior (superior) ST elevation in I, aVL, -III, and -aVF. The evolving infarct is evidenced by loss/notching of R and/or evolving Q waves in I, aVL, and possibly –V2, –V3.

Acute LAD occlusion proximal to the first diagonal adds to the changes mentioned above for the acute ST-T and evolving QRS changes in leads V1–V5, along with many added labels for these infarcts. Terms such as septal, anteroseptal, anterior, strictly anterior, anteroapical, apical and anterolateral are all in wide usage to describe the ECG/VCG changes in V1–V5 that result from LAD occlusion. A combination of these terms is used to indicate extension of the infarct to more than one region, along with additional terms such as large, extensive or massive. A significant simplification occurs when the size modifiers summarized in Table 16.3, namely, probable small, small, moderate, large and very large, are used along with the simple descriptor "anterior," to describe the spectrum of changes that occurs with occlusion in this arterial system. When major ST-T changes of injury and/or ischemia are also present, modifiers, such as "hyperacute," "acute" or "recent" are appropriate. When there are changes of anteroapical infarct with inferior involvement, then adding the term "with inferior extension" or using "anteroapical inferior" are appropriate but "apical" with size modifiers is simpler. The reader is reminded that to assess the extent of the anatomic change, the ECG/VCG changes considered must include not only ST-T and initial Q-wave vectors, but loss of mid-to-later QRS vectors as well. The interaction of these criteria in the quantification of anterior infarct is discussed in more detail in Sect. 16.3. Serial ECGs of a typical moderately sized acute anterior infarct are shown in Fig. 16.18. The QRS MI size, score of the day 15 ECG, the interaction with the individual criteria met and the distribution of the associated infarct in relation to the 12 segment LV of this patient's score worksheet are shown in Fig. 16.19. The 24-lead ECG and the MRI images of a small acute and large late acute anterior infarct are shown in Figs. 16.25 and 16.26. ECG/VCGs of a moderate size and a very large old anterior infarct with angiographic correlations are shown in Figs. 16.30 and 16.31.

16.4.3.2 Anterior Infarct with Associated Left Anterior-Superior Fascicular Block, LAFB

Eight percent of the patients in the authors' ventriculographic series with visible anterior infarct and LAD coronary artery occlusion had an associated clear-cut left anterior-superior fascicular block (LAFB), by criteria advocated by the Bethesda Conference Task Force1 on Standardization of terminology [128]. Figure 16.8 shows a simulation of the sequence of activation seen in these patients. The major difference seen in the ECG/VCGs of these patients in comparison to those with normal conduction and anterior infarct are:

(a) QRS prolonged to 105–110 ms (110–140 ms when evidence of LVH is present);
(b) qR pattern in aVL with wide separation of initial 30 ms vectors from the terminal 30 ms vectors; and
(c) Mean frontal QRS axis −45° to −110°, depending on the size of the infarct.

The important ECG/VCG features for the diagnosis of this combination of fascicular block and infarct are the wide divergence of initial and terminal vectors in the frontal plane. This is particularly evident in the larger infarcts. Grant and Dodge [16, 41] postulated that these changes initially described by First [129] "may be due to a block in the superior division(s) of the left bundle." The important ventriculographic feature which relates to the ECG and VCG is that in no instance in the Rancho Los Amigos Hospital, University of Southern California (Rancho/USC) series of this group was the entire anterosuperior base akinetic (infarcted). It follows that this region, which is activated late and unopposed, will produce prominent late superior posterior vectors. The absence of this vector effectively excludes the diagnosis of left anterior-superior fascicular block. This is unlike left inferior-posterior fascicular block (LIFB), where the inferior base, which produces terminal inferior vectors in this conduction abnormality, is commonly infarcted. A typical clinical example of a patient who developed a left anterior-superior fascicular block (LAFB) and complete RBBB from a very large acute anterior infarct, where the QRS MI size score suggests involvement of 36% of the LV, is shown in Fig. 16.20.

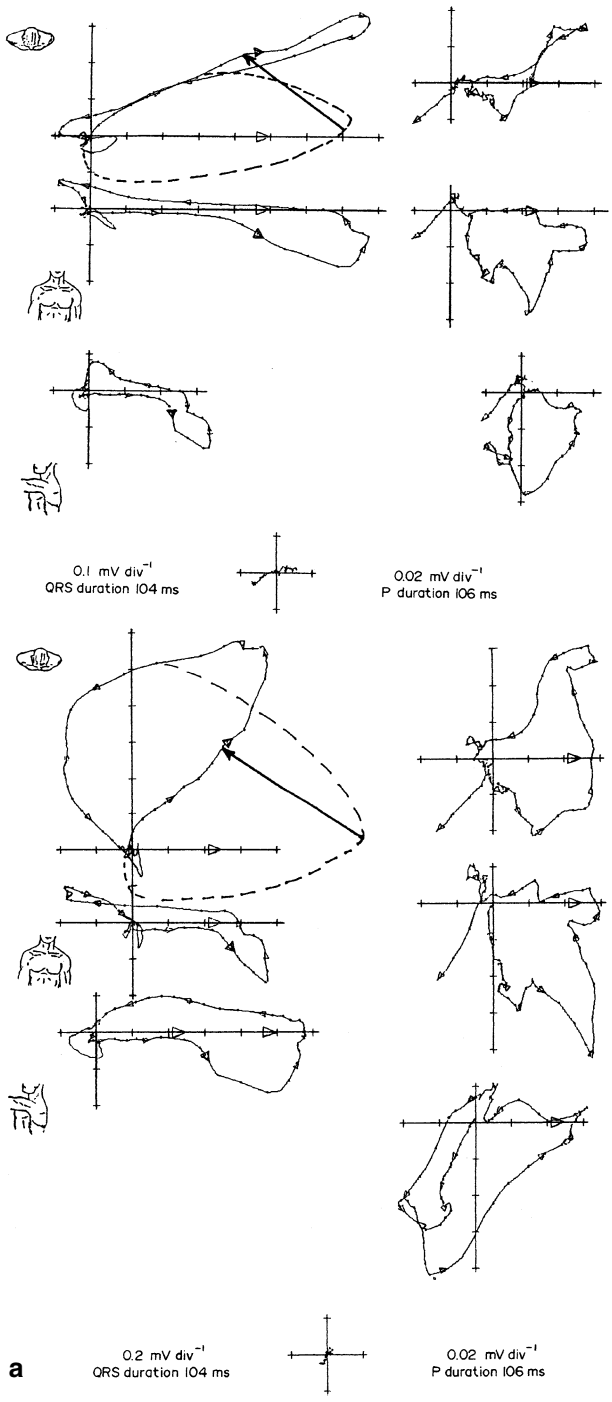

Figure 16.30 (Continued)

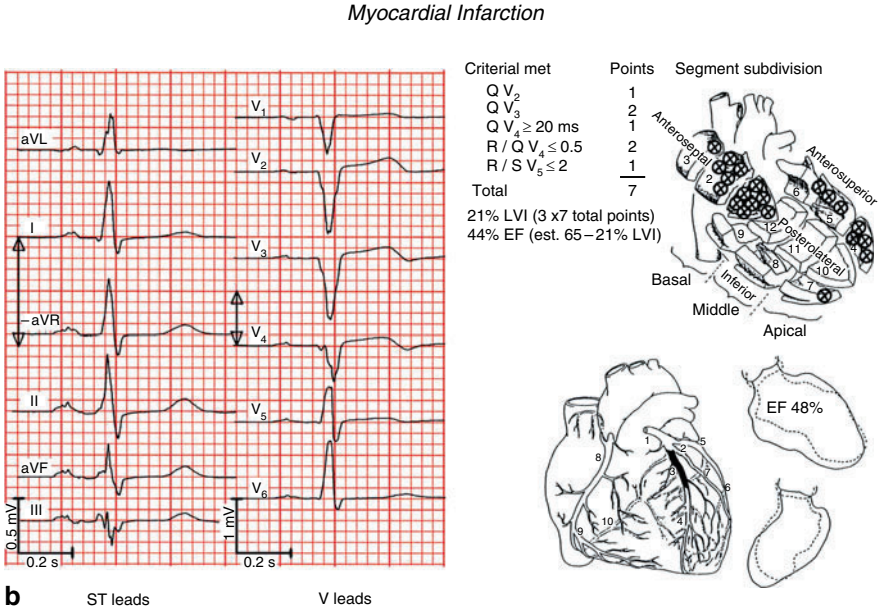

Figure 16.30

(a) The Cube VCG is the *upper half* of the figure and the McFee in the *lower half*. The horizontal, frontal and left sagittal QRS-T loops are to the *left*; P loops and the initial 10 ms of the QRS at higher gain are to the *right of each set*. Time marks are every 2 ms, the *small arrows* every 10 ms, and the *large arrow* at the 40 ms vector. The calibration is indicated below the Cube and McFee QRS-T VCGs on the *left* and P VCGs on the *right*. This 54-year-old man with a history of a previous infarct shows significant loss of initial anterior and apical forces. The dotted line represents the average VCG for each lead system recorded from 97 age-matched normal males. The peak magnitude of this QRS deformity in each is indicated by the *solid line* and *arrowhead*. The peak magnitude and the duration for each lead system, transferred to the nomogram in Fig. 16.12, yields the following: For the Cube, 0.3 mV for 60 ms estimates the infarct size as 6 cm and the ejection fraction (EF) as 47%. For the McFee, 0.9 mV for 50 ms estimates an 8 cm infarct and an EF of 42%. (b) Note limb leads are in the orderly (Cabrera) sequence from the top down, aVL, I, -aVR, II, aVF, III. The ECG here and the VCGs shown in (a) are signal averaged from 1 ms digitized data. The gain is indicated at the bottom of each panel. There are abnormal Qs V2–V4 and further loss of R waves, V4, V5 yielding 7 ECG points as shown above with an estimated infarct size of 21% LV and estimated EF of 44%. These criteria using the autopsy validated distribution from the QRS MI size score shown in Fig. 16.16 yield the prediction of local infarct as shown in the *upper right*. The *lower* figures show the findings of single vessel LAD occlusion at angiography, and the localized anteroapical infarct shown on biplane ventriculograms with an ejection fraction of 48%.

16.4.4 Non-Dominant Circumflex Occlusion and Typical Posterolateral Infarcts

The typical serial ECG changes of a large acute posterolateral infarct with apical extension consistent with occlusion of a large obtuse marginal branch of a non-dominant LCX coronary artery are shown in Fig. 16.21. Note that the ST changes in this example reflect predominantly posterior and apical injury and ischemia. The evolving QRS shows major loss of posterior and leftward apical vectors that, by the QRS MI size score, involves 27% of the LV. The activation sequence relating to a similar infarct, but smaller with less apical extension, is shown in Fig. 16.4. ECG/VCGs with angiographic correlations of similar healed small and moderate old posterolateral infarcts from patients in the Rancho/USC CAD database with LCX occlusion are shown in Figs. 16.32 and 16.33. Note that in these two more typical examples of posterolateral infarct, the QRS changes are limited to the mid and terminal QRS. Lesions in this location, as in the example shown in Fig. 16.33b, extend onto the inferior surface (and/or apex) in about one third of cases. They produce acute

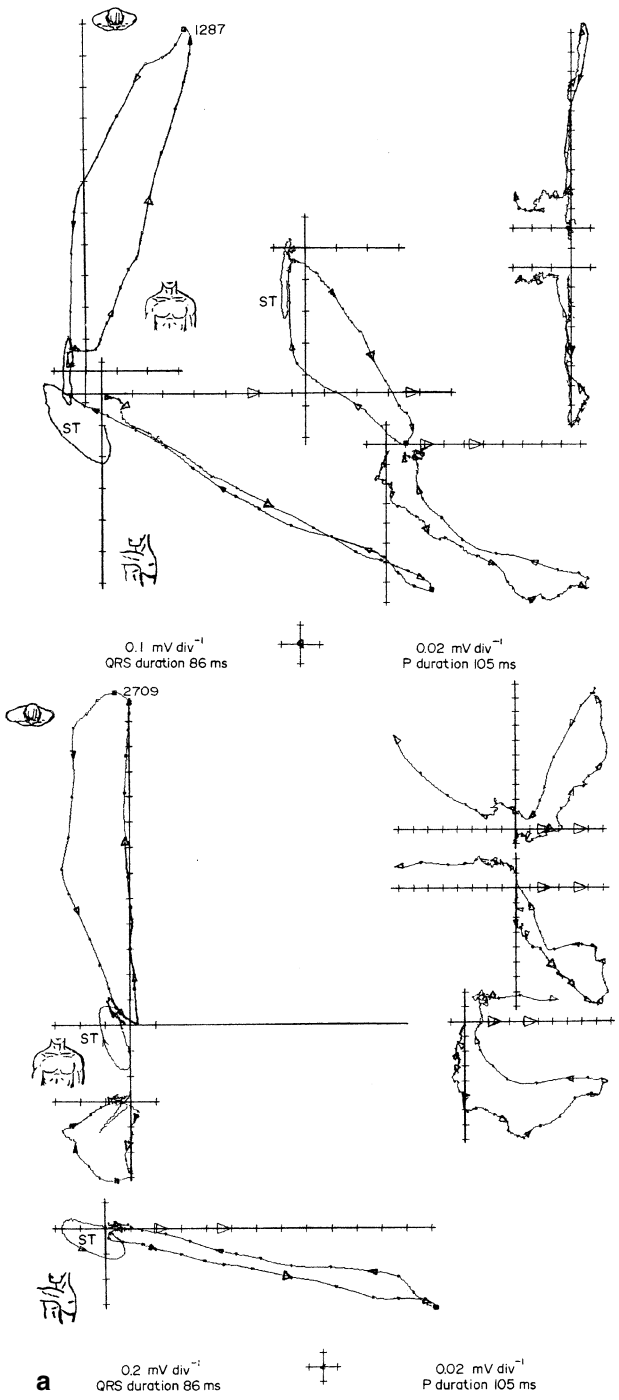

Figure 16.31 (Continued)

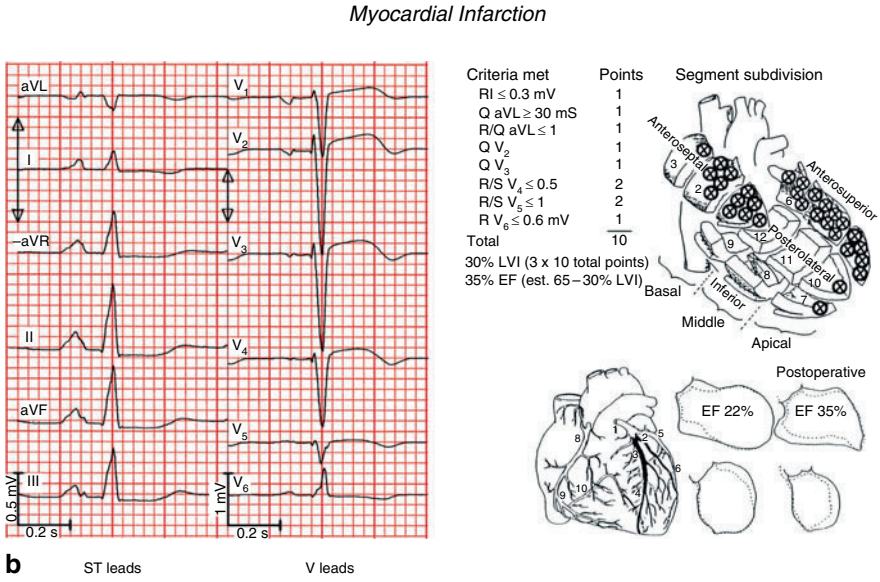

Figure 16.31

(a) The Cube VCG is the *upper half* of the figure and the McFee in the *lower half*. This 64-year-old man had a history of a single acute myocardial infarct prior to his angiogram. The P loops displayed to the *right* of both lead systems demonstrate major increases in left atrial voltage and activation times indicative of major LV diastolic dysfunction. There is increased posterior QRS voltage of both VCG lead systems consistent with the clinical history of hypertension. The initial right atrial voltages were also mildly increased and the QRS frontal axis is shifted rightward from where it would be expected with LVH. These are consistent with the acute course and the post-infarct period, which had been complicated by congestive heart failure. There is major loss of initial anterior and leftward vectors in both VCGs. Compared to the VCG loops of early LVH, the Cube has lost 0.6 mV for 60 ms and the McFee 1.3 mV for 60 ms. When transferred to the nomogram of Fig. 16.12 this yields a predicted infarct size of 9 and 11 cm, respectively, and an EF of 38% and 32% respectively. (b) Note limb leads are in the orderly (Cabrera) sequence from the *top down*, aVL, I, -aVR, II, aVF, III. The ECG demonstrates a large anterior infarct and increased posterior voltage suggestive of LVH. There is a rightward shift of the frontal axis to +75 unexpected for LVH, but a common finding in large anterior infarcts with major anterosuperior wall involvement. In this case, as in most, the frontal QRS does not show wide separation of initial and terminal 30 ms vectors and the QRS duration here is 86 ms. Thus inferior fascicular disease is most unlikely and its blood supply is normal. The total ECG score for infarct of 10 would be indicative of 30% LV infarct pathologically, and would predict an EF of 35%. It is noteworthy that no infarct was distributed to the inferior or posterolateral wall at the apex by the observed QRS criteria. A large thin walled anteroapical aneurysm was present with a LV EF of 22%, large LV volumes and high end diastolic pressures. Following resection of the aneurysm there was significant return of inferior wall motion at the apex indicative of "tethering" and improvement in EF to 35%.

ST-T changes in inferior (and/or left-sided) leads, and evolve variable small-to-significant Q waves in aVF, II, -aVR, I and V6 (see Sect. 16.4.9).

16.4.5 Right Coronary Occlusion and Typical Inferior Infarcts

The right coronary artery supplies the AV nodal artery in 85–90% of patients. This artery takes origin from the crux or "U-turn" in the right coronary at the origin of the posterior-inferior descending branch of this artery. This AV nodal artery terminates in a "T," one limb of which supplies the AV node, while the other limb supplies the bundle of His and the first 1–2 cm of the left bundle [130]. Thus, transient AV block is common with right coronary occlusion and in part

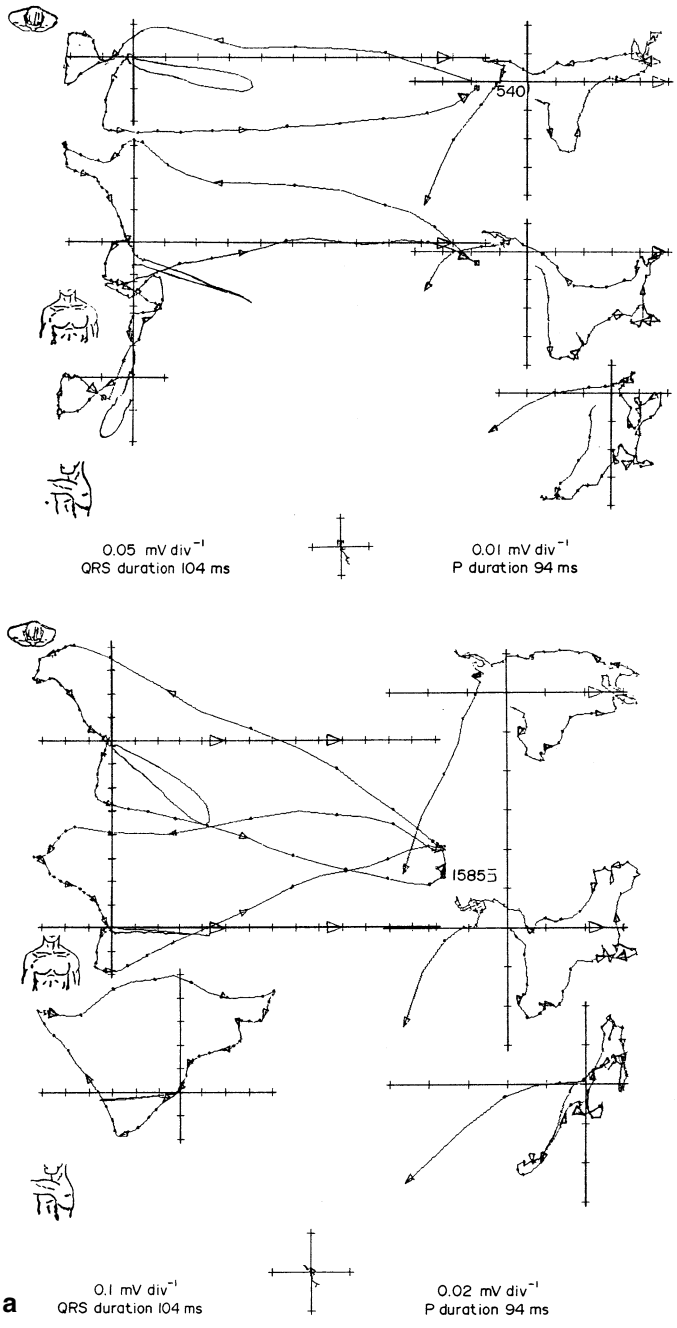

Figure 16.32 **(Continued)**

due to the dual and variable blood supply to the region, His bundle and left bundle branch conduction abnormalities are less common. This region has a dual and variable blood supply. The other artery which supplies it is the first septal perforator from the left anterior descending coronary artery. The proximal left bundle is more often supplied by the AV nodal branch of the right coronary. Acute infarction and recent onset left bundle branch block is associated with recent inferior infarct more often than with anterior infarct [37].

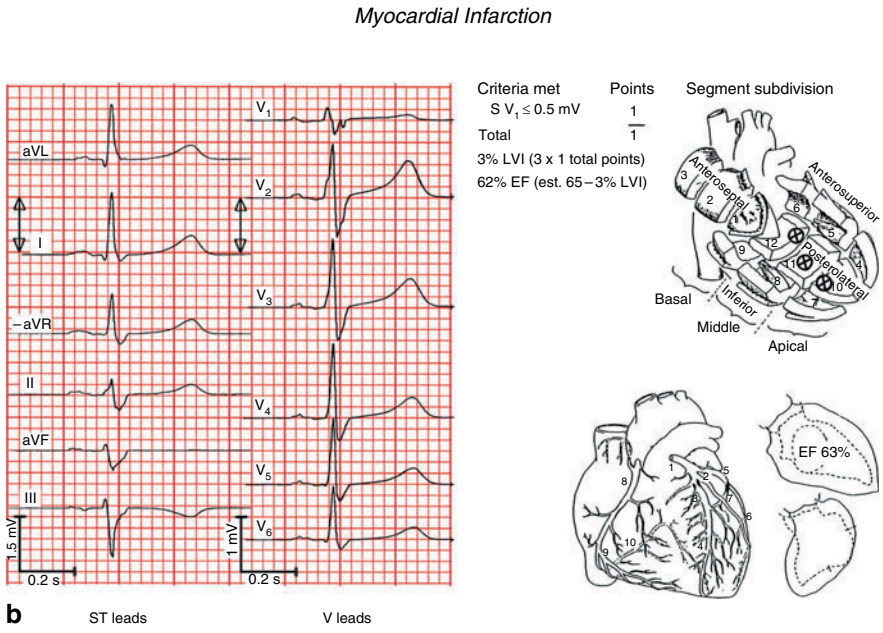

Figure 16.32

(a) The Cube VCG is the *upper half* of the figure and the McFee in the *lower half*. The main abnormality seen here is a shift of the mid and late QRS vectors superior and anterior to their usual location. The QRS loop in the left sagittal projection is inscribed clockwise particularly evident in the McFee system, and the terminal displacement anterior is clearly abnormal in the Cube. The P vectors for both right and left atria, and the ST-T vectors are normal. The deformity in the Cube is 0.2 mV for 50 ms, and in the McFee is 0.5 mV for 40 ms. From the nomogram (Fig. 16.12) these changes are predictive of a 4 cm and a 5 cm infarct respectively and an EF of 55% and 52%. Both VCG systems have leads on the back and in general are more sensitive to posterolateral infarct from LCX occlusion than the 12-lead ECG. (b) Note limb leads are in the orderly (Cabrera) sequence from the *top down*, aVL, I, -aVR, II, aVF, III. The ECG has abnormal left axis and only 1 point (3% LVI) for posterolateral infarction. There was total occlusion as shown of the LCX just proximal to the obtuse marginal branch and on the LAO ventriculogram a small posterolateral infarct at the junction of the middle and basal segments of the posterolateral wall. Many angiographic laboratories do not routinely report a left anterior oblique (LAO) ventriculogram. Small posterolateral infarcts are easily overlooked in the traditional RAO ventriculogram. Except for a faint double contour on the RAO ventriculogram in this case, there is no reflection of this infarct on the RAO systolic contours. It is also noteworthy that abnormal left axis deviation is seen with little support angiographically for superior fascicular disease. Occlusive arteriographic disease was identified as shown in the proximal LAD, but it was less than 70% and no regional wall motion abnormalities were noted. In this case, the VCG changes which correspond well to the lesion found suggest that the axis change is a straightforward expression of the loss of basal posterior-inferior vectors.

The inferior-posterior fascicles of the left bundle through the distal third of their course are supplied from septal branches of the posterior (inferior) descending and the first posterolateral branches of the RCA. The fascicles are variably vulnerable to disruption with right coronary occlusion and inferior infarction. Eighty five percent of patients with inferior MI from RCA occlusion develop the ECG/VCG changes of peri-infarction/inferior fascicular block (LIFB) described below. The changes due to this conduction abnormality must first be reviewed in order to understand the changes seen with right coronary occlusion and inferior infarct. This group of patients has the following evidence of LIFB:

(a) Twenty ms prolongation of QRS to 100–120 ms, which may be intermittent in the early stages of acute inferior infarction.

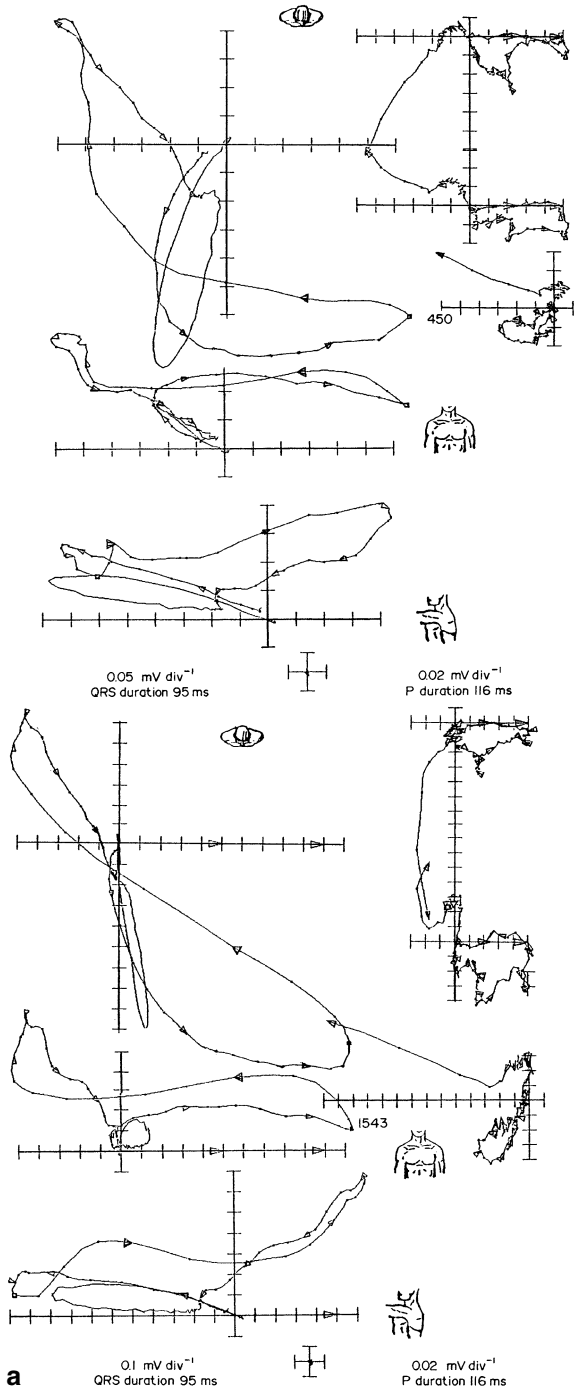

Figure 16.33 (Continued)

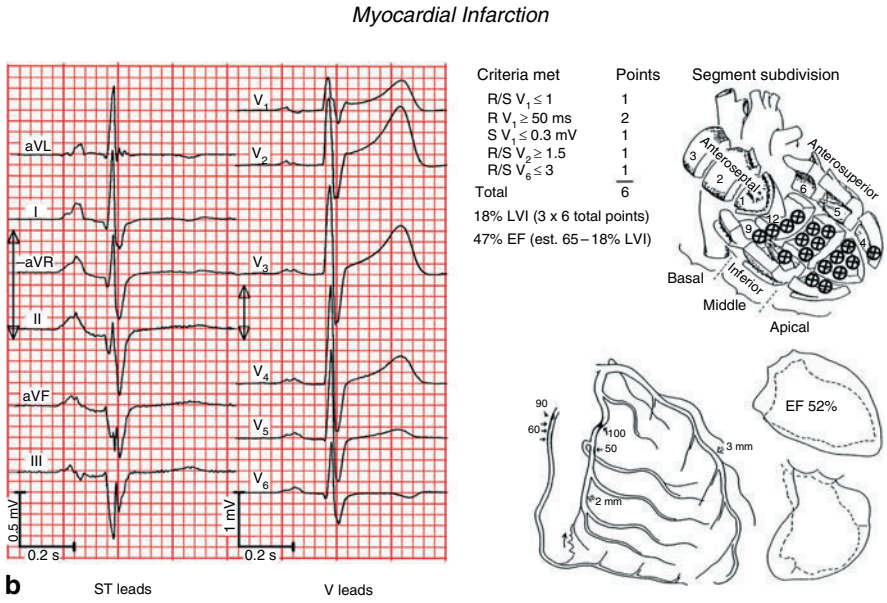

Figure 16.33

(a) The Cube VCG is the *upper half* of the figure and the McFee in the *lower half*. P vectors here show a modest increase in left atrial activation times (P duration 116 ms) and leftward vectors consistent with mild to moderate LV dysfunction. There is significant loss of posterior and leftward vectors in both lead systems with significant inferior losses from 20 ms onward. The frontal plane is not that of inferior fascicular (peri-infarction) block in that the initial QRS vectors are irregular and terminal vectors are not directed inferior and rightward. The QRS duration is less than 100 ms and is much more suggestive of posterolateral infarct with inferior extension from a codominant LCX occlusion, rather than RCA disease. The large T vector is directed anterior and somewhat rightward and superior predominantly away from the posterolateral wall or LCX distribution. The deformities from the average normal loop are 0.6 mV/50 ms in the Cube and 0.8 mV/50 ms for the McFee. The nomogram of 16.12 predicts an 8 cm lesion for each, and an EF of 42%. (b) Note limb leads are in the orderly (Cabrera) sequence from the *top down*, aVL, I, -aVR, II, aVF, III. The 12 lead ECG in this case above as in the earlier Fig. 16.32b shows abnormal left axis with a Q in aVL and I that might suggest left anterior fascicular block. The lack of a prominant inferior initial 30 ms vector and of a prominant superior terminal 30 ms vector of 0.8 mV or more in aVF and aVL are inconsistent with this diagnosis as is a QRS duration of <100 ms. In this case the left axis, as in Fig. 16.32b, is a simple subtraction effect from significant inferior extension of a moderate sized posterolateral infarct from occlusion of codominant LCX, proximal to four prominent marginal branches. The LAD is free of disease and there is little support for the hypothesis that the left axis deviation is due to anterior fascicular conduction delay. Six points are generated by the ECG/QRS score for infarct size, all indicating posterolateral infarct with inferior and apical extension. The predicted infarct size is 18% LV with a predicted EF of 47%.

(b) Patients with very small infarcts from right coronary occlusion have the ECG/VCG changes of LIFB, described in Chap. 15, with an open frontal plane loop as seen in Fig. 16.34a. They have wide separation of the initial 30 ms and terminal 30 ms of Grant and Dodge's [16, 41] peri-infarction block, which they suggested "was probably due to a block in the inferior fascicles."

(c) The initial vectors are seen as a smooth arc superior and leftward, with no high frequency notches or splintering in the smooth abnormal Q, and are consistent with early unopposed propagation through a normal anterosuperior wall.

(d) The high frequency notching and irregularities are in the mid- and terminal vectors, consistent with activation fronts traversing the areas around the late activated and infarcted inferior wall.

(e) Finally, for years it has been observed that the classic Q wave of inferior infarction occasionally disappears after a typical course of infarction. When this happens, the QRS usually returns to a more normal duration of 80–90 ms,

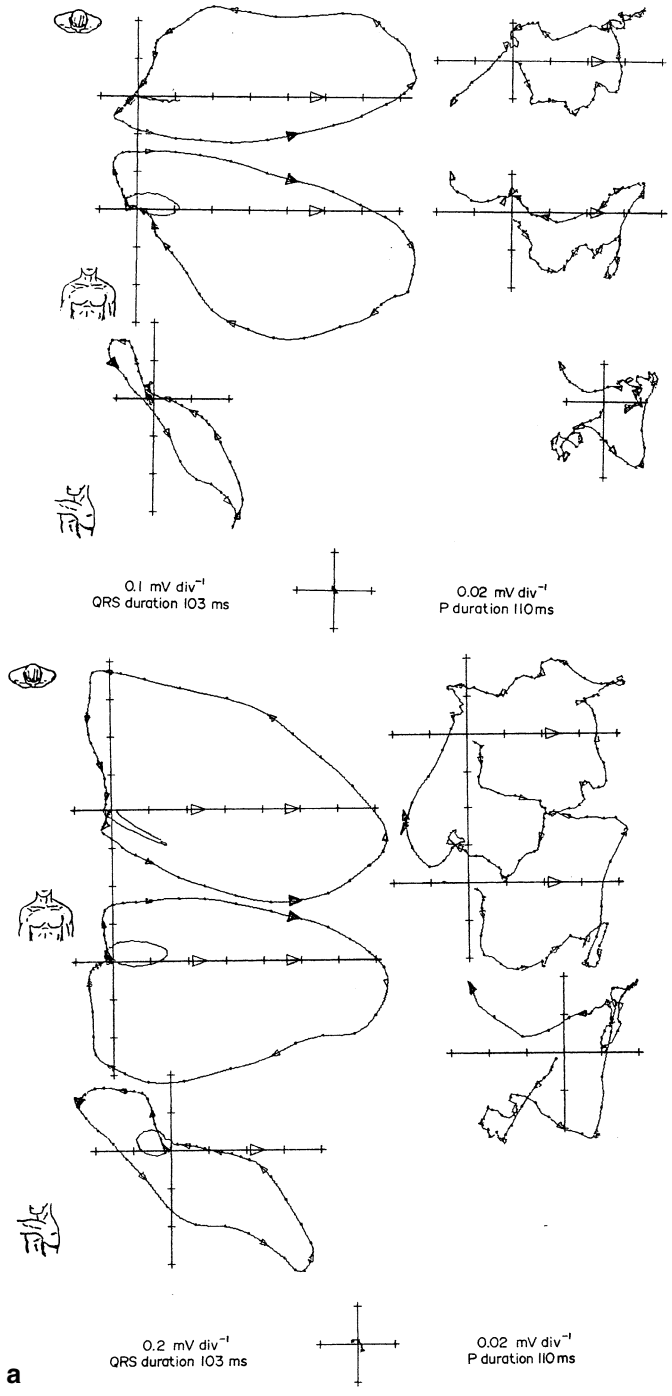

Figure 16.34 (Continued)

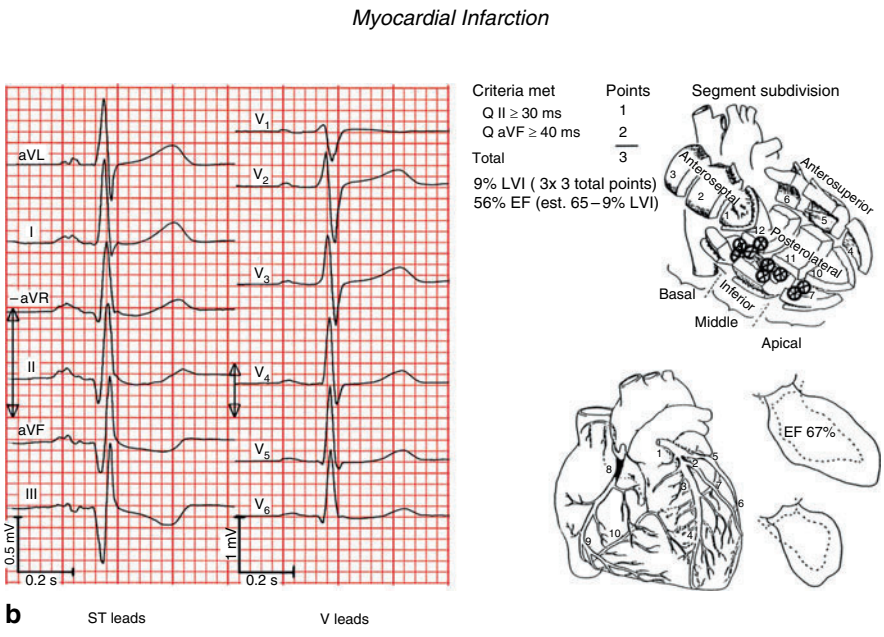

Figure 16.34

(a) Cube (*top*) and McFee (*bottom*) sets of VCGs from a 60 year old man with the history of prior infarct is typical of a number of patients from the Rancho series with RCA occlusion and small or no visible infarcts. The QRS duration is 103 ms. The frontal plane initial and terminal 30 ms QRS vectors are widely separated in both. In those with no visible wall motion abnormalities, and in simulations of inferior fascicular block, the initial arc superior swings far to the *left*, as is seen here. It crosses the horizontal plane (and the *X* axis in the frontal plane) at 35 ms on the average. The peak left voltage occurs at 40–45 ms. When there is little or no infarction of the inferior base or middle segments, the terminal inferior vectors which arise from this region are well preserved as seen here. The inferior amplitude is 2/3 of the leftward amplitude on the average. This ratio should be used in construction of the non-infarct loop for estimating inferior infarct size in the presence of this conduction abnormality. When this ratio is used for this patient, small infarcts are predicted by both lead systems of 2–3 cm with a predicted EF of 60%. The P vectors are entirely normal, indicating little or no LV diastolic dysfunction. (b) Note limb leads are in the orderly (Cabrera) sequence from the *top down*, aVL, I, -aVR, II, aVF, III. Because the initial and terminal 10 ms are nearly perpendicular to the frontal plane, the QRS duration appears shorter than the 103 ms recorded in the VCG and seen in the precordial leads. Since the electrophysiological variable we look for in measuring QRS duration is total time of ventricular excitation it is important to measure it in the lead where it is longest. In general, ECG analysis from three orthogonal or eight simultaneous standard leads eliminates this ambiguity. The wide separation of initial and terminal 30 ms vectors is also evident in the frontal plane. Three points are accumulated for inferior infarct from the QRS score which represents 9% LV infarcted and 56% EF.

and the axis shifts superiorly. These findings support the Grant and Dodge hypothesis that a "block in the inferior fascicles" was transient and has now disappeared. The decrease in QRS duration is due to the return to normal conduction. A significant axis shift to the left, superiorly, would result from the disappearance of the LIFB and a further axis shift superiorly from the inferior infarct. This would be proportional to the infarct size, with loss of late inferior QRS vectors from the base of the inferior LV wall, which activates normally during the late QRS.

The serial ECG changes of a patient with a typical acute inferior infarction from right coronary occlusion, and who evolves the changes of LIFB, described above, is shown in Fig. 16.22. A 24-lead ECG and MRI image of a small inferior infarct

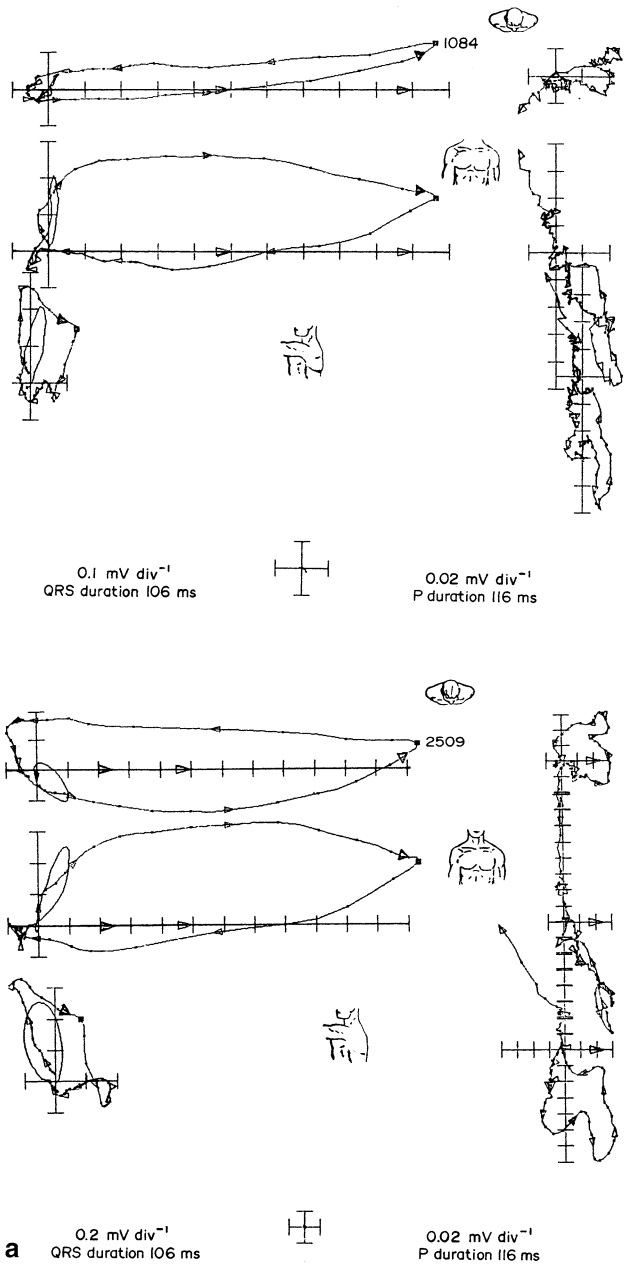

Figure 16.35 **(Continued)**

from occlusion of the posterior-inferior descending distal branch of the right coronary artery is shown in Fig. 16.28. A large inferior infarct with significant posterolateral and apical extension is seen in Fig. 16.35. Typical ECG/VCGs of patients with small and large inferior infarcts are presented in Figs. 16.34a and 16.36a, along with the biplane ventriculograms from these same subjects (Figs. 16.34b and 16.36b).

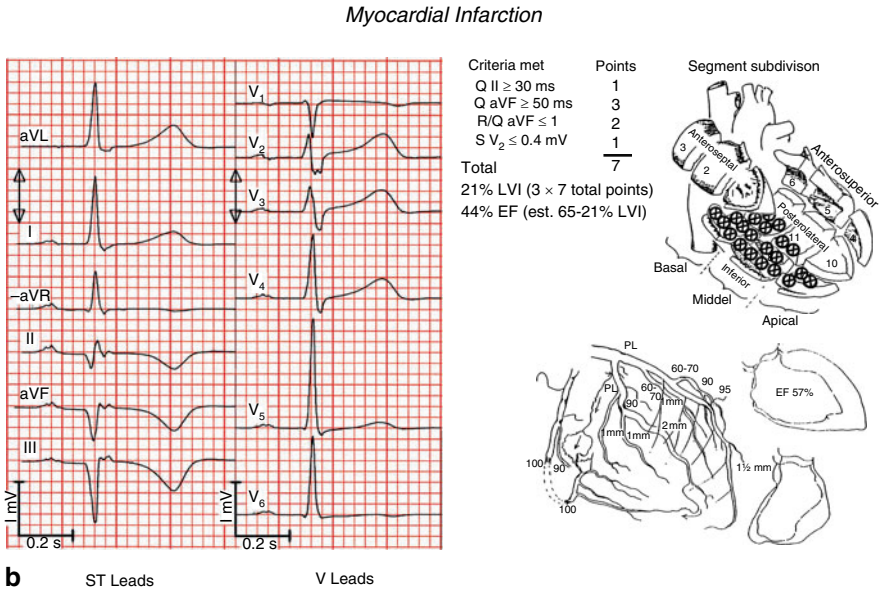

Figure 16.35

(a) The Cube VCG is the *upper half* of the figure and the McFee in the lower half. This 56-year-old man has Cube and McFee VCG changes typical of the occasional patient with RCA occlusion and large inferior infarct involving most of the inferior wall, with some posterolateral wall and inferior septal extension. There is a slight decrease in initial anterior and terminal posterior vectors resulting in a flattened horizontal plane loop. The QRS duration is 106 ms, initial and terminal 30 ms are widely separated, with the initial vector superior as one would expect with RCA occlusion and inferior fascicular (peri-infarction) block. The terminal inferior rightward vector expected with this conduction, while very diminutive because of the extensive infarction of the segments producing it, is still visible. The initial arc leftward remains superior for 50 and 48 ms respectively and is indicative of significant inferoapical extension. In reconstructing the expected loop for inferior fascicular block by the rule of inferior vectors equal to 2/3 of the maximal leftward vector, it is evident that most of the inferior middle and basal segments are infarcted. Deformities of 0.6,mV/50 ms and 1.4 mV/50 ms yield transferred to the nomogram (Fig. 16.12) estimates of 8 and 10 cm and estimates of EF of 42% and 35%. The left atrial activation times are indicative of mild to moderate left atrial overload, but the voltage is only at the upper limits of normal, which is unusual considering the evidence for large inferior infarct. This suggests that infarct size may be overestimated. (b) Note limb leads are in the orderly (Cabrera) sequence from the *top down*, aVL, I, -aVR, II, aVF, III. The small terminal rightward and inferior 30 ms vector which is widely separated from the initial 30 ms vector is evident in the frontal plane ECG. The QRS infarct size score accumulated 7 points for inferior infarct and distributes them into the inferior wall with significant extension into the apex and onto the posterolateral wall and predicts an EF of 44%. When the systolic and diastolic left ventriculogram center lines were superimposed, there is an akinetic segment involving the same regions predicted by the QRS score. The remaining LV contracted vigorously producing an unusually good ejection fraction (57%) for an infarct of this size.

16.4.5.1 Right Ventricular Infarction

Subsequent to proximal RCA occlusion, right ventricular (RV) infarction has been shown [130, 131] to be about as common as LV infarction. The completed infarct in the right ventricle, however, is patchy, macroscopic and multifocal. The lack of confluent localized visible scar probably accounts for the statement in older pathology literature that RV infarct is uncommon. Also, the absence of a large confluent scar can be evoked to account for the fact that, until recently, no QRS changes of RV infarct have been elucidated in the ECG/VCG. Based on the location of RV potentials in body-surface map data, and the proximity of the RV base to the sternum, it was to be expected that both the acute ST-T and evolving QRS changes

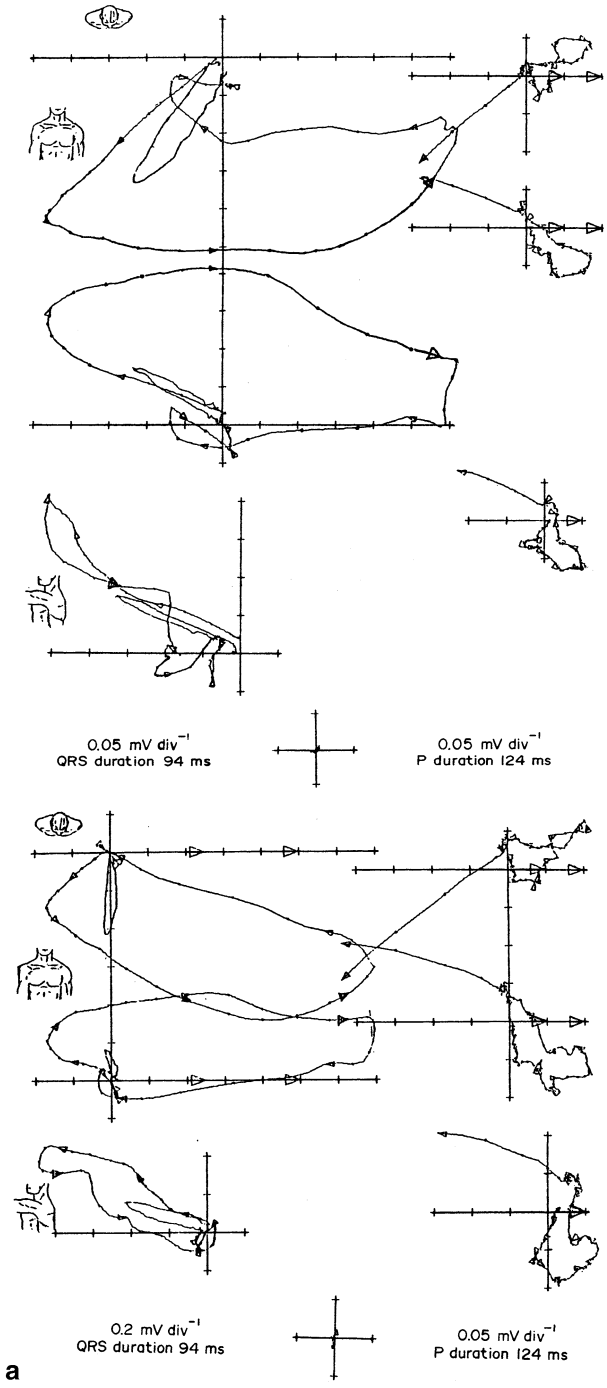

Figure 16.36 (Continued)

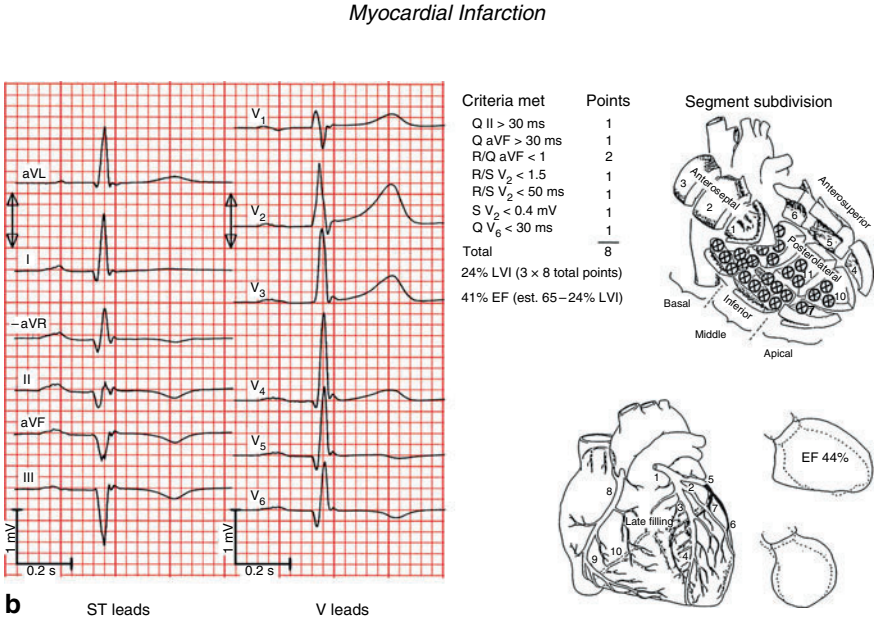

Figure 16.36

(a) The Cube VCG is the *upper half* of the figure and the McFee in the *lower half*. This VCG combines many of the changes of large posterolateral infarct seen in Fig. 16.33a, b and large inferior infarct of Fig. 16.35a, b. The QRS changes of inferior fascicular conduction delay are less well documented, although much of the small terminal 30 ms vector is opposite the initial 30 ms vector, and the QRS duration is 100 ms. Assuming the basic activation of inferior fascicular block, and reconstructing a non-infarct loop using the 2/3 rule and a normal average left voltage, deformities of 0.5 mV/60 ms and 0.8 mV/50 ms are seen in the Cube and McFee respectively. Infarcts of 8 and 7.5 cm are read from the nomogram (Fig. 16.12) in which case EFs of 42% and 44% would be expected. If normal conduction is assumed, the infarct sizes would be 1–2 cm smaller and the predicted ejection fractions would be 45–50%. (b) Note limb leads are in the orderly (Cabrera) sequence from the *top down*, aVL, I, -aVR, II, aVF, III. The main point of interest in QRS scoring this ECG for infarct size is to note the "notched" Q in F. This leads to a Q duration of only 30 ms when one measures to the point on the baseline directly above the peak of the "notch." Notching this early in the Q is unlikely in inferior fascicular delay where a "smooth" Q is usual in the presence of a normal anterosuperior wall. A "notched" Q in F in normal conduction is usually the result of border effects from inferior extension of anterior or posterolateral infarcts into the apical and middle segments of the inferior wall. In this case 8 QRS points accrued and the criteria distributed the infarct more into the base that was found at ventriculography, and underestimated the apical involvement, although the overall estimate of infarct size and EF were appropriate.

of RV infarct would be most marked in V4R, V3R and V1. The abnormal changes of RV infarct are also prominent in lower midchest and right parasternal leads. A series of papers [132–134], which have been reviewed by Kulbertus et al. [135], reported that an ST segment in V4R elevated by as little as 0.05 mV (0.5 mm at a gain of 10 mm = 1 mV) is a highly sensitive and specific marker of acute RV infarction. Carson and associates [136] reported vectorcardiographic changes in the ST-T vectors in seven patients with acute RV infarction in association with inferior infarction. They suggested that a rightward and anterior ST vector of magnitude ≥0.15 mV was a good discriminator between these 7 patients and 20 others with acute inferior infarction and no evidence of RV infarction on cardiac scintigraphic studies. Geft and coworkers [134] also reported that elevated ST segments in precordial leads V1–V3 may be caused by RV, rather than anterior LV infarction. The magnitude of the ST change in this event decreases from right to left and there are no evolving abnormal Q

waves in these precordial leads. It is also not surprising that the time-course of the peak amplitude, or even the presence of these acute ST changes, is short and must be looked for attentively to make accurate assessment of the extent of RV infarction.

With the advent of the balloon catheter for right-heart catheterization, the measurement of right-sided hemodynamics has become routinely available in present-day coronary-care units. The clinical evidence for RV infarction is often acute right-heart failure. In the presence of normal left-heart filling pressures and RV failure, there is increased RV diastolic filling pressure, increased right atrial (central venous) pressure and ECG/VCG changes of right atrial overload. Since single inferior infarcts of the left ventricle from an RCA occlusion are rarely large, it follows that LV failure with a high left-atrial filling pressure is, indeed, also rare. The low-cardiac-output state seen in these patients is thus very likely a result of RV failure, not left, and the LV is usually volume-depleted owing to a low output from the right heart. In the adult P wave, 0.1 mV amplitude anteriorly in V1, V2, or Z and 0.175 mV amplitude inferiorly in aVF or *Y* exceeds the 98% upper limits of normal (see Table 16.1), and should be read as suggesting right-atrial overload. Acute and transient P-wave voltage amplitudes of 0.2 mV in V1, and V2 (and *Z*) and as much as 0.3 mV in aVF (and *Y*) can be seen in this circumstance, from acute right-atrial overload (RAO).

Morgera and coworkers [137] reported on a pathology series of patients with RV infarct in association with inferior infarct in whom right precordial leads V3R-V6R had been recorded serially along with a standard 12-lead ECG. Twenty-one subjects with pathoanatomically confirmed inferior LV infarct and variable degrees of RV infarct were compared to nine patients with necrosis limited to the inferior LV. Specificity studies also included 82 subjects of similar age and sex distribution without clinical evidence of heart disease, for whom V3R-V6R had been recorded in addition to the standard 12-lead ECG. In the normal subjects, an rS complex was seen in V3R in 100% and in V4R in 91% (rSr' was seen in 6%). On the other hand, QS or Qr in V3R and V4R were specific markers of RV infarct in this small number of autopsy-validated patients (specificity 100%, sensitivity 78%). This group also confirmed that ST elevation ≥0.05 mV in these leads did not occur in the normal subjects, and ST elevation of ≥ 0.1 mV was not seen in the acute stage of the patients with inferior infarction limited to the LV. Zehender and associates [138] in a large clinical series of 200 consecutive patients with acute inferior infarction, confirmed the high sensitivity and specificity of the 0.1 mV of ST elevation in V4R for the diagnosis of acute RV infarction. The relative risk of in-hospital mortality was 7.7 for those with this finding.

In summary, the changes of right atrial overload are seen in conjunction with acute inferior infarction without a history of prior infarct, and suggest RV involvement in the infarct. Prominent ST elevation in V1, especially if accompanied by decreasing or depressed ST amplitude in V2–V4, would further confirm the suspicion of acute RV infarction, even in the absence of a low-output state. If ST amp ≥0.1 mV is seen in V3R and V4R [138], the diagnosis of acute RV infarct is confirmed with a high specificity (88%), sensitivity (78%) and diagnostic accuracy (83%). QS or qR complexes usually evolve in these same leads. Furthermore, the peak ST-segment elevation in these leads, while of short duration, appears to be a reliable measure of the extent of RV involvement.

16.4.6 Dominant Left Circumflex Occlusion and Typical Posterolateral Inferior Infarcts

When the left posterior circumflex supplies the posterior (inferior) descending coronary artery, three locations of infarction occur based on the site of the occlusion as follows:

(a) Acute occlusion of the dominant LCX distal to the main marginal take-off produces acute inferior ST-T changes of LV posterolateral and inferior infarction and evolution of an LIFB pattern indistinguishable from the typical acute distal RCA occlusion described above. On the other hand, the changes in right precordial leads V1, V3R, V4R of acute RV infarction exclude acute LCX occlusion.
(b) Obtuse marginal occlusion produces identical changes to those described earlier for non dominant LCX with infarction of the posterolateral mesial region. In one third of these, there is some extension onto the inferior wall and posterolateral apex.
(c) The group of patients with proximal occlusion of the left dominant posterior circumflex produces a wide range of infarcts from small to very large, involving both the posterolateral and inferior walls.

In the author's (RHS) Rancho/USC database, all of those who had significant infarction met the ECG/VCG criteria for left inferior (posterior) fascicular block (LIFB) described above. A typical ECG/VCG from a patient with these changes is presented in Fig. 16.35.

16.4.7 Differential Diagnosis of Poor R-Wave Progression in Leads V1–V6

Pulmonary emphysema, right or left ventricular hypertrophy, anterior preexcitation (Wolff-Parkinson-White (WPW) pattern) and diffuse infiltrative or myopathic processes are all well-known causes of poor R-wave progression in right precordial leads. In general, consideration of these pathologies sets in motion the differential diagnostic process in the interpretation of the ECG/VCG that will separate out such causes of decreased or absent R waves in V1–V3 from anterior infarction.

In pulmonary emphysema, the generalized low voltage, and in particular the significant attenuation of anterior, leftward and inferior vectors, are volume-conductor effects. Owing to the pulmonary overexpansion, there is an increase in the AP diameter, an elevation of the sternum and ribs anteriorly, a lowering of the diaphragms which "peel off" from the inferior surface of the heart and a downward and posterior displacement of the heart. In addition to these major geometric changes, there is a decrease in the conductivity of lungs resulting from the changes secondary to the emphysema. The displacement of the ribs with their ECG/VCG recording locations upward and anteriorly, along with displacement of the heart downward and posteriorly, significantly increases the distance from the heart to all the precordial recording electrodes. These two factors decrease field strength remarkably to all the usual precordial-lead recording sites. The loss of contact of the heart with the diaphragm decreases the inferior field strength of the ventricles as a result, but the atria, especially the right atrium, have a direct conductor (the vena cava) into the abdomen and to the left-leg recording electrode. The net effect of all of these changes in patients with otherwise normal hearts is to shift the mean P vector so that it is directed inferiorly, while the mean QRS vector is directed posteriorly with generalized low-voltage QRS amplitudes. These are the classic ECG/VCG changes of pulmonary emphysema [139] and rarely lead to a problem in diagnosis. Anteroapical infarct with loss of anterior, leftward and inferior vectors can result in similar or identical QRS changes including generalized low voltage. LV infarct of this degree is generally associated with high-frequency notching of the early to mid-QRS and with significant left atrial overload (LAO) including a leftward shift in the mean frontal-plane P axis. The absence of a vertical frontal P vector and an increase in P duration of ≥120 ms effectively excludes emphysematous changes, and the presence of ST-T changes, of anteroapical injury and ischemia, if seen, makes it much more likely that the QRS changes described, together with LAO, are a result of infarction.

Patients with moderate to severe right ventricular hypertrophy (RVH) may have qR changes in right precordial leads without anatomic evidence of an anterior infarct which it mimics. When these changes occur in patients under the age of 25–30, the chance that they are a result of infarction is slight. The presence of moderate to severe right atrial overload (RAO) as defined in Tables 16.1 and 16.2, and the absence of LAO especially when associated with right axis deviation, effectively excludes anterior infarct as a cause of these changes even in the older patients. Conversely, in older patients, when initial and/or mid-QRS notching is widely observed, abnormal Q waves are seen in other leads and definite LAO is seen. Even if the ECG signs of RVH and RAO are noted, it is now highly probable that the q of the qR in V1 and V2 is caused by an anterior infarct.

In 10–15% of patients with left ventricular hypertrophy (LVH), there are decreased or absent initial R waves in V1 and perhaps to V2 and V3, without anatomic evidence of anterior infarct. There is also an increased incidence of infarction in the presence of LVH. It is important, therefore, to assess the presence or absence of each, alone or in combination. Since prognosis is a function of the severity of the LVH and the size of the infarct, it is important to quantify both. If the ECG/VCG signs of LVH (i.e., increased voltage, duration, repolarization changes or LAO) are present, the absence of initial R waves in V1–V3 may not represent anterior infarct, especially in the absence of signs of infarction in other ECG/VCG leads. It has been found appropriate to suppress anterior infarct points from V1 and V2 when scoring for infarct size if the ECG/VCG signs of LVH are present [140]. Notched initial vectors or a qrS pattern is not present in these leads with LVH alone, and when present in V1 or V2, should be tabulated as one point each in the infarct score. For any ECG QRS point score for infarct size of more than three obtained from the rest of the ECG, the probability that

absent R waves in V1–V2 are a result of infarct, even if smoothly transcribed, increases to more than 90%, and they should therefore be tabulated.

Anterior pre-excitation can produce absent initial R waves in V1–V3. Since by definition this form of WPW pattern is pre-excitation of the anterior wall (either the septum or right ventricle) via direct accessory pathways from the right atrium, it follows that the PR interval is particularly short and the delta wave from the pre-excitation is unusually prominent, making the diagnosis of WPW pattern straightforward.

The differentiation of the infiltrative and myopathic processes as a cause of poor R-wave progression in right precordial leads is usually made on clinical grounds. These entities should be considered when widespread splintering of the QRS is seen along with significant atrial overload, especially LAO, and increased QRS duration associated with a dilated left ventricle, without the voltage changes of ventricular hypertrophy. When the myopathic process involves the peripheral conduction, as it often does, an atypical wide complex LBBB pattern is commonly seen along with abnormal left or right axis deviation. This is not a confounder in the differential diagnosis of poor R-wave progression.

16.4.8 Differential Diagnosis of Prominent Anterior (and Rightward) Forces

Abnormal initial and/or terminal R waves in V1 or V2, and prominent S waves in V5 and V6 are seen routinely in moderate to severe RVH and quite commonly in posterolateral infarct. Two thirds of the latter do not have inferior or leftward Q waves, and the differentiation of prior posterolateral infarct from RVH cannot be made securely on the basis of QRS changes alone. When the prominent anterior and rightward QRS changes are associated with abnormal inferior or leftward Q waves and abnormal posterior/inferior ischemic ST-T changes, they pose little problem in the differential diagnosis. The case for evolved prior posterolateral infarct becomes quite secure if the mean T vector is anterior, there is no right axis shift in the frontal plane, RAO (right atrial overload) is absent and definite LAO (left atrial overload) is present. In this case, the QRS score for infarct size can be applied with confidence even in the absence of abnormal inferior and leftward Q waves. Conversely, in the presence of even "probable RAO" by the criteria of Tables 16.1 and 16.2, the diagnosis of posterolateral infarct is much less reliable and its quantification by the QRS score is unreliable. When the following requirements are satisfied:

(a) Criteria for definite RAO are present,
(b) The QRS axis in the frontal plane is oriented to the right, and
(c) The mean T axis is directed posteriorly,

then the likelihood of RVH is very high and the likelihood of posterolateral infarct very low.

The QRS score is reliable for estimating anterior and inferior infarct size, providing that points from all R/S ratio criteria in V4–V6 are suppressed as well as all posterolateral points in V1 and V2. The probability modifiers as indicated in Table 16.3 should also be used.

16.4.9 Differential Diagnosis of Abnormal Inferior Q Waves and ST Vectors

Abnormally acute ST-T vectors, together with evolving significant Q waves in II and aVF, and the changes of inferior-posterior fascicular block described earlier, occur in 85% of patients with RCA occlusion and local inferior wall motion abnormalities. These ECG changes also occur in 5% of those with RCA occlusion and no wall motion abnormalities. This is presumed to be a result of small focal lesions disrupting the inferior fascicle. In the latter case, the ST-T change is much less prominent. The Q wave, as it develops, is consistently smoothly inscribed.

Abnormal initial superior QRS vectors evolve in 15% of patients with acute LAD coronary occlusion and anterior infarction. With a mid to distal acute LAD occlusion, the risk area localizes to the apex with the usual "wrap around" of the distal LAD onto the apical third of the inferior wall. This is associated with a variable acute ST vector directed

inferiorly and leftward. From a quick review of the spatial relationships of the heart in Fig. 16.1, it is clear that the apical third of the anterosuperior wall is facing almost entirely left while the inferior apical third faces directly inferiorly. The acute ST change and the evolving QRS changes of infarction are simple subtraction effects. For the evolving infarct, there is a loss of initial inferior QRS vectors because of the loss of activation fronts from the inferior extension of the infarct and dominance of the normal superior activation fronts and their normal superior vectors. The Q waves are usually shallow, irregular, slurred and/or notched and the QRS does not show the wide separation of initial and terminal 30 ms vectors, or the 20 ms increase in QRS duration seen with typical RCA occlusion and the inferior fascicular block pattern.

Acute LCX occlusion and consequent visible posterolateral infarct on biplane ventriculograms is associated with some inferior extension in about one third of cases. This produces abnormal acute inferior, as well as posterolateral, ST-T vectors, while abnormal initial superior QRS vectors with an abnormal left axis evolve. Abnormal Q waves may appear in inferior leads, especially lead III and aVF (but usually not in lead II). This is also a simple subtraction effect, as described above. Typically, the abnormal initial QRS waves in this instance are notched or slurred with a normal QRS duration. They are distinguished from the abnormal but smooth inferior Q waves, wide separation of initial and terminal 30 ms vectors and slightly prolonged QRS of inferior-posterior fascicular block as seen so commonly with the infarcts from RCA occlusion.

16.4.10 Summary of Electrocardiographic Changes Following Acute Coronary Occlusion

In summary for this section, the early minutes of acute coronary occlusion and evolving acute infarction produce a major shift in the ST segment that is vectorially related to the region undergoing acute ischemic injury (Table 16.5). There is:

(a) Prominent superior and slightly leftward and posterior ST vector deviation for proximal occlusion of the first large diagonal branch of the LAD;
(b) Moderate anterior, inferior and leftward ST vector deviation for mid to distal acute LAD occlusion with the usual prominent "wrap around" of the distal LAD onto the inferior apex;
(c) Prominent anterior, superior and leftward ST vector deviation for acute proximal LAD occlusion;
(d) Prominent posterior and moderate leftward (± minimal inferior) ST vector deviation with acute proximal LCX occlusion;
(e) Prominent posterior and moderate inferior ST vector deviation with acute proximal left dominant LCX occlusion. This specific ST change also occurs in acute proximal occlusion of the rare, very right dominant RCA with a large posterolateral branch perfusing most of the posterolateral wall and a diminutive LCX. In this case, local ST amp ≥0.1 mV in V3R and V4R due to RV infarction excludes LCX occlusion. If the occlusion in the RCA is distal, the two are indistinguishable; and
(f) Inferior, ± leftward, and ± posterolateral ST deviation of acute distal RCA occlusion.

The magnitude of the peak ST change is related to the extent of myocardial area at risk. From a review of Fig. 16.9 and Chap. 18, the acute injury process of acute infarction can be seen as a continuous process throughout systole and diastole. It follows that the "primary" localized acute injury currents will be superimposed on the "secondary" ST-T changes of RBBB, LBBB, pre-excitation, RVH, and LVH. When adjusted for the secondary ST-T changes of each, the residual ST-T displacement vector of the localized acute injury can still be recovered. This is dealt with in detail for LBBB and ventricular pacing for patients with acute infarction in Sect. 16.5.5.2.

As the infarction process progresses, if circulation to the affected region is reestablished either spontaneously, by clot lysis, or balloon dilatation, the ST segment returns toward or to normal in a matter of seconds to minutes. The ST-T wave also becomes terminally inverted as the healing infarct evolves. By day 1 post infarction, a large T vector evolves directed away from the infarcted region. In chronic infarct, the T vector tends to decrease in magnitude being

Table 16.5

Summary of local ECG lead ST deviation changes of acute myocardial infarction from occlusion of the Left Anterior Descending, Left Circumflex and Right Coronary arteries

7 Culprit risk areas in the 3 coronary arteries
1. Proximal left anterior descending
Anterior ST deviation V1, ***V2***, **V3***, V4 and
Superior ST deviation ***-aVF, -III***, aVL, I
2. Main diagonal LAD
Superior ST deviation ***-aVF, -III***, aVL, I
Minor or no anterior ST deviation V1, V2, V3
3. Mid to distal LAD
Anteroapical ST deviation V3 ***V4, V5***, V6 and
Inferoapical ST deviation aVF, ***II, -aVR***, I
4. Non-dominant LCX
Posterolateral ST Deviation V1, ***V2, V3***, V4, V6 and
Less Inferior ST Deviation III, aVF, II
5. Left dominant LCX
Posterior and Inferior ST Deviation about equal
in V1, ***V2, V3***, V4, V6 and aVL, ***III, aVF***, II
6. Proximal RCA
Inferior ST deviation aVL, **V4R**, ***III, aVF***, II
Less or no Posterior ST Deviation V1, V2, V3
7. Distal RCA
Inferior ST deviation aVL, ***III, aVF***, II, None V4R
Less or no posterior ST deviation V1, V2, V3

* ***Italics/Bold*** indicates usual leads with maximum deviation

in general directed posteriorly and rightward in anterior infarct, superiorly and leftward with inferior infarct, and anteriorly with posterolateral infarct. It is important to recognize further that there are effects other than infarction that produce major changes in repolarization. Since repolarization is a passive process linked to depolarization, it follows that any major change in depolarization such as left or right bundle branch block or pre-excitation, for example, has major "secondary" effects on repolarization (Chap. 14). The 3D spatial vector of the ST and T electric fields is directly opposite the late activated terminal half of the QRS in both RBBB and LBBB. Likewise, moderate to severe right and left ventricular hypertrophy have their ST and T vector fields opposite to their mean QRS vector. Electrolyte abnormalities (for specifics see Chap. 18) also have a major generalized effect on repolarization, as well as variable effects on depolarization.

16.5 Bundle Branch Block and Infarction

16.5.1 Essential Principles

In the consideration of bundle branch block (BBB) and infarction, the following important points should be noted. In the first place, complete disruption of either the right or left bundle from coronary disease produces an uncoupling in time of the excitation of one side of the heart from the other, separating right from left ventricular excitation. Also, a predictable activation sequence occurs with each. Finally, when the activation sequence is taken into account, an associated local

infarct produces additional deformities in the resultant surface ECG/VCG which are predictable. The location of an infarct can still be determined, and its size predicted. During an acute infarction, the primary ST-T changes of acute ischemia/injury are add-ons to the secondary effects of the bundle branch blocks. When the secondary effects are adjusted for, the direction and magnitude of residual ST-T deviation is predictive of the location of the acute infarction and its size and/or extent. In the light of the current knowledge of activation, primary and secondary repolarization, coronary anatomy and infarct distribution and size, it is no longer appropriate to say "in the presence of left bundle branch block no statement can be made about the presence or absence of myocardial infarction."

16.5.2 Validation Studies in Bundle Branch Blocks

The pathoanatomic studies correlating infarct size at autopsy and ECG point score for infarct size, reported by the authors [18, 30–34] and described earlier, excluded patients with ECG evidence of conduction defects, ventricular hypertrophy or emphysema. The angiographic correlations did not. For those subjects with complete RBBB and LBBB discussed in this section, the validation consists of coronary and biplane ventricular angiographic correlations from the (Rancho/USC database) databank, as shown in Figs. 16.30–16.37, and Figure 16.41. The authors are also indebted to the large body of clinical [37, 141–146], epidemiologic [147–150] and anatomic [18, 151, 152] correlations reported in the literature. In pathoanatomic correlations with BBB, the presence of RBBB is generally unambiguous. However, it is difficult to establish from the literature the true incidence of, and therefore the pathoanatomic correlations with, complete LBBB. Most reports in the literature use the original Wilson/NYHA [53] criteria for LBBB which includes a QRS duration of ≥120 ms. On the other hand, Grant and Dodge [16] pointed out that in intermittent LBBB the QRS duration is 140–160 ms in patients with a QRS duration of 80–100 ms in the normally conducted beats. A QRS duration of <140 ms is uncommon in typical LBBB and durations of 170–180 ms occur in many. As these authors point out, those ECGs with intermediate durations of 120–130 ms are often atypical and many have the wide separation of initial and terminal 30 ms vectors typical of the fascicular (or "peri-infarction") blocks. When the published ECG (and VCG) records of LBBB are reviewed, it seems evident that about half of these records with QRS ≥120 ms meet the criteria of fascicular blocks with QRS prolongation. The prolongation appears to be due in part to LVH. The authors estimate the incidence of complete LBBB by the criteria defined by Grant and Dodge (which conform to the authors' data) to be about half that reported in most of the series cited. Horan, Flowers et al. [153] also point out that the reported autopsy correlations of ECG/VCG changes of infarct in patients with so-called LBBB suffer significantly from this admixture of fascicular blocks and complete LBBB. It is not possible from the published data, except in a few instances, to separate out these subgroups and their specific associated pathoanatomic lesions.

In our hands, those patients with an ECG/VCG pattern resembling LBBB with a QRS duration <140 ms, but meeting the Wilson criterion of QRS duration ≥120 ms, usually have LV overload and local infarction which produces the initial and mid-QRS changes reminiscent of LBBB. Indeed, as Grant and Dodge previously observed, it has been found in the patients studied by the authors that even in many of those with LV conduction delay of the left type with QRS duration ≥140 ms, the ECG/VCG will show wide separation of initial and terminal vectors without mid-QRS notching and slowing of transcription. This is atypical for LBBB and more consistent with fascicular block, usually anterior (superior) combined with severe LVH. These patients will have increased LV dimensions at ventriculography. In both subsets, the ECG score and the VCG criteria for infarct size and location, which assume LBBB is not present, will perform well in predicting the angiographic change.

16.5.3 Incidence and Prognosis of BBB in Patients with Coronary Artery Disease

16.5.3.1 Incidence of Preexisting or Recent Onset RBBB

In the series of Hiss and Lamb [154], complete RBBB was found 52 times (0.1%) in 44,213 healthy US Air Force personnel under 25 years of age (whereas LBBB was not seen in this age-group). Acquired RBBB below the age of 50 occurred

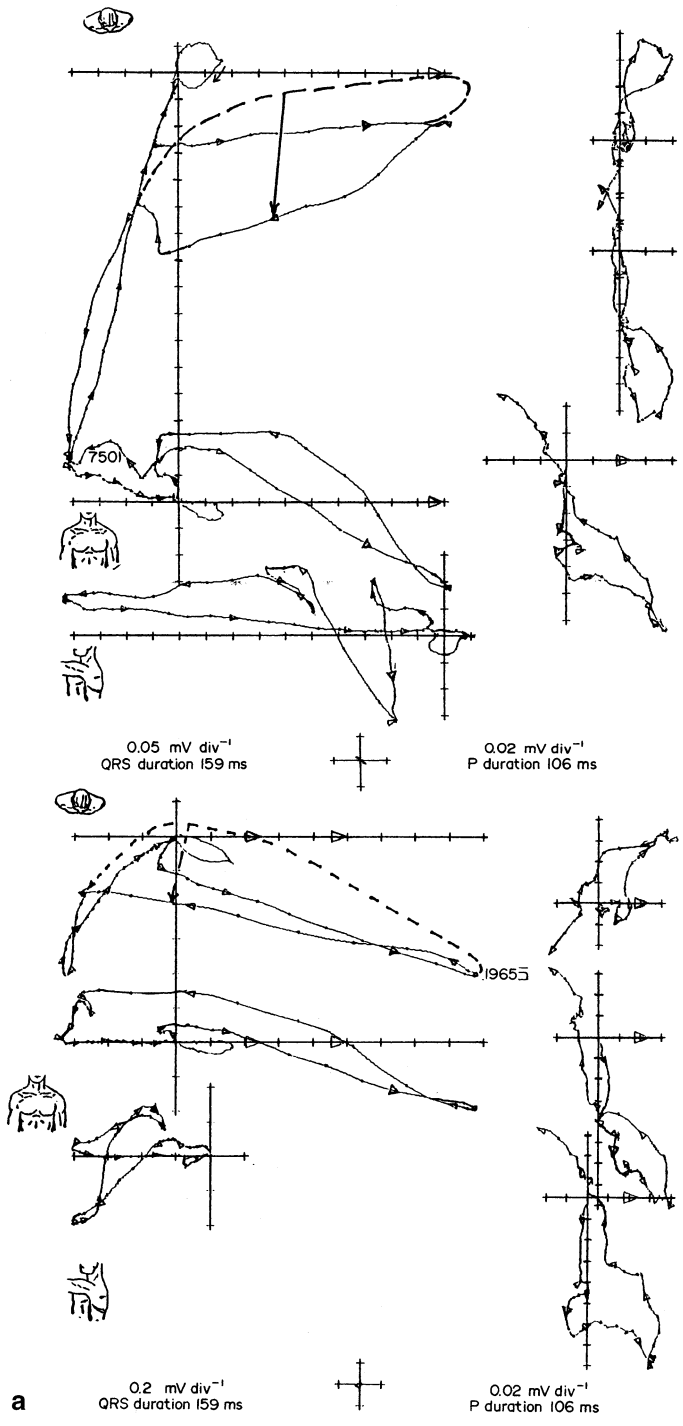

Figure 16.37 (Continued)

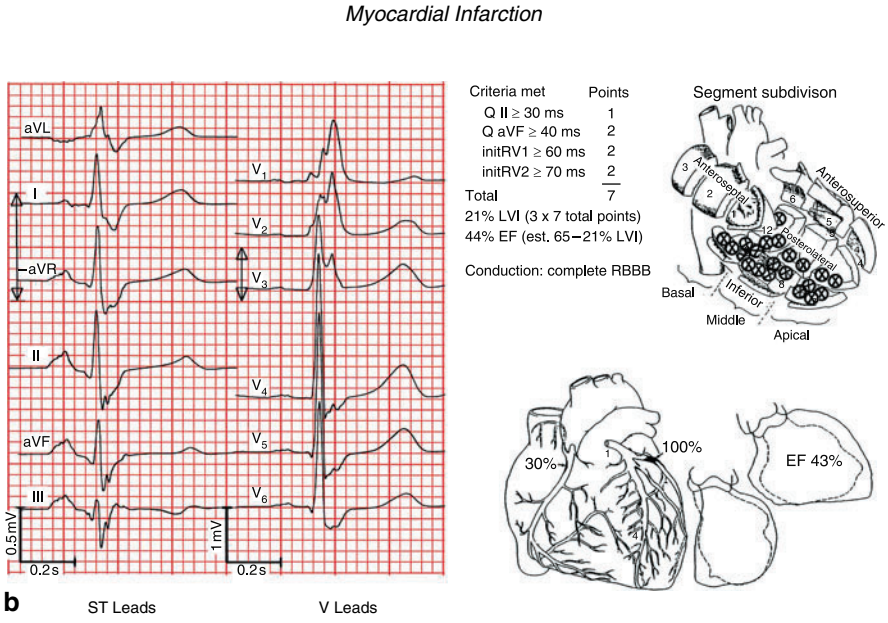

Figure 16.37

(a) The Cube VCG is the upper half of the figure and the McFee in the lower half. This 55-year-old woman apparently had preexisting right bundle branch block (RBBB). Prior to angiograms done because of angina she had the VCGs recorded. In both lead systems, the VCG inscription is atypical for RBBB in that the 45–80 ms vectors are written in a clockwise fashion in the horizontal and left sagittal planes instead of counterclockwise. The usual VCG change for this interval is shown by the *dotted lines* in both lead systems. It is perhaps more anatomically consistent to say that after the peak leftward vector, i.e., at apical breakthrough of LV activation, the vector fails to swing toward the free posterolateral LV wall before it is overridden by the late RV activation. The latter change is the stereotypical change seen in RBBB even in the presence of severe RV hypertrophy. These subtleties in phase of the surface ECG signal are difficult if not impossible to appreciate from visual inspection of conventional 12 lead ECGs. They can be mathematically defined easily in simultaneous digitized orthogonal lead or 12 lead ECG data. The specific change described and the presence of an abnormal superior initial 34 ms vector are strong VCG evidence for infarction of the posterolateral-inferior wall from this codominant LCX occlusion, as shown on these illustrations the magnitude and duration of the deformities in each lead system, transferred to the nomogram (Fig. 16.12), yielded an estimate of infarct size of 6 cm and an EF of 48%. (b) Note limb leads are in the orderly (Cabrera) sequence from the *top down*, aVL, I, -aVR, II, aVF, III. Since the 1st edition of this book chapter we, the authors, have developed and validated QRS infarct size scores for RBBB. LAFB ± RBBB, LVH and LBBB (see Appendix A). The score for RBBB as shown above, in addition to 3 points for abnormal Qs II, aVF (as noted in 1st edition) gives 2 points each for V1, V2 wide initial R, increasing the points to 7 (21% LVI) for posterolateral-inferior infarct and a 44% EF.

in 0.6% of US Air Force pilots [155], and 13% of these (0.08% of the total) were found to have coronary artery disease at angiography. All but a small percent of the remainder had entirely normal angiographic findings and hemodynamics, normal exercise tests and performance, normal electrophysiologic studies, and were returned to flying status. Right bundle branch block is, per se, not incompatible with long life. On the other hand, when it occurs as the result of an acute myocardial infarct, it is usually an ominous sign [37]. The survival rate is reduced to less than one fourth of that expected for acute myocardial infarction as a whole owing to the extensive infarction that usually produces this conduction abnormality. In the setting of acute infarction, RBBB is more common than LBBB. It occurs as a new event in 7% of all patients with acute infarction. In the large majority of cases, it is a result of very proximal LAD coronary

artery occlusion with an anterior infarction, which is usually very large, with significant basal septal involvement. Only occasionally (<0.35% of acute infarcts) it is caused by RCA occlusion with inferior and basal septal infarction. Infarction in any of the three arterial distributions can occur in patients with stable long-standing RBBB. Since the presence of the block does not affect prognosis and infarct size does, it becomes very important in terms of management to be able to evaluate infarct size in the presence of this conduction abnormality. Only then can it reasonably be predicted whether the patient has a good prognosis and can be expected to go back to high levels of activity, or whether the patient must expect serious limitation of functional reserve and must plan activity and possible return to gainful employment accordingly.

16.5.3.2 Incidence of Preexisting or Recent Onset Complete LBBB

Hiss and Lamb [154] found 0% incidence of LBBB in 44,231 otherwise healthy US Air Force personnel below the age of 25. Acquired LBBB also occurred much less often in the pilot population below 50 years of age than RBBB [155], namely 0.1% as compared to 0.6%. Significant coronary disease was found at angiography in 22% of subjects with LBBB (0.02% of the total) compared to 13% for RBBB (0.08% of the total). In both groups, all but a small percentage of the remainder were found to have normal angiography, hemodynamics, electrophysiological studies and exercise performance, and were returned to flying status. In patients with angiographically documented coronary artery disease, the incidence of LBBB in the Rancho/USC and Duke University databanks using the Wilson (and NYHA) definition of LBBB was 1.7%. Using the more appropriate criteria from the Grant and Dodge report [16] that include a QRS duration of ≥140 ms, the incidence was 1%.

In earlier reports [37], LBBB was seen as a new event in 2–3% of patients with an acute myocardial infarction. In the current aging populations, 5–6% of patients presenting to chest pain centers who evolve an acute infarction have LBBB on their admission ECG (see Sect. 16.5.5.2 below).

16.5.3.3 Prognosis

In the US Air Force study, RBBB, while being more common as an incidental finding, was also more common as an acquired finding on follow-up examination. It was four times more often associated with newly diagnosed coronary disease at angiography than acquired LBBB. In both groups, over three fourths of these pilots had normal coronary arteries, normal stress hemodynamics and were allowed to remain on flying status. Long-term survival in epidemiological studies of the general populations of subjects with either RBBB or LBBB is decreased threefold over age-matched cohorts [147–150]. It was concluded that the survival was more closely related to the underlying heart disease and other risk factors than to the presence of the block *per se*.

In asymptomatic subjects, or in those suspected of coronary disease who have preexisting RBBB or LBBB on the ECG/VCG, there is a different admixture of patients with no infarcts or small infarcts with normal LV function, and patients with very large infarcts or ischemic myopathy and very poor LV function. Since prognosis is much more closely related to the severity of the underlying heart disease than to the presence or absence of BBB, it becomes important for both management and prognosis to be able to evaluate the presence, size and location of the infarct. Patients with recent onset LBBB in the setting of acute infarction have, in general, small infarcts, although a few are very large. Such patients have been found to have the same survival rate as age-matched subjects without BBBs [37]. It is not surprising that they have a threefold improved short-term survival rate compared to those with an acute infarct and recent onset of RBBB, most of whom have large anterior infarcts.

16.5.4 Myocardial Infarction and RBBB

In uncomplicated RBBB, the abnormal right ventricular depolarization produces a stereotypic repolarization pattern. These secondary ST-T changes are seen as displacement of the ST segment to the left and posteriorly, directly opposite to

the terminal right and anterior QRS of delayed RV depolarization. The prominent T-wave (and vector field) follows the ST segment to the left and posteriorly. The early ST-T changes of acute anterior, posterolateral, or inferior infarction superimposed on the secondary repolarization of RBBB are readily discernible. There are subtle but important changes in the initial 60 ms of the QRS with this abnormality. The most important is a 5°–10° shift of the initial forces anteriorly and superiorly owing to loss of normal posteriorly directed vectors from the right septal surface and loss of normal early inferior vectors in the right ventricle. This, however, has no important effect on criteria for quantifying healed anterior infarcts. It does have major effects on criteria for posterolateral infarct and minor, but important, effects for inferior infarct with inferior-posterior fascicular block discussed in Sect. 16.5.4.4 below.

16.5.4.1 Left Anterior Descending Occlusion, Anterior Infarction and RBBB

When an anterior superior infarct has produced the RBBB, as discussed in the recent onset block described above, the infarct is usually large to very large. On the other hand, when it occurs in a patient with a long-standing congenital or stable RBBB the infarct can be of any size. Thus, the distribution of the size of the infarct is weighted to the end of the scale from large to very large. Nevertheless, the criteria for prior (healed) or acute anterior infarct described in this chapter perform quite well as predictors of the size of this infarct as seen on biplane ventriculograms.

16.5.4.2 Left Anterior Descending Occlusion, Anterior Infarction. RBBB and LAFB

The left anterior-superior fascicles of the left bundle and the right bundle are both supplied by the LAD coronary artery. It is not surprising, therefore, that this combination of blocks and infarction is relatively common. See Fig. 16.19 for an example of a very large acute anterior infarct in which these conduction abnormalities developed. The left anterior (superior) fascicular block (LAFB) produces changes described in the section on typical anterior infarct. The presence of the additional RBBB does not significantly alter the ability of the ECG and VCG criteria to localize and size anterior infarcts and to predict biplane angiographic change.

16.5.4.3 Circumflex Occlusion, Posterolateral Infarction and RBBB

It is theoretically possible for a very dominant circumflex coronary that also provides a major blood supply to the septum to be etiologically involved in the production of RBBB. Four percent of all recent onset RBBBs are associated with recent inferior infarction. Since 10–15% of all inferior infarcts are the result of total occlusion of a dominant circumflex, it follows that 0.4–0.7% of all recent onset RBBBs would be associated with a recent occlusion of a dominant circumflex and a recent inferior posterolateral infarction. In fact, such a finding has never been documented in the authors' centers, but Grant and Dodge [143] reported a preexisting posterolateral infarct in 6 out of 80 (7.5%) subjects with intermittent RBBB. On the other hand, we have noted that acute chest pain patients with RBBB who have >0.2 mV posterior ST deviation in two leads of V1–V3 have a high probability of having an acute LCX occlusion.

Circumflex occlusion with posterolateral infarction in patients who also have a preexisting RBBB does occur as an isolated lesion. Since initial forces are displaced somewhat anteriorly by the RBBB, a QRS vector loop which is entirely anterior occurs occasionally without any infarction at angiography or autopsy. The changes in QRS described above for RBBB replicate the criteria for posterolateral infarct listed in the ECG score for infarct size, Fig. 16.16, in the absence of the infarction. Thus, posterolateral points by the ECG QRS score are completely unreliable in the presence of RBBB and should not be used. In patients with large posterolateral infarcts, with apical and inferior extension, the abnormal loss of R and/or Q waves in I, V4, V5 and V6 and in inferior leads may be the most reliable sign of this lesion. Unfortunately, these leads are not usually involved with the more usual small posterolateral infarcts. VCG changes (especially with the Cube lead system – see Chap. 11) are, however, still reliable predictors of infarct size with ventriculographic posterolateral wall motion abnormalities from circumflex occlusion. Irregularities of the 20–60 ms vectors, with anterior displacement that produces a clockwise initial inscription of the horizontal plane VCG (Fig. 16.37), are indicators of

localized posterolateral infarction and RBBB. Statistically adequate numbers of these patients to test significance do not exist in the authors' database. Nevertheless, the amount of deformity from the usual counterclockwise initial inscription of the horizontal plane loop has been predictive of the size of posterolateral lesions as seen angiographically in this small number of patients.

16.5.4.4 RCA Occlusion, Inferior Infarction, RBBB and LIFB

In those patients with stable preexisting RBBB (and the few patients with recent onset RBBB) and acute RCA occlusion, the significant ST inferior deviation of acute inferior ischemia/injury (≥0.1 mV) is superimposed on a minor secondary ST elevation (0.05 mV) of RBBB (for a total of ≥0.15 mV). In the evolved/healed inferior infarct, LIFB (inferior-posterior fascicular block), as defined earlier in this chapter, is nearly always present. In these situations, with a normal anterosuperior wall and apex, the criteria for inferior infarct are nearly as effective as if the RBBB were not present. RBBB itself produces early loss of inferior forces (from the absent early activation inferior right ventricle). Thus, there is a slight increase (3%LV) in the inferior QRS MI size score and overestimation of inferior infarct size in the presence of RBBB.

On the other hand, in the somewhat more common situation where the RBBB has been caused by a large anterior infarct, the presence of an inferior infarction is more difficult to deduce and the infarct size is less reliably estimated. The reasons are the same as if the RBBB were not there, namely, inferior Q waves as evidence for inferior infarction, with or without inferior-posterior fascicular block, are dependent upon an intact anterosuperior wall for their production. When a large anterior infarct is also present, there is a major decrease in anterosuperior wall vectors needed to produce abnormal superior vectors. However, the major loss of leftward vectors from the apical involvement of the large anterior infarct is still present. When inferior infarction is present together with a large anterior infarct (with or without RBBB), the anterior infarct is rarely missed by the criteria for infarct size presented in this chapter. Its size, however, may be underestimated. The presence of a separate posterolateral infarct from circumflex occlusion or a significant posterolateral extension of an inferior infarct is suspected in RBBB plus inferior fascicular block by the same criteria described in Sect. 16.5.4.3 above for RBBB alone.

16.5.5 Myocardial Infarction and LBBB

Recent onset LBBB, when seen, is usually intermittent, rate-dependent, and associated with a high degree of intranodal block. The diagnosis of prior infarct, or the estimation of its size, is rarely a problem in this context because the LBBB is intermittent and the more normal conducted beats are available for analysis. In preexisting or persistent LBBB in patients with chronic angina pectoris or a previously documented infarct, many of the ECG/VCGs exhibiting a LBBB configuration will be atypical. Those with a mild increase in QRS duration of 120–130 ms, small or absent R in V1, V2, notched R in V5 or V6, LVH, and/or with the criteria for superior or inferior-posterior fascicular block, that is, wide separation of initial and terminal 30 ms vectors, are readily analyzed as to presence and size of infarct by the criteria presented in this chapter. In the absence of clinical idiopathic cardiomyopathy in the current aging population, LBBB with QRS ≥ 140 ms will be present in 4–5% of the subset with angina or documented coronary artery disease. Of this subset 40–50% of the "typical" LBBB, as described in detail below, will usually be associated with calcification at the base of the heart around the aortic and mitral rings and/or multiple proximal coronary occlusions involving both the LAD and the right coronary arteries.

16.5.5.1 Secondary ST-T of LBBB Modified by a Local Acute Myocardial Infarction

In the current aging population of patients presenting to chest pain centers, there is an increasing incidence (4–5%) of LBBB, and a similar incidence of ventricular pacing with LBBB type morphology. It has been observed that patients

presenting with these LBBB morphologies and signs and symptoms of acute myocardial infarction are significantly less likely to undergo early intervention for coronary reperfusion [156]. The window of opportunity to salvage threatened myocardium is 4–6 h from onset of symptoms [157]. Consequently, a rapid and accurate diagnosis of AMI has become essential. Those with symptoms, normal conduction, and ECG ST deviations of acute myocardial infarction (AMI), in the absence of contraindications, are managed with immediate thrombolytic therapy or percutaneous coronary angioplasty of the acutely occluded artery. However, for those with LBBB morphologies, methodological limitations and conflicting reliabilities of various proposed ECG criteria have resulted in their limited acceptance. This has improved since Sgarbossa et al. and Sgarbossa/Wagner established three electrocardiographic criteria with independent value in the diagnosis of AMI in patients with chest pain and LBBB, which have begun to be more widely utilized. The criteria are (1) STj elevation ≥500 μV in any lead and discordant with the QRS complex, and (2) STj depression V1, V2 or V3 ≥ 100 μV, (3) STj elevation ≥ 100 μV in any lead with upright QRS. A scoring system is utilized.

An improvement in both sensitivity and specificity was found by Polizos and Selvester [156] when they reported a LBBB "10% rule" for the ratio of STj to the |R-S| amplitude. In a control population of 94 chest pain patients documented to be non-ischemia or acute infarction, the STj deviation was 10% of the |R-S| amplitude ±200 μV in anterior-posterior leads V1, V2, V3 and ±100 μV in all other leads for 1094/1128 leads giving a specificity of 97%. The sensitivity was 79% (76/96) for the patients with LBBB morphology, QRS ≥ 140 ms and documented acute myocardial infarction (AMI) who exceeded the biomarker thresholds confirmatory of the clinical suspicion of possible acute infarction. Figure 16.38 panel A illustrates the implementation of the 10% rule. There was a
reasonable distribution of STj deviations exceeding the 10% ratio consistent with acute anterior, inferior, posterolateral, and apical MIs of the 76 in the following contiguous lead pair(s): Anterior STj deviation beyond the 10% rule in anterior-posterior leads V1, V2, V3 of ±200 μV in 26 (34%) consistent with anterior AMI, and posterior STj deviations in 11 (15%) consistent with posterolateral AMI; +100 μV inferior in inferior-superior leads II, aVF, III, aVL in 21 (27%) consistent with inferior AMI; −100 μ V base-apex leads I, aVR, V4, V5, V6 in 18 (24%) consistent with acute apical and/or global subendocardial ischemia. Twelve of the 76 did not meet the Sgarbossa-Wagner criteria for acute injury/ischemia. It was also noted that the 10% rule for localizing ST changes of acute MI worked as well for those with single chamber RV pacing which usually has atypical LBBB morphology and a QRS duration ≤140 ms.

16.5.5.2 Activation Sequence in LBBB and Regional Healed Infarcts

The incidence of LBBB in the subset of the aging population with angina, history of infarct and documented coronary artery disease is 5–6%. A normal ventriculogram will be seen in 1–2% despite definite angiographic coronary disease, and a diffuse myopathic change will be seen on the ventriculogram in 20–30% of this subset. A typical LBBB with QRS duration ≥140 ms (≥130 ms for females) now represents 2–3% of patients with documentable coronary artery disease and either single or multiple local infarcts. The computer simulation of the total-body ECG during depolarization and repolarization was used to unravel the complex interactions of hypertrophy, infarcts (single and multiple) and ischemia and injury, in RBBB and LBBB. The following discussion of ventricular activation in typical LBBB is presented as a basis for the development of the criteria for infarcts in all of the three main coronary distributions.

A better appreciation of this topic can be gained if the activation sequence of LBBB, summarized in 3-plane isochrone maps in Fig. 16.39, is reviewed along with the distribution of the infarcts associated with LAD, LCX and RCA occlusion shown in Fig. 16.3. These are the major determinants of ECG/VCG changes of healed infarct plus LBBB. A short review of the activation in LBBB is given here as a basis for understanding these changes. For the first 50 ms of LBBB, the activation fronts are developing simultaneously anteriorly in the right ventricle and posteriorly on the right septal surface in its apical and middle segments as indicated from Fig. 16.6A and 16.39. As RV breakthrough of the anterior fronts occurs at about 10 ms, there is a rapid shift of the resultant QRS vector posteriorly since it is dominated by the enlarging posteriorly directed fronts in the anteroseptal wall of the left ventricle. This produces the **first in a series of QRST changes** typical of LBBB, namely a small, short-duration initial vector directed anteriorly and leftward, and sets the stage for all the others.

In the absence of LVH, it requires about 40 ms for this rapidly enlarging posteriorly directed wavefront to traverse the septum in the lower portion. A hole then develops in these septal fronts and remains for next 30–40 ms as the Purkinje

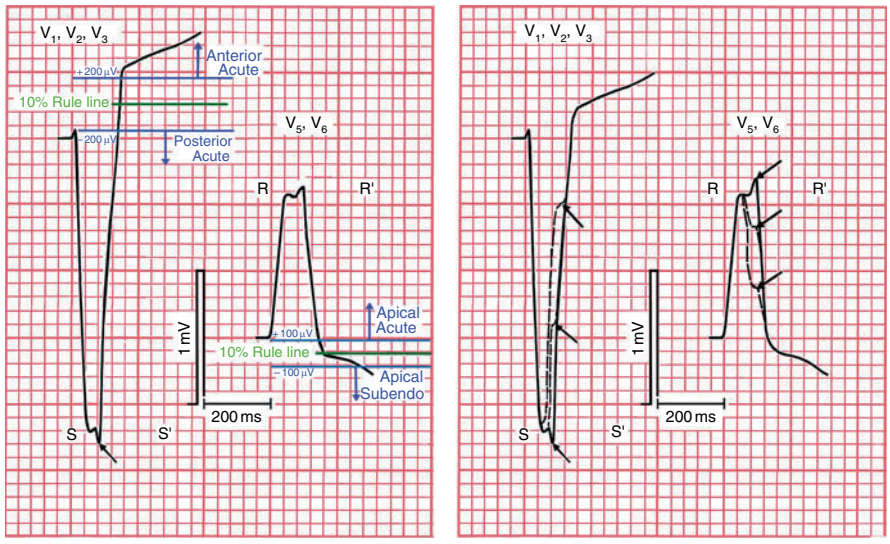

Figure 16.38

Pane a. For acute myocardial infarction with LBBB the 10% *rule line* represents the expected STJ opposite the absolute value of R-S. The 98% confidence limit is ±200 μV for V1, V2, V3 and ±100 μV in V5, V6, and limb leads. In patients with persistent ischemic chest pain, STJ deviation in 2 or more contiguous leads exceeding these thresholds, the diagnosis of acute myocardial infarction can be made with 97% specificity. The extent of the evolving infarction and its location are a function of the number of leads with ST deviation exceeding thresholds directed outward from the center of the local epicardial region in jeopardy. Pane b. For prior infarct size with LBBB this diagram depicts visually R,R′,S, and S′ used in the QRS scoring system The S in V1 or V2 and the R in V5 or V6 represent change in direction of mean QRS vector (and electric field) at the breakthrough of septal activation on the left septal surface (see Fig. 16.39). This occurs near the first 1/3 of the QRS (at 45–70 ms) when activation fronts propagating through the septum from the *right side* arrive at the *left* and a hole develops in the previously continuous activation front. As the fronts propagate outward in the septum, their area directed posterior remains rather constant (from 70 to 95 ms.) resulting in "slow mid QRS conduction," one of the "classic" criteria for diagnosis of LBBB. It follows that an S′ in V1 or V2 and the R′ in V5 or V6 is the change in direction of the mean QRS vector that occurs near the 2/3 point of the QRS with breakthrough of activation at the apex of the LV. This may show up as a definite S′ or R′, but may be only a slurring of terminal QRS as shown. For the purpose of the infarct size score, any extra notching in the mid QRS between the R and R′ should be ignored. When a definite inflection point does not occur at the 1/3 or 2/3 point in any designated V lead, the time when it occurs in the others is transferred to the lead in question and the R, R′, S, or S′ amplitude is taken at this point.

network on the left side is being entered. This produces the **second QRST change typical of LBBB**, that is a slurred notch develops at about 50 ms into the QRS, best seen in anterior leads V1, V2, and Z and in left leads I, V5, V6 and *X*. Activation progresses outward in the septum enlarging the hole in a ring of active surface of about the same surface area directed from anterior to posterior in the remaining basal, superior, inferior and apical septum. A review of the LBBB activation in Fig. 16.39 with special attention to the 50–80 ms isochrones in the lower left sagittal view will account for the ring of active fronts and their average direction that remain relatively unchanged for this period of time. This adds **the third change of typical LBBB**, namely, mid-QRS slowing of transcription to the notch just described, which is also seen in the same leads as the slurred notch. As the left Purkinje network in the midseptal region is entered, activation spreads rapidly out in the endocardium. At 60–90 ms from the QRS onset, fronts are developing in the subendocardium and mural myocardium of the superior and inferior walls and much of the apex, especially anteriorly. Besides the broad

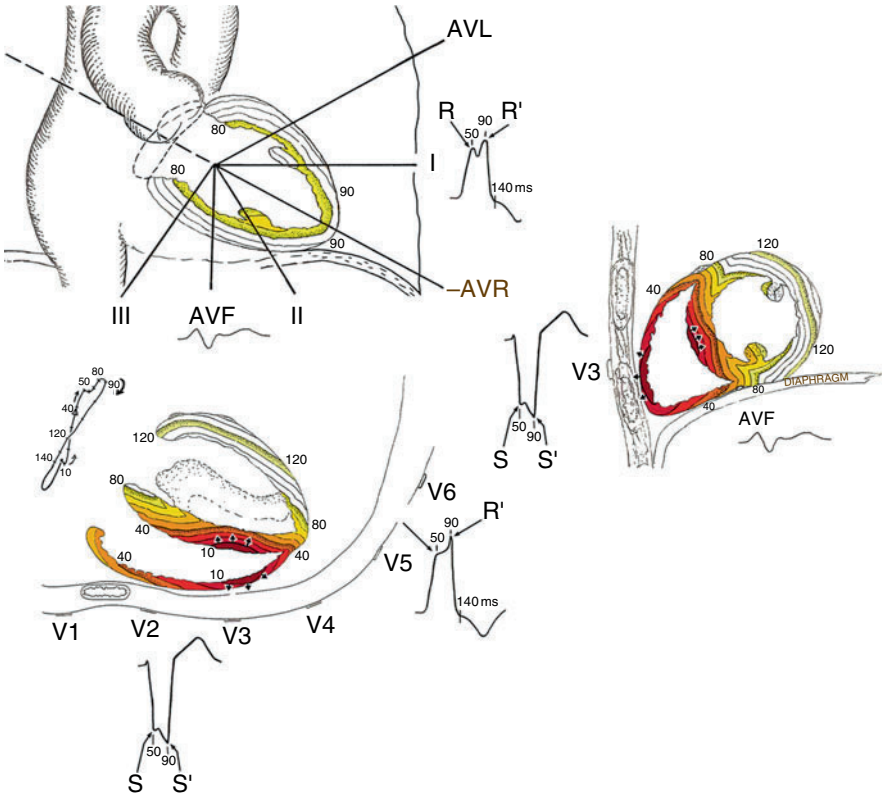

Figure 16.39

Activation sequences (10 ms isochrones) for LBBB in horizontal, frontal and left sagittal planes with QRS changes of a healed myocardial infarct in any local perfusion bed of the three major coronary arteries and their branches. See Figs. 16.38 and 16.40 for details of the how the typical LBBB QRS complexes shown in this figure are changed of infarction involving infarction in the local regions supplied by the 3 main coronary arteries or thneir branches.

fronts propagating in the left ventricle, the only unopposed front at this time is that developing leftward in the apex. This produces a shift leftward in the QRS vector, reaching a peak at about 100 ms, as apical LV breakthrough of activation fronts occurs. This produces the **fourth change typical of complete LBBB**, namely, a second peak in the QRS amplitude, usually higher than the first and following the mid-QRS slowing and notch just described. This change too is best seen in anterior and leftward leads. As this peak is receding, the activation fronts that have been developing on the posterolateral wall are also beginning to decrease in size. The prolated ellipsoid shape of the LV and the smaller diameter of the LV at the mitral valve and adjacent basal segments accounts for the following. Posteriorly directed fronts in the most basal portions of the superior, inferior walls meet and merge on the most basal part of the posterolateral free wall prior to the posterior and leftward directed fronts in the apical and middle posterolateral segments. This produces the **fifth change typical of LBBB**; namely, clockwise inscription of the QRS loop in the horizontal plane. In an LV wall of normal thickness, this activation takes 40–50 ms for a total QRS duration of 140–150 ms (**the sixth classic feature of LBBB**). Since the propagation velocity in human myocardium is 3–4 mm/10 ms, any increase in septal or and posterolateral wall thickness will increase total QRS duration (i.e., for every 2 mm added to the septum and to the posterolateral wall (or 4 mm total), 10–13 ms is added to the total QRS duration).

In uncomplicated LBBB, the balance of superior and inferior wall vectors, where large wavefronts are present throughout much of the QRS, is such that the mean frontal-plane axis is at or near zero degrees with a very narrow frontal-plane

Left bundle branch block QRS MI size score criteria

LBBB QRS-Score

Lead	Criteria	Pts	Max pts
Anterosuperior wall*			
I	R/Q ≤ 1.5	1	1*
	R/S ≤ 1.5		
aVL	Q ≥ 50 ms	2	4*
	Q ≥ 40 ms	1	
	R/S ≤ 0.5	2	
	R/Q ≤ 0.5		
	R/S ≤ 1	1	
	R/Q ≤ 1		
Inferior wall			
II	Q ≥ 40 ms	2	3
	Q ≥ 30 ms	1	
	R/Q ≤ 0.5	1	
	R/S ≤ 0.5		
aVF	Q ≥ 50 ms	2	3
	Q ≥ 40 ms	1	
	R/Q ≤ 0.5	1	
	R/S ≤ 0.5		
Anteroseptal wall*			
V1	NCHINIT40	1	3**
	R ≥ 0.3 mV	2	
	R ≥ 30 ms		
	R ≥ 0.2 mV	1	
	R ≥ 20 ms		
V2	NCHINIT40	1	3**
	R ≥ 0.4 mV	2	
	R ≥ 30 ms		
	R ≥ 0.3 mV	1	
	R ≥ 20 ms		
Posterlateral wall			
V1	S/S' ≥ 2.0	3	3
	S/S' ≥ 1.5	2	
	S/S' ≥ 1.25	1	
V2	S/S' ≥ 2.5	3	3
	S/S' ≥ 2.0	2	
	S/S' ≥ 1.5	1	
Apical 4 segments			
I	any Q	1	2
	R ≤ 0.2 mV		
	R/Q ≤ 1	1	
	R/S ≤ 1		
V5	any Q	1	4
	R/R' ≥ 2	2	
	R/R' ≥ 1	1	
	R/S ≤ 2		
	R ≤ 0.5 mV	1	
V6	Q ≥ 20 ms	1	4
	R/R' ≥ 2	2	
	R/R' ≥ 1	1	
	R/S ≤ 2		
	R ≤ 0.6 mV	1	
Total Points _____			33

12 LV Segments

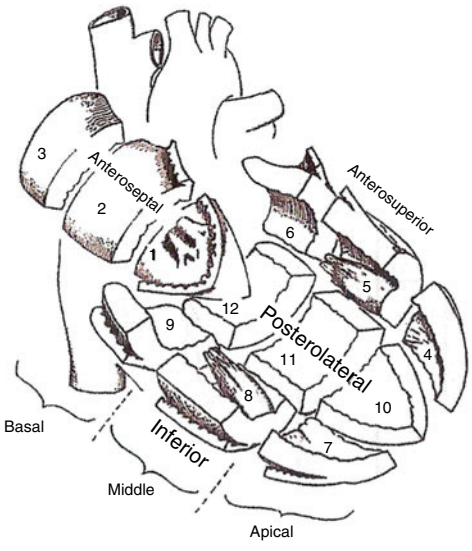

Short-axis View of Middle 4 Segments

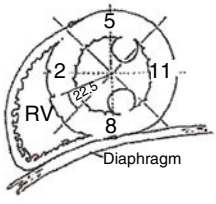

LBBB QRS Score Instructions

Age normalize all amplitude criteria to age 55 by increasing them 1%/yr age 20-54 and decreasing them 1%/yr for >55 yrs.
For females further decrease by 10% all QRSdur and QRSamp criteria.
Circle each QRS criteria.
If >1 criterion in bracket (box) met, select one with most points.

Criteria Definitions

NCHINIT40 = Notch in initial 40 ms
The definitions of S, S', R and R' are shown below.

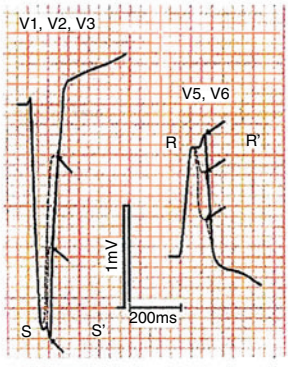

Additional Rules

* Exclude anteroseptal points if right atrial overload (suggesting RVH) is present (P positive amplitude in V1 or V2 P ≥ 0.1 mV or aVF P ≥ 0.175 mV).

** Exclude anterosuperior points if right axis deviation is present (mean QRS axis ≥90°).

Total QRS points _____ *3 = _____ % LV MI

Figure 16.40

projection of the loop. This **is the seventh QRST change typical of uncomplicated LBBB**. Any shift beyond ±20° represents disruption of this balance of vectors, either from missing myocardium or further disruption of the more distal Purkinje conduction. The latter is rare in recent onset LBBB in patients with coronary artery disease, but is common in the congestive cardiomyopathies where the myopathic autoimmune process also extensively involves the peripheral Purkinje

system. Marked left axis or right axis shifts have been reported as markers of the process. **The eighth classic change of LBBB** relates to repolarization, which is directly linked to the very abnormal depolarization. ST-T vectors in LBBB are directed opposite to those of QRS in all projections.

In summary, with respect to **superimposed myocardial infarction on LBBB**, the first 50 ms of ventricular depolarization is dominated by the septum and right ventricle (see Fig. 16.39); the middle 50 ms is dominated by the paraseptal areas of the left ventricle adjacent to the septum, namely, the anterosuperior, anteroapical and inferior walls; and the last 50 ms is made up of activation fronts in the posterolateral wall of the left ventricle. It follows that **anterior infarction** will result in loss of initial posteriorly directed anteroseptal vectors unmasking the early anterior RV forces with the resultant increase in initial anterior vector magnitude and duration. There will also be a significant increase in high-frequency notching and slurring in the initial QRS as the activation fronts encounter the patchy interdigitation of scar and normal myocardium at the border of the infarct. **Anterosuperior extension** of the anterior infarct will deform the early to mid-QRS vectors inferiorly with a mean axis shift inferiorly. Significant **anteroapical extension** of the anterior infarct will result in a loss of leftward vectors and a loss of the second peak of R in I, V5, V6, and *X* with a shift of the mean axis to being almost directly posterior (and/or rightward and inferior if major anterosuperior extension is also present). Details of the QRS MI size score to reflect these changes due to infarct and to quantify infarct size are presented in Sect. 16.5.5. **Inferior infarction** from posterior-inferior descending artery (PDA) occlusion, usually as the result of RCA occlusion, results in loss of inferior vectors in the early to mid-QRS and significant displacement of these vectors superiorly from their usual location, as seen in typical LBBB. **Posterolateral infarct** from occlusion of a non-dominant LCX, results in an attenuation of the late posterior vectors and a shift of the mid to terminal QRS anterior vectors. **Posterolateral-inferior infarct** from a left dominant LCX, or a rare very dominant RCA occlusion with a large distal posterolateral branch and a diminutive LCX, has a simple combination effect on the QRS of inferior and posterolateral infarct just described. These changes are defined more explicitly for each of the three major coronary distributions in Appendix B, Fig. 16.39, and in the three sub-sections of the Sect. 16.5.5 to follow.

16.5.5.3 LAD Occlusion, Anterior Infarction and LBBB

Figure 16.41a, b is an example of a patient who at the time of angiography had two areas of infarction: a large anterior infarct with inferoapical extension from proximal LAD coronary occlusion and a second moderate-sized inferior infarct from RCA occlusion. The ECG/VCG shows changes of atypical LBBB with a QRS duration of 197 ms. In this case, the P vectors seen to the right of the VCG plots show significant abnormalities. The P duration is increased to 133 ms. The initial right atrial vectors are mildly increased in amplitude above normal anterior and inferior component limits, indicative of mildly decreased RV diastolic compliance consistent with mild RV and pulmonary hypertension. The left atrial activation times are significantly increased and voltage amplitude directed leftward and posteriorly is greatly increased (3–4 times normal), which is consistent with a major decrease in diastolic compliance in the left ventricle such as might be seen with severe LV dysfunction from extensive infarction and compensatory hypertrophy.

In the uncomplicated LBBB, all of the QRS except for the first 10–15 ms is directed leftward and posteriorly owing to the posteriorly directed fronts in the septum and the left ventricle. In this case, infarction in the anteroseptal area and apex has two effects. First, notching and slurring is seen especially in V4, V5 and V6 in the initial 50–60 ms, which in uncomplicated LBBB is usually smoothly written. Second, there is increased amplitude and duration of the initial anterior forces or vectors owing to infarction in the septum which allows the anteriorly directed fronts in the right ventricle to dominate. In this case, the first 30 ms are smoothly written with an increased anterior amplitude. This suggests, along with the mild RAO changes, that mild RVH might be responsible for some of this change. Typically, significant septal involvement would produce a broad slurred and notched R wave in V1 and V2 and a prominent, prolonged, irregular initial anterior vector loop in the VCG, in addition to the other features of LBBB. The magnitude and duration of the anterior vectors is related to the size or extent of septal involvement.

The LV apex is extensively infarcted in this patient as it often is in anterior infarcts. There is a significant loss of leftward vectors from 60 to 100 ms when the apex is expected to be activated. This is the usual marker of the presence of

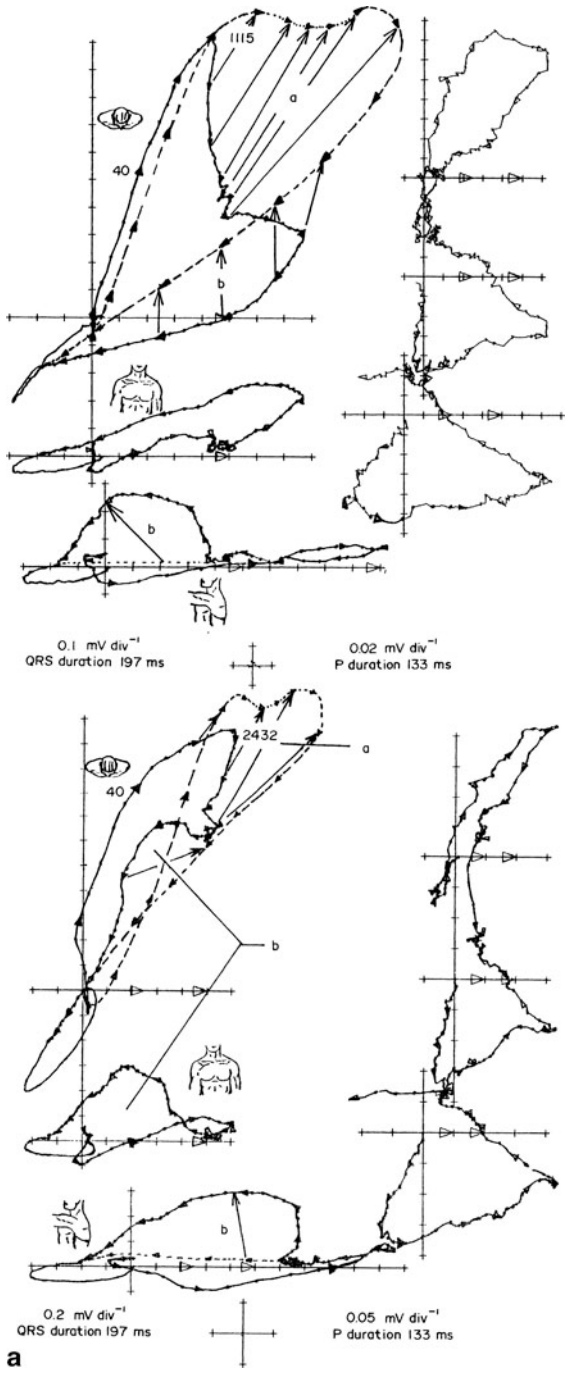

Figure 16.41 **(Continued)**

apical extension of this infarct in LBBB. Again, the more extensive the apical involvement, the greater the loss of expected leftward vectors and the longer this deformity lasts. The anterosuperior wall also demonstrates significant involvement. This produces a loss of early superior vectors with a consequent inferior shift of the initial QRS. The two VCGs for this first infarct (see Fig. 16.41a for details) showed major deformities in the early and mid QRS that when transferred to

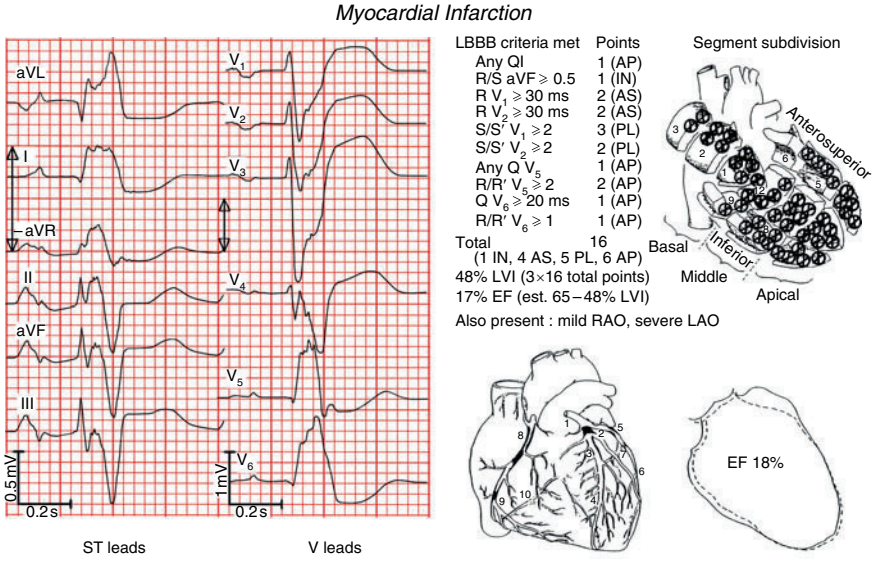

Figure 16.41

(a) The Cube VCG (*top*) and the McFee (*bottom*) are from a 59-year-old man who had a history of two myocardial infarcts. After the first infarct the ECG and VCG demonstrated a large anterior infarct and normal conduction. Coronary angiograms and biplane Vgrams revealed major 3 vessel disease, 100% LAD, and a large anterior infarct. The patient declined surgery and was symptomatically well controlled on medical management. Three years later he suffered a second infarct and had the VCGs shown here. A second angiogram demonstrated 100% RCA occlusion in the interim and a moderate sized inferior infarct. These VCGs demonstrate a very atypical LBBB with QRS duration of 197 ms. VCGs for typical LBBBs of 197 ms duration are shown in *dotted lines*. The specific changes are discussed in the text in the sections on LAD occlusion, anterior infarct, and LBBB and on RCA occlusion, inferior infarct and LBBB. Infarct #1, shows major deformities (a) of the initial 2/3rds of the QRS in both lead systems, i.e., 0.7 mV/100 ms for the Cube and 1.1 mV/100 ms for the McFee. From the nomogram (Fig. 16.12) a large anteroapical infarct is estimated for both VCGs of 12 cm and 40% involvement of the LV perimeter. Infarct #2 produced deformities (b) in the latter 1/3 of the QRS of 0.3 mV/50 ms and 0.5 mV/50 ms. When transferred to the nomogram (Fig. 16.12) resulted in an estimate for the inferior posterolateral infarct of 6 cm for each VCG and 20% LV involvement angiographically. The sum of 60% of the LV perimeter predicts an LVEF of 18%. (b) Note limb leads are in the orderly (Cabrera) sequence from the *top down*, aVL, I, -aVR, II, aVF, III. Using the version of the LBBB QRS MI size scoring system shown in Appendix B, a total of 16 points or 48% LV infarct is accumulated. As seen in the *upper middle panel* above, this predicted a 17% EF, and distributed the damage into the anterior (septal/superior), apex, inferior, and posterolateral walls as shown. These criteria picked up the anterosuperior and inferior wall involvement seen on the angiogram, and predicted well by the VCGs as shown in (a). A left anterior oblique ventriculogam was not available to evaluate the posterolateral changes predicted by this version of the LBBB QRS MI size scoring system.

the nomogram (Fig. 16.12) estimated a large anterior infarct of 12 cm and 45% of the LV perimeter. For the second infarct, there is displacement of the terminal 80 ms vectors sharply superiorly and anteriorly from their usual location with LBBB. This is most evident on the Cube lead system and on the 12 lead ECG as prominent S′ in the inferior leads, an abnormal left axis and a broad slurred S" V1–V3. These findings are indicative of a moderately sized basal posterolateral-inferior infarct in addition to the large anterior one described above (see Fig. 16.41a, b and legends for details). When the magnitude and duration of the VCG changes of both infarcts are transferred to the nomogram, 65% of the perimeter of the LV on the RAO ventriculogram is predicted be involved with infarction and the ejection fraction is predicted to be 14%.

Losses from the septum, apex and superior wall each contribute to the total sum of the criteria for the QRS MI size score for anterior infarct size in LBBB seen here in Fig. 16.41b and tabulated from Appendix B. A total of 9 points (27% LV) for anteroapical infarction and 7 points (21% LV) for a posterolateral-inferior infarct were scored. The total is 16 points for 48% LV infarcted and an estimated LV ejection fraction of 17%. Appendix B.

16.5.5.4 Differential Diagnosis of LBBB and Prominent Anterior Forces

Left ventricular hypertrophy is often associated with superior fascicular block, and can have a total QRS duration of greater than 140–160 ms. If the fascicular block is associated with or is the result of a moderate anterior apical infarct, as it often is, it may produce a QRS morphology (large notched RR′ V4, V5, V6) quite suggestive of complete LBBB as are small R waves in V1, V2 and Z. A second moderate posterolateral infarct would produce a prominent wide R wave in V1, V2 mimicking a LBBB + anteroseptal infarct. Wide separation of frontal plane (limb leads) initial and terminal 30 ms vectors, as described by Grant and Dodge [91], effectively identifies this combination of changes. The associated infarcts are usually large, and the ECG QRS score and the nomogram for VCG infarct size will give reliable estimates of angiographic regional wall motion abnormalities and global function.

A second major change that mimics some of the changes described above for LBBB and anterior infarct is RVH in the presence of complete LBBB. The increase of anterior, rightward and inferior vectors for the first 70–80 ms from RVH produces a shift in the LBBB vectors. This results in sharp, smooth, and widened initial anterior vectors with increased amplitude in leads V1, V2, and Z similar to those described above for anterior infarct. It also displaces the 20–80 ms vectors to the right and inferiorly. This decreases the initial leftward vector in I, aVL, V5, V6 and *X*. As a result, in some cases Q waves are produced in these leads, again mimicking anterior infarction with apical and superior wall extension. There are two major features that can be used in the differential diagnosis of these changes. First, in right-sided overload, the degree of RAO parallels the degree of RV overload. When even mild to moderate RAO is present, by the criteria described in Table 16.2, the likelihood increases greatly that the changes described above are in fact caused by RV overload. The second feature that serves as a marker of RV overload in this situation is the presence of a sharp, smooth abnormal initial anterior vector loop of 0.3 mV or more, lasting 20 ms or longer. The magnitude and duration of this deformity, as well as the severity of the RAO, is related to the degree of RV overload. In summary, the presence of RAO and the absence of notching in the initial vectors reasonably exclude anterior infarction as a cause for the changes described above.

Significant confounding can occur with LBBB owing to coronary disease which is associated with extensive infarction, primary or secondary LV overload, left-heart failure, and severe LAO. Significant right-heart failure, RAO and RV overload are then the secondary results which can produce additive effects in the presence of anterior infarct as far as increased amplitude and duration of initial anterior QRS vectors are concerned. However, even so, the information exists in the ECG/VCG, as it did in the case presented in Fig. 16.41 to provide a reasonable basis for unscrambling each of these effects and in most cases assessing the relative contribution of each to the final ECG/VCG changes observed.

16.5.5.5 Circumflex Coronary Occlusion, Posterolateral Infarction and LBBB

Only in the presence of a dominant circumflex coronary artery would the blood supply to the proximal left bundle be influenced by total occlusion of this vessel. This anatomy occurs in 10–15% of all human hearts. Since a significant percentage of recent onset LBBBs are as a result of inferior infarction, theoretically 8–10% of these (1% of the total) are the result of total circumflex occlusion. These infarcts could be expected to produce a combination of inferior and posterolateral effects as described above. No such combination was identified in the authors' database of single-vessel circumflex occlusions, but an example of such changes is presented in the case shown in Fig. 16.41. This patient with RCA occlusion appeared to have significant posterolateral extension of the inferior infarct. Appendix B.

16.5.5.6 RCA Occlusion, Inferior Infarct and LBBB

Figure 16.41, discussed earlier, shows an example of a patient who had LBBB and a moderate inferior-posterolateral infarct from total RCA occlusion in addition to a large anterior infarct and total LAD occlusion. The activation of the base of the septum and the base of the inferior and posterolateral walls are separated in time in LBBB from the apical and midseptum. Therefore much of the area perfused by the RCA is activated after that perfused by the LAD, and separate QRS deformities can be identified for each as shown in the figure. In this case, the late deformity, superior and anterior to that seen in typical LBBB, results from local losses, inferiorly and posteriorly. The uncoupling in time of the activation of septal and free wall fronts in LBBB has produced less cancellation and more reliable estimates of multiple infarct size in the presence of this conduction abnormality than in normal conduction.

16.6 Future Advances in ECG Diagnosis and Imaging of Infarction

There are two areas in the ECG/VCG diagnosis of infarction where as yet the possibilities have not been fully exploited: the very early quantification of area at risk in acute infarction and the quantification of infarct size and residual ischemic area at risk in the considerable number of patients with the complex mix of chamber enlargement, BBB and single or multiple infarcts in the various coronary distributions. It is likely that both management and prognosis in these patients will continue to be tightly bound to infarct size and the extent of ischemia or mass of myocardium at risk. The computer simulation of ventricular excitation and recovery is expected to be an important tool in the further clarification of these complex interactions involved in the manifold combinations of regional ischemia, infarction, chamber enlargement and conduction abnormalities (both minor and major).

From reported studies with the model of the authors [159–161], some aspects of which were detailed in this chapter, this exploration is expected to move into larger numbers of simultaneously recorded leads, probably 16–32 with at least two or three of these leads recorded on the back of the thorax. Small multilead ECG recording systems with onboard computer analysis of these 16–32 leads are well within the capability of twenty-first century technology. The computer model, clinical and cardiac MRI, and postmortem validation studies will be used to provide the optimal lead array, digitizing rates, location of these leads and criteria for quantifying regional acute ischemia and chronic infarct size in the presence of normal conduction, various conduction abnormalities, chamber enlargement and variations in torso geometry, conductivity, and heart or coronary anatomy.

With respect to acute coronary care, the future may see more optimal use of three simultaneous quasi-orthogonal monitoring leads with online identification and continuous monitoring of the area of myocardium at risk, including (a) its extent, (b) the size of the evolving infarct in the risk area, and (c) intermittent conduction change and ectopic activity related to the perfusion bed of the area at risk or at a distance. These would all involve straightforward extensions of existing knowledge. The rapid advances in miniaturization of electronic and computer chip components make it realistic to expect this quantitative capability to be resident in online computer monitoring systems, ambulance recorders and highly portable long-term ambulatory physiological monitoring devices.

Noninvasive ECG imaging with inverse isochrone and potential mapping of endocardium, and epicardium from a few centers has appeared [162]. Inverse imaging of the electromotive surface of the propagating wave of excitation using "smart" constraints of the solution is in process in a few centers as well. The three-dimensional color graphic imaging of the heart and infarct geometry for a specific patient, along with direct imaging of the wave of excitation of the atria and ventricles and the recovery process specific for that patient, are also direct extensions of these modeling efforts and automated signal processing and analysis technology. From this type of imaging, it is possible to visualize, directly, regional, and transmural extent of ischemia and infarction, wall thickness and details of local excitation and recovery. This would include delayed or fractionated excitation potentials and areas of slow conduction. Direct visualization of reentrant pathways and their anatomic substrate would also be a direct outgrowth of such developments. The compelling advantage of working first-hand with the heart's own ECG signal is that these noninvasive measurements can be repeated as often as needed with little or no discomfort or risk to the patient. Indeed, continuous monitoring of many ECG leads and algorithmic processing of the information requires only adaptation of existing technology and carefully controlled validation studies.

APPENDIXES

Suuplemental Data APPENDIX A: QRS-Score Criteria

Lead	RBBB Criteria	Pts	LAFB Criteria	Pts	LAFB + RBBB Criteria	Pts	LVH Criteria	Pts	No Confounders Criteria	Pts	Max Pts
I	Q ≥ 30 ms	1	Q ≥ 30 ms	1	Q ≥ 30 ms	1	Q ≥ 30 ms	1	Q ≥ 30 ms	1	
	R/Q ≤ 1	1	R/Q ≤ 1	1	R/Q ≤ 1	1	R/Q ≤ 1	1	R/Q ≤ 1	1	2
	R ≤ 0.2 mV		R ≤ 0.2 mV		R ≤ 0.2 mV		R ≤ 0.2 mV		R ≤ 0.2 mV		
II	Q ≥ 40 ms	2	Q ≥ 40 ms	2	Q ≥ 40 ms	2	Q ≥ 40 ms	2	Q ≥ 40 ms	2	2
	Q ≥ 30 ms	1	Q ≥ 30 ms	1	Q ≥ 30 ms	1	Q ≥ 30 ms	1	Q ≥ 30 ms	1	
aVL	Q ≥ 30 ms	1	Q ≥ 40 ms	1	Q ≥ 40 ms	1	Q ≥ 40 ms	1	Q ≥ 30 ms	1	2
	R/Q ≤ 1	1	R/Q ≤ 1	1	R/Q ≤ 1	1	R/Q ≤ 1	1	R/Q ≤ 1	1	
aVF	Q ≥ 50 ms	3	Q ≥ 50 ms	3	Q ≥ 50 ms	3	Q ≥ 60 ms	3	Q ≥ 50 ms	3	
	Q ≥ 40 ms	2	Q ≥ 40 ms	2	Q ≥ 40 ms	2	Q ≥ 50 ms	2	Q ≥ 40 ms	2	
	Q ≥ 30 ms	1	Q ≥ 30 ms	1	Q ≥ 30 ms	1	Q ≥ 40 ms	1	Q ≥ 30 ms	1	5
	R/Q ≤ 1	2	R/Q ≤ 1	2	R/Q ≤ 1	2	R/Q ≤ 1	2	R/Q ≤ 1	2	
	R/Q ≤ 2	1	R/Q ≤ 2	1	R/Q ≤ 2	1	R/Q ≤ 2	1	R/Q ≤ 2	1	
V1	Q ≥ 50 ms	2			Q ≥ 50 ms	2	any QR				(2)
Ant.	any Q	1	any QR	1	any Q	1	(or QS if *)	1	any Q	1	1
	R ≤ 20 ms						.04S notch				
V1			R/S ≥ 1	1		1	R/S ≥ 1	1	R/S ≥ 1	1	
Post.	Init R ≥ 60 ms	2	Init R ≥ 50 ms	2	Init R ≥ 60 ms	2	Init R ≥ 50 ms	2	Init R ≥ 50 ms	2	
	Init R ≥ 1.5 mV		Init R ≥ 1 mV		Init R ≥ 1.5 mV		Init R ≥ 1 mV		Init R ≥ 1 mV		4
Exclude if :	Init R ≥ 50 ms	1	Init R ≥ 40 ms	1	Init R ≥ 50 ms	1	Init R ≥ 40 ms	1	Init R ≥ 40 ms	1	
	Init R ≥ 1.0 mV		Init R ≥ 0.7 mV		Init R ≥ 1.0 mV		Init R ≥ 0.7 mV		Init R ≥ 0.7 mV		
			Q&S ≤ 0.2 mV	1			Q&S ≤ 0.2 mV	1	Q&S ≤ 0.2 mV	1	
V2	Q ≥ 50 ms	2			Q ≥ 50 ms	2					(2)
Ant.	any Q	1	any QR	1	any Q	1	any QR	1	any Q	1	1
	R ≤ 10 ms		R ≤ 10 ms		R ≤ 10 ms		(or QS if *)		R ≤ 10 ms		
	R ≤ 0.1 mV		R ≤ 0.1 mV		R ≤ 0.1 mV		.04S notch		R ≤ 0.1 mV		
V2			R/S ≥ 1.5	1			R/S ≥ 1.5	1	R/S ≥ 1.5	1	
Post.	Init R ≥ 70 ms	2	R ≥ 60 ms	2	Init R ≥ 70 ms	2	R ≥ 60 ms	2	R ≥ 60 ms	2	
	Init R ≥ 2.5 mV		R ≥ 2 mV		Init R ≥ 2.5 mV		R ≥ 2 mV		R ≥ 2 mV		4
Exclude if :	Init R ≥ 50 ms	1	R ≥ 50 ms	1	Init R ≥ 50 ms	1	R ≥ 50 ms	1	R ≥ 50 ms	1	
	Init R ≥ 2.0 mV		R ≥ 1.5 mV		Init R ≥ 2.0 mV		R ≥ 1.5 mV		R ≥ 1.5 mV		
			Q&S ≤ 0.3 mV	1		1	Q&S ≤ 0.3 mV	1	Q&S ≤ 0.3 mV	1	
V3	Q ≥ 30 ms	2	Q ≥ 30 ms	2	Q ≥ 30 ms	2	QR+Q ≥ 30 ms	2	Q ≥ 30 ms	2	
	R ≤ 10 ms		R ≤ 10 ms		R ≤ 10 ms		.04S notch		R ≤ 10 ms		2
	Q ≥ 20 ms	1	Q ≥ 20 ms	1	Q ≥ 20 ms	1	any QR	1	Q ≥ 20 ms	1	
	R ≤ 20 ms		R ≤ 20 ms		R ≤ 20 ms		(or QS if *)		R ≤ 20 ms		
V4	Q ≥ 20 ms	1	Q ≥ 20 ms	1	Q ≥ 20 ms	1	Q ≥ 20 ms	1	Q ≥ 20 ms	1	
	R/Q ≤ 0.5	2	R/Q ≤ 0.5	2	R/Q ≤ 0.5	2	R/Q ≤ 0.5	2	R/Q ≤ 0.5	2	
	R/S ≤ 0.5		R/S ≤ 0.5		R/S ≤ 0.5		R/S ≤ 0.5		R/S ≤ 0.5		
	R/Q ≤ 1	1	R/Q ≤ 1	1	R/Q ≤ 1	1	R/Q ≤ 1	1	R/Q ≤ 1	1	3
	R/S ≤ 1		R/S ≤ 1		R/S ≤ 1		R/S ≤ 1		R/S ≤ 1		
	R ≤ 0.5 mV		R ≤ 0.5 mV		R ≤ 0.5 mV		R ≤ 0.5 mV		R ≤ 0.5 mV		
	.04R notch		.04R notch		.04R notch		.04R notch		.04R notch		
V5	Q ≥ 30 ms	1	Q ≥ 30 ms	1	Q ≥ 30 ms	1	Q ≥ 30 ms	1	Q ≥ 30 ms	1	
	R/Q ≤ 1	2	R/Q ≤ 1	2	R/Q ≤ 1	2	R/Q ≤ 1	2	R/Q ≤ 1	2	
	R/S ≤ 1		R/S ≤ 1		R/S ≤ 1		R/S ≤ 1		R/S ≤ 1		
	R/Q ≤ 2	1	R/Q ≤ 2	1	R/Q ≤ 2	1	R/Q ≤ 2	1	R/Q ≤ 2	1	3
	R/S ≤ 2		R/S ≤ 1.5		R/S ≤ 1.5		R/S ≤ 2		R/S ≤ 2		
	R ≤ 0.6 mV		R ≤ 0.6 mV		R ≤ 0.6 mV		R ≤ 0.6 mV		R ≤ 0.6 mV		
	.04R notch		.04R notch		.04R notch		.04R notch		.04R notch		
V6	Q ≥ 30 ms	1	Q ≥ 30 ms	1	Q ≥ 30 ms	1	Q ≥ 30 ms	1	Q ≥ 30 ms	1	
	R/Q ≤ 1	2	R/Q ≤ 1	2	R/Q ≤ 1	2	R/Q ≤ 1	2	R/Q ≤ 1	2	
	R/S ≤ 1		R/S ≤ 1		R/S ≤ 1		R/S ≤ 1		R/S ≤ 1		
	R/Q ≤ 3	1	R/Q ≤ 3	1	R/Q ≤ 3	1	R/Q ≤ 3	1	R/Q ≤ 3	1	3
	R/S ≤ 3		R/S ≤ 2		R/S ≤ 2		R/S ≤ 3		R/S ≤ 3		
	R ≤ 0.6 mV		R ≤ 0.6 mV		R ≤ 0.6 mV		R ≤ 0.6 mV		R ≤ 0.6 mV		
	.04R notch		.04R notch		.04R notch		.04R notch		.04R notch		
Total	Points		Points		Points		Points		Points		32

For each QRS-score point scored to the left, circle the numbers to the right in the same row which shows the %LV scar in each of the 12 LV segments.

% LV Scar in 12 LV Segments

Ant-Sep 1	2	3	Ant-Sup 4	5	6	Inf 7	8	9	Postlat 10	11	12
			1	1					1		
			1	1	1						
						2	2	2			
							2	1			
			2	1							
			1	2							
						3	2	2			
						2	2	2			
							2	1			
							1	3			
							1	2			
2	2	2									
	1	2									
									1	1	1
					1	1	1		1	1	1
						1			1	1	
								1		1	1
2	2	2									
	1	2									
								1		1	1
						1	1		1	2	1
								1	1	1	
								1		1	1
2	2	1		1							
1	1			1							
1	1		1								
2	1		1	1		1					
1	1		1								
1	1		1								
2	1		1	1		1					
1			1	1							
			1			1			2		
						1			2	2	
						1			1	1	

For each 1% scar place an X in corresponding LV segment to right to show scar location

QRS Score Instructions

1. Select column with appropriate conduction (tan highlights show differences in criteria between conduction types).
2. Age normalize all amplitude criteria to age 55 by increasing them 1%/yr age 20-54 and decreasing them 1%/yr for >55 yrs.
3. For females further decrease by 10% all QRSdur and QRSamp criteria.
4. Circle each QRS criteria met; if >1 criterion in a box met, select one with most points.

Waveform Definitions

Init R = Initial R

.04R notch = notch in initial 40 ms

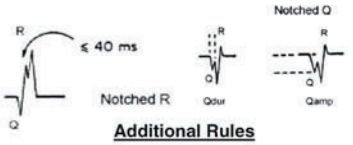

Additional Rules

*(for LVH) if ≥ 4 anterior/apical QRS points present (other than QS), then count QS in V1-V3.

**(for posterolateral criteria) exclude if right atrial overload present (suggesting RVH) if P positive amplitude in V1 or V2 P≥0.1 mV or aVF P≥0.175 mV.

12 LV Segments

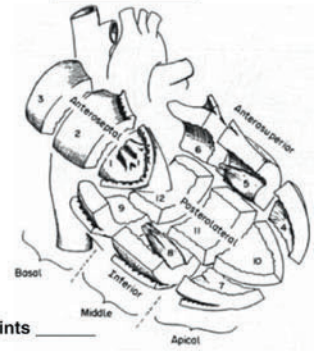

Total QRS points _____

***3 =** _____ **% LV scar**

References

1. Hurst, J.W., Current status of clinical electrocardiography with suggestions for the improvement of the interpretive process. *Am. J. Cardiol.*, 2003;**92**: 1072–1079.
2. Foundation, T.N., The Nobel Prize in Physiology or Medicine 1963. 2007 [cited January 7, 2008]; Available from: http://nobelprize.org/nobel_prizes/medicine/laureates/1963/.
3. Overton, E., The general muscle- and nerve physiology – Second Notice – The indispensability of natrium (or lithium) ions for muscle contraction. *Arch. Ges. Physiol.*, 1902; **92**: 346.
4. Smith, F.M., The ligation of coronary arteries with electrocardiographic study. *Arch. Int. Med.*, 1918;**22**: 8–27.
5. Pardee, H.E.B., An electrocardiographic sign of coronary artery obstruction. *Arch. Int. Med.*, 1920;**26**: 244–257.
6. Otto, H.L., The ventricular electrocardiogram. An experimental study. *Arch. Int. Med.*, 1929;**43**: 335–350.
7. Barnes, A.R., Study of the R-T interval in myocardial infarction. *Am. Heart J.*, 1929;**5**: 142–171.
8. Wilson, R.N., A.G. MacLeod, and P.S. Barker, The distribution of action and injury displayed by heart muscle and other excitable tissues. *Scientific Series*, vol. X. Ann Arbor, MI: University of Michigan Press, 1933.
9. Wilson, F.N, F.D. Johnston, A.G. MacLeod, et al., Electrocardiograms that represent the potential variations of a single electrode. *Am. Heart J.*, 1933;**9**: 447–471.
10. Wilson, F.N., F.D. Johnston, F.F. Rosenbaum, et al., Einthoven's triangle, the theory of unipolar electrocardiographic leads, and the interpretation of the precordial electrocardiograms. *Am. Heart J.*, 1946;**32**: 277–310.
11. Braunwald, E. and P.R. Maroko, The reduction of infarct size – an idea whose time (for testing) has come. *Circulation*, 1974;**50**: 206–209.
12. Holland, R.P. and H. Brooks, Precordial and epicardial surface potentials during Myocardial ischemia in the pig. A theoretical and experimental analysis of the TQ and ST segments. *Circ. Res.*, 1975;**37**: 471–480.
13. Holland, R.P., H. Brooks, and B. Lidl, Spatial and nonspatial influences on the TG-ST segment deflection of ischemia. Theoretical and experimental analysis in the pig. *J. Clin. Invest.*, 1977;**60**: 197–214.
14. Braunwald, E. and P.R. Maroko, ST-segment mapping. Realistic and unrealistic expectations. *Circulation*, 1976;**54**: 529–532.
15. Janse, M.J., ST segment mapping and infarct size. *Cardiovasc. Res.*, 2000;**45**: 190–193.
16. Grant, R.P. and H.T. Dodge, Mechanisms of QRS complex prolongation in man; left ventricular conduction disturbances. *Am. J. Med.*, 1956;**20**: 834–852.
17. Wagner, G.S., M.J. Cowan, N.C. Flowers, L.E. Ginzton, R.E. Ideker, M.M. Laks, R.H. Selvester, and S.R. Swiryn, Nomenclature of myocardial wall segments. Committee report. Computerized Interpretation of the ECG VIII. *Proceedings of the Engineering Foundation Conference*, vol. 222, R.H. Selvester, Editor. New York, 1983.
18. Ideker, R.E., G.S. Wagner, W.K. Ruth, et al., Evaluation of a QRS scoring system for estimating myocardial infarct size. II. Correlation with quantitative anatomic findings for anterior infarcts. *Am. J. Cardiol.*, 1982;**49**: 1604–1614.
19. Horan, L.G., N.C. Flowers, and J.C. Johnson, Significance of the diagnostic Q wave of myocardial infarction. *Circulation*, 1971;**43**: 428–436.
20. Henry, W.L., A. DeMaria, H. Feigenbaum, R. Kerber, N. Nanda, R.L. Popp, D. Sahn, N.B. Schiller, A.I. Tajik, and A.E. Weyman, Identification of myocardial wall segments: Report of the ASE Committee on Nomenclature and Standards, Raleigh, NC: American Society of Echocardiography, 1982.
21. Zinn, W.J. and R.S. Cosby, Myocardial infarction; a re-evaluation of the diagnostic accuracy of the electrocardiogram. *Am. J. Med.*, 1950;**8**: 177–179.
22. Johnson, W.J., R.W. Anchor, H.B. Burchell, and J.E. Edwards, Unrecognized myocardial infarction; a clinicopathologic study. *AMA Arch. Intern. Med.*, 1959;**103**: 253–261.
23. Woods, J.D., W. Laurie, and W.G. Smith, The reliability of the electrocardiogram in myocardial infarction. *Lancet*, 1963;**2**: 265–269.
24. Anderson, J.L., Chair Writing Committee, ACC/AHA 2007 guidelines for the management of patients with Unstable Angina/Non-ST-Elevation myocardial infarction. A report of the American College of Cardiology/American Heart Association task force on practice guidelines (Writing Committee to revise the 2002 guidelines for managing UA/NonSTEMI). *JACC*, 2007;**50**(No 7): e1–157.
25. Selvester, R.H., Nomina anatomica contradicta. Especially as relates to the heart and electrocardiology. *J. Electrocardiol*, 1992;**25**: 157–162.
26. Reimer, K.A. and R.B. Jennings, The "wavefront phenomenon" of myocardial ischemic cell death. II. Transmural progression of necrosis within the framework of ischemic bed size (myocardium at risk) and collateral flow. *Lab. Invest*, 1979;**40**: 633–644.
27. Christian, T.F., R.S. Schwartz, and R.J. Gibbons, Determinants of infarct size in reperfusion therapy for acute myocardial infarction. *Circulation*, 1992;**86**: 81–90.
28. Reimer, K.A., J.E. Lowe, and M.M. Rasmussen, The wavefront phenomenon of ischemic cell death. 1. Myocardial infarct size vs. duration of coronary occlusion in dogs. *Circulation*, 1977;**56**: 786–794.
29. Selvester, R.H. and M.E. Sanmarco, Infarct size in hi-gain, hi-fidelity VCGs and serial ventriculograms in patients with proven coronary artery disease, in *Modern Electrocardiology*, Z. Antaloczy, Editor. Amsterdam: Exerpta Medica, 1978, pp. 523–528.
30. Wagner, G.S., C.J. Freye, S.T. Palmeri, S.F. Roark, N.C. Stack, R.E. Ideker, F.E. Harrell Jr., and R.H. Selvester, Evaluation of a QRS scoring system for estimating myocardial infarct size. I. Specificity and observer agreement. *Circulation*, 1982;**65**: 342–347.
31. Palmeri, S.T., D.G. Harrison, F.R. Cobb, K.G. Morris, F.E. Harrell, R.E. Ideker, and R.H. Selvester, A QRS scoring system for assessing left ventricular function after myocardial infarction. *N. Engl. J. Med.*, 1982;**306**: 4–9.
32. Roark, S.F., R.E. Ideker, G.S. Wagner, D.R. Alonso, S.P. Bishop, C.M. Bloor, D.A. Bramlet, J.E. Edwards, J.T. Fallon, G.J. Gottlieb, D.B. Hackel, H.R. Phillips, K.A. Reimer, W.J. Rogers, W.K. Ruth, R.M. Savage, R.D. White, and R.H. Selvester, Evaluation of a QRS scoring system for estimating myocardial infarct size.

III. Correlation with quantitative anatomic findings for inferior infarcts. *Am. J. Cardiol.*, 1983;**51**: 382–389.
33. Ward, R.M., R.D. White, R.E. Ideker, et al., Evaluation of a QRS scoring system for estimating myocardial infarct size. IV. Correlation with quantitative anatomic findings for posterolateral infarcts. *Am. J. Cardiol.*, 1984;**53**: 706–714.
34. Ideker, R.E., G.S. Wagner, and R.H. Selvester, Anatomic validation of computer model ECG criteria for infarct size and location, in *Computeized Interpretation of ECG VII, Proceedings of the Engineering Foundation Conference*, M.M. Laks, Editor. New York: Engineering Foundation, 1982, pp. 147–152.
35. Daniel, T.M., J.P. Boineau, and D.C. Sabiston Jr., Comparison of human ventricular activation with a canine model in chronic myocardial infarction. *Circulation*, 1971;**44**: 74–89.
36. Cox, J.L., T.M. Daniel, and J.P. Boineau, The electrophysiologic time-course of acute myocardial ischemia and the effects of early coronary artery reperfusion. *Circulation*, 1973;**48**: 971–983.
37. Lie, K.I., H.J. Wellens, and R.M. Schuilenburg, Bundle branch block and acute myocardial infarction, in *The Conduction System of the Heart: Structure, Function, and Clinical Applications*, H.J. Wellens, K.I. Lie, and M.J. Janse, Editors. Philadelphia, PA: Lea and Febiger, 1976, p. 666.
38. Mullins, C.B. and J.M. Atkins, Prognoses and management of venticular conduction blocks in acute myocardial infarction. *Mod. Concepts Cardiovasc. Dis.*, 1976;**45**: 129–133.
39. Marriott, H.J. and P. Hogan, Hemiblock in acute myocardial infarction. *Chest*, 1970;58: 342–344.
40. Rosenbaum, M.B., The hemiblocks: diagnostic criteria and clinical significance. *Mod. Concepts Cardiovasc. Dis.*, 1970;**39**: 141–146.
41. Grant, R.P., *ClinicalElectrocardiography, the Spatial Vector Approach*, New York: McGraw-Hill, 1957.
42. Durrer, D., R.T. Van Dam, F.L. Meijler, R.C. Arzbaecher, E.J. Muller, and G.E. Freud, Electrical activation and membrane action potentials of the perfused normal human heart. *Circulation*, 1966;**34**: 412–422.
43. Durrer, D., R.T. van Dam, G.E. Frued, F.L. Meijler, and J.P. Roos, Excitation of the human heart, in *Electrical Activity of the Heart*, C.C. Thomas, Editor. Springfield: C.C. Thomas, 1969, p. 53.
44. Durrer, D., R.T. van Dam, G.E. Freud, M.J. Janse, F.L. Meijler, and R.C. Arzbaecher, Total excitation of the isolated human heart. *Circulation*, 1970;**41**: 899–912.
45. Selvester, R.H. and J.C. Solomon, Optimal ECG electrode sites and criteria for detection of asymptomatic coronary artery disease at rest and with exercise. *USAFSAM Technical Report*, 1984;**85–47**: 80–98.
46. Spach, M.S., R.C. Barr, C.F. Lanning, and P.C. Tucek, Origin of body surface QRS and T wave potentials from epicardial potential distributions in the intact chimpanzee. *Circulation*, 1977;**55**: 268–268. *of IEEE. Computer Society*, 1982, pp. 87–90.
47. Burgess, M.J., K. Millar, and J.A. Abildskov, Cancellation of electrocardiographic effects during ventricular recovery. *J. Electrocardiol.*, 1969;**2**: 101–107.
48. Burgess, M.J., K. Millar, and J.A. Abildskov, The geometry of ventricular repolarization boundaries. *Am. Heart J.*, 1970;**79**: 524–530.
49. Burgess, M.J., L.S. Green, K. Millar, R. Wyatt, and J.A. Abildskov, The sequence of normal ventricular recovery. *Am. Heart J.*, 1972;**84**: 660–669.
50. Abildskov, J.A., M.J. Burgess, K. Millar, R. Wyatt, and G. Baule, The primary T wave – a new electrocardiographic waveform. *Am. Heart J.*, 197;**81**: 242–249.
51. Abildskov, J.A., A.K. Evans, R.L. Lux, and M.J. Burgess, Ventricular recovery properties and QRST deflection area in cardiac electrograms. *Am. J. Physiol.*, 1980;**239**: H227–31.
52. Abildskov, J.A., L.S. Green, A.K. Evans, and R.L. Lux, The QRST deflection area of electrograms during global alterations of ventricular repolarization. *J. Electrocardiol.*, 1982;**15**: 103–107.
53. Spach, M.S. and R.C. Barr, Ventricular intramural and epicardial potential distributions during ventricular activation and repolarization in the intact dog. *Circ. Res.*, 1975;**37**: 243–257.
54. Selvester, R.H., R. Kalaba, C.R. Collier, R. Bellman, and H. Kagiwada, A digital computer model of the vectorcardiogram with distance and boundary effects: simulated myocardial infarction. *Am. Heart J.*, 1967;**74**: 792–808.
55. Selvester, R.H., J.C. Solomon, and T.L. Gillespie, Digital computer model of a total body electrocardiographic surface map. An adult male-torso simulation with lungs. *Circulation*, 1968;**38**: 684–690.
56. Solomon, J.C. and R.H. Selvester, Simulation of measured activation sequence in the human heart. *Am. Heart J.*, 1973;**85**: 518–524.
57. Selvester, R.H., J.C. Solomon, and D. Sapoznikov, Computer simulation of the electrocardiogram, in *Computer Techniques in Cardiology*, L.D. Cady, Editor. Washington, DC: Marcel Decker, Inc., 1979, pp. 417–453.
58. Selvester, R.H., M.E. Sanmarco, J.C. Solomon, and G.S. Wagner, Methods of determining infarct size, ECG: QRS change, in *Myocardial Infarction: Measurement and Intervention*, G.S. Wagner, Editor. Hague: Martinus Nijhoff, 1982, p. 23.
59. Wilson, F.N., A.G. Macleod, P.S. Barker, and F.D. Johnston, The determination and the significance of the areas of the ventricular deflections of the electrocardiogram. *Am. Heart J.*, 1934; **19**: 46.
60. Wilson, F.N., A.G. Macleod, and P.S. Barker, The potential variations produced by the heart beat at the apices of Einthoven's triangle. *Am. Heart J.*, 1931;**7**: 207–211.
61. Burger, H.C., A theoretical elucidation of the notion ventricular gradient. *Am. Heart J.*, 1957;**53**: 240–246.
62. Fruehan, C.T., B. Crain, M.J. Burgess, K. Millar, and J.A. Abildskov, Observations concerning the validity of the ventricular gradient concept. *Am. Heart J.*, 1969;**78**: 796–801.
63. Schafer, H., A. Pena, and P. Scholmerich, Der Monophasische Aktionsstrom von Spitze und Basis des Warmbluterherzens und die Theorie der T-Welle des EKG. *Pflugers Arch.*, 1943;**246**: 728–745.
64. Ling, G. and R.W. Gerard, The normal membrane potential of the frog Sartorius fibers. *J. Cell. Comp. Physiol.*, 1949;**34**: 383–395.
65. Hoffman, B.F. and E.E. Suckling, Relationship between cardiac cellular potentials and the deflections of the electrogram. *Am. J. Physiol.*, 1952;**171**: 737.
66. Hoffman, B.F., C.Y. Kao, and E.E. Suckling, Refractoriness in cardiac muscle. *Am. J. Physiol.*, 1957;**190**: 473–482.
67. Hoffman, B.F. and P.F. Cranefield, *Electrophysiology of the Heart*, New York: McGraw-Hill, 1960.
68. Brady, A.J. and J.W. Woodbury, Effects of sodium and potassium on repolarization in frog ventricular fibers, in *The Electrophysiology of the Heart*, H. Hecht, Editor. Ann. N.Y. Acad. Sci., 1957, p. 687.

69. Hoffman, B.F., P.F. Cranefield, E. Lepeschkin, B. Surawicz, and H.C. Herrlich, Comparison of cardiac monophasic action potentials recorded by intracellular and suction electrodes. *Am. J. Physiol.*, 1959;**196**: 1297–1301.
70. Autenrieth, G., B. Surawicz, and C.S. Kuo, Sequence of repolarization on the ventricular surface in the dog. *Am. Heart J.*, 1975;**89**: 463–469.
71. Scher, A.M. and A.C. Young, The pathway of ventricular depolarization in the dog. *Circ. Res.*, 1956;**4**: 461–469.
72. Scher, A.M. and A.C. Young, Ventricular depolarization and the genesis of QRS. *Ann. N.Y. Acad. Sci.*, 1957;**65**: 768–778.
73. Scher, A.M., A.C. Young, A.L. Malmgren, and R.R. Paton, Spread of electrical activity through the wall of the ventricle. *Circ. Res.*, 1953;**1**: 539–547.
74. Durrer, D. and L.H. Van Der Twell, Spread of activation in the left ventricular wall of the dog. I. *Am. Heart J.*, 1953;**46**: 683–691.
75. van Dam, R.Th. and D. Durrer, Experimental study on the intramural distribution of the excitability cycle and on the form of the epicardial T wave in the dog heart in situ. *Am. Heart J.*, 1961;**61**: 537–542.
76. Kootsey, J.M. and E.A. Johnson, The Origin of the T wave. *CRC Crit. Rev. Bioeng.*, 1980;**4**: 233–270.
77. Gussak, I. and C. Antzelevitch, Editors. *Cardiac Repolarization, Bridging Basic and Clinical Science*. Totowa, NJ: Humana Press, 2003.
78. Arnsdorf, M.F. and E.K. Louie, The ECG: spatial and non spatial determinants of the extracellularly recorded potential with emphasis on the TQ-ST segment, in *Myocardial Infarction, Measurement and Intervention*, G.S. Wagner, Editor. The Hague: Martinus Nijhoff, 1980, p. 51.
79. Janse, M.J., J. Cinca, H. Morena, J.W. Fiolet, A.G. Kleber, G.P. de Vries, A.E. Becker, and D. Durrer, The "border zone" in myocardial ischemia. An electrophysiological, metabolic, and histochemical correlation in the pig heart. *Circ. Res.*, 1979;**44**: 576–588.
80. Harken, A.H., C.H. Barlow, W.R. Harden, and B. Chance, Two and three dimensional display of myocardial ischemic "border zone" in dogs. *Am. J. Cardiol.*, 1978;**42**: 954–959.
81. Simson, M.B., W. Harden, C. Barlow, and A.H. Harken, Visualization of the distance between perfusion and anoxia along an ischemic border. *Circulation*, 1979;**60**: 1151–1155.
82. Cox, J.L., V.W. McLaughlin, N.C. Flowers, and L.G. Horan, The ischemic zone surrounding acute myocardial infarction. Its morphology as detected by dehydrogenase staining. *Am. Heart J.*, 1968;76: 650–659.
83. Harumi, K., M.J. Burgess, and J.A. Abildskov, A theoretic model of the T wave. *Circulation*, 1966;**34**: 657–668.
84. Thiry, P.S. and R.M. Rosenberg, On electrophysiological activity of the normal heart. *J. Franklin Inst.*, 1974;**297**: 377.
85. Miller, W.T. and D.B. Geselowitz, Simulation studies of the electrocardiogram. I. The normal heart. *Circ. Res.*, 1978;**43**: 301–315.
86. Miller, W.T. 3rd and D.B. Geselowitz, Simulation studies of the electrocardiogram. II. Ischemia and infarction. *Circ. Res.*, 1978;**43**: 315–323.
87. Selvester, R.H., J.C. Solomon, and G.D. Tolan, Fine grid computer simulation of QRS-T and criteria for the quantitation of regional ischemia. *J. Electrocardiol.*, 1987;**20**(Suppl. 1–8).
88. Maroko, P.R., P. Libby, J.W. Covell, B.E. Sobel, J. Ross Jr., and E. Braunwald, Precordial S-T segment elevation mapping: an atraumatic method for assessing alterations in the extent of myocardial ischemic injury. The effects of pharmacologic and hemodynamic interventions. *Am. J. Cardiol.*, 1972;**29**: 223–230.
89. Akiyama, T., M. Hodges, T.L. Biddle, B. Zawrotny, and C. Vangellow, Measurement of S-T segment elevation in acute myocardial infarction in man. Comparison of a precordial mapping technique and the Frank vector system. *Am. J. Cardiol.*, 1975;**36**: 155–162.
90. Wikswo, J.P. Jr., S.C. Gundersen, W. Murphy, A.K. Dawson, and R.F. Smith, Sequential QRS vector subtractions in acute myocardial infarction in humans. Time course and relationship to serial changes in serum CK-MB concentration. *Circ. Res.*, 1981;**49**: 1055–1062.
91. Sederholm, M., P. Grottum, L. erhardt, and J. Kjekshus, Quantitative assessment of myocardial ischemia and necrosis by continuous vectorcardiography and measurement of creatine kinase release in patients. *Circulation*, 1983;**68**: 1006–1012.
92. Aldrich, H.R., N.B. Wagner, J. Boswick, A.T. Corsa, M.G. Jones, P. Grande, K.L. Lee, and G.S. Wagner, Use of initial ST-segment deviation for prediction of final electrocardiographic size of acute myocardial infarcts. *Am. J. Cardiol.*, 1988;**61**: 749–753.
93. Friedman, H.H., *Diagnostic Electgrocardiography and Vectorcardiography*. San Francisco, CA: McGraw-Hill, 1971.
94. Benchimol, A., *Vectorcardiography*. Baltimore, MD: Wilkins & Wilkins, 1973.
95. Eisenstein, I., M.E. Sanmarco, W.L. Madrid, and R.H. Selvester, Electrocardiographic and vectorcardiographic diagnosis of posterior wall myocardial infarction. Significance of the T wave. *Chest*, 1985;**88**: 409–416.
96. Selvester, R.H., J.C. Solomon, K. Baron, H.A. Saetre, and M.H. Ellestad, Optimal electrode sites and crriteria for detection of asymptomatic coronary artery disease detection: update 1990. *USAF Armstrong Laboratory Technical Report*, 1991:0029: 8–48.
97. Ellestad, M.H., Personal communication.
98. Nelson, G.R., P.F. Cohn, and R. Gorlin, Prognosis in medically-treated coronary artery disease: influence of ejection fraction compared to other parameters. *Circulation*, 1975;**52**: 408–412.
99. Coronary artery surgery study (CASS): a randomized trial of coronary artery bypass surgery. Survival data. *Circulation*, 1983;**68**: 939–950.
100. Heikkila, J., P.G. Hugenholtz, and B.S. Tabakin, Prediction of left heart filling pressure and its sequential change in acute myocardial infarction from the terminal force of the P wave. *Br. Heart J.*, 1973;**35**: 142–151.
101. Wickline, S.A. and J.J. McNamara, Vectorcardiographic quantification of infarct size in baboons. *Circulation*, 1978;**57**: 910–920.
102. Cowan, M.J., D.D. Reichenbach, R.A. Bruce, and L. Fisher, Estimation of myocardial infarct size by digital computer analysis of the VCG. *J. Electrocardiol.*, 1982;**15**: 307–316.
103. Cowan, M.J., R.A. Bruce, and D.D. Reichenbach, Estimation of inferobasal myocardial infarct size by late activation abnormalities of the QRS complex. *Am. J. Cardiol.*, 1984;**54**: 726–732.
104. Anderson, C.I., D.G. Harrison, N.C. Stack, N.B. Hindman, R.E. Ideker, S.T. Palmeri, R.H. Selvester, and G.S. Wagner, Evaluation of serial QRS changes during acute inferior myocardial infarction using a QRS scoring system. *Am. J. Cardiol.*, 1983;**52**: 252–256.
105. DePace, N.L., A.S. Iskandrian, A.H. Hakki, S.A. Kane, and B. Segal, Use of QRS scoring and thallium-201 scintigraphy to assess left ventricular function after myocardial infarction. *Am. J. Cardiol.*, 1982;**50**: 126–128.

106. Madrid, W.L., M.M. Laks, and R.H. Selvester, Evaluation of the performance of a Hewlett Packard program for myocardial infarct size determination. Computerized Interpretation of the Electrocardiogram, in *Engineering Foundation Conference*, Santa Barbara, CA, 1983.
107. Madrid, W.L., N.B. Hindman, G.S. Wagner, and R.H. Selvester, Infarct size by on-line computer analysis of ECG in a bedside microprocessor ECG cart, in Computers in Cardiology, *Proceedings of the IEEE Computer Society*, Los Angeles, CA, 1984, pp. 325–328.
108. Hindman, N.B., D.D. Schocken, M. Widmann, W.D. Anderson, R.D. White, S. Leggett, R.E. Ideker, T. Hinohara, R.H. Selvester, and G.S. Wagner, Evaluation of a QRS scoring system for estimating myocardial infarct size. V. Specificity and method of application of the complete system. *Am. J. Cardiol.*, 1985;**55**: 1485–1490.
109. Engblom, H., G.S. Wagner, R.M. Setser, R.H. Selvester, T. Billgren, J.M. Kasper, C. Maynard, O. Pahlm, H. Arheden, and R.D. White, Quantitative clinical assessment of chronic anterior myocardial infarction with delayed enhancement magnetic resonance imaging and QRS scoring. *Am. Heart J.*, 2003;**146**: 359–366.
110. Engblom, H., E. Hedstrom, E. Heiberg, G.S. Wagner, O. Pahlm, and H. Arheden, Size and transmural extent of first-time reperfused myocardial infarction assessed by cardiac magnetic resonance can be estimated by 12-lead electrocardiogram. *Am. Heart J.*, 2005;**150**: 920.
111. Kleber, A.G., M.J. Janse, F.J. van Capelle, and D. Durrer, Mechanism and time course of S-T and T-Q segment changes during acute regional myocardial ischemia in the pig heart determined by extracellular and intracellular recordings. *Circ. Res.*, 1978;**42**: 603–613.
112. Shaw, R.M. and Y. Rudy, Electrophysiologic effects of acute myocardial ischemia: a theoretical study of altered cell excitability and action potentialduration. *Cardiovasc. Res.*, 1997;**35**: 256–272.
113. Reimer, K.A., R.B. Jennings, F.R. Cobb, et al., Animal models for protecting ischemic myocardium: results of the NHLBI Cooperative Study. Comparison of unconscious and conscious dog models. *Circ. Res.*, 1985;**56**: 651–665.
114. Anderson, S.T., M. Wilkins, W.D. Weaver, R.H. Selvester, and G.S. Wagner, Electrocardiographic phasing of acute myocardial infarction. *J. Electrocardiol.*, 1992;**25**(Suppl. 3–5).
115. Wilkins, M.L., A.D. Pryor, C. Maynard, et al., An electrocardiographic acuteness score for quantifying the timing of a myocardial infarction to guide decisions regarding reperfusion therapy. *Am. J. Cardiol.*, 1995;**75**: 617–620.
116. Heden, B., R. Ripa, E. Persson, Q. Song, C. Maynard, P. Leibrandt, T. Wall, T.F. Christian, S.C. Hammill, S.S. Bell, O. Pahlm, and G.S. Wagner, A modified Anderson-Wilkins electrocardiographic acuteness score for anterior or inferior myocardial infarction. *Am. Heart J.*, 2003;**146**: 797–803.
117. Wagner, G., T. Lim, L. Gettes, A. Gorgels, M. Josephson, H. Wellens, S. Anderson, R. Childers, P. Clemmensen, P. Kligfield, P. Macfarlane, O. Pahlm, and R. Selvester, Consideration of pitfalls in and omissions from the current ECG standards for diagnosis of myocardial ischemia/infarction in patients who have acute coronary syndromes. *Cardiol. Clin.*, 2006;**24**: 331–342.
118. Corey, K.E., C. Maynard, O. Pahlm, M.L. Wilkins, S.T. Anderson, M.D. Cerqueira, A.D. Pryor, M.H. Raitt, R.H. Selvester, J. Turner, W.D. Weaver, and G.S. Wagner, Combined historical and electrocardiographic timing of acute anterior and inferior myocardial infarcts for prediction of reperfusion achievable size limitation. *Am. J. Cardiol.*, 1999;**83**: 826–831.
119. Sejersten, M., R.S. Ripa, C. Maynard, P. Grande, H.R. Andersen, G.S. Wagner, and P. Clemmensen, DANAMI-2 Investigators. Timing of ischemic onset estimated from the electrocardiogram is better than historical timing for predicting outcome after reperfusion therapy for acute anterior myocardial infarction: a DANish trial in Acute Myocardial Infarction 2 (DANAMI-2) substudy. *Am. Heart J.*, 2007;**154**(61): e1–8.
120. Engblom, H., B. Heden, E. Hedstrom, G. Wagner, and H. Arheden, ECG Estimate Of Ischemic Acuteness and Time from Pain Onset for Predicting Myocardial Salvage in Patients Undergoing Primary Percutaneous Coronary Intervention. *Circulation*, 2007;**116**: II 528 (abstr).
121. Sclarovsky, S., A. Mager, J. Kusniec, E. Rechavia, A. Sagie, R. Bassevich, and B. Strasberg, Electrocardiographic classification of acute myocardial ischemia. *Isr. J. Med. Sci.*, 1990;**26**: 525–531.
122. Birnbaum, Y., R.A. Kloner, S. Sclarovsky, C.P. Cannon, C.H. McCabe, V.G. Davies, B.L. Zaret, F.J. Wackers, and E. Braunwald, Distortion of the terminal portion of the QRS on the admission electrocardiogram in acute myocardial infarction and correlation with infarct size and long-term prognosis (Thrombolysis in Myocardial Infarction 4 Trial). *Am. J. Cardiol.*, 1996;**78**: 396–403.
123. Birnbaum, Y., I. Herz, S. Sclarovsky, B. Zlotikamien, A. Chetrit, L. Olmer, and G.I. Barbash, Prognostic significance of the admission electrocardiogram in acute myocardial infarction. *J. Am. Coll. Cardiol.*, 1996;**27**: 1128–1132.
124. Sejersten, M., Y. Birnbaum, R.S. Ripa, C. Maynard, G.S. Wagner, and P. Clemmensen, ;ANAMI-2 Investigators. Influences of electrocardiographic ischaemia grades and symptom duration on outcomes in patients with acute myocardial infarction treated with thrombolysis versus primary percutaneous coronary intervention: results from the DANAMI-2 trial. *Heart*, 2006;**92**: 1577–1582.
125. Ripa, R.S., L. Holmvang, C. Maynard, M. Sejersten, P. Clemmensen, P. Grande, B. Lindahl, B. Lagerqvist, L. Wallentin, and G.S. Wagner, Consideration of the total ST-segment deviation on the initial electrocardiogram for predicting final acute posterior myocardial infarct size in patients with maximum ST-segment deviation as depression in leads V1 through V3. A FRISC II substudy. *J. Electrocardiol.*, 2005;**38**: 180–186.
126. Pahlm-Webb, U., O. Pahlm, S. Sadanandan, R.H. Selvester, and G.S. Wagner, A new method for using the direction of ST-segment deviation to localize the site of acute coronary occlusion: the 24-view standard electrocardiogram. *Am. J. Med.*, 2002;**113**: 75–78.
127. Engelen, D.J., A.P. Gorgels, E.C. Cheriex, E.D. De Muinck, A.J. Ophuis, W.R. Dassen, J. Vainer, V.G. van Ommen, and H.J. Wellens, Value of the electrocardiogram in localizing the occlusion site in the left anterior descending coronary artery in acute anterior myocardial infarction. *J. Am. Coll. Cardiol.*, 1999;**34**: 389–395.
128. Surawicz, B., H. Uhley, R. Borun, et al., Task Force 1: Standardization of terminology and interpretation. *Am J Cardiol.*, 1978: **41**: 130–45
129. First, S.R., R.H. Bayley, and D.R. Bedford, Peri-infarction block; electrocardiographic abnormality occasionally resembling bundle branch block and local ventricular block of other types. *Circulation*, 1950;**2**: 31–36.

130. Isner, J.M. and W.C. Roberts, Right ventricular infarction complicating left ventricular infarction secondary to coronary heart disease. Frequency, location, associated findings and significance from analysis of 236 necropsy patients with acute or healed myocardial infarction. *Am. J. Cardiol.*, 1978;**42**: 885–894.
131. Ratliff, N.B, and D.B. Hackel, Combined right and left ventricular infarction: Pathogenesis anc clinicalpathologic correlations. *Am. J. Cardiol.*, 1980;**45**: 217–221.
132. Cohn, J.N., N.H. Guiha, M.I. Broder, and C.J. Limas, Right ventricular infarction. Clinical and hemodynamic features. *Am. J. Cardiol.*, 1974;**33**: 209–214.
133. Klein, H.O., T. Tordjman, R. Ninio, P. Sareli, V. Oren, R. Lang, J. Gefen, C. Pauzner, E. Di Segni, D. David, and E. Kaplinsky, The early recognition of right ventricular infarction: diagnostic accuracy of the electrocardiographic V4R lead. *Circulation*, 1983;**67**: 558–565.
134. Geft, I.L., P.K. Shah, L. Rodriguez, S. Hulse, J. Maddahi, D.S. Berman, and W. Ganz, ST elevations in leads V1 to V5 may be caused by right coronary artery occlusion and acute right ventricular infarction. *Am. J. Cardiol.*, 1984;**53**: 991–996.
135. Kulbertus, H.E., P. Rigo, and V. Legrand, Right ventricular infarction: Pathophysiology, diagnosis, clinical course, and treatment. *Mod. Concepts Cardiovas. Dis.*, 1985;**54**: 1.
136. Carson, W., Y.Z. Tseng, P.J. Huang, C.D. Tseng, and T.L. Wu, Vectorcardiographic features of acute right ventricular infarction. *J. Electrocardiol.*, 1984;**17**: 253–261.
137. Morgera, T., E. Alberti, F. Silvestri, C. Pandullo, M.T. Della Mea, and F. Camerini, Right precordial ST and QRS changes in the diagnosis of right ventricular infarction. *Am. Heart J.*, 1984;**108**: 13–18.
138. Zehender, M., W. Kasper, E. Kauder, M. Schonthaler, A. Geibel, J. Olschewski, and H. Just, Right ventricular infarction as an independent predictor of prognosis after acute inferior myocardial infarction. *N. Engl. J. Med.*, 1993;**328**: 981–988.
139. Selvester, R.H. and H.B. Rubin, New criteria for electrocardiographic diagnosis of emphysema and cor pulmonale. *Am. Heart J.*, 1965;**69**: 437–447.
140. Freye, C.J., N.B. Wagner, C.M. Howe, N.C. Stack, R.E. Ideker, R.H. Selvester, and G.S. Wagner, Evaluation of a QRS scoring system for estimating myocardial infarct size. VIII. Specificity in a control group with left ventricular hypertrophy and proposal of a new scoring system for use with this confounding factor. *J. Electrocardiol*, 1992;**25**: 19–23.
141. Norris, R.M. and M.S. Croxson, Bundle branch block in acute myocardial infarction. *Am. Heart J.*, 1970;**79**: 728–733.
142. Bauer, G.E., Development of bundle branch block. *Am. J. Cardiol.*, 1964;**14**: 346–351.
143. Dodge, H.T. and R.P. Grant, Mechanisms of QRS complex prolongation in man; right ventricular conduction defects. *Am. J. Med.*, 1956;**21**: 534–550.
144. Scott, R.C., Left bundle branch block–a clinical assessment. III. *Am. Heart J.*, 1965;**70**: 813–829.
145. Scott, R.C., Left bundle branch block–a clinical assessment. II. *Am. Heart J.*, 1965;**70**: 691–712.
146. Scott, R.C., Left bundle branch block–a clinical assessment. I. *Am. Heart J.*, 1965;**70**: 535–566.
147. Ostrander, L.D. Jr., Bundle branch block: an epidemiological study. *Circulation*, 1964;**30**: 872.
148. Edmands, R.E., An epidemiological assessment of bundle-branch block. *Circulation*, 1966;**34**: 1081–1087.
149. Schneider, J.F., H.E. Thomas Jr., B.E. Kreger, P.M. McNamara, and W.B. Kannel, Newly acquired left bundle-branch block: the Framingham study. *Ann. Intern. Med.*, 1979;**90**: 303–310.
150. Schneider, J.F., H.E. Thomas, B.E. Kreger, P.M. McNamara, P. Sorlie, and W.B. Kannel, Newly acquired right bundle-branch block: The Framingham Study. *Ann. Intern. Med.*, 1980;**92**: 37–44.
151. Rhoads, D.V., J.E. Edwards, and R.D. Pruitt, The electrocardiogram in the presence of myocardial infarction and intraventricular block of the left bundlebranch block type. A clinical pathologic study. *Am. Heart. J.*, 1961;**62**: 735–745.
152. Haft, J.I., M.V. Herman, and R. Gorlin, Left bundle branch block: etiologic, hemodynamic, and ventriculographic considerations. *Circulation*, 1971;**43**: 279–287.
153. Horan, L.G., N.C. Flowers, and W.J. Tolleson, Thomas JR: The significance of diagnostic Q waves in the presence of bundle branch block. *Chest*, 1970;**58**: 214–220.
154. Hiss, R.G. and L.E. Lamb, Electrocardiographic findings in 122,043 individuals. *Circulation*, 1962;**25**: 947–961.
155. Hickman, J.R. and G.M. McGranahan Jr., Clinical aerospace cardiology, in *Fundamentals of Aerospace and Flight Medecine*, R.L. DeHart, Editor. Philadelphia, PA: Lea & Febiger, 1985, p. 421.
156. Polizos, G. and R.H. Selvester, Left bundle branch block and acute myocardial infarction: Diagnosis and location. abstract in AHA Scientific Sessions. *Circulation*, 2003.
157. Rogers, W.J., L.J. Bowlby, N.C. Chandra, W.J. French, J.M. Gore, C.T. Lambrew, R.M. Rubison, A.J. Tiefenbrunn, and W.D. Weaver, Treatment of myocardial infarction in the United States (1990 to 1993). Observations from the National Registry of Myocardial Infarction. *Circulation*, 1994;**90**: 2103–2114.
158. Sgarbossa, E.B., S.L. Pinski, A. Barbagelata, D.A. Underwood, K.B. Gates, E.J. Topol, R.M. Califf, and G.S. Wagner, Electrocardiographic diagnosis of evolving acute myocardial infarction in the presence of left bundle-branch block. GUSTO-1 (Global Utilization of Streptokinase and Tissue Plasminogen Activator for Occluded Coronary Arteries) Investigators. *N. Engl. J. Med.*, 1996;**334**: 481–487.
159. Tolan, G.T., R.H. Selvester, and J.C. Solomon, Optimal ECG electrode sites and criteria for detection of asymptomatic coronary artery disease. Computer ECG Analysis: towards Standardization, in *3rd International Conference on Common Standards for Quantitative Electrocardiography*, Amsterdam: North Holland Publ. Co. 1985.
160. Selvester, R.H., J.C. Solomon, and R.B. Pearson, ECG body surface map criteria for quantifying infarct, as derived from computer simulations, in *3rd International Symposium on Body Surface Mapping*. Dordrecht: Martinus Nijhoff, Publ. Co., 1985.
161. Solomon, J.C., R.H. Selvester, and G.T. Tolan, *Forward ECG simulation. Proceedings of the Society for Computer Si006Dulation. in 5th Annual Multiconference, Society for Computer Simulation*, San Diego, 1986.
162. Ramanathan, C., R.N. Ghanem, P. Jia, K. Ryu, and Y. Rudy, Noninvasive electrocardiographic imaging for cardiac electrophysiology and arrhythmia. *Nat. Med.*, 2004;**10**: 422–428.

17 Ventricular Repolarization: Theory and Practice in Non-Ischemic Myocardium

Borys Surawicz

P. W. Macfarlane, A. van Oosterom, O. Pahlm, P. Kligfield, M. Janse, J. Camm (eds.), *Comprehensive Electrocardiology*, DOI 10.1007/978-1-84882-046-3_17,

17.1 Introduction

Of all components of the electrocardiogram (ECG), the ST segment and the T wave are subject to the greatest potential misinterpretation because the line dividing normal from abnormal is not sharp, and because the patterns of abnormal repolarization resulting from structural derangements and functional disturbances are similar to each other. The amplitudes of ST and T deflections can be measured accurately, but the normal ranges are wide and the absolute values are not meaningful unless related to the QRS amplitude. Also, a meaningful interpretation of the direction of the T wave vector in one or more planes requires correlations with the mean QRS vector or the vector of one of the QRS components; for example, terminal slurred portion of QRS in right bundle branch block. The greatest difficulties of interpretation may be caused by problems related to the timing, and involve the following questions:

1. When does the ST segment end and the T wave begin?
2. Where does the T wave end and the U wave begin?
3. How does one differentiate the terminal dip of the T wave from a depressed TU junction or a negative TU segment?

Electrocardiography is abundant in descriptive terms. The depression of the ST segment is pictured as trough-, sickle-, claw-, plane-, or wing-like. Various forms of T waves bear such designations as notched, diphasic, coved, saddlelike, blunted, dimpled, cloven, tent-shaped, and so on [1]. It is apparent that the evaluation of the ST segment and the T wave is frequently based on descriptive rather than measurable properties, and that the electrocardiographic diagnoses are frequently made on the basis of visual impressions rather than detailed measurements.

Cellular electrophysiology has made an important contribution to the understanding of the processes controlling ventricular repolarization. The uniform changes in the shape and duration of the ventricular action potential can adequately explain most of the metabolic and pharmacological effects on repolarization [2]. However, other types of ST segment and T wave changes are caused predominantly by the changes in the sequence of repolarization. Such changes may be either primary or secondary to the changes in the sequence of depolarization. The latter may not involve changes in the shape and duration of the ventricular action potential. Accordingly, assumptions underlying the interpretation of T wave changes concern the basic shape of the ventricular action potential, the local difference between action potential durations and the sequences of activation.

Figure 17.1 shows the electrocardiogram (ECG) and the right ventricular endocardial monophasic action potential (MAP), recorded with a suction electrode in man. It can be seen that the MAP ends near the end of the T wave, that the ST segment corresponds to the early slower phase of repolarization, and that the T wave corresponds to the more

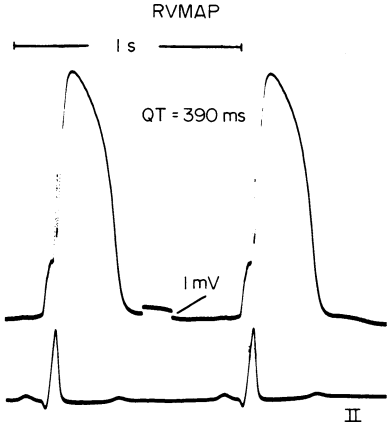

Figure 17.1

Normal right ventricular monophasic action potentials (RVMAP) and normal electrocardiogram (ECG) in a patient with mitral stenosis. (After Shabetai et al. [3]. © American Heart Association, Dallas, Texas. Reproduced with permission.)

rapid terminal portion of repolarization. More detailed correlations between the morphology of repolarization in the ECG and in the single fibers have been performed in isolated perfused rabbit hearts. With the exception of a shorter QRS duration (i.e., 35 ms as opposed to 80 ms), the morphology of the ECG complex in the rabbit and man is similar [4, 5]. Our correlations of simultaneously recorded ventricular transmembrane action potentials (TAPs) and ECGs in isolated perfused rabbit hearts showed that action potentials (APs) of varying shape and duration terminated near the end of the T wave. A shorter duration of the AP was accompanied by a shorter QT interval, and a longer duration of the AP was accompanied by a longer QT interval in the ECG. A prolonged plateau was associated with a longer duration of the ST segment, and a shorter plateau with a shorter duration of the ST segment. The increased velocity of the initial portion of repolarization was associated with a deviation of the ST segment from the baseline, and a steeper slope of terminal repolarization with a more abrupt descent of the T wave; that is, "peaking." A slower slope of repolarization, approaching a straight line, was associated with a wide, poorly defined T wave of low amplitude; a prolongation of the terminal portion of repolarization was accompanied by the appearance of a prominent U wave and fusion of T and U waves [2]. Such abnormalities were induced by changes in heart rate, body temperature, electrolyte imbalance, and drugs, and were reversible when the underlying metabolic or pharmacological abnormality disappeared. It follows that an accurate interpretation of the ECG requires information regarding the metabolic status and the drug intake of the patient.

17.2 ST Segment

17.2.1 Duration

The isoelectric course of the ST segment is caused by the relatively long flat slope of ventricular repolarization during phase 2 (plateau) of the AP. The duration of the ST segment tends to parallel the duration of ventricular AP, and the rate-dependent changes in the duration of the ST segment reflect the rate-dependent changes in the duration of the plateau of the ventricular AP [6]. The parallel relation between the durations of the ST segment and the plateau of ventricular AP is exemplified by the effects of the extracellular calcium concentration. Both the plateau of the AP and the ST segment lengthen during hypocalcemia and shorten during hypercalcemia. However, the T wave remains unchanged, provided the slope of terminal repolarization and the sequence of repolarization are not changed. Figure 17.2 shows a simultaneous recording of the MAP and ECG in a patient with hypocalcemia due to hypoparathyroidism. Both the amplitude and the polarity of the T wave remain unchanged when the ST segment shortens after the administration of calcium. It can be seen that the ST segment shortening is associated with shortening of the plateau but without change in the slope of phase 3 (see Chap. 3 for definitions). As a rule, hypocalcemia and hypercalcemia do not change the polarity of the T wave, but a few exceptions have been found in patients in whom severe hypocalcemia caused flattening or inversion of the T wave in the leads with an upright QRS complex [7–9].

Aside from the effects of heart rate, catecholamines, calcium, and several class III antiarrhythmic drugs the changes in the duration of the ventricular AP are seldom a result of, solely or predominantly, changes in the duration of the plateau. Under most other conditions that alter the duration of the AP, changes in the duration of the plateau are associated with a concomitant change in the slope of the plateau, and usually with the changes in the slope of phase 3. For example, digitalis and hypokalemia shorten phase 2 and prolong phase 3, while class 1A antiarrhythmic drugs, e.g., quinidine and disopyramide, prolong both the phase 2 and the phase 3 of the ventricular AP.

17.2.2 Deviations from the Baseline

Theoretically, the absence of ST segment deviation from the baseline implies an absence of significant potential differences during phase 2 of ventricular repolarization. Even under normal circumstances, this condition is not always fulfilled, particularly at the onset of repolarization. Figure 17.3 is a schematic diagram in which the ECG is derived from the potential difference between two APs hypothetically attributed to the first and the last ventricular fiber depolarized during recording of a single QRS complex. In the derived ECG, the configuration of the ST segment and T wave is determined by the potential difference during repolarization. The diagram shows that after the end of depolarization, some potential

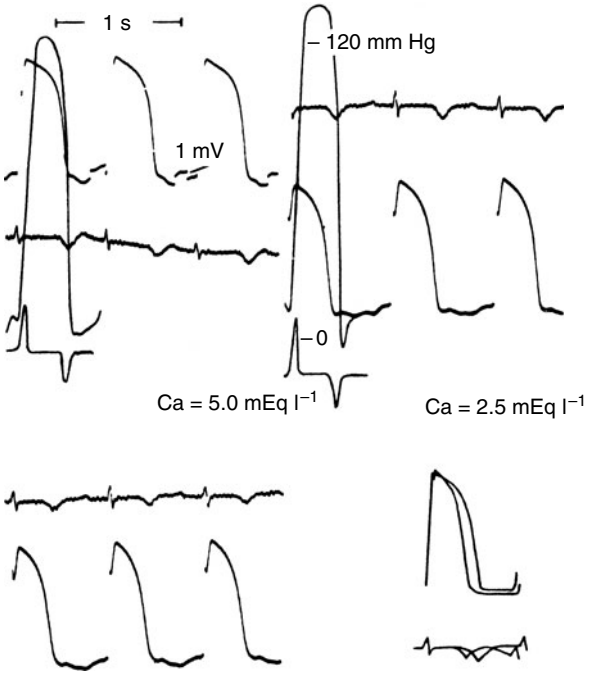

Figure 17.2

Effect of the administration of $CaCl_2$ to a patient with hypoparathyroidism (*top left*). Plasma calcium is 2.5 mEq l^{-1}. Phase 2 of the right ventricular MAP and the ST segment in lead II are prolonged. Retouched tracings of left ventricular pressure and its first derivative are superimposed on the first complex (*top right*). After intravenous administration of 0.7 g of $CaCl_2$, plasma calcium concentration is 5.0 mEq l^{-1}. Note shortening of phase 2 of the right ventricular MAP and of the ST segment and increased left ventricular pressure and first derivative. (After Shabetai et al. [3]. © American Heart Association, Dallas, Texas. Reproduced with permission.)

differences do exist before the onset of uniform depolarization to the level of the plateau. This interval is short but it may cause deviation of the junction (J depression) and of the early portion of the ST segment. As a result of this, measurements of ST segment deviation are usually made about 60–80 ms after the end of the QRS complex when all ventricular fibers are expected to be depolarized (discharged) to the same membrane potentials indicated by two superimposed segments of repolarization (phase 3) before the onset of rapid repolarization. Mapping studies have shown that the ST segment may be appropriately modeled as a single current dipole directed toward the apex of the heart, unaltered by the heart rate [10]. The potential difference between the rapid repolarizations (phase 3) is responsible for the T wave. Afterward, all fibers are "at rest" (charged) and potential differences are absent [11].

17.2.2.1 ST Deviations in the Absence of Ischemia (Secondary Repolarization Changes)

The two diagrams in Fig. 17.3c explain why the entire ST segment or its major portion may deviate from the baseline in the absence of myocardial ischemia. The diagram on the left shows the mechanism of repolarization abnormalities secondary to conduction delay, indicated by a prolonged interval between the upstrokes of the first and the last APs. The longer conduction time lengthens the QRS complex and enhances the potential differences during the entire repolarization. This happens because some of the early depolarized fibers begin to pass through the rapid phase 3 repolarization while the late depolarized fibers will be still at the level of the plateau. In the diagram, potential differences (arrow) persist throughout the entire repolarization phase and therefore the entire ST segment deviates from the baseline. Secondary ST segment changes are usually accompanied by secondary T wave changes.

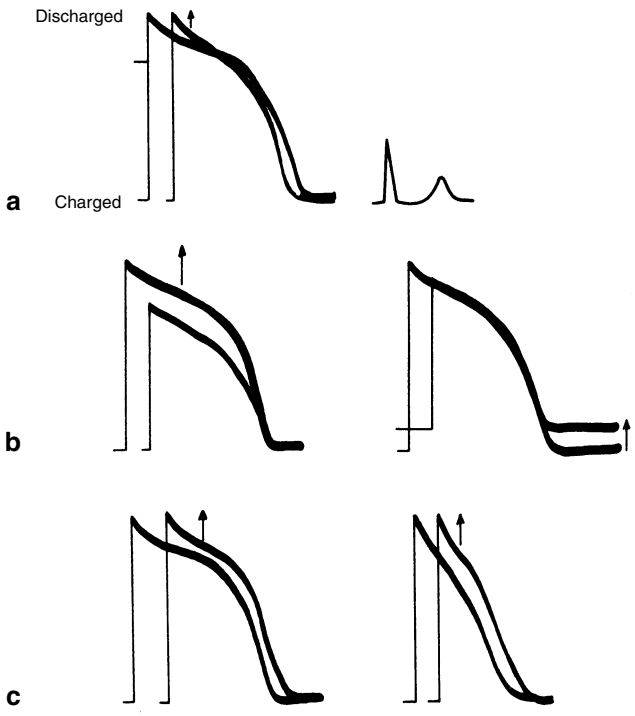

Figure 17.3
Schematic diagrams: (a) the normal electrocardiogram is derived from the potential differences between two ventricular APs; (b) the potential differences responsible for systolic and diastolic currents of injury; (c) potential differences responsible for secondary repolarization abnormalities to the left and changes in the repolarization slope (e.g., digitalis effect) to the right. (After Surawicz and Saito [11]. © Yorke Medical Group, Magazine Division, New York. Reproduced with permission.)

17.2.2.2 ST Deviations Arising from Primary Repolarization Abnormalities in the Absence of Ischemia

The diagram on the right in Fig. 17.3c shows the mechanisms of primary repolarization abnormalities caused by APs in which potential differences persist during most or all of repolarization because the slope of repolarization during phase 2 is steeper than normal. This mechanism will cause deviation of the ST segment from the base line in the absence of ischemia or any changes in the sequences of depolarization. The short ventricular AP with a steep slope of repolarization shown in this diagram depicts changes induced by digitalis or tachycardia. This may be one of the mechanisms of ST segment depression during exercise-induced tachycardia in the absence of myocardial ischemia.

17.2.2.3 Depression of the ST Segment

ST depression in precordial leads reflects a posteriorly directed deviation of the ST-segment vector. Several mechanisms of such deviation are shown in schematic diagrams in Fig. 17.4. In the upper left diagram, the crosshatched area represents a region of subendocardial ischemia or infarction that causes a systolic and a diastolic current of injury; the former results in depression of the ST segment (solid arrow) and the latter in elevation of the baseline (dashed arrow). It has been shown that ST segment depression during ischemia correlated well with the decrease in subendocardial blood flow and presence of perfusion defects in scintigrams as well as wall motion abnormalities in the echocardiogram (see Chap. 18).

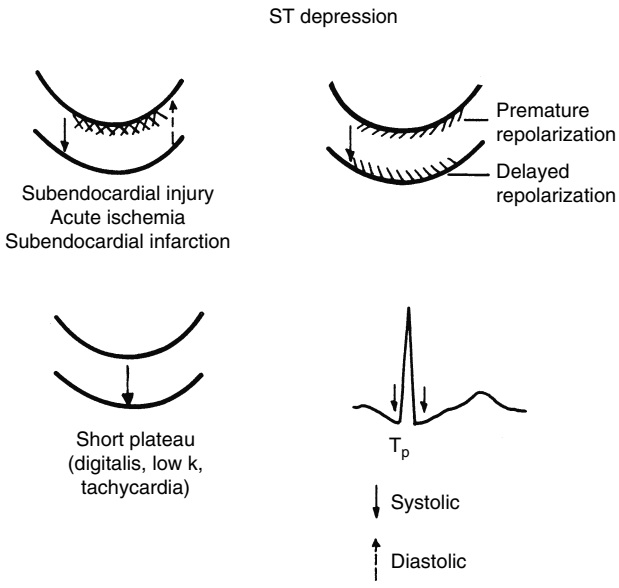

Figure 17.4

Diagram of several mechanisms of ST-segment depression. The direction of the arrows indicates the flow of current and not the ST-segment vector. See text for explanation. (After Surawicz and Saito [11]. © Yorke Medical Group, Magazine Division, New York. Reproduced with permission.)

In the upper right diagram, secondary ST segment depression is a result of delayed repolarization in the subepicardial region, or alternatively because of premature repolarization in the subendocardial region. In the lower left diagram, ST segment deviation occurs in the absence of injury or conduction delay, because of the uniform shortening of phase 2 (plateau) of the ventricular AP; owing to the effect of digitalis, hypokalemia, or tachycardia, for example.

Finally, the lower right diagram shows that the depression of ST segment may be caused by atrial repolarization represented by a negative T wave of the P wave (T_P), which is inscribed during the interval between the two arrows. Note that the ST depression is relative to P onset and would not be measured as such by a computer program using QRS onset as a baseline reference. The inscription of atrial repolarization during the ST segment has been documented in man during the recording of atrial MAP using suction electrodes [3] (Fig. 17.5). In Fig. 17.5, the negative T_P wave causes an upsloping course of the PR segment. This pattern helps to recognize false positive ST depression, even though it may be caused not only by a negative T_P wave but also by a P wave superimposed on a U wave.

17.2.2.4 Elevation of the ST Segment

ST elevation in precordial leads reflects an anteriorly directed deviation of the ST segment vector. Several mechanisms of such deviation are shown in the schematic diagrams in Fig. 17.6. In the diagram on the left, the crosshatched region represents a region of subepicardial injury, infarction, pericarditis [12], cardiac tumor [13], or transient ischemia during variant angina pectoris. The resulting systolic and diastolic currents of injury will cause elevation of the ST segment (solid arrow) and depression of the baseline (dashed arrow). In the diagram on the right, secondary ST segment elevation is a result of either delayed repolarization in the subendocardial region, or alternatively from premature repolarization of the subepicardial region. The latter phenomenon is the commonly assumed mechanism of a normal male pattern in young males Another cause of ST segment elevation is an abnormal atrial repolarization; that is, an upright Ta wave [14].

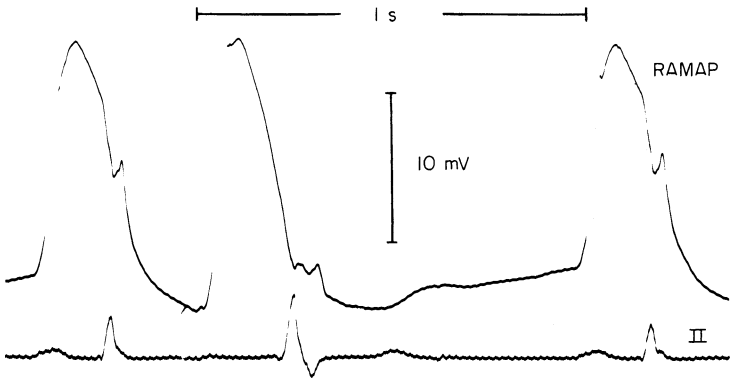

Figure 17.5

Effect of rate on the right atrial monophasic action potential (RAMAP). The duration of the RAMAP cannot be accurately measured because the QRS artifact distorts phase 3. However, phase 2 is not distorted. Phase 2 is longer in the sinus beats (first and third potentials) than in the atrial premature beat (second potential) with aberrant ventricular conduction. The tracing shows also that atrial repolarization continues during the inscription of the QRS complex and ST segment. (After Shabetai et al. [3]. © American Heart Association, Dallas, Texas. Reproduced with permission.)

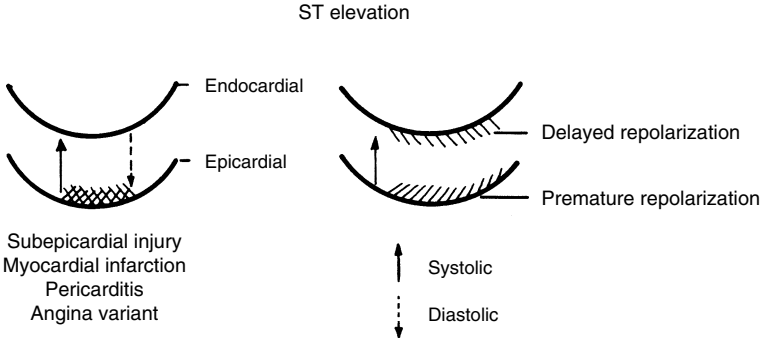

Figure 17.6

Diagram of several mechanisms of ST-segment elevation. The direction of the arrows indicates the flow of current and not the ST-segment vector. See text for explanation. (After Surawicz and Saito [11]. © Yorke Medical Group, Magazine Division. Reproduced with permission.)

17.2.2.5 ST Segment Depression-Normal Variant

A slightly downsloping or horizontal ST segment depression may occur as an apparent normal variant in the absence of myocardial ischemia, digitalis, hypokalemia, or secondary repolarization abnormalities. At rest, in the routine ECG, this occurs more commonly in women than in men [15–17]. However, during ambulatory monitoring, transient ST segment depression from 0.1 to 0.4 mV, lasting from 30 s to 2 h was recorded in 15 of 50 normal male volunteers who were 35–59 years old [18].

17.2.2.6 ST Segment Elevation-Normal Variant and Acute Pericarditis

In some individuals, particularly young men, ST segment elevation occurs as a normal variant [19–23]. The term early or premature repolarization is frequently applied to this pattern [22, 23] although in most cases this is a normal male pattern

(see below). The latter term implies that the ST segment shift is attributed to the shortening of ventricular APs in some epicardial regions. A rapid early repolarization in these regions may be expected to produce potential differences resulting in a "current of injury" and a consequent elevation of the ST segment. In partial support of this theory are the observations that exercise and isoproterenol [23, 24] abolish the ST segment elevation presumably as a result of diminished difference between ventricular AP durations [25]. However, mapping studies have not substantiated the rationale for the term "early repolarization" because in normal young volunteers, the overlap between the onset of ventricular repolarization and the end of QRS ranged from 4 to 16 ms. Further, there was no significant correlation between these values and ST segment deviation in the precordial leads [26].

The pattern of "early repolarization" may simulate the early pattern of acute pericarditis, possibly because both may be caused by a similar mechanism. In both patterns, the inscription of the ST segment begins before QRS forces have returned to baseline [12, 22] but the ST elevation in pericarditis is usually present in both limb and precordial leads, while in the pattern of "normal variant," ST elevation is confined more frequently to only the precordial leads [23]. Also, the T-wave amplitude in the left precordial leads tends to be greater in persons with "normal variant" than in patients with acute pericarditis [27].

17.2.2.7 ST Segment: Effect of Gender and Age

Anecdotal differences between ventricular repolarization in males and females have been observed for a long time, but only recently quantitatively defined. The typical male pattern prevails in young males and the typical female in ca 80% of women of all ages and in elderly males [28, 29]. The pattern is usually best expressed in the precordial lead with the tallest T wave, and the measurable descriptors are the level of J point and the angle of the ascent of the ST segment. In the male pattern, which is often labeled as premature or early repolarization variant (see above), the J point is situated more than 0.1 mV above the baseline, and the ST segment ascends at an angle > 20°. In the female pattern, the J point is situated less than 0.1 mV above the baseline, most often on the baseline, and the angle of the ST ascent is < 20°, most often close to 0°. The indeterminate patter, present in about 10–20% of men and women is characterized by J point as in male and the ST segment as in female pattern. Typical patterns are shown in Fig. 17.7 and the distribution of patterns in both genders from childhood to old age is shown in Fig. 17.8.

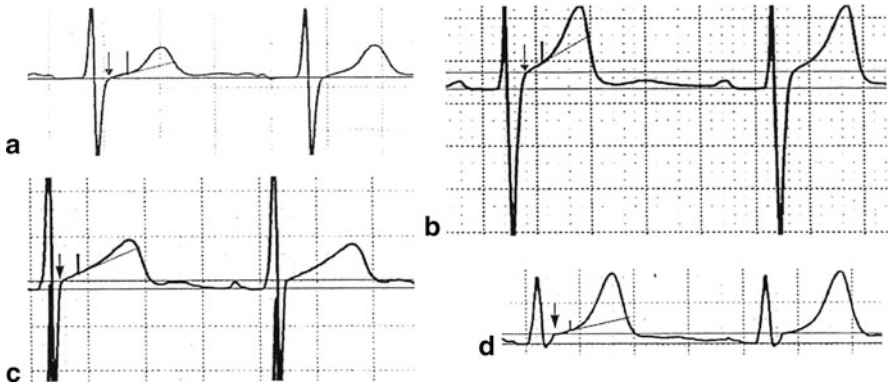

Figure 17.7

Method of pattern determination in representative ECG complexes of lead V3. The two horizontal lines represent the Q–Q line and the line parallel to the Q–Q line at the level of the J point, respectively. The arrow marks the J point; the short ventricle line marks the point 60 ms after the J point; the oblique line connects the J point with the above point (see text). (a) Female pattern: the J point is at the level of the Q–Q line, and the ST angle is 19°. (b) Male pattern: the J point is > 0.1 mV above the Q–Q line, and the ST angle is 36°. (c) Variant of the male pattern in which the T wave ascends at the J point; the J point is > 0.1 mV above the Q–Q line, and the angle between the line parallel to the Q–Q line at the level of the J point and the ascent of the T wave is 29°. (d) Indeterminate pattern: the J point is > 0.1 mV above the Q–Q line, and the ST angle is 15°. (From Surawicz et al., 2002 [29]. © *J. Am. Coll Cardiol*. Reproduced with permission.)

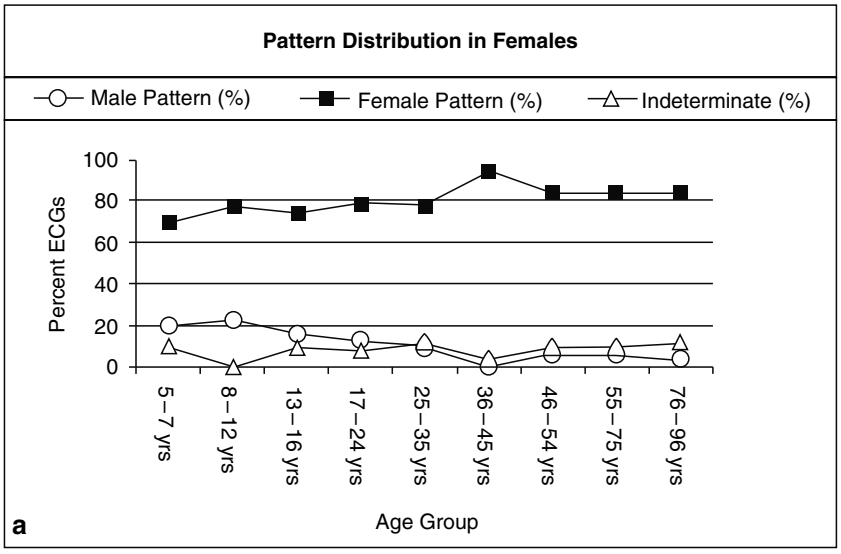

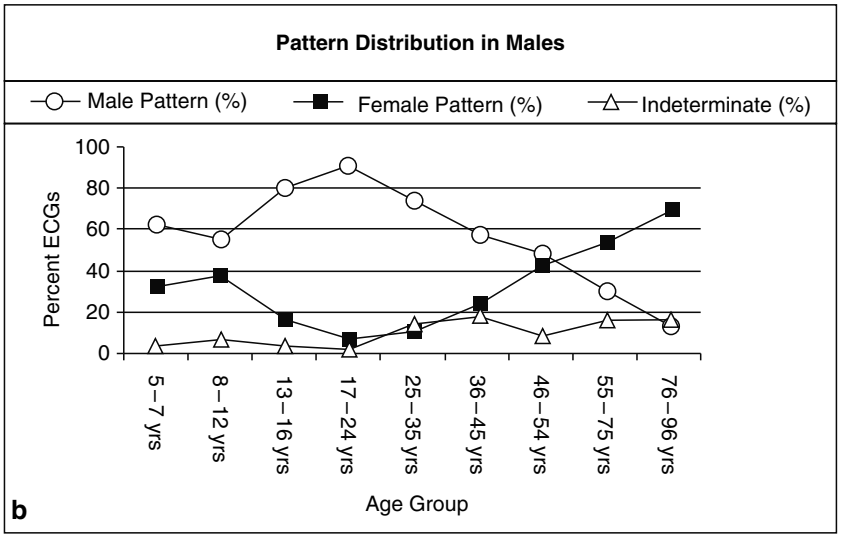

Figure 17.8

Pattern distribution in different age groups of females and males. (From Surawicz et al., 2002 [29]. © J. Am. Coll. Cardiol. Reproduced with permission.)

17.2.2.8 Alternans of the Depressed and the Elevated ST Segment

Alternans of the ST segment is known to occur both in experimental animals and in man. The alternans pattern may consist of an alternating depth of ST segment depression, or an alternating amplitude of ST segment elevation. To the best of the author's knowledge, an alternation of ST segment depression and elevation has not been reported.

The most common cause of the alternans of the ST segment is myocardial ischemia [30–34]. Alternans of an elevated ST segment was observed also in man during hyperkalemia [35] and in a cyanotic infant [36]. Alternation in the degree of ST segment depression was observed following critical decrease of flow in the left main coronary artery in dogs, in association with alternation of blood pressure, stroke volume, and occasionally with alternation of T wave [31]. In the pig,

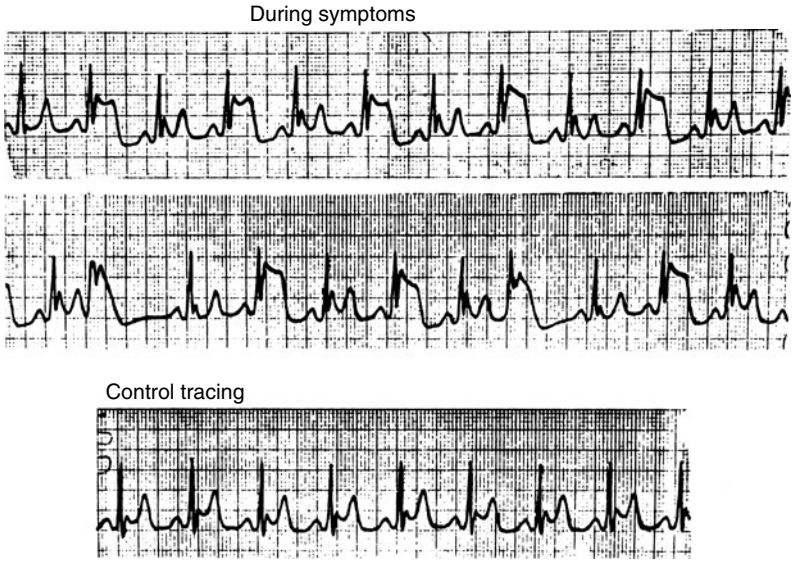

Figure 17.9

Electrocardiogram of a patient recorded from a continuous coronary-care unit monitor lead during an episode of Prinzmetal angina. Note the striking 2:1 electrical alternans involving the ST segment. A control tracing (for comparison) was taken with the same leads immediately after the pain subsided. (After Williams et al. [32]. © American College of Physicians, Philadelphia, Pennsylvania. Reproduced with permission.)

ST segment alternans was observed not only after coronary artery ligation but also during reperfusion [37]. The alternans of the ST segment elevation in man is not uncommon during attacks of vasospastic angina pectoris (Fig. 17.9), but has not been reported in the presence of ST segment elevation resulting from myocardial infarction [38].

More than one hypothetical mechanism can be postulated to explain the alternans of the ST segment elevation or depression in association with the alternans of contractile force. However, the most plausible mechanism appears to be an alternans of the slope of phase 2 (plateau) of the ventricular AP. Such an alternans has been observed in the records of MAPs registered simultaneously with electrograms during ST segment alternans produced by occlusion of the left anterior descending coronary artery (LAD) artery in dogs [31]. In some cases, the alternans appeared to occur also at the level of resting membrane potential [33].

17.3 T Wave

17.3.1 General Considerations: Ventricular Gradient

The T wave represents the uncanceled potential differences of ventricular repolarization. Since most of the electromotive forces generated during cardiac activity undergo cancellation, the area of the T wave is estimated to represent only 1–8% or less of the total time–voltage product of the heart [39, 40]. As will be discussed later in this section, the normal sequences of ventricular repolarization and the anatomic sites of the uncanceled potential differences responsible for the T wave in the normal heart are still not known.

The analysis of the T wave may be approached by relating the T-wave area to the QRS area. Wilson et al. pointed out that if all ventricular action potentials had the same magnitude and the same duration, the net area of the ventricular complex (QRS and T) should be zero [41]. However, in the normal heart, the mean QRS vector and the mean T vector form a narrow angle, and the area of the ventricular complex has a positive value. This indicates that in some parts of the ventricles, the intensity, or the duration of activity, must be greater than in others. This difference of activity was designated

as the ventricular gradient. The ventricular gradient points from the parts of the ventricle with greater duration of activity toward the parts with the lesser duration [41, 42]. The main source of the ventricular gradient is the nonhomogeneous duration of recovery; that is, the difference in duration of action potentials in different parts of the ventricles [41–44]. Several other sources of expected differences between the QRS area and the T area in the surface ECG (changes in the position or orientation of cardiac fibers during activity, and the nonlinear relation between the source of potentials and the surrounding field) appear to play only a negligible role in the genesis of the ventricular gradient [39, 45].

The concept of ventricular gradient developed by Wilson et al. applied only to a small unit of two adjacent fibers with different AP durations [41]. Subsequently, Gardberg and Rosen extended the validity of the concept to a strip of turtle ventricle [46]. In this preparation, the area of the electrogram was determined by differences in the rate of repolarization, but was not dependent on the path of excitation [46]. The presence of ventricular gradient in the entire heart can be demonstrated after an application of a brief and very strong electric shock that depolarizes simultaneously all ventricular elements. This shock causes a T wave without a QRS complex, and the area of this T wave represents the pure ventricular gradient [47]. The application of such shocks to dogs produced a large, upright T wave in leads II and III, and suggested an overall direction of repolarization from the apex to the base of the heart [47]. The principle of the independence of ventricular gradient of the sequence of activation has been reaffirmed in a study of QRST isoarea maps utilizing 192 electrodes [48] The same conclusion was reached by the mathematical analysis of a theoretical model in which propagation occurred under uniform isotropic conditions and the action potentials were identical except for possible variations in the duration of plateau [49].

It has been shown that compared to depolarization, repolarization generates more dipolar electrical fields [50]. However, our present knowledge of the spatial and temporal characteristics of the normal recovery process is still very incomplete. Studies of local electrograms and local effective refractory periods indicate that the general order of recovery is approximately the same as the order of activation [41, 45, 47, 51]. However, the QRST area in the local electrograms is seldom zero, even when the records are made with very closely spaced bipolar electrodes [63]. This indicates that inhomogeneities of repolarization occur within very small distances over the entire surface of the heart, and most probably within the entire ventricular wall [2].

Studies utilizing suction electrodes to record MAPs on the ventricular surface in dogs suggested a complex and geographically nonuniform sequence of ventricular repolarization [52], which had a tendency to shorten progressively in progressively later activated areas. This shortening appeared to be determined by the time of activation rather than by the site of activation [76] (Table 17.1.). Accordingly, the relation of the. MAP duration on the ventricular surface agreed with the direction of ventricular gradient [52]. Several studies utilizing refractory periods to estimate the sequence of repolarization reported similar recovery properties [53, 54]. It was shown that the sequence of recovery at the epicardial level was similar to the sequence of normal activation, but the sequence of excitation and recovery differed at the endocardium with some basal areas recovering excitability earlier than the apex in spite of later activation [55–57]. Also, in humans, body-surface mapping utilizing 192 electrocardiographic leads showed that the normal sequences of ventricular excitation and recovery were similar, and that the potential-difference boundaries with stable locations were widely distributed during later portions of the T wave [54].

With regard to the transmural sequence of excitation, early studies showed that the functional refractory period in the canine ventricle was approximately 15 ms longer in the subendocardial than in the subepicardial layers [58] (Fig. 17.10). Subsequently, more detailed studies confirmed that the normal sequence of recovery proceeded from epicardium to

Table 17.1

Relation between the duration of the monophasic action potential (MAP) expressed as a percentage of longest MAP in each dog and the activation time on the ventricular surface

Group	Activation time (ms)	Number of dogs	Number of APs	Duration average ± SD	Differences between groups
I	8–20	14	46	95.1 ± 3.4	III*
II	21–30	17	97	94.4 ± 4.5	III**
III	> 31	21	41	92.5 ± 4.7	I*, II**

*$p < 0.01$; **$p < 0.05$

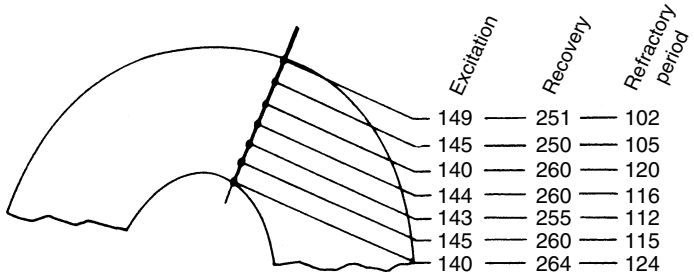

Figure 17.10

Excitation times, recovering times, and refractory period on the endocardial–epicardial axis in the posterolateral left ventricular wall. The times shown are in milliseconds after atrial stimulation. Findings are representative of five experiments in which comparable measurements were made shortly after thoracotomy and without pericardial incision over the ventricles. Excitation was earliest at the endocardium, and endocardial refractory periods were longer than those near the epicardium, as has been previously established. (After Abildskov [55]. © American Heart Association, Dallas, Texas. Reproduced with permission.)

endocardium [55, 59]. It has been shown that action potentials from scattered myocytes, assumed to represent mainly the intramural action potentials, were longer than both the subendocardial or the subepicardial action potentials, and approximated more closely than the latter, the QT duration in the guinea pig heart [60].

The mechanisms responsible for the differences between the duration of repolarization in different regions of the ventricles remains to be identified. Wilson et al. considered two possible explanations: first, the inherent characteristics of the fibers; or second, the effects created by different environmental influences; for instance, differences in innervation, blood supply, or temperature [51]. In the canine and human ventricle, the temperature on the epicardial surface exceeds the temperature of the endocardium by 0.5–0.7°C [61, 62]. However, several studies have shown conclusively that the ventricular gradient cannot be attributed entirely, or even predominantly, to these temperature differences [61–63]. It has also been shown that ventricular gradient is not caused by increased pressure in the subendocardial regions because, in patients with severe hypertension, marked and rapid lowering of blood pressure with hexamethonium did not alter the ventricular gradient [2].

The magnitude of the ventricular gradient depends on factors that still remain unknown [63]. The inhomogeneous behavior of repolarization may represent an inherent property of the myocardium, because an upright T wave and a high gradient are present even in isolated papillary muscles or muscle strips [45]. It appears likely that some of the "inherent" AP duration differences in the ventricular myocardium result from electrotonic interactions during ventricular repolarization. An attempt to estimate these influences by comparing refractory periods during repeated stimulation (drives) at single ectopic sites, and during fusion drives from two ectopic sites, showed that refractory periods were as much as 10 ms shorter when a fusion occurred within 1 mm of the test site; an effect probably arising from electrotonic interactions [64].

Another factor proposed as an explanation of the differences in AP duration in different portions of ventricular myocardium is the difference in the thickness of the ventricular wall in different portions of the ventricles and the septum [65].

Numerous studies have demonstrated that local changes in the duration of recovery can alter the amplitude, duration, and polarity of the T wave without changes in the QRS complex. Regional changes in the duration of recovery produced by cooling and warming have resulted in predictable deviations of the T-wave vector from the area with the longer duration toward the area with the shorter duration of the recovery period [41, 46, 47, 66–69]. Calculations based on experimental data have shown that small alterations in the local form of the AP may cause large percentile changes in the configuration of the T wave [39]. This means that the ventricular gradient is very sensitive to local differences in the duration of repolarization and that the T wave may be considered as "some kind of special detector for differences in repolarization of the various parts of the ventricle" [39].

Experimental and clinical studies in our laboratory have provided certain estimates of the magnitude of repolarization changes required to alter the T-wave morphology or the T vector. Isoproterenol (2 mcg ml^{-1}) administered into four different vessels of anesthetized open-chest dogs induced T-wave changes without QRS changes. By correlating these

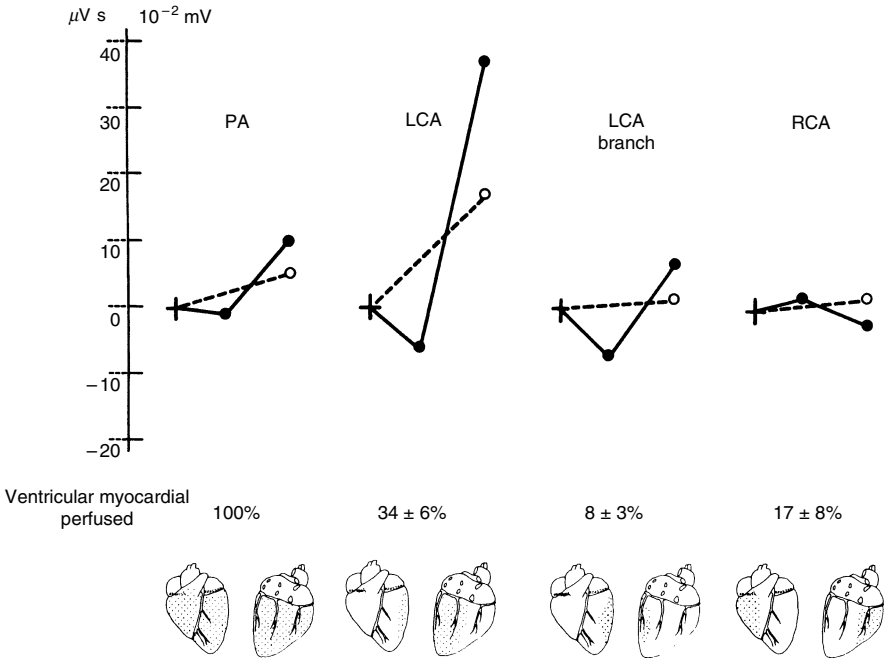

Figure 17.11

Late (steady-state) effect of isoproterenol (ISP) on T-wave amplitude in 10^{-2} mV (*solid line*) and T-wave area in μVs (*broken line*) in four groups of experiments. The points represent average change from control values. In each panel, the proximal solid dot represents the a_1T amplitude and the distal solid dot the a_2T amplitude; a_1 and a_2 refer apices of a bifid T wave. The lower part shows the percentage of the ventricular myocardial mass perfused with ISP. The ISP-perfused area of the ventricles is indicated by the dotted area in the diagram under each number. In each panel, the anterior surface of the heart is shown on the left and the posterior surface on the right. PA, pulmonary artery (group I); LCA, left circumflex coronary artery (group II); LCA branch, left circumflex coronary artery branch (group III); and RCA, right coronary artery (group IV). (After Autenrieth et al. [69]. © American Heart Association, Dallas, Texas. Reproduced with permission.)

T-wave changes with the changes in the duration of MAPs recorded with suction electrodes and with the tissue mass perfused with isoproterenol, it was possible to demonstrate that a significant change in T-wave amplitude in orthogonal leads occurred when MAP shortened by 18:+/−8 ms in the portion of left ventricular wall comprising about 8% of ventricular myocardium [25]. As expected, T-wave changes were greater when MAP shortening of similar magnitude extended over a mass comprising about 34% of ventricular myocardium (Fig. 17.11). However, other results from the same study showed that the magnitude of T-wave change was not proportional to the mass of tissue with the uniformly shortened repolarization. Some of these discrepancies were attributed to cancellation, and some to an uneven contribution of different repolarization regions to the T wave [25]. Subsequently, changes in the duration of MAP on the anterior and posterior walls of the dog ventricle were correlated with changes in T-wave polarity and duration of the QT interval after:

1. Left stellate-ganglion transection,
2. Right stellate-ganglion stimulation, and
3. Administration of isoproterenol before or after these procedures.

Left stellate-ganglion transection and right stellate-ganglion stimulation produced similar changes in T-wave polarity, but the former prolonged and the latter shortened the QT interval. All procedures changed the duration of the MAP and the QT interval in the same direction [25]. The reversal of T-wave polarity induced by left stellate-ganglion transection, right

stellate-ganglion stimulation, or the administration of isoproterenol after left stellate-ganglion transection was associated with an average change of 13–17 ms in the difference between the MAP durations on the anterior and posterior ventricular walls. Isoproterenol restored to normal the neurogenic T-wave abnormalities produced by left stellate-ganglion transection and right stellate-ganglion stimulation. The drug shortened the previously prolonged MAP more than the normal MAP, and the normal MAP more than the previously shortened MAP. This study confirmed that the T wave is a sensitive indicator of relatively small changes (<20 ms) in the sequence of ventricular repolarization, and also explained the mechanism by which isoproterenol "normalized" the primary T-wave abnormalities [25].

In a parallel clinical study, the effects of isoproterenol on the T wave were compared with the effects of atropine or pacing at the same rate [70]. In 37 patients, isoproterenol reversed the T-wave polarity from negative to positive, while the T-wave abnormality persisted after atropine or pacing following an identical rate increase. The average QT shortening with isoproterenol was 20 ms greater than that with atropine or pacing. This suggested that a lengthening of repolarization by 20 ms in some portion of ventricular myocardium might have been responsible for the inversion of T wave. A similar value was obtained in a different manner in 29 patients with left ventricular hypertrophy (LVH) pattern and negative T waves in the left precordial leads. In 18 of these patients, the negative T wave persisted after the administration of isoproterenol and in 11, the T wave became upright. In the patients in whom the T wave became upright, the QRS duration averaged 85 ms and in patients in whom the T wave remained negative, the QRS duration averaged 106 ms. Since QT shortening produced by isoproterenol was the same in both groups, it was concluded that conduction delay by 21 ms was responsible for the secondary T-wave inversion in the left precordial leads [70].

17.3.2 Normal Configuration and Direction

The configuration of the normal T wave is largely determined by the asynchrony of the phase 3 of ventricular repolarization duration of ventricular TAPs. In the theoretical model deriving ventricular complex in the ECG by the algebraic subtraction of 2 APs in Fig. 17.3, the T wave would be upright when the terminal AP ends before the initial AP, isoelectric when both APs end simultaneously and inverted when the initial AP ends before the terminal AP. Notwithstanding the obvious limitations of such a simplistic model, it proved to be applicable in the derivation of T-wave polarity in local bipolar electrograms. The study of Taggart et al. [71] showed an excellent correlation between T-wave polarity in the local electrogram in the intact pig heart in vivo and the T wave of the ECG-like waveform derived by the subtraction of 2 MAPs recorded at the sites of the corresponding electrode. The successful reproduction of T-wave configuration in this model appears to reflect two general properties of ventricular repolarization, i.e., the simple dipolar nature of the generated electrical fields and the smooth electrotonic modulation of the AP duration during impulse propagation.

In our two studies, the average maximum differences of the MAP duration on the ventricular surface in dogs were 22 ± 9 ms [72] and 27 ± 10 ms [72]. The reported differences of MAP durations on the surface of the isolated cat heart averaged 25 ms [73]. These values suggest that the differences of AP durations on the entire surface may be greater than the transmural differences of refractory period [58].

Some indication of the approximate maximum differences between AP durations in an individual dog can be obtained from the relation between the timing of the T-wave apex and the repolarization slope of the MAP. The T wave results from many simultaneous local gradients between APs during repolarization. The peak of the T wave is expected to coincide with the maximum of these local gradients. The maximum local gradient between two APs during repolarization may be expected during the inscription of the steepest repolarization slope of the AP, which terminates earlier. If this consideration is applied to the entire heart, the peak of the T wave should not occur before the onset of rapid repolarization in some portion of the ventricle. This, in turn, suggests that the duration of the interval between the peak of the T wave (aT) and the end of the T wave (eT) bears a certain relation to the dispersion of repolarization in the entire heart. In our study, the interval between aT (second peak if the T wave was bifid) and eT in leads II or *Y* averaged 33 ± 12 ms. The precise relation between the dispersion of repolarization and the aT–eT interval is not known, but, knowing the repolarization slope of the individual MAP, the probable upper limits of dispersion in an individual case were calculated. An example of such a calculation is illustrated in Fig. 17.12, which shows one ventricular complex from Fig. 17.13.

In Fig. 17.13, the MAP at the anterior base ends 17 ms before the end of the T wave, and the MAP at the posterior base ends 33 ms before the end of the T wave. Thus, the dispersion of repolarization between these two MAPs was 16 ms. The shape of the T waves was derived from the plot of "potential differences" produced by superposition of these two MAPs

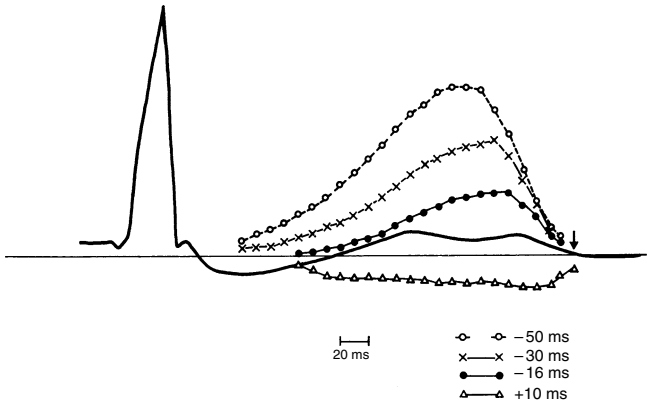

Figure 17.12

Magnified ventricular complex from Fig. 17.13 (solid trace) with an additional four different T waves derived from the "potential differences" between two superimposed MAPs illustrated in Fig. 17.13. The solid circles mark the T wave derived from the MAPs superimposed in the same sequence as they occurred in the experiment (MAP at the anterior base ends 17 ms and MAP at the posterior base 33 ms before the end of the T wave). Other T waves represent "potential differences" between MAPs of the same configuration but after shortening or lengthening, phase 2 of the MAP at the posterior base. The T wave marked by crosses was constructed after the MAP at the posterior base was shortened by 14 ms; this increased the eMAP–eT difference (e denotes end) between these two MAPs from 16 to 30 ms. The T wave marked by empty circles is constructed after the MAP at the posterior base was shortened by 34 ms; this increased the eMAP–eT difference between these two MAPs to 50 ms. The T wave marked by triangles was constructed after the MAP duration at the posterior base was increased by 26 ms; this altered the eMAP–eT sequence between these two MAPs and produced a negative T wave. Note that the aT–eT interval (second peak) of the recorded T wave is 40 ms, and that the aT–eT intervals of the derived T waves are 44 ms (dispersion 16 ms), 55 ms (dispersion 30 ms), and 75 ms (dispersion 50 ms). (After Autenrieth et al. [52]. © Mosby, St Louis, Missouri. Reproduced with permission.)

when the dispersion of repolarization was unchanged (16 ms) and when the dispersion was shortened or prolonged by "shortening" or "lengthening" the MAP at the posterior base. Fig. 17.12 shows that, unlike the recorded T wave, the derived T waves had only one peak. The timing of this peak is within the observed range of aT–eT intervals when the dispersion of repolarization is 10, 16, or 30 ms, but it occurs earlier than observed in any experiment when the dispersion is 50 ms. This suggests that the dispersion of repolarization in dogs is less than 50 ms; that is, less than the duration of the QRS complex [75].

In the study of Yanowitz, Preston, and Abildskov [74], unilateral stellate-ganglion stimulation was followed by an apparent lengthening of the QT interval. This suggested that certain APs terminate after the end of the T wave but do not generate deflections, because they end simultaneously and undergo cancellation [74]. Fig. 17.14 shows that in our study of dogs, there was no evidence to support such "silent repolarization" on the ventricular surface, since all MAPs terminated during the inscription of T wave. The same results were obtained from studies on the rabbit and man [76].

The normal T wave in humans is always positive in lead I, nearly always positive or isoelectric in lead II, and positive, negative, or diphasic in leads III and a VF. The normal angle between the T-wave axis and QRS axis seldom exceeds 80°. The angle tends to be more narrow in persons with a vertical QRS axis, and wider in persons with horizontal QRS axis [42]. Immediately after birth and during the first few days of life, the T wave is usually upright in the right precordial leads but afterward it becomes negative in the leads extending from V_4R to V_2, and sometimes to V_3. The gradual change from a negative to positive T wave in these leads occurs during childhood and adolescence. In the majority of the normal adults, the T wave is upright in the leads V_2 to V_6. A "juvenile pattern" is an ECG with negative T waves in the right precordial leads occur in young adults without heart disease. The term implies a failure of normal evolution from the childhood pattern to the adult pattern. Several studies of normal persons below age 40 have shown that negative T waves in leads V_2 and V_3 occur more frequently in black than in white persons. In young, healthy black persons, negative T

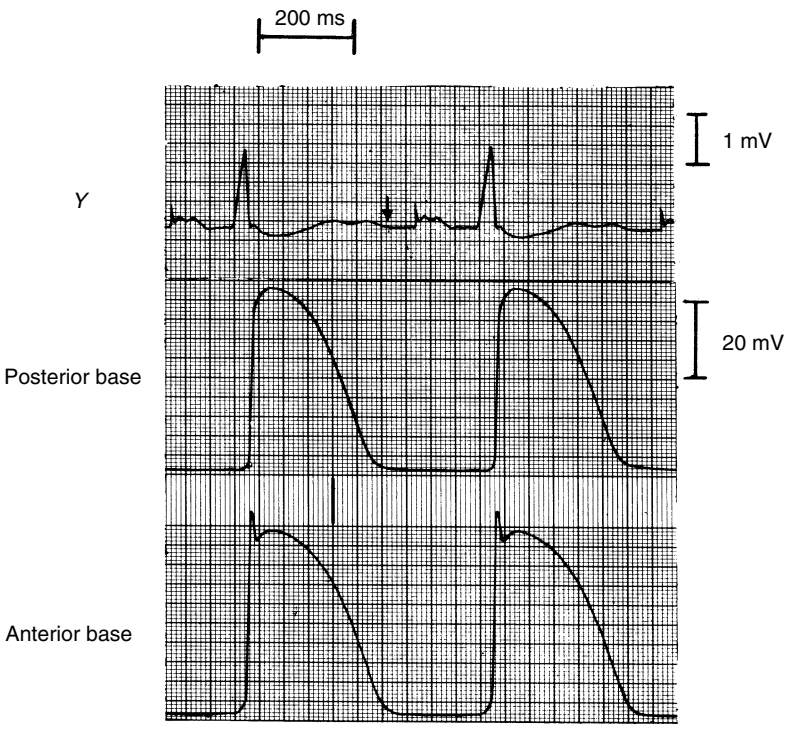

	Activation time ms	Duration ms
Anterior base	29	274
Posterior base	35	252

Figure 17.13

Typical example of the differences between two MAPs from two different sites. The T wave is upright and bifid. The arrow marks the end of the T wave. Heart rate is kept constant by atrial pacing. (After Autenrieth et al. [52]. © Mosby, St Louis, Missouri. Reproduced with permission.)

waves may occasionally be present even in the leads V_4 and V_5. However, in persons above age 40, the negative T waves in the right precordial leads rarely indicate a juvenile pattern.

Another rare normal variant is an isolated negative T wave in the midprecordial leads V_3 and/or V_4. In such cases, the T wave tends to be diphasic rather than frankly negative. In cases of isolated negative or biphasic T wave in the midprecordial leads occurring in the absence of heart disease, the area of the T wave abnormality over the precordium is small, and shifting the electrodes downward will usually reveal an upright T wave.

Consistent with the smooth course of phase 3 of the ventricular AP, the T wave is smooth and rounded, and contains little frequency content in excess of 10 cycles s^{-1}. The apex of the T wave is reached after an interval amounting to 68–84% of the QT interval [6]. As a rule, the ascent of the normal T wave is longer than the descent, whereas the ascent of the U wave is shorter than its descent (Fig. 17.15, see below). The apex configuration of the T wave helps to differentiate between the T wave and the P wave, which usually displays notches that are indicative of higher frequency components. However, when the T wave is notched in the precordial leads, a second summit may be as pointed as a P wave.

The duration of the Q–aT interval depends on the heart rate in the same manner as the QT interval, but the duration of the interval from the apex to the end of the T wave (aT–eT interval) changes normally only slightly with changes in

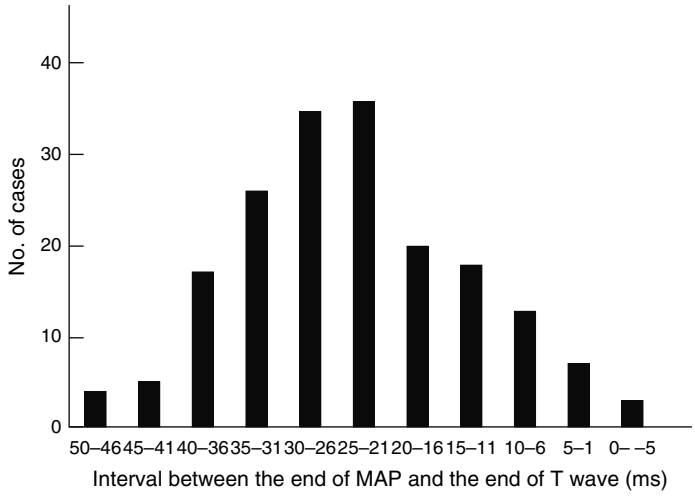

Figure 17.14

Distribution of the intervals between the end of the monophasic action potential (MAP) and the end of the T wave in 178 tracings. (After Autenrieth et al. [52]. © Mosby, St Louis, Missouri. Reproduced with permission.)

Figure 17.15

The difference between the configuration of the T wave and the U wave in a normal ECG. The consecutive vertical lines from left to right show the beginning, apex, and end of the T wave, followed by the beginning, apex, and end of the U wave. Note that the ascent of the T wave is longer than its descent – that is, similar to the course of repolarization of ventricular and Purkinje fibres – whereas the ascent of the U wave is shorter than its descent. The duration of the QT interval is 420 ms; the duration of the QU interval is 680 ms. (Reproduced from Surawicz: U wave: facts, hypotheses, misconceptions, and misnomers. *J. Cardiovasc. Electrophysiol.* 1998;9: 1117–1126, © Wiley, Reproduced with permission.)

rate [4]. Thus, the difference between the intervals at a rate of 50 min^{-1} and at a rate of 100 min^{-1}, averaged 70 ms for the end of the QRS–aT interval and 15 ms for the aT–eT interval [4].

Vectorcardiography is a major alternative way of expressing electrical activity during repolarization. Vectorcardiography may have certain advantages over the ECG because it can record the sense of rotation, the speed of inscription, and the form of the T loop expressed by Chou et al. [75] as length–width ratio (L/W ratio).

The studied characteristics of the T loop have included:

1. The direction of the maximal vector in the frontal, horizontal, and right sagittal planes,
2. The magnitude of the maximal vector in each plane,
3. The L/W ratio,
4. The rotation of the T loop in each plane,
5. The speed of inscription, and
6. The QRS/T angle.

The normal T loop [75] in adults is a long ellipse with the L/W ratio of >2.6 (average 7.16 ± 4.18). The amplitude of the maximal vector lies in the range 0.2–0.75 mV (mean 0.5 mV in frontal and horizontal planes, and 0.4 mV in the right sagittal plane). The normal T-wave loop is directed to the left, anteriorly, and inferiorly. In the horizontal plane, the T-loop inscription is characteristically counterclockwise, occasionally not definable because of a very narrow loop, and rarely clockwise. In the right sagittal plane, it is clockwise and very rarely counterclockwise with a narrow loop. In the frontal plane it is either clockwise or counterclockwise. As a rule, the inscription of the efferent portion of the loop is slower than that of the afferent portion of the loop. The QRST angle shows marked variation in horizontal and right sagittal planes but is usually < 28° in the frontal plane. The spatial QRST angle ranges from 26 to 134° [75].

17.3.3 Classification of T-Wave Abnormalities

The concept of ventricular gradient allows one to define the primary and the secondary T-wave abnormalities according to their independence or dependence on changes in the QRS complex [41, 76, 77]. A "secondary" T wave is a deflection, which would follow a given QRS complex if ventricular recovery properties were uniform. Therefore, the area of primary T wave is equal to ventricular gradient and the primary T wave describes variations of the ventricular gradient as a function of time [54]. The concept was tested in a theoretical model consisting of 1,675 elements of left ventricular myocardium [78]. The satisfactory feature of this model was that the derived secondary T waves under zero-gradient conditions were independent of the sequence of activation. However, in another series of correlations the derived primary T wave was compared with the T wave generated by means of total instantaneous depolarization. The two waveforms were closely related but by no means identical. Calculations of this type suggest that although the concept of primary and secondary T waves may be clinically applicable, the accurate quantitative analysis of the components of repolarization is difficult to perform.

Table 17.2 shows that primary abnormalities may be caused first, by a uniform alteration in the shape or duration of all ventricular APs without a change in the sequence of repolarization [60]; and second, nonuniform changes in shape or duration of the ventricular APs resulting in an altered sequence of repolarization [79]. Abnormal T waves may also be caused by various combinations or primary and secondary mechanisms, as presented in Table 17.2.

Certain types of primary T-wave abnormalities are labeled as "functional" or "nonspecific." Neither of these two categories can be precisely defined. Functional T-wave abnormalities are usually aggravated by hyperventilation and corrected by reassurance, potassium [80], and isoproterenol administration. Functional abnormalities reportedly occur more frequently in blacks and in young persons with anxiety or psychiatric disorders [81, 82]. The present criteria for separating "functional" from "organic" T-wave abnormalities are based more on the results of clinical evaluation rather than on any particular electrocardiographic characteristics [2].

Table 17.2
Classification of T-wave abnormalities

Sequence of depolarization	Shape and duration of ventricular AP	Sequence of repolarization	Type of abnormality
Abnormal	Normal	Abnormal	Secondary
Normal	Uniformly abnormal	Normal	Primary
Normal	Nonuniformly abnormal	Abnormal	Primary

The term nonspecific implies an abnormality of unknown cause. This term is popular among electrocardiographers, but is usually unsatisfactory to the physician who receives the report [84]. The use of the term nonspecific abnormalities should decline with increasing recognition of various specific causes of T-wave abnormalities. In practice, it is helpful to follow the term nonspecific by some clarifying descriptor, e.g., minor, slight, compatible with myocardial ischemia, etc.

The term "rapidly reversible primary T-wave abnormality" has been introduced to characterize a category of primary T-wave abnormalities, which disappear spontaneously with changes in posture or heart rate, or within minutes after the administration of certain drugs. Rapidly reversible T-wave abnormalities are not synonymous with "labile" T-wave abnormalities, which only represent cases of spontaneous variability. The category of rapidly reversible primary T-wave abnormalities includes most cases with functional and nonspecific T-wave abnormalities, but does not exclude T-wave abnormalities in patients with documented heart disease or with abnormalities caused by known extracardiac factors.

17.3.4 Secondary T-Wave Abnormalities

In theory, secondary T-wave abnormalities can be recognized by measuring ventricular gradient planimetrically, or by correlating the sequence of depolarization with the sequence of repolarization in the maps of local MAPs on the body torso. Neither method is practical. Haws and Lux [83] have shown that the time from the onset of activation to the V_{max} of T wave in the unipolar electrograms in dogs correlated with the duration of APs with an accuracy of up to 24 ms. This method of estimating APD simplifies the interpretation of precordial mapping in humans. Yamaki et al. [84] applied this method to differentiate between secondary and primary T-wave changes using an array of unipolar body surface leads. Secondary T-wave abnormalities can be expected under any condition of altered sequence of depolarization. In practice, the recognition of secondary T-wave abnormalities is not difficult when the T-wave vector deviates in a direction opposite to that of the main QRS vector in the presence of ventricular hypertrophy, or left bundle branch block patterns. Also, a secondary T-wave is directed opposite to the slow terminal QRS component in the presence of right bundle branch block, and opposite to the delta wave in the presence of a ventricular preexcitation pattern. However, the recognition of the secondary T-wave abnormalities may be difficult in the presence of conduction disturbances accompanied by independent primary T-wave abnormalities such as peri-infraction block, hyperkalemia, or quinidine-like antiarrhythmic drugs. An illustrative example of secondary T-wave changes is shown in Fig. 17.16 from a subject with Wolff–Parkinson–White syndrome and varying degree of preexcitation. Planimetric measurement showed that in all complexes the QRST area was approximately the same.

In the typical "left ventricular strain pattern," the T wave is inverted and the ST segment is depressed in leads in which the QRS area is positive; that is, usually in left precordial leads, and limb leads I and II. If the QRS complex is upright in lead III, the T wave is inverted in all three limb leads ("concordant left ventricular strain pattern"). In some cases, the T wave is upright in lead I but inverted only in one or more of the left precordial leads and in lead aVL. The secondary T wave abnormalities caused by left ventricular hypertrophy reflect an abnormally wide QRST angle in both the frontal and the horizontal planes in the presence of an unchanged ventricular gradient. During typical evolution of the left ventricular strain pattern, the phase of T wave lowering precedes the stage of inversion. When the T wave is low but upright, the

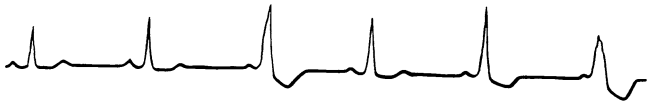

Figure 17.16

Example of secondary T-wave changes caused by ventricular preexcitation. The consecutive ventricular electrocardiographic complexes represent conduction without preexcitation (*first complex*), during presumed maximal preexcitation (*last complex*), and varying degrees of fusion complexes. Note widening of the QRS/T angle and association of T-wave changes with depression of ST segment whereas the QRST area is approximately the same in all complexes. (Reproduced with permission from Suracwicz, B., *Electrophysiological Basis of Electrocardiogram and Cardiac Arrhythmias*. Williams & Wilkins, Baltimore, MD, 1995, p. 584.)

secondary abnormalities of T wave amplitude should be suspected when the QRST angle is abnormally wide or when the T wave amplitude is less than about 10–15% of the R-wave amplitude. In patients with arterial hypertension, the changes in the magnitude of secondary T wave abnormalities sometimes correlate with the efficacy of hypertension treatment.

In patients with aortic valve disease, the evolution of the secondary T-wave abnormalities tends to parallel the progression of left ventricular hypertrophy and dilatation. However, in young patients with uncomplicated aortic regurgitation, T waves may remain upright in the leads with increased amplitude of R wave. The same may be observed in other conditions associated with the so-called left ventricular diastolic overload pattern; for example, ventricular septal defect with a large left-to-right shunt, or patent ductus arteriosus.

In a typical pattern of "right ventricular hypertrophy and strain," for example, in patients with pulmonary valvular stenosis, tetralogy of Fallot, or severe pulmonary hypertension, T wave inversion and ST segment depression are present usually in leads in which the QRS area is positive – leads II, III, and right precordial leads. In such cases the QRST angle is wide, and the T wave is upright in the leads in which the QRS area is negative – lead I, and the left precordial leads. In the presence of acute cor pulmonale (pulmonary embolism, for example), transient T-wave changes are probably primary and not secondary. In patients with chronic lung disease and deep S waves in the limb and left precordial leads, the T wave tends to be in an opposite direction to the main QRS axis.

In the presence of right bundle branch block, the T-wave vector is oriented opposite to the vector of the terminal wide QRS component. The constancy of QRST area in many cases of intermittent right bundle branch block, or during progression from incomplete to complete right bundle branch block, has generally validated the concept of ventricular gradient.

In the presence of left bundle branch block, the T wave is usually directed oppositely to the main QRS axis. Therefore, the negative T waves in the leads with a deep S wave are indicative of additional primary T-wave abnormalities (Fig. 17.17). However, the persistence of an upright T wave in leads with a tall R wave-lead I or V_6 does not have the same implication since it may simply result from lowering of a T wave that had been taller in the absence of left bundle branch block, or other unexplained factors. Secondary T-wave inversion owing to left bundle branch block is usually associated with a depressed ST segment and the ascending limb of the inverted T wave being steeper than the descending limb [42].

In the vectorcardiogram of a left ventricular hypertrophy pattern, the T loop shifts rightward, inferiorly, and either anteriorly or posteriorly; the spatial QRST angle increases, the T loop becomes wider and therefore the L/W ratio decreases. The T-loop inscription in the frontal plane is counterclockwise in approximately one-third of all patients. In 75% of patients with clockwise horizontal T loops, the T loop is located within the 90–180° quadrant although only 40% of T loops located within this quadrant are inscribed clockwise. Left bundle branch block produces changes in T loops similar to those in left ventricular hypertrophy. In right ventricular hypertrophy (RVH), the T-loop vector shifts posteriorly but maintains the leftward orientation; it becomes wider and the L/W ratio decreases [85]; the rotation in the horizontal plane is frequently clockwise and in the right sagittal plane, counterclockwise. The T-loop changes in right bundle branch block [86, 87] are also similar to those in right ventricular hypertrophy.

17.3.5 Primary T-Wave Abnormalities

17.3.5.1 Ventricular Transmembrane Action Potentials

T-wave abnormalities caused predominantly by uniform changes in the shape or duration of ventricular transmembrane action potentials include abnormalities of ventricular repolarization induced by drugs or abnormal electrolyte concentrations. The majority of such abnormalities can be attributed to changes in the slope of phase 3 alone, or to combined changes in the slope of phase 2 and 3 of the ventricular AP.

17.3.5.2 Cardiac Glycosides

The principal abnormalities of ventricular repolarization produced by digitalis are the result of shortening of phase 2, decreased slope of phase 3, and absolute shortening of the ventricular AP. The earliest ECG change in repolarization

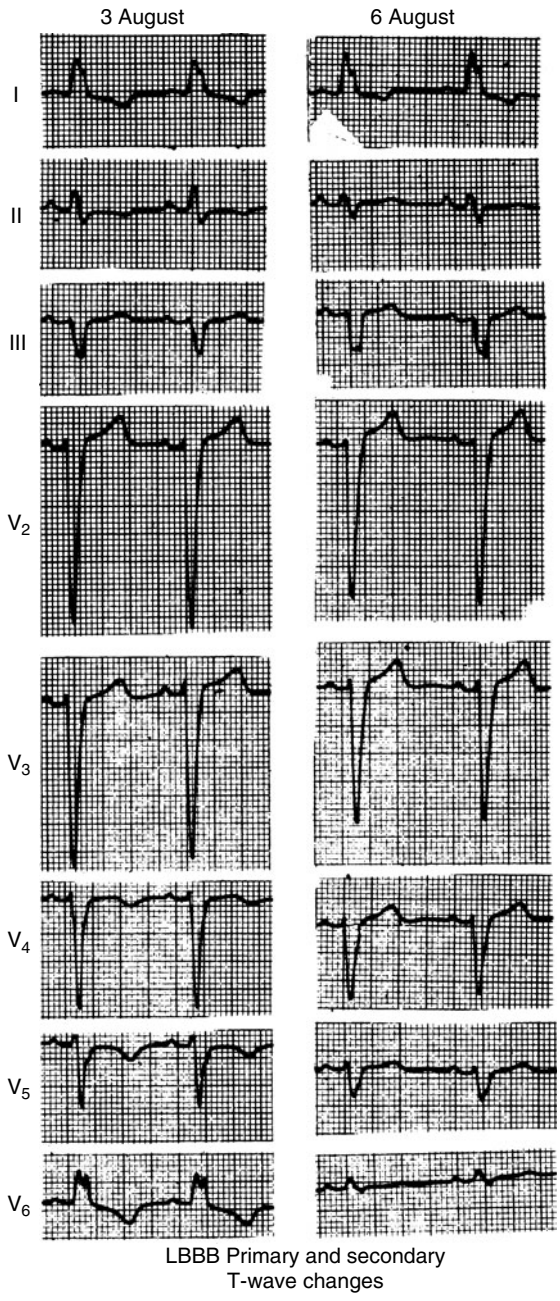

Figure 17.17

Electrocardiograms of a patient with left bundle branch block (LBBB) and myocardial infarction. The negative T waves in V_4–V_5 on August 3 represent primary T-wave abnormalities that are no longer present on August 6.

produced by digitalis consists of a decrease in T-wave amplitude and shortening of the QT_c interval. These changes are followed by the depression of the ST segment, decrease in the ventricular gradient, and inversion of the T wave. Although lowering of the T wave can occur without the depression of the ST segment, the inversion of the T wave is nearly always associated with ST depression. Initially, the entire ST segment is slightly depressed, but later the terminal portion becomes more depressed, making an angle of about 90° with the ascending limb of the T wave (Fig. 17.18).

Figure 17.18

Electrocardiograms of a patient who received a last maintenance dose of 0.1 g of digitalis leaf on August 6. Note diphasic T wave and depression of ST segment, which makes an angle of almost 90° with ascending limb of T wave in the first two tracings. Digitalis effect on the ECG disappeared within 6 weeks (bottom trace). (Reproduced from Surawicz and Lasseter [90]. © Grune and Stratton, New York. Reproduced with permission.)

Later the ST segment has a steep downward course and the T wave appears diphasic (negative–positive). These changes are usually most pronounced in leads that have the highest QRS complex [42].

The effects of digitalis on ventricular repolarization may simulate the patterns of left ventricular hypertrophy, acute ischemia, and various nonspecific repolarization abnormalities. The abnormalities of repolarization produced by digitalis are frequently more pronounced at rapid rather than at slow heart rates, possibly because phase 2 of the AP is shortened more at rapid heart rates [86, 87]. The ST abnormalities produced by digitalis during exercise-induced tachycardia are similar to changes attributed to acute myocardial ischemia. Thus, digitalis may cause a false positive exercise test.

In addition to the usual T-wave abnormalities, digitalis may produce two atypical patterns: pointed inverted T waves [42] and peaking of the terminal T-wave portion [90]. The pointed inverted T wave is similar to the T wave arising from myocardial ischemia or pericarditis, but is associated with shortened QT_c interval. This interval is usually normal in pericarditis and prolonged in myocardial ischemia. Peaking of the terminal portion of the T wave was observed in about 10% of patients receiving digitalis and was sometimes, but not always, related to increased plasma K^+ concentration [88, 89].

Although in an individual patient digitalis administration usually produces progressive ECG changes, there is no satisfactory correlation between the dose and such changes. The individual variations depend on the underlying ECG pattern and the rhythm. In some patients, the effects of digitalis on repolarization cannot be recognized even in the presence of toxicity manifested by nausea, vomiting, or ectopic complexes [90]. With the advent of routine measurements of blood digoxin concentrations there has been an appreciable decline in digitalis toxicity and marked ECG abnormalities.

17.3.5.3 Class IA Antiarrhythmic Drugs

Increasing doses of quinidine progressively increase the QRS duration. The most pronounced ECG changes are produced by quinidine, the use of which has markedly declined, but the ECG effects are most characteristic for a type 1A drug.

Typically, the entire QRS complex widens uniformly, but sometimes the widening predominantly affects the terminal portion. In the absence of QRS widening, quinidine produces primary T-wave changes but in the presence of a wide QRS, the T-wave abnormalities may be a result of a combination of primary and secondary changes. Quinidine prolongs the duration of the T wave and QT_c interval. In leads with upright T waves, the T wave initially becomes lower and later becomes notched or slightly inverted; in leads with inverted T waves, the T wave becomes less deeply inverted. These T-wave alterations usually occur without concomitant depression or elevation of the ST segment, but are accompanied by an increased U-wave amplitude [42, 91]. When QRS widening becomes pronounced, the secondary T-wave changes may alter the T-wave vector; usually the T-wave vector moves in the direction opposite the wide portion of the QRS complex. The peak effect of quinidine on the ECG occurs within about 2–4 h after the oral administration of the drug. This effect is reduced by about 50% after 12 h.

The T-wave changes produced by quinidine and other antiarrhythmic drugs in class 1A category can be attributed to the prolongation and decreased slope of phase 3 in ventricular AP [5]. The latter effect also explains the increase in the U-wave amplitude, although lowering of plasma K^+ concentration, which may be produced by quinidine, can contribute to this effect [92].

Abnormalities of ventricular repolarization produced by doses of quinidine that result in plasma-quinidine concentrations of less than about 5.0 mgl^{-1} are difficult to distinguish from various nonspecific T wave abnormalities. However, the combination of the QRS, T- and U-wave changes produced by higher doses results in a fairly specific ECG pattern. Digitalis exaggerates quinidine-induced abnormalities of repolarization by lowering the T-wave amplitude and increasing the U-wave amplitude. In addition, digitalis shortens phase 2 of the ventricular AP and causes depression of the ST segment. Therefore, the combination of digitalis and quinidine produces an ECG with a depressed ST segment, low T wave, and a prominent U wave. This pattern is indistinguishable from the pattern produced by severe hyperkalemia [93]. It has been mentioned earlier that quinidine does not depress the ST segment, probably because phase 2 of the ventricular AP is not appreciably altered by the drug. In contrast to digitalis, quinidine may prevent the appearance of ST depression during exercise and thus may contribute to a false-negative response to exercise [94].

Procainamide and ajmaline alter the ECG in the same manner as quinidine, but the effect of the customary maintenance dosages is usually less pronounced. In patients treated with 1–2 g of procainamide per day, the QRS interval becomes wider, the QT_c is prolonged, the T wave becomes notched, and the U-wave amplitude may be increased [95–97]. Like quinidine, the combination of procainamide with digitalis produces an ECG pattern simulating hypokalemia. Procainamide is a shorter-acting drug than quinidine; therefore, its effect on the ECG appears earlier and persists for a shorter time.

Disopyramide prolongs QRS and QT intervals and causes primary and secondary T-wave changes similar to those produced by quinidine and procainamide.

17.3.5.4 Class III drugs

Class III action prolongs T-wave duration most often by blocking one of the potassium channels, but it may be produced by other mechanisms, such as increased inward sodium current. Some of the potassium channel–blocking drugs in this category are sotalol, amiodarone, bretylium, dofetilide [98], ibutilide [99], sematilide [100], and almokalant [101]. On the ECG, these drugs prolong the QT and JT interval without QRS prolongation (with the exception of amioadorone) and exhibit the property of reversed use dependence.

17.3.5.5 Phenothiazines

The effects of phenothiazines on ventricular repolarization are very similar to those of quinidine. Studies of the phenothiazine effect on the canine ventricular AP have shown that these drugs prolong the duration of phase 3 and either do not change or shorten the duration of phase 2 [102]. These effects explain the quinidine-like repolarization abnormalities in the ECG induced by therapeutic doses of chlorpromazine and thioridazine.

Several phenothiazine derivatives produce dose-dependent reversible abnormalities of ventricular repolarization. These abnormalities occur most commonly after the administration of thioridazine. They are apparently less pronounced

after chlorpromazine and even less so after trifluoperazine [103]. The earliest ECG change produced by phenothiazines consists of lengthening of the QT_c interval, and widening, blunting, and notching of the T wave. Higher doses produce lowering and inversion of the T wave in the standard limb and precordial leads [104, 105]. The effects may be more pronounced in the right than in the left precordial leads. Sometimes, lengthening of the QT_c interval may occur in the absence of appreciable T-wave abnormalities. The U-wave amplitude is frequently increased, but ST changes are usually absent.

17.3.5.6 Hyperkalemia

Peaking of the T wave is the earliest electrocardiographic manifestation of hyperkalemia (Fig. 17.19). Peaking occurs when the plasma K^+ concentration exceeds 5.5 $mEq l^{-1}$, usually before the ECG shows any measurable alteration of the QRS complex [106–108]. The diagnosis of hyperkalemia cannot be made with certainty on the basis of T-wave changes alone. The characteristic tall, steep, narrow, and pointed T wave was found in only 22% of patients with hyperkalemia [109]. In the remainder of patients, the tall T waves were very similar to tall T waves in patients with bradycardia, psychiatric disorders, cerebrovascular accidents, left ventricular diastolic overload, subendocardial ischemia, and in some individuals with no apparent abnormalities. When the tall, peaked T wave is the only electrocardiographic abnormality produced by hyperkalemia, and the duration of the QRS complex and of the ST segment is normal, the QT_c interval is either normal or decreased. In the presence of a pattern of advanced hyperkalemia with a wide QRS complex, the T wave may lack its characteristic peaked and narrow configuration, probably because the T-wave abnormalities secondary to intraventricular conduction disturbances obscure the primary T-wave changes caused by the increased steepness of phase 3 of the AP.

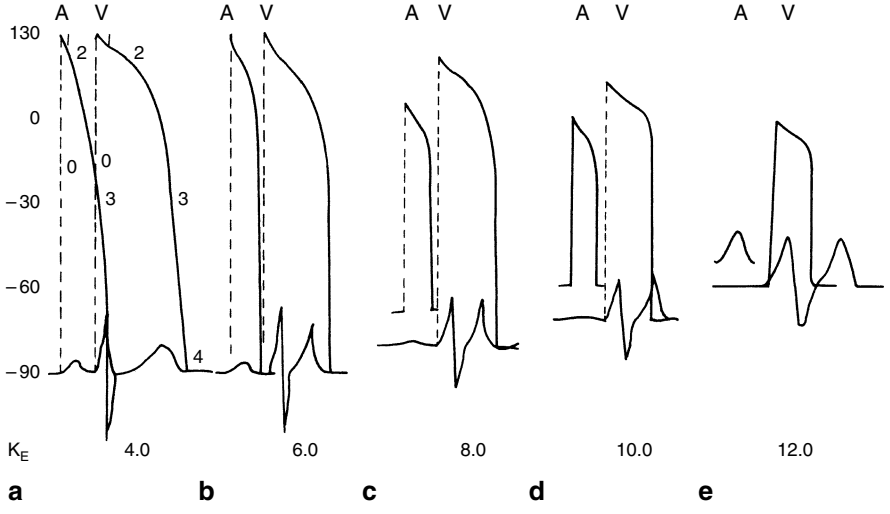

Figure 17.19

Diagram of an atrial (A) and a ventricular (V) action potential (AP) superimposed on the electrocardiogram. The numbers on the left designate the transmembrane potential in millivolts (mV) and the numbers at the bottom, the extracellular concentration of potassium (K_E) in milliequivalents per liter (mEq l^{-1}). In tracings (a) and (b), the resting membrane potential (RMP) is −90 mV, whereas the total amplitude of the AP is 130 mV because the upstroke overshoots the 0 potential by +40 mV. Note the shortening of the AP, the increased velocity of phase 3, the progressive decrease in RMP, and in the amplitude of the AP with increasing K_E. The most rapid upstroke of the AP is shown as a line interrupted by wide spaces ((a) and (b)); the slowest upstroke is shown as a continuous line (atrial AP in (d) and ventricular AP in (e)). Note the decreasing upstroke velocity and the increasing duration of the QRS complex with increasing K_E. In (a) and (b), the atrial and the ventricular AP have the same RMP and the same amplitude, whereas in (c) and (d), the RMP of the atrial AP is less negative than the RMP of the ventricular AP, and the amplitude of the atrial AP is lower than that of the corresponding ventricular AP. See text for further discussion. (After Surawicz [9]. © Mosby, St Louis, Missouri. Reproduced with permission.)

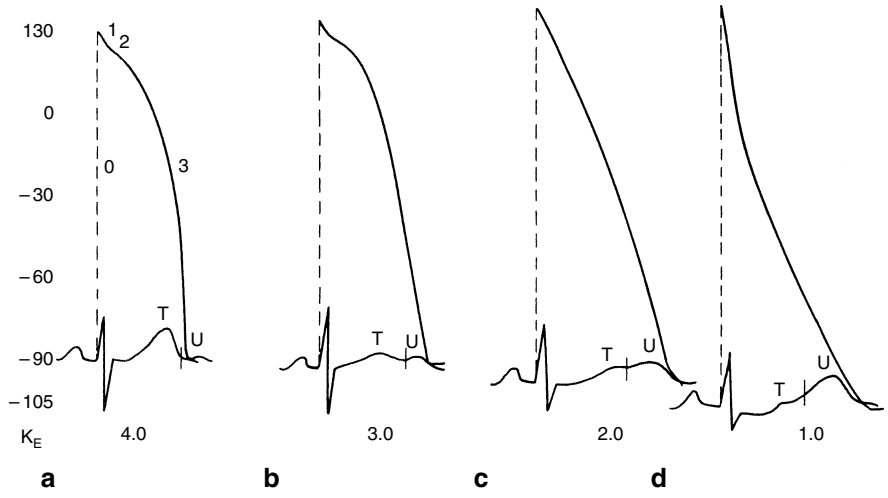

Figure 17.20

Diagram of the ventricular AP superimposed on the electrocardiogram for extracellular concentration of potassium (KE) of (a) 4.0, (b) 3.0, (c) 2.0, and (d) 1.0 ml^{-1}. The numbers on the left designate the transmembrane potential in millivolts, as in Fig. 15.18. The RMP, the amplitude of the AP, and the overshoot in the control tracing (a) are the same as for the ventricular AP in Fig. 17.19. Note the progressively increasing velocity of phase 2, decreasing velocity of phase 3, and increasing duration of the AP. Furthermore, note the progressive increase in the RMP (more negative), and the increasing amplitude of the AP. The electrocardiographic changes are described in the text. (After Surawicz [9]. © Mosby, St Louis, Missouri. Reproduced with permission.)

17.3.5.7 Hypokalemia

The changes in the shape of the AP (Fig. 17.20) are reflected in the ECG as a progressive depression of the ST segment, a decrease in the T-wave amplitude and an increase in the U-wave amplitude in the standard limb and precordial leads. As long as the T wave and the U wave are separated by a notch, the duration of the QT interval is unchanged [93, 110] In more advanced stages of hypokalemia, the T wave and the U wave are fused and an accurate measurement of the QT interval is not possible.

It has been suggested that in hypokalemia, the U wave is superimposed on the gradually increasing diastolic potential produced by the prolonged duration of the ventricular repolarization [111]. If this assumption is correct, then the progressive increase in U-wave amplitude in hypokalemia may be more apparent than real. This concept finds some support in the observations that the intervals from the onset of the QRS complex to the apex and the end of the U wave (Q–aU and Q–eU. intervals) are not altered during the development and regression of the pattern of hypokalemia [9].

17.3.5.8 Combination of Abnormal Potassium and Calcium Concentration

In patients with hypokalemia and hypocalcemia, the ECG shows a prolonged ST segment and a prominent "repolarization" wave, which consists of T + U waves. This is owing to a prolongation of both phase 2 and phase 3 of the AP [4] (Fig. 17.21). The recognition of the hypokalemia pattern in the presence of hypocalcemia may be facilitated by the administration of calcium, which shortens the ST segment and separates the T wave from the U wave [93]. The combination of hypocalcemia and hyperkalemia, which frequently occurs in patients with uremia, can be recognized by the presence of a prolonged ST segment and a peaked, narrow T wave.

An increased extracellular concentration of calcium decreases the duration of phase 2 and the ventricular AP becomes similar to the normal atrial AP [112]. In patients with hypercalcemia, the ST segment is short or absent, and the QT_c

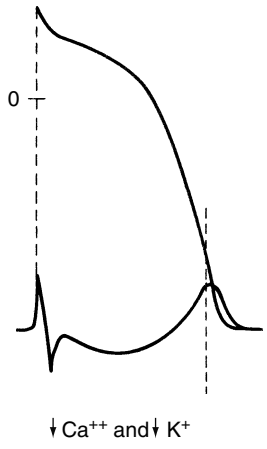

Figure 17.21

Ventricular AP and electrocardiogram from isolated perfused rabbit heart (retraced) during perfusion with low-calcium, low-potassium Krebs–Henscleit solution. Note the prolonged duration of phase 2 and slow slope of phase 3. The corresponding ECG changes are prolonged and depressed ST segment, and wide repolarization T + U wave. The interrupted vertical line bisecting the apex of the T wave represents the end of mechanical systole.

interval is shortened. However, the U-wave amplitude is either normal or increased. In patients with hypercalcemia and hypokalemia, the ECG shows a short ST segment and a prominent repolarization wave, which consists of T + U waves (9).

17.3.6 T-Wave Abnormalities Caused by Nonhomogeneous Repolarization

This category of primary T-wave abnormalities [113] accounts for the largest number of structural and functional disturbances of ventricular repolarization. Characteristically, these abnormalities affect only the T wave and do not alter either the course or the duration of the ST segment. In the normal ECG, the apex of the T wave is reached at the time corresponding to 68–84% of the entire QT interval [6]. The duration of the Q–aT interval depends on the heart rate in the same manner as that of the QT interval, but the duration of the interval from the apex to the end of the T wave (aT–eT interval) is similar in all normal persons and changes only slightly with changes in rate [6]. Thus, the difference between the intervals at a rate of 50 min^{-1} and at a rate of 100 min^{-1} averaged 70 ms for the end of the QRS–aT interval and 15 ms for the aT–eT interval [6].

T-wave abnormalities owing to asynchronous repolarization may be associated with a prolonged or normal QT_c interval. The QT_c lengthening is usually attributed to some regional increase in the AP duration. Primary T-wave abnormalities as a result of nonhomogeneous repolarization are frequently associated with an increased duration of the aT–eT interval. This suggests that the regional alterations of AP duration may arise from differences in the duration of phase 3.

17.3.6.1 Syndrome X

The label of syndrome X has been pinned to several different groups of patients who have in common angina-like chest pain and no evidence of obstructive disease in the large coronary artery branches. In some of these groups there is evidence of either myocardial ischemia induced by stress or abnormal vasomobility of coronary microvessels. Some individuals with this syndrome have inverted T waves in many leads. In one study of such patients, the presence of symmetrical inverted T waves at rest was associated with a coronary vasoconstrictor response to cold pressor test [114]. In other studies, evidence of myocardial ischemia was present in some but not in all patients with syndrome X and abnormal T waves. Also, presence of stress-induced ST segment depression in patients with syndrome X occurs with and without myocardial

ischemia. Lactate metabolism, oxygen saturation in the coronary sinus, regional myocardial perfusion, and left ventricular wall motion abnormalities in these patients may be or may be not abnormal [114–119].

17.3.6.2 Pericarditis

The T-wave vector in patients with pericarditis is usually directed to the right and superiorly. In typical cases, the T wave becomes inverted in all standard leads with the exception of leads aVF and V_1. The T-wave inversion usually persists after the disappearance of ST abnormalities and is attributed to superficial myocarditis (epicarditis). Unlike myocardial infarction, the interval between the nadir of the negative T wave and its end is usually not prolonged, and the duration of the QT_c interval is normal [12]. The direction of the T-wave vector in pericarditis suggests prolongation of activity in the damaged fibers. Histological studies suggest that the damage is limited to a thin subepicardial layer of myocardium. Accordingly, pericarditis appears to represent an example of a large T-wave abnormality produced by a relatively small mass of abnormal myocardium extending over a wide surface area.

17.3.6.3 Other T-Wave Abnormalities Attributed to Myocardial Damage

The primary "coronary" or "postischemic" T-wave pattern with a normal ST segment, abnormal T vector, pointed T wave, and prolonged QT interval may appear in patients with various types of pathologic processes, including, among others, pulmonary embolism, acute cor pulmonale, myocardial tumor, abscess, and acute myocarditis caused by diphtheria, brucellosis, malaria, trichinosis, rheumatic fever, mumps, measles, scrub typhus, and various other infections [42, 120]. Similar T-wave changes may be caused by acute and chronic cardiomyopathy of obscure etiology [121], Friedreich's ataxia [122, 123], chest trauma [124], lightning stroke [125], various poisons, e.g., phosphorus [126], carbon monoxide [127], venoms, adder bite [128], scorpion sting [129], and certain drugs e.g., emetine, chloroquine, plasmoquin, antimony compounds, lithium, and arsenicals [66, 110]. These abnormalities are probably caused by transient or permanent prolongation of repolarization in certain regions of the heart. They usually regress slowly after the recovery from the disease or after the elimination of the noxious agent from the body. Some of these T-wave abnormalities may not be a result of organic myocardial damage but may arise from functional, neurogenic repolarization changes precipitated by the disease. For instance, in one patient with abnormal T waves attributed to myocardial damage produced by scorpion sting, autopsy did not reveal cardiac abnormalities and the ECG changes were thought to be a result of excessive catecholamine liberation [129]. T-wave abnormalities in patients with primary myocardial disease are usually secondary to QRS abnormalities produced by hypertrophy. However, in some patients, primary T-wave abnormalities precede the appearance of changes in duration, amplitude, or axis of the QRS complex [121, 130–132]. The mechanism of such T-wave abnormalities is unknown. A study by Coltart and Meldrum [133] demonstrated that the ventricular AP from a muscle band excised in a patient with hypertrophic cardiomyopathy had a slow slope of phase 3. The duration of this AP was 498 ms as compared to an average duration of 302 ms in eight control human subjects. This observation would adequately explain the primary T-wave abnormalities and prolonged QT_c interval in patients with hypertrophic obstructive cardiomyopathy.

Primary T-wave abnormalities frequently occur also in patients with mitral insufficiency owing to mitral valve prolapse [134] and with mitral insufficiency owing to a floppy mitral valve in patients with Marfan's syndrome [133]. In the majority of patients with mitral insufficiency owing to the former, the T waves are flat or inverted in leads II and III, and the QT_c interval is prolonged [135–137]. The mechanism of these T-wave abnormalities is obscure. Myocardial ischemia is unlikely because these changes frequently occur in children and in young adults. In two young patients with such T-wave abnormalities and atypical chest pain, coronary arteriograms were normal [138]. It is possible that the T-wave abnormalities in this syndrome are caused by the similar factors that produce T-wave abnormalities in familial cardiomyopathy. This is because the mitral valve prolapse is associated with localized dysfunction of the left ventricular myocardium. On the other hand, it is conceivable that T-wave abnormalities are a result of prolonged repolarization in the abnormal left ventricular ridge described in this syndrome [136].

17.3.6.4 ECG Pattern of Cerebrovascular Accident

In 1954, Burch et al. identified a specific electrocardiographic pattern peculiar to certain patients with cerebrovascular accident (CVA) [139]. This pattern occurs most frequently in patients with intracranial hemorrhage [139–145] but has been also found in patients with other intracranial lesions, such as cerebral venous thrombosis, acute cerebral infarction [144], head injuries [145], neurosurgical procedures, and cryohypophysectomy [2].

Patients with the typical ECG pattern (Fig. 17.22) have one or more of the following abnormalities:

1. Prolongation of the QT_c interval by 20% or more,
2. T-wave amplitude exceeding 0.5 mV, and
3. U-wave amplitude exceeding 0.15 mV.

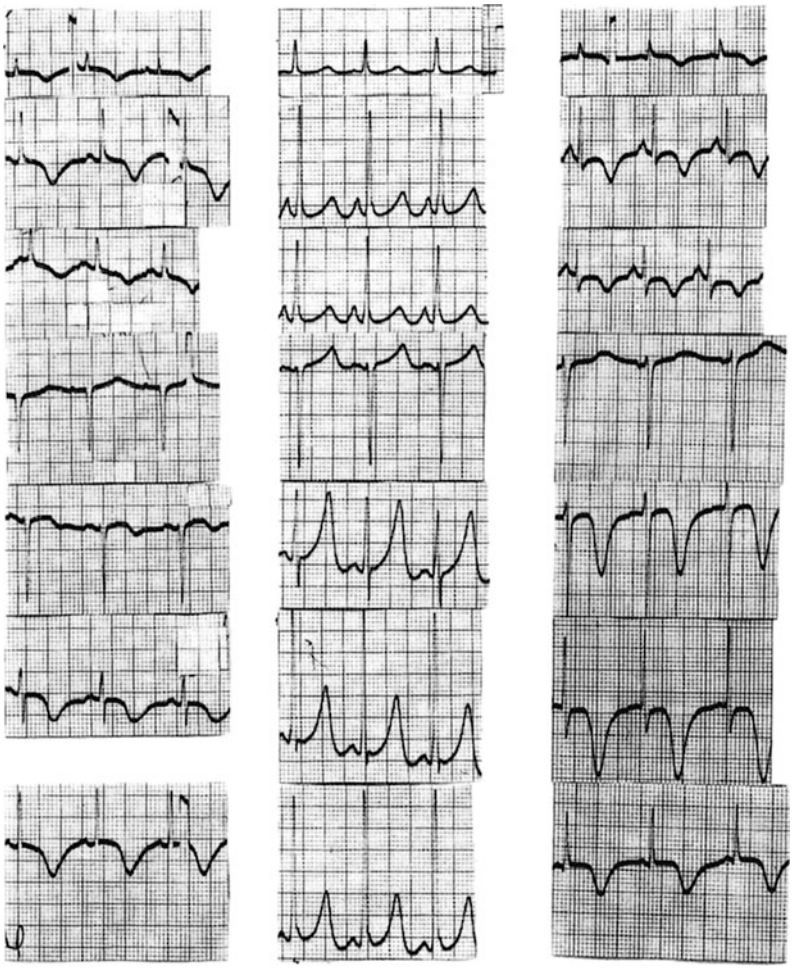

Figure 17.22

Three examples of ECG pattern in patients with subarachnoid hemorrhage. Note, prolonged QT and increased amplitude of negative (*left and right*) upright (*middle*) T wave.

ECGs with these abnormalities can be classified into five types:

1. Type I – QT_c is prolonged and T-wave amplitude is increased,
2. Type II – QT_c is prolonged and U-wave amplitude is increased,
3. Type III – only the QT_c interval is prolonged,
4. Type IV – T-wave and U-wave amplitudes are increased, and
5. Type V – the QT_c interval is prolonged and both T-wave and U-wave amplitudes are increased.

All of these patterns, particularly the "giant" T waves or "massive T inversion" may be caused by many other factors, such as electrolyte imbalance, hypertrophy, intraventricular conduction disturbances, myocardial infarction or ischemia [146–148], bradycardia, second- or third-degree atrioventricular (AV) block [147–149], and acute disease of abdominal viscera [150]. After the elimination of all patients with the above disorders, a CVA pattern was found in 60 of among approximately 45,000 ECGs recorded during the 4-year period 1965–1969 [151]. Of these, 48 patients with this pattern had intracranial lesions; in three patients, the pattern was attributed to hypothermia, and in one patient, to myxedema coma. In one patient, the pattern was recorded 1 day prior to a hypertensive crisis secondary to pheochromocytoma; in six patients without heart disease, the cause of CVA pattern was not established. The combination of long QT and increased T-wave amplitude (type 1) occurred in 78% of patients with the "CVA pattern" while other types were less common [2].

Schindler and Surawicz [151] also studied the prevalence of the CVA in various central nervous system (CNS) disorders. The CVA pattern was present in 32% of patients with intracranial hemorrhage, in 10% of patients with primary intracranial neoplasm, and in 7% of patients with acute cerebral thrombosis and increased intracranial pressure. The pattern was found only in one patient with hypertensive encephalopathy and in one of 32 patients with brain metastases. In two patients, the pattern appeared after cryohypophysectomy (Fig. 17.23). In these patients, the procedure also produced a transient diabetes insipidus. The CVA pattern and the diabetes insipidus regressed in both patients within a few weeks. Subsequently, the appearance of the CVA pattern after cryohypophysectomy in several other patients was observed. These observations suggest that the CVA pattern may arise from the injury of the hypothalamus. This hypothesis would

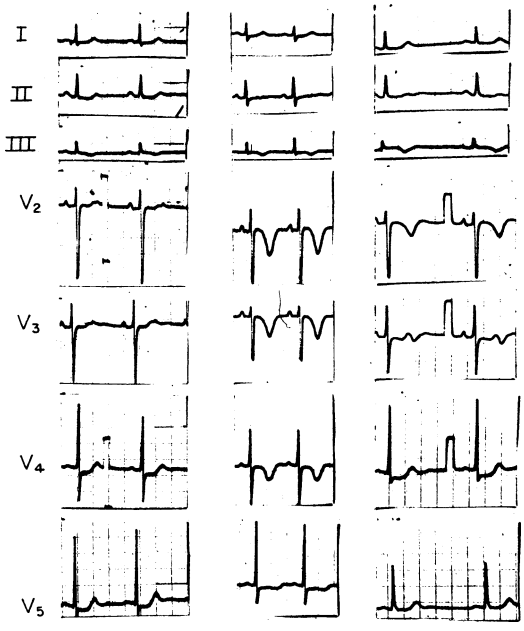

Figure 17.23

Electrocardiogram of a 52-year old woman, receiving 0.25 mg maintenance dose of digoxin, before (*left*) 3 days (*middle*), and 18 days (*right*) after cryohypophysectomy. (After Surawicz [2]. © Grune and Stratton, New York. Reproduced with permission from: Surawicz B, Knoebel SK. Long QT: good, bad and indifferent? J Am Coll Cardiol 1984;4: 398.)

explain the relatively high prevalence of this pattern in patients with subarachnoid hemorrhage because hypothalamic lesions occur frequently after the rupture of aneurysms of the anterior and posterior communicating arteries. In the study of Crompton, hemorrhagic lesions in the hypothalamus were present in 22 of 32 patients with a ruptured anterior communicating artery and in 19 of 27 patients with a ruptured posterior communicating artery [152]. Studies by Jenkins et al. demonstrated functional disturbances of hypothalamic function in the majority of patients with ruptured intracranial aneurysm [153].

Millar and Abildskov have shown that minor repolarization abnormalities (low or notched T waves, prolonged QT_c interval, and ST depression) occur more frequently in patients with various CNS disorders than in a control population [154]. In another study, T-wave inversion without prolongation of the QT_c interval occurred in 15% of patients with meningitis and intracranial space-occupying lesions [153]. These two studies suggest that many patients with CNS disease have less distinct T-wave abnormalities than the typical pattern described by Burch et al. [139].

17.3.6.5 Other T-Wave Abnormalities Associated With an Apparent Dysfunction of the Autonomic Nervous System

T-wave abnormalities in patients with various dysfunctions of the autonomic nervous system are probably caused by the effects of nonhomogeneous sympathetic stimulation on ventricular repolarization [2]. Such a mechanism may explain T-wave abnormalities preceding hypertensive crisis owing to pheochromocytoma, or abnormalities arising from adrenal and pituitary insufficiency [2]. Typically, the T waves in patients with endocrine disorders become normal after the correction of the hormonal deficiency. In patients with pituitary insufficiency, the correction of T-wave abnormalities may require several months of hormone replacement therapy. However, transient reversal to normal can be achieved by small doses of intravenously administered isoproterenol (Fig. 17.24).

Visceral reflexes are thought to be responsible for the rapidly reversible T-wave changes present in some patients with acute abdominal processes (cholecystitis, peritonitis, appendicitis, pancreatic necrosis, and ileus) [42]. These ECG abnormalities may simulate myocardial ischemia in patients without pathologic abnormalities of the heart and coronary vessels [155, 156].

T-wave abnormalities occur frequently in patients with acute and subacute pancreatitis [157]. This may be caused in some cases by pericarditis or myocardial necrosis induced by circulating enzymes from the damaged pancreas [158–161]. Also, a T-wave pattern resembling the CVA pattern, namely a wide, deeply inverted T wave and prolonged QT_c interval, was recorded in 10 of 106 patients after transabdominal truncal vagotomy for the treatment of peptic ulcer disease [162]. The authors of this report suggested that the ECG abnormalities could be a result of vagal reflex causing central autonomic stimulation or to catecholamine release in response to the parasympathetic stimulation [162].

Other neurogenic T-wave abnormalities have been reported with spinal cord injury [163] and in association with electroconvulsive therapy [164].

17.3.6.6 Giant and Global Negative T Waves

The designation of negative T wave as giant or global is based on impression rather than on specific measurements of the depth and with of the T wave. The term "global" was used by Walder and Spodick [165] who found such pattern in 100 cases among approximately 30,000 consecutive routine ECGs they interpreted. Eighty two of these patients were women. The QTc interval was prolonged. The most common causes were myocardial ischemia and central nervous system disorders. Other conditions included pericarditis, myocarditis, apicalhypertrophic cardiomyopathy (Fig. 17.25), cardiac metastases, carotid endarterectomy, cocaine abuse, and pheochromocytoma. In some cases, no associated condition was apparent. After following these patients for up to 11 years, the authors [166] concluded that their long-term prognosis depended on the underlying or associated disease, and that the striking diffuse T-wave changes per se do not imply poor prognosis. Brsic et al. [167] reported a series of 17 patients (all women) with "global" T-wave inversion with "ischemic" chest pain, normal coronary arteriograms, and intact left ventricular function [168]. In another series of nine patients (all women), the pattern was associated with acute cardiogenic but nonischemic pulmonary edema [169]. The ECG changes gradually resolved within 1 week and had no immediate prognostic implications. Another cause of "global" T inversion

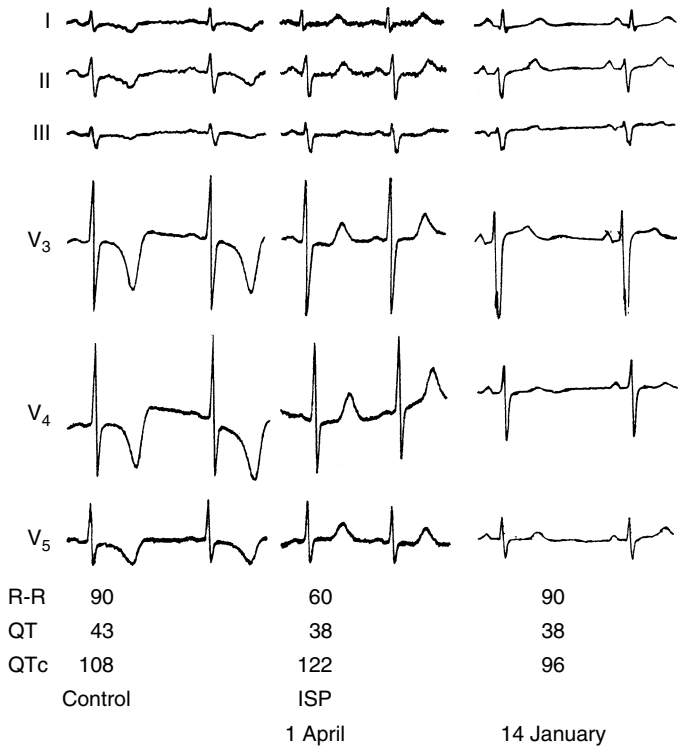

Figure 17.24

Electrocardiogram of a 43-year old man with pituitary insufficiency and no evidence of heart disease. In the control tracing on April 1, the T wave is inverted before, and upright after the administration of 1.5 μg of isoproterenol (ISP). The T wave became upright within 9.5 months after the onset of treatment with prednisone and thyroid (January 14, following year). At the latter date, the heart rate is the same as in the control electrocardiographic tracing of April 1, but the QT interval is 0.05 s shorter. The QT interval on January 14 is the same as the QT interval after the administration of ISP on April 1. (After Daoud et al. [70]. © Yorke Medical Group, Magazines Division, New York. Reproduced with permission.)

is the presence of complete A-V block. In patients with hypertrophic cardiomyopathy, reports from Japan [170] indicate that patients with giant negative T waves have hypertrophy confined to the left ventricular apex, mild symptoms, and few adverse prognostic features. The study of Alfonso et al. [171], however, showed that patients in the West with giant negative T waves have a wider clinical spectrum and that their prognosis is not different from that of patients without such T waves.

17.3.6.7 Isolated T-Wave Inversion of Adults

Another rare variant is an isolated negative T wave in the midprecordial leads V_3 and V_4. In such cases the T wave tends to be diphasic rather than frankly negative. This pattern occurs sometimes in the absence of heart disease. Under these circumstances the region in which the T wave is abnormal over the precordium is small, and a slight downward shift of the electrode usually reveals an upright T wave. In a series of 86 consecutive patients with isolated T-wave inversion reported by Okada et al. [172], 23 had no symptoms and represented a normal variant [172]. The remaining 63 patients had chest pain, and most of them had coronary artery disease. The presence or absence of structural heart disease could be differentiated by recording additional precordial leads. In the absence of heart disease, the area of negative T waves extended downward and rightward and in patients with heart disease, leftward and upward [172].

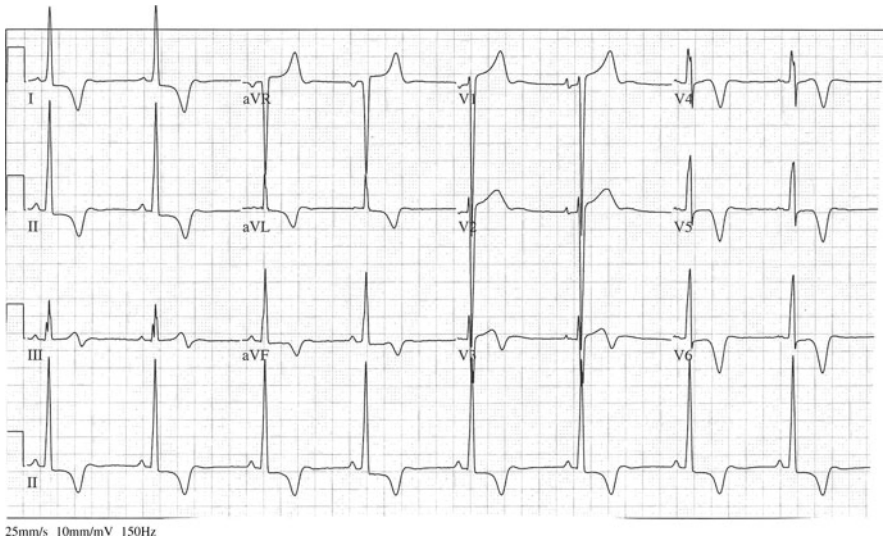

Figure 17.25
Electrocardiogram of a 40-year old woman with apical hypertrophic cardiomyopathy and normal coronary arteries.

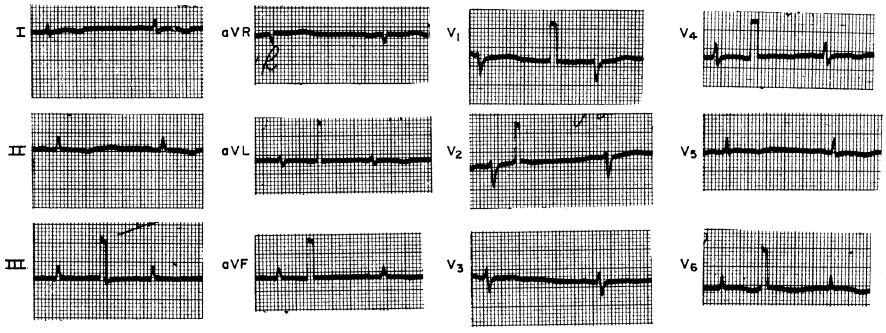

Figure 17.26
Typical ECG pattern of a patient with untreated myxedema. (After Surawicz and Mangiardi, The electrocardiogram in endocrine and metabolic disorders, in *Clinical Electrocardiographic Correlations*, J.E. Rios, Editor. Philadelphia, PA: © Davis, 1977, pp. 243–66. Reproduced with permission.)

17.3.6.8 Hypothyroidism

Hypothyroidism usually causes a decrease of T-wave amplitude attributed to the low voltage caused by myxedema (Fig. 17.26). T-wave inversion can also occur, probably owing to pericarditis [42]. The T-wave abnormalities regress within weeks or months after start of specific treatment [42, 173, 174]. Sometimes, however, the abnormalities subside within days or even within 24 h [174]. Rapid regression suggests that at least in some cases, the T-wave abnormalities in hypothyroidism may be related to abnormal function of the autonomic nervous system rather than to the effect of myxedema on the myocardium or to pericarditis.

17.3.6.9 T-Wave Abnormalities Attributed to Fear, Anxiety, and Nervous Tension

Fear, especially fear of operation [175], anxiety, worry, or longing suggested by hypnosis, and other emotional factors may produce T-wave abnormalities in persons without heart disease. Berman et al. found lowering or inversion of the T wave in 5 of 14 normal persons in an anxiety fear situation induced by hypnotic suggestion [176]. These abnormalities have usually been associated with tachycardia. Ljung attributed T-wave abnormalities induced by "fright" to hyperventilation [177]. Others ascribed the T-wave changes produced by fear and anxiety to sympathetic stimulation [175] or to abnormal "sensitivity" of the myocardium to adrenaline [178]. It has been shown that T-wave abnormalities in anxious patients may disappear after reassurance and rest, even without change in heart rate [179].

Several studies reported T-wave abnormalities in a vaguely defined syndrome of neurocirculatory asthenia (NCA) characterized by tachycardia, hyperventilation, labile blood pressure, and low effort tolerance. However, it has been shown conclusively that NCA is not associated with a characteristic ECG pattern [180–184]. In many patients with NCA, abnormal T waves are associated with tachycardia and therefore may arise from excessive sympathetic stimulation [185], but sometimes T-wave abnormalities appear when the heart rate is slow and disappear when the rate increases following the administration of nitrates and atropine, or when the subject is in an upright position [105].

17.3.6.10 Transient T-Wave Abnormalities Arising from Extracardiac Factors

This category of T-wave abnormalities includes changes attributed to transient asynchrony of repolarization produced by a variety of factors acting on a normal or an abnormal heart.

Hyperventilation

In the author's study, hyperventilation (HV) produced T-wave inversion in at least one of several simultaneously recorded ECG leads in 73% of randomly selected healthy students. In some of the author's subjects, T-wave abnormalities were more pronounced after 20 s than after 60 s of HV (Fig. 17.27). Others reported similar observations [186, 187]. The study of Biberman et al. suggests that the true incidence of T-wave abnormalities during HV may be underestimated unless multiple ECG leads are monitored during the HV [188].

The study of Biberman et al. showed that the T-wave abnormalities produced by HV could not be attributed to alkalosis [188], changes in plasma sodium, potassium, calcium, or magnesium concentrations, or changes in heart position. The T-wave abnormalities produced by HV were always accompanied by tachycardia but could not be attributed solely to a critical increase in heart rate. This conclusion is in agreement with previous studies in which the T wave became inverted after HV but remained upright when tachycardia was induced by exercise [189, 190], intravenous administration of propantheline [190], or breathing air containing 5% CO_2 [191, 192].

The transient T-wave inversion that occurs during HV was similar to the transient T-wave abnormalities produced by isoproterenol infusion [190]. The T-wave abnormalities produced by HV were attributed to an asynchronous shortening of ventricular repolarization during the early phase of sympathetic stimulation [190]. In keeping with this hypothesis are the observations that T-wave abnormalities produced by HV can be prevented by pretreatment with propranolol [193, 194], and that the suppression of T-wave abnormalities by propranolol is not attributable to the prevention of tachycardia because after the administration of atropine with propranolol, the heart rate increased but the T wave remained upright [195].

Orthostatic Abnormalities

In the upright position, ventricular gradient decreases, QRST angle widens [193], and T-wave changes occur in the majority of normal young individuals [194]. However, the incidence of unequivocal orthostatic T-wave abnormalities varies in different patient groups. Lepeschkin and Surawicz found an abnormal orthostatic ECG only in 3% of individuals with a negative exercise test but in 30% of persons with junctional ST depression and in 23% of patients with ischemic heart disease and positive exercise tests [41]. In patients with NCA, orthostatic T-wave abnormalities occurred in 63% of women and 30% of men [185].

Transient orthostatic T-wave abnormalities have been attributed to increased sympathetic activity [184]. This hypothesis is supported by the observation that adrenergic blockade increases the ventricular gradient and decreases the QRST

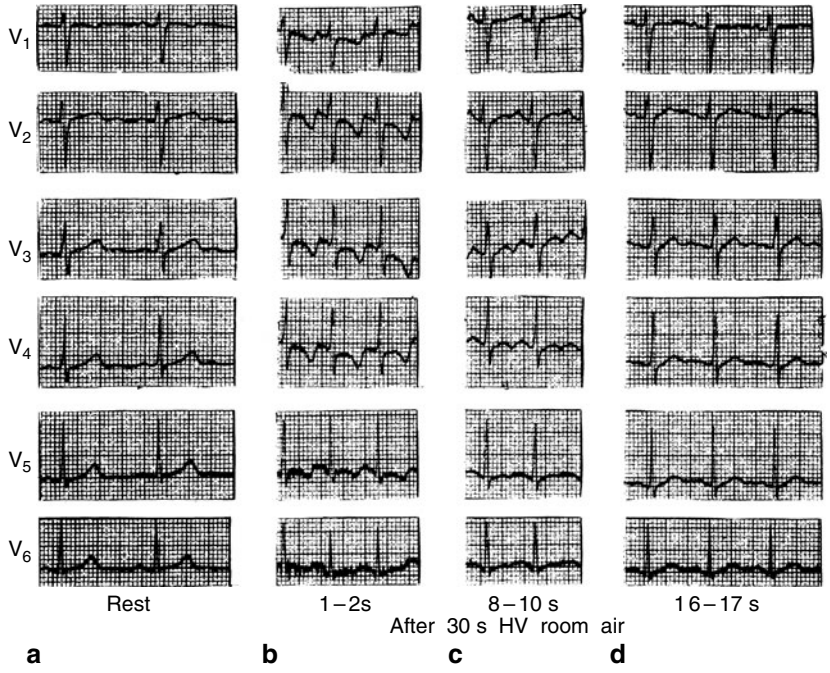

Figure 17.27

Simultaneously recorded ECG leads V_1–V_6 (paper speed 25 m ms^{-1}) in a 21-year old student. (a) control, before hyperventilation (HV): R–R = 85, QT = 38, QT_c = 41; (b) during first 2 s after 30 s of HV: R–R = 44, QT = 32, QT_c = 48; (c) during eighth and tenth second: R–R = 44, QT = 30, QT_c = 45; (d) during sixteenth to seventeenth second: R–R = 56, QT = 32, QT_c = 43. Note that the R–R intervals in (b) and (c) are the same, but in (c) the QT and QTc intervals are shorter and the T waves less inverted. (After Biberman et al. [188]. © Mosby, St Louis, Missouri. Reproduced with permission.)

angle in the upright position [193]. Similarly, intravenous administration of propranolol prevents orthostatic T-wave abnormalities [196–198]. Propranolol blocks an increase in heart rate that occurs after standing up, but the suppression of the orthostatic T-wave changes is apparently not solely a result of the decrease in heart rate [196].

Postprandial Abnormalities

A decrease in T-wave amplitude or T-wave inversion in leads I, II, V_2–V_4 occurs frequently within 30 min after a meal of about 1,200 calories [199]. Postprandial T-wave abnormalities occurred in 3.9% of 2,000 young healthy airmen [200]. These abnormalities may arise from lowering of plasma K^+ concentration, tachycardia, and possibly sympathetic stimulation. It has been shown that various nonspecific T-wave abnormalities frequently disappear when the ECG is recorded after fasting [201].

Postextrasystolic Abnormalities

The cause of occasional primary T-wave changes in the first and sometimes also in the second or third postextrasystolic beats is not known (Fig. 17.28). Asynchrony of repolarization has been suggested as the cause in a case of postextrasystolic T-wave inversion associated with prolongation of QT interval [202]. The postextrasystolic T-wave changes apparently occur more frequently in patients with heart disease than in normal persons [202–204], but the reason for this association is not obvious.

Post-tachycardia Abnormalities

In about 20% of patients with paroxysmal tachycardia, the normal T wave becomes inverted for hours or days after the termination of the attack [42] or interruption of tachycardia by ablation. This may occur after ventricular [205] or

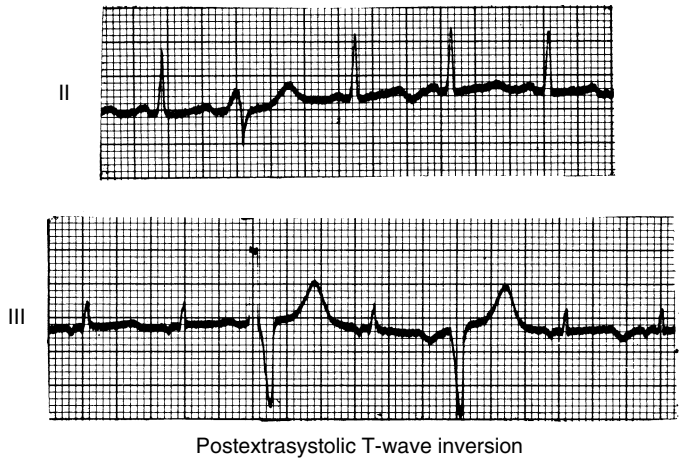

Figure 17.28

Postextrasystolic T-wave inversion in a person with no evidence of heart disease and a normal ECG except for ventricular premature complexes.

supraventricular tachycardias [206], and is unrelated to the age of the patient or to the presence or absence of heart disease. In a 21-year-old patient with normal hemodynamic findings and a normal coronary arteriogram, T-wave inversion in leads II, III, and V_3–V_6 persisted for 19 days after termination of a tachycardia [206]. The cause of the long duration of the "post-tachycardia syndrome" is not clear, but the abnormalities usually persist longer than would be expected on the basis of physiological adjustment to the new rate.

Induced and Accidental Hypothermia: Cooling of the Posterior Wall of the Heart

Profound hypothermia alters depolarization and repolarization, but moderate hypothermia may produce T-wave abnormalities without appreciable QRS changes. Homogeneous cooling of the entire heart causes the expected increase in the T-wave duration without change in polarity. Such patterns have been observed in patients with accidental hypothermia [207]. Cooling the posterior wall of the heart by drinking iced water usually produces deviation of the T-wave vector anteriorly and superiorly with the resulting T-wave inversion in leads II and III [42]. This effect is a result of the local prolongation of repolarization in the cooled area of the ventricle.

Abnormalities Produced by Injection of Contrast into Coronary Arteries

Injection of ionic contrast into coronary arteries produces transient prolongation of the QT_c interval and changes in the T-wave morphology. These T-wave changes are sometimes associated with prolongation of the QRS complex, but in most cases they are primary. As a rule, the T-wave vector is directed away from the area perfused by the contrast [208, 209]. These T-wave changes have been attributed to the regional prolongation of repolarization caused by the high sodium concentration in the contrast medium [210], or the medium's calcium-binding properties [211]. The author and coworkers have shown that transient T-wave abnormalities, which occur during injection of the contrast into the right coronary artery, were associated with prolongation of the ventricular MAP in the right ventricle without changes in the MAP in the left ventricle [3] (Fig. 17.29).

Abnormalities Produced by Ventricular Pacing

Ventricular pacing frequently produces T-wave inversion in the nonpaced sinus impulses. These T-wave changes occur without changes in the QRS duration. The T-wave abnormalities increase with increased duration of pacing and the amount of energy used for pacing [212, 213]. The site of stimulation determines the vector of the T wave. After pacing the endocardial surface of the right ventricle or the epicardial surface and the apex of the left ventricle, abnormal T waves appear predominantly in leads II, III, and V_3–V_5 but after pacing the right ventricular outflow tract, the T-wave inversions

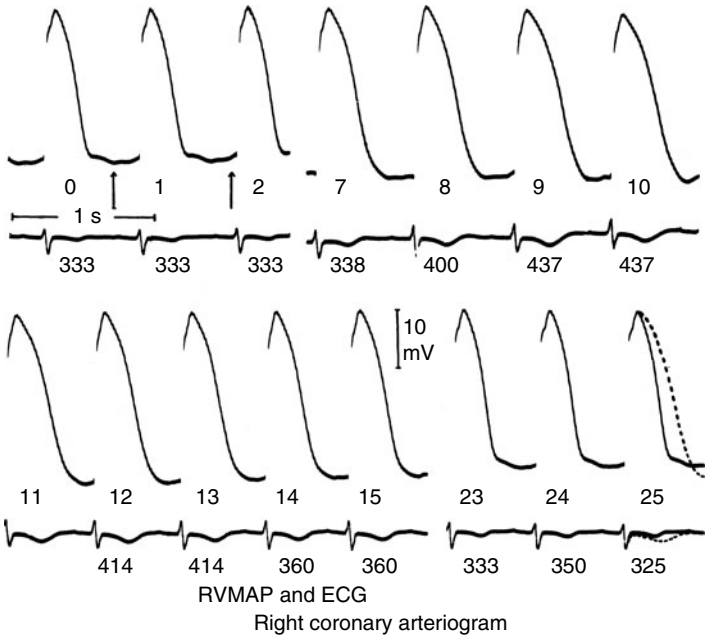

Figure 17.29

Right ventricular monophasic action potential (TVMAP) and lead II recorded during injection of 4 ml of 75% Hypaque (diatrizoate) into the right coronary artery. Arrows mark the onset and end of the injection. The consecutive 25 beats after the injection are numbered. The numbers under the T wave represent the QT intervals in milliseconds. See text for further discussion. The MAP and electrocardiogram of the tenth beat are superimposed on those of the 25th beat. (After Shabetai et al. [3]. © American Heart Association, Dallas, Texas. Reproduced with permission.)

occur mainly in leads V_1 and V_2 [212]. Recently, Shvilkin et al. [214] reported that a combination of positive T wave in aVL, positive or isoelectric T wave in lead I, and maximal T-wave inversion in precordial leads greater than T-wave inversion in lead III was 92% sensitive and 100% specific for postpacing T-wave changes. The duration of the T-wave abnormalities after pacing depends on the duration of pacing. In some cases, T-wave abnormalities persisted for 1 or 2 years after the termination of pacing. T-wave changes do not appear after atrial pacing or after ventricular pacing during the ventricular refractory period [214]. Thus, the T-wave abnormalities appear to be related to the presence of abnormal depolarization in the stimulated area. It may be assumed that T-wave abnormalities are produced by prolongation of repolarization in the vicinity of the pacing electrode, but the mechanism of such prolongation is unknown. It has been reported that T-wave abnormalities produced by pacing are not reversible after oral administration of potassium or after an increase in heart rate with isoproterenol.

Abnormalities Following Preexcitation and Left Bundle Branch Block. Cardiac "Memory"

Transient T-wave abnormalities have been found in patients with intermittent preexcitation [215–217] and intermittent left bundle branch block [218, 219]. These abnormalities apparently persist for a variable amount of time after the disappearance of the left bundle branch block or preexcitation pattern respectively. Similar abnormalities have not been recorded in patients with intermittent right bundle branch block. The most consistent and conspicuous T-wave abnormality after disappearance of a left bundle branch block pattern has been recorded in right precordial leads [219–221], but in one study [219], abnormalities in the limb leads were present also in approximately 50% of patients. The natural history of this phenomenon has not been studied adequately and the clinical significance of such T-wave abnormalities is debatable [219]. The appearance of primary T-wave abnormalities following cessation of pacing, normalization of intraventricular conduction, and disappearance of secondary T-wave abnormalities has been considered by Rosenbaum

et al. as a possible manifestation of repolarization "memory" [213]. This hypothesis implies that the abnormal sequence of activation is "remembered" following the return of a normal activation pattern.

Normal Variants and Unexplained T-Wave Abnormalities

T-wave abnormalities have been found in 0.5–4.2% of normal persons in various population groups [82, 221, 222]. The largest group of individuals without heart disease has been studied by Hiss and Lamb [82]. In their study of 122,043 men, aged 16–50 years, the overall incidence of T-wave abnormalities was 11.5/1,000 with the highest incidence in the youngest and the oldest age groups. T-wave abnormalities occurred most frequently in the lateral precordial leads and least frequently in lead I. However, in the studies reported by Fisch, ST or T abnormalities were absent in 776 normal individuals below the age of 25 years but were present in 15.7% of 671 persons older than 65 years [223]. A study of 12 asymptomatic men, aged 18–19 years, selected on the basis of flat, notched, or inverted T waves in the precordial leads, showed that this group had higher systolic blood pressure and higher plasma noradrenaline concentration than an age-matched control group with normal T waves [224].

Major unexplained T-wave abnormalities – deeply inverted T waves – were observed in about 2 out of 1,000 [225], and 7 out of 1,000 patients [84] in two large groups of hospital patients, and in about 4 out of 1,000 in a large group of life-insurance applicants. Pruitt et al. found no evidence of heart disease in 3 of 62 patients with deeply inverted (at least 5 mm) T waves [226]. Life-insurance statistics report a 226% increase in mortality in persons with major T-wave abnormalities and a 166% increase in mortality in persons with minor T-wave abnormalities [85]. This increased mortality suggests that a group of persons with isolated T-wave abnormalities may represent a mixture of persons with abnormalities unrelated to heart disease and persons with clinically silent or "atypical" ischemic heart disease [83].

17.3.6.11 Tests Employed in the Recognition of Rapidly Reversible T-Wave Abnormalities

This discussion will be limited to the methods used in the differential diagnosis of primary T-wave abnormalities attributed to nonhomogeneous repolarization. These abnormalities may be arbitrarily divided into three types:

1. Rate-dependent abnormalities associated with normal or slow heart rate,
2. Rate-dependent abnormalities associated with rapid heart rate, and
3. Abnormalities independent of heart rate.

Detection of T-Wave Abnormalities Associated with Normal or Slow Heart Rate

In certain patients without heart disease, primary T-wave abnormalities appear only at normal or slow heart rates and disappear after a certain critical increase in rate. Several patients have been observed in whom primary negative T waves became upright after a certain critical increase of heart rate with exercise, hyperventilation, pacing, and administration of atropine or isoproterenol. This type of purely rate-dependent T-wave abnormality can be identified most conclusively with atrial pacing while the effects of exercise, hyperventilation, and isoproterenol may be attributed to the sympathetic stimulation, and the effects of atropine on the vagolytic action of the drug. It has been suggested that T-wave abnormalities, which disappear after the administration of vagolytic drugs, are caused by vagal reflex [227, 228]. However, the suppression of T-wave abnormalities by atropine or Pro-Banthine is more likely to be a result of a nonspecific increase in heart rate rather than to the specific vagolytic action of the drug. The vagolytic drugs do not exert a specific effect on normal repolarization. In persons with normal T waves, atropine decreases the T-wave amplitude [229], but this decrease is proportional to the increase in heart rate [230] and, therefore, is probably caused by tachycardia. Although in some patients with nonspecific T-wave abnormalities atropine may reverse the abnormality, in the majority of patients atropine either does not change or may even exaggerate the abnormal T-wave pattern [70, 231].

Detection of T-Wave Abnormalities Associated with Rapid Heart Rate

Various nonspecific T-wave abnormalities are frequently associated with tachycardia and disappear when the heart rate becomes slower. The effect of sympatholytic drugs on the T wave may be in part owing to the slowing of heart rate. Numerous studies have shown that certain T-wave abnormalities may be abolished by the administration of ergotamine, dihydroergotamine, or propranolol. It has been reported that the intravenous administration of 10–20 mg propranolol

abolishes ST and T abnormalities at rest and prevents the orthostatic and exercise-induced changes in patients without heart disease but not in patients with T-wave abnormalities arising from myocardial ischemia or myocarditis [199]. Beta-blocking agents decrease heart rate but their effect on the orthostatic and hyperventilation-induced T-wave abnormalities is apparently not exclusively owing to the slowing of the heart rate [193, 195].

Detection of Rapidly Reversible Rate-Independent T-Wave Abnormalities

Administration of Potassium Salts

A moderate increase in the concentration of potassium can change an abnormally low or a negative T wave into an upright T wave without change in heart rate. Several investigators have administered about 10 g of potassium salts orally in order to differentiate the T-wave abnormalities produced by structural heart diseases from various functional and nonspecific abnormalities. This procedure may be diagnostically useful because oral administration of potassium does not alter the angle between the mean spatial QRS and T-wave vector in persons with a normal T wave and in patients with myocardial infarction or left ventricular hypertrophy. However, potassium restores to normal the QRST angle in persons with T-wave abnormalities, which are not a result of heart disease. The administration of potassium salts in order to differentiate functional abnormalities from abnormalities arising from organic disease is apparently not safe because ventricular tachycardia, ventricular fibrillation, and asystole have been reported to follow such tests [2].

Administration of Isoproterenol

In persons with normal T waves, isoproterenol (ISP) administered at a rate of 3–6 mcg min^{-1} for 4–6 min produced a biphasic effect [188]. During the early phase of the infusion, the T-wave amplitude decreased in all subjects, and in 10 of 11, the previously upright T wave became negative in one or more of leads I, II, or V_3–V_6. The maximum T-wave inversion usually occurred 30–40 s after beginning the ISP infusion. Subsequently, the T wave became upright and the U-wave amplitude increased. After approximately 2 min of ISP infusion, the T-wave amplitude was similar to the control and in some cases even greater than before the ISP infusion. The initial decrease of T-wave amplitude was always associated with an increase in heart rate but without an appreciable change in QT interval. As a result, the QT_c interval was increased. The subsequent increase of T-wave amplitude was associated with a significant decrease in QT and QT_c intervals but an insignificant decrease in the R–R interval. Accordingly, the T-wave inversion was associated with the hysteresis of the QT interval (Fig. 17.30). This was attributed to an asynchronous shortening of ventricular repolarization.

The effect of ISP on the sequence of normal repolarization suggested to Daoud et al. that it may be of interest to study the effect of the drug on the abnormal T wave. Isoproterenol was administered at the rate of 2–6 μg min^{-1} for 30–90 s to 80 patients with various types of T-wave abnormalities. The ISP infusion increased the heart rate by 27–55 (average 37) beats min^{-1} [70]. In patients with secondary T-wave abnormalities arising from hypertrophy and bundle branch block and in patients with primary T-wave abnormalities after myocardial infarction or pericarditis, administration of ISP altered only the amplitude and not the polarity of the T wave. In these patients, the ISP effect was similar to the effect of tachycardia produced by atropine or pacing [93]. However, in patients with various primary T-wave abnormalities and a normal QRS complex, ISP transiently shifted the abnormal T-wave vector to the left and anteriorly by 60–180° and "normalized" the ECG (Fig. 17.31).

Our studies favor the hypothesis that ISP reverses the primary T-wave abnormalities by an asynchronous shortening of the AP. The effect of ISP on ventricular repolarization is probably a result of beta adrenergic stimulation because it can be blocked by pronethalol without any changes in heart rate [232]. Our studies suggest that the rapidly reversible primary T-wave abnormalities probably result from some regional deficiency of sympathetic stimulation and that ISP has a greater absolute shortening effect on AP in the areas with deficient stimulation than in the areas with normal responses to sympathetic stimulation. This hypothesis is supported by our studies in dogs, which showed that ISP changed T-wave polarity and restored the control T-wave configurations after both left stellate-ganglion transection and right stellate-ganglion stimulation. In each case, ISP produced unequal shortening of the MAP on the anterior and posterior walls of the ventricle and thereby restored the normal relation between their durations. After left stellate-ganglion transection, ISP shortened the previously prolonged MAP more than it did the control MAP; after right stellate-ganglion stimulation, ISP shortened the control MAP more than the previously shortened MAP [25] (Fig. 17.32).

If the results of our experiments in dogs are applicable to man, normalization of the T wave after the administration of ISP may be expected in all cases of primary T-wave changes induced by regional shortening of ventricular APs or regional lengthening of ventricular APs provided that the latter are susceptible to the shortening effect of the drug. We assume that

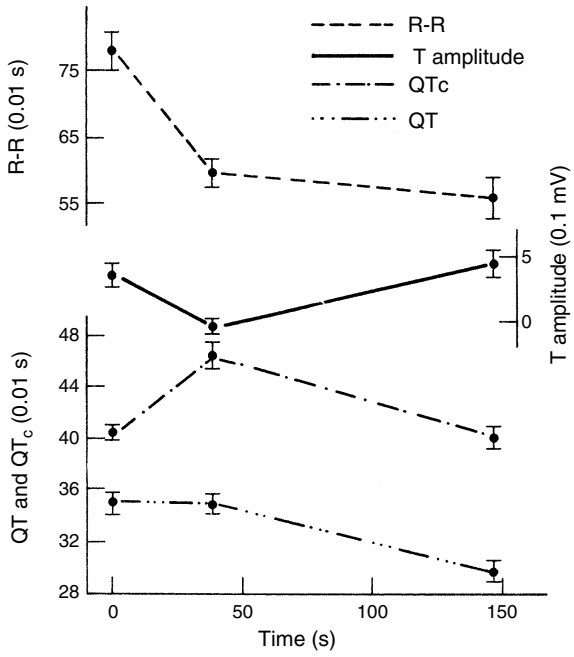

Figure 17.30

Changes in R–R, T amplitude, QT, and QT_c during isoproterenol administration to 11 healthy volunteers. Each point designates the mean value, and each vertical bar, the standard error. (After Biberman et al. [188]. © Mosby, St Louis, Missouri. Reproduced with permission.)

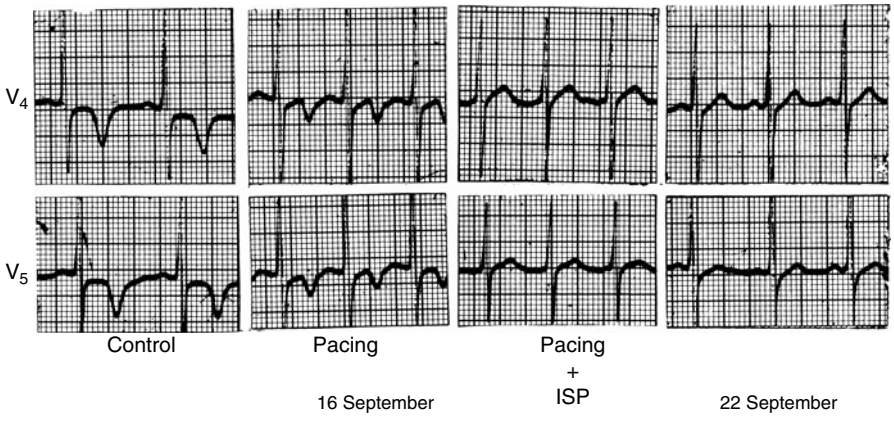

Figure 17.31

Electrocardiogram of a 55-year old man with diabetes mellitus, increased left ventricular end-diastolic pressure, and normal coronary arteriogram, before (control), during atrial pacing, and during pacing and isoproterenol (ISP) infusion. Note the effect of ISP on the T wave. The QT interval during pacing with isoproterenol is 34, and without isoproterenol is 32. (After Daoud et al. [70]. © Yorke Medical Group, Magazine Division, New York. Reproduced with permission.)

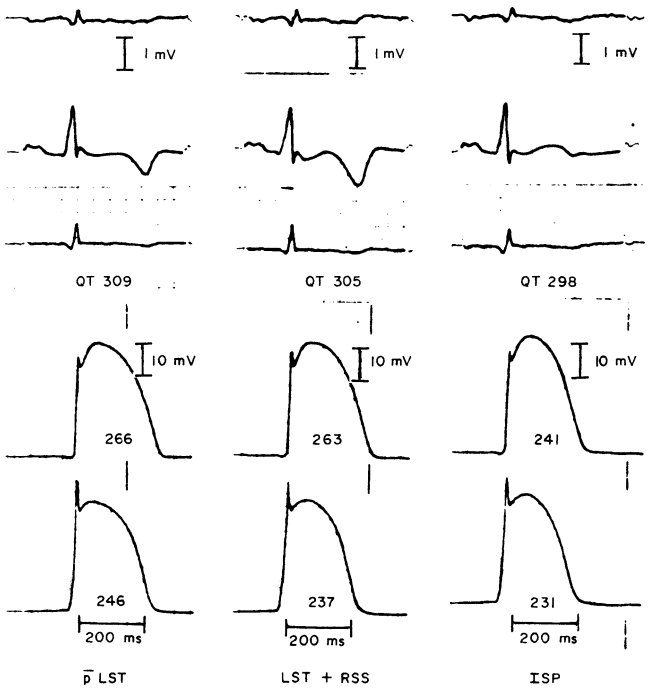

Figure 17.32

From top to bottom, leads *X*, *Y*, and *Z* and MAP on the posterior and anterior walls of the left ventricle. Effects of left ventricular stellate-ganglion transection (LST) alone (*left panel*), subsequent right stellate-ganglion stimulation (RSS) (*middle panel*), and the administration of isoproterenol (ISP) (3 μg) after right stellate-ganglion stimulation (*right panel*). See text for further discussion. (After Kuo and Surawicz [76]. © Yorke Medical Group, Magazines Division, New York. Reproduced with permission.)

one or both of these two mechanisms account for the high incidence of isoproterenol-induced T-wave normalization in persons with T-wave abnormalities of diverse origins and with different QT intervals [70].Conversely, the lack of T-wave normalization in patients after myocardial infarction or pericarditis [70] may be attributed to an inadequate shortening effect of isoproterenol on the abnormally prolonged APs [232]. The effect of sympathetic stimulation on reversal of T-wave polarity from negative to positive is not limited to isoproterenol. It is seen often during exercise, e.g., during stress tests in the absence of myocardial ischemia. Similarly during dobutamine infusion T-wave normalization is reported to indicate viable myocardium in patients after recent myocardial infarction [233].

17.3.7 T Wave Alternans

Electrical and mechanical alternans may be concurrent or dissociated from each other. At the cellular level, mechanical alternans in the ventricular myocardium is usually accompanied by an alternating shape of the ventricular action potential. T-wave alternans is usually associated with a long QT interval [234–237]. In the majority of published cases, the alternating T wave occupied nearly the entire diastolic interval [234–239].

Also, T-wave alternans experimentally produced by stellate-ganglion stimulation in anesthetized and vagotomized cats [235], or by hypocalcemia in dogs [240, 241], was associated with prolonged QT interval.

Lepeschkin suggested that T-wave alternans was a result of the alternans of ventricular AP associated with alternation of the diastolic intervals [242]. A close proximity to preceding repolarization exerts a shortening effect on AP duration [243]. Consequently, the diastolic interval after a short AP increases and the AP becomes longer. In the author's laboratory, T-wave alternans occurred simultaneously with ventricular AP alternans in the isolated perfused rabbit heart when the

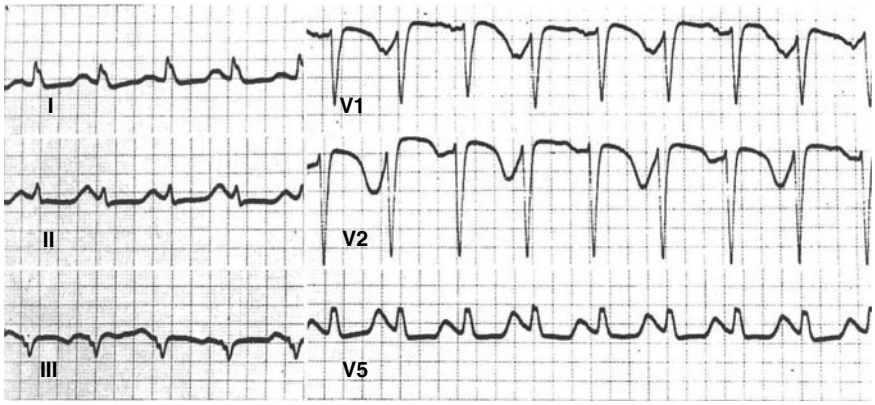

Figure 17.33

T-wave alternans in a 60-year old woman with severe hypocalcemia and history of hypocalcemic tetany. (From Aravindakshan and Surawicz B et al. [246] © Elsevier, Inc. Reproduced with permission.)

AP duration was prolonged by cooling quinidine or a combination of hypocalcemia and hypokalemia. In each case, the mechanism suggested by Lepeschkin [241] could account for the T-wave alternans. However, this may not be the only mechanism of T-wave alternans since experimental T-wave alternans can occur in the absence of appreciable QT lengthening, and conversely, alternans of the AP duration cannot always be explained by alternans of the diastolic intervals (personal observations and examples given by Kleinfeld et al. [244].

T-wave alternans depends on critical shortening of the diastolic interval when the duration of the ventricular AP exceeds the cycle length. Therefore a QT interval occupying nearly the entire cycle length can be seen in many cases of repolarization alternans associated with a long QT interval (Fig. 17.33). T-wave alternans with a long QT has been reported in some of the following conditions: congenital long-QT syndrome, hypocalcemia, treatment with quinidine, hypokalemia, hypokalemia with hypocalcemia, and hypomagnesemia and after defibrillation. It may also be unexplained.

In addition to the manifest alternans, on the ECG, subtle alternans forms may become detectable by digital processing techniques. It has been shown that these subtle forms of alternans are associated with increased susceptibility to inducible ventricular tachyarrhythmias in patients with coronary artery disease and nonischemic cardiomyopathy and therefore may represent a noninvasive marker of electrical instability [245].

17.3.8 ST–T Abnormalities

As a result of the differences in the underlying mechanisms, the behavior of the ST segment and of the T wave differ under a variety of conditions discussed earlier. For example, hypocalcemia usually causes lengthening of the ST segment without T-wave changes. Conversely, moderate hyperkalemia causes T-wave changes without appreciable change of ST segment duration. Although myocardial ischemia frequently produces both ST segment and T-wave changes, our studies have shown that during exercise, the behavior of the T wave bears no relation to the behavior of the ST segment [246].

In spite of the fundamental differences in the genesis of the ST segment and the T wave, electrocardiographers frequently use the expression ST–T changes to describe the patterns associated with the alterations of these two repolarization components. One of the reasons for using this definition is the lack of a distinct point of demarcation between the end of the ST segment and the onset of T wave. Another reason is a common occurrence of concomitant ST and T-wave abnormalities associated with either the secondary repolarization abnormalities such as left ventricular hypertrophy or left bundle branch block (Fig. 17.3c), or the primary repolarization abnormalities caused by shortening of the plateau of the ventricular AP; for example, tachycardia, digitalis, or hypokalemia (Fig. 17.3c). Nevertheless, it is the author's opinion that in many cases the electrocardiographic diagnosis gains in precision when the ST segment, the T wave, and also the U wave are analyzed as separate components rather than as an expression of an integrated process of "repolarization."

17.3.9 Prognostic Value of the Descriptors of T-Wave Morphology

Numerous studies in the recent literature have explored the prognostic value of various computerized descriptors of T-wave characteristics, e.g., morphology analysis [246], heterogeneity of ventricular repolarization [247], principal components of the T-wave vector loop [248], and spatial T-wave deviation [249, 250]. The clinical usefulness of these analyses will depend on their comparison with more conventional electrocardiographic and clinical parameters.

17.4 U Wave

The purpose of this section is to review briefly some concepts of U-wave genesis and the clinical significance of this ECG deflection, which owes its designation to Einthoven. Compared to other components of the ECG, the U wave has been less intensely investigated and its mechanism is still poorly understood [251]. Some of the reasons for this are its low amplitude, the difficulty of separating it from the T wave and/or the P wave, particularly at rapid rates, and its uncertain clinical significance. The experimental animal models are also difficult to interpret because various diastolic deflections recorded in local electrograms do not necessarily have the same timing as the U wave recorded in the human surface ECG.

17.4.1 Identification of the U Wave

This discussion will be limited to a deflection, which is usually detectable at slow or moderate heart rates in the surface ECG [252]. It is inscribed during protodiastole; that is, it coincides with the isovolumic relaxation. The interval between the end of the T wave and the apex of the U wave is usually about 100 ms. It is of interest that this interval is little affected by the heart rate [6].

The distinction between the U wave and the T wave may become difficult when the T wave is notched, diphasic, or prolonged. In such cases, various degrees of fusion between the T wave and the U wave may occur. In hypokalemia, the initial portion of ventricular repolarization (phase 2) is shortened and the terminal portion (phase 3) is prolonged. These changes result in the disappearance of the isolelectric ST segment, obliteration of the apex of the T wave, and a shift of the major repolarization deflection toward early diastole. It appears that the U wave proper becomes fused with this repolarization component and evolves into the largest deflection during repolarization. If the notch between T and U persists, the QT interval is not prolonged. A complete fusion results in a large T+U complex. In cases with true QT prolongation caused by delayed repolarization in certain portions of the myocardium, the T wave also merges with the U wave but the resulting T–U deflection has a different configuration from the T–U complexes during hypokalemia. This occurs because instead of lifting the U wave to prominence, the T wave tends to encroach upon the U wave, which becomes less distinct or unrecognizable. Thus, differences in the morphology of the T+U complex reveal the differences in the pathogenesis. However, in most cases in clinical electrocardiography, the T wave can be distinguished from the U wave using published and suggested maneuvers [253]. Among these, timing the apices of the waves in question, correlation with the second sound, or incisura of the arterial pulse, and in some cases, the administration of calcium salts intravenously, tend to be most helpful [253].

17.4.2 Relation Between the U Wave and Other Deflections of the ECG

In a number of patients with left ventricular hypertrophy, the U wave is inverted in the left precordial leads. Frequently, when the blood pressure of these patients is lowered, the U wave becomes upright; this is usually associated with a decrease in the QRS amplitude. Similarly, in acute myocardial ischemia during exercise, an increase in QRS amplitude and U-wave inversion frequently occur simultaneously. In these cases, the common cause of increased QRS amplitude and the U-wave inversion may be the increase in the intracardiac blood volume

In both left and right ventricular hypertrophy (LVH and RVH, respectively), the axis of the U wave tends to be directed opposite to the main QRS axis; that is, the U wave is negative in the left precordial leads in LVH and negative in the right precordial leads in RVH. Typically, in such cases, the U-wave vector parallels that of the T wave. In some cases of LVH,

the U wave is inverted in the leads where the T wave is upright. The independent behaviors of the T wave and U wave also become obvious during transient changes in T-wave polarity associated with myocardial ischemia or changes in systemic vascular resistance.

17.4.3 ST Segment

Ordinarily, the U wave shows no correlation with the ST segment but during acute ischemia or development of the left ventricular "strain" pattern, ST depression and U-wave inversion may occur concomitantly.

17.4.4 U-Wave Amplitude

The U-wave amplitude tends to be inversely proportional to the R–R interval. At heart rates exceeding about 90–100 min^{-1}, the U wave becomes indistinct [252]. Its amplitude is increased by interventions associated with positive inotropic effect, such as catecholamines, hypercalcemia, and digitalis. As mentioned above, a prolonged phase 3 of the ventricular AP, e.g., during hypokalemia or quinidine administration, increases the U-wave amplitude. Presumably, this is by superposition of the U wave on the repolarization potentials inscribed during the late portion of the prolonged AP. The U-wave amplitude is diminished during tachycardia and hyperkalemia. A negative inotropic effect appears to cause a decrease in U-wave amplitude. In hypocalcemia, the U wave is not detectable but the cause is difficult to determine because of the prolonged QT interval.

17.4.5 The Negative U Wave

The negative U wave seldom occurs in the absence of heart disease or other electrocardiographical abnormalities. Holzmann and Zurukzoglu [254] found that 197 of 200 patients with a negative U wave had heart disease. Of 100 patients reported by Ameur-Hendrich et al. [255], 99 had heart disease and 1 had anemia.

In the study of Kishida et al. of 488 patients with a negative U wave, this was the only electrocardiographic abnormality in 25 (5.1%) of patients [256]. In an additional 34 (7%) of the patients, the electrocardiogram was normal at rest and became abnormal after exercise. In the study of Holzmann and Zurukzoglu [254], the U wave was the only abnormality in 19.5% of their patients, most of whom had hypertension. In patients with hypertension, a negative U wave was the only abnormality in 9 out of 45 patients in the study of Georgopoulos et al. [257], and in 1 out of 66 in the study of Kemp et al. [258]. The above studies refer to patients with purely negative U waves only. Lambert included patients with a depressed T–U junction and diphasic U wave but this apparently did not decrease the specificity of the pattern since all but 3 of 245 patients had organic heart disease [259].

U-wave inversion has also been reported during attacks of variant angina [260]. In a study of 38 patients in whom angina was induced by ergonovine maleate, transient U-wave inversion was apparent in 17 with ST elevation in the precordial leads but only 3 of 21 with ST elevation in the inferior leads. In the 17 subjects who had spasm of the LAD coronary artery, the lead that most frequently exhibited U-wave inversion was V_4 (94%), which also showed ST elevation in 82%. In this study, negative U waves frequently occurred without ST elevation. This caused the authors to suggest that such a finding may be a result of ischemia in areas marginal to the central ischemic zone or of recovery from temporary ischemia.

With respect to exercise testing, it was shown that U-wave inversion could be induced in patients with stenosis of the LAD coronary artery [261]. The sensitivity was low at 21% but the specificity was high, being 93%.

In the study of Kishida et al. [256], systemic hypertension was the primary diagnosis in the largest number of patients (Table 17.3).

Previous studies have shown that, in patients with hypertension, the regression of U-wave inversion was associated with lowering of blood pressure [257, 258]. Kishida et al. [256] reviewed the records of 130 patients in whom the U wave changed polarity from negative to positive or vice versa in the same lead within a period of less than 1 year (Fig. 17.34). In 107 patients, the change from a negative to a positive U wave occurred during the course of medical treatment, and in 23 patients, the change in polarity occurred after a surgical procedure; in 9 within 1 week after kidney transplantation; in

Table 17.3

Primary clinical diagnosis of 488 patients with a negative U wave

	Total[a]	Percentage
Valvular heart disease	75 (48)	15.4
Pure aortic	43 (25)[b]	
Pure mitral	15 (12)[c]	
Combined aortic and mitral	17 (11)[d]	
Congenital heart disease	12 (9)	2.5
Coronary artery disease	162 (33)	33.2
Myocardial infarction; acute	7 (0)	
Old	61 (20)	
Angina pectoris	94 (13)	
Hypertension	193 (28)	39.5
Chronic renal failure	43 (14)	
Cerebrovascular disease	8 (0)	
Peripheral vascular disease	23 (1)	
Without above complications	119 (13)	
Primary cardiomyopathy	4 (3)	0.8
Hyperthyroidism	7 (0)	1.4
No manifest heart disease	35 (0)	7.2
	488 (121)	100

[a]Number of patients on digitalis are shown in parentheses
[b]Predominant aortic regurgitation – 35
[c]Predominant mitral regurgitation – 11
[d]Aortic + mitral regurgitation – 10

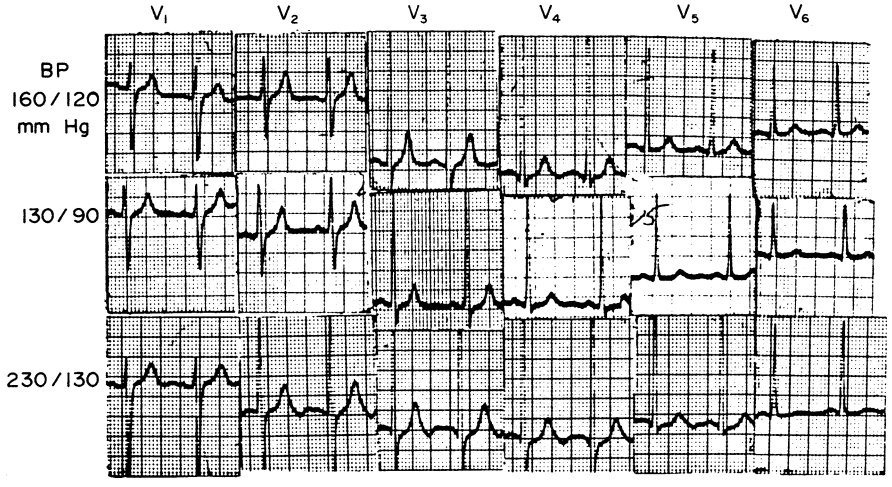

Figure 17.34

An example of reversible U-wave inversion related to blood-pressure changes in an adult with hypertension. The U wave is negative in leads V_3 and V_4 in the upper row and in leads V_2–V_5 in the lower row. In the middle row, the U wave is isoelectric or positive in all leads, and the QRS amplitude is lower in most leads compared to that in the upper and lower rows. BP denotes the blood pressure. (After Kishida et al. [256]. © Yorke Medical Group, Magazines Division, New York. Reproduced with permission.)

6 within 1 week after insertion of aortic or mitral valve prosthesis; and in 8 within 1 month after coronary artery-aorta saphenous bypass graft.

In 29 patients with systemic hypertension and a normal QRS duration, the change in U-wave polarity occurred more than once in the course of a follow-up period of less than 1 year. Each appearance of the negative U waves in these patients was associated with a significant increase in systolic and diastolic blood pressure without significant changes in heart rate, QRS duration, or the duration of QT_c, $Q–aU_c$ (aU denotes the U-wave apex), and QU_c intervals.

No consistent change was found in the pattern of T wave or ST segment changes associated with the change in U-wave polarity. These results suggest that changes in U-wave polarity are independent of electrophysiological processes that control the level of the ST segment and the morphology of the T wave. However, these conclusions do not apply to U-wave inversion associated with transient exercise-induced myocardial ischemia since such patients were not included in this group.

The decrease in QRS amplitude accompanying the change from a negative to upright or isoelectric U wave is a consistent finding in patients with hypertensive and valvular heart disease [256]. Fu et al. [262] recorded echocardiograms in hypertensive patients in whom handgrip caused inversion of the U wave as well as an increase in QRS amplitude. They showed that these changes were associated with an increase in left ventricular dimension. These observations implicate left ventricular dilatation as the possible cause of the U-wave inversion and the associated increase in the QRS amplitude. The increase in QRS amplitude in the dilated ventricle may be attributed to the Brody effect resulting from the increase in intracavitary blood volume at the end of diastole. The association between the negative U wave and the increased diastolic dimension or volume of the left ventricle implicates stretch as a possible cause of U-wave inversion [256]. It has been shown that left ventricular relaxation was prolonged in patients with hypertension [263] and either prolonged or incomplete in patients with myocardial ischemia [264]. Abnormalities in ventricular relaxation have also been reported in patients with aortic and mitral regurgitation [265].

17.4.5.1 Timing of the Negative U Wave

Watanabe suggested that the longer duration of the T–aU interval in patients with left bundle branch block favored the Purkinje fiber repolarization theory of U-wave genesis [255]. In our opinion, the delayed appearance of the U wave in relation to ventricular repolarization is of no help in establishing the mechanism of the U wave, because the finding could be owing to either delayed repolarization of the Purkinje fibers in the left ventricle or to delayed relaxation of the left ventricle. The role of prolonged QT_c in the absence of QRS prolongation has been examined. It was observed that patients with a LVH pattern and negative T waves in leads I, aVL, and $V_4–V_6$ tended to have greater QRS amplitude and a longer QT interval than patients with a less wide QRS–T angle. In this group of patients in whom QRS duration was normal, the U wave appeared later when the QT_c interval was longer. This finding suggests that the timing of the U wave is influenced by the total duration of ventricular repolarization and not by the pattern or duration of ventricular depolarization as suggested by Watanabe [266]. Similar conclusions can be drawn from the study of Ferrero and Maeder [267] who found that the T–aU intervals in patients with right bundle branch block were significantly longer in patients with RVH than in those without hypertrophy or with LVH. This suggests that the delayed U-wave timing was caused by some factors directly related to myocardial hypertrophy, rather than to the delayed activation of the Purkinje fibers.

17.4.6 Theories of U-Wave Genesis

17.4.6.1 Repolarization of Purkinje Fibers

Since the AP duration in the Purkinje fibers is longer than in the ventricular muscle fibers, it has been suspected that the U wave may be caused by the repolarization of Purkinje fibers. One of the difficulties with this concept is the small mass of the conducting tissue. Lepeschkin [268] listed the following observations, which would be difficult to reconcile with the Purkinje fiber theory:

1. Amphibia have U waves but no Purkinje fibers;
2. The configuration of the normal U wave does not conform to the Purkinje fiber repolarization pattern because the descent is longer than the ascent; (Fig. 17.15) and
3. Dependence on mechanical events as exemplified by the relation of the U wave to the preceding P wave during atrioventricular dissociation, bradycardia, postextrasystolic pauses, exercise, digitalis, and catecholamines.

Additional arguments against the Purkinje fiber theory are as follows:

1. The time difference between the end of the T wave and apex of the U wave is nearly constant within the range of heart rates between 60–90 min^{-1}; in this range, the AP duration differences between Purkinje and ventricular fibers should be greater when the rate is slower;
2. In patients with right bundle branch block, the timing of the U wave correlated better with the presence of RVH than with intraventricular conduction [267]; and
3. The results of Kishida et al. [256] showed no consistent difference between the direction of the U-wave vector in the presence of right bundle branch block and left bundle branch block.

17.4.6.2 Ventricular Repolarization Theory

If it is assumed that the U wave arises from a delay in repolarization in some portion of the ventricle, e.g., the papillary muscle, then the corresponding deflection must be designated as a part of the T wave rather than a U wave. However, if the terminal repolarization is prolonged, the U-wave amplitude may be increased owing to superposition of the T wave and U wave. In these cases, the deflection corresponding to the timing of the U wave may become the most prominent component of ventricular repolarization.

17.4.6.3 Mechanoelectrical Coupling

This is the most likely cause of a U wave of normal amplitude. It has been shown that stretch prolongs terminal repolarization in single fibers [269] and therefore may be expected to produce an ECG deflection after the T wave. Its vector may be determined by the sequence of ventricular relaxation. Changes in U-wave polarity may be attributed to changes in the sequence of relaxation. This would explain the mechanism of U-wave inversion in patients with hypertension or aortic regurgitation. In patients with acute ischemia, changes in U-wave polarity may be explained by an abnormal relaxation pattern during protodiastole known as protodiastolic shortening or "aftercontraction."

Recently, further support for a mechanoelectrical mechanism as the cause of inverted U waves has come from Choo and Gibson [270]. They studied the relationship between ECG hypertrophy and ventricular function using M-mode echocardiography and apex cardiography in 73 patients with LVH. Thirty eight of these cases had secondary ST–T changes together with U-wave inversion, 20 had LVH with ST–T changes, and 15 had LVH without ST–T or U-wave changes. The main findings were that U-wave inversion was related to a prolonged isovolumic relaxation period, delayed mitral valve opening relative to minimum cavity dimension, and reduced diastolic wall thinning rate. In the absence of U-wave inversion, LVH with secondary ST–T changes was weakly related to diastolic abnormalities. The authors noted that when U-wave inversion was present, a significant increase in transverse dimension occurred (almost one-third of the total for diastole) during the period between minimum dimension and left ventricular filling. Since the volume was constant during this period, other dimensions must have reduced, "implying the presence of incoordinate relaxation." Thus U-wave inversion appears to be linked to a mechanical event, the latter being thought by Choo and Gibson to be the more likely primary cause, if indeed there is a mechanoelectrical coupling.

Recently, Di Bernardo and Murray explored the hypotheses of U-wave genesis in a computer model of left ventricular repolarization, which exhibited an afterdepolarization. They investigated separately the effect of the amplitude of the afterpotential, dispersion of repolarization, and the timing of the afterpotential relative to the principal component on the 12-leadelectrocardiogram. They found that delaying repolarization in different regions of the heart could not explain

the U wave. However, U-wave polarity and other characteristics of the U wave could be explained by the presence of afterpotentials. In their model, U-wave inversion correlated with an abnormal afterpotential timing [271].

Further studies are needed to clarify the genesis of normal and abnormal U waves.

References

1. Surawicz, B., Primary and secondary T wave changes. *Heart Bull.*, 1966;**15**: 31–35.
2. Surawicz, B., The pathogenesis and clinical significance of primary T wave abnormalities, in *Advances in Electrocardiography*, R.C. Schlant and J.W. Hurst, Editors. New York: Grune and Stratton, 1972, 377–421.
3. Shabetai, R., B .Surawicz, and W. Hammill, Monophasic action potentials in man. *Circulation*, 1968;**38**: 341–352.
4. Surawicz, B., E.Lepeschkin, H.C. Herrlich, and B.F. Hoffman, Effect of potassium and calcium deficiency on the monophasic action potential, electrocardiogram and contractility of isolated rabbit hearts. *Am. J. Physiol.*, 1959;**196**: 1302–1307.
5. Gettes, L.S., B. Surawicz, and J.C. Shiue, Effect of high K, low K, and quinidine on QRS duration and ventricular action potential. *Am. J. Physiol.*, 1962;**203**: 1135–1140.
6. Lepeschkin, E. and B. Surawicz, The duration of the Q-U interval and its components in electrocardiograms of normal persons. *Am. Heart J.*, 1953;**46**: 9–20.
7. Ljung, O., The electrocardiogram in hypocalcemia, with special reference to the T wave. *Acta Med. Scand.*, 1949;**136**: 56–70.
8. Reynolds, T.B., H.E. Martin, and R.E.Homann, Serum electrolytes and the electrocardiogram. *Am. Heart J.*, 1951;**42**: 671–681.
9. Surawicz, B., Relationship between electrocardiogram and electrolytes. *Am. Heart J.*, 1967;**73**: 814–834.
10. Mirvis, D.M. and J. Marin-Garcia, Effects of tachycardia with normal and ectopic ventricular activation on S-T segment potential and patterns in the dog. *J. Electrocardiol.*, 1985;**18**: 223–231.
11. Surawicz, B. and S. Saito, Exercise testing for detection of myocardial ischemia in patients with abnormal electrocardiograms at rest. *Am. J. Cardiol.*, 1978;**41**: 943–951.
12. Surawicz, B. and K.C. Lasseter, Electrocardiogram in pericarditis. *Am. J. Cardiol.*, 1970;**26**: 471–474.
13. Harris, T.R., G.D. Copeland, and D.A. Brody, Progressive injury current with metastatic tumor of the heart. Case report and review of the literature. *Am. Heart J.*, 1965;**69**: 392–400.
14. Puletti, M., M. Curione, F. Pozzar, G. Righetti, and G. Jacobellis, Atrial repolarization: its role in ST elevation. *J. Electrocardiol.* 1979;**12**: 321–324.
15. Gubner, R., Determinants of ischemic electrocardiographic abnormalities and chest pain. Part II – The exercise electrocardiogram test. *J. Occup. Med.*, 1961;**3**: 110–120.
16. Surawicz, B., QRS, ST segment, T wave and U-wave specificity for myocardial ischemia and infarction, in *Clinical Strategies in Ischemic Heart Disease*, E. Corday and H.J.C. Swan, Editors. Baltimore, MD: Williams and Wilkins, 1979, pp. 160–165.
17. Lepeschkin, E. and B. Surawicz, Characteristics of true-positive and false-positive results of electrocardiographic Master two-step exercise test. *N. Engl. J. Med.*, 1958;**258**: 511–520.
18. Armstrong, W.F., J.W. Jordan, S.N. Morris, and P.L. McHenry, Prevalence and magnitude of S-T segment and T wave abnormalities in normal men during continuous ambulatory electrocardiography. *Am. J. Cardiol.*, 1982;**49**: 1638–1642.
19. Shipley, R.A., and W.R. Hallaran, The four lead electrocardiogram in two hundred normal men and women. *Am. Heart J.*, 1936;**11**: 325–345.
20. Goldman, M.J., RS-T segment elevation in mid- and left precordial leads as a normal variant. *Am. Heart J.*, 1953;**46**: 817–820.
21. Wasserburger, R.H. and W.J. Alt, The normal RS-T segment elevation variant. *Am. J. Cardiol.*, 1961;**8:** 184–192.
22. Kambara, H. and J. Phillips, Long-term evaluation of early repolarization syndrome (normal variant RS-T segment elevation). *Am. J. Cardiol.*, 1976;**38**: 157–161.
23. Spodick, D.H., Differential characteristics of the electrocardiogram in early repolarization and acute pericarditis. *N. Engl. J. Med.*, 1976;**295**: 523–526.
24. Morace, G., L. Padeletti, M.C. Porciani, and F.Fantini, Effect of isoproterenol on the "early repolarization" syndrome. *Am. Heart J.*, 1979;**97**: 343–347.
25. Kuo, C.S. and B. Surawicz, Ventricular monophasic action potential changes associated with neurogenic T wave abnormalities and isoproterenol administration in dogs. *Am. J. Cardiol.*, 1976;**38**: 170–177.
26. Mirvis, D.M., Evaluation of normal variations in S-T segment patterns by body surface isopotential mapping: S-T segment elevation in absence of heart disease. *Am. J. Cardiol.*, 1982; **50**: 122–128.
27. Ginzton, L.E. and M.M. Laks, The differential diagnosis of acute pericarditis from the normal variant: new electrocardiographic criteria. *Circulation*, 1982;**65:** 1004–1009.
28. Bidoggia, H., J.P. Maciel, N. Capalozza, S. Mosca, E.J. Blaksley, E. Valverede, G. Bertran, P. Arini, B.S.C. Biaggetti, and R.A. Quinteiro, Sex differences on the electrocardiographic pattern of cardiac repolarization: possible role of testosterone. *Am. Heart J.*, 2000;**140**: 678–683.
29. Surawicz, B. and R.S. Parikh, Prevalence of male and female patterns of early ventricular repolarization in the normal ECG of males and females from childhood to old age. *J. Am. Coll. Cardi*ol., 2002;**40**: 1870–1876.
30. Hellerstein, H.K. and I.M. Liebow, Electrical alternation in experimental coronary artery occlusion. *Am. J. Physiol.*, 1950;**60**: 366–374.
31. Roselle, H.A., R.S. Crampton, and R.B.Case, Alternans of the depressed S-T segment during coronary insufficiency: its relation to mechanical events. *Am. J. Cardiol.*, 1966;**18**: 200–207.
32. Williams, R.R., G.S. Wagner, and R.H. Peter, ST segment alternans in Prinzmetal's angina: a report of two cases. *Ann. Intern. Med.*, 1974;**81**: 51–54.
33. Nakashima, M., H. Hashimoto, M. Kanamaru, T. Nagaya, M. Hashizume, and H. Oishi, Experimental studies and clinical

report on the electrical alternans of ST segment during myocardial ischemia. *Jpn. Heart J.*, 1978;**19**: 396–408.
34. Puletti, M., M. Curione, G. Righetti, and G. Jacobellis, Alternans of the ST segment and T wave in acute myocardial infarction. *J Electrocardiol.*, 1980;**13**: 297–300.
35. Levine, H.D., S.H. Wanzer, and J.P. Merrill, Dialyzable currents of injury in potassium intoxication resembling myocardial infarction or pericarditis. *Circulation*, 1956;**13**: 29–36.
36. Chung, E.K., Principles of cardiac arrhythmias. Baltmore, MD: Williams and Wilkins, 1971, pp. 385–395.
37. Liechti, M., M. Gertsch, A. Kleber, and U. Althaus, Experimenteller Myokardinfarkt beim Schwein: Einfluss von, Probeligatur und Revaskularisierung auf die ST -Strecke im epikardialen Ekg. und auf die Haufigkeit von Kammerflimmern. *Schweiz. Med. Wochensch.*, 1977;**107**: 1552–1554.
38. Rozanski, J.J. and M. Kleinfeld, ST segment alternans in Prinzmetal's angina and associated ventricular arrhythmias. *Circulation*, 1976;**53/54** (Suppl. 2): 77.
39. Schaefer, H. and H.G. Haas, Electrocardiography, in *Handbook of Physiology*, vol. 1, section 2: Circulation, W. F. Hamilton and P. Dow, Editors. Washington, DC: American Physiological Society, 1962, pp. 323–415.
40. Burgess, M.J., K. Millar, and J.A. Abildskov, Cancellation of electrocardiographic effects during ventricular recovery. *J. Electrocardiol.*, 1969;**2**: 101–107.
41. Wilson, F.N., A.G. Macleod, and P.S. Barker, The *T* deflection of the electrocardiogram. *Trans. Assoc. Am. Physicians*, 1931;**46**: 29–38.
42. Lepeschkin, E., *Modern Electrocardiography.* Baltimore, MD: Williams and Wilkins, 1951, pp. 307, 420.
43. Harumi, K., M.J. Burgess, and J.A. Abildskov, A theoretic model of the T wave. *Circulation*, 1966;**34**: 657–668.
44. Ashman, R. and E. Byer, The normal human ventricular gradient. I. Factors which affect its direction and its relation to the mean QRS axis. *Am. Heart J.*, 1943;**25**: 16–57.
45. Haas, H.G., Ein Beitrag zur Theorie des Ventrikelgradienten. *Cardiologia*, 1960; **36**: 321–336.
46. Gardberg, M. and I.L. Rosen, Monophasic curve analysis and the ventricular gradient in the electrogram of strips of turtle ventricle. *Circ. Res.*, 1959;**7**: 870–875.
47. Van Dam, R. and D. Durrer, The T wave and ventricular repolarization. *Am. J. Cardiol.*, 1964;**14**: 294–300.
48. Abildskov, J.A., P. Urie, R. Lux, J. R. Burgess, and R.Wyatt R, Body surface distribution of QRST area. *Adv. Cardiol.*, 1978;**21**: 59–64.
49. Plonsey, R., A contemporary view of the ventricular gradient of Wilson. *J. Electrocardiol.*, 1979;**12**: 337–341.
50. Brody, D.A., D.M. Mirvis, R.E. Ideker, et al., Relative' dipolar behavior of the equivalent T wave generator: quantitative comparison with ventricular excitation in the rabbit heart. *Circ. Res.*, 1977;**40**: 263–268.
51. Wilson, F.N., F.F. Rosenbaum, and F.D. Johnston, Interpretation of the ventricular complex of the electrocardiogram. *Adv. Intern. Med.*, 1947;**2**: 1–63.
52. Autenrieth, G., B. Surawicz, and C.S. Kuo, Sequence of repolarization on the ventricular surface in the dog. *Am. Heart J.*, 1975;**89**: 463–469.
53. Burgess, M. J., L.S. Green, K. Millar, R. Wyatt, and J.A. Abildskov, The sequence of normal ventricular recovery. *Am. Heart J.*, 1972;**84**: 660–669.
54. Abildskov, J.A., M.J. Burgess, R.L. Lux, R. Wyatt, and G.M. Vincent, The expression of normal ventricular repolarization in the body surface distribution of T potentials. *Circulation*, 1976;**54**: 901–906.
55. Abildskov, J.A., The sequence of normal recovery of excitability in the dog heart. *Circulation*, 1975;**52**: 442–446.
56. Franz, M.R. et al., Monophasic action potential mapping in human subjects with normal electrocardiograms: direct evidence for the genesis if the T wave. *Circulation*, 1987;**75**: 379–386.
57. Cowan, J.C. et al., Sequence of epicardial repolarization and configuration of the T wave. *Br. Heart J.*, 1988;**60**: 424–433.
58. van Dam, R.Th. and D. Durrer, Experimental study on the intramural distribution of the excitability cycle on the form of the epicardial T wave in the dog heart in situ. *Am. Heart J.*, 1961;**61**: 537–542.
59. Spach, M.S. and R.C Barr, Ventricular intramural and epicardial potential distributions during ventricular activation and repolarization in the intact dog. *Circ. Res.*, 1975;**37**: 243–257.
60. Watanabe, T., P.M. Rautaharju, and T.F. McDonald, Ventricular action potentials, ventricular extracellular potentials, and the ECG of guinea pig. *Circ. Res.*, 1985;**57**: 362–373.
61. Engelking, R. and W Bienroth, Untersuchungen tiber den intramuralen Temperaturgradienten des Herzens und seinen Einfluss auf das Elektrokardiogramm. *Cardiologia*, 1959;**34**: 147–163.
62. Reynolds, E W. Jr.and P.N. Yu, Transmyocardial temperature gradient in dog and man: relation to the polarity of the T wave of the electrocardiogram. *Circ. Res.*, 1964;**15**: 11–19.
63. Abel, H., I. Briske, R. Engelking, W. Gartner, and H. Schaefer, L'action des gradients de temperature de la paroi du ventricule sur Ie gradient ventriculaire dans I'electrocardiogramme. *Acta Cardiol.*, 1958;**13**: 278–298.
64. Toyoshima, H. and M.J. Burgess, Electrotonic interaction during canine ventricular repolarization. *Circ. Res.*, 1978;**43**: 348–356.
65. Abel, H. and H. Loeper, Transverse sections of myocardial fibers and the T wave. Z. *Kardiol.*, 1973;**62**: 380–387 (article in German).
66. Burgess, M.J., K. Hammi, and J.A. Abildskov, Application of a theoretic T wave model to experimentally induced T wave abnormalities. *Circulation*, 1966;**34**: 669–678.
67. Hoff, H.E. and L H. Nahum, The factors determining the direction of the T wave: the effect of heat and cold upon the dextro- and levocardiogram. *Am. J. Physiol.*, 1941;**131**: 700–709.
68. Toyoshima, H., M. Prinzmetal, M. Horiba, et al., The nature of normal and abnormal electrocardiograms. *Arch. Intern. Med.*, 1965;**115**: 4–16.
69. Autenrieth, G., B. Surawicz, C.S. Kuo, and M. Arita, Primary T wave abnormalities caused by uniform and regional shortening of ventricular monophasic action potential in dog. *Circulation.* 1975;**51**: 668–676.
70. Daoud, F,S., B. Surawicz, and L.S. Gettes, Effect of isoproterenol on the abnormal T wave. *Am. J. Cardiol.*, 1972;**30**: 810–819.
71. Taggart, P, et al., Interplay between adrenaline and interbeat interval on ventricular repolarisation in intact heart in vivo. *Cardiovasc. Res.*, 1990;**24**: 884–895.
72. Kuo, C-S., J.P. Amlie, K. Munakata, C.P. Reddy, and B. Surawicz, Dispersion of monophasic action potential durations and activation times during atrial pacing, ventricular pacing, and ventricular premature pacing stimulation in canine ventricles. *Cardiovasc. Res.*, 1983;**17**: 152–161.

73. Sarachek, N.S, J. Roberts, and J.J. Leonard, A new method to measure non-uniformity in the intact heart. *J. Electrocardiol.*, 1972;**5**: 341–348.
74. Yanowitz, F., J.B. Preston, and J.A. Abildskov, Functional distribution of right and left stellate innervation to the ventricles: production of neurogenic electrocardiographic changes by unilateral alterations of sympathetic tone. *Circ. Res.*, 1966;**18**: 416–428.
75. Chou T C, Helm R A, Lach R, The significance of a wide TsE loop. *Circulation*, 1964; **30**: 400-410.
76. Kuo, C.S. and B. Surawicz, Relationship of transmembrane action potential form to the T wave and T loop, in *Vectorcardiography 3*, B.F. Hoffman and R.I.Hamby, Editors. Amsterdam: North-Holland, 1976, pp.67–74.
77. Wilson, F.N, F.D. Johnston, and I.G.W. Hill, The form of the electrocardiogram in experimental myocardial infarction. IV. Additional observations on the later effects produced by ligation of the anterior descending branch of the left coronary artery. *Am. Heart J.*, 1935;**10**: 1025–1041.
78. Horan, L.G., R.C. Hand, J.C. Johnson, M.R. Sridharan, T.B. Rankin, and N.C. Flowers, A theoretical examination of ventricular repolarization and the secondary T wave. *Circ. Res.*, 1978;**42**: 750–757.
79. Hecht, H H., Some observations and theories concerning the electrical behavior of heart muscle. *Am. J. Med.*, 1961;**30**: 720–746.
80. Wasserburger, R.H. and R.J. Corliss, Value of oral potassium salts in differentiation of functional and organic T wave changes. *Am J. Cardiol.*, 1962;**10:** 673–687.
81. Hiss, R.G. and L.E. Lamb, Electrocardiographic findings in 122,043 individuals. *Circulation*, 1962;**25**: 947–961.
82. Friedberg, C.K. and Zager A, "Nonspecific" ST and T wave changes. *Circulation*, 1961;**23**: 655–661.
83. Haws, C.W. and R.L. Lux, Correlation between in vivo transmembrane action potential durations and activation-recovery intervals from electrograms. *Circulation*, 1990;**81**: 281–288.
84. Yamaki, M., et al., Relation between recovery sequence estimated from body surface potentials and T wave shape in patients with negative T waves and normal subjects. *Circulation*, 1992;**85**:1768–1774.
85. Hamby, R.I., I. Hoffman, and E. Glassman, The T loop in right ventricular hypertrophy. *Dis. Chest*, 1969;**55**: 105–109.
86. Rubler, S., I. Hoffman, W.D. Franklin, and R.C. Taymor, The T loop in right bundle branch block: a vectorcardiographic study of 82 cases. *Am. Heart J.*, 1968;**76**: 217–226.
87. Hoffman, B.F., Effects of digitalis on electrical activity of cardiac fibers, in *Digitalis*, C. Fisch, and Surawicz B, Editors. New York: Grune and Stratton, 1969 pp. 93–109.
88. Levine, H.D. and E.T. Angelakos, Late peaking of the T wave as a digitalis effect. *Am. Heart J.*, 1964;**68**: 320–324.
89. Tandowsky, R M., N. Anderson, and J.K. Vandeventer, An electrocardiographic and clinical study of various so-called cardiac drugs. *Am. Heart J.*, 1944;**28**: 298–310.
90. Surawicz, B. and K C Lasseter, Effect of drugs on the electrocardiogram. *Prog. Cardiovasc. Dis.* 1970;**13**: 26–55.
91. Sagall, E.L., C.D Horn, and J.E.F. Riseman, Studies on the action of quinidine in man. I. Measurement of the speed and duration of the effect following oral and intramuscular administration. *Arch. Intern. Med.*, 1943;**71**: 460–473.
92. Lee, Y.C., Quinidine intoxication: an experimental study of the effect of molar sodium lactate and potassium chloride. *Am. Heart J.*, 1960;**60**: 785–798.
93. Surawicz, B, Lepeschkin, E, The electrocardiographic pattern of hypopotassemia with and without hypocalcemia. *Circulation*, 1953;**8**: 801–828.
94. Freedberg A S, J.E.F. Riseman, and E.D. Spiegl., Objective evidence of the efficacy of medicinal therapy in angina pectoris. *Am. Heart J.*, 1941;**22**: 494–518
95. Kayden, H.J., B.B. Brodie, J.M. Steele, Procaine amide: a review. *Circulation*, 1957;**15**: 118–126.
96. McCord, M.C, J.T. Taguchi, A study of the effect of procaine amide hydrochloride in supraventricular arrhythmias. *Circulation*, 1951;**4**: 387–393.
97. Zapata-Diaz J, E. Cabrera, and R. Mendez, An experimental and clinical study on the effects of procaine amide (Pronestyl) on the heart. *Am. Heart J.*, 1952;**43**: 854–870.
98. Rasmussen, H.S., M.J.Allen, K.J. Blackburn, G.S. Butrous, and H.W. Dalrymple, Dofetilide, a novel class III antiarrhythmic agent. *J. Cardiovasc. Pharmacol.*, 1992;**20** (Suppl. 2): S96–105.
99. Di Marco, J.P., The ibutilde for atrial arrhythmias study group cardioversion of atrial flutter by intravenous ibutilide: a new class III antiarrhythmic agent. *J. Am. Coll. Cardiol.*, 1991;**17**: 324A.
100. Wong, W., H.N. Pavlou, U.M. Birgesdorfer, D.E. Hilleman, S.M. Mohuddin, and D.M. Roden, Pharmacology of the class III antiarrhythmic agent sematilide in patients with arrhythmias. *Am. J. Cardiol.*, 1992;**69**: 206–212.
101. Carmeliet, E., Use-dependent block and use-dependent unblock of the delayed rectifier K+ current by almokalant in rabbit ventricular myocytes. *Circ. Res.*, 1993;**73**: 857–868.
102. Arita, M. and B. Surawicz, Electrophysiologic effects of phenothiazines on canine cardiac fibers. *J. Pharmacol. Exp. Ther.*, 1973;**184**: 619–630.
103. Kelly, H.G., J.E. Fay, and S.G.Laverty, Thioridazine hydrochloride (Mellaril): its effect on the electrocardiogram and a report of two fatalities with electrocardiographic abnormalities. *Can. Med. Assoc. J.*, 1963;**89**: 546–554.
104. Alexander, S., R. Shader, and L. Grinspoon, Electrocardiographic effects of thioridazine hydrochloride (Mellaril). *Lahey Clin. Found. Bull.*, 1967;**16**: 207–215.
105. Wendkos, M.H., The influence of autonomic imbalance on the human electrocardiogram. I. Unstable T waves in precordial leads from emotionally unstable persons without organic heart disease. *Am. Heart J.*, 1944;**28**: 549–567.
106. Butcher, W.A., K.G. Wakim, H.E. Essex, R.D. Pruitt, and H.B. Burchell, The effect of changes in concentration of cations on the electrocardiogram of the isolated perfused heart. *Am. Heart J.*, 1952;**43**: 801–814.
107. Levine, H.D., J.P. Vazifdar, B. Lown, J.P. Merrill, 'Tent-shaped" T waves of normal amplitude in potassium intoxication. *Am. Heart J.*, 1952;**43**: 437–450.
108. Winkler, A.W., H.E. Hoff, and P.K. Smith, Electrocardiographic changes and concentration of potassium in serum following intravenous injection of potassium chloride. *Am. J. Physiol.*, 1938;**124**: 478–483.
109. Braun, H.A., B. Surawicz, and S.T. Bellet, waves in hyperpotassemia: their differentiation from simulating T waves in other conditions. *Am. J. Med. Sci.*, 1955;**230**:147–156.
110. McAllen, P.M., The electrocardiogram associated with low levels of serum potassium. *Br. Heart J.*, 1951;**13**: 159–166.

111. Sjostrand,T., The electrocardiogram in hypopotassemia. *Acta Med. Scand.*, 1955;**151**: 73–83.
112. Hoffman, B.F. and E.E. Suckling, Effect of several cations on transmembrane potentials of cardiac muscle. *Am. J. Physiol.*, 1956;**186**: 317–324.
113. Abildskov, JA., M.J. Burgess, K. Millar, R.Wyatt, and G. Baule, The primary T wave – a new electrocardiographic waveform. *Am. Heart J.*, 1971;**81**: 242–249.
114. Montorsi, P., F. Fabbiochi, A. Loaldi, L. Annoni, A. Polese, N. De Cesare, and M. Guazzi, Coronary adrenergic hyperactivity in patients with syndrome X and abnormal electrocardiogram at rest. *Am. J. Cardiol.*, 1991;**68**: 1698–1703.
115. Camici, P.G, P. Marraccini, R. Lorenzoni, G. Burrigoli, N. Pecori, and A. Perissonotto, E. Ferrannini, A. L'Abate, and M. Marzilli, Coronary hemodynamics and myocardial metabolism in patients with syndrome X response to pacing stress. *J Am. Coll. Cardiol.*, 1991;**171**: 1461–1470.
116. Cannon, R.O., P.G. Camici, and S.E. Epstein, Pathophysiological dilemma of syndrome X. *Circulation*, 1992;**85**: 883–892.
117. Niboyannopoulos, P., J.C. Kaski, and A. Crake Maseri, Absence of myocardial dysfunction during stress in patients with syndrome X. *J. Am. Cardiol.*, 1991;**18**:1461–1470.
118. Tousoulis, D., T. Crake, D.C. Lefroy, A.R. Galassi, and A. Maseri, Left ventricular hypercontractility and ST segment depression in patients with syndrome X. *J. Am. Coll. Cardiol.*, 1993;**22**: 1607–1613.
119. Tweddel, A.C., W. Martin, and I. Hutton, Thallium scans in syndrome X. Br. Heart J., 1992;**68**: 48–50.
120. Levine, H.D., Non-specificity of the electrocardiogram associated with coronary artery disease. *Am. J. Med.*, 1953;**15**:344–355.
121. Stapleton, J.F., J.P. Segal, and W.P.Harvey, The electrocardiogram of myocardopathy. *Prog. Cardiovasc. Dis.*, 1970;**13**: 217–239.
122. Evans, W. and G. Wright, The electrocardiogram in Friedreich disease. *Br. Heart J.*, 1942;**4**: 91–102.
123. Nadas, A.S., M.M. Alimurung, and L.A. Sieracki, Cardiac manifestations of Friedreich's ataxia. *N. Engl. J. Med.*, 1951;**244**: 239–244.
124. Dolara, A., P. Morando, and M. Pampaloni, Electrocardiographic findings in 98 consecutive non-penetrating chest injuries. *Dis. Chest*, 1967;**52**: 50–56.
125. Burda, C.D., Electrocardiographic changes in lightning stroke. *Am. Heart J.*, 1966;**72**: 521–524.
126. Diaz-Rivera, R.S., F. Ramos-Morales, M.R. Garcia-Palmieri, and E A. Ramirez, The electrocardiographic changes in acute phosphorous poisoning in man. *Am. J. Med. Sci.*, 1961;**241**: 758–765.
127. Cosby, R.S. and M. Bergeron, Electrocardiographic changes in carbon monoxide poisoning. *Am. J. Cardiol.*, 1963;**11**: 93–96.
128. Chadha, J.S., D.W. Ashby, and J.O. Brown, Abnormal electrocardiogram after adder bite. *Br. Heart J.*, 1968;**30**: 138–140.
129. Gueron, M., J. Stern, and W. Cohen, Severe myocardial damage and heart failure in scorpion sting. Report of five cases. *Am. J. Cardiol.*, 1967;**19**: 719–726.
130. Bahl, O.P., T.J. Walsh, and E. Massie, Electrocardiography and vectorcardiography in idiopathic hypertrophic subaortic stenosis. *Am. J. Med. Sci.*, 1970;**259**: 262–271.
131. Bowers, D., An electrocardiographic pattern associated with mitral valve deformity in Marfan's syndrome. *Circulation*, 1961;**23**: 30–33.
132. Braudo, M., E.D. Wifle, and J.D. Keith, A distinctive electrocardiogram in muscular subaortic stenosis due to ventricular septal hypertrophy. *Am. J. Cardiol.*, 1964;**14**: 599–607.
133. Coltart, D.J. and S.J. Meldrum, Hypertrophic cardiomyopathy. An electrophysiological study. *Br. Med. J.*, 1970;**4**: 217–218.
134. Barlow J B, Bosman C K, Pocock W A, Marchand P, Late systolic murmurs and non-ejection ("mid-late") systolic clicks. Analysis of 90 patients. *Br. Heart J.* 1968; **30**: 203–18.
135. Bittar, N. and J.A. Sosa, The billowing mitral valve leaflet: report on fourteen patients. *Circulation*, 1968;**38**: 763–770.
136. Ehlers, K.H., M.A. Engle, R. Levin, H.Grossman, and R.J. Fleming, Left ventricular abnormality with late mitral insulficiency and abnormal electrocardiogram. *Am. J. Cardiol.*, 1970;**26**: 333–340.
137. Hancock, E.W. and K.Cohn, The syndrome associated with midsystolic click and late systolic murmur. *Am. J. Med.*, 1966;**41**: 183–196.
138. Stannard, M., J.G. Sloman, W.S.C.Hare, and A J. Goble, Prolapse of the posterior leaflet of the mitral valve: a clinical, familial, and cineangiographic study. *Br. Med. J.*, 1967;**3**: 71–74.
139. Burch G E, R. Meyers, and J.A. Abildskov, A new electrocardiographic pattern observed in cerebrovascular accidents. *Circulation*, 1954;**9**: 719–723.
140. Abildskov, J.A., K. Millar, M.J. Burgess, and W Vincent, The electrocardiogram and the central nervous system. *Prog. Cardiovasc. Dis.*, 1970;**13**: 210–216.
141. Cropp, G.J. and G.W. Manning, Electrocardiographic changes simulating myocardial ischemia and infarction associated with spontaneous intracranial hemorrhage. *Circulation*, 1960;**22**: 25–38.
142. Fentz, V. and J. Gormsen, Electrocardiographic patterns in patients with cerebrovascular accidents. *Circulation*, 1962;**25**: 22–28.
143. Hersch, C., Electrocardiographic changes in subarachnoid haemorrhage, meningitis, and intracranial space-occupying lesions. *Br. Heart J.*, 1964;**26**: 785–793.
144. Levine, H.J. and N.W. White, Unusual ECG patterns in rupture of vertebral artery aneurysm. *Arch. Intern. Med.*, 1962;**110**: 523–525.
145. Shuster, S., The electrocardiogram in subarachnoid haemorrhage. *Br. Heart J.*, 1960;**22**: 316–320.
146. Fisch, C, Giant negative T wave. *J. Indiana State Med. Assoc.*, 1961;**54**: 1664–1665.
147. Ippolito, T.L., J.S. Blier, and T.T. Fox, Massive T wave inversion. *Am. Heart J.*, 1954;**48**: 88–94.
148. Jacobson, D. and V.Schrire, Giant T wave inversion. *Br. Heart J.*, 1966;**28**: 768–775.
149. Szilagyi, N. and S L. Solomon, Variations in the form of the T wave in a case of partial heart block. *Am. Heart J.*, 1959;**8**: 637–644.
150. Dolara, A. and L.Pozzi, Electrical alteration of T wave without change in QRS complex. *Br. Heart J.*, 1971;**33**: 161–163.
151. Schindler, S.C. and B. Surawicz, Clinical significance of the ECG pattern with prolonged Q- T c interval, and increased T or U amplitude (CVA pattern). *Am. J. Cardiol.*, 1967;**19**: 148. [Abstract.]
152. Crompton, M.R., Hypothalamic lesions following the rupture of cerebral berry aneurysms. *Brain*, 1963;**86**: 301–314.
153. Jenkins,J.S., M. Buckell, A.B. Carter, and S. Westlake, Hypothalamic-pituitary-adrenal function after subarachnoid haemorrhage. *Br. Med. J.*, 1969;**4**: 707–709.
154. Millar, K. and J.A. Abildskov, Notched T waves in young persons with central nervous system lesions. *Circulation*, 1968;**37**: 597–603.

155. Averbuck,S.H., Acute generalized postoperative peritonitis simulating coronary artery occlusion. *J. Mt. Sinai Hosp.(NY)*, 1942;**8**: 335–340.
156. Fulton, M.C. and H.J.L. Marriott, Acute pancreatitis simulating myocardial infarction in the electrocardiogram. *Ann. Intern. Med.*, 1963;**59**: 730–732.
157. Gottesman. J., D. Casten, and A.J Beller, Changes in the electrocardiogram induced by acute pancreatitis. *J. Am. Med. Assoc.*, 1943;**123**: 892–894.
158. Kiessling, C.E., R.S. Schaaf, and A.M. Lyle, A study of T wave changes in the electrocardiograms of normal individuals. *Am. J. Cardiol.*, 1964;**13**: 598–602.
159. Lieberman, J.S., A. Taylor, and I.S. Wright, The effect of intravenous trypsin administration on the electrocardiogram of the rabbit. *Circulation*, 1954;**10**: 338–342.
160. Pollock, A.V., C.A. Bertrand, Electrocardiographic changes in acute pancreatitis. *Surgery*, 1956;**40**: 951–960.
161. Spritzer, H.W, C.R. Peterson, R.C. Jones, and E.L. Overholt, Electrocardiographic abnormalities in acute pancreatitis: two patients studied by selective coronary arteriography. *Mil. Med.*, 1969;**134**: 687–693.
162. Gallivan, G.J., H. Levine, and A.J. Canzonetti, Ischemic electrocardiographic changes after truncal vagotomy. *J. Am. Med. Assoc.*, 1970;**211**: 798–801.
163. Lehmann, K.G., A.H. Shandling, A.U. Yusi, and V.F Froelicher, Altered ventricular repolarization in central sympathetic dysfunction associated with spinal cord injury. *Am J. Cardiol*, 1969;**63**:1498–1504.
164. O'Brien, K.E, N. Pastis, and J.B.Conti, Diffuse T wave inversions associated with electroconvulsive therapy. *Am J. Cardiol.*, 2004;**93**: 1573–1574.
165. Walder, L.A. and D.H. Spodick, Global T wave inversion. *J. Am. Coll. Cardiol.*, 1991;**17**:1479–1485.
166. Walder, D.A. and D.H. Spodick, Global T wave inversion: long-term follow-up. *J. Am. Coll. Cardiol.*, 1993;**21**: 1652–1656
167. Brscic, E., A. Brusca, P. Presbiterio, F. Orzan, R. Conte, and E. Rosettoni, Ischemic chest pain and global T wave inversion in women with normal coronary arteriograms. *Am. J. Cardiol.*, 1997;**80**: 245–247.
168. Littmann, L., Large T wave inversion and QT prolongation associated with pulmonary edema: a report of nine cases. *J. Am. Coll. Cardiol.*, 1999;**34**: 1106–1110.
169. Suzuki, J., R. Shimamoto, J. Nishikawa, et al., Morphological onset and early diagnosis in apical hypertrophic cardiomyopathy: a long-term analysis with nuclear magnetic resonance imaging. *J. Am. Coll. Cardiol.*, 1999;**33**: 146.
170. Sakamoto, T., K. Amano, Y. Hada, et al., Asymmetric apical hypertrophy: ten year's experience. *Postgrad. Med. J.*, 1986;**62**: 567–570.
171. Alfonso, F., P. Nihoyannopolous, J. Stewart, S. Dickie, R. Lemery, and W.J. McKenna, Clinical significance of giant negative T waves in hypertrophic cardiomyopathy. *J. Am. Coll. Cardiol.*, 1990;**15**: 965–971.
172. Okada, M., M.Yotsukara, T. Shimada, and K. Ishikawa, Clinical implications of isolated T wave inversion in adults: electrocardiographic differentiation of the underlying causes of the phenomenon. *J. Am. Coll. Cardiol.*,1994;**24**: 739–745.
173. Urschel, D.L. and G.E. Gates, Mean spatial vectorcardiography: the T vector changes in hypothyroidism. *Am. Heart J.*, 1953;**45**: 611–622.
174. Zondek, H., The electrocardiogram in myxoedema. *Br. Heart J.*, 1964;**26**: 227–232.
175. Mainzer, F., L'influence de l'anxiete sur l'electrocardiogramme: son importance dans l'ectrocardiographie pratique. *Cardiologia*, 1958;**32**: 362–374.
176. Berman, R., E. Simonson, and W. Heron, Electrocardiographic effects associated with hypnotic suggestion in normal and coronary sclerotic individuals. *J. Appl. Physiol.*, 1954;**7**: 89–92.
177. Ljung, O., Alterations in the electrocardiogram as a result of emotionally stimulated respiratory movements especially with reference to the so-called "fright electrocardiogram." *Acta Med. Scand.*, 1951;**141**: 221–229.
178. Mitchell, J.H. and A.P. Shapiro, The relationship of adrenalin and T wave changes in the anxiety state. *Am. Heart J.*, 1954;**48**: 323–330.
179. Magendantz, H., and J. Shortsleeve, Electrocardiographic abnormalities inpatients exhibiting anxiety. *Am. Heart J.*, 1951;**42**: 849–857.
180. Kannel ,W.B., T.R. Dawber, and M.E. Cohen, The electrocardiogram in neurocirculatory asthenia (anxiety, neurosis or neurasthenia): a study of 203 neurocirculatory asthenia patients and 757 healthy controls in the Framingham study. *Ann. Intern. Med.*, 1958;**49**: 1351–1360.
181. Logue, R.B., J.F. Hanson, and W.A. Knight, Electrocardiographic studies in neurocirculatory asthenia. *Am. Heart J.*, 1944;**28**: 574–577.
182. Wendkos, M.H. and R.B. Logue, Unstable T waves in leads II and III in persons with neurocirculatory asthenia. *Am. Heart J.*, 1946;**31**: 711–723.
183. Wheeler, E.O., Emotional stress: cardiovascular disease and cardiovascular symptoms. in *The Heart*, 2nd edn., J.W. Hurst and R.B. Logue, Editors. New York: McGraw-Hill, 1970, pp. 1414–1422.
184. White, P.D., M.E. Cohen, and W.P.Chapman, The electrocardiogram in neurocirculatory asthenia, anxiety neurosis, or effort syndrome. *Am. Heart J.*, 1947;**34**: 340–344.
185. Levander-Lindgren, M., Studes in neurocirculatory asthenia (Da Costa's syndrome). I. Variations with regard to symptoms and some pathophysiological signs. *Acta Med. Scand.*, 1962;**172**: 665–676.
186. Lewis, B.I., Mechanism and management of hyperventilation syndromes. *Biochem. Clin.*, 1964;**4**: 89–96.
187. Crede, R.H., N.C. Chivers, and A.P. Shapiro, Electrocardiographic abnormalities associated with emotional disturbances. A case report. *Psychosom. Med.*, 1951;**13**: 277–288.
188. Biberman, L., R.N. Sarma, and B. Surawicz, T wave abnormalities during hyperventilation and isoproterenol infusion. *Am. Heart J.*, 1971;**81**: 166–174.
189. Salvetti, A., P.L. Cella, P. Arrigoni, and D. Biancalana, Comportamento della fase di ripolarizzazione ventricolare dopo sforza e dopo iperventilazione volontaria in giovani sani. *Cuore Circ.*, 1964;**48**: 192–208.
190. Yu, P.N., B.J.B. Yim, and C.A. Stanfield, Hyperventilation syndrome. *Arch. Intern. Med.*, 1959;**103**: 902–913.
191. Christensen, B.C., Studies on hyperventilation. II. Electrocardiographic changes in normal man during voluntary hyperventilation. *J. Clin. Invest.*, 1946;**25**: 880–889.
192. Christensen, B.C., Variations in the carbon dioxide tension in the arterial blood and the electrocardiogram in man. *Acta Physiol. Scand.*, 1946;**12**: 389–396.

193. Schweitzer, P., T. Hildebrand, H. Klvanova, S. Simko, E. Galajdova, and J. Gregorova, Der Einfluss der adrenergen Blockade auf die orthostatischen Veriinderungen der Integralvektoren von QRS. T sowie des Ventrikelgradienten bei Patienten mit neurozirkulatorischer Asthenie und Thyreotoxikose. Z. *Kreislaufforsch.*, 1967;**56**: 316–325.
194. Hiss, R.G., G.B. Smith Jr., and L.E. Lamb, Pitfalls in interpreting electrocardiographic changes occurring while monitoring stress procedures. *Aerosp. Med.*, 1960;**31**: 9–18.
195. Furberg, C. and C.F. Tengblad, Adrenergic beta receptor blockade and the effect of hyperventilation on the electrocardiogram. *Scand. J. Clin. Lab. Invest.*, 1966;**18**: 467–472.
196. Pentimone, F., A. Pesola, A. L'Abbate, A. Smorfa, and C. Siusti, Effetto del propanolol sulle modificazioni elettocardiografiche secondarie alla prova da iperventillazione volontaria ed alla prova ortostatica. *Cuore Circ.*, 1967;**51**: 79–93.
197. Furberg, C., Adrenergic beta-blockade and electrocardiographical ST-T changes. *Acta Med. Scand.*, 1967;**181**: 21–32.
198. Nordenfelt, O., Orthostatic ECG changes and the adrenergic beta-receptor blocking agent, Propanolol (Inderal). *Acta Med. Scand.*, 1965;**178**: 393–401.
199. Simonson, E. and C.A. McKinlay, The meal test in clinical electrocardiography. *Circulation*, 1950;**1**: 1006–1016.
200. Sears, G.A and G.W. Manning, Routine electrocardiography: postprandial T wave changes. *Am. Heart J.*, 1958;**56:** 591.
201. Sleeper, J.C. and E.S.Orgain, Differentiation of benign from pathologic T waves in the electrocardiogram. *Am. J. Cardiol.*, 1963;**11**: 338–347.
202. Mann, R.H. and H.B. Burchell, The significance of T wave inversion in sinus beats following ventricular extrasystoles. *Am Heart J.*, 1954;**47**: 504–513.
203. Paparella, N., F. Ouyang, G.Fuca, K.H. Kuch, R.Cappalo, and P.Alboni, Significance of newly acquired negative T wave after interruption of paroxysmal reentrant supraventricular tachycardia with narrow QRS complex. *Am. J. Cardiol.*, 2000;**85**: 261–263.
204. Levine, H.D., B. Lown, and R.B.Streeper, The clinical significance of postextrasystolic T wave changes. *Circulation*, 1952;**6**: 538–548.
205. Meyer, P. and C. Schmidt, Troubles postextrasystoliques de la repolarisation. *Arch. Mal. Coeur Vaiss.*, 1949;**42**: 1175–1180.
206. Graybiel, A. and P.D. White, Inversion of the T wave in lead I or II of the electrocardiogram in young individuals with neurocirculatory asthenia with thyrotoxicosis, in relation to certain infections, and following paroxysmal ventricular tachycardia. *Am. Heart J.*, 1935;**10**: 34–54.
207. Kernohan, R.J., Post-paroxysmal tachycardia syndrome. *Br. Heart J.*, 1969;**31**: 803–806.
208. Trevino, A., B. Razi, and B.M. Beller, The characteristic electrocardiogram of accidental hypothermia. *Arch. Intern. Med.*, 1971;**127**: 470–473.
209. MacAlpin, R.N., W.A.Weidner, A.A. Kattus Jr., and W.N. Hanafee, Electrocardiographic changes during selective coronary cineangiography. *Circulation*, 1966;**34**: 627–637.
210. Smith, R.F., J.W. Harthorne, and C.A. Sanders, Vectorcardiographic changes during intracoronary injections. *Circulation*, 1967;**36**: 63–76.
211. Wolf, G.L. and J.W. Hirshfeld Jr., Changes in QTc interval induced with Renografin-76 and Hypaque-76 during coronary arteriography. *J. Am. Coll. Cardiol.*, 1983;**1**: 1489–1492.
212. Chatterjee, K., A. Harris, G. Davies, and A. Leatham, Electrocardiographic changes subsequent to artificial ventricular depolarization. *Br. Heart J.*, 1969;**31**: 770–779.
213. Rosenbaum, M.B., H.H. Blanco, M.V. Elizari, J.O. Lazzari, and J.M. Davidenko, Electrotonic modulation of the T wave and cardiac memory. *Am. J. Cardiol.*, 1982;**50**: 213–222.
214. Shvilkin, A., K.L. Kalon, M.R. Rosen, and M.E. Josephson, T-vector direction differentiates postpacing from ischemic T wave inversion in precordial leads. Circulation, 2005; **111**: 969–974.
215. Nicolai, P., J.L. Medvedowsky, M. Delaage, C. Barnay, E. Blache, and A. Pisapia, Wolff-Parkinson-White syndrome: T wave abnormalities during normal pathway conduction. *J. Electrocardiol.*, 1981;**14**: 295–300.
216. Kalbfleisch, S.J., J. Sousa, R. El Atassi, et al., Repolarization abnormalities after catheter ablation of accessory atrioventricular connections with radiofrequency current.*J. Am. Coll. Cardiol.*, 1991;**18**: 761.
217. Surawicz, B., Transient T wave abnormalities after cessation of ventricular pre-excitation. Memory of what? *J. Cardiovasc. Electrophysiol.*, 1996;**7**: 51–59.
218. Engel, T.R., R.Shah, L.A. DePodesta, W.S. Frankl, and R.L. Krause, T wave abnormalities of intermittent left bundle branch block. *Ann. Intern. Med.*, 1978;**89**: 204–206.
219. Denes, P., A. Pick, R.H. Miller, R.J. Pietras, and K.M. Rosen, A characteristic precordial repolarization abnormality with intermittent left bundle branch block. *Ann. Intern. Med.*, 1978;**89**: 55–57.
220. Surawicz, B., Transient T wave abnormalities in intermittent bundle branch block. *Am. J. Cardiol.*, 1982;**50**: 363–364.
221. Stewart. C.B and G.W. Manning, A detailed analysis of the electrocardiograms of 500 R.C.A.F. aircrew. *Am. Heart J.*, 1944;**27**: 502–523.
222. Viscidi, P.C. and A.J. Geiger, Electrocardiographic observations on 500 unselected young adults at work. *Am. Heart. J.*, 1943;**26**: 763–768.
223. Fisch, C., The electrocardiogram in the aged, in *Geriatric Cardiology*, R.J. Noble and D.A. Rothbaurn, Editors. Philadelphia, PA: Davis, 1981, pp. 63–74 (Brest, A.N. Editor, *Cardiovasc. Clin.*, **12**).
224. Atterhog, J.H., K. Eliasson, and P. Hjemdahl, Sympathoadrenal and cardiovascular responses to mental stress, isometric handgrip and cold pressor test in asymptomatic young men with primary T wave abnormalities in the electrocardiogram. *Br. Heart J.*, 1981;**46**: 311–319.
225. Littmann, D., Abnormal electrocardiograms in the absence of demonstrable heart disease. *Am. J. Med.*, 1948;**5**: 337–350.
226. Pruitt, R.D., C.H. Klakeg, and L.E Chapin, Certain clinical states and pathologic changes associated with deeply inverted T waves in the precordial electrocardiogram. *Circulation*, 1955;**11**: 517–530.
227. Kaufman, J.M. and R. Lubera, Preoperative use of atropine and electrocardiographic changes. Differentiation of ischemic from bilary-induced abnormalities. *J. Am. Med. Assoc.*, 1967;**200**: 197–200.
228. Wasserburger, R.H. and T.H. Lorenz, The effect of hyperventilation and pro-banthine on isolate RS-T segment and T wave abnormalities. *Am. Heart J.*, 1956;**51**: 666–683.
229. Leitner, St. J. and H. Steinlin, Untersuchungen iiber den Einfiuss des vegetativen Nervensystems auf das Elektrocardiogrammrn. *Arch. Kreislaufforsch.*, 1943;**13**: 62–96.

230. Dauchot, P. and J.S. Gravenstein, Effects of atropine on the electrocardiogram in different age groups. *Clin. Pharmacol. Ther.*, 1971;**12**: 274–280.
231. Sparks H V Jr, Hollenberg M, Carriere S, Funkenstein D, Zakheim R M, Barger A C, Sympathomimetic drugs and repolarization of ventricular myocardium of the dog. *Cardiovasc. Res.* 1970; **4**: 363–70.
232. Kuo, C.S., D.F. Butler, C.M. Chen, and B. Surawicz, Pathogenesis of post-ischemic T wave abnormalities. *Am J. Cardiol.*, 1974;**33**: 149. [Abstract.]
233. Salustri, A., P. Garyfallidis, A. Elhendy, M. Ciavatti, J.H. Cornel, A. Gemelli, F.J. Ten Cate, J.R.T.C Roelandt, and P.M. Fioretti, T wave normalization during dobutamine echocardiography for diagnosis of viable myocardium. *Am. J. Cardiol.*, 1995;**75**: 505–507.
234. Hiejima, K. and T.Sano, Electrical alternans of TU wave in Romano-Ward syndrome. *Br. Heart J.*, 1976;**38**: 767–770.
235. Schwartz, P.J. and A. Malliani, Electrical alternation of the T wave: clinical and experimental evidence of its relationship with the sympathetic nervous system and with the long Q-T syndrome. *Am. Heart J.*, 1975;**89**: 45–50.
236. Saitoh, H., J.C. Bailey, and B. Surawicz, Alternans of action potential after abrupt shortening of cycle length: differences between dog Purkinje and ventricular muscle fibers. *Circ Res.*, 1988;**62**: 1027.
237. Surawicz, B. and C. Fisch, Cardiac alternans: diverse mechanisms and clinical manifestations. *J. Am Coll. Cardiol.*, 1989;**20**: 483–499.
238. Sharma, S, K.G. Nair, and H.A. Gadekar, Romano-Ward prolonged QT syndrome with intermittent T wave alternans and atrioventricular block. *Am Heart J.*, 1981;**101**: 500–501.
239. Fisch C, Edmands R E, Greenspan K, T wave alternans: An association with abrupt rate change. *Am. Heart J.* 1971; **81**: 817–821.
240. Navarro-Lopez, F., J. Cinca, G. Sanz, J. Magriiia, and A. Betriu, Isolated T wave alternans elicited by hypocalcemia in dogs. *J. Electrocardiol.*, 1978;**11**: 103–108.
241. Surawicz B., Effect of Ca on duration of Q-T interval and ventricular systole in dog. *Am. J. Physiol.*, 1963;**205**: 785–789.
242. Lepeschkin, E., Electrocardiographic observations on the mechanism of the electrical alternans of the heart. *Cardiologia*, 1950;**16**: 278–287.
243. Gettes,L.S., N. Morehouse,and B. Surawicz, Effect of premature depolarization on the duration of action potentials in Purkinje and ventricular fibers of the moderator band of the pig heart: role of proximity and the duration of the preceding action potential. *Circ. Res.*, 1972;**30**: 55–66.
244. Kleinfeld, M., E. Stein, and C.E. Kossmann, Electrical alternans with emphasis on recent observations made by means of single-cell electrical recording. *Am. Heart J.*, 1963;**65**: 495–500.
245. Surawicz, B., in *Chou's Electrocardiography in Clinical Practice*, B. Surawicz and T. Knilans, Editors. Philadelphia, PA: WB Saunders, 2001, p.562.
246. Aravindakshan, V., B. Surawicz, and R.D. Allen, Electrocardiographic exercise test in patients with abnormal T waves at rest. *Am. Heart J.*, 1977;**93**: 706–714.
247. Zabel, M., A. Burak, T. Klingenheben, M.R. Franz, S.H. Hohenloser, and M. Malik, Analysis of 12-lead T wave morphology for risk stratification after myocardial infarction. *Circulation*, 2000;**102**:1252–1572.
248. Zabel, M., M. Malik, K. Hnatkova, V. Papademetriou, R.D. Fletcher, and M. R. Franz, Analysis of T wave morphology from the 12-lead electrocardiogram for prediction of long-term prognosis in male US veterans. *Circulation*, 2002;**106**; 1066–1070.
249. Okin, P.M., R.B. Devereux, R.R. Fabsitz, E.T. Lee, J.M. Galloway, and B.V. Howard, Principal component analysis of the T wave and prediction of cardiovascular mortality in American Indians. The Strong Heart Study. *Circulation*, 2002;**105**: 714–719.
250. Rautaharju P M, Nelson J C, Kronmal R A, Zhang Z M, Robbins J, Gottdiener J S, Furberg C D, Manolio T, and Fried L, Usefulness of T-axis deviation as an independent risk indicator for cardiac events in older men and women free from coronary heart disease (The cardiovascular health study). *Am J Cardiol* 2001; **88**: 118–123.
251. Surawicz. B., Is the U wave in the electrocardiogram a mechano-electric phenomenon? in *Cardiac Mechano-Electric Feedback and Arrhythmias. From Pipette to Patient*, P. Kohl, F. Sachs, and M.R. Franz, Editors. Philadelphia, PA: Elsevier, pp. 179–190.
252. Surawicz, B., U-wave: facts, hypotheses, misconceptions and misnomers. *J. Cardiovasc. Electrophysiol.*, 1999;**8**: 1117–1126.
253. Lepeschkin, E. and B. Surawicz,. The measurement of the Q-T interval of the electrocardiogram. *Circulation*, 1952;**6**: 378–388.
254. Holzmann, M. and W. Zurukzoglu, Die klinishe Bedeutung der negativen und diphasischen U-Wellen in menschlichen Ekg. *Cardiologia*, 1955;**27**: 202–214.
255. Ameur-Hendrich, C., G. Cordier, F. Hessel, J.P. Chemouny, and G. Laval, Onde U negative a valeur diagnostique et prognostique. A propos de 100 cas. *Ann. Cardiol. Angeiol.*, 1976;**25**: 103–110.
256. Kishida, H., J.S. Cole, and B. Surawicz, Negative U wave: a highly specific but poorly understood sign of heart disease. *Am. J. Cardiol.*, 1982;**49**: 2030–2036.
257. Georgopoulos. A.J., W.L. Proudfit, and I.H. Page, Relationship between arterial pressure and negative U waves in electrocardiograms. *Circulation*, 1961;**23**: 675–680.
258. Kemp, R.L., B. Surawicz, J.C. Bettinger, H. Gottlieb, and S. Bellet, Prognostic significance of negative U waves in the, electrocardiogram in hypertension. *Circulation*, 1957;**15**: 98–101.
259. Lambert, J., Clinical study of the abnormalities of the terminal complex TU-U of the electrocardiogram. *Circulation*, 1957;**15**: 102–104.
260. Miwa, K., T. Murakami, H. Kambara, and C. Kawai, U wave inversion during attacks of variant angina. *Br. Heart J.*, 1983;**50**: 378–382.
261. Gerson, M.C., J.F. Phillips, S.N. Morris, and P.L. McHenry, Exercise-induced U wave inversion as a marker of stenosis of the left anterior descending coronary artery. *Circulation*, 1979;**60**: 1014–1020.
262. Fu, L.T., N. Takahashi, M. Yamamoto, M. Kuboki, and S. Koyama, Handgrip induced negative U-wave in electrocardiogram of hypertensive subjects. *Jpn. Heart J.*, 1981;**22**: 59–73.
263. Hanrath,P., D.G. Mathey, R. Siegert, and W. Bleifeld, Left ventricular relaxation and filling pattern in different forms of left ventricular hypertrophy: an echocardiographic study. *Am. J. Cardiol.*, 1980;**45**: 15–23.
264. Mann, T., S. Goldberg, G H. Mudge Jr., and W.Grossman, Factors contributing to altered left ventricular diastolic properties during angina pectoris. *Circulation*, 1979; **59**: 14–20.
265. Rousseau, M.F., H. Pouleur, J.M.R Detry, and L.A. Brasseur, Impaired left ventricular relaxation in patients with aortic or mitral regurgitation *Am. J. Cardiol.*, 1982;**49**: 990. [Abstract.]

266. Watanabe, Y. and I.M. De Azevedo, Electrocardiographic correlation of bundle branch block and the U wave. *J. Electrocardiol.*, 1979;**6**: 215–220.
267. Ferrero, C. and J. Maeder, Bloc de branche droite: diagnostic de l'hypertrophie ventriculaire droite par la chronologie de l'onde V. *Schweiz. Med. Wochenschr.*, 1970;**100**: 190–192.
268. Lepeschkin, E., Physiologic basis of the U wave, in *Advances in Electrocardiography*, R.C. Schlant and J.W. Hurst, Editors. New York: Grune and Stratton, 1972, pp. 431–447.
269. Dudel, J. and W. Trautwein, Das Aktionspotential und Mechanogramm des Herzmuskels unter dem Einfluss der Dehnung. *Cardiologia*, 1954;**25**: 344–362.
270. Choo, M.H. and D.G.Gibson, U waves in ventricular hypertrophy: possible demonstration of mechano-electrical feedback. *Br. Heart J.*, 1986;**55**: 428–433.
271. Di Bernardo, D. and A. Murray, Origin of the electrocardiogram of U-waves and abnormal U-wave inversion. *Cardiovasc Res.*, 2002;**53**: 202–208.

18 Ventricular Repolarization in Myocardial Ischemia and Myocardial Infarction: Theory and Practice

Borys Surawicz

P. W. Macfarlane, A. van Oosterom, O. Pahlm, P. Kligfield, M. Janse, J. Camm (eds.), *Comprehensive Electrocardiology*, DOI 10.1007/978-1-84882-046-3_18,

18.1 Physiologic and Biochemical Processes Responsible for the Electrocardiographic Alterations During Myocardial Ischemia and Myocardial Infarction

The dominant effects of ischemia during the first few minutes are cellular K^+ loss, extracellular K^+ accumulation, and acidosis, resulting in rapid depolarization, inexcitability, and loss of active tension development. After a latency period of several minutes, there is a second phase of K^+ loss, increase in free cytosolic Ca^{2+}, electrical cell-to-cell uncoupling, and development of ischemic contracture [1].

Normally, the cell maintains a balance between influx and efflux of K^+. The influx occurs mainly through the Na^+/K^+ pump that has been assumed to function normally within the first 10–15 min of ischemia [2, 3]. Thus, the increase in extracellular K^+ must be attributed to an increased K^+ efflux taking place passively as a consequence of the K concentration gradient and through gated K^+ channels. One of the suggested causes of K^+ loss is the intracellular acidosis causing efflux of inorganic phosphate and lactate and carrying K^+ out of the cells [4, 5]. Increased K^+ efflux contributes to shortening of the action potential (AP) [6–8]. There is evidence that the K_{ATP} channel plays an important role in the K^+ loss during myocardial ischemia [9].

The resting membrane potential (RMP) decreases within minutes after experimental coronary occlusion [10–12]. During acute global ischemia in the perfused guinea pig heart, the RMP decreased within 15 min from −82 to −49.5 mV. This degree of depolarization could be accounted for by an extracellular K^+ level of 15 mM. This means that RMP approached the estimated K equilibrium potential [4].

Along with depolarization, the upstroke velocity of the AP decreases. A frequent precursor of the loss of excitability (when the RMP falls below about −60 mV) in the ischemic myocardium is electrical alternans.

During the healing phase of myocardial infarction (MI), encompassing the first 2 weeks, the fibers in the surviving epicardial muscle are arranged in closely packed fascicles but an increase in fibrous tissue sometimes separates individual muscle fibers. The RMP and AP amplitudes are frequently decreased, but in most surviving fibers RMP is more negative than −60 to −70 mV, implying that the slow conduction depends on the depressed sodium current rather than on calcium current [9]. Conduction velocity in the epicardial zone overlying the infarct is decreased as a result of the above-mentioned depressed Na channel and altered anatomical fiber arrangement [13]. At most sites, within the infarcted region, the effective refractory period is prolonged with depressed excitability and increased dispersion of both excitability and refractoriness [14, 15].

The characteristics of APs of the surviving endocardial cells from human infarcts have been studied in tissues resected during cardiac surgery. In all aspects, the APs, the extracellular electrograms, and the structural abnormalities have resembled the respective counterparts from the experimental animal models [9].

18.2 Systolic and Diastolic Currents of Injury

Figure 17.3b in the preceding chapter shows two mechanisms of ST segment displacement encountered in myocardial ischemia: first, the shortening and decreased amplitude of the AP, and second, depolarization, i.e., less negative resting membrane potential. The shortening and decreased amplitude causes potential differences during repolarization that is electrical systole, and this results in a systolic current of injury. The depolarization causes potential differences during electrical diastole and results in a diastolic current of injury. The left arrow in Fig. 17.3b shows that the potential difference produced by the systolic current of injury displaces the ST segment and the right arrow shows that the potential difference produced by the diastolic current of injury displaces the baseline. Both effects influence the ECG in the same manner (see below).

18.3 ST Segment Deviations Arising from Epicardial or Endocardial Injury

Figure 18.1 is a diagrammatic representation of the effects of epicardial and endocardial injury on the ST segment in the standard limb or anterior precordial leads of the ECG. Epicardial injury may cause elevation of the ST segment and depression of the baseline, whereas subendocardial injury may cause the depression of the ST segment and the elevation

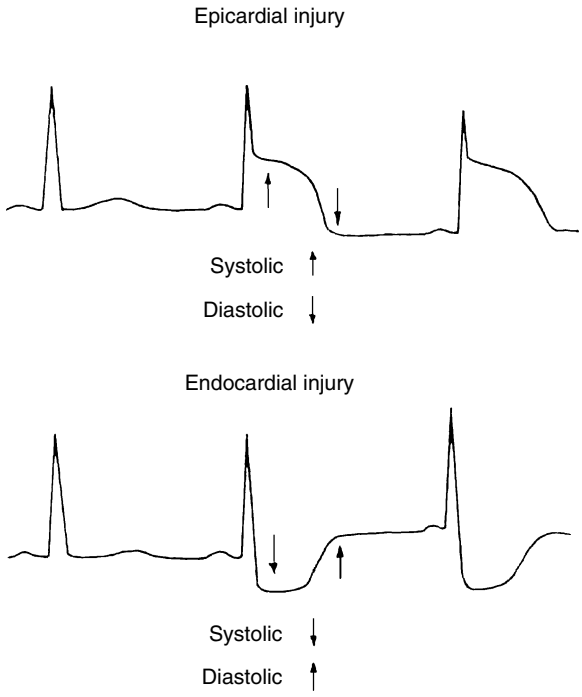

Figure 18.1

Diagram illustrating the effects of subepicardial and subendocardial injury on the ST segment and the baseline of the electrocardiogram. The direction of the arrows indicates the flow of the injury current and not the direction of the ST segment vector. For explanation see text. With permission from Surawicz B and Saito S: Exercise testing for detection of myocardial ischemia in patients with abnormal electrocardiograms at rest. *Am. J. Cardiol.*, 1978;41: 943–951.

of the baseline. The conventional ECG recorded with alternating current (ac)-coupled amplifiers does not reveal displacement of the baseline and therefore does not differentiate between the ST segment displacement caused by the systolic and that caused by the diastolic current of injury [16].

Studies using the magnetocardiogram which records the same currents as the ECG but, unlike the ECG, responds to direct current, have been helpful in separating the systolic from the diastolic "current of injury" [17]. The magnetocardiogram also showed that ST depression during exercise-induced ischemia is a result of baseline shift, produced by a steady injury current which flows during the entire cardiac cycle but is interrupted during the ST interval [18].

Several studies have shown that the major change after coronary occlusion in dogs is the "diastolic injury current" owing to depolarization in the ischemic areas, while the shortening of AP during acute ischemia makes only a small contribution to the ST segment displacement. In the isolated perfused pig heart, TP (baseline) depression occurred within 1.5 min and ST elevation within 4 min after occlusion of the left anterior descending (LAD) coronary artery [3, 19]. It has been shown that the injury current arises at the ischemic border [20] which in the study of Coronel et al. [19] consisted of interdigitated normal and ischemic zones sharply demarcated from each other. Potential gradients at the "electrical border" between the ischemic and normal myocardium in the dogs during LAD coronary artery occlusion measured 12–20 mV [21].

In patients with acute myocardial infarction, isopotential body-surface mapping has shown early appearance of repolarization potentials, i.e., −21.3+/−:4.6 ms before the end of the QRS complex in patients with anterior infarction and 34.6:+/−12.4 ms before the end of the QRS complex in patients with inferior infarction [3]. The topographic configuration of the isopotential maps was relatively simple, and in patients with both types of infarction, the pattern was compatible with a single-dipole equivalent cardiac generator [22]. For additional discussion of the systolic and diastolic injury currents, see Chap. 17.

Acute injury pattern is an electrocardiographic term that defines an abnormal ST segment elevation in 2 or more adjacent standard 12 leads except lead aVR. The term is derived from an injury current flowing between an injured, i.e., depolarized tissue and a normally polarized tissue (see above). The most common cause of injury current and the corresponding injury pattern is acute myocardial ischemia, e.g., during thrombotic, embolic, or spastic coronary occlusion. It needs to be emphasized that acute injury is not synonymous with acute myocardial infarction (MI). An acute injury pattern may appear as a precursor of MI, concomitantly with a pattern of acute MI, or in the presence of pre-existing MI pattern. Transient injury current producing a similar ECG injury pattern may result from pressure exerted by the pericardial fluid during acute pericarditis.

As a rule, the vector of the deviated ST segment is directed toward the site of ischemia. Thus, ischemia or infarction of the anterior wall causes ST segment elevation in the anterior precordial leads, whereas ischemia or infarction of the inferior wall causes ST segment elevation in the "inferior leads" (see below).

An ST segment depression in the anterior precordial leads usually indicates a subendocardial or nontransmural ischemia or infarction unless it is reciprocal to ST segment elevation in leads II, III and aVF (see below).

Kornreich et al. [23] used 120 leads to construct body-surface potential map in 131 patients with acute myocardial infarction. They found that the most abnormal ST segment elevations and depressions at each location of myocardial infarction were localized outside the standard precordial lead positions. This study supports the prevailing notion that larger numbers of electrodes such as employed during mapping of the torso can improve the diagnostic accuracy of the ECG.

18.4 Localization of the Site of Ischemia

18.4.1 Anterior Wall Myocardial Infarction and Occlusion of Left Anterior Descending (LAD) Coronary Artery

In patients with acute injury associated with anterior MI, ST segment elevation is usually present in leads I, aVL, variable number of precordial leads (usually 2–6), and occasionally in lead II. Examples of various types of anterior MI, i.e., anterior, anterior-superior, anterolateral, and anterior-inferior are shown in Figs. 18.2–18.8. Differences in type depend to some extent on the site of left anterior descending (LAD) coronary artery occlusion.

Birnbaum et al. [24] attempted to predict the level of obstruction of the LAD artery in patients with acute anterior infarction. The culprit lesions were proximal to the first diagonal branch of the artery in 59 patients and distal to that artery in 38 patients. When the ST segment was elevated in the anterior precordial leads, the presence of ST segment elevation in leads I and aVL was predictive of a proximal lesion in 87% of cases; its absence was predictive of a distal lesion in 73%. The presence of reciprocal ST segment depression in the inferior leads was also suggestive of a proximal lesion (Figs. 18.2–18.4, 18.6, and 18.7). In agreement with the above observations, unpublished studies from the author's laboratory showed that the ST segment elevation after the LAD occlusion distal to the takeoff of the first septal perforator and the first diagonal artery usually involves leads V_{2-4} (Fig. 18.8), whereas a more proximal obstruction involves, in addition, leads aVL and/or V_{5-6} (Figs. 18.2–18.7).

In patients with an anterior MI, ST segment elevation in lead V_1 occurs less frequently than in leads V_2 and V_3. The presence of ST segment elevation in lead V_1 suggests that the conal branch of the right coronary artery is either absent or small and therefore does not reach the intraventricular septum [25]. Conversely, the absence of ST segment elevation in lead V_1 during acute anterior MI suggests the presence of a large conal branch of the right coronary artery protecting the septum from a transseptal MI [25].

Occlusion of the LAD artery "wrapped" around the apex could be recognized by the presence of ST segment elevation and Q wave in the "inferior" leads during the early stage of infarction [25] (Fig. 18.5).

In patients with anterior MI, reciprocal ST segment depression is present usually in leads III and aVF (Figs. 18.2, 18.3, 18.6, and 18.7) and often in lead aVR (Figs. 18.4, 18.7, and 18.9). Reciprocal ST segment depression tends to be absent in lead aVF when the LAD coronary artery is occluded distally [26].

Occlusion of the first diagonal branch of LAD coronary artery causes ST elevation mainly in leads I and aVL and fewer changes in the precordial leads [28–30] (Fig. 18.9).

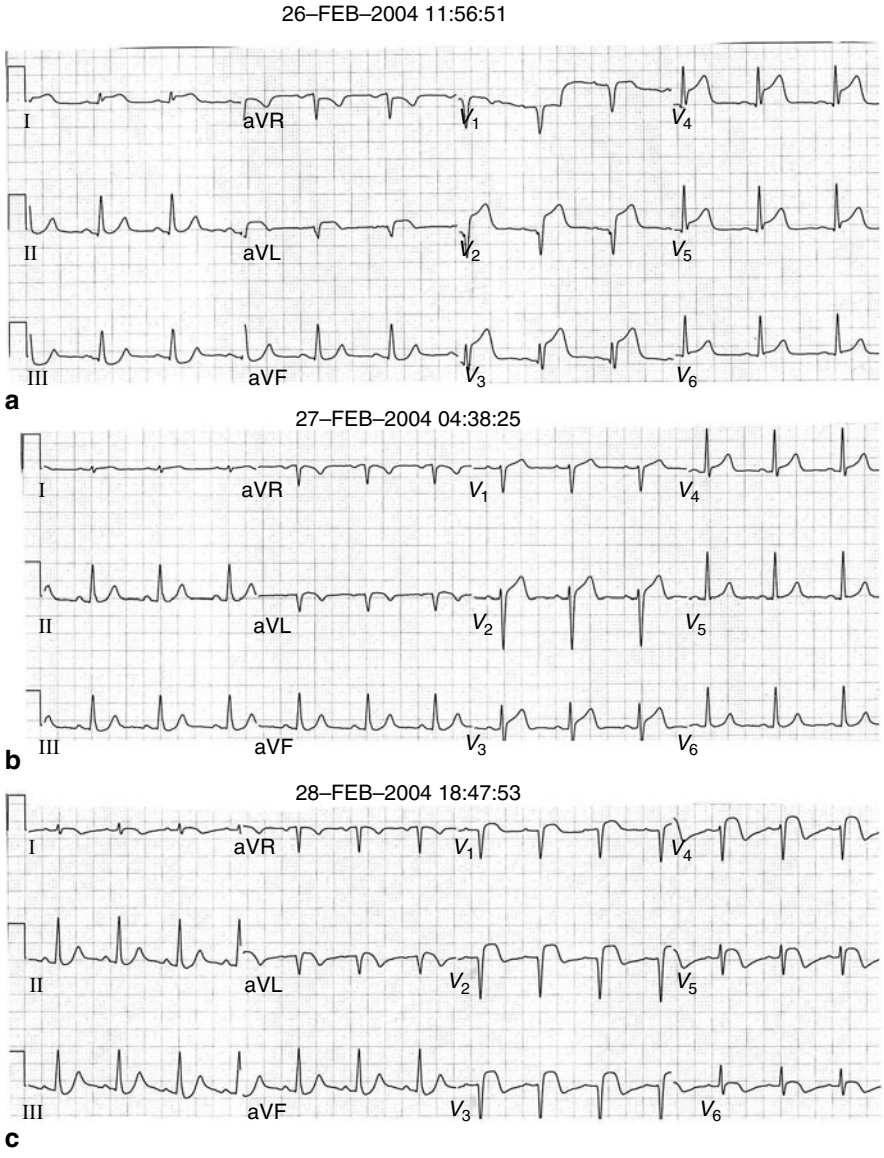

Figure 18.2

Electrocardiogram of a 51-year-old man with acute anterior-superior myocardial infarction caused by total occlusion of left anterior descending coronary artery proximal to the first septal perforator and the first diagonal branch; there was also 40% occlusion of the first obtuse marginal branch of the left circumflex artery and 70% occlusion of the right coronary artery. Kinesis involved large portion of the anterior wall and the apex. with an estimated left ventricular ejection fraction of 15%. In (a): ST elevation in leads aVL and $V_{1–6}$, with reciprocal ST depression in leads III and aVR. In (b): one day later "pseudonormalization" with slight ST elevation in the leads $V_{2–3}$ and T wave inversion in lead aVL as the only abnormalities. In (c): on the following day when chest pain resolved. ST elevation and T wave inversion in leads I, aVL and $V_{1–6}$ with reciprocal ST depression in the leads III, aVF compatible with the evolution of the infarction pattern. Incipient T wave inversion in leads a VL, $V_{2–6}$.

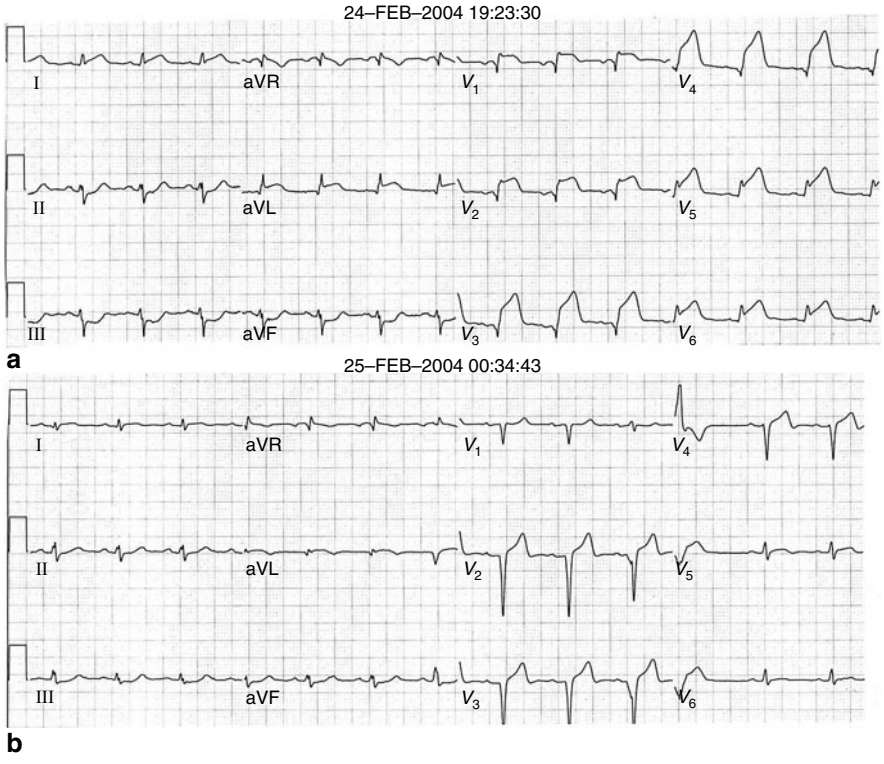

Figure 18.3

Electrocardiogram of a 52-year-old man with acute anterior-superior myocardial infarction caused by "very proximal" total occlusion of left anterior descending coronary artery before first septal perforator. Other lesions included: 60% occlusion of the proximal left circumflex artery and 50% proximal occlusion of the right coronary artery., Large portion of the anterior wall including apex was akinetic with an estimated left ventricular ejection fraction of 25%. In (a): Q waves in leads aVL, $V_{1–4}$, ST elevation in I, aVL and $V_{1–6}$ with reciprocal ST-depression in leads II, III, aVF. In (b), 5 h later after percutaneous intervention: Q waves in aVL, $V_{1–3}$, slight residual ST deviation with an incipient T wave inversion in lead V_4.

Occlusion of the main septal branch causes ST elevation in leads V_1 and V_2 and reciprocal ST segment depression in leads II, III, aVF, V_5, and V_6. Assali et al. [27] observed that persistent ST segment depression in leads $V_{5–6}$ in survivors of anterior MI was associated with increased left ventricular filling pressure and a restrictive left ventricular filling pattern.

18.5 Inferior Wall MI

In the presence of acute injury associated with inferior MI, ST segment is elevated in leads II, III, aVF, and, occasionally, in leads $V_{5–6}$ (Figs. 18.10 and 18.11).

It has been reported that ST segment elevation in lead V_6 occurred in all cases of left circumflex artery occlusion; and ST elevation in lead V_3R was present in 82% of cases with occluded right coronary artery [31]. In one study [32], the presence of ST segment elevation in lead V_6 in patients with acute inferior myocardial infarction was associated with larger infarct size and greater incidence of complications. Also, mortality in patients with inferior MI was increased when maximal ST segment elevation occurred in leads $V_{4–6}$ and not in lead III [33]. ST segment elevation in lead VI may be caused by the presence of right ventricular MI which can be suspected also when in the presence of anterior MI reciprocal ST segment depression in lead VI is absent [34–36].

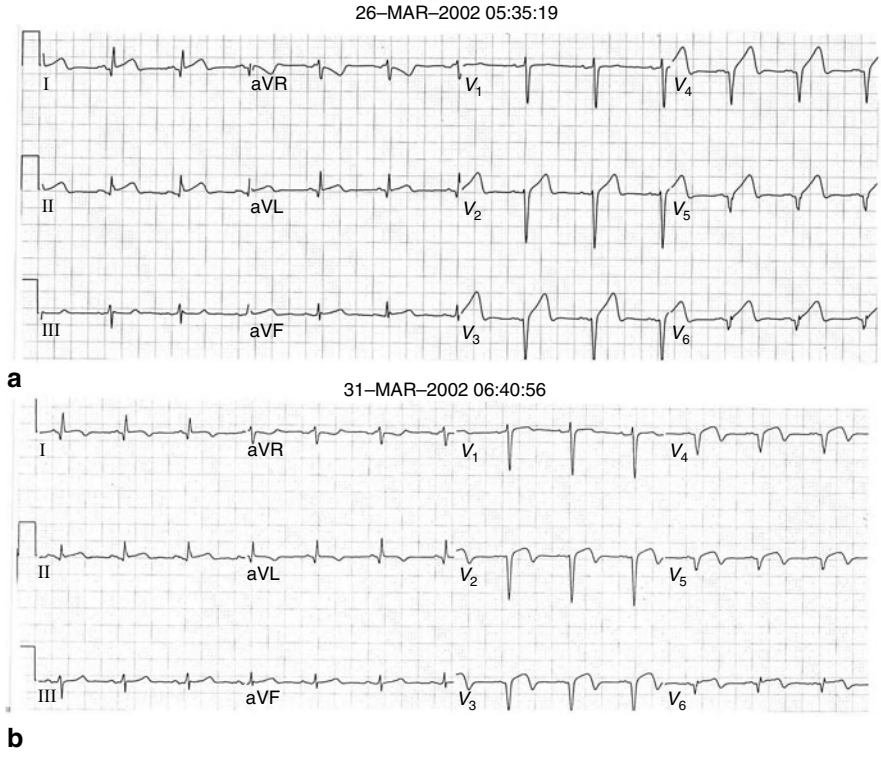

Figure 18.4

Electrocardiogram of a 47-year-old woman with anterolateral myocardial infarction (MI) caused by total occlusion of left anterior descending coronary artery in midportion associated with 50–70% occlusion of the co-dominant left anterior circumflex artery. Anterior wall and apex were akinetic with an estimated left ventricular ejection fraction of 30%. In (a): Q waves with ST elevation in leads I, aVL, $V_{3–6}$ and reciprocal ST depression in aVR. In (b) 5 days later after an emergent percutaneous intervention evolution of ECG pattern of anterior MI with T wave inversion in leads I, aVL and $V_{2–6}$. Residual ST elevation is present in the above leads.

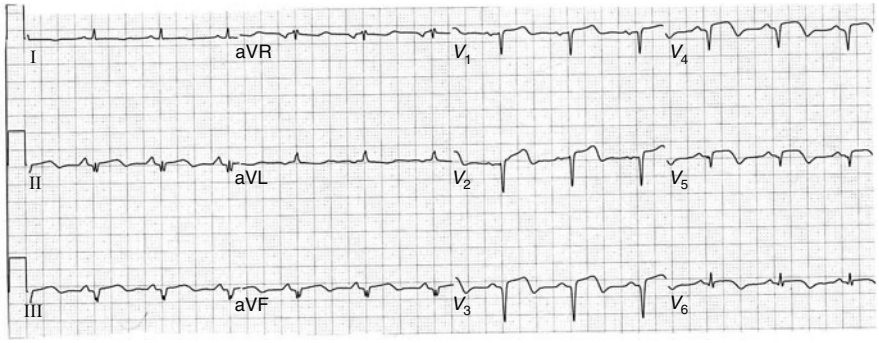

Figure 18.5

Electrocardiogram of a 70-year-old woman with acute anterior and inferior myocardial infarction caused by complete occlusion of left anterior descending coronary artery proximal to the first septal perforator and to the first diagonal branch without appreciable abnormalities in the remaining large coronary branches. A large portion of anterior wall was akinetic, including apex and an adjoining area of the inferior wall with an estimated left ventricular ejection fraction of 15%. Note Q waves and ST elevation in leads II, III, aVF, $V_{1–5}$ and incipient T wave inversion in leads II, III, $V_{3–6}$. No reciprocal ST depression in the available leads.

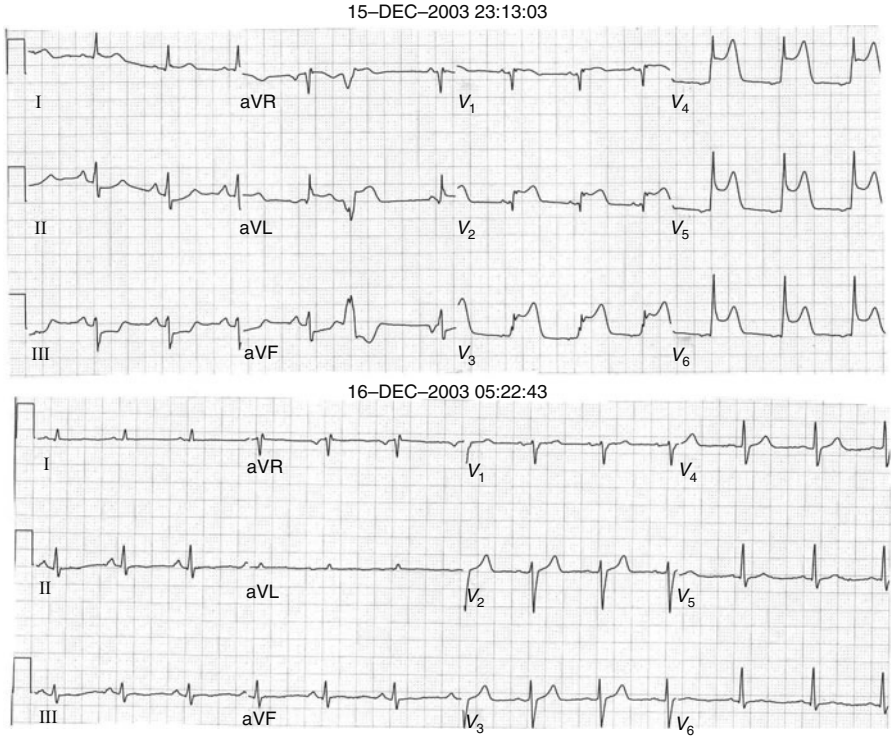

Figure 18.6

Electrocardiogram of a 51-year-old woman with acute anterior myocardial infarction caused by "very proximal" total occlusion of left anterior descending coronary artery without appreciable obstructions in the remaining large coronary branches. Substantial portion of the anterior wall was akinetic, including the apex, and the estimated left ventricular ejection fraction was 20%. On top: Q wave and ST elevation in leads I, aVL, $V_{2–6}$ and reciprocal ST depression in leads III, aVF and aVR. At the bottom 6 h later ECG is normal after percutaneous intervention.

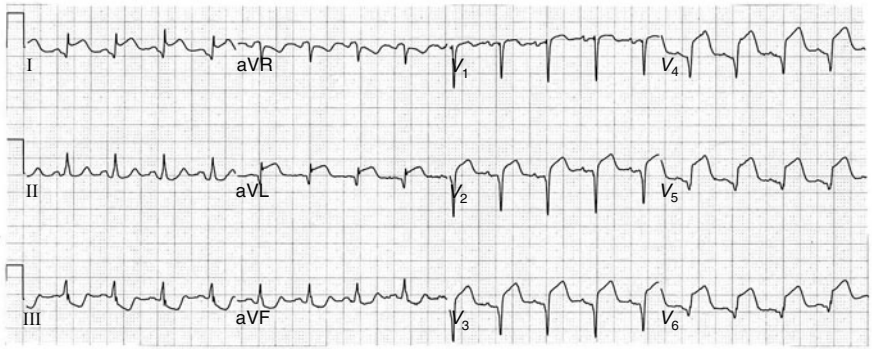

Figure 18.7

Electrocardiogram of a 56-year-old woman with acute anterior-superior-lateral myocardial infarction caused by occlusion of proximal left anterior descending coronary artery and occlusion of first marginal branch of left circumflex artery. There was severe anteroapical hypokinesis and mild inferior hypokinesis with estimated left ventricular ejection fraction of 20%. In A. before intervention Q wave in lead V_2, ST elevation in I, aVL, $V_{2–6}$ with reciprocal ST depression in leads III, aVF.

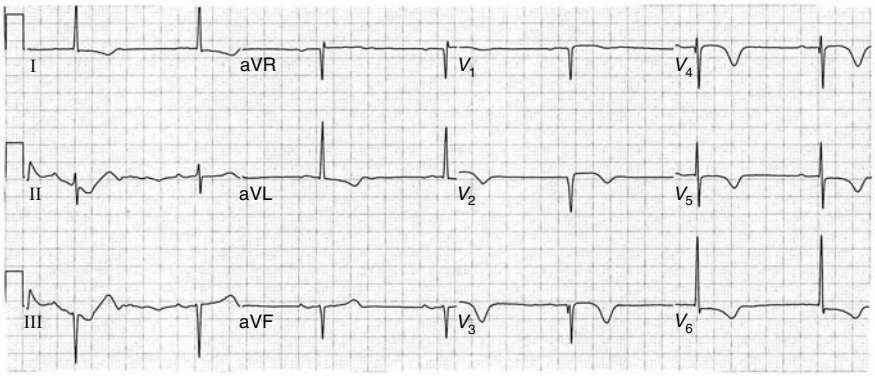

Figure 18.8

Electrocardiogram of a 94-year-old woman 1 day after an acute anterior myocardial infarction (MI) caused by occlusion of left anterior descending coronary artery distal to the first septal perforator and to the first diagonal branch. Other major coronary branches were free of disease. There was apical and adjoining inferior wall hypokinesis with estimated left ventricular ejection fraction of 40% Note: Q waves in leads $V_{1–3}$, small Q in lead V_4, ST elevation in leads V_1–V_3 and T wave inversion in leads I, aVL and $V_{1–6}$. This is an example of a relatively small MI with symmetrical negative T waves present in a larger number of leads than the leads with Q waves and ST elevation.

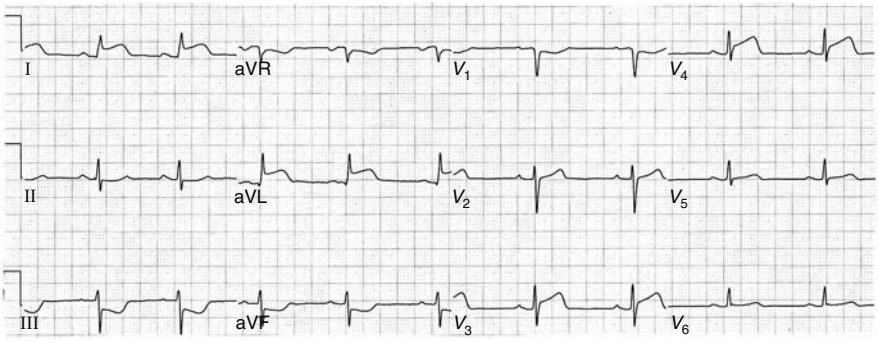

Figure 18.9

Electrocardiogram of a 47-year-old woman caused by complete occlusion of a large diagonal branch of the left anterior descending (LAD) coronary artery; there was also a 30% occlusion of the proximal LAD coronary artery; other major coronary branches were free of disease. Ventriculogram revealed anterior and apical akinesis with estimated left ventricular ejection fraction of 30%. Note: ST elevation in leads I, aVL, $V_{4–5}$ with reciprocal ST depression in leads III, aVF and aVR.

Reciprocal ST segment depression is usually present in leads I and aVL, often in one or more precordial leads, and predominantly in leads $V_{2–3}$ [31] (Fig. 18.10). The presence of ST depression in lead V_1 indicates either a reciprocal change alone or an association with posterior wall MI.

In a study of 16,521 patients with inferior MI, ST segment depression in the precordial leads was present in 61.1% of cases [36]. Reciprocal ST segment depression occurred more frequently in patients with larger MI, greater wall motion abnormalities, and was associated with higher mortality [37, 38]. The magnitude of the sum of ST depression voltage in leads $V_{1–6}$ added significant independent prognostic information with the risk of 30-day mortality increasing by 36% for every 0.5 mV of precordial ST segment depression [34].

In the study of 1,155 patients with inferior MI who took part in the Global Utilization of Streptokinase and TPA for Occluded Arteries Study (GUSTOI-I), subjects with maximum ST segment depression in leads $V_{4–6}$ had more often three-vessel disease than those without precordial ST segment depression or those with ST segment depression in leads

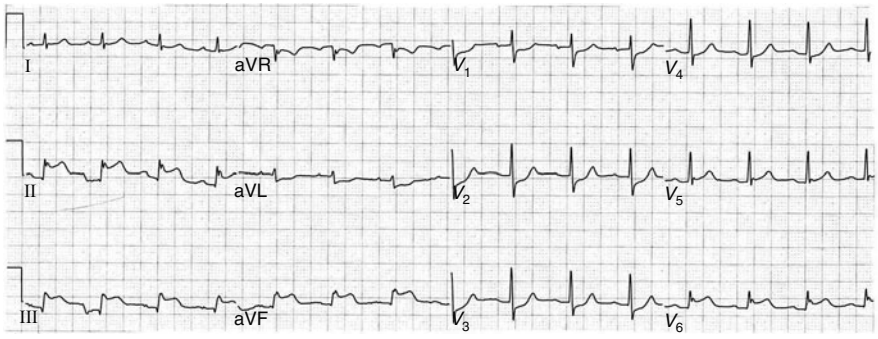

Figure 18.10

Electrocardiogram of a 69-year-old man with acute inferior and posterior myocardial infarction attributed to occlusion of mid-right coronary artery and mid-left anterior circumflex artery. Left anterior descending coronary artery was free of disease. There was inferior, lateral and posterior hypokinesis with an estimated left ventricular ejection fraction of 50% Electrocardiogram shows Q wave in leads II and III with tall R waves in leads $V_{1–2}$, ST elevation in leads II, III, aVF and ST depression in leads aVR, $V_{1–3}$.

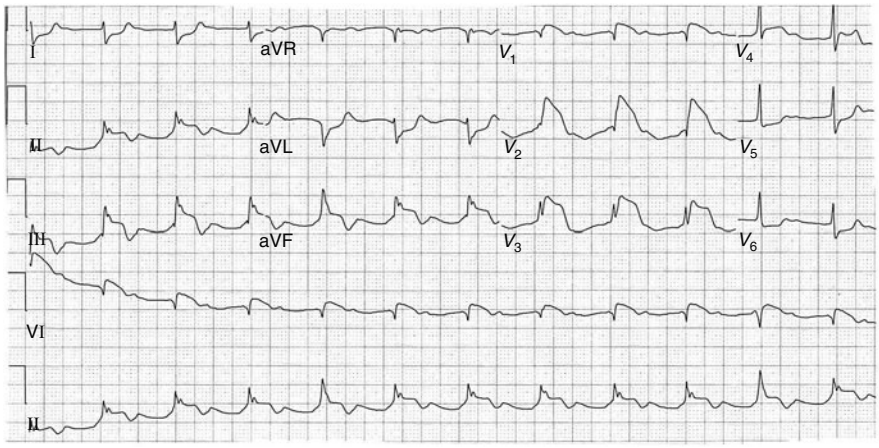

Figure 18.11

Electrocardiogram of a 58-year-old woman with documented acute myocardial infarction of inferior wall and right ventricle caused by total occlusion of proximal right coronary artery associated with nonobstructive disease of left circumflex and left anterior descending coronary arteries. Note: ST elevation in leads II, III, $V_{1–4}$ with reciprocal ST depression in leads I, aVL and $V_{5–6}$. The course was complicated by ventricular fibrillation, intraaortic balloon insertion and emergent coronary artery bypass surgery.

V_1–V_3 [39]. Patients with maximum depression in leads $V_{1–3}$ had larger infarction as estimated by peak creatine kinase, probably due to posterior or posterobasal extension [40].

18.6 Differences Between Inferior MI Caused by Right and Left Circumflex Occlusion

In patients with inferior myocardial infarction caused by occlusion of the right or the circumflex coronary artery with ST segment elevation in leads II, III, and aVF, the presence of additional elevation of ST segment in the "lateral" precordial

leads (V_5, V_6) and/or leads I and aVL was a fairly sensitive and specific marker for left circumflex coronary artery occlusion [40] which accounts for about 18% of cases of inferior MI [41].

In these patients, ST segment in lead I is more likely to be isoelectric or elevated rather than depressed as in most patients with occluded RCA [41].

Huey et al. [42] compared the ECGs of 40 consecutive patients with acute MI caused by left circumflex artery occlusion with those of 107 patients with right coronary artery (RCA) occlusion. In the patients with inferior MI, the presence of ST segment elevation in one or more of leads I, aVL, V_5, and V_6 was highly suggestive of the left circumflex artery occlusion.

Depression of ST segment in leads V_{1-3}, as shown in Fig. 18.10, tends to indicate large posterolateral perfusion defect [32, 43] and is more often associated with occlusion of circumflex artery (71%) than of RCA occlusion (40%) [30]. Chia et al. [44] found that an ST II/III ratio of 1 or an isoelectric ST segment in lead I represented sensitive and specific markers of left circumflex artery occlusion whereas an ST II/III ratio <1 (ST segment elevation in III greater than in II) and ST depression in lead I were sensitive and specific markers of RCA occlusion. Bairey et al. [40] reported that ST segment elevation in the lateral leads identified circumflex artery occlusion as the cause of inferior MI. In patients with inferior MI, ST segment elevation in lead III exceeding that in lead II, particularly when combined with ST segment elevation in lead V_1 is predictive of occlusion of the RCA proximal to the acute margin of the heart. Herz et al. [45] reported the same results with an added finding that in patients with RCA occlusion reciprocal ST depression in lead aVL was greater than in lead I.

18.7 Lateral, Inferior Lateral and Posterolateral Myocardial Infarction

Localization of ST segment elevation and reciprocal ST segment depression varies in patients with lateral MI, depending on the extent and location of the MI. Typically, ST segment elevation in patients with inferior-lateral MI is present in leads II, III, aVF, and V_6. In many cases, however, ST elevation extends to the right of lead V_6, i.e., leads V_{3-5}. However, the lead with maximal ST segment elevation is usually V_6 or V_5. Reciprocal ST segment depression may be present in leads I, VI, aVL, and V_{1-4} but may also be absent.

In patients with posterolateral MI, ST segment elevation is either absent or present in leads V_{5-6}. Reciprocal ST segment depression occurs usually in leads V_{1-3}. Elevation of ST segment >2 mm in leads V_5 and V_6 correlated with an artery (right or circumflex) supplying a large territory of the myocardium with an expected high ischemic burden [45]. ST segment elevation in posterior leads V_7 through V_9 in patients with an inferior MI was associated with a high incidence of posterolateral wall motion abnormalities, large infarct size, low left ventricular ejection fraction, and high incidence of adverse effects after discharge [46].

In patients with a so-called true posterior MI, i.e., without ECG evidence of inferior and/or lateral MI, ST segment elevation may be present in leads V_{7-9} and reciprocal ST segment depression in leads V_{1-3} [41]. Routine recording of leads V_{7-9} has been recommended in patients with suspected MI but non-diagnostic 12-lead ECG [47–49].

In patients with high lateral MI caused by occlusion of the left circumflex coronary artery, the ST segment is usually elevated in leads I, aVL, and V_{5-6} and is depressed in leads III, aVF, and, occasionally, in lead VI. An abnormally tall R wave in lead V_1-consistent with posterior infarction – also suggests left circumflex artery occlusion.

18.8 Acute Injury Pattern in the Right Precordial Leads and Right Ventricular Infarction and Other Causes

Isolated infarction of the RV free wall seldom occurs [9, 41, 50]. Symptomatic RV MI causing serious hemodynamic complications is usually associated with an acute MI of the inferior or inferoposterior wall. Pathologic studies showed that RV infarction is present in 14–36% of patients with inferior LV Q-wave MI, but no major RV MI is seen in hearts with isolated anterior MI [41, 52–54]. A small portion of the RV, however, was involved with equal frequency in anterior and inferior (posterior) LV infarction.

ST segment elevation in the right precordial leads V_3R and V_4R usually signifies presence of RV MI [51]. In patients with RV MI, ST segment elevation may extend to additional right precordial leads V_5R and V_6R [52–55] and sometimes to precordial leads V_1–V_4 [53] (Fig. 18.11).

In the presence of inferior MI, diagnosis of RV MI is supported by a discordant pattern of ST segment elevation in V_1 and ST segment depression in V_2 [56]. ST segment elevation in leads V_3R–V_4R may be present in patients with acute anterior MI but will seldom extend to lead V_5R [51]. Also, when the ST segment elevation caused by acute anterior MI is present in leads V_3R to V_5R, the magnitude of ST segment elevation diminishes from V_3R to V_5R whereas in the presence of RV MI, ST segment elevation is either the same or increases from V_3R to V_5R [51].

Lead V_4R appears to be most useful among precordial leads in recognition of RV MI. Zehender et al. [57] found ST segment elevation in lead V_4R in 107 (54%) out of 200 consecutive patients with acute inferior infarction. Using autopsy findings, coronary angiography, hemodynamic measurements, and noninvasive imaging, they found that ST segment elevation in lead V_4R had a sensitivity of 88% and diagnostic accuracy of 83% in the diagnosis of the associated acute RV MI.

Braat et al. [58] emphasized the transient nature of the ST elevation in the supplementary leads because this finding was no longer present within 19 h after the onset of chest pain. Saw et al. [59] reported that ST elevation in III > II was more sensitive than ST elevation in lead V_4R in diagnosing RV MI. Menown et al. [60] found that body surface mapping provides improved classification of patients with acute MI of inferior wall, right ventricle, and posterior wall as compared with right ventricular or posterior leads alone.

In patients with RSR' pattern in the right precordial leads and absent anterior infarction, ST segment elevation may be caused by septal ischemia, or by RV MI [52–55]. Other causes of such pattern where the ST segment elevation include the syndrome associated with sudden cardiac death described by Brugada [61] and arrhythmogenic right ventricular dysplasia. The Brugada syndrome [62] consists of RBBB, persistent ST segment elevation in leads $V_{1–3}$ and sudden cardiac death affecting predominantly male gender. Some forms of this syndrome are intermittent and asymptomatic with transient normalization of the ECG. Typically, the ST segment elevation has a saddle back or a coved appearance [63]. The elevation is augmented by selective stimulation of alpha adrenergic or muscarinic receptors or by class 1A antiarrhythmic drugs [64] and vagal activity [65] but reduced by beta adrenergic stimulation or alpha adrenergic block [66]. Many of these patients have no evidence of structural heart disease. Similar ECG pattern was present in young male Southeast Asians who died unexpectedly during sleep [67] and in patients with familial cardiomyopathy (arrhythmogenic RV dysplasia) involving the RV and the conducting system [68–70]. Common to these conditions is QRS widening confined to selected leads with ST segment elevation and normal QRS duration in remote leads such as I and V_6 [71]. Most commonly, ST elevation occurs in leads $V_{1–3}$, but cases with ST elevation in the inferior leads have been reported [72].

In patients with RV dysplasia, the shape of the terminal QRS portion in the right precordial leads has been likened to the Greek letter epsilon. The pattern of right bundle branch block with ST segment elevation in the right precordial leads is not entirely specific for either right ventricular ischemia or Brugada syndrome because more often it is present in other conditions [73].

18.9 Left Main Coronary Artery Obstruction

In two studies of patients with anterior MI, ST elevation in aVR greater than in lead V_1 was found to be predictive of left main coronary artery obstruction [74, 75]. This requires further confirmation.

18.10 Coronary Spasm, Unstable Angina Pectoris, and Non-Q-Wave Myocardial Infarction*

Acute injury pattern is the diagnostic marker of coronary spasm, and the lead distribution of ST segment deviation during coronary spasm is the same as during myocardial ischemia caused by other types of coronary occlusion. ST segment elevation has been reported also in patients with syndrome x, normal coronary angiograms, and suspected spasm of coronary arterioles [76]. In patients with unstable angina pectoris [77] and non-Q-wave MI [78], acute injury pattern is present in the minority of cases.

*Current nomenclature; non-ST elevation myocardial infarction (NSTEMI)

18.11 ST Segment Changes as a Guide to Thrombolytic and Percutaneous Intervention Therapy

The indication for an emergent thrombolytic therapy of a suspected acute MI is based on the presence of ST segment elevation greater than 0.1 mV in two limb or two or more anatomically contiguous precordial leads. In the cases of pre-existing ST segment elevation such as in LBBB, the same rule applies when the availability of the basic pattern allows the recognition of the ST shift [79] (Fig. 18.12).

Regression of ST segment elevation parallels recanalization [80–82], and incomplete resolution of ST segment elevation is a powerful independent predictor of early mortality [83–86]. Also, in patients with acute MI treated with direct angioplasty, a rapid decrease of ST segment elevation was observed in patients with myocardial reperfusion, but not in those with no-reflow phenomenon [87]. Re-elevation of ST segment is a sign of limited myocardial salvage and suggests extensive myocardial damage [88–92]. In some cases, in the presence of anterior ischemia, transient increase in ST segment elevation (attributed to adenosine release) preceding and following the decrease during the first hour has no adverse consequences [93, 94]. The magnitude of ST segment elevation, measured as a sum of ST-shift voltages, is related to the severity of myocardial ischemia and not to the size of the area at risk [95], but the localization of the ST segment elevation predicts the site of the future loss of QRS voltages.

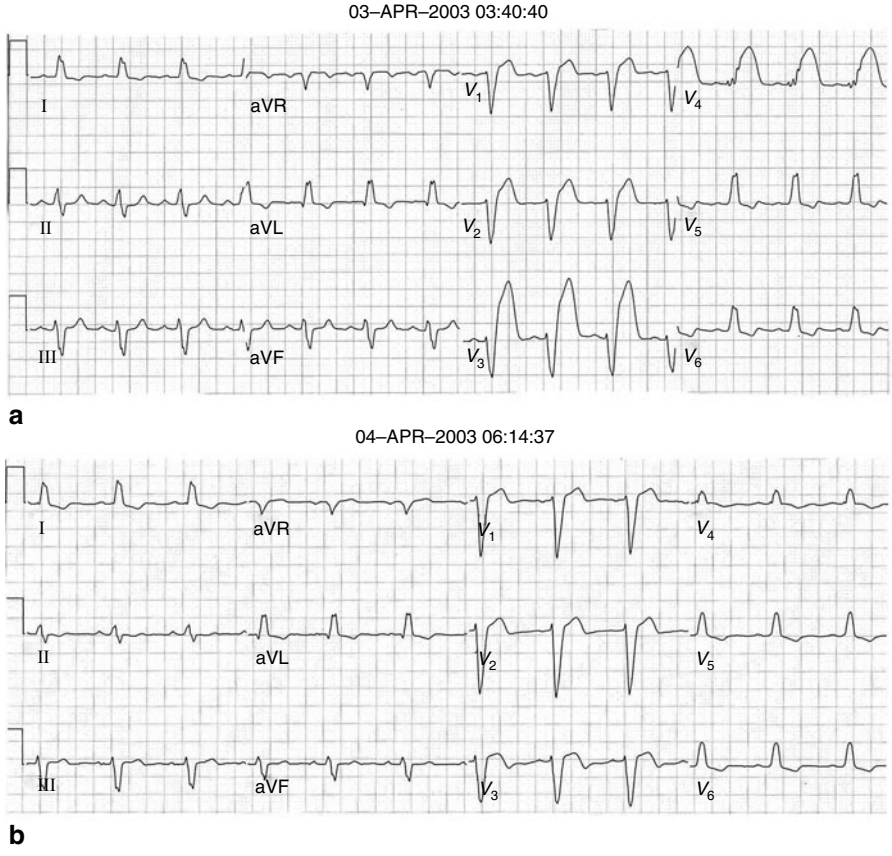

Figure 18.12

Electrocardiogram of a 58-year-old man with left bundle branch block (LBBB) and acute anterior myocardial infarction (MI). In (a), in addition to secondary ST and T changes of LBBB, there is primary ST elevation in leads V_{2-4}-indicative of acute injury pattern. No reciprocal ST depression is discernible. In (b), after percutaneous intervention, primary ST elevation subsided, but primary T-wave inversion in leads V_{2-3} is compatible with evolution of anterior MI pattern.

The depression of the ST segment may be reciprocal or indicative of an additional, presumably subendocardial ischemia. Shah et al. [96] evaluated the prognostic significance of the resolution of ST segment depression in patients with acute MI after thrombolytic treatment. They compared patients with ST segment depression resolving simultaneously with ST segment elevation (simultaneous group) and patients with ST segment depression persisting after ST segment elevation resolution (independent group). In-hospital mortality was significantly higher in the independent group than in the simultaneous group and a control group without ST segment depression. In other studies, early resolution of ST segment elevation was associated with improved wall motion [97] and salvage index [98].

18.12 ST Segment Shift During Percutaneous Coronary Angioplasty

Balloon occlusion of the coronary artery during angioplasty lasts usually from 1 to 3 min. The behavior of ST segment during PTCA is the same as during spontaneous myocardial ischemia but the magnitude of ST segment elevation expressed in percent of QRS amplitude tends to be smaller. Also, the average number of leads with ST segment elevation and those with reciprocal ST segment depression tends to be smaller during PTCA than during acute ischemia. The maximal ST segment elevation during balloon occlusion of LAD coronary artery is located in lead V_2, V_3, or V_4 [99], and during occlusion of RCA in the lead III. During occlusion of diagonal branch of LAD coronary artery maximal ST segment elevation may be located in lead aVL. The results of occlusion of left circumflex coronary artery vary. In about one third of cases, ST segment shift in the standard 12 lead ECG is absent, in another third, ST segment elevation is present in one or more standard leads, and in the remaining one third of cases there is ST segment depression in leads V_{2-3} which is believed to represent a reciprocal change of ST segment elevation localized in the back [99].

In theory, the absence of ST segment displacement at the site of presumed acute injury may be due to cancellation by a contralateral ST segment displacement in an opposite direction but in practice such mechanism is difficult to verify. The nonhomogeneous intensity of ischemia detracts from the accuracy of localizing the site of ischemia. Thus, it has been shown that a balloon occlusion of the partially stenotic left anterior descending coronary artery caused a reversible ST segment elevation in the left precordial leads when the collateral circulation was poor or absent. However, the same procedure in similar patients with good collateral circulation produced ST segment depression in the same leads [100]. Studies during coronary artery angioplasty showed that the site of impaired perfusion could be identified with greater accuracy using a larger array of precordial leads. For instance, ST segment elevation in the left axillary and back leads was specific for occlusions of left circumflex and diagonal branches. The ST segment elevation in lead V_3R was present in 82% of cases with occluded right coronary artery. It has been shown that in patients with acute first anterior myocardial infarction caused by left anterior descending coronary artery lesion, treated with rapid reperfusion by angioplasty, the ST segment behavior has a predictive value. Kobayashi et al. [101] found that the recovery of the left ventricular systolic function was better in patients in whom ST segment elevation resolved than in those in whom it did not. Also, Santoro et al. [102] reported that reduction in ST segment elevation after direct coronary angioplasty was the only independent predictor of left ventricular function recovery. In a more recent collaborative CADILLAC study of 700 patients with prior percutaneous intervention (PCI), ST segment resolution was found to be a strong independent predictor of both survival and freedom from reinfarction [103]. Watanabe et al. [104] found that persistent ST segment elevation present 30 min after primary percutaneous transluminal coronary angioplasty was a highly specific electrocardiographic marker of impaired reperfusion in patients with acute MI. Also in the study by Feldman et al. [105], incomplete (<50%) resolution of ST elevation was a marker of more extensive myocardial damage. It has been suggested to use ST segment resolution as a surrogate end point in reperfusion trials of acute myocardial infarction [106]. Microvascular injury has been suspected to be the cause of persistent ST segment elevation after primary angioplasty for acute myocardial infarction [107, 108].

18.13 Persistent ST Segment Elevation After Myocardial Infarction

Persistent ST segment elevation that lasts more than 1 month after the onset of acute MI is the most helpful sign of nonviable myocardium [109]. The mechanism of such ST segment elevation is poorly understood. A prevailing hypothesis attributes ST displacement to an injury current generated during systole at the junction of the aneurysm with

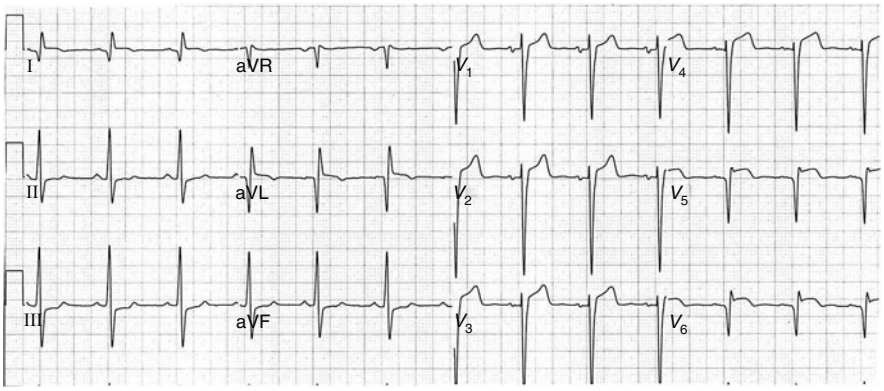

Figure 18.13

Electrocardiogram of a 61-year-old woman recorded 20 years after anterior myocardial infarction and development of a large calcified ventricular aneurysm with an apical thrombus and an estimated left ventricular election fraction of 15%. The left anterior descending coronary artery was atretic and diffusely diseased whereas the left circumflex and the right coronary artery harbored mild luminal irregularities. Note: Q waves in leads I, aVL, $V_{5–6}$ and ST elevation in the above leads as well as in leads $V_{1–4}$.

the surrounding myocardium. According to this theory, the outward (paradoxical) bulging of the aneurysm produces undue tension at the junction of the aneurysm and normal tissue, resulting in injury (depolarization) of the surviving myocardium next to the border of the aneurysm [110].

After healing of myocardial infarction, ST segment elevation persists in about 60% of patients with anterior infarction (Fig. 18.13) and in about 5% of patients with inferior myocardial infarction [111]. Persistent ST segment elevation correlates with the presence of asynergy. It has been shown that ST segment elevation developed during balloon inflation coincident with the new appearance of hypocontractility in a region of previously normal motion [112] and that there was a close association between the magnitude and extent of ST segment elevation and the extent of asynergy [112]. The most sensitive marker for anterior wall hypocontractility was ST segment elevation in lead V_2 and for inferior wall hypocontractility ST segment elevation in lead III.

The widely held notion that the persistent ST segment elevation is a marker of ventricular aneurysm has not been supported by the recent studies. Radionuclide imaging has shown similar global and regional wall motion abnormalities in patients with and without persistent ST segment elevation after myocardial infarction [113]. If the aneurysm is defined as a "full thickness scar that exhibits a localized convex protrusion during both phases of the cardiac cycle," two-dimensional echocardiography showed that the persistent ST segment elevation correlates with dyskinesia rather than with aneurysm [114]. The well established relation between the persistent ST segment elevation and the paradoxical motion of left ventricular (LV) myocardium [114], suggests that stretch may play role in the process, but the mechanism by which stretch, might cause ST segment displacement has not been elucidated. The study of Toyofuku et al. [115] supports the hypothesis that stretch can cause ST segment elevation in the absence of ischemia. These investigators reported that in patients with arrhythmogenic right ventricular dysplasia (ARVD) who had no coronary artery disease, ST segment elevation was induced by exercise. In their study, significant ST segment elevation in the right precordial leads developed in 11 of 17 (65%) patients with severe right ventricular asynergy; the finding proved to be helpful in diagnosing ARVD noninvasively.

In some patients with dyskinesis, the ST segment becomes elevated after exercise and after cardiac surgery. The phenomenon of ST segment elevation reappearing during exercise-induced ischemia has been reproduced in pigs with a 1-month-old MI [116]. In this model, acute ischemia adjacent to chronic infarction induced ST segment elevation at the surface of the scar despite the virtual absence of viable tissue in the infarction. This suggests a passive ST segment potential transmission from the ischemic peri-infarction area through the infarction.

18.14 Aneurysmectomy

The results of aneurysmectomy have not helped to locate the site of abnormal potential differences [117–119]. In one study of 74 ECGs with ST segment elevation before aneurysmectomy, the pattern remained unchanged in 60.8%, improved in 25.7% and became more pronounced in 13.5% of cases after aneurysmectomy. The average ST segment amplitude after aneurysmectomy in several studies was reduced by only one quarter. Engel et al. [117] found that after encircling endocardial ventriculotomy, ST segment elevation was unchanged. This suggested that the ST segment elevation did not originate in the injured tissue adjacent to the aneurysm. However, the authors admitted the possibility that the encircling procedure could have created new zones of injury.

Anatomic correlations confirm the angiographic findings. In 64 cases of autopsy-proven ventricular aneurysm, the ECG location of the infarction correlated well with the anatomic site of the aneurysm [118]. Among the patients in whom the ECG was recorded more than 30 days after the onset of infarction, 79% of 50 patients with an anterior aneurysm and 50% of 13 patients with a posterior (inferior) aneurysm had persistent ST segment elevation in the appropriate leads. Among 290 patients with an LV pseudoaneurysm, the incidence of ST segment elevation was 20% [119].

Among patients undergoing surgical resection of a ventricular aneurysm [117], the anatomic localization determined at the time of operation was correctly predicted by the ECG changes. Of 26 patients, 21 had abnormal Q waves and 22 had persistent ST segment elevation. Those with wide distribution of the abnormal Q waves had large aneurysms, but the size of the infarction could not be predicted by the magnitude of the ST segment elevation. After aneurysmectomy, there was usually a decrease in QRS duration and an increase in R wave amplitude. The number of leads with abnormal Q waves was reduced, and in some cases Q waves disappeared in all leads. The ST segment elevation also tended to decrease, and in about one third of cases it disappeared after aneurysmectomy. It can be concluded, therefore, that the ECG is a fairly sensitive tool for detecting ventricular aneurysms, particularly at the more common anterior location.

18.15 ECG Findings Predictive of Cardiac Rupture

Oliva et al. [120] retrospectively and prospectively examined ECGs of 70 patients with cardiac rupture after MI. Patients with rupture had a significantly higher incidence of pericarditis, which was detectable on the ECG by progressive or recurrent ST segment elevation in the absence of recurrent ischemia. In patients with anterior infarction, free wall rupture did not occur when the ECG changes of infarction were confined to leads V_1 and V_2. When the anterior wall adjacent to the septum ruptured, the ECG showed changes in leads V_1 through V_4. Of 30 patients with an inferior infarction, 27 had additional involvement of the adjacent lateral wall, or posterior wall, or both. Altogether, 55 patients (79%) had multisegment infarcts, with a mid-lateral or high lateral component in 88%.

Figueras et al. [121] examined clinical and ECG features in patients who died of an acute MI with and without LV free wall rupture. Risk factors of an early rupture included advanced age and first transmural anterior infarction without conduction abnormalities or heart failure. ST segment elevation on admission was higher in patients with early rupture (1 day) than in those with later rupture. On day 2 the ST segment elevation decreased less in patients with the subsequent late rupture (>2 days) than in those without rupture. Among the entire group of 93 patients with rupture, the site of rupture was anterior in 38%, posterior in 33%, and lateral in 29%. Evidence of pericarditis was rarely seen except for extensive pericardial adhesions in ten patients who died late (>4 days). A reported pattern predictive of free cardiac rupture was ST elevation in lead aVL on admission [122] whereas the reported risk factors for the development of ventricular septal defect were: age, female gender, and absence of previous angina. In another study of patients with anterior infarction, less ST segment depression in lead III was a predictor of post-MI ventricular septal defect [123].

18.16 ST Segment Elevation: Normal Variant and Acute Pericarditis (See ❯ Chap. 17)

18.16.1 Other Causes of ST Segment Elevation

Persistent multilead ST segment elevation is present in patients with spinal cord injury at C5 to C6 levels, i.e., lesions which completely disrupt cardiac sympathetic influences [124]. These changes were reversed by low doses of infused

Table 18.1

Less Common Causes of ST Segment Elevation

Pulmonary embolism and acute cor pulmonale (usually lead III)
Cardiac tumor
Acute aortic dissection [126]
After mitral valvuloplasty [127]
Pancreatitis, gall bladder disease [128–130] and other catastrophic illnesses [131].
Myocarditis [132]
Septic shock
Anaphylactic reaction [133]
Hyperkalemia ("dialyzable current of injury")
With any marked QRS widening, e.g., antidepressant drug overdose [134] or class IC antiarrhythmic drugs [135, 136]
After transthoracic cardioversion [137, 138]

isoproterenol. Although the mechanism of ST segment elevation in these patients has not been clarified, the findings demonstrate that normal sympathetic tone modulates the course and/or sequence of ventricular repolarization.

Normal "male" pattern with elevated J point and ST segment elevation, mainly in right precordial, is attributed to the effect of testosterone [125] and probably encompasses most cases of a normal variant inappropriately dubbed as "premature repolarization" (see Chap. 17). Less common causes of ST-segment elevation (Table 18.1) which are encountered less frequently than the conditions discussed in the preceding text.

18.16.2 Reciprocal ST Changes in Acute Myocardial Infarction

ST depression in the presence of ST elevation can be a result of either a process which caused the injury current responsible for ST elevation (that is, a true reciprocal change), or the presence of an independent additional area of injury in another location. The magnitude and distribution of ST depression in the baseline ECG of patients with acute coronary syndrome is a strong predictor of cardiac morbidity and mortality [139]. Existence of reciprocal ST depression is supported by experimental studies.

In dogs with anterior myocardial infarction following occlusion of the LAD coronary artery, tachycardia increased ST segment elevation in the anterior precordial leads concomitantly with an increase of reciprocal ST segment depression [140]. It has been shown that a subendocardial lesion associated with ST segment elevation in subendocardial electrograms causes a reciprocal ST segment depression in the epicardial electrograms as long as a layer of nonischemic epicardial muscle is present. However, when ischemia becomes transmural, ST segment elevation occurs in the epicardial electrograms [141].

During acute ischemia, reciprocal ST segment depression is present in all patients with inferior myocardial infarction and in 70% of patients with anterior myocardial infarction. In the cases in which the magnitude of ST segment elevation is small because the overall amplitude of the complex is low, reciprocal ST segment depression may be more conspicuous than the culprit ST segment elevation.

Echocardiographic studies showed that remote-wall changes did not correlate with reciprocal ST segment depression, a finding which is compatible with a true reciprocal change [142]. In other studies, nuclear imaging suggested that reciprocal change indicates an additional region of remote ischemia [143]. Also, angiographic studies performed within 2 weeks of acute myocardial infarction in 84 patients with inferior myocardial infarction showed that patients with anterolateral ST segment depression had larger infarcts and greater incidence of multivessel disease [111]. In the same study, the absence of reciprocal ST segment depression "virtually precluded multivessel disease." Also, in patients with anterior infarction, ST segment depression in inferior leads occurred in 45% of cases and was associated with more extensive infarction, increased morbidity and greater incidence of multivessel coronary disease [144].

During evolution of inferior-wall infarction associated with ST segment elevation in lead III, an absent or disproportionately small reciprocal ST segment elevation in lead V_2 was suggestive of an associated infarction of the right ventricle [145] (Fig. 18.11).

The same principle was shown to be applicable when anterior myocardial infarction caused by occlusion of the left anterior descending coronary artery was accompanied by ischemia of the inferior wall [143]. The latter was caused by either continuation of the occluded left anterior descending coronary artery beyond the apex of the heart onto the inferior wall of the left ventricle, or left anterior descending coronary artery supplying collaterals to the previously infarcted inferior wall. Under such circumstances the ST segment elevation in the anterior precordial leads was associated with either attenuation or reversal of the reciprocal ST segment depression in the "inferior" leads [146].

Boden and Spodick [147] listed the following causes of ST depression in the precordial leads in addition to reciprocal changes in the presence of inferoposterior or inferoseptal or basal (high lateral) acute MI: (1) myocardial ischemia or non-Q-wave infarction; (2) posterior ("transmural") or posteroseptal acute MI, and (3) "benign" reciprocal changes (presumably a normal variant).

18.17 Absence of the Expected Reciprocal ST Segment Deviation

In the presence of the three common types of Q-wave myocardial infarction, i.e., anterior, lateral, and inferior, ST segment elevation is usually associated with reciprocal ST depression in one or more of the standard 12 leads. In the presence of posterior or anterior subendocardial myocardial infarction, the acute injury pattern is manifested by ST segment depression in one or more of the standard leads, and the reciprocal ST segment elevation may be present only in the back in the case of subendocardial infarction, and may be difficult to detect in the anterior leads in the case of posterior infarction because of the low amplitude of ST segment deviation caused by remote location of infarction.

The apparent lack of expected reciprocal ST segment depression in the presence of ST segment elevation in one or more standard precordial leads may be attributed to some of the following factors: (1) Failure to examine leads aVR and V_1 which are probably relatively close to the posterobasal part of the left ventricle; these leads are often less carefully examined than the other ten leads, and therefore the differences between normal and abnormal patterns in these leads may be less recognizable (Fig. 18.4); (2) Difficulty of recognition caused by low amplitude of the ventricular complex in the leads with expected ST segment deviation; (3) Obfuscation by secondary ST segment deviations caused by intraventricular conduction disturbance (Fig. 18.12) or ventricular hypertrophy; common cause is wide terminal QRS deflection in the presence of incomplete or complete RBBB; (4) Co-existence of acute anterior and inferior injury patterns; and (5) Diffuse ST segment elevation in the early stage of anterior infarction with transient extension of ST segment elevation into the territory facing the inferior leads. (Fig. 18.5) Associated pericarditis (Fig. 18.14); It has been suggested [148] that disappearance of reciprocal ST segment depression or appearance of ST segment elevation in the leads with previous ST segment depression may facilitate in some cases the diagnosis of infarction-related pericarditis.

18.18 Hyperacute T Wave Pattern

Pointed tall or deeply negative "coronary" T waves associated with prolonged QT interval may appear either before or after the onset of ST segment shift (Figs. 18.2 and 18.6). These T wave abnormalities are attributed to prolongation of activity in the ischemic regions of the ventricle [9, 149]. In some cases the increase in T wave amplitude may be modest and not easily recognized [150]. In the presence of posterior infarction tall upright T waves in the precordial leads are similar to "hyperacute" T waves during acute anterior ischemia but usually are less transient.

18.19 Postischemic T Wave Abnormalities

In patients with myocardial infarction or unstable angina pectoris, pointed "coronary" T waves appear when the primary deviation of the ST segment has begun to subside. This is attributed to prolongation of activity in the regions of the ventricle immediately adjoining the area of infarction [151]. The abnormal T wave after myocardial infarction is frequently called the: "ischemic" T wave. However, the same term has been also used to designate the pattern of acute myocardial ischemia which is associated with shortening of the QT interval and deviation of the ST segment from baseline. Since lengthening of the QT interval appears later when the injury becomes subacute or chronic, Lepeschkin [152] proposed

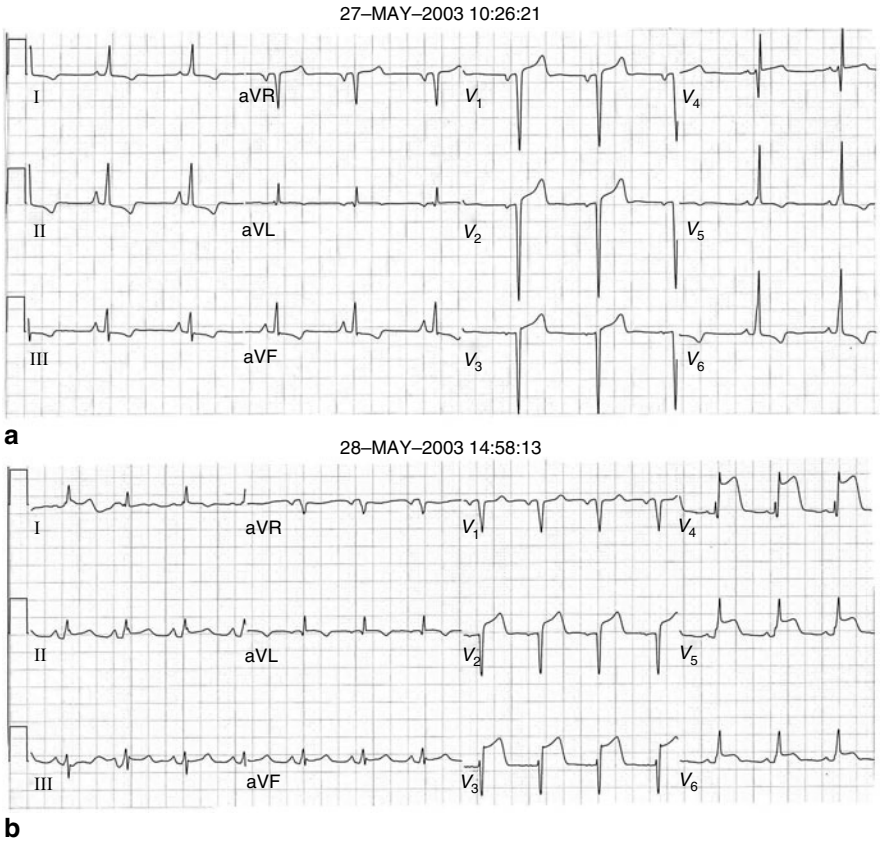

Figure 18.14

Electrocardiogram of a 40-year-old man with hypertension and three-vessel coronary artery disease. In (a) before coronary artery bypass operation, ECG shows left ventricular hypertrophy pattern with secondary ST and T changes. In (b) on the first post-operative day, ST elevation in II, III, $V_{2–6}$ attributed to postoperative pericarditis. No definite reciprocal ST depression is discernible. The above ST changes regressed 1 day later (not shown).

the term "postischemic T wave pattern". In dogs with myocardial infarction, T wave inversion appears within 2 to 3 days after coronary ligation and is associated with an average 24 ms increase in the functional refractory period at the ischemic site [153]. This suggests lengthening of the ventricular AP in this area, a finding which is supported by experimental data. The possible cause of such a lengthening is not known. The proposed theories include changes in the ionic composition of the partly damaged fibers, a decreased temperature owing to depressed mechanical activity [152], or altered function of repolarizing membrane currents. There is no experimental confirmation of any of these theories. The postischemic T wave abnormalities which appear during exercise-induced or a spontaneous attack of angina pectoris usually regress within minutes, but after myocardial infarction, such changes may persist for several days, weeks, months or years.

The vector of abnormal T waves tends to be directed away from the area of abnormal (prolonged) repolarization; that is negative T waves in leads V_1–V_4 in anterior infarction in V_2–V_5, V_6 in anterolateral infarction in V_1 or V_2–V_4 and I, aVL in antero-superior infarction, in I, aVL, and V_5–V_6 in lateral infarction, in II, III and aVF in inferior infarction and an upright T waves in right precordial leads in posterior infarction. However, the correlation between the distribution of T wave abnormalities and localization of myocardial lesions is not as reliable as the correlation between the distribution of Q waves and the region of myocardial infarction (Fig. 18.8). Therefore, it is not advisable to attempt to localize regions of ischemia or fibrosis based on the T wave vector alone in the absence of QRS abnormalities produced by infarction.

In the differential diagnosis of abnormal T wave following T wave characteristics suggest the presence of myocardial ischemia or non-Q-wave MI: (1) T wave is preceded by a horizontal ST segment; (2) T wave is nearly symmetrical and

deep; (3) T wave abnormalities occur in several contiguous leads; (4) QT interval is prolonged. The specificity of diagnosis increases with the increasing number of the above features. In patients with giant negative T waves (see Chap. 17) the presence of coronary artery disease is suggested by the absence of left ventricular hypertrophy and the symmetry of the T wave [154].

In most cases, the T wave abnormalities tend to persist longer than the ST segment deviations. Kloner reported that negative T waves became normal concurrently with the disappearance of wall motion abnormalities within 6 months after coronary angioplasty, presumably owing to the recovery of the stunned (hypoperfused) or hibernating (damaged) but capable of recovery myocardium [155]. The primary "coronary" or postischemic T wave pattern without ST deviation, an abnormal T wave vector, pointed T wave, and prolonged QT interval may appear in patients with various types of pathologic processes discussed in Chap. 17.

18.20 Evolution of ECG Pattern of Acute ST-Elevation Myocardial Infarction (STEMI)**

In a classic sequence of events, during MI the first ECG change is the "hyperacute" T wave followed by ST segment elevation, Q waves (possibly abnormal R waves), decreased ST segment elevation with the beginning of T wave inversion, and return of the ST segment to baseline with symmetric T wave inversion and a prolonged QT interval. During the course of the transition from ST elevation to T wave inversion, a stage of pseudonormalization may occur when the ST segment deviation subsides and the T wave inversion has not yet occurred (see Fig. 18.2). This classic sequence of events is often altered in various ways, particularly in patients undergoing thrombolytic therapy or primary coronary angioplasty (see Figs. 18.3 and 18.6).

The incidence of transient "hyperacute" T wave changes is low even when the ECG is monitored from the time of the onset of symptoms. The patterns of ST segment elevation are described earlier. As a rule, the ST segment elevation is recorded in a larger number of leads than in those with a developing abnormal Q wave. The extent, magnitude, and time course of ST elevation and the associated reciprocal ST segment depression are highly variable. In most cases the initial ST segment elevation decreases markedly during the first 7 to 12 h after the onset of chest pain [90, 156] and subsides within a few days. Mills et al. [157] found that the ST segment elevation resolved within 2 weeks in 90% of patients with inferior infarction and in only 40% of those with anterior infarction. The modern treatment of acute MI has changed the course of ST segment evolution, but the significance of persistent ST segment elevation as a marker of suspected ventricular aneurysm has remained unchanged (see above).

Abnormal T waves are usually more symmetric and more pointed than normal T waves. They are sometimes called "coronary" T waves and are usually associated with lengthening of the QT interval. Pointed "coronary" T waves appear before or after the primary elevation of the ST segment has begun to subside. In the presence of an elevated ST segment the site at which the T wave descent begins to form can be recognizes by the presence of a notch at the summit of repolarization wave (Figs. 18.4 and 18.5). When the notch deepens, the negative deflection is formed. This negative deflection has a characteristic shape known as cove plane T wave [9]. With the increasing descent of the ST segment, the area of the negative T wave increases. When the ST segment becomes horizontal, a symmetric sharply inverted T wave of varying amplitude is inscribed. Such T waves are distinctly different from the secondary T waves of ventricular hypertrophy or intraventricular conduction disturbances but may be indistinguishable from T wave abnormalities caused by other processes (Fig. 18.15; also see Chap. 17).

18.21 Prognostic Implications of Abnormal Repolarization During Acute Myocardial Infarction

The absolute magnitude of the ST segment elevation at hospital admission was found to be of significant prognostic importance [158]. In patients with an inferior infarction, the amplitude of the ST segment elevation was predictive of in-hospital development of a high degree AV block [159]. The degree of reciprocal ST segment depression also was related to infarct size and mortality independent of the ST segment elevation with both anterior and inferior infarctions.

** Previously known as acute Q-wave MI

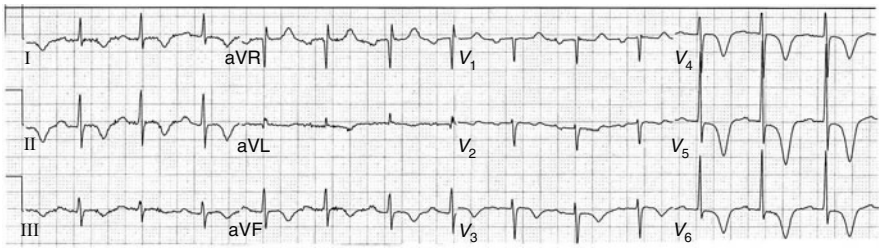

Figure 18.15

Electrocardiogram of a 70-year-old woman with pulmonary edema and normal coronary arteries shows deeply inverted symmetrical T waves of "coronary" configuration in leads I, II, III, aVF and V_3.

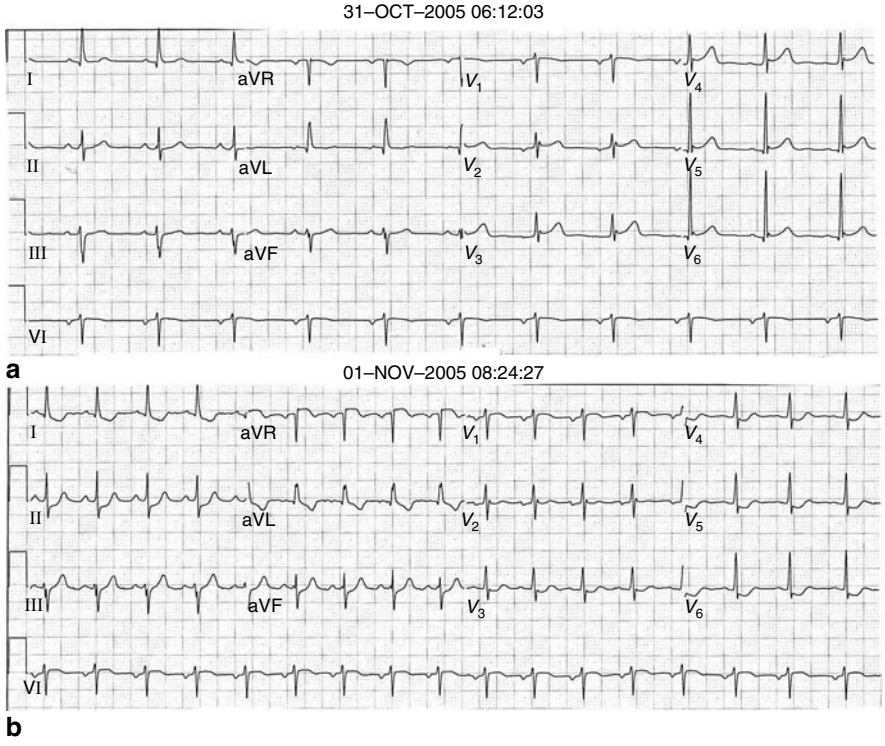

Figure 18.16

Electrocardiogram of a 72-year-old woman before and after carotid endarterectomy with post-operative chest pain. In (a), normal ECG. In (b), during chest pain ST depression in leads I, II, aVL, $V_{3–6}$ with reciprocal ST-elevation in leads aVR and V_1. See text.

T wave abnormalities also have predictive value [160–162]. In one study of patients with acute Q-wave MI, those with ST segment elevation of >2 mm and positive T waves had large infarcts, but a low incidence of recurrent ischemia [162]. In another study [161] persistent negative T waves in leads with Q waves in the chronic stage of MI indicated transmural infarction with a thin fibrotic layer, whereas positive T waves indicated a nontransmural infarct containing viable myocardium within the damaged myocardium. Tamura et al. [163] found that normalization of negative T waves in the infarct-related leads during healing of acute anterior infarction occurred in patients with small infarct and was suggestive of functional recovery of viable myocardium. Lanzelotti et al. [164] reported that persistent negative T waves after first

acute MI were independently associated with a worse outcome whereas Q wave regression was of no long-term prognostic importance. Also among patients with non-ST segment elevation acute coronary syndromes, those with abnormal T waves had a significantly greater incidence of adverse effects [165].

18.22 Angina Pectoris

Stress-induced angina is often associated with ST depression in anterior and inferior leads attributed to subendocardial ischemia. Figure 18.16 shows that these changes are associated with reciprocal ST elevation in leads aVR and V_1. This subject is covered in greater detail in the chapter dealing with stress testing.

18.23 Silent Myocardial Ischemia

Silent myocardial ischemia is observed in patients with asymptomatic coronary artery disease, in patients with symptomatic angina and painless periods and after myocardial infarction [166, 167, 170]. Electrocardiographic manifestations of silent ischemia usually consist of horizontal or downsloping ST segment depression recorded during exercise test or ambulatory monitoring. Silent ST segment elevation may occur but is uncommon.

The review of literature by Rozanski and Berman [170] disclosed that among patients with coronary artery disease, about one third of the episodes of ST segment depression observed during exercise testing occur silently. Ambulatory ECG monitoring in patients with history of angina pectoris and an abnormal exercise test showed that about 75% of the episodes of ST segment depression are silent. The frequency of silent or symptomatic myocardial ischemia follows a typical circadian rhythm, with the highest frequency of the episodes in the morning hours [171, 172].

18.24 QT-Interval

During acute myocardial ischemia QT interval may shorten, lengthen or remain unchanged [31].

18.25 U Wave

During acute myocardial ischemia U wave may become inverted or increase in amplitude. The former occurs more often. In patients with anterior infarction, U wave may become inverted in anterior leads and in those with inferior MI in inferior leads. Transient U wave inversion may be caused, however, not only by regional myocardial ischemia but also by elevation of blood pressure [173, 174] (see Chap. 17).

References

1. Cascio, W.E., G.X. Yan, and A.G. Kleber, Passive electrical properties, mechanical activity and extracellular potassium in arterially perfused and ischemic rabbit ventricular muscle. *Circ. Res.*, 1990;**66**: 1461–1473.
2. Jennings, R.B., K.A. Reimer, M.L. Hill, and S.E. Mayer, Total ischemia in dog hearts in vitro. 1. Comparison of high energy phosphate production, utilization and depletion and of adenosine nucleotide catabolism in total ischemia in vitro vs severe ischemia in vivo. *Circ. Res.*, 1981: 892–900.
3. Janse, M.J., H. Cinca, J. Morena, et al., The "border zone" in myocardial ischemia. An electrophysiological, metabolic and histochemical correlation in the pig heart. *Circ. Res.*, 1979;**44**: 576–588.
4. Kleber, A.G, Resting membrane potential, extracellular potassium activity and intracellular sodium activity during acute global ischemia in isolated perfused guinea pig hearts. *Circ. Res.*, 1983;**52**: 442–450.
5. Kleber, A.G., C.B. Riegger, and M.J. Janse, Extracellular K+ and H+ in early ischemia: mechanisms and relation to changes in impulse propagation. *J. Moll. Cell. Cardiol.*, 1987;**19**: 35–44.
6. Vleugels, A., J. Vereecke, J. Van der Heyden, and E. Carmeliet, Ionic currents during hypoxia in voltage-clamped ventricular muscle. *Circ. Res.*, 1980;**47**: 501–508.
7. Isenberg, G., J. Vereecke, G. Van der Heyden, and E. Carmeliet, The shortening of the action potential by DNP in guinea pig ventricular myocytes is mediated by an increase of a-time dependent K+ conductance. *Pfluegers Archiv.*, 1983;**397**: 251–259.

8. Van der Heyden, G., J. Vereecke, and R. Carmeliet, The effect of cyanide on the K current in guinea pig ventricular myocytes. *Basic Res. Cardiol.*, 1985;**80**: 93–96.
9. Surawicz, B., *Electrophysiological Basis of ECG and Cardiac Arrhythmias*. Baltimore, MD: Williams and Wilkins, 1995.
10. Samson, W.E. and A.M. Scher, Mechanism of ST segment alteration during acute myocardial injury. *Circ. Res.*, 1960;**8**: 780–787.
11. Downar, E., M.J. Janse, and D. Durrer, The effect of acute coronary artery occlusion on subepicardial transmembrane potential in the intact porcine heart. *Circulation*, 1977;**56**: 217–224.
12. Kleber, A.G., M.J. Janse, P.J. Van Capelle, and D. Durrer, Mechanisms and time course of ST and TQ segment changes during acute regional myocardial ischemia in the pig heart determined by extracellular and intracellular recordings. *Circ. Res.*, 1978;**42**: 603–613.
13. Janse, M.J. and A.L. Wit, Electrophysiological mechanisms of ventricular arrhythmias resulting from myocardial ischemia and infarction. *Physiol. Rev.*, 1989;**69**: 1049–1150.
14. Michelson, E.L., J.F. Spear, and E.N. Moore, Strength-interval relations in a chronic canine model of myocardial infarction. Implications for the interpretation of electrophysiologic studies. *Circulation*, 1981;**63**: 1158–1165.
15. Gardner, P., P.C. Ursell, J.J. Fenoglio, and A.L. Wit, Electrophysiological and anatomical basis for fractionated electrograms recorded from healed myocardial infarcts. *Circulation*, 1985;**72**: 596–611.
16. Taccardi, B., Changes in cardiac electrogenesis following coronary occlusion, in Coronary Circulation and Energetics of the Myocardium, G. Marchetti and B. Taccardi, Editors. Karger, Basel, 1967, pp. 259–267.
17. Cohen, D. and L.A. Kaufman, Magnetic determination of the relationship between the S-T segment shift and the injury current produced by coronary artery occlusion. *Circ. Res.*, 1975;**36**: 414–425.
18. Cohen, D., P. Savard, R.D. Rifkin, E. Lepeschkin, and W.E. Strauss, Magnetic measurement of the S-T and T-Q segment shifts in humans; Part II: Exercise-induced S-T segment depression. *Circ. Res.*, 1983;**53**: 274–279.
19. R. Coronel, F.J. Wilms-Schopman, T. Opthof, F.J. van Cappelle, and M. Janse, Injury current and gradients of diastolic stimulation threshold, TQ potential and extracellular potassium concentration during acute regional ischemia in the isolated perfused pig heart. *Circ. Res.*, 1991;**68**: 1241–1249.
20. Smith, G.T., G. Geary, W. Ruf, T.H. Roelofs, J.J. McNamara, Epicardial mapping and electrocardiographic models of myocardial ischemic injury. *Circulation*, 1979;**60**: 930–938.
21. Cinca, J., J. Figueras, G. Senador, E. Garcia-Moreno, A. Salas, and J. Rius, Transmural DC electrograms after coronary artery occlusion and latex embolization in pigs. *Am. J. Physiol.*, 1984;**246**: H475–H482.
22. Mirvis, D.M., Body surface distribution of repolarization forces during acute myocardial infarction. Isopotential and isoarea mapping. *Circulation*, 1980;**62**: 878–887.
23. Kornreich, F., T.J. Montague, and P.M. Rautaharju, Body surface potential mapping of ST segment changes in acute myocardial infarction. Implications for ECG enrollment criteria for thrombolytic therapy. *Circulation*, 1993;**87**: 773–782.
24. Birnbaum, Y., S. Sclarovsky, A. Solodky, et al., Prediction of the level of left anterior descending coronary artery obstruction during anterior wall acute myocardial infarction by the admission electrocardiogram. *Am. J. Cardiol.*, 1993;**72**: 823–826.
25. Ben-Gal, T., I. Herz, A. Solodky, et al., Acute anterior wall myocardial infarction entailing ST segment elevation in lead V_1; electrocardiographic and angiographic correlations. *Clin. Cardiol.*, 1998;**21**: 399–404.
26. Engelen, D.J.M., A.P.M. Gorgels, E.C. Cheriex, et al., ECG criteria differentiating between proximal versus distal occlusion of the left anterior descending coronary artery. *J. Am. Coll. Cardiol.*, 1997;**30**: 430A (abstr).
27. Assali, A., S. Sclarovsky, I. Herz, et al., Persistent ST segment depression in precordial leads V_5–V_6 after Q-wave anterior wall myocardial infarction is associated with restrictive physiology of the left ventricle. *J. Am. Coll. Cardiol.*, 2000;**35**: 352–357.
28. Lew, A.S., H. Hod, B. Cercek, P.K. Shah, and W. Ganz, Inferior ST segment changes during acute anterior myocardial infarction; a marker of the presence or absence of concomitant inferior wall ischemia. *J. Am. Coll. Cardiol.*, 1987;**30**: 519–526.
29. Iwasaki, K., S. Kusachi, T. Kita, and G. Taniguchi, Prediction of isolated first diagonal branch occlusion by 12-lead electrocardiography; ST segment shift in I and aVL. *J. Am. Coll. Cardiol.*, 1994;**23**: 1557–1561.
30. Surawicz, B., C.M. Orr, J.B. Hermiller, K.D. Bell, R.P. Pinto, QRS changes during percutaneous transluminal coronary angioplasty and their possible mechanisms. *J. Am. Coll. Cardiol.*, 1997;**30**: 452–458.
31. Tsuka, Y., T. Sugiura, A. Yoshiteru, et al., Clinical characteristics of ST segment elevation in lead V_6 in patients with Q-wave acute inferior wall myocardial infarction. *Coron. Art. Dis.*, 1999;**10**: 465–469.
32. Birnbaum, Y., I. Herz, S. Sclarovsky, et al., Prognostic significance of precordial ST segment depression on admission electrocardiogram in patients with inferior wall myocardial infarction. *J. Am. Coll. Cardiol.*, 1996;**28**: 313–318.
33. Wong, C.K., B. Freedman, G. Bautovich, et al., Mechanism and significance of precordial ST segment depression during inferior wall acute myocardial infarction associated with severe narrowing of the dominant right coronary artery. *Am. J. Cardiol.*, 1993;**71**: 1025–1030.
34. Shah, P.K., M. Pichler, D.S. Berman, et al., Non-invasive identification of a high risk subset of patients with acute inferior myocardial infarction. *Am. J. Cardiol.*, 1980;**48**: 915–921.
35. Goldberg, H.L., J.S. Borer, J.S. Jacobstein, et al., Anterior ST depression in inferior myocardial infarction; indicator of posterolateral infarction. *Am. J. Cardiol.*, 1981;**48**: 1009–1015.
36. Peterson, E.D., W.R. Hathaway, K.M. Zabel, et al., Prognostic significance of precordial ST segment depression during inferior myocardial infarction in the thrombolytic era:results in 16,521 patients. *J. Am. Coll. Cardiol.*, 1996;**28**: 305–312.
37. Bates, E.R., P.M. Clemmensen, R.M. Califf, et al., Precordial ST segment depression predicts a worse prognosis in inferior infarction despite reperfusion therapy. *J. Am. Coll. Cardiol.*, 1990;**16**: 1538–1544.
38. Kosuge, M., K. Kimura, T. Ishikawa, et al., New electrocardigraphic criteria predicting the site of coronary artery occlusion in inferior wall acute myocardial infarction. *Am. J. Cardiol.*, 1998;**82**: 1318–1322.

39. Birnbaum, Y., G.S. Wagner, G.I. Barbash, et al., Correlation of angiographic findings and right (V_1 to V_3) versus (V_4 to V_6) precordial ST segment depression in inferior wall acute myocardial infarction. *Am. J. Cardiol*., 1999;**83**: 143–148.
40. Bairey, C.N., P.K. Shah, A.S. Lew, et al., Electrocardiographic differentiation of occlusion of the left circumflex versus right coronary artery as a cause of inferior acute myocardial infarction. *Am. J. Cardiol*., 1997;**79**: 182–186.
41. Casas, R.E., H.J.L. Mariott, and D.L. Glancy, Value of leads V_7–V_9 in diagnosing posterior wall acute myocardial infarction and other causes of tall R waves in $V_{1–2}$. *Am. J. Cardiol*., 1997;**80**: 508–509.
42. Huey, B.L., G.A. Beller, D.L. Kaiser, and R.S. Gibson, A comprehensive analysis of myocardial infarction due to circumflex artery occlusion; comparison with infarction due to right coronary artery and left anterior descending artery occlusion. *J. Am. Coll. Cardiol*., 1988;**12**: 1156–1166.
43. Nagahama, Y., T. Sugiura, K. Takehana, et al., PQ segment depression in acute Q wave inferior wall myocardial infarction. *Circulation*, 1995;**91**: 641–645.
44. Chia, B.L., J.W.L. Yip, H.C. Tan, and Y.T. Lim, Usefulness of ST elevation II/III ratio and ST deviation in lead I for identifying the culprit artery in inferior wall acute myocardial infarction. *Am. J. Cardiol*., 2000;**86**: 341–343.
45. Herz, I., A.R. Assali, Y. Adler, A. Solodky, S.L. Sclarovsky, New electrocardiographic criteria for predicting either the right or left circumflex artery as the culprit coronary artery in inferior wall acute myocardial infarction. *Am. J. Cardiol*., 1997;**88**: 1343–1345.
46. Assali, A.R., S. Sclarovsky, I. Herz, et al., Comparison of patients with inferior wall acute myocardial infarction with versus without ST segment elevation in leads V_5 and V_6. *Am. J. Cardiol*., 1998;**81**: 81–83.
47. Dunn, R.F., H.N. Newman, L. Bernstein, et al., The clinical features of isolated circumflex coronary artery disease. *Circulation*, 1984;**69**: 477–484.
48. Agarwal, J.B., K. Khaw, and F. Aurignac, Lo Curto. Importance of posterior chest leads in patients with suspected myocardial infarction, but non-diagnostic routine 12-lead electrocardiogram. *Am. J. Cardiol*., 1999;**83**: 323–326.
49. Zalenski, R.J., R.J. Rydman, E.P. Sloan, et al., ST segment elevation and the prediction of hospital life-threatening complications. The role of right ventricular and posterior leads. *J. Electrocardiol*., 1998;**31**(Supplement): 164–171.
50. Matetzky, S., D. Freimark, M.S. Feinberg, et al., Acute myocardial infarction with isolated ST segment elevation in posterior chest leads V 7–9. *J. Am. Coll. Cardiol*., 1999;**34**: 748–753.
51. Chou, T.C., J. van der Bel-Kahn, J. Allen, et al., Electrocardiographic diagnosis of right ventricular infarction. *Am. J. Med*., 1981;**70**: 1175–1181.
52. Braat, S.H., A.P.M. Gorgels, F.W. Bar, H.J. Wellens, et al., Value of the ST-T segment in lead V_4 in inferior wall acute myocardial infarction to predict the site of coronary artery occlusion. *Am. J. Cardiol*., 1988;**62**: 140–142.
53. Kataoka, H., K. Kanzaki, and Y. Mikuriya, An ECG marker of underlying right ventricular conduction delay in the hyperacute phase of right ventricular infarction or ischemia. *J. Electrocardiol*., 1990;**23**: 369–372.
54. Geft, I.L., P.K. Shah, L. Rodriguez, et al., ST elevations in leads V_1 to V_5 may be caused by right coronary artery occlusion and acute right ventricular infarction. *Am. J. Cardiol*., 1984;**53**: 991–996.
55. Forman, M.B., J. Goodin, B. Phelan, H. Kopelman, and R. Virmani, Electrocardiographic changes associated with isolater right ventricular infarction. *J. Am. Coll. Cardiol*., 1984;**4**: 640–643.
56. Mak, K.H., B.L. Chia, A.F. Tan, and T. Johan, Simultaneous ST segment elevation in lead V_1 and depression in lead V_2. A discordant ECG pattern indicating right ventricular infarction. *J. Electrocardiol*., 1994;**22**: 203–207.
57. Zehender, M., W. Kasper, E. Kauder, et al., Right ventricular infarction as an independent predictor of prognosis after acute inferior myocardial infarction. *N. Engl. J. Med*., 1993;**328**: 981–988.
58. Braat, S., P. Brugada, C. De Zwaan, J.M. Coenegracht, and H.J. Wellens, Value of electrocardiogram in diagnosing right ventricular infarction in patients with an acute inferior wall myocardial infarction. *Br. Heart J*., 1983;**49**: 368–372.
59. Saw, J., C. Davies, A. Fung, J.J. Spinelli, and J. Jue, Value of ST elevation in lead III greater than lead II in inferior wall acute myocardial infarction for predicting in-hospital mortality and diagnosing right ventricular infarction. *Am. J. Cardiol*., 2001;**87**: 448–450.
60. Menown, I.B.A., J. Allen, M.C.C. Anderson, and A.A.J. Adgey, Early diagnosis of right ventricular or posterior infarction associated with inferior wall left ventricular acute myocardial infarction. *Am. J. Cardiol*., 2000;**85**: 934–938.
61. Brugada, J. and P. Brugada, Further characterization of the syndrome of right bundle branch block, ST segment elevation and sudden death. *J. Cardiovasc. Electrophysiol*., 1997;**8**: 325–331.
62. Brugada, P. and J. Brugada, Right bundle branch block, persistent ST segment elevation and sudden cardiac death: A distinct clinical and electrocardiographic syndrome. *J. Am. Coll. Cardiol*., 1992;**20**: 1391–1395.
63. Atarashi, H., S. Ogawa, K. Harumi, et al., Characteristics of patients with right bundle branch block and ST segment elevation in right precordial lead. *Am. J. Cardiol*., 1996;**78**: 581–585.
64. Ailings, M. and A. Wilde, "Brugada" syndrome. Clinical data and suggested pathophysiological mechanism. *Circulation*, 1999;**99**: 666–671.
65. Wung, S.F. and B. Drew, New electrocardiographic criteria for posterior wall acute myocardial ischemia validated by a percutaneous transluminal coronary angioplasty. Model of acute myocardial infarction. *Am. J. Cardiol*., 2001;**87**: 970–974.
66. Miayazaki, T., H. Mitamura, H. Miyoshi, et al., Autonomic and antiarrhythmic drug modulation of ST segment elevation in patients with Brugada syndrome. *J. Am. Coll. Cardiol*., 1996;**27**: 1061–1064.
67. Nademanee, K., G. Veerakul, S. Nimmannit, et al., Arrhythmogenic marker for the sudden unexplained death in Thai men. *Circulation*, 1997;**96**: 2595–2598.
68. Marcus, F.I., G.H. Fontaine, et al., Right ventricular dysplasia; A report of 24 adult cases. *Circulation*, 1982;**65**: 384–389.

69. Corrado, D., A. Nava, G. Guja, et al., Familial cardiomyopathy underlies syndrome of right bundle branch block, ST segment elevation and sudden death. *J. Am. Coll. Cardiol.*, 1996;**27**: 443–448.
70. Tada, H., N. Aihara, T. One, et al., Arrhythmogenic right ventricular cardiomyopathy underlies syndrome of right bundle branch block, ST segment elevation, and sudden death. *Am. J. Cardiol.*, 1998;**81**: 519–523.
71. Marcus, F.I. and G. Fontaine, Arrhythmogenic right ventricular dysplasia/cardiomyopathy: a review Pacing. *Clin. Electrophysiol.*, 1995;**18**: 1298–1314.
72. Takagi, M., N. Aihara, H. Takaki, et al., Clinical characteristics of patients with spontaneous or inducible ventricular fibrillation without apparent heart disease presenting with J wave and ST segment elevation in inferior leads. *J. Cardiovasc. Electrophysiol.*, 2000;**11**: 844–848.
73. Surawicz, B., Brugada syndrome: manifest, concealed, "asymptomatic", suspected and simulated. *J. Am. Coll. Cardiol.*, 2001;**38**: 775–777.
74. Yamaji, H., K. Iwasaki, S. Kusachi, et al., Prediction of acute left main coronary artery obstruction by 12 lead electrocardiography. ST segment elevation in lead aVR with less ST segment elevation in lead V_1. *J. Am. Coll. Cardiol.*, 2001;**38**: 1338–1354.
75. Gaitonde, R., N. Sharma, S. Al-Hasan, J.M. Miller, V. Jayachandran, and V.G. Kalaria, Prediction of significant left main coronary artery stenosis by the 12-lead electrocardiogram in patients with rest angina pectoris and the withholding of clopidogrel therapy. *Am. J. Cardiol.*, 2003;**92**: 846–848.
76. Mukarami, H., K. Urabe, and M. Nishimura, Inappropriate microvascular constriction produced transient ST segment elevation in patients with syndrome X. *J. Am. Coll. Cardiol.*, 1998;**32**: 1287–1292.
77. DeServi, H., E. Arbustini, F. Marsico, et al., Correlation between clinical and morphologic findings in unstable angina. *Am. J. Cardiol.*, 1996;**11**: 128–131.
78. Huey, B., M. Gheorghiade, R.S. Crampton, et al., Acute non-Q wave myocardial infarction with early ST segment elevation: Evidence for spontaneous coronary reperfusion and implications for thrombolytic trials. *J. Am. Coll. Cardiol.*, 1987;**9**: 18–25.
79. Stark, K., M.W. Krucoff, B. Schryver, and K.M. Kent, l: Quantification of ST segment changes during coronary angioplasty in patients with left bundle branch block. *Am. J. Cardiol.*, 1991;**67**: 1219–1222.
80. Blanke, H., H. Scherff, K.R. Karsch, et al., Electrocardiographic changes after streptokinase-induced recanalization in patients with acute left anterior descending artery obstruction. *Circulation*, 1983;**68**: 406–412.
81. Fernandez, A.R., R.F. Sequeira, S. Chakko, et al., ST segment tracking for rapid determination of patency of the infarct-related artery in acute myocardial infarction. *J. Am. Coll. Cardiol.*, 1995;**26**: 675–683.
82. Veldkamp, R.F., S. Sawchak, J.E. Pope, et al., Performance of an automated real-time ST segment analysis program to detect coronary occlusion and reperfusion. *J. Electrocardiol.*, 1996;**29**: 257–263.
83. Schroeder, R., K. Wegscheider, K. Schroder, R. Dissman, and W. Meyer-Sabelle, Extent of early ST segment elevation resolution. A strong predictor of outcome in patients with acute myocardial infarction and a sensitive measure to compare thrombolytic regimens. *J. Am. Coll. Cardiol.*, 1995;**26**: 1657–1664.
84. Pepine, C.J., Prognostic markers in thrombolytic therapy: Looking beyond mortality. *Am. J. Cardiol.*, 1996;**78**: 24.
85. Krucoff, M.W., M.A. Croll, J.E. Pope, et al., Continuous 12-lead ST segment recovery analysis in the TAMI 7 study. *Circulation*, 1993;**88**: 437–446.
86. Mauro, F., P. Maggioni, M.G. Francos, et al., A simple electrocardiographic predictor of outcome of patients with acute myocardial infarction treated with a thrombolytic agent. *J. Am. Coll. Cardiol.*, 1994;**24**: 600–606.
87. Santoro, G.M., R. Valenti, P. Buoanamici, et al., Relation between ST segment changes and myocardial perfusion evaluated by myocardial contrast echocardiography in patients with acute myocardial infarction treated with direct angioplasty. *Am. J. Cardiol.*, 1988;**82**: 932–936.
88. Krucoff, M.W., A.R. Parente, R.K. Bottner, et al., Stability of multilead ST segment "fingerprints" over time after percutaneous transluminal coronary angioplasty and its usefulness in detecting reocclusion. *Am. J. Cardiol.*, 1988;**61**: 1232–1237.
89. Kondo, M., K. Tamura, H. Tania, et al., Is ST segment re-elevation associated with reperfusion an indicator of marked myocardial damage after thrombolysis? *J. Am. Coll. Cardiol.*, 1993;**21**: 62–67.
90. Essen, R., W. Merx, and S. Effert, Spontaneous course of ST segment elevation in acute anterior myocardial infarction. *Circulation*, 1979;**59**: 105–112.
91. Ochiai, M., T. Isshiki, Y. Hirose, et al., Myocardial damage after successful thrombolysis is associated with the duration of ST-re-elevation at reperfusion. *Clin. Cardiol.*, 1995;**18**: 321–327.
92. Kosuge, M., K. Kimura, T. Ishikawa, et al., Relation of absence of ST re-elevation immediately after reperfusion and success of reperfusion with myocardial salvage. *Am. J. Cardiol.*, 1997;**80**: 1080–1083.
93. Schechter, M., B. Rabinowitz, B. Beker, et al., Additional ST segment elevation during the first hour of thrombolytic therapy: an electrocardiographic sign predicting a favorable clinical outcome. *J. Am. Coll. Cardiol.*, 1992;**20**: 1460–1464.
94. Doevendans, P.A., A.P. Gorgels, R. van der Zee, et al., Electrocardiographic diagnosis of reperfusion during thrombolytic therapy in acute myocardial infarction. *Am. J. Cardiol.*, 1995;**75**: 1206–1210.
95. Steg, P.G., M. Faraggi, D. Himbertt, et al., Comparison using dynamic vectorcardiography and MIBI SPECT of ST segment changes and myocardial MIBI uptake during percutaneous transluminal coronary angioplasty of the left anterior descending coronary artery. *Am. J. Cardiol.*, 1995;**75**: 998–1002.
96. Shah, A., G.S. Wagner, R.M. Califf, et al., Comparative prognostic significance of simultaneous versus independent resolution relative to ST segment elevation during acute myocardial infarction. *J. Am. Coll. Cardiol.*, 1997;**30**: 1478–1483.
97. Andrews, J., I.T. Straznicky, J.K. French, et al., for the HERO-1 investigators. ST segment recovery adds to the assessment of TIMI 2 and 3 flow in predicting infarct wall motion after thrombolytic therapy. *Circulation*, 2000;**101**: 2138–2143.
98. Dong, J., G. Ndrepepa, C. Schmitt, et al., Early resolution of ST segment elevation correlates with myocardial salvage assessed by Tc-99m Sestamibi scintigraphy in patients with acute myocardial infarction after mechanical or thrombolytic reperfusion therapy. *Circulation*, 2002;**105**: 2946–2949.

99. Shah, A., G.S. Wagner, C.L. Green, et al., Electrocardiographic differentiation of the ST segment depression of acute myocardial injury due to the left circumflex artery occlusion from that of myocardial ischemia of nonocclusive etiologies. *Am. J. Cardiol.*, 1997;**78**: 512–513.
100. MacDonald, R.G., J.A. Hill, R.L. Feldman, ST segment response to acute coronary occlusion. Coronary hemodynamic and angiographic determinants of direction of ST segment shift. *Circulation*, 1986;**74**: 973–979.
101. Kobayashi, N., N. Ohmura, I. Nakada, et al., Further ST elevation at reperfusion by direct percutaneous transluminal coronary angioplasty predicts poor recovery of left ventricular systolic function in anterior wall AMI. *Am. J. Cardiol.*, 1997;**79**: 862–866.
102. Santoro, G.M., D. Antoniucci, R. Valenti, et al., Rapid reduction of ST segment elevation after successful direct angioplasty in acute myocardial infarction. *Am. J. Cardiol.*, 1997;**80**: 865–869.
103. McLaughlin, M.G., G.W. Stone, E. Aymong, et al., Prognostic utility of comparative methods for assessment of ST segment resolution after primary angioplasty for acute myocardial infarction. The controlled Abciximab and device investigation to lower late angioplasty complications (CADILLAC) Trial. *J. Am. Coll. Cardiol.*, 2004;**44**: 215–223.
104. Watanabe, J., S. Nakamura, T. Sugiura, et al., Early identification of impaired myocardial reperfusion with serial assessment of ST segments after percutaneous transluminal coronary angioplasty during acute myocardial infarction. *Am. J. Cardiol.*, 2001;**88**: 956–959.
105. Feldman, L.J., P. Coste, A. Furber, et al., for the French Optimal STenting (FROST)-2 investigators. Incomplete resolution of ST segment elevation is a marker of transient microcirculatory dysfunction after stenting for acute myocardial infarction. *Circulation*, 2003;**107**: 2684–2689.
106. Brodie, B., T.D. Stuckey, C. Hansen, et al., Relation between electrocardiographic ST segment resolution and early and late outcomes after primary percutaneous coronary intervention for acute myocardial infarction. *Am. J. Cardiol.*, 2005;**95**: 343–348.
107. Claeys, M.J., J. Bosmans, L. Veenstra, et al., Determinants and prognostic implications of persistent ST segment elevation after primary angioplasty for acute myocardial infarction. *Circulation*, 1999;**99**: 1972–1977.
108. Matetzky, S., G. Novikov, L. Gruberg, et al., The significance of persistent ST elevation after primary PTCA. *J. Am. Coll. Cardiol.*, 1999;**34**: 1932–1938.
109. Cokkinos, D.V., G.L. Hallman, D.A. Cooley, O. Zamalloa, and R.D. Leachman, Left ventricular aneurysm: analysis of electrocardiographic features and postresection changes. *Am. Heart J.*, 1971;**82**: 149–157.
110. Chou, T.C., Electrocardiography, in Clinical Practice 1996; 4th ed: Philadelphia, PA: WB Saunders.
111. Roubin, G.S., W.F. Shen, M. Nicholson, et al., Anterolateral ST segment depression in acute inferior myocardial infarction. *Am. Heart J.*, 1984;**107**: 1177–1182.
112. Cohen, M., S.J. Scharpf, and K.P. Rentrop, Prospective analysis of electrocardiographic variables as markers for extent and location of acute wall motion abnormalities observed during coronary angioplasty in human subjects. *J. Am. Coll. Cardiol.*, 1987;**10**: 17–24.
113. Lindsay, J., R.C. Dewey, B.S. Talesnick, and N.G. Nolan, Relation of ST segment elevation after healing of acute myocardial infarction to the presence of ventricular aneurysm. *Am. J. Cardiol.*, 1984;**54**: 84–86.
114. Arvan, S. and M.A. Varat, Persistent ST segment elevation and left ventricular wall abnormalities. A 2 dimensional echocardiographic study. *Am. J. Cardiol.*, 1984;**53**: 1542–1546.
115. Toyofuku, M., H. Takaki, K. Sunagawa, et al., Exercise-induced ST elevation in patients with arrhythmogenic right ventricular dysplasia. *J. Electrocardiol.*, 1999;**32**: 1–8.
116. Cinca, J., A. Bardaji, A. Carreno, et al., ST segment elevation at the surface of a healed myocardial infarction in pigs: conditions for passive transmission from the ischemic peri-infarction zone. *Circulation*, 1995;**91**: 1552–1559.
117. Engel, T.R., R. Caine, P.R. Kowey, and J.O. Finnegan, ST segment elevation with ventricular aneurysm. *J. Electrocardiol.*, 1984;**17**: 75–77.
118. Dubnow, M.H., H.B. Burchell, and J.L. Titus, Post-infarction ventricular aneurysma clinicopathologic and electrocardiographic study of 80 cases. *Am. Heart J.*, 1965;**70**: 753–760.
119. Frances, C., A. Romero, and D. Grady, Left ventricular pseudoaneurysm. *J. Am. Coll. Cardiol.*, 1998;**32**: 537–541.
120. Oliva, P.B., S.C. Hammill, and W.D. Edwards, Cardiac rupture, a clinically predictable complication of acute myocardial infarction: report of 70 cases with clinico-pathologic correlations. *J. Am. Coll. Cardiol.*, 1993;**22**: 720–726.
121. Figueras, J., A. Curos, J.M. Cortodellas, and J. Soler-Soler, Relevance of electrocardiographic findings, heart failure and infarct site in assessing and timing of left ventricular free wall rupture during acute myocardial infarction. *Am. J. Cardiol.*, 1995;**76**: 543–547.
122. Yoshino, H., M. Yotsukara, K. Yano, et al., Cardiac rupture and admission electrocardiography in acute anterior myocardial infarction: Implication of ST elevation in aVL. *J. Electrocardiol.*, 2000;**33**: 49–53.
123. Birnbaum, Y., G.S. Wagner, K.B. Gates, et al., Clinical and electrocardiographic variables associated with increased risk of ventricular septal defect in acute anterior myocardial infarction. *Am. J. Cardiol.*, 2000;**86**: 830–834.
124. Lehmann, K.G., A.H. Shandling, A. Yusi, and V.F. Froelicher, Altered ventricular repolarization in central sympathetic dysfunction associated with spinal cord injury. *J. Am. J. Cardiol.*, 1989;**63**: 1498–1504.
125. Surawicz, B. and S.R. Parikh, Prevalence of male and female patterns of early ventricular repolarization in the normal ECG of males and females from childhood to old age. *J. Am. Coll. Cardiol.*, 2002;**40**: 1870–1876.
126. Hirata, K., M. Kyushima, and H. Asato, Electrocardiographic abnormalities in patients with acute dissection. *Am. J. Cardiol.*, 1995;**76**: 1207–1212.
127. Ludman, P.F., D. Hildick-Smith, A. Harcombe, and L.M. Shapiro, Transient ST segment changes associated with mitral valvuloplasty using the Inoue balloon. *Am. J. Cardiol.*, 1997;**79**: 1704–1705.
128. Patel, J., A. Mohaved, and W.C. Reeves, Electrocardiographic and segmental wall motion abnormalities in pancreatitis mimicking myocardial infarction. *Clin. Cardiol.*, 1994;**17**: 505–509.

129. Chandraratna, P.A.M., A. Nimalasurya, C.L. Reid, S. Cohn, and S.H. Rahimtoola, Left ventricular asynergy in acute myocarditis. Simulation of acute myocardial infarction. *JAMA*, 1983;**250**: 1428–1430.
130. Dec, G.W., H. Waldman, J. Southern, et al., Viral myocarditis mimicking acute myocardial infarction. *J. Am. Coll. Cardiol.*, 1992;**20**: 85–89.
131. Thomas, I., J. Mathew, V.P. Kumar, R. Cooper, and J. Ferlinz, Electrocardiographic changes in catastrophic abdominal illness mimicking acute myocardial infarction. *Am. J. Cardiol.*, 1987;**59**: 1224–1225.
132. Chida, K., S.I. Ohkawa, and Y. Esaki, Clinicopathologic characteristics of elderly patients with persistent ST segment elevation and inverted T waves: Evidence of insidious or healed myocarditis? *J. Am. Coll. Cardiol.*, 1995;**25**: 1641–1649.
133. Rich, M.W., Myocardial injury caused by an anaphylactic reaction to ampicillin/sulbactam in a patient with normal coronary arteries. *Tex. Heart Inst. J.*, 1998;**25**: 194–197.
134. Bolognesi, R., D. Tsialtas, P.E. Vasini, M. Conti, and C. Manca, Abnormal ventricular repolarization mimicking myocardial infarction after heterocycling antidepressant overdose. *Am. J. Cardiol.*, 1997;**79**: 242–245.
135. Nakamura, W., K. Segawa, H. Ito, and N. Yoshimoto, Class IC antiarrhythmic drugs, flecainide and pilsicainide, produce ST segment elevation simulating inferior myocardial ischemia. *J. Cardiovasc. Electrophysiol.*, 1998;**9**: 585–558.
136. Krishanan, S. and M.E. Josephson, ST segment elevation induced by class IC antiarrhythmic agents: underlying electrophysiologic mechanisms and insight into drug-induced proarrhythmia. *J. Cardiovasc. Electrophysiol.*, 1998;**9**: 1167–1174.
137. Kok, L.C., M.A. Mitchell, D.E. Haines, J.P. Mounsey, and J.P. Di Marco, Transient ST elevation after transthoracic cardioversionn in patients with hemodynamically unstable ventricular tachyarrhythmia. *Am. J. Cardiol.*, 2000;**85**: 877–881.
138. Wang, K., R.W. Asinger, and H.J.L. Marriott, ST segment elevation in conditions other than acute myocardial infarction. *N. Engl. J. Med.*, 2003;**349**: 2128–2135.
139. Kaul O, We-Ching C, Harrington RA, Wagner GS, et al. for the PARAGON-A and GUSTO-IIb Investigators. Prognostic value of ST segment depression in acute coronary syndromes: Insights from PARAGON-A applied to GUSTO-IIb. *J. Am. Coll. Cardiol.*, 2001;**38**: 64–71.
140. Mirvis, D.M., J.L. Wilson, and K.B. Ramanathan, Effects of experimental myocardial infarction on the ST segment response to tachycardia. *J. Am. Coll. Cardiol.*, 1985;**6**: 665–673.
141. Guyton, R.A., J.H. McClenathan, G.E. Newman, and L.L. Michaelis, Significance of subendocardial S-T segment elevation caused by coronary stenosis in the dog. *Am. J. Cardiol.*, 1977;**40**: 373–380.
142. Camara, E.J.N., N. Chandra, P. Ouyang, S.H. Gottlieb, and E.P. Shapiro, Reciprocal ST change in acute myocardial infarction. Assessment by electrocardiography and echocardiography. *J. Am. Coll. Cardiol.*, 1983;**2**: 251–257.
143. Pichler, M., P.K. Shah, T. Peter, et al., Wall motion abnormalities and electrocardiographic changes in acute transmural myocardial infarction: Implications of reciprocal ST segment depression. *Am. Heart J.*, 1983;**106**: 1003–1009.
144. Haraphongse, M., S. Tanomsup, and B.I. Jugdutt, Inferior ST segment depression during acute anterior myocardial infarction: Clinical and angiographic correlations. *J. Am. Coll. Cardiol.*, 1984;**4**: 467–476.
145. Lew, A.S., P. Laramee, P.K. Shah, J. Maddahi, T. Peter, and W. Ganz, Ratio of ST segment depression in lead V_2 to ST segment elevation in lead aVF in evolving inferior acute myocardial infarction; an aid to recognition of right ventricular ischemia. *Am. J. Cardiol.*, 1986;**57**: 1047–1051.
146. Lew, A.S., H. Hod, B. Cercek, P.K. Shah, and W. Ganz, Inferior ST segment changes during acute anterior myocardial infarction. A marker of the presence or absence of concomitant inferior wall ischemia. *J. Am. Coll. Cardiol.*, 1987;**10**: 519–526.
147. Boden, W.E. and D.H. Spodick, Diagnostic significance of precordial ST segment depression. *Am. J. Cardiol.*, 1989;**63**: 358–361.
148. Oliva, P.B., S.C. Hammill, and W.D. Edwards, Electrocardiographic diagnosis of postinfarction regional pericarditis. *Circulation*, 1993;**88**: 896–904.
149. Wilson, F.N., A.G. Macleod, and P.S. Barker, The T deflection of the electrocardiogram. *Trans. Assoc. Am. Phys.*, 1931;**46**: 29–38.
150. Goldberger, A.L., Hyperacute T waves revisited. *Am. Heart J.*, 1982;**104**: 888–890.
151. Wilson, F.N., F.F. Rosenbaum, and F.D. Johnston, Interpretation of the ventricular complex of the electrocardiogram. *Adv. Intern. Med.*, 1947;**2**: 1–63.
152. Lepeschkin, E., *Modern Electrocardiography*. Baltimore, MD: Williams and Wilkins, 1951, pp. 307, 420.
153. Kleber, A.G., M.F. Janse, F.J.L. van Capelle, and D. Durrer, Mechanism and time course of S-T and T-Q segment changes during acute regional myocardial ischemia in pig heart determined by extracellular and intracellular recordings. *Circ. Res.*, 1978;**42**: 603–613.
154. Otrusinik, R., M.A. Alpert, C.R. Hamm, et al., Factors predicting coronary artery disease in patients with giant negative T waves. *Am. J. Cardiol.*, 2000;**85**: 873–875.
155. Kloner, R.A., Inverted T waves. An electrocardiographic marker of stunned or hibernating myocardium in man? *Circulation*, 1990;**82**: 1060–1061.
156. Zmyslinski, R.W., T. Akiyama, T.L. Biddle, et al., Natural course of S-T segment and QRS complex in patients with acute anterior myocardial infarction. *Am. J. Cardiol.*, 1979;43: 29–34.
157. Mills, R.M., E. Young, R. Gordon, et al., Natural history of S-T segment elevation in acute myocardial infarction. *Am. J. Cardiol.*, 1975;**35**: 609–614.
158. Willems, J.L., R.J. Willems, G.M. Willems, et al., Significance of initial ST segment elevation and depression for the management of thrombolytic therapy in acute myocardial infarction. *Circulation*, 1990;**82**: 1147–1158.
159. Birnbaum, Y., S. Sclarovsky, and I. Herz, Admission clinical and electrocardiographic characteristics predicting in-hospital development of high-degree atrioventricular block in inferior acute myocardial infarction. *Am. J. Cardiol.*, 1997;**80**: 1134–1138.
160. Hochrein, J., F. Sun, K.S. Pieper, et al., Higher T wave amplitude associated with better prognosis in patients receiving thrombolytic therapy for acute myocardial infarction (a GUSTO-I substudy). *Am. J. Cardiol.*, 1998;**81**: 1078–1084.
161. Sclarovsky-Benjaminov, F., S. Sclarovsky, and Y. Birnbaum, The predictive value of the electrocardiographic pattern of acute Q-wave myocardial infarction for recurrent ischemia. *Clin. Cardiol.*, 1995;**18**: 710–715.
162. Maeda, S., T. Imai, K. Kuboki, et al., Pathologic implications of restored positive T waves and persistent negative T waves after Q wave myocardial infarction. *J. Am. Coll. Cardiol.*, 1996;**28**: 1514–1518.

163. Tamura, A., K. Nagase, Y. Mikurya, et al., Significance of spontaneous normalization of negative T waves in infarct-related leads during healing of anterior wall acute myocardial infarction. *Am. J. Cardiol*., 1999;**84**: 1341–1344.
164. Lanzellotti, P., P.L. Gerard, H.E. Kulbertus, and L.A. Pierard, Persistent negative T waves in the infarct-related leads as an independent predictor of poor long-term prognosis after acute myocardial infarction. *Am. J. Cardiol*., 2002;**90**: 833–837.
165. Jacobsen, M.D., G.S. Wagner, L. Holmvang, P.W. Macfarlane, U. Nasllund, P. Grande, and P. Clemmensen, on behalf of the TRIM investigators. Clinical significance of abnormal T waves in patients with non-ST segment elevation acute coronary syndromes. *Am. J. Cardiol*., 2001;**88**: 1225–1229.
166. Chierchia, S., M. Lazzari, B. Friedman, C. Brunelli, and A. Maseri, Impairment of myocardial perfusion and function during painless myocardial ischemia. *J. Am. Coll. Cardiol*., 1983;**1**: 294–330.
167. Deanfield, J.E., M. Shea, P. Ribiero, et al., Transient ST segment depression as a marker of myocardial ischemia during daily life. *Am. J. Cardiol*., 1984;**54**: 1195–1200.
168. Maseri, A., Role of coronary artery spasm in symptomatic and silent myocardial ischemia. *J. Am. Coll. Cardiol*., 1987;**9**: 249–262.
169. von Arnim, T., B. Hoffling, M. Schreiber, et al., Characteristics of episodes of ST elevation or ST depression during ambulatory monitoring in patients subsequently undergoing coronary angiography. *Br. Heart J*., 1985;**54**: 484–488.
170. Rozanski, A. and D.S. Berman, Silent myocardial ischemia: I. Pathophysiology, frequency of occurrence and approaches toward detection. *Am. Heart J*., 1987;**114**: 615–626.
171. Quyumi, A., C.M. Wright, L.J. Mockus, and K.M. Fox, How important is history of chest pain in determining the degree of ischemia in patients with angina pectoris? *Br. Heart J*., 1985;**54**: 22–26.
172. Rocco, M.B., J. Barry, S. Campbell, et al., Circadian variation of transient myocardial ischemia in patients with coronary artery disease. *Circulation*, 1987;**75**: 395–400.
173. Gerson, M.C., J.F. Phillips, S.N. Morris, and P.L. McHenry, Exercise-induced U wave inversion as a marker of stenosis of the left anterior descending coronary artery. *Circulation*, 1979;**60**: 1014–1020.
174. Kishida, H., J.S. Cole, and B. Surawicz, Negative U wave: A highly specific but poorly understood sign of heart disease. *Am. J. Cardiol*., 1982;**49**: 2030–2036.

19 The QT Interval

Wojciech Zareba · Iwona Cygankiewicz

P. W. Macfarlane, A. van Oosterom, O. Pahlm, P. Kligfield, M. Janse, J. Camm (eds.), *Comprehensive Electrocardiology*, DOI 10.1007/978-1-84882-046-3_19,

19.1 Introduction

The QT interval in an electrocardiogram is a global reflection of complex processes governing the repolarization of ventricular myocardium. Most frequent concerns regarding the QT interval relate to its prolongation whereas QT shortening is relatively rare. QT interval prolongation may result from inherited long QT syndrome (LQTS), but more frequently is observed in the course of ischemic and nonischemic cardiomyopathies, or can be induced by drugs or abnormal electrolyte/metabolic disorders [1–10]. The LQTS is characterized by prolongation of the QT interval on the electrocardiogram and is associated with an increased propensity to ventricular tachyarrhythmias that can lead to cardiac events such as syncope, cardiac arrest, or sudden death [1–6]. The LQTS is a pure electrical disorder, which became a paradigm to understand QT interval and repolarization in general, and its role in cardiac electrophysiology. In particular, clinical observations in LQTS patients and related basic science research have led to a better understanding of the role of repolarization in cardiac arrhythmias and cardiac electrophysiology. Recognition of the association between QT prolongation and risk of torsades de pointes (TdP) ventricular tachycardia (VT) has lead to increasing interest in evaluating QT prolongation as a surrogate marker of cardiac arrhythmias, first in congenital LQTS, second, in drug-induced abnormalities of repolarization, and in more common conditions as well as in healthy subjects [1–6, 10].

In this chapter, we aim to provide an overview of current concepts on ventricular repolarization and its pathophysiology, describe clinical and electrocardiographic aspects of QT interval analysis, explore prognostic significance of repolarization abnormalities, describe clinical aspects of drug-induced repolarization abnormalities, and describe dynamic features of the QT interval.

19.2 QT Interval and Ventricular Repolarization

19.2.1 Long QT Syndrome (LQTS) as a Paradigm for Understanding Ventricular Repolarization

During the last decades, several mutations in specific genes encoding cardiac ion channels have been identified in patients with the congenital form of LQTS [11–22]. These mutations cause alterations in the ion-channel proteins leading to abnormalities in ion-channel function that prolong ventricular repolarization (Fig. 19.1). The KVLQT1 (LQT1) gene [11, 14] encodes a potassium channel protein (α-subunit) that when coexpressed with a protein (β-subunit) from the minK (KCNE1; LQT5) gene produces a reduction in the slowly activating, delayed rectifier (repolarizing) potassium current (I_{Ks}). The reduction in I_{Kr} (rapidly activating delayed rectifier) current is caused by mutations in the HERG (LQT2) gene [11, 12] regulating the major pore-forming subunit or by mutations in the MiRP1 (LQT6) gene coding the putative regulatory subunit of the I_{Kr} channel. The SCN5A (LQT3) sodium channel gene [13] mutations cause abnormal inactivation of sodium channel with an inward leakage of sodium ions during the repolarization phase contributing to QT prolongation. There are currently 12 different genes recognized as causing QT prolongation (Table 19.1). About

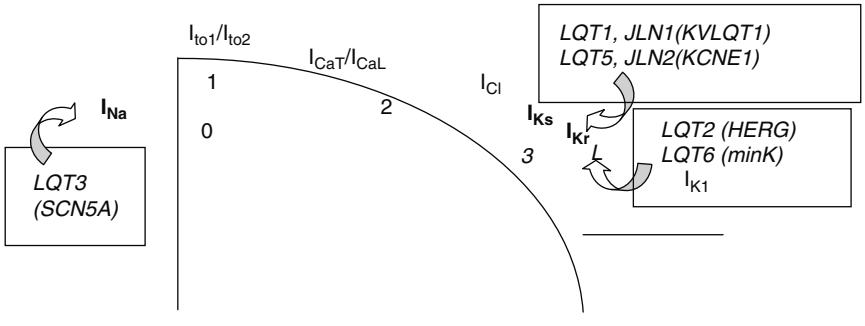

Figure 19.1
Schematic presentation of action potential with key ion currents and related long QT syndrome (LQTS) genes.

Table 19.1

Genetic types of the Long QT Syndrome (LQTS)

Genotype	Chromosome	Affected gene	Channel protein	Ion-channel current
LQT1	11	KCNQ1	Four α-subunits each with six membrane spanning segments	$\downarrow I_{Ks}$
LQT2	7	KCNH2	Four α-subunits each with six membrane spanning segments	$\downarrow I_{Kr}$
LQT3	3	SCN5A	One α-subunit with 24 membrane spanning segments	$\uparrow I_{Na}$
LQT4	4	Ankyrin-B (ANK2)	Sodium pump and Na/Ca exchanger	I_{Na}[a]
LQT5	21	KCNE1	β-subunit of KCNQ1 with one membrane spanning segment	$\downarrow I_{Ks}$
LQT6	21	KCNE2	β-subunit of KCNH2 with one membrane spanning segment	$\downarrow I_{Kr}$
LQT7	17	KCNJ2	Two membrane spanning segments	$\downarrow I_{K1}$
LQT8	6	CACNA1C	One α_1-subunit with 24 membrane spanning segments	$\uparrow I_{Ca}$
LQT9	3	CAV3 (Caveolin)	Altered gating kinetics of $Na_v1.5$	I_{Na}[a]
LQT10	11	SCN4B	β-subunit of SCN5A with one membrane spanning segment	$\uparrow I_{Na}$
LQT11	7	AKAP9	A-kinaze anchor protein	$\downarrow I_{Ks}$[a]
LQT12	20	SNTA1	Sodium current (SCN5A) regulator	$\uparrow I_{Na}$[a]

[a]Channel-related proteins, these are not proteins forming channels

60–70% of genetically tested patients have mutations found in one of the recognized causative genes [22]. It is estimated that among patients with known genotype, LQT1 and LQT2 account for the majority (87%) of cases of congenital LQTS, LQT3 accounts for 8%, whereas LQT5 and LQT6 are extremely rare accounting for less than 5% of LQTS cases [11]. The remaining types of LQTS: LQT4 [15], LQT7 [16], LQT8 [17], LQT9 [18], LQT10 [19], LQT11 [20], and LQT12 [21] are extremely rare conditions accounting when combined for less than 1% of clinical LQTS cases, but their importance should not be underappreciated since they provide crucial insight into mechanisms of cardiac repolarization. Identification of some of these rare forms has led to recognizing the role of not only ion-channel proteins but also proteins associated with and regulating ion-channel function in repolarization.

19.2.2 Ion-Channel Function and Arrhythmogenesis

There are significant differences in repolarization in the various layers of the myocardium, with the epicardial cells having the shortest action potential duration, endocardial cells having an intermediate duration, and M cells having the longest action potential duration [23–25]. QT duration on ECG represents the longest repolarization in the M cell zone. This physiologic transmural dispersion of repolarization usually does not lead to TdP. However, proarrhythmic states may arise as a result of specific gene mutations or actions of medications causing selective action potential prolongation in certain areas of the heart (usually M cells) that lead to increased transmural repolarization gradients (Fig. 19.2) [25]. This increased transmural gradient may contribute to reentrant arrhythmias leading to TdP. It is worth stressing that not all drugs prolonging repolarization cause TdP. For example, amiodarone is known to prolong QT duration, but since this drug is not increasing transmural heterogeneity of repolarization (or it might decrease it), TdP is not observed in patients taking this drug. Similarly, the novel compound ranolazine may increase QT duration but simultaneously decreases heterogeneity of repolarization. Interestingly, both of these drugs are mild calcium and sodium channel blockers, which might contribute to a decreased propensity to proarrhythmias [26].

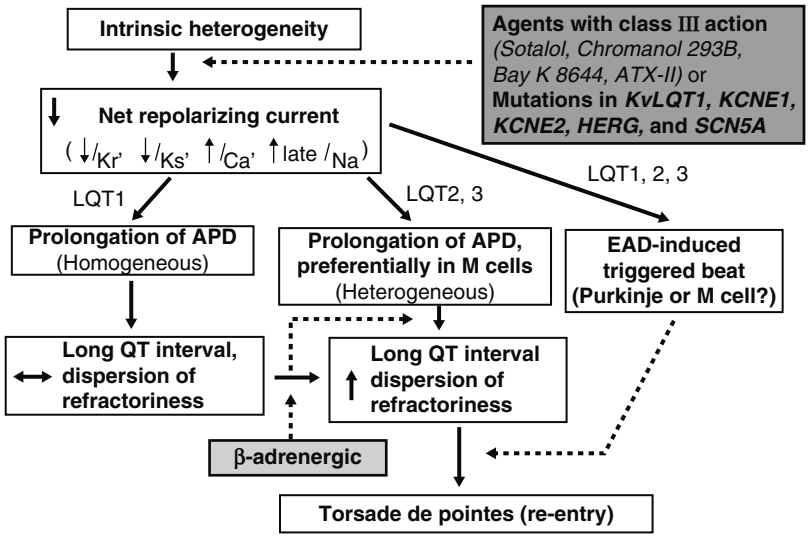

Figure 19.2

Proposed cellular and ionic mechanisms for the long QT syndrome. APD, action potential duration; EAD, early after depolarization (Antzelevitch et al. [25]. © Elsevier Limited. Reproduced with permission).

Recent progress in the understanding of ion-channel structure and function has provided evidence for the mechanisms associated with HERG channel and I_{Kr} current abnormalities [27–29]. Numerous medications cause QT prolongation by blocking I_{Kr} due to their binding affinity to sites within the HERG channel cavity, while others may cause abnormal trafficking of proteins forming the channel from inside the cell toward the cellular membrane. Abnormal trafficking of channel proteins may result in a decreased number of channels in the cellular membrane or expression of dysfunctional channels [29]. Some of the proteins do not reach the membrane at all, and some reach it as imperfect, defective proteins that are not fully functional, therefore unable to pass the expected number of potassium ions through the pore of the channel. LQT2 patients as well as patients who never had an LQTS diagnosed but might have genetic polymorphism of HERG protein are particularly prone to developing QT prolongation due to drugs blocking this channel. Other individuals with normal function and structure of the channel who develop drug-induced QT prolongation might have an affinity to experience an entrapment of the drug molecule within the pore of the channel causing decreased outward potassium current.

Although dysfunction of different ion channels has been found to cause inherited forms of LQTS, the HERG channel conducting I_{Kr}, the rapid delayed rectifier current, seems to play a critical role in drug-induced QT prolongation and TdP [10, 30–32]. Numerous medications including some antiarrhythmics, antihistamine, antibiotics, psychotropic, and gastrointestinal prokinetic drugs have been found to block I_{Kr}. The reason for so many different drugs blocking the same channel is found in a different molecular structure and dysfunction of the channel caused by prolonged entrapment of drug molecules in the channel cavity leading to enhanced binding affinity of the drug to the sites in the channel [27–29]. The other potassium channels have a protective mechanism (a proline-X- proline sequence in S6 domain) that reduces the volume of the channel cavity precluding drug molecules to be trapped there. The HERG channel does not have proline residues in the S6 location and, therefore, this channel is more prone to bind drug molecules inside the channel with subsequent blocking of the channel and reduction in I_{Kr} current. Since not all drugs that block I_{Kr} produce TdP, other mechanisms might be involved in the proarrhythmic response including other actions of the drugs. Amiodarone and verapamil are examples of I_{Kr} blockers that are not associated with increased risk of TdP possibly due to concomitant blocking of calcium channels or homogenous prolongation of repolarization in various layers of the myocardium.

Transmural dispersion of repolarization seems to play the most important role in arrhythmogenesis in both drug-mediated and congenital forms of LQTS [24, 25]. There is a physiologic transmural dispersion of repolarization with M cells showing the longest action potential duration, epicardial cells the shortest, and endocardial cells intermediate

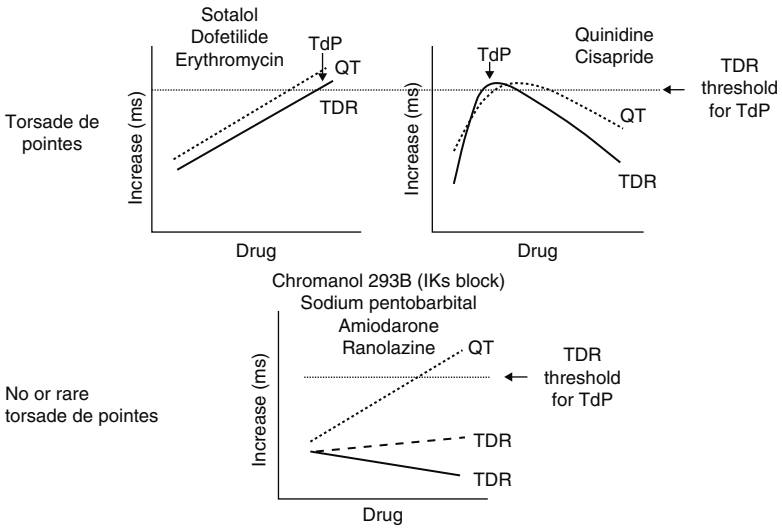

Figure 19.3

Correspondence between changes in QT interval and transmural dispersion of repolarization, and propensity for development of torsade de pointes (Antzelevitch et al. [25]. © Elsevier Limited. Reproduced with permission).

action potential duration. The magnitude of this physiologic transmural dispersion of repolarization is not sufficient to cause conditions leading to TdP, unless there is selective prolongation of the action potential in one of the layers (M cells) due to action of drugs or due to a specific genetic mutation (Fig. 19.3). This excessive prolongation increases the magnitude of transmural gradient of repolarization, which may cause functional block and reentry in response to a premature beat [24, 25].

19.3 QT Interval

19.3.1 QT Interval Measurement

The routine QT interval measurements in ECGs are used to assess global repolarization duration. The QT interval includes the QRS complex, nevertheless, the entire QT interval is considered as a measure of repolarization since the repolarization process already takes place during the QRS complex for early activated regions of myocardium. The QT interval should be measured from the onset of the QRS complex to the offset of the T wave, defined as a deflection point terminating the descending arm of the T wave usually at the level of isoelectric line or as the nadir between the T and U waves [33, 34]. When T and U waves are merged or when the T wave has a bifid appearance with two components of the T wave, clinicians might have difficulties where to identify the end of the repolarization segment. In such a case, careful inspection of repolarization duration in all 12 leads might be helpful in determining proper approach to quantify QT interval in such situation, or a QTU duration is sometimes reported with proper acknowledgment that the measurement includes a second component that might be part of the T wave or superimposed U wave (Fig. 19.4). In case of repolarization morphologies with the presence of a second component of T wave or U wave, some investigators suggest using the rule that U wave usually should be at least 150 ms behind the peak of the T wave, whereas closer deflections might be considered as the second component of the T wave [35, 36]. However, there are no systematic data validating this rule. There is no doubt that complex patterns of repolarization usually reflect more heterogeneous repolarization patterns which are likely to contribute to arrhythmogenic conditions. Identifying the end of theT wave and measurement of QT may lead to quite

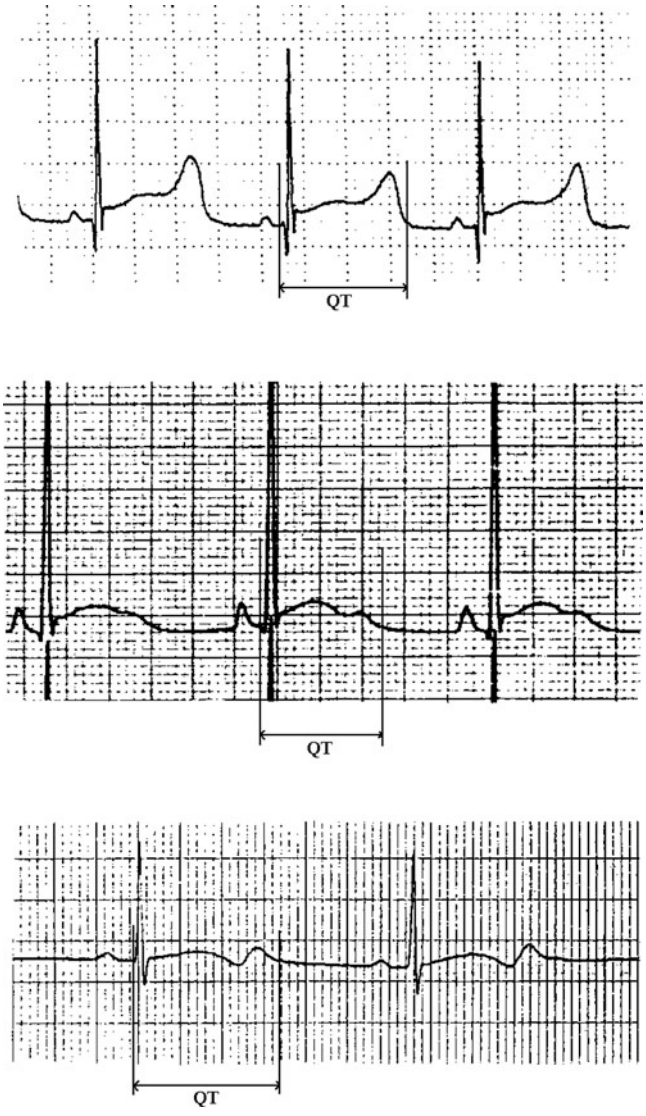

Figure 19.4
QT interval measurement in different T wave morphologies.

significant differences based on the experience of the reader, as it was shown by Viskin et al. [37] who demonstrated that only about 40% of internists and 70% of cardiologists were able to measure it properly in comparison to measurements done by a group of experts.

19.3.2 Lead Selection for QT Duration

Physiologically, the optimal method of measuring the QT in ECG is to take the earliest onset of the QRS complex in any of 12 leads and the latest offset of the T wave in any of the 12 leads, reflecting global duration of the repolarization process [38]. This approach is rarely exercised in manual measurements since it is time consuming and in most cases does not provide major benefit on top of routine measurements done in lead II. In some cases with borderline QT prolongation,

careful investigation of repolarization duration and morphology in all leads might help identify QT prolongation and repolarization abnormalities.

Automatic algorithms evaluating repolarization duration might also utilize the concept of a so-called global lead represented as a superimposition of all 12 leads in the ECG [38]. The QT interval in such presentation is measured from the earliest onset of the QRS complex in any lead to the latest offset in any lead verified visually with all T wave ends superimposed.

The QT duration varies among standard 12 leads, and QT dispersion has been measured in numerous studies as a possible marker of arrhythmogenic conditions [39, 40]. However, due to conceptual and methodological limitations of QT dispersion, this method has not been approved as a standard tool in clinical practice or in drug studies. Interlead differences in repolarization morphology rather than just QT duration seem to better reflect the complexity of repolarization process [40–44]. Interlead differences in repolarization morphology could be quantified utilizing various methods including principal component analysis, area-based analysis of repolarization segment, and other methods [41–44]. Principal component analysis of the repolarization segment allows quantifying the length $(\lambda 1)$ and width $(\lambda 2)$ of the T wave loop [41, 43]. The roundness of the T-loop in its preferential plane $(\lambda 2/\lambda 1)$ has been considered as an index of increased T wave complexity.

19.3.3 Adaptation of QT Duration to Heart Rate

In 1920, Bazett described a curvilinear association between the QT and RR intervals and the formula based on his observation $(QTc = QT/(RR^{1/2}))$ is most frequently used [45]. The Fridericia's [46] formula $(QTc = QT/(RR^{1/3}))$ is increasingly used especially in studies evaluating the effects of medications on the QT interval. Both these formulae adjust the QT interval to the conditions seen for a heart rate of 60 bpm. Bazett's QTc formula has limitations of overestimating repolarization duration at fast heart rates and underestimating it at slow heart rates. Fridericia's formula causes less misjudgment, however, clinicians are not comfortable in using this formula on a daily basis due to a need of cubic root equation and more importantly due to limited clinical data on normal values and the diagnostic and prognostic significance of this measurement. Few other QTc formulae were proposed including (1) Framingham [47] – a more linear formula $(QTc = QT + 0.154(1 - RR))$; (2) Hodges et al. [48] – utilizing the heart rate $(QTc = QT + 1.75(\text{heart rate} - 60))$; (3) Rautaharju et al. [49] – where QT is entered in milliseconds and where the formula is different for males and females depending on age: for all females and males <15 and >50 years $QTI = QT(HR + 100)/656$ ms and for males 15–50 years: $QTI = (100 \times QT)/((656/(1 + 0.01HR)) + 0.4\,\text{age} - 25)$; and Karjalainen et al. [50] – where both QT and RR are entered in milliseconds, and it varies by heart rate: for heart rate <60 bpm, $QT_{Nc} = (QT \times 392)/(0.116\,RR + 277)$; for heart rate 60–99 bpm $QT_{Nc} = (QT \times 392)/(0.156\,RR + 236)$; and for heart rate ≥ 100 bpm, $QT_{Nc} = (QT \times 392)/(0.384\,RR + 99)$. All of these formulas tend to adjust well for the QT/RR association; however, each has some limitations. The QTc formulae provide good estimation of QT duration at heart rates close to the normal resting range of 55–75 bpm as observed in the vast majority of ECGs. However, below and above those limits there could be room for misclassification of the QTc value. Heart rates below 55 bpm or above 75–80 bpm are usually recorded using Holter recordings and exercise testing and for these ranges of heart rates, the Fridericia's (cubic) formula is of preference due to its simplicity of application, although other more complex formulae including Rautaharju's or Karjalainen's could be used.

For evaluation of ECGs recorded off and on a drug, the analysis of QT/RR regression with the subject-specific QT/RR relationship plots is of increasing use [51, 52]. One could also use the so-called RR-bin method that relies on measurement of QT intervals in absolute value for matched RR intervals for recordings off and on drugs without a need of using correction formulas [53]. The QT/RR subject-specific method and the RR-bin approach are particularly valuable when evaluating drugs affecting heart rates.

19.3.4 Normal QTc Values for Age and Gender

QT interval duration is different according to age and gender. Table 19.1 shows proposed normal and abnormal QTc values (using Bazett heart rate correction) by age and gender [54]. Women and children have longer duration of repolarization than men (Table 19.2).

Table 19.2

QTc values by age and gender

QTc value (sec)	Children 1–15 years	Men	Women
Normal	< 0.44	< 0.43	< 0.45
Borderline	0.44–0.46	0.43–0.45	0.45–0.46
Prolonged	> 0.46	> 0.45	> 0.46

Adapted with permission from Ref [54].

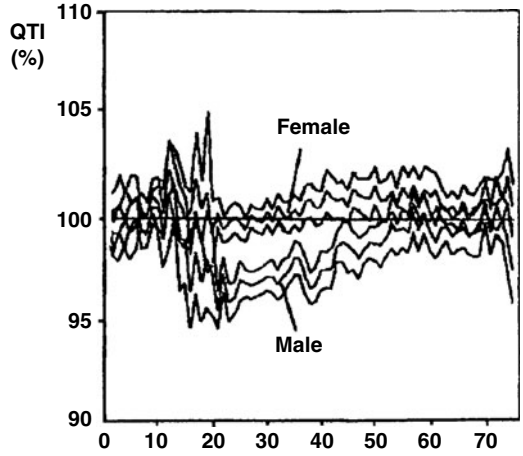

Figure 19.5

Age and sex-related pattern of QTI (QT index by Rautaharju) (Rautaharju et al. [49]. © Pulsus Group Inc. Reproduced with permission).

Rautaharju et al. [49] demonstrated that a sex-related difference in QT is due to a shorter QT duration in men than women at age 15–55 years, not because of QT prolongation in women (Fig. 19.5). Slower heart rate in men is one of the important factors contributing to this difference, but it is postulated that other important modulators include different density of potassium ion channels in male versus female myocardium, effects of female hormones contributing to longer QT duration in women, or possibly the effect of male hormones contributing to their shorter QT duration. Sex-related differences in repolarization are also observed for parameters describing T wave morphology with men having a steeper ascending arm of the T wave than women [55]. Women dominate cases of drug-induced torsade de pointes and long QT cases in adulthood which is explained by a longer QTc in women than men.

19.3.5 QT Prolongation and Risk of Cardiac Arrhythmias and Mortality

The risk of arrhythmic events is significantly associated with QT prolongation in LQTS [1–6]. For every 10 ms increase of QTc duration, there is 5% exponential increase of the risk of cardiac events [1]. Therefore, a patient showing an increase in QTc duration from 440 to 500 ms has a 34% increase in the risk of cardiac events (60 ms difference indicates 1.05^6 = 1.34). Figure 19.6 shows the association between QTc interval and risk of aborted cardiac arrest or death in LQTS patients evaluated during adulthood from age 18 to 40 years [56]. Subjects with QTc > 500 ms are particularly prone to developing cardiac events. Genotype–phenotype correlations indicate that about a third of LQTS carriers have normal or borderline QTc values [2–4]. These observations indicate that the magnitude of QTc duration is not the sole factor when evaluating the risk of arrhythmic events. In the case of drug-induced QTc prolongation, the QTc duration above 500 ms or prolongation by more than 60 ms in response to a drug indicates an increased risk of TdP [57].

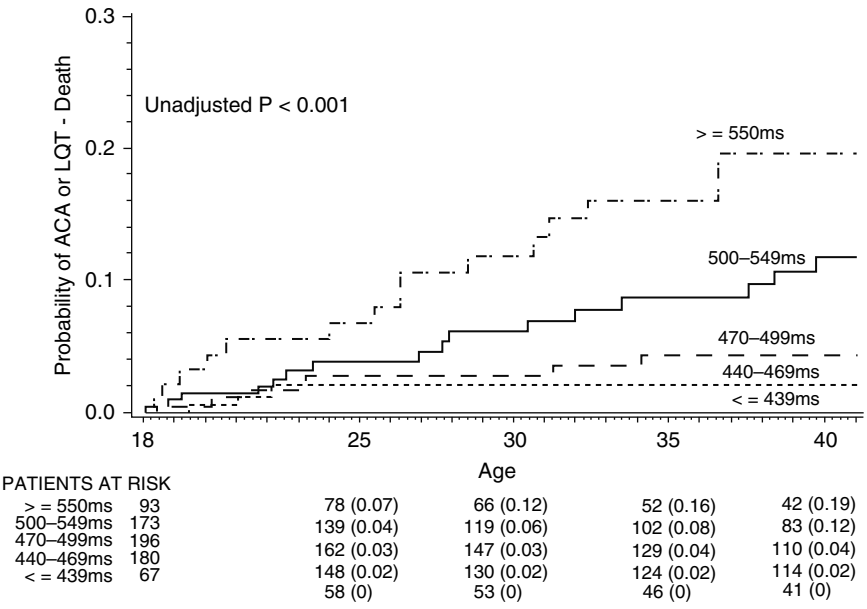

Figure 19.6

Cumulative probability of cardiac events by QTc duration in adult LQTS patients (Sauer et al. [56]. © Elsevier Limited. Reproduced with permission).

QT prolongation is also considered as a risk factor in non-LQTS subjects. The Rotterdam Study [58], a prospective population-based cohort study of 3,105 men and 4,878 women aged 55 years and older, demonstrated that an abnormally prolonged QTc interval (>450 ms in men, >470 ms in women) was associated with a threefold increased risk of sudden cardiac death after adjustment for age, gender, body mass index, hypertension, cholesterol/high-density lipoprotein ratio, diabetes mellitus, myocardial infarction, heart failure, and heart rate (Figure 19.9). The Framingham study did not show an association of baseline QTc prolongation with total mortality, sudden death, or coronary mortality [59]. The Cardiovascular Health Study [60], on the other hand, showed an association between a QTc interval of >450 ms and total mortality, and in the Strong Heart Study [61], a QTc interval of ≥ 460 ms was associated with a twofold increased risk of cardiac and total mortality.

Data regarding the predictive value of QT interval prolongation in patients with coronary disease and heart failure are controversial [62–68]. In a recent study of Attar et al. [63], 682 individuals underwent diagnostic coronary angiography of whom 17 (2.5%) died or had a nonfatal myocardial infarction during 1-year follow-up. In multivariate analysis, QRS duration, extent of coronary disease, and prolonged corrected QT peak interval were independently associated with events. However, most of the studies are not able to confirm practical usefulness of QT prolongation for predicting cardiac events in patients with underlying coronary disease and cardiomyopathy since these conditions alter repolarization and QT prolongation is reflecting more a severity of the disease than the risk of cardiac events [64–68].

19.3.6 Changes in T wave Morphology

The T wave morphology varies among LQTS patients and this variation could be related to the type of affected ion channel, the magnitude of ion-channel dysfunction, as well as other factors including age, heart rate, and the status of the autonomic nervous system. It has been recognized that specific genetic types of LQTS could be associated with distinct ECG patterns of repolarization [69]. Figure 19.7 shows specific patterns associated with distinct genetic types of the disorder: LQT1 characterized by wide, broad-based T waves, LQT2 usually showing low-amplitude and frequently notched

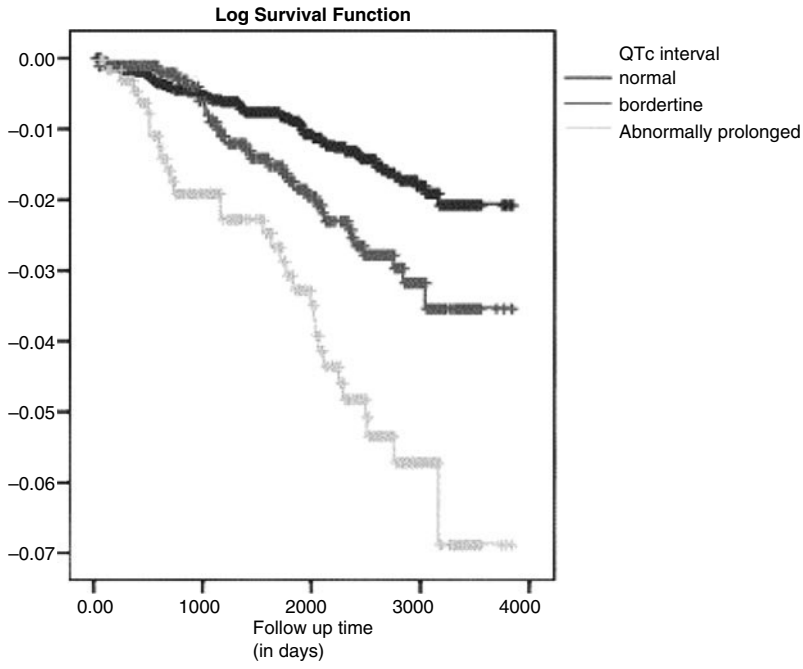

Figure 19.7

Risk of sudden death and QTc in elderly subjects enrolled in the Rotterdam study (Straus et al. [58]. © Elsevier Limited, Oxford, UK. Reproduced with permission).

T waves, and LQT3 characterized by a relatively long ST segment followed by a peaked, frequently tall, T wave. The abnormal T wave morphology might be particularly useful in diagnosing patients with borderline QTc duration (420–470 ms). In such patients, presence of an abnormal (notched, flat) T wave may indicate the possibility of LQTS.

The HERG gene mutation encodes the I_{Kr} current (the current most frequently affected by drugs) and is associated with decreased T wave amplitude with increased presence of notches [69, 70]. Similar observations could be made when evaluating drug-induced changes in repolarization. Drug-induced changes in T wave morphology reflect changes in the transmural gradient of repolarization with propensity to arrhythmogenesis (Fig. 19.8) [71, 72]. Therefore, identification of drug-induced changes in repolarization morphology in clinical studies should always trigger attention since those changes may indicate a propensity to proarrhythmia.

19.4 Drug-Induced QT Prolongation

Numerous cardiac and noncardiac drugs have been found to prolong the QTc interval duration and cause TdP (Table 19.3). Most of them directly block the I_{Kr} current, while others exert such action if administered together with a drug affecting the function of the cytochrome P-450 enzymatic system. The quinidine-induced sudden deaths and subsequently the results of the CAST trial brought further attention to the proarrhythmic effects of antiarrhythmic drugs [73]. In the early 1990s, the adverse effects of terfenadine (an antihistamine drug) brought much attention to the possibility of noncardiac drugs being associated with torsade de pointes and sudden cardiac death [74]. Terfenadine, an anithistamine agent, blocks the I_{Kr} current (also blocking sodium current and the L-type calcium channel) causing a mean 6 ms QTc prolongation, which should not have clinical implications. Cardiac events were reported in patients taking terfenadine, almost exclusively when used in combination with other medications (ketoconazole, antibiotics) also metabolized by the same enzymatic system of the cytochrome P-450 3A4. Such a combination causes increase in plasma concentration of terfenadine due to inhibition of its metabolism by a concomitantly administered drug with subsequent substantial QTc

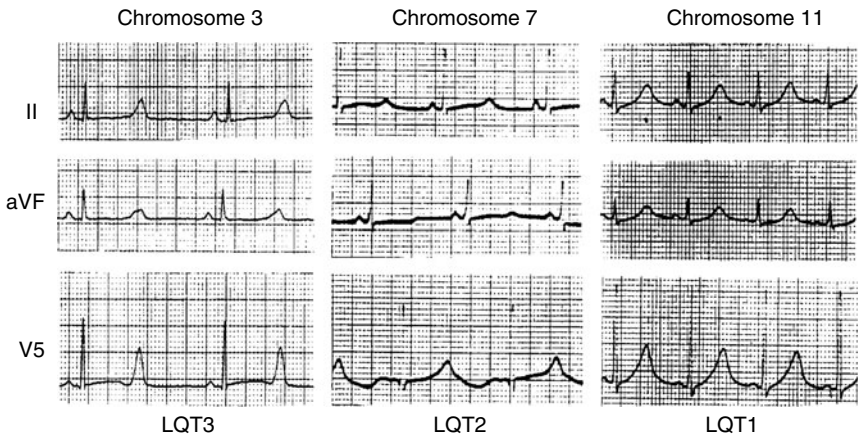

Figure 19.8

T wave morphology in ECG recordings from leads II, aVF, and V5 from patients with LQT1, LQT2, and LQT 3 (Moss et al. [69], © American Heart Association, Dallas, Texas, Reproduced with permission).

Table 19.3

Drugs that prolong the QT interval

Category	Drugs
Antihistamines	Astemizole, terfenadine
Anti-infectives	Amantadine, clarithromycin, chloroquine, erythromycin, grepafloxacin, moxifloxacin, pentamidine, sparfloxacin, trimethoprim-sulfamethoxazole
Antineoplastics	Tamoxifen
Antiarrhythmics	Quinidine, sotalol, procainamide, amiodarone, bretylium, disopyramide, flecainide, ibutilide, moricizine, tocainide, dofetilide
Antilipemic agents	Probucol
Calcium channel blockers	Bepridil
Diuretics	Indapamide
Gastrointestinal agents	Cisapride
Hormones	Fludrocortisone, vasopressin
Antidepressants	Amitriptyline, amoxapine, clomipramine, imipramine, nortriptyline, protriptyline
Antipsychotic	Chlorpromazine, haloperidol, perphenazine, quetiapine, risperidone, sertindole, thioridazine, ziprasidone, doxepin, methadone

prolongation (>60 ms in majority of reported cases) and TdP. Among noncardiac drugs, several antipsychotic drugs block I_{Kr} current and cause QTc prolongation and some of them were reported to be associated with sudden death [75].

Based on transmural recordings from perfused wedge preparations [71, 72] it was postulated that the peak of the recorded T wave coincides with the end of repolarization in the epicardium and the end of the T wave with the end of repolarization in the M cell zone, thus measurement of the T peak – T end duration and its ratio to the QT interval was proposed to reflect transmural dispersion, at least in the experimental setting. Liu et al. [76] applied this approach effectively in laboratory conditions identifying drugs prone to induce TdP ❯ Figure 19.9. ❯ Figure 19.10 shows drug-induced changes in the TpTe/QT ratio for drugs known to cause QT prolongation and TdP in comparison to drugs with no such effect. These findings provide the foundation for applying T wave morphology for identifying patients prone to developing TdP.

Drug-induced QT prolongation and TdP usually occur in susceptible individuals; ❯ Table 19.4 lists common factors predisposing to QT prolongation and TdP [77]. Females have faster resting heart rates and longer QTc intervals than

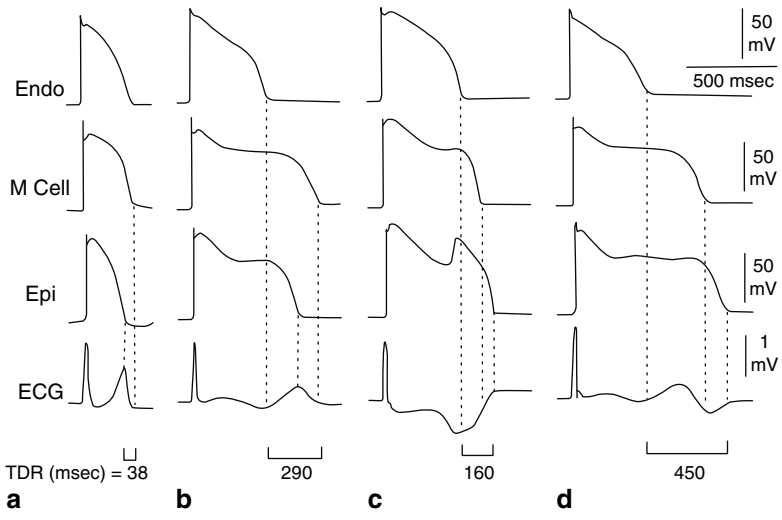

Figure 19.9

Transmural dispersion of action potentials and changes in T wave morphology on ECG. (a) Normal T wave with normal transmural gradient of repolarization. (b) Biphasic T wave: increase in transmural gradient with end of endocardial action potential coinciding with negative phase of T wave. (c) Inverted T wave: epicardial layer shows longest repolarization duration contributing to increased and inverted transmural gradient. (d) Polyphasic T wave with markedly increased transmural gradient: negative phases of T wave coincide with end of action potential in endocardial and M cell layers (Emori et al. [72]. © Wiley–Blackwell. Reproduced with permission).

men, and not surprisingly about 70% of cases of drug-induced TdP are found in women [77]. The elderly and patients with underlying heart diseases (cardiomyopathies), those with electrolyte abnormalities, especially hypokalemia and bradycardia, are at particularly increased risk for drug-induced QT prolongation and TdP. In some patients, there is evidence for a genetic predisposition to drug-induced QT prolongation although there are not yet data supporting that all cases are genetically predetermined [78].

The Food and Drug Administration (FDA) in the United States and the Committee for Proprietary Medicinal Products (CPMP) of the European Agency for the Evaluation of Medicinal Products mandate evaluating the potential QT prolonging effects of all new drugs undergoing regulatory approval [79, 80]. Each drug has to be evaluated individually after full considerations of risks associated with the drug in relationship to benefit of the drug for the population at risk. A number of drugs which show some QT prolonging effects in Phase I or Phase II studies might require further testing in a so-called Thorough QT Study. The Thorough QT Study consists of repeated monitoring of QT and RR parameters as well as T wave morphology during administration of a tested drug and during administration of moxifloxacin, an antibiotic with known QT prolonging effect considered as a positive control (to validate the ability of the ECG core lab to detect the expected repolarization changes). Drugs with QT prolongation showing upper confidence intervals exceeding 10 ms might require additional safety measures during the next phases of development, possibly requiring specific labeling about the QT prolonging effect, or may not be recommended for entering the market.

19.5 Dynamics of QT Interval

The QT interval may be influenced by several factors including heart rate, sympathovagal balance, metabolic and electrolyte changes, disease entities, or drugs. Heart rate dependency of the repolarization process represents a form of repolarization dynamics appreciated already in the 1920s by several researchers including Bazett and Fridericia who described the QT/RR relationship and established the first heart rate correction formulae [45, 46]. It is well accepted

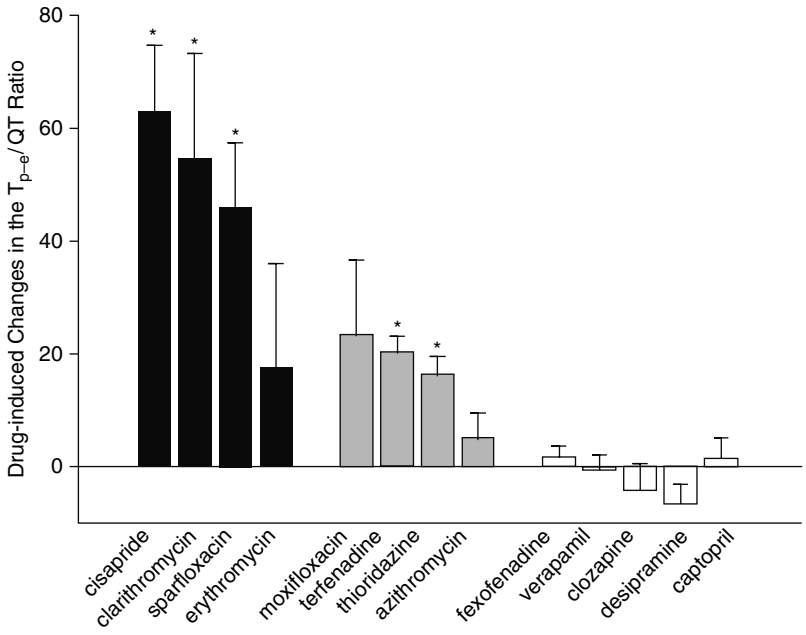

Figure 19.10

Maximal drug-induced change in TpTe/QT ratio at concentrations <100-fold of their free therapeutic plasma concentration. The black bars represent the compounds that resulted in significant QT prolongation accompanied by the development of EAD, R-on-T extrasystoles, and torsades de pointes (TdP); the gray bars represent the compounds that led to a significant increase in the QT interval but without EAD and EAD-dependent phenomena; and the blank bars represent the negative compounds. * indicates $p < 0.05$ when compared with the control value of the compound (Liu et al. [76]. © Elsevier Limited. Reproduced with permission).

Table 19.4

Factors associated with increased risk of QT prolongation and torsades de pointes (TdP)

Prolonged QTc
Female sex
Advanced age
Bradycardia
Hypokalemia
Hypomagnesemia
Congestive heart failure (low EF)
Cardiac arrhythmias
Combinations of drugs (cytochrome P450 enzymes inhibitors)
Genetic polymorphisms of gene coding cardiac ion channels or enzymes in liver metabolising drugs

that during controlled exercise the uncorrected QT interval shortens with decreasing RR intervals. In case of progressively increasing or decreasing heart rate, the QT interval shows a linear correlation with heart rate within physiological limits. However, in cases of abrupt RR changes, the QT interval does not change adequately, and a lag of QT adaptation to changing heart rate is frequently observed. It is also recognized that RR interval changes in the form of a "short–long cycle" may precede the onset of VT. The presence of this sequence might prolong action potential duration (reflected as QT prolongation on surface ECG), facilitating early after depolarizations and triggering TdP VT.

Advances in Holter technology in recent years have allowed for continuous tracking of RR intervals and corresponding QT intervals and brought an increased interest in the analysis of the dynamic behavior of repolarization. Changes in not only duration but also in morphology of the QT interval have been explored within the last decade. This dynamic behavior of repolarization could be evaluated by identifying specific patterns of the QT and RR intervals' relationship in long-term recordings, by measuring beat-to-beat QT or T wave variability, and by measuring 2:1 pattern of variability defined as T wave alternans (TWA) [81].

19.5.1 Methods to Assess QT/RR Dynamics

Adjustment of the QT to changing heart rate is a dynamic phenomenon consisting of fast adaptation and slow adaptation phases. Franz et al. [82] showed that after a rapid change in heart rate, the fast adaptation phase of repolarization usually lasts 30–60 s followed by a 2-min slow adaptation. This adjustment also seems highly individual and among other factors is dependent on the nature of heart rate changes. Repolarization adapts faster to increasing heart rate than it does to decreasing heart rate. This differential response is known as repolarization hysteresis [83]. Measures of repolarization hysteresis are proposed for diagnosing LQTS patients who usually show a larger difference in QT duration between exercise and recovery than control subjects [84].

Several methods have been developed to describe the dynamicity of repolarization [85–87], however, QT/RR slope is increasingly used, mainly due to incorporation of the algorithm into commercial Holter software. Repolarization dynamics are then measured by the slope of the linear regression between QT and RR intervals (Fig. 19.11). To compute the QT/RR slope, RR and QT intervals included in 30- or 60-s epoch of ECG are calculated and averaged to diminish possible influence of erroneous measurements and to decrease the effect of sudden and short-acting changes in RR on QT interval duration [88]. These averaged QT and RR intervals may be then linearly fitted from the period of prolonged recording, typically 24 h of Holter. Measurement of slope is usually performed separately for both the QT apex (QTa) and QT end (QTe). In contrast to the short beat-to-beat QT interval adaptation and hysteresis, the QT/RR slope refers to overall behavior of QT in response to changes in RR. Steeper slope indicates excessive prolongation of QT at longer RR cycle lengths and adequate or excessive shortening of QT at shorter RR cardiac cycles (Fig. 19.11). Flat slope indicates that QT interval is less dependent on the RR cycle and fails to adequately shorten at faster heart rates (shorter cycle). Both of these features might contribute to an increased risk of arrhythmias. Steeper QT/RR indicates decreased vagal

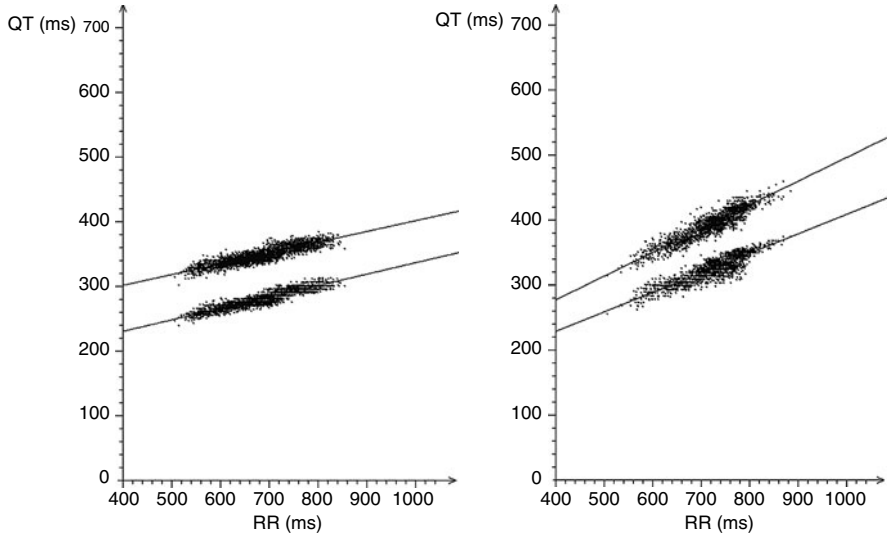

Figure 19.11
Example of repolarization dynamics measured by QT/RR slopes.

tone and increased sympathetic activity, which might contribute to a higher vulnerability of myocardium to arrhythmias. At the cellular level, sympathetic stimulation prolongs ventricular refractoriness. Therefore, abnormal QT slope represents increased vulnerability of myocardial substrate to its modulation by the autonomic nervous system. Lengthening of the QT at slower rates might be associated with arrhythmogenic increase in dispersion of refractoriness in the myocardium while excessive shortening of QT at fast heart rates might facilitate arrhythmia by diminished heterogeneity of refractoriness. QT dynamics reflects both the rate dependence of ventricular repolarization as well as the modulation of this dependence by a variety of factors such as autonomic nervous system, hormones, metabolic equilibrium, disease entities, and drugs. As significant diurnal variation of QT/RR was reported, QT/RR is usually evaluated separately for day and night time [89].

19.5.2 Clinical Factors Influencing QT/RR Slope

QT dynamicity is known to be influenced by a variety of clinical covariates. Advanced age was related to abnormal QT/RR dynamicity in healthy subjects [89], however, in patients with cardiac diseases, as shown in other studies, this relationship was absent or weak [90, 91]. It is most likely that advanced age and underlying heart disease influence repolarization parameters to a higher degree than age itself. Gender-related changes in repolarization parameters have been reported for several decades showing that women have longer QTc interval duration, and that women are more prone to develop torsade de pointes arrhythmias. Consequently, women tend to present higher QT/RR slopes than men, suggesting that QT dynamicity (both QT and RR duration) is influenced not only by autonomic nervous tone but also by other factors like hormones, and gender-specific differences in repolarizing currents [87, 89, 92, 93]. Hormone-related changes in QT/RR behavior were observed in subsequent phases of menstrual cycle [94] as well as during estrogen replacement therapy [95].

The QT/RR slope was found to be a strong marker of existing cardiac pathology. Abnormal QT dynamicity was observed in different populations including patients with long QT syndrome, ischemic heart disease, dilated and hypertrophic cardiomyopathy, congestive heart failure, mitral valve prolapse, hypertension, TakoTsubo syndrome, obstructive sleep apnea, or diabetes – all of the settings known to present some degree of impaired autonomic nervous system control [96–107].

Merri et al. [96] were the first to develop a Holter-based algorithm to assess the QT/RR relationship, and to report that patients with LQTS have a significantly increased relationship between repolarization duration and preceding sinus cycle length with an exaggerated prolongation of QT interval at slower heart rates. In this relatively small study, 16 subjects with LQTS were compared with ten matched healthy volunteers. Each RTm interval (the interval from R peak to the maximum amplitude of a T wave) was coupled to the RR interval of the preceding beat to avoid problems related with identification of Q wave onset and T wave end. The mean value for RTm/RR slope was significantly ($p = 0.003$) higher in LQTS patients (0.21 ± 0.08) than in normal subjects (0.14 ± 0.03) (Fig. 19.12).

An abnormal QT/RR relationship indicates an exaggerated delay in repolarization with prolonged cycle length. In these cases, the T wave of the beat immediately following a long pause may have a bizarre configuration and prolongation of the QT interval, and reflect the presence of afterdepolarizations contributing to triggered ventricular arrhythmias. This pattern may explain bradycardia-related occurrence of TdP in LQTS patients. In patients with LQTS heterogeneous channel, abnormalities may contribute to differences in the QT/RR relationship. Some reports indicate that patients with LQTS may be characterized by flatter than normal QT/RR slopes [108].

Lower values of QTa/RR (QTa – QTapex duration) slopes were observed in patients with idiopathic ventricular fibrillation (VF) [109, 110]. The decrease in QT/RR slopes was particularly prominent at night time, which may contribute to the nocturnal occurrence of VF in this subset of patients. On the other hand, inappropriate QT shortening at higher rates may also result in a lower slope. A similar pattern with significantly reduced QT/RR slopes at night time was observed also in patients with Brugada syndrome. Of note, QT/RR slopes were significantly decreased in patients with spontaneous Brugada syndrome as compared to those with induced Brugada ECG pattern [111].

Coronary artery disease may influence repolarization dynamics by alteration of the autonomic nervous system as well as by structural changes in myocardium. Among patients with coronary artery disease, higher slopes are observed in patients with multi-vessel as compared to single-vessel coronary patients [112]. In patients with diseased hearts, impaired dynamicity of repolarization may be related to the degree of left ventricular dysfunction and may progress with severity of symptoms in patients with heart failure [90, 100, 102]. In general, patients with congestive heart failure present steeper

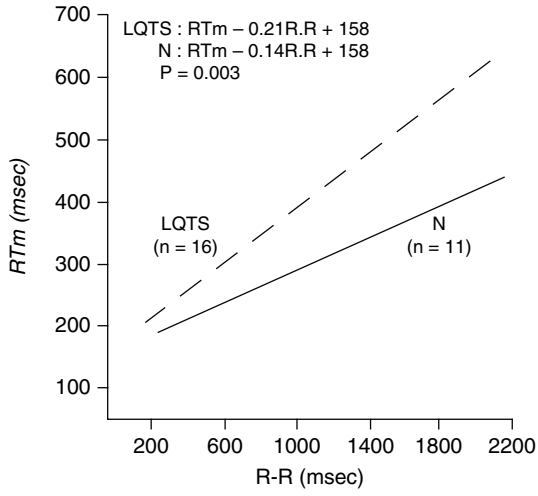

Figure 19.12

Mean regression RTm/RR lines for one normal subject (N) and 16 patients with LQTS. The RTm/RR slope is significantly larger in the LQTS patients than in the normal subjects (Merri et al. [96]. © American Heart Association, Dallas, Texas. Reproduced with permission).

slopes not only than healthy subjects but also than those with coronary disease [100]. This finding may be related to both more advanced structural changes expressed by low ejection fraction and also by coexisting impairment of the autonomic nervous system. Alteration in autonomic nervous system functioning may also explain the loss of the typical night–day variation in QT/RR slope reported in healthy subjects (Fig. 19.13).

Studies on the influence of reperfusion treatment on repolarization dynamics provide further insight into the potential mechanism underlying the observation about the relationship between steeper QT slopes and arrhythmic events in postinfarction patients. Bonnemeier et al. [113] found that in patients with first acute myocardial infarction undergoing PCI procedures, the QT/RR slopes were significantly increased in patients with TIMI 2 flow subgroup whereas they remained constant in those with complete reperfusion. Patients with increased QT/RR slopes after PCI more frequently presented with major arrhythmic events during a 1-year follow-up. Therefore, the authors concluded that impaired QT dynamicity reflects an altered electrical restitution after incomplete reperfusion PCI, potentially providing a substrate for life-threatening arrhythmias. Such an incomplete reperfusion might affect ventricular repolarization by directly influencing electrophysiological properties or interplaying with autonomic nervous tone (Fig. 19.14).

19.5.3 Prognostic Value of QT/RR Slopes

Evaluation of the repolarization process limited to QT interval duration in a surface ECG only may not correspond to what happens in the period directly preceding malignant arrhythmias. Abrupt changes in QT behavior were observed in patients with life-threatening arrhythmias on Holter monitoring. Singh et al. [114] reported an abrupt increase in the QT/RR slope associated with a prolonged QTc and reduced heart rate variability in the interval immediately preceding the onset of VF that led to cardiac arrest in a 71-year-old man with hypertension and chronic renal failure. QT/RR slope increased from 0.032 at 60 min before VF to 0.293 as observed 10 min before cardiac arrest (Fig. 19.15). Similarly, Sredniawa et al. [115] described an abrupt increase in QT/RR slope (from 0.223 to 0.483) in the period preceding a burst of frequent ventricular ectopic beats on Holter monitoring in coronary patients with documented cardiac arrest due to sustained VT. Transitory QT lengthening may express a temporal imbalance of the autonomic nervous system that may lead to heterogeneity of the ventricular refractory periods and may predispose to the development of reentry phenomena.

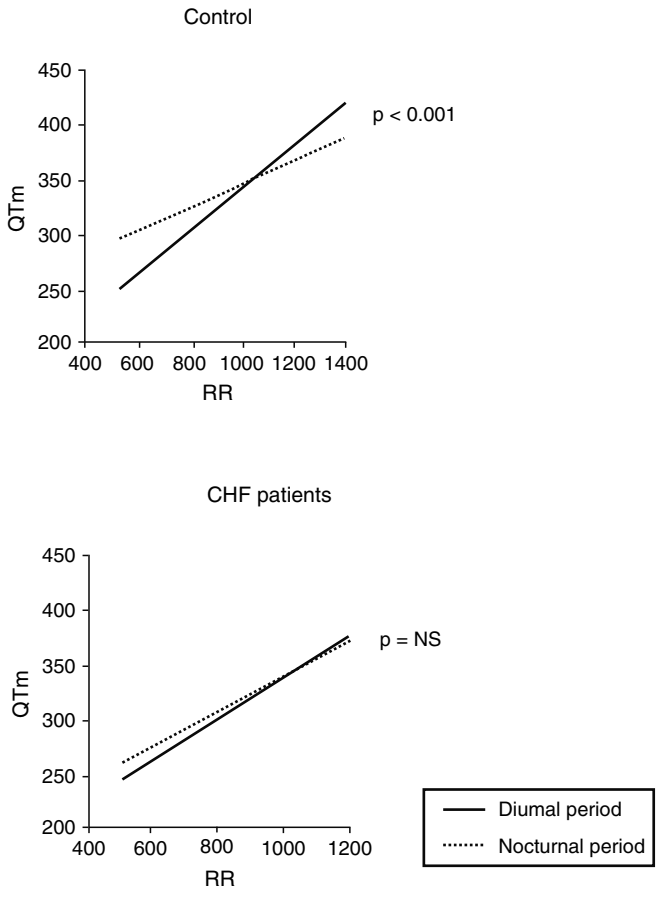

Figure 19.13

Circadian modulation of QTm rate dependence in control patients (top panel) and in CHF patients (bottom panel). In the CHF group, the physiological circadian modulation of QTm rate dependence is lacking. CHF: congestive heart failure; solid lines: diurnal period; dotted lines: nocturnal period (Faber et al. [100]. © Wiley–Blackwell. Reproduced with permission from reference).

Several investigators evaluated the prognostic value of QT dynamics in predicting cardiac and arrhythmic events. In 1999, Extramiana et al. [98] compared postinfarction patients with a history of VT and positive programmed electrical stimulation with a control group without VT history, negative electrophysiologic study and arrhythmia-free 3-year survival after myocardial infarction. The analysis showed significantly enhanced QT dynamicity in postinfarction patients with a history of VT. In this group, QT/RR slopes were much higher than in control subjects within the three assessed circadian periods (awake, sleep, morning awakening). Furthermore, the difference was even more pronounced during awaking hours – a period considered as the high-risk time for sudden death occurrence (0.251 vs. 0.179 in VT and control groups, respectively). Of note, neither static QT parameters nor HRV parameters, potentially indicating abnormal autonomic nervous system modulation, could differentiate the VT group from controls.

Strong evidence of the prognostic value of QT/RR slopes in prediction of sudden death was provided by the GREPI study (Groupe d'Etude du Pronostic de l'Infarctus du myocarde) published in 2002 [116]. This multicenter, prospective study including 256 patients with acute myocardial infarction demonstrated that abnormal QT/RR evaluated nine to 14 days after infarction is an independent risk marker for sudden death during an average 7-year follow-up. As no normal limits of QT/RR exist, patients with QT/RR values corresponding to upper quartile were arbitrary defined as a high-risk subgroup. Steeper QT/RR slope (>0.18 during daytime) was associated with total mortality as well as with sudden death,

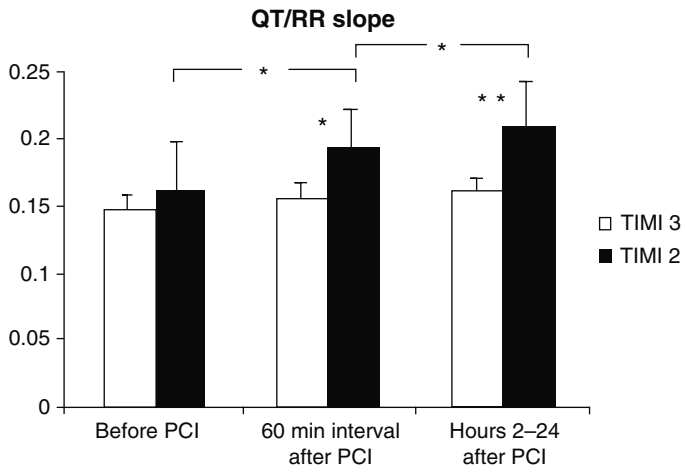

Figure 19.14

QT/RR slope, in the first hour after PCI, and in interval from hour 2 to 24 after PCI in patients with TIMI 2 and 3 flow (Bonnemeier et al. [113], © American Heart Association, Dallas, Texas. Reproduced with permission).

indicating that excessive shortening at fast rates and/or excessive lengthening at slow rates may contribute to arrhythmic events (Fig. 19.16). The increased QT/RR slope was the most powerful predictor when tested simultaneously with clinical variables in the Cox multivariate model. It is worth emphasizing that the hazard ratio for sudden death was three times higher than for mortality of all causes (hazard ratio: 6.07 vs. 2.25, respectively). At the same time, other ECG stratifiers like SDNN and late potentials did not provide any prognostic information. Interestingly, only daytime, but not nighttime, QT slopes were predictive for events during follow-up.

In the EMIAT (European Myocardial Infarct Amiodarone Trial) study, QT dynamicity was assessed in postinfarction patients with LVEF <= 40% and was compared between patients with arrhythmic cardiac death (ACD) and non-ACD during a mean of 21 months follow-up [117]. The QT slopes were significantly higher in the cardiac death group, but only increased morning QT/RR slope differentiated patients with arrhythmic versus non- ACD (QT/RR slope: 0.272 vs. 0.239, respectively). Therefore, QT dynamicity not only discriminated postinfarction patients who died of cardiac death from survivors but also predicted the type of death. Other data from the EMIAT trial indicated that chronic amiodarone treatment affects the QT/RR relationship and the lack of treatment-related QT/RR changes predicts arrhythmic death [118].

Another study in postinfarction patients [87] documented higher QT/RR slopes in patients who died versus survived during a 3-year follow-up (0.187 vs. 0.139, $p < 0.001$). As in this case, increased QT/RR slope was associated with high risk of mortality and sudden death only in univariate analysis, the authors developed an additional novel parameter: QT/RR variability ratio, defined as SDQT/SDNN remained the only significant multivariate risk stratifier among all studied repolarization measures.

Several noninvasive Holter-based parameters were documented as strong risk markers in postinfarction patients, but arrhythmic risk stratification in patients with dilated cardiomyopathy and/or heart failure is still an open, unanswered issue. Even though the majority of noninvasive parameters predicts arrhythmic events in post-MI patients, these parameters fail to be independent markers in patients with DCM, and data in patients with heart failure are scarce and conflicting.

Pathak et al. [119] demonstrated that increased QT/RR slope (>0.28) assessed over 24 h was predictive for sudden death in patients with chronic heart failure class II–III due to ischemic (43%) or idiopathic (57%) cardiomyopathy with mean LVEF 28%. It is worth emphasizing that similar to studies in postinfarction patients, abnormal QT dynamicity was more related with sudden death than with total mortality. The hazard ratio of 24-h QT dynamicity (QTe) was over 50% higher for sudden death than for total mortality (HR = 3.4 vs. 2.2 in univariate analysis). A study by Watanabe et al. [120] confirmed that impaired QT dynamics is an independent risk marker in patients with heart failure followed for an average

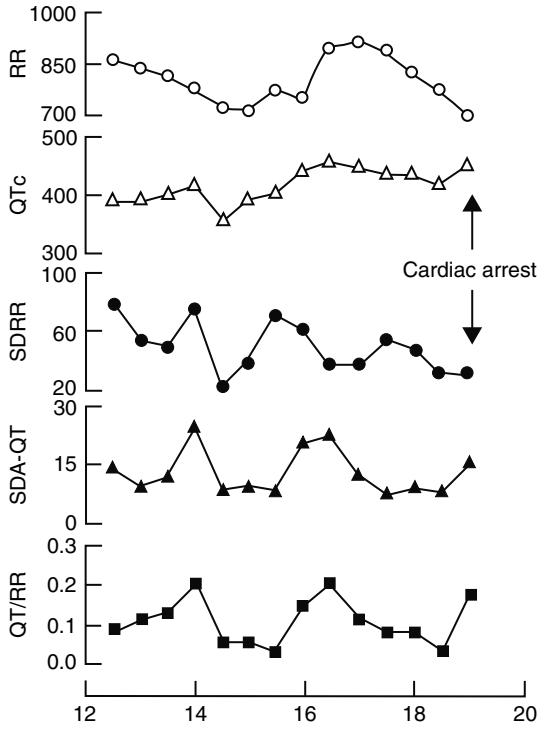

QT/RR slope and SDRR in the hour preceding the terminal rhythm

Time(min)	*QT/RR slope*	*SDRR (ms)*
−60	0.032	43.2
−50	0.043	37.3
−40	0.068	56.8
−30	0.026	40.5
−20	0.018	25.3
−10	0.293	33.1

SDRR, standard deviation of consecutive RR intervals over 5 min intervals.

Figure 19.15

Half-hourly distribution of electrophysiological parameters assessed preceding cardiac arrest. SDRR: standard deviation of the consecutive RR intervals over 5-min segments; SDA-QT: standard deviation of the average of consecutive uncorrected QT intervals over 5-min segments; QTc: corrected QT interval; QT/RR: the slope of the regression line between the QT and RR intervals (Singh et al. [114]. © BMJ Publishing Group Ltd. Reproduced with permission).

of 34 months. Similar to other studies increased QT/RR slope (>0.17 over the day) was a stronger predictor of sudden death than cardiac death (HR 11.2 vs. 4.73, respectively).

Analysis of repolarization dynamics was performed in the MUSIC study [121], which analyzed 542 patients with mild to moderate heart failure (49% with ischemic cardiomyopathy; mean LVEF 37%). The mean value of QTa/RR slope was 0.172 and QT/RR was 0.193. During the 44-month follow-up there were 119 deaths including 47 sudden deaths. Non-survivors were characterized by steeper QT/RR slopes. In this study, increased QT/RR slopes during the daytime (>0.20 for QTa and >0.22 for QTe) were independently associated with increased total mortality during an average 44-month follow-up (hazard ratio = 1.57 and 1.58 for QTa and QT, respectively) (Fig. 19.17). None of the dynamic repolarization parameters was associated with increased risk of sudden death.

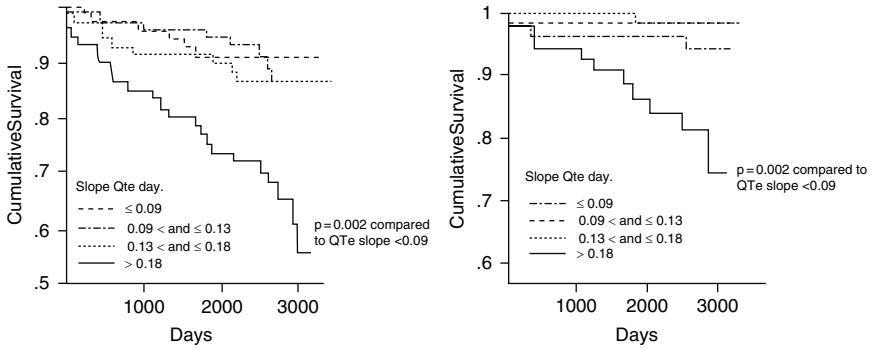

Figure 19.16

Event-free curves of total mortality (left) and sudden death (right) according to daytime slope of QTe/RR using the Kaplan Meier method (Chevalier et al. [116]. © Wiley–Blackwell. Reproduced with permission).

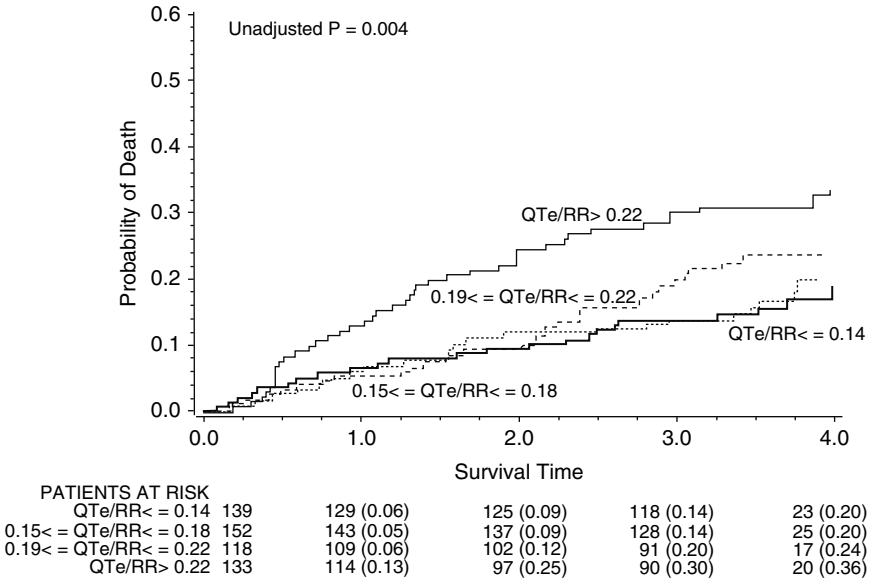

Figure 19.17

Probability of death according to the QTe/RR slope value in patients with congestive heart failure (Cygankiewicz et al. [121]. © Wiley–Blackwell. Reproduced with permission).

Independent prognostic value of QT dynamicity in patients with idiopathic dilated cardiomyopathy was reported by Iacoviello et al. [90] who found that abnormal QT dynamicity was significantly associated with arrhythmic events (VT/VF or SCD) during a mean 39-month follow-up. At multivariate analysis only the QT slope (>0.19) decreased LVEF (Left Ventricular Ejection Fraction) and nsVT (non-sustained Ventricular Tachycardia) were independent predictors of poor outcome.

In summary for the section on QT/RR dynamics, there is increasing evidence that abnormal QT/RR slope is a powerful predictor of cardiac events, mainly mortality in various groups of patients with ischemic heart disease and nonischemic cardiomyopathies. Modern Holter technology provides algorithms for computing QT/RR slope automatically with very much needed preprocessing and filtering that aims to decrease the effects of outliers and effects of instantaneous changes of QT and RR behavior. However, it is worth pointing out that apart from the overall pattern of QT/RR behavior, there is

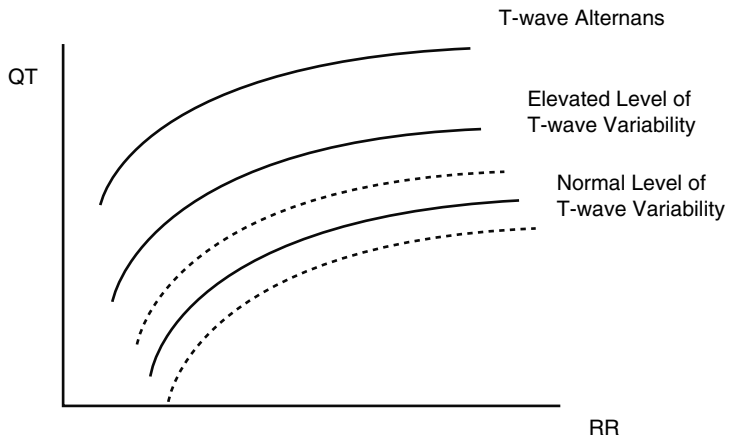

Figure 19.18

Conceptual link between ECG measures of myocardial vulnerability: QT/RR relationship, T wave (or QT) variability and T wave alternans (TWA) (Zareba [122]. © Wiley–Blackwell. Reproduced with permission).

an increased interest in exploring beat-to-beat changes in the QT interval (QT variability), especially since such instantaneous changes might lead to development of life-threatening ventricular tachyarrhythmias. QT dynamics expressed as overall QT/RR slope representing overall underlying substrate for arrhythmia might be complemented by analysis of QT variability reflecting transient changes in vulnerability of myocardium to arrhythmias.

19.6 QT Variability

The QT interval being influenced by a variety of factors may change not only in terms of its duration but also morphology. QT variability is an ECG phenomenon consisting of beat-to-beat changes in repolarization duration and morphology appearing without the 2:1 pattern typical for TWA. These beat-to-beat changes in the T wave amplitude and shape as well as in QT duration, similar to what was observed in the case of QT dynamics, can be analyzed by several novel computerized ECG methods enabling for detection and quantification of subtle, microvolt-level changes, which otherwise remain undetected by the naked eye.

In a healthy heart, there is some small level of beat-to-beat variation of action potential duration which could be elevated by autonomic stimuli, a disease process, or effects of drugs [122]. The QT variability is dependent on both QT and RR duration and either QT prolongation, RR shortening, or both occurring simultaneously might contribute to excessive QT variability and in the case of further challenges to TWA (Fig. 19.18). Along the line of this concept, TWA occur in most of the healthy subjects if heart rate exceeds 120–140 bpm, and this is why exercise-induced TWA are evaluated in a range of heart rates not exceeding 110 bpm.

19.6.1 Methods of QT Variability Assessment

In 1997, Berger and coworkers published a new method to assess the QT variability which they named QT lability [123]. A time-stretching algorithm was developed to quantify changes in repolarization duration and morphology. Beat-to-beat QT interval variability was measured on the basis of 256-s records of surface ECGs. A QT variability index was calculated as the logarithm of the ratio of normalized QT variance to heart rate variance. Using this algorithm, the authors documented that patients with dilated cardiomyopathy had higher QT variability as compared to control subjects (Fig. 19.19).

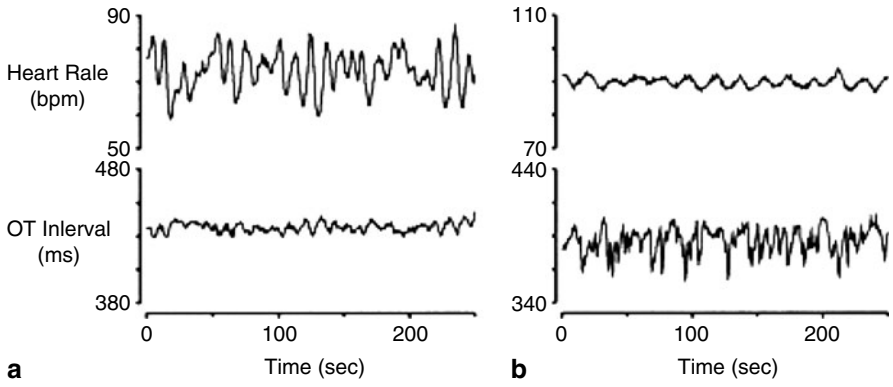

Figure 19.19

Left part of the figure (a) shows normal subject [with high HRV and low QTV], while (b) is the patient with dilated cardiomyopathy [low HRV and high QTV].

Changes in heart rate and heart rate variability influence changes in the QT interval; however, QT variability cannot be entirely explained by changes in the autonomic nervous system. It is likely that beat-to-beat changes in action potential duration are dependent on instantaneous changes in ion-channel activity or the number of channels involved in the repolarization process. Even with a stable RR interval, there is a possibility of repolarization changes due to variations in the number of channels involved [124]. Myocardial conditions might alter the number of channels involved and changes in cycle length might further potentiate beat-to-beat variability of repolarization.

Exact detection of the end of the T wave is one of the main limitations of a proper assessment of QT-related parameters. Random noise, baseline wandering, and respiration modulation of T wave shape may influence the beat-to-beat QTe evaluation. Our group developed a T wave endpoint-independent method to quantify repolarization variability based on a wavelet transformation. The wavelet-based method showed that LQTS patients (SCN5A carriers) have significantly increased repolarization variability both in time and amplitude as compared to noncarriers [125]. Recently, we focused on a time-domain technique quantifying T wave variability (TWV) based on a beat-to-beat change in T wave amplitude without a need to identify the end of the T wave. As shown in Fig. 19.20, the variation of mean amplitude inside each of the four windows encompassing the repolarization segment (T1–T4) is analyzed across beats, and the level of variability is computed in each window based on the estimated variance of the average amplitude across beats in the selected window. The square-root value is reported and expressed in microvolt. The prognostic significance of this method was validated in the MADIT II cohort [126].

19.6.2 Clinical Factors Influencing QT Variability

Increased QT variability has been demonstrated in patients with heart failure, dilated cardiomyopathy, hypertrophic cardiomyopathy, coronary disease, LQTS as well as in patients with anxiety, depression, and panic disorders [127–133]. There are also data indicating that cocaine use may increase QT variability in a dose-dependent manner [134]. QT variability increases prior to drug-induced torsade de pointes in experimental conditions [135, 136]. QT variability was also reported to be influenced by external factors such as air pollution [137].

Little is known about the clinical covariates influencing QT variability. In the original paper by Berger et al. [123], no differences were found in QT variability between patients with ischemic and nonischemic dilated cardiomyopathy. Several reports indicate that QTVI (QT variability index) depends more on NYHA functional class than on LVEF, indicating that QT variability might be more related to disintegration of the autonomic nervous system than to structural changes in myocardium [98, 99]. Long-term treatment with beta-blockers (metoprolol or carvedilol) in patients with congestive heart failure in NYHA class II–III was documented to significantly reduce QTVI as compared to placebo [138]. Not only pharmacotherapy but also reperfusion may influence QT variability. As documented by Bonnemeier et al. [139], successful

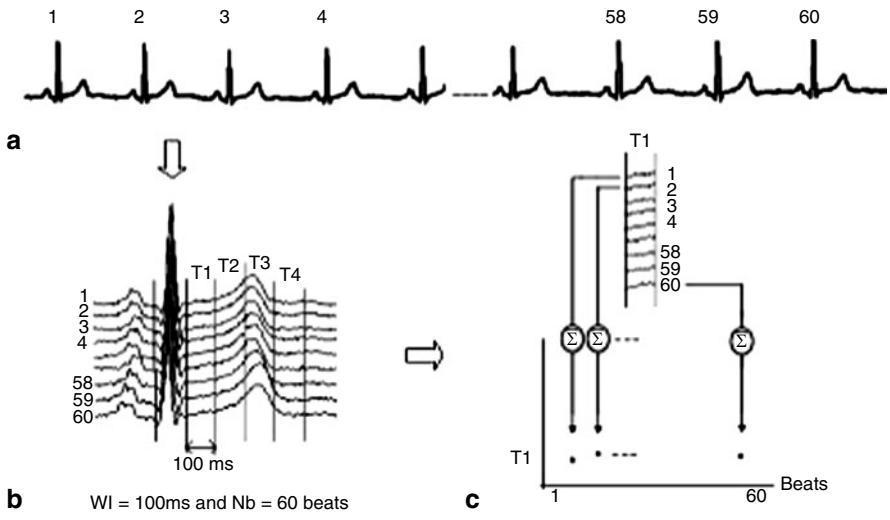

Figure 19.20

Schematic presentation of the ECG processing for the measurements of T wave amplitude variability. (a) A set of 60 continuous cardiac beats are identified; (b) the beats are aligned based on the QRS beginning and the repolarization segment is windowed using 100 ms duration interval (T1–T4), (c) mean amplitude of each beat inside each window (T1–T4) are computed and plotted across beats, this panel represents the computation for T1 only (Couderc et al. [126]. © Oxford University Press. Reproduced with permission).

reperfusion resulted in a significant decrease in QT variability in patients with TIMI 2 and 3 flow grade. Interestingly, patients who experienced major arrhythmic events (sudden death, survived sudden death due to VF or sustained VT) during a 1-year follow-up were characterized by significantly higher mean 24-h QT variability (QTcSD 26.7 ± 2.9 vs. 25.4 ± 2.9, $p < 0.05$). This observation indicates that despite the opening of the infarct-related artery, impaired microcirculation may lead to persistent repolarization liability being an electrophysiological substrate for arrhythmic events.

19.6.3 Prognostic Value of QT Variability

The first study to demonstrate the usefulness of QT variability (assessed according to Berger' algorithm) in recognition of elevated arrhythmic risk was published in 1998 by Atiga et al. [140]. This study analyzed QTVI in 95 patients undergoing electrophysiological study. The QTVI was higher in patients with structural heart disease than in controls (−0.7 ± 0.7 vs. −1.1 ± 0.5, $p < 0.05$), and higher in patients who died suddenly during a 2-year follow-up than in other patients with heart disease (0.0 ± 0.6 vs. −0.8 ± 0.5, $p < 0.05$). After adjustment for significant clinical covariates, increased QTVI (≥0.1) was the only parameter identifying patients at risk of arrhythmic events (OR = 12.5, $p = 0.004$). The event-free survival rate was 67% for patients with QTVI ≥ 0.1 as compared to 85% with those with QTVI <0.1. It is important to emphasize that QTVI outperformed the following parameters tested simultaneously in studied patients as a predictor: QT dispersion, TWA during atrial pacing, VT inducibility, SAECG, HRV, and ejection fraction.

Berger's algorithm was applied by our group to the MADIT II population to investigate whether abnormal QT repolarization is related to spontaneous VT/VF detected by ICD (141). In this study, QT variability was assessed in a 10-min resting ECG recording. A high-risk QT variability subgroup was defined by identifying patients from the highest (>75th percentile) QTVI distribution. The beat-to-beat QT variability algorithm applied to MADIT II patients showed an independent prognostic value of QTVI (> −0.52 log units) to predict an increased risk of arrhythmic events in postinfarction patients with severe left ventricular dysfunction (EF <30%). The mean QTVI and QTVN (QT variability numerator) were significantly higher in subjects requiring an appropriate therapy for VF/VT during a mean of 21 ± 12 months of follow-up (−0.80± vs. −0.94 ± 0.60, $p = 0.037$; and 0.39 ± 0.59 vs. 0.25 ± 0.56, $p = 0.001$ for QTVI and QTVN, respectively).

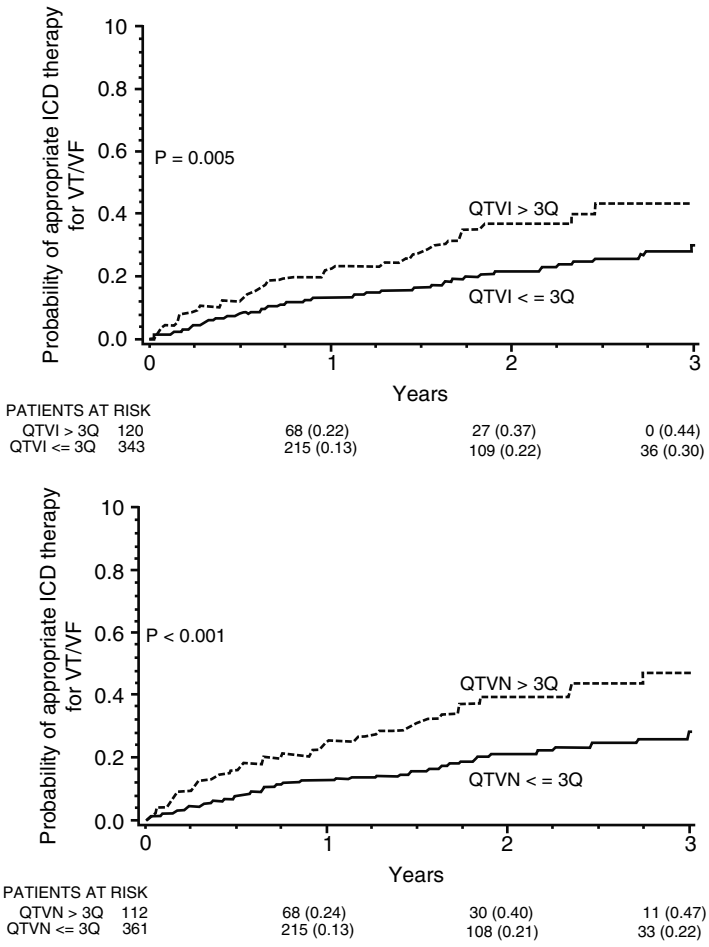

Figure 19.21

Cumulative probability of first appropriate defibrillator therapy for ventricular tachycardia (VT) or ventricular fibrillation (VF) in patients with QT variability numerator (QTVN) in the highest quartile versus lower three quartiles for QT variability index (QTVI) (top panel) and QTVN (bottom panel) (Haigney et al. [141]. © Elsevier Limited. Reproduced with permission).

Of the subjects in the highest quartile for QTVI, 37% experienced an episode of VT/VF as compared to 22% in the lower three quartiles. An even stronger difference was observed in respect to QTVN (40 vs. 22%, $p < 0.001$) (Fig. 19.21). Multivariate Cox analysis showed that both QTVI and QTVN were independent risk factors for VT/VF (HR = 1.80 and 2.18, respectively), after adjustment for significant clinical covariates. It is worth emphasizing that neither low ejection fraction nor inducibility of VT/VF during programmed ventricular stimulation was a significant predictor of spontaneous VT/VF. Additional analysis focusing on survival showed that increased QTVI was related to a higher incidence of death within the defibrillator arm.

Recently, we developed a new method to quantify repolarization variability focusing on the variability of T wave amplitude in scalar ECGs instead of analyzing the variability of QT interval duration. Our newly developed method to estimate TWV was tested in a group of 275 ICD patients from the MADITII trial. TWV >0.59 μV was an independent risk predictor of ICD therapy for VT or fibrillation. Patients with increased TWC had 47% probability of appropriate ICD therapy as compared to 29% in those with TWV <= 59 μV during a mean 3-year follow-up (Fig. 19.22). Concordance of the findings by two different methods (Berger's and ours) support the observation that the phenomenon of QT variability exists and might be considered as a risk stratifier [126].

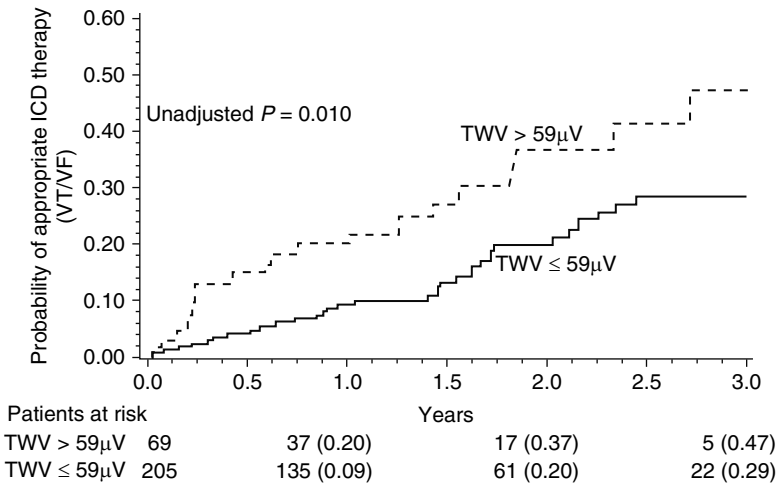

Figure 19.22

Cumulative probability of VT/VF requiring ICD therapy in MADIT II patients (Couderc et al. © Oxford University Press. Reproduced with permission).

More and more attention is recently paid to patients with relatively preserved LVEF. Due to advancement in modern treatment, this population of patients is growing, and despite a lower incidence of sudden death in patients with significantly depressed LVEF, the absolute number of patients experiencing sudden death in absolute values is very high. As recently documented by Piccirillo et al. [142], abnormal QT variability can identify the sudden cardiac death high-risk group among asymptomatic patients with only mild to moderate left ventricular dysfunction. In a group of 396 patients with congestive heart failure due to ischemic cardiomyopathy with LVEF between 35 and 40% and NYHA class I, QTVI greater or equal to the 80th percentile (−0.47) indicated an independent high risk for SCD with HR of 4.6 (1.5–13.4, $p = 0.006$). This finding might suggest that abnormal QT variability may serve as a marker to identify possible candidates for ICD therapy among patients with a moderately depressed LVEF. However, this requires further prospective studies.

In comparison to the QT/RR slope analyses where computer algorithms take advantage of averaging a series of beats, the methodology of quantifying beat-to-beat QT or TWV requires very robust identification of repolarization in consecutive beats. Although QT measurement on a beat-to-beat basis is of primary interest, it is frequently difficult to accomplish in ambulatory recordings due to challenges in identifying the end of the T waves. Both the above mentioned methods, QT variability/lability developed by Berger et al. [123] and TWV developed by Couderc et al. [126], do not require precise identification of the T wave end since they both rely on quantifying QT and T wave morphology on a beat-to-beat basis. Despite these advances in signal processing, it has to be recognized that there are limitations of quantifying beat-to-beat QT or TWV in recordings with flat T waves, in recordings with non-sinus rhythms, frequent arrhythmias, or excessive noise.

TWA is yet another parameter reflecting beat-to-beat changes in T wave morphology and there is a large body of literature describing the electrophysiologic understanding of this electrical phenomenon and clinical applications in the risk stratification of ventricular arrhythmias and sudden death. This broad topic was purposefully not covered by this chapter, which specifically focused on the QT interval and its dynamics.

19.7 Summary

During the last decade, we have observed increasing interest in analysis of the QT interval, which is considered an important ECG parameter reflecting the complexity of ventricular repolarization driven by an interplay of ion-channel activity, myocardial cell connectivity, disease processes (ischemia, hypertrophy), and external factors including drugs. Despite the 100 years of science and clinical practice in electrocardiography, there is still room for improvement in developing

reproducible methods of manual and automatic measurements of the QT interval. Computerized method quantifying QT duration and T wave morphology are increasingly used in everyday practice and in drug safety studies. There also is an increasing appreciation for T wave morphology that offers additional clinically relevant information in addition to QT duration, particularly in electrical disorders of the heart and drug safety concerns. Evaluation of static measures of QT interval duration and T wave morphology is increasingly accompanied by analyses of dynamic features of the QT interval behavior that could be quantified by measuring QT adaptation to changing heart rate, QT or T wave variability, as well as TWA. These dynamic measures of repolarization seem particularly promising in the risk stratification of mortality in patients with ischemic heart diseases and patients with cardiomyopathies.

References

1. Moss, A.J., P.J. Schwartz, R.S. Crampton, et al., The long QT syndrome. Prospective longitudinal study of 328 families. *Circulation*, 1991;**84**: 1136–1144.
2. Vincent, G.M., K.W. Timothy, M. Leppert, et al., The spectrum of symptoms and QT intervals in carriers of the gene for the long-QT syndrome. *N. Engl. J. Med.*, 1992;**327**: 846–852.
3. Zareba, W., A.J. Moss, S. le Cessie, et al., Risk of cardiac events in family members of patients with long QT syndrome. *J. Am. Coll. Cardiol.*, 1995;**26**: 1685–1691.
4. Zareba, W., A.J. Moss, P.J. Schwartz, et al., Influence of genotype on the clinical course of the long-QT syndrome. International Long-QT Syndrome Registry Research Group. *N. Engl. J. Med.*, 1998;**339**: 960–965.
5. Priori, S.G., P.J. Schwartz, C. Napolitano, et al., Risk stratification in the long-QT syndrome. *N. Engl. J. Med.*, 2003;**348**: 1866–1874.
6. Zareba, W. and I. Cygankiewicz, Long QT syndrome and short QT syndrome. *Prog. Cardiovasc. Dis.*, 2008;**51**: 264–278.
7. Schouten, E.G., J.M. Dekker, P. Meppelink, et al., QT interval prolongation predicts cardiovascular mortality in an apparently healthy population. *Circulation*, 1991;**84**: 1516–1523.
8. Sohaib, S.M., O. Papacosta, R.W. Morris, et al., Length of the QT interval: determinants and prognostic implications in a population-based prospective study of older men. *J Electrocardiol.*, 2008;**41**: 704–710.
9. Piotrowicz, K., W. Zareba, S. McNitt, and A.J. Moss, Repolarization duration in patients with conduction disturbances after myocardial infarction. *Am. J. Cardiol.*, 2007;**99**: 163–168.
10. Zareba, W., Drug induced QT prolongation. *Cardiol. J.*, 2007;**14**: 523–533.
11. Splawski, I., J. Shen, K.W. Timothy, et al., Spectrum of mutations in long-QT syndrome genes: KVLQT1, HERG, SCN5A, KCNE1, and KCNE2. *Circulation*, 2000;**102**: 1178–1185.
12. Curran, M.E., I. Splawski, K. Timothy, et al., A molecular basis for cardiac arrhythmia: HERG mutations cause long QT syndrome. *Cell*, 1995;**80**: 795–803.
13. Wang, Q., J. Shen, I. Splawski, et al., SCN5A mutations cause an inherited cardiac arrhythmia, long QT syndrome. *Cell*, 1995;**80**:805–811.
14. Wang, Q., M.E. Curran, I. Splawski, et al., Positional cloning of a novel potassium channel gene: KVLQT1 mutations cause cardiac arrhythmias. *Nat. Genet.*, 1996;**12**:17–23.
15. Mohler, P.J., J.J. Schott, A.O. Gramolini, et al., Ankyrin-B mutation causes type 4 long-QT cardiac arrhythmia and sudden cardiac death. *Nature*, 2003;**421**:634–639.
16. Plaster, N.M., R. Tawil, M. Tristani-Firouzi, et al., Mutations in Kir2.1 cause the developmental and episodic electrical phenotypes of Andersen's syndrome. *Cell*, 2001;**105**:511–519.
17. Splawski, I., K.W. Timothy, L.M. Sharpe, et al., Ca(V)1.2 calcium channel dysfunction causes a multisystem disorder including arrhythmia and autism. *Cell*, 2004;**119**:19–31.
18. Medeiros-Domingo, A., T. Kaku, D.J. Tester, et al., SCN4B-encoded sodium channel beta4 subunit in congenital long-QT syndrome. *Circulation*, 2007;**116**: 134–142.
19. Vatta, M., M.J. Ackerman, B. Ye, et al., Mutant caveolin-3 induces persistent late sodium current and is associated with long-QT syndrome. *Circulation*, 2006;**114**:2104–2112.
20. Chen, L., M.L. Marquardt, D.J. Tester, et al., Mutation of an A-kinase-anchoring protein causes long-QT syndrome. *Proc. Nat. Acad. Sci. USA*, 2007;**104**:20990–20995.
21. Ueda, K., C. Valdivia, A. Medeiros-Domingo, et al., Syntrophin mutation associated with long QT syndrome through activation of the nNOS-SCN5A macromolecular complex. *Proc. Natl. Acad. Sci. USA*, 2008;**105**: 9355–9360.
22. Napolitano, C., S.G. Priori, P.J. Schwartz, et al., Genetic testing in the long QT syndrome: development and validation of an efficient approach to genotyping in clinical practice. *JAMA*, 2005;**294**: 2975–2980.
23. Fadi, A.G., G.X. Yan, C. Antzelevitch, and D.S. Rosenbaum, Unique topographical distribution of M cells underlies reentrant mechanism of torsades de pointes in the long-QT syndrome. *Circulation*, 2002;**105**: 1247–1253.
24. Antzelevitch, C., and W. Shimizu, Cellular mechanisms underlying the long QT syndrome. *Curr. Opin. Cardiol.*, 2002;**17**: 43–51.
25. Antzelevitch, C. Role of transmural dispersion of repolarization in the genesis of drug-induced torsades de pointes. *Heart Rhythm*, 2005;**2**: S9–S15.
26. Antzelevitch, C., L. Belardinelli, A.C. Zygmunt, et al., Electrophysiologic effects of ranolazine: a novel anti-anginal agent with antiarrhythmic properties. *Circulation*, 2004;**110**: 904–910.
27. Moss, A.J. and R.S. Kass, Long QT syndrome: from channels to cardiac arrhythmias. *J. Clin. Invest.*, 2005;**115**: 2018–2024.
28. Keating, M.T. and M.C. Sanguinetti, Molecular and cellular mechanisms of cardiac arrhythmias. *Cell*, 2001;**104**: 569–580.
29. Sanguinetti, M.C., C. Jiang, M.E. Curran, and M.T. Keating, A mechanistic link between an inherited and an acquired cardiac arrhythmia: *HERG* encodes the IKr potassium channel. *Cell*, 1995;**81**: 299–307.

30. Roden, D.M., R.L. Woosley, and R.K. Primm, Incidence and clinical features of the quinidine-associated long QT syndrome: implications for patient care. *Am. Heart. J.*, 1986;**111**: 1088–1093.
31. Kay, G.N., V.J. Plumb, J.G. Arciniegas, et al., Torsades de pointes: the long-short initiating sequence and other clinical features: observations in 32 patients. *J. Am. Coll. Cardiol.*, 1983;**2**: 806–817.
32. Makkar, R.R., B.S. Fromm, R.T. Steinman, et al., Female gender as a risk factor for torsades de pointes associated with cardiovascular drugs. *JAMA*, 1993;**270**: 2590–2597.
33. Moss, A, Measurement of the QT interval and the risk associated with QTc interval prolongation: a review. *Am. J. Cardiol.*, 1993;**72**: 23B–25B.
34. Goldenberg, I, A.J. Moss, and W. Zareba, QT interval: how to measure it and what is "normal". *J. Cardiovasc. Electrophysiol.*, 2006;**17**: 333–336.
35. Lepeschkin, E., The U wave of the electrocardiogram. *Mod. Concepts Cardiovasc. Dis.*, 1969;**38**: 39–45.
36. Pérez Riera, A.R., C. Ferreira, C.F. Filho, et al., The enigmatic sixth wave of the electrocardiogram: the U wave. *Cardiol. J.*, 2008;**15**: 408–421.
37. Viskin, S., U. Rosovski, A.J. Sands, et al., Inaccurate electrocardiographic interpretation of long QT: the majority of physicians cannot recognize a long QT when they see one. *Heart Rhythm*, 2005;**2**: 569–574.
38. Kligfield, P., L.S. Gettes, J.J. Bailey, et al., Recommendations for the standardization and interpretation of the electrocardiogram: part I: the electrocardiogram and its technology a scientific statement from the American Heart Association Electrocardiography and Arrhythmias Committee, Council on Clinical Cardiology; the American College of Cardiology Foundation; and the Heart Rhythm Society endorsed by the International Society for Computerized Electrocardiology. *J. Am. Coll. Cardiol.*, 2007;**49**: 1109–1127.
39. Zareba, W., A.J. Moss, S. le Cessie, Dispersion of ventricular repolarization and arrhythmic cardiac death in coronary artery disease. *Am. J. Cardiol.*, 1994;**74**: 550–553.
40. Zareba, W., Dispersion of repolarization: time to move beyond QT dispersion. *Annals of Noninvasive Electrocardiol.*, 2000;**5**: 373–381.
41. Priori, S.G., D.W. Mortara, C. Napolitano, et al., Evaluation of the spatial aspects of T-wave complexity in the long-QT syndrome. *Circulation*, 1997;**96**: 3006–3012.
42. Zareba, W., A.J. Moss, and J. Konecki. TU wave area-derived measures of repolarization dispersion in the long QT syndrome. *J. Electrocardiol.*, 1998;**30**(Suppl.): 191–195.
43. Okin, P.M., R.B. Devereux, R.R. Fabsitz, et al., Principal component analysis of the T wave and prediction of cardiovascular mortality in American Indians: the Strong Heart Study. *Circulation*, 2002;**105**: 714–719.
44. Couderc, J.P., S. McNitt, J. Xia, et al., Repolarization morphology in adult LQT2 carriers with borderline prolonged QTc interval. *Heart Rhythm*, 2006;**3**: 1460–1466.
45. Bazett, H.C., An analysis of time relations of electrocardiograms. *Heart*, 1920;**7**: 353–367.
46. Fridericia, L.S., Duration of systole in electrocardiogram. *Acta. Med. Scandinav.*, 1920;**53**: 469–475.
47. Sagie, A., M.G. Larson, R.J. Goldberg, et al., An improved method for adjusting the QT interval for heart rate (the Framingham Heart Study). *Am. J. Cardiol.*, 1992;**70**: 797–801.
48. Hodges, M., D. Salerno, and D. Erlien, Bazett's QT correction reviewed: evidence that a linear QT correction for heart rate is better. *J. Am. Coll. Cardiol.*, 1983;**1**: 694.
49. Rautaharju, P.M., S.H. Zhou, S.Wong, et al., Sex differences in the evolution of electrocardiographic QT interval with age. *Can. J. Cardiol.*, 1992;**8**: 690–695.
50. Karjalainen, J., M. Viitasalo, M. Manttari, et al., Relation between QT intervals and heart rates from 40-to 120 beats/min in rest electrocardiogram of men and a simple method to adjust QT interval values. *J. Am. Coll. Cardiol.*, 1994;**23**: 1547–1553.
51. Batchvarov, V.N., A. Ghuran, P. Smetana, et al., QT-RR relationship in healthy subjects exhibits substantial intersubject variability and high intrasubject stability. *Am. J. Physiol. Heart Circ. Physiol.*, 2002;**282**: H2356–H2363.
52. Malik, M., K. Hnatkova, and V. Batchvarov, Differences between study-specific and subject-specific heart rate corrections of the QT interval in investigations of drug induced QTc prolongation. *Pacing Clin. Electrophysiol.*, 2004;**27**: 791–800.
53. Extramiana, F., P. Maison-Blanche, A. Haggui, et al. Control of rapid heart rate changes for electrocardiographic analysis: implications for thorough QT studies. *Clin. Cardiol.*, 2006;**29**: 534–539.
54. Moss, A.J. and J. Robinson. Clinical features of the idiopathic long QT syndrome. *Circulation*, 1992;**85**(Suppl. 1): I140–I144.
55. Lehmann, M.H. and H.Yang, Sexual dimorphism in the electrocardiographic dynamics of human ventricular repolarization: characterization in true time domain. *Circulation*, 2001;**104**: 32–38.
56. Sauer, A.J., A.J. Moss, S. McNitt, et al., Long QT syndrome in adults. *J. Am. Coll. Cardiol.*, 2007;**49**: 329–337.
57. Fenichel, R.R., M. Malik, C. Antzelevitch, et al., Drug-induced Torsade de Pointes and implications for drug development. *J. Cardiovasc. Electrophysiol.*, 2004;**15**: 475–495.
58. Straus, S.M., J.A. Kors, M.L. De Bruin, et al., Prolonged QTc interval and risk of sudden cardiac death in a population of older adults. *J. Am. Coll. Cardiol.*, 2006;**47**: 362–367.
59. Goldberg, R.J., J. Bengtson, Z.Y. Chen, et al., Duration of the QT interval and total and cardiovascular mortality in healthy persons (the Framingham Heart Study experience). *Am. J. Cardiol.*, 1991;**67**: 55–58.
60. Robbins, J., J.C. Nelson, P.M. Rautaharju, and J.S. Gottdiener, The association between the length of the QT interval and mortality in the cardiovascular health study. *Am. J. Med.*, 2003;**115**: 689–694.
61. Okin, P.M., R.B. Devereux, B.V. Howard, et al., Assessment of QT interval and QT dispersion for prediction of all-cause and cardiovascular mortality in American Indians: the Strong Heart Study. *Circulation*, 2000;**101**: 61–66.
62. Algra, A., J.G. Tijssen, J.R. Roelandt, et al., QTc prolongation measured by standard 12-lead electrocardiography is an independent risk factor for sudden death due to cardiac arrest. *Circulation*, 1991;**83**: 1888–1894.
63. Attar, M.N., K. Wong, D.G. Groves, et al., Clinical implications of QRS duration and QT peak prolongation in patients with suspected coronary disease referred for elective cardiac catheterization. *Ann. Noninvasive Electrocardiol.*, 2008;**13**: 106–112.
64. Davey, P., QT interval and mortality from coronary artery disease. *Prog. Cardiovasc. Dis.*, 2000;**42**: 359–384.

65. Davey, P., QT interval lengthening in cardiac disease relates more to left ventricular systolic dysfunction than to autonomic function. *Eur. J. Heart Fail.*, 2000;**2**: 265–271.
66. Montanez, A., J.N. Ruskin, P.R. Hebert, et al., Prolonged QTc interval and risks of total and cardiovascular mortality and sudden death in the general population: a review and qualitative overview of the prospective cohort studies. *Arch. Intern. Med.*, 2004;**164**: 943–948.
67. Breidthardt, T., M. Christ, M. Matti, et al., QRS and QTc interval prolongation in the prediction of long-term mortality of patients with acute destabilised heart failure. *Heart*, 2007;**93**: 1093–1097.
68. Zareba, K.M., H.J. Shenkman, and J.D. Bisognano, Predictive value of admission electrocardiography in patients with heart failure. *Congest. Heart Fail.*, 2008;**14**: 173–179.
69. Moss, A.J., W. Zareba, J. Benhorin, et al., ECG T-wave patterns in genetically distinct forms of the hereditary long QT syndrome. *Circulation*, 1995;**92**: 2929–2934.
70. Zhang, L., K.W. Timothy, G.M. Vincent, et al., Spectrum of ST-T-wave patterns and repolarization parameters in congenital long-QT syndrome: ECG findings identify genotypes. *Circulation*, 2000;**102**: 2849–2855.
71. Yan, G.X. and Antzelevitch C., Cellular basis for the normal T wave and the electrocardiographic manifestations of the long-QT syndrome. *Circulation*, 1998;**98**: 1928–1936.
72. Emori, T. and C. Antzelevitch Cellular basis for complex T waves and arrhythmic activity following combined I_{Kr} and I_{Ks} block. *J. Cardiovasc. Electrophysiol.*, 2001;**12**: 1369–1378.
73. The CAST Investigators. Increased mortality due to encainide or flecainide in a randomized trial of arrhythmia suppression after myocardial infarction. *N. Engl. J. Med.*, 1989;**321**: 406–412.
74. Woosley, R.L., Y. Chen, J.P. Freiman, and R.A. Gillis. Mechanism of the cardiotoxic actions of terfenadine. *JAMA*, 1993;**269**: 1532–1536.
75. Glasman, A.H. and T.J. Biggert. Antipsychotic drugs: prolonged QTc interval, torsade de point sudden death. Am. J. Psychiatry, 2001;**158**(1): 774–782.
76. Liu, T, B.S. Brown, Y. Wu, et al., Blinded validation of the isolated arterially perfused rabbit ventricular wedge in preclinical assessment of drug-induced proarrhythmias. *Heart Rhythm*, 2006;**3**: 948–956.
77. Makkar, R.R., B.S. Fromm, R.T. Steinman, et al., Female gender as a risk factor for torsades de pointes associated with cardiovascular drugs. *JAMA*, 1993;**270**: 2590–2597.
78. Roden, D.M. and P.C. Viswanathan. Genetics of acquired long QT syndrome. *J. Clin. Invest.*, 2005;**115**: 2025–2032.
79. Haverkamp, W., G. Breithardt, A.J. Camm, et al., The potential for QT prolongation and proarrhythmia by non-antiarrhythmic drugs: clinical and regulatory implications: report on a policy conference of the European Society of Cardiology. *Eur. Heart J.*, 2000;**21**: 1216–1231.
80. International Conference on Harmonisation; guidance on E14 clinical evaluation of QT/QTc interval prolongation and proarrhythmic potential for non-antiarrhythmic drugs; availability. *Fed. Regist.*, 2005;**70**: 61134–61135.
81. Zareba, W. and A. Bayes de Luna, QT dynamics and variability. *Ann. Noninvasive Electrocardiol.*, 2005;**10**: 256–262.
82. Franz, M.R., C.D. Swerdlow, L.B. Liem, et al., Cycle length dependence of human action potential in vivo. Effects of single extrastimuli, sudden sustained rate acceleration and deceleration, and different steady-state frequencies. *J. Clin. Invest.* 1988;**82**: 972–979.
83. Lau, C.P., A.R. Freedman, S. Fleming et al., Hysteresis of the ventricular paced QT interval in response to abrupt changes in pacing rate. *Cardiovasc. Res.*, 1988;**22**: 67–72.
84. Krahn, A.D., G.J. Klein, and R.Yee, Hysteresis of the RT interval with exercise. A new marker for the long QT syndrome? *Circulation*, 1997;**96**: 1551–1556.
85. Merri, M., M. Alberti, and A.J. Moss, Dynamic analysis of ventricular repolarization duration from 24 hour Holter recordings. *IEEE Trans. Biomed. Eng.*, 1993;**40**: 1219–1225.
86. Homs, E., V. Marti, J. Offndo, et al., Automatic measurement of corrected QT interval in Holter recordings: comparison of its dynamic behavior in patients after myocardial infarction with and without life-threatening arrhythmias. *Am. Heart. J.*, 1997;**134**(2 Pt 1): 181–187.
87. Jensen, B.T., C.E. Larroude, L.P. Rasmussen, et al., Beat-to-beat QT dynamics in healthy subjects. *Ann. Noninvasive Electrocardiol.*, 2004;**9**: 3–11.
88. Badilini, F., P. Maison-Blanche, R. Childers et al., QT interval analysis on ambulatory electrocardiogram recordings. A selective beat averaging approach. *Med. Biol. Eng. Comput.*, 1999;**37**: 71–79.
89. Extramiana, F., P. Maison-Blanche, F. Badilini et al., Circadian modulation of QT-rate dependence in healthy volunteers: gender and age differences. *J. Electrocardiol.*, 1999;**32**: 33–43.
90. Iacoviello, M., C. Forleo, P. Guida, et al., Ventricular repolarization dynamicity provides independent prognostic information toward major arrhythmic events in patients with idiopathic dilated cardiomyopathy. *J. Am. Coll. Cardiol.*, 2007;**50**: 225–231.
91. Jensen, B.T., S.Z. Abildstrom, C.E. Larroude, et al., QT dynamics in risk stratification after myocardial infarction. *Heart Rhythm*, 2005;**2**: 357–364.
92. Stramba-Badiale, M., E. Locati, A. Martinelli, et al., Gender and the relationship between ventricular repolarization and cardiac cycle length during 24-hour Holter recordings. *Eur. Heart. J.*, 1997;**18**: 1000–1006.
93. Sredniawa, B., A. Musialik-Lydka, P. Jarski, et al., Circadian and sex-dependent QT dynamics. *Pacing Clin. Electrophysiol.*, 2005;**28**(Suppl. 1): S211–S216.
94. Nakagawa, M., T. Ooie, N. Takahashi, et al., Influence of menstrual cycle on QT dynamics. *Pacing Clin. Electrophysiol.*, 2006;**29**: 607–613.
95. Vrtovec, B., V. Starc, and H. Meden-Vrtovec, The effect of estrogen replacement therapy on ventricular repolarization dynamics in healthy postmenopausal women. *J. Electrocardiol.*, 2001;**34**: 227–283.
96. Merri, M., A.J. Moss, J. Benhorin, et al., Relation between ventricular repolarization duration and cardiac cycle length during 24 hour Holter recordings. Findings in normal patients and patients with long QT syndrome. *Circulation*, 1992;**85**: 1816–1821.
97. Perkiomaki, J.S., W. Zareba, A. Nomura, et al., Repolarization dynamics in patients with long QT syndrome. *J. Cardiovasc. Electrophysiol.*, 2002;**13**: 651–656.

98. Extramiana, F., N. Neyroud, H. Huikuri, et al., QT interval and arrhythmic assessment after myocardial infarction. *Am. J. Cardiol*., 1999;**83**: 266–269.
99. Savelieva, I., Y.G. Yap, G.Yi, et al., Relation of ventricular repolarization to cardiac cycle length in normal subjects, hypertrophic cardiomyopathy and patients with myocardial infarction. *Clin. Cardiol*., 1999;**22**: 649–654.
100. Faber, T.S., A. Grom, M. Schopflin, et al., Beat-to-beat assessment of QT/RR ratio in severe heart failure and overt myocardia ischemia: a measure of electrical integrity in diseased hearts. *Pacing Clin. Electrophysiol*., 2003;**26**: 836–842.
101. Roche, F., J.M. Gaspoz, I. Court-Fortune, et al., Alteration of QT rate dependence reflects cardiac autonomic imbalance in patients with obstructive sleep apnea syndrome. *Pacing Clin. Electrophysiol*., 2003;**26**: 1446–1453.
102. Pellerin, D., P. Maison Blanche, F. Extramiana, et al., Autonomic influences on ventricular repolarization in congestive heart failure. *J. Electrocadiol*., 2001;**34**: 35–40.
103. Lang, C.C., J.M. Neilson, and A.D. Flapan. Abnormalities of the repolarization characteristics of patients with heart failure progress with symptom severity. *Ann. Noninvasive Electrocardiol*., 2004;**9**: 257–264.
104. Digeos-Hasnier, S., X. Copie, O. Paziaud, et al., Abnormalities of ventricular repolarization in mitral valve prolapse. *Ann. Noninvasive Electrocardiol*., 2005;**10**: 297–304.
105. Bonnemeier, H., J. Ortak, F. Bode, et al., Modulation of ventricular repolarization in patients with transient left ventricular apical ballooning: a case control study. *J. Cardiovasc. Electrophysiol*., 2006;**17**: 1340–1347.
106. Lieb, W., C. Voss, J. Ortak, et al., Impact of diabetes on QT dynamicity in patients with and without myocardial infarction: the KORA Family Heart Study. *Pacing Clin. Electrophysiol*., 2007;**30**: S183–S187.
107. Valensi, P.E., N.B. Johnson, P. Maison-Blanche, et al., Influence of autonomic neuropathy on heart rate dependence of ventricular repolarization in diabetic patients. *Diabetes Care*, 2002;**25**: 918–923.
108. Nakagawa, M., T. Iwao, S. Ishida, et al., Dynamics of QT interval in a patient with long QT syndrome and a normal QT interval. *Jpn. Circ. J*., 1998;**62**: 215–218.
109. Fujiki, A., M. Suago, K. Nishida, et al., Repolarization abnormality in idiopathic ventricular fibrillation: assessment using 24-hour QT-RR and QTa-RR relationship. *J. Cardiovasc. Electrophysiol*. 2004;**15**: 59–63.
110. Tavernier, R., L. Jordaens, F. Haerynck, et al., Changes in the QT interval and its adaptation to rate, assessed with continuous electrocardiographic recordings in patients with ventricular fibrillation, as compared to normal individuals without arrhythmias. *Eur. Heart J*., 1997;**18**: 994–999.
111. Pierre, B., D. Babuty, P. Paret, et al., Abnormal nocturnal heart rate variability and QT dynamics in patients with Brugada syndrome. *Pacing Clin. Electrophysiol*., 2007; **30**(Suppl. 1): 188–191.
112. Yavuz, B., A. Deniz, G. Abali, et al., Impaired ventricular electrical stability and sympathetic hyperactivity in patients with multivessel coronary artery disease. *Coron. Artery Dis*., 2007;**18**: 241–245.
113. Bonnemeier, H., U.K.W. Wiegand, F. Bode, et al., Impact of infarct-related artery flow on QT dynamicity in patients undergoing direct percutaneous coronary intervention for acute myocardial infarction. *Circulation*, 2003;**108**: 2979–2986.
114. Singh, J.P., P. Sleight, A. Kardos, and G. Hart, QT interval dynamics and heart rate variability preceding a case of cardiac arrest. *Heart*, 1997;**77**: 375–377.
115. Sredniawa, B., P. Jarski, A. Musialik-Lydka, et al., QT dynamics and the risk of sudden arrhythmic cardiac death In ischemic heart disease. *Pacing Clin. Electrophysiol*., 2004;**27** (Pt 1): 827–828.
116. Chevalier, P., H. Burri, P. Adeleine, et al., QT dynamicity and sudden death after myocardial infarction: results of long term follow up study. *J. Cardiovasc. Electrophysiol*., 2002;**14**: 227–233.
117. Milliez, P., A. Leenhardt, P. Maison Blanche, et al., Usefulness of ventricular repolarization dynamicity in patients with ischemic cardiomyopathy (from the European Myocardial Infarct Amiodarone Trial). *Am. J. Cardiol*., 2005;**95**: 821–826.
118. Smetana, P., E. Pueyo, K. Hnatkowa, et al., Individual pattern of dynamic QT/RR relationship in survivors of acute myocardial infarction and their relationship to antiarrhythmic efficacy of amiodarone. *J. Cardiovasc. Electrophysiol*., 2004;**15**: 1147–1154.
119. Pathak, A., D. Curnier, J. Fourcade, et al., QT dynamicity: a prognostic factor for sudden death in chronic heart failure. *Eur. J. Heart Fail*., 2005;**7**: 269–275.
120. Watanabe, E., T. Arakawa, T. Uchiyama, et al., Prognostic significance of circadian variability of RR and QT intervals and QT dynamicity in patients with chronic heart failure. *Heart Rhythm*, 2007;**4**: 999–1005.
121. Cygankiewicz, I., W. Zareba, R. Vazquez, et al., Prognostic value of QT/RR slope in predicting mortality in patients with congestive heart failure. *J. Cardiovasc. Electrophysiol*., 2008;**19**: 1066–1072.
122. Zareba, W., QT-RR slope: dynamics of repolarization in the risk stratification. *J. Cardiovasc. Electrophysiol*., 2003;**14**: 234–235.
123. Berger, R.D., E.K. Kasper, K.L. Baughman, et al., Beat-to-beat QT interval variability. Novel evidence for repolarization lability in ischemic and nonischemic dilated cardiomyopathy. *Circulation*, 1997;**96**: 1557–1565.
124. Zareba, W., F. Badilini, and A.J. Moss, Automatic detection of spatial and dynamic heterogeneity of repolarization. *J. Electrocardiol*., 1994;**27**(Suppl.): 66–72.
125. Couderc, J.P., W. Zareba, L. Burattini, and A.J. Moss, Beat-to-beat repolarization variability in LQTS patients with SCN5A sodium channel gene mutation. *Pacing Clin. Electrophysiol*., 1999;**22**: 1581–1592.
126. Couderc, J.P., W. Zareba, S. McNitt, et al., Repolarization variability in the risk stratification of MADIT II patients. *Europace*, 2007;**9**: 717–723.
127. Goldenberg, I., J. Mathew, A.J. Moss, et al., Corrected QT variability in serial electrocardiograms in long QT syndrome: the importance of the maximum corrected QT for risk stratification. *J. Am. Coll. Cardiol*., 2006;**48**: 1047–1052.
128. Vrtovec, B., V. Starc, and R. Starc, Beat-to-beat QT interval variability in coronary patients. *J. Electrocardiol*., 2000;**33**: 119–25.
129. Cuomo, S., F. Marciano, M.L. Migaux, et al., Abnormal QT interval variability in patients with hypertrophic cardiomyopathy: can syncope be predicted? *J. Electrocardiol*., 2004;**37**: 113–119.
130. Hiromoto, K., H. Shimizu, T. Mine, et al., Correlation between beat-to-beat QT interval variability and impaired left ventricular function in patients with previous myocardial infarction. *Ann. Noninvasive Electrocardiol*., 2006;**11**: 299–305.
131. Desai, N., D.S. Raghunandan, M. Mallavarapu, et al., Beat-to-beat heart rate and QT variability in patients with congestive

cardiac failure: blunted response to orthostatic challenge. *Ann. Noninvasive Electrocardiol*. 2004;**9**: 323–329.
132. Yeragani, V.K., M. Tancer, and T. Uhde, Heart rate and QT interval variability: abnormal alpha-2 adrenergic function in patients with panic disorder. *Psychiatry*, 2003;**121**: 185–196.
133. Carney, R.M., K.F. Freedland, P. Stein, et al., Effects of depression on QT interval variability after myocardial infarction. *Psychosomatic Medicine*, 2003;**65**: 177–180.
134. Haigney, M.C., S. Alam, S. Tebo, et al., Intravenous cocaine and QT variability. *J. Cardiovasc. Electrophysiol*., 2006;**17**: 610–616.
135. Thomsen, M.B., P.G. Volders, J.D. Beekman, et al., Beat-to-beat variability of repolarization determines proarrhythmic outcome in dogs susceptible to drug-induced Torsades de Pointes. *J. Am. Coll. Cardiol*., 2006;**48**: 1268–1276.
136. Thomsen, M., A. Oros, M. Schoenmakers, et al., Proarrhythmic electrical remodeling is associated with increased beat-to-beat variability of repolarization. *Cardiovasc. Res*., 2007;**73**: 521–530.
137. Henneberger, A., W. Zareba, A. Ibald-Mulli, et al., Repolarization changes induced by air pollution in ischemic heart disease patients. *Environ. Health. Perspect*., 2005;**113**: 440–446.
138. Piccirillo, G., R. Quaglione, M. Nocco et al., Effects of long-term beta-blocker (metoprolol or carvedilol) therapy on QT variability in subjects with chronic heart failure secondary to ischemic cardiomyopathy. *Am. J. Cardiol*. 2002;**90**: 1113–1117.
139. Bonnemeier, H., F. Hartmann, U.K. Wiegand, et al., Course and prognostic implications of QT interval and QT variability after primary coronary angioplasty in acute myocardial infarction. *J. Am. Coll. Cardiol*., 2001;**37**: 44–50.
140. Atiga, W.L., Calkins, H., Lawrence, J.H., et al., Beat-to-beat repolarization lability identifies patients at risk for sudden cardiac death. *J. Cardiovasc. Electrophysiol*., 1998;**9**: 899–908.
141. Haigney, M.C., W. Zareba, P.J. Gentlesk, et al., and the MADIT II Investigators. QT interval variability and spontaneous ventricular tachycardia or fibrillation in the Multicenter Automatic Defibrillator Implantation Trial (MADIT) II patients. *J. Am. Coll. Cardiol*., 2004;**44**: 1481–1487.
142. Piccirillo, G., D. Magri, S. Matera, et al. QT variability strongly predicts sudden cardiac death in asymptomatic subjects with mild or moderate left ventricular dysfunction: a prospective study. *Eur. Heart. J*. 2007;**28**: 1344–1350.

20 Miscellaneous Electrocardiographic Topics

J.E. Madias

P. W. Macfarlane, A. van Oosterom, O. Pahlm, P. Kligfield, M. Janse, J. Camm (eds.), *Comprehensive Electrocardiology*, DOI 10.1007/978-1-84882-046-3_20,

20.1 Introduction

A chapter, entitled as this one is, aims at providing a systematic presentation on a number of topics, which are either not included elsewhere in this book, or they receive a cursory treatment as mere components of an overall exposition. In the first category, one could consider the attenuation of ECG voltage resulting from the development of peripheral edema of varying etiology [1], while in the second the giant T waves could represent an example of a topic included here, but also mentioned under ST-T changes found in chapters about myocardial infarction, ischemia, intraventricular conduction abnormalities or ventricular hypertrophy. In such a venture some redundancy is inevitable, but overall it proves to be beneficial. Some ECG abnormalities, which were included in this chapter in the first Edition, became so pervasive as to deserve their separate handling (e.g., QT interval, Chap. 19). Many ECG topics, not considered previously, had to be included in this Edition because of their expanding role in the practice of medicine. Finally, one should envisage that undescribed ECG changes and associations are still awaiting detection, and thus a chapter like this is open-ended in terms of its contents, and serves as a "gate" or "filter" for what eventually becomes established. The author is much indebted to Professor C.Y. Chen and the late Professor K. Harumi, authors of this chapter in the first Edition, for the aid received from their original text and associated references, and for the marvelous panel of their figures, most of which have been retained.

20.2 Electrolyte, Acid Base, and Blood Abnormalities

Imbalances of the various cations, and disturbances in the acid-base, blood gas, and hemoglobin concentration affect the ECG most often in a nonspecific fashion, although occasionally may produce characteristic changes, as in the alterations of K^+ and Ca^{2+}.

Electrophysiologic properties of myocardial cells depend on the movement of electrolytes across their membranes, setting up ionic currents [2, 3]. Table 20.1 summarizes the effects of various types of electrolyte imbalance on the transmembrane action potential, which result in ECG changes of depolarization (P wave and QRS complex), repolarization (ST segment and T wave), and impulse generation and conduction.

In the clinical domain, the characteristic ECGs resulting from electrolyte imbalance are encountered in patients with malabsorption, starvation, various endocrinopathies and sizeable loss of electrolytes due to severe vomiting, diarrhea, burns, diabetic ketoacidosis, and diuretic therapy. Patients with renal failure are the ones most frequently troubled by electrolyte imbalance. Among all the electrolyte disorders, changes in serum K^+ are the most prevalent, leading to alterations in the ECG and occasionally serious cardiac rhythm and conduction disturbances.

20.2.1 Hyperkalemia

20.2.1.1 P Wave, QRS Complex, and Conduction Disturbance

Normally the extracellular concentration of K^+ (3.5–5.0 mEq L^{-1}) is much lower than the intracellular K^+ (140 mEq L^{-1}), and thus the intracellular to extracellular concentration gradient of this cation can be easily increased or decreased by small changes in the serum K^+ [2, 3]. An increase in the extracellular K^+ concentration and the consequent decrease of this gradient will rapidly decrease the resting membrane potential, the magnitude of the action potential, and the maximum rate of rise of phase 0 $(dV/dt)_{max}$, the last resulting from its dependence on the resting membrane potential (Fig. 20.1). Also, since the conduction velocity in the Purkinje fibers and cardiac muscle is determined primarily by $(dV/dt)_{max}$, and this is reduced in hyperkalemia (↑K), conduction through the heart will be depressed [4]. During phase 4, the membrane potential is approximately compatible with the equilibrium potential of K^+. If there is an excess of extracellular K^+, as in ↑K, the membrane potential is reduced according to the Nernst equation [2]. ↑K, however, produces a biphasic effect on the atrioventricular (AV) conduction system, with mild degrees accelerating the AV conduction, and severe ↑K (≥7.5 mEq L^{-1}) depressing it. In experimental studies, conduction is most rapid at a K^+ level of ~6.0–6.5 mEq L^{-1}. This enhancing effect of mild ↑K may improve conduction in patients with sinus rhythm and AV block, or accelerate the ventricular response in atrial fibrillation [4–6]. Severe ↑K may produce all kinds of AV blocks,

Table 20.1
Effects of K^+ and Ca^{2+} on electrophysiological properties

	Hyperkalemia	Hypokalemia	Hypercalcemia	Hypocalcemia
Phase 0				
Upstroke rate of rise (d*V*/d*t*)	Decreased	Unchanged or increased	Decreased	Increased
Action potential Amplitude	Decreased	Increased		
Phase 2				
Plateau of action Potential	Shortened	Prolonged	Shortened	Prolonged
Phase 3				
Action potential Duration	Shortened	Prolonged	Shortened	Prolonged
Phase 4				
Resting membrane Potential	Decreased	Increased Decreased (≤2 mEq)	Unchanged	Unchanged
Pacemaker activity	Enhanced (5.5–6 mEq) Depressed (≥7 mEq)	Enhanced	Increased	Increased
Conductivity	Enhanced (5.5–6 mEq) Depressed (≥7 mEq)	Depressed	Decreased	Increased

although high-degree AV block is infrequent. Electrophysiological studies show that the sites of AV block in ↑K are at the atrionodal, nodal-His or His-Purkinje regions, and that the N (true nodal) regions are relatively insensitive to it [7].

The action of increased serum K^+ on the various types of cardiac fibers may be nonuniform [5], with the atrial fibers being more sensitive than the ventricular myocardium. Intra-atrial conduction is depressed in ↑K (7.0–7.5 mEq L^{-1}), resulting in wide and flattened P waves (Table 20.2), and in severe ↑K (≥9 mEq L^{-1}), intra-atrial conduction is markedly slowed and the P waves often disappear (Fig. 20.2), leading to the so-called sinoventricular rhythm. In this condition, where absence of P waves hinders its differentiation from complete AV block, there is no influence of ↑K on the sinus pacemaker properties, and conduction from the sinus node to the ventricular fibers is maintained.

Intraventricular conduction is also affected by ↑K, and its mild to severe forms lead to diffuse widening of the QRS complexes, often simulating all kinds of bundle branch blocks (Fig. 20.2). Left anterior or posterior fascicular blocks may be observed transiently [8], and might be caused by the nonuniform effects of ↑K on the intraventricular conduction [9]. The same mechanism may be responsible for the pseudoinfarctional QRS patterns occasionally noted and mistaken for real myocardial infarcts (MI). Also a reduction of cardiac excitability manifest as an increase in the threshold or failure to capture by an electronic pacemaker has been noted with ↑K, involving the atrium or the ventricle [10–12]. Indeed, failure to capture the atrium with preservation of capture of the ventricle in DDD pacemaking attests to the greater sensitivity of the former to ↑K [11]. With levels of serum $K^+ \geq 8$ mEq L^{-1} a sine-wave pattern may appear [13], consisting of a wide QRS complex with an inverted T wave leading to ventricular fibrillation and cardiac standstill.

20.2.1.2 ST Segment and T Wave

Increase in the extracellular K^+ concentration (≥6.0 mEq L^{-1}) shortens the duration of the action potential, mainly by increasing the steepness of phase 2 [9] (Fig. 20.1). This action of K^+ may depend on an increase of K^+

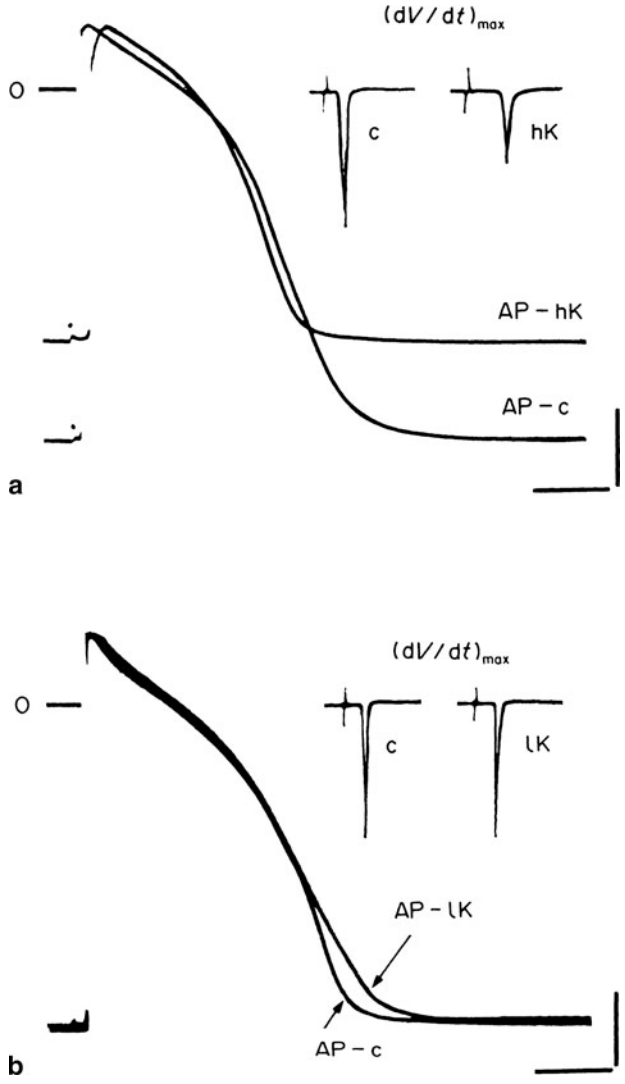

Figure 20.1

Action potentials from the guinea pig's heart: (a) action potentials in normal (2.7 mM) and altered Tyrode's solution (K^+; 8.0 mM) are depicted. In a higher concentration of K^+, the resting membrane potential and the maximum upstroke velocity of phase 0 are reduced, and the duration of repolarization is shortened (c, control; hK, higher concentration of K^+; AP, action potential); (b) action potentials in normal (K^+; 2.7 mM) and altered Tyrode's solution (K^+; 1.0 mM) are depicted. In a lower concentration of K^+ (lK), the resting membrane potential and the maximum upstroke velocity are unchanged, while the duration of repolarization is slightly prolonged.

conductance (gK) [3]. These changes in the shape of the action potential are probably the reason for the shortening of the QT interval and the peaked tent-shaped T wave, which is the most common and the sole ECG sign of serum K^+ concentrations between 5.5 and 6.5 mEq L^{-1}. The corresponding change in the vectorcardiogram is a linear T wave loop. The T wave changes are more frequently seen in leads II, III and in the precordial leads, and are nonspecific for ↑K, since they are also seen in many other conditions, i.e., myocardial ischemia, bradycardia, and subjects with early repolarization (Fig. 20.3). In differentiating acute ischemic syndromes from ↑K, the regional presence in the former with normal or prolonged QTc, in contrast to the diffuse occurrence in the latter of similarly appearing T waves with shortened

Table 20.2

ECG abnormalities in hyperkalemia

	Abnormalities
P and QRS waves	Flat and broad P wave (7–7.5 mEq L^{-1}) Disappearing P wave (8–9 mEq L^{-1}) Widening of QRS wave (≥6.5 mEq L^{-1}) Sine-wave patterns of QRS wave (≥8–9 mEq L^{-1}) Cardiac arrest (8 mEq L^{-1} or higher)
ST segment and T waves	Tent-shaped T wave (≥5.5 mEq L^{-1}) Shortening QT_c interval (≥5.5 mEq L^{-1}) Opposing T wave (8–9 mEq L^{-1}) Depression or elevation of ST segment (6.5–7.5 mEq L^{-1})
Conduction and impulse formation	Accelerated AV conduction (5.5–6 mEq L^{-1}) Slow AV conduction (≥7–7.5 mEq L^{-1}) Failure of cardiac capture by artificial pacemaker (6–7.5 mEq L^{-1}) Reversible fascicular block (6.5–7.5 mEq L^{-1}) Reentrant ectopic beats (7.5–8.5 mEq L^{-1}) Ventricular fibrillation (8–9 mEq L^{-1})

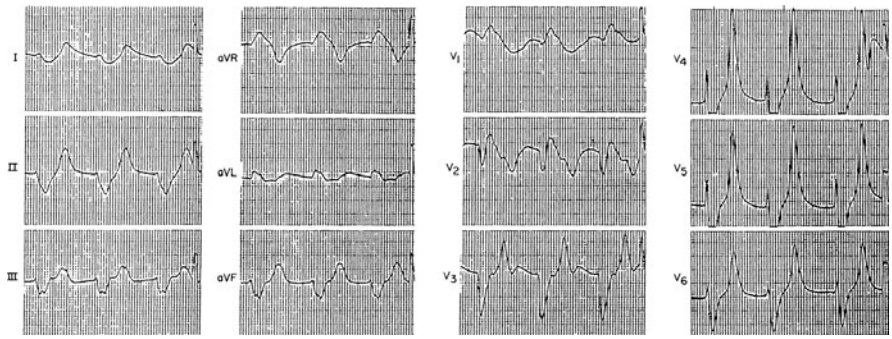

Figure 20.2

The ECG was recorded from a patient suffering from severe chronic renal failure, and advanced hyperkalemia (serum K^+ level was 8.3 mEq L^{-1}). The characteristic sinoventricular rhythm (no discernible P waves), and the intraventricular conduction disturbance, simulating right bundle branch block, are shown.

QTc, is helpful [2]. Occasionally, the tent-shaped T waves may be of normal amplitude, [14], and this should be kept in mind so that ↑K is not overlooked. In severe ↑K (7.5 mEq L^{-1}), the T wave changes may be associated with widening of the QRS and a decrease in the amplitude of the R waves. The T wave changes in advanced ↑K may be secondary to intraventricular conduction disturbances [13, 15], rather than due to the alteration of the action potential. In very severe ↑K, an inverted T wave with a wide QRS complex may be observed and may be followed by the development of ventricular tachycardia, fibrillation, and asystole [16].

ST segment depression, and even rarely ST segment elevation, may be observed in ↑K, probably as a result of the shortening of the plateau of the action potential and the decrease of diastolic potential (Fig. 20.1). ST segment elevation indistinguishable from a current of injury has been recognized for a long time, and has led to numerous reports in the literature of ↑K, simulating acute MI [17]; in such cases correction of ↑K has abolished the pseudoinfarctional ECG pattern, hence the expression "dialyzable currents of injury" has been coined to characterize these transient ECG alterations [18]. The ST segment elevation probably is due to inhomogeneous depolarization of different myocardial territories, resulting

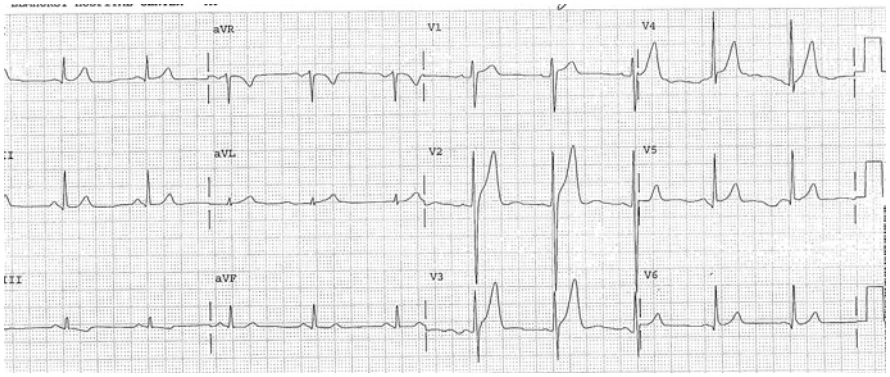

Figure 20.3

ECG changes simulating hyperkalemia in a 27-year old healthy male subject, due to early repolarization; automated systems often interpret these changes as due to "metabolic or ischemic abnormalities". A QTc of 358 ms was present, in the absence of hypercalcemia, or hyperkalemia.

in voltage gradients and current flow between these regions. A pseudoinfarctional ST segment elevation has been noted in a hypokalemic patient undergoing rapid K^+ replenishment, and while she was still hypokalemic (K^+: 3.0 mEq L^{-1}) (Fig. 20.4), and it was attributed to the reduction of the intracellular to extracellular gradient, not unlike what occurs with true serum ↑K [19]. Finally, it should be always kept in mind that profound ↑K may be encountered without ECG manifestations [20].

20.2.2 Hypokalemia

20.2.2.1 P Wave and QRS Complex

Increase in the resting membrane potential and the amplitude of the action potential are mediated by a progressive decrease of serum K^+ at a level ~2.7 mEq L^{-1}, although with even lower concentrations, the conduction velocity might be reduced, indicating a decrease in resting membrane potential and prolongation of repolarization [2]. Thus, with severe hypokalemia (↓K), the amplitude and the duration of the QRS increase (Table 20.3). The widened QRS complexes indicate that the intraventricular conduction disturbance is due to a generalized slowing of conduction in the peripheral conduction system and/or myocardium. The amplitude and duration of the P waves also are usually increased in ↓K, as seen in leads II, III and aVF, with such changes resembling P-pulmonale, or "pseudo P-pulmonale" found in left atrial abnormality.

20.2.2.2 ST Segment and T and U Waves

The earliest abnormalities consequent to a modest reduction of the serum K^+ are those of repolarization, and are commonly appreciated in the ECG. Electrophysiologically, there is an increase in the action potential duration. Further lowering of K^+ leads to shortening of the plateau phase of the action potential, and a progressively steeper slope of phase 2. This change in the slope of the action potential, mediated by decreased conductance, can occur with milder ↓K (2.7–2.4 mEq L^{-1}), but it is associated with insignificant effect on the resting potential.

The ECG (usually leads II, III and V_2–V_4) reveals abnormalities of the ST segment, T and U waves, which constitute the most common and helpful changes for the detection of ↓K (Table 20.3). The amplitude of the T and U wave reflect relatively accurately the levels of the deficit in the serum concentration of K^+ (Fig. 20.5). The diagnosis of ↓K in patients

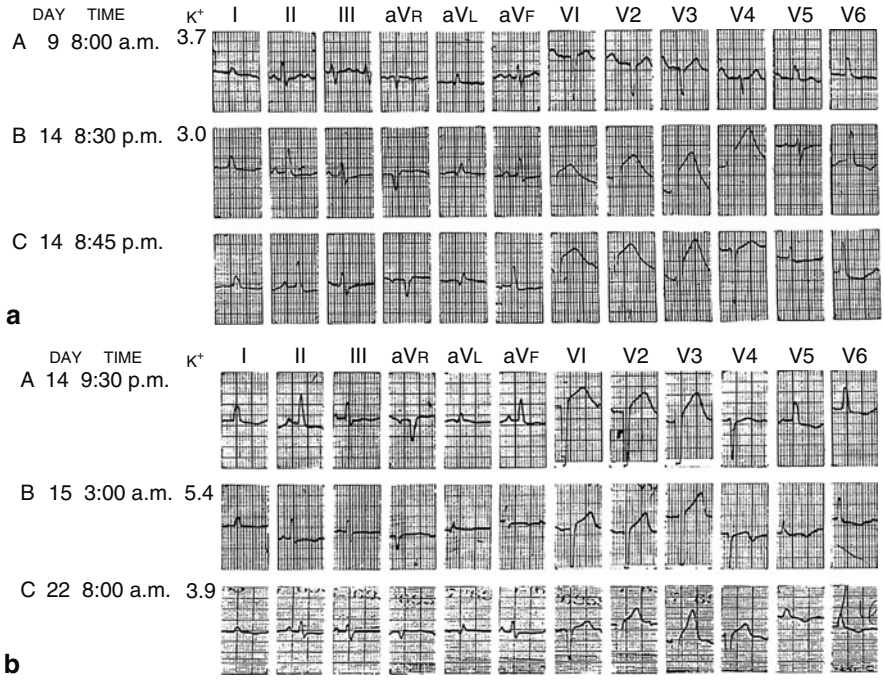

Figure 20.4

(a) ST segment elevation, simulating an acute myocardial infarction in a 65-year-old woman, which persisted for a few hours while she was receiving K^+ supplementation for hypokalemia resulting from intravenous hyperalimentation. (b) The highest serum K^+ recorded in this patient was 5.4 mEq L^{-1}, at which time the ST segment elevation had resolved. (Reproduced from Ref. [19]. With permission of the *Journal of Electrocardiology*.)

Table 20.3

ECG abnormalities in hypokalemia

	Abnormalities
P and QRS waves	Increased QRS wave amplitude Increased QRS wave duration Increased P wave amplitude Increased P wave duration
ST segment, T and U waves	Prominent U wave Flat or inverted T wave ST segment depression
Conduction and impulse formation	Atrial premature contractions Atrial tachycardia Supraventricular tachycardia AV junctional rhythm AV dissociation First degree AV block Ventricular premature contractions Bidirectional ventricular tachycardia Ventricular fibrillation

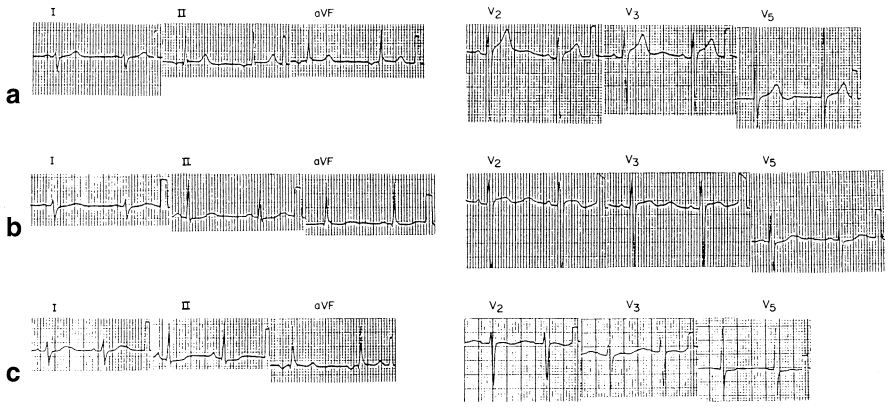

Figure 20.5

ECG changes at different degrees of hypokalemia, in a patient with primary aldosteronism: (a) Na 147 mEq L^{-1}, K 4.3 mEq L^{-1}, Cl 106 mEq L^{-1}; (b) Na 146 mEq L^{-1}, K 2.8 mEq L^{-1}, Cl 98 mEq L^{-1}; (c) Na 147 mEq L^{-1}, K 1.7 mEq L^{-1}, Cl 97 mEq L^{-1}. With increasing ↓K the T wave becomes lower and the U wave taller.

can be facilitated by employing ST segment depression ≥0.05 mV, U wave amplitude >0.1 mV, and U wave amplitude >T wave amplitude in the same lead as the other criteria, with the frequency of a positive diagnosis paralleling the severity of ↓K [21]. The depressed ST segment and the low or inverted T wave may fuse with the prominent U wave in ↓K without significant changes of QT or QU intervals. In severe ↓K, the ST segment depression is accompanied by a prominent U wave and a dwarfed T wave.

The effects of ↓K on the Purkinje fibers differ from those on the ventricular fibers, prolonging the plateau phase in the former and shortening it in the latter, thus increasing the difference between the action potential durations [22]; this difference in the sensitivity of Purkinje and myocardial fibers to ↓K might underlie the development of the U wave.

20.2.2.3 Conduction and Impulse Generation

A clinically relevant effect of ↓K is the enhancement of automaticity of latent pacemakers, which is probably mediated by the acceleration of the decay of pacemaker current (i_{K2}) in the Purkinje fibers resulting from a decreased K^+ conductance [3]. Accordingly, unifocal or multifocal ectopic beats have been found in experimental and clinical studies. Common cardiac arrhythmias at serum K^+ levels ≤3.0 mEq L^{-1} are atrial premature beats, atrial tachycardia with or without AV block, supraventricular tachycardia, AV junctional rhythm and AV junctional parasystole. However, in a study employing ambulatory ECG monitoring of hypertensive patients without coronary artery disease treated with diuretics, K^+ levels of 2.5 to 3.4 mEq L^{-1} were not associated with arrhythmias [23]. The important issue of whether mild to moderate ↓K *per se* is arrhythmogenic has not been resolved thus far conclusively, but even resolution of this matter may not be clinically relevant most of the time, in terms of the need for correction of ↓K; patients usually present with clusters of conditions and abnormal tests, and in that setting management should be individualized and mostly in favor of K^+ replenishment [24]. The duration of the action potential is prolonged in severe ↓K (Fig. 20.1), making it more likely for a propagated simple ectopic ventricular impulse to fall into the vulnerable period of the fused TU complex, and easily initiate reentrant arrhythmias by a complex interplay of ectopy and depressed conduction. In such a setting, "torsade de pointes" (TdP), the unusual multidirectional ventricular tachycardia characteristic of ↓K [25], may emerge; in fact ↓K is an important cause of acquired long QT syndrome, and associated TdP. ↓K also causes arrhythmias due to enhanced automaticity. The enhancement of digitalis-induced arrhythmias by ↓K has been known for a long time and thus it is recommended that serum K^+ be kept between 4.5 and 5.0 mEq L^{-1} [26]. Also, arrhythmias occur in the interplay of ↓K and myocardial ischemia [27]. Significant AV and intraventricular conduction disturbances secondary to ↓K have been noted in patients, with 1° AV block appearing at serum K^+ levels ≤2.7 mEq L^{-1}, and variable degrees of AV block at levels ≤1.01 mEq L^{-1} [2, 28].

20.2.3 Hypercalcemia and Hypocalcemia

20.2.3.1 P Wave and QRS Complex

The resting potential, the amplitude of the action potential, or the shape of phase 3 are not significantly affected even with extremes of serum Ca^{2+} concentrations (1.2–20.8 mEq L^{-1}) [29]. Primarily, an abnormal Ca^{2+} level impacts the ventricular repolarization. However, severe hypercalcemia (↑Ca) reduces the upstroke and conduction velocities in ventricular muscle fibers, and increases the QRS duration, in contrast to hypocalcemia (↓Ca), which decreases the QRS duration [2, 30]. An increased amplitude of the QRS complex, suggesting an increase in the ventricular muscle mass, has been observed with ↑Ca [31]. Furthermore, the duration of the T wave was significantly prolonged in patients with hyperparathyroidism. Abnormal serum Ca^{2+} concentrations have no discernible effect on the P wave. All degrees of AV block can be seen with ↑Ca [2]. Also sinus node dysfunction and tachy-brady syndrome have been described with ↑Ca [32, 33].

20.2.3.2 ST Segment and T Wave

↑Ca shortens the duration of phase 2 of the action potential in all cardiac fibers (Table 20.1) and increases the amplitude of the plateau, a feature enhanced by increased catecholamines [2, 34]. Consequently, the duration of the action potential and the effective refractory period are decreased. Phase 2 of the action potential should be prolonged since, as per the Nernst equation, ↑Ca increases the inward calcium current. However, ↑Ca actually produces a rapid repolarization, probably resulting from the simultaneous enhancement of the K^+ outward current [3]. As the slope of phase 2 and its duration are reflected in the shape of the ST segment of the ECG, the shortening of Q-oT (onset of QRS complex to onset of T wave) and Q-aT (onset of the QRS complex to the apex of the T wave) are the most common early ECG abnormalities in ↑Ca [35] (Fig. 20.6); the total duration of ventricular repolarization does not decrease though, and thus ↑Ca has less effect on the QTc or QU intervals [36, 37]. Occasionally in ↑Ca, the onset of the T wave appears to be at the J-point [38]. An Osborn-like wave has been described with ↑Ca [39]. Short QTc is frequently encountered, particularly in young subjects without ↑Ca (Fig. 20.3) [38], sometimes bordering the measurements seen in patients with the short QT interval syndrome [40]. However, an increased T wave duration has been documented with ↑Ca [31]. By contrast, ↓Ca increases the duration of plateau phase (Table 20.1), leading to prolongation of the ST segment and QT interval, which are both early ECG signs of ↓Ca [2]. In both ↑Ca and ↓Ca, the effect on the QT interval is primarily exerted on the ST segment [2]. The T wave morphology can be affected in both ↑Ca and ↓Ca [2]. Barring the confounding influence of other electrolyte abnormalities, the change of the Q-oTc interval duration may significantly correlate with the serum Ca^{2+} level [41]. The duration of the T wave is not usually affected by ↓Ca, but its amplitude is decreased or sometimes it becomes flattened (Fig. 20.6). The combined ↓Ca and hyperkalemia of renal failure produces ST segment prolongation with narrow-based tall T waves [2]. ↓Ca may mimic acute MI with ST elevation, reciprocal ST segment depression, and regional contraction abnormalities; all these abate with calcium and vitamin D_3 therapy [42]; coronary spasm is implicated in this condition.

20.2.3.3 Conduction and Impulse Generation

Although cardiac arrhythmias and 1° AV block are infrequent in ↓Ca and ↑Ca [5], extreme ↓Ca can produce sinus bradycardia with intermittent sinoatrial block, 2:1 AV block and complete AV block [43, 44], especially in children, and ventricular fibrillation (VF) [45], while ventricular tachycardia and VF have also occurred with ↑Ca [46, 47]. Moreover, torsade de pointes has occurred with both ↓Ca and ↑Ca [48, 49].

The hereditary prolonged QT syndrome and the prolonged QT interval seen with ischemic heart disease are predisposing factors for VF. A possible explanation for the absence of cardiac arrhythmias in sodium EDTA induced ↓Ca with prolonged QT interval [50] is that ↓Ca produces a uniform prolongation of repolarization, thus preventing reentry. Continuous injection of calcium chloride until death in animal experiments led to a change in AV conduction, followed by VF [51].

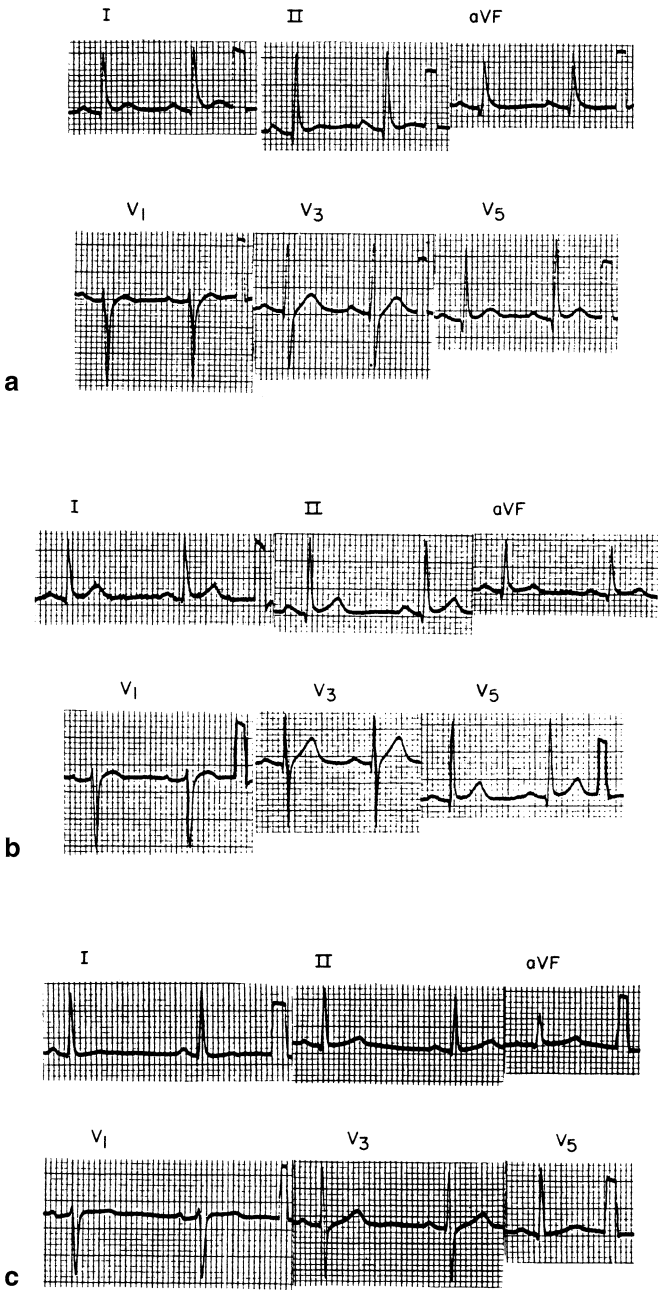

Figure 20.6

ECG changes at different serum Ca^{2+} levels. (a) 7.2 mEq L^{-1}; (b) 4.2 mEq L^{-1}; (c) 2.6 mEq L^{-1}.

In hyperparathyroidism with severe ↑Ca, sinus arrest, Wenckebach 2° AV block and atrial fibrillation have been reported [52, 53]. ↑Ca also may accentuate digitalis-induced ectopy. Finally, the interaction between K^+ and Ca^{2+}, in which ↑Ca reverses the conduction abnormality and cardiac arrhythmias induced by ↑K, has been put to therapeutic use.

20.2.4 Hypomagnesemia and Hypermagnesemia

Clinically encountered abnormalities of serum Mg^{2+} do not affect the action potential significantly. However, the combination of hypomagnesemia (↓Mg), ↓K and digitalis intoxication can lead to cardiac arrhythmias [2, 26]. The influence of ↓Mg in digitalis-induced arrhythmias may be related to the role of Mg^{2+} as a cofactor for membrane sodium and potassium (Na^+–K^+) adenosine triphosphatase, which maintains mitochondrial integrity [54]. Nevertheless, hypomagnesemic patients have suffered paroxysmal VF in the absence of digitalis therapy [55]. ↓Mg in patients with alcoholic heart disease leads to ECG changes similar to the ones noted with ↑K (slightly widened QRS complexes, mild ST depression, peaked T waves and prolonged QT intervals) [56]. Simultaneous correction of ↓Mg and ↓K, in cases of ↓K resistant to adequate replenishment of K^+, is required [24, 26]. Depressed AV conduction with severe hypermagnesemia (↑Mg) may be due to slowing of the velocity of the upstroke of the action potential. In attributing changes in the ECG to ↑Mg, attention should be paid to the associated electrolyte and metabolic disorders [2]. Whether ↓Mg and ↑Mg are arrhythmogenic has not as yet been determined [57].

20.2.5 Sodium

The amplitude of the action potential, and the upstroke velocity, increase with hypernatremia (↑Na) and decrease with hyponatremia (↓Na) [2]. However, since the concentrations of Na^+ required to change the ECG are usually incompatible with life, no ECG abnormalities are encountered with the range of changes seen in the clinical setting [2]. Widened QRS due to intraventricular conduction disturbances resulting from ↑K is shortened by ↑Na, and further prolonged by ↓Na [2].

20.2.6 Lithium

Li^+ readily replaces intracellular K^+, and in patients treated for bipolar depression, may cause minor T wave abnormalities, sinus bradycardia and sinus node dysfunction, with stimulation testing revealing that only the sinus node is reversibly affected by this cation [58]. High Li^+ levels (>1.2 mEq L^{-1}) are also associated with prolongation of PR interval and other AV blocks, ventricular arrhythmias, reversible diffuse T wave inversions, and QTc interval prolongation [59]. The T wave inversions may be due to intracellular displacement of K^+ by Li^+, and respond to K^+ administration. The SA and AV node dysfunction are attributed to alterations of Ca^{2+} flux caused by Li^+. Frequent recording of the ECG, particularly in patients with renal failure or concomitant therapy with β-blockers and Ca^{2+} channel inhibitors, could detect treated patients with over-range Li^+ levels [59].

20.2.7 Hypertonicity and Hypotonicity

Cardiac cells become hyperpolarized and reveal a decrease in action potential upstroke by hypertonic sucrose and other type of solutions [60, 61], and this slows conduction probably because of the widened resting-threshold membrane potential gradient. In canine cardiac Purkinje fibers, hypertonicity increases the action potential duration [61], and in ventricular fibers from guinea pigs and cats, it leads to disappearance of phase 3 of the action potential [60]. Information on hypotonicity is lacking. An anisotonic solution application on the heart causes T wave changes. However, in the clinical setting changes in osmolarity occur in various combinations with alterations in electrolytes, pH, and oxygenation, and thus the impact on electrophysiology and the ECG is variable.

20.2.8 pH

It is difficult to evaluate the effects of pH changes on the ECG, since acidosis and alkalosis are closely linked to alterations in the serum concentration of K^+ and Ca^{2+}. Resting membrane potential and repolarization of canine Purkinje fibers were little affected by a pH of 6.8, while decreasing the bicarbonate concentration to 12 mM independent of acidosis led to an

increase in the action potential duration [62]. In diseases leading to metabolic and respiratory acidosis, an increase in the amplitude of the T wave would be expected, while alkalosis would lead to flattening or even inversion of T waves [63]. The above are stated by extrapolation from results of human experimentation with voluntary hyperventilation, exercise, and ingestion of Na bicarbonate and ammonium chloride. Alkalosis and acidosis increase the pacing threshold [12].

20.2.9 Oxygen and Carbon Dioxide

Hypoxemia ($\downarrow PaO_2$), rise of PaO_2 through breathing of high oxygen concentrations, hypercapnia ($\uparrow PaCO_2$), and hypocapnia ($\downarrow PaCO_2$) are encountered in patients with respiratory and metabolic conditions; thus inevitably alterations in pH and concentrations of serum electrolytes also occur. $\downarrow PaO_2$ in canine experiments leads to sinus tachycardia [64], while normal human subjects develop reduction of the T wave amplitude and in patients with coronary artery disease, similar T wave changes develop and are associated with ST segment depression [65]. Atrial and ventricular extrasystoles are rare in the absence of cardiac pathology. There is no literature on breathing high oxygen concentrations under normobaric conditions and the ECG, although data on ECG with hyperventilation may be only tangentially relevant, due to the associated $\downarrow PaCO_2$. $\uparrow PaCO_2$ increased QTc interval and QT dispersion in normal subjects [66], and in dogs caused an increase in respiratory sinus arrhythmia, in contrast to the decrease produced by $\downarrow PaO_2$ [67]. $\downarrow PaCO_2$ induced by voluntary hyperventilation led to mild increase in heart rate, and a decrease in the mean amplitude of the T waves [68]. Up to 15% of apparently healthy subjects had nonspecific ST-T changes with hyperventilation [69].

20.2.10 Anemia and Polycythemia

ECG changes in anemia (↓Hb) and polycythemia (↑Hb) are partially modulated by underlying cardiac pathology. Thus, chronic ↓Hb results in high output failure, cardiac dilatation, and resultant increase in the amplitude of QRS complexes. ↓Hb may also lead to left ventricular hypertrophy on the ECG in renal transplant recipients [70], and low heart rate variability in patients with stable coronary heart disease [71]. ↑Hb with its prothrombotic effects may lead to MI or pulmonary embolism, with corresponding ECG changes. ↓Hb and ↑Hb lead to increase and decrease in the amplitude of QRS complexes correspondingly, both in animal experiments and human subjects [72, 73].

20.3 Atmospheric Pressure Changes

Exposure to high altitude (hypoxemic stress) impacts normal subjects and patients, producing pulmonary hypertension, which is reversible on return to low altitudes. At 4,700 m altitude, normal subjects showed striking low frequency (0.04–0.06 Hz) heart rate oscillations during sleep, which correlated with low frequency (0.05 Hz) respiratory oscillations consistent with an unstable cardiopulmonary control system, not merely attributable to increased sympathetic modulation of heart rate [74]. The same high altitude, as simulated in a hypobaric chamber, had no impact on ventricular stimulation thresholds, thus ensuring the safety of pacing in pacemaker patients exposed to high altitude [75]. At a simulated altitude of 4,500 m, an increase in myocardial blood flow by 62% was documented in normal subjects inhaling a hypoxic gas mixture, expected to induce myocardial ischemia in patients with coronary artery disease (CAD); however, airplane travel corresponds to exposure to an altitude of ~2,000 m (cabin pressure in most airplanes during flight), does not lead to changes in myocardial blood flow, and thus it is tolerated even by patients with CAD [76]. However, all the above reflect changes imparted by associated hypoxemia. Apnea due to underwater diving results in bradycardia and increase in R wave amplitude [77], and scuba diving may lead to ECG signs of right ventricular hypertrophy, sinus bradycardia, and sinus arrhythmia [78]. Premature atrial and ventricular beats may occur even in normal subjects during deep breath-hold dive [79]. Two other influences are included herein, although they are not experienced necessarily in association with changes in increases in atmospheric pressure: (1) The Bezold-Jarisch reflex involves a marked increase in vagal efferent discharge to the heart with profound bradycardia-hypotension responses, and can occur with many ordinary activities [80], various pathologies, and medical procedures; and (2) face immersion increases heart rate variability

via an increase in vagal activity [81], and total body immersion in cold water increases QT dispersion in normal subjects, particularly older persons[82].

20.4 Gravity Changes

Aerial combat and space travel entails changes in gravity exerted on the body. In experiments with normal subjects, employing a special aircraft, increase in gravity (1.7–1.8 G) led to increase in the R wave of Z lead, while decrease in gravity resulted in the opposite effect. The mechanism by which gravity changes the amplitude of QRS complexes appears to be dependent on alterations in thoracic and heart geometry, thoracic conductivity, and the heart-electrode distance [83]. Sustained high gravity acceleration led to tall narrow-based T waves 1 min after the stress period; since hyperkalemia was found immediately after stress, its role in the T wave changes is implicated, although adrenergic stimulation is also a possible alternative cause [84].

20.5 Temperature Changes

20.5.1 Hypothermia

Low body temperature imparts characteristic changes to the ECG. These include sinus bradycardia, prolonged PR, QRS, and QTc intervals, and the "Osborn waves", i.e., slowly inscribed camel-hump like deflections of the J point in the same direction as the QRS complexes, bridging the end of the QRS and the beginning of the ST segment, seen most prominently in leads facing the left ventricle and in the inferior limb leads [85–89] (Fig. 20.7). The amplitude and duration of the J waves bear some relationship to the fall of the body temperature. Flat or even inverted T waves appear when the J waves become very prominent. The resultant QRS complex widening is occasionally misinterpreted as an intraventricular conduction delay or right bundle branch block. The prolongation of the PR interval suggests a slowed conduction in the atria and the AV junction. Atrial arrhythmias encountered include junctional rhythm, atrial flutter, and atrial fibrillation [90], with the latter being the most common, particularly with temperatures below 32°C; ventricular extrasystoles and ventricular fibrillation also occur with temperatures below 28°C [91]. Body shivering, even when not visually noticeable, results in intermittent or continuous baseline oscillation (Fig. 20.7). Rewarming abolishes both the arrhythmias and the "Osborn waves", although the latter may persist in an attenuated form for 12–24 h [87].

It has been thought that the "Osborn waves" may represent a current of injury, or early repolarization in a ventricular territory while delayed depolarization is under way in some other territory, or due to delayed ventricular depolarization [86, 92]. These waves are not pathognomonic of hypothermia, and may also be seen in patients with cerebral injuries, e.g., subarachnoid hemorrhage [93, 94], hypothalamic lesions, Prinzmetal's angina or other types of myocardial ischemia, infarction, coronary angioplasty [95] (Fig. 20.8), hypercalcemia [35], and as a normal variant [89]. These waves often simulate ischemic injury [16], resulting in problems in the differential diagnosis. Also, regional epicardial cooling of the heart in canine experiments led to "Osborn waves" indistinguishable from the ECG changes of Brugada pattern [96], suggesting a pathophysiological similarity of the two conditions, due to activation of transient outward current (Ito) [97]. A J wave is caused by the transmural (epicardial–endocardial) voltage gradient resulting from a prominent action potential notch in the epicardial, but not in the endocardial, cells. Hypothermia-related delayed conduction of action potential from the endocardial cells to epicardium also moves a latent J wave out of the QRS complex, making it even more prominent [98]. Experimental cooling of the ventricle causes T wave inversion [96], also seen in clinical hypothermia (Fig. 20.7).

20.5.2 Hyperthermia

Warming of the inside of the heart causes T wave changes [86]; this may have relevance in therapeutic ablations, where an increased temperature is produced in different heart chambers. Fever causes sinus tachycardia with or without nonspecific ST-T changes. Since fever accompanies many underlying pathologies, it is difficult to evaluate the effect of fever per

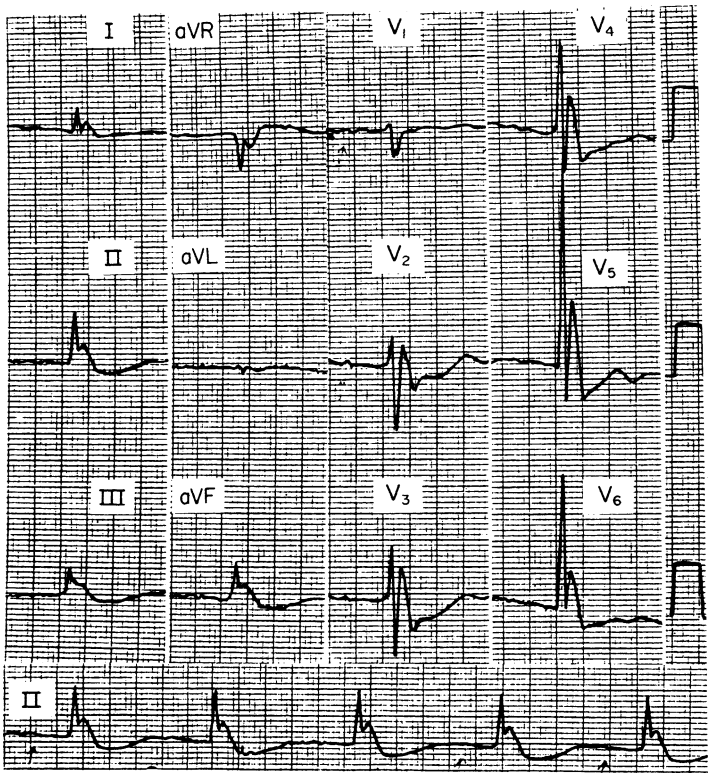

Figure 20.7

An ECG recorded from a patient with hypothermia, whose body temperature was below 32° C. "Osborn waves" in all leads, sinus bradycardia and 1° AV block (rhythm strip, lead II), low T waves, prolonged QT interval, and intermittent baseline oscillation from somatic muscle tremor are evident.

se on the ECG. All types of arrhythmias, from trivial to life threatening, have been described with febrile illnesses. The ECG phenotype in Brugada syndrome is temperature-dependent, and thus it may emerge with fever, in association with arrhythmias and T wave alternans [99–101]. Paroxysmal atrial fibrillation with fever most probably is due to an intercurrent illness. Malignant hyperthermia may lead to sudden death [102], and since anesthesia is a frequent precipitant, close ECG monitoring is emphasized [103].

20.6 Endocrine Disorders

Frequently, it is the ECG that alerts the physician to the fact that what is perceived initially as a primary cardiac disorder is indeed a secondary cardiac involvement of a systemic affliction [16]. Endocrine disorders impact the heart by direct and indirect ways producing occasionally pathognomonic ECG appearances.

20.6.1 Thyroid Heart Diseases

Deficiency or excess of thyroid hormones exert direct effects on the cardiac electrical activity, leading to changes in the ECG; in addition, the secondary activation of the sympathetic nervous system (SNS) influences indirectly the heart's electrical activity [104, 105]. Direct effects of hyperthyroidism (↑TH) on the sinoatrial node fibers of the rabbit included shortening of the action potential duration (APD) and increase in the diastolic rate of depolarization, while the opposite

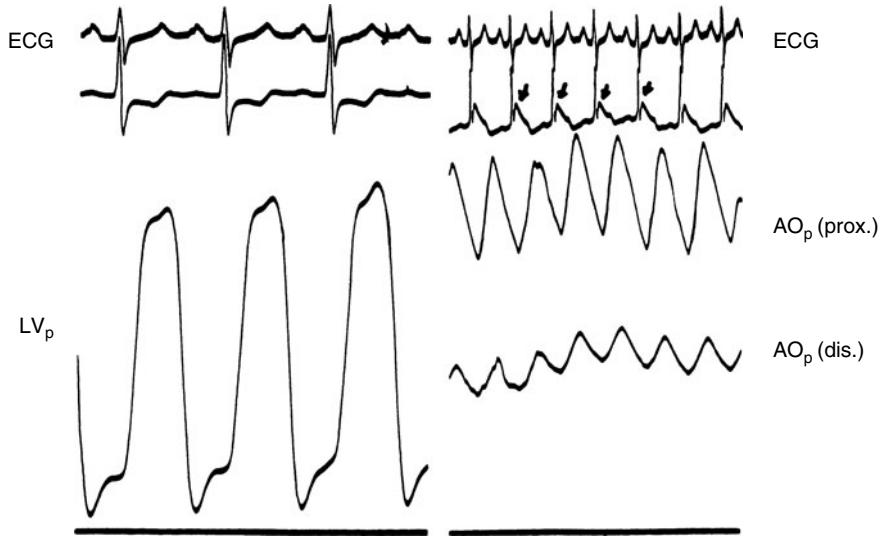

Figure 20.8

Inflation of the balloon during percutaneous transluminal coronary angioplasty induced regional myocardial ischemia; note arrows pointing to "Osborn waves" in ECG lead V_5. (AOp, aortic pressure: prox., proximal; dis., distal; LVp, left ventricular pressure).

was observed in hypothyroid animals [106]. ↑TH also induced shortening of the APD of atrial fibers [106, 107], AV conduction and functional refractory period, with opposite effects in hypothyroidism (↓TH). ↑TH prolonged APD in canine Purkinje fibers [108], and shortened it in guinea pigs [109], while in ventricular papillary muscle from rabbits, ↑TH prolonged APD at slow rates and shortened it at rapid stimulation [110]. It can be speculated that the lowered stimulation threshold for repetitive atrial activity in the hyperthyroid rabbit [107] and the shortened refractory period of atrial cells [105] are etiologically linked to the frequent association of atrial fibrillation (AF) and clinical ↑TH. The effect of thyroid hormone on sinoatrial, atrial and AV nodal fibers appears to be direct, and independent of the influence of the SNS.

20.6.2 Hyperthyroidism

20.6.2.1 Arrhythmias

Atrial arrhythmias encountered in ↑TH include sinus tachycardia, AF, and atrial flutter in descending order of frequency [111]. Sinus tachycardia is persistent throughout the 24 h, and its rate reflects the severity of ↑TH [105, 112, 113]. AF reversed to normal sinus rhythm in 62% of patients, but this occurs with some delay, or follows establishment of euthyroidism by several months [114]. Persisting AF in patients rendered euthyroid may require cardioversion [114], and may reflect the presence of comorbidity. A role for subclinical ↑TH in facilitating emergence of AF has been identified [115]. Young thyrotoxic patients rarely have AF [116]. Prospective data on the above are lacking. Paroxysmal atrial tachycardia, and premature atrial and ventricular beats are rare [111]. The Wolff-Parkinson-White ECG pattern is more frequent in hyperthyroid subjects than in the general population [2, 117]. Paradoxical intraatrial conduction disturbances, manifesting as prolongation and notching of P waves, and 1°, 2° and 3° AV block are also found [105, 112, 113]. The AV block, which often precedes the emergence of atrial fibrillation, is also paradoxical since canine experiments have documented enhanced AV conduction (see Sect. 20.6.1) [111]. Even intraventricular conduction blocks can occur, most commonly left anterior fascicular block and right bundle branch block (RBBB) [111, 113]. These changes are reversible with management of ↑TH [111, 113].

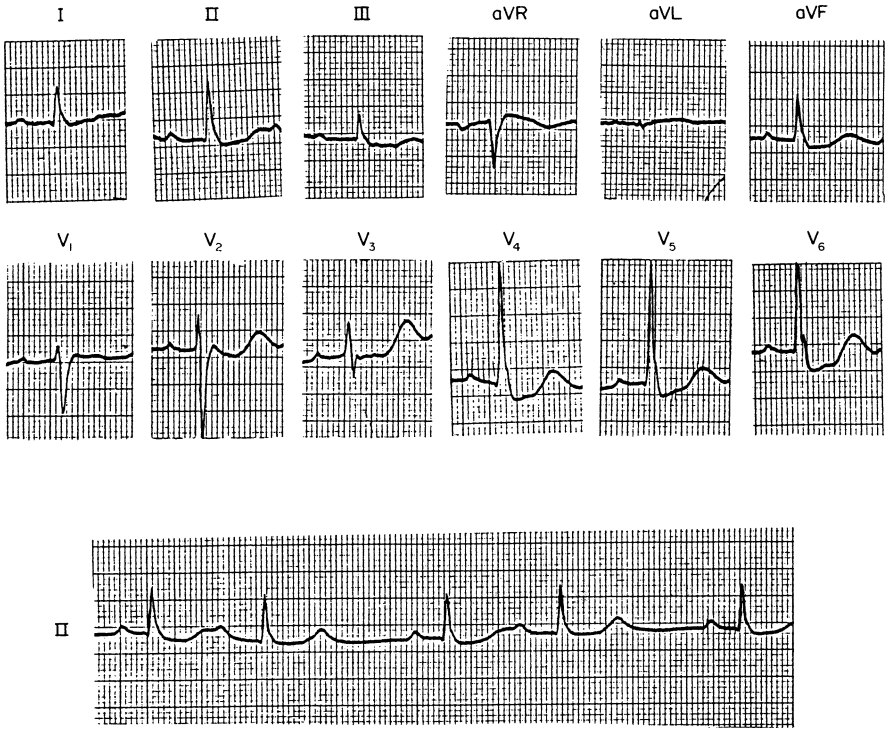

Figure 20.9
ECG recorded in a patient during an episode of thyrotoxic periodic paralysis, showing marked ST-T changes and QT interval prolongation (*upper* panel), and periods of Mobitz II 2° AV block (*lower* panel).

20.6.2.2 P Wave, QRS Complex, ST Segment, T Wave

Increased amplitude of QRS complexes and P waves, simulating left ventricular hypertrophy and P-pulmonale may be seen with ↑TH, and can lead to such erroneous diagnoses. Perhaps these increased amplitudes are due to the influence of the thyroid hormone, or the aroused SNS [104], or the rapid heart rates per se [118]. Nonspecific ST-T abnormalities were observed in 25% of patients with hyperthyroidism, particularly in women 20–30 years old [112, 113].

While a shortened QT interval was detected in hyperthyroid patients by some [112], others have observed prolonged QTc in patients with ↑TH, with a good positive relationship between the QTc interval and serum levels of tri-iodothyronine, thyroxine, and tri-iodothyronine uptake, but not heart rate, suggesting that a direct effect of elevated thyroid hormones on the myocardium must be at play [119].

Thyrotoxic periodic paralysis is characterized by episodic weakness and paralysis of skeletal muscles. In a study of this syndrome, serum K^+ was ≤2.8 mEq L^{-1} in all patients during paralysis and the ECGs showed sinus arrest and 2° AV block in a few patients (Fig. 20.9), while none had extrasystoles [120]; nevertheless, ventricular fibrillation has been reported during periodic paralysis [121]. Other typical ECG features are sinus tachycardia, high QRS voltage, and prominent U waves [122–124].

20.6.3 Hypothyroidism

A combination of sinus bradycardia and low-voltage P, QRS and T waves (Fig. 20.10) is seen in the ECG of patients with ↓TH [105]. These changes may be related to the direct effects of low levels of circulating thyroid hormones on the

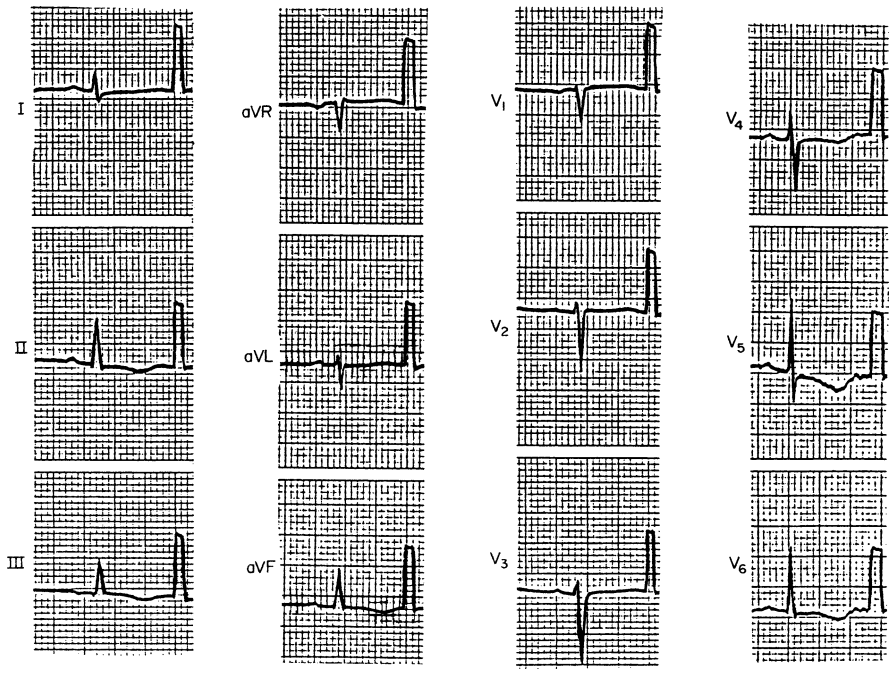

Figure 20.10
ECG of a 40-year-old woman with hypothyroidism.

myocardium, associated pericarditis or pericardial effusion, intracardiac and extracardiac deposits of myxomatous material. The frequently prolonged QT interval associated with low T wave amplitude may render the accurate measurement of the QT interval problematic [111]. The low-voltage ECG does not correlate with pericardial effusion [125], suggesting that other causes for this may be implicated.

The incidence of AV and intraventricular conduction blocks (particularly incomplete and complete RBBB) is greater by a factor of 3 in patients with myxedema than in the general population [105, 126], but complete AV block associated with syncope is less common [127]. Both sinus bradycardia and 1° AV block improve with the administration of thyroid hormone. Atrial flutter, AF, and nodal tachycardia, are rarely seen. Ventricular tachycardia in association with syncope in patients with myxedema coma has been reported [128, 129]. An increased rate of reentrant ventricular tachycardias may be due to the prolonged action potential duration [130].

20.6.4 Parathyroid Diseases

Hyperparathyroidism and hypoparathyroidism, along with many other mechanisms, lead to hypercalcemia and hypocalcemia respectively with ECG changes caused by these biochemical abnormalities (see Sect. 20.2.3).

20.6.5 Hypothalamus and Pituitary Gland

The hypothalamus is the center of autonomic sympathetic and vagal control of the heart. Animal experiments with stimulation of the hypothalamus led to arrhythmias and repolarization abnormalities, and its injury may be the reason for the characteristic T wave changes in subarachnoid hemorrhage (see Sect. 20.7) [111]. Pituitary insufficiency is associated with T wave abnormalities and prolonged QTc, but no changes in the QRS complex or ST segment; these T wave changes, which are similar to those seen in adrenal insufficiency and myxedema, are abolished transiently with isoproterenol, and

usually disappear with hormonal therapy [131]. There are no specific electrophysiologic or ECG abnormalities noted with acromegaly, but the 50–80% incidence of ECG changes, arrhythmias and conduction disturbances encountered with this disease are secondary to the associated cardiac hypertrophy and cardiomyopathy. Changes noted include ST segment depression and T wave inversion, septal Q waves, left axis deviation, increased QT dispersion, conduction abnormalities, atrial and ventricular ectopic beats, sick sinus syndrome, supraventricular and ventricular tachycardias, and late potentials in signal averaged ECG [132–134]. AF or sinus tachycardia in acromegaly should prompt evaluation of associated hyperthyroidism.

20.6.6 Cushing's Disease and Cushing's Syndrome

High levels of cortisol secretion are associated with hypertension and accelerated atherosclosis with resultant changes in the ECG; left ventricular hypertrophy with inverted T waves has also been described in Cushing's syndrome [135]. An increase in the PR and QTc intervals has been observed with cortisol hypersecretion [104].

20.6.7 Hyperaldosteronism and Hypoaldosteronism

Aldosterone hypersecretion (Crohn's disease) leads to hypertension and hypervolemia associated with increased QRS complexes, and ECG signs of hypokalemia (see Sect. 20.2.2). In cases of hypoaldosteronism (Addison's disease), the ensuing hyperkalemia leads to all the expected ECG changes (see Sect. 20.2.1) [136]. Sinus bradycardia, low ECG voltage, low or inverted T waves, and prolonged QTc are also seen with Addison's disease. Adrenal insufficiency in rats and cats did not alter the resting or action potentials [137].

20.6.8 Pheochromocytoma

A large variety of ECG abnormalities has been noted in patients with pheochromocytoma. Sinus tachycardia, left ventricular hypertrophy, sinus node dysfunction with intermittent sinus arrest and AV-nodal escape rhythm, are found; also ST segment depression, elevation, and inverted, upright, and sometimes positive "giant T waves" diagnostic of acute myocardial infarction (MI) have been documented. The postulated mechanisms for these changes include "catecholamine myocarditis", myocardial infarction, hypertrophic, apical (Japanese), dilated and "tako-tsubo" cardiomyopathies, and coronary vasospasm [138–140]. Other findings include a decreased low frequency component of heart rate variability, "pseudo-P-pulmonale" due to high circulating catecholamines, frequent premature ventricular beats, monomorphic ventricular tachycardia, torsade de pointes, and long QT interval [38, 141–144, 146, 147].

20.6.9 Diabetes Mellitus

In experimental diabetic animals, sinus bradycardia, prolongation of the sinus node recovery time, inhomogeneity of atrial conduction and AV nodal block, have been found [148]. In diabetic patients without hypertension and coronary artery disease (CAD), diffuse T wave abnormalities are frequently noted. Also the expected ECG changes due to hyperkalemia with diabetic ketoacidosis are seen, while hypokalemia, and its attendant ECG changes may ensue with intracellular influx of K^+ following therapy of acidosis (alkali, fluids, and insulin). Transient deep T wave inversions with prolonged QT interval may be present during therapy of diabetic acidosis while serum K^+ is normal. These are attributed to a central nervous system abnormality coinciding with sensorial disturbances [149]. Sulfonylurea attenuates the magnitude of ST segment elevation during an acute myocardial infarction, leading to inappropriate withholding of thrombolytic therapy [150]. Diabetic patients with CAD have a higher risk of developing silent myocardial ischemia (ST segment depression) during exercise than non-diabetic patients [151]. Autonomic neuropathy in diabetic individuals results in a decrease in heart rate variability and a disappearance of the heart rate dependency of the QT interval, a plausible mechanism for the increased risk of ventricular arrhythmias and sudden death in such patients [152].

The most frequent conduction disorders in type 2 diabetes are RBBB and left anterior fascicular block [153]. Hypoglycemia can induce angina and silent myocardial ischemia with classic ST-T changes, in diabetic patients with and without CAD, which are abolished with glucose administration [154, 155]. Hyperglycemia increases the pacing threshold [12].

20.7 Neurological and Neuromuscular Diseases

20.7.1 Cerebrovasular Accidents

An increased incidence mainly of repolarization ECG abnormalities, e.g., flat, large broad inverted, and rarely positive "giant T waves", depressed or elevated ST segments, prominent U waves, and prolonged QT intervals are noted in patients with cerebrovascular accidents (CVA) [156, 157], particularly in those with subarachnoid or intracerebral hemorrhage, who show more severe such changes [158, 159]. Similar ECG abnormalities are seen with ischemic strokes, neurosurgical procedures, head injuries, meningitis, epilepsy, and intracranial tumors. Prolonged QT intervals are associated with the risk of torsade de pointes [160, 161]. The prevalence of ECG abnormalities with subarachnoid hemorrhage has been reported to be 50–90% [159–166]. The ECG changes resemble those of myocardial ischemia (Fig. 20.11), with wide and deeply inverted T waves noted usually in leads I, aVL, and left precordial leads, although the QRS complexes are not usually altered [164, 167]. Q waves may occasionally develop and in combination with ST segment elevation (Fig. 20.11) simulate the ECG of patients with acute MI [168, 169]. In the latter, usually the duration of the T wave and QT interval is shorter, and the amplitude smaller. These ECG abnormalities may be either short-lived or persist for several weeks [169, 170]. Arrhythmias are noted in >75% of patients, and include sinus bradycardia and tachycardia, atrial and ventricular extrasystoles and atrial fibrillation (AF) [168, 171, 172]. Often it is not clear whether the last is the consequence or the cause of a CVA [173]. After acute CVA ambulatory 7-day ECG monitoring surpassed the standard ECG and 24-h Holter

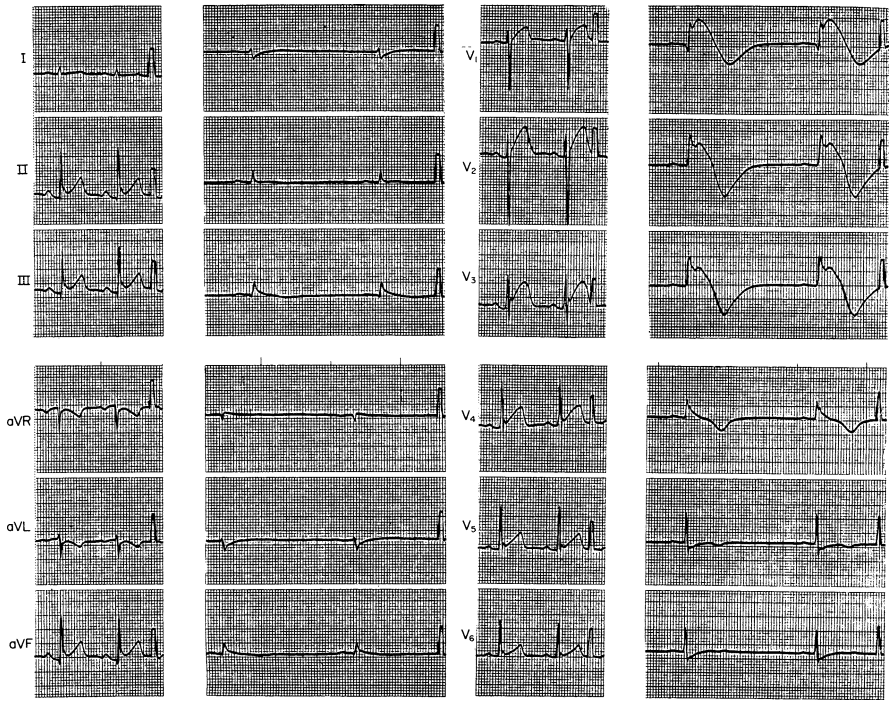

Figure 20.11

Marked bradycardia with precordial ST segment elevation and giant T wave inversions resembling changes seen in the acute phase of myocardial infarction, in serial ECGs recorded in the acute stage of subarachnoid hemorrhage.

monitoring, in the detection of AF [174]. All varieties of AV blocks have been encountered with CVAs [175]. Heart rate variability decreases and heart rate increases after the acute phase of CVA [176].

The exact cause of these ECG changes has not been delineated, but it appears that cerebrovascular pathology leads to myocardial injury [177]. Moreover it appears that specific brain lesions lead to specific ECG abnormalities; e.g., insular lesions were related to sinus tachycardia, ectopic beats, and ST elevation, with right insular lesions related to AF, atrioventricular block, ectopic beats, and inverted T waves, and right insular lesions, compared with left or no insular lesions, increased the odds of death within 3 months independent of stroke severity and age [178]. Postmortem study of hearts revealed interruption of myocyte bundles and disarray of myocyte architecture with more severe such changes in patients who had tall inverted or peaked T waves [157]. Also focal subendocardial hemorrhagic lesions were found in some patients who died of subarachnoid hemorrhage [179], and prospective studies with a variety of intracranial lesions documented subendocardial hemorrhage in 40% and epicardial hemorrhage or myocytolysis in 8% of patients [180]. The rise of the myocardial biomarker troponin I, noted in patients with neurological syndromes, further supports the occurrence of cardiac damage [181]. This direct proof of heart injury is also corroborated by evidence for regional wall motion abnormalities in ventriculographic and echocardiographic studies [182–184]. The arrhythmias and ECG changes, observed after manipulation of the circle of Willis during surgical procedures in humans and experimental animals, provide evidence that a pathophysiologic link between the central nervous system and the heart is at play [185].

Mechanistically the T wave changes have been attributed to functional repolarization abnormalities [186, 187], structural heart disturbances [188], parasympathetic nerve stimulation [189], and surge of sympathetic tone and catecholamine release [190]. Animal studies have demonstrated that infusions of catecholamines and stimulation of hypothalamus and insula produce the same hemodynamic alterations and necrotic myocardial lesions seen in subarachnoid hemorrhage [168, 191]; these lesions appear similar to those seen in patients with pheochromocytoma (see Sect. 20.6.8) or cocaine abuse, conditions previously linked to sympathetic stimulation [192]. Of course it is possible that this sympathetic arousal leads to myocardial damage mediated by increase in the myocardial oxygen demands in patients with neurologic syndromes and coronary artery disease. Nevertheless, autopsies in patients with head trauma or subarachnoid hemorrhage have identified myocardial injury in the presence of normal coronary arteries [190, 193]. It is also hypothesized that the myocardial lesions found at autopsy are caused by disturbances in the cardiac contraction pattern resulting from abnormal excitation of the origins of the autonomic nerves at the central nervous system mediated by the extravasation of blood [157]. The bulk of evidence indicates that sympathetic arousal is the pathophysiologic mechanism for myocardial damage, via a direct effect or an intense coronary vasoconstrictive influence [192]. This is further corroborated by animal studies showing that adrenergic blockade, reserpine, and occasionally, atropine prevented the ECG abnormalities [180].

20.7.2 Seizures

At least a dozen electrophysiological disorders (torsade de pointes, Brugada syndrome, long-, and short-QT syndromes and arrhythmogenic right ventricular dysplasia) as well as cardiogenic syncope, often masquerade as “epilepsy” or “seizures” in both the adult and pediatric population, emphasizing the importance of the ECG and continuous ECG monitoring in unraveling many of the above diagnostic conundrums [194]. On the other hand, the higher incidence of sudden death in epilepsy than in the normal population points to ventricular tachyarrhythmias as the possible culprit. The reduction of high frequency and increase of low frequency values in heart rate variability in the frequency domain analysis in such patients suggests that increased sympathetic activity may be the incriminating factor [195].

20.7.3 Neuromuscular Diseases

Friedreich’s ataxia, progressive muscular dystrophy and myotonic muscular dystrophy (MD) are hereditary neuropathic diseases associated with cardiomyopathy. MD is associated with very slow pulse, high incidence of all types of AV block, Q waves and slurring of the QRS complexes resulting from changes in the intraventricular conduction, left axis deviation,

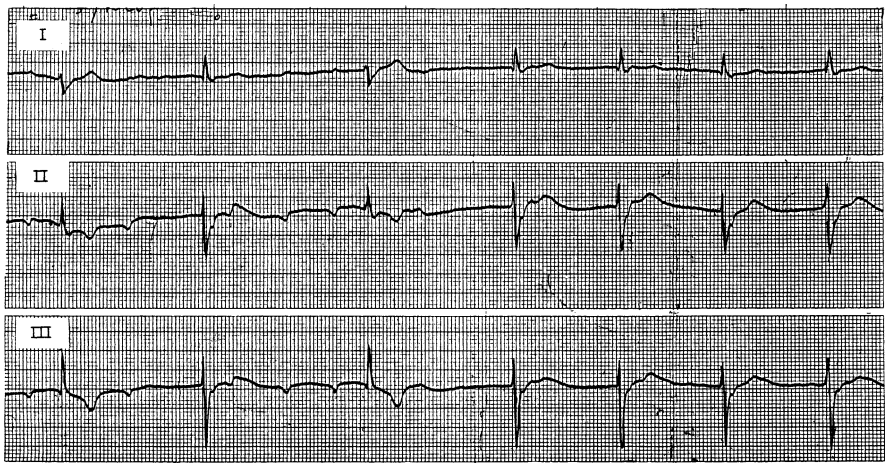

Figure 20.12
An ECG from a patient with myotonic dystrophy during syncopal seizure, showing complete AV block and AV junctional escape rhythm.

P waves of low amplitude, ST segment abnormalities, and flat or inverted T waves [196, 198, 199]. Most frequent cardiac manifestations of this disease are conduction abnormalities (Fig. 20.12) for which electronic pacing is often required (Fig. 20.13).

Atrial arrhythmias also occur more frequently (flutter and fibrillation) than ventricular arrhythmias. An association of the frequency of arrhythmias and conduction disturbances with the severity of the disease has been documented [199]. In spite of the high prevalence of conduction abnormalities in MD, the incidence of complete heart block is lower than expected [200, 201]. A tall R wave in V_1 is seen in Duchenne muscular dystrophy. Cardiac involvement in facioscapulohumeral MD was characterized by myocardial thickening in the echocardiogram and incomplete right bundle branch block, ST elevation in V_2–V_4, and tall T waves in V_3–V_5 [202, 203]. Short and prolonged QTs are seen in different forms of MD [204].

20.8 Thoracic Diseases

20.8.1 Thoracic Skeletal Abnormalities

Posterior depression of the sternum and costal cartilages (pectus excavatum) (PEX) may be associated with ECG changes, which are not specific for the condition and are attributed to the compression and leftward displacement of the heart between the sternum and the spine. These ECG changes, which may not necessarily signify any cardiac abnormality, include non-ischemic and ischemic type T wave inversions (Fig. 20.14), late transition of the precordial QRS complexes with the Q waves in V_1–V_4 simulating an anterior myocardial infarction (MI), complete right bundle branch block (RBBB), an rSr' pattern in lead V_1, and a negative P wave in lead V_1, similar to that of lead aVR; this last finding may be due to the direction of the atrial depolarization vector away from the V_1 position, because of the leftward displacement of the heart [205–208]. PEX was associated with incomplete blockade of the bundle of His, ventricular extrasystoles, Wolff-Parkinson-White syndrome, and mitral valve prolapse (MVP) (97% of cases) [209]. With thoracic deformities, the distance of the heart from certain precordial electrodes may increase or decrease, resulting in low or high QRS complexes. Paroxysmal tachycardias have been described in association with PEX [206], but as in patients with MVP, it is uncertain whether they are truly related to the condition. In patients

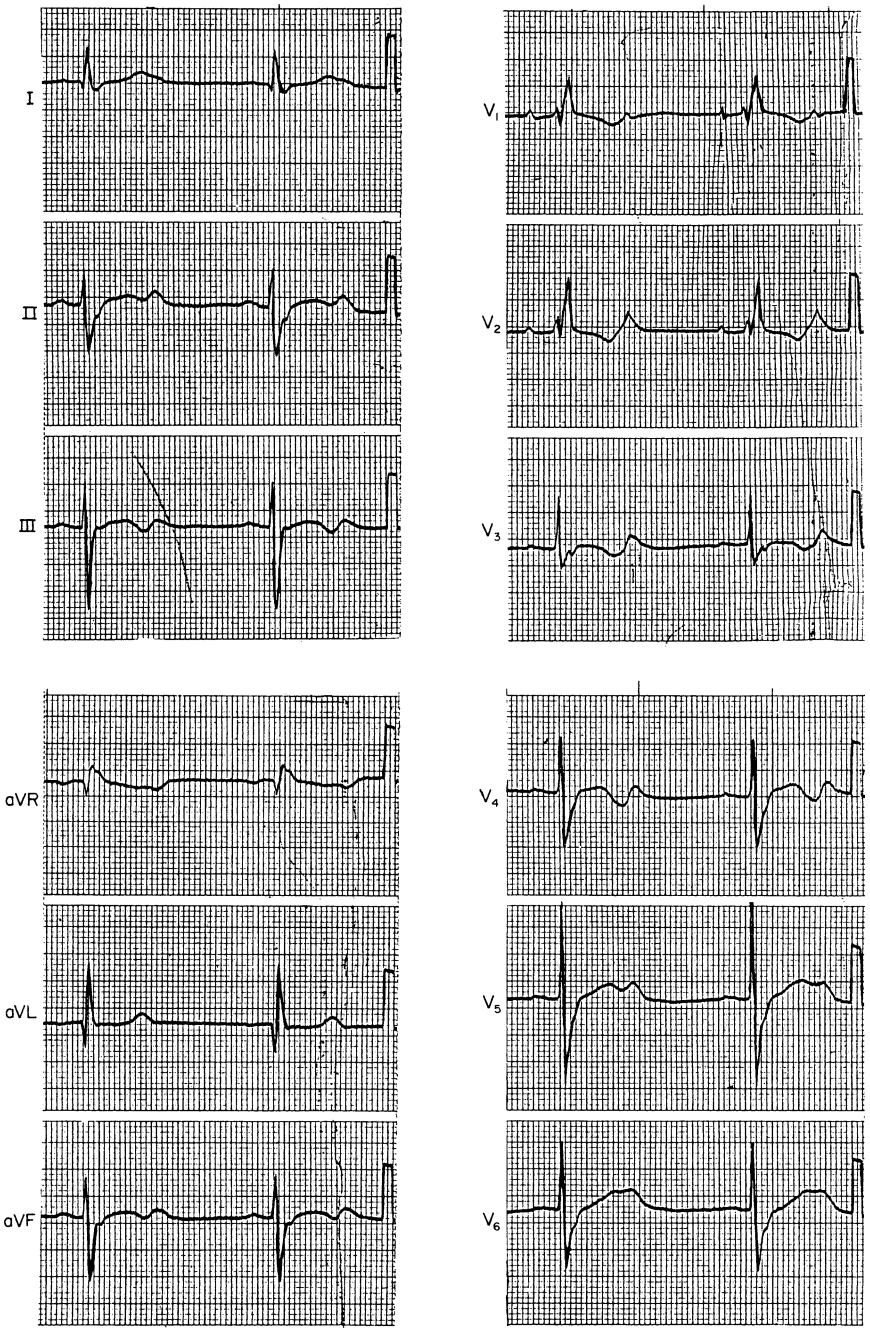

Figure 20.13

The ECG obtained after recovery from syncopal seizure of the same patient as in Fig. 20.12, shows marked sinus bradycardia, prolonged QT interval, prominent U wave, 1° AV block, and complete right bundle branch block with left anterior fascicular block (frontal QRS axis of −60°). This patient underwent implantation of an artificial pacemaker.

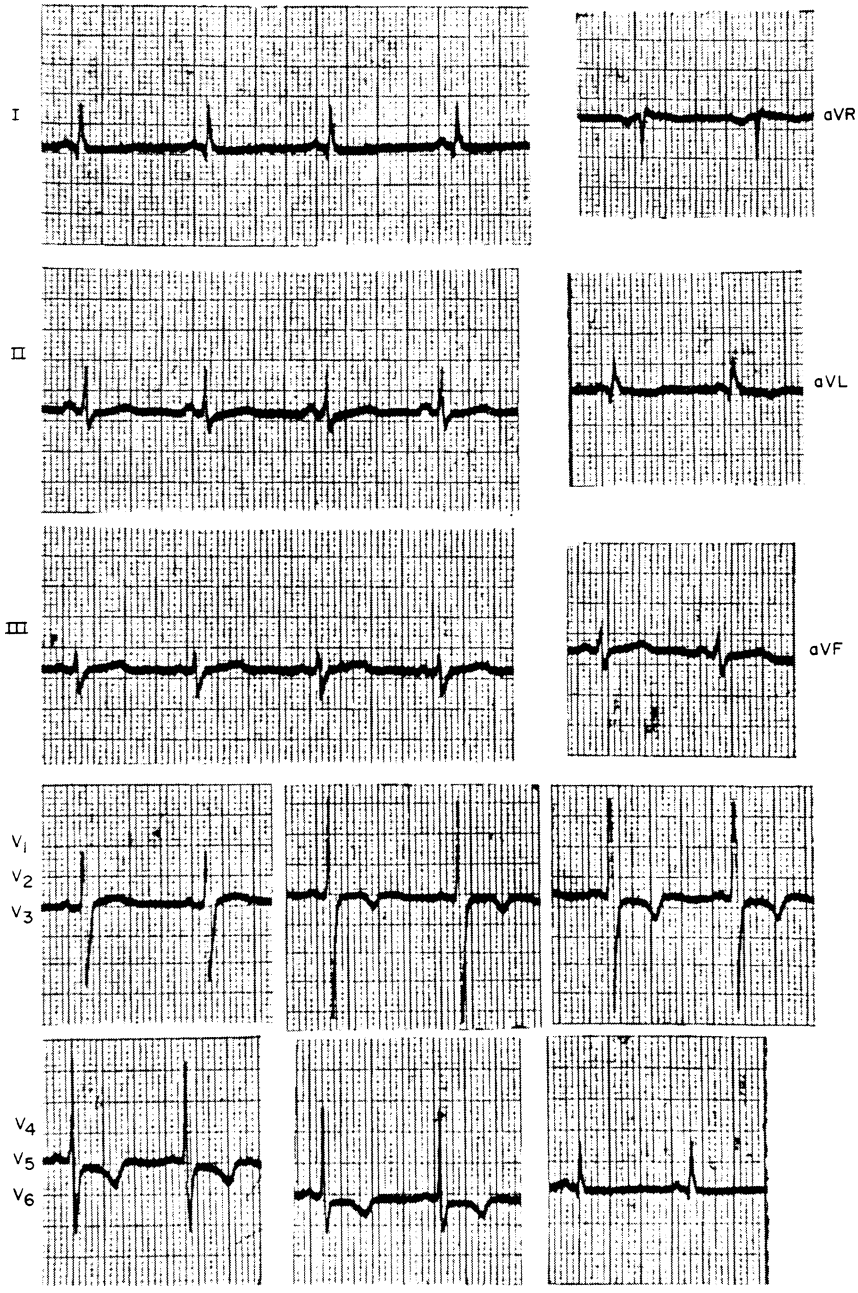

Figure 20.14
ECG of a patient with pectus excavatum showing ischemic-appearing T waves in the precordial leads.

with the "straight back syndrome", in which the heart is compressed and leftwardly displaced between a "straightened" dorsal spine and the unaffected sternum, ECG changes similar to those described in patients with PEX have been noted. Noninfarctional Q waves in the inferior leads or severe frontal QRS left axis deviation has been observed [86]. Severe degrees of kyphosis, scoliosis or kyphoscoliosis are accompanied by deranged lung function, hypoxemia, and pulmonary hypertension. In such situations, the ECG changes may be related to chronic cor pulmonale (see

Sect. 20.9.1). An association of thoracic skeletal abnormalities and MVP has been documented [210]; also it has been postulated that MVP may be an acquired condition caused by a growth disproportion between the heart and the chest cavity [211].

20.8.2 Parenchymal Lung Diseases

Chronic obstructive lung disease (COPD) and its clinical expressions of bronchitis and emphysema may lead to a decrease in the ECG voltage, particularly in the limb leads; also the precordial leads may show an attenuated ECG voltage, especially in the left precordial leads, which partially may be due to the increase of the distance of the heart from the recording electrodes. Of course this occurs when there is a lung-inflated consequence of the underlying pathology, as in emphysema. Theoretically, in asthma, lung hyperinflation also may be present episodically. In severe asthma, transient sinus tachycardia, right axis deviation, right atrial enlargement, right ventricular hypertrophy, ventricular premature complexes, and RBBB were noted, and correlated with the degree of airway obstruction [212]. Asthmatics show reversible inferior T wave inversions [213], and increase in heart rate and decrease in heart rate variability, when exposed to ambient coarse particles [214]. The presence of hypoxia ($\downarrow O_2$), hypercapnea ($\uparrow CO_2$), respiratory acidosis, alkalosis or exacerbations of COPD may set the stage for more ECG abnormalities to appear (see Sects. 20.2.8 and 20.2.9). The frontal QRS axis is vertical or rightward, and poor R wave progression in the precordial leads is noted simulating an anterior MI. Both are due to the downward displacement of the diaphragm resulting in an anatomical, and thus an electrical, vertical heart position and a high placement of the precordial leads relative to the heart [38, 86]. In addition, right ventricular dilatation contributes to the leftward shift of the transition zone. P waves are tall in leads II, III, and aVF with a vertical or rightward frontal axis, due to the heart's vertical position; P-R segment and ST segment depressions in the same leads are due to exaggerated atrial repolarization [38]. Some of the above changes are stable in established COPD, or transient, as in patients with asthmatic attacks. Exercise, even when associated with $\downarrow O_2$, does not cause myocardial repolarization abnormalities (altered QTc dispersion) in patients with COPD [215]; others, however, have documented increase in QTc dispersion with $\downarrow O_2$ and $\uparrow CO_2$, and decrease of QTc dispersion with partial correction of $\downarrow O_2$ [216].

Theoretically lung tissue, particularly in its hyperinflated state, is a poor electrical conductor and should produce an increase in ECG potentials based on its increased impedance [217]. However, this may be offset by the increase in the heart surface-electrode distance due to hyperinflation. When acute or chronic cor pulmonale ensues, the expected ECG pictures emerge (see Sects. 20.9.1 and 20.9.2). Extensive atelectasis and infiltration due to pneumonia, pleural effusions, and other complications are expected to influence the ECG further. The ECG voltage is routinely attenuated in patients cared for in respiratory critical care units (Fig. 20.15).

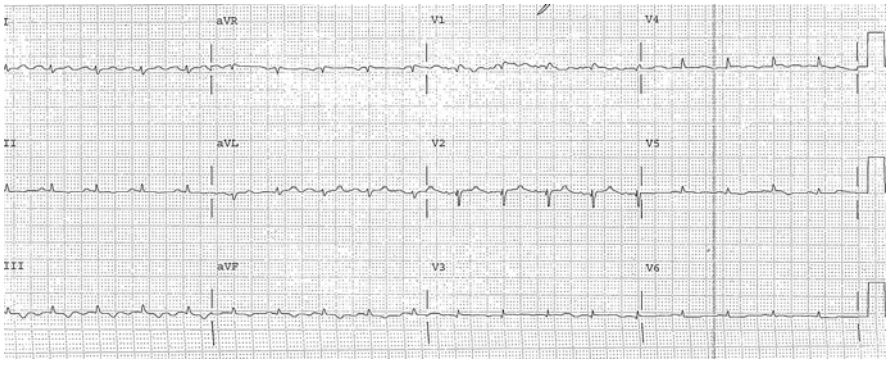

Figure 20.15

ECG of a 74-year-old woman hospitalized in the Respiratory Intensive Care Unit. The chest X-ray showed infiltrates and atelectases, an endotracheal tube in place, bilateral pleural effusions and cardiomegaly. The echocardiogram showed normal size and function of the left ventricle, and enlarged hypocontractile right ventricle with pulmonary hypertension. Note the low ECG voltage, tachycardia, and a frontal QRS axis of 95°.

COPD is associated with atrial and ventricular arrhythmias, particularly multifocal atrial tachycardia, which typically is seen in elderly patients with severe decompensation [218]. Although not firmly established, the mechanism of this arrhythmia may be delayed afterdepolarizations leading to triggered activity [218]. Several factors may be potentially arrhythmogenic in patients with COPD, including $\downarrow O_2$, $\uparrow CO_2$, acid-base disturbances, cor pulmonale and the use of sympathomimetic drugs, methylxanthines, digitalis, preexisting cardiopulmonary pathology, conscious sedation, endotracheal intubation, anesthesia, invasive procedure and surgery. Cough related syncope has been traced to inappropriate chronotropic response to hypotension [219].

20.8.3 Sleep Apnea/Hypopnea Syndrome

Marked obesity and COPD, with associated $\downarrow O_2$, $\uparrow CO_2$, and oropharyngeal obstruction, result in the sleep apnea/hypopnea syndrome (SAS), which is associated with autonomic nervous system dysfunction and culminates in pulmonary hypertension, and heart disease. ECG changes noted in SAS include sinus tachycardia, bradycardia, arrhythmia and arrest, supraventricular and ventricular couplets and tachycardia, nocturnal ST segment depression, 2° AV block Mobitz II, high ULF, VLF, LF components and high LF/HF, but low HF values in spectral analysis of heart rate variability, and increased QTc dispersion [220–222]. Continuous positive airway pressure therapy and bariatric surgery ameliorates or eradicates all or many of the above [222, 223]. Heart rate tachograms derived from Holter ECG monitoring can be used, in lieu of polysomnography, to detect SAS [224].

20.8.4 Lung Congestion and Lavage

In pulmonary edema, reduced ECG voltage is noted, due to the short-circuiting effect on the cardiac potentials from the congested lungs surrounding the heart; this phenomenon can be exploited in monitoring patients for congestive heart failure; however, the interplay of cardiac volume changes during episodes of acute pulmonary edema may offset the attenuation of ECG complexes, leading to unchanged ECG potentials [225]. Lung lavage, particularly of the left lung, used in the therapy of pulmonary proteinosis, results in attenuated ECG potentials [226].

20.8.5 Pneumothorax and Pneumopericardium

The ECG of pneumothorax and pneumomediastinum simulates appearances found in cardiac pathology [227–231], with the left pneumothorax producing a decrease in QRS and T wave voltage, inverted T waves in the precordial leads, and right frontal QRS axis deviation [231], which leads to an increase in the voltage of the R wave in lead III (Fig. 20.16). Occasionally right pneumothorax may not produce discernible ECG changes but when it does, the transitional zone moves to the left, T waves decrease in the right precordial leads, R and T waves increase in the left precordial leads, and can simulate anterior MI [232]. In left pneumothorax, the transitional zone is unchanged, but the voltages of QRS and T waves in the precordial leads and the R waves in V_4–V_6 decrease. Tension pneumothorax may alter the ECG in unexpected ways and may imitate other pathologies, particularly pulmonary embolism, and MI. The underlying mechanisms for these ECG findings are probably the drastic positional changes of the heart, and the resultant change in its distance from the recording electrodes due to alterations (particularly with left pneumothorax) in the intrathoracic volume conductor properties, overloading of the right ventricle, and a rotation of the heart. Pneumomediastinum can cause T wave inversions [233].

20.8.6 Pleural and Mediastinal Effusions

Pleural effusion, depending on its size and location, results in lung and heart displacement, influencing the ECG appearance. When it is left-sided and large, attenuation of QRS complexes and R waves and pseudo-infarctional Q waves are

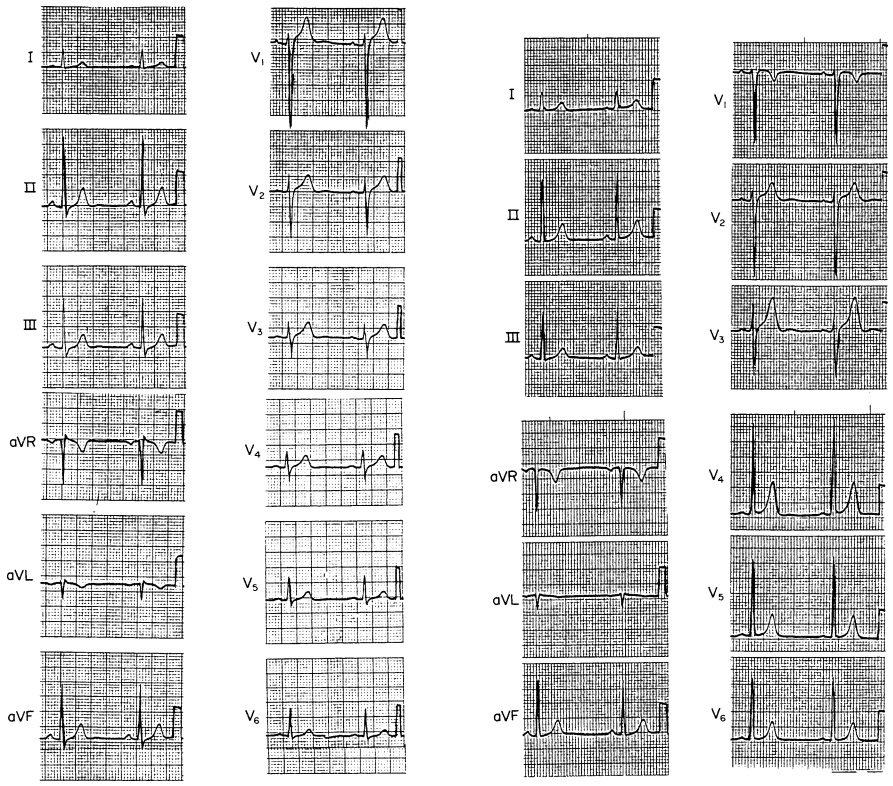

Figure 20.16

ECG in spontaneous left pneumothorax showing reduced QRS voltage in V_3–V_6 (*left* panel), with increased voltage after recovery (*right* panel).

observed, mediated by an increase in the heart-electrode distance and the short-circuiting of heart's potentials due to the intervening fluid [217, 234]. In addition to pathological causes, pleural effusion may follow intrathoracic procedures [234] and insertion of central venous catheters (CVC), the latter employed for hemodynamic monitoring, hemodialysis, or facilitation of monitoring the intracardiac P wave via the CVC [235]. ECG changes are further affected when pleural effusion is combined with pericardial effusion.

20.8.7 Pleural Disease

Thickening of pleura due to inflammatory, infectious (tuberculosis) and neoplastic diseases, or radiation therapy, particularly involving the left side of the thorax is associated with attenuation of the ECG voltage. Often these pleural changes are coupled with pleural effusion, resulting in further loss in ECG voltage.

20.8.8 Aortic Dissection

Acute or chronic aortic dissection can lead to a spectrum of complications (outflow tract stenosis, aortic valve and coronary insufficiency, and myocardial infarction [MI], with suggestive ECG abnormalities). The ECG may be normal or indicative of prior pathologies. Typical of the ECG in acute aortic dissection is its fluidity in time as the clinical picture evolves. Differentiation of aortic dissection from acute MI is imperative, to avoid administration of thrombolytic therapy [236].

20.9 Pulmonary Hypertension

Pulmonary hypertension may arise acutely or gradually, be transient or progressive, and be primary, or secondary to lung or heart disease. Paralleling this variability in pathology, a spectrum of ECG changes is observed reflecting functional or structural alterations of the right ventricle and atrium. ECG changes observed in pulmonary hypertension are also modulated by other intercurrent conditions and left ventricular and atrial pathology.

20.9.1 Chronic Cor Pulmonale

Chronic conditions including COPD, other pulmonary diseases, congenital heart disease, recurrent pulmonary embolism, left ventricular systolic and diastolic dysfunction, obstructive sleep apnea syndrome, and primary pulmonary hypertension lead to chronic cor pulmonale. The ECG of chronic cor pulmonale includes frontal right axis QRS deviation, tall R waves in V_1–V_3, early R wave progression (counterclockwise rotation), R/S ≥ 1 in V_1, R amplitude in V_1 ≥ 5 mm, R/S V_5 ≤ 1, incomplete or complete right bundle branch block (RBBB), T wave inversion in V_1–V_3, and P pulmonale [237]; rarely ST segment depression or elevation in inferior leads is seen [238]. Chronic cor pulmonale with evidence of right ventricular hypertrophy and/or dilatation is occasionally presenting as reversed R wave progression, where the R waves decrease progressively from V_1 or V_2 to V_3–V_6. Arrhythmias encountered include sinus tachycardia, supraventricular and ventricular extrasystoles, atrial flutter and fibrillation, and multifocal atrial tachycardia.

20.9.2 Acute Cor Pulmonale and Pulmonary Embolism

All the above conditions culminating in chronic cor pulmonale may also cause acute cor pulmonale, which by definition is transient, although it can evolve to the chronic type. Pulmonary embolism, transient heart failure, or rise of left ventricular afterload, can lead to acute cor pulmonale. The ECG is not sensitive or specific for the recognition of pulmonary embolism, and changes and their severity depend on time and the frequency of recording, the size and location of the embolus and its hemodynamic consequences, and preexisting pulmonary and/or heart diseases [16]. The latter may complicate the diagnosis by either accentuating or masking the ECG abnormalities. The most frequent ECG abnormalities in patients with pulmonary embolism reported in three series were clockwise cardiac rotation and sinus tachycardia [239], RBBB and sinus tachycardia [240], and T wave inversion in the right precordial leads [241]. Also, the ECG was found to be normal in 72% and 27% of the patients with PEM [242, 243]. Other ECG findings include P-pulmonale, right axis deviation (RAD) and left axis deviation (LAD), an S_1Q_3 pattern, Q waves in leads III and aVF (but not II), S waves in leads I and aVL, R > 0.5 mV or R/S ratio >1 in lead V_1, QR pattern in lead V_1, nonspecific ST-T changes, 1° AV block, atrial and ventricular premature beats, and atrial flutter and fibrillation [86, 244–247]. The ST-T changes include T wave inversion in leads III and aVF, in addition to those in precordial leads, and ST segment elevation in leads III, aVR and V_1. ST-T changes in limb and precordial leads may be due to the right ventricular conduction disturbances, myocardial ischemia resulting from low cardiac output and/or pulmonary hypertension, and in some patients underlying coronary artery disease. In pulmonary embolism, ECG changes are transient, as compared to myocardial infarction (MI); also T wave inversions constitute an early feature, while they appear later in MI. An otherwise unexplainable episode of atrial fibrillation occasionally may be due to acute pulmonary embolism. The SIQ3T3 pattern, thought in the past, and even by some today, to be pathognomonic of pulmonary embolism [244] (Fig. 20.17), has been found to be equally prevalent in patients with and without this condition [246]. It is postulated that the SIQ3T3 pattern is due to left posterior fascicular block, mediated by selective stretch of the posterior part of the septum due to the high right ventricular pressure, leading to conduction delay in the posteroinferior fibers of the left bundle. Accordingly, LAD, which is twice as frequent as RAD, may be due to selective stretching of the anterosuperior branch of the left bundle [248]. Also the SIQ3T3 pattern may be due to mere right ventricular dilatation and change in this chamber's position relevant to the left ventricle and/or thorax.

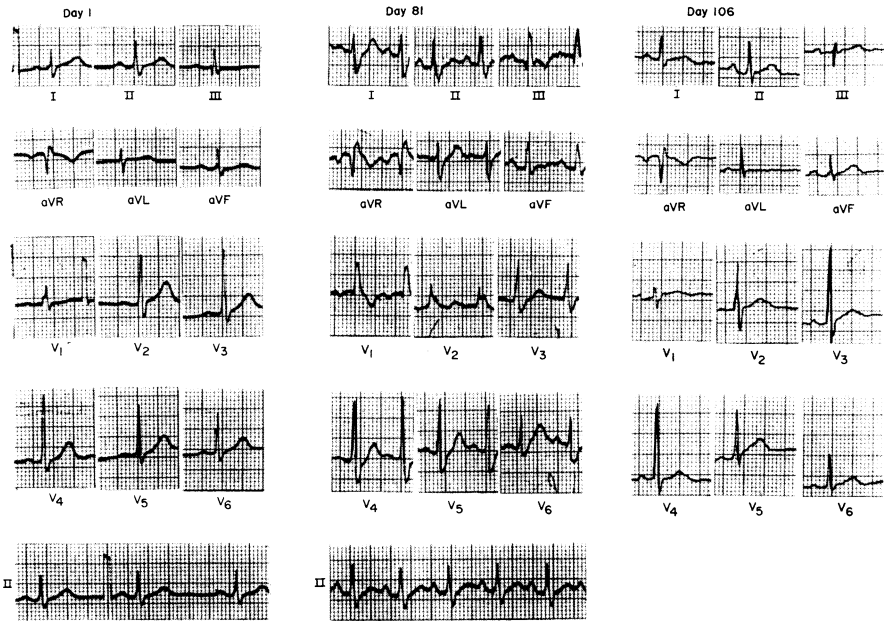

Figure 20.17

The ECG on day 1 before the occurrence of acute pulmonary embolism, showed normal axis and incomplete right bundle branch block (RBBB). The ECG on day 81, the day of the event, showed sinus tachycardia, marked right axis deviation, $S_1Q_3T_3$ pattern, complete RBBB, and T inversion in leads V_1 and V_2. The ECG on day 106, 1 month after successful thrombolytic treatment, showed a normal axis and no sign of right heart overload.

Right ventricular pressure overload may direct the initial left septal force superiorly and the terminal QRS vector rightwardly, resulting in a Q wave in lead III and an S wave in lead I, respectively; the same mechanism may also lead to a clockwise rotation of the heart along its longitudinal axis, i.e., a leftward displacement in the transitional zone of the precordial leads. The occasional appearance of Q waves is due to marked changes in the position of the left and right ventricle due to the latter's dilatation. Incomplete or complete RBBB with RAD is also attributed to the acute right ventricular dilatation.

Since the above ECG changes are nonspecific for acute right ventricular strain due to pulmonary embolism, they should be differentiated from those of normals, inferior or anterior MI or ischemia, extensive pneumonia, massive atelectasis, chronic cor pulmonale, pneumothorax, and large pleural effusion. A previous ECG available for comparison [86], and the repetition of the ECG, has enhanced its sensitivity in diagnosing pulmonary embolism [249]. Accordingly, a shift in the axis even if it remains within the normal limits may be indicative of pathology. Pulmonary embolism with severe hemodynamic consequences has been linked to precordial T wave inversions [250], and high ECG scores consisting of a number of weighted ECG findings described above [251].

20.10 Mitral Valve Prolapse Syndrome

Degeneration or myxomatous infiltration of the mitral leaflets leads to their characteristic abnormal systolic sagging, known as mitral valve prolapse [104]. The ECG in patients with MVP can be normal, but various arrhythmias and nonspecific ST-T changes, involving mostly the inferior leads, may be present in 15–42% of patients [86, 252], often misinterpreted as ischemic in origin. The T wave abnormalities may be confined only to the precordial leads (Fig. 20.18), or may be diffuse. While the T wave inversions may vary spontaneously, exercise may normalize them, and inhalation of amyl nitrate

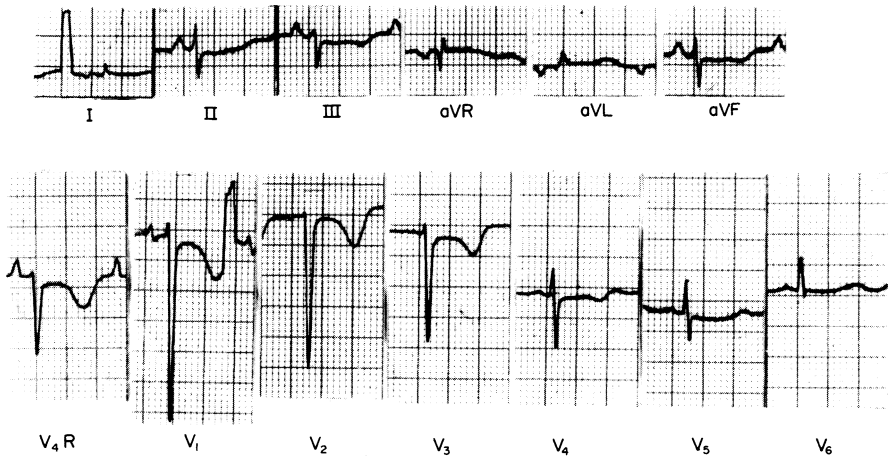

Figure 20.18
ECG of a patient with mitral valve prolapse (MVP) showing ischemic-appearing T wave inversion in precordial leads V_1–V_4, with a prolonged QT interval.

will accentuate them or convert flat to inverted T waves. An ECG false-positive exercise response, with marked ST segment depression during exercise or on recovery, is not at all uncommon, with a 53% incidence reported in one series [253]. Other ECG abnormalities occasionally noted are prolongation of the QT interval (Fig. 20.18), prominent U waves and abnormal Q waves without evidence of infarction [86]. Heart rate variability in patients with MVP was not different than in control subjects, but the QT duration was increased; also the QT/RR slope revealed an increased nocturnal rate dependence, which might explain the risk of arrhythmic events in these patients [254].

The pathogenesis of flattened or inverted T waves is still elusive, although ischemia or even infarction of the papillary muscle and the adjacent myocardium is implicated [255]. It has been postulated that the underlying mechanism might be the increased traction to the papillary muscle(s) exerted by the billowing leaflet(s) via the attached chordae, which thus interferes with the rather tenuous vascular supply of the region.

Studies with Holter monitoring show that patients with MVP have a higher incidence of supraventricular and ventricular arrhythmias than normal subjects [255–259]. Arrhythmias noted run the gamut from atrial, junctional, or ventricular extrasystoles to paroxysmal supraventricular tachycardia, premature ventricular extrasystoles in a bigeminal, trigeminal, or R-on-T patterns, or even ventricular tachycardia and fibrillation [86, 104]. It is believed that the latter is the cause of syncope or sudden death in some patients with MVP [86, 104, 260]. Possible predisposing mechanisms for arrhythmias in patients with MVP could be the mechanical stress to which the left atrium and ventricle are subjected, an underlying myocardial ischemia, as evidenced by the nonspecific ST-T abnormalities, possible coexisting bypass tracts, usually left-sided which would precipitate reentrant tachycardias, and a QT-interval prolongation [86]. Although it cannot be denied that arrhythmias in patients with MVP may be associated with an increased risk of sudden death, the previously reported increased incidence probably had been due to a selection bias (study of patients with the most severe form of the syndrome) [261]. In the same vein, the occurrence of complex ventricular arrhythmias in some patients with MVP may be a reflection of their underlying consequent mitral regurgitation, and not due to the syndrome per se, since such arrhythmias are common in patients with nonischemic hemodynamically significant mitral regurgitation, regardless of the specific etiology [262].

20.11 Infectious Heart Diseases

The heart can be affected by any of the entire range of infectious agents. Depending on the topography of physiological and structural derangements and the subsequent pathophysiological consequences, as for example in endocarditis, viral

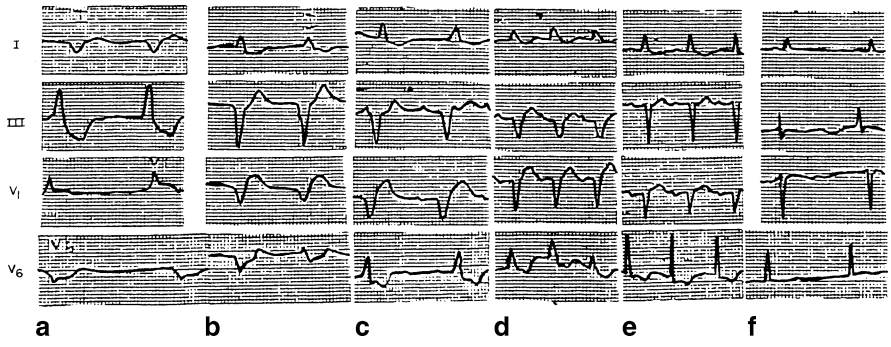

Figure 20.19

Serial ECG changes in acute viral myocarditis: (a) junctional escape rhythm with RBBB-type intraventricular conduction defect (IVCD) and ST abnormality; (b) junctional escape rhythm with LBBB-type IVCD; (c) normal sinus rhythm with LBBB-type IVCD; (d) sinus tachycardia with LBBB; (e) sinus tachycardia with normal QRS morphology; (f) atrial fibrillation with normal QRS morphology.

myocarditis, echinococcosis, syphilis, Chagas disease, and others, the gamut of arrhythmias, conduction abnormalities, and evidence of chamber hypertrophy/dilatation may be seen in the ECG.

20.11.1 Myocarditis

While most cases of acute "idiopathic" myocarditis are probably due to viruses [263], any infectious organism or toxic agent can cause this condition. ECG changes of acute viral myocarditis are frequent but nonspecific, and consist of diffuse low voltage, ST-T abnormalities, QT interval prolongation, sinus tachycardia, atrial and ventricular arrhythmias, and AV and intraventricular conduction defects (Fig. 20.19) [86]. The ST segment and T wave changes may be related to the associated pericarditis. A "fulminant" form of myocarditis is seen in association with Q waves plus ST segment elevation, and heralds a rapidly fatal course; in general, abnormal QRS complexes and left bundle branch block are markers of poor survival and sudden cardiac death [264]. Frequently "idiopathic" ventricular tachycardia is linked to macroscopic and/or microscopic ventricular abnormalities of myocarditis [265].

Acute rheumatic fever, still of major prevalence in developing countries, may lead to "rheumatic carditis", a form of "pan-carditis" with involvement of endocardium, and pericardium, but also with a "myocarditis" component. The most frequent encounter in such patients is 1° AV block (Fig. 20.20), with 2° AV block of the Wenckebach type or complete AV block occurring rarely. The length of P-R interval does not bare any relationship with the severity of the carditis, or the eventual occurrence of valvular sequelae [266].

Rarely a patient with acute MC may show changes suggestive of myocardial infarction (ST segment elevation, reciprocal ST segment depression, or even Q waves). A possible myocarditis should be suspected when a previously healthy young adult presents with serious atrial or ventricular arrhythmias, high-degree AV block, intraventricular conduction disturbances, or cardiac arrest (Figs. 20.19, 20.21 and 20.22).

20.11.2 Chagas Disease

Chagas disease, a progressive disease leading to congestive heart failure and a variety of ECG abnormalities is essentially endemic in Central and South America. A study of symptomatic seropositive patients revealed an incidence of arrhythmias, including extrasystoles, of 100%. 1° or 2° AV block occurred in 14.3%, 3° AV block in 2.5%, atrial fibrillation in 18.6%, ventricular extrasystoles in 75.2%, right bundle branch block (RBBB) in 39.8% and left anterior fascicular block (LAFB) in 38.6% of patients, with the last two being the most commonly occurring conduction defects [267]. Another study of

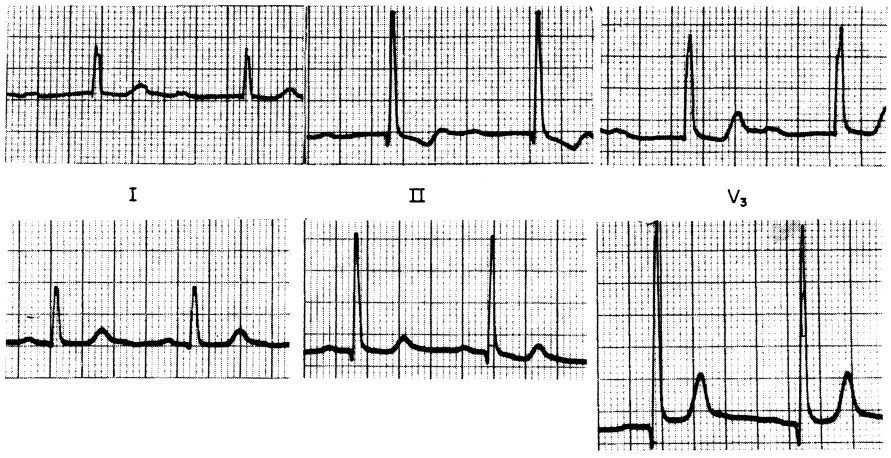

Figure 20.20
Marked PR prolongation (0.46 s) during the acute phase of rheumatic fever (*upper* trace) has returned to normal AV conduction 4 days later (*lower* trace).

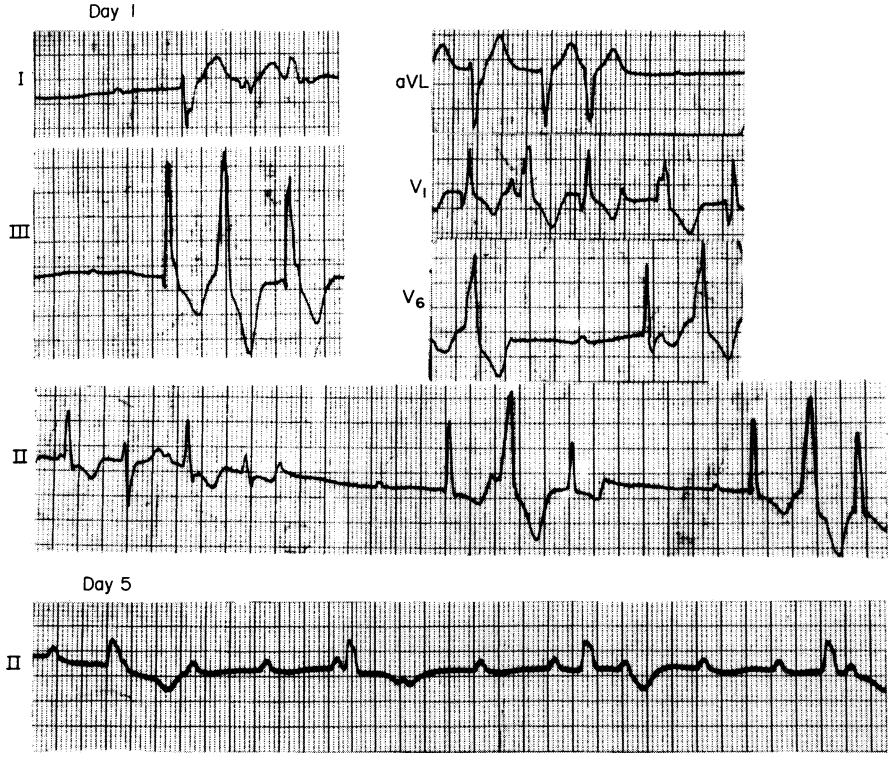

Figure 20.21
ECG showing AV dissociation and frequent VPCs during the acute phase of viral myocarditis. Four days later, the ECG rhythm has changed to complete AV block with a normal atrial rate.

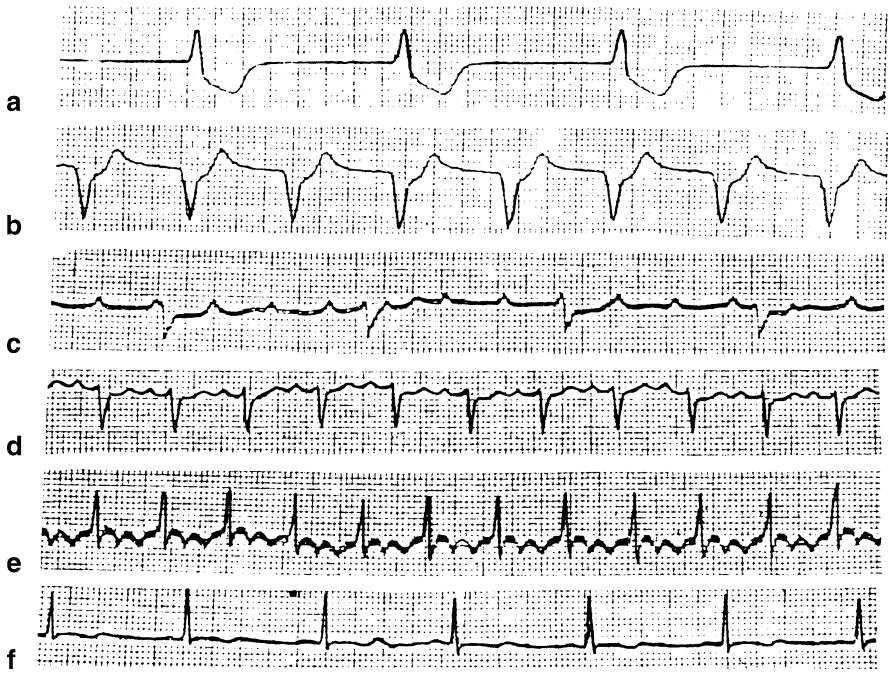

Figure 20.22

Serial ECG changes in acute viral myocarditis: (a) idioventricular rhythm; (b) accelerated idioventricular rhythm; (c) complete AV block; (d) sinus tachycardia with left axis deviation; (e) atrial flutter with right axis deviation; (f) atrial fibrillation.

seropositive subjects showed that RBBB was also the most commonly found ECG abnormality [268]. An incidence of RBBB of 9.3% versus 1.3%, and of LAFB of 9.3% versus 3.9% were the only significant differences between asymptomatic Chagas seropositive and seronegative subjects, while the most frequently occurring ECG finding in these two groups was a T wave change (11.2% vs. 9.1%, respectively) [267]. An early cardio-vagal dysfunction was documented in asymptomatic seropositive subjects regardless of ECG appearance, based on a large panel of tests, suggesting that such change may be useful for identification of subclinical disease [269]. Abnormal values for heart rate turbulence have been noted in patients with Chagas disease [270].

20.12 Connective Tissue Diseases

Connective tissue diseases, e.g., lupus erythematosus, scleroderma, rheumatoid arthritis, etc., frequently impact the cardiovascular system, leading to a variety of cardiac sequelae, and ECG abnormalities. Thus, patients with rheumatoid arthritis were found to have increased sympathetic activity [271]; the signal averaged ECG in patients with scleroderma revealed late potentials in the absence of overt cardiac disease [272], which could be related to the high incidence of ventricular arrhythmias and sudden death in this disorder. In Marfan's syndrome, atrial and ventricular extrasystoles and T wave changes were detected [273]; in patients with systemic lupus erythematosus, atrial and ventricular arrhythmias, 1° AV block, and acquired complete heart block, along with a myriad of ECG abnormalities depending on the associated cardiac complications have been found [274]. Q waves, ST segment changes, increased P wave terminal force, conduction defects, and features of cor pulmonale (see Sect. 20.9.1) were found in patients with connective tissue diseases [275, 276].

20.13 Cardiomyopathy

20.13.1 Hypertrophic Cardiomyopathy

The ECG is abnormal in 93% of patients with hypertrophic cardiomyopathy showing left ventricular hypertrophy (LVH), pseudoinfarctional Q waves, abnormalities of the P waves, ST segments, or T waves, QTc prolongation, and atrial and ventricular arrhythmias, irrespective of the presence of left ventricular outflow obstruction; however, none of these findings is diagnostic of the disease [277, 278]. Left atrial enlargement (LAE), secondary to either poor left ventricular compliance or mitral regurgitation was more common than right atrial enlargement [278]; P-pulmonale noted in patients with HCM may be of the "pseudo-P pulmonale" type, occasionally seen with LAE [86]. LVH, mostly associated with secondary T wave inversion, was present in 81% of patients [278]. ECG LVH may reflect primary involvement of the left ventricular myocardium or hypertrophy in response to the outflow tract obstruction [279]. A frontal axis superior to 0° noted in 52% of patients might have been related to LVH. [278]. The most common ECG findings in hypertrophic cardiomyopathy are the ST segment and T wave abnormalities [86, 277], which may be of the nonspecific type, or those secondary to LVH and conduction defects. Sinoatrial or AV blocks are uncommon [86, 280, 281], with a 4% incidence of complete AV block, requiring permanent pacemaking [278]. T wave alternans (TWA) was more frequent in patients with hypertrophic cardiomyopathy than in hypertensive LVH, and there was a correlation of TWA with myocardial disarray and/or fibrosis, the maximal numbers of successive ventricular ectopic beats and episodes of nonsustained ventricular tachycardia (VT), reflecting myocardial electrical instability [282, 283]. Longer QRS and QT intervals are consequences of increased left ventricular mass in patients with hypertrophic cardiomyopathy, while abnormalities in the T wave complexity index, QT dispersion, activation-recovery interval and its dispersion, and duration of the signal in the terminal portion of the QRS predicted cardiogenic syncope [284].

Pseudoinfarctional Q waves, the most distinctive ECG abnormality in hypertrophic cardiomyopathy (Figs. 20.23–20.25), are more commonly seen in the anterolateral than the inferior leads [278], and may be due to ventricular septal hypertrophy, septal fibrosis, or abnormal septal activation caused by disarray of the myofibrils [86, 285]. These abnormal Q waves, seen in both the obstructive and non obstructive types of hypertrophic cardiomyopathy have no apparent relationship to the severity of the outflow tract obstruction [86], and they may change in amplitude, or even disappear during the course of the disease [285]. It is intriguing that the segmental muscle hypertrophy of hypertrophic cardiomyopathy produces Q waves similar to those resulting from muscle necrosis. A study employing intracoronary electrograms identified the mechanisms of Q wave generation in hypertrophic cardiomyopathy to be both transmural myocardial fibrosis and altered direction of resultant initial vectors due to disproportionate hypertrophy of septal and/or free wall, unopposed by apical forces; areas of fibrosis were associated with regional contraction abnormalities while hypertrophic territories were not [286]. The above were corroborated by newly appearing and disappearing Q waves after alcohol septal ablations in patients with hypertrophic cardiomyopathy [287]. Occasionally patients with hypertrophic cardiomyopathy can suffer a true myocardial infarction (Fig. 20.26).

Atrial fibrillation (AF) has been reported to occur in 7–45% of the patients, while atrial and ventricular premature beats were found in 9–27% when employing 24 h ambulatory ECG monitoring [86, 278, 280]. VT was observed in 4% of patients (Fig. 20.27a) during Holter monitoring [278], with a higher incidence reported in other literature [86, 280, 281]. AF and the Wolff-Parkinson-White syndrome are more commonly associated with certain genetic mutations in patients with hypertrophic cardiomyopathy. Nonsustained VT particularly in the young has a poor prognosis, and sustained VT and ventricular fibrillation are rarely documented [288]. Invasive electrophysiology studies have little advantage over non-invasive risk stratification [289], and along with a host of risk factors, both need to be considered for prophylactic implantation of an automatic defibrillator [288, 289].

20.13.2 Dilated Cardiomyopathy

The most common ECG findings in patients with dilated cardiomyopathy are left ventricular hypertrophy (LVH) and left atrial enlargement (LAE) [86]. The pathophysiologic pathways leading to dilated cardiomyopathy are ever expanding.

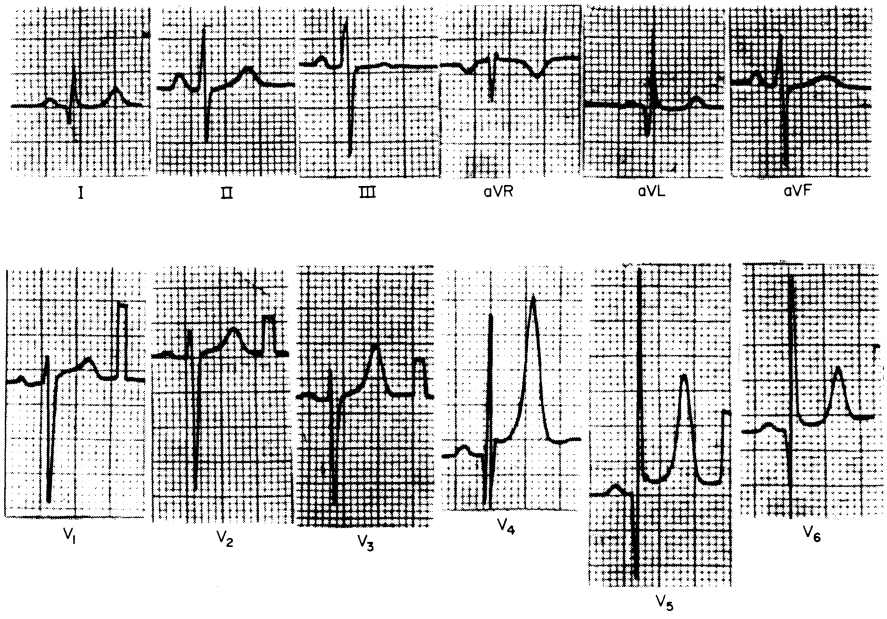

Figure 20.23

Pseudoinfarctional Q waves in leads I, aVL, and V_4–V_6, with evidence of left ventricular hypertrophy in a patient with HCM.

A newly described form of apical dilated cardiomyopathy ("takotsubo") induced by acute physical and psychological stress leads to ST segment elevation, diffuse T wave inversion, and prolonged QT interval indistinguishable from acute myocardial infarction syndrome [290–292]. A reversible arrhythmogenic dilated cardiomyopathy due to tachyarrhythmias, mainly atrial fibrillation (AF) [293], but rarely even due to "chronic" sustained ventricular tachycardia [294] should be kept in mind. Arrhythmogenic right ventricular dysplasia may lead to right and rarely left ventricular dilated cardiomyopathy [295]. Right ventricular hypertrophy (RVH) and biventricular hypertrophy/dilatation (BVH) are commonly documented by echocardiography or autopsy, although are not always paired with suggestive ECG findings. The ECG cannot distinguish hypertrophy from dilatation [296]. Although BVH due to congenital heart disease is occasionally associated with the Katz–Wachtel pattern [297] characterized by large diphasic QRS complexes in the standard bipolar leads, BVH may lead to a reduction of QRS voltage or an almost normal ECG due to cancellation [2]. The author has observed large diphasic QRS complexes in the precordial leads in patients with BVH, while a normal-sized diphasic QRS complex in these leads is a normal finding [297]. An R/S ratio ≥1 in V_1 is the most sensitive among the conventional ECG criteria of RVH [298]. Diastolic overload is associated with LVH in the ECG, and tall symmetrical T waves with some ST segment elevation (not commented upon by the author) of upward concave type, in contrast to ST segment depression and inverted T waves, found with systolic overload [299]. Diffuse myocardial fibrosis may be the mechanism of the reduced QRS voltage in dilated cardiomyopathy. This attenuation of QRS complexes may involve only the limb leads, while the precordial leads may be normal or prominent in amplitude and show poor R wave progression in patients with dilated cardiomyopathy, or congestive heart failure (Fig. 20.27b) [300, 301]. Low voltage ECG in patients with peripheral edema is seen in spite of the cardiac dilatation (see Sect. 20.25.6). Also the amplitude of cardiac signals, acquired by body surface potential mapping, decreased by approximately 30% after partial left ventriculotomy [302].

Pseudoinfarctional Q waves in patients with dilated cardiomyopathy may be seen, although with lower frequency than in dilated cardiomyopathy; such Q waves are mostly present in the right and mid-precordial leads (Fig. 20.27b), and are probably due to LVH and/or intraventricular conduction defects (IVCD) [86, 303, 304]. IV conduction defects, particularly left bundle branch block (LBBB) (Fig. 20.28), are common in dilated cardiomyopathy, with incidences varying between 9% [305] and 44% [86, 300, 303, 306]. LBBB is so prevalent that its presence, particularly in patients

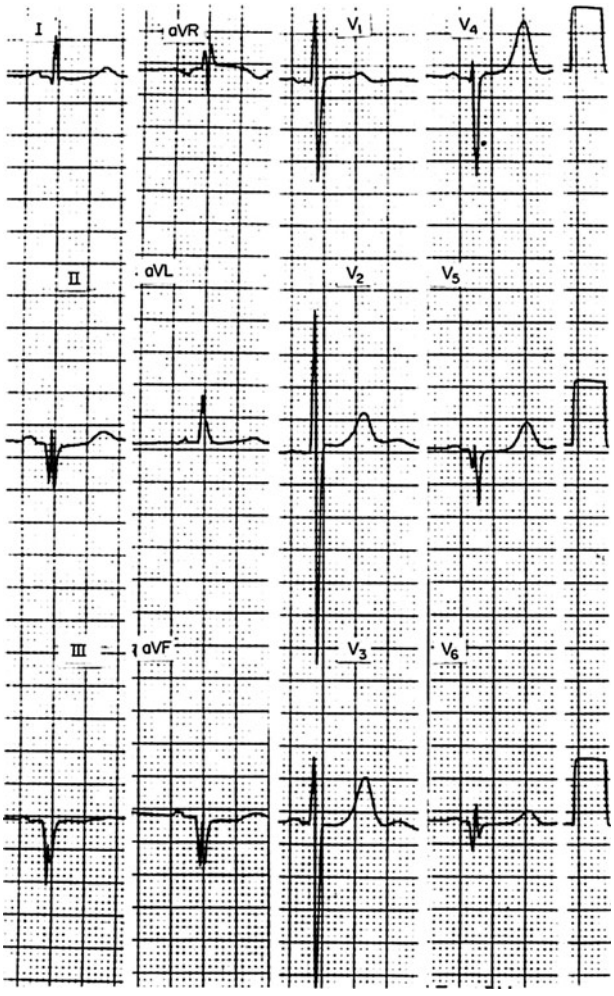

Figure 20.24

Pseudoinfarctional Q waves in leads II, III, aVF, V_5 and V_6, and reversed R wave progression in V_1–V_4 in a patient with documented HCM.

younger than 40 years of age, would support the diagnosis of the disease. An association of extreme frontal right axis deviation with the LBBB has been noted in some patients, and may indicate extreme severity of dilated cardiomyopathy [307]. QRS duration and its perturbations are employed as a predictor, in the monitoring of patients with dilated cardiomyopathy, and their response to resynchronization therapy [308–310]. Heart rate turbulence (onset and slope), microvolt-level T-wave alternans, abnormal baroreflex sensitivity and heart rate variability are powerful independent predictors of ventricular tachyarrhythmic events in patients with dilated cardiomyopathy [311, 312]. Commonly, the prolongation of the QRS complexes, in the absence of typical features of either LBBB or right bundle branch block, qualifies for the diagnosis of IVCD (Fig. 20.29). Most of the ST segment and T wave changes seen in the left precordial leads in dilated cardiomyopathy are nonspecific or secondary to LVH, IVCD, or digitalis effect. Atrial arrhythmias, particularly AF (Fig. 20.29), and ventricular arrhythmias are common in this disease. ECGs pertaining to employment of pacing, implantable cardioverter/defibrillators, and resynchronization therapy, with changes associated with their advanced operational features and occasional malfunction, are frequently encountered in patients with dilated cardiomyopathy [313].

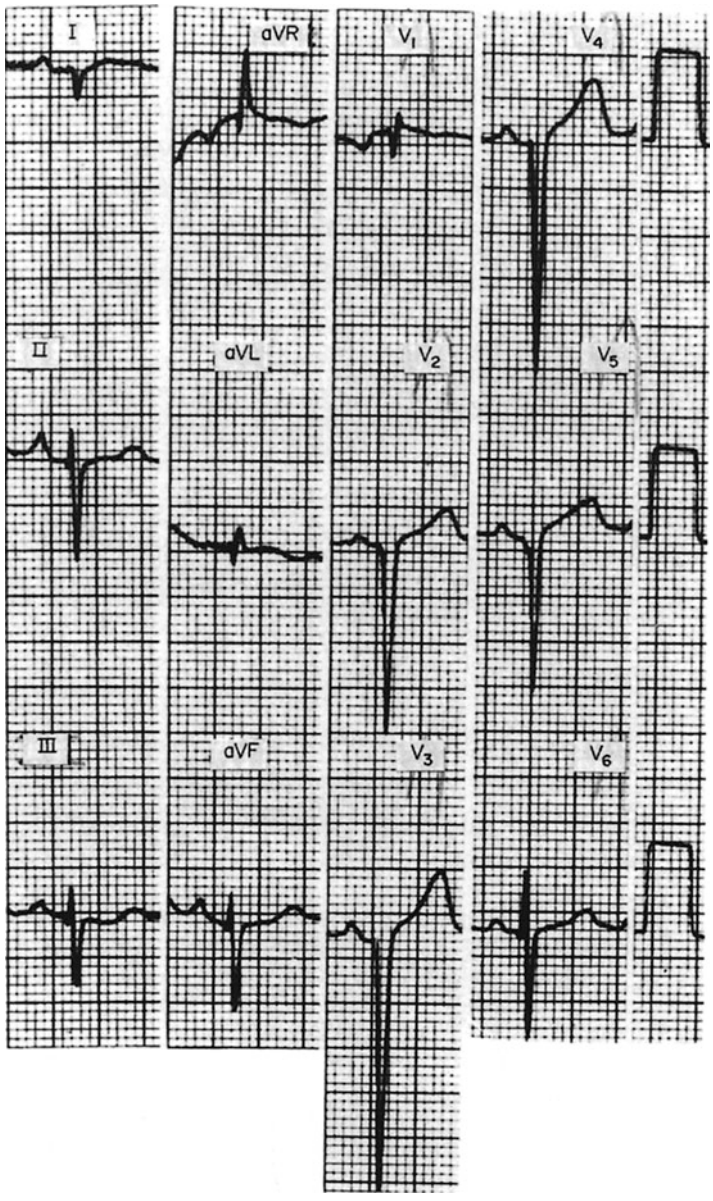

Figure 20.25
Pseudoinfarctional Q waves in V_1–V_5 in a patient with documented HCM.

20.13.3 Restrictive Cardiomyopathy

Restrictive cardiomyopathy is characterized by low-voltage QRS complexes, left and right atrial enlargement, LVH, nonspecific ST-T changes, AV conduction defects, IVCD, and arrhythmias, particularly AF [2]. Pseudoinfarctional Q waves and low voltage ECG complexes are noted in amyloid heart disease [2, 314], while body surface potential maps revealed correlation of the amplitude of positive potentials on the anterior and lateral chest wall with disease severity, and prolongation of ventricular activation time [315]. It is possible that the low voltage in advanced stages of restrictive cardiomyopathy

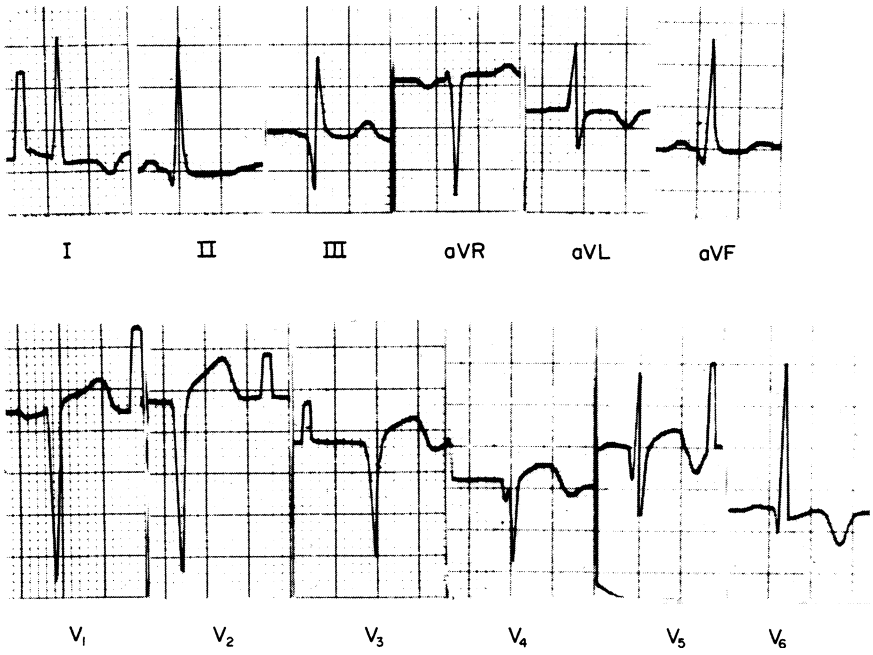

Figure 20.26
ECG of a patient with documented HCM complicated by acute anterior myocardial infarction.

may be in part related to the associated peripheral edema (see Sect. 20.25.6). Other infiltrative diseases causing restrictive cardiomyopathy are Fabry disease [316], hemochromatosis, in which chelation therapy restores the amplitude of QRS complexes [317], hypereosinophilia [318], mucopolysaccharide (Hurler's) and glycogen storage (Pompe's) diseases [319]. The last is associated with very high QRS complexes, possibly related to high extracellular resistance [2].

20.14 Cardiac Transplantation

ECG changes at some point after cardiac transplantation (CT) are seen in approximately 75% of patients, consisting of bundle branch block, atrial flutter or fibrillation, and ventricular arrhythmias with coronary vasculopathy [320]. A direct association of increase in QTc duration over time with mortality has been identified [321]. However, with contemporary treatment, ECG changes develop only in severe forms of rejection. Diffuse low QRS voltage, loss of precordial R wave amplitude, right axis deviation, 1° AV block progressing to nodal rhythm, atrial arrhythmias, and occasionally ischemic ST segment changes are looked for in the monitoring of patients following CT [322, 323]. However, these changes are nonspecific, and particularly in reference to the QRS voltage, attenuation has not correlated with acute rejection [324]; pericardial and pleural effusions, or other complications in the post cardiac transplantation course could also be the cause of low QRS voltage [325]. Linear or nonlinear analyses of heart rate variability provide detection of acute rejection following allograft CT [326]. Increased QTc dispersion, independent of the reduction of the ejection fraction, has been found in patients with post CT coronary vasculopathy [327]. However, increase in QTc dispersion and right bundle branch block have not been found to discriminate between patients with and without biopsy-proven cellular rejection [328–330], although a trend has been noted linking increased QTc dispersion and rejection, calling for a change of management [330]. The study of the frequency content of the ECG has been found useful for the detection of rejection, and its management, while changes in QRS or signal averaged ECG were noncontributory [331, 332]. Analysis of the ventricular evoked response obtained by programmed electrical stimulation may be suitable for detection and monitoring of cardiac allograft rejection [333].

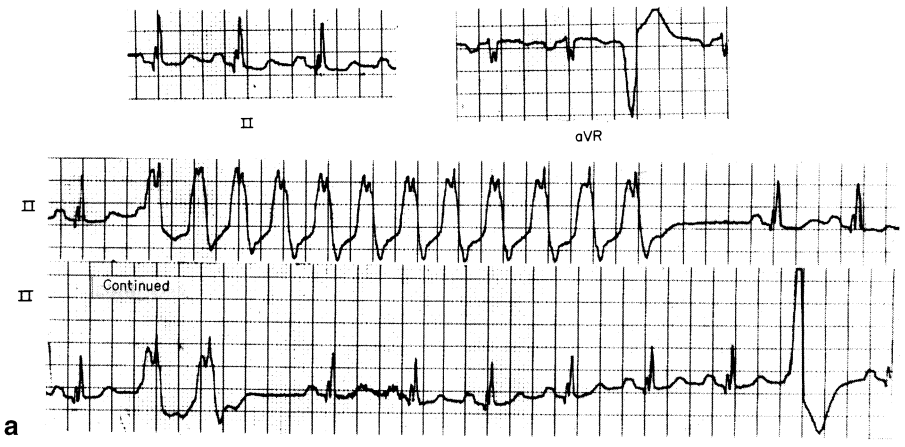

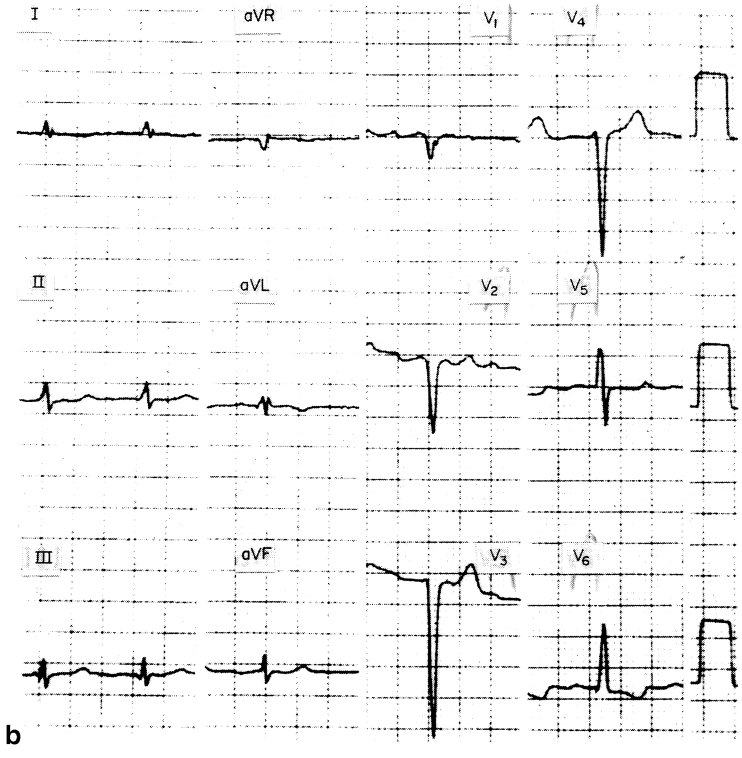

Figure 20.27

(a) Ventricular tachycardia in a patient with documented hypertrophic cardiomyopathy. (b) ECG of a patient with autopsy-proven idiopathic congestive cardiomyopathy, simulating an old anteroseptal myocardial infarction. The low voltage in standard leads is the result of pericardial effusion, which often appears not to have involved the precordial leads in patients with enormous QRS complexes prior to the development of the effusion.

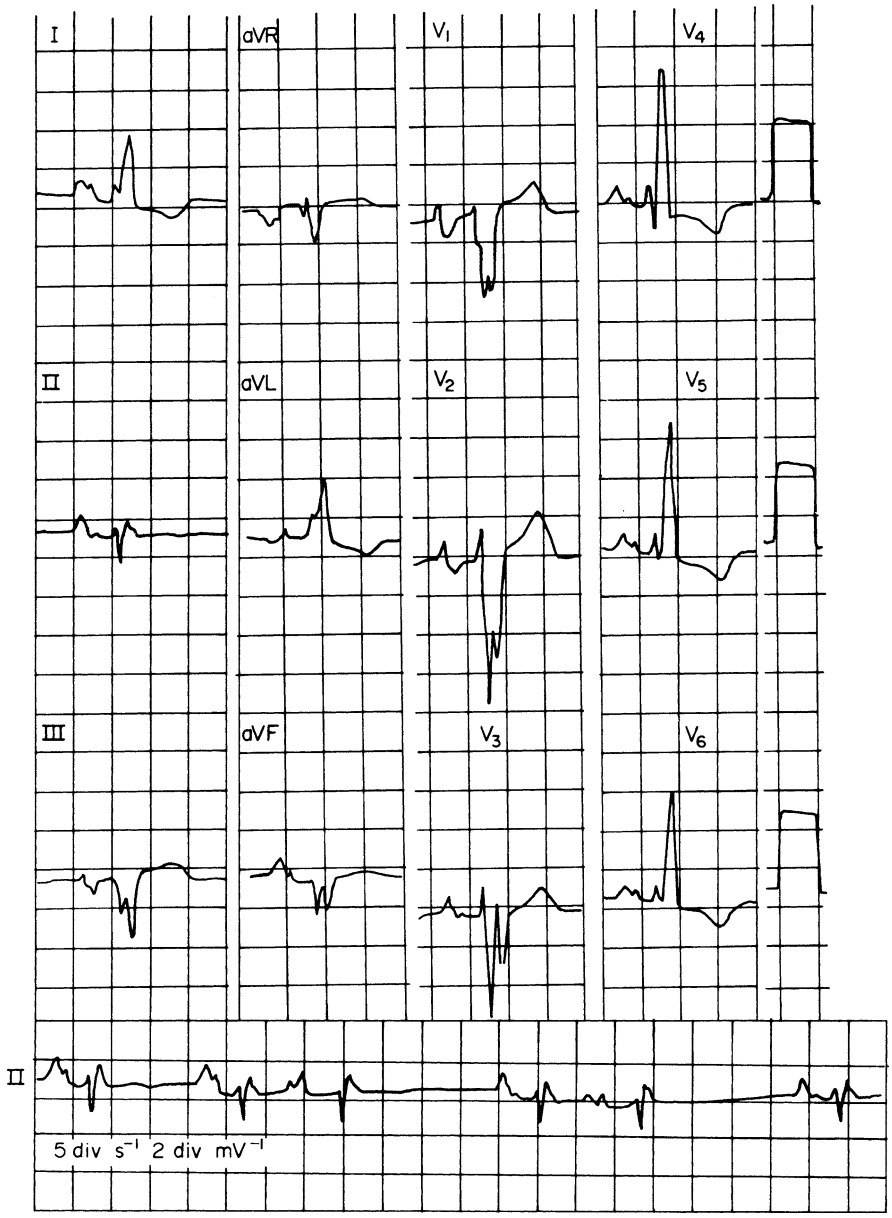

Figure 20.28
ECG showing left atrial enlargement and LBBB in a patient with dilated cardiomyopathy.

20.15 Heart Injury

Trauma to the heart and large vessels may lead to ECG changes, which depend on the nature of injury and the particular anatomic site of cardiac involvement. Blunt trauma to the chest wall can involve the underlying heart in "commotio cordis", "contusio cordis", and "steering wheel injury" where experimental work and clinical experience has shown the gamut of ECG abnormalities occurring, with various outcomes from sudden death due to ventricular fibrillation (VF), to quick, but sometimes more protracted, recovery [334]. Atrial and ventricular arrhythmias, AV and intraventricular

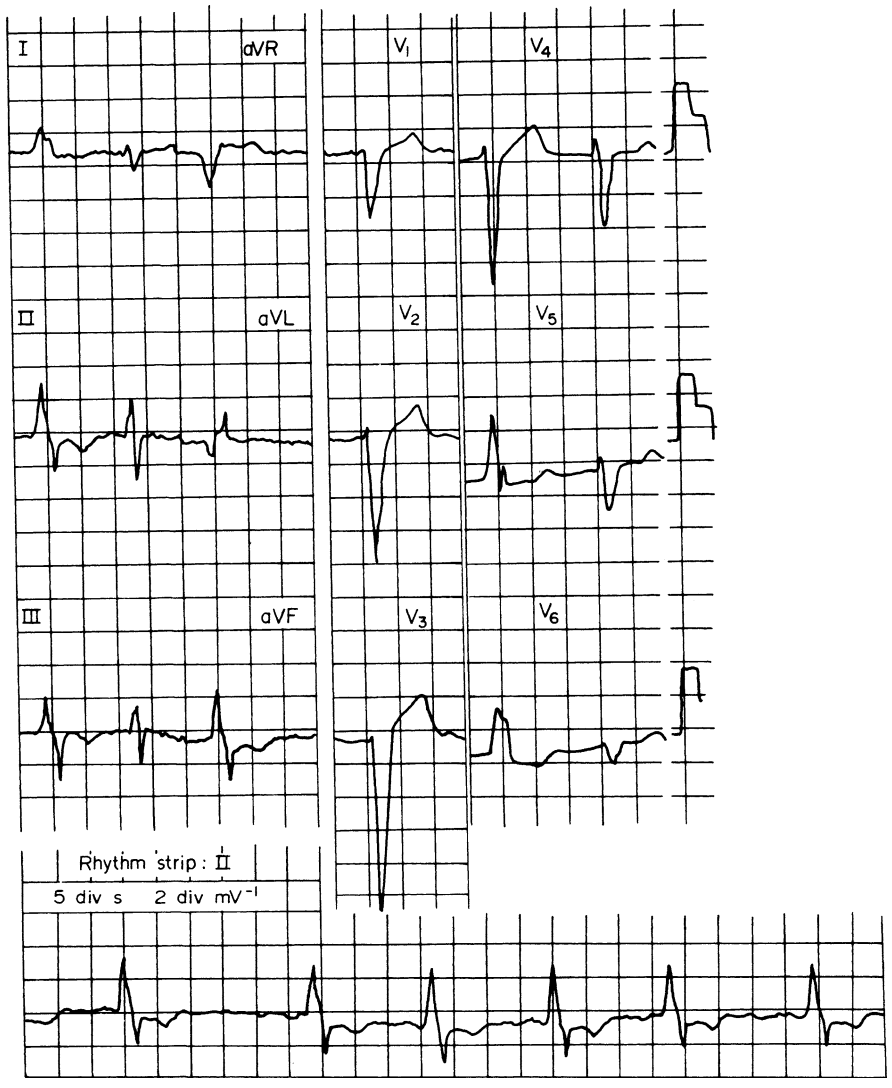

Figure 20.29
Atrial fibrillation and LBBB-like IVCD in a patient with dilated cardiomyopathy.

conduction disturbances, evidence of pericarditis, pericardial effusion and frank myocardial infarction (MI) (resulting from damage to the myocardium itself or the perfusing coronary artery) are found. Some of the above may be noted only transiently, while others may leave a permanent change on the ECG. Attenuated ECG complexes or such changes becoming more pronounced in serial ECGs indicate hemopericardium, which is often expanding rapidly. Minor repolarization ECG changes may be seen in "contusio cordis", which can be followed by ventricular pseudoaneurysm and sudden cardiac death. Similar changes lasting for a few hours can be seen in boxers [335]. Involvement of valves leads to atrial and myocardial after effects, which manifest as progressive ECG changes as the pathophysiology of cavity enlargements evolves.

A variety of arrhythmias result from electrical injuries including the effect of lightning to the heart, with the alternating current being worse than the direct current at the same voltage. Current of high frequencies is not damaging, and the vulnerability of patients varies with the degree of skin resistance. Levels of current intensity (approximately 80 mA is fatal), duration of exposure, and its trajectory passing through the heart, determine the seriousness of the outcome.

Sinus tachycardia, ST segment elevation, nonspecific ST-T changes, prolonged QTc interval, atrial and ventricular tachycardia, VF, conduction abnormalities, and MI can occur with low and high voltage electrical injuries; QTc prolongation results only from direct lightning hits, and for MI coronary vasospasm is implicated [336, 337]. The transient collapse, noted in some victims, implies that VF may be occasionally reversible. After exposure in survivors, sinus tachycardia and non-specific ST-T changes can be seen in the ECG, which partially may be due to underlying myocardial injury [337].

After electroconvulsive therapy, no new persisting ECG changes were found even in patients with prior cardiac disease [338]. Internal cardioversion of atrial fibrillation may lead to prolongation of QTc [339]. Brief ST segment elevation may follow external DC cardioversion [340]. Internal and external cardioversion of ventricular arrhythmias resulted in brief sinus bradycardia, supraventricular and rare ventricular tachycardias [341]. The external and internal defibrillation during procedures or after implantation of automatic defibrillators, has the potential rarely to cause epicardial injury, or biochemical evidence of necrosis [342–344].

20.16 Pericardial Diseases

Acute and chronic diseases of the pericardium produce various ECG abnormalities, some of which are nonspecific, while others are very distinctive of the underlying pathology.

20.16.1 Pericarditis

Acute pericarditis causes diffuse ST segment elevation and T wave inversion, attributed to subepicardial myocarditis or myocardial damage along with the type involving the pericardium per se (Fig. 20.30). Although the condition is usually generalized, local or loculated pericarditis occasionally occurs and results in regional ST-T changes. Four stages of evolutionary ST segment and T wave changes have been described in association with acute pericarditis [120, 345]: (a) stage 1: diffuse ST elevation in almost all leads except aVR and possibly V_1, i.e., absence of reciprocal changes; (b) stage 2: return of ST junction to the baseline, with diminishing amplitude of the T wave; (c) stage 3: inversion of

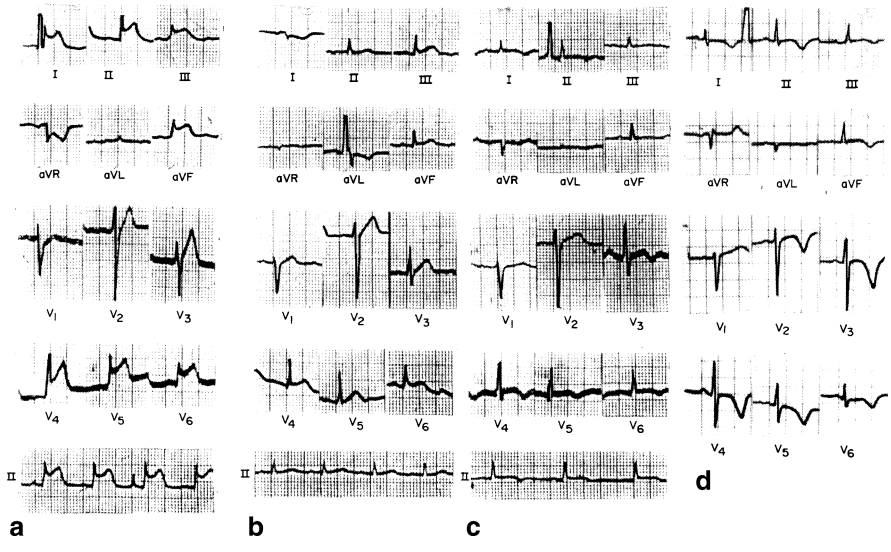

Figure 20.30
Serial ECG changes in a patient with acute viral pericarditis: (a) Diffuse ST elevation seen on day 1; (b) Normal ST segment and T wave seen on day 2; (c) Normal ST segment, but the T wave begins to be inverted on day 3; (d) Marked T wave inversion seen on day 16.

the T wave with an isoelectric ST segment; and (d) stage 4: return of the T wave to its normal pattern. One or more stages may be absent, or features of one stage may be intermingled with features of another, depending on the frequency of observation, severity of the disease, and time interval between the recording and the onset of illness. Although characteristic ST segment displacement has been reported in ≥90% of the cases of the disease, the sensitivity and specificity of ECG changes in the diagnosis of acute pericarditis are very difficult to evaluate [345]. The typical ST segment and T wave abnormalities are more often seen in acute purulent pericarditis than in the type resulting from tuberculosis, uremia, or as a complication of acute myocardial infarction (MI) either shortly after inception, or later (Dressler's syndrome). Perhaps the associated QRST alterations of the subacute or chronic MI explain the apparent paucity of characteristic ST-T changes of pericarditis in Dressler's syndrome, although others feel that the latter has truly decreased in incidence in the thrombolytic era [346]. Etiology of pericarditis and the extent of the associated myocardial damage determine the duration of the ECG changes [86]. Thus, while purulent pericarditis is likely to be associated with persistent ECG abnormalities, the ST segment displacement in acute viral or idiopathic pericarditis may return usually to normal within a week. However the succeeding T wave inversion may last longer, perhaps for weeks or months, even in patients who have fully recovered.

Other less frequent and specific ECG findings in acute pericarditis include a depressed PR segment, and atrial arrhythmias, both of which are probably responses to atrial injury. Some PR segment depression (occasionally up to 200 μV) is the normal expression of atrial repolarization (secondary) and may extend into the ST segment and T wave [347]; consequently, the exaggerated PR segment should be viewed as a primary alteration of the atrial repolarization, and is encountered in 23% of patients with clinically silent pericarditis, particularly with inflammatory pericardial involvement [348].

The ST segment displacement observed in acute pericarditis should be differentiated from those occurring in acute MI, ST elevation in healthy young people caused by vagotonia, and early repolarization. In reference to the differentiation from acute MI [349], the following are helpful: (a) There is no reciprocal ST segment depression in acute pericarditis – ST depression is only seen in lead aVR (Figs. 18.25 and 20.30), and rarely in leads V_1, III and aVL; (b) Less severe ST segment elevation (usually <0.4 mV) occurs in pericarditis, but more leads are involved; (c) Upward concave ST segment elevation, rather than upward convex ST segment elevation, is observed in pericarditis; (d) During the period of ST segment elevation, the T wave remains upright in pericarditis, until the ST segment returns to the isoelectric line; (e) More diffuse but less deep T wave inversion occurs in pericarditis; and (f) The QT interval in pericarditis is normal. Regarding the differentiation of pericarditis from early repolarization, it has been reported that the ratio of ST segment elevation to the corresponding upright T wave is higher in the former than in the latter [350] (Fig. 20.30).

20.16.2 Pericardial Effusion

Low QRS voltage is traditionally thought to be due to the "insulating" effect of fluid or fibrin deposits [86], or changes in the electrical properties of the pericardium, although an alternative explanation is that of a short-circuiting effect of the fluid enveloping the heart [351]. There is continuing debate about the correlation of the presence of low voltage ECG or the degree of QRS attenuation and the magnitude of pericardial effusion and it appears that the interplay of the above is complex [352]. Generalized low QRS voltage with electrical alternans is seen with large pericardial effusions, and is attributed to a swinging motion of the heart maintaining a two-beat periodicity [86, 353].

20.16.3 Pericardial Tamponade

There are no specific ECG changes of pericardial tamponade; however the low voltage ECG in tamponade may be due to the associated (usually large) PE although a possible compressive effect of the increased pericardial pressure reducing the ventricular volume has also been implicated [354].

20.16.4 Pericardial Constriction

ECG changes with chronic pericardial constriction include all the above findings seen in pericarditis, particularly the T wave inversion seen in its third stage, and the low QRS voltage found with pulmonary embolism [355]; the depth of T waves has been felt to correlate with the degree of myocardial-pericardial adherence [356], and may have implications on the feasibility of surgical pericardial "stripping".

20.17 Heart Tumors

A variety of benign and malignant primary and metastatic heart tumors are associated with Q waves, ST segment deviations, T wave inversions, conduction abnormalities, and atrial and ventricular arrhythmias. ECG changes may simulate all appearances of myocardial ischemia and infarction [357, 358]. The entire range of ECG changes of pericarditis (see Sect. 20.16) may be seen with tumor invasion of the pericardium [359]. Cardiac rhabdomyomas associated with tuberous sclerosis may show ECG evidence of right or left ventricular hypertrophy depending on the ventricular cavity involved, in the absence of pressure overload or cardiac enlargement, with such changes disappearing with regression of the tumors [360]. Atrial myxomas lead mainly to P-mitrale (broad P waves in lead II and enhanced terminal force of P waves in lead V_1) [361].

20.18 Electrical Alternans

Electrical alternans, i.e. a regular alternating change in the configuration or magnitude and axis of the ECG complexes, arising from the same pacemaker, and associated with a stable R-R interval, is an extracardiac phenomenon [86]. It may involve the P, QRS or T waves, and when all these three occur together, "total electrical alternans" is said to be present. ST segment alternans occasionally occurs in the setting of variant angina [362], myocardial infarction [363], exercise testing [364], or during coronary angioplasty [365], and even alternans in conduction can occur. P, T, and U wave, and ST segment alternans is rare, while QRS alternans, with or without T wave change, is the most common pattern.

Pericardial effusion, with or without cardiac tamponade, is the most common clinical cause of electrical alternans (see Sect. 20.16.2) (Fig. 20.31), and is often associated with low ECG voltage and tachycardia. QRS alternans may also occur in hypertensive heart disease with left ventricular hypertrophy, coronary artery disease (CAD), and supraventricular tachycardia associated with the Wolff-Parkinson-White syndrome (WPW). Alternating WPW pattern might be misinterpreted as QRS alternans (Fig. 20.32), although the mechanism obviously is different (pseudo-alternans). In pericardial effusion or cardiac tamponade, electrical alternans most likely results from cardiac displacement in the pericardial sac as well as the reduction of the restraining interference of the lungs on the heart [366]. In the absence of pericardial effusion or cardiac tamponade, the possible mechanism of electrical alternans is an alternation in the pattern

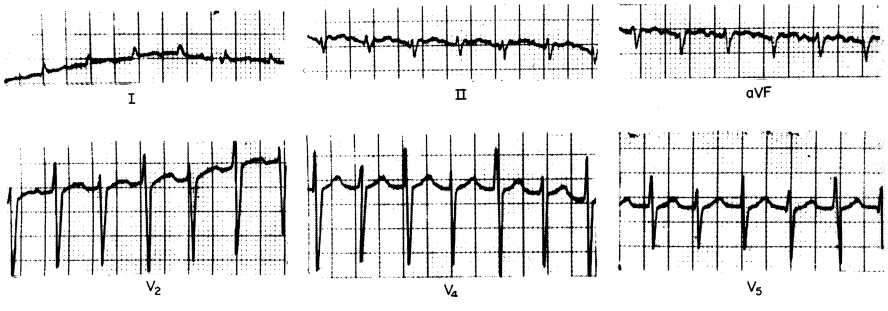

Figure 20.31
QRS alternans in a patient with complicated large pericardial effusion due to a hepatoma.

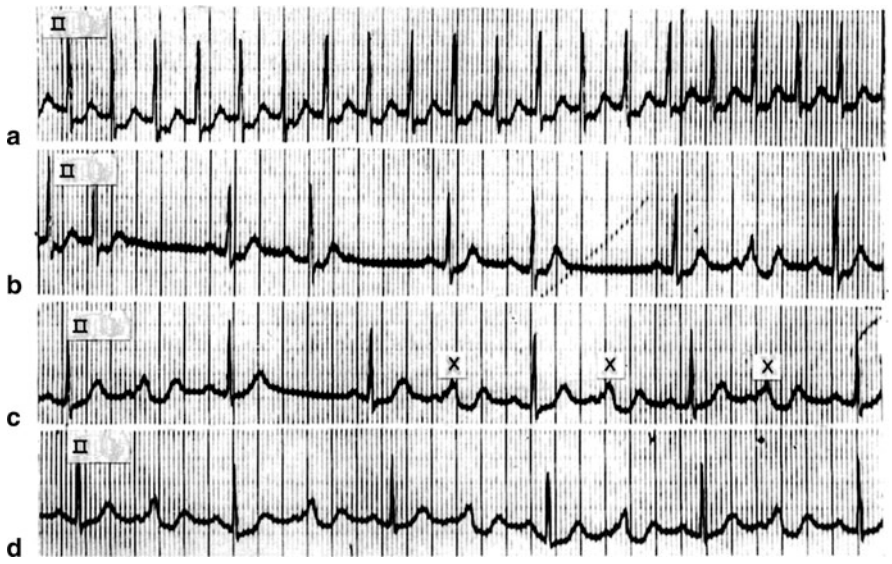

Figure 20.32

QRS alternans in a patient with alternating WPW ECG pattern (lead II (b, c, d). Note the regularity of the P–P interval, and the xs indicating the QRSs with preexcitation).

of depolarization, which is the consequence of the inhomogeneous refractory phase of the myocardium [367]. However, this should be termed "depolarization alternans" and the implication is that this is a cardiac rather than extracardiac phenomenon. Currently T wave alternans, expressed in μV, has been employed in research and practice [368]; particularly its application during exercise testing is touted as useful for evaluation of patients with CAD, or for selection of patients for implantation of cardioverter/defibrillators [369].

20.19 Cardiac Memory

T wave changes can be thought of as primary, implying a change in ventricular gradient, like the ones caused by electrolytic or ischemic disturbances, or secondary, due to changes in the ventricular depolarization sequence, as in bundle branch block (BBB) or sequence of repolarization as in some forms of left ventricular hypertrophy. Experimental work [370–372] and the repolarization changes noted in left bundle branch block (LBBB) and right ventricular pacing led to the proposition that a change in the sequence of ventricular activation may also induce variation in the duration of the excited state resulting in a change in the ventricular gradient, i.e. emergence of "primary" or "pseudoprimary" T wave abnormalities [373–375]. Such T wave changes are unlike the secondary changes that are seen as "obligatory" components of LBBB or right ventricular pacing, and have the following characteristics: they develop gradually; a long time may be needed for maximal effect to appear and subsequently to dissipate, and a shorter time for these to take place when the heart has been previously exposed to BBB or pacing. They are manifest during return to normal activation; and their direction is the same as that of the inciting abnormal QRS complexes (Fig. 20.33). These "pseudoprimary" T wave changes may also be seen in some cases of transient complete AV block with wide QRS complexes, single or combined fascicular blocks, preexcitation, after tachycardias especially ventricular, following premature ventricular beats (VPBs) (Fig. 20.34a) and premature atrial beats (Fig. 20.35) and even after myocardial infarction [375]. It has been stated that with single VPBs, cardiac memory can be detected when the VPBs are interpolated (Fig. 20.34a) or they are followed by a non-fully compensatory period (Fig. 20.34b), while it does not occur or is barely detected with fully compensatory periods; however, occasionally evidence of memory is seen in association with a fully compensatory period (Fig. 20.36). Also the change in the T wave may require a few beats for full return to the appearance present prior to the VPCs.

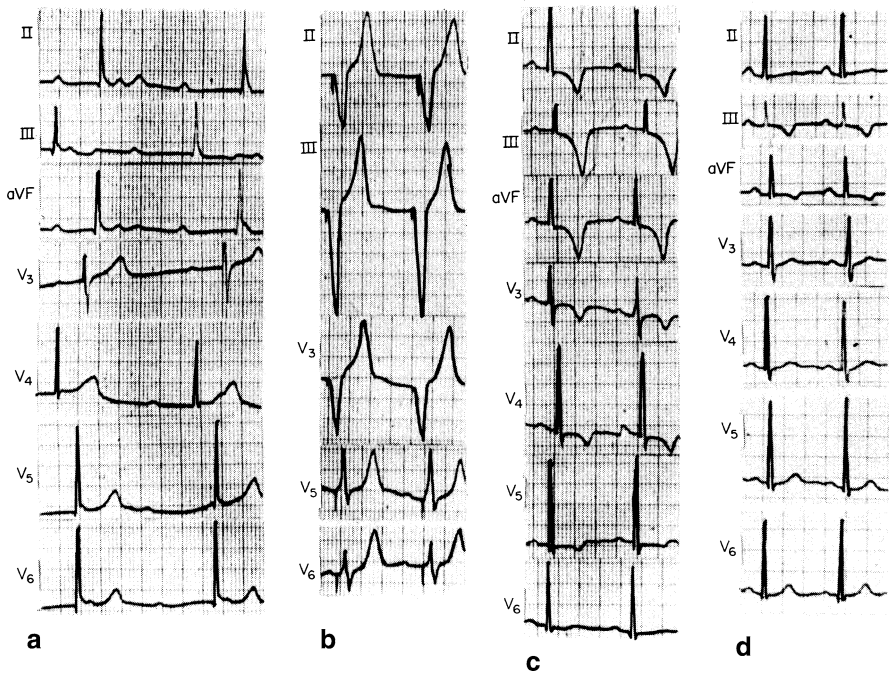

Figure 20.33

(a) ECG of a patient with acute myocarditis shows complete AV block. (b) ECG shows RV pacing rhythm. (c) ECG 6 days later, after discontinuation of the pacemaker, shows remarkable T wave inversion in leads II, III, aVF, V_3–V_6, with the T waves in the same direction as the wide QRSs during RV pacing. (d) ECG further 4 days later has returned to normal.

Multiple single VPBs may gradually enhance the observed post-VPB T wave changes. Evidence for cardiac memory is ubiquitous in both standard ECGs, exercise stress ECGs, and Holter monitoring tracings (Figs. 20.34 and 20.35).

The mechanism, by which the ventricular gradient is affected when the sequence of ventricular activation changes as in LBBB, has been thought to be an electrotonic modulation occurring during cardiac activation, accelerating repolarization at sites where depolarization starts, and delaying it at sites where it terminates [375]. A cumulative modulation of the T wave change ensues, which can be appreciated in serial ECGs, and suggests some form of "storage", simulating "memory". Such change may persist for days or weeks after the discontinuation of the inciting stimulus. Although the mechanism of these T wave changes has been debated for a long time, the existence of cardiac memory is not any more disputed, and is currently viewed as a form of remodeling via similar processes determining memory in the central nervous system [374, 376–378]. Cardiac memory consequent to pacing has been shown to depend on changes in ionic currents, and the distinction between secondary and "pseudoprimary" T wave changes is becoming less clear, since pacing for example alters slightly the post-pacing QRS complexes, which are not exactly as they appeared prior to the initiation of artificial cardiac stimulation [378].

The clinical significance of these T wave changes was and still is the object of controversy [377–379]. The post PVB T wave abnormality is a case in point, where arguments persist as to whether it reflects latent pathology, or merely it is a consequence of cardiac memory [377–379]. The same applies to T wave changes in the intrinsic ventricular capture beats in patients with intermittent pacing (Fig. 20.37), and whether this signifies underlying pathology, injury to the myocardium, or merely "an ECG curiosity" [378, 379]. In terms of the causative mechanism, T wave change after a VPB could also be due to myocardial ischemia resulting from post-ectopic potentiation of ventricular contraction, transiently increasing regional myocardial oxygen demands [380, 381]. A way to discriminate between the T wave changes due to cardiac memory and those reflecting ischemic alterations regardless of the coronary artery involved has been reported, and relies on the polarity and amplitude of the T waves in particular ECG leads [382].

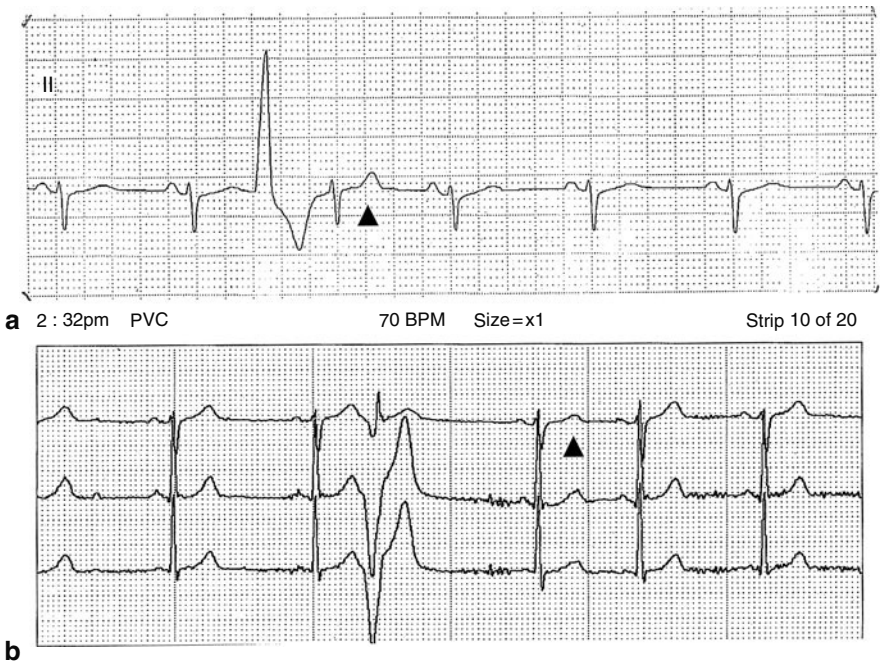

Figure 20.34

(a) ECG of a 66-year-old man with hypertension, and normal coronary arteries and left ventricular function shows T wave changes after an interpolated VPB (arrowhead) (b) A Holter ECG recording of a 53-year-old man with normal coronary arteries and left ventricular function complaining of palpitations reveals post VPB T wave changes (arrowhead).

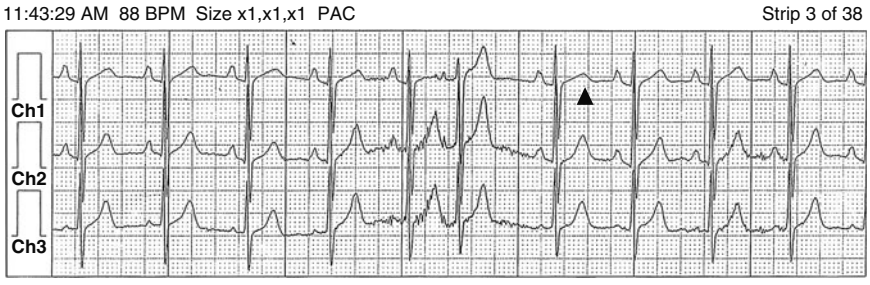

Figure 20.35

Holter ECG of a 54-year-old man with complaints of dizziness and a normal exercise treadmill/thallium-201 test shows post premature atrial beat (PAB) lowering of the T wave (arrowhead) to the direction of the predominant QRS forces of the PAB.

20.20 Gastrointestinal Disease

A number of diseases of abdominal organs (pancreatitis, cholecystitis, duodenal ulcer disease) are associated with ECG changes, mainly nonspecific ST-T changes; however, occasionally the ECG changes are more impressive, i.e., deep T wave inversion and ST segment elevation of ≥ 1.0 mm, and rarely Q waves simulating myocardial ischemia or infarction [383, 384]. ST-T changes in patients with gastrointestinal diseases may occasionally represent a normal variant. In esophageal disorders in particular, due to the frequent presentation with chest pain indistinguishable from the one due

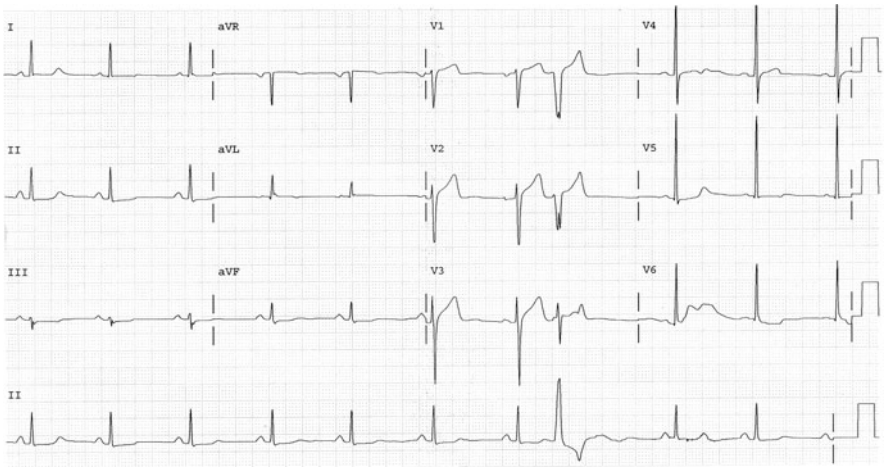

Figure 20.36

ECG of a 65-year-old man with hypertension and left ventricular hypertrophy in his echocardiogram, shows T wave enhancement post VPB (arrowhead) to the direction of the predominant QRS forces of the VPB.

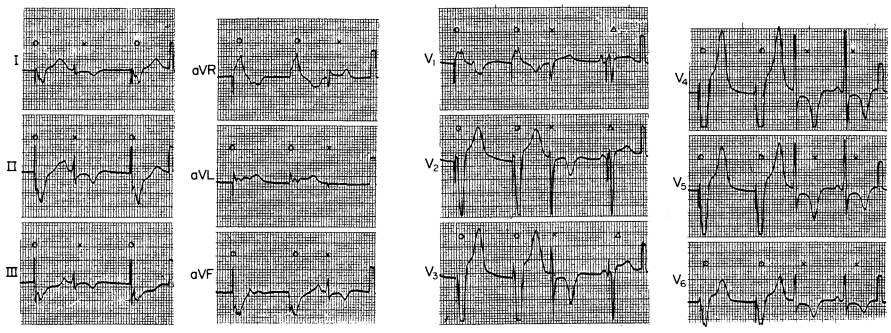

Figure 20.37

In a 72-year-old woman with sick sinus syndrome, demand artificial pacing (DDI) produced conducted beats (x), with deeply inverted T waves. Note the similarity in the directions of the inverted T and the paced QRS complex (o, paced beat; Δ, fusion beat).

to myocardial ischemia, evaluation of ECG changes is problematic [16]. Although real myocardial ischemia has been occasionally attributed to esophageal reflux, ECG changes did not occur with decrease in the esophageal pH [385]. Upper gastrointestinal endoscopy is associated with sinus tachycardia, ST segment depression, and in some patients, evidence of myocardial ischemia by cardiac scintigraphy [386]; no protective effect was documented by sedation or supplemental oxygen, and the tachycardia rather than hypoxemia was found to be the mediator of ST segment depression [387, 388]. Myocardial ischemia with ST segment depression or elevation during colonoscopy (under conscious sedation and without supplementary oxygen) may be associated with tachycardia and/or hypoxemia, while probably viscerocardiac reflexes may be contributing to the pathogenesis of myocardial ischemia [389]. In general, arousal of the sympathetic nervous system, sinus tachycardia, atrial and ventricular ectopy, and ST segment deviations are noted, particularly in elderly patients and/or those with cardiac disease, and supplemental oxygen, sedation, and monitoring during and after endoscopic procedures is recommended. A frequent affliction, the "irritable bowel syndrome" is associated with palpitations [390], and functional gastric dilatation may present with atypical chest pain and dramatic T wave inversions, resolving with gastric decompression [391].

20.21 Renal Disease and Hemodialysis

Renal diseases, with the culminating coronary artery disease and hypertension, may lead to all the commonly encountered ECG abnormalities of these complications. Patients with renal failure and pericarditis/pericardial effusion may have the expected ECG changes (see Sect. 20.16), and those with end stage disease show increase in ECG voltage after hemodialysis, most probably due to alleviation of fluid overload [392–394]. Patients with renal failure suffer an excessive mortality, particularly cardiovascular in nature and due to sudden death [395], and their ECGs reveal abnormal late potentials [396], decreased heart rate variability [397], and prolongation of the P wave and QTc intervals [398, 399]. Some of these changes may become accentuated with hemodialysis but a confounding influence contributing to these abnormalities may be the fluid shifts which such patients experience [400].

20.22 Psychiatric Disease

Psychiatric disease aggravates the condition of patients with coronary artery disease or heart failure. In addition, psychiatric disease, in the absence of cardiac disease, increases mortality. Psychiatric disorders are linked to autonomic dysregulations, and heart rate variability (HRV) is reduced in patients with major depression, panic disorders, Alzheimer's disease, and schizophrenia [401]. The magnitude of HRV reduction correlates with the severity of the depression and there is suspicion that these dysregulations are partly responsible for the increased mortality in patients with psychiatric disease. Mostly reduced parasympathetic activity, but also elevated sympathetic activities have been found in psychiatric patients. Antidepressive therapy with serotonin reuptake inhibitors has failed to improve the prognosis of these patients. Anorexia nervosa, bulimia, depression, anxiety, and panic attacks prolong QTc, while weight recovery in patients with anorexia nervosa reduces the increased QT duration and QT dispersion [402]. Such patients with psychiatric disease and QT abnormalities should be evaluated for underlying hypokalemia [403]. Certain antipsychotic drugs cause T wave changes and QTc prolongation and confer an arrhythmic risk to patients with psychiatric disease [404]. Although ECG screening of all patients with psychiatric disease is felt not to be cost-effective, the high prevalence of electrophysiologic abnormalities in such patients and the importance of monitoring such prognostic parameters, as the above, and their response to drug therapy, emphasizes the importance of routine use of the ECG [405].

20.23 Non-Specific ST-T Changes

The "non-specific ST-T changes" designation is employed widely by electrocardiographers, mostly without adherence to specific criteria. Implicitly this diagnosis encompasses "mild" ST-T alterations for some, while others refer to criteria (<0.1 mV ST segment elevation or depression with or without flattened or inverted T waves <0.5 mV) [406]. Although such changes can be found as a normal variant, or as a response to many drugs, other environmental influences or substances, and in a large array of pathological conditions, most often there is no explanation for their presence. Since many causes lead to similar ECG appearances, the designation "non-specific ST-T changes" in describing these changes is appropriate. The term "non specific" is employed in contrast to "specific", e.g. the tall T waves of hyperkalemia; however, even "specific" changes can occasionally occur without a specific inciting pathology. Interpretation of ST-T changes should always take into consideration the clinical context. A partial list of conditions causing non specific ST-T changes, contained in a book, includes 90 items [406].

Non specific ST-T changes are frequently the reason for cardiology consultation (e.g. in healthy pregnant women) (Fig. 20.38) (see Sect. 20.27), and the cause for anxiety or iatrogenic disease, in normal subjects [407]. Only up to 8% of patients presenting to an emergency department with chest pain and normal ECG or non specific ST-T changes were diagnosed with an acute myocardial infarction [408]. Also, transient ST segment changes were found in up to 8% of patients' ambulatory ECG recordings in the absence of coronary artery disease [409]. Non specific ST-T changes were detected in ambulatory ECG monitoring after meals, with the Valsalva maneuver, and with a change in body position [410].

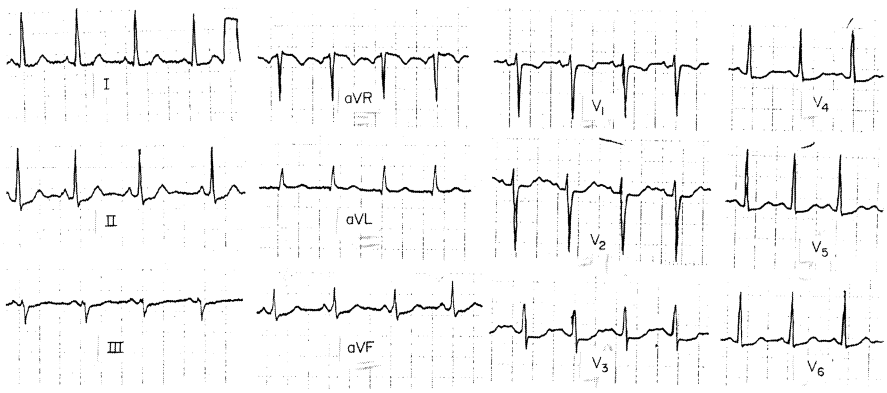

Figure 20.38

ECG of a young woman 24 weeks pregnant who was referred for evaluation after a heart murmur was detected; this turned out to be a functional murmur, and echocardiography showed a hyperdynamic normal-sized heart.

Variation in anatomical position of the heart and the spread of excitation and repolarization may generate a wide range of normalcy. Multiple gradients of repolarization are generated, with cancellation from simultaneously recovering territories, resulting in the appearance of what is called normal ST-T waves. When cardiac activation is abnormal, such gradients are altered, their cancellation patterns are different, and the associated changes in the shape of action potentials (particularly the slope and duration of phases 2 and 3) conspire to produce ST-T wave abnormalities. These types of changes, called "secondary" changes, are due to abnormal activation seen with bundle branch blocks or ventricular hypertrophies, in distinction from "primary" ST-T wave abnormalities resulting from alterations of the recovery process per se. [131]. Examples of the latter are changes imparted by various cardiac and non-cardiac conditions, and drugs. Non specific ST-T changes may be similar in morphology and amplitude to the above "primary" and "secondary" changes.

20.24 Giant and Low Voltage ECG Complexes and Waves

The "giant" ECG voltage characterization is often employed without criteria, although it is occasionally used for high amplitude T waves, e.g., T amplitude >1.0 mV is considered a diagnostic demarcation [406]. Conventionally, low voltage ECG is diagnosed when the QRS peak to peak voltage is ≤0.5 mV in the limb leads and ≤1 mV in the precordial leads.

20.24.1 Giant R Waves

Giant R waves are noted transiently with myocardial infarction (MI) (Fig. 20.39) [411], Prinzmetal's angina (Fig. 20.40) [412], and during exercise stress testing (Fig. 20.41) [413]. Often they appear as monophasic QRS complexes with merging of the QRS and ST segment, some widening of QRS, and in the presence of tachycardia may simulate ventricular tachycardia [414]. Mechanistically, giant R waves may represent intraventricular (unopposed) ventricular conduction delay [415].

20.24.2 Positive Giant T Waves

If positive or negative T waves >1.0 mV are considered as "giant", their incidence is frequent. Positive "giant T waves" are seen with electrolytic abnormalities, Prinzmetal's angina, hyperacute phase of MI, hyperkalemia, and rarely cerebrovascular accidents [406]. Transient positive giant T waves are seen in leads V_1–V_3 in posterior MI, left ventricular hypertrophy

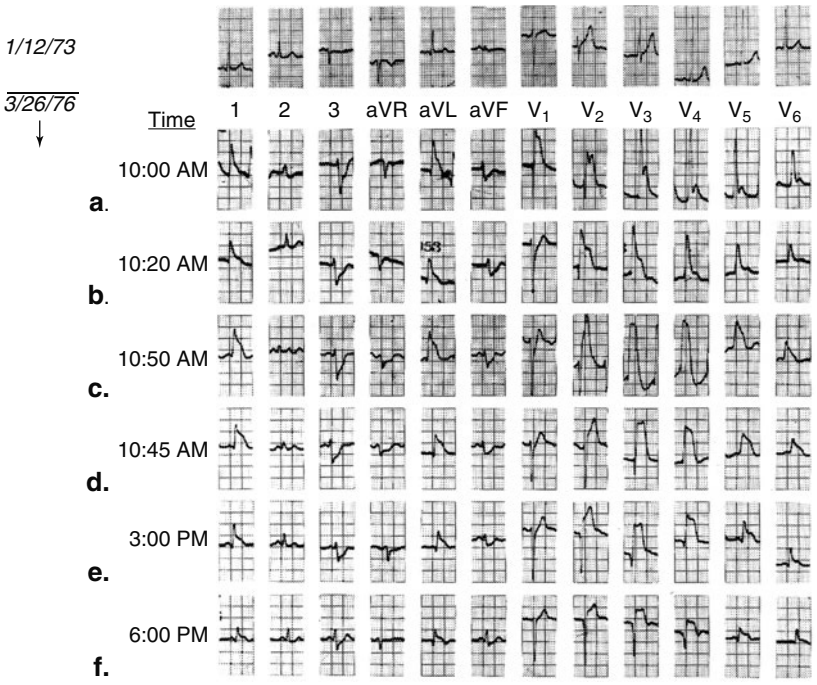

Figure 20.39

ECG of a 43-year-old man who presented minutes after onset of chest pain; an acute myocardial infarction (MI) was associated with early changes in the amplitude and duration of the QRS complexes before the emergence of the classic ECG changes of MI. (Reproduced from Ref. [411]. With permission of the *Journal of Electrocardiology*.)

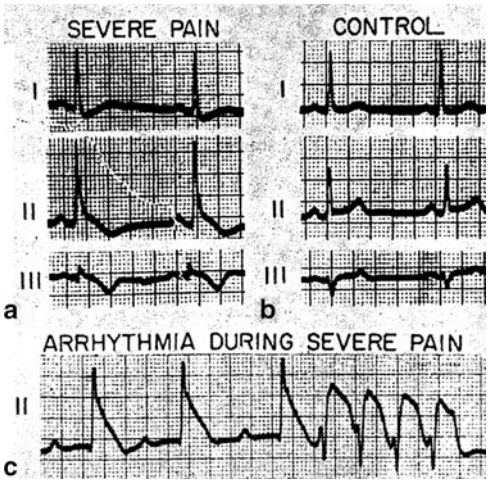

Figure 20.40

ECG of a 42-year-old man, subjected to anginal attacks of Prinzmetal's angina; increase in the amplitude of the R wave particularly in lead II (a) in comparison with the resting ECG (b) occurred and was followed by ST segment elevation. A burst of ventricular tachycatrdia occurred at the peak of the attack (c). (Reproduced from Ref. [412]. With permission of the *Journal of the American Medical Association*.)

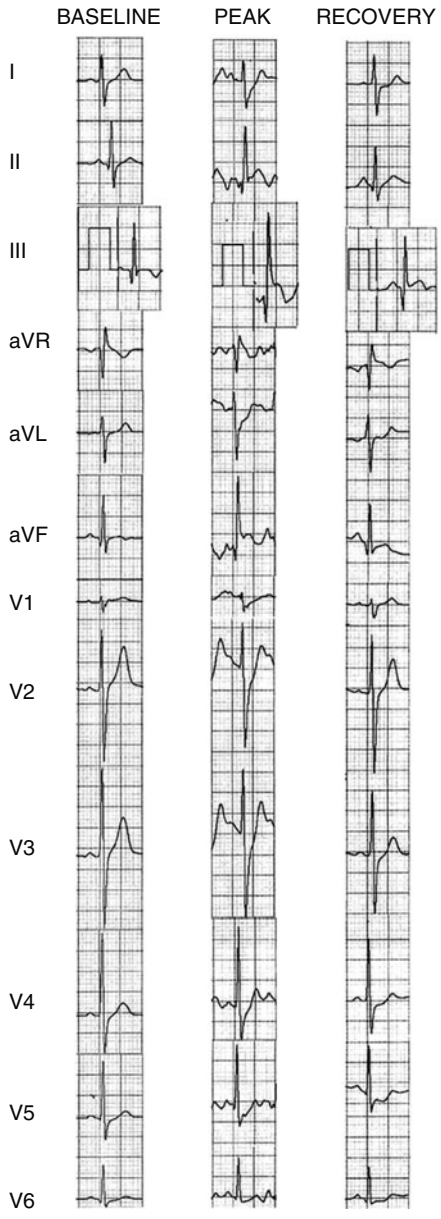

Figure 20.41

Exercise stress ECG from a 39-year-old man who showed transient increase in the amplitude of R-wave in leads II, III, and aVF; cardiac enzymes did not rise after the stress test, coronary arteriography revealed three-vessel coronary artery disease with an occluded right coronary artery, and a left ventricular ejection fraction of 75% with mild hypokinesis of the inferior ventricular wall. (Reproduced from Ref. [413]. With permission of the *Journal of Electrocardiology*.)

and left bundle branch block, and in left precordial leads in association with aortic and mitral regurgitation and other left ventricular volume overload states [299]. Positive giant T waves are very occasionally encountered in the early phase of acute pericarditis, or as a normal variant in early repolarization with occasionally marked (Fig. 20.3), but most often modest, ST segment elevation. Automated ECG interpretation often ascribes the positive giant T waves to "metabolic abnormalities".

20.24.3 Negative Giant T Waves

Many clinical entities are associated with negative "giant T waves", pointing to a common underlying ventricular repolarization disturbance [416–421], but with diverse pathophysiological underpinnings, or rarely as a normal variant in young subjects [406], particularly of the black race. A variety of morphologies of the negative giant T waves are encountered in different leads and in different patients associated with abnormalities in the ST segment and prolongation of the QT interval. Deeply inverted T waves and QT prolongation, both being abnormalities of ventricular repolarization, often coexist in many conditions. T wave morphology is not expected to change from a diffuse increase of the action-potential duration, which results however in a QT prolongation, as in hypocalcemia. On the other hand, T wave changes imply underlying regional differences in the repolarization duration. However, minor local dispersion of the action potential is often accompanied by QT prolongation. Theoretically the negative giant T waves could be due to shortening of the action potentials somewhere in the ventricles. In general, negative giant T waves are almost always associated with some QT prolongation, but the separation of the ECG entities of negative giant T waves with and without QT interval prolongation may be useful. Furthermore, mild QT interval prolongation may not have the same diagnostic and prognostic significance as marked QT prolongation. The particulars of prolonged congenital and acquired long QT interval are dealt with in Chap. 19, while here the focus is mainly on the negative giant T waves.

20.24.3.1 Myocardial Infarction and Ischemic Heart Disease

Symmetrical negative giant T waves are frequently found in patients with MI in the subacute phase and beyond, and in leads overlying the infarcted territory. Also, they are seen in non-ST segment elevation or non-Q wave MIs (Fig. 20.42), angina pectoris, and variant angina [422–425]. Some prolongation of the QT interval is seen in the above conditions, suggesting a repolarization delay of the ischemic territory, and explains the interest in employing the QT interval as a prognostic index [426–428].

20.24.3.2 Ventricular Hypertrophy and Hypertrophic Cardiomyopathy

Occasionally, secondary negative giant T waves are seen in leads V_1–V_4 with right ventricular hypertrophy (RVH) [416], particularly in association with the acute right ventricular pressure overload of pulmonary embolism. Similar T waves in leads V_4–V_6, with less impressive changes in the limb leads, and tall R waves in V_2 and V_3 resembling the pattern of RVH are noted in the "Japanese" hypertrophic cardiomyopathy with confinement of hypertrophy to the apical region (Figs. 20.43 and 20.44) [429–431]. The above ECG picture evolves gradually over the course of many years and then

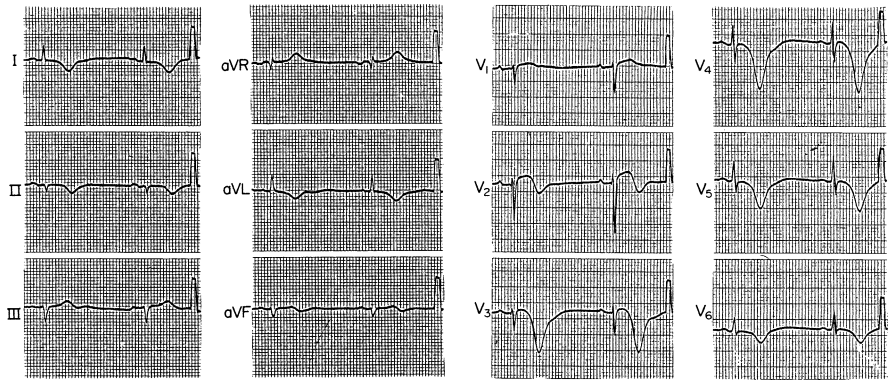

Figure 20.42
Negative "giant T waves" in the ECG recorded from a 70-year-old woman with anterior and inferior myocardial infarction.

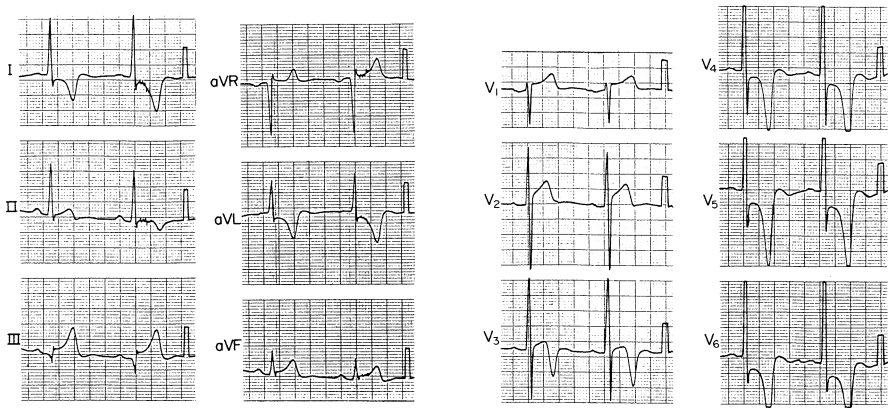

Figure 20.43
ECG showing negative "giant T-waves" in a 55-year-old man with apical hypertrophic cardiomyopathy.

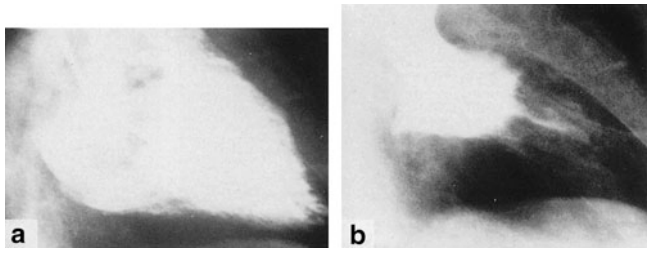

Figure 20.44
Ventriculogram at end diastole (a) and end systole (b) of the patient whose ECG is shown in Figs. 20.43 and 18.44.

may persist for a long time. Some QT interval prolongation, attributed to a recovery delay of the abnormal hypertrophic myocardium, is usually seen in these patients. Similar T wave abnormalities may be found in other cardiomyopathies [277, 432].

20.24.3.3 Central Nervous System

Negative giant T waves resembling changes found in MI may be seen in patients with cerebral pathology, e.g. brain tumors, or subarachnoid hemorrhage (Fig. 20.45), [418, 433–441]. Frequently, pronounced QT interval prolongation and occasionally abnormal Q waves are also noted. Similar ECG changes have been reported in brain surgery and cranial injuries [442, 443]. Subarachnoid hemorrhage and lesions in the frontal cortex and basal portion of the brain are frequent correlates of these ECG abnormalities, and are probably due to abnormal autonomic nervous system discharges and electrolyte or other metabolic problems (see Sect. 20.7.1).

20.24.3.4 Electrolyte Abnormalities

Myocardial repolarization disturbances are frequently linked to abnormal serum electrolyte concentration [13, 419]; prominent U waves with hypokalemia and QT prolongation with hypocalcemia are prime examples. Such conditions are rarely associated with significant T wave abnormalities, since they exert a diffuse influence on the myocardium. Nevertheless in severe or chronic K^+ or Ca^{2+} deficiencies, deeply inverted T waves, marked ST segment changes, and ventricular arrhythmias have been noted [25, 416, 444]. The underlying mechanism appears to be the changes in the membrane or

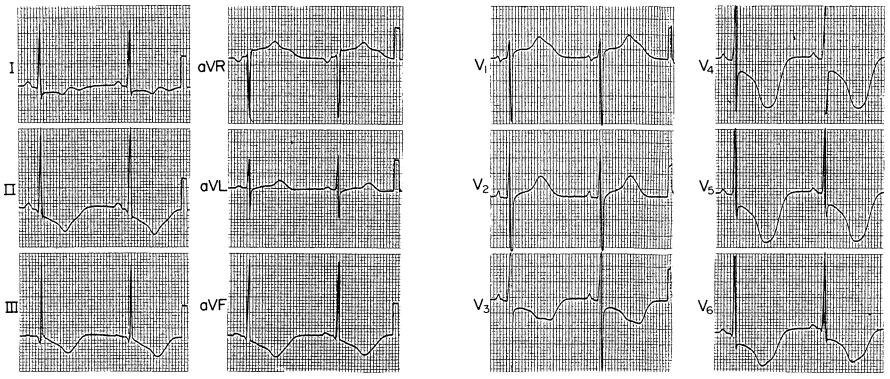

Figure 20.45

Giant negative T-waves with prolonged QTU-interval in a 55-year-old woman with subarachnoid hemorrhage, resembling myocardial ischemia (compare with Figs. 20.42 and 18.43).

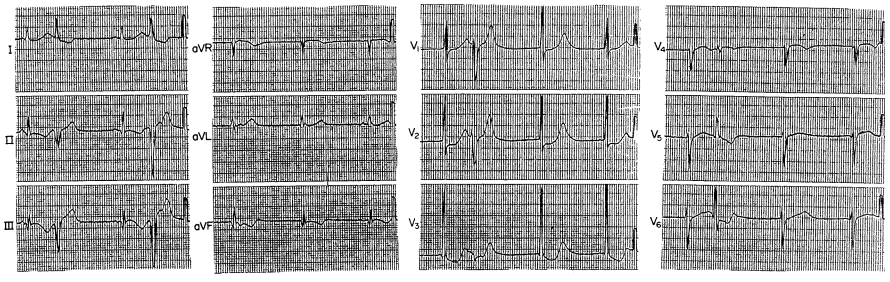

Figure 20.46

Markedly prolonged QT interval, ST-T abnormalities, and negative T waves in leads II, III and aVF. T-waves seen in a 62-year-old woman with an inferior myocardial infarction, potassium of 2.5 mEq L^{-1}, and digoxin level of 1.8 ng mL^{-1}. The T wave was normalized after these values became normal.

intracellular distribution of ions and an enhanced sensitivity to sympathetic activity. Myocardial ischemia, infarction and high serum digoxin level may complicate the picture further (Fig. 20.46).

20.24.3.5 Sympathetic Nerves and Catecholamines

Clinical doses of catecholamines administered to normal subjects lead to sinus tachycardia, minor changes in the morphology of QRS complex, and flattening of the T waves [445, 446]; these are partly caused by the β_2-mediated lowering of the serum potassium level [446, 447]. Slight shortening in the action potential duration of normal ventricular muscle has been observed with isoproterenol [448–450], but such changes could alter the ECG drastically. Negative giant T waves can be generated with unilateral stimulation of the stellate ganglion or local application of catecholamines [451–454]. Right and left sympathetic nerves innervate the anterior and posterior aspects of the ventricles, respectively [455], and thus when either of the right and left sides is stimulated, a small local difference in repolarization leads to T wave changes.

In contrast, high doses of catecholamines superimposed on myocardial pathology or electrolyte abnormalities could influence the ECG markedly [456, 457]. Accordingly, negative giant T waves can be produced by experimental isoproterenol infusions combined with a high calcium environment [458]. Repeated or chronic catecholamine exposure may have somewhat different outcomes from that of acute single dose administration. Negative giant T waves have been

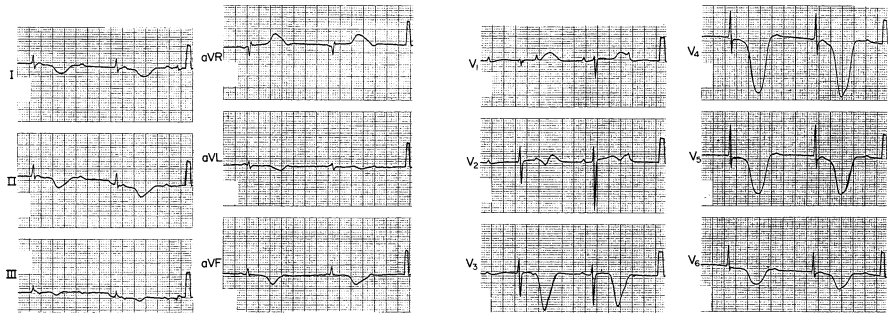

Figure 20.47
ECG of a 76-year-old woman with complete AV block and giant negative T-waves.

reported with pheochromocytoma [459, 460], and it is probable that the effect of catecholamines is modified by underlying myocardial ischemia, abnormalities in electrolyte distribution, or other reasons. Also catecholamines could induce focal toxic "myocarditis" and cardiomyopathy [461, 462].

20.24.3.6 AV Block and Heart-Rate Change

Occasionally in bradycardia, in the setting of advanced AV block, negative giant T waves with marked QT prolongation have been observed (Fig. 20.47) [416, 417]. Bizarre repolarization waves are most likely to occur after Adams-Stokes attacks resulting from tachyarrhythmias, where abnormalities in the recovery process are, in turn, considered to predispose to ventricular arrhythmias (VT) and initiate repeated attacks over a period of time. Hence, it is often difficult to determine which is the primary event. Similar repolarization abnormalities have been seen in association with torsades de pointes [463, 464], suggesting a common underlying mechanism; this atypical VT is caused by certain antiarrhythmic drugs and other agents (see Chap. 19).

Post-tachycardia inverted T waves, not necessarily with marked QT prolongation, have been observed after the termination of supraventricular or ventricular tachycardia [465, 466]. Inverted T waves, not always of the "giant" variety, have been observed also after artificial ventricular pacing [467, 468], but since the pacing rate inducing them is not high (as in the post-tachycardia states) the mechanism is different (see Sect. 20.19). Of similar mechanism are the changes noted after transient or intermittent LBBB [469], and radiofrequency catheter ablation of accessory bypass tracts [470]; in the latter case the T wave changes secondary to such tracts are replaced after ablation by the "memory" primary T wave changes [471].

20.24.3.7 Antiarrhythmic Drugs and Miscellaneous Conditions

The list of drugs leading to ST-T changes, with QT prolongation and ventricular arrhythmias, is perpetually expanding. Association with negative giant T waves is not reported with all such drugs, but since they cause long QTc or ventricular arrhythmias, they are considered as potential causes of giant T waves. Since these agents primarily prolong the QT interval, they are dealt with in Chap. 19. During angiography (see Sect. 20.29.6) and surgical procedures [472–476], low temperature and tissue injuries may also be responsible for pronounced ST-T abnormalities.

20.24.4 Low Voltage ECG

The "low voltage ECG" is characterized by a decrease in amplitude of all components of the ECG curve; thus the P waves, the QRS complex and the T waves are of low amplitude, although diagnostic criteria conventionally refer only to the

QRS complexes. Traditionally the list of conditions associated with the low voltage ECG includes among others, obesity, emphysema, pneumothorax, pericardial and pleural effusions, infiltrative heart disease, multiple MIs, and myocarditis [477]; also other factors can induce such ECG changes (see Sect. 20.25.6).

20.25 Extracardiac Factors

Amplitude, morphology, and orientation of the various components of the ECG curve are influenced by a number of factors exerting an effect beyond the heart's surface. What is recorded at the body surface are "residual currents" after the extracardiac influences (pericardial, and body volume conductor) have exerted their effects on the currents emanating from the heart [217]. Additionally, the intracavitary blood volume influences the potentials recorded at the body surface [478].

20.25.1 Heart-Electrode Distance

Distance of the heart from the chest wall (and therefore from the recording electrode), irrespective of the intervening tissues and organs, affects the surface ECG voltage [479]. The prime example of such influence is the large voltages recorded in the precordial leads in comparison with the unipolar limb leads [480]. The drop of ECG voltage is precipitous, as the "exploring" electrode is positioned at gradually increasing distances from the heart, and this relationship follows the inverse square law. The increase in the V_4–V_6 QRS voltage in tachycardia may be due to the enhanced closeness of the heart's "centroid" to the chest wall precipitated by a reduction of its volume due to tachycardia [118]; hypovolemia leading to an underfilling of the heart may exert a similar influence. These associations are discordant to what is expected as a result of "Brody effect" [478].

20.25.2 Body Habitus

Anthropometric designations of ectomorphic, mesomorphic, or endomorphic with their attendant different amount and proportion and distribution of muscle and fat, have an effect on the appearance of ECG, which is exerted via the variation in the heart-electrode distance (see Sect. 20.25.1), and heart position (see Sect. 20.25.3). The chest configuration also influences potentials. The ECG of emaciated patients may show enormous deflections in all leads [481], while thin-chested individuals have such changes only in precordial leads [482]. Both factors prevent great losses in potentials on the way to the body surface (Wilson's "proximity effect") [480]. Muscular or obese (see Sect. 20.26) individuals, or those with large cylindrical chests have attenuated potentials. Consequently knowledge of the patient's height, weight, and body build is useful in accurately interpreting the ECG.

20.25.3 Heart Position

The anatomical versus "electrical" heart positions should be viewed as distinct, with the former however influencing the latter. There is a relation between the ECG and the anatomical position of the heart in the thorax [479]; thus a vertical position of the QRS loop is found with a vertical anatomical axis of the heart, as seen in lean subjects and/or with a low-positioned diaphragm, while a leftward rotation of the loop is seen with transversely placed heart in association with a raised diaphragm in a stocky individual and/or with a prominent abdomen. In a person with average body build the anatomic and electrical orientation of the heart is from upper right to lower left. In slender tall individuals the heart is anatomically more vertical and shows a vertical axis [482], while it is more horizontal in heavy-set corpulent subjects who have more squat hearts [481]. Occasionally, there is a discordance of the anatomical and electrical axes of the heart.

Rotations of the body and heart can be about the sagittal body axis (e.g. dextrocardia), the anatomical longitudinal axis of the heart or the long axis of the body, or the transverse axis (anterior or posterior position of the apex).

The last is associated with low QRS voltage in the frontal plane, as with emphysema. Similar changes are seen in congestive heart failure (CHF), and can be attributed to the left ventricular posterior displacement due to right ventricular dilatation in patients with CHF [301]. Even Q waves can be found in some ECG leads as a result of an unusual position of the heart. The P waves and T waves are also affected, and the R/S ratios may be changed markedly. Physiological and pathological changes in the position of the diaphragm, i.e. pregnancy (see Sect. 20.27), obesity (see Sect. 20.26), ascites, and tumors may resemble the ECG appearances of deep expiration, while emphysema, asthma, and wasting mimic the state of deep inspiration. All these changes can be compounded by pathological alterations, thus becoming atypical. The "electrical centers" or "centers of gravity" of the atrial and ventricular depolarization and their relationship to various positions of surface electrodes determine the ECG appearance [481].

20.25.4 Body Posture

Different body positions influence the ECG, since they change the relationship of the heart with the recording electrodes; this may apply particularly for lateral decubitus and for prone, in contrast to supine, body positions. Both stable ECGs in the supine, sitting, and standing positions, using the standard and the Mason-Likar exercise testing electrode "hook-up" [483, 484] (Fig. 20.48), and decrease in the R wave amplitude in the standing position has been reported [485]. A heart rate increase is expected by assuming the sitting and standing positions [484, 485]. Nevertheless, mild T wave changes and alterations of repolarization occur with change in position [486]. Also, non-specific ST-T changes, tall P waves in leads II and III, and right QRS frontal axis deviation have been recorded in young patients with a labile autonomic nervous system on assuming the upright position [481]. Since the ECG is routinely recorded in a supine body posture, changes are expected mostly in ambulatory ECG recordings, where drastic variation of the entire PQRST curve has been noted with

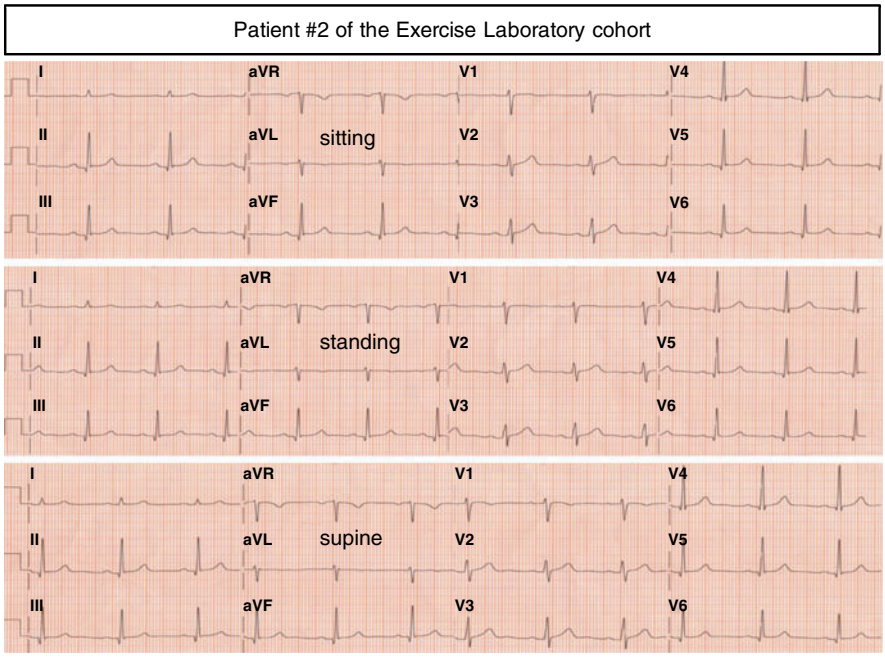

Figure 20.48
ECGs in the sitting, standing and supine positions, employing the Mason-Likar electrode "hook-up", from a patient undergoing a Bruce treadmill exercise stress test, were similar in appearance. (Reproduced from Ref. [484]. With permission of the *Journal of Electrocardiology*.)

different body postures [487]. Lying on the right or left side, or the prone position produces expected ECG alterations (shift of the entire PQRST three dimensional vector loop toward the lowest body point). The R wave in V_5 increases in amplitude in the left decubitus position [479]. Absence of changes in the amplitude and frontal axis of QRS complexes in the standard bipolar ECG leads with lying on the right and left sides is indicative of pathology causing fixation of the heart in the thorax (adhesive pericardiomediastinitis) [488]. Also, the inelastic dilated lungs of an emphysematous patient can lead to a "fixation" of the heart in the thorax, leading to a stable ECG, unaffected by changes in the body position [481]. Perhaps recording of the ECG in the standing position, in a patient who complains of orthostatic symptoms, may be more informative of his/her condition than the traditional recording in the supine position; ECGs recorded during "tilt table" testing may not be equivalent to those recorded in self-supported standing patients, and thus the latter should also be employed [484].

20.25.5 Respiration

The frontal QRS axis is deflected to the right in inspiration and to the left in expiration [489] (Fig. 20.49). Lead III is particularly affected, and its positivity of P, R, and T waves may be increased, or be reversed especially in deep inspiration and expiration respectively [482]. Of diagnostic significance for non existing inferior myocardial infarction is the conversion of a considerable Q wave to a nonpathological q wave or even to an R wave in lead III, during deep inspiration. Also morphological changes are seen in the QRS complex related to the projection of a changed loop in its 3D space orientation, on the recording thoracic electrode lattice. Of course, the outcome of deep inspiration depends on the amplitude and polarity of waves and complexes at expiration. ECG changes due to respiration reflect a special and reproducible change in the heart's position (see Sect. 20.25.3), [489] along with other electrophysiological influences not examined herein.

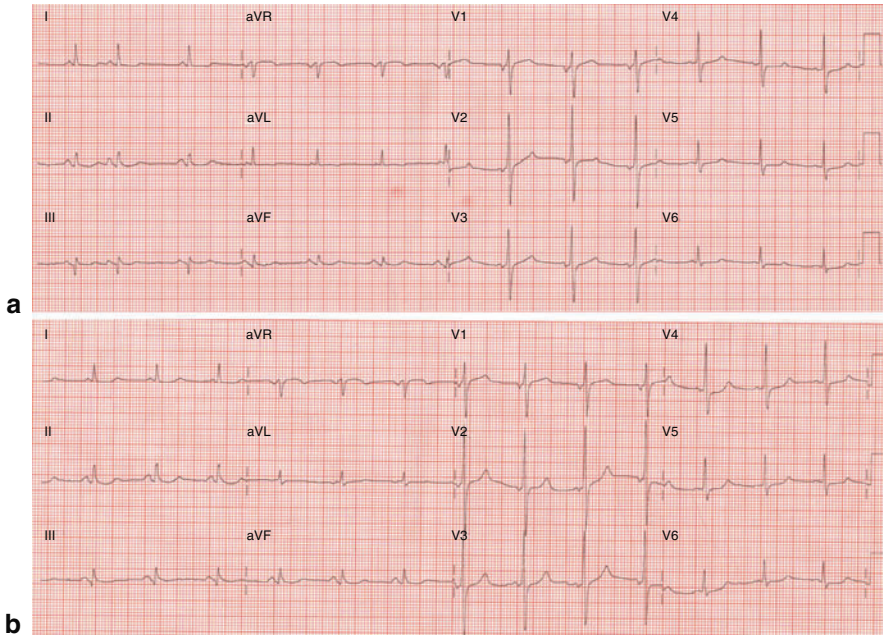

Figure 20.49

ECGs of a 63-year-old patient with history of coronary artery disease and chronic obstructive lung disease, obtained in the supine position at the points of modest expiration (a) and inspiration (b) showing a corresponding shift of the frontal QRS axis from 20° to 52°.

20.25.6 Peripheral Edema

Peripheral edema of varying etiology (sepsis, pneumonia, chronic obstructive lung disease, congestive heart failure [CHF], end stage-renal failure) leads to attenuation of all parts of the ECG curve [1, 490], which is more prominent in the limb and lateral precordial leads. Some of these changes do not necessarily reach the point of "low voltage" ECG. Peripheral edema in supine patients involves more the dorsal torso due to gravity. Also, due to the eccentric anterior/lateral position of the heart in the chest, V_5 and V_6 are much more affected than V_1 and V_2 (Fig. 20.50). Weight gain due to peripheral edema correlates well with the reduction of the amplitude of QRS complexes [1]. Augmentation of the ECG voltage (the inverse phenomenon) has also been observed with treatment of peripheral edema due to CHF [491, 492] (Fig. 20.51), or after hemodialysis [493, 494]. The attenuation of the QRS complexes in the limb leads reflect the overall (peripheral/distal changes) while the changes in the precordial leads reflect also the influence of peripheral edema on local thoracic ECG expression [1]. Clinical consequence of this phenomenon is the false negative ECG diagnosis of left ventricular hypertrophy [495], as well as atrial abnormalities [496].

The attenuation of the ECG voltage with peripheral edema appears to be due to a decreased electrical impedance of the passive volume conductor influencing the transfer of cardiac potentials from the surface of the heart to the recording sites [1, 217]. Other consequences of peripheral edema are shortening of the QRS and the QT intervals, which are attributed to a measurement failure in detection of early onset and late offset of these intervals resulting from the overall attenuation of the ECG curves [497, 498]. There may be clinical implications of these shortenings of the QRS and QT durations for patients with heart failure and peripheral edema who are being considered for cardioverter/defibrillator implantation, or biventricular resynchronization pacing [490]. Continuous impedance monitoring incorporated in the permanent pacemakers can be employed to monitor the intrathoracic edema in patients with heart failure [499]; the principle involved is similar to the one discussed above to explain the changes in the ECG amplitude with peripheral edema, although applied locally.

20.26 Obesity

Traditionally low voltage ECG comes to mind in association with obesity, resulting from increase in the distance of the heart from the recording electrodes due to the excess of adipose tissue. In addition, some influence must be exerted by the resistivity characteristics of the fat, which may increase the amplitude of body surface potentials [217]. The condition also tends to shift the frontal axis to the left, due to elevation of the diaphragm (see Sect. 20.25.3); such a shift may lead to a false diagnosis of an inferior myocardial infarction [500]. Increases in the QRS amplitude, QRS duration, QTc and PR intervals, and heart rate have also been reported in obesity [501]; increase in the cardiac workload leading to left ventricular hypertrophy may be the reasons for this. ECG abnormalities change after bariatric surgery for obesity but are not eliminated [502]. Liquid protein diets result in QTc or QTUc prolongation, ST-T abnormalities, left axis deviation, torsade de pointes, and ventricular fibrillation [503, 504].

20.27 Pregnancy

Although pregnancy is associated with augmented blood volume and cardiac output, the ECG of most pregnant women is normal. In the late stages of pregnancy, sinus tachycardia is frequently present, and the frontal QRS axis gradually shifts leftward or towards horizontal, or rarely even rightward due to elevation of the left hemidiaphragm, consequent to uterine enlargement [505]. Also with advancing pregnancy, atrial and ventricular premature beats are common. In young women during pregnancy, first onset of reentrant supraventricular tachycardias (RSVT) is rare, but symptoms of recurrent RSVT are exacerbated [506]. AV conduction defects are extremely rare, and they are of the 2° AV block

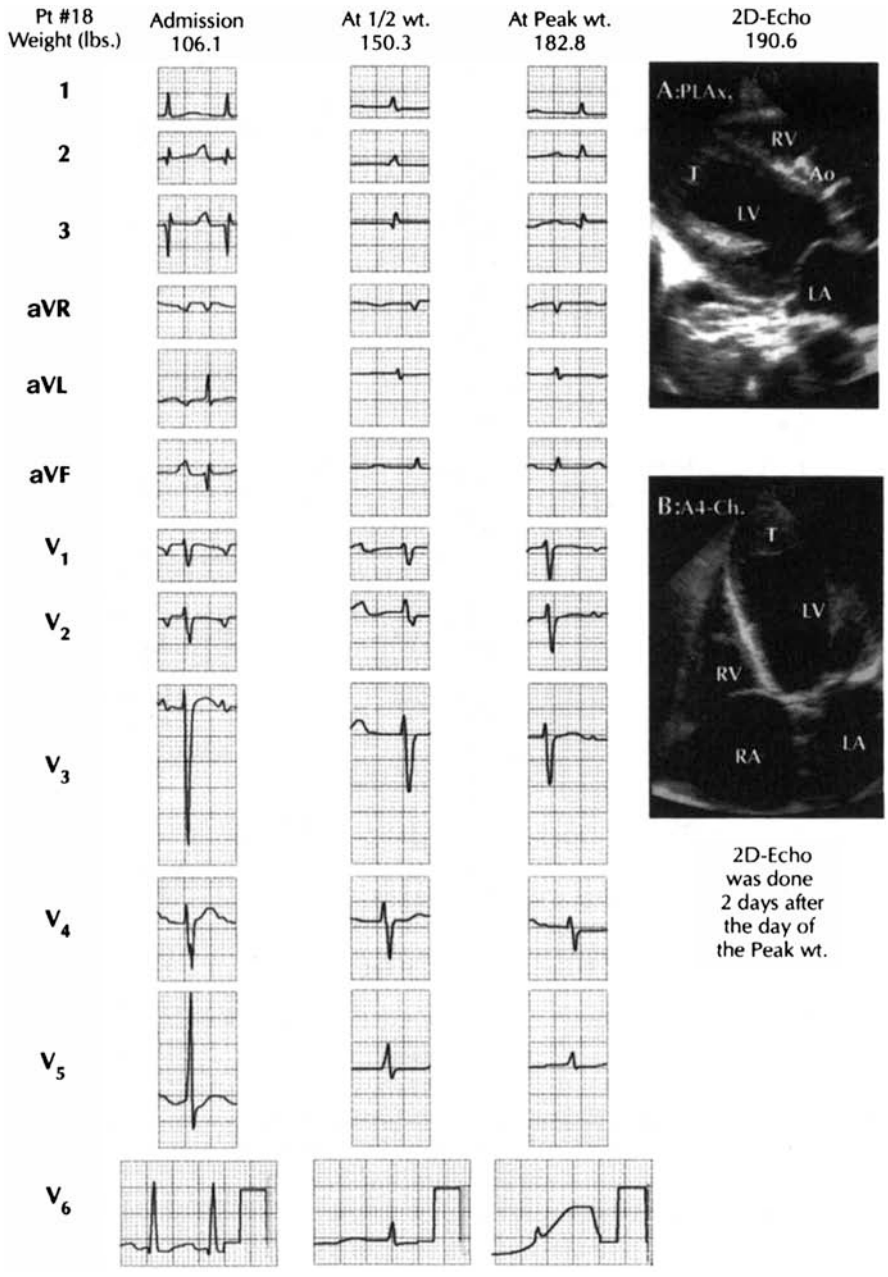

Figure 20.50

ECGs of a 53-year-old man who had suffered pneumonia and sepsis and in the process had fluid overload gaining 84.5 lbs showed gradual attenuation of the voltage of his ECGs; an echocardiogram obtained close to the date of the peak fluid accumulation showed that there was no pericardial effusion to account for the attenuated ECG voltage. (Reproduced from Ref. [1]. With permission of the *Journal of the American College of Cardiology*.)

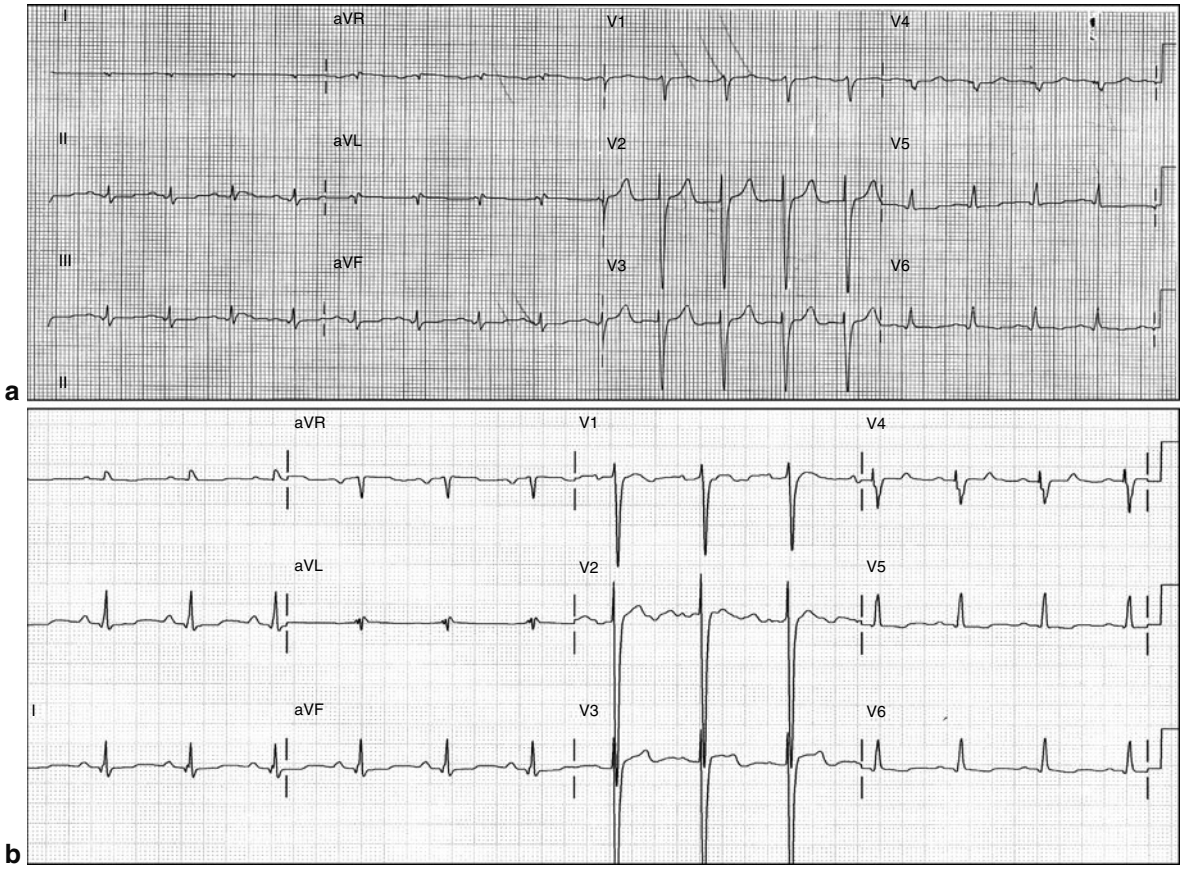

Figure 20.51

ECGs of a 54-year-old man with congestive heart failure who lost 48 lbs in the course of 2 weeks in response to diuresis, showed augmentation of the voltage of his discharge ECG (b) in comparison with the one from his admission (a). (Reproduced from Ref. [492]. With permission of the *Congestive Heart Failure*.)

of Wenckebach type [507]. Increase in size and mass of the left ventricle, as assessed by echocardiography, is occasionally associated with QRS voltage compatible with left ventricular hypertrophy.

Transient ST segment depression with flat or inverted T waves may be registered in both the limb and precordial leads (Fig. 20.38) [508], and such changes are abolished after delivery but may recur with succeeding pregnancies [509]. Follow-up for 20–30 years of women with such changes has not disclosed any pathology. A cause for these ST-T changes has not been found, and myocardial ischemia does not appear to be contributory. Occasionally Q waves with inverted T waves may occur in the limb leads in older patients, suggestive of an inferior myocardial infarction [500] (see Sect. 20.25.3), but such changes are not registered in aVF and are abolished by deep breathing.

Peripartum cardiomyopathy, a form of an idiopathic congestive cardiomyopathy characteristic of pregnancy, is manifest in a few women during the last month of gestation or the first few months after delivery. It is associated with cardiomegaly and all the hallmarks of heart failure (see Sect. 20.13.2). Nonspecific ST segment depression and T wave inversions are seen in the ECG of patients afflicted with this condition.

Cardiovascular abnormalities in pregnant women such as hypertension, rheumatic heart disease, congenital heart disease, and obstructive cardiomyopathy may become aggravated, by the increased circulatory load. The ECG tends to show changes in keeping with these associated diseases, occasionally expressing right and/or left ventricular hypertrophy.

20.28 Fetal Electrocardiography

The fetal ECG (FECG), albeit initially of low signal-to-noise ratio and poor quality of tracings, has permitted the detection of the fetal heart rate [510]; the fetal and maternal heart rates are independent of each other in the absence of pathology [511]. To obtain analyzable tracings, amplification of the fetal heart currents is necessary [512], since such currents are expected to be miniscule at the maternal abdominal surface due to the large distance between their source and the recording electrodes, and the short-circuiting effect of the amniotic fluid. The fetal ECG has important clinical applications [513]. Directly applied fetal electrodes and computerized signal-enhancement techniques [514] have led to improvement in the quality of tracings [515]. This, in turn, has provided the basis for correlative studies of ECG parameters (P, QRS, ST amplitudes, heart rate variability) with the condition of the fetus as assessed by laboratory data such as blood gas analysis, blood pH, or hemoglobin content [516]. As a minimum, digital signal processing techniques applied to maternal abdominal fetal ECGs (› Fig. 20.52) can improve monitoring and analysis of fetal heart rate [517, 518]. A study of the PR–RR relationship during normal labor found both positive and negative relationship between P-R and R-R intervals, but the latter did not discriminate between bradycardia with or without hypoxemia [519]. The problem of fetal ECG extraction is being addressed by a multitude of innovative techniques [520, 521]. In some of these studies, the intrapartum fetal ECG is obtained by fetal scalp electrodes [522]. Modern fetal electrocardiography has extended its scope to monitoring and analysis of the fetal ST waveforms [519].

20.29 Food, Drink and Other Compounds

20.29.1 Prandial and Postprandial Changes

The effect of eating solid food and drinking fluids, both cold and hot, on the ECG has been reported; changes occur in the T waves with cold [523] and hot drinks, and supraventricular tachyarrhythmias, focal atrial tachycardia, atrial fibrillation, and ischemic ST segment changes have been elicited [524–527]. The arrhythmogenic influences may be due to neural or local sensitivity of the atria or pulmonary veins, while the ST segment changes may partially reflect coronary vasospasm. Water ingestion in normals increased cardiac vagal control, but this is not seen in the elderly, transplant recipients, or subjects with autonomic failure [528]. Tachyarrhythmias, syncope, and silent myocardial ischemia have been observed with swallowing, belching and mastication [529–531]. Post-prandially, exertional angina indicates obstructive coronary artery disease, rest angina reflects an unexplained myocardial oxygen supply deficit [532], and heart rate variability assessment suggests diminished vagal activity [533]. Starvation in ex-prisoners of wars increased QTc duration and dispersion [534], and in patients with anorexia nervosa, enhanced heart rate variability due to increased vagal control was detected [535]; QTc abnormalities in the latter were abolished with oral potassium administration and refeeding [536, 537].

20.29.2 Alcohol

Alcohol drinking induces, in healthy subjects, sinus tachycardia, atrial and ventricular ectopic beats, and prolongation of the P-R, QRS and QTc intervals [538]. The interplay of pathology and alcohol drinking in patients may exacerbate the above, and can cause more abnormalities. Rarely, heavy alcohol drinking leads to myocardial infarction [539]. Sinus

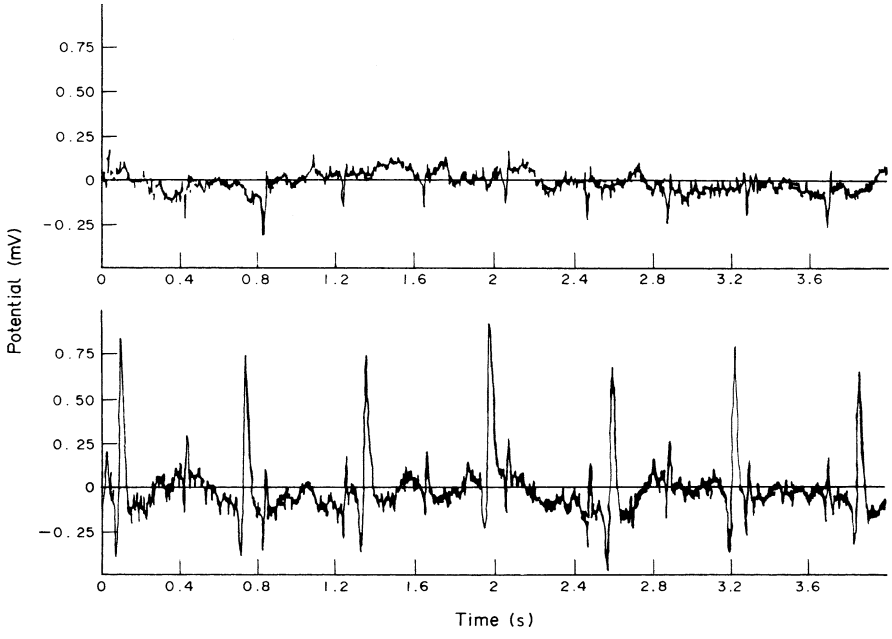

Figure 20.52
The lower tracing shows the abdominal ECG containing maternal and fetal ECG signals. The upper tracing shows the fetal ECG obtained after mathematical treatment to remove the maternal signal. (After van Oosterom. In: Ruttkay I, Macfarlane P, eds. *Electrocardiology* 83, 1984, 175. © Excerpta Medica, Amsterdam. Reproduced with permission.)

tachycardia and decrease in heart rate variability is determined by the aldehyde dehydrogenase-2 genotype and is probably mediated by catecholamine secretion [540]. Heavy alcohol drinking may render an implantable cardioverter defibrillator transiently ineffective [541]. Signal averaging of the P waves identifies patients who are prone to alcohol-induced paroxysmal atrial fibrillation [542]. Alcohol withdrawal may culminate in a catecholamine-driven state characterized by ST segment depressions and release of myocardial enzymes [543].

20.29.3 Caffeine

The effective and functional antegrade and retrograde refractory periods of the atrioventricular node decrease after coffee ingestion, most probably due to a rise in catecholamines [544]. In normal adults, even high dose caffeine does not affect the heart rate or cause atrial or ventricular ectopy [545]. Caffeine did not increase the rate of PVCs, ventricular couplets, and ventricular tachycardia in patients with a recent myocardial infarction [546], or even among patients with known life-threatening arrhythmias [547]; also coffee was not associated with risk of atrial fibrillation or flutter [548]. In patients referred with symptomatic idiopathic ventricular premature beats (VPBs), caffeine restriction did not result in significant change in the frequency of VPBs [549].

20.29.4 Tobacco

Smokers have elevated mean heart rates, mediated by sympathetic stimulation, while the vagal cardiac control is not altered. Thus, no change in respiratory sinus arrhythmia is detected [550]. However, environmental tobacco exposure in nonsmokers led to a decrement in the heart rate variability [551]. In ambulatory ECG studies, smokers had a higher heart rate and prevalence of supraventricular and ventricular extrasystoles than non-smokers, and

smoking cessation led to reversion of these differences [552]. Electrophysiologic studies at baseline and after smoking showed an increase in heart rate and improved atrioventricular conduction both in patients on and off beta-blockers, suggesting a direct effect of sympathomimetic action of smoking; also atrial and ventricular arrhythmias were not increased by smoking [553]. In the absence of an arrhythmogenic substrate, smoking does not induce late potentials in smokers [554].

20.29.5 Drugs

The tricyclic anti-depressants, not favored any more for treatment of depression, mediate their cardiovascular side effects via a quinidine-like influence and anticholinergic action, leading to sinus bradycardia, prolongation of P-R, QRS and QTc intervals, 2° and 3° AV blocks, and torsade de pointes [555, 556]. Premonitory ECG features of cardiac toxicity include QRS duration >100 ms, and a rightward shift of the terminal 40 ms frontal axis of the QRS vector [556]. Arrhythmias, nonspecific ST-T changes, QTc prolongation and decrease in the amplitude of the QRS complexes have been described with some chemotherapeutic drugs [557]. Although cardiomyopathy due to anthracycline-related toxicity and lethal arrhythmias is well recognized, many other chemotherapeutic drugs are associated with bradycardia, ischemic ST-T changes, myocardial infarction, and serious arrhythmias [16]. The electrophysiologic and ECG effects of drugs are beyond the scope of this chapter; also drug-induced prolongation of QTc is dealt with in Chap. 19.

20.29.6 Contrast Agents

Employment of contrast agents in cardiac catheterization is associated with frequent ECG changes, like inversion or peaking of the T waves in the inferior leads, prolongation of the QTc and QRS complexes, and significant ST segment shifts [558]. Transient bradycardia, sinus arrest, and various degrees, including complete AV blocks, are encountered. Ventricular fibrillation is reported in 0.6% to 1.3% of patients [559]. Hyperosmolarity mediates partly the toxicity of contrast agents, while transiently induced hypocalcemia may contribute to ventricular fibrillation [560]. Newer contrast agents are lower in osmolarity, and have a lower calcium-binding potential, thus resulting in fewer ECG changes and arrhythmias, including ventricular fibrillation [561].

20.29.7 Illicit Drugs

Amphetamines and cocaine may be associated with ECG changes suggestive of ischemia most probably mediated by a strong sympathomimetic influence, although coronary vasospasm may also be contributing particularly with cocaine [562]. An abundance of literature, mainly case reports, documents occurrence of ST segment deviations, atrial and ventricular arrhythmias, myocardial infarction, QTc prolongation, and decrease in heart rate variability with the use of cocaine.

20.29.8 Poisons

CO poisoning results in ST-T changes reflective of myocardial ischemia, which could culminate in myocardial infarction [563, 564], and may require hyperbaric oxygen administration [565]. CO, in contrast to cyanide, which commonly coexist in exhaust fumes and smoke, led to slowing of AV conduction and ventricular repolarization in animal experiments [566]. Organophosphates lead to acetylcholine accumulation with resultant sinus tachycardia, bradycardia, ST-T changes, prolonged QTc, atrial fibrillation, monomorphic ventricular tachycardia (VT), torsade de pointes, and ventricular fibrillation (VF) [567, 568]. The commonest heavy metal poisoning is with arsenic, and is associated with T wave inversion,

QTc prolongation, torsade de pointes, and VF [569]. Emetine results in a host of ECG changes including T wave alterations, and prolongation of PR, QRS and QT intervals [570]. Antimony poisoning produces flattening and/or inversion of T waves and prolongation of the QTc, particularly in large doses and with prolonged exposure [571]. Poisoning can result from herbal agents used singly in the context of alternative medicine, or by interacting with conventional medications. Bradycardia, heart blocks and VT result from oleander, a cardiac glycoside containing plant [572]. Many toxins from scorpion venoms activate sodium channels and the sympathetic nervous system; scorpion envenomation resulted in 1° atrioventricular block, intraventricular conduction disturbances, predominantly right bundle branch block, reversible ventricular repolarization changes, and arrhythmias [573].

20.30 Physical Activities

20.30.1 Exercise

Exercise and its lack impart certain changes in the ECG. The rapid increase in the heart rate early during exercise is typical of underconditioning, with a much slower heart rate rise encountered in fit individuals. In a study of monozygotic twin pairs discordant for physical fitness, the ones who engaged in more physical activities had ECG evidence of left ventricular hypertrophy (LVH), not corroborated by echocardiography [574]; this suggests a different role of ECG in the assessment of effects of exercise beyond that of the anatomic LVH. Heart rate at 1 or 2 min of recovery after exercise is a prognostic index of mortality [575] and morbidity and should be employed unfailingly. Heart rate variability increases with exercise, even after a single such session or mild exercise in sedentary individuals [576]. T wave alternans during exercise is rarely found in normal subjects [577]. In view of the prognostic importance of the long QTc interval, physicians should look for it when evaluating normal subjects embarking in an exercise program. Swimming, jogging, running, mild, moderate, or heavy exercise, the isotonic or isometric nature of exercise, and the age, sex, weight, and sedentary status of healthy subjects and patients, all are factors influencing the ECG derived diagnostic and prognostic parameters.

20.30.2 Bathing

Bathing and showering is associated with tachycardia, atrial and ventricular extrasystoles and even ventricular tachycardia, particularly in the elderly and during winter [578]; the ambient temperature, the temperature of the bathing water and underlying pathology are influential. Heart rate variability showed changes in the elderly during hot bathing with the LF/HF ratio in the frequency domain analysis decreasing, which suggests a decrease in sympathetic tone predisposing to syncope. The high ambient temperatures of sauna bathing with its resultant reduction in the intraventricular volume is associated with increases in the magnitudes of the R and Q waves in lead Z, and of the S wave in lead X, which contradict the Brody effect [478, 579]. Showering or bathing lead to changes in the autonomic nervous tone, while addition of light exercise in predisposed individuals may lead to myocardial ischemia [580]. Cold packs on the chest wall cause nonspecific ST-T changes [406].

20.30.3 Athlete's Heart

The range of athletic activities is wide, encompassing increase of strength or endurance objectives, length of involvement, status (amateur to elite) and intensity. ECG changes are seen in athletes, in subjects with "athlete's heart", and in athletes with heart disease. These distinctions should be kept in mind. Vagally mediated sinus bradycardia, sinus arrhythmia, escape rhythms (both atrial and ventricular), incomplete right bundle branch block, various atrial and ventricular arrhythmias, all degrees of AV blocks are noted, with the disappearance of many of the above under stress, attesting to the non pathological nature of these findings [581, 582]. Other ECG features often seen in athletes include increased amplitude of Q, R, and S waves, ST segment changes, and T wave flattening or inversion, often mimicking LVH or cardiomyopathy [583]. The ECG is more sensitive in diagnosing athlete's heart than the imaging modalities focusing on change in left ventricular dimensions and myocardial wall thickness. Reversibility of LVH is seen in the ECG of athletes

undergoing detraining, who also experience resolution of ventricular extrasystoles and episodes of ventricular tachycardia, and absence of cardiac events at follow-up; all these support the notion that LVH and these rhythm disturbances are of benign nature, or they represent another expression of AH [584]. QT duration and QT dispersion do not increase in athletes, as they do in patients with LVH due to hypertension, even in the presence of LVH [585, 586]. Heart rate variability is increased in athletes [582]. The ECG is used in screening individuals who potentially could be "athletes" – see Chap. 13.

20.31 Bodily Functions

20.31.1 Sleep

ECGs during sleep may normally show isorhythmic AV dissociation, marked bradycardia, sinus arrhythmia, sinus nodal blocks, 1° and 2° Mobitz AV blocks, and supraventricular and ventricular beats; atrial extrasystoles are less frequent, and ventricular extrasystoles are more frequent, than during wakefulness, while both increase with age [587]. In Holter ECG recordings, long asymptomatic pauses are occasionally seen during sleep, but these should not lead to interventions. Recumbent episodes at night, while awake, cannot be distinguished from sleep in the evaluation of such recordings. Heart rate variability changes during sleep, and is related to changes in the encephalogram and cycles of rapid, and non-rapid, eye movement sleep [588], while QT interval duration increases [589]. Sleep deprivation results in increased sympathetic and decreased parasympathetic cardiovascular modulation [590].

20.31.2 Diurnal Changes

The ECG is subject to diurnal changes; thus the heart rate, cardiac refractoriness and conduction, pacing and defibrillation thresholds, heart rate variability indices, QT duration, QT dispersion and T wave alternans show diurnal variability [591]. Autonomic tone mediated physiologic variations, during eating, sleeping, and exercise result in day-to-day fluctuations in pacing threshold [12], while some have not found a role of the autonomic tone for such variation [592]. Studies of the reproducibility of ECGs over time have disclosed diurnal changes, e.g., the P wave duration and PR interval show a significant circadian variation in healthy subjects [593]. These variations require that the "time" factor is considered in the analysis of electrophysiological and ECG test results, and may provide an explanation for the clustering of clinical "events" at particular time windows. These diurnal changes of electrophysiological/ECG variables are influenced by a large number of factors, e.g. age effect on QT intervals [594], and cardiac pathology.

20.31.3 Sexual Activity

Sexual activity may precipitate ischemic ST segment changes [595] and ventricular arrhythmias [596] in patients with coronary artery disease. In normal subjects, sexual activity leads to sinus tachycardia, equal to 60–70% of maximum predictive value, persisting longer in women [597], and affecting the post exercise heart rate recovery for at least 2 h after sexual activity [598]. All the above changes are modulated by the arousal of the sympathetic nervous system, which exerts an effect on all electrophysiologic and ECG parameters.

20.31.4 Belching, Nausea, Vomiting

Atrial arrhythmias, including atrial fibrillation, can be precipitated by esophageal stimulation during swallowing and belching [599]. Ischemic like ST depression and T wave inversion can be found in patients experiencing nausea [600]. Spontaneous or self-induced vomiting is associated with prolonged QTc, although inter-current pathology or electrolyte abnormalities are confounding factors [601].

20.31.5 Urination and Defecation

Situational syncope is diagnosed with bradycardia immediately after urination or defecation [602]. Profound sinus bradycardia due to increased vagal tone, while straining during a bowel movement, could result in severe cerebral and myocardial hypoperfusion with cardiac arrest, particularly in elderly patients. Syncope during straining is rarely associated with advanced AV blocks necessitating implantation of a permanent pacemaker [603]. Defecation syncope may also occur in patients in the context of alternation of intrinsic and pacemaker rhythms, requiring reprogramming of the device [604].

20.32 Aging

Aging attenuates the ECG potentials [481]; such changes in the precordial leads may be offset by the reduced thickness of the chest wall, bringing the heart closer to the recording electrodes. An increased incidence of atrial and ventricular ectopic beats, bundle branch blocks, pathological and non-pathological Q waves, T wave inversion and atrial fibrillation is seen, which is probably due to morphological and histological changes of the cardiac musculature, or associated ischemia and infarction. [605]; indeed differentiating such changes due to aging per se from those due to pathology is difficult [606]. Such changes in the atria with fibro-fatty regional replacement may be the substrate initiating and maintaining atrial fibrillation [607].

20.33 Gender

ECG is influenced by gender; accordingly left ventricular hypertrophy employs for its diagnosis different thresholds for amplitude criteria for the two sexes. Conversely, the performance of different ECG criteria differs between men and women [608]. The amplitude in some precordial leads is influenced by the positioning of electrodes in relation to the left breast [609]. The amplitude of ST segment and duration of QTc intervals varied among the three phases of the menstrual cycle [610]. P-R intervals are longer in men, while women have higher resting heart rates, longer QTc intervals and steeper slope of 24 h QT/RR dynamics, explaining their greater susceptibility to torsades de pointes during treatment with drugs that prolong QT interval [611, 612]. Further data relating to the influence of gender on the ECG can be found in Chap. 13.

20.34 Anthropometric Parameters

Anthropometric parameters influence the ECG. Thus the height, weight, configuration of different body parts, abdominal circumference, fat percentage, presence of obesity (see Sect. 20.26), and body habitus (see Sect. 20.25.2) need to be considered in research and practice. The magnitude of spatial atrial vectors has shown the greatest variability in reference to anthropometric parameters [613].

20.35 Race and Ethnicity

Race and ethnicity lead to differences in the ECG. The normal T wave amplitudes were greater in Chinese than in Americans, except for lead V_1, which was greater in Americans than in Chinese [614]. The prevalence of early transition in precordial leads, high R wave in lead V_1, and R and T wave amplitudes differed in various ethnic groups; also the incidence of left ventricular hypertrophy would be overestimated for some ethnic groups using fixed R wave amplitude criteria [615]. The prevalence of 1° AV block and ventricular extrasystoles is higher, and intraventricular blocks and atrial fibrillation lower, in African than Caucasian Americans [616–619]. The early repolarization pattern is more

common in young black athletic males [620], and routine criteria for left ventricular hypertrophy do not apply to black Africans [621].

20.36 Normal Variants

It has long been recognized that inappropriate ECG interpretation has consequences often creating ECG-based cardiac invalidism [407]. Usually this is due to non-adherence to established ECG criteria of normalcy and/or lack of knowledge on normal variants on the part of the human interpreter. For professionals relying on automated ECG interpretations, problems arise with the occasional error in measurements, or employment of inappropriate diagnostic criteria by the automated algorithm. These problems could be easily corrected and are gradually being addressed.

20.36.1 P Waves

P wave abnormalities are often diagnosed inappropriately; the mere presence of a late negativity of the P wave in lead V_1 (area <1.0 mm^3) is a normal finding. "Left atrial enlargement" was ubiquitously present according to the interpretation of some of the earlier automated systems. Appearance of "transient P-pulmonale" is often seen in association with increased heart rate [120, 481, 482], and it is a normal response to exercise. Wandering atrial pacemaker, particularly in association with sinus bradycardia is a common finding in the young. Also "AV nodal" and "low atrial" activity with isorhythmic AV dissociation are commonly encountered. Many of the above are seen both in standard ECGs and Holter ECG recordings.

20.36.2 QRS Complexes

Notches, r′, rounding of peaks, W, or M-shaped QRS complexes, without increase in their duration, can be seen normally, although they are also encountered in patients with hypertension, septal fibrosis or as residuals from prior small myocardial infarctions. Elevated or depressed ST or PR segments due to atrial repolarization may hamper the measurement of the QRS duration. Some borderline QRS widening may disappear with exercise. The QRS duration in neonates is shorter than in adults [2]. Qs in QRS complexes in III may decrease or disappear with inspiration, or as a result of minor rightward shift of the frontal QRS axis during inspiration or exercise [482]. Deep but narrow Qs in inferior and lateral leads, often in association with large QRS complexes mimicking those encountered in left ventricular hypertrophy, are seen in normal adolescents and young adults, particularly male. Also Qs or QS, without associated ST segment and T changes in leads I and aVL may not be pathological in subjects with a vertical heart [481]. The pattern of "early transition" characterized by R/S > 1 in V_2–V_4 is frequently found in healthy subjects [615], often with a vertical QRS axis, while the "poor R-wave progression in V_1–V_2" ("pseudoinfarct" pattern), or with a QS in V_1 and V_2 (interpreted by some automated ECG interpretation algorithms as suggestive of anteroseptal myocardial infarction), are mostly not associated with such pathology [622]. Low voltage ECG in the limb leads or throughout all ECG leads, is occasionally a normal variant, while low voltage in leads V_3 and V_4 in women may be due to the underlying breast [609]. Transient augmentation in the QRS amplitude can be brought about by an increase in the heart rate in the setting of narrow QRS complex tachycardia [118]. Frontal QRS axes, −30° to 45° in the young, and more commonly 100° to 120° in the old, without identifiable cardiac pathology, are occasionally found.

20.36.3 ST Segment and T Waves

ST segment elevation, usually concave upwards starting from an r′ and an elevated J point with upright tall T waves involving particularly V_2–V_4, occasionally only II, III, and aVF, or rarely all ECG leads are seen in normal subjects and comprise the "early repolarization" normal variant (Figs. 20.3 and 20.53). The ST segment elevation decreases in amplitude with mild exercise, as witnessed in the stress laboratory. The peaked T wave associated with early repolarization

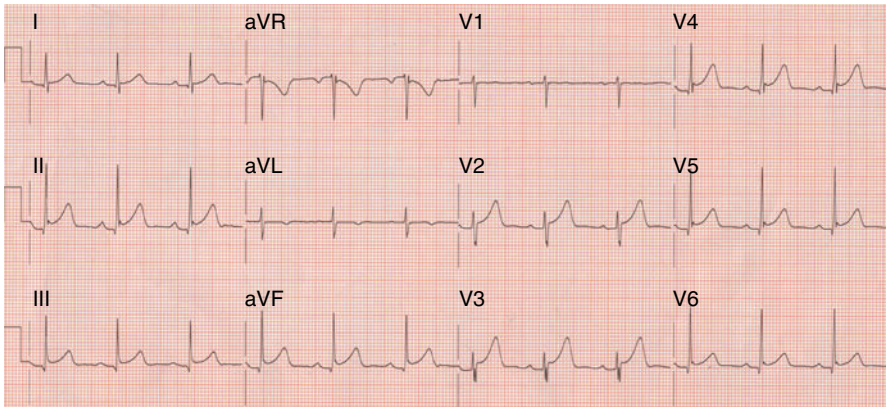

Figure 20.53

ECG of a 37-year-old man with atypical for angina chest pain with a negative maximal exercise stress/thallium test, showing ST segment elevation of early repolarization type, involving all ECG leads, save for aVR, aVL, and V_1.

mimics the one seen with hyperkalemia, but it is asymmetrical and not narrow-based; this T wave is often attributed to "metabolic abnormalities" by automated ECG interpretation systems. Although this ST segment elevation pattern is more common in the young, male, and particularly black individual [620, 623], it can be found in many other groups, and can be rarely associated with T wave inversion and notching of the downstroke of the R waves [624, 625]. The ST changes are stable, not accompanied by reciprocal ST depressions except in aVR, often diffuse as those noted in pericarditis, in contrast to those of ischemia or myocardial infarction. PR segment depression, thought to be due to atrial wall injury, and lower T wave amplitudes, changing over time, differentiate pericarditis from early repolarization. Although the characterization of early repolarization implies an overlapping of cardiac activation and recovery, this was not found with body surface isopotential mapping [626]. The similarities in the ECG of early repolarization, the "Osborn waves" of hypothermia, and the Brugada pattern have led to a reexamination of the mechanism of early repolarization. The cellular and ionic characteristics of Brugada pattern and early repolarization raise the possibility that the latter may not be benign after all, and that individuals with early repolarization may be at risk for life threatening arrhythmias under certain conditions [627]. The so-called post tachycardia syndrome is also characterized by ST depression [482], sometimes deeper than the ones of "nonspecific ST-T changes".

T-wave inversion, commonly seen in children, can be found mainly in leads V_1–V_3, in young or even middle age normal subjects, particularly women. The term "persistent juvenile pattern" is often used to describe such changes in adults [628], and has led to unnecessary coronary arteriography in normal individuals presenting with complaints of chest pain. Occasionally these T wave inversions are very deep [406], particularly in young black males. T wave inversion is noted in some leads, depending on the T wave axis. Shortened QTc mimicking hypercalcemia or digitalis effect is common in young healthy individuals (Fig. 20.3), but occasionally seen in older adults. The congenital short QTc interval syndrome [40] is much shorter (<300 ms), than the one described herein.

20.36.4 Heart Rhythm and Conduction

Sinus arrhythmia is seen in all ages, and not necessarily in the presence of sinus bradycardia. Sinus tachycardia is frequent, and is occasionally unpleasant to some healthy subjects, who seek evaluation. Sinus bradycardia, rare PACs and PVCs, are found in normal subject. PR interval <120 ms suggestive of accelerated AV conduction is common, particularly in young subjects (Fig. 20.54), with PR intervals even as low as 90 ms, especially in association with rapid heart rates; this is not due to Lown–Levine–Ganong syndrome, which should be diagnosed only in association with supraventricular

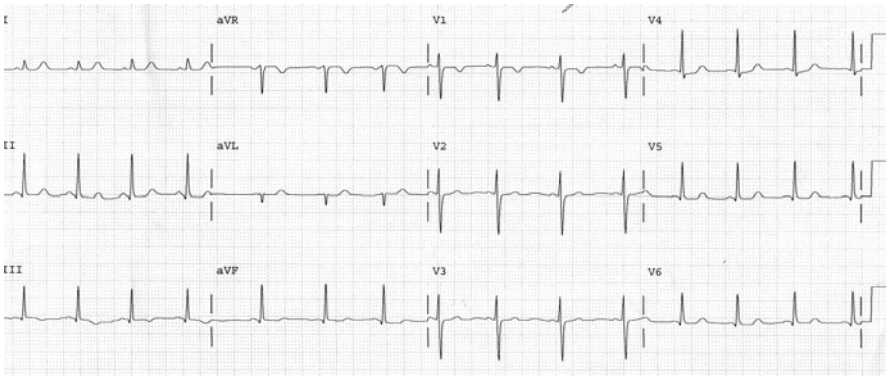

Figure 20.54

ECG of a 29-year-old healthy lady showing a PR interval of 113 ms, with a sinus rhythm at a rate of 87 beats. min^{-1}, and with a frontal P wave axis of 58° and a QRS axis of 69°. T waves in V_1–V_3 suggest a "persistent juvenile" pattern.

arrhythmias [629]. Mild to significant prolongation of PR interval, or Mobitz II AV block, particularly during sleep, are seen in normal young subjects [630].

20.37 Artifactual ECG Abnormalities

Artifactual ECG abnormalities are common, have many sources, and may result in confusion and difficulty in interpretation. When the ECG is in disagreement with the clinical state, an inquiry about ECG artifacts is in order.

20.37.1 Improper Electrode Positioning

Improper limb electrode positioning, particularly involving the reversal of the right and left arm electrodes, is frequent. The distortions of the ECG resulting from electrode misplacement are illustrated in Fig. 20.55 [631]. Reversal of the right arm and left leg electrodes creates the pattern of an inferior MI (Fig. 20.56) [632]. The reversal of the leg electrodes does not change the ECG appearance, since the potential on the right and left ankles is similar while it does not matter on which leg the grounding electrode is placed. All types of artifactual ECG can be suspected by the marked difference in the morphology of the complexes in leads I and V_6 (Fig. 20.57), save for the one shown in Fig. 20.55d. Although the changing polarity of leads I and aVR and the alteration of the other limb leads mimics dextrocardia (except in Fig. 20.55d), the unaltered V_1–V_6 leads can aid in the differentiation of artifactual ECGs from the ECG of dextrocardia (Fig. 20.57).

With multi-channel ECG recorders, the inappropriate sequence in the positioning of V_1–V_6 electrodes leads to confusing ECG artifacts, with unaltered limb leads. The reversal(s) of electrodes at various points of the V_1–V_6 sequence result(s) in different patterns of R wave progression and/or regression (Fig. 20.58). More frequent is the placement of all precordial electrodes higher (most common) or lower than their proper position. This has necessitated, when quantitative ECGs are employed serially, inclusion of a separate analysis of the limb leads [633]. Placing V_1–V_6 higher than appropriately on the thorax, results in poor R wave progression and mimics anterior myocardial infarction or RBBB or rSR pattern [632]. Problems with the recording of V_1–V_6 may arise in women when some of these leads are placed above or below the left breast [609], or when this is done with some variation in serial recordings. A device has been described to facilitate correct V_1–V_6 lead placement [634].

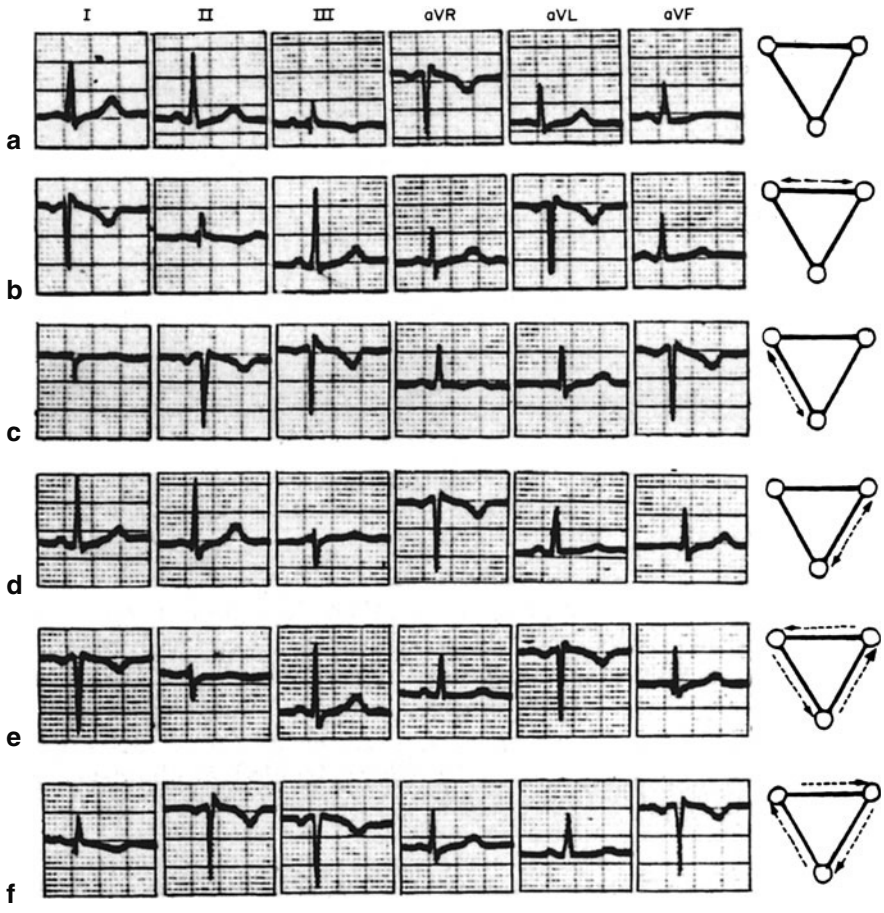

Figure 20.55
Various patterns of ECG resulting from the incorrect positioning of limb electrodes: (a) normal; (b) reversed positioning of arm leads; (c) reversed positioning of the right arm and left leg leads; (d) reversed positioning of left-sided limb leads; (e) counterclockwise incorrect positioning of upper and lower limb leads; (f) clockwise incorrect placement of upper and lower limb leads. (After Marriott [631]. © Williams and Wilkins, Baltimore, Maryland. Reproduced with permission.)

20.37.2 Muscle Tremor and Other Movements During ECG Recording

Parkinsonism, the extrapyramidal syndrome, or shivering, result in muscle tremor distorting the isoelectric line, which by its coarse and fine undulations, may mimic atrial flutter (Figs. 20.59 and 20.60), or atrial fibrillation. The irregularity of the undulating baseline differentiates artifacts from atrial flutter. However, if the artifactual undulations of the baseline are regular, it may be problematic to differentiate artifacts superimposed on a regular atrial rhythm, from atrial flutter transmitted to the ventricles with a fixed AV block. Muscle tremor with sinus arrhythmia or other irregular rhythms may be mistaken for atrial fibrillation. Undulations from muscle tremor or insufficient relaxation of the peripheral musculature are of irregular frequency and amplitude, and may affect the limb leads more than the precordial leads. Applying the limb leads electrodes in the proximal part of the limbs may be necessary in patients with intense tremor. If the muscular tremor can be traced to cold environment, the ECG should be recorded in a room with an appropriate temperature. Sometimes AC interference or other electrical or mechanical artifacts, regular or quasi-regular, will have a similar effect on the ECG. Movements of the body or the attached electrodes cause coarse changes and shifts or wandering of the baseline. Body

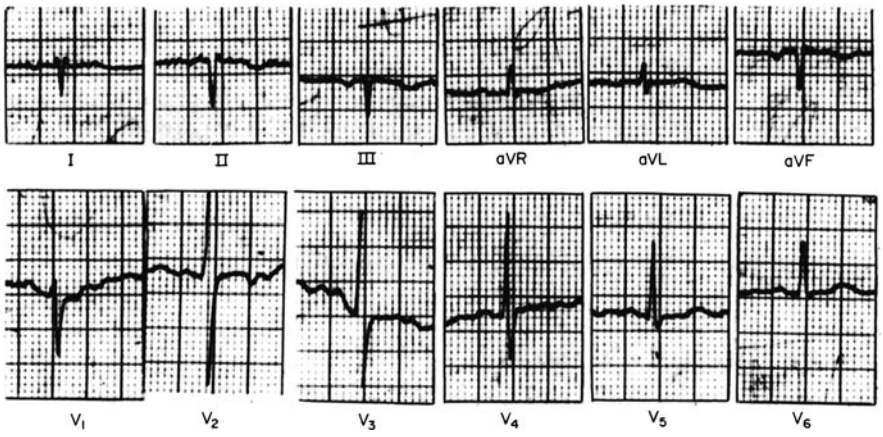

Figure 20.56

Artifactual ECG resulting from the interchange of right arm and left leg lead connections.

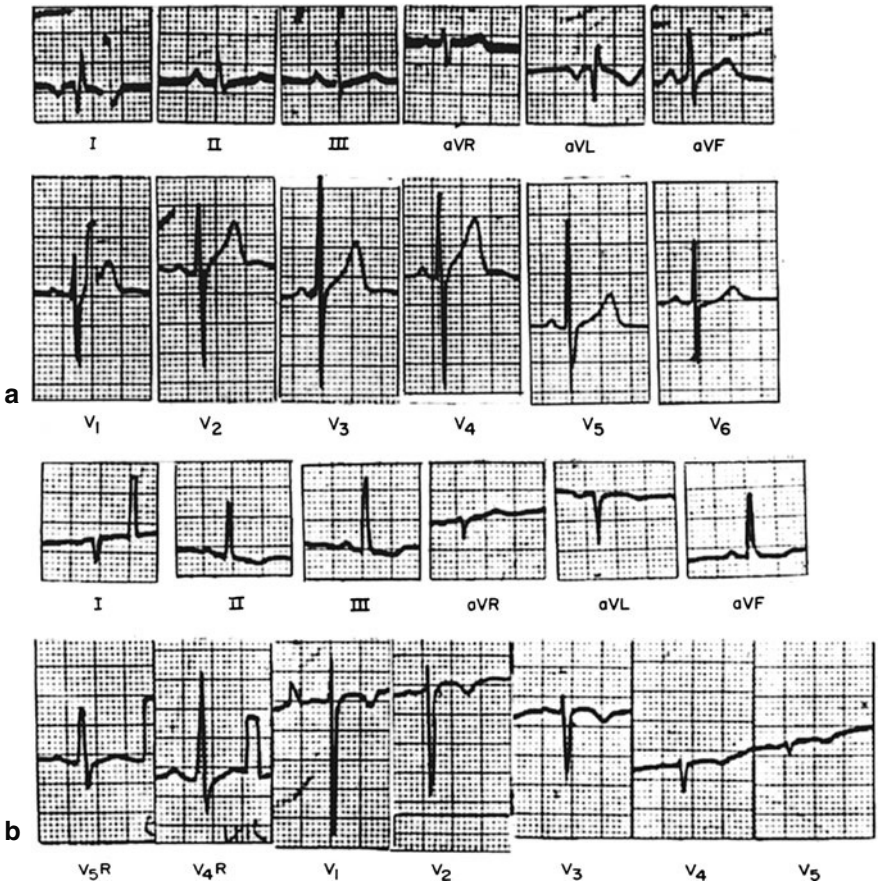

Figure 20.57

(a) Artifactual ECG resulting from the reversal of right and left arm electrodes; (b) ECG correctly recorded in a young lady with dextrocardia, where there is a similarity between leads I and V_6. Leads from the right chest wall display larger QRS complexes than the ones from leads V_4 and V_5.

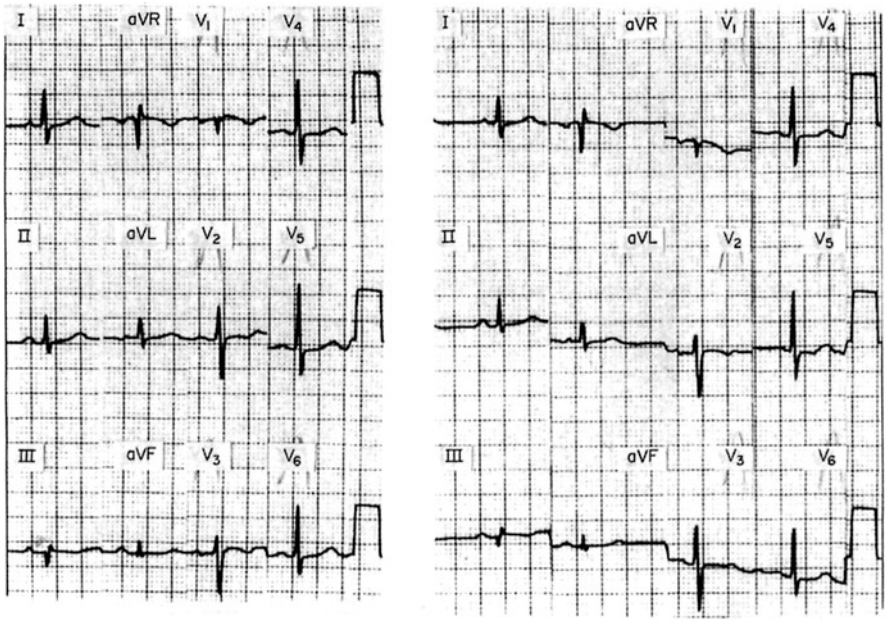

Figure 20.58

***Left* panel: artifactual ECG resulting from the reversed electrode positioning of V_2 and V_3, using a three-channel ECG recorder; *right* panel: electrode positioning error has been corrected.**

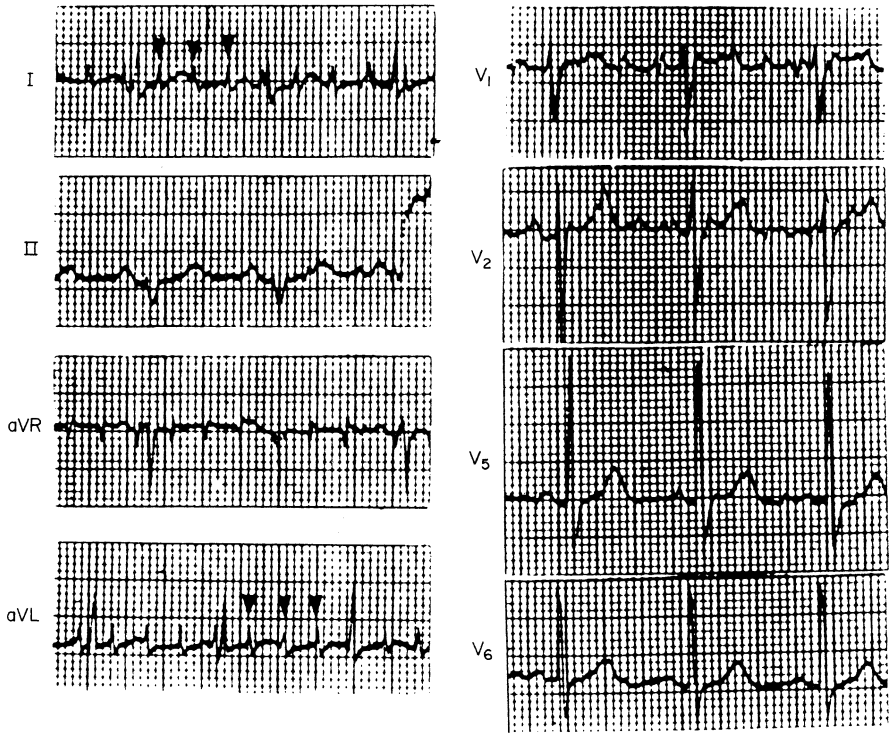

Figure 20.59

Artifactual ECG, mimicking atrial flutter, resulting from tremor of limbs in a patient possibly suffering from the extrapyramidal syndrome.

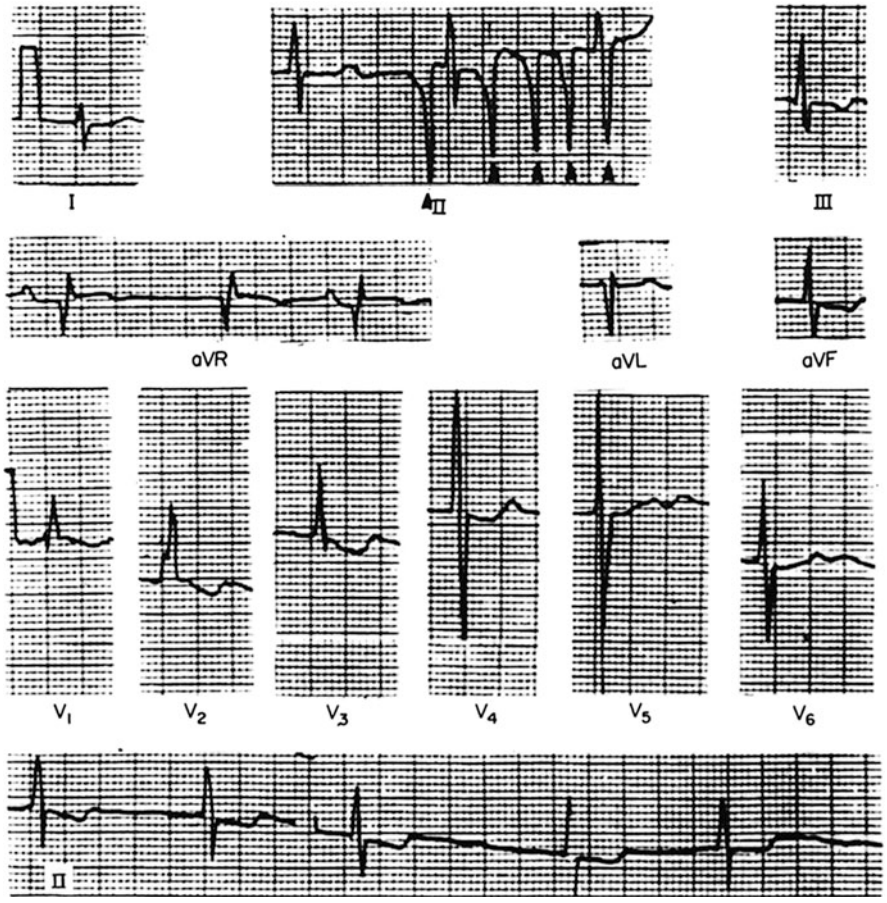

Figure 20.60
Artifactual ECG (lead II) resulting from vigorous tremor of limbs.

movements and poor skin-electrode contact may mimic arrhythmias, leading to improper therapies including implantation of devices [635]. Asymptomatic "pseudo-torsade de pointes" ventricular tachycardia has been recorded on telemetry in a patient with Parkinson's disease during urination [636]. Some of these artifacts can be traced to the respiratory movements, which if excessive in a particular patient, may necessitate recording the ECG with held respiration. Scrutinizing the ECG and the circumstances of its acquisition often resolve these mimicries, although repeating the ECG recording may occasionally be necessary. For ambulatory recordings, the multi-lead devices are preferred since occasionally 1 or 2 of the employed leads are uninterpretable due to artifacts.

20.37.3 Inappropriate Damping of the Stylus of the ECG Recorder

Inappropriate damping of the stylus of the ECG recorder will create distortion of signals. In an era of digital recorders, this applies only to equipment producing paper strip ECG recordings still in use. An underdamping causes an overshoot on the upswing and downswing of the signals (Fig. 20.61), and increase of the amplitude of all rapid deflections, i.e., the Q, R, and S waves. In contrast, overdamping will record sharp angles or fast deflections with low fidelity

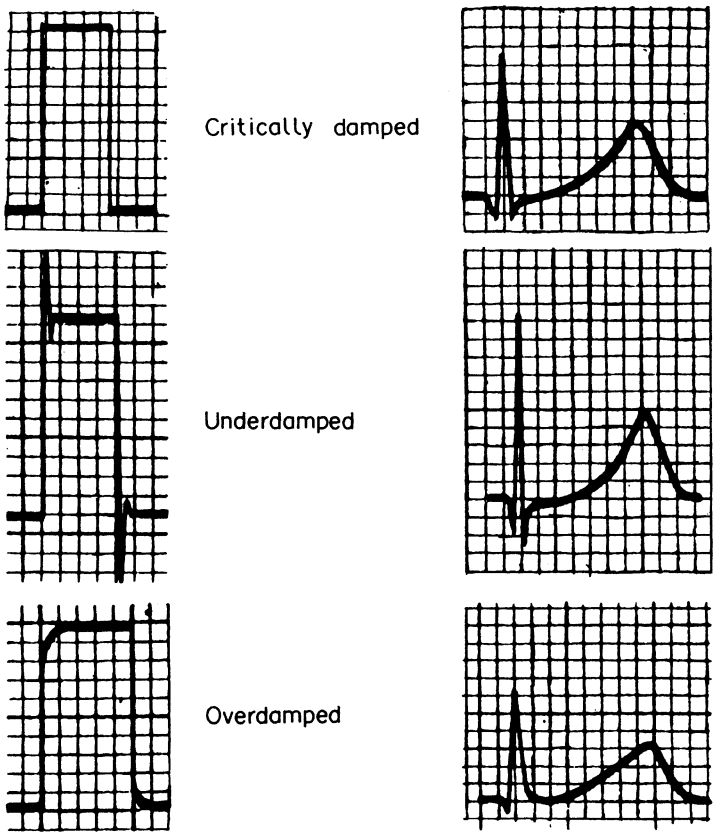

Figure 20.61
The shape calibrations and corresponding different ECG morphologies resulting from critical damping, underdamping and overdamping of the stylus.

(Fig. 20.61), all notches will become slurred, the QRS complexes may appear widened, and the ST segment falsely depressed (Fig. 20.62).

20.37.4 Wrong Speed or Wrong Switching During the ECG Recording

By recording at a faster chart paper speed, e.g., 50 mm/s, all components of the ECG appear widened (Fig. 20.63). This is occasionally intended for more accurate manual measurement of time intervals; however, if this is done by error it may confuse an inexperienced interpreter, unaware of the change. Diagnoses like prolonged P wave duration, 1° AV block, intraventricular conduction delay, prolonged QTc have been entertained prior to the reviewer noting the recording speed. Similar problems are encountered in continuous ambulatory ECG recorders due to mechanical malfunction. Another unusual artifactual ECG may occasionally be produced when a single-channel recorder is used and one fails to switch to the "V" lead position during precordial ECG recording, thus in turn generating a record with all $V_1 - V_6$ leads being similar to lead aVF (Fig. 20.64). These artifacts, which may cause difficulty in interpretation, can be traced to an inexperienced operator of the ECG equipment, when an ECG technician is not available.

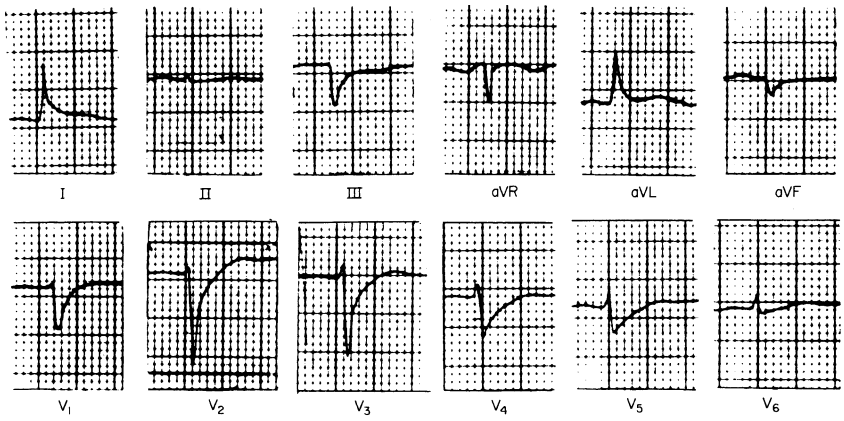

Figure 20.62
Artifactual ECG resulting from an overdamped stylus.

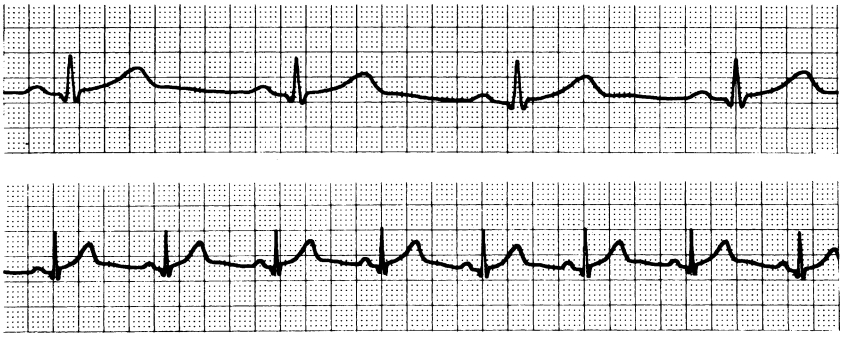

Figure 20.63
"Artifactual" ECG caused by higher recording speed (50 mm s^{-1}) (*upper* panel), also shown at normal speed (25 mm s^{-1}) in the *lower* panel.

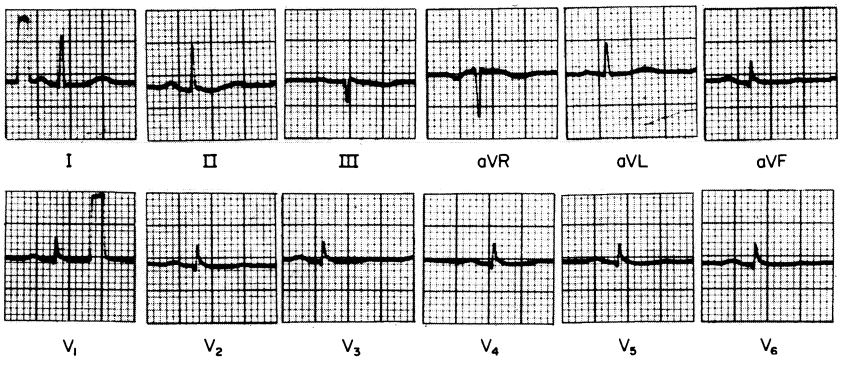

Figure 20.64
V_1–V_6 are similar to lead aVF, in an artifactual ECG caused by faulty switching during the recording of the precordial ECG leads.

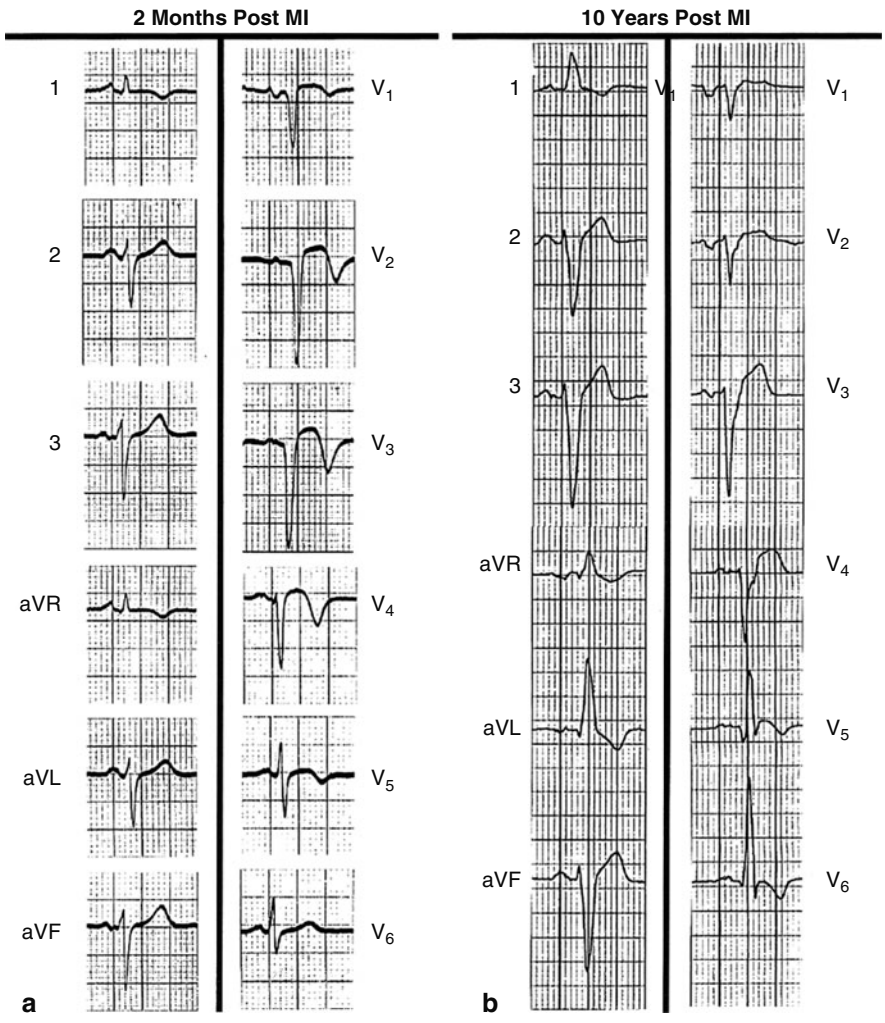

Figure 20.65

ECG of a 55-year-old man who had suffered an extensive anterior myocardial infarction 10 years earlier (a) showing persistent ST segment elevation in lead V_5 (b) in the presence of left bundle branch block suggestive of a primary repolarization abnormality due to a ventricular aneurysm (consider this figure with Fig. 20.66). (Reproduced from Ref. [640]. With permission of the *Journal of Electrocardiology*.)

20.37.5 Electric and Magnetic Fields

Sensing of the electromagnetic fields produces artifacts in the ECG. Proper grounding of the electrocardiograph and the patient prevents the characteristic fixed amplitude 50 or 60 Hz undulations of the electrical ac power lines, and higher frequencies from other electrical equipment in the environment. Magnetic fields are generated with the interaction of electrical power and the lead wires, and appear as a high frequency noise in the ECG; this distortion can be prevented by aligning all the lead wires with the patient's body in the head to foot axis. When feasible, unplugging some of the electrical devices (including the patient's bed), in the environment where the ECG is being recorded, contributes to an artifact-free record; similarly unplugging the electrocardiograph itself and operating it in "battery mode" is advisable.

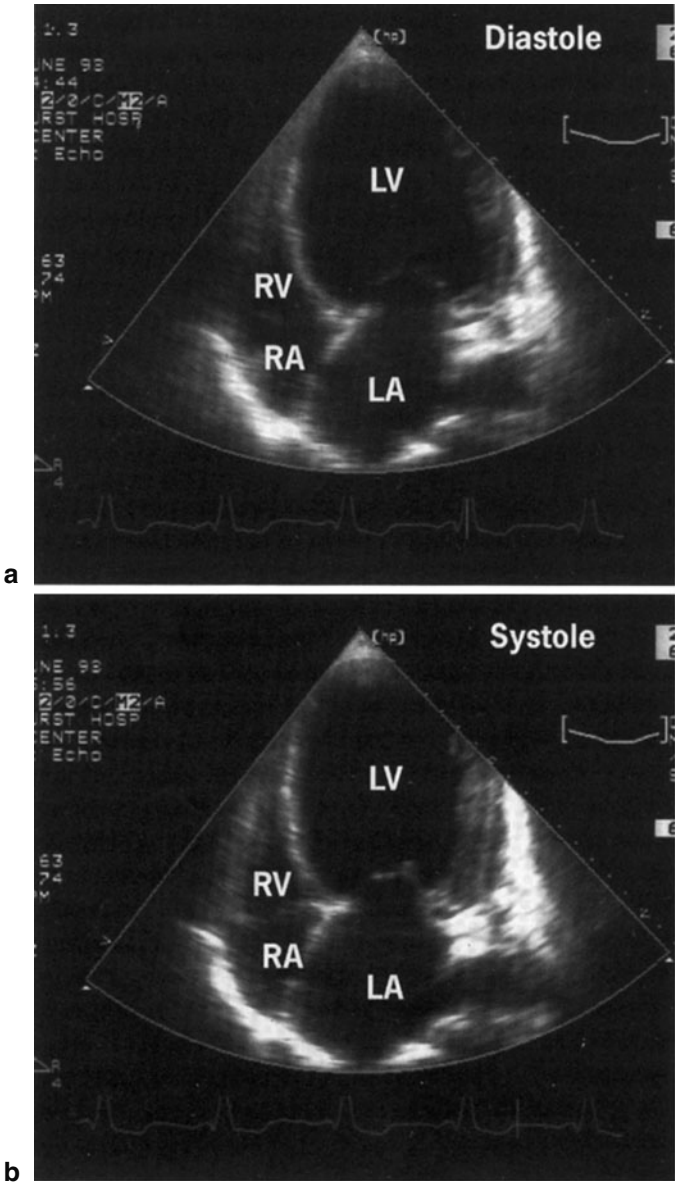

Figure 20.66

An echocardiogram (four-chamber view) of the patient, whose ECG is shown in Fig. 66, revealing an enormous ventricular aneurysm (VA). During systole (a) and diastole (b) the septum is thin and akinetic due to the VA, while the lateral wall displays thickening during systole. LV = left ventricle; RV = right ventricle; LA = left atrium; RA = right atrium. (Reproduced from Ref. [640]. With permission of the *Journal of Electrocardiology*.)

20.37.6 Other Sources of Artifactual ECGs

Unintentionally recording the ECG with an increased or decreased calibration for the entire ECG or only the precordial leads may create diagnostic problems in busy places, where scrutiny of the records is not routine. Unintentional under,

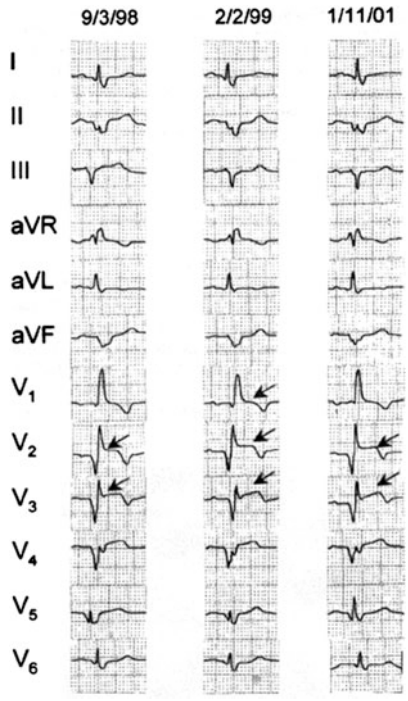

Figure 20.67

ECG of a 67-year-old woman who had suffered an anterior myocardial infarction complicating by a ventricular aneurysm who had persistent ST segment elevation in leads V_1–V_3, suggestive of a primary repolarization change in the presence of right bundle branch block. (Reproduced from Ref. [641]. With permission of the *Annals of Noninvasive Electrocardiology*.)

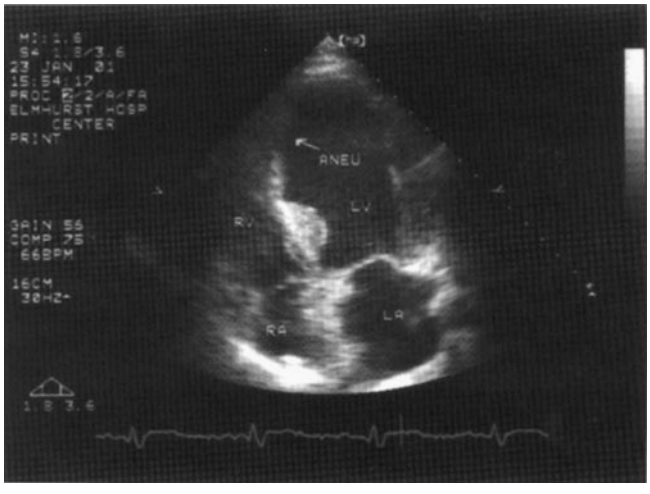

Figure 20.68

An echocardiogram (four-chamber view) of the patient whose ECG is shown in Fig. 20.67, revealing a large ventricular aneurysm. (Reproduced from Ref. [641]. With permission of the *Annals of Noninvasive Electrocardiology*.)

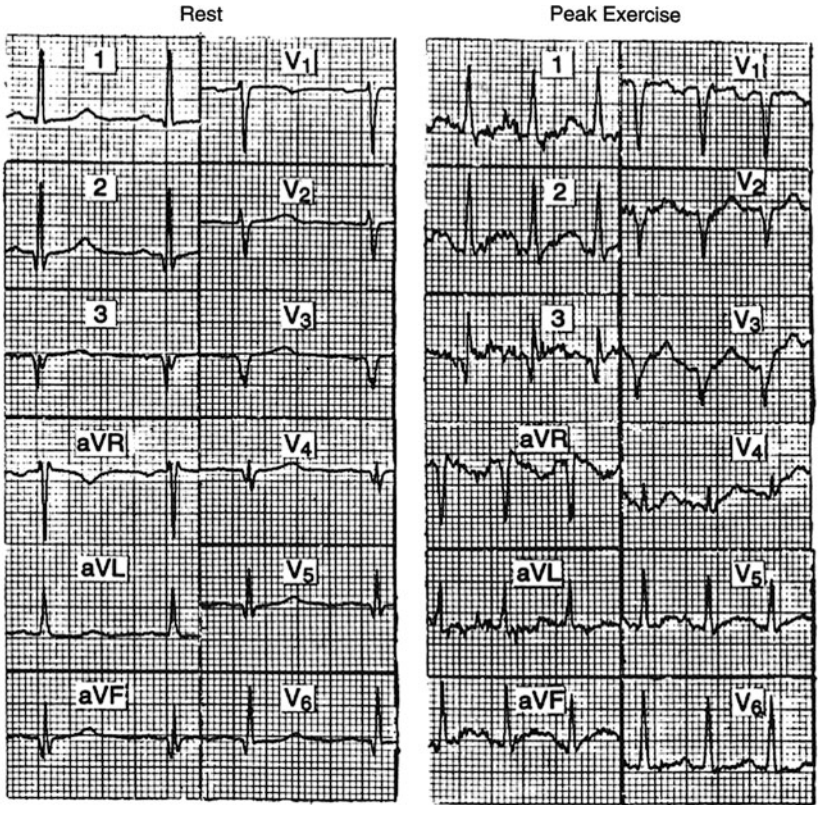

Figure 20.69

Comparison of ECGs from rest, peak exercise stress test (94% of maximal predicted heart rate) and recovery phases of a 62-year-old woman did not disclose ischemic changes; note the enormous change in the P wave at peak exercise suggestive of left atrial abnormality. Compare with Fig. 20.70. (Reproduced from Ref. [642]. With permission of the *Journal of Electrocardiology*.)

or over-calibration may be more of a problem when there is no automated interpretation provided by the ECG apparatus, since the latter's algorithm detects such alterations. Then "low voltage" ECG, left ventricular hypertrophy, P wave abnormalities, or major changes from previous tracings are diagnosed, before the recording mistake is detected.

20.38 Automated ECG Interpretation

Automated ECG interpretation is widely available in commercial electrocardiographs; both a routine and extended ECG interpretation can be generated instantly, with the hardcopy reports including different sets of ECG data measurements. Instant provision of measurements provides an advantage over manual assessment of the ECG when clinical decisions need to be implemented rapidly [637]. However, the presence of artifacts often complicates matters to the point that measurements become unreliable. Also, even with correct measurements, the final ECG diagnosis is often erroneous, but this is correctable by adopting appropriate criteria, or upgrading the algorithmic component dealing with the measurements-interpretation coupling. Thus, current experience shows that problems with automated ECG interpretation systems can be reduced to "inaccurate diagnoses" based on "accurate measurements". However, even today, automated ECG interpretation must be subject to human over-reading [638, 639]. Further discussion on this topic can be found in Chap. 37.

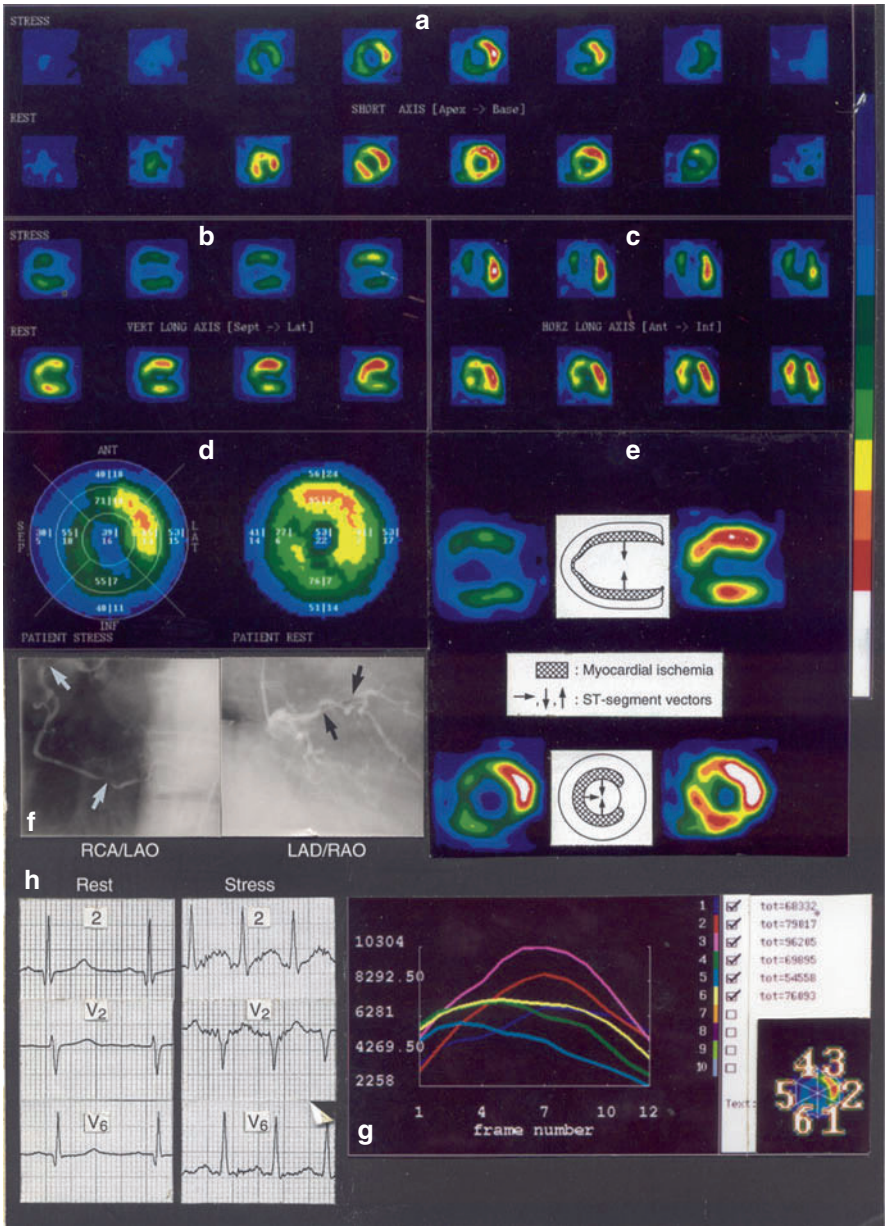

Figure 20.70

Thallium myocardial imaging of the patient whose ECGs are shown in Fig. 20.69, revealing severe reversible perfusion defects involving many myocardial territories (A–D) selected ECG leads from the exercise stress test (H) severe stenosis of the right and left anterior descending coronary arteries on coronary arteriography (F) and the vectorial conceptualization explaining the association of ischemia in myocardial territories opposite each other with false negative exercise ECG due to electrical cancellation. (Reproduced from Ref. [642]. With permission of the *Journal of Electrocardiology*.)

20.39 New Ideas in Elecrocardiography

As the ever-expanding discovery of new ECG associations with various clinical entities goes on, new insights come to light. Some ECG "curiosities" start as such, and eventually find their way into the main stream of electrocardiography by

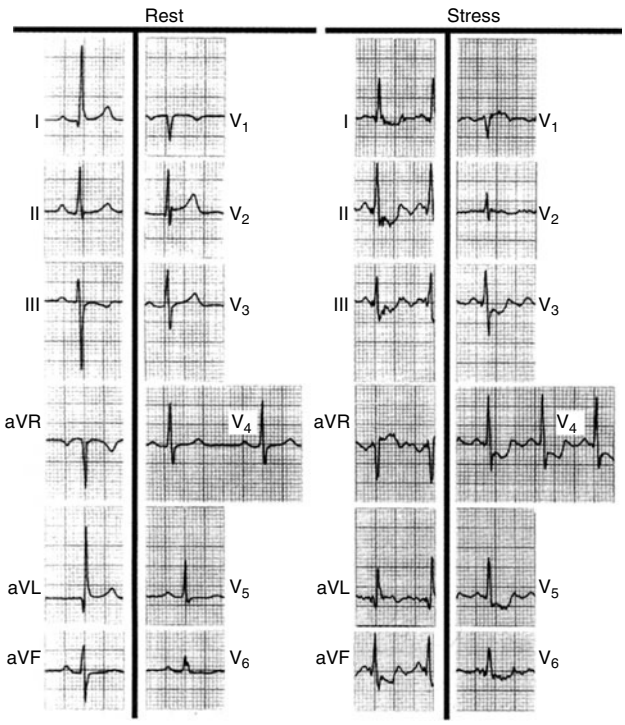

Figure 20.71

Comparison of ECGs from rest, and peak exercise stress test of a 72-year-old man with severe three-vessel coronary artery disease showing ischemic changes. Compare with Fig. 20.72. (Reproduced from Ref. [643]. With permission of *Clinical Cardiology*.)

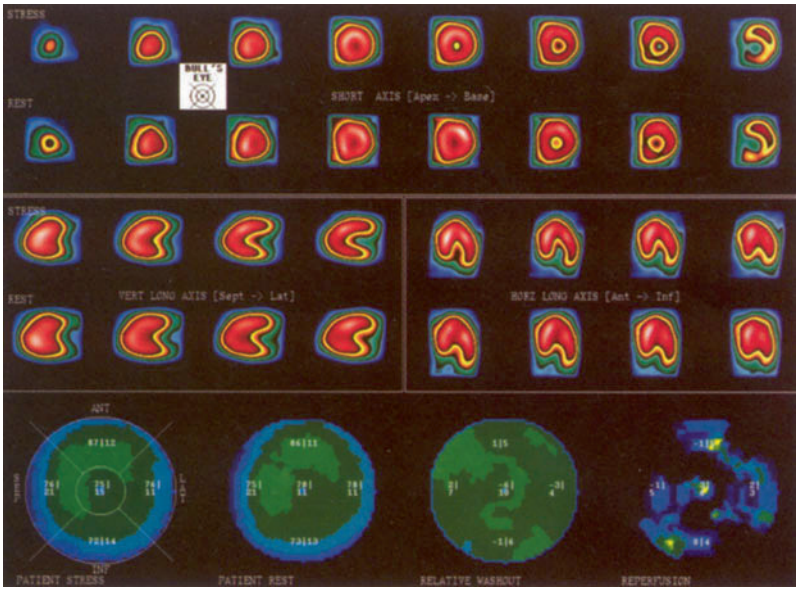

Figure 20.72

Thallium myocardial imaging of the patient whose ECGs are shown in Fig. 20.70 revealing falsely negative appearances due to balanced severe myocardial ischemia. (Reproduced from Ref. [643]. With permission of *Clinical Cardiology*.)

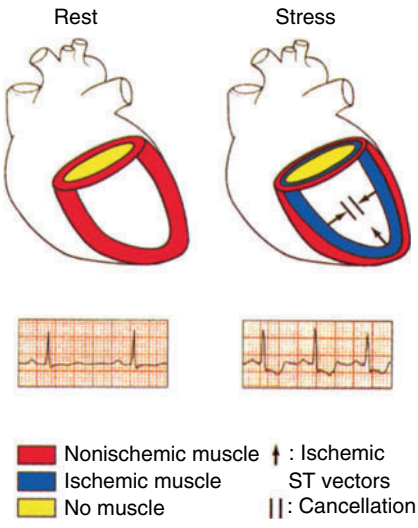

Figure 20.73

Consider this figure with Figs. 20.71 and 20.72. A schematic explaining the mechanism of a false negative for ischemia thallium myocardial scintigram (due to balanced ischemia) in association with a true positive stress ECG; although electrical cancellation of ST segment depression occurs for most of the ischemic ventricle, the area of the ischemic apex remains unopposed by muscular ischemic tissue, thus rendering the stress ECG positive. (Reproduced from Ref. [643]. With permission of *Clinical Cardiology*.)

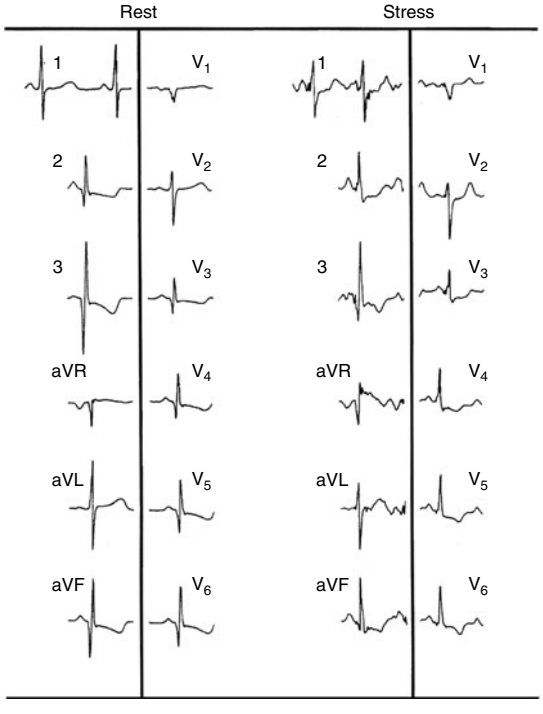

Figure 20.74

Comparison of ECGs from rest, and peak exercise stress test of a 40-year-old woman with a previous inferior myocardial infarction revealed a transient reduction or disappearance of the infarctional Q waves in the stress ECG. Consider this figure with Fig. 20.75. (Reproduced from Ref. [644]. With permission of *Journal of Electrocardiology*.)

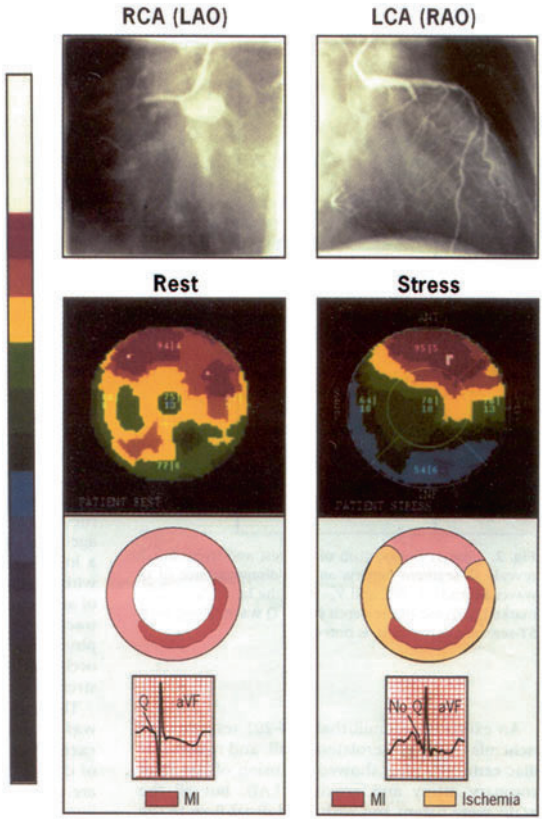

Figure 20.75

Consider this figure with Fig. 20.74 Coronary arteriograms showed occluded right coronary artery (RCA) and left circumflex coronary artery, while the left anterior descending coronary artery had a 50% (LCA). Thallium myocardial scintigraphy disclosed severe reversible perfusion defects affecting among others the territory opposite the region of the old infarct (MI). The schematic explains the mechanism of transient disappearance of infarctional Q waves due to the transient incapacitation of the area opposite the MI, temporarily incapable to pull the early QRS vector away from the MI, and thus generate the Q wave. (Reproduced from Ref. [644]. With permission of the *Journal of Electrocardiology*.)

being diagnostically useful. A few such examples include the diagnosis of left ventricular aneurysm in the presence of left bundle branch block from the ST segment elevation in the leads V_4–V_6 (Figs. 20.65 and 20.66) [640], left ventricular aneurysm in the presence of right bundle branch block from the ST segment elevation in the leads V_1–V_3 (Figs. 20.67 and 20.68) [641], an explanation for the false negative ECG diagnosis of exercise induced ischemia due to cancellation of the ST segment vectors from ischemic myocardial territories opposite each other ("ischemic ST segment counterpoise") (Figs. 20.69 and 20.70) [642], the false negative diagnosis of myocardial ischemia by myocardial scintigraphy in association with a positive exercise ECG (Figs. 20.71 and 20.72), and the role of the apical ischemia in producing such a discrepancy (Fig. 20.73) [643], and the transient reduction or disappearance of Q-waves from an old myocardial infarction due to exercise-induced ischemia in the territory opposite the infarct (Figs. 20.74 and 20.75) [644]. The employment of intracardiac electrograms obtained via a "saline ECG lead" from a central venous catheter for the detection of P waves (Fig. 20.76) [645] or the diagnosis of arrhythmias, is another example of an idea awaiting routine use.

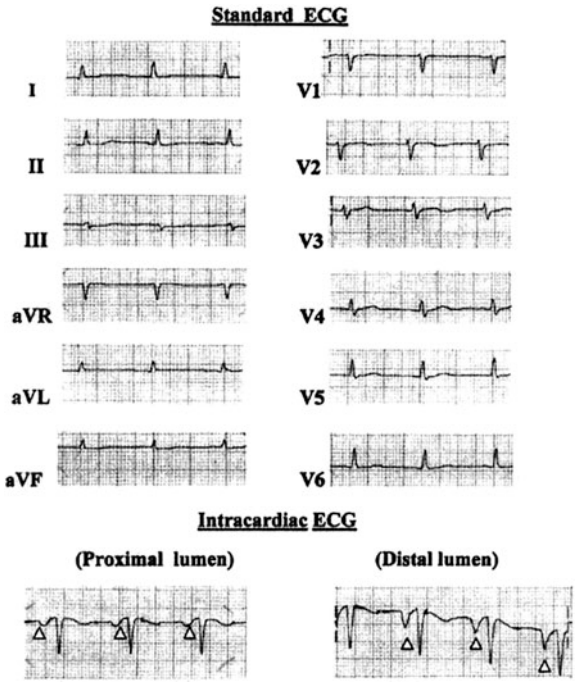

Figure 20.76

Standard ECG of a 68-year-old woman with chronic renal failure and sepsis who suffered peripheral edema, showing attenuated ECG voltage and invisible P waves. Electrical connection of the one of the "V" leads with her saline-filled central venous (jugular) catheter enable recording of the P waves (Δ). Note the larger P waves recorded via the distal lumen versus the proximal lumen ("proximity effect"). (Reproduced from Ref. [645]. With permission of *American Journal of Cardiology*.)

References

1. Madias, J.E., R. Bazaz, H. Agarwal, M. Win, and L. Medepalli, Anasarca mediated attenuation of the amplitude of electrocardiogram complexes. A description of a heretofore unrecognized phenomenon. *J. Am. Coll. Cardiol.*, 2001;**38**: 756–764.
2. Surawicz, B., *Electrophysiologic Basis of ECG and Cardiac Arrhythmias*. Baltimore, MD: Williams & Wilkins, 1995.
3. Noble, D., *The Initiation of the Heart Beat*, 2nd edn. Oxford: Clarendon Press, 1979.
4. Fisch, C., S.B. Knoebel, H. Feigenbaum, K. Greenspan, Potassium and the monophasic action potential, electrocardiogram, conduction and arrhythmias. *Prog. Cardiovasc. Dis.*, 1966;**8**: 387–418.
5. Fisch, C., Relation of electrolyte disturbances to cardiac arrhythmias. *Circulation*, 1973;**47**: 408–419.
6. Ettinger, P.0., T.J. Regan, and H.A. Oldewurtel, Hyperkalemia, cardiac conduction, and the electrocardiogram. A review. *Am. Heart J.*, 1974;**88**: 360–371.
7. Watanabe, Y. and L.S. Dreifus, Interactions of quinidine and potassium on atrioventricular transmission. *Circ. Res.*, 1967;**20**: 434–446.
8. O'Neil, J.P. and E.K. Chung, Unusual electrocardiographic finding-Bifascicular block due to hyperkalemia. *Am. J. Med.*, 1976;**61**: 537–540.
9. Sekiya, S., S. Ichikawa, T. Tsutsumi, K. Harumi, Nonuniform action potential durations at different sites in canine left ventricle. *Jpn. Heart J.*, 1983;**24**: 935–945.
10. O'Reilly, M.V., D.P. Murnaghan, and M.B. Williams, Transvenous pacemaker failure induced by hyperkalemia. *J. Am. Med. Assoc.*, 1974;**228**: 336.
11. Barold, S.S., M.D. Falkoff, L.S. Ong, and R.A. Heinle, Hyperkalemia-induced failure of atrial capture during dual-chamber cardiac pacing. *J. Am. Coll. Cardiol.*, 1987;**10**: 467–469.
12. Dohrmann, M.L. and N.F. Goldschlager, Myocardial stimulation threshold in patients with cardiac pacemakers: Effect of physiologic variables, pharmacologic agents, and lead electrodes. *Cardiol. Clin.*, 1985;**3**: 527–537.
13. Surawicz, B., Relationship between electrocardiogram and electrolytes. *Am. Heart J.*, 1967;**73**: 814–834.
14. Levine, H.D., J.P. Vazifdar, B. Lown, J.P. Merrill, "Tent-shaped" T waves of normal amplitude in potassium intoxication. *Am. Heart J.*, 1952;**43**: 437–450.
15. Surawicz, B., H. Chlebus, and A. Mazzoleni, Hemodynamic and electrocardiographic effects of hyperpotassemia: Differences in response to slow and rapid increases in concentration of plasma K^+. *Am. Heart J.*, 1967;**73**: 647–664.

16. Van Mieghem, C., M. Sabbe, and D. Knockaert, The clinical value of the ECG in noncardiac conditions. *Chest*, 2004;**125**: 1561–1576.
17. Moulik, P.K., C. Nethaji, and A.A. Khaleeli, Misleading electrocardiographic results in patients with hyperkalemia and diabetic ketoacidosis. *BMJ*, 2002;**325**: 1346–1347.
18. Levine, H.D., S.H. Wanzer, and J.P. Merrill, Dialyzable currents of injury in potassium intoxication resembling acute myocardial infarction or pericarditis. *Circulation*, 1956;**13**: 29–36.
19. Madias, J.E. and N.E. Madias, Hyperkalemia-like ECG changes simulating acute myocardial infarction in a patient with hypokalemia undergoing potassium replacement. *J. Electrocardiol.*, 1989;**22**: 93–97.
20. Szerlip, H.M., J. Weiss, and I. Singer, Profound hyperkalemia without electrocardiographic manifestations. *Am. J. Kidney Dis.*, 1986;**7**: 461–465.
21. Surawicz, B., H.A. Braun, W.B. Crum, R.L. Kemp, S. Wagner, and S. Bellett, Quantitive analysis of the electrocardiographic patterns of hypopotassemia. *Circulation*, 1957;**16**: 750–763.
22. Gettes, L. and B. Surawicz, Effects of low and high concentrations of potassium on the simultaneously recorded Purkinje and ventricular action potentials of the perfused pig moderator band. *Circ. Res.*, 1968;**23**: 717–729.
23. Madias, J.E., N.E. Madias, and H.P. Gavras, Nonarrhythmogenicity of diuretic-induced hypokalemia. Its evidence in patients with uncomplicated hypertension. *Arch. Intern. Med.*, 1984;**144**: 2171–2176.
24. Cohn, J.N., P.R. Kowey, P.K. Whelton, and L.M. Prisant, New guidelines for potassium replacement in clinical practice: A contemporary review by the National Council on potassium in clinical practice. *Arch. Intern. Med.*, 2000;**160**: 2429–2436.
25. Krikler, D.M. and P.V.L. Curry, Torsade de pointes, an atypical ventricular tachycardia. *Br. Heart J.*, 1976;**38**: 117–120.
26. Leier, C.V., L. Dei Cas, and M. Metra, Clinical relevance and management of the major electrolyte abnormalities in congestive heart failure: Hyponatremia, hypokalemia, and hypomagnesemia. *Am. Heart J.*, 1994;**128**: 564–574.
27. Burton, D.R., Hypokalemia. *Clinical Physiology of Acid-Base and Electrolyte Disorders*, 4th edn. New York: McGraw-Hill, 1994, pp. 776–822.
28. Paes de Carvalho, A. and W.B. Langan, Influence of extracellular potassium levels on atrioventricular transmission. *Am. J. Physiol.*, 1963;**205**: 375–381.
29. Weidmann, S., Effects of calcium ions and local anaesthetics on electrical properties of Purkinje fibres. *J. Physiol. (Lond.)* 1955;**129**: 568–582.
30. Temte, J.V. and L.D. Davis, Effect of calcium concentration on the transmembrane potentials of Purkinje fibers. *Circ. Res.*, 1967;**20**: 32–44.
31. Lind, L. and S. Ljunghall, Serum calcium and the ECG in patients with primary hyperparathyroidism. *J. Electrocardiol.*, 1994;**27**: 99–103.
32. Shah, A.P., A. Lopez, R.Y. Wachsner, S.K. Meymandi, A.K. El-Bialy, and A.M. Ichiuji, Sinus node dysfunction secondary to hyperparathyroidism. *J. Cardiovasc. Pharmacol. Ther.*, 2004;**9**: 145–147.
33. Carpenter, C. and M.E. May, Case report: Cardiotoxic calcemia. *Am. J. Med. Sci.*, 1994;**307**: 43–44.
34. Reuter, H. and H. Scholz, The regulation of the calcium conductance of cardiac muscle by adrenaline. *J. Physiol. (Lond.)* 1977;**264**: 49–62.
35. Nierenberg, D.W. and B.J. Ransil, Q-aTc interval as a clinical indicator of hypercalcemia. *Am. J. Cardiol.*, 1979;**44**: 243–248.
36. Bronsky, D., A. Dubin, S.S. Waldstein, and D.S. Kushner, Calcium and the electrocardiogram. II. The electrocardiographic manifestations of hyperparathyroidism and of marked hypercalcemia from various other etiologies. *Am. J. Cardiol.*, 1961;**7**: 833–839.
37. Ellman, H., H. Dembin, and N. Seriff, The rarity of shortening of the QT interval in patients with hypercalcemia. *Crit. Care Med.*, 1982;**10**: 320–322.
38. Wagner, G.S., *Marriott's Practical Electrocardiography*, 10th edn. Philadelphia, PA: Lippincott Williams & Wilkins, 2001.
39. Sridharan, M.R. and L.G. Horan, Electrocardiographic J wave of hypercalcemia. *Am. J. Cardiol.*, 1984;**54**: 672–673.
40. Gussak, I., P. Brugada, J. Brugada, et al., Idiopathic short QT interval: A new clinical syndrome. *Cardiology*, 2000;**90**: 99–102.
41. Nekvasil, R., J. Stejskal, and A. Tuma, Detection of early onset neonatal hypocalcaemia in low birth weight infants by QTc and Q-oTc interval measurement. *Acta Paediatr. Acad. Sci. Hung.*, 1980;**21**: 203–210.
42. Lehmann, G., I. Deisenhofer, G. Ndrepepa, and C. Schmitt, ECG changes in a 25-year-old woman with hypocalcemia due to hypoparathyroidism. Hypocalcemia mimicking acute myocardial infarction. *Chest*, 2000;**118**: 260–262.
43. Johnson, J.D. and R. Jennings, Hypocalcemia and cardiac arrhythmias. *Am. J. Dis. Child* 1968;**115**: 373–376.
44. Griffin, J.H., Neonatal hypocalcemia and complete heart block. *Am. J. Dis. Child*, 1965;**110**: 672–675.
45. Kambara, H., B.J. Iteld, and J. Phillips, Hypocalcemia and intractable ventricular fibrillation. (Letter.) *Ann. Intern. Med.* 1977;**86**: 583–584.
46. Chang, C.J., S.A. Chen, C.T. Tai, et al., Ventricular tachycardia in a patient with primary hyperparathyroidism. *Pacing Clin. Electrophysiol.*, 2000;**23**: 534–537.
47. Kiewiet, R.M., H.H. Ponssen, E.N. Janssens, and P.W. Fels, Ventricular fibrillation in hypercalcaemic crisis due to primary hyperparathyroidism. *Neth. J. Med.*, 2004;**62**: 94–96.
48. Akiyama, T., J. Batchelder, J. Worsman, H.W. Moses, and M. Jedlinski, Hypocalcemic Torsades de Pointes. *J. Electrocardiol.*, 1989;**22**: 89–92.
49. Kearney, P., M. Reardon, and J. O'Hare, Primary hyperparathyroidism presenting as torsades de pointes. *Br. Heart J.*, 1993;**70**: 473.
50. Surawicz, B., M.G. MacDonald, V. Kaljot, and J.C. Bettinger, Treatment of cardiac arrhythmias with salts of ethylenediamine tetraacetic acid (EDTA). *Am. Heart J.*, 1959;**58**: 493–503.
51. Hoff, H.E., P.K. Smith, and A.W. Winkler, Electrocardiographic changes and concentration of calcium in serum following intravenous injection of calcium chloride. *Am. J. Physiol.*, 1939;**125**: 162–171.
52. Johnson, J.D. and R. Jennings, Hypocalcemia and cardiac arrhythmias. *Am. J. Dis. Child*, 1968;**115**: 373–376.
53. Voss, D.M. and E.H. Drake, Cardiac manifestations of hyperparathyroidism, with presentation of a previously unreported arrhythmia. *Am. Heart J.*, 1967;**72**: 235–239.
54. Seelig, M.S., Myocardial loss of functional magnesium. I. Effect on mitochondrial integrity and potassium retention. *Recent Adv. Stud. Cardiac Struct. Metab.*, 1972;**1**: 615–625.

55. Loeb, H.S., R.J. Pietras, R.M. Gunnar, and J.R. Tobin Jr., Paroxysmal ventricular fibrillation in two patients with hypomagnesemia. *Circulation*, 1968;**37**: 210–215.
56. Seelig, M.S., Electrocardiographic patterns of magnesium depletion appearing in alcoholic heart disease. *Ann. N. Y. Acad. Sci.*, 1969;**162**: 906–917.
57. Surawicz, B., Is hypomagnesemia or magnesium deficiency arrhythmogenic? *J. Am. Coll. Cardiol.*, 1989;**14**: 1093–1096.
58. Wellens, H.J., V.M. Cats, and D.R. Duren, Symptomatic sinus node abnormalities following lithium carbonate therapy. *Am. J. Med.*, 1975;**59**: 285–287.
59. Chih-Hsin, H., L. Ping-Yen, C. Jyh-Hong, Y. Tzung-Lieh, T. Hsiang-Yi, and L. Li-Jen, Electrocardiographic abnormalities as predictors for over-range lithium levels. *Cardiology*, 2005;**103**: 101–106.
60. Hermsmeyer, K., R. Rulon, and N. Sperelakis, Loss of the plateau of the cardiac action potential in hypertonic solutions. *J. Gen. Physiol.*, 1972;**59**: 779–793.
61. Bailey, J.C., Electrophysiological effects of hypertonic sucrose solutions on canine cardiac Purkinje fibers. *Circ. Res.*, 1981;**49**: 1112–1118.
62. Spitzer, K.W. and P.M. Hogan, The effects of acidosis and bicarbonate on action potential repolarization in canine cardiac Purkinje fibers. *J. Gen. Physiol.*, 1979;**73**: 199–218.
63. Barker, P.S., E.L. Schrader, and E. Ronzoni, The effects of alkalosis and of acidosis upon the human electrocardiogram. *Am. Heart J.*, 1939;**17**: 169–186.
64. Madias, J.E., K.M. Venkataraman, L.T. Synder, P.S. Vokonas, and W.B. Hood Jr., Experimental myocardial infarction. XI. Circulatory effects of hypoxia in intact conscious dogs with coronary occlusion. *Am. J. Cardiol.*, 1974;**23**: 796–802.
65. Broch, O.J., Calibrated hypoxemia test in normal subjects and coronary patients. II. The relation between ECG changes and oxygen saturation of blood. *Acta Med. Scand.*, 1972;**191**: 185–190.
66. Kiely, D.G., R.I. Cargill, and B.J. Lipworth, Effects of hypercapnia on hemodynamic, inotropic, lusitropic, and electrophysiologic indices in humans. *Chest*, 1996;**109**: 1215–1221.
67. Yasuma, F., M. Hirai, and J.I. Hayano, Differential effects of hypoxia and hypercapnia on respiratory sinus arrhythmia in conscious dogs. *Jpn. Circ. J.*, 2001;**65**: 738–742.
68. Rutherford, J.J., T.H. Clutton-Brock, and M.J. Parkes, Hypocapnia reduces the T wave of the electrocardiogram in normal human subjects. *Am. J. Physiol. Regul. Integr. Comp. Physiol.*, 2005;**289**: R148–R155.
69. Alexopoulos, D., J. Christodoulou, T. Toulgaridis, et al., Repolarization abnormalities with prolonged hyperventilation in apparently healthy subjects: Incidence, mechanisms and affecting factors. *Eur. Heart J.*, 1996;**17**: 1432–1437.
70. Rigatto, C., R. Foley, J. Jeffery, et al., Electrocardiographic left ventricular hypertrophy in renal transplant recipients: Prognostic value and impact of blood pressure and anemia. *J. Am. Soc. Nephrol.*, 2003;**14**: 462–468.
71. Gehi, A., J. Ix, M. Shlipak, S.S. Pipkin, and M.A. Whooley, Relation of anemia to low heart rate variability in patients with coronary heart disease (from the Heart and Soul Study). *Am. J. Cardiol.*, 2005;**95**: 1474–1477.
72. Nelson, C.V., P.W. Rand, E.T. Angelakos, and P.G. Hugenholtz, Effect of intracardiac blood on the special vectorcardiogram. 1. Results in the dog. *Circ. Res.*, 1972;**31**: 95–104.
73. Rosenthal, A., N.J. Restieauz, and S.A. Feig, Influence of acute variations in hematocrit on the QRS complex of the Frank electrocardiogram. *Circulation*, 1971;**44**: 456–465.
74. Lipsitz, L.A., F. Hashimoto, and L.P. Lubowsky, Heart rate and respiratory rhythm dynamics on ascent to high altitude. *Br. Heart J.*, 1995;**74**: 390–396.
75. Weilenmann, D., F. Duru, M. Schonbeck, et al., Influence of acute exposure to high altitude and hypoxemia on ventricular stimulation thresholds in pacemaker patients. *Pacing Clin. Electrophysiol.*, 2000;**23**: 512–515.
76. Kaufmann, P.A., C. Schirlo, V. Pavlicek, et al., Increased myocardial blood flow during acute exposure to simulated altitudes. *J. Nucl. Cardiol.*, 2001;**8**: 158–164.
77. Pan, A.W., J. He, Y. Kinouchi, H. Yamaguchi, and H. Miyamoto, Blood flow in the carotid artery during breath-holding in relation to diving bradycardia. *Eur. J. Appl. Physiol. Occup. Physiol.*, 1997;**75**: 388–395.
78. Mukerji, B., M.A. Alpert, and V. Mukerji, Right ventricular alterations in scuba divers: Findings on electrocardiography and echocardiography. *South Med. J.*, 2000;**93**: 673–676.
79. Ferrigno, M., B. Grassi, G. Ferretti, et al., Electrocardiogram during deep breath-hold dives by elite divers. *Undersea Biomed. Res.*, 1991;**18**: 81–91.
80. Rocha, I., E.I. de Oliveira, K.M. Spyer, and L.S. Carvalho, Interaction of the Bezold-Jarisch reflex with the urinary bladder function. *Rev. Port Cardiol.*, 2000;**19**: 977–988.
81. Hayashi, N., M. Ishihara, A. Tanaka, T. Osumi, and T. Yoshida, Face immersion increases vagal activity as assessed by heart rate variability. *Eur. J. Appl. Physiol. Occup. Physiol.*, 1997;**76**: 394–399.
82. Chu, C.S., T.H. Lin, Y.H. Lu, et al., Cold effect on qt dispersion in healthy subjects. *Kaohsiung J. Med. Sci.*, 2002;**18**: 236–240.
83. Saltykova, M., A. Capderou, O. Atkov, et al., Variations of intrathoracic amount of blood as a reason of ECG voltage changes. *Ann. Noninv. Electrocardiol.*, 2003;**8**: 321–332.
84. Whinnery, J.E., Acceleration induced voltage variations in the electrocardiogram during exhaustive simulated aerial combat maneuvering. *Aviat. Space Environ. Med.*, 1982;**53**: 147–152.
85. Osborn, J.J., Experimental hypothermia. Respiratory and blood pH changes in relation to cardiac function. *Am. J. Physiol.*, 1953;**175**: 389–398.
86. Surawitz, B. and T.K. Knilans,*Chou's Electrocardiography in Clinical Practice. Adult and Pediatric*, 5th edn. Philadelphia, PA: WB Saunders, 2001.
87. Okada, M., F. Nishimura, H. Yoshino, M. Kimura, and T. Ogino, The J wave in accidental hypothermia. *J. Electrocardiol.*, 1983;**16**: 23–28.
88. Gussak, I., P. Bjerregaard, T.M. Egan, and B.R. Chaitman, ECG phenomenon called the J wave. History, pathophysiology, and clinical significance. *J. Electrocardiol.*, 1995;**28**: 49–58.
89. Solomon, A., R.A. Barish, B. Browne, and E. Tso, The electrocardiographic features of hypothermia. *J. Emerg. Med.*, 1989;**7**: 169–173.
90. Strohmer, B. and M. Pichler, Atrial fibrillation and prominent J (Osborn) waves in critical hypothermia. *Int. J. Cardiol.*, 2004;**96**: 291–293.
91. Danzl, D.F. and R.S. Pozos, Accidental hypothermia. *N. Engl. J. Med.*, 1994;**331**: 1756–1760.
92. Trevino, A., B.M. Razi, B. Beller, and S. Antonio, The characteristic electrocardiogram of accidental hypothermia. *Arch. Intern. Med.*, 1971;**127**: 470–473.

93. Abbott, J.A. and M.D. Cheitlin, The non-specific camel-hump sign. *J. Am. Med. Assoc.*, 1976;**235**: 413–414.
94. Carrillo-Esper, R., L. Limon-Camacho, H.L. Vallejo-Mora, et al., Non-hypothermic J wave in subarachnoid hemorrhage. *Circulation*, 2004;**72**: 125–129.
95. Scherlag, B.J., C.G. Gunn, E.J. Berbari, and R. Lazzara, Peri-infarction block (1950)-Late potential (1980): Their relationship, significance and diagnostic implications. *Am. J. Cardiol.*, 1985;**55**: 839–841.
96. Nishida, K., A. Fujiki, K. Mizumaki, et al., Canine model of Brugada syndrome using regional epicardial cooling of the right ventricular outflow tract. *J. Cardiovasc. Electrophysiol.*, 2004;**15**: 936–941.
97. Fish, J.M. and C. Antzelevitch, Link between hypothermia and the Brugada syndrome. *J. Cardiovasc. Electrophysiol.*, 2004;**15**: 942–944.
98. Yan, G.X. and C. Antzelevitch, Cellular basis for the electrocardiographic J wave. *Circulation*, 1996;**93**: 372–379.
99. Wakita, R., I. Watanabe, Y. Okumura, et al., Brugada-like electrocardiographic pattern unmasked by fever. *Jpn. Heart J.*, 2004;**45**: 163–167.
100. Sanchez, J.M. and A.M. Kates, Brugada-type electrocardiographic pattern unmasked by fever. *Mayo. Clin. Proc.*, 2004;**79**: 273–274.
101. Morita, H., S. Nagase, K. Kusano, and T. Ohe, Spontaneous T wave alternans and premature ventricular contractions during febrile illness in a patient with Brugada syndrome. *J. Cardiovasc. Electrophysiol.*, 2002;**13**: 816–818.
102. Ryan, J.F. and L.G. Tedeschi, Sudden unexplained death in a patient with a family history of malignant hyperthermia. *J. Clin. Anesth.*, 1997;**9**: 66–68.
103. Jantzen, J.P., K. Erdmann, and P.P. Kleemann, Malignant hyperthermia susceptibility-successful management with a "stressfree" technique. *Acta Anaesthesiol. Belg.*, 1987;**38**: 107–113.
104. Zipes, D.P., P. Libby, R.O. Bonow, and E. Braunwald, *Braunwald's Heart Disease: A Textbook of Cardiovascular Medicine*, 7th edn. Philadelphia, PA: Elsevier Saunders, 2005.
105. Polikar, R., A.G. Burger, U. Scherrer, and P. Nicod, The thyroid and the heart. *Circulation*, 1993;**87**: 1435–1441.
106. Johnson, P.N., A.S. Freedberg, and J.M. Marshall, Action of thyroid hormone on the transmembrane potentials from sino atrial cells and atrial muscle cells in isolated atria of rabbits. *Cardiology*, 1973;**58**: 273–289.
107. Arnsdorf, M.F. and R.W. Childers, Atrial electrophysiology in experimental hyperthyroidism in rabbits. *Circ. Res.*, 1970;**26**: 575–581.
108. Jaeger, J.M., S.R. Houser, A.R. Freeman, J.F. Spann Jr., Effect of thyroid hormone on canine cardiac Purkinje fiber transmembrane potential. *Am. J. Physiol.*, 1981;**240**: H934–H940.
109. Binah, O., I. Rubinstein, and E. Gilat, Effects of thyroid hormone on the action potential and membrane currents of guinea pig ventricular myocytes. *Pflugers Arch.*, 1987;**409**: 214–216.
110. Sharp, N.A., D.S. Neel, and R.L. Parsons, Influence of thyroid hormone levels on the electrical and mechanical properties of rabbit papillary muscle. *J. Mol. Cell. Cardiol.*, 1985;**17**: 119–132.
111. Surawicz, B. and M.L. Mangiardi, Electrocardiogram in endocrine and metabolic disorders, in Clinical Electrocardiographic Correlations, J.C. Rios, Editor. Davis, Philadelphia, PA, 1977, pp. 243–266.
112. Hoffman, I. and R.D. Lowrey, The electrocardiogram in thyrotoxicosis. *Am. J. Cardiol.*, 1960;**6**: 893–904.
113. Benker, V.G., H. Preiss, H. Kreusen, et al., Ekg Veriinderungen bei Hyperthyreose. Untersuchungen an 542 patienten. *Z. Kardiol.*, 1974;**63**: 799–811.
114. Nakazawa, H., K. Sakurai, N. Hamada, N. Momotani, and K. Ito, Management of atrial fibrillation in the post-thyrotoxic state. *Am. J. Med.*, 1982;**72**: 903–906.
115. Sawin, C.T., Subclinical hyperthyroidism and atrial fibrillation. *Thyroid*, 2002;**12**: 501–503.
116. Pilapil, V.R. and D.G. Watson, Electrocardiogram in hyperthyroid children. *Am. J. Dis. Child*, 1970;**119**: 245–248.
117. Sanghvi, L.M. and K. Banerjee, Wolff-parkinson White syndrome associated with thyrotoxicosis. *Am. J. Cardiol.*, 1961;**8**: 431–437.
118. Wakimoto, H., N. Izumida, Y. Asano, et al., Augmentation of QRS wave amplitudes in the precordial leads during narrow QRS tachycardia. *J. Cardiovasc. Electrophysiol.*, 2000;**11**: 52–60.
119. Harumi, K. and T. Ouichi, Q-T prolongation syndrome (in Japanese). *Naika Mook* No.20. Tokyo. Kinbara, 1981: 210.
120. Lepeschkin, E., *Modern Electrocardiography*, vol. I. Baltimore, MD: Williams & Wilkins, 1951.
121. Fisher, J., Thyrotoxic periodic paralysis with ventricular fibrillation. *Arch. Intern. Med.*, 1982;**142**: 1362–1364.
122. Shih-Hua, L., Thyrotoxic periodic paralysis. *Mayo. Clin. Proc.*, 2005;**80**: 99–105.
123. Hsu, Y.J., Y.F. Line, T. Chau, J.T. Liou, S.W. Kuo, and S.H. Line, Electrocardiographic manifestations in patients with thyrotoxic periodic paralysis. *Am. J. Med.*, 2003;**326**: 128–132.
124. Boccalandro, C., L. Lopez, F. Boccalandro, and V. Lavis, Electrocardographic changes in thyrotoxic periodic paralysis. *Am. J. Cardiol.*, 2003;**91**: 775–777.
125. Kerber, R.E. and B. Sherman, Echocardiographic evaluation of pericardial effusion in myxedema. Incidence and biochemical and clinical correlations. *Circulation*, 1975;**52**: 823–827.
126. Vanhaelst, L., P. Neve, P. Chailly, and P.A. Bastenie, Coronary disease in hypothyroidism: Observations in clinical myxoedema. *Lancet*, 1967;**2**: 800–802.
127. Lee, J.K. and J.A. Lewis, Myxoedema with complete A-V block and Adams-Stokes disease abolished with thyroid education. *Br. Heart J.*, 1962;**24**: 253–256.
128. Hansen, J.E., Paroxysmal ventricular tachycardia associated with myxedema. A case report. *Am. Heart J.*, 1961;**61**: 692–697.
129. Macaulay, M.B. and R.J. Shepherd, Syncope in myxoedema due to transient ventricular fibrillation. *Postgrad. Med. J.*, 1971;**47**: 361–363.
130. Sun, Z.Q., W.A. Ojamaak-Coetzee, M. Artman, and I. Klein, Effects of thyroid hormone on action potential and repolarizing currents in rat ventricular myocytes. *Am. J. Physiol.*, 2000;**278**: E302–E307.
131. Surawicz, B., The pathogenesis and clinical significance of primary ST-T wave abnormalities, in Advances in electrocardiography, R.C. Schlant and J.W. Hurst, Editors. Grune and Stratton, New York, 1972.
132. Clayton, R.N., Cardiovascular function in acromegaly. *Endocr. Rev.*, 2003;**24**: 272–277.
133. Ciulla, M., M. Arosio, M.V. Barelli, et al., Blood pressure-independent cardiac hypertrophy in acromegalic patients. *J. Hypertens.*, 1999;**17**: 1965–1969.

134. Herrmann, B.L., C. Bruch, B. Saller, et al., Acromegaly: Evidence for a direct relation between disease activity and cardiac dysfunction in patients without ventricular hypertrophy. *Clin. Endocrinol. (Oxf.)*, 2002;**56**: 595–602.
135. Sugihara, N., M. Shimizu, Y. Kita, et al., Cardiac characteristics and postoperative courses in Cushing's syndrome. *Am. J. Cardiol.*, 1992;**69**: 1475–1480.
136. Bhattacharyya, A., S. Jagadeesan, R.J. Wolstenholme, and D.J. Tymms, Acute adrenocortical crisis and an abnormal electrocardiogram. *Hosp. Med.*, 1999;**60**: 908–909.
137. Rovetto, M.J. and A.M. Lefer, Electrophysiologic properties of cardiac muscle in adrenal insufficiency. *Am. J. Physiol.*, 1970;**218**: 1015–1019.
138. Bruch, C., N. Dagres, H. Wieneke, C. Herborn, K. Brandt-Mainz, and R. Erbel, Sinus node dysfunction with intermittent sinus arrest and AV-nodal escape rhythm as initial manifestation of pheochromocytoma. *Z. Kardiol.*, 2002;**91**: 81–87.
139. Dinckal, M.H., V. Davutoglu, S. Soydinc, and A. Kirilmaz, Phaeochromocytoma-induced myocarditis mimicking acute myocardial infarction. *Int. J. Clin. Pract.*, 2003;**57**: 842–843.
140. Takeno, Y., S. Eno, T. Hondo, K. Matsuda, and Z. Zushi, Pheochromocytoma with reversal of tako-tsubo-like transient left ventricular dysfunction: A case report. *J. Cardiol.*, 2004;**43**: 281–287.
141. Minami, J., M. Todoroki, T. Ishimitsu, and H. Matsuoka, Changes in heart rate variability before and after surgery in patients with pheochromocytoma. *Auton. Neurosci.*, 2004;**111**: 144–146.
142. Tzemos, N., G.P. McNeill, R.T. Jung, and T.M. MacDonald, Post exertional broad complex tachycardia in a normotensive patient: A rare presentation of phaeochromocytoma. *Scott. Med. J.*, 2001;**46**: 14–15.
143. Roshan, J., O.K. George, S. Vineet, P.V. George, and V.J. Jose, Torsade de pointes in a case of pheochromocytoma-an unusual presentation of an uncommon disease. *Indian Heart J.*, 2004;**56**: 248–249.
144. Viskin, S., R. Fish, A. Roth, P.J. Schwartz, and B. Belhassen, Clinical problem-solving. QT or not QT? *N. Engl. J. Med.*, 2000;**343**: 352–356.
145. Lopes, H.F., H.B. Silva, C. Frimm Cde, L.A. Bortolotto, G. Belotti, and F. Pileggi, A false diagnosis of hypertrophic myocardiopathy in pheochromocytoma. *Arq. Bras. Cardiol.*, 1995;**65**: 167–169.
146. Schuiki, E.R., R. Jenni, F.W. Amann, and W.H. Ziegler, A reversible form of apical left ventricular hypertrophy associated with pheochromocytoma. *J. Am. Soc. Echocardiogr.*, 1993;**6**: 327–331.
147. Salvador, M., F. Begasse, J. Guittard, and B. Chamontin, Value of the study of electrocardiographic P wave in pheochromocytoma. *Arch. Mal. Coeur. Vaiss.*, 1992;**85**: 39–43.
148. Senges, J., J. Brachmann, D. Pelzer, C. Hasslacher, E. Weihe, and W. Kubler, Altered cardiac automaticity and conduction in experimental diabetes mellitus. *J. Mol. Cell. Cardiol.*, 1980;**12**: 1341–1351.
149. Surawicz, B. and M.L. Mangiardi, Electrocardiogram in endocrine and metabolic disorders. *Cardiovasc. Clin. North Am.*, 1977;**77**: 243–246.
150. Huizar, J.F., L.A. Gonzalez, J. Alderman, and H.S. Smith, Sulfonylureas attenuate electrocardiographic ST-segment elevation during an acute myocardial infarction in diabetics. *J. Am. Coll. Cardiol.*, 2003;**42**: 1017–1021.
151. Ditchburn, C.J., J.A. Hall, M. de Belder, A. Davies, W. Kelly, and R. Bilous, Silent myocardial ischaemia in patients with proved coronary artery disease: A comparison of diabetic and non-diabetic patients. *Postgrad. Med. J.*, 2001;**77**: 395–398.
152. Coumel, P., N. Johnson, F. Extramiana, P. Maison-Blanche, and P. Valensi, Electrocardiographic changes and rhythm problems in the diabetic. *Arch. Mal. Coeur. Vaiss.*, 2000;**93**: 59–66.
153. Rodriguez-Moran, M. and F. Guerrero-Romero, Electrocardiographic changes and cardiovascular risk factors in patients with type-2 diabetes. *Salud. Publica. Mex.*, 1999;**41**: 12–17.
154. Pezzilli, R., P. Broccoli, P. Billi, and B. Barakat, Silent myocardial ischemia induced by hypoglycemia. *Panminerva. Med.*, 1998;**40**: 347–349.
155. Matsunaga, R., J. Miura, and T. Fujito, Ischemic change on electrocardiogram induced by hypoglycemia in a diabetic patient. *Jpn. Circ. J.*, 1998;**62**: 142–145.
156. Burch, G.E., R. Meyers, and J.A. Abildskov, A new electrocardiographic pattern observed in cerebrovascular accidents. *Circulation*, 1954;**9**: 719–723.
157. Makino, T. and R. Okada, A clinicopathological study of the T wave changes of the subarachnoidal hemorrhage (SAH). *Jpn. Heart J.*, 1982;**23** (Suppl I): 546–548.
158. Fentz, V. and J. Gormsen, Electrocardiographic patterns in patients with cerebrovascular accidents. *Circulation*, 1962;**25**: 22–28.
159. Shuster, S., The electrocardiogram in subarachnoid haemorrhage. *Br. Heart J.*, 1960;**22**: 316–320.
160. Di Pasquale, G., A. Andreoli, M. Lusa, et al., Cardiologic complications of subarachnoid hemorrhage. *J. Neurosurg. Sci.*, 1998;**42** (suppl 1): 33–36.
161. Di Pasquale, G., G. Pinelli, A. Andreoli, et al., Torsade de pointes and ventricular flutter-fibrillation following spontaneous cerebral subarachnoid hemorrhage. *Int. J. Cardiol.*, 1988;**18**: 163–172.
162. Cropp, G.J. and G.W. Manning, Electrocardiographic changes simulating myocardial ischemia and infarction associated with spontaneous intracranial hemorrhage. *Circulation*, 1960;**22**: 25–38.
163. Hersch, C., Electrocardiographic changes in subarachnoid haemorrhage, meningitis, and intracranial space-occupying lesions. *Br. Heart J.*, 1964;**26**: 785–793.
164. Hunt, D., C. McRae, and P. Zapf, Electrocardiographic and serum enzyme changes in subarachnoid hemorrhage. *Am. Heart J.*, 1969;**77**: 479–488.
165. Eisalo, A., J. Periisalo, and P.I. Halonen, Electrocardiographic abnormalities and some laboratory findings in patients with subarachnoid haemorrhage. *Br. Heart J.*, 1972;**34**: 217–226.
166. Harumi, K., Unpublished data. Yokohama: Showa University.
167. Surawicz, B., Electrocardiographic pattern of cerebrovascular accident. *J. Am. Med. Assoc.*, 1966;**197**: 913–914.
168. Valeriano, J. and J. Elson, Electrocardiographic changes in central nervous system disease. *Neurol. Clin.*, 1993;**11**: 257–272.
169. Brouwers, P.J., E.F. Wijdicks, D. Hasan, et al., Serial electrocardiographic recording in aneurysmal subarachnoid hemorrhage. *Stroke*, 1989;**20**: 1162–1167.

170. Dimant, J. and D. Grob, Electrocardiographic changes and myocardial damage in patients with acute cerebrovascular accidents. *Stroke*, 1977;**8**: 448–455.
171. Brit ton, M., U. de Faire, C. Helmers, K. Miah, and C. Ryding, Wester P0. Arrhythmias in patients with acute cerebrovasculardisease. *Acta Med. Scand.*, 1979;**205**: 425–428.
172. Norris, J.W. and V.C. Hachinski, Intensive care management of stroke patients. *Stroke*, 1976;**7**: 573–577.
173. Oppenheimer, S.M., D.F. Cechetto, and V.C. Hachinski, Cerebrogenic cardiac arrhythmias: Cerebral electrocardiographic influences and their role in sudden death. *Arch. Neurol.*, 1990;**47**: 513–519.
174. Jabaudon, D., J. Sztajzel, K. Sievert, T. Landis, and R. Sztajzel, Usefulness of ambulatory 7-day ECG monitoring for the detection of atrial fibrillation and flutter after acute stroke and transient ischemic attack. *Stroke*, 2004;**35**: 1647–1651.
175. Van der Ark, G., Cardiovascular changes with acute subdural hematoma. *Surg. Neurol.*, 1975;**3**: 305–308.
176. Lakusic, N., D. Mahovic, T. Babic, and D. Sporis, Changes in autonomic control of heart rate after ischemic cerebral stroke. *Acta Med. Croatica.*, 2003;**57**: 269–273.
177. Apak, I., K. Iltumur, Y. Tamam, and N. Kaya, Serum cardiac troponin T levels as an indicator of myocardial injury in ischemic and hemorrhagic stroke patients. *Tohoku. J. Exp. Med.*, 2005;**205**: 93–101.
178. Christensen, H., G. Boysen, A.F. Christensen, and H.H. Johannesen,. Insular lesions, ECG abnormalities, and outcome in acute stroke. *J. Neurol. Neurosurg. Psychiat.*, 2005;**76**: 269–271.
179. Greenhoot, J.H and D.D. Reichenbach, Cardiac injury and subarachnoid hemorrhage. A clinical, pathological, and physiological correlation. *J. Neurosurg.*, 1969;**30**: 521–531.
180. Connor, R.C.R., Heart damage associated with intracranial lesions. *Br. Med. J.*, 1968;**3**: 29–31.
181. Dixit, S., M. Castle, R.P. Velu, et al., Cardiac involvement in patients with acute neurologic disease. *Arch. Intern. Med.*, 2000;**160**: 3153–3158.
182. Connor, R.C.R., Heart damage associated with intracranial lesions. *BMJ*, 1968;**3**: 29–31.
183. Pollick, C., B. Cujec, S. Parker, and C. Tator, Left ventricular wall motion abnormalities in subarachnoid hemorrhage: An echocardiographic study. *J. Am. Coll. Cardiol.*, 1988;**12**: 600–605.
184. Kono, T., H. Morita, T. Kuroiwa, H. Onaka, H. Takatsuka, and A. Fujiwara, Left ventricular wall motion abnormalities in patients with subarachnoid hemorrhage: Neurogenic stunned myocardium. *J. Am. Coll. Cardiol.*, 1994;**24**: 636–640.
185. Pool, J.L., Vasocardiac effects of the circle of Willis. *AMA Arch. Neurol. Psychiat.*, 1957;**78**: 355–368.
186. Eisalo, A., J. Periisalo, and P.I. Halonen, Electrocardiographic abnormalities and some laboratory findings in patients with subarachnoid haemorrhage. *Br. Heart J.*, 1972;**34**: 217–226.
187. Pine, D.S., Tierney L Clinical problem-solving: A stressful interaction. *N. Engl. J. Med.*, 1996;**334**: 1530–1534.
188. Beard, E.F., J.W. Robertson, and R.C.L. Robertson, Spontaneous subarachnoid hemorrhage simulating acute myocardial infarction. *Am. Heart J.*, 1959;**58**: 755–759.
189. Doshi, R. and G. Neil-Dwyer, A clinicopathological study of patients following a subarachnoid hemorrhage. *J. Neurosurg.*, 1980;**52**: 295–301.
190. Tokgözoglu, S.L., M.K. Batur, M.A. Topçuoglu, O. Saribas, S. Kes, and A. Oto, Effects of stroke localization on cardiac autonomic balance and sudden death. *Stroke*, 1999;**30**: 1307–1311.
191. Jacob, W.A., A. van Bogaert, and M.H.A. De Groodt-Lasseel, Myocardial ultrastructure and haemodynamic reactions during experimental subarachnoid haemorrhage. *J. Mol. Cell. Cardiol.*, 1972;**4**: 287–298.
192. Shanlin, R.J., M.J. Sole, M. Rahimifar, C.H. Tator, and S.M. Factor, Increased intracranial pressure elicits hypertension, increased sympathetic activity, electrocardiographic abnormalities and myocardial damage in rats. *J. Am. Coll. Cardiol.*, 1988;**12**: 727–736.
193. McLeod, A.A., G. Neil-Dwyer, C.H.A. Meyer, P.L. Richardson, J. Cruickshank, and J. Bartlett, Cardiac sequelae of acute head injury. *Br. Heart J.*, 1982;**47**: 221–226.
194. Ackerman, M.J., Cardiac causes of sudden unexpected death in children and their relationship to seizures and syncope: Genetic testing for cardiac electropathies. *Semin. Pediatr. Neurol.*, 2005;**12**: 52–58.
195. Evrengul, H., H. Tanriverdi, D. Dursunoglu, et al., Time and frequency domain analyses of heart rate variability in patients with epilepsy. *Epilepsy Res.*, 2005;**63**: 131–139.
196. Griffith, T.W., On myotonia. *Q. J. Med.*, 1912;**5**: 229–247.
197. Evans, W., The heart in myotonia atrophica. *Br. Heart J.*, 1944;**6**: 41–47.
198. Church, S.C., The heart in myotonia atrophica. *Arch. Intern. Med.*, 1967;**119**: 176–181.
199. **O**lofsson, B.-O., H. Forsberg, S. Andersson, P. Bjerle, A. Henriksson, and I. Wedin, Electrocardiographic findings in myotonic dystrophy. *Br. Heart J.*, 1988;**59**: 47–52.
200. DeWind, L.T. and R.J. Jones, Cardiovascular observations in dystrophia myotonica. *J. Am. Med. Assoc.*, 1950;**144**: 299–303.
201. Petkovich, N.J., M. Dunn, and W. Reed, Myotonia dystrophica with A-V dissociation and Stokes-Adams attacks. A case report and review of the literature. *Am. Heart J.*, 1964;**68**: 391–396.
202. Finstere, J., C. Stollberger, and G. Meng, Cardiac involvement in facioscapulohumeral muscular dystrophy. *Cardiology*, 2005;**103**: 81–83.
203. Finsterer, J. and C. Stollberger, Cardiac involvement in primary myopathies. *Cardiology*, 2000;**94**: 1–11.
204. Berlit, P. and B. Stegaru-Hellring, The heart in muscular dystrophy: An electrocardiographic and ultrasound study of 20 patients. *Eur. Arch. Psychiat. Clin. Neurosci.*, 1991;**241**: 177–180.
205. De-Oliveira, J.M., M.P. Sambhi, and H.A. Zimmerman, The electrocardiogram in pectus excavatum. *Br. Heart J.*, 1958;**20**: 495–501.
206. Elisberg, E.I., Electrocardiographic changes associated with pectus excavatum. *Ann. Intern. Med.*, 1958;**49**: 130–141.
207. Wachtel, F.W., M.M. Ravitch, and A. Grishman, The relation of pectus excavatum to heart disease. *Am. Heart J.*, 1956;**52**: 21–37.
208. Dressier, W. and H. Roesler, Electrocardiographic changes in funnel chest. *Am. Heart J.*, 1950;**40**: 877–883.
209. Iakovlev, V.M., G.I. Nechaeva, and I.A. Viktorova, Clinical function of the myocardium and cardio- and hemodynamics in patients with pectus carinatum deformity. *Ter. Arkh.*, 1990;**62**: 69–72.
210. Kumar, U.K. and K.V. Sahasranam, Mitral valve prolapse syndrome and associated thoracic skeletal abnormalities. *J. Assoc. Physicians India*, 1991;**39**: 536–539.
211. Raggi, P., T.Q. Callister, N.J. Lippolis, and D.J. Russo, Is mitral valve prolapse due to cardiac entrapment in the chest cavity? A CT view. *Chest*, 2000;**117**: 636–642.

212. Chazan, R. and W. Droszcz, Electrocardiographic changes in patients with airway obstruction. *Pol. Arch. Med. Wewn.*, 1992;**87**: 237–241.
213. Efthimiou, J., A.B. Hassan, O. Ormerod, and M.K. Benson, Reversible T-wave abnormality in severe acute asthma: An electrocardiographic sign of severity. *Respir. Med.*, 1991;**85**: 195–202.
214. Gong, H. Jr., W.S. Linn, S.L. Terrell, et al., Altered heart-rate variability in asthmatic and healthy volunteers exposed to concentrated ambient coarse particles. *Inhal. Toxicol.*, 2004;**16**: 335–343.
215. Smith, R.P., M.K. Johnson, J. Ashley, S.T. Rudkin, and R.J. White, Effect of exercise induced hypoxaemia on myocardial repolarisation in severe chronic obstructive pulmonary disease. *Thorax*, 1998;**53**: 572–576.
216. Sarubbi, B., V. Esposito, V. Ducceschi, et al., Effect of blood gas derangement on QTc dispersion in severe chronic obstructive pulmonary disease: Evidence of an electropathy? *Int. J. Cardiol.*, 1997;**58**: 287–292.
217. Rudy, Y., The electrocardiogram and its relationship to excitation of the heart, in Physiology and Pathophysiology of the Heart, N. Sperelakis, Editor, 3rd edn. Kluwer, The Netherlands, 1995, p. 201.
218. McCord, J. and S. Borzak, Multifocal atrial tachycardia. *Chest*, 1998;**113**: 203–209.
219. Benditt, D.G., N. Samniah, S. Pham, et al., Effect of cough on heart rate and blood pressure in patients with "cough syncope". *Heart Rhythm*, 2005;**2**: 807–813.
220. Alonso-Fernandez, A., F. Garcia-Rio, M.A. Racionero, et al., Cardiac rhythm disturbances and ST-segment depression episodes in patients with obstructive sleep apnea-hypopnea syndrome and its mechanisms. *Chest*, 2005;**127**: 15–22.
221. Aydin, M., R. Altin, A. Ozeren, L. Kart, M. Bilge, and M. Unalacak, Cardiac autonomic activity in obstructive sleep apnea: Time-dependent and spectral analysis of heart rate variability using 24-hour Holter electrocardiograms. *Tex. Heart Inst. J.*, 2004;**31**: 132–136.
222. Nakamura, T., K. Chin, R. Hosokawa, et al., Corrected QT dispersion and cardiac sympathetic function in patients with obstructive sleep apnea-hypopnea syndrome. *Chest*, 2004;**125**: 2107–2114.
223. Valencia-Flores, M., A. Orea, M. Herrera, et al., Effect of bariatric surgery on obstructive sleep apnea and hypopnea syndrome, electrocardiogram, and pulmonary arterial pressure. *Obes. Surg.*, 2004;**14**: 755–762.
224. Stein, P.K., S.P. Duntley, P.P. Domitrovich, P. Nishith, and R.M. Carney, A simple method to identify sleep apnea using Holter recordings. *J. Cardiovasc. Electrophysiol.*, 2003;**14**: 467–473.
225. Madias, J.E., Amplitude of the electrocardiographic QRS complexes during and after severe pulmonary edema. *Ann. Noninvasive Electrocardiol.*, 2004;**9**: 192–197.
226. Rudy, Y., R. Wood, R. Plonsey, and J. Liebman, The effect of high lung conductivity on electrocardiographic potentials. Results from human subjects undergoing bronchopulmonary lavage. *Circulation*, 1982;**65**: 440–445.
227. Master, A.M., The electrocardiographic changes in pneumothorax in which the heart has been rotated: The similarity of some of these changes to those indicating myocardial involvement. *Am. Heart J.*, 1928;**3**: 472–483.
228. Littman, D., Electrocardiographic phenomena associated with spontaneous pneumothorax and mediastinal emphysema. *Am. J. Med. Sci.*, 1946;**212**: 682–690.
229. Armen, R.N. and T.V. Frank, Electrocardiogram patterns in pneumothorax. *Dis. Chest*, 1949;**15**: 709–719.
230. Copeland, R. and G. Omenn, Electrocardiographic changes suggestive of coronary artery disease in pneumothorax. Their reversibility with upright posture. *Arch. Intern. Med.*, 1970;**125**: 151–153.
231. Walston, A., D.L. Brewer, and C.S. Kitchens, The electrocardiographic manifestations of spontaneous left pneumothorax. *Ann. Intern. Med.*, 1974;**80**: 375–379.
232. Maheshwari, M. and S.R. Mittal, Right-sided pneumothorax simulating anterior wall myocardial infarction. *Indian Heart J.*, 2004;**56**: 73.
233. Sakabe, K., N. Fukuda, K. Wakayama, T. Nada, H. Shinohara, and Y. Tamura, Spontaneous pneumomediastium: A cause of T-wave inversion in electrocardiogram. *Int. J. Cardiol.*, 2004;**94**: 123–126.
234. Osswald, S., M. Roelke, S.S. O'Nunain, et al., Electrocardiographic pseudo-infarct patterns after implantation of cardioverter-defibrillators. *Am. Heart J.*, 1995;**129**: 265–272.
235. Madias, J.E., Comparison of P-waves recorded on the standard electrocardiogram, the "Lewis lead", and "saline-filled central venous catheter"-based intracardiac electrocardiogram. *Am. J. Cardiol.*, 2004;**94**: 474–478.
236. Eriksen, U.H., H. Molgaard, J. Ingerslev, and T.T. Nielsen, Fatal hemostatic complications following erroneous thrombolytic therapy in patients with suspected acute myocardial infarction. *Ugeskr. Laeger.*, 1993;**155**: 1392–1394.
237. Caruso, G., G.M. Trovato, A. Corsaro, and V. Sciuto, Correlative evaluation of electrocardiographic changes and spirometric parameters in pulmonary cardiopathy secondary to chronic obstructive bronchopneumopathy. *Recenti. Prog. Med.*, 1989;**80**: 468–470.
238. Lewczuk, J., Suggestive characteristics of inferior wall heart infarct in the EKG of patients with chronic cor pulmonale. *Pneumonol. Pol.*, 1989;**57**: 373–376.
239. Cutforth, R.H. and S. Oram, The electrocardiograms in pulmonary embolism. *Br. Heart J.*, 1958;**20**: 41–60.
240. Weber, D.M. and J.H. Phillips Jr., A re-evaluation of electrocardiographic changes accompanying acute pulmonary embolism. *Am. J. Med. Sci.*, 1966;**251**: 381–398.
241. Stein, P.D., J.E. Dalen, K.M. Mclntyre, A.A. Sasahara, N.K. Wenger, and P.W. Willis III, The electrocardiograms in acute pulmonary embolism. *Prog. Cardiovasc. Dis.*, 1975;**17**: 2 47–57.
242. Hildner, F.J. and R.S. Ormond, Accuracy of the clinical diagnosis of pulmonary embolism. *J. Am. Med. Assoc.*, 1967;**202**: 567–570.
243. Ullman, E., W.J. Brady, A.D. Perron, et al., Electrocardiographic manifestations of pulmonary embolism. *Am. J. Emerg. Med.*, 2001;**19**: 514–519.
244. McGinn, S. and P.D. White, Acute cor pulmonale resulting from pulmonary embolism. Its clinical recognition. *J. Am. Med. Assoc.*, 1935;**104**: 1473–1480.
245. Sasahara, A., T.M. Hyers, C.M. Cole, et al. (eds.), The urokinase-pulmonary embolism trial. A national cooperative study. *Circulation*, 1973;**47** (Suppl. II): 1–12.
246. Chan, T.C., G.M. Vilke, M. Pollack, et al., Electrocardiographic manifestations: Pulmonary embolism. *J. Emerg. Med.*, 2001;**21**: 263–270.

247. Panos, R.J., R.A. Barish, W.W. Depriest, et al., The electrocardiographic manifestations of pulmonary embolism. *J. Emerg. Med.*, 1988;**6**: 301–307.
248. Lynch, R.E., P.D. Stein, and T.A. Bruce, Leftward shift of frontal plane QRS axis as a frequent manifestation of acute pulmonary embolism. *Chest*, 1972;**61**: 443–446.
249. Sreeram, N., E.C. Cheriex, J.L. Smeets, A.P. Gorgels, and H.J. Wellens, Value of the 12-lead electrocardiogram at hospital admission in the diagnosis of pulmonary embolism. *Am. J. Cardiol.*, 1994;**73**: 298–303.
250. Ferrari, E., A. Imbert, T. Chevalier, A. Mihoubi, P. Morand, and M. Baudouy, The ECG in pulmonary embolism: Predictive value of negative T waves in precordial leads-80 case reports. *Chest*, 1997;**111**: 537–543.
251. Daniel, K.R., D.M. Courtney, and J.A. Kline, Assessment of cardiac stress from massive pulmonary embolism with 12-lead ECG. *Chest*, 2001;**120**: 474–481.
252. Procacci, P.M., S.V. Savran, S.L. Schreiter, and A.L. Bryson, Prevalence of clinical mitral-valve prolapse in 1169 young women. *N. Engl. J. Med.*, 1976;**294**: 1086–1088.
253. Massie, B., E.H. Botvinick, D. Shames, M. Taradash, J. Werner, and N. Schiller, Myocardial perfusion scintigraphy in patients with mitral valve prolapse. *Circulation*, 1978;**57**: 19–26.
254. Digeos-Hasnier, S., X. Copie, O. Paziaud, et al., Abnormalities of ventricular repolarization in mitral valve prolapse. *Ann. Noninvasive Electrocardiol.*, 2005;**10**: 297–304.
255. Barlow, J.B. and W.A. Pocock, The problem of non ejection systolic clicks and associated mitral systolic murmurs: Emphasis on the billowing mitral leaflet syndrome. *Am. Heart J.*, 1975;**90**: 636–655.
256. DeMaria. A.N., E.A. Amsterdam, L.A. Vismara, A. Neumann, and D.T. Mason, Arrhythmias in the mitral valve prolapse syndrome. Prevalence, nature, and frequency. *Ann. Intern. Med.*, 1976;**84**: 656–660.
257. Devereux, R.B., J.K. Perloff, N. Reichek, and M.E. Josephson, Mitral valve prolapse. *Circulation*, 1976;**54**: 3–14.
258. Josephson, M.E., L.N. Horowitz, and J.A. Kastor, Paroxysmal supraventricular tachycardia in patients with mitral valve prolapse. *Circulation*, 1978;**57**: 111–115.
259. Winkle, R.A., M.G. Lopes, J.W. Fitzgerald, D.J. Goodwin, J.S. Schroeder, and D.C. Harrison, Arrhythmias in patients with mitral valve prolapse. *Circulation*, 1975;**52**: 73–81.
260. Shappell, S.D., C.E. Marshall, R.E. Brown, and T.A. Bruce, Sudden death and the familial occurrence of the mid-systolic click, late systolic murmur syndrome. *Circulation*, 1973;**48**: 1128–1134.
261. Kramer, H.M., P. Kligfield, R.B. Devereux, D.D. Savage, and R. Kramer-Fox, Arrhythmias in mitral valve prolapse. Effect of selection bias. *Arch. Intern. Med.*, 1984;**144**: 2360–2364.
262. Kligfield, P., C. Hochreiter, H. Kramer, et al., Complex arrhythmias in mitral regurgitation with and without mitral valve prolapse: Contrast to arrhythmias in mitral valve prolapse without mitral regurgitation. *Am. J. Cardiol.*, 1985;**55**: 1545–1549.
263. Lansdown, A.B.G., Viral infections and diseases of the heart. *Prog. Med. Virol.*, 1978;**24**: 70–113.
264. Morgera, T., A. Di Lenarda, L. Dreas, et al., Electrocardiography of myocarditis revisited: Clinical and prognostic significance of electrocardiographic changes. *Am. Heart J.*, 1992;**124**: 455–467.
265. Morgera, T., A. Salvi, E. Alberti, F. Silvestri, and F. Camerini, Morphological findings in apparently idiopathic ventricular tachycardia. An echocardiographic haemodynamic and histologic study. *Eur. Heart J.*, 1985;**6**: 323–334.
266. Feinstein, A.R., H.F. Wood, M. Spagnuolo, et al., Rheumatic fever in children and adolescents. A long-term epidemiologic study of subsequent prophylaxis, streptococcal infections, and clinical sequelae. VII. Cardiac changes and sequelae. *Ann. Intern. Med.*, 1964;**60** (Suppl. 5): 87–123.
267. Acquatella, H., F. Catalioti, J.R. Gomez-Mancebo, V. Davalos, and L. Villalobos, Long-term control of Chagas disease in Venezuela: Effects on serologic findings, electrocardiographic abnormalities and clinical outcome. *Circulation*, 1987;**76**: 556–562.
268. Maguire, J.H., K.E. Mott, J.S. Lehman, et al., Relationship of electrocardiographic abnormalities and seropositivity to Trypanosoma cruzi within a rural community in Northeast Brazil. *Am. Heart J.*, 1983;**105**: 287–294.
269. Villar, J.C., H. Leon, and C.A. Morillo, Cardiovascular autonomic function testing in asymptomatic T. cruzi carriers: A sensitive method to identify subclinical Chagas' disease. *Int. J. Cardiol.*, 2004;**93**: 189–1895.
270. Francis, J., M.A. Watanabe, and G. Schmidt, Heart rate turbulence: A new predictor for risk of sudden cardiac death. *Ann. Noninvasive Electrocardiol.*, 2005;**10**: 102–109.
271. Evrengul, H., D. Dursunoglu, V. Cobankara, et al., Heart rate variability in patients with rheumatoid arthritis. *Rheumatol. Int.*, 2004;**24**: 198–202.
272. Paradiso, M., M. Di Franco, A. Musca, et al., Ventricular late potentials in systemic sclerosis: Relationship with skin involvement. *J. Rheumatol.*, 2002;**29**: 1388–1392.
273. Algom, M., Z. Schlesinger, J. Madjar, S. Tal, D. Krakowsky, and K. Fried, Cardiovascular, skeletal and ophthalmologic manifestations in patients with Marfan's syndrome. *Isr. J. Med. Sci.*, 1989;**25**: 261–263.
274. Ansari, A., P.H. Larson, and H.D. Bates, Cardiovascular manifestations of systemic lupus erythematosus: Current perspective. *Prog. Cardiovasc. Dis.*, 1985;**27**: 421–434.
275. Laitinen, O., E. Kentala, and M. Leirisalo, Electrocardiographic findings in patients with connective tissue disease. *Scand. J. Rheumatol.*, 1978;**7**(4): 193–198.
276. Bagirova, V.V. and G.G. Bagirova, Cor pulmonale in various collagen diseases. *Kardiologiia*, 1978;**18**: 127–131.
277. Savage, D.D., S.F. Seides, C.E. Clark, et al., Electrocardiographic findings in patients with obstructive and nonobstructive hypertrophic cardiomyopathy. *Circulation*, 1978;**58**: 402–408.
278. Chen, C.Y. and W.G. Liang, Electrocardiographic patterns in patients with idiopathic hypertrophic cardiomyopathy. *Chin. Med. J.*, 1984;**33**: 393–402.
279. Braudo, M., E.D. Wigle, and J.D. Keith, A distinctive electrocardiogram in muscular subaortic stenosis due to ventricular septal hypertrophy. *Am. J. Cardiol.*, 1964;**14**: 599–607.
280. McKenna, W.J., S. Chetty, C.M. Oakley, and J.F. Goodwin, Arrhythmias in hypertrophic cardiomyopathy: Exercise and 48 hour ambulatory electrocardiographic assessment with and without beta adrenergic blocking therapy. *Am. J. Cardiol.*, 1980;**45**: 1–5.
281. Savage, D.D., S.F. Seides, B.J. Maron, D.J. Myers, and S.E. Epstein, Prevalence of arrhythmias during 24-hour electrocardiographic monitoring and exercise testing in patients with obstructive and nonobstructive hypertrophic cardiomyopathy. *Circulation*, 1979;**59**: 866–875.
282. Kon-No, Y., J. Watanabe, Y. Koseki, et al., Microvolt T wave alternans in human cardiac hypertrophy: Electrical instability and

abnormal myocardial arrangement. *J. Cardiovasc. Electrophysiol.*, 2001;**12**: 759–763.
283. Kuroda, N., Y. Ohnishi, A. Yoshida, A. Kimura, and M. Yokoyama, Clinical significance of T-wave alternans in hypertrophic cardiomyopathy. *Circ. J.*, 2002;**66**: 457–462.
284. Barletta, G., C. Lazzeri, F. Franchi, R. Del Bene, and A. Michelucci, Hypertrophic cardiomyopathy: Electrical abnormalities detected by the extended-length ECG and their relation to syncope. *Int. J. Cardiol.*, 2004;**97**: 43–48.
285. Frank, S. and E. Braunwald, Idiopathic hypertrophic subaortic stenosis. Clinical analysis of 126 patients with emphasis on the natural history. *Circulation*, 1968;**37**: 759–788.
286. Koga, Y., A. Yamaga, K. Hiyamuta, H. Ikeda, and H. Toshima, Mechanisms of abnormal Q waves in hypertrophic cardiomyopathy assessed by intracoronary electrocardiography. *J. Cardiovasc. Electrophysiol.*, 2004;**15**: 1402–1408.
287. Runquist, L.H., C.D. Nielsen, D. Killip, P. Gazes, and W.H. Spencer III, Electrocardiographic findings after alcohol septal ablation therapy for obstructive hypertrophic cardiomyopathy. *Am. J. Cardiol.*, 2002;**90**: 1020–1022.
288. Babuty, D., L. Fauchier, D. Nguyen, et al., Arrhythmias of primary hypertrophic cardiomyopathy *Arch. Mal. Coeur. Vaiss.*, 2003;**96**: 7–15.
289. Behr, E.R., P. Elliott, and W.J. McKenna, Role of invasive EP testing in the evaluation and management of hypertrophic cardiomyopathy. *Card. Electrophysiol. Rev.*, 2002;**6**: 482–486.
290. Kawai, S., H. Suzuki, H. Yamaguchi, et al., Ampulla cardiomyopathy ("Takotsubo" cardiomyopathy)-reversible left ventricular dysfunction: With ST segment elevation. *Jpn. Circ. J.*, 2000;**64**: 156–159.
291. Wittstein, I.S., D.R. Thiemann, J.A. Lima, et al., Neurohumoral features of myocardial stunning due to sudden emotional stress. *N. Engl. J. Med.*, 2005;**352**: 539–548.
292. Pavin, D., H. Le Breton, and C. Daubert, Human stress cardiomyopathy mimicking acute myocardial syndrome. *Heart*, 1997;**78**: 509–511.
293. Jonkaitiene, R. and V. Mizariene, Arrhythmogenic dilated cardiomyopathy. *Medicina (Kaunas)*, 2003;**39**: 673–676.
294. Matsuura, Y., W. Chin, T. Kurihara, et al., Tachycardia-induced cardiomyopathy: A case report. *J. Cardiol.*, 1990;**20**: 509–518.
295. Marcus, F.I. and G. Fontaine, Arrhythmogenic right ventricular dysplasia/cardiomyopathy: A review. *Pacing Clin. Electrophysiol.*, 1995;**18**: 1298–1314.
296. Mirvis, D.M., *Electrocardiography. A physiological Approach*. St. Louis, MO: Mosby, 1993.
297. Katz, L.N. and H. Wachtel, The diphasic QRS type of electrocardiogram in congenital heart disease. *Am. Heart J.*, 1937;**13**: 202–206.
298. Loperfido, F., A. Digaetano, P. Santarelli, et al., The evaluation of left and right ventricular hypertrophy in combined ventricular overload by electrocardiography: Relationship with the echocardiographic data. *J. Electrocardiol.*, 1982;**15**: 327–334.
299. Cabrera, E. and J.R. Monroy, Systolic and diastolic loading of the heart. II. Electrocardiographic data. *Am. Heart J.*, 1952;**43**: 669–686.
300. Hamby, R.I. and F. Raia, Electrocardiographic aspects of primary myocardial disease in 60 patients. *Am. Heart J.*, 1968;**76**: 316–328.
301. Goldberger, A., A specific ECG triad associated with congestive heart failure. *Pacing Clin. Electrophysiol.*, 1982;**5**: 593–599.
302. Trobec, R., B. Gersak, and R. Hren, Body surface mapping after partial left ventriculotomy. *Heart Surg. Forum*, 2002;**5**: 187–192.
303. Marriott, H.J.L., Electrocardiographic abnormalities, conduction disorders and arrhythmias in primary myocardial disease. *Prog. Cardiovasc. Dis.*, 1964;**7**: 99–114.
304. Tavel, M.E. and C. Fisch, Abnormal Q waves simulating myocardial infarction in diffuse myocardial diseases. *Am. Heart J.*, 1964;**68**: 534–537.
305. Flowers, N.C. and L.G. Horan, Electrocardiographic and vectorcardiographic features of myocardial disease, in Myocardial Disease, N.O. Fowler, Editor. Grune and Stratton, New York, 1973, pp. 181–211.
306. Stapleton, J.F., J.P. Segal, and W.P. Harvey, The electrocardiogram of myocardiopathy. *Prog. Cardiovasc. Dis.*, 1970;**13**: 217–239.
307. Childers, R., S. Lupovich, M. Sochanski, and H. Konarzewska, Left bundle branch block and right axis deviation: A report of 36 cases. *J. Electrocardiol.*, 2000;**33** Suppl: 93–102.
308. Zimetbaum, P.J., A.E. Buxton, W. Batsford, et al., Electrocardiographic predictors of arrhythmic death and total mortality in the multicenter unsustained tachycardia trial. *Circulation*, 2004;**110**: 766–769.
309. Shamim, W., M. Yousufuddin, M. Cicoria, D.G. Gibson, A.J. Coats, and M.Y. Henein, Incremental changes in QRS duration in serial ECGs over time identify high risk elderly patients with heart failure. *Heart*, 2002;**88**: 47–51.
310. Molhoek, S.G., L. VAN Erven, M. Bootsma, P. Steendijk, E.E. Van Der Wall, and M.J. Schalij, QRS duration and shortening to predict clinical response to cardiac resynchronization therapy in patients with end-stage heart failure. *Pacing Clin. Electrophysiol.*, 2004;**27**: 308–313.
311. Francis, J., M.A. Watanabe, and G. Schmidt, Heart rate turbulence: A new predictor for risk of sudden cardiac death. *Ann. Noninvasive Electrocardiol.*, 2005;**10**: 102–109.
312. Hohnloser, S.H., T. Klingenheben, D. Bloomfield, O. Dabbous, and R.J. Cohen, Usefulness of microvolt T-wave alternans for prediction of ventricular tachyarrhythmic events in patients with dilated cardiomyopathy: Results from a prospective observational study. *J. Am. Coll. Cardiol.*, 2003;**41**: 2220–2224.
313. Saksena, S. and A.J. Camm, *Electrophysiological Disorders of the Heart*. Philadelphia, PA: Elsevier Churchill Livingstone, 2005.
314. Rahman, J.E., E.F. Helou, R. Gelzer-Bell, et al., Noninvasive diagnosis of biopsy-proven cardiac amyloidosis. *J. Am. Coll. Cardiol.*, 2004;**43**: 410–415.
315. Kinoshita, O., M. Hongo, M. Takeda, and M. Sekiguchi, Body surface potential maps in patients with familial amyloid polyneuropathy. *J. Electrocardiol.*, 1993;**26**: 301–309.
316. Linhart, A., J.C. Lubanda, T. Palecek, et al., Cardiac manifestations in Fabry disease. *J. Inherit. Metab. Dis.*, 2001;**24** Suppl 2: 75–83.
317. Baudouy, P., P. Lombrail, I. Azancot, A. Piekarski, E. Martin, and R. Slama, Adiastole caused by a secondary cardiac hemochromatosis. Successful treatment with an iron chelating agent. *Arch. Mal. Coeur. Vaiss.*, 1983;**76**: 1240–1246.
318. Moiseev, S.V., E.N. Semenkova, and N.P. Shatkovskii, Heart involvement in hypereosinophilia: The restrictive or the dilated type? *Ter. Arkh.*, 1989;**61**: 79–81.
319. Bonnet, D., P. Rustin, A. Rotig, et al., Metabolic and genetic investigations in childhood cardiomyopathies. *Arch. Mal. Coeur. Vaiss.*, 1999;**92**: 1509–1514.

320. Hoskova, L., I. Malek, R. Krausova, M. Podzimkova, and J. Pirk, Electrocardiographic changes after heart transplantation. *Vnitr. Lek.*, 2002;**48** Suppl 1: 72–75.
321. Kolasa, M.W., J.C. Lee, J.E. Atwood, R.R. Marcus, and R.E. Eckart, Relation of QTc duration heterogeneity to morality following orthotopic heart transplantation. *Am. J. Cardiol.*, 2005;**95**: 431–432.
322. Stinson, E.B., E. Dong Jr, C.P. Hieber, J.S. Schroeder, and N.E. Shumway, Cardiac transplantation in man. I. Early rejection. *J. Am. Med. Assoc.*, 1969;**207**: 2233–2242.
323. Carzolari, V., A. Angelini, C. Basso, et al., Histologic findings in the conduction system after cardiac transplantation and correlation with electrocardiographic findings. *Am. J. Cardiol.*, 1999;**4**: 756–759.
324. Cooper, D.K., R.G. Charles, A.G. Rose, et al., Does the electrocardiogram detect early acute heart rejection. *Heart Transplant.*, 1985;**4**: 546–549.
325. Jamieson, S.W., B.A. Reitz, P.E. Oyer, C.P. Bieber, E.B. Stinson, and N.E. Shumway, Current management of cardiac transplant recipients. *Br. Heart J.*, 1979;**42**: 703–708.
326. Izrailtyan, I., J.Y. Kresh, R.J. Morris, et al., Early detection of acute allograft rejection by linear and nonlinear analysis of heart rate variability. *J. Thorac. Cadiovasc. Surg.*, 2000;**20**: 737–745.
327. Ali, A., M.R. Mehra, F.S. Malik, et al., Insights into ventricular repolarization abnormalities in cardiac allograft vasculopathy. *Am. J. Cardiol.*, 2001;**87**: 367–368.
328. Gao, S.Z., S.A. Hunt, V. Wiederhold, et al., Characteristics of serial electrocardiograms in heart transplant recipients. *Am. Heart J.*, 1991;**122**: 771–774.
329. Sandhu, J.S., E.I. Curtiss, W.P. Follansbee, et al., The scalar electrocardiogram of the orthotopic heart transplant recipient. *Am. Heart J.*, 1990;**119**: 917–923.
330. Eckart, R.E., M.W. Kolasa, N.A. Khan, M.D. Kwan, and M.E. Peele, Surface electrocardiography and histologic rejection following orthotopic heart transplantation. *Ann. Noninvas. Electrocardiol.*, 2005;**10**: 60–64.
331. Haberl, R., M. Weber, H. Reichenspurner, et al., Frequency analysis of the surface electrocardiogram for recognition of acute rejection after orthotopic cardiac transplantation in man. *Circulation*, 1987;**76**: 101–108.
332. Bernadic, M. and I. Sulkova, Classical electrocardiography and the Wigner distribution in the detection of rejection of heart transplants. *Bratisl. Lek. Listy.*, 2000;**101**: 223–225.
333. Zupan, I., B. Vrtovec, U.D. Breskvar, and T. Gabrijelcic, Noninvasive monitoring of rejection therapy based on intramyocardial electrograms after orthotopic heart transplantation. Initial experience with 14 cases. *Int. Immunopharmacol.*, 2005;**5**: 59–65.
334. Madias, C., B.J. Maron, J. Weinstock, N.A. Estes III, and M.S. Link, Commotio cordis-sudden cardiac death with chest wall impact. *J. Cardiovasc. Electrophysiol.*, 2007;**18**: 115–122.
335. Bianco, M., F. Colella, A. Pannozzo, et al., Boxing and "commotio cordis": ECG and humoral study. *Int. J. Sports Med.*, 2005;**26**: 151–157.
336. Franzius, C., H. Meyer-Hofmann, and A.E. Lison, Myocardial infarct and rhabdomyolysis after a high-voltage accident with successful resuscitation. *Dtsch. Med. Wochenschr.*, 1997;**122**: 400–406.
337. Lichtenberg, R., D. Dries, K. Ward, W. Marshall, and P. Scanlon, Cardiovascular effects of lightning strikes. *J. Am. Coll. Cardiol.*, 1993;**21**: 531–536.
338. Dec, W.G. Jr., T.A. Stern, and C. Welch, The effects of electroconvulsive therapy on serial electrocardiograms and serum cardiac enzyme values. *J. Am. Med. Assoc.*, 1985;**253**: 2525–2529.
339. Boriani, G., C. Valzania, M. Biffi, et al., Increase in QT/QTc dispersion after low energy cardioversion of chronic persistent atrial fibrillation. *Int. J. Cardiol.*, 2004;**95**: 245–250.
340. Chun, P.K., J.E. Davia, and D.J. Donohue, ST-segment elevation with elective DC cardioversion. *Circulation*, 1981;**63**: 220–224.
341. Eysmann, S.B., F.E. Marchlinski, A.E. Buxton, and M.E. Josephson, Electrocardiographic changes after cardioversion of ventricular arrhythmias. *Circulation*, 1986;**73**: 73–81.
342. Liaudet, L., R. Kehtari, and J.F. Enrico, Myocardial lesion secondary to defibrillation. Literature review and practical implications *Rev. Med. Suisse. Romande.*, 1993;**113**: 933–943.
343. Joglar, J.A., D.J. Kessler, P.J. Welch, et al., Effects of repeated electrical defibrillations on cardiac troponin I levels. *Am. J. Cardiol.*, 1999;**83**: 270–272.
344. Avitall, B., S. Port, R. Gal, et al., Automatic implantable cardioverter/defibrillator discharges and acute myocardial injury. *Circulation*, 1990;**81**: 1482–1487.
345. Spodick, D.H., Electrocardiogram in acute pericarditis. Distributions of morphologic and axial changes by stages. *Am. J. Cardiol.*, 1974;**33**: 470–474.
346. Shahar, A., H. Hod, G.M. Barabash, E. Kaplinsky, and M. Motro, Disappearance of a syndrome: Dressler's syndrome in the era of thrombolysis. *Cardiology*, 1994;**85**: 255–258.
347. Sapin, P.M., G. Koch, M.B. Blauwet, J.J. McCarthy, S.W. Hinds, and L.S. Gettes, Identification of false positive exercise tests with use of electrocardiographic criteria: A possible role for atrial repolarization waves. *J. Am. Coll. Cardiol.*, 1991;**18**: 127–135.
348. Kudo, Y., F. Yamasaki, Y. Doi, and T. Sugiura, Clinical correlates of PR-segment depression in asymptomatic patients with pericardial effusion. *J. Am. Coll. Cardiol.*, 2002;**39**: 2000–2004.
349. Hull, E., The electrocardiogram in pericarditis. *Am. J. Cardiol.*, 1961;**7**: 21–32.
350. Ginzton, L.E. and M.M. Laks, The differential diagnosis of acute pericarditis from the normal variant: New electrocardiographic criteria. *Circulation*, 1982;**65**: 1004–1009.
351. Spodick, D.H., "Low voltage ECG" and pericardial effusion; practical and conceptual problems. *Chest*, 1979;**75**: 113–114.
352. Spodick, D.H., Low voltage with pericardial effusion: Complexity of mechanisms. *Chest*, 2003;**124**: 2044–2045.
353. Surawicz, B. and C. Fisch, Cardiac alternans: Diverse mechanisms and clinical manifestations. *J. Am. Coll. Cardiol.*, 1992;**20**: 483–499.
354. Bruch, C., A. Schmermund, N. Dagres, et al., Changes in QRS voltage in cardiac tamponade and pericardial effusion: Reversibility after pericardiocentesis and after anti-inflammatory drug treatment. *J. Am. Coll. Cardiol.*, 2001;**38**: 219–226.
355. Dalton, J.C., R.J. Pearson, and P.D. White, Constrictive pericarditis: A review and long term follow-up of 78 cases. *Ann. Intern. Med.*, 1956;**45**: 445–458.
356. Evans, W. and F. Jackson, Constrictive pericarditis. *Br. Heart J.*, 1952;**14**: 53–59.
357. Abe, S., N. Watanabe, S. Ogura, et al., Myocardial metastasis from primary lung cancer: Myocardial infarction-like ECG changes and pathologic findings. *Jpn. J. Med.*, 1991;**30**: 213–218.
358. Tremel, F., O. Orliaguet, J.E. Lanney, O. Guenot, and E. Arnaud Crozat, Metastasis stimulating a myocardial infarction. *Arch. Mal. Coeur. Vaiss.*, 2003;**96**: 59–61.

359. Hammerschmidt, S., C. Pohlink, H. Wirtz, and T. Rother, Alternating electric heart axis in a patient with small cell lung cancer. *Dtsch. Med. Wochenschr.*, 2004;**129**: 19–22.
360. Shiono, J., H. Horigome, S. Yasui, T. Miyamoto, et al., Electrocardiographic changes in patients with cardiac rhabdomyomas associated with tuberous sclerosis. *Cardiol. Young*, 2003;**13**: 258–263.
361. Komiya, N., S. Isomoto, M. Hayano, T. Kugimiya, and K. Yano, The influence of tumor size on the electrocardiographic changes in patients with left atrial myxoma. *J. Electrocardiol.*, 2002;**35**: 53–57.
362. Rozanski, J.J. and M. Kleinfeld, Alternans of the ST segment of T wave. A sign of electrical instability in Prinzmetal's angina. *Pacing Clin. Electrophysiol.*, 1982;**5**: 359–365.
363. Puletti, M., C. Borgia, S.M. Erba, G. Jacobellis, and M. Curione, ST segment alternams in myocardial infarct: Apropos of a case. *G Ital. Cardiol.*, 1983;**13**: 208–211.
364. Rozanski, J.J. and M. Kleinfeld, Occurrence of ST segmental electrical alternans during exercise test. *Pacing Clin. Electrophysiol.*, 1981;**4**: 339–340.
365. Sochanski, M., T. Feldman, K.G. Chua, A. Benn, and R. Childers, ST segment alternans during coronary angioplasty. *Cathet. Cardiovasc. Diagn.*, 1992;**27**: 45–48.
366. Usher, B.W. and R.L. Popp, Electrical alternans: Mechanism in pericardial effusion. *Am. Heart J.*, 1972;**83**: 459–463.
367. Hamburger, W.W., L.N. Katz, and O. Saphir, Electrical alternans: A clinical study with a report of two necropsies. *J. Am. Med. Assoc.*, 1936;**106**: 902–905.
368. Gehi, A.K., R.H. Stein, L.D. Metz, and J.A. Gomes, Microvolt T-wave alternans for the risk stratification of ventricular tachyarrhythmic events: A meta-analysis. *J. Am. Coll. Cardiol.*, 2005;**46**: 75–82.
369. Bloomfield, D.M., R.C. Steinman, P.B. Namerow, et al., Microvolt T-wave alternans distinguishes between patients likely and patients not likely to benefit from implanted cardiac defibrillator therapy: A solution to the Multicenter Automatic Defibrillator Implantation Trial (MADIT) II conundrum. *Circulation*, 2004;**110**: 1885–1889.
370. Burgess, M.J., L.S. Green, K. Millar, and J.A. Abildskov, The sequence of normal ventricular recovery. *Am. Heart J.*, 1972;**84**: 660–669.
371. Autenreith, G., B. Surawicz, and C.S. Kuo, Sequence of repolarization on the ventricular surface in the dog. *Am. Heart J.*, 1975;**89**: 463–469.
372. Abildskov, J.A., Effects of activation sequence on the local recovery of ventricular excitability in the dog. *Circ. Res.*, 1976;**38**: 240–243.
373. Toyoshima, H. and M.J. Burgess, Electrotonic interaction during canine ventricular repolarization. *Circ. Res.*, 1978;**43**: 348–356.
374. Rosenbaum, M.B., H.H. Blanco, M.V. Elizari, J.O. Lizzari, and J.M. Davidenko, Electrotonic modulation of the T wave and cardiac inemory. *Am. J. Cardiol.*, 1982;**50**: 213–222.
375. Rosenbaum, M.B., H.H. Blanco, M.V. Elizari, J.O. Lizzari, and H.M. Vetulli, Electrotonic modulation of ventricular repolarization and cardiac memory, in Frontiers of Cardiac Electrophysiology, M.B. Rosenbaum and M.V. Elizari, Editors. Nijhoff, Boston, MA, 1983, pp. 67–99.
376. Hoffman, B.F., Electrotonic modulation of the T wave. *Am. J. Cardiol.*, 1982;**50**: 361–362.
377. Surawicz, B., Transient T wave abnormalities in intermittent bundle branch block. *Am. J. Cardiol.*, 1982;**50**: 363–364.
378. Rosen, M.R., What is cardiac memory? *J. Cardiovasc. Electrophysiol.*, 2000;**11**: 1289–1293.
379. Surawicz, B., What is cardiac memory? *J. Cardiovasc. Electrophysiol.*, 2001;**12**: 390–391.
380. Chung, E.K., *Principles of Cardiac Arrhythmias*, 3rd edn. Philadelphia,PA: Williams & Wilkins, 1983, pp. 348–349.
381. Ranganathan, N., V. Sivaciyan, and R.C. Chisholm, Effects of post-extrasystolic potentiation on systolic time intervals. *Am. J. Cardiol.*, 1978;**42**: 14–22.
382. Shvilkin, A., K.K.L. Ho, M.R. Rosen, and M.E. Josephson, T-vector direction differentiates postpacing from ischemic T-wave inversion in precordial leads. *Circulation*, 2005;**111**: 969–974.
383. Colleran, J.A., V. Papademetriou, P. Narayan, et al., Electrocardiographic abnormalities suggestive of myocardial ischemia during upper gastrointestinal bleeding. *Am. J. Cardiol.*, 1995;**75**: 312–314.
384. Khairy, P. and P. Marsolais, Pancreatitis with electrocardiographic changes mimicking acute myocardial infarction. *Can. J. Gastroenterol.*, 2001;**15**: 522–526.
385. Wani, M. and S. Hishon, ECG record during changes in oesophageal pH. *Gut*, 1990;**31**: 127–128.
386. Christensen, M., H.W. Hendel, V. Rasmussen, et al., Endoscopic retrograde cholangiopancreatography causes reduced myocardial blood flow. *Endoscopy*, 2002;**34**: 797–800.
387. Rosenberg, J., K. Stausholm, I.B. Andersen, et al., No effect of oxygen therapy on myocardial ischaemia during gastroscopy. *Scand. J. Gastroenterol.*, 1996;**31**: 200–205.
388. Patterson, K.W., N. Noonan, N.W. Keeling, et al., Hypoxemia during outpatient gastrointestinal endoscopy: The effects of sedation and supplemental oxygen. *J. Clin. Anesth.*, 1995;**7**: 136–140.
389. Holm, C., M. Christensen, V. Rasmussen, et al., Hypoxaemia and myocardial ischaemia during colonoscopy. *Scand. J. Gastroenterol.*, 1998;**33**: 769–772.
390. Jones, R. and S. Lydeard, Irritable bowel syndrome in the general population. *BMJ*, 1992;**304**: 87–90.
391. Frais, M.A. and K. Rodgers, Dramatic electrocardiographic T-wave changes associated with gastric dilatation. *Chest*, 1990;**98**: 489–490.
392. Ishikawa, K., T. Nagasawa, and H. Shimadu, Influence of hemodialysis on electrocardiographic wave forms. *Am. Heart J.*, 1979;**97**: 5–11.
393. Madias, J.E. and V. Narayan, Augmentation of the amplitude of electrocardiographic QRS complexes immediately after hemodialysis: A study of 26 hemodialysis sessions of a single patient, aided by measurements of resistance, reactance, and impedance. *J. Electrocardiol.*, 2003;**36**: 263–271.
394. Madias, J.E., P waves in patients with changing edematous states: Implications on interpreting repeat P wave measurements in patients developing anasarca or undergoing hemodialysis. *Pacing Clin. Electrophysiol.*, 2004;**27**: 749–756.
395. Urso, S., M. Garozzo, F. Milone, and G. Battaglia, Cardiovascular risk markers in hemodialysis patients. *Int. J. Artif. Organs*, 2004;**27**: 1083–1090.
396. Morales, M.A., C. Gremigni, P. Dattolo, et al., Signal-averaged ECG abnormalities in haemodialysis patients. Role of dialysis. *Nephrol. Dial. Transplant.*, 1998;**13**: 668–673.
397. Fukuta, H., J. Hayano, S. Ishihara, et al., Prognostic value of heart rate variability in patients with end-stage renal disease on chronic haemodialysis. *Nephrol. Dial. Transplant.*, 2003;**18**: 318–325.

398. Tezcan, U.K., B. Amasyali, I. Can, et al., Increased P wave dispersion and maximum P wave duration after hemodialysis. *Ann. Noninvasive Electrocardiol.*, 2004;**9**: 34–38.
399. Suzuki, R., K. Tsumura, T. Inoue, H. Kishimoto, and H. Morii, QT interval prolongation in the patients receiving maintenance hemodialysis. *Clin. Nephrol.*, 1998;**49**: 240–244.
400. Madias, J.E., Increases in P-wave duration and dispersion after hemodialysis are totally (or partially) due to the procedure-induced alleviation of the body fluid overload: A hypothesis with strong experimental support. *Ann. Noninvasive Electrocardiol.*, 2005;**10**: 129–133.
401. Birkhofer, A., G. Schmidt, and H. Forstl, Heart and brain – the influence of psychiatric disorders and their therapy on the heart rate variability. *Fortschr. Neurol. Psychiatr.*, 2005;**73**: 192–205.
402. Mont, L., J. Castro, B. Herreros, et al., Reversibility of cardiac abnormalities in adolescents with anorexia nervosa after weight recovery. *J. Am. Acad. Child Adolesc. Psychiat.*, 2003;**42**: 808–813.
403. Vanderdonckt, O., M. Lambert, M.C. Montero, B. Boland, and C. Brohet, The 12-lead electrocardiogram in anorexia nervosa: A report of 2 cases followed by a retrospective study. *J. Electrocardiol.*, 2001;**34**: 233–242.
404. Reilly, J.G., S.A. Ayis, I.N. Ferrier, S.J. Jones, and S.H. Thomas, QTc-interval abnormalities and psychotropic drug therapy in psychiatric patients. *Lancet*, 2000;**355**: 1048–1052.
405. Hollister, L.E., Electrocardiographic screening in psychiatric patients. *J. Clin. Psychiat.*, 1995;**56**: 26–29.
406. Goldberger, A.L., *Myocardial Infarction. Electrocardiographic Differential Diagnosis*, 4th edn. St. Louis, MO: Mosby Year Book, 1991.
407. Goldman, M.J., Normal variants in the electrocardiogram leading to cardiac invalidism. *Am. Heart J.*, 1960;**59**: 71–77.
408. Brady, W.J. and D. Roberts, and F. Morris, The nondiagnostic ECG in the chest pain patient: Normal and nonspecific initial ECG presentations of acute MI. *Am. J. Emerg. Med.*, 1999;**17**: 394–397.
409. Quyyumi, A.A., Current concepts of pathophysiology, circadian patterns, and vasoreactive factors associated with myocardial ischemia detected by ambulatory electrocardiography. *Cardiol. Clin.*, 1992;**10**: 403–415.
410. Bertolet, B.D., A.F. Boyette, C.A. Hofmann, et al., Prevalence of pseudoischemic ST-segment changes during ambulatory electrocardiographic monitoring. *Am. J. Cardiol.*, 1992;**70**: 818–820.
411. Madias, J.E., The earliest electrocardiographic sign of acute transmural myocardial infarction. *J. Electrocardiol.*, 1977;**10**: 193–196.
412. Prinzmetal, M., A. Ekmekci, R. Kennamer, J.K. Kwoczynski, H. Shubin, and H. Toyoshima, Variant form of angina pectoris, previously undelineated syndrome. *J. Am. Med. Assoc.*, 1960;**174**: 1794–1800.
413. Madias, J.E. and M. Attari, Exercise-triggered transient R-wave enhancement and ST-segment elevation in II, III, and aVF ECG leads: A testament to the "plasticity" of the QRS complex during ischemia. *J. Electrocardiol.*, 2004;**37**: 121–126.
414. Madias, J.E., Ventricular tachycardia-like complexes in acute myocardial infarction. *Chest*, 1985;**88**: 644.
415. Barnhill, J.E., J.P. Wikswo Jr, A.K. Dawson, et al., The QRS complex during transient myocardial ischemia: Studies in patients with variant angina pectoris and in a canine preparation. *Circulation*, 1985;**71**: 901–911.
416. Jacobson, D. and V. Schrire, Giant T wave inversion. *Br. Heart J.*, 1966;**28**:768–775, 417.
417. Wyss, S., M. Holzmann, F. Schaub, G. Forster, and E. Hohnloser, Abnorme Repolarisationsbilder nach Adams-Stokes'schen Anfällen. *Cardiologia*, 1962;**40**: 169–190.
418. Yamour, B.J., M.R. Sridharan, J.F. Rice, and N.C. Flowers, Electrocardiographic changes in cerebrovascular hemorrhage. *Am. Heart J.*, 1980;**99**: 294–300.
419. Surawicz, B. and E. Lepeschkin, The electrocardiographic pattern of hypopotassemia with and without hypocalcemia. *Circulation*, 1953;**8**: 801–823.
420. Vincent, G.M., J.A. Abildskov, and M.J. Burgess, QT interval syndromes. *Prog. Cardiovasc. Dis.*, 1974;**16**: 523–530.
421. Fowler, N.O., D. McCall, T.-C. Chou, J.C. Holmes, and I.B. Nanenson, Electrocardiographic changes and cardiac arrhythmias in patients receiving psychotropic drugs. *Am. J. Cardiol.*, 1976;**37**: 223–230.
422. Pruitt, R.D., E.W. Dennis, and S.A. Kinard, The difficult electrocardiographic diagnosis of myocardial infarction. *Prog. Cardiovasc. Dis.*, 1963;**6**: 85–106.
423. Cook, R.W., J.E. Edwards, and R.D. Pruitt, Electrocardiographic changes in acute subendocardial infarction, I and II. *Circulation*, 1958;**18**: 603–622.
424. Ogawa, H., K. Hiramori, K. Haze, et al., Classification of non-Q-wave myocardial infarction according to electrocardiographic changes. *Br. Heart J.*, 1985;;**4**: 473–478.
425. Miwa, K., H. Kambara, C. Kawai, and T. Murakami, Two electrocardiographic patterns with or without transient T-wave inversion during recovery periods of variant anginal attacks. *Jpn. Circ. J.*, 1983;**47**: 1415–1422.
426. Taylor, G.J., R.S. Crampton, R.S. Gibson, P.T. Stebbins, M.T.G. Waldman, and G.A. Beller, Prolonged QT interval at onset of acute myocardial infarction in predicting early phase ventricular tachycardia. *Am. Heart J.*, 1981;**102**: 16–24.
427. Ahnve, S., E. Gilpin, E.B. Madsen, V. Froelicher, H. Henning, and J. Ross Jr., Prognostic importance of QTc interval at discharge after acute myocardial infarction: A multicenter study of 865 patients. *Am. Heart J.*, 1984;**108**: 395–400,
428. Wheelan, K., J. Mukharji, R.E. Rude, et al., Sudden death and its relation to QT interval prolongation after acute myocardial infarction: Two-year follow-up. *Am. J. Cardiol.*, 1986;**57**: 745–750.
429. Sakamoto, T., C. Tei, M. Murayama, et al., Giant T wave inversion as a manifestation of asymmetrical apical hypertrophy (AAH) of the left ventricle. Echocardiographic and ultrasono-cardiotomographic study. *Jpn. Hearl J.*, 1976;**17**: 611–629.
430. Yamaguchi, H., T. Ishimura, S. Nishiyama, et al., Hypertrophic nonobstructive cardiomyopathy with giant negative T waves (apical hypertrophy). Ventriculographic and echocardiographic features in 30 patients. *Am. J. Cardiol.*, 1979;**44**: 401–412.
431. Kereiakes, D., D.J. Anderson, L. Crouse, and K. Chatterjee, Apical hypertrophic cardiomyopathy. *Am. Heart J.*, 1983;**105**: 855–856.
432. Ino, T., M. Iwahara, K. Nishimoto, et al., Infantile hypertrophic cardiomyopathy with QT prolongation. *Jpn. Heart J.*, 1986;**27**: 893–899.
433. Abildskov, J.A., K. Millar, M.J. Burgess, and W. Vincent, The electrocardiogram and the central nervous system. *Prog. Cardiovasc. Dis.*, 1970;**13**: 210–216.

434. Hammer, W.J., A.J. Luessenhop, and A.M. Weintraub, Observations on the electrocardiographic changes associated with subarachnoidal hemorrhage with special reference to their genesis. *Am. J. Med.*, 1975;**59**: 427–433.
435. Levine, H.D., Non-specificity of the electrocardiogram associated with coronary artery disease. *Am. J. Med.*, 1953;**15**: 344–355.
436. Hurch, G.E., R. Meyers, and J.A. Abildskov, A new electrocardiographic pattern observed in cerebrovascular accidents. *Circulation*, 1954;**9**: 719–723.
437. Cropp, G.J. and G.W. Manning, Electrocardiographic changes simulating myocardial ischemia and infarction associated with spontaneous intracranial hemorrhage. *Circulation*, 1960;**22**: 25–38.
438. Hersch, C., Electrocardiographic changes in subarachnoidal haemorrhage, meningitis, and intracranial space occupying lesions. *Br. Heart J.*, 1965;**26**: 785–793.
439. Miura, T., K. Tsuchihashi, E. Yoshida, K. Kobayashi, K. Shimamoto, and O. Iimura, Electrocardiographic abnormalities in cerebrovascular accidents. *Jpn. J. Med.*, 1984;**23**: 22–26.
440. Jachuck, S.J., P.S. Ramani, F. Clark, and R.M. Kalbag, Electrocardiographic abnormalities associated with raised intracranial pressure. *Br. Med. J.*, 1975;**1**: 242–244.
441. Goldstein, D.S., The electrocardiogram in stroke: Relationship to pathophysiological type and comparison with prior tracings. *Stroke*, 1979;**10**: 253–259.
442. Hayashi, S., J. Watanabe, S. Miyagawa, S. Tamakuma, and H. Nagaki, Studies of electrocardiographic patterns in cases with neurosurgical lesions. *Jpn. Heart J.*, 1961;**2**: 92–111.
443. Hrunninkhuis, L.G.H., Electrocardiographic abnormalities suggesting myocardial infarction in a patient with severe cranial trauma. *Pacing Clin. Electrophysiol.*, 1983;**6**: 1336–1340.
444. Tamura, K., T. Tamura, S. Yoshida, M. Inui, and N. Fukuhara, Transient recurrent ventricular fibrillation due to hypopotassemia with special note on the U wave. *Jpn. Heart J.*, 1967;**8**: 652–660.
445. Lepeschkin, E., H. Marchet, G. Schroeder, et al., Effect of epinephrine and norepinephrine on the electrocardiogram of 100 normal subjects.*Am. J. Cardiol.*, 1960;**5**: 594–603.
446. Mashima, S., Effects of insulin on the electrocardiogram. *Jpn. Heart J.*, 1960;**1**: 56–71.
447. Struthers, A.D., J.L. Reid, R. Whitesmith, and J.C. Rodger, Effect of intravenous adrenaline on electrocardiogram, blood pressure, and serum potassium. *Br. Heart J.*, 1983;**49**: 90–93.
448. Prinzmetal, M., Y. Hashimoto, A. Hayashi, et al., Effects of propranolol and epinephrine on the electrophysiology of the heart. *Jpn. Heart J.*, 1970;**11**: 478–488.
449. Giotti, A., F. Ledda, and P.F. Mannaioni, Effects of noradrenaline and isoprenaline, in combination with IX and p receptor blocking substances, on the action potential of cardiac Purkinje fibres. *J. Physiol. (Lond.)*, 1973;**229**: 99–113.
450. Nathan, D. and G.W. Heeler Jr., Electrophysiologic correlates of the inotropic effects of isoproterenol in canine myocardium. *J. Mol. Cell. Cardiol.*, 1975;**7**: 1–15.
451. Ueda, H., Y. Yanai, S. Murao, et al., Electrocardiographic and vectorcardiographic changes produced by electrical stimulation of the cardiac nerves. *Jpn. Heart J.*, 1964;**5**: 359–372.
452. Yanowitz, F., J.H. Preston, and J.A. Abildskov, Functional distribution of right and left stellate innervation to the ventricles. Production of neurogenic electrocardiographic changes by unilateral alteration of sympathetic tone. *Circ. Res.*, 1966;**18**: 416–428.
453. Murayama, M., K. Harumi, S. Mashima, K. Shimomura, and S. Murao, Prolongation of ventricular action potential due to sympathetic stimulation. *Jpn. Heart J.*, 1977;**18**: 259–265.
454. Autenrieth, G., H. Surawicz, C.S. Kuo, and M. Arita, Primary T wave abnormalities caused by uniform and regional shortening of ventricular monophasic action potential in dog. *Circulation*, 1975;**51**: 668–676.
455. Randall, W.C., M. Szentivanyi, J.H. Pace, J.S. Wechsler, and M.P. Kaye, Patterns of sympathetic nerve projections onto the canine heart. *Circ. Res.*, 1968;**22**: 315–323.
456. Piscatelli, R.L. and L.M. Fox, Myocardial injury from epinephrine overdosage. *Am. J. Cardiol.*, 1968;**21**: 735–737.
457. Wexler, H., J. Kuaity, and E. Simonson, Electrocardiographic effects of isoprenaline in normal subjects and patients with coronary atherosclerosis. *Br. Heart J.*, 1971;**33**: 759–764.
458. Murayama, M., S. Mashima, K. Shimomura, K. Takayanagi, Y.Z. Tseng, and S. Murao, An experimental model of giant negative T wave associated with QT prolongation produced by combined effect of calcium and isoproterenol. *Jpn. Heart J.*, 1981;**22**: 257–265.
459. Sayer, W.J., M. Moser, and T.W. Mattingly, Pheochromocytoma and the abnormal electrocardiogram. *Am. Heart J.*, 1954;**48**: 42–53.
460. Cheng, T.O. and T.T. Bashour, Striking electrocardiographic changes associated with pheochromocytoma. *Chest*, 1976;**70**: 397–399.
461. Van Vliet, P.D., H.B. Hurchell, and J.L. Titus, Focal myocarditis associated with pheochromocytoma. *N. Engl. J. Med.*, 1966;**274**: 102–108.
462. Rona, G., Catecholamine cardiotoxicity. *J. Mol. Cell Cardiol.*, 1985;**17**: 291–306.
463. Dessertenne, F., La tachycardie ventriculaire a deux foyers opposes variables. *Arch. Mal. Coeur. Vaiss.*, 1966;**59**: 263–272.
464. Soffer, J., L.S. Dreifus, and E.L. Michelson, Polymorphous ventricular tachycardia associated with normal and long QT intervals. *Am. J. Cardiol.*, 1982;**49**: 2021–2029.
465. Kernohan, R.J., Post-paroxysmal tachycardia syndrome. *Br. Heart J.*, 1969;**31**: 803–806.
466. Myerson, R.M. and A.H. Clagett Jr., Transient inversion of T waves after paroxysmal tachycardia. *J. Am. Med. Assoc.*, 1952;**148**: 193–196.
467. Tsutsumi, T., K. Izumo, S. Sekiya, and K. Harumi, Post-pacing T loop abnormalities. *Jpn. Heart J.*, 1985;**26**: 897–908.
468. Richter von Arnauld, H.P., H. Kirsch, C. Gauwerky, and K.W. Westermann, Schrittmacherarrhythmie durch ungewohnliche T-Welleninhibierung bei einem externen Demand-Schrittmacher. *Z. Kreilaufforsch.*, 1974;**63**: 637–642.
469. Denes, P., A. Pick, R.H. Miller, R.J. Pietras, and K.M. Rosen, A characteristic precordial repolarization abnormality with intermittent left bundle-branch block. *Ann. Intern. Med.*, 1978;**89**: 55–57.
470. Wood, M.A., J.P. DiMarco, and D.E. Haines, Electrocardiographic abnormalities after radiofrequency catheter ablation of accessory bypass tracts in the Wolff-Parkinson-White syndrome. *Am. J. Cardiol.*, 1992;**70**: 200–204.
471. Surawicz, B., Transient T wave abnormalities after cessation of ventricular preexcitation: Memory of what? *J. Cardiovasc. Electrophysiol.*, 1996;**7**: 51–59.

472. MacAlpin, R.N., W.A. Weidner, A.A. Kattus Jr., and W.N. Hanafee, Electrocardiographic changes during selective coronary cineangiography. *Circulation*, 1966;**34**: 627–637.
473. Klein, H.O., H. Gross, and I.L. Rubin, Transient electrocardiographic changes simulating myocardial infarction during open-heart surgery. *Am. Heart J.*, 1970;**79**: 463–470.
474. Martin, G.R. and P. Stanger, Transient prolongation of the QTc interval after balloon valvuloplasty and angioplasty in children. *Am. J. Cardiol.*, 1986;**58**: 1233–1235.
475. Hultgren, H.N., M. Miyagawa, W. Buch, and W.W. Angell, Ischemic myocardial injury during cardiopulmonary bypass surgery. *Am. Heart J.*, 1973;**85**: 167–176.
476. Benchimol, A., K.B. Desser, and J.A. Schumacher, Electrocardiographic changes during selective aortocoronary saphenous vein bypass graft angiography in man. *Am. J. Cardiol.*, 1973;**31**: 23–29.
477. Toshima, H., Y. Ohkita, and M. Shingu, Clinical features of acute coxsackie B viral myocarditis. *Jpn. Circ. J.*, 1979;**43**: 441–444.
478. Brody, D.A., A theoretical analysis of intracavitary blood mass influence on the heart-lead relationship. *Circ. Res.*, 1956;**4**: 731–738.
479. Feldman, T., K.M. Borow, A. Neumann, R.M. Lang, and R.W. Childers, Relation of electrocardiographic R-wave amplitude to changes in left ventricular chamber size and position in normal subjects. *Am. J. Cardiol.*, 1985;**55**: 1168–1174.
480. Wilson, F.N., F.D. Johnston, F. Rosenbaum, et al., The precordial electrocardiogram. *Am. Heart J.*, 1944;**27**: 19–85.
481. Holzmann, M., *Clinical Electrocardiography. A Textbook for Practitioners and Students*. Translated by Douglas Robertson, London: Staples Press, 1952.
482. Sodi-Pallares and R.M. Calder, *New Bases of Electrocardiography*. St. Louis, MO: The CV Mosby, 1956.
483. Mason, R.E. and I. Likar, A new system of multiplelead exercise electrocardiography. *Am. Heart J.*, 1966;**71**: 196–205.
484. Madias, J.E., Comparability of the standing and supine standard electrocardiograms, and standing, sitting, and supine stress electrocardiograms. *J. Electrocardiol.*, 2006;**39**(2): 142–149.
485. Jones, A.Y., C. Kam, K.W. Lai, et al., Changes in heart rate and R-wave amplitude with posture. *Chin. J. Physiol.*, 2003;**46**: 63–69.
486. Yeragani, V.K., R. Pohl, V.C. Jampala, R. Balon, J. Kay, and G. Igel, Effect of posture and isoproterenol on beat-to-beat heart rate and QT variability. *Neuropsychobiology*, 2000;**41**: 113–123.
487. Pharand, C., J.B. Nasmith, J.C. Rajaonah, B. Dube, and A.R. LeBlanc, Distinction between myocardial ischemia and postural changes in continuous ECG monitoring based on ST-segment amplitude and vector orientation-preliminary results. *Can. J. Cardiol.*, 2003;**19**: 1023–1029.
488. Dieuaide, F.R.,The ECG as an aid in the diagnosis of adhesive pericardial mediastinitis. *Arch. Int. Med.*, 1925;**35**: 362–370.
489. Ruttkay-Nedecky, I., Effects of respiration and heart position on the cardiac electric field, in The Theoretical Basis of Electrocardiology, C.V. Nelson and D.B. Geselowitz, Editors. Clarendon Press, Oxford, 1976, p. 120.
490. Madias, J.E., The Impact of changing edematous states on the QRS duration: Implications for cardiac resynchronization therapy and implantable cardioverter/defibrillator implantation *Europace*, 2005;**7**: 158–164.
491. Ishikawa, K., A.S. Berson, and H.W. Pipberger, Electrocardiographic changes due to cardiac enlargement. *Am. Heart J.*, 1971;**81**: 635–643.
492. Madias, J.E., Standard electrocardiographic and signal-averaged electrocardiographic changes in congestive heart failure. *Congest. Heart Fail.*, 2005;**11**: 266–271.
493. Fuenmayor, A.J., C.J. Vasquez, A.M. Fuenmayor, et al., Hemodialysis changes the QRS amplitude in the electrocardiogram. *Int. J. Cardiol.*, 1993;**41**: 141–145.
494. Madias, J.E. and V. Narayan, Augmentation of the amplitude of electrocardiographic QRS complexes immediately following hemodialysis: A study of 26 hemodialysis sessions of a single patient, aided by measurements of resistance/reactance/impedance. *J. Electrocardiol.*, 2003;**36**: 263–271.
495. Madias, J.E., Concealment of electrocardiographically based diagnosis of left ventricular hypertrophy by anasarca. *Am. J. Hypertens.*, 2004;**17**: 897–903.
496. Madias, J.E., Masking of the diagnoses of P-pulmonale, P-mitrale, and biatrial abnormality by anasarca peripheral edema. *Congest. Heart Fail.*, 2006;**12**(1): 20–24.
497. Madias, J.E., Significance of shortening of the mean QRS duration of the standard electrocardiogram in patients developing peripheral edema. *Am. J. Cardiol.*, 2002;**89**: 1444–1446.
498. Madias, J.E., QTc Interval in patients with changing edematous states: Implications on interpreting repeat QTc interval measurements in patients with anasarca of varying etiology, and those undergoing hemodialysis. *Pacing Clin. Electrophysiol.*, 2005;**28**: 54–61.
499. Belalcazar, A. and R. Patterson, Monitoring lung edema using the pacemaker pulse and skin electrodes. *Physiol. Meas.*, 2005;**26**: S153–S163.
500. Srar, G.W., G.W. Wagner, S.V. Behar, et al., Vectocardiographic criteria for the diagnosis of inferior myocardial infarction. *Circulation*, 1974;**49**: 829–836.
501. Frank, S., J.A. Colliver, and A. Frank, The electrocardiogram in obesity: Statistical analysis of 1,029 patients. *J. Am. Coll. Cardiol.*, 1986;**7**: 295–299.
502. Valencia-Flores, M., A. Orea, and M. Herrera, Effect of bariatric surgery on obstructive sleep apnea and hypopnea syndrome, electrocardiogram, and pulmonary arterial pressure. *Obes. Surg.*, 2004;**14**: 755–762.
503. Singh, B.N., T.D. Gaarder, T. Kanegae, M. Goldstein, J.Z. Montgomerie, and H. Mills, Liquid protein diets and torsade de pointes. *J. Am. Med. Assoc.*, 1978;**240**: 115–119.
504. Brown, J.M., J.F. Yetter, M.J. Spicer, and J.D. Jones, Cardiac complications of protein-sparing modified fasting. *J. Am. Med. Assoc.*, 1978;**240**: 120–122.
505. Bhagwat, A.R. and P.J. Engel, Heart disease and pregnancy. *Cardiol. Clin.*, 1995;**13**: 163–168.
506. Lee, S.H., S.A. Chen, T.J. Wu, et al., Effects of pregnancy on first onset and symptoms of paroxysmal supraventricular tachycardia. *Am. J. Cardiol.*, 1995;**76**: 675–678.
507. Copeland, G.D. and T.N. Stern, Wenckebach periods in pregnancy and puerperium. *Am. Heart J.*, 1958;**56**: 291–298.
508. Veille, J.C., D.W. Kitzman, and A.E. Bacevice, Effects of pregnancy on the electrocardiogram in healthy subjects during strenuous exercise. *Am. J. Obstet. Gynecol.*, 1996;**175**: 1360–1364.
509. Oram, S., *Clinical Heart Disease*, 2nd edn. London: Heinemann, 1981, p. 703.
510. Cremer, M., Ueber die direkte Ableitung der Aktionsstrome des mensch lichen Herzens vom Oesophagus und iiber das Elektrokardiogramm des Fotus. *Munchener. Med. Woch. MMW Muench. Med. Wochenschr.*, 1906;**53**: 811–813.

511. de Smoler, P.E., H.C. Smith, and S. Karchmer, Correlation of fetal heart rate, maternal heart rate, and age of pregnancy. *Am. J. Obstet. Gynecol.*, 1975;**121**: 62–65.
512. Maekawa, M. and J. Toyoshima, The foetal electrocardiogram on the human subject. *Acta Sch. Med. Univ. Kioto*, 1930;**12**: 519–520.
513. Advances in fetal electrocardiography. *J. Perinat. Med.*, 1986;**14**: 345–452.
514. Van Oosterom, A., Spatial filtering of the fetal electrocardiogram. *J. Perinat. Med.*, 1986;**14**: 411–419.
515. Jenkins, H.M.L., Technical progress in fetal electrocardiography-A review. *J. Perinat. Med.*, 1986;**14**: 365–370.
516. Murray, H.G., The fetal electrocardiogram: Current clinical developments in Nottingham. *J. Perinat. Med.*, 1986;**14**: 399–404.
517. Cerrutti, S., G. Baselli, S. Civardi, et al., Variability analysis of the fetal heart rate signals as obtained from abdominal electrocardiographic readings. *J. Perinat. Med.*, 1986;**14**: 445–452.
518. Luzietti, R., R. Erkkola, U. Hasbargen, et al., European Community Multicentre Trial "Fetal ECG Analysis During Labour": The P-R interval. *J. Perinat. Med.*, 1997;**25**: 27–34.
519. Rosen, K.G., Fetal electrocardiogram waveform analysis in labour. *Curr. Opin. Obstet. Gynecol.*, 2005;**17**: 147–150.
520. Assaleh, K. and H. Al-Nashash, A novel technique for the extraction of fetal ECG using polynomial networks. *IEEE Trans. Biomed. Eng.*, 2005;**52**: 1148–1152.
521. Mochimaru, F., Y. Fujimoto, and Y. Ishikawa, The fetal electrocardiogram by independent component analysis and wavelets. *Jpn. J. Physiol.*, 2004;**54**: 457–463.
522. Tongsong, T., A. Iamthongin, C. Wanapirak, et al., Accuracy of fetal heart-rate variability interpretation by obstetricians using the criteria of the National Institute of Child Health and Human Development compared with computer-aided interpretation. *J. Obstet. Gynaecol. Res.*, 2005;**31**: 68–71.
523. Becker, A. and H.K. Hellerstein, Effects of drinking iced water on the T loop of the spatial vectorcardiogram and on the spatial ventricular gradient. *J. Electrocardiol.*, 1969;**2**: 145–157.
524. Scardi, S. and C. Pandullo, Supraventricular tachyarrhythmia of a variable degree of atrial synchronization caused by drinking cold water. *G. Ital. Cardiol.*, 1985;**15**: 454–455.
525. Gillinov, A.M. and T.W. Rice, Prandial atrial fibrillation: Off-pump pulmonary vein isolation with hiatal hernia repair. *Ann. Thorac. Surg.*, 2004;**78**: 1836–1838.
526. Ng, G.A., E.W. Lau, and M.J. Griffith, Temperature-sensitive focal atrial tachycardia in the left atrium. *J. Cardiovasc. Electrophysiol.*, 2000;**11**: 324–327.
527. Tanabe, T. and Y. Goto, Unstable angina pectoris-changes in the ST-T segment during daily activities such as bathing, eating, defecating and urinating. *Jpn. Circ. J.*, 1983;**47**: 451–458.
528. Routledge, H.C., S. Chowdhary, J.H. Coote, and J.N. Townend, Cardiac vagal response to water ingestion in normal human subjects. *Clin. Sci. (Lond.)*, 2002;**103**: 157–162.
529. Farb, A. and S.A. Valenti, Swallow syncope. *Md. Med. J.*, 1999;**48**: 151–154.
530. Wilmshurst, P.T., Tachyarrhythmias triggered by swallowing and belching. *Heart*, 1999;**81**: 313–315.
531. Shea, M.J., J.E. Deanfield, R.A. Wilson, C.M. Delandsheere, and A.P. Selwyn, Silent myocardial ischemia during mastication. *Am. J. Med.*, 1987;**82**: 357–360.
532. Figueras, J., B.N. Singh, W. Ganz, and H.J. Swan, Haemodynamic and electrocardiographic accompaniments of resting postprandial angina. *Br. Heart J.*, 1979;**42**: 402–409.
533. Lu, C.L., X. Zou, W.C. Orr, and J.D. Chen, Postprandial changes of sympathovagal balance measured by heart rate variability. *Dig. Dis. Sci.*, 1999;**44**: 857–861.
534. Corovic, N., Z. Durakovic, and M. Misigoj-Durakovic, Dispersion of the corrected QT interval in the electrocardiogram of the ex-prisoners of war. *Int. J. Cardiol.*, 2003;**88**: 279–283.
535. Galetta, F., F. Franzoni, F. Prattichizzo, M. Rolla, G. Santoro, and F. Pentimone, Heart rate variability and left ventricular diastolic function in anorexia nervosa. *Adolesc. Health*, 2003;**32**: 416–421.
536. Franzoni, F., E. Mataloni, R. Femia, and F. Galetta, Effect of oral potassium supplementation on QT dispersion in anorexia nervosa. *Acta Paediatr.*, 2002;**91**: 653–656.
537. Swenne, I., Heart risk associated with weight loss in anorexia nervosa and eating disorders: Electrocardiographic changes during the early phase of refeeding. *Acta Paediatr.*, 2000;**89**: 447–452.
538. Lorsheyd, A., D.W. de Lange, M.L. Hijmering, et al., PR and OTc interval prolongation on the electrocardiogram after binge drinking in healthy individuals. *Neth. J. Med.*, 2005;**63**: 59–63.
539. Gowda, R.M., I.A. Khan, B.C. Vasavada, and T.J. Sacchi, Alcohol-triggered acute myocardial infarction. *Am. J. Ther.*, 2003;**10**: 71–72.
540. Nishimura, F.T., T. Fukunaga, H. Kajiura, et al., Effects of aldehyde dehydrogenase-2 genotype on cardiovascular and endocrine responses to alcohol in young Japanese subjects. *Auton. Neurosci.*, 2002;**102**: 60–70.
541. Papaioannou, G.I. and J. Kluger, Ineffective ICD therapy due to excessive alcohol and exercise. *Pacing Clin. Electrophysiol.*, 2002;**25**: 1144–1145.
542. Steinbigler, P., R. Haberl, B. Konig, and G. Steinbeck, P-wave signal averaging identifies patients prone to alcohol-induced paroxysmal atrial fibrillation. *Am. J. Cardiol.*, 2003;**91**: 491–494.
543. Denison, H., S. Jern, R. Jagenburg, C. Wendestam, and S. Wallerstedt, ST-segment changes and catecholamine-related myocardial enzyme release during alcohol withdrawal. *Alcohol.* 1997;**32**: 185–194.
544. Gould, L., C.V. Reddy, K.C. Oh, et al., Electrophysiologic properties of coffee in man. *J. Clin. Pharmacol.*, 1979;**19**: 46–55.
545. Newcombe, P.F., K.W. Renton, P.M. Rautaharju, C.A. Spencer, and T.J. Montague, High-dose caffeine and cardiac rate and rhythm in normal subjects. *Chest*, 1988;**94**: 90–94.
546. Myers, M.G. and L. Harris, High dose caffeine and ventricular arrhythmias. *Can. J. Cardiol.*, 1990;**6**: 95–98.
547. Graboys, T.B., C.M. Blatt, and B. Lown, The effect of caffeine on ventricular ectopic activity in patients with malignant ventricular arrhythmia. *Arch. Intern. Med.*, 1989;**149**: 637–639.
548. Frost, L. and P. Vestergaard, Caffeine and risk of atrial fibrillation or flutter: The Danish Diet, Cancer, and Health Study. *Am. J. Clin. Nutr.*, 2005;**81**: 578–582.
549. Newby, D.E., J.M. Neilson, D.R. Jarvie, and N.A. Boon, Caffeine restriction has no role in the management of patients with symptomatic idiopathic ventricular premature beats. *Heart*, 1996;**76**: 355–357.
550. Hirsch, J.A., B. Bishop, and J.L. York, Role of parasympathetic (vagal) cardiac control in elevated heart rates of smokers. *Addict. Biol.*, 1996;**1**: 405–413.

551. Pope, C.A. 3rd, D.J. Eatough, D.R. Gold, et al., Acute exposure to environmental tobacco smoke and heart rate variability. *Environ. Health Perspect.*, 2001;**109**: 711–716.
552. Aparici, M., A.L. Fernandez Gonzalez, and J. Peteiro, 24-hour ambulatory electrocardiographic registry: Differences between smokers and non-smokers and habit breaking effects. *Med. Clin. (Barc.)*, 1993;**100**: 125–127.
553. Peters, R.W., N.L. Benowitz, S. Valenti, G. Modin, and M.L. Fisher, Electrophysiologic effects of cigarette smoking in patients with and without chronic beta-blocker therapy. *Am. J. Cardiol.*, 1987;**60**: 1078–1082.
554. Sperry, R.E., J.L. Vacek, and G.S. Smith, The effects of smoking on the signal-averaged electrocardiogram in normal subjects. *Chest*, 1991;**99**: 121–122.
555. Harrigan, R.A. and W.J. Brady, ECG abnormalities in tricyclic antidepressant ingestion. *Am. J. Emerg. Med.*, 1999;**17**: 387–393.
556. Groleau, G., R. Jotte, and R. Barish, The electrocardiographic manifestations of cyclic antidepressant therapy and overdose: A review. *J. Emerg. Med.*, 1990;**8**: 597–605.
557. Frishman, W.H., H.M. Sung, H.C. Yee, et al., Cardiovascular toxicity with cancer chemotherapy. *Curr. Probl. Cardiol.*, 1996;**21**: 225–286.
558. Hanley, P.C., D.R. Holmes Jr, P.R. Julsrud, et al., Use of conventional and newer radiographic contrast agents in cardiac angiography. *Prog. Cardiovasc. Dis.*, 1986;**28**: 435–448.
559. Zukerman, L.S., T.D. Friehling, N.M. Wolf, et al., Effect of calcium-binding additives on ventricular fibrillation and repolarization changes during coronary angiography. *J. Am. Coll. Cardiol.*, 1987;**10**: 1249–1253.
560. Brennan, E., P.R. Mahrer, and V.J. Aharonian, Incidence and presumed etiology of ventricular fibrillation during coronary angioplasty. *Am. J. Cardiol.*, 1991;**67**: 769–770.
561. Missri, J. and R.M. Jeresaty, Ventricular fibrillation during coronary angiography: Reduced incidence with nonionic contrast media. *Cathet. Cardiovasc. Diagn.*, 1990;**19**: 4–7.
562. Lange, R.A. and L.D. Hillis, Cardiovascular complications of cocaine use. *N. Engl. J. Med.*, 2001;**345**: 351–8.
563. Satran, D., C.R. Henry, C. Adkinson, C.I. Nicholson, Y. Bracha, and T.D. Henry, Cardiovascular manifestations of moderate to severe carbon monoxide poisoning. *J. Am. Coll. Cardiol.*, 2005;**45**: 1513–1516.
564. Lee, D., T.L. Hsu, C.H. Chen, S.P. Wang, and M.S Chang, Myocardial infarction with normal coronary artery after carbon monoxide exposure: A case report. *Zhonghua Yi Xue Za Zhi (Taipei)*, 1996;**57**: 355–359.
565. Weaver, L.K., R.O. Hopkins, K.J. Chan, et al., Hyperbaric oxygen for acute carbon monoxide poisoning. *N. Engl. J. Med.*, 2002;**347**: 1057–1067.
566. Katzman, G.M. and D.G. Penney, Electrocardiographic responses to carbon monoxide and cyanide in the conscious rat. *Toxicol. Lett.*, 1993;**69**: 139–153.
567. Saadeh, A.M., N.A. Farsakh, and M.K. Al-Ali, Cardiac manifestations of acute carbamate and organophosphate poisoning. *Heart*, 1997;**77**: 461–464.
568. Karki, P., J.A. Ansari, S. Bhandary, and S. Koirala, Cardiac and electrocardiographical manifestations of acute organophosphate poisoning. *Singapore Med. J.*, 2004;**45**: 385–389.
569. Vahter, M. and G. Concha, Role of metabolism in arsenic toxicity. *Pharmacol. Toxicol.*, 2001;**89**: 1–5.
570. Pain, A. and A. Wingfield, Electrocardiographic changes due to emetine therapy. *Trans. R. Soc. Trop. Med. Hyg.*, 1968;**62**: 221–226.
571. Chulay, J.D., H.C. Spencer, and M. Mugambi, Electrocardiographic changes during treatment of leishmaniasis with pentavalent antimony (sodium stibogluconate). *Am. J. Trop. Med. Hyg.*, 1985;**34**: 702–709.
572. Mashour, N.H., G.I. Lin, and W.H. Frishman, Herbal medicine for the treatment of cardiovascular disease, clinical considerations. *Arch. Intern. Med.*, 1998;**158**: 2225–2234.
573. Gonzalez-Romero, S., J.A. Gonzalez-Hermosillo, A. Gonzalez, M.E. Flores, and G. Mijangos Vargas, The electrocardiographic changes in patients stung by scorpions. *Arch. Inst. Cardiol. Mex.*, 1991;**61**: 15–20.
574. Hannukainen, J.C., U.M. Kujala, J. Toikka, et al., Cardiac structure and function in monozygotic twin pairs discordant for physical fitness. *J. Appl. Physiol.*, 2005;**99**: 535–541.
575. Shetler, K., R. Marcus, V.F. Froelicher, et al., Heart rate recovery: Validation and methodologic issues. *J. Am. Coll. Cardiol.*, 2001;**38**: 1980–1987.
576. Raczak, G., G.D. Pinna, M.T. La Rovere, et al., Cardiovagal response to acute mild exercise in young healthy subjects. *Circ. J.*, 2005;**69**: 976–980.
577. Turitto, G., E.B. Caref, G. El-Attar, et al., Optimal target heart rate for exercise-induced T-wave alternans. *Ann. Noninvasive Electrocardiol.*, 2001;**6**: 123–128.
578. Chiba, T., M. Yamauchi, N. Nishida, T. Kaneko, K. Yoshizaki, and N. Yoshioka, Risk factors of sudden death in the Japanese hot bath in the senior population. *Forensic Sci. Int.*, 2005;**149**: 151–158.
579. Ishikawa, K., C. Shirato, and A. Yanagisawa, Electrocardiographic changes due to sauna bathing. Influence of acute reduction in circulating blood volume on body surface potentials with special reference to the Brody effect. *Br. Heart J.*, 1983;**50**: 469–475.
580. Tanabe, T. and Y. Goto, Unstable angina pectoris-changes in the ST-T segment during daily activities such as bathing, eating, defecating and urinating. *Jpn. Circ. J.*, 1983;**47**: 451–458.
581. Pokan, R., M. Huonker, M. Schumacher, et al., ECG of the athlete's heart. *Acta Med. Austriaca*, 1994;**21**: 76–82.
582. Langdeau, J.B., L. Blier, H. Turcotte, G. O'Hara, and L.P. Boulet, Electrocardiographic findings in athletes: The prevalence of left ventricular hypertrophy and conduction defects. *Can. J. Cardiol.*, 2001;**17**: 655–659.
583. Pelliccia, A., F.M. Di Paolo, and B.J. Maron, The athlete's heart: Remodeling, electrocardiogram and preparticipation screening. *Cardiol. Rev.*, 2002;**10**: 85–90.
584. Biffi, A., B.J. Maron, L.Verdile, et al., Impact of physical deconditioning on ventricular tachyarrhythmias in trained athletes. *J. Am. Coll. Cardiol.*, 2004;**44**: 1053–1058.
585. Turkmen, M., I. Barutcu, A.M. Esen, et al., Assessment of QT interval duration and dispersion in athlete's heart. *J. Int. Med. Res.*, 2004;**32**: 626–632.
586. Lonati, L.M., G. Magnaghi, C. Bizzi, and G. Leonetti, Patterns of QT dispersion in athletic and hypertensive left ventricular hypertrophy. *Ann. Noninvasive Electrocardiol.*, 2004;**9**: 252–256.
587. Masini, V., M. Rocchi, and M. Santini, Dynamic ECG in normal subjects. *G Ital. Cardiol.*, 1980;**10**: 1267–1279.
588. Zhuang, Z., X. Gao, and S. Gao, The relationship of HRV to sleep EEG and sleep rhythm. *Int. J. Neurosci.*, 2005;**115**: 315–327.

589. Molnar, J., F. Zhang, J. Weiss, F.A. Ehlert, and J.E. Rosenthal, Diurnal pattern of QTc interval: How long is prolonged? Possible relation to circadian triggers of cardiovascular events. *J. Am. Coll. Cardiol.*, 1996;**27**: 76–83.
590. Zhong, X., H.J. Hilton, G.J. Gates, et al., Increased sympathetic and decreased parasympathetic cardiovascular modulation in normal humans with acute sleep deprivation. *J. Appl. Physiol.*, 2005;**98**: 2024–2032.
591. Guo, Y.F. and P.K. Stein, Circadian rhythm in the cardiovascular system: Considerations in non-invasive electrophysiology. *Card. Electrophysiol. Rev.*, 2002;**6**: 267–272.
592. Schuchert, A., G. Behrens, and T. Meinertz, Diurnal variations of the ventricular pacing threshold in patients with cardiac pacemakers are not related to changes in autonomic tone. *Am. J. Cardiol.*, 2000;**86**: 226–229.
593. Dilaveris, P.E., P. Farbom, V. Batchvarov, A. Ghuran, and M. Malik, Circadian behavior of P-wave duration, P-wave area, and PR interval in healthy subjects. *Ann. Noninvasive Electrocardiol.*, 2001;**6**: 92–97.
594. Yeragani, V.K., R. Berger, R. Pohl, and R. Balon, Effect of age on diurnal changes of 24-hour QT interval variability. *Pediatr. Cardiol.*, 2005;**26**: 39–44.
595. Drory, Y., I. Shapira, E.Z. Fisman, and A. Pines, Myocardial ischemia during sexual activity in patients with coronary artery disease. *Am. J. Cardiol.*, 1995;**75**: 835–837.
596. Drory, Y., E.Z. Fisman, Y. Shapira, and A. Pines, Ventricular arrhythmias during sexual activity in patients with coronary artery disease. *Chest*, 1996;**109**: 922–924.
597. Masini, V., E. Romei, and A.T. Fiorella, Dynamic electrocardiogram in normal subjects during sexual activity. *G. Ital. Cardiol.*, 1980;**10**: 1442–1448.
598. Sztajzel, J., M. Periat, V. Marti, P. Krall, and W. Rutishauser, Effect of sexual activity on cycle ergometer stress test parameters, on plasmatic testosterone levels and on concentration capacity. A study in high-level male athletes performed in the laboratory. *J. Sports Med. Phys. Fitness*, 2000;**40**: 233–239.
599. Wilmshurst, P.T., Tachyarrhythmias triggered by swallowing and belching. *Heart*, 1999;**81**: 313–315.
600. Lowenstein, L. and A. Hussein, Transient ischemic ECG changes in a patient with acute cholecystitis without a history of ischemic heart disease. *Harefuah*, 2000;**138**: 449–450.
601. Contaldo, F., M.R. Di Paolo, C. Mazzacano, G. Di Biase, and D. Giumetti, Hypopotassemia and prolongation of the Q-T interval in a patient with severe malnutrition caused by bulimia and post-prandial vomiting. *Recenti. Prog. Med.*, 1990;**81**: 266–268.
602. Brignole, M., Neurally-mediated syncope. *Ital. Heart J.*, 2005;**6**: 249–255.
603. Mikhail, M.S., D. Thangathurai, J.F. Viljoen, and P.A. Chandraratna, Atrioventricular block secondary to straining. *Crit. Care Med.*,1987;**15**: 705–706.
604. Rudas, L., A. Kardos, L. Halmai, T. Torok, I. Pap, and Z. Hegedus, Defecation syncope following pacemaker implantation. *Orv. Hetil.*, 1997;**138**: 81–82.
605. Molander, U., D.K. Dey, V. Sundh, and B. Steen, ECG abnormalities in the elderly: Prevalence, time and generation trends and association with mortality. *Aging Clin. Exp. Res.*, 2003;**15**: 488–493.
606. Roffe, C., Ageing of the heart. *Br. J. Biomed. Sci.*, 1998;**55**: 136–148.
607. Becker, A.E., How structurally normal are human atria in patients with atrial fibrillation? *Heart Rhythm*, 2004;**1**: 627–631.
608. Alfakih, K., K. Walters, T. Jones, J. Ridgway, A.S. Hall, and M. Sivananthan, New gender-specific partition values for ECG criteria of left ventricular hypertrophy: Recalibration against cardiac MRI. *Hypertension*, 2004;**44**: 175–179.
609. Colaco, R., P. Reay, C. Beckett, T.C. Aitchison, and P.W. Mcfarlane, False positive ECG reports of anterior myocardial infarction in women. *J. Electrocardiol.*, 2000;**33** Suppl: 239–244.
610. Endres, S., K.A. Mayuga, A. Cristofaro, T. Taneja, J.J. Goldberger, and A.H. Kadish, Menstrual cycle and ST height. *Ann. Noninvasive Electrocardiol.*, 2004;**9**: 121–126.
611. James, A.F., S.C. Choisy, and J.C. Hancox, Recent advances in understanding sex differences in cardiac repolarization. *Prog. Biophys. Mol. Biol.*, 2007;**94**(3): 265–319.
612. Sredniawa, B., A. Musialik-Lydka, P. Jarski, Z. Kalarus, and L. Polonski, Circadian and sex-dependent QT dynamics. *Pacing Clin. Electrophysiol.*, 2005;**28** Suppl 1:S211–S216.
613. Regecova, V. and D. Andrasyova, Relation between anthropometric indicators and electrocardiogram variability. *Vnitr. Lek.*, 2002;**48**: Suppl 1: 120–129.
614. Xie, Z., C. Wang, and M. Li, Electrocardiographic T-wave amplitude of normal population and its correlation with age, sex and race. *Hunan Yi Ke Da Xue Xue Bao*, 1999;**24**: 335–340.
615. Mansi, I.A. and I.S. Nash, Ethnic differences in electrocardiographic amplitude measurements. *Ann. Saudi. Med.*, 2004;**24**: 459–464.
616. Upshaw, C.B. Jr., Comparison of the prevalence of first-degree atrioventricular block in African-American and in Caucasian patients: An electrocardiographic study III. *J. Natl. Med. Assoc.*, 2004;**96**: 756–760.
617. Simpson, R.J. Jr, W.E. Cascio, P.J. Schreiner, R.S. Crow, P.M. Rautaharju, and G. Heiss, Prevalence of premature ventricular contractions in a population of African American and white men and women: The Atherosclerosis Risk in Communities (ARIC) study. *Am. Heart J.*, 2002;**143**: 535–540.
618. Upshaw, C.B. Jr., Lower prevalence of intraventricular block in African-American patients compared with Caucasian patients: An electrocardiographic study II. *J. Natl. Med. Assoc.*, 2003;**95**: 818–824.
619. Upshaw, C.B. Jr., Reduced prevalence of atrial fibrillation in black patients compared with white patients attending an urban hospital: An electrocardiographic study. *J. Natl. Med. Assoc.*, 2002;**94**: 204–208.
620. Klatsky, A.L., R. Oehm, R.A. Cooper, N. Udaltsova, and M.A. Armstrong, The early repolarization normal variant electrocardiogram: Correlates and consequences. *Am. J. Med.*, 2003;**115**: 171–177.
621. Niakara, A., N. Ouedraogo, L.V. Nebie, N.J. Kabore, and C.A. Megnigbeto, Routine electrocardiographic criteria for the diagnosis of left ventricular hypertrophy: Performance in Black Africans. *Ann. Cardiol. Angeiol. (Paris)*, 2002;**51**: 193–198.
622. MacAlpin, R.N., Clinical significance of QS complexes in V_1 and V_2 without other electrocardiographic abnormality. *Ann. Noninvasive Electrocardiol.*, 2004;**9**: 39–47.
623. Kambara, H. and J. Phillips, Long-term evaluation of early repolarization syndrome (normal variant RS-T segment elevation). *Am. J. Cardiol.*, 1976;**38**: 157–156.
624. Mirvis, D.M., Evaluation of normal variation in S-T segment patterns by body surface isopotential mapping: S-T segment elevation in absence of heart disease. *Am. J. Cardiol.*, 1982;**50**: 122–128.

625. Mirvis, D.M., The electrogenesis of terminal QRS notches in normal subjects. *J. Electrocardiol.*, 1983;**16**: 113–121.
626. Mirvis, D.M., Evaluation of normal variation in S-T segment patterns by body surface isopotential mapping: S-T segment elevation in absence of heart disease. *Am. J. Cardiol.*, 1982;**50**: 122–128.
627. Gussak, I. and C. Antzelevitch, Early repolarization syndrome: Clinical characteristics and possible cellular and ionic mechanisms. *J. Electrocardiol.*, 2000;**33**: 299–309.
628. Page, H.L. Jr and W.B. Campbell, Electrocardiography: Persistent juvenile T wave pattern. *J. Tenn. Med. Assoc.*, 1974;**67**: 306.
629. Lown, B., W.F. Ganong, and S.A. Levine, The syndrome of short P-R interval, normal QRS complex and paroxysmal rapid heart action. *Circulation*, 1952;**5**: 693–706.
630. Brodsky, M., D. Wu, P. Denes, C. Kanakis, and K.M. Rosen, Arrhythmias documented by 24 hour continuous electrocardiographic monitoring in 50 male medical students without apparent heart disease. *Am. J. Cardiol.*, 1977;**39**: 390–395.
631. Marriott, H.J.L., *Practical Electrocardiography*. Baltimore, MD: Williams & Wilkins, 1983, pp. 33–35.
632. Peberdy, M.A. and J.P. Ornato, Recognition of electrocardiographic lead misplacements. *Am. J. Emerg. Med.*, 1993;**11**: 403–405.
633. Madias, J.E., A comparison of 2-lead, 6-lead, and 12-lead ECGs in patients with changing edematous states: Implications for the employment of quantitative electrocardiography in research and clinical applications. *Chest*, 2003;**124**: 2057–2063.
634. Herman, M.V., D.A. Ingram, J.A. Levy, J.R. Cook, and R.J. Athans, Variability of electrocardiographic precordial lead placement: A method to improve accuracy and reliability. *Clin. Cardiol.*, 1991;**14**: 469–476.
635. Knight, B.P., F. Pelosi, G.F. Michaud, et al., Clinical consequences of electrocardiographic artifact mimicking ventricular tachycardia. *N. Engl. J. Med.*, 1999;**341**: 1270–1274, 278**.**
636. Krantz, M.J. and J.A. Garcia, Pseudo-torsade de pointes with underlying wandering pacemaker. *Clin. Cardiol.*, 2005;**28**: 355.
637. Ripa, R.S., E. Persson, B. Heden, et al., Comparison between human andautomated electrocardiographic waveform measurements for calculating the Anderson-Wilkins acuteness score in patients with acute myocardial infarction. *J. Electrocardiol.*, 2005;**38**: 96–99.
638. Poon, K., P.M. Okin, and P. Kligfield, Diagnostic performance of a computer-based ECG rhythm algorithm. *J. Electrocardiol.*, 2005;**38**: 235–238.
639. Hamilton, R.M., A.B. Houston, K. McLeod, and P.W. Macfarlane, Evaluation of pediatric electrocardiogram diagnosis of ventricular hypertrophy by computer program compared with cardiologists. *Pediatr. Cardiol.*, 2005;**26**: 373–378.
640. Madias, J.E., A. Kaminetsky, and N. Sonlanki, Myocardial infarction-induced ventricular aneurysm in the presence of complete left bundle branch block. *J. Electrocardiol.*, 1999;**32**: 179–183.
641. Madias, J.E., R. Ashtiani, H. Agarwal, V.K. Narayan, M. Win, and A. Sinha, Diagnosis of ventricular aneurysm and other severe segmental left ventricular dysfunction consequent to a myocardial infarction in the presence of right bundle branch block: ECG correlates of a positive diagnosis made via echocardiography and/or contrast ventriculography. *Ann. Noninvasive Electrocardiol.*, 2005;**10**: 53–59.
642. Madias, J.E., M. Mahjoub, and J. Valance, The paradox of negative exercise stress ECG/positive thallium scintigram. Ischemic ST-segment counterpoise as the underlying mechanism. *J. Electrocardiol.*, 1996;**29**: 243–248.
643. Madias, J.E., P. Knez, and M.T. Win, True-positive exercise electrocardiogram/false-negative thallium-201 scintigram: A proposal of a mechanism for the paradox. *Clin. Cardiol.*, 2000;**23**: 625–629.
644. Madias, J.E., B. Manyam, M. Khan, V. Singh, and C. Tziros, Transient disappearance of Q waves of previous myocardial infarction due to exercise-induced ischemia of the contralateral noninfarcted myocardium. *J. Electrocardiol.*, 1997;**30**: 97–103.
645. Madias, J.E., V. Narayan, and M. Attari, Detection of P waves via a "saline-filled central venous catheter electrocardiographic lead" in patients with low electrocardiographic voltage due to anasarca. *Am. J. Cardiol.*, 2003;**91**: 910–914.

21 The Electrocardiogram in Congenital Heart Disease

Jerome Liebman

P. W. Macfarlane, A. van Oosterom, O. Pahlm, P. Kligfield, M. Janse, J. Camm (eds.), *Comprehensive Electrocardiology*, DOI 10.1007/978-1-84882-046-3_21,

21.1 Introduction

The electrocardiogram in congenital heart disease has often been discussed in terms of specific types of electrocardiograms for specific types of lesions. Indeed, in the pages, which follow, certain such relationships do occur. However, the relationships are usually based upon specific mechanisms, some of which are well understood (including cardiovascular hemodynamics) and some of which are not. Close analysis reveals that most of the time the electrocardiogram is not specific for a specific lesion, but that the hemodynamics determine the changes from normal. An exception is the abnormal superior vector associated with endocardial cushion defect. Therefore, an understanding of the electrocardiogram of infants, children and young adults with congenital heart diseases necessitates an understanding of the hemodynamics of the various lesions. Consequently, accompanying the discussion of each lesion will be a brief delineation of pertinent hemodynamics. Since these hemodynamics are usually not contaminated by effects of coronary artery disease, the related atrial and ventricular hypertrophy tends to be relatively "pure" as compared to hypertrophy in the older adult. On the other hand, there are specific problems which complicate matters in infants and children, particularly the problem of the heart being so large in relation to the chest – the proximity effect. [(1–6)] This proximity effect not only accentuates anterior over posterior sources in terms of magnitude but may significantly distort the orientation of the various sources differently in different parts of the chest [1–6]. These effects plus lung effects and various inhomogeneities appear to be particularly important in children [7–12]. Another problem relates to the often considerable differences in normal values from one age-group to another, particularly in early infancy [8, 9, 11–13]. Appropriate statistics for electrocardiography must also be utilized [14, 15].

Despite the obvious differences between infants and, children on the one hand and the older adult on the other, the basic principles of the electrocardiographic interpretations are not different per se [10]. Furthermore, there are no differences in basic principles when interpreting the electrocardiogram of people with congenital heart disease. The interpretation must be based upon known physics, physiology and pathology [3, 4, 8, 10].

The term electrocardiography is used for

(a) The two lead systems of standard electrocardiography with scalar display, namely the standard limb leads and the precordial leads [8, 9]
(b) Orthogonal electrocardiography with scalar and/or vector display [16–20]
(c) Electrocardiographic body surface potential mapping (BSPM) [21, 22]

In this chapter, standard electrocardiography, and Frank system [16] and McFee–Parungao system [17] orthogonal electrocardiography, will be utilized, often contiguously. In all figures showing simultaneous X, Y and Z scalars, the paper speed is 50 div s^{-1}. It seems probable that some form of BSPM is part of the future of electrocardiography, but its inclusion in this chapter will be minimal; it is discussed in detail in Chaps. 31 and 32.

The approach to interpretation of the electrocardiogram must also reflect improvements in the understanding of anatomical, physical and electrophysiological phenomena. Terminology, as much as possible, must be based upon appropriate principles, the past not being revered simply because of usage. The term "axis deviation," for example, is not appropriate since "axis" as utilized, refers to the mean QRS vector in the frontal plane. There are many areas of the heart being depolarized early, other areas late and other areas later yet. These areas cannot be averaged.

The only axes of use are the X, Y and Z axes, representing left-right, inferior-superior, and anterior-posterior directions. Although, there are many areas of interpretation where understanding is deficient, pattern reading is not generally reliable. Perhaps, the major element necessary for appropriate interpretation of hypertrophy is the knowledge of the sequence of activation "what is being depolarized and when" [8–10, 21–26].

A most useful way to appreciate "what is being depolarized and when" (while interpreting the standard electrocardiogram), is to utilize vector analysis, despite the known inaccuracies. Each lead on the chest, for example, is best viewed as a projection of the cardiac vector (see Chaps. 10, 11, and 13), despite the fact that this projection is distorted by many things, including proximity effects and various inhomogeneities. The vector loop in the frontal plane of standard electrocardiography is only minimally useful even though proximity distortion is not a factor, particularly because of the very poor X axis as represented in lead I. This poor X axis is the major distorting factor in Burger's scalene triangle [27]. The vector loop in the horizontal plane of standard electrocardiography is extremely useful, however, despite the distortion of the cardiac vector. For an explicit description of the simple methodology for construction of the vector loop from

standard limb or precordial leads, see previous publications [8–10]. Considerable reference will be made in this chapter to such vector loops – hence the use of terms such as "terminal vector" in the standard ECG.

The electrocardiographer must also have available all normal values for the various types of useful parameters, including the quantitative limits for specific leads. These values must be utilized within the guidelines of appropriate statistics [13, 14]. The normal limits of the ECG in infants and children are discussed in Chap. 13 and a comprehensive list of tables is presented in the Appendices. Many of these tables were produced as a result of the work of the author [8, 9]. A separate paper dealing with statistical treatment of data has also been prepared by the author and is presented in the Appendices. For convenience a small summary table of principal limits of normality is presented in the Table 21.1.

In the following pages, common and otherwise important congenital cardiac diseases will be discussed and representative electrocardiograms will be illustrated. Whenever pertinent, the hemodynamics will be illustrated utilizing the box diagram, as shown for a normal child [28, 29] in Fig. 21.1.

21.2 Atrial Septal Defect (Ostium Secundum Type)

Atrial septal defect (ASD) is not a disease usually recognized in early infancy [28]. Since compliance of the right ventricle in the newborn period is diminished as compared to that of the left ventricle, there is no left-to-right shunt at that time. At the same time, there is no stimulus to prevent the newborn's pulmonary arterioles and small muscular arteries (resistance vessels) from maturing normally (rapidly) into thin-walled, very compliant vessels. Such "adult-type" vessels can allow up to three to four times normal flow without increasing pulmonary artery pressure. In the first weeks to months after birth, as compliance of the right ventricle slowly increases compared to that of the left ventricle, a left-to-right shunt develops, albeit very slowly. As the left-to-right shunt slowly increases, selective hypertrophy gradually develops so that the ventricle is conditioned to prevent congestive heart failure. The hypertrophy causes a decrease in compliance of the right ventricle resulting in the slow development of the left-to-right shunt because of "feed back" mechanisms. By the time a large left-to-right shunt is present through the ASD, the resistance vessels are thin-walled and the pulmonary artery pressure is rarely more than 35–40 mm Hg systolic. The consequence is a right ventricle, which is complaint, is a little thicker than normal, but is dilated. Very few children with atrial septal defect are diagnosed as such between 1 and 2 years of age. Most then remain very stable throughout childhood. The box diagrams Fig. 21.2 for atrial septal defect include the volume of work in each chamber. There is increased volume of work of both the right atrium and right ventricle (although there is increased volume entering the left atrium, it immediately goes through the nonrestrictive ASD so that there is no increased work for the left atrium).

Table 21.1

Approximate upper limits of normal subjects used as a pediatric ECG "ready-reckoner" (ECG standards 95%)

Age	Heart rate (beats min^{-1})	PR (s)	QRS (s)	QT (s)	V_5		aVF		V_2	
					R	S	R	S	R	S
0–24 h	145	0.12	0.08	0.32	18.0	24.0				
1–7 days	175	0.12	0.08	0.31	19.3	16.2	10.5	3.1	31.1	34.1
8–30 days	190	0.11	0.07	0.30	27.0	12.3	12.4	3.8	29.0	25.7
1–3 months	190	0.13	0.08	0.28	20.7	12.7	13.8	3.1	27.4	34.1
3–6 months	179	0.13	0.08	0.30	25.5	15.4	18.5	3.4	28.6	26.5
6–12 months	177	0.13	0.08	0.30	24.7	8.0	16.4	3.7	24.4	30.1
1–3 years	163	0.15	0.08	0.31	27.7	7.0	16.6	3.8	22.5	32.1
3–5 years	132	0.15	0.08	0.38	30.0	5.8	16.7	3.0	22.8	28.8
5–8 years	115	0.16	0.08	0.37	31.2	6.6	14.8	3.4	22.0	35.3
8–12 years	107	0.17	0.08	0.42	30.0	4.4	17.8	3.7	16.9	35.6
12–16 years	102	0.16	0.08	0.42	26.7	5.0	19.7	3.8	18.4	41.0

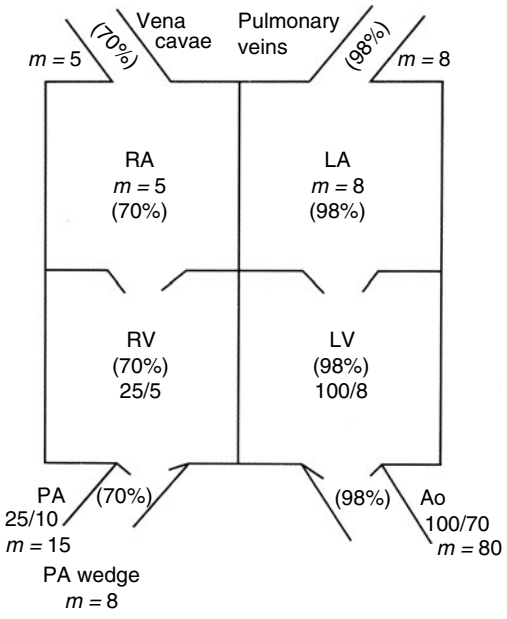

Figure 21.1

Hemodynamics of a normal child, utilizing the box diagram: RA, right atrium; RV, right ventricle; PA, pulmonary artery; PA wedge, pulmonary artery wedge (an estimate of pulmonary venous pressure); LA, left atrium; LV, left ventricle; Ao, aorta; *m*, mean pressure. Numbers indicate pressures in mm Hg. Numbers in parentheses are percentage oxygen saturations.

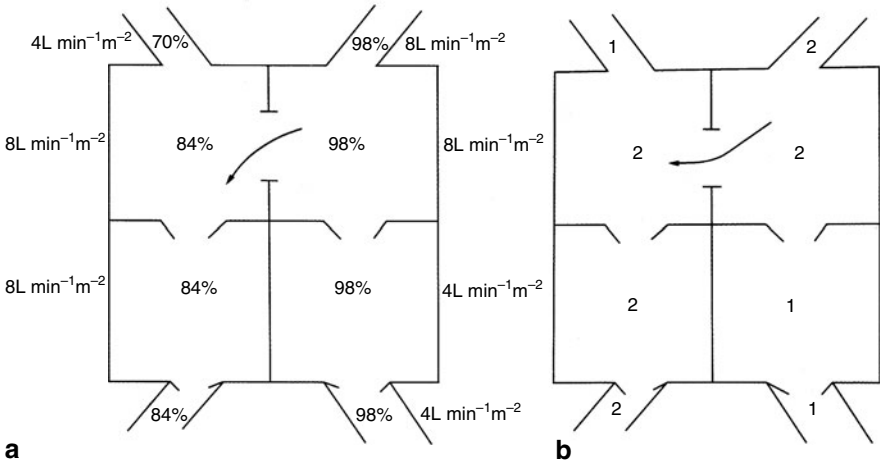

Figure 21.2

Box diagrams of atrial septal defect (ASD). In (a), the volume in each blood vessel and chamber is in 1 min^{-1} m^{-2}. It is assumed that 41 min^{-1} m^{-2} is the normal cardiac output. Note the increase in oxygen saturation (expressed as percentages) at the atrial level. The calculated pulmonary:systemic (P:S) flow ratio is 2:1. In (b), ASD is shown, utilizing the normal cardiac output as 1 unit of cardiac output. Therefore, 1 unit returns to the venae cavae and 1 unit goes across the ASD, resulting in 2 units of volume in the RA, 2 units in the RV, 2 units in the PA, 2 units in the pulmonary veins (PV), 2 units in the LA, 1 unit in the LV, and 1 unit in the Ao. Therefore, this box diagram delineates an ASD with a 2:1 P:S flow ratio as in (a).

All of the above is for the most common ASD (the secundum type). The dynamics of partial anomalous pulmonary venous return and the sinus venosus type of ASD are identical, as is the electrocardiogram. The exception is that in the sinus venosus lesion the pacemaker is frequently not sinus but is low atrial or atrioventricular (AV) junctional. The ostium primum type of ASD will be discussed later in this chapter.

21.2.1 Right Atrial Enlargement

Right atrial enlargement (RAE) is a term which does not attempt to distinguish between hypertrophy and dilatation. The most useful criteria for RAE are the following.

(a) Standard electrocardiography (ECG) [8, 9, 30–32]:
  (i) Increased magnitude of first portion of P wave in lead II (mainly inferior)
  (ii) Increased magnitude of first portion of P wave in lead V_1.(mainly anterior) and
  (iii) Increased negative magnitude of P wave in lead V_1 if lead V_2 is mainly anterior
(b) Orthogonal electrocardiography (VCG) [8, 9, 33, 34]:
  (i) Increased magnitude of P anterior
  (ii) Increased spatial vector magnitude (SVA) at the time of maximum P anterior
  (iii) Increased P magnitude inferior

21.2.2 Right Ventricular Hypertrophy with Terminal Right Conduction Delay

Criteria for right ventricular hypertrophy (RVH) are many [8, 9, 35], with the most sensitive being an increased magnitude of the terminal QRS vector to the right, and analysis of the direction of inscription of the vector loop in the horizontal plane. It is appropriate at this time to delineate all the criteria for RVH, while being more specific about ASD. Then, for other defects where pure RVH is present, reference can be made to these criteria.

21.2.2.1 RVH Criterion 1 – Direction of Inscription of QRS Vector Loops

The direction of inscription of the QRS vector loop in the frontal plane of standard electrocardiography is not generally useful. A clockwise-inscribed frontal plane loop is the norm in all infants and is present in 62% of teenagers [35]. Analysis of the horizontal plane, however, is very useful. In ASD, the RVH is not usually severe, with the initial QRS loop being inscribed normally to the right and anterior, after which the direction of inscription is to the left and anterior. The terminal vector then may or may not become posterior, but if it does, the magnitude of the posterior QRS vector is usually very small. The variation is considerable even when the amount of pulmonary blood flow is essentially the same from case to case. Sometimes the vector remains so far anterior that a clockwise-inscribed vector loop results. The terminal QRS vector to the right is frequently, but not always, greater than normal, but since the QRS projection posteriorly is usually small or nonexistent, the terminal vector in the standard ECG crosses the projection of the V_4R and V_1 lead vectors. The result is a terminal r or R in those leads. The terminal vector is usually inscribed quite slowly, so that the ECG diagnosis is RVH with terminal right conduction delay [36–39]. Figures 21.3 and 21.4 illustrate this.

Plates 21.1 and 21.2 are BSPMs of the same child as in Fig. 21.4. These maps were recorded with 180 electrodes. Plate 21.1 is from 36 to 46 ms of the QRS; while Plate 21.2 is from 48 to 58 ms. On the side is the color scale, from 0 to −2, 550 μ V, and from 0 to +2, 640 μ V. At the bottom is a magnitude factor, which represents the total of the instantaneous value from each of the 180 electrodes. The frontal and horizontal plane vectorcardiograms, derived from appropriate leads from among the 180, are also simultaneously drawn. The red dots each indicate the six maps of the QRS BSPM 2 ms apart. As with the scale factor, the yellow to orange to red are negative values, while the increasing intensity green to red are positive values. Each map (from clavicle to waist) is divided into four sections. The left border is the right axillary line and the right border is also the right axillary line. Therefore, the viewer should consider the maps as the chest unrolled. Therefore, the four sections are the right anterior chest, left anterior chest, left posterior chest and right posterior chest.

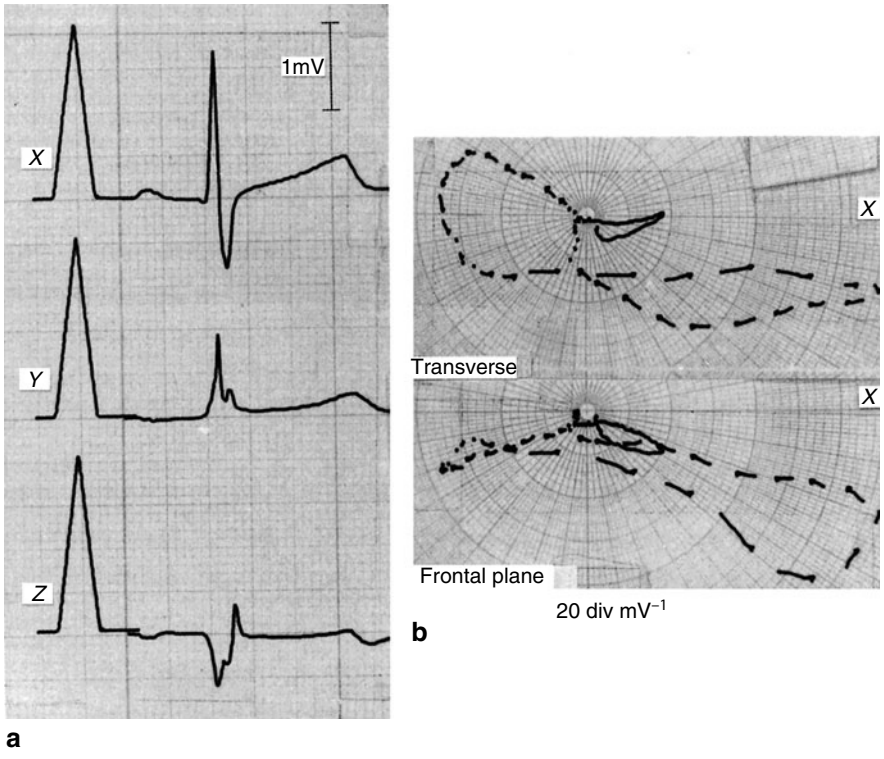

Figure 21.3

Frank-system orthogonal electrocardiogram with (a), simultaneous *X*, *Y* and *Z* orthogonal scalars plus (b), horizontal and frontal plane vectorcardiograms. In this and all similar figures of this article, the scalar ECG traces are at 50 div s^{-1}. The large regular peaks preceding the traces in (a) are the standardizations. The direction of inscription in (b) is away from the "hook" on each mark; e.g., mainly clockwise in the frontal plane. The patient is a 15-year-old male with a sinus venosus type of ASD, including partial anomalous pulmonary venous return to the superior vena cava. The diagnosis of RVH with terminal right conduction delay was straightforward and typical, just as in ASD secundum. Note, however, that the P vector (lead *Y*) is superior, a low atrial pacemaker being common in sinus venosus ASD. (After Liebman et al. [8]. © Williams and Wilkins, Baltimore, MD. Reproduced with permission.)

Note in Plate 21.1 at 38 ms that there is a notch (just to the left of the sternum) in the positive zone. This notch gradually expands, becoming less and less positive, so that it eventually loses positivity. At 48 ms, an extension of the negative has fitted into the notch (Plate 21.2), which continues to expand in area and magnitude. This entire process depicts epicardial right ventricular breakthrough. It has begun very late and is very prolonged, typical of atrial septal defect. The average normal time for epicardial right ventricular breakthrough is 25 ms, with the negative extension being from the right superior area rather than the central superior zone. In addition, after the onset of breakthrough there is considerable positivity to the right and anteriorly, arising from the right ventricle. This is not seen in the normal subject. We have documented previously [37–39] that in right bundle branch block there is no epicardial right ventricular breakthrough. In the past, it has been stated that in atrial septal defect, there is incomplete right bundle branch block. Our BSPM data clearly documents that the diagnosis in ASD is RVH with terminal right conduction delay, and that there is no right bundle branch block.

Obviously, in RVH in general there is a spectrum based upon the severity of the hemodynamics. Therefore, it is not considered useful to describe types of RVH. (With ASD, there is a spectrum even with very little variation in hemodynamics.) It is also not considered useful to diagnose volume overload versus pressure overload on the basis of the type of activation sequence. Any diagnostic criteria that have been developed to do so most likely indicate differences in severity.

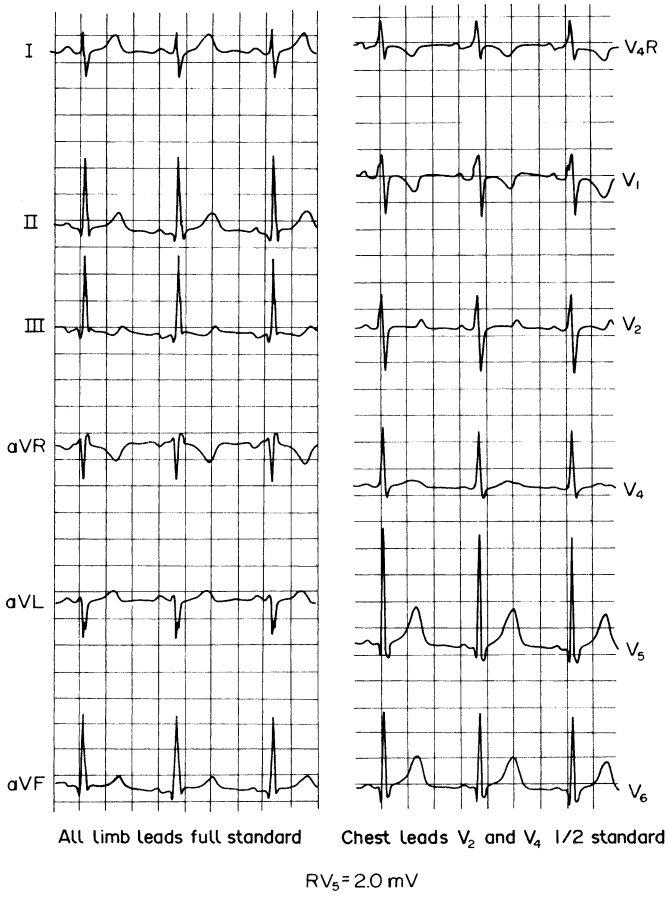

Figure 21.4
Standard ECG (with six simultaneous leads in limb and chest leads) of a 9½-year-old boy with a large secundum ASD. This type of ECG is unusual for an ASD. Note that the R waves in V_4R, V_1, V_2 are prolonged in duration (in V_2 above 0.03 s). In this child's VCG, the diagnosis of RVH with terminal right conduction delay was straightforward although the terminal vector was posterior (and well to the right). Why there was not a prominent terminal vector the right in the standard ECG is not clear, but the reason why there is no terminal R in the right chest leads is because the rightward posterior or terminal projection was too far posterior to cross the projections of the V_4R and V_1 lead vectors (see Fig. 21.5). (After Liebman et al. [8]. © Williams and Wilkins, Baltimore, MD. Reproduced with permission.)

A terminal right conduction delay from right ventricular volume overload, is likely in ASD, although mild to moderate pulmonic stenosis may result in an almost identical ECG [40].

21.2.2.2 RVH Criterion 2 – Initial QRS Vector Loop to the Left and Anterior

This is uncommon except in severe RVH. This criterion is unlikely to be met in ASD, where the RVH is not marked.

21.2.2.3 RVH Criterion 3 – Main or Mean QRS Horizontal Plane Vector to the Right

This is only found when RVH is severe enough, and therefore is not usually seen in ASD.

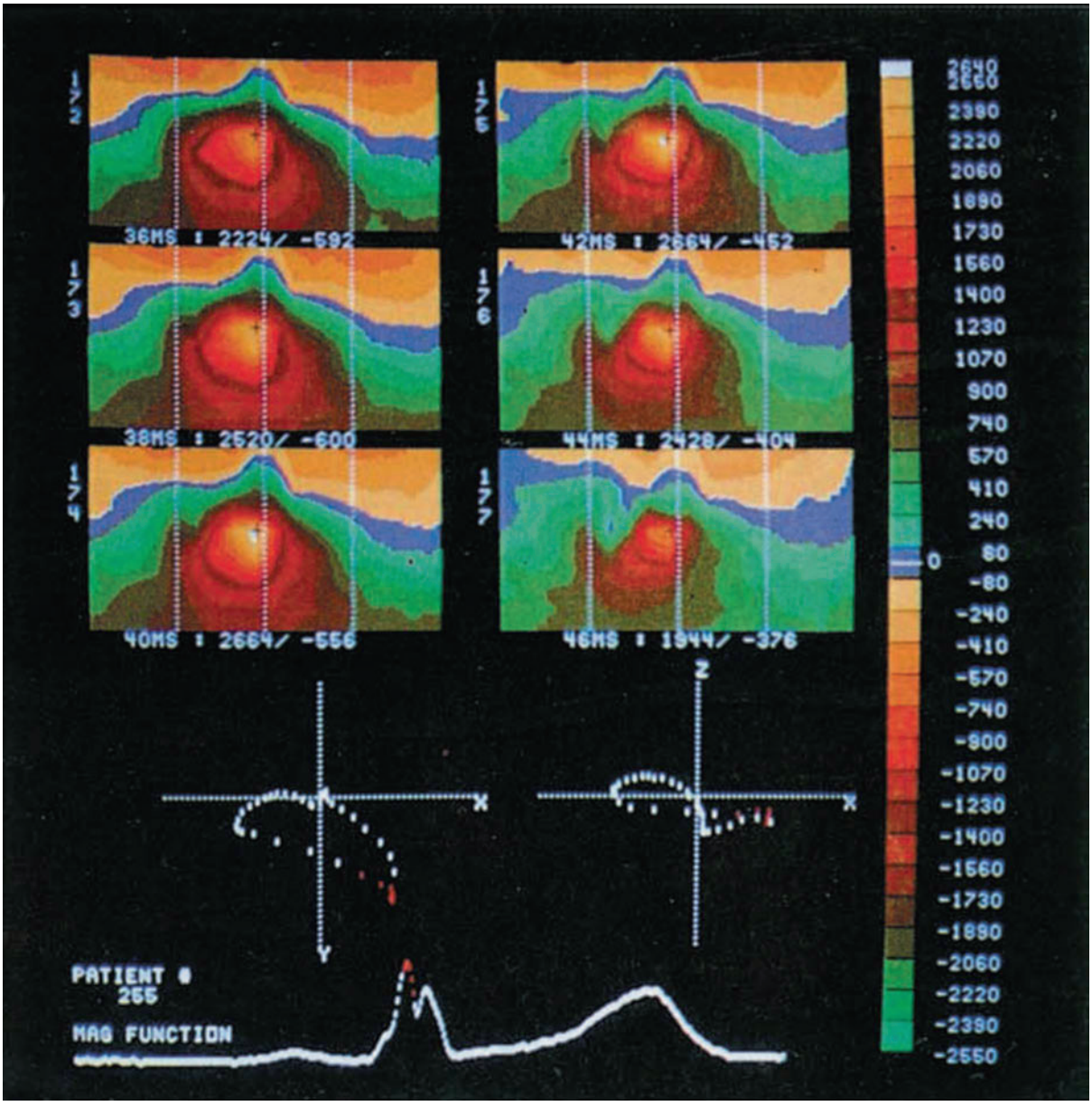

Plate 21.1

Body-surface potentia map of the subject of Fig. 21.4 from 36–45 ms of the QRS (See Sect. 21.2.2.1 for detail).

21.2.2.4 RVH Criterion 4 – Main or Mean QRS Vector Abnormally Anterior

This is common, but by itself is an unreliable sign of RVH. Proximity effect, particularly in preschool children, or in the presence of chest deformities such as pectus excavatum, may cause overreading of RVH. This is so, on occasion, even in older children.

As an important aside, note that main QRS vectors are much more meaningful than are mean vectors. In utilizing main vectors, the electrocardiographer is considering activation sequences. In RVH, there may be two main vectors: the first vector to the left and anterior, the second (terminal) vector to the right and posterior (or anterior). The result is that after 1 month, and certainly after 2 months of age, the presence of two main vectors provides a criterion for RVH. If the first vector is abnormally to the left, then additional left ventricular hypertrophy (LVH) must be diagnosed. However,

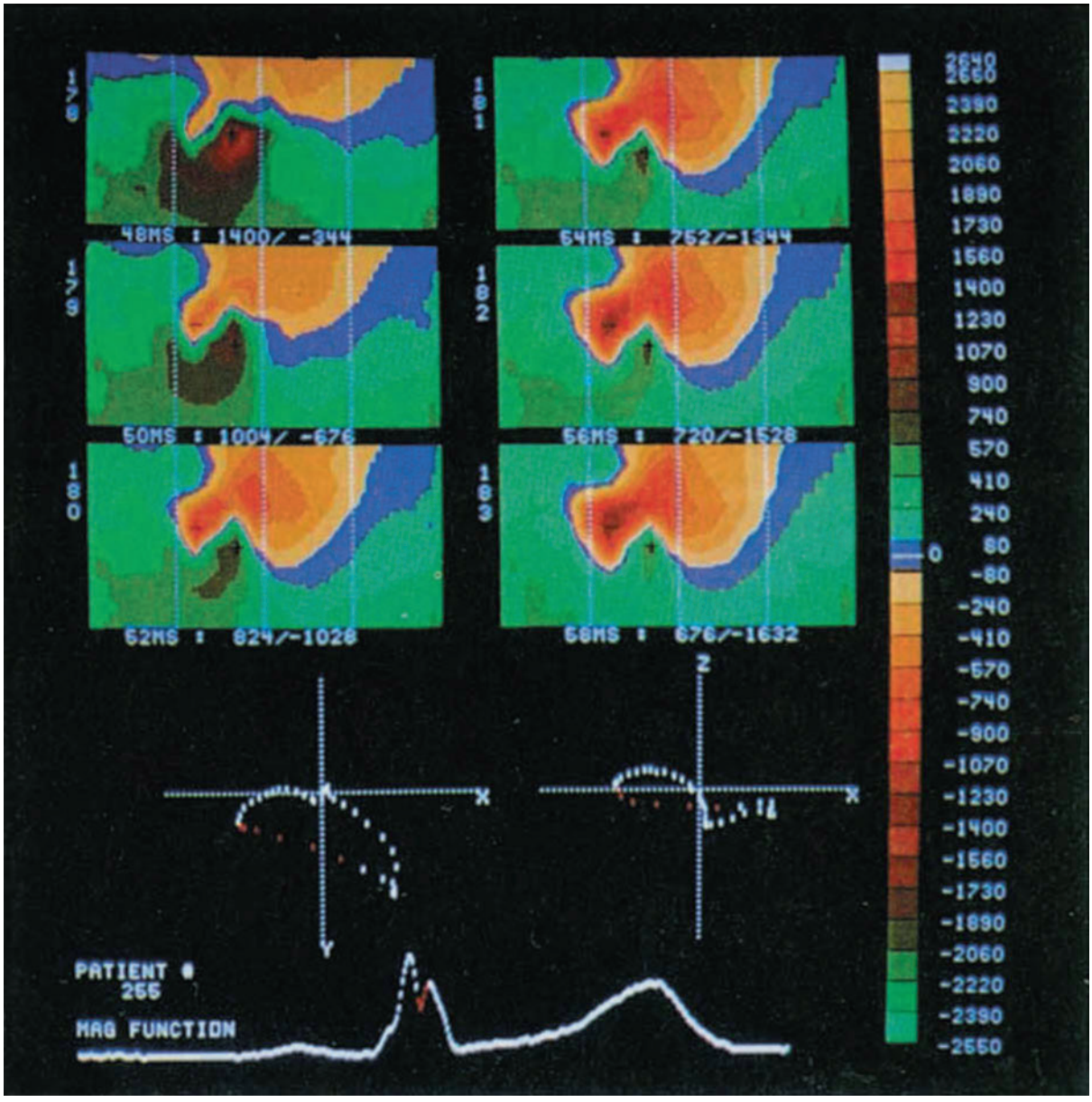

Plate 21.2

Body-surface potentia map of the subject of Fig. 21.4 from 45–58 ms of the QRS (See Sect. 21.2.2.1 for details).

it must be appreciated that this LVH may be diagnosed inappropriately in ASD, since the anterior right ventricle, because of its increased volume, may cause a proximity effect artifact in leads V_5 and V_6.

21.2.2.5 RVH Criterion 5 – Mean QRS Vector in the Frontal Plane to the Right

This has been called right axis deviation (RAD), a standard ECG term which is not appropriate. The use of axis deviation as a parameter for diagnosis is not recommended since the only true orthogonal axes are the X, Y and Z axes.

If RAD is present in the standard 12-lead ECG with nothing else to suggest RVH, a mean QRS to the right should be ignored. As with Burger's scalene triangle [27], the X axis of lead I is poor. The prominent S in lead I may be owing to distortion of the right-left lead by superior-inferior forces, often present without a prominent S in lead V_5. In orthogonal electrocardiography, a mean vector to the right is a reliable indicator of RVH.

21.2.2.6 RVH Criterion 6 – Increased Magnitude of Terminal Rightward QRS Vector Loop

This is manifested by an increased terminal X to the right, or a deep S in V_5, and is the most sensitive measurement criterion for RVH [35]. To be certain of its reliability, a deep S in V_6 as well is helpful.

21.2.2.7 RVH Criterion 7 – A Terminal r or R′ in V_4R and V_1

This has been the most misunderstood criterion for RVH (particularly in ASD), and points out a major reason why pattern reading, or the identification of a particular criterion in one lead, may be fraught with error. Figure 21.5 is explanatory. A terminal r or R in V_4R or V_1 indicates only that the terminal projection crosses the perpendicular to the V_4R or V_1 lead vector. When the terminal QRS vector is markedly posterior, a large terminal vector to the right is necessary in order to cross the perpendicular to the V_4R or V_1 lead vector, whereas when the terminal vector is minimally posterior, or is anterior, only a small magnitude terminal QRS vector to the right is necessary to cross the perpendicular to the V_4R or V_1 lead vector. In ASD, where the terminal vector is of decreased magnitude posteriorly, the characteristic terminal r or R is expected. In normal people, because of large variation in how far posterior the main body of the vector "loop" projects, as well as how much to the anterior the most rightward portion of the terminal QRS vector extends, it is difficult to correlate the magnitude of the terminal r or R′. This helps explain the normal variant rsŕ in the right chest leads, particularly when

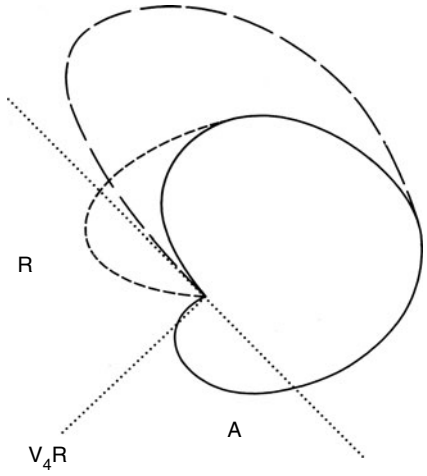

Figure 21.5

A diagrammatic representation of a transverse vector loop with two different terminal vectors: A, anterior; R, right. The V_4R lead axis is depicted as well as the perpendicular to the projection of the V_4R lead (*dotted line*). Both terminal vectors extend about equally to the right, with the more posterior projection (*dashes*) slightly further to the right. The more anterior terminal vector (*bold dashes*) crosses the perpendicular to the V_4R lead axis, as well as the perpendicular to the V_1 lead axis (not depicted). Therefore, for the more anterior terminal rightward vector, V_4R (and V_1) would project on those chest leads as rSr′ complexes, whereas for the more posterior terminal rightward vector, V_4R (and V_1) would project on those chest leads as rS complexes. (After Liebman et al. [8]. © Williams and Wilkins, Baltimore, MD. Reproduced with permission.)

there is not a deep S in V_5 and V_6, and when the S (Z axis posterior) is relatively small. The deeper the S in V_2, the more significant is the r′ in V_4R and V_1 as an indicator of RVH.

There are times when, in the right chest leads, there is a small voltage terminal r in V_4R and/or V_1 without a deep S in V_5. This is likely to represent a proximity effect and is usually a normal variant. (Despite the fact that is represents a proximity effect, it may also be the only clue, in a particular tracing, to the diagnosis of mild RVH.) An orthogonal electrocardiogram with vector display will usually help determine whether RVH is present.

The rsŕ or rsŔ has, of course, been called "incomplete right bundle branch block" by the majority of electrocardiographers. Clearly this is incorrect, for the reasons described above. Furthermore, even though in ASD there is right ventricular dilatation and terminal right conduction delay on the ECG of almost all patients, there is no right bundle branch block. This has been documented in the body-surface potential map in that there is definite epicardial right ventricular breakthrough [37–39] (Plate 21.1). (In order to make sure that there is no confusion with the terminology of the past, the author has discarded the term "incomplete right bundle branch block," even when it is truly present, in favor of the term partial right bundle branch block (partial RBBB). Partial RBBB, in congenital heart diseases, is usually seen as a consequence of certain types of cardiac surgery and is only infrequently seen in the nonoperative state [37–39]. It is very rare for children with ASD who have not undergone operation to have partial RBBB.)

21.2.2.8 RVH Criterion 8 – Increased Magnitude of Z Anterior

This is only relatively reliable. It is necessary to be cautious about the tall initial r or R. It is easy to overread RVH where there is a tall spiking R wave of brief duration as part of an RS complex. Most of the time, particularly in the preschool child, the cause is a proximity effect because the heart is so close to the chest wall at those ages. It is preferred that the duration of the initial QRS (e.g., R in V_1) be at least 30 ms in order to suggest the diagnosis of RVH. Although an increased R/S ratio in V_1 is commonly used to diagnose RVH, it is a very soft unreliable sign. (Z anterior corresponds to an R wave in V_1, V_2, in the orthogonal ECG, e.g., Fig. 21.3.)

21.2.2.9 RVH Criterion 9 – Increased Magnitude of Y Inferior

This involves a tall R in aVF. It may be part of severe RVH but is not a factor in ASD.

21.2.2.10 RVH Criterion 10 – Increased Magnitude of Z Posterior

This is a deep S in V_1, V_2. It may be part of severe RVH in the presence of a clockwise-inscribed horizontal plane "loop" terminating well posterior, but it is not a factor in ASD.

21.2.2.11 RVH Criterion 11 – Abnormal Ratios of Specific Magnitudes

An example of this is an increased ratio of the magnitude of Z anterior to Z posterior (a weak criterion) and/or an increased ratio of the magnitude of X terminal right to X left (an excellent criterion). Normal standards for orthogonal electrocardiography are present for many, although not all, age groups and very few standards are available for the standard 12-lead ECG. The concept, however, must always be considered. It is particularly useful in the presence of abnormally low voltage from various causes, including lung disease. However, overreading of RVH in the standard ECG is very common when the R/S ratio in lead V_1 is utilized, as mentioned above. The error appears especially when the tall initial R is of brief duration, presumably part of a proximity effect. Proximity effect is most common in the preschool child, but can be recognized at all ages.

21.2.2.12 RVH Criterion 12 – Increased Magnitude of the Terminal R in AVR

This is a reliable criterion, but when present the diagnosis is usually obvious from other criteria.

21.2.2.13 RVH Criterion 13 – Increased Magnitude of the Maximal Spatial Vector to the Right

This is known as MSVR. In general it is an excellent criterion, but it is not useful in ASD (see Sect. 21.5).

21.2.2.14 RVH Criterion 14 – Abnormally Prolonged QRS Duration

On average, the QRS is prolonged, but the variation is so great that the criterion is only of limited value. Most often, a clearly prolonged QRS duration is part of RBBB, but, occasionally, it is seen as part of ASD, with considerable terminal right conduction delay.

21.2.2.15 RVH Criterion 15 – T-Wave Abnormality

This is not useful in ASD (see Sect. 21.5).

21.2.2.16 RVH Criterion 16 – ST Segment Abnormality

With severe RVH, ST-segment abnormality may occur, although it is not as common or extensive as in severe LVH. The abnormal ST-segment vector is directed posterior and to the left, so that it is recognized in the standard ECG as ST depression in the right chest leads. It is not expected in ASD.

21.2.2.17 RVH Criterion 17 – T Vector Anterior Leftward

An upright T wave in leads V_4R and V_1 after age 72 h is abnormal, and is indicative of RVH. It does not appear to occur in ASD.

21.3 Atrial Septal Defect (Ostium Primum Type)

This condition is considered here without mitral valve abnormality. The horizontal plane electrocardiogram of the ostium primum defect without mitral regurgitation is identical to that of the ostium secundum type [41]. All else being equal, the amount of RVH is dependent upon the amount of left-to-right shunt. However, because this is an endocardial cushion defect, an abnormally superior vector loop is present (Fig. 21.6). (The term "abnormally superior vector" is utilized instead of the inaccurate and inappropriate term, "left axis deviation.") It is specifically defined, in the frontal plane, as initial inferior, usually rotating counterclockwise, and terminally superior. In addition to the premise that axis deviation is a term that is inaccurate and not useful (mean vector is preferred), a normal mean vector is usually further to the left than is the abnormally superior vector. Another term commonly used is left anterior hemiblock, since the electrocardiogram is identical. However, here the term left anterior hemiblock is reserved for that of an abnormally superior vector loop which develops after a disease or surgical injury, in situations where the ECG was previously known to demonstrate a normal inferior vector.

The genesis of the congenital abnormally superior vector almost always implies an endocardial cushion defect, even when it is part of other congenital lesions such as tricuspid atresia or double outlet right ventricle. It can also be part of the Noonan syndrome, for reasons not completely clear, although there may be some left ventricular cardiomyopathy in patients with Noonan's syndrome.

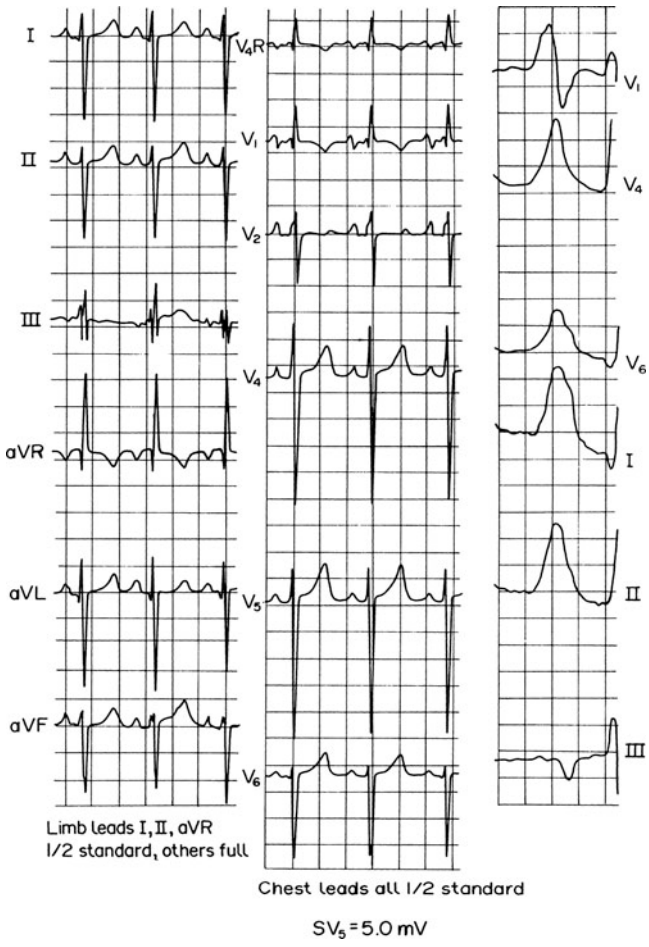

Figure 21.6

Standard ECG in a 2½-year-old child with a large ASD of the ostium primum type. On the right is a simultaneous recording of the P wave in leads V_1, V_4, V_6, I, II, III at 4 x standard and 100 mms^{-1} for purposes of atrial analysis. The first portion of the P wave is of increased magnitude inferiorly and anteriorly, so that there is right atrial enlargement. No left atrial enlargement is present. There is the classical abnormally superior maximum QRS vector of endocardial cushion defects (with initial QRS inferior, as it must be to make the diagnosis). There is more marked RVH than is usual, yet right ventricular pressure is only minimally above normal. (After Liebman et al. [8].)

Whether the left anterior branch has been surgically injured or whether the abnormally superior vector is congenital as in patients with endocardial cushion defect, BSPMs have shown late and prolonged superior activation [42]. The genesis of the initial inferior activation is related to the fact that whereas the left side of the septum is activated by the posterior branch of the left bundle, the initial superior vector in the normal person is the result of activation of the left anterior branch of the left bundle. Therefore, when there is a true "abnormally superior vector loop" or left anterior hemiblock, the normal initial superior activation does not occur. The consequence is an initial inferior vector [43, 44].

21.4 Single Atrium

The true single atrium is rare, but since it includes the area of the ostium primum, an endocardial cushion defect is part of the lesion. Therefore, an abnormally superior vector is present.

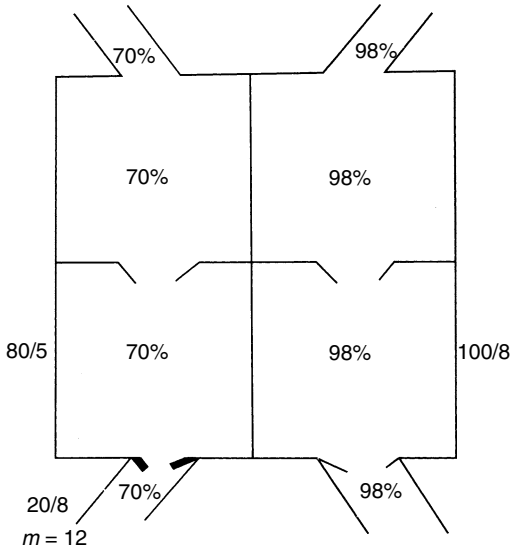

Figure 21.7
Box diagram of pulmonic stenosis with intact ventricular septum. The oxygen saturations are normal. The right ventricular pressure is elevated, in this case to near systemic level.

21.5 Pulmonic Stenosis with Intact Ventricular Septum

Pulmonic stenosis (PS) is, almost invariably, purely valvular. Infundibular pulmonic stenosis, when present as the only lesion, is believed to have been associated with a ventricular septal defect (VSD), which had previously closed. Occasionally, an anomalous right ventricular muscle bundle could have been the cause of the PS, although here too, a VSD has often been present. The spectrum of severity in valvular PS is from a trivial narrowing with minimal or no increase in right ventricular pressure (RV pressure), to that of extremely severe narrowing resulting in suprasystemic pressure in the right ventricle. The hemodynamics, therefore, is that of pure pressure overloading of the right ventricle (Fig. 21.7). Occasionally with suprasystemic RV pressure there is a right-to-left shunt at the atrial level through a foramen ovale. The hemodynamic consequence is cyanosis and less than normal volume in the right ventricle. The pressure and volume in the left ventricle remain normal.

RAE is expected with increased pressure overload of the right ventricle, since compliance of the right ventricle is diminished. RVH is common in PS and the various criteria for RVH from Sect. 21.2.2 in the presence of PS are discussed here.

21.5.1 RVH Criterion 1 in Pulmonic Stenosis

In the mildest PS, the ECG may be normal. With slightly increased RV pressure, the activation sequence remains normal, with an increased QRS terminal vector to the right, often associated with a decreased posterior projection. Therefore, there will be a terminal r or R in V_4R and/or V_1, since the terminal vector crosses the V_4R and/or V_1 lead vectors (Fig. 21.8). This can occur, of course, without terminal right conduction delay, but the latter is sometimes present in the RVH of the pure pressure load hypertrophy of PS. As expected, since there is a spectrum of severity of valvular PS, the RVH severity varies. As the PS increases, the maximum QRS vector is less posterior and the terminal vector is more to the right so that the horizontal plane may show a crossed loop with two main vectors. With increased severity, the vector loop is almost entirely anterior, with a clockwise direction of inscription (Fig. 21.9). Rarely, in severe PS, the terminal QRS vector is markedly posterior with a clockwise direction of QRS loop inscription. With increased severity, the initial QRS is to the

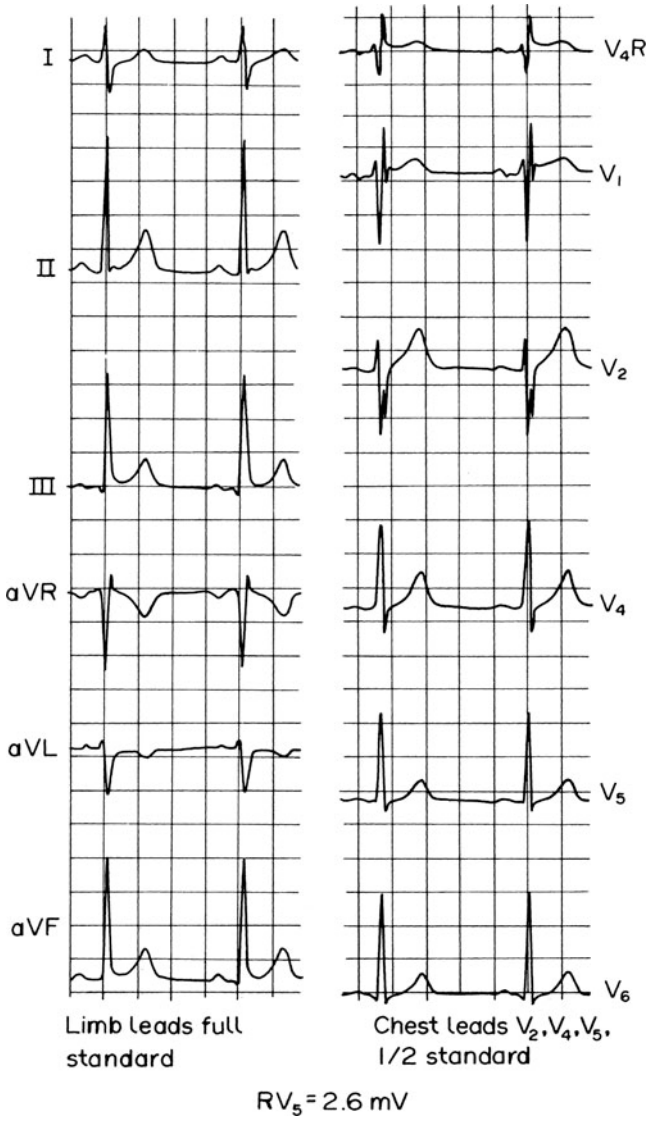

Figure 21.8
Standard 12-lead ECG of a 17-year-old male who had surgery for moderately severe valvular pulmonic stenosis (PS), via the pulmonary artery. The right ventricle was not entered and RBBB did not develop. The RVH gradually decreased until it stabilized with this ECG. Mild residual PS remains. There is trivial RVH on the basis of the anterior T vector and terminal R′ in V_4R and V_1. (After Liebman et al. (1982). © Williams and Wilkins, Baltimore, MD. Reproduced with permission.)

left and anterior, suggesting suprasystemic right ventricular pressure [40] (Fig. 21.10). The mechanism for the initial QRS to the left in severe pulmonic stenosis has been hypothesized utilizing body surface potential maps [24, 45, 46].

21.5.2 RVH Criterion 2 in Pulmonic Stenosis

When the PS is very severe, the initial QRS is frequently to the left and anterior. Suprasystemic pressure must then be considered, although the mechanism can only be hypothesized. The ECG of initial QRS activation is due mainly to four

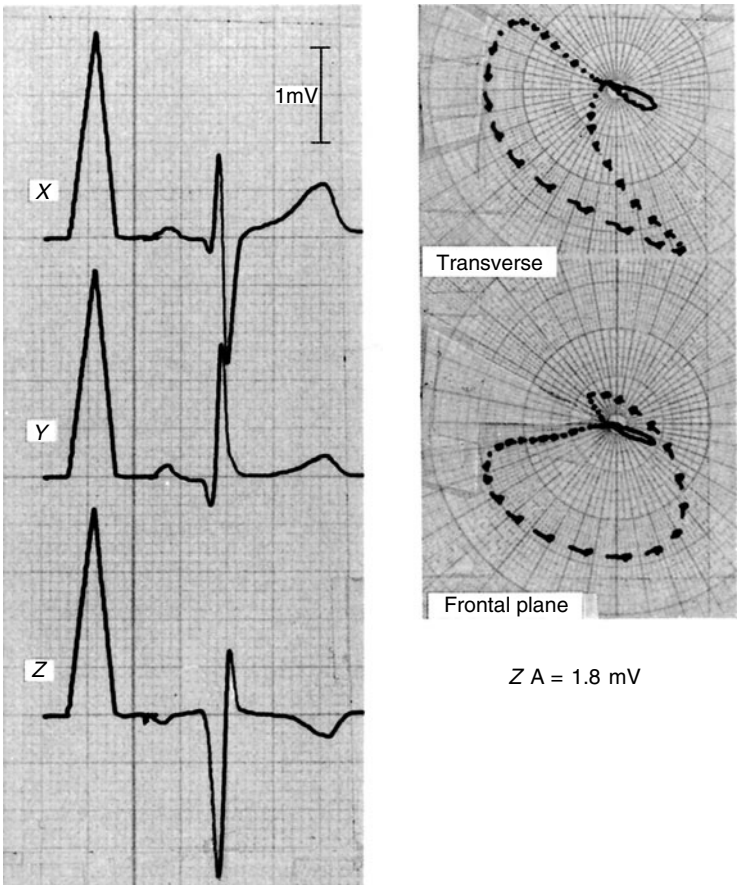

Figure 21.9

Frank-system orthogonal ECG of a 20-month-old female with valvular PS and RV pressure just under systemic level. The initial QRS is to the right, consistent with the RV pressure being less than suprasystemic. The wide open clockwise vector indicates considerable RVH. There are two main vectors, the first to the left and anterior, the second to the right and posterior. The magnitude left is within normal limits so that additional LVH is not present. (In the standard ECG, the initial vector to the left may be *above* the 95th percentile and additional LVH diagnosed, yet the cause in this case is only a proximity effect because the right ventricle is so large that the V_5 lead is too close to it. This artifact is *less* likely in the Frank or axial (McFee–Parungao) orthogonal ECG systems). (After Liebman et al. [8]. © Williams and Wilkins, Baltimore, MD. Reproduced with permission.)

components, namely the left septum 1/2 to 2/3 down the septum, the free posterior wall adjacent to the left septum, the right septum (somewhat more inferior than the left septum), and the right ventricular endocardium. (A fifth area responsible for initial superior activation has been discussed above.) Immediately following is activation of the free anterior wall including the portion near the septum. Rotation of the septum owing to the high RV pressure appears to be an insignificant factor in the presence of pressure overloading, so that aspects of initial activation as described above appear most important. Right septal hypertrophy could also be a factor, but this cannot be anatomically documented. The most likely hypothesis is that the marked hypertrophy of the anterior wall inferior to the position of normal initial activation extends to the left of the position of normal initial activation. It is also possible that the sequence of initial activation has changed so that different components become more important. The answers may not be easily available, but perhaps they will be found through detailed studies involving endocardial and epicardial mapping in humans. Body surface mapping appears to have confirmed the above hypothesis [45, 46].

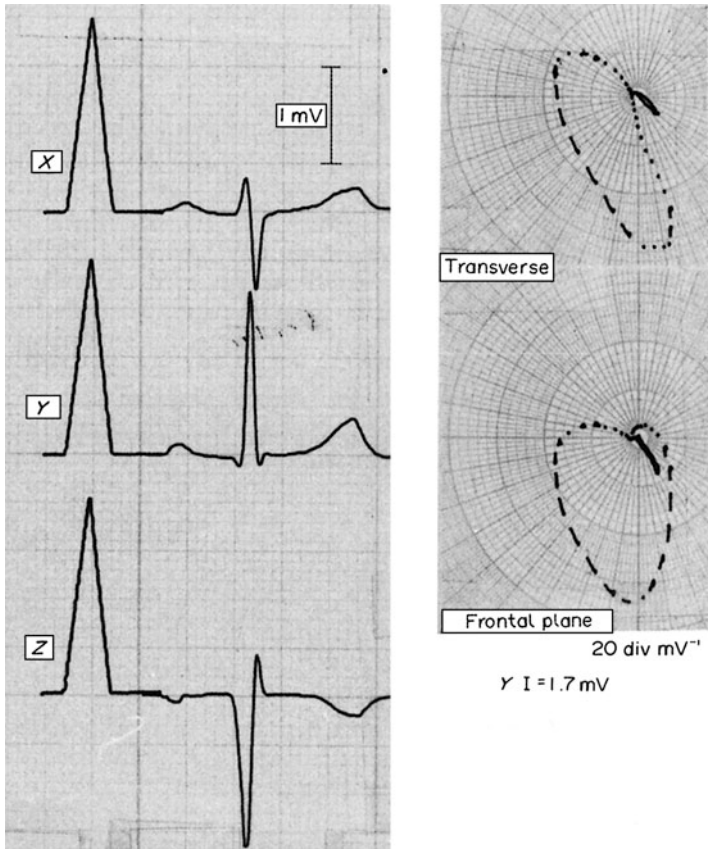

Figure 21.10

Frank-system orthogonal ECG of a 3-year-old female with valvular PS and RV pressure above systemic level. The initial QRS to the left is consistent with suprasystemic RV pressure, although not all patients with PS and intact ventricular septum and initial QRS to the left have suprasystemic pressure. However, when initial QRS is *not* to the left, the suprasystemic RV pressure is not likely to be present.

Occasionally the initial leftward QRS vector is far enough to the left so that the V_4R and/or V_1 lead vectors are not crossed. The result is a qR complex in those leads. The qR in V_4R and V_1, therefore, provides another indication of severity. A qR in V_2, because the initial QRS vector is to the left and posterior, is also very occasionally seen and is an indication of even greater severity. Usually in such patients, however, the VCG does not demonstrate this vector to be to the left and posterior (because V_2 is not reliably comparable to lead Z).

21.5.3 RVH Criterion 6 in Pulmonic Stenosis

This criterion is the single most reliable criterion of RVH and in known PS has been shown to provide at least as good an index for estimation of RV pressure as the more tediously calculated MSVR [35].

21.5.4 RVH Criterion 7 in Pulmonic Stenosis

As described above, an rsŕ or rsŔ pattern is very common in the ECG associated with pure valvular PS even though there is pressure overload. With increased severity of the PS, the right chest leads demonstrate a pure R (because the vector is mostly anterior) or a qR when the initial QRS is well to the left.

21.5.5 RVH Criterion 13 in Pulmonic Stenosis

In PS this criterion has been used as a specific predictor of the RV pressure in valvular PS with intact ventricular septum. Present data indicates a correlation coefficient of 0.65 to 0.70 for the Frank system (lower with McFee–Parungao) [35], although the originally published data claimed much higher correlation. In any case, the confidence interval for specific patients is so wide that the criterion is best used considering the individual patient as his or her own control, just as for magnitude of the terminal QRS vector to the right; e.g., when looking for change over a period of time.

21.5.6 RVH Criteria 16 and 17 in Pulmonic Stenosis

With very severe PS, ST-T abnormality may be present. There may be ST depression in the right chest leads and/or the T vector may be abnormally posterior and, usually, to the left. Very occasionally, the T vector may even be to the right so that the T is inverted from V_4R to V_5 (Fig. 21.11). The deviation of T from QRS is less in the frontal than horizontal planes. A special T abnormality must be mentioned which is not related to severity and is not well understood. An anterior leftward T vector is abnormal after age 72 h (T upright V_4R, V_1, V_2, as well as V_5, V_6) (Fig. 21.12). This empiric indication of RVH may be present in mild PS even in the presence of a normal QRS.

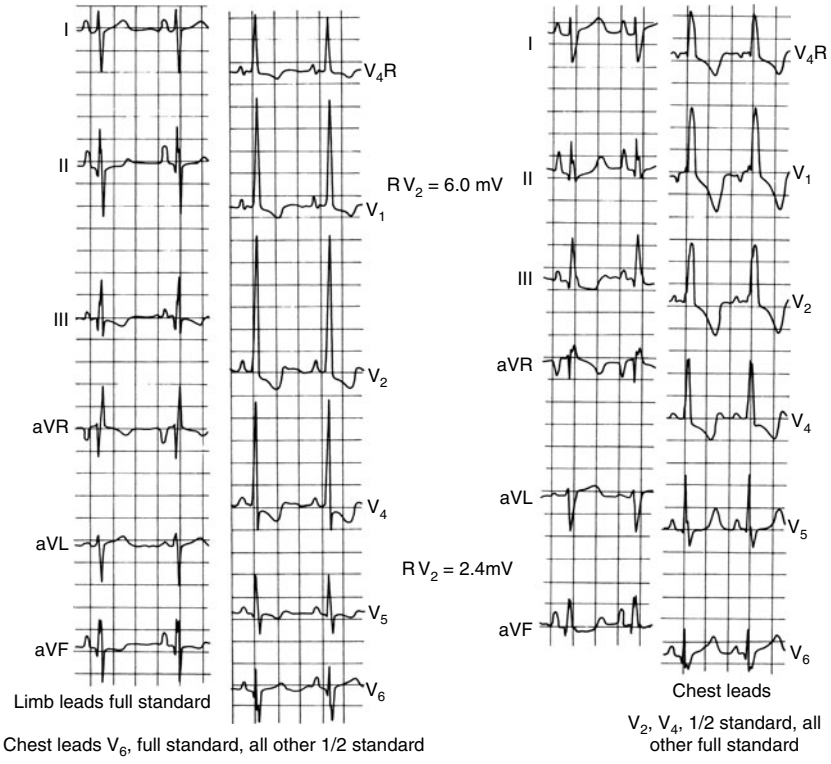

Figure 21.11

Standard ECG before (left) and after (right) surgery in a 22-month-old male with severe PS and suprasystemic RV pressure. Note that initial QRS is *not* to the left (a rare exception) but there is marked ST and T abnormality so that the T vector is to the right and posterior. Right atrial hypertrophy is also present. Following surgery (the surgeon had to enter the right ventricular outflow tract via the pulmonary artery) advanced RBBB developed. (A few years later, the RBBB resolved.) (After Liebman *et al*. [8]. © Williams and Wilkins, Baltimore, Maryland. Reproduced with permission.)

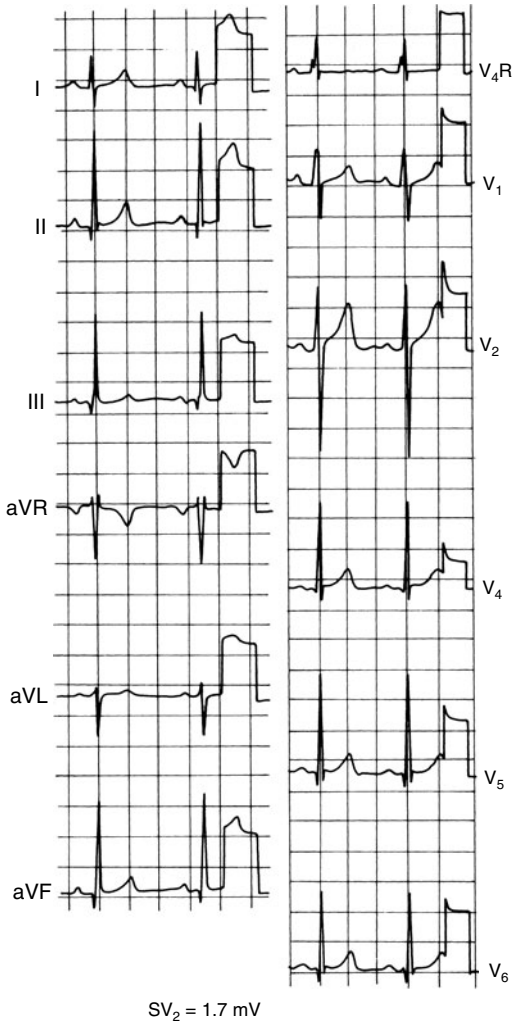

Figure 21.12
Note the anterior T waves in right chest lead, an unexplained indication of RVH after 72 hours of age.

21.6 Total Anomalous Pulmonary Venous Return to the Right Atrium

This condition, known as TAPVR, comes in two major varieties, with or without pulmonary venous obstruction. In either case, the RVH is severe, so that the hemodynamic variations are not considered pertinent to this section. In the majority of patients after early infancy, there is no significant pulmonary venous obstruction. Almost invariably, the four pulmonary veins drain into a common pulmonary venous trunk, which has not been normally incorporated into the left atrium. Drainage is then via a systemic vein, frequently primitive, to the right superior vena cava, left superior vena cava or coronary sinus, and thereafter, to the right atrium. The result (see Fig. 21.13) is a tremendous volume overload of the right side of the heart. As with atrial septal defect, and for similar reasons, there is only moderate elevation of RV pressure, although since the increase in pulmonary blood flow is obligatory and early, there may be a significant RV pressure elevation in some cases. Another significant aspect is that, because there has been decreased volume into the left atrium and left ventricle in utero, as well as after birth, the left atrium and left ventricle may be small. In addition embryologically, since the common trunk has not been incorporated into the primitive left atrium, the resulting left atrium

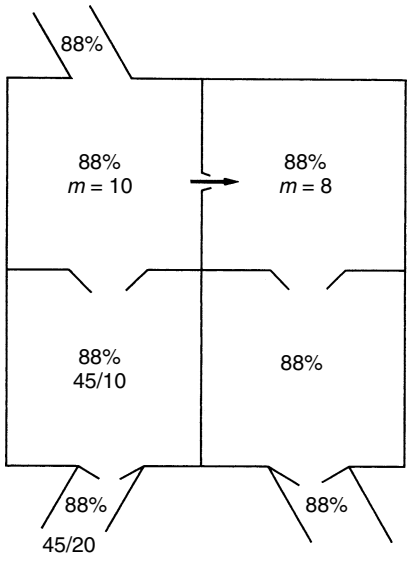

Figure 21.13

Box diagram in total anomalous pulmonary venous return (TAPVR) with low pulmonary vascular resistance, so that the pulmonary artery pressure is only minimally elevated. The common pulmonary venous trunk (posterior to left atrium) drains into a systemic vein and then into the superior vena cava. Therefore there is a very large volume overload into the right atrium and ventricle estimated as at least four times normal. The left atrium is embryologically small and the left ventricle may also be small, contributing to the marked RVH. The ventricular septum usually bows into the left ventricle.

may be very small. In patients with pulmonary venous obstruction, the usual anatomy is that the systemic vein from the common trunk drains below the diaphragm to the portal vein or even hepatic vein. The pulmonary venous obstruction is in the liver and is intense. The increase in volume work of the right ventricle may be minimal, but because of the severe elevation of pulmonary venous pressure in utero, the pulmonary vascular resistance is greatly elevated. Usually, the pulmonary artery pressure is suprasystemic. In both the unobstructed and obstructed types of TAPVR, the former mainly because of volume overload, the latter mainly because of pressure overload, the RVH is severe (Fig. 21.14). The small left ventricle adds to the RVH. The two types of TAPVR cannot be separated on the basis of the ECG. With increased volume and pressure in the right atrium, as well as decreased compliance of the right ventricle, RAE is usually considerable.

21.6.1 RVH Criterion 1 in TAPVR

The initial QRS is usually to the left and may be posterior. At the time of activation of the free walls of each ventricle, the right ventricle usually dominates. More often than not, the maximum QRS vector does not ever go posterior, so that after reaching a brief maximal deflection to the left, the vectors are anterior and to the right. A clockwise horizontal plane vector usually results, with the main vector well to the right and anterior.

21.6.2 RVH Criterion 2 in TAPVR

For the reasons described for severe PS in Sect. 21.5.2, the initial QRS is usually to the left and anterior. In addition, the large volume right ventricle together with the small left ventricle results in the lower septum bowing into the left ventricle. Consequently, the initial QRS is often even posterior as well as to the left (Fig. 21.15).

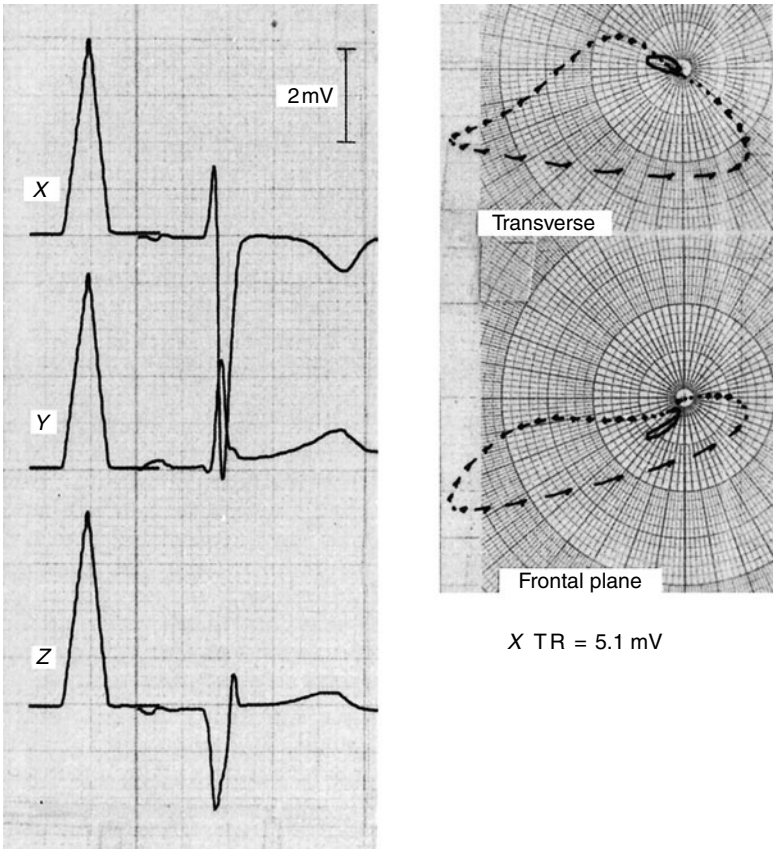

Figure 21.14

McFee-Parungao system orthogonal ECG and vector loops of a seven year old male with TAPVR and low pulmonary vascular resistance. The magnitude of the terminal vector of the right (XTR) is remarkably large, even for the McFee-Parungao system, where voltages are greater than in the Frank system. The T vector to the right and posterior, is very abnormal although there was only volume overload. In the standard ECG, the T wave was inverted from $V_Y r$ through V_6 (After Liebman et al. [8]. © Williams and Wilkins, Baltimore, MD (1982). Reproduced with permission).

21.7 Hypoplastic Left Ventricle Syndrome

In the most severe form of the hypoplastic left ventricle syndrome, there is little or no left ventricular cavity, with no blood in it. There is a hypoplastic ascending aorta, aortic atresia and mitral atresia. Therefore, all pulmonary venous flow must go through a usually restrictive atrial opening into the right atrium, right ventricle and pulmonary artery. There is a high pulmonary vascular resistance, so that there is a right-to-left shunt through a patent ductus arteriosus into the descending aorta. Therefore, even in cases where the hypoplastic left ventricle syndrome is less severe, for example, with aortic stenosis and/or mitral stenosis intead of atresia, the RVH is severe (Fig. 21.16). There is marked volume and pressure overload, to which is added the small left ventricle.

In addition to RAE, there is marked left atrial enlargement (LAE) as well. The left atrial pressure is very high and there is volume overload, with the only egress being the restrictive atrial opening.

The direction of inscription of the QRS vector loop and the initial portion are similar to those of the marked RVH of total anomalous pulmonary venous return. In approximately half of the children with hypoplastic left ventricle syndrome, the initial QRS is posterior as well as to the left (Fig. 21.17). Very infrequently the initial QRS is to the right. Rarely, the

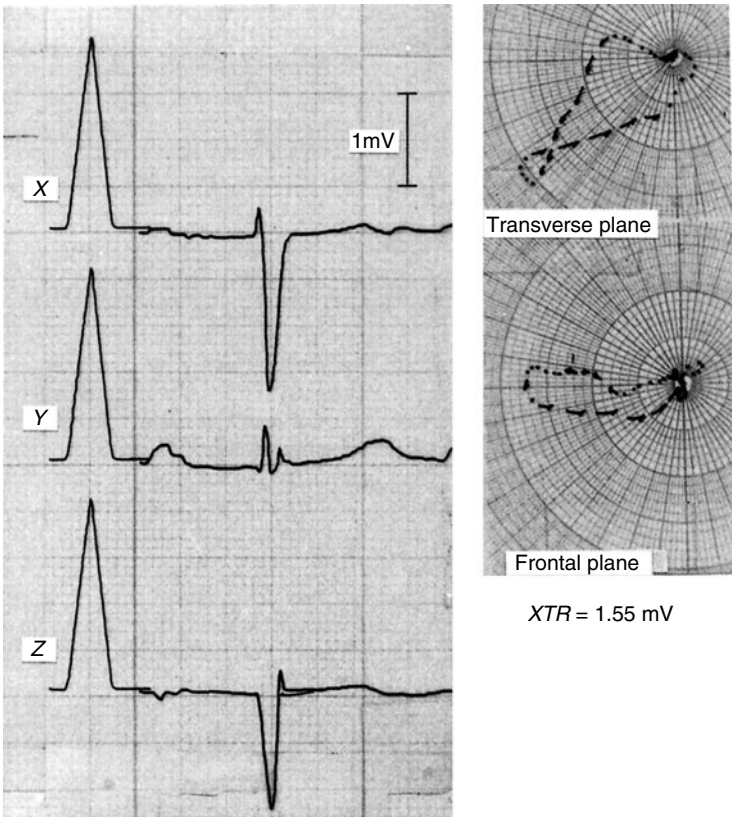

Figure 21.15

Frank system orthogonal ECG and vector loops of a 16 month old male with TAPVR to the superior vena cava and low pulmonary vascular resistance. There was marked right ventricular volume overload as in figure 21.14. The initial QRS is to the left, indicating the severity of the RVH, but it is also posterior, consistent with even more severe RVH. The fact that the septum is bowed into the left ventricle contributes to this unusual QRS (After Liebman et al. [8]. © Williams and Wilkins, Baltimore, MD (1982). Reproduced with permission).

ECG may show good left chest potentials [47], most likely because of the large volume right ventricle extending well to the left, providing a proximity effect.

21.8 Complicated Coarctation of the Aorta

The most common combination of lesions making up this syndrome is that of severe coarctation of the aorta (in the normal position near the left subclavian artery) together with a ventricular septal defect and/or patent ductus arteriosus. Although the pulmonary vascular resistance after birth remains high, the resistance to flow through the coarctation is even greater, so that there is an early left-to-right shunt. Consequently, the left ventricle is hypertrophied and dilated owing to great pressure and volume work. Nonetheless, the ECG often demonstrates pure RVH (Fig. 21.18). It is believed that the effects in utero are responsible. Prior to birth, the right ventricle, working against the newborn's very high pulmonary vascular resistance, sends blood through the ductus arteriosus and then, presumably, through the coarctation. It is hypothesized that prior to birth this extra work of the right ventricular myocardium results in cellular hyperplasia, which persists after birth. Thus, there is hypertrophy of more cells. In addition, because of left ventricular failure after birth, there is a high pulmonary venous pressure, resulting in pulmonary hypertension. Although simple coarctation is

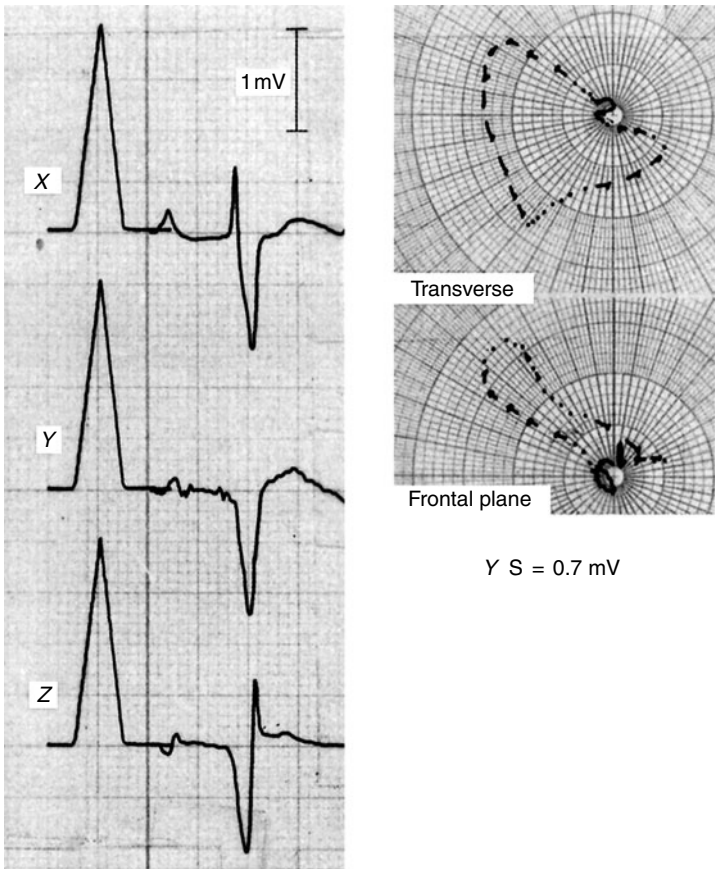

Figure 21.16
Frank system orthogonal ECG with vector loops of a five day old male with the hypoplastic LV syndrome. The initial QRS is to the left, is part of the severe RVH. There is also ST abnormality as manifested in the unclosed ST segment directed posterior in the transverse plane. The elevation of ST in the Z lead is derived from the same observation. The frontal plane is unusual being entirely superior. It is not related to an "abnormally superior QRS vector" since the initial QRS is not inferior. Explanations can only be hypothesized (After Liebman et al. [8]. © Williams and Wilkins, Baltimore, MD (1982). Reproduced with permission).

expected to have pure LVH, the infant with severe narrowing occasionally has pure RVH. Although this usually changes to LVH in a few months, occasionally it may persist (Fig. 21.19). Many years after successful surgery for simple coarctation of the aorta BSPM has shown mild RVH in many [48]. The mechanism is believed to be cellular hyperplasia with hypertrophy shortly after birth.

21.9 Transposition of the Great Arteries with Intact Ventricular Septum

The hemodynamics of transposition of the great arteries is one of constant change after birth. In most cases, the anatomy demonstrates in addition only a foramen ovale, no atrial septal defect, with minimal left-to-right shunt and right -to-left shunt at that level. The ductus arteriosus, because of low systemic PO_2, remains open for a variable, but brief, period of days, allowing some low-oxygen blood to go from the aorta to the pulmonary artery. Pulmonary vascular resistance does not decrease as rapidly as in normal babies, so that pulmonary blood flow (and thus left ventricular flow) is only a little above normal. Left ventricular pressure (LV pressure) gradually decreases over the first few days. On balance, the work of the left ventricle is a little above normal and this, together with the right ventricle working against systemic pressure,

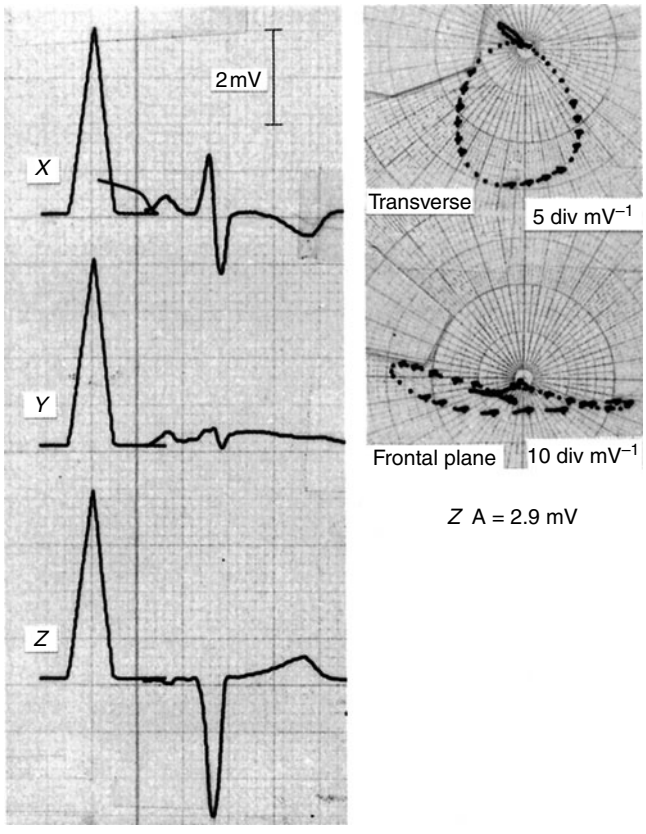

Figure 21.17

Frank system orthogonal ECG with vector loops in a six year old female with the hypoplastic left ventricle syndrome (unusually old for this condition). The RVH is severe with the initial QRS vector directed left and posterior (as in half such babies) and the T vector to the right posterior (After Liebman et al. [8]. © Williams and Wilkins, Baltimore, MD (1982). Reproduced with permission).

usually results in a normal vectorcardiogram (Fig. 21.20). Occasionally, there is some right ventricular hypertrophy. After successful balloon atrial septostomy, the pulmonary vascular resistance usually decreases and the ductus arteriosus closes. There is then significant bi-directional shunting at the atrial level. The volume of work of the systemic right ventricle is above normal and that of the left ventricle is very much increased. However, because of the low pulmonary vascular resistance, LV pressure is quite low; for example, 40 mm Hg. Therefore, pure, often considerable, RVH can be expected (Fig. 21.21). Then, if an "atrial switching" operation, such as the Mustard or Senning procedure, is successfully accomplished, the result is that left ventricular volume is normal with low left ventricular pressures. Consequently, the RVH is now severe (Fig. 21.22). In many such patients, there is significant pulmonic stenosis, but the expected additional LVH is often not recognized. After successful arterial switching surgery (now a standard of care), the electrocardiogram usually gradually normalizes.

21.10 Tetralogy of Fallot

In tetralogy of Fallot (TOF), by definition, there is a nonrestrictive ventricular septal defect (so that the RV and LV pressures are equal), with pulmonic stenosis being severe enough so that resistance to flow into the pulmonary artery is greater than resistance to flow into the aorta. The result is a right-to-left shunt. Although an overriding aorta is not necessary to create the hemodynamics, it is usually present in the embryological TOF. In the maximally severe TOF,

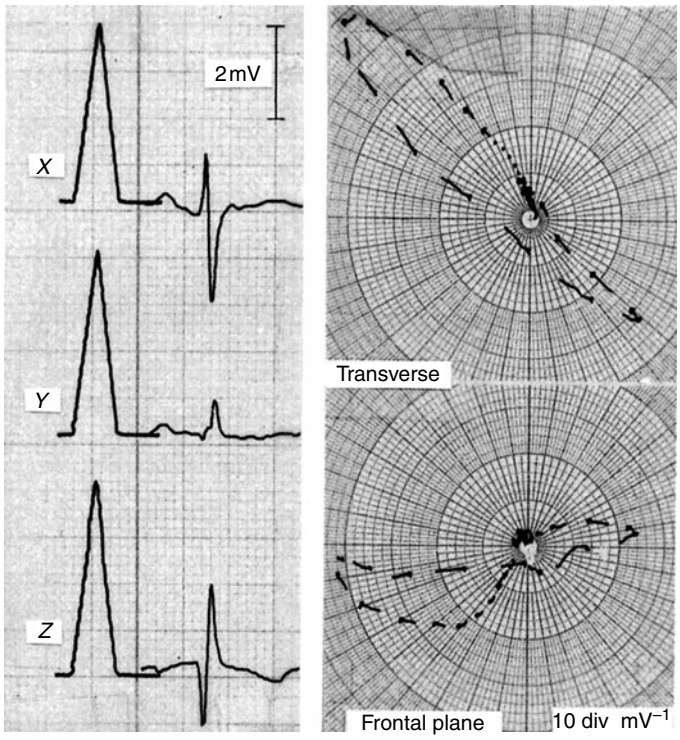

Figure 21.18

Frank system orthogonal ECG with vector loops in a three month old male with coarctation of the aorta, ventricular septal defect and mitral stenosis. The RVH is considerable. The horizontal plane vector loop is clockwise with the large terminal right vector (XTR) markedly posterior. (The large terminal right posterior projection is part of the RVH. The diagnosis of additional LVH would be an error). (After Liebman et al. [8]. © Williams and Wilkins, Baltimore, MD (1982). Reproduced with permission).

there is pulmonary atresia, so that 100% of right ventricular blood goes from right to left through the VSD. The pulmonary blood flow is then by way of a ductus arteriosus or bronchial arteries. A typical moderately severe TOF, with 50% of right ventricular blood going from right to left through the VSD, is depicted in Fig. 21.23.

Right ventricular volume work is normal, at systemic pressure, while left ventricular volume work is less than normal, at normal pressure. Pure RVH, therefore, is expected. (Note that if a systemic-pulmonary artery shunt is created, there is increased left ventricular volume work to accompany the RV pressure work) so that LVH may also develop.

With regard to the effect on atria, RAE is usually found in TOF. The effect on ventricles is discussed according to the criteria laid down in Sect. 21.2.2.

21.10.1 RVH Criterion 1 in TOF

Because the hypertrophy is usually severe, the RVH is much as described for severe valvular PS with intact ventricular septum. An exception is that in the most severe form, often associated with the lowest arterial oxygen saturation, the clockwise-inscribed vector loop turns quickly to the right (after beginning to the left) before terminating markedly posterior. The result in the standard ECG is often that the only QRS complexes where R > S are V_4R and V_1 (Figs. 21.24 and 21.25). Occasionally, the only complex with R > S is V_4R, so that unless there is an orthogonal VCG, the diagnosis of RVH may be difficult to make. Careful vector analysis of the chest leads, however, should reveal that the horizontal plane is rotated clockwise (Fig. 21.26).

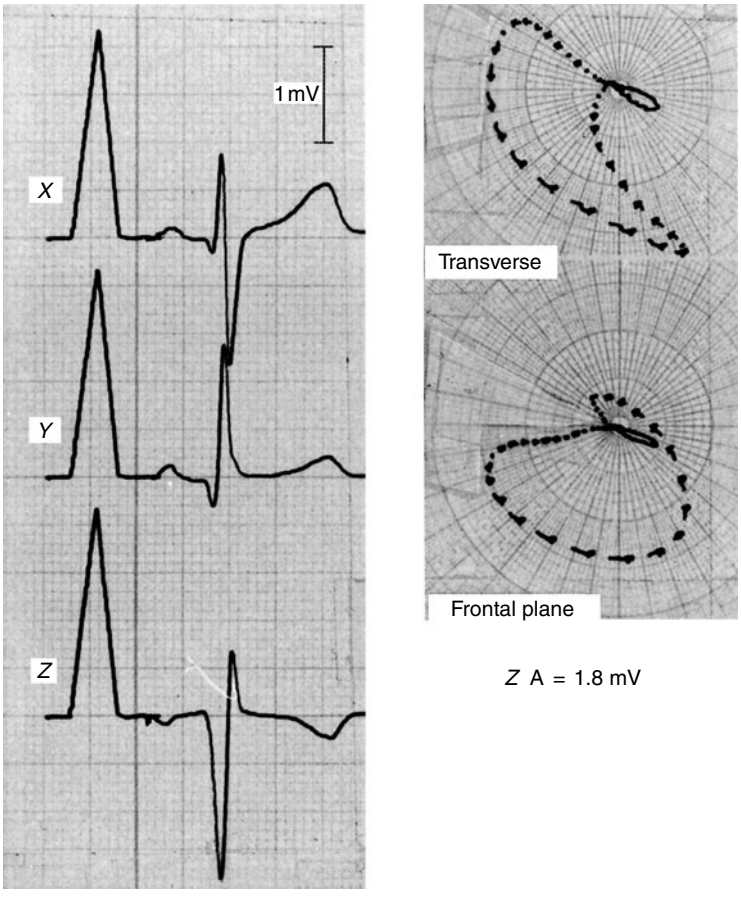

Figure 21.19

Frank system orthogonal ECG with vector loops in a 21 year old female with severe simple coarctation of the aorta. The diagnosis is RVH with no evidence for additional LVH.

21.10.2 RVH Criterion 2 in TOF

The initial QRS vectors are usually to the left and anterior (Figs. 21.27 and 21.28) since the RVH is severe.

21.10.3 RVH Criterion 9 in TOF (R in AVF)

The abnormally tall R in aVF by itself, in the presence of prominent left chest potentials, suggests the diagnosis of left ventricular hypertrophy since the more inferior ventricle is the left ventricle. However, it is an error, in the presence of significant RVH, to diagnose additional LVH when an abnormally tall R in aVF is present. In this case, the prominent inferior vector is part of RVH, presumably from hypertrophy of the inferior right ventricle. This criterion is extremely common in the presence of TOF (Fig. 21.24).

21.10.4 RVH Criterion 16 and 17 in TOF

ST-T abnormally (with the T vector well to the right and posterior) is very unusual in TOF, even when very severe, but can occur (Fig. 21.25).

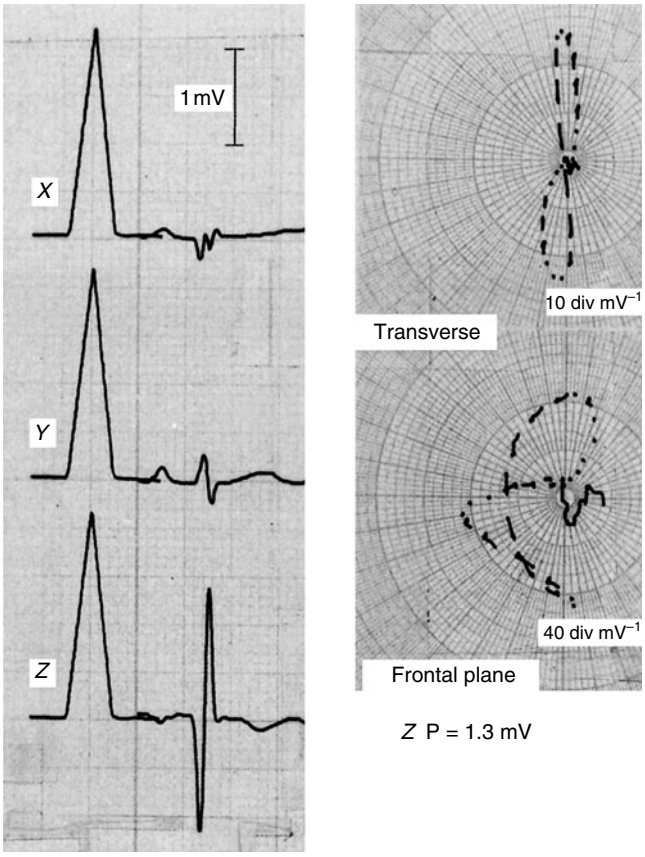

Figure 21.20
Frank system orthogonal ECG with vector loops in a five day old with simple transposition of the great arteries with intact ventricular septum (the frontal plane vector loop is at 40 div(mv^{-1}) (so that voltage is quite low). The ECG is normal (very unusual).

21.11 Obstruction of Outflow From the Left Atrium

This includes congenital mitral stenosis (multiple varieties), supravalvular stenosing ring, and cor triatriatum. All of these have the same pathophysiology, unrelated to the varying embryology. The cause of the RVH is elevation of pulmonary venous pressure. Should the obstruction be significant in the newborn period, when the fetal thick-walled pulmonary arterioles remain, the RVH may be severe. Should the obstruction become significant later in life, it may take time, as the pulmonary arterioles become more muscular once again, before significant RVH develops. Both left and right atrial hypertrophy (LAE and RAE, respectively) will be present [8, 33, 49–53]. The reliability of the reading of LAE is only fair although reliability of reading RAE is very good.

21.12 Nonrestrictive LV-RV Communication with Pulmonary Vascular Disease

An example of this is ventricular septal defect. The degree of RAE or RVH depends upon the severity of the pulmonary vascular disease, just as in tetralogy of Fallot, where the degree of RAH or RVH depends upon the severity of the pulmonic stenosis. The box diagram in Fig. 21.29 is explanatory.

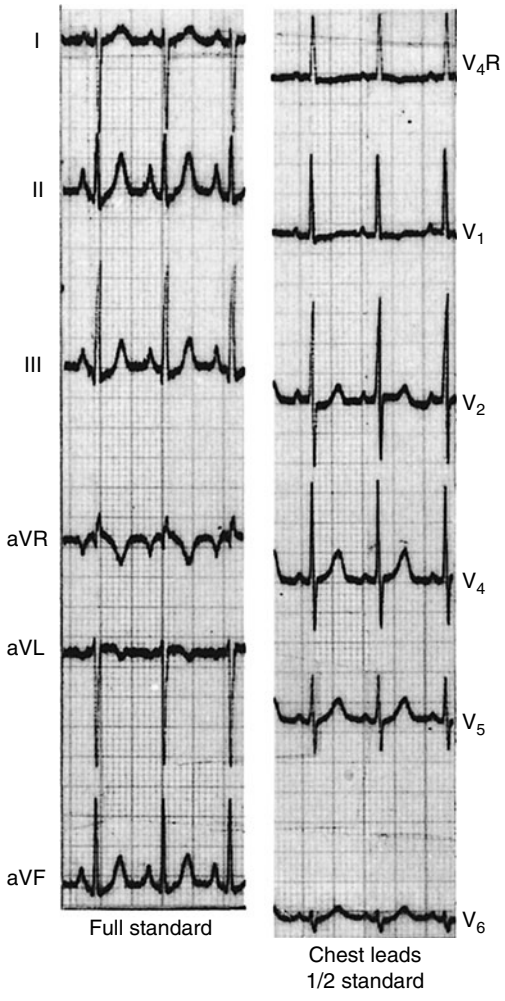

Figure 21.21

Standard ECG in a three month old male with simple transposition of the great arteries and intact ventricular septum. A balloon atrial septostomy had been done in the newborn period. The RVH is moderate. Note that the initial QRS is to the left. Right atrial hypertrophy is present on the basis of the first part of the P wave inferior and anterior having a large magnitude.

However, in patients with large ventricular septal defect, there is likely to have been a period before the pulmonary vascular disease developed when there was significant left-to-right shunt. Therefore, there may be less RVH than in TOF, owing to previous hemodynamics.

21.13 Patent Ductus Arteriosus

In pediatrics, the isolated patent ductus arteriosus (PDA) must be discussed in two contexts. First, there is the PDA associated with the newborn, usually prematurely born, often with respiratory distress syndrome; and second, there is PDA that is congenitally open, and manifest after the newborn period. The ductus in the former is presumed to be kept open mainly because of the hypoxia associated with the pulmonary disease. The flow through it is from left-to-right, so that the left atrium and left ventricle are enlarged. However, because of the high pulmonary venous pressure

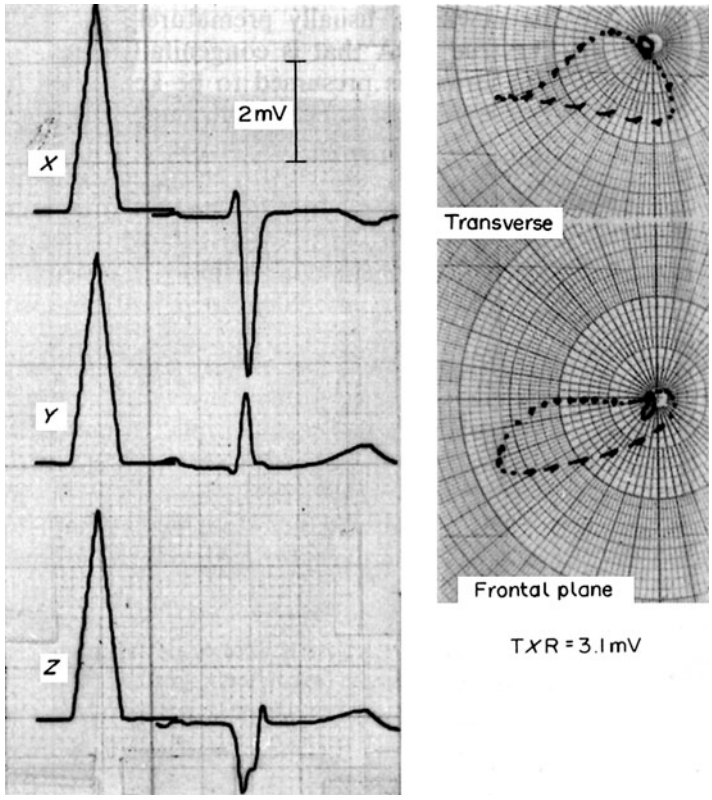

Figure 21.22

Frank-system orthogonal ECG in a 6-year-old female with transposition of the great arteries who had undergone a successful atrial switching procedure (Mustard) in the first year of life. As is typical, the RVH is very severe with initial QRS to the left, most of the clockwise-inscribed QRS vector loop to the right and the T vector posterior right. After successful Mustard operations, the right ventricle is at systemic level, and the left ventricle is usually at less than half systemic level. (After Liebman et al. [8]. © Williams and Wilkins, Baltimore, MD. Reproduced with permission.)

as well as the lung disease per se, there is likely to be significant pulmonary hypertension. Therefore, the right ventricle is involved as well. In addition, the prematurely born baby has a very low voltage and has less of the newborn's right ventricular dominance [54]. Finally, the ductus tends to open and close, the hemodynamics changing rapidly. Consequently, the ECG is not reliably useful in evaluation. The ECG is very useful, however, in the evaluation of the "true" congenital PDA.

The left-to-right shunt through the "true" PDA is not usually significant until a number of weeks after birth, related to a more gradual decrease in pulmonary vascular resistance than in normal babies. The ductus itself, because of its length, has considerable resistance, so that the majority of PDAs are associated with no more than moderate pulmonary hypertension and usually less. The work of the heart is, therefore, volume work of the left ventricle (Fig. 21.30).

There is left atrial enlargement (LAE), a term which does not attempt to distinguish between hypertrophy and dilatation. The most useful criteria for LAE are the following [8, 33, 49–53]:

(a) Standard electrocardiography [3, 16, 17, 29–31]:
  (i) Increased duration of second portion of P wave (i.e., when P is m-shaped)
  (ii) Increased P terminal force in V_1 (>0.003 mVs)
  (iii) Increased time between first and second peak of P

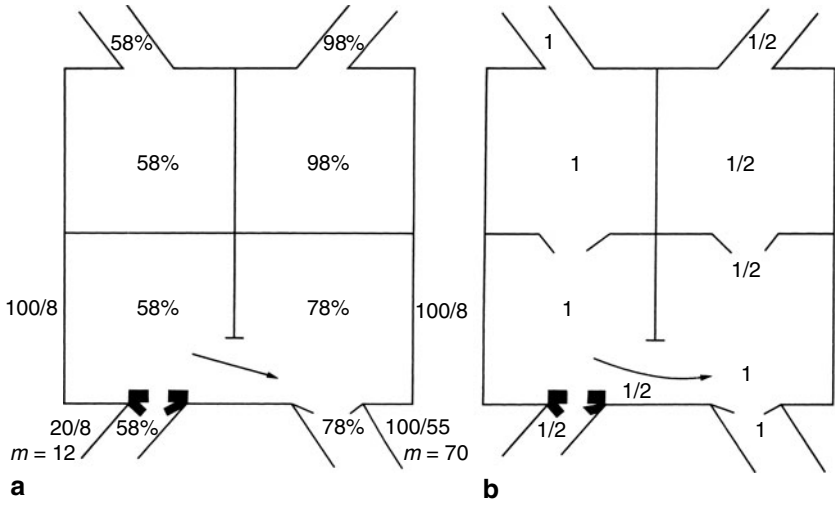

Figure 21.23

Box diagram typical of tetralogy of Fallot. In (a), the right and left ventricular pressures are equal. Resistance to flow past the severe pulmonary stenosis is much greater than is systemic artery vascular resistance. Therefore, there is considerable right-to-left shunt and no left-to-right shunt. The systemic arterial oxygen saturation is only 78%. In (b), the outputs into the pulmonary artery and aorta, and volumes in each entering great vein and each chamber are delineated. The right ventricle at systemic pressure sends blood through the severely stenotic right ventricular outflow tract and into the aorta as well. Only one-half normal volume enters the left ventricle, which sends less than the normal volume into the aorta at normal pressure. Therefore, the ECG is that of pure RVH.

(b) Orthogonal electrocardiography [3, 32–34]:
- (i) Increased P terminal force
- (ii) Increased duration second portion of P
- (iii) Increased magnitude posterior of second portion of P
- (iv) Increased time between first and second peak of P
- (v) Increased spatial magnitude at the time of maximum posterior (SVP)

21.13.1 Left Ventricular Hypertrophy

Criteria for left ventricular hypertrophy are many [35], with the most sensitive being an increased magnitude posterior in the presence of a normally inscribed horizontal plane vector loop. It is appropriate at this time to delineate all the criteria for LVH while being more specific about PDA. Then, for other defects where pure LVH is present, reference can be made to these criteria.

21.13.1.1 LVH Criterion 1 – Direction of Inscription of QRS Vector Loops

The QRS vector loops may have exactly the same configuration as in the normal, so that after infancy there is a normal initial QRS vector to the right and anterior, followed by the vector being increasingly to the left, first anterior, then clearly posterior, ending slightly to the right and posterior. However, the spatial voltage will be larger than normal. (Occasionally, particularly in severe hypertrophy, the most distal portion of the loop is to the left, but inscribed clockwise. The genesis of this is presumed to be an intraventricular conduction abnormality involving the left bundle, associated with fibrosis.) A newborn with a wide-open counterclockwise-inscribed vector loop indicates LVH no matter what the voltage.

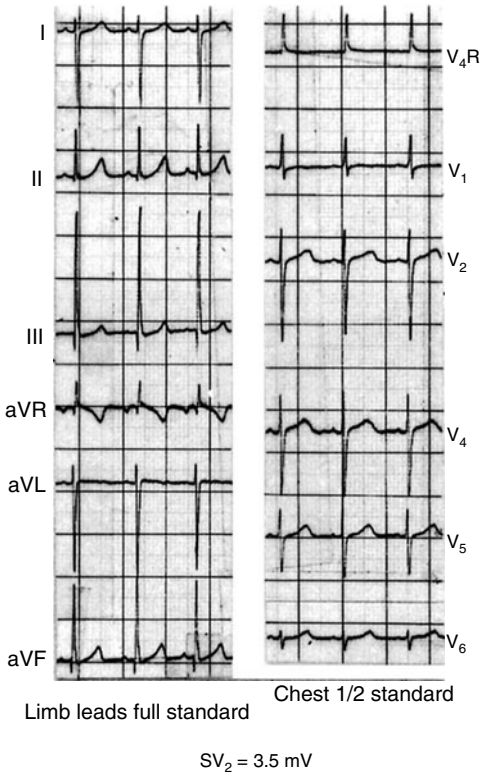

Figure 21.24

Standard ECG of a 4½-year-old male with TOF and marked RVH. There is a wide open clockwise horizontal plane vector loop which extends quickly to the right and posterior. The loop is not shown but can be derived from the standard ECG as discussed in Chap. 11. The posterior projection is very large (3.5 mV) (not part of LVH) and there is also a prominent inferior vector, seen frequently in TOF.

The direction of inscription in the frontal plane usually remains clockwise. Only occasionally does LVH cause counterclockwise inscription in the frontal plane, usually in older children with very severe LVH, but the maximum QRS vector will still be mainly inferior.

In PDA, the initial QRS vector is usually normally rightward and anterior, with normal horizontal plane direction of inscription and increased voltage both to the left and posterior.

21.13.1.2 LVH Criterion 2 – Initial QRS vector

An initial QRS vector to the left and anterior [45, 46, 55, 56] (a manifestation of severe LVH) is not usually seen in PDA. However, a large initial QRS to the right and anterior, and frequently superior, is very common. This is left septal hypertrophy, not LVH per se. (Proximity effect, particularly in the preschool child, may cause a prominent initial anterior vector, sometimes also rightward, contributing to an erroneous diagnosis of left septal hypertrophy.)

21.13.1.3 LVH Criterion 3 – Abnormally Posterior Angle of the Main or Mean QRS Vector

This is only a fair sign of LVH because of so much normal variability.

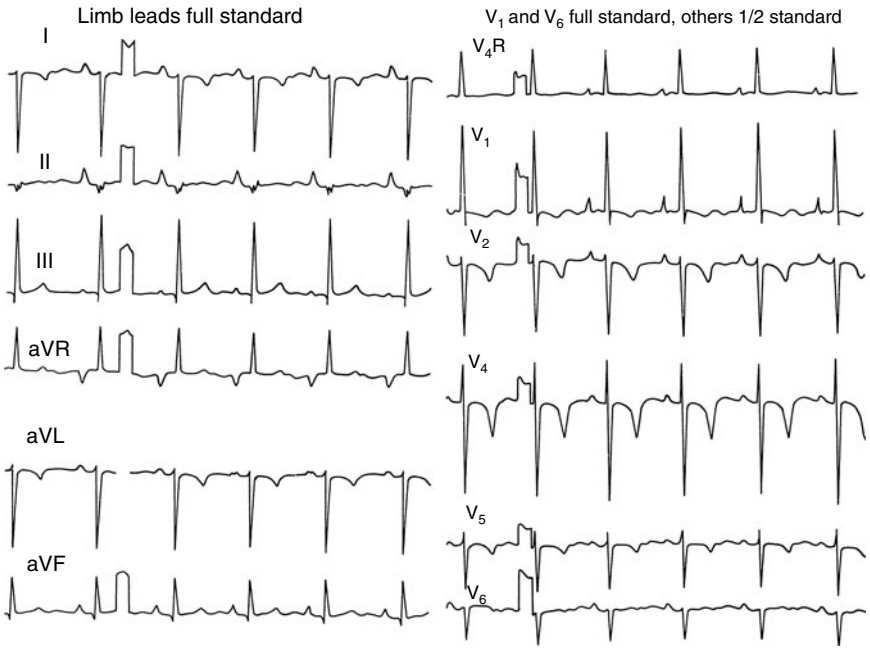

Figure 21.25

Standard ECG of a 10-year-old with severe TOF and very severe RVH (as well as right atrial hypertrophy). What is unusual for TOF is the marked T abnormality, the T being to the right and posterior. The maximum QRS vector is also posteriorly directed (and to the right) as in Fig.21.24.

21.13.1.4 LVH criterion 4 – Horizontal Plane Vector Loop Progressing Rapidly from Anterior to Posterior

This causes the loop to be posterior by about 20 ms. The differential diagnosis is anterior myocardial infarction, rare in children, so that the criterion is excellent.

21.13.1.5 LVH Criterion 5 – Increased Magnitude of Leftward QRS Vector

This gives increased X to the left and tall R in V_5, V_6. This is an excellent sign of LVH. If V_6 is greater than V_5, even though neither is above 97.5 percentile, LVH should be considered. In the latter, a very wide, broad leftward loop has been projected, which remains to the left for a long time.

21.13.1.6 LVH Criterion 6 – Increased Magnitude of Inferior QRS Vector

This leads to increased Y inferior and a tall R in aVF. In the presence of a normal horizontal plane vector loop with good left chest potential (which need not be abnormally high), a clearly large inferior vector suggests LVH. The left ventricle is the more inferior ventricle. However, pure marked RVH is frequently associated with a large inferior vector, but, as noted above, even mild RVH or LVH can be associated with a high magnitude inferior vector.

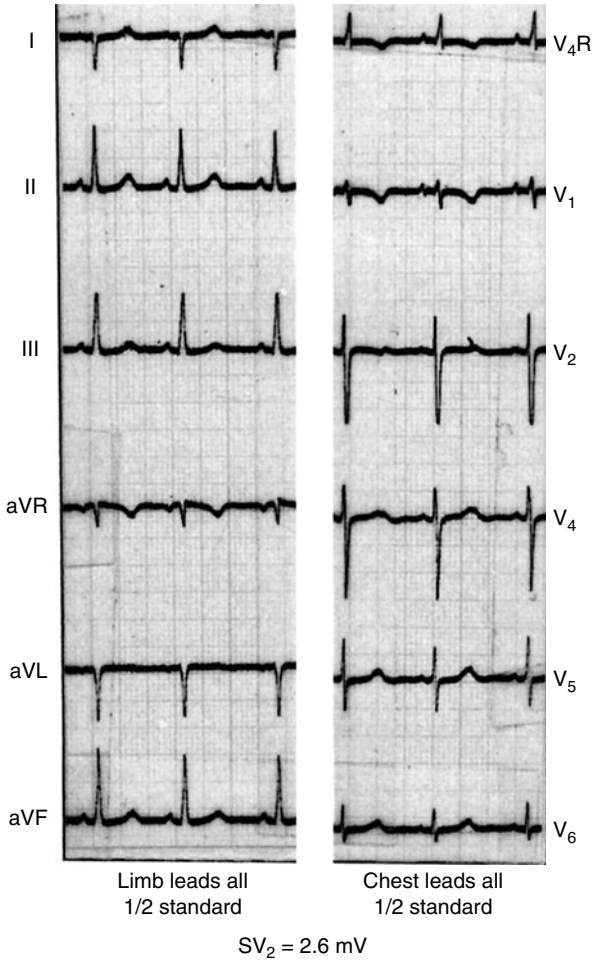

Figure 21.26

Standard ECG of a 5-year-old female with TOF and moderately severe RVH. As in Figs. 21.24 and 21.25, the initial QRS is to the left and the QRS transverses quickly to the right and posterior. The difference here is that not only does V_2 demonstrate rS, but so does V_1. Therefore, without V_4R (and/or the orthogonal ECG) RVH would be difficult to diagnose. Note that all leads are half standard size. (After Liebman et al. [8]. © Williams and Wilkins, Baltimore, MD. Reproduced with permission.)

21.13.1.7 LVH Criterion 7 – Increased Magnitude of Posterior QRS Vector

This means increased Z posterior, with a deep S in V_1, V_2. The abnormally posterior maximum QRS vector is probably the single best criterion for LVH (although lung disease, with high residual volume, may cause decreased anterior forces, and therefore, an abnormally posterior vector) [57]. In severe RVH, a clockwise-inscribed horizontal plane vector loop may terminally swing far posterior, so that additional LVH is sometimes diagnosed. This would be in error for in such a case the genesis of the posterior forces is presumed to be late posterior right ventricular potentials occurring after the left ventricle has completed activation. If, with a counterclockwise horizontal plane vector loop, the X left and Z posterior are at the upper limit of normal in magnitude, LVH is likely. A Z posterior at the upper limit of normal together with a quite small X left may be part of an abnormally posterior horizontal plane QRS vector angle and is a weak sign of LVH.

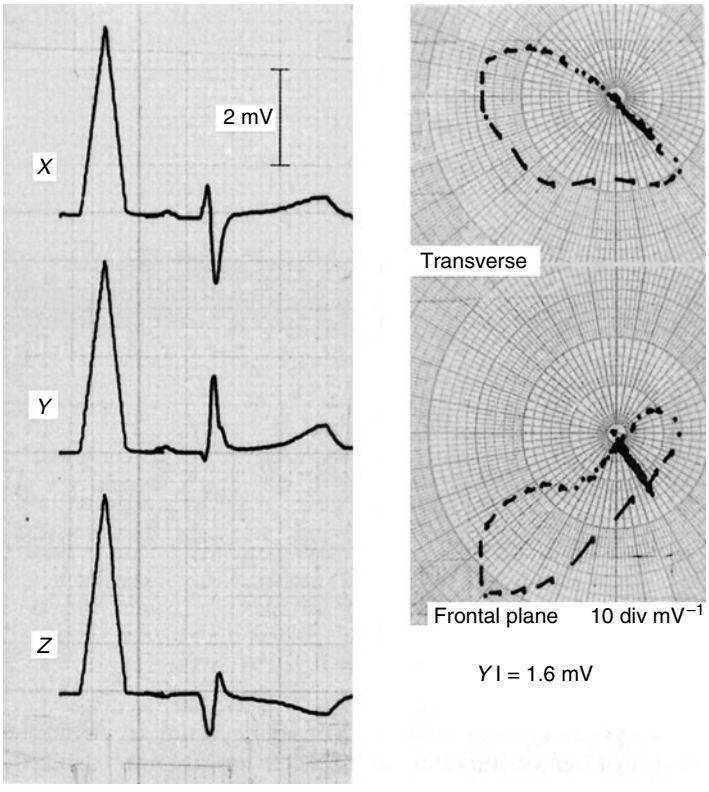

Figure 21.27

Frank-system orthogonal ECG of a 4-year-old with TOF. As is typical, the direction of inscription is wide open clockwise with the initial QRS to the left. The T in the horizontal plane overlays the initial QRS. (After Liebman et al. [8]. © Williams and Wilkins, Baltimore, MD. Reproduced with permission.)

21.13.1.8 LVH Criterion 8 – Increased Magnitude of Terminal Rightward QRS Vector in the Presence of an Abnormally Posterior Maximum QRS Vector

This is frequently a manifestation of posterobasal LVH rather than combined ventricular hypertrophy. However, it is often not possible to distinguish the difference.

21.13.1.9 LVH Criterion 9 – Abnormal Ratios of Specific Magnitudes

An example of this is a decreased magnitude of the ratio of Z anterior to Z posterior. Other ratios are less reliable. It is particularly useful in the presence of low voltage from various causes. The major differential is that of lung disease with a high residual volume. A good clue is that, in lung disease, the X left is also decreased in magnitude, more than merely by the low voltage per se, since there is frequently air in the lateral left chest wall in cystic fibrosis [57] as well as in the anterior chest.

21.13.1.10 LVH Criterion 10 – Increased Magnitude of R in aVL

This is a reliable criterion, but, when met, the diagnosis is usually obvious from other criteria. An important note of caution is that in the presence of an abnormally superior maximum QRS vector, the magnitude of R in aVL will be

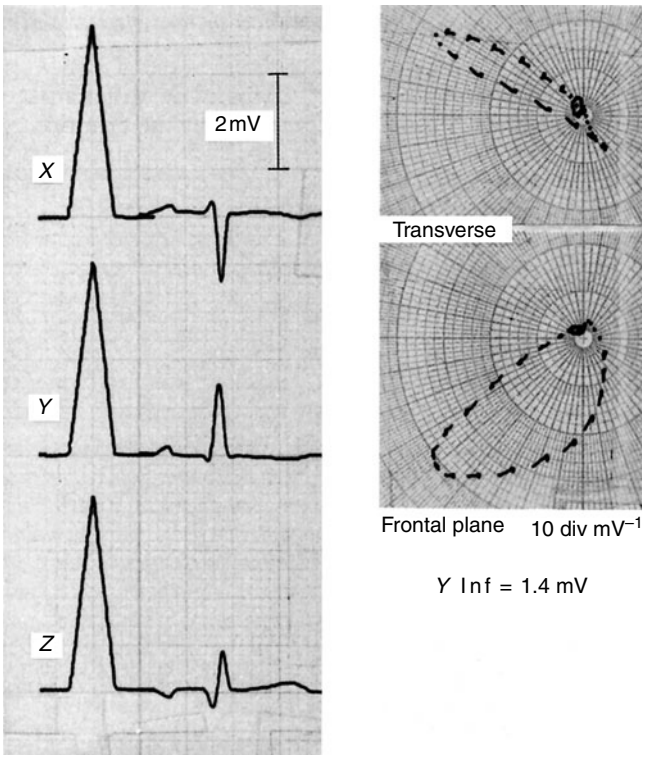

Figure 21.28

Frank-system orthogonal ECG of a 1-day-old baby boy with a maximal TOF, which indicates non-restrictive VSD, pulmonary atresia and 100% right-to-left shunt. The pulmonary blood flow in the 1-day-old child was via a small ductus arteriosus. The RVH is severe with a wide open clockwise vector loop (normal for this age), but with most of the terminal vector to the right and posterior. The T vector is to the right and posterior, but that could be normal for this age.

increased because the direction of the vector is similar to that of the lead vector for aVL; in such cases, therefore, the criterion cannot be utilized.

21.13.1.11 LVH Criterion 11 – Increased Magnitude of the Maximal Spatial Vector to the Left (MSVL)

This is, in general, an excellent criterion, but the measurement of Z posterior by itself is probably just as good, and simpler. (See Sect. 21.14 for specific use.)

21.13.1.12 LVH Criterion 12 – Abnormally Prolonged QRS Duration

On average, the QRS is prolonged, but the criterion is only fair because the variation is so great.

21.13.1.13 LVH Criterion 13 – T-Wave Abnormality

There are two types of T-wave abnormality. The first, very common in PDA, is a large magnitude T vector in the normal direction (increased left and/or inferior). By itself the criterion is not useful, for tall T waves can be present in many

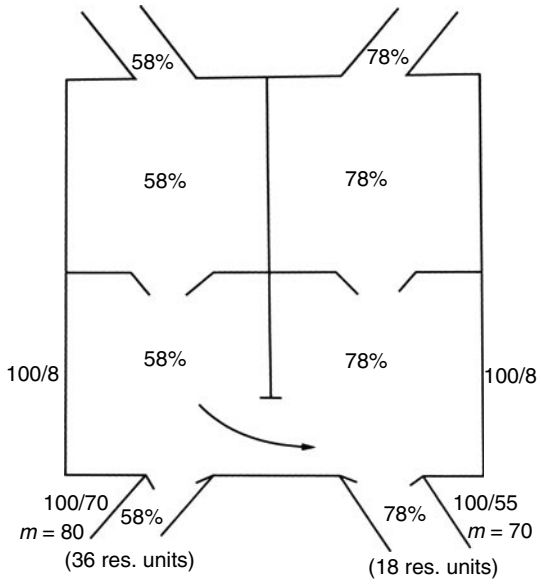

Figure 21.29

Box diagram of a patient with non-restrictive VSD and pulmonary vascular disease, so that resistance to flow into the pulmonary artery is higher than resistance to flow into the aorta. The amount of right-to-left shunt is exactly the same as in the patient with TOF depicted in Fig. 21.23. Oxygen saturations are given as percentage values.

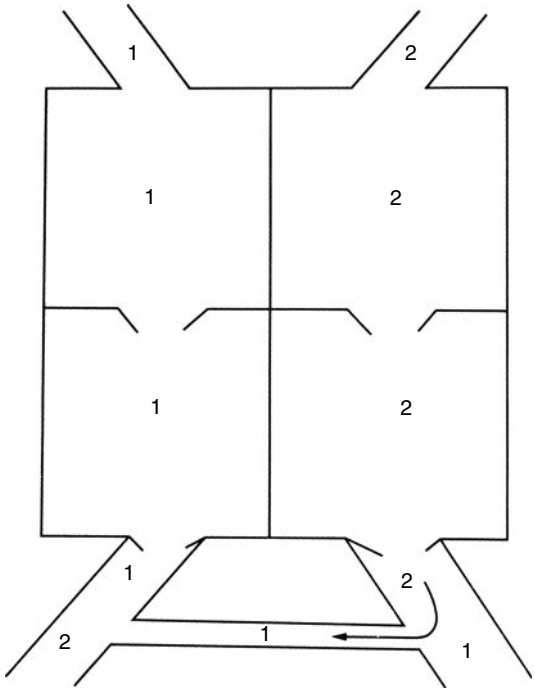

Figure 21.30

Box diagram of a patient with a patent ductus arteriosus and moderate left-to-right shunt (2/1 pulmonary/systemic flow ratio). On the basis of the volume work alone, there is pure LVH. However, the larger the ductus, the greater the pulmonary artery (and thus right ventricular) pressure.

situations including hyperkalemia. It is also not an indication of severity. Although often present in volume overloading, tall T waves can also be present in patients with pressure overloading.

The second type of T-wave abnormality is that of a wide deviation of T from QRS (i.e., increased QRS-T angle). When LVH is severe, the T vector is more anterior and less to the left. In the most severe cases, the T vector will be so much to the anterior that the T waves are upright in the right chest leads. If, in addition, the T vector is to the right, the T in the left chest leads will also be negative. Although this type of T abnormality has been associated with severe pressure overload, it is also seen in the pure volume overload of PDA when the left-to-right shunt is very large. Severity of the hypertrophy, perhaps with fibrosis, seems to be the cause, rather than the type of hemodynamics, for example, pressure versus volume overloading. A low-voltage T vector may have similar significance to that of a wide QRS-T angle.

21.13.1.14 LVH criterion 14 – ST-Segment Abnormality

When the T-wave abnormality is severe, there will usually also be ST-segment abnormality, manifested by depression in the X leads (V_5, V_6) and sometimes elevation in V_4R and V_1. ST depression inferiorly, in Y or aVF, may also be present. As in the T-wave abnormality, ST-segment abnormality has usually been associated with severe pressure overload, but severe volume overload, as in a large shunt PDA or aortic regurgitation, may also be responsible.

21.14 Aortic Stenosis (Valvular)

Whereas PDA provides the prototype for left ventricular volume overload, aortic stenosis (AS) provides the example usually given for pure pressure overload. However, valvular stenosis, because of the frequent narrow pulse pressure causing less coronary perfusion when severe and the need for perfusion of very thick muscle, has the additional problem of that poor perfusion (Fig. 21.31).

The ECG criteria of importance in aortic stenosis are the following.

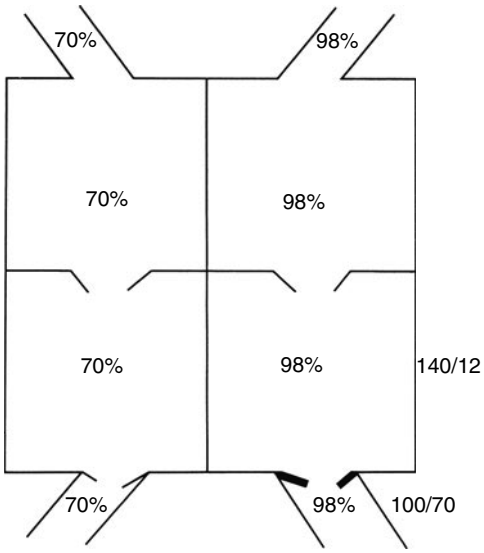

Figure 21.31

Box diagram of a patient with pure valvular aortic stenosis. The oxygen saturations are normal. The amount of stenosis is moderate in this case, with a 40 mm systolic gradient. Note that the end-diastolic pressure in the left ventricle is, as is typical, only somewhat elevated. Although there is consequent elevation of the left atrial pressure, there is usually, no dilatation.

21.14.1 LVH Criterion 1 in Aortic Stenosis

The direction of inscription of the vector loop is typical of that in LVH, but there are a number of important specifics for this lesion. First, the more severe the stenosis, the more likely is the initial QRS to be oriented to the left and anterior [45, 46, 55, 56] (Fig. 21.32). Second, in the more severe cases, the QRS forces are often directed posterior so early that anterior myocardial infarction may not be able to be differentiated (Fig. 21.33). Third, posterobasal LVH is common, although there seems to be little or no relationship to severity (Fig. 21.32). Fourth, in severe cases, the vector turns posterior very early, then turns laterally so that there is a crossed (figure-of-eight) loop. It may be that the posterobasal area is being activated early, as in left bundle branch block (LBBB). Under any circumstance it is likely that considerable

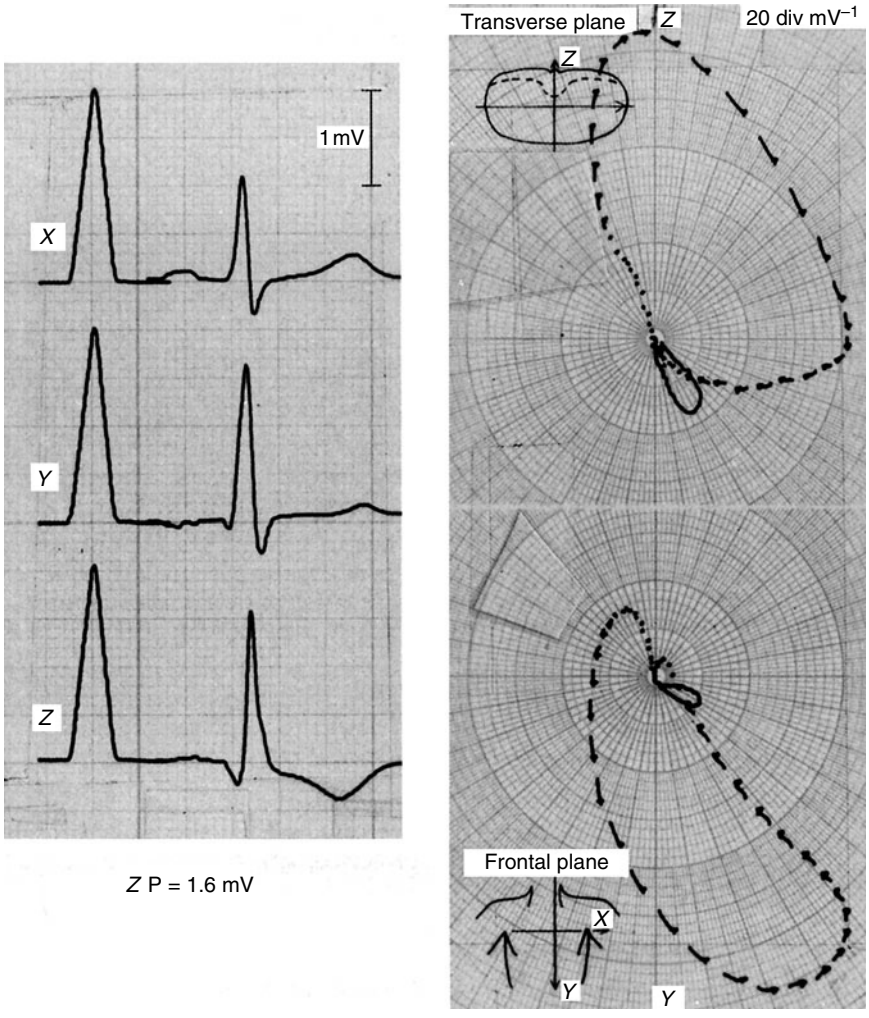

Figure 21.32

Frank-system orthogonal ECG of an 18-year-old male operated upon one year previously for severe valvular aortic stenosis. The QRS had not significantly changed, although the T-vector had been further to the right. (Note that, as is usual, the frontal plane vector loop is wide open and clockwise inscribed, despite the severe LVH). (After Liebman et al [8]. © Williams and Wilkins, Baltimore, MD. Reproduced with permission.)

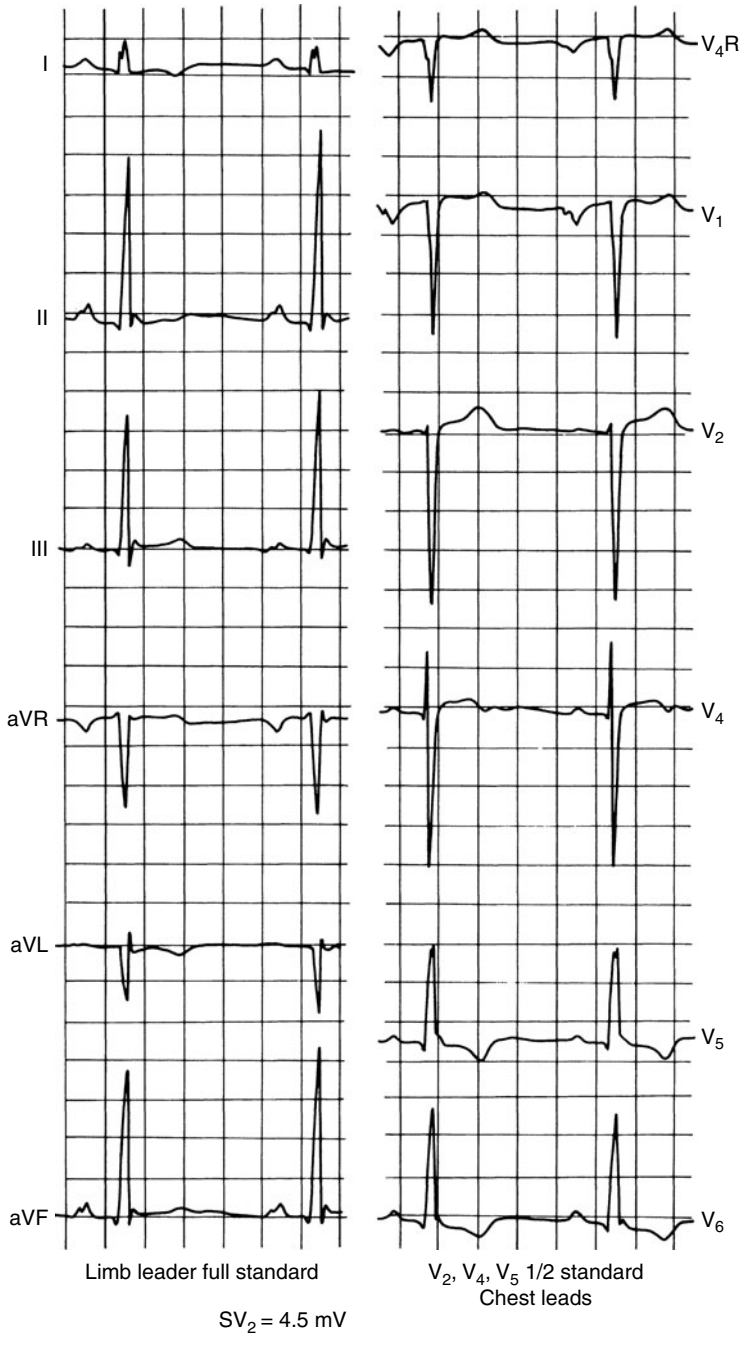

Figure 21.33

Standard ECG of an 18-year-old male with severe coarctation of the aorta (operated upon successfully at age 2 years) and two further operations for severe valvular aortic stenosis. The first operation was a valvotomy and the second for aortic valve replacement. The initial QRS is to the right, anterior, superior (normal). The horizontal plane direction of inscription in the ECG appears to be counterclockwise with considerable midportion slowing, but with the VCG the vector goes well posterior before going to the left as in many patients with left bundle branch block (LBBB). Nonetheless, the diagnosis is intraventricular conduction abnormality as part of marked LVH since the initial QRS is normal. (The T vector is well to the right and posterior, very abnormal, and could be part of either severe LVH or LBBB). (After Liebman et al. [8]. © Williams and Wilkins, Baltimore, MD. Reproduced with permission.)

fibrosis is present. If the initial QRS is to the right, then intraventricular conduction abnormality (perhaps due to fibrosis) is suggested, as part of severe LVH (Fig. 21.33). If the initial QRS is to the left, then differentiation from LBBB may not be possible.

21.14.2 LVH Criterion 2 in Aortic Stenosis

The initial QRS activation includes at least five major components:

(a) The left septum, 1/2 to 2/3 down the septum
(b) The posterior free wall of the left ventricle near the left septum where activation begins, stimulated by the posterior branch of the left bundle
(c) The right septum, stimulated by a branch of the right bundle from the base of the anterior papillary muscle
(d) The right ventricular endocardium, stimulated by branches from the right bundle via the moderator band
(e) Up the septum from stimulation by the left anterior branch of the left bundle, which causes the normal QRS to be initially superior left or right and anterior or posterior.

As stated above, in severe valvular AS, the initial QRS is frequently to the left. Data [56] shows that in a series of 70 patients severe enough to need surgery, the initial QRS was to the left in half, and when it was to the right, the magnitude was small. In another series of 63 catheterized patients, 41 had systolic gradients less than 50 mm Hg, of which, in 37 the initial QRS was to the right. Of 22 who had systolic gradients greater than 50 mm Hg and/or need surgery, the initial QRS was to the right in only three. The etiology of the initial QRS vector to the left in the more severe cases is not known, but it could be hypothesized that hypertrophy of the free posterior wall near the left septum may provide the answer. Studies in BSPM [45, 46] have confirmed this hypothesis. Fibrosis of the left septum, which could surely cause the initial QRS to be to the left, has not been confirmed in pathologic studies. Left septal hypertrophy is not usually seen in valvular aortic stenosis, but is frequently recognized in fixed subvalvular stenosis, where the initial QRS to the left is very unusual.

21.14.3 LVH Criterion 4 in Aortic Stenosis

This criterion, which involves the QRS vector turning posterior very rapidly (so that anterior myocardial infarction is in the differential diagnosis) is common in significant aortic stenosis (Fig. 21.33).

21.14.4 LVH Criterion 7 in Aortic Stenosis

An increased magnitude of the Z posterior is an excellent parameter. Correlations of peak LV pressure with the magnitude of the Z posterior in the Frank system gives an estimated R value of 0.65 for prediction of the pressure. The confidence interval is wide, however, so that it is beneficial using only the patient himself or herself as his or her own control. As severity increases, the magnitude of Z posterior increases (Fig. 21.34).

21.14.5 LVH Criterion 8 in Aortic Stenosis

This is common in significant aortic stenosis, where the prominent terminal vector to the right and posterior occurs without pulmonary hypertension or other evidence of a hypertrophied right ventricle (Fig. 21.32), and suggests posterobasal LVH.

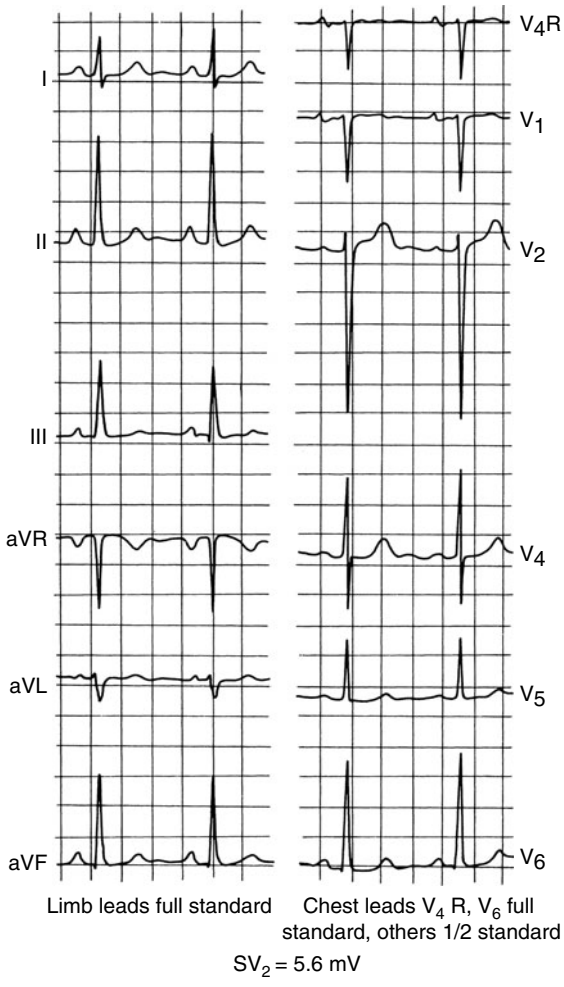

Figure 21.34

Standard ECG of a 16-year-old male with severe aortic stenosis. There is minimal if any ST-segment abnormality, and the T-wave abnormality is minimal, with the maximum T vector being well anterior, but not to the left. The initial QRS is minimally to the right. The posterior projection is of extremely large magnitude. Another sign of LVH in this ECG is that the magnitude of the *X* left in V_6 is at least as great as in V_5. (After Liebman et al. [8]. © Williams and Wilkins, Baltimore, MD. Reproduced with permission.)

21.14.6 LVH Criterion 11 in Aortic Stenosis

This measure, at one time, was considered to have a very strong correlation with LV pressure, but data indicates that its usefulness is essentially the same as for the magnitude of the Z posterior (Frank system). However, as a parameter for LVH per se, it is an excellent parameter.

21.14.7 LVH Criterion 13 in Aortic Stenosis

There may be a T-wave abnormality in significant valvular aortic stenosis without ST-segment abnormality. The T vector may be markedly anterior, although still to the left (Fig. 21.32), and on occasion the T vector magnitude may be

increased. Neither abnormality is worrisome, but if the T vector is to the right as well as anterior, and if the T vector magnitude is decreased, then there is great concern indicating the need for immediate intervention. This can be compared to the presence of secondary T-wave abnormalities in LVH in the adult (see Chap. 15).

21.14.8 LVH Criterion 14 in Aortic Stenosis

Depressed ST segment in the left chest or X leads and/or aVF (Y leads) indicate that perfusion may not be adequate for the great mass of left ventricular muscle. (ST-segment abnormalities, particularly with a low-magnitude T vector and/or T vector to the right, usually indicates the need for immediate surgery or balloon valvuloplasty). This finding, it should be made clear, is not because of severe pressure overload, but because of "severity" per se. It can occur in association with a large PDA or severe aortic regurgitation, as an example.

21.15 Aortic Stenosis (Fixed, Subvalvular)

Everything stated above for valvular aortic stenosis holds for fixed subvalvular aortic stenosis except for one difference, for which no explanation is available. This relates to the initial QRS vector, which, in severe cases, is only rarely to the left. In fact, it may be abnormally to the right, as in left septal hypertrophy (Fig. 21.35). As part of the same studies cited above [55, 56], seven of eight patients with fixed subvalvular aortic stenosis, a systolic gradient greater than 50 mm Hg and needing surgery, had initial QRS vectors directed to the right and anterior of greater magnitude than normal.

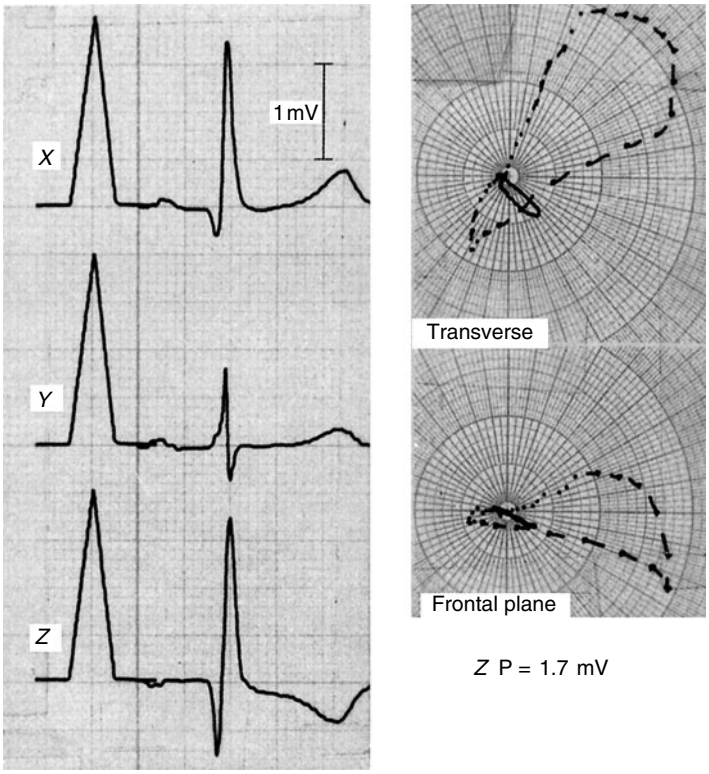

Figure 21.35
Frank-system orthogonal ECG of a 14-year-old male with subvalvular aortic stenosis. Note the typical large magnitude initial QRS to the right and anterior.

21.16 Cardiomyopathy

Primary cardiomyopathies (congestive or restrictive) are part of this discussion, whereas hypertrophic cardiomyopathies (with or without obstruction) are not. Cardiomyopathies per se are usually not considered congenital. However, an increasing number of infants are being recognized, often with primary cardiomyopathy, without systemic disease. Many are familial. Of the familial cardiomyopathies (including what used to be termed endocardial fibroelastosis), an increasing number of affected infants are being documented as having specific abnormalities of mitochondrial energy metabolism. It is not the purview of this section to delineate these diseases; just two things will be pointed out. First, the majority, when severe, have LVH with ST and T abnormalities as previously described, although LBBB may be present. Second (a critical piece of information) is, that the patient and the electrocardiogram are almost invariably categorized as normal in the newborn period. One reported family where all five children had severe cardiomyopathy [58] provides information of particular interest. The electrocardiogram, followed from the newborn period in three of the five, became abnormal at 2 months of age, before the patients' disease became clinically evident shortly thereafter. Another sibling had been evaluated on many occasions, with normal electrocardiograms, only to become ill as a teenager, with severe LVH and ST-segment and T-wave abnormality along with severe congestive heart failure.

21.17 Coarctation of the Aorta After Infancy

Isolated coarctation of the aorta is almost always located in the same place, near the origin of the original ductus arteriosus, and near the left subclavian artery. Although some patients with this anatomy can be very ill in early infancy, with heart failure and pulmonary hypertension, the majority of patients with simple coarctation after infancy are not associated with congestive heart failure. There will also usually not be very much elevation of left ventricular end-diastolic, and thus pulmonary venous, pressure. Therefore, pulmonary hypertension is not expected. Consequently, the ECG demonstrates pure LVH. In addition, because there is high aortic pressure (Fig. 21.36), coronary flow and perfusion are

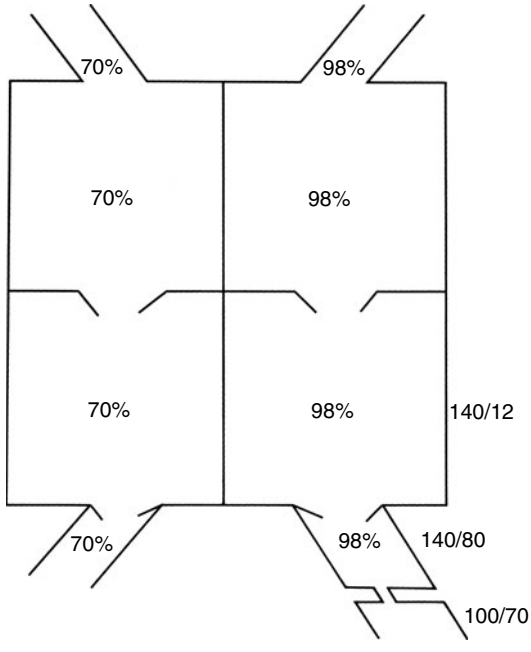

Figure 21.36

Box diagram of a patient with simple coarction of the aorta, of moderate severity, with 40 mm systolic gradient and moderate increase in left ventricular end-diastolic pressure. Unlike the situation in valvular of subvalvular aortic stenosis (see Fig. 21.31), the driving force for coronary blood flow is high, so that myocardial perfusion is usually adequate.

adequate. Therefore, ST-segment and T-wave abnormalities are usually not present. Although the type of LVH is usually not distinctive, it is very common to have posterobasal LVH. As part of the posterobasal LVH the terminal vector to the right may be so great that there is often a terminal r or R in V_4R and V_1. Such standard ECG's have often erroneously been diagnosed as "incomplete right bundle branch block." In many teenagers and young adults, many years after successful coarctation surgery, rsr' is often recognized. This has been shown using BSPM to reflect RVH, as described above [48]. The mechanism is believed to be hypertrophy of more cells (hyperplasia) shortly after birth.

21.18 Anomalous Origin of the Left Coronary Artery in the Older Child

When the left coronary artery originates from the pulmonary artery and the right coronary artery originates from the aorta normally, the coronary flow depends upon the development of adequate intercoronary collaterals and the extent of lowering of pulmonary vascular resistance. There are children with this anomaly who progress through infancy without transmural myocardial infarction [59], presumably because intercoronary collaterals are adequate, resulting in considerable flow from the right coronary system into the left coronary artery system. Since pulmonary vascular resistance is normal, flow is through the left coronary artery into the pulmonary artery, resulting in left-to-right shunt. The latter per se results in volume work in the left ventricle so that there may be LVH. In addition, there is some "steal" from the left ventricle into the pulmonary artery causing some left ventricular disease, though usually not enough to result in ST-segment and T-wave abnormality. Finally, because of the steal from the myocardium there may be papillary muscle dysfunction and significant mitral regurgitation. The result is even more severe LVH, with no special aspects that specifically point to the diagnosis of anomalous left coronary artery from the pulmonary artery. (On the other hand, if there are not enough intercoronary collaterals and/or the left coronary artery is very small, there is little flow into the left coronary artery system. The result is very poor perfusion of the left ventricular myocardium so that there is LVH with ST-T abnormality. However, this latter ECG is not pure, since there will usually also be anterolateral wall myocardial infarction as manifested by a deep broad Q in lead aVL.)

21.19 Congenital Mitral Regurgitation

There are many causes of isolated congenital mitral regurgitation, with no other cardiac abnormalities, although it is always necessary to rule out an anomalous left coronary artery. Among these, the diagnosis of endocardial cushion defect with pure mitral regurgitation is not common. Therefore, the frontal plane vector is inferior and the severity of the LVH (due to a pure volume overload) (Figs. 21.37 and 21.38), depends upon the magnitude of the regurgitation.

Of particular interest for discussion is the magnitude of the regurgitation of the abiotrophy of the mitral valve associated with Marfan's syndrome, which may result in extremely severe mitral regurgitation in infancy. The LVH is extremely severe, often with ST-T abnormalities, even though the hypertrophy is caused by a pure volume overload. After infancy, the mitral regurgitation in Marfan's syndrome is usually mild and is associated with prolapsed mitral valve.

A second lesion for discussion is the pure mitral regurgitation associated with prolapsed mitral valve [60] (Fig. 21.39). This is also a congenital lesion, often familial (mother and daughter), even though the diagnosis is rarely made before the immediate preschool period. In childhood, the mitral regurgitation is rarely enough to cause LVH on the ECG. Nonetheless, T-wave abnormality is very common, the T vector being markedly anterior and sometimes superior as well [60] (Fig. 21.40). Strikingly, an electrocardiogram taken a few hours later may be normal, the variation with time being remarkable. Prominent U waves are often present. There are hypotheses for the etiology of the T-wave abnormality, but there is no knowledge. LVH is not responsible.

21.20 Congenital Aortic Regurgitation

Congenital aortic regurgitation is a lesion which varies in severity from the trivial to the moderately severe. The LVH on the ECG depends upon the severity of the leak. The most severe cases are often not caused by valve problems per se but

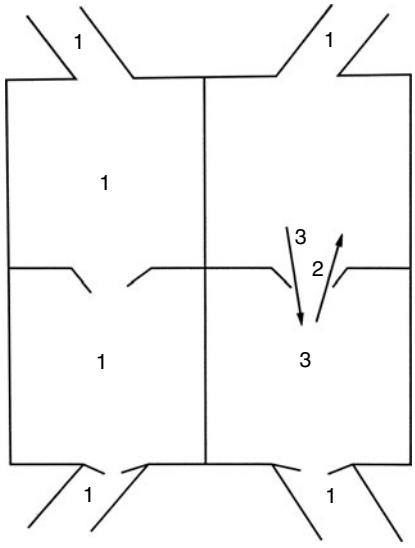

Figure 21.37

Box diagram of a patient with moderate mitral valve regurgitation so that for each unit of blood ejected into the aorta, two units regurgitate into the left atrium. The result is three times normal volume of the left atrium (so that there is left atrial dilatation) and three times normal volume work of the left ventricle. LAH and LVH are expected.

by a "tunnel" – a fistula between the root of the aorta and the left ventricular outflow tract. The sinuses of valsalva are not involved, with aneurysm caused by ruptured sinus of valsalva being mainly a disease of adulthood. One type of T-wave abnormality, common in congenital aortic regurgitation, is a large magnitude T vector in the normal direction. This T-wave abnormality is of little concern. On occasion, in severe cases, there may be the more common ST-T abnormality of great concern, similar to that seen in severe aortic stenosis, even though aortic regurgitation causes volume overload (Fig. 21.41). Commonly present in aortic regurgitation is a large initial QRS vector to the right and anterior, providing evidence of left septal hypertrophy.

21.21 Systemic Arterial Fistula

Cerebral arterial fistula is included in this discussion. The hemodynamics are similar to that of patent ductus arterious without pulmonary hypertension. There is pure volume overload of the left ventricle, although there may be enough increased systemic venous flow to the superior venacava to cause additional RVH.

21.22 Coronary Arterial Fistula

Coronary arterial fistula is a special type of systemic arterial fistula. Pure LVH occurs only when the fistula is into the left ventricle or left atrium, and such cases are rare [61]. In addition to the LVH, there may be ST-T abnormality, which is not related to hypertrophy per se, but to inadequate perfusion. When the fistula is into the right side of the heart there may be RVH owing to the right heart volume overload.

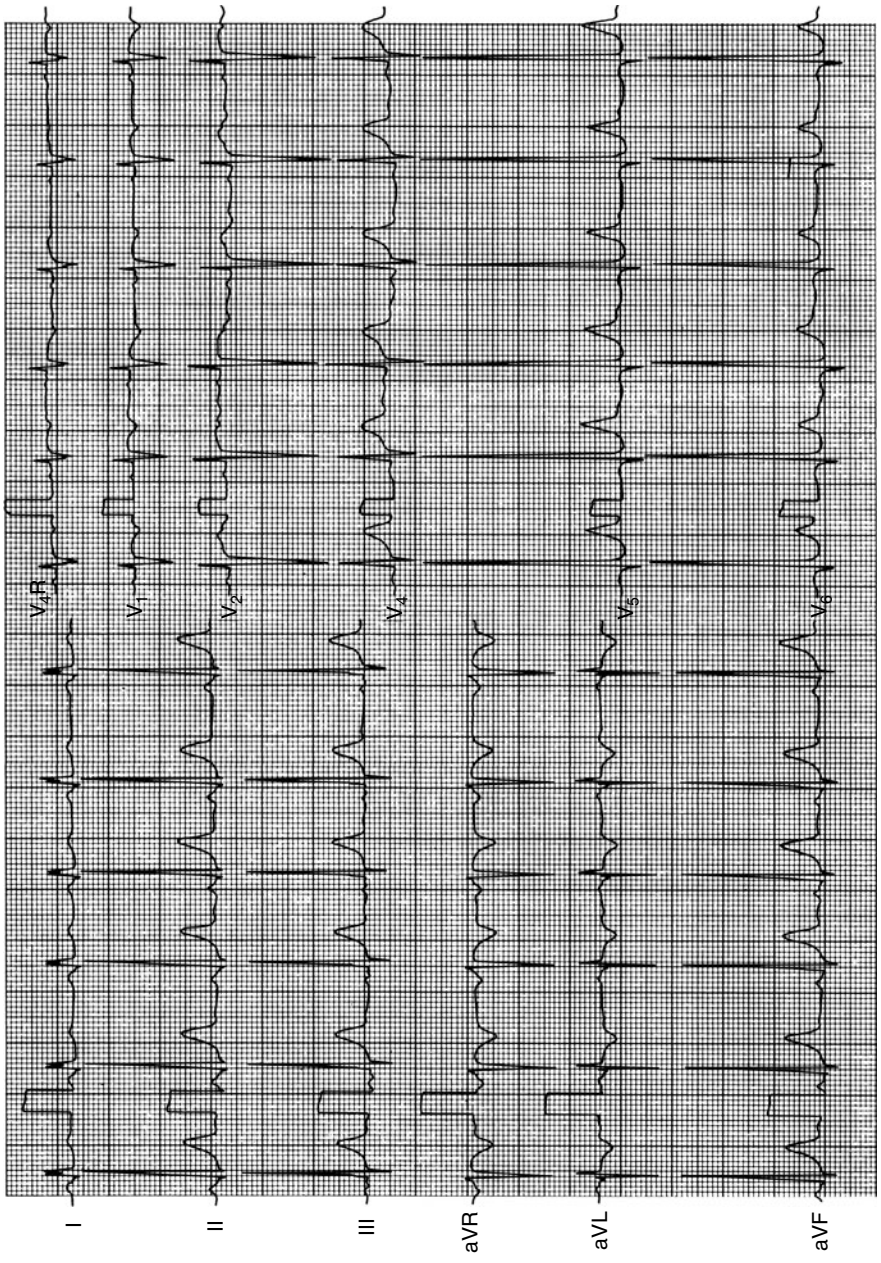

Figure 21.38

Standard ECG of a 9-year-old female with severe congenital mitral regurgitation. Angiography demonstrated considerable dilatation of the left atrium and left ventricle. The left atrial enlargement is diagnosed because of the very prolonged second part of the P wave (see Fig 21.50 for enlargement). There is a left septal hypertrophy (increased magnitude of initial QRS forces to the right and anterior) while the QRS loop is wide open and inscribed counterclockwise with increased magnitude posteriorly to left. (QRS loop is not shown here.)

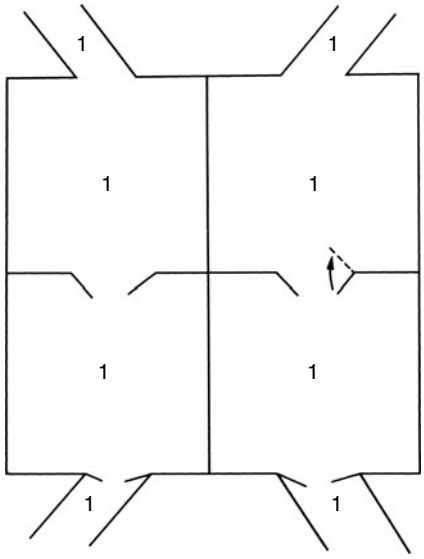

Figure 21.39

Box diagram of a patient with prolapsed mitral valve (almost always the posterior leaflet). This diagram depicts no significant regurgitation. The actual leak may be nonexistent and, in children, rarely more than minimal. An important exception is the rare infant with severe mitral regurgitation associated with Marfan's syndrome.

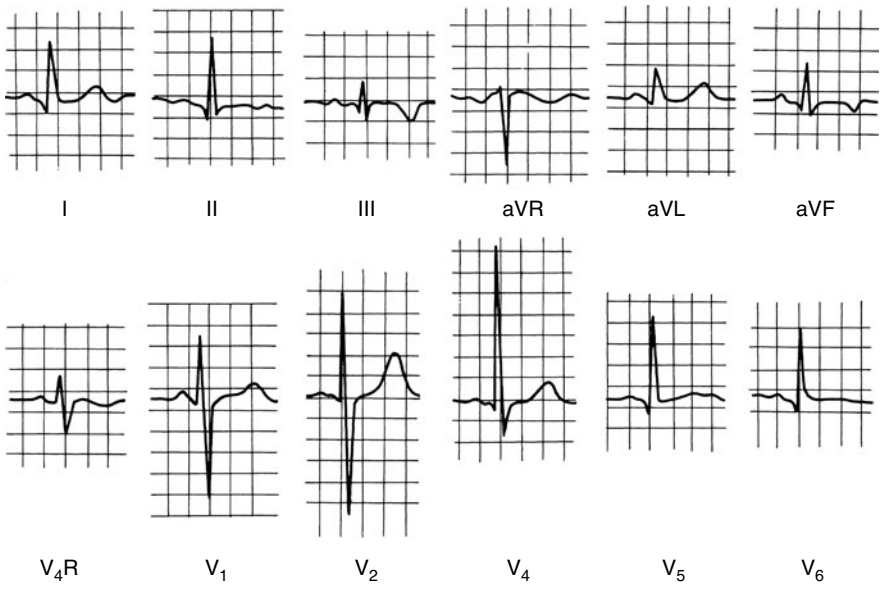

Figure 21.40

Standard ECG of an 11-year-old female with prolapsed mitral valve and trivial mitral regurgitation. The T vector is abnormally anterior and superior. There is no LVH. (After Liebman et al. [8]. © Williams and Wilkins, Baltimore, MD. Reproduced with permission.)

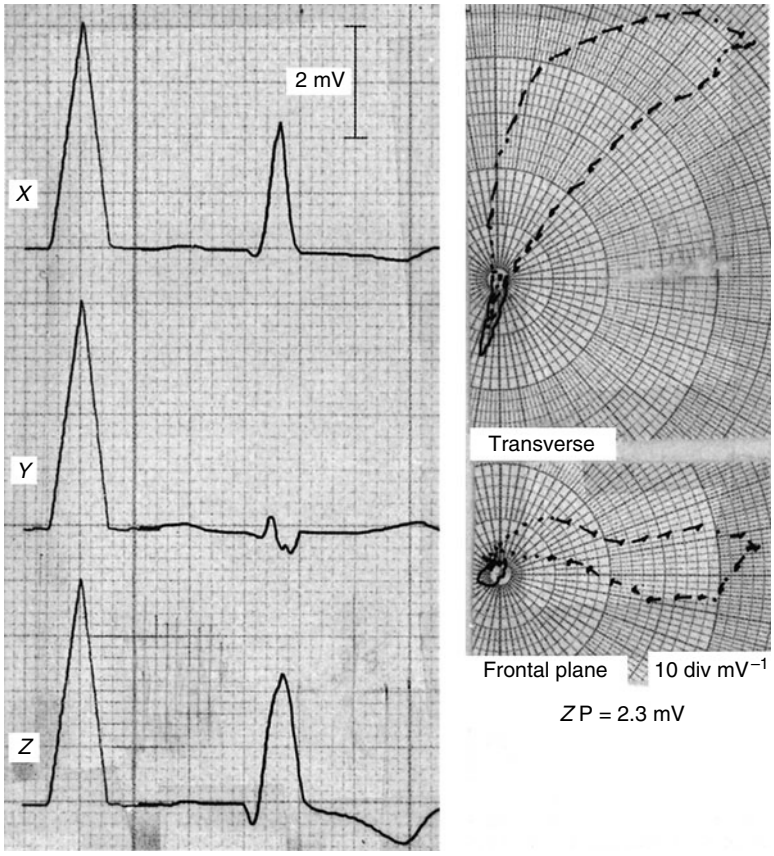

Figure 21.41

Frank-system orthogonal ECG in a 23-year-old male who had been operated upon at age 18 years for severe aortic regurgitation. The operation was a plication and aortic stenosis was created. The left ventricle was not entered. The T direction, opposite to the direction of the QRS vector, was present *before* surgery and is part of the severe LVH. The QRS vector turns posteriorly so quickly that anterior myocardial infarction had to be considered. The reason for the mainly superior QRS vector is not known. (After Liebman et al. [8]. © Williams and Wilkins, Baltimore, MD. Reproduced with permission.)

21.23 Hypoplastic Right Ventricle with Pulmonary Atresia

The box diagram in Fig. 21.42 describes the hemodynamics of hypoplastic RV with pulmonary atresia. Note that a ventricular septal defect is not part of the lesion. Since no blood can leave the right ventricle, the entire systemic cardiac output goes right to left through an atrial opening. Babies with this lesion are "patent ductus dependent," with the only pulmonary artery blood flow coming from the aorta via the ductus. The flow then drains from the lungs, via the pulmonary veins, to the left atrium. Therefore, if as in Fig. 21.42, the pulmonary artery blood flow is half of the normal systemic blood flow, then the left atrium and left ventricle handle 3/2 times the normal volume. The volume overload of the left ventricle, as well as the hypoplastic right ventricle, results in an ECG that demonstrates considerable LVH (Fig. 21.43). Since, prior to surgery, the patients are newborns, the LVH is often diagnosed mainly on the basis of the direction of inscription of the vector loop, which is wide open as seen in the frontal plane and counterclockwise inscribed in the transverse view. Specific magnitude increases may also be present, but conduction abnormalities and ST-T abnormalities are usually not. As a result of the hypoplastic right ventricle, the septum and left ventricle are differently positioned from normal, which must be considered in making ECG interpretations.

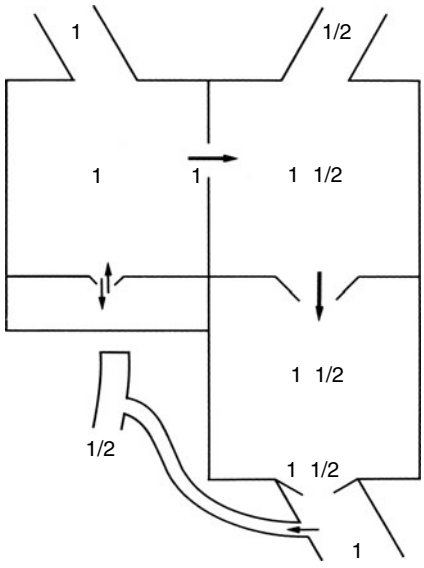

Figure 21.42

Box diagram of a patient with hypoplastic right ventricle and pulmonary atresia. This is a ductal-dependent lesion, the entire pulmonary blood flow coming via the ductus arteriosus. Presuming half normal pulmonary blood flow, the left atrium and left ventricle each handle 1½ units of volume. Therefore, there is marked LVH on account of the increased volume work of the left ventricle, plus the hypoplastic right ventricle.

Surgery is absolutely necessary for the patient's survival, including relief of right ventricular outflow obstruction and, more important, a systemic pulmonary artery connection. The latter causes even more volume load on the left ventricle. Should the surgery result in an increased volume of the right ventricle, the ECG only rarely reflects it. The surgical systemic-pulmonary connection accentuates the LVH.

21.24 Hypoplastic Right Ventricle with Tricuspid Atresia

The box diagram in Fig. 21.44 describes the hemodynamics of hypoplastic RV with tricuspid atresia. In this case, a ventricular septal defect is present (although spontaneous closure is common). Since no blood can enter the right ventricle through the atretic tricuspid valve, the entire systemic cardiac output goes through an atrial opening into the left atrium and left ventricle. Flow then goes left to right through the VSD to enter the right ventricle and pulmonary artery. As in the hypoplastic right ventricle with pulmonary atresia, if there is one-half normal pulmonary blood flow, left ventricular volume work is 3/2 times normal. Consequently, with the hypoplastic right ventricle and the left ventricular volume overload, there is considerable LVH on the ECG. LVH in the newborn period is often diagnosed on the basis of the direction of inscription of the vector loop – wide open with counterclockwise inscription in the transverse plane. With aging, specific magnitude increases become more important, and with the need for a systemic to pulmonary artery shunt procedure, the LVH becomes more severe.

Two aspects of the ECG are of great interest. The first is that usually the frontal plane will demonstrate an abnormally superior QRS vector typical of that in endocardial cushion defects (Figs. 21.45 and 21.46). Studies have shown that the ventricular septal defect is almost always posterior [62] and is believed to be an endocardial cushion defect. (On the other hand, in the presence of tricuspid atresia with transposition, the frontal plane QRS vector is inferiorly directed and associated with an anterior VSD [62].) The second aspect of the ECG of great interest is the occasional unusual ECG suggesting left lateral well fibrosis with initial QRS to the right and extending posterior before going left [8] (Fig. 21.46). The latter has not been seen in newborns in the author's experience, so it is presumed that it is acquired,

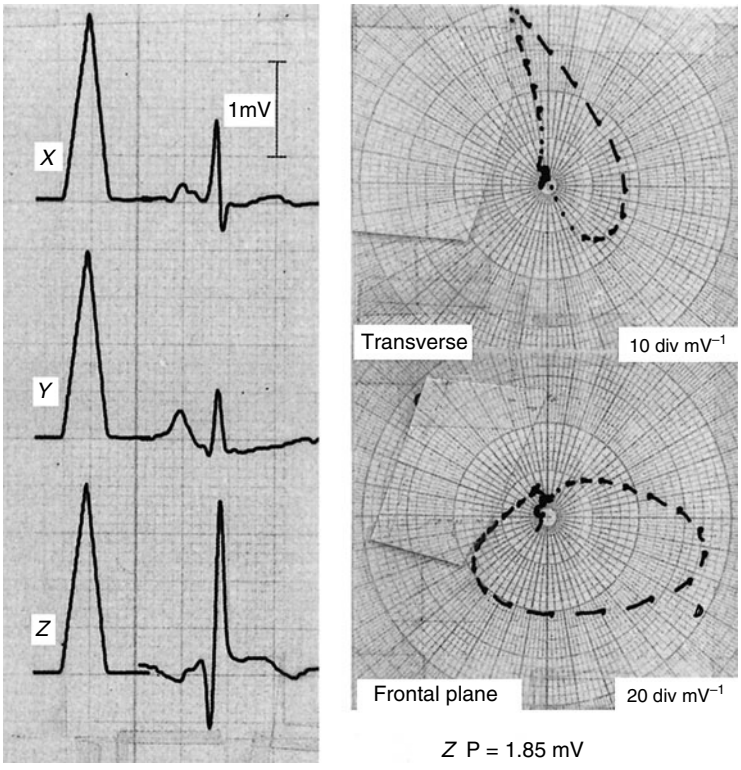

Figure 21.43

Frank-system orthogonal ECG of a 1-day-old male baby with hypoplastic right ventricle and pulmonary atresia. Note the wide open counterclockwise direction of inscription in the horizontal plane, indicative of LVH in a newborn. Note also the large magnitude of the first portion of the P wave (lead *Y*, inferior; lead Z, anterior) indicative of RAH. (After Liebman et al. [8]. © Williams and Wilkins, Baltimore, MD. Reproduced with permission.)

in association with the longstanding volume overload. Left ventricular cardiomyopathy is relatively common, part of the same etiology.

As with the hypoplastic right ventricle with pulmonary atresia, the proper ECG interpretation may be impeded by the different position of the septum and left ventricle, although the LVH per se is easily diagnosed in both.

21.25 Biventricular (Combined Ventricular) Hypertrophy

For further information see Liebman et al. [8].

21.25.1 Left Ventricular Disease with Pulmonary Venous Hypertension

Any of the lesions described above with pure LVH may be associated with elevated pulmonary venous pressure, and thus pulmonary hypertension (Fig. 21.47). Therefore, RVH can be present in addition to LVH. When the left ventricular dysfunction occurs in the newborn period, at which time the pulmonary arterioles are still thick walled, pulmonary venous hypertension causes pulmonary artery hypertension more quickly and more severely. Should the left ventricular disease be treated, medically or surgically, so that dysfunction becomes less, then the RVH may resolve even though there is enough left ventricular abnormality to continue to cause LVH.

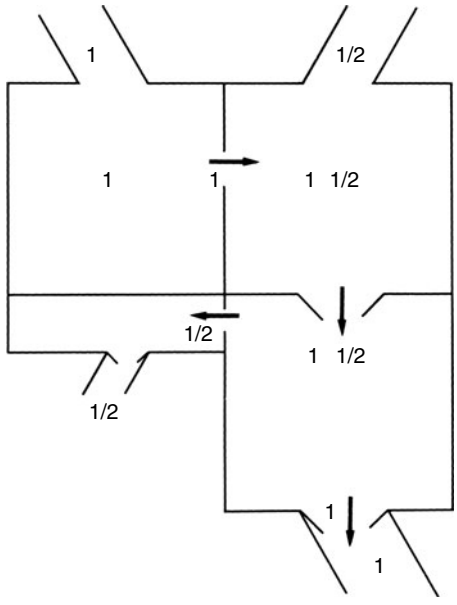

Figure 21.44

Box diagram of a patient with hypoplastic right ventricle and tricuspid atresia. The pulmonary blood is dependent upon the left-to-right shunt through the VSD. Presuming half normal pulmonary blood flow, the left atrium and left ventricle each handle 1½ units of volume. Therefore there is LVH for two reasons. (The VSD is almost always posterior in the endocardial cushion position).

21.25.2 Two Separate Lesions with Dynamics for LVH and RVH

There are numerous cardiac lesions, which predispose to the presence of biventricular (combined ventricular) hypertrophy. These are now discussed.

21.25.2.1 Ventricular Septal Defect

The prototype of biventricular hypertrophy (BVH) is the ventricular septal defect. Before discussing the electrocardiogram in ventricular septal defect (VSD), some aspects of the physiology and pathophysiology must be discussed. By definition, in the largest defects (nonrestrictive), the RV pressure is the same as that of the left ventricle. Therefore, in the absence of pulmonary stenosis, systemic level pulmonary hypertension is present. The determination of shunting depends, in such cases, on the difference in vascular resistance in the pulmonary and systemic circulations. As a result of transmission of systemic pressure into the pulmonary resistance vessels, the newborn's arterioles mature slowly. It is usually only after some weeks that a left-to-right shunt becomes significant. A baby of six weeks may have a nonrestrictive VSD with a pulmonary to systemic flow ratio of 3/1. The left ventricle and left atrium have three times normal blood flow, so that there is LAE and LVH. The right ventricle shares in some of the volume overload, although much of the increased pulmonary artery blood flow reaches the pulmonary artery via a left ventricular thrust almost directly into the pulmonary artery. RVH is certainly present, however, because of the high pressure. With increasingly smaller sized defects, the right ventricular and pulmonary artery pressures are, perhaps, 3/4, 2/3, or even 1/2, systemic level, irrespective of the amount of left-right shunt. In fact, despite the restrictive nature of the defects, the pulmonary to systemic flow ratio can still be large, for example, 3/1 or more, because of low pulmonary vascular resistance. When the defects are so restrictive that

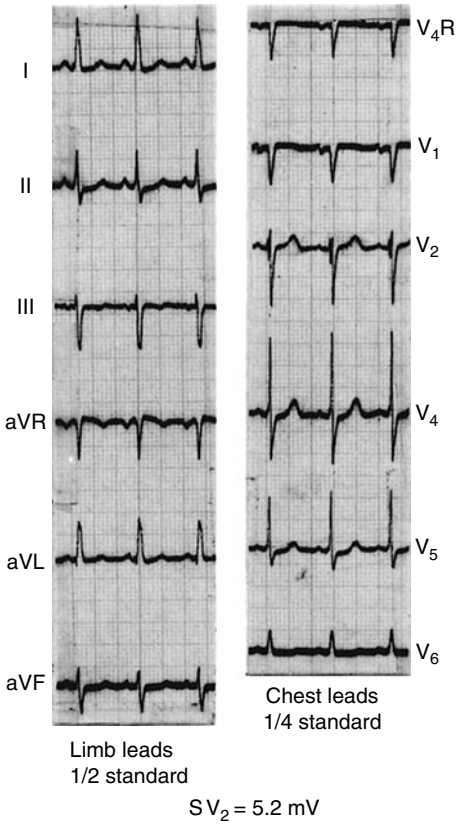

Figure 21.45

Standard ECG of a 19-month-old male with hypoplastic right ventricle and tricuspid atresia, who had had a systemic to pulmonary artery shunt because the VSD had spontaneously closed. The horizontal plane is wide open with counterclockwise inscription in the transverse plane and the voltages to the left and posterior are of very great magnitude. LVH is considerable although there is no ST-T abnormality. There is also an abnormally superior maximum QRS vector, since the VSD had been in the endocardial cushion defect position. (After Liebman et al. [8]. © Williams and Wilkins, Baltimore, MD. Reproduced with permission.)

the pressure is less than half systemic, including normal, it is unusual after infancy for the pulmonary to systemic flow ratio to be more than 2/1. This is because the small size of the defect itself provides too much resistance to blood flow to allow a large left-to-right shunt. Finally, to add to the complexity of the ECG interpretation, there is the problem of the lesion being dynamic. First, the defect tends to become smaller with age, and second, in large defects, where surgery is not undertaken till after early infancy, pulmonary vascular disease may occasionally develop.

In summary, VSD is a lesion which is expected to cause BVH. The volume overload is mainly left ventricular, although the right ventricle shares in it, albeit less so (Figs. 21.48 and 21.49). There is also right ventricular pressure overload, dependent upon the size of the defect, since the larger the defect the greater the magnitude of the right ventricular and pulmonary artery hypertension. Therefore, prediction of the amount of left-to-right shunt through the VSD is based mainly on the amount of LVH, whereas prediction of the size of the defect and thus the amount of pulmonary hypertension is based mainly on the amount of RVH. This predictability is reasonable in the first year of life, but because of the problem of the dynamic nature of the lesion, becomes less reliable after that. In general, when only LVH is present, the defect is quite restrictive, so that there is little or no pulmonary hypertension present. When there is only RVH, there should be concern that the defect is large, perhaps with an increased pulmonary vascular resistance, so that there is little left-to-right shunt.

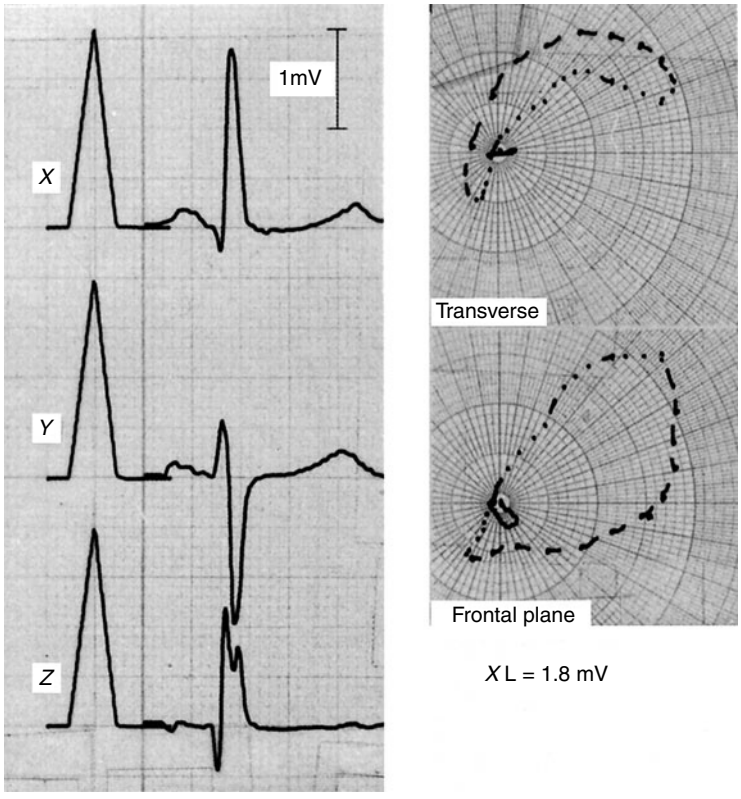

Figure 21.46

Frank-system orthogonal ECG of a 9-year-old female with hypoplastic right ventricle and tricuspid atresia, who had had no surgery. The frontal plane QRS vector loop is typical, beginning inferior, and rotating counterclockwise, mainly superior. The transverse plane demonstrates considerable conduction abnormality. The initial QRS portion is to the right and anterior, then swings posterior while still well to the right, so that the QRS is inscribed clockwise. A left lateral wall myocardial infarction must be considered (but autopsy 4 years later, death following the Fontan procedure, demonstrated no infarction). The left ventricle was myopathic, however, with considerable hypertrophy and replacement fibrosis. (After Liebman et al. [8]. © Williams and Wilkins, Baltimore, MD. Reproduced with permission.)

The degree of BVH should reflect the amount of left-to-right shunt and the size of the defect, but accuracy can only be approximate.

A VSD may also cause combined atrial enlargement. The larger the left-to-right shunt, the larger the volume overload of the left atrium. Meanwhile, the higher the RV pressure, the less is the compliance of the right ventricle, so that RAE may be present. The most commonly recognized, however, is pure LAE because the volume overload of the left atrium is dominant.

21.25.3 Biatrial Enlargement

For further discussion see Liebman et al. [8] and Ishikawa et al. [34]. Simultaneous registration of various leads is particularly useful in diagnosing biatrial enlargement (BAE) (Fig. 21.50), particularly when the magnitude is increased (e.g., four times normal standard) and the speed of the paper is 100 mm s^{-1}. The author has usually utilized simultaneous

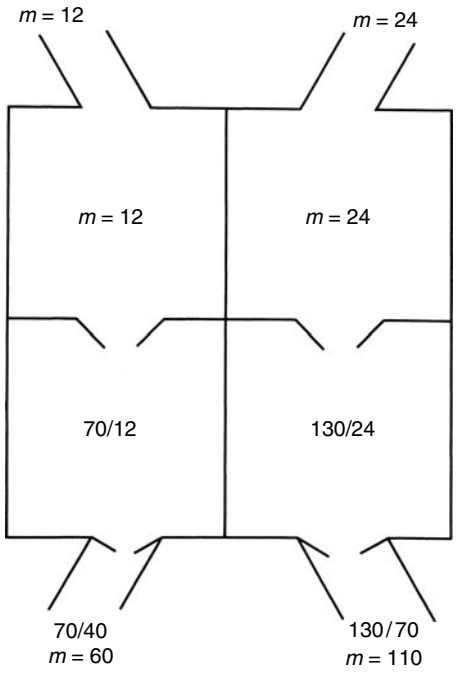

Figure 21.47

Box diagram of a patient with left ventricular cardiomyopathy and secondary pulmonary hypertension. The left ventricular end-diastolic pressure is 24 mm Hg, so that there is elevated pulmonary venous pressure (*m* = mean pressure in mm Hg). Reflex pulmonary hypertension may result.

leads V_1, V_4, V_6, I, II and III, but other combinations can be useful. It is important to be able to delineate the first portion of the P wave (especially along its inferior and anterior lead axes) from the terminal portion (to the left). If only three simultaneous leads are available, leads II, V_1 and V_5 or V_6 would usually be most useful.

The most useful criteria for BAE are the following.

(a) Standard ECG:
- (I) Increased P magnitude inferior and/or anterior (first part) plus an increased duration of P (the latter owing to increased duration of second part of P)
- (II) Increased P magnitude inferior and/or anterior (first part) plus increased magnitude posterior (second part)
- (III) Increased P magnitude inferior and/or anterior (first part) plus increased P terminal force
- (IV) Increased P magnitude inferior and/or anterior (first part) plus increased time between first and second peaks (the latter in normal infants is usually not more than 0.02 s apart, and in adolescents, rarely exceeds 0.04 s [3])

(b) Orthogonal ECG:
- (I) Increased P magnitude inferior and/or anterior (first part) plus increased duration of P (owing to increased duration second part)
- (II) Increased spatial vector magnitude of P anterior (SVA) plus increased duration of P
- (III) Increased P magnitude inferior and/or anterior (first part) and/or SVA plus increased magnitude posterior (second part)
- (IV) Increased P magnitude inferior and/or anterior (first part) and/or SVA plus increased magnitude of P spatial vector posterior
- (V) Increased P magnitude inferior and/or anterior (first part) and/or SVA plus increased time between peaks
- (VI) Increased P magnitude inferior and/or anterior (first part) and/or SVA plus increased P terminal force

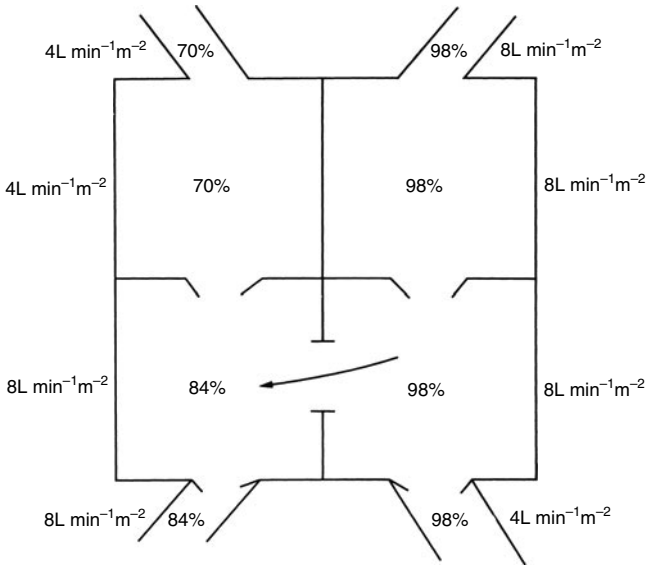

Figure 21.48

Box diagram of a child with a VSD with left-to-right shunt so that the P/S flow ratio is 2/1 (P, pulmonary flow:S, systemic flow). The systemic cardiac output is normal. There is an increase in oxygen saturation in the right ventricle.

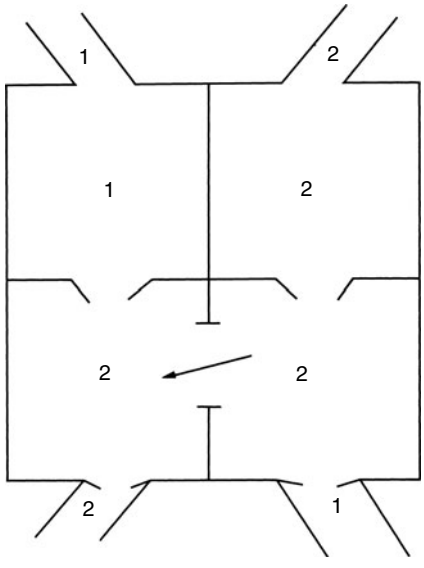

Figure 21.49

Box diagram of same child as in Fig. 21.48, with a 2/1 P/S flow ratio. The left atrium and left ventricle each has twice normal volume, while the left ventricle must eject blood into the right ventricle, although some is ejected directly into the pulmonary artery. There is LVH and there *may* be some additional mild RVH based on the passive volume work of the right ventricle. However, the larger the VSD, the higher the RV pressure, so that RVH is expected.

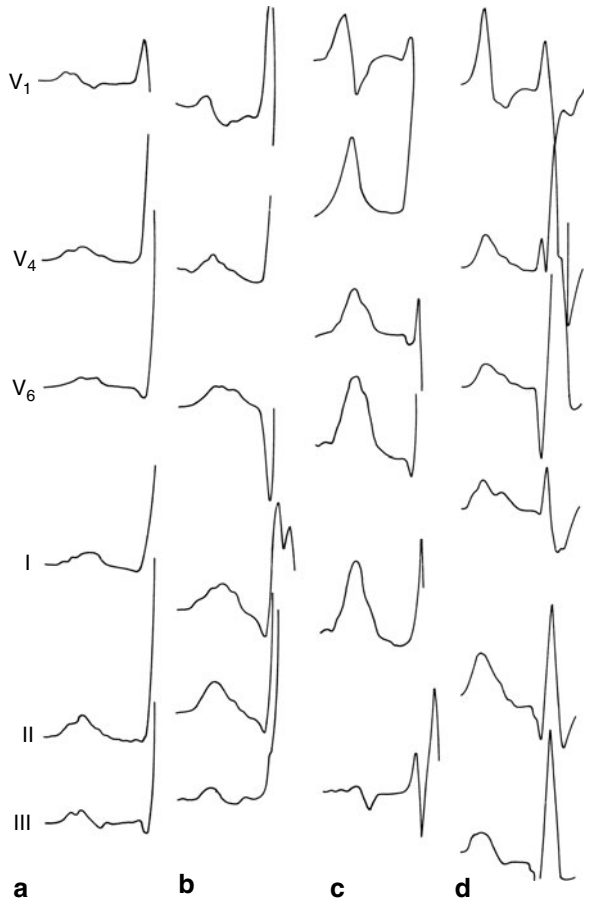

Figure 21.50

Four representative ECGs for P-wave analysis. The simultaneous tracings of leads V_1, V_4, V_6, I, II and III are recorded at 100 mm s^{-1} and at four times standard calibration. The first ECG (a) is normal, (b) shows LAH, (c) shows RAH and (d) shows BAH. (After Liebman et al. [8]. © Williams and Wilkins, Baltimore, MD. Reproduced with permission.)

The fact that there is a dynamic reason to have BVH does not necessarily mean that there should be combined atrial hypertrophy (BAH). Neither or only one atrium may be enlarged or hypertrophied. Volume overload, of course, causes atrial enlargement, whereas decreased ventricular compliance, as with ventricular pressure overload or cardiomyopathy, causes mainly atrial hypertrophy. In general, RAH is much better recognized with the ECG than is LAH. Obviously, also, RAH or LAH may be present without hypertrophy of the ventricle on the same side. The prime examples are the expected RAH in the presence of the hypoplastic right ventricle syndrome and the expected LAH in the presence of the hypoplastic left ventricle syndrome.

21.25.4 Criteria for Biventricular Hypertrophy

Biventricular hypertrophy and relevant criteria are discussed further in Liebman et al. [8].

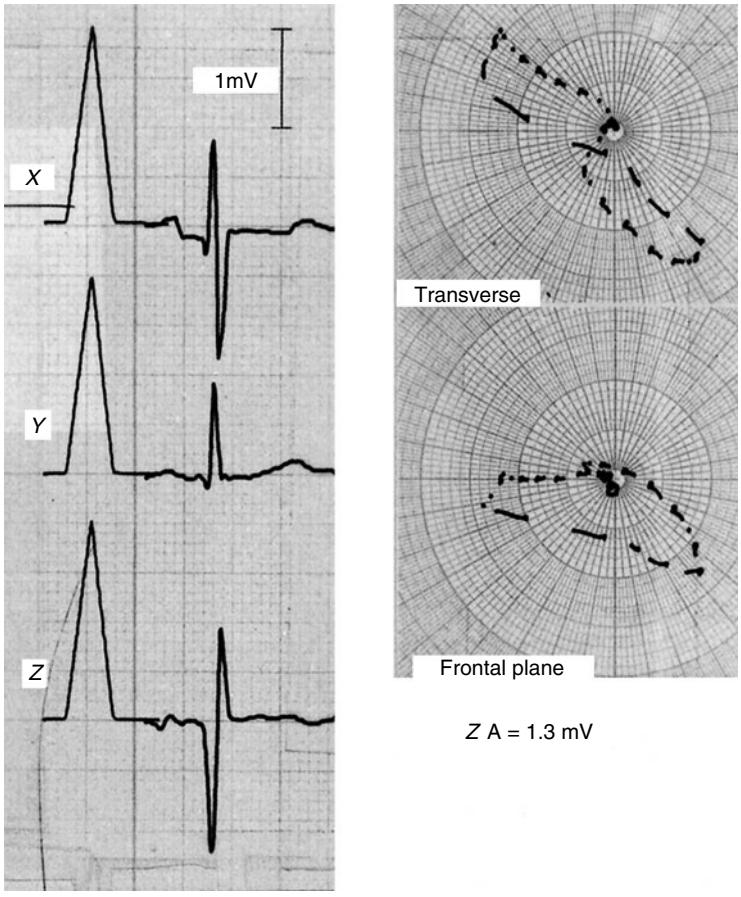

Figure 21.51

Frank-system orthogonal ECG of a 5½-week-old baby boy with TOF. There are two main vectors, the first being to the left and anterior, the second to the right and posterior. From the activation sequence, RVH is clear. There is no additional LVH, since the first main vector is not abnormally to the left. (After Liebman et al. [8]. © Williams and Wilkins, Baltimore, MD. Reproduced with permission.)

21.25.4.1 BVH Criterion 1 – Direction of Inscription of QRS Vector Loops

(a) There are many variations of BVH where the direction of inscription is particularly useful. The presence of two main vectors in the transverse plane often provides excellent evidence. The most common situation is that of the first vector being abnormally to the left as well as anterior and the second vector being abnormally to the right as well as posterior. After 1 month of life, RVH is definite (Fig. 21.51), and LVH is additionally diagnosed if the leftward vector is of increased magnitude. (An increased magnitude posterior QRS vector in this situation is not enough.) Most commonly, the first limb of the QRS vector loop is inscribed counterclockwise and the second limb clockwise.

(b) The activation sequence may be exactly as normal, with a wholly counterclockwise transverse QRS loop and large magnitude leftward and/or posterior projections. (In the newborn period, such a loop indicates LVH without abnormal magnitudes.) However, if the anterior projection is also very large and prolonged, then additional RVH is diagnosed. In the same situation, if the terminal right QRS magnitude is increased, RVH should also be suggested; but if the corresponding vector is abnormally posterior, then the large rightward vector may indicate posterobasal LVH rather than additional RVH (Fig. 21.52).

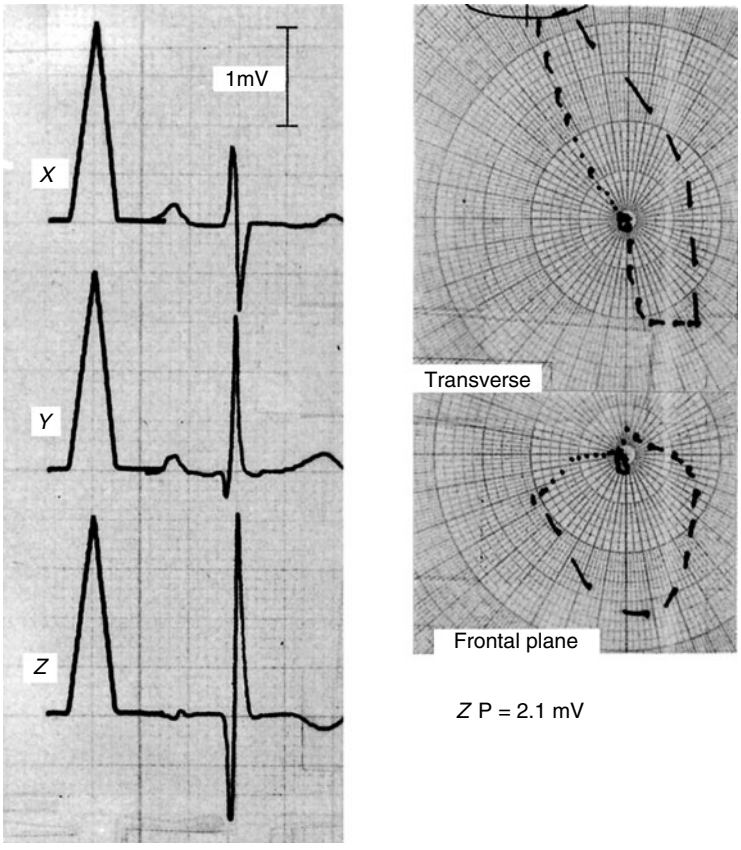

Figure 21.52
Frank-system orthogonal ECG of a three-week-old baby boy with a large VSD and large left-to-right shunt at an unusually early age. Both the posterior and inferior projections are of increased magnitude. LVH is clear, and the terminal projection to the right is also of increased magnitude, so that additional RVH is likely. It is possible, however, that the terminal projection to the right may be due to posterobasal LVH. (After Liebman et al. [8]. © Williams and Wilkins, Baltimore, MD. Reproduced with permission.)

(c) If the transverse plane is inscribed wholly clockwise, pure RVH is the usual diagnosis; but if it is also abnormally to the left, additional LVH should be considered (Fig. 21.53). However, this latter diagnosis can be an error, since a large dilated right ventricle can cause considerable proximity effect upon the lead projections on the left chest. A definite error is to diagnose additional LVH if, with the presence of a wholly clockwise transverse plane loop, there is a large terminal rightward posterior projection. This terminal posterior projection is probably derived from the right ventricle after the left ventricle has completed activation, and is a manifestation of severe RVH.

21.25.4.2 BVH Criterion 2 – Decreased QRS Magnitude Posteriorly and/or to the Left, with a Large Terminal QRS Vector to the Right

These provide excellent criteria with the caution that a terminal right posterior QRS vector may be a possible manifestation of posterobasal LVH instead of additional RVH. In the standard ECG, the BVH may be missed, even though it is clearly

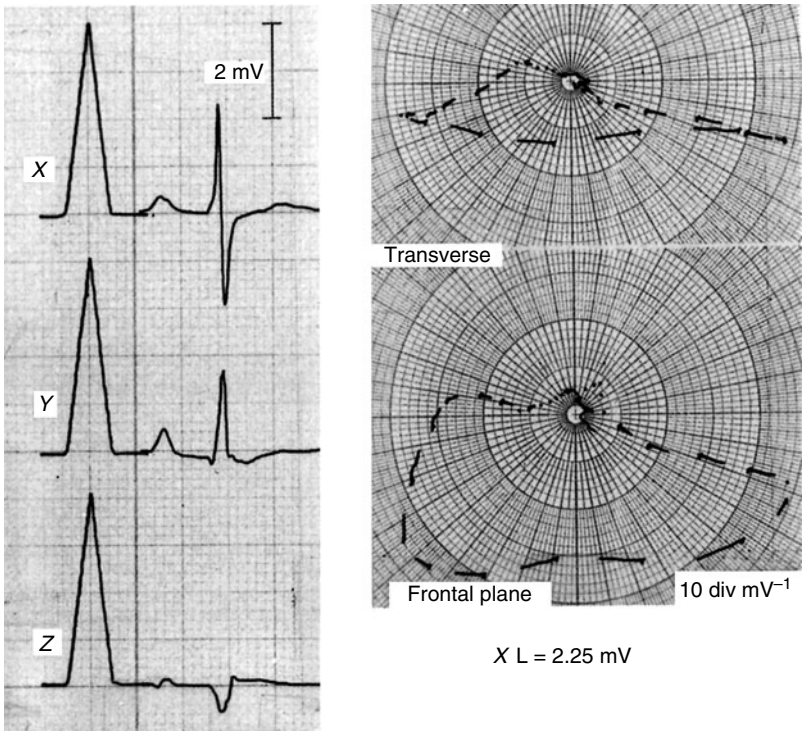

Figure 21.53
Frank-system orthogonal ECG in a 4-month-old baby boy with a large VSD and large left-to-right shunt. There are two main vectors in the transverse plane, although the inscription is wholly clockwise, indicative of RVH. The magnitude to the left is increased indicative of additional LVH. It is unlikely that the latter is caused by the proximity effect, although the very large heart in the small chest of a baby makes it possible. (After Liebman et al. [8]. © Williams and Wilkins, Baltimore, MD. Reproduced with permission.)

present in the Frank- or McFee-system orthogonal VCG. The abnormally posterior QRS vector may cause the projection of the large terminal rightward vector not to cross the perpendiculars to leads V_4R and V_1. If, on the standard ECG, there is a deep S wave in V_5 or V_6, then the lack of a terminal r or R in V_4R or V_1 is not missed, except that, for reasons unknown, the large terminal QRS vector to the right may be present in the VCG, without a deep S in V_5 or V_6 in the standard ECG.

21.25.4.3 BVH Criterion 3 – Increased Magnitude Anterior Along with Definite Evidence for LVH

The anterior portion provides only a soft sign for additional RVH. The initial anterior limb should be broad and of at least 0.03 s duration (after infancy). A large initial rightward anterior QRS vector could be caused by left septal hypertrophy, whereas a tall spiking initial anterior vector reflected in the right chest leads is commonly caused by proximity effect – particularly in preschool children.

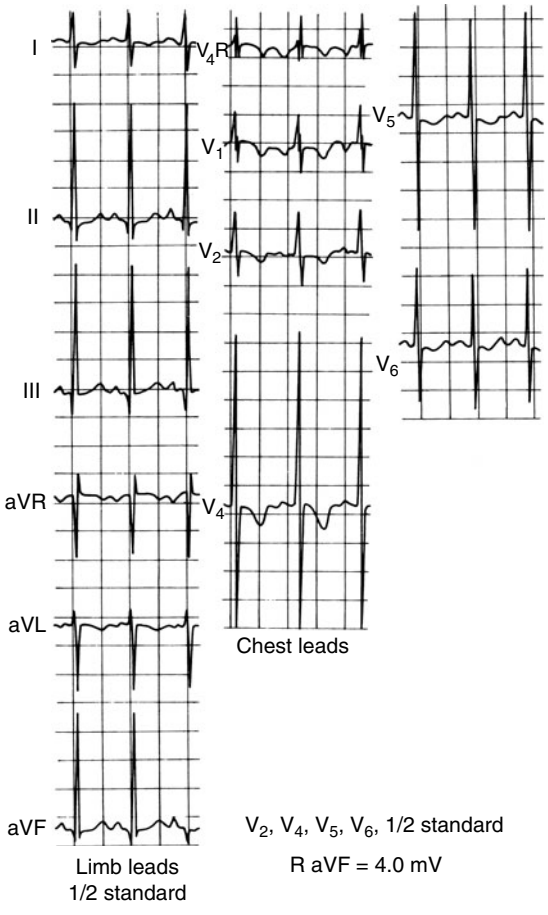

Figure 21.54

Standard ECG of a 2-month-old baby boy with a large VSD and large left-to-right shunt. The voltages are exceptionally high. In lead V_4, the combined QRS magnitude is greater than 10.0 mV. The QRS appearances in V_4, V_5 demonstrate the Kaltz-Wachtel phenomenon.

21.25.4.4 BVH Criterion 4 – Increased Magnitude Inferior Vector (Increased Y Inferior, Tall R in aVF) in the Presence of RVH as Diagnosed in the Transverse Plane

In the presence of good left ventricular potential and the absence of very severe RVH, additional LVH can be considered. However, if the RVH is severe, the increased magnitude inferior is part of the RVH. Such an ECG is common, for example, in tetralogy of Fallot.

21.25.4.5 BVH Criterion 5 – Katz-Wachtel phenomenon

This is a "pattern" and is not generally useful, although it is commonly discussed, particularly in relation to ventricular septal defect. It was originally described as "tall R and S waves in the mid-chest leads, together with tall R and S waves in two of the three 'bipolar' standard limb leads [63]." The biphasic nature of the QRS was believed to be caused by the

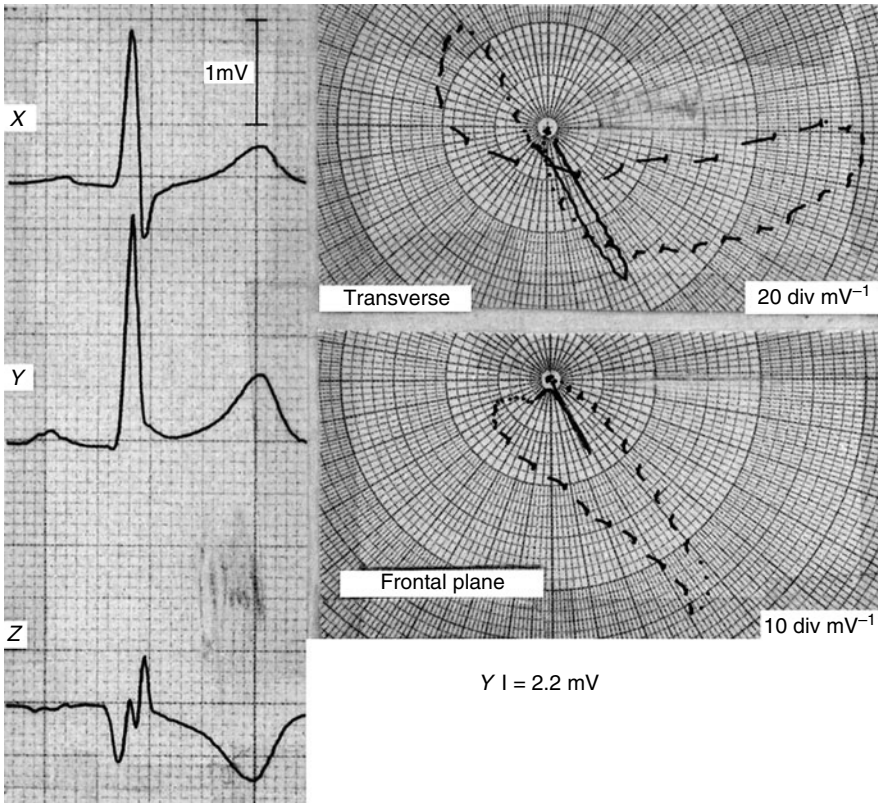

Figure 21.55
Frank-system orthogonal ECG of a 17-year-old with a small VSD (once significantly larger). LVH is present on the basis of the increased magnitude inferior vector. The activation sequence, where the QRS vector moves to the right without going posterior, indicates RVH. There is also some terminal right conduction delay. The mild BVH reflects previous dynamics. (After Liebman et al. [8]. © Williams and Wilkins, Baltimore, MD. Reproduced with permission.)

opening in the septum, but of course that is not true. The manifestation of BVH is that of a wide-open counterclockwise transverse plane vector loop with the first limb markedly anterior and the second decidedly posterior (Fig. 21.54).

21.25.4.6 BVH Criterion 6 – Definite ECG Evidence of Hypertrophy of One Ventricle, with Suggested ECG Evidence of Hypertrophy for the Other

This is a nonspecific but valid criterion, and an overlap of much that has been said above.

21.25.4.7 BVH Criterion 7 – ST and T Abnormality

With the present level of knowledge, ST and T abnormality in the presence of hypertrophy indicates severity, but cannot be used to diagnose hypertrophy per se.

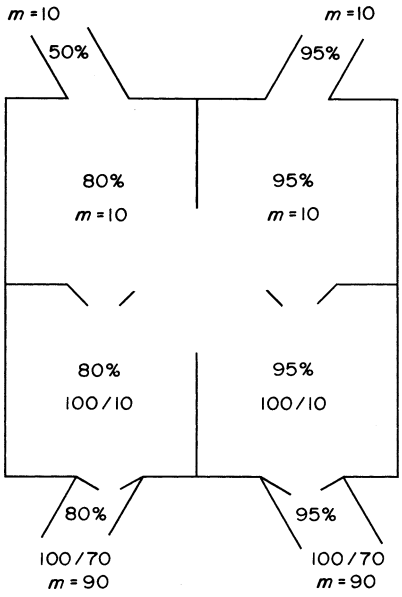

Figure 21.56

Box diagram of a patient with complete AV canal. Note the communication among all four chambers. Left and right atrial pressures are equal, and LV and RV pressures are equal. There must be systemic level pulmonary hypertension. In this case, there is a large left-to-right shunt at the atrial level, although severe mitral and/or tricuspid regurgitation is possible.

21.25.4.8 Addendum

As a result of the dynamic nature of the lesion, BVH may be recognized although the lesion has become very small. The ECG thus reflects previous dynamics (Fig. 21.55).

21.25.5 False-Positive Criteria for BVH

21.25.5.1 BVH Criterion 8 – Mean QRS Vector to the Right in the Frontal Plane of Standard ECG in the Presence of Definite LVH

The LVH is best diagnosed in the chest leads, the transverse plane, but the mean QRS vector to the right may help in diagnosing additional RVH. However, it is often an artifact of the poor lead I, so it is not reliable. However, if present in Frank or McFee vectorcardiograms, the horizontal plane would show the large terminal vector to the right, as well, and BVH would be the correct diagnosis.

21.25.5.2 BVH Criterion 9 – Clockwise Inscription of the Frontal Plane in the Presence of Definite LVH

This is similar to criterion 8 and is not an indicator of BVH since the clockwise frontal plane in the standard ECG is normal in most children.

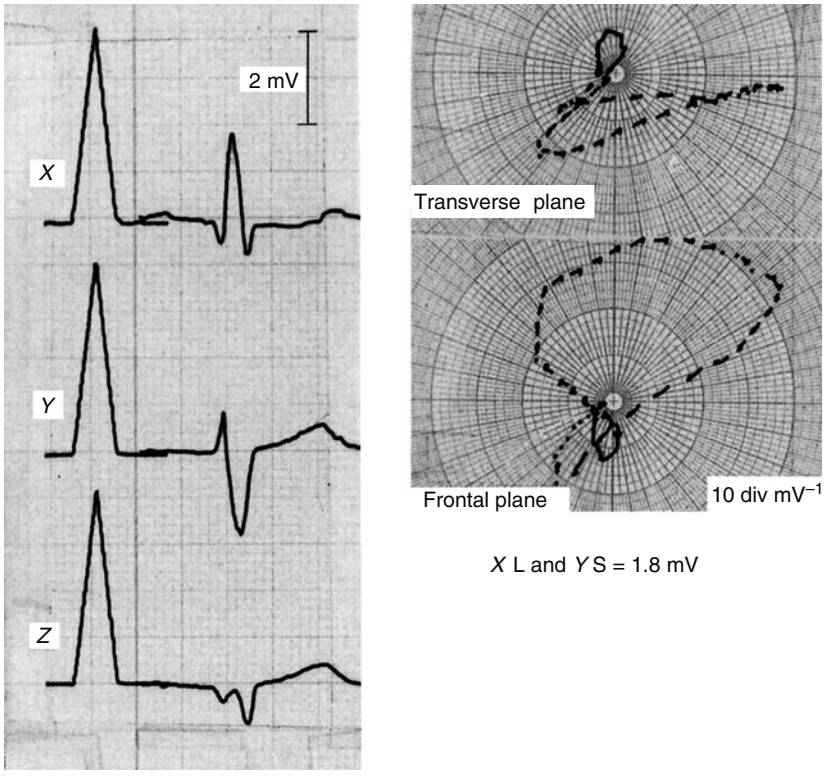

Figure 21.57

Frank-system orthogonal ECG of a 15-month-old female with a partial AV canal. There is a large left-to-right shunt at both the atrial and ventricular levels with the RV pressure at 2/3 systemic level. There is a typical "abnormally superior vector" and BVH. The RVH is diagnosed on the basis of the mainly clockwise-inscribed anterior loop, as seen in the transverse plane, with the increased QRS magnitude projection to the left.

21.25.5.3 BVH Criterion 10 – Mean QRS Vector to the Left in the Frontal Plane in the Presence of Definite RVH

Frequently, the inscription in the frontal plane will be counterclockwise. This is only a fair sign unless there is increased magnitude to the left (R in lead I or aVL). But this, too, is unreliable since a leftward frontal vector causes the projection on lead aVL to increase in magnitude.

21.25.5.4 BVH Criterion 11 – Abnormally Superior Maximum QRS Vector in the Presence of Definite RVH

This is not a sign of BVH, for the abnormally superior vector indicates a conduction defect involving the left anterior branch of the left bundle. The abnormally superior vector may also cause the R wave in lead I and/or aVL to be of increased magnitude.

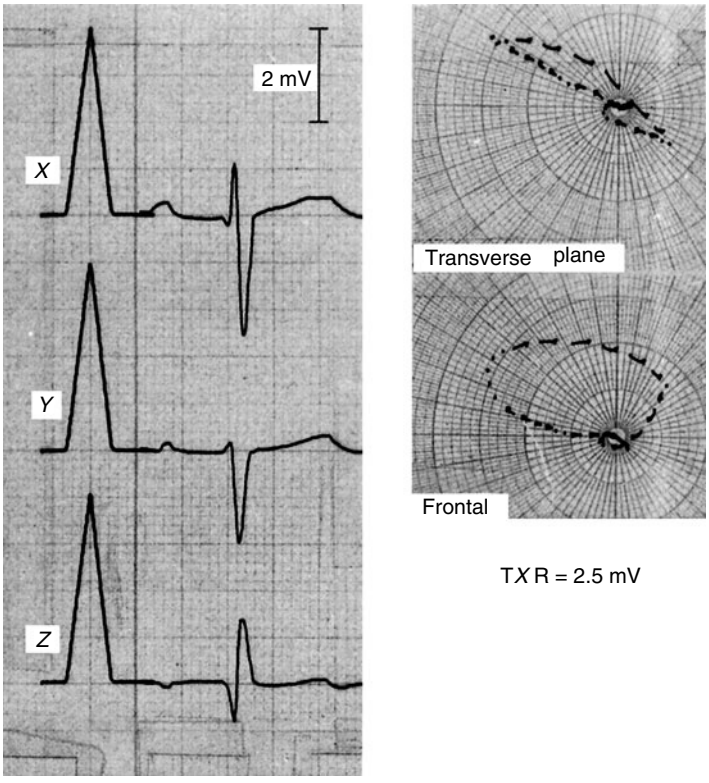

Figure 21.58

Frank-system orthogonal ECG of a 5-year-old male with complete AV canal and increased pulmonary vascular resistance. There is a small left-to-right and right-to-left shunt plus significant mitral regurgitation. There is a typical "abnormally superior QRS vector." Although RVH is marked, with the very large terminal QRS vector to the right, additional LVH is suggested because the transverse plane loop is inscribed counterclockwise. (After Liebman et al. [8]. © Williams and Wilkins, Baltimore, MD. Reproduced with permission.)

21.26 Atrioventricular Canal

No matter how extensive the endocardial cushion defect, whether a simple ostium primum defect without mitral regurgitation, or a simple VSD in the endocardial cushion position, a complete atrioventricular (AV) canal, or any intermediate form, an abnormally superior maximum QRS vector is expected. Only very occasionally is such a vector not present (the uncommon exception being especially seen in Down syndrome).

In the Complete AV canal, the shunting is complex and may be in diastole as well as systole. Diastolic flow can be right to left, from right atrium to left ventricle, or left to right, from left atrium to right ventricle. Systolic flow is from left atrium to right atrium as well as left ventricle to right ventricle. Left-to-right atrial flow may also occur in diastole. Since a nonrestrictive ventricular septal communication is usually part of the lesion, by definition, there is left-to-right shunt at the ventricular level as long as pulmonary vascular resistance is less than systemic vascular resistance. Mitral regurgitation and, less often, tricuspid regurgitation may also be part of the lesion. The left-to-right shunt at the ventricular level as well as mitral regurgitation cause left ventricular volume overload, whereas left ventricle to right atrial communication and left-to-right shunting at the atrial level cause right ventricular volume overload. Tricuspid regurgitation also causes right ventricular volume overload. Since there is systemic pressure in the right ventricle and pulmonary artery, there is also

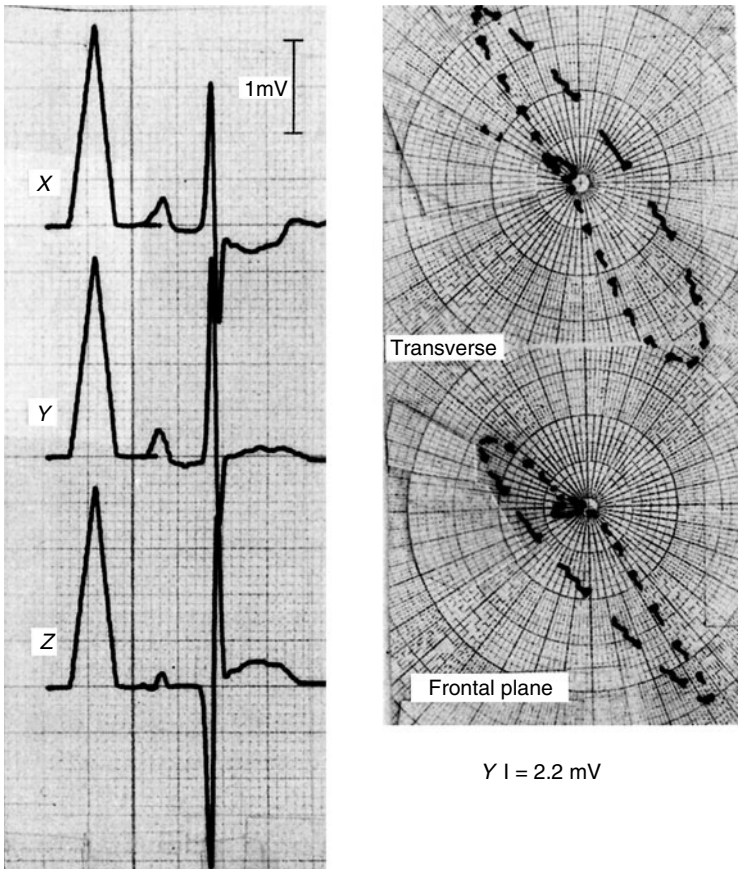

Figure 21.59

Frank-system VCG of a 6-week-old baby girl with a true truncus arteriosus and elevated pulmonary vascular resistance. The left-to-right shunt was small. The VCG loop exhibits counterclockwise inscription in the transverse plane. There is also a large inferior vector as well as prominent anterior and posterior forces. BVH is present, although the LVH is dominant. The hemodynamics have not been well predicted. (After Liebman et al. [8]. © Williams and Wilkins, Baltimore, MD. Reproduced with permission.)

RV pressure overload (Fig. 21.56). It should be evident that it would be very difficult on the basis of the ECG per se to predict the hemodynamics (Figs. 21.57 and 21.58). The information must be complementary to other aspects of the clinical picture. Even patients with little or no left-to-right shunt because of pulmonary vascular disease may have LVH in addition to the marked RVH if there is mitral regurgitation, or if the left ventricle is reflecting previous hemodynamics. BVH can, of course, occur in a variety of lesions besides the above.

21.27 Large PDA (and the Common A-P Window)

The PDA with left-to-right shunt, as described previously, is associated with LVH. However, in the presence of larger PDA (and the connection is shorter), the resistance to flow through it decreases and the pressure in the pulmonary artery increases. The nonrestrictive PDA is quite uncommon and is associated, by definition, with systemic pressure pulmonary

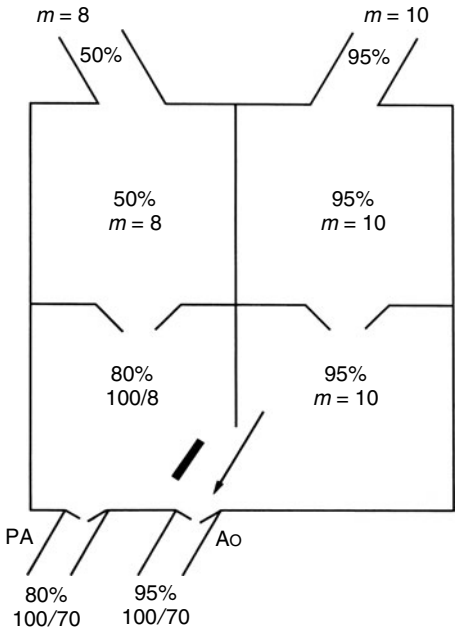

Figure 21.60

Box diagram of a patient with double outlet right ventricle (DORV) where the VSD is subaortic. As a result of the double conus, there is usually considerable muscle separating the origin of the aorta and pulmonary artery. Therefore, very little of the right ventricle blood goes into the aorta and the patient is usually quite pink, acting like one with a simple large VSD.

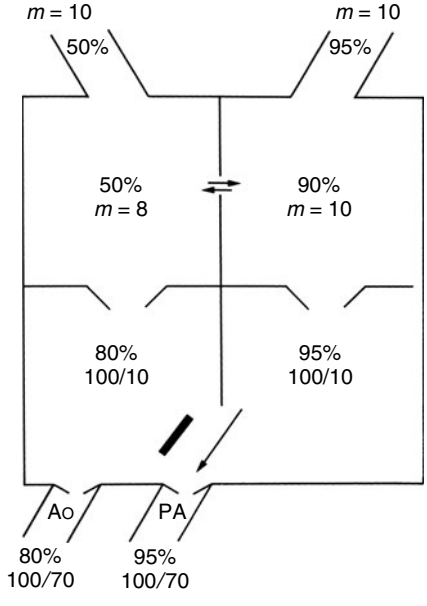

Figure 21.61

Box diagram of a patient with DORV where the VSD is subpulmonic (Taussig-Bing complex). As a result of the double conus, there is considerable muscle separating the origin of the aorta and pulmonary artery. Therefore, very little of the right ventricle blood goes out through the pulmonary artery. The physiology is that of transposition of the great arteries with RV and pulmonary artery pressures at systemic level.

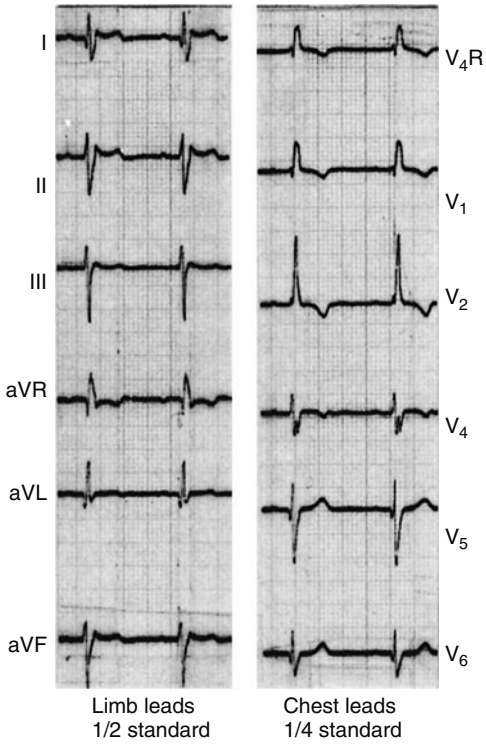

Figure 21.62

Standard ECG recorded postoperatively from a 6½-year-old male with DORV. There is RBBB. The abnormally superior maximum QRS vector was present preoperatively as well, as in some patients with DORV where the VSD is subaortic and in the endocardial cushion position.

hypertension. The higher the pulmonary artery pressure, the more likely it is that there will be additional RVH. The same principles, of course, hold for the A-P window, which is usually nonrestrictive.

21.28 Left Ventricle to Right Atrial Shunt

This is an unusual form of VSD where the defect is above the tricuspid valve ring. Consequently, left ventricular flow through the defect is into the right atrium. There are important differences from that of the more common VSD (from left ventricle to right ventricle), for no matter how large the defect, there is no transmission of systemic pressure into the right ventricle. Therefore, on that basis, there is less likely to be RVH. On the other hand, since all the left-to-right flow is into the right atrium, then all of the left-to-right flow must passively flow from the right atrium into the right ventricle. Therefore, on this latter basis, RVH is *more* likely. There is none of the aspect encountered in the more common VSD where some of the left-to-right shunt flows directly from the left ventricle to the pulmonary artery. Obviously, the presence or absence of RVH in this lesion is not very helpful in estimating pulmonary hypertension. RAE, on the other hand, is definitely more likely than in the common VSD.

21.29 Ostium Primum ASD with Mitral Regurgitation

The hemodynamics of this lesion are quite straightforward. With a larger left-to-right shunt, the RVH with terminal right conduction delay is greater, as in the secundum ASD. With considerable mitral regurgitation, the LVH is great.

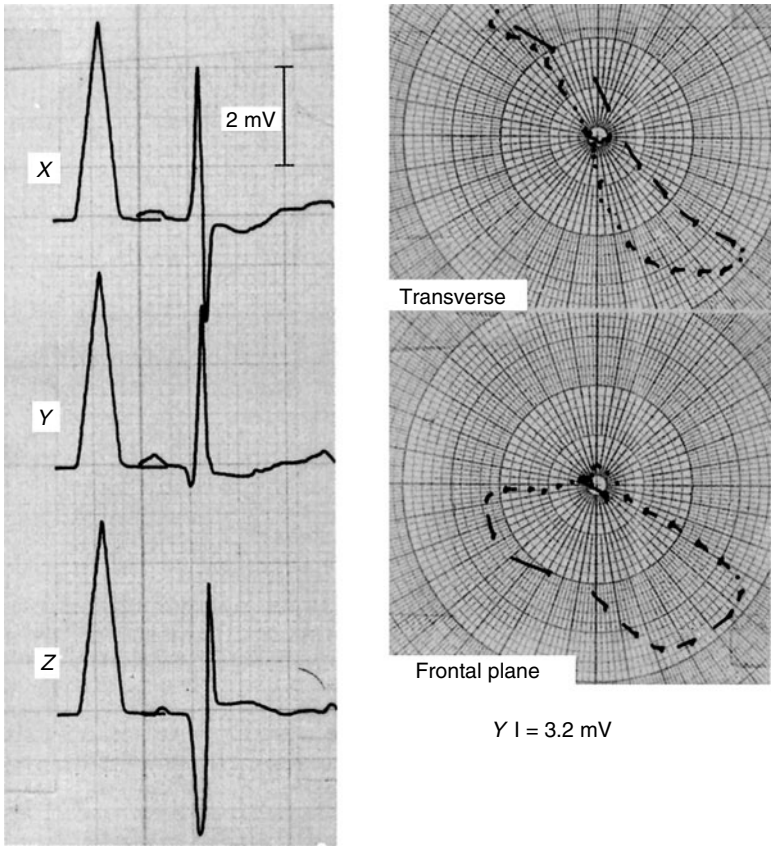

Figure 21.63

Frank-system orthogonal ECG in a 9-week-old male with simple severe coarction of the aorta, and who is not in congestive heart failure. There is considerable LVH with large magnitude inferior and leftward vectors in the presence of a counterclockwise-inscribed transverse plain "loop." However, there is also considerable RVH since the terminal QRS vector to the right (2.0 mV) is abnormally large.

However, if the ostium primum opening is large, the regurgitant flow acts as though it is going directly into the right atrium, and some actually does. Therefore, unlike pure mitral regurgitation, LAH is not present. It is present only when the ostium primum opening is small, while the mitral regurgitation is considerable.

21.30 True Truncus Arteriosus

Since the VSD is very large, RV pressure is at systemic level and since, in infancy, in the most common type I truncus, pulmonary vascular resistance is low, the left ventricle provides most of the work of the increase in pulmonary blood flow. BVH is, therefore, part of the lesion. In general, just as in large VSD, with low pulmonary vascular resistance, the left ventricle dominates, and if pulmonary vascular resistance is increased, the right ventricle dominates. Pulmonary vascular disease frequently develops very rapidly, so that the progression to pure RVH on the ECG is ominous. However, particularly because of varying streaming patterns from left ventricle to right ventricle and left ventricle to aorta or pulmonary artery, predictability is not reliable (Fig. 21.59).

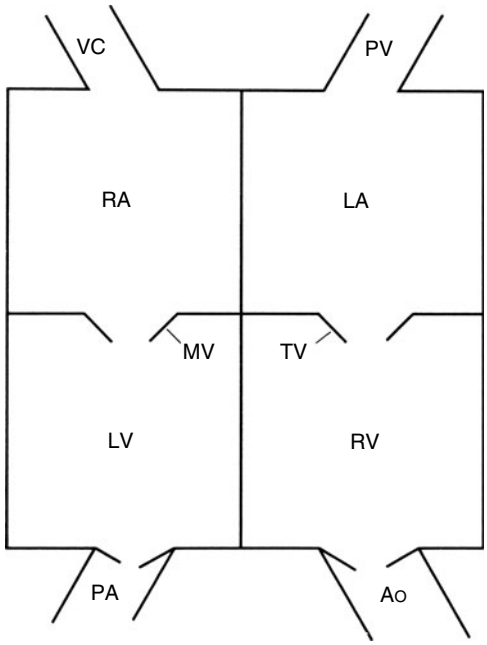

Figure 21.64

Box diagram of a patient with ventricular inversion and no other abnormality. The right atrium drains into the right-sided left ventricle and then the pulmonary artery (which is posterior). The left atrium drains into the left-sided right ventricle and then the aorta (which is anterior). Note that the mitral valve stays with the left ventricle and the tricuspid valve stays with the right ventricle.

21.31 Double Outlet Right Ventricle

The dynamics of this lesion are of great interest and very variable, because of variable anatomy. The VSD may be subaortic (Fig. 21.60) so that the patient acts like that of a simple nonrestrictive VSD, with LVH dominant on the ECG. There may be severe pulmonic stenosis in addition to the non-restrictive VSD so that the patient may be cyanotic, acting like that of TOF. Pure RVH may be present, but if so, usually with much more left chest potential than in TOF. There may even be BVH despite the severe PS. The VSD may be subpulmonic so that the pathophysiology is like that of transposition with large VSD (Fig. 21.61). (Additional pulmonic stenosis in the presence of the subpulmonic VSD is not common.) The VSD can also be not preferentially committed to either great artery, in which case, LVH is likely to be dominant; the VSD can be restrictive so that in addition to RVH, the additional LVH may be very severe, even with ST-T abnormality. Finally, particularly when in the subaortic position, the VSD is commonly an endocardial cushion type, resulting in an abnormally superior maximum QRS vector on the ECG (Fig. 21.62).

21.32 Coarctation of the Aorta Late in Infancy

The electrocardiogram in simple severe coarctation of the aorta in infancy is of great interest. It is known that in early infancy pure RVH is common because of the dynamics in utero plus, in those with congestive heart failures, there is pulmonary hypertension secondary to pulmonary venous hypertension. However, even after increased pulmonary venous pressure is no longer present and after the expected LVH has finally developed, additional RVH may persist for a long time. The explanation is again, presumed to be related to, the dynamics in utero and attendant cellular hyperplasia [48] (Fig. 21.63).

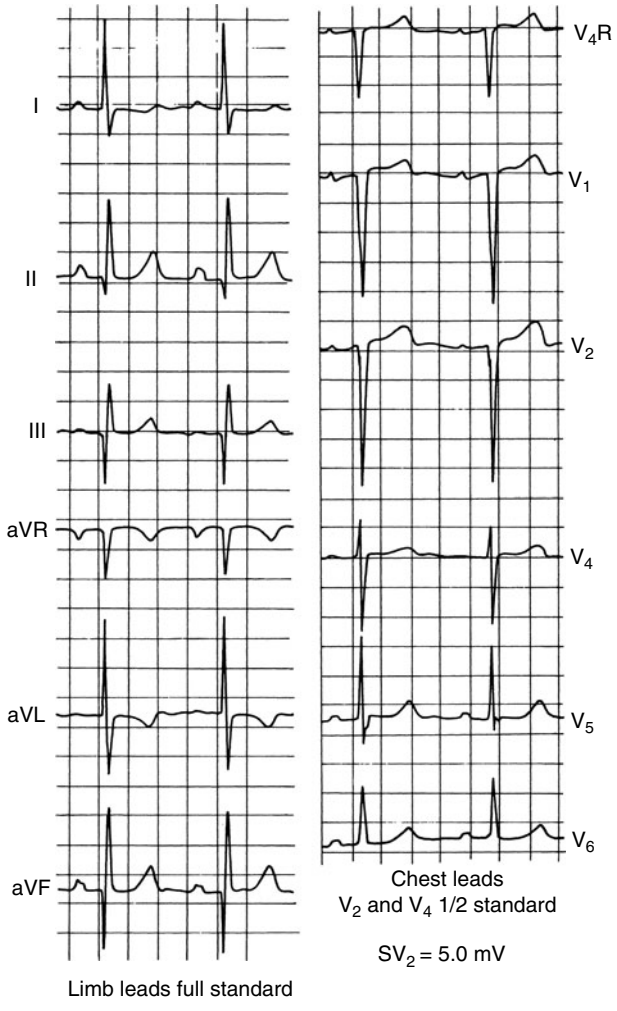

Figure 21.65

Standard ECG of an 11½-year-old male with ventricular inversion (L transposition) and, as the only other abnormality, left AV valve (tricuspid) regurgitation. The initial QRS activation is straight to the left and only slightly anterior. There is a very large magnitude initial superior vector. There is a wide open counterclockwise direction of inscription, with the magnitude posterior very large. LVH is diagnosed, although this is a right ventricle on the left side. (After Liebman et al. [8]. © Williams and Wilkins, Baltimore, MD. Reproduced with permission.)

21.33 Special Lesions

There are a number of lesions where the ECG is of particular interest.

21.33.1 Ventricular Inversion

In this lesion, the right atrial blood goes into the right-sided left ventricle, from which the pulmonary artery arises. The left atrial blood enters the left-sided right ventricle from which the aorta arises (Fig. 21.64). Although ventricular

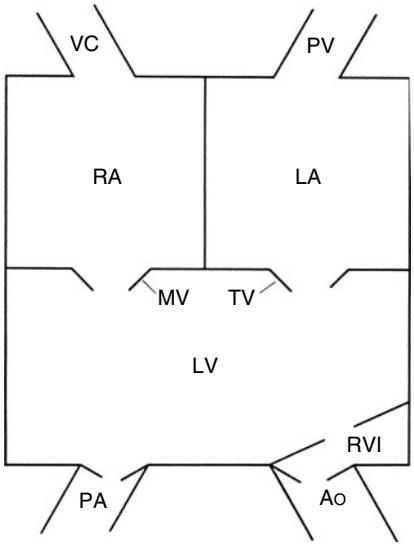

Figure 21.66

Box diagram of a patient with ventricular inversion and a single ventricle. Although seeimingly complex, it is really quite similar to that of Fig. 21.64. There is aplasia of the body of the right ventricle, however, so that only the right ventricular infundibulum (RVI) remains.

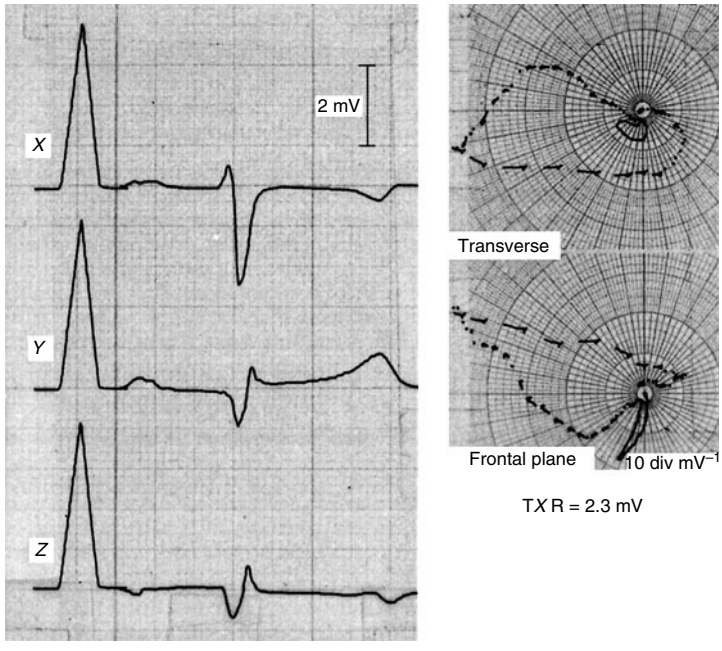

Figure 21.67

Frank-system orthogonal ECG of a 24-year-old male with single ventricle (SV), who had pulmonary artery banding procedure at the age of 4 years. The SV is of the most common type with ventricular inversion and L transposition. There is no AV valve regurgitation. Note that the initial superior vector is very large and that the initial QRS forces are to the left and very slightly posterior. There is marked "RVH" associated with the pulmonary artery band.

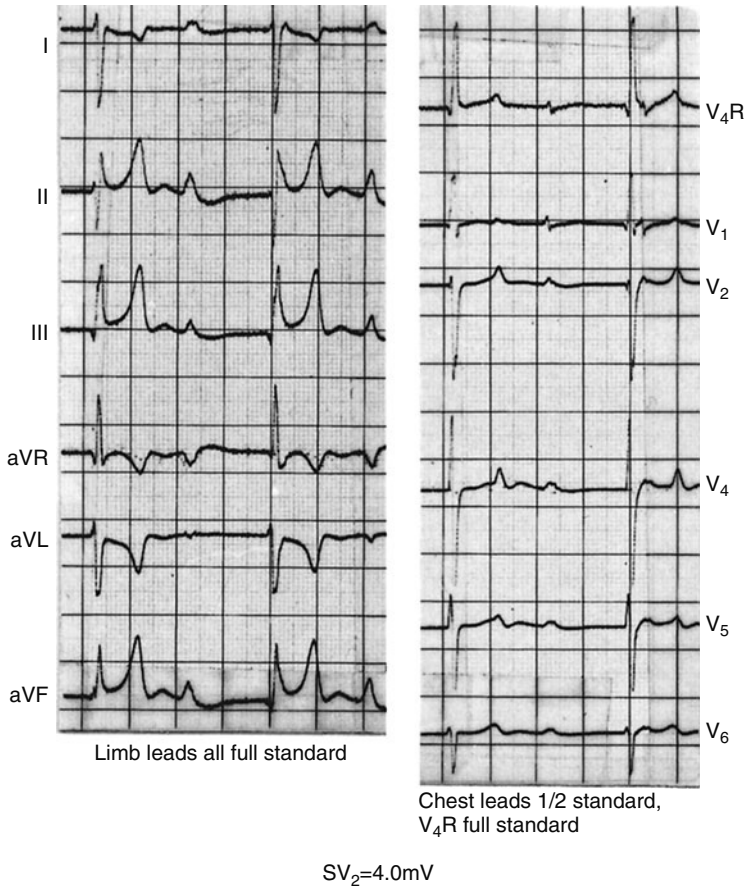

Figure 21.68

Standard ECG of same patient as in Fig. 21.67 4 years previously (there was no significant difference). Although the initial QRS is to the left and slightly posterior, the large magnitude initial QRS superior force seen in the VCG is not reflected in the ECG. Note that the patient has complete AV block, a finding which is very common in ventricular inversion.

inversion can be associated with no other anomalies, usually something else is present, such as ventricular septal defect, left-sided atrioventricular valve insufficiency or pulmonic stenosis. However, the most common abnormality is actually a variety of single ventricle (see Sect. 21.33.2). Obviously, the ECG must reflect the hemodynamics of the particular abnormalities, but of special interest is initial QRS activation. The left bundle branches are on the right side, since the left ventricle is on the right side, and, of course, the right bundle branch is on the left side. Therefore, the vector of initial QRS activation may be from right to left depending upon other aspects of initial activation. The anatomy of the ventricles is such that the septum is almost vertical rather than at an angle. Therefore, the expected right-to-left activation is usually *not* to the left and posterior, although this can occur. It is usually straight left. This usually produces q waves in V_4R and V_1, but not V_2 (although this can occur), but, of course, no small q wave in V_5 and V_6. Meanwhile, because of the vertical septum, initial activation is straight up the septum, so that in the superior inferior leads (for example, aVF) there is often a large initial Q wave (Fig. 21.65). This may even be the larger magnitude wave in lead aVF; or be entirely superior. This is of course not an abnormally superior vector for, to make that diagnosis, the initial QRS vector must be inferior.

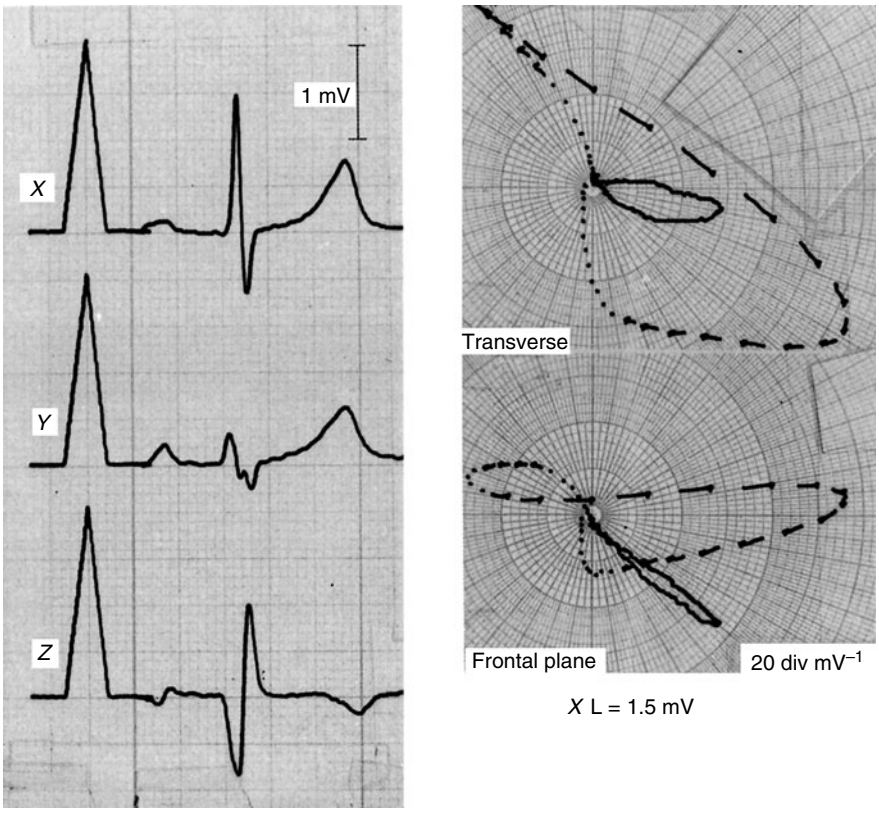

Figure 21.69

Frank-system orthogonal ECG of a 6½-year-old male with single ventricle, no ventricular inversion and D loop transposition of the great arteries. The initial QRS loop is normal and the standard ECG, as well as the Frank-system ECG, gave no clue to single ventricle. There was a large left-to-right shunt. The ECG shows enough terminal right conduction delay to suggest partial RBBB. Complete repair (septation) had been successfully accomplished. (After Liebman et al. [8]. © Williams and Wilkins, Baltimore, MD. Reproduced with permission.)

21.33.2 Single Ventricle

By definition, in single ventricle, both AV valves enter one ventricle even if one of the AV valves is atretic. By far the most common single ventricle is, in actual fact, a form of ventricular inversion with an unusual abnormality; that of hypoplasia of the body of the right ventricle. As a result of the ventricular inversion, the single left ventricle is on the right and a right ventricular infundibulum (connected by the bulboventricular foramen) is on the left. The pulmonary artery arises on the right from the single left ventricle, whereas the aorta arises on the left from the right ventricular infundibulum (Fig. 21.66). The classical initial QRS of ventricular inversion may be present (Figs. 21.67 and 21.68), but other than that there are no other reliable electrocardiographic clues to single ventricle. The conduction system is, however, very specifically known [64].

There used to be a dictum that single ventricle is associated electrocardiographically with deep S waves in all the precordial leads. This presupposed that single ventricle was caused by an absent septum, with all else normal. That type of

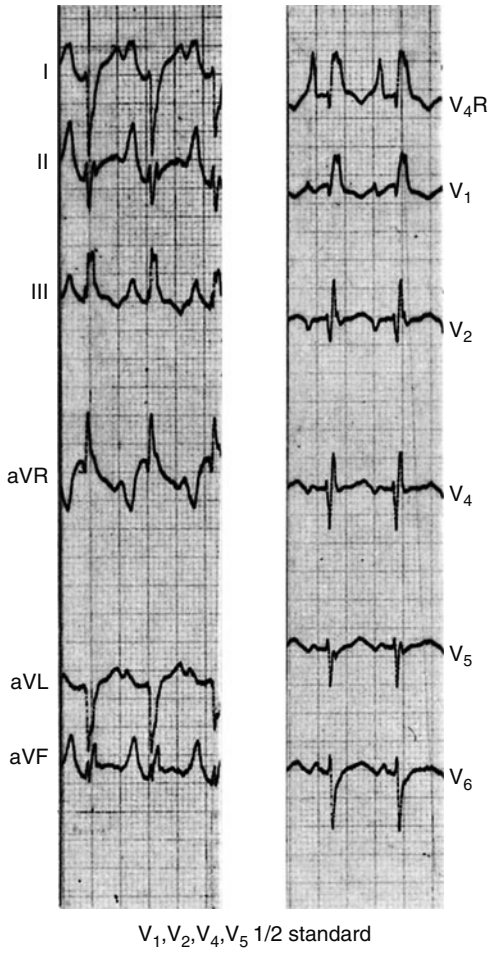

Figure 21.70

Standard ECG of an 18-month-old female with Ebstein's anomaly. There is marked RAH (note tall P in leads II and V_4R). The QRS complex demonstrates a prominent terminal vector to the right and anterior which is inscribed very slowly (advanced RBBB).

single ventricle is quite rare, and even when present, such an ECG is not usually found (Fig. 21.69). In general, however, for most varieties of single ventricle, severe PS is associated with pure RVH, and BVH is likely to indicate that severe PS is not present.

21.33.3 Ebstein's Anomaly

Ebstein's anomaly is very variable in its anatomy and severity. The tricuspid valve is very abnormal and there is displacement of the valve into the right ventricle. The result is a small ineffective functioning right ventricle. Intracavitary electrocardiography reveals a right ventricular electrocardiogram at a varying distance on the right atrial side of the valve. The degree of tricuspid regurgitation varies from none to considerable, and the amount of right-to-left shunt at the atrial level varies from none to considerable.

The electrocardiogram usually demonstrates right atrial hypertrophy, which is often marked. In addition, there is advanced RBBB because of the abnormal development and position of the bundle (Lev, M., personal communication) (Fig. 21.70), with the generalized voltage often less than usual for advanced RBBB. (There may be great variation in the

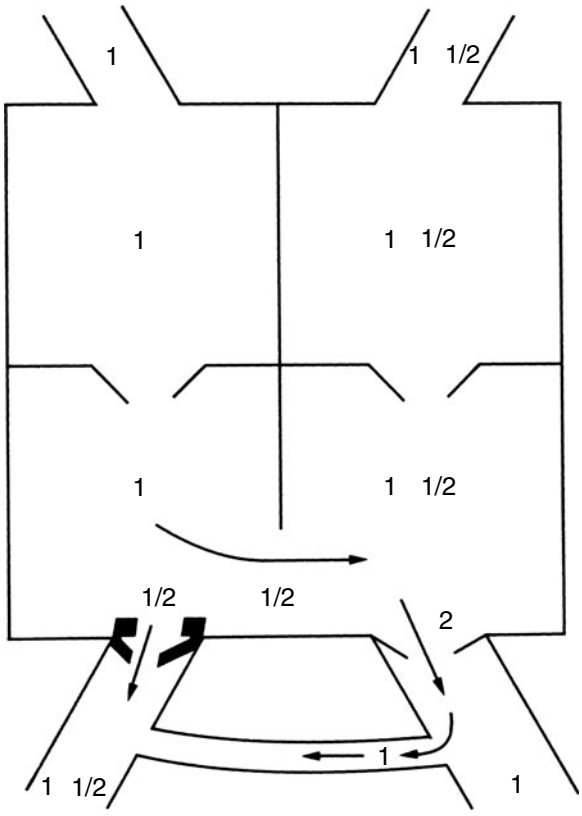

Figure 21.71

Box diagram of a patient with TOF who has had a systemic-pulmonary shunt surgically placed. In the unoperated patient with TOF (Fig. 21.23) where the pulmonary blood flow is one-half normal, the left ventricle handles between one-half normal and normal volume, depending upon how much right ventricular blood flows into the aorta directly. For a shunt where one unit of cardiac output flows from aorta to pulmonary artery, the entire volume must be handled by the left ventricle. Therefore, the left ventricle handles between 1½ and 2 times normal volume, depending upon how much right ventricular blood flows into the aorta directly.

degree and variety of RBBB in Ebstein's anomaly.) Finally, in a large number of cases, there is evidence for an accessory connection usually entering the anterior high lateral portion of the right ventricle. The resulting electrocardiogram is that of the classical pre excitation and simulation of LBBB. Even without the Wolff-Parkinson-White (WPW) syndrome, atrial arrhythmias are very common.

21.33.4 Dextrocardia

Interpretation of the electrocardiogram is very difficult, not so much because the heart is in the right chest, but because of the complex anatomic relationship of the chambers often present. In the presence of abdominal situs inversus, there is atrial situs inversus and usually there is no pathology. In that situation, when there is a cardiac abnormality, interpretation

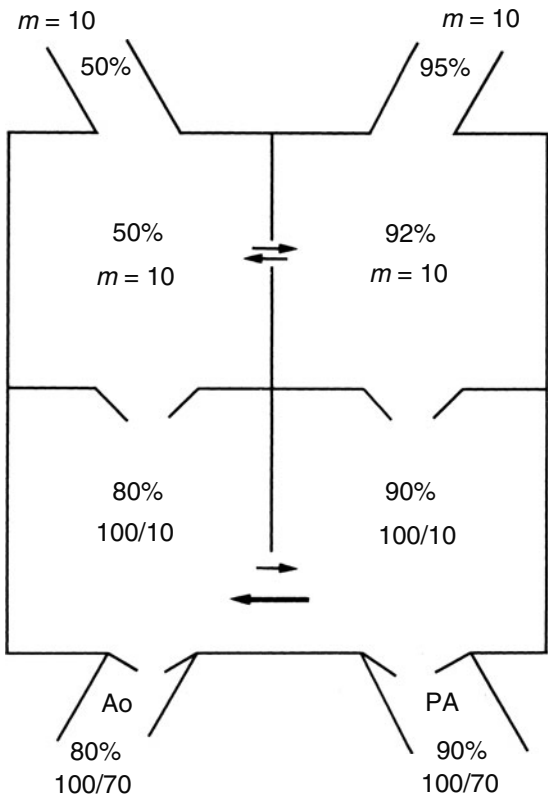

Figure 21.72

Box diagram of a patient with transposition of the great arteries (TGA) with a nonrestrictive VSD. The right and left ventricular and, of course, aorta and pulmonary artery systolic pressures are equal. (Should pulmonary stenosis be present, the ventricular pressures would be unaffected, but pulmonary artery pressures would be less. Should the VSD be smaller, then LV pressure would be less). The flow patterns through the atrial and ventricular openings are complex. The amount of left-to-right and right-to-left shunt theoretically should be equal, but the difficult calculations rarely come out that way. With low pulmonary vascular resistance, the expected is a larger left atrial to right atrial shunt at the atrial level, and a larger right-to-left shunt at the ventricular level. In the above box diagram, there is a small right-to-left shunt and trivial left-to-right shunt at the atrial level, plus a small right-to-left shunt and a large left-to-right shunt at the ventricular level. In this case pulmonary vascular resistance is high.

of the electrocardiogram is not difficult. On the other hand, normal abdominal situs together with normal atrial situs are usually associated with complex disease. A particular use of the electrocardiogram has been to determine the relationship of the atria to each other. However, there may be many errors for many reasons, including the frequent left atrial pacemaker. Since the left atrium is on the same side as that of the stomach bubble, the chest x-ray provides a far more reliable method than does the ECG. If there is a transverse liver, however, the ECG is extremely helpful.

On the other hand, by utilizing the initial QRS forces, ventricular relationships are often readily determined with the electrocardiogram [65]. For example, in situs inversus, if the initial QRS vector is directed to the left, anterior and superior, then it is surmised that the morphologic left ventricle is to the right of the morphologic right ventricle, and that this morphologic ventricle is also posterior to the morphologic right ventricle. Thus, this information can be utilized in deciding which ventricle is hypertrophied and can also be used in a complementary way in interpreting

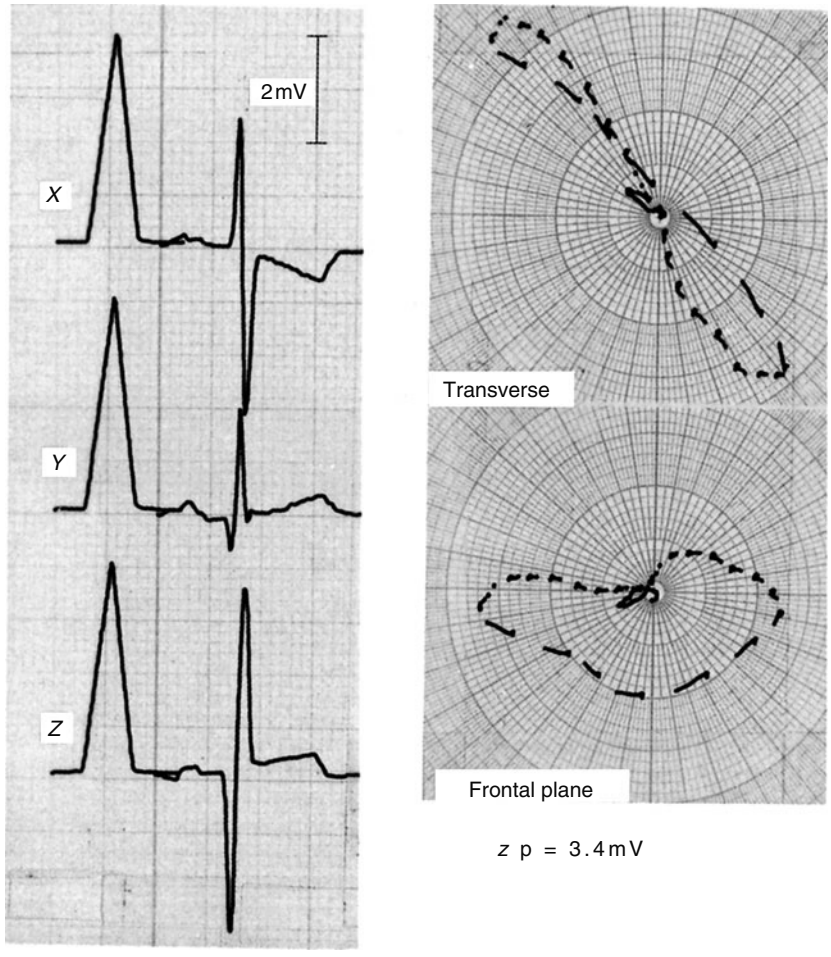

Figure 21.73

McFee–Parungao (axial) system orthogonal ECG in a 3½-month-old baby girl with TGA and a large VSD. There are two main vectors, the first to the left and anterior (with the QRS magnitude left above normal) and the second to the right and posterior. BVH is clear. (After Liebman et al. [8]. © Williams and Wilkins, Baltimore, MD. Reproduced with permission.)

echocardiographic, cardiac catheterization, and angiographic data. Although the above type of analysis can be very useful, it must be remembered that unpredictable rotations as well as hypertrophy may cause many errors.

21.33.5 Tetralogy of Fallot with Systemic-Pulmonary Shunt

As described in Sect. 21.10, TOF is a lesion associated with pure RVH. The addition of a systemic-pulmonary shunt provides left ventricular volume work and increased left-sided potential (Fig. 21.71). The ECG is very sensitive in this regard. If a child is born with an embryologic TOF but less severe pulmonic stenosis, there may be left-to-right shunt. Such a patient may show BVH. It is then common as the child grows older for the pulmonic stenosis to become more severe, the child to become cyanotic from the right-to-left shunt, the left-to-right shunt to disappear and the ECG to show pure RVH. Then such a patient may need a systemic-pulmonary shunt, and once again develop BVH. In terms of the major parameter of the LVH in this situation, an increased posterior QRS projection is not useful for reasons described previously. An increased magnitude to the left, particularly as part of a vector loop with two main vectors, is very reliable.

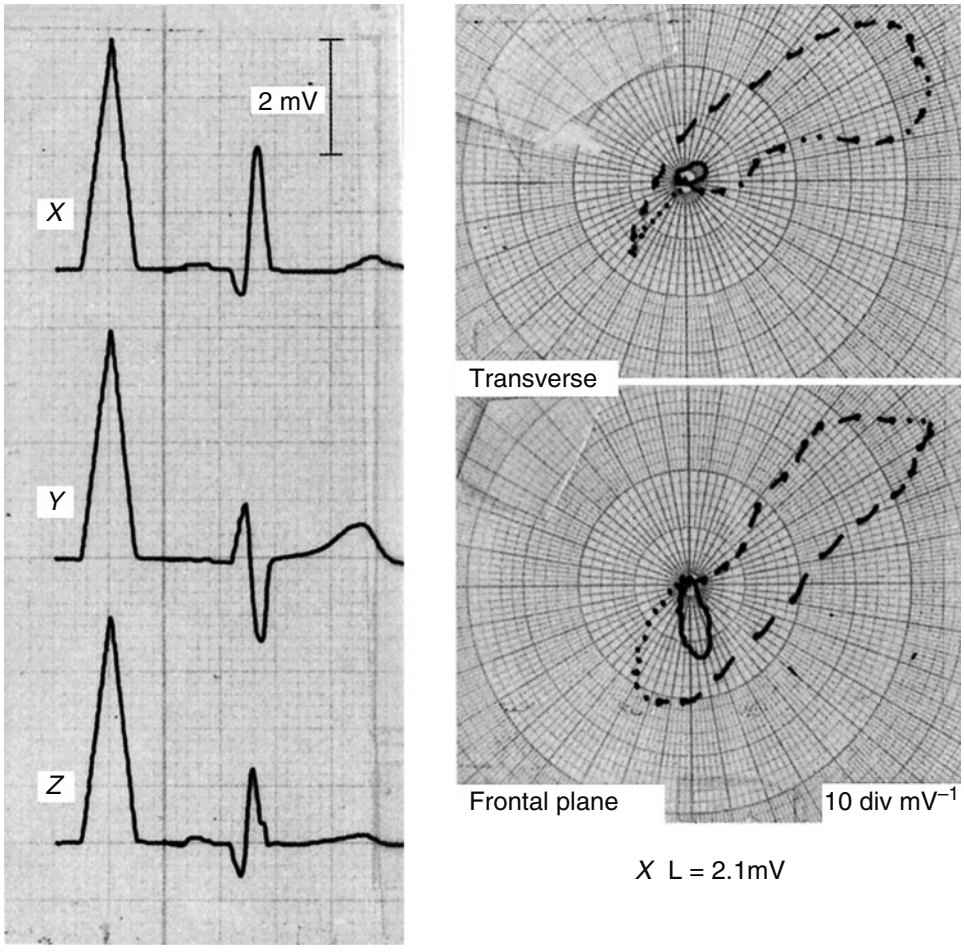

Figure 21.74

Frank-system orthogonal ECG in a 3-year-old asymptomatic female referred to a heart murmur (caused by considerable mitral regurgitation). There was a significant left-to-right atrial shunt at the pulmonary artery level owing to retrograde flow from the large right coronary artery into the left coronary artery by way of intercoronary collaterals. The left coronary artery drained into the left pulmonary artery. An area of the left lateral left ventricular wall did not contract. The initial QRS is to the right, anterior, superior, but then extends to the right and posterior before extending left. (It would appear that the posterobasal left ventricle is depolarizing before any left lateral wall). In the *X* lead, the initial QRS right is prolonged. Left lateral and myocardial infarction is the diagnosis, owing to anomalous left coronary artery (ALCA). (ALCA with manifest infarction in the older child is not common. Usually, the infarctions occur in infants with fewer intercoronary collaterals). (After Liebman et al. [8]. © Williams and Wilkins, Baltimore, MD. Reproduced with permission.)

21.33.6 Transposition of the Great Arteries with Large VSD

Since the right ventricle is the systemic ventricle, it is at systemic pressure; RVH is, therefore, expected. If a VSD is present and is nonrestrictive, the left ventricle is also at systemic pressure. Should pulmonary vascular resistance be low, then there will be considerably increased pulmonary blood flow and increased volume work of the left ventricle (Fig. 21.72) so that BVH may be present on the ECG (Fig. 21.73). Should there be a high pulmonary vascular resistance, there is less pulmonary blood flow and pure RVH is more likely. It is said that significant pulmonic stenosis lends itself to additional LVH, presumably because of high LV pressure as well as continued increased volume. Experience shows, however, that

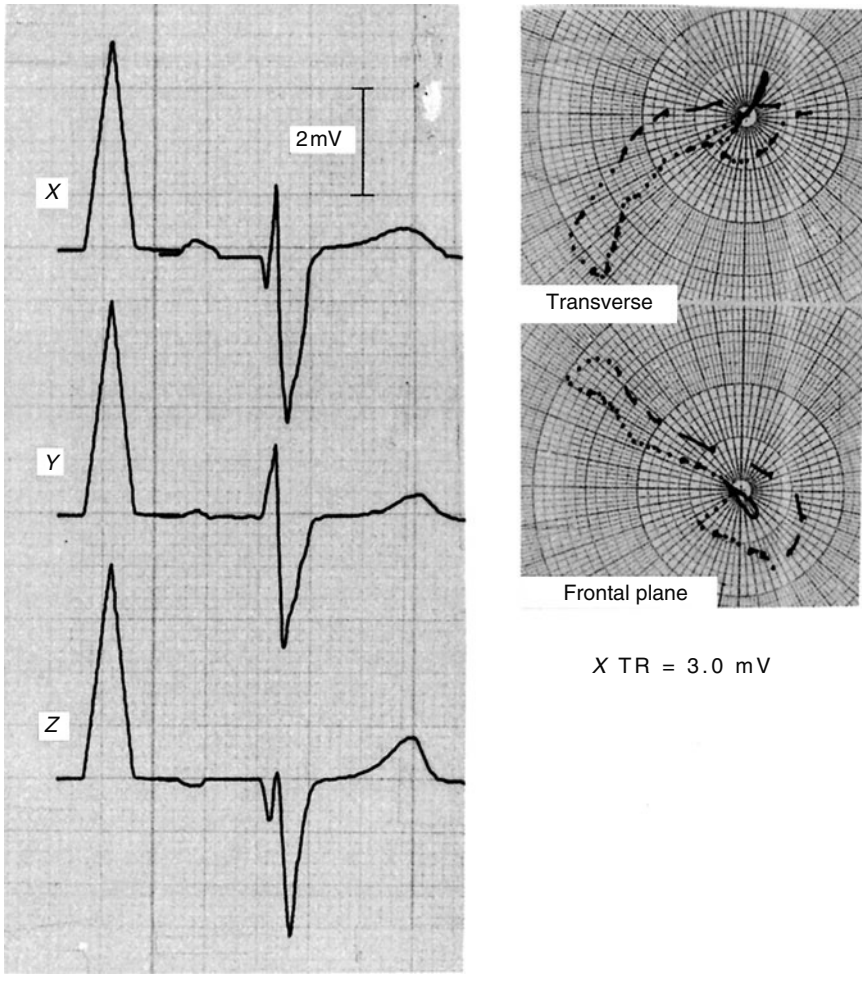

Figure 21.75

McFee–Parungao system orthogonal ECG of a 5-year-old male who had had complete repair for TOF 1 year previously. There is a large terminal vector loop to the right and anterior, which is very slowly inscribed. There is advanced RBBB. In the frontal plane, the initial QRS force is inferior, and most of the vector loop is superior, so that there is an "abnormally superior maximum QRS vector." Since this patient, prior to surgery, had a normal inferior maximum QRS vector with initial superior QRS forces, it is preferable to term this left anterior division block (left anterior hemiblock).

the finding is unreliable because with the increasing pulmonic stenosis, left ventricular volume decreases, resulting in less LVH. On the other hand, in the presence of an intact ventricular septum, PS results in increased LV pressure, so there is hemodynamic reason for *more* LVH.

21.33.7 Anomalous Left Coronary Artery in the Infant

Babies born with anomalous left coronary artery are recognized almost invariably by 3 months of age. The hearts are large, congestive heart failure is considerable and the ECG documents a left lateral wall myocardial infarction (Fig. 21.74). As a result of lack of opposition from lateral wall potentials, the initial QRS stays to the right for a long time as the QRS vector turns posterior. The ECG differential is that of left septal hypertrophy, but in the latter, the duration is not great and the QRS vector turns to the left before traversing posterior. The latter is readily recognized with the vector loop display

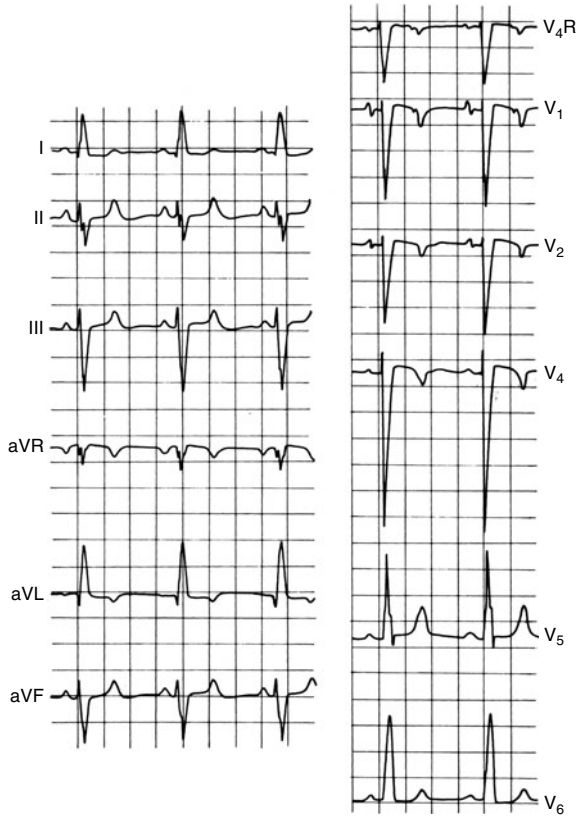

Figure 21.76

Standard ECG of a 2-year-old female with TGA, a large VSD in the endocardial cushion area and pulmonic stenosis (the typical abnormally superior maximum QRS vector had been present prior to surgery). A Mustard procedure had been done, and attempts had been made to relieve some of the pulmonic stenosis via the pulmonary artery, so that some of the left ventricular outlow area was excised. The ECG result included partial LBBB. The initial QRS is to the left and anterior and there is midventricular slowing. There is no T-wave abnormality (A VCG would be needed, however, for better delineation).

but is difficult to be sure of with a standard ECG. The lesion where a similar ECG may be seen is that of the hypoplastic right ventricle with tricuspid atresia, but the abnormally superior maximum QRS vector in the latter is distinctive (see Fig. 21.46).

21.33.8 Postoperative RBBB, Left Anterior Hemiblock and LBBB

Postoperative RBBB is very common, is usually advanced, but can be partial. Only infrequently is the advanced RBBB caused by damage to the proximal right bundle. Most often it is because of damage to the right bundle after ventriculotomy with incision into the moderator band. Although traditional definitions would allow the ECG interpretation of "complete" RBBB for all such patients, we have recently documented, utilizing body-surface potential mapping, that there is a great spectrum of "complete" RBBB [66]. Therefore, the term advanced RBBB appears to be more appropriate. Occasionally, the advanced RBBB is associated with an abnormally superior maximum QRS vector not present prior to surgery, in which

case it is presumed that the left anterior branch of the left bundle has been damaged (Fig. 21.75). Postoperative partial RBBB is also often recognized.

Postoperative advanced LBBB is becoming increasingly common, particularly as more complex lesions are being surgically corrected and as the need to enter the left ventricle in order to facilitate such surgery increases (Fig. 21.76).

References

1. Rush, S., *An Atlas of Heart-Lead Transfer Coefficients*. Hanover, NH: University Press of New England, 1975.
2. Rudy, Y. and R. Plonsey, The eccentric spheres model as the basis for the study of the role of geometry and inhemogeneites in electrocardiography. *IEEE Trans. Biomed. Eng.*, 1979;**26**: 392.
3. Rudy, Y., R. Plonseyi, and J. Liebman, The effects of variations in conductivity and geometrical parameters on the electrocardiogram using an eccentric spheres model. *Circ. Res.*, 1979;**44**: 104–111.
4. Rudy, Y. and R. Plonsey, A comparison of volume conductor and source geometry effects on body surface and epicardial potentials. *Circ. Res.*, 1980;**46**: 283.
5. Rudy, Y. and R. Plonsey, Comments on the effects of variations in the size of the heart on the magnitude of ECG potentials. *J. Electrocardiol.*, 1980;**13**: 79.
6. Ishikawa, K., A.S. Berson, and H.W. Pipberger, Electrocardiographic changes due to cardiac enlargement. *Am. Heart J.*, 1971;**81**: 635.
7. Rudy, Y., R.Wood, R. Plonsey, and J. Liebman, The effects of high lung conductivity on electrocardiographic potentials. *Circulation*, 1982;**65**: 440–445.
8. Liebman, J., R. Plonsey, and P.C.Gillette, Editors, *Pediatric Electrocardiography*. Baltimore, MD: Williams and Wilkins, 1982.
9. Liebman, J. and R. Plonsey, Electrocardiology in heart disease, in *Infants, Children and Adolescents*, 2nd edn., Chapter 3, A.J. Moss, F.H. Adams, and G.C. Emmanouilides, Editors. Baltimore, MD: Williams and Wilkins, 1983, pp. 18–61.
10. Liebman, J. and R. Plonsey, Basic principles for understanding electrocardiography. *Paediatrican*, 1973;**2**: 251–268.
11. Davignon, A., P. Rautaharju, E. Boiselle E, et al., Normal electrocardiogrophic standards for infants and children. *Pediatr. Cardiol.*, 1979;**I**: 133–152.
12. Macfarlane, P.W. and T.D.V. Lawrie, Tables of normal limits, in *Comprehensive Electrocardiology*, Vol. 3. New York: Pergamon Press, 1989, pp. 1442–1526.
13. Liebman, J., Tables of normal limits for standard and orthogonal pediatric ECG, in *Comprehensive Electrocardiology*, Vol. 3. New York: Pergamon Press, 1989, pp. 1475–1494, 1509–1517.
14. Downs, T.D. and J. Liebman, Statistical methods for vectorcardiographic directions. *IEEE Trans. Biomed. Eng.*, 1969;**16**: 87–94.
15. Liebman, J., Linear and directional statistics, in *Comprehensive Electrocardiology*, Vol. 3. New York: Pergamon Press, 1989, pp. 1522–1526.
16. Frank, E., An accurate, clinically practical system for spatial vectorcardiography. *Circulation*, 1956;**13**: 737–749.
17. McFee. R. and A. Parungoa,. An orthogonal lead system for clinical electrocardiography. *Am. Heart J.*, 1961;**62**: 93–100.
18. Young, E., J. Liebman, and A.S. Nadas, The normal vectorcardiogram in children. *Am. J Cardiol.*, 1960;**5**: 457–463.
19. Hugenholtz, P.G. and J.Liebman, The orthogonal vectorcardiogram in 100 normal children (Frank system) with some comparative data recorded by the cube system. *Circulation*, 1962;**26**: 891–901.
20. Rautaharju, P.M., A. Davignon, F. Soumis, et al., Evolution of QRS-T relationships from birth to adolescence in Frank lead orthogonal electrocardiograms of 1492 normal children. *Circulation*, 1979;**60**: 196–204.
21. Taccardi, B., Distribution of heart potentials on the thoracic surface of normal human subjects. *Circ. Res.*, 1963;**12**: 341–352.
22. Liebman, J., C.W. Thomas, Y. Rudy, and R. Plonsey, Electrocardiographic body surface potential maps of the QRS of normal children. *J. Electrocardiol.*, 1981;**12**: 249–260.
23. Liebman, J., The electrocardiogram of the future, body surface potential mapping (Keynote Lecture), in *21st International Congress on Electrocardiography*, Yokohama, Japan, July 4–7, 1994; *Jpn. Heart J.*, 1994;**35**(Suppl. 1): 69–73.
24. Liebman, J., The body surface potential map in congenital heart disease, in *Einthoven 2002: 100 years of Electrocardiography*, M.J. Schalij, et al., Editors. Leiden: The Einthoven Foundation, 2002, pp. 215–220.
25. Durrer, D., R.Th. van Dam, G.E. Freud, M.J. Janse, F.L. Meijler, and R.C. Arzbaecher, Total excitation of the isolated human heart. *Circulation*, 1970;**41**: 899–912.
26. Scher, A.M. and M.S. Spach, Cardiac depolarization and repolarization and the electrocardiogram, in *Handbook of Physiology, Section 2: The Cardiovascular System, Vol. I: The Heart*, R.M. Berne, N. Speralakis, and S.R. Geiger, Editors. Bethesda, MD: American Physiological Society, 1979, pp. 357–392.
27. Burger, H.C. and J.L. van Milaan, Heart vector and leads, Part II. *Br. Heart J.*, 1947;**9**: 154–160.
28. Liebman, J., G. Borka, and S. Hirschfeld, The heart, in *Care of the High Risk Neonate*, M.H. Klaus and A.A. Fanaroff, Editors. Philadelphia, PA: Saunders, 1979, pp. 294–323.
29. Nadas, A.S. and D.C. Fyler, *Pediatric Cardiology*, 3rd edn. Philadelphia, PA: Saunders, 1972.
30. Spach, M.S., T.D. King, R.C. Barr, D.E. Boaz, M.N. Morrow, and S. Herman-Giddens, Electrical potential distribution surrounding the atria during depolarization and repolarization of the dog. *Circ. Res.*, 1969;**24**: 857–873.
31. Puech, P., The P wave: correlations of surface and intra-atrial electrograms, in *Complex Electrocardiography 2*, C. Fisch, Editor. Philadelphia, PA: Davis, 1974; *Cardivasc. Clin.*, 1974;**6**(1).
32. Reynolds, J.L., The electrocardiographic recognition of right atrial abnormality in children. *Am. Heart J.*, 1971;**81**: 748–759.
33. Ferrer, P.L. and R.C. Ellison. The Frank scalar atrial vectorcardiogram in normal children. *Am. Heart J.*, 1974;**88**: 467–475.
34. Ishikawa, K., P.M. Kini, and H.V.P. Pipberger, Wave analysis in 2464 orthogonal electrocardiograms from normal subjects and patients with atrial overload. *Circulation*, 1973;**48**: 565–574.

35. Lee, M H., J. Liebman, and W.Mackay. Orthogonal electrocardiograph correlation study of 100 children with pure cardiac defects, in *Vectorcardiography 3*, **I**. Hoffman and R.I. Hamby, Editors. Amsterdam: North-Holland, 1976, pp. 181–198.
36. Zhou, S. H., J. Liebman, A.M. Dubin, et al., Using 12-lead ECG and synthesized VCG in detection of right ventricular hypertrophy with terminal right conduction delay versus partial RBBB in the pediatric population. *J. Electrocardiol.*, 2001;**34**(Suppl.): 249–257.
37. Liebman, J., Y. Rudy, P.J. Diaz, et al., Body surface potential mapping: partial right bundle branch block vs right ventricular hypertrophy with terminal right conduction delay. *J.Am. Coll. Cardiol.*, 1984;**3**: 496.
38. Liebman, J., C.W. Thomas, Y. Rudy, et al., Partial right bundle-branch block vs right ventricular hypertrophy with terminal conduction delay. Differentiation using a color-displayed body-surface potential mapping system, in *Electrocardiology 83*, **I**. Ruttkáy-Nedecky and P.MacFarlane, Editors. Amsterdam: Excerpta Medica, 1984, pp. 218–225.
39. Liebman, J., Y. Rudy, and C.W. Thomas. RVH with terminal right conduction delay versus partial right bundle branch block (utilizing body surface potential maps), in *Fundamental and Pediatric Electrocardiography*, J. Liebman, R. Plonsey, and Y. Rudy, Editors. Boston, MA: Nijhoff, 1986, pp. 389–398.
40. Mehran-Pour, M., A.Whitney, J. Liebman, et al., Quantification of the Frank and McFee-Parungao orthogonal electrocardiogram in valvular pulmonic stenosis. Correlations with hemodynamic measurement. *J. Electrocardiol.*, 1979;**12**: 69–76.
41. Liebman, J. and A.S. Nadas, The vectorcardiogram on the differential diagnosis of atrial septal defect in children. *Circulation*, 1960;**72**: 956–975.
42. Spach, M.S., J.P. Boineau, E.C. Long, et al., Genesis of the vectorcardiogram (electrocardiogram) in endocardial cushion defects, in *Vectorcardiography – 1965*, I. Hoffman and R.C. Taymor, Editors. Amsterdam: North-Holland, 1966, pp. 307–326.
43. Liebman, J., R. Plonsey, and Y. Rudy, *Pediatric and Fundamental Electrocardiography*. Boston, MA: Martinus Nijhoff, 1987.
44. Liebman. J., C.W. Thomas, and Y. Rudy, Conduction abnormalities and ventricular hypertrophy, in *Body Surface Electrocardiographic Mapping*, D. Mirvis, Editor. Boston, MA: Kluwer Academic, 1988, pp. 153–166.
45. Liebman, J., The initial QRS left as part of severe obstructive hypertrophy. Body surface potential mapping in children with severe aortic stenosis and pulmonic stenosis, in *Proceedings of the 24th International Congress on Electrocardiology*, Bratislava, June 24–28, 1997, p. 53.
46. Liebman, J., What's old, what's new in non-arrhythmia electrocardiology. Annual Harumi Lecture of the International Society of Computerization, in *Electrocardiology (ISCE)*, April 30, 2004; *J Electrocardiol.*, 2004;**37**(Suppl.): 152–165.
47. Strong, W B., J. Liebman, and E. Perrin, Hypoplastic left ventricle syndrome. Electrocardiographic evidence of left ventricular hypertrophy. *Am. J. Dis. Child.*, 1970;**120**: 511–514.
48. Liebman, J., C.W.Thomas, and Y. Rudy, ECG body surface potential mapping many years after successful surgery for coarctation of the aorta. *J. Electrocardiol.*, 1993;**26**: 25–41.
49. Macruz, R., J.K. Perloff, and R.B. Case, A method for the electrocardiographic recognition of atrial enlargement. *Circulation*, 1958;**17**: 882–889.
50. Morris J.J. Jr., E.H. Estes Jr., R.E. Whalen, et al., P wave analysis in valvular heart disease. *Circulation*, 1964;**29**: 242–252.
51. Banerjea, J.C. and S.K. Mukherjee, Some observations in left atrial enlargement in the electrocardiogram. *Indian Heart J.*, 1978;**20**: 264.
52. Ishikawa, K. and H.V. Pipberger, Critical evaluation of the twin peaked P wave (pseudo-P mitrale) in orthogonal electrocardiograms. *J. Electrocardiol.*, 1980;**13**: 181–184.
53. Ferrer, P.L. and R.C. Ellison, Detection of atrial overload in congenital heart disease by the Frank scalar atrial vectorcardiogram. *Circulation*, 1973;**48**(Suppl. IV): 82. [Abstract.]
54. Liebman, J., H.C. Romberg, and T.D. Downs, The Frank QRS vectorcardiogram in the premature infant, in *Vectorcardiography 1965*, I. Hoffman and R.C. Taymor, Editors. Amsterdam: North-Holland, 1966.
55. Liebman, J., R. Plonsey, and J.L. Ankeney, The initial QRS vector in ventricular hypertrophy, in *Proceedings of the IXth International Congress on Electrocardiology*, Tokyo, 1982; *Jpn. Heart J.*, 1982;**23**(Suppl. 1): 480–482.
56. Ankeney, J.L., T.S. Tzeng, and J. Liebman, Surgical therapy for congenital aortic valvular stenosis: a 23 year experience. *J. Thorac. Cardiovasc. Surg.*, 1983;**85**: 41–48.
57. Liebman, J., C.F. Doershuk, C. Rapp, et al., The vectorcardiogram in cystic fibrosis. Diagnostic significance and correlation with pulmonary function tests. *Circulation*, 1967;**35**: 552–567.
58. Lee, M.H., J. Liebman, A.G. Steinberg, E.V. Perrin, and V.Whitman, Familial occurrence of endocardial fibroelastosis in three siblings, including identical twins. *Pediatrics*, 1973;**52**: 402–411.
59. Liebman, J., H.K. Hellerstein, J.L. Ankeney, et al., The problem of the anomalous left coronary artery arising from the pulmonary artery in older children. *N. Engl. J. Med.*, 1963;**269**: 486–494.
60. Sreenivasan, V.V., J. Liebman, D.S. Linton, et al., Posterior mitral regurgitation in girls possibly due to posterior papillary muscle dysfunction. *Pediatrics*, 1968;**42**: 276–290.
61. Agusti, R., J. Liebman, J.Ankeney, et al., Congenital right coronary artery to left atrium fistula. *Am J. Cardiol.*, 1967;**19**: 428–433.
62. Bharati, S. and M. Lev, The conduction system in tricuspid atresia with and without regular (d-) transposition. *Circulation*, 1977;**56**: 423–439.
63. Katz, L.N. and H. Wachtel, The diphasic QRS type of electrocardiogram in congenital heart disease. *Am. Heart J.*, 1937;**13**: 202–206.
64. Bharati, S. and M. Lev, The course of the conduction system in single ventricle with inverted (L-) loop and inverted (L-) transposition. *Circulation*, 1975;**51**: 723–730.
65. Liebman, J., S.L. Miller, and I.H. Gessner. The initial QRS vector in children, in *Vectorcardiography*, 2 edn., I. Hoffman, Editor. Amsterdam: North-Holland, 1971, pp. 645–648.
66. Liebman, J., Y. Rudy, P. Diaz, et al., The spectrum of right bundle branch block as manifested in electrocardiographic body surface potential maps. *J. Electrocardiol.*, 1984;**17**: 329–346.

22 Electrocardiography in Adult Congenital Heart Disease

Paul Khairy · Ariane J. Marelli

P. W. Macfarlane, A. van Oosterom, O. Pahlm, P. Kligfield, M. Janse, J. Camm (eds.), *Comprehensive Electrocardiology*, DOI 10.1007/978-1-84882-046-3_22,

22.1 Introduction

Adult congenital heart disease (ACHD) is a growing subspecialty of cardiology with a rapidly expanding patient population [1–4]. In an earlier era, more than half of all children born with congenital defects died before reaching adulthood [5]. With current care, nearly 90% of such infants are expected to thrive into their adult years [1, 3, 6]. In North America, outpatient visits in ACHD tertiary care centers increased by 400% in 1999 and continue to rise [3].

Despite these successes, it is now appreciated that early surgical interventions were "reparative" and not "curative." Symptoms and complications may surface many years after quiescent courses in childhood. As such, meticulous clinical assessment and follow-up is warranted. As the growing population of survivors with ACHD ages and health needs rise, an increasing number of caregivers will be exposed to such patients at some point in their careers. The 12-lead electrocardiogram (ECG) remains an invaluable cornerstone in the clinical appraisal of adults with congenital heart disease that, in certain circumstances, provides diagnostic and/or prognostic information. It is, therefore, timely and appropriate that a chapter be dedicated to this topic.

In Chap. 21, detailed ECG criteria associated with congenital heart defects in children and their hemodynamic consequences were extensively reviewed. Isolated lesions of the left and right ventricular outflow tracts have also been addressed elsewhere. This chapter provides a clinical perspective to ECG interpretation in ACHD, emphasizing practical and pathognomonic ECG findings in the more frequent congenital defects encountered in adults, stressing the particularities associated with adults as opposed to children. As a result of hemodynamic or hypoxic stress imposed by the original cardiac malformation and/or postoperative sequelae from reparative surgery [7], arrhythmias figure prominently among the issues encountered in ACHD [8]. Thus, when discussing ECG findings for the varied pathologies, examples of associated common arrhythmias will be presented. First, an overview of the conduction system and its variations in congenital heart disease will be provided to facilitate an understanding of ECG patterns in ACHD.

22.2 Anatomy of the Conduction System in Congenital Heart Disease

22.2.1 Sinus Node

In the morphologically normal heart, a spindle-shaped sinus node is usually located epicardially in the sulcus terminalis, at the junction between the venous portion of the right atrium and the base of the right atrial appendage. Normal sinus activation, therefore, results in a typical P-wave axis between 15° and 75°. Most patients with congenitally malformed hearts have normally positioned atrial chambers, or "atrial situs solitus." This arrangement is usually associated with normal sinus node location. The position of the sinus node may, however, vary with the atrial chambers and their appendages.

22.2.2 Juxtaposition of the Atrial Appendages

Juxtaposition of the atrial appendages refers to a condition whereby both atrial appendages are located on the same side of the arterial pedicle rather than each being ipsilateral to its respective atrium. Right juxtaposition, with the left atrial appendage on the right side, adjacent to the right atrial appendage, is exceedingly rare and not associated with a malpositioned sinus node. However, left juxtaposition is more common and is accompanied by a displaced sinus node. While the sulcus terminalis remains an important landmark, the sinus node is more anteriorly positioned and may be located inferior to the crista terminalis [9]. Left juxtaposition may herald an abnormal ventriculoarterial connection, such as discordant or double outlet right ventricle, and is frequently found in tricuspid atresia [10].

22.2.3 Situs Inversus and Heterotaxy Syndromes

In "atrial situs inversus," the atria are positioned in mirror-image fashion, with the right atrium and its sinus node on the individual's left side. Consequently, the P-wave axis shifts to between 105° and 165°, with a P-wave that is often negative in lead I and most positive in lead III.

Heterotaxy syndromes refer to disorders of lateralization whereby the arrangement of abdominal and thoracic viscera differ from situs solitus and situs inversus. These syndromes are often associated with severe congenital cardiac malformations, and although there is much variability, are generally characterized as either right atrial isomerism (asplenia syndrome) or left atrial isomerism (polysplenia syndrome). Patients with right atrial isomerism often have two separate sinus nodes, at the junctions of right- and left-sided superior vena cavae with atrial chambers [11, 12]. On the ECG, this is often reflected by a P-wave axis that fluctuates as the prevailing pacemaker shifts from one sinus node to the other (Fig. 22.1) [13]. In contrast, the majority of hearts with left atrial isomerism do not have a histologically recognizable sinus node. When present, it is hypoplastic and located posteroinferiorly, far from the orifice of the superior vena cava [12, 14]. As a result, slow atrial rates and junctional escape rhythms are common (Fig. 22.2) [14].

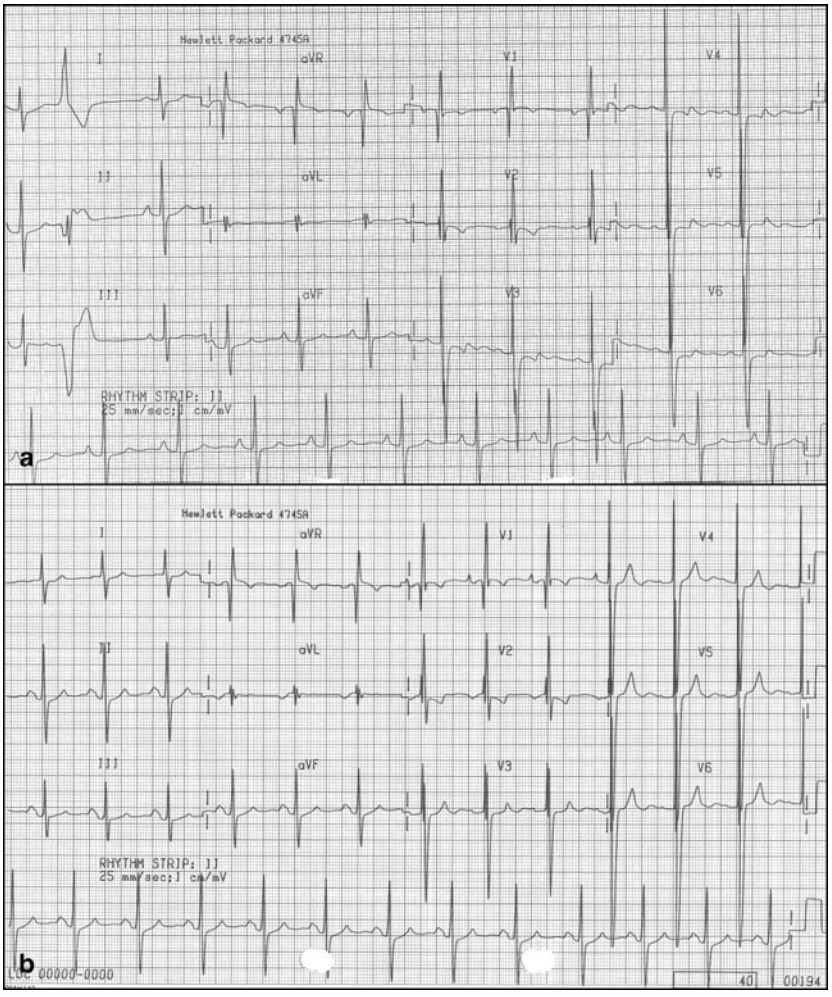

Figure 22.1

12-lead electrocardiogram (ECGs) of a 37-year-old man with heterotaxy syndrome of the asplenia type. Note the difference in P-wave axis and morphology between panels a and b, indicating a shift in the governing pacemaker. In panel a, the P-wave axis is 65° and is positive in lead I, monophasic in the inferior leads, and predominantly negative in lead V1. In panel b, the P-wave axis is 90°, notched in the inferior leads, and predominantly positive in lead V1.

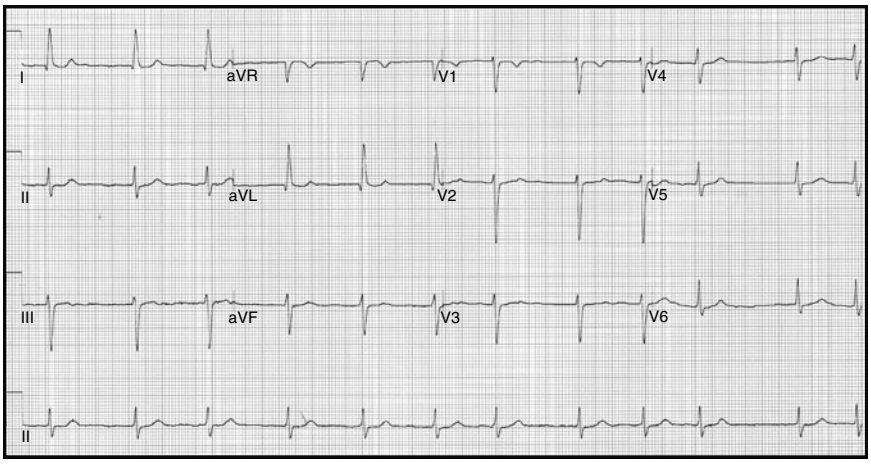

Figure 22.2

A 12-lead ECG of a 42-year-old woman with heterotaxy syndrome of the polysplenia type. Note the absence of clearly identifiable P-waves. The irregular rate suggests underlying atrial fibrillation. However, multiple cardioversion attempts failed to interrupt this rhythm, even briefly. A junctional rhythm was present at birth and sinus node function was never confirmed.

22.2.4 AV Node and His-Purkinje System

In normal hearts, the atrioventricular (AV) node is located at the apex of Koch's triangle, delimited on one side by the septal leaflet of the tricuspid valve and on another side by the tendon of Todaro that extends from the Eustachian valve (guarding the opening of the inferior vena cava) to the central fibrous body. The mouth of the coronary sinus forms the base of this triangle. The common bundle, or bundle of His, extends from the AV node and is the only pathway of myocardial continuity between the atria and the ventricles. In simple septal defects and/or valvar stenosis, the AV conduction system generally assumes its normal pattern. However, displacement of the AV conduction system occurs in congenital defects associated with malaligned atrial and ventricular septae, discordant AV arrangements, and single ventricles.

22.2.5 AV Canal Defect

Atrioventricular canal defects (AVCD) are associated with a displaced AV conduction system, as the compact AV node occupies an inferior position outside of Koch's triangle, anterior to the mouth of the coronary sinus and adjacent to where posterior rims of atrial and ventricular septae unite [15–17]. The common bundle extends along the lower rim of the ventricular septum. This inferior course and the relative hypoplasia of the left anterior hemifascicle gives rise to the superior QRS axis typical of AVCD [18, 19].

22.2.6 Congenitally Corrected Transposition of the Great Arteries

In "congenitally corrected" transposition of the great arteries, or L-TGA, atrioventricular and ventriculo-arterial discordance coexist such that the atrial situs is normal but the right ventricle is sub-aortic and leftward and the left ventricle is sub-pulmonary and rightward. L-TGA is associated with marked displacement of the AV conduction system. The AV node is located outside of Koch's triangle, displaced anteriorly and slightly more laterally [20, 21]. An elongated common bundle of His runs medially toward the septum to the site of fibrous continuity between the right-sided mitral valve and the pulmonary artery. The common bundle then courses along the anterior rim of the pulmonary valve and, if a ventricular septal defect (VSD) is present, continues along its upper rim [20, 21].

22.2.7 Tricuspid Atresia

Patients with tricuspid atresia have an imperforated fibrous AV connection. The septal leaflet of the tricuspid valve that normally forms one border of Koch's triangle is absent. Therefore, the usual anatomic landmarks demarcating the location of the AV node cannot be applied. Pathologic studies in tricuspid atresia have suggested that the compact AV node is typically situated on the floor of the right atrium, adjacent to an abnormally formed central fibrous body [22, 23]. A small "dimple" lined with endocardium is found just anterior to the mouth of the coronary sinus and has been considered to indicate the theoretical site of the absent tricuspid valve [22]. The AV node is found within the confines of the coronary sinus, tendon of Todaro, and right atrial "dimple." It pierces the central fibrous body to become the penetrating bundle of His, along the left side of the septum. The remaining course of the His-Purkinje system is related to some extent on the presence and location of associated VSDs. In general, the His-bundle is further leftward and away from more anterior septal defects [23].

22.2.8 Other Forms of Single Ventricle Physiology

In considering the course of the conduction system and potential for AV block in other types of single ventricle physiology, it is important to note the type of ventricular looping and whether the dominant ventricle is right or left. The most conspicuous abnormalities in the location of the AV conduction system occur in single ventricles with AV discordance and AVCD. In the case of an L-looped single left ventricle, two AV nodes may be present, with a posterior node that does not usually make contact with the ventricular septum [17]. The elongated course of the common bundle renders it susceptible to fibrous degeneration and complete AV block [24]. With ventricular D-looping and a dominant right ventricle, the AV node is positioned within its usual landmarks and the common bundle enters the ventricular septum directly [25].

22.3 Electrocardiography in Adult Congenital Heart Disease (ACHD)

22.3.1 Ostium Secundum Atrial Septal Defect

Defects of the atrial septum constitute at least 30% of all congenital heart disease seen in adults and ostium secundum atrial septal defect (ASD) is twice more prevalent in females than males (4). Adults with a secundum-type ASD most commonly have underlying sinus rhythm. However, the incidence of atrial fibrillation and/or flutter with unrepaired ASDs is approximately 20% and increases with age [26, 27]. Surgical closure may decrease the occurrence of atrial arrhythmias, but appears less effective in older individuals [26–29]. Gatzoulis et al. [26] retrospectively reviewed 218 adults with surgical closure of an isolated ASD. Over a mean postoperative follow-up of 3.8 years, 60% of patients with preoperative atrial flutter or fibrillation continued to have arrhythmias and 2.3% developed new-onset arrhythmias. All patients with persistent and new arrhythmias were over 40 years of age at surgery. Attie et al. [27] randomized 521 adults 40 years and older to surgical ASD closure versus medical therapy. Over a median of 7.3 years, new-onset atrial flutter or fibrillation occurred in 7.4% and 8.7% of patients with surgical and medical therapy, a nonsignificant difference.

The impact of transcatheter ASD device closure remains to be determined. One retrospective study of 132 patients found that all persistent arrhythmias remained after closure [29]. Of those with prior paroxysmal atrial tachyarrhythmias, two-thirds were free of symptomatic recurrence at a mean of 17 months. The incidence of symptomatic paroxysmal and persistent atrial fibrillation or flutter was 17 and 11%/year, respectively. Age $\geqslant$ 55 years was a risk factor for atrial tachyarrhythmias after transcatheter device closure.

A typical ECG in the adult with an ASD has a QRS complex with an rSr′ or rsR′ configuration over the right precordial leads [30–39]. This is likely a manifestation of right ventricular overload rather than a true conduction delay in the right bundle branch [40]. In contrast to a sharp and narrow r′ not exceeding 5 mm in the rSr′ pattern found in 2.4% of normal hearts, the r′ associated with an ASD is broader and somewhat slurred [32, 34]. As a result of prolonged terminal forces, QRS duration is lengthened but often remains within the upper limit of normal. However, a complete right bundle branch

block pattern is not infrequent with increasing age. Also, q-waves in the inferior leads are occasionally observed although poorly defined.

While PR prolongation is seen in 6–19% of patients, progression toward higher degree AV block is uncommon [39, 41, 42], with complete AV block rarely reported [43]. The QRS axis is usually between 0° and 180° and is often vertical. Right axis deviation is commonly seen in adults with associated pulmonary vascular disease [44, 45]. In contrast, left axis deviation is rare but has been described in some hereditary forms such as Holt–Oram syndrome [43, 46]. In older individuals, it may represent an acquired left anterior fascicular block. ECG criteria for right atrial enlargement are met in approximately 35% of patients [30, 32–34, 36–39].

A notch near the apex of the R-wave in the inferior leads, termed "crochetage," has been correlated with ASD [35]. In a study of 1,560 adults and adolescents including 459 normal subjects and 1,101 patients with various forms of congenital heart disease, this pattern was identified in 73.1% of those with ASDs [47]. Among patients with ASDs, its incidence increased with larger anatomic defects or greater left-to-right shunts, even in the presence of pulmonary hypertension. The specificity of this sign in diagnosing ASD was 92% when present in all three inferior limb leads. Early disappearance of this pattern was observed in 35.1% of surgically repaired patients, although the right bundle branch block pattern persisted. In a second study, the "crochetage" pattern was observed in at least one inferior limb lead in 31.7% of preoperative patients with a secundum ASD [48]. The specificity of the "crochetage pattern" for detecting a secundum ASD was 86.1% and > 92% when present in at least one and in all three inferior limb leads, respectively. Typical ECG features are depicted in Figs. 22.3 and 22.4.

22.3.2 Ventricular Septal Defect

Ventricular septal defects (VSD) are the most common congenital heart malformation in the pediatric population, but often close spontaneously or cause symptoms of congestive heart failure that prompt surgical intervention prior to adulthood [49]. Although a VSD can occur anywhere along the interventricular septum, effects on the conduction system and arrhythmias in unoperated patients are most likely related to hemodynamic consequences, not specific location [50]. Adults most commonly present with small restrictive VSDs or large unrestrictive VSDs with Eisenmenger's complex.

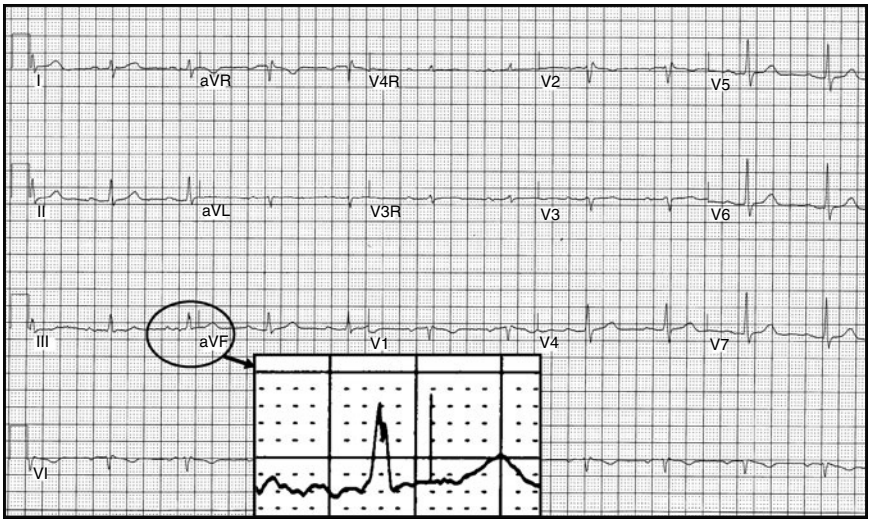

Figure 22.3
15-lead ECG in a 53-year-old woman with a secundum atrial septal defect (ASD). Note the rSr′ QRS pattern over the right precordial leads, with a broad and slurred r′. The QRS axis is vertical and the PR interval measures 200 ms. Encircled and magnified in the insert is the "crochetage" pattern over the inferior leads, characterized by a notch near the R-wave apex.

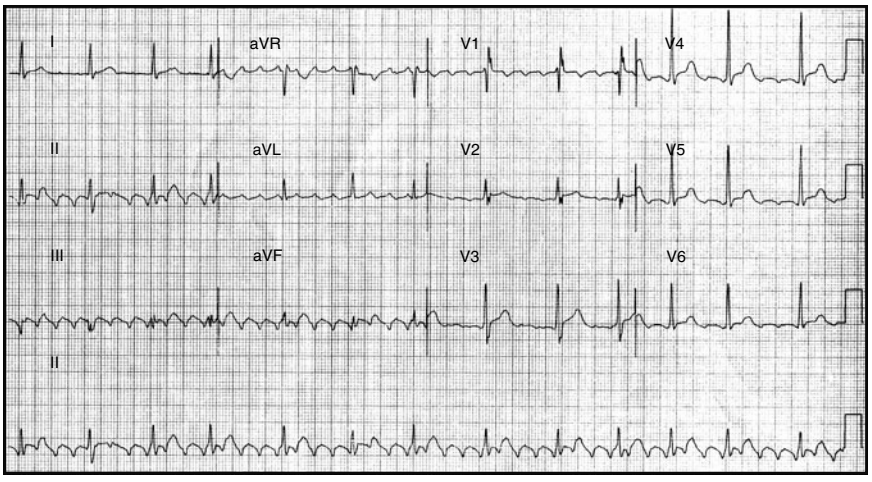

Figure 22.4

12-lead ECG in a 58-year-old man with a secundum ASD. Intra-atrial reentrant tachycardia developed 21 years after surgical repair. Note the classic "saw tooth" pattern of flutter waves with a cycle length of 230 ms and variable AV conduction, compatible with typical counterclockwise atrial flutter. The patient underwent successful transcatheter ablation of the cavotricuspid isthmus.

Either way, defects of the membranous septum, or "perimembranous" VSDs, are located in the left ventricular outflow beneath the aortic valve and account for the majority of VSDs [4].

In a review comparing 439 patients with unoperated VSDs to a control population, a higher prevalence of isolated premature ventricular contractions (PVC), couplets, and multiform PVCs was noted [50]. Non-sustained or sustained ventricular tachycardia occurred in 5.7% of patients. The most powerful independent predictor for high-grade ectopy was higher mean pulmonary artery pressure. Despite these ventricular arrhythmias, sudden cardiac death is reportedly uncommon but has been described in patients with cardiac hypertrophy and progressive fibrosis of the conduction system [51–54]. In patients with surgically repaired VSDs, late sudden death occurs in about 4% [55, 56]. Risk factors for mortality include age greater than 5 years at time of surgery, pulmonary vascular resistance greater than 7 Woods units, and complete heart block [56]. Transcatheter VSD closure is an alternative to surgery in selected patients. Although long-term follow-up is not yet available, complete heart block is a recognized complication [57–59].

Electrocardiographic findings in isolated VSDs are highly dependent on the hemodynamic effects of the left-to-right shunt, i.e., degree of left ventricular volume overload and right ventricular pressure overload. Small defects often produce normal tracings, with the exception of increased ventricular ectopy and the occasional rsr′ pattern over the right precordial leads [60, 61]. Large VSDs are associated with right and sometimes left atrial enlargement, with broad notched P-waves in leads I and II and negative terminal forces in lead V1. The PR interval is normal or mildly prolonged [60, 61]. The QRS axis usually shifts moderately rightward and evidence for biventricular hypertrophy is found in 23–61% of cases [62]. As shown in Fig. 22.5, the Katz–Wachtel phenomenon may be seen, with large equiphasic RS complexes over the midprecordial leads [63]. The R-wave amplitude in V1 may meet right ventricular hypertrophy criteria and deep Q-waves may be present over the lateral precordial leads. A right bundle branch block has been reported in 30–60% of patients and appears independent of whether the VSD was repaired through an atrial or ventricular incision [56, 64, 65]. Right bundle branch block with left-axis deviation is seen in 3–15% of patients [56, 65]. First-degree AV block occurs in about 10% of patients and the incidence of complete heart block on long-term follow-up is 1–3% [56, 65].

Eisenmenger's complex refers to flow reversal across a VSD when pulmonary vascular resistance exceeds systemic levels. Evidence for biventricular hypertrophy is often lacking, as right ventricular hypertrophy and pulmonary hypertension predominate. In adults, rightward QRS axis deviation is often present, as are peaked P-waves in lead II and tall monophasic R-waves in V1 [66, 67].

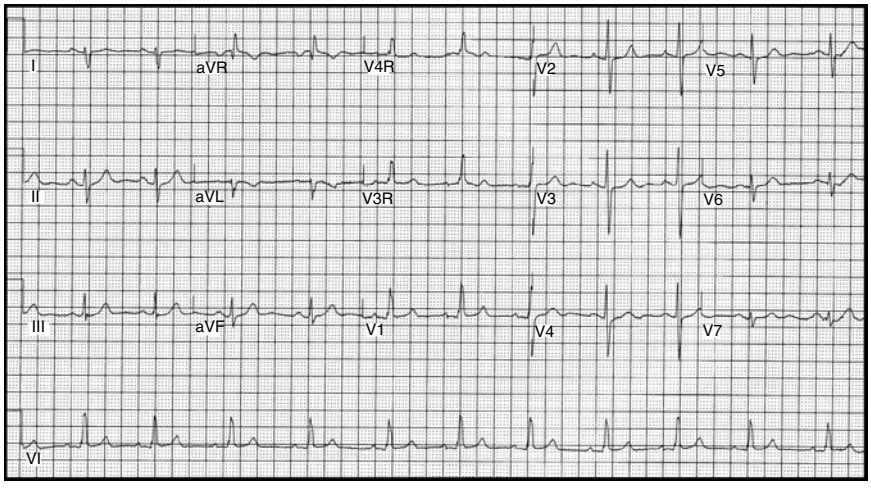

Figure 22.5

15-lead ECG in a 45-year-old woman with a moderate ventricular septal (VSD). Note the broad notched P-wave in lead II, normal PR interval, and right axis deviation. The R-wave amplitude in V1 meets right ventricular hypertrophy criteria. "Katz–Wachtel" phenomenon is present, with large equiphasic RS complexes over the mid-precordial leads that reflect biventricular hypertrophy.

22.3.3 Atrioventricular Canal Defect

The most common presentations of AVCD in adulthood are either a partial defect, consisting of a primum ASD and cleft mitral valve, or surgically repaired complete AVCD. Less commonly, an unoperated patient with a complete AVCD that includes a large primum ASD, inlet VSD, and cleft mitral valve presents with Eisenmenger's physiology or with spontaneous closure of the inlet VSD by way of aneurysm formation. In addition to ECG findings associated with the displaced AV conduction system, electrocardiographic findings reflect the dominant physiology of the defect, e.g., large left-to-right atrial shunt and mitral regurgitation in partial AVCD and Eisenmenger's physiology in an unrepaired complete AVCD [4].

Following surgical repair of AVCD, atrial fibrillation or flutter may develop in 5% of patients [68, 69]. Persistent complete AV block occurs in 1–7% in the immediate postoperative period and approximately 2% thereafter [69–72]. Prolonged infra-Hisian conduction time may be a marker for increased risk of late AV block, even in the presence of a normal PR interval [73]. Although increased ventricular ectopy has been described in up to 30% of patients, complex ventricular arrhythmias occur most commonly in the setting of left ventricular dysfunction [69].

Distinctive ECG features in the adult with AVCD, displayed in Fig. 22.6, involve the PR interval, right ventricular activation pattern, and QRS axis. First-degree AV block is present in over 50% of patients and is most commonly due to intraatrial conduction delay, although acquired postoperative AV block may occur [73–78]. In 18 patients with AVCD, electrophysiologic studies revealed supra-Hisian first-degree AV block in five patients, and intraatrial conduction delay in the majority [55]. The QRS pattern in right precordial leads may be similar to ostium secundum ASD, with delay in right ventricular activation. Interestingly, this is thought to result from conduction along a longer than normal right bundle branch that emanates from the inferiorly displaced common bundle; not from delayed parietal conduction [74].

As previously mentioned, a superior QRS axis is a hallmark of AVCD with left axis deviation that may be moderate or extreme. Q-waves are present in leads I and aVL and S waves in II, III, and aVF that characteristically have a notched upstroke [74–77]. Nonetheless, an intermediate QRS axis and right axis deviation have been described. One study assessed the QRS axis in 135 patients with typical AVCD and 9 patients with atypical forms of AVCD characterized by a well-formed atrial septum, milder downward displacement of the AV valves, and shorter length of the ostium primum defect [79]. All nine patients with atypical AVCD had an unusual mean frontal QRS axis compared with 6 of 135 patients (4%) with typical

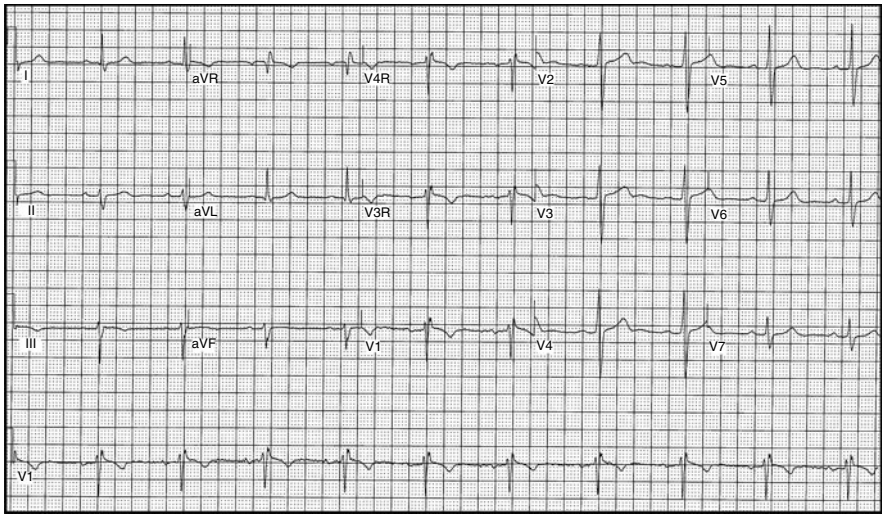

Figure 22.6

15-lead ECG in a 42-year-old man with a surgically repaired Atrioventricular canal defects (AVCD). Note the rSr′ QRS pattern over the right precordial leads, similar to secundum ASD. The PR interval is prolonged and the typical superior QRS axis is present. S-waves in leads II, III, and aVF have a characteristically notched upstroke.

AVCD. It was, therefore, speculated that this atypical morphology, supposedly related to the degree of posteroinferior displacement of the conduction system, explained in part the observed differences in QRS axis.

22.3.4 Patent Ductus Arteriosus

Most patients with moderate or large patent ductus arteriosus (PDA) will have undergone ductal ligation in infancy. The majority of adults with PDA fall into one of two categories: a fortuitously discovered PDA on echocardiography or Eisenmenger's physiology with irreversible pulmonary vascular obstructive disease [4]. In the former case, the ECG is expected to be normal, whereas in the latter case, ECG findings are dominated by Eisenmenger's physiology. In patients with a moderate size PDA, sinus rhythm is usually present although atrial fibrillation may occur in older individuals [80, 81]. Evidence for left atrial enlargement may be present and PR prolongation is found in 10–20% [82]. The QRS axis is generally normal. Left ventricular volume overload may be characterized by deep S-waves in V1 and tall R-waves in leads V5 and V6 that are accompanied by nonspecific repolarization changes [81, 82].

22.3.5 Pulmonary Stenosis

The obstruction of the right ventricular outflow tract can occur at the level of the pulmonary valve, below, or above it, either in the main pulmonary artery trunk or at one or both of its branches. As a group, these lesions represent a spectrum of unoperated and postoperative anomalies that are among the most commonly encountered in the adult with congenital disease. Isolated congenital valvar pulmonary stenosis is reported to occur in 10% of all patients with congenital heart disease. In adults, pulmonary atresia, supravalvar, and branch pulmonary artery stenosis are commonly encountered in the setting of tetralogy of Fallot (TOF). Congenital branch pulmonary artery stenosis can occur in isolation but is not usually associated with substantial right ventricular pressure overload. ECG features of primary infundibular stenosis or double-chambered right ventricle vary depending on the presence or absence of an associated VSD and/or concomitant valvar pulmonary stenosis [4].

Criteria for right ventricular hypertrophy in the presence of valvar pulmonary stenosis were extensively reviewed in a previous chapter. In general, the severity of pulmonary stenosis correlates with the R to S ratio in leads V1 and V6, and R-wave amplitude in lead V1 [83, 84]. The PR interval is typically normal but prolongation may reflect increased right atrial size and pressure [85, 86]. High amplitude peaked P-waves in lead II are commonly found in severe pulmonary stenosis, but not consistently so [87]. The QRS axis may be normal with mild pulmonary stenosis but is deviated rightward with moderate or severe obstruction. The degree of right axis deviation is positively correlated with right ventricular pressure [83].

22.3.6 Aortic Coarctation

Complications of operated and unoperated adult patients with aortic coarctation include left ventricular hypertrophy, systemic hypertension, heart failure, aortic dissection, premature coronary artery disease, and cerebrovascular events [88, 89]. In a population-based study, only 1 of 536 survivors with aortic coarctation repair died suddenly during the first 20 years of follow-up [90]. However, with longer-term follow-up, nine sudden deaths occurred, two of which resulted from aortic rupture. All seven sudden presumably arrhythmic deaths transpired in patients with advanced ventricular dysfunction [90].

In adults with uncomplicated aortic coarctation, the ECG usually exhibits normal sinus rhythm. Unlike children with concomitant left-to-right interatrial shunts, left but not right atrial enlargement is often seen [91]. The PR interval is usually normal and the QRS axis is normal or displaced leftward. Persistent right ventricular hypertrophy beyond infancy is rare. Left ventricular hypertrophy commonly occurs, with the most sensitive ECG criterion being increased QRS voltage [92], as demonstrated in Fig. 22.7.

22.3.7 Ebstein's Anomaly

In Ebstein's anomaly, the tricuspid valve is displaced apically, creating an "atrialized" portion of the right ventricle that is morphologically and electrically right ventricle but functionally right atrium [93]. Differences in clinical presentation

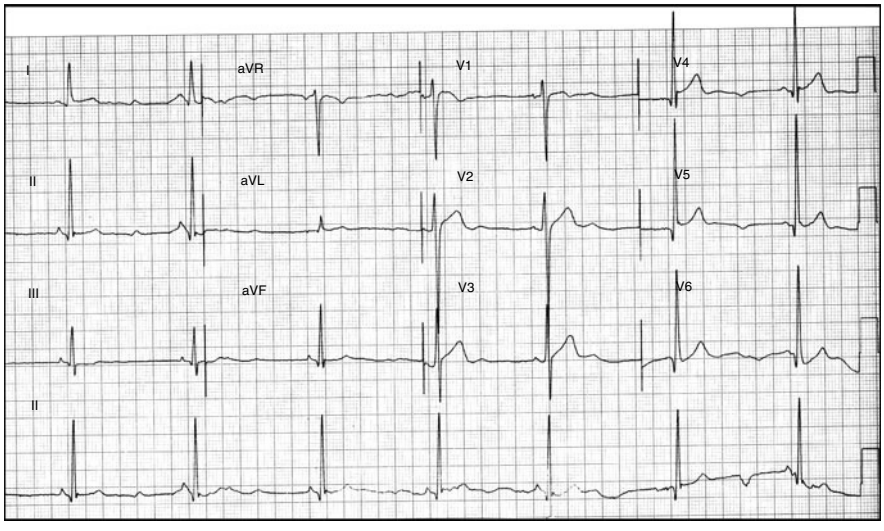

Figure 22.7

12-lead ECG in a 26-year-old man with aortic coarctation surgically repaired at 6 years of age, with recoarctation repair at 17 years. Note the voltage criteria for left ventricular hypertrophy with an R-wave in lead II > 2.0 mV, R-wave in lead V5 > 3.0 mV, and sum of S-wave in lead V1 and R-wave in lead V5 or V6 > 3.5 mV. The QRS duration exceeds 90 ms.

result from a wide spectrum of lesion severity as determined by degree of tricuspid leaflet tethering, relative proportion of atrialized and true right ventricle, and presence or absence of right ventricular outflow tract obstruction. A patent foramen ovale or secundum ASD is a common associated feature. The presence of tricuspid regurgitation with an enlarged right atrium, left-to-right shunting, and accessory pathways provide the substrate for most atrial arrhythmias. Mechanical stimulation of the "atrialized" ventricle may provoke ventricular arrhythmias, but spontaneous ventricular tachycardia is otherwise uncommon in the absence of associated malformations [94].

The ECG is invaluable in the adult with Ebstein's anomaly for clinical diagnosis, detection of accessory pathways, and characterization of arrhythmias, as exemplified in Figs. 22.8 and 22.9. Indeed, accessory AV and atriofascicular pathways are found in 25% and are more often right-sided and multiple than accessory pathways in structurally normal hearts [93, 95, 96] ventricular tachyarrhythmias including AV reciprocating tachycardia, ectopic atrial tachycardia, and atrial fibrillation or flutter occur in 30–40% of patients, constituting the most common presentation in adolescents and adults [97, 98]. Tolerance to tachyarrhythmia is dependent on the severity of Ebstein's malformation that can range from mild and asymptomatic to severe, with associated tricuspid regurgitation, cyanosis, and hemodynamic compromise. The role of arrhythmias in the etiology of sudden death, reported in 3–4% of patients [97], remains poorly defined. Sudden death may occur from severe cyanosis or from rapid conduction of atrial fibrillation or flutter to the ventricles via high risk or multiple pathways [96].

In Ebstein's anomaly, P-waves are characteristically tall and broad due to prolonged conduction in the enlarged right atrium and have been coined "Himalayan" [99, 100]. First-degree AV block is often present as a result of intraatrial conduction delay, with a PR interval than can be markedly prolonged [101]. Naturally, the PR interval may be shortened in the presence of an accessory AV or atriofascicular pathway. As the right ventricle is diminutive, low amplitude QRS complexes are characteristically seen over the right precordial leads [102, 103]. Due to the "atrialized" portion of the right ventricle, the QRS complex typically exhibits right ventricular conduction delay of the right bundle branch

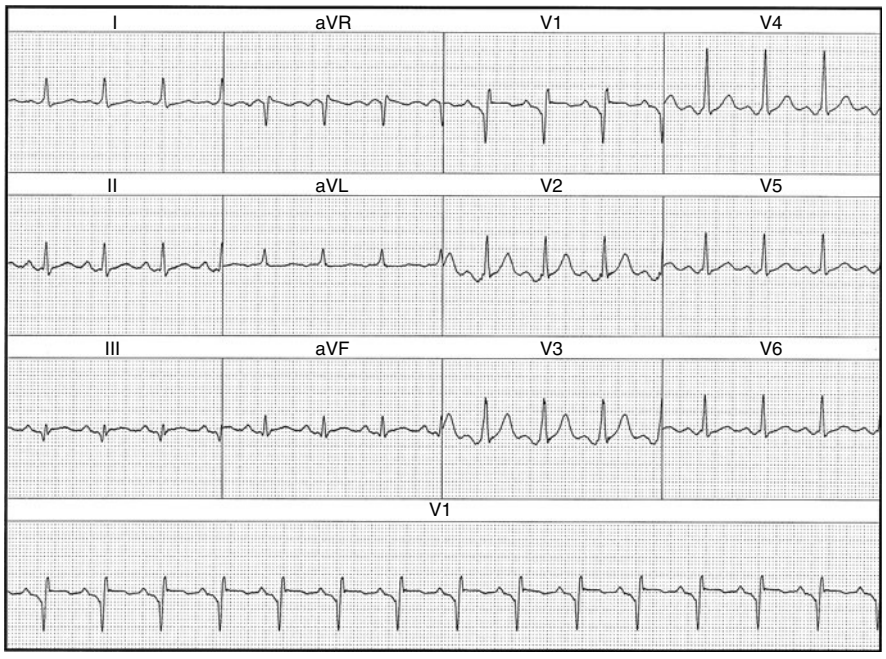

Figure 22.8

12-lead ECG in a 39-year-old man with Ebstein's anomaly and palpitations. Note the short PR interval, delta wave, and wide QRS complex consistent with ventricular preexcitation. The delta wave axis (i.e., negative in leads V1, III, and aVF and positive in leads I and aVL) suggests a right-sided posteroseptal accessory pathway. This pathway was deemed "high risk" as preexcited atrial fibrillation up to 245 bpm occurred. It was successfully ablated.

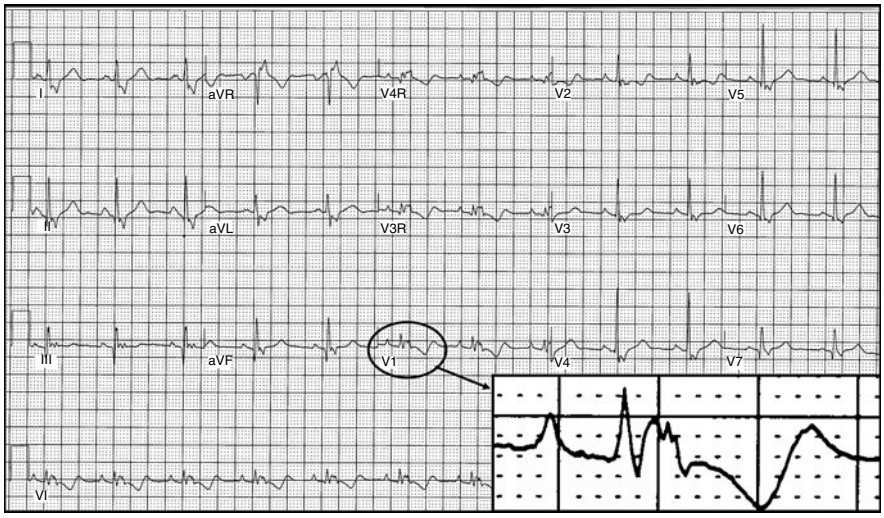

Figure 22.9

15-lead ECG in a 33-year-old woman with Ebstein's anomaly. Encircled and magnified in the insert, a low-amplitude multiphasic "bizarre" QRS complex is seen over the right precordial leads with a right bundle branch block pattern. P-waves are broad and somewhat tall. The QRS axis is normal and Q-waves are notable in leads V1, II, III, and aVF.

type that is often atypical and multiphasic [99–101]. In unoperated patients with Ebstein's anomaly, signal-averaged ECGs almost universally identify late potentials that correspond to delayed conduction across the "atrialized" right ventricle [104].

In the absence of ventricular preexcitation, the QRS axis is generally normal but occasionally leftward [105, 106]. In about 50% of patients, Q-waves are noted in lead V1 and may extend as far as lead V4 [107, 108]. T-wave inversion in leads V1–V4 is also common [107, 108]. Q-waves may be present in leads II, III, and aVF [105, 107]. It has been hypothesized that these Q-waves reflect right ventricular intracavitary potentials resulting from the inferior and leftward displacement of the tricuspid valve [107].

22.3.8 Surgically Corrected Tetralogy of Fallot

Tetralogy of Fallot is the most common cyanotic heart disease, accounting for approximately 10% of all congenital heart malformations [109]. Corrective surgery has been performed for over 40 years with excellent results [110]. However, atriotomies are commonly performed, predisposing to the late development of intraatrial reentrant tachycardia (IART) [111, 112]. Patients with IART may have typical isthmus-dependent flutter and/or incision-related macroreentrant circuits [113–116]. Development of IART may herald worsening ventricular function and tricuspid regurgitation [111, 112, 117, 118]. Moreover, sudden cardiac death is the single most common cause of mortality late after repair [119]. In a cohort study of 793 patients with repaired TOF followed for 35 years, 10% developed atrial flutter, 11.9% experienced sustained ventricular tachycardia (Fig. 22.10), and 8.3% died suddenly [112]. Very few arrhythmic events occurred the first 5–10 years following corrective surgery. Thereafter, a slow but steady decline in freedom from atrial and ventricular arrhythmias and sudden cardiac death was observed [112, 120–122].

In adults with surgically corrected TOF, baseline sinus rhythm is commonly seen, with P-waves of normal axis, duration, and amplitude, although somewhat peaked [123–128]. The QRS axis is typically normal or rightwardly displaced with underlying right ventricular hypertrophy. In the presence of a right bundle branch block, criteria for right ventricular hypertrophy include an R′ in V1 $\geqslant$ 15 mm and right axis deviation of the initial vector that represents unblocked

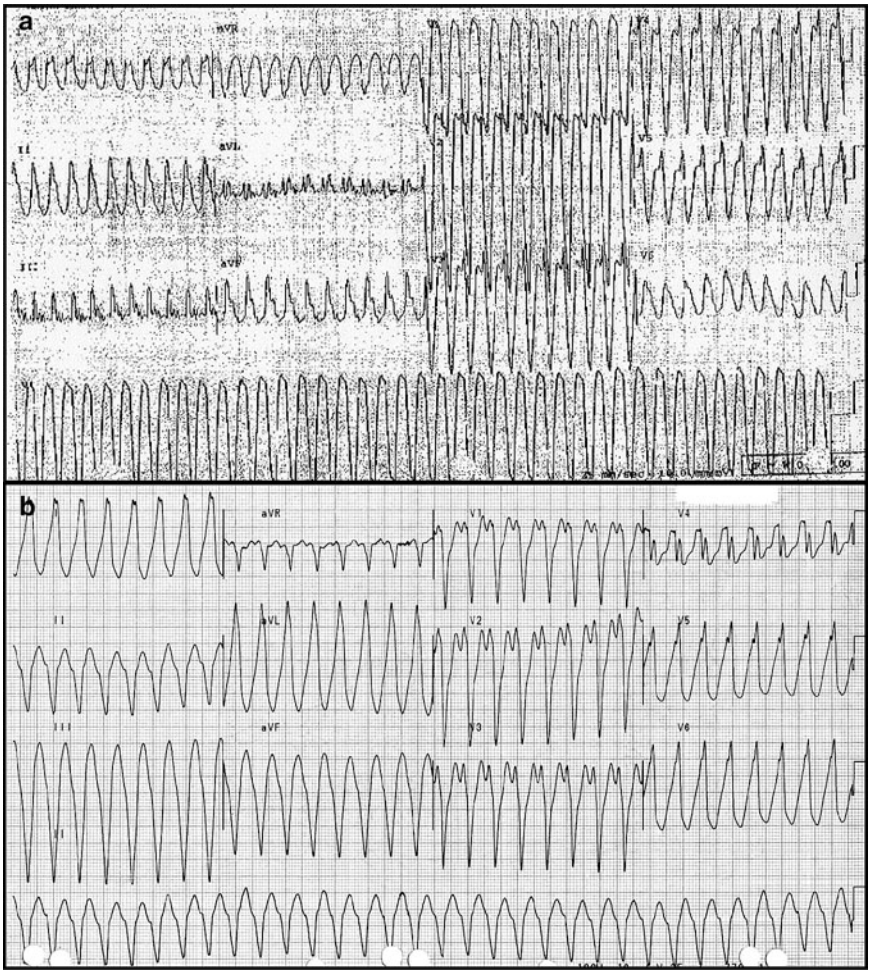

Figure 22.10

ECG examples of clinical monomorphic ventricular tachycardia in adults with corrected tetralogy of Fallot. In Panel a, a 34-year-old man with surgically repaired tetralogy of Fallot presented with a wide-complex tachycardia at 240 bpm. Left bundle branch block morphology and inferior axis reflect the typical right ventricular outflow tract origin. Panel b depicts ventricular tachycardia at 195 bpm in a 46-year-old man with surgically repaired tetralogy of Fallot. While the QRS complex is of left bundle branch morphology, consonant with a right ventricular source, the superior QRS axis suggests an origin remote from the outflow tract.

forces [129, 130]. Left axis deviation should raise the suspicion of an associated AVCD, although left anterior hemiblock may be present in 5–10% of adults [124, 131]. Right bundle branch block is the rule following repair, even in the absence of a ventriculotomy incision [123–126]. Early lengthening of the QRS interval post TOF repair results from surgical injury to the right bundle branch and myocardium [132], whereas later broadening reflects right ventricular dilation [133, 134].

Given the small but undeniable risk of ventricular arrhythmias and sudden cardiac death post TOF repair, considerable efforts have been directed toward identifying predictors allowing stratification of patients into high- and low-risk categories. In the largest cohort study to date [112], a QRS interval $\geqslant$ 180 ms (RR 8.8), as shown in Fig. 22.11, and an annual increase in QRS duration (RR 1.1 for each 1 ms increase/year) were independent risk factors for sustained ventricular tachycardia. Patients with ventricular tachycardia or sudden cardiac death were more likely to have increased

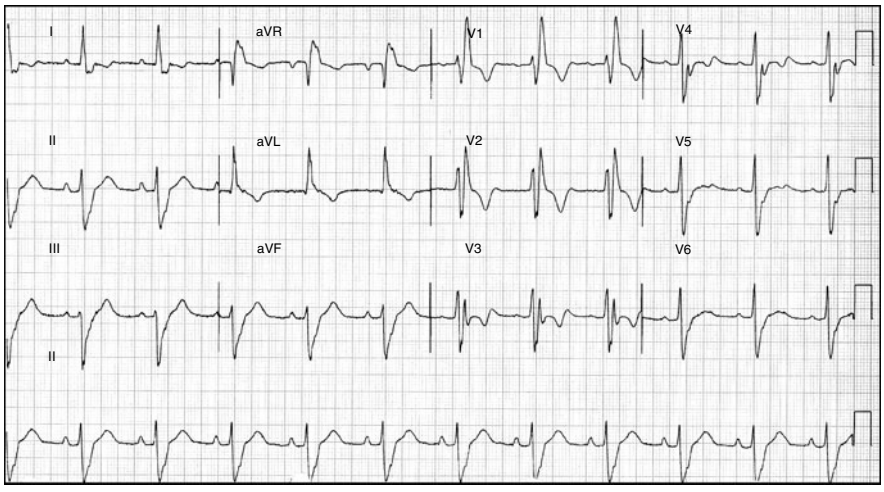

Figure 22.11

12-lead ECG of a 50-year-old man with surgically repaired tetralogy of Fallot. Note the characteristic right bundle branch block morphology. The QRS duration of 192 ms is associated with increased risk for ventricular arrhythmias and sudden death. The tall R′ in V1 and deep S-waves in V5 and V6 suggest right ventricular hypertrophy in the context of mild residual pulmonary stenosis. First-degree AV block and left axis deviation are also present.

cardiothoracic ratios, at least moderate pulmonary and tricuspid regurgitation, and peripheral pulmonary stenosis. A greater degree of QT dispersion was also noted, believed to reflect increased heterogeneity in myocardial repolarization. Other reported risk factors have included frequent ectopic beats [135], increased right ventricular systolic pressures [121, 136, 137], complete heart block [121, 138], and increased JT dispersion [139, 140]. The induction of sustained ventricular tachycardia on electrophysiologic study is a powerful independent predictor of susceptibility to clinical ventricular tachycardia or sudden death [141].

22.3.9 Congenitally Corrected Transposition of the Great Arteries

Patients with isolated L-TGA may remain asymptomatic and undiagnosed well into their adult years. As depicted in Fig. 22.12, the 12-lead ECG can provide critically important diagnostic information. The anatomy of the conduction system in L-TGA was previously reviewed, explaining the vulnerable AV conduction system with its fragile common bundle. In a study of 107 patients with L-TGA, complete AV block occurred in 22% [142]. Risk of AV block was estimated to be 2% per year, irrespective of associated anomalies. On electrophysiologic testing, the site of AV block was found to be above or within the area that generated His-like electrograms [143–145]. This finding is consistent with clinical and pathological observations: a stable narrow QRS escape rhythm often accompanies complete AV block [142] and fibrosis of the common bundle is noted histologically [144, 146, 147]. As the AV node and elongated bundle appear particularly susceptible to catheter or surgical trauma, caution should be exercised with manipulation to these areas. Complete AV block follows surgical repair of an associated VSD in over 25% of patients [142, 148–150].

L-TGA has also been referred to as "ventricular inversion," as the ventricles and associated bundle branches are reversed. The sinus node is positioned in its usual location such that the P-wave axis and morphology are typically normal. However, the ventricular septum that is normally activated from left-to-right is depolarized in the opposite direction, producing the ECG pattern characteristic of L-TGA [151–154]. The usual "septal" q-waves over left precordial leads and small initial R-waves over the right precordial leads are absent. Instead, Q-waves are present over the right precordial leads, consonant with right-to-left septal activation. Moreover, as the septum is activated in a superior direction, Q-waves, which

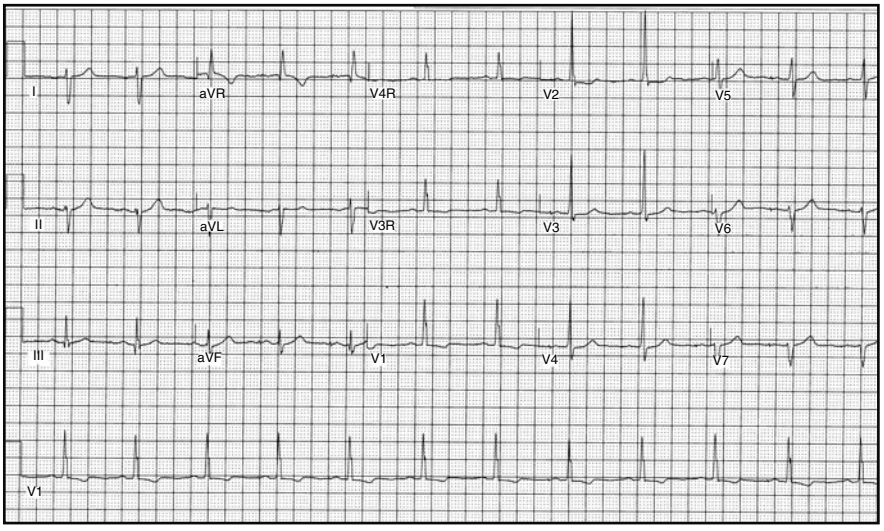

Figure 22.12

15-lead ECG of a 25-year-old man with L-TGA. Note the first-degree AV block, normal P-wave axis, left QRS axis deviation, and absent septal q-waves. Broad Q-waves are seen over the right precordial leads. In inferior leads, Q-waves are deepest in lead III. T-waves are positive in all precordial leads.

are not uncommonly broad, are seen in leads III and aVF, typically most pronounced in lead III. Thus, left axis deviation is the rule. Interestingly, in > 80% of patients, positive T-waves are present over all precordial leads, attributed to the side-by-side nature of the inverted ventricles [151–154]. In patients with associated Ebstein's malformation of the tricuspid valve, left-sided accessory pathways may be present [155–158].

22.3.10 Complete Transposition of the Great Arteries and Intraatrial Baffle

In "complete" transposition of the great arteries, or D-TGA, the atrioventricular relationship is preserved but ventriculoarterial discordance is present. D-TGA accounts for 5–7% of all congenital cardiac malformations [109]. In the absence of a shunt allowing for mixing between parallel systemic and pulmonary circulations, D-TGA is incompatible with life. In 1959, Senning introduced an intraatrial baffle repair redirecting systemic and pulmonary venous return without grafts or prostheses [159]. In 1964, Mustard described an alternate technique for intraatrial baffle repair using a pericardial patch [160]. Although arterial switch surgery [161] has supplanted atrial correction as the procedure of choice, the majority of adults with D-TGA have had intraatrial baffle repairs. Late arrhythmic complications include sinus node dysfunction, atrial tachyarrhythmias, and sudden cardiac death [90, 162–169].

Of 478 patients with Mustard repairs, the actuarial rate of loss of sinus rhythm was 39% at 10 years and 60% at 20 years [165]. By 20 years after repair, atrial flutter had occurred in 24%. Loss of coordinated atrial activity and rapid ventricular rates can result in severe symptoms and hemodynamic compromise. Atrial arrhythmias are associated with impaired ventricular function [170, 171] and increased risk of sudden death in some, but not all, studies [172]. In a retrospective multicenter case-control study that identified 47 patients with D-TGA and Mustard or Senning surgery who experienced sudden death, risk factors included the presence of symptoms of arrhythmia or heart failure and history of documented atrial fibrillation or flutter [173]. ECG criteria, chest X-ray, and Holter findings were not predictive of sudden death and medical therapy and pacemakers were not found to be protective.

Characteristic ECG findings, exemplified by Figs. 22.13 and 22.14, are found in adults with D-TGA and intraatrial baffle repair [174, 175]. As sinus node dysfunction is highly prevalent, atrial and junctional rhythms may be seen. In simple D-TGA, AV node function is preserved. However, intraatrial conduction delay may result in a prolonged PR interval.

Figure 22.13

15-lead ECG of a 29-year-old woman with D-TGA and Mustard procedure. Note the normal PR interval, right axis deviation, and right ventricular hypertrophy. Absent q-waves, small r-waves, and deep S-waves over leads V5–V7 reflect the diminutive left ventricle. A pacemaker was implanted for sinus node dysfunction; bipolar atrial pacing spikes precede the eighth and 11th P-wave.

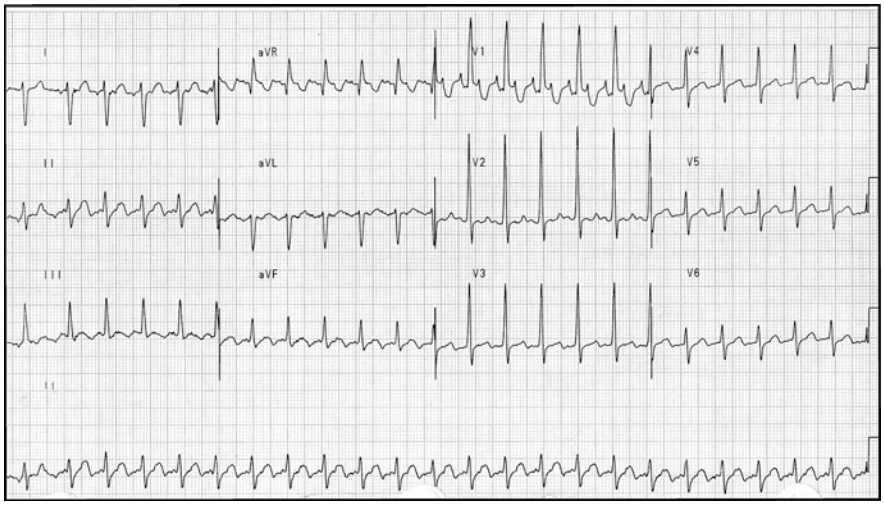

Figure 22.14

12-lead ECG in a 38-year-old woman with D-TGA and Mustard procedure. Note the intraatrial reentrant tachycardia (IART) cycle length of 215 ms with 2:1 AV conduction. Right axis deviation, right ventricular hypertrophy, and a diminutive left ventricle are also present.

AV block is more common in the presence of surgical repair of an associated VSD and/or tricuspid regurgitation [176]. Despite corrected physiology, the right ventricle remains systemically positioned. Thus, ECG criteria for right ventricular hypertrophy are usually present, with right axis deviation [174, 175]. Right atrial enlargement may likewise be present [174]. Conversely, the subpulmonary left ventricle is diminutive with decreased terminal forces reflected in the absence of q-waves, small r-waves, and deep S-waves over the left precordial leads.

22.3.11 Single Ventricle Physiology with Fontan Surgery

Developed in 1971 as surgical palliation for tricuspid atresia, the Fontan procedure has undergone multiple modifications to become the procedure of choice for various forms of single ventricle physiology [177]. Atrial arrhythmias after the Fontan procedure are among the more challenging problems in the field of adult congenital electrophysiology. These arrhythmias occur in the context of single functional ventricles and may be associated with substantial morbidity and mortality. Rapid hemodynamic deterioration and heart failure can ensue. Depending on the particular type of repair, IART or atrial fibrillation may occur in up to 57% of patients [178]. Tachycardia circuits can be complex and/or multiple [113, 116, 179, 180]. Patients with failing Fontans and refractory atrial arrhythmias should be considered for surgical conversion to a lateral tunnel or extracardiac conduit with concomitant arrhythmia surgery [181–185]. On short- to medium-term follow-up, advantages of the extracardiac in comparison to the intracardiac lateral tunnel Fontan include a decreased incidence of sinus node dysfunction [186], although not consistently so [187].

Given the heterogeneity of the multiple morphologic types of single ventricles, the ECG appearance is highly variable. At mid-term follow-up, sinus node dysfunction occurs in 13–16% of patients with classic Fontans (i.e., right atrium to pulmonary artery anastamosis) and increases with duration of follow-up [188–190]. In patients with tricuspid atresia, the PR interval is usually normal with tall and broad P-waves. Left axis deviation is characteristic [191–194], as shown in Fig. 22.15. In the absence of a functional right ventricle, left ventricular forces are unopposed, as manifested by small r-waves and deep S-waves over the right precordial leads and tall R-waves over the left precordial leads.

In the most common subtype of double-inlet left ventricle, i.e., with ventriculo-arterial discordance, AV conduction is often abnormal, with PR prolongation and increased risk of complete heart block [195, 196]. As in L-TGA, Q-waves are absent over the left precordial leads and may be present over the right precordial leads. Q-waves may also be seen in leads II, III, and aVF [195, 197]. In a series of 18 patients with univentricular hearts of right ventricular morphology, 12 had double inlet, four absent right, and two absent left AV connections [198]. ECG revealed right ventricular hypertrophy in all and 11 had a superior frontal QRS axis. An example of an ECG in an adult with a hypoplastic left ventricle is provided in Fig. 22.16.

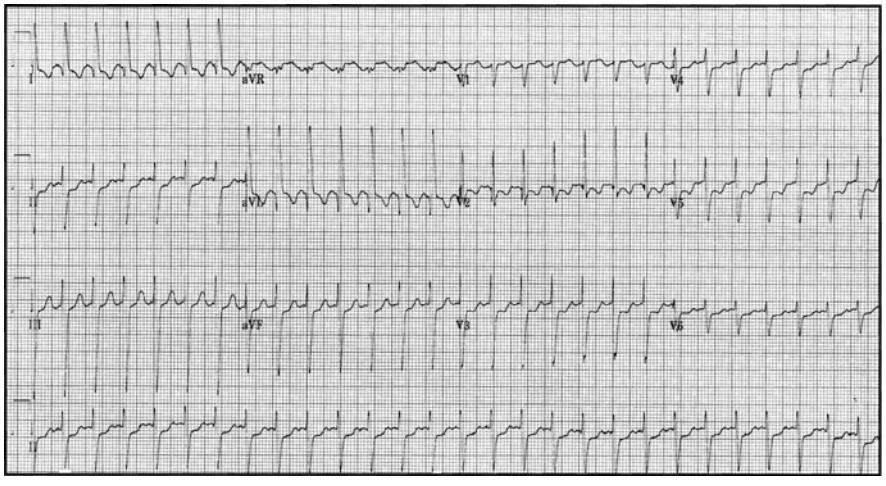

Figure 22.15

12-lead ECG in a 31-year-old woman with tricuspid atresia, ASD, and VSD, status post old-style Fontan later revised to an extracardiac conduit with a right atrial Maze procedure. An IART with a ventricular response rate of 167 bpm was electrically cardioverted. Note the characteristic left axis deviation.

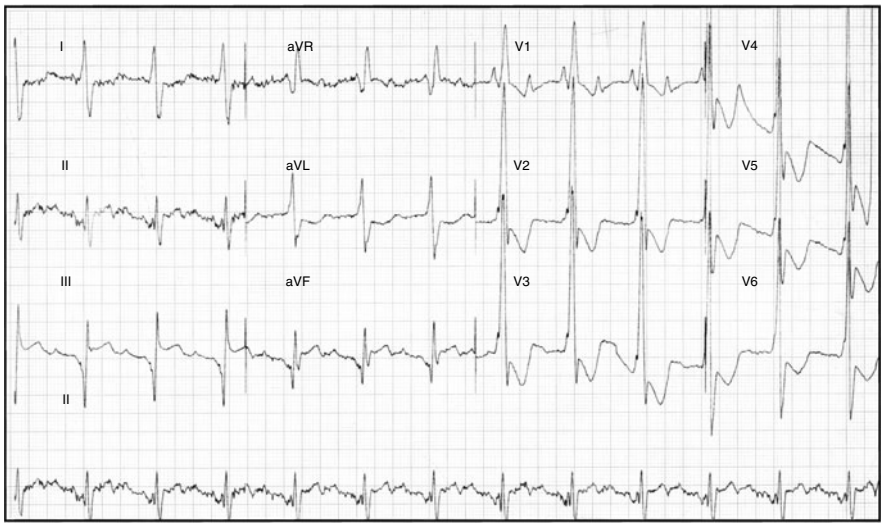

Figure 22.16
12-lead ECG in a 24-year-old man with mitral atresia and hypoplastic left ventricle status post old-style Fontan. Note the IART at a cycle length of 370 ms with 2:1 AV conduction. Right ventricular hypertrophy criteria are met and the frontal QRS axis is superior, typical of univentricular hearts of right ventricular morphology.

22.3.12 Cardiac Malpositions

In dextrocardia with situs inversus, also called mirror-image dextrocardia, the ventricles are inverted, as are the viscera and the atria. The heart usually functions normally and the diagnosis is often fortuitous. In mesocardia, the heart is centrally located in the chest with normal atrial and visceral anatomy. The apex is central or rightwardly displaced on chest radiography. Typically, no associated cardiac malformations are present. When dextrocardia with situs solitus occurs, as illustrated in Fig. 22.17, the ventricles are inverted, but not the viscera or atria. Associated severe cardiac malformations are typical [4].

The ECG is of considerable diagnostic importance in dextrocardia with situs inversus. As previously discussed, the right atrium and sinus node are positioned on the patient's left side, yielding a P-wave axis that remains inferiorly oriented but rightwardly displaced. In the absence of an ectopic focus, P-waves are upright in aVR and inverted in I and aVL [199–202]. Ventricular depolarization and repolarization occur in an inverse fashion. In lead I, the QRS is predominantly negative with T-wave inversion. Right precordial leads resemble the left precordial leads of normal hearts, aVL resembles aVR, and vice versa. Thus, left ventricular hypertrophy is manifested by tall R-waves in V1 and V2. Right ventricular hypertrophy is reflected by deeper Q-waves and small R-waves in lead I and taller R-waves over right lateral chest leads (e.g., V5R and V6R) [199, 200].

22.3.13 Coronary Anomalies

Isolated ectopic or anomalous origins of the coronary arteries are seen in 0.6–1.5% of patients undergoing coronary angiography [203]. The prognosis is favorable if the anomalous coronary artery does not course between the pulmonary artery and aorta. The most common anomalies are not associated with myocardial ischemia and include ectopic origin of the left circumflex artery from the right sinus of Valsalva; anomalous origin of the right coronary artery from the left sinus, and anomalous origin of the left main coronary artery from the right sinus. In coronary-cameral fistulas, the ECG is typically normal until volume overload of the receiving chamber occurs with or without ischemic changes related to coronary steal [204–206].

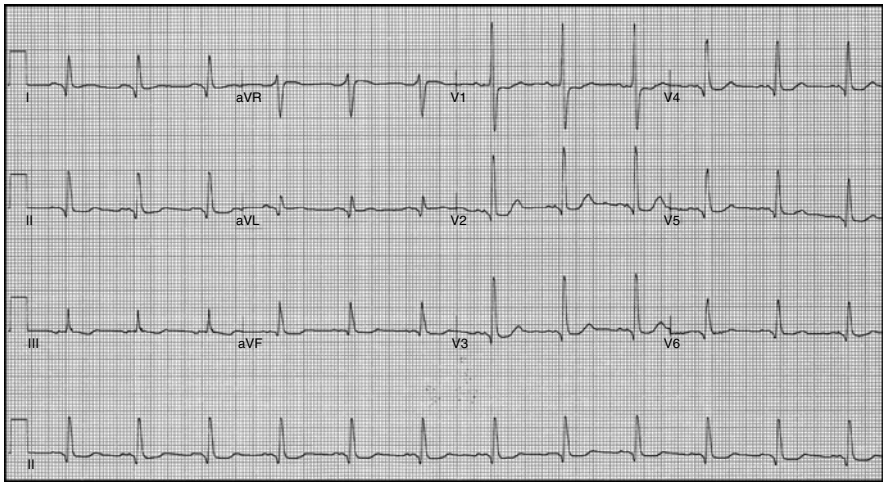

Figure 22.17

12-lead ECG in a 45-year-old man with situs solitus, dextrocardia, anomalous pulmonary venous return, single atrium, and pulmonary stenosis. The P-wave vector is directed leftward and somewhat inferiorly, with an axis of 30° that is consistent with atrial situs solitus and normal position of the sinus node. Note the reverse R-wave progression pattern, with decreasing amplitude from leads V1 to V6. The pathologic Q-wave in lead I may reflect right ventricular hypertrophy in the setting of pulmonary stenosis.

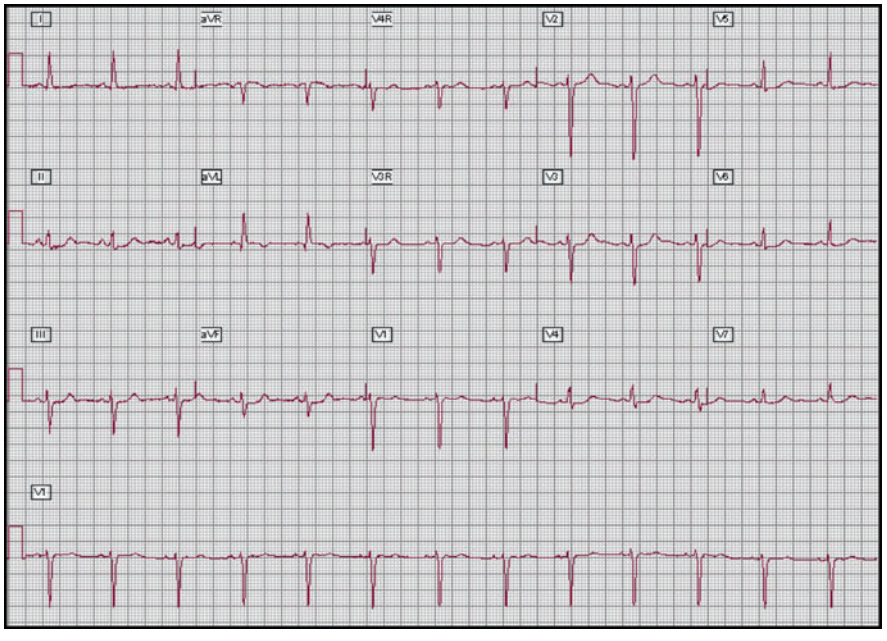

Figure 22.18

15-lead ECG in a 35-year-old woman with anomalous origin of the left coronary artery from the pulmonary artery. She presented with chest pain at 13 years of age and underwent a Takeuchi repair. Note the loss of R-wave amplitude with no R-wave progression over precordial leads V1–V3, consistent with an old anteroseptal myocardial infarction.

The ECG is useful in the diagnosis of anomalous origin of the left coronary artery from the pulmonary trunk. This is the most common anomaly associated with myocardial ischemia, with 25% of cases surviving to adolescence or adulthood [207]. As a result of decreased perfusion pressure and hypoxemic blood flow through the left coronary artery, anterolateral myocardial infarction usually occurs prior to the clinical recognition of this entity. The 12-lead ECG, therefore, displays pathologic Q-waves in leads I, aVL, and V4–V6 that are typically deep [208–214]. In addition, the posterobasal portion of the left ventricle appears to selectively hypertrophy [211]. This may result in left axis deviation, a pattern consistent with left ventricular hypertrophy, and nonspecific repolarization changes [208–211, 214]. Anteroseptal myocardial infarction patterns have also been described, as depicted in Fig. 22.18.

References

1. Perloff, J.K. and C.A. Warnes, Challenges posed by adults with repaired congenital heart disease. *Circulation*, 2001;**103**(21): 2637–2643.
2. Warnes, C.A., R. Liberthson, G.K. Danielson, et al., Task force 1: the changing profile of congenital heart disease in adult life. *J. Am. Coll. Cardiol.*, 2001;**37**(5): 1170–1175.
3. Gatzoulis, M.A., S. Hechter, S.C. Siu, and G.D. Webb, Outpatient clinics for adults with congenital heart disease: increasing workload and evolving patterns of referral. *Heart*, 1999;**81**(1):57–61.
4. Marelli, A. and Moodie D. Adult congenital heart disease, in *Textbook of Cardiovascular Medicine*, 2nd edn., E. Topol, Editor. Philadelphia, PA: Lippincott Williams & Wilkins, 2002, pp. 709–731.
5. Moller, J.H., K.A. Taubert, H.D. Allen, E.B. Clark, and R.M. Laurer, Cardiovascular health and disease in children: current status. *Circulation*, 1994;**89**: 923–930.
6. Gatzoulis, M.A. and G.D. Webb, Adults with congenital heart disease: a growing population, in *Diagnosis and Management of Adult Congenital Heart Disease*, M.A. Gatzoulis and G.D. Webb, From chapter P.E.F. Daubeney, Editors. London: Churchill Livingston, 2003, pp. 3–6.
7. Kanter, R.J. and A. Garson, Jr., Atrial arrhythmias during chronic follow-up of surgery for complex congenital heart disease. *Pacing Clin. Electrophysiol.*, 1997;**20**(2 Pt 2): 502–511.
8. Engelfriet, P., E. Boersma, E. Oechslin, et al., The spectrum of adult congenital heart disease in Europe: morbidity and mortality in a 5 year follow-up period. *Eur. Heart J.*, 2005; **26**(21): 2325–2333.
9. Ho, S.Y., J.L. Monro, and R.H. Anderson, Disposition of the sinus node in left-sided juxtaposition of the atrial appendages. *Br. Heart J.*, 1979;**41**(2): 129–132.
10. Anjos, R.T., S.Y. Ho, and R.H. Anderson, Surgical implications of juxtaposition of the atrial appendages. A review of forty-nine autopsied hearts. *J. Thorac. Cardiovasc. Surg.*, 1990;**99**(5): 897–904.
11. Rossi, L., S. Montella, C. Frescura, and G. Thiene, Congenital atrioventricular block in right atrial isomerism (asplenia). A case due to atrionodal discontinuity. *Chest*, 1984;**85**(4):578–580.
12. Dickinson, D.F., J.L. Wilkinson, K.R. Anderson, A. Smith, S.Y. Ho, and R.H. Anderson, The cardiac conduction system in situs ambiguus. *Circulation*, 1979;**59**(5): 879–885.
13. Wren, C., F.J. Macartney, and J.E. Deanfield, Cardiac rhythm in atrial isomerism. *Am. J. Cardiol.*, 1987;**59**(12): 1156–1158.
14. Momma, K., A. Takao, and T. Shibata, Characteristics and natural history of abnormal atrial rhythms in left isomerism. *Am. J. Cardiol.*, 1990;**65**(3): 231–236.
15. Moorman, A.F.M., F. de Jong, M.M.F.J. Denyn, and W.H. Lamers. Development of the cardiac conduction system. *Circ. Res.*, 1998;**82**: 629–644.
16. Anderson, R.H. and S.Y. Ho, The morphology of the specialized atrioventricular junctional area: the evolution of understanding. *Pacing Clin. Electrophysiol.*, 2002;**25**(6): 957.
17. Anderson, R.H. and S.Y. Ho, The morphology of the cardiac conduction system. *Novartis Found. Symp.*, 2003;**250**: 6–17.
18. Campbell, R.M., M. Dick, P. Hees, and D.M. Behrendt, Epicardial and endocardial activation in patients with endocardial cushion defect. *Am. J. Cardiol.*, 1983;**51**(2): 277–281.
19. Borkon, A.M., D.R. Pieroni, P.J. Varghese, C.S. Ho, and R.D. Rowe. The superior QRS axis in ostium primum ASD: a proposed mechanism. *Am. Heart J.*, 1975;**90**(2): 215–221.
20. Anderson, R.H., R. Arnold, and J.L. Wilkinson, The conducting system in congenitally corrected transposition. *Lancet*, 1973;**1**(7815): 1286–1288.
21. Anderson, R.H., A.E. Becker, R. Arnold, and J.L. Wilkinson, The conducting tissues in congenitally corrected transposition. *Circulation*, 1974;**50**(5): 911–923.
22. Guller, B., J.W. DuShane, and J.L. Titus. The atrioventricular conduction system in two cases of tricuspid atresia. *Circulation*, 1969;**40**(2): 217–226.
23. Bharati, S. and M. Lev, The conduction system in tricuspid atresia with and without regular (d-) transposition. *Circulation*, 1977;**56**(3): 423–429.
24. Bharati, S. and M. Lev, The course of the conduction system in single ventricle with inverted (L-) loop and inverted (L-) transposition. *Circulation*, 1975;**51**(4): 723–730.
25. Wilkinson, J.L., D. Dickinson, A. Smith, and R.H. Anderson, Conducting tissues in univentricular heart of right ventricular type with double or common inlet. *J. Thorac. Cardiovasc. Surg.*, 1979;**77**(5): 691–698.
26. Gatzoulis, M.A., M.A. Freeman, S.C. Siu, G.D. Webb, and L. Harris, Atrial arrhythmia after surgical closure of atrial septal defects in adults. *N. Engl. J. Med.*, 1999;**340**(11): 839–846.
27. Attie, F., M. Rosas, N. Granados, C. Zabal, A. Buendia, and J. Calderon, Surgical treatment for secundum atrial septal defects in patients > 40 years old. A randomized clinical trial. *J. Am. Coll. Cardiol.*, 2001;**38**(7): 2035–2042.
28. Donti, A., M. Bonvicini, and A. Placci, et al., Surgical treatment of secundum atrial septal defect in patients older than 50 years. *Ital. Heart J.*, 2001;**2**(6): 428–432.
29. Silversides, C.K., S.C. Siu, P.R. McLaughlin, et al., Symptomatic atrial arrhythmias and transcatheter closure of atrial septal defects in adult patients. *Heart*, 2004;**90**(10): 1194–1198.

30. Zufelt, K., H.C. Rosenberg, M.D. Li, and G.I. Joubert, The electrocardiogram and the secundum atrial septal defect: a reexamination in the era of echocardiography. *Can. J. Cardiol.*, 1998;**14**(2): 227–232.
31. Tan, K.T., A. Takao, A. Hashimoto, and T. Sato, Electrocardiogram of secumdum type atrial septal defect simulating endocardial cushion defect. *Br. Heart. J.*, 1975;**37**(2): 209–215.
32. Mori, H., K. Mikawa, T. Niki, T. Nagao, and S. Matsumo, QRS waves of the spatial velocity electrocardiogram in atrial septal defect. *Jpn. Heart J.*, 1972;**13**(5): 407–417.
33. Boineau, J.P., M.S. Spach, and C.R. Ayers, Genesis of the electrocardiogram in atrial septal defect. *Am. Heart J.*, 1964;**68**: 637–651.
34. Dreifus, L.S., S. Bender, H. Goldberg, and D.F. Downing, The electrocardiogram in atrial septal defect. *Dis. Chest*, 1959;**36**: 521–527.
35. Rodriguez-Alvarez, A., G. Martinez De Rodriguez, A.M. Goggans, et al., The vectorcardiographic equivalent of the "crochetage" of the QRS of the electrocardiogram in atrial septal defect of the ostium secundum type. Preliminary report. *Am. Heart J.*, 1959;**58**: 388–394.
36. Burch, G.E. and N. Depasquale, The electrocardiogram and ventricular gradient in atrial septal defect. *Am. Heart J.*, 1959;**58**(2): 190–203.
37. Toscano Barboza, E., R.O. Brandenburg, and H.J. Swan, Atrial septal defect; the electrocardiogram and its hemodynamic correlation in 100 proved cases. *Am. J. Cardiol.*, 1958;**2**(6): 698–713.
38. Milnor, W.R. and C.A. Bertrand, The electrocardiogram in atrial septal defect; a study of twenty-four cases, with observations on the RSR'-V1 pattern. *Am. J. Med.*, 1957;**22**(2): 223–233.
39. Barber, J.M. and O. Magidson, Atrial septal defect with special reference to the electrocardiogram. *Br. Heart J.*, 1950;**12**(2): 203–204.
40. Sung, R.J., D.M. Tamer, A.S. Agha, A. Castellanos, R.J. Myerburg, and H. Gelband, Etiology of the electrocardiographic pattern of "incomplete right bundle branch block" in atrial septal defect: an electrophysiologic study. *J. Pediatr.*, 1975;**87**(6 Pt 2): 1182–1186.
41. Anderson, P.A., M.C. Rogers, R.V. Canent Jr., and M.S. Spach, Atrioventricular conduction in secundum atrial septal defects. *Circulation*, 1973;**48**(1): 27–31.
42. Clark, E.B. and J.D. Kugler, Preoperative secundum atrial septal defect with coexisting sinus node and atrioventricular node dysfunction. *Circulation*, 1982;**65**(5): 976–980.
43. Emanuel, R., K. O'Brien, J. Somerville, K. Jefferson, and M. Hegde, Proceedings: association of secundum atrial septal defect with abnormalities of atrioventricular conduction or left axis deviation: a new syndrome. *Br. Heart J.*, 1976;**38**(5): 536.
44. Yamaki, S., T. Horiuchi, M. Miura, Y. Suzuki, E. Ishizawa, and T. Takahashi, Pulmonary vascular disease in secundum atrial septal defect with pulmonary hypertension. *Chest*, 1986; **89**(5): 694–698.
45. Heath, D., H.F. Helmholz Jr., H.B. Burchell, J.W. Dushane, and J.E. Edwards, Graded pulmonary vascular changes and hemodynamic findings in cases of atrial and ventricular septal defect and patent ductus arteriosus. *Circulation*, 1958; **18**(6): 1155–1166.
46. Emanuel, R., K. O'Brien, J. Somerville, K. Jefferson, and M. Hegde, Association of secundum atrial septal defect with abnormalities of atrioventricular conduction or left axis deviation. Genetic study of 10 families. *Br. Heart J.*, 1975;**37**(10): 1085–1092.
47. Heller, J., A.A. Hagege, B. Besse, M. Desnos, F.N. Marie, and C. Guerot, "Crochetage" (notch) on R wave in inferior limb leads: a new independent electrocardiographic sign of atrial septal defect. *J. Am. Coll. Cardiol.*, 1996;**27**(4): 877–882.
48. Cohen, J.S., D.J. Patton, and R.M. Giuffre, The crochetage pattern in electrocardiograms of pediatric atrial septal defect patients. *Can. J. Cardiol.*, 2000;**16**(10): 1241–1247.
49. Therrien, J., A. Dore, W. Gersony, et al., CCS Consensus Conference 2001 update: recommendations for the management of adults with congenital heart disease. Part I. *Can. J. Cardiol.* 2001;**17**(9): 940–959.
50. Liberman, L., S. Kaufman, M. Alfayyadh, A.J. Hordof, and H.D. Apfel, Noninvasive prediction of pulmonary artery pressure in patients with isolated ventricular septal defect. *Pediatr. Cardiol.*, 2000;**21**(3): 197–201.
51. Cohle, S.D., E. Balraj, and M. Bell, Sudden death due to ventricular septal defect. *Pediatr. Dev. Pathol.*, 1999;**2**(4): 327–332.
52. Sarubbi, B., L.M. Gerlis, S.Y. Ho, and J. Somerville, Sudden death in an adult with a small ventricular septal defect and an aneurysmal membranous septum. *Cardiol. Young*, 1999;**9**(1): 99–103.
53. Byard, R.W., Ventricular septal defect and sudden death in early childhood. *J. Paediatr. Child Health*, 1994;**30**(5): 439–440.
54. Smith, N.M. and S.Y. Ho, Heart block and sudden death associated with fibrosis of the conduction system at the margin of a ventricular septal defect. *Pediatr. Cardiol.*, 1994;**15**(3): 139–142.
55. Fournier, A., M.L. Young, O.L. Garcia, D.F. Tamer, and G.S. Wolff, Electrophysiologic cardiac function before and after surgery in children with atrioventricular canal. *Am. J. Cardiol.*, 1986;**57**(13): 1137–1141.
56. Moller, J.H., C. Patton, R.L. Varco, and C.W. Lillehei, Late results (30 to 35 years) after operative closure of isolated ventricular septal defect from 1954 to 1960. *Am. J. Cardiol.*, 1991;**68**(15): 1491–1497.
57. Knauth, A.L., J.E. Lock, S.B. Perry, et al., Transcatheter device closure of congenital and postoperative residual ventricular septal defects. *Circulation*, 2004;**110**(5): 501–507.
58. Thanopoulos, B.D. and M.L. Rigby, Outcome of transcatheter closure of muscular ventricular septal defects with the Amplatzer ventricular septal defect occluder. *Heart*, 2005;**91**(4): 513–516.
59. Pedra, C.A., S.R. Pedra, C.A. Esteves, F. Chamie, L.A. Christiani, and V.F. Fontes, Transcatheter closure of perimembranous ventricular septal defects. *Expert Rev. Cardiovasc. Ther.*, 2004;**2**(2): 253–264.
60. Papadopoulos, C., Y.C. Lee, and L. Scherlis, Isolated ventricular septal defect. Electrocardiographic, vectorcardiographic and catheterization data. *Am. J. Cardiol.* 1965;**16**(3): 359–368.
61. Toscano-Barboza, E., and J.W. Dushane, Ventricular septal defect: correlation of electrocardiographic and hemodynamic findings in 60 proved cases. *Am. J. Cardiol.*, 1959;**3**(6): 721–732.
62. Riggs, T., S. Mehta, S. Hirschfeld, G. Borkat, and J. Liebman, Ventricular septal defect in infancy: a combined vectorgraphic and echocardiographic study. *Circulation*, 1979;**59**(2): 385–394.
63. Katz, L.N. and H. Wachtel, The diphasic QRS type of electrocardiogram in congenital heart disease. *Am. Heart J.*, 1937;**13**: 22.
64. Kidd, L., D.J. Driscoll, W.M. Gersony, et al., Second natural history study of congenital heart defects: results of treatment of patients with ventricular septal defects. *Circulation*, 1993;**87**(Suppl. 1): I-38–I-59.
65. Blake, S., E. Chung, H. Wesley, and K. Hallidie-Smith, Conduction defects, ventricular arrhythmias, and late death after

surgical closure of ventricular septal defect. *Br. Heart J.*, 1982;**47**: 305–315.
66. Cantor, W.J., D.A. Harrison, J.S. Moussadji, et al., Determinants of survival and length of survival in adults with Eisenmenger syndrome. *Am. J. Cardiol.*, 1999;**84**(6): 677–681.
67. Saha, A., K.G. Balakrishnan, P.K. Jaiswal, et al., Prognosis for patients with Eisenmenger syndrome of various aetiology. *Int. J. Cardiol.*, 1994;**45**(3): 199–207.
68. Vetter, V.L. and L.N. Horowitz, Electrophysiologic residua and sequelae of surgery for congenital heart defects. *Am. J. Cardiol.*, 1982;**50**(3): 588–604.
69. Daliento, L., G. Rizzoli, M.C. Marchiori, et al., Electrical instability in patients undergoing surgery for atrioventricular septal defect. *Int. J. Cardiol.*, 1991;**30**(1): 15–21.
70. McGrath, L.B. and L. Gonzalez-Lavin, Actuarial survival, freedom from reoperation, and other events after repair of atrioventricular septal defects. *J. Thorac. Cardiovasc. Surg.*, 1987;**94**(4): 582–590.
71. Culpepper, W., J. Kolff, C.Y. Lin, et al., Complete common atrioventricular canal in infancy – surgical repair and postoperative hemodynamics. *Circulation*, 1978;**58**(3): 550–558.
72. Rastelli, G.C., P.A. Ongley, J.W. Kirklin, and D.C. McGoon, Surgical repair of the complete form of persistent common atrioventricular canal. *J. Thorac. Cardiovasc. Surg.*, 1968;**55**(3): 299–308.
73. Jacobsen, J.R., P.C. Gillette, B.N. Corbett, M. Rabinovitch, and D.G. McNamara, Intracardiac electrography in endocardial cushion defects. *Circulation*, 1976;**54**(4): 599–603.
74. Boineau, J.P., E.N. Moore, and D.F. Patterson, Relationship between the ECG, ventricular activation, and the ventricular conduction system in ostium primum ASD. *Circulation*, 1973;**48**(3): 556–564.
75. Feldt, R.H., J.W. DuShane, and J.L. Titus, The atrioventricular conduction system in persistent common atrioventricular canal defect: correlations with electrocardiogram. *Circulation*, 1970;**42**(3): 437–444.
76. Durrer, D., J.P. Roos, and R.T. van Dam, The genesis of the electrocardiogram of patients with ostium primum defects (ventral atrial septal defects). *Am. Heart J.*, 1966;**71**(5): 642–650.
77. Coelho, E., S. Sequerra Amran, and E.S.A. Bordalo, Electrocardiogram and vectorcardiogram of ostium secundum and ostium primum. *Cardiologia*, 1960;**37**: 319–330.
78. Waldo, A.L., G.A. Kaiser, F.O. Bowman Jr., and J.R. Malm, Etiology of prolongation of the P-R interval in patients with an endocardial cushion defect. Further observations on internodal conduction and the polarity of the retrograde P wave. *Circulation*, 1973;**48**(1): 19–26.
79. Suzuki, K., Y. Murakami, K. Tatsuno, et al., Atypical form of atrioventricular septal defect without left axis deviation: relation between morphology and unusual QRS axis. *Br. Heart J.*, 1993;**70**(2): 180–184.
80. Cosh, J.A., Patent ductus arteriosus; a follow-up study of 73 cases. *Br. Heart J.*, 1957;**19**(1): 13–22.
81. Marquis, R.M., H.C. Miller, R.J. McCormack, M.B. Matthews, and A.H. Kitchin, Persistence of ductus arteriosus with left to right shunt in the older patient. *Br. Heart J.*, 1982;**48**(5): 469–484.
82. Mirowski, M., F. Arevalo, G.A. Medrano, and F.A. Cisneros, Conduction disturbances in patent ductus arteriosus. A study of 20 cases before and after surgery with determination of the P-R index. *Circulation*, 1962;**25**: 807–813.
83. Danilowicz, D., J.I. Hoffman, and A.M. Rudolph, Serial studies of pulmonary stenosis in infancy and childhood. *Br. Heart J.*, 1975;**37**(8): 808–818.
84. Rasmussen, K. and S.J. Sorland, Prediction of right ventricular systolic pressure in pulmonary stenosis from combined vectorcardiographic data. *Am. Heart J.*, 1973;**86**(3): 318–328.
85. Yahini, J.H., M.J. Dulfano, and M. Toor, Pulmonic stenosis. A clinical assessment of severity. *Am. J. Cardiol.*, 1960;**5**: 744–757.
86. Macruz, R., J.K. Perloff, and R.B. Case, A method for the electrocardiographic recognition of atrial enlargement. *Circulation*, 1958;**17**(5): 882–889.
87. Abrahams, D.G. and P. Wood, Pulmonary stenosis with normal aortic root. *Br. Heart J.*, 1951;**13**(4): 419–448.
88. Vriend, J.W. and B.J. Mulder, Late complications in patients after repair of aortic coarctation: implications for management. *Int. J. Cardiol.*, 2005;**101**(3): 399–406.
89. Toro-Salazar, O.H., J. Steinberger, W. Thomas, A.P. Rocchini, B. Carpenter, and J.H. Moller, Long-term follow-up of patients after coarctation of the aorta repair. *Am. J. Cardiol.*, 2002;**89**(5): 541–547.
90. Silka, M.J., B.G. Hardy, V.D. Menashe, and C.D. Morris. A population-based prospective evaluation of risk of sudden cardiac death after operation for common congenital heart defects. *J. Am. Coll. Cardiol.*, 1998;**32**(1): 245–251.
91. Gaum, W.E., T.C. Chou, and S. Kaplan, The vectorcardiogram and electrocardiogram in supravalvular aortic stenosis and coarctation of the aorta. *Am. Heart J.*, 1972;**84**(5): 620–628.
92. Glancy, D.L., A.G. Morrow, A.L. Simon, and W.C. Roberts, Juxtaductal aortic coarctation. Analysis of 84 patients studied hemodynamically, angiographically, and morphologically after age 1 year. *Am. J. Cardiol.*, 1983;**51**(3): 537–551.
93. Ho, S.Y., D. Goltz, K. McCarthy, et al., The atrioventricular junctions in Ebstein malformation. *Heart*, 2000;**83**(4): 444–449.
94. Smith, W.M., J.J. Gallagher, C.R. Kerr, et al., The electrophysiologic basis and management of symptomatic recurrent tachycardia in patients with Ebstein's anomaly of the tricuspid valve. *Am. J. Cardiol.*, 1982;**49**(5): 1223–1234.
95. Hebe, J., Ebstein's anomaly in adults. Arrhythmias: diagnosis and therapeutic approach. *Thorac. Cardiovasc. Surg.*, 2000;**48**(4): 214–219.
96. Attie, F., M. Rosas, M. Rijlaarsdam, et al., The adult patient with Ebstein anomaly. Outcome in 72 unoperated patients. *Medicine* (Baltimore), 2000;**79**(1): 27–36.
97. Celemajer, D., C. Bull, J. Till, et al., Ebstein's anomaly: presentation and outcome from fetus to adult. *J. Am. Coll. Cardiol.*, 1994;**23**: 170–176.
98. Gentles, T., A. Calder, P. Clarkson, and J. Neutze, Predictors of long-term survival with Ebstein's anomaly of the tricuspid valve. *Am. J. Cardiol.*, 1992;**69**: 377–381.
99. Hernandez, F.A., R. Rochkind, and H.R. Cooper, The intracavitary electrocardiogram in the diagnosis of Ebstein's anomaly. *Am. J. Cardiol.*, 1958;**1**(2): 181–190.
100. Van Lingen, B. and S.R. Bauersfeld, The electrocardiogram in Ebstein's anomaly of the tricuspid valve. *Am. Heart J.*, 1955;**50**(1): 13–23.
101. Macruz, R., J. Tranchesi, M. Ebaid, F. Pileggi, A. Romero, and L.V. Decourt, Ebstein's disease. Electrovectorcardiographic and radiologic correlations. *Am. J. Cardiol.*, 1968;**21**(5): 653–660.
102. Kastor, J.A., B.N. Goldreyer, M.E. Josephson, et al., Electrophysiologic characteristics of Ebstein's anomaly of the tricuspid valve. *Circulation*, 1975;**52**(6): 987–995.

103. Genton, E. and S.G. Blount Jr., The spectrum of Ebstein's anomaly. *Am. Heart. J.*, 1967;**73**(3): 395–425.
104. Tede, N.H., K. Shivkumar, J.K. Perloff, et al., Signal-averaged electrocardiogram in Ebstein's anomaly. *Am. J. Cardiol.*, 2004; **93**(4): 432–436.
105. Follath, F. and K.A. Hallidie-Smith, Unusual electrocardiographic changes in Ebstein's anomaly. *Br. Heart J.*, 1972;**34**(5): 513–519.
106. Schiebler, G.L., P. Adams Jr., R.C. Anderson, K. Amplatz, and R.G. Lester, Clinical study of twenty-three cases of Ebstein's anomaly of the tricuspid valve. *Circulation*, 1959;**19**(2): 165–187.
107. Bialostozky, D., G.A. Medrano, L. Munoz, and R. Contreras, Vectorcardiographic study and anatomic observations in 21 cases of Ebstein's malformation of the tricuspid valve. *Am. J. Cardiol.*, 1972;**30**(4): 354–361.
108. Kumar, A.E., D.C. Fyler, O.S. Miettinen, and A.S. Nadas, Ebstein's anomaly. Clinical profile and natural history. *Am. J. Cardiol.*, 1971;**28**(1): 84–95.
109. Brickner, M.E., L.D. Hillis, and R.A. Lange, Congenital heart disease in adults. Second of two parts. *N. Engl. J. Med.* 2000;**342**(5): 334–342.
110. Lillehei, C.W., M. Cohen, and H.E. Warden, Direct vision intracardiac surgical correction of the tetralogy of Fallot, pentalogy of Fallot, and pulmonary atresia defects: report of the first ten cases. *Ann. Surg.*, 1955;**142**: 418–445.
111. Li, W. and J. Somerville, Atrial flutter in grown-up congenital heart (GUCH) patients. Clinical characteristics of affected population. *Int. J. Cardiol.*, 2000;**75**(2–3): 129–137.
112. Gatzoulis, M.A., S. Balaji, S.A. Webber, et al., Risk factors for arrhythmia and sudden cardiac death late after repair of tetralogy of Fallot: a multicentre study. *Lancet*, 2000;**356**(9234): 975–981.
113. Delacretaz, E., L.I. Ganz, K. Soejima, et al., Multi atrial macro-re-entry circuits in adults with repaired congenital heart disease: entrainment mapping combined with three-dimensional electroanatomic mapping. *J. Am. Coll. Cardiol.*, 2001;**37**(6): 1665–1676.
114. Nakagawa, H., N. Shah, K. Matsudaira, et al., Characterization of reentrant circuit in macroreentrant right atrial tachycardia after surgical repair of congenital heart disease: isolated channels between scars allow "focal" ablation. *Circulation*, 2001;**103**(5): 699–709.
115. Triedman, J.K., M.E. Alexander, B.A. Love, et al., Influence of patient factors and ablative technologies on outcomes of radiofrequency ablation of intra-atrial re-entrant tachycardia in patients with congenital heart disease. *J. Am. Coll. Cardiol.*, 2002;**39**(11): 1827–1835.
116. Triedman, J.K., K.J. Jenkins, S.D. Colan, J.P. Saul, and E.P. Walsh, Intra-atrial reentrant tachycardia after palliation of congenital heart disease: characterization of multiple macroreentrant circuits using fluoroscopically based three-dimensional endocardial mapping. *J. Cardiovasc. Electrophysiol.*, 1997;**8**(3): 259–270.
117. Harrison, D.A., S.C. Siu, F. Hussain, C.J. MacLoghlin, G.D. Webb, and L. Harris, Sustained atrial arrhythmias in adults late after repair of tetralogy of fallot. *Am. J. Cardiol.*, 2001;**87**(5): 584–588.
118. Therrien, J., S.C. Siu, L. Harris, et al., Impact of pulmonary valve replacement on arrhythmia propensity late after repair of tetralogy of Fallot. *Circulation*, 2001;**103**(20): 2489–2494.
119. Gillette, P.C. and A. Garson Jr., Sudden cardiac death in the pediatric population. *Circulation*, 1992;**85**(Suppl. 1): 164–169.
120. Nollert, G., T. Fischlein, S. Bouterwek, C. Bohmer, W. Klinner, and B. Reichart, Long-term survival in patients with repair of tetralogy of Fallot: 36-year follow-up of 490 survivors of the first year after surgical repair. *J. Am. Coll. Cardiol.*, 1997;**30**(5): 1374–1383.
121. Jonsson, H., T. Ivert, L.A. Brodin, and R. Jonasson, Late sudden deaths after repair of tetralogy of Fallot. Electrocardiographic findings associated with survival. *Scand. J. Thorac. Cardiovasc. Surg.*, 1995;**29**(3): 131–139.
122. Bricker, J.T., Sudden death and tetralogy of Fallot. Risks, markers, and causes. *Circulation*, 1995;**92**(2): 158–159.
123. Roberts, D.L., H.R. Wagner, and E.C. Lambert, The electrocardiogram in tetralogy of Fallot. *J. Electrocardiol.*, 1972;**5**(2): 155–161.
124. Feldt, R.H., J.W. DuShane, and J.L. Titus, The anatomy of the atrioventricular conduction system in ventricular septal defect and tetralogy of fallot: correlations with the electrocardiogram and vectorcardiogram. *Circulation*, 1966;**34**(5): 774–782.
125. Landtman, B. and M.D. Wolf, Total correction of tetralogy of Fallot: II. Changes in the electrocardiogram following surgery. *Circulation*, 1965;**31**: 394–402.
126. Mirowski, M., A. Mehrizi, and H.B. Taussig, The electrocardiogram in patients with both great vessels arising from the right ventricle combined with pulmonary stenosis. An analysis of 22 cases with special reference to the differential diagnosis from the tetralogy of Fallot. *Circulation*, 1963;**28**: 1116–1127.
127. Depasquale, N.P. and G.E. Burch, The electrocardiogram, vectorcardiogram, and ventricular gradient in the tetralogy of Fallot. *Circulation*, 1961;**24**: 94–109.
128. Pileggi, F., J. Bocanegra, J. Tranchesi, et al., The electrocardiogram in tetralogy of Fallot: a study of 142 cases. *Am. Heart J.*, 1960;**59**: 667–680.
129. Gardberg, M. and I.L. Rosen, The electrocardiogram and vectorcardiogram in right ventricular hypertrophy and right bundle branch block. *Dis. Chest.*, 1959;**36**: 407–422.
130. Milnor, W.R. Electrocardiogram and vectorcardiogram in right ventricular hypertrophy and right bundle-branch block. *Circulation*, 1957;**16**(3): 348–367.
131. DiSciascio, G. and L.M. Bargeron Jr., The electrocardiogram in tetralogy of Fallot with complete atrioventricular canal. *Tex. Heart Inst. J.*, 1982;**9**(2): 163–167.
132. Norgard, G., M.A. Gatzoulis, F. Moraes, et al., Relationship between type of outflow tract repair and postoperative right ventricular diastolic physiology in tetralogy of Fallot: implications for long-term outcome. *Circulation*, 1996;**94**(12): 3276–3280.
133. Gatzoulis, M.A., J.A. Till, J. Somerville, and A.N. Redington, Mechanoelectrical interaction in tetralogy of Fallot. QRS prolongation relates to right ventricular size and predicts malignant ventricular arrhythmias and sudden death. *Circulation*, 1995;**92**(2): 231–237.
134. Till, J.A., M.A. Gatzoulis, J.E. Deanfield, J. Somerville, W. Gregory, and A.N. Redington, Evolution of QRS prolongation following repair of tetralogy of Fallot: implications for symptomatic arrhythmia and sudden death. *Circulation*, 1995;**92** (Suppl.): 1707.
135. Harrison, D.A., L. Harris, S.C. Siu, et al., Sustained ventricular tachycardia in adult patients late after repair of tetralogy of Fallot. *J. Am. Coll. Cardiol.*, 1997;**30**(5): 1368–1373.
136. Garson, A. Jr., M.R. Nihill, D.G. McNamara, and D.A. Cooley, Status of the adult and adolescent after repair of tetralogy of Fallot. *Circulation*, 1979;**59**: 1232–1240.

137. Katz, N.M., E.H. Blackstone, J.W. Kirklin, and A.D. Pacifico, Late survival and symptoms after repair of tetralogy of Fallot. *Circulation*, 1982;**65**: 403–410.
138. Hokanson, J.S. and J.H. Moller, Significance of early transient complete heart block as a predictor of sudden death late after operative correction of tetralogy of Fallot. *Am. J. Cardiol.*, 2001;**87**(11): 1271–1277.
139. Berul, C.I., S.L. Hill, R.L. Geggel, et al., Electrocardiographic markers of late sudden death risk in postoperative tetralogy of Fallot children. *J. Cardiovasc. Electrophysiol.*, 1997;**8**(12): 1349–1356.
140. Vogel, M., J. Sponring, S. Cullen, J.E. Deanfield, and A.N. Redington, Regional wall motion and abnormalities of electrical depolarization and repolarization in patients after surgical repair of tetralogy of Fallot. *Circulation*, 2001;**103**(12): 1669–1673.
141. Khairy, P., M.J. Landzberg, M.A. Gatzoulis, et al., Value of programmed ventricular stimulation after tetralogy of Fallot repair: a multicenter study. *Circulation*, 2004;**109**(16): 1994–2000.
142. Huhta, J.C., J.D. Maloney, D.G. Ritter, D.M. Ilstrup, and R.H. Feldt, Complete atrioventricular block in patients with atrioventricular discordance. *Circulation*, 1983;**67**(6): 1374–1377.
143. Daliento, L., D. Corrado, G. Buja, N. John, A. Nava, and G. Thiene, Rhythm and conduction disturbances in isolated, congenitally corrected transposition of the great arteries. *Am. J. Cardiol.*, 1986;**58**(3): 314–318.
144. Gillette, P.C., U. Busch, C.E. Mullins, and D.G. McNamara, Electrophysiologic studies in patients with ventricular inversion and "corrected transposition". *Circulation*, 1979;**60**(4): 939–945.
145. Amikam, S., J. Lemer, Y. Kishon, E. Riss, and H.N. Neufeld, Complete heart block in an adult with corrected transposition of the great arteries treated with permanent pacemaker. *Thorax*, 1979;**34**(4): 547–549.
146. Foster, J.R., A.N. Damato, L.E. Kline, M. Akhtar, and J.N. Ruskin, Congenitally corrected transposition of the great vessels: localization of the site of complete atrioventricular block using his bundle electrograms. *Am. J. Cardiol.*, 1976;**38**(3): 383–387.
147. Rosen, K.M., H.S. Loeb, R.M. Gunnar, and S.H. Rahimtoola, Mobitz type II block without bundle-branch block. *Circulation*, 1971;**44**(6): 1111–1119.
148. de Leval, M.R., P. Bastos, J. Stark, J.F. Taylor, F.J. Macartney, and R.H. Anderson, Surgical technique to reduce the risks of heart block following closure of ventricular septal defect in atrioventricular discordance. *J. Thorac. Cardiovasc. Surg.*, 1979;**78**(4): 515–526.
149. McGrath, L.B., J.W. Kirklin, E.H. Blackstone, A.D. Pacifico, J.K. Kirklin, and L.M. Bargeron, Jr., Death and other events after cardiac repair in discordant atrioventricular connection. *J. Thorac. Cardiovasc. Surg.*, 1985;**90**(5): 711–728.
150. Hwang, B., F. Bowman, J. Malm, and E. Krongrad, Surgical repair of congenitally corrected transposition of the great arteries: results and follow-up. *Am. J. Cardiol.*, 1982;**50**(4): 781–785.
151. Victorica, B.E., B.L. Miller, and I.H. Gessner, Electrocardiogram and vectorcardiogram in ventricular inversion (corrected transposition). *Am. Heart J.*, 1973;**86**(6): 733–744.
152. Okamura, K., A. Takao, A. Hashimoto, S. Hosoda, and K. Mimori, Electrocardiogram in corrected transposition of the great arteries with and without associated cardiac anomalies. *J. Electrocardiol.*, 1973;**6**(1): 3–10.
153. Fernandez, F., J. Laurichesse, L. Scebat, and L. Lenegre, Electrocardiogram in corrected transposition of the great vessels of the bulbo-ventricular inversion type. *Br. Heart J.*, 1970;**32**(2): 165–171.
154. Namin, E.P., R.A. Arcilla, and B.M. Gasul, The vectorcardiogram and electrocardiogram in corrected transposition of the great vessels. *Dis. Chest.*, 1963;**44**: 313–314.
155. Bokeriia, L.A., A. Revishvili, and M.M. Makhmudov, Syndrome of ventricular preexcitation and corrected transposition of the great vessels with insufficiency of the arterial atrioventricular valve of the Ebstein anomaly type. *Kardiologiia*, 1984;**24**(12): 94–95.
156. Rogers, J.H. Jr. and P.S. Rao, Ebstein's anomaly of the left atrioventricular valve with congenital corrected transposition of the great arteries. Diagnosis by intracavitary electrocardiography. *Chest*, 1977;**72**(2): 253–256.
157. Brugada, J., V. Valls, R. Freixa, et al., Radiofrequency ablation of a posteroseptal atrioventricular accessory pathway in a left-sided tricuspid ring with Ebsteinlike anomaly in a patient with congenitally corrected transposition of the great arteries. *Pacing Clin. Electrophysiol.*, 2000;**23**(1): 133–136.
158. Keller, N. and M.R. Soorensen, Corrected transposition of the great arteries with a left-sided Ebstein-like anomaly and WPW-syndrome. A case diagnosed by two-dimensional echocardiography. *Ugeskr Laeger*, 1981;**143**(31): 1971–1972.
159. Senning, A., Surgical correction of transposition of the great vessels. *Surgery*, 1959;**45**: 966–980.
160. Mustard, W.T., Successful two stage correction of transposition of the great vessels. *Surgery*, 1964;**55**: 469–472.
161. Jatene, A.D., V.F. Fontes, P.P. Paulista, et al., Anatomic correction of transposition of the great vessels. *J. Thorac. Cardiovasc. Surg.*, 1976;**72**(3): 364–370.
162. Wilson, N.J., P.M. Clarkson, B.G. Barratt-Boyes, et al., Long-term outcome after the mustard repair for simple transposition of the great arteries. 28-year follow-up. *J. Am. Coll. Cardiol.*, 1998;**32**(3): 758–765.
163. Janousek, J., T. Paul, I. Luhmer, M. Wilken, J. Hruda, H.C. Kallfelz, Atrial baffle procedures for complete transposition of the great arteries: natural course of sinus node dysfunction and risk factors for dysrhythmias and sudden death. *Z. Kardiol.*, 1994;**83**(12): 933–938.
164. Gatzoulis, M.A., J. Walters, P.R. McLaughlin, N. Merchant, G.D. Webb, and P. Liu, Late arrhythmia in adults with the mustard procedure for transposition of great arteries: a surrogate marker for right ventricular dysfunction? *Heart*, 2000;**84**(4): 409–415.
165. Gelatt, M., R.M. Hamilton, B.W. McCrindle, et al., Arrhythmia and mortality after the Mustard procedure: a 30-year single-center experience. *J. Am. Coll. Cardiol.*, 1997;**29**(1): 194–201.
166. Stark, J., M.J. Tynan, K.W. Ashcraft, E. Aberdeen, and D.J. Waterston, Obstruction of pulmonary veins and superior vena cava after the Mustard operation for transposition of the great arteries. *Circulation*, 1972;**45**(Suppl. 1): 1116–1120.
167. Benatar, A., R. Tanke, M. Roef, E.J. Meyboom, and H.J. Van de Wal, Mid-term results of the modified Senning operation for cavopulmonary connection with autologous tissue. *Eur. J. Cardiothorac. Surg.*, 1995;**9**(6): 320–324.
168. Kirjavainen, M., J.M. Happonen, and I. Louhimo, Late results of Senning operation. *J. Thorac. Cardiovasc. Surg.*, 1999;**117**(3): 488–495.

169. Khairy, P., M.J. Landzberg, J. Lambert, and C.P. O'Donnell, Long-term outcomes after the atrial switch for surgical correction of transposition: a meta-analysis comparing the Mustard and Senning procedures. *Cardiol. Young.*, 2004;**14**(3): 284–292.
170. Puley, G., S. Siu, M. Connelly, et al., Arrhythmia and survival in patients > 18 years of age after the mustard procedure for complete transposition of the great arteries. *Am. J. Cardiol.*, 1999;**83**(7): 1080–1084.
171. Li, W., J. Somerville, D.G. Gibson, and M.Y. Henein, Disturbed atrioventricular electromechanical function long after Mustard operation for transposition of great arteries: a potential contributing factor to atrial flutter. *J. Am. Soc. Echocardiogr.*, 2001;**14**(11): 1088–1093.
172. Sarkar, D., C. Bull, R. Yates, et al., Comparison of long-term outcomes of atrial repair of simple transposition with implications for a late arterial switch strategy. *Circulation*, 1999;**100**(Suppl. 19): II176–II181.
173. Kammeraad, J.A., C.H. van Deurzen, N. Sreeram, et al., Predictors of sudden cardiac death after Mustard or Senning repair for transposition of the great arteries. *J. Am. Coll. Cardiol.*, 2004;**44**(5): 1095.
174. Khoury, G.H., R.M. Shaher, R.S. Fowler, and J.D. Keith, Preoperative and postoperative electrocardiogram in complete transposition of the great vessels. *Am. Heart J.*, 1966;**72**(2): 199–205.
175. Shaher, R.M. and D.C. Deuchar, The electrocardiogram in complete transposition of the great vessels. *Br. Heart J.*, 1966;**28**(2): 265–275.
176. Bharati, S. and M. Lev, The conduction system in simple, regular (D-), complete transposition with ventricular septal defect. *J. Thorac. Cardiovasc. Surg.*, 1976;**72**(2): 194–201.
177. Fontan, F. and E. Baudet, Surgical repair of tricuspid atresia. *Thorax*, 1971;**26**(3): 240–258.
178. Gatzoulis, M.A., M.D. Munk, W.G. Williams, and G.D. Webb, Definitive palliation with cavopulmonary or aortopulmonary shunts for adults with single ventricle physiology. *Heart*, 2000;**83**(1): 51–57.
179. Love, B.A., K.K. Collins, E.P. Walsh, and J.K. Triedman, Electroanatomic characterization of conduction barriers in sinus/atrially paced rhythm and association with intra-atrial reentrant tachycardia circuits following congenital heart disease surgery. *J. Cardiovasc. Electrophysiol.*, 2001;**12**(1): 17–25.
180. Triedman, J.K., M.E. Alexander, C.I. Berul, L.M. Bevilacqua, and E.P. Walsh, Electroanatomic mapping of entrained and exit zones in patients with repaired congenital heart disease and intra-atrial reentrant tachycardia. *Circulation*, 2001;**103**(16): 2060–2065.
181. Setty, S.P., K. Finucane, J.R. Skinner, and A.R. Kerr, Extracardiac conduit with a limited maze procedure for the failing Fontan with atrial tachycardias. *Ann. Thorac. Surg.*, 2002;**74**(6): 1992–1997.
182. Petko, M., R.J. Myung, G. Wernovsky, et al., Surgical reinterventions following the Fontan procedure. *Eur. J. Cardiothorac. Surg.*, 2003;**24**(2): 255–259.
183. Agnoletti, G., A. Borghi, G. Vignati, and G.C. Crupi, Fontan conversion to total cavopulmonary connection and arrhythmia ablation: clinical and functional results. *Heart*, 2003;**89**(2): 193–198.
184. Mavroudis, C., C.L. Backer, B.J. Deal, C. Johnsrude, and J. Strasburger, Total cavopulmonary conversion and maze procedure for patients with failure of the Fontan operation, *J. Thorac. Cardiovasc. Surg.*, 2001;**122**(5): 863–871.
185. Mavroudis, C., B.J. Deal, and C.L. Backer, The beneficial effects of total cavopulmonary conversion and arrhythmia surgery for the failed Fontan. *Semin. Thorac. Cardiovasc. Surg. Pediatr. Card. Surg. Annu.*, 2002;**5**: 12–24.
186. Nurnberg, J.H., S. Ovroutski, V. Alexi-Meskishvili, P. Ewert, R. Hetzer, and P.E. Lange, New onset arrhythmias after the extracardiac conduit Fontan operation compared with the intraatrial lateral tunnel procedure: early and midterm results. *Ann. Thorac. Surg.*, 2004;**78**(6): 1979–1988.
187. Kumar, S.P., C.S. Rubinstein, J.M. Simsic, A.B. Taylor, J.P. Saul, and S.M. Bradley, Lateral tunnel versus extracardiac conduit Fontan procedure: a concurrent comparison. *Ann. Thorac. Surg.*, 2003;**76**(5): 1389–1396.
188. Cohen, M.I., G. Wernovsky, V.L. Vetter, et al., Sinus node function after a systematically staged Fontan procedure. *Circulation*, 1998;**98**(Suppl. 19): II352–II358.
189. Manning, P.B., J.E. Mayer Jr., G. Wernovsky, S.B. Fishberger, and E.P. Walsh, Staged operation to Fontan increases the incidence of sinoatrial node dysfunction. *J. Thorac. Cardiovasc. Surg.*, 1996;**111**(4): 833–839.
190. Chan, D.P., D.A. Bartmus, W.D. Edwards, and C.B. Porter, Histopathologic abnormalities of the sinus node compared with electrocardiographic evidence of sinus node dysfunction after the modified Fontan operation: an autopsy study of 14 cases. *Tex. Heart Inst. J.*, 1992;**19**(4): 278–283.
191. Davachi, F., R.V. Lucas Jr., and J.H. Moller, The electrocardiogram and vectorcardiogram in tricuspid atresia. Correlation with pathologic anatomy. *Am. J. Cardiol.*, 1970;**25**(1): 18–27.
192. Gamboa, R., W.M. Gersony, and A.S. Nadas, The electrocardiogram in tricuspid atresia and pulmonary atresia with intact ventricular septum. *Circulation*, 1966;**34**(1): 24–37.
193. Neill, C.A. and A.J. Brink, Left axis deviation in tricuspid atresia and single ventricle; the electrocardiogram in 36 autopsied cases. *Circulation*, 1955;**12**(4): 612–619.
194. Kroop, I.G. and A. Grishman, The variability of the electrocardiogram in congenital tricuspid atresia. *J. Pediatr.*, 1950;**37**(2): 231–237.
195. Davachi, F. and J.H. Moller, The electrocardiogram and vectorcardiogram in single ventricle. Anatomic correlations. *Am. J. Cardiol.*, 1969;**23**(1): 19–31.
196. Shaher, R.M., The electrocardiogram in single ventricle. *Br. Heart J.*, 1963;**25**: 465–473.
197. Elliott, L.P., H.D. Ruttenberg, R.S. Eliot, and R.C. Anderson, Vectorial analysis of the electrocardiogram in common ventricle. *Br. Heart J.*, 1964;**26**: 302–311.
198. Shinebourne, E.A., K.C. Lau, G. Calcaterra, and R.H. Anderson, Univentricular heart of right ventricular type: clinical, angiographic and electocardiographic features. *Am. J. Cardiol.*, 1980;**46**(3): 439–445.
199. Momma, K. and L.M. Linde, Cardiac rhythms in dextrocardia. *Am. J. Cardiol.*, 1970;**25**(4): 420–427.
200. Campbell, M. and D.C. Deuchar, Dextrocardia and isolated laevocardia. II. Situs inversus and isolated dextrocardia. *Br. Heart J.*, 1966;**28**(4): 472–487.
201. Mirowski, M., C.A. Neill, H.T. Bahnson, and H.B. Taussig, Negative P waves in lead I in dextroversion: differential diagnosis from mirror-image dextrocardia, with a report of a successful

closure of a ventricular septal defect in a patient with dextroversion associated with agenesis of the right lung. *Circulation*, 1962;**26**: 413–420.
202. Campbell, M. and G. Reynolds, The significance of the direction of the P wave in dextrocardia and isolated laevocardia. *Br. Heart J.*, 1952;**14**(4): 481–488.
203. Click, R., D. Holmes, R. Vlietstra, A. Kosinski, and R. Kronmal, Anomalous coronary arteries: location, degree of atherosclerosis and effect on survival-a report from the Coranary Artery Surgery Study. *J. Am. Coll. Cardiol.*, 1989;**13**(3): 531–537.
204. Haravon, A., M. Franklin, and M.J. Krauthamer, Congenital coronary artery to left ventricle fistula with angina pectoris. Coronary steal syndrome? *N. Y. State. J. Med.*, 1972;**72**(17): 2196–2200.
205. Moro-Serrano, C., J. Martinez, A.H. Madrid, et al., Ventricular tachycardia in a patient with congenital coronary arteriovenous fistula. *Am. Heart J.*, 1992;**124**(2): 503–505.
206. McNamara, J.J. and R.E. Gross, Congenital coronary artery fistula. *Surgery*, 1969;**65**(1): 59–69.
207. Wilson, C., P. Dlabal, R. Holeyfield, C. Akins, and D. Knauf, Anomalous origin of left coronary artery from pulmonary artery: case reports and review of literature concerning teenagers and adults. *J. Thorac. Cardiovasc. Surg.*, 1977;**73**(6): 887–893.
208. Perry, L.W. and L.P. Scott, Anomalous left coronary artery from pulmonary artery: report of 11 cases; review of indications for and results of surgery. *Circulation*, 1970;**41**(6): 1043–1052.
209. Flaherty, J.T., M.S. Spach, J.P. Boineau, R.V. Canent, Jr., R.C. Barr, and D.C. Sabiston Jr., Cardiac potentials on body surface of infants with anomalous left coronary artery (myocardial infarction). *Circulation*, 1967;**36**(3): 345–358.
210. Vanderhauwaert, L.G., G.L. Stalpaert, and L. Verhaeghe, Anomalous origin of the left coronary artery from the pulmonary artery; a therapeutic problem. *Am. Heart. J.*, 1965;**69**: 538–543.
211. Burch, G.E. and Depasquale N.P., The anomalous left coronary artery: an experiment of nature. *Am. J. Med.*, 1964;**37**: 159–161.
212. Rudolph, A.M., N.L. Gootman, N. Kaplan, and M. Rohman, Anomalous left coronary artery arising from the pulmonary artery with large left-to-right shunt in infancy. *J. Pediatr.*, 1963;**63**: 543–549.
213. Cumming, G.R. and C.C. Ferguson, Anomalous origin of the left coronary artery from the pulmonary artery, functioning as a coronary arteriovenous fistula. *Am. Heart J.*, 1962;**64**: 690–695.
214. Keith, J.D., The anomalous origin of the left coronary artery from the pulmonary artery. *Br. Heart J.*, 1959;**21**(2): 149–161.

Section 6

Cardiac Arrhythmias

23 Cellular Electrophysiological and Genetic Mechanisms of Cardiac Arrhythmias

Andrew L. Wit · Michael R. Rosen

P. W. Macfarlane, A. van Oosterom, O. Pahlm, P. Kligfield, M. Janse, J. Camm (eds.), *Comprehensive Electrocardiology*, DOI 10.1007/978-1-84882-046-3_23,

23.1 Introduction

Cardiac arrhythmias result from abnormalities in the rate, regularity or site of origin of the cardiac impulse or disturbance in the conduction of that impulse such that the normal sequence of activation of atria and ventricles is altered [1]. Thus, arrhythmias result from abnormalities in the initiation of impulses or in conduction of these impulses through the heart [2, 3]. Such alterations in impulse initiation or conduction are readily apparent in recordings of extracellular signals from the heart, in the form of either the electrocardiogram or more direct electrographic recordings from the atria and ventricles. However, the recording of the transmembrane electrical events of the individual myocardial cells with microelectrodes has provided the information necessary for understanding the mechanisms that are responsible for the arrhythmias. The importance of this approach was recognized in the 1960s by Hoffman and Cranefield [2]. Although arrhythmias may have many different pathological causes, in the final analysis all arrhythmias are the consequence of critical alterations in the cellular electrophysiology. How these changes in cellular electrophysiology occur, what they are, and how they cause arrhythmias are the subject of this chapter.

Much of the discussion is focused on abnormalities in the membrane currents that flow across the sarcolemma and that determine the transmembrane resting and action potential. The reader is therefore advised to consult ❯ Chap. 3, which describes the normal properties of the membrane channels and currents, before reading this chapter.

23.2 Arrhythmias Caused by Abnormal Impulse Initiation

The term "impulse initiation" is used to indicate that an electrical impulse can arise in a single cell or group of closely coupled cells through depolarization of the cell membrane, and once initiated, spread through the rest of the heart (impulse conduction). Impulse initiation occurs because of localized changes in the ionic currents, which flow across the membranes of individual cells. There are two major causes for the impulse initiation that may result in arrhythmias: automaticity and triggered activity. Each has its own unique cellular mechanisms resulting in membrane depolarization. Automaticity is the result of spontaneous (diastolic) phase 4 depolarization (see ❯ Fig. 23.1) that can occur *de novo*, whereas triggered activity is caused by afterdepolarizations, which require a preceding action potential for their induction. These different cellular mechanisms result in arrhythmias that have very different characteristics in their mode of onset, their rate, and their response to interventions such as external pacemakers and drugs.

23.2.1 Automaticity

It is convenient to subdivide automaticity into two categories, normal and abnormal. Normal automaticity is found in the primary pacemaker of the heart –the sinus node – as well as certain subsidiary or latent pacemakers which can become the pacemaker if the function of the sinus node is compromised. Impulse initiation is a normal function of these latent pacemakers. Abnormal automaticity, whether the result of experimental interventions or pathology, only occurs in cardiac cells when major changes occur in their transmembrane potentials. This property is not confined to any specific latent pacemaker but may occur anywhere in the heart. Arrhythmias characterized by abnormalities in the rate, regularity or site of origin of the cardiac impulse can result from either normal or abnormal automaticity.

23.2.1.1 Normal Automaticity

The cause of normal automaticity in the sinus node is a spontaneous decline in the transmembrane potential during diastole, referred to as phase 4 or diastolic depolarization (❯ Fig. 23.1). When the depolarization reaches threshold potential, a spontaneous action potential (impulse) is initiated. The fall in membrane potential during phase 4 reflects a gradual shift in the balance between inward and outward membrane currents in the direction of the net inward (depolarizing) current.

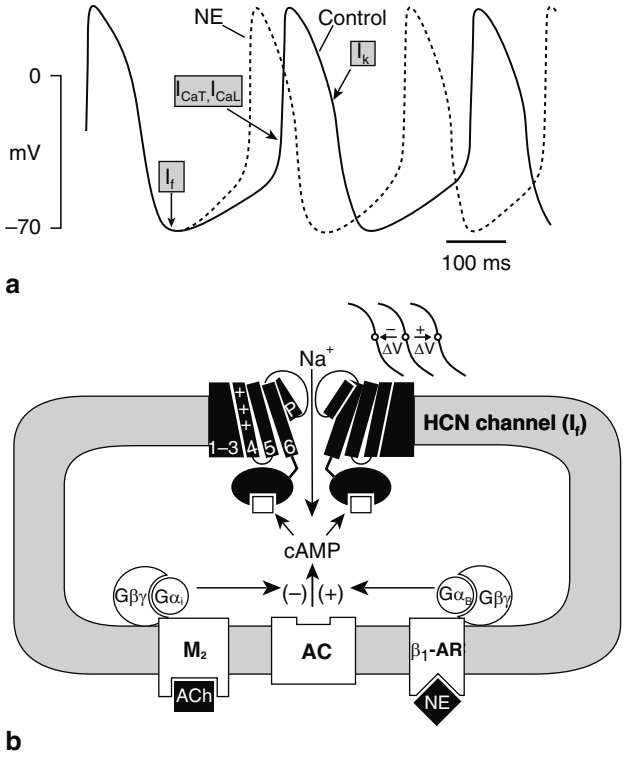

Figure 23.1

***Panel A*: Representation of sinoatrial node action potential (Control: solid lines) and some of the ion channels that contribute to it. I_f is activated on hyperpolarization and provides inward current during phase 4. T- and L-type Ca currents are initiated towards the end of phase 4: the latter also contributes the major current to the upstroke of the action potential. Delayed rectifier current (I_K) is responsible for repolarization. The acceleratory effects of norepinephrine (NE) are shown as broken lines. Note the prominent increase in phase 4, reflecting the actions of NE on I_f. *Panel B*: Cartoon of the pacemaker channel. There are six transmembrane spanning domains: when the channel in the open position, Na is the major ion transmitted. Cyclic AMP binding sites are present near the amino terminus. Also depicted are β_1-adrenergic (B1-AR) and M2-muscarinic receptors, providing, respectively, norepinephrine and acetylcholine binding sites. Via G-protein coupling these regulate adenylyl cyclase (AC) activity which in turn regulates intracellular cAMP levels, determining availability of the second messenger for binding and for channel modulation (Reproduced with permission from Biel et al. (2002)).**

The specific properties of the pacemaker current which causes phase 4 depolarization have been studied with voltage-clamp techniques. These investigations have shown that diastolic depolarization results from the initiation on of an inward current, I_f, that is activated after repolarization of the action potential is complete [4, 5]. As shown in Fig. 23.1 several currents contribute to phase 4 depolarization and to the sinus node action potential, but the process is initiated by the pacemaker current I_f [5]. The channel carrying I_f, which is an inward sodium current, activates as the membrane hyperpolarizes. For this reason, it was designated "funny current" or I_f [4, 5]. The cartoon in Fig. 23.1 also depicts the α subunit of the HCN (hyperpolarization-activated, cyclic nucleotide gated) channel that carries I_f [5]. HCN has four isoforms, designated as HCN1–4. The predominant isoform in sinus node is HCN4 and in ventricle, HCN2. HCN3 is not found in heart. A cyclic-AMP binding site on the HCN channel permits catecholamines to modulate activation. It is largely this property that regulates the autonomic responsiveness of the cardiac pacemaker. Figure 23.1 also demonstrates that other channels contribute to the voltage-time course of the pacemaker potential, including inward calcium current [6] and outward potassium current.

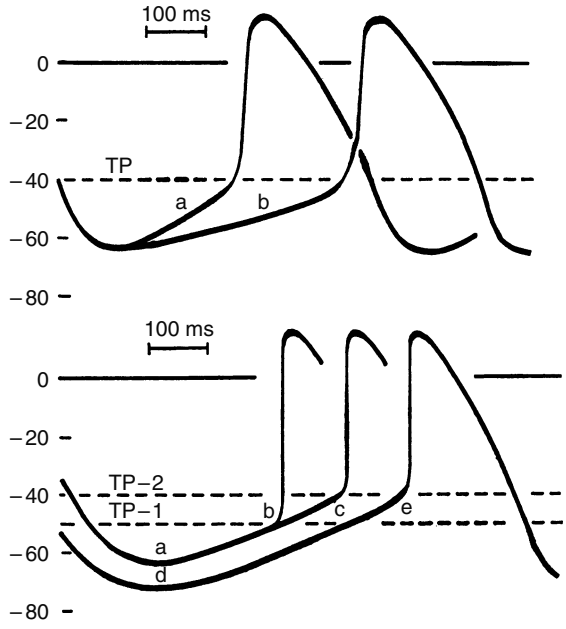

Figure 23.2

Transmembrane action potential recorded from a sinus node fiber showing the mechanism responsible for impulse initiation and its change in frequency. In the upper diagram, trace "a" shows phase 4 depolarization (normal automaticity) that carries membrane potential to the threshold potential TP, after which action potential upstroke occurs. Trace "b" shows how a decrease in the slope or rate of phase 4 depolarization increases the time required for the transmembrane potential to reach threshold, and thereby slows the rate. The lower diagram shows how changes in maximum diastolic potential or threshold potential affects rate when the slope of phase 4 depolarization remains unchanged. Changing threshold potential from TP-1 to TP-2 increases the time required for phase 4 depolarization to bring membrane potential to the TP (trace "b" to "c") and slows the rate. Increasing maximum diastolic potential from "a" to "d" has a similar effect (Reproduced with permission after Hoffman and Cranefield (1960) © McGraw Hill, New York).

The intrinsic rate at which sinus node pacemaker cells initiate impulses is determined by three factors:

(a) The maximum diastolic potential which is maintained by the outward potassium current, I_{k1} and the Na/K pump:
(b) The threshold potential, at which the action potential upstroke is initiated; and
(c) The rate or slope of phase 4 depolarization (Fig. 23.2), which is determined by the properties of the pacemaker current [7].

A change in any one of these three factors will alter the time required for phase 4 depolarization to carry the membrane potential from its maximum diastolic level to threshold, and thereby alter the rate of impulse initiation. For example, if the maximum diastolic potential increases (becomes more negative), as may be induced by vagal nerve stimulation, spontaneous depolarization to threshold potential will take longer and the rate of impulse initiation will fall. Conversely, a decrease in the maximum diastolic potential will tend to increase the rate of impulse initiation. Similarly, changes in threshold potential or changes in the slope of phase 4 depolarization will alter the rate of impulse initiation (Fig. 23.2) [7]. Such alterations in the rate of impulse initiation in the sinus node may lead to arrhythmias as discussed below.

In addition to the sinus node, normal cardiac cells with pacemaking capability are located in parts of the atria (plateau fibers along the crista terminalis and interatrial septum [8]), in the atrioventricular (AV) junctional region [9–11] and in the His-Purkinje system [7]. Yet, there is a hierarchy of a pacemaker activities in the heart such that the sinus nodes initiate

impulses most rapidly and the distal Purkinje system most slowly [12–14]. The membrane currents causing spontaneous diastolic depolarization at ectopic sites have been studied most thoroughly in Purkinje fibers also, using voltage-clamp techniques [15, 16]. We can best understand the hierarchy of pacemaker function by contrasting pacemaker current (I_f) and the sinus node and in the ventricles. We stress that I_f is present throughout the heart, although it activates at the most positive potentials in sinus node while in myocardium it activates at levels negative to the physiologic range of membrane potentials(N-150 mL). These differences in activation are in part determined by HCN isoforms (HCN_4 predominates in sinus node, HCN_2 in ventricle and in part by other properties. For example in the neonatal ventricle activation is more positive than in adult, and a shift to more negative activation voltages occurs with growth and development [17].

In the normal heart, the intrinsic rate of impulse initiation by the sinus node is higher than that of other potentially automatic cells. Hence, latent pacemakers are excited by impulses propagated from the sinus node before they can depolarize spontaneously to threshold potential. Not only are latent pacemakers prevented from initiating an impulse because they are depolarized before they have a chance to fire, but also the diastolic (phase 4) depolarization of the latent pacemaker cells is actually inhibited because they are repeatedly depolarized by the impulses from the sinus node [12, 18]. This inhibition can be demonstrated easily by suddenly stopping the sinus by, for example, vagal stimulation. Impulses then usually arise from a subsidiary pacemaker, but that impulse initiation is generally preceded by a long period of quiescence [19]. Impulse initiation by subsidiary pacemakers begins at a low rate and only gradually speeds up to a final steady rate which is, however, still slower than the rate of the original sinus rhythm.

The quiescent period following termination of the sinus rhythm reflects the inhibitory influence exerted on the subsidiary pacemaker by the dominant sinus node pacemaker. This inhibition is called overdrive suppression. Overdrive suppression has been best characterized in microelectrode studies on isolated Purkinje fiber bundles exhibiting pacemaker activity (Fig. 23.3) [18]; it is the result of driving a pacemaker cell faster than its intrinsic spontaneous rate and is mediated by enhanced activity of the Na^+ K^+ exchange pump. During normal sinus rhythm, the sinus node drives the latent pacemakers at a faster rate than their normal automatic rate. As a result, the intracellular sodium concentration of the latent pacemakers is increased to a higher steady-state level than would be the case were the pacemaker firing at its own intrinsic rate. This is the result of sodium ions entering the cell during each action-potential upstroke. The rate of activity of the sodium pump is largely determined by the intracellular sodium concentration [20], so that pump activity is enhanced during high rates of stimulation [18]. Since the sodium pump usually moves more Na^+ outward than K^+

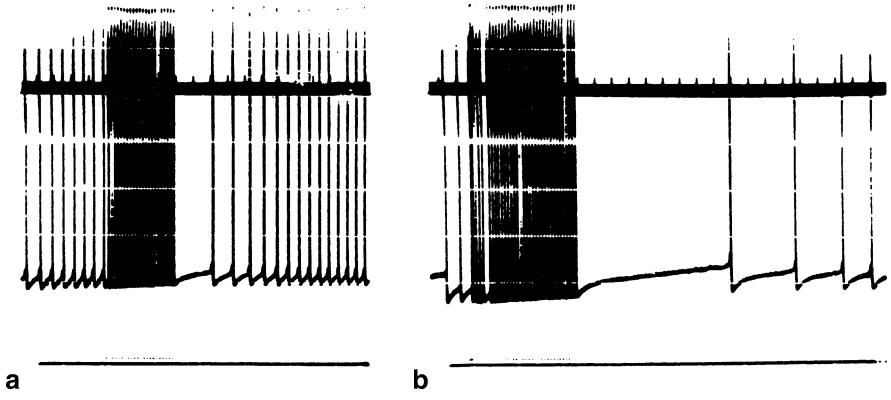

Figure 23.3

Overdrive suppression of normal automaticity in a Purkinje fiber. The first eight action potentials in (a) occur spontaneously at the intrinsic firing rate of the Purkinje fiber. Note the phase 4 depolarization preceding the upstroke or the action potential. A period of rapid stimulation is then imposed for 25 s at the end of which there is a short quiescent period followed by the reappearance of the spontaneous rhythm with gradually increases to the control rate. In (b) a longer period of overdrive is followed by prolonged quiescence and a far slower rate than the control rate. Stimulus pulses are shown in the bottom traces and the time marks in the top traces occur at 5 ms intervals (Reproduced with permission after Cranefield (1975) © Futura, Mount Kisco, New York).

inward, it generates a net outward (hyperpolarizing) current across the cell membrane [21]. When subsidiary pacemaker cells are driven faster than their intrinsic rate (such as by the sinus node), the enhanced outward pump current suppresses spontaneous impulse initiation in these cells, which, as described above is dependent on the net inward current (Fig. 23.3). When the dominant (overdrive) pacemaker is stopped, this suppression is responsible for the period of quiescence which lasts until the intracellular Na^+ concentration, and hence the pump current becomes small enough to allow subsidiary pacemaker cells to depolarize spontaneously to threshold. Intracellular sodium concentration decreases during the quiescent period, because sodium is constantly being pumped out of the cell and little is entering [22]. Intracellular Na^+ and pump current continue to decline after the first spontaneous impulse, resulting in gradual increases in the discharge rate of the subsidiary pacemaker. The higher the rate, or the longer the duration of overdrive, the greater is the enhancement of pump activity, so that the period of quiescence following the cessation of overdrive is directly related to the rate and duration of overdrive (Fig. 23.3) [18].

The sinus node, itself, can also be overdrive-suppressed if it is driven at a rate more rapid than its intrinsic rate [23, 24]. Thus, there may be a quiescent period after termination of a rapid ectopic tachycardia before the sinus rhythm resumes [25]. However, when overdrive suppression of the normal sinus node occurs, it is of lesser magnitude than that of subsidiary pacemakers overdriven at comparable rates [23]. As described above, overdrive suppression of pacemaker fibers depends on sodium entering the fibers during phase 0 of the action potential, stimulating sodium pump activity. In the sinus node, the action-potential upstroke is largely dependant on slow inward current carried by calcium, and far less sodium enters the fiber during the upstroke than occurs in latent pacemaker cells such as Purkinje fibers. As a result, the activity of the sodium pump is probably not increased to the same extent in sinus node cells after a period of overdrive and, therefore, there is less overdrive suppression. The relative resistance of the normal sinus node to overdrive suppression may be important in enabling it to remain as the dominant pacemaker even when its rhythm is transiently perturbed by external influences (such as transient shifts of the pacemaker to an ectopic site). The diseased sinus node, however, may be much more easily overdrive-suppressed [26].

Another mechanism that may suppress subsidiary pacemakers, in addition to overdrive suppression, is the electronic interaction among pacemaker cells and the nonpacemaker cells in the surrounding myocardium [27] (Fig. 23.4). This mechanism may be particularly important in suppressing AV nodal automaticity [28]. AV nodal cells have intrinsic pacemaker activity that may be nearly as rapid as that in the sinus node. This can be demonstrated in small pieces of the AV node superfused in a tissue chamber [9]. Such pacemaker activity is not easily overdrive-suppressed, probably for the same reasons discussed above for the sinus node. However, the pacemaker activity of the AV node may be suppressed by axial current flowing through the connections between the node and the surrounding atrial cells (Fig. 23.4). The atrial cells have resting potentials which are more negative that those of the nodal cells and are not latent pacemakers. As a result of the more negative potentials of the atrial cells, current flow between them and the nodal cells should be in a direction which prevents spontaneous phase 4 depolarization of the latter. This current flow is apparently sufficient to prevent nodal automaticity despite the paucity of the intercellular junctions in the nodal region. The same mechanisms might be operative in the other regions of the atria where latent pacemaker cells may be surrounded by nonpacemaker cells, or in the distal Purkinje system where the Purkinje fibers are in contact with working ventricular muscle [27].

Arrhythmias caused by the normal automaticity of the cardiac fibers may occur for several different reasons. Such arrhythmias might result simply from an alteration in the rate of impulse initiation by the normal sinus node pacemaker without the shift of impulse origin to an ectopic site; sinus bradycardia and tachycardia are such arrhythmias. The cellular mechanisms which can change the rate of impulse initiation have been described above.

A shift in the site of impulse initiation to one of the regions where subsidiary pacemakers are located is another factor which results in arrhythmias caused by a normal automatic mechanism. This would be expected to happen when any of the following occurs:

(a) The rate of the sinus node pacemaker falls considerably below the intrinsic rates of the subsidiary pacemakers;
(b) Inhibitory electrotonic influences between nonpacemaker and pacemaker cells are interrupted;
(c) Impulse initiation in subsidiary pacemaker cells is enhanced.

The rate at which the sinus node activates subsidiary pacemakers may be decreased in a number of situations. Impulse initiation by the sinus node may be slowed or completely inhibited by heightened activity in the parasympathetic nervous

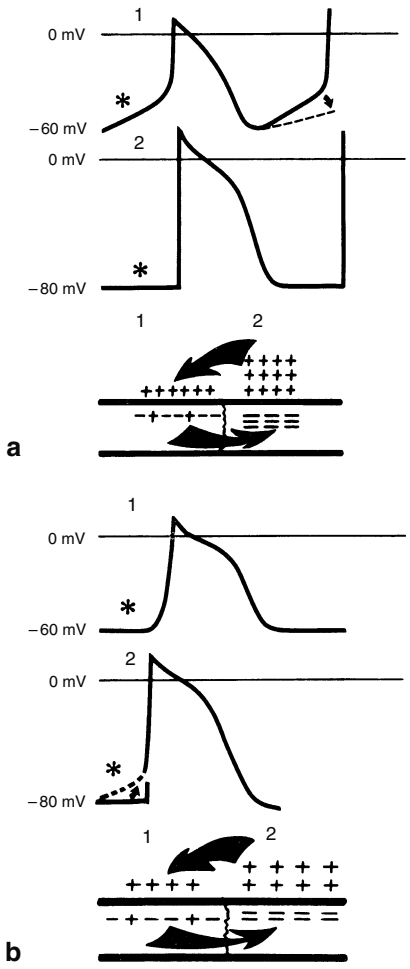

Figure 23.4

Part (a) is a diagrammatic representation of the effects of current flow from a cell with a high resting potential on the spontaneous diastolic depolarization of a cell with a lower resting potential; *1*, the transmembrane potential of a cell with a maximum diastolic potential of −60 mV and spontaneous diastolic depolarization (*); *2*, the transmembrane potential of an adjacent cell with a steady maximum diastolic potential −80 mV(*). Below it is a schematic representation of the membrane during the diastolic period. Since 1 has a lower potential across the membrane than 2, there is a flow of positive charge from 2 to 1 in extracellular space and from 1 to 2 in intracellular space, tending to oppose the decrease in membrane potential. Part (b) shows the interaction between: *1*, a cell with a steady low membrane potential of −60 mV and *2*, a cell with a higher membrane potential but spontaneous diastolic depolarization. Below is a schematic representation of the membrane during the diastolic period. Current (positive charge) flows from the cell with the higher membrane potential 1 in extracellular space and from 1 to 2 in intracellular space. This has a depolarizing effect on 2 and accelerates spontaneous diastolic depolarization while having some hyperpolarizing effects on 1.

system [29], or as a result of sinus node disease [13]. Alternatively, there may be block of impulse conduction from the sinus node to the atria or block of conduction from the atria to the ventricles. Under any of the above conditions there may be "escape" of a subsidiary pacemaker as a result of the removal of overdrive suppression by the sinus pacemaker. As stated earlier, there is a natural hierarchy of intrinsic rates of subsidiary pacemakers, with atrial pacemakers having faster intrinsic rates than ventricular pacemakers [12–14, 30]. Once overdrive suppression is removed, the pacemaker with the

faster rate becomes the site of impulse origin after sinus node inhibition [12]. As a result, there is a tendency for ectopic rhythms to arise in the atria or the AV junction when the sinus node impulse initiation is impaired or when there is sinus exit block. During AV block, the pacemaker will be in the AV junction or ventricular specialized conducting system, depending on the site of the block. The His bundle has a faster intrinsic rate than the more distally located Purkinje fibers [14]. Sometimes, however, pathologic processes that are responsible for the suppression of impulse initiation in the sinus node also suppress pacemaking in the atria and AV junction, so ectopic impulses may occur in the ventricular conducting system. This may occur during the sick sinus syndrome where ectopic ventricular beats, rather than junctional beats sometimes occur during the period of sinus bradycardia or arrest [31].

Any event which decreases intercellular coupling among latent pacemaker cells and surrounding nonpacemaker cells also removes inhibitory influences on the latent pacemakers [27]. Coupling might be reduced by fibrosis which can separate myocardial fibers. For example, fibrosis in the atrial aspect of the AV junctional region that results in heart block might release nodal pacemakers from electrotonic suppression by surrounding atrial cells and permit them to become the dominant pacemakers of the ventricle. Uncoupling might also be caused by factors which increase the intracellular Ca^{2+} [32] since intracellular calcium levels control coupling resistance among myocardial cells. This might result, for example, from treatment with digitalis [33], which inhibits the Na/K pump and sodium extrusion, and thus increases calcium levels in the cell [34].

Subsidiary pacemaker activity also may be enhanced, causing impulse initiation to shift to ectopic sites, even when sinus node function is normal. Norepinephrine released locally from sympathetic nerves steepens the slope of diastolic depolarization of latent pacemaker cells [10, 35], and diminishes the inhibitory effects of overdrive [36]. Localized effects may occur in the absence of sinus node stimulation [37]. Therefore, sympathetic stimulation may enable membrane potential of ectopic pacemakers to reach threshold before they are activated by an impulse from the sinus node, resulting in ectopic premature impulses or automatic rhythms. From studies of isolated tissues superfused with catecholamines and from studies on sympathetic stimulation in dogs, it appears that the limit for automatic rates generated by subsidiary pacemakers in the atria is close to 200 min^{-1} [38], and in the Purkinje fibers of the ventricles around 120 min^{-1} [39]. Normal automaticity enhanced by sympathetic stimulation, therefore, probably does not cause very rapid ventricular rhythms although it might cause atrial tachycardia.

The flow of current between partially depolarized myocardium and normally polarized latent pacemaker cells, also might enhance automaticity [40]. The mechanism has been proposed to be a cause of the ectopic beats that arise in the ventricle [41]. Ischemia causes a reduction in membrane potential of the affected cells. Thus, at the border of an ischemic area there is a transition, which might be quite abrupt, between depolarized and normal tissue. As a result of the differences in membrane potential, depolarizing current is expected to flow into the normal area and if cells in this area have some spontaneous diastolic depolarization (Purkinje fibers adjacent to the infarct) it would be enhanced, possibly to an extent sufficient to cause spontaneous impulse initiation (Fig. 23.4).

Inhibition of the electrogenic sodium-potassium pump results in a net increase in inward current during diastole because of the decrease in outward current normally generated by the pump and, therefore, increases automaticity in subsidiary pacemakers. This might occur after adenosine triphosphate (ATP) is depleted during prolonged hypoxia or ischemia or in the presence of toxic concentrations of digitalis [42]. A decrease in the extracellular potassium level also enhances normal automaticity [43], as does acute stretch [44].

Working atrial and ventricular myocardial cells do not normally show spontaneous diastolic depolarization. However, if left unstimulated for long intervals atrial myocardium can depolarized to lower membrane potentials at which abnormal automaticity (see below) is initiated [45]. This membrane depolarization is attributed to two causes: (1) in the absence of frequent stimulation the hyperpolarizing effect of the Na/K pump is lost; (2) The inward rectifying current I_{k1} which is responsible for maintaining a high membrane potential is weak in atrium [46]. In contrast, ventricular myocardium does not initiate spontaneous impulses even when it is not excited for long periods of time by propagated impulses. Although, Na/K pump function is minimal in this setting, there is a prominent I_{k1} in ventricle which maintains cells at a high membrane potential.

Neither atrial nor ventricular myocardium expresses pacemaker currents at the normal range of membrane potentials, although the pacemaker current, I_f, is present in myocardium, activating at membrane potentials around −150 mV, far outside the physiologic range [47]. Interestingly, in settings of myocardial hypertrophy [48] and failure [49] the activation of I_f shifts to more positive voltages, within the physiologic range. This has led to the suggestion [50] that some arrhythmias occurring in clinical disease may in fact result from an I_f-based automatic mechanism.

23.2.1.2 Abnormal Automaticity

In some instances of cardiac disease, the resting potentials of the atrial or ventricular myocardial cells are reduced. The same reduction can be achieved experimentally. When membrane potential is less than about −60 mV, spontaneous diastolic depolarization may occur and cause repetitive impulse initiation [51–53]. This is called "abnormal automaticity." Likewise, cells such as those in the Purkinje system which are normally automatic at high levels of membrane potential also show abnormal automaticity when the membrane potential is reduced (Fig. 23.5) [54, 55]. However, if a low level of membrane potential is the only criterion used to identify abnormal automaticity, the automaticity of the sinus node would have to be considered abnormal. Therefore, an important distinction for abnormal automaticity is that the membrane potentials of fibers showing this type of activity are markedly reduced from their own normal level.

At the low level of membrane potential at which abnormal automaticity occurs, it is likely that at least some of the ionic currents causing the automatic activity are not the same as those causing normal automatic activity. A likely cause of automaticity at membrane potentials of around −50 mV is deactivation of K^+ current I_{k1} [56]. This current under normal control conditions produces repolarization of the membrane after the upstroke of an action potential. In addition, the spontaneously occurring action potentials usually have upstrokes dependant on slow inward Ca^{2+} current [55] because the fast inward Na^+ current is inactivated at the low levels of membrane potential.

The decrease in membrane potential of cardiac cells required for abnormal automaticity to occur may be induced by a variety of factors related to cardiac disease. The causes of a low resting potential are best considered in terms of the Goldman-Hodgkin-Katz equation [57] which closely approximates the resting potential V_r of working myocardial cells over a wide range of extra cellular K^+ concentrations.

$$V_r = \frac{RT}{F} \ln \left(\frac{[K]_o + P_{Na}/P_K[Na]_o}{[K]_i + P_{Na}/P_K[Na]_i} \right)$$

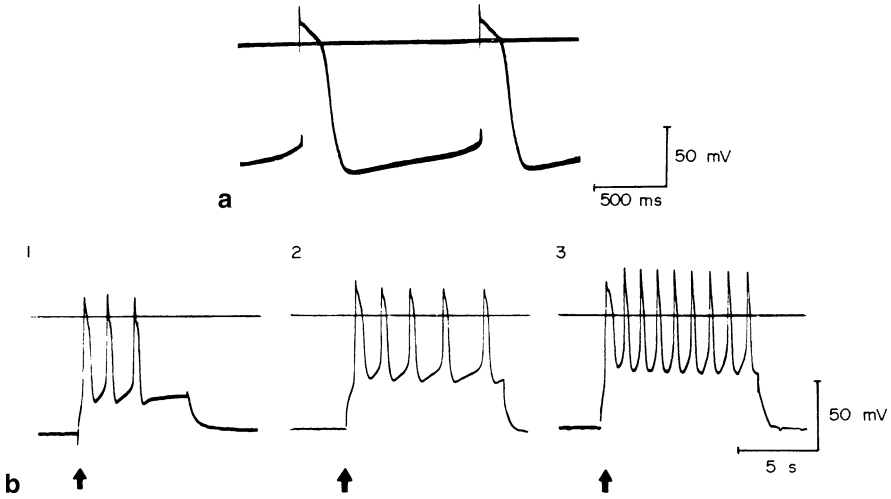

Figure 23.5

Normal and abnormal automaticity in a canine Purkinje fiber. Part (a) shows automatic firing of a Purkinje fiber with a maximum diastolic potential of −85 mV. Part (b) shows the abnormal automaticity that can occur when membrane potential is decreased: in 1, the fiber is depolarized (at the arrow) to a membrane potential of −45 mV by injecting a long lasting current pulse through a microelectrode and three automatic action potentials occur, in 2, a larger amplitude current pulse at the arrow reduces membrane potential to −40 mV, resulting in more sustained automatic activity; in 3, a still larger current pulse at the arrow reduces membrane potential to −30 mV and automatic activity occurs at a still faster rate. Automaticity in atrial and ventricular muscle also occur when the membrane potential is decreased in a similar way (Reproduced with permission after Wit and Friedman (1975) © American Medical Association, Chicago, Illinois).

where R is the gas constant, F is the Faraday, T is the absolute temperature, $[K]_o$ and $[K]_i$ are the extracellular and intracellular K^+ concentrations, respectively; P_{Na}/P_k is the ratio of the permeability coefficients for Na^+ and K^+, and $[Na]_o$ and $[Na]_i$ are the extracellular and intracellular Na^+ concentrations, respectively.

The several ways in which the resting potential can be less negative according to this equation are that $[K]_o$ might be increased, $[K]_i$ might be decreased, or the ratio P_{Na}/P_K might be increased following either an increase in P_{Na} (sodium permeability of the sarcolemma) or a decrease in P_K (potassium permeability of the sarcolemma). Any one of these changes would by itself cause the resting potential to decline and more than one change might occur in diseased cell [58].

Although an increase in extracellular potassium concentration can reduce membrane potential, automatic firing in working atrial, ventricular, and Purkinje fibers usually does not occur when $[K]_o$ is elevated because of the increase in K^+ conductance (and, hence, net outward current) that results from an increase in $[K]_o^+$ [59]. However, atrial fibers in the mitral valve [60] and fibers in the AV node may have automatic activity even when $[K]_o$ is markedly elevated. A decrease in $[K]_i$ has been shown to occur in the Purkinje fibers which survive on the endocardial surface of infarcts and this decreases persists for at least 24 h after coronary occlusion [61]. The reduction in $[K]_i$ undoubtedly contributes to the low membrane potential in these cells, although changes in membrane conductance are also responsible [61]. These Purkinje fibers have abnormal automaticity [62, 63]. Preparations of diseased atrial and ventricular myocardium from human hearts show phase 4 depolarization and abnormal automaticity at membrane potentials in the range −50 to −60 mV [64–66]. It has been proposed that a decrease in membrane potassium conductance, P_K, is an important cause of the low membrane potentials in the atrial fibers [65].

Myocardial fibers with low resting potentials will not fire automatically if the sinus node drives them faster than their intrinsic abnormal, automatic rate. An abnormal automatic focus should manifest itself and cause an arrhythmia when the sinus rate decreases below the intrinsic rate of the focus or when the rate of the focus increases above that of the sinus node, as was discussed for latent pacemakers with normal automaticity. A similar interplay between maximum diastolic potential, threshold potential and rate of phase 4 depolarization determines the rate of impulse initiation by the abnormal pacemaker. However, there is an important distinction between the effects of the dominant sinus pacemaker on the two kinds of foci, that is abnormal automaticity is *not* overdrive-suppressed to the same extent as the normal automaticity that occurs at high levels of membrane potential [67–69]. Moreover, the extent of suppression of spontaneous diastolic depolarization by overdrive is directly related to the level of membrane potential at which the automatic rhythms occur [68, 69] (Fig. 23.6). For example, Purkinje fibers showing automaticity at membrane potentials of −60 to −70 mV still manifest some overdrive suppression, although less than those fibers with automaticity at −90 mV. Automaticity in Purkinje fibers with membrane potentials less than −60mV is only slightly suppressed by short periods of overdrive. These differences in the effects of overdrive may be related to the reduction in the amount of sodium entering the cell membrane as potential decreases, and therefore, the degree to which the sodium- potassium pump is stimulated. (As the

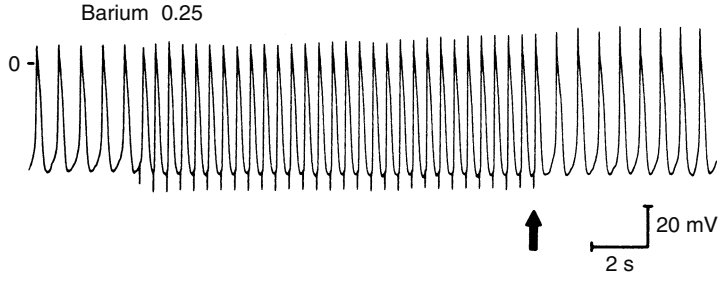

Figure 23.6

Effects of overdrive stimulation on abnormal automaticity occurring at a membrane potential of −52 mV. Abnormal automaticity was caused by adding 0.25 mmol $BaCl_2$ to the Tyrode's superfusate. The control cycle length is 810 ms. Stimulation cycle is 500 ms and the period of stimulation is denoted by the stimulus artifacts. The stimulation was stopped at the arrow. Note the absence of overdrive suppression (Reproduced with permission after Dangman and Hoffman (1982) © Futura, Mount Kisco, New York).

membrane potential is reduced and the Na^+ channels inactivated there is a decrease in the fast inward sodium current and hence a decrease in activation of the pump [70].) For markedly depolarized tissue showing no suppression after brief periods of overdrive, long periods of rapid overdrive can suppress automaticity either because Na^+ can enter the cell through the slow channel to stimulate the pump [70] or because calcium entering during the upstroke of slow response action potentials is exchanged for sodium, thereby elevating $[Na]_i$ [71].

At normal sinus rates there may be little overdrive suppression of pacemakers with abnormal automaticity. As a result of the lack of overdrive suppression, even transient sinus pauses or occasional long sinus cycle lengths may permit the ectopic focus to capture the heart for one or more beats. On the other hand, an ectopic pacemaker with normal automaticity would probably be quiescent during relatively short, transient sinus pauses because they are overdrive- suppressed. It is possible that the depolarized level of membrane potential at which abnormal automaticity occurs might cause entrance block into focus and prevent it form being overdriven by the sinus node [72]. This would lead to parasystole, an example of an arrhythmia caused by a combination of an abnormality of impulse conduction and initiation (discussed in more detail later in this chapter).

The firing rate of an abnormally automatic focus might also be enhanced above that of the sinus node, leading to arrhythmias in the absence of sinus node suppression or conduction block between the focus and surrounding myocardium. The automatic rate is a direct function of the level of membrane potential– the greater the depolarization, the faster the rate [51–55]. Experimental studies have shown firing rates in muscle and Purkinje fibers of 150–200 min^{-1} at membrane potentials less that −50 mV and these rates appear to be sufficiently rapid to enable these pacemakers to control the heart. Catecholamines also increase abnormal automaticity ll[73].

23.2.1.3 Some Clinical Characteristics of Arrhythmias Caused by Automaticity

Thus far, we have considered the influences of the sinus node pacemaker on subsidiary pacemakers with different automatic mechanisms. The sinus node probably exerts an inhibitory effect on the normal automatic mechanism by overdrive but has lesser inhibitory effects on the abnormal one. These known effects of overdrive on pacemaker mechanisms might sometimes be of use in distinguishing automatic arrhythmias caused by triggered activity or reentry (see Sect. 23.2.2) in the in situ heart, or in distinguishing arrhythmias caused by normal automaticity from those caused by abnormal automaticity [68]. If a tachycardia is caused by normal automaticity it could be predicted that the rate of tachycardia should be suppressed immediately after it is overdriven by electrical stimulation, even when the overdrive period is relatively short (Fig. 23.7). The transient pause after overdrive should be followed by a gradual speeding up of the ectopic rhythm until the original rate is resumed. The duration of the transient pause and the time required for resumption of the original ratel+ is directly related to the rate and duration of overdrive. It is important to stress, however, that the tachycardia is not terminated but only suppressed transiently. This behavior is a result of the increased activity of the sodium-potassium pump discussed previously. During overdrive of atrial or sinus tachycardias, acetylcholine may be released from electrically stimulated nerve endings and contribute further to the overdrive suppression [74].

The characteristic behavior of normally automatic pacemakers has been demonstrated in some clinical and experimental electrophysiological studies on both atrial and ventricular tachycardias [75, 76]. On the other hand, tachycardias caused by abnormal automaticity should not be suppressed by overdrive, unless the overdrive period is long and the rate fast [68]. The difficulty in suppressing such tachycardias by overdrive stems from a lesser amount of Na^+ entering the cells, as previously mentioned. Short periods of overdrive can even result in a transient speeding of the tachycardia rate (overdrive acceleration) [68]. Accelerated idioventricular rhythms or tachycardia in canine myocardial infarction are not easily overdrive-suppressed and therefore may be caused by abnormal automaticity [76].

In addition to overdrive, the response of the rhythm to programmed premature stimuli applied to the heart is sometimes useful in determining the mechanism of clinical arrhythmias [77]. Of major importance is the fact that automatic rhythms caused by either normal or abnormal automaticity cannot be terminated by premature impulses (nor can they be started by premature impulses–in contrast, see effects of stimuli on triggered activity and on reentry discussed in Sect. 23.2.2). Other than that, premature impulses induced at different times during diastole may transiently perturb the rhythm during the subsequent few cycles. Detailed descriptions of the effects of premature impulses in automatic impulse initiation have been published [78–80].

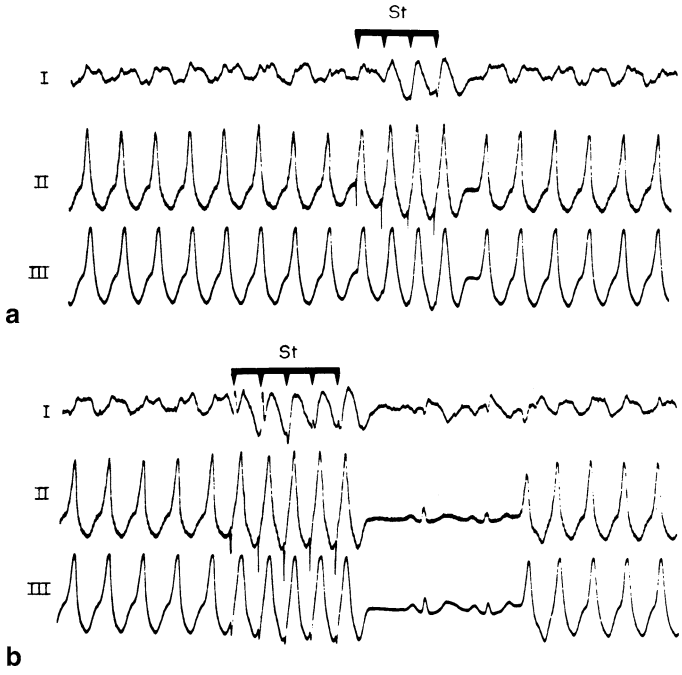

Figure 23.7

Effects of overdrive on ventricular tachycardia that may be caused by automaticity. Leads I, II, and III of the ECG are shown. In (a), a burst of rapid stimuli St is followed by a short pause and then recurrence of tachycardia, In (b), a burst of five stimuli is followed by a greater suppression of tachycardia, allowing the occurrence of two sinus beats. Tachycardia then reappears (Reproduced with permission after Fontaine et al. (1984) © Futura, Mount Kisco, New York).

23.2.2 Afterdepolarizations and Triggered Activity

Afterdepolarizations are oscillations in membrane potential that are induced by, and follow, an action potential. These oscillations are divided into two categories: early afterdepolarizations, which precede full repolarization of the membrane; and delayed afterdepolarizations, which follow full repolarization. Both of these types of afterdepolarizations are, in turn, capable of initiating arrhythmias referred to as "triggered" [81]. Triggered arrhythmias must be initiated by a conducted or stimulated action potential (the trigger) and cannot arise during a period of quiescence such as that caused by sinus node inhibition [82]. This contrasts with normal or abnormal automaticity which have just been described.

23.2.2.1 Early Afterdepolarizations

Early afterdepolarizations most frequently occur during repolarization of an action potential which has been initiated from a high level of membrane potential (usually −75 to −90 mV). They may appear as an oscillation at the plateau level of membrane potential or later during phase 3 of repolarization. Under certain conditions these oscillations can lead to a second upstroke or action potential (see Fig. 23.8). When the oscillation is large enough, the decrease in membrane potential leads to an increase in inward (depolarizing) current and a second action potential occurs prior to complete repolarization of the first.

This second action potential occurring during repolarization is triggered in the sense that is evoked by an early afterdepolarization which, in turn is induced by the preceding action potential. Without the preceding action potential there would be no second upstroke. The second action potential may also be followed by other action potentials, all occurring at the low level of membrane potential characteristic of the plateau of phase 3 (Fig. 23.8). The sustained rhythmic activity

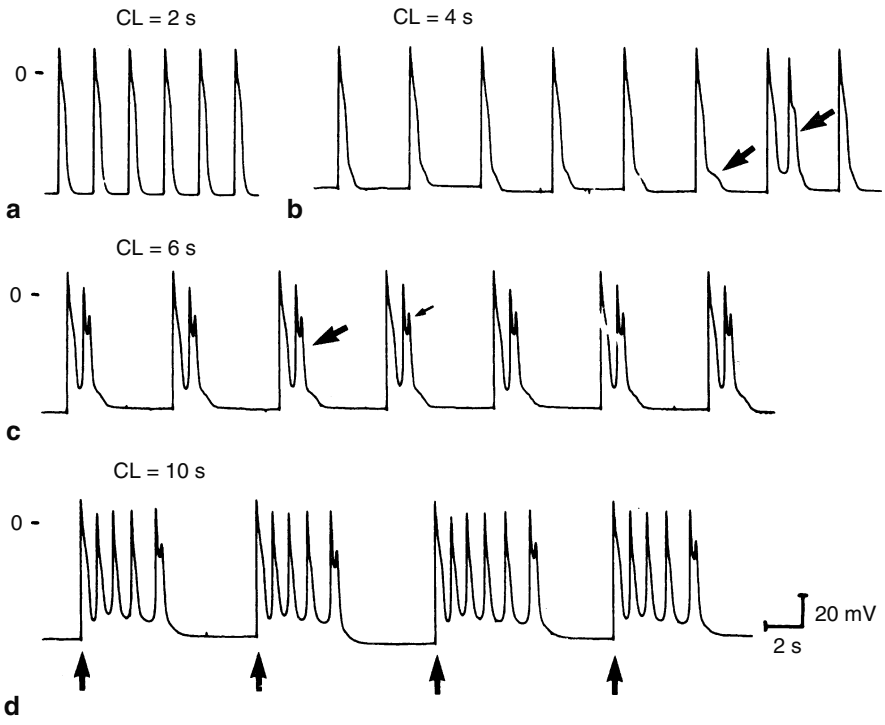

Figure 23.8

Early afterdepolarizations in Purkinje fibers. Part (a) shows the transmembrane potential recorded from a Purkinje fiber stimulated at a cycle length (CL) of 2 s. Repolarization appears to be normal. In (b), when CL is increased to 4 s, an early afterdepolarization appears during phase 3 of repolarization (*arrow*). At the right a second upstroke or triggered action potential arises from the early afterdepolarization (*arrow*). In (c), at a CL of 6 s, a single triggered action potential (arrow) occurs during phase 3 of each stimulated action potential. An early afterdepolarization also occurs during the plateau of the triggered action potential (*small arrow*). In (d), at a CL of 10 s, a burst of triggered action potentials occurs during phase 3 of each stimulated action potential (arrows point to stimulated action potentials) (Reproduced with permission after Damiano and Rosen (1984) © American Heart Association, Dallas, Texas).

that ensues may continue for a variable number of impulses and may terminate when the increase in membrane potential associated with repolarization of the initiating action potential returns membrane potential to a high level. Triggered activity may occur again when the next action potential is initiated from the high level membrane potential. Sometimes repolarization to this high level may not occur, and membrane potential may remain at the plateau level or at a level intermediate between the plateau and the resting potential. The sustained rhythmic activity may then continue at the reduced level of membrane potential.

There are some conceptual difficulties associated with triggered activity caused by early afterdepolarizations [81]. According to the definition of triggered activity, there is no problem in characterizing the second action potential that is induced by an early afterdepolarization and occurs during repolarization as being triggered. However, if a series of action potentials arises following this premature upstroke and before the cell repolarizes to a high resting potential, it might be wondered whether these action potentials are triggered or whether they occur only because the membrane potential has been shifted into a region where abnormal automatic activity occurs. The previous section pointed out how abnormal automaticity occurs at reduced membrane potentials. Certainly, based on the response of the sustained rhythm to pacing (see below), it is not readily differentiated from abnormal automaticity occurring at low membrane potentials. It is for this reason the authors think it appropriate to suggest that only the first action potential is triggered and the remaining are automatic. As a result, the major differentiation between triggered and abnormally automatic rhythms may be that the

former result from interruption of repolarization by an oscillation (which is triggered) and the latter from depolarization of the membrane to the same range of potentials. Hence, the inciting events differ but the subsequent rhythm may be the same.

The ionic mechanisms which cause early afterdepolarizations likely result from abnormalities in the repolarizing membrane currents. During the plateau phase of the action potential, the rate of membrane repolarization is very slow and the net repolarizing membrane current is very small. This net current is outward throughout the range of membrane potentials between zero and the resting potential [59]. The net repolarizing current results from an imbalance between inward and outward currents. The inward current component includes a background Na^+ current, Na^+ current flowing through incompletely inactivated sodium channels [83] and the slow inward Ca^{2+} current [84]. The major outward currents are carried by potassium via rapidly activating (I_{Kr}) and slowly activating (I_{Ks}) delayed rectifier currents, which are voltage gated [85]. Also contributing to outward membrane current in the plateau range is the electrogenic sodium-potassium pump [86]. Normally the net outward membrane current shifts membrane potential progressively in a negative direction and the final rapid phase of action-potential repolarization takes place. An early afterdepolarization might occur if there is a shift in the current-voltage relationship resulting in a region of net inward current during the plateau range of membrane potentials. This would retard or prevent repolarization [59] and might lead to a secondary depolarization during the plateau phase or phase 3 if regenerative inward current is activated. The second upstroke and any subsequent action potentials that arise from the low levels of membrane potential during the plateau are Ca^{2+}-dependant; that is, the inward current responsible for the upstroke flows through the Ca^{2+} channel because that fast channel is inactivated [55]. Action potentials which arise during phase 3 might have upstrokes caused by current flowing through partially reactivated fast sodium channels or a combination of slow and fast channels. More recent research has suggested that either a Ca window current [87] alterations in Ca loading and Na/Ca exchange current [88] and/or calmodulin kinase activity [89] also may contribute to early afterdepolarizations.

Conditions that increase the inward current components or decrease the outward current components during repolarization are expected to induce the shift in the current- voltage relationship which causes early afterdepolarizations. Experimental drugs such as aconitine [90] and veratridine [91] cause early afterdepolarizations probably by increasing Na^+ conductance during the plateau phase. Although these drugs are not clinically important, their effects demonstrate that if similar increases in conductance were caused by cardiac pathology, triggered activity would occur. Early afterdepolarizations can also occasionally be seen in Purkinje fibers superfused with normal Tyrode's solution soon after they have been excised from the heart. These early afterdepolarizations might be caused by relatively nonspecific inward current flowing via incompletely healed cuts made at the ends of fibers, or through other regions injured by stretching or crushing during the dissection [82]. This suggests the interesting possibility that mechanical injury or stretch of Purkinje fibers in situ might cause triggering. Stretch of the cardiac fibers in the ventricles might occur in heart failure or in ventricular aneurysms. Mechanical injury might also occur in the area of an infarct or aneurysm.

Early afterdepolarizations leading to triggered activity in isolated cardiac preparations may also be caused by factors which are present in the heart in situ under some pathological conditions. Among these factors are hypoxia [92], high pCO_2 [93] and high concentrations of catecholamines [94]. Data are not yet available which elucidate how they exert their effects. Since catecholamines, hypoxia, and elevated pCO_2 may be present in an ischemic or infarct regions of the ventricles, it is possible that early afterdepolarization may cause some of the arrhythmias which occur soon after myocardial ischemia.

Some drugs that have been used clinically and that markedly prolong the time course for repolarization, such as the β-receptor blocking drug sotalol [95] and the antiarrhythmic *N*-acetyl procainamide [96], also cause early afterdepolarizations and triggered activity. These drugs have been shown to cause cardiac arrhythmias that may be triggered in experimental animals and in patients [97] (see Fig. 23.9). Single triggered impulses occurring as a result of early afterdepolarizations should induce premature depolarizations having fixed coupling intervals to the preceding beat (since they occur during repolarization of an action potential accompanying the preceding beat). Hence, a bigeminal rhythm would occur if each action potential caused by propagation of the normal sinus impulse were followed by a second upstroke caused by an early afterdepolarization. If a train of triggered action potentials occurs during repolarization, it would be expected to cause a paroxysm of tachycardia with the first impulse of tachycardia having a fixed coupling interval to the preceding eat. Tachycardias would terminate when repolarization of the triggering action potential occurs. Usually, the rate of activity during the repolarization of the triggering action potentials slows gradually before termination. Thus termination of the triggered tachycardias might be expected to be preceded by gradual slowing of the tachycardias.

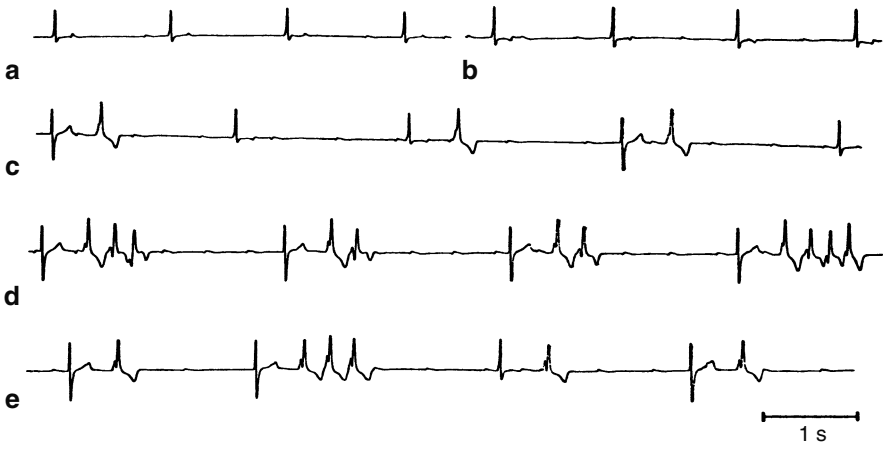

Figure 23.9

Ventricular arrhythmias that might be caused by early afterdepolarizations in the dog (a), the control electrocardiogram of a dog with experimentally induced heart block; (b) and (c), traces after 50 mg kg^{-1} *N*-acetyl procainamide (NAPA) was injected intravenously; (d) and (e), traces taken after 100 mg kg^{-1} NAPA was administered. NAPA prolongs Purkinje fiber action potential duration, causing early afterdepolarization and triggered activity. In (c) coupled ventricular premature depolarizations caused by the NAPA are evident. In (d) and (e), short runs of ventricular tachycardia can be seen. The first impulse of tachycardia has a relatively fixed coupling to the QRS (Reproduced with permission after Dangman and Hoffman (1981) © Williams and Wilkins, Baltimore, Maryland).

Since the occurrence of early afterdepolarizations is facilitated by a decrease in the net repolarizing current, a slowing of the rate at which the triggering action potentials are elicited might also favor the occurrence of the afterdepolarizations (Fig. 23.8). As the drive rate slows, action potential duration is prolonged, reflecting a decrease in net outward current. It, therefore, seems likely that some tachycardias which occur after a period of bradycardia might be caused by early afterdepolarizations [98]. It is likely that tachycardias in patients with the congenital and acquired long QT interval syndromes (in which there is prolonged repolarization) are triggered [91]. Certainly, experimental animal studies [99, 100] as well as the clinical literature [101] point to early afterdepolarizations and triggered activity as a cause of torsades de pointes, the characteristic and often lethal arrhythmia of congenital and acquired LQTS. The clinical applicability of this mechanism was most dramatically brought home by the SWORD trial [102], in which d- Sotalol, a drug that blocks the HERG channel that carries I_{Kr} was found to cause excess deaths in a population of post-myocardial infarction patients.

It is instructive to attempt to predict the effects of stimulation of the heart on triggered arrhythmias caused by early afterdepolarizations, since various stimulation protocols are used in attempts to determine the mechanisms causing clinical arrhythmias. Overdrive stimulation during sinus rhythm should prevent occurrence of paroxysmal triggered tachycardias since rapid stimulation usually decreases the duration of the action potential; that is, an action potential of short duration does not favor the occurrence of early afterdepolarizations. However, once overdrive pacing is stopped, the paroxysms of tachycardias might spontaneously reappear as action potential duration again lengthens. The response of the triggered tachycardias to overdrive (during tachycardia) is similar to the response of abnormal automaticity to overdrive [103]; these rhythms are not easily terminated or suppressed by brief periods of overdrive but are suppressed transiently by periods of pacing in the range of 2–3 min. The tachyarrhythmias induced by early afterdepolarizations are not terminated readily by single interpolated stimulated impulses, but can be reset in much the same way as automatic rhythms. The similar response to overdrive pacing of the tachyarrhythmias induced by early afterdepolarizations and of abnormal automaticity is further evidence that the two phenomena are caused by a similar mechanism as mentioned above.

23.2.2.2 Delayed Afterdepolarizations

Delayed afterdepolarizations are oscillations in membrane potential that occur after repolarization of an action potential and are induced by that action potential (Fig. 23.10). One or more oscillations may occur after each action potential. Delayed afterepolarizations may be subthreshold, but when they are large enough to bring the membrane potential to the threshold of a regenerative inward current, a nondriven (triggered) impulse arises which may also be followed by an afterdepolarization. The impulse is said to be triggered since it would not have occurred without the preceding action potential [55, 81, 82].

Delayed afterdepolarizations occur under a number of conditions in which there is either a large increase in the intracellular calcium, or an abnormality in the sequestration or release of calcium by the sarcoplasmic reticulum, or a combination of the two. One of the most widely recognized causes is toxic concentrations of cardiac glycosides [104–107]. Cardiac glycosides inhibit the Na^+-K^+ pump thereby leading to an increase in $[Na]_i$. This in turn increases the intracellular Ca^{2+} through a Na^+-Ca^{2+} exchange mechanism [108]. Delayed afterdepolarizations caused by digitalis can occur in Purkinje fibers and in working atrial and ventricular muscle fibers although Purkinje fibers seem to develop them at lower drug concentrations [107]. Other experimental maneuvers which inhibit the Na^+-K^+ pump also increase the intracellular calcium and cause delayed afterdepolarizations similar to those induced by digitalis. A prime example is exposure of cardiac fibers to a K^+-free extracellular environment [109].

Catecholamines can cause delayed afterdepolarizations [10, 110, 111], and delayed afterdepolarizations and triggered activity induced by catecholamine have been described in atrial fibers of the mitral valve [111] and coronary sinus [10], as well as other regions of the atria [82]. Ventricular muscle fibers and Purkinje fibers also can develop delayed afterdepolarizations in the presence of high concentrations of catecholamines [110, 111].

Delayed afterdepolarizations may also occur in the absence of drugs or catecholamines. They have been identified in fibers in the upper pectinate muscles bordering the crista terminalis in the rabbit heart [112], in hypertrophied ventricular myocardium [113], in human atrial myocardium [45], in Purkinje fibers surviving on the subendocardial surface of canine infarcts [114], and in atrial fibers in sleeves of myocardium extending into the pulmonary veins (in which early afterdepolarizations also have described) [115]. Triggered activity in the pulmonary veins has been hypothesized as a likely cause of paroxysmal atrial fibrillation [115, 116]. The exact relationship of hypertrophy or ischemia to the occurrence of delayed afterdepolarizations in not known yet in any detail, but in the former uptake and release of calcium by sarcoplasmic reticulum may be abnormal [117] and in the latter there may be an increase in $[Ca]_i$ secondary to an increase in $[Na]_i$ [118].

The mechanisms by which elevated intracellular Ca^{2+} causes delayed afterdepolarizations have been explored in studies utilizing voltage-clamp techniques to control the depolarization of the membrane and to measure ionic currents [109, 119–123]. Delayed afterdepolarizations result from a transient inward current which is activated by repolarization after a depolarizing voltage-clamp pulse (Fig. 23.11). The voltage clamp pulse is somewhat comparable to an action potential. Increasing the magnitude of the depolarization in the plateau voltage range increases the magnitude of the current and causes the peak to be reached more rapidly. The transient inward current also increases in amplitude with increasing duration of the voltage clamp pulse or increasing pulse frequency (see below). All these changes in the characteristics of the clamp pulse may lead to an increase in $[Ca^{2+}]_i$, at least partly from an increase in the slow inward

Figure 23.10

Delayed afterdepolarizations caused by catecholamines recorded from an atrial fiber in an isolated, superfused preparation of canine coronary sinus tissue. The afterdepolarization amplitude is increasing with each stimulated impulse until it reaches threshold and causes triggered activity, as indicated by the black arrows at the right.

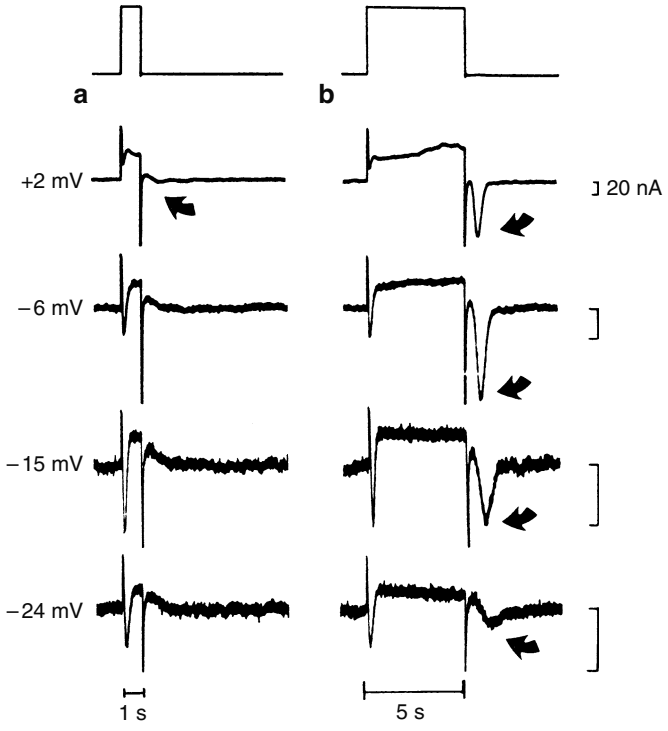

Figure 23.11

Some characteristics of the transient inward current in calf Purkinje fibers. The preparation was exposed to 1 μm strophanthidin, Traces a and b show the protocol. The membrane potential was clamped at a holding potential of −41 mV and depolarizing voltage-clamp pulses were imposed for either 1 s (a) or 5 s (b). The depolarization ranged from −24 to +2 mV as indicated on the left side of the figure. The membrane currents recorded during this clamp protocol are shown in each column. The transient inward (TI) current responsible for delayed afterdepolarizations is indicated by the arrows. The TI current is larger after longer duration voltage clamp pulses and after pulses to around −6 mV (Reproduced with permission after Lederer and Tsien (1976) © Cambridge University Press, London).

current [124]. The amplitude of the transient inward current is maximal at membrane potentials of −50 to −70 mV and decreases at both lower and higher membrane potentials, Thus, the transient inward current is significantly different from the pacemaker currents which cause automatic rhythms.

From these characteristics of the transient inward current, it can be predicted that the following will lead to an increase in delayed afterdepolarization amplitude and cause triggered activity:

(a) An increase in the amplitude and/or duration of the action-potential plateau [114];
(b) An increase in the frequency at which action potentials are induced;
(c) A decrease in the resting membrane potential in muscle or Purkinje fibers from normal levels around −80 mV to −90 mV to less than −70 mV [125].

The link between the depolarization pulse (whether caused by voltage clamp or by an action potential) and the subsequent transient inward current may involve release and reuptake of calcium from the sarcoplasmic reticulum. Normally, release is initiated by the depolarization phase of the action potential and reuptake is complete by the end of the action potential. However, if the sarcoplasmic reticulum is overloaded with calcium, it may not be able to take up all the calcium and/or there may be secondary release of calcium after repolarization [126]. Certainly, spontaneous Ca^{2+} release from the

sarcoplasmic reticulum has been demonstrated both in single cardiac myocytes and in isolated cardiac trabeculae. Moreover, the occurrence of propagating Ca^{2+} waves in myocytes that induce delayed afterdepolarizations has been reported and validated [127].

The increased level of cytoplasmic calcium has been proposed to alter sarcolemmal permeability, causing activation of a nonspecific membrane channel that allow an inward rush of positive charge carried mainly by sodium, such that the delayed afterdepolarization occurs [128]. However, there are some dissenting opinions concerning the mechanism for the inward current during the afterdepolarization. It has also been proposed that this current results from electrogenic exchange of intracellular calcium for extracellular sodium that results in the net transfer into the cell of positive charge in the form of sodium ions, to generate an inward current [122, 129].

Delayed afterdepolarizations may not be large enough to reach threshold, in which case triggered activity does not occur. As indicated previously, triggering may result in fibers showing subthreshold afterdepolarization if the rate at which the fiber is driven is increased (Fig. 23.12a). In cardiac fibers with a single afterdepolarization following each action potential, the amplitude of the afterdepolarization increases as the drive rate increases (unlike early afterdepolarizations which have the opposite relationship). At a sufficiently rapid drive rate the afterdepolarization attains a sufficient amplitude to reach threshold and triggering occurs (Fig. 23.12a). A decrease in the length of even a single drive cycle, that is, a premature impulse, may increase the amplitude of the afterdepolarization of the action potential that follows the short cycle. As the premature impulse occurs earlier and earlier after the previous impulse, the amplitudes of the afterdepolarizations which follow the premature impulses increase and may reach threshold, initiating triggered activity (Fig. 23.12b). The likelihood of a premature impulse initiating triggered activity increases at more rapid basic drive rates. In cardiac Purkinje fibers made digitalis toxic, at least two afterdepolarizations are usually present at relatively slow rates of drive. The first afterdepolarization is larger than the second. As the drive cycle length is decreased to around 500 ms, the amplitude of the first oscillation increases to its maximum and triggered activity may occur. If it does not occur and the drive cycle length is decreased further, the amplitude of the second afterdepolarization increases while the first declines, and triggered action potentials may arise from the second oscillation [130].

The increase in amplitude of delayed afterdepolarizations with increasing drive rate is also probably responsible for perpetuation of triggered activity once the nondriven action potential has occurred. Since the first nondriven action potential arises from the peak of a delayed afterdepolarization, the coupling interval between the upstroke of this triggered action potential and the upstroke of the triggering action potential is usually shorter than the drive cycle length which caused the first triggered impulse; that is, the first triggered action potential is, itself, premature. Hence, the afterdepolarization following the first nondriven action potential will be larger and a second triggered action potential will, therefore, occur at a short coupling interval. The process thus perpetuates itself.

There may be some differences in the characteristics of triggered activity caused by delayed afterdepolarizations, depending upon the cause. The initial period of triggered activity caused by catecholamines in atrial fibers is often characterized by a gradual decrease in the cycle length after which a relatively constant cycle length occurs [10, 131]. This decrease in cycle length may be accompanied by a decrease in maximum diastolic potential, (at least partly caused by accumulation of K^+ outside the cell during rapid activity owing to restricted diffusion in the extracellular space [132, 133]). The decrease in maximum diastolic potential contributes to the gradual acceleration in the rate of triggered activity since the rate increases as membrane potential decreases in the same way as we described for normal automaticity. Similar characteristics for triggered activity caused by factors other than catecholamines have also been described in atrial, ventricular, and Purkinje fibers. On the other hand, during triggered activity in Purkinje fibers exposed to toxic amounts of digitalis, there is not usually a gradual increase in rate, but rather, the maximum triggered rate is attained after a few impulses [134].

Triggered activity often terminates spontaneously. When catecholamine-induced triggered activity in atrial fibers of the coronary sinus terminates, the rate usually slows gradually before termination. This gradual slowing is accompanied by a progressive increase in the maximum diastolic potential. A delayed afterdepolarization usually follows the last triggered impulse [10, 131]. The spontaneous termination of triggered activity in canine coronary sinus fibers (and probably also in other types of cardiac fibers) is caused, at least in part, by an increase in the rate of electrogenic sodium extrusion [131]. Sodium pump activity is enhanced by the increase in intracellular Na^+ concentration which results from the increase in Na^+ influx during the rapid period of triggered activity. The increase in outward sodium pump current increases the maximum diastolic potential and reduces the rate of triggered activity; a sufficient increase in sodium pump current terminates the triggered activity [131]. Triggered activity caused by digitalis toxicity probably stops by another mechanism. Termination of a triggered burst is usually not associated with gradual slowing and hyperpolarization but often

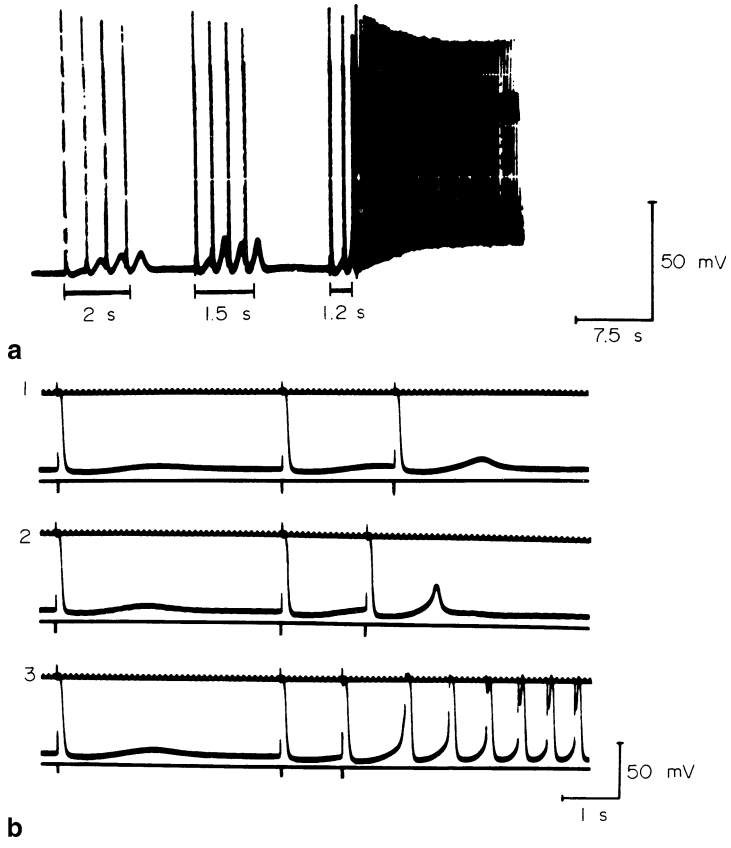

Figure 23.12

Part (a) shows the effects of stimulus rate on afterdepolarization amplitude. Part (b) shows the effects of premature stimulation on afterdepolarization amplitude and triggering. The transmembrane potentials shown were recorded from an atrial fiber in the canine coronary sinus superfused with Tyrode's solution containing norepinephrine. In (a), the cycle length is indicated beneath each group of impulses. The afterdepolarization following the last driven impulse has an amplitude of 10 m in the first case and 17 mV in the second. In the third case, sustained rhythmic activity is triggered. The rate is too rapid for the individual upstrokes to be apparent. Maximum diastolic potential decreases during the initial period of triggered activity. In (b), the bottom trace in each panel shows the stimulus pulses. Each panel shows the last two impulses of a series of ten impulses, driven at a cycle length of 4 s, that did not cause triggering. A premature impulse is then induced at progressively shorter coupling intervals. The amplitude of the afterdepolarizations during the basic drive varied from 2 to 6 mV. In *1*, the afterdepolarization following premature action potential induced 2 s after the last basic action potential has an amplitude of 11 mV. In *2*, at a shorter premature coupling interval of 1.4 s, the amplitude of the afterdepolarization following premature action potential is 31 mV. In *3*, at a shorter premature coupling of 1 s triggered activity occurs following the premature action potential (Reproduced with permission after Wit and Cranefield (1977) © American Heart Association, Dallas, Texas).

by speeding of the rate, a decrease in action potential amplitude and membrane depolarization. Termination is probably not related to activity of the Na^+ pump since the pump is inhibited by the digitalis, but may be caused by Na^+ or Ca^+ accumulation in the cell secondary to the rapid rate. A decreased transmembrane concentration gradient to either Na^+ or Ca^+ might diminish the afterdepolarization and finally lead to cessation of activity.

Since, as mentioned before, electrical stimulation of the heart is one way in which mechanisms of clinical arrhythmias have been studied, it is worth reviewing the effects of stimulation on triggered activity caused by delayed afterdepolarizations. Triggered tachycardias may be initiated by either an increase in heart rate or by premature impulses as described

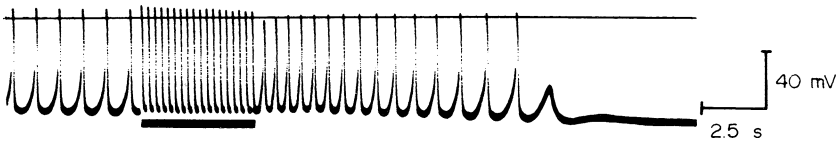

Figure 23.13

Termination of triggered activity by overdrive stimulation. At the left the transmembrane potential from an atrial fiber in the canine coronary sinus is shown during a period of triggered activity. Rapid overdrive stimulation was accomplished during the period that is underlined. Immediately following this overdrive, the rate of triggered activity is accelerated. Later there is a gradual slowing of the rate and a simultaneous increase in maximum diastolic potential until triggered activity stops (Reproduced with permission after Wit et al. (1981) © American Heart Association, Dallas, Texas).

above, and therefore triggered arrhythmias might be started by stimulating the heart. Triggered activity can also be terminated by either premature or overdrive stimulation. It is sometimes possible to terminate triggered activity with a single premature stimulus [60]. Such a premature impulse is followed by an increased afterhyperpolarization which, in turn, is followed by an afterdepolarization that does not reach threshold because it arises from the more negative membrane potential of the preceding afterhyperpolarization. More frequently, premature impulses will simply reset the triggered rhythm in much the same way as they reset automatic rhythms. The ability of premature impulses to terminate triggered activity is increased if they are preceded by a period of rapid drive [135].

Triggered activity can also be terminated by overdrive (Fig. 23.13). The effects of overdrive are dependant both on its rate and duration. During a short period of overdrive at a rate only moderately faster than the triggered rate there is often a decrease in the maximum diastolic potential; following the period of overdrive the rate of the triggered activity may be faster than it was before overdrive, perhaps because of the decrease in maximum diastolic potential. This postoverdrive acceleration is similar to the acceleration which can occur during abnormal automaticity. The accelerated rate then slows, and maximum diastolic potential increases until preoverdrive values are attained. If either the rate or duration of overdrive is increased to a critical degree, the decline in maximum diastolic potential during overdrive is greater as is the postoverdrive acceleration. In cardiac fibers in which triggered activity is caused by factors other than digitalis, such as catecholamines, the maximum diastolic potential then increases and the rate gradually slows until activity stops (Fig. 23.13). The increase in maximum diastolic potential and the slowing and termination of triggered activity following a period of overdrive are caused by enhanced activity of the electrogenic sodium pump. This enhanced activity results from a transient increase in intracellular Na^+ caused by the increased number of action potentials during overdrive. The increased outward pump current following overdrive increases maximum diastolic potential and slows the rate as discussed above for spontaneous termination of triggered activity [131].

Although overdrive stimulation also terminates triggered activity caused by digitalis, the mechanism for the termination may not involve enhanced electrogenic Na^+ pump activity, since the pump is inhibited by the presence of digitalis. Termination caused by overdrive usually is associated with depolarization rather than hyperpolarization and generally occurs within several beats after the overdrive [135]. Termination may be caused by an increase in intracellular Na^+ or Ca^+ resulting from the increased number of action potentials during the overdrive.

23.3 Abnormalities of Repolarization and Their Genetic Determinants

As was demonstrated in Chap. 3, the past decade has seen a vast increment in our understanding of the molecular determinants of ion channels. Figure 23.14 demonstrates how either a decrease in outward current or an increase in inward current may result in prolongation of repolarization and an arrhythmia. Note that the prolonged repolarization in itself is not arrhythmogenic unless it initiates dispersion of repolarization sufficient to facilitate reentry and/or is associated with an early afterdepolarization that, in turn, initiates triggered activity.

We now appreciate that ion channelopathies associated with genetic or acquired alterations in channel structure can alter repolarization importantly and give rise to arrhythmias. A major impetus to this understanding came from the

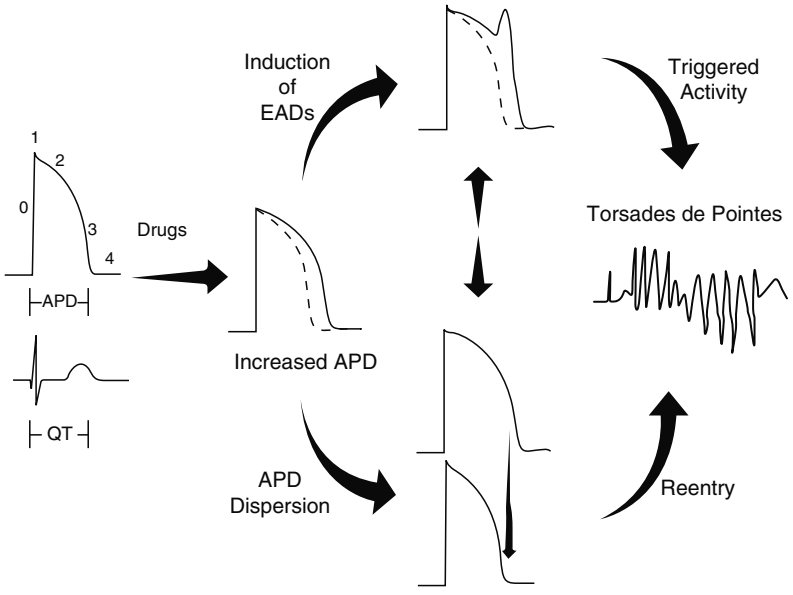

Figure 23.14

Potential mechanisms underlying the induction of torsades de pointes by drugs that prolong repolarization. Depicted here is an increase in action potential duration (APD) induced by drugs. As a result there can be the generation of early afterdepolarizations (EAD) and/or increased dispersion of APD. EAD can induce triggered activity and excess APD dispersion can induce reentry. Both mechanisms can result in torsades de pointes (Reproduced with permission from Ebert et al. (1998)).

pioneering work of Schwartz and colleagues on the congenital long QT syndrome (LQTS) [136, 137]. Their work demonstrated that syndromes resulting from autosomal dominant inheritance resulted in long QT intervals on ECG, syncope, and death from an arrhythmia having the characteristic torsades de pointes morphology [136, 137]. We now understand that rather than a single disease entity characterized by a long QT interval on the electrocardiogram, lesions occur that are literally family-specific in potassium and sodium channels [138–141]. With regard to the potassium channels, two potassium channel pore-forming or α-subunits, (KvLQT1 and HERG) have been implicated in the LQT_1 and LQT_2 syndromes, respectively, while two beta subunits, minK and MiRP1 are involved in LQT_5 and LQT_6 respectively. In addition, the sodium channel, SCN5A has been found associated with the LQT3 syndrome. All these subunits contribute to the genesis of the arrhythmias in LQTS, although via different mechanisms. The K channels involved normally carry repolarizing currents, but lose function in LQTS such that there is a decrease in outward current through the ion channel in question, thereby prolonging the duration of repolarization. In contrast, the Na channel manifests an increase in inward current during the plateau of the action potential, giving rise to prolongation of repolarization.

The initial gene identified as associated with LQTS was the KvLQT1 gene [138] in which intragenic deletions, missense mutations, deletion mutations and insertion mutations all have been described (see [139] for summary). This family of abnormalities was incorporated in the LQT1 family of channelopathies. Based on the association of the beta-subunit, minK to impart normal function to KvLQT1, it was also hypothesized and later demonstrated [140] that mutations in minK can also contribute to LQTS (LQT5).

The second major potassium channel involved in LQTS was the HERG channel (LQT2). Intragenic deletions, missense mutations and duplications [139] all have been implicated here. The potassium channel subunit MiRP1 – largely associated with HERG – also has been shown to express missense mutations contributing to LQTS [141] (LQT6).

The remaining channelopathy noted has not been in a potassium channel, but in the sodium channel, SCN5A (LQT3). Missense mutations and intragenic deletions [139] have been shown to contribute to the persistence of inward current during the plateau of the action potential here.

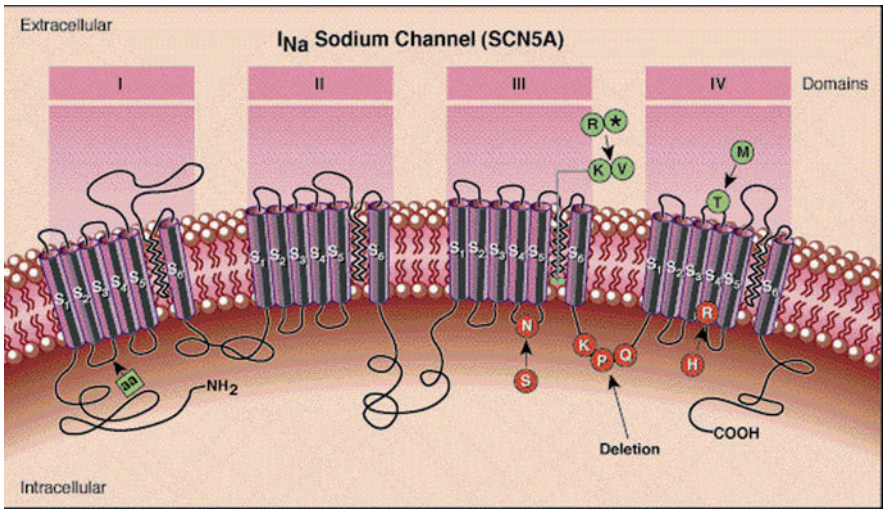

Figure 23.15

The predicted secondary structure of the cardiac sodium channel and locations of mutations causing idiopathic ventricular fibrillation (IVF) and chromsosome-3-linked long –QT syndrome (LQT). The channels consist of four putative transmembrane domains (DI-DIV), with each domain containing six transmembrane segments (S1-S-6). IVF mutations are shown in green and LQT- associated mutations in red (Reproduced with permission from Chen et al. (1998)).

It is interesting to note that lesions close in locus to those in the SCN5A channel are not uniquely associated with LQTS (Fig. 23.15). Rather, it has been demonstrated that in the Brugada syndrome, in which there is also familial inheritance, mutations in SCN5A are associated with a loss of function or rapid recovery from inactivation of the sodium channels. The arrhythmia is expressed far more in young adult males than in females and has shown a particular predilection for Asian populations [141, 142]. Hence subtle differences among loci in the SCN5A channel in Brugada's syndrome and LQTS result in major differences in terms of age, gender, and phenotypic expression of the arrhythmia seen.

A final arrhythmia to be mentioned is familial atrial fibrillation. The familial inheritance is well-established here, linkages to chromosomes 6 and 10 have been identified and abnormalities in at least one ion channel (I_{ks}) and the $KvLQT_1$ and mink subunits have been noted [143]. It is probable however that this information represents only a subset of patients with familial atrial fibrillation.

23.4 Alterations in Refractory Period

After the upstroke of the action potential, the sodium channels are inactivated, and the fast sodium current ceases to flow. Inactivation of the inward Ca^{2+} current and activation of outwardly directed potassium currents bring about repolarization. The sodium channels remain inactivated throughout the action potential plateau until repolarization increases membrane potential levels negative to about −60 mV. Inactivation is then gradually removed as repolarization continues. Complete removal of inactivation occurs when membrane potential returns to around −90 mV. During the plateau, when Na^+ channels are inactivated, the cell cannot be excited. The period during which the cell cannot respond to an impulse by initiating a propagated action potential is referred to as the "effective refractory period." During the latter phase of repolarization, progressive removal of inactivation allows increasingly large sodium currents to flow through the still partially inactivated sodium channels when the cells are excited. This is the "relative refractory period." The rate of rise of action potentials initiated during the relative refractory period is reduced because the Na^+ channels are only partially reactivated. Hence, the conduction velocity of these "premature" action potentials is low. In cells with slow response action potentials (sinus and AV nodes or depolarized myocardial fibers), the effective refractory period and recovery of

excitability persists until after complete repolarization. Removal of inactivation of slow channels is time dependent as well as voltage-dependent, and as result the relative refractory period extends well into diastole.

Alterations of both the effective and relative refractory periods may contribute to the occurrence of reentry in several different ways. First, as indicated previously, a decrease in the effective refractory period can decrease the size of reentrant circuits enabling them to exist in many localized areas of the heart. In fact, if the effective refractory period is decreased sufficiently, more than one reentrant circuit can exist at a time in some regions [144, 145]. The effective refractory period of atrial muscle, for example, is decreased by the acetylcholine released during vagal stimulation. As a result, reentry in atrial muscle causing atrial fibrillation is more easily induced during vagal stimulation [146]. Many reentrant circuits probably exist simultaneously during this arrhythmia [144]. Action potential duration and effective refractory are decreased in the ventricle during the early minutes of acute ischemia [147], or in some of the ventricular muscle cells in chronically ischemic areas, probably contributing to the occurrence of reentry [148]. Action potential duration and the effective refractory period of Purkinje fibers just distal to a site of conduction block may be decreased by the effects of electrotonic interactions with muscle proximal to the site of block, enabling reentrant impulses to reexcite the Purkinje regions [149].

Marked differences in refractory periods of closely adjacent regions may contribute to the initiation of reentry by causing localized block of premature impulses – a mechanism for the transient or unidirectional block discussed earlier. Inhomogeneities in the effective refractory periods in adjacent regions occur in the atria during vagal stimulation because of the irregular distribution of nerve endings [150], and in the ventricle and Purkinje system during acute or chronic ischemia [62, 148]. Moreover, recent data suggest that with healing of myocardial infarct there is a sprouting of sympathetic nerves growing in areas that had been totally or partially demonstrated as a result of ischemia [151]. Depending in the distribution of this neural growth, increased heterogeneity of sympathetic input may occur.

When the effective refractory period of adjacent regions are sufficiently different, conduction of an early premature impulse may block in the region with the longest refractory periods but may proceed slowly through the relatively refractory myocardium in the region with the shorter refractory period (Fig. 23.22). The slowly conducting impulse may return to excite tissue just distal to the region of block and then reexcite tissue proximal to the site of block. Sufficient time must elapse during propagation to permit this region proximal to the site of block to recover excitability. Inhomogeneities in refractory periods are also a probable cause of reentry initiated by early premature impulses in the sinus and AV nodes [152, 153].

23.5 Abnormal Impulse Conduction and Reentry

The second major cause of arrhythmias is abnormal impulse conduction. One means whereby conduction abnormalities can cause arrhythmias has already been discussed, namely, the escape of subsidiary pacemakers that occur when there is sinoatrial, or atrioventricular block. Abnormal impulse conduction can also cause reentrant excitation, a mechanism for arrhythmias that does not depend on pacemaker activity.

Before discussing abnormalities of impulse propagation it is important to review the normal propagation of the cardiac impulse. As a general rule it is understood that propagation is more rapid in fibers and through fiber bundles of large diameter than of small diameter [7]. However, given that the cell membrane is a good insulator, it is imperative that for propagation to proceed intercellular sites be present that have low resistances, permitting the flow of electrical current and of signaling molecules from cell to cell. These sites are the so-called gap junctions, regions at which the membranes of adjacent cells are closely apposed [154]. Examination of such sites reveals the presence of intercellular channels, whose anatomy is contributed to by one hemichannel provided by each cell (Fig. 23.16). Each hemichannel is referred to as a connexon, each of which is formed by a rosette-like pattern of 6 transmembrane spanning proteins called connexins. A number of connexins occur in the cells of the body: those most numerous in heart are connexins 43 (most prominent in atrial and ventricular myocardium), 45 (most prominent in the sinoatrial node and the ventricular conducting system), and 40 (most prominent in sinoatrial node and atrial myocardium and ventricular conducting system)[155]. Gap junctional density is greatest at the longitudinal ends of myocytes, thereby facilitating propagation along the long axes of cardiac fibers. Gap junctions are also seen at the lateral margins of myocytes, but given their lower density, current flow transversely is a fraction of that longitudinally [154].

It is the combination of low resistance junctions and the upstroke velocity of an arriving action potential that contributes most immediately to the propagation of the cardiac impulse. However, the relationship between number of

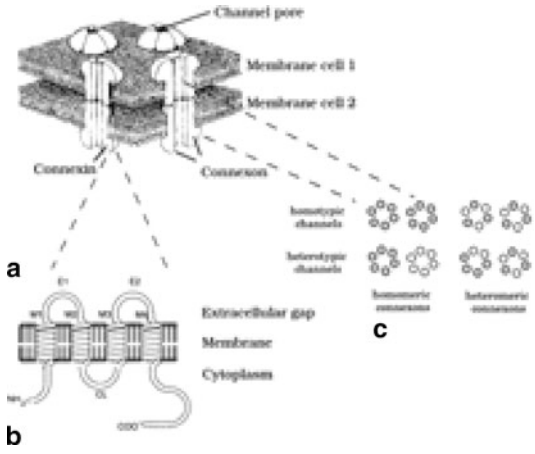

Figure 23.16

Schematic illustration of gap junction structure. (a) Part of a gap junction plaque showing several channels interconnecting two cells and the composition of an individual channel from two half-channels (connexons) which are composed of connexin proteins. (b) Secondary structure of a single connexin protein. (c) Scheme explaining the composition of homotypic and heterotypic channels from homomeric and heteromeric connexons (Reproduced with permission from van Veen et al. (2001)).

connexins present in any region of the heart and conduction velocity is complex, because there is a large margin of safety within the system. Specifically in myocardium it appears that the preponderance of connexins must be lost before conduction begins to slow [156]. Hence, extensive pathology must be present before a change is seen in the propagation of the cardiac impulse.

During sinus rhythm, the cardiac impulse usually dies out after the sequential activation of the atria and ventricles, because it is surrounded by tissue that it recently excited and which is therefore, refractory. A new impulse must arise in the sinus node for subsequent activation. Under special conditions the propagating impulse may not die out after complete activation of the heart but it may persist to reexcite (reenter) the atria or ventricles after the end of the refractory period [157]. The underlying principles that enable this reentrant excitation to occur can be illustrated with a simple experimental model consisting of a ring of excitable tissue. This model was first studied by physiologists during the early twentieth century and the results of these studies provided much of the basic information which has led to an understanding of reentrant mechanisms [158, 159]. In fact, more is being learned even today from studies on simple rings [160]. As shown in Fig. 23.17, if a ring of excitable tissue is stimulated at one point, two waves of excitation progress in opposite directions around the ring, but only one excitation of the ring occurs since the waves collide and die out. By temporarily applying pressure near the site of stimulation, however, an excitation can be induced to progress in only one direction. If the compression then is removed restoring conduction in this region, the impulse can then propagate around the ring, reenter tissue it previously excited and continue to circulate. Circular conduction of this kind has also been called circus movement.

Reentry does not occur normally in the heart. The pattern of conduction and the dying out of each impulse of sinus origin might be represented by the diagram in Fig. 23.17a. It is apparent that for reentry to occur a region of block must be present, at least, transiently. The block is necessary to provide the return pathway for the impulse to reenter the region it is to reexcite. Transient block, causing reentry, can occur in the heart after premature excitation (see below). Reentry also may occur when there is permanent block, but the block then must be unidirectional. In the ring experiment shown in Fig. 23.17, identical circus movement would occur if, instead of transient compression, permanent unidirectional conduction block were present. This means that conduction is blocked in one direction (from right to left in the diagram) but can proceed in the other (from left to right). It is obvious that if permanent block occurred in both directions reentry could not occur. Unidirectional block often occurs in cardiac fibers in which excitability and conduction are depressed. The electrophysiological mechanisms are discussed later in this chapter.

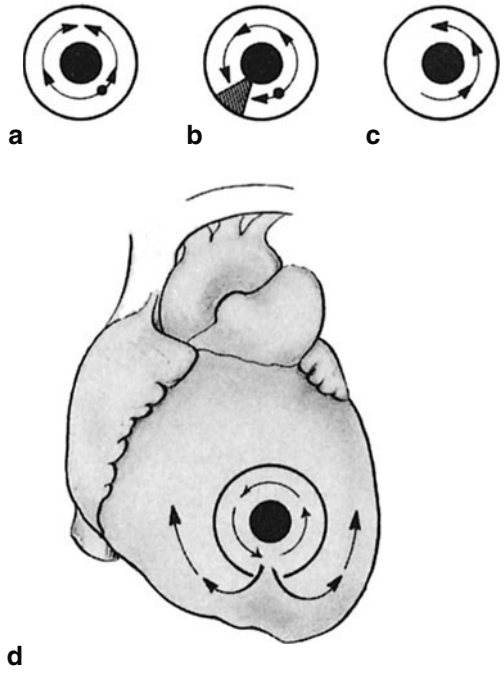

Figure 23.17

Schematic representation of reentry in a ring of cardiac tissue. The pattern of impulse propagation is indicated by the arrows and the small dot indicates the area in which the ring is stimulated. In (a), impulses propagate away from the point of stimulation in both directions and collide; no reentry occurs. In (b), in which the shaded area was compressed, the impulse propagates around in the ring in any one direction. Immediately, after stimulation the compression was relieved. Part (c) shows the circulating impulse returning to its point of origin and then continuing around the loop. Identical reentry would occur if the cross-hatched area were a region of permanent unidirectional conduction block, with the conduction block in the right-to-left direction. Part (d) shows how reentry in a loop of the kind described in (a)–(c) can cause arrhythmias if located in the heart. In this example, the loop is composed of ventricular muscle which is functionally separated from the rest of the ventricles along most of its border (bold line), perhaps as a result of fibrosis, but in functional continuity with the ventricles at its lower end. The arrows in (d) show how excitation waves propagate into the ventricles from continuously circulating impulses to cause ventricles tachycardia (Reproduced with permission after Wit (1979) © Excerpta Medica, Amsterdam).

In addition, for reentry to occur, the impulse must always find excitable tissue in the direction in which it is propagating. This requires the conduction time around the loop to be longer than the effective refractory period of the cardiac fibers that compromise the loop. If it is not, conduction of the reentering impulse would block. Normal heart muscle (excluding nodal fibers) has a refractory period which ranges from about 150–500 ms and a conduction velocity of at least 0.5–2.0 ms^{-1}. Therefore, the impulse conducting at a normal velocity of at least 0.5 ms^{-1} in reentrant pathway must conduct for at least 150 ms before it can return and reexcite a region it previously excited. This means the conduction pathway must be at least 7.5 cm long for reentry to occur in cardiac fibers with normal conduction and refractory properties. Such long reentrant pathways, functionally isolated from the rest of the heart, rarely exist. Clearly, the length of the pathway necessary for reentry can be shortened if the conduction velocity is slowed and/or the refractory period is reduced. For example, if conduction velocity is slowed to 0.05 ms^{-1}(as can occur in diseased cardiac fibers or in the normal sinus or AV node) the reentrant circuit need be no more than 7.5 mm in length. Circuits of this size can readily exist in the heart. Therefore, slowed conduction in combination with unidirectional block is a prerequisite which permits reentry to occur.

The "loop" of tissue which enables reentry to occur is called the reentrant circuit. It can be located almost anywhere in the heart and can assume a variety of sizes and shapes. The circuit may be an anatomical structure such as a ring of

cardiac fibers in the peripheral Purkinje system. The circuit may also be functional and its existence, size, and shape be determined by electrophysiological properties of cardiac cells rather than anatomy. The size and location of an anatomical by defined reentrant circuit obviously remains fixed and results in what may be called "ordered reentry." The size and reentrant circuits dependent on functional properties rather than anatomy may also be fixed but they also may change with time leading to random reentry. Random reentry is probably most often associated with atrial or ventricular fibrillation, whereas ordered reentry can cause most other types of arrhythmias [3].

23.5.1 Mechanisms for Slow Conduction

There can be a number of causes for the slow conduction and block which predispose to the occurrence of reentry. The speed at which impulses propagate in cardiac fibers is dependent on certain features of their transmembrane action potentials and passive electrical properties [161]. Alterations in either (by cardiac pathology) can result in reentrant arrhythmias. An important feature of the transmembrane potential of working (atrial and ventricular) myocardial and Purkinje fibers which governs speed of propagation is the magnitude of the inward sodium current flowing through the fast sodium channels in the sarcolemma during the active potential upstroke and the rapidity with which this current reaches maximum intensity. The magnitude of this current flow determines the amplitude of phase 0 of the action potential; the speed of development of current flow is reflected in the rate at which the cell depolarizes (V_{max} of phase 0) [162]. The depolarization phase or upstroke of the action potential may be considered as resulting from the opening of specialized membrane channels (fast sodium channels) through which sodium ions rapidly pass form the extracellular fluid into the cell (Fig. 23.18). The process of channel opening and closing has been described in a model devised by Hodgkin and Huxley for the nerve action potential [163]. According to this model, two "gates" control the passage of sodium ions through the channel. One gate m moves rapidly to open the channel; the other gate h moves slowly to close the channel. For an action potential to be initiated, a large enough area of membrane must be depolarized rapidly to threshold potential so that enough sodium channels are opened to give rise to the regenerative inward sodium current (m gates opened). After the upstroke of the action potential the sodium channels inactivate and the fast sodium current ceases to flow (h gates closed)(Fig. 23.18).

The inward sodium current causes conduction of the cardiac impulse as follows: Impulse conduction occurs from one cell exciting the next by means of local currents which flow ahead of the action potential. These local currents depolarize the membrane potential to threshold potential to elicit the action potential. This process is illustrated in Fig. 23.19. An action potential is elicited at site A and is accompanied by a rapid inward sodium current I_{Na}. Part of this inward current flows along the fiber towards site B, which has not yet been excited. This intracellular flow is called the axial current I_a. Site A is the current source and site B, the current sink. The current at site B exits through the membrane either as capacitive current I_c which depolarizes the membrane potential or as membrane current flowing through ionic channels I_i. If the depolarization caused by the capacitive current is large enough to bring the membrane to its threshold potential an action potential will occur at site B. When the resting membrane resistance r_m (determined by channels that conduct ionic current near the resting potential) is high, a larger portion of the current passes out as capacitive current and is, therefore, more effective in eliciting an action potential. Also, when the resting membrane resistance is high, more axial current spreads for a longer distance along the fiber and excites more distant areas. There is also intracellular resistance to the axial current flow r_a which determines how far axial current spreads and its effectiveness in depolarizing the membrane at a distance. The cytoplasm offers minimal resistance to the spread of axial current. A larger portion of the resistance is located at the intercellular connections between myocardial fibers-gap junctions of the intercalated disks. Although extracellular resistance to current flow has an influence, it is normally significantly less than intracellular resistance.

The conduction velocity depends both on how much capacitive current flows out at unexcited sites ahead of the propagating wavefront and the distance at which the capacitive current can bring membrane potential to threshold. One important factor which influences the amount of axial and, therefore, capacitive current is the amount of fast inward current generated by the propagating action potential. A reduction of this inward current, leading to a reduction in the rate or amplitude of depolarization, may decrease axial current flow, slow conduction and lead to conduction block. Such a reduction may result from inactivation of sodium channels (Fig. 23.18). The intensity of the inward Na^+ current

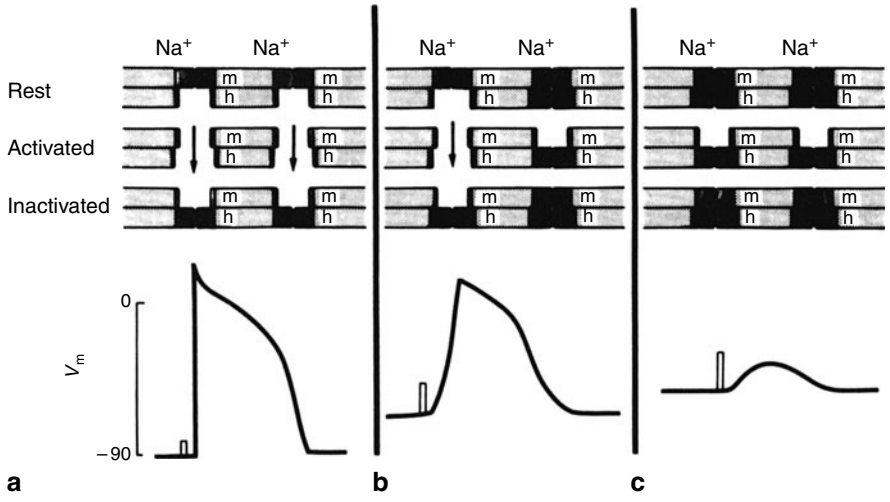

Figure 23.18

Schematic depiction of the Na^+ channels in the sarcolemma at rest, in the activated state and in the inactivated state. The "gates", m and h control channels opening and closing, respectively. At the bottom of the figure are representative action potentials. In (a) at a resting potential of −90 mV, most of the Na^+ channels can be activated causing an action potential with rapid upstroke. Activation is represented by open channels and the arrow depicting inward Na^+ current. When the membrane depolarizes during the upstroke of the action potential, the channels inactivate; the diagram shows that they are closed. In (b), resting potential is reduced to −70 mV and about 50% of the Na^+ channels cannot be activated. A depressed fast-response action potential with a slow upstroke occurs when the cell is excited because the inward Na^+ current is decreased. In (c), at a resting potential less than −60 mV; Na^+ channels cannot be activated and an action potential might not be elicited (Reproduced with permission after Wit and Rosen (1981) © American Heart Association, Dallas, Texas).

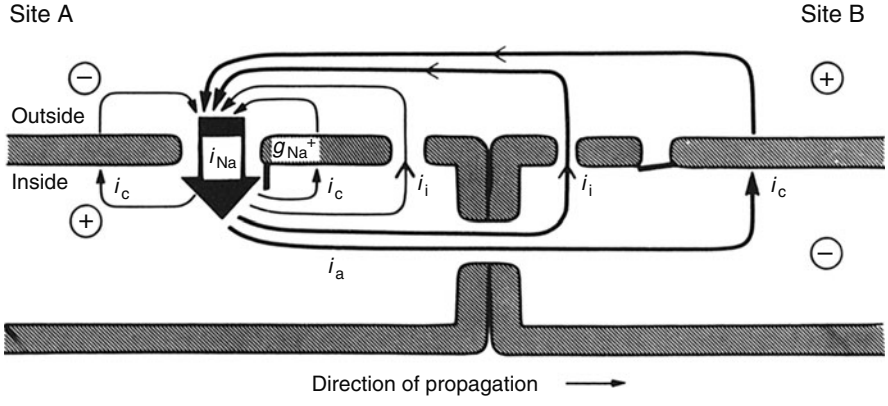

Figure 23.19

Schematic diagram of the propagation of an action potential along a cardiac muscle fiber: i_{Na}, sodium current; I_a, axial current i_c, capacitive current: I_i, ionic current: g_{Na+}, conductivity of the membrane to Na ions. The larger arrow indicates the large inrush of Na ions (I_{Na}) through membrane channels during the upstroke (Reproduced with permission after Frame and Hoffman (1984) © Nijhoff, The Hague).

depends on the fraction of Na^+ channels which are open when the cell is excited and the size of the Na^+ electrochemical potential gradient (relative concentration of Na^+ outside the cell, in the extracellular space, compared to Na^+ concentration inside the cell) [84, 164]. The fraction of Na^+ channels available for opening is determined largely by the level of membrane potential at which an action potential is initiated. Na^+ channels are inactivated either after the upstroke of an action potential or if the steady-state resting membrane potential is reduced. Immediately after the upstroke cardiac fibers are inexcitable because of Na^+ channel inactivation at the positive level of membrane potential. During repolarization progressive removal of inactivation allows increasingly large Na^+ currents to flow through the still partially inactivated Na^+ channels when the cells are excited. The inward Na^+ current and rate of rise of action potentials initiated during this relative refractory period are reduced because the Na^+ channels are only partly reactivated [164]. Hence the conduction velocity of these premature action potentials is low. Premature activation of the heart can therefore induce reentry because premature impulses conduct slowly in regions of the heart where the cardiac fibers are not completely repolarized (where Na^+ channels are to some extent inactivated) and their conduction may block in regions where cells have not repolarized to about −60 mV. Hence the prerequisites for reentry – slow conduction and block – can be brought about by premature activation.

Reentry might also occur in cardiac cells with persistently low levels of resting potential (which may be between −60 and −70 mV) caused by disease. At these resting potentials, a significant fraction of the Na^+ channels is inactivated, and therefore unavailable for activation by a depolarizing stimulus. The magnitude of the net inward current during phase 0 of the action potential is reduced and consequently both the speed and amplitude of the upstroke is diminished, decreasing axial current flow and slowing conduction significantly. Such action potentials with upstrokes dependent on inward current flowing via partially inactivated Na^+ channels are sometimes referred to as "depressed fast responses" (Fig. 23.18). Further depolarization and inactivated of the Na^+ channel may decrease the excitability of cardiac fibers to such an extent that they may become a site of unidirectional conduction block [1]. Thus in a diseased region there may be some area of slow conduction and some area of conduction block, possibly depending on the level of resting potential. The combination may cause reentry.

After the upstroke of the action potential, membrane potential begins to return to the resting level during phase 1 repolarization because the sodium channels are inactivated and the fast (depolarizing) sodium current ceases to flow. However, this return is slowed by a second inward current which is smaller and slower than the fast sodium current and probably is carried by both sodium and calcium ions [165] (Fig. 23.20). This secondary inward current flows through so-called slow channels that are distinct from the fast sodium channels. The threshold for activation of the slow inward current is in the range of −30 to −40 mV compared with −60 to −70 mV for the fast sodium current. This current inactivates much more slowly than the fast sodium current and gradually diminishes as the cell repolarizes. Under special conditions, it may also underlie the occurrence of the slow conduction that causes reentrant arrhythmias [49]. Although, the fast sodium current may be largely inactivated at membrane potentials near −50 mV, the slow inward current is not activated and is still available for activation [43, 84, 165]. Under certain conditions in cells with resting potentials less than −60 mV (such as when membrane conductance is very low or when catecholamines are present), this normally weak slow inward current may give rise the regenerative depolarization characteristic of a propagated action potential. This propagated action potential, dependent on slow inward current alone, is "the slow response" (Fig. 23.20) [55]. Since this inward current is weak, conduction velocity is slow and both unidirectional and bidirectional conduction block may occur [163]. Slow response action potentials can occur in diseased cardiac fibers with low resting potentials but they also occur in some normal tissue of the heart, such as cells of the sinus and AV nodes where the maximum diastolic potential is normally less than about −70 mV [55, 166].

The slow conduction and block necessary for reentry can also be caused by factors other than the decrease in inward current accompanying a decrease in membrane potential. These other factors tend to decrease the magnitude and spread of axial current along the myocardial fiber. An increased resistance to axial current flow, which is expressed as "effective axial resistance" (resistance to current flow in the direction of propagation which is dependent on the intracellular and extracellular resistivities) may decrease conduction velocity [167, 168]. Whether an increase in extracellular resistance to current flow sufficient to impair conduction and cause arrhythmias occurs during pathological states is not yet known. It is likely, however, that sufficient increases in intracellular resistance can occur. Although the intracellular resistance depends on both the resistance of the cytoplasm and the resistance at the gap junctions which couple cells together, the change in intracellular resistance causing arrhythmias probably results mainly from changes in junctional resistance.

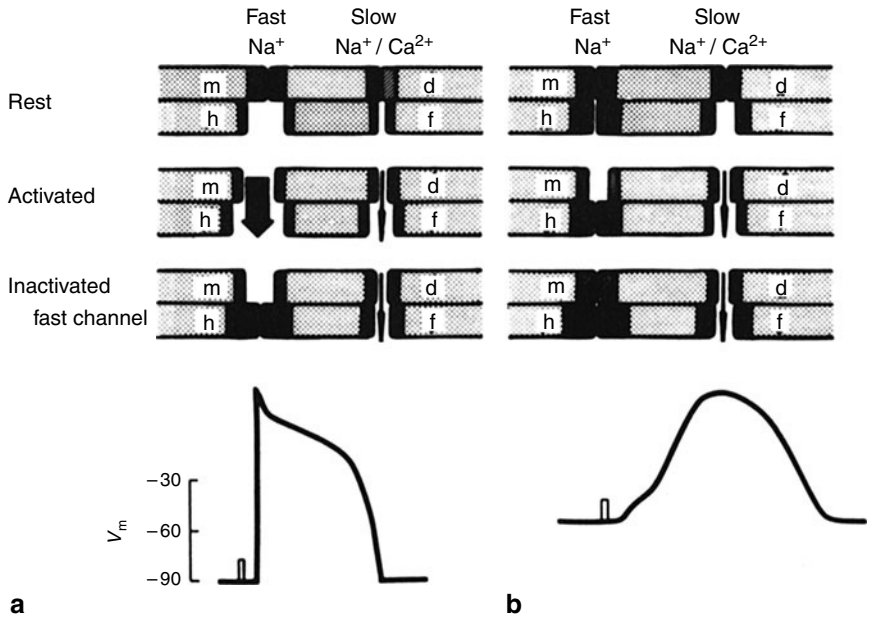

Figure 23.20

Schematic depiction of the sarcolemma containing the fast Na' channels and the slow Na^+/Ca^{2+} channels. The "gates" m and h control Na^+ channel opening and closing, respectively. The "gates" d and f control Ca^{2+} channel opening and closing, respectively. Representative action potentials are shown at the bottom of the figure. In (a), the normal action potential, elicited from a resting potential of −90 mV is shown. At rest, both fast and slow channels are inactivated (represented by closed channels). After the fiber is stimulated the channels are activated (represented by open channels) and fast inward Na^+ current (*large arrows*) and slow inward Na^+/Ca^{2+} current (*small arrows*) cause the action potential upstroke and plateau. The fast channel inactivates before the slow channel. In (b), in a cell with a resting potential of −50 mV, the fast Na^+ channels are not activated when the fiber is stimulated. The slow channels can still be activated and current can pass through them to cause slow response action potentials (Reproduced with permission after Wit and Rosen (1981) © American Heart Association, Dallas, Texas).

During conduction of the impulse, axial current flows from one myocardial cell to the adjacent cell through the gap junctions at the intercalated disks (which normally have a relatively low resistance) [161] and, therefore, the resistance, extent and distribution of these junctions have a profound influence on conduction. This influence can be seen even in normal atrial or ventricular myocardium. In regions where cardiac muscle fibers are closely packed together and arranged parallel to each other in a uniform manner, conduction in the direction parallel to the myocardial fiber orientation (along the long axis of the myocardial fibers) is much more rapid than in the direction perpendicular to the long axis (Fig. 23.21) [167–169]. This property is known as anisotropy. Conduction perpendicular to the long axis of the fibers can be slow as $0.1\,ms^{-1}$ even though resting and action potentials of the muscles fibers are normal. The slow conduction is caused by an effective axial resistivity which is higher in the direction perpendicular to fiber orientation than parallel to fiber orientation. This higher axial resistivity results in part from fewer and shorter intercalculated disks connecting myocardial fibers in a side-to-side direction than in the end-to-end direction. Conduction in normal ventricular myocardium can, therefore, be slow enough to cause reentry as will be discussed in more detail later.

Pathological alterations in anatomy may also cause slow conduction by increasing axial resistance through effects on coupling between cells. Fibrosis in the heart separates myocardial fibers, reducing the number of disk connections and decreasing the extent or area of connections that remain (see Fig. 23.22a). An example is the effect of fibrosis, resulting from infarction, on the myocardial fibers in the infracted region. The broad, wide disks which occur at the longitudinal ends of normal cells no longer are present because of the deformation of the cells by the connective tissue. Only short

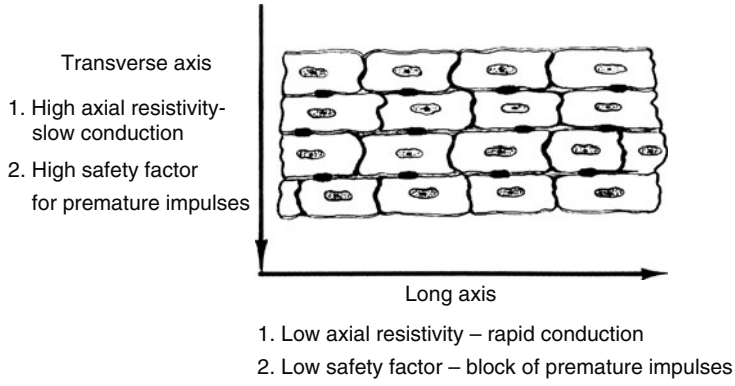

Figure 23.21

Influence of anisotropic structure of cardiac muscle on conduction velocity. In the uniformly anisotropic cardiac muscle [137, 138] shown, the myocardial fibers are arranged parallel to each other and are packed closely together. Intercalated disks join cardiac cells both at their ends and in a side-to-side direction. The disks joining the fibers in the end-to-end direction are usually broad and numerous resulting in a low axial resistivity in this direction, whereas the disks connecting cells in a side-to-side direction are short and sometimes sparse, resulting in a higher axial resistivity in this direction. The high safety factor for premature impulses in the transverse axis means that, in this direction, premature impulses are not easily blocked (Reproduced with permission after Gardner et al. (1984) © Lea & Febiger, Philadelphia, Pennsylvania).

segments of intercalculated disks remain in some regions. Conduction is very slow despite the presence of normal resting potentials, probably because there is a high resistance to current flow through the shortened disks [170].

A combination of reduction in gap junctions plus microfibrosis occurring between myocytes is responsible for the slow conduction and reentry seen in, for example, healing myocardial infarction [171, 172]. In addition, the formation of gap junctions along the lateral margins of cells that had been uncoupled during the acute phase of ischemia can favor current flow from cell to cell along the lateral margins [173, 174]. Resultant very slow transverse conduction to the point of discontinuous propagation is a mechanism whereby reentry has been shown to occur (summarized in [175]). In addition to structural changes, a rise in intracellular calcium can slow conduction by increasing resistance to current flow through gap junctions in the disks, since calcium levels profoundly affect the resistance of the gap junction [176]. This may occur during prolonged periods of ischemia [177]. Cardiac glycosides also increase resistance at the disk by increasing intracellular calcium [33].

The effective axial resistivity is also dependent on the size and shape of the myocardial cells (Fig. 23.23). Resistance to current flow may increase markedly and conduction may be slowed in regions where cells branch or where there are abrupt increases in cell size or number. A detailed description of the mechanisms is given by Spach et al. [167, 168], and Joyner et al. [178, 179]. Some discussion of these factors can also be found in Sect. 23.5.2.

23.5.2 Unidirectional Block of Impulse Conduction

According to the model illustrated in Fig. 23.17, unidirectional conduction block (block of conduction in one direction along a bundle of cardiac fibers, while conduction in the other direction is maintained) is necessary for the occurrence of many kinds of reentry. Unidirectional block in part of the circuit leaves a return pathway through which impulse conducts to reenter previously excited areas. There are a number of mechanisms that might cause unidirectional block, some of which have been demonstrated directly and others of which are the products of theoretical considerations. The mechanisms involve changes in both active and passive properties of the cardiac cells.

The unidirectional block needed for the initiation of the reentrant tachycardia may be transient, as exemplified by block of a premature impulse that initiates a reentrant tachycardia. The conduction of an impulse, which is sufficiently

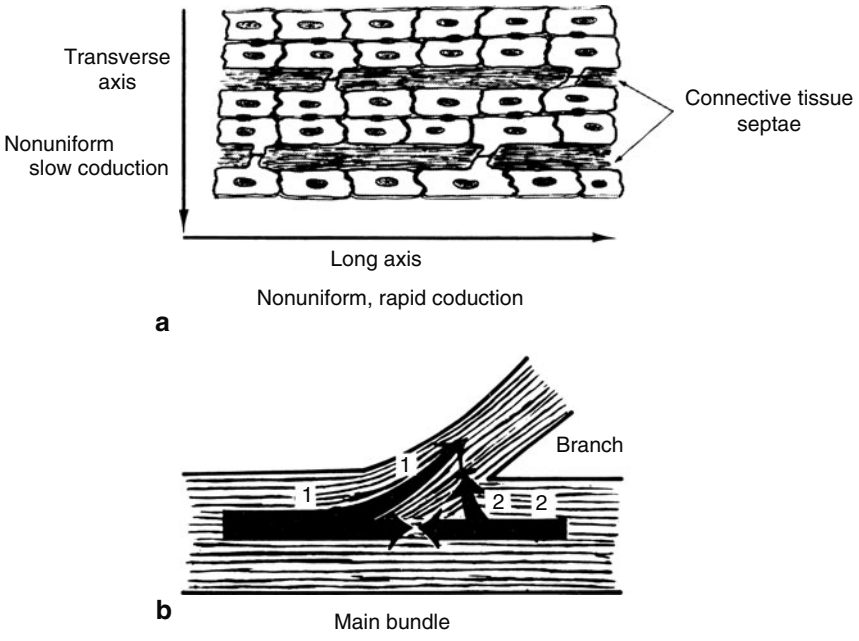

Figure 23.22

Influences of myocardial structure on impulse conduction. Part (a) shows the separation of myocardial fiber bundles that can result from fibrosis. This may reduce the number of disk connections, thereby slowing impulse conduction. Part (b) shows how branching of a fiber bundle can influence propagation. The lines within the main bundle and the branch indicate the orientation of the myocardial fibers. Conduction occurs in the direction of the long axis of the fibers when the impulse conducts along the main bundle into the branch as indicated by *arrow 1*. Conduction in this direction is not influenced by the presence of the branch. When an impulse conducts from the main bundle into the branch as indicated by *arrow 2*, there is a sudden change in fiber orientation in the direction of propagation so that the impulse must conduct transversely to the long axis of the fibers as it enters the branch. The sudden increase in axial resistivity caused by the change might cause block, particularly when there is some depression of the action-potential upstroke (Reproduced with permission from Gardner et al. (1984) © Lea & Febiger, Philadelphia, Pennsylvania).

premature, is blocked where it encounters cells that are not excitable because of incomplete repolarization but may continue to propagate in other regions of the reentrant pathway if the fibers are more fully repolarized and, therefore, excitable (see Sect. 23.5.3). Functionally, the region where the premature impulse blocks is a region of unidirectional block if it can be excited later, after it has recovered excitability, by an impulse propagated from another direction as shown in Fig. 23.24.

Unidirectional conduction block in a reentrant circuit can also be persistent and independent of premature activation. In a bundle of atrial, ventricular or Purkinje fibers with normal electrophysiological properties, an impulse can conduct rapidly in either direction. However, there is usually some asymmetry in the conduction velocity and as a consequence, conduction in one direction may take slightly longer than in the other direction [1, 55, 161]. This is of no physiological significance. The asymmetry of conduction can be the result of several factors. Bundles of cardiac muscle are composed of interconnecting myocardial fibers (cells), packed in a connective tissue matrix. These calls have differing diameters and branch frequently. An impulse conducting in one direction encounters a different sequence of changes in cell diameter, branching and frequency and distribution of gap junctions than it does when traveling in the opposite direction. The "configuration of the pathways" in each direction is not the same [55]. As mentioned above, these structural features influence conduction by affecting the axial current. Theoretical analyses indicate that the conduction velocity of an impulse passing abruptly from a fiber of small diameter to one of large diameter transiently slows at the junction because the larger cable results in a larger sink in longitudinal axial current (there is more membrane for this current to depolarize to threshold if

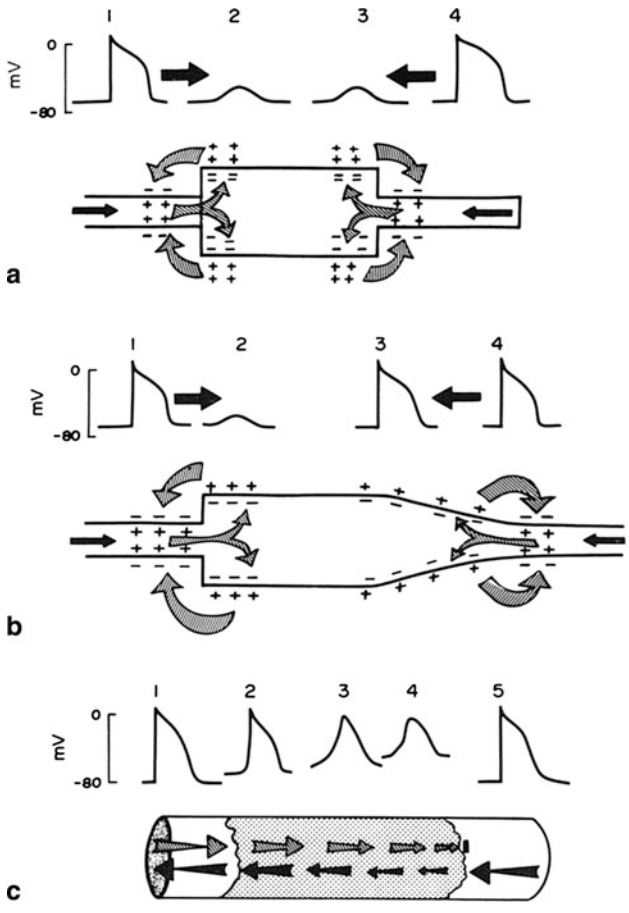

Figure 23.23

Mechanisms for unidirectional conduction block. Part (a) shows the effects on conduction of a small diameter fiber coupled to a large diameter fiber. When the impulse is conducting (*solid arrows*) from left to right there is a sudden increase in membrane area which the current flow (*shaded arrows*) must depolarize to threshold for conduction to continue. If the membrane is not depolarized to threshold, conduction blocks as indicated by action potential 2 (above). The change in membrane area in (a) is symmetrical, that is, the large diameter cable is connected at its other end to another small diameter cable. Therefore, an impulse conducting from right to left in the diagram would also block. Part (b) shows an asymmetrical nonuniformity that might cause unidirectional block. Conduction from left to right blocks at the region where there is an abrupt increase in the cable diameter as in (a) (see the action potentials). However the transition from large to small cable at the opposite end is gradual. An impulse conducting from right to left can still depolarize the membrane to threshold despite a gradual increase in membrane area (see text). Part (c) shows unidirectional block caused by asymmetrical depression of the action-potential upstroke. The stippled region represents a poorly perfused part of the cable between two normal regions. During conduction from left to right, the action potentials are progressively more depressed. Normal action potential 1 can excite 2, 2 excites 3 and 3 excites 4, but the slowly rising low-amplitude upstroke of 4 does not generate sufficient axial current to bring membrane potential of *5* to threshold and conduction blocks. In the opposite direction, the large amplitude action potential at *5* generates sufficient current to excite 4. Impulse conduction continues through the depressed region to the opposite end where the upstroke of action potential 2 is large enough to excite the normal adjacent area 1.

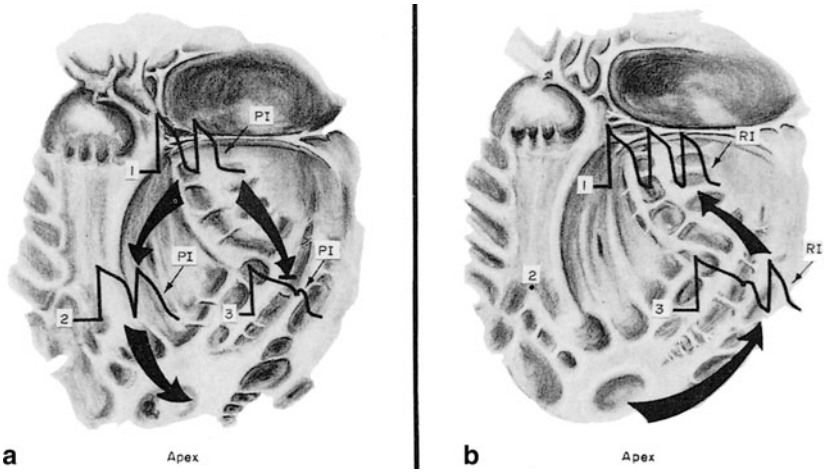

Figure 23.24

Mechanism for functional unidirectional conduction block and initiation of reentry in the subendocardial Purkinje network surviving over an area of extensive myocardial infarction [154]. Both (a) and (b) show the endocardial surface of the left anterior papillary muscle (to the left) and the anterior interventricular septum (to the right). Subendocardial Purkinje fibers in different regions have action potentials with different durations and refractory periods. Action potentials recorded at sites 1 and 2 have shorter durations and refractory periods than at site 3. In (a), an early premature impulse PI arising at 1 conducts into regions where action potentials have a longer duration (conduction pathways indicated by large arrows). The action potential at 3 is longer than at 2. Consequently the premature impulse can excite cells at 2 but conduction blocks at 3. This area becomes a site of unidirectional block because as shown in (b), the premature impulse, after conducting through 2 arrives at 3 when these cells are excitable. It excites the cells at 3 in the retrograde direction and then returns to its site of origin (1) as a reentrant impulse RI (Reproduced with permission after Wit et al. (1974) © Mosby, St Louis, Missouri).

conduction of the impulse is to continue) [161, 178–181]. A similar slowing occurs when an impulse conducts into a region where there is an abrupt increase in branching of the myocardial syncytium; conduction transiently slows because of the larger current sink provided by the increased membrane area that must be depolarized. In the opposite direction, it can be predicted that conduction will speed transiently at the junction between larger and smaller cable because the smaller sink for axial current results in more rapid depolarization of the membrane to threshold [161, 178–180]. Theoretically, if there is a large enough difference in the diameter of the two cables, an impulse conducting in the small fiber will block at the junction with the larger fiber while in the opposite direction, excitation will proceed from the large diameter fiber to the small one [180]. For this model to explain unidirectional block, once the abrupt change in cell diameter or membrane area has occurred it does not return to its original one. In the heart, however, it is more likely that the properties are more or less the same on each side of the region through which the asymmetrical conduction has occurred [180]. If the abnormalities of that region are symmetrical around its midpoint (an abrupt increase in fiber diameter followed later by an abrupt decrease (Fig. 23.23a), block would occur irrespective of direction. An asymmetrical uniformity is necessary for one-way conduction [181]. For example, there may be an abrupt increase in fiber diameter or effective axial resistance R_i followed by a gradual return to the original diameter (Fig. 23.23b). In this model, block would occur in the direction in which there is an abrupt increase in the sink for the reasons described above. However, in the opposite direction the gradual increase in diameter would not cause block because the axial current would actually increase (there is a decrease in R_i as the cable diameter is increased as well as an increase in transmembrane current because of the larger membrane area) [180] (Fig. 23.23).

It is doubtful, however, that abrupt changes of the magnitude required to cause block of the normal action potential exist because the safety factor for conduction is large; that is, there is a large excess of activating current over that required for propagation [161]. Dodge and Cranefield have pointed out that "only if an action potential is a relatively weak stimulus and the unexcited area is not easily excited will plausible changes in membrane resistance, cell diameter, or intercellular

coupling block"[181]. There is the necessity for interaction of abnormal action potentials and decreased excitability with the preexisting anatomical impediments. When the resting potential of muscle fiber or Purkinje bundle is decreased, the reduced action potential upstroke results in a decreased axial current as described above and, therefore, the action potential is a weak stimulus. The normal directional differences in conduction are then exaggerated. At a critical degree of depression, conduction may fail in one direction while being maintained in the other (although it may be markedly slowed). At this critical degree of depression the reduced axial current is not sufficient to depolarize the membrane to threshold where the current sink is increased because of the structural changes described above, but the axial current is still more than adequate during conduction in the opposite direction (Fig. 23.23c).

It also has been proposed that block may occur at branching points where there is an abrupt change in the orientation of the myocardial fibers if there is a sudden increase of axial resistivity [168]. For example, an impulse conducting along a muscle bundle in a direction parallel to the fiber orientation (low effective axial resistivity) may conduct into a branch of that bundle; at the branching point the orientation of the myocardial fiber may be perpendicular to the original direction of conduction and therefore, the effective axial resistivity suddenly becomes high (Fig. 23.22b). Therefore, it seems that a sufficient decrease in axial current caused by depression of the action potential upstroke could result in conduction block of the impulse entering the branch from the direction in which there is the marked change in the fiber orientation, but no block from the opposite direction (Fig. 23.22).

Although the possible mechanisms for unidirectional conduction block discussed so far all involved important influences on conduction of the structure of muscle bundles, unidirectional block is most likely to occur when action potential upstrokes are depressed. Asymmetrical depression of the upstroke may also be an important factor that causes unidirectional conduction block irrespective of anatomy [55]. Such asymmetrical depression of the action potential might occur because of asymmetrical distribution of a pathological event. As a simple example, the action-potential upstrokes in a bundle of fibers may be diminished as a result of a reduction of perfusion after coronary occlusion, but reduction may be more severe towards one end of the bundle than the other (Fig. 23.23). A propagating impulse consisting of an action potential with the normal upstroke velocity enters the poorly perfused region and propagates through this region with decrement. That is, as it conducts from the less depressed to the more severely depressed end, the action-potential upstroke velocity and amplitude progressively decrease, as does the axial current caused by the upstroke [7]. When the impulse arrives at the opposite end of the depressed segment of the bundle with normal action potentials, the weak axial current may not be sufficient to depolarize the membrane to threshold. Conduction, therefore, blocks even though the normally perfused region is excitable. Conduction in the opposite direction, however, might still occur. The large axial current generated by the normal action potential flows for a considerable distance through the depressed region. These cells, in turn, may be able to excite adjacent fibers in the direction of propagation (Fig. 23.23c).

23.5.3 Reentrant Arrhythmias

It has been indicated above that reentry can occur in different regions of the heart, utilizing either anatomical or functional pathways. It has also been shown that slow conduction and block may have a number of different cellular mechanisms. Conceivably, any of these mechanisms may occur in either an anatomical or functional reentrant pathway. Several examples of reentry caused by the different mechanisms will now be provided.

23.5.3.1 Anatomical Pathways

Reentrant excitation caused by the slow conduction and block which accompany depression of the action potential upstroke (either because of premature excitation or because of a persistent reduction in the resting membrane potential) may occur in gross anatomically distinct circuits (around an anatomical obstacle). Reentrant excitation involving an anatomically distinct circuit and obstacle is exemplified by reentry in a loop of cardiac fiber bundles such as the loop of Purkinje fiber bundles in the distal conduction system illustrated in Fig. 23.25a. In this model of an anatomic circuit, slow conduction and unidirectional block are caused by reducing the steady-state level of the resting potential [182]. The unidirectional block (shaded area) is located near the origin of branch B in the loop of Purkinje fiber bundles; an impulse cannot conduct through this area in the anterograde direction but it can in the retrograde direction. Slow conduction

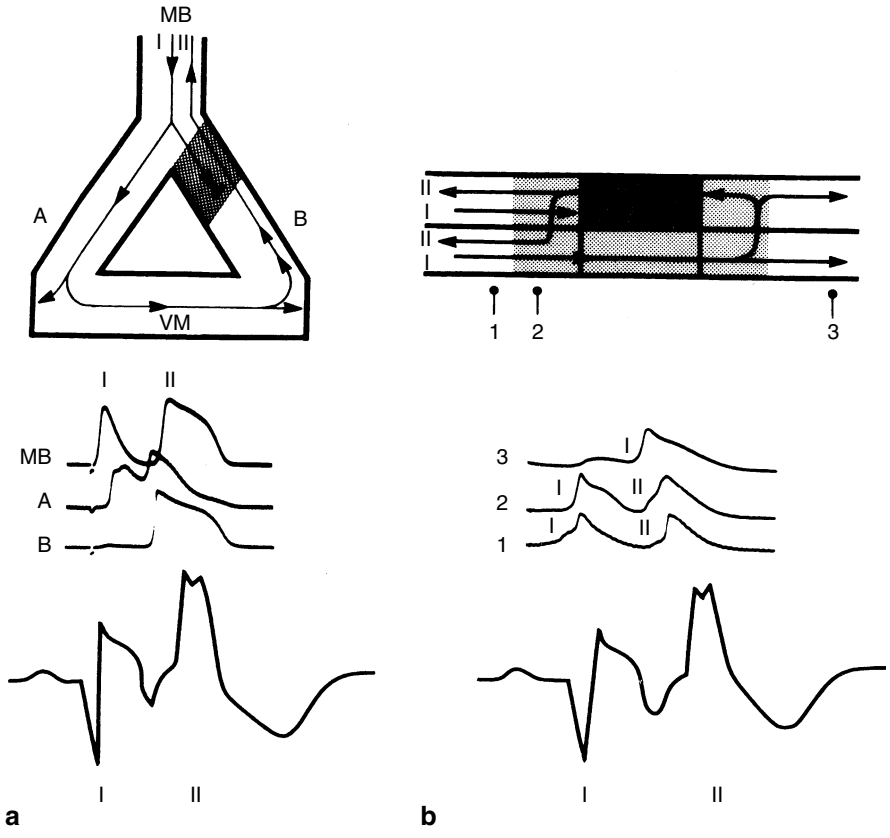

Figure 23.25

A possible mechanism for reentry in an anatomical pathway comprised of Purkinje fiber bundles and ventricular muscle. Part (a) shows a main bundle of Purkinje fibers (MB) which divides into two branches A and B before terminating on ventricular muscle (VM). A severely depressed area in which unidirectional conductional block occurs in the anterograde direction is located in branch B (shaded area). Conduction is slow throughout the rest of the loop because the Purkinje fibers have low resting potentials, and consequently, their action potentials have slow upstrokes. The arrows indicate the sequence of activation of the loop by the conducting impulse: *arrow I* represents an impulse of sinus origin entering the loop; *arrow II* is the reentering impulse leaving the loop (details of the mechanism by which reentry occurs are given in the text). Action potentials recorded from MB and branches A and B are shown below, together with an example of how the ECG might appear. Action potential I was recorded from the main bundle (MB) as impulse I entered the loop; the action potentials in A and B were recorded from Purkinje bundles A and B as the impulse conducted around the loop; and the action potential II in the MB trace was recorded from the main bundle when the impulse reexcited it. Impulse I would cause ventricular depolarization I on the ECG and impulse II would cause a ventricular extrasystole (ventricular depolarization II). Part (b) shows, at the top, how reentry can occur even in a single bundle of muscle or Purkinje fibers by the mechanism of reflection. The diagram depicts two adjacent fibers in a bundle. The entire shaded area is depressed and depression in the darker area of the upper fiber is so severe that unidirectional conduction block occurs there. The arrows indicate the sequence of activation in the bundle. Arrows labeled I show the impulse entering the bundle. Conduction of the impulse blocks in the fiber at the top in the severely depressed region but continues in the fiber at the bottom which is not as depressed. The impulse conducts transversely from the bottom fiber to the top fiber, once past the region *of* severe depression. It then conducts retrogradely through this severely depressed region in the top bundle. Arrows labeled II show the reentrant impulse returning to reexcite the left end *of* the bundle (see text). Action potentials recorded from sites 1, 2 and 3 in the lower fiber are shown below: action potentials labeled I were recorded as the impulse conducted from left to right; action potentials labeled II were recorded as the impulse returned to its origin. The bottom trace shows how such events might appear on the ECG (Reproduced with permission after Wit and Bigger (1975) © American Heart Association, Dallas, Texas).

occurs in the rest of the loop because of the low resting potentials. An impulse conducting into the loop via the main Purkinje fiber bundle (arrow showing impulse I) blocks near the origin of branch B and can enter only branch A through which it conducts slowly into the ventricular muscle (VM). The impulse then can invade branch B at its myocardial end. This branch had not been excited initially because of the unidirectional block at its origin and so the impulse can still conduct in a retrograde direction in branch B, through the region of unidirectional block, and then reexcite the main bundle from which it entered the loop (arrows showing impulse II).

The reentering impulse (II) will, of course, block if it returns to the main bundle while the fibers in that region are still effectively refractory. Hence, there is the necessity for slow conduction around the loop (slow conduction in only part of the loop, such as in the area of unidirectional block, would also suffice). The region of unidirectional block is necessary to prevent one part of the loop (branch B) from being invaded by the anterograde impulse and so provides a return excitable pathway for the reentering impulse as mentioned before.

When the reentrant impulse returns to the main bundle it may travel throughout the conduction system to reactivate the ventricles, causing a premature ventricular depolarization. It also may reinvade the bundle of Purkinje fibers through which it originally excited the ventricular muscle (branch A) and once again propagate back through the reentrant pathway. This may result in a continuous circling of the impulse around the loop and a tachycardia.

If conduction in this pathway – the loop of Purkinje fibers and ventricular muscle – is not sufficiently slow to permit reentry or if there is no strategically located site of unidirectional block, reentry might still be induced by premature activation. If the cardiac fibers are activated prematurely, before they have completely recovered excitability, the premature impulse will conduct slowly and unidirectional block may result because of the low safety margin for conduction in partially refractory tissue. Premature activation may, therefore, lead to reentry of kind illustrated in Fig. 23.25.

Anatomic circuits also might be formed by bundles of surviving muscle fibers in healed infarcts or in fibrotic regions of the atria or ventricles. The critical slow conduction and block may be caused by depressed transmembrane potentials such as in the atria of hearts with cardiomyopathy [183] or in increased effective axial resistivity such as in healed infarcts [170]. Gross anatomical circuits are also involved in reentry utilizing the bundle branch which may cause ventricular tachycardia [184], reentry utilizing an accessory AV connecting pathway which may cause supraventricular tachycardia [185], and reentry around the tricuspid ring which may cause atrial flutter [186]. The specific mechanisms involved are discussed in the publications referenced.

23.5.3.2 Functional Pathways

Gross anatomical loops and anatomical obstacles are not a prerequisite for the occurrence of reentry. Reentry caused by slow conduction and unidirectional block can also occur in unbranched bundles or "sheets" of muscle fibers. A kind of reentry called reflection occurs in unbranched bundles of Purkinje fibers in which conduction is slow because the resting and action potentials are depressed (Fig. 23.25b) [1, 55]. During reflection, excitation occurring slowly in one direction along a bundle of fibers and is followed by excitation occurring in the opposite direction. The returning (reflected) impulse may be caused by reentry owing to functional longitudinal dissociation of the bundles [135].

Antzelevitch, Jalife and Moe described another mechanism which may cause reflection [187, 188]. Slow conduction does not occur along the entire bundle because of depressed transmembrane potentials, but rather there is a delayed activation of part of the bundle, resulting from electronic excitation of a region distal to an inexcitable segment (Fig. 23.26). The segment, may be rendered inexcitable by a depressed resting potential and subsequent inactivation of the sodium current channels. If a segment of a bundle of Purkinje fibers is inexcitable and will not generate action potentials, impulses conducting along the bundle will block at that segment (Fig. 23.26a, A). The blocked action potential, however, can generate axial current flow through the inexcitable segment of the fiber bundle which can act as a passive cable. The electronic manifestation of the blocked impulse decays along the cable in the inexcitable segment according to the length constant which is dependant to a large extent on the intracellular and extracellular resistances to current flow. If the inexcitable segment is sufficiently short relative to the length constant (less than 2 mm in the experiments of Antzelevitch et al. [187] and Jalife and Moe [188]), the current flow across the gap can depolarize the excitable fibers distal to the inexcitable region and can excite an action potential (Fig. 23.26a). The magnitude of delay of the action potential is dependant to a large extent on the time-course and amplitude of the electrotonic current flow. The action potential initiated distal to the point of block not only will conduct distally along the fiber but can also itself cause retrograde axial current flow through

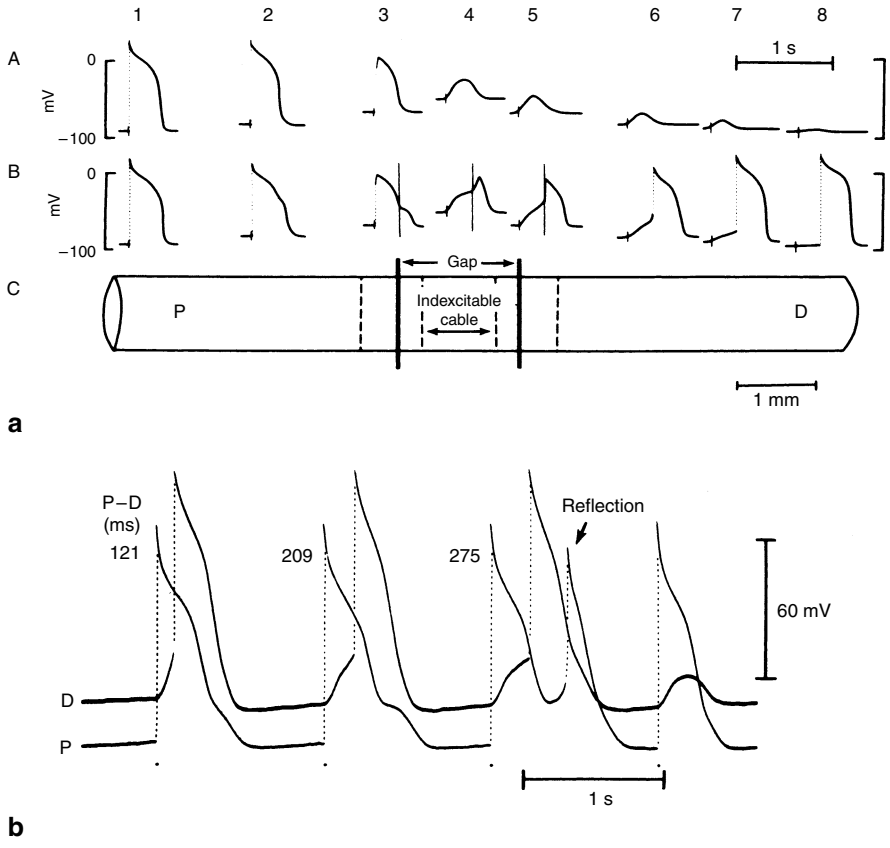

Figure 23.26

Part (a) is a schematic representation of block and conduction across an inexcitable segment of a Purkinje fiber bundle. The bundle is represented in C. The inexcitable segment of the cable with a low membrane potential shown here was produced experimentally by exposing this central segment to a superfusion solution that mimicked an ischemic environment. An impulse initiated in the proximal segment P propagates to the border of the inexcitable region and conduction blocks there (action potentials 1, 2 and 3 in A and B). Axial current flows through the inexcitable cable, depolarizing electrotonically the membrane fibers distal (D) to the inexcitable region (action potentials 4, 5, 6, 7 in A). Depolarization may be large enough to bring the distal membrane to threshold, causing an action potential distal to the inexcitable region (potential 5, 6, 7 in B). When conduction across the inexcitable region is successful, axial current generated from the distal action potential may also flow back towards the proximal region through the gap. This current flow has a depolarizing effect as evidenced in action potential 3 in B; note the alteration in repolarization of this action potential that resembles an early afterdepolarization (Reproduced with permission after Antzelevitch and Mae (1981) © American Heart Association. Dallas, Texas). Part (b) shows the case when this reaches threshold, the axial current being sufficiently large, and causes an action potential during repolarization. Two action potentials are shown, one recorded from the proximal (P) and the other from the distal (D) side of the inexcitable region. Conduction delay between P and D increases with each stimulated impulse, from 121 to 275 ms. Note the delay in repolarization in the P trace after the second action potential. This reaches threshold after the third action potential (with 275 ms delay) resulting in an action potential arising during phase 3 of repolarization (labeled "reflection") (Reproduced with permission from Antzelevitch (1983) © Saunders, Philadelphia, Pennsylvania).

the inexcitable gap to depolarize the part of the fiber proximal to the gap at the site of the original block. If the sum of excitation timed in both directions across the inexcitable gap exceeds the refractory period of the proximal segment, an action potential will be elicited that propagates retrogradely along the fiber (Fig. 23.26b). This reflected action potential reenters the part of the bundle that already was excited. Thus impulse transmission in both directions occurs over the same pathway unlike the types of reentry discussed previously. Reflection resulting from delays in activation caused by electrotonic transmission might be limited to areas where damage to the myocardial fiber is focal, as if the damage is too extensive electrotonic transmission across the inexcitable area would fail.

Another mechanism that can cause reentry in functional pathways is the "leading circle" mechanism originally described by Allessie et al. in experiments on atrial muscle [189–191]. Reentry is initiated by precisely timed premature impulses in regions which are activated normally at regular rates of stimulation. Initiation of reentry is made possible by the different refractory periods of atrial fibers in close proximity to one another [189]. The premature impulse that initiates reentry blocks in fibers with long refractory periods and conducts in fibers with shorter refractory periods, eventually returning to the initial region of block after excitability recovers there. The impulse may then continue to circulate around a central area which is kept refractory because it is constantly bombarded by impulses propagating toward it from all sides of the circuit (Fig. 23.27). This central area provides a functional obstacle that prevents excitation from propagating across the fulcrum of the circuit. The circumference of the smallest (leading) circle around the functional obstacle may be as little as 6–8 mm and is a pathway in which the efficacy of stimulation of the circulating wavefront is just sufficient

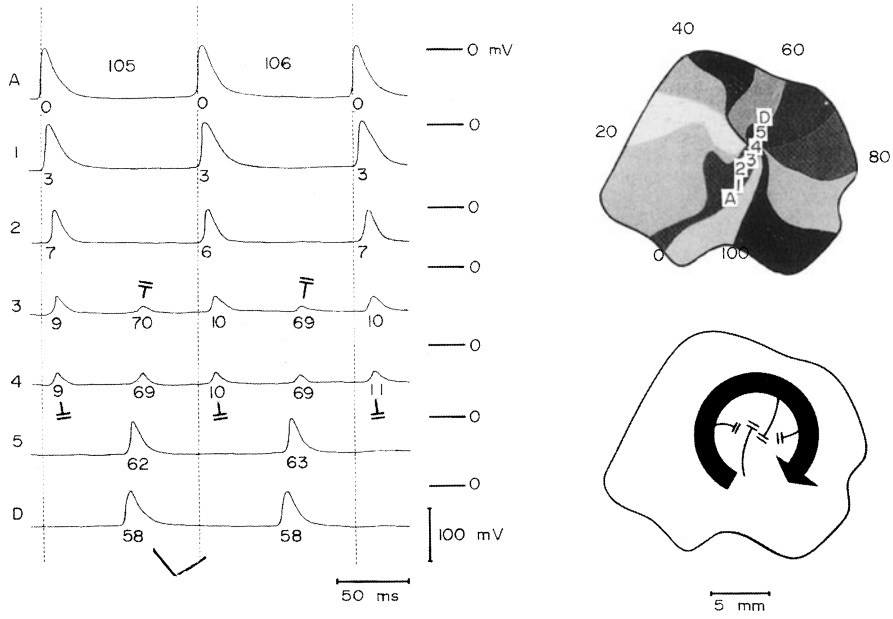

Figure 23.27

Reentry in isolated left atrial myocardium by the leading circle mechanism. At the right, above, is the map of the activation pattern of the atrium during circus movement. The impulse rotates continuously in a clockwise direction; each number and different shading indicates the time in milliseconds during which a given region is activated. Activation proceeds from 0 to 100 ms and one complete revolution takes 100 ms. At the left, the membrane potentials of seven fibers (marked A, D and 1–5) located on a straight line through the center of the circus movement are shown (the locations from which these action potentials were recorded are indicated on the map at the upper right). These records show that the fibers in the, central point of the circuit (3 and 4) show double responses of subnormal amplitude during circus movement. These responses result from conduction of the impulse from the circulating wave toward the center. At the lower right the activation pattern during circus movement is given schematically. It shows the circuit with the converging wavelets in the center (Reproduced with permission after Allessie et al. (1976) © American Heart Association, Dallas, Texas).

to excite the tissue ahead. This tissue is still in its relative refractory phase. Conduction through the functional reentrant circuit is slowed, therefore, because impulses are propagating in partially refractory tissue. Single circuits of this kind might cause atrial tachycardia or flutter [192]. Functional reentrant circuits of the leading circle type may change their size and location and if they do, would fall under the general category of random reentry. Changes in size may result from changes in refractory period, as would be expected to occur if autonomic (particularly parasympathetic) activity increases. The existence of multiple circuits is made possible by conditions which shorten the refractory period and/or depress conduction velocity and thereby decrease the minimal dimensions of the leading circuit. Multiple circuits of the leading circle type may be the cause of atrial fibrillation during which "reentry occurs over numerous loops of various size and position wandering over the excitable surface" [144]. Functional reentrant circuits of the leading circle type might also occur in the ventricles as a result of similar mechanisms, and might even cause fibrillation.

The anisotropic properties of atrial and ventricular myocardium also may predispose to functional reentrant circuits [167, 171] as described previously how conduction velocity varies depending on the direction of impulse propagation relative to the long axis of the myocardial fibers; slow conduction occurs perpendicular to the long axis while more rapid conduction occurs parallel to this axis. In addition, although it may seem paradoxical, some experimental studies on isolated tissue have shown that despite more rapid conduction, early premature impulses block more readily in the direction of the long axis because the safety factor is lower in the direction of lower axial resistivity [167]. There is, however, some controversy concerning this point [193]. More detailed discussion on this subject has been published [167, 168, 193]. As a result of this heterogeneity of conduction, early premature impulses may block in some regions but conduct slowly through others. Conduction may be slow enough to allow the impulse eventually to excite areas of initial block and a functional reentrant circuit is established (Fig. 23.28).

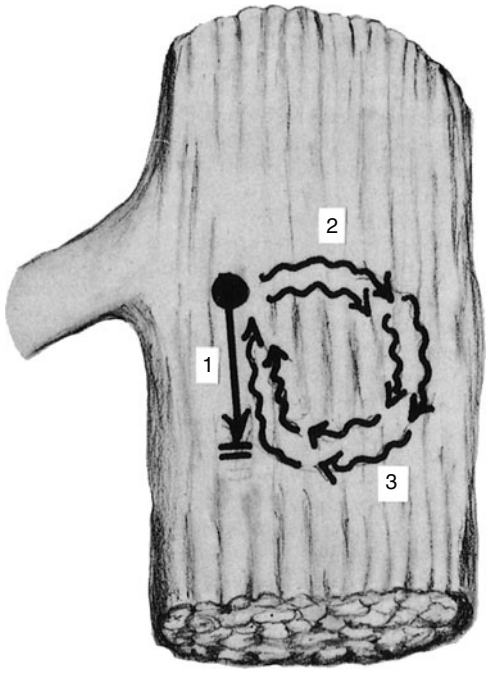

Figure 23.28

Diagram of reentry caused by anisotropic properties of cardiac muscle. An atrial trabeculum is shown. The direction of the long axis of the myocardial fibers is indicated by the lines. Conduction of an early stimulated premature impulse at the site where the dot is located blocks in the direction of the long axis of the myocardial fibers. Block is indicated by arrow 1 and horizontal lines. Conduction of the premature impulse in the direction perpendicular to the long axis does not block but proceeds slowly (*arrow 2*), returning to the site of block after this region has recovered excitability (*arrow 3*).

An additional factor to be considered here is spiral wave reentry. Initially described as a physical-chemical phenomenon the principle behind spiral wave reentry is that for any rotating wave, the lip of the wave creates a spiral in moving through a surrounding medium [194]. The importance of this phenomenon may be appreciated by referring to leading circle reentry (Fig. 23.27) where the core around which reentry occurs is rendered permanently inexcitable by centripetally conducting wavelets. In the leading circle setting, excitability is an essential determinant of reentry. However, wavefront curvature is also a critical factor in maintaining functional reentry [195] as even in the presence of excitable tissue, once a critical curvature is reached a wavefront may cease to propagate. In spiral wave reentry, the core is excitable (as opposed to the leading circle) but it is not excited: hence the fundamental difference between the two forms of reentry. Contributing to the occurrence of spiral wave reentry are such factors as tissue anisotropy, fibrosis and blood vessels [196].

23.5.3.3 Clinical Characteristics of Reentrant Excitation

Although it once was thought that arrhythmias caused by reentrant excitation could be distinguished readily from arrhythmias caused by other mechanisms either by their electrocardiographic characteristics or by the effects of clinical interventions, it now appears that this is not the case. For example, spontaneously occurring premature depolarizations occurring with fixed coupling to a preceding beat were thought to result mainly from reentrant excitation [197]. The coupling interval represented the time elapsed while the impulse was conducted through the reentrant circuit before reemerging to excite the heart. The coupling interval was fixed because the conduction pathway and conduction velocity did not change. However, it is now understood that conduction velocity through reentrant circuits can vary from beat to beat [1] and that the circuits sometimes may change in size, resulting in reentrant premature depolarizations with variable degrees of coupling. Furthermore, premature depolarizations with fixed coupling also to result from mechanisms other than reentry. One such example is triggered activity, described previously. Moreover, electrotonic interactions between conducted impulses and parasystolic foci also can cause fixed coupling [198, 199]. This mechanism will be explained in more detail in Sect. 23.6 dealing with arrhythmias caused by a combination of abnormalities of impulse initiation and impulse conduction.

Another distinguishing feature of reentrant tachycardias was believed to be their initiation by spontaneous or stimulated premature impulses occurring at critical cycle lengths. Yet it is now recognized that triggered activity can be induced in the same way. Properly timed premature impulses may initiate reentry by causing the necessary slow conduction and/or transient conduction block, if they are not present during the regular rhythm. Either or both may occur when the premature impulse encroaches on the relative refractory period of the tissue in the potential reentrant circuit. Overdrive stimulation also may cause reentry by inducing slow conduction or block. Reentry may be induced in either anatomical or functional circuits.

The influence of stimulated impulses on established tachycardias has also been considered to be a way in which reentrant excitation might be differentiated from other mechanisms causing arrhythmias. In general, it had been thought that termination of tachycardias by single stimulated premature impulses or by a period of overdrive stimulation (again, occurring at critical cycle lengths) identified reentry. However, it has been discussed how stimulation of the heart may not always affect reentrant tachycardias in this predicted way. The influence of stimulated impulses on reentry depends to a large extent on whether reentry is occurring in anatomical or functional circuits and whether or not an "excitable gap" is present in the circuit. The term "excitable gap" is used to describe a region in the reentrant circuit which has had the chance to recover full excitability before arrival of the reentering impulse [200]. During reentry caused by the leading circle mechanism in tissue with relatively uniform properties of conduction and refractoriness, no fully excitable gap exists because the crest of the reentrant impulse is conducting in the relatively refractory tissue it previously excited [189–191]. It is, therefore, very difficult for premature impulses induced by stimuli outside the reentrant circuit to penetrate the circuit and influence the tachycardia (Fig. 23.29a). This may account for the failure of stimulated premature impulses to terminate rapid atrial flutter [201], or some sustained ventricular tachycardias which nevertheless for other reasons are believed to be caused by reentry [202].

On the other hand, there may often be an excitable gap in a circuit defined by anatomy in which the conduction time around the circuit takes longer than the full recovery time of cardiac fibers comprising the circuit. A properly timed premature impulse can then enter the circuit. The stimulated impulse might conduct around the circuit in the same way as the reentering impulse, thereby resetting the tachycardia, or it may block conduction of the reentering impulse and

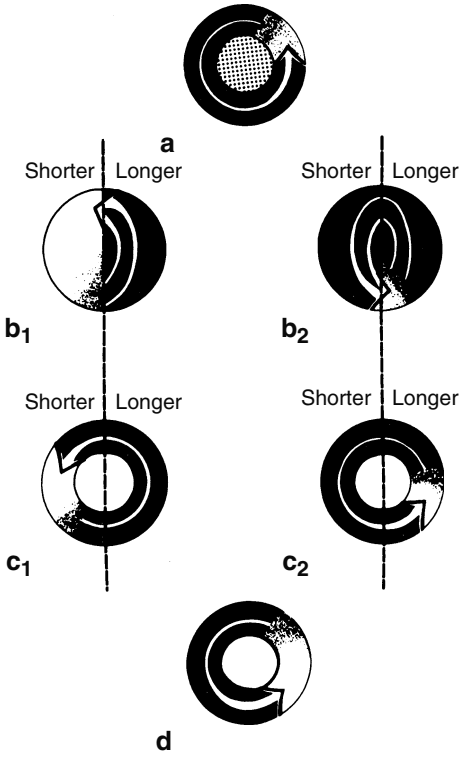

Figure 23.29

Schematic representation of the effects of stimulated impulses on reentry in circuits with different properties. Black areas represent refractory tissue, dotted areas partially refractory tissue and white areas an excitable gap. Part (a) shows leading circle reentry over a functional pathway in which refractoriness is sufficiently uniform that there is no fully excitable gap. Parts (b_1) and (b_2) show functional pathway with an area of long refractoriness and an area of short refractoriness. In (b_1), an excitable gap is present in the area with the short refractory period at the time the reentering impulse shown by the arrow is conducting in the region with the longer refractory period. The excitable gap is absent in (b_2) when the reentrant impulse is conducting through the region with the shorter refractory period. Parts (c_1) and (c_2) show an anatomic pathway with a region of long refractoriness and a region of short refractoriness. In (c_1), an excitable gap exists in the region with the short refractory period while the reentering impulse, shown by the arrow, is conducting in the region with the longer refractory period. In (c_2), an excitable gap is absent when the reentering impulse conducts through the region with the shorter refractory period (c_2). Part (d) shows an anatomically defined pathway that is long enough in relation to the duration of refractoriness so that all parts of the pathway have a fully excitable gap (Reproduced with permission after Frame and Hoffman (1984) © Nijhoff, The Hague).

terminate the tachycardia. Termination of the tachycardia would be expected to occur when conduction of the stimulated impulse blocks in the circuit in the anterograde direction and collides with the reentering impulse in the retrograde direction (Fig. 23.29d). These two examples of the possible lack of effect of stimulated impulses on leading circle reentry and termination of reentry in an anatomical pathway represents opposite extremes. Excitable gaps also may exist in functional circuits if there are large differences in the refractory periods or conduction velocities in different parts of the circuit [200]. A premature impulse then might be able to enter the circuit during the excitable gap in the region with the shorter refractory period while the reentrant impulse is conducting in the region with the longer refractory period or slower conduction velocity (Fig. 23.29b). Conversely, no excitable gap exists in the circuit while the reentering impulse is conducting through the region with the shorter refractory period or more rapid conduction velocity. Some forms of atrial flutter, supraventricular tachycardias and ventricular tachycardias which can be terminated by premature impulses may

be caused by reentry in functional circuits with an excitable gap. Excitable gaps might also be absent in some anatomic circuits if the impulse is conducting in relatively refractory tissue throughout the circuit because of a long refractory period or a short path length (Fig. 23.29c_2) [200]. A means for considering the mechanism of an arrhythmia via its response to specific form of programmed electrical stimulation has been described by Waldo and associates [201, 202] as transient entrainment. By pacing at cycle lengths that permit capture of an arrhythmia and observing the characteristics of the paced beats as well as the pattern of interruption and reinitiation of the arrhythmias, reentry can be diagnosed with a high degree of certainty.

Overdrive stimulation can also terminate reentry when the stimulated impulses penetrate the reentrant circuit and block conduction [203]. The presence or absence of a fully excitable gap may also influence the effects of overdrive for the same reason discussed for single stimulated impulses.

23.6 Simultaneous Abnormalities of Impulse Initiation and Conduction

Abnormalities of impulse initiation and conduction are expected to coexist under certain conditions. Action potentials initiated by spontaneous diastolic depolarization or delayed afterdepolarizations may conduct very slowly or block if they arise at sufficiently low membrane potentials caused by diastolic depolarization [204, 205] Threshold potential also shifts to more positive values when the rate of diastolic depolarization is slow, ensuring that the action potentials arise from low membrane potentials. These action potentials have slow upstrokes and reduced amplitudes resulting from partial inactivation of the sodium channel. Slow conduction of the impulse arising from the abnormality in initiation may cause reentry [204]. Impulses propagating into regions with spontaneous diastolic depolarization or delayed afterdepolarization may also conduct slowly (and reenter) if they enter these regions late in the diastolic cycle, at a time when membrane potential has markedly deceased. If they invade these regions early in the cycle, prior to phase 4 depolarization, they will conduct more normally. The interrelationship between diastolic depolarization and conduction could be a cause of rate-dependent changes in conduction such as the appearance of right bundle branch block at long cycle lengths [206]. Impulses arising during phase 4 depolarization might also conduct more rapidly than normal, even when there is partial inactivation of the inward current if threshold potential is not shifted, since the amount of depolarizing current necessary to initiate an action potential would be reduced. This enhancement of conduction might occur when diastolic depolarization is relatively small.

The second major example of coexisting abnormalities of conduction and automaticity is the parasystolic focus. The existence of such a focus depends on the presence of entry block. The likelihood that the spontaneous impulses generated by the parasystolic focus will excite the heart depends on the ability of these impulses to propagate from the focus to surrounding fibers. If, because of marked phase 4 depolarization, the focus generates small, slowly rising action potentials, these may not be able to propagate or may propagate quite slowly. The degree of exit block thus might depend on the magnitude of phase 4 depolarization in the focus [3].

If a parasystolic focus with normal automaticity is coupled in an appropriate manner to the surrounding cardiac fiber, propagating activity of those fibers may influence the firing of the focus even though there is entry block [198, 199]. This may occur if there are electrotonic effects of the propagating impulses on phase 4 depolarization of the focus. Electrotonic current spread from action potentials arriving in the vicinity of the focus tends to depolarize the fibers in the focus during diastole (axial current flows toward the focus). The resulting subthreshold depolarization early in diastole inhibits subsequent phase 4 depolarization (possibly by inactivating the voltage dependent I_f), while late in diastole it shifts the membrane potential enough to cause activation of the fast inward current and thus accelerates firing (Fig. 23.30). During phase 4 depolarization membrane resistance increases [43]. For this reason, as the action potential arrives at the site of entry block later and later during phase 4 depolarization of fibers in the parasystolic focus, it will cause a progressively larger change in their membrane potential. As the synchrony between the focus and the dominant rhythm changes and the propagating impulse arrives progressively later during phase 4, the cycle of the parasystolic focus will increase to a maximum, abruptly decrease to a minimum and then progressively increase to the control value [199]. This type of interaction between the dominant rhythm and the rhythm of the parasystolic focus means the parasystolic rhythms may show fixed or variable coupling or other complex interactions with the sinus rhythm. These are discussed in greater detail elsewhere [199]. Although electrotronic interactions are also expected to occur between the dominant

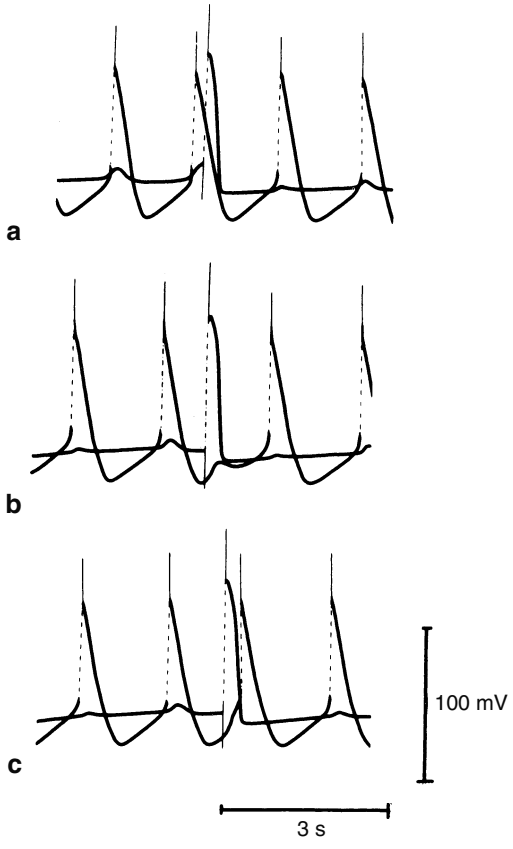

Figure 23.30

Electrotonic interaction between propagated impulses and a parasystolic focus. In each part, transmembrane potentials recorded at two different sites are shown. The top traces in each show stimulated action potentials that cannot propagate into and excite a parasystolic focus; automatic firing in this focus is shown in the bottom traces. The focus also has a high grade of exit block as indicated by the failure of an action potential to occur in the top trace following a spontaneous impulse in the focus. The only action potentials seen in the top trace result from propagation from another site. In (a), the propagating impulse (top trace) occurs shortly after the impulse in the parasystolic focus and does not influence it. In (b), the propagating impulse occurs early during phase 4 depolarization in the focus. Electrotonic current spread from this impulse causes a subthreshold depolarization early in diastole and this slows the rate of subsequent phase 4 depolarization. In (c), the propagating impulse occurs late in diastole of the parasystolic focus. Electrotonic current spread from the impulse accelerates the terminal portion of phase 4 depolarization and accelerates firing (Reproduced with permission after Jalife and Moe (1976) © American Research Association, Dallas, Texas).

rhythm and parasystolic focus with abnormal automaticity, the effects of the interactions cannot be predicted without an understanding of the voltage-dependence of the conductance causing the abnormal phase 4 depolarization.

23.7 Conclusion

The information we have discussed here on arrhythmogenic mechanisms has been derived mainly from experimental laboratory studies on isolated cardiac tissues and to a lesser extent from studies of intact animals, of ion channels and of the genetic determinants of specific arrhythmias. Approximately 20 years ago, in the first edition of this text, we wrote "there is a good possibility that pharmacological agents can be developed to modify the operation of these channels and

suppress or abolish the arrhythmogenic mechanism"[207]. We stated this because we believed that "since the different mechanisms [for arrhythmias] utilize different channels with different properties, drugs which act specifically on one another of the mechanisms can be developed. Hence, rational therapy of arrhythmias in the future will consist in identifying the mechanism for a clinical arrhythmia by a specific clinical test and then selecting an appropriate drug to suppress that mechanism"[207].

Simply stated, we were naïve. As the CAST [208] and SWORD [102] trials have effectively demonstrated, attempts to use basic and clinical information available at the time to devise rational approaches to pharmacologic therapy resulted in excess mortality. This is not to say that newer and more selective and safer molecules will not be developed: but it is to admit that the goal is far more daunting than we had expected. In the meantime, the use of interventional techniques such as ablation [209] has had a high degree of success in selected arrhythmias and the advent of cardioverter-defibrillators has clearly improved the duration of life [210]. In other words, the device industry has provided interventions and expectations that pharmacology has not yet been able to deliver.

The final ingredient in our therapeutic mix is provided by the nascent field of gene and cell therapy. Although approaches here are very much in their infancy, early results hold out some promise that repair and replacement of, and therapy for, arrhythmogenic tissues may be within reach [211–216]. And having stated this, we very much still believe in our concluding statement of 20 years ago: "rational therapy of arrhythmias in the future will consist in identifying the mechanism for a clinical arrhythmia by a specific clinical test and then selecting an appropriate [intervention] to suppress that mechanism"[207].

Acknowledgements

The authors would like to thank Ms. Laureen Pagan for her careful attention to the preparation of this manuscript and Mr. Richard Haynes for illustration assistance.

References

1. Cranefield, P.F., A.L. Wit, and B.F. Hoffman, Genesis of cardiac arrhythmias. *Circulation*, 1973;**47**: 190–204.
2. Hoffman, B.F. and P.F. Cranefield, The physiological basis of cardiac arrhythmias. *Am. J. Med.*, 1964;**37**: 670–684.
3. Hoffman, B.F. and M.R. Rosen, Cellular mechanisms for cardiac arrhythmias. *Circ. Res.*, 1981;**49**: 1–15.
4. DiFrancesco, D. and C. Ojeda, Properties of the current i_f in the sino-atrial node of the rabbit compared with those of the current i_k in Purkinje fibers. *J. Physiol. London*, 1980;**308**: 35–37.
5. Biel, M., A. Schneider, and C. Wahl, Cardiac HCN channels: structure, function, and modulation. *Trends Cardiovas. Med.*, 2002;**12**: 206–212.
6. Yanagihara, K. and H. Irisawa, Potassium current during the pacemaker depolarization in rabbit sinoatrial node cell. *Pflügers Arch.*, 1980;**388**: 255–260.
7. Hoffman, B.F. and P.F. Cranefield, *Electrophysiology of the Heart*. New York: McGraw-Hill, 1960.
8. Hogan, P.M. and L.D. Davis, Evidence for specialized fibers in the canine atrium. *Circ. Res.*, 1968;**23**: 387–396.
9. Kokubun, S., M. Nishimura, A. Noma, and A. Irisawa, The spontaneous action potential of rabbit atrioventricular node cells. *Jpn. J. Physiol.*, 1980;**30**: 529–540.
10. Wit, A.L. and P.F. Cranefield, Triggered and automatic activity in the canine coronary sinus. *Circ. Res.*, 1977;**41**: 435–445.
11. Wit, A.L., J.J. Fenoglio Jr., B.M. Wagner, and A.L. Bassett, Electrophysiological properties of cardiac muscle in the anterior mitral valve leaflet and the adjacent atrium in the dog: possible implications for the genesis of atrial dysrhythmias. *Circ. Res.*, 1973;**32**: 731–745.
12. Vassalle, M., The relationship among cardiac pacemakers: overdrive suppression. *Circ. Res.*, 1977;**41**: 269–277.
13. Erlanger, J. and J.R. Blackman, A study of relative rhythmicity and conductivity in various regions of the auricles of the mammalian heart. *Am. J. Physiol.*, 1907;**19**: 125–174.
14. Hope, R.R., B.J. Scherlag, N. EI-Sherif, and R. Lazzara, Hierarchy of ventricular pacemakers. *Circ. Res.*, 1976;**39**: 883–888.
15. DiFrancesco, D., A new interpretation of the pace-maker current in calf Purkinje fibers. *J. Physiol. London*, 1981;**314**: 359–376.
16. DiFrancesco, D., A study of the ionic nature of the pace-maker current in calf Purkinje fibers. *J. Physiol. London*, 1981;**314**: 377–393.
17. Qu, J., A. Barbuti, L. Protas, B. Santoro, I.S. Cohen, and R.B. Robinson, HCN2 overexpression in newborn and adult ventricular myocytes: distinct effects on gating and excitability. *Circ. Res.*, 2001;**89**: E8–E14.
18. Vassalle, M., Electrogenic suppression of automaticity in sheep and dog Purkinje fibers. *Circ. Res.*, 1970;**27**: 361–377.
19. Vassalle, M., D.L. Caress, A.J. Slovin, and J.H. Stuckey, On the cause of ventricular asystole during vagal stimulation. *Circ. Res.*, 1967;**10**: 228–241.

20. Glitsch, H.G., Characteristics of active Na transport in intact cardiac cells. *Am. J. Physiol*., 1979;**236**: H189–H199.
21. Gadsby, D.C. and P.F. Cranefield, Direct measurement of changes in sodium pump current in canine cardiac Purkinje fibers. *Proc. Natl. Acad. Sci. USA* 1979;**76**: 1783–1787.
22. January, C.T. and H.A. Fozzard, The effects of membrane potential, extracellular potassium and tetrodotoxin on the intracellular sodium ion activity of sheep cardiac muscle. *Circ. Res*., 1984;**54**: 652–665.
23. Jordan, J.L., I. Yamaguchi, W.J. Mandel, and A.E. McCullen, Comparative effects of overdrive on sinus and subsidiary pacemaker function. *Am. Heart J*., 1977;**93**: 367–374.
24. Kodama, I., J. Goto, S. Ando, J. Toyama, and K. Yamada, Effects of rapid stimulation on the transmembrane action potentials of rabbit Sinus node pacemaker cells. *Circ. Res*., 1980;**46**: 90–99.
25. Gang, E.S., J.A. Reiffel, F.D. Livelli Jr., J.T. Bigger Jr., Sinus node recovery times following the spontaneous termination of supraventricular tachycardia and following atrial overdrive pacing: a comparison. *Am. Heart J*. 1983;**105**: 210–215.
26. Breithardt, G., L. Seipel, and F. Loogen, Sinus node recovery time and calculated sinoatrial conduction time in normal subjects and patients with sinus node dysfunction. *Circulation*, 1977;**56**: 43–50.
27. Van Capelle, F.J.L. and D. Durrer, Computer simulation of arrhythmias in a network of coupled excitable elements. *Circ. Res*., 1980;**47**: 454–466.
28. Wit, A.L. and P.F. Cranefield, Mechanisms of impulse initiation in the atrioventricular junction and the effects of acetylstrophanthidin. *Am. J. Cardiol*., 1982;**49**: 921.
29. Toda, N. and T.C. West, Changes in sino-atrial node transmembrane potentials on vagal stimulation of the isolated rabbit atrium. *Nature*, 1965;**205**: 808–809.
30. Erlanger, J. and A.D. Hirschfelder, Further studies on the physiology of heart block in mammals. *Am. J. Physiol*., 1906;**15**: 153–206.
31. Ferrer, M.I., *The Sick Sinus Syndrome*. Mount Kisco, NY: Futura, 1974.
32. Dahl, G. and G. Isenberg, Decoupling of heart muscle cells: correlation with increased cytoplasmic calcium activity and with changes of nexus ultrastructure. *J. Membr. Biol*., 1980;**53**: 63–75.
33. Weingart, R., The actions of ouabain on intercellular coupling and conduction velocity in mammalian ventricular muscle. *J. Physiol. London*, 1977;**264**: 341–365.
34. Ellis, D., The etTects of external cations and ouabain on the intracellular sodium activity of sheep heart Purkinje fibers. *J. Physiol. London*, 1977;**273**: 211–240.
35. Tsien, R.W., EtTect of epinephrine on the pacemaker potassium current of cardiac Purkinje fibers. *J. Gen. Physiol*., 1974;**64**: 293–319.
36. Pliam, M.B., D.J. Krellenstein, M. Vassalle, and C.M. Brooks, The influence of norepinephrine, reserpine and propranolol on overdrive suppression. *J. Electrocardiol*., 1975;**8**: 17–24.
37. Armour, J.A., G.R. Hageman, and W.C. Randall, Arrhythmias induced by local cardiac nerve stimulation. *Am. J. Physiol*., 1972;**223**: 1068–1075.
38. Randall, W.C., Sympathetic control of the heart, in, ed. *Neural Regulation of the Heart*, WC Randall, Editor. New York: Oxford University Press, 1977, pp. 45–94.
39. Vassalle, M., M.J. Levine, and J.H. Stuckey, On the sympathetic control of ventricular automaticity; the effects of stellate ganglion stimulation. *Circ. Res*., 1968;**23**: 249–258.
40. Katzung, B.G., L.M. Hondeghem, and A.O. Grant, Cardiac ventricular automaticity induced by current of injury. *Pflügers Arch*., 1975;**360**: 193–197.
41. Janse, M.J. and F.J.L. van Capelle, Electrotonic interactions across an inexcitable region as a cause of ectopic activity in acute regional myocardial ischemia. A study in intact porcine and canine hearts and computer models. *Circ. Res*., 1982;**50**: 527–537.
42. Rosen, M.R., H. Gelband, C. Merker, and B.F. Hoffman, Mechanisms of digitalis toxicity: effects of ouabain on phase four of canine Purkinje fiber transmembrane potentials. *Circulation*, 1973;**47**: 681–689.
43. Vassalle, M., Cardiac pacemaker potentials at different extra- and intracellular K concentrations. *Am. J. Physiol*., 1965;**208**: 770–775.
44. Deck, K.A., Anderungen des Ruhepotentials und der Kabeleigenschaften von Purkinje 'Faden bei der Dehnung. *Pflügers Arch*., 1964;**280**: 131–140.
45. Mary-Rabine, L., A.J. Hordof, P. Danilo Jr., J.R. Maim, and M.R. Rosen, Mechanisms for impulse initiation in isolated human atrial fibers. *Circ. Res*., 1980;**47**: 267–277.
46. Hoppe, U.C. and D.J. Beuckelmann, Characterization of the hyperpolarization-activated inward current in isolated human atrial myocytes. *Cardiovasc. Res*., 1998;**38**: 788–801.
47. Yu, H., F. Chang, and I.S. Cohen, Pacemaker current I_f in adult canine cardiac ventricular myocytes. *J. Physiol*., 1995;**485**: 469–483.
48. Cerbai, E., M. Barbieri, and A. Mugelli, Occurrence and properties of the hyperpolarization-activated current I_f in ventricular myocytes from normotensive and hypertensive rats during aging. *Circulation*, 1996;**94**: 1674–1481.
49. Cerbai, E., R. Pino, F. Porciatti, G. Sani, M. Toscano, M. Maccherini, G. Giunti, and A. Mugelli, Characterization of the hyperpolarization-activated current, I_f, in ventricular myocytes from human failing heart. *Circulation*, 1997;**95**: 568–571.
50. Cerbai, E., L. Sartiani, P. DePaoli, R. Pino, M. Maccherini, F. Bizzarri, F. DiCiolla, G. Davoli, G. Sani, and A. Mugelli, The properties of the pacemaker current I_f in human ventricular myocytes are modulated by cardiac disease. *J. Mol. Cell Cardiol*., 2001;**33**: 441–448.
51. Katzung, B.G. and J.A. Morgenstern, Effects of extracellular potassium on ventricular automaticity and evidence for a pacemaker current in mammalian ventricular myocardium. *Circ. Res*., 1977;**40**: 105–111.
52. Imanishi, S. and B. Surawicz, Automatic activity in depolarized guinea pig ventricular myocardium: characteristics and mechanisms. *Circ. Res*., 1976;**39**: 751–759.
53. Brown, H.F. and S.J. Noble, Membrane currents underlying delayed rectification and pace-maker activity in frog atrial muscle. *J. Physiol. London*, 1969;**204**: 717–736.
54. Imanishi, S., Calcium-sensitive discharges in canine Purkinje fibers. *Jpn. J. Physiol*., 1971;**21**: 443–463.
55. Cranefield, P.F., *The Conduction of the Cardiac Impulse: The Slow Response and Cardiac Arrhythmias*. Mount Kisco, NY: Futura, 1975.
56. Noble, D. and R.W. Tsien, The kinetics and rectifier properties of the slow potassium current in cardiac Purkinje fibers. *J. Physiol. London*, 1968;**195**: 185–214.
57. Hodgkin, A.L. and B. Katz, The effect of sodium ions on the electrical activity of the giant axon of the squid. *J. Physiol. London*, 1949;**108**: 37–77.

58. Gadsby, D.C. and A.L. Wit, Electrophysiologic characteristics of cardiac cells and the genesis of cardiac arrhythmias, in *Cardiac Pharmacology*, RD Wilkersen, Editor. New York: Academic Press, 1981, pp. 229–274.
59. Gadsby, D.C. and P.F. Cranefield, Two levels of resting potential in cardiac Purkinje fibers. *J. Gen. Physiol*., 1977; **70**:725–746.
60. Wit, A.L. and P.F. Cranefield, Triggered activity in cardiac muscle fibers of the simian mitral valve. *Circ. Res*., 1976;**38**: 85–98.
61. Dresdner, K.P., R.P. Kline, and A.L. Wit, Cytoplasmic K^+ and Na^+ activity in subendocardial canine Purkinje fibers from one day old infarcts using double-barrel ion selective electrodes: comparison with maximum diastolic potential. *Biophys. J*., 1985;**47**: 463a.
62. Friedman, P.L., J.R. Stewart, and A.L. Wit, Spontaneous and induced cardiac arrhythmias in subendocardial Purkinje fibers surviving extensive myocardial infarction in dogs. *Circ. Res*., 1973;**33**: 612–626.
63. Lazzara, R., N. EI-Sherif, and B.J. Scherlag, Electrophysiological properties of canine Purkinje cells in one-day-old myocardial infarction. *Circ. Res*., 1973;**33**: 722–734.
64. Hordof, A.J., R. Edie, J.R. Maim, B.F. Hoffman, and M.R. Rosen, Electrophysiological properties and response to pharmacologic agents of fibers from diseased human atria. *Circulation*, 1976;**54**: 774–779.
65. Ten Eick, R.E. and D.H. Singer, Electrophysiological properties of diseased human atrium. I. Low diastolic potential and altered cellular response to potassium. *Circ. Res*., 1979;**44**: 545–557.
66. Singer, D.H., C.M. Baumgarten, and R.E. Ten Eick, Cellular electrophysiology of ventricular and other dysrhythmias: studies on diseased and ischemic heart. *Prog. Cardiovasc. Dis*., 1981;**24**: 97–156.
67. Carmeliet, E., The slow inward current: non-voltage-clamp studies, in *The Slow Inward Current and Cardiac Arrhythmias*, D.P. Zipes, J.C. Bailey, and V. Elharrar, Editors. The Hague: Nijhoff, 1980, pp. 97–110.
68. Hoffman, B.F. and K.H. Dangman, Are arrhythmias caused by automatic impulse generation? in *Normal and Abnormal Conduction In the Heart*, A. Paes de Carvalho, B.F. Hoffman, M. Lieberman, Editors. Mount Kisco, NY: Futura, 1982, pp. 429–448.
69. Dangman, K.H. and B.F. Hoffman, Studies on overdrive stimulation of canine cardiac Purkinje fibers: maximal diastolic potential as a determinant of the response. *J. Am. Coll. Cardiol*., 1983;**2**: 1183–1190.
70. Falk, R.T. and I.S. Cohen, Membrane current following activity in canine cardiac Purkinje fibers. *J. Gen. Physiol*., 1984;**83**: 771–799.
71. Mullins, L.J., *Ton Transport in Heart*. New York: Raven, 1981.
72. Ferrier, G.R. and J.E. Rosenthal, Automaticity and entrance block induced by focal depolarization of mammalian ventricular tissues. *Circ. Res*., 1980;**47**: 238–248.
73. Hume, J. and B.G. Katzung, Physiological role of endogenous amines in the modulation of ventricular automaticity in the guinea-pig. *J. Physiol. London*, 1980;**309**: 275–286.
74. Lange, G., Action of driving stimuli from intrinsic and extrinsic sources on in situ cardiac pacemaker tissues. *Circ. Res*., 1965;**17**: 449–459.
75. Goldreyer, B.N., J.J. Gallagher, and A.N. Damato, The electrophysiologic demonstration of atrial ectopic tachycardia in man. *Am. Heart J*., 1973;**85**: 205–215.
76. Le Marec, H., K.H. Dangman, P. Danilo Jr., and M.R. Rosen, An evaluation of automaticity and triggered activity in the canine heart one to four days after myocardial infarction. *Circulation*, 1985;**71**: 1224–1236.
77. Wellens, H.J.J., Value and limitations of programmed electrical stimulation of the heart in the study and treatment of tachycardias. *Circulation*, 1978;**57**: 845–853.
78. Bonke, F.I.M., L.N. Bouman, H.E. vap Rijn, Change of cardiac rhythm in the rabbit after an atrial premature beat. *Circ. Res*., 1969;**24**: 533–544.
79. Klein H.O., D.H. Singer, B.F. Hoffman, Effects of atrial premature systoles on sinus rhythm in the rabbit. *Circ. Res*., 1973;**32**: 480–491.
80. Klein, H.O., P.F. Cranefield, and B.F. Hoffman, Effect of extrasystoles on idoventricular rhythm. *Circ. Res*., 1972;**30**: 651–615.
81. Cranefield, P.F., Action potentials, afterpotentials, and arrhythmias. *Circ. Res*., 1977;**41**: 415–423.
82. Wit, A.L., P.F. Cranefield, and D.C. Gadsby, Triggered activity, in *The Slow Inward Current and Cardiac Arrhythmias*, D.P. Zipes, J.C. Bailey, and V. Elharrar, Editors. The Hague: Nijhoff, 1980, pp. 437–454.
83. Attwell, D., I. Cohen, D. Eisner, M. Ohba, and C. Ojeda, The steady state lTX-sensitive ("window") sodium current in cardiac Purkinje fibers. *Pftügers Arch*., 1979;**379**: 137–142.
84. Reuter, H., Properties of two inward membrane currents in the heart. *Annu. Rev. Physiol*., 1979;**41**: 413–424.
85. Jurkiewicz, N.K. and M.C. Sanguinetti, Rate-dependent prolongation of cardiac action potentials by a methanesulfonanilide class III antiarrhythmic agent. Specific block of rapidly activating delayed rectifier K+ current by dofetilide. *Circ. Res*., 1993;**72**: 75–83.
86. Gadsby, D.C. and P.F. Cranefield, Electrogenic sodium extrusion in cardiac Purkinje fibers. *J. Gen. Physiol*., 1979;**73**: 819–837.
87. January, C. and J.M. Riddle, Early afterdepolarizations: mechanisms of induction and block. A role for the L type Ca current. *Circ. Res*., 1989;**64**: 977–990.
88. Volders, P.G., A. Kulcsar, M.A. Vos, K.R. Sipido, H.J. Wellens, R. Lazzara, and B. Szabo, Similarities between early and delayed after depolarizations induced by isoproterenol in canine ventricular myocytes. *Cardiovasc. Res*., 1997;**34**: 348–359.
89. Wu, Y., D.M. Roden, and M.E. Anderson, CaM kinase inhibition prevents development of the arrhythmogenic transient inward current. *Circ. Res*., 1999;**84**: 906–912.
90. Schmidt, R.F., Versuche mit Aconitin zum Problem der spontanen Erregungsbildung im Herzen. *Pftügers Arch*., 1960;**271**: 526–536.
91. Matsuda, K., B.F. Hoffman, C.N. Ellner, M. Katz, C.Mc. Brooks, Veratrine induced prolongation of repolarisation in the mammalian heart, in *Proceeding of the 19th International Physiological Congress*, Montreal, 1953, pp. 596–597.
92. Trautwein, W., U. Gottstein, and J. Dudel, Der Aktionsstrom der Myokardfaser im Sauerstoffmangel. *Pflügers Arch*., 1954:**260**: 40–60.
93. Coraboeuf, E. and J. Boistel, L'action des taux eleves de gaz carbonique sur Ie tissu cardiaque, etudiee a l'aide de microelectrodes intracellulaires. *C. R. Soc. Bioi. Paris*, 1953;**147**: 654–665.
94. Brooks, C.Mc., B.F. Hoffman, E.E. Suckling, and O. Orias, *Excitability of the Heart*. New York: Grune and Stratton, 1955.
95. Strauss, H.C., J.T. Bigger Jr., and B.F. Hoffman, Electrophysiological and beta-receptor blocking effects of MJ 1999 on dog and rabbit cardiac tissue. *Circ. Res*., 1970;**26**: 661–678.

96. Dangman, K.H. and B.F. Hoffman, *In vivo* and *in vitro* antiarrhythmic and arrhythmogenic effects of *N*-acetyl procainamide. *J. Pharmacol. Exp. Ther*., 1981;**217**: 851–862.
97. Elonen, E., P.J. Neuvonan, L. Tarssanen, and R. Kala, Sotalol intoxication with prolonged Q-T interval and severe tachyarrhythmias. *BMJ*, 1979;**1**: 1184.
98. Krikler, D.M. and P.V.L. Curry, *Torsatk de pointes*: an atypical ventricular tachycardia. *Br. Heart J*., 1976;**38**: 117–120.
99. Brachmann, J., B.J. Scherlag, L.Y. Rosenshtraukh, R. Lazzara, Bradycardia-dependent triggered activity: relevance to drug-induced multiform ventricular tachycardia. *Circulation*, 1983;**68**: 846–856.
100. Volders, P.G., K.R. Sipido, M.A. Vos, R.L. Spatjens, J.D. Leunissen, E. Carmeliet, H.J. Wellens, Downregulation of delayed rectifier K(+) currents in dogs with chronic complete atrioventricular block and acquired torsades de pointes. *Circulation*, 1999;**100**: 2455–2461.
101. Belardinelli, L., C. Antzelevitch, M.A. Vos, Assessing predictors of drug-induced torsade de pointes. *Trends Pharmacol. Sci*., 2003;**24**: 619–625.
102. Pratt, C.M., A.J. Camm, W. Cooper, P.L. Friedman, D.J. MacNeil, K.M. Moulton, B. Pitt, P.J. Schwartz, E.P. Veltri, and A.L. Waldo, Mortality in the survival with oral D-sotalol (SWORD) trial: why did patients die? *Am. J. Cardiol*., 1998;**81**: 869–876.
103. Damiano, B.P. and M.R. Rosen, Effects of pacing on triggered activity induced by early afterdepolarizations. *Circulation*, 1984;**69**: 1013–1025.
104. Rosen, M.R., H. Gelband, and B.F. Hoffman, Correlation between effects of ouabain on the canine electrocardiogram and transmembrane potentials of isolated Purkinje fibers. *Circulation*, 1973;**47**: 65–72.
105. Ferrier, G.R., J.H. Saunders, and C. Mendez, A cellular mechanism for the generation of ventricular arrhythmias by acetylstrophanthidin. *Circ. Res*., 1973;**32**: 600–609.
106. Davis, L.D., Effect of changes in cycle length on diastolic depolarization produced by ouabain in canine Purkinje fibers. *Circ. Res*., 1973;**32**: 206–214.
107. Ferrier, G.R., Digitalis arrhythmias: role of oscillatory afterpotentials. *Prog. Cardiovasc. Dis*., 1977;**19**: 459–474.
108. Akera, T. and T.M. Brody, The role of Na^+, K^+ ATPase in the inotropic action of digitalis. *Pharmacol. Rev*., 1977;**29**: 187–220.
109. Eisner, D.A. and W.J. Lederer, Inotropic and arrhythmogenic effects of potassium-depleted solutions on mammalian cardiac muscle. *J. Physiol. London*, 1979;**294**: 255–277.
110. Nathan, D. and G.W. Beeler Jr., Electrophysiologic correlates of the inotropic effects of isoproterenal in canine myocardium. *J. Mol. Cell. Cardiol*., 1975;**7**: 1–15.
111. Dangman, K.H., P. Danilo Jr., A.J. Hordof, L. Mary-Rabine, R.F. Reder, and M.R. Rosen, Electrophysiologic characteristics of human ventricular and Purkinje fibers. *Circulation*, 1982;**65**: 362–368.
112. Saito, T., M. Otoguro, and T. Matsubara, Electrophysiological studies on the mechanism of electrically induced sustained rhythmic activity in the rabbit right atrium. *Circ. Res*., 1978;**42**: 199–206.
113. Aronson, R.S., Afterpotentials and triggered activity in hypertrophied myocardium from rats with renal hypertension. *Circ. Res*., 1981;**48**: 120–127.
114. EI-Sherif, N., W.B. Gough, R.H. Zeiler, and R. Mehra, Triggered ventricular rhythm in I-day-old myocardial infarction in the dog. *Circ. Res*., 1983;**52**: 566–579.
115. Chen, Y.J., S.A. Chen, M.S. Chang, and C.I. Lin, Arrhythmogenic activity of cardiac muscle in pulmonary veins of the dog: implication for the genesis of atrial fibrillation. *Cardiovas. Res.* 2000;**48**: 265–273.
116. Haissaguerre, M., P. Jais, D.C. Shah, A. Takahashi, M. Hocini, G. Quiniou, S. Garrigue, A. Le Mouroux, P. Le Metayer, and J. Clementy, Spontaneous initiation of atrial fibrillation by ectopic beats originating in the pulmonary veins. *N. Engl. J. Med*., 1998;**339**: 659–666.
117. Braunwald, E., J. Ross Jr., and E.H. Sonnenblick, *Mechanisms of Contraction of the Normal and Failing Heart*. Boston, MA: Little, Brown, 1976.
118. Clusin, W.T., M. Buchbinder, A.K. Ellis, R.S. Kemoff, J.C. Giacomini, and D.C. Harrison, Reduction of ischemic depolarization by the calcium blocker diltiazem. Correlation with improvement of ventricular conduction and early arrhythmias in the dog. *Circ. Res*., 1984;**54**: 10–20.
119. Kass, R.S., R.W. Tsien, and R. Weingart, Ionic basis of transient inward current induced by strophanthidin in cardiac Purkinje fibres. *J. Physiol. London*, 1978;**281**: 209–226.
120. Kass, R.S., W.J. Lederer, R.W. Tsien, and R. Weingart, Role of calcium ions in transient inward currents and after contractions induced by strophanthidin in cardiac Purkinje fibres. *J. Physiol. London*, 1978;**281**: 187–208.
121. Vassalle, M. and A. Mugelli, An oscillatory current in sheep cardiac Purkinje fibers. *Circ. Res*., 1981;**48**: 618–631.
122. Karagueuzian, H.S. and B.G. Katzung, Voltage-damp studies of transient inward current and mechanical oscillations induced by ouabain in ferret papillary muscle. *J. Physiol. London*, 1982;**327**: 255–271.
123. Tseng, G.N. A.L. Wit, Characteristics of a transient inward current causing catecholamine induced triggered atrial tachycardia. *Circulation*, 1984;**70**(Suppl. II): 221.
124. Reuter, H., The dependence of slow inward current in Purkinje fibres on the extracellular calcium-concentration. *J. Physiol. London*, 1967;**192**: 479–492.
125. Ferrier, G.R., Effects of transmembrane potential on oscillatory afterpotentials induced by acetylstrophanthidin in canine ventricular tissues. *J. Pharmacol. Exp. Ther*., 1980;**215**: 332–341.
126. Tsien, R.W., R.S. Kass, and R. Weingart, Cellular and subcellular mechanisms of cardiac pacemaker oscillations. *J. Exp. Biol*., 1979;**81**: 205–215.
127. Ter Keurs, H.E.D.J. and P.A. Boyden, Ca^{2+} and arrhythmias, in *Foundations of Cardiac Arrhythmias*, P.M. Spooner and M.R. Rosen, Editors. New York: Marcel Dekker Inc, 2000, pp. 287–317.
128. Colquhoun, D., E. Neher, H. Reuter, and C.F. Stevens, Inward current channels activated by intracellular Ca in cultured cardiac cells. *Nature*, 1981;**294**: 752–754.
129. Arlock, P. and B.G. Katzung, Effects of sodium substitutes on transient inward current and tension in guinea-pig and ferret papillary muscle. *J. Physiol. London*, 1985;**360**: 105–120.
130. Rosen, M.R. and P. Danilo Jr., Digitalis-induced delayed afterdepolarizations, in *The Slow Inward Current and Cardiac Arrhythmias*, D.P. Zipes, J.C. Bailey, and V. Elharrar Editors. The Hague: Nijhoff, 1980, pp. 417–435.
131. Wit, A.L., P.F. Cranefield, and D.C. Gadsby, Electrogenic sodium extrusion can stop triggered activity in the canine coronary sinus. *Circ. Res*., 1981;**49**: 1029–1042.

132. Kline, R.P., M.S. Siegal, J. Kupersmith, and A.L. Wit, Effects of strophanthidin on changes in extracellular potassium during triggered activity in the arrhythmic canine coronary sinus. *Circulation*, 1982;**66**(Suppl. 2): 356.
133. Kline, R.P. and M. Morad, Potassium efflux in heart muscle during activity: extracellular accumulation and its implications. *J. Physiol.*, 1978;**280**: 537–558.
134. Rosen, M.R. and R.F. Reder, Does triggered activity have a role in the genesis of cardiac arrhythmias? *Ann. Intern. Med.*, 1981;**94**: 794–801.
135. Moak, J.P. and M.R. Rosen, Induction and termination of triggered activity by pacing in isolated canine Purkinje fibers. *Circulation*, 1984;**69**: 149–162.
136. Schwartz, P.J., The idiopathic long, Q.T., syndrome: progress and questions. *Am. Heart J.*, 1985;**109**: 399–411.
137. Schwartz, P.J., Prevention of the arrhythmias in the long QT syndrome. in *Medical Management of Cardiac Arrhythmias*, H.E. Kulbertus, Editor. Edinburgh: Churchill Livingston, 1986, pp. 153–156.
138. Keating, M.T., D. Atkinson, C. Dunn, K. Timothy, G.M. Vincent, and M. Leppert, Linkage of a cardiac arrhythmia, the long QT, and the Harvey ras-1 gene. *Science*, 1991;**252**: 704–706.
139. Towbin, J.A. and K. Schwartz, Genetic approaches and familial arrhythmias, in *Foundations of Cardiac Arrhythmias*, P.M. Spooner and M.R. Rosen, Editors. New York: Marcel Dekker Inc, 2000, pp. 665–699.
140. Splawski, I., M. Tristani-Firouzi, M.H. Lehmann, M.C. Sanguinetti, and M.T. Keating, Mutations in the hminK gene cause long QT syndrome and suppress I_{Ks} function. *Nat. Genet.*, 1997;**17**: 338–340.
141. Abbott, G.W., F. Sesti, I. Splawski, M.E. Buck, M.H. Lehmann, K.W. Timothy, M.T. Keating, and S.A. Goldstein, MiRP1 forms I_{Kr} potassium channels with HERG and is associated with cardiac arrhythmia. *Cell*, 1999;**97**: 175–187.
142. Chen, Q., G.E. Kirsch, D. Zhang, R. Brugada, J. Brugada, P. Brugada, D. Potenza, A. Moya, M. Borggrefe, G. Breithardt, R. Ortiz-Lopez, Z. Wang, C. Antzelevitch, R.E. O'Brien, E. Schulze-Bahr, M.T. Keating, J.A. Towbin, and Q. Wang, Genetic basis and molecular mechanism for idiopathic ventricular fibrillation. *Nature* 1998;**392**: 293–296.
143. Ellinor, P.T. and C.A. Macrae, The genetics of atrial fibrillation. *J. Cardiovasc. Electrophysiol.*, 2003;**14**: 1007–1009.
144. Moe, G.K., On the multiple wavelet hypothesis of atrial fibrillation. *Arch. Int. Pharmacodyn.*, 1962;**140**: 183–188.
145. Moe, G.K., W.C. Rheinboldt, and J.A. Abildskov, A computer model of atrial fibrillation. *Am. Heart J.*, 1964; **67**: 200–220.
146. Coumel, P., P. Attuel, J. Lavallee, D. Flammang, J.F. Leclercq, and R. Slama, Syndrome d'arythmie auriculaire d'origine vagale. *Arch. Mal. Coeur Vaiss.*, 1978;**71**: 645–656.
147. Janse, M.J. and A.G. Kleber, Electrophysiological changes and ventricular arrhythmias in the early phase of regional myocardial ischemia. *Circ. Res.*, 1981;**49**: 1069–1081.
148. Myerburg, R.J., H. Gelband, K. Nilsson, et al., Long term electrophysiological abnormalities resulting from experimental myocardial infarction in cats. *Circ. Res.*, 1977;**41**: 73–84.
149. Sasyniuk, B.I. and C. Mendez, A mechanism for reentry in canine ventricular tissue. *Circ. Res.*, 1971;**28**: 3–15.
150. Alessi, R., M. Nusynowitz, J.A. Abildskov, G.K. Moe, Nonuniform distribution of vagal effects on the atrial refractory period. *Am. J. Physiol.*, 1958;**194**: 406–410.
151. Zhou, S., L.S. Chen, Y. Miyauchi, M. Miyauchi, S. Kar, S. Kangavari, M.C. Fishbein, B. Sharifi, and P.S. Chen, Mechanisms of cardiac nerve sprouting after myocardial infarction in dogs. *Circ. Res.*, 2004;**95**: 76–83.
152. Mendez, C. and G.K. Moe, Demonstration of a dual A-V nodal conduction system in the isolated rabbit heart. *Circ. Res.*, 1966;**19**: 378–393.
153. Allessie, M.A. and F.I.M. Bonke, Direct demonstration of sinus node reentry in the rabbit heart. *Circ. Res.*, 1979;**44**: 557–568.
154. Severs, N.J., S.R. Coppen, E. Dupont, H.I. Yeh, Y.S. Ko, T. Matsushita, Gap junction alterations in human cardiac disease. *Cardiovasc. Res.*, 2004;**62**: 368–377.
155. van Veen, A.A., H.V. van Rijen, and T. Opthof, Cardiac gap junction channels: modulation of expression and channel properties. *Cardiovasc. Res.*, 2001;**51**: 217–229.
156. Thomas, S.P., J.P. Kucera, L. Bircher-Lehmann, Y. Rudy, J.E. Saffitz, A.G. Kleber, Impulse propagation in synthetic strands of neonatal cardiac myocytes with genetically reduced levels of connexin43. *Circ. Res.*, 2003;**92**: 1209–1216.
157. Wit, A.L. and P.F. Cranefield, Reentrant excitation as a cause of cardiac arrhythmias. *Am. J. Physiol.*, 1978;**235**: H1–H17.
158. Mines, G.R., On circulating excitations in heart muscles and their possible relation to tachycardia and fibrillation. *Trans. R. Soc. Can.*, 1914; Ser. 3, 8: Sect. IV, 43–52.
159. Mayer, A.G., Rhythmical pulsation in Scyphomedusae-II. *Carnegie Inst. Washington. Papers Tortugas Lab.*, 1908;**I**: 113–131.
160. Page, R.L., L.H. Frame, and B.F. Hoffman, Circus movement in the tricuspid ring: an in vitro model. *J. Am. Coll. Cardiol.*, 1984;**3**: 478.
161. Fozzard, H.A., Conduction of the action potential, in *Handbook of Physiology. Section* 2: *The Cardiovascular System*, vol. I, *The Heart*, R.M. Berne and N. Sperelakis, Editors. Bethesda, MD: American Physiological Society, 1979, pp. 335–356.
162. Carmeliet, E. and J. Vereecke, Electrogenesis of the action potential and automaticity, in *Handbook of Physiology. Section* 2: *The Cardiovascular System*, vol. I, *The Heart*, R.M. Berne and N. Sperelakis, Editors. Bethesda, MD: American Physiological Society, 1979, pp. 269–334.
163. Hodgkin, A.L., *The Conduction of the Nervous Impulse*. Springfield, IL: Thomas, 1964.
164. Weidmann, S., The effect of the cardiac membrane potential on the rapid availability of the sodium-carrying system. *J. Physiol. London*, 1955;**127**: 213–224.
165. Tsien, R.W., Calcium channels in excitable cell membranes. *Annu. Rev. Physiol.* 1983;**45**: 341–358.
166. Zipes, D.P. and C. Mendez, Action of manganese ions and tetrodotoxin on atrioventricular nodal transmembrane potentials in isolated rabbit hearts. *Circ. Res.*, 1973;**32**: 447–454.
167. Spach, M.S., W.T. Miller 3rd, D.B. Geselowitz, R.C. Barr, J.M. Kootsey, and E.A. Johnson, The discontinuous nature of propagation in normal canine cardiac muscle: evidence for recurrent discontinuities of intracellular resistance that effect the membrane currents. *Circ. Res.*, 1981;**48**: 39–54.
168. Spach, M.S., W.T. Muller 3rd, P.C. Dolber, J.M. Kootsey, J.R. Sommer, C.E. Mosher Jr., The functional role of structural complexities in the propagation of depolarization in the atrium of the dog: cardiac conduction disturbances due to discontinuities of effective axial resistivity. *Circ. Res.*, 1982;**50**: 175–191.
169. Clerc, L., Directional differences of impulse spread in trabecular muscle from mammalian heart. *J. Physiol. London*, 1976;**2S5**: 335–346.

170. Ursell, P.C., P.I. Gardner, A. Albala, J.J. Fenoglio Jr., A.L. Wit, Structural and electrophysiological changes in the epicardial border zone of canine myocardial infarcts during infarct healing. *Circ. Res.*, 1985;**56**: 436–451.
171. Spach, M.S. and P.C. Dolber, Relating extracellular potentials and their derivatives to anisotropic propagation at a microscopic level in human cardiac muscle. Evidence for electrical uncoupling of side-to-side fiber connections with increasing age. *Circ. Res.*, 1986;**58**: 356–371.
172. Spach, M.S., P.C. Dolber, and J.F. Heidlage, Influence of the passive anisotropic properties on directional differences in propagation following modification of the sodium conductance in human atrial muscle. A model of reentry base on anisotropic discontinuous propagation. *Circ. Res.*, 1988;**62**: 811–832.
173. Spach, M.S. and M.E. Josephson, Initiating reentry: the role of nonuniform anisotropy in small circuits. *J. Cardiovasc. Electrophysiol.*, 1994;**5**: 182–209.
174. Lake, F.R., K.J. Cullen, N.H. de Klerk, M.G. McCall, D.L. Rosman, Atrial fibrillation and mortality in an elderly population. *Aust. NZ J. Med.*, 1989;**19**: 321–326.
175. Antzelevitch, C. and M.S. Spach, Impulse conduction: continuous and discontinuous, in *Foundations of Cardiac Arrhythmias*, P.M. Spooner and M.R. Rosen, Editors. New York: Marcel Dekker Inc, 2000, pp. 205–241.
176. Page, E. and Y. Shibata, Permeable junctions between cardiac cells. *Annu. Rev. Physiol.*, 1981;**43**: 431–441.
177. Wojtczak, J., Contractures and increase in internal longitudinal resistance of cow ventricular muscle induced by hypoxia. *Circ. Res.*, 1979;**44**: 88–95.
178. Joyner, R.W., Effects of the discrete pattern of electrical coupling on propagation through an electrical syncytium. *Circ. Res.*, 1982;**50**: 192–200.
179. Joyner, R.W., R. Veenstra, D. Rawling, and A. Chorro, Propagation through electrically coupled cells. Effects of a resistive barrier. *Biophys. J.*, 1984;**45**: 1017–1025.
180. Goldstein, S.S. and W. Rail, Changes of action potential shape and velocity for changing core conductor geometry. *Biophys. J.*, 1974;**14**: 731–757.
181. Dodge, F.A. and P.F. Cranefield, Nonuniform conduction in cardiac Purkinje fibers, in *Normal and Abnormal Conduction in the Heart*, A. Paes de Carvalho, B.F. Hoffman, and M. Lieberman, Editors. Mount Kisco, NY: Futura, 1982, pp. 379–395.
182. Wit, A.L., P.F. Cranefield, and B.F. Hoffman, Slow conduction and reentry in the ventricular conducting system II. Singly and sustained circus movement in networks of canine and bovine Purkinje fibers. *Circ. Res.*, 1972;**30**: 11–22.
183. Boyden, P.A., L.P. Tilley, A. Albala, S.K. Liu, J.J. Fenoglio Jr., and A. Wit, Mechanisms for atrial arrhythmias associated with cardiomyopathy: a study of feline hearts with primary myocardial disease. *Circulation*, 1984;**69**: 1036–1047.
184. Moe, G.K., C. Mendez, J. Han, and A.V. Aberrant, Impulse propagation in the dog heart: a study of functional bundle branch block. *Circ. Res.*, 1965;**16**: 261–286.
185. Gallagher, J.J., M. Gilbert, R.H. Svenson, W.C. Sealy, J. Kasell, A.G. Wallace, Wolff-Parkinson-White syndrome: the problem, evaluation, and surgical correction. *Circulation*, 1975;**51**: 767–785.
186. Frame, L.H., R.L. Page, P.A. Boyden, and B.F. Hoffman, A right atrial incision that stabilizes reentry around the tricuspid ring in dogs. *Circulation*, 1983;**68**(Suppl. 3): 361.
187. Antzelevitch, C., J. Jalife, G.K. Moe, Characteristics of reflection as a mechanism of reentrant arrhythmias and its relationship to parasystole. *Circulation*, 1980;**61**: 182–191.
188. Jalife, J. and G.K. Moe, Excitation, conduction, and reflection of impulses in isolated bovine and canine cardiac Purkinje fibers. *Circ. Res.*, 1981;**49**: 233–247.
189. Allessie, M.A., F.I.M. Bonke, and F.J.G. Schopman, Circus movement in rabbit atrial muscle as a mechanism of tachycardia II. The role of nonuniform recovery of excitability in the occurrence of unidirectional block, as studied with multiple microelectrodes. *Circ. Res.*, 1976;**39**: 168–177.
190. Allessie, M.A., F.I.M. Bonke, and F.J.G. Schopman, Circus movement in rabbit atrial muscle as a mechanism of tachycardia. *Circ. Res.*, 1973;**33**: 54–62.
191. Allessie, M.A., F.I.M. Bonke, and F.J.G. Schopman, Circus movement in rabbit atrial muscle as a mechanism of tachycardia. III. The "Leading Circle" concept: a new model of circus movement in cardiac tissue without the involvement of an anatomical obstacle. *Circ. Res.*, 1977;**41**: 9–18.
192. Allessie, M.A., W.J.E.P. Lammers, F.I.M. Bonke, and J. Hollen, Intra-atrial reentry as a mechanism for atrial flutter induced by acetylcholine and rapid pacing in the dog. *Circulation*, 1984;**70**: 123–135.
193. Van Capelle, F.J.L., *Slow conduction and cardiac arrhythmias*, thesis. Amsterdam: University of Amsterdam, 1983.
194. Davidenko, J.M., A.V. Pertsov, R. Salomonsz, W. Baxter, and J. Jalife, Stationary and drifting spiral waves of excitation in isolated cardiac muscle. *Nature*, 1992;**355**: 349–351.
195. Winfree, A.T., *When Time Breaks Down*. Princeton, NJ: Princeton University Press, 1987.
196. Janse, M.J. and E. Downer, Reentry, in *Foundations of Cardiac Arrhythmias*, P.M. Spooner and M.R. Rosen, Editors. New York: Marcel Dekker Inc, 2000, pp. 449–477.
197. Katz, L.N. and A. Pick, *Clinical Electrocardiography. I. The Arrhythmias* Philadelphia, PA: Lea & Febiger, 1956.
198. Jalife, J. and G.K. Moe, A biologic model of parasystole. *Am. J. Cardiol.*, 1979;**43**: 761–772.
199. Jalife, J. and G.K. Moe, Effect of electrotonic potentials on pacemaker activity of canine Purkinje fibers in relation to parasystole. *Circ. Res.*, 1976;**39**: 801–808.
200. Frame, L.H. and B.F. Hoffman, Mechanisms of tachycardia, in *Tachycardias*, B. Surawicz, C. Pratrap Reddy, and E.N. Prystowsky, Editors. Boston, MA: Nijhoff, 1984, pp. 7–36.
201. Waldo, A.L., W.A.H. Maclean, R.B. Karp, N.T. Kouchoukos, and T.N. James, Entrainment and interruption of atrial flutter with atrial pacing: studies in man following open heart surgery. *Circulation*, 1977;**56**: 737–745.
202. Waldo, A.L., Atrial flutter: entrainment characteristics. *J. Cardiovasc. Electrophysiol.*, 1997;**8**: 337–352.
203. Josephson, M.E., L.N. Horowitz, A. Farshidi, S.R. Spielman, E.L. Michelson, A.M. Greenspan, Sustained ventricular tachycardia: evidence for protected localized reentry. *Am. J. Cardiol.*, 1978;**42**: 416–424.
204. Singer, D.H., R. Lazzara, and B.F. Hoffman, Interrelationships between automaticity and conduction in Purkinje fibers. *Circ. Res.*, 1967;**21**: 537–558.
205. Saunders, J.H., G.R. Ferrier, G.K. Moe, Conduction block associated with transient depolarizations induced by acetylstrophanthidin in isolated canine Purkinje fibers. *Circ. Res.*, 1973;**32**: 610–617.

206. Rosenbaum, M.B., J.O., Lazzari, and M.V. Elizara, The role of phase 3 and phase 4 block in clinical electrocardiography, in *The Conduction System of the Heart: Structure, Function and Clinical Implications*, H.J.J. Wellens, K.I. Lie, M.J. Janse, Editors. Leyden: Stenfert Kroese, 1976, pp. 126–142.
207. Wit, A.L. and M.R. Rosen, Cellular electrophysiological mechanisms of cardiac arrhythmias, in *Comprehensive Electrocardiology, Theory and Practice in Health and Disease*, vol. 2, P.W. MacFarlane and T.D. Veitch Lawrie, Editors. Elmsford, NY: Pergamon Press, 1989, Chapter 20, pp. 801–841.
208. Akhtar, M., G. Breithardt, A.J. Camm, P. Coumel, M.J. Janse, R. Lazzara, R.J. Myerburg, P.J. Schwartz, A.L. Waldo, H.J. Wellens, et al., CAST and beyond implications of the cardiac arrhythmia suppression trial. Task force of the working group on arrhythmias of the European society of cardiology. *Circulation*, 1990;**81**: 1123–1127.
209. Manolis, A.S., P.J. Wang, and N.A. Estes 3rd, Radiofrequency catheter ablation for cardiac tachyarrhythmias. *Ann. Intern. Med.*, 1994;**121**: 452–461.
210. Moss, A.J., A. Vyas, H. Greenberg, R.B. Case, W. Zareba, W.J. Hall, M.W. Brown, S.A. McNitt, and M.L. Andrews, MADIT-II Research Group. Temporal aspects of improved survival with the implanted defibrillator (MADIT-II). *Am. J. Cardiol.*, 2004;**94**: 312–315.
211. Plotnikov, A.N., E.A. Sosunov, J. Qu, I.N. Shlapakova, E.P. Anyukhovsky, L. Liu, M.J. Janse, P.R. Brink, I.S. Cohen, R.B. Robinson, P. Danilo Jr., and M.R. Rosen, Biological pacemaker implanted in canine left bundle branch provides ventricular escape rhythms that have physiologically acceptable rates. *Circulation*, 2004;**109**: 506–512.
212. Potapova, I., A. Plotnikov, Z. Lu, P. Danilo Jr., V. Valiunas, J. Qu, S. Doronin, J. Zuckerman, I.N. Shlapakova, J. Gao, Z. Pan, A.J. Herron, R.B. Robinson, P.R. Brink, M.R. Rosen, and I.S. Cohen, Human mesenchymal stem cells as a gene delivery system to create cardiac pacemakers. *Circ. Res.*, 2004;**94**: 952–959.
213. Murata, M., E. Cingolani, A.D. McDonald, J.K. Donahue, E. Marbán, Creation of a genetic calcium channel blocker by targeted gem gene transfer in the heart. *Circ. Res.*, 2004;**95**: 398–405.
214. Kehat, I., L. Khimovich, O. Caspi, A. Gepstein, R. Shofti, G. Arbel, I. Huber, J. Satin, J. Itskovitz-Eldor, and L. Gepstein, Electromechanical integration of cardiomyocytes derived from human embryonic stem cells. *Nat. Biotechnol.*, 2004;**22**: 1282–1289.
215. Dobert, N., M. Britten, B. Assmus, U. Berner, C. Menzel, R. Lehmann, N. Hamscho, V. Schachinger, S. Dimmeler, A.M. Zeiher, F. Grunwald, Transplantation of progenitor cells after reperfused acute myocardial infarction: evaluation of perfusion and myocardial viability with FDG-PET and thallium SPECT. *Eur. J. Nucl. Med. Mol. Imaging*, 2004;**31**: 1146–1151.
216. Wollert, K.C., G.P. Meyer, J. Lotz, S. Ringes-Lichtenberg, P. Lippolt, C. Breidenbach, S. Fichtner, T. Korte, B. Hornig, D. Messinger, L. Arseniev, B. Hertenstein, A. Ganser, and H. Drexler, Intracoronary autologous bone-marrow cell transfer after myocardial infarction: the BOOST randomised controlled clinical trial. *Lancet*, 2004;**364**: 141–148.

24 Clinical Cardiac Electrophysiology

Andrew C. Rankin · F. Russell Quinn · Alan P. Rae

P. W. Macfarlane, A. van Oosterom, O. Pahlm, P. Kligfield, M. Janse, J. Camm (eds.), *Comprehensive Electrocardiology*, DOI 10.1007/978-1-84882-046-3_24,

24.1 Introduction

Clinical cardiac electrophysiology (EP) techniques, involving intracardiac recording and electrical stimulation, have been of major importance in elucidating the mechanisms of cardiac arrhythmias. They not only have led to improved interpretation of the surface electrocardiogram (ECG) but have evolved to play a major role in the therapy of tachycardias. This role has changed in recent years, with a decline in EP-guided therapy for ventricular tachyarrhythmias but an increase in diagnostic use prior to curative catheter ablation.

24.2 History of Clinical Electrophysiology

Direct recording of intracavitary electrograms was first reported in 1945 by Lenègre and Maurice [1]. Developments in recording techniques subsequently permitted the registration of these potentials from all the cardiac chambers [2–5]. Although the integration of the atrioventricular (AV) conducting system had been described in 1906 by Tawara [6], the His-bundle electrogram was not recorded until 1958 by Alanis, Gonzalez, and Lopez in the isolated canine heart [7]. His-bundle recordings in man were obtained using an electrode catheter in 1960 [8], but the standard endocardial catheter technique for recording a His-bundle potential was first described by Scherlag and coworkers in 1969 [9]. Subsequently, electrode catheter recordings of electrograms from the sinus node [10] and from accessory AV pathways [11] have been obtained.

Initially, the major clinical application of "His-bundle electrocardiography" was as a descriptive method for the diagnosis of AV conduction disturbances [12, 13]. Subsequently electrophysiological techniques were used to assess sinoatrial disease [14], and the development of programmed electrical stimulation to initiate tachycardia allowed the study of the mechanisms of arrhythmias.

The induction of ventricular fibrillation by electrical currents was demonstrated as early as 1899 by Prevost and Battelli [15], but the electrical induction and termination of arrhythmias essentially started in the early 1950s. Reentry as a mechanism for tachyarrhythmias was proposed initially by Mines [16] and the presence of potential substrate for reentry was identified by Moe and coworkers [17] in 1956. Subsequently, in 1963, the initiation and termination of supraventricular tachycardia was demonstrated in a canine model [18]. A seminal study by Durrer et al. [19] in 1967 demonstrated that supraventricular tachycardia could be initiated and terminated by the introduction of premature beats in patients with the Wolff-Parkinson-White syndrome. Evidence for the reentrant basis for the majority of paroxysmal supraventricular tachycardias was provided by Bigger and Goldreyer using a systematic approach with programmed stimulation and His-bundle recording [20]. These techniques were translated to patients with ventricular tachycardia in 1972 by Wellens et al. [21] who suggested that the mechanism underlying this arrhythmia was also reentry [22]. A macroreentrant mechanism was described by Akhtar and colleagues in 1976 with the demonstration of the "V_3 phenomenon" or bundle branch reentrant beat [23], although clinically occurring tachycardias of this type are uncommon [24]. The microreentrant basis for the majority of ventricular tachycardias in patients with underlying coronary artery disease was demonstrated in a series of studies from Josephson and Horowitz and coworkers [25–28].

The ability to reproducibly initiate ventricular arrhythmias by programmed electrical stimulation, using repetitive extrastimuli with varying coupling intervals, led to EP-guided drug therapy. The arrhythmia would be induced in the drug-free state, and then the effect of drug therapy on subsequent inducibility was used to select long-term treatment. Non-randomized studies appeared to support this practice [29, 30] but more recent randomized studies have not confirmed benefit from this approach [31–34], leading to the virtual demise of the electrophysiology study as the determinant of therapy for life-threatening arrhythmias. At the same time, the development of catheter ablation techniques has increased the use of clinical electrophysiology testing to identify the targets for this curative therapy [35].

24.3 Methodology

24.3.1 Electrophysiological Equipment

At its most basic, a clinical EP study requires equipment to allow recording of cardiac activity and delivery of electrical stimulation to the heart. A standard ECG recorder, a temporary external pacing unit, and a transvenous pacing catheter would suffice for a simple EP study, such as the measurement of the sinus node recovery time in the evaluation of the sick sinus syndrome. However, such simple procedures are now rarely performed, and modern clinical electrophysiology equipment is designed to undertake more complex studies, with recordings from multiple intracardiac electrode catheters, and programmed electrical stimulation for the induction and investigation of tachyarrhythmias.

In a modern EP system, dedicated computer systems have replaced multi-channel analogue chart- and tape-recorders. Surface electrodes and intracardiac catheters are connected to the computer system via an electrically isolated patient-interface unit. Multiple ECG leads and intracardiac electrograms can be displayed on-screen, stored to hard disk, or printed out. The simultaneous display of the signals with several surface ECGs permits the evaluation of the timing and morphology of the surface signals relative to the intracardiac electrograms. Usually, at least three approximately orthogonal surface leads are displayed, with additional limb and precordial ECG leads if required for tachycardia morphology analysis. For routine studies, bipolar intracardiac signals are amplified and band-pass filtered in the frequency range 30–500 Hz, which allows optimum definition of the intracardiac electrograms. Additional information can be obtained from unipolar electrograms, using either Wilson's central terminal or an electrode catheter placed distant from the heart, e.g., in the inferior vena cava, as the reference potential. By using different filtering of the unipolar potential, essentially the same as a standard ECG (0.5–25 Hz), valuable information can be obtained from the electrogram morphology, not only the timing [36].

For studies involving the assessment of refractory periods and tachycardia induction, simple temporary pacing units are not sufficient, and a more sophisticated programmable stimulator is required. This should provide isolated outputs to prevent leakage currents that might cause arrhythmias, with the capability of delivering at least three extrastimuli at independently variable intervals during spontaneous or paced rhythms, and with provision for a wide range of paced cycle lengths.

The studies should be performed in a dedicated EP laboratory, cardiac catheterization laboratory, or procedure room with fluoroscopy. In addition, it should be emphasized that the personnel should have the necessary specialist training and that full resuscitative equipment should be available. Recommendations have been published for training and clinical competence in invasive electrophysiology studies [37, 38].

24.3.2 The Electrophysiology Study

Patients are studied in the post-absorptive state with no, or only mild, sedation (e.g., with benzodiazepines). If patients have been on antiarrhythmic drugs, these should be withdrawn prior to study for a period of at least five half-lives, if arrhythmia induction is planned. Other cardioactive drugs that are not used as antiarrhythmics may be continued.

Electrode catheters are inserted percutaneously using standard catheterization techniques under local anesthesia, and are positioned in selected areas of the heart under fluoroscopic guidance (Fig. 24.1). Depending on the type of study and the intracardiac recordings required, two to five catheters are usually inserted. The conventional EP catheter is quadripolar, which allows the distal pair of electrodes to deliver the stimuli for pacing and the proximal pair of electrodes to obtain bipolar electrogram recordings. Pre-shaped curves aid the placement of catheters in different positions in the heart. There are large varieties of specialized electrode catheters in routine use. For example, a multipolar tricuspid annulus catheter may aid ablation of atrial flutter (Fig. 24.1c), and a circular multipolar catheter may be used to guide pulmonary vein isolation (Fig. 24.1d). Ablation catheters are deflectable to aid their placement, and have a larger electrode at their tip, usually 4 mm. Larger 8 mm tip, or irrigated tip, catheters are also used, to create larger and deeper lesions.

The number of catheters, and the site of placement, varies depending on the clinical requirements. If the only clinical question is whether or not a ventricular arrhythmia is inducible then a single quadripolar catheter to the right ventricular

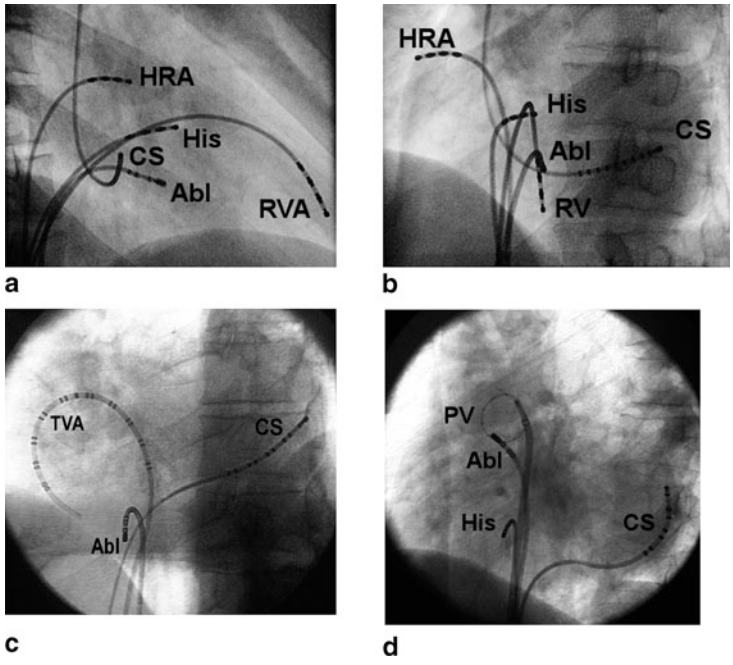

Figure 24.1

Radiographs of EP catheters. (a) Right Anterior Oblique (RAO) and (b) Left Anterior Oblique (LAO) views of catheters placed for a diagnostic and RF ablation procedure. Catheters have been positioned to high right atrium (HRA), tricuspid annulus to record a His-bundle potential (His), coronary sinus (CS), right ventricular apex (RVA), and for ablation of AV nodal slow pathway (Abl). (c) Multipolar catheters placed at tricuspid valve annulus (TVA), coronary sinus (CS), and an ablation catheter (Abl) placed across the cavo-tricuspid isthmus for ablation of atrial flutter (LAO view). (d) Pulmonary vein (PV) catheter placed via a transseptal sheath at the right upper pulmonary vein to guide the ablation catheter (Abl) during a pulmonary vein isolation procedure. Catheters also positioned at coronary sinus (CS) and His bundle (His), seen in LAO view.

(RV) apex may suffice, but if further assessment of cardiac electrophysiology or diagnosis is required then more catheters are used. Many EP laboratories have routinely placed three catheters (high right atrial, His bundle, and RV apex) for an initial study, with a fourth catheter placed in the coronary sinus to provide recordings from left atrium and ventricle when investigating supraventricular tachycardia (Fig. 24.1a, b). With the expanding indications for electrophysiological procedures, catheter choice and placement have become more specific, to maximize the diagnostic information required to proceed to ablation and to avoid unnecessary catheter use, in order to reduce complications and cost [39]. Much time was previously spent on assessments of the electrophysiological properties of the heart, which now may be omitted to concentrate on the identification and ablation of the arrhythmia substrate. For example, a single catheter approach has been described for left-sided accessory pathway ablation, omitting all EP assessment prior to ablation [40].

24.3.2.1 His-Bundle Recording

The cornerstone of EP testing has been a stable, accurate His-bundle recording. To achieve this, a multipolar catheter is inserted via the femoral vein and is manipulated across the tricuspid valve into the right ventricle. While maintaining clockwise torque to hold the catheter against the tricuspid ring, the catheter is slowly withdrawn until the His-bundle signal between the atrial and ventricular electrograms is recorded (Fig. 24.2). With a proximal His-bundle recording, the atrial and ventricular components of the electrogram should be of nearly equal amplitude. The normal His-bundle deflection is 10–25 ms in duration and, in the absence of a bypass pathway, the HV interval should be at least 35 ms.

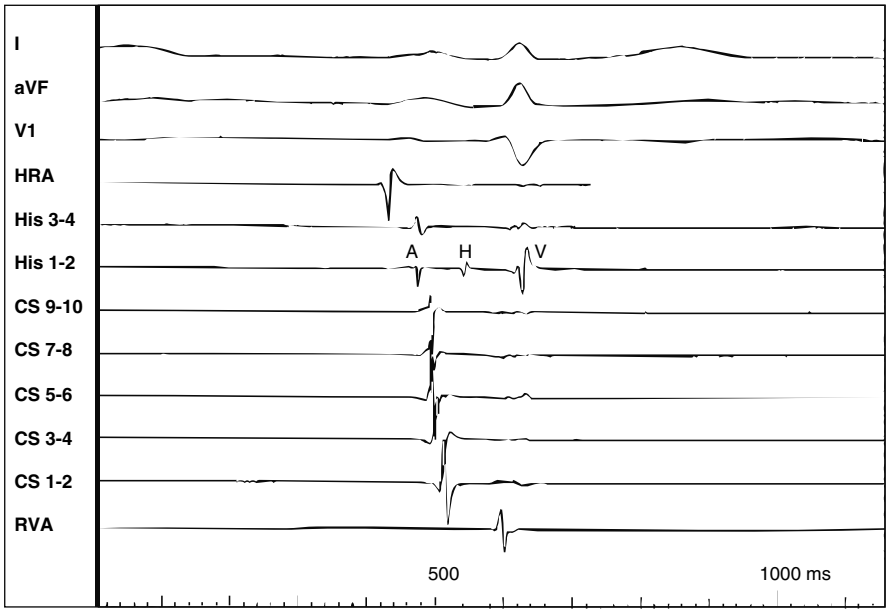

Figure 24.2

Recordings in sinus rhythm. Three ECG leads (I, aVF, and V1) and intracardiac bipolar electrograms from high right atrium (HRA), proximal and distal electrodes of the His-bundle catheter (His 3-4, 1-2), pairs of electrodes of a decapolar catheter in the coronary sinus (CS 1-10), and right ventricular apex (RVA) are shown. Atrial activation begins in the high right atrium, followed by septal activation at the His and then spreading across the left atrium.

If this interval is less than 35 ms, the deflection may be a right bundle branch potential. Validation may be obtained by selective His-bundle pacing – the interval between stimulus and ventricular component should be identical to the basal HV interval [41].

24.3.2.2 Intracardiac Chamber Recording

A right atrial catheter may be positioned at the superior posterolateral region near the sinus node (Fig. 24.1a, b). The left atrium can be entered directly from the right atrium through a patent foramen ovale or by means of a trans-septal procedure, but in most cases left atrial stimulation and recording are obtained from a catheter positioned in the coronary sinus (Figs. 24.1 and 24.2). This is of particular value with supraventricular tachycardia, when an accessory pathway is suspected, and a catheter with multiple electrodes, e.g., octapolar or decapolar, is placed in the coronary sinus to facilitate mapping. The coronary sinus catheter was previously most commonly inserted from above (Fig. 24.1a, b), via the left antecubital, subclavian, or right internal jugular veins, but increasingly the femoral vein approach is used, deploying a deflectable multipolar catheter (Fig. 24.1c, d). Some laboratories use the coronary sinus catheter to pace the atria, and hence dispense with the right atrial catheter, in order to simplify procedures [39]. The standard catheter position in the right ventricle is with the tip in the RV apex, because it provides a stable, easily reproducible site. The RV outflow tract is also utilized, particularly for arrhythmia induction. For certain studies, such as ventricular stimulation or tachycardia mapping, a left ventricular (LV) electrode catheter is required [42]. It is inserted by the standard retrograde arterial approach usually from the femoral artery but occasionally by means of a brachial arteriotomy. Access to the LV can also be achieved by crossing the mitral valve after a trans-septal puncture, and in some cases epicardial pacing of the LV can be obtained via a branch of the CS. LV catheterization during routine EP studies is not standard.

24.3.2.3 Stimulation

Pacing and programmed stimulation is normally performed with rectangular stimuli having a 1–2 ms pulse width and an amplitude of twice the late diastolic threshold. The electrode catheters are positioned in appropriate regions of low threshold for stimulation. In general, these thresholds should be less than 2 mA, 1 mA, and 4 mA for catheters positioned in the right atrium, right ventricle, and coronary sinus, respectively. Repositioning of catheters, and interventions such as antiarrhythmic therapy, may alter stimulation thresholds and these should be rechecked after such maneuvers. Changing thresholds may influence certain electrophysiological parameters such as refractory periods. Although the use of pulse amplitude of twice the diastolic threshold is a routine practice in many laboratories, some investigators have advocated using higher pulse amplitudes, since an increase in current strength may facilitate the induction of ventricular tachyarrhythmias by permitting the introduction of extrastimuli at shorter coupling intervals [43]. However, in some patients, ventricular arrhythmias were not inducible at the higher strength although an arrhythmia was induced at twice the diastolic threshold [44]. A major concern with the use of high pulse amplitudes is the possibility of an increased induction of nonclinical arrhythmias [45].

24.3.3 Electrophysiology Study Protocols

An EP study protocol must be flexible and should be selected in accordance with the particular problem to be evaluated. Unfortunately, there has been little standardization in study protocols between laboratories, particularly in relation to ventricular stimulation, and this has contributed to the concerns about the evidence base for its clinical utility. However, while EP-guided therapy for ventricular arrhythmias has declined, the role of the electrophysiology study in the diagnosis of tachycardia and the identification of a substrate for ablation has increased. The baseline diagnostic information obtained will depend on the number of catheters placed, and the stimulation protocols utilized, but may include an assessment of the AV conduction system, evaluation of the refractory periods of its components and induction, definition of mechanism, and termination of tachyarrhythmia.

24.3.3.1 Baseline AV Conduction Intervals

(a) *PA interval and intra-atrial conduction times*

The depolarization of the atrium usually occurs earliest in the region of the sinus node either at the high right atrium, the node itself or the mid-lateral aspect of the right atrium [46]. The PA interval, measured from the onset of the P wave in the surface ECG to the atrial electrogram recorded from the His-bundle electrode (AV junction) catheter is a measure of the intra-atrial conduction time [47]. It is not sensitive to changes in autonomic tone. The sequence of atrial activation times at various right and left atrial sites may be more useful than the PA interval. An example of a normal atrial activation pattern is shown in Fig. 24.2 and an example of an abnormal pattern during atrioventricular re-entrant tachycardia (AVRT) is shown in Fig. 24.3.

(b) *AH interval*

Since the depolarization of the AV node cannot be demonstrated using standard electrophysiological techniques, the AH interval is employed for the functional evaluation of AV nodal conduction. The AH interval is measured from the first high-frequency deflection in the atrial electrogram recorded from the His-bundle catheter to the first deflection of the His-bundle electrogram (Fig. 24.2). The normal range of the AH interval is 60–125 ms. The AH interval is markedly influenced by changes in autonomic tone. The AH interval shortens with sympathetic stimulation and lengthens with parasympathetic (vagal) stimulation. Therefore, it may vary profoundly during an EP study depending on the balance of autonomic tone in relation to the patient's level of sedation, anxiety, and other factors.

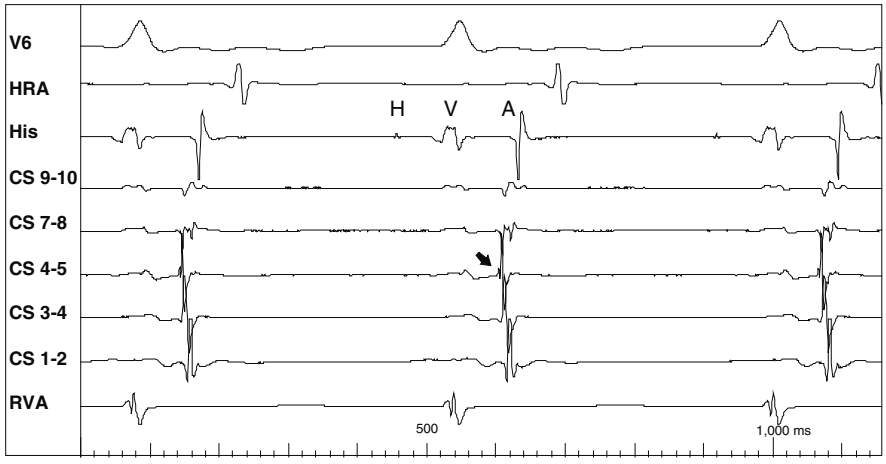

Figure 24.3

Atrioventricular (AV) tachycardia, with a left-sided accessory pathway. Electrograms from high right atrium (HRA), His-bundle catheter (His), a decapolar coronary sinus catheter (CS 1-10), and RV apex. Earliest atrial activation (arrowed) is recorded from the middle pair of electrodes of the coronary sinus catheter (CS 4-5), indicating a left-sided pathway.

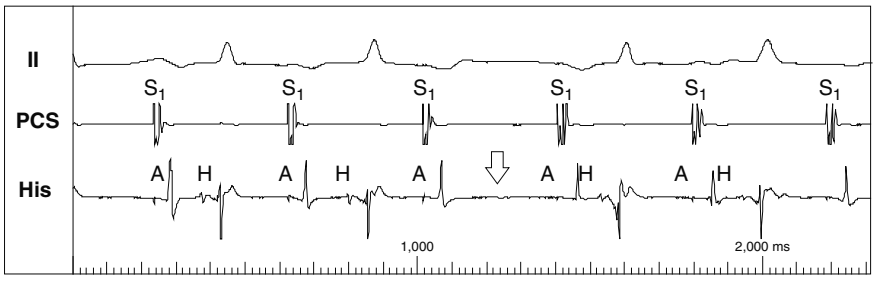

Figure 24.4

Wenckebach-type AV block with atrial pacing. The drive cycle length (S_1-S_1) is 390 ms, pacing from proximal coronary sinus electrodes (PCS). The AH interval increases until block occurs (arrow) of AV nodal conduction.

During atrial pacing at increasing rates (incremental pacing), the normal physiological response is a progressive lengthening in the AH interval at successive rates until AV nodal block occurs. This block occurs usually at rates of 130–170 beats per minute (bpm) and has Wenckebach periodicity, with beat-to-beat AH prolongation prior to block (Fig. 24.4). With alterations in autonomic tone, however, physiological AV nodal block can occur in normal individuals outside this range. At more rapid atrial pacing rates 2:1 or higher degrees of AV nodal block can occur (Fig. 24.4b). The development of AV nodal Wenckebach periods at cycle lengths of 600 ms or longer raises the possibility of a conduction disturbance, especially if they persist after the administration of atropine. AV nodal block at cycle lengths of 300 ms or shorter is suggestive of enhanced AV nodal conduction, sometimes called Lown-Ganong-Levine syndrome [48]. Whether this syndrome merely constitutes one end of the spectrum of AV nodal conduction or is caused by the presence of an atrio-His accessory pathway bypassing part or all of the AV node remains speculative [49].

(c) *HV interval*

The HV interval, a measure of infranodal conduction, assesses conduction through the His bundle, the bundle branches, and the terminal Purkinje system. The normal His-bundle width is 10–25 ms. The total HV interval is measured from the

first deflection of the His bundle to the earliest indication of ventricular activation either in the surface or intracardiac leads (Fig. 24.2). For adults, the HV interval ranges from 35 to 55 ms. An interval less than 35 ms suggests that either the electrogram is obtained from the right bundle branch, or there is an accessory AV connection bypassing at least part of the His-Purkinje system. The HV interval is not influenced by autonomic tone and should not vary within or between studies. With atrial pacing, the HV interval normally remains constant, although at high-paced rates HV interval lengthening with infra-His block may occur in normal individuals. The development of functional bundle branch or complete infra-His block can also occur because of abrupt shortening of the paced cycle length. The facilitation of AV nodal conduction, for instance by catecholamine stimulation, permitting the penetration of impulses into the His-Purkinje system can also increase the likelihood of functional His-Purkinje block.

(d) *Intraventricular conduction*

To measure intraventricular conduction, endocardial mapping of both ventricles is required, which is not usually part of a routine study. The Q-RVA conduction time may be measured, from the onset of ventricular activation to the RV apical electrogram, but is of limited clinical value, in contrast to the QRS duration from the surface ECG, which may have prognostic value [50].

(e) *Ventriculoatrial conduction*

In the absence of an accessory pathway, ventriculoatrial (VA) conduction utilizes the normal AV conduction system retrogradely. VA conduction may be absent in normal individuals with intact anterograde conduction and conversely may be present in patients with anterograde AV block [51]. In general, AV conduction is better than VA conduction.

During incremental ventricular pacing, in the majority of patients, VA conduction time progressively lengthens until the development of VA block, although the degree of prolongation of VA conduction is relatively less than that seen with AV conduction. The site of retrograde VA block may be located in either the His-Purkinje system or the AV node, but since retrograde His-bundle electrograms are only infrequently recorded during ventricular pacing, this localization can only be inferred indirectly. As with AV conduction, the retrograde His-Purkinje system is sensitive to abrupt changes in cycle length.

24.3.3.2 Refractory Period Assessment

The refractory periods of the cardiac chambers and the components of the AV conduction system are evaluated by the technique of premature stimulation. Refractoriness is influenced by several factors including the intensity of the extrastimuli and the cycle length of the spontaneous or paced rate at which the refractory period is measured. There is a basic difference in the responses of myocardium and nodal tissue to increasing rate or increasing prematurity: in atrial or ventricular muscle there is a decrease in the refractory periods, in contrast to the AV node where there is an increase in refractory intervals and conduction time (decremental conduction).

By convention, the notation used is as follows: S_1 is the basic stimulus and S_2 is the first premature stimulus; S_1-S_1 is the paced cycle length; S_1-S_2 is the coupling interval between the last complex of the paced cycle and the premature stimulus S_2. The corresponding notations for the atrial, His-bundle, and ventricular electrograms are A_1-A_1 and A_1-A_2, H_1-H_1 and H_1-H_2, and V_1-V_1 and V_1-V_2, respectively (e.g., Fig. 24.5).

(a) *Effective refractory period*

The effective refractory period (ERP) is defined as the longest premature coupling interval, S_1-S_2, which fails to produce a propagated response. For the atrium, therefore, the ERP is the longest S_1-S_2, which fails to produce an A_2 (Fig. 24.5c); the AV nodal ERP is the longest A_1-A_2, which fails to produce an H_2 (Fig. 24.5b); and the ERP of the His-Purkinje system is the longest H_1-H_2, which fails to elicit a ventricular response. The ERP of the components of the AV conduction system, except for the AV node, shorten with decreasing drive cycle lengths.

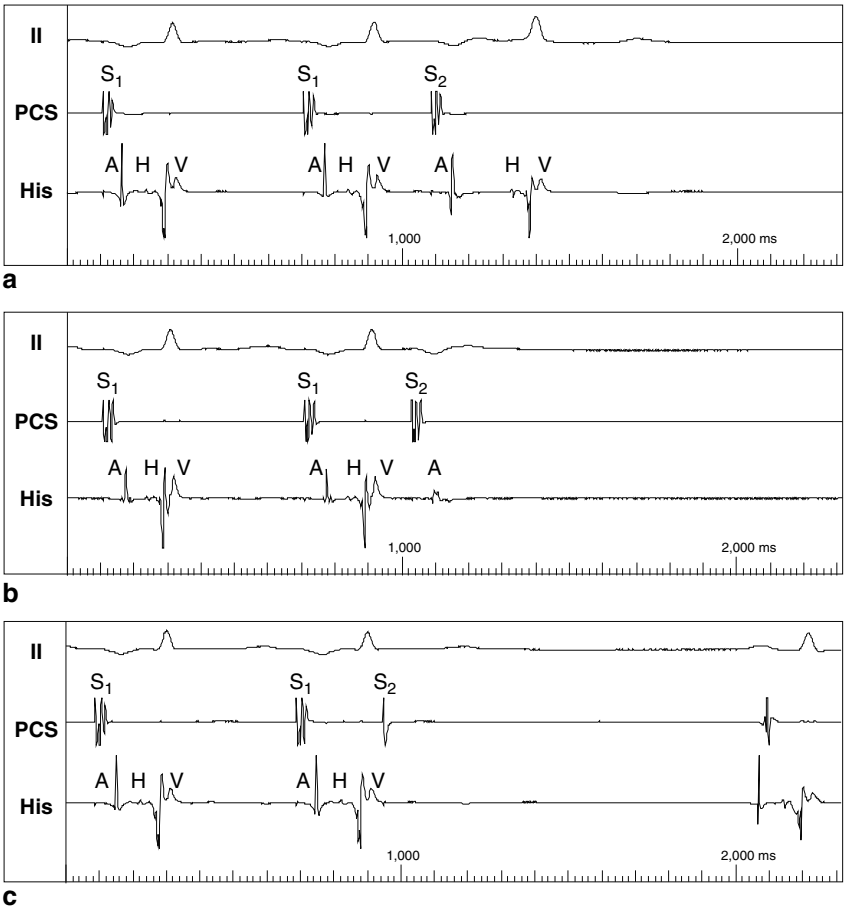

Figure 24.5

Responses to atrial premature beats. Following an 8-beat drive train, S_1-S_1, cycle length 600 ms, from proximal coronary sinus electrodes (PCS), a premature stimulus is delivered (S_1-S_2). With a coupling interval of 380 ms (a) there is prolongation of the AH interval, compared to during the drive train. With a shorter coupling interval of 320 ms (b) the AV nodal effective refractory period (ERP) is reached and there is block of conduction, with only atrial capture - note the absence of a His potential, demonstrating that the block is at the level of the AV node. When the coupling interval is shortened further to 260 ms (c) the atrium is also refractory, with no atrial capture.

(b) *Relative refractory period*

The relative refractory period (RRP) is the longest premature coupling interval at which delay in conduction (prolongation of conduction time) of the extrastimulus occurs. The RRP of the atrium is, therefore, the longest S_1-S_2 at which S_2-A_2 is greater than S_1-A_1, For the AV node, the RRP is the longest A_1-A_2 at which A_2-H_2 is greater than A_1-H_2 and the RRP of the His-Purkinje system is the longest H_1-H_2 at which H_2-V_2 is greater than H_1-V_2.

(c) *Functional refractory period*

In contrast to the ERP and the RRP, the functional refractory period (FRP) is an indication of the conduction within tissue, not the refractoriness of the tissue. Although a misnomer, the term refractory period has remained in conventional usage.

The FRP is defined as the shortest output-coupling interval produced by a tissue in response to programmed extrastimulation. The atrial FRP is the shortest A_1-A_2 produced by any S_1-S_2. The AV nodal FRP is the shortest H_1-H_2 in response to any A_1-A_2 and the FRP of the His-Purkinje system is the shortest V_1-V_2 in response to any H_1-H_2. Frequently, the FRP of the AV node is longer than the ERP of the His-Purkinje system preventing measurement of the His-Purkinje ERP.

(d) *Programmed atrial premature stimulation*

Programmed atrial stimulation is performed by scanning diastole with a premature stimulus introduced initially late in diastole after 6–10 beats of either spontaneous rhythm or an atrial drive cycle. The coupling interval of the premature stimulus is progressively shortened by 10–20 ms. The introduction of premature stimuli in the atrium in the region of the sinus node during sinus rhythm permits the evaluation of the sinoatrial conduction time (see Chap. 26).

Decreasing the coupling interval of atrial premature stimuli produces progressive delay in AV nodal conduction manifested by lengthening of the A_2-H_2 interval (Fig. 24.6). The H_1-H_2 interval initially shows progressive shortening in response to shortening of the A_1-A_2 interval until a nadir is reached, when the increase in AH interval is greater than the decrease in A_1-A_2, followed by a slow increase in the H_1-H_2 intervals. By definition, this nadir corresponds to the FRP of the AV node. Further shortening of A_1-A_2 may produce block in the AV node (ERP of the AV node).

Changes in the cycle length of the drive train tend to have a variable effect on the FRP, but with shortening of the drive train cycle length, there is invariably a lengthening of the ERP of the AV node [52]. The probability, therefore, of

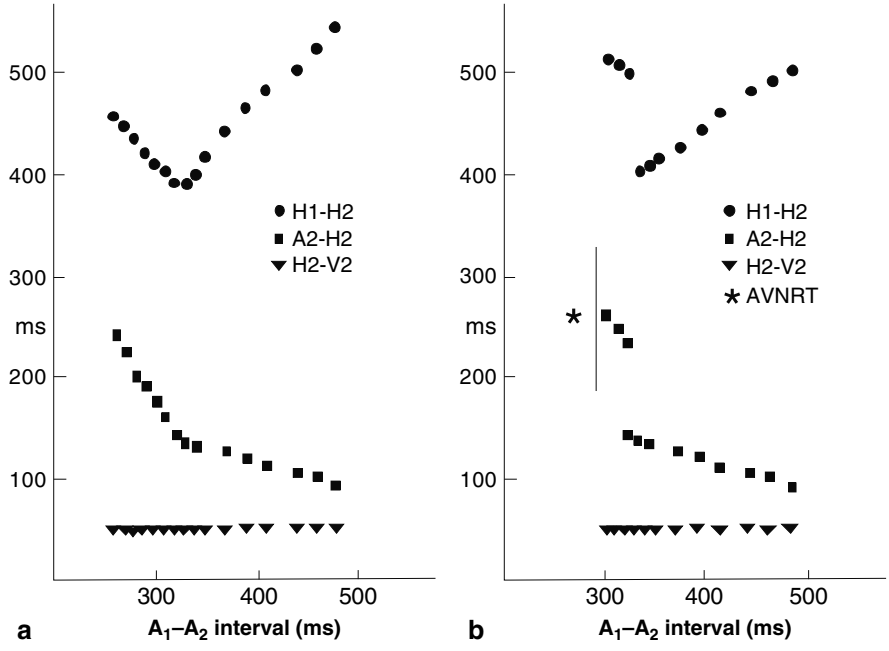

Figure 24.6

Responses of the AV conduction system to atrial extrastimuli in a normal individual (a) and a patient with dual AV nodal physiology (b). With progressive shortening of the coupling interval (A_1-A_2) there is initial associated shortening of the H_1-H_2 interval, but as the A_1-A_2 shortens further there is relatively greater increase in the AH interval, which results in prolongation of the H_1-H_2 interval. In the normal individual (a) a minimum value of the H_1-H_2 interval is reached (380 ms), which is the functional refractory period (FRP) of the AV node. The presence of dual AV nodal pathways (b) is shown by a sudden increase in the AH (and correspondingly the HV) intervals. At a critical delay, this is associated with the initiation of AV nodal reentrant tachycardia (AVNRT) (asterisk).

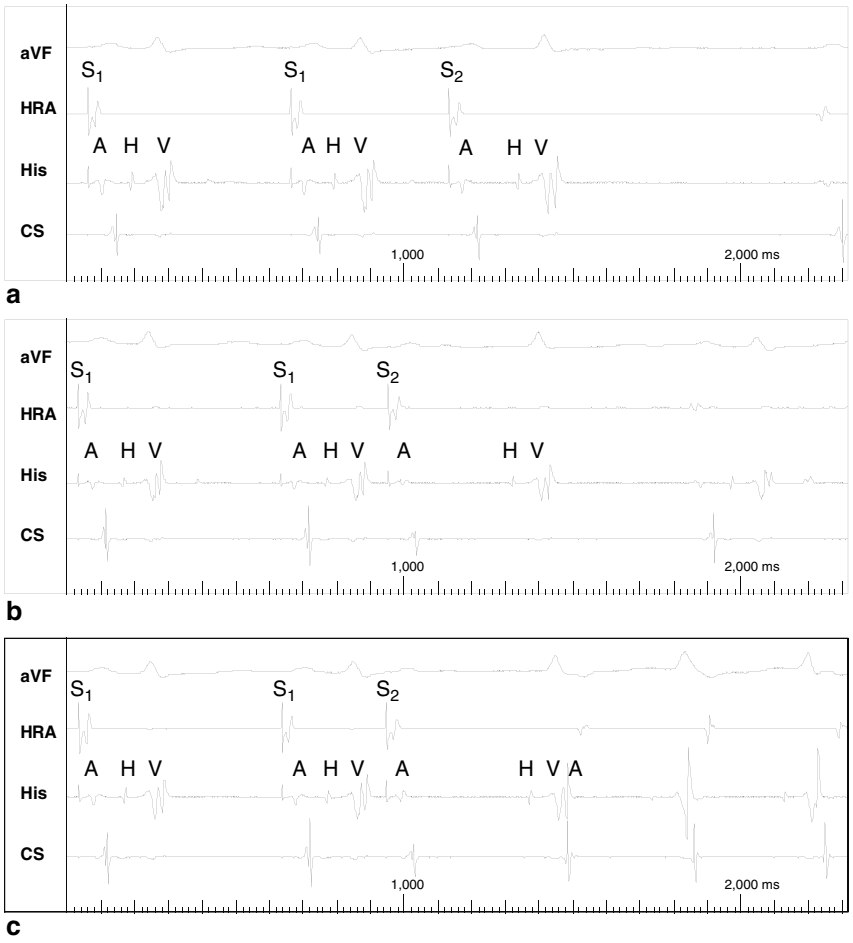

Figure 24.7

Responses to atrial premature beat demonstrating dual AV nodal pathways and initiation of AVNRT. With a relatively long coupling interval of 470 ms (a) there is conduction down the fast pathway, with a normal AH interval. With a short coupling interval of 320 ms (b) there is marked prolongation of the AH interval, indicating conduction down the slow pathway. With further shortening of the coupling interval to 310 ms (c) there is initiation of AVNRT. Surface lead aVF and electrograms from high right atrium (HRA), His bundle, and coronary sinus (CS) are shown.

encountering the ERP of the AV node is increased by employing faster drive trains. In a proportion of patients, especially those with AV nodal reentrant tachycardia (AVNRT), the response to atrial premature stimulation demonstrates a discontinuous curve suggesting two electrophysiologically distinct AV nodal pathways [53, 54]. In patients with dual pathways, the AH interval progressively grows longer until there is a sudden "jump" in the AH interval in response to a small decrement in the premature coupling interval (Figs. 24.6 and 24.7). This sudden increase in AH interval reflects block in the "fast" AV nodal pathway, which has a longer refractory period than the "slow" pathway. The presence of dual AV nodal pathways in itself does not imply the presence of AVNRT but only the potential substrate. In some patients, dual AV nodal pathways may not be manifest in the baseline state but can be exposed by alterations in autonomic tone or with drug therapy [55]. Despite the presence of discontinuity in AV conduction, retrograde VA conduction commonly is continuous [53]. However, the finding of discontinuous retrograde conduction curves in a minority of patients identified differences in the site of atrial insertion, with the slow pathway retrograde activation via the area of the coronary sinus os and the fast pathway in the region of the His-bundle recording [56]. This anatomical differentiation

between the pathways provides the basis of selective slow pathway ablation in the treatment of AVNRT [57]. Further experience has revealed the potential complexities of arrhythmia substrate with a diversity of AV nodal pathways described [58, 59].

In contrast to the AV node, there is usually no change in conduction in the His-Purkinje system to atrial premature stimulation (Fig. 24.6). Uncommon patterns of response include progressive delay in conduction with lengthening of the HV interval, an abrupt change in the HV interval, and complete block of infranodal conduction. The development of aberrant conduction or block within the His-Purkinje system is more likely during sinus rhythm or longer drive train cycle lengths because the refractoriness of the tissue is directly related to the preceding cycle length. At slower rates, the relative or ERPs may then be longer than the FRP of the AV node. Conduction delay or block within the His-Purkinje system therefore is not necessarily an abnormal response. Functional delay or block in the right bundle tends to occur more frequently than in the left bundle.

(e) *Programmed ventricular premature stimulation*

Programmed ventricular stimulation is performed in a similar manner to atrial stimulation. Ventricular stimuli are introduced after 6–10 beats of spontaneous rhythm or a ventricular drive train at progressively shorter coupling intervals until ventricular refractoriness occurs. For routine studies, ventricular stimulation is performed at the RV apex. The ventricular ERP at the apex is usually less than 300 ms and, in an otherwise normal ventricle, refractoriness varies little at other sites.

Retrograde refractory periods may be difficult to determine because the His-bundle electrogram is frequently obscured by the ventricular electrogram. With progressive shortening of the V_1-V_2 (S_1-S_2) interval, the retrograde His-bundle electrogram H_2 may emerge from the ventricular electrogram, and with further shortening the V_2-H_2 interval will progressively lengthen until either ventricular refractoriness or retrograde His-Purkinje block occurs. Not infrequently, in the latter circumstances, with further shortening of V_1-V_2, the H_2 will reappear because of proximal conduction delay (gap phenomenon: see Sect. 24.3.3.2.f). Retrograde AV nodal conduction (H_2-A_2) may show either progressive slowing of conduction with an increasing H_2-A_2 interval, or an almost constant relatively short H_2-A_2 interval, or discontinuous curves analogous to the anterograde dual AV nodal pathways. Retrograde atrial activation in the absence of an accessory pathway is usually first observed in the His-bundle electrogram (Fig. 24.8).

Ventricular premature stimulation can induce a variety of repetitive responses. AV nodal echo beats in relation to retrograde dual pathways may be initiated, although a sustained tachycardia rarely occurs. Frequently, in patients with normal conduction, the "V_3 phenomenon," or bundle branch reentrant beat, (Fig. 24.9) may be observed [23]. This repetitive ventricular response is caused by the development of a macro-reentrant circuit involving the His bundle and bundle branches. Block in the right bundle branch is followed by retrograde conduction of the impulse by the left bundle with retrograde conduction to the His bundle and subsequent completion of the reentrant circuit by

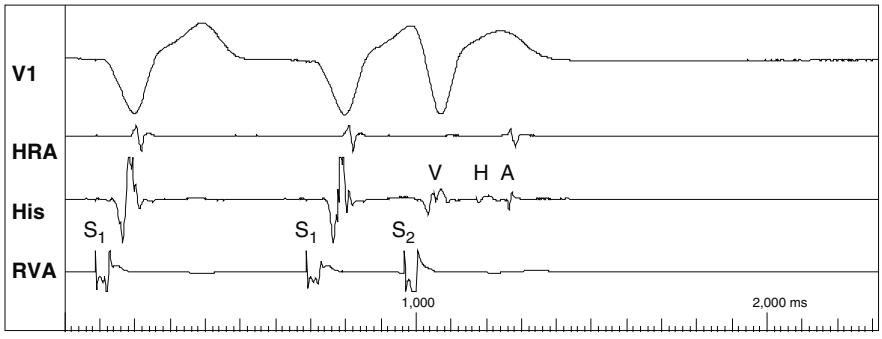

Figure 24.8

Retrograde conduction in response to a ventricular premature beat. Following the ventricular extrastimulus, coupling interval 280 ms, retrograde His bundle and atrial activation are seen.

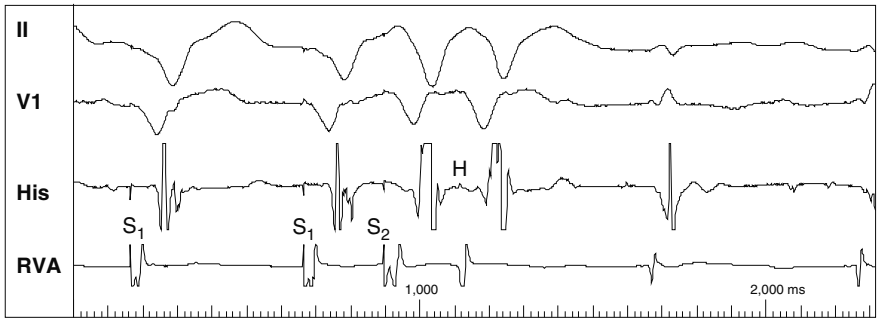

Figure 24.9

Bundle branch reentrant beat in response to a single ventricular extrastimulus. Following the extrastimulus (S2), coupling interval 230 ms, there is retrograde His-bundle activation (H) preceding the reentrant beat, which has a left bundle branch block morphology.

anterograde conduction down the now-recovered right bundle branch. Therefore, the repetitive response has a left bundle branch block morphology with an HV interval the same or longer than the HV interval observed during sinus rhythm.

(f) *Gap phenomenon*

During programmed extrastimulation, block of the impulse may occur but then be followed by the resumption of conduction with shorter coupling intervals of the premature stimuli. This is known as the gap phenomenon. It is caused by the development of conduction delay proximal to the site of block, allowing the distal tissue to recover and conduct [60]. For example, as A_1-A_2 is shortened, block may occur at the level of the His bundle. With further shortening of A_1-A_2, the resulting increase in the A_2-H_2 interval produces lengthening of the H_1-H_2 such that it exceeds the refractory period of the distal tissue with the resumption of conduction. Several gaps have been identified in relation to the components of the AV conduction system, both in the anterograde [60, 61] and retrograde directions [62]. The gap phenomenon is a physiological response and is not of pathological significance.

24.3.3.3 Induction, Definition of Mechanism, and Termination of Tachyarrhythmias

The stimulation protocol used to induce tachycardia will depend on the specific arrhythmia. Programmed stimulation of the ventricle can induce ventricular tachycardia or fibrillation, and this has been used to guide therapy and assess risk (Figs. 24.10 and 24.11). A common protocol would use up to three extrastimuli (S_2, S_3, S_4), at two drive cycle-lengths (S_1-S_1, e.g., 600 ms and 450 ms) at two ventricular sites, such as RV apex and outflow tract. However, a variety of other protocols have been used, with different drive cycle lengths and number of extrastimuli [63]. More aggressive protocols, with faster drive rates and increased number of extrastimuli, particularly if tightly coupled, may induce nonspecific arrhythmia, such as ventricular fibrillation [64]. The diversity of protocols, and the concerns about the specificity of induced arrhythmia, have contributed to the decline in the clinical use of ventricular stimulation. Induced tachycardia may be terminated by further ventricular stimulation, either extrastimuli or overdrive pacing (Fig. 24.10b) [63]. There is the risk of causing acceleration of the arrhythmia, particularly if the tachycardia is fast (Fig. 24.11b). With respect to other tachycardias, supraventricular tachycardias may be induced by atrial or ventricular extrastimuli, and atrial arrhythmias can be induced by atrial extrastimuli or rapid atrial pacing. Catecholamine stimulation, using isoproterenol infusion, may be necessary for arrhythmia induction. Tachycardia induction, diagnosis, and termination, and techniques of mapping to identify targets for ablation, are discussed further below, and in Chaps. 23 and 25.

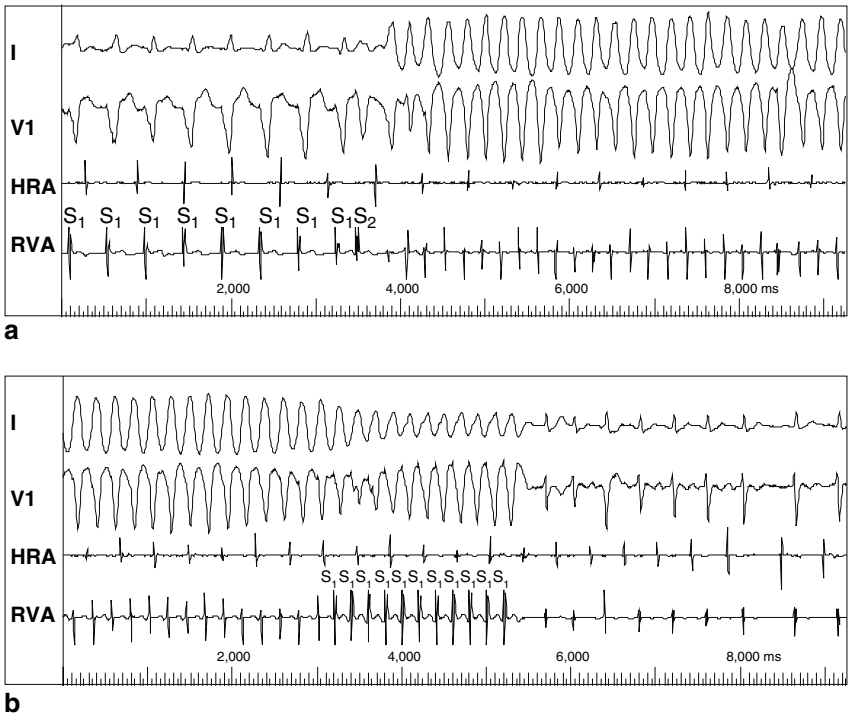

Figure 24.10

Initiation and termination of sustained ventricular tachycardia. Following an 8-beat drive train, cycle length 450 ms, a single premature ventricular beat, coupling interval 250 ms, initiates VT (a). There is ventricular-atrial dissociation, as seen in the recording from high right atrium (HRA). A burst of rapid ventricular pacing (b) terminates the VT and restores normal sinus rhythm.

24.3.4 Safety of Electrophysiological Testing

Clinical cardiac electrophysiological testing involves invasive techniques and therefore has a potential for complication, which is inherent in any cardiac catheterization procedure. Venous thrombosis is the most common complication, with an incidence ranging between 0.5 and 2.5% [65, 66]. Factors which may influence the development of thrombosis include not only the patient population being studied but also specific aspects of the procedure, such as the use of systemic anticoagulation and the duration the electrode catheters are in situ [65, 66]. Arterial injury occurs in 0.1–0.4% of patients either because of local trauma during attempts at arterial cannulation or inadvertently during femoral venous catheterization [66]. Cardiac perforation has been observed in 0.2% of patients, although tamponade was less common and emergency pericardiocentesis was required only rarely [67]. The risk of complications has increased with the addition of ablation procedures to the diagnostic EP study, which may include complications specific to the procedure, such as inadvertent AV block with ablation of AV nodal pathways, or thromboembolic complications with left-sided ablations, or pericardial tamponade with transseptal puncture [68, 69]. In a prospective study of nearly 4,000 procedures, the risk of complications increased from 1.1% for diagnostic EP procedures to 3.1% with radiofrequency ablation [70]. Risk was increased with older age patients and with the presence of systemic disease. The target of ablation also increases the risk, with higher complications for AVNRT compared to AVRT, and for scar-related VT compared to idiopathic VT [68]. Pulmonary vein isolation and left atrial ablation for atrial fibrillation may also expose the patient to increased risk of up to 6%, including specific risks like pulmonary vein stenosis and atrio-esophageal fistula [71, 72].

Complications specifically related to ventricular stimulation studies, such as the induction of heart block or nonclinical arrhythmias, are usually transient and not of clinical importance, despite the need for cardioversion in

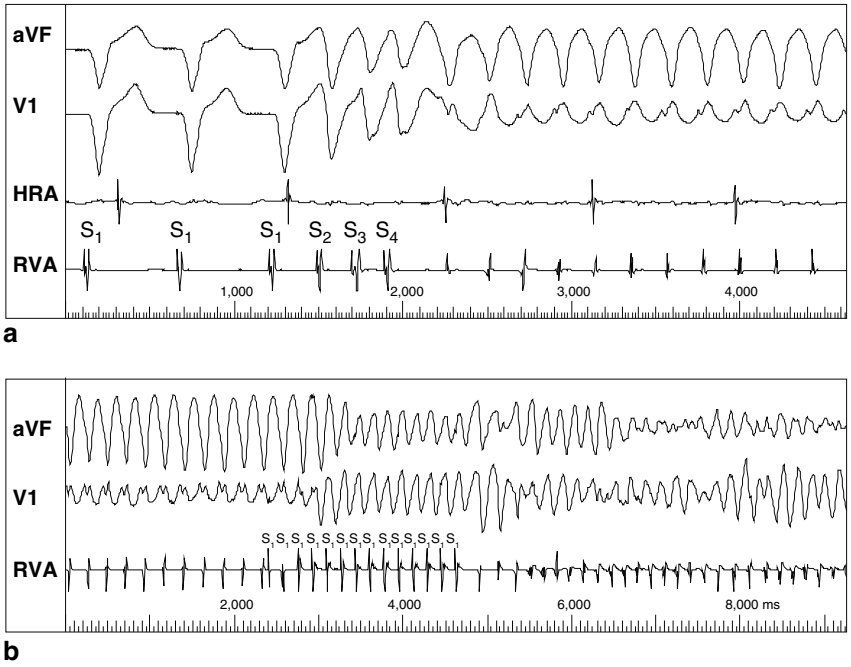

Figure 24.11
Initiation of VT with triple extrastimuli (a), and acceleration to ventricular fibrillation with burst pacing (b).

over 50% of these patients [66]. The risk of death during EP testing is low (0.1–0.2%), despite the induction of malignant ventricular arrhythmias.

24.5 Indications for Electrophysiology Studies

The indications for EP studies can be considered in three categories:

1. Diagnostic – to determine the mechanism of an arrhythmia, either tachycardia or bradycardia
2. Therapeutic – to identify the substrate of the arrhythmia prior to ablation, or to guide therapy selection
3. Risk stratification – to determine the risk of life-threatening arrhythmia

The role of EP testing in each of these categories has changed, due to progress in diagnostic methodologies, the results of clinical studies and the advances in treatment options. For example, implantable event-recorders now have an important role in the diagnosis of unexplained syncope [73], and often replace the relatively nonspecific invasive EP study [74]. The exception may be patients with syncope and prior myocardial infarction (MI), where induction of monomorphic VT can indicate an arrhythmic etiology. However, there is evidence of benefit from the implantable defibrillator in many such patients without the need for an EP study [75], further reducing the role of invasive testing. There is clearly overlap between the diagnostic and the therapeutic indications in that establishing the diagnosis may lead to curative catheter ablation. With respect to risk stratification, the value of the EP study in predicting adverse outcome has been questioned, because of the recognition of persisting risk of sudden death despite a negative EP study in a variety of conditions, including ventricular arrhythmias occurring post-infarction [31], or associated with dilated cardiomyopathy [76] or Brugada syndrome [77]. When considering specific arrhythmias, each of these categories (diagnosis, therapy, and risk assessment) may have a role.

24.5.1 Diagnosis of Arrhythmias

24.5.1.1 Bradycardia

The role of invasive EP studies in the diagnosis of bradycardias has declined in recent years. The ACC/AHA/HRS 2008 pacing guidelines include the measurement of HV interval ($\geqslant$ 100 ms), the diagnosis of infranodal conduction block post-MI and the presence of major abnormalities of sinus node function as factors in the decision as to whether to implant a permanent pacemaker in selected situations [78]. Assessment of sinoatrial dysfunction and AV conduction disease is described in Chaps. 26 and 28 respectively.

24.5.1.2 Tachycardia

The specific diagnostic electrophysiological procedures undertaken will depend on the clinical question and therapeutic aim, usually determined by the previously documented arrhythmia. Tachycardias with narrow QRS complexes are described as supraventricular tachycardias, and include atrial and junctional tachycardias. The latter include AVRT, utilizing an accessory pathway, and AVNRT, whose substrate is dual AV nodal pathways. Wide-complex tachycardias may also be supraventricular, with aberrant AV conduction such as bundle branch block or pre-excitation, but may be ventricular in origin. The surface ECG has limitations in diagnosing such broad complex tachycardias, and invasive electrophysiological studies may be of particular value in this context.

(a) *Identification of substrate*

In a patient with supraventricular tachycardia, the presence of a substrate for reentry, such as an accessory pathway, may be manifest by an abnormal intracardiac activation sequence of either atrial or ventricular electrograms. For example, in the presence of pre-excitation, the earliest ventricular activation during sinus rhythm will be at the site of the ventricular insertion of the pathway (Fig. 24.12), or with a concealed pathway the earliest atrial activation during ventricular pacing may be used to identify the site of the pathway. The most common pathway location is left-sided, in which case the

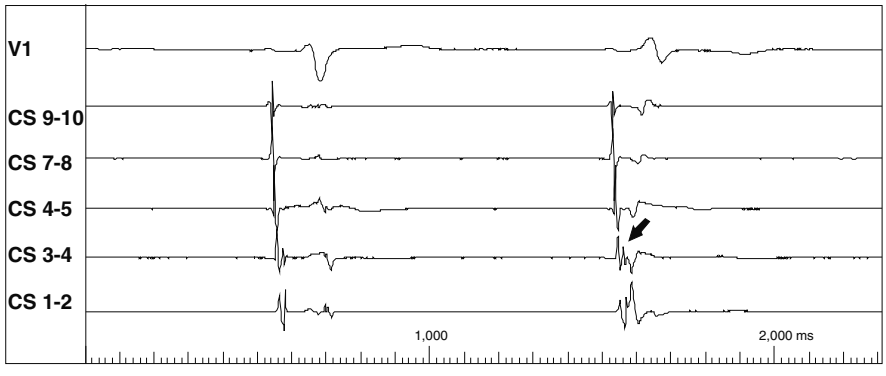

Figure 24.12
Intermittent pre-excitation with a left-sided accessory pathway. The first beat is not pre-excited and left ventricular (LV) activation in the coronary sinus (CS) electrograms is late. The second beat is pre-excited, with a delta wave on the surface ECG (V1), and earliest ventricular activation is recorded from the distal coronary sinus electrodes (arrowed) indicating a left-lateral accessory pathway.

earliest activation will be identified from the coronary sinus catheter electrograms. If the activation sequences are normal during sinus rhythm and ventricular pacing, with earliest retrograde atrial activation recorded at the His-bundle catheter, then atrial programmed stimulation may identify the presence of dual AV nodal physiology, as the substrate for AVNRT (Fig. 24.7). The identification of the tachycardia substrate may allow curative catheter ablation. If there is neither an accessory pathway nor AVNRT, then an atrial arrhythmia is likely, and it may be necessary to induce the tachycardia to allow mapping and ablation. However, if typical atrial flutter has been documented, it is not necessary to induce the arrhythmia, since it is recognized that the cavo-tricuspid isthmus is an essential component of the reentry circuit and the target for ablation.

(b) *Mechanisms of tachycardia*

Reentry is the most common mechanism underlying clinical sustained tachyarrhythmias. It is a characteristic of reentrant arrhythmias that they can be initiated by premature beats. Atrial reentrant and junctional tachycardias, AVNRT or AVRT, can commonly be initiated by atrial premature beats. The latter tachycardias are dependent on critical delay in the AV conduction induced by the premature beat, which allows subsequent retrograde conduction up the accessory pathway or the fast retrograde AV nodal pathway. Ventricular premature beats may also induce AVRT, and infrequently AVNRT, or may initiate reentrant ventricular tachycardia (Fig. 24.10), particularly in the presence of a ventricular substrate such as scarring from an old MI. Less commonly, arrhythmias are due to focal increased automaticity, or to triggered activity. Tachycardias that originate from an automatic focus may be less likely to be inducible by programmed stimulation but may be initiated by catecholamine stimulation, using an infusion of isoproterenol, a β-adrenoceptor agonist. Triggered arrhythmias, which may depend on oscillations of intracellular calcium induced by preceding beats, may also be initiated by pacing protocols.

(c) *Atrial activation during tachycardia*

Once a sustained tachycardia has been induced, the mechanism may be clear from the atrial activation timing and sequence. With typical ("slow–fast") AVNRT, atrial activation may be coincident with or precede ventricular activation, and the earliest atrial activation is commonly seen from the His-bundle catheter (Fig. 24.7). With AVRT, the atrial activation sequence is determined by the site of the accessory pathway, and is commonly eccentric (Fig. 24.3), although a paraseptal pathway may have a retrograde activation sequence similar to that via the normal conducting system. Atrial tachycardia may remain a differential diagnosis of such tachycardias, and electrophysiological maneuvers have been described, which may aid the diagnosis. A ventricular premature beat timed to coincide with the His-bundle electrogram can alter the timing of the atrial activation only in the presence of an accessory pathway, since retrograde conduction via the normal conducting system will be refractory (Fig. 24.13). Differentiating between an atrial tachycardia and AVNRT or AVRT can be achieved by observing the responses following cessation of a short burst of ventricular pacing, faster than the tachycardia rate and with 1:1 VA conduction [79]. With atrial tachycardia, on termination of ventricular pacing the retrograde atrial signal is followed by an atrial tachycardia beat, which conducts to the ventricle – an A-A-V response – whereas AVNRT and AVRT show an A-V response (Fig. 24.14). There are limitations to this technique, including a "pseudo A-A-V" response in patients with AVNRT and long HV intervals, when identification of A-H or A-A-H responses is more accurate [80]. Differentiation between atypical AVNRT from AVRT utilizing a posterior paraseptal accessory pathway may be aided by the appearance of V-H-A with ventricular premature beats in the former [81]. The presence of a concealed paraseptal pathway can be assessed in sinus rhythm by pacing via the His-bundle catheter and comparing the retrograde atrial activation timing with His-bundle capture and local ventricular capture [82]. Atrial flutter has a faster atrial rate and is characterized by intermittent AV conduction, commonly 2:1. The atrial activation sequence is typically counterclockwise around the tricuspid annulus. Ventricular tachycardia may have retrograde conduction to the atria, with earliest activation at the His-bundle catheter, or there may be VA dissociation.

(d) *Entrainment*

The evidence of the reentrant basis of the majority of clinical atrial and ventricular tachycardias came from studies of the phenomenon of entrainment [83]. Waldo et al, in a series of studies initially of post-operative atrial flutter [84] and

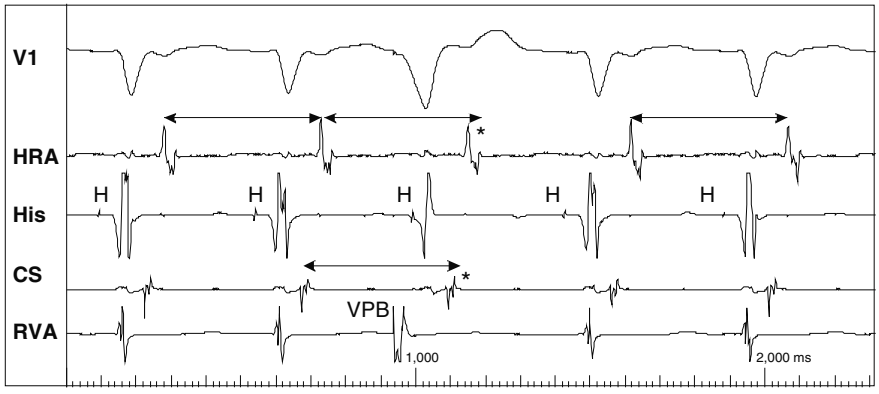

Figure 24.13

His-coincident ventricular premature beat (VPB) during atrio-ventricular reentrant tachycardia (AVRT). A premature stimulus in the right ventricle pulls ventricular activation earlier, timing with the anterograde activation of the His bundle. The following atrial activation (asterisks) occurs at an interval shorter than the tachycardia cycle length (arrows). This confirms the presence of an accessory pathway, since the normal conducting system would be refractory and unable to conduct retrogradely.

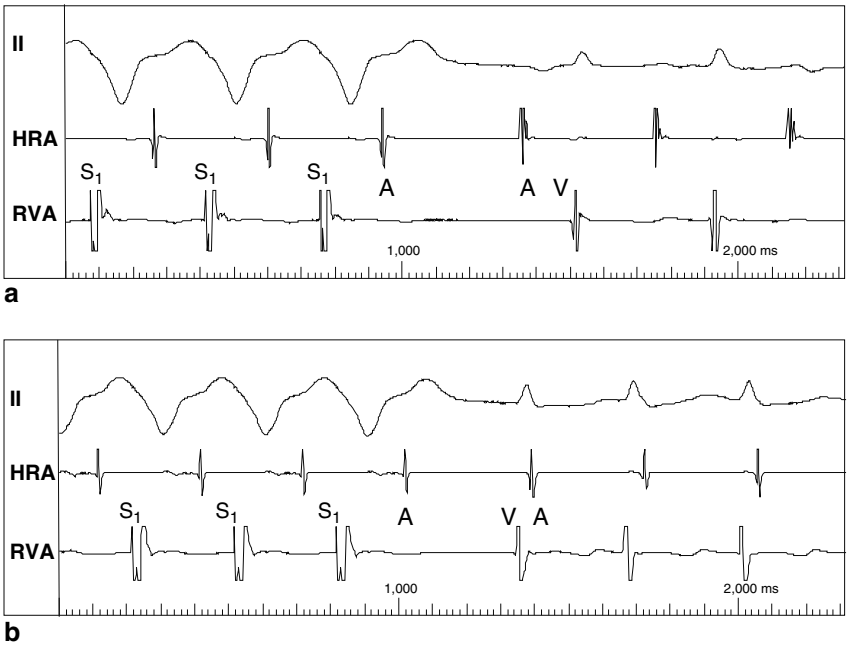

Figure 24.14

A technique for the diagnosis of atrial tachycardia. During atrial tachycardia (a), following termination of ventricular pacing with retrograde atrial activation, there is a A-A-V response. During AVNRT (b) there is a A-V-A response.

subsequently of supraventricular [85] and ventricular tachycardia [86], described three criteria for entrainment: (1) constant fusion during the transient entrainment of a tachycardia except for the last captured beat (which was entrained but not fused), (2) progressive fusion at different entrainment rates, and (3) interruption of the tachycardia associated with local conduction block followed by activation from a different direction [85]. A fourth criterion was added based on the electrogram equivalent of progressive fusion [87]. Demonstration that any of these criteria were met by pacing during a sustained tachycardia was evidence of a reentrant mechanism.

The demonstration of entrainment required that the reentry circuit had an excitable gap, allowing capture from pacing outside of the circuit. Local activation sequences within the tachycardia circuit were unchanged, with the rate increased to that of the pacing, but the surface electrogram was a fusion of the morphologies determined by the local pacing site and the tachycardia. Since the last paced beat entered the circuit but the output did not fuse with a subsequent paced beat, the beat following pacing had the morphology of the tachycardia but was at the pacing cycle length (Fig. 24.15). The degree of fusion varied depending on the pacing rate, with the morphology more closely resembling that of the paced beats with increased rate (progressive fusion). At a critical rate, the paced impulse may collide with the tachycardia wavefront producing block and termination of the tachycardia. Subsequent activation was from the direction of pacing, and had a shorter coupling interval.

With the development of mapping techniques it became apparent that if the pacing site was within the reentry circuit then none of the criteria could be met, so-called "concealed entrainment" [88] or "entrainment with concealed fusion". In this case the morphology and activation sequences of the entrained rhythm would be identical to the tachycardia, but at the pacing rate. The local return cycle would be at the tachycardia cycle length, and not the pacing rate (Fig. 24.16). A prolonged return cycle indicates that the pacing site was not within the reentry circuit [89]. The demonstration of concealed entrainment may be of value in confirming a site for successful catheter ablation [90, 91].

(e) *Syncope of undetermined etiology*

The role of EP studies in the diagnosis of syncope has diminished, but may still be of value in selected patients [74, 92, 93]. Tilt testing to diagnose neurocardiogenic syncope and implanted loop recorders to allow correlation between symptoms and cardiac rhythm have contributed to the decline in the use of invasive studies. The expanding indications for implantable devices to treat ventricular arrhythmias have reduced the need to demonstrate inducible ventricular arrhythmias in patients in whom they are suspected. The clinical significance of an induced arrhythmia or an identified conduction abnormality may be uncertain, reflecting the low sensitivity and specificity of EP testing. The diagnostic yield is particularly low in the absence of structural heart disease [94, 95].

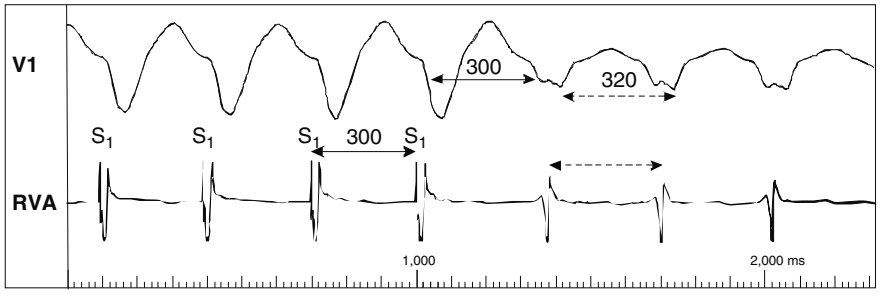

Figure 24.15

Entrainment of ventricular tachycardia. During pacing at cycle length 300 ms the ECG has a different morphology compared to during tachycardia. The beat following the last stimulus is at the pacing cycle length, but has the morphology of the tachycardia. Pacing cycle length indicated by filled arrow, and tachycardia cycle length by interrupted arrows.

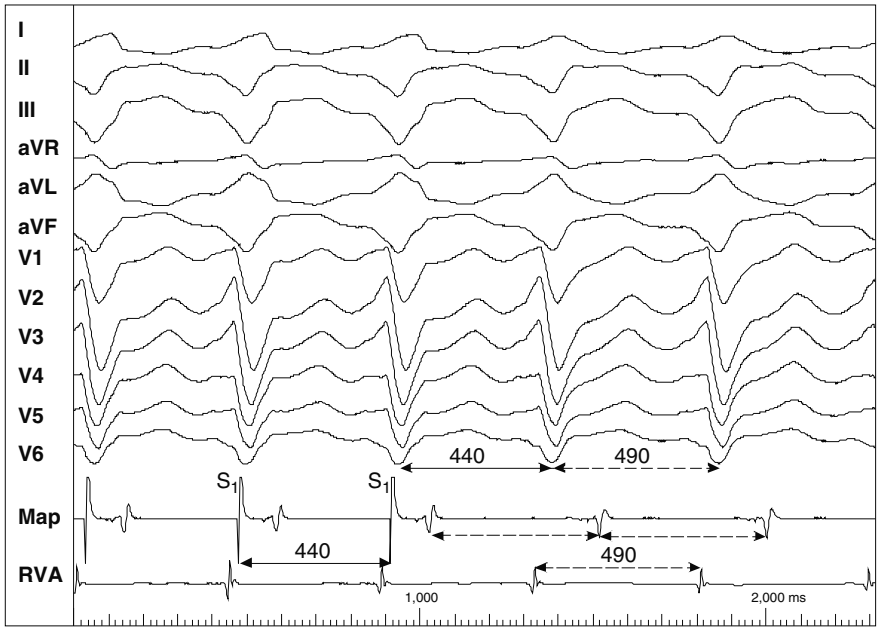

Figure 24.16

Concealed entrainment. Pacing using the mapping catheter (Map) at cycle length 440 ms produces an ECG morphology nearly identical to that during tachycardia. The return cycle of the local electrogram recorded from the mapping catheter is at almost the tachycardia cycle length (interrupted arrows). This is consistent with pacing within the reentry circuit, and the delay between the stimulus and the ventricular activation, as indicated by the surface ECG, suggests the site is at the entrance to an area of slow conduction.

24.5.2 Therapeutic Role of Electrophysiology Studies

24.5.2.1 Catheter Ablation

A major change in the role of EP studies has followed the development of catheter ablation for the curative treatment of cardiac arrhythmias [35, 96, 97]. Techniques and principles developed for the diagnosis of arrhythmias now are applied in a more specific manner to identify the substrate for ablation. A more anatomical, rather than electrophysiological, approach may be applied to the ablation of some arrhythmias, including AVNRT [98], atrial flutter [99] or fibrillation [100], and ventricular tachycardia [101]. Technologies have been developed to aid the mapping of complex arrhythmia substrates, and are described in Chap. 25. However, many arrhythmias can be successfully treated by catheter ablation using conventional electrophysiological techniques to aid the mapping and identification of the ablation target, using the following methods.

(a) *Earliest activation.* The site of successful ablation of an accessory pathway or a focal atrial or ventricular tachycardia is usually determined by the identification of the site of earliest activation (Figs. 24.3 and 24.17). The use of unipolar signals from the distal ablation catheter (filtered like a standard ECG) is of value, as the presence of an R wave identifies a site unlikely to be successful, whereas successful sites have a QS pattern (Fig. 24.18) [102].

(b) *Pace mapping.* This is based on the principle that pacing at the site of origin of the tachycardia should produce the identical ECG morphology to the clinical arrhythmia. It is of value in the ablation of focal ventricular tachycardia, such as RV outflow tachycardia (Fig. 24.17). One advantage is the option to continue mapping in the absence of the arrhythmia, particularly if the tachycardia is poorly tolerated by the patient.

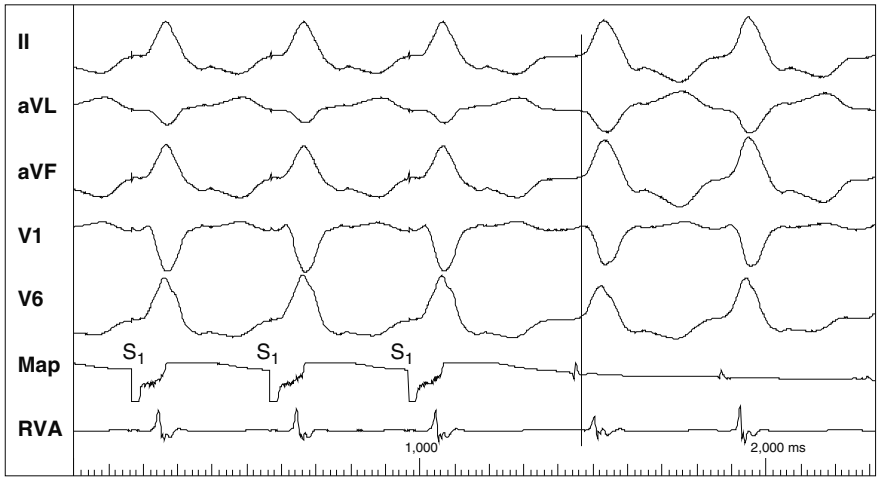

Figure 24.17

Pace mapping at a site of early activation during RV outflow tachycardia. Pacing through the mapping catheter (Map) produces a morphology nearly identical to that during tachycardia. The local activation at this site is early, preceding the onset of the QRS complexes (vertical line).

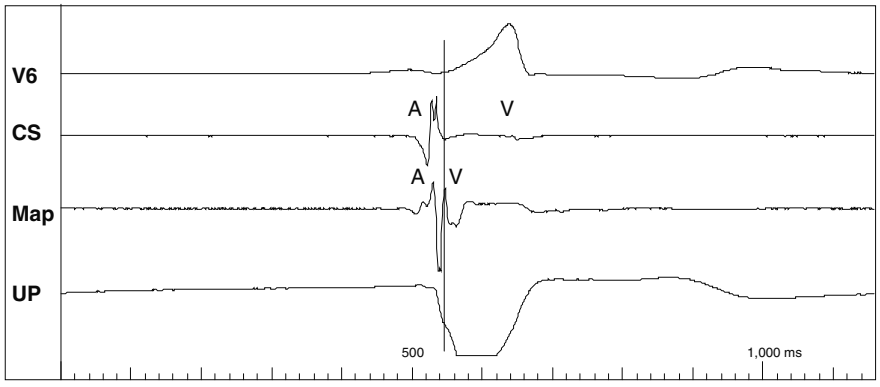

Figure 24.18

Site of ablation of an accessory pathway. The ventricular activation recorded from the coronary sinus (CS) catheter indicates that LV activation is late. Mapping catheter (Map) is at a site on the RV annulus where ventricular activation is earlier, preceding the onset of the delta wave (vertical line). The unipolar signal has a PQS morphology, consistent with the site of the pathway, indicating a likely successful site for ablation.

(c) *Electrogram-guided ablation.* For a number of tachycardias, the above methods may be of limited value, particularly if the substrate is a macro-reentrant circuit, and specific characteristics of potentially successful ablation sites have been described. Examples include (1) AVNRT, where a characteristic complex signal with a slow pathway potential has been described [57], (2) Mahaim tachycardia, which uses an atrio-fascicular bypass tract, and can be ablated on the tricuspid annulus guided by a Mahaim potential [103, 104], and (3) Idiopathic LV (fascicular) tachycardia, where ablation is guided by Purkinje and pre-Purkinje potentials [105, 106].

(d) *Entrainment mapping.* With reentrant arrhythmias, activation mapping may be of limited value, and the aim is to identify a component of the circuit, which may be the site of successful ablation. The demonstration of "entrainment with concealed fusion" as described above, may identify an area within the circuit, or a prolonged post-pacing interval may provide evidence that the site is outside the circuit and therefore unlikely to be a successful ablation

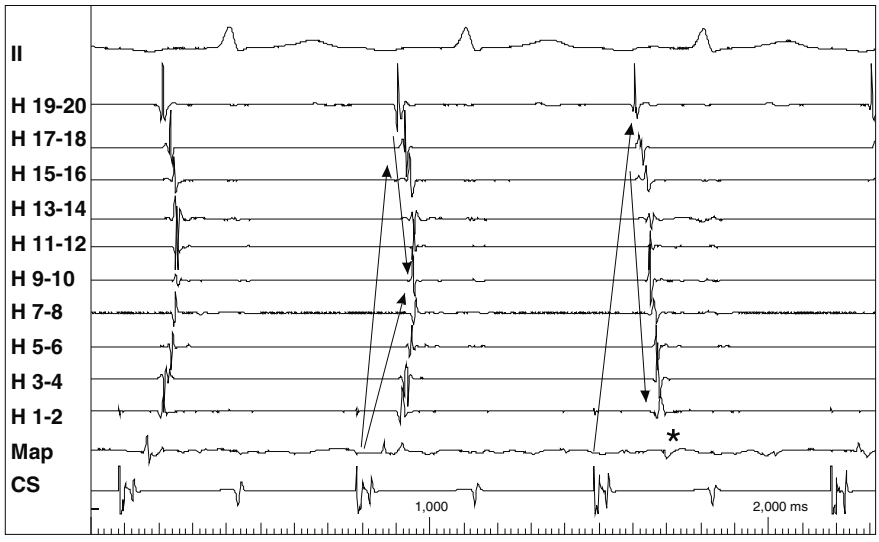

Figure 24.19

Cavo-tricuspid isthmus block during radiofrequency ablation for atrial flutter. A double-decapolar "Halo" catheter (H 1-20) is recording activation from around the tricuspid annulus, during pacing from the coronary sinus (CS) catheter. In the first two beats, there is activation around the annulus in both clockwise and counterclockwise directions, indicated by the arrows. During the third beat, there is only counterclockwise activation, indicating isthmus block. This is confirmed by the local electrogram from the mapping catheter (Map) at the site of the ablation, which becomes widely split (asterisk).

site. Such "entrainment mapping" may be of particular value in identifying sites for ablation in atrial and ventricular reentrant tachycardias, [89, 90, 107].

(e) *Assessment of ablation success.* EP techniques can be used to assess whether a catheter ablation has been successful in a number of ways. In the case of an accessory pathway, the absence of abnormal ventricular or atrial activation indicates successful pathway block. Non-inducibility of tachycardia is the end-point for ablation of AVNRT, or reentrant VT. With AVNRT, it is not necessary to abolish slow pathway conduction since persisting dual AV nodal physiology but non-inducibility of AVNRT is an acceptable end-point, correlating with long-term benefit [57]. Abolition of spontaneous or isoproterenol-induced arrhythmia, such as automatic tachycardias like RVOT tachycardia, may indicate success. In atrial flutter, in which the cavo-tricuspid isthmus is part of the reentrant circuit, termination of the arrhythmia during ablation by itself did not correlate with good long-term outcome [108], whereas demonstration of bi-directional isthmus block post-ablation indicated long-term benefit [109]. Thus, in this case, successful ablation can be performed in the absence of the arrhythmia, using the change in atrial activation recorded from a multipolar tricuspid annulus catheter (Fig. 24.1c) during coronary sinus pacing as the indication of isthmus block (Fig. 24.19).

24.5.2.2 Guidance of Therapy

The practice of EP-guided drug therapy for ventricular arrhythmias has now largely been abandoned. The ability to induce life-threatening arrhythmias by ventricular stimulation [21], led to the premise that the EP study could be used to assess the efficacy of drug therapy [30, 110]. During the 1980s, much time was spent in EP labs performing multiple ventricular stimulation studies in patients with prior ventricular arrhythmias. When sustained arrhythmia was induced at baseline in a drug-free state, re-induction was attempted following intravenous drug administration, commonly procainamide [111]. Oral drug treatment was then initiated and EP studies were repeated at intervals, depending on the response [112].

Such serial drug testing took many days, or weeks if amiodarone was also tested. Observational data indicated that patients whose arrhythmias were non-inducible on drug therapy [29], or whose tachycardia rate was slowed to improve hemodynamic tolerability [113–115], had a better outcome compared to those who continued to have inducible life-threatening arrhythmia. However, randomized studies have failed to confirm the prognostic benefit from EP-guided drug therapy [34, 116, 117]. In addition, there was evidence that patients whose arrhythmias were non-inducible may remain at risk of life-threatening arrhythmia recurrence [31, 118]. In addition, data from the AVID registry indicated that stable VT may not be a benign arrhythmia, with a mortality of over 30% at 3 years [119]. There are also concerns regarding the specificity of induced arrhythmias in relation to the stimulation protocols [64] and the day-to-day reproducibility of the technique [120, 121]. The development of the implantable cardioverter defibrillator (ICD) provided a superior therapy to dug treatment for high-risk patients [116].

It has been suggested that an EP study may be of value in identifying those patients with VT who may respond to antitachycardia pacing (ATP) [63]. However, reproducibility of response to ATP is variable, and may not be predictive [122]. In particular, induced fast VT had a lower success rate of ATP, but studies have shown a high percentage success (73%) with spontaneous fast VT [123, 124]. In addition, survivors of cardiac arrest from VF, without prior documented clinical VT, may have recurrent monomorphic VT, which is poorly predicted by EP studies [125], and which may be successfully terminated by ATP [123].

24.5.3 Risk Stratification

The role of EP testing in risk stratification remains controversial. The ability of the EP study to induce life-threatening arrhythmia may offer a method to identify patients at high risk of sudden death, of particular value in those patients who have not yet had an arrhythmia but have been identified as being at risk.

24.5.3.1 Wolff-Parkinson-White Syndrome

In patients with the Wolff-Parkinson-White syndrome there is a recognized risk of sudden death. A minority of patients have an accessory pathway with a short refractory period allowing a rapid ventricular response to atrial flutter or fibrillation [126], which may degenerate from pre-excited atrial fibrillation to ventricular fibrillation [127]. Noninvasive testing, including ambulatory monitoring and exercise testing [128], may reveal intermittent pre-excitation, indicating a relatively long accessory pathway refractory period, in up to 20%, but in the majority of patients the properties of their pathway cannot be determined without invasive EP assessment. A pathway ERP of less than 270 ms, or the shortest RR interval less than 250ms during induced atrial fibrillation, identified increased risk [129]. In symptomatic patients, this is less of an issue, since catheter ablation can be curative and removes the risk from the pathway. The asymptomatic patient presents more of a dilemma. Conventional wisdom has been that the risk to an asymptomatic patient is low and does not merit even the low risk associated with catheter ablation. However, recent reports have challenged this view, providing evidence to support a more aggressive approach to ablation in the asymptomatic patient [130, 131].

24.5.3.2 Ventricular Arrhythmias

(a) *Post-myocardial infarction*

Sudden death due to lethal ventricular arrhythmia continues to be a major cause of mortality following MI. The peri-infarct area of myocardium provides a substrate for reentrant arrhythmias. Although ventricular fibrillation (VF) is commonly the identified fatal arrhythmia, there is evidence that the initial arrhythmia is often fast monomorphic ventricular tachycardia (VT), which then degenerates into VF. Thus, ventricular stimulation may induce VT or VF in survivors of cardiac arrest post-MI. Such potentially lethal arrhythmias may also be inducible in patients who have not yet had a cardiac arrest, and therefore may identify those at risk. The initiation of VT or VF has been shown to identify a population of post-infarction patients at risk of sudden death by spontaneous development of ventricular tachyarrhythmias

[132, 133]. With the availability of the ICD, there is a need to identify high-risk patients likely to benefit from expensive device therapy post-MI, so-called primary prevention. Studies utilizing combinations of risk factors, including LV dysfunction, non-sustained VT, and inducibility, have shown that it is possible to identify a high-risk population which can benefit from the ICD [134]. The Multicenter Automatic Defibrillator Implantation Trial (MADIT) [135] and the Multicenter Unsustained Tachycardia Trial (MUSTT) [116] required an EP study with inducible VT and showed mortality benefit with the ICD. However, MADIT II required only LV dysfunction post-MI as an entry criterion, without the need to demonstrate inducibility of arrhythmia, and showed a 31% reduction in the risk of death post-MI with the ICD [75]. In this study, 82% of patients who received an ICD had an EP study, and unexpectedly, ICD therapy for VF was less common in inducible than in noninducible patients [32]. Furthermore, the induction of VF was less predictive of subsequent arrhythmia than the induction of monomorphic VT, confirming the relatively nonspecific nature of induced VF. Finally, observational data from the MUSTT registry showed that patients post-MI who did not have inducible arrhythmia at EP study had a similar mortality to those who had inducible VT/VF [31], providing further evidence against the role of invasive EP testing following MI.

(b) *Cardiomyopathy*

Sudden death from ventricular arrhythmia is a cause of mortality in both dilated and hypertrophic cardiomyopathy. While EP studies to induce ventricular arrhythmia have been advocated for both these conditions, there is now recognition that ventricular stimulation is of limited value, due to its unacceptably low sensitivity and specificity [136, 137]. However, the finding of paced electrogram fractionation may be of prognostic value [138, 139]. Non-inducibility at EP study in patients with dilated cardiomyopathy may be even less predictive of freedom from sudden death than in the post-MI patients [136]. Mortality benefit from the ICD has been shown in patients with heart failure, including dilated cardiomyopathy, without the requirement of an EP study [140]. In hypertrophic cardiomyopathy, indications for the ICD are based on clinical risk factors, including family history, syncope, septal thickness, non-sustained VT, or hemodynamical instability at exercise testing [141].

Arrhythmogenic right ventricular dysplasia or cardiomyopathy (ARVC) is a genetically linked abnormality affecting the RV predominantly and is characterized by monomorphic ventricular tachycardia and a risk of sudden death [142]. EP-guided therapy has been shown to be of clinical value, but suffers from the same limitations as in the post-MI situation, and there is increasing use of the ICD, without a prior EP study [143, 144].

(c) *Arrhythmogenic channelopathies*

A major advance in recent years has been the increased understanding of genetic disorders, which may cause life-threatening arrhythmia due to electrophysiological changes at the level of ion channels and receptors, in the absence of structural heart disease. These include the long QT syndrome, Brugada syndrome, and catecholaminergic polymorphic ventricular tachycardia. Ventricular stimulation has little role in the management of these conditions [145, 146], except in the Brugada syndrome, where it remains controversial. This is a condition characterized by baseline ECG abnormalities (RBBB with ST elevation) and can cause lethal ventricular arrhythmias [147, 148]. The only treatment is an ICD. Inducible arrhythmia has been shown to be of value in the identification of risk by some [149], but not confirmed by others [77, 150].

References

1. Lenègre, J. and P. Maurice, De quelques resultats obtenus par la dérivation directe intracavitaire des courants électriques de l'oreillette et du ventricle droits. *Arch. Mal. Coeur Vaiss.*, 1945;**38**: 298–302.
2. Battro, A. and H. Bidoggia, Endocardiac electrocardiogram obtained by heart catheterization in man. *Am. Heart J.*, 1947;**33**: 604–632.
3. Hecht, H.H., Potential variations of the right auricular and ventricular cavities in man. *Am. Heart J.*, 1946;**32**: 39–51.
4. Zimmerman, H.A. and H.K., Hellerstien, Cavity potentials of the human ventricles. *Circulation*, 1951;**3**: 95–104.
5. LeVine, H.D. and W.T. Goodale, Studies in intracardiac electrography in man; IV. The potential variations in the coronary venous. *Circulation*, 1950;**2**: 48–59.

6. Tawara, S., *Das Reizleitungssystem des Säugetierherzens. Ein Anatomisch-Histologische Studie über das Atrioventrikularbundel und die Purkinjeschen Fäden*. Jena, Germany: Verslag Gustav Fischer, 1906.
7. Alanis, J., H. Gonzalez, and E. Lopez, The electrical activity of the bundle of His. *J. Physiol.*, 1958;**142**: 127–140.
8. Giraud, G., P. Puech, H. Latour, and J. Hertault, Variations de potentiel liées à l'activité du système de conduction auriculo-ventriculaire chez l'homme. *Arch. Mal. Coeur Vaiss.*, 1960;**53**: 757–776.
9. Scherlag, B.J., S.H. Lau, R.H. Helfant, et al., Catheter technique for recording His bundle activity in man. *Circulation*, 1969;**39**: 13–18.
10. Reiffel, J.A., E. Gang, J. Gliklich, et al., The human sinus node electrogram: A transvenous catheter technique and a comparison of directly measured and indirectly estimated sinoatrial conduction time in adults. *Circulation*, 1980;**62**: 1324–1334.
11. Prystowsky, E.N., K.F. Browne, and D.P. Zipes, Intracardiac recording by catheter electrode of accessory pathway depolarization. *J. Am. Coll. Cardiol.*, 1983;**1**: 468–470.
12. Damato, A.N., S.H. Lau, R. Helfant, et al., A study of heart block in man using His bundle recordings. *Circulation*, 1969;**39**: 297–305.
13. Narula, O.S., B.J. Scherlag, P. Samet, and R.P. Javier, Atrioventricular block. Localization and classification by His bundle recordings. *Am. J. Med.*, 1971;**50**: 146–165.
14. Mandel, W., H. Hayakawa, R. Danzig, and H.S. Marcus, Evaluation of sino-atrial node function in man by overdrive suppression. *Circulation*, 1971;**44**: 59–66.
15. Prevost, J.-L. and F. Battelli, La mort par les courants electriques: Courants alternatifs à haute tension. *J. Physiol. Pathol. Gen.*, 1899;**1**: 427.
16. Mines, G.R., On dynamic equilibrium in the heart. *J. Physiol. (London)*, 1913;**46**: 349–383.
17. Moe, G.K., J.B. Preston, and H. Burlington, Physiologic evidence for a dual A-V transmission system. *Circ. Res.*, 1956;**4**: 357–375.
18. Moe, G.K., W. Cohen, and R.L. Vick, Experimentally induced paroxysmal A-V nodal tachycardia in the dog. *Am. Heart J.*, 1963;**65**: 87–92.
19. Durrer, D., L. Schoo, R.M. Schuilenburg, and H.J. Wellens, The role of premature beats in the initiation and the termination of supraventricular tachycardia in the Wolff-Parkinson-White syndrome. *Circulation*, 1967;**36**: 644–662.
20. Bigger, J.T., Jr. and B.N. Goldreyer, The mechanism of supraventricular tachycardia. *Circulation*, 1970;**42**: 673–688.
21. Wellens, H.J., R.M. Schuilenburg, and D. Durrer, Electrical stimulation of the heart in patients with ventricular tachycardia. *Circulation*, 1972;**46**: 216–226.
22. Wellens, H.J., D.R. Duren, and K.I. Lie, Observations on mechanisms of ventricular tachycardia in man. *Circulation*, 1976;**54**: 237–244.
23. Akhtar, M., A.N. Damato, W.P. Batsford, et al., Demonstration of re-entry within the His-Purkinje system in man. *Circulation*, 1974;**50**: 1150–1162.
24. Lloyd, E.A., D.P. Zipes, J.J. Heger, and E.N. Prystowsky, Sustained ventricular tachycardia due to bundle branch reentry. *Am. Heart J.*, 1982;**104**: 1095–1097.
25. Josephson, M.E., L.N. Horowitz, A., Farshidi, and J.A. Kastor, Recurrent sustained ventricular tachycardia. 1. Mechanisms. *Circulation*, 1978;**57**: 431–440.
26. Josephson, M.E., L.N. Horowitz, and A. Farshidi, Continuous local electrical activity. A mechanism of recurrent ventricular tachycardia. *Circulation*, 1978;**57**: 659–665.
27. Horowitz, L.N., M.E. Josephson, and A.H. Harken, Epicardial and endocardial activation during sustained ventricular tachycardia in man. *Circulation* 1980;**61**: 1227–1238.
28. Josephson, M.E., L.N. Horowitz, A. Farshidi, et al., Sustained ventricular tachycardia: Evidence for protected localized reentry. *Am. J. Cardiol.*, 1978;**42**: 416–424.
29. Wilber, D.J., H. Garan, D. Finkelstein, et al., Out-of-hospital cardiac arrest. Use of electrophysiologic testing in the prediction of long-term outcome. *N. Engl. J. Med.*, 1988;**318**: 19–24.
30. Horowitz, L.N., M.E. Josephson, A. Farshidi, et al., Recurrent sustained ventricular tachycardia 3. Role of the electrophysiologic study in selection of antiarrhythmic regimens. *Circulation*, 1978;**58**: 986–997.
31. Buxton, A.E., K.L. Lee, L. DiCarlo, et al., Electrophysiologic testing to identify patients with coronary artery disease who are at risk for sudden death. Multicenter Unsustained Tachycardia Trial Investigators. *N. Engl. J. Med.*, 2000;**342**: 1937–1945.
32. Daubert, J.P., W. Zareba, W.J. Hall, et al., Predictive value of ventricular arrhythmia inducibility for subsequent ventricular tachycardia or ventricular fibrillation in Multicenter Automatic Defibrillator Implantation Trial (MADIT) II patients. *J. Am. Coll. Cardiol.*, 2006;**47**: 98–107.
33. Brodsky, M.A., L.B. Mitchell, B.D. Halperin, M.H. Raitt, and A.P. Hallstrom Prognostic value of baseline electrophysiology studies in patients with sustained ventricular tachyarrhythmia: The Antiarrhythmics Versus Implantable Defibrillators (AVID) trial. *Am. Heart J.*, 2002;**144**: 478–484.
34. Mason, J.W., A comparison of electrophysiologic testing with Holter monitoring to predict antiarrhythmic-drug efficacy for ventricular tachyarrhythmias. Electrophysiologic Study versus Electrocardiographic Monitoring Investigators. *N. Engl. J. Med.*, 1993;**329**: 445–451.
35. Morady, F., Radio-frequency ablation as treatment for cardiac arrhythmias. *N. Engl. J. Med.*, 1999;**340**: 534–544.
36. Stevenson, W.G. and K. Soejima, Recording techniques for clinical electrophysiology. *J. Cardiovasc. Electrophysiol.*, 2005;**16**: 1017–1022.
37. Campbell, R.W., R. Charles, J.C. Cowan, et al., Clinical competence in electrophysiological techniques. *Heart*, 1997;**78**: 403–412.
38. Tracy, C.M., M. Akhtar, J.P. DiMarco, et al., American College of Cardiology/American Heart Association 2006 Update of the Clinical Competence Statement on invasive electrophysiology studies, catheter ablation, and cardioversion: A report of the American College of Cardiology/American Heart Association/American College of Physicians Task Force on Clinical Competence and Training. *Circulation*, 2006;**114**:1654–1668.
39. Ng, G.A., E.W. Lau, and M.J. Griffith, A streamlined "3-catheter" approach in the electrophysiological study and radiofrequency ablation of narrow complex tachycardia. *J. Intervent. Card. Electrophysiol.*, 2002;**7**: 209–214.
40. Kuck, K.H. and M. Schluter, Single-catheter approach to radiofrequency current ablation ofleft-sided accessory pathways

in patients with Wolff-Parkinson-White syndrome. *Circulation*, 1991;**84**: 2366–2375.
41. Narula, O.S., B.J. Scherlag, and P. Samet, Pervenous pacing of the specialized conducting system in man. His bundle and A-V nodal stimulation. *Circulation*, 1970;**41**: 77–87.
42. Michelson, E.L., S.R. Spielman, A.M. Greenspan, et al., Electrophysiologic study of the left ventricle: Indications and safety. *Chest*, 1979;**75**: 592–596.
43. Herre, J.M., D.E. Mann, J.C. Luck, et al., Effect of increased current, multiple pacing sites and number of extrastimuli on induction of ventricular tachycardia. *Am. J. Cardiol.*, 1986;**57**: 102–107.
44. Morady, F., L.A. Dicarlo, Jr., L.B. Liem, R.B. Krol, and J.M. Baerman, Effects of high stimulation current on the induction of ventricular tachycardia. *Am. J. Cardiol.*, 1985;**56**: 73–78.
45. Kennedy, E.E., L.E. Rosenfeld, C.A. McPherson, S.I. Stark, and W.P. Batsford, Mechanisms and relevance of arrhythmias induced by high-current programmed ventricular stimulation. *Am. J. Cardiol.*, 1986;**57**: 598–603.
46. Josephson, M.E., D.L. Scharf, J.A. Kastor, and J.G. Kitchen, Atrial endocardial activation in man. Electrode catheter technique of endocardial mapping. *Am. J. Cardiol.*, 1977;**39**: 972–981.
47. Bekheit, S., J.G. Murtagh, P. Morton, and E. Fletcher, Measurements of sinus impulse conduction from electrogram of bundle of His. *Br. Heart J.*, 1971;**33**: 719–724.
48. Benditt, D.G., L.C. Pritchett, W.M. Smith, A.G. Wallace, and J.J. Gallagher, Characteristics of atrioventricular conduction and the spectrum of arrhythmias in Lown-Ganong-Levine syndrome. *Circulation*, 1978;**57**: 454–465.
49. Wiener, I., Syndromes of Lown-Ganong-Levine and enhanced atrioventricular nodal conduction. *Am. J. Cardiol.*, 1983;**52**: 637–639.
50. Kashani, A., and S.S. Barold, Significance of QRS complex duration in patients with heart failure. *J. Am. Coll. Cardiol.*, 2005;**46**: 2183–2192.
51. Gupta, P.K., and J.I. Haft, Retrograde ventriculoatrial conduction in complete heart block: Studies with His bundle electrography. *Am. J. Cardiol.*, 1972;**30**: 408–411.
52. Denes, P., D. Wu, R. Dhingra, R.J. Pietras, and K.M. Rosen, The effects of cycle length on cardiac refractory periods in man. *Circulation*, 1974;**49**: 32–41.
53. Denes, P., D. Wu, R.C. Dhingra, R. Chuquimia, and K.M. Rosen, Demonstration of dual A-V nodal pathways in patients with paroxysmal supraventricular tachycardia. *Circulation*, 1973;**48**: 549–555.
54. Scheinman, M.M. and Y. Yang, The history of AV nodal reentry. *Pacing Clin. Electrophysiol.*, 2005;**28**: 1232–1237.
55. Wu, D., P. Denes, R. Bauernfeind, et al., Effects of atropine on induction and maintenance of atrioventricular nodal reentrant tachycardia. *Circulation*, 1979;**59**: 779–788.
56. Sung, R.J., H.L. Waxman, S. Saksena, and Z. Juma, Sequence of retrograde atrial activation in patients with dual atrioventricular nodal pathways. *Circulation*, 1981;**64**: 1059–1067.
57. Jackman, W.M., K.J. Beckman, J.H. McClelland, et al., Treatment of supraventricular tachycardia due to atrioventricular nodal reentry, by radiofrequency catheter ablation of slow-pathway conduction. *N. Engl. J. Med.*, 1992;**327**: 313–318.
58. Heidbuchel, H. and W.M. Jackman, Characterization of subforms of AV nodal reentrant tachycardia. *Europace*, 2004;**6**: 316–329.
59. Nawata, H., N. Yamamoto, K. Hirao, et al., Heterogeneity of anterograde fast-pathway and retrograde slow-pathway conduction patterns in patients with the fast-slow form of atrioventricular nodal reentrant tachycardia: Electrophysiologic and electrocardiographic considerations. *J. Am. Coll. Cardiol.*, 1998;**32**: 1731–1740.
60. Wu, D., P. Denes, R. Dhingra, and K.M. Rosen, Nature of the gap phenomenon in man. *Circ. Res.*, 1974;**34**: 682–692.
61. Akhtar, M., A.N. Damato, W.P. Batsford, et al., Unmasking and conversion of gap phenomenon in the human heart. *Circulation*, 1974;**49**: 624–630.
62. Akhtar, M., A.N. Damato, A.R. Caracta, W.P. Batsford, and S.H. Lau, The gap phenomena during retrograde conduction in man. *Circulation*, 1974;**49**: 811–817.
63. Josephson, M.E., *Clinical Cardiac Electrophysiology. Techniques and Interpretations*, 4th Edition, Philadelphia, PA: Lippincott Williams & Williams, 2008.
64. Brugada, P., M. Green, H. Abdollah, and H.J. Wellens, Significance of ventricular arrhythmias initiated by programmed ventricular stimulation: The importance of the type of ventricular arrhythmia induced and the number of premature stimuli required. *Circulation*, 1984;**69**: 87–92.
65. DiMarco, J.P., H. Garan, and J.N. Ruskin, Complications in patients undergoing cardiac electrophysiologic procedures. *Ann. Intern. Med.*, 1982;**97**: 490–493.
66. Horowitz, L.N., H.R. Kay, S.P. Kutalek, et al., Risks and complications of clinical cardiac electrophysiologic studies: A prospective analysis of 1,000 consecutive patients. *J. Am. Coll. Cardiol.*, 1987;**9**: 1261–1268.
67. Horowitz, L.N., Safety of electrophysiologic studies. *Circulation*, 1986;**73**: II28–II31.
68. Hindricks, G., The Multicentre European Radiofrequency Survey (MERFS): Complications of radiofrequency catheter ablation of arrhythmias. The Multicentre European Radiofrequency Survey (MERFS) investigators of the Working Group on Arrhythmias of the European Society of Cardiology. *Eur. Heart J.*, 1993;**14**: 1644–1653.
69. Scheinman, M.M. and S. Huang, The 1998 NASPE prospective catheter ablation registry. *Pacing Clin. Electrophysiol.*, 2000;**23**: 1020–1028.
70. Chen, S.A., C.E. Chiang, C.T. Tai, et al., Complications of diagnostic electrophysiologic studies and radiofrequency catheter ablation in patients with tachyarrhythmias: An eight-year survey of 3,966 consecutive procedures in a tertiary referral center. *Am. J. Cardiol.*, 1996;**77**: 41–46.
71. Cappato, R., H. Calkins, S.A. Chen, et al., Worldwide survey on the methods, efficacy, and safety of catheter ablation for human atrial fibrillation. *Circulation*, 2005;**111**: 1100–1105.
72. Quinn, F.R. and A.C. Rankin, Atrial fibrillation ablation in the real world. *Heart*, 2005;**91**: 1507–1508.
73. Boersma, L., L. Mont, A. Sionis, E. Garcia, and J. Brugada, Value of the implantable loop recorder for the management of patients with unexplained syncope. *Europace*, 2004;**6**: 70–76.
74. Strickberger, S.A., D.W. Benson, I. Biaggioni, et al., AHA/ACCF Scientific Statement on the evaluation of syncope. *Circulation*, 2006;**113**: 316–327.
75. Moss, A.J., W. Zareba, W.J. Hall, et al., Prophylactic implantation of a defibrillator in patients with myocardial infarction and reduced ejection fraction. *N. Engl. J. Med.*, 2002;**346**: 877–883.

76. Grimm, W., J. Hoffmann, V. Menz, K. Luck, and B. Maisch, Programmed ventricular stimulation for arrhythmia risk prediction in patients with idiopathic dilated cardiomyopathy and nonsustained ventricular tachycardia. *J. Am. Coll. Cardiol.*, 1998;**32**: 739–745.
77. Kanda, M., W. Shimizu, K. Matsuo, et al., Electrophysiologic characteristics and implications of induced ventricular fibrillation in symptomatic patients with Brugada syndrome. *J. Am. Coll. Cardiol.*, 2002;**39**: 1799–1805.
78. Epstein, A.E., J.P. DiMarco, K.A. Ellenbogen, et al., ACC/AHA/HRS 2008 Guidelines for Device-Based Therapy of Cardiac Rhythm Abnormalities: a report of the American College of Cardiology/American Heart Association Task Force on Practice Guidelines (Writing Committee to Revise the ACC/AHA/NASPE 2002 Guideline Update for Implantation of Cardiac Pacemakers and Antiarrhythmia Devices): developed in collaboration with the American Association for Thoracic Surgery and Society of Thoracic Surgeons. Circulation 2008;117: e350–408.
79. Knight, B.P., A. Zivin, J. Souza, et al., A technique for the rapid diagnosis of atrial tachycardia in the electrophysiology laboratory. *J. Am. Coll. Cardiol.*, 1999;**33**: 775–781.
80. Vijayaraman, P., B.P. Lee, G. Kalahasty, M.A. Wood, and K.A. Ellenbogen, Reanalysis of the "pseudo A-A-V" response to ventricular entrainment of supraventricular tachycardia: Importance of his-bundle timing. *J. Cardiovasc. Electrophysiol.*, 2006;**17**: 25–28.
81. Owada, S., A. Iwasa, S. Sasaki, et al., "V-H-A Pattern" as a criterion for the differential diagnosis of atypical AV nodal reentrant tachycardia from AV reciprocating tachycardia. *Pacing Clin. Electrophysiol.*, 2005;**28**: 667–674.
82. Hirao, K., K. Otomo, X. Wang, et al., Para-Hisian pacing. A new method for differentiating retrograde conduction over an accessory AV pathway from conduction over the AV node. *Circulation*, 1996;**94**: 1027–1035.
83. Waldo, A.L., From bedside to bench: Entrainment and other stories. *Heart Rhythm*, 2004;**1**: 94–106.
84. Waldo, A.L., W.A. MacLean, R.B. Karp, N.T. Kouchoukos, and T.N. James, Entrainment and interruption of atrial flutter with atrial pacing: Studies in man following open heart surgery. *Circulation*, 1977;**56**: 737–745.
85. Waldo, A.L., V.J. Plumb, J.G. Arciniegas, et al., Transient entrainment and interruption of the atrioventricular bypass pathway type of paroxysmal atrial tachycardia. A model for understanding and identifying reentrant arrhythmias. *Circulation*, 1983;**67**: 73–83.
86. Waldo, A.L., R.W. Henthorn, V.J. Plumb, and W.A. MacLean, Demonstration of the mechanism of transient entrainment and interruption of ventricular tachycardia with rapid atrial pacing. *J. Am. Coll. Cardiol.*, 1984;**3**: 422–430.
87. Henthorn, R.W., K. Okumura, B. Olshansky, et al., A fourth criterion for transient entrainment: The electrogram equivalent of progressive fusion. *Circulation*, 1988;**77**: 1003–1012.
88. Okumura, K., R.W. Henthorn, A.E. Epstein, V.J. Plumb, and A.L. Waldo, Further observations on transient entrainment: Importance of pacing site and properties of the components of the reentry circuit. *Circulation*, 1985;**72**: 1293–1307.
89. Stevenson, W.G., H. Khan, P. Sager, et al., Identification of reentry circuit sites during catheter mapping and radiofrequency ablation of ventricular tachycardia late after myocardial infarction. *Circulation*, 1993;**88**: 1647–1670.
90. Waldo, A.L. and R.W. Henthorn, Use of transient entrainment during ventricular tachycardia to localize a critical area in the reentry circuit for ablation. *Pacing Clin. Electrophysiol.*, 1989;**12**: 231–244.
91. Morady, F., A. Kadish, S. Rosenheck, et al., Concealed entrainment as a guide for catheter ablation of ventricular tachycardia in patients with prior myocardial infarction. *J. Am. Coll. Cardiol.*, 1991;**17**: 678–689.
92. Brignole, M., P. Alboni, D. Benditt, et al., Guidelines on management (diagnosis and treatment) of syncope. *Eur. Heart J.*, 2001;**22**: 1256–1306.
93. Brignole, M., P. Alboni, D.G. Benditt, et al., Guidelines on management (diagnosis and treatment) of syncope—update 2004. *Europace*, 2004;**6**: 467–537.
94. Gulamhusein, S., G.V. Naccarelli, P.T. Ko, et al., Value and limitations of clinical electrophysiologic study in assessment of patients with unexplained syncope. *Am. J. Med.*, 1982;**73**: 700–705.
95. Linzer, M., E.H. Yang, N.A. Estes, III, et al., Diagnosing syncope. Part 2: Unexplained syncope. Clinical Efficacy Assessment Project of the American College of Physicians. *Ann. Intern. Med.*, 1997;**127**: 76–86.
96. Jackman, W.M., X.Z. Wang, K.J. Friday, et al., Catheter ablation of accessory atrioventricular pathways (Wolff-Parkinson-White syndrome) by radiofrequency current. *N. Engl. J. Med.*, 1991;**324**: 1605–1611.
97. Calkins, H., J. Sousa, R. el Atassi, et al., Diagnosis and cure of the Wolff-Parkinson-White syndrome or paroxysmal supraventricular tachycardias during a single electrophysiologic test. *N. Engl. J. Med.*, 1991;**324**: 1612–1618.
98. Epstein, L.M., M.D. Lesh, J.C. Griffin, R.J. Lee, and M.M. Scheinman, A direct midseptal approach to slow atrioventricular nodal pathway ablation. *Pacing Clin. Electrophysiol.*, 1995;**18**: 57–64.
99. Kirkorian, G., E. Moncada, P. Chevalier, et al., Radiofrequency ablation of atrial flutter. Efficacy of an anatomically guided approach. *Circulation*, 1994;**90**: 2804–2814.
100. Pappone, C., S. Rosanio, G. Oreto, et al., Circumferential radiofrequency ablation of pulmonary vein ostia: A new anatomic approach for curing atrial fibrillation. *Circulation*, 2000;**102**: 2619–2628.
101. Soejima, K., M. Suzuki, W.H. Maisel, et al., Catheter ablation in patients with multiple and unstable ventricular tachycardias after myocardial infarction: Short ablation lines guided by reentry circuit isthmuses and sinus rhythm mapping. *Circulation*, 2001;**104**: 664–669.
102. Haissaguerre, M., J.F. Dartigues, J.F. Warin, et al., Electrogram patterns predictive of successful catheter ablation of accessory pathways. Value of unipolar recording mode. *Circulation*, 1991;**84**: 188–202.
103. McClelland, J.H., X. Wang, K.J. Beckman, et al., Radiofrequency catheter ablation of right atriofascicular (Mahaim) accessory pathways guided by accessory pathway activation potentials. *Circulation*, 1994;**89**: 2655–2666.
104. Heald, S.C., D.W. Davies, D.E. Ward, C.J. Garratt, and E. Rowland, Radiofrequency catheter ablation of Mahaim tachycardia by targeting Mahaim potentials at the tricuspid annulus. *Br. Heart J.*, 1995;**73**: 250–257.
105. Nakagawa, H., K.J. Beckman, J.H. McClelland, et al., Radiofrequency catheter ablation of idiopathic left ventricular

tachycardia guided by a Purkinje potential. *Circulation*, 1993;**88**: 2607–2617.
106. Nogami, A., S. Naito, H. Tada, et al., Demonstration of diastolic and presystolic Purkinje potentials as critical potentials in a macroreentry circuit of verapamil-sensitive idiopathic left ventricular tachycardia. *J. Am. Coll. Cardiol.*, 2000;**36**: 811–823.
107. Stevenson, W.G., P.T. Sager, and P.L. Friedman, Entrainment techniques for mapping atrial and ventricular tachycardias. *J. Cardiovasc. Electrophysiol.*, 1995;**6**: 201–216.
108. Calkins, H., A.R. Leon, A.G. Deam, et al., Catheter ablation of atrial flutter using radiofrequency energy. *Am. J. Cardiol.*, 1994;**73**: 353–356.
109. Poty, H., N., Saoudi, M. Nair, F. Anselme, and B. Letac, Radiofrequency catheter ablation of atrial flutter. Further insights into the various types of isthmus block: Application to ablation during sinus rhythm. *Circulation*, 1996;**94**: 3204–3213.
110. Fisher, J.D., H.L. Cohen, R. Mehra, et al., Cardiac pacing and pacemakers II. Serial electrophysiologic-pharmacologic testing for control of recurrent tachyarrhythmias. *Am. Heart J.*, 1977;**93**: 658–668.
111. Waxman, H.L., A.E. Buxton, L.M. Sadowski, and M.E. Josephson, The response to procainamide during electrophysiologic study for sustained ventricular tachyarrhythmias predicts the response to other medications. *Circulation*, 1983;**67**: 30–37.
112. Breithardt, G., L. Seipel, R.R. Abendroth, and F. Loogen, Serial electrophysiological testing of antiarrhythmic drug efficacy in patients with recurrent ventricular tachycardia. *Eur. Heart J.*, 1980;**1**: 11–24.
113. Waller, T.J., H.R. Kay, S.R. Spielman, et al., Reduction in sudden death and total mortality by antiarrhythmic therapy evaluated by electrophysiologic drug testing: criteria of efficacy in patients with sustained ventricular tachyarrhythmia. *J. Am. Coll. Cardiol.*, 1987;**10**: 83–89.
114. Borggrefe, M., H.J. Trampisch, and G. Breithardt, Reappraisal of criteria for assessing drug efficacy in patients with ventricular tachyarrhythmias: Complete versus partial suppression of inducible arrhythmias. *J. Am. Coll. Cardiol.*, 1988;**12**: 140–149.
115. Handlin, L.R., W.N. Brodine, H. Gibbs, and J.L. Vacek, Slowing of ventricular tachycardia as a possible endpoint for serial drug testing at electrophysiological study. *Pacing Clin. Electrophysiol.*, 1992;**15**: 864–869.
116. Buxton, A.E., K.L. Lee, J.D. Fisher, et al., A randomized study of the prevention of sudden death in patients with coronary artery disease. Multicenter Unsustained Tachycardia Trial Investigators. *N. Engl. J. Med.*, 1999;**341**: 1882–1890.
117. Lee, K.L., G. Hafley, J.D. Fisher, et al., Effect of implantable defibrillators on arrhythmic events and mortality in the multicenter unsustained tachycardia trial. *Circulation*, 2002;**106**: 233–238.
118. Morady, F., L. DiCarlo, S. Winston, J.C. Davis, and M.M. Scheinman, Clinical features and prognosis of patients with out of hospital cardiac arrest and a normal electrophysiologic study. *J. Am. Coll. Cardiol.*, 1984;**4**: 39–44.
119. Raitt, M.H., E.G. Renfroe, A.E. Epstein, et al., "Stable" ventricular tachycardia is not a benign rhythm: Insights from the antiarrhythmics versus implantable defibrillators (AVID) registry. *Circulation*, 2001;**103**: 244–252.
120. McPherson, C.A., L.E. Rosenfeld, and W.P. Batsford, Day-to-day reproducibility of responses to right ventricular programmed electrical stimulation: Implications for serial drug testing. *Am. J. Cardiol.*, 1985;**55**: 689–695.
121. Mann, D.E., V. Hartz, E.A. Hahn, and M.J. Reiter, Effect of reproducibility of baseline arrhythmia induction on drug efficacy predictions and outcome in the Electrophysiologic Study Versus Electrocardiographic Monitoring (ESVEM) trial. *Am. J. Cardiol.*, 1997;**80**: 1448–1452.
122. Schaumann, A., M.F. von zur, B. Herse, B.D. Gonska, and H. Kreuzer, Empirical versus tested antitachycardia pacing in implantable cardioverter defibrillators: A prospective study including 200 patients. *Circulation*, 1998;**97**: 66–74.
123. Wathen, M.S., M.O. Sweeney, P.J. DeGroot, et al., Shock reduction using antitachycardia pacing for spontaneous rapid ventricular tachycardia in patients with coronary artery disease. *Circulation*, 2001;**104**: 796–801.
124. Wathen, M.S., P.J. DeGroot, M.O. Sweeney, et al., Prospective randomized multicenter trial of empirical antitachycardia pacing versus shocks for spontaneous rapid ventricular tachycardia in patients with implantable cardioverter-defibrillators: Pacing Fast Ventricular Tachycardia Reduces Shock Therapies (PainFREE Rx II) trial results. *Circulation*, 2004;**110**: 2591–2596.
125. Raitt, M.H., G.L. Dolack, P.J. Kudenchuk, J.E. Poole, and G.H. Bardy, Ventricular arrhythmias detected after transvenous defibrillator implantation in patients with a clinical history of only ventricular fibrillation. Implications for use of implantable defibrillator. *Circulation*, 1995;**91**: 1996–2001.
126. Wellens, H.J. and D. Durrer, Wolff-Parkinson-White syndrome and atrial fibrillation. Relation between refractory period of accessory pathway and ventricular rate during atrial fibrillation. *Am. J. Cardiol.*, 1974;**34**: 777–782.
127. Klein, G.J., T.M. Bashore, T.D. Sellers, et al., Ventricular fibrillation in the Wolff-Parkinson-White syndrome. *N. Engl. J. Med.*, 1979;**301**: 1080–1085.
128. Jezior, M.R., S.M. Kent, and J.E. Atwood, Exercise testing in Wolff-Parkinson-White syndrome: Case report with ECG and literature review. *Chest*, 2005;**127**: 1454–1457.
129. Blomstrom-Lundqvist, C., M.M. Scheinman, E.M. Aliot, et al., ACC/AHA/ESC guidelines for the management of patients with supraventricular arrhythmias-executive summary. *J. Am. Coll. Cardiol.*, 2003;**42**: 1493–1531.
130. Pappone, C., V. Santinelli, S. Rosanio, et al., Usefulness of invasive electrophysiologic testing to stratify the risk of arrhythmic events in asymptomatic patients with Wolff-Parkinson-White pattern: Results from a large prospective long-term follow-up study. *J. Am. Coll. Cardiol.*, 2003;**41**: 239–244.
131. Pappone, C., F. Manguso, R. Santinelli, et al., Radiofrequency ablation in children with asymptomatic Wolff-Parkinson-White syndrome. *N. Engl. J. Med.*, 2004;**351**: 1197–1205.
132. Richards, D.A., D.V. Cody, A.R. Denniss, et al., Ventricular electrical instability: A predictor of death after myocardial infarction. *Am. J. Cardiol.*, 1983;**51**: 75–80.
133. Richards, D.A., K. Byth, D.L. Ross, and J.B. Uther, What is the best predictor of spontaneous ventricular tachycardia and sudden death after myocardial infarction? *Circulation*, 1991;**83**: 756–763.
134. Bailey, J.J., A.S. Berson, H. Handelsman, and M. Hodges, Utility of current risk stratification tests for predicting major arrhythmic events after myocardial infarction. *J. Am. Coll. Cardiol.*, 2001;**38**: 1902–1911.
135. Moss, A.J., W.J. Hall, D.S. Cannom, et al., Improved survival with an implanted defibrillator in patients with coronary disease at high risk for ventricular arrhythmia. Multicenter Automatic

Defibrillator Implantation Trial Investigators. *N. Engl. J. Med.*, 1996;**335**: 1933–1940.

136. Chen, X., M. Shenasa, M. Borggrefe, et al., Role of programmed ventricular stimulation in patients with idiopathic dilated cardiomyopathy and documented sustained ventricular tachyarrhythmias: Inducibility and prognostic value in 102 patients. *Eur. Heart J.*, 1994;**15**: 76–82.
137. Behr, E.R., P. Elliott, and W.J. McKenna, Role of invasive EP testing in the evaluation and management of hypertrophic cardiomyopathy. *Card. Electrophysiol. Rev.*, 2002;**6**: 482–486.
138. Saumarez, R.C. and A.A. Grace, Paced ventricular electrogram fractionation and sudden death in hypertrophic cardiomyopathy and other non-coronary heart diseases. *Cardiovasc. Res.*, 2000;**47**: 11–22.
139. Saumarez, R.C., L. Chojnowska, R. Derksen, et al., Sudden death in noncoronary heart disease is associated with delayed paced ventricular activation. *Circulation*, 2003;**107**: 2595–2600.
140. Bardy, G.H., K.L. Lee, D.B. Mark, et al., Amiodarone or an implantable cardioverter-defibrillator for congestive heart failure. *N. Engl. J. Med.*, 2005;**352**: 225–237.
141. Elliott, P.M., J. Poloniecki, S. Dickie, et al., Sudden death in hypertrophic cardiomyopathy: Identification of high risk patients. *J. Am. Coll. Cardiol.*, 2000;**36**: 2212–2218.
142. Kies, P., M. Bootsma, J. Bax, M.J. Schalij, and E.E. van der Wall, Arrhythmogenic right ventricular dysplasia/cardiomyopathy: Screening, diagnosis, and treatment. *Heart Rhythm*, 2006;**3**: 225–234.
143. Corrado, D., L. Leoni, M.S. Link, et al., Implantable cardioverter-defibrillator therapy for prevention of sudden death in patients with arrhythmogenic right ventricular cardiomyopathy/dysplasia. *Circulation*, 2003;**108**: 3084–3091.
144. Wichter, T., M. Paul, C. Wollmann, et al., Implantable cardioverter/defibrillator therapy in arrhythmogenic right ventricular cardiomyopathy: Single-center experience of long-term follow-up and complications in 60 patients. *Circulation*, 2004;**109**: 1503–1508.
145. Bhandari, A.K., W.A. Shapiro, F. Morady, et al., Electrophysiologic testing in patients with the long QT syndrome. *Circulation*, 1985;**71**: 63–71.
146. Sumitomo, N., K. Harada, M. Nagashima, et al., Catecholaminergic polymorphic ventricular tachycardia: Electrocardiographic characteristics and optimal therapeutic strategies to prevent sudden death. *Heart*, 2003;**89**: 66–70.
147. Brugada, J., P. Brugada, and R. Brugada, The syndrome of right bundle branch block ST segment elevation in V1 to V3 and sudden death—the Brugada syndrome. *Europace*, 1999;**1**: 156–166.
148. Wilde, A.A., C. Antzelevitch, M. Borggrefe, et al., Proposed diagnostic criteria for the Brugada syndrome: Consensus report. *Circulation*, 2002;**106**: 2514–2519.
149. Brugada, P., R. Brugada, L. Mont, et al., Natural history of Brugada syndrome: The prognostic value of programmed electrical stimulation of the heart. *J. Cardiovasc. Electrophysiol.*, 2003;**14**: 455–457.
150. Priori, S.G., C. Napolitano, M. Gasparini, et al., Natural history of Brugada syndrome: Insights for risk stratification and management. *Circulation*, 2002;**105**: 1342–1347.

25 Intracardiac Mapping

Oliver R. Segal · Michael Koa-Wing · Julian Jarman · Nicholas Peters · Vias Markides · D. Wyn Davies

P. W. Macfarlane, A. van Oosterom, O. Pahlm, P. Kligfield, M. Janse, J. Camm (eds.), *Comprehensive Electrocardiology*, DOI 10.1007/978-1-84882-046-3_25,

25.1 Catheter-Based Mapping Techniques

25.1.1 The Development of Catheter-Based Mapping Techniques

Following the inception of cardiac catheterization in the 1940s, catheter-based techniques were developed to record electrical activity from the endocardial surface using electrode catheters. One of the first exponents of this technique was Scherlag, who used electrode catheters to record activity from the His bundle in man [1]. At the same time, programmed electrical stimulation was being developed by Wellens' group, to both induce and terminate supraventricular tachycardias (SVT) in patients with Wolff-Parkinson-White Syndrome [2], and then later in patients with ventricular tachycardia (VT) [3]. Catheter recordings were then used to determine the refractory periods of the atria, ventricles, and the His–Purkinje tissue, and the functional characteristics of the A-V conducting system. This led to the investigation of the effects of pharmacological agents on these functional parameters and their efficacy in terminating and preventing arrhythmias.

The use of multiple catheters inside the heart allowed investigators to compare activation timings at different sites and represented the first step in mapping arrhythmias. This simple technique allowed the approximate localization of accessory pathways in patients with Wolff-Parkinson-White Syndrome and, subsequently, led Josephson et al. to describe endocardial mapping techniques for VT arising from the left ventricle [4]. However, the use of single or multiple catheters for mapping arrhythmias has important limitations. It is usually only applicable to sustained, monomorphic arrhythmias that are hemodynamically stable where there is time for sequential mapping. Furthermore, the spatial resolution of individual catheters may not be sufficient to elucidate the mechanism or substrate and origin of complex arrhythmias, especially infarct-related VT. To overcome these limitations in VT, some investigators developed criteria for identifying sites critical for arrhythmogenesis during sinus rhythm, namely, the presence of abnormal fractionated electrograms [5–7].

25.1.2 Conventional Contact Catheter Mapping

Intracardiac mapping using conventional contact catheters remains the cornerstone of diagnostic electrophysiology and ablation. The placement of catheters in different cardiac chambers with simultaneous recording enables determination of the origin of many types of arrhythmia. However, considerable knowledge and experience is required to interpret this information, and many different techniques designed to tackle the same forms of tachycardia have evolved.

25.1.3 Vascular Access

The placement of catheters within the right heart and coronary sinus requires cannulation of a central vein. The right and left femoral veins are typically used for the placement of most catheters, although the subclavian veins may be particularly useful for the placement of electrodes within the coronary sinus.

Access to the left atrium and ventricle can be obtained either via the retrograde trans-aortic route (although mapping of the left atrium using this technique is usually difficult) or via the transseptal route, where puncture of the intra-atrial septum is usually required unless a patent foramen ovale or atrial septal defect is present, in which case access may be achieved directly. Importantly, once catheters are placed within the left-sided circulation, anticoagulation with heparin is required to prevent thrombotic and embolic complications.

25.1.4 Contact Catheters

A variety of diagnostic catheters are available from many different manufacturers. In their simplest form, they comprise a fixed-curve bipolar catheter, with which it is possible to both record electrical activity and pace the heart using a bipolar or unipolar configuration.

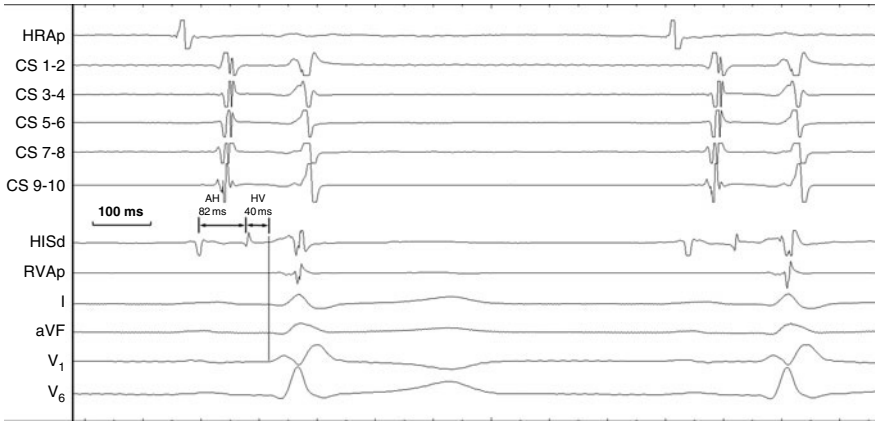

Figure 25.1

Typical electrograms recorded from a conventional diagnostic electrophysiology study. Abbreviations: AH, interval between septal atrial and His electrograms; CS, coronary sinus; Hisd, distal His bundle electrogram; HRA, high right atrium; HV, interval between the His electrogram and the earliest ventricular activity inscribed from any intracardiac or surface lead, in this case, V_1, which demonstrates right bundle branch block to be present; RVAp, proximal right ventricular apical electrogram. Four ECG leads are labeled conventionally.

However, fixed curve quadripolar catheters are typically used for recording electrical activity from the high right atrium, the AV node/bundle of His, and the apex of the right ventricle (Fig. 25.1). The addition of the two extra electrodes provides more electrical information from the chamber in which they have been placed, and this in turn provides greater information to gauge the direction of activation within a cardiac chamber. In addition, this offers the ability to pace and record simultaneously from closely adjacent electrodes. A quadripolar catheter placed at the bundle of His may also be able to record electrical potentials from the proximal right bundle branch, which is useful in some circumstances.

In contrast, a multipolar catheter, such as a decapolar catheter, is typically used for recording electrical activity within the coronary sinus, enabling the length of the vein to be spanned by the recording electrodes. The coronary sinus is the only place where left atrial and ventricular activity can be recorded from standard venous cannulation. It is therefore logical to obtain as much information as possible from a single catheter so that, for example, in patients with left-sided accessory pathways, a decapolar catheter within the coronary sinus lies close to the mitral annulus, facilitating pathway localization. Some centres now routinely use deflectable diagnostic decapolar catheters for use within the coronary sinus, which can make cannulation of the coronary sinus from the femoral route significantly easier.

Specialized multipolar mapping catheters are available that have been designed to guide specific types of catheter ablation. The "Halo" catheter is a 20-pole deflectable curvilinear mapping catheter, which is designed to sit around the tricuspid valve annulus and is used most frequently during typical atrial flutter ablation, although it can be useful in any procedure in which global right atrial recording is required or to guide the localization of right-sided accessory pathways [8]. The "Lasso" catheter is also a multipolar, curvilinear mapping catheter designed to sit at the os of the pulmonary veins to guide the ablation of atrial fibrillation (AF) by pulmonary venous isolation.

25.2 Recording Systems

A system that simultaneously records the standard 12 surface ECG waveforms in addition to a large number of channels for recording intracardiac signals is necessary for performing diagnostic and therapeutic electrophysiological procedures. A number of different recording systems are commercially available, and signals are amplified and filtered over a wide and variable frequency range (from under 1 Hz to 200 kHz), digitized, displayed, and stored.

25.3 Electrogram Recording and Morphology

Electrical activity within the heart can be recorded with unipolar or bipolar configurations. Unipolar electrograms are recorded between a single pole from within the heart and a distant pole typically located intravascularly but outside the heart to minimize surface electrical noise generated by skeletal muscle or an alternating current power supply.

The morphology of unipolar electrograms provides information about the direction of the wavefront of activation coming toward or away from the catheter by the same principle as seen on the standard surface ECG. A wavefront that comes toward the catheter will produce a positive deflection, while a negative deflection occurs when the wavefront travels away from it. Thus, when attempting to map a focal tachycardia, i.e., a tachycardia that originates from a specific focus and propagates centrifugally, a QS morphology indicates the location of the focus. Accordingly, an RS morphology is recorded from all other sites. There are important caveats to this rule that include the need for adequate tissue contact, minimal high-pass filtering, and the presence of "far-field" electrograms that can obscure small amplitude signals. Examples of the latter include ventricular far-field signals recorded from the overlying right atrial appendage or ventricular electrograms from healthy tissue obscuring small potentials from zones of slow conduction within reentrant VT circuits. Bipolar signals also provide information on wavefront propagation, but here, the orientation of the bipole relative to wavefront propagation is a major determinant of the signal shape.

The majority of intracardiac recordings are made with bipolar electrograms. Although their morphology provides limited information about wavefront direction, they indicate the time of local endocardial activation better than unipolar signals.

25.4 Catheter Mapping

Sites critical to the maintenance of a tachycardia can be elucidated by careful interpretation of surface ECG morphology and electrogram timing in combination with specialized pacing maneuvers. In addition, pacing is routinely used to initiate and terminate tachycardias, and the type of pacing maneuver that succeeds in doing so can give information about the likely substrate of the arrhythmia. For instance, arrhythmias that are readily and repeatedly induced using programmed stimulation are most frequently a result of reentry. Triggered rhythms may require appropriate drugs or sometimes physical maneuvers, such as straight leg raising, to aid inducibility.

The process of arrhythmia diagnosis depends significantly on the interpretation of electrogram timing. As bipolar recordings are used in the majority of cases, electrogram morphology is not usually considered in this diagnostic process, although sometimes the combination of unipolar and bipolar recordings are helpful, for example, in ablation of typical right atrial flutter (see below). Usually, complimentary methods of mapping are used to help in the diagnosis of arrhythmias. These are described below.

25.4.1 Activation Sequence Mapping

During focal tachycardias, the origin of the tachycardia is the site at which the earliest electrogram can be localized. This site is found using a roving mapping catheter, and the timing of successive electrograms recorded from this catheter are compared with a stable and relevant reference signal, be it another intracardiac electrogram or surface ECG feature. For instance, focal atrial tachycardias can be mapped by comparing the roving catheter electrogram to the earliest P wave onset on the surface ECG during tachycardia or perhaps to the electrogram recorded from a stable catheter placed within either atrium. If unipolar recording is utilized with minimal high-pass filtering, the presence of a QS morphology belies the source of the tachycardia. In another example, activation mapping can be used to locate the focus of idiopathic VT occurring in structurally normal hearts, especially when these tachycardias arise in the right or left ventricular outflow tracts. One approach to mapping these tachycardias is to progressively move two mapping and ablation catheters and compare electrogram timings between the two catheters that are gradually moved to the site with the earliest activation.

Arrhythmias that are caused by reentry do not have an "earliest" or "latest" signal as there is continuous electrical activity around a barrier to conduction, be it a fixed or functional barrier or a combination of the two. Nevertheless,

activation mapping is still useful in locating sites critical to tachycardia maintenance in reentrant arrhythmias as long as the operator has knowledge of the substrate that supports these arrhythmias. In the case of infarct-related ventricular tachycardia, the circuit is composed of a "systolic" portion in essentially healthy myocardium and a "diastolic" portion in which activation proceeds along a corridor of diseased tissue, usually at the infarct scar border zone and protected by fixed or functional block (see below). Electrograms recorded from this area are found prior to the earliest onset of the QRS complex on the surface ECG. The "diastolic" pathway is the narrowest part of the VT reentrant circuit and the target for ablation. Electrograms occurring in diastole are searched for as they may indicate the location of the diastolic pathway (DP), which is critical to arrhythmia maintenance. However, electrograms in diastole may also represent recordings from blind-ending "bystander" pathways that are not required for tachycardia but usually lie close to the tachycardia's "diastolic" pathway. Specialized pacing maneuvers are required to make this differentiation, which are outlined in detail below.

25.4.2 Pacemapping

The principle of pacemapping is that stimulation at the site of origin of a tachycardia produces a 12-lead ECG that is identical to the tachycardia itself. Stimulation must be performed at a similar cycle length to tachycardia, otherwise localized conduction characteristics may alter ECG morphology. Although bipolar pacing is employed most often for this, it must be remembered that endocardial capture can be from either of the two poles.

Pacemapping is most helpful when used, in addition to activation mapping, in mapping focal tachycardias occurring in structurally normal hearts. As the rest of the myocardium has normal conduction characteristics, pacing at the focus of the arrhythmia should result in a surface ECG morphology identical to tachycardia, or, more commonly, to ectopy arising from the same site. It is important to examine all 12 leads of the surface ECG during tachycardia/ectopy and pacing, and even the smallest difference in P or QRS shape can imply that the catheter is not exactly on the focus. One disadvantage of this technique is that the artifact caused by the pacing stimulus can hamper this comparison.

It is important to also be aware that in the presence of structural heart disease, for instance in infarct-related ventricular tachycardia, areas of "functional block" exist during tachycardia but not during sinus rhythm [9, 123]. These areas act as barriers to conduction protecting an area of myocardium to allow reentry. This is important in post-myocardial infarction (MI) VT and in typical atrial flutter [10]. Therefore, pacemapping from sinus rhythm in these scenarios would produce very different ECG morphologies to those during tachycardia, indicative of different activation sequences.

25.4.3 Entrainment Mapping

This method of mapping is reserved for reentrant arrhythmias. Reentrant circuits typically have "fast" and "slow" components, the latter allowing time for tissue that would otherwise be refractory to recover, permitting the circuit to continue. As described, the different components of these circuits may be separated by fixed anatomical obstacles or zones of functional block. As the activation wavefront travels around the circuit, it encounters continuously excitable tissue ahead of it. This area of tissue that exists between the advancing head of the activation wavefront and the retreating, refractory tail is known as the "excitable gap." It is believed that all macro-reentrant circuits contain such an excitable gap, although the size and conduction characteristics within it may vary not only between different types of reentrant arrhythmia but even at different locations within an individual circuit [11, 124].

Pacing maneuvers may therefore interact with the excitable gap, and the resulting change to activation indicates whether stimulation occurred within the circuit or from outside. It can even discriminate between pacing from the true diastolic pathway and bystander areas (see below).

A single premature extrastimulus may "reset" a reentrant circuit. Resetting is the term used to describe the effect that a premature stimulus has when it reaches the circuit and encounters excitable tissue, the excitable gap. It will both collide with the previous tachycardia wavefront in a retrograde (antidromic) direction and advance the orthodromic activation of the tachycardia [12–14]. The circuit will be "reset" if the excitable gap is fully excitable. The return cycle is the interval between the extrastimulus and the onset of the next beat of tachycardia, and its properties define the characteristics of the excitable gap as this interval corresponds with the time required to reach the circuit, conduct through it, and exit it.

Entrainment, therefore, refers to the ability to continuously reset a tachycardia circuit with pacing at a cycle length just shorter than tachycardia (overdrive pacing). The presence of fusion between the native tachycardia and the paced complex defines entrainment and ensures that activation wavefronts from pacing are interacting with the tachycardia circuit, and is strongly supportive of a reentrant mechanism [15–17]. Focal arrhythmias cannot manifest fusion during overdrive pacing, and tachycardia is suppressed or accelerated by this maneuver.

Entrainment has been described in atrial flutter [18], reentrant atrial tachycardia [19], atrioventricular reentry [17], and reentrant ventricular tachycardia [20–24], and has also been demonstrated in patients with atrioventricular nodal reentrant tachycardia (AVNRT) [20, 25]. Observations during pacing proximal to the site of slow conduction in a reentrant circuit led Waldo's group to propose first a set of three criteria [26], and subsequently a fourth criterion for transient entrainment [21], as follows:

1. The presence of constant fusion beats on the ECG while pacing during tachycardia, at a constant rate that is faster than the tachycardia and that fails to interrupt it, except for the last paced beat that is entrained but not fused.
2. The demonstration of progressive fusion while pacing during tachycardia at two rates that are faster than the tachycardia but do not terminate it.
3. The interruption of a tachycardia during pacing at a rate faster than that of the tachycardia is associated with localized conduction block to a site for one beat, followed by activation of that site by the next pacing impulse from a different direction and with a shorter conduction time.
4. While pacing during tachycardia from a constant site at two rates, both of which are faster than the tachycardia and do not interrupt it, a change in electrogram morphology at, and conduction to, an electrogram recording site is observed.

However, successful entrainment in itself does not prove that the pacing site is located within the circuit, simply that reentry exists. In order to determine whether the pacing site is in such a location, further examination of the fused ECG complexes, the return cycle interval, and the relationship of the pacing stimulus to intracardiac electrograms are required and are outlined below.

Pacing from within a protected part (usually the "diastolic" portion) of the circuit entrains the circuit without change to the surface ECG morphology, as the stimulated orthodromic wavefronts follow exactly the same pathway as the tachycardia wavefronts. This is termed entrainment with concealed fusion or concealed entrainment [27]. The antidromic wavefront from the stimulus collides with the native tachycardia wavefront within the boundaries of the protected pathway and, therefore, does not interrupt the outer portion of activation responsible for the majority of ECG morphology. However, pacing at a connected bystander site will also entrain with concealed fusion.

When pacing within the tachycardia circuit, the return cycle approximates the tachycardia cycle length (TCL) (within 30 ms). Consequently, if pacing from a bystander position, the return cycle is longer than the tachycardia cycle length. However, the return cycle alone cannot discriminate between outer systolic portions of the circuit and the narrow diastolic isthmuses. It is therefore necessary to examine the interval between the pacing stimulus and a fixed reference point, for instance, the stimulus-QRS interval in the setting of reentrant VT (described later).

It should be noted that overdrive pacing must be performed at a cycle length close to that of tachycardia due to the possibility that a shorter pacing cycle length may provoke decremental conduction within the circuit, thereby altering the intervals described above.

25.5 Alternative Mapping Technologies

To overcome the limitations of conventional mapping techniques, principally the ability to record electrogram data from small parts of each cardiac chamber and the usual need for sustained tachycardia, alternative mapping approaches have been developed. They are based on two principles. Electroanatomic mapping systems collect sequential electrogram data from an entire cardiac chamber if necessary to define the underlying electrical substrate, while noncontact and basket catheter mapping systems are designed to collect global electrogram data from even a single cardiac cycle.

25.5.1 Defining the Electrical Substrate Using Electroanatomic Mapping

Electroanatomic systems (CARTO, LocaLisa, Realtime Position Management, and NavX System) [28–31] correlate activation with acquired chamber geometries. They are not suitable for activation mapping during unstable rhythms, but data acquired during sinus rhythm can be used to target ablation.

In creating a global activation map by sequentially collecting activation times on a three-dimensional geometry of a cardiac chamber or chambers, the entire circuit of macro-reentrant arrhythmia can be visualized. Using voltage data, these systems can delineate scar, thereby highlighting the important scar boundary regions where, for instance, VT diastolic pathway activity predominates. Focal or linear lines of ablation can then be created at these regions to abolish reentrant circuits, the latter typically extended to electrically silent areas, for example, the mitral valve annulus or dense scar. This method overcomes the need for mapping during tachycardia by defining potential arrhythmogenic substrates.

25.5.2 Electroanatomic Mapping

The CARTO™ system (Biosense Webster, Diamond Bar, California, USA) works on the principle that a metal coil placed in a magnetic field will generate an electrical current. The magnitude of this current depends on the coil's orientation within the magnetic field and the field's strength. In this system, the coil is located in a specialized catheter tip and three magnets of varying strength are arranged under the patient. The catheter acts as a locator as it is dragged along the endocardial surface, and electrogram data is acquired at each point to facilitate sequential creation of isochronal and voltage maps. Therefore, as with conventional contact catheter techniques, detailed activation mapping of hemodynamically unstable VT is not possible using this system. Instead, substrate mapping (voltage data) and pacemapping during sinus rhythm are employed to identify areas thought to be critical to tachycardia maintenance. These mapping systems also offer the benefit of catheter navigation, thereby limiting x-ray exposure to both patients and medical personnel.

Electroanatomical mapping has been used for mapping and ablation of a range of supraventricular arrhythmias including focal and reentrant atrial tachycardias [32, 33], atrial flutter [31, 34], and accessory pathway ablation [35]. In addition, it has also been extensively used in the treatment of unstable infarct-related ventricular tachycardia using voltage maps created during sinus rhythm [36–39], which hitherto had essentially been "unmappable" using conventional techniques.

25.5.3 LocaLisa

LocaLisa is a non-fluoroscopic catheter location system [29] that utilizes the principle that when an external current is applied across a medium with predictable impedance, a voltage drop occurs [29]. The electrical field strength at a particular point is proportional to the relative position within the medium.

Three orthogonal skin electrode pairs are attached to the patient to produce three-dimensional currents. A 1 mA current is passed between electrodes to create a high-frequency transthoracic electric field. When catheters are moved within the electrical field, sensors incorporated into the catheter tip detect changes in voltage. Each electrode pair emits slightly different signals between 30 and 32 kHz, which are detected by the sensor catheters. Signals are then processed, and the components of different frequencies can be differentiated. The amplitude of each electrical signal is then recorded digitally. The three-dimensional position of any intracardiac catheter can then be computed from the field strength along each orthogonal axis. Sites of interest and previous catheter positions, such as radiofrequency ablation sites, can be marked and used for reference. The system has been used in ablating atrial tachycardia and atrial flutter [40–42], and has also been used to guide pulmonary vein isolation for patients with atrial fibrillation [43].

25.5.4 Global Data Acquisition from a Single Cardiac Cycle

Global mapping systems (basket catheter mapping and noncontact mapping (NCM)) [44, 45] were developed to provide simultaneous data from an entire cardiac chamber from just a single beat of sinus rhythm or tachycardia.

This ability allowed rapid and detailed mapping of an entire VT circuit without the need for tachycardia to be sustained, and such systems are therefore ideally suited for mapping complex and poorly tolerated arrhythmias, such as infarct-related VT.

25.5.5 Basket Catheter Mapping

The basket or multielectrode mapping catheter consists of eight equidistant collapsible splines, or arms, each with four or eight electrode pairs creating a 32–64-bipolar-electrode catheter. A suitably sized basket is deployed via a guiding sheath into the relevant chamber, enabling endocardial mapping.

Studies in swine have shown that this technology is capable of rapidly generating isochronal endocardial maps [46, 47], and unipolar pacing can be performed from each of the electrodes for both pacemapping or entrainment. It has been used to map focal and macro-reentrant atrial tachycardias, atrial arrhythmias in congenital heart disease, and idiopathic outflow tract VT [48–51]. However, there have been relatively few studies using this form of mapping technology to guide VT ablation in man. This is because nonuniform, unpredictable, and relatively uncontrollable spline contact limits spatial resolution of complex activation in structural heart disease and limits the ability to perform pacemapping and entrainment in severely deformed ventricles [45].

25.6 Noncontact Mapping

Noncontact mapping (NCM) is dependent on three important mathematical principles: the Laplace equation, the boundary element method, and the classic solid angle theory [52–55].

Laplace calculated that the voltage measured at an outer boundary (e.g., the endocardium) can be applied to a formula that accurately calculates the voltage everywhere inside a chamber cavity – the Laplace equation [52]. Cavitary potentials are a summation of the electric potential from around the entire endocardial surface and dependent on the distance from each endocardial source point, a principle known as spatial averaging.

The boundary element method describes the process in which a simple formula applied to multiple elements within a boundary and then combined, can provide an accurate assessment of information along the whole boundary [52]. Thus, when calculating voltage from an endocardial surface, the endocardium is divided into multiple elements and a simple expression for voltage and current is applied to each element to estimate the electrical behavior within and between each element. These estimates are combined for an accurate depiction of endocardial potentials.

The classic solid angle theory [53, 54] describes the phenomenon that changes in cardiac potential are detected earliest by an electrode in closest proximity to the source of activation. This site has the greatest negative potential change that decreases with distance. If position and orientation of each electrode is known, the site of origin and sequential activation within a cardiac chamber can be determined [55]. The use of the boundary element method as an inverse solution to Laplace's equation has enabled the reconstruction of surface endocardial electrograms from intracavitary potentials and led to the development of multielectrode intracavitary probes.

Using a collapsible multielectrode array (MEA) with a braid of 64 wires woven around an 8 ml balloon (recreating 3,360 virtual endocardial electrograms), three-dimensional chamber geometries are constructed on a computer workstation. Far-field electrogram data from the array are fed into the amplifier system, sampled at 1.2 kHz, and filtered. A ring electrode on the proximal shaft of the 9F array catheter in the inferior vena cava (IVC) is used as a reference for unipolar electrogram recordings. Because the far-field electrograms detected by the array are of low amplitude and frequency, the potentials are enhanced and resolved mathematically. This allows the construction of high-resolution endocardial isopotential and isochronal maps. Using a locator signal, the system can also guide a contact mapping and ablation catheter, with limited need for fluoroscopy, to points on the virtual endocardium that may be suitable sites for ablation.

The system has been used to map macro-reentrant VT complicating ischemic heart disease, where it has proved valuable in identifying the target diastolic pathway and guiding its ablation [44, 56], and has also mapped other VTs in normal hearts [57, 58]. With the array deployed in the atrium, the noncontact system can delineate the substrates

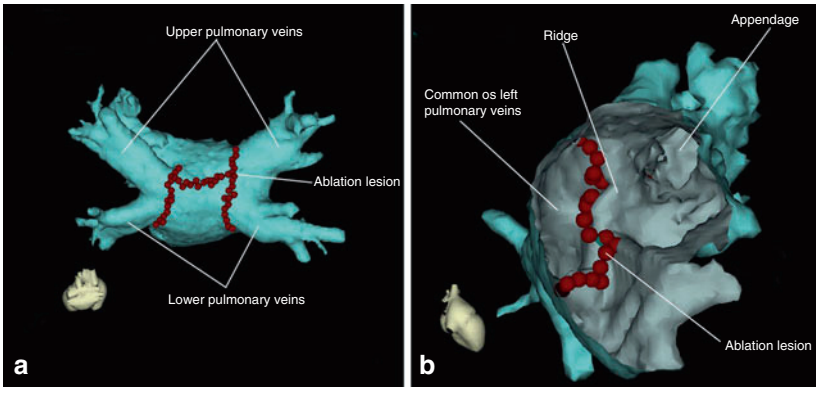

Figure 25.2
(a) External view of digitally derived anatomy of left atrium and pulmonary veins with linear ablation lesions depicted in red. (b) Internal view of digitally derived anatomy of left atrium showing the os of a common left pulmonary vein and the entrance into the left atrial appendage. Linear ablation lesions are depicted in red.

of focal [59], macro-reentrant atrial tachycardia [60], focally initiated atrial fibrillation [61, 62], and atrial fibrillation and typical atrial flutter [63–65], and guide mapping and ablation of tachycardias due to intra-atrial reentry after Fontan surgery [66].

25.6.1 CARTO Merge™

The CARTO Merge™ system integrates computed tomography (CT) or magnetic resonance imaging (MRI) digital images of the heart structures into the mapping study so that a patient's actual anatomy and the conventional mapping geometry can be combined.

Once the images are imported into the CARTO system, each cardiovascular structure can be identified and segmented out until the structures of interest, for example, the left atrium and pulmonary veins, are selected and retained. Its three-dimensional hull is then integrated into the mapping study at the time of the procedure. Using fluoroscopy, fixed anatomical landmarks are identified and acquired as geometric location points. These points are then registered with their corresponding sites on the CT/MRI image, and the two then "merged" together so that the catheter tip can be navigated on-screen within the digital anatomical image (Fig. 25.2).

Electroanatomical mapping with CT/MRI image integration is particularly useful in performing ablation procedures in which anatomical information is important, such as ablation of AF, and in patients with complex anatomy, such as those with congenital heart disease.

25.6.2 EnSite Verismo™ Segmentation Tool

This software works in a similar way to the CARTO Merge software, although direct integration of the mapping data with the CT/MR-derived images is just becoming available.

25.7 Conventional Mapping for Specific Arrhythmias

25.7.1 Mapping of Atrioventricular Nodal Reentrant Tachycardia (AVNRT)

In patients with AVNRT, during performance of an anterograde conduction curve, a jump in AH conduction (indicating anterograde block in the "fast" AV nodal pathway and conduction via a slow pathway) will initiate AVNRT in 70% of

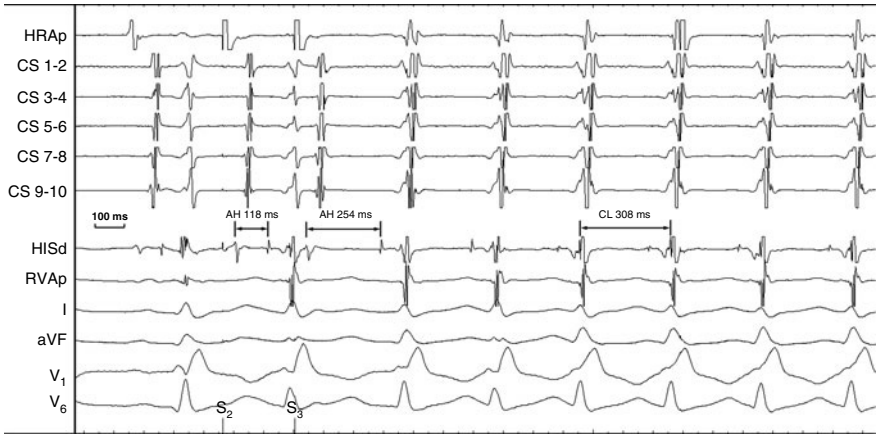

Figure 25.3

Abbreviations: AVNRT, atrioventricular nodal reentry tachycardia; CL, cycle length; otherwise as for Fig. 25.1. Initiation of typical slow-fast AVNRT by two premature atrial extrastimuli (S_1 & S_2) delivered during sinus rhythm. A jump in AH interval is seen after S_2, which is followed by typical slow-fast AVNRT (see text) at a cycle length of 308 ms.

patients (Fig. 25.3). A minimum 50 ms increase in the AH interval after a 10–20 ms shortening in the A1A2 interval is required for a "jump" to be diagnostic. However, single echo beats, i.e., a single cycle of anterograde conduction over the slow pathway followed by retrograde conduction over the fast pathway, are normal. The administration of isoprenaline or atropine may allow AVNRT to be sustained following further pacing. It should also be noted that variants of typical (slow-fast) AVNRT exist, in which the conduction properties and refractory periods overlap such that a jump may not be observed. It is standard practice to proceed to ablation only when tachycardia is readily and repeatedly inducible predominantly, so that a clear end point is provided, i.e., a lack of inducibility following ablation. If tachycardia cannot be induced despite the maneuvers described above, it is advisable not to proceed and to repeat the procedure at a later date.

Typical AVNRT consists of a long AH interval and synchronous, or nearly synchronous, atrial and ventricular conduction with a short VA interval. The latter reflects rapid retrograde fast pathway conduction coincident with rapid anterograde His–Purkinje activation. The presence of bundle branch block will cause HV prolongation and delay of ventricular electrograms depending on which bundle branch is affected but cycle length will not be affected. Retrograde atrial activation should occur in a concentric pattern during typical AVNRT.

Atypical AVNRT (fast-slow) in which anterograde conduction occurs over the fast pathway and retrograde via the slow pathway results in a "long RP" tachycardia on the ECG with corresponding change in intracardiac electrogram. The earliest atrial activation is typically more posteroinferior than in slow-fast AVNRT reflecting the relative location of the slow and fast pathways. The same surface appearance can be produced by orthodromic AVRT with a slowly conducting accessory pathway and low atrial tachycardia with 1:1 AV conduction.

Finally, if a narrow complex tachycardia is induced with an eccentric retrograde atrial activation pattern, either AVRT or AVNRT with a bystander accessory pathway is present. The latter, which is a rare entity, would be expected to demonstrate a degree of fusion between the retrograde activation via the accessory pathway and the fast AV nodal pathway. During any apparent junctional reentry tachycardia, it is important to examine for the presence of an accessory pathway. Sensed, single ventricular extrastimuli are introduced during tachycardia at shorter intervals until one produces ventricular depolarization that is synchronous with the His bundle electrogram. At this point, the ventricular stimulus cannot conduct retrogradely over the AV node as the His bundle is activating anterogradely. Therefore, if this maneuver alters the timing of the subsequent atrial electrogram from that anticipated, an accessory pathway should be suspected. However, this phenomenon is dependent on the size of the excitable gap present, intraventricular conduction properties, the site of pacing, and location of the accessory pathway. In typical AVNRT, the excitable gap is usually relatively small and the RV apical catheter, a considerable distance from the circuit. Therefore, the advancement of atrial activation can only occur with extremely premature extrastimuli. In contrast, an accessory-pathway-mediated tachycardia utilizes the His–Purkinje

system, and therefore the circuit is much closer to the RV catheter. This phenomenon has been developed into a useful tool known as the preexcitation index (PI), to aid discrimination of different types of accessory-pathway-mediated AVRT and AVNRT [67]. The PI is defined as the tachycardia cycle length minus the longest coupled ventricular extrastimulus to result in advancement of atrial activation. A PI of >100 ms is typically seen with AVNRT, 75 ms or greater with left free wall accessory pathways, and <45 ms with septal APs [67]. Finally, failure to advance atrial activation with ventricular extrastimuli does not exclude AVRT, especially if the accessory pathway has decremental properties, or is located on the left free wall.

The response to entrainment is a further additional pacing maneuver that is useful to discriminate between different types of SVT. When AVNRT or AVRT is entrained from the ventricle, it will typically terminate with a V-A-V response, i.e., the last entrained atrial activation will return directly to the ventricle as there are two pathways connecting atrium to ventricle. However, when an atrial tachycardia, which by definition is not dependent on conduction via the AV node or ventricles for maintenance, is entrained, it will typically demonstrate a V-A-A-V response as the last entrained A will subsequently block anterogradely in the AV node. There are important distinctions to this rule, especially if atrial tachycardia occurs in the presence of dual AV node physiology.

The post-pacing interval (PPI) following entrainment (ventricular pacing) is also extremely useful to help differentiate AVNRT from AVRT. This interval represents the time taken to travel to the circuit from the pacing site, once around the circuit, and then the time back to the recording site. Thus, if the tachycardia cycle length (TCL) is subtracted from the PPI, this interval represents twice the time to conduct to and from the circuit, thereby giving a useful indication of how far away the circuit is. It is important to remember that the prematurity of the ventricular pacing results in decrementation elsewhere, especially in the AV node, so the previous definition of PPI-TCL is not entirely accurate. Nevertheless, this calculation has been shown to be extremely useful in differentiating atypical AVNRT from AVRT utilizing a septal accessory pathway, in which the former all had a PPI-TCL of >115 ms [68]. This technique has subsequently been refined to account for decrementation at the AV node [69, 125].

Once AVNRT has been confirmed and if appropriate given the patient's symptomatology, modification of the slow pathway can be performed to permanently interrupt the circuit. Different methods have been described to effect slow pathway modification based on analysis of electrograms [70, 71] or by anatomical guidance [72, 73]. Usually, a combination of these techniques is used. During sinus rhythm, a deflectable ablation catheter is advanced in the RAO (right anterior oblique) projection into the base of the right ventricle at the infero-posterior part of Koch's triangle and withdrawn slowly until small atrial electrograms are identified, typically later than those recorded at the His catheter [74]. The catheter is then moved progressively superiorly on the septal tricuspid annulus until a so-called "dome and spike" morphology is seen, thought to indicate an atrial electrogram closely followed by a slow pathway potential. It is not uncommon to find such potentials in alternative positions depending on the course of the right posterior extension of the AV node. Fairly frequently, this includes sites superior to the coronary sinus os. Successful slow pathway modification, usually associated with an irregular junctional rhythm during RF energy delivery, can be achieved at these sites. The presence of slow junctional activity during energy delivery tends to indicate a successful ablation site. The exact cause of this phenomenon is not clear, but is thought to be due to the effects of thermal injury on inputs to the AV node. It is almost always seen with energy delivery at successful sites at which its duration is longer, but is also seen in up to 65% of unsuccessful sites [75]. Thus, although lack of junctional activity during energy delivery almost invariably suggests an ineffective application, the converse is not necessarily true. Therefore, it is common practice not to continue energy delivery at sites in which junctional activity is not observed after approximately 15 s, and to proceed with caution if the rhythm is rapid, as this may indicate proximity to the compact AV node.

There is increasing risk of inadvertent heart block as the compact AV node is approached [76]. As such, it is absolutely critical that continuous radiographic screening and electrogram analysis is performed during energy delivery so that it can be immediately terminated should the catheter be displaced, AH prolongation is seen, there is absence of atrial depolarization during junctional rhythm, or AV block occurs. Occasionally, ablation within the coronary sinus ostium itself or even less commonly on the left side of the atrial septum is required to achieve successful ablation.

Mid-septal ablation sites appear to be associated with a higher and earlier occurrence of junctional rhythm and higher success rates than more posterior sites [77]. The cycle length of junctional activity during slow pathway ablation (around 500 ms) tends to be longer than that observed with fast pathway ablation (around 400 ms) [78], although there remains some debate about this [74]. Rates below 350 ms suggest proximity to the compact AV node and are associated with the development of conduction block [79].

25.7.2 Wolff-Parkinson-White Syndrome and Concealed Accessory Pathways

In patients with the Wolff-Parkinson-White Syndrome, the accessory pathway can be localized before the diagnostic electrophysiology study using surface electrocardiographic features. Analysis of the delta wave vector and QRS polarity has enabled the construction of various algorithms to help predict the ventricular insertion site of these pathways [80–86]. Morphological ECG analysis is however dependent on the degree of preexcitation, which is dependent on a combination of heart rate, pathway location, and AV nodal function. Atrial pacing during EP study can maximize preexcitation, thereby aiding analysis.

25.7.2.1 Mapping

A standard four-wire electrophysiology study is generally performed using catheters placed at the high right atrium, His bundle area, coronary sinus, and right ventricular apex (Fig. 25.4).

If the ECG in sinus rhythm is normal, the presence of eccentric atrial activation during ventricular pacing should alert the operator to the possibility of a "concealed" accessory pathway, which is capable of only retrograde conduction and, therefore, does not cause ventricular preexcitation. If the earliest anterograde ventricular activation or retrograde atrial activation is recorded from the coronary sinus, the CS (coronary sinus) catheter should then be positioned such that the earliest atrial or ventricular electrograms can be recorded and are "bracketed" by later electrograms on either side of this site. The electrode site recording the earliest A or V electrogram then becomes a useful target for more detailed mapping and ablation. The same principle can be applied to the tricuspid valve annulus using Halo catheters for the localization of right-sided accessory pathways [8].

Atrial and ventricular pacing is performed to characterize the accessory pathway refractory period, induce tachycardia, and to exclude the presence of other arrhythmias. The operator should be alert to the possibility of alternative SVT, for example, atrial tachycardia and AVNRT being conducted with a bystander accessory pathway. It is therefore important that scanning ventricular extrastimuli and responses to entrainment, as described previously, are analyzed to confirm the properties of the circuit being examined.

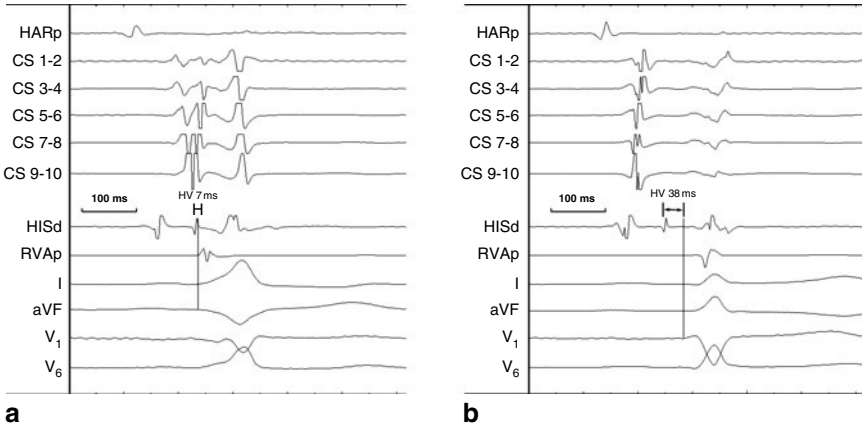

Figure 25.4

(a) Electrograms recorded from a patient with preexcitation by a right-sided pathway. Abbreviations as for Fig. 25.1. The earliest ventricular activation is seen at the right ventricular apex with a very short HV interval. Delta waves are seen at the QRS onset. (b) Electrograms from the patient recorded in Fig. 25.2a after successful ablation of the accessory pathway. The QRS and HV interval are now normal. The increased AV interval is most obviously seen in the CS electrograms.

Once tachycardia has been induced, it is important to attempt to prove that it is accessory pathway mediated. Prolongation of the V-A interval that occurs with the development of bundle branch block ipsilateral to the site of the accessory pathway confirms this. This is also demonstrated by a His synchronous ventricular extrastimulus that terminates tachycardia without atrial capture, or delays the subsequent atrial electrogram.

More detailed mapping of the site of an accessory pathway is facilitated using a deflectable mapping and ablation catheter, usually with a 4 mm tip. Right-sided pathways are mapped along the tricuspid annulus typically from a femoral approach, although a subclavian approach may occasionally be required for greater catheter stability in some right free wall pathways. Left-sided pathways may be mapped from within the coronary sinus (especially postero-septal pathways), using a retrograde trans-aortic approach or via transseptal puncture, the latter being used most commonly for mapping and ablating left lateral pathways. Mapping itself can be performed during sinus rhythm, atrial or ventricular pacing, and orthodromic or antidromic AVRT depending on which of these provides the best identification of the earliest atrial or ventricular activation electrogram.

Bipolar recording is typically used, and the earliest atrial or ventricular electrogram recorded from the mapping catheter is continuously compared to a fixed reference point. In anterogradely conducting accessory pathways, this is often the earliest delta wave onset on the surface ECG. For concealed pathways, a fixed atrial electrogram is used, for example, the earliest atrial electrogram recorded on the CS catheter. In addition to this, morphological electrogram features are also analyzed including electrogram stability indicating tissue contact, the interval between atrial and ventricular components, and the presence of a high-frequency depolarization between these components. The latter may represent a "pathway potential," but it must be possible to dissociate this from both atrial and ventricular components of the electrogram to be sure of this. When mapping in an antero-septal or mid-septal location, the His depolarization must also be considered as a possible cause. A balanced signal, i.e., an electrogram in which the atrial and ventricular components have similar amplitude, suggests true apposition to the AV ring. However, accessory pathways can be successfully ablated from the atrial or ventricular sides of the annulus. Furthermore, pathways can lie obliquely across the AV ring such that the atrial and ventricular insertion sites are not obviously radiographically contiguous. Unipolar pacing can play an important role in the mapping of accessory pathways in which the presence of a QS morphology indicates the location of the pathway insertion site. The differentiation of atrial and ventricular components at sites close to the pathway is sometimes difficult and can be facilitated using atrial extrastimuli or burst pacing causing accessory pathway block.

Mapping of septal accessory pathways presents the additional hazard of the adjacent AV nodal structures, and even greater care must be taken during energy delivery. Postero-septal accessory pathways account for 25–30% of all accessory AV connections [87], and although equally successfully treated by catheter ablation, are often associated with long procedural times. This is related to the complexity of the anatomy of the postero-septal region in addition to the difficulty in delivering adequate energy deep in the postero-septal space. In the majority of cases and in spite of the morphology of the surface ECG, postero-septal accessory pathway electrograms can be reached from a right-sided approach, either at the right postero-septal right atrium or within the proximal coronary sinus. However, mapping of the left-sided postero-septal region is required in some cases. Some of these pathways lie epicardially, and catheters must be maneuvered into subbranches of the coronary venous system, especially if diverticulae are present, in which case retrograde coronary sinus angiography beforehand can be very useful. Accessory pathways arising in the anterior or mid-septum are less common (approximately 6–7%) and frequently conduct anterogradely. Due to the proximity of such pathways to the AV node and its connections, atrial and ventricular activation sequences (depending on which chamber is being paced) can closely mimic each other making differentiation difficult. The technique of para-Hisian pacing can be useful in this regard. Pacing at low outputs captures only adjacent ventricular muscle, which, in the absence of an accessory pathway, conducts relatively slowly to the His–Purkinje system before proceeding retrogradely to the atrium. Pacing at high outputs, however, captures the His bundle itself, leading to rapid retrograde conduction. If an adjacent septal accessory pathway is present, rapid conduction to the atrium will occur regardless of whether low or high outputs are used. This technique can be used both diagnostically prior to ablation as well as a confirmatory test following ablation. A similar technique can be performed with pacing from the base and apex of the right ventricle, the latter lying adjacent to the distal ramifications of the His–Purkinje system allowing rapid retrograde conduction.

Right free wall accessory pathways present their own special difficulties. Mapping of this portion of the tricuspid valve annulus is hampered by the difficulty in manipulating catheters such that they slide along the annulus smoothly and in achieving stability at sites of interest. The use of a multipolar circumferential catheter that sits around the annulus may sometimes be necessary to help localize and bracket the pathway region [8], and the use of catheter sheaths can

greatly enhance stability. Furthermore, right free wall pathways may often be multiple, especially when Ebstein's anomaly is present in which identification of the true AV groove may prove extremely difficult. Occasionally, mapping from the ventricular side of the AV groove is necessary to ablate these pathways, which is achieved using the catheter inversion technique.

25.7.3 Atrial Flutter

Typical atrial flutter is a macro-reentrant circuit within the right atrium. Although very high success rates are now achieved routinely using ablation for this arrhythmia, the precise substrate that underlies it remains unclear. It is accepted that the tricuspid valve annulus forms the anterior boundary of the circuit and that a critical slowly conducting isthmus [88] exists between this and the inferior vena cava, the Eustachian ridge, and the ostium of the coronary sinus, and is targeted for ablation [89, 90]. The exact nature of the posterolateral barrier of the circuit remains less clear and relates to the crista terminalis and whether this represents a zone of fixed or functional block. Nevertheless, detailed mapping of the circuit is infrequently required if typical surface ECG features are present during tachycardia, including a regular "saw-tooth" pattern of atrial activity with negative polarity in the inferior limb leads and positive polarity in lead V1. If these features are present, many operators will not attempt the initiation of tachycardia or further mapping and proceed directly to ablation across the isthmus. However, if mapping is required, a circumferential multipolar catheter placed *en face* to the tricuspid valve annulus aids significantly. As the name suggests, counterclockwise atrial flutter (accounting for approximately 90% of typical atrial flutter [91]) demonstrates counterclockwise activation and importantly septal activation that proceeds in a caudo-cranial direction. Clockwise flutter demonstrates septal activation in the opposite direction. If required, entrainment using atrial pacing from the isthmus will confirm this if concealed fusion is manifest on the surface ECG. Demonstration of concealed entrainment from this region, in which there is a long stimulus to F wave interval [92], ensures that ablation that transects this region will prevent the arrhythmia recurring.

25.7.3.1 Mapping to Guide Radiofrequency Ablation

There are several different mapping strategies that can be adopted to aid typical atrial flutter ablation. One practice is to place a quadripolar catheter in the coronary sinus, a multipolar curvilinear "Halo" catheter around the tricuspid valve annulus, and a pentapolar 8 mm tip deflectable ablation catheter across the isthmus. The latter has four electrodes at the tip and a fifth along the shaft of the catheter to act as a reference electrode within the IVC to record unipolar signals from the isthmus (see below). An additional pole in the IVC acts as an indifferent electrode enabling unipolar mapping electrograms to be generated from the ablation catheter to more accurately guide ablation.

Ablation can be performed either during atrial flutter or, if in sinus rhythm, during pacing from the coronary sinus. The deflectable ablation catheter is passed into the base of the right ventricle such that it abuts the inferior aspect of the tricuspid valve annulus at a 5 to 6 o'clock position in an LAO (left anterior oblique) 30° projection. The desired electrogram recorded at the start of the procedure should demonstrate a large ventricular component and a small atrial signal. During continuous energy delivery, the ablation catheter is then withdrawn slowly into the right atrium across the isthmus ensuring good tissue contact and maintenance of the 5 or 6 o'clock position in the LAO projection. Electrograms recorded from the catheter tip are analyzed during ablation at each site to look for the development of split potentials indicating the creation of a line of block. As the catheter reaches the Eustachian ridge and the junction of the isthmus and the IVC, the catheter is de-flexed to maintain good apposition with the tissue surface. This may need confirmatory views in an RAO 30° projection. Care must be taken during ablation at this region, which is often painful for the patient. In addition, the catheter can suddenly fall back within the IVC, at which point energy delivery must be ceased immediately.

If performed during atrial flutter, it is expected that the arrhythmia will terminate during this procedure. However, this does not necessarily mark the end point of the procedure. Once sinus rhythm has occurred, continuous pacing from the coronary sinus is performed and electrograms from the Halo catheter are examined. Prior to the completion of a line of block across the isthmus, activation from the coronary sinus proceeds in two wavefronts across the superior and inferior aspects of the tricuspid valve annulus producing a fusion pattern with latest atrial activation at the lateral wall. This is demonstrated by a "chevron" pattern of atrial electrograms along the Halo catheter. The creation of a continuous line of block across the isthmus prevents activation proceeding along the inferior aspect of the right atrium with propagation

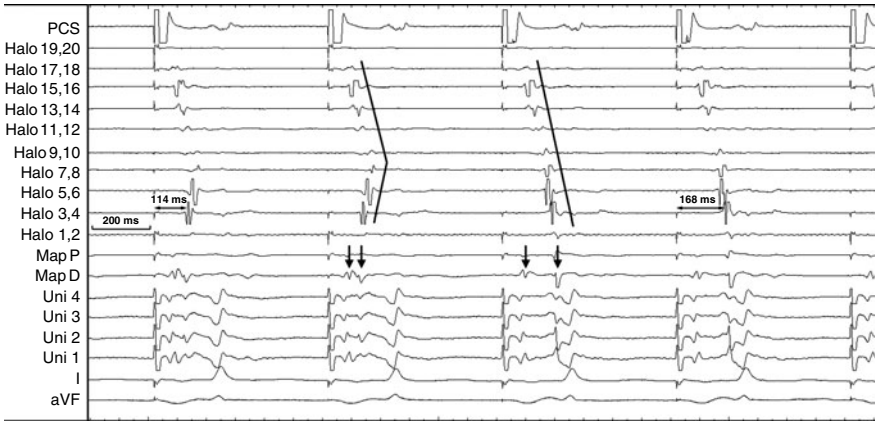

Figure 25.5

Abbreviations: Halo, electrograms recorded from a 20-pole curvilinear catheter (the "Halo") placed around the tricuspid annulus; Map P & Map D, electrograms recorded from the proximal and distal map bipoles, respectively; PCS, proximal CS electrogram; Uni, unipolar electrograms recorded between each of the mapping/ablation catheter's four poles and an indifferent electrode in the inferior vena cava. The development of block to clockwise conduction during radiofrequency ablation seen by straightening of the chevron of the Halo electrograms (see text). Also note the separation of two components of the Map electrograms as block develops, most easily seen in Map P & Map D in this example.

occurring exclusively in a counterclockwise direction. This is manifest by a straightening of the chevron into a line of atrial electrograms with the earliest at the septal side of the Halo catheter (its proximal poles) and the latest recorded from the Halo's distal poles just lateral to the line of block that has been created (Fig. 25.5). This appearance indicates the presence of unidirectional block in the clockwise direction. However, unidirectional block alone as an end point is not sufficient to prevent long-term recurrence [89]. To explore for bidirectional block, pacing is then performed from different bi-poles (typically poles 1,2 and 5,6 or 7,8) on the Halo catheter. If counterclockwise block is also present, the Halo will activate in an exclusively clockwise direction and, when pacing from the distal poles 1,2, a longer interval will be measured between the pacing stimulus and the CS electrogram than when pacing from the more proximal poles.

Another indication of isthmus block is the finding of equally spaced split potentials from each of the mapping catheter's electrodes when it is placed along the line of block. When the line of block is incomplete, these split potentials can guide the operator to the point where conduction persists. This will be identified by a location where the electrogram is relatively normal and of greater amplitude than the neighboring treated tissue, and the two components of the split potential will be closer together (and even continuous) than the split potentials from the other poles betraying nearby conduction across the line of block.

Alternatively, this procedure can be performed using bipolar electrogram recording only from the ablation catheter looking for signal degradation during energy delivery and the creation of double potentials across the isthmus. If necessary, the expense of the procedure can be limited by performing the procedure without a catheter in the coronary sinus during tachycardia or sinus rhythm. Pacing from either side of the line is performed by advancing the Halo catheter across the isthmus, with the tip either within the coronary sinus itself or against the interatrial septum. This technique however requires repeated movement and repositioning of the Halo catheter, which adds to the complexity of the procedure and to the interpretation of the timing of the intracardiac signals. It is even possible to perform the entire procedure with just an ablation and coronary sinus catheter.

25.7.3.2 Atypical Atrial Flutter

This group of reentrant tachycardias can occur in the left or right atrium and are most commonly seen in the context of organic heart disease, previous cardiac surgical intervention, or previous linear atrial ablation, rather than in the

structurally normal heart. The circuits that underlie such tachycardias are dependent on the presence of fixed anatomical barriers and lines of functional block. Gaps in the latter may lead to atypical circuits, and generally the use of advanced mapping systems (contact or noncontact) can significantly aid diagnosis and ablation. However, conventional mapping techniques can be utilized, especially activation mapping and entrainment. As with typical atrial flutter, a multipolar circumferential catheter can be extremely useful for mapping around the tricuspid valve annulus and right atrial free wall. Atypical reentrant left atrial flutters are fairly frequently encountered following linear ablation for atrial fibrillation. Due to the complexity of the underlying substrate, mapping these arrhythmias is often helped by an advanced mapping system.

25.7.4 Focal Atrial Tachycardias

Focal atrial tachycardias are most commonly present in the middle age, and although they can arise from any site within the left or right atrium, they are most commonly right sided [93], especially related to the crista terminalis (Fig. 25.6). A small proportion of patients will have multiple foci. The majority are thought to be due to abnormal automaticity and, therefore, susceptible to the effects of the autonomic nervous system. As such, drugs such as isoproterenol may be necessary for induction, and programmed stimulation may not be useful although overdrive pacing can be used for tachycardia termination. Conversely, triggered or micro-reentrant focal atrial tachycardias are inducible with programmed stimulation, which, in the case of the former, may cause tachycardia acceleration.

Analysis of P wave morphology on the surface ECG, if available, is invaluable prior to intracardiac mapping to determine the general location of the focus. If tachycardia is sustained, activation mapping using a roving 4 mm tip deflectable mapping catheter is the preferred technique, utilizing the P wave onset as the fixed reference point and unipolar recording looking for a QS complex at the site of the focus. As with atrial flutter, multipolar catheters placed in relevant parts of the atrium can significantly aid this technique. Once the focus has thought to have been identified, entrainment mapping can be used for confirmation. In addition to these techniques and especially in the case of non-sustained tachycardia, pacemapping can be performed comparing paced P waves with those of tachycardia. For obvious reasons, it is necessary that sufficient AV block has occurred at some point during tachycardia such that an unperturbed P wave can be seen without interference from an adjacent QRS complex. It is also important that the lowest output to achieve local capture is used to prevent recruitment of larger areas of myocardium. This technique can feasibly be performed even if only a single culprit ectopic has previously been recorded, but in these cases, the use of noncontact mapping is extremely helpful. This

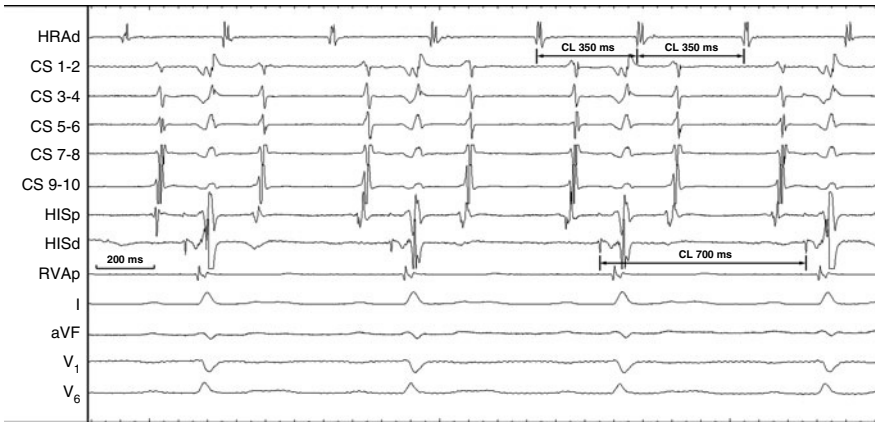

Figure 25.6

Abbreviations: HISp, proximal His electrogram; HRAd, distal HRA electrogram; otherwise as for Fig. 25.1. A right atrial tachycardia of CL 350 ms conducted with 2:1 AV block producing a ventricular CL of 700 ms. Note that right atrial activation (in HRA) is well in advance of left atrial activation (in CS channels) confirming a right atrial (or SVC) origin.

mapping technique, described in detail below, simultaneously records activity from an entire cardiac chamber, enabling localization of a focus from a single ectopic beat. Electroanatomical mapping of stable sustained atrial tachycardias can aid the identification of the source.

25.7.5 Atrial Fibrillation

It is only relatively recently that ablative techniques have been developed to prevent the recurrence of atrial fibrillation (AF) [70]. Initial interest focused purely on the role of ectopy arising from the pulmonary veins and ablation to isolate them from the left atrium [94]. This strategy alone is not sufficient to effect a cure in many patients, especially those with persistent or permanent AF. For those, further techniques have been developed to compartmentalize the left atrium in an effort to prevent reentry [95], a strategy not dissimilar to the surgical Maze procedure [96].

Mapping of AF itself is not necessary for these ablation strategies to be performed. If pulmonary vein isolation is desired, circumferential mapping catheters can be placed at the ostia of the pulmonary veins to guide ostial or antral ablation and to establish the presence of entry and exit block facilitated by pacing outside and from within the vein, respectively. A purely anatomical approach relies on the creation of contiguous linear lesions, something that is really only possible using a three-dimensional mapping system (see below). Apart from testing the completeness of block across these lines, which is not necessarily recommended by all proponents, pacing and mapping is not required.

More recently, however, focus has shifted to modification of the underlying substrate that is thought to support AF. These techniques, including that recently proposed by Nademanee et al. [97], have sought to identify areas of complex fractionated electrograms during AF within regions of the left and right atria to be used as target sites for ablation. The underlying hypothesis is that these areas represent zones of slow conduction and turning points responsible for the reentrant wavelets of AF. Nademanee et al. reported that 95% of the patients had sinus rhythm restored without cardioversion during the procedure using this technique and 91% of patients were free from all arrhythmia at 1 year. It remains to be seen whether these results can be duplicated, or tested prospectively in a randomized controlled trial. However, the future of AF ablation may involve much more detailed intracardiac mapping than is necessary for those techniques most commonly practiced at present.

25.7.5.1 Focally Initiated Atrial Fibrillation

In most patients with AF, episodes are initiated by ectopic depolarization originating from within the muscular sleeves of a pulmonary vein (PV) or veins. In some patients, AF is also perpetuated by a rapidly firing focus within these muscular sleeves [94, 98]. Both these processes can be identified by mapping within the PVs. The "normal" PV activation sequence of atrial followed by PV electrograms is reversed during "culprit" PV activity. Ablation to disconnect such a PV should prevent the recurrence of AF, but the recognition that multiple PVs can generate AF at different times means that most ablation procedures will aim to disconnect all PVs. Occasionally, such foci may be identified in non-pulmonary veins sites, such as the superior vena cava or coronary sinus and vein/ligament of Marshall. Identification of the approximate location of these foci may be possible prior to the procedure using P wave vector analysis, including those arising from the pulmonary veins [99].

25.7.6 Conventional Diagnostic Electrophysiology Study for Ventricular Tachycardia and Ventricular Stimulation Studies

It is recommended that coronary angiography is performed prior to attempts to initiate VT in patients in whom coronary heart disease is either suspected or known because of increased risk of inducing unstable rhythms or VF in patients who might have critical coronary heart disease. When significant coronary artery disease is identified, revascularization should be undertaken before proceeding to further electrophysiological evaluation.

As for the investigation of SVT, quadripolar diagnostic catheters are placed at the right ventricular apex, His bundle area, and the high right atrium. Catheters at these three positions provide electrogram data that enables rapid discrimination between ventricular and supraventricular arrhythmias (especially preexcited tachycardias or those conducted

Figure 25.7

Abbreviations: as for other figures with conventional 12-lead ECG labeling. A drive train of eight paced beats is delivered to the right ventricular outflow tract (RVOT) at a CL of 400 ms. Two premature stimuli (S2 & S3) are then delivered, initiating VT. This has a similar but not identical morphology to the paced beats, suggesting that it originates somewhere from the RVOT.

with aberrancy) or tachycardias arising from the AV junction. Due to the risk of inducing hemodynamically unstable arrhythmias, remote self-adherent defibrillation electrodes fitted to the patient and connected to an external defibrillator during the study are mandatory. In some centres, it is routine to also have invasive blood pressure monitoring during such a study to enable rapid assessment of an arrhythmia's hemodynamic status, especially when ablation is planned.

Baseline intervals are measured as before with special consideration paid to the presence of bundle branch block and HV prolongation during sinus rhythm, which will alter the appearance of induced supraventricular arrhythmias. Ventricular pacing should be performed using the extrastimulus technique to exclude the presence of a concealed accessory pathway, as described previously. Pacing is performed at twice diastolic threshold as higher current delivery may prevent VT induction [100]. VT initiation is performed using the Wellens protocol [3]. During this, sustained or non-sustained ventricular arrhythmias may be observed following the introduction of extrastimuli to the right ventricular apex and, if necessary, the right ventricular outflow tract (RVOT) (Fig. 25.7), thereby increasing the sensitivity of the protocol [101]. Pacing is discontinued when a sustained ventricular arrhythmia is induced and blood pressure and the patient's conscious level recorded. External DC cardioversion should be immediately available if VF or hemodynamically unstable VT is induced. The addition of drugs such as isoproterenol may also be required.

It is important to be aware that the risk of inducing non-clinical VT or VF increases with the use of multiple extrastimuli so that, under those circumstances, the specificity of the test is reduced, although the sensitivity increases [102]. Knowledge of the pre-procedural clinical arrhythmia is thus important in the interpretation of such findings.

25.7.7 Mapping of Ventricular Tachycardia

The preferred method for mapping ventricular tachycardia depends on the underlying substrate and, therefore, the likely mechanism of the arrhythmia. VT occurring in the structurally normal heart, also known as idiopathic VT, can arise from several different sites. The commonest are from the right ventricular outflow tract and the left posterior fascicle, although left ventricular outflow tachycardias occur commonly. VT occurring in the context of structural heart disease also has a wide variety of subtypes and mechanisms including infarct-related/ischemic VT (reentry), bundle branch reentrant VT, VT associated with right ventricular dysplasia, Chagasic heart disease (reentrant or triggered), and is in association with dilated cardiomyopathy. In the following sections, we focus on the commonest VT subtypes, namely, idiopathic RVOT tachycardia, bundle branch reentry, and post-myocardial infarction VT.

25.7.7.1 Idiopathic Right Ventricular Outflow Tract Tachycardia

RVOT tachycardia accounts for approximately 10% of patients presenting with VT. They are focal in nature due to cyclic c-AMP-mediated triggered activity and typically present as a repetitive monomorphic tachycardia, i.e., characterized by frequent ventricular ectopy and salvoes of non-sustained VT interspersed with sinus rhythm [103, 104]. They most commonly originate from the septal portion of the RVOT below the pulmonary valve, but other locations have been identified including the anterior, posterior, and free walls of the RVOT, and from the epicardial surface. Although all forms typically manifest an LBBB (left bundle branch block) and inferior axis morphology on the surface ECG, there is a wide degree of subtle heterogeneity to other ECG features, such as the presence of notching, precordial R transition, and QRS frontal axis [51, 105, 106]. Although frequently incessant, induction may be facilitated by programmed stimulation or with the administration of isoproterenol.

Mapping may be performed conventionally, with a basket catheter or with complex mapping systems. Noncontact mapping can be particularly useful if RVOT ectopy is infrequent. Conventional mapping is performed using a standard quadripolar catheter at the RVA (right ventricular apex) for programmed stimulation and as a timing reference with one or two 4 mm tip deflectable mapping and ablation catheters in the RVOT. Following analysis of surface ECG morphology, the ablation catheter or catheters are navigated to the region of interest and a combination of activation mapping and pacemapping is used to locate the exact origin of tachycardia. Unipolar recording at the site of origin will display a QS morphology. Activation mapping is referenced to either the RVA catheter electrogram or preferably to the earliest ventricular onset on the surface ECG. However, due to the size of the catheter tip, activation mapping alone cannot be relied upon and a perfect pacematch should be sought before proceeding to ablation. Pacemapping should be performed at diastolic threshold, or just above, and at similar rates to tachycardia to enable direct comparison (Fig. 25.8).

25.7.7.2 Bundle Branch Reentrant VT

This form of VT most commonly occurs in the setting of idiopathic dilated cardiomyopathy and is usually manifest with an LBBB morphology. Most patients have complete or a partial bundle branch block pattern on the surface

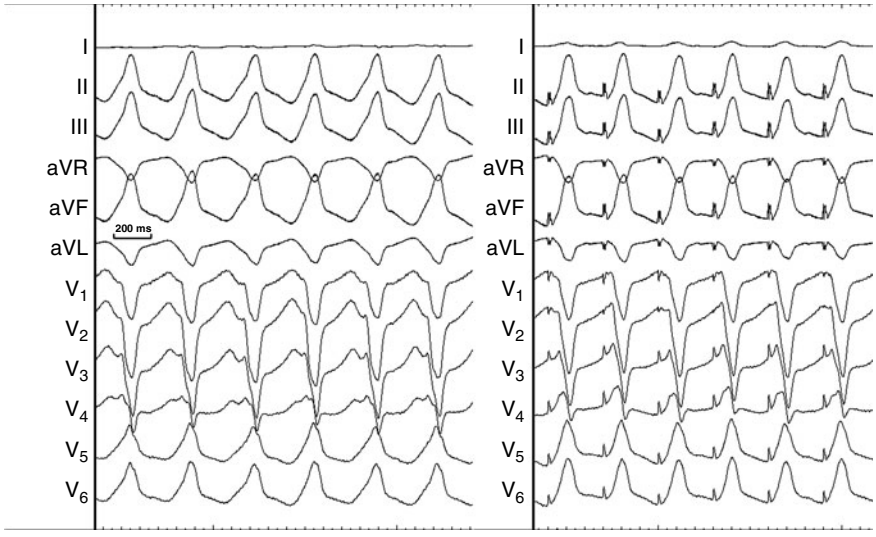

Figure 25.8

Pacemapping of RVOT tachycardia. The 12-lead ECG of tachycardia is in the left panel, and the attempt at pacemapping is in the right panel. The CL is the same in both. The QRS morphologies are similar but not identical. There are differences seen in leads V_4 and slightly in V_3, V_5, and V_6, suggesting that the catheter needs to be moved to a nearby location to produce a perfect pacematch in all 12 leads.

ECG and a prolonged HV interval (75–80 ms) [107]. However, this probably reflects slow conduction rather than true block, which would preclude this arrhythmia. The macro-reentrant circuit that underlies this VT consists of retrograde conduction in the left bundle branch (LBB) followed by anterograde conduction via the right bundle branch (RBB). The circuit is completed via ventricular muscle between the distal ends of the bundle branches. In a minority of patients, an RBBB (right bundle branch block) form,which has an identical circuit but in the opposite direction is seen.

Induction is effected by programmed stimulation using extrastimuli and is dependent on achieving a critical conduction delay in the His–Purkinje network. Occasionally, atrial pacing or drugs that slow His–Purkinje conduction may be required (isoproterenol, Class IA agents). Mapping is performed with catheters at the RVA, His bundle, RBB, and preferably LBB. Activation should proceed from His bundle to RBB to RVA to LBB. Spontaneous changes in the V-V interval are preceded and predicted by change in the H-H interval. Ablation of the right bundle or sometimes left bundle branch terminates the tachycardia and prevents the arrhythmia recurring.

25.7.7.3 Infarct-Related Ventricular Tachycardia

Ventricular tachycardia is most commonly seen in the setting of underlying coronary artery disease with prior remote myocardial infarction (MI) and is due to macro-reentry within or at the border of the MI scar. Mapping of infarct-related VT using conventional methods continues to present significant challenges. This is related to several factors including hemodynamic intolerance, the size of the ventricles (and therefore the difficulty in navigating catheters to sites of interest), the complexity of the underlying circuit, and the difficulty in identifying its critical diastolic portion. Although once offered in an attempt to cure VT, it is now recognized that despite successful ablation, new VT occurs in a large proportion of patients during follow-up [56]. As such, ablation is now mostly performed in patients with existing implantable cardioverter defibrillators (ICDs) experiencing frequent ICD shocks, or using substrate ablation techniques during sinus rhythm (SR) (see below).

Determination of an endocardial exit site of a specific VT using morphological features of the surface ECG is less reliable than for VT in the structurally normal heart, largely due to the influence of scar and the frequent development of functional conduction block to complete the tachycardia circuit. However, three algorithms, which attempt this, enabling rapid localization of a VT to an approximate region of the left or right ventricle prior to insertion of catheters have been published [108–110].

Due to its reentrant mechanism, infarct-related VT is usually inducible by programmed stimulation. With conventional mapping, both activation and entrainment mapping techniques are needed to delineate the reentrant circuit. Pacemapping during sinus rhythm is unreliable in identifying either the diastolic pathway or exit site regions for the reasons outlined below.

Complex mapping systems can be particularly helpful in characterizing these complex substrates, especially when mapping hemodynamically unstable or non-sustained VT. In the former, electroanatomic substrate mapping during sinus rhythm may be deployed to identify regions of scar, the infarct border zone, and corridors of myocardium within dense scar that have persistent but impaired conduction. These regions are then targeted for ablation using linear lesions that are connected to electrically silent areas. In non-sustained VT, noncontact mapping offers the only realistic method of identifying key parts of the circuit, even from a single cardiac cycle.

25.7.8 Conventional Mapping of Infarct-Related VT

Continuous surface 12-lead ECG recording is mandatory in these studies both for approximate determination of VT exit site location as well for activation, pacemapping, and entrainment mapping. A quadripolar catheter is typically positioned at the RVA for programmed stimulation and termination and as a timing reference. Access to the left ventricle is achieved using either the retrograde trans-aortic or transseptal approaches. Each offers an advantage in reaching some parts of the LV more easily. It is advantageous to continuously monitor systemic and pulmonary arterial blood pressure throughout the procedure, as elevation of pulmonary artery pressure during VT is the first sign of hemodynamic deterioration and indicates the need to terminate VT and allow recovery during sinus rhythm before VT is re-induced and mapped again.

25.7.8.1 Activation Mapping

Once the clinical VT has been initiated, a mapping catheter is advanced to the approximate exit site region. From this reference point, the aim is to identify the critical diastolic pathway region of the circuit characterized by low-amplitude, high-frequency, fractionated electrograms that occur during diastole. Such electrograms are not specific for the critical diastolic pathway and may also be found at inner and outer loop sites as well as at bystander regions. These cannot be differentiated from the central common pathway using activation mapping alone; these require complimentary pacing techniques. To further complicate matters, a significant proportion of circuits have diastolic pathway regions located intramurally or subepicardially that are not identifiable using endocardial mapping techniques. Once identified, entrainment mapping is utilized to prove whether or not they are critical to circuit maintenance.

25.7.8.2 Pacemapping

In contrast to VT in the context of a structurally normal heart, pacemapping is not reliable in the setting of healed myocardial infarction. This is due to the necessity for functional lines of block to maintain the VT circuit. Functional block is not present during sinus rhythm [111, 112] so that paced activation wavefronts during sinus rhythm can propagate across these areas, resulting in a different surface QRS morphology [113].

25.7.8.3 Entrainment Mapping of VT

Pacing during VT, however, can be utilized to determine the portion of the circuit where the catheter is situated. During VT, pacing from a site remote to the circuit will collide with the reentrant wavefront, resulting in fusion with a resultant change in surface QRS morphology. The presence of constant QRS fusion during pacing defines entrainment and ensures that activation wavefronts from pacing are interacting with the tachycardia circuit. Criteria for recognition of entrainment during VT are summarized in Table 25.1.

The post-pacing interval (PPI) is the interval after the last paced extrastimulus that entrains VT and the next depolarization at the pacing site [27]. When pacing within the tachycardia circuit, the PPI approximates the tachycardia cycle length. Consequently, if pacing from a bystander position, the PPI is longer than VT cycle length. However, the PPI alone cannot discriminate between outer systolic portions of the circuit and the narrow diastolic isthmuses.

Pacing from within the diastolic portion of the circuit entrains the circuit without change to the surface QRS morphology, as the paced orthodromic wavefront activates the circuit in an identical sequence as the VT wavefronts. This is called concealed fusion or concealed entrainment [27]. The antidromic wavefront from the stimulus collides with the VT wavefront within the boundaries of the diastolic pathway and, therefore, does not interrupt the systolic portion of activation responsible for QRS morphology. Pacing at a bystander site within areas of scar adjacent to and connecting to the critical diastolic pathway will also entrain the tachycardia without change in the surface QRS morphology. These locations can be distinguished by analysis of the intervals between the diastolic electrograms, the pacing stimuli, and QRS onset. When pacing from the critical diastolic pathway, the interval between the diastolic electrogram and the QRS onset will be identical to the interval between the pacing stimulus and the QRS onset because the respective activation wavefronts travel over the same path. In the case of a bystander pathway, this is activated from the critical diastolic pathway while

Table 25.1

Criteria for demonstrating entrainment of VT

1. Fixed fusion at a given paced cycle length
2. Progressive fusion at faster paced cycle lengths
3. Resumption of the VT on cessation of pacing with a non-fused QRS complex
4. For tachycardia in which fusion on the ECG is not observed: Fixed fusion demonstrated by analysis of the electrograms at the site of origin

Table 25.2
Characteristics of entrainment from the diastolic pathway of a VT circuit

1. Entrainment with concealed fusion
2. Post-pacing interval = VT cycle length ±30 ms
3. Stimulus-QRS = Electrogram-QRS
4. Stimulus-QRS/VT cycle length = 31–70%
5. Isolated potential during VT

activation continues along the critical diastolic pathway to the exit site to generate the QRS complex. When pacing from a bystander location, the activation wavefront has to travel back to reach the critical diastolic pathway before then proceeding to generate an identical QRS morphology. Therefore, the pacing-QRS interval is longer than the electrogram-QRS interval in a bystander pathway. However, such pathways do indicate that the mapping catheter is close to the ablation target of the critical diastolic pathway.

The stimulus-QRS interval is the conduction time from the pacing site to the VT exit site. It is therefore short when near the exit and longer at the entry site or from within the diastolic pathway. Therefore, the ratio of the stimulus-QRS interval as a proportion of the VT cycle length can help determine the location of the pacing site from sites within the inner loop. Characteristics of entrainment from the diastolic pathway are shown in Table 25.2.

The utility of these pacing maneuvers has been demonstrated in the work of El Shalakany et al. in which ablation sites were compared using the following criteria: an exact QRS match during entrainment, a return cycle within 10 ms of the VT cycle length, and the presence of presystolic potentials with the E-QRS interval less than or equal to 10 ms of the stimulus-to-QRS (S-QRS) interval. When all three criteria were met, VT could be terminated with a single radiofrequency lesion in all patients, whereas the lesion was almost invariably unsuccessful when all three criteria were not met [114].

25.7.9 VT Ablation Using Complex Mapping Systems

Initial data from series using noncontact mapping to guide VT ablation have been encouraging with high initial success rates. Schilling et al. [44] used noncontact mapping to target VT and achieved an initial success rate of 77% of all VT in which diastolic pathway activity was mapped. Strickberger's group [115] successfully ablated 15 of 19 targeted VT (78%). The remaining 4 VT could not be ablated due to inability to maneuver the catheter to the target site, proximity of the target site to the bundle of His, or due to a complication causing termination of the procedure. On follow-up, VT recurrence was significantly reduced, as was the requirement for defibrillator therapy. In the 12 patients with ICDs implanted prior to ablation, defibrillator therapy frequency was reduced from 19 ± 32 per month to 0.6 ± 1.4 per month in 1 month of follow-up.

The CARTO system was used by Soejima et al. [36] to generate voltage maps during sinus rhythm to target VT ablation. VT was induced and, if possible, a potential reentrant isthmus was identified. If unstable, pacemapping along the low voltage border of scar was performed looking for an identical pacematch to that of the induced VT in addition to a stimulus to QRS delay of greater than 40 ms. Standard RF, irrigated, or cooled-tip catheter energy was delivered to these sites during sinus rhythm; then short ablation lines were created extending from these sites parallel to the scar border zone over 1–2 cm until pacing at 10 mA at 2 ms stimulus strength failed to capture in that region. If the target site was within 2–3 cm of the mitral annulus, lesions were extended to the annulus to interrupt a potential submitral isthmus, as first demonstrated by Wilber et al. [116]. Programmed stimulation was repeated, and if VT was re-induced, further mapping and ablation was repeated with RF lines extended. Electrically unexcitable scar (EUS) was identified in all 14 patients, and all 20 VT circuit isthmuses were located adjacent to these regions. However, it was difficult to discriminate between low-amplitude, fractionated electrograms that represented scar and those that indicated the diastolic pathway. Nevertheless, RF ablation lines connecting selected EUS regions abolished all inducible VTs in 10 patients (71%) and spontaneous VT was markedly reduced during follow-up (142 ± 360 to 0.9 ± 2.0 episodes per month).

25.7.10 Mapping and Ablation of Hemodynamically Unstable VT

As described above, conventional mapping is not feasible for unstable ventricular arrhythmias. Several groups have published series on the use of substrate mapping during sinus rhythm and noncontact mapping of unstable VT followed by rapid termination.

25.7.10.1 Electroanatomic Mapping

Marchlinski et al. used the CARTO system to produce voltage maps of the LV with the creation of linear ablation lines from areas of dense scar (defined by a voltage amplitude of <0.5 mV) to areas of normal endocardium or anatomic boundaries [37]. In addition, ECG morphology during VT and pacemapping in SR guided sites of ablation. Nine of 16 patients had VT in the context of healed MI, and the remaining had dilated cardiomyopathy. Thirteen patients had poorly tolerated VT and of these, seven had VT-inducible post-ablation, five of which were fast VT only. All patients had ICDs, and during follow-up of median 8 months (range 3–36), only two patients with unstable VT had a recurrence, giving a success rate in this subset of 85%. Up to 87 RF lesions were required per patient, mean 54.6 ± 24.1 per patient.

Arenal et al. studied 18 patients considered to have unmappable VT, either because the target VT was not inducible or the target VT was not tolerated [38]. A further six patients with well-tolerated VT were studied to enable activation mapping and entrainment for comparison. The authors hypothesized that low-amplitude electrograms with an isolated, delayed component (E-IDC) along scar border were more specific for VT isthmus' slow conduction than low-amplitude electrograms alone (commonly found along scar border). Such electrograms were characterized by double or multiple components separated by very-low-amplitude signals and could be found in sinus rhythm. Again, the CARTO system was used to generate voltage maps (complete scar defined as voltage ≤0.1 mV, dense scar as voltage ≥0.1 mV and ≤0.5 mV), and E-IDC located during SR or RVA pacing were marked on the map for rapid location, with areas up to 1 cm around these sites then explored and labeled. When complete, pacemapping was performed starting at sites with the latest isolated, delayed component (E-LIDC) and moving to adjacent sites when pacemapping was not identical to clinical VT. Attempts at VT induction were performed at E-IDC sites with an identical pacematch, to look for presystolic or mid-diastolic electrograms during VT and to examine the stimulus-to-QRS interval. Concealed entrainment was attempted when the VT was sufficiently well tolerated. Ablation was then performed at all sites with E-IDC at which pacemapping reproduced the target VT and the stimulus-to-QRS interval was ≥50 ms, or at any E-IDC site that became mid-diastolic during VT. Between 1 and 35 RF lesions were applied per patient, and none of the six patients with hemodynamically unstable VT was inducible after ablation. Of the 18 patients with unmappable VT, two patients had a recurrence of their clinical VT during follow-up and a further five patients had a recurrence of a previously unrecorded VT.

Most recently, Brunckhorst et al. have used another marker of slow conduction to help identify targets for VT ablation during sinus rhythm [39]. Twelve patients were studied in whom 51 VT were inducible. All clinical VT were resistant to drug therapy causing ICD shocks in all. Stimulus-to-QRS interval (S-QRS) delays were analyzed during pacemapping at multiple areas in the left ventricle. Pacing was performed at 890 sites (74 ± 23 per patient) of which 93% of sites achieved capture. There was no S-QRS delay at 56% of pacing sites, a delay of ≥40 ms at 44%, and a delay of ≥80 ms at 15% of sites, the latter two groups usually being clustered together. The areas of conduction delay were compared to locations of target areas (areas within 2 cm of a reentrant isthmus, defined by entrainment and ablation) and overlapped in 13 of 14 cases. Sites with a delay ≥80 ms were more frequently in a target area, although a close pacematch was only seen in 41% of sites in these areas and an exact match in only 9%. Furthermore, 46% of sites with a close pacing match were outside the target area, emphasizing the limitations of pacemapping of VT in patients with structural heart disease. Ablation was performed at a mean of 10 ± 3 sites in the target area, rendering seven patients non-inducible at the end of the procedure and at least one VT was abolished in a further five patients. Over 6 months follow-up, three patients died and VT recurred at the time of death in two of these patients. The remaining nine patients remained free from VT despite a mean of 18 ± 16 VT episodes in the 6 months prior to ablation.

Although having limitations, these techniques have allowed the treatment of patients deemed unsuitable for conventional ablation. They have also improved our understanding of the subtleties of the underlying substrate that support scar-related VT.

25.7.10.2 Noncontact Mapping

Della Bella et al. have reported on the use of noncontact mapping to guide ablation of hemodynamically unstable VT in 17 patients, of whom 11 had infarct-related VT [117]. VT was induced and terminated after 15–20 s, and activation analyzed off-line. Ablation was performed in SR either by a line across the diastolic pathway (DP) (if identified) or around the exit point. If the patient was non-inducible at the end of the procedure, an ICD was not implanted. Separating out the different underlying etiologies, an exit point was defined in all 21 post-MI VT and DP activity identified in 17 (80%). Successful ablation was achieved in 67% of VT and in 53% of patients, with a partial success in one further patient. Ablation was not performed, or was unsuccessful in 42% of patients, and importantly, the success rate of ablation was higher with linear lesions across the DP (78%) compared with encircling lesions around the exit (16%).

During follow-up, seven out of nine successfully ablated patients remained free from arrhythmia recurrence, as did the patient with a partial success, and all remained free of the target VT. ICD shock frequency was significantly reduced. The results from this study demonstrate that noncontact-mapping-guided ablation of unstable VT is feasible with success highly dependent on the identification of DP activity, as with stable VT [44]. However, in patients with frequent ICD shocks from rapid, hemodynamically unstable VT, this technology does provide a therapeutic option if drug therapy is limited.

25.7.11 Epicardial Mapping of VT

Access to the epicardium can be obtained either from the coronary sinus and its tributaries, through the coronary arteries, or through direct pericardial puncture. The use of multipolar electrodes in the former can help facilitate positioning of endocardial catheters [118]. Intracoronary guide-wire mapping using standard angioplasty guidewires recording unipolar signals has also been reported to guide intracoronary ethanol ablation [126]. Pericardial puncture with direct epicardial mapping was originally described in the treatment of VT in the context of Chagasic heart disease [120]. However, it has now been used successfully in conjunction with substrate mapping of the endocardium in infarct-related VT [121, 122].

25.8 Conclusions

Intracardiac mapping has revolutionized our understanding of the mechanisms of abnormal arrhythmias and led directly to curative procedures in the majority through ablation. Intracardiac mapping techniques are based on analysis of electrogram timing (and, in some cases, morphology) during sinus rhythm, pacing, and during tachycardia in conjunction with morphological features and timing of surface ECG features. Conventional diagnostic electrophysiology is further based on three basic types of mapping: activation mapping, pacemapping, and entrainment. Complex mapping systems now exist that enable mapping of electrophysiological data from an entire cardiac chamber or from a single beat of tachycardia, so that previously "unmappable" rhythms may now be successfully treated.

References

1. Scherlag, B.J., S.H. Lau, R.H. Helfant, et al., Catheter technique for recording His bundle activity in man. *Circulation*, 1969;**39**: 13–18.
2. Durrer, D., L. Schoo, R.M. Schuilenburg, et al., The role of premature beats in the initiation and the termination of supraventricular tachycardia in the Wolff-Parkinson-White syndrome. *Circulation*, 1967;**36**: 644–662.
3. Wellens, H.J., R.M. Schuilenburg, and D. Durrer, Electrical stimulation of the heart in patients with ventricular tachycardia. *Circulation*, 1972;**46**: 216–226.
4. Josephson, M.E., L.N. Horowitz, and A. Farshidi, Continuous local electrical activity. A mechanism of recurrent ventricular tachycardia. *Circulation*, 1978;**57**: 659–665.
5. Cassidy, D.M., J.A. Vassallo, J.M. Miller, et al., Endocardial catheter mapping in patients in sinus rhythm: Relationship to underlying heart disease and ventricular arrhythmias. *Circulation*, 1986;**73**: 645–652.
6. Cassidy, D.M., J.A. Vassallo, A.E. Buxton et al., Catheter mapping during sinus rhythm: relation of local electrogram duration to ventricular tachycardia cycle length. *Am. J. Cardiol.*, 1985;**55**: 713–716.

7. Cassidy, D.M., J.A. Vassallo, A.E. Buxton, et al., The value of catheter mapping during sinus rhythm to localize site of origin of ventricular tachycardia. *Circulation*, 1984;**69**: 1103–1110.
8. Wong, T., W. Hussain, V. Markides, et al., Ablation of difficult right-sided accessory pathways aided by mapping of tricuspid annular activation using a Halo catheter: Halo-mapping of right sided accessory pathways. *J. Interv. Card. Electrophysiol.*, 2006;**16**: 175–182.
9. Stevenson, W.G., P.T. Sager, P.D. Natterson, et al., Relation of pace mapping QRS configuration and conduction delay to ventricular tachycardia reentry circuits in human infarct scars. *J. Am. Coll. Cardiol.*, 1995;**26**: 481–488.
10. Liu, T.Y., C.T. Tai, B.H. Huang, et al., Functional characterization of the crista terminalis in patients with atrial flutter: implications for radiofrequency ablation. *J. Am. Coll. Cardiol.*, 2004;**43**: 1639–1645.
11. Peters, N.S., J. Coromilas, M.S. Hanna, et al., Characteristics of the temporal and spatial excitable gap in anisotropic reentrant circuits causing sustained ventricular tachycardia. *Circ. Res.*, 1998;**82**: 279–293.
12. Almendral, J.M., N.J. Stamato, M.E. Rosenthal, et al., Resetting response patterns during sustained ventricular tachycardia: relationship to the excitable gap. *Circulation*, 1986;**74**: 722–730.
13. Almendral, J.M., M.E. Rosenthal, N.J. Stamato, et al., Analysis of the resetting phenomenon in sustained uniform ventricular tachycardia: incidence and relation to termination. *J. Am. Coll. Cardiol.*, 1986;**8**: 294–300.
14. Rosenthal, M.E., N.J. Stamato, J.M. Almendral, et al., Resetting of ventricular tachycardia with electrocardiographic fusion: incidence and significance. *Circulation*, 1988;**77**: 581–588.
15. Almendral, J.M., C.D. Gottlieb, M.E. Rosenthal, et al., Entrainment of ventricular tachycardia: explanation for surface electrocardiographic phenomena by analysis of electrograms recorded within the tachycardia circuit. *Circulation*, 1988;**77**: 569–580.
16. MacLean, W.A., V.J. Plumb, and A.L. Waldo, Transient entrainment and interruption of ventricular tachycardia. *Pacing Clin. Electrophysiol.*, 1981;**4**: 358–366.
17. Waldo, A.L., V.J. Plumb, J.G. Arciniegas, et al., Transient entrainment and interruption of the atrioventricular bypass pathway type of paroxysmal atrial tachycardia. A model for understanding and identifying reentrant arrhythmias. *Circulation*, 1983;**67**: 73–83.
18. Waldo, A.L., W.A. MacLean, R.B. Karp, et al., Entrainment and interruption of atrial flutter with atrial pacing: studies in man following open heart surgery. *Circulation*, 1977;**56**: 737–745.
19. Henthorn, R.W., V.J. Plumb, J.G. Arciniegas, et al., Entrainment of "ectopic atrial tachycardia": evidence for re-entry. *Am. J. Cardiol.*, 1982;**49**: 920.
20. Brugada, P., A.L. Waldo, and H.J. Wellens, Transient entrainment and interruption of atrioventricular node tachycardia. *J. Am. Coll. Cardiol.*, 1987;**9**: 769–775.
21. Henthorn, R.W., K. Okumura, B. Olshansky, et al., A fourth criterion for transient entrainment: the electrogram equivalent of progressive fusion. *Circulation*, 1988;**77**: 1003–1012.
22. Okumura, K., B. Olshansky, R.W. Henthorn, et al., Demonstration of the presence of slow conduction during sustained ventricular tachycardia in man: use of transient entrainment of the tachycardia. *Circulation*, 1987;**75**: 369–378.
23. Waldo, A.L., R.W. Henthorn, V.J. Plumb, et al., Demonstration of the mechanism of transient entrainment and interruption of ventricular tachycardia with rapid atrial pacing. *J. Am. Coll. Cardiol.*, 1984;**3**: 422–430.
24. Waldo, A.L. and R.W. Henthorn, Use of transient entrainment during ventricular tachycardia to localize a critical area in the reentry circuit for ablation. *Pacing Clin. Electrophysiol.*, 1989;**12**: 231–244.
25. Portillo, B., J. Mejias, N. Leon-Portillo, et al., Entrainment of atrioventricular nodal reentrant tachycardias during overdrive pacing from high right atrium and coronary sinus. With special reference to atrioventricular dissociation and 2:1 retrograde block during tachycardias. *Am. J. Cardiol.*, 1984;**53**: 1570–1576.
26. Okumura, K., R.W. Henthorn, A.E. Epstein, et al., Further observations on transient entrainment: importance of pacing site and properties of the components of the reentry circuit. *Circulation*, 1985;**72**: 1293–1307.
27. Stevenson, W.G., H. Khan, P. Sager, et al., Identification of reentry circuit sites during catheter mapping and radiofrequency ablation of ventricular tachycardia late after myocardial infarction. *Circulation*, 1993;**88**: 1647–1670.
28. Gepstein, L., G. Hayam, and S.A. Ben Haim, A novel method for nonfluoroscopic catheter-based electroanatomical mapping of the heart. In vitro and in vivo accuracy results. *Circulation*, 1997;**95**: 1611–1622.
29. Wittkampf, F.H., E.F. Wever, R. Derksen, et al., LocaLisa: new technique for real-time 3-dimensional localization of regular intracardiac electrodes. *Circulation*, 1999;**99**: 1312–1317.
30. de Groot, N., M. Bootsma, E.T. van der Velde, et al., Three-dimensional catheter positioning during radiofrequency ablation in patients: first application of a real-time position management system. *J. Cardiovasc. Electrophysiol.*, 2000;**11**: 1183–1192.
31. Ventura, R., T. Rostock, H.U. Klemm, et al., Catheter ablation of common-type atrial flutter guided by three-dimensional right atrial geometry reconstruction and catheter tracking using cutaneous patches: a randomized prospective study. *J. Cardiovasc. Electrophysiol.*, 2004;**15**: 1157–1161.
32. Kottkamp, H., G. Hindricks, G. Breithardt, et al., Three-dimensional electromagnetic catheter technology: electroanatomical mapping of the right atrium and ablation of ectopic atrial tachycardia. *J. Cardiovasc. Electrophysiol.*, 1997;**8**: 1332–1337.
33. Marchlinski, F., D. Callans, C. Gottlieb, et al., Magnetic electroanatomical mapping for ablation of focal atrial tachycardias. *Pacing Clin. Electrophysiol.*, 1998;**21**: 1621–1635.
34. Nakagawa, H. and W.M. Jackman, Use of a three-dimensional, nonfluoroscopic mapping system for catheter ablation of typical atrial flutter. *Pacing Clin. Electrophysiol.*, 1998;**21**: 1279–1286.
35. Worley, S.J., Use of a real-time three-dimensional magnetic navigation system for radiofrequency ablation of accessory pathways. *Pacing Clin. Electrophysiol.*, 1998;**21**: 1636–1645.
36. Soejima, K., M. Suzuki, W.H. Maisel, et al., Catheter ablation in patients with multiple and unstable ventricular tachycardias after myocardial infarction: short ablation lines guided by reentry circuit isthmuses and sinus rhythm mapping. *Circulation*, 2001;**104**: 664–669.
37. Marchlinski, F.E., D.J. Callans, C.D. Gottlieb, et al., Linear ablation lesions for control of unmappable ventricular tachycardia in patients with ischemic and nonischemic cardiomyopathy. *Circulation*, 2000;**101**: 1288–1296.

38. Arenal, A., E. Glez-Torrecilla, M. Ortiz, et al., Ablation of electrograms with an isolated, delayed component as treatment of unmappable monomorphic ventricular tachycardias in patients with structural heart disease. *J. Am. Coll. Cardiol.*, 2003;**41**: 81–92.
39. Brunckhorst, C.B., W.G. Stevenson, K. Soejima, et al., Relationship of slow conduction detected by pace-mapping to ventricular tachycardia re-entry circuit sites after infarction. *J. Am. Coll. Cardiol.*, 2003;**41**: 802–809.
40. Leonelli, F.M., G. Tomassoni, M. Richey, et al., Usefulness of three-dimensional non-fluoroscopic mapping in the ablation of typical atrial flutter. *Ital. Heart J.*, 2002;**3**: 360–365.
41. Leonelli, F.M., G. Tomassoni, M. Richey, et al., Ablation of incisional atrial tachycardias using a three-dimensional nonfluoroscopic mapping system. *Pacing Clin. Electrophysiol.*, 2001;**24**: 1653–1659.
42. Natale, A., L. Breeding, G. Tomassoni, et al., Ablation of right and left ectopic atrial tachycardias using a three-dimensional nonfluoroscopic mapping system. *Am. J. Cardiol.*, 1998;**82**: 989–992.
43. Macle, L., P. Jais, C. Scavee, et al., Pulmonary vein disconnection using the LocaLisa three-dimensional nonfluoroscopic catheter imaging system. *J. Cardiovasc. Electrophysiol.*, 2003;**14**: 693–697.
44. Schilling, R.J., N.S. Peters, and D.W. Davies, Feasibility of a noncontact catheter for endocardial mapping of human ventricular tachycardia. *Circulation*, 1999;**99**: 2543–2552.
45. Schalij, M.J., F.P. van Rugge, M. Siezenga, et al., Endocardial activation mapping of ventricular tachycardia in patients: first application of a 32-site bipolar mapping electrode catheter. *Circulation*, 1998;**98**: 2168–2179.
46. Aiba, T., W. Shimizu, A. Taguchi, et al., Clinical usefulness of a multielectrode basket catheter for idiopathic ventricular tachycardia originating from right ventricular outflow tract. *J. Cardiovasc. Electrophysiol.*, 2001;**12**: 511–517.
47. Eldar, M., D.G. Ohad, A.J. Greenspon, et al., Percutaneous multielectrode endocardial mapping and ablation of ventricular tachycardia in the swine model. *Adv. Exp. Med. Biol.*, 1997;**430**: 313–321.
48. Yamane, T., S. Miyanaga, K. Inada, et al., A focal source of atrial fibrillation in the superior vena cava: isolation and elimination by radiofrequency ablation with the guide of basket catheter mapping. *J. Interv. Card. Electrophysiol.*, 2004;**11**: 131–134.
49. Nishida, K., A. Fujiki, H. Nagasawa, et al., Complex atrial reentrant circuits evaluated by entrainment mapping using a multielectrode basket catheter. *Circ. J.*, 2004;**68**: 168–171.
50. Zrenner, B., G. Ndrepepa, M.A. Schneider, et al., Mapping and ablation of atrial arrhythmias after surgical correction of congenital heart disease guided by a 64-electrode basket catheter. *Am. J. Cardiol.*, 2001;**88**: 573–578.
51. Yoshida, Y., M. Hirai, Y. Murakami, et al., Localization of precise origin of idiopathic ventricular tachycardia from the right ventricular outflow tract by a 12-lead ECG: a study of pace mapping using a multielectrode "basket" catheter. *Pacing Clin. Electrophysiol.*, 1999;**22**: 1760–1768.
52. Sigl, R., *Introduction to Potential Theory: Fundamental Mathematical and Physical Topics for the Study of Physical Geodesy*. Tunbridge Wells: Abacus Press, 1973.
53. Plonsey, R., An extension of the solid angle potential formulation for an active cell. *Biophys. J.*, 1965;**5**: 663–667.
54. Scher, A. and M. Spach, Cardiac depolarization and repolarization and the electrogram, in *Handbook of Physiology*, R.M. Berne, Editor. Bethesda, MD: American Physiological Society, 1979, p. 37.
55. Colli-Franzone, P., L. Guerri, C. Viganotti, et al., Potential fields generated by oblique dipole layers modeling excitation wavefronts in the anisotropic myocardium. Comparison with potential fields elicited by paced dog hearts in a volume conductor. *Circ. Res.*, 1982;**51**: 330–346.
56. Segal, O.R., A.W. Chow, V. Markides, et al., Long-term results after ablation of infarct-related ventricular tachycardia. *Heart Rhythm*, 2005;**2**: 474–482.
57. Betts, T.R., P.R. Roberts, S.A. Allen, et al., Radiofrequency ablation of idiopathic left ventricular tachycardia at the site of earliest activation as determined by noncontact mapping. *J. Cardiovasc. Electrophysiol.*, 2000;**11**: 1094–1101.
58. Chen, M., B. Yang, J. Zou, et al., Non-contact mapping and linear ablation of the left posterior fascicle during sinus rhythm in the treatment of idiopathic left ventricular tachycardia. *Europace*, 2005;**7**: 138–144.
59. Segal, O.R., V. Markides, P. Kanagaratnam, et al., Multiple distinct right atrial endocardial origins in a patient with atrial tachycardia: mapping and ablation using noncontact mapping. *Pacing Clin. Electrophysiol.*, 2004;**27**: 541–544.
60. Tai, C.T., T.Y. Liu, P.C. Lee, et al., Non-contact mapping to guide radiofrequency ablation of atypical right atrial flutter. *J. Am. Coll. Cardiol.*, 2004;**44**: 1080–1086.
61. Schneider, M.A., G. Ndrepepa, B. Zrenner, et al., Noncontact mapping-guided catheter ablation of atrial fibrillation associated with left atrial ectopy. *J. Cardiovasc. Electrophysiol.*, 2000;**11**: 475–479.
62. Markides, V., R.J. Schilling, A.W.C. Chow, P. Kanagaratnam, D. Lamb, N.S. Peters, and D.W. Davies, Non-contact mapping of the human left atrium to guide ablation of focal atrial fibrillation. *Circulation*, 2000;**102**(18 Suppl. II): 575.
63. Schilling, R.J., A.H. Kadish, N.S. Peters, et al., Endocardial mapping of atrial fibrillation in the human right atrium using a non-contact catheter. *Eur. Heart J.*, 2000;**21**: 550–564.
64. Schilling, R.J., N.S. Peters, J. Goldberger, et al., Characterization of the anatomy and conduction velocities of the human right atrial flutter circuit determined by noncontact mapping. *J. Am. Coll. Cardiol.*, 2001;**38**: 385–393.
65. Schumacher, B., W. Jung, T. Lewalter, et al., Verification of linear lesions using a noncontact multielectrode array catheter versus conventional contact mapping techniques. *J. Cardiovasc. Electrophysiol.*, 1999;**10**: 791–798.
66. Betts, T.R., P.R. Roberts, S.A. Allen, et al., Electrophysiological mapping and ablation of intra-atrial reentry tachycardia after Fontan surgery with the use of a noncontact mapping system. *Circulation*, 2000;**102**: 419–425.
67. Miles, W.M., R. Yee, G.J. Klein, et al., The preexcitation index: an aid in determining the mechanism of supraventricular tachycardia and localizing accessory pathways. *Circulation*, 1986;**74**: 493–500.
68. Michaud, G.F., H. Tada, S. Chough et al., Differentiation of atypical atrioventricular node re-entrant tachycardia from orthodromic reciprocating tachycardia using a septal accessory pathway by the response to ventricular pacing. *J. Am. Coll. Cardiol.*, 2001;**38**: 1163–1167.
69. Gonzalez-Torrecilla, E., A. Arenal, F. Atienza, et al., First postpacing interval after tachycardia entrainment with correction for atrioventricular node delay: a simple maneuver for differential diagnosis of atrioventricular nodal reentrant tachycardias

versus orthodromic reciprocating tachycardias. *Heart Rhythm*, 2006;**3**: 674–679.
70. Haissaguerre, M., F. Gaita, B. Fischer, et al., Elimination of atrioventricular nodal reentrant tachycardia using discrete slow potentials to guide application of radiofrequency energy [see comments]. *Circulation*, 1992;**85**: 2162–2175.
71. Jackman, W.M., K.J. Beckman, J.H. McClelland, et al., Treatment of supraventricular tachycardia due to atrioventricular nodal reentry, by radiofrequency catheter ablation of slow-pathway conduction. *N. Engl. J. Med.*, 1992;**327**: 313–318.
72. Jazayeri, M.R., S.L. Hempe, J.S. Sra, et al., Selective transcatheter ablation of the fast and slow pathways using radiofrequency energy in patients with atrioventricular nodal reentrant tachycardia [see comments]. *Circulation*, 1992;**85**: 1318–1328.
73. Wathen, M., A. Natale, K. Wolfe, et al., An anatomically guided approach to atrioventricular node slow pathway ablation. *Am. J. Cardiol.*, 1992;**70**: 886–889.
74. Hintringer, F., J. Hartikainen, D.W. Davies, et al., Prediction of atrioventricular block during radiofrequency ablation of the slow pathway of the atrioventricular node. *Circulation*, 1995;**92**: 3490–3496.
75. Jentzer, J.H., R. Goyal, B.D. Williamson, et al., Analysis of junctional ectopy during radiofrequency ablation of the slow pathway in patients with atrioventricular nodal reentrant tachycardia. *Circulation*, 1994;**90**: 2820–2826.
76. Willems, S., H. Shenasa, H. Kottkamp, et al., Temperature-controlled slow pathway ablation for treatment of atrioventricular nodal reentrant tachycardia using a combined anatomical and electrogram guided strategy. *Eur. Heart J.*, 1996;**17**: 1092–1102.
77. Poret, P., C. Leclercq, D. Gras, et al., Junctional rhythm during slow pathway radiofrequency ablation in patients with atrioventricular nodal reentrant tachycardia: beat-to-beat analysis and its prognostic value in relation to electrophysiologic and anatomic parameters. *J. Cardiovasc. Electrophysiol.*, 2000;**11**: 405–412.
78. Schumacher, B., J. Tebbenjohanns, D. Pfeiffer, et al., Junctional arrhythmias in radiofrequency modification of the atrioventricular node. *Z. Kardiol.*, 1995;**84**: 977–985.
79. Lipscomb, K.J., A.M. Zaidi, A.P. Fitzpatrick, et al., Slow pathway modification for atrioventricular node re-entrant tachycardia: fast junctional tachycardia predicts adverse prognosis. *Heart*, 2001;**85**: 44–47.
80. Iturralde, P., V. Araya-Gomez, L. Colin, et al., A new ECG algorithm for the localization of accessory pathways using only the polarity of the QRS complex. *J. Electrocardiol.*, 1996;**29**: 289–299.
81. d'Avila, A., J. Brugada, V. Skeberis, et al., A fast and reliable algorithm to localize accessory pathways based on the polarity of the QRS complex on the surface ECG during sinus rhythm. *Pacing Clin. Electrophysiol.*, 1995;**18**: 1615–1627.
82. Xie, B., S.C. Heald, Y. Bashir, et al., Localization of accessory pathways from the 12-lead electrocardiogram using a new algorithm. *Am. J. Cardiol.*, 1994;**74**: 161–165.
83. Arruda, M.S., J.H. McClelland, X. Wang, et al., Development and validation of an ECG algorithm for identifying accessory pathway ablation site in Wolff-Parkinson-White syndrome. *J. Cardiovasc. Electrophysiol.*, 1998;**9**: 2–12.
84. Chiang, C.E., S.A. Chen, W.S. Teo, et al., An accurate stepwise electrocardiographic algorithm for localization of accessory pathways in patients with Wolff-Parkinson-White syndrome from a comprehensive analysis of delta waves and R/S ratio during sinus rhythm. *Am. J. Cardiol.*, 1995;**76**: 40–46.
85. Fitzpatrick, A.P., R.P. Gonzales, M.D. Lesh, et al., New algorithm for the localization of accessory atrioventricular connections using a baseline electrocardiogram [published erratum appears in *J. Am. Coll. Cardiol.* 1994 Apr;23(5):1272]. *J. Am. Coll. Cardiol.*, 1994;**23**: 107–116.
86. Diker, E., M. Ozdemir, U.K. Tezcan, et al., QRS polarity on 12-lead surface ECG. A criterion for the differentiation of right and left posteroseptal accessory atrioventricular pathways. *Cardiology*, 1997;**88**: 328–332.
87. Jackman, W.M., X.Z. Wang, K.J. Friday, et al., Catheter ablation of accessory atrioventricular pathways (Wolff-Parkinson-White syndrome) by radiofrequency current. *N. Engl. J. Med.*, 1991;**324**: 1605–1611.
88. Feld, G.K., M. Mollerus, U. Birgersdotter-Green, et al., Conduction velocity in the tricuspid valve-inferior vena cava isthmus is slower in patients with type I atrial flutter compared to those without a history of atrial flutter. *J. Cardiovasc. Electrophysiol.*, 1997;**8**: 1338–1348.
89. Nakagawa, H., R. Lazzara, T. Khastgir, et al., Role of the tricuspid annulus and the eustachian valve/ridge on atrial flutter. Relevance to catheter ablation of the septal isthmus and a new technique for rapid identification of ablation success [see comments]. *Circulation*, 1996;**94**: 407–424.
90. Olgin, J.E., J.M. Kalman, L.A. Saxon, et al., Mechanism of initiation of atrial flutter in humans: site of unidirectional block and direction of rotation. *J. Am. Coll. Cardiol.*, 1997;**29**: 376–384.
91. Saoudi, N., F. Cosio, A. Waldo, et al., A classification of atrial flutter and regular atrial tachycardia according to electrophysiological mechanisms and anatomical bases; a Statement from a Joint Expert Group from The Working Group of Arrhythmias of the European Society of Cardiology and the North American Society of Pacing and Electrophysiology. *Eur. Heart J.*, 2001;**22**: 1162–1182.
92. Feld, G.K., R.P. Fleck, P.S. Chen, et al., Radiofrequency catheter ablation for the treatment of human type 1 atrial flutter. Identification of a critical zone in the reentrant circuit by endocardial mapping techniques [see comments]. *Circulation*, 1992;**86**: 1233–1240.
93. Chen, S.A., C.T. Tai, C.E. Chiang, et al., Focal atrial tachycardia: reanalysis of the clinical and electrophysiologic characteristics and prediction of successful radiofrequency ablation. *J. Cardiovasc. Electrophysiol.*, 1998;**9**: 355–365.
94. Haissaguerre, M., P. Jais, D.C. Shah, et al., Spontaneous initiation of atrial fibrillation by ectopic beats originating in the pulmonary veins. *N. Engl. J. Med.*, 1998;**339**: 659–666.
95. Pappone, C., S. Rosanio, G. Oreto, et al., Circumferential radiofrequency ablation of pulmonary vein ostia: a new anatomic approach for curing atrial fibrillation. *Circulation*, 2000;**102**: 2619–2628.
96. Cox, J.L., R.B. Schuessler, D.G. Lappas, et al., An 8 1/2-year clinical experience with surgery for atrial fibrillation. *Ann. Surg.*, 1996;**224**: 267–273.
97. Nademanee, K., J. McKenzie, E. Kosar, et al., A new approach for catheter ablation of atrial fibrillation: mapping of the electrophysiologic substrate. *J. Am. Coll. Cardiol.*, 2004;**43**: 2044–2053.
98. Lau, C.P., H.F. Tse, and G.M. Ayers, Defibrillation-guided radiofrequency ablation of atrial fibrillation secondary to an atrial focus. *J. Am. Coll. Cardiol.*, 1999;**33**: 1217–1226.

99. Lee, S.H., C.T. Tai, W.S. Lin, et al., Predicting the arrhythmogenic foci of atrial fibrillation before atrial transseptal procedure: implication for catheter ablation [In Process Citation]. *J. Cardiovasc. Electrophysiol.*, 2000;**11**: 750–757.
100. Morady, F., L.A. Dicarlo Jr., L.B. Liem, et al., Effects of high stimulation current on the induction of ventricular tachycardia. *Am. J. Cardiol.*, 1985;**56**: 73–78.
101. Doherty, J.U., M.G. Kienzle, H.L. Waxman, et al., Programmed ventricular stimulation at a second right ventricular site: an analysis of 100 patients, with special reference to sensitivity, specificity and characteristics of patients with induced ventricular tachycardia. *Am. J. Cardiol.*, 1983;**52**: 1184–1189.
102. Herre, J.M., D.E. Mann, J.C. Luck, et al., Effect of increased current, multiple pacing sites and number of extrastimuli on induction of ventricular tachycardia. *Am. J. Cardiol.*, 1986;**57**: 102–107.
103. Lerman, B.B., K. Stein, E.D. Engelstein, et al., Mechanism of repetitive monomorphic ventricular tachycardia. *Circulation*, 1995;**92**: 421–429.
104. Lerman, B.B., L. Belardinelli, G.A. West, et al., Adenosine-sensitive ventricular tachycardia: evidence suggesting cyclic AMP-mediated triggered activity. *Circulation*, 1986;**74**: 270–280.
105. Jadonath, R.L., D.S. Schwartzman, M.W. Preminger, et al., Utility of the 12-lead electrocardiogram in localizing the origin of right ventricular outflow tract tachycardia. *Am. Heart J.*, 1995;**130**: 1107–1113.
106. Dixit, S., E.P. Gerstenfeld, D.J. Callans, et al., Electrocardiographic patterns of superior right ventricular outflow tract tachycardias: distinguishing septal and free-wall sites of origin. *J. Cardiovasc. Electrophysiol.*, 2003;**14**: 1–7.
107. Tchou, P., M. Jazayeri, S. Denker, et al., Transcatheter electrical ablation of right bundle branch. A method of treating macroreentrant ventricular tachycardia attributed to bundle branch reentry. *Circulation*, 1988;**78**: 246–257.
108. Kuchar, D.L., J.N. Ruskin, and H. Garan, Electrocardiographic localization of the site of origin of ventricular tachycardia in patients with prior myocardial infarction. *J. Am. Coll. Cardiol.*, 1989;**13**: 893–903.
109. Miller, J.M., F.E. Marchlinski, A.E. Buxton, et al., Relationship between the 12-lead electrocardiogram during ventricular tachycardia and endocardial site of origin in patients with coronary artery disease. *Circulation*, 1988;**77**: 759–766.
110. Segal, O.R., A.W. Chow, T. Wong, et al., A novel algorithm for determining endocardial VT exit site from 12 lead surface ECG characteristics in human, infarct-related ventricular tachycardia. *J. Cardiovasc. Electrophysiol.*, 2007;**18**: 161–168.
111. Callans, D.J., M. Zardini, C.D. Gottlieb, et al., The variable contribution of functional and anatomic barriers in human ventricular tachycardia: an analysis with resetting from two sites. *J. Am. Coll. Cardiol.*, 1996;**27**: 1106–1111.
112. Ciaccio, E.J., M.M. Scheinman, V. Fridman, et al., Dynamic changes in electrogram morphology at functional lines of block in reentrant circuits during ventricular tachycardia in the infarcted canine heart: a new method to localize reentrant circuits from electrogram features using adaptive template matching. *J. Cardiovasc. Electrophysiol.*, 1999;**10**: 194–213.
113. Morady, F., A. Kadish, S. Rosenheck, et al., Concealed entrainment as a guide for catheter ablation of ventricular tachycardia in patients with prior myocardial infarction. *J. Am. Coll. Cardiol.*, 1991;**17**: 678–689.
114. El Shalakany, A., T. Hadjis, P. Papageorgiou, et al., Entrainment/mapping criteria for the prediction of termination of ventricular tachycardia by single radiofrequency lesion in patients with coronary artery disease. *Circulation*, 1999;**99**: 2283– 2289.
115. Strickberger, S.A., B.P. Knight, G.F. Michaud, et al., Mapping and ablation of ventricular tachycardia guided by virtual electrograms using a noncontact, computerized mapping system. *J. Am. Coll. Cardiol.*, 2000;**35**: 414–421.
116. Wilber, D.J., D.E. Kopp, D.N. Glascock, et al., Catheter ablation of the mitral isthmus for ventricular tachycardia associated with inferior infarction. *Circulation*, 1995;**92**: 3481–3489.
117. Della, B.P., R. De Ponti, J.A. Uriarte, et al., Catheter ablation and antiarrhythmic drugs for haemodynamically tolerated post-infarction ventricular tachycardia; long-term outcome in relation to acute electrophysiological findings. *Eur. Heart J.*, 2002;**23**: 414–424.
118. de Paola, A.A., W.D. Melo, M.Z. Tavora, et al., Angiographic and electrophysiological substrates for ventricular tachycardia mapping through the coronary veins. *Heart*, 1998;**79**: 59–63.
119. Wong, T., A.W. Chow, V. Markides, R.J. Schilling, N.S. Peters, and D.W. Davies, Human ventricular tachycardia ablation guided by intracoronary artery guide-wire mapping. *Pacing Clin. Electrophysiol.*, 2002;**25**: 524.
120. Sosa, E., M. Scanavacca, A. d'Avila, et al., Endocardial and epicardial ablation guided by nonsurgical transthoracic epicardial mapping to treat recurrent ventricular tachycardia. *J. Cardiovasc. Electrophysiol.*, 1998;**9**: 229–239.
121. Cesario, D.A., M. Vaseghi, N.G. Boyle, et al., Value of high-density endocardial and epicardial mapping for catheter ablation of hemodynamically unstable ventricular tachycardia. *Heart Rhythm*, 2006;**3**: 1–10.
122. Schweikert, R.A., W.I. Saliba, G. Tomassoni, et al., Percutaneous pericardial instrumentation for endo-epicardial mapping of previously failed ablations. *Circulation*, 2003;**108**: 1329–1335.
123. Segal, O.R., A.W. Chow, N.S. Peters and D.W. Davies, Mechanisms that initiate ventricular tachycardia in the infarcted human heart. *Heart Rhythm*, 2010;**7**: 57–64.
124. Segal, O.R., A.W. Chow, V. Markides, D.W. Davies and N.S. Peters, Characterisation of the effects of single ventricular extrastimuli on endocardial activation in human, infarct-related ventricular tachycardia. *J. Am. Coll. Cardiol.*, 2007;**49**: 1315–1323.
125. Segal, O.R., L.J. Gula, A.C. Skanes, A.D. Krahn, R. Yee and G.J. Klein, Differential ventricular entrainment – a maneuver to differentiate AV node reentrant tachycardia from orthodromic reciprocating tachycardia. *Heart Rhythm*, 2009;**6**: 493–500.
126. Segal, O.R., T. Wong, A.W. Chow, J. Jarman, R.J. Schilling, V. Markides, N.S. Peters and D.W. Davies, Intra-coronary guidewire mapping – A novel technique to guide ablation of human ventricular tachycardia. *J. Interv. Card. Electrophysiol.*, 2007;**18**: 143–154.

26 Sinus and Atrial Arrhythmias

F. Russell Quinn · Andrew D. McGavigan · Andrew C. Rankin

P. W. Macfarlane, A. van Oosterom, O. Pahlm, P. Kligfield, M. Janse, J. Camm (eds.), *Comprehensive Electrocardiology*, DOI 10.1007/978-1-84882-046-3_26,

26.1 Introduction

Although rarely fatal, disorders of sinus node function and atrial arrhythmias are causes of much morbidity. They are the most common causes of clinical bradyarrhythmias and tachyarrhythmias, respectively. Sinus node dysfunction accounts for over half of permanent pacemaker implants worldwide [1], while atrial fibrillation occurs secondary to the progression of most cardiac conditions [2]. The sinus node and the atrium are closely related, both anatomically and functionally, and disorders of one interfere with the functioning of the other. This fact is of particular relevance to the electrocardiographic study of sinus and atrial activity.

The electrocardiographic diagnosis both of sinus disorders and atrial arrhythmias depends on the P wave as evidence of atrial activation, since sinus node activity itself is not recorded on the surface ECG. The presence or absence of P waves, their morphology and timing, including their relation to ventricular activation as manifest by the PR interval, provide sufficient information for the diagnosis of most sinus and atrial disturbances. While the application of invasive electrophysiological techniques to the assessment of sinus node function [3, 4] and atrial arrhythmias [5] has provided a wealth of information about their origins and the mechanisms underlying arrhythmias in general, it is now recognized that non-invasive studies, including electrocardiography and ambulatory monitoring, are sufficient for the investigation of the majority [6, 7]. Invasive electrophysiological study may be useful for cases in which there are diagnostic or management problems [8], and as a prelude to curative catheter ablation. With catheter ablation techniques playing an increasing role in the management of certain atrial arrhythmias, there has been renewed interest in P wave morphology on the surface ECG as a guide to the origin and mechanism of focal and reentrant atrial rhythm disturbances.

26.2 Normal Sinus Rhythm and Sinus Arrhythmias

26.2.1 Electrophysiology of the Sinus Node

Activation of the normal cardiac cycle originates in the sinus node, a small discrete mass of specialized pacemaker (P) cells situated at the junction of the high right atrium (HRA) and superior vena cava [9, 10]. Sinus nodal cells are characterized by a membrane potential of around −60 mV at its most negative; that is, they are relatively depolarized compared to other non-nodal cardiac tissues which have a membrane potential of −80 to −100 mV [11]. At such a potential, fast sodium channels are largely inactivated and the action potential of the P cells is dependent on slower inward calcium currents [12, 13]. On repolarization after an action potential, slow spontaneous depolarization occurs during diastole until threshold is reached and another action potential occurs. This diastolic depolarization is often described as the pacemaker potential, or phase 4 of the action-potential cycle. Several ion currents have been implicated in the pacemaker potential, including potassium conductances, the hyperpolarization-activated cation current, I_f [14] and the sustained inward current, I_{st} [12, 15]. In addition, rhythmic release of calcium from intracellular stores, and its subsequent reuptake, may also play a role in generating the pacemaker potential [16]. Other cardiac tissues may also exhibit pacemaker potentials, notably atrioventricular (AV) nodal and Purkinje-fiber cells, but at a slower rate than in the sinus node. Thus, the rate of sinus firing determines the rate of the rest of the heart. In the absence of a sinus beat, however, these lower pacemakers may generate "escape" rhythms.

The activity originating in the sinus nodal cells is conducted out to the surrounding atrium through transitional (T) cells, which have electrophysiological properties intermediate between the pacemaker cells and the quiescent atrial tissue [17]. The site of the primary pacemaker may shift between groups of pacemaker cells within the sinus node, or into the T cells or even the atrium. Disorders of sinus function may result from a failure of impulse generation by the nodal (P) cells, or a failure of conduction of the impulse from sinus to atrial cells, via the T cells [4].

Figure 26.1

Sinus rhythm: (a) normal sinus rhythm, 72 bpm; (b) sinus bradycardia, 36 bpm; (c) sinus tachycardia, 114 bpm; (d) sinus arrhythmia, rate 66 bpm on inspiration, 38 bpm on expiration. ECG leads shown on each strip recording.

26.2.2 Normal Sequence of Atrial Activation and P Wave Morphology

The cardiac impulse in normal sinus rhythm originates in the sinus node, spreads directly to the right atrium and thence to the left atrium, before being conducted through the AV node and His-Purkinje system to the ventricles. This activation sequence is clearly seen in electrophysiological studies using multiple sites for intracardiac recordings. Atrial activation occurs first in the high right atrium, followed by the low right atrium at the AV junction, before it is seen in the proximal and finally the distal coronary sinus electrograms, the latter representing left atrial activation. Activation of the His bundle is then detected, followed by spread of excitation to the ventricles (see Fig. 24.2). The origin of the atrial activation in the HRA determines the P wave axis, the normal axis being from 0 to +90°. Thus, the P wave is usually upright in leads I, II and aVF, and inverted in aVR. In the horizontal plane, the activation from right to left produces upright P waves in the left-sided chest leads V_3–V_6. The P wave may also be upright in V_1–V_2, but is more commonly inverted or biphasic. Normal sinus rhythm has regular P waves, preceding the QRS complexes by a constant PR interval of 120–200 ms (Fig. 26.1a). The P wave configuration should be constant in any given lead, other than minor changes in axis with respiration.

26.2.3 Autonomic Control of Sinus Rate

The sinus node has both sympathetic and parasympathetic innervations which control the rate of sinus firing by altering the rate of depolarization of the pacemaker potential. The parasympathetic vagal influence is dominant at rest, slowing the intrinsic rate, as shown by the increase in heart rate with atropine [18]. Sympathetic innervation and circulating catecholamines increase heart rate during exercise and stress. Autonomic tone has a major influence on sinus node function and an awareness of this fact is important in the assessment of sinus node dysfunction.

Variations of autonomic tone may also cause the location of the pacemaker to shift within the sinus node, or to an ectopic atrial focus. As vagal discharge slows the pacemaker cells, another region under less vagal control may take over pacing. The P wave configuration may change only slightly with "wandering sinus pacemaker," but with "wandering atrial pacemaker" the P wave morphology and axis will change, as beats originate from ectopic atrial foci.

26.2.4 Normal Sinus Heart Rate

The normal heart rate in the adult is widely accepted as 60–100 beats per minute (bpm), lower than this being defined as bradycardia, and faster as tachycardia. However, not all physicians would agree with this stated range. A WHO/ISFC Task Force [19] thought that the inherent rate of the sinoatrial (SA) node had a "representative" range of 50–100 bpm. Spodick et al. measured the resting heart rate of 500 consecutive asymptomatic subjects, who were aged 50–80 years, and were free from cardiac medication. They found a range (2 standard deviations below and above the mean) of 46–93 bpm for men, and 51–95 bpm for women [20]. There was no association between age and the resting heart rate. Others have reported similar findings with ageing in healthy subjects, but in those with heart disease the resting heart rate falls with age (reviewed by Brignole [21]).

26.2.5 Sinus Bradycardia

A sinus rate of <60 bpm is defined as sinus bradycardia. Normal P waves precede each QRS complex with a constant PR interval (Fig. 26.1b). Sinus bradycardia occurs in normal children [22] and adults [23, 24] during sleep, with heart rate commonly down to 30–40 bpm and also in athletes, owing to enhanced vagal tone [25]. Vagal overactivity may also be pathophysiological, producing profound sinus bradycardia during vasovagal episodes or acute inferior myocardial infarction [26]. Unexplained sinus bradycardia is the most common manifestation of sinus node dysfunction [21, 27, 28].

26.2.6 Sinus Tachycardia

The electrocardiographic features of sinus tachycardia are a heart rate of >100 bpm with a normal P wave morphology and axis and a normal PR interval (Fig. 26.1c). Sinus tachycardia is normal in young children, while in adults it is seen in response to neural or hormonal influences. Physiological or pathological stresses, such as physical exercise, anxiety, fever, hypotension, heart failure or thyrotoxicosis all cause sinus tachycardia. The rate may be transiently slowed by carotid sinus massage. The rate of sinus tachycardia may be up to 200 bpm in young adults during maximal exercise. Maximal heart rate on exercise tends to decrease with age [29], an approximate guide being 208-(0.7 × age) bpm [30].

26.2.7 Sinus Arrhythmia

During normal sinus rhythm the P-P interval is relatively constant, but variations, termed sinus arrhythmia, may occur. This is a common arrhythmia, usually arising from physiological variations in autonomic tone [22, 23]. There is phasic variation in the P-P interval, the difference in sinus cycle length being ≥120 ms, with normal P waves and PR interval (Fig. 26.1d). It is most commonly related to the respiratory cycle, with an increase in sinus rate during inspiration owing to reflex inhibition of vagal tone and a slowing of rate with expiration [31]. Non-respiratory sinus arrhythmia may also occur, secondary to heart disease, for example, acute myocardial infarction or digoxin toxicity.

A further form of variation in sinus rate, known as ventriculophasic sinus arrhythmia, is noted when there is prolongation of a sinus cycle which has no corresponding ventricular contraction. This is most commonly seen in complete AV block (Fig. 26.2) [32]. The P-P interval of a cycle which includes a QRS complex is shorter than the following cycle which does not. A similar lengthening of P-P interval may be noted following a premature ventricular contraction with a compensatory pause. Proposed mechanisms for ventriculophasic sinus arrhythmia include mechanical and/or hemodynamic effects of ventricular systole on the sinus node and changes in baroreceptor-mediated vagal activity. In an interesting study, de Marchena et al. studied the phenomenon in patients who had received a cardiac transplant [33]. The P-P interval of the recipient's retained atrial tissue (which has preserved vagal innervation to its sinus node, but lacks flow in its sinus node artery) was found to be independent of the donor heart's ventricular activity. This lack of ventriculophasic effect suggests that hemodynamic rather than autonomic effects on the sinus node may be most important.

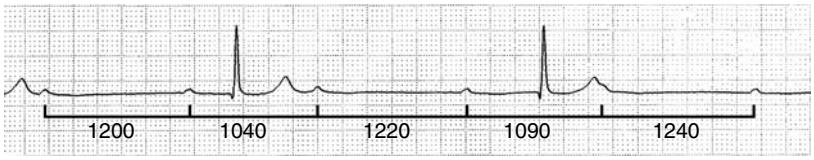

Figure 26.2
Ventriculophasic sinus arrhythmia. Cardiac monitor tracing in a patient with complete heart block and a narrow-complex escape rhythm, showing variations in the atrial rate in response to ventricular systole – the P-P intervals (indicated in ms) which contain a QRS complex are shorter than those which do not.

26.2.8 Inappropriate Sinus Tachycardia and Postural Orthostatic Tachycardia Syndrome

Inappropriate sinus tachycardia, also referred to as chronic nonparoxysmal sinus tachycardia, occurs in otherwise healthy people and is apparently a result of increased automaticity of the sinus node, due to defective autonomic control [34, 35]. The clinical features are of resting sinus tachycardia, and an exaggerated response to minimal activity, in the absence of other causes, such as hyperthyroidism, heart failure, anaemia, cardioactive drugs, or infection. The electrocardiogram shows P waves with an axis and morphology corresponding to those during sinus rhythm. Ambulatory monitoring or exercise testing shows a gradual onset and termination of the tachycardia. A related, and often overlapping, condition is the postural orthostatic tachycardia syndrome (POTS) which is characterised by an increase in the sinus rate by 30 bpm, or to greater than 120 bpm, when the patient stands up from a supine position. This increase in heart rate occurs in the absence of significant orthostatic hypotension [35]. These conditions may persist for months or years, and can cause troublesome symptoms but have a good prognosis. Treatments often include volume expansion, beta-blockers and other peripherally- or centrally-active agents to modify vascular tone. Studies of catheter-based modification of the sinus node have generally yielded disappointing long-term results [35].

26.2.9 Sinus Node Reentrant Tachycardia

Sinus node reentrant tachycardia accounts for around 5–15% of supraventricular tachycardias and is characterized by a modest increase in heart rate to 100–150 bpm, P waves which are similar, though not necessarily identical, to those during sinus rhythm and a RP/PR ratio of >1 [36–38]. As with other reentrant tachycardias, it can be initiated and terminated during electrophysiological study by premature atrial stimuli [39]. The atrial activation sequence is identical to that during sinus rhythm, originating in the HRA. It is not usually associated with sinus node dysfunction and is seen more commonly during electrophysiological study than as a spontaneous arrhythmia [40]. If treatment is required, sinus node reentrant tachycardia can be managed with drugs or by ablative therapy [38].

26.3 Sinus Node Dysfunction

Disturbance of sinus node function is a common cause of symptomatic arrhythmias and may be a result of a failure of sinus automaticity, or of a failure of propagation of the impulse from the sinus node to the atrium (SA block), or a combination of both. There are many etiological or associated conditions and the cause of sinus node dysfunction may be classified as intrinsic, related to pathological changes in sinus and atrial tissue, or extrinsic, with disturbance of sinus function being attributable to the influence of other factors, commonly autonomic overactivity, or cardioactive drugs [41]. Both intrinsic and extrinsic forms may be chronic, with slow progression, or acute, with sudden onset usually related to predisposing factors such as ischemia, inflammation, surgical trauma or drugs.

In view of the multifactorial etiology of sinus node dysfunction, it is not surprising that no single underlying histological abnormality has been identified, but rather a variety of findings have been reported. In most cases, the

node is of normal size with marked loss of nodal cells and replacement by fibrosis. With normal ageing, the sinus node undergoes striking loss of myocardial cells, with an increase in fibrous tissue [42]. In patients with sinus node dysfunction, there may be virtual total fibrosis of the node, with the proportion of nodal cells being as low as 5%. By contrast to these fibrotic nodes of normal size, the sinus node may be hypoplastic, presumably as a congenital abnormality [43]. Rarely, the node appears to be morphologically normal, with fibrosis or fatty infiltration around the nodal tissue [44]. Fibrotic involvement of atrium itself and AV nodal regions is commonly found in patients with sinus nodal fibrosis [42, 43], consistent with the common coexistence of AV conduction abnormalities [45, 46], or atrial tachyarrhythmias [47]. Acute sinus node dysfunction may result from inflammatory involvement of the node in pericarditis [48] or myocardial infarction, but only rarely is it a result of atheroma or thrombosis of the sinus node coronary artery branch itself [42, 43]. The sinus node can also be affected by systemic infiltrative conditions, such as amyloidosis [49] and hemochromatosis [50], leading to sinus node dysfunction, and a variety of arrhythmias.

In addition to abnormal autonomic influences as extrinsic causes of sinus dysfunction, it has been hypothesized that an abnormal response to the regulatory influence of adenosine, locally released by active myocardium, may underlie intrinsic sinus node disease [51]. Evidence to support an increased sensitivity to adenosine comes from the demonstration of marked bradycardia and sinus pauses produced by intravenous adenyl compounds [52], and the therapeutic response to theophylline, an adenosine antagonist, in some patients [53, 54]. Finally, the possibility of an autoimmune mechanism has been raised by the finding of autoantibodies against sinus node in over 25% of patients with sinus dysfunction or bradycardia [55].

26.3.1 Sick Sinus Syndrome

The term "sick sinus syndrome" was first coined in the 1960s by Lown [56], to describe acute sinus disturbance after cardioversion, and was subsequently applied by Ferrer [57] to patients with chronic SA dysfunction. Although, strictly, it should be confined to patients with intrinsic sinus node dysfunction, the term has been commonly applied to any patient with symptoms attributable to disorders of sinus node function [58, 59]. The clinical picture of sick sinus syndrome includes a variety of arrhythmias [21, 27] with multifactorial etiologies [59]. The sick sinus syndrome may be diagnosed in symptomatic patients with any of the following electrocardiographic findings:

(a) Inappropriate sinus bradycardia,
(b) Sinus arrest with or without an ectopic atrial or junctional escape rhythm,
(c) Sinoatrial exit block,
(d) Alternating bradycardia and atrial tachyarrhythmia (the "bradycardia-tachycardia syndrome") [47, 60].

In addition, chronic atrial fibrillation with slow ventricular response in the absence of drug therapy usually indicates underlying sinoatrial dysfunction, and attempts at cardioversion typically produce a slow, unstable rhythm [56]. In patients with sinus node dysfunction there is commonly depression of the lower latent pacemakers and the failure of "escape" rhythms results in symptomatic bradycardia. Abnormalities of AV conduction are also found in over half of patients with sick sinus syndrome [45, 46], although more recent evidence suggests that in those with intact AV conduction, it remains stable with time, especially in those without concomitant bundle branch block [61]. Carotid sinus hypersensitivity may mimic, or unmask, sinus node dysfunction [62, 63].

The bradycardia-tachycardia syndrome comprises about half of the patients with sick sinus syndrome [59]. Symptoms may occur with the tachycardia, commonly atrial fibrillation or flutter, or especially with the bradycardia, as long pauses may result following spontaneous termination of the tachycardia (Fig. 26.3). The tachycardia may simply be predisposed to by the bradycardia, occurring as an "escape" arrhythmia, and may be suppressed by atrial pacing [64]. In other cases, the finding of atrial histopathology [42] indicates that atrial arrhythmias may be the result of the general pathological process. It is probable that the development of atrial arrhythmias is the natural progression of the condition [65], but this progression occurs only very slowly [66].

Figure 26.3
Ambulatory monitor tracing, showing a pause of 4 s after spontaneous termination of atrial fibrillation in the bradycardia-tachycardia syndrome. The pause is followed by a junctional escape beat.

Figure 26.4
Sinus arrest, as seen on ambulatory monitor tracing. The lower trace is continuous with the upper trace. After two sinus beats there is a pause of 4.9 s, followed by an ectopic atrial escape beat (*arrowhead*). The first spontaneous sinus beat (*) occurs after a total of 6.9 s. A further pause of 3.4 s occurs, followed by a junctional escape beat.

26.3.2 Sinus Arrest

Failure of impulse formation by the sinus node results in the absence of atrial activation and a pause is seen on the ECG (Fig. 26.4). Sinus arrest may produce periods of ventricular asystole of variable duration, depending on the time taken for recovery of sinus automaticity, or appearance of an escape rhythm from a lower pacemaker. Since the regular sinus discharge has been interrupted, the duration of the pause has no arithmetical relation to the basic sinus cycle length.

26.3.3 Sinoatrial Block

Block of SA conduction may result in the failure of atrial depolarization, despite continuing sinus automaticity. Sinoatrial block may be classified as first degree, second degree or third degree, with delayed conduction, intermittent or complete block, analogous to AV block. Only second-degree SA block can be diagnosed from the ECG, although first-degree conduction delay may be assessed by electrophysiological study. Second-degree SA block can be further subclassified as type I (Wenckebach) or type II, which is again analogous to second-degree AV block. Type II SA block is the most frequently

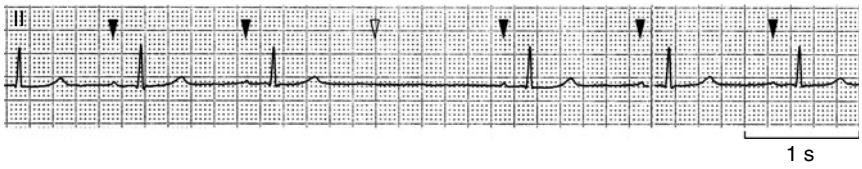

Figure 26.5

Sinoatrial block (type II). The sinus pause is twice the preceding sinus cycle length (P waves are indicated by filled *arrowheads*), owing to exit block of sinus activity preventing the expected P wave (*open arrowhead*).

seen, with intermittent block occurring without preceding conduction delay. This is in contrast to AV block, where type I second-degree block is the more common. Sinoatrial block is diagnosed from the ECG by the intermittent absence of the P wave and subsequent QRS complex. The duration of the pause is an exact multiple of the preceding sinus cycle length, since sinus activity continues despite the failure of atrial activation (Fig. 26.5). Type I (Wenckebach) SA block has increasing delay in SA conduction with successive beats until there is failure of atrial activation and an absent P wave. Since sinus activity is not apparent on the ECG, the diagnosis is established by a progressive decrease in P-P interval prior to the dropped beat, owing to the characteristic periodicity of the Wenckebach phenomenon, whereby, although conduction is progressively delayed, the beat-by-beat increment in delay decreases [67]. The pause with type I SA block will, therefore, be less than twice the preceding P-P interval.

26.3.4 Diagnosis of Sinus Node Dysfunction

The investigation of patients with suspected sick sinus syndrome must be directed to the demonstration of abnormalities of sinus function and the establishment of the correlation between the patient's symptoms and the arrhythmias. The rhythm abnormalities are often intermittent and the resting ECG may be normal. The likelihood of detecting arrhythmias is increased by longer periods of ECG recording, and ambulatory Holter monitoring reveals the diagnosis in many more patients [68, 69]. The development of implanted loop recorders has allowed more prolonged ECG monitoring (up to 3 years) and can increase the diagnostic yield in patients with normal baseline tests [70, 71]. The results of these tests, however, must be interpreted carefully since sinus bradycardia, sinus arrest and SA block may all be normal findings [24], particularly in young people [22, 23] or athletes [25]. Sinus pauses of >2 s are generally abnormal and indicate sinus node dysfunction [72, 73], but it is important to document the relationship of the patient's symptoms to an arrhythmia, as asymptomatic pauses do not require treatment [74].

Abnormal heart-rate responses to exercise [75], atropine [76, 77] or isoprenaline [77, 78] are common in the sick sinus syndrome, although these tests are of questionable clinical utility [21]. The combination of atropine (0.04 mg/kg) and propranolol (0.2 mg/kg) produces complete autonomic blockade and reveals the intrinsic heart rate (IHR), which has a well-defined normal range that decreases with age [79]. The IHR can be predicted from a linear regression equation:

$$\text{IHR} = 118.1 - (0.57 \times \text{age})$$

Patients with intrinsic sinus node dysfunction have an abnormally slow IHR, whereas it is normal in those with extrinsic vagally-induced dysfunction [80, 81]. The effects of carotid sinus pressure should also be determined (Fig. 26.6). Carotid sinus hypersensitivity is present in around 33% of patients with sick sinus syndrome, although the two conditions appear to be pathophysiologically distinct [21].

In the majority of patients, noninvasive investigation is sufficient to establish the diagnosis of sick sinus syndrome [6, 7, 81]. Invasive testing is now seldom employed in this context, however in some circumstances it may help clarify the clinical diagnosis. For example, in patients with syncope thought to be due to sick sinus syndrome in whom ambulatory ECG monitoring has failed to record an event, the demonstration of markedly abnormal sinus node function in an invasive electrophysiology study may support the diagnosis and strengthen the case for implantation of a permanent pacemaker [4, 7]. The most commonly used tests involve atrial pacing to measure sinus automaticity (the sinus node recovery

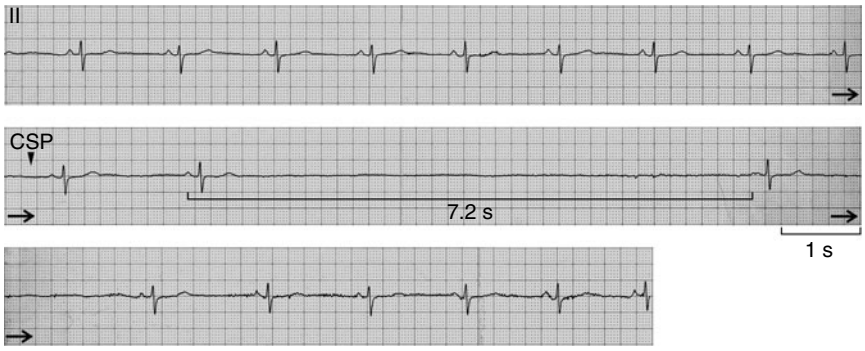

Figure 26.6

Carotid sinus hypersensitivity. Traces are continuous. Carotid sinus pressure (CSP) results in sinus suppression, with a pause of 7.2 s.

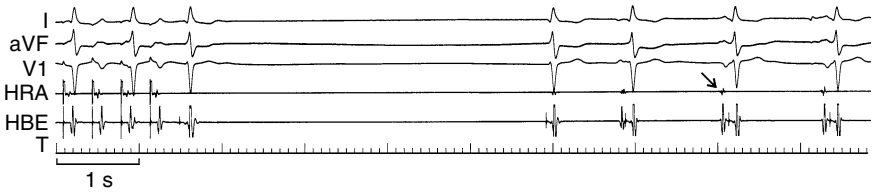

Figure 26.7

Sinus node recovery time (SNRT). Following cessation of atrial pacing at a cycle length of 350 ms for 30 s, there is a pause of 6.9 s before the first spontaneous sinus beat (*arrowed*). The figure shows surface leads I, aVF and V1, and intracardiac recordings from the high right atrium (HRA) and His bundle electrogram (HBE). Time-bar (T) indicates seconds (large divisions).

time) and sinoatrial conduction (SA conduction time). Direct sinus node recordings [4, 82, 83] have added greatly to the understanding of the electrophysiological abnormalities in the sick sinus syndrome [84] but are not in routine clinical use [21]. The main invasive tests of sinus node function will be outlined below, but for more in depth reviews, the reader is directed elsewhere [4, 85–87].

26.3.5 Electrophysiological Assessment of Sinus Node Function

26.3.5.1 Sinus Node Recovery Time

Since the automaticity of cardiac pacemaker cells may be transiently suppressed by pacing at rates faster than their own firing rate [88], an assessment of sinus automaticity can be obtained by examining the time taken for recovery following a period of overdrive suppression by rapid atrial pacing [3]. The interval from the last paced P wave to the first spontaneous sinus P wave is the sinus node recovery time (SNRT). If sinus node dysfunction is present, the depression of automaticity is manifest by prolongation of the SNRT [3, 4, 89]. The resultant pause may be of several seconds duration in patients with sick sinus syndrome (Fig. 26.7).

It is apparent that the duration of the pause following atrial pacing will also depend on the basic sinus cycle length (SCL): the slower the heart rate the longer the expected pause. The SNRT may be corrected for heart rate in a number of ways, the commonest being to subtract the mean SCL (corrected sinus node recovery time, CSNRT = SNRT – SCL) [90]. Different ranges of normal have been suggested by different investigators [85, 87], but a CSNRT > 550 ms is generally considered to be abnormal. Another commonly applied correction is the expression of the SNRT as a percentage of the SCL (normal SNRT/SCL × 100 < 150%) [85, 86].

In addition to the SNRT, further assessment of sinus function can be obtained by examining the atrial rhythm for several beats following pacing. While the first post-pacing pause is usually the longest, many patients with sinus dysfunction exhibit sudden prolongation of subsequent cycles [77]. Such "secondary pauses" are indicative of sinus node dysfunction and do not occur in normal individuals [91]. Pauses which are multiples of the basic SCL are a result of SA exit block. Secondary pauses may be the only manifestation of sinus dysfunction during electrophysiological study [77, 91]. The total recovery time (TRT) for the sinus cycle to return to stable prepacing values can also be taken as an indication of sinus function, and should be <5 s [77, 85].

26.3.5.2 Sinoatrial Conduction Time

An estimate of SA conduction may be obtained by examining the responses to atrial pacing, since a paced atrial activation must travel retrogradely into the sinus node and the subsequent sinus activity must then be conducted out to the atrium. Two methods of measuring the SA conduction time (SACT) are commonly used. The Strauss method [92] introduces atrial premature stimuli following successive runs of eight spontaneous sinus cycles (each impulse designated A_1). If the paced atrial extrastimulus (A_2) is introduced at an appropriate time in mid-diastole, it will penetrate the sinus node before it has fired spontaneously, and depolarize the pacemaker, which is then reset. The return cycle (the time from the paced atrial extrastimulus to the first spontaneous sinus beat, A_3) will be the sum of the time taken for the beat to conduct into the node, the basic SCL following reset and the SA exit conduction time. Thus $A_2A_3 = A_1A_1 + SACT$, where SACT is the total conduction time into and out of the node.

The method of Narula [93] is simpler, employing an 8-beat train of atrial pacing (A_p) at a slow rate (<10 bpm above the sinus rate). The return cycle to the first sinus beat (A) is then measured, and the total SACT calculated as A_pA-post-pacing SCL. This method attempts to overcome one problem with the Strauss method – if there is any significant degree of sinus arrhythmia, then error will be introduced into the estimation of the SACT. The Narula method assumes that a short eight-beat train of slow atrial pacing effectively stabilizes the SCL, without significant suppression of automaticity.

The two methods for estimating SA conduction give similar, but not identical, values for SACT [83, 93, 94], and a fairly wide range of normal values for total SACT have been reported (from 200 to 344 ms, reviewed in [85]).

26.3.5.3 Sinus Node Refractoriness

Another technique which has been used for the assessment of sinus node function is the measurement of the retrograde sinus node effective refractory period (SNERP) [95]. Eight-beat trains of atrial pacing are followed by single extrastimuli of increasing prematurity and the return cycle A_2A_3 is plotted against the coupling interval A_1A_2. The SNERP is taken as the longest coupling interval that is followed by an interpolated beat. There appears to be clear separation between values of SNERP in normal individuals and in patients with sinus dysfunction (325 as opposed to 522 ms) [95]. A limitation of this technique is that the SNERP could only be measured in 75% of patients in one study [87].

26.3.5.4 Direct Sinus Node Recording

The development of catheter techniques to record directly from the region of the sinus node in humans [4, 82, 84] has allowed the validation of the indirect assessments of sinus node function [4, 83, 84]. The technique involves the placement of a multipole catheter in the proximity of the sinus node and, with appropriate amplification and filtering, a sinus node electrogram (SNE) can be recorded. The direct SNE parallels the membrane potential changes seen in sinus pacemaker cells, with a slow diastolic depolarization (phase 4) prior to the upstroke (phase 0) of the sinus action potential, which precedes the rapid upstroke of atrial depolarization. The SACT is measured from the onset of sinus node depolarization to the onset of atrial activation, and is less than around 120 ms in normal individuals [83, 84, 96]. An additional measurement, the duration of sinus node depolarization (SND_d), can be determined from direct sinus node recordings, and is usually <150 ms in normal subjects. A $SND_d \geq 200$ ms can indicate the presence of significant sinus node dysfunction [4].

The role of the SNE in the investigation of sinus node dysfunction is doubtful as the placement of the catheter is relatively time-consuming, and recordings can be obtained in only 80% of patients and are seldom stable [86]. The technique, however, has provided some fascinating insights into the interpretation of results from indirect assessment of sinus function. For example, many patients with long pauses after rapid atrial pacing, who are considered to have a prolonged SNRT, have in fact been found to have continuing sinus activity, as shown by the SNE, the pauses arising from SA exit block preventing atrial activation [97, 98].

26.3.5.5 Clinical Role of Electrophysiological Testing

The main limitations of electrophysiological assessment of sinus node dysfunction are the low sensitivity of the tests and the variable clinical significance of abnormalities if found. Abnormalities of the measurement of SNRT and SACT have sensitivities of only about 50% or less in symptomatic patients with sinus node dysfunction [8, 85, 99]. The sensitivity is improved if both tests are combined, and the specificity of the tests is good, being of the order of 75–95% [6, 8]. Autonomic blockade may increase the sensitivity of the electrophysiological tests [87, 100, 101], and particularly aids in the identification of those patients with intrinsic sinus dysfunction [81]. Both sensitivity and specificity are best in symptomatic patients, especially those with syncope, but are less helpful in asymptomatic patients [102]. Thus, with respect to establishing a diagnosis, electrophysiological testing may support the clinical suspicion of sinus node dysfunction if abnormalities are found, but cannot be used to exclude sinus node disease, given the limited sensitivity of the tests. In addition, since the prognosis of patients with sinus node dysfunction is good [66, 102, 103] and does not appear to be altered by pacemaker implantation [74, 103], the finding of sinus node dysfunction in itself does not mandate therapeutic intervention [74, 104].

The correlation of arrhythmia with symptoms is most important, but is not always possible to achieve even with ambulatory monitoring [69]. Invasive investigation of patients with syncope of undetermined origin reveals sinus node disease in about 10% of cases [8] and other electrophysiological abnormalities may be detected in up to 75% [105]. A presumed diagnosis of sick sinus syndrome can be made if major abnormalities of sinus node function (e.g., a SNRT $>$ 3 s) are demonstrated in an electrophysiology study and other causes for the patient's symptoms have been ruled out [7, 21]. Other supporting findings on non-invasive testing include: persistent daytime HR $<$ 40 bpm, often with little variation in HR; second degree SA block; prolonged sinus pauses (which are not vagally-mediated); abnormal intrinsic HR; and severe chronotropic incompetence [21].

In patients with the bradycardia-tachycardia syndrome, in whom monitoring may have failed to demonstrate significant pauses, there is good correlation between pauses observed after atrial pacing and those occurring on spontaneous termination of tachycardia [106]. Other patients with documented bradycardia-tachycardia syndrome may be symptomatic from the tachyarrhythmia rather than the bradycardia and antiarrhythmic therapy may be more appropriate than pacing. Electrophysiological testing can indicate whether drug therapy may worsen sinus dysfunction, meriting prophylactic pacemaker implantation. Full electrophysiological study may also demonstrate inducible tachyarrhythmias, such as ventricular tachycardia, as the true cause of symptoms in some patients with suspected sinus disease [105].

Finally, assessment of AV conduction is important in patients with sick sinus syndrome for whom a single-chamber atrial (AAI) pacemaker is planned. This is usually assessed at the time of pacemaker implantation, rather than in a separate electrophysiology study, and if AV conduction is normal, with 1:1 AV conduction at atrial pacing rates of ≥120 bpm, then AAI pacing is generally appropriate. It should be noted that serial electrophysiological studies after single-chamber atrial pacemaker implantation have shown that AV conduction may subsequently deteriorate in patients requiring additional antiarrhythmic therapy [107].

26.4 Atrial Arrhythmias

Atrial arrhythmias are common and may occur in patients without heart disease as well as being a feature of most cardiovascular conditions. They are of major clinical importance, and can be associated with significant morbidity, but are only rarely fatal in themselves. The majority may be diagnosed without invasive investigation on the basis of the surface ECG

[108–110]. Satisfactory pharmacological management is often achieved, although there is an increasing role for curative catheter ablation for several types of atrial arrhythmias (see Chap. 24, [108]).

26.4.1 Mechanisms of Atrial Arrhythmias

Tachyarrhythmias, in general, result from either abnormal impulse generation, such as abnormal automaticity and triggered activity, or abnormal impulse conduction, resulting in reentrant circuits [111].

Automatic atrial arrhythmias are a consequence of abnormal foci which have inherent pacemaker properties and thus generate arrhythmias spontaneously if their firing rate exceeds that of the sinus node. The pacemaker current, I_f, may contribute to this phenomenon in human atrial tissue [112]. Foci of abnormal automaticity can occur in a variety of sites, including within the vena cava and pulmonary veins [113, 114], and the arrhythmias they produce can be paroxysmal or incessant.

Triggered activity, by contrast, results from early or delayed afterdepolarizations which follow preceding action potentials [115]. These may reach threshold and result in further action potentials. Afterdepolarizations are a result of transient inward currents [116, 117] which are activated by oscillations of intracellular calcium in conditions of calcium overload, such as can be induced by cardiac glycosides or catecholamines. It is likely that triggered activity underlies arrhythmias caused by digoxin toxicity [118]. Intracellular calcium is also increased by repetitive stimulation which may induce afterdepolarizations.

Reentry is the commonest mechanism of cardiac arrhythmia generation, and can be dependent on a macro-reentrant circuit, such as in AV nodal reentrant tachycardia (AVNRT) and AV reciprocating tachycardia (AVRT), or on micro-rentrant circuits as in fibrillation (see Chaps. 24 and 27). Within the atria, structural or functional lines of block can exist which create the conditions necessary for macro-reentry [119]. The classic example is that of "typical" (cavo-tricuspid isthmus-dependent) flutter, as discussed in Sect. 26.8.

The underlying mechanisms of tachycardias may be differentiated electrocardiographically to some extent, but more particularly by the responses to pacing and premature stimulation. Characteristically, reentrant tachycardias are reproducibly initiated and terminated by premature stimuli, whereas automatic tachycardias are not [120]. The latter may display suppression and reset of the automatic focus in response to premature stimuli, followed by a noncompensatory pause. Triggered activity is more difficult to differentiate as it may be initiated and terminated by pacing [118].

Based on these mechanistic considerations, most regular atrial arrhythmias can be classified into two broad groups – *Focal atrial tachycardia*, where activation spreads from a central point and is due to an automatic, triggered, or micro-reentrant mechanism; and *Macro-reentrant atrial tachycardia*, where conduction is occurring around a defined circuit [119]. *Atrial fibrillation* is distinct and characterized by relatively chaotic atrial activation, driven by complex mechanisms including multiple circuit reentry [218], and irregular ventricular activity (when AV conduction is intact).

26.4.2 General Electrocardiographic Features of Atrial Arrhythmias

Focal atrial arrhythmias may originate at any site in the atria, frequently remote from the sinus node. The morphology of atrial activation usually differs from the P wave observed in sinus rhythm, and depends on the site of origin [121]. The P wave vector and morphology can be used to predict the site of origin of an ectopic rhythm [122] (see Sect. 26.6), although some limitations exist [121, 123, 124] and accurate localization can only be obtained with certainty by intracardiac mapping [125].

Reentrant atrial tachycardias are generally initiated by spontaneous atrial premature beats, the initial P wave usually differing from subsequent P waves during the tachycardia. Unlike the junctional reentrant tachycardias (i.e., AVNRT and AVRT), initiation of atrial tachycardia is independent of AV nodal conduction and may be initiated by atrial beats which block proximal to the His bundle [123].

Atrial arrhythmias have often been defined with respect to the atrial rate, distinguishing between atrial tachycardia (100–250 bpm), flutter (250–350 bpm) or fibrillation (400–600 bpm). However, atrial rate alone cannot be considered a rigid diagnostic criterion as exceptions may occur. For example, the atrial rate in atrial flutter may be slower, particularly

in the presence of antiarrhythmic drugs, or faster, as rates of over 400 bpm have been documented [126]. Transition may occur between atrial arrhythmias, with atrial flutter or tachycardia converting to fibrillation [127, 128]. Intermediate forms may also be seen (termed "flutter fibrillation") where organized atrial activity can be recorded from some areas of the atrium but not others [129].

Focal and reentrant atrial arrhythmias can be incessant, defined as being present for at least 90% of the monitored time. The rate may vary during the day, increasing on exercise and slowing during sleep [130]. Incessant tachycardias can occur in young people with otherwise normal hearts and may cause heart failure due to "tachycardiomyopathy" [131]. In such cases, successful ablation of the arrhythmia can be curative and lead to a sustained improvement in cardiac function [132–134].

26.5 Atrial Premature Complexes

26.5.1 Overview

The commonest atrial arrhythmia is the atrial premature complex (APC), also known as an atrial extrasystole or atrial ectopic beat. These atrial impulses are characterized by their prematurity, occurring before the next expected sinus beat, and abnormal P-wave morphology, owing to their ectopic origin (Fig. 26.8). With respect to terminology, the terms

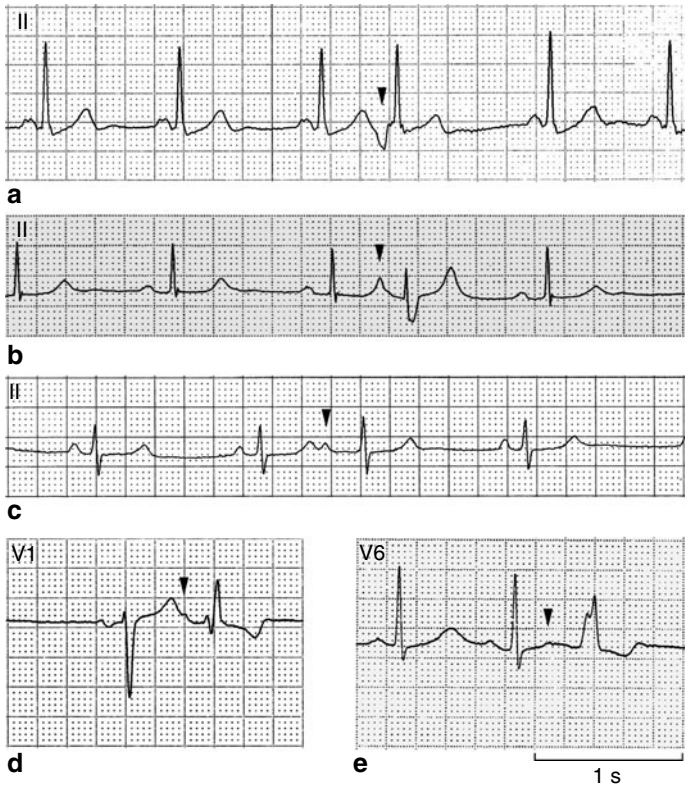

Figure 26.8

Atrial premature complexes (APCs, indicated by *arrowheads*). Part (a) shows an APC with a clearly abnormal P wave. Part (b) shows an APC superimposed on the preceding T wave, with aberrant conduction to the ventricles. In part (c), an APC occurs with a prolonged PR interval, and a less than compensatory pause. Parts (d) and (e) show APCs conducted with right bundle branch block, and left bundle branch block, respectively.

atrial "premature complex" and "extrasystole" clearly refer to an extra, premature beat, whereas atrial "ectopic" defines the site of origin but not the timing of the beat. An atrial ectopic, for example, may occur as an escape beat following a sinus pause, and so the term includes both premature and escape rhythms. It is, therefore, a less specific term and thus the others are to be preferred.

Atrial premature complexes are common and occur in normal individuals of all ages [22, 23, 135, 136]. Their frequency increases with age, being found in 13% of healthy boys [22], 56% of male medical students [23] and in 75–88% of adult males, although frequent APCs occur only rarely (2–6%) [135, 136]. They are more common in patients with cardiac disease; for example APCs can be found in 94% of patients with mitral stenosis [137]. They are exacerbated by fatigue, stress, caffeine, tobacco and alcohol [135]. They rarely cause symptoms requiring treatment although, occasionally, frequent early or blocked APCs may cause an effective bradycardia – the extrasystolic beat has a low stroke volume owing to inadequate ventricular filling and is followed by a postectopic pause, or has no associated ventricular systole. In atrial bigeminy, for instance, the pulse rate may effectively be halved (Fig. 26.9). In sick sinus syndrome, an APC may be followed by symptomatic sinus pauses owing to sinus node suppression. The more important clinical relevance of APCs, however, is their role in triggering other arrhythmias. Most reentrant supraventricular tachycardias, including atrial flutter, are initiated by APCs (Fig. 26.10). Suppression of APCs may therefore be an important part of the prophylactic treatment of these arrhythmias, and can often be achieved with beta-blockers or calcium channel antagonists [108].

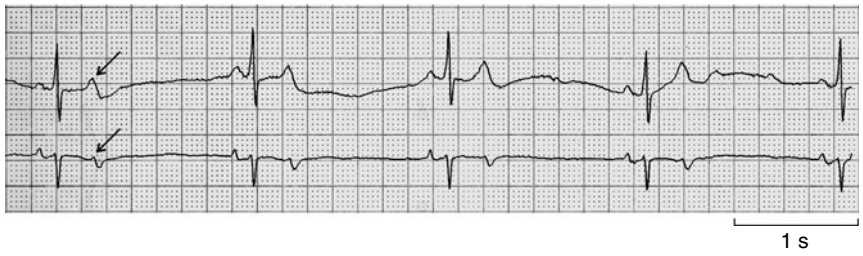

Figure 26.9

Ambulatory monitor tracing showing atrial bigeminy, with blocked atrial premature complexes (*arrowed* for first complex). This results in effective bradycardia, with a ventricular rate of 39 bpm.

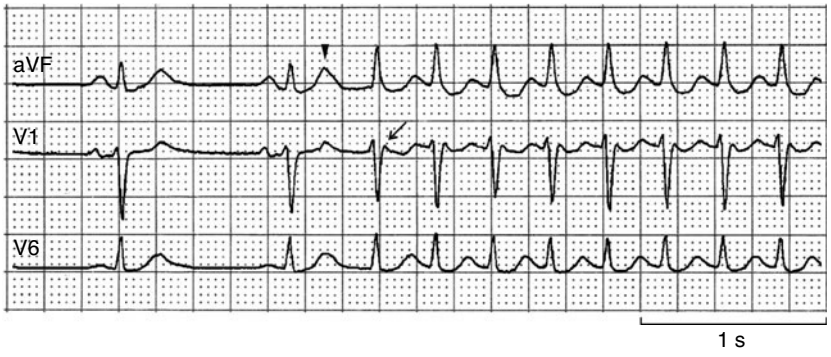

Figure 26.10

Atrial premature complex initiating AV nodal reentrant tachycardia (AVNRT). The APC (*arrowhead*) is partly obscured by the preceding T wave and has a long PR interval due to conduction via the AV nodal slow pathway. Typical AVNRT occurs, with P waves almost coincident with the QRS complex. The presence of atrial activity can be inferred from the characteristic development of a "pseudo-R′ wave" (*arrowed*) in lead V1.

26.5.2 Electrocardiographic Features

The relationship of an APC to ventricular activation will depend on its site of origin, its prematurity and the refractoriness of the AV node. The PR interval may be normal, or even short if the ectopic atrial activity is close to the AV node [138]. However, when an APC occurs early in diastole, close to the refractory period of the AV node, conduction may be delayed with resultant prolongation of the PR interval (Fig. 26.8c). When the APC occurs even earlier, it may find that the AV node is refractory, preventing impulse conduction to the ventricles. Such a "blocked" atrial extrasystole may be obscured by the preceding T wave (Fig. 26.9), and the following postextrasystolic pause may be incorrectly diagnosed as owing to sinus arrest.

The pause which follows an APC is most commonly a consequence of sinus resetting, as the premature atrial activity depolarizes not only the atria but also the sinus node. As a result, the pause is less than compensatory, the sinus node having fired earlier than expected. Thus the P-P interval flanking the APC is less than twice the basic cycle length (Fig. 26.8a–c). This is in contrast to the pause following most ventricular premature complexes which do not interfere with sinus activity; the next sinus beat occurs as expected and the pause is fully compensatory, the P-P interval being equal to twice the basic cycle length. A compensatory pause can occasionally be seen after an APC when the atrial ectopic activity collides with the sinus impulse in the perinodal tissue, preventing the spread of the sinus beat to the atria but without resetting the pacemaker. Rarely, an APC may encounter SA entrance block in the perinodal tissue but the exit of the sinus beat is unaffected. The APC is thus interpolated between two consecutive sinus beats, although the sinus P-P interval is usually slightly prolonged.

While an APC produces abnormal atrial activation, conduction below the AV node is usually normal with a resultant narrow QRS complex, in the absence of preexisting bundle branch block. Aberrant conduction may occur, however, as the impulse may reach the His Purkinje system while it is still relatively refractory from the preceding beat. Refractoriness of the conducting system is related directly to the preceding cycle length, a slower rate being associated with a longer refractory period. This is in contrast to AV nodal refractoriness, which increases with increasing rate. Aberrant conduction is therefore most likely to occur when a premature beat with a short coupling interval follows a longer interval, owing either to bradycardia or to a pause. This is termed the Ashman phenomenon [139]. For this reason, aberrant conduction may be seen with atrial bigeminy, where every extrasystolic cycle is preceded by a postextrasystolic pause. The refractory period of the right bundle branch is generally longer than that of the left and so right bundle branch block (RBBB) is the commonest configuration seen when an APC is aberrantly conducted (Fig. 26.8d). Less commonly, left bundle branch block (LBBB) may occur (Fig. 26.8e), particularly at faster rates, since at shorter cycle lengths the refractory period of the left bundle may exceed that of the right [140].

In an individual with frequent APCs there is usually a relatively constant interval between the APC and the preceding sinus beat. Such a constant coupling interval may indicate a reentrant mechanism underlying the premature impulse, such as intra-atrial or AV nodal echoes. This is in contrast to the rarely seen atrial parasystole [141, 142] when an automatic focus produces atrial beats independent of the sinus activity. Since the rate of atrial parasystole differs from that of sinus rhythm, the APCs have no fixed relation to the sinus beats. Atrial premature complexes commonly occur singly and sporadically, but may occur following every second or third sinus beat, producing bigeminy and trigeminy, respectively (see Fig. 26.9). Multiple APCs may occur consecutively; the occurrence of six or more APCs is considered to be a burst of nonsustained atrial tachycardia (Fig. 26.11).

Figure 26.11
Ambulatory monitor tracing showing non-sustained atrial tachycardia.

26.6 Focal Atrial Tachycardia

26.6.1 Overview

Focal atrial tachycardia is usually non-sustained and asymptomatic and is often an incidental finding on ambulatory monitoring. It has a prevalence of 0.34% in the general population and is higher in those with a history of palpitations [143]. Symptomatic sustained atrial tachycardia accounts for up to 17% of patients undergoing electrophysiology (EP) study for supraventricular tachycardia (SVT), with no sex preponderance [144–146]. There appears to be a bimodal distribution with peaks in the pediatric age group and in the elderly. This probably reflects different mechanisms of arrhythmogenesis in these groups, with AT due to increased automaticity being prevalent in the young and micro-reentry being more common with increasing age [146–148]. Pharmacological treatment is often unsuccessful, and curative radiofrequency ablation should be considered at an early stage. Ablation is associated with success rates of between 69% and 100% [146, 149–151], with recurrence rates of 7% [148].

26.6.2 The Electrocardiogram in the Diagnosis of Focal Atrial Tachycardia

Focal AT produces a narrow-complex tachycardia (or wide-complex in the presence of fixed or rate-related bundle branch block). The surface electrocardiogram provides clues to the diagnosis and helps differentiate it from sinus tachycardia and other causes of SVT. Important features are the mode of onset and termination, the R-P relationship and the P wave vector.

Abrupt onset or a short 4–5 beat "warm-up" period helps distinguish AT from sinus tachycardia, AVNRT and AVRT. Similarly, termination is usually abrupt (unlike sinus tachycardia) or displays a short "cool down phase" (unlike AVNRT or AVRT). Termination with block in the AV node (ending on a P wave) effectively excludes AT [152].

AT usually has a long RP interval (defined as >50% of RR interval), distinguishing it from typical AVNRT and most forms of AVRT. This is a useful indicator, but it is important to remember that there are exceptions to this rule. For example, delay in AV nodal conduction during rapid AT may cause prolongation of the PR interval producing a short-RP tachycardia. Similarly, atypical AVNRT, and AVRT utilizing a decremental accessory pathway as the retrograde limb, may produce a long-RP tachycardia. Other features of the RP relationship may help distinguish AT from other forms of SVT. In AT, AV nodal and ventricular activation are passive and not necessary for tachycardia maintenance. As such, the relationship between atrial and ventricular activity is not fixed and variation in the RP interval supports the diagnosis of AT [152–154] although multiple or decremental accessory pathways may display a similar variation in RP relationship. Higher degrees of AV block can also occur, for example in digoxin toxicity [155, 156] where the resulting arrhythmia is commonly referred to as "paroxysmal atrial tachycardia (PAT) with block."

Clues may also be gained from the P wave vector. A positive P wave in the inferior leads makes AT more likely, as a superiorly directed vector is characteristic in AVNRT and common in AVRT. However, a superior vector is seen in focal AT with origins from inferior structures such as the inferior annuli, CS os or low crista terminalis. All these features may aid in the diagnosis of AT, but ultimately, differentiation from other causes of supraventricular tachycardia may not be possible until the time of diagnostic EP study.

26.6.3 P Wave Morphology

P wave morphology is determined by point of origin and subsequent pattern of atrial activation. As such, analysis of the P wave provides information on the site of origin of focal AT, as activation spreads radially with the origin as the epicenter. However, the spatial resolution of the P wave is only 17 mm [124], and as such, P wave morphology can only be used to localize to a general region of interest. Fortunately, AT foci display characteristic anatomical distributions with clustering at several structures and therefore localizing to a general area is often sufficient to direct more detailed mapping at EP study. A useful algorithm has been developed to predict the site of origin of focal AT based on the P wave morphology, with a reported accuracy of 93% when compared to the anatomical site of successful ablation [157].

The P wave on the surface ECG is often obscured by fusion with the preceding T wave, in some cases giving the appearance of a junctional tachycardia [158]. Administration of adenosine or a short burst of ventricular pacing to induce

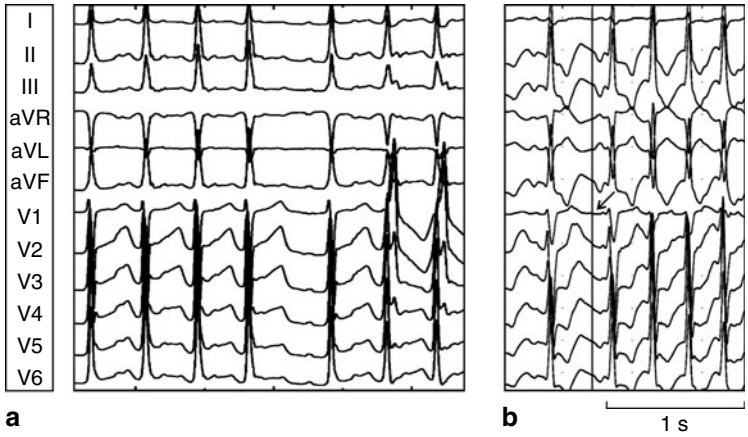

Figure 26.12

Assessment of P wave morphology in atrial tachycardia (AT). In part (a), intravenous adenosine has been administered. P wave morphology is clearly seen following transient AV block. The focus is right parahisian with a largely isoelectric P wave in lead V1 and positive P wave in the inferior leads. Part (b) illustrates the importance of assessing the initial P wave vector in determining the origin of an atrial tachycardia. The vertical line represents the onset of the P wave in the limb leads. The characteristic isoelectric component of V1 (*arrowed*) observed in AT from the os of the coronary sinus may have been missed if the P wave onset was not clearly defined. The ECG shows demonstrates the other features of AT from this site, with typical negative P wave in the inferior leads and a negative transition across the chest leads.

transient AV block may be necessary to remove T-P fusion (Fig. 26.12a). It is important to limit analysis to clearly defined P waves and to include the initial vector which may be isoelectric and easily missed (Fig. 26.12b). Increasing the sweep speed to 50 or 75 mm/s and the amplitude to 50 mm/mV better defines small changes in vector and is a useful tool when analyzing P wave morphology. Characteristic features of P wave morphology have been described for most common foci and are a function of the anatomic relationship of these foci and normal propagation away from the focus. As such, the utility of the P wave in localization is limited in those with structural heart disease or previous atrial surgery or extensive atrial ablation.

26.6.4 Localizing Tachycardia Focus to the Left or Right Atrium

P wave morphology is useful in differentiating left from right atrial foci. This is a function of the anatomical relationship of the atria, with the left atrium being a more posterior and leftward structure than the right atrium. As such, leads V1 and aVL are useful discriminators [122]. Activation from right atrial foci spread leftwards, and a positive or biphasic P wave in aVL has a positive predictive accuracy of 83% and negative predictive value of 85%. In contrast, a positive P wave in V1 is a feature of left atrial foci as activation spreads anteriorly and rightward. It provides a sensitivity and specificity for a left atrial focus of 93% and 88% respectively [122]. Specificity is reduced by the virtue that foci arising from the high crista terminalis in the right atrium can display a positive P wave in this lead. Analysis of the sinus rhythm P wave can help in this situation. As the sinus node complex is located in the high crista [159], the tachycardia P wave morphology should be similar to the sinus P wave if site of origin is the high crista, but will be markedly different if tachycardia focus is of left atrial origin [122].

It is perhaps unsurprising that foci arising from septal structures provide exceptions to these rules, as activation wavefront progresses both left and rightward and a variety of P wave morphologies have been reported [160–163]. However, careful analysis of the initial vector may often help differentiate a right from left atrial origin. For example, tachycardias originating from the coronary sinus (CS) ostium [163] or right septal region [160, 161] often have an initial negative or

isoelectric vector in lead V1, which is in keeping with a right atrial origin (Fig. 26.12b). Missing this initial component may lead to misclassification of the P wave as positive, localizing the focus to the wrong chamber. It is therefore essential that careful analysis of the entire P wave is performed.

Using this simple tool, it is possible to define the focus to the left or right atrium with a high degree of accuracy. However, further localization is possible as specific anatomical locations are associated with characteristic P wave morphologies, which are discussed below.

26.6.5 Right Atrium

26.6.5.1 Crista Terminalis

Up to 50% of right atrial tachycardias arise from the crista terminalis [149]. This structure extends the entire length of the right atrium inserting supero-medially into the inter-atrial septum near Bachmann's bundle and being contiguous with the Eustachian ridge inferiorly. It is therefore not surprising that there is some variation in P wave morphology along its length. Low cristal sites are usually associated with an negative P wave in lead V1 [149]. However, high and mid-cristal foci often display a biphasic P wave morphology in V1 with an initial positive vector followed by a negative component (Fig. 26.13a), although, as discussed above, a completely positive morphology is sometimes present and in this situation one should consider the morphology of the sinus P wave [122, 149, 164]. Lead aVL displays marked variation in morphology, but lead I is positive and aVR negative in the majority of cases [164]. The inferior leads display different vectors depending on the position of the tachycardia focus along the length of the crista. P waves are positive inferiorly in high cristal foci and isoelectric or negative in more inferior cristal sites.

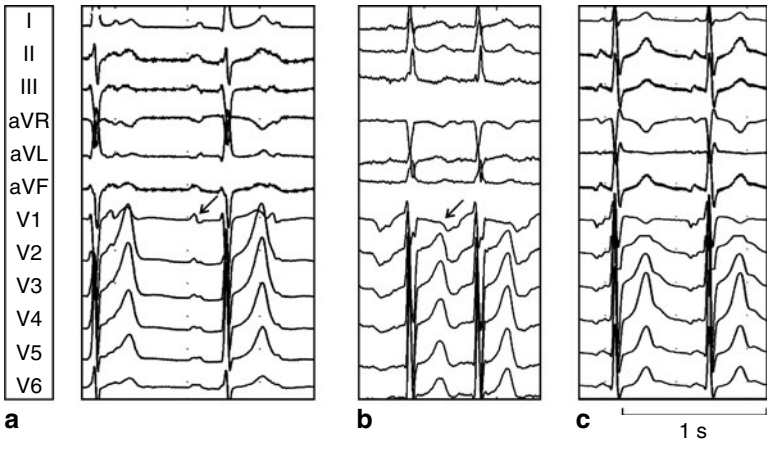

Figure 26.13

Surface electrocardiograms illustrating focal atrial tachycardias from different right atrial sites. Part (a) shows the characteristic P wave morphology of a high cristal focus being positive/negative biphasic in lead V1 (*arrowed*), negative in aVR and positive in lead I. A positive P wave vector in the inferior leads localizes the focus to the high crista terminalis. Part (b) illustrates an inferior tricuspid annulus (TA) focus. The P wave is negative in lead V1 (*arrowed*), and positive in lead I. P waves are isoelectric/negative inferiorly, localizing to the infero-anterior TA. Part (c) shows P wave morphology of a right atrial appendage focus, displaying a negative vector in lead V1, becoming increasingly positive across the precordial leads. P waves are positive in the inferior leads. Morphology from this site is similar to the superior TA, given its close anatomical proximity.

26.6.5.2 Tricuspid Annulus

The tricuspid annulus (TA) is a less common site for focal AT, comprising 13% of right atrial tachycardias in a series by Morton et al. [165]. The TA is an anterior and a relatively rightward structure, and as such, the P wave is characteristically negative in lead V1 and positive in leads I and aVL [164, 165], except for the rare cases of tachycardia arising from the septal TA, where the P wave will have an isoelectric component. The majority of foci arise from the infero-anterior TA and negative or iso-electric P waves are usual in the inferior leads (Fig. 26.13b). Positive P waves inferiorly indicate a superior TA focus.

26.6.5.3 CS Ostium

Tachycardias arising from the CS os account for 7% of all focal atrial tachycardia [163] and display a characteristic P wave morphology similar to that of the flutter wave of typical counter-clockwise isthmus dependent flutter. This is a function of the close proximity to the usual exit site of flutter with both displaying an initial negative or isoelectric component in lead V1 which is characteristic of foci arising from the septum. This initial negative vector is followed by a positive deflection which may become more negative across the precordial leads (Fig. 26.12b). The CS os is an inferior structure, and atrial activation is therefore in a superior direction with resultant negative P waves in the inferior leads [160, 163].

26.6.5.4 Right Atrial Appendage

The right atrial appendage is an uncommon site for focal AT. Insights into P wave morphology can be gained from a series of seven patients by Roberts-Thomson and colleagues [166]. P waves were negative in lead V1 in all patients, in keeping with the relative anterior and rightward position of the appendage. P wave vector became progressively more positive across the precordial leads and generally displayed an inferior axis (Fig. 26.13c).

26.6.5.5 The Inter-atrial Septum

Focal AT has been described from several septal structures other than the CS os both on the right and left sides. These include the triangle of Koch, the right and left perinodal regions and the septal insertion of the crista terminalis [149, 160–162]. In general, P wave duration is relatively short, reflecting a short total atrial activation time due to simultaneous activation of both the right and left atria. Lead V1 displays an initial negative or isoelectric component (Fig. 26.12a), followed by a positive deflection with right septal sites, and is usually completely positive in left septal foci. The inferior leads help further localize right septal sites, with anteroseptal sites displaying a positive P wave, and negative P waves being a feature of mid-septal sites.

26.6.6 Left Atrium

26.6.6.1 Pulmonary Veins

The pulmonary veins are a common site for focal AT, especially the superior veins [167, 168]. The veins are a posterior and leftward structure and the P wave is characteristically positive in V1 and across the other chest leads. Left-sided veins are further from the septum and total atrial activation time is longer than for foci originating in the right-sided veins. As a result, the P wave in left atrial foci display a longer P wave duration and are characteristically notched in the inferior leads (Fig. 26.14a) [167]. Given the relative anatomical relationship of the veins, the lateral limb leads help distinguish right from left pulmonary venous foci. Lead I is usually positive in right-sided veins and isoelectric or negative in the left veins. In contrast, lead aVL is a poor discriminator. The P wave vector in the inferior limb leads help discriminate between the upper and lower veins, being more positive in superior venous foci.

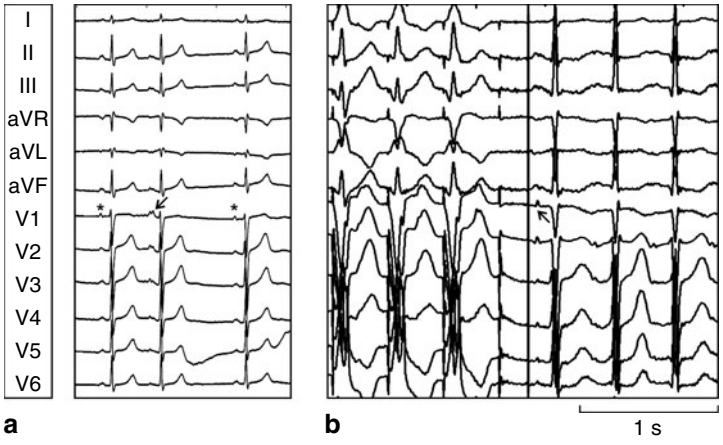

Figure 26.14

Surface electrocardiograms illustrating focal atrial tachycardias from left atrial sites. Part (a) shows the characteristic P wave morphology from a left superior pulmonary vein focus (*arrowed*) between two sinus beats (*). Lead V1 is positive and notched. Note the notched positive P waves in the inferior leads. Part (b) illustrates an atrial tachycardia arising from the aorto-mitral continuity. A burst of ventricular pacing has produced transient AV block which allows clear definition of the P wave (*vertical line*). Note the initial negative deflection in lead V1 (*arrowed*).

26.6.6.2 Mitral Annulus

Focal AT arising from the mitral annulus is well described, with the most common area being the supero-medial aspect at the aorto-mitral continuity [169, 170]. In keeping with its fairly midline anatomical position, this site typically displays a short P wave duration. The P wave in lead V1 is biphasic with an initial negative deflection followed by a positive vector, which becomes progressively more isoelectric across the precordial leads (Fig. 26.14b). P waves are usually negative in leads I and aVL and weakly positive in the inferior leads [169, 170].

26.6.6.3 Other Left Atrial Foci

P wave morphology of tachycardia arising from the left septum has already been discussed. Other uncommon sites of tachycardia reported in the literature are the left atrial appendage [122, 168] and the body of the coronary sinus [171–173]. Foci arising from the left atrial appendage display a similar P wave morphology to left sided pulmonary vein foci given their close anatomical proximity, with the exception of deeply negative P waves in leads I and aVL. Tachycardias originating from the CS musculature display a positive P wave in lead V1 and across the precordial leads.

26.7 Multifocal Atrial Tachycardia

26.7.1 Overview

Multifocal atrial tachycardia (MAT), or "chaotic atrial tachycardia," is characterized by an atrial rate of greater than 100 bpm and discrete P waves of at least three different morphologies [174, 175]. The prevalence of MAT in hospitalized patients is 0.05–0.32%, and it characteristically occurs in severely ill elderly patients, in particular those with acute exacerbations of pulmonary disease [174–176]. Other associations include hypoxemia, pulmonary embolism, electrolyte

disturbance, and administration of theophylline or beta-agonist therapy [175, 177–179]. There is a high associated mortality, related to the underlying disease [174, 175, 180]. Multifocal atrial tachycardia may also be found uncommonly in children, where it may occur in the absence of underlying disease [175, 181]. In children, it is rarely associated with atrial fibrillation and is commonly self-limiting in nature.

The cornerstones of management are treatment of the underlying condition, correction of hypoxia and electrolyte abnormalities (in particular, hypokalemia), and discontinuation of medications thought to exacerbate the arrhythmia. The arrhythmia generally resolves as the patient's condition improves, but if pharmacological treatment is required, then the agents with the most evidence of efficacy are metoprolol [182] and intravenous magnesium [183]. Several other drug treatments have been reported, but generally in small trials, often without adequate control groups (reviewed by McCord and Borzak [175]). If MAT is refractory to medical treatment, then the ventricular rate can be controlled by catheter ablation of the AV junction combined with ventricular pacing [184], or catheter ablation to modify AV conduction [185].

MAT is thought to be due to triggered activity caused by delayed afterdepolarizations [118, 177, 186]. Although direct evidence for this is lacking, the fact that MAT is seen in conditions of calcium overload (e.g., high catecholamine states, and in the presence of phosphodiesterase inhibition), and can be suppressed by magnesium, supports triggered activity as the underlying mechanism. Magnesium is thought to have membrane-stabilizing effects, reducing afterdepolarizations. MAT is not a manifestation of digoxin toxicity [174, 176, 180].

26.7.2 The Electrocardiogram in MAT

By definition, at least three different P wave morphologies are seen on the surface ECG, separated by isoelectric intervals, and there is irregular variation in the P–P interval [174]. The multiple P-wave morphologies suggest a multifocal atrial origin, although a single focus with multiple exit pathways or intra-atrial conduction disturbances cannot be excluded. The irregular rhythm of MAT may mimic atrial fibrillation. There is a relation between MAT and other atrial arrhythmias, since in about half of patients it is either preceded by atrial flutter or fibrillation, or these arrhythmias subsequently develop [176, 180].

26.8 Macro-Reentrant Atrial Tachycardia

26.8.1 Overview

In contrast to the point source origin of focal AT with passive activation of the rest of the atrium, macro-reentrant AT is defined as a re-entrant circuit which can be entrained from at least two sites > 2 cm apart [119]. Entrainment is the transient increase in the rate of the tachycardia to match that of the overdrive paced rate (see Chap. 24) [187–190]. On termination of pacing, the tachycardia reverts to its basic cycle length. Entrainment provides evidence of a reentrant circuit which has an excitable gap that can be penetrated by the paced impulse. The paced beat repeatedly resets the tachycardia resulting in a decrease in the tachycardia cycle length to that of the paced drive cycle. The morphology of the atrial complexes changes during entrainment owing to fusion beats resulting from collision of the paced impulse with the preceding tachycardia wavefront. When pacing ceases, the last entrained beat does not manifest fusion since there is no impulse collision. At a critical paced rate, the pacing wavefront blocks in both directions and the reentrant tachycardia is interrupted [187–190].

Macro-reentrant circuits usually have a central barrier to conduction and an area of slow conduction, producing the excitable gap necessary for macro-reentry. Historically, the classification of atrial macro-reentry, also commonly referred to as atrial flutter, has been conflicting, and recent attempts have been made to standardize nomenclature [119, 191]. Scheinman et al. [191], propose a classification with three main divisions – right atrial cavo-tricuspid isthmus (CTI) dependent flutter, right atrial non-CTI dependent flutter and left atrial flutter. The former is commonly referred to as typical flutter, with the latter two often called atypical flutters.

Typical flutter (right atrial CTI-dependent) accounts for around 90% of macro-reentrant atrial tachycardia, with an increasing prevalence with advancing age to a peak incidence of 0.6% in those over 80 years [192, 193]. Atrial fibrillation and flutter often co-exist, and share the same risk factors, both being more prevalent in the elderly, in males and those with structural heart disease, hypertension, chronic pulmonary disease or an acute illness [192, 194]. It may also be associated with toxic or metabolic conditions, such as alcohol excess or thyrotoxicosis. Right atrial non-CTI dependent flutter or left atrial flutter, often grouped together as the atypical flutters, are less common and usually patients have a prior history of atrial surgery, catheter ablation procedures, valvular heart disease or congenital heart disease [119, 195, 196], although spontaneous scarring causing a flutter circuit in the right atrial free wall has recently been reported in the absence of traditional risk factors [197].

The clinical significance of atrial flutter depends on the ventricular rate and the severity of underlying heart disease. In the acute setting, cardioversion can be achieved by external DC shock, atrial overdrive pacing or pharmacological agents (reviewed by Blomstrom-Lundqvist et al. [108], Wellens [198], Lee et al. [193]). Satisfactory pharmacological control of the ventricular rate in atrial flutter by blocking AV nodal conduction is often more difficult to achieve than it is in atrial fibrillation. Chronic therapy with Class Ia, Ic or III antiarrhythmic agents in an attempt to maintain sinus rhythm is only moderately successful and can be associated with proarrhythmia, such as torsades de pointes (with Class III agents) or 1:1 AV conduction during flutter (Class Ia and Ic agents) [108, 198].

The recognition of the anatomical substrates for macro-reentry and advances in catheter ablation have revolutionized the management of atrial flutter in the last 10–15 years. Linear ablation to interrupt the macro-reentrant circuit can be curative, with a high success rate for typical (CTI-dependent) flutter and a low rate of recurrence, particularly if bi-directional isthmus conduction block is demonstrated [108, 193]. Ablation should be considered early in the management of recurrent or persistent typical flutter. Indeed, a randomized comparison of first-line radiofrequency ablation with antiarrhythmic drug therapy has shown better maintenance of sinus rhythm, fewer hospitalizations, and better quality of life in those who underwent ablation [199]. Ablation is also having an increasing role in the management of "atypical" flutters, facilitated by the development of new endocardial mapping technologies [200–203].

26.8.2 The Electrocardiogram in the Differentiation of Macro-Reentrant from Focal Atrial Tachycardia

The rate of tachycardia does not help differentiate a focal from macro-reentrant mechanism. Although focal AT is usually associated with lower rates than macro-reentry [146], cycle length is highly variable in focal AT and rates can be as high as 340 bpm [204]. Similarly, although macro-reentrant tachycardia usually displays high rates, marked delay in conduction may produce much slower tachycardia cycle lengths.

Careful examination of the flutter or P wave and analysis of the intervening P-P interval may be of value. They may be obscured by the QRS or T wave and maneuvers to cause transient AV block may be required to unmask the atrial activity (Fig. 26.15). Atrial activation is largely passive in focal AT, but, by definition, there is atrial activation over the whole tachycardia cycle length in atrial macro-reentry. As such, continuous activity is often seen in the 12 lead ECG, with no isoelectric period between the flutter waves ("saw-tooth" waveform, Fig. 26.16). However, there may be no obvious discernible isoelectric period in short cycle length focal AT and it is not always present in flutter. Despite these limitations, a high atrial rate or lack of an isoelectric component should alert the physician to the possibility of a macro-reentrant mechanism.

26.8.2.1 Electrocardiographic Features of Typical (CTI-Dependent) Flutter

Typical flutter is a macro-reentrant circuit confined to the right atrium. It is bounded by the tricuspid annulus anteriorly and by the caval veins, the Eustachian ridge and the crista terminalis posteriorly. An obligate part of the circuit is the cavo-tricuspid isthmus [205, 206]. Linear ablation within this isthmus by radiofrequency ablation is curative with a high success rate. In 90% of patients with typical flutter, activation is counterclockwise around this circuit [119], with

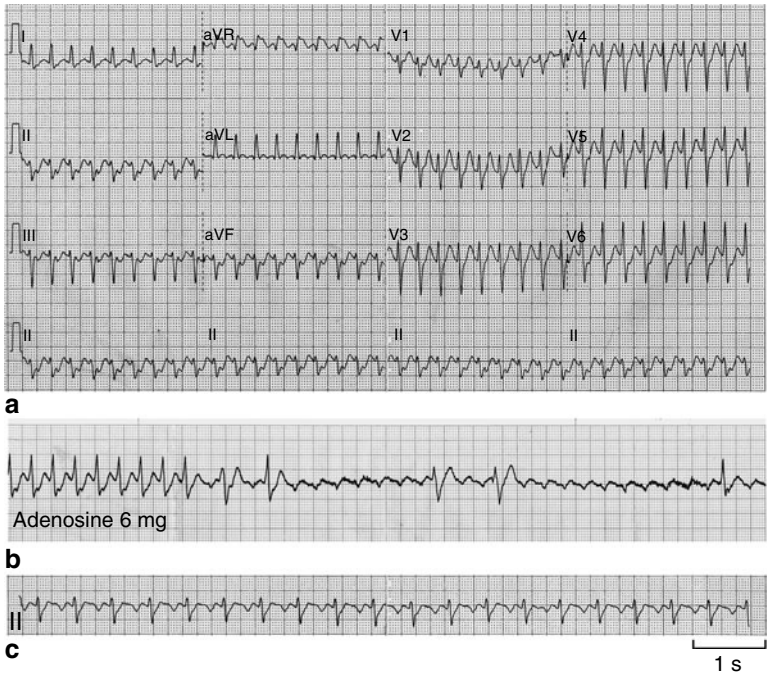

Figure 26.15

Narrow-complex tachycardia (a), with a rate of 218 bpm. Intravenous adenosine (b) reveals flutter waves. After initial drug treatment, 2:1 AV conduction results, with a ventricular rate of 110 bpm (c).

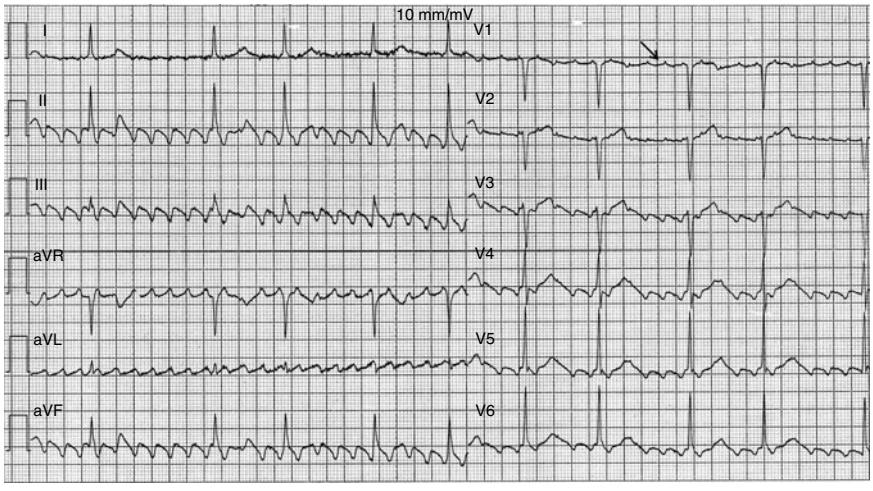

Figure 26.16

Typical counterclockwise cavotricuspid isthmus-dependent atrial flutter with isoelectric/positive P wave in lead V1 (*arrowed*) and negative "saw tooth" flutter waves in the inferior leads.

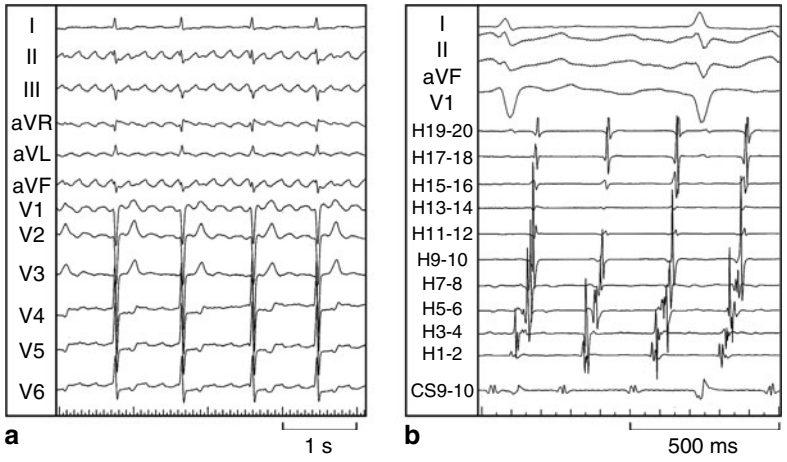

Figure 26.17

Characteristic flutter wave morphology of clockwise cavotricuspid isthmus-dependent atrial flutter. Part (a) shows negative flutter waves in lead V1 and positive flutter waves in the inferior leads. Part (b) shows surface leads I, II, aVF and V1, and intracardiac recordings from electrode pairs (H1-2 to H19-20) of a 20-pole "Halo" catheter lying around the tricuspid annulus (see Fig. 24.1c), and the proximal poles of a catheter lying in the coronary sinus (CS9-10). Atrial activation travels in a clockwise direction from the distal poles of the Halo catheter (H1-2) to the proximal poles (H19-20).

the activation wavefront exiting the CTI medially near the CS os [207], activating the posterior and septal aspects of the right atrium in a superior direction, with later inferior activation of the lateral wall. This gives rise to a characteristic appearance on the ECG with negative saw-tooth flutter waves in the inferior leads (Fig. 26.16). Lead V1 displays a pattern similar to that seen in focal AT arising from the CS os [163], with an initial isoelectric component followed by a positive vector. The flutter waves become progressively more negative across the precordial leads. These features are highly specific for counterclockwise CTI-dependent flutter [119]. In 10% of patients with CTI-dependent flutter, activation is in the opposite direction (clockwise). Flutter wave morphology is reversed with positive saw tooth pattern in the inferior leads and lead V1 displaying a negative vector (Fig. 26.17), although other morphologies have been reported [208].

The atrial rate in typical flutter ranges from 240 to 340 bpm, which is often almost exactly 300 bpm. The AV node rarely conducts as rapidly and so AV block is usually seen, commonly with 2:1 AV conduction, giving a ventricular rate of 150 bpm. The diagnosis of atrial flutter with 2:1 block should always be considered when a regular tachycardia of 150 bpm is identified. Higher degrees of AV conduction block can also be seen, for example in the presence of nodal blocking agents, with a ratio of 4:1, or rarely 3:1 (Fig. 26.16). The preference for even multiples of conduction – 2:1 or 4:1 – may be due to two levels of block in the AV node [209]. Rarely, very rapid ventricular rates are found as a result of 1:1 AV conduction (Fig. 26.15). This may arise because of the presence of an accessory pathway with a short refractory period, but may also occur with enhanced AV nodal conduction [210, 211], or because of slowing of the flutter rate by medication.

26.8.2.2 Electrocardiographic Features of Atypical (Non-CTI-Dependent) Flutter

The 12 lead ECG is of less use in localizing other forms of atrial macro-reentry. Flutter wave amplitude is often low in atypical flutter, regardless of the site of the circuit. Analysis of flutter wave morphology in leads V1 and V2 may be of some use, as left atrial flutters tend to display a positive flutter waves in these leads [212].

26.9 Atrial Fibrillation

26.9.1 Overview

Atrial fibrillation has been called the "grandfather of atrial arrhythmias" [213]. It was first described as a distinct rhythm in humans in the 1900s [214], but irregularities of the pulse associated with valvular heart disease had been recognized centuries before [215]. It is the commonest sustained arrhythmia in adults, may occur in normal hearts or as a feature of all types of cardiovascular diseases, and is associated with significant morbidity and mortality. A number of schemes for classifying AF have been proposed (e.g., [216]), but were of limited clinical utility. Current international guidelines recommend a simple classification, with paroxysmal, persistent and permanent AF [217]. It recognizes "*first detected*" AF, which may present itself in a number of ways – from a clearly defined, symptomatic episode, to an incidental finding on a routine ECG. If the arrhythmia is recurrent and each episode spontaneously reverts to sinus rhythm within 7 days, it is termed "*paroxysmal*". If it does not terminate spontaneously, AF is classed as "*persistent*" (usually lasting > 7 days). Persistent AF may respond to electrical or pharmacological cardioversion, or may go on to become "*permanent*" (e.g., lasting > 1 year) which is resistant to cardioversion. The classification also recognizes "*secondary*" AF, when the arrhythmia occurs as a consequence of another condition, for example acute myocardial infarction, pericarditis, cardiac surgery, or lower respiratory tract infection.

26.9.2 Mechanisms of Atrial Fibrillation

The electrophysiological mechanisms responsible for the initiation and maintenance of atrial fibrillation have been the subject of extensive experimental work [218]. Insights have been gained at single cell and whole tissue levels, as well as through computer modeling and clinical studies. Advancements in the understanding of the arrhythmia have led to novel therapeutic approaches that, in some cases, can offer the hope of a cure.

26.9.2.1 Focal Triggers of AF

Recent work has demonstrated that paroxysms of AF are frequently triggered by foci of ectopic activity in the sleeves of muscular tissue which extend into the proximal portions of the pulmonary veins [114]. This tissue is in electrical continuity with the left atrium, and it is proposed that a rapidly firing source within the vein can lead to fibrillatory conduction in the atrium ("focal trigger"). In some cases, continued activity of the focus may be required to sustain the arrhythmia ("focal driver"), whilst in others the fibrillation is self-sustaining within the atria. The underlying mechanism of the focal ectopic activity is as yet unclear, with possibilities including increased automaticity, triggered activity and micro-reentry, and indeed these mechanisms may not be mutually exclusive. The recognition of these focal initiators has led to the development of catheter ablation techniques for the treatment of AF. These were initially directed at ablating the ectopic focus itself, but have now evolved to aim for electrical isolation of all four pulmonary veins, with or without other lesions in the atria [219, 220] (see Chap. 24). Focal triggers have also been described in other venous structures, including the superior vena cava [113], the vein of Marshall [221] and the coronary sinus [172], and these may also be amenable to catheter ablation.

26.9.2.2 Tissue Substrate for Sustained AF

The mechanisms responsible for sustained fibrillatory conduction within the atria have also been the subject of much research. It has been proposed on the basis of experimental work and computer modeling that fibrillation develops when a wavefront becomes fractionated and produces multiple random reentrant wavelets [222, 223]. These wavelets would generate disorganized, chaotic atrial activity on the surface ECG. This theory requires a critical mass of atrial tissue to sustain several reentrant waves, and has been supported by the demonstration of such multiple wavelets resulting from intra-atrial reentry of the leading-circle type [224]. Further support comes from the observation that a surgical procedure

to "compartmentalize" conduction in the left atrium (the Maze procedure) can cure chronic AF, presumably by preventing reentrant waves from being sustained [225]. However, more recent studies have proposed that in fact a single high frequency stably rotating spiral wave ("mother rotor"), usually in the left atrium, can lead to the activation pattern seen in AF (reviewed by Jalife et al. [226]).

26.9.2.3 Atrial Electrical Remodeling

It has been observed that the longer a patient has been in AF, the harder it is to restore and maintain sinus rhythm [227]. This observation has been confirmed in studies employing rapid atrial pacing in goats to induce AF – when AF was initially induced, it would self-terminate after a short time, but when repeatedly induced it would eventually lead to sustained fibrillation [228]. This has been encapsulated in the phrase "AF begets AF," and the underlying process is referred to as electrical remodeling. Studies have shown that AF leads to a marked shortening of the atrial effective refractory period, along with dispersion of refractoriness, and both factors may facilitate reentry within the atria. The underlying ionic mechanisms for these phenomena have been investigated in animal models and changes in a number of ion channel conductances have been implicated (reviewed by Nattel et al. [229]).

26.9.2.4 Influence of the Autonomic Nervous System on AF

There is a complex relationship between sympathetic and parasympathetic activity and atrial electrophysiology. The autonomic nervous system has been implicated in the triggering and maintenance of AF, and, by altering AV nodal conduction, can also affect the ventricular rate. Vagal stimulation can reduce markedly the action potential duration and effective refractory period of atrial cells [230], and this can occur in a spatially heterogeneous fashion [231]. This leads to increased dispersion of refractoriness and conditions which could facilitate wavelet reentry. In animal experiments, intense vagal stimulation can promote induction of AF by atrial extrastimuli [231, 232]. Adrenergic stimulation and high catecholamine states can increase atrial ectopy, which may trigger episodes of AF (reviewed by Olshansky [233]). This mechanism may be of particular relevance in postoperative patients who develop AF.

Clinical observations of patients with paroxysmal AF (PAF) lead Coumel to propose that some have "vagotonic" PAF, usually initiated during sleep or after meals; while some have "adrenergic" PAF, predominantly occurring after exercise or other high catecholamine states (e.g., see [234], reviewed by Olshansky [233]). Those classed as "vagotonic" appear less likely to benefit from catheter-based pulmonary vein isolation as a treatment for PAF [235]. Other studies of catheter ablation for AF have shown that in around a third of patients, delivery of radiofrequency energy to some areas of the posterior left atrium results in intense vagal stimulation (e.g., causing sinus bradycardia, asystole or AV block) and elimination of such reflexes correlates with increased freedom from AF recurrence [236]. These sites may correspond to areas of vagal innervation via ganglia lying within fat pads behind the left atrium [233].

26.9.3 Epidemiology of AF

Both the prevalence and incidence of AF double with every decade beyond the age of 50 years [2]. The prevalence rises from 0.5% in the 6th decade of life to just under 9% in the 9th decade [237], and the lifetime risk of developing AF in those over the age of 40 years is 1 in 4 [238]. At any age, the arrhythmia is commoner in men than in women, and other significant risk factors include heart failure, hypertension, valvular heart disease, coronary artery disease, diabetes mellitus and hyperthyroidism [2, 239–241]. Atrial fibrillation occurs in about 10–20% of patients with acute myocardial infarction and is associated with more extensive infarction and higher mortality [217, 242]. Long-term moderate alcohol intake does not appear to lead to AF, but higher levels of consumption do significantly increase its incidence [243], and an alcoholic binge can precipitate an acute episode [244, 245]. In a minority of cases, no associated medical condition is identified and these patients are considered to have "lone" AF [246, 247].

A number of the conditions which predispose to AF may do so through the "final common pathway" of increased left atrial pressure and consequent dilatation of that chamber [248, 249]. Given the proposed mechanisms for AF, this step may be crucial in providing the necessary substrate to sustain the arrhythmia. Several other echocardiographic findings are commoner in patients with AF (e.g., increased left ventricular size, mitral annular calcification), although often they are "markers" for other predisposing conditions, rather than risk factors in themselves. However, after correcting for other risk factors, reduced fractional shortening and left ventricular hypertrophy, as well as increased left atrial size, do appear to be independent predictors of AF [250].

Non-rheumatic atrial fibrillation is associated with a two- to seven-fold increase in the risk of stroke, and in the presence of rheumatic heart disease, this risk is even higher (around 17 times the risk of age-matched controls) [2, 217, 237]. AF is also associated with an increased incidence of heart failure [251] and overall mortality is doubled, although some of this increased risk can be attributed to underlying heart disease [217].

26.9.4 Electrocardiographic Features of Atrial Fibrillation

The atrial activity in atrial fibrillation is very rapid and irregular, and is seen on the surface ECG as chaotic fibrillatory ("f") waves at rates of up to 600 min^{-1} (Fig. 26.18). P waves are absent as no coordinated atrial activity occurs. The amplitude of the atrial fibrillatory waves may vary, being described as "coarse" or "fine" fibrillation. There is no correlation between the fibrillatory wave amplitude and atrial size on echocardiography or etiology of heart disease [252].

The ventricular rate is dependent on the conduction properties of the AV node and is usually rapid, unless there is preexisting, or drug-induced, AV nodal conduction delay (Fig. 26.18). The ventricular rhythm is characteristically irregularly irregular, which reflects not only the irregularities of the atrial activity, but also the conduction through the AV node. Some atrial impulses may penetrate the node but are blocked at different levels without being conducted to the ventricles. The consequent refractoriness influences the conduction of subsequent atrial impulses through the AV node, the extent of the delay depending on the degree of penetration of the preceding impulse. The effect of such concealed conduction on ventricular rate is demonstrated by the fact that the ventricular rate during rapid atrial pacing may be greater than the rate once atrial fibrillation is initiated [253]. Clinically, regularization of the ventricular rhythm may be

Figure 26.18
Ventricular rate in atrial fibrillation. In part (a) there is a controlled rate (66 bpm) due to treatment with a beta blocker. Part (b) shows AF with a slow ventricular response (36 bpm) in a patient on no cardioactive medication (suggestive of sick sinus syndrome). A rapid ventricular response (102 bpm) is seen in part (c).

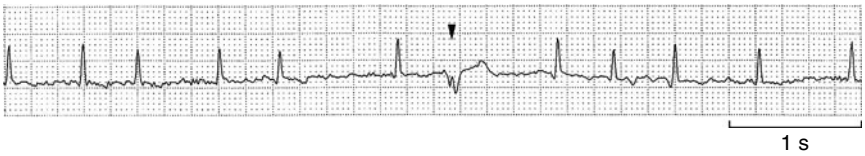

Figure 26.19

Aberrant conduction in atrial fibrillation due to rate-dependent refractoriness of the conducting system (the Ashmann phenomenon). An aberrantly conducted beat (*arrowhead*) occurs close to a beat which was preceded by a long interval.

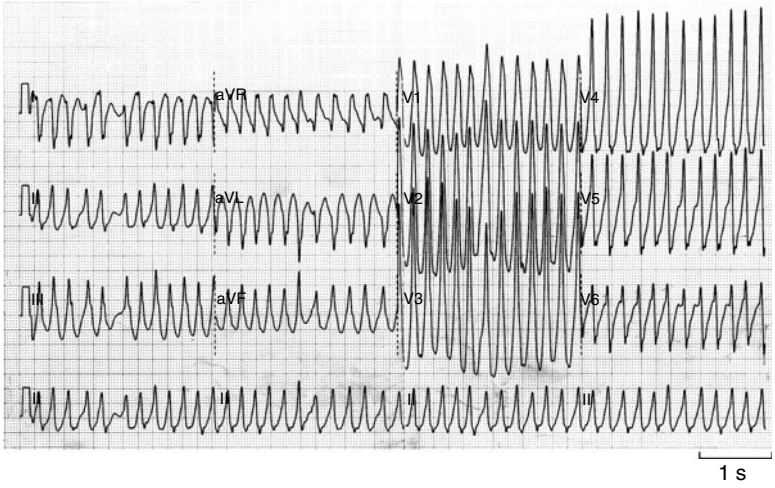

Figure 26.20

Preexcited atrial fibrillation in the Wolff-Parkinson-White syndrome. The ventricular rate is rapid (282 bpm) and the complexes are broad and preexcited due to conduction down an accessory pathway.

observed with third-degree AV block and a junctional or ventricular escape rhythm or in digoxin toxicity, owing to the development of a junctional rhythm.

The QRS complex is normally narrow, unless aberrant conduction is present. Intermittent aberrancy (sometimes called "phasic aberrant ventricular conduction") presents a particular diagnostic problem in atrial fibrillation since neither prematurity nor rate may distinguish between aberrancy and ventricular ectopics. Electrocardiographic criteria have been described to differentiate between aberrancy and ectopy based on QRS morphology and axis [254]. The aberrant morphology is usually RBBB, reflecting the relative refractory periods of the bundle, and it may exhibit the "Ashman phenomenon" (Fig. 26.19, see Sect. 26.5.2). Less commonly, LBBB may occur, but at shorter cycles and independent of preceding cycle length [140]. A ventricular complex may be followed by a short "compensatory pause" even in atrial fibrillation, owing to retrograde penetration of the AV node inhibiting the next conducted beat [255].

An alternative, but less common, reason for broad complexes in atrial fibrillation is conduction via an accessory pathway in Wolff-Parkinson-White (WPW) syndrome (Fig. 26.20). This diagnosis is important as the excessively rapid ventricular rate may lead to ventricular fibrillation, particularly if AV nodal blocking drugs are given which may enhance conduction down the bypass pathway [256]. Although reentrant tachycardia is the most common arrhythmia in such patients, there appears to be an increased incidence of atrial flutter and fibrillation [257]. Patients with WPW syndrome who exhibit preserved antegrade conduction via their accessory pathway at short cycle lengths (for example during exercise or rapid atrial pacing) are at particular risk of sudden death, and the treatment of choice is ablation of the pathway [217].

References

1. Kusumoto, F.M., and N. Goldschlager, Cardiac pacing. *N. Engl. J. Med.*, 1996;**334**: 89–97.
2. Kannel, W.B., P.A. Wolf, E.J. Benjamin, and D. Levy, Prevalence, incidence, prognosis, and predisposing conditions for atrial fibrillation: population-based estimates. *Am. J. Cardiol.*, 1998;**82**: 2N–9N.
3. Mandel, W., H. Hayakawa, R. Danzig, and H.S. Marcus, Evaluation of sino-atrial node function in man by overdrive suppression. *Circulation*, 1971;**44**: 59–66.
4. Reiffel, J.A. and M.J. Kuehnert, Electrophysiological testing of sinus node function: diagnostic and prognostic application-including updated information from sinus node electrograms. *Pace Clin. Electrophysiol.*, 1994;**17**: 349–365.
5. Callans, D.J., D. Schwartzman, C.D. Gottlieb, and F.E. Marchlinski, Insights into the electrophysiology of atrial arrhythmias gained by the catheter ablation experience: "learning while burning, Part II." *J. Cardiovasc. Electrophysiol.*, 1995;**6**: 229–243.
6. Brignole, M., P. Alboni, D.G. Benditt, L. Bergfeldt, J.J. Blanc, P.E.B. Thomsen, et al., Guidelines on management (diagnosis and treatment) of syncope – update 2004. The task force on syncope, European Society of Cardiology. *Europace*, 2004;**6**: 467–547.
7. Epstein, A.E., J.P. DiMarco, K.A. Ellenbogen, N.A.M. Estes III, R.A. Freedman, L.S. Gettes, et al, ACC/AHA/HRS 2008 guidelines for device-based therapy of cardiac rhythm abnormalities: a report of the American College of Cardiology/American Heart Association Task Force on Practice Guidelines (Writing Committee to revise the ACC/AHA/NASPE 2002 guideline update for implantation of cardiac pacemakers and antiarrhythmia devices). *J. Am. Coll. Cardiol.*, 2008;**51**: e1–e62.
8. Benditt, D.G., C.C. Gornick, D. Dunbar, A. Almquist, and S. Pool-Schneider, Indications for electrophysiologic testing in the diagnosis and assessment of sinus node dysfunction. *Circulation*, 1987;**75**: III93–102.
9. James, T.N., Structure and function of the sinus node, AV node and His bundle of the human heart: part I-structure. *Prog. Cardiovasc. Dis.*, 2002;**45**: 235–267.
10. Sanchez-Quintana, D., J.A. Cabrera, J. Farre, V. Climent, R.H. Anderson, and S.Y. Ho, Sinus node revisited in the era of electroanatomical mapping and catheter ablation. *Heart*, 2005;**91**: 189–194.
11. Irisawa, H., T. Nakayama, and A. Noma, Membrane currents of single pacemaker cells from rabbit S-A and A-V nodes, in D. Noble and T. Powell, Editors. London: Academic Press, 1987, pp. 167–186.
12. Mitsuiye, T., Y. Shinagawa, and A. Noma, Sustained inward current during pacemaker depolarization in mammalian sinoatrial node cells. *Circ. Res.*, 2000;**87**: 88–91.
13. Mangoni, M.E., B. Couette, E. Bourinet, J. Platzer, D. Reimer, J. Striessnig, et al., Functional role of L-type Cav1.3 Ca^{2+} channels in cardiac pacemaker activity. *Proc. Natl. Acad. Sci. U.S.A.*, 2003;**100**: 5543–5548.
14. Stieber, J., F. Hofmann, and A. Ludwig, Pacemaker channels and sinus node arrhythmia. *Trends Cardiovasc. Med.*, 2004;**14**: 23–28.
15. Cho, H.S., M. Takano, and A. Noma, The electrophysiological properties of spontaneously beating pacemaker cells isolated from mouse sinoatrial node. *J. Physiol. (Lond.)*, 2003;**550**: 169–180.
16. Vinogradova, T.M., V.A. Maltsev, K.Y. Bogdanov, A.E. Lyashkov, and E.G. Lakatta, Rhythmic Ca^{2+} oscillations drive sinoatrial nodal cell pacemaker function to make the heart tick. *Ann. N.Y. Acad. Sci.*, 2005;**1047**: 138–156.
17. Bleeker, W.K., A.J. Mackaay, M. Masson-Pevet, L.N. Bouman, and A.E. Becker, Functional and morphological organization of the rabbit sinus node. *Circ. Res.*, 1980;**46**: 11–22.
18. Morton, H.J. and E.T. Thomas, Effect of atropine on the heart-rate. *Lancet*, 1958;**2**: 1313–1315.
19. WHO/ISFC Task Force, Definition of terms related to cardiac rhythm. *Am. Heart J.*, 1978;**95**: 796–806.
20. Spodick, D.H., P. Raju, R.L. Bishop, and R.D. Rifkin, Operational definition of normal sinus heart rate. *Am. J. Cardiol.*, 1992;**69**: 1245–1246.
21. Brignole, M., Sick sinus syndrome. *Clin. Geriatr. Med.*, 2002;**18**: 211–227.
22. Scott, O., G.J. Williams, and G.I. Fiddler, Results of 24 hour ambulatory monitoring of electrocardiogram in 131 healthy boys aged 10 to 13 years. *Br. Heart J.*, 1980;**44**: 304–308.
23. Brodsky, M., D. Wu, P. Denes, C. Kanakis, and K.M. Rosen, Arrhythmias documented by 24 hour continuous electrocardiographic monitoring in 50 male medical students without apparent heart disease. *Am. J. Cardiol.*, 1977;**39**: 390–395.
24. Bjerregaard, P., Mean 24 hour heart rate, minimal heart rate and pauses in healthy subjects 40–79 years of age. *Eur. Heart J.*, 1983;**4**: 44–51.
25. Talan, D.A., R.A. Bauernfeind, W.W. Ashley, C. Kanakis Jr., and K.M. Rosen, Twenty-four hour continuous ECG recordings in long-distance runners. *Chest*, 1982;**82**: 19–24.
26. Adgey, A.A., J.S. Geddes, H.C. Mulholland, D.A. Keegan, and J.F. Pantridge, Incidence, significance, and management of early bradyarrhythmia complicating acute myocardial infarction. *Lancet*, 1968;**2**: 1097–1101.
27. Alpert, M.A. and G.C. Flaker, Arrhythmias associated with sinus node dysfunction. Pathogenesis, recognition, and management. *JAMA*, 1983;**250**: 2160–2166.
28. Adan, V. and L.A. Crown, Diagnosis and treatment of sick sinus syndrome. *Am. Fam. Physician*, 2003;**67**: 1725–1732.
29. Sheffield, L.T., J.H. Holt, and T.J. Reeves, Exercise graded by heart rate in electrocardiographic testing for angina pectoris. *Circulation*, 1965;**32**: 622–629.
30. Tanaka, H., K.D. Monahan, and D.R. Seals, Age-predicted maximal heart rate revisited. *J. Am. Coll. Cardiol.*, 2001;**37**: 153–156.
31. Yasuma, F. and J. Hayano, Respiratory sinus arrhythmia: why does the heartbeat synchronize with respiratory rhythm? *Chest*, 2004;**125**: 683–690.
32. Rosenbaum, M.B. and E. Lepeschin, The effect of ventricular systole on auricular rhythm in auriculoventricular block. *Circulation*, 1955;**11**: 240–261.
33. de Marchena, E., M. Colvin-Adams, J. Esnard, M. Ridha, A. Castellanos, and R.J. Myerburg, Ventriculophasic sinus arrhythmia in the orthotopic transplanted heart: mechanism of disease revisited. *Int. J. Cardiol.*, 2003;**91**: 71–74.
34. Bauernfeind, R.A., F. Amat-y-Leon, R.C. Dhingra, R. Kehoe, C. Wyndham, and K.M. Rosen, Chronic nonparoxysmal sinus

tachycardia in otherwise healthy persons. *Ann. Intern. Med.*, 1979;**91**: 702–710.
35. Brady, P.A., P.A. Low, and W.K. Shen, Inappropriate sinus tachycardia, postural orthostatic tachycardia syndrome, and overlapping syndromes. Pace Clin. Electrophysiol., 2005;**28**: 1112–1121.
36. Narula, O.S., Sinus node re-entry: a mechanism for supraventricular tachycardia. *Circulation*, 1974;**50**: 1114–1128.
37. Sperry, R.E., K.A. Ellenbogen, M.A. Wood, M.K. Belz, and B.S. Stambler, Radiofrequency catheter ablation of sinus node reentrant tachycardia. *Pace Clin. Electrophysiol.*, 1993;**16**: 2202–2209.
38. Gomes, J.A., D. Mehta, and M.N. Langan, Sinus node reentrant tachycardia. *Pace Clin. Electrophysiol.*, 1995;**18**: 1045–1057.
39. Gomes, J.A., R.J. Hariman, P.S. Kang, and I.H. Chowdry, Sustained symptomatic sinus node reentrant tachycardia: incidence, clinical significance, electrophysiologic observations and the effects of antiarrhythmic agents. *J. Am. Coll. Cardiol.*, 1985;**5**: 45–57.
40. Damato, A.N., Clinical evidence for sinus node reentry, in *The Sinus Node: Structure, Function and Clinical Relevance*, F.I.M. Bonke, Editor. The Hague: Nijhoff, 1978, pp. 379–388.
41. Bashour, T.T., Classification of sinus node dysfunction. *Am. Heart J.*, 1985;**110**: 1251–1256.
42. Thery, C., B. Gosselin, J. Lekieffre, and H. Warembourg, Pathology of sinoatrial node. Correlations with electrocardiographic findings in 111 patients. *Am. Heart J.*, 1977;**93**: 735–740.
43. Evans, R. and D.B. Shaw, Pathological studies in sinoatrial disorder (sick sinus syndrome). *Br. Heart J.*, 1977;**39**: 778–786.
44. Bharati, S., A. Nordenberg, R. Bauernfiend, J.P. Varghese, A.G. Carvalho, K. Rosen, et al., The anatomic substrate for the sick sinus syndrome in adolescence. *Am. J. Cardiol.*, 1980;**46**: 163–172.
45. Rosen, K.M., H.S. Loeb, M.Z. Sinno, S.H. Rahimtoola, and R.M. Gunnar, Cardiac conduction in patients with symptomatic sinus node disease. *Circulation*, 1971;**43**: 836–844.
46. Narula, O.S., Atrioventricular conduction defects in patients with sinus bradycardia. Analysis by His bundle recordings. *Circulation*, 1971;**44**: 1096–1110.
47. Kaplan, B.M., R. Langendorf, M. Lev, and A. Pick, Tachycardia-bradycardia syndrome (so-called "sick sinus syndrome"). Pathology, mechanisms and treatment. *Am. J. Cardiol.*, 1973;**31**: 497–508.
48. Demoulin, J.C. and H.E. Kulbertus, Histopathological correlates of sinoatrial disease. *Br. Heart J.*, 1978;**40**: 1384–1389.
49. Hwang, Y.T., C.D. Tseng, J.J. Hwang, K.L. Hsu, F.T. Chiang, Y.Z. Tseng, et al., Cardiac amyloidosis presenting as sick sinus syndrome and intractable heart failure: report of a case. *J. Formos. Med. Assoc.*, 1993;**92**: 283–287.
50. Wang, T.L., W.J. Chen, C.S. Liau, and Y.T. Lee, Sick sinus syndrome as the early manifestation of cardiac hemochromatosis. *J. Electrocardiol.*, 1994;**27**: 91–96.
51. Watt, A.H., Sick sinus syndrome: an adenosine-mediated disease. *Lancet*, 1985;**1**: 786–788.
52. Benedini, G., C. Cuccia, R. Bolognesi, A. Affatato, G. Gallo, E. Renaldini, et al., Value of purinic compounds in assessing sinus node dysfunction in man: a new diagnostic method. *Eur. Heart J.*, 1984;**5**: 394–403.
53. Benditt, D.G., D.W. Benson Jr., J. Kreitt, A. Dunnigan, M.R. Pritzker, L. Crouse, et al., Electrophysiologic effects of theophylline in young patients with recurrent symptomatic bradyarrhythmias. *Am. J. Cardiol.*, 1983;**52**: 1223–1229.
54. Alboni, P., C. Menozzi, M. Brignole, N. Paparella, G. Gaggioli, G. Lolli, et al., Effects of permanent pacemaker and oral theophylline in sick sinus syndrome the THEOPACE study: a randomized controlled trial. *Circulation*, 1997;**96**: 260–266.
55. Maisch, B., U. Lotze, J. Schneider, and K. Kochsiek, Antibodies to human sinus node in sick sinus syndrome. *Pace Clin. Electrophysiol.*, 1986;**9**: 1101–1109.
56. Lown, B., Electrical reversion of cardiac arrhythmias. *Br. Heart J.*, 1967;**29**: 469–489.
57. Ferrer, M.I., The sick sinus syndrome in atrial disease. *JAMA*, 1968;**206**: 645–646.
58. Bigger, J.T. Jr. and J.A. Reiffel, Sick sinus syndrome. *Annu. Rev. Med.*, 1979;**30**: 91–118.
59. Rubenstein, J.J., C.L. Schulman, P.M. Yurchak, and R.W. DeSanctis, Clinical spectrum of the sick sinus syndrome. *Circulation*, 1972;**46**: 5–13.
60. Short, D.S., The syndrome of alternating bradycardia and tachycardia. *Br. Heart J.*, 1954;**16**: 208–214.
61. Andersen, H.R., J.C. Nielsen, P.E. Thomsen, L. Thuesen, T. Vesterlund, A.K. Pedersen, et al., Atrioventricular conduction during long-term follow-up of patients with sick sinus syndrome. *Circulation*, 1998;**98**: 1315–1321.
62. Walter, P.F., I.S. Crawley, and E.R. Dorney, Carotid sinus hypersensitivity and syncope. *Am. J. Cardiol.*, 1978;**42**: 396–403.
63. Davies, A.B., M.R. Stephens, and A.G. Davies, Carotid sinus hypersensitivity in patients presenting with syncope. *Br. Heart J.*, 1979;**42**: 583–586.
64. Sutton, R. and R.A. Kenny, The natural history of sick sinus syndrome. *Pace Clin. Electrophysiol.*, 1986;**9**: 1110–1114.
65. Ferrer, M.I., The etiology and natural history of sinus node disorders. *Arch. Intern. Med.*, 1982;**142**: 371–372.
66. Simonsen, E., J.S. Nielsen, and B.L. Nielsen, Sinus node dysfunction in 128 patients. A retrospective study with follow-up. *Acta Med. Scand.*, 1980;**208**: 343–348.
67. Denes, P., L. Levy, A. Pick, and K.M. Rosen, The incidence of typical and atypical A-V Wenckebach periodicity. *Am. Heart J.*, 1975;**89**: 26–31.
68. Crook, B.R., P.M. Cashman, F.D. Stott, and E.B. Raftery, Tape monitoring of the electrocardiogram in ambulant patients with sinoatrial disease. *Br. Heart J.*, 1973;**35**: 1009–1013.
69. Reiffel, J.A., J.T. Bigger Jr., M. Cramer, and D.S. Reid, Ability of Holter electrocardiographic recording and atrial stimulation to detect sinus nodal dysfunction in symptomatic and asymptomatic patients with sinus bradycardia. *Am. J. Cardiol.*, 1977;**40**: 189–194.
70. Krahn, A.D., G.J. Klein, R. Yee, and C. Norris, Final results from a pilot study with an implantable loop recorder to determine the etiology of syncope in patients with negative noninvasive and invasive testing. *Am. J. Cardiol.*, 1998;**82**: 117–119.
71. Reiffel, J.A., R. Schwarzberg, and M. Murry, Comparison of autotriggered memory loop recorders versus standard loop recorders versus 24-hour Holter monitors for arrhythmia detection. *Am. J. Cardiol.*, 2005;**95**: 1055–1059.
72. Kantelip, J.P., E. Sage, and P. Duchene-Marullaz, Findings on ambulatory electrocardiographic monitoring in subjects older than 80 years. *Am. J. Cardiol.*, 1986;**57**: 398–401.
73. Molgaard, H., K.E. Sorensen, and P. Bjerregaard, Minimal heart rates and longest pauses in healthy adult subjects on two occasions eight years apart. *Eur. Heart J.*, 1989;**10**: 758–764.

74. Mazuz, M. and H.S. Friedman, Significance of prolonged electrocardiographic pauses in sinoatrial disease: sick sinus syndrome. *Am. J. Cardiol*., 1983;**52**: 485–489.
75. Abbott, J.A., D.S. Hirschfeld, F.W. Kunkel, M.M. Scheinman, and G. Modin, Graded exercise testing in patients with sinus node dysfunction. *Am. J. Med*., 1977;**62**: 330–338.
76. Dhingra, R.C., F. Amat-y-Leon, C. Wyndham, P. Denes, D. Wu, R.H. Miller, et al., Electrophysiologic effects of atropine on sinus node and atrium in patients with sinus nodal dysfunction. *Am. J. Cardiol*., 1976;**38**: 848–855.
77. Strauss, H.C., J.T. Bigger, A.L. Saroff, and E.G. Giardina, Electrophysiologic evaluation of sinus node function in patients with sinus node dysfunction. *Circulation*, 1976;**53**: 763–776.
78. Cleaveland, C.R., R.E. Rangno, and D.G. Shand, A standardized isoproterenol sensitivity test. The effects of sinus arrhythmia, atropine, and propranolol. *Arch. Intern. Med*., 1972;**130**: 47–52.
79. Jose, A.D. and D. Collison, The normal range and determinants of the intrinsic heart rate in man. *Cardiovasc. Res*., 1970;**4**: 160–167.
80. Jordan, J.L., I. Yamaguchi, and W.J. Mandel, Studies on the mechanism of sinus node dysfunction in the sick sinus syndrome. *Circulation*, 1978;**57**: 217–223.
81. Szatmary, L.J., Autonomic blockade and sick sinus syndrome. New concept in the interpretation of electrophysiological and Holter data. *Eur. Heart J*., 1984;**5**: 637–648.
82. Hariman, R.J., E. Krongrad, R.A. Boxer, M.B. Weiss, C.N. Steeg, and B.F .Hoffman, Method for recording electrical activity of the sinoatrial node and automatic atrial foci during cardiac catheterization in human subjects. *Am. J. Cardiol*., 1980;**45**: 775–781.
83. Gomes, J.A., P.S. Kang, and N. El Sherif, The sinus node electrogram in patients with and without sick sinus syndrome: techniques and correlation between directly measured and indirectly estimated sinoatrial conduction time. *Circulation*, 1982;**66**: 864–873.
84. Reiffel, J.A., E. Gang, J. Gliklich, M.B. Weiss, J.C. Davis, J.N. Patton, et al., The human sinus node electrogram: a transvenous catheter technique and a comparison of directly measured and indirectly estimated sinoatrial conduction time in adults. *Circulation*, 1980;**62**: 1324–1334.
85. Josephson, M.E., *Sinus Node Function. Clinical Cardiac Electrophysiology: Techniques and Interpretations*, 4th edn. Philadelphia, PA: Lippincott Williams & Wilkins, 2008, pp. 69–92.
86. Reiffel, J.A., Electrophysiologic evaluation of sinus node function. *Cardiol. Clin*., 1986;**4**: 401–416.
87. Yee, R. and H.C. Strauss, Electrophysiologic mechanisms: sinus node dysfunction. *Circulation*, 1987;**75**: III12–III18.
88. Vassalle, M., The relationship among cardiac pacemakers. Overdrive suppression. *Circ. Res*., 1977;**41**: 269–277.
89. Narula, O.S., P. Samet, and R.P. Javier, Significance of the sinus-node recovery time. *Circulation*, 1972;**45**: 140–158.
90. Mandel, W.J., H. Hayakawa, H.N. Allen, R. Danzig, and A.I. Kermaier, Assessment of sinus node function in patients with the sick sinus syndrome. *Circulation*, 1972;**46**: 761–769.
91. Benditt, D.G., H.C. Strauss, M.M. Scheinman, V.S. Behar, and A.G. Wallace, Analysis of secondary pauses following termination of rapid atrial pacing in man. *Circulation*, 1976;**54**: 436–441.
92. Strauss, H.C., A.L. Saroff, J.T. Bigger Jr., and E.G. Giardina, Premature atrial stimulation as a key to the understanding of sinoatrial conduction in man. Presentation of data and critical review of the literature. *Circulation*, 1973;**47**: 86–93.
93. Narula, O.S., N. Shantha, M. Vasquez, W.D. Towne, and J.W. Linhart, A new method for measurement of sinoatrial conduction time. *Circulation*, 1978;**58**: 706–714.
94. Breithardt, G. and L. Seipel, Comparative study of two methods of estimating sinoatrial conduction time in man. *Am. J. Cardiol*., 1978;**42**: 965–972.
95. Kerr, C.R. and H.C. Strauss, The measurement of sinus node refractoriness in man. *Circulation*, 1983;**68**: 1231–1237.
96. Juillard, A., F. Guillerm, H.V. Chuong, A. Barrillon, and A. Gerbaux, Sinus node electrogram recording in 59 patients. Comparison with simultaneous estimation of sinoatrial conduction using premature atrial stimulation. *Br. Heart J*., 1983;**50**: 75–84.
97. Asseman, P., B. Berzin, D. Desry, D. Vilarem, P. Durand, C. Delmotte, et al., Persistent sinus nodal electrograms during abnormally prolonged postpacing atrial pauses in sick sinus syndrome in humans: sinoatrial block vs. overdrive suppression. *Circulation*, 1983;**68**: 33–41.
98. Asseman, P., B. Berzin, D. Desry, J.J. Bauchart, R. Reade, O. Leroy, et al., Postextrasystolic sinoatrial exit block in human sick sinus syndrome: demonstration by direct recording of sinus node electrograms. *Am. Heart J*., 1991;**122**: 1633–1643.
99. Fujimura, O., R. Yee, G.J. Klein, A.D. Sharma, and K.A. Boahene, The diagnostic sensitivity of electrophysiologic testing in patients with syncope caused by transient bradycardia. *N. Engl. J. Med*., 1989;**321**: 1703–1707.
100. Kang, P.S., J.A. Gomes, and N. El Sherif, Differential effects of functional autonomic blockade on the variables of sinus nodal automaticity in sick sinus syndrome. *Am. J. Cardiol*., 1982;**49**: 273–282.
101. Bergfeldt, L., H. Vallin, M. Rosenqvist, P. Insulander, R. Nordlander, and H. Astrom, Sinus node recovery time assessment revisited: role of pharmacologic blockade of the autonomic nervous system. *J. Cardiovasc. Electrophysiol*., 1996;**7**: 95–101.
102. Gann, D., A. Tolentino, and P. Samet, Electrophysiologic evaluation of elderly patients with sinus bradycardia: a long-term follow-up study. *Ann. Intern. Med*., 1979;**90**: 24–29.
103. Shaw, D.B., R.R. Holman, and J.I. Gowers, Survival in sinoatrial disorder (sick-sinus syndrome). *Br. Med. J*., 1980;**280**: 139–141.
104. Dhingra, R.C., F. Amat-y-Leon, C. Wyndham, P.C. Deedwania, D. Wu, P. Denes, et al., Clinical significance of prolonged sinoatrial conduction time. *Circulation*, 1977;**55**: 8–15.
105. Teichman, S.L., S.D. Felder, J.A. Matos, S.G. Kim, L.E. Waspe, and J.D. Fisher, The value of electrophysiologic studies in syncope of undetermined origin: report of 150 cases. *Am. Heart J*., 1985;**110**: 469–479.
106. Gang, E.S., J.A. Reiffel, F.D. Livelli Jr., and J.T. Bigger Jr., Sinus node recovery times following the spontaneous termination of supraventricular tachycardia and following atrial overdrive pacing: a comparison. *Am. Heart J*., 1983;**105**: 210–215.
107. van Mechelen, R., A. Segers, and F. Hagemeijer, Serial electrophysiologic studies after single chamber atrial pacemaker implantation in patients with symptomatic sinus node dysfunction. *Eur. Heart J*., 1984;**5**: 628–636.
108. Blomstrom-Lundqvist, C., M.M. Scheinman, E.M. Aliot, J.S. Alpert, H. Calkins, A.J. Camm, et al., ACC/AHA/ESC guidelines for the management of patients with supraventricular arrhythmias – executive summary. A report of the American college

of cardiology/American heart association task force on practice guidelines and the European society of cardiology committee for practice guidelines (writing committee to develop guidelines for the management of patients with supraventricular arrhythmias) developed in collaboration with NASPE-Heart Rhythm Society. *J. Am. Coll. Cardiol.*, 2003;**42**: 1493–1531.

109. Chen, S.A., C.T. Tai, C.E. Chiang, and M.S. Chang, Role of the surface electrocardiogram in the diagnosis of patients with supraventricular tachycardia. *Cardiol. Clin.*, 1997;**15**: 539–565.
110. Obel, O.A. and A.J. Camm, Supraventricular tachycardia. ECG diagnosis and anatomy. *Eur. Heart J.*, 1997;**18**(Suppl. C): 2–11.
111. Hoffman, B.F. and M.R. Rosen, Cellular mechanisms for cardiac arrhythmias. *Circ. Res.*, 1981;**49**: 1–15.
112. Zorn-Pauly, K., P. Schaffer, B. Pelzmann, P. Lang, H. Machler, B. Rigler, et al., If in left human atrium: a potential contributor to atrial ectopy. *Cardiovasc. Res.*, 2004;**64**: 250–259.
113. Tsai, C.F., C.T. Tai, M.H. Hsieh, W.S. Lin, W.C. Yu, K.C. Ueng, et al., Initiation of atrial fibrillation by ectopic beats originating from the superior vena cava: electrophysiological characteristics and results of radiofrequency ablation. *Circulation*, 2000;**102**: 67–74.
114. Haissaguerre, M., P. Jais, D.C. Shah, A. Takahashi, M. Hocini, G. Quiniou, et al., Spontaneous initiation of atrial fibrillation by ectopic beats originating in the pulmonary veins. *N. Engl. J. Med.*, 1998;**339**: 659–666.
115. Wit, A.L. and M.R. Rosen, Afterdepolarizations and triggered activity: distinction from automaticity as an arrhythmogenic mechanism, in *The Heart and Cardiovascular System*, H.A. Fozzard, E. Haber, R.B. Jennings, A.M. Katz, and H.E. Morgan, Editors. New York: Raven Press, 1992, pp. 2113–2163.
116. Lederer, W.J. and R.W. Tsien, Transient inward current underlying arrhythmogenic effects of cardiotonic steroids in Purkinje fibres. *J. Physiol. (Lond.)*, 1976;**263**: 73–100.
117. Fedida, D., D. Noble, A.C. Rankin, and A.J. Spindler, The arrhythmogenic transient inward current iTI and related contraction in isolated guinea-pig ventricular myocytes. *J. Physiol. (Lond.)*, 1987;**392**: 523–542.
118. Rosen, M.R. and R.F. Reder, Does triggered activity have a role in the genesis of cardiac arrhythmias? *Ann. Intern. Med.*, 1981;**94**: 794–801.
119. Saoudi, N., F. Cosio, A. Waldo, S.A. Chen, Y. Iesaka, M. Lesh, et al., Classification of atrial flutter and regular atrial tachycardia according to electrophysiologic mechanism and anatomic bases: a statement from a joint expert group from the Working Group of Arrhythmias of the European Society of Cardiology and the North American Society of Pacing and Electrophysiology. *J. Cardiovasc. Electrophysiol.*, 2001;**12**: 852–866.
120. Wellens, H.J., Value and limitations of programmed electrical stimulation of the heart in the study and treatment of tachycardias. *Circulation*, 1978;**57**: 845–853.
121. MacLean, W.A., R.B. Karp, N.T. Kouchoukos, T.N. James, and A.L. Waldo, P waves during ectopic atrial rhythms in man: a study utilizing atrial pacing with fixed electrodes. *Circulation*, 1975;**52**: 426–434.
122. Tang, C.W., M.M. Scheinman, G.F. Van Hare, L.M. Epstein, A.P. Fitzpatrick, R.J. Lee, et al., Use of P wave configuration during atrial tachycardia to predict site of origin. *J. Am. Coll. Cardiol.*, 1995;**26**: 1315–1324.
123. Wu, D., P. Denes, F. Amat-y-Leon, R.C. Chhablani, and K.M. Rosen, Limitation of the surface electrocardiogram in diagnosis of atrial arrhythmias. Further observations on dissimilar atrial rhythms. *Am. J. Cardiol.*, 1975;**36**: 91–97.
124. Man, K.C., Chan, K.K., P. Kovack, R. Goyal, F. Bogun, M. Harvey, et al., Spatial resolution of atrial pace mapping as determined by unipolar atrial pacing at adjacent sites. *Circulation*, 1996;**94**: 1357–1363.
125. Josephson, M.E., D.L. Scharf, J.A. Kastor, and J.G. Kitchen, Atrial endocardial activation in man. Electrode catheter technique of endocardial mapping. *Am. J. Cardiol.*, 1977;**39**: 972–981.
126. Wells, J.L. Jr., W.A. MacLean, T.N. James, and A.L. Waldo, Characterization of atrial flutter. Studies in man after open heart surgery using fixed atrial electrodes. *Circulation*, 1979;**60**: 665–673.
127. Killip, T. and J.H. Gault, Mode of onset of atrial fibrillation in man. *Am. Heart J.*, 1965;**70**: 172–179.
128. Bennett, M.A. and B.L. Pentecost, The pattern of onset and spontaneous cessation of atrial fibrillation in man. *Circulation*, 1970;**41**: 981–988.
129. Cosio, F.G., F. Arribas, and M. Lopez-Gil, Electrophysiologic findings in atrial fibrillation, in *Atrial Fibrillation: Mechanisms and Management*, R.H. Falk and P.J. Podrid, Editors. Philadelphia, PA: Lippincott-Raven, 1997, pp. 397–410.
130. Scheinman, M.M., D. Basu, and M. Hollenberg, Electrophysiologic studies in patients with persistent atrial tachycardia. *Circulation*, 1974;**50**: 266–273.
131. Shinbane, J.S., M.A. Wood, D.N. Jensen, K.A. Ellenbogen, A.P. Fitzpatrick, and M.M. Scheinman, Tachycardia-induced cardiomyopathy: a review of animal models and clinical studies. *J. Am. Coll. Cardiol.*, 1997;**29**: 709–715.
132. Walker, N.L., S.M. Cobbe, and D.H. Birnie, Tachycardiomyopathy: a diagnosis not to be missed. *Heart*, 2004;**90**: e7.
133. Calo, L., L. Sciarra, R. Scioli, F. Lamberti, M.L. Loricchio, C. Pandozi, et al., Recovery of cardiac function after ablation of atrial tachycardia arising from the tricuspid annulus. *Ital. Heart J.*, 2005;**6**: 652–657.
134. Raungratanaamporn, O., K. Bhuripanyo, R. Krittayaphong, C. Sriratanasathavorn, S. Raungratanaamporn, C. Kangkagate, et al., Reversibility of tachycardiomyopathy after successful radiofrequency catheter ablation: intermediate results. *J. Med. Assoc. Thai.*, 2001;**84**: 258–264.
135. Orth-Gomer, K., C. Hogstedt, L. Bodin, and B. Soderholm, Frequency of extrasystoles in healthy male employees. *Br. Heart J.*, 1986;**55**: 259–264.
136. Folarin, V.A., P.J. Fitzsimmons, and W.B. Kruyer, Holter monitor findings in asymptomatic male military aviators without structural heart disease. *Aviat. Space Environ. Med.*, 2001;**72**: 836–838.
137. Ramsdale, D.R., N. Arumugam, S.S. Singh, J. Pearson, and R.G. Charles, Holter monitoring in patients with mitral stenosis and sinus rhythm. *Eur. Heart J.*, 1987;**8**: 164–170.
138. Waldo, A.L., K.J. Vitikainen, G.A. Kaiser, J.R. Malm, and B.F. Hoffman, The P wave and P-R interval. Effects of the site of origin of atrial depolarization. *Circulation*, 1970;**42**: 653–671.
139. Gouaux, J.L. and R. Ashman, Auricular fibrillation with aberration simulating ventricular paroxysmal tachycardia. *Am. Heart J.*, 1947;**34**: 366–373.
140. Fisch, C., D.P. Zipes, and P.L. McHenry, Rate dependent aberrancy. *Circulation*, 1973;**48**: 714–724.
141. Chung, K.Y., T.J. Walsh, and E. Massie, Combined atrial and ventricular parasystole. *Am. J. Cardiol.*, 1965;**16**: 462–464.

142. Eliakim, M., Atrial parasystole. Effect of carotid sinus stimulation, Valsalva maneuver and exercise. *Am. J. Cardiol.*, 1965;**16**: 457–461.
143. Poutiainen, A.M., M.J. Koistinen, K.E. Airaksinen, E.K. Hartikainen, R.V. Kettunen, J.E. Karjalainen, et al., Prevalence and natural course of ectopic atrial tachycardia. *Eur. Heart J.*, 1999;**20**: 694–700.
144. Rodriguez, L.M., C. De Chillou, J. Schlapfer, J. Metzger, X. Baiyan, A. van den Dool, et al., Age at onset and gender of patients with different types of supraventricular tachycardias. *Am. J. Cardiol.*, 1992;**70**: 1213–1215.
145. Porter, M.J., J.B. Morton, R. Denman, A.C. Lin, S. Tierney, P.A. Santucci, et al., Influence of age and gender on the mechanism of supraventricular tachycardia. *Heart Rhythm*, 2004;**1**: 393–396.
146. Chen, S.A., C.E. Chiang, C.J. Yang, C.C. Cheng, T.J. Wu, S.P. Wang, et al., Sustained atrial tachycardia in adult patients. Electrophysiological characteristics, pharmacological response, possible mechanisms, and effects of radiofrequency ablation. *Circulation*, 1994;**90**: 1262–1278.
147. von Bernuth, G., W. Engelhardt, H.H. Kramer, H. Singer, P. Schneider, H. Ulmer, et al., Atrial automatic tachycardia in infancy and childhood. *Eur. Heart J.*, 1992;**13**: 1410–1415.
148. Chen, S.A., C.T. Tai, C.E. Chiang, Y.A. Ding, and M.S. Chang, Focal atrial tachycardia: reanalysis of the clinical and electrophysiologic characteristics and prediction of successful radiofrequency ablation. *J. Cardiovasc. Electrophysiol.*, 1998;**9**: 355–365.
149. Kalman, J.M., J.E. Olgin, M.R. Karch, M. Hamdan, R.J. Lee, and M.D. Lesh "Cristal tachycardias": origin of right atrial tachycardias from the crista terminalis identified by intracardiac echocardiography. *J. Am. Coll. Cardiol.*, 1998;**31**: 451–459.
150. Natale, A., L. Breeding, G. Tomassoni, K. Rajkovich, M. Richey, S. Beheiry, et al., Ablation of right and left ectopic atrial tachycardias using a three-dimensional nonfluoroscopic mapping system. *Am. J. Cardiol.*, 1998;**82**: 989–992.
151. Anguera, I., J. Brugada, M. Roba, L. Mont, L. Aguinaga, P. Geelen, et al., Outcomes after radiofrequency catheter ablation of atrial tachycardia. *Am. J. Cardiol.*, 2001;**87**: 886–890.
152. Knight, B.P., M. Ebinger, H. Oral, M.H. Kim, C. Sticherling, F. Pelosi, et al., Diagnostic value of tachycardia features and pacing maneuvers during paroxysmal supraventricular tachycardia. *J. Am. Coll. Cardiol.*, 2000;**36**: 574–582.
153. Benditt, D.G., E.L. Pritchett, W.M. Smith, and J.J. Gallagher, Ventriculoatrial intervals: diagnostic use in paroxysmal supraventricular tachycardia. *Ann. Intern. Med.*, 1979;**91**: 161–166.
154. Knight, B.P., A. Zivin, J. Souza, M. Flemming, F. Pelosi, R. Goyal, et al., A technique for the rapid diagnosis of atrial tachycardia in the electrophysiology laboratory. *J. Am. Coll. Cardiol.*, 1999;**33**: 775–781.
155. Lown, B., N.F. Wyatt, and H.D. Levine, Paroxysmal atrial tachycardia with block. *Circulation*, 1960;**21**: 129–143.
156. Storstein, O. and K. Rasmussen, Digitalis and atrial tachycardia with block. *Br. Heart J.*, 1974;**36**: 171–176.
157. Kistler, P.M., K.C. Roberts-Thomson, H.M. Haqqani, S.P. Fynn, S. Singarayar, J.K. Vohra, et al, P-wave morphology in focal atrial tachycardia - development of an algorithm to predict the anatomical site of origin. *J. Am. Coll. Cardiol.*, 2006;**48**: 1010–1017.
158. Zipes, D.P., W.E. Gaum, B.C. Genetos, R.D. Glassman, J. Noble, and C. Fisch, Atrial tachycardia without P waves masquerading as an A-V junctional tachycardia. *Circulation*, 1977;**55**: 253–260.
159. Boineau, J.P., T.E. Canavan, R.B. Schuessler, M.E. Cain, P.B. Corr, and J.L. Cox, Demonstration of a widely distributed atrial pacemaker complex in the human heart. *Circulation*, 1988;**77**: 1221–1237.
160. Chen, C.C., C.T. Tai, C.E. Chiang, W.C. Yu, S.H. Lee, Y.J. Chen, et al., Atrial tachycardias originating from the atrial septum: electrophysiologic characteristics and radiofrequency ablation. *J. Cardiovasc. Electrophysiol.*, 2000;**11**: 744–749.
161. Frey, B., G. Kreiner, M. Gwechenberger, and H.D. Gossinger, Ablation of atrial tachycardia originating from the vicinity of the atrioventricular node: significance of mapping both sides of the interatrial septum. *J. Am. Coll. Cardiol.*, 2001;**38**: 394–400.
162. Marrouche, N.F., A. SippensGroenewegen, Y. Yang, S. Dibs, and M.M. Scheinman, Clinical and electrophysiologic characteristics of left septal atrial tachycardia. *J. Am. Coll. Cardiol.*, 2002;**40**: 1133–1139.
163. Kistler, P.M., S.P. Fynn, H. Haqqani, I.H. Stevenson, J.K. Vohra, J.B. Morton, et al., Focal atrial tachycardia from the ostium of the coronary sinus: electrocardiographic and electrophysiological characterization and radiofrequency ablation. *J. Am. Coll. Cardiol.*, 2005;**45**: 1488–1493.
164. Tada, H., A. Nogami, S. Naito, M. Suguta, M. Nakatsugawa, Y. Horie, et al., Simple electrocardiographic criteria for identifying the site of origin of focal right atrial tachycardia. *Pace Clin. Electrophysiol.*, 1998;**21**: 2431–2439.
165. Morton, J.B., P. Sanders, A. Das, J.K. Vohra, P.B. Sparks, and J.M. Kalman, Focal atrial tachycardia arising from the tricuspid annulus: electrophysiologic and electrocardiographic characteristics. *J. Cardiovasc. Electrophysiol.*, 2001;**12**: 653–659.
166. Roberts-Thomson, K.C., P.M. Kistler, A.D. McGavigan, R.J. Hillock, I.H. Stevenson, S. Spence, et al., Focal atrial tachycardias arising from the right atrial appendage: electrocardiographic and electrophysiological characteristics and radiofrequency ablation. *J. Cardiovasc. Electrophysiol.*, 2007;**18**(4): 367–372.
167. Kistler, P.M., P. Sanders, S.P. Fynn, I.H. Stevenson, A. Hussin, J.K. Vohra, et al., Electrophysiological and electrocardiographic characteristics of focal atrial tachycardia originating from the pulmonary veins: acute and long-term outcomes of radiofrequency ablation. *Circulation*, 2003;**108**: 1968–1975.
168. Hachiya, H., S. Ernst, F. Ouyang, H. Mavrakis, J. Chun, D. Bansch, et al., Topographic distribution of focal left atrial tachycardias defined by electrocardiographic and electrophysiological data. *Circ. J.*, 2005;**69**: 205–210.
169. Kistler, P.M., P. Sanders, A. Hussin, J.B. Morton, J.K. Vohra, P.B. Sparks, et al., Focal atrial tachycardia arising from the mitral annulus: electrocardiographic and electrophysiologic characterization. *J. Am. Coll. Cardiol.*, 2003;**41**: 2212–2219.
170. Gonzalez, M.D., L.J. Contreras, M.R. Jongbloed, J. Rivera, T.P. Donahue, A.B. Curtis, et al., Left atrial tachycardia originating from the mitral annulus-aorta junction. *Circulation*, 2004;**110**: 3187–3192.
171. Tritto, M., M. Zardini, R. De Ponti, and J.A. Salerno-Uriarte, Iterative atrial tachycardia originating from the coronary sinus musculature. *J. Cardiovasc. Electrophysiol.*, 2001;**12**: 1187–1189.

172. Volkmer, M., M. Antz, J. Hebe, and K.H. Kuck, Focal atrial tachycardia originating from the musculature of the coronary sinus. *J. Cardiovasc. Electrophysiol.*, 2002;**13**: 68–71.
173. Badhwar, N., J.M. Kalman, P.B. Sparks, P.M. Kistler, M. Attari, M. Berger, et al., Atrial tachycardia arising from the coronary sinus musculature: electrophysiological characteristics and long-term outcomes of radiofrequency ablation. *J. Am. Coll. Cardiol.*, 2005;**46**: 1921–1930.
174. Shine, K.I., J.A. Kastor, and P.M. Yurchak, Multifocal atrial tachycardia. Clinical and electrocardiographic features in 32 patients. *N. Engl. J. Med.*, 1968;**279**: 344–349.
175. McCord, J. and S. Borzak, Multifocal atrial tachycardia. *Chest*, 1998;**113**: 203–209.
176. Lipson, M.J. and S. Naimi, Multifocal atrial tachycardia (chaotic atrial tachycardia). Clinical associations and significance. *Circulation*, 1970;**42**: 397–407.
177. Marchlinski, F.E. and J.M. Miller, Atrial arrhythmias exacerbated by theophylline. Response to verapamil and evidence for triggered activity in man. *Chest*, 1985;**88**: 931–934.
178. Strickberger, S.A., C.B. Miller, and J.H. Levine, Multifocal atrial tachycardia from electrolyte imbalance. *Am. Heart J.*, 1988;**115**: 680–682.
179. Levine, J.H., J.R. Michael, and T. Guarnieri, Multifocal atrial tachycardia: a toxic effect of theophylline. *Lancet*, 1985;**1**: 12–14.
180. Wang, K., B.L. Goldfarb, F.L. Gobel, and H.G. Richman, Multifocal atrial tachycardia. *Arch. Intern. Med.*, 1977;**137**: 161–164.
181. Bisset, G.S. III, S.F. Seigel, W.E. Gaum, and S. Kaplan, Chaotic atrial tachycardia in childhood. *Am. Heart J.*, 1981;**101**: 268–272.
182. Arsura, E., A.S. Lefkin, D.L. Scher, M. Solar, and S. Tessler, A randomized, double-blind, placebo-controlled study of verapamil and metoprolol in treatment of multifocal atrial tachycardia. *Am. J. Med.*, 1988;**85**: 519–524.
183. McCord, J.K., S. Borzak, T. Davis, and M. Gheorghiade, Usefulness of intravenous magnesium for multifocal atrial tachycardia in patients with chronic obstructive pulmonary disease. *Am. J. Cardiol.*, 1998;**81**: 91–93.
184. Tucker, K.J., J. Law, and M.J. Rodriques, Treatment of refractory recurrent multifocal atrial tachycardia with atrioventricular junction ablation and permanent pacing. *J. Invasive Cardiol.*, 1995;**7**: 207–212.
185. Ueng, K.C., S.H. Lee, D.J. Wu, C.S. Lin, M.S. Chang, and S.A. Chen, Radiofrequency catheter modification of atrioventricular junction in patients with COPD and medically refractory multifocal atrial tachycardia. *Chest*, 2000;**117**: 52–59.
186. Levine, J.H., J.R. Michael, and T. Guarnieri, Treatment of multifocal atrial tachycardia with verapamil. *N. Engl. J. Med.*, 1985;**312**: 21–25.
187. Watson, R.M. and M.E. Josephson, Atrial flutter. I. Electrophysiologic substrates and modes of initiation and termination. *Am. J. Cardiol.*, 1980;**45**: 732–741.
188. Waldo, A.L., W.A. MacLean, R.B. Karp, N.T. Kouchoukos, and T.N. James, Entrainment and interruption of atrial flutter with atrial pacing: studies in man following open heart surgery. *Circulation*, 1977;**56**: 737–745.
189. Greenberg, M.L., T.A. Kelly, B.B. Lerman, and J.P. DiMarco, Atrial pacing for conversion of atrial flutter. *Am. J. Cardiol.*, 1986;**58**: 95–99.
190. Waldo, A.L., Atrial flutter: entrainment characteristics. *J. Cardiovasc. Electrophysiol.*, 1997;**8**: 337–352.
191. Scheinman, M.M., Y. Yang, and J. Cheng, Atrial flutter: Part II Nomenclature. *Pace Clin. Electrophysiol.*, 2004;**27**: 504–506.
192. Granada, J., W. Uribe, P.H. Chyou, K. Maassen, R. Vierkant, P.N. Smith, et al., Incidence and predictors of atrial flutter in the general population. *J. Am. Coll. Cardiol.*, 2000;**36**: 2242–2246.
193. Lee, K.W., Y. Yang, and M.M. Scheinman, Atrial flutter: a review of its history, mechanisms, clinical features, and current therapy. *Curr. Probl. Cardiol.*, 2005;**30**: 121–167.
194. Vidaillet, H., J.F. Granada, P.H. Chyou, K. Maassen, M. Ortiz, J.N. Pulido, et al., A population-based study of mortality among patients with atrial fibrillation or flutter. *Am. J. Med.*, 2002;**113**: 365–370.
195. Kalman, J.M., G.F. VanHare, J.E. Olgin, L.A. Saxon, S.I. Stark, and M.D. Lesh, Ablation of "incisional" reentrant atrial tachycardia complicating surgery for congenital heart disease. Use of entrainment to define a critical isthmus of conduction. *Circulation*, 1996;**93**: 502–512.
196. Chugh, A., H. Oral, K. Lemola, B. Hall, P. Cheung, E. Good, et al., Prevalence, mechanisms, and clinical significance of macroreentrant atrial tachycardia during and following left atrial ablation for atrial fibrillation. *Heart Rhythm*, 2005;**2**: 464–471.
197. Stevenson, I.H., P.M. Kistler, S.J. Spence, J.K. Vohra, P.B. Sparks, J.B. Morton, et al., Scar-related right atrial macroreentrant tachycardia in patients without prior atrial surgery: electroanatomic characterization and ablation outcome. *Heart Rhythm*, 2005;**2**: 594–601.
198. Wellens, H.J., Contemporary management of atrial flutter. *Circulation*, 2002;**106**: 649–652.
199. Natale, A., K.H. Newby, E. Pisano, F. Leonelli, R. Fanelli, D. Potenza, et al., Prospective randomized comparison of antiarrhythmic therapy versus first-line radiofrequency ablation in patients with atrial flutter. *J. Am. Coll. Cardiol.*, 2000;**35**: 1898–1904.
200. Tai, C.T., T.Y. Liu, P.C. Lee, Y.J. Lin, M.S. Chang, and S.A. Chen, Non-contact mapping to guide radiofrequency ablation of atypical right atrial flutter. *J. Am. Coll. Cardiol.*, 2004;**44**: 1080–1086.
201. Della, B.P., A. Fraticelli, C. Tondo, S. Riva, G. Fassini, and C. Carbucicchio, Atypical atrial flutter: clinical features, electrophysiological characteristics and response to radiofrequency catheter ablation. *Europace*, 2002;**4**: 241–253.
202. Jais, P., M. Hocini, R. Weerasoryia, L. Macle, C. Scavee, F. Raybaud, et al., Atypical left atrial flutters. *Card. Electrophysiol. Rev.*, 2002;**6**: 371–377.
203. Olshansky, B., Advances in atrial flutter mapping: what goes around comes around. *J. Cardiovasc. Electrophysiol.*, 2004;**15**: 415–417.
204. Mehta, A.V. and L.L. Ewing, Atrial tachycardia in infants and children: electrocardiographic classification and its significance. *Pediatr. Cardiol.*, 1993;**14**: 199–203.
205. Olgin, J.E., J.M. Kalman, A.P. Fitzpatrick, and M.D. Lesh, Role of right atrial endocardial structures as barriers to conduction during human type I atrial flutter. Activation and entrainment mapping guided by intracardiac echocardiography. *Circulation*, 1995;**92**: 1839–1848.
206. Kalman, J.M., J.E. Olgin, L.A. Saxon, W.G. Fisher, R.J. Lee, and M.D. Lesh, Activation and entrainment mapping defines the tricuspid annulus as the anterior barrier in typical atrial flutter. *Circulation*, 1996;**94**: 398–406.
207. Schwartzman, D., D.J. Callans, C.D. Gottlieb, S.M. Dillon, C. Movsowitz, and F.E. Marchlinski, Conduction block in the inferior vena caval-tricuspid valve isthmus: association with

outcome of radiofrequency ablation of type I atrial flutter. *J. Am. Coll. Cardiol.*, 1996;**28**: 1519–1531.
208. Saoudi, N., M. Nair, A. Abdelazziz, H. Poty, A. Daou, F. Anselme, et al., Electrocardiographic patterns and results of radiofrequency catheter ablation of clockwise type I atrial flutter. *J. Cardiovasc. Electrophysiol.*, 1996;**7**: 931–942.
209. Besoain-Santander, M., A. Pick, and R. Langendorf, A-V conduction in auricular flutter. *Circulation*, 1950;**2**: 604–616.
210. Kennelly, B.M. and G.K. Lane, Electrophysiological studies in four patients with atrial flutter with 1:1 atrioventricular conduction. *Am. Heart J.*, 1978;**96**: 723–730.
211. Moleiro, F., I.J. Mendoza, V. Medina-Ravell, A. Castellanos, and R.J. Myerburg, One to one atrioventricular conduction during atrial pacing at rates of 300/minute in absence of Wolff-Parkinson-White Syndrome. *Am. J. Cardiol.*, 1981;**48**: 789–796.
212. Bochoeyer, A., Y. Yang, J. Cheng, R.J. Lee, E.C. Keung, N.F. Marrouche, et al., Surface electrocardiographic characteristics of right and left atrial flutter. *Circulation*, 2003;**108**: 60–66.
213. Selzer, A., Atrial fibrillation revisited. *N. Engl. J. Med.*, 1982;**30**6: 1044–1045.
214. Lewis, T., Auricular fibrillation: a common clinical condition. *Br. Med. J.*, 1909;**2**: 1528.
215. McMichael, J., History of atrial fibrillation 1628–1819 Harvey – de Senac – Laennec. *Br. Heart J.*, 1982;**48**: 193–197.
216. Levy, S., G. Breithardt, R.W. Campbell, A.J. Camm, J.C. Daubert, M. Allessie, et al., Atrial fibrillation: current knowledge and recommendations for management. Working Group on Arrhythmias of the European Society of Cardiology. *Eur. Heart J.*, 1998;**19**: 1294–1320.
217. Fuster V., L.E. Rydén, D.S. Cannom, H.J. Crijns, A.B. Curtis, K.A. Ellenbogen, et al, ACC/AHA/ESC 2006 guidelines for the management of patients with atrial fibrillation: a report of the American College of Cardiology/American Heart Association Task Force on Practice Guidelines and the European Society of Cardiology Committee for Practice Guidelines (Writing Committee to Revise the 2001 Guidelines for the Management of Patients With Atrial Fibrillation). *J. Am. Coll. Cardiol.*, 2006;**48**:e149–246.
218. Nattel, S., New ideas about atrial fibrillation 50 years on. *Nature*, 2002;**415**: 219–226.
219. Quinn, F.R. and A.C. Rankin, Atrial fibrillation ablation in the real world. *Heart*, 2005;**91**: 1507–1508.
220. Oral, H., Mechanisms of atrial fibrillation: lessons from studies in patients. *Prog. Cardiovasc. Dis.*, 2005;**48**: 29–40.
221. Hwang, C., T.J. Wu, R.N. Doshi, C.T. Peter, and P.S. Chen, Vein of marshall cannulation for the analysis of electrical activity in patients with focal atrial fibrillation. *Circulation*, 2000;**101**: 1503–1505.
222. Moe, G.K., On the multiple wavelet hypothesis of atrial fibrillation. *Arch. Int. Pharmacodyn. Ther.*, 1962;**140**: 183–188.
223. Moe, G.K., W.C. Rheinboldt, and J.A. Abildskov, A computer model of atrial fibrillation. *Am. Heart J.*, 1964;**67**: 200–220.
224. Allessie, M.A., W.J.P. Lammers, and F.I.M. Bonke, Experimental evaluation of Moe's multiple wavelet hypothesis of atrial fibrillation, in *Cardiac Electrophysiology and Arrhythmias*, D.P. Zipes and J. Jalife, Editors. Orlando, FL: Grune and Statton, 1985, pp. 265–275.
225. Cox, J.L., R.B. Schuessler, and J.P. Boineau, The development of the Maze procedure for the treatment of atrial fibrillation. *Semin. Thorac. Cardiovasc. Surg.*, 2000;**12**: 2–14.
226. Jalife, J., O. Berenfeld, and M. Mansour, Mother rotors and fibrillatory conduction: a mechanism of atrial fibrillation. *Cardiovasc. Res.*, 2002;**54**: 204–216.
227. Ricard, P., S. Levy, J. Trigano, F. Paganelli, E. Daoud, K.C. Man, et al., Prospective assessment of the minimum energy needed for external electrical cardioversion of atrial fibrillation. *Am. J. Cardiol.*, 1997;**79**: 815–816.
228. Wijffels, M.C., C.J. Kirchhof, R. Dorland, and M.A. Allessie, Atrial fibrillation begets atrial fibrillation. A study in awake chronically instrumented goats. *Circulation*, 1995;**92**: 1954–1968.
229. Nattel, S., A. Shiroshita-Takeshita, B.J. Brundel, and L. Rivard, Mechanisms of atrial fibrillation: lessons from animal models. *Prog. Cardiovasc. Dis.*, 2005;**48**: 9–28.
230. Euler, D.E., B. Olshansky, and S.Y. Kim, Reflex vagal control of atrial repolarization. *Am. J. Physiol.*, 1996;**271**: H870–H875.
231. Alessi, R., M. Nusynowitz, J.A. Abildskov, and G.K. Moe, Nonuniform distribution of vagal effects on the atrial refractory period. *Am. J. Physiol.*, 1958;**194**: 406–410.
232. Euler, D.E. and P.J. Scanlon, Acetylcholine release by a stimulus train lowers atrial fibrillation threshold. *Am. J. Physiol.*, 1987;**253**: H863–H868.
233. Olshansky, B., Interrelationships between the autonomic nervous system and atrial fibrillation. *Prog. Cardiovasc. Dis.*, 2005;**48**: 57–78.
234. Coumel, P., Clinical approach to paroxysmal atrial fibrillation. *Clin. Cardiol.*, 1990;**13**: 209–212.
235. Oral, H., A. Chugh, C. Scharf, B. Hall, P. Cheung, S. Veerareddy, et al., Pulmonary vein isolation for vagotonic, adrenergic, and random episodes of paroxysmal atrial fibrillation. *J. Cardiovasc. Electrophysiol.*, 2004;**15**: 402–406.
236. Pappone, C., V. Santinelli, F. Manguso, G. Vicedomini, F. Gugliotta, G. Augello, et al., Pulmonary vein denervation enhances long-term benefit after circumferential ablation for paroxysmal atrial fibrillation. *Circulation*, 2004;**109**: 327–334.
237. Wolf, P.A., R.D. Abbott, and W.B. Kannel, Atrial fibrillation as an independent risk factor for stroke: the Framingham Study. *Stroke*, 1991;**22**: 983–988.
238. Lloyd-Jones, D.M., T.J. Wang, E.P. Leip, M.G. Larson, D. Levy, R.S. Vasan, et al., Lifetime risk for development of atrial fibrillation: the Framingham Heart Study. *Circulation*, 2004;**110**: 1042–1046.
239. Benjamin, E.J., D. Levy, S.M. Vaziri, R.B. D'Agostino, A.J. Belanger, and P.A. Wolf, Independent risk factors for atrial fibrillation in a population-based cohort. The Framingham Heart Study. *JAMA*, 1994;**271**: 840–844.
240. Tsang, T.S., Y. Miyasaka, M.E. Barnes, and B.J. Gersh, Epidemiological profile of atrial fibrillation: a contemporary perspective. *Prog. Cardiovasc. Dis.*, 2005;**48**: 1–8.
241. Forfar, J.C., H.C. Miller, and A.D. Toft, Occult thyrotoxicosis: a correctable cause of "idiopathic" atrial fibrillation. *Am. J. Cardiol.*, 1979;**44**: 9–12.
242. Rathore, S.S., A.K. Berger, K.P. Weinfurt, K.A. Schulman, W.J. Oetgen, B.J. Gersh, et al., Acute myocardial infarction complicated by atrial fibrillation in the elderly: prevalence and outcomes. *Circulation*, 2000;**101**: 969–974.
243. Djousse, L., D. Levy, E.J. Benjamin, S.J. Blease, A. Russ, M.G. Larson, et al., Long-term alcohol consumption and the risk of atrial fibrillation in the Framingham Study. *Am. J. Cardiol.*, 2004;**93**: 710–713.

244. Koskinen, P., M. Kupari, H. Leinonen, and K. Luomanmaki, Alcohol and new onset atrial fibrillation: a case-control study of a current series. *Br. Heart J.*, 1987;**57**: 468–473.
245. Thornton, J.R., Atrial fibrillation in healthy non-alcoholic people after an alcoholic binge. *Lancet*, 1984;**2**: 1013–1015.
246. Brand, F.N., R.D. Abbott, W.B. Kannel, and P.A. Wolf, Characteristics and prognosis of lone atrial fibrillation. 30-year follow-up in the Framingham Study. *JAMA*, 1985;**254**: 3449–3453.
247. Kopecky, S.L., B.J. Gersh, M.D. McGoon, J.P. Whisnant, D.R. Holmes Jr., D.M. Ilstrup, et al., The natural history of lone atrial fibrillation. A population-based study over three decades. *N. Engl. J. Med.*, 1987;**317**: 669–674.
248. Henry, W.L., J. Morganroth, A.S. Pearlman, C.E. Clark, D.R. Redwood, S.B. Itscoitz, et al., Relation between echocardiographically determined left atrial size and atrial fibrillation. *Circulation*, 1976;**53**: 273–279.
249. Aronow, W.S., K.S. Schwartz, and M. Koenigsberg, Prevalence of enlarged left atrial dimension by echocardiography and its correlation with atrial fibrillation and an abnormal P terminal force in lead V1 of the electrocardiogram in 588 elderly persons. *Am. J. Cardiol.*, 1987;**59**: 1003–1004.
250. Vaziri, S.M., M.G. Larson, E.J. Benjamin, and D. Levy, Echocardiographic predictors of nonrheumatic atrial fibrillation. The Framingham Heart Study. *Circulation*, 1994;**89**: 724–730.
251. Wang, T.J., M.G. Larson, D. Levy, R.S. Vasan, E.P. Leip, P.A. Wolf, et al., Temporal relations of atrial fibrillation and congestive heart failure and their joint influence on mortality: the Framingham Heart Study. *Circulation*, 2003;**107**: 2920–2925.
252. Morganroth, J., L.N. Horowitz, M.E. Josephson, and J.A. Kastor, Relationship of atrial fibrillatory wave amplitude to left atrial size and etiology of heart disease. An old generalization re-examined. *Am. Heart J.*, 1979;**97**: 184–186.
253. Cohen, S.I., S.H. Lau, W.D. Berkowitz, and A.N. Damato, Concealed conduction during atrial fibrillation. *Am. J. Cardiol.*, 1970;**25**: 416–419.
254. Wellens, H.J., F.W. Bar, and K.I. Lie, The value of the electrocardiogram in the differential diagnosis of a tachycardia with a widened QRS complex. *Am. J. Med.*, 1978;**64**: 27–33.
255. Pritchett, E.L., W.M. Smith, G.J. Klein, S.C. Hammill, and J.J. Gallagher, The "compensatory pause" of atrial fibrillation. *Circulation*, 1980;**62**: 1021–1025.
256. Klein, G.J., T.M. Bashore, T.D. Sellers, E.L. Pritchett, W.M. Smith, and J.J. Gallagher, Ventricular fibrillation in the Wolff-Parkinson-White syndrome. *N. Engl. J. Med.*, 1979;**301**: 1080–1085.
257. Campbell, R.W., R.A. Smith, J.J. Gallagher, E.L. Pritchett, and A.G. Wallace, Atrial fibrillation in the preexcitation syndrome. *Am. J. Cardiol.*, 1977;**40**: 514–520.

27 Clinical Electrophysiological Mechanisms of Tachycardias Arising from the Atrioventricular Junction

Demosthenes G. Katritsis · A. John Camm

P. W. Macfarlane, A. van Oosterom, O. Pahlm, P. Kligfield, M. Janse, J. Camm (eds.), *Comprehensive Electrocardiology*, DOI 10.1007/978-1-84882-046-3_27,

27.1 Atrioventricular Junctional Tachycardias

27.1.1 Definitions

Junctional tachycardias originate in the AV junction, i.e., the AV node and its approaches [1, 2]. Tachycardias originating in the AV junction can be classified into two types according to their underlying electrophysiological mechanism. The first type is caused by reentry movement in the region of the AV node and the adjacent perinodal tissue. It is therefore called atrioventricular nodal reentrant tachycardia (AVNRT). The second type comprises tachycardias that are caused by enhanced automaticity or triggered activity in the AV junction [1]. The term AV junction refers to a part of the atrioventricular specialized conducting system consisting of the transitional cell zone, the AV node and its extensions, and the penetrating part of the bundle of His [3–5]. Approximately one half of narrow QRS tachycardias are due to AV junctional reentry, and one third is due to reentry over accessory atrioventricular connections [1, 2]. In the absence of preexcitation during sinus rhythm, the most frequent cause of regular supraventricular tachycardia is reentry within the atrioventricular junction.

27.2 Atrioventricular Nodal Reentrant Tachycardia

27.2.1 Aetiology and Mechanism

Atrioventricular nodal reentrant tachycardia (AVNRT) is thought to result from reentry in the region of the AV junction. However, the precise anatomical site of the circuit and the pathways involved have not yet been established.

27.2.2 Conventional Concepts

The suggestion that circus movement in the atrioventricular node can be a mechanism for supraventricular tachycardia was made as early as 1913 [6]. The concept of dual AV nodal pathways dates from 1956 when Moe and colleagues [7] demonstrated evidence of a dual AV conduction system in dogs. They noted a sudden increase in the AV conduction time when a premature atrial impulse was delivered at a critical coupling interval after a regular extrastimuli series.

Denes et al. [8] in 1973 ascribed episodes of paroxysmal supraventricular tachycardia to AV node reentry due to the presence of dual atrioventricular nodal pathways. It was postulated that a dual conduction system was present, one having a faster conduction time and longer refractory period and the other having a slower conduction time and shorter refractory period (Fig. 27.1). At a critical coupling interval, the premature impulse blocks in the faster pathway and conducts in the still excitable slow pathway, causing a sudden jump in the AV conduction time. Following this, the impulse returns to the atria, supposedly via the fast pathway, which has then recovered, and an atrial reciprocal response or "echo" beat or sustained tachycardia results (Fig. 27.2) [8, 9]. Rosen et al. [10], using His bundle recordings and the atrial extrastimulus method, demonstrated sudden prolongation of the AH interval in a patient with dual atrioventricular nodal pathways. These discontinuities in AH conduction can be displayed by plotting A_2-H_2 conduction times or H_1-H_2 intervals against A_1-A_2 intervals giving the "antegrade conduction curve" (Fig. 27.3) [11]. Normally, the AV node displays a gradual conduction time prolongation with atrial extrastimulation, thus resulting in smooth conduction curves with a progressive increment of the AH or HH intervals (Fig. 27.4) [11]. A sudden increment of AV nodal conduction time results in a discontinuous curve. The portion of the curve to the right of the sudden increment was described as reflecting fast (or beta) pathway conduction time and that to the left as slow (or alpha) pathway conduction (Fig. 27.3). An increase in H_1-H_2 of >50 ms for a decrease in A_1-A_2 of 10-20 ms was arbitrarily considered conduction "jump" reflecting the presence of dual AV nodal pathways [12–14].

Discontinuous refractory period curves, however, may not be present in all patients with AVNRT. Antegrade dual pathways are demonstrable in approximately 75% of patients with tachycardia [12, 14], and AVNRT may occur in the presence of continuous AV nodal conduction curves [15–17]. Conversely, antegrade dual pathways can be demonstrated in subjects without tachycardia [13, 18]. In children undergoing electrophysiological studies, up to 35% may have discontinuous curves [19, 20]. Similarly, people without tachycardia may exhibit discontinuous curves on antegrade or retrograde

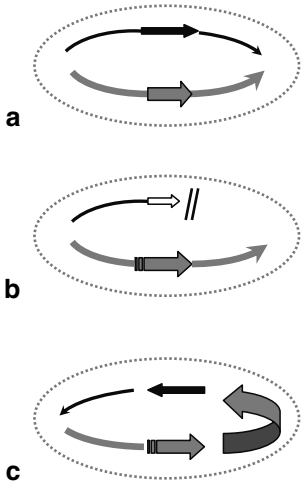

Figure 27.1

Theoretical depiction of the AV nodal reentrant circuit. During sinus rhythm (a) the impulse penetrates both the fast and the slow pathway. A premature beat results in conduction block of the fast pathway and propagation through the slow (b). An earlier impulse encounters more delay in the slow pathway in a way that the blocked fast pathway has recovered when the now retrograde impulse arrives and tachycardia begins (c).

activation [21, 22]. It seems, therefore, that mere presence of AV nodal duality even in conjunction with AV echos is not enough to predispose to paroxysmal tachycardia.

In 5–10% of patients with AV nodal reentry, antegrade conduction is thought to proceed over the fast pathway and retrograde conduction over the slow pathway and may result in an incessant form of AVNRT [23, 24]. In these patients, antegrade conduction curves are not discontinuous. This pattern of conduction as well as the incessant nature can also be seen in the presence of concealed septal accessory pathways with decremental properties [25]. Depending on the orientation of the reentrant circuit, therefore, AVNRT has been traditionally classified into *slow-fast* or typical form and into *fast-slow* or atypical form.

27.2.3 Recent Developments

The concept of dual AV junctional pathways can provide explanations for many aspects of the electrophysiological behavior of these tachycardias, but several obscure points remain. These pathways have not been demonstrated histologically, and the exact circuit responsible for the reentrant tachycardia is unknown [26, 27]. Recently, exciting information from the ablation laboratory and the surgical theatre has appeared regarding the nature of the AVNRT circuit, although several questions still remain unsettled.

There has been considerable evidence that more than two pathways may be involved in the AVNRT circuit. Triple AV nodal pathways have been described [28, 29], and dual AV nodal conduction may persist in patients in whom AVNRT was abolished by catheter ablation [30]. Indeed, electrophysiologic demonstration of multiple discontinuities in the AV node conduction curve suggests the presence of multiple anterograde AV node pathways (Fig. 27.5), although not all of them are involved in the initiation and maintenance of AVNRT [31]. In a series of 550 patients with AVNRT described by Tai et al., 36 patients had multiple anterograde and retrograde AV nodal pathways that constituted the substrates of multiple reentry circuits [32]. Hwang et al. [33] have also described 17 patients with the fast-slow or slow-slow forms of AVNRT in whom the slow-fast form was also inducible. This finding clearly suggests the potential existence of multiple slow pathways in certain patients in whom several different forms of AVNRT may coexist. There have also been reports of patients demonstrating evidence of multiple pathways following radiofrequency ablation of both the slow [33] and the fast pathway [34]. We have also reported on a patient with slow-fast AVNRT in whom, during radiofrequency ablation

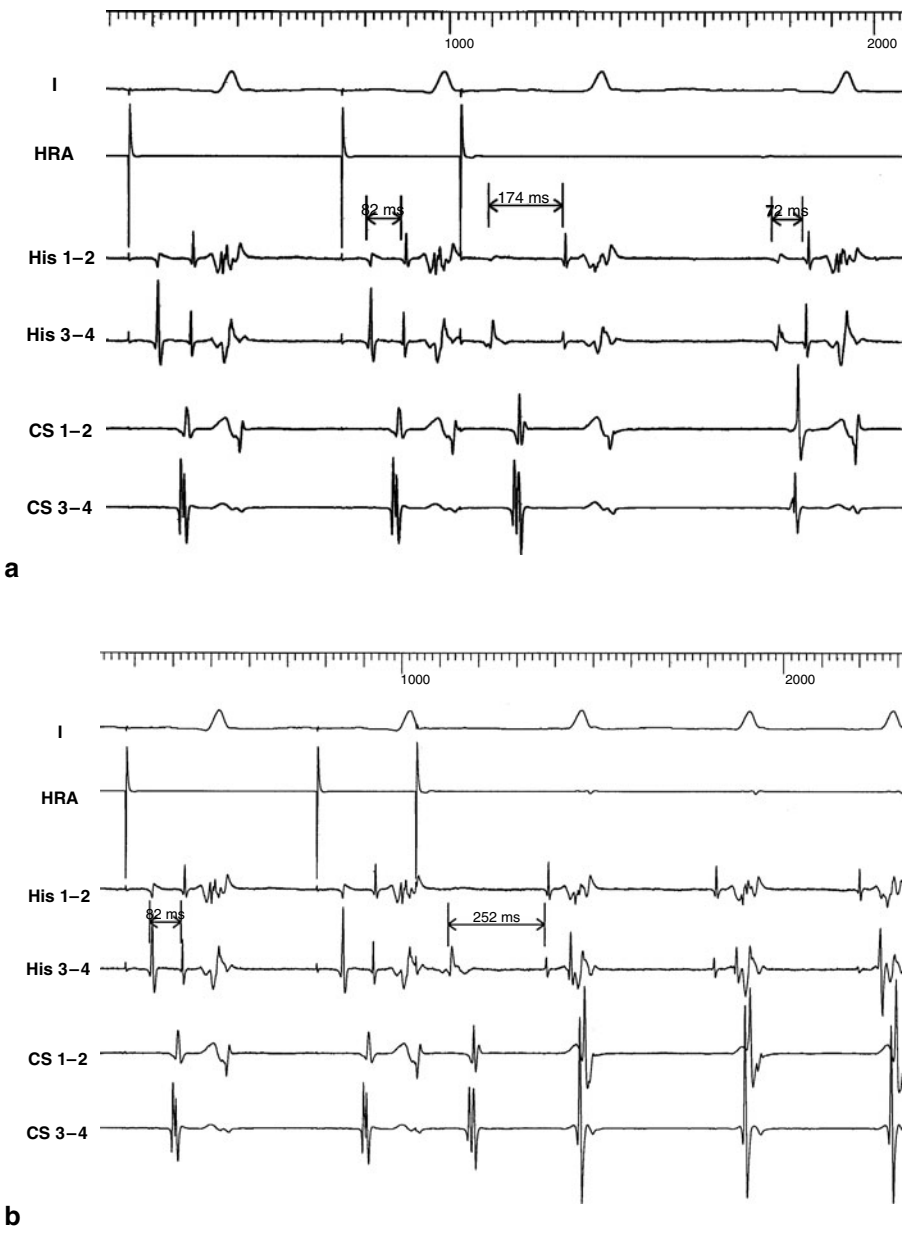

Figure 27.2

Anterograde jump and initiation of slow-fast AVNRT with atrial extrastimuli. At ventricular pacing cycle length of 500 s, a ventricular extrastimulus is delivered at 260 ms (a) with resultant decremental conduction through the fast pathway (AH = 174 ms). At a coupling interval of 240 ms (b) there is a conduction jump with AH = 252 ms and tachycardia is induced. Note that atrial electrograms are superimposed on the ventricular ones, but on His bundle 3–4 electrogram, the atrial electrogram preceeds the ventricular one. I: lead I of the surface ECG, HRA: high right atrium, His: His bundle, CS: coronary sinus.

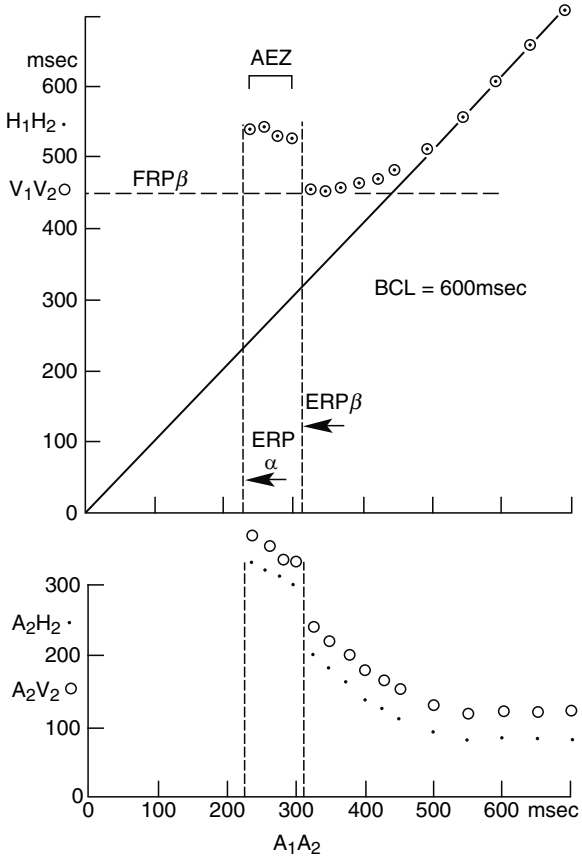

Figure 27.3

Anterograde conduction curves from a patient with "slow-fast" AVNRT. The sudden increase of AH (jump) indicates refractoriness of the fast (beta) pathway and conduction through the slow (alpha) pathway. Please see text for details. (From Ward and Camm [11]. © Edward Arnold, London. Reproduced with permission.)

of his slow pathway, retrograde activation was continuously alternating from a fast to a slow pathway producing alternating tachycardia cycles during both the anterior and posterior (or slow-slow) (Fig. 27.6) forms of tachycardia [35]. In another report, the initiation of fast-slow AVNRT was dependent on sudden A-H prolongation, indicating antegrade conduction over a slow pathway that shortened during the ensuing beats [36]. It seems therefore that, at least according to conventional definitions, a group of such pathways may be involved in the reentrant circuit [31, 32, 37].

There has also been a long debate whether the adjacent atrial tissue constitutes an obligate part of the reentrant circuit or an "upper common pathway" is present within subatrial nodal structures in the triangle of Koch. Early studies have demonstrated dissociation of the atrium during AVNRT and provided evidence in favor of the presence of a common pathway [38, 39], with decremental conduction properties [40], without any participation of the atrium. High-resolution mapping of the triangle of Koch in canine hearts has demonstrated that reentrant ventricular echo beats did not require the perinodal tissue [41] and AVNRT has been recorded in a patient during atrial fibrillation [42]. However, observations based on conventional electrophysiology studies have questioned the confinement of the AVNRT circuit to the AV node and suggested that the retrograde fast pathway may not involve normal AV nodal tissue. Schuger et al. [43] have shown that after concealed antegrade impulse penetration, the retrograde fast pathway in AVNRT exhibits an abrupt transition from full excitability to absolute refractoriness unlike AV nodal tissue. This "all or none" type of conduction had also been described in other studies [44–46]. Experimental and clinical studies presented evidence of perinodal involvement in the tachycardia circuit [47, 48], and slow pathway radiofrequency ablation in patients with AVNRT also

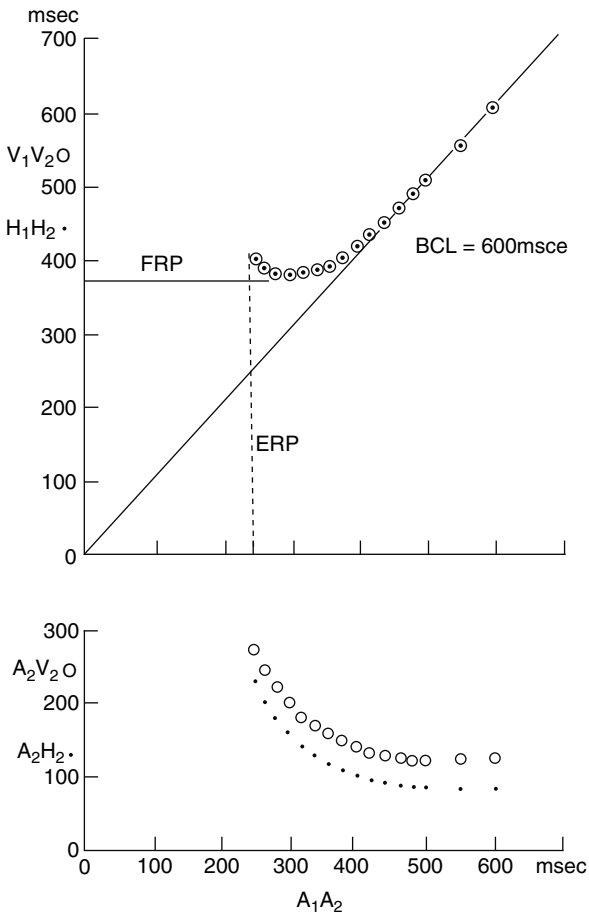

Figure 27.4

Normal anterograde conduction curves. Please note the gradual increase of AH intervals with shortening of the coupling intervals A_1A_2. ERP and FRP are the effective and functional refractory periods of the AV node. (From Ward and Camm [11]. © Edward Arnold, London. Reproduced with permission.)

resulted in persistent nondecremental retrograde conduction [49]. McGuire et al. [50] have demonstrated two types of presumed slow-fast AVNRT, corresponding to the A and B types previously described by the same group [51]. In the anterior type, the earliest atrial activity was recorded before ventricular activation and recorded near the His bundle, whereas in the posterior type, ventriculoatrial (VA) intervals were longer and the earliest atrial activity was recorded near the coronary sinus (CS) ostium. Although the different atrial activation sequences may be explained by intranodal circuits with different atrial exits, differences in ventriculoatrial intervals and tachycardia cycle lengths (TCLs) of the two tachycardias in each patient suggested different circuits for each tachycardia. This implies that a common pathway of AV nodal tissue is not present above the reentrant circuit and suggests that perinodal atrium forms part of the circuit. Recent observations have also documented that the majority of patients with AVNRT have multiple heterogenous sites of early atrial activation during the arrhythmia rather than a focal breakthrough site, thus arguing against the concept of an anatomically discrete pathway [52]. It has been therefore postulated that the so-called "proximal common pathway" is probably a broad area allowing fast and slow pathways to have different retrograde exit sites [52, 53]. A recent study with direct recording of the AV nodal electrograms and correlation with histology has showed that the AV nodal reentry occurs in the complex network of nodal and transitional cells and in the rim of surrounding atrial cells [54].

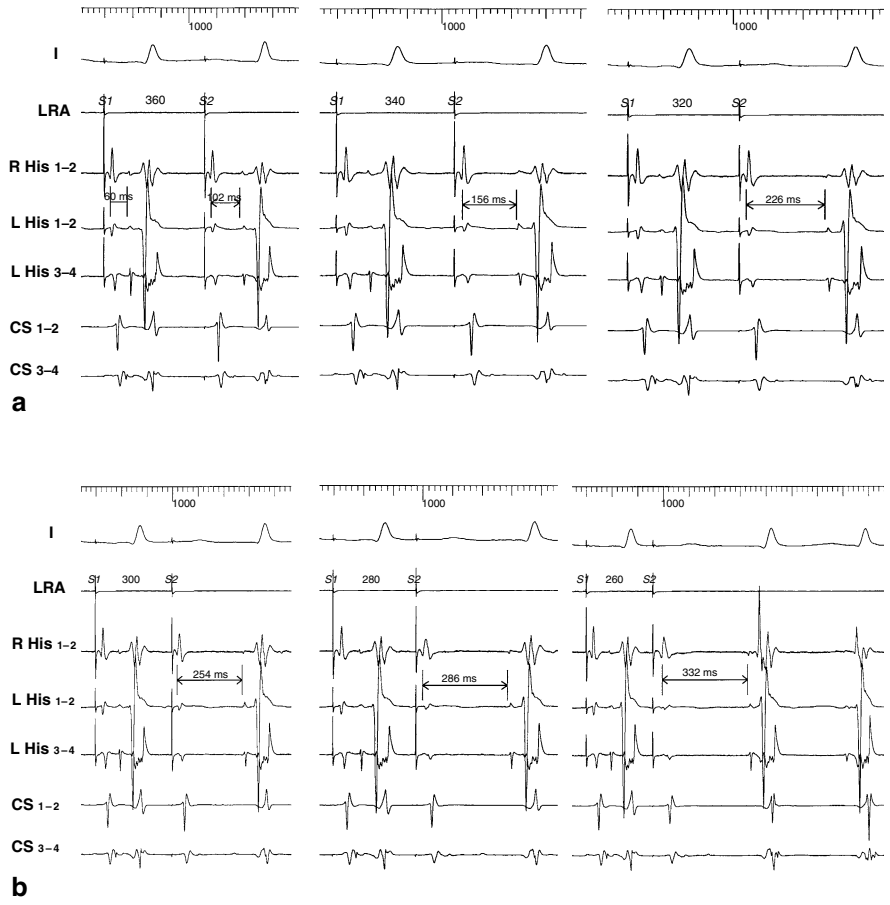

Figure 27.5

Multiple conduction jumps (a) and decrement before tachycardia initiation (b), indicating the presence of more than one "slow" pathway. I: ECG lead, LRA: low right atrium, RHis: His bundle recorded from the right septum, LHis: His bundle recorded from the left septum, CS: coronary sinus.

Controversy also exists regarding the so-called lower common pathway, i.e., the tissue between the tachycardia circuit and the His bundle [40, 55, 56]. The conduction time over the lower common pathway has been usually estimated by subtracting the H-A interval during tachycardia from that during ventricular pacing at the same cycle length and considered a measurable interval in the majority of typical AVNRT cases [40]. Studies utilizing para-Hisian pacing, however, have failed to detect evidence of a lower common pathway in typical slow-fast AVNRT, as opposed to fast-slow or slow-slow AVNRT, and have actually used its presence to contribute toward the differential diagnosis between those forms of the tachycardia [55, 56].

Finally, the possibility of functional as opposed to anatomic reentry has also been raised. As already discussed, the demonstration of dual AV nodal characteristics is not a prerequisite for the induction of AVNRT, and successful ablation of the slow pathway does not necessitate changes in AV nodal duality characteristics and slow pathway electrophysiological parameters [57, 58]. The AV junction anatomical structure contains the conditions for the existence of functional pathways. A deep central portion is surrounded by successive layers of myocardium that gradually merge with atrial myocardium [59, 60]. In the region located anteriorly to the coronary sinus os, the terminal atrial tissue overlaps the AV node, showing a smooth rather than abrupt transition [61]. This area has the lowest velocity among cardiac tissues, including the node itself, demonstrates a high level of automaticity, and has characteristics of functional longitudinal

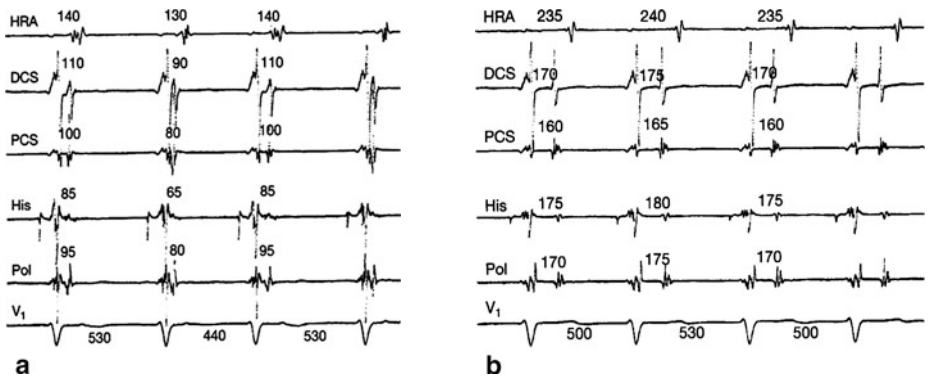

Figure 27.6

Anterior slow-fast AVNRT (a) and posterior slow-fast or slow-slow AVNRT (b) with alternating retrograde conduction intervals. This recording was obtained during slow pathway ablation and indicates AVNRT circuits alternatively using two different pathways in the retrograde direction. (From Katritsis et al. [35]. © John Wiley & Sons. Reproduced with permission.) V_1: ECG lead, HRA: high right atrium, His: His bundle, Pol: ablating catheter, DCS: distal coronary sinus, PCS: proximal coronary sinus.

dissociation [3, 61, 62]. Jalife [63] has shown that conduction jump and reentry can occur in a nonhomogeneous linear structure if conduction occurs electrotonically across an area of block and has demonstrated dual pathway responses in isolated Purkinje fibers. It seems that tissue anisotropy, because of fiber orientation heterogenicity and consequent anisotropic conduction or spatial inhomogeneity of refractoriness, may contribute to different electrophysiological characteristics [64, 65] as well as pharmacological responses of functional pathways that, given the right conditions, might constitute the antegrade and retrograde limbs of the circuit [66, 67].

27.2.4 Proposed Models of the AVNRT Circuit

There is now evidence suggesting that AVNRT most probably results from reentry in various locations in the AV nodal and atrial perinodal area. The old model of the reentrant circuit comprised by two anatomically distinct limbs confined to the AV node is too oversimplified to represent reality. It is also debatable whether the two antegrade pathways seen in the majority of patients with AVNRT are the same two pathways used in the reentry circuit during tachycardia [68].

Wu and colleagues [69] have proposed that the slow pathway is the compact node and its posterior input of transitional cells, whereas the retrograde fast pathway is the anterior superficial group of transitional cells. Keim et al. [70] have proposed a more comprehensive model: the AV node, at least in patients with AVNRT, containing fibers capable of different conduction velocity. The fastest of the fast fibers and the slowest of the slow run at opposite edges of the AV node, superiorly and inferiorly, respectively, whereas the fibers between them are responsible for normal antegrade conduction without participation in the arrhythmia. Transitional nodal or atrial fibers constitute the upper connection of those two fiber sets. Patterson and Scherlag [68] have proposed a combined anatomic and functional model based on several hypotheses: transitional cells are the normal input for the fast pathway, AV Wenckebach behavior is due to another group of transitional cells (mid pathway), and fast pathway AV conduction during sinus rhythm and VA conduction during AVNRT are different. Spach and Josephson [71] have adopted a purely anisotropic model. The genesis of AVNRT is attributed to nonuniform anisotropy due to sparse side-to-side coupling between cells in the triangle of Koch. However, although anisotropic properties of the transitional cells do have a certain role in the genesis of this arrhythmia, anisotropic reentry as such cannot be accounted for the typical electrophysiologic characteristics of dual AV nodal conduction and AVNRT [72, 73].

27.2.5 The Role of Inferior Nodal Extensions

We have recently proposed a new model based on the description of the inferior nodal extensions [74, 75]. In 1906, Tawara described inferior extensions of the AV node in the human heart [76]. Later Becker and colleagues provided histological evidence of both rightward and leftward inferior extensions and speculated that they may be involved in slow pathway conduction [4, 77, 78]. The inferior nodal extensions are basically part of the AV node and facilitate atrial inputs that also contain transitional cells connecting atrial myocardium with the nodal extensions. Recent experimental studies in the rabbit heart have related the inferior (posterior) extension with slow pathway conduction properties [79–82], and histopathologic examination of the septum following successful ablation of the slow pathway in the human has demonstrated interruption of a long right inferior atrial extension [83]. We have shown that atrial inputs to the AV node can be studied in the human and have examined their electrophysiological properties in patients with and without discontinuous AV conduction curves [74, 75]. Fourteen patients without AVRT (atrioventricular reentrant tachycardia) or AV conduction jumps were studied by simultaneous recording of right- and left-sided His bundle electrograms during multisite atrial pacing. When atrial pacing resulted in conduction through the slow pathway, left inferoparaseptal pacing produced shorter stimulus to His intervals (St-H), as compared to low right atrial pacing. The difference between St-H at maximum decrement and St-H at constant pacing was significantly smaller during left inferoparaseptal than low right atrial pacing [74]. These findings are compatible with the observation that the leftward inferior extension is much shorter in length than the rightward inferior extension [78, 79], and suggest that the inferior atrial extensions are involved in "slow pathway" conduction. We have also studied ten patients with AV conduction jumps and inducible slow-fast AVNRT, before and after successful slow pathway ablation [75]. Simultaneous His bundle recordings from right and left sides of the septum were made during right and left inferoparaseptal pacing. Longer stimulus to His intervals was measured during right inferoparaseptal pacing compared to left inferoparaseptal pacing, at similar coupling intervals during AVNRT induction. Post-ablation, St-H intervals at maximum AV nodal conduction decrement were similar during right inferoparaseptal and left inferoparaseptal pacing, at similar coupling intervals. Pre-ablation, differences between St-H intervals at AVNRT induction or maximum AV conduction decrement (indicating slow pathway conduction) and constant cycle length pacing (indicating fast pathway conduction) for right His recordings with right inferoparaseptal pacing were significantly greater than differences measured with left His during left inferoparaseptal pacing. Post-ablation, these differences disappeared. Resetting of AVNRT with a left inferoparaseptal extrastimulus was achieved in seven of ten patients and indicated the presence of an atrio-nodal connection that is operating on the left side of the septum and allows the advancement of the next His bundle electrogram.

Thus, the electrophysiologic characteristics of the right and left inferior atrial inputs to the human AV node in patients with AVNRT and their response to slow-pathway ablation provide further evidence that the inferior nodal extensions represent the anatomic substrate of the slow pathway. Nodal decremental conduction might represent a fusion between a decrementally conducting AV node as well as activation through the inferior inputs. The demonstration of a jump indicates a shift of activation through the inferior extensions that now act as the "slow pathway." Whether other superior extensions or the compact node itself [79, 80] might be responsible for the "fast pathway" is not known. Superior atrial inputs to the node have not been histologically demonstrated. However, the existence of multiple atrial inputs to the node is now established [84], and one might speculate that yet undefined superior extensions may also play a role in initial "fast pathway" conduction. There has been now considerable evidence that the right and left inferior extensions of the human AV node and the atrio-nodal inputs they facilitate may provide the anatomic substrate of the slow pathway, and a comprehensive model of the tachycardia circuit for all forms of atrioventricular nodal reentrant tachycardia based on the concept of atrio-nodal inputs has been proposed (Fig. 27.7) [85].

27.3 The Electrocardiogram

Typically, AVNRT is a narrow, complex tachycardia, i.e., QRS duration is less than 120 ms (Fig. 27.8), unless aberrant conduction, usually of the RBBB type, or a previous conduction defect exists. The QRS is normal in contour, but tachycardia-related ST depression may be seen during and after the event. The RR interval is regular, although some

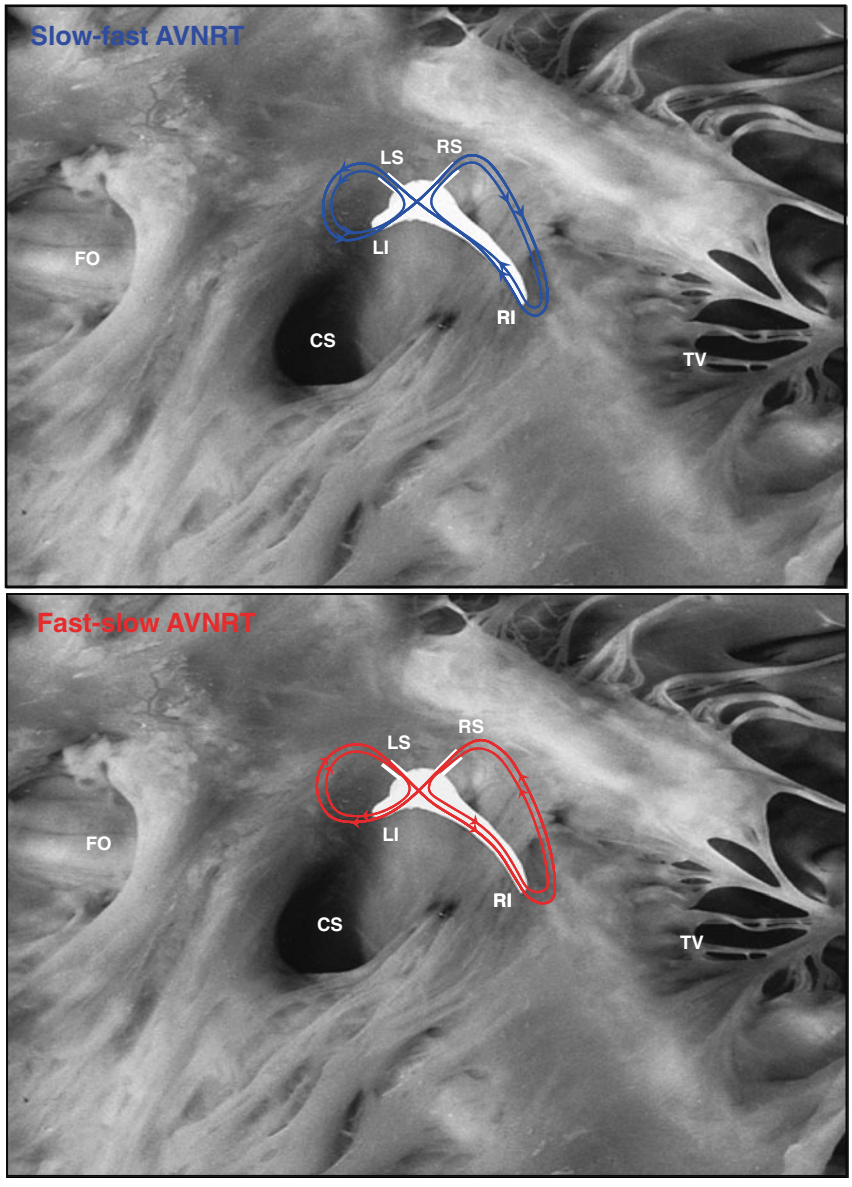

Figure 27.7

(a) Proposed circuit of slow-fast AVNRT. Right- or left-sided circuits may occur with antegrade conduction through the inferior inputs (slow pathway conduction) and retrograde conduction through the superior inputs (fast pathway conduction). Theoretical possibilities are for a right-sided circuit, a left-sided circuit, simultaneous right and left circuits, and figure-of-eight reentry. Overlapping lines indicate possibilities of alternating operating circuits. The site of earliest retrograde atrial activation also depends on the relative length of left and right superior atrial inputs. (b) Proposed circuit of fast-slow AVNRT. Circuits may occur with antegrade conduction through the superior inputs (fast pathway conduction), and retrograde conduction through the inferior inputs (slow pathway conduction). Possibilities are as in slow-fast but in the opposite direction. The site of earliest retrograde atrial activation depends on the relative length of left and right inferior atrial inputs. (c) Proposed circuit of slow-slow AVNRT. The circuit travels antegradely through the right inferior input and retrogradely through the left inferior input, although theoretically the opposite might also occur (please see text for details). (Adapted with kind permission from Katritsis and Becker.[85]) RS: right superior input, LS: left superior input, RI: right inferior input, LI: left inferior input, CS: coronary sinus, TV: tricuspid valve, FO: foramen ovale.

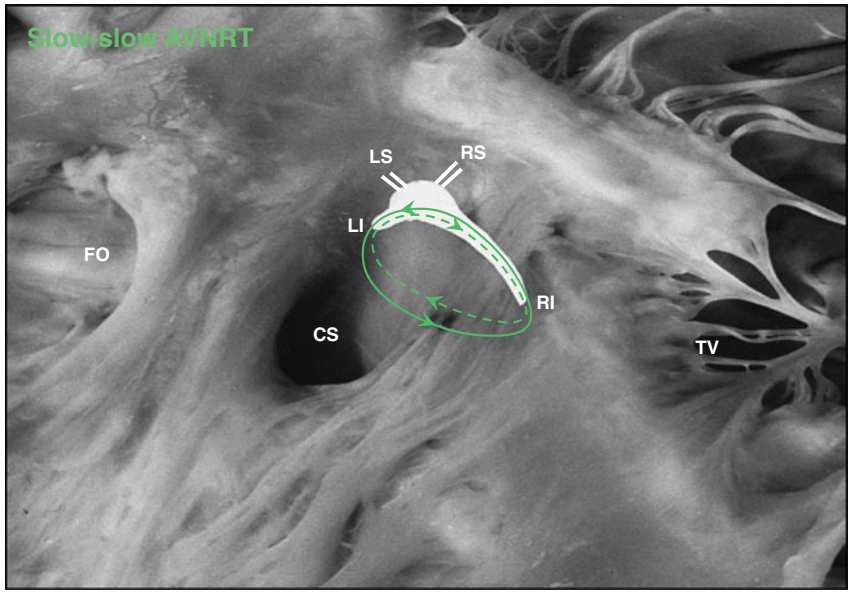

c

Figure 27.7 (Continued)

variation due to changes in AV nodal conduction time (as mainly determined by the slow pathway conduction characteristics) may be seen.

Abnormal (retrograde) P′ waves are constantly related to the QRS and, in the majority of cases, are indiscernible or very close to the QRS complex (RP′/RR < 0.5). Thus P′ waves are either masked by the QRS complex or seen as a small terminal P′ wave that is not present during sinus rhythm (Figs. 27.8 and 27.9). In the atypical form of AVNRT (fast-slow), P′ waves are clearly visible before the QRS, i.e., RP′/P′R > 0.75 (Fig. 27.10), denoting a "*long RP tachycardia*," and are negative in leads II, III, aVF, and V_6 but positive in V_1. P′ waves are shallow in the inferior leads in the rare form of anterior fast-slow AVNRT [86]. Although AV dissociation is usually not seen, it can occur since neither the atria (or, more precisely, the majority of atrial tissue) nor the ventricles are necessary for the reentry circuit. If the tachycardia is initiated by atrial ectopic beats, the initial (ectopic) P′ wave usually differs from the subsequent (retrograde) P′ waves.

27.4 Electrophysiologic Study

27.4.1 Antegrade and Retrograde AV Conduction Curves

Discontinuous AV conduction curves (A_1-A_2/H_1-H_2 or A_1-A_2/A_2-H_2) are suggestive of the presence of antegrade dual AV junction pathway [12]. As previously discussed, discontinuous refractory period curves may not be necessarily demonstrated in all patients with AVNRT. In addition, the mere presence of AV nodal duality is not enough to predispose to paroxysmal tachycardia. Conventionally, an increase of at least 50 ms (conduction jump) in the AH interval for a decrease of 10 ms in the coupling interval (A_1-A_2) is considered to reflect dual AV nodal (or, more precisely, junctional) pathways. Failure to demonstrate dual pathways in patients with AVNRT may occur due to several factors as follows.

1. The functional refractory period of the atrium limits the prematurity with which extrastimuli can encounter the AV node [13], or the refractory periods of the slow and fast pathways are similar. Stimulation at faster rates or the introduction of multiple extrastimuli is required in these cases in order to decrease atrial refractoriness or merely dissociate the two pathways [16].

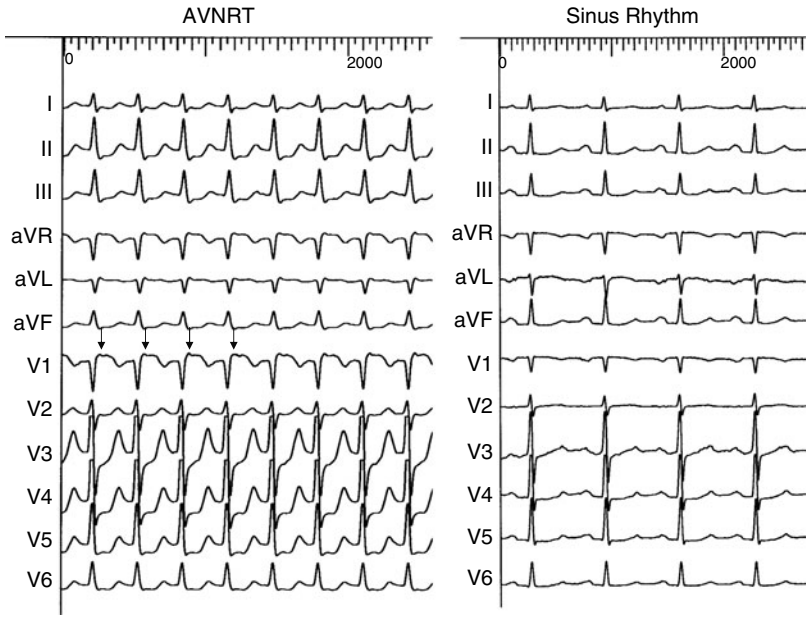

Figure 27.8

12-lead ECG during "slow-fast" AVNRT. Note that small P′ waves that are seen during tachycardia (arrows) are not present during sinus rhythm.

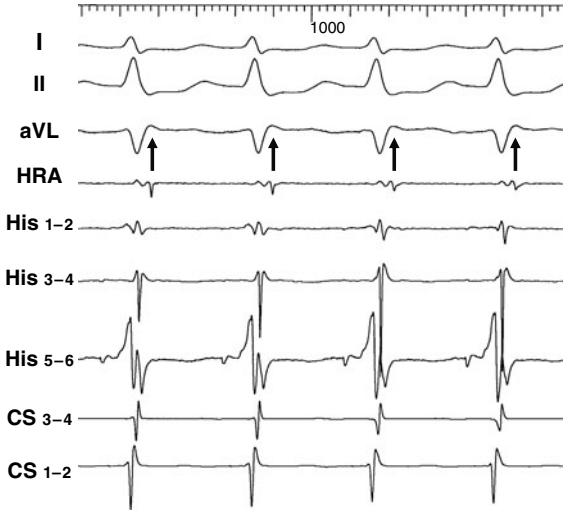

Figure 27.9

Slow-fast AVNRT from the same patient as in Fig. 27.8. Small P′ waves at the end of QRS correspond to retrograde atrial conduction (*arrows*). I: ECG lead, II: lead II of the surface ECG, aVL: lead aVL of the surface ECG, HRA: high right atrium, His: His bundle, CS: coronary sinus.

2. The slow pathway has a longer antegrade refractory period than the fast one, thus preventing the demonstration of a jump, as happens with the fast-slow variety of AVNRT. Retrograde stimulation curves in these patients may demonstrate a jump if the retrograde refractory period of the fast pathway exceeds the retrograde refractory period of the slow one [23].

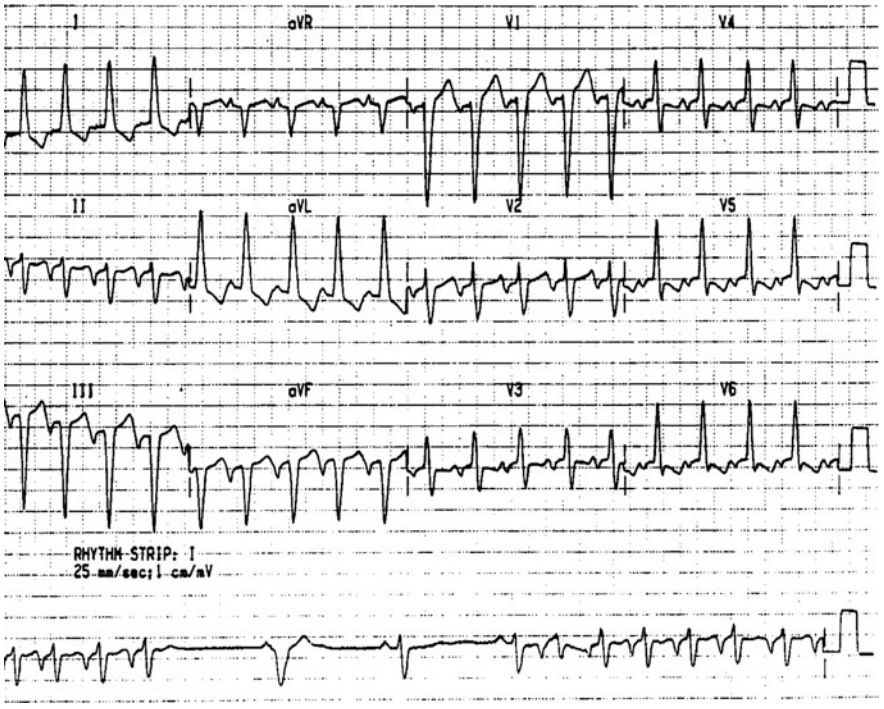

Figure 27.10
12-lead ECG during fast-slow AVNRT. Note the prolonged R-P′ and the incessant nature of the tachycardia.

Ventricular extrastimulation frequently demonstrates continuous VA conduction curves with either fixed or minimal prolongation of the VA interval in patients with typical slow-fast AVNRT [87–89]. This has been traditionally accepted to reflect retrograde fast pathway conduction [90]. Decremental conduction or retrograde jumps may also occur. During retrograde stimulation curves, it is often difficult to obtain recordings of the retrograde His bundle potential. In the literature, retrograde conduction properties of the fast and slow pathways have been derived indirectly by analyzing the conduction curves (V_1-V_2/A_1-A_2). Thus, in case of discontinuous retrograde curves, the longest V_1-V_2 interval in which conduction fails in the fast pathway is assumed to be the retrograde effective refractory period of the fast pathway, and the shortest attainable A_1-A_2 interval on the fast pathway conduction curves (i.e., to the right of discontinuity) is assumed to be its functional refractory period. Similarly, the analysis of the curves on the left of discontinuity, which represent a slow pathway conduction, provides the refractory periods of the slow pathway [24, 53]. This method assumes that no other causes of discontinuities in VA conduction, such as intraventricular conduction delays, exist.

As a rule, at least two cycle lengths (usually 600 and 400 ms) should be studied both antegradely and retrogradely. On certain occasions, the application of two or three extrastimuli may be necessary to expose slow pathway conduction or to induce critical conduction delay required for the initiation of reentry.

27.4.2 Initiation of Tachycardia

The initiation of AVNRT in the electrophysiology laboratory can be accomplished by atrial or ventricular extrastimulation. These modes of induction have been explained according to the conventionally accepted mechanism, although, as previously discussed, this may not be the case.

27.4.2.1 Slow-Fast AVNRT

According to conventionally accepted mechanisms, the requirements for the induction of AVNRT are blocked in an antegrade fast pathway conduction with continued conduction in a slow pathway with critical AV nodal (AH) delay, followed by retrograde conduction over the fast pathway [91]. A critical AV node conduction is necessary in order to allow the antegradely blocked fast pathway to recover and resume retrograde conduction, leading to the occurrence of an atrial echo beat. Depending, therefore, on both critical antegrade delay and retrograde conduction properties, the echo zones may not coincide with the entire slow pathway conduction curves. Sustained reentry requires the ability for repetitive antegrade slow pathway and repetitive retrograde fast pathway conduction.

A *single atrial extrastimulus* can initiate the slow-fast form of tachycardia by producing antegrade block in the fast pathway while conducting through the slow one (Fig. 27.2). If the tachycardia is induced during the conduction of antegrade AV conduction curves, usually a typical decrement (jump) precedes the initiation of tachycardia, but this is not always seen. If the atrial pacing length has already reached antegrade fast pathway refractoriness, with resultant antegrade AV conduction exclusively over the slow pathway, tachycardia initiation is associated by smooth rather than discontinuous AV node conduction curves. *Double or triple atrial extrastimuli* or *incremental atrial pacing* may occasionally be required for tachycardia induction [16]. At critical atrial pacing rates, either a jump or an atypical Wenckebach periodicity or even both can be seen [92]. At faster pacing cycle lengths, the conduction time of one pathway may be prolonged with simultaneous lengthening of the refractoriness of the other pathway. Consequently, the resultant atrial echo zone is widened, and self-initiation (i.e., without an atrial extrastimulus) of sustained reentry may become possible at shorter pacing lengths. Rarely, atrial extrastimuli or even sinus beats may produce simultaneous fast and slow pathway conduction, resulting in double ventricular responses [93]. Repetition of such a phenomenon produces a paroxysmal form of non-reentrant tachycardia [94, 95].

Ventricular extrastimuli or *incremental ventricular pacing* may also initiate slow-fast reentry, but much less commonly than atrial stimulation. In one third of patients, tachycardia can be initiated by ventricular extrastimuli [90]. This mode of tachycardia initiation requires that the slow pathway has a retrograde refractory period longer than that of the fast pathway. Consequently, the ventricular extrastimulus blocks in the slow pathway and is conducted over the fast one, thus preventing the demonstration of any retrograde jump. Retrograde refractoriness of the His–Purkinje system appears to be an important limiting factor with respect to initiation by ventricular pacing.

27.4.2.2 Fast-Slow AVNRT

Ventricular extrastimuli may cause initiation of tachycardia after blocking the fast pathway and conducted retrogradely over the slow pathway. After the attainment of a critical VA conduction delay (H_2-A_2), the impulse is conducted through the fast pathway in the antegrade direction and produces a ventricular echo. The ventricular echo zone may or may not coincide with the entire retrograde slow pathway conduction curves since the ventricular or the His–Purkinje tissue may exhibit conduction delay in response to ventricular extrastimulation, thereby precluding maintenance of critical H_2-A_2 delay. When tachycardia is induced during retrograde curves, its initiation is usually preceded by a sudden jump in ventriculoatrial conduction times. If, however, the ventricular pacing length has already reached retrograde fast pathway refractoriness with resultant retrograde VA conduction exclusively over the slow pathway, tachycardia initiation is associated by smooth rather than discontinuous VA conduction curves. *Incremental ventricular pacing* can also induce tachycardia of this form with a mechanism analogous to the one described previously for the slow-fast form.

Atrial extrastimuli can initiate tachycardia of this form only if the slow pathway has an antegrade refractory period longer than that of the fast pathway being incapable of antegrade conduction. Sudden increment of AV conduction, therefore, is not noted in this case. The critical AV node conduction delay required for the initiation of an atrial echo or sustained reentry is minimal, since the A_1-H_2 interval is within the range of antegrade fast pathway conduction times. When the slow pathway has markedly prolonged antegrade refractoriness relative to that of the fast pathway (wide window), late atrial premature beats or spontaneous acceleration of the sinus rate can easily induce AV node reentry of the fast-slow form. This may explain the incessant nature of this tachycardia.

The initiation of an AV junctional reentry tachycardia of any form is therefore dependent on several factors such as the effective refractory periods of the two pathways, the functional refractory periods of the atrium or the ventricle, and the number of the delivered extrastimuli or the cycle length of the basic pacing drive. Both atrial and ventricular incremental pacing may facilitate initiation of AV node reentry tachycardia of either form [12]. In certain occasions, isoprenaline infusion or atropine may be necessary to modulate the autonomic tone and allow the induction and sustenance of tachycardia [96].

27.4.3 Effect of Stimulation During Tachycardia

A late single atrial extrastimulus may fail to depolarize the entire atria or, if the atria are depolarized, may fail to penetrate the reentrant circuit causing a compensatory pause without affecting the cycle length of the tachycardia. Earlier extrastimuli may penetrate the reentrant circuit, resulting in premature depolarization of the atria and termination of the tachycardia. Resetting of the tachycardia may also occur, although rarely, because atrial refractoriness usually does not allow adequately early extrastimuli. The latter usually happens in AVNRTs with cycle lengths more than 300 ms, unless the stimulation is carried out very close to the AV node (Fig. 27.11). Faster AVNRTs usually require two extrastimuli or rapid atrial pacing to stop.

Ventricular extrastimuli behave in a similar manner. A very important point typical of AVNRTs is the inability of His-synchronous ventricular extrastimuli to capture the atrium and advance or delay the subsequent atrial activation or reset the whole tachycardia cycle. Ventricular extrastimulation is very important for the differential diagnosis, as will be discussed later.

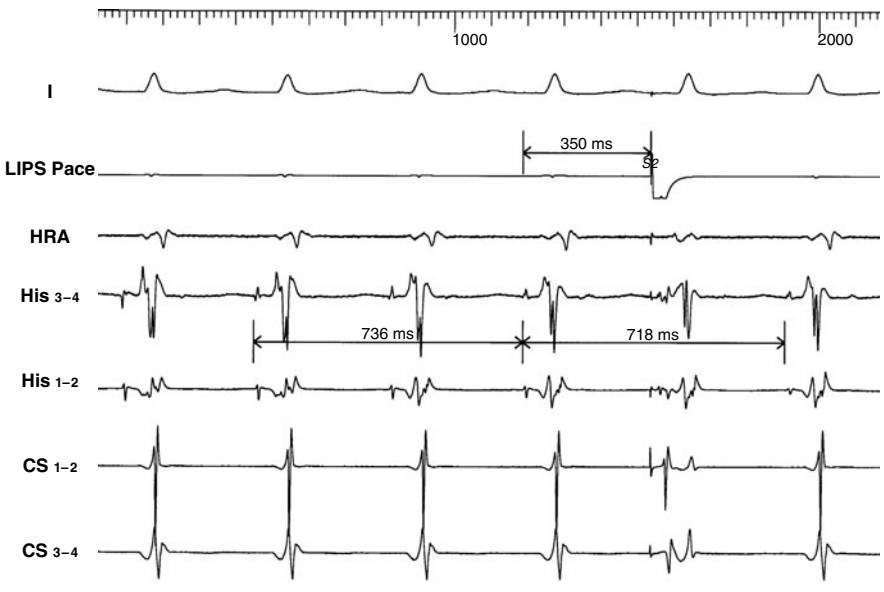

Figure 27.11

Resetting of slow-fast AVNRT. The tachycardia cycle length is 365 ms. An atrial extrastimuli is delivered from the left inferoparaseptal area very close to the His area, 350 ms following the His bundle activation, and results in resetting of the next His bundle electrogram. I: ECG lead, HRA: high right atrium, His: His bundle, CS: coronary sinus, LIPS: left inferoparaseptal pacing.

27.5 Electrophysiologic Forms of AVNRT

According to the conventional description of a dual AV junctional pathway, AVNRT has been traditionally classified as slow-fast or typical AVNRT, and fast-slow or atypical AVNRT. The fast pathway of the reentry circuit runs superiorly and anteriorly in the triangle of Koch, whereas the slow pathway runs inferiorly and posteriorly close to the coronary sinus ostium [70]. Indeed, detailed endocardial mapping in patients with AVNRT has demonstrated that in the majority of slow-fast cases of AVNRT, the site of earliest atrial activation is close to the apex of Koch's triangle, near the AV node–His bundle junction, i.e., anterior to the node [44, 97]. Thus, the earliest retrograde A, whenever atrial electrograms are separated from ventricular ones, occurs in the His bundle electrogram, followed by the ostium of the coronary sinus, distal coronary sinus, and high right atrium [14, 97]. Depolarization of the distal coronary sinus may also be simultaneous or slightly later than in the high right atrium. However, the recognition of the fact that all forms of AVNRT may present with atypical retrograde atrial activation has made classification attempts more complicated, and a universally accepted scheme does not exist. Most authors, however, would accept the following classification:

1. In *typical or slow-fast form* of AVNRT, the onset of atrial activation appears prior, at the onset, or just after the QRS complex, thus maintaining an atrial-His/His-atrial ratio A-H/H-A > 1 (Fig. 27.2). In particular, the following criteria are considered as diagnostic for the slow-fast form of AVNRT: an A-H/H-A ratio > 3 [44], a VA interval measured from the onset of ventricular activation on the surface ECG to the earliest deflection of the atrial activation in the His bundle electrogram < 60 ms, or a VA interval measured at the high right atrium < 95 ms [98]. Although, typically, the earliest retrograde atrial activation is being recorded at the His bundle electrogram, cases of posterior retrograde fast pathways, i.e., with posterior earliest retrograde atrial activation at the CS [99] have been described.
2. In *atypical or fast-slow form* of AVNRT (approximately 5–10% of all AVNRT cases), retrograde atrial electrograms begin well after ventricular activation with an A-H/H-A ratio < 1, indicating that retrograde conduction is slower than antegrade conduction [24]. The VA interval measured from the onset of ventricular activation on surface ECG to the earliest deflection of the atrial activation in the His bundle electrogram is > 60 ms, and in the high right atrium > 100 [100]. In the majority of fast-slow cases, the site of earliest atrial activation is posterior to the AV node near the orifice of the coronary sinus [49, 101]. However, anterior and mid-forms of fast-slow AVNRT have also been described [33, 86].
3. In the *slow-slow form*, the A-H/H-A ratio is > 1 but the VA interval is > 60 ms, suggesting that two slow pathways are utilized for both anterograde and retrograde activation [33, 102]. Usually, but not always, earliest atrial activation is at the posterior septum (coronary sinus ostium) [33, 102]. The so-called *posterior or type B* AVNRT can be demonstrated in approximately 2% of patients with the anterior form of slow-fast AVNRT [50]. In posterior tachycardia, the VA times (as measured from the onset of ventricular activity to the onset of atrial activity by whichever electrode recorded the earliest interval) may be prolonged, ranging from 76 to 168 ms [50]. The atrial-His/His-atrial ratio, however, remains more than one. Some cases of posterior slow-fast AVNRT may actually represent the slow-slow form [26, 99]. Since conduction times are sensitive to autonomic changes, attempts to classify the AVNRT forms according to retrograde atrial activation sequence and the possibility of demonstrating a lower common pathway, have appeared [56]. We know now that all forms of AVNRT (slow-fast, fast-slow, and slow-slow) may display anterior, posterior, and middle retrograde activation patterns [86]. Heterogeneity of both fast and slow conduction patterns has been well described, and in certain patients all forms of AVNRT may be inducible [33, 86].

27.6 Differential Diagnosis

27.6.1 Narrow-QRS Tachycardia

In the presence of a narrow QRS tachycardia, AVNRT should be differentiated from atrial tachycardia or orthodromic atrioventricular reentrant tachycardia (AVRT) due to an accessory pathway, i.e., tachycardia using the AV node for antegrade conduction and the accessory pathway for retrograde conduction.

27.6.1.1 AVNRT versus Atrial Tachycardia

Simple pacing maneuvers can be utilized in order to exclude reentrant or triggered atrial tachycardias. If there is demonstration of change in (1) AA interval when a ventricular extrastimulus is delivered during tachycardia, (2) tachycardia termination by a ventricular extrastimulus that did not conduct to the atrium, (3) constant His-atrial interval of the return cycle after the introduction of a premature atrial impulse with a wide range of coupling intervals during tachycardia, and (4) ventricle to atrium to His sequence during retrograde initiation of tachycardia, then the aetiology is other than atrial tachycardia [103–105]. In particular, the atrial response upon cessation of ventricular pacing associated with 1:1 ventriculoatrial conduction during tachycardia can distinguish between atrial tachycardia and AVNRT or AVRT. Atrial tachycardia is associated with an A-A-V response, whereas AVNRT or AVRT produce an A-V response [104]. The difference in the AH interval between atrial pacing and the tachycardia may also allow differentiation of AVNRT from atrial tachycardia. A Δ A-H >40 ms indicates AVNRT, whereas in atrial tachycardia this difference is <10 msec [105]. This concept is discussed later under the differential diagnosis of AVNRT vs. AVRT.

27.6.1.2 AVNRT versus AVRT due to Accessory Pathways

The eccentric retrograde atrial activation during ventricular stimulation or tachycardia and the demonstration of continuous AV or VA conduction curves usually characterizing nonseptal concealed accessory pathways, differentiate this form of atrioventricular reentry from AVNRT. Care is needed, however, since AVNRT is now known to occur with eccentric atrial activation and, in addition, decremental septal pathways may mimic AVNRT especially of the fast-slow or slow-slow forms (Fig. 27.12). Septal pathways may have the property of decremental conduction [106, 107] and normal atrial retrograde activation during tachycardia. These tachycardias tend to be incessant [108, 109]. The documentation of preexcited beats as well as AV dissociation and the induction of bundle branch block (BBB) during tachycardia may assist the differential diagnosis. The demonstration of AV block or AV dissociation during tachycardia is characteristic of AVNRT excluding the presence of an accessory pathway [110, 111]. Similarly, the development of bundle branch block either spontaneously or after the introduction of ventricular extrastimuli during AVNRT does not change the AA or HH intervals. Although the first VV interval may be prolonged for one cycle due to HV prolongation associated with the development of BBB, the subsequent cycles of tachycardia are identical to the basic tachycardia cycle length. A significant change in the VA interval with the development of bundle branch block is diagnostic of orthodromic AVRT and localizes the pathway to the same side as the block [112].

In general, septal ventriculoatrial interval < 70 ms is diagnostic of slow-fast AVNRT provided that atrial tachycardia has been excluded [113, 114]. In the case of relatively delayed retrograde conduction that allows the identification of retrograde P waves, ECG criteria can be applied for diagnosis. The presence of a pseudo r′ wave in lead V1 or a pseudo S wave in leads II, III, and aVF was indicative of anterior AVNRT with an accuracy of 100%. A difference of RP′ intervals in lead V_1 and III > 20 ms was indicative of posterior AVNRT rather than AVRT due to a posteroseptal pathway [115].

In septal decremental pathways, ventricular extrastimuli introduced while the His bundle is refractory during tachycardia may advance or delay subsequent atrial activation (extranodal capture), whereas in slow-fast AVNRT, either anterior or posterior, atrial activity is not perturbed. Atrial capture at a time when the His bundle is refractory implies the presence of an accessory pathway (Fig. 27.13) [116]. In practice, the extrastimulus has to be delivered coincident with the His potential or up to 50 ms before this [117]. Failure to reset the atria (Fig. 27.14) suggests, but does not prove, that an accessory pathway is not present or that it is relatively far from the site of premature stimulation (e.g., right ventricular stimulation in the presence of a left free wall pathway) [118]. Theoretically, it is possible that resetting of the atrium might be a result of an increase in conduction time over such a pathway of a magnitude equal to the interval by which the extrastimulus preceded atrial activation, but such a coincidence is rare. In addition, at the time of His bundle activation, the accessory pathway may be refractory and resetting by ventricular extrastimuli may not be seen. Failure to demonstrate resetting, therefore, does not exclude an anomalous septal pathway with decremental properties. Thus,

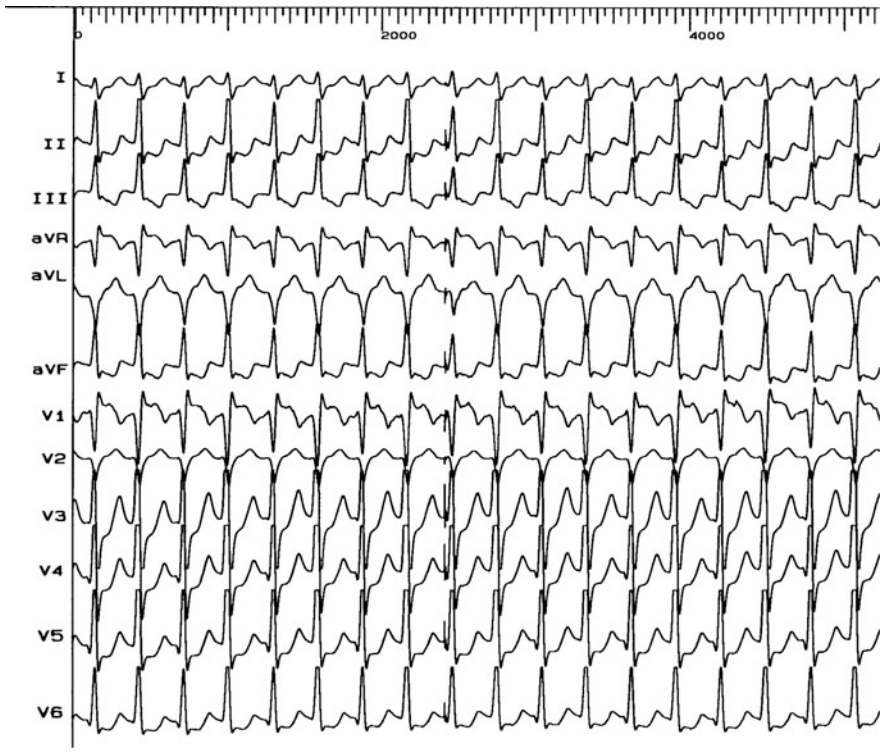

Figure 27.12
12-lead ECG during atrioventricular reentrant tachycardia due to a posteroseptal accessory pathway.

resetting or termination of the tachycardia with His-refractory ventricular extrastimuli is a specific but not highly sensitive criterion for differential diagnosis. Additional criteria have therefore been suggested. Using ventricular-induced atrial preexcitation, Miles et al. [119] devised a preexcitation index for the differentiation of AVNRT and AVRT using an accessory pathway. Progressively premature right ventricular extrastimuli (V_2) were introduced during tachycardia, and the difference between the tachycardia cycle length and the longest V_1V_2 at which atrial preexcitation occurred defined the preexcitation index. Atrial preexcitation occurred in 10% of 22 patients with AVNRT compared with 89% of 55 patients with AVRT. A preexcitation index of 100 ms or greater characterized AVNRT, whereas an index less than 45 ms characterized AVRT using a septal pathway. Left free wall pathways had indices of 75 ms or greater. In another report of 16 patients with AVNRT and 23 patients with AVRT studied at St. George's Hospital in London, the ratio between the minimum ventriculoatrial interval during tachycardia and ventricular pacing was 0.32–0.27 in AVNRT, 0.48–0.71 in AVRT using a left free wall pathway, 0.91–1.08 in posteroseptal pathways, 0.94–1.29 in anteroseptal pathways, and 1.53–1.68 in right free wall pathways [114]. A difference in the VA interval during tachycardia and right apical ventricular pacing > 90 ms has also been reported to differentiate patients with AVNRT from those with AVRT [120]. The difference between the ventriculoatrial interval obtained during apical pacing and that obtained during posterobasal pacing (ventriculoatrial index) can also discriminate between patients with posteroseptal pathways (> 10 ms) and patients with nodal retrograde conduction (< 5 ms) [121].

Miller et al. [122] found the His to atria (HA) intervals to offer more precise discrimination. Their criterion is the difference between His to atrial intervals during pacing and during tachycardia (ΔHA). In 84 patients, a retrograde His was present in 93% of them and the ΔHA was > 0 ms in AVNRT and < −27 ms in orthodromic AVRT incorporating a septal accessory pathway. Thus, an intermediate value of ΔHA = −10 ms had 100% sensitivity, specificity, and predictive accuracy in differentiating the two forms of tachycardia. Parahisian pacing and the change in timing and sequence of retrograde atrial activation between His and proximal right bundle branch capture and noncapture has also been

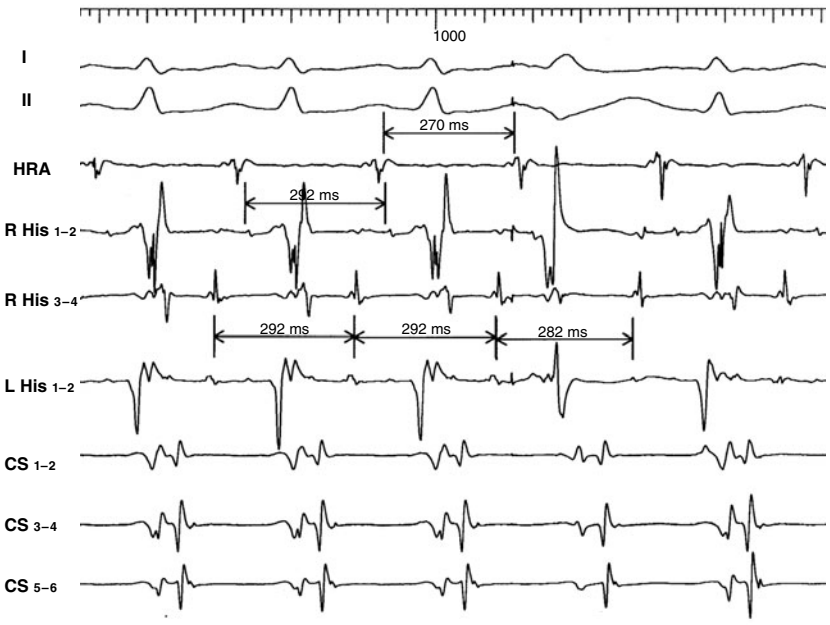

Figure 27.13

Resetting of atrioventricular reentrant tachycardia due to a left posteroseptal accessory pathway. The tachycardia cycle length is 292 ms. At 270 ms, a ventricular extrastimulus is delivered at a time when the His bundle is expected to be refractory and resets the next atrial electrogram (from 292 to 282 ms). I, II: ECG leads, HRA: high right atrium, RHis: His bundle recorded from the right septum, LHis: His bundle recorded from the left septum, CS: coronary sinus.

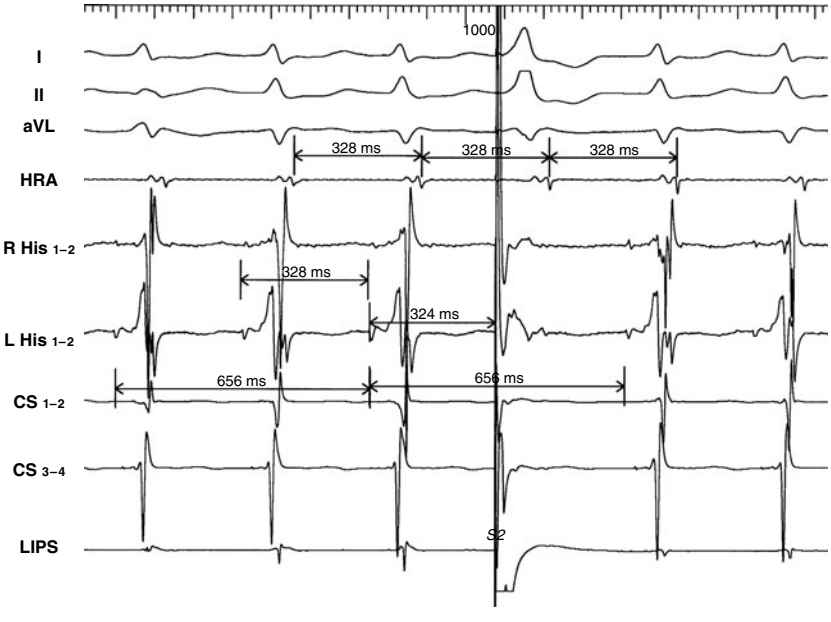

Figure 27.14

No resetting of AVNRT. Absence of resetting with para-Hisian pacing from the right septum. I, II, aVL: ECG leads, HRA: high right atrium, RHis: His bundle recorded from the right septum, LHis: His bundle recorded from the left septum, CS: coronary sinus, RIPS: right inferoparaseptal area.

used for differentiation between AV nodal and septal pathway retrograde conduction [123]. The response is considered extranodal when the retrograde atrial activation during His bundle capture is the same as during ventricular capture without His bundle capture. These techniques, however, require recording of both antegrade and retrograde His bundle activation.

The difference in the AH interval between atrial pacing and the tachycardia may also allow differentiation of atypical AVNRT from other types of long RP tachycardias. A ΔA-H > 40 ms indicates AVNRT, whereas in atrial tachycardia, this difference is <10 msec [105].

Right apical stimulation is relatively close to the insertion of a septal accessory pathway as opposed to the AV junction. Thus, ventricular fusion during resetting or entrainment of tachycardia has been reported to occur in patients with AVRT due to septal pathways but not with AVNRT [124]. Michaud et al. [100] have proposed two additional criteria for differential diagnosis. The ventriculoatrial (VA) interval and tachycardia cycle length (TCL) were measured during tachycardia, and entrainment of the tachycardia was accomplished with right apical ventricular pacing. The intervals between the last ventricular pacing stimulus and the last entrained atrial depolarization during tachycardia (SA) as well as the post-pacing interval were considered. All patients with AVNRT had SA-VA intervals > 85 ms and PPI-TCL intervals > 114 ms [100]. Conventional entrainment techniques do not take into account pacing induced incremental AV nodal conduction (ie in the post-pacing A-H) that may alter the PPI. Thus, Gonzalez-Torrecilla et al [126], "corrected" the PPI-TCL difference by subtracting from it the difference: postpacing AH interval minus basic AH interval. The presence of a corrected PPI-TCL < 110 msec indicated AVRT. Entrainment through basal RV pacing away from the septum may produce prolonged PPI-TCL intervals in the absence of a septal pathway due to the distance of the RV base from the AV node (activation occurs retrogradely through the distal His-Purkinje system) and has been found superior to apical entrainment for diagnostic purposes [127]. A differential (between base and apex) corrected PPI-TCL >30 msec or a differential VA interval > 20 msec has been reported to predict AVNRT very reliably [128]. The main advantage of this technique is that the differential VA interval could be calculated from the last paced beat in case the tachycardia was terminated after transient entrainment.

It should be noted that in clinical practice, pacing or other maneuvers cannot be applied to all cases and multiple criteria have to be used for the differential diagnosis of narrow complex tachycardias with atypical characteristics [113].

27.6.2 Wide-WRS Tachycardia

In the presence of wide-QRS tachycardia, when ventricular tachycardia is excluded, antidromic atrioventricular reentrant tachycardia should be differentiated from AVNRT with a bystanding accessory pathway, and the possibilities of AVNRT or atrial tachycardia with aberrant conduction due to bundle branch block should also be considered.

27.6.2.1 AVNRT with a bystanding Accessory Pathway versus Antidromic AVRT

Antidromic AVRT, i.e., tachycardia utilizing the accessory pathway for antegrade conduction and the AV node for retrograde conduction, may be induced in approximately 6% of the patients with accessory pathways located in the left or right free wall, or the anterior septum at an adequate distance from the AV node [125]. In some cases, atrioventricular junctional reentry may be the underlying mechanism of the preexcited tachycardia and the possibility of AVNRT conducting over a bystanding accessory pathway should be considered in the presence of transition from narrow to wide complex tachycardia of a similar cycle length and without disturbing the HH intervals [129]. In this case, atrial extrastimuli fail to induce advancement of the following preexcited QRS complex, the next retrograde His bundle deflection where apparent, and the subsequent atrial deflection, as may happen in the presence of a macroreentrant loop [130].

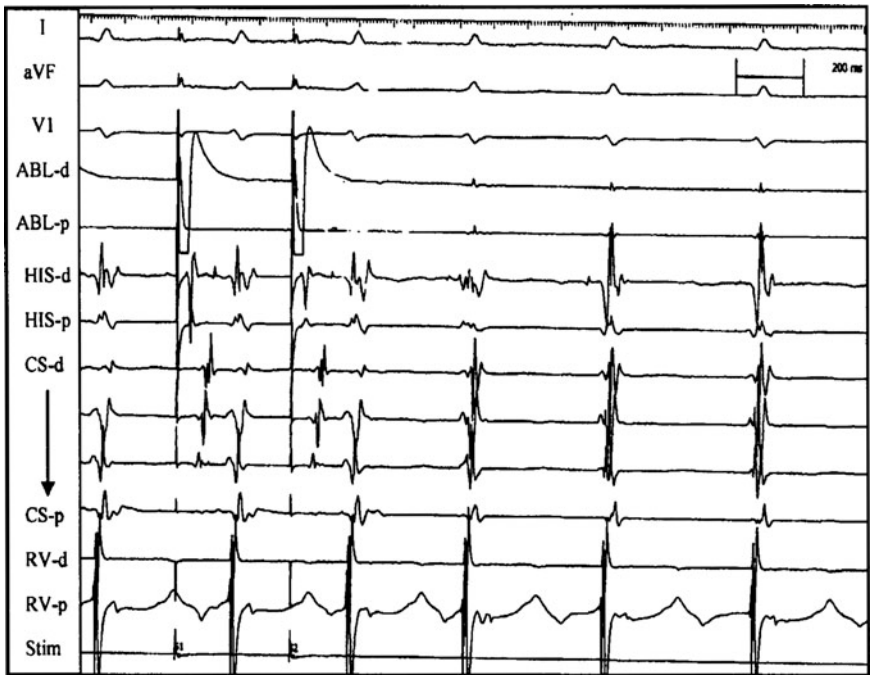

Figure 27.15

Junctional tachycardia initiated with atrial pacing. Although there is a prolonged AH interval during tachycardia, the first tachycardia beat conducts without AH delay. (Reproduced from Hamdan et al. [136] with kind permission.) I, aVF, V_1: ECG leads, ABL: ablation catheter, His: His bundle, CS: coronary sinus, RV: right ventricle, Stim: stimulation channel.

27.7 Non-Reentrant AV Junctional Tachycardias

27.7.1 Non-Paroxysmal Junctional Tachycardias

The term *non-paroxysmal junctional tachycardia was* initially used to denote junctional rhythms of gradual onset and termination with a rate between 70 and 130 beats/min [131]. This tachycardia was frequently diagnosed in the past, and considered to be a typical example of a digitalis-induced arrhythmia [132]. Non-paroxysmal junctional tachycardia usually occurs in patients with underlying heart disease, such as myocardial infarction, or after open-heart surgery, although it can occur rarely in apparently normal persons [133, 134].

Most cases of non-paroxysmal junctional tachycardia, especially the digitalis-induced, are caused by delayed after-depolarizations and triggered activity in the AV node [135]. In these patients, tachycardia can be induced by atrial ectopics or atrial pacing. Enhanced automaticity can also occur however, as suggested by the ability of this tachycardia in some patients to accelerate with enhanced sympathetic tone.

27.8 Focal Junctional Tachycardia

Focal junctional tachycardias have been also called automatic junctional tachycardias since the dominant (but not the only) mechanism is enhanced automaticity [136].

27.8.1 Pediatric Population

These tachycardias were first described in the pediatric population as junctional ectopic tachycardias [137] or His bundle tachycardias [138]. They may occur as a congenital arrhythmia [138–140] or early after infant open-heart surgery [141, 142]. The focus of the tachycardia seems to be localized in the lower part of the AV junction or, most probably, within the His bundle. They are dangerous forms of arrhythmia refractory to medical therapy, overdrive pacing, and DC cardioversion. Diagnosis is made on the ECG, which shows a narrow QRS tachycardia with slower and dissociated P waves. In electrophysiology study, there is a normal HV interval and normal AV conduction curves [139, 143].

27.8.2 Adults

In adult patients, the tachycardia is associated with a structurally normal heart and the prognosis is usually benign [144, 145].

The usual electrocardiographic finding is a narrow QRS tachycardia with AV dissociation. Occasionally, the tachycardia might be irregular, thus resembling atrial fibrillation. In the electrophysiology laboratory, the arrhythmia is not inducible by programmed electrical stimulation, thus making reentry an unlikely mechanism. It is, however, sensitive to isoproterenol administration, and in some cases, rapid atrial or ventricular pacing may result in tachycardia induction, suggesting abnormal automaticity or triggered activity as the other possible mechanism. During tachycardia, there is a normal or increased HV interval with atrioventricular dissociation that is interrupted by frequent episodes of ventriculoatrial conduction with earliest atrial activation in the posteroseptal, anteroseptal, or midseptal regions. At times, the mode of tachycardia induction resembles a double AV nodal response that is characteristic of AVNRT (Fig. 27.15) [136].

References

1. Camm, A.J. and D. Katritsis, The diagnosis of tachyarrhythmias, in *Heart Disease*, 2 edn., D.G. Julian, A.J. Camm, K.M. Fox, R.J.C. Hall, and P.A. Poole-Wilson, Editors. Philadelphia, PA: Saunders, 1996, pp. 6606–6621.
2. Josephson, M.E. and H.J. Wellens, Electrophysiologic evaluation of supraventricular tachycardia. *Cardiol. Clin.*, 1997;**15**: 567–586.
3. Anderson, R.H., M.J. Janse, F.J.L. Van Capelle, et al., A combined morphological and electrophysiological study of the atrioventricular node of the rabbit heart. *Circulation* 1974;**35**: 909–922.
4. Becker, A.E. and R.H. Anderson, Morphology of the human atrioventricular junctional area, in *The Conduction System of the Heart. Structure, Function and Clinical Implications*, H.J.J. Wellens, K.I. Lie, and M.J. Janse, Editors. Leiden: HE Stenfert Kroese BV, 1976; pp. 263–286.
5. Racker, D.K., Atrioventricular node and input pathways: A correlated gross anatomical and histological study of canine atrioventricular junctional region. *Anat. Rec.*, 1989;**224**: 336–354.
6. Mines, G.R., On dynamic equilibrium of the heart. *J. Physiol.*, 1913;**46**: 349–354.
7. Moe, G.K., J.B. Preston, and H. Burlington, Physiologic evidence of a dual AV transmission system. *Circ. Res.*, 1956;**4**: 357–375.
8. Denes, P., R.C. Dhingra, R. Chuquimia, et al., Demonstration of dual AV nodal pathways in patients with paroxysmal supraventricular tachycardia. *Circulation*, 1973;**48**: 549–555.
9. Mendez, C., J. Han, P.D. Carcia de Jalon, et al., Some characteristics of ventricular echoes. *Circ. Res.*, 1965;**16**: 561–581.
10. Rosen, K.M., A. Mehta, and R.A. Miller, Demonstration of dual atrioventricular nodal pathways in man. *Am. J. Cardiol.*, 1974;**33**: 13–18.
11. Ward, D.E. and A.J. Camm, *Clinical Electrophysiology of the Heart*. London: E Arnold, 1987.
12. Katritsis, D.G. and A.J. Camm, Classification and differential diagnosis of atrioventricular nodal re-entrant tachycardia. *Europace*, 2006;**8**: 29–36.
13. Denes, P., D. Wu, R. Dhingra, et al., Dual atrioventricular nodal pathways. A common electrophysiological response. *Br. Heart J.*, 1975;**37**: 1069–1076.
14. Josephson, M.E. and J.A. Kastor, Supraventricular tachycardia: Mechanisms and management. *Ann. Intern. Med.*, 1977;**87**: 346–358.
15. Tai, C.T., S.A. Chen, C.E. Chiang, et al., Complex electrophysiological characteristics in atrioventricular nodal re-entrant tachycardia with continuous atrioventricular node function curves. *Circulation*, 1997;**95**: 2541–2547.
16. Kuo, C.T., K.H. Lin, N.J. Cheng, et al., Characterization of atrioventricular nodal reentry with continuous atrioventricular node conduction curve by double atrial extrastimulation. *Circulation*, 1999;**99**: 659–665.
17. Sheahan, R.G., G.J. Klein, R. Yee, C.A. Le Feuvre, and A.D. Krahn, Atrioventricular node reentry with 'smooth' AV

node function curves: A different arrhythmia substrate? *Circulation*, 1996;**93**: 969–972.
18. Levites, R. and J.I. Haft, Evidence suggesting dual AV nodal pathways in patients without supraventricular tachycardias. *Chest*, 1975;**67**: 36–42.
19. Thapar, M.K. and P.C. Gillette, Dual atrioventricular nodal pathways: A common electrophysiologic response in children. *Circulation*, 1979;**60**: 1369–1374.
20. Casta, A., G.S. Wolff, A.V. Mehta, et al., Dual atrioventricular nodal pathways: A benign finding in arrhythmia-free children with heart disease. *Am. J. Cardiol.*, 1980;**46**: 1013–1018.
21. Brugada, P., B. Heddle, M. Green, et al., Initiation of atrioventricular nodal reentrant tachycardia in patients with discontinuous anterograde atrioventricular nodal conduction curves with and without documented supraventricular tachycardia: Observations on the role of discontinuous retrograde conduction curve. *Am. Heart J.*, 1984;**107**: 685–697.
22. Reyes, W., S. Milstein, A. Dunnigan, et al., Indications for modification of coexisting dual atrioventricular node pathways in patients undergoing surgical ablation of accessory atrioventricular connections. *J. Am. Coll. Cardiol.*, 1991;**17**: 1561–1567.
23. Wu, D., P. Denes, F. Amay-y-Leon, et al., An unusual variety of atrioventricular nodal re-entry due to retrograde dual atrioventricular nodal pathways. *Circulation*, 1977;**56**: 50–59.
24. Sung, R.J., J.L. Styperek, R.J. Myerburg, and A. Castellanos, Initiation of two distinct forms of atrioventricular nodal reentrant tachycardia during programmed ventricular stimulation in man. *Am. J. Cardiol.*, 1978;**42**: 404–415.
25. Coumel, P., P. Attuel, and J.F. Leclercq, Permanent form of junctional reciprocating tachycardia: Mechanism, clinical and therapeutic implications, in *Cardiac Arrhythmias: Electrophysiology, Diagnosis and Management*, O.S. Narula, Editors. Baltimore, MD: Williams and Wilkins, 1979, pp. 347–363.
26. Otomo, K., Z. Wang, R. Lazarra, and W.M. Jackman, Atrioventricular nodal reentrant tachycardia: Electrophysiological characteristics of four forms and implications for the reentrant circuit, in *Cardiac Electrophysiology: From Cell to Bedside*, 3rd edn., D.P. Zipes and J. Jalife, Editors. Philadelphia, PA: WB Saunders Company, 1999, pp. 504–521.
27. Kwaku, K.F. and M.E. Josephson, Typical AVNRT. An update on mechanisms and therapy. *Card. Electrophysiol. Rev.*, 2002;**6**: 414–421.
28. Swiryn, S., R. Bauernfeind, E. Palileo, B. Strasberg, C.E. Duffy, and K.M. Rosen, Electrophysiologic study demonstrating triple antegrade AV nodal pathways in patients with spontaneous and/or induced supraventricular tachycardia. *Am. Heart J.*, 1982;**103**: 168–174.
29. Sublettt, K.L. and O. Fujimura, Atrioventricular node reentry that utilizes triple nodal pathways. *Am. Heart J.*, 1992;**124**: 777–779.
30. Lee, M.A., F. Morady, A. Kadish, et al., Catheter modification of the atrioventricular junction with radiofrequency energy for control of atrioventricular nodal reentry tachycardia. *Circulation*, 1991;**83**: 827–835.
31. Tai, C.T., S.A. Chen, C.E. Chiang, et al., Multiple anterograde atrioventricular node pathways in patients with atrioventricular node reentrant tachycardia. *J. Am. Coll. Cardiol.*, 1996;**28**: 725–731.
32. Tai, C.T., S.A. Chen, C.E. Chiang, et al., Electrophysiologic characteristics and radiofrequency catheter ablation in patients with multiple atrioventricular nodal reentry tachycardias. *Am. J. Cardiol.*, 1996;**77**: 52–58.
33. Hwang, C., D.J. Martin, J.S. Goodman, et al., Atypical atrioventricular node reciprocating tachycardia masquerading as tachycardia using a left-sided accessory pathway. *J. Am. Coll. Cardiol.*, 1997;**30**: 218–225.
34. Mitrani, R.D., L.S. Klein, F.K. Hackett, D.P. Zipes, W.M. Miles, Radiofrequency ablation of atrioventricular node reentrant tachycardia: Comparison between fast (anterior) and slow (posterior) pathway ablation. *J. Am. Coll. Cardiol.*, 1992;**21**: 432–435.
35. Katritsis, D., A. Slade, A.J. Camm, E. Rowland, Atrioventricular junctional reentrant tachycardia utilising multiple retrograde fibres during ablation of the slow pathway. *Clin. Cardiol.*, 1993;**16**: 889–891.
36. Fujiki, A., S. Yoshida, K. Mizumaki, and S. Sasayama, Fast-slow type of atrioventricular nodal reentrant tachycardia: Horizontal dissociation of the AV node during tachycardia. *Pacing Clin. Electrophysiol.*, 1988;**11**: 1559–1565.
37. Ward, D.E. and C. Garratt, Atrioventricular nodal reentrant tachycardia. Is there a third pathway? *J. Electrophysiol.*, 1993;**4**: 62–67.
38. Bauernfeind, R.A., D. Wu, P. Denes, and K.M. Rosen, Retrograde block during dual pathway atrioventricular nodal reentrant paroxysmal tachycardia. *Am. J. Cardiol.*, 1978;**42**: 499–505.
39. Ko, P.T., G.V. Naccarelli, S. Gulamhusein, E.N. Prystowski, D.P. Zipes, and G.J. Klein, Atrioventricular dissociation during paroxysmal junctional tachycardia. *PACE*, 1981;**4**: 670–678.
40. Miller, J.M., M.E. Rosenthal, J.A. Vassalo, and M.E. Josephson, Atrioventricular nodal reentrant tachycardia: Studies on upper and lower "common pathways". *Circulation*, 1987;**75**: 930–940.
41. Loh, P., J.M. de Bakker, M. Hocini, B. Thibault, R.N. Hauer, and M.J. Janse, Reentrant pathway during ventricular echoes is confined to the atrioventricular node: High-resolution mapping and dissection of the triangle of Koch in isolated, perfused canine hearts. *Circulation*, 1999;**100**: 1346–1353.
42. Chen, J. and M.E. Josephson, Atrioventricular nodal tachycardia occurring during atrial fibrillation. *J. Cardiovasc. Electrophysiol.*, 2000;**11**: 812–815.
43. Schuger, C.D., R.T. Steinman, and M.H. Lehmann, Recovery of retrograde fast pathway excitability in the atrioventricular node reentrant circuit after concealed antegrade impulse penetration. *J. Am. Coll. Cardiol.*, 1991;**17**: 1129–1137.
44. Akhtar, M., A.N. Damato, J. Ruskin, et al., Antegrade and retrograde conduction characteristics in three patterns of paroxysmal atrioventricular junctional reentrant tachycardia. *Am. Heart J.*, 1978;**95**: 22–42.
45. Gomes, J.A.C., M.S. Dhatt, N.S. Rubenson, and A.N. Damato, Electrophysiologic evidence for selective retrograde utilization of a specialized conducting system in atrioventricular nodal reentry tachycardia. *Am. J. Cardiol.*, 1979;**43**: 687–698.
46. Wu, D., J.S. Hung, C.T. Kuo, K.S. Hsu, and W.B. Shieh, Effects of quinidine on atrioventricular nodal reentrant paroxysmal tachycardia. *Circulation*, 1981;**64**: 823–831.
47. Yamabe, H., Y. Shimasaki, O. Honda, Y. Kimura, and Y. Hokamura, Demonstration of the exact anatomic tachycardia circuit

in the fast-slow form of atrioventricular nodal reentrant tachycardia. *Circulation*, 2001;**104**: 1268–1273.

48. Iinuma, H., L.S. Dreifus, T. Mazgalev, R. Price, and E.L. Michelson, Role of the perinodal region in atrioventricular nodal reentry: Evidence in an isolated rabbit heart preparation. *J. Am. Coll. Cardiol.*, 1983;**2**: 465–473.
49. Kay, G.N., A.E. Epstein, S.M. Dailey, and V.J. Plumb, Selective radiofrequency ablation of the slow pathway for the treatment of atrioventricular nodal reentrant tachycardia. Evidence for involvement of perinodal myocardium within the reentrant circuit. *Circulation*, 1992;**85**: 1675–1688.
50. McGuire, M.A., K.-C. Lau, D.C. Johnson, D.A. Richards, J.B. Uther, and D.L. Ross, Patients with two types of atrioventricular junctional (AV nodal) reentrant tachycardia. Evidence that a common pathway of nodal tissue is not present above the reentrant circuit. *Circulation*, 1991;**83**: 1232–1246.
51. Ross, D.L., D.C. Johnson, A.R. Dennis, M.J. Cooper, D.A. Richards, and J.B. Uther, Curative surgery for atrioventricular junctional ("AV nodal") reentrant tachycardia. *J. Am. Coll. Cardiol.*, 1985;**6**: 1383–1392.
52. Anselme, F., B. Hook, K. Monahan, et al., Heterogeneity of retrograde fast-pathway conduction pattern in patients with atrioventricular nodal reentry tachycardia: Observations by simultaneous multisite catheter mapping of Koch's triangle. *Circulation*, 1996;**93**: 960–968.
53. Sung, R.J., H.L. Waxman, S. Saksena, and Z. Juma, Sequence of retrograde atrial activation in patients with dual atrioventricular nodal pathways. *Circulation*, 1981;**64**: 1059–1067.
54. Loh, P., S.Y. Ho, T. Kawara, et al., Reentrant circuits in the canine atrioventricular node during atrial and ventricular echoes: Electrophysiological and histological correlation. *Circulation*, 2003;**108**: 231–238.
55. Heidbuchel, H., H. Ector, and F. Van de Werf, Prospective evaluation of the length of the lower common pathway in the differential diagnosis of various forms of AV nodal reentrant tachycardia. *Pacing Clin. Electrophysiol.*, 1998;**21**: 209–216.
56. Heidbuchel, H. and W.M. Jackman, Characterization of subforms of AV nodal reentrant tachycardia. *Europace*, 2004;**6**: 316–329.
57. Gianfranchi, L., M. Brignole, P. Delise, et al., Modification of antegrade slow pathway is not crucial for successful catheter ablation of common atrioventricular nodal reentrant tachycardia. *Pacing Clin. Electrophysiol.*, 1999;**22**: 263–267.
58. Manolis, A.S., P.J. Wang, and N.A. Estes 3rd., Radiofrequency ablation of slow pathway in patients with atrioventricular nodal reentrant tachycardia. Do arrhythmia recurrences correlate with persistent slow pathway conduction or site of successful ablation? *Circulation*, 1994;**90**: 2815–2819.
59. Zipes, D.P., C. Mendez, and G.K. Moe, Evidence for summation and voltage dependency in rabbit atrioventricular nodal fibers. *Circ. Res.*, 1973;**32**: 170–177.
60. Efimov, I.R. and T.N. Mazgalev, High-resolution, three-dimensional fluorescent imaging reveals multilayer conduction pattern in the atrioventricular node. *Circulation*, 1998;**98**: 54–57.
61. Spach, M.S., M. Lieberman, J.G. Scott, R.C. Barr, E.S. Johnson, and J.M. Kootsey, Excitation sequences of the atrial septum and the AV node in isolated hearts of the dog and rabbit. *Circulation*, 1971;**29**: 156–172.
62. Tse, W.W., Transmembrane potentials of canine AV junctional tissues. *Am. Heart J.*, 1986;**11**: 1100–1105.
63. Jalife, J., The sucrose gap preparation as a model of AV nodal transmission: Are dual pathways necessary for reciprocation and AV nodal "echoes"? *PACE*, 1983;**6**: 1106–1110.
64. Spach, M.S., Anisotropic structural complexities in the genesis of reentrant arrhythmias. *Circulation*, 1991;**84**: 1447–1450.
65. Malik, M. and A.J. Camm, Complexity of AV nodal function: Complex nodal structure or complex behavior of nodal elements? *PACE*, 1998;**11**: 425–433.
66. Spach, M.S., W.T. Miller, D.B. Geselowitz, R.C. Barr, J.M. Kootsey, E.A. Johnson, The discontinuous nature of propagation in normal canine cardiac muscle: Evidence for recurrent discontinuities of intracellular resistance that affect the membrane currents. *Circ. Res.*, 1981;**48**: 39–54.
67. Paes de Carvallho, A. and D.F. de Almeida, Spread of activity through the atrioventricular node. *Circ. Res.*, 1960;**8**: 801–809.
68. Patterson, E. and B.J. Scherlag, Anatomic and functional fast atrioventricular conduction pathway. *J. Cardiovasc. Electrophysiol.*, 2002;**13**: 945–949.
69. Wu, D., S.-J. Yeh, C.-C. Wang, M.-S. Wen, H.-J. Chang, F.-C. Lin, Nature of dual atrioventricular node pathways and the tachycardia circuit as defined by radiofrequency ablation technique. *J. Am. Coll. Cardiol.*, 1992;**20**: 884–895.
70. Keim, S., P. Werner, M. Jazayeri, M. Akhtar, and P. Tchou, Localization of the fast and slow pathways in atrioventricular nodal reentrant tachycardia by intraoperative ice mapping. *Circulation*, 1992;**86**: 919–925.
71. Spach, M.S. and M.E. Josephson, Initiating reentry: The role of nonuniform anisotropy in small circuits. *J. Cardiovasc. Electrophysiol.*, 1994;**5**: 182–209.
72. Hocini, M., P. Loh, S.Y. Ho, et al., Anisotropic conduction in the triangle of Koch of mammalian hearts: Electrophysiologic and anatomic correlations. *J. Am. Coll. Cardiol.*, 1998;**31**: 629–636.
73. Patterson, E. and B.J. Scherlag, Decremental conduction in the posterior and anterior AV nodal inputs. *J. Interv. Card. Electrophysiol.*, 2002;**7**: 137–148.
74. Katritsis, D.G., A.E. Becker, K.A. Ellenbogen, E. Giazitzoglou, S. Korovesis, and A.J. Camm, The right and left inferior extensions of the atrioventricular node may represent the anatomic substrate of the slow pathway in the human. *Heart Rhythm*, 2004;**1**: 582–586.
75. Katritsis, D.G., A.E. Becker, K.A. Ellenbogen, E. Giazitzoglou, S. Korovesis, and A.J. Camm, Effect of slow pathway ablation in atrioventricular nodal reentrant tachycardia on the electrophysiologic characteristics of the inferior atrial inputs to the human atrioventricular node. *Am. J. Cardiol.* 2006;**97**: 860–865.
76. Tawara, S., *Das Reitzleitungssystem des Säugetierherzens: Eine anatomisch-histologische Studie über das Atrioventrikularbundel und die Purkinjeschen Fäden*. Jena, Germany: Gustav Fischer, 1906; pp. 135–136.
77. Inoue, S. and A.E. Becker, Posterior extensions of the human compact atrioventricular node: A neglected anatomic feature of potential clinical significance. *Circulation*, 1998;**97**: 188—193.
78. Waki, K., J.S. Kim, and A.E. Becker, Morphology of the human atrioventricular node is age dependent: A feature of potential clinical significance. *J. Cardiovasc. Electrophysiol.*, 2000;**11**: 1144—1151.

79. Khalife, K., J. Billette, D. Medkour, et al., Role of the compact node and its posterior extension in normal atrioventricular nodal conduction, refractory, and dual pathway properties. *J. Cardiovasc. Electrophysiol.*, 1999;**10**: 1439–1451.
80. Lin, L.J., J. Billette, D. Medkour, M.C. Reid, M. Tremblay, and K. Khalife, Properties and substrate of slow pathway exposed with a compact node targeted fast pathway ablation in rabbit atrioventricular node. *J. Cardiovasc. Electrophysiol.*, 2001;**12**: 479–486.
81. Reid, M.C., J. Billette, K. Khalife, and R. Tadros, Role of compact node and posterior extension in direction-dependent changes in atrioventricular nodal function in rabbit. *J. Cardiovasc. Electrophysiol.*, 2003;**14**: 1342–1350.
82. Dobrzynski, H., V.P. Nikolski, A.T. Sambelashvili, et al., Site of origin and molecular substrate of atrioventricular junctional rhythm in the rabbit heart. *Circ. Res.*, 2003;**93**: 1102–1110.
83. Inoue, S., A.E. Becker, R. Riccardi, and F. Gaita, Interruption of the inferior extension of the compact atrioventricular node underlies successful radio frequency ablation of atrioventricular nodal reentrant tachycardia. *J. Interv. Card. Electrophysiol.*, 1999;**3**: 273–277.
84. Antz, M., B.J. Scherlag, K. Otomo, et al., Evidence for multiple atrio-AV nodal inputs in the normal dog heart. *J. Cardiovasc. Electrophysiol.*, 1998;**9**: 395–408.
85. Katritsis, D.G. and A. Becker, The Circuit of Atrioventricular Nodal Reentrant Tachycardia: a Proposal. *Heart Rhythm*. 2007;**4**: 1354–1360.
86. Nawata, H., N. Yamamoto, K. Hirao, et al., Heterogeneity of anterograde fast-pathway and retrograde slow-pathway conduction patterns in patients with the fast-slow form of atrioventricular nodal re-entrant tachycardia: Electrophysiologic and electrocardiographic considerations. *J. Am. Coll. Cardiol.*, 1998;**32**: 1731–1740.
87. Gomes, J.A.C., M.S. Dhatt, A.N. Damato, M. Akhtar, and C.A. Holder, Incidence, determinants and significance of fixed retrograde conduction in the region of the atrioventricular node: Evidence for retrograde atrioventricular nodal bypass tracts. *Am. J. Cardiol.*, 1979;**44**: 1089–1098.
88. Wu. D., Dual atrioventricular nodal pathway: A reappraisal. *PACE*, 1982;**5**: 72–77.
89. Wu, D., P. Denes, F. Amat-Y-Leon, et al., Clinical electrocardiographic and electrophysiological observations in patients with paroxysmal supraventricular tachycardia. *Am. J. Cardiol.*, 1978;**41**: 1045–1051.
90. Wu, D., H.C. Kou, S.J. Yeh, F.C. Lin, and J.S. Hung, Determinants of tachycardia induction using ventricular stimulation in dual pathway atrioventricular nodal reentrant tachycardia. *Am. Heart J.*, 1984;**108**: 44–55.
91. Denes, P., D. Wu, F. Amat-y-Leon, R. Dhingra, C. Wyndham, and K.M. Rosen, The determinants of atrioventricular nodal reentrance with premature atrial stimulation in patients with dual AV nodal pathways. *Circulation*, 1977;**56**: 253–259.
92. Wu, D., P. Denes, R. Dhingra, et al., Determinants of fast and slow pathway conduction in patients with dual AV nodal pathways. *Circ. Res.*, 1975;**36**: 782–790.
93. Wu, D., P. Denes, R. Dhingra, R. Pietras, and K.M. Rosen, New manifestations of dual AV nodal pathways. *Eur. J. Cardiol.*, 1975;**2**: 459–466.
94. Csapo. G., Paroxysmal nonrentrant tachycardia due to simultaneous conduction in dual atrioventricular nodal pathways. *Am. J. Cardiol.*, 1979;**43**: 1033–1045.
95. Kim, S.S., R. Lal, and R. Ruffy, Paroxysmal nonrentrant supraventricular tachycardia due to simultaneous fast and slow pathway conduction in dual atrioventricular nodal pathways. *J. Am. Coll. Cardiol.*, 1987;**10**: 456–461.
96. Huycke, E.C., W.T. Lai, N.X. Nguyen, E.C. Keung, and R.J. Sung, Role of intravenous isoproterenol in the electrophysiologic induction of atrioventricular node reentrant tachycardia in patients with dual atrioventricular nodal pathways. *Am. J. Cardiol.*, 1989;**64**: 1131–1137.
97. Amat-y-Leon, F., R. Dhingra, D. Wu, P. Denes, C. Wyndham, and K.M. Rosen, Catheter mapping of retrograde atrial activation. Observations during ventricular pacing and AV nodal re-entrant paroxysmal tachycardia. *Br. Heart J.*, 1976;**38**: 355–362.
98. Benditt, D.G., E.L.C. Pritchett, W.M. Smith, and J.J. Gallagher, Ventriculoatrial intervals: Diagnostic use in paroxysmal supraventricular tachycardias. *Ann. Intern. Med.*, 1979;**91**: 161–166.
99. Engelstein, E.D., K.M. Stein, S.M. Markowitz, and B.B. Lerman, Posterior fast atrioventricular node pathways: Implications for radiofrequency catheter ablation of atrioventricular node reentrant tachycardia. *J. Am. Coll. Cardiol.*, 1996; **27**: 1098–1105.
100. Michaud, G.F., H. Tada, S. Chough, et al., Differentiation of atypical atrioventricular node re-entrant tachycardia from orthodromic reciprocating tachycardia using a septal accessory pathway by the response to ventricular pacing. *J. Am. Coll. Cardiol.*, 2001;**38**: 1163–1167.
101. Jazayeri, M.R., S.L. Hempe, J.S. Sra, et al., Selective transcatheter ablation of the fast and slow pathways using radiofrequency energy in patients with atrioventricular nodal reentrant tachycardia. *Circulation*, 1992;**85**: 1318–1328.
102. Goldberger, J., R. Brooks, and A. Kadish, Physiology of "atypical" atrioventricular junctional reentrant tachycardia occurring following radiofrequency catheter modification of the atrioventricular node. *Pacing Clin. Electrophysiol.*, 1992;**15**: 2270–2282.
103. Taniguchi, Y., S.J. Yeh, M.S. Wen, C.C. Wang, and D. Wu, Atypical atrioventricular nodal reentry tachycardia with atrioventricular block mimicking atrial tachycardia: Electrophysiologic properties and radiofrequency ablation therapy. *J. Cardiovasc. Electrophysiol.*, 1997;**8**: 1302–1308.
104. Knight, B.P., A. Zivin, J. Souza, et al., A technique for the rapid diagnosis of atrial tachycardia in the electrophysiology laboratory. *J. Am. Coll. Cardiol.*, 1999;**33**: 775–781.
105. Man, K.C., M. Niebauer, E. Daoud, et al., Comparison of atrial-His intervals during tachycardia and atrial pacing in patients with long RP tachycardia. *J. Cardiovasc. Electrophysiol.*, 1995;**6**: 700–710.
106. Farre, J., D.L. Ross, I. Wiener, F.W. Bar, E.J. Vanagt, H.J.J. Wellens, Reciprocal tachycardias using accessory pathways with long conduction times. *Am. J. Cardiol.*, 1979;**44**: 1099–1109.
107. Atie, J., P. Brugada, J. Brugada, et al., Longitudinal dissociation of atrioventricular accessory pathways. *J. Am. Coll. Cardiol.*, 1991;**17**: 161–166.

108. Sung, R.J., Incessant supraventricular tachycardia. *PACE*, 1983;**6**: 1306–1326.
109. Coumel, P., Functional reciprocating tachycardias. The permanent and paroxysmal forms of AV nodal reciprocating tachycardias. *J. Electrocardiol*., 1975;**8**: 79–90.
110. Vassalo, J.A., D.M. Cassidy, and M.E. Josephson, Atrioventricular nodal supraventricular tachycardia. *Am. J. Cardiol*., 1985;**56**: 193–195.
111. Yeh, S.-J., T. Yamamoto, F.-C. Lin, and D. Wu, Atrioventricular block in the atypical form of junctional reciprocating tachycardia: Evidence supporting the atrioventricular node as the site of reentry. *J. Am. Coll. Cardiol*., 1990;**15**: 385–392.
112. Kerr, C.R., J.J. Gallagher, and L.D. German, Changes in ventriculoatrial intervals with bundle branch block aberration during reciprocating tachycardia in patients with accessory atrioventricular pathways. *Circulation*, 1982;**66**: 196–201.
113. Knight, B.P., M. Ebinger, H. Oral, et al., Diagnostic value of tachycardia features and pacing maneuvers during paroxysmal supraventricular tachycardia. *J. Am. Coll. Cardiol*., 2000;**36**: 574–582.
114. Crozier, I., S. Wafa, D. Ward, and J. Camm, Diagnostic value of comparison of ventriculoatrial interval during junctional tachycardia and right ventricular apical pacing. *PACE*, 1989;**12**: 942–953.
115. Tai, C.T., S.A. Chen, C.E. Chiang, et al., A new electrocardiographic algorithm using retrograde P waves for differentiating atrioventricular node reentrant tachycardia from atrioventricular reciprocating tachycardia mediated by concealed accessory pathway. *J. Am. Coll. Cardiol*., 1997;**29**: 394–402.
116. Spurrell, R.A.J., D.M. Krikler, and E. Sowton, Concealed bypass of the atrioventricular node in patients with supraventricular tachycardia revealed by intracardiac electrical stimulation and verapamil. *Am. J. Cardiol*., 1974;**33**: 590–595.
117. Ross, D.L. and J.B. Uther, Diagnosis of concealed accessory pathways in supraventricular tachycardia. *PACE*, 1983;**7**: 1069–1085.
118. Benditt, D.G., D.W. Benson, A. Dunnigan, et al., Role of extrastimulus site and tachycardia cycle length in inducibility of atrial preexcitation by premature ventricular stimulation during reciprocating tachycardia. *Am. J. Cardiol*., 1987;**60**: 811–819.
119. Miles, W.M., R. Yee, G.J. Klein, D.P. Zipes, and E.N. Prystowsky, The preexcitation index: An aid in determining the mechanism of supraventricular tachycardia and localizing accessory pathways. *Circulation*, 1986;**74**: 493–500.
120. Tai, C.T., S.A. Chen, C.E. Chiang, and M.S. Chang, Characteristics and radiofrequency catheter ablation of septal accessory atrioventricular pathways. *Pacing Clin. Electrophysiol*., 1999;**22**: 500–511.
121. Martinez-Alday, J.D., J. Almendral, A. Arenal, et al., Identification of concealed posteroseptal Kent pathways by comparison of ventriculoatrial intervals from apical and posterobasal right ventricular sites. *Circulation*, 1994;**89**: 1060–1067.
122. Miller, J.M., M.E. Rosenthal, C.D. Gottlieb, J.A. Vassalo, and M.E. Josephson, Usefulness of the ΔHA interval to accurately distinguish atrioventricular nodal reentry from orthodromic septal bypass tract tachycardias. *Am. J. Cardiol*., 1991;**68**: 1037–1044.
123. Hirao, K., K. Otomo, X. Wang, et al., Para-Hisian pacing. A new method for differentiating retrograde conduction over an accessory AV pathway from conduction over the AV node. *Circulation*, 1996;**94**: 1027–1035.
124. Ormaetxe, J.M., J. Almendral, A. Arenal, et al., Ventricular fusion during resetting and entrainment of orthodromic supraventricular tachycardia involving septal accessory pathways. Implications for the differential diagnosis with atrioventricular nodal reentry. *Circulation*, 1993;**88**: 2623–2631.
125. Packer, D.L., J.J. Gallagher, and E.N. Prystowsky, Physiological substrate for antidromic reciprocating tachycardia. Parequisite characteristics of the accessory pathway and atrioventricular conduction system. *Circulation*, 1992;**85**: 574–588.
126. González-Torrecilla, E., A. Arenal, F. Atienza, J. Osca, J. García-Fernández, A. Puchol, A. Sánchez, and J. Almendral, First postpacing interval after tachycardia entrainment with correction for atrioventricular node delay: a simple maneuver for differential diagnosis of atrioventricular nodal reentrant tachycardias versus orthodromic reciprocating tachycardias. *Heart Rhythm*. 2006;**3**: 674–679.
127. Veenhuyzen, G.D., K. Coverett, F.R. Quinn, J.L. Sapp, A.M. Gillis, R. Sheldon, D.V. Exner, and L.B. Mitchell, Single diagnostic pacing maneuver for supraventricular tachycardia. *Heart Rhythm*. 2008;**5**: 1152–1158.
128. Segal, O.R., L.J. Gula, A.C. Skanes, A.D. Krahn, R. Yee, and G.J. Klein, Differential ventricular entrainment: a maneuver to differentiate AV node reentrant tachycardia from orthodromic reciprocating tachycardia. *Heart Rhythm*. 2009;**6**: 493–500.
129. Smith, W.M., A. Broughton, M.J. Reiter, D.W. Benson, A.O. Grant, J.J. Gallagher, Bystander accessory pathway during AV node reentrant tachycardia. *PACE*, 1983;**6**: 537–543.
130. Atie, J., P. Brugada, J. Brugada, et al., Clinical and electrophysiologic characteristics of patients with antidromic circus movement tachycardia in the Wolff-Parkinson-White syndrome. *Am. J. Cardiol*., 1990;**66**: 1082–1091.
131. Pick, A. and P. Dominguez, Nonparoxysmal A-V nodal tachycardia. *Circulation*, 1967;**16**: 1022–1031.
132. Dreifus, L.S., M. Katz, Y. Watanabe, et al., Clinical significance of disorders of impulse formation and conduction in the atrioventricular junction. *Am. J. Cardiol*., 1963;**11**: 384–391.
133. Rosen, K.M., Junctional tachycardia: Mechanisms, diagnosis, differential diagnosis and management. *Circulation*, 1973;**67**: 654–664.
134. Palileo, E.V., R.A. Brauernfeind, S.P. Swiryn, C.R. Wyndham, K.M. Rosen, Chronic nonparoxysmal junctional tachycardia. *Chest*, 1981;**80**: 106–108.
135. Rosen, M.R., C. Fisch, B.F. Hoffman, P. Danilo, D.E. Lovelace, J.B. Knoebel, Can accelerated atrioventricular junctional escape rhythms be explained by delayed afterdepolarizations? *Am. J. Cardiol*., 1980;**45**: 1272–1284.
136. Hamdan, M.H., N. Badhwar, and M.M. Scheinman, Role of invasive electrophysiologic testing in the evaluation and management of adult patients with focal junctional tachycardia. *Card. Electrophysiol. Rev*., 2002;**6**: 431–435.
137. Garson, A. and P.C. Gillette, Junctional ectopic tachycardia in children: Electrocardiography, electrophysiology and pharmacologic response. *Am. J. Cardiol*., 1979;**44**: 298–302.
138. Coumel, P., J.E. Fifelle, P. Attuel, et al., Tachycardia focale hissiennes congenitales. Etudes cooperative de sept cas. *Arch. Mal. Coeur*., 1976;**69**: 899–909.

139. Villain, E., V.L. Vetter, J.M. Garcia, J. Herre, A. Cifarelli, A. Garson Jr., Evolving concepts in the management of congenital junctional ectopic tachycardia. A multicenter study. *Circulation*, 1990;**81**: 1544–1549.
140. Wren, C. and R.W. Campbell, His bundle tachycardia-arrhythmogenic and antiarrhythmic effects of therapy. *Eur. Heart J.*, 1987;**8**: 647–650.
141. Walsh, E.P., J.P. Saul, G.F. Sholler, et al., Evaluation of a staged treatment protocol for rapid automatic junctional tachycardia after operation for congenital heart disease. *J. Am. Coll. Cardiol.*, 1997;**29**: 1046–1053.
142. Gillette, P.C., Diagnosis and management of postoperative junctional ectopic tachycardia. *Am. Heart J.*, 1989;**118**: 192–194.
143. Wren, C., Incessant tachycardias. *Eur. Heart J.*, 1998;**19**(Suppl E): E32–E36.
144. Ruder, M.A., J.C. Davis, M. Eldar, J.A. Abbott, J.C. Griffin, J.J. Seger, and M.M. Scheinman, Clinical and electrophysiologic characterization of automatic junctional tachycardia in adults. *Circulation*, 1986;**73**: 930–937.
145. Scheinman, M.M., R.P. Gonzalez, M.W. Cooper, M.D. Lesh, R.J. Lee, and L.M. Epstein, Clinical and electrophysiologic features and role of catheter ablation techniques in adult patients with automatic atrioventricular junctional tachycardia. *Am. J. Cardiol.*, 1994;**74**: 565–572.

28 Atrioventricular Dissociation

Anton P.M. Gorgels · Frits W. Bär · Karel Den Dulk† · Hein J.J. Wellens

† Deceased

P. W. Macfarlane, A. van Oosterom, O. Pahlm, P. Kligfield, M. Janse, J. Camm (eds.), *Comprehensive Electrocardiology*, DOI 10.1007/978-1-84882-046-3_28,

28.1 Introduction

28.1.1 Definitions

The atrioventricular (AV) conduction system has the property of anterograde AV conduction in case of supraventricular activation of the heart, and in many instances of retrograde VA conduction, in case the heart is dominated by ventricular activation. AV dissociation is the phenomenon of independent activation of the atria and the ventricles. Different mechanisms for its occurrence exist, but the common denominator is the absence of the usual antegrade AV relation or retrograde VA relation. AV dissociation can be (1) complete or incomplete, (2) continuous or intermittent, and (3) structural or functional. When AV dissociation is incomplete, occasional AV or VA conducted beat is termed a capture beat (Fig. 28.1). AV dissociation is not synonymous to AV block, the latter being just one of the mechanisms for AV dissociation [1].

28.1.2 Types

Three types of AV dissociation can be differentiated.

(a) AV dissociation may be found in the presence of a slow sinus or atrial rhythm, where the atrial rate is below the AV junctional or ventricular escape rhythm in combination with second-degree or incomplete block in the anterograde and retrograde direction. If the AV dissociation is incomplete, this could be the result of intermittent anterograde capture of sinus (or atrial) impulses or of intermittent capture of retrogradely conducted ventricular (Fig. 28.2) or AV junctional escape beats. Complete AV dissociation is diagnosed when complete block in both directions is present.

(b) The second type is found in the presence of an AV junctional or ventricular rhythm with rate above the sinus (or atrial) rate in combination with second (Fig. 28.3) or third (Fig. 28.4) degree block in the retrograde direction.

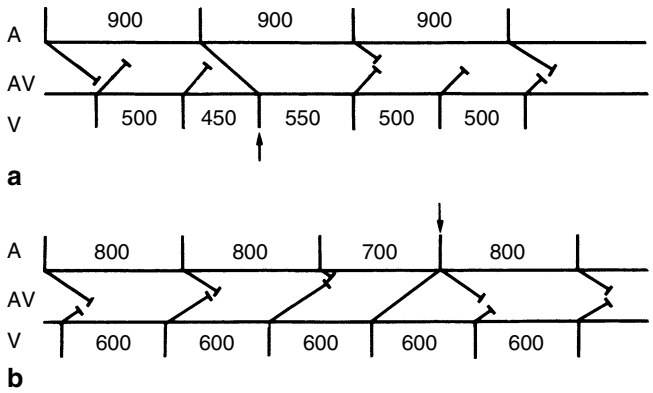

Figure 28.1

The ladder diagrams illustrate incomplete AV dissociation during ventricular tachycardia. Part (a) demonstrates occasional atrial capture of the ventricle (arrow), while part (b) shows occasional ventricular capture of the atrium (arrow). In (a), there is retrograde block of the atrioventricular conduction system (AV) during ventricular tachycardia (cycle length 500 ms). The second atrial impulse from the left is able to capture the ventricle, because at that time there is no retrograde invasion of the AV conduction system. Part (b) shows the opposite. Anterograde conduction of atrial impulses is not possible during the existing ventricular tachycardia. However, a retrograde capture (fourth ventricular impulse) can arise if concealed anterograde penetration of the atrial impulse is absent. In this illustration, it can be seen that this impulse gives an echo beat back to the ventricle due to a dual AV nodal pathway.

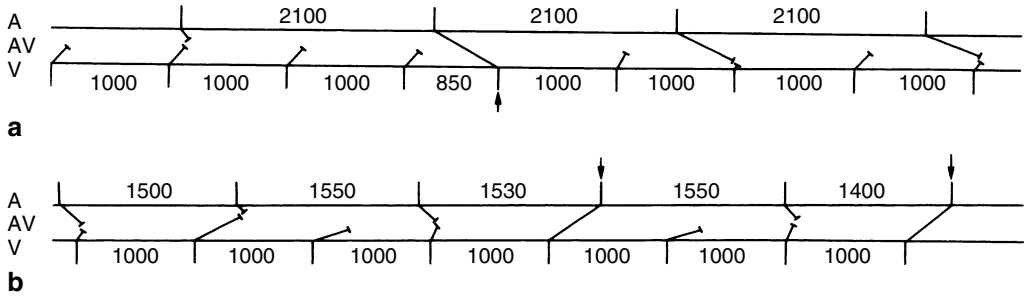

Figure 28.2

The ladder diagrams illustrate intermittent capture (arrows) during sinus bradycardia: (a), anterograde capture and (b), retrograde capture. In (a), the ventricular escape rhythm is not able to conduct in the retrograde direction. Because of the feasibility of anterograde conduction, the second beat from the left of the slow atrial rhythm captures the ventricle. In (b), anterograde conduction of the slow atrial rhythm is not possible. No retrograde conduction is present in the third and sixth ventricular escape beats. The fifth and eighth ventricular beats from the left are able to capture the atrium (arrows) because at that time anterograde concealed penetration from the atrium is absent. No echo beat is seen, because there is no dual AV nodal pathway as was present in Fig. 28.1.

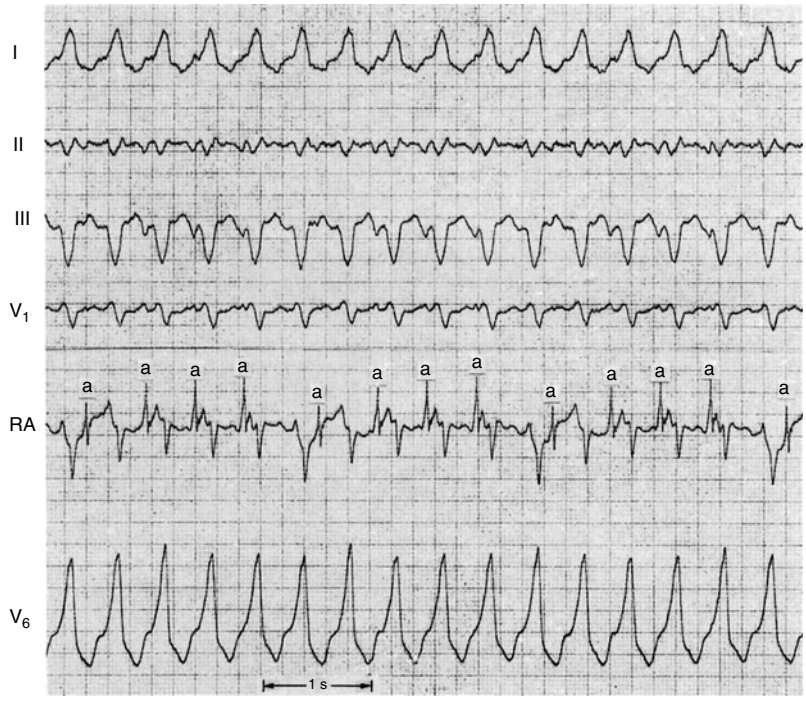

Figure 28.3

Simultaneously recorded five-channel ECG and a right-atrial endocavitary recording illustrating a rather rare example of 5:4 retrograde VA conduction in a patient with ventricular tachycardia. As can be seen in this case, leads II and V_1 are often helpful in detecting P waves on the surface ECG (RA: right atrium, a: atrial endocavitary signal).

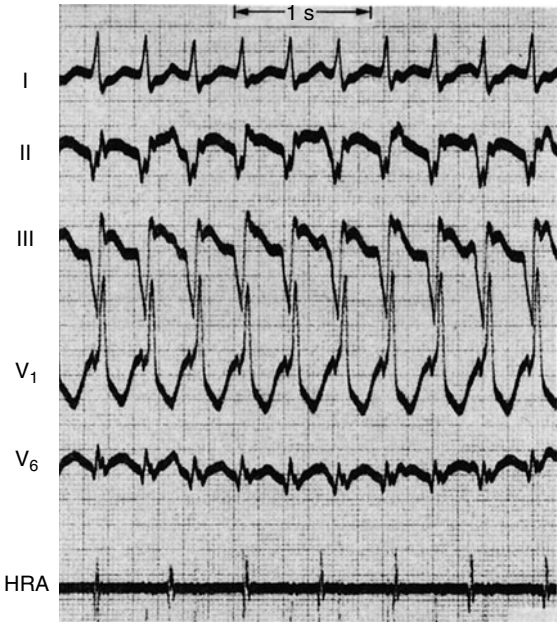

Figure 28.4

This five-channel ECG shows a tachycardia with a rate of 150 beats min^{-1} (bmp). The endocavitary atrial recording (HRA) indicates complete AV dissociation with a ventricular rate higher than the atrial rate. The P waves are also clearly visible in lead II. The finding of complete AV dissociation is extremely suggestive of the presence of ventricular tachycardia.

In the presence of normal anterograde conduction, capture beats can frequently be seen at lower rates of the accelerated ventricular (or AV junctional) rhythm (Fig. 28.5). Higher ventricular (or AV junctional rates usually do not allow anterograde conduction (complete AV dissociation). This form of AV dissociation is clinically important in tachycardias with a wide QRS complex. It helps to differentiate a supraventricular tachycardia with aberrant conduction from a ventricular tachycardia [1]. AV dissociation in wide QRS tachycardias is diagnostic of ventricular tachycardia. Approximately 50% of ventricular tachycardias have complete AV dissociation. In the other 50%, 1:1, 2:1, or Wenckebach type, VA conduction is present [2–5]. Capture or fusion beats are also of help in differentiating supraventricular tachycardia with aberrant conduction from ventricular tachycardia. However, their occurrence is rare (6%) [2].

(c) The third and most important type of AV dissociation is AV block. Block describes delay or failure of impulse propagation. Varying degrees of block exist. AV block is usually classified as first-, second-, or third-degree block according to the severity of the conduction disturbance [6]. AV block will be discussed in detail, because it is the most frequent cause of AV dissociation and its presence has important clinical implications.

28.2 History of Atrioventricular Block

In 1827, Robert Adams [7] opposed Morgagni's hypothesis [8] that the brain was the cause of seizures in patients with bradycardia. He stated that perhaps the heart was the cause of the bradycardia and the neurological symptoms were the subsequent result. Many disagreed with Adams, but William Stokes [9] concluded in 1846 that Adams' concept was correct. The term heart block was introduced by Gaskell [10, 11] in 1882. Einthoven [12] demonstrated the first case of AV block on an electrocardiogram. Wenckebach [13], Hay [14], and Mobitz [15] described and classified several types of AV

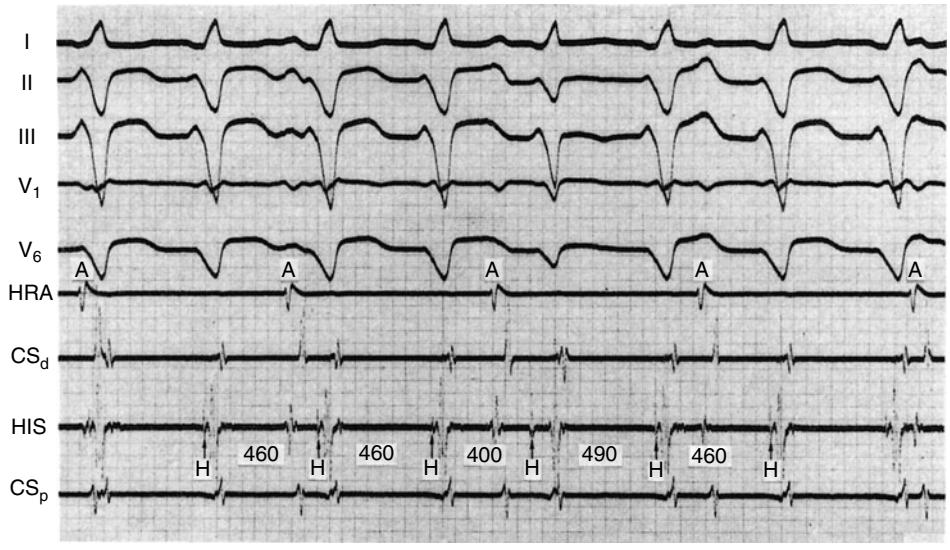

Figure 28.5

Recording of a ventricular tachycardia with a rate of approximately 135 bmp. The HH intervals are 460 ms. The fifth beat from the left is a little earlier than expected with an HH interval of 400 ms. The QRS configuration is also different. The intracardiac recordings indicate that this premature beat is a fusion between an anterogradely conducted (capture) beat and impulse formation in the ventricle (HRA, high right atrium; CS_d, distal coronary sinus; HIS, His bundle; CS_p, proximal coronary sinus).

block. In the following years, many other clinical and experimental studies were published [16–19]. The introduction of intracardiac recordings [20] made possible more precise determination of location of block in humans.

28.3 Classification of Atrioventricular Block

28.3.1 First-Degree AV Block

This represents a prolongation of the AV conduction time (PR interval) beyond 0.2 s. However, every atrial impulse is conducted to the ventricle. Therefore the term block should be avoided. These criteria can be applied only in the presence of a regular sinus or atrial rhythm. The normal PR interval is age-dependent. In younger patients, the PR interval is shorter due to sympathetic tone. The PR interval is also shortened during exercise.

28.3.2 Second-Degree AV Block

This is diagnosed when some of the atrial impulses are not conducted to the ventricle. Second-degree block can be subdivided into the following categories.

28.3.2.1 Mobitz Type I (Wenckebach) Block

In this form of second-degree AV block, the PR interval in several successive beats becomes progressively prolonged, resulting in the dropping on one ventricular depolarization due to failure of conduction. The subsequent PR interval is shortened (Fig. 28.6) [13, 15, 21].

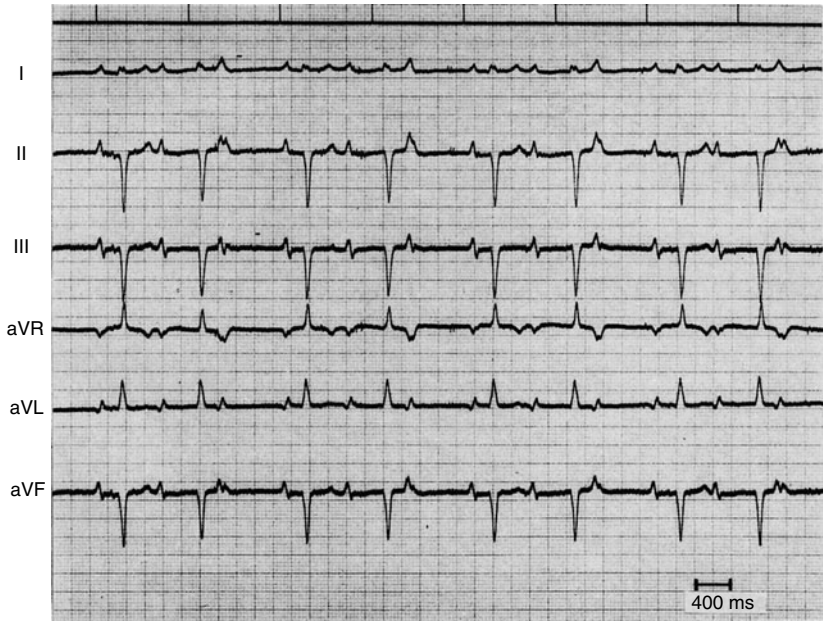

Figure 28.6
Six-channel ECG recording illustrating a Mobitz type I AV block in the AV node or His bundle (narrow QRS complex). Statistically, there is an 8:1 chance that the block is situated in the AV node.

28.3.2.2 Mobitz Type II Block

In this type of second-degree AV block, there is a sudden failure of one or more atrial impulses to be conducted during maintenance of a constant PR interval (Fig. 28.7) [15–21].

28.3.2.3 Higher Degree AV Block

In 2:1 AV block, every second atrial impulse is not propagated to the ventricle (Fig. 28.8). High-degree or advanced AV block, such as 3:1 or 4:1 block, or occasional conducted impulses can exist [22].

28.3.2.4 Third-Degree (Complete) AV Block

In third-degree (complete) AV block, no atrial impulses are propagated to the ventricle (Fig. 28.9).

28.4 Methodology for Determining the Site of a Block

The conduction defect can be present in the AV node, His bundle, bundle branches, or at multiple sites. Determination of the location of the type of block has important consequences in terms of prognosis and treatment.

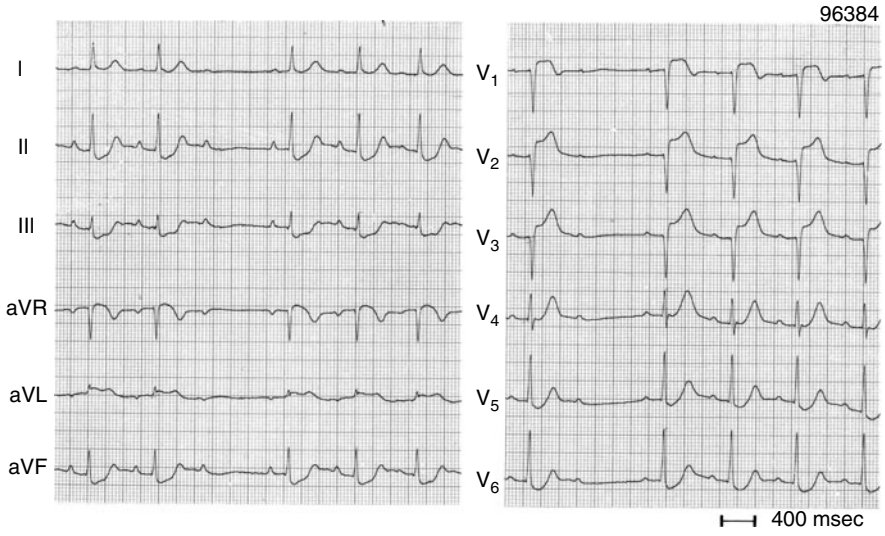

Figure 28.7

Twelve-lead ECG of a patient with Mobitz II block in acute anteroseptal infarction. The third P wave in the left panel and the second P wave in the right panel are suddenly blocked. The QRS width is narrow, suggesting a conduction problem within the His bundle.

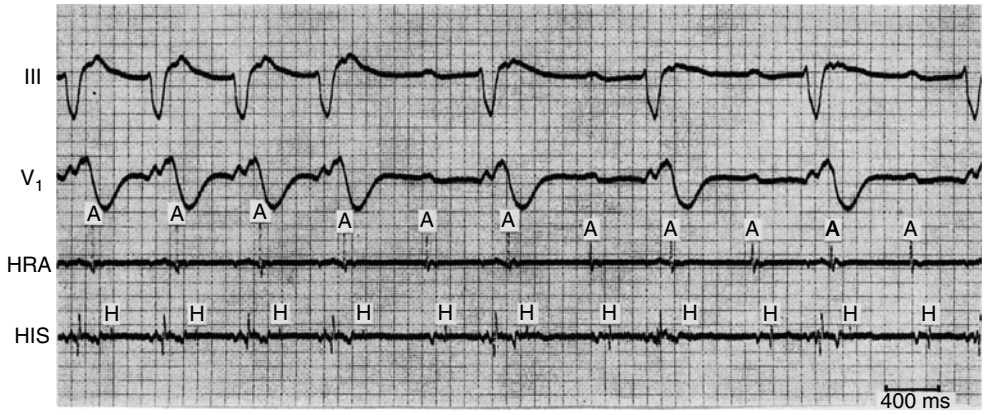

Figure 28.8

In this recording, leads III, V_1, high rate atrium (HRA), and His-bundle lead (HIS) are shown. On the left side of the figure, sinus tachycardia at a rate of 105 bpm with 1:1 conduction is present. First-degree AV block is seen with an AH interval of 120 ms (normal 50–120 ms) and an HV interval of 260 ms (normal 35–55 ms). The sudden change from 1:1 to 2:1 AV block develops without further prolongation of the preceding HV interval. The His recording proves that AV block is located distal to His, because every atrial activation is followed by a His signal. The presence of block in the bundle branches is suggested by the QRS width (±220 ms) in the surface ECG. The configuration in lead V_1 indicates the presence of a right bundle branch block and the negative QRS complex in lead III is in favor of a left anterior fascicular block.

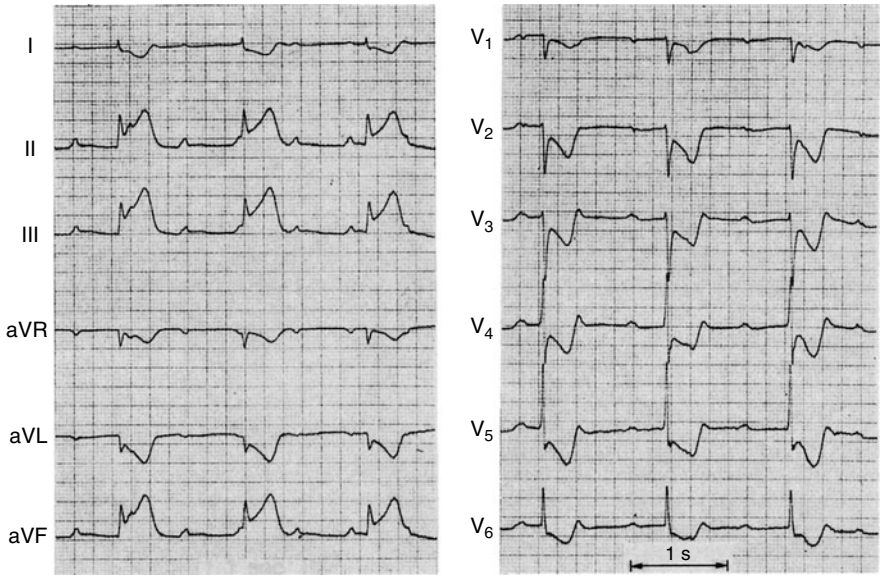

Figure 28.9

This ECG shows an extensive acute infero posterior wall myocardial infarction with third-degree block situated in the AV node and an AV nodal escape rhythm (narrow QRS complexes) of 38 bpm. In acute inferior myocardial infarction, AV block can occur due to vagal stimulation. Usually, the sinus rate is then also low. In this illustration, the sinus rate is approximately 100 bpm, which makes it unlikely that the AV conduction disturbance is caused by vagal influences.

28.4.1 The Value of the Electrocardiogram

28.4.1.1 PR Interval

The PR interval is the time between the beginning of the P wave and the beginning of the QRS complex, and as such, gives an indication of AV conduction.

AV conduction delay or block can be present in the atrium, AV node, His bundle, bundle branches or Purkinje fibers, but the actual site cannot be determined from the surface ECG. PR prolongation of more than 0.3 s is very suggestive of conduction delay in the AV node, but a PR interval between 0.2 and 0.3 s has no indicative value as to the site of block. Block can also be simultaneously present at different levels of the conduction system.

28.4.1.2 QRS Complex

Puech et al. [23], Narula [24], and Schuilenburg [25] found in their studies that the width of the conducted QRS complex gives an indication of the site of block.

28.4.1.3 Conducted Beats: Narrow QRS Complexes

QRS complexes of less than 0.12 s usually signify that the block is located in the AV node or His bundle (Fig. 28.10). A rare exception of a narrow, conducted QRS complex in the presence of trifascicular disease is the coincidence of identical conduction delay in both bundle branches, resulting in PR prolongation and a narrow QRS complex.

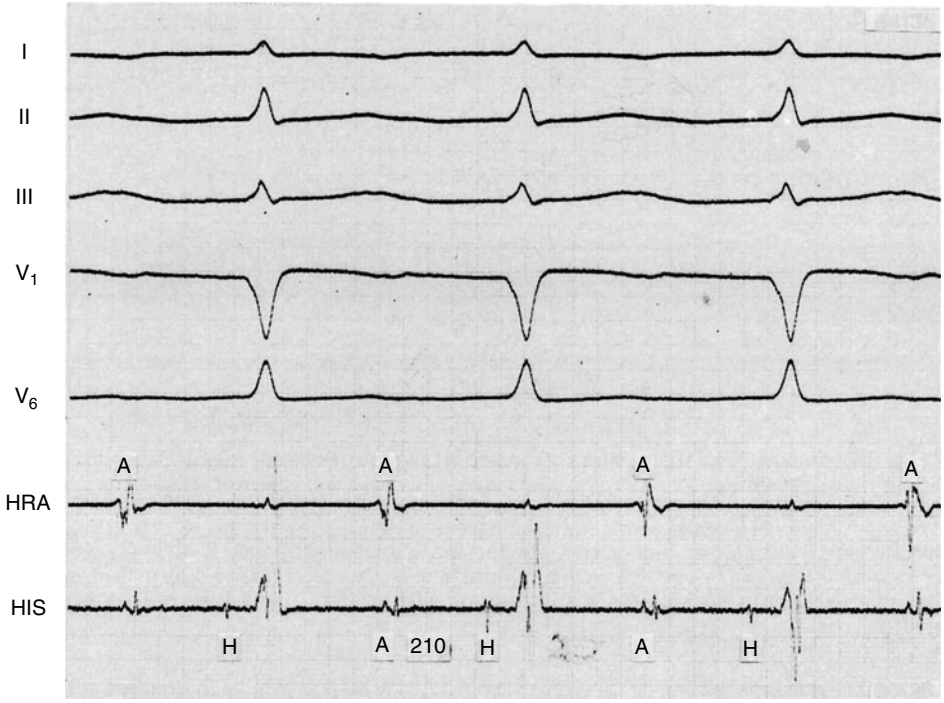

Figure 28.10

Leads I, II, III, V_1, and V_6 are shown in combination with the intracardiac recordings from high right atrium (HRA) and His bundle (HIS). Paper speed is 100 mm/s. First-degree AV block is present. Because of the prolonged AH time of 210 ms, the conduction delay is located in the AV node. This might have been expected from the surface ECG because of the narrow QRS complexes (0.09 s).

28.4.1.4 Conducted Beats: Widened QRS Complexes

QRS complexes ⩾0.12 s do not allow any conclusions to be drawn as to the site of block. A significant group of patients has a combination of AV nodal or intra-Hisian block associated with an intraventricular conduction defect (Fig. 28.11), while others have block in the bundle branches (Fig. 28.8). However, AV block with widened QRS complexes in the setting of an extensive anterior wall infarction is frequently associated with bilateral bundle branch block (Fig. 28.12) [26–28].

28.4.1.5 Escape Rhythm

In patients with third-degree block situated in the AV node, 65% have an escape rhythm with a narrow QRS complex, while 35% have a wide QRS complex [29–31]. All patients with trifascicular block have a wide QRS escape rhythm.

Although Adams–Stokes attacks cannot be predicted on the ECG, patients having wide QRS complexes with a slow escape rate are most prone to syncopal attacks, because distal block has a slow (25–45 bpm) and unreliable escape rhythm with long periods of asystole (Fig. 28.13) [32]. The escape rate in the AV node is usually higher and reliable (40–60 bpm). Sometimes the escape rhythm is faster than expected (Fig. 28.14). These accelerated idioventricular rhythms (AIVR) have rates between 60 and 125 bpm, and are commonly seen in the reperfusion phase of an acute myocardial infarction. AIVR is a very specific reperfusion arrhythmia with a specificity of more than 80% and a positive predictive value of more than 90% [33–35]. AIVR is probably caused by reperfusion damage. It is a transient, self-terminating arrhythmia that does not need treatment. It usually has no major hemodynamic consequences, and it is not a precursor of more malignant

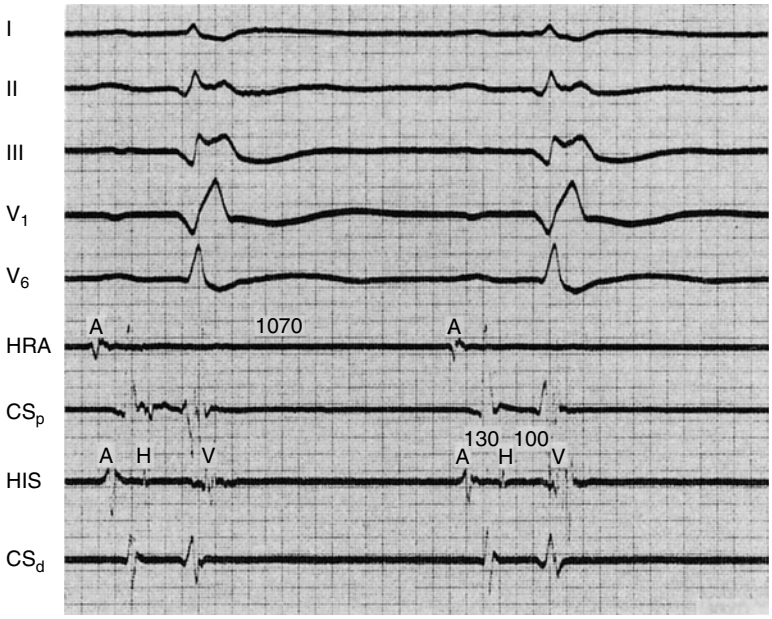

Figure 28.11

Five surface and four intracardiac recordings illustrating that the first-degree AV block arises from conduction delay at two levels. The AH interval is slightly prolonged (130 ms). The most important delay is present in the distal conduction system (HV interval = 100 ms). This last finding is an indication for pacemaker implantation.

arrhythmias. Engelen et al. [36] showed a relation between the number and duration of AIVR's and the recovery of left ventricular function following reperfusion. In that study, it was also found that after percutaneous coronary intervention, AIVR was less frequent than after reperfusion due to fibrinolytic treatment.

28.4.2 The Value of Diagnostic Interventions

28.4.2.1 Noninvasive Methods

Noninvasive interventions can be useful for detecting the location of block. These interventions include the following.

Atropine

Atropine, when given intravenously in a dosage of 0.5–1 mg, has an accelerating effect on the sinus rate, which can produce further deterioration of AV conduction. On the other hand, the drug improves impulse conduction through the AV node [24]. Because of the delicate balance of these two effects, it is not surprising that the outcome of atropine administration is not completely predictable, since it depends on the variable responses of impulse formation and conduction (Fig. 28.15). When given to patients with AV nodal conduction problems, atropine can shorten the PR interval or diminish the degree of block. In patients with a conduction problem below the AV node, no effect on conduction is seen although sometimes a more severe degree of block is provoked by the increase of the sinus rate.

Ajmaline

A latent conduction defect, present in the bundle branches, can be uncovered by ajmaline (50 mg intravenously) because this drug depresses conduction below the AV node [37–39].

This test is dangerous, however, because it can result in ventricular asystole (for explanation see Sect. 28.4.1.5). Ajmaline should be given only after introducing an external ventricular pacemaker. The second rare, but more serious,

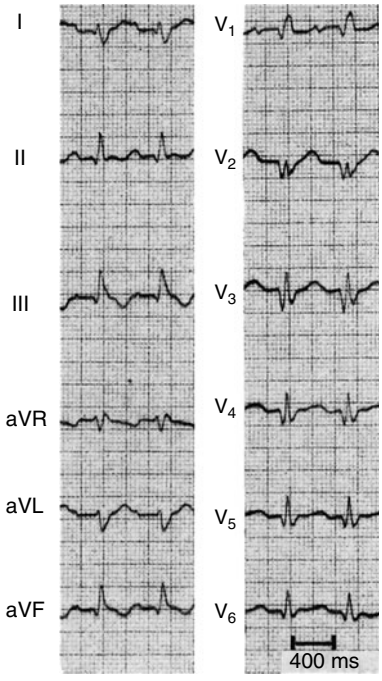

Figure 28.12

Twelve-lead ECG of a patient with an extensive anteroseptal myocardial infarction and trifascicular conduction problems which were acquired during the infarction. Lead V_1 shows a QR pattern typical of septal involvement of the infarct in combination with a complete right bundle branch block. Right axis deviation suggests block in the posterior fascicle of the left bundle, while the PR prolongation (0.26 s) is most likely caused by additional block in the third bundle – the anterior fascicle of the left bundle. Intracardiac recordings showed a normal AH interval and a prolonged HV interval indicating that conduction delay indeed was located below the His bundle. Mortality is extremely high (86%) due to the extensive muscle damage, which can be indirectly derived from the above-mentioned conduction defects.

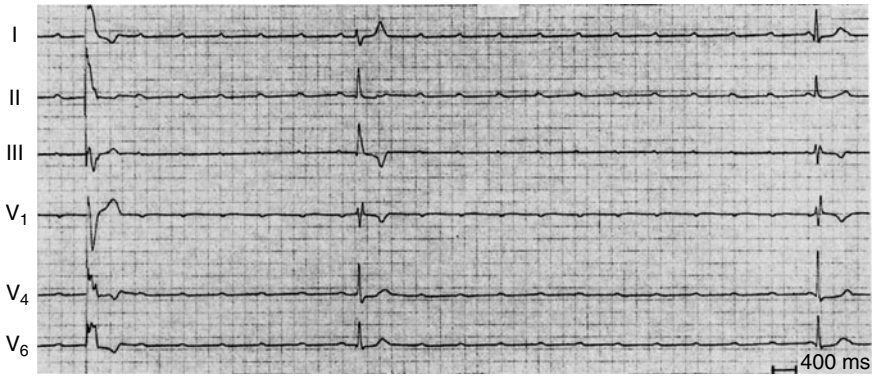

Figure 28.13

ECG recording demonstrating third-degree AV block in a patient with Lev's disease. The external pacemaker rate was gradually turned down and switched off. After the last paced beat, long periods of ventricular asystole can be seen.

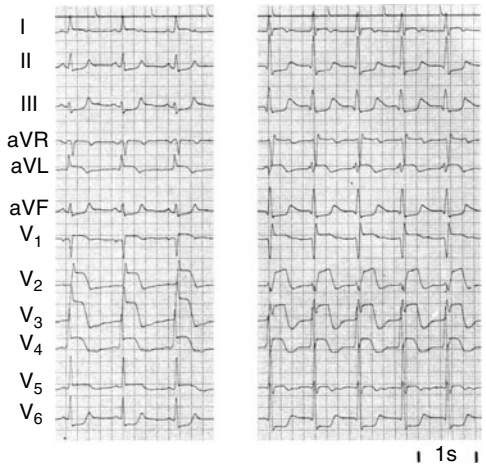

Figure 28.14

Left panel. Twelve-lead ECG of a patient with an acute anteroseptal infarction. Right panel. Accelerated idioventricular rhythm (AIVR) with a configuration suggesting an origin in the basal septal part of the left ventricle, that is, the infarcted area. Typically, AIVR in this setting starts with a long coupling interval and has regular R–R intervals.

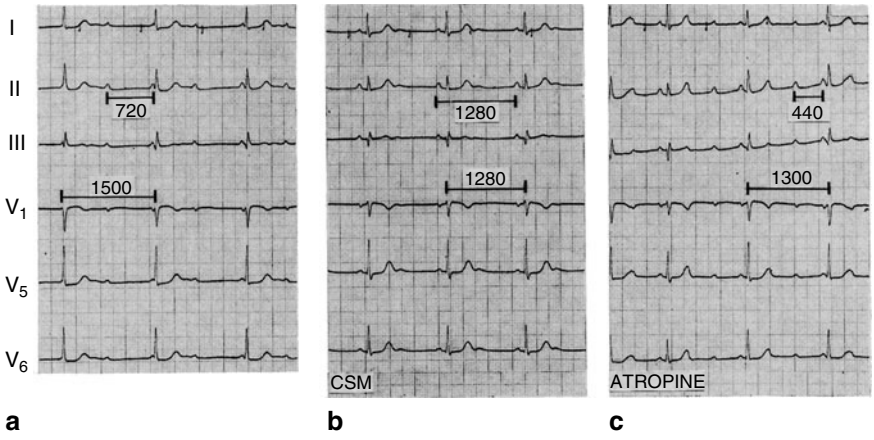

Figure 28.15

Six surface ECG leads of a patient with distal AV conduction disturbance. In (a) third-degree block is present. Because of the narrow QRS escape rhythm, the conduction problem is located in the AV node or the His bundle. P–P interval is 720 ms and R–R interval 1500 ms. In (b) carotid sinus massage (CMS) is performed. In proximal AV block, further depression of AV nodal conduction would therefore be expected. However, the significant slowing of the sinus rate allows the AV node to propagate every P wave to the ventricle and to restore normal conduction. In (c) atropine was given. In proximal AV block, atropine improves AV nodal conduction. In this case, the important decrease in P–P interval (440 ms) prevents normal conduction. The two opposite effects result in second-degree AV block. It can be deduced that the second beat from the left is conducted because it comes earlier than expected and its configuration is identical to that in the conducted beats in (b) and different from the escape beats in (a). The rate of the escape rhythm has increased slightly with the R–R interval shortening from 1500 to 1300 ms.

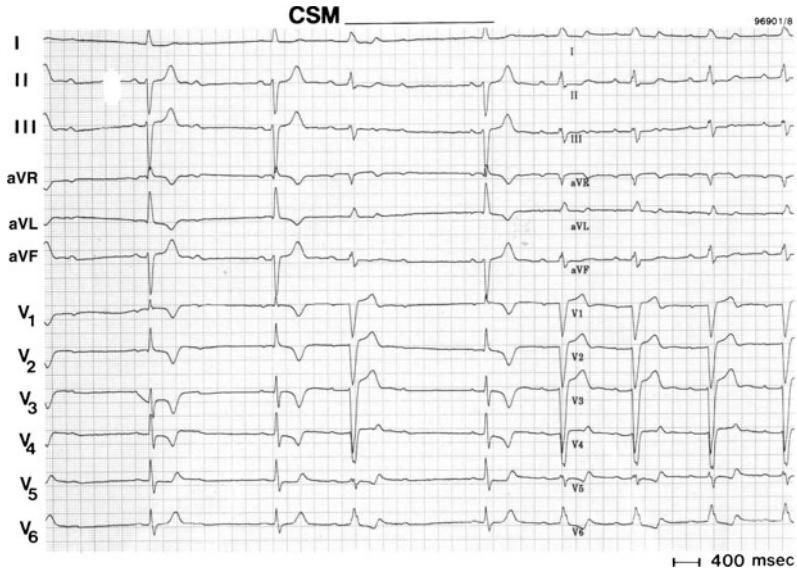

Figure 28.16

Twelve-lead ECG showing a complex arrhythmia due to distal conduction disease in a patient after aortic valve replacement. Advanced AV block present with the first 2 QRS complexes show incomplete right bundle branch block and left axis deviation (anterior fascicular block). The 3d QRS complex is conducted with a prolonged PR interval and shows left bundle branch block. A fourth beat with the initial configuration is seen, followed, due to carotid sinus massage (CSM)–induced mild slowing of the sinus rate, by 1:1 conduction with prolonged PR intervals and left bundle branch block.

complication that has been described is ventricular fibrillation. Therefore, sound advice is to restrict this test to special cases only.

Vagal maneuvers

Vagal maneuvers, such as carotid sinus massage, have the opposite effect to atropine and produce further prolongation of the PR interval or provoke second-degree block in the AV node, whereas no effect is seen in distal block [24]. However, the vagal maneuver can give concomitant AV nodal conduction delay in those patients having conduction problems in the His–Purkinje system [40]. Furthermore, conduction may be restored in both types of block because of slowing of the sinus rate (Figs. 28.15 and 28.16). Therefore, vagal maneuvers are of less value for differentiation among various sites of block.

Vagal maneuvers can depress, and atropine or exercise can accelerate, the escape rhythm in the AV node during third-degree block. They do not usually have much influence on escape rhythm below the AV node.

Exercise

Exercise has an adrenergic effect on the heart, which is comparable to atropine. During exercise, sinus rate increases and AV nodal conduction improves. In patients with conduction problems in the His bundle or bundle branches, exercise may enhance the degree of block due to increase of the sinus rate (Fig. 28.17). Occasionally, in patients with bridging of one of the coronary arteries, block can also develop during exercise [41].

28.4.2.2 Invasive Methods

Atrial pacing

Atrial pacing will produce further prolongation of the PR interval, and can result in a higher degree of AV nodal block in patients with AV nodal disease. In contrast to this, the effect of atrial pacing on infranodal block is

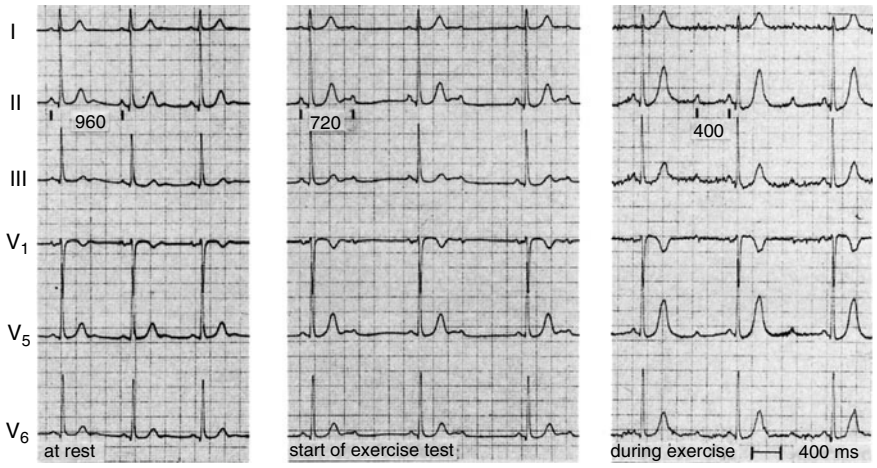

Figure 28.17

Six-lead ECG of a 54-year-old male, who exercised on a treadmill. A sudden change from 1:1 to 2:1 AV conduction was found at sinus rates more than 65 bpm, as well as a change to 3:1 AV conduction at sinus rates above 145 bpm. In this patient, the His bundle is the most likely location of block, because the PR interval of the (probably) conducted P wave remained constant (0.15 s) and the QRS complex was narrow (0.09 s).

minor. Patients with first-degree block in the His–Purkinje system will usually maintain 1:1 conduction at high atrial rates [24].

The escape rhythm can be suppressed by ventricular stimulation in patients with third-degree AV block in or distal to the His bundle (Fig. 28.13). The escape rhythm in AV nodal block is not so easily suppressed by ventricular pacing.

There is no difference in respect of the reaction to atropine, exercise, and artificial pacing of the atrium in a normal heart [42–44]. The same holds also for the diseased heart. This is true for first-degree as well as for second-degree block [45–48].

The His-bundle ECG

The most appropriate method for determining the site of block is His-bundle recording [20, 25, 49–58]. Using this approach, the intra-atrial (PA) conduction time can be measured. This is the time between the onset of the P wave on the surface ECG (or the intracavitary high right-atrial ECG) and the first rapid deflection of the atrial wave in the His-bundle recording (see Fig. 28.5) AV nodal conduction is measured as the AH time (the time between the atrial wave and the beginning of the His-bundle spike on the His-bundle recording). The HV time is the time from the beginning of the His-bundle spike to the earliest onset of activation of the ventricle. PA time varies between 25 and 45 ms, AH time between 50 and 120 ms and HV time between 35 and 55 ms. The width of the His-bundle potential is 15–20 ms [46, 54, 55, 59–65]. A full discussion on His-bundle ECG recording is presented in Chap. 24.

Electrophysiological investigations are of great help in the presence of AV block and widened QRS complexes. Such recordings allow us to find the exact location of block (Figs. 28.11 and 28.18), to predict the likelihood of asystole, and to determine the reliability of the escape rhythm. His-bundle recordings may be required to identify those patients at risk of developing complete block, because in patients with bifascicular block, abnormal conduction of the remaining fascicle may also be present. It has been shown that AV conduction delays may exist in the absence of PR prolongation or other electrocardiographic abnormalities [46].

A His-bundle recording is, however, not a routine procedure because it is a time-consuming and invasive investigation [66]. The level of the conduction defect can roughly be estimated by studying the PR interval, QRS duration, and AV relationship on the surface ECG in the majority of cases [67–69].

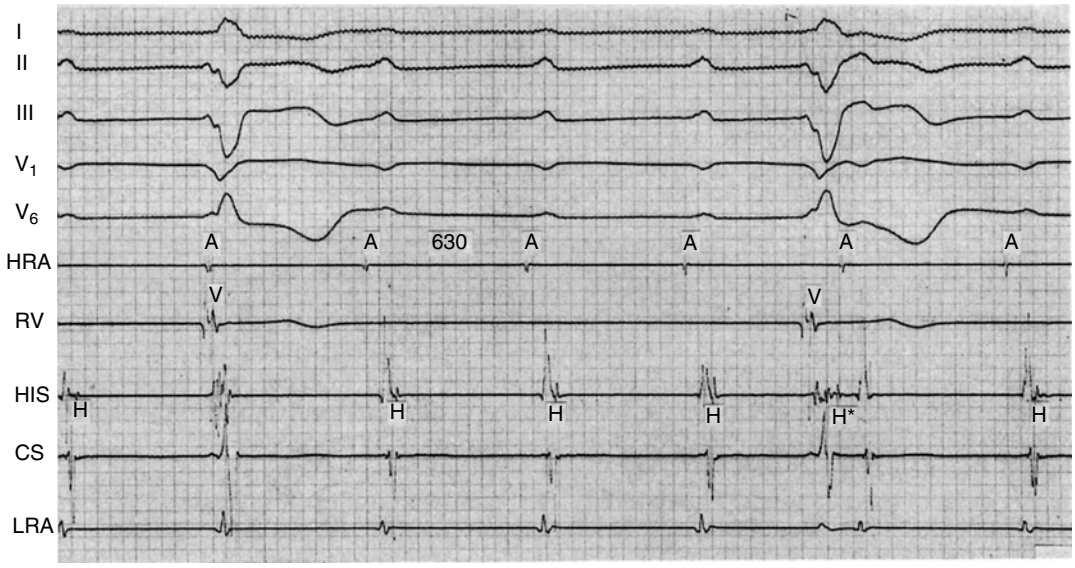

Figure 28.18

This recording is taken from a patient with Adams–Stokes attacks due to paroxysmal complete AV block. It shows five surface leads and five intracardiac recordings. The His-bundle electrogram shows that every atrial signal is followed by a His deflection, indicating that block is located distal to His. The rate of the ventricular escape rhythm is only 26 bpm. The second escape beat is retrogradely conducted to the His bundle. The next atrial event is blocked proximal to the His bundle because of retrograde concealed penetration of the AV node (HRA, high right atrium; RV, right ventricle; HIS, His bundle; CS; coronary sinus; LRA, low right atrium; interval given in milliseconds).

For the clinician, a knowledge of whether the site of the block is above or below the His bundle is probably sufficient. Invasive and noninvasive methods for determining the site of block will be discussed in detail for all three types of conduction disturbances.

28.5 Incomplete Block

28.5.1 First-Degree AV Conduction Delay

In the following discussion, the term first-degree AV "block" will be avoided, as there is no block but rather delay in conduction.

In first-degree AV conduction delay, the site of the delay is most frequently located in the AV node, but can also be found infranodally (Table 28.1). Some patients have PR prolongation due to intra-atrial conduction delay. The P wave will then be widened and markedly diminished in voltage [70]. In these cases there may be no impaired conduction in the AV nodal or His–Purkinje system. However, intra-atrial conduction delay is often related to atrial arrhythmia [70].

PR prolongation greater than 0.2 s has no value as far as locating the site of block is concerned. However, a PR interval greater than 0.3 s is very suggestive of a delay within the AV node. Narula et al. [24] stated that in 79% of all cases with prolonged PR interval, the conduction delays were located at more than one site, although the AV node was the dominant site of delay (83%). Delay at a single site was noted in the atrium in 3%, in 11% in the AV node, and in the His–Purkinje system in 7%. Puech et al. [29] reported conduction disturbances at multiple sites in only 20% of their cases.

A narrow QRS complex suggests that block is located in the AV node (Fig. 28.10). First-degree AV conduction delay in combination with a wide QRS complex is most commonly associated with a conduction defect in the bundle

Table 28.1
Incidence of the location of block in first degree AV-block [29]

	AV node	Intra-Hisian	Bundle branches
Narrow WRS compex (< 0.12 s)	87%	13%	
Wide QRS complex (⩾ 0.12 s)	22%	12%	66%

branches (Figs. 28.8 and 28.11). However, frequently (66%) block is present at two levels, especially in those with left bundle branch block [29, 30, 68, 69, 71, 72]. When PR prolongation and left bundle branch block are found together, block is predominantly located in the common bundle (Fig. 28.7) [29, 71, 72]. Complete right bundle branch block with first-degree AV conduction delay, without extreme right or left axis deviation, is associated with conduction delay in the left bundle branch in only 40% of the cases. All other patients have additional conduction problems in the AV node or His bundle. The combination of first-degree AV conduction delay and bifascicular block (right bundle branch block and left anterior or posterior fascicular block) is commonly a result of a conduction delay in the third bundle branch (Fig. 28.12), although in rare cases the conduction delay can be located in the AV node [71, 72].

In patients where the ECG shows a PR prolongation and a wide QRS complex, His-bundle studies should be performed. HV intervals of more than 75 ms are an indication for pacemaker implantation [73, 74], because in patients with these findings, total AV block and syncope will probably shortly appear due to progressive disease of the conduction system. In contrast to this, first-degree AV nodal delay carries a good prognosis. In such cases, pacing is not indicated.

It has to be realized that occasional prolongation of PR time is found in apparently normal subjects [43, 75, 76]. PR intervals up to 0.28 s were found in 1.6% of 19,000 healthy aviators [3, 77]. A 10-year follow-up study showed that none of these people had progression of their first-degree AV block [78].

Interventions such as atropine (Fig. 28.15) and exercise will decrease PR interval in patients with AV nodal conduction delay. On the other hand, carotid sinus massage produces further prolongation of the PR interval, or can give second-degree block when the conduction delay is present in the AV node. Carotid sinus massage, when performed in patients with first-degree block in the His–Purkinje system, does not generate second-degree block. In patients with AV nodal disease, atrial pacing at rates above 130 bpm will either produce further prolongation of the PR interval or second-degree block. In the presence of HV prolongation, atrial pacing at rapid rates usually maintains 1:1 AV conduction without further prolongation of the HV interval. Only occasionally does second-degree infranodal block develop.

28.5.2 Second-Degree AV Block

Table 28.2 presents the incidence of second-degree block at the various sites.

28.5.2.1 Mobitz Type I (Wenckebach) Block

The classic type I second-degree block is characterized by a progressive lengthening of the PR interval until a P wave is blocked. The PR interval is longest in the beat preceding the blocked P wave and the shortest after the dropped beat. The maximum PR increment occurs between the first and second conducted beat. In the following conducted cycles, the increment of PR interval gradually diminishes, resulting in a lessening of the PR interval increment (Figs. 28.6 and 28.18).

The explanation for this type of conduction defect is probably that the progressive delay is caused by increasing fatigue of the AV node or distal conduction system until a block occurs. Presumably, each impulse arrives earlier in the relative refractory phase of the conduction system (see Chap. 3). Therefore, the impulse is conducted more slowly, until it reaches the absolute refractory phase. After the dropped beat, the conduction system has partially recovered, resulting in a shorter PR interval. The Wenckebach phenomenon can be observed in any portion of depressed conduction system [13, 67, 79–82]. However, this classic pattern of Wenckebach block is seen infrequently (14%) [83, 84]; it is seen more often in patients with higher conduction ratios such as 4:3 or 5:4. Conduction ratios such as 7:6 are normally associated

Table 28.2

Incidence of the location in second-degree AV block [29]

	AV node	Intra-Hisian	Bundle branches
Mobitz type I (Wenckebach)	72%	9%	19%
Mobitz type II		20%	80%
2:1 block	27%	23%	50%

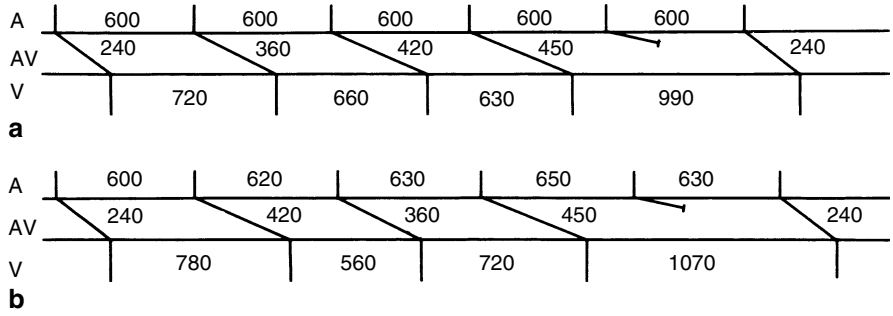

Figure 28.19

Part (a) represents a typical 5:4 Wenckebach sequence. Progressive lengthening of the AV interval is present. The increment of the AV interval becomes smaller from beat to beat, decreasing from 120 to 30 ms over the first four cycles. This results in shortening of the R–R intervals. Part (b) also shows a Wenckebach sequence. The behavior of this block is atypical. In other words, although there is a gradual prolongation, the AV interval changes unpredictably from beat to beat. The atypical behavior of the Wenckebach sequence is in this case caused by the change in atrial rate.

with an atypical behavior. They show progressive PR prolongation with unpredictable changes in increment. This is called atypical Wenckebach (Fig. 28.19).

The explanations for the atypical Wenckebach behavior have been described by Langendorf and others [83–93], and are as follows.

(a) Changes in sinoatrial rate which influence the PR interval. This is probably the most important explanation. The change in sinoatrial rate could be caused by a change in cardiac output caused by the Wenckebach sequence.
(b) Interpolated atrial premature contractions causing changes in AV conduction [89].
(c) Reentry or premature impulses giving rise to concealed premature depolarization of conduction tissue [86–88, 90–93]. Concealed conduction may lead to an unanticipated prolongation of PR interval or blocked P waves after a Wenckebach pause, because partial penetration of an impulse into the conduction system influences the subsequent impulse conduction. The degree of penetration of a blocked impulse can sometimes be inferred from its effect on subsequent events. Atypical Mobitz type I block is seen intranodally as frequently as infranodally [94].

Location of type I block is rather unpredictable and requires His-bundle studies, especially when the conduction disturbance is associated with wide QRS complexes [94, 95]. Minimal increment in the PR interval suggests distal block, but it is not diagnostic.

Significant prolongation of the PR interval during the Wenckebach cycles suggests AV nodal block. Second-degree block located in the AV node has a relatively benign course in patients without organic heart disease and does not produce syncope [96, 97]. In contrast to this, distal second-degree block requires pacemaker implantation [98].

First-degree and second-degree type I block can be present in normal subjects especially during sleep [75, 99–104]. A 6% incidence of spontaneous Wenckebach periods during sleep has been reported in healthy students without apparent heart disease. In none of these subjects were symptoms or progression of block observed in a 6-year follow-up period [101]. The same was found in athletes, where there was a 9% incidence of Wenckebach periods [76, 100–103, 105]. However, the

benign prognosis of this type of block is not confirmed in all studies. During prospective analysis of 16 infants with second-degree type I AV block, seven of them had progression to third-degree block, and one of these seven experienced syncopal attacks [102].

Intervention procedures are not helpful for the differential diagnosis between normal and diseased subjects [45–48].

28.5.2.2 Mobitz Type II Block

Mobitz type II second-degree AV block is characterized by a sudden failure of a P wave to be conducted to the ventricle without PR prolongation in the preceding beats (Figs. 28.7 and 28.20). This type of block is always located below the AV node (Table 28.1). The nonconducted P wave will be followed by a His-bundle signal. Sometimes a "split" His can be seen in the His-bundle recording in the presence of His-bundle disease. In the rare case of a proximal His-bundle defect, the His signal will not be seen after the P wave, but preceding every QRS complex thereby fallaciously simulating AV nodal block [46, 106, 107]. In patients having disease of the bundle branches, widened QRS complexes are present [24], while the PR interval is usually normal or slightly prolonged [79]. One-third of the cases of chronic second-degree block have the typical behavior of Mobitz type II AV block. A finding of Mobitz type II block is always an indication for pacemaker implantation, because it is usually permanent and often progresses to complete AV block [108].

With respect to interventions during second-degree Mobitz type I or II AV block, atropine and exercise can enhance AV conduction and restore 1:1 conduction. Such a finding is suggestive of AV nodal block. If distal block is present, sometimes the reverse effect can be seen and progression of block will appear because of an increase in sinus rate without improvement of conduction of the His–Purkinje system [40]. The opposite is seen after carotid sinus massage.

In AV nodal block, atrial pacing will produce further progression of AV block, while in His–Purkinje system block, minor changes are seen in PR and HV intervals.

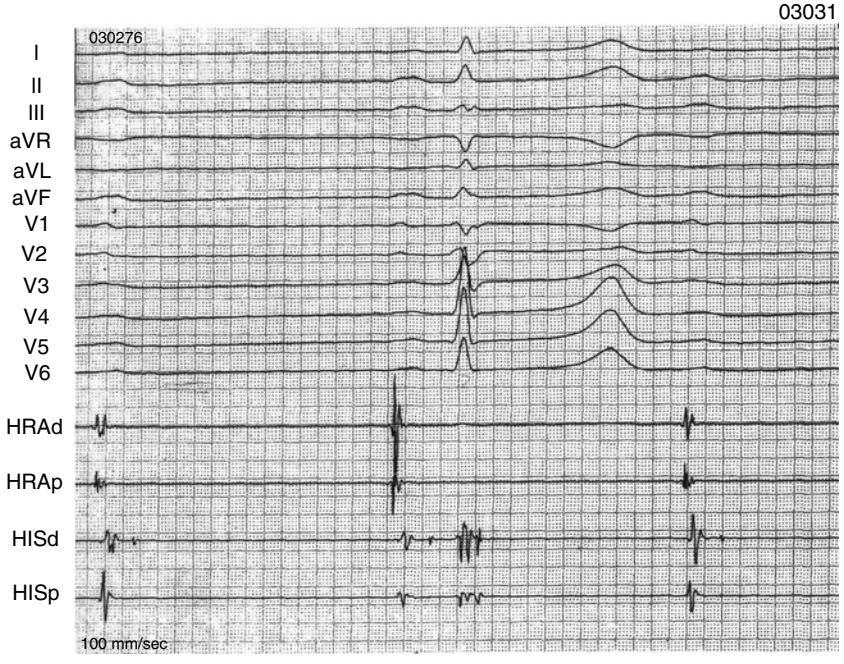

Figure 28.20

Twelve-lead surface ECG combined with intracavitary recordings from the same patient, as in Fig. 28.7, shows the location of the block distal from the His bundle.

Differentiation between type I and II is important with respect to management, because type II block is always indicative of distal disease. Distinction between types of block can be difficult if there is only a minimal increment in PR interval before and after a dropped beat or in the presence of 2:1 block. In these patients, exercise or atropine may clarify the situation by provoking Wenckebach periods due to higher sinus rates. Vagal maneuvers may produce a higher degree of block and indicate which is the underlying type of block.

28.5.2.3 2:1 or Higher Degree AV Block

Several terms are used for this type of block such as advanced AV block [22] and severe or high-degree block [109]. In 2:1 block, every second P wave is conducted to the ventricle (Fig. 28.8). These cases cannot be distinguished as type I or type II unless two consecutively conducted beats are seen, such as during temporary 3:2 block or 1:1 conduction (Fig. 28.8) [96]. Changes in conduction can be secondary to slight alterations of the vagal tone [30].

With respect to interventions in this group, carotid sinus massage, if applied with caution, may be clinically useful in indicating the site of block. Increase of block in the AV node is suggestive of an AV nodal conduction problem, while decrease of block indicates distal block because of slowing of the sinus rate. In rare cases with bradycardia-dependent distal block (phase 4 block – see Chap. 23), carotid sinus massage aggravates block [56, 110]. Atropine and exercise have the opposite effect to vagal stimulation [30, 47, 48, 111].

The interesting phenomenon of ventriculophasic arrhythmias in digitalis intoxication should be mentioned. Excess of digitalis can produce all three types of block in the AV node [112, 113]. Second-degree AV block as a manifestation of digitalis intoxication most commonly shows the Wenckebach type of block or a constant type of 2:1, 3:1, or 4:1 block. During 2:1 AV conduction, the P–P interval embracing the QRS complex [114] differs from the P-P interval without a QRS complex [114]. This is possibly the result of a change in autonomic tone during the cardiac cycle [115, 116].

28.6 Complete Block (Third-Degree AV Block)

In complete block, no atrial impulses are propagated to the ventricle. Third-degree or complete AV block can be located at all three sites of the conduction system [61, 72, 117]. (Table 28.3). The location of block cannot be predicted from the escape rhythm. However, during the acute phase of a myocardial infarction the site of infarction provides indirect information as to the site of block. Myocardial infarction located in the inferior wall can give AV nodal block (Fig. 28.9), while damage located in the anteroseptal wall indicates that the conduction disorders are in the bundle branches (Fig. 28.12) [26, 28, 118]. If the rate of the escape rhythm is more or less the same as the atrial rate, it can be difficult to distinguish this "isorhythmic dissociation" from sinus rhythm with 1:1 conduction to the ventricle. An example of such a problem is given in Fig. 28.21.

Interventions can be performed in patients where the origin of block is unclear. In contrast to findings during distal block, exercise and atropine [47, 48] can increase rate in the AV node significantly or can restore first- or second-degree AV block [30, 32, 60, 118–120]. Atrial pacing does not help in further differentiation between sites of block. Ventricular pacing has to be carried out with caution because subsidiary pacemakers are readily suppressed by ventricular stimulation and can produce long episodes of asystole. Such a finding is suggestive of distal block. Carotid sinus massage may slow the AV nodal escape rhythm, but can produce second-degree block instead of third-degree block in distal conduction disturbances due to slowing of the sinus rate with late arrival of the impulses at the distal conduction system, giving them more time to recover [121, 122].

Table 28.3

Incidence and location of block in third-degree AV block [29]

Escape rhythm	AV node	Intra-Hisian	Bundle branches
Narrow QRS complex (<0.12 s)	48%	52%	
Wide QRS complex (⩾0.12 s)	11%	5%	84%

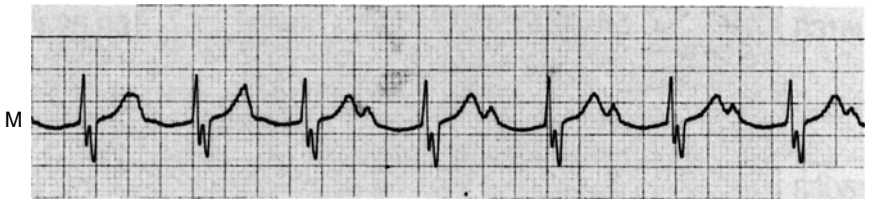

Figure 28.21
The rhythm in this tracing is either sinus rhythm with first-degree AV block or "isorhythmic dissociation," that is, a situation where, in the presence of complete block, rates at atrial and ventricular level are more or less identical. In this registration, careful measurement will show that the PR intervals of the first two beats are longer than the other PR intervals, which could fit with an isorhythmic dissociation. However, the sinus rate of the first two beats is higher, causing further lengthening of PR interval. The key for making the correct diagnosis is that the R–R interval of the first beats is also shorter. Therefore, a relation between atrium and ventricle must be present. If complete block were present, the ventricular rate would not have been influenced. This proves that sinus rhythm with first-degree AV block is the correct diagnosis.

28.7 Etiology of Atrioventricular Block

Multiple pathological processes can affect the conduction system. The common causes of AV block are the following.

28.7.1 Fibrosis

The most frequent cause of AV block (40–50%)[123] is fibrosis of the specialized conduction system due to progressive sclerosis of the ventricular septum and the surrounding tissues [16, 123–126]. This is also called Lenègre and Lev disease. It is a typical disease of the elderly. These patients can have normal coronary arteries [127–131].

28.7.2 Ischemic Heart Disease

The second important cause of AV block (40%) is ischemic heart disease. Two out of five occurrences are chronic [130] and three out of five can be found in the setting of an acute myocardial infarction (Figs. 28.9 and 28.13) [132–135]. In approximately 19% of patients having an acute myocardial infarction, AV block develops (8% first degree, 5% second degree and 6% third degree) [136–138]. Only a few patients have exercise-related ischemic AV block.

28.7.3 Drugs

Digitalis [112, 114, 139–141] can create different degrees of AV nodal block, especially when given in a toxic dosage (Fig. 28.22). Other drugs which can create AV nodal block are verapamil, amiodarone, diphenylhydantoin [142], and beta-blocking agents [143]. Quinidine and other class I drug [144] can produce block in the His–Purkinje system.

28.7.4 Vagal Influences

Not uncommonly, vagal reactions, for example, due to pain (Fig. 28.9) or during carotid sinus massage, can produce complete AV block, sometimes with longer ventricular asystole [145–148]. In elderly patients, the presence of hypersensitive carotid sinus syndrome can produce profound fall in arterial pressure and marked slowing in heart rate either by slowing of the sinus rate and/or the development of second-degree or third-degree AV block [147, 149, 150]. This may or may not be combined with a vagal vasodilatory effect.

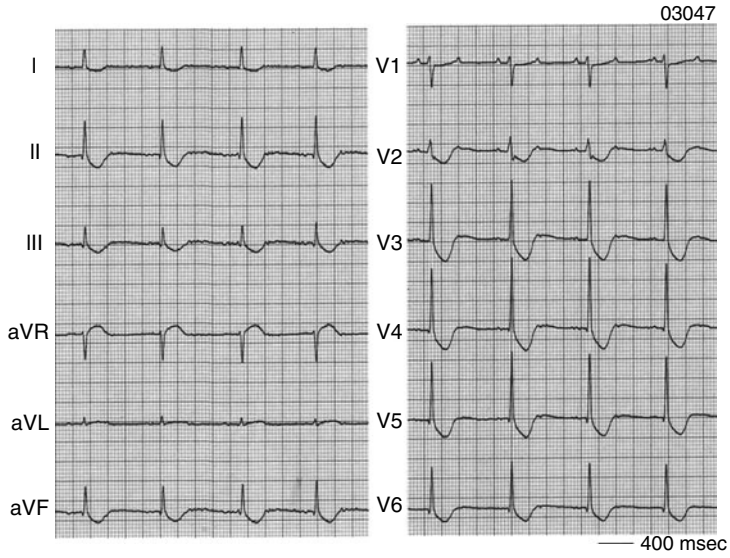

Figure 28.22
Atrial tachycardia with 2:1 AV conduction in digitalis intoxication. After dissipation of the digitalis compound from the blood, sinus rhythm with normalization of the AV conduction and the ST segments reoccurred.

28.7.5 Valvular Disease

Disease of the aortic or mitral valve with a calcified valve ring (rheumatic, congenital bicuspid, or other) can give rise to block in the His bundle. This is frequently seen in aortic stenosis. When the aortic valve is severely calcified, the deposits can extend down into the ventricular septum and advanced or complete block may develop (Fig. 28.16) [125, 130, 151].

28.7.6 Postsurgery

Replacement of a calcified aortic or mitral valve [5], closure of a ventricular septal defect, or other surgical traumas can result in AV block [19, 134, 152–156].

28.7.7 Congenital Disease

Complete AV block may also be congenital occurring as an isolated finding or, in half of the patients, in association with congenital malformations of the heart [152, 154, 157–167]. Most patients with congenital block have their conduction disturbance in the AV node and some of them in the His bundle [72, 153, 159, 168]. Microscopic studies suggest that there is a failure of the atrial myocardium to contact the AV region or a congenital separation between the AV node and the His–Purkinje system caused by an alteration in the development of the AV node [19, 120, 125, 130, 153, 169–175].

28.7.8 Cardiomyopathy

Any type of block can coexist with any type of cardiomyopathy as in amyloidosis, sarcoidosis (Fig. 28.23) [176], and hypertrophic obstructive cardiomyopathy [125, 130, 177–179].

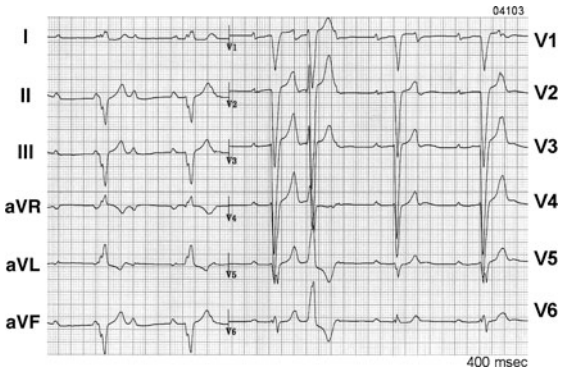

Figure 28.23
Twelve-lead ECG of a male with documented cardiac sarcoidosis, involving the distal conduction system. Sinus rhythm is present with complete AV block and a slow escape rhythm suggesting an origin in the inferior part of the right ventricle.

28.7.9 Myocarditis

Myocarditis can be bacterial, like acute rheumatic fever, diphtheria or Lyme disease, or viral [180–192]. AV block developing in this setting is a sign of a poor prognosis in the evolution of the disease [125, 130].

28.7.10 Potassium

High potassium levels [193, 194] can create AV block at plasma levels above 6.5 $mEql^{-1}$.

28.7.11 Others

An association of AV block with muscular and neuromuscular heredodegenerative syndromes is known [124, 125, 195–197]. In myotonic muscular dystrophy, Kearns–Sayre syndrome [198], Erb's dystrophy (limb-girdle), and peroneal muscular atrophy with or without symptoms of pacemaker implantation should be considered because there may be unpredictable progression of AV conduction disease [199, 200]. Cardiac tumors, primary [201] or metastatic [202], after chemotherapy [203] and radiation [204], cysts [125, 205], myocardial bridging [41], and traumas [125, 206] have been described as rare causes of AV block. Also in the congenital long QT syndrome the conduction system may be involved and functional 2:1 block and bundle branch block was described [207].

28.8 Age and Sex

Campbell [208] found in patients with chronic third-degree AV block that age varied between 50 and 70 years and that males predominated in a ratio of 4:1. In Ide's series [209], peak incidence occurred between 70 and 80 years of age and the ratio of males to females was 5:2. Elderly women are predilected to distal lesions due to degenerative calcified infiltrations in that area. They are three times more likely to have block in that region compared to men [210, 211].

28.9 Clinical Features

Clinical features are dependent on ventricular rate during the presence of AV block. First-degree and most types of second-degree AV block do not produce symptoms. An exception is the Mobitz type II second-degree AV block, where

sudden longer episodes of ventricular asystole can produce syncope. Higher degrees of second-degree block (3:1 or 4:1 AV block) with lower ventricular rates may give symptoms similar to those of third-degree block. These patients can develop dizziness or syncopal attacks (Adams–Stokes attacks). Syncope is usually caused by transient ventricular asystole, but ventricular tachycardia or fibrillation can also be the etiology of the complaints [29, 52, 56, 212–215]. Fatigue, dyspnea or cardiac asthma, and angina can be present in patients with marginal myocardial reserve or coronary circulation at rates of 40–50 bpm or lower [71, 72, 216–218]. Generally, in contrast to the patients with chronic and stable third-degree block, those with paroxysmal episodes of third-degree block have most complaints.

28.10 Therapy

Only in those patients who are symptomatic, or who will have a high chance of becoming symptomatic, is therapy needed. This can be atropine, isoproterenol, or artificial pacing. Atropine and isoproterenol are useful for short-term treatment. Atropine can be given to patients having a severe vagal reaction which, for example, is not uncommon in the acute stage of an inferior wall infarction (Fig. 28.9). In the other patients, a temporary or permanently implanted pacemaker may be indicated. When drugs play a role in the presence of the AV block, the drug should be discontinued, or at least the dosage should be lowered or a pacemaker implanted if it is important to continue the use of the drug. Isoproterenol is sometimes helpful as an acute temporary treatment prior to insertion of a temporary pacemaker in patients having bock in the His–Purkinje system.

AV block located below the AV node, that is, in the His bundle or bundle branches, is associated with a high incidence of sudden asystole [219–223]. Most investigators agree that patients with bifascicular block with HV prolongation and neurological symptoms should be paced [224–226]. If the HV interval exceeds 75 ms, pacing is indicated even without the presence of neurological complaints [227].

Each patient should be evaluated individually. If any doubt exists, other possible causes of syncope must be excluded prior to pacemaker implantation [215]. In patients with syncopal attacks due to AV conduction problems, long term ambulatory rhythm monitoring is very useful to confirm the diagnosis (see Chap. 39)

Approaches to treatment of patients with chronic AV conduction disturbances can be summarized as follows [228].

28.10.1 Normal PR Interval

The HV interval can be prolonged in patients with a normal PR interval. The HV interval should be measured in symptomatic patients with bifascicular block. If the HV interval is prolonged, pacemaker implantation should be considered. The incidental finding at electrophysiological study of a markedly prolonged HV interval (greater than or equal to 100 ms) in asymptomatic patients is a class IIa indication for pacemaker implantation.

28.10.2 First-Degree AV Delay

Asymptomatic first-degree AV delay is treated conservatively. Even asymptomatic conduction delay with bifascicular block is considered a class III indication for pacemaker insertion. First-degree AV delay with symptoms suggestive of pacemaker syndrome and documented alleviation of symptoms with temporary AV pacing is a class IIa indication for pacemaker treatment [229, 230].

28.10.3 Second-Degree AV Block

No pacemaker is indicated in asymptomatic type I second-degree AV block at the supra-Hisian (AV nodal) level not known to be intra or infra-Hisian. Type II second-degree AV block is a pacemaker indication. Also the non-physiological induction of distal AV block at electrophysiological study is a class IIa indication. After the acute phase of myocardial infarction, transient advanced second-degree AV block and associated bundle branch block should be treated with a

pacemaker. If the site of block is uncertain, an electrophysiological study may be necessary. Persistent second-degree block at the AV nodal level is considered a class IIb indication for a pacemaker.

28.10.4 Third-Degree AV Block

A pacemaker must be used in case of intermittent or permanent third-degree AV block and also in alternating bundle branch block. Also, after the acute phase of myocardial infarction, distal AV block is a pacemaker indication.

28.11 Prognosis

The prognosis of heart block depends on the causative factor. Before the existence of artificial pacemakers, the average life expectancy following discovery of complete chronic heart block varied between 2.5 and 7 years [136, 138, 208]. Since restoration of the heartbeat by artificial pacing was made possible, the prognosis of patients having chronic AV block is much better [231]. At the present time, pulse generators last well beyond 5–10 years. The prognosis of patients with serious underlying cardiac or other diseases is therefore related to this disease [135, 232–236] while the pacemaker patient without serious underlying disease has the same mortality rate as the general population [232].

In patients with ischemic heart disease, inferior wall infarction is the most frequent cause of AV block; less often it can be found in extensive anterior wall infarctions. In patients with an inferior infarct, block is located in the AV node [118, 237]. When third-degree AV nodal block develops, the patients usually have a reliable escape rhythm and are not threatened by asystole. In nearly all cases, the conduction disturbance disappears within 1–2 weeks. In the prereperfusion era the in-hospital mortality of patients with inferior wall infarction in combination with second- or third-degree AV block was 22% compared to 9% in patients with an inferior infarct and normal AV conduction or first-degree AV block [26, 238–245]. This difference in mortality is probably a result of larger infarct size.

Patients with an extensive anterior wall infarction have a conduction problem in the bundle branches. This is associated with a poor prognosis. Block can be fatal, because of long periods of asystole due to an unreliable escape rhythm arising in the ventricle when third-degree block is present [18, 133, 238, 246]. However, the major cause of death is the extent of the myocardial damage [26, 238, 243, 245]. Cardiac pacing will, therefore, not change the mortality but it can prevent Adams–Stokes attacks [133, 241]. In the prereperfusion era development of right bundle branch block in setting of such an infarct had an in-hospital mortality of 67%, right bundle branch block in combination with left anterior fascicular block 72%, and in combination with left posterior fascicular block 86% (Fig. 28.12). Ninety-five percent of the patients with trifascicular block died [241]. The incidence rates of complete heart block resulting from AMI have not changed over time [247, 248]. Early reperfusion either by thrombolytic therapy or percutaneous coronary intervention can reverse ischemia related conduction disturbances, but they remain an indicator of higher risk [247–254].

In the general population, asymptomatic subjects with bifascicular block statistically carry little risk of developing total block and dying. Conduction studies are not necessary [255, 256]. In the selected group of hospital inpatients with this phenomenon, however, prognosis is compromised. This is probably related to the prognosis of the underlying disease. In a retrospective study, McAnulty et al. [257] found a 5-year morality of 55%. Narula [258] and Gupta [259] also stated in their prospective studies that there was a positive correlation with both mortality and complete block inpatients with bifascicular block.

In another prospective study, Kulbertus recorded in 32% progression to complete block in 5 years [260]. He found that although bifascicular block is related to a high incidence of death, it is not related to the conduction disturbance itself, but to other (e.g., cardiac) causes.

References

1. WHO/ISFC Task Force, Definition of terms related to cardiac rhythm. *Am. Heart J.*, 1978;**95**: 796–806.
2. Wellens, H.J.J., F.W. Bär, E.J. Vanagt, P. Brugada, and J. Farré, The differentiation between ventricular tachycardia and supraventricular tachycardia with aberrant conduction: the value of the 12-lead electrocardiogram, in *What's New in Electrocardiography?* H.J.J. Wellens and H.E. Kulbertus, Editors. The Hague: Nijhoff, 1981, pp. 184–199.

3. Touboul, P., C. Clément, J. Magrina, Y. Tessier, and J.P. Delhaye, Enregistrement de l'activité électrique du tissue de conduction auriculo-ventriculaire au cours des tqchycqrdies ventriculaires. *Arch. Mal. Coeur Vaiss.*, 1972;**65**: 1409–1421.
4. Carcia Civera, R., R. Sanjuan, J.A. Ferrero, R. Blanquer, R. Llacer, and J. Llavador, Valor del Hisiograma en el diagnostico defferencial de las taquicardias ventriculares. *Rev. Esp. Cardiol.*, 1975;**28**: 191.
5. Wellens, H.J.J, D.R. Düren, E. Downar, and K.I. Lie, Mechanism, V-A conduction and QRS configuration in ventricular tachycardia in man. *Circulation*, 1975;**51–52**(Suppl. II): 137.
6. Kastor, J.A., Atrioventricular block. *N. Engl. J. Med.*, 1975;**292**: 462–465, 572–574.
7. Adams, R., Cases of diseases of the heart, accompanied with pathological observations. *Dublin Hosp. Rep.*, 1827;4: 353–453.
8. Morgagni, J.B,. *De Sedibus et Causis Morborum*, 2nd edn. Padua: Remondini, 1765.
9. Stokes, W., Observations on some cases of permanently slow pulse. *Dublin Q. J. Med. Sci.*, 1846;**2**: 73–85.
10. Gaskell, W.H., On the rhythm of the heart of the frog, and on the nature of the action of the vagus nerve. *Philos. Trans. R. Soc. Lond.*, 1882;**173**: 993–1033.
11. Gaskell, W.H., On the innervation of the heart, with especial reference to the heart of the tortoise. *J. Physiol. (London)*, 1883;**4**: 43–127.
12. Einthoven, W., Le télécardiogramme. *Arch. Int. Physiol.*, 1906–1907;**4**: 132–164.
13. Wenckebach, K.F., Zur Analyse des unregelmässigen Pulses. *Z. Klin. Med.*, 1899;**37**: 475–488.
14. Hay, J., Bradycardia and cardiac arrhythmia produced by depression of certain of the functions of the heart. *Lancet*, 1906;**1**: 139–143.
15. Mobitz, W., Über die unvollständige Störung der Erregungsüberleiting zwischen Vorhof und Kammer des menschlichen Herzens. *Z. Gesamte Esp. Med.*, 1924;**41**: 180–237.
16. Yater, W.M. and V.H. Cornell, Heart block due to calcareous lesions of the bundle of His: review and report of a case with delaited histopathologic study. *Ann. Intern. Med.*, 1935;**8**: 777–789.
17. Besoain-Santander, M., A. Pick, and R. Langendorf, AV conduction in auricular flutter. *Circulation*, 1950;2: 604–616.
18. Julian, D.G., P.A. Valentine, and G.G. Miller, Disturbances of rate, rhythm and conduction in acute myocardial infarction. *Am. J. Med.*, 1964;**37**: 915–927.
19. Lev, M., The pathology of complete atrioventricular block. *Prog. Cardiovasc. Dis.*, 1964;**6**: 317–326.
20. Scherlag, B.J., S.H. Lau, R.H. Helfant, W.D. Berkowitz, E. Stein, and A.N. Damato, Catheter technique for recording His bundle activity in man. *Circulation*, 1969;**39**: 13–18.
21. Mobitz, W., Über den partiellen Herzblock. *Z. Klin. Med.*, 1928;**107**: 449–462.
22. Watanabe, Y. and L.S. Dreifus, Levels of concealment in second degree and advanced second degree AV-block. *Am. Heart J.*, 1972;**84**: 330–347.
23. Puech, P. and R. Grolleau, Localization of AV block, in *The Cardiac Arrhythmias*, P. Peuch and R. Slama, Editors. Paris: Roussel UCLAF, 1979, p. 139.
24. Narula, O.S., Atrioventricular block, in *Cardiac Arrhythmias: Electrophysiology, Diagnosis and Management*, O.S. Narula, Editors. Baltimore, MD: Williams and Wilkins, 1979, pp. 85–113.
25. Schuilenburg, R.M. and D. Durrer, Conduction disturbances located within the His bundle. *Circulation*, 1972;**45**: 612–628.
26. Lie, K.I., H.J. Wellens, R.M. Schuilenburg, A.E. Becker, and D. Durrer, Factors influencing prognosis of bundle branch block complicating acute antero-septal infarction. The value of His bundle recordings. *Circulation*, 1974;**50**: 935–941.
27. Sutton, R. and M. Davies, The conduction system in acute myocardial infarction complicated by heart block. *Circulation*, 1968;**38**: 987–992.
28. Rosen, K.M., H.S. Loeb, R. Chuquimia, M.Z. Sinno, S.H. Rahimotoola, and R.M. Gunnar, Site of heart block in acute myocardial infarction. *Circulation*, 1970;**42**: 925–933.
29. Puech, P., R. Grolleau, and C. Guimond, Incidence of different types of A-V block and their localization by His bundle recordings, in *The Conduction System of the Heart*, H.J.J. Wellens, K.I. Lie, and M.J. Janse, Editors. Leiden: Stenfert Kroese, 1976, pp. 467–484.
30. Narula, O.S., Current concepts of atrioventricular block, in *His Bundle Electrocardiography and Clinical Electrophysiology*, A.S. Narula, Editor. Philadelphia, PA: Davis, 1975, pp. 139–175.
31. Rosen, K.M., R.C. Dhingra, H.S. Loeb, and S.H. Rahimtoola, Chronic heart block in adults. Clinical and electrophysiological observations. *Arch. Intern. Med.*, 1973;**131**: 663–672.
32. Levy, A.M., A.J. Camm, and J.F. Keane, Multiple arrhythmias detected during nocturnal monitoring in patients with congenital complete heart block. *Circulation*, 1977;**55**: 247–253.
33. Goldberg, S., A.J. Greenspon, P.L. Urban, B. Muza, B. Berger, P. Walinsky, P. Maroko, Reperfusion arrhythmia: a marker of restoration of antegrade flow during intracoronary thrombolysis for acute myocardial infarction. *Am. Heart J.*, 1983;**105**: 26–32.
34. Gorgels, A.P., M.A. Vos, I.S. Letsch, E.A. Verschuuren, F.W. Bar, J.H. Janssen, and H.J.J. Wellens, Usefulness of the accelerated idioventricular rhythm as a marker for myocardial necrosis and reperfusion during thrombolytic therapy in acute myocardial infarction. *Am. J. Cardiol.*, 1988;**61**: 231–235.
35. Gressin, V., Y. Louvard, M. Pezzano, and H. Lardoux, Holter recording of ventricular arrhythmias during intravenous thrombolysis for acute myocardial infarction. *Am. J. Cardiol.*, 1992;69: 152–159.
36. Engelen, D.J., V. Gressin, M.W. Krucoff, D.A. Theuns, C. Green, E.C. Cheriex, P. Maison-Blanche, W.R. Dassen, H.J. Wellens, and A.P. Gorgels, Usefulness of frequent arrhythmias after epicardial recanalization in anterior wall acute myocardial infarction as a marker of cellular injury leading to poor recovery of left ventricular function. *Am. J. Cardiol.*, 2003;**92**: 1143–1149.
37. Puech, P., M. Blondeau, P. Bohyn, et al., L'évolution des blocs de branche vers le bloc auriculo-ventriculair complet. *Acta Cardiol.*, 1976;**21**(Suppl.): 33–66.
38. Slama, R., G. Motté, and R. Grolleau, Paroxysmal atrioventricular block, in *The Cardiac Arrhytmias*, P. Puech and R. Slama, Editors. Paris: Roussel UCLAF, 1979, p. 151.
39. Guérot, C.L., A. Coste, P.E. Valère, and R. Tricot, Lé'preuve à l'Ajmaline dans le diagnostic du bloc auriculo-ventriculaire paroxistyque. *Arch. Mal. Cœur Vaiss.*, 1973;**66**: 1241–1253.
40. Schuilenberg, R.M. and D. Durrer Rate-dependency of functional block in the human His bundle and bundle branch-Purkinje system. *Circulation*, 1973;**48**: 526–540.
41. Den Dulk, K., P. Brugada, S. Braat, B. Heddle, and H.J.J. Wellens, Myocardial bridging as a cause of paroxysmal atrioventricular block. *J. Am. Coll. Cardiol.*, 1983;**1**: 965–969.

42. Manning, G.W. and G.A. Sears, Postural heart block. *Am. J. Cardiol*., 1962;**9**: 558–563.
43. Scherf, D. and J.H. Dix, The effects of posture on A-V conduction. *Am. Heart J*., 1952;**43**: 494–506.
44. Lister, J.W., E. Stein, B.D. Kosowsky, S.H. Lau, and A.N. Damato, Atrioventricular conduction in man: effect of rate, exercise, isoproterenol and atropine on the P-R interval. *Am. J. Cardiol*., 1965;**16**: 516–523.
45. Gupta, P.K., E. Lichtstein, and K. Chadda, Electrophysiological features of complete AV block within the His bundle. *Br. Heart J*., 1973;**35**: 610–615.
46. Narula, O.S., Conduction disorders in the AV transmission system, in *Cardiac Arrhythmias*, L.S. Dreifus and W. Likoff, Editors. New York: Grune and Stratton, 1973, pp. 259–291.
47. Schweitzer, P. and H. Mark, The effect of atropine on cardiac arrhythmias and conduction. Part 1., *Am. Heart J*., 1980;**100**: 119–127.
48. Schweitzer, P. and H. Mark, The effect of atropine on cardiac arrhythmias and conduction. Part 2., *Am. Heart J*., 1980;**100**: 255–261.
49. Mahaim, I., *Les Maladies Organiques du Faisceau de His-Tawara*. Paris: Masson, 1931.
50. Yater, W.M., V.H. Cornell, and T. Claytor, Auriculoventricular heart block due to bilateral bundle-branch lesions. *Arch. Intern. Med*., 1936;**57**: 132–173.
51. Lenègre, J., Bilateral bundle branch block. *Cardiologia*, 1966;**48**: 134–147.
52. Schuilenburg, R.M. and D. Durrer, Observations on atrioventricular conduction in patients with bilateral bundle branch block. *Circulation*, 1970;**41**: 967–979.
53. Rosen, K.M., Evaluation of cardiac conduction in the cardiac catheterisation laboratory. *Am. J. Cardiol*., 1972;**30**: 701–703.
54. Dhingra, R.C., K.M. Rosen, and S.H. Rahimtoola, Normal conduction intervals and responses in sixty-one patients using His bundle recording and atrial pacing. *Chest*, 1973;**64**: 55–59.
55. Schuilenburg, R.M., *Observations on atrioventricular conduction in man using intracardiac electrocardiography and stimulation*, thesis. Amsterdam: Swado Offset, 1974.
56. Schuilenburg, R.M. and D. Durrer, Problems in the recognition of conduction disturbances in the His bundle. *Circulation*, 1975;**51**: 68–74.
57. Wellens, H.J.J., Value and limitations of programmed electrical stimulation of the heart in the study and treatment of tachycardias. *Circulation*, 1978;**57**: 845–853.
58. Ohkawa, S.-I., Sugiura, M., Itoh, Y., et al., Electrophysiologic and histologic correlations in chronic complete atrioventricular block. *Circulation*, 1981;**64**: 215–231.
59. Damato, A.N. and S.H. Lau, Clinical value of the electrogram of the conduction system. *Prog. Cardiovasc. Dis*., 1970;**13**: 119–140.
60. Narula, O.S., B.J. Sherlag, P. Samet, and R.P. Javier, Atrioventricular block. Localization and classification by His bundle recordings. *Am. J. Med*., 1971;**50**: 146–165.
61. Narula, O.S., R.P. Javier, P. Samet, and L.C. Maramba, Significance of His and left bundle recordings from the left heart in man. *Circulation*, 1970;**42**: 385–396.
62. Damato, A.N., J.J. Gallagher, R.N. Schnitzler, and S.H. Lau, Use of His bundle recordings in understanding A-V conduction disturbances. *Bull. N. Y. Acad. Med*., 1971;**47**: 905–922.
63. Castellanos, A. Jr., C.A. Castillo, and A.S. Agha, Contribution of His bundle recordings to the understanding of clinical arrhythmias. *Am. J. Cardiol*., 1971;**28**: 499–508.
64. Puech, P. and R. Grolleau, *L'Activité du Faisceau de His Normale et Pathologique*. Paris: Sandoz, 1972.
65. Bekheit, S., P. Morton, J.G. Murtagh, and E. Fletcher, Comparison of sinoventricular conduction hn children and adults using bundle of His electrograms. *Br. Heart J*., 1973;**35**: 507–515.
66. Ross, D.L., J. Farre, F.W.H.M. Bär, et al., Comprehensive clinical electrophysiologic studies in the investigation of documented or suspected tachycardias. Time, staff, problems and costs. *Circulation*, 1980;**61**: 1010–1016.
67. Narula, O.S., L.S. Cohen, P. Samet, J.W. Lister, B.J. Scherlag, and F.J. Hildner, Localization of A-V conduction defects in man by recording of the His bundle electrogram. *Am. J. Cardiol*., 1970;**25**: 228–237.
68. Narula, O.S. and P. Samet, Significance of first degree A-V block. *Circulation*, 1971;**43**: 772–773.
69. Levites, R. and J.I. Haft, Significance of first degree heart block (prolonged P-R interval) in bifascicular block. *Am. J. Cardiol*., 1974;**34**: 259–264.
70. Narula, O.S., M. Runge, and P. Samet, Second degree Wenckebach type AV block due to block within the atrium *Br. Heart J*., 1972;**34**: 1127–1136.
71. Puech, P., Atrioventricular block: the value in intracardiac recordings, in *Cardiac Arrhythmias*, D.M. Krikler and J.F. Goodwin, Editors. Philadelphia, PA: Saunders, 1975, p. 81.
72. Guimond, C. and P. Puech, Intra-His bundle blocks (102 cases). *Eur. J. Cardiol*., 1976;**4**: 481–493.
73. Fisher, J.D., H.L. Cohen, M.M. Kay, and D. Seinfeld, The complete His bundle study. *Clin. Res*., 1977;**25**: 648A.
74. Dhingra, R.C., E. Palileo, B. Strasberg, et al., Significance of the HV interval in 517 patients with chronic bifascicular bloc. *Circulation*, 1980;**64**: 1265–1271.
75. Johnson, R.L., K.H. Averill, and L.E. Lamb, Electrocardiographic findings in 67,375 asymptomatic subjects: VII. Atrioventricular block. *Am. J. Cardiol*., 1960;**6**: 153–177.
76. Viitasalo, M.T., R. Kala, and A. Eisalo, Ambulatory electrocardiographic recording in endurance athletes. *Br. Heart J.*, 1982;**47**: 213–220.
77. Graybiel, Q., R.A. McFarland, D.C. Gates, and V.A. Webster, Analysis of the electrocardiograms obtained from 1000 young healthy aviators. *Am. Heart J*., 1944;**27**: 524–549.
78. Packard, J.M., J.S. Graettinger, and A. Gaybiel, Analysis of the electrocardiograms obtained from 1000 young healthy aviators: ten year follow-up. *Circulation*, 1954;**10**: 384–400.
79. Narula, O.S. and P. Samet, Wenckebach and Mobitz type II A-V block due to block within the His bundle and bundle branches. *Circulation*, 1970;**41**: 947–965.
80. Dreifus, L.S., Y. Watanabe, R. Haiat, and D. Kimbiris, Atrioventricular block. *Am. J. Cardiol*., 1971;**28**: 371–380.
81. Kretz, A. and H.O. DaRuos, Experimental Luciani-Wenckebach phenomenon in the anterior and posterior divisions of the left bundle branch of the canine heart. *Am. Heart J*., 1972;**84**: 513–524.
82. Wennemark, J.R. and J.P. Bandura, Microelectrode study of Wenckebach periodicity in canine Purkinje fibers. *Am J. Cardiol*., 1974;**33**: 390–398.
83. Friedman, H.S., J.A.C Gomes, and J.I. Haft, An analysis of Wenckebach periodicity. *J. Electrocardiol*., 1975;**8**: 307–315.
84. Denes, P., L. Levy, A. Pick, and K.M. Rosen, The incidence of typical and atypical A-V Wenckebach periodicity. *Am. Heart J*., 1975;**89**: 26–31.

85. Wenckebach, K.F. and H. Winterberg, *Die Unregelmässige Hertztätigkeit*. Leipzig: Wilhelm Engelmann, 1927, p. 305.
86. Langendorf, R. and J.S. Mehlman, Blocked (nonconducted) A-V nodal premature systoles imitating first and second degree A-V block. *Am. Heart J.*, 1947;**34**: 500–506.
87. Rosen, K.M., S.H. Rahimtoola, and R.M. Gunnar, Pseudo A-V block secondary to premature nonpropagated His bundle depolarizations. Documentation by His bundle electrocardiography. *Circulation*, 1970;**42**: 367–373.
88. Lindsay, A.E. and L. Schamroth, Atrioventricular junctional parasystole with concealed conduction simulating second degree atrioventricular block. *Am. J. Cardiol.*, 1973;**31**: 397–399.
89. Watanabe, Y., Atrioventricular block (in Japanese). *Saishin Igaku*, 1970;**25**: 799–805.
90. Watanabe, Y. and L.S. Dreifus, Inhomogeneous conduction in the A-V node. A model for re-entry. *Am. Heart J.*, 1965;**70**: 505–514.
91. Watanabe, Y. and L.S. Dreifus, Second degree atrioventricular block. *Cardiovasc. Res.*, 1967;**1**: 150–158.
92. Fisch, C., D.P. Zipes, and P.L. McHenry, Electrocardiographic manifestations of concealed junctional ectopic impulses. *Circulation*, 1976;**53**: 217–223.
93. Littmann, L. and R.H. Svenson, Concealed re-entry: a mechanism of atrioventricular nodal alternating Wenckebach periodicity. *Circulation*, 1982;**65**: 1269–1275.
94. El-Sherif, N., J. Aranda, B. Befeler, and R. Lazzara, Atypical Wenckebach periodicity simulating Mobitz II AV block. *Br. Heart J.*, 1978;**40**: 1376–1383.
95. Scherlag, B.J., N. El-Sherif, and R. Lazarra, Experimental model for study of Mobitz type II and paroxysmal atrioventricular block. *Am. J. Cardiol.*, 1974;**34**: 309–317.
96. Langendorf, R. and A. Pick, Atrioventricular block, type II (Mobitz)—Its nature and clinical significance. *Circulation*, 1968;**38**: 819–821.
97. Strasberg, B., F. Amat-Y-Leon, R.C. Dhingra, et al., Natural history of chronic second-degree atrioventricular nodal block. *Circulation*, 1981;**63**: 1043–1049.
98. Donoso, E., L.N. Adler, and C.K. Friedberg, Unusual forms of second-degree atrioventricular block, including Mobitz type-II block, associated with the Morgagni-Adams-Stokes syndrome. *Am. Heart. J.*, 1964;**67**: 150–157.
99. Grossman, M., Second degree heart block with Wenckebach phenomenon: its occurrence over a period of several years in a young healthy adult. *Am. Heart J.*, 1958;**56**: 607–610.
100. Meyles, I., E. Kaplinsky, J.H. Yahini, N. Hanne-Paparo, and H.N. Neufeld, Wenckebach A-V block: a frequent feature following heavy physical training. *Am. Heart J.*, 1975;**90**: 426–430.
101. Brodsky, M., D. Wu, P. Denes, C. Kanakis, and K.M. Rosen, Arrhythmias documented by 24 hour continuous electrocardiographic monitoring in 50 male medical students without apparent heart disease. *Am. J. Cardiol.*, 1977;**39**: 390–395.
102. Young, D., R. Eisenberg, B. Fish, and J.D. Fisher, Wenckebach atrioventricular block (Mobitz type I) in children and adolescents. *Am. J. Cardiol.*, 1977;**40**: 393–399.
103. Otsuka, K., Y. Ichimaru, and T. Yanaga, Studies of arrhythmias by 24 hour polygraphic recordings: relation between atrioventricular block and sleep states. *Am. Heart J.*, 1983;**105**: 934–940.
104. Dickinson, D.F. and O. Scott, Ambulatory electrocardiographic monitoring in 100 healthy teenage boys. *Br. Heart J.*, 1984;**51**: 179–183.
105. Zeppilli, P., R. Fenici, M. Sassara, M.M. Pirrami, and G. Gaselli, Wenckebach second degree A-V block in top-ranking athletes: an old problem revisited. *Am. Heart J.*, 1980;**100**:281–294.
106. Langendorf, R., H. Cohen, and E.G. Gozo Jr., Observations on second degree atrioventricular block, including new criteria for the differential diagnosis between type I and type II block. *Am. J. Cardiol.*, 1972;**29**: 111–119.
107. Goodfriend, M.A. and S.S. Barold, Tachycardia-dependent and bradycardia-dependent Mobitz type II atrioventricular block within the bundle of His. *Am. J. Cardiol.*, 1974;**33**: 908–913.
108. Gilchrist, A.R., Clinical aspects of high-grade heart-block. *Scott. Med. J.*, 1958;**3**: 53–75.
109. Friedberg, C.K., Disturbance in conduction: heart block and bundle branch block, in *Diseases of the Heart*, C.K. Friedberg, Editor. Philadelphia, PA: Saunders, 1966, pp. 583–639.
110. Jonas, E.A., B.D. Kosowsky, and K. Ramaswamy, Complete His-Purkinje block produced by carotid sinus massage: report of a case. *Circulation*, 1974;**50**: 192–197.
111. Narula, O.S., Wenckebach type I and type II atrioventricular block (revisited), in *Complex Electrocardiography*, vol. 2, C. Fisch, Editor, Philadelphia, PA: Davis, 1974, pp. 137–136.
112. Gaultier, M., E. Fournier, M.L. Efthymiou, J.P. Frejaville, P. Jouannot, and M. Dentan, Intoxication digitalique aigue (70 observations). *Bull. Soc. Med. Hop. Paris*, 1968;**119**: 247–274.
113. Smith, T.W. and J.T. Willerson, Suicidal and accidental digoxin ingestion. Report of five cases with serum digoxin level correlations. *Circulation*, 1971;**44**: 29–36.
114. Vanagt, E.J. and H.J.J. Wellens, The electrocardiogram in digitalis intoxication, in *What's New in Electrocardiography?* H.J.J. Wellens and H.E. Kulbertus, Editors. The Hague: Nijhoff, 1981, pp. 315–343.
115. Roth, I.R. and B. Kisch, The mechanism of irregular sinus rhythm in auriculoventricular heart block. *Am. Heart J.*, 1947;**36**: 257–276.
116. Rosenbaum, M.B. and E. Mepeschkin, The effects of ventricular systole on auricular rhythm in auriculoventricular block. *Circulation*, 1955;**11**: 240–261.
117. Narula, O.S., B.J. Sherlag, R.P. Javier, F.J. Hildner, and P. Samet, Analysis of the Q-V conduction defect in complete heart block utilizing His bundle electrograms. *Circulation*, 1970;**41**: 437–448.
118. Lie, K.I., H.J.J. Wellens, R.M. Schuilenburg, and D. Durrer Mechanism and significance of widened QRS complexes during complete atrioventricular block in acute inferior myocardial infarction. *Am. J. Cardiol.*, 1974;**33**: 833–889.
119. Narula, O.S. and P. Samet, Effect of atropine and glucagons on A-V nodal and His bundle pacemakers in man. *Circulation*, 1971;**44** (Suppl. II): 205.
120. Kelly, D.T., S.J. Brodsky, M. Mirowski, L.J. Krovetz, and R.D. Rowe, Bundle of His recording in congenital complete heart block. *Circulation*, 1972;**45**: 277–281.
121. Tavazzi, L., J.A. Salerno, M. Chimienti, M. Ray, and P. Bobba, Electrophysiological mechanisms of the paroxysmal atrioventricular block, in *Diagnosis, and Treatment of Cardiac Arrhythmias*, A. Bayes and J. Cosin, Editors. Oxford: Pergamon, 1980, pp. 415–430.
122. Narula, O.S. and N. Shantha, Atrioventricular block: clinical concepts and His bundle electrocardiography, in *Cardiac Arrhythmias: Their Mechanisms, Diagnosis, and Management*, W.J. Mandel, Editor. Philadelphia, PA: Lippencott, 1980, p. 437.

123. Zoob, M. and K.S. Smith, The aetiology of complete heart-block. *Br. Med. J.*, 1963;**2**: 1149–1153.
124. Lenègre, J., Etiology and pathology of bilateral bundle branch block in relation to complete heart block. *Prog. Cardiovasc. Dis.*, 1964;**6**: 409–444.
125. Lev, M., Anatomic basis for atrioventricular block. *Am. J. Med.*, 1964;**37**: 742–748.
126. Lev, M., P.N. Unger, K.M. Rosen, and S. Bharati The anatomic substrate of complete left bundle branch block. *Circulation*, 1974;**50**: 479–486.
127. Lenégre, J., Les blocks auriculo-ventriculaires complets chroniques. Etude des causes et des lesions à propos de 37 cas. *Mal. Cardiol. Vasc.*, 1962;**3**: 311–343.
128. Davies, M.J., A histological study of the conduction system in complete heart block. *J. Pathol.*, 1967;**94**: 351–358.
129. Rosenbaum, M.B., M.V. Elizari, J.O. Lazzari, G.J. Nau, R.J. Levi, and M.S. Halpern, Intraventricular trifascicular blocks. Review of the literature and classification. *Am. Heart J.*, 1969;**78**: 450–459.
130. Harris, A., M. Davies, D. Redwood, A. Leatham, and H. Siddons, Aetiology of chronic heart bock: a clinico-pathological correlation in 65 cases. *Br. Heart J.*, 1969;**31**: 206–218.
131. Rosenbaum, M.B., The hemiblocks: diagnostic and clinical significance. *Mod. Concepts Cardiovasc. Dis.*, 1970;**39**: 141–146.
132. Begg, F.R., G.J. Margovern, W.J. Cushing, E.M. Kent, and D.L. Fisher, Selective cine coronary arteriography in patients with complete heart block. *J. Thorac. Cardiovasc. Surg.*, 1969;**57**: 9–16.
133. Escher, D.J.W., The use of artificial pacemakers in acute myocardial infarction, in *Controversy in Cardiology: The Practical Clinical Approach*, E.K. Chung, Editor. New York: Springer, 1976, p. 51.
134. Furman, S., Cardiac pacing and pacemakers I. Indications for pacing bradyarrhythmias. *Am. Heart J.*, 1977;**93**: 523–530.
135. Simon, A.B. and A.E. Zloto, Atrioventricular block: natural history after permanent ventricular pacing. *Am. J. Cardiol.*, 1978;**41**: 500–507.
136. Penton, G.B., H. Miller, and S.A. Levine, Some clinical features of complete heart block. *Circulation*, 1956;**13**: 801–824.
137. Wright, J.C., M.R. Hejtmancik, G.R. Herrmann, and A.H. Shields, A clinical study of complete heart block. *Am. Heart J.*, 1956;**52**: 369–378.
138. Rowe, J.C. and P.D. White, Complete heart block: a follow-up study. *Ann. Intern. Med.*, 1958;**49**: 260–270.
139. Mason, D.T., R. Zelis, G. Lee, J.L. Hughes, J.F. Spann Jr., and E.A. Amsterdam, Current concepts and treatment of digitalis toxicity. *Am. J. Cardiol.*, 1971;**27**: 546–559.
140. Przybyla, A.C., K.L. Paulay, E. Stein, and A.N. Damato, Effects of digoxin on atrioventricular conduction patterns in man. *Am. J. Cardiol.*, 1974;**33**: 344–350.
141. Rosen, M.R., A.L. Wit, and B.F. Hoffman, Electrophysiology and pharmacology of cardiac arrhythmias. IV. Cardiac antiarrhythmic and toxic effects of digitalis. *Am. Heart J.*, 1975;**89**: 391–399.
142. Wit, A.L., M.R. Rosen, and B.F. Hoffmann, Electrophysiology an pharmacology of cardiac arrhythmias. VIII. Cardiac effects of diphenylhydantoin B. *Am. Heart J.*, 1975;**90**: 397–404.
143. Wit, A.L., B.F. Hoffman, and M.R. Rosen, Electrophysiology and pharmacology of cardiac arrhythmias. IX. Cardiac electrophysiologic effects of beta arenergic receptor stimulation and blockade. Part B. *Am. Heart J.*, 1975;**90**: 665–675.
144. Hoffman, B.F., M.R. Rosen, and A.L. Wit, Electrophysiology and pharmacology of cardiac arrhythmias. VII. Cardiac effects of quinidine and procaine amide. B. *Am. Heart J.*, 1975;**90**: 117–122.
145. Mackenzie, J., Definition of the term "heart-block". *Br. Med. J.*, 1906;**2**: 1107–1021.
146. Weiss, S. and E.B. Ferris Jr., Adams-Stokes syndrome with transient heart block of vagovagal reflex origin: mechanism and treatment. *Arch. Intern. Med.*, 1934;**54**: 931–951.
147. Weiss, S. and J.P. Baker, The carotid sinus reflex in health and disease: its rôle in the causation of fainting and convulsions. *Medicine*, 1933;**12**: 297–354.
148. Strasberg, B., W. Lam, S. Swiryn, et al., Symptomatic spontaneous paroxysmal AV nodal block due to localized hyperresponsiveness of the AV node to vagotonic reflexes. *Am. Heart J.*, 1982;**103**: 795–801.
149. Lown, B. and S.A. Levine, The carotid sinus: clinical value of its stimulation. *Circulation*, 1961;**23**: 766–789.
150. Lesser, L.M. and N.K. Wenger, Carotid sinus syncope. *Heart Lung*, 1976;**5**: 453–456.
151. Sanoudos, G. and G.E. Reed, Late heart block in aortic valve replacement. *J. Cardiovasc. Surg.*, 1974;**15**: 475–478.
152. Griffiths, S.P., Congenital complete heart block. *Circulation*, 1971;**43**: 615–617.
153. Rosen, K.M., A. Metha, S.H. Rahimtoola, R.A. Miller, Sites of congenital and surgical heart block as defined by His bundle electrocardiography. *Circulation*, 1971;**44**: 833–841.
154. Furman, S. and D. Young, Cardiac pacing in children and adolescents. *Am. J. Cardiol.*, 1977;**39**: 550–558.
155. Hofschire, P.J., D.M. Nicoloff, and J.H. Moller, Postoperative complete heart block in 64 children treated with and without cardiac pacing. *Am. J. Cardiol.*, 1977;**39**: 559–562.
156. Kim, M.H., G.M. Deeb, K.A. Eagle, D. Bruckman, F. Pelosi, H. Oral, C. Sticherling, R.L. Baker, S.P. Chough, K. Wasmer, G.F. Michaud, B.P. Knight, S.A. Strickberger, and F. Morady, Complete atrioventricular block after valvular heart surgery and the timing of pacemaker implantation. *Am. J. Cardiol.*, 2001;**87**: 649–651, A10.
157. Yabek, S.M., R.E. Swensson, and J.M. Jarmakani, Electrocardiographic recognition of sinus node dysfunction in children and young adults. *Circulation*, 1977;**56**: 235–239.
158. Williams, W.G., T. Izukawa, P.M. Olley, G.A. Trusler, and R.D. Rowe, Permanent cardiac pacing in infants and children. *PACE*, 1978;**1**: 439–447.
159. Reid, J.M., E.N. Coleman, and W. Doig, Complete congenital heart block. Report of 35 cases. *Br. Heart J.*, 1982;**48**: 236–239.
160. Blake, R.S., E.E. Chung, H. Wesley, and K.A. Hallidie-Smith, Conduction defects, ventricular arrhythmias, and late death after surgical closure of ventricular septal defect. *Br. Heart J.*, 1982;**47**: 305–315.
161. Furman, S. and G. Robinson, The use of an intracardiac pacemaker in the correction of total heart block. *Surg. Forum*, 1958;**9**: 245–248.
162. Paul, M.H., A.M. Rudolph, and A.S. Nadas, Congenital complete atrioventricular block: problems of clinical assessment. *Circulation*, 1958;**18**: 183–190.
163. Elmqvist, R. and A. Senning, An implantable pacemaker for the heart, in *Medical Electronics Proceedings of the 2nd International Conference on Medical Electronics*, C.N. Smyth, Editor. London: Iliffle, 1960, pp. 253–254.

164. Zoll, P.M., H.A. Frank, L.R.N. Zarsky, A.J. Linenthal, and A.H. Belgard, Long-term electrical stimulation of the heart for Stokes-Adams disease. *Ann. Surg.*, 1961;**154**: 330–346.
165. Kantrowitz, A., R. Cohen, H. Raillard, J. Schmidt, and D.S. Feldman, The treatment of complete heart block with an implanted controllable pacemaker. *Surg. Gynecol. Obstet.*, 1962;**115**: 415–420.
166. Nakamura, F.F. and A.S. Nada, Complete heart block in infants and children. *N. Engl. J. Med.*, 1964;**270**: 1261–1268.
167. Lemberg, L., A. Castellanos Jr., and B. Berkovits, Pacemaking on demand in AV block. *J. Am. Med. Assoc.*, 1965;**191**: 12–14.
168. Nasrallah, A.T., P.C. Gillette, and C.E. Mullins, Congenital and surgical atrioventricular block within the His bundle. *Am. J. Cardiol.*, 1975;**36**: 914–920.
169. Feldt, R.H., J.W. DuShane, and J.L. Titus, The atrioventricular conduction system in persistent common atrioventricular canal defect. Correlation with electrocardiogram. *Circulation*, 1970;**42**: 437–444.
170. Lev, M., J. Silverman, F.M. Fitzmaurice, M.H. Paul, D.E. Cassels, and R.A. Miller Lack of connection between the aria and the more peripheral conduction system in congenital atrioventricular block. *Am. J. Cardiol.*, 1971;**27**: 481–490.
171. Ferris, J.A.J. and W.A. Aherne, Cartilage in relation to the conduction tissue of the heart in sudden death. *Lancet*, 1971;**9**: 64–66.
172. Lev, M., Cuadros, H., and M.H. Paul, Interruption of the atrioventricular bundle with congenital atrioventricular block. *Circulation*, 1971;**43**: 703–710.
173. Anderson, R.H., A.E. Becker, R. Arnold, and J.L. Wilkinson, The conducting tissues in congenitally corrected transposition. *Circulation*, 1974;**50**: 911–923.
174. James, T.N., M.S. Spencer, and J.C. Kloepfler, De subitaneis mortibus, XXI. Adult onset syncope with comments on the nature of congenital heart block and the morphogenesis of the human atrioventricular septal junction. *Circulation*, 1976;**54**: 1001–1009.
175. Anderson, R.H., A.C.G. Wenick, T.G. Losekoot, and A.E. Becker, Congenitally complete heart block: developmental aspects. *Circulation*, 1977;**56**: 90–101.
176. Smedema, J.P., G. Snoep, M.O. van Kroonenburgh, R.J. van Geuns, E.C. Cheriex, A.P. Gorgels, and H.J. Crijns, The additional value of gadolinium-enhanced MRI to standard assessment for cardiac involvement in patients with pulmonary sarcoidosis. *Chest*, 2005;**128**: 1629–1637.
177. Rosen, K.M., S.H. Rahimtoola, S. Bharati, and M. Lev, Bundle branch block with intact atrioventricular conduction. Electrophysiologic and pathologic correlations in three cases. *Am. J. Cardiol.*, 1973;**32**: 783–793.
178. Matlof, H.J., J.C. Zener, and D.C. Harrison, Idiopathic hypertrophic subaortic stenosis and heart block. Cycle-to-cycle variation as a function of alteration in preload and afterload. *Am. J. Cardiol.*, 1973;**32**: 719–722.
179. Bashour, F.A., T. MacConnel, W. Skinner, and M. Hanson, Myocardial sarcoïdosis. *Dis. Chest*, 1968;**53**: 413–420.
180. Bernstein, M., Auriculoventricular dissociation following scarlet fever: report of a case. *Am. Heart J.*, 1938;**16**: 582–586.
181. Menon, T.B. and C.K.P. Rao, Tuberculosis of the myocardium causing complete heart block. *Am. J. Pathol.*, 1945;**21**: 1193–1196.
182. Logue, R.B. and J.F. Hanson, Complete heart block in German measles. *Am. Heart J.*, 1945;**30**: 205–207.
183. Rosenberg, D.H., Electrocardiographic changes in epidemic parotitis (mumps). *Proc. Soc. Exp. Biol. Med.*, 1945;**58**: 9–11.
184. Rantz, L.A., W.W. Spink, and P.J. Boisvert, Abnormalities in the electrocardiogram following haemolytic streptococcus sore throat. *Arch. Intern. Med.*, 1946;**77**: 66–79.
185. Clark, N.S., Complete heart block in children. Report of three cases possibly attributable to measles. *Arch. Dis. Child*, 1948;**23**: 156–162.
186. Engle, M.A., Recovery from complete heart block in diphtheria. *Pediatrics*, 1949;**3**: 222–233.
187. Kaindl, F. and K. Rummelhardt, Zur Therapie rezidivierender Adams-Stokes-Anfälle. *Wien. Klin. Wochenschr.*, 1956;**68**: 583–584.
188. Shee, J.C., Stokes-Adams attacks due to toxoplasma myocarditis. *Br. Heart J.*, 1964;**26**: 151–153.
189. Kleid, J.J., E.S. Kim, B. Brand, S. Eckles, and G.M. Gordon, Heart block complicating acute bacterial endocarditis. *Chest*, 1972;**61**: 301–303.
190. Lim, C.-H., C.C.S Toh, B.-L. Chia, and L.-P. Low, Stokes-Adams attacks due to acute non-specific myocarditis. *Am. Heart J.*, 1975;**90**: 172–178.
191. Wray, R. and M. Iveson, Complete heart block and systemic lupus erythematosus. *Br. Heart J.*, 1975;**37**: 982–983.
192. Lev, M., S. Bharati, F.G. Hoffman, and L. Leight, The conduction system in rheumatoid arthritis with complete atrioventricular block. *Am. Heart J.*, 1975;**90**: 78–83.
193. Surawicz, B., Relationship between electrocardiogram and electrolytes. *Am. Heart J.*, 1967;**73**: 814–834.
194. Fisch, C., Relation of electrolyte disturbances to cardiac arrhythmias. *Circulation*, 1973;**47**: 408–419.
195. Clark, D.S., R.J. Myerburg, A.R. Morales, B. Befeler, F.A. Hernandez, and H. Gelband, Heart block in Kearns-Sayre syndrome. Electrophysiologic-pathologic correlation. *Chest*, 1975;**68**: 727–730.
196. Sanyal, S.K. and W.W. Johnson, Cardiac conduction abnormalities in children with Duchenne's progressive muscular dystrophy: electrocardiographic features and morphologic correlates. *Circulation*, 1982;**66**: 853–863.
197. Komajda, M., R. Frank, J. Vedel, G. Fontaine, J.-C. Petitot, and Y. Grosgogeat Intracardiac conduction defects in dystrophia myotonica: electrophysiological study of 12 cases. *Br. Heart J.*, 1980;**43**: 315–320.
198. Schwartzkopff, B., H. Frenzel, B. Losse, M. Borggrefe, K.V. Toyka, W. Hammerstein, R. Seitz, M. Deckert, and G. Breithardt, Heart involvement in progressive external ophthalmoplegia (Kearns-Sayre syndrome): electrophysiologic, hemodynamic and morphologic findings, *Z. Kardiol.*, 1986;**75**: 161–169.
199. Hiromasa, S., T. Ikeda, K. Kubota, et al., Myotonic dystrophy: ambulatory electrocardiogram, electrophysiologic study, and echocardiographic evaluation. *Am. Heart J.*, 1987;**113**: 1482–1488.
200. Stevenson, W.G., J.K. Perloff, J.N. Weiss, and T.L. Anderson Facioscapulohumeral muscular dystrophy: evidence for selective, genetic electrophysiologic cardiac involvement. *J. Am. Coll. Cardiol.*, 1990;**15**: 292–299.
201. Arai, T., C. Kurashima, S. Wada, K. Chida, and S. Ohkawa, An unusual site for the AV node tumor: report of two cases. *Cardiovasc. Pathol.*, 1999;**8**: 325–328.
202. Van Hare, G.F., C.K. Phoon, F. Munkenbeck, C.R. Patel, D.L. Fink, and N.H. Silverman, Cardiac involvement by non-Hodgkin's lymphoma: an unusual presentation of heart conduction disturbances. *Pacing Clin. Electrophysiol.*, 1994;**17**: 1561–1564.

203. Ando, M., T. Yokozawa, J. Sawada, Y. Takaue, K. Togitani, N. Kawahigashi, M. Narabayashi, K. Takeyama, R. Tanosaki, S. Mineishi, Y. Kobayashi, T. Watanabe, I. Adachi, and K. Tobinai, Cardiac conduction abnormalities in patients with breast cancer undergoing high-dose chemotherapy and stem cell transplantation. *Bone Marrow Transplant.*, 2000;**25**: 185–189.
204. Kaplan, B.M., A.J. Miller, S. Bharati, M. Lev, and I. Martin Grais, Complete AV block following mediastinal radiation therapy: electrocardiographic and pathologic correlation and review of the world literature. *J. Interv. Card. Electrophysiol.*, 1997;**1**: 175–188. Review.
205. James, T.N., D.J.L. Carson, and T.K. Marshall, De subitaneis mortibus, I, Fibroma compressing His bundle. *Circulation*, 1973;**48**: 428–433.
206. Rosen, K.M., R. Heller, A. Ehsani, and S.H. Rahimtoola, Localization of site of traumatic heart block with His bundle recordings. Electrophysiologic observations regarding the nature of "split" H potentials. *Am. J. Cardiol.*, 1972;**30**: 412–417.
207. Gorgels, A.P., F. Al Fadley, L. Zaman, M.J. Kantoch, and Z. Al Halees, The long QT syndrome with impaired atrioventricular conduction: a malignant variant in infants. *J. Cardiovasc. Electrophysiol.*, 1998;**9**: 1225–1232.
208. Campbell, M., Complete heart block. *Br. Heart J.*, 1944;**6**: 69–92.
209. Ide, L.W., The clinical aspects of complete auriculoventricular heart block: a clinical analysis of 71 cases. *Ann. Intern. Med.*, 1950;**32**: 510–523.
210. Pomerance, A., Pathological and clinical study of calcification the mitral valve ring. *J. Clin. Pathol.*, 1970;**23**: 354–361.
211. Narula, O.S. and P. Samet, Predilection of elderly females for intra-His bundle (BH) blocks. *Circulation*, 1974;**50**(Suppl. III): 195.
212. Escher, D.J.W. and S. Furman, Pacemaker therapy for chronic rhythm disorders. *Prog. Cardiovasc. Dis.*, 1972;**14**: 459–474.
213. Conklin, E.F., S. Giannelli Jr., and T.F. Nealon Jr., Four hundred consecutive patients with permanent transveneous pacemakers. *J. Thorac. Cardiovasc. Surg.*, 1975;**69**: 1–7.
214. Wellens, H.J.J., P. Brugada, and F.W.H.M. Bär, The role of intraventricular conduction disorders in precipitating sudden death. *Ann. N. Y. Acad. Sci.*, 1982;**382**: 136–142.
215. Ezri, M., B.B. Lerman, F.E. Marchlinski, A.E. Buxton, and M.E. Josephson, Electrophysiologic evaluation of syncope in patients with bifascicular block. *Am. Heart J.*, 1983;**106**: 693–697.
216. Concklin, E.F. and S. Giannelli Jr., Four hundred consecutive patients with permanent transveneous pacemakers. *J. Thorac. Cardiovasc. Surg.*, 1975;**69**: 1.
217. Havia, T., M. Arstila, H. Wendelen, and R. Heinonen, Permanent endocardial pacing. An analysis of 90 patients. *Acta med. Scand.*, 1976;**596**: 7–11.
218. Sixth semi-annual clinical evaluation report to the United States Nuclear Regulatory Commission, Medtronic Inc. Medtronic implantable demand isotopic pulse generator, Laurens-Alcatel model 9000. 1976.
219. Ranganathan, N., R. Dhurandhar, J.H. Phillips, and E.D. Wigle, His bundle electrogram in bundle-branch block. *Circulation*, 1972;**45**: 282–294.
220. Hunt, D., J.T. Lie, J. Vohra, and G. Sloman, Histopathology of heart block complicating acute myocardial infarction: correlation with the His bundle electrogram. *Circulation*, 1973;**48**: 1252–1261.
221. Lichstein, E., P.K. Gupta, K.D. Chadda, H.-M. Liu, and M. Sayeed, Findings of prognostic value in patients with incomplete bilateral bundle branch block complicating acute myocardial infarction. *Am. J. Cardiol.*, 1973;**32**: 913–918.
222. Nasrallah, A.T. and E.F. Beard, Intra-his bundle block complicating acute inferior myocardial infarction. *Chest*, 1976;**69**: 420–422.
223. Kourtesis, P., E. Lichstein, K.D. Chadda, and P.K. Gupta, Incidence and significance of left anterior hemiblock complicating acute inferior wall myocardial infarction. *Circulation*, 1976;**53**: 784–787.
224. Lichstein, E., P.K. Gupta, and K.D. Chadda, Indications for pacing in patients with chronic bifascicular block. *PACE*, 1978;**1**: 540–543.
225. Kastor, J.A., Cardiac electrophysiology: hemiblocks and stopped hearts. *N. Engl. J. Med.*, 1978;**299**: 249–251.
226. Fisher, J.D., H.E. Kulbertus, and O.S. Narula, Panel discussion: the prognostic value of the H-V interval. *PACE*, 1978;**1**: 132–139.
227. McAnulty, J.H, S.H. Rahimtoola, E.S. Murphy, et al., A prospective study of sudden death in "high-risk" bundle branch block. *N. Engl. J. Med.*, 1978;**299**: 209–215.
228. Gregoratos, G., J. Abrams, A.E. Epstein, R.A. Freedman, D.L. Hayes, M.A. Hlatky, R.E. Kerber, G.V. Naccarelli, M.H. Schoenfeld, M.J. Silka, S.L. Winters, R.J. Gibbons, E.M. Antman, J.S. Alpert, G. Gregoratos, L.F. Hiratzka, D.P. Faxon, A.K. Jacobs, V. Fuster, and S.C. Smith Jr., American College of Cardiology/American Heart Association Task Force on Practice Guidelines/North American Society for Pacing and Electrophysiology Committee to Update the 1998 Pacemaker Guidelines.
229. Connelly, D.T. and D.M. Steinhaus, Mobitz type I atrioventricular block: an indication for permanent pacing? *Pacing Clin. Electrophysiol.*, 1996;**19**: 261–264.
230. Barold, S.S., Indications for permanent cardiac pacing in first-degree AV block: class I, II, or III? *Pacing Clin. Electrophysiol.*, 1996;**19**: 747–751.
231. Glikson, M., J.A. Dearani, L.K. Hyberger, H.V. Schaff, S.C. Hammill, and D.L. Hayes, Indications, effectiveness, and long-term dependency in permanent pacing after cardiac surgery. *Am. J Cardiol.*, 1997;**80**: 1309–1313.
232. Wohl, A.J., N.J. Laborde, J.M. Atkins, C.G. Blomqvist, and C.B. Mullins, Prognosis of patients permanently paced for sick sinus syndrome. *Arch. Intern. Med.*, 1976;**136**: 406–408.
233. Lichstein, E., C. Ribas-Meneclier, D. Naik, K.D. Chadda, P.K. Gupta, and H. Smith Jr., The natural history of trifascicular disease following permanent implantation: significance of continuing changes in atrioventricular conduction. *Circulation*, 1976;**54**: 780–783.
234. Furman, S., V. Parsonnet, M. Bilitch, and D. Escher, Fate of patients with permanent pacemakers. *Circulation*, 1977;**56**(Suppl. III): 12.
235. Nolan, S.P., R.S. Crampton, L.B. McGuire, R.C. McGann, H.C. Holz, and W.H. Muller Jr., Factors influencing survival of patients with permanent cardiac pacemackers. *Ann. Surg.*, 1977;**185**: 122–127.
236. Ginks, W., R. Sutton, H. Siddons, and A. Leatham, Unsuspected coronary artery disease as cause of chronic atrioventricular block in middle age. *Br. Heart J.*, 1980;**44**: 699–702.
237. Resnekov, L., Pacemaking and acute myocardial infarction. *Impulse*, 1978;**11**: 1.
238. Col, J.J. and S.L. Weinberg, The incidence and mortality of intraventricular conduction in acute myocardial infarction. *Am. J. Cardiol.*, 1972;**29**: 344–350.

239. Atkins, J.M., S.J. Leshin, G. Blomqvist, and C.B. Mullins, Ventricular conduction blocks and sudden death in acute myocardial infarction. Potential indications for pacing. *N. Engl. J. Med.*, 1973;**288**: 281–284.
240. Waugh, R.A., G.S. Wagner, T.L. Haney, R.A. Rosati, and J.J. Morris, Jr., Immediate and remote prognostic significance of fascicular block during myocardial infarction. *Circulation*, 1973;**47**: 765–775.
241. Lie, K.I., *Acute myocardial infarction in the coronary care unit: Factors influencing its immediate prognosis*, thesis. Amsterdam: Peco, 1974.
242. Lie, K.I., H.J.J. Wellens, and R.M. Schuilenberg, Bundle branch block and acute myocardial infarction, in *The Conduction System of the Heart: Structure, Function and Clinical Implications*, H.J.J. Wellens, K.I. Lie, and M.J. Janse, Editors. Leiden: Stenfert Kroese, 1976, pp. 662–672.
243. Mullins, C.B. and J.M. Atkins, Prognoses and management of ventricular conduction blocks in acute myocardial infarction. *Mod. Concepts Cardiovasc. Dis.*, 1976;**45**: 129–133.
244. Tans, A.C., K.I. Lie, and D. Durrer, Clinical setting and prognostic significance of high degree atrioventricular block in acute inferior myocardial infarction: a study of 144 patients. *Am. Heart J.*, 1980;**99**: 4–8.
245. Juma, Z., A. Castellanos, and R.J. Myerburg, Prognostic significance of the electrocardiogram in patients with coronary heart disease, in *What's New in Electrocardiography?* H.J.J. Wellens and H.E. Kulbertus, Editors. The Hague: Nijhoff, 1981, pp. 1–22.
246. Meltzer, L.E. and J.B. Kitchell, The incidence of arrhythmias associated with acute myocardial infarction. *Prog. Cardiovasc. Dis.*, 1966;**9**: 50–63.
247. Goldberg R. J., J.C. Zevallos, J. Yarzebski, J.S. Alpert, J.M. Gore, Z. Chen, and J.E. Dalen, Prognosis of Acute Myocardial Infarction Complicated by Complete Heart Block (the Worcester Heart Attack Study. *Am. J. Cardiol.*, 1992;**69**: 1139–1141.
248. Archbold R.A., J.W. Sayer, S. Ray, P. Wilkinson, K. Ranjadayalan, and A.D. Timmis, Frequency and prognostic implications of conduction defects in acute myocardial infarction since the introduction of thrombolytic therapy. *Eur. Heart J.*, 1998;**19**: 893–898.
249. Sgarbossa E.B., S.L. Pinski, E.J. Topol, R.M. Califf, A. Barbagelata, S.G. Goodman, K.B. Gates, C.B. Granger, D.P. Miller, D.A. Underwood, and G.S. Wagner, Acute myocardial infarction and complete bundle branch block at hospital admission: clinical characteristics and outcome in the thrombolytic era. GUSTO-I Investigators. Global Utilization of Streptokinase and t-PA [tissue-type plasminogen activator] for Occluded Coronary Arteries *J. Am. Coll. Cardiol.*, 1998;**31**: 105–110.
250. Harpaz D., S. Behar, S. Gottlieb, V. Boyko, Y. Kishon, and M. Eldar, for the SPRINT Study Group and the Israeli Thrombolytic Survey Group, Complete atrioventricular block complicating acute myocardial infarction in the thrombolytic era. *J. Am. Coll. Cardiol.*, 1999;**34**: 1721–1728.
251. Spencer F.A., S. Jabbour, D. Lessard, J. Yarzebski, S. Ravid, V. Zaleskas, M. Hyder, J.M. Gore, and R.J. Goldberg, Two–decade-long trends (1975–1997) in the incidence, hospitalization, and long-term death rates associated with complete heart block complicating acute myocardial infarction: A community-wide perspective. *Am. Heart J.*, 2003;**145**: 500–507.
252. Aplin M., T. Engstrøm, N.G. Vejlstrup, P. Clemmensen, C. Torp-Pedersen, L. Køber, and on behalf of the TRACE Study Group, Prognostic importance of complete atrioventricular block complicating acute myocardial infarction. *Am. J. Cardiol.*, 2003;**92**: 853–856.
253. Meine T.J., S.M. Al-Khatib, J.H. Alexander, C.B. Granger, H.D. White, R. Kilaru, K. Williams, E.M. Ohman, E. Topol, and R.M. Califf, Incidence, predictors, and outcomes of high-degree atrioventricular block complicating acute myocardial infarction treated with thrombolytic therapy. *Am. Heart J.*, 2005;**149**: 670–674.
254. Ho K.W., T.H. Koh, P. Wong, S.L. Wong, Y.T. Lim, S.T. Lim, and L.F. Hsu, Complete atrioventricular block complicating acute anterior myocardial infarction can be reversed with acute coronary angioplasty. *Ann. Acad. Med. Singapore*, 2010;**39**: 254–257.
255. Lister, J.W., R.S. Kline, and M.E. Lesser, Chronic bilateral bundle branch block. Long-term observations in ambulatory patients. *Br. Heart J.*, 1977;**39**: 203–207.
256. Kulbertus, H.E., F. de Leval-Rutten, M. Dubois, and J.M. Petit, Prognostic significance of left anterior hemiblock with right bundle branch block in mass screening. *Am. J. Cardiol.*, 1978;**41**: 385.
257. McAnulty, J.H., S. Kauffman, E. Murphy, D.G. Kassebaum, and S.H. Rahimtoola, Survival in patients with intraventricular conduction defects. *Arch. Intern. Med.*, 1978;**138**: 30–35.
258. Narula, O.S., D. Gann, and P. Samet, Prognostic value of H-V interval in patients with right bundle branch block (RBBB) and left axis deviation (LAD): follow-up observations from one to six years. *Circulation*, 1974;**50**(Suppl. III): 56.
259. Gupta, P.K., E. Lichstein, and K.D. Chadda, Follow-up studies in patients with right bundle branch block and left anterior hemiblock: significance of H-V interval. *J. Electrocardiol.*, 1977;**10**: 221–224.
260. Kulbertus, H.E., The magnitude of risk of developing complete heart block in patients with LAD-RBBB. *Am. Heart J.*, 1973;**86**: 278–279.

29 Ventricular Tachycardia

Guy Fontaine · Alain Coulombe · Jèrôme Lacotte · Robert Frank

P. W. Macfarlane, A. van Oosterom, O. Pahlm, P. Kligfield, M. Janse, J. Camm (eds.), *Comprehensive Electrocardiology*, DOI 10.1007/978-1-84882-046-3_29,

29.1 Introduction

Ventricular arrhythmias are an important topic in cardiology and are frequently observed in clinical practice. They present in different forms ranging from benign ventricular extrasystoles to ventricular tachycardia and fibrillation which may lead to sudden death.

The latter group has been the focus of major interest in recent years. Such arrhythmias are usually observed as a complication of coronary artery disease and are responsible for about 500,000 deaths a year in North America. Autopsy findings often show minimal lesions or chronic scars, which suggest that some of these deaths are entirely the result of an arrhythmia and that the treatment of these severe ventricular arrhythmias should be one of the major objectives of modern electrophysiology. This is especially true now that significant advances have been made in the following areas:

- The synthesis of new antiarrhythmic drugs
- The effectiveness of implantable defibrillators
- The benefit of catheter ablation techniques

This chapter on ventricular arrhythmias has been arbitrarily divided into two parts: the first deals with ventricular extrasystoles and the second, with ventricular tachycardia and fibrillation. This is, of course, an artificial distinction and the same pathological situations may be discussed according to whether they present clinically as a form of isolated ventricular extrasystoles or ventricular tachycardia. This latter form is not necessarily a sign of disease's progression, as patients may show one or the other arrhythmia from the beginning.

It might be necessary to consider first the electrophysiological mechanisms of these arrhythmias. It should be emphasized that there are probably significant differences between those observed in an electrophysiological bath with microelectrodes in normal animal tissues placed in artificial electrophysiological conditions, and those which are the substrate of human pathology. Although the relationship between these two approaches remains uncertain, both the cellular electrophysiological and clinical aspects will be discussed.

29.1.1 Cellular Electrophysiological Mechanisms of Arrhythmias

The electrophysiological mechanisms of cardiac arrhythmias at cellular level can be divided into three main groups; namely, increased automaticity, triggered activity, and reentry.

29.1.2 Increased automaticity

Increased automaticity corresponds with an increase in the normal phenomena of automaticity, and is the result of a slow diastolic depolarization in phase 4 of the action potential [1]. The activation of the adjacent nonspecific myocardium is the result of an electrotonic effect occurring when the resting potential of the automatic cells reaches its threshold. In abnormal automaticity, the resting potential is less negative (−60 mV) than in normal His-Purkinje fibers (−90 mV). In pathological conditions, every ventricular myocardial fiber [2] may exhibit this abnormal rapid automaticity. At these low potentials, which correspond to partial depolarization, the rapid sodium channel is inactivated. The ionic mechanism on which this abnormal activity is most dependent may be influenced by a number of factors. In particular, myocardial ischemia, which increases the extracellular potassium concentration, may lead to this type of abnormal automaticity when a certain level of myocardial depolarization is reached.

In addition, the partial depolarization which inactivates the rapid sodium channel can cause a conduction defect which suppresses the physiological inhibition of automatic activity by a more rapid rhythm arising from the sinus node. This is the case in complete atrioventricular block [1].

29.1.3 Triggered activity

Triggered activity is the term used to describe a possible mechanism whereby, a cardiac arrhythmia does not occur spontaneously in resting fibers, but arises only after electrical stimulation [3]. It is immediately apparent that this cellular electrophysiological phenomenon, which is distinct from re-entry, may pose a diagnostic problem in clinical electrophysiology where the same property of triggering and termination is considered to be a criterion of re-entry.

Two types of triggered activity have been described [4, 5] and have been restudied and developed in cellular electrophysiology [6, 7]. One is the result of early after-depolarization occurring on the plateau phase of the action potential, or in phase 3, corresponding to the T wave of the surface ECG [6, 8]. The other is owing to delayed after-depolarization occurring at the end of phase 3 or the beginning of phase 4 of the action potential, corresponding to the end of the T wave, or the remaining part of the diastolic period. The latter has been particularly well studied in atrial tissues [9].

Early after-depolarization has also been observed in myocardial ischemia as a result of hypoxia or increase in the partial pressure of carbon dioxide. It is characterised by an abrupt "hump" in the action potential at the end of phase 2, which may trigger another action potential. This action potential therefore may occur at a low or at a high membrane potential level although the initial potential of the first stimulated beat had a normal resting potential (−75 to −80 mV). Early after-depolarization is, however, considered as being "triggered" because it is only observed if a stimulated potential which initiates the sequence is present. This phenomenon is facilitated by slow pacing while fast pacing can abolish it. After the triggered action potential at a low resting membrane potential, repetitive activity, known as oscillatory after-depolarization becomes possible [6].

Low level early after-depolarization occurs at low membrane potentials suggesting intervention of the calcium window current underlie by L-type Ca^{2+} channel, triggering slowly conducted action potential. High level early after-depolarization occurring at high membrane potentials are triggered by an increase of the window sodium current often giving rise to bursts of fast conducted re-excitations [10, 11]. Following the formation of thrombus in cardiac cavities or coronaries, the serine protease thrombin is formed and can reach the myocardial tissue by the active process of extravasation. It was recently shown that thrombin markedly increases the window sodium current, and thus may induce high level EAD that underlies Torsades de pointes [12].

Sodium channel mutations (E1295K and ΔKPQ) responsible for a familial form of long QT syndrome (LQTS-3) result in notable increase in window sodium current [13]. Activity arising from low level early after-depolarisations is generally short-lived as the fibers return to a normal potential after a few oscillations.

Delayed after-depolarization is observed at the end of repolarization of the stimulated potentials in fibers placed under special electrophysiological conditions in which the presence of steroid or glucoid cardiotonics seem to play an important role (Fig. 29.1). The stimulated action potential is first followed by depolarization, but it then returns to an even more negative value of resting potential than the basal resting membrane potential (hyperpolarization). This is followed by a wave which comprises the delayed after-potential or several oscillatory potentials and which has a less-negative value that may return to the value of the fiber's resting potential if its amplitude is small. If the amplitude is large enough, the peak of the wave created by the delayed after-depolarization will reach the threshold level and an action potential will be initiated. Depending on local conditions, these potentials may fade away, after having initiated a new depolarization and another delayed after-depolarization which is unable to reach the threshold of depolarization. However, if the threshold of depolarization is reached, a second action potential will be triggered and so on. Once triggered, this repetitive activity can continue for a long period of time (several hours). A warming-up phenomenon is often observed with an acceleration of the rate of depolarization. It is the activity related to this delayed after-depolarization which can cause diagnostic difficulties with tachycardia resulting from re-entry.

There are different means by which a delayed after-depolarization may reach threshold level. It may result from the rate of stimulation; that is, if the first stimulus induces an after-depolarization which does not attain the threshold value, there will be no propagation. However, the following stimulation, if sufficiently early in the cycle, will produce an increase in the amplitude of its after-depolarization which may or may not reach the threshold value. The next stimulus will again increase the amplitude of its after-depolarization, until eventually it reaches the threshold value, thereby generating a propagated action potential. That is to say that acceleration of the pacing rate will increase the amplitude of the delayed after-depolarization and the number of the propagated triggered action potentials, and will decrease their coupling interval: the faster the pacing rate, the faster the rate of the triggered rhythm.

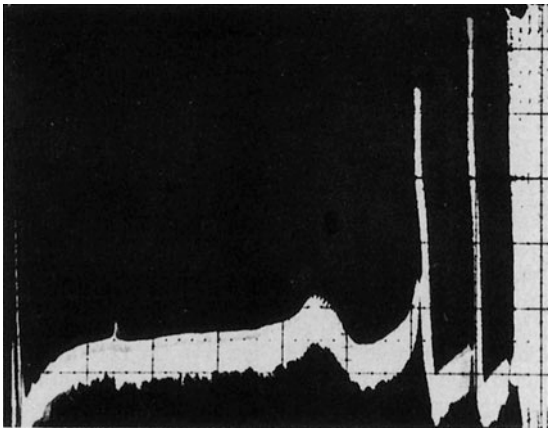

Figure 29.1
Delayed after-depolarization occurring in sheep Purkinje fibers following hypokalemia ($2.7\,\mu mol\,l^{-1}$) and the addition of a toxic amount of ouabain. The first oscillation is subthreshold, the second one reaches threshold and is followed by the beginning of triggered action potentials (Courtesy of Dr F. Fillette).

The same sequence of events may be observed after a premature stimulation during an artificially driven rhythm. The amplitude of the delayed depolarization and its prematurity both increase when the stimulus is delivered earlier in the cycle. This is a notable feature and will be referred to later in the discussion on the mechanism of arrhythmias in clinical electrophysiology. It explains the warming-up phenomenon; its action potential gives rise to a new delayed after-depolarization earlier in the cycle and of greater amplitude, which then plays the same role as an extrastimulus for the following potential.

At the cellular level, delayed-after-depolarizations are favoured by high intracellular calcium load and are due to the activation of calcium-dependent transient inward current (Iti). Various ionic conductances can underlie Iti [14, 15]. It can be a calcium-activated nonselective cationic channel [16], or calcium-dependent chloride current [17] but in most cases it is the Na-Ca exchanger when it removes calcium from the cytosol that generated Iti [18, 19]. The molecular nature of Iti takes into account that both the occurrence and amplitude of delayed-after-depolarization increase in conditions characterized by an enhanced intracellular calcium load such as rapid stimulation rate or beta-adrenergic stimulation. In failing myocardium, the altered excitation-contraction coupling process results in an abnormal intracellular calcium homeostasis that can favour delayed-after-depolarization [20].

29.1.4 Re-entry

The third fundamental mechanism of arrhythmias is the re-entry phenomenon [21]. Well known in clinical studies of the Wolff-Parkinson-White (WPW) syndrome, it has been extended to the field of ventricular tachycardia, as the myocardium behaves in a similar way during programmed pacing [22]. There are three essential conditions for the initiation of re-entry, as follows:

- The presence of two separate conduction pathways with different functional electrophysiological properties.
- Unidirectional block (usually induced by the preceding beat and located at the junction between healthy and pathological myocardium).
- A conduction delay hindering the activation front from encountering excitable myocardium beyond the site of the block.

Reentry phenomena have different clinical expressions, depending on whether they have microreentry (between Purkinje fibers and healthy myocardium), or macroreentry circuits (involving the bundle branches in case of dilated cardiomyopathy and/or a larger amount of myocardium) [23–25].

At that time, it was difficult to accept that conduction could be sufficiently delayed for the propagation time of the activation front to exceed the duration of the refractory period of the tissues located distal to the block. This was because calculations showed that it required delays about 100 times the normal value for this phenomenon to be possible [26]. In fact, this was only demonstrated partially by the recording of delayed potentials occurring in the diastolic period 250 ms after the onset of QRS complexes in experimental acute ischemic tissue [27]. These delayed potentials were observed in the animal and later in humans in diverse pathological conditions, and their behavior during premature stimulation showed unusual phenomena commonly observed in the nodo-Hisian conduction system [28, 29]. These time-dependent properties support the explanation of the mechanism of ventricular tachycardia initiation; that is, the prematurity of the extrastimulus increases the conduction time in abnormally slow conducting fibers, so allowing the most delayed potentials to transmit the activation to adjacent myocardium in the same way that stimulation of fibers in a zone of markedly delayed conduction enables reactivation of the adjacent myocardium [30–33]. Experimental studies have demonstrated the phenomenon of reentry by mapping the first cycles of an ischemic ventricular tachycardia [34, 35].

These mechanisms are important in clinical arrhythmias because ventricular tachycardia can be initiated and terminated by programmed pacing, or by bursts of rapid pacing. However, the demonstration of triggered activity unrelated to reentry has raised the problem of distinguishing between these two mechanisms.

It has also been demonstrated that programmed pacing is able to initiate ventricular arrhythmias in only a small number of cases in the acute phase of myocardial infarction, a situation in which it was thought that both increased automaticity and reentry could play a role.

On the other hand, intraventricular reentry is probably the only operative mechanism in sustained chronic ventricular tachycardia in the chronic phase after myocardial infarction. In clinical practice, the phenomena of extrasystoles, and even ventricular tachycardia can be triggered by pacing methods in severe digitalis overdose. However, pacing methods are often used to prevent bradycardias or atrioventricular blocks induced by digitalis [36].

Finally, focal reexcitation phenomena may be observed when the repolarization of adjacent fibers is asynchronous, a condition favored by beta-adrenergic stimulation or acute ischemia [35].

A delayed activation of normal myocardium after pacing in a zone where late potentials were recorded was reported in 1978 by Fontaine et al [31]. This again reinforced the concept of reentrant phenomenon in heart muscle and definitely excluded the mechanism of triggered activity. In patients at the chronic phase of myocardial infarction, De Bakker demonstrated the presence of a "zig-zag" slow conduction pattern, in which wave fronts could travel perpendicular to the fiber direction ensheathed by collagenous septa [37].

29.1.5 Criteria for Discriminating Between Cellular Electrophysiological and Clinical Mechanisms of Tachycardia

The main difficulty concerning the respective mechanisms of reentry and phenomena of triggered activity is the paucity of discriminating methods which can be used both in cellular and clinical electrophysiology. It was noted above that the induction and termination of tachycardia by programmed stimulation may be observed in both situations, but there is one way of differentiating the two mechanisms. In tachycardias triggered by delayed after-depolarization, the coupling interval of the first propagated potential decreases with increasing prematurity of the initiating extrasystole. Indeed, the moment at which delayed after-depolarization reaches the threshold becomes more premature as the coupling interval of the extrastimulus decreases. Conversely, in reentry, the coupling interval of the first propagated potential which initiates the tachycardia increases as the prematurity of the extrastimulus increases. This is owing to the conduction-time increase in the zone of delayed conduction.

Using these criteria, a retrospective study of 425 patients investigated in the authors' clinical electrophysiological laboratory in which tachycardia could be initiated and terminated by programmed pacing, showed that in 33 patients tachycardia originated in the atrium, whilst in 79 patients the point of origin was ventricular. Seven patients with atrial

tachycardia and only one with ventricular tachycardia had positive evidence in favor of a mechanism of triggered activation. In addition, in five of the patients with atrial tachycardia and in the patient with ventricular tachycardia, the administration of intravenous verapamil terminated the tachycardia and prevented its reinitiation.

These results suggest that the role played by a triggered activity in the clinical situation is quite modest especially as far as the ventricular arrhythmias are concerned [38].

29.2 Ventricular Extrasystoles

Ventricular extrasystoles (VES) result from premature depolarization of the myocardium distal to the atrioventricular junction; that is, below the bifurcation of the His bundle. They may, therefore, arise from either of the two ventricles or from the interventricular septum. Recently, triggers of VES and of ventricular fibrillation (VF) were found in various locations within the Purkinje network in patients presenting with recurrent VF without underlying cardiac disease and were successfully treated by radiofrequency catheter ablation [39].

29.2.1 Clinical features

From the clinical standpoint it is useful to distinguish between asymptomatic VES detected during clinical examination and confirmed by ECG, and symptomatic VES which are not necessarily the most dangerous, but which can have important effects on the quality of life.

Ventricular extrasystoles may be totally asymptomatic, but often they cause symptoms such as palpitations, a sensation of a missed beat, of cardiac arrest or of strong beats. Less commonly, when VES are frequent or in salvos, the patient may experience dizziness, angina, hypotension and finally tachyarrhythmia cardiomyopathy.

It is important to inquire about the patient's general health and lifestyle, in order to assess as accurately as possible the functional disturbance and the frequency of symptoms, as well as to detect any predisposing factors such as exercise, anxiety, stimulants (tobacco, alcohol, coffee, and so on), sleep disturbances, hypoxia, physical stress, drug administration, and so forth.

On examination, VES cause an irregular heart beat and changes in the intensity of the heart sounds. A systolic murmur may be detected. Organic aortic systolic murmurs decrease in intensity during the extra systolic beat but are accentuated during the following systole (contraction produced by the strong normal beat following the compensatory pause).

The hemodynamic effects of VES include the following [40]:

- Reduction in left ventricular systolic pressures (prematurity dependent)
- Increase in the length of diastole (postextrasystolic compensatory pause) resulting in an increase of stroke volume of the following systole (Fig. 29.2)
- Abnormal valve motion (premature closure, mitral valve prolapse, decreased valve opening, and so on) clearly demonstrated by echocardiography

29.2.1.1 Relationship to the P wave

Diagnosis and study of VES depend on the analysis of the ECG. Ventricular extrasystoles are premature, wide QRS complexes (usually > 120 ms) followed by a T wave with an axis opposite to that of the QRS. Characteristically, VES are not preceded by P waves. As the P wave is not easily detected in some leads, simultaneous multichannel recordings are useful in distinguishing VES from atrial and junctional extrasystoles with aberrant conduction. As a rule, VES are completely dissociated from the preceding atrial activity but they may be followed by a retrograde P wave (Fig. 29.3).

A bipolar sternal lead recording with the "right arm" electrode on the manubrium and "left arm" electrode on the xiphoid process may help to show the P waves. Another more sensitive method of recording the atrial activity is to use an esophageal or an endocardial lead (Fig. 29.2).

Figure 29.2

Left ventricular extrasystole recorded during an endocardial study: CS, coronary sinus showing the atrial and the ventricular component of the ECG; RV 1–2, RV 3–4, Quadripolar catheter positioned in the infundibular area; LV, left ventricle showing that the activation commences first in this ventricle; RVa, apex of the right ventricle; AP, arterial pressure recorded on the radial artery. The second arrow indicates the drop of end-diastolic blood pressure.

29.2.1.2 Morphology

It is often difficult to distinguish VES from supraventricular or junctional extrasystoles with ventricular aberration resulting from a decrease in conduction in the intraventricular conduction system. Conversely, VES arising just above the division of the His bundle will give rise to narrow QRS complexes, suggesting supraventricular activity [41]. In addition, an extrasystole occurring at the appropriate time may lead to a narrow QRS complex in the case of fusion with a normal ventricular activation, but showing bundle branch block ipsilateral to the site of origin of the extrasystole.

The morphology of VESs may generally indicate their site of origin. Appearances of right bundle branch block are observed in left ventricular extrasystoles. The arrhythmia arises within the right ventricle or septum when left bundle branch block appearances are recorded, the site being apical when the QRS is negative in leads I, II and III, and basal when positive in these leads [42]. Right-sided VES always give rise to appearances of left-sided delay whilst left-sided VES (base of interventricular septum) could show appearances of right- or left-sided delay [43].

The morphology of VES may be unchanged from one extrasystole to the next (Fig. 29.3), or they may vary (Fig. 29.4), in an unpredictable manner (polymorphic extrasystoles). Polymorphism must be distinguished from possible fusion between very late VES and normal depolarization (QRS complex preceded by a normal P wave with shortened PR interval and an intermediate QRS morphology).

29.2.1.3 Chronology

Ventricular extrasystoles may be divided into two types according to their relationship to the preceding QRS complex; namely, those with a short coupling interval occurring near to or on the peak of the T wave (R-on-T phenomenon) and late VES with long coupling intervals (Fig. 29.5). These intervals may be fixed (varying less than 80 ms) suggesting parasystole (Fig. 29.6) [41, 44]; that is, the interectopic interval is approximately a multiple (>1) of a fixed interval.

The following types of VES may be distinguished from the analysis of their relationship to the sinus beats.

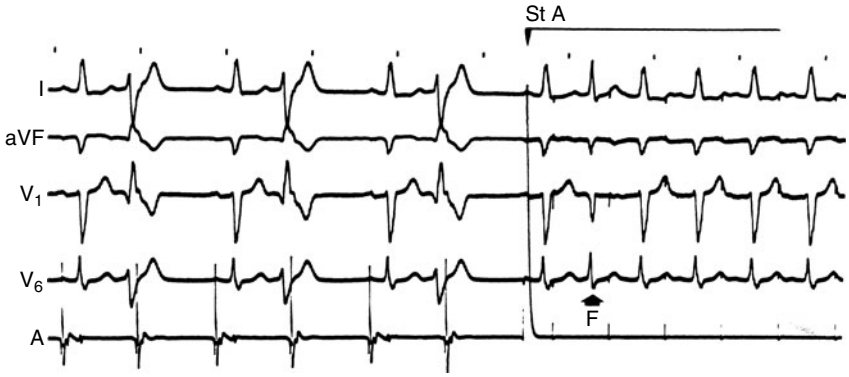

Figure 29.3

Bigeminy is visible at the beginning of the tracing. Tracing A represents the endocardial atrial electrogram. In this case, atrial activity is not modified by the extrasystoles which are therefore followed by a full compensatory pause. On the right, there is atrial pacing (St A) at a period longer than the coupling interval of extrasystoles, resulting in complete disappearance of extrasystoles. A fusion beat F is observed at the beginning of atrial pacing.

Figure 29.4

Polymorphic ventricular extrasystoles recorded during open chest surgery. Note the existence of multiple fragmented potentials on the epicardial leads E_1-E_3 preceding runs of extrasystoles which end with highly fragmented complexes (stars). RV is the potential recorded from the epicardium of the right ventricle. Note the major asynchrony between the two ventricles. RA is the atrial endocardial lead. Each atrial activity is preceded by the stimulation artifact.

- VES with a compensatory pause (Fig. 29.3) is the most common type. The interval between the sinus beat preceding the extrasystole, and the VES itself added to that following the VES, corresponds to two normal periods (retrograde conduction to the atrium and normal anterograde depolarization are blocked).
- In VES with retrograde conduction which recycles the sinus node, the pause following the VES is equal to the normal sinus period (Fig. 29.7 (b)).
- Interpolated VES do not affect the normal period. These VES are not conducted to the atrium and the normal sinus depolarization which follows is not blocked in refractory, junctional tissues (Fig. 29.7 (a)).

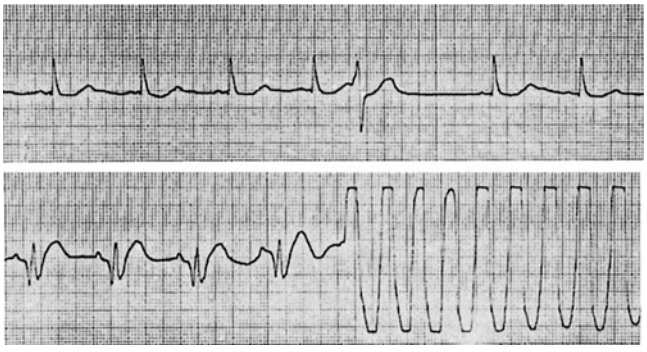

Figure 29.5
The top panel illustrates an extrasystole with a relatively short coupling interval. The bottom panel shows an extrasystole with a relatively long coupling interval initiating a run of sustained ventricular tachycardia.

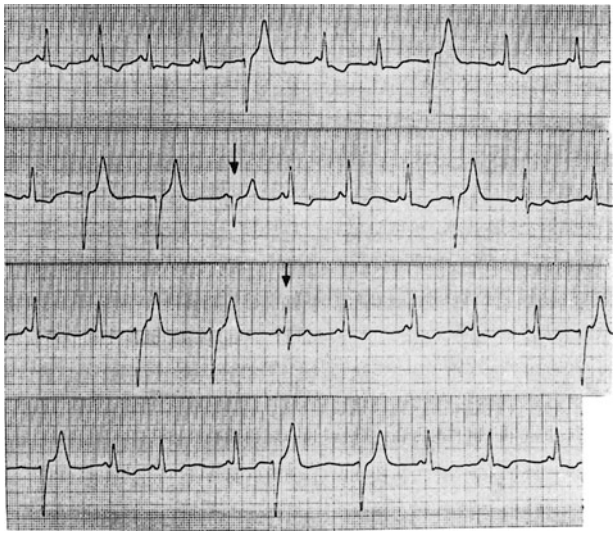

Figure 29.6
Parasystolic focus interfering with sinus rhythm. The interval measurements demonstrate that this focus is not completely protected from the supraventricular beats. The strips are continuous running from top to bottom. The arrows indicate fusion beats.

Other ECG appearances may also be observed [41]:

- The VES may be followed by AV junctional escape (Fig. 29.7 (c)).
- The VES may have a visible retrograde conduction. In this case, a P′ wave, usually negative in lead II, is situated in the ST segment or T wave.
- The VES may have a ventricular echo. Here, the abnormal activation is conducted retrogradely to the atrium and then returns to the ventricle without the intervention of sinus node activity. Ventricular extrasystoles are followed by either a normal or widened (aberration) ventricular complex with a fixed coupling interval which may be preceded by a P′ wave and is often followed by a compensatory pause.

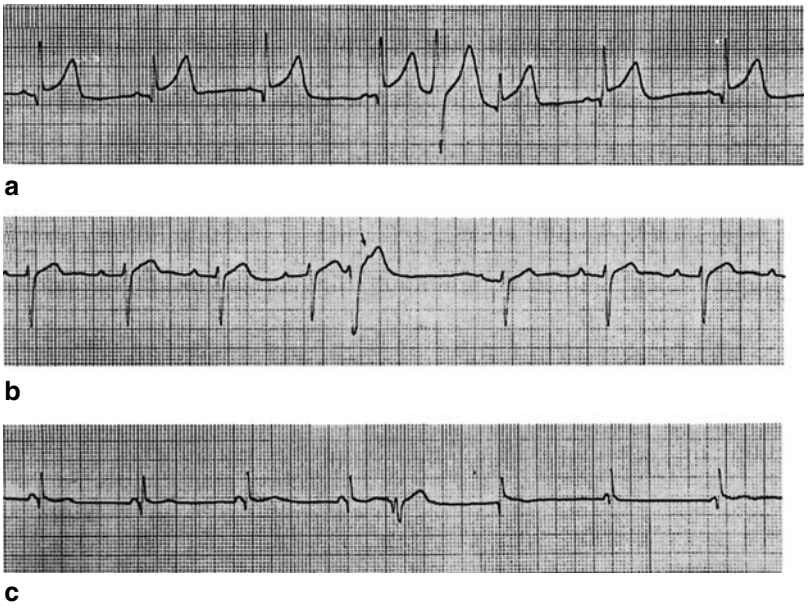

Figure 29.7

Part (a) illustrates an interpolated extrasystole; part (b) shows an extrasystole with an atrial retrograde conduction (arrow) and part (c) shows an extrasystole fol1owed by a junctional escape.

Finally, when VES are repeated with a fixed coupling interval, it is possible to record the following:

- Ventricular bigeminy when one ventricular extrasystole follows each normal complex (Fig. 29.3).
- Ventricular trigeminy when one ventricular extrasystole occurs following every two normal beats (in fact, trigeminy literally corresponds to one normal complex following every two VES).
- A salvo defined as three or more successive VES (Fig. 29.2).
- When more than three successive VES are recorded, it is sometimes called ventricular tachycardia (VT), or a burst of VT (Fig. 29.8).

29.2.2 Endocavitary studies

Electrophysiological investigations (Chap. 24) are rarely indicated for the study of VES in themselves, but the latter could be undertaken during electrophysiological studies indicated for other reasons. Ventricular extrasystoles always precede the H potential on His-bundle recordings. In case of ventriculoatrial conduction, they are followed by a retrograde atrial electrogram.

However, it could be important to study the behavior of VES during atrial pacing. In some, cases, the VES are suppressed beyond a critical pacing rate. This rate is not stable with time, but an appropriate level could be found in certain patients and this could be used to prevent VES in the long-term, using an atrial pacemaker system (Fig. 29.3).

Pace mapping [45] is a technique of endocavitary pacing, which may be carried out in sinus rhythm (and sometimes during tachycardia). Its object is to duplicate the configuration of VT and so define its site of origin. However, this technique also has its limitations [46].

29.2.3 Management

Management is the major problem of VES. The prognosis is closely related to the presence of underlying cardiac disease, especially ischemic cardiomyopathy. Although the vast majority of VES are benign, even in cases with underlying cardiac

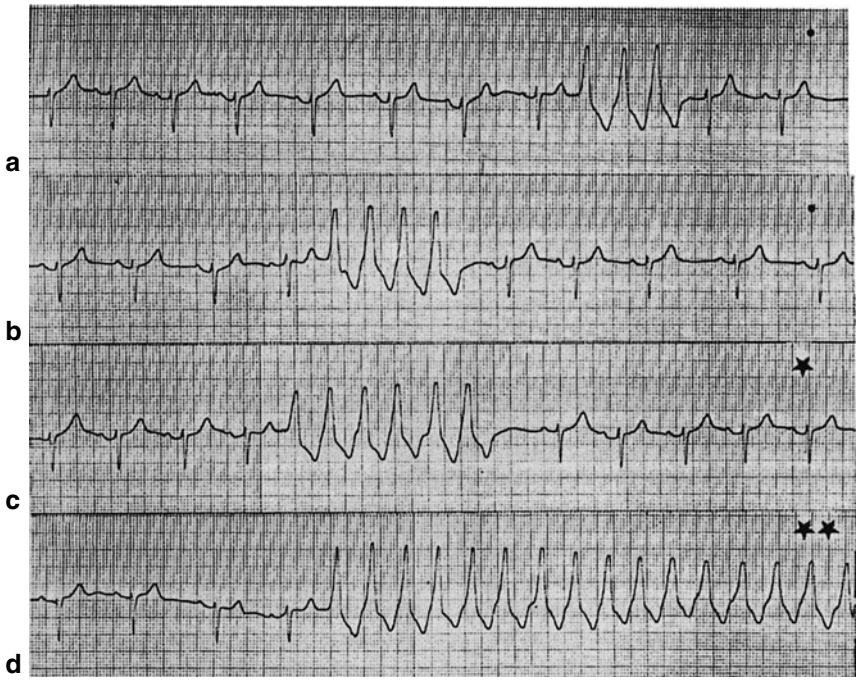

Figure 29.8

Difficulties in the definition of ventricular tachycardia are exemplified in these ECGs. There are salvos of three (a) or four (b) ectopic ventricular beats; a burst of extrasystoles, alternatively regarded as a short run of ventricular tachycardia is seen in (c) and the beginning of a sustained episode of ventricular tachycardia in (d).

disease, others are markers of potentially dangerous arrhythmias and indicate a high risk of sudden death. Investigation and treatment must take these two facts into consideration.

Some investigations provide information about the arrhythmia itself, whilst other, mainly noninvasive, techniques (echocardiography, angiography, exercise-stress testing, Holter monitoring and scintigraphy) may provide clues to the underlying cause of the arrhythmia. As a general rule, only cases of potentially lethal arrhythmias, or patients with history of cardiac arrest or "resuscitated sudden deaths" are referred for electrophysiological investigation and coronary angiography for evaluation of the risks of ventricular tachycardia or ventricular fibrillation (VF).

29.2.4 VES in normal subjects with apparently healthy hearts

Ventricular extrasystoles in "normal" persons are often called "idiopathic." The widespread use of Holter monitoring (Chap. 33) has shown that this arrhythmia is very common and may be observed in nearly all cases when the period of observation is long enough (73% in 48 h monitoring) [47–51]. The frequency of VES increases with age and other factors which must be considered when assessing the prognosis.

A number of workers, including Rosenbaum [42] have described the following characteristic features of "benign" VES: vertical axis, left bundle branch block pattern, large R waves in leads II and III, fixed, long coupling intervals, secondary ST-T wave changes (sloping ST depression and T wave of opposite polarity to the QRS), isolated and infrequent VES.

Electrophysiological studies and epicardial mapping have shown that these VES arise in the upper part of the right side of the interventricular septum (Fig. 29.9), also called right ventricular outflow tract VES. They usually disappear on exercise and are only recorded on Holter monitoring when the spontaneous rhythm slows [47, 52].

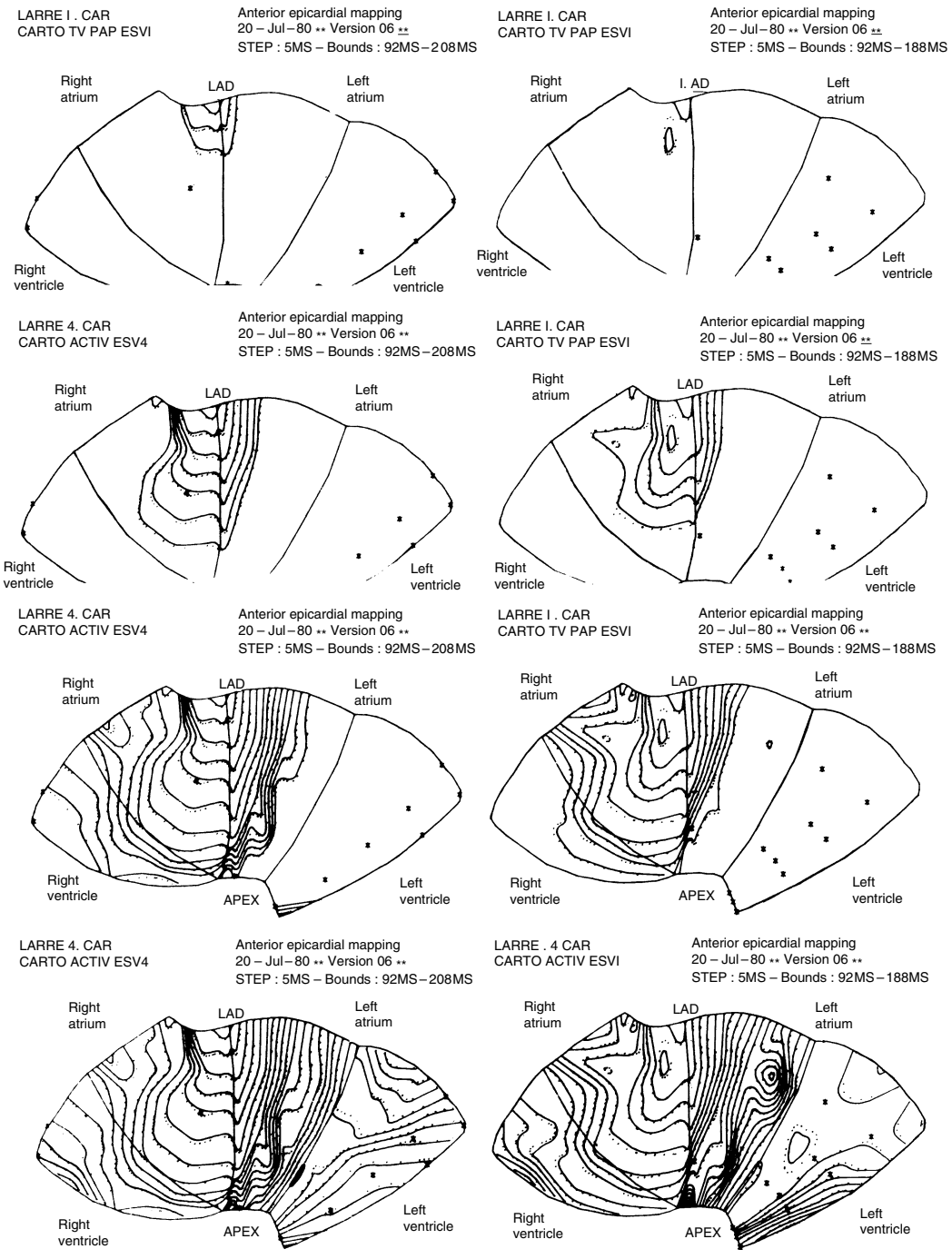

Figure 29.9

Spread of activation is shown on epicardial maps during normal sinus rhythm on the right, and on the left during an extrasystole arising from the upper part of the septum. The latter could lead to paroxysmal episodes of extrasystoles or runs of ventricular tachycardia, which could in some very rare cases be treated by a surgical approach if antiarrhythmic therapy had failed. In sinus rhythm, epicardial activation is first seen in the free wall of the right ventricle in the anteroparaseptal area. On the left, the earliest epicardial activation is noted at the origin of the left anterior descending (LAD) coronary artery. In all maps, the time interval between isochrones is 5 ms.

This concept of "benign" VES must be interpreted with caution but it remains useful when the arrhythmia is totally asymptomatic in patients without apparent cardiac disease. Treatment is unnecessary [53] in most cases but therapy may be required for psychological reasons in some patients. These VES are particularly common in women and may be poorly tolerated. To complicate matters, most classic antiarrhythmic drugs are ineffective. This explains the use of drugs aimed more at relieving symptoms than at treating the arrhythmia; formerly, patients were prescribed sedatives, or usually, as second-line therapy, relatively weak antiarrhythmic agents such as beta blockers or verapamil. Nowadays, the use of radiofrequency ablation [54] or powerful antiarrhythmic drugs (class I, like flecainide) which are easy to use in healthy hearts, has completely transformed the lives of these patients.

Identical VES have been reported to come more rarely from the left ventricular outflow tract, the aortic sinus of Valsalva or the trunk of the pulmonary artery [55]. The VES morphology in precordial leads, especially the presence of a transition complex, is a good first approximation regarding the location of the successful ablation site [56].

Ventricular extrasystoles observed during the period of awakening, or during or immediately after exercise in apparently normal patients, are also very common. The autonomic nervous system is thought to play a major role in their initiation [57–59]. The frequency of this type of VES varies with age [57]. They are observed on Holter recording when the patient awakes, and tend to become more frequent on exercise but disappear during sleep. This arrhythmia does not seem to be a marker for a latent coronary artery disease and is not associated with an increased risk of sudden death [52, 57, 59, 60].

Treatment is based on the underlying physiopathogenic mechanism of the arrhythmia and so beta blockers are considered appropriate first-line drugs. As most patients require long-term therapy, beta blocker with a 24 h duration of action, some of which also have weak class I antiarrhythmic effects, are to be preferred.

Even in patients with "normal" hearts, short coupling intervals [61], changing morphologies, complex interaction (bigeminy, ventricular tachycardia) and predisposing factors (sleep, exercise, postexercise) may be observed without higher risk of potentially lethal arrhythmia or sudden death [62], especially when the VES are infrequent and the patients are young [47–49, 52, 63].

Nevertheless, frequent (over 5/h or 10/1000 sinus beats) and/or polymorphic VES, aggravated by exercise in patients over 40 years old are suggestive of coronary artery disease, even in the absence of cardiovascular risk factors. They appear to be associated with a higher risk of sudden death and coronary events [49, 50, 58, 63–65] although this premise is not universally accepted [60, 66].

The presence of cardiovascular risk factors increases the predictive value of these VES especially that of complex VES [58–60, 63–67].

29.2.5 VES and coronary artery disease

It is useful to distinguish VES occurring in the acute phase of myocardial infarction (the first 10 days) from those observed in chronic coronary insufficiency (with or without previous infarction).

29.2.5.1 Acute phase of myocardial infarction (Lown's classification)

Electrocardiogram monitoring in the coronary care unit has shown that VES are very common and are nearly always present [68–70]. Different classifications have been proposed for assessing the prognosis but the best known is that of Lown [53, 71], as shown in Table 29.1.

This classification distinguishes dangerous arrhythmias (grade 2 and over) from apparently benign arrhythmias. Although some points are debatable, especially the significance of grade 5, this classification is still used [68, 72, 73].

High-grade VES (that is, frequent and repetitive VES) do not seem to be related to the site of infarction but are related to its size [74, 75]. These VES (especially grade 5) seem to increase the risk of VT [68], but effective treatment of them has not been shown to prevent VT or VF as these particular arrhythmias seem to have different triggering factors.

No significant correlation has been found between ventricular arrhythmias (VES, VT and VF) observed in the acute phase and those observed after hospital discharge (after 3 weeks) [76], probably because they have different mechanisms;

Table 29.1
Lown's classification of ventricular extra-systoles (VES) [53, 71]

Grade	Type of VES
0	no VES
1a	isolated, rare VES (>1 mn-1 or >30 h)
1b	infrequent VES (>1 mn-1 but <30 h)
2	frequent monomorphic VES (>30 h)
3	frequent polymorphic VES
4a	Couplets
4b	triplets or salvos > 3
5	R-on-T phenomenon

namely, reentry in the chronic phase and increased automaticity in the acute phase [77]. However, the more serious repetitive VES observed in the acute phase are also probably as a result of reentry [74].

The treatment in the acute phase is now well established. When the arrhythmia exceeds grade 1 (l b for some authors) treatment with intravenous (IV) lidocaine is recommended [71, 78]. This drug is effective and has only a slightly depressive effect on contractility and conduction. In addition, its time of action is short. Therefore, this drug is easier to handle in the case of negative inotropic effects. On the other hand, IV administration with an electric pump is mandatory in order to have a constant infusion rate.

In the rare cases of complete or relative inefficacy or major side effects (usually owing to overdosage), drugs with the least-negative inotropic effects are to be preferred. In the authors' experience IV amiodarone is very useful as it has both an antianginal and powerful antiarrhythmic action without depression of the activation process or myocardial contractility. It may be administered intravenously by continuous infusion (2 g in 24 h). Bolus injection is dangerous because of the hypotensive effect of the excipient. Oral administration with high loading doses (1.2 g per day for the first 4 days) is also well tolerated and reduces the delay of onset of action [79].

Other antiarrhythmic agents, especially the class I drugs were used in the 80s but their negative inotropic effects must not be overlooked. They are best administered by slow IV infusion, preferably with an electric syringe, again to ensure a constant infusion rate.

29.2.5.2 The chronic phase

The problem of management of VES is more difficult at the chronic phase of myocardial infarction.

There is a need to determine the following:

- The best means of detecting the VES and assessing their severity;
- The most appropriate moment after infarction at which to perform the study;
- The prognosis of the arrhythmia detected and the risks of sudden death or progression of the coronary artery disease;
- The best treatment and effective prophylaxis against more serious arrhythmias.

Some of these questions have now been answered. Most workers agree that all patients at risk should undergo at least one 24 h Holter ECG before hospital discharge, sometimes associated with an exercise test. If repeated or performed after the third week postinfarction, the test does not seem to provide any additional information [80] despite the fact that the frequency and complexity of VES may increase up to the sixth month [81].

It is more difficult to assess the severity and prognosis. Lown's classification remains useful: grade 2 or more complex arrhythmias must be carefully managed while complex VES are associated with a higher risk of sudden death [53] [82–85] or cardiac death [63, 86, 87].

Holter monitoring seems to be more useful than exercise-stress testing in the evaluation of these arrhythmias but the two methods are complementary [80, 88]. Exercise testing may show an increase in the number of VES as well as changes in the ST segment.

In order to assess the prognosis, the arrhythmias must be interpreted in a wider context, taking into account a number of other factors. First, factors related to the cardiac rhythm must be considered. These are as follows.

- Low ejection fraction and raised left ventricular end diastolic pressure [53, 89–94];
- The frequency of VES appears to be proportional to the mean sinus rate [47, 95];
- Aggravation during exercise has been known to be a poor prognostic factor for a long time [47] but is not a constant finding in uncomplicated myocardial infarction without global left ventricular dysfunction [80];
- Second, cardiac factors should be considered: the severity of coronary artery disease is difficult to dissociate from ventricular arrhythmias. The following factors play a role;
- Previous myocardial infarction;
- ST changes on exercise-stress testing have been shown to be more sensitive than Holter monitoring [80, 95, 96];
- Segmental abnormalities of wall motion [84, 92, 93, 97];
- The number of diseased vessels [92], although this factor is not universally accepted [84, 93].

On the other hand, the site of infarction does not seem to be important [51] although some workers do not agree [53]. Finally, the clinical context and the patient's mental condition have to be taken into consideration. The roles of the autonomic nervous system and of certain hormonal and humoral factors, though not fully understood, are certainly not completely divorced from the mechanism of some arrhythmias [53].

The presence of complex and frequent VES after myocardial infarction seems to be associated with higher mortality, especially as a result of sudden arrhythmic death, and also appears to be independent of other factors [83, 86, 87, 90, 93, 94, 98]. The risk is maximal during the first six months and then gradually decreases [81, 99].

A cooperative study on a group of 804 cases [100] studied by Holter monitoring was able to indicate, after univariate analysis, that it was possible to classify these patients into three groups at risk of sudden death over a two-year period. Two electrocardiographic markers are considered: number of VES per hour and the presence or absence of runs (i.e., three or more VES in a row). In the first grade, defined as patients having less than three VES per hour and no runs, the two-year mortality rate is 8%; in the second, which consisted of patients having more than three VES per hour, or having runs, the mortality rate increases to 16%; in the third group, composed of patients having more than three VES per hour and runs, the mortality rate increases to 37%.

Other investigators have proposed electrophysiological studies shortly after the acute phase of myocardial infarction for these high-risk patients. The recording of repetitive ventricular responses to a single extrastimulus may help identify the subgroup with a high risk of sudden arrhythmic death [91].

About 90% of complex VES can now be effectively controlled by antiarrhythmic drugs, the number of which is continually increasing [94]. However, the role of VES in the induction of more severe arrhythmias is still not clear, and the suppression of VES has not been shown to protect patients from sudden death [53, 70, 94, 97]. Some drugs suppress VES without reducing the risk of sudden arrhythmic death. Other drugs seem to reduce the risk with only a partial but perhaps adequate, effect on the VES [41, 51, 53, 82]. Beta blockers belong to this latter group.

It is, nevertheless, rational to treat patients with complex, frequent, repetitive VES at rest or at exercise, irrespective of whether they are associated with other bad prognostic factors such as previous infarction and poor ventricular function [51, 86, 89, 90]. The benefits of treatment are less obvious in patients who have suffered small, uncomplicated infarcts and who have rare, monomorphic VES [47, 53, 89].

Patients in whom an effective antiarrhythmic treatment is most useful are included in the subgroup with salvos or short coupled VES [101]. In a study of 140 patients including two thirds with coronary artery disease, the suppression of salvos and most of the isolated extrasystoles led to a marked decrease in the annual rate of sudden arrhythmic death from 40 to 2.8%. This result was even more impressive in the subgroup of patients with a reduced ejection fraction in which

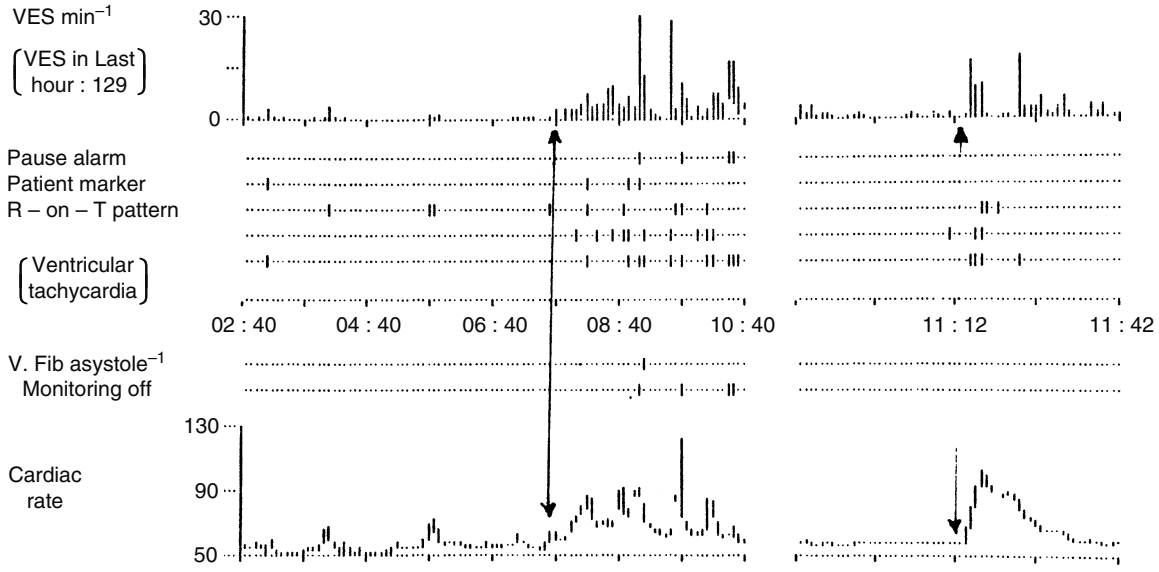

Figure 29.10

Computerized bedside monitoring report showing premature ventricular contraction (VES min^{-1}), in a patient with ventricular extrasystoles after myocardial infarction. The vertical arrows indicate that during the awakening period (7.40 a.m.), the basic cardiac rate (lower curve) increases, to be followed by a concomitant increase in the frequency of premature ventricular contractions. (V.Fib, ventricular fibrillation.)

the control of ventricular arrhythmias led to a decrease in the annual risk of sudden arrhythmic death from 80 to less than 5%.

Several methods of evaluating the efficacy of treatment have been proposed, all based to a certain degree on repeated bedside or Holter monitoring and/or exercise-stress testing (Fig. 29.10). These investigations are used to determine the most effective drug with least side effects. Beta blockers in combination with amiodarone have the advantage of associating an antianginal and an antiarrhythmic effect (Fig. 29.11) [79].

29.2.6 Chronic coronary insufficiency without infarction

Spontaneous or exercise-induced VES are generally recognized as having an important predictive value in patients with coronary artery disease. VES induced or aggravated by exercise are usually associated with more severe, multivessel disease [78, 96, 102] often associated with abnormalities of regional-wall function [59]. The risk of sudden death or of further ischemic events is higher. A reduction in the frequency of VES on exercise also seems to have the same significance [58]. It is, therefore, logical to treat these arrhythmias especially when they are complex and associated with ST changes on exercise-stress testing. Infrequent monomorphic VES, on the other hand, require only regular follow-up.

29.2.7 Other cardiac diseases

Most cardiac diseases are associated with a higher risk of ventricular arrhythmias and sudden death. The relationship between these two factors has often been studied and the efficacy of antiarrhythmic therapy evaluated. Three main types of cardiac disease may be distinguished: cardiomyopathies, mitral valve prolapse, and aortic valve disease.

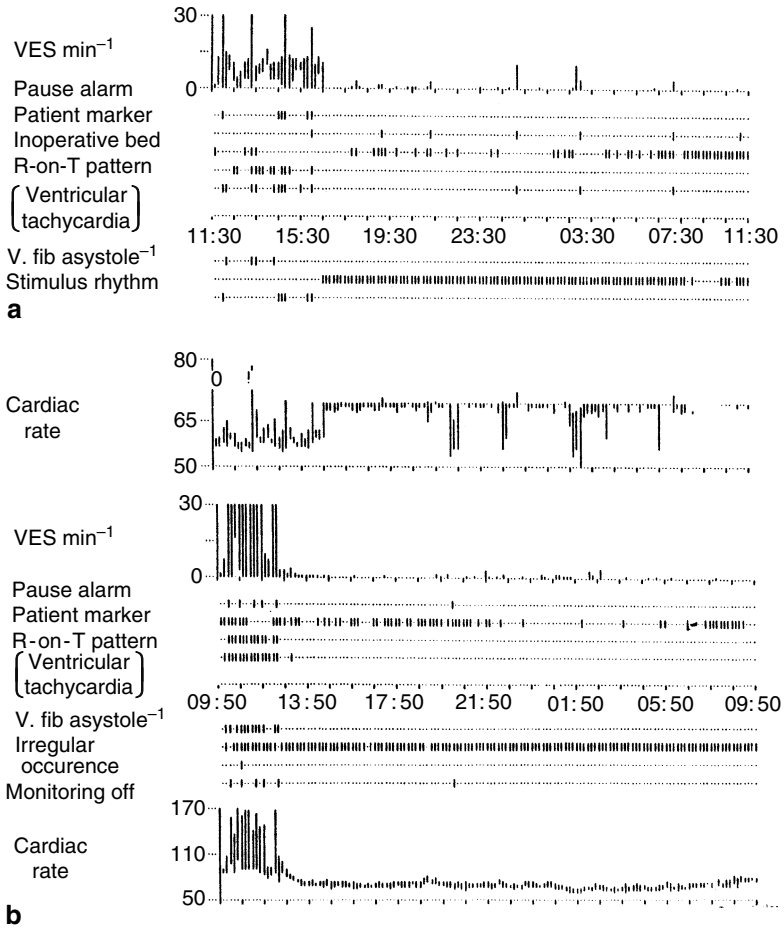

Figure 29.11

A study of the effect of two opposite antiarrhythmic methods in the treatment of premature ventricular contraction (VES min^{-1}) in two patients in the chronic phase of myocardial infarction. In (a), ventricular extrasystoles are suppressed by increasing the patients cardiac rate from 55 to 70 min^{-1} by a temporary pacemaker. In (b), sinus tachycardia related extrasystoles (on the left) are suppressed after administration of acebutolol which produces a decrease in the cardiac rate from 120 to 65 min^{-1}, with complete disappearance of the premature ventricular contractions.

29.2.7.1 VES and cardiomyopathies

The study of ventricular arrhythmias in cardiomyopathy is difficult because of the poor definition of the frontiers of this condition. Cardiomyopathy may, however, be broadly divided into three subgroups: hypertrophic cardiomyopathy (HCM), dilated cardiomyopathy (DCM), and restrictive cardiomyopathy (RCM).

Hypertrophic cardiomyopathy has been studied in more depth than the other forms. The incidence and prognosis of arrhythmias seem to be the same, whether the hypertrophy is diffuse or localized to the interventricular septum (asymmetric septal hypertrophy), with or without obstruction (HOCM). Ventricular extrasystoles are common, especially on Holter monitoring, and the incidence varies from 80 to 90% [103–105]. The arrhythmia is severe (frequent and/or polymorphic, grade 2 or more in Lown's classification) in about half the patients [104–106]. There is little correlation between symptoms and the severity of the arrhythmia. Ventricular arrhythmias are commonly asymptomatic and often occur at night [103–105]. Holter monitoring is the investigation of choice for detecting these arrhythmias, the presence of which,

in the experience of most workers increases the risk of sudden death [103, 104, 107, 108]. A family history of sudden death, especially in young patients, and asymptomatic VT on Holter monitoring are two factors which help identify a subgroup of patients at high risk [103, 106, 109] requiring antiarrhythmic therapy or a prophylactic implantation of an ICD [110]. The classical treatment of HCM is beta-blocker therapy but it is not 100% effective in preventing sudden death [106, 111]. Of note, verapamil is the gold standard treatment of atrial fibrillation in hypertrophic cardiomyopathy [112].

Ventricular extrasystoles are also more frequent and complex in DCM and RCM than in so-called "normal" hearts. They become more severe as the disease progresses in association with the increased risk of sudden death. However, the presence of ventricular arrhythmias does not appear to be an independent prognostic criterion [113–115], and its treatment remains subject to caution. Numerous mutations have been reported, encoding for sarcomeric protein genes, some conveying either favorable or adverse prognosis [116].

29.2.7.2 Mitral valve prolapse

Mitral valve prolapse is the most common form of valvular disease (5 to 15% of the general population) and is easily diagnosed by echocardiography. Ventricular arrhythmias are commonly observed in association (60 to 70% of cases) and they may be complex. In the majority of subjects this is an obviously benign condition, but a small number are at high risk from of severe arrhythmias. Holter monitoring is a more sensitive means of identifying these patients than the standard ECG [117, 118]. There is no correlation between the severity of the arrhythmia and the clinical symptoms or the valvular lesions [117–119]. High-risk patients may show ST-T wave changes in the posterior and/or lateral leads [119, 120] and frequent VES (over 400 per 24 h) [117]. The clinical context seems to play an important role.

The arrhythmias often seem to be influenced by the sympathetic nervous system, with a reduction of the number of VES during the night and an increase on exercise [119]. Considering the high incidence of mitral valve prolapse, it is probable that a number of cases of sudden death in young asymptomatic patients are the result of high-grade ventricular arrhythmias, especially VF [121], but this hypothesis has never been clearly demonstrated [122] and no consistent predictor of sudden cardiac death (SCD) has been found. However, the presence of a myocardial dysfunction or a severe mitral regurgitation is correlated with a poor outcome.

Antiarrhythmic treatment is logical in high-risk patients. Beta-blockers are indicated in obvious adrenergic-induced arrhythmias.

29.2.7.3 Aortic valve disease

The frequency and complexity of VES in aortic stenosis or regurgitation without associated coronary artery disease are comparable with those in HCM. Ventricular extrasystoles are usually asymptomatic [123], and unrelated to the transvalvular pressure gradient in aortic stenosis, or to the severity of the leak in aortic regurgitation [124]. Arrhythmias seem to be more common in dilated ventricles [125] when the ejection fraction is low and the peak systolic stress increases [73, 126]. The frequency of these VES seems to paradoxically increase after valve replacement. This behavior is not related to any preoperative feature of the disease.

Myocardial dysfunction is thought to be an important causal factor [73], but the treatment of these arrhythmias remains controversial. Some authors believe antiarrhythmic therapy to be mandatory [126] while others question its efficacy in this type of pathology [73].

In conclusion, the management of VES is clearly dependent on the type and severity of the underlying cardiac disease. An accurate assessment of the risk of "degeneration" of the arrhythmia is essential in each condition and each patient. This remains difficult and further study of the mechanisms involved in the initiation of life-threatening arrhythmias, the cause of most sudden deaths, is required.

29.3 Ventricular Tachycardias

Ventricular tachycardia is defined as a tachycardia originating below the bifurcation of the His bundle and consisting of at least three successive complexes, occurring with a frequency between 100 and 250 per minute (Fig. 29.8) [127, 128].

29.3.1 Diagnosis

The diagnosis of ventricular tachycardia is generally established by study of the ECG recording. In most cases, this diagnosis is relatively simple. However, at times, it can be extremely difficult or misleading even for experts. The most common problem is distinguishing ventricular tachycardia from supraventricular tachycardia with aberration or more complex situations like the involvement of an accessory pathway. As the consequences of these alternative diagnoses may be very different from a therapeutic point of view, it may sometimes be necessary to confirm the diagnosis by esophageal recordings, or by endocavitary investigation [128–131] without delaying the DC shock in case of poorly tolerated arrhythmia.

29.3.1.1 Electrocardiographic features

The characteristic features of VT are the following:

- Regular tachycardia with a rate usually between 100 and 200 beats/min,
- Wide deformed monomorphic ventricular complexes (QRS > 0.12 s), and
- Anterograde atrioventricular dissociation.

Atrial activity

The atrial rhythm depends on the sinus node and is usually slower than rapid rhythm of the VT (Fig. 29.12). However, retrograde ventriculoatrial conduction is often observed with the ventricular activation conducted 1:1 to the atrium, or with retrograde block of different degrees.

In order to confirm VT, the P waves capable of capture or fusion must be carefully identified. This may be difficult using classical surface recordings and a bisternal lead or an esophageal recording may help in the diagnosis. This occurrence of fusion indicates that a ventricular focus has been modified by an external influence, usually supraventricular, but which may also be of ventricular origin. Capture of the ventricle by the supraventricular rhythm with a normal QRS complex implies an atrial origin of the activation. However, extrasystoles arising from the contralateral site of origin of the VT can also normalize the QRS width.

There are exceptions to the above. Atrial rhythm is not always slower and dissociated from the ventricular rhythm. This may be the case in two situations:

- There may be retrograde conduction. Therefore, ventricular tachycardia should be differentiated from atrial or junctional tachycardia with 1:1 conduction with either functional bundle branch block or preexcitation.
- The atrial activity may be atrial fibrillation or an isorhythmic atrial tachycardia.

Conversely atrial activation at a slower rate dissociated during tachycardia with wide QRS complexes, is not always a ventricular tachycardia. A tachycardia originating in the His bundle associated with bundle branch block and retrograde block may also give the same appearances.

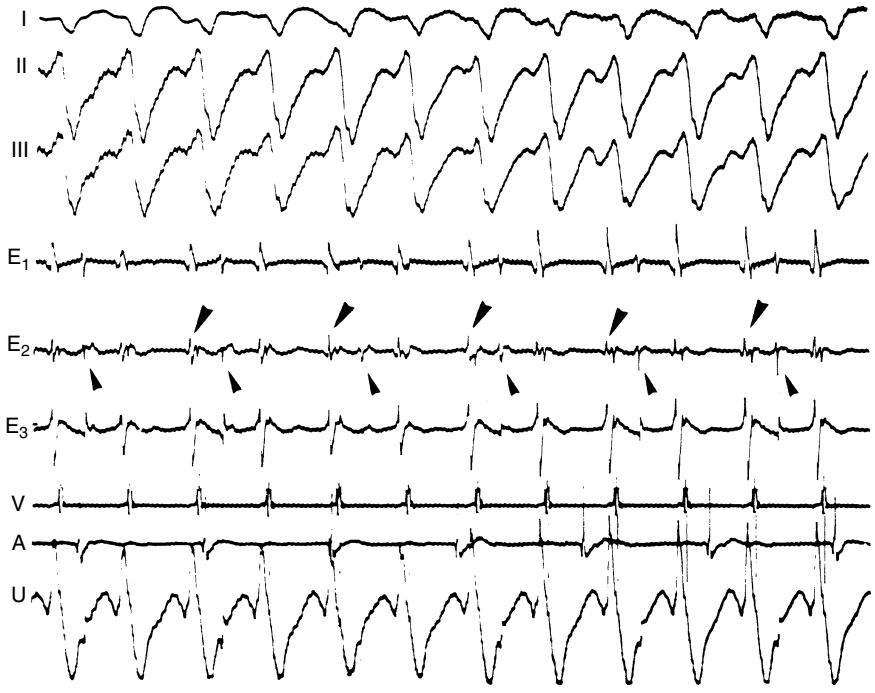

Figure 29.12

An episode of sustained ventricular tachycardia recorded during epicardial mapping. E_I, E_2, E_3 are the epicardial leads. The atrial rhythm (A) is completely dissociated from the ventricular rhythm (V) recorded on the anterior aspect of the right ventricle. In this patient with arrhythmogenic right ventricular dysplasia, the moving epicardial probe (E) records a phenomenon of 2: 1 Mobitz II block in the ventricle. The delayed potential stressed by the upward directed arrows appears on one of the other beats, and follows a normal synchronous beat indicated by the downward oriented arrow. U is the unipolar recording from the bipolar roving probe.

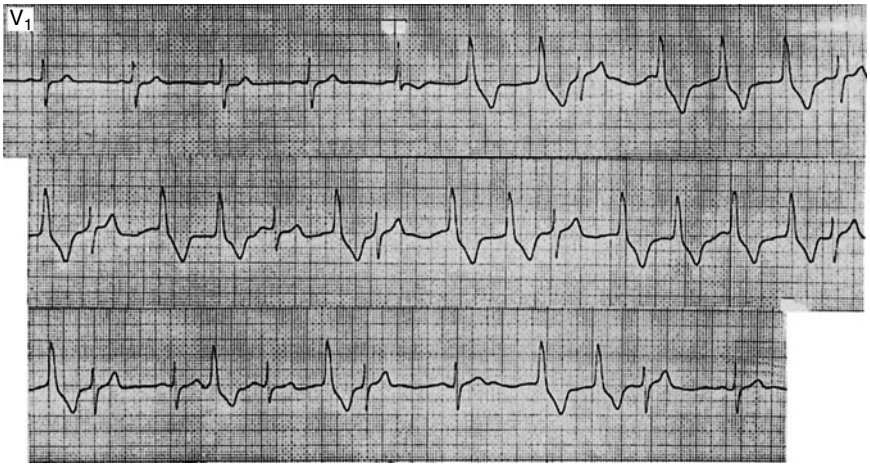

Figure 29.13

Accelerated idioventricular rhythm with a fusion beat owing to simultaneous activation between the supraventricular activity and the ventricular rhythm. The strips are recorded continuously, beginning with the top panel.

Ventricular activity

The ventricular rhythm may be as follows:

- Irregular (ventricular tachyarrhythmia), posing the difficult differential diagnosis of a Kent bundle with a short refractory period in atrial fibrillation (pseudoventricular tachycardia);
- Slower (< 100 beats/min), in cases of accelerated idioventricular rhythm (Fig. 29.13) or on account of treatment; or
- Faster (> 200 beats/min), with a regular large-amplitude sinusoidal wave called "ventricular flutter."

29.3.1.2 Electrocardiographic discrimination between VT and SVT

In the case of a wide complex tachycardia (WCT), a SVT may simulate a VT because of:

- A rate dependent bundle branch block aberration
- An accessory pathway with fast atrioventricular conduction
- Some electrolyte disorders (i.e. hyperkalemia) or antiarrhythmic drugs widening the QRS complex (especially class I).

Many algorithms based on ECG features have been published in the last two decades [140, 141] to improve the differential diagnosis between SVT and VT when major criteria like capture and fusion phenomenon or atrioventricular dissociation are missing or dubious. Before using these complex algorithms, the first step of clinical evaluation is to look for the presence of the following abnormalities on previously recorded ECGs (in sinus rhythm) if available:

– LBBB or RBBB
– Ventricular preexcitation
– VES with the same morphology as the WCT.

Other criteria like QRS axis and QRS duration generally provide a small contribution to the diagnosis. However, a QRS axis rotation between −90° and −180° is considered as very specific of a ventricular origin, whereas other deviations can be achieved by both VT and SVT. Concerning QRS duration, a value above 140ms was found to have a very high specificity for VT, even if antiarrhythmic drug administration (class Ia and Ic especially) during SVT or conduction through an accessory pathway may widen the ventricular complex up to 140–160ms. Conversely, VT arising from the ventricular septum or from the His-Purkinje system in patients without structural heart disease is known to give relatively "narrow" WCT. These data suggest that there is no reliable measure able to discriminate SVT from VT, even if a QRS duration of more than 140 ms has a high specificity in the absence of antiarrhythmic drugs or Wolff-Parkinson-White syndrome.

The main step in the differential diagnosis is ultimately based on the analysis of QRS morphology during WCT, which can be divided into LBBB or RBBB pattern according to the polarity of QRS in lead V_1:

- When V_1 has a RBBB morphology, monophasic R wave or biphasic qR and Rs patterns are very suggestive of VT whereas a triphasic ventricular complex like rSr', rsr', rSR' or rsR' is more consistent with an aberration in conduction. At the same time, an R/S ratio < 1 in V_6 is expected during a WCT related to SVT. Classical patterns for VT in V_6 are rS, QS or an R exclusive wave (Fig. 29.14).
- When V_1 has an LBBB morphology, the discrimination criteria are mainly based on the beginning of the QRS complex. When the depolarization is transmitted from the atrium to the ventricle through the His-Purkinje network, the QRS complex keeps a sharp onset even in the presence of aberrant conduction. Conversely, the ventricular depolarization of a VT through undifferentiated or scar tissue is supposed to give a slow rising or descending wave at the onset of the QRS complex. Criteria like R wave duration longer than 30 ms or an interval between the onset of the QRS to the S wave nadir of at least 60 ms in V_1, are highly correlated with a ventricular origin [142]. In V_6, the common pattern encountered during SVT is R exclusive or RR', with the lack of an initial q wave. In the case of VT, the usual morphologies are QR or QS (Fig. 29.15).

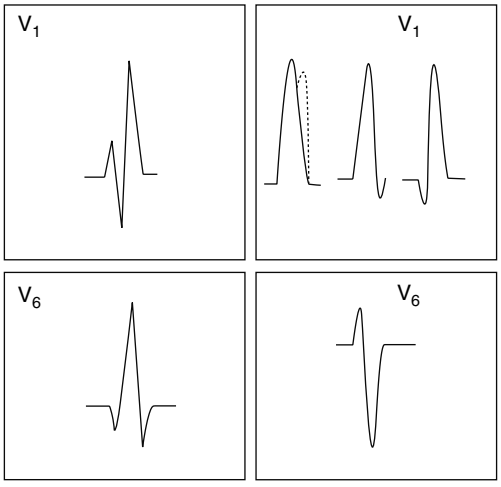

Figure 29.14
Classical morphologies of QRS in V_1 and V_6 encountered in case of SVT (left patterns) and VT (right patterns) with a RBBB pattern.

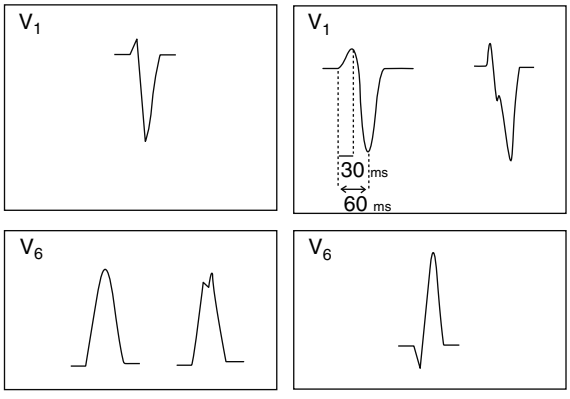

Figure 29.15
Classical morphologies of QRS in V_1 and V_6 encountered in case of SVT (left patterns) and VT (right patterns) with a LBBB pattern. R duration above 30 ms and interval between the onset of the QRS to the S wave nadir of at least 60 ms in V_1 suggest VT.

This analysis of QRS morphology during WCT may seem so difficult to carry out that some authors have suggested to look for more simple features like:

- lack of RS complex in precordial leads, highly suggestive of a VT according to Brugada [140], especially in the presence of a long interval between the onset of the QRS to the S wave nadir of at least 60 ms in V_1 (specificity = 100%);
- negative or positive concordance from V_1 to V_6 (all precordial leads predominantly positive or negative) is very uncommon in SVT except in the presence of an accessory pathway.

In case of an uncertain diagnosis, especially during administration of antiarrhythmic drugs (given the risk of false positive criteria for VT), the ultimate step for WCT discrimination is the use of vagal maneuvers (carotid sinus massage or valsalva maneuver for instance) of parasympathomimetic drugs.

29.3.1.3 Results of endocavitary investigations during VT

Endocavitary electrophysiological investigations can be of diagnostic and therapeutic value when the VT is well tolerated and does not require immediate cardioversion. Electrophysiological studies usually confirm the diagnosis of VT, and in addition define the atrial rhythm (sinus, retrograde, ectopic).

In the His-bundle recording in VT, the His potential H' is dissociated from P waves and related to the QRS complex. The timing of H' with respect to the QRS is variable, but it is usually situated within or just after the QRS complex. This is an argument in favor of VT. However, a WPW syndrome with reciprocating tachycardia involving Mahaim fibers in the retrograde direction may pose a difficult differential diagnosis with VT.

A programmable stimulator is used to deliver 2 ms pulse duration stimuli at twice the diastolic threshold (around 2 mA), this amplitude being sometimes increased up to five times the threshold value. The stimuli can be directed to any of the three catheters through a remote-controlled switch box. Two stimulators should be available, one preset for tachycardia interruption and the other for programmed pacing during the investigation.

Ventricular tachycardia may be initiated by either atrial or ventricular pacing. In the former, the maneuvers involve introducing two or three atrial extrastimuli with increasing prematurity into a basal sinus cycle. When this is ineffective, coupled extrastimuli at increasing prematurity are introduced on a fixed atrial paced rhythm. Finally, overdrive pacing up to the Wenckebach point can be used. Ventricular pacing, includes the following:

- Asynchronous ventricular pacing at an increasing rate, from 70 to 200 beats/min;
- Coupled ventricular stimulation, then paired ventricular extrastimuli during sinus rhythm at increasing prematurity until the effective refractory period (erp) is reached and eventually three to five premature stimulations up to the erps (Fig. 29.16);
- Paired ventricular stimulation which is repeated at fixed basic ventricular rate at 100, 130 and 150 beats/min;
- Bursts of rapid ventricular pacing with each stimulus eliciting a ventricular response for a period of 3–7 s;
- Pharmacological injection of isoproterenol [143].

In fact, protocols and definitions of VT vary from group to group. Selected protocols have been summarized in Table 29.2. Some groups use different intensities of stimulation or different sites of stimulation [144, 145]. However, these protocols are very controversial [146, 147] especially as some groups use them to test the effectiveness of treatment.

Different sorts of response may be elicited by the above pacing maneuvers. These include the following:

- Simple repetitive ventricular responses with an identical configuration to the paced beat. This type of response is physiological and corresponds to re-entry from branch to branch and has no pathological significance [148].
- Initiation of sustained ($\geq$ 30 s) or nonsustained ($<$ 30 s) VT that comprises at least three successive complexes. The frequency, configuration and electrical axis enable VT to be classified as "clinical" when identical to the spontaneous recorded VT, or "nonclinical" when otherwise. However, nonclinical VT may in fact correspond to a clinical VT which has not been recorded.
- Rapid and poorly tolerated VT or ventricular fibrillation must be defibrillated when the patient has lost consciousness.

29.3.2 Etiologies

The cause of VT may be deduced from clinical examination of the patient and from the results of different complementary investigations. In patients without clinically obvious cardiac disease, investigations may be limited to standard electrocardiography, stress testing, echocardiography, and eventually myocardial scintigraphy. In patients with obvious underlying cardiac disease, it may be necessary to perform right and left ventriculography, as well as coronary arteriography. The most common pathologies are outlined in the following subsections.

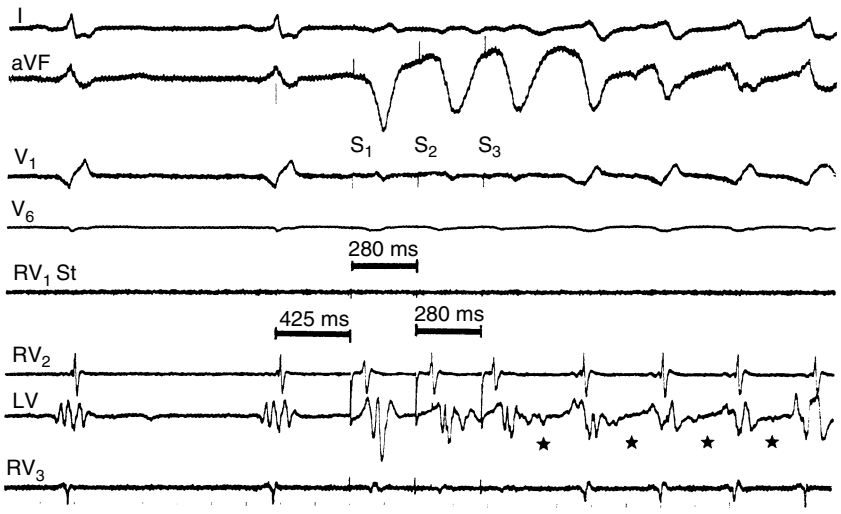

Figure 29.16

Induction of sustained ventricular tachycardia by three premature stimuli S_1, S_2, S_3 during sinus rhythm, in a patient in the chronic phase of myocardial infarction. RV_1, RV_2, RV_3 are recorded from the right ventricle. LV indicates the endocardial bipolar lead in an abnormal zone of the left ventricle showing fragmentation, both during sinus rhythm and during programmed pacing. When ventricular tachycardia is elicited, note the fragmentation of delayed potential bridging diastole (stars).

29.3.2.1 Coronary artery disease

Coronary artery disease occurs in about 80% of cases. Acute myocardial infarction is often complicated by polymorphic ventricular arrhythmias which explained the high mortality previously associated with acute myocardial infarction [149]. Ventricular arrhythmias may also be observed after a delay of 10 to 15 years following the initial infarct and may be the only clinical sign of a ventricular aneurysm [150, 151]. In this group of patients, the association with cardiac failure is a poor prognostic factor.

During the last decade, several major studies have clearly demonstrated the benefit of the ICD in the secondary [152–154] and primary prevention [155–157] of sudden cardiac death compared with an optimal treatment including ACE and beta-blockers, sometimes completed with an antiarrhythmic drug strategy guided by an electrophysiologic testing. A major challenge in the management of patients with CAD remains the definition of subgroups at high risk of SCD. Major criteria in this risk stratification strategy are, a previous history of SCD or spontaneous sustained VT, and left ventricular ejection fraction of 30% or less one month after an acute coronary syndrome. Conversely, prevention of ventricular arrhythmias by ICD or drugs in patients with preserved systolic function still remains unclear.

During the early phase after myocardial infarction (40 days), ICD shows no benefit in terms of survival among high risk patients with reduced left ventricular ejection fraction of 35% or less and depressed heart-rate variability.

According to these trials, indications for ICD implantation [110] in patients with a coronary heart disease are:

- Spontaneous sustained VT with impaired left ventricular ejection fraction,
- Syncope of undetermined origin with clinically relevant, hemodynamically significant sustained VT or VF induced at electrophysiological study when drug therapy is ineffective, not tolerated, or not preferred (bad compliance on long term),
- Coronary disease, prior myocardial infarction, left ventricular dysfunction, and inducible VF or sustained VT at electrophysiological study that is not controlled by a Class I antiarrhythmic drug,
- Spontaneous sustained VT that is not amenable to other treatments,

Table 29.2

Protocols of programmed pacing and definition of ventricular tachycardia (VT)

Study	Programmed pacing	Definition of VT
Mason and Winkle [134]	A1 atrial stimulation V1 ventricular stimulation extrastimulus V2, V2-V3, V2-V3-V4, V2-V3-V4-V5 V1,V2,V3 stimulation burst of VT RV1 + LV2 isoproterenol	Sustained for > 15 s Nonsustained: 6–15 complexes.
Mann et al [135]	ventricular stimulation (apex + septum) extrastimulus V2, V2-V3, V2-V3-V4, V2-V3-V4-V5 stimulation (500 ms) + extrastimulus burst of VT.	sustained for > 1 min or necessitating intervention for termination (poor hemodynamic tolerance) nonsustained > 6 beats, spontaneous termination within one minute.
Doherty and Josephson [136]	atrial A1, A1-A2, A1-A2-A3, stimulation extrastimulus V2, V2-V3, V2-V3-V4 ventricular pacing V2, V2-V3 other site isoproterenol	
Ruskin et al [137]	atrial A1, A1-A2, stimulation V1 ventricular stimulation extrastimulus V2, V2-V3 burst (RV) of VT	sustained VT: 100 narrow nonspontaneous complexes nonsustained VT > 5 complexes and < 100 complexes repetitive ventricular response, 3 or 4 extrasystoles.
Vandepol et al [138]	V2, V1-V2, V1-V2-V3 during sinus rhythm burst (multiple site) of VT	sustained VT > 1 min, nonspontaneous termination nonsustained VT > 3 complexes < 1 min, spontaneous termination
Perrot et al [131]	A1-A2, A1-A2, -A3 atrial stimulation ventricular stimulation with V1-V2, V1-V2-V3 extrastimuli pacing from 70 to 100 min-1.	nonsustained VT > 5 complexes at a rate of > 100 min-1 for < 1 min, spontaneous termination, sustained VT > 1 min, frequency > 100 min-1.
Livelli et al [139]	A1-V2, A1-V2-V3 atrial stimulation V1-V2, V1-V2-V3 during sinus rhythm burst (apex, infundibulum RV) of VT.	sustained VT: nonspontaneous termination (necessitate intervention) nonsustained VT > 3 complexes, but spontaneous termination.
Fisher [132]	A1-A2, A1-A2-A3 atrial stimulation + V1-V2-V3, V1-V2-V3-V4 burst of VT isoproterenol	VT > 3 ventricular complexes with a frequency > 100 min-1.
Josephson et al [2]	A1-A2, V1-V2-V3 during sinus rhythm and pacing (multiple sites, sometimes right sided, sometimes left sided).	sustained VT > 30 s or termination by extrastimuli or shock (when poorly tolerated) nonsustained VT: spontaneous termination before 10 complexes.
Breithardt et al [215]	V1-V2, V1-V2-V3 during sinus rhythm and ventricular pacing (120, 140, 160, 180 min-1) burst of VT from 10 to 20 s (180 to 220 min-1).	sustained VT > 30 s or necessitating intervention for termination nonsustained VT: spontaneous termination within 30 s.

- Patients with left ventricular ejection fraction ≤30%, at least one month post myocardial infarction and three months post coronary artery revascularization surgery.

29.3.2.2 Dilated cardiomyopathy

Dilated cardiomyopathy (4% of cases) is generally associated with normal coronary arteriography [158]. Ventricular arrhythmias, especially VT and ventricular fibrillation, are some of the lethal complications of this condition. These

arrhythmias may be very varied, usually polymorphic, and have a poor prognosis. Sudden death is commonly observed an average of three years after the clinical onset of the arrhythmias, unless the natural outcome is shortened by other complications of this condition such as embolism and chronic heart failure. However, some cases of dilated cardiomyopathy (DCM) progress very slowly, with some patients surviving more than ten years. Some of these cases of dilated cardiomyopathy may be of viral origin [159]. In patients with DCM, primary prevention of SCD is more and more based on ICD, often combined with a resynchronization device [160, 161]. Indications are comparable with those concerning CAD.

29.3.2.3 Hypertrophic cardiomyopathy

Hypertrophic cardiomyopathy (HCM) is generally diagnosed in young and apparently healthy subjects, some of whom may practice sport at a high level, which may explain some of the sudden deaths in this group [162]. Some investigators [106] reported an incidence of 66% of severe ventricular arrhythmias and 19% of sustained VT in a series of 99 patients with hypertrophic cardiomyopathy. During a three-year follow-up period, six cases of cardiac arrest were observed, two of which were the result of ventricular fibrillation. The annual mortality of patients with VT was 8.6% compared to only 1% in patients without this arrhythmia. Arrhythmias were more commonly observed at night time, perhaps because of nocturnal sinus bradycardia. Another form of hypertrophic cardiopathy has been described [163] involving only the apex of the ventricle, characterized by deeply inverted T waves in the left precordial leads (see Chap. 20). The diagnosis is confirmed by angiography which shows characteristic obliteration of the apex of the left ventricle. Although ventricular arrhythmias were reported for a long time in patients with HCM, the magnitude of ventricular arrhythmias and their relation with SCD have become more fully understood following a larger use of ICDs [164].

Current indications from both the American College of Cardiology and the European Society of Cardiology [110] for ICD implantation are listed below:

- Cardiac arrest
- Spontaneous sustained VT
- Family history of SCD and HCM
- Unexplained syncope
- Extreme LV hypertrophy with septal wall thickness ≥ 30 mm
- Hypotensive blood pressure response to exercise
- Nonsustained VT (Holter).

The significance of LV outflow tract obstruction has been demonstrated after many small studies had previously reported conflicting results. In 2003, Maron et al published a large study of 1101 patients followed for a mean of 6.3 ± 6.2 years [165]. Patients with obstruction (defined as a basal gradient of at least 30 mm Hg) have an increased risk of SCD (RR = 1.9; p = 0.01), but the low annual rate of death (1.5% vs 0.9%) gives a poor predictive value to this criterion beside risk stratification and is not sufficient alone to justify an ICD implantation.

Management of HCM may also change in the next few years in terms of risk stratification with the contribution of genetics and in terms of treatment due to a more widespread use of percutaneous alcohol septal ablation. However, the impact of this recent technique on the general course of the disease is unknown.

29.3.2.4 Mitral valve prolapse

Mitral valve prolapse (Barlow syndrome) is commonly complicated by ventricular arrhythmias. Ventricular extrasystoles are observed in almost 50% of cases [117]. Salvos of extrasystoles and sustained VT may also be recorded. However, although mitral valve prolapse is a relatively common condition, ventricular arrhythmias leading to VT are rare. Nevertheless, 25 cases of sudden death were reported in one review in 1979 [166]. The typical presentation is a woman of about 40 years of age with polymorphic VES and VT with a right bundle branch block configuration. The ECG shows characteristic ST-segment changes with inversion of the T wave in the left precordial leads. These forms of mitral valve prolapse are usually associated with mitral regurgitation.

No clinical or electrocardiographic criterion appears to be valuable in determining patients with a high-risk of SCD. The only indication for an ICD implantation is in secondary prevention [167].

29.3.2.5 Arrhythmogenic right ventricular dysplasia

Arrhythmogenic right ventricular dysplasia [168–170] arises from an abnormality in the development of a part of the right ventricular myocardium. There is a progressive alteration of the subendocardial and mediomural fibers leading to fibroadipose degeneration. The general structure of the myocardium is usually preserved but the adipose cells seem, progressively, to replace the myocardial fibers. The disease progresses very slowly in most cases with preservation of strands of healthy or partially degenerated myocardial fibers within the adipose tissue, interconnecting with some strands in the subendocardial layers. The network of fibers may be the site of delayed conduction and the origin of delayed potentials favoring the initiation of VT by reentry (› Fig. 29.17). Major complications are ventricular arrhythmias, mainly VT, with the risk of sudden cardiac death, and congestive heart failure. This appears when right ventricular enlargement impairs left ventricle filling or when left ventricle itself is directly affected by the disease, masquerading as a dilated cardiomyopathy. Factors defining the prognosis have been clearly described by Hulot [171]: 130 patients were followed during 8.1 ± 7.8 years - 24 deaths occurred of which 21 were of a cardiovascular origin (progressive heart failure for 14 patients, sudden death for the remaining 7 patients). Multivariate analysis showed that right ventricular failure, left ventricular dysfunction and ventricular tachycardia identified high-risk subjects. Treatment strategy remains unclear in the absence of large prospective studies and a combined therapy is generally required, based on anti-arrhythmic drugs and catheter ablation [172], sometimes coupled with an ICD. Indications for defibrillator implantation are still debated except in cases of secondary prevention [167]. Two retrospective, non randomized studies have recently been published which demonstrated a better outcome in high risk patients implanted with an ICD [173, 174]. In case of frequent episodes of VT requiring external or post ICD implantation defibrillation shocks, radiofrequency catheter ablation or DC ablation remains the therapy of choice [172]. At the time of symptomatic congestive heart failure, heart transplantation or right ventricular cardiomyoplasty [175] has to be planned.

29.3.2.6 Uhl's anomaly

Uhl's anomaly [176] is an anatomically similar condition to arrhythmogenic right ventricular dysplasia, but is associated with severe dilatation of the right heart and characteristic thinning of certain zones of the free wall of the right ventricle. The latter occurs to such a degree that, in some cases, no myocardium is observed between the epicardial and endocardial layers. Severe forms of this condition have been described as "parchment heart" and are associated with a very poor prognosis, with death intervening in the first days or weeks of life. However, there are some rare adult forms which may, like arrhythmogenic right ventricular dysplasia, lead to attacks of VT and sudden death.

29.3.2.7 Brugada syndrome

Brugada syndrome, recently described in 1992, is characterized by a "coved" ST segment elevation in right precordial leads in generally young patients with structurally normal hearts. It is correlated with a high incidence of sudden arrhythmic deaths related to ventricular fibrillation [177]. This specific ECG pattern is the consequence of a mutation on a gene encoding for the sodium channel, leading to an imbalance between the outward potassium current and the inward sodium channel generating an electric gradient between epicardial and endocardial layers during ventricular repolarization. Sudden cardiac death risk is predicted by personal and familial presentation and by the onset of ventricular fibrillation during programmed ventricular stimulation. Screening parents and siblings is mandatory due to the autosomal dominant transmission of mutations described. In high-risk patients and in secondary prevention, an ICD implantation is required [177].

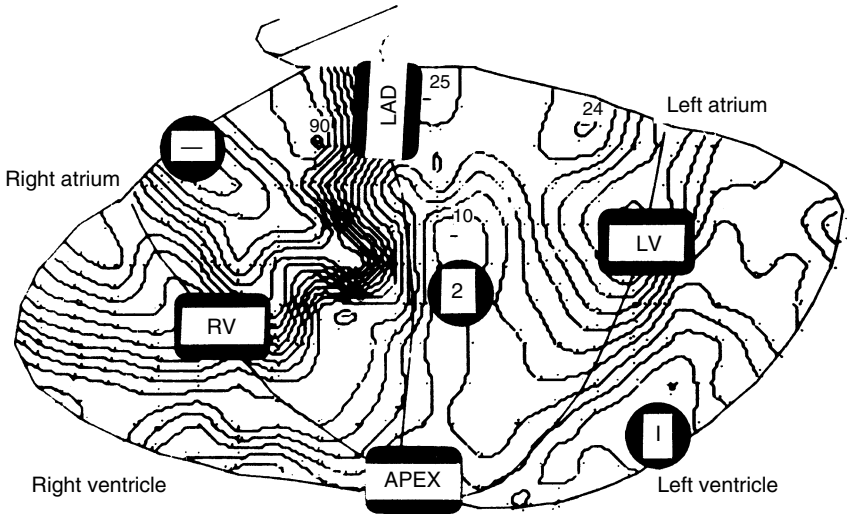

Figure 29.17

Epicardial map showing the activation pattern in a patient with arrhythmogenic right ventricular dysplasia. The first activated area (1) is situated on the posterodiaphragmatic aspect of the left ventricle. The second area (2) of excitation appears also abnormally on the anterior aspect of the left ventricle. The right ventricle shows major delay of conduction as indicated by tightly packed isochrones. The latest activated area is located near the AV groove in the area indicated by the minus sign. This place was also the area where the VT originated. LAD indicates the left anterior descending artery.

29.3.2.8 Idiopathic VT

Idiopathic VT is observed in clinically normal hearts and is generally the only symptom present. The arrhythmia starts as VES which become progressively more frequent, leading to sustained VT of the same configuration. These VES and VT mainly arise from:

- the right ventricular outflow tract (RVOT), giving a pattern of LBBB with a normal QRS axis [178] and less frequently from the left ventricular outflow tract (LVOT) or the aortic root with a RBBB pattern [56]. These are the most common type of VES or VT, occurring generally in young patients in the absence of overt cardiac disease, especially after having excluded an arrhythmogenic right ventricular cardiomyopathy which gives VES with the same morphology. Long term prognosis is generally good, except for the risk of developing a tachyarrhythmia cardiomyopathy, but medical treatment including class I or class II anti-arrhythmic drugs is required in symptomatic patients or in case of repetitive VES. These forms of VT are frequently very difficult to initiate and impossible to terminate by programmed pacing but are sensitive to isoprenaline infusion. Radiofrequency catheter ablation is performed when drugs are ineffective or badly tolerated, with a high level of success [179].
- the left Purkinje network system, also called "fascicular VT", usually seen in young patients with clinically normal hearts experiencing episodes of VT with a particular ECG pattern showing right bundle branch block with left axis deviation. This arrhythmia is frequently misleading suggesting at first sight a supraventricular tachycardia with functional aberration. Electrophysiological studies, however, demonstrate a typical VT. This arrhythmia could in many cases be triggered by ventricular or even atrial pacing. Endocardial mapping shows that the origin of the VT is located in the left inferior paraseptal area, with a presystolic potential recorded on the Purkinje system [180]. It is surprising that this arrhythmia can be reproducibly stopped by an IV verapamil (10 mg) injection. Radiofrequency catheter ablation is required in case of drug refractory VT.

29.3.2.9 Cardiac tumors

Cardiac tumors [181] may present with recurrent VT. They are rare in adults but should be suspected in cases of childhood VT. The tumors are more commonly primary than secondary. They usually give rise to polymorphic forms of VT, the clinical characteristics of which depend on the site of the lesion. Prognosis is usually very poor except in rhabdomyoma in which some cases of spontaneous regression have been reported. Cardiac fibromas are basically benign tumors but local extension of the lesion may lead to death. Surgery may be possible in some cases, but it may be very difficult or impossible to resect the tumor from the interventricular septum.

29.3.2.10 Catecholamine-induced polymorphic VT

Catecholamine-induced polymorphic ventricular tachycardia is usually seen in childhood [182]. This is a rare form of VT which occurs in clinically normal hearts, almost exclusively on effort, despite a normal QT interval. These arrhythmias always occur in identical conditions after acceleration of the sinus rhythm owing to exercise or emotion. Sinus tachycardia leads to a junctional tachycardia and then VES or bigeminy which trigger polymorphic and often bidirectional VT. This finally degenerates to rapid polymorphic VT at a rate of about 300 beats/min accompanied by syncope. The arrhythmia may be reproduced during an exercise-stress test or isoproterenol infusion, and can cause sudden death. The treatment of choice seems to be beta blockade and amiodarone. Nevertheless, further studies are required to assess long-term results of this treatment.

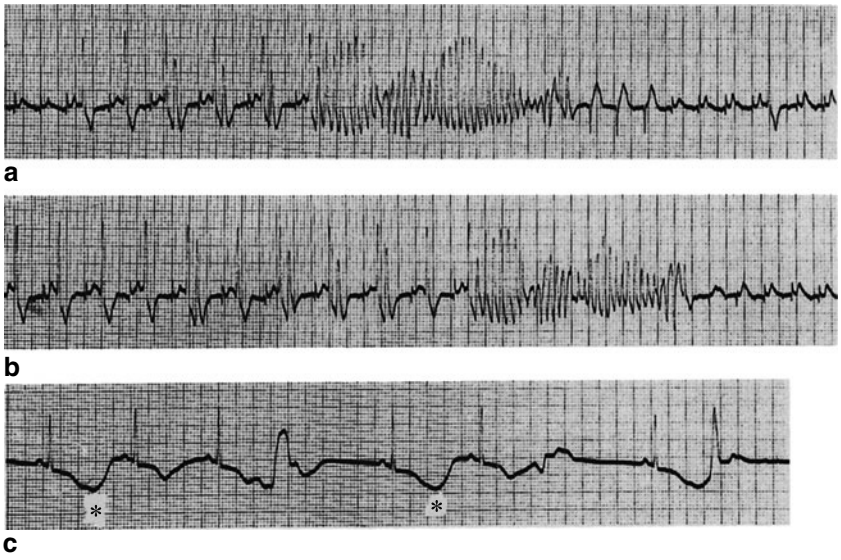

Figure 29.18

Two episodes of Torsades de pointes recorded at a very slow speed which shows the crescendo type of ventricular arrhythmias. First, in (a), there are two single extrasystoles, and then two extrasystoles following each sinus beat. Thereafter, the typical features of Torsades de pointes, which ends spontaneously, can be seen. Note the giant T wave on the last three beats before the re-establishment of the basic rhythm. The same pattern is also observed on tracing (b) recorded in the same patient. Tracing (c) is from a different patient. Note the huge deformation of the last part of the T wave, denoted by an asterisk, sometimes leading to an extrasystole. These giant waves are the harbingers of Torsades de pointes.

29.3.2.11 Torsade de pointes (TdP)

The term Torsade de pointes (TdP), chosen by Dessertenne, corresponds with a continuously changing morphology of the QRS (Fig. 29.18) during a VT run, with a cyclic decrease in the amplitude of the ventriculograms with a periodic rotation of QRS axis [183]. Such a polymorphic VT occurs in patients with long QT syndromes, induced by drugs or genetically inherited, with the risk of syncope during the episode and the possibility of conversion into ventricular fibrillation. Endocardial recordings show fragmented potential during QRS complexes initiating TdP, then followed by twisting electrograms with a pattern of double spikes at the time of QRS axis rotation [184]. The first hypothesis reported was the presence of two foci of activation firing simultaneously with varying degrees of fusion, but subsequently the spiral wave activity theory was confirmed following the in vitro experiments led by Davidenko [185]. Using high resolution optical mapping, he demonstrated that the core position of the arrhythmia was moving at every beat in a single direction, giving a pattern of TdP, or in various directions, leading to VF. Good results have been reported with IV injection of magnesium sulphate to prevent recurrence. It appears to be as effective as isoproterenol but without the undesirable side effects of the latter [186]. "Quinidine-like" (class I) antiarrhythmics are contraindicated in torsades de pointes with long QT intervals. Similarly, defibrillation is indicated only when torsades de pointes degenerates into VF.

29.3.2.12 Congenital long-QT syndrome

The congenital long-QT syndrome is a rare condition which may lead to attacks of polymorphic VT described as torsade de pointes, preceded by a very abnormal lengthening of the corrected QT (QTc) interval (calculated from Bazett's formula), associated with a U wave leading to a dimpled appearance at the end of the T wave.

Two subgroups have been defined:

- The Lange-Nielsen syndrome, described in 1957, which associates ventricular arrhythmias and ST changes with deafness, transmitted in the autosomal recessive mode; and
- The Romano-Ward syndrome, in which deafness is absent and which is transmitted in the autosomal dominant mode.

These congenital long QT syndromes correspond with mutations involving sodium or potassium channels and are classified into seven types from LQT1 to LQT7 [187]. However, sporadic cases do occur without a familial context. Syncope occurs during exercise or emotion. The QT interval is prolonged during the appearance of VES at the end of the repolarization associated with alternating changes in amplitude of the ST segment. This leads to very rapid bursts of tachycardia with cardiovascular collapse and loss of consciousness. Electrophysiological studies show prolongation of the refractory period with a large variation in its value from one point to another in the ventricle. The prognosis, conditioned by the symptoms, the QTc duration and the mutation identified, varies from less than 5% of major cardiac event at 5 years under treatment to more than 50% in high risk patients [188]. Treatment strategy is based on beta-blocker therapy for every patient with a long ST syndrome, avoiding QT prolonging drugs and sports. ICD implantation is required in secondary prevention or in case of bad observance or poor efficacy of beta-blockers [167]. Permanent cardiac pacing has limited indications, and is mostly used for rate support in cases of symptomatic bradycardia under treatment. Parents and siblings should be screened by ECG and genotypic analysis is mandatory.

29.3.2.13 Bouveret VT

"Bouveret ventricular tachycardia" (Parkinson-Papp) affects young patients without obvious myocardial disease [189]. It comprises runs of monomorphic VT, suggesting a point of origin in the upper part of the interventricular septum, as has been shown by epicardial mapping performed in a few cases. This diagnosis can only be retained after a complete cardiological checkup to exclude any other cardiac disease, remembering that sometimes VT may be the only presenting symptom of a cardiac disease for many years.

The classification of some idiopathic right ventricular tachycardias with left bundle branch block configuration and a normal or right axis, is imprecise. The prognosis is usually good [178]. However, some patients may be very disabled by these episodes of tachycardia.

29.3.3 Treatment of ventricular tachycardia

All forms of VT should be treated to restore sinus rhythm. The clinical tolerance of VT depends, above all, on the underlying myocardial condition, a factor which partially determines the urgency of treatment and therapeutic choice.

29.3.3.1 Termination methods

Pharmacodynamic methods

The most widely used intravenous antiarrhythmic agents (Tables 29.3 and 29.4) are beta blockers, procainamide, disopyramide and amiodarone (if VT is well tolerated). Lidocaine and mexiletine are mainly used to prevent VT in the acute phase of myocardial infarction, suppressing, or at least decreasing, the frequency of VES.

Endocavitary pacing

Ventricular tachycardia may rarely be terminated by atrial extrastimuli but one, two or three right ventricular extrastimuli are usually more effective. This is an elegant method of terminating VT and has the advantage that it can be used to predict the efficacy of antiarrhythmic therapy (no negative inotropic effect).

Defibrillation and cardioversion

External DC shock is normally used when the patient has lost consciousness or after a short-lasting general anaesthetic. The electrical energy delivered ranges from 80 to 300 J [190]. When VT has a tendency to recur, during transport or in the operating theatre, adhesive defibrillation electrodes may be used which reduce the discomfort and increase the margin of safety. Repetitive shocks must be used with caution in patients with a low ejection fraction, especially in dilated cardiomyopathy and acute myocardial infarction. In all cases, the lowest amount of electrical energy possible should be used, to avoid local changes in ionic concentration and cellular damage.

29.3.3.2 Termination strategy

The strategy used to terminate attacks of VT depends mainly on the condition of the patient on admission to hospital. If VT is very rapid, and poorly tolerated with cardiovascular collapse and syncope, immediate direct current shock is required, with or without anaesthetic, depending on whether or not the patient is conscious.

When VT is better tolerated, with the risk of cardiac failure in the short term, an antiarrhythmic agent with a rapid onset of action has to be used, despite the possibility of a negative inotropic effect and the need for cardiovascular resuscitation.

When VT is well tolerated, the drug of choice is amiodarone which has the great advantage of having no negative inotropic effects, providing that it is injected over a 5–10 min period at a dose of 300–400 mg. However, if VT is well tolerated and an electrophysiological laboratory is available, electrical stimulation techniques are to be preferred to drug therapy. Endocavitary catheters can be used to confirm the diagnosis of VT and then terminate the majority of attacks by programmed pacing techniques. A catheter left at the apex of the ventricle allows better control if VT occurs.

29.3.3.3 Prevention of recurrence

Once an attack has been terminated, measures must be taken to prevent a recurrence and to assess the effectiveness of antiarrhythmic therapy. A distinction should be drawn between VT in the acute phase of myocardial infarction

Table 29.3

Properties of administration of the most widely used intravenous antiarrhythmic agents

Class	Antiarrhythmic Effects	Properties	Drug	Effect On MI[b]		Side effects	Dosage[c]		Interval Between Successive doses (h)	Antiarrhythmic effectiveness
				Ch	In		iv	PO per 24 h (mg)		
Ia	Membrane Stabilizer	Quinidine-like	quinidine	+	–	cardiac GI		600 Q base	6–12	2.5 g ml^{-1}
			procainamide	+	–	cardiac GI	50–100 mg min^{-1} 600 mg $24h^{-1}$	4 at 8g	4	4–10 g ml^{-1}
			disopyramide	+	–	anticholenergic cardiac	1.5 mg kg^{-1} in 5 min	400–600	6	3–8 ml^{-1}
			ajmaline	–	–	cardiac	1 mg kg^{-1} min^{-1}			
Ib		lidocaine-like	lidocaine	0	–	neurologic, GI cardiac in case of rapid injection	50 mg iv 2000 mg J ES			
			mexiletine	0	–	neurologic GI, cardiac in case of rapid injection	250 mg in 10 min 1200 mg J ES	600–800	8	0.5 at 2g ml^{-1}
			aprindine	0	–	neurologic, GI, hepatitis, hematologic	rarely used	100	12	1 at 2 μ g ml^{-1}
			tocainide	0	–	GI, neurologic	0.5–0.75 mg kg min^{-1} for 15 min	1200–1800	8	6 at 12 μ g ml^{-1}
Ic			encainide	0	–	cardiac, occular, GI	0.75–1 mg kg^{-1} in 15 min	75–225	8	14 mg ml-1 per os
			flecainide	0	–	cardiac, neurologic, occular, GI	1–2 mg kg^{-1} for 5 min then 1.5–2 mg kg^{-1}	300–400	12	0.2–1 g ml^{-1}
			propafenone	–	–	cardiac, GI	1 mg kg^{-1} in 2 min	300–1200	8	0.5–2 g ml^{-1}

Table 29.3 (Continued)

Class	Antiarrhythmic Effects	Properties	Drug	Effect On MI[b]		Side effects	Dosage[c]		Interval Between Successive doses (h)	Antiarrhythmic effectiveness
				Ch	In		iv	PO per 24 h (mg)		
II	Beta inhibiting action	ISA +	propanolol	–	–	cardiac, arterial, sexual		80–480	6–8	
		ISA +	acebutolol	–	–	bronchiectatic		400–800	8	
		ISA -	nadolol	–	–			80–240	24	
			atenolol	–	–			50–100	12	
III	Anti thyroid like effect And Prolongation of the repolarization phase of the action potential duration		amiodarone	–	–	photo-sensitization corneal deposits, cardiac, GI, thyroid, neurologic pulmonary fibrosis	150 mg in 10 min 900 mg J^{-1}	200–600	24	
			bretylium			hypotension, GI	5 mg kg^{-1} iv then 1–2 mg min^{-1}	600	6	0.5–1.5 μ ml^{-1}
	Beta effect ISA[a]		sotalol	–	–/0	cardiac peripheral vascular obstructive pulmonary	0.5mg kg-1	160–480	24	
IV	Calcium blockers		verapamil	–	–	cardiac, GI neurologic cutaneous	10 mg in 1 min	120–480	8	
			diltiazem	–	–	cardiac, cutaneous GI, hepatic		180–360	6–8	
			bepridil	–	–	GI, cutaneous cardiac	3 mg kg^{-1}	400–1000	8	
I+			cibenzoline		–	cardiac, GI	1 mg kg^{-1} in 2 min	260–390	6	200–400 mg ml^{-1}
III+										
IV										

a. ISA, intrinsic sympathomimetic activity. b. Ch., chronotropic; In., inotropic c iv, intravenous route; PO, per os; ES, electrical seringua.

Table 29.4

Properties and administration of beta-blocking agents

ISA[a]	ESA[b] (quinidine-like)	Drug	Proteic binding (%)	Daily dosage (mg)	Interval between successive doses (h)
0	+ + +	propranolol	90	120–480	8
+	+	acebutolol	30	200–1200	12
++	+	alprenolol	85	150–600	6
++	+	oxprenolol	80	160–320	6
0	±	timolol	30	10–60	8
0	0	atenolol	5	100–300	12
0	0	metoprolol	12	100–400	6–8
0	0	nadolol	30	80–160	24
+ + +	0	pindolol	45	15–45	6–8
0	0	sotalol	0	160–480	> 24
0	0	labetalol			

[a] ISA, intrinsic sympathomimetric activity. [b] ESA, extrinsic sympathomimetric activity.

Table 29.5

Classification of antiarrhythmic drugs [191]

Class	Mechanism	Example
Ia	Sodium channel blockade	quinidine, ajmaline, procainamide
Ib	Sodium channel blockade	lidocaine, mexiletine, tocainide
Ic	Sodium channel blockade	flecainide, propafenone
II	Beta blockade	propranolo, metorprolol
III		amiodarone, sotalol
IV	Calcium channel blockade	verapamil, diltiazem

and chronic VT which occurs usually after the first week following infarction, but which may also be observed in cardiomyopathy, ventricular dysplasia, idiopathic aneurysm, mitral valve prolapse, tumors of the heart, and so forth.

Palliative methods

Cellular electrophysiological techniques have been used to classify the different antiarrhythmic drugs into four main groups [191], as shown in Table 29.5. A full discussion on the drug therapy for the treatment of VT is beyond the scope of this book. However, commonly used drugs are outlined below and further references to the advantages and disadvantages (side effects) of each are provided.

Amiodarone is widely used [192] having some advantages, such as a long half-life, but with commonly occurring side effects [193–204].

Although beta blockers do not have a direct antiarrhythmic effect, apart from sotalol, they may prevent extrasystoles induced by the autonomic nervous system by decreasing the heart rate; for example, VES occurring on waking or during exercise have a reduced frequency when treated with beta-blocking agents [205].

Verapamil [206] is a calcium antagonist which has no effect on VT except in the special case described above where VT occurs in young patients with right bundle branch block and left axis deviation.

29.3.3.4 Strategy for the use of palliative methods for the treatment of chronic recurrent VT

Ventricular tachycardia is a potentially dangerous arrhythmia which has to be controlled by antiarrhythmic therapy. Patients may be divided into two groups. The first group are those considered as low-risk cases, in whom the arrhythmia is perceived, is not too rapid, is infrequent and monomorphic. In these moderately symptomatic cases, amiodarone may be given at a moderate dose from 400–600 mg daily, before reducing to the maintenance dosage. The common class I antiarrhythmic drugs are selected by successive therapeutic trials. Treatment is prescribed orally and its effectiveness confirmed by Holter monitoring.

When VT is life-threatening, that is, there are frequent attacks of rapid polymorphic VT, degenerating to VF and associated with syncope or functional angina, the patient should not be discharged from hospital until the arrhythmia is well controlled. As the frequency of attacks may be greatly variable, it is not practical to wait for spontaneous recurrence of the arrhythmia and, therefore, provocative methods are used to trigger an attack, essentially by programmed pacing maneuvers.

Electrophysiological provocation tests are performed under the same conditions as those in which VT could be induced initially [49, 131, 136, 206–210], bearing in mind that these are not the usual conditions in which the patient lives. The choice of the most effective drug is made on the results of repeated provocative-pacing tests during drug therapy, which implies that VT can be inducible. Different criteria are used by different groups of workers which makes comparison of results difficult. First of all, there is no agreed definition in a recurrent tachycardia of its sustained or nonsustained character. Different protocols for electrical stimulation are used, stimulating different zones and cardiac chambers (Fig. 29.19).

Nevertheless, in the subgroup of patients at high risk, programmed pacing methods seem to have made an important contribution to their treatment. However, the pacing protocol must be performed under clearly defined conditions. Some groups have based their results on studies performed in the electrophysiological laboratory with antiarrhythmic drugs administered parenterally. A judicious selection of these drugs allows assessment of two or three of them at each investigation. However, the eventual effectiveness of the same drug administered orally may be different. Therefore, it may be preferable to test antiarrhythmic drugs given only orally, which implies retesting the patient after each therapeutic trial, when the concentration of the drug has reached therapeutic levels. This is time consuming and expensive.

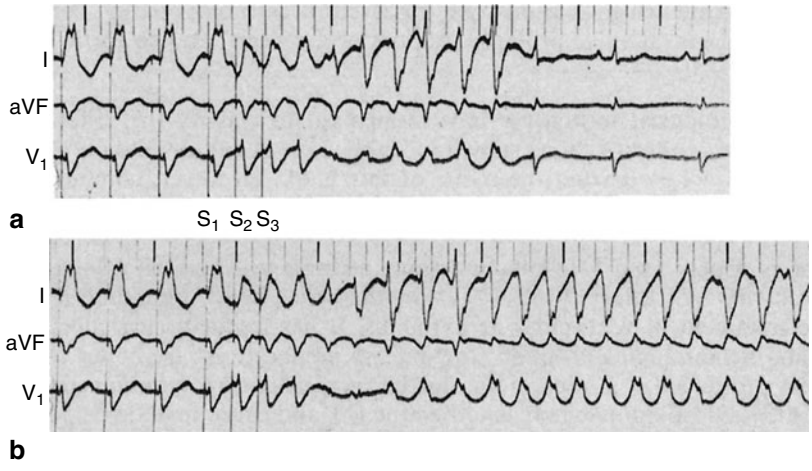

Figure 29.19

Part (a) shows the induction of nonsustained ventricular tachycardia by two premature stimuli S_2 and S_3, following a regular driven cycle. The tachycardia stops after 3 s. On tracing (b), recorded in the same patient, the same protocol induces a sustained episode of ventricular tachycardia. This suggests that each procedure has to be repeated several times, taking into consideration only the highest-grade arrhythmia obtained.

In addition to electrophysiological investigation, the authors' policy is to perform exercise-stress testing. This allows an evaluation of the antiarrhythmic effect on remaining VES and, above all, aims to confirm the absence of VT during exercise.

The absence of VT on repeated 24-hour Holter recordings during antiarrhythmic therapy seems to be a reliable prognostic factor [211]. This is an important investigation as the patient is assessed under everyday living conditions [212].

Whatever the results with the different antiarrhythmic drugs used, there seem to be two major factors which influence the risk of sudden or cardiac death as follows:

- Myocardial function, which may be assessed by the New York Heart Association functional classification – patients in stage IV have a higher risk of sudden and cardiac death [213, 214];
- The ability to trigger VT despite antiarrhythmic therapy [207, 215].

However, several points must be remembered. First, all antiarrhythmic drugs may aggravate or even provoke ventricular arrhythmias. This has been reported with quinidine, procainamide [216], amiodarone [217], disopyramide, propranolol, pendolol, mexiletine, tocainide, aprindine, propafenone [218, 219], encainide [220] and flecainide [221, 222]. Secondly, most antiarrhythmic agents have potentially dangerous hemodynamic effects, especially in severe cardiac disease. The risk is even higher when several antiarrhythmics are used in association [223]. Finally, any exacerbation of a stable arrhythmia should alert the physician to an aggravation of myocardial function.

Inefficacy of antiarrhythmic therapy

A number of precautions must be observed before confirming that an antiarrhythmic drug is inefficient. Sufficient time must be allowed for the plasma concentrations to reach therapeutic levels. When drug dosage is not readily available, this interval is estimated to be about five times the drug's half-life. In the case of amiodarone, which has a very long half-life compared to other antiarrhythmic drugs, the delay would be unacceptably long and so measures are taken to shorten it by using loading doses (up to 1200 mg of amiodarone per day). When an antiarrhythmic agent is judged to be ineffective, drugs of a different group should be tried if necessary in association with drugs of another group or subgroup (e.g., quinidine, mexiletine or beta blocker, flecainide, etc.) [224].

The implantable defibrillator

The implantable defibrillator is a considerable technological achievement. It was originally designed to prevent sudden death due to ventricular fibrillation, but it is now often used to treat rapid resistant VT [226, 227]. This device is capable of storing energy of 25–30 J in a capacitor which charges when the arrhythmia occurs. An internal electric shock is delivered after an interval of less than 30 s following the onset of the arrhythmia. The theoretical total capacity is 100 shocks. Several improvements have been made to the original design. Defibrillation was initially performed using a spring electrode positioned in the superior vena cava and another patch-shaped metallic electrode positioned at the apex of the left ventricle. This design has been replaced by two epicardial patches, and since 1991, by an intracardiac coil-shaped electrode, including bipolar sensing and pacing distal electrodes for tachycardia interruption and bradycardia prevention. A microcomputer stores the number of shocks delivered, the electrograms of each arrhythmia detected, and the amount of energy remaining. The use of this device is indicated for patients with ventricular arrhythmias which start as VF, and for VT interruption.

When the patients cannot be treated by antiarrhythmic drugs, surgical ablation of the arrhythmogenic substrate, the first radical treatment, is seldom used nowadays, due to its risks of complications. It has been superseded by transcutaneous catheter ablation techniques [228, 229].

29.3.3.5 Radical treatment

There are two radical methods of treating VT: surgery and by definitive medical treatment, namely, catheter ablation using radiofrequency methods, or sometimes fulguration.

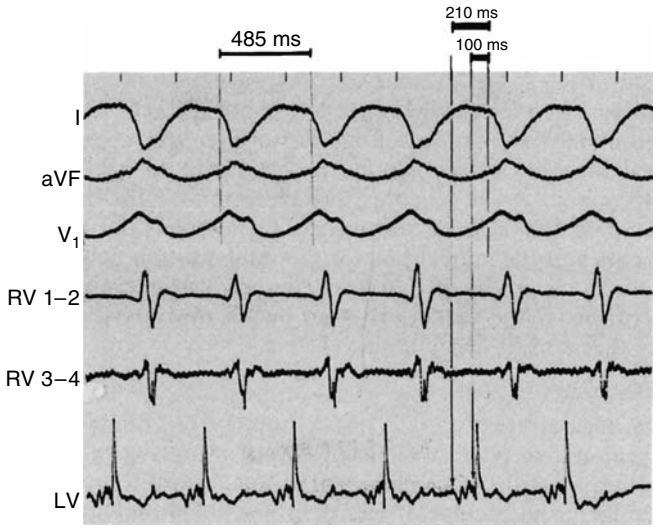

Figure 29.20

Endocardial mapping during ventricular tachycardia using a bipolar catheter located inside the left ventricle. Fragmented activity is seen on this lead (LV). A large potential is observed 100 ms before the onset of the surface QRS complex. Note also that fragmented activity is also obtained 210 ms before QRS complexes. The right ventricle is activated later, confirming that the tachycardia originates on the left side of the heart. RV 1–2 and RV 3–4 are two bipolar tracings from a bipolar right ventricular lead.

Surgery

The surgical treatment of VT is reviewed by Fontaine et al. [230]. The classical treatment of VT complicating coronary artery disease involved two main techniques: aneurysmectomy based on the perioperative findings and myocardial revascularization by coronary bypass grafting (saphenous vein or mammary artery). However, these two methods were not always effective as VT recurred in 30 to 40% of operated patients. New surgical techniques have been developed in the late seventies, based on the result of preoperative endocardial and perioperative epicardial mapping (simple ventriculotomy, encircling endocardial ventriculotomy, subendocardial excision, cryosurgery, and perioperative laser).

The site of origin of VT is determined either preoperatively or perioperatively. The former uses an endocardial recording catheter. The results depend on the thorough manipulation of the catheter within the left ventricle, usually around a myocardial scar. This method involves the following processes:

- the recording of fragmented low-amplitude diastolic potentials usually detected in the zone of the aneurysm [129, 231] which indicate areas of abnormal conduction but which do not actually determine the site of origin,
- the recording of the earliest potential during induced VT (Fig. 29.20), and
- the reproduction of the morphology of the documented VT by stimulation at different points within the ventricle.

The perioperative method involves endocardial mapping and, above all, endocavitary recording during induced VT to determine the earliest potential during the arrhythmia (Fig. 29.9) (during normothermia). The point of breakthrough of VT can thereby be determined with more accuracy in order to guide the surgical action (Figs. 29.4 and 29.12).

The use of techniques based on electrophysiology should be adapted to the type of anatomopathological lesion. An important case is the ventricular aneurysm [232]. After opening the aneurysm, endocavitary mapping is performed. This may be followed by various alternatives as follows:

- Encircling endocardial ventriculotomy [233, 234] with the aim of interrupting the reentrant phenomenon without too much damage to the healthy myocardium;

- Subendocardial resection;
- Cryosurgery aimed at destroying or excluding the zone of abnormal conduction by freezing; and later,
- The use of preoperative laser treatment with the same objective as cryosurgery, but whose action is more rapid and less traumatic;
- Cardiomyoplasty.

These techniques may be associated with excision of the fibrous wall of the ventricular aneurysm, which gives an improved ventricular ejection fraction by remodelling the left ventricle. In addition, myocardial revascularization may be indicated [235, 236].

Other pathologies [237] and their treatments include the following:

- Arrhythmogenic right ventricular dysplasia which can be treated by simple ventriculotomy or resection of the dysplasic zones if not too extensive [238–240];
- Dilated cardiomyopathy with ventricular arrhythmias which can be treated by simple ventriculotomy when the patient's condition permits;
- Ventricular arrhythmias complicating cardiac tumors which can sometimes be cured when the tumor is resectable, although benign primary cardiac tumors are rare in adults; and
- Idiopathic VT, which can be treated by simple ventriculotomy or subendocardial excision;
- Catheter ablation.

After localizing the point of origin of VT by endocardial mapping with a mapping catheter, the arrhythmia may then be treated by applying a destructive energy at the distal electrode of the same catheter. Fulguration was the first to be applied, using the energy of an external cardiac defibrillator. It has been substituted by the thermal energy of radiofrequency ablation in the early 90's for safety reasons and for improved accuracy. The acute efficacy of this technique is tested by using the usual protocols of provocative pacing to try to reinitiate clinical VT immediately after the ablation and then ten days later. This later investigation seems to have a better predictive value.

The fulguration technique proved to be a very successful method in an evaluation of a series of 38 consecutive cases [241, 242]. It has the advantage of being applicable to patients for whom surgery has been refused because of their poor general condition and the extent of myocardial damage [243]. Owing to its excellent results, this technique has been extended to less critical cases. However, the method is long and difficult, and several sessions are necessary in half of the cases. It is also necessary to use antiarrhythmic drugs in 50% of the patients. Nevertheless, improvements should be possible in order to produce optimal results.

In practice, radical forms of treatment of VT are indicated in the following situations [244]: cases of VT with proven resistance to different antiarrhythmic agents and documented spontaneous recurrences, and cases of VT treated effectively by antiarrhythmic drugs but in which there is a surgical indication for myocardial revascularization. Ventriculotomy, plication of an aneurysm, or cryosurgery may be the associated methods in the latter situation.

References

1. Vassale, M., Physiological basis of normal and abnormal automaticity. In: Rosenbaum MB, Elizari MV, eds. Frontiers of Cardiac Electrophysiology. The Hague: Nijhoff, 1983:120–43.
2. Josephson, M.E., L.N. Horowitz, A. Farshidi, et al., Recurrent sustained ventricular tachycardia. 1. Mechanisms. *Circulation*, 1978;**57**: 431–40.
3. Cranefield, P.F., Ventricular fibrillation. *N. Engl. J. Med.*, 1973;**289**: 732–6.
4. Bozler, E., The initiation of impulses in cardiac muscle. *Am. J. Physiol.*, 1943;**138**: 273–82.
5. Segers, M., Le role des potentiels tardifs du coeur. Mem. Acad. *R. Med. Belg*, 1941;**1**: 1–30.
6. Cranefield, P.F., Action potentials, afterpotentials, and arrhythmias. *Circ. Res.*, 1977;**41**: 415–23.
7. Cranefield, P.F. and R.S. Aronson, Initiation of sustained rhythmic activity by single propagated action potentials in canine cardiac Purkinje fibers exposed to sodium-free solution or to ouabain. *Circ. Res.*, 1974;**34**: 477–81.
8. Cranefield, P.F., Triggered arrhythmias. In: Rosenbaum MB, Elizari MV, eds. *Frontiers of Cardiac Electrophysiology*. The Hague: Nijhoff, 1983:182–94.
9. Wit, A.L., P.A. Boyden, D.C. Gadsby, et al., Triggered activity as a cause of atrial arrhythmias. In: Narula OS, ed. *Cardiac*

Arrhythmias: Electrophysiology, Diagnosis and Management. Baltimore, Maryland: Williams and Wilkins, 1979:14–31.
10. Coraboeuf, E., E. Deroubaix, and A. Coulombe, Acidosis-induced abnormal repolarization and repetitive activity in isolated dog Purkinje fibres. *J. Physiol.*, (Paris) 1980;**76**: 97–106.
11. Coulombe, A., E. Coraboeuf, C. Malecot, et al., Role of the "Na window" current and other ionic currents in triggering early after-depolarizations and resulting re-excitations in Purkinje fibers. In: Zipes DP, Jalife J, eds. *Cardiac Electrophysiology and Arrhythmias*. Orlando: Grune & Stratton, 1985:43–49.
12. Pinet, C., B. Le Grand, G.W. John, et al., Thrombin facilitation of voltage-gated sodium channel activation in human cardiomyocytes: Implications for ischemic sodium loading. *Circulation*, 2002;**106**: 2098–2103.
13. Abriel, H., C. Cabo, X.H. Wehrens, et al., Novel arrhythmogenic mechanism revealed by a long-QT syndrome mutation in the cardiac Na(+) channel. *Circ. Res.*, 2001;**88**: 740–745.
14. January, C.T. and H.A. Fozzard, Delayed afterdepolarizations in heart muscle: mechanisms and relevance. *Pharmacol. Rev.*, 1988;**40**: 219–227.
15. Wit, A.L. and M.R. Rosen, Afterdepolarizations and triggered activity: distinction from automaticity as an arrhythmogenic mechanism. In: Fozzard HA, Habert E, Jennings RB, Katz AM, Morgan HE, eds. *The Heart and Cardiovascular System: Scientific Foundations 2nd ed*. New York, NY: Raven Press, 1992:2113–2163.
16. Colquhoun, D., Neher, E., Reuter, H., et al., Inward current channels activated by intracellular Ca in cultured cardiac cells. *Nature*, 1981;**294**: 752–754.
17. Zygmunt, A.C., R.J. Goodrow, and C.M. Weigel, INaCa and ICl(Ca) contribute to isoproterenol-induced delayed after depolarizations in midmyocardial cells. *Am. J. Physiol.*, 1998;**275**: H1979–H1992.
18. Lipp, P. and L. Pott, Transient inward current in guinea-pig atrial myocytes reflects a change of sodium-calcium exchange current. *J. Physiol.*, 1988;**397**: 601–630.
19. Benardeau, A., S.N. Hatem, C. Rucker-Martin, et al., Contribution of Na + /Ca2+ exchange to action potential of human atrial myocytes. *Am. J. Physiol.*, 1996;**271**: H1151–H1161.
20. Pogwizd, S.M., K. Schlotthauer, L. Li, et al., Arrhythmogenesis and contractile dysfunction in heart failure: Roles of sodium-calcium exchange, inward rectifier potassium current, and residual beta-adrenergic responsiveness. *Circ. Res.*, 2001;**88**: 1159–1167.
21. Moe, G.K. and C. Mendez, The physiologic basis of reciprocal rhythm. *Prog. Cardiovasc. Dis.*, 1966;**8**: 461–482.
22. Wellens, H.J., D.R. Duren, and K.I. Lie., Observations on mechanisms of ventricular tachycardia in man. *Circulation*, 1976;**54**: 237–244.
23. Richards, D.A., G.J. Blake, J.F. Spear, et al., Electrophysiologic substrate for ventricular tachycardia: correlation of properties in vivo and in vitro. *Circulation*, 1984;**69**: 369–381.
24. Welch, W.J., B. Strasberg, A. Coelho, et al., Sustained macroreentrant ventricular tachycardia. *Am. Heart. J.*, 1982;**104**: 166–169.
25. Lloyd, E.A., D.P. Zipes, J.J. Heger, et al., Sustained ventricular tachycardia due to bundle branch reentry. *Am. Heart. J.*, 1982;**104**: 1095–1097.
26. Rosen, M.R. and P.J. Danilo, The electrophysiological basis for cardiac arrhythmias. In: Narula OS, ed. *Cardiac Arrhythmias: Electrophysiology, Diagnosis and Management*. Baltimore, Maryland: Williams and Wilkins, 1979:3–13.
27. Boineau, J.P. and J.L. Cox, Slow ventricular activation in acute myocardial infarction. A source of re-entrant premature ventricular contractions. *Circulation*, 1973;**48**: 702–713.
28. El-Sherif, N., B.J. Scherlag, R. Lazzara, et al., Re-entrant ventricular arrhythmias in the late myocardial infarction period. 1. Conduction characteristics in the infarction zone. *Circulation*, 1977;**55**: 686–702.
29. El-Sherif, N., R.R. Hope, B.J. Scherlag, et al., Re-entrant ventricular arrhythmias in the late myocardial infarction period. 2. Patterns of initiation and termination of re-entry. *Circulation*, 1977;**55**: 702–719.
30. Fontaine, G., G. Guiraudon, and R. Frank, Intramyocardial conduction defects in patients prone to chronic ventricular tachycardia. I. The post-excitation syndrome in sinus rhythm. In: Sandoe E, Julian DG, Bell JW, eds. *Management of Ventricular Tachycardia*. Role of Mexiletine. Amsterdam: *Excerpta. Medica.*, 1978:39–55.
31. Fontaine, G., G. Guiraudon, and R. Frank, Intramyocardial conduction defects in patients prone to ventricular tachycardia. II. A dynamic study of the post-excitation syndrome. In: Sandoe E, Julian DG, Bell JW, eds. Management of Ventricular Tachycardia. Role of Mexiletine. Amsterdam: *Excerpta. Medica.*, 1978:56–66.
32. Fontaine, G., G. Guiraudon, and R. Frank, The pathophysiology of chronic disturbances of ventricular rhythm. In: Masoni A, Alboni E, eds. Cardiac Electrophysiology Today. London: Academic Press, 1982:251–71.
33. Fontaine, G., G. Guiraudon, and R. Frank, Intramyocardial conduction defects in patients prone to ventricular tachycardia. In: Sandoe E, Julian DG, Bell JW, eds. Management of Ventricular Tachycardia. Role of Mexiletine. Amsterdam: *Excerpta. Medica.*, 1978:67–79.
34. Wit, A.L., M.A. Allessie, F.M. Bonke, et al., Excitation of the infarcted canine heart during initiation of ventricular tachycardia by premature impulses. *Circulation*, 1980;**62** (Suppl. 3): 195.
35. Janse, M.J., F.J. van Capelle, H. Morsink, et al., Flow of "injury" current and patterns of excitation during early ventricular arrhythmias in acute regional myocardial ischemia in isolated porcine and canine hearts. Evidence for two different arrhythmogenic mechanisms. *Circ. Res.*, 1980;**47**: 151–165.
36. Motte, G., Digitalis-induced ventricular arrhythmias. Apropos of oscillating post-potentials. *Arch. Mal. Coeur. Vaiss.*, 1979;**72**: 311–316.
37. de Bakker, J.M., F.J. van Capelle, M.J. Janse, et al. Slow conduction in the infarcted human heart. 'Zigzag' course of activation. *Circulation*, 1993;**88**: 915–926.
38. Brugada, P., H.J.J. Wellens, The role of triggered activity in clinical arrhythmias. In: Rosenbaum MB, Elizari MV, eds. *Frontiers of Cardiac Electrophysiology*. The Hague: Nijhoff, 1983: 195–216.
39. Haissaguerre, M., D.C. Shah, P. Jais, et al., Role of Purkinje conducting system in triggering of idiopathic ventricular fibrillation. *Lancet.*, 2002;**359**: 677–678.
40. Schamroth, L., *The Disorders of Cardiac Rhythm*. Oxford: Blackwell, 1971.
41. Zipes, D.P., Specific arrhythmias: Diagnosis and treatment. In: Braunwald E, ed. Heart Disease: A Textbook of Cardiovascular Medicine. Philadelphia: Saunders, 1984:683–743.
42. Rosenbaum, M.B., Classification of ventricular extrasystoles according to form. *J. Electrocardiol.*, 1969;**2**: 289–297.

43. Josephson, M.E., L.N. Horowitz, A. Farshidi, et al., Recurrent sustained ventricular tachycardia. 4. Pleomorphism. *Circulation*, 1979;**59**: 459–468.
44. Krishnaswami, V. and A.R. Geraci, Permanent pacing in disorders of sinus node function. *Am. Heart. J.*, 1975;**89**: 579–585.
45. Josephson, M.E., L.N. Horowitz, A. Farshidi, et al., Recurrent sustained ventricular tachycardia. 2. Endocardial mapping. *Circulation*, 1978;**57**: 440–447.
46. Josephson, M.E., H.L. Waxman, F.E. Marchlinski, et al., Electrocardiographic features of ectopic impulse formation. Specificity of ventricular activation patterns. In: Josephson ME, Wellens HJJ, eds. *Tachycardias: Mechanisms, Diagnosis, Treatment*. Philadelphia, Pennsylvania: Lea and Febiger, 1984: 363–386.
47. Coumel, P., When should ventricular extrasystole be treated?. *Presse Med* 1983;**12**: 2663–2665.
48. Brodsky, M., D. Wu, P. Denes, et al., Arrhythmias documented by 24 hour continuous electrocardiographic monitoring in 50 male medical students without apparent heart disease. *Am. J. Cardiol.*, 1977;**39**: 390–395.
49. Rodstein, M., L. Wolloch, and R.S. Gubner, Mortality study of the significance of extrasystoles in an insured population. *Circulation*, 1971;**44**: 617–625.
50. Hinkle, L.E., Jr., S.T. Carver, and M. Stevens, The frequency of asymptomatic disturbances of cardiac rhythm and conduction in middle-aged men. *Am. J. Cardiol*, 1969;**24**: 629–650.
51. Medvedowsky, J.L., C. Barnay, C.Massat, Evolution des arythmies ventriculaires après infarctus du myocarde. Intérêt des enregistrements électrocardiographiques de longue durée. Résultats préliminaires. *Arch. Mal. Coeur. Vaiss.*, 1981;**74**: 809–819.
52. Kennedy, H.L. and S.J. Underhill, Frequent or complex ventricular ectopy in apparently healthy subjects: a clinical study of 25 cases. *Am. J. Cardiol.*, 1976;**38**: 141–148.
53. Lown, B., Sudden cardiac death: the major challenge confronting contemporary cardiology. *Am. J. Cardiol.*, 1979;**43**: 313–328.
54. Rodriguez, L.M., J.L. Smeets, C. Timmermans, et al., Predictors for successful ablation of right- and left-sided idiopathic ventricular tachycardia. *Am. J. Cardiol.*, 1997;**79**: 309–314.
55. Tanner, H., G. Hindricks, P. Schirdewahn, et al., Outflow tract tachycardia with R/S transition in lead V3: six different anatomic approaches for successful ablation. *J. Am. Coll. Cardiol.*, 2005;**45**: 418–423.
56. Ouyang, F., P. Fotuhi, S.Y. Ho, et al., Repetitive monomorphic ventricular tachycardia originating from the aortic sinus cusp: electrocardiographic characterization for guiding catheter ablation. *J. Am. Coll. Cardiol.*, 2002;**39**: 500–508.
57. Faris, J.V., P.L. McHenry, J.W. Jordan, et al., Prevalence and reproducibility of exercise-induced ventricular arrhythmias during maximal exercise testing in normal men. *Am. J. Cardiol.*, 1976;**37**: 617–622.
58. Udall, J.A. and M.H. Ellestad, Predictive implications of ventricular premature contractions associated with treadmill stress testing. *Circulation*, 1977;**56**: 985–989.
59. McHenry, P.L., S.N. Morris, M. Kavalier, et al., Comparative study of exercise-induced ventricular arrhythmias in normal subjects and patients with documented coronary artery disease. *Am. J. Cardiol.*, 1976;**37**: 609–616.
60. Crow, R., R. Prineas, and H. Blackburn, The prognostic significance of ventricular ectopic beats among the apparently healthy. *Am. Heart. J.*, 1981;**101**: 244–248.
61. Viskin, S., R. Rosso, O. Rogowski, et al., The "Short-Coupled" Variant of Right Ventricular Outflow Ventricular Tachycardia: A Not-So-Benign Form of Benign Ventricular Tachycardia? *Journal of Cardiovascular Electrophysiology*, 2005;**16**: 1–5.
62. Fontaine, G.H., P. Fornes, J.L. Hebert, et al., Ventricular tachycardia in arrhythmogenic right ventricular cardiomyopathies. In: Zipes DP, Jalife J, eds. *Cardiac electrophysiology: from cell to bedside*. Syracuse, New York: Saunders, 2004:588–600.
63. Hinkle, L.E., S.T. Carver, D.C. Argyros, The prognostic significance of ventricular premature contractions in healthy people and in people with coronary heart disease. *Acta. Cardiol.*, 1974;**18** Suppl: 5–32.
64. Rabkin, S.W., F.A. Mathewson, and R.B. Tate, Relationship of ventricular ectopy in men without apparent heart disease to occurrence of ischemic heart disease and sudden death. *Am. Heart. J.*, 1981;**101**: 135–142.
65. The coronary drug project: Post-infarction electrocardiographic findings and prognosis. *Circulation*, 1971; **44** (Suppl. 2):154.
66. Kennedy, H.L., J.E. Pescarmona, R.J. Bouchard, et al., Coronary artery status of apparently healthy subjects with frequent and complex ventricular ectopy. *Ann. Intern. Med.*, 1980;**92**: 179–185.
67. Chiang, B.N., L.V. Perlman, M. Fulton, et al., Predisposing factors in sudden cardiac death in Tecumseh, Michigan. A prospective study. *Circulation*, 1970;**41**: 31–37.
68. de Soyza, N., J.K. Bissett, J.J. Kane, et al., Ectopic ventricular prematurity and its relationship to ventricular tachycardia in acute myocardial infarction in man. *Circulation*, 1974;**50**: 529–33.
69. Campbell, R.W., A. Murray, and D.G. Julian, Ventricular arrhythmias in first 12 hours of acute myocardial infarction. Natural history study. *Br. Heart. J.*, 1981;**46**: 351–357.
70. Vismaria, L.A., A.N. DeMaria, J.L. Hughes, et al., Evaluation of arrhythmias in the late hospital phase of acute myocardial infarction compared to coronary care unit ectopy. *Br. Heart. J.*, 1975;**37**: 598–603.
71. Lown, B. and M. Wolf, Approaches to sudden death from coronary heart disease. *Circulation*, 1971;**44**: 130–142.
72. Roberts, R., H.D. Ambos, C.W. Loh, et al., Initiation of repetitive ventricular depolarizations by relatively late premature complexes in patients with acute myocardial infarction. *Am. J. Cardiol.*, 1978;**41**: 678–683.
73. von Olshausen, K., F. Schwarz, J. Apfelbach, et al., Determinants of the incidence and severity of ventricular arrhythmias in aortic valve disease. *Am. J. Cardiol.*, 1983;**51**: 1103–1109.
74. Juillard, A., A. Bouajina, B. Frechon, et al., Significance of repetitive ventricular extrasystoles in the acute phase of myocardial infarction. *Arch. Mal. Coeur. Vaiss.*, 1984;**77**: 121–127.
75. Roberts, R., A. Husain, H.D. Ambos, et al., Relation between infarct size and ventricular arrhythmia. *Br. Heart. J.*, 1975;**37**: 1169–1175.
76. de Soyza, N., Bennett, F.A., Murphy, M.L., et al., The relationship of paroxysmal ventricular tachycardia complicating the acute phase and ventricular arrhythmia during the late hospital phase of myocardial infarction to long-term survival. *Am. J. Med.*, 1978;**64**: 377–381.
77. Fazzini, P.F., F. Marchi, and P. Pucci, Effects of verapamil in ventricular premature beats of acute myocardial infarction. *Acta. Cardiol.*, 1978;**33**: 25–29.
78. Wyman, M.G., Prevention of primary ventricular fibrillation in acute myocardial infarction. *Am. J. Cardiol.*, 1972; **29**:298.

79. Tonet, J.L., P. Lechat, R. Frank, et al., Electrocardiographic effects and antiarrhythmic action of 1200 mg of oral amiodarone per day. *Ann. Cardiol. Angeiol.*, (Paris) 1984; **33**:309–315.
80. DeBusk, R.F., D.M. Davidson, N. Houston, et al., Serial ambulatory electrocardiography and treadmill exercise testing after uncomplicated myocardial infarction. *Am. J. Cardiol.*, 1980;**45**: 547–554.
81. Moss, A.J., J.J. DeCamilla, H.P. Davis, et al., Clinical significance of ventricular ectopic beats in the early posthospital phase of myocardial infarction. *Am. J. Cardiol.*, 1977;**39**: 635–640.
82. Vismara, L.A., E.A. Amsterdam, D.T. Mason, Relation of ventricular arrhythmias in the late hospital phase of acute myocardial infarction to sudden death after hospital discharge. *Am. J. Med.*, 1975;**59**: 6–12.
83. The coronary drug project: Prognostic importance of premature beats following myocardial infarction. Experience in the coronary drug project. *JAMA*, 1973;**223**: 1116–1124.
84. Califf, R.M., J.M. Burks, and V.S. Behar, et al., Relationships among ventricular arrhythmias, coronary artery disease, and angiographic and electrocardiographic indicators of myocardial fibrosis. *Circulation*, 1978;**57**: 725–732.
85. Ruberman, W., E. Weinblatt, C.W. Frank, et al., Ventricular premature beats and mortality of men with coronary heart disease. *Circulation*, 1975;**52**: III 199–203.
86. Horowitz, L.N. and J. Morganroth, Can we prevent sudden cardiac death? *Am. J. Cardiol.*, 1982;**50**: 535–538.
87. Moss, A.J., H.T. Davis, J. DeCamilla, et al., Ventricular ectopic beats and their relation to sudden and nonsudden cardiac death after myocardial infarction. *Circulation*, 1979;**60**: 998–1003.
88. Laurent, M., B. Miane, C. Almange, et al., Comparison of data from exercise tests and continuous electrocardiographic recording in patients with ventricular extrasystole. Apropos of 131 cases. *Arch. Mal. Coeur. Vaiss.*, 1982;**75**: 653–662.
89. Davis, H.T., J. DeCamilla, L.W. Bayer, et al., Survivorship patterns in the posthospital phase of myocardial infarction. *Circulation*, 1979;**60**: 1252–1258.
90. Schulze, R.A., Jr., H.W. Strauss, and B. Pitt, Sudden death in the year following myocardial infarction. Relation to ventricular premature contractions in the late hospitals phase and left ventricular ejection fraction. *Am. J. Med.*, 1977;**62**: 192–199.
91. Greene, H.L., P.R. Reid, and A.H. Schaeffer, The repetitive ventricular response in man. A predictor of sudden death. *N. Engl. J. Med.*, 1978;**299**: 729–734.
92. Calvert, A., B. Lown, and R. Gorlin, Ventricular premature beats and anatomically defined coronary heart disease. *Am. J. Cardiol.*, 1977;**39**: 627–634.
93. Uretz, E.F., P. Denes, N. Ruggie, et al., Relation of ventricular premature beats to underlying heart disease. *Am. J. Cardiol.*, 1984; **53**:774–80.
94. Bigger, J.T., Jr., F.M. Weld, and L.M. Rolnitzky, Which postinfarction ventricular arrhythmias should be treated? *Am. Heart. J.*, 1982;**103**: 660–666.
95. Winkle, R.A., The relationship between ventricular ectopic beat frequency and heart rate. *Circulation*, 1982;**66**: 439–46.
96. Helfant, R.H., R. Pine, V. Kabde, et al., Exercise-related ventricular premature complexes in coronary heart disease. Correlations with ischemia and angiographic severity. *Ann. Intern. Med.*, 1974;**80**: 589–592.
97. Schulze, R.A., Jr., J. Rouleau, P. Rigo, et al., Ventricular arrhythmias in the late hospital phase of acute myocardial infarction. Relation to left ventricular function detected by gated cardiac blood pool scanning. *Circulation*, 1975;**52**: 1006–1011.
98. Ruberman, W., E. Weinblatt, and J.D. Goldberg, et al., Ventricular premature beats and mortality after myocardial infarction. *N. Engl. J. Med.*, 1977;**297**: 750–757.
99. Moss, A.J., J. DeCamilla, F. Engstrom, et al., The posthospital phase of myocardial infarction: identification of patients with increased mortality risk. *Circulation*, 1974;**49**: 460–466.
100. Moss, A.J., Update of postinfarction-risk stratification: physiologic variables. *Ann. N. Y. Acad. Sci.*, 1984;**427**: 280–285.
101. Graboys, T.B., Premature ventricular contractions. In: Harrison DC, ed. *Cardiac Arrhythmias: A Decade of Progress*. Boston, Massachusetts: Hall, 1981:567.
102. Zaret, B.L. and C.R.J Conti, Exercise-induced ventricular irritability: Hemodynamic and angiographic correlations. *Am. J. Cardiol.*, 1972;**29**: 298.
103. Bjarnason, I., T. Hardarson, and S. Jonsson, Cardiac arrhythmias in hypertrophic cardiomyopathy. *Br. Heart. J.*, 1982;**48**: 198–203.
104. Savage, D.D., S.F. Seides, B.J. Maron, et al., Prevalence of arrhythmias during 24-hour electrocardiographic monitoring and exercise testing in patients with obstructive and nonobstructive hypertrophic cardiomyopathy. *Circulation*, 1979;**59**: 866–875.
105. Ingham, R.E., Rossen, R.M., Goodman, D.J., et al., Ambulatory electrocardiographic monitoring in idiopathic hypertrophic subaortic stenosis. *Circulation*, 1975;**52** (Suppl. 2): 93.
106. Maron, B.J., Savage, D.D., Wolfson, J.K., et al., Prognostic significance of 24 hour ambulatory electrocardiographic monitoring in patients with hypertrophic cardiomyopathy: a prospective study. *Am. J. Cardiol.*, 1981;**48**: 252–257.
107. Maron, B.J., W.C. Roberts, and S.E. Epstein, Sudden death in hypertrophic cardiomyopathy: a profile of 78 patients. *Circulation*, 1982;**65**: 1388–1394.
108. Weiss, A.N., C.L. Jobe, T. Gordon, et al., Relationship of premature ventricular contractions and left ventricular hypertrophy to sudden cardiac death. *Circulation*, 1969;**40** (Suppl. 3): 213.
109. Doi, Y.L., W.J. McKenna, S. Chetty, et al., Prediction of mortality and serious ventricular arrhythmia in hypertrophic cardiomyopathy. An echocardiographic study. *Br. Heart. J.*, 1980;**44**: 150–157.
110. Maron, B.J., W.J. McKenna, G.K. Danielson, et al., American College of Cardiology/European Society of Cardiology Clinical Expert Consensus Document on Hypertrophic Cardiomyopathy. A report of the American College of Cardiology Foundation Task Force on Clinical Expert Consensus Documents and the European Society of Cardiology Committee for Practice Guidelines. *Eur. Heart. J.*, 2003;**24**: 1965–1991.
111. McKenna, W.J., S. Chetty, C.M. Oakley, et al., Exercise electrocardiographic and 48 hour ambulatory electrocardiographic monitor assessment of arrhythmia and off beta blocker therapy in hypertrophic cardiomyopathy. *Am. J. Cardiol.*, 1979;**43**: 420.
112. Bonow, R.O., T.M. Frederick, S.L. Bacharach, et al., Atrial systole and left ventricular filling in hypertrophic cardiomyopathy: effect of verapamil. *Am. J. Cardiol.*, 1983;**51**: 1386–1391.
113. Huang, S.K., J. Jones, and P. Denes, Significance of ventricular tachycardia in primary congestive cardiomyopathy. *Am. J. Cardiol.*, 1982;**49**: 1006.
114. Fuster, V., B.J. Gersh, E.R. Giuliani, et al., The natural history of idiopathic dilated cardiomyopathy. *Am. J. Cardiol.*, 1981;**47**: 525–531.

115. Silverman, K.J., G.M. Hutchins, and B.H. Bulkley, Cardiac sarcoid: a clinicopathologic study of 84 unselected patients with systemic sarcoidosis. *Circulation*, 1978;**58**: 1204–1211.
116. Charron, P., J.F. Forissier, M.E. Amara, et al., Accuracy of European diagnostic criteria for familial hypertrophic cardiomyopathy in a genotyped population. *Int. J. Cardiol.*, 2003;**90**: 33–38; discussion 38–40.
117. Winkle, R.A., M.G. Lopes, J.W. Fitzgerald, et al., Arrhythmias in patients with mitral valve prolapse. *Circulation*, 1975;**52**: 73–81.
118. DeMaria, A.N. The syndrome of mitral valve prolapse: problems and perspectives. *Ann. Intern. Med.*, 1976;**85**: 525–526.
119. Leclercq, J.F., M.C. Malergue, D. Milosevic, et al., Ventricular arrhythmias and mitral valve prolapse. A study of 35 cases. *Arch. Mal. Coeur. Vaiss.*, 1980;**73**: 276–287.
120. Campbell, R.W., M.G. Godman, G.I. Fiddler, et al., Ventricular arrhythmias in syndrome of balloon deformity of mitral valve. Definition of possible high risk group. *Br. Heart. J.*, 1976;**38**: 1053–1057.
121. Rakowski, H., M.B. Waxman, R.W. Wald, et al., Mitral valve prolapse and ventricular fibrillation. *Circulation*, 1975;**52** (Suppl. 2): 93.
122. Boudoulas, H., S.F. Schaal, J.M. Stang, et al., Mitral valve prolapse: cardiac arrest with long-term survival. *Int. J. Cardiol.*, 1990;**26**: 37–44.
123. Kligfield, P., C. Hochreiter, H. Kramer, et al., Complex arrhythmias in mitral regurgitation with and without mitral valve prolapse: contrast to arrhythmias in mitral valve prolapse without mitral regurgitation. *Am. J. Cardiol.*, 1985;**55**(13 Pt 1): 1545–1549.
124. Kennedy, H.L., S.J. Underhill, P.F. Poblete, et al., Ventricular ectopic beats in patients with aortic valve disease. *Circulation*, 1975;**52** (Suppl. 2): 202.
125. Khaja, F., A. Rastogi, J.F. Brymer, et al., Coronary anatomy and left ventricular size: Determinants of ventricular arrhythmias in aortic valve disease. *Circulation*, 1982;**66** (Suppl. 2): 355.
126. Schilling, G., T. Finkbeiner, P. Elberskirch, et al., Incidence of ventricular arrhythmias in patients with aortic valve replacement. *Am. J. Cardiol.*, 1982;**49**: 894.
127. Guerot, C., P.E. Valere, A. Castillo-Fenoy, et al., Tachycardia by branch-to-branch reentry. *Arch. Mal. Coeur. Vaiss.*, 1974;**67**: 1–11.
128. Motte, G. and R. Slama, Les Tachycardies Ventriculaires. Paris: Lab. Servier, 1979.
129. Kastor, J.A., L.N. Horowitz, A.H. Harken, et al., Clinical electrophysiology of ventricular tachycardia. *N. Engl. J. Med.*, 1981;**304**: 1004–1019.
130. Fillette, F., G. Fontaine, and Y. Grosgogeat, Ventricular tachycardia. Study methods and status of current knowledge. *Arch. Mal. Coeur. Vaiss.*, 1982;**75**: 501–505.
131. Perrot, B., B. Thiel, F. Cherrier, et al., Results of the systematic application of ventricular stimulation methods. *Arch. Mal. Coeur. Vaiss.*, 1984;**77**: 262–272.
132. Fisher, J.D., Ventricular tachycardia–practical and provocative electrophysiology. *Circulation*, 1978;**58**: 1000–1007.
133. Scheinman, M.M., Induction of ventricular tachycardia: a promising new technique or clinical electrophysiology gone awry? *Circulation*, 1978; **58**:998–999.
134. Mason, J.W. and R.A. Winkle, Electrode-catheter arrhythmia induction in the selection and assessment of antiarrhythmic drug therapy for recurrent ventricular tachycardia. *Circulation*, 1978;**58**: 971–985.
135. Mann, D.E., J.C. Luck, J.C. Griffin, et al., Induction of clinical ventricular tachycardia using programmed stimulation: value of third and fourth extrastimuli. *Am. J. Cardiol.*, 1983;**52**: 501–506.
136. Doherty, J.U., M.E. Josephson, Role of electrophysiologic testing in the therapy of ventricular arrhythmias. *Pacing Clin. Electrophysiol.*, 1983;**6**: 1070–1083.
137. Ruskin, J.N., J.P. DiMarco, and H. Garan, Out-of-hospital cardiac arrest: electrophysiologic observations and selection of long-term antiarrhythmic therapy. *N. Engl. J. Med.*, 1980;**303**: 607–613.
138. Vandepol, C.J., A. Farshidi, S.R. Spielman, et al., Incidence and clinical significance of induced ventricular tachycardia. *Am. J. Cardiol.*, 1980;**45**: 725–731.
139. Livelli, F.D., Jr. J.T. Bigger, J.A. Reiffel, et al., Response to programmed ventricular stimulation: sensitivity, specificity and relation to heart disease. *Am. J. Cardiol.*, 1982;**50**: 452–458.
140. Brugada, P., J. Brugada, L. Mont, et al., A new approach to the differential diagnosis of a regular tachycardia with a wide QRS complex. *Circulation*, 1991;**83**: 1649–1659.
141. Wellens, H.J., F.W. Bar, and K.I. Lie, The value of the electrocardiogram in the differential diagnosis of a tachycardia with a widened QRS complex. *Am. J. Med.*, 1978;**64**: 27–33.
142. Kindwall, K.E., J. Brown, and M.E. Josephson, Electrocardiographic criteria for ventricular tachycardia in wide complex left bundle branch block morphology tachycardias. *Am. J. Cardiol.*, 1988;**61**: 1279–1283.
143. Reddy, C.P. and L.S. Gettes, Use of isoproterenol as an aid to electric induction of chronic recurrent ventricular tachycardia. *Am. J. Cardiol.*, 1979;**44**: 705–713.
144. Doherty, J.U., Kienzle, M.G., Waxman, H.L., et al., Programmed ventricular stimulation at a second right ventricular site: an analysis of 100 patients, with special reference to sensitivity, specificity and characteristics of patients with induced ventricular tachycardia. *Am. J. Cardiol.*, 1983;**52**: 1184–1189.
145. Morady, F., D. Hess, and M.M. Scheinman, Electrophysiologic drug testing in patients with malignant ventricular arrhythmias: importance of stimulation at more than one ventricular site. *Am. J. Cardiol.*, 1982;**50**: 1055–1060.
146. Swerdlow, C.D., J. Blum, R.A. Winkle, et al., Decreased incidence of antiarrhythmic drug efficacy at electrophysiologic study associated with the use of a third extrastimulus. *Am. Heart. J.*, 1982;**104**: 1004–1011.
147. Graboys, T.B., The stampede to stimulation–numerators and denominators revisited relative to electrophysiologic study of ventricular arrhythmias. *Am. Heart. J.*, 1982;**103**: 1089–1090.
148. Akhtar, M., The clinical significance of the repetitive ventricular response. *Circulation*, 1981;**63**: 773–775.
149. Grenadier, E., Alpan, G., Maor, N., et al., Polymorphous ventricular tachycardia in acute myocardial infarction. *Am. J. Cardiol.*, 1984;**53**: 1280–1283.
150. Cohen, M., I. Wiener, A. Pichard, et al., Determinants of ventricular tachycardia in patients with coronary artery disease and ventricular aneurysm. Clinical, hemodynamic, and angiographic factors. *Am. J. Cardiol.*, 1983;**51**: 61–64.
151. Medvedowsky, J.L., C. Barnay, C. Arnaud, et al., Course of ventricular arrhythmias following myocardial infarction. Results of a 2-year follow-up. *Arch. Mal. Coeur. Vaiss.*, 1984;**77**: 754–765.
152. A comparison of antiarrhythmic-drug therapy with implantable defibrillators in patients resuscitated from near-fatal ventricular

arrhythmias. The Antiarrhythmics versus Implantable Defibrillators (AVID) Investigators. *N. Engl. J. Med.*, 1997;**337**: 1576–1583.
153. Kuck, K.H., R. Cappato, J. Siebels, et al., Randomized comparison of antiarrhythmic drug therapy with implantable defibrillators in patients resuscitated from cardiac arrest: the Cardiac Arrest Study Hamburg (CASH). *Circulation*, 2000;**102**: 748–754.
154. Connolly, S.J., M. Gent, R.S. Roberts, et al., Canadian implantable defibrillator study (CIDS): a randomized trial of the implantable cardioverter defibrillator against amiodarone. *Circulation*, 2000;**101**: 1297–1302.
155. Buxton, A.E., K.L. Lee, J.D. Fisher, et al., A randomized study of the prevention of sudden death in patients with coronary artery disease. Multicenter Unsustained Tachycardia Trial Investigators. *N. Engl. J. Med.*, 1999;**341**: 1882–1890.
156. Moss, A.J., W. Zareba, W.J. Hall, et al., Prophylactic implantation of a defibrillator in patients with myocardial infarction and reduced ejection fraction. *N. Engl. J. Med.*, 2002;**346**: 877–883.
157. Moss, A.J., W.J. Hall, D.S. Cannom, et al., Improved survival with an implanted defibrillator in patients with coronary disease at high risk for ventricular arrhythmia. Multicenter Automatic Defibrillator Implantation Trial Investigators. *N. Engl. J. Med.*, 1996;**335**: 1933–1940.
158. Leclerq, J.F., P. Maisonblanche, B. Cauchemez, et al., Ventricular rhythm disorders in congestive myocardiopathy. *Arch. Mal. Coeur. Vaiss.*, 1984;**77**: 937–945.
159. Johnson, R.A., I. Palacios, Dilated cardiomyopathies of the adult (first of two parts). *N. Engl. J. Med.*, 1982;**307**: 1051–1058.
160. Bardy, G.H., K.L. Lee, D.B. Mark, et al., Amiodarone or an implantable cardioverter-defibrillator for congestive heart failure. *N. Engl. J. Med.*, 2005;**352**: 225–237.
161. Bristow, M.R., Saxon, L.A., Boehmer, J., et al., Cardiac-resynchronization therapy with or without an implantable defibrillator in advanced chronic heart failure. *N. Engl. J. Med.*, 2004;**350**: 2140–2150.
162. Maron, B.J., J. Shirani, L.C. Poliac, et al., Sudden death in young competitive athletes. Clinical, demographic, and pathological profiles. *JAMA*, 1996;**276**: 199–204.
163. Yamaguchi, H., T. Ishimura, S. Nishiyama, et al., Hypertrophic nonobstructive cardiomyopathy with giant negative T waves (apical hypertrophy): ventriculographic and echocardiographic features in 30 patients. *Am. J. Cardiol.*, 1979;**44**: 401–412.
164. Maron, B.J., W.K. Shen, M.S. Link, et al., Efficacy of implantable cardioverter-defibrillators for the prevention of sudden death in patients with hypertrophic cardiomyopathy. *N. Engl. J. Med.*, 2000;**342**: 365–373.
165. Maron, M.S., I. Olivotto, S. Betocchi, et al., Effect of left ventricular outflow tract obstruction on clinical outcome in hypertrophic cardiomyopathy. *N. Engl. J. Med.*, 2003;**348**: 295–303.
166. Jeresaty, R.M. *Mitral Valve Prolapse*. New York: Raven, 1979.
167. Gregoratos, G., J. Abrams, A.E. Epstein, et al. ACC/AHA/NASPE 2002 Guideline update for implantation of cardiac pacemakers and antiarrhythmia devices: summary article: a report of the American College of Cardiology/American Heart Association Task Force on Practice Guidelines (ACC/AHA/NASPE Committee to Update the 1998 Pacemaker Guidelines). *Circulation*, 2002;**106**: 2145–2161.
168. Marcus, F.I., G.H. Fontaine, G. Guiraudon, et al., Right ventricular dysplasia: a report of 24 adult cases. *Circulation*, 1982;**65**: 384–398.
169. Fontaine, G., G. Guiraudon, R. Frank, et al., The arrhythmogenic right ventricular dysplasia syndrome. In: Hayase S, Murao S, MacArthur C, eds. *Cardiology*. Amsterdam: Excerpta Medica, 1979: 955–958.
170. Vedel, J., R. Frank, G. Fontaine, et al., Recurrent ventricular tachycardia and parchment right ventricle in the adult. Anatomical and clinical report of 2 cases. *Arch. Mal. Coeur. Vaiss.*, 1978;**71**: 973–981.
171. Hulot, J.S., X. Jouven, J.P. Empana, et al., Natural history and risk stratification of arrhythmogenic right ventricular dysplasia/cardiomyopathy. *Circulation*, 2004;**110**: 1879–1884.
172. Fontaine, G., J. Tonet, Y. Gallais, et al., Ventricular tachycardia catheter ablation in arrhythmogenic right ventricular dysplasia: a 16-year experience. *Curr. Cardiol. Rep.*, 2000;**2**: 498–506.
173. Corrado, D., L. Leoni, M.S. Link, et al., Implantable cardioverter-defibrillator therapy for prevention of sudden death in patients with arrhythmogenic right ventricular cardiomyopathy/dysplasia. *Circulation*, 2003;**108**: 3084–3091.
174. Wichter, T., M. Paul, C. Wollmann, et al., Implantable cardioverter/defibrillator therapy in arrhythmogenic right ventricular cardiomyopathy: single-center experience of long-term follow-up and complications in 60 patients. *Circulation*, 2004;**109**: 1503–1508.
175. Chachques, J.C., P.G. Argyriadis, G. Fontaine, et al., Right ventricular cardiomyoplasty: 10-year follow-up. *Ann. Thorac. Surg.*, 2003;**75**: 1464–1468.
176. Uhl, H.S. A previously undescribed congenital malformation of the heart: almost total absence of the myocardium of the right ventricle. *Bull. Johns. Hopkins Hosp.*, 1952;**91**: 197–209.
177. Antzelevitch, C., P. Brugada, M. Borggrefe, et al., Brugada syndrome: report of the second consensus conference: endorsed by the Heart Rhythm Society and the European Heart Rhythm Association. *Circulation*, 2005;**111**: 659–670.
178. Buxton, A.E., H.L. Waxman, F.E. Marchlinski, et al., Right ventricular tachycardia: clinical and electrophysiologic characteristics. *Circulation*, 1983;**68**: 917–927.
179. Wen, M.S., Y. Taniguchi, S.J. Yeh, et al., Determinants of tachycardia recurrences after radiofrequency ablation of idiopathic ventricular tachycardia. *Am. J. Cardiol.*, 1998; **81**: 500–503.
180. Tsuchiya, T., K. Okumura, T. Honda, et al., Significance of late diastolic potential preceding Purkinje potential in verapamil-sensitive idiopathic left ventricular tachycardia. *Circulation*, 1999;**99**: 2408–2413.
181. McAllister, H.A. and J.J. Fenoglio, *Tumors of Cardiovascular System*. A.F.I.P: Bethesda, Maryland, 1978.
182. Lucet, V., J. Fidelle, D. Do N'Goc, et al., Catecholaminergic polymorphic ventricular tachycardia in children. Differential diagnosis of epilepsy. *Presse. Med.*, 1983;**12**: 102.
183. Dessertenne, F., Ventricular tachycardia with 2 variable opposing foci. *Arch. Mal. Coeur. Vaiss.*, 1966; **59**: 263–272.
184. Fontaine, G., A new look at torsades de pointes. *Ann. N. Y. Acad. Sci.*, 1992;**644**: 157–177.
185. Davidenko, J.M., Spiral wave activity: a possible common mechanism for polymorphic and monomorphic ventricular tachycardias. *J. Cardiovasc. Electrophysiol.*, 1993;**4**: 730–746.
186. Tzivoni, D., A. Keren, A.M. Cohen, et al., Magnesium therapy for torsades de pointes. *Am. J. Cardiol.*, 1984; **53**:528–30.
187. Chiang, C.E. and D.M. Roden, The long QT syndromes: genetic basis and clinical implications. *J. Am. Coll. Cardiol.*, 2000;**36**: 1–12.

188. Priori, S.G., P.J. Schwartz, C. Napolitano, et al., Risk stratification in the long-QT syndrome. *N. Engl. J. Med.*, 2003;**348**: 1866–1874.
189. Sebastien, P., M. Waynberger, P. Beaufils, et al., Isolated ventricular tachycardia without patent cardiopathy. *Arch. Mal. Coeur. Vaiss.*, 1976;**69**: 919–928.
190. Weaver, W.D., L.A. Cobb, M.K. Copass, et al., Ventricular defibrillation - a comparative trial using 175-J and 320-J shocks. *N. Engl. J. Med.*, 1982;**307**: 1101–116.
191. Vaughan-Williams, E.M., Interet des etudes experimentales d'anti-arythmiques et leur application clinique. *Coeur. Med. Interne.*, 1978;**17**: 471–489.
192. Borggrefe, M., L. Seipel, G. Breithardt, Effect of amiodarone on ventricular tachycardia. In: Breithardt G, Loogen F, eds. *New Aspects in the Medical Treatment of Tachyarrhythmias*. Munich: Urban and Schwarzenberg, 1983: 177–185.
193. Fogoros, R.N., K.P. Anderson, R.A. Winkle, et al., Amiodarone: clinical efficacy and toxicity in 96 patients with recurrent, drug-refractory arrhythmias. *Circulation*, 1983;**68**: 88–94.
194. Finerman, W.B., Jr., A. Hamer, T. Peter, et al., Electrophysiologic effects of chronic amiodarone therapy in patients with ventricular arrhythmias. *Am. Heart. J.*, 1982;**104**: 987–996.
195. Frank, R., G. Fontaine, P. Blanc, Les methodes provocatives dans l'etude de l'amiodarone per os dans les tachycardies ventriculaires et celles du syndrome de Wolff-Parkinson-White. *Colloque sur L'amiodarone*. Paris: Lab. Labaz, 1977: 35–42.
196. Morady, F., M.M. Scheinman, D.S. Hess, Amiodarone in the management of patients with ventricular tachycardia and ventricular fibrillation. *Pacing Clin. Electrophysiol.*, 1983;**6**: 609–615.
197. Morady, F., M.M. Scheinman, E. Shen, et al., Intravenous amiodarone in the acute treatment of recurrent symptomatic ventricular tachycardia. *Am. J. Cardiol.*, 1983;**51**: 156–159.
198. Waxman, H.L., W.C. Groh, F.E. Marchlinski, et al., Amiodarone for control of sustained ventricular tachyarrhythmia: clinical and electrophysiologic effects in 51 patients. *Am. J. Cardiol.*, 1982;**50**: 1066–1074.
199. Rakita, L. and S.M. Sobol, Amiodarone in the treatment of refractory ventricular arrhythmias: Importance and safety of initial high-dose therapy. *JAMA*, 1983;**250**: 1293–1295.
200. Nademanee, K., B.N. Singh, J. Hendrickson, et al., Amiodarone in refractory life-threatening ventricular arrhythmias. *Ann. Intern. Med.*, 1983;**98**: 577–584.
201. Heger, J.J., E.N. Prystowsky, W.M. Jackman, et al., Clinical efficacy and electrophysiology during long-term therapy for recurrent ventricular tachycardia or ventricular fibrillation. *N. Engl. J. Med.*, 1981;**305**: 539–545.
202. Morady, F., M.J. Sauve, P. Malone, et al., Long-term efficacy and toxicity of high-dose amiodarone therapy for ventricular tachycardia or ventricular fibrillation. *Am. J. Cardiol.*, 1983;**52**: 975–979.
203. Marcus, F.I., G.H. Fontaine, R. Frank, et al., Clinical pharmacology and therapeutic applications of the antiarrhythmic agent amiodarone. *Am. Heart. J.*, 1981;**101**: 480–493.
204. Kosinski, E.J., J.B. Albin, E. Young, et al., Hemodynamic effects of intravenous amiodarone. J *Am. Coll. Cardiol.*, 1984;**4**: 565–570.
205. Glasser, S.P., P.I. Clark, A.R. Laddu, Comparison of the antiarrhythmic effects of acebutolol and propranolol in the treatment of ventricular arrhythmias. *Am. J. Cardiol.*, 1983;**52**: 992–995.
206. Belhassen, B., H.H. Rotmensch, S. Laniado, Response of recurrent sustained ventricular tachycardia to verapamil. *Br. Heart. J.*, 1981;**46**: 679–682.
207. Frank, R., G. Fontaine, R. Coutte, et al., Reproducibilité des arythmies ventriculaires déclenchées avant et après imprégnation médicamenteuse. Valeur prédictive de l'effet anti-arythmique. *Arch. Mal. Coeur. Vaiss.*, 1981;**74**: 79–86.
208. Horowitz, L.N., M.E. Josephson, A. Farshidi, et al., Recurrent sustained ventricular tachycardia 3. Role of the electrophysiologic study in selection of antiarrhythmic regimens. *Circulation*, 1978;**58**: 986–997.
209. Mason, J.W., C.D. Swerdlow, R.A. Winkle, et al., Programmed ventricular stimulation in predicting vulnerability to ventricular arrhythmias and their response to antiarrhythmic therapy. *Am. Heart. J.*, 1982;**103**: 633–639.
210. Swerdlow, C.D., G. Gong, D.S. Echt, et al. Clinical factors predicting successful electrophysiologic-pharmacologic study in patients with ventricular tachycardia. *J. Am. Coll. Cardiol.*, 1983;**1**: 409–416.
211. Vlay, S.C., C.H. Kallman, and P.R. Reid, Prognostic assessment of survivors of ventricular tachycardia and ventricular fibrillation with ambulatory monitoring. *Am. J. Cardiol.*, 1984;**54**: 87–90.
212. Platia, E.V., S.C. Vlay, P.R. Reid, A comparison of the predictive value of programmed electrical stimulation and the Holter monitoring in patients with malignant ventricular arrhythmias. *Am. J. Cardiol.*, 1982;**49**: 928.
213. Swerdlow, C.D., R.A. Winkle, J.W. Mason, Determinants of survival in patients with ventricular tachyarrhythmias. *N. Engl. J. Med.*, 1983;**308**: 1436–1442.
214. Buxton, A.E., F.E. Marchlinski, H.L. Waxman, et al., Prognostic factors in nonsustained ventricular tachycardia. *Am. J. Cardiol.*, 1984;**53**: 1275–1279.
215. Breithardt, G., Seipel, L., R.R. Abendroth, et al., Serial electrophysiological testing of antiarrhythmic drug efficacy in patients with recurrent ventricular tachycardia. *Eur. Heart. J.*, 1980;**1**: 11–24.
216. Kang, P.S., J.A. Gomes, and N. El-Sherif, Procainamide in the induction and perpetuation of ventricular tachycardia in man. *Pacing Clin. Electrophysiol.*, 1982;**5**: 311–322.
217. Sclarovsky, S., R.F. Lewin, O. Kracoff, et al., Amiodarone-induced polymorphous ventricular tachycardia. *Am. Heart. J.*, 1983;**105**: 6–12.
218. Connolly, S.J., R.E. Kates, C.S. Lebsack, et al., Clinical pharmacology of propafenone. *Circulation*, 1983;**68**: 589–596.
219. Connolly, S.J., R.E. Kates, C.S. Lebsack, et al., Clinical efficacy and electrophysiology of oral propafenone for ventricular tachycardia. *Am. J. Cardiol.*, 1983;**52**: 1208–1213.
220. Seipel, L. and G. Breithardt, Propafenone–a new antiarrhythmic drug. *Eur. Heart. J.*, 1980;**1**: 309–313.
221. Kulbertus, H.E., The arrhythmogenic effects of antiarrhythmic agents. In: Befeler B, ed. *Selected Topics in Cardiac Arrhythmias*. Mount Kisco, New York: Futura, 1980: 113–119.
222. Velebit, V., P. Podrid, B, Lown, et al., Aggravation and provocation of ventricular arrhythmias by antiarrhythmic drugs. *Circulation*, 1982;**65**: 886–894.
223. Block, P.J. and R.A. Winkle, Hemodynamic effects of antiarrhythmic drugs. *Am. J. Cardiol.*, 1983;**52**: 14C–23C.
224. Leclercq, J.F. and P. Coumel, Les indications cliniques des différentes drogues dans les arythmies rebelles. *Ther. Umsch.*, 1982;**39**: 128–136.

225. Zipes, D.P., J.J. Heger, W.M. Miles, et al., Synchronous intracardiac cardioversion. *Pacing Clin. Electrophysiol.*, 1984;**7**: 522–533.
226. Mirowski, M., P.R. Reid, M.M. Mower, et al., The automatic implantable cardioverter-defibrillator. *Pacing Clin. Electrophysiol.*, 1984;**7**: 534–540.
227. Mirowski, M., P.R. Reid, R.A. Winkle, et al., Mortality in patients with implanted automatic defibrillators. *Ann. Intern. Med.*, 1983;**98**: 585–588.
228. Fisher, J.D., S.G. Kim, S. Furman, et al., Role of implantable pacemakers in control of recurrent ventricular tachycardia. *Am. J. Cardiol.*, 1982;**49**: 194–206.
229. Hartzler, G.O., Electrode catheter ablation of focal ventricular tachycardia. *J. Am. Coll. Cardiol.*, 1983;**1**: 595.
230. Fontaine, G., G. Guiraudon, R. Frank, et al., The surgical treatment of cardiac arrhythmias. In: Befeler B, ed. *The Management of Cardiac Arrhythmias*, 1979.
231. Josephson, M.E., L.N. Horowitz, A. Farshidi, Continuous local electrical activity. A mechanism of recurrent ventricular tachycardia. *Circulation*, 1978;**57**: 659–665.
232. Harken, A.H., L.N. Horowitz, M.E. Josephson, Comparison of standard aneurysmectomy and aneurysmectomy with directed endocardial resection for the treatment of recurrent sustained ventricular tachycardia. *J. Thorac. Cardiovasc. Surg.*, 1980;**80**: 527–534.
233. Guiraudon, G., G. Fontaine, R. Frank, et al., Circular exclusion ventriculotomy. Surgical treatment of ventricular tachycardia following myocardial infarction. *Arch. Mal. Coeur. Vaiss.*, 1978;**71**: 1255–1262.
234. Guiraudon, G., G. Fontaine, R. Frank, et al., Surgical treatment of chronic ventricular tachycardias. The concept of arrhythmogenic area. In: Masoni A, Alboni P, eds. *Cardiac Electrophysiology Today*. London: Academic Press, 1982: 325–347.
235. Horowitz, L.N., A.H. Harken, J.A. Kastor, et al., Ventricular resection guided by epicardial and endocardial mapping for treatment of recurrent ventricular tachycardia. *N. Engl. J. Med.*, 1980;**302**: 589–593.
236. Cohen, M., M. Packer, and R. Gorlin, Indications for left ventricular aneurysmectomy. *Circulation*, 1983;**67**: 717–722.
237. Fontaine, G., G. Guiraudon, and R. Frank, Surgical management of ventricular tachycardia not related to myocardial ischemia. In: Josephson ME, Wellens HJJ, eds. *Tachycardias: Mechanisms, Diagnosis and Treatment*. Philadelphia, Pennsylvania: Lea and Febiger, 1984: 451–473.
238. Fontaine, G., R. Frank, J.L. Tonet, et al., Arrhythmogenic right ventricular dysplasia: a clinical model for the study of chronic ventricular tachycardia. *Jpn. Circ. J.*, 1984;**48**: 515–538.
239. Trigano, J.A., H. Nasta, J.L. Michaud, et al., Resistant ventricular tachycardia caused by right ventricular dysplasia. A case of surgical recovery reported 6 years after intervention. *Arch. Mal. Coeur. Vaiss.*, 1983;**76**: 852–857.
240. Guiraudon, G.M., G.J. Klein, S.S. Gulamhusein, et al., Total disconnection of the right ventricular free wall: surgical treatment of right ventricular tachycardia associated with right ventricular dysplasia. *Circulation*, 1983;**67**: 463–470.
241. Scheinman, M.M. and F. Morady, E.N. Shen, Interventional electrophysiology: Catheter ablation techniques. *Clin. Prog. Pacing. Electrophysiol.*, 1983;**1**: 375–381.
242. Fontaine, G., R. Frank, J.L. Tonet, et al., Treatment of resistant ventricular tachycardia with endocavitary fulguration and antiarrhythmic therapy, compared to antiarrhythmic therapy alone: experience in 111 consecutive cases with a mean follow-up of 18 months. *Tex. Heart. Inst. J.*, 1986;**13**: 401–418.
243. Josephson, M.E. Catheter ablation of arrhythmias. *Ann. Intern. Med.*, 1984;**101**: 234–237.
244. Fontaine, G., G. Guiraudon, R. Frank, et al., When is surgery of ventricular tachycardia indicated? *Nouv. Presse. Med.*, 1981;**10**: 3539–3540.

30 Atrial Tachycardias in Infants, Children, and Young Adults with Congenital Heart Disease

Parvin C. Dorostkar · Jerome Liebman

P. W. Macfarlane, A. van Oosterom, O. Pahlm, P. Kligfield, M. Janse, J. Camm (eds.), *Comprehensive Electrocardiology*, DOI 10.1007/978-1-84882-046-3_30,

30.1 Introduction

Atrial tachycardias comprise a minority of all supraventricular tachycardias in pediatric patients. Mechanistically, these tachycardias present a multiple of different types of tachycardias that originate and sustain in the atria and often express themselves as tachycardias in association with a rapid ventricular response in the younger patient. Atrial tachycardias can be categorized into three basic mechanistic universes: those that are automatic in nature, those that are triggered in nature, and those that are reentrant in nature.

Differentiation of the three different types of atrial tachycardias is important and can sometimes be difficult. In general, abnormalities of impulse formation, that is, atrial automatic tachycardia and/or atrial triggered tachycardia, tend to express beat-to-beat variability and have been associated with a "warm-up, cool-down phenomenon." In contrast, abnormalities of impulse propagation include atrial tachycardias that are reentrant in nature and tend to have a fixed atrial rate with either a fixed or variable ventricular response. These individuals usually present with an inappropriately fast heart rate with little heart rate variability.

In contrast to atrial tachycardias that are associated with abnormalities of impulse formation, abnormalities of impulse propagation, as stated above, use a reentrant circuit within the atrium as their primary mechanism. This tachycardia usually occurs in patients with congenital heart disease, especially those who have had surgery for either repair or palliation of the underlying heart defect. The tachycardia responds transiently to atrial pacing and cardioversion and can sometimes be suppressed with antiarrhythmic medications. In most recent years, this tachycardia has proven to be responsive to ablative therapies and has been the subject of much study.

The first part of this chapter will focus on the clinical evaluation and treatment of automatic atrial tachycardia, while the second part dwells on atrial reentrant tachycardias. Representative electrophysiologic tracings and maps are interspersed.

30.1.1 Automatic/Triggered Atrial Tachycardias

Automatic or ectopic atrial tachycardias are caused by abnormal impulse formation where one or a few closely associated cells generate an atrial impulse faster than that of the sinus node. The arrhythmia has unique clinical features in that it usually occurs in a structurally normal heart. It classically expresses some degree of heart rate variability, and is often incessant. Because of its persistent nature, this tachycardia can be associated with a cardiomyopathy [1–3]. Automatic tachycardias rare also difficult to treat, because they are often resistant to medications and/or chemical or electrical cardioversion.

Automatic atrial tachycardias are thought to be focal in nature, depolarizing the atrium in a spreading fashion originating from the rapidly firing, abnormal focus. The exact underlying pathophysiology of automatic activity is not well understood. It is thought that the cells express abnormally rapid depolarization resulting in a faster pacemaker rate than that the sinus node. This tachycardia comprises approximately 15% of newly diagnosed supraventricular tachycardias in the pediatric population and comprises only 5% of all supraventricular tachycardias in the adult age group. Because the atrial rate is variable and sometimes only marginally above the sinus tachycardia rate, patients with this type of tachycardia may go undiagnosed for several years until they present with ventricular dysfunction associated with cardiomyopathy. Cardiomyopathy is more likely to occur in patients with higher heart rates (150–176 beats per minute), but may occasionally occur in patients with lower heart rates (90–136 beats per minute) [4]. When this happens, it is possible that the tachycardia is misdiagnosed as sinus tachycardia before a final diagnoses can be made. Myocardial dysfunction is noted to be present in about 50% of patients with ectopic atrial tachycardia. Automatic activity tends to be associated with either spontaneous diastolic Phase IV depolarization or abnormalities in repolarization of Phase III of the action potential. The location of the focus can be discerned by critical evaluation of the P-wave morphology suggesting direction of depolarization. Ectopic atrial tachycardias arising from the right atrium or the right atrial appendage are directed to the left and, usually, inferior, so that there are positive P-waves in leads I, II, III, and aVF, very similar to those in sinus rhythm. However, the P-wave morphology is usually distinctly different from that in sinus rhythm, although the non-electrophysiology physician may call it "sinus like." In contrast, ectopic atrial tachycardias from the left-sided atrium express a P-wave morphology very different from those seen in sinus rhythm. The P-wave is directed to the right and

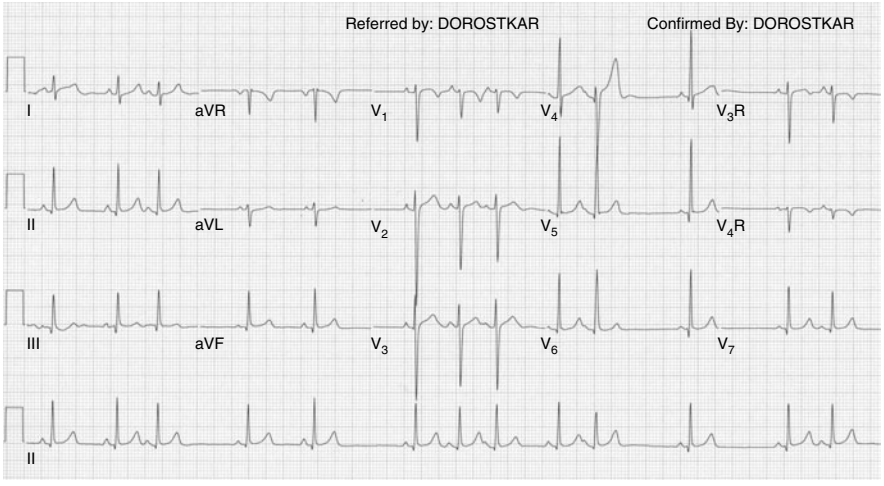

Figure 30.1

Eight-year-old male referred for evaluation of an irregular heartbeat. Note that the ECG shows episodic salvos of a triggered atrial tachycardia arising from the right atrium as evidenced by P-waves that are positive in I, II, III, and aVF.

inferior so that the P-waves of ectopic atrial tachycardia arising from the left atrium express negative P-waves in I and aVL and usually positive P-waves in II, III, and aVF.

Electrocardiographic and monitored rhythm recordings characteristic of automatic atrial tachycardia are highly variable. Heart rates range from just above the sinus rate to as fast as 300 beats per minute. In addition, this tachycardia exhibits multiple varied behaviors including the classic warm-up and cool-down behavior; expressed salvoes of beats anywhere from three beats to several seconds in duration; as well as variable atrioventricular relationships with transmission of conduction to the ventricles varying from one to one conduction to first-degree, second-degree, and "apparent" third-degree atrioventricular block or multilevel block through the atrioventricular node. Atrial tachycardia rates associated with automatic atrial tachycardia vary highly; in addition, the tachycardia heart rate, as stated above, can vary in association with the degree of atrioventricular node transmission to the ventricle (Fig. 30.2). There may also be a wide complex QRS owing to aberrant ventricular conduction. As these tachycardias, typically, have "a mind of their own," they tend to express themselves with variable rates in a persistent fashion. Higher levels of atrioventricular conduction block can usually be seen while the patient is sleeping and, therefore, a Holter monitor of the heptum of such patients might be helpful in elucidating the diagnostic expression and behavior of the automatic atrial tachycardia (Fig. 30.2). Adenosine can be used as a tool to diagnose automatic atrial tachycardia, as it causes transient atrioventricular node block. In the majority of cases, the tachycardia itself is not sensitive to adenosine and, therefore, P-waves can be dissociated from the ventricles unmasking the atrial tachycardia during transient atrioventricular node block with P-waves, lone-standing. A minority of automatic atrial tachycardias are sensitive and responsive to adenosine and will terminate, usually inscribing a QRS complex as the last expressed electrogram before they resume their activities a few seconds later. Electrical or chemical cardioversion may be transiently effective, but the tachycardia usually resumes. Automatic tachycardias tend to be variably initiated and are not responsive to extra-stimulation techniques or overdrive pacing in regards to initiation or termination of the tachycardia. Triggered activity is thought to be associated with delayed afterdepolarization; these tachycardias express their own behavior independent of pacing maneuvers and are difficult to induce and/or terminate with traditional electrophysiologically mediated pacing techniques.

As stated above, ectopic atrial tachycardia may arise either from the right or the left atrium. Although the origin of ectopic atrial tachycardia appears to be widely distributed throughout both atria, there is some suggestion that automaticity or increased triggered activity may have a propensity to arise near atrial appendages, or in and around atrial extensions into pulmonary veins. The reasons for this distribution are unclear, but there appears to be some association with the expression of HNK-1 antigen, which has become known as a marker for specialized conduction tissues during cardiac development [5, 6]. In a study by Blom-Gitinberger, investigators demonstrated an association between the

Figure 30.2

Newborn infant with a virtually incessant atrial tachycardia that showed multilevel block on the 24 h Holter recordings.

HNK-1 antigen expression and a propensity to develop automaticity [6]. However, the stimulus for automaticity expression and, therefore, tachycardia expression remains poorly understood.

Electrophysiologic testing can be performed to confirm the diagnosis of a suspected ectopic atrial tachycardia and can be especially meaningful if the patient has an associated myopathy, as it offers a potential cure if a successful ablation can be achieved [6, 7]. Activation sequence mapping can be done with newer mapping technologies, which delineate detailed localization of the automatic focus so that ablation can be successful (Fig. 30.4). Should a successful ablation occur, echocardiography can then be used to follow ventricular function, which will often return to normal. Both systolic and diastolic dysfunction improve over time if successful ablation is achieved. As stated above, usually cardiomyopathy is observed in patients with higher heart rates as compared to those with lower heart rates [4].

Pharmacologic management of patients with atrial ectopic tachycardias is often quite challenging. An initial approach with rate control should be tried to maximize optimal hemodynamics. Though desirable, rhythm control is difficult and often fraught with challenging side effects from antiarrhythmic medications. Since medications, that provide rate control,

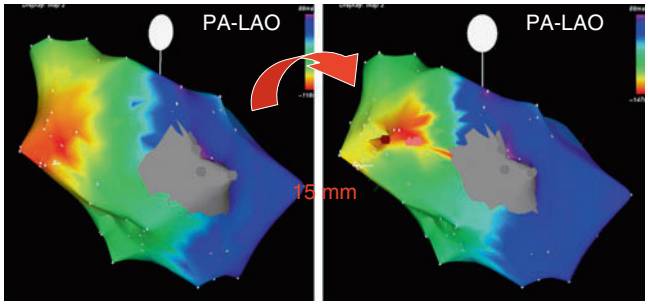

Figure 30.3

Eleven-year-old male with incessant atrial tachycardia mapped to the posterolateral left atrium and successfully ablated; bright red color denotes areas of earliest atrial activation as noted by the color bar; gray denotes absent atrial signals consistent with the orifice of the left atrial appendage; note that centric activation of the left atrium away from the mapped dominant tachycardia pacemaker.

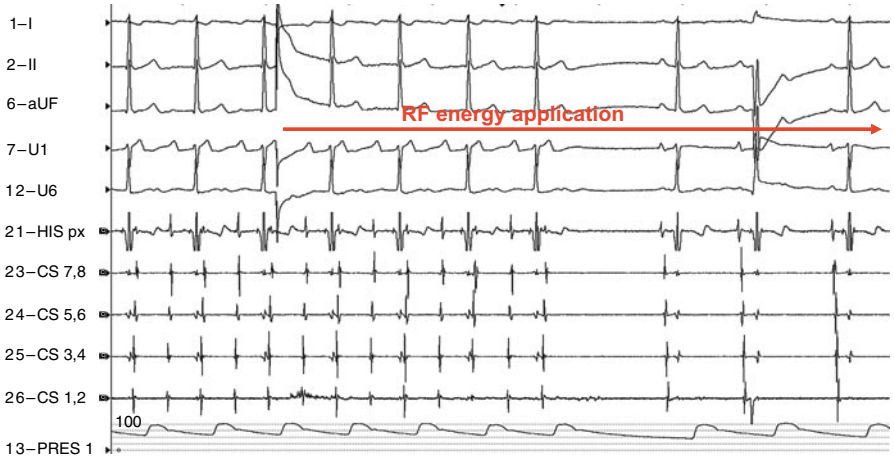

Figure 30.4

Successful radiofrequency energy application in an 11-year-old male with incessant atrial tachycardia, mapped in the left atrium.

including beta-blockers and digoxin, seem to be well tolerated in the pediatric population, these drugs are chosen as a first-line option. In addition to rate control, by suppressing automaticity, beta blockers appear to control ectopic atrial tachycardia in about 20% of cases. Ultimately, successful suppression of tachycardia occurs in about 50% of cases, often utilizing multiple medications. Class IC (Flecainide and/or Propafenone) and/or Class III (Sotalol) agents are favorably used for atrial ectopic tachycardias that present a challenge in regards to control. Verapamil has been commonly cited for rate control in the adult literature, but is less commonly used in pediatrics. This drug is thought to suppress triggered activity. Thus, verapamil may offer both rate control and rhythm control. However, calcium channel blockers are contraindicated in the infant, as they are associated with asystole, probably related to the infant's poorly differentiated endoplasmic reticulum and therefore, inability to benefit form the drug's actions.

The natural history of ectopic atrial tachycardia is variable. When it occurs in younger neonates and infants, the tachycardia seems to regress spontaneously in about 50% of cases. However, when the patients are older and present with cardiomyopathy, the tachycardia tends to be more persistent and requires more aggressive intervention.

Though surgical techniques were employed effectively for drug-resistant ectopic atrial tachycardia throughout the 1980s, the advent of radiofrequency energy application changed the outcomes. The earliest attempts to ablate ectopic atrial tachycardia using transvenous methods occurred in 1984 using direct DC energy. Further developments in technology introduced the application of radiofrequency energy as an intervention. When used appropriately, this intervention tends to underscore the relatively benign course and good outcomes in association with high success rates for ablation of this type of tachycardia. The success rate with currently available technology for the ablation of ectopic atrial tachycardia is now greater than 90% with a relatively low complication rate. Nowadays, patients who present with ventricular failure due to an atrial tachycardia are promptly managed with electrophysiologic study and catheter ablation using either radiofrequency or cryoablative energy. This otherwise malignant arrhythmia can now, be often-cured (Figs. 30.3 and 30.4).

Multifocal atrial tachycardia, also known as chaotic atrial tachycardia, is a rare form of automatic atrial tachycardia, where there is more than one focus firing rapidly [8]. Multifocal atrial tachycardia is mostly a condition seen in adults, particularly with cor pulmonale or chronic obstructive pulmonary disease [10]. Multifocal atrial tachycardia is frequently idiopathic in nature, although it has been associated, in rare cases, with Macrocephaly-Cutis Marmorata Telangiectatica Congenita [9] and other rare diseases. When it occurs in the postoperative period, it is often very difficult to control and may require aggressive therapy including early consideration of radiofrequency ablation of the atrioventricular node for rate control. Classic ECG (electrocardiogram) findings include P-waves that are irregularly inscribed at heart rates greater than 100 beats per minute. There may be three or more different P-wave morphologies. The ventricular response to such a tachycardia can be quite varied. Rate-related bundle branch block can be seen after short–long or after long–short ventricular responses due to variable ventricular transmission of the rapid impulses in the atrium.

The clinical course of multifocal atrial tachycardia in children includes spontaneous resolution of the tachycardia in 50–80% of the cases by 12–18 months of age. Rarely, during the time in which the multifocal atrial tachycardia is expressed, there may be progressive cardiomyopathy and sudden cardiac death, presumably associated with rapid ventricular conduction [11, 12]. Multifocal atrial tachycardia tends to be quite resistant to medical management, even aggressive pharmacologic therapy. Traditionally, beta-blockers or digoxin can be used for rate control and, sometimes, can suppress atrial and ventricular irritability. However, rhythm control is usually quite difficult in these patients. Combinations of medications have been used with limited success, including amiodarone [13]. As a last resort, ablation of the atrioventricular node can be performed to control the rate in patients who are severely symptomatic. In this case, careful consideration of the aggressive approach to the hemodynamic compromise should be weighed as the patient will most likely require a pacemaker for the rest of his/her life. Most telling is that once the tachycardia has resolved, the recurrence risk is quite low as the tachycardia does not reoccur during later life.

Regardless, short of ablation therapy, medical management of both rhythm control and rate control appears to be challenging in patients with a triggered and/or automatic atrial tachycardia. With the advent of radiofrequency energy application and/or (now) cryo-ablation, the cure rate for atrial tachycardia remains high and especially hopeful for those patients suffering from associated myocardial dysfunction.

30.1.2 Reentrant Atrial Tachycardias

As stated above, in contrast to atrial tachycardias associated with abnormalities of impulse formation, abnormalities of impulse propagation use a reentrant circuit within the atrium as their primary mechanism. The history related to the development of understanding of atrial reentrant tachycardias is of particular interest. The traditional term for atrial reentrant tachycardia is atrial flutter. The term "flutter" originates from the Anglo-Saxon word "floterian," meaning to move or flap wings rapidly without flying or to move with quick vibrations or undulations. This descriptive term was fist used by a British physiologist, MacWilliams, in 1887 while looking at a dog atrium [14]. In 1905, there was a first recording of atrial flutter by William Richie using an ink-polygraph recorder in a patient with complete atrioventricular block [15], which was followed in 1910 by a first-time recording of atrial flutter in the same patient using an electrocardiograph [16]. Einthoven in 1906 had reported a similar phenomenon in his laboratory from a patient 1.5 km away [17]. The most

clear electrocardiographic recordings of atrial flutter were made in 1913 by Sir Thomas Lewis who described a classic saw-toothed pattern with negative deflections in leads II and III [18]. Once this arrhythmia was acknowledged, many investigators began to hypothesize and study its mechanism with two basic schools of thought predominating: Is the primary mechanism one of automaticity (abnormal impulse formation, as believed by Lewis) or reentry (abnormal impulse propagation)? Works by Mayer with the Scyphomedusae (1906), Mines (1913), and Garrey (1914) suggested reentry as a primary mechanism. In 1921, after a series of canine experiments, Lewis changed his mind and supported the notion that atrial flutter was supported by reentry [19]. Since mapping techniques were crude at the time, controversy continued to exist. Clinically, different ECG patterns of flutter were noted raising further questions in regards to the underlying mechanism. Telling work by Cabrera and Sodi-Pallares in 1947 showed that atrial flutter was a result of consecutive regular activation fronts oriented in the sagittal plane using data obtained from ECG and VCG recordings [20]. Despite these experiments, several clinical observations suggested that atrial flutter may be arising from a single focus firing rapidly. In a classic paper by Puech et al. in 1970, the authors identified two types of flutter: the common type, where P-waves were negative in II, III, and aVF; and the "rare" type, where flutter waves were best expressed in leads I and aVL [21]. Even though these studies showed that activation of the right atrium during common flutter preceded cranially along the interatrial septum and then caudally along the free wall of the right atrium, with the left atrium being activated at the same time as during septal activation, the question of reentry versus automaticity was not clearly answered from these studies. Finally, several ongoing studies by Waldo et al. in 1977 both in the canine sterile pericarditis model and in postoperative patients demonstrated that the mechanism for atrial flutter was reentrant and, thus, an abnormality of impulse propagation. These investigators used entrainment techniques to support the notion of reentry as opposed to automaticity as the underlying mechanism for flutter. Using epicardial electrode recordings, four electrophysiological criteria were identified with each of them sufficient to demonstrate circuit movement tachycardia incorporating an excitable gap [22–32]. Waldo also made a distinction between the two types of atrial flutter: Type 1, easily influenced by programmed pacing, and Type 2, which was infrequently seen, faster, and not easily influenced by rapid atrial pacing. In 1978, Wyndham was the first to report that atrial flutter could be interrupted using a self-activated radiofrequency generator [33]. Once identified as reentrant in mechanism, the quest to understand a more detailed mechanism continued. Pastelin et al. were able to identify that cutting the medial and posterior bundles in the atrium interrupted atrial flutter [34]. The role of anatomic and functional barriers was investigated including the proposed role of an area of slow conduction [35, 36]. Other investigators looked at the type of atrial reentry demonstrating that it was macroreentrant [37] and dependent on myocyte interconnections [38]. Another experimental model suggested that atrial reentry was possible without an area of slow conduction [39]. In the same year (1986), Guy Fontaine used radiofrequency energy in two patients to treat atrial flutter [40]. Further work demonstrated that the expression of atrial flutter was related to the time course of postoperative pericarditis. At the same time, the role of double potentials and fractionated atrial signals was interrogated by Cosio et al. suggesting that these signals were associated with areas of slow conduction [41] and that they provided an opportunity to study the reentrant mechanism further. Finally, after electrical fulguration was shown to be effective in the late 1980s [42], Feld et al. showed that atrial flutter was amenable to radiofrequency ablation in 1992 [43], targeting areas of slow conduction. As the quest to understand more complex types of atrial reentrant tachycardia continues, technology supports and parallels better understanding of the underlying mechanisms that can, therefore, support better outcomes in patients.

The observation that atrial tachycardias are more common in the postoperative patient with congenital heart disease has resulted in several investigators focusing on the role of surgical incisions in the expression of atrial reentrant tachycardia. It was thought that atrial reentry in these patients was also subeustachian isthmus dependent, although subsequently this observation has been scrutinized further to show that there are a variety of complex reentrant rhythms present in the patient with postoperative congenital heart disease.

30.1.3 Atrial Anatomy: Lessons from Atrial Flutter in Animal Models and Adult Patients with Heart Disease

Anatomic studies evaluated the role of the crista terminalis of the right atrium, which is located in the sulcus terminalis located in the right atrium inferior to the superior caval vein. The sinus node rests within the crista terminalis and supports the initiation of the sinus impulse. The origination of the impulse that initiates atrial flutter was thought to be the sinus node [35], but it is now accepted that any premature beat originating anywhere in the myocardium can serve as the

initiator of atrial reentry as long as a supportive substrate is present. There is also a school of thought that atrial flutter is a later manifestation of atrial fibrillation once given the opportunity to organize. In general, right atrial pacemaker activity is thought to originate from along the sulcus terminalis, whereas premature atrial beats from the left atrium are thought to originate from the pulmonary veins. The right atrium is largely smooth-walled and derived from the embryologic sinus venosus. In contrast, the left atrium is formed from the anlage of the pulmonary veins. There is a fold between the right pulmonary veins and the superior vena cava known as the "Waterston groove." The orifice of the inferior vena cava (IVC) and coronary sinus have fibrous continuity with only variable amounts of myocardial tissue bridging the right and the left atrium superficially [44]. Posteriorly, the right and the left atrium are separated by a groove that is filled with fibro-fatty tissue; only anteriorly, there is a distinct band of muscle that passes from the anteromedial aspect of the right atrium and superior vena cava to the left atrium, known as Bachman's bundle [45]. In the right atrium, the pectinate muscles run obliquely toward the right atrial appendage. In contrast, in the left atrium, myocardial fibers encircle the pulmonary veins and to some degree the mitral valve annuals. Several natural orifices exist in the right atrium including the superior vena cava, inferior vena cava, atrial septum, tricuspid valve, coronary sinus, and right atrial appendage orifice. This geometry plays a crucial role during activation sequences involved while atrial reentry occurs, like posing selective lines of block or activating conduction pathways during expression of atrial reentrant tachycardias.

Atrial reentrant tachycardias, classically referred to as atrial flutter, have now been accepted to involve abnormalities of impulse propagation that occur within either atria. Although primarily thought to be associated with right atrial disease, atrial reentrant arrhythmias can occur involving the right, the left, or both atria. Even though atrial flutter/atrial reentrant tachycardia is a common arrhythmia seen in the adult population, this arrhythmia is much more rare in the pediatric population and usually occurs in patients with underlying cardiac abnormalities, especially those who have undergone surgery for correction or palliation of congenital heart disease. In patients with underlying cardiac abnormalities, this arrhythmia, though rare, poses a challenge with regards to diagnosis, management, and therapy. In addition, this arrhythmia is often associated with significant morbidity and mortality in young patients with structural or functional heart disease.

Improved understanding of atrial reentrant tachycardias has allowed for differentiation of different types of atrial reentry in most recent years. Both clinical and experimental studies and observations over the last 10–15 years have been able to delineate the electrophysiologic circuit(s) that support macroreentry in atrial reentrant tachycardias. It has been shown that atrial reentry most commonly occurs in the right atrium. It is a self-sustaining circuit, and usually occurs in patients with either structural or functional heart disease. Continued study of atrial reentry defined the role of the crista terminalis as an anisotropic barrier to conduction during the common forms of atrial flutter. It has also been shown that the tricuspid valve annulus serves as an anterior anatomic barrier, supporting this "classic" reentrant loop. Finally, abnormal automaticity of the crista terminalis, the remnants of the cardinal veins, the sinus venosus and pulmonary veins have been shown to serve as triggers to express premature electrical activity that subsequently serves as the initiating factor for the expression of atrial reentry. Further research has demonstrated that intrinsic anisotropic properties of the right atrial wall related to the trabeculations of the right atrium and the number and distribution of gap junctions or connexin proteins support expression of atrial reentry. There is no doubt that the expression of atrial reentry is multifactorial, but the tachycardia seems to be more present in the right atrium, especially in patients who have either functional or congenital abnormalities of the right atrium.

The debate in regards to the underlying mechanism of atrial flutter continued for several decades until a variety of experimental animal models of atrial reentrant tachycardia were developed and demonstrated that, indeed, atrial flutter and/or atrial reentrant tachycardia is an abnormality of impulse propagation supporting reentry inside the atria (mostly the right atrium). In addition to delineating the underlying mechanism for atrial reentry tachycardia, these models supported a better understanding of the exact reentrant loop and conduction behavior during atrial tachycardia. Evaluation of a variety of anatomic structures in association with the expression of the atrial reentrant tachycardia became the next subject of intensive study. Most recently, with the advent of catheter-based mapping and ablation techniques, atrial reentrant tachycardias have been further characterized and studied in regards to distribution, expression, reentrant loop and insight into the roles of specific anatomic structures and/or surgical incisions.

In 1947, Rosenblueth and Garcia-Ramos developed a model of intercaval crush injury to study atrial flutter [46]. This model served to support the notion that nonconductive barriers were necessary for the induction and sustenance of intra-atrial reentrant tachycardias. The observation that the extension of the injury to the tricuspid valve annulus terminated the arrhythmia was essential to understanding that this particular arrhythmia was reentrant in nature and

required an isthmus. A second surgical model developed by Frame et al. [39] used a posterior intercaval incision that was y-shaped and demonstrated that the reentry was around the tricuspid ring sustaining flutter. In this model, it was demonstrated that the tricuspid valve annulus forced activation in a circular manner around the tricuspid valve annulus. A model of acetylcholine-induced tachycardia developed by Allessie et al. described the refractoriness of atrial tissue and its role in the support of atrial reentry in the right atrium [37]. It was thought that functional refractoriness played a critical role in determining propagation of reentrant wavefronts in the right atrium. Secondly, the sterile pericarditis model of atrial flutter assessed and proved the relative importance of anatomic boundaries, functional refractoriness, and the role of anatomic barriers in the expression of atrial reentry [22, 28, 30–32]. It appeared that in several of these models, nonconductive barriers were crucial for the expression of reentry and that some of these barriers were functional in nature. Several other models then undiscovered the importance of endocardial structures, both anatomically and functionally.

Finally, in a canine model, Boineau [35] demonstrated that the crista terminalis was crucial in regards to expression of the common type of atrial flutter in adults. This model demonstrated the interaction between anisotropic conduction and the complex geometry of the right atrium with regards to common atrial slutter expression. In addition, this model was extended by several investigators who further elucidated the role of anisotropy and conduction velocity change along the crista terminalis. It was, therefore, thought that the cellular basis for observed directional preferences for longitudinal conduction in the crista terminalis may very well be associated with the role of gap junctions and cell-to-cell interactions favoring conduction in one direction and, therefore, suggesting that anisotropy plays a critical role in the expression of atrial reentry [47–54].

30.1.4 Intra-Atrial Reentry in the Postoperative Patient with Congenital Heart Disease

Intra-atrial tachycardia has carried many names in the past, including the traditional name of atrial flutter [49, 50]. Reentrant in nature, this tachycardia uses a variety of reentrant loops, in contrast to common atrial flutter, which uses the subeustachian isthmus as a critical component of its reentrant loop. Common atrial flutter usually depicts a tachycardia cycle length of around 200 ms and inscribes P-waves that are negative in II, III, and aVF. In contrast, intra-atrial tachycardia, which typically occurs in the post-operative patient, expresses a broad range of tachycardia cycle lengths and P-wave morphologies [55]. This tachycardia has been denoted as such because the reentrant tachycardia may use reentrant circuits that are not similar to that found in common atrial flutter. Even though the tricuspid valve subeustachian isthmus can be involved in the expression of postoperative intra-atrial reentrant tachycardia in the patient with congenital heart disease, there appear to be other reentrant pathways or loops, sometimes involving the atriotomy, or other anatomic boundaries. About one third to one fourth of patients with congenital heart disease, especially those who have had either surgery or palliation for congenital heart disease, will develop or have a propensity to develop sustained atrial tachycardia that can be demonstrated using programmed stimulation [56–58]. Only about 8% of patients who develop atrial reentrant tachycardias have anatomically and functionally normal hearts, with over 80% having associated repaired or unrepaired congenital heart disease [56] (Table 30.1).

In regards to intra-atrial reentry tachycardia in the postoperative patient, two key surgical models have served to improve our understanding of the atrial reentrant tachycardia in the postoperative patient with pediatric heart disease.

Table 30.1

Atrial tachycardia incidence in pediatric patients

Repaired congenital heart disease	60
Palliated congenital heart disease	13
Unoperated congenital heart disease	8
Normal heart	8
Cardiomyopathy	6
Rheumatic heart disease	4
Others	2

From Garson et al. (1985).

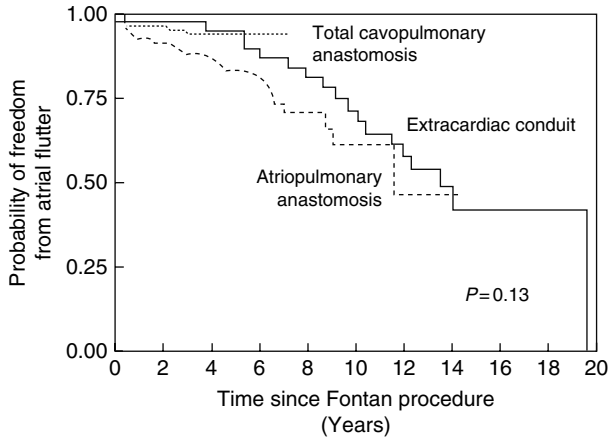

Figure 30.5

The Kaplan–Meier curve depicts probability of experiencing no atrial tachycardias after Fontan operation with respect to time and type of Fontan operation performed.

The first of these models was one developed by Cronin et al. [59, 60], which involved a sham Mustard operation. Rodefeld et al. [61–65] also developed a sham model of a lateral tunnel variety of the Fontan procedure (Fig. 30.5). In both of these models, it was felt that a common pathway for most of the observed tachycardias was in the free wall of the right atrium and that the tachycardia resolved when connecting the atriotomy to either the tricuspid valve annulus or the superior vena cava. These studies also found that the inclusion of the crista terminalis in the suture line aggravated the propensity of atrial tachycardia expression.

30.2 Epidemiology

In general, intra-atrial reentrant tachycardia in patients with congenital heart disease occurs in patients who have had significant manipulation or alterations of the right atrium, most often associated with surgery for heart disease [56]. Most of these surgeries include surgery for either atrial septal defect or ventricular septal defect repair, Mustard or Senning operations for the transposition of the great arteries (TGA), and those surgeries involving palliative procedures for single-ventricle physiology. In addition, there is a significant incidence of atrial tachycardia in association with lesions such as Tetralogy of Fallot and/or Ebstein's Anomaly. Of particular challenge is atrial tachycardia in the postoperative patient after a Fontan operation. Because of single-ventricle physiology and an often underlying myopathy, atrial tachycardia in these patients is hemodynamically poorly tolerated. Gelatt showed that 14–29% of patients after Fontan operation had atrial tachycardia at a mean follow-up of 4 years [57, 58]. One of the primary predictors of atrial tachycardia expression was the presence of atrial tachycardia in the immediate postoperative period. Another study showed that 16% of patients had atrial tachycardia at 5-year follow-up and appeared to correlate the expression of atrial tachycardia to the presence of extensive atrial baffling, and co-related the type of repair with arrhythmia expression [66]. Finally, a study from the Mayo Clinic demonstrated a prevalence of 17% at a 5-year follow-up with associated risk factors including perioperative arrhythmia, age at operation, and atrioventricular valve dysfunction [67]. It appears that about 40% of Fontan survivors have atrial tachycardia at a 10-year follow-up (Fig. 30.5). Although the overall prevalence of atrial tachycardia is lower in those patients undergoing total cavopulmonary connection, these patients are not completely free of the atrial arrhythmias. The incidence of atrial arrhythmias seems higher in patients with complex heart disease, there is a documented incidence of 14% in patients undergoing atrial septal defect repair. In addition, atrial arrhythmias may be associated with sinus node dysfunction as a cofactor [68–70]. The Mustard procedure has been quoted to have an incidence of 43% of atrial tachycardia with 16% having recurrent atrial arrhythmias. Patients who have undergone the Mustard procedure have an increased risk of atrial tachycardia with an incidence of 27% at 20 years, and have an increased risk of sudden death of 6.5% at a mean follow-up period of 11.6 years [57, 58]. It appears that atrial tachycardia may be associated with concordant

sinus node dysfunction, as shown by a study of patients with atrial flutter after Tetralogy of Fallot [71] or atrial septal defect repair [69], superimposed on a genetic propensity.

30.3 Clinical Symptoms

Symptoms associated with intra-atrial reentry tachycardia in patients with postoperative heart disease are quite varied, ranging from no symptoms, to palpitations, to hemodynamic collapse, to sudden cardiac death thought to be associated with concomitant rapid conduction and ventricular dysfunction. From clinical observations, it is obvious that the presence of atrial tachycardia adds significant morbidity and mortality to postoperative patients. Especially in patients with single-ventricle physiology, the added burden of atrial arrhythmias is significant. In these patients, early postoperative arrhythmias were poorly tolerated, particularly atrial fibrillation and junctional ectopic tachycardia. Peters et al. observed that more than half of all patients who died in the perioperative period had atrial tachycardias [72].

Late postoperative arrhythmias are associated with higher right atrial pressures measured both early and late after the operation and worse ventricular function. Late arrhythmias may be the first manifestation of anatomic obstruction, which should be investigated promptly. In these patients with atrial arrhythmias, atrial thrombi can also be frequently noted, requiring aggressive anticoagulation.

30.4 Treatment of Atrial Tachycardia

The treatment of atrial tachycardias is challenging in patients with postoperative congenital heart disease [71, 73–80]. The acute treatment of atrial tachycardias depends on the clinical symptoms and associated cardiac defect(s). Once suspected, the patient should undergo full evaluation including documentation and definition of the arrhythmia with a 12-lead electrocardiogram and interrogation of intracardiac structures for thrombus formation and cardiac function [81]. Depending on the clinical arrhythmia, patients will often have associated cardiomyopathy. Patients with underlying complex congenital heart disease have an increased risk of intracardiac thrombus formation, especially during expression of the atrial tachycardia. Careful evaluation of intracardiac stasis or thrombus is essential prior to proceeding with plans for either chemical or electrical cardioversion to normal sinus rhythm. Acute conversion of an atrial tachycardia can be achieved in most cases where the mechanism of the tachycardia is supported by reentry. In these cases, either chemical cardioversion with Ibutilide (0.01 mg/kg/dose repeated 2 times after 5–10 min) can be tried. In these patients, it is of prime importance that the patient's electrolytes are evaluated for hypomagnesemia or hypokalemia. A defibrillator should be available with experienced staff, since Ibutilide can cause Torsades de Pointe in association with QTc prolongation, which can be exacerbated in the presence of hypokalemia or hypomagnesemia and/or concomitant myopathy.

Chronic treatment of atrial tachycardias can be achieved with Class IA, IIC, or III antiarrhythmic agents, antitachycardia pacing devices, or with a more promising and more permanent approach of electrophysiologic study with ablation. Medical management of these arrhythmias is additionally hampered, because most antiarrhythmic medications affect myocardial function, which is often depressed in patients after cardiac surgery. It appears that Sotalol may have a beneficial effect on both acute and chronic tachycardia control [82, 83]. Antitachycardia pacing has also proven to be promising, though not always successful. Often patients exhibit multiple tachycardias or are unresponsive to pacing maneuvers perhaps due to the relative small excitable gap of the reentrant loop [78, 84–86]. Antitachycardia pacing has been reported to be associated with lethal pro-arrhythmias in selected patients, so that patient selection is critical. If there is significant myopathy and a normal atrioventricular node, rapid conduction with cardiovascular compromise is more likely [85, 87–89].

Ablation procedures offer the potential for cure for patients with postoperative atrial tachycardias. Initial evaluation and outcome of electrophysiologic study with ablation was less than optimal because traditional mapping techniques were hampered by poor definition of the underlying anatomic defect(s), associated postoperative distortions and scars that are not visualized with current fluoroscopic techniques, and poor understanding of the tachycardia mechanism. In addition, traditional techniques are limited in their in-ability to outline and display impulse propagation. These limitations hindered the clinician's understanding of the complexity of the tachycardia mechanism and the identification of critical areas

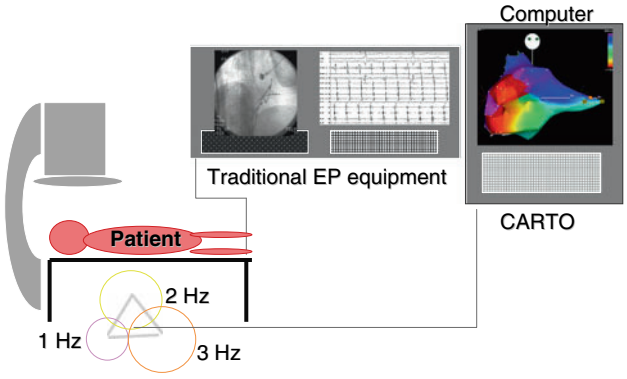

Figure 30.6

An artistic representation of the technical setup in the cardiac catheterization laboratory involving traditional electrophysiologic mapping and ablation equipment, complimented by a computer-based three-dimensional mapping system allowing study and ablation of complex arrhythmias.

for successful ablative therapy [76, 80, 90–97]. Newer mapping techniques (Fig. 30.6) supported by better understanding of the tachycardia mechanism and improved electrophysiologic techniques, including entrainment mapping promise improved outcomes. Therefore, newer approaches offer hope for cure of these reentrant tachycardias [98, 99].

30.4.1 Mechanisms of Postoperative Atrial Reentrant Tachycardias

In a small cohort of 21 consecutive patients with congenital heart disease, who were admitted to the University of California between 6/97 and 12/98 and to Rainbow Babies and Children's Hospital at Case Western Reserve University between 6/99 and 12/2000, a total of 33 atrial tachycardias were studied in the electrophysiology laboratory using advanced mapping techniques. All patients had documented clinical atrial tachycardia in association with postoperative congenital heart disease. Patients underwent electrophysiologic study under sedation, and in addition to the traditional electrophysiologic approach, patients underwent mapping of the clinical tachycardia using the non-fluoroscopic electroanatomic mapping (EAM) system (using CARTO) [98, 99]. Atrial tachycardia was induced using atrial overdrive pacing, atrial extrastimulation techniques, and/or isoproterenol infusion, when needed. The electroanatomic map was carefully interrogated for (1) activation sequences; (2) areas of low voltage (<0.03 mV), to identify areas that could be associated with diseased tissue and/or scar, supporting a barrier(s) for intra-atrial reentry tachycardia; (3) double potentials, which may reflect areas of slow conduction or functional and/or structural lines of conduction block. Entrainment techniques were used to define the mechanism and to identify a critical tachycardia isthmus.

Traditional electrophysiologic catheters were used to perform fluoroscopic mapping followed by electroanatomic mapping. The superior vena cava to (systemic venous) atrial junction and the inferior vena cava (IVC) to (systemic venous) atrial junction were mapped and marked with a three-dimensional ring or a tag. When possible, the His position was also tagged. In five of six patients with D-transposition of the great arteries (TGA) status post atrial switch operation, the pulmonary venous atrium was mapped from the arterial side as well. When present, double potentials and areas of scar were tagged during mapping and data acquisition.

Entrainment mapping was used to characterize each tachycardia circuit. After consistent capture was ensured, the intracardiac electrograms and the surface 12-lead ECG (electrocardiogram) were carefully interrogated to evaluate activation sequences compared to the native tachycardia. If the post-pacing interval (PPI) equaled the tachycardia cycle length and was associated with changes in either intracardiac activation sequences or surface P-wave morphology, the paced location was considered to demonstrate fusion and, therefore, labeled as manifest entrainment. These areas were considered less optimal for ablation. Concealed entrainment was present when (a) the post-pacing interval, defined as the stimulus

artifact to the onset of the next atrial electrogram recorded from the pacing bipoles, was ⩽30 ms of the tachycardia cycle length, (b) the intracardiac activation sequences were identical during pacing as compared to those during spontaneous tachycardia, and (c) the surface P-wave morphology was identical to the paced P-wave morphology. Areas of manifest and concealed entrainment were marked on the constructed three-dimensional image created by the EAM. Only areas with concealed entrainment were targeted for the radiofrequency energy application. Patients were subdivided into two cohorts: those with simple atriotomies (such as those seen after ASD [atrial septal defect], VSD [ventricular septal defect], AVSD [atrioventricular septal defect], or TOF [tetralogy of fallot] repair) and those with more complex atriotomies, as found in patients after Mustard or Senning operation and/or surgery for single-ventricle physiology.

30.4.2 Intra-Atrial Tachycardias Associated with a *Simple Atriotomy*

In patients with simple atriotomies ($N = 12$), one underwent correction of an atrial septal defect(s) (ASD), five underwent correction of an ASD and ventricular septal defect(s) (VSD), and one underwent complete atrioventricular septal defect (AVSD) repair. Five of these had a single tachycardia that was mapped and ablated. The sixth patient (with an ASD and VSD) had two separate tachycardias, of which both were mapped and ablated. Of these seven tachycardias, four had tachycardias involving the cavotricuspid isthmus and all were successfully ablated in the subeustachian isthmus. The other three tachycardias were successfully ablated by creating lesions from either anterior double potentials to the IVC ($N = 2$), where the tachycardia was revolving around an anterior barrier, or from the posterolateral right atrial wall double potentials to the IVC, where the tachycardia was found to revolve around a posterolateral barrier (Fig. 30.7).

There were three patients with Tetralogy of Fallot. Two of these three patients had a single tachycardia. These tachycardias were successfully ablated by creating lesions from anterior double potentials to the IVC in one and from the posterolateral right atrial wall to the IVC in another, which recurred 18 months later. Repeat mapping of the same tachycardia revealed a "Figure-of-8" (previously missed) and was successfully ablated between a suspected atriotomy (mapped double potentials) and the posterolateral wall, and the posterolateral wall and the IVC. The third patient had three different tachycardias, all of which were successfully ablated; ablative lesions were successful in the subeustachian isthmus for a subeustachian-dependent tachycardia, between anterior double potentials and the IVC for an incisional tachycardia and between the posterolateral wall and the IVC for a free wall atrial tachycardia.

The remaining three patients had simple atriotomies for Ebstein's anomaly of the tricuspid valve, Marfan's syndrome, and L-TGA with a VSD; all patients had a single atrial tachycardia. Two of these tachycardias were successfully ablated in the subeustachian isthmus. The patient with Ebstein's anomaly received multiple ablative lesions in the subeustachian isthmus, which did not result in tachycardia termination. Retrospective evaluation revealed a "Figure-of-8" tachycardia with a common isthmus between an anterior atriotomy and posterolateral double potentials. This complex mechanism was not recognized at the time of the study (Fig. 30.8).

In those patients where the posterolateral right atrial free wall provided a pivot area for the tachycardia (5 of 16 tachycardias), the EAM revealed a reentrant circuit that was distinctly different from classic clockwise or counterclockwise flutter around the tricuspid valve. Impulse propagation occurred around the valve, but these activation sequences were driven by a circuit that was primarily located laterally and posteriorly and almost perpendicular to the frontal plane. In these patients, entrainment from the subeustachian isthmus exhibited manifest entrainment, confirming that the subeustachian isthmus was not critical to the reentrant loop. Successful ablation of these tachycardias was achieved by ablation of an area that bridged the posterolateral right atrial free wall (behind the crista terminalis) to the IVC in all five patients (Fig. 30.7).

Three other tachycardias were noted to propagate around an anterior barrier. In one patient, the tachycardia was thought to be isthmus dependent, but unsuccessful ablation of the subeustachian isthmus was thought to be due to the inability to achieve a transmural lesion or due to poor understanding of the underlying mechanism. Only a traditional ablation catheter was used.

In summary, patients with a simple atriotomy demonstrated four different tachycardia mechanisms: subeustachian isthmus dependent (7/16 or 44%), reentry around posterolateral double potentials (4/16 or 25%), reentry around anterior double potentials (3/16 or 19%), and "Figure-of-8" tachycardia (2/16 or 12%) with a common isthmus located between mapped double potentials either laterally or anteriorly and another anatomic barrier such as the tricuspid valve.

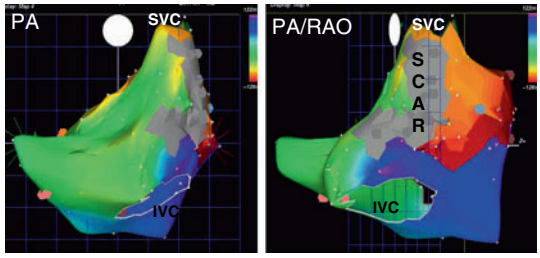

Figure 30.7

These activation maps of the right atrium in a 37-year-old male after atrial septal defect repair confirm non-isthmus-dependent atrial tachycardia. Shown are PA (posteroanterior) and RAO (right anterior oblique) projections displaying that the atrial tachycardia was mapped to revolve around a lateral scar within the right atrium in a counterclockwise fashion.

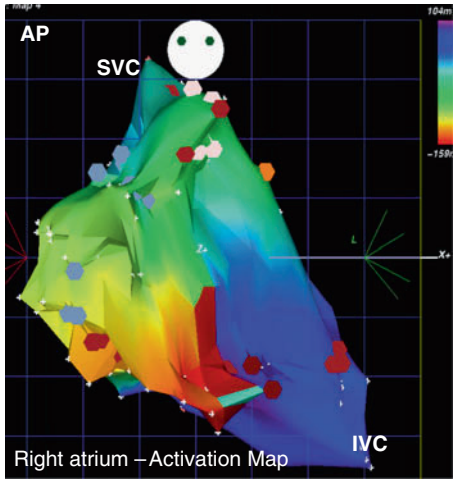

Figure 30.8

Figure-of-8 loop atrial tachycardia in a patient after simple atriotomy for tricuspid valve surgery for Ebstein's anomaly.

30.4.3 Intra-Atrial Tachycardias Associated with *Complex Atriotomies*

30.4.3.1 Patients after Atrial Switch Operation

Thirteen of the 17 tachycardias were mapped in six patients after an atrial switch operation. Two of these patients had a single tachycardia that was successfully ablated in the subeustachian isthmus on the pulmonary venous side. This tachycardia traversed the isthmus arising posteroseptally on the pulmonary venous side, inscribing a clockwise propagation pattern moving anteriorly and superiorly, and then descending to the posteroseptal area. The systemic venous atrial side was passively activated by the reentrant wavefront as it traversed the upper and mid-septal portions (Fig. 30.9). A third patient had two tachycardias. One of these tachycardias appeared to be focal in nature. The EAM of this tachycardia revealed passive activation of the systemic venous atrium from the posteroseptal area, where the post-pacing interval was identical to the tachycardia cycle length. Because of patient size (5 years old), the pulmonary venous atrium was not accessed. However, the patient had recurrent tachycardia with a different cycle length and surface ECG morphology

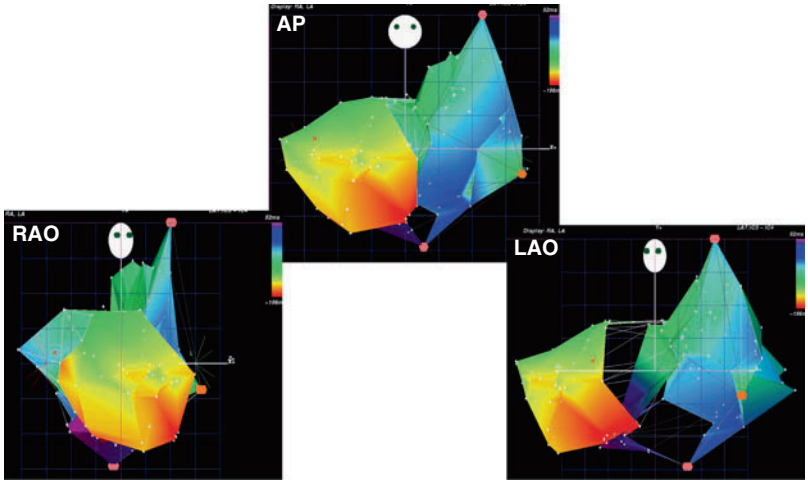

Figure 30.9

These activation maps of the systemic and pulmonary venous atrium of a 26-year-old female with transposition after atrial switch operation confirm that the atrial reentrant tachycardia is primarily confined to the pulmonary venous atrium (earliest activation is in red) with passive activation of the systemic venous atrium. Some areas of the atria could not be mapped due to technical difficulties.

about 8 months later. This tachycardia was then successfully ablated with lesions in the posteroseptal area of the anatomic right atrium on the pulmonary venous side; there has been no recurrence in over 4 years.

The remaining three patients had multiple tachycardias (one patient each had two, three, and four different atrial tachycardias, respectively). The subeustachian isthmus served as the successful ablation site in only one of these tachycardias. Of the remaining tachycardias ($N = 8$), six were successfully ablated either in the systemic venous atrium ($N = 4$), or the posterolateral wall of the pulmonary venous atrium ($N = 1$), or between the posterolateral systemic venous atrial free wall and the IVC ($N = 1$). Two tachycardias were not ablated due to procedure length and/or poor understanding of the mechanism of tachycardia.

30.4.3.2 Patients After Fontan Operation

Four of 17 tachycardias were mapped in three patients' status after a Fontan operation. All of these patients had an atriopulmonary connection ("classic" Fontan connection for tricuspid atresia, $N = 2$, and for double inlet left ventricle, $N = 1$). In two patients, a single intra-atrial reentry tachycardia was addressed. Successful ablation occurred in the area between a suspected atriotomy and an atrial septal defect patch in one patient and in the area between posterolateral double potentials and the IVC in the other. The third patient had at least two tachycardias; neither could be successfully ablated.

30.4.4 "Figure-of-8" Intra-Atrial Tachycardias

"Figure-of-8" tachycardias were noted to occur more often (25%) in patients with complex atriotomies. "Figure-of-8" tachycardia with a common isthmus in the systemic venous atrium (Fig. 30.10) involved clockwise propagation around a scar and/or double potentials in the right lateral free wall and counterclockwise propagation around anterior atrial

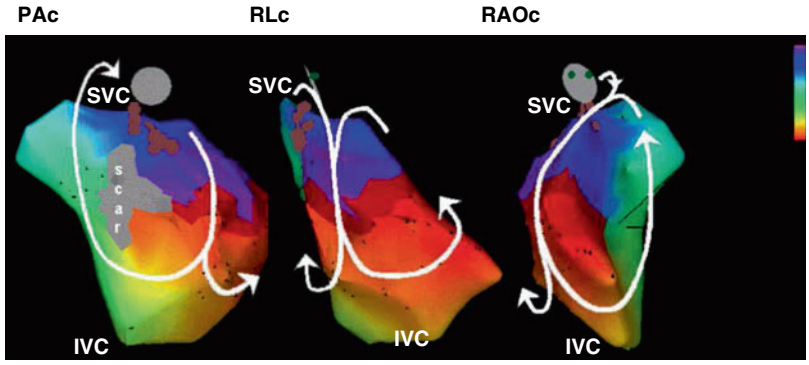

Figure 30.10

Figure-of-8 loop atrial tachycardia in a 13-year-old male patient after complex atriotomy for transposition of the great arteries and atrial switch operation (Mustard operation at 2 years of age).

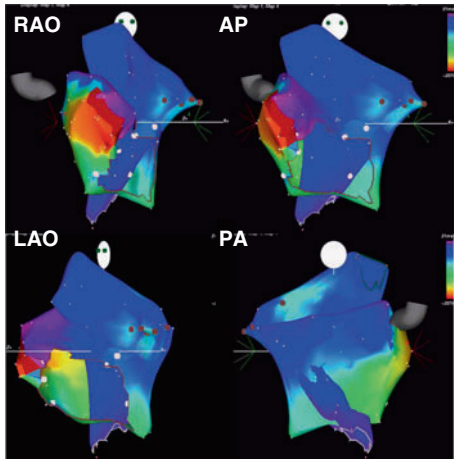

Figure 30.11

Figure-of-8 loop atrial tachycardia in an 18-year-old male patient after complex atriotomy for transposition of the great arteries and atrial switch operation (Mustard operation at 2 years of age). Shown is the electroanatomic map of both atria.

incisions (lower pant leg). A long ablative lesion bridging the superior and inferior pant leg resulted in successful ablation with no recurrence in more than 4 years.

"Figure-of-8" tachycardia in the pulmonary venous side involved counterclockwise propagation around the mitral valve annulus and clockwise around double potentials recorded on the lateral right free wall of the pulmonary venous atrium. Successful ablation was achieved from the posterolateral right free wall of the pulmonary venous atrium to the mitral valve (Fig. 30.11).

Another two "Figure-of-8" tachycardias were noted in patients after the Fontan operation. One of these demonstrated a common isthmus between an anterior atriotomy and an ASD patch and was successfully ablated. The second "Figure-of-8" tachycardia could not be ablated presumably because a transmural lesion could not be achieved. Ablative lesions from the right atrial posterolateral wall to both the IVC and the tricuspid valve dimple did not result in successful ablation of the tachycardia. This patient has had no clinical recurrence, however, after 8 months of follow-up.

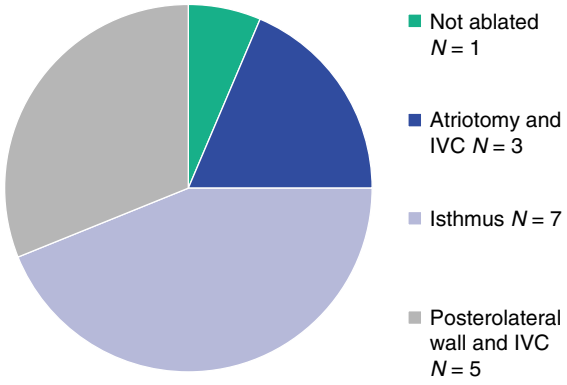

Figure 30.12

Summary of locations of successful ablation of atrial reentrant tachycardias in patients after a simple atriotomy. Atriotomies included those for ASD repair, VSD repair, TOF repair, AVSD repair, Ebstein's anomaly, and ventricular inversion. Note that the subeustachian isthmus was critical in supporting reentry in 44% of atrial tachycardias.

30.4.5 Role of the Subeustachian Area (Classic Flutter Isthmus)

In patients with postoperative atrial tachycardia, only 33% of reentry tachycardias involved the subeustachian isthmus as a critical part of the reentrant loop (Fig. 30.12). These findings are in contrast to those of Chan et al. [52]. This discrepancy in observation can be explained by several factors. Our patient population included patients with complex atrial surgery; the Chan study included patients with a simple atriotomy only. We used EAM in our study, allowing for more precise evaluation of the reentrant circuit. Our findings also differ somewhat from those of Collins et al. [100] and Love et al. [99], who noted that the subeustachian isthmus was critical to 57% of patients after atrial switch operation, whereas we noted that only 24% of these tachycardias involved the subeustachian isthmus. Regardless, our study confirms that intra-atrial reentry tachycardia in postoperative patients more often involves other crucial areas, such as the posterolateral right atrial wall [7, 9, 18]. We believe that the observed differences are due to the inclusion of a wider spectrum of congenital heart diseases and perhaps, more intensive evaluation of the tachycardia.

Another isthmus frequently mapped and successfully targeted for ablation was between posterolateral double potentials and the IVC. This isthmus is also recognized in adult patients with unusual types of atrial reentry tachycardia. Our study demonstrates that this reentrant atrial tachycardia is fairly common in patients after repair for congenital heart disease, involving an atriotomy that supports this unique reentrant substrate. Finally, a less common isthmus was between an anterior atriotomy and the IVC, and is in congruence with other studies. The implications of these findings for mapping and ablation suggest that subeustachian ablation may be more successful in patients after simple, rather than complex, atriotomy for congenital heart disease, and that other isthmuses could be crucially involved in postoperative reentry tachycardia and may even coexist.

The type and complexity of the reentry tachycardia varied with the type and complexity of the surgical repair. For simple atriotomies, multiple circuit tachycardias were less common than in patients with complex atriotomies (Figs. 30.12 and 30.13).

30.5 Long-Term Follow-Up of Patients with Atrial Tachycardia

Even with the use of advanced imaging techniques, the long-term success rate for our patients is 71% at a mean follow-up of 29 ± 17 months and at least 25% of patients (5/21) required repeat procedures. Failures may be due to inability to create transmural lesions (especially in patients after the Fontan operation), limited ability to reach critical areas (i.e., pulmonary venous atrium), or other limiting factors (i.e., procedure time and patient tolerance).

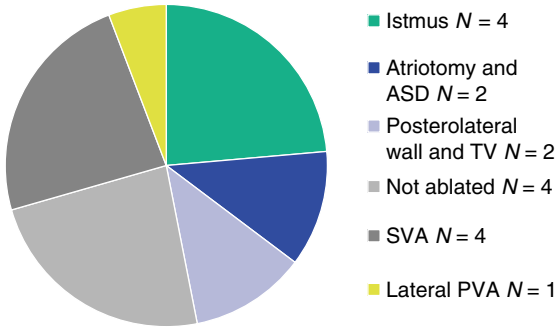

Figure 30.13

Summary of locations of successful ablation of atrial reentrant tachycardias in patients after a complex atriotomy. Atriotomies included those for Senning operation, Mustard operation, Bidirectional Glenn operation, and Fontan surgery. Note that the subeustachian isthmus was critical in supporting reentry in 24% of atrial tachycardias.

In summary, there are variety of different mechanisms of tachycardias in postoperative patients, some inscribing complicated reentrant loops such as "Figure-of-8" atrial reentry tachycardia. Because patients with congenital heart disease encompass a heterogeneous population and because surgical techniques are variable and the anatomy of the expressed disease so complicated, we found the use of multiple complementary approaches to be of great benefit to successful treatment of these postoperative tachycardias.

References

1. Garson, A. Jr. and P.C. Gillette, Junctional ectopic tachycardia in children: electrocardiography, electrophysiology and pharmacologic response. *Am. J. Cardiol.*, 1979;**44**: 298–302.
2. Gillette, P.C. and A. Garson Jr., Electrophysiologic and pharmacologic characteristics of automatic ectopic atrial tachycardia. *Circulation*, 1977;**56**: 571–575.
3. Garson, A. Jr., P.C. Gillette, and D.G. McNamara, Supraventricular tachycardia in children: clinical features, response to treatment, and long-term follow-up in 217 patients. *J. Pediatr.*, 1981;**98**: 875–882.
4. Fishberger, S.B., S.D. Colan, J.P. Saul, J.E. Mayer Jr., and E.P. Walsh, Myocardial mechanics before and after ablation of chronic tachycardia. *Pacing Clin. Electrophysiol.*, 1996;**19**: 42–49.
5. Blom, N.A., J. Ottenkamp, M.C. Deruiter, A.C. Wenink, and A.C. Gittenberger-de Groot, Development of the cardiac conduction system in atrioventricular septal defect in human trisomy 21. *Pediatr. Res.*, 2005;**58**: 516–520.
6. Blom, N.A., A.C. Gittenberger-de Groot, M.C. DeRuiter, R.E. Poelmann, M.M. Mentink, and J. Ottenkamp, Development of the cardiac conduction tissue in human embryos using HNK-1 antigen expression: possible relevance for understanding of abnormal atrial automaticity. *Circulation*, 1999;**99**: 800–806.
7. Walsh, E., Ablation of ectopic atrial tachycardia in children, in *Radiofrequency Catheter Ablation of Cardiac Arrhythmias*, 2nd edn., S.K.S. Huang and D.J. Wilber, Editor. Armonk, NY: Futura, 2000, pp. 115–138.
8. Liberthson, R.R. and S.D. Colan, Multifocal or chaotic atrial rhythm: report of nine infants, delineation of clinical course and management, and review of the literature. *Pediatr. Cardiol.*, 1982;**2**: 179–184.
9. Garavelli, L., K. Leask, C. Zanacca, S. Pedori, G. Albertini, E. Della Giustina, G.F. Croci, C. Magnani, G. Banchini, J. Clayton-Smith, M. Bocian, H. Firth, J.A. Gold, and J. Hurst, MRI and neurological findings in macrocephaly-cutis marmorata telangiectatica congenita syndrome: report of ten cases and review of the literature. *Genet. Couns.*, 2005;**16**: 117–128.
10. Shine, K.I., J.A. Kastor, and P.M. Yurchak, Multifocal atrial tachycardia. Clinical and electrocardiographic features in 32 patients. *N. Engl. J. Med.*, 1968;**279**: 344–349.
11. Salim, M.A., C.L. Case, and P.C. Gillette, Chaotic atrial tachycardia in children. *Am. Heart J.*, 1995;**129**: 831–833.
12. Dodo, H., R.M. Gow, R.M. Hamilton, and R.M. Freedom, Chaotic atrial rhythm in children. *Am. Heart J.*, 1995;**129**: 990–995.
13. Zeevi, B., M. Berant, S. Sclarovsky, and L.C. Blieden, Treatment of multifocal atrial tachycardia with amiodarone in a child with congenital heart disease. *Am. J. Cardiol.*, 1986;**57**: 344–345.
14. MacWilliams, J., Fibrillar contraction of the heart. *J. Physiol.*, 1887;**8**: 296.
15. Ritchie, W., Complete heart block with dissociation of the action of the auricles and ventricles. *Proc. R. Soc. Edinburgh.*, 1905;**25**: 1085.
16. Jolly, W.A. and W.T. Ritchie, Auricular flutter and fibrillation. 1911. *Ann. Noninvasive Electrocardiol.*, 2003;**8**: 92–96.
17. Einthoven, W., Le telecardiogramme. *Arch. Int. Physiol.*, 1906;**4**: 132.

18. Lewis, T., Observations upon a curious and not uncommon form of extreme acceleration of the auricle: auricular flutter. *Heart*, 1913;**4**: 171.
19. Lewis, T.D.D. and T.T. Iliescu. A demonstration of circus movement in clinical flutter of the auricles. *Heart*, 1921;**8**: 341.
20. Cabrera, E.S.-P.D., Discusion del movimiento circular y prueba directa de su existencia en el flutter auricular clinico. *Arch. Inst. Cardiol. Mex.*, 1947;**17**: 850.
21. Puech, P., H. Latour, and R. Grolleau, Flutter and his limits. *Arch. Mal. Coeur Vaiss.*, 1970;**63**: 116–144.
22. Waldo, A.L., Atrial flutter. New directions in management and mechanism. *Circulation*, 1990;**81**: 1142–1143.
23. Olshansky, B., K. Okumura, P.G. Hess, and A.L. Waldo, Demonstration of an area of slow conduction in human atrial flutter. *J. Am. Coll. Cardiol.*, 1990;**16**: 1639–1648.
24. Waldo, A.L., Clinical evaluation in therapy of patients with atrial fibrillation or flutter. *Cardiol. Clin.*, 1990;**8**: 479–490.
25. Henthorn, R.W., Y. Rudy, and A.L. Waldo, Evolving concepts regarding the role of tissue structure in arrhythmogenesis in the infarcted human heart. *J. Am. Coll. Cardiol.*, 1990;**15**: 1608–1609.
26. Henthorn, R.W., K. Okumura, B. Olshansky, V.J. Plumb, P.G. Hess, and A.L. Waldo, A fourth criterion for transient entrainment: the electrogram equivalent of progressive fusion. *Circulation*, 1988;**77**: 1003–1112.
27. Waldo, A.L., W.A. MacLean, T.B. Cooper, N.T. Kouchoukos, and R.B. Karp, Use of temporarily placed epicardial atrial wire electrodes for the diagnosis and treatment of cardiac arrhythmias following open-heart surgery. *J. Thorac. Cardiovasc. Surg.*, 1978;**76**: 500–505.
28. Waldo, A.L., W.A. MacLean, R.B. Karp, N.T. Kouchoukos, and T.N. James, Entrainment and interruption of atrial flutter with atrial pacing: studies in man following open heart surgery. *Circulation*, 1977;**56**: 737–745.
29. Olshansky, B., K. Okumura, R.W. Henthorn, and A.L. Waldo, Characterization of double potentials in human atrial flutter: studies during transient entrainment. *J. Am. Coll. Cardiol.*, 1990;**15**: 833–841.
30. Waldo, A.L., R.W. Henthorn, A.E. Epstein, and V.J. Plumb, Significance of transient entrainment in pacing treatment of tachyarrhythmias. *Arch. Mal. Coeur Vaiss.*, 1985;**78** Spec No: 23–28.
31. Waldo, A.L., R.W. Henthorn, A.E. Epstein, and V.J. Plumb, Diagnosis and treatment of arrhythmias during and following open heart surgery. *Med. Clin. North Am.*, 1984;**68**: 1153–1169.
32. Waldo, A.L., Mechanisms of atrial fibrillation, atrial flutter, and ectopic atrial tachycardia—a brief review. *Circulation*, 1987;**75**: III37–III40.
33. Wyndham, C.R., D. Wu, P. Denes, D. Sugarman, S. Levitsky, and K.M. Rosen, Self-initiated conversion of paroxysmal atrial flutter utilizing a radio-frequency pacemaker. *Am. J. Cardiol.*, 1978;**41**: 1119–1122.
34. Pastelin, G., R. Mendez, and G.K. Moe, Participation of atrial specialized conduction pathways in atrial flutter. *Circ. Res.*, 1978;**42**: 386–393.
35. Boineau, J.P., R.B. Schuessler, C.R. Mooney, C.B. Miller, A.C. Wylds, R.D. Hudson, J.M. Borremans, and C.W. Brockus, Natural and evoked atrial flutter due to circus movement in dogs. Role of abnormal atrial pathways, slow conduction, nonuniform refractory period distribution and premature beats. *Am. J. Cardiol.*, 1980;**45**: 1167–1181.
36. Inoue, H., H. Matsuo, K. Takayanagi, and S. Murao, Clinical and experimental studies of the effects of atrial extrastimulation and rapid pacing on atrial flutter cycle. Evidence of macro-reentry with an excitable gap. *Am. J. Cardiol.*, 1981;**48**: 623–631.
37. Allessie, M.A., W.J. Lammers, I.M. Bonke, and J. Hollen, Intra-atrial reentry as a mechanism for atrial flutter induced by acetylcholine and rapid pacing in the dog. *Circulation*, 1984;**70**: 123–135.
38. Spach, M.S., W.T. Miller III, P.C. Dolber, J.M. Kootsey, J.R. Sommer, C.E. Mosher Jr., The functional role of structural complexities in the propagation of depolarization in the atrium of the dog. Cardiac conduction disturbances due to discontinuities of effective axial resistivity. *Circ. Res.*, 1982;**50**: 175–191.
39. Frame, L.H., R.L. Page, and B.F. Hoffman, Atrial reentry around an anatomic barrier with a partially refractory excitable gap. A canine model of atrial flutter. *Circ. Res.*, 1986;**58**: 495–511.
40. Fontaine, G., C. Moro-Serrano, L. Menezes-Falcao, M. Todorova, R. Frank, J.L. Tonet, and Y. Grosgogeat, Anti-tachycardia radiofrequency pacemakers. Experience with 44 cases. *Arch. Mal. Coeur Vaiss.*, 1986;**79**: 1696–1702.
41. Cosio, F.G., F. Arribas, J. Palacios, J. Tascon, and M. Lopez-Gil, Fragmented electrograms and continuous electrical activity in atrial flutter. *Am. J. Cardiol.*, 1986;**57**: 1309–1314.
42. Saoudi, N., G. Atallah, G. Kirkorian, and P. Touboul, Catheter ablation of the atrial myocardium in human type I atrial flutter. *Circulation*, 1990;**81**: 762–771.
43. Feld, G.K., R.P. Fleck, P.S. Chen, K. Boyce, T.D. Bahnson, J.B. Stein, C.M. Calisi, and M. Ibarra, Radiofrequency catheter ablation for the treatment of human type 1 atrial flutter. Identification of a critical zone in the reentrant circuit by endocardial mapping techniques. *Circulation*, 1992;**86**: 1233–1240.
44. Anderson, R.H. and A.E. Becker, *Cardiac Anatomy: An Integrated Text and Colour Atlas*: London: Gower Medical Publishing; 1980.
45. Bachmann, G., The interauricular time interval. *Am. J. Physiol.*, 1916;**41**: 309.
46. Rosenblueth, A. and J. Garcia-Ramos, Studies on flutter and fibrillation. II. The influence of artificial obstacles on experimental auricular flutter. *Am. Heart J.*, 1947;**33**: 677–684.
47. Waldo, A.L., The interrelationship between atrial fibrillation and atrial flutter. *Prog. Cardiovasc. Dis.*, 2005;**48**: 41–56.
48. Waldo, A.L., Mechanisms of atrial flutter and atrial fibrillation: distinct entities or two sides of a coin? *Cardiovasc. Res.*, 2002;**54**: 217–229.
49. Saoudi, N., F. Cosio, A. Waldo, S.A. Chen, Y. Iesaka, M. Lesh, S. Saksena, J. Salerno, and W. Schoels, Classification of atrial flutter and regular atrial tachycardia according to electrophysiologic mechanism and anatomic bases: a statement from a joint expert group from the Working Group of Arrhythmias of the European Society of Cardiology and the North American Society of Pacing and Electrophysiology. *J. Cardiovasc. Electrophysiol.*, 2001;**12**: 852–866.
50. Saoudi, N., F. Cosio, A. Waldo, S.A. Chen, Y. Iesaka, M. Lesh, S. Saksena, J. Salerno, and W. Schoels, A classification of atrial flutter and regular atrial tachycardia according to electrophysiological mechanisms and anatomical bases; a Statement from a Joint Expert Group from The Working Group of Arrhythmias of the European Society of Cardiology and the North American Society of Pacing and Electrophysiology. *Eur. Heart J.*, 2001;**22**: 1162–1182.

51. Tomita, Y., K. Matsuo, J. Sahadevan, C.M. Khrestian, and A.L. Waldo, Role of functional block extension in lesion-related atrial flutter. *Circulation*, 2001;**103**: 1025–1130.
52. Chan, D.P., G.F. Van Hare, J.A. Mackall, M.D. Carlson, and A.L. Waldo, Importance of atrial flutter isthmus in postoperative intra-atrial reentrant tachycardia. *Circulation*, 2000;**102**: 1283–1289.
53. Waldo, A.L., Treatment of atrial flutter. *Heart*, 2000;**84**: 227–232.
54. Uno, K., K. Kumagai, C.M. Khrestian, and A.L. Waldo, New insights regarding the atrial flutter reentrant circuit: studies in the canine sterile pericarditis model. *Circulation*, 1999;**100**: 1354–1360.
55. Muller, G.I., B.J. Deal, J.F. Strasburger, and D.W. Benson Jr., Electrocardiographic features of atrial tachycardias after operation for congenital heart disease. *Am. J. Cardiol.*, 1993;**71**: 122–124.
56. Garson, A. Jr., M. Bink-Boelkens, P.S. Hesslein, A.J. Hordof, J.F. Keane, W.H. Neches, and C.J. Porter, Atrial flutter in the young: a collaborative study of 380 cases. *J. Am. Coll. Cardiol.*, 1985;**6**: 871–878.
57. Gelatt, M., R.M. Hamilton, B.W. McCrindle, R.M. Gow, W.G. Williams, G.A. Trusler, and R.M. Freedom, Risk factors for atrial tachyarrhythmias after the Fontan operation. *J. Am. Coll. Cardiol.*, 1994;**24**: 1735–1741.
58. Gelatt, M., R.M. Hamilton, B.W. McCrindle, M. Connelly, A. Davis, L. Harris, R.M. Gow, W.G. Williams, G.A. Trusler, and R.M. Freedom, Arrhythmia and mortality after the Mustard procedure: a 30-year single-center experience. *J. Am. Coll. Cardiol.*, 1997;**29**: 194–201.
59. Cronin, C.S., T. Nitta, M. Mitsuno, F. Isobe, R.B. Schuessler, J.P. Boineau, and J.L. Cox, Characterization and surgical ablation of acute atrial flutter following the Mustard procedure. A canine model. *Circulation*, 1993;**88**: II461–II471.
60. Nitta, T., R.B. Schuessler, M. Mitsuno, C.K. Rokkas, F. Isobe, C.S. Cronin, J.L. Cox, and J.P. Boineau, Return cycle mapping after entrainment of ventricular tachycardia. *Circulation*, 1998;**97**: 1164–1175.
61. Bromberg, B.I., R.B. Schuessler, S.K. Gandhi, M.D. Rodefeld, J.P. Boineau, and C.B. Huddleston, A canine model of atrial flutter following the intra-atrial lateral tunnel Fontan operation. *J. Electrocardiol.*, 1998;**30**(Suppl. 1): 85–93.
62. Gandhi, S.K., B.I. Bromberg, M.D. Rodefeld, R.B. Schuessler, J.P. Boineau, J.L. Cox, and C.B. Huddleston, Spontaneous atrial flutter in a chronic canine model of the modified Fontan operation. *J. Am. Coll. Cardiol.*, 1997;**30**: 1095–1103.
63. Rodefeld, M.D., S.K. Gandhi, C.B. Huddleston, B.J. Turken, R.B. Schuessler, J.P. Boineau, J.L. Cox, and B.I. Bromberg, Anatomically based ablation of atrial flutter in an acute canine model of the modified Fontan operation. *J. Thorac. Cardiovasc. Surg.*, 1996;**112**: 898–907.
64. Gandhi, S.K., B.I. Bromberg, M.D. Rodefeld, R.B. Schuessler, J.P. Boineau, J.L. Cox, and C.B. Huddleston, Lateral tunnel suture line variation reduces atrial flutter after the modified Fontan operation. *Ann. Thorac. Surg.*, 1996;**61**: 1299–1309.
65. Rodefeld, M.D., B.I. Bromberg, R.B. Schuessler, J.P. Boineau, J.L. Cox, and C.B. Huddleston, Atrial flutter after lateral tunnel construction in the modified Fontan operation: a canine model. *J. Thorac. Cardiovasc. Surg.*, 1996;**111**: 514–526.
66. Fishberger, S.B., G. Wernovsky, T.L. Gentles, K. Gauvreau, J. Burnett, J.E. Mayer Jr., and E.P. Walsh, Factors that influence the development of atrial flutter after the Fontan operation. *J. Thorac. Cardiovasc. Surg.*, 1997;**113**: 80–86.
67. Durongpisitkul, K., C.J. Porter, F. Cetta, K.P. Offord, J.M. Slezak, F.J. Puga, H.V. Schaff, G.K. Danielson, and D.J. Driscoll, Predictors of early- and late-onset supraventricular tachyarrhythmias after Fontan operation. *Circulation*, 1998;**98**: 1099–1107.
68. Bink-Boelkens, M.T., A. Bergstra, A.H. Cromme-Dijkhuis, A. Eygelaar, M.J. Landsman, and E.L. Mooyaart, The asymptomatic child a long time after the Mustard operation for transposition of the great arteries. *Ann. Thorac. Surg.*, 1989;**47**: 45–50.
69. Bink-Boelkens, M.T., K.J. Meuzelaar, and A. Eygelaar, Arrhythmias after repair of secundum atrial septal defect: the influence of surgical modification. *Am. Heart J.*, 1988;**115**: 629–633.
70. Bink-Boelkens, M.T., H. Velvis, J.J. van der Heide, A. Eygelaar, and R.A. Hardjowijono, Dysrhythmias after atrial surgery in children. *Am. Heart J.*, 1983;**106**: 125–130.
71. Roos-Hesselink, J., M.G. Perlroth, J. McGhie, and S. Spitaels, Atrial arrhythmias in adults after repair of tetralogy of Fallot. Correlations with clinical, exercise, and echocardiographic findings. *Circulation*, 1995;**91**: 2214–2219.
72. Peters, N.S. and J. Somerville, Arrhythmias after the Fontan procedure. *Br. Heart J.*, 1992;**68**: 199–204.
73. Douglas, D.E., C.L. Case, C.O. Shuler, and P.C. Gillette, Successful radiofrequency catheter ablation of atrial muscle reentry tachycardia in a young adult. *Clin. Cardiol.*, 1995;**18**: 51–53.
74. Balaji, S., C.L. Case, R.M. Sade, and P.C. Gillette, Arrhythmias and electrocardiographic changes after the hemi-Fontan procedure. *Am. J. Cardiol.*, 1994;**73**: 828–829.
75. Balaji, S., T.B. Johnson, R.M. Sade, C.L. Case, and P.C. Gillette, Management of atrial flutter after the Fontan procedure. *J. Am. Coll. Cardiol.*, 1994;**23**: 1209–1215.
76. Case, C.L., P.C. Gillette, D.E. Douglas, and R.A. Liebermann, Radiofrequency catheter ablation of atrial flutter in a patient with postoperative congenital heart disease. *Am. Heart J.*, 1993;**126**: 715–716.
77. Flinn, C.J., G.S. Wolff, M. Dick II, R.M. Campbell, G. Borkat, A. Casta, A. Hordof, T.J. Hougen, R.E. Kavey, J. Kugler, et al., Cardiac rhythm after the Mustard operation for complete transposition of the great arteries. *N. Engl. J. Med.*, 1984;**310**: 1635–1638.
78. Porter, C.B., J. Fukushige, D.L. Hayes, M.D. McGoon, M.J. Osborn, and F.J. Puga, Permanent antitachycardia pacing for chronic atrial tachyarrhythmias in postoperative pediatric patients. *Pacing Clin. Electrophysiol.*, 1991;**14**: 2056–2057.
79. Porter, C.J. and A. Garson, Incidence and management of dysrhythmias after Fontan procedure. *Herz*, 1993;**18**: 318–327.
80. Baker, B.M., B.D. Lindsay, B.I. Bromberg, D.W. Frazier, M.E. Cain, and J.M. Smith, Catheter ablation of clinical intraatrial reentrant tachycardias resulting from previous atrial surgery: localizing and transecting the critical isthmus. *J. Am. Coll. Cardiol.*, 1996;**28**: 411–417.
81. Feltes, T.F. and R.A. Friedman, Transesophageal echocardiographic detection of atrial thrombi in patients with nonfibrillation atrial tachyarrhythmias and congenital heart disease. *J. Am. Coll. Cardiol.*, 1994;**24**: 1365–1370.
82. Beaufort-Krol, G.C. and M.T. Bink-Boelkens, Sotalol for atrial tachycardias after surgery for congenital heart disease. *Pacing Clin. Electrophysiol.*, 1997;**20**: 2125–2129.
83. Beaufort-Krol, G.C. and M.T. Bink-Boelkens, Effectiveness of sotalol for atrial flutter in children after surgery for congenital heart disease. *Am. J. Cardiol.*, 1997;**79**: 92–94.

84. Fukushige, J., C.B. Porter, D.L. Hayes, M.D. McGoon, M.J. Osborn, and R.E. Vlietstra, Antitachycardia pacemaker treatment of postoperative arrhythmias in pediatric patients. *Pacing Clin. Electrophysiol.*, 1991;**14**: 546–556.
85. Rhodes, L.A., E.P. Walsh, W.J. Gamble, J.K. Triedman, and J.P. Saul, Benefits and potential risks of atrial antitachycardia pacing after repair of congenital heart disease. *Pacing Clin. Electrophysiol.*, 1995;**18**: 1005–1016.
86. Rhodes, L.A., E.P. Walsh, and J.P. Saul, Conversion of atrial flutter in pediatric patients by transesophageal atrial pacing: a safe, effective, minimally invasive procedure. *Am. Heart J.*, 1995;**130**: 323–327.
87. Gillette, P.C., D.G. Wampler, C. Shannon, and D. Ott, Use of cardiac pacing after the Mustard operation for transposition of the great arteries. *J. Am. Coll. Cardiol.*, 1986;**7**: 138–141.
88. Duster, M.C., M.T. Bink-Boelkens, D. Wampler, P.C. Gillette, D.G. McNamara, and D.A. Cooley, Long-term follow-up of dysrhythmias following the Mustard procedure. *Am. Heart J.*, 1985;**109**: 1323–1326.
89. Gillette, P.C., D.G. Wampler, C. Shannon, and D. Ott, Use of atrial pacing in a young population. *Pacing Clin. Electrophysiol.*, 1985;**8**: 94–100.
90. Lesh, M.D., J.M. Kalman, and M.R. Karch, Use of intracardiac echocardiography during electrophysiologic evaluation and therapy of atrial arrhythmias. *J. Cardiovasc. Electrophysiol.*, 1998;**9**: S40–S47.
91. Kalman, J.M., J.E. Olgin, M.R. Karch, M. Hamdan, R.J. Lee, and M.D. Lesh, "Cristal tachycardias": origin of right atrial tachycardias from the crista terminalis identified by intracardiac echocardiography. *J. Am. Coll. Cardiol.*, 1998;**31**: 451–459.
92. Olgin, J.E., J.M. Kalman, M. Chin, C. Stillson, M. Maguire, P. Ursel, and M.D. Lesh, Electrophysiological effects of long, linear atrial lesions placed under intracardiac ultrasound guidance. *Circulation*, 1997;**96**: 2715–2721.
93. Lesh, M.D., J.M. Kalman, L.A. Saxon, and P.C. Dorostkar, Electrophysiology of "incisional" reentrant atrial tachycardia complicating surgery for congenital heart disease. *Pacing Clin. Electrophysiol.*, 1997;**20**: 2107–2111.
94. Kalman, J.M., J.E. Olgin, L.A. Saxon, R.J. Lee, M.M. Scheinman, and M.D. Lesh, Electrocardiographic and electrophysiologic characterization of atypical atrial flutter in man: use of activation and entrainment mapping and implications for catheter ablation. *J. Cardiovasc. Electrophysiol.*, 1997;**8**: 121–144.
95. Kalman, J.M., J.E. Olgin, L.A. Saxon, W.G. Fisher, R.J. Lee, and M.D. Lesh, Activation and entrainment mapping defines the tricuspid annulus as the anterior barrier in typical atrial flutter. *Circulation*, 1996;**94**: 398–406.
96. Kalman, J.M., G.F. VanHare, J.E. Olgin, L.A. Saxon, S.I. Stark, and M.D. Lesh, Ablation of 'incisional' reentrant atrial tachycardia complicating surgery for congenital heart disease. Use of entrainment to define a critical isthmus of conduction. *Circulation*, 1996;**93**: 502–512.
97. Olgin, J.E., J.M. Kalman, A.P. Fitzpatrick, and M.D. Lesh, Role of right atrial endocardial structures as barriers to conduction during human type I atrial flutter. Activation and entrainment mapping guided by intracardiac echocardiography. *Circulation*, 1995;**92**: 1839–1848.
98. Dorostkar, P.C., J. Cheng, and M.M. Scheinman, Electroanatomical mapping and ablation of the substrate supporting intraatrial reentrant tachycardia after palliation for complex congenital heart disease. *Pacing Clin. Electrophysiol.*, 1998;**21**: 1810–1819.
99. Love, B.A., K.K. Collins, E.P. Walsh, and J.K. Triedman, Electroanatomic characterization of conduction barriers in sinus/atrially paced rhythm and association with intra-atrial reentrant tachycardia circuits following congenital heart disease surgery. *J. Cardiovasc. Electrophysiol.*, 2001;**12**: 17–25.
100. Collins, K.K., B.A. Love, E.P. Walsh, J.P. Saul, M.R. Epstein, and J.K. Triedman, Location of acutely successful radiofrequency catheter ablation of intraatrial reentrant tachycardia in patients with congenital heart disease. *Am. J. Cardiol.*, 2000;**86**: 969–974.

Section 7

Body-Surface Isopotential Mapping

31 Body Surface Potential Mapping Techniques

Robert L. Lux

P. W. Macfarlane, A. van Oosterom, O. Pahlm, P. Kligfield, M. Janse, J. Camm (eds.), *Comprehensive Electrocardiology*, DOI 10.1007/978-1-84882-046-3_31,

31.1 Introduction – History and Technology

Body surface potential mapping is an extension of conventional electrocardiography that acknowledges the fact that cardiac electrical fields – the voltage distributions and current flow patterns arising from cardiac currents – exist everywhere within and on the body surface. Waller, Einthoven, Wilson, and many of the early electrocardiographers recognized that the electrocardiogram could be measured from any body surface site and that the measured signals were different at each site, but because of limitations in recording technology, they could measure only one or at best a few sites at a time. The evolution of electronic amplifiers and the advent and access of laboratory computers during the late 1960s made possible the recording of many ECGs at a time, thus allowing the *mapping* of spatial distributions of potential. The sequence of these distributions defines what has come to be known as the body surface potential map. Unlike *scalar* electrocardiography which relies on interpretation of waveform features including amplitudes, durations, and morphologies of the different electrocardiographic waves, body surface potential mapping focuses on the magnitude, location, and migration of potential extrema as well as the shape and dynamics of isopotential contours throughout the cardiac cycle.

Body surface potential mapping (BSPM) is a subset of the more general field of cardiac mapping that includes the *direct* study of cardiac fields measured in the intracavitary space, intramurally within the myocardium, and on epicardial and endocardial surfaces. While body surface mapping is completely noninvasive and makes use of passive or active electrodes placed on the body surface, direct cardiac mapping techniques are invasive and require insertion of catheter mounted arrays (balloons, baskets) in the cavities, multipolar catheters placed in the coronary veins, multipolar needles inserted directly into the myocardium, or "sock" or patch mounted arrays of electrodes for use on the epicardium at the time of open chest surgery. In all cases, the objective is to assess the 2D and 3D distributions of potential or current on and within the myocardium, thus the more the recording sites, the greater the resolution and ability to characterize the underlying cardiac electrical sources. In this chapter, we shall focus exclusively on BSPM.

The original rationale for BSPM was that the ability to visualize the dynamic patterns of cardiac generated potentials was hypothesized to provide a more complete picture of the underlying electrical sources of the heart than that provided by the limited view of six "unipolar" precordial leads and the six limb/augmented leads of which only two are independent. This, in turn, would provide better means to detect and characterize the underlying disease, namely infarction, ischemia, abnormalities of conduction, hypertrophy, and cardiomyopathy. A secondary, more powerful rationale was that the rapidly developing methodology of inverse electrocardiography offered an opportunity for body surface map data to be used to calculate, estimate, characterize, or localize the electrical sources within the heart. In fact, the work of Ramanathan et al. and others in recent years has shown the feasibility of generating reliable estimates of cardiac electrograms and extracted information such as depolarization (activation) sequence and repolarization (recovery) sequence derived from measured body surface maps and measured torso and organ geometries and resistivities [1].

In point of fact, largely because of the expense of custom recording equipment and the consideration that computing power needed for processing and display was available only as expensive, laboratory computing systems, the early mapping efforts in the 1970s and early 1980s were relegated almost exclusively to the laboratory. Additionally, the rapid evolution of ultrasonic imaging of the heart began to provide inexpensive, noninvasive means of detecting cardiac abnormalities, including wall motion abnormalities (infarction and ischemia), valve dysfunction, wall thickness (hypertrophy), and conduction defects (bundle branch block). This new technology siphoned energy and rationale for body surface mapping, leaving electrophysiology and arrhythmias as the major remaining areas of study. Nevertheless, BSPM continues to be used, particularly as a means to better characterize heart disease and, more recently, as a means to facilitate localization key circuits in arrhythmias.

31.2 Recording Techniques

Body surface mapping systems include an electrode array, electronics for amplification, and recording of the ECG data, computing resources for preprocessing the recorded ECGs, displaying them in a variety of formats, and for analyzing the signals for purposes of detection, classification, or monitoring changes in cardiac electrophysiological state.

31.2.1 Electrode Arrays

Most early mapping was done using regular arrays (fixed numbers of columns and rows) of passive metal electrodes, typically chlorided silver, attached to individual strips of nylon, rubber, or other substrate material. Conventional electrode paste was routinely used to enhance electrical contact with the skin and double-sided adhesive strips or "doughnuts" were used to hold the electrodes in place. At least one group used polished insect pins attached to individual wires to record signals and another group devised a vest embedded with active dry electrodes – electrodes that have preamplifiers mounted directly on the metal. The objective of these designs was to obtain high quality and low noise signals while minimizing the time needed to apply the electrode arrays.

In the early days of mapping, little was known about redundancy of electrocardiographic information in the sense of correlation between sites, and hence mappers used large numbers of electrodes (242, 192, 128, 64, etc.). As body surface potential map databases grew and as experience and understanding of distributions demonstrated that there was considerable redundancy in these signals, several groups focused on "limited" or "reduced" lead systems to maximize capture of information while reducing the costs associated with large numbers of leads and the associated electronics and computing needed to manage the data. This topic will be addressed later in this chapter.

Several techniques have been developed to facilitate and speed up the process of applying the electrodes to patients. These include the use of strips of electrodes with double sided adhesive, inflatable vests in which electrodes are embedded on the inner surfaces, arrays of electrodes supported by a mechanical shell and adjustable to fit each torso, and strips of electrodes attached to the patient via suction. Most electrode systems use and require use of electrode gel for purposes of ensuring good electrode–skin contact, but others have reported success using active dry electrodes that eliminate the need for electrode gel.

31.2.2 Electronics

Mapping systems require the need for amplification of the small (~2 mV magnitude) signals, analog-to-digital (A/D) converters to convert the amplified voltages into numerical representation for later processing, and a means to store these samples from each of the electrodes. The basis of all electrocardiographic recording is the electronic amplifier tailored for bioelectric signals having maximum amplitudes of 2 mV. During the late 1960s and early 1970s, such amplifiers were readily available, but not configured in size and cost to permit assemblies of the hundreds needed for the "simultaneous" recording, essential for mapping. Several groups developed their own custom amplifier systems using low noise, high performance integrated circuits that allowed packaging of tens of individual amplifiers on each circuit board. The addition of individual *sample and hold* circuits made possible the "simultaneous" sampling of data from all amplifiers, important for maintaining temporal integrity of the data. Another important contribution to the technology was the use of analog *multiplexers*, integrated circuits that allowed signals from multiple amplifiers to be switched into one data stream that could then be fed to one A/D converter. This innovation drastically reduced the system cost by eliminating the need for expensive A/D converters for each channel. The stream of digital samples was then stored in computer memory or directly to disk using double buffering techniques and finally to digital tape. Early systems were limited to short recording times, typically just a few seconds, a consequence of the limits of available computing technologies and storage media. Present systems, both custom laboratory systems and the few commercially available, can record continuously to memory or disk for long periods of time.

31.2.3 Computer Processing and Display

The advent of laboratory computers and later, the availability of personal computers, made possible the extensive processing, analysis, and display of body surface potential map data. For each multichannel recording, individual signals had to be calibrated, adjusted for baseline drift, filtered if there were excessive noise, or estimated or interpolated from other signals if the signal were excessively noisy or "missing", often a problem when hundreds of leads and connectors were considered. The signature presentation of body surface potential data is the isopotential contour map, in which potentials for each sample time are displayed as contour maps on geometric representations of the torso. Data in Fig. 31.1 show

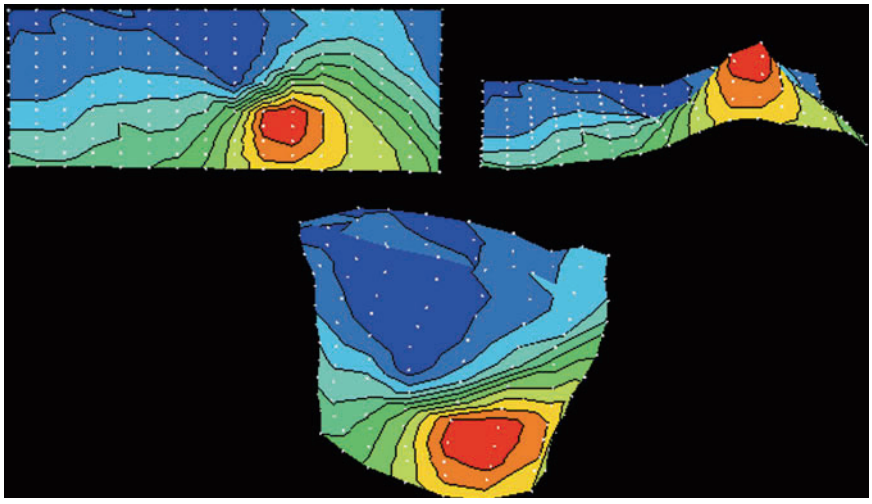

Figure 31.1
Examples of isopotential contour map displays from the early QRS of a normal subject. On the upper left panel is a stylized 2D contour plot showing an array of 12 rows by 16 columns (192 sites) that represent a torso surface. The *top* and *bottom* edges of the rectangle correspond to the levels of the sternal notch and umbilicus, respectively. The *vertical midline* of the array corresponds to the vertical anterior thoracic midline and the *left* and *right* edges of the display correspond to the spine. On the upper right panel is the same data as displayed in the left panel except with vertical modulation of the potential, thus showing positive and negative extrema as "mountain peaks" and "valleys". The bottom panel shows the same data now presented on a 3D torso model. Contours are colored from blue (*negative*) to red (*positive*).

the same "frame" (sample) early in the QRS of a normal subject using a flat 2D array (upper left) as well as a 3D torso array (bottom). A third presentation of the same data (upper right), the orthographic projection, shows the potential distributions as "mountains and valleys" and is useful in enhancing magnitude differences and changes at the expense of extrema localization. An example of early, mid, and late "frames" within the sequence of QRS maps of a normal subject is shown in Fig. 31.2. The features of these maps used to describe them include the location and movement of the positive and negative extrema (trajectories) and the shape, steepness (gradient), and levels of isopotential contours. A variety of scaling techniques is used including *linear*, in which contours are spaced at fixed intervals, *normalized* in which a fixed number of contours is drawn for each map and which is useful for displaying data having low amplitude or widely varying amplitude, and *logarithmic* spacing for widely varying amplitudes. Additionally, since positive and negative potentials may be quite disparate in magnitude, it is often helpful to use *separate scaling* for positive and negative potentials. Such scaling options offer flexibility in assessing pattern and/or amplitude differences or changes.

31.3 Lead Systems for Recording and Estimating Body Surface Potential Maps

Since the objectives of electrocardiographic body surface potential mapping are measurement, analysis, and the use of **distributions**, measurement explicitly requires extensive spatial sampling. In contrast to the conventional 12 lead ECG and VCG techniques, which were developed from empirical considerations as well as representations of the electrical activity of the heart as a simple dipole, mapping lead systems were designed to measure "all" available ECG information.

Lead systems have been characterized as "complete" or "limited" (also referred to as "reduced lead systems"), the former implying the actual sampling of "all" data and the latter implying the sampling of a small number of sites for approximating or estimating complete distributions to a prespecified level of accuracy. Since mapping has been relegated primarily to research laboratories, there have never been standards for lead systems. Thus, there is a great variety in the

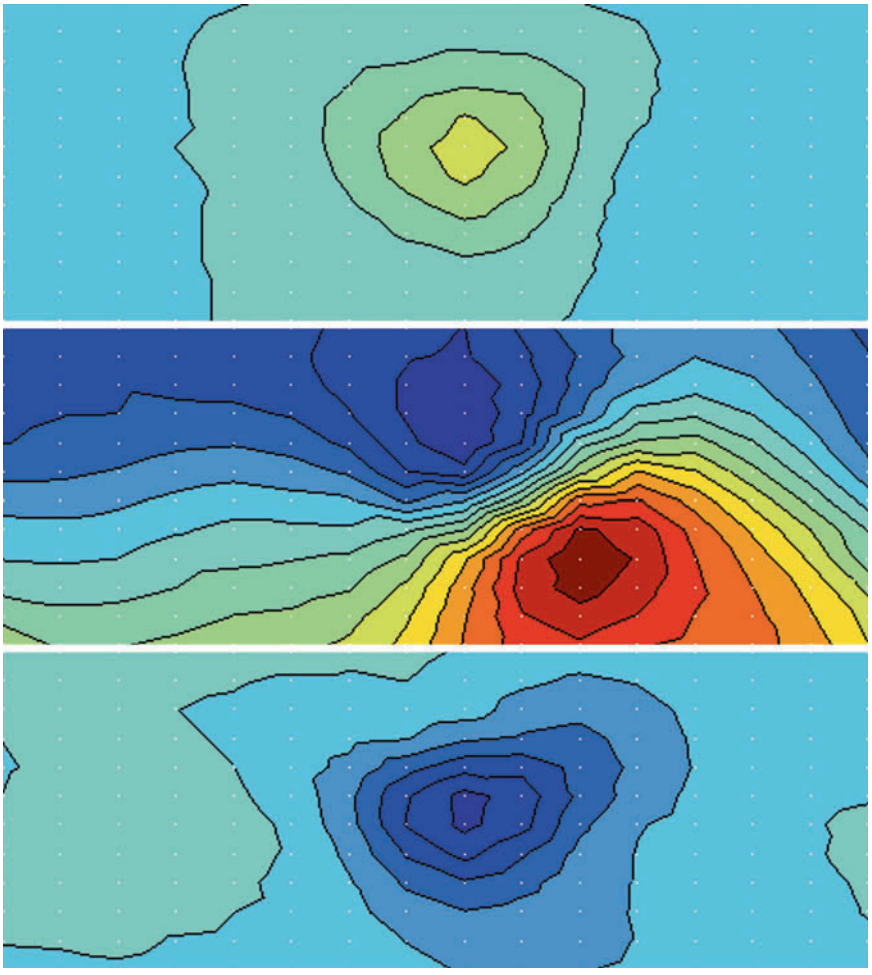

Figure 31.2
Three QRS "frames" (isopotential distributions) from a normal subject showing early, mid, and late distributions.

number and placement of recording sites. "Complete" sampling lead systems published in the literature include provision to measure 64, 120, 128, 192, and 242 body surface sites. Since the purpose of extensive sampling is to define the spatial character of the cardiac generated potentials, these systems are designed to sample most of the thoracic surface. In most systems, electrodes are placed in evenly separated rows and columns over the thorax. Modifications to this basic arrangement include increased spatial sampling density in the precordial region (doubling the number of rows and columns in this region) and reduced sampling density on the posterior surface (halving the number of rows and/or columns) and placement of leads lower on the torso and higher, including the shoulders. It is important to note that the rationale for a particular lead system is dictated by the presumption that all ECG information will be sampled. Also, however, lead systems may be tied to the type of displays used. Complete lead systems were used initially because of the lack of knowledge concerning the detailed spatial character of ECG distributions or the extent of redundancy. By measuring data at all sites, direct display of the distributions and later analysis demonstrated that, for practical purposes, complete sampling was not necessary. This led to the development of a variety of "limited lead" systems for estimating complete maps [2–4]. The mechanisms by which complete ECG distributions may be "derived" from such limited lead sets include interpolation, modeling, and estimation.

31.3.1 Interpolation

Interpolation relies on mathematical formulae that provide smooth approximations to data within the regions between measurement sites. Simple linear or bilinear interpolation may be used, or curve or surface fitting may be applied. Another interpolation approach is to assume a periodic structure for the data, a strictly correct assumption when applied to the circumferential aspect of the torso. This permits use of Fourier series to build interpolation polynomials from which potentials may be approximated at unmeasured sites [5].

31.3.2 Modeling

Modeling approaches rely on physical characteristics of measurement sites – geometric location, conductivity of the torso, and its inhomogeneity – in conjunction with the field equations that *model* the problem to predict aspects of the distributions in unmeasured regions.

31.3.3 Estimation

Estimation techniques, on the other hand, utilize information obtained from complete lead systems in order to develop statistical transformations for estimating unmeasured data from that measured at limited lead sites. Ultimately, potentials $\boldsymbol{\Phi_u}$ at N_u unmeasured sites, are to be estimated from potentials $\boldsymbol{\Phi_m}$ at N_m measured sites, by a linear transformation, T, such that

$$\Phi_u = T\Phi_m$$

Theoretically, a perfect transformation exists for each subject and each cardiac state. However, an average transformation may function sufficiently well to permit its use in a practical system. In one implementation of this approach, the transformation, T, may be determined as the linear, least mean squared error estimator given by

$$T = K_{um}K_{mm}^{-1}$$

where, K_{um} is the cross covariance matrix between unmeasured and measured sites and K_{mm} is the covariance matrix of measured sites defined using the expectation operator, E, as

$$K_{um} = E\left[\left(\Phi_u - \overline{\Phi_u}\right)\left(\Phi_m - \overline{\Phi_m}\right)^T\right]$$

and

$$K_{mm} = E\left[\left(\Phi_m - \overline{\Phi_m}\right)\left(\Phi_m - \overline{\Phi_m}\right)^T\right]$$

where

$$K = \begin{bmatrix} K_{mm} & K_{mu} \\ K_{um} & K_{mm} \end{bmatrix}$$

In general, the covariance between any two sites i and j, k_{ij} is given by

$$k_{ij} = E\left[\left(p_i - \overline{p_i}\right)\left(p_j - \overline{p_j}\right)\right] = \rho_{ij}\sigma_i\sigma_j$$

in which ρ_{ij} is the correlation coefficient between potentials at sites i and j, σ_i and σ_j are the potential standard deviations at sites i and j. Regardless of the method for assigning potentials to the unmeasured sites, a variety of error criteria for assessing the adequacy of lead systems have been developed which permit selection of lead systems to suit one's needs. These criteria include root-mean-square (rms) error, correlation coefficient, peak error, and others, all of which compare estimated data with that obtained from a complete lead system. Depending on the number and placement of leads, estimation errors approaching the system and recording noise levels are possible. This approach has formed the basis for estimating BSPMs and even the 12 lead ECG from small numbers of leads.

31.4 Utilization of Body Surface Potential Map Information

There are two primary uses of map data, both ultimately aimed at understanding and characterizing normal and abnormal cardiac electrophysiology. The first and original use relates to the characterization of cardiac state, specifically with respect to disease, by direct correlation of map features with independent documentation of cardiac physiology and pathology. With regard to this use, emphasis is placed on practical application of measurements for improved, noninvasive diagnosis as compared to the 12 lead ECG. The second use of map data relates to the validation and assessment of forward and inverse models and concentrates on estimation of myocardial current distributions from which underlying physiology can be inferred. The latter is discussed elsewhere in this text and will not be described here. Regarding the former, utilization of map information is accomplished through visual assessment and/or quantitative approaches that permit rigorous analyses, particularly those involving statistical methods. Examples of these now follow.

Since the first maps were recorded, simple observation of the potential distributions has been the primary means of analysis. The sequence of distributions, including dynamics, relative magnitudes and trajectories of positive and negative extrema, and morphology of contours provide a rich characterization of each heart cycle. Classical features of maps on patients with old infarcts, bundle branch blocks, ectopic activation, WPW, etc., provide sufficient information for simple, "eyeball" classification which is often not as clear using the 12 lead ECG alone. For example, cardiac events leading to a marginally abnormal Q wave in a 12 lead examination would likely have a more definitive representation in maps, namely a negative extremum with signature temporal and spatial characteristics. In WPW, a delta wave – small deflection preceding and merging with the QRS – in the 12 lead, is transformed to an early negative extremum, whose location indirectly points to the location of the accessory pathway on the A-V ring. Ectopic ventricular beats and VT exhibit map patterns that consistently identify the location of early depolarization. The latter two illustrations characterize the "atlas" approach to map analysis in which map patterns originating from known cardiac location, whether epicardial, endocardial, or septal and both atrial and ventricular, are catalogued and then used for comparison to patterns from unknown activations [6–8]. Maps obtained from patients having a variety of cardiac pathologies are described in the following chapter. However, a brief introduction to the methods of qualitatively interpreting map distributions might be useful.

31.4.1 Qualitative Analysis

The elementary interpretation of potential distributions follows that of conventional ECGs. During the QRS, a positive wave in a unipolar lead is indicative of an approaching activation front and a negative wave reflects a receding front. Hence, Q or S waves signify receding wave fronts as viewed from the measurement site, whereas R or R′ waves are indicative of wave fronts approaching the site. In isopotential contour maps obtained during depolarization, body surface regions that are negative primarily reflect the perspective of receding depolarization surfaces, whereas regions that are positive are those which "see" approaching depolarization surfaces. During repolarization, the polarity is reversed, as is the interpretation.

In order to illustrate interpretation of map distributions, two examples are presented. The map in ❯ Fig. 31.3 shows data *early* in the QRS of a patient with an old anterior wall myocardial infarct. The dominant anterior negative extremum and left, posterolateral positive extremum, result from a depolarization surface oriented along a dominant anterior to posterior axis. This pattern persists throughout much of the QRS and the lack of anterior positivity is consistent with the loss of active, anterior wall myocardium.

The sequence of map frames shown in ❯ Fig. 31.4 shows potential distributions, *early*, mid, and late in the QRS of a patient with right bundle branch block. *The early (top) left to right axis (blue to yellow) of the potential distribution is indicative of a depolarization surface oriented in a left to right direction and would signify early left ventricular depolarization. The mid QRS transitional distribution shows a posterior-to-anterior distribution, likely dominated by LV endocardial-to-epicardial depolarization. The late QRS pattern (bottom) shows a right inferior to left superior axis and suggests a right ventricular depolarization pattern.*

Similar interpretations can be applied to ECGs and body surface maps during *repolarization*, with the exception that polarity reversal must be taken into account. In unipolar ECGs, positive T waves are measured at sites that, on the average, observe recovery receding from them. Contrariwise, negative T waves are detected at sites which observe recovery

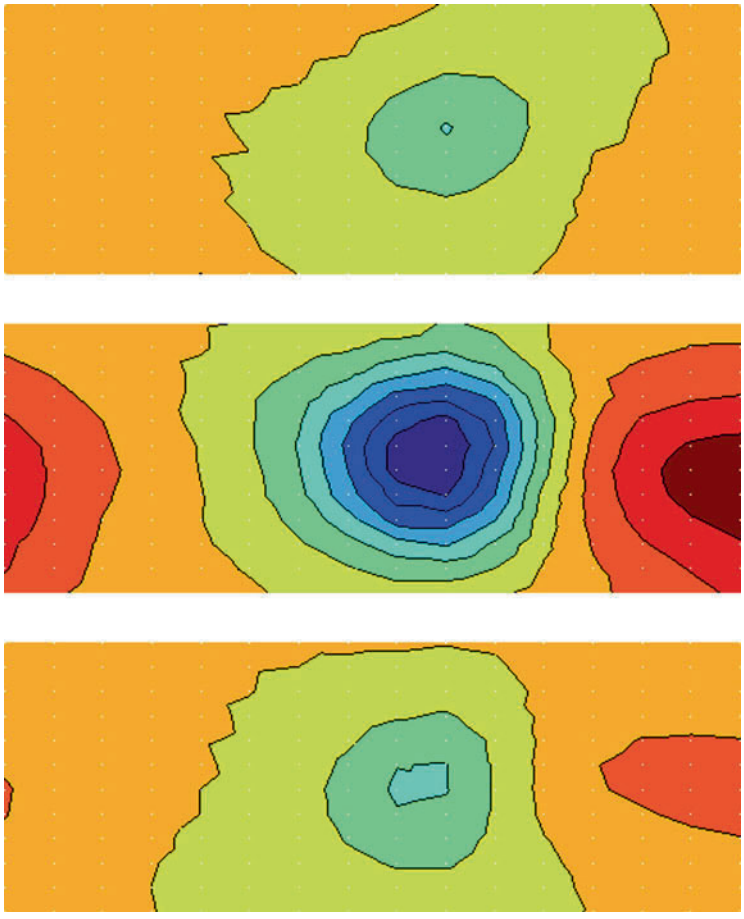

Figure 31.3
Three QRS frames from a patient with old anterior myocardial infarction.

approaching them. In maps, positive regions are indicative of sites which, on average, observe repolarization receding and negative regions occur where recovery is approaching. A potential distribution during recovery of a normal subject is shown in Fig. 31.5. This distribution, which is quite static in pattern, shows a dominant right superior to left inferior axis on the anterior thoracic surface. This is consistent with the predominant epicardial to endocardial distribution of recovery observed in the normal heart following supraventricular activation.

It should be stressed at this point that the qualitative interpretation of potential distributions is correct in a general sense, although it is far from exact. The potential observed at any site results from a complex superposition of the effects of all active cardiac currents. The complexity of both the cardiac generator as well as the body volume conductor make exact interpretation difficult, if not impossible. The anisotropic, inhomogeneous, time varying nature of the active and passive tissue underscores the difficulty of carrying out unambiguous interpretation of map data from a qualitative approach.

31.4.2 Quantitative Analyses of Body Surface Maps

The simplest quantitative approaches to map analysis are those that assign numerical values to visually observable features. Thus, the *trajectories* of positive and/or negative extrema may be parameterized into x, y coordinates varying with time.

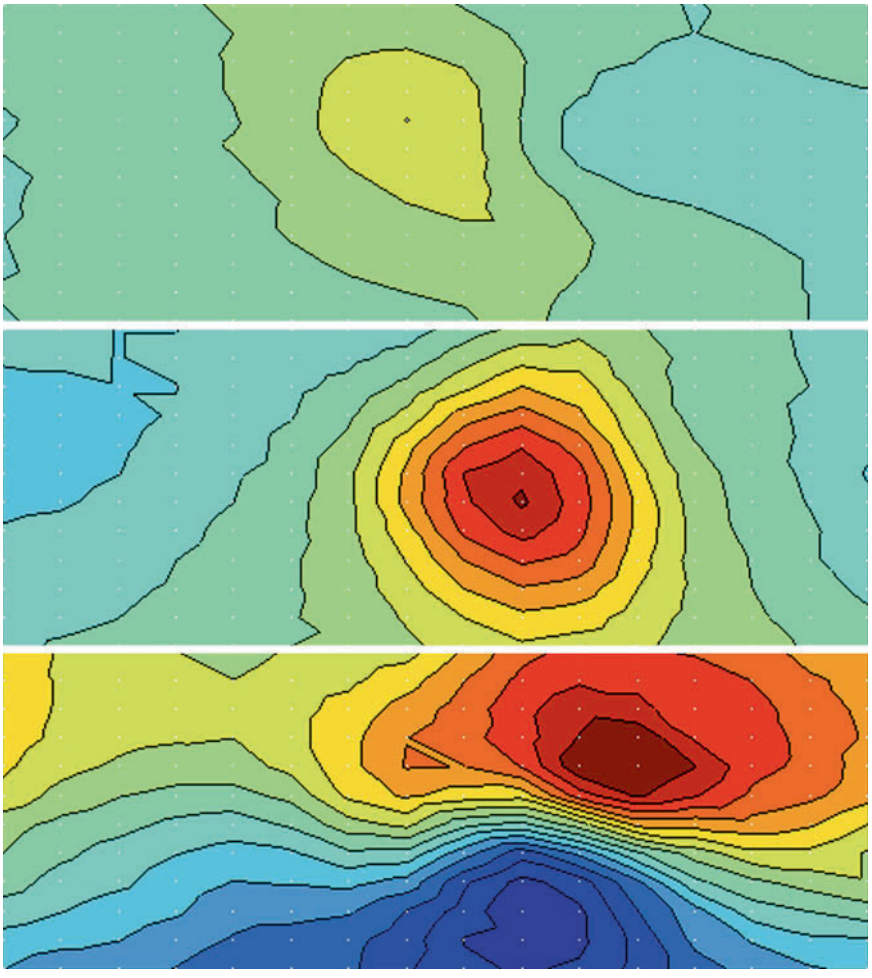

Figure 31.4
Three QRS frames from a patient with old right bundle branch block.

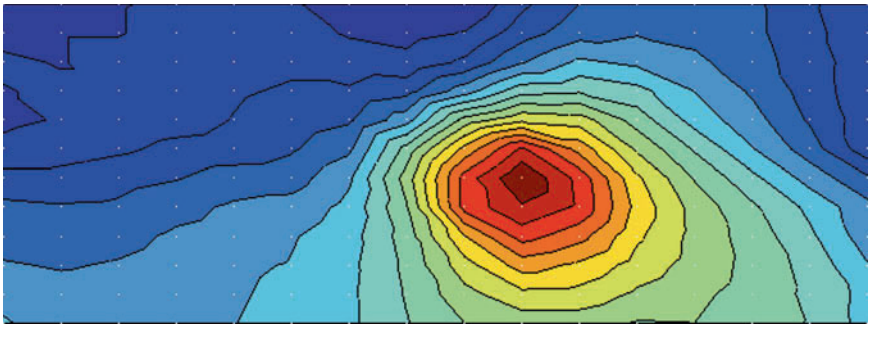

Figure 31.5
A T wave isopotential map from a normal subject.

The magnitudes of the extrema may be plotted against time. Then statistics of these features, such as the mean or peak values may then be used for conventional statistical analysis in order to establish classification rules or to demonstrate differences between classes of maps.

31.4.3 Distributions of ECG Integrals (Areas)

Another class of quantitative map features makes use of so-called integrals or areas. Segments of the sequence of maps may be integrated and displayed as distributions. Thus, QRS, STT, and QRST integral maps are obtained by integrating all ECGs over the QRS, STT, or QT intervals, respectively, and displaying their distributions. Other specialized areas have been used, including the ST_{60} in which integration is carried out over the 80 ms following the "end" of QRS, or the "Q zone" map in which the first 30 ms of the QRS is integrated.

There are two ways of interpreting integral distributions, one based on purely signal theoretic considerations and one based on theoretical aspects of cardiac electrophysiology. Thus, the QRS integral distribution may be thought of as the average QRS potential distribution, which it would be if all values determined from the integration are divided by the interval of integration. In addition, it would be the distribution that would result if all cardiac fibers depolarized "simultaneously" with the same dipole direction and strength they normally have. Of course, such an activation sequence is not possible. All other area distributions may be thought of as average distributions for the interval over which the integration was performed. These integrals have been shown to be useful in assessing cardiac state or its change.

The more powerful, theoretic interpretation of areas originated with the concept of the "ventricular gradient" first proposed by Frank Wilson [9]. He argued that in the presence of a homogeneous distribution of action potentials, that is, identical recovery properties, the integral of any ECG over the QT interval should be zero. A corollary to this, suggests that since the measured QRST area distribution is not zero, and, moreover, almost independent of activation sequence, it reflects disparity of recovery properties, that is, action potential shape and duration. Though the exact relationship between QRST area and disparity of recovery properties has not been established, it is clear that a significant one exists. Since the distribution of recovery properties is known to play an important role in some mechanisms of arrhythmogenesis, QRST area distributions may play an important role in assessing a patient's vulnerability to ventricular arrhythmias. This has been explored by several groups that relate QRST integral distributions to vulnerability [10–13]. Moreover, Plonsey and Geselowitz have provided a theoretical justification for Wilson's original work [14, 15].

The same theory that predicts that the QRST area should reflect the distribution of recovery properties suggests that the QRS area distribution should reflect the distribution of activation sequence. Experimental support for this hypothesis has been documented and the measurement may prove useful in diagnosing abnormalities of conduction. As a consequence of the relationships of QRS area to activation sequence and QRST area to recovery properties, it follows that the STT area should reflect recovery sequence.

The body surface distributions of QRS, STT, and QRST integrals obtained from a normal subject are illustrated in Fig. 31.6. Interpretation of these distributions in terms of average activation sequence, recovery sequence, and recovery properties follows along lines similar to those used for interpreting isopotential maps. The superior-right to inferior-left anterior axis of the QRS area distribution is consistent with the dominant direction of depolarization of the left ventricle, namely endocardium to epicardium that presents itself, on average, along a base to apex axis. The facts that the distribution of the STT areas is similar to that of the QRS and that the polarity associated with recovery is reversed compared to depolarization provide evidence that recovery sequence is opposite to that of activation. This epicardial to endocardial sequence of recovery in a normal heart following supraventricular activation is well documented. Finally, the distribution of QRST areas is supportive of the previously observed epicardial to endocardial gradient of recovery properties. In summary, the distributions of deflection integrals provide important information concerning the underlying electrophysiological processes in the heart. These indices and analyses of their spatial character are being examined for utility in providing insight into arrhythmia vulnerability, the extent and nature of conduction defects, as well as other abnormalities of activation and recovery.

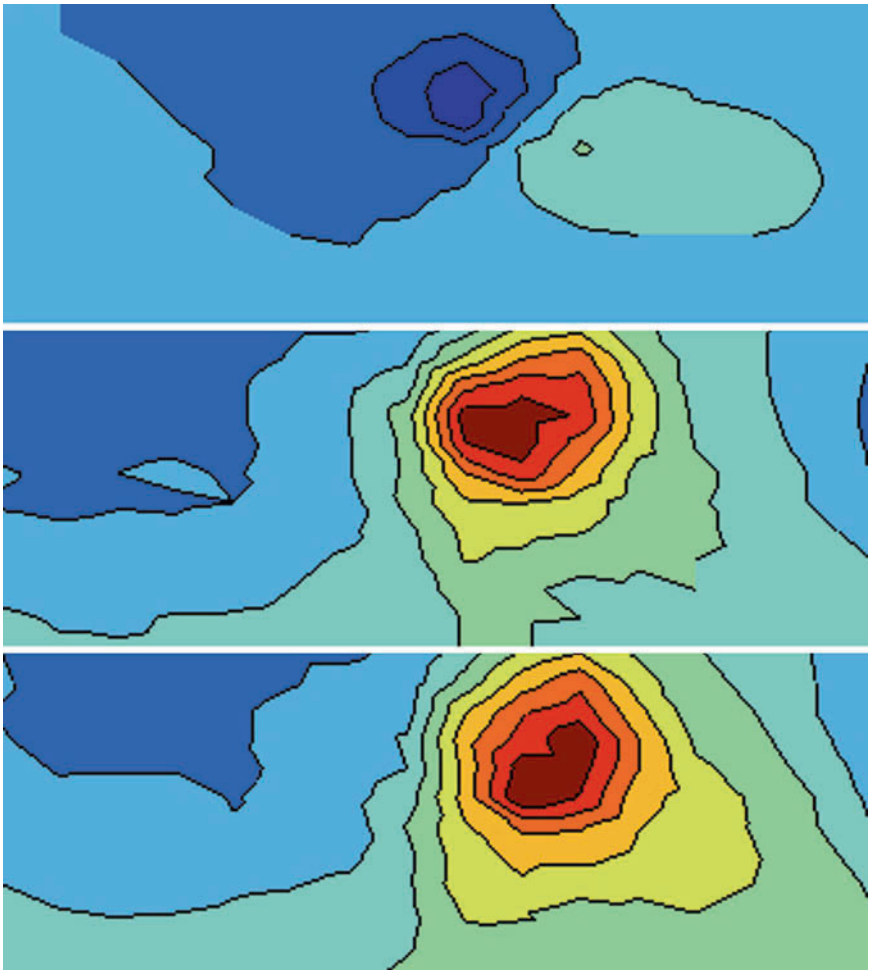

Figure 31.6
QRS, STT, and QRST integral maps from a normal subject.

31.5 Statistical Representation of Body Surface Maps

Another approach to quantitative characterization of maps is the use of mathematical or statistical representation [16, 17]. In this technique, maps are characterized using mathematical or statistically derived basis functions. All the data from a patients map, the complete sequence of potential distributions, may be represented as an n-dimensional vector that can be used to reconstruct the original maps within a prespecified error. The advantage of this technique over other, quantitative characterizations, is that the representation features are independent and common to all maps and all patients. The vector of representing parameters may be used to compare maps on a beat-to-beat basis within one patient, between patients, or between classes of patients. Furthermore, independence of the parameters greatly simplifies the statistical analysis. The technique has been particularly useful in the non-invasive diagnosis of a variety of classes of heart disease for which diagnostic performance of the 12 lead ECG is ineffective.

In this approach, each map frame (potential distribution) is represented as a linear combination (weighted sum) of 12 *independent*, normalized basis functions. Specifically, if **P**(k) is the k^{th} sample in time of an N dimensional potential vector (map frame), then such a representation is expressed as

$$P(k) = \sum_{i=1}^{N} \alpha_i(k)\Phi_i$$
$$\Phi_i \bullet \Phi_i = \delta_{ij} = \left\{ \begin{array}{l} 0, i \neq j \\ 1, i = j \end{array} \right\}$$

where the set of basis vectors $\{\Phi\}$ can be any N dimensional mathematical functions. An efficient representation, the so-called Karhunen–Loeve transformation, derives these functions, statistically, from samples of the data that one wants to represent. For the above maps, the covariance matrix, K, can be defined as

$$K = E[(P - \overline{P})(P - \overline{P})^T]$$

while the solution of the classical "eigenvalue equation"

$$|\lambda_i I - K\Phi_i| = 0$$

leads to solutions of sets eigenvector and eigenvalue pairs, $\{\Theta\}$ and $\{\lambda\}$. These can be calculated from covariance matrices and average potential vectors estimated from large data sets (hundreds of subjects or patients and hundreds of map frames from each subject). Once obtained, for each potential vector, P(k), the coefficient "wave forms" α_i(k) can be obtained from

$$\alpha_i(k) = P(k) \bullet \Phi_i$$

Thus, the sequence of measured map frames, {**P**(k)} can be replaced by the set of coefficient "wave forms," $\{\alpha_i(k)\}$ and since there is considerable redundancy in body surface potential maps, only a few, N≈10 or 15 basis functions are needed to represent the entire BSPM. The first three *spatial* body surface eigenvectors for a large set of normal and abnormal body surface maps are shown in Fig. 31.7. These spatial distributions were statistically derived from a set of over 20,000 map frames obtained from maps on over 400 patients and normal subjects. The result of the representation is to convert each frame of 192 potentials that defines the torso potential distribution at a given instant, to a set of 12 numbers. This 16:1 reduction in data removes spatial dependence or redundancy in the distributions. Importantly, the representation process is reversible in the sense that the 12 representation variables, in combination with the 12 feature distributions, may be used to reconstruct the original, measured distribution to an error of only .044 mV rms. The effect of this spatial representation procedure is to replace the sequence of map frames of a complete BSPM with a set of 12 waveforms that are the time varying weights of each of the feature frames. The process of representation can be continued for the time domain, that is, the coefficient waveforms can be represented by basis functions derived from the coefficient waveforms, $\{\alpha_i(k)\}$, The overall effect of first spatial and then temporal representation is to replace the original BSPM (100,000 potential measurements/QRST) with an equivalent set of 216 independent variables. This "vector" of 216 parameters represents the original BSPM in the sense that from it, the original BSPM may be reconstructed to a high level of accuracy. This vector of representation parameters may then be used in classical statistical strategies for classifying or comparing map data, whether beat-to-beat within one patient, patient-to-patient, or class-to-class.

31.6 Summary

The long history of body surface potential mapping, will likely continue. The rapid developments in anatomic imaging, inverse technologies, and computing speed and power will almost certainly lead to practical systems for rapid, non-invasive, or minimally invasive assessment of cardiac electrophysiology. BSPM will play a critical role in that it is the body surface potentials that ultimately are transformed into estimates of myocardial depolarization and repolarization sequences that form the basis for understanding and characterizing regional cardiac electrophysiology, arrhythmias, and disease.

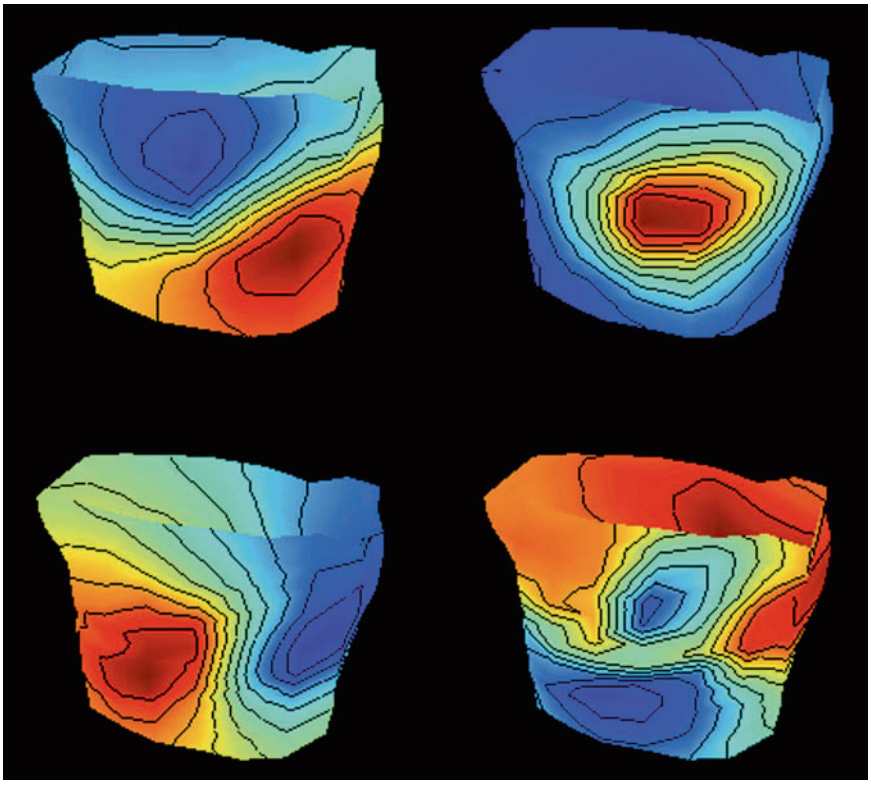

Figure 31.7

First four *normalized* spatial eigenvectors calculated from a covariance matrix estimated using data from normal subjects and patients with a variety of cardiac diseases.

Acknowledgement

The author wishes to acknowledge Dr. Robert S. MacLeod of the University of Utah who developed the Map3D program used to display the BSPM data that are illustrated in this chapter.

References

1. Ramanathan, C., R.N. Ghanem, P. Jia, et al., Noninvasive electrocardiographic imaging for cardiac electrophysiology and arrhythmia. *Nat. Med.*, Apr 2004;**10**(4): 422–428.
2. Barr, R.C., M.S. Spach, and G.S. Herman-Giddens, Selection of the number and positions of measuring locations for electrocardiography. *IEEE Trans. Biomed. Eng.*, Mar 1971;**18**(2): 125–138.
3. Lux, R.L., M.J. Burgess, R.F. Wyatt, et al., Clinically practical lead systems for improved electrocardiography: comparison with precordial grids and conventional lead systems. *Circulation*, Feb 1979;**59**(2): 356–363.
4. Lux, R.L., C.R. Smith, R.F. Wyatt, et al., Limited lead selection for estimation of body surface potential maps in electrocardiography. *IEEE Trans. Biomed. Eng.*, May 1978;**25**(3): 270–276.
5. Monro, D.M., Interpolation methods for surface mapping. *Comput. Programs Biomed.*, Apr 1980;**11**(2): 145–157.
6. SippensGroenewegen, A., R.N. Hauer, N.M. van Hemel, et al., Atlas of paced body surface QRS integral maps for localization of the site of origin of postinfarction ventricular tachycardia. *J. Electrocardiol.*, 1994;**27**(Suppl): 105–112.
7. SippensGroenewegen, A., H.A. Peeters, E.R. Jessurun, et al., Body surface mapping during pacing at multiple sites in the human atrium: P-wave morphology of ectopic right atrial activation. *Circulation*, Feb 3 1998;**97**(4): 369–380.
8. SippensGroenewegen, A., F.X. Roithinger, H.A. Peeters, et al., Body surface mapping of atrial arrhythmias: atlas of paced P wave integral maps to localize the focal origin of right atrial tachycardia. *J Electrocardiol.*, 1998;**31**(Suppl): 85–91.

9. Wilson, F.N., A.G. MacLeod, P.S. Barker, et al., The determination and significance of the areas of the ventricular deflections of the electrocardiogram. *Am. Heart J.*, 1934;**10**: 46.
10. Urie, P.M., M.J. Burgess, R.L. Lux, et al., The electrocardiographic recognition of cardiac states at high risk of ventricular arrhythmias. An experimental study in dogs. *Circ. Res.*, March 1978;**42**(3): 350–358.
11. Lux, R.L., P.M. Urie, M.J. Burgess, et al., Variability of the body surface distributions of QRS, ST-T and QRST deflection areas with varied activation sequence in dogs. *Cardiovasc. Res.*, Oct 1980;**14**(10): 607–612.
12. Abildskov, J.A., QRST area maps and cardiac arrhythmias. *J. Am. Coll. Cardiol.*, Nov 15 1989;**14**(6): 1537–1538.
13. Hubley-Kozey, C.L., L.B. Mitchell, M.J. Gardner, et al., Spatial features in body-surface potential maps can identify patients with a history of sustained ventricular tachycardia. *Circulation*, Oct 1 1995; **92**(7): 1825–1838.
14. Plonsey, R., A contemporary view of the ventricular gradient of Wilson. *J. Electrocardiol.*, Oct 1979;**12**(4): 337–341.
15. Geselowitz, D.B., The ventricular gradient revisited: relation to the area under the action potential. *IEEE Trans. Biomed. Eng.*, Jan 1983;**30**(1): 76–77.
16. Evans, A.K., R.L. Lux, M.J. Burgess, et al., Redundancy reduction for improved display and analysis of body surface potential maps. II. Temporal compression. *Circ. Res.*, July 1981;**49**(1): 197–203.
17. Lux, R.L., A.K. Evans, M.J. Burgess, et al., Redundancy reduction for improved display and analysis of body surface potential maps. I. Spatial compression. *Circ. Res.*, July 1981;**49**(1): 186–196.

32 Body Surface Potential Mapping

Luigi de Ambroggi · Alexandru D. Corlan

P. W. Macfarlane, A. van Oosterom, O. Pahlm, P. Kligfield, M. Janse, J. Camm (eds.), *Comprehensive Electrocardiology*, DOI 10.1007/978-1-84882-046-3_32,

32.1 Introduction

Body-surface potential maps (BSPMs) present the distribution of cardiac potentials on the chest surface during the cardiac cycle. They provide the spatial as well as the temporal and amplitude components of cardiac electrical activity, whereas the ECG scalar waveforms present only the time–voltage variation in a given lead point.

When an excitation wavefront spreads through atrial or ventricular heart muscle, it generates bioelectric currents, which distribute themselves to all conducting tissues in the body. This wavefront is a thin layer of heart muscle separating resting from excited areas. For the sake of simplicity, reference is made to the "classical" electrical model [1], according to which an excitation front is considered to be equivalent to a uniform dipole layer, where the dipole axis is everywhere orthogonal to the front; moreover, the tissue resistivity is supposed to be homogeneous. According to this model, currents arise from the anterior aspect of the front, flow through the thorax, and finally point to the posterior aspect of the front. Figure 32.1 illustrates the distributions of the currents and potentials, in a horizontal thoracic section, arising from an excitation wavefront in the ventricular septum. The locations of the potential maximum and minimum on the thoracic surface are correlated with the topography and orientation of the wavefront. According to the traditional solid angle theory, a potential maximum in a given area on the chest surface indicates that an excitation wave is pointing toward that area; a potential minimum indicates that the posterior or negative aspect of the wavefront is seen from the area where the minimum is present.

However, the relationship between surface potential distribution and wavefront shape is sometimes very complex. In fact, the potential distribution at the surface depends on the location, number, and geometry of the wavefronts in the thorax, the geometry of the torso, and the inhomogeneities of the conducting medium (cardiac and extracardiac tissues). For example, several excitation waves may be travelling simultaneously through the right and left ventricle, giving rise to a complex distribution of currents and potentials. Also, when an excitation wave spreading from the endocardium reaches the epicardial surface, a hole appears in the advancing wavefront. Through this hole or "window," the currents reenter the heart. If a window is close to the chest wall, a new potential minimum appears on the thoracic surface, in addition to those already present. A similar hole appears in the excitation wavefront when a portion of ventricular wall cannot be activated, because of a local myocardial infarction. In this case too, a potential minimum appears on the chest surface in the region facing the infarcted area. A further cause of complexity arises from the fact that the dipole density is not uniform on the surface of the wavefront, in that a wavefront spreading along fibers generates more current per unit area than a wavefront spreading across fibers [2, 3].

During repolarization, currents proportional to transmembrane potential gradient from the M-cell region flow toward the epicardium and endocardium, the former being of higher amplitude [4, 5]. This amounts to numerous small dipoles distributed in the whole mass of the myocardium. The orientation of these dipoles remains mostly unchanged during repolarization, and their amplitudes change relatively synchronously. Localized repolarization changes further add to the complexity of the body-surface potentials in heart disease.

Every excitation wave and every portion of repolarizing tissue in the heart influence the potential distribution on the entire body surface. It follows that information on the electrical activity of the heart can be recorded not only from the points commonly explored by conventional ECG and VCG leads, but also from the entire body surface. BSPMs provide all the information available on the entire chest surface.

32.2 History

The first example of a potential map was published by A. Waller in 1889 [6], on the basis of 10–20 ECG recordings from the surface of the human body; the potential distribution resembled that which would have appeared if a dipole had been located in the heart. Later, a few attempts to determine surface potential distributions were made by several authors with rudimentary techniques.

In 1951, Nahum et al. [7] published the first description of isopotential line distribution on the thoracic surface at successive instants during the cardiac cycle in man. They did not detect the simultaneous presence of several maxima and minima but observed that the surface potential distribution was much more complicated than that likely to result from an equivalent dipolar generator. In the 1960s, Taccardi [8, 9] described the instantaneous distribution of heart potentials during ventricular activation in dogs and in normal human subjects. These investigations clearly showed that several potential

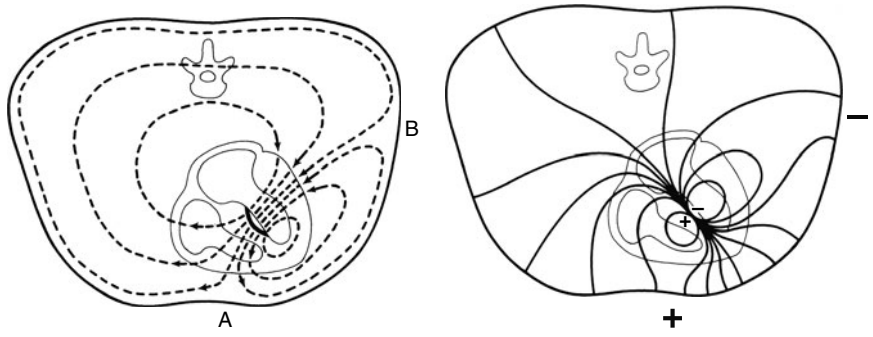

Figure 32.1

***Left*: Schematic drawing of a horizontal section of the human thorax illustrating the pathway of the currents, which arise from an excitation wavefront (solid line in septum) spreading through the septum in a left-to-right direction. A indicates the area where the current lines reach the surface; B indicates the area from which the currents dip into the thorax pointing to the posterior aspect of the wavefront. *Right*: Potential distribution in the same thoracic section and at the same instant. The plus sign indicates the location of the potential maximum on the surface (corresponding to point A); the minus sign indicates the location of the potential minimum (corresponding to point B).**

maxima and minima may be simultaneously present on the body surface during part of the QRS interval; moreover, an attempt was made to correlate the location of surface maxima and minima with the probable location of excitation wavefronts in the ventricles. The complexity of surface potential patterns, although not physically incompatible with a dipolar source, strongly suggested that a more complex electrical model of the heart should be adopted in order to account for the potential distributions found on the human and canine trunk.

Since then, BSPMs have been recorded from normal subjects (newborns and adults), cardiac patients, and experimental animals by many investigators in different countries.

32.3 Methods

Many lead systems have been used to record BSPMs throughout the world differing in the number of leads as well as in electrode location on the thorax. In theory, the optimal lead system should have a number of leads large enough to detect all details of the potential distribution on the torso surface. However, transformation methods have been proposed to estimate BSPM in a particular lead system from the BSPM data measured by using another lead system [10].

Techniques for recording, processing, and displaying the potential maps are illustrated in Chap. 31.

Different methods of analysis of BSPMs have been used to extract relevant information. These are described below.

32.3.1 Instantaneous BSPMs

The distribution of chest potentials in each instant of the cardiac cycle can be analyzed qualitatively, by visual inspection, or quantitatively by considering a number of numerical parameters relating to location, amplitude, and migration of potential maxima and minima.

32.3.2 Integral Maps

Since differences between maps of normal subjects and patients cannot easily be quantified by inspection of the sequence of instantaneous potential distributions, the potential–time integral maps have been considered. This approach has been proved to allow a reduction in the amount of data to be analyzed without substantial loss of information [11]. With this method, only a few maps are required to represent a cardiac cycle (QRS, ST-T, QRST, or other intervals for particular

purposes). In addition, this technique permits the calculation of average maps for groups of subjects without the need for time-phase alignment.

An approximation of the potential time integral, relating to a given interval of the cardiac cycle, is obtained by computing, at each lead point, the algebraic sum of all the instantaneous potential values throughout the interval considered, multiplied by the sampling interval. The values, expressed in mVms, are transferred to a diagram representing the thoracic surface explored, and isointegral contour lines can be drawn (Fig. 32.2).

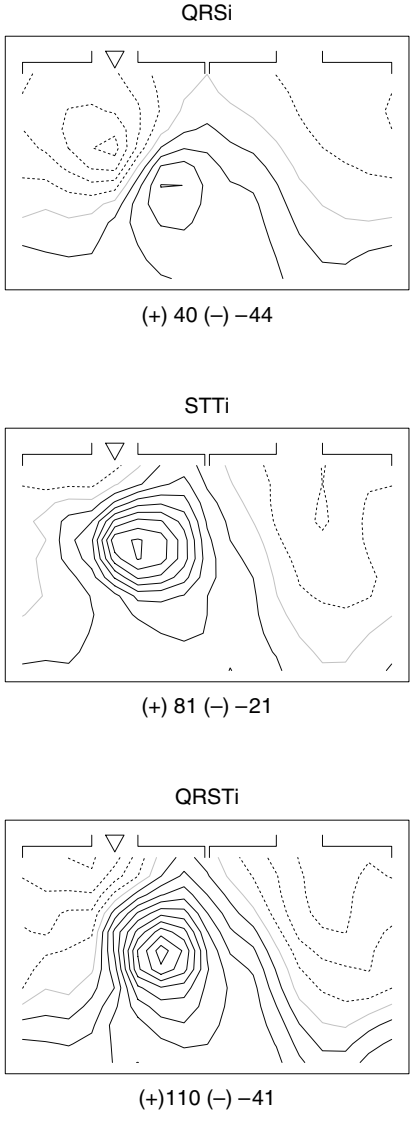

Figure 32.2

Integral maps in a normal subject during the QRS interval (*top*) ST-T interval (*middle*) and QRST interval (*bottom*). The left half of each map represents the anterior face of the thorax, the right half represents the posterior face. Continuous dark lines represent positive isointegrals, dashed lines represent negative isointegrals. The grey continuous line represents the zero integral line. The legend under each map indicates by (+) the maximum integral value on the respective map, by (–) the minimum integral value and (:) the gradient between isointegral lines, in 10 mVms.

32.3.3 Principal Component Analysis

Reduction of the information in body-surface ECG recordings can be achieved by decomposing individual integral maps or population-wide sets of recordings or the matrix of potentials in time over an interval (such as the ST-T) into components, which are independent of (noncorrelated to) each other. For example, singular value decomposition of the matrix of instantaneous repolarization potentials in time can be written as a sum of components each consisting of a potential distribution on the body surface, changing in time. The relative spatial distribution of the potentials of each component is constant, and the only thing that changes in time is the general amplitude of the component.

Figure 32.3 shows the first four components of the ST-T potentials in a normal subject. The first component contains normally over 75% of the potential amplitude, and is probably due to the general transmural gradient of the ventricular action potential. The second component is usually opposed (inversely correlated) to the QRS integral and likely corresponds to the repolarization gradient secondary to the depolarization sequence. The relative contribution of the first or

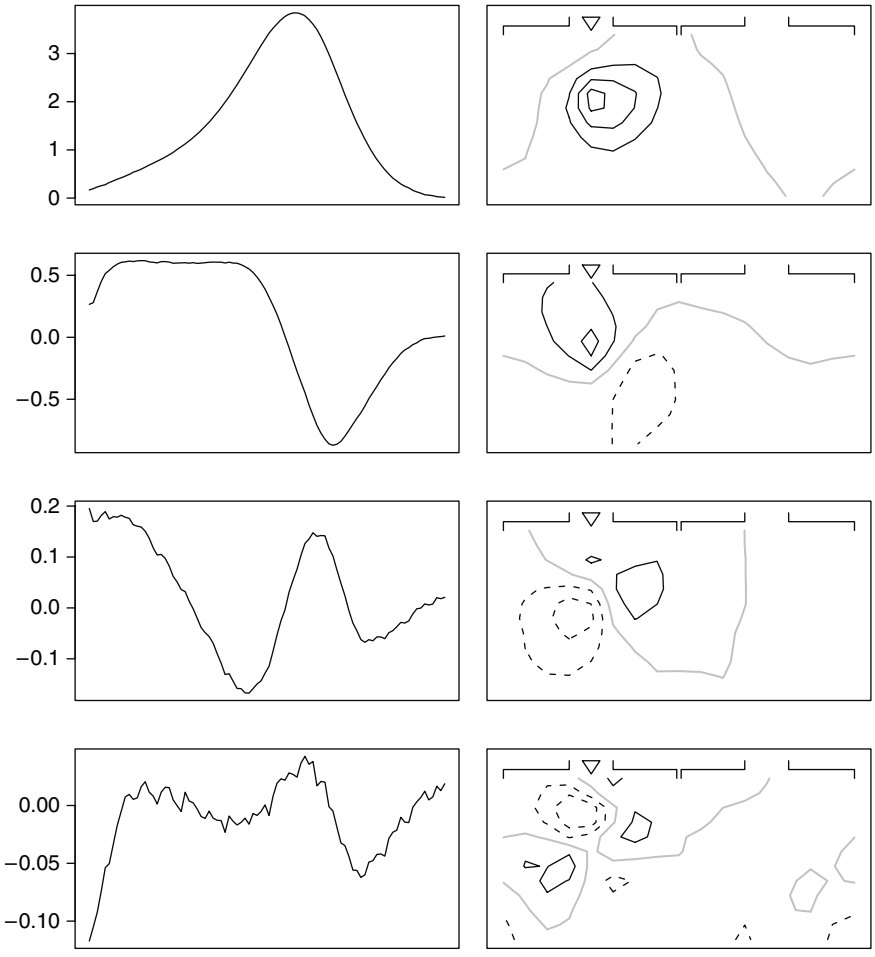

Figure 32.3

The first four components resulting from singular value decomposition of the matrix of instantaneous repolarization potentials versus time in a normal recording. Each component is represented by the body-surface potential distribution (*right*) (distance between isopotential lines is arbitrary) and the variation of its amplitude in time (*left*) (time on *x*-axis and relative amplitude on *y*-axis). The first component is at the *top*, the fourth at the *bottom*.

first two components to the repolarization potentials is decreased in most pathological states and may be indicative of the presence of arrhythmogenic repolarization heterogeneity.

Reduction of the information in body-surface ECG recordings to a few numerical indices can be achieved by analysing individual recordings or population-wide sets of recordings into components that are independent of (not correlated to) each other. One method is principal component analysis in which a set of signals, either instantaneous body-surface distributions at different instants in time, or time-based signals from different leads, or integral maps in a group of individuals are decomposed into eigenvectors (components, usually sets of potentials) and eigenvalues (numbers which quantify the contribution of each eigenvector to the general variability of the overall data). Ventricular repolarization is particularly suitable to this type of analysis, as most of the variability of normal repolarization potentials in most instants over the ST-T interval can be described by a single component.

32.3.4 Autocorrelation Maps

Autocorrelation (AC) maps are square matrices of values between -1.0 and 1.0, which represent the correlation coefficients of every pair of instantaneous potential distributions from a set of successive instants in time [12]. The same time interval appears on both coordinates of the map and the matrix is symmetrical with respect to the first diagonal. Values on the first diagonal are always 1.0, representing correlations of each instantaneous map with itself.

Autocorrelation maps reflect only phenomena taking place in the ECG source (myocardium) and are very little influenced by the geometry of the volume conductor (thorax) that connects it to the lead system [13]. AC maps are very sensitive to variations in the activation sequence. For example, Figs. 32.4 and 32.5 show recordings in two healthy individuals in whom the 12 lead ECGs and QRS integral maps look very much alike, but differences in the activation sequence are evident in the instantaneous potential maps, especially in the AC maps.

The AC map of the ST-T interval is normally quite close to 1 as the normal repolarization pattern shows little change, apart from the amplitude. The extent of change can be quantified by choosing the map at the peak of T (on the root mean square signal) as a reference map and calculating the average difference from one of the lines that goes through that instant on the AC map over the S-T peak and T peak-end intervals. We call these average differences the early and late repolarization deviation indices (ERDI and LRDI), respectively.

32.4 Normal Maps

32.4.1 Atrial Excitation and Recovery

At the onset of atrial excitation, a potential minimum is generally observed near the right sterno-clavicular joint, in the right supraclavicular region, or in the right mammary area (Fig. 32.6a) [14, 15]. The potential maximum or minimum is here defined as a point on the thoracic surface where the potential value is higher or lower in relation to all the surrounding points. Mirvis [16] did not observe a clear-cut minimum, but only a broad area of negative low-level potentials over the upper back and the right chest during the initial phase of atrial excitation. A potential maximum is initially located either in the right submammary area or in the lower sternal region (Fig. 32.6b). During the subsequent stages of atrial activation, the maximum moves leftward, gradually reaching the left mammary region, the left lateral chest wall and, in some cases, the dorsal region (Fig. 32.6c). The minimum moves slightly downward. During the leftward migration of the maximum, a secondary potential maximum sometimes appears on the left lateral wall of the thorax. The movement of the potential maximum from right to left is most likely correlated with the spread of the excitation wavefronts from the right to the left atrium.

During atrial recovery (Fig. 32.6d), surface potential maps resemble those recorded in the early stages of atrial excitation, but with reverse polarity [15–17]. A potential minimum is generally located on the sternal and left mammary region and a maximum on the right shoulder both in adults and infants. This finding suggests that repolarization advances through the atrial walls in approximately the same order as does excitation. This is in agreement with experimental data, demonstrating that the atrial regions that depolarize first are also the first to recover [18].

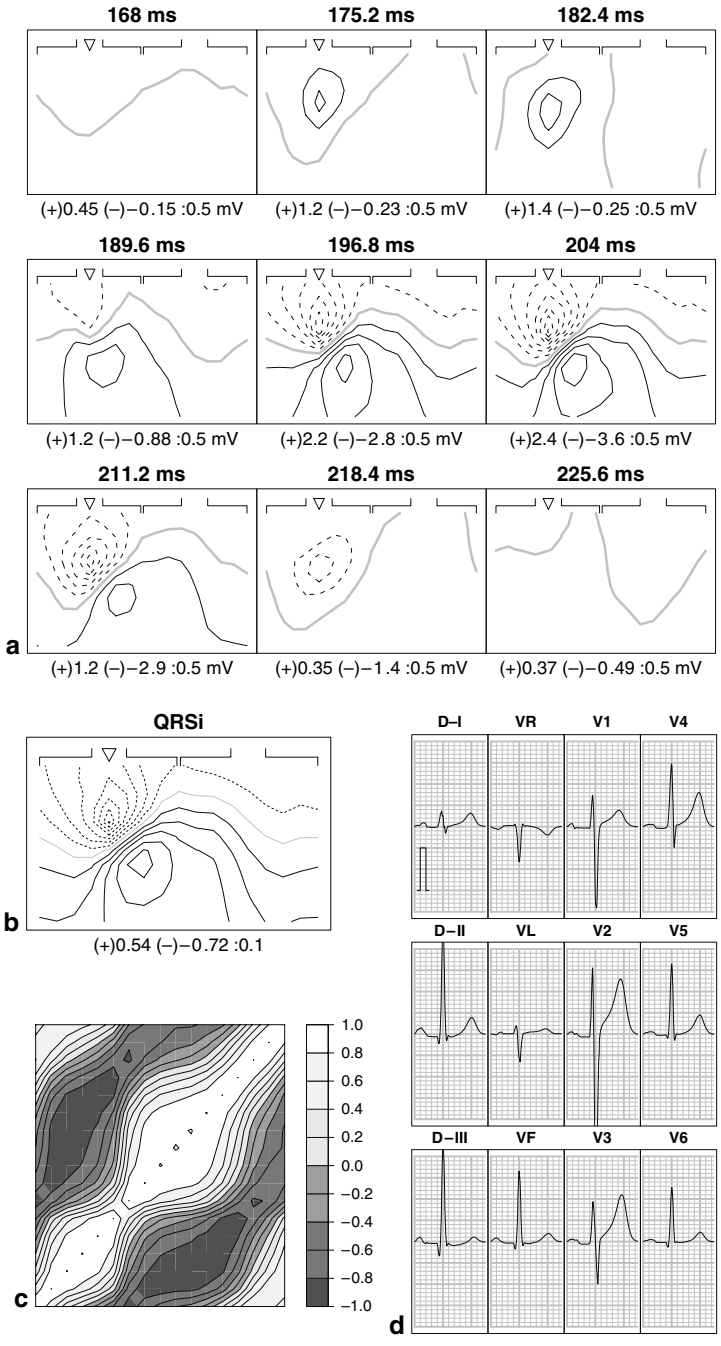

Figure 32.4

Different representations of depolarization potentials of the same cardiac cycle in a normal subject. (a) Successive, instantaneous potential maps during the QRS; conventions are as in Fig. 32.2, except that the lines are isopotential and are measured in mV; the label above each map indicates the timing of the instantaneous map. (b) Integral map with the same conventions as in Fig. 32.2. (c) Autocorrelation map of the QRS interval; the same time interval is on both *x*- and *y*-axis, and each point on the map represents the correlation coefficient between instantaneous potential distributions at the instants of its *x*- and *y*-coordinates, using shades of gray from black for −1.0 to white for 1.0, as indicated on the scale at right. (d) Standard ECG reconstructed from leads corresponding to the standard ECG leads, extracted from the body-surface lead system.

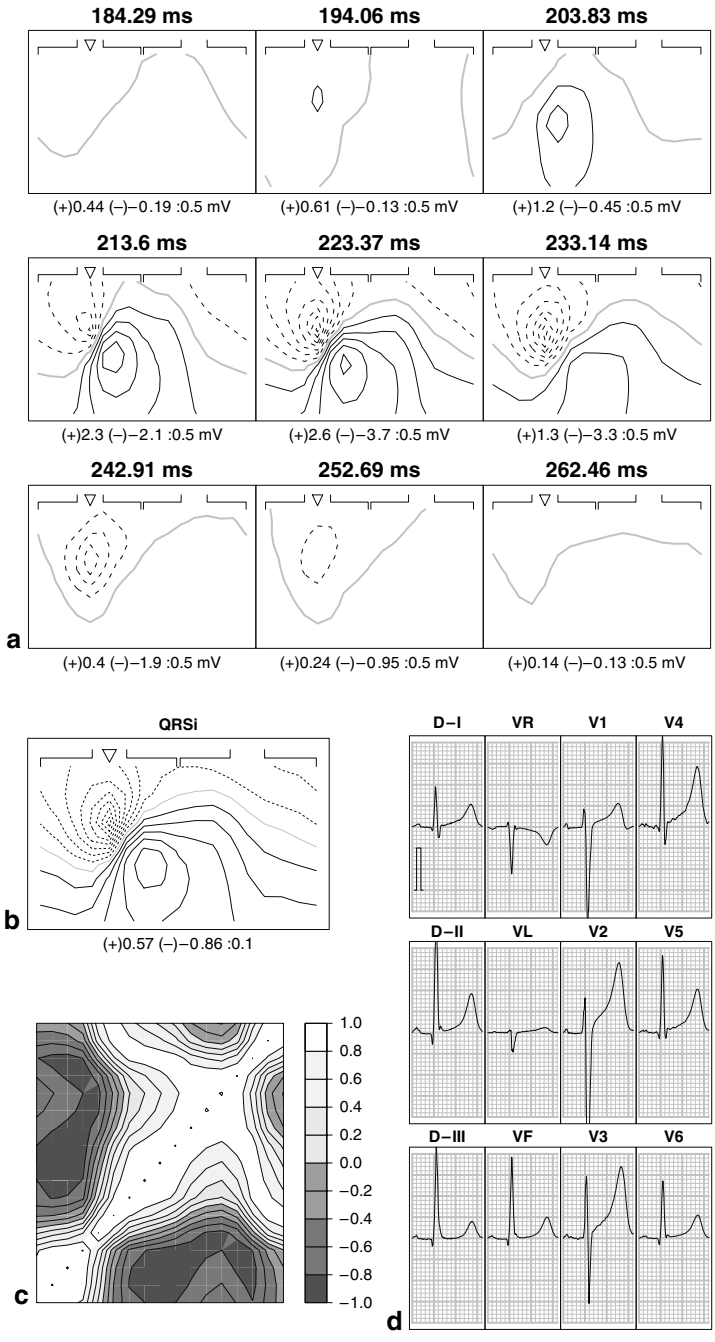

Figure 32.5

The same representations of ventricular activation as in Fig. 32.4, for one cardiac cycle in a different healthy individual. This recording was selected from a set of 236 in healthy people as a recording with an almost identical QRS integral as that in Fig. 32.4. Note the similarity of the 12-lead ECG, the visible differences in the instantaneous potentials and the striking differences in the AC map.

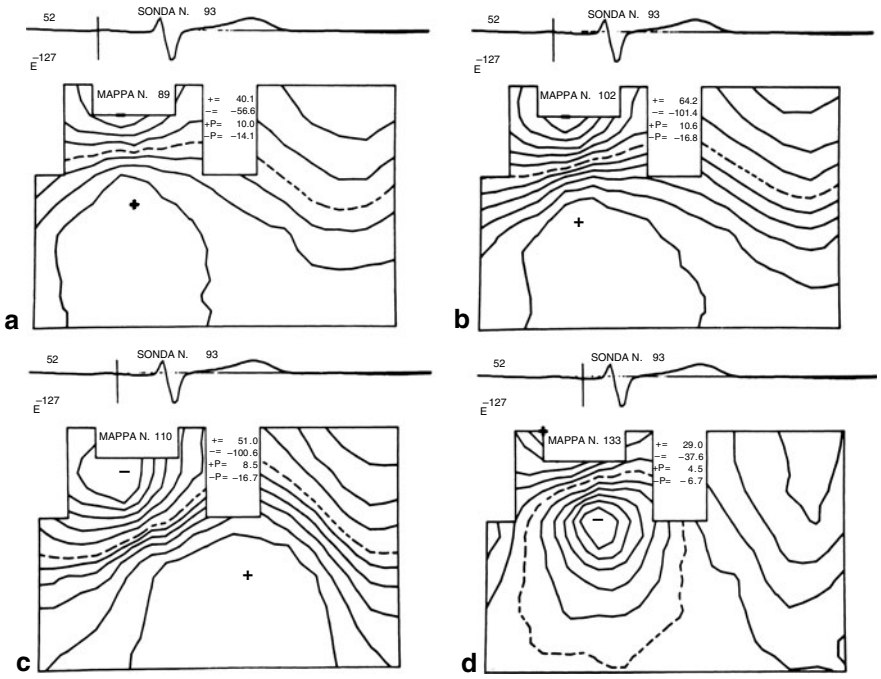

Figure 32.6

Averaged surface maps relating to atrial activation and recovery in a normal subject, at the instants or time indicated by the vertical line crossing the ECG at top of each figure. The time interval between the (a) and (d) is 88 ms. The zero equipotential line is dashed. The plus and minus signs indicate the value of the positive and negative peaks in microvolts; +P and −P indicate the step (in microvolts) between adjacent positive and negative equipotential lines.

32.4.2 Ventricular Activation

Body-surface potential distributions during ventricular excitation have been described by many investigators in adults [9, 19–21], children [22, 23], and infants [24, 25].

The main features of maps observed in adults are as follows. At the beginning of the QRS, a potential maximum appears in the upper or mid-sternal area, and a minimum is generally located in a lower position on the left thoracic wall or on the back (Fig. 32.7a). This potential pattern can be related to septal excitation, which occurs in a predominantly left-to-right direction [26, 27] and probably also to right ventricular free wall activation.

Later, the minimum migrates dorsally. In 25% of subjects, the migration is discontinuous: a separate low-amplitude dorsal minimum appears before the left lateral initial minimum has disappeared. Thus, in these subjects, two distinct minima are simultaneously present during the initial 15–20 ms of QRS [28]. The minimum then moves toward the right shoulder and finally appears in the right clavicular area (Fig. 32.7a, b). In some cases, the minimum moves horizontally around the back and reaches the right axillary region. This behavior has been observed particularly in subjects with left axis deviation in the standard 12-lead ECG. Meanwhile, the maximum migrates downward to the left mammary region (Fig. 32.7c). The events described above are temporally related to the spread of excitation in an endo-epicardial direction through the walls of both ventricles, with a mean direction from base to apex.

Thereafter, a new minimum often appears in the midsternal area (60% of cases in the authors' studies), at 14–44 ms after the onset of ventricular activation (Fig. 32.7d). This minimum is considered to be the surface manifestation of the right ventricular breakthrough, that is, of the presence of a "window" in the advancing wavefront, through which the currents reenter the heart. In the following instants, the sternal minimum and the right clavicular minimum merge to form a single, broad anterior negative area (Fig. 32.7e). In about 40% of the cases, the sternal minimum does not appear as a separate entity, and the sternal area becomes negative as a result of the migration of the main minimum.

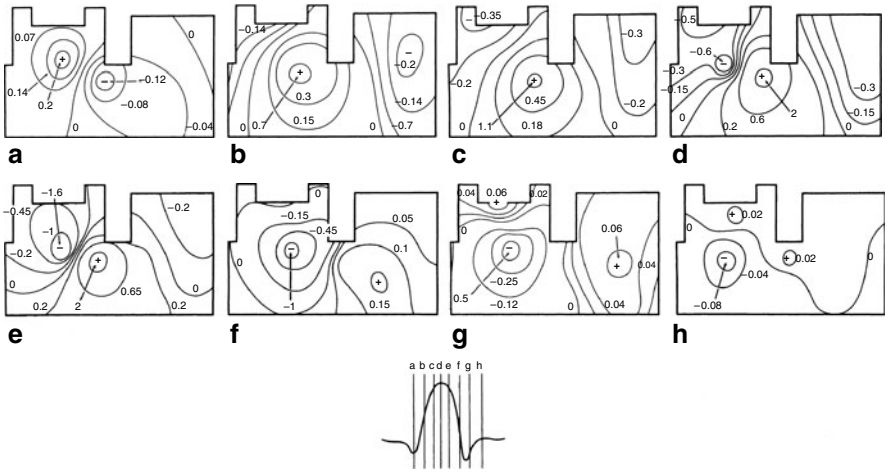

Figure 32.7

Body-surface potential maps during normal ventricular activation. Each map refers to the instant or time indicated by the vertical line crossing the ECG (*bottom*). The potential values are expressed in millivolts.

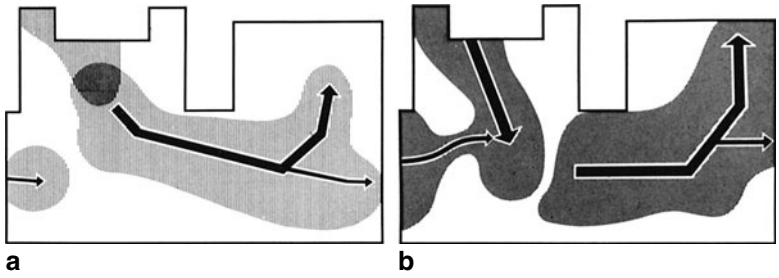

Figure 32.8

The shaded areas encompass all locations of the potential maxima (a) and minima (b) throughout the QRS interval in 50 normal subjects. The *arrows* indicate the main direction of migration of the principal maximum (a) and minimum (b). (After Taccardi et al. [15]. © Clarendon, Oxford. Reproduced with permission.)

Later, the maximum moves toward the left thoracic wall and then dorsally (Fig. 32.7f). In about 55% of adults, a new maximum appears in the upper sternal area during the last 20–30 ms of the QRS interval (Fig. 32.7g). In the great majority of cases, the second maximum appears while the dorsal maximum is still present, the time overlap being 10–30 ms. These potential patterns most likely indicate the presence of two separate excitation waves travelling through the heart. The dorsal maximum may be related to the activation of the posterobasal portions of the ventricles, and the upper sternal maximum to the excitation of the crista supraventricularis and pulmonary infundibulum. The time relationships between the two maxima may provide some indirect information about the time-course of excitation waves in the heart.

Green et al. [21] defined the range of normal body-surface potentials in a large population (1,113 subjects, aged 10–80 years) as a function of age, sex, and body habitus. On average, QRS potentials decreased with increasing age. Potential pattern distributions remained constant from 10 to 40 years; about 30% of the subjects older than 40 years had early negative potentials recorded more diffusely over the right thorax. This resulted in more vertically oriented zero equipotential lines. Only minor differences concerning QRS potential amplitude and distributions were noted when male and female subjects were compared within groups of similar age and body habitus.

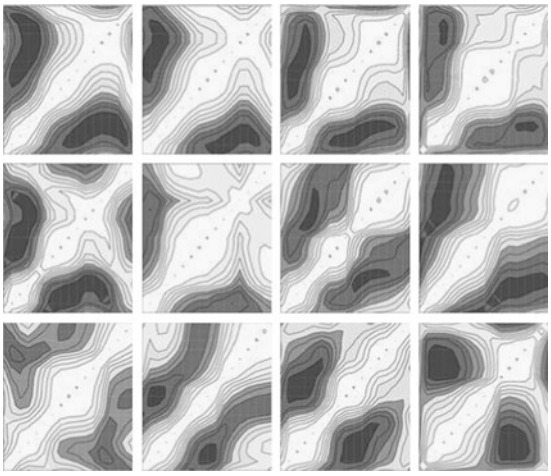

Figure 32.9

AC maps of body-surface recordings during the QRS interval in 12 healthy individuals, which are representative of the normal variability of ventricular depolarization. Same conventions as in Fig. 32.4c.

Interindividual variability is due to variability of the thorax conductor [29] and source variability [30]. Normal variability of the ventricular activation may be due to the well-known variability of the conduction system.

We computed AC maps in 236 normal recordings from the dataset of Dr. F. Kornreich (Vrije University of Brussels, Belgium). We sorted them using divisive clustering analysis taking the correlation coefficient as a measure of distance between AC maps. Twelve prototype cases spanning the whole spectrum of variability of AC maps of normal activation are shown in Fig. 32.9. In each activation AC map, the size of white ($R > 0.8$) regions along the main diagonal corresponds to periods of relative stability of body-surface distribution of potentials (apart from amplitude). Sometimes, these regions are distinct, as the transition from one pattern to the next is sudden (as in types 3 and 4), while in other cases, it is less distinct, as the transition is gradual (as in type 10). Usually, three such phases can be identified, the first two being separated by the ventricular breakthrough. The dark region, which occurs symmetrically between the first two phases, corresponds to the relatively opposed disposition of potential extrema on the body surface before and after ventricular breakthrough. The third phase corresponds to activation of the basal regions of the ventricles and pulmonary infundibulum and has a very variable relationship with the first two.

The amplitudes and surface distributions of time integrals during ventricular activation were firstly reported by Montague et al. [31] in 40 men and 15 healthy women and subsequently by many other authors. The QRS integral map is characterized by a dipolar distribution with a minimum in the mid-sternal area and a maximum in the left mammary-axillary region (Fig. 32.2).

In children, the main features of the maps are similar to those observed in adults. There are, however, minor differences; for instance, the sternal maximum during the last stage of QRS was present only in a small percentage of children [22], but invariably appeared during peak inspiration in the series of subjects studied by Flaherty [32]. According to Liebman et al. [23], the location of the terminal maximum can be right superior-anterior, anterior-superior, or right posterior, probably suggesting that the end of activation is in the right ventricular outflow tract, in the superior septum, or in the posterobasal left ventricle.

In newborn infants, Tazawa and Yoshimoto [24] observed that during ventricular excitation, the initial potential maximum migrated to the right instead of moving to the left and dorsally as in normal adults. This behavior of the maximum was attributed to the physiological predominance of the right ventricle in the newborn heart. Benson et al. [25] described the evolution of the surface potential during ventricular excitation and recovery in the first year of life. There was a progression of change in the body-surface QRS potential distribution: at birth. A single QRS maximum migrated to the right during the second half of QRS; at several months of age, the initial maximum evolved into two maxima: one moving to the right, and the other to the left; at 9–12 months of age, the initial maximum moved to the left lateral

thorax, while the right maximum almost disappeared. Moreover, the age-related changes of the QRS maps were associated with similar changes on the repolarization maps; with increasing age, movement of both the excitation and the recovery positive potentials to the right chest progressively disappeared.

32.4.3 Ventricular Repolarization

Sizeable recovery potentials usually appear at the surface of the body before the end of the QRS interval [14] (Fig. 32.7h). This finding was confirmed and quantified by Spach et al. [33], who also reported that the time overlapping of excitation and recovery potentials varied in different age groups, being greater in younger classes (8–12 and 20–29 years). In some subjects, the overlap lasted for 12–28 ms. The first signs of repolarization consist of a potential maximum, which generally appears on the sternal area, on the left precordium or, in a few cases, even more laterally, on the left axillary region (Fig. 32.7h). In the latter case, the maximum soon moves toward the central anterior chest area (Fig. 32.10a). During the early phase of recovery, the minimum is often ill-defined. The most negative areas can be found anywhere around the maximum, in the anterior lower part of the torso, in the lateral wall, or in the back [14].

This potential distribution is essentially in agreement with that described by Spach [33] in subjects 8–60 years old during the first 50 ms of ventricular recovery. Within 100–150 ms from the onset of ST the most negative potentials concentrate in an area covering the right scapular region, the right shoulder, the clavicular, and the upper sternal regions (Fig. 32.10). In a minority of adult subjects, the most negative areas are located in the right clavicular or scapular regions from the beginning of repolarization. During the T wave the minimum is consistently found in the right clavicular or scapular areas and the maximum in the precordial region [12, 14]. Slight shifts of the potential extrema are usually observed during the entire T interval (Fig. 32.10).

In a large normal population, Green et al. [21] observed that ST-T potentials decreased with age in both sexes. Moreover, in female subjects over the age of 40, there were more extensive low-level negative potentials over the precordium during the ST segment than in men. On the other hand, male subjects consistently showed greater T potential amplitudes.

The early repolarization deviation index (ERDI, see Sect. 32.3.4) is about twice as high as in females compared to males [34]. LRDI is higher in males. As the correlation coefficients between instantaneous potentials in the same subject are invariant to the features of the thorax conductor [13], it proves that gender differences in repolarization potentials are not entirely due to the systematic anatomical differences in thorax shape and conductivity between the genders, but must be due, at least in part, to differences in myocardial repolarization gradients.

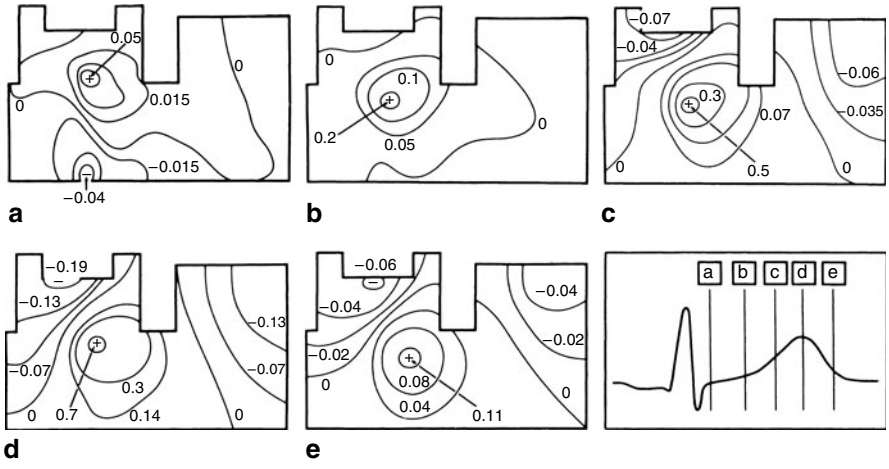

Figure 32.10

Body-surface maps during normal ventricular recovery. Each map refers to the instant or time indicated by the vertical line intersecting the ECG. (After Taccardi et al. [15]. © Clarendon, Oxford. Reproduced with permission.)

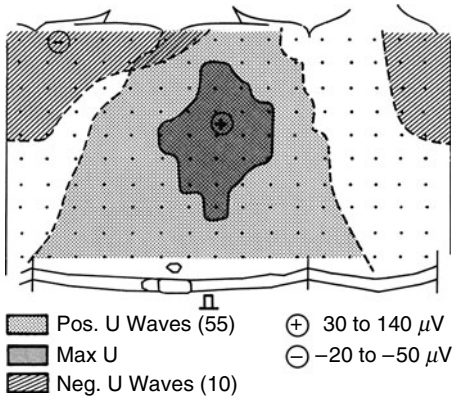

Figure 32.11

Location or potential maxima and minima during the U wave in 55 normal subjects aged 8–60 years. (After Spach et al. [17]. © American Heart Association, Dallas, Texas. Reproduced with permission.)

The integral maps of QRST deflections are thought to provide valuable information on the ventricular recovery process [35]. Areas of QRST deflection mainly reflect the intrinsic recovery properties and are largely independent of the ventricular excitation sequence. Actually, at the body surface, negative QRST integrals should be recorded from areas facing myocardial regions with longer recovery durations, whereas positive values are recorded from the thoracic surface facing cardiac regions with shorter recovery durations.

In normal subjects the ST-T and the QRST integral maps show a bipolar distribution of the values with a minimum on the right clavicular–upper sternal areas and a maximum on the mammary region (Fig. 32.2).

A few descriptions of accurate recordings of potential distributions during the U wave have been reported [17, 36, 37]. Spach and associates [17] studied 11 children aged 1–7 years and 55 subjects aged 8–60. In the 11 children, no measurable U wave was found. In the remaining subjects, positive U-wave potentials were located within a broad area on the anterior and left lateral chest surface (Fig. 32.11); the magnitude of the potential maximum varied from 30 to 140 μV. The highest U voltages were confined to the precordial area where the highest T voltages occurred. In most subjects, the specific locations of T-wave and U-wave maxima were coincident; in 17 subjects, the U-wave maximum was slightly to the right of the T-wave maximum. Clear-cut negative U waves were found in only 10 of the 55 subjects. The negative peaks varied from −20 to −50 μV and occurred on the right clavicular or scapular areas (Fig. 32.11).

32.5 BSPM in Heart Disease

32.5.1 Ischemic Heart Disease

32.5.1.1 Myocardial Infarction

Descriptions of the potential distribution on the body surface in patients with anterior or inferior myocardial infarction (MI) have been published by many authors [38–53].

An attempt was made to define quantitatively the characteristic features and the range of variation of surface maps in anterior and inferior myocardial infarction during ventricular activation and recovery [38].

In patients with anterior MI (Fig. 32.12), at the onset of ventricular activation, the potential minimum was located in the sternal or left mammary region. In some patients, the minimum lay outside the area where the minima were located in normal subjects. In MI patients, the minimum remained confined to a limited zone on the anterior chest wall throughout the QRS interval, whereas in normal subjects, it migrated leftward and dorsally.

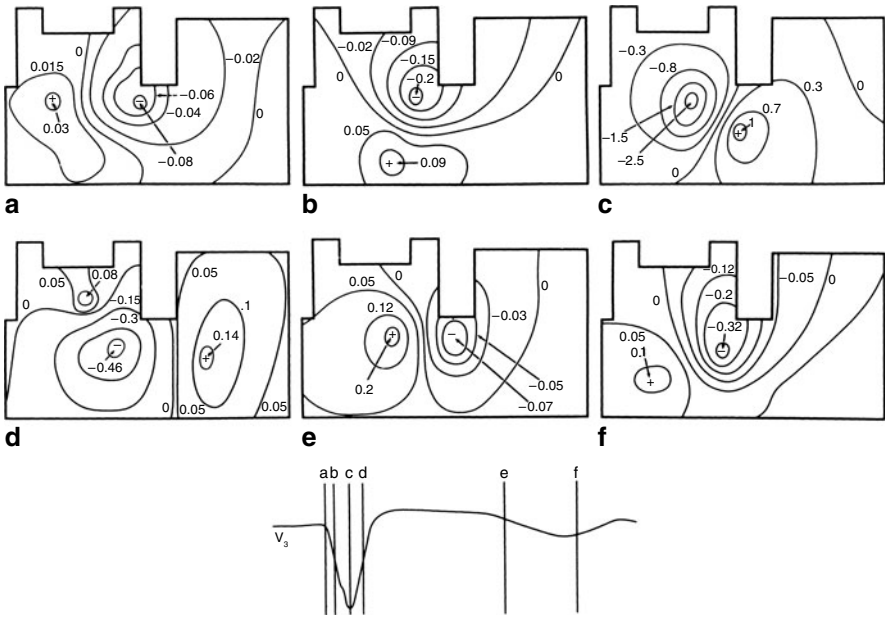

Figure 32.12

Body-surface maps in a subject with anterior MI. Each map refers to the instant of time indicated by the vertical fine crossing the ECG. Potential values are expressed in millivolts.

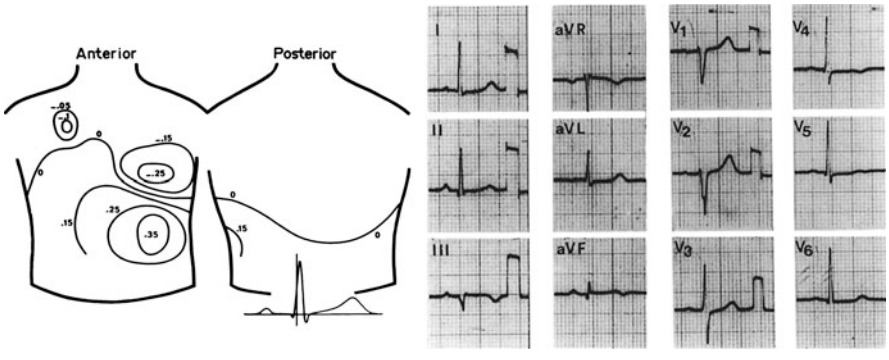

Figure 32.13

Body-surface map of a patient with an old anterior MI not revealed by the 12-lead ECG. During the early phases of the QRS interval an abnormal potential minimum is present on the left mammary region above the area explored by the standard precordial leads.

The persistence of a negative area on the anterior chest surface could be ascribed to the presence of an infarcted region in the underlying ventricular wall. This region did not depolarize and thus acted as a current sink. Occasionally, the minimum was located above the area explored by conventional precordial leads; in these cases, as in Fig. 32.13, the l2-lead ECG did not reveal any sign of anterior MI although there are suspicious changes in the inferior leads III, aVF, and the anterolateral leads V4–V6. In 13 subjects with anterior MI, the highest absolute value of the potential minimum varied between 1.06 and 4.77 mV (mean 2.78 ± 0.3) and was significantly higher than in normal subjects ($p < 0.01$).

At the onset of ventricular activation, the location of the potential maximum was normal in the majority of cases. However, the migration of the maximum was clearly abnormal, as could be expected since the area through which the maximum should normally have passed during its migration was occupied by the potential minimum. During the first 30 ms of ventricular activation the behavior of the maximum varied. In the majority of cases, it moved superiorly toward the neck, then posteriorly toward the left scapular region, and finally reached the left axillary region; in other patients (Fig. 32.12), the maximum migrated inferiorly on the anterior chest wall and reached the left axillary region; in two cases, in which the maximum was located in the left submammary region, it stayed in the same area. These various trajectories were probably related to the different extent and topography of the infarction. During the following phases of ventricular excitation the behavior of the potential maximum was within normal limits. The highest value reached by the potential maximum was significantly lower than that observed in normal subjects (mean 1.29 mV ± 0.23 standard error; $p < 0.01$). Moreover, the highest positive value was reached later than in normal subjects ($p < 0.01$), occurring between 30 and 66 ms (mean 41.8 ± 2.6).

At the beginning of the ST interval, the surface potential values were very low and the potential minimum was ill-defined, whereas the maximum was usually well developed, as occurs in normal subjects. The electronegative areas were located either on the left lateral wall of the chest, or on the lower part of the back, or both. These features are similar to those observed in normals. During the T interval, a clear-cut minimum generally appeared in the left mammary or submammary region. This location is definitely abnormal (see Fig. 32.10). In some patients, another minimum was simultaneously present in a normal area; that is, the upper sternal region. The location of the T minimum over the precordial area facing the infarction could be explained by assuming that the infarcted area did not generate recovery currents of its own and acted as a sink for repolarization currents originating in the surrounding, uninjured myocardial tissues. The highest values reached by the recovery maximum were significantly lower than in normal subjects ($p < 0.01$), whereas the highest values reached by the minimum were significantly higher ($p < 0.01$).

During the ST interval and the initial portion of the T wave, the recovery maximum was located within the normal area on the anterior chest wall (Fig. 32.12e). During the second half of the T wave, in the majority of cases, the potential maxima moved away from the area where they had appeared (Fig. 32.12f), and mainly scattered over the anterior lower thoracic surface. This late migration of the potential maximum was not observed in any of the normal subjects. This phenomenon is quantified by the late repolarization deviation index (LRDI, see Sect. 32.3.4), which increases in non-ischemic ventricular hypertrophy [54] as well as in old myocardial infarction compared to normal [55], even when adjusted for gender, being higher in males [34].

In the 14 cases of inferior myocardial infarction (Fig. 32.14), the potential minimum was located within or near the normal area at the beginning of the QRS interval. It then moved to the inferior half of the posterior or anterior chest wall, thus passing beyond the limits of the normal scatter for the relevant instants of time. At 20 ms, the minimum was located outside the normal area in the great majority of patients. The low position of the minimum, which was observed in all patients with inferior MI at 20–30 ms, was most likely related to the presence of an infarcted area in the diaphragmatic wall of the heart. This area of non-depolarizing tissue acted as a "window" through which the depolarization currents generated by normal cardiac muscle reentered the heart.

During the following instants, the minimum migrated toward the midsternal region in some patients; in the other patients (Fig. 32.14b), a new separate minimum appeared in the sternal region between 22 and 42 ms after the beginning of the QRS interval, while the first minimum was disappearing. Here, as in normal subjects, the sternal minimum was attributed to right ventricular breakthrough.

The highest absolute value of the negative potential varied between 0.45 and 1.67 mV (mean 1.3 ± 0.1) and was significantly lower than in the authors' normal subjects ($p < 0.01$). The low absolute value reached by the sternal minimum could be explained by the fact that the solid angle viewing the negative aspect of the wavefront from the sternum was smaller than in normal conditions because the wavefront did not extend over the entire diaphragmatic wall of the heart. In the authors' experience, in patients with inferior myocardial infarction, the behavior of the potential maximum during the QRS interval (Fig. 32.14), its area of distribution, and its highest absolute value were within normal limits.

At the beginning of the ST interval, electronegative areas could be found on the lower half of the trunk anteriorly and posteriorly, as in normal subjects. During the T wave, the recovery minimum moved to or remained in the inferior half of the trunk (Fig. 32.14e). The abnormally low location of the minimum during the T wave could be ascribed to the presence of an infarcted area in the diaphragmatic wall of the heart, which acted as a sink for recovery currents.

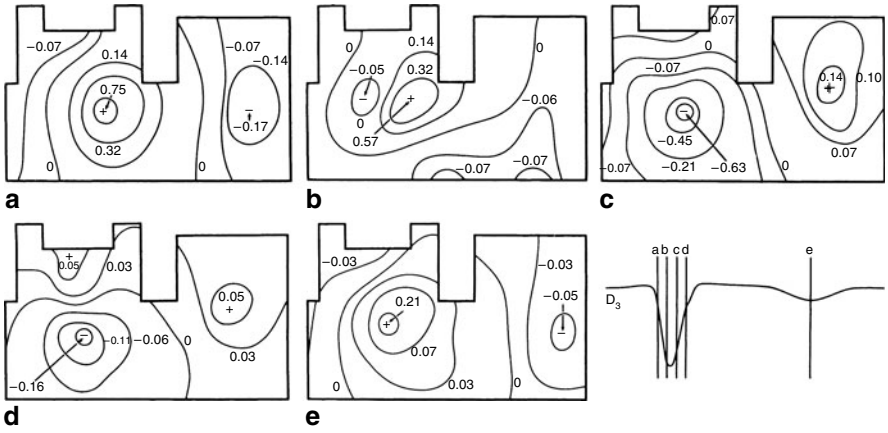

Figure 32.14

Body-surface map of a patient with inferior MI. Each map refers to the instant of time indicated by the vertical line crossing the ECG. Potential values are expressed in millivolts. The time interval between successive bars is 15 ms.

The location of the recovery maximum was within the normal area, i.e., the sternal or left mammary region, during the entire recovery process (Fig. 32.14e). The highest absolute values reached by the recovery maximum and minimum were not significantly different from those observed in normal subjects.

Potential patterns similar to those mentioned above were also described by Vincent and coworkers [43] in 28 subjects with inferior MI. These authors were also able to detect on BSPMs the characteristic features of inferior infarction in eight patients, whose ECGs had returned to normal or were nondiagnostic for the previous infarction. Similar findings were obtained by Osugi et al. [47].

Hirai et al. [48] described an abnormal location of the minimum at 15 ms into the QRS in 26 of the 32 cases of anterior myocardial infarction with a normal 12-lead ECG.

The possibility of detecting signs of myocardial infarction by means of body-surface mapping, even when the conventional ECG was within normal limits, was also demonstrated by Flowers et al. [41, 42]. Using departure maps, abnormalities of potential distribution were found in patients with anterior or inferior MI at the onset of ventricular excitation (corresponding to the Q wave in the conventional ECG) and during the mid-phases and late phases of the QRS interval [41].

Ohta et al. [46] compared body-surface maps with left ventriculographic findings in 24 patients with old inferoposterior MI. Using the departure-map technique as proposed by Flowers [41], they found surface potential abnormalities owing to infarction during specific phases of the QRS interval and in specific areas on the chest surface, depending on the location and extent of ventricular asynergy. In particular, some patients with inferior MI and, in addition, severe asynergy of the anterior, apical, or septal segments but without ECG or VCG signs of anterior MI, exhibited definite abnormalities of departure maps, which were different from those related to purely inferior MI.

De Ambroggi et al. [39] recorded BSPMs in 30 patients with old inferior myocardial infarction. Of these, 15 had no signs of necrosis in the conventional ECG. A number of variables relative to the instantaneous potential distribution and to integral maps were considered. The most accurate diagnostic criterion was derived from the integral values of the first 40 ms of QRS, with a sensitivity of 73% in patients without signs of necrosis in the 12-lead ECG, and of 100% in patients with pathological Q waves in the ECG, with a specificity of 83%.

In non-Q myocardial infarction of the anterolateral wall, the integral maps of the first 40 ms of QRS provided a good sensitivity (67%) in detecting signs (areas of values two standard deviations lower than normal) of the old necrosis in a group of patients with normal ECG [40].

Medvegy et al. recorded BSPM in 45 patients with documented non-Q-wave MI [52]. The main abnormality revealed by BSPM was the loss of electrical potential, but different features were characteristic for each region of the heart, so that they were suitable for the detection and localization of non-Q-wave MI, in the clinical setting of unstable coronary artery disease.

32.5.1.2 Acute Myocardial Infarction

Since the late 1970s, a simplified method of electrocardiographic mapping has been widely used in acute MI in order to obtain data on the infarct size and to assess the efficacy of various therapeutic interventions aimed at limiting myocardial injury [56].

The simplified method consists in recording 35–70 ECGs from the left hemithorax and in calculating the sum of the amplitudes of ST-segment elevations at all electrode sites, and the number of points with ST elevation. Similar procedures have also been used to evaluate the appearance of pathological Q waves and the reduction of R waves on the thoracic area explored.

The use of thoracic maps for assessing infarct size is based on experimental observations in animals demonstrating that any intervention that provokes an extension or reduction of the epicardial ischemic areas produces similar variations of the precordial areas, in which ST elevation is recorded [57, 58]. The use of these simplified methods of electrocardiographic mapping for assessing the extent of the infarction has aroused much criticism [59, 60]. In fact, there are several factors, other than the dimensions of the infarct, which can influence the ST segment elevation and, to a lesser extent, the QRS complex. These factors consist of local intraventricular conduction disturbances, electrophysiological changes in the myocardium outside the ischemic area, electrical cancellation phenomena, intra-extracellular electrolyte levels, pericarditis, heart rate, and autonomic nervous system activity. Despite the above considerations, the method does offer some definite advantages in monitoring patients with acute MI, in that it can reveal variations in the extent and severity of the ischemic process earlier than other methods, such as enzyme levels and myocardial scanning.

A description of the ST-T potential distribution on the entire chest surface in acute MI was reported by Mirvis [61], who observed a characteristic early appearance of the repolarization potentials in both anterior and inferior MI, with a longer than normal overlap between final excitation and recovery potential patterns. During the ST-T interval, the potential distributions were characterized in anterior MI by a single maximum on the left anterior chest that remained fixed in location but increased in amplitude as repolarization progressed; in inferior MI, there was a single minimum generally located on the left anterior-superior thorax, with positive potentials covering the lower thoracic portions.

The distribution of QRS and ST potentials in acute inferior myocardial infarction (mean 76 h after the onset of symptoms) has been studied by Montague et al. [62]. They computed integral maps in a group of 36 patients with acute inferior MI, and found negative areas over much of the inferior torso with extension of the positivity to the superior torso, during the first half of the QRS interval (Q zone); conversely, the ST segment integral map was characterized by abnormally positive inferior distributions and concomitant negative precordial distributions. Moreover, patients with right ventricular involvement tended to have a greater area of negative Q zone over the right anterior inferior thorax and greater inferior and rightward extension of ST segment positivity as compared with patients with exclusive left ventricular infarction. Thus, in acute inferior MI, BSPMs make it possible to detect definite abnormalities of both depolarization and repolarization potentials, which indicate right ventricular involvement.

More recently, Menown et al. [63] confirmed the ability of BSPMs (using 80 leads) to improve, with respect to conventional ECG, the classification of inferior acute MI with posterior or right ventricular wall involvement.

The same group demonstrated that the BSPM diagnostic algorithm detected acute MI with higher sensitivity than a 12-lead ECG diagnostic algorithm or a physician's interpretation, without loss of specificity [64]. They also showed the superiority of BSPM versus the 12-lead ECG in detecting acute MI in the presence of left bundle branch block (LBBB) [65].

32.5.1.3 Myocardial Ischemia

In angina patients, the resting ECG is very often normal between attacks. This can indicate that cardiac electrogenesis is normal or that there are electrical abnormalities, which are not revealed by the conventional ECG because they are too small, or because they are projected to surface areas not explored by conventional leads.

In several patients with proven angina pectoris and a normal resting ECG, surface maps exhibited an abnormal distribution of recovery potentials [66]. In these patients, the location of the potential minimum during recovery was outside the normal range during some phases of the ST segment and of the T wave, often on the lower left lateral region of the chest (Fig. 32.15a).

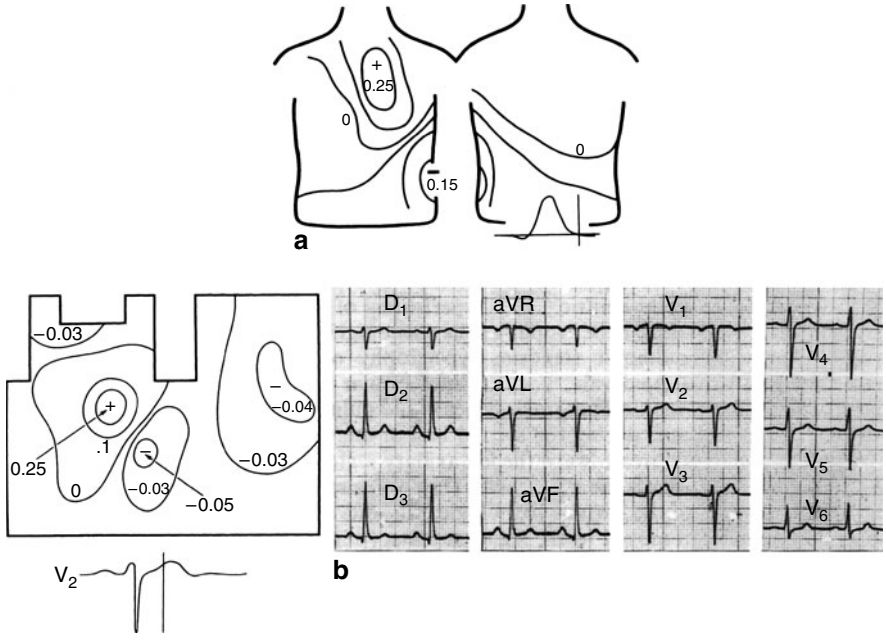

Figure 32.15

(a) BSPM of a patient with angina and normal resting ECG. The map refers to the early ST interval, as indicated by the vertical line crossing the ECG. This potential pattern lasted about 200 ms. Potential values are expressed in millivolts. (b) BSPM at the instant indicated by the vertical line crossing the ECG, in a patient with angina but normal T waves on the resting ECG. The map shows a complex potential distribution with one maximum and two minima.

During the entire ST-T interval the potential maximum was located within the normal area in most patients with angina. Only in a few subjects was the location of the maximum abnormal during the final phases of ventricular recovery. In some of these patients with angina and a normal resting ECG, a complex potential distribution was observed (Fig. 32.15b), with one maximum and one minimum located normally and a second minimum placed in an abnormal position.

In a study [67] performed on 14 patients with stable angina and a normal resting ECG, the analysis of BSPMs was extended to a new series of quantitative aspects; that is, temporal evolution during the ST-T interval of the highest potential on the chest, lowest potential, highest potential difference, integral of the absolute value of the potential function extended over the entire chest surface, and the percentage of the total thoracic area with positive potentials. By deriving a number of voltage-related variables from these time functions and by submitting them to multivariate analysis, it was possible to separate more than 90% of the ischemic patients from normal subjects. It has been shown [68] that, in some patients with typical angina but no evidence of MI, QRS potentials can differ from normal at some chest locations, which are not explored by the standard 12 leads.

BSPMs were also used to study the potential variations before, during, and after coronary angioplasty (PTCA). During balloon inflation in the anterior descending or right coronary artery, specific changes of QRS instantaneous and integral maps were observed, suggesting a regional conduction delay due to myocardial ischemia [69].

Shenasa et al. [70] demonstrated potential patterns 40 ms after QRS end during inflation that were specific to the three major coronary arteries dilated. The left anterior descending coronary artery was associated with the largest ST-segment shifts with a precordial maximum and negative potentials over the back; for the right coronary artery, negative potentials covered the upper left torso with a left mid-axillary minimum and positive potentials over the rest of the torso; for the left circumflex coronary artery, negative potentials covered the anterior torso with a precordial minimum and positive potentials over the back. These changes disappeared rapidly after balloon deflation. Thus, BSPMs provide a comprehensive

approach for the evaluation of electrocardiographic changes and the development of optimal leads for the detection of acute occlusion of a coronary artery.

BSPMs were also used to evaluate the clinical efficacy of PTCA and were proved useful to detect restenosis [71].

32.5.1.4 Exercise Maps

Potential maps have been obtained during exercise in normal subjects and patients with angina.

Some authors [72] recorded ECGs from 16 points located on the left anterior thorax, using traditional methods. This technique should be more appropriately considered as a system of multiple precordial leads rather than surface mapping. The 16-lead system, however, has shown greater sensitivity than 12 standard leads or three orthogonal leads [73], although this has not been confirmed by other groups.

Other investigators studied the instantaneous potential distribution on the anterior thorax [74, 75] or on the entire chest [76–79]. A complete and accurate study on the QRS and ST-T wave changes induced by exercise was performed by Spach's group in healthy subjects [76]. These authors were able to obtain high-quality potential maps during exercise without averaging ECG waveforms, by using their system for calculating total body potential distributions from 24 chest leads. Exercise induced consistent changes in potential patterns. During the first 20 ms of QRS, the minimum stayed on the lower left chest, while, in the resting condition, it gradually migrated toward the upper back. In mid-QRS, the magnitude of the anterior potential maximum was approximately 60% of that observed in the map at rest while the duration of the QRS interval usually increased (2–10 ms) at peak exercise. On the basis of these findings, it was suggested that the decrease in the magnitude of the precordial potential maximum in the midportion of QRS (R wave in lead V5) might result from changes in the sequence of activation of the ventricles, rather than from blood volume variations (Brody effect).

In the early stage of ventricular repolarization (early ST segment), a potential minimum usually developed on the lower left thorax during exercise. This minimum generally decreased in magnitude in a short time after exercise. During the subsequent instants of the ST interval, the lower left precordial region became less negative and was usually positive by the early portion of the T wave. At the peak of the T wave the potential pattern showed slight changes during and after exercise with respect to the resting condition. However, the amplitude did change considerably. In particular, immediately after exercise, the magnitude of T-wave potentials increased rapidly, reaching its highest value 30–90 s after the end of exercise, before gradually decreasing; in some subjects, the potential values were still higher than resting values 10 min after exercise.

In patients with angina, Simoons and Block [77] reported some typical changes induced by exercise. The recovery minimum was located in the lower part of the left side of the chest and attained −90 μV or more 60 ms after the end of the QRS complex. This repolarization pattern was found in 21 out of 25 coronary patients, but in none of the normal subjects (sensitivity 84%, specificity 100%).

Yanowitz et al. [79] recorded BSMs before and after exercise in 25 males with documented coronary disease. By considering the integrals of the first 80 ms of the ST interval, they found abnormal negative values in 18 cases. Moreover, in 25% of the cases, BSPMs after exercise showed maximal depression of the ST-segment area at sites not sampled by the leads usually employed in exercise testing. This finding suggests that BSPMs may increase the sensitivity of the exercise testing for coronary disease.

32.5.2 Right Ventricular Hypertrophy

Hypertrophy may involve various portions of the right ventricle in different forms of heart disease. In children BSPMs were recorded in the following types of right ventricular hypertrophy (RVH) [80]: dilation of right ventricle and hypertrophy of the crista supraventricularis owing to secundum atrial septal defect; hypertrophy of the entire right ventricle, including the outflow tract, secondary to valvular pulmonic stenosis; hypertrophy of the proximal portion of the right ventricle between the tricuspid valve and the infundibular stenosis, with normal thickness of the right ventricular wall in the outflow tract, beneath the pulmonary valve (tetralogy of Fallot).

While, in normal subjects, during the second half of the QRS interval, the potential maximum moves from the precordial area toward the left axillary region and then to the back, in all patients with RVH, it migrated toward the right chest.

The movement of the maximum on the right thorax was different according to the various pathological conditions [80]. In atrial septal defect (ostium secundum) the maximum moved to the right mammary region, finally reaching the upper sternal region. In tetralogy of Fallot with infundibular stenosis, the maxima migrated toward the right lateral thoracic wall. In valvular pulmonic stenosis, the maximum migrated on the anterior right chest toward the upper central area, as in atrial septal defect; the potential values, however, were markedly higher.

These surface potential patterns were correlated with the spread of excitation through the right ventricular wall, as determined in the same patients at surgery. In all three types of RVH, the activation wavefront moved on the epicardial surface in a rightward direction. In atrial septal defect, the latest epicardial events were recorded along the atrioventricular groove and gave rise to a right-chest maximum. However, after completion of epicardial excitation on the right ventricle, a potential maximum persisted over the upper sternal area. This terminal maximum was probably related to an activation wavefront spreading through the upper part of the septum and the crista supraventricularis, which is most likely hypertrophied in right ventricular volume overload.

In valvular pulmonic stenosis, as the wavefront moved laterally across the right ventricular free wall, it produced a maximum over the right chest while a minimum was positioned over the left precordium. The terminal excitation wavefront spread superiorly through the outflow tract of the right ventricle and gave rise to the upper sternal maximum.

In tetralogy of Fallot, after right ventricular breakthrough occurred, the wavefront moved laterally toward the atrioventricular groove and produced a maximum over the lower mid-right chest with a minimum in the left precordial region. The latest portions of the right ventricle to be depolarized were along the lateral inferior part of the atrioventricular groove. The final orientation of the wavefront was such that it resulted in a maximum in the right axillary region with a minimum over the central chest. Thus, maps enable the different types of RVH to be recognized to a greater extent than does the 12-lead ECG.

Body-surface maps in adult patients with RVH owing to mild-to-moderate valvular pulmonic stenosis were obtained by Sohi et al. [81]. Using departure maps, they observed a delayed appearance of the sternal negativity, which is usually related to right ventricular breakthrough, and an abnormal positivity located in the upper anterior chest.

32.5.3 Left Ventricular Hypertrophy

Body-surface maps in patients with left ventricular hypertrophy (LVH) owing to mild-to-moderate aortic stenosis were studied by Sohi et al. [81], using the departure-map technique. They observed an abnormal delay of early negativity on the anterior right chest and a potential maximum on the upper anterior chest, which peaked later and lasted longer than normal.

An assessment of left ventricular mass in patients with LVH was attempted by Holt et al. [82] on the basis of chest-surface potential distribution. They used a mathematical model in which the ventricles and the septum were represented by 12 dipoles. The dipole activity was assumed to be proportional to the amount of viable myocardium in that region; the strength of each dipole as a function of time was determined by measuring potentials at 126 locations on the thoracic surface and by applying suitable transfer coefficients. A good correlation was found between left ventricular mass determined by angiography and that determined by surface potentials ($r = 0.85$). Moreover, the correlation coefficient was much higher using BSMs than other electrocardiographic recordings (12 standard ECG leads or VCG).

Yamaki et al. [83] used BSPMs recorded with 87 leads to determine the severity of LVH in 57 patients with concentric hypertrophy and in 30 with left ventricular dilatation. A number of parameters related to QRS voltages and ventricular activation time were measured, and some of them were proven useful in determining the severity of LVH.

Kornreich et al. [84] studied BSPMs during the entire cardiac cycle (PQRST) in 122 patients with LVH. Best classification results were achieved with ST-T features, followed by features from the P wave, QRS, and PR segment. Cumulative use of ST-T and P features yielded a specificity of 94% with a sensitivity of 88%.

Hirai et al. [85] studied QRST integral maps in patients with LVH (10 with aortic stenosis, 12 with aortic regurgitation, and 22 with hypertrophic cardiomyopathy). Abnormalities in patients with hypertrophic cardiomyopathy were manifest even in mild LVH and a greater disparity of repolarization was found in hypertrophic cardiomyopathy than in LVH due to aortic valve disease.

We reported the results on BSPMs recorded in 16 patients with LVH due to aortic stenosis, focusing on the analysis of ventricular repolarization, with the aim of searching for subtle alterations not revealed by the usual ECG processing, which are likely to reflect ventricular repolarization heterogeneities [54].

The classical signs of LVH in the standard ECG (increased QRS voltage and ST-T changes) are reflected on BSPMs as (1) increased amplitude of the QRS integral map and of the STT integral map, (2) relatively low amplitude of the QRST integral map, due to the cancellation between the depolarization and repolarization potentials, and (3) opposing aspects of the QRS and STT integral maps.

In order to detect possible minor electrical disparities of repolarization not apparent from visual inspection of the ST-T and QRST maps, we analyzed the morphology of all the recorded ST-T waves, using principal component analysis. In our patients, the "similarity index," defined as the first eigenvalue divided by the sum of all eigenvalues, was slightly but significantly lower than in control subjects (0.73 vs 0.77; $p = 0.027$), suggesting the presence of a degree of heterogeneity of repolarization higher than in the normals. The repolarization deviation indices were also computed, as described in the methods. In our LVH patients, the changes during early repolarization, as reflected by ERDI, were similar to those observed in our control group and also in the larger group of 159 normal subjects from the database of Dr. F. Kornreich (Vrije University of Brussels, Belgium). Then, we focused on the analysis of the T peak-T end period, during which possible heterogeneities of repolarization should be more likely to be detected. The LRDI was significantly higher ($p = 0.005$) in LVH patients than in normals. The values of similarity index and LRDI found in LVH patients suggest a higher than normal degree of repolarization heterogeneity, not detected by the usual electrocardiographic analysis.

32.5.4 Right Bundle Branch Block

Several types of potential patterns have been observed in patients with right bundle branch block (RBBB) [86–88]. During the initial phases of ventricular activation, the surface potential distribution was similar to that observed in normal subjects with a maximum located on the sternal or left mammary region and a minimum on the left chest wall or in the dorsal regions (Fig. 32.16b). The sternal minimum, which indicates right ventricular breakthrough and which occurs in normal subjects 14–44 ms after the onset of the QRS complex, did not appear. Only at a later stage (38–70 ms after the onset of ventricular activation) did a second minimum appear, which, however, was located in an abnormal position, that is, in the left mammary region (Fig. 32.16d). It should be noted that this second minimum usually occurred to the right of the potential maximum located on the left precordium. This maximum was attributed to the spread of excitation through the left ventricular wall, while the delayed minimum was interpreted as the result of excitation arriving on the surface of the left ventricle, most probably in the left paraseptal region or in the apical area.

Shortly after the appearance of the second minimum, a new potential maximum appeared on the right precordium (Fig. 32.16c). This led to a complex potential distribution with two maxima (left and right) and two minima (on the right clavicular region and on the left precordial area), indicating the simultaneous presence of two excitation waves spreading into the left and right ventricles. Subsequently, the two negative areas merged, while the left maximum shifted to the back (Fig. 32.16g) and eventually disappeared, as in normal subjects, about 80 ms after the onset of the QRS complex. Thus, during the final stages of the QRS interval, only the signs of delayed right ventricular activation persisted, with a maximum on the right anterior chest wall and a minimum on the left precordial area (Fig. 32.17a–c). At the end of the QRS complex, early recovery potentials could often be observed before the last excitation potentials disappeared. Usually, the activation maximum and minimum shifted slightly to the right, and the recovery maximum appeared in the left mammary region, giving rise to patterns with three extrema (Fig. 32.17d). Later, only two extrema remained: the recovery minimum in the sternal or right mammary region and the recovery maximum in the left mammary area (Fig. 32.17e). This pattern persisted throughout the ST and T intervals (Fig. 32.17f) and approximately represented a mirror image of the potential distribution observed during the last phases of ventricular activation.

In some patients, a different behavior of the potential maximum and minimum was observed during the midportion of QRS; that is, the anterior maximum, after reaching the precordial area, did not complete its leftward migration but reverted to the sternal region and then moved to the right precordium, thereby taking over the role of the second maximum observed in typical RBBB. The second minimum did not appear in the left parasternal region to the right of the maximum, as in typical cases, but to its left, in the external part of the left mammary region. The electrophysiological mechanism giving rise to this peculiar sequence of potential patterns observed could not be identified.

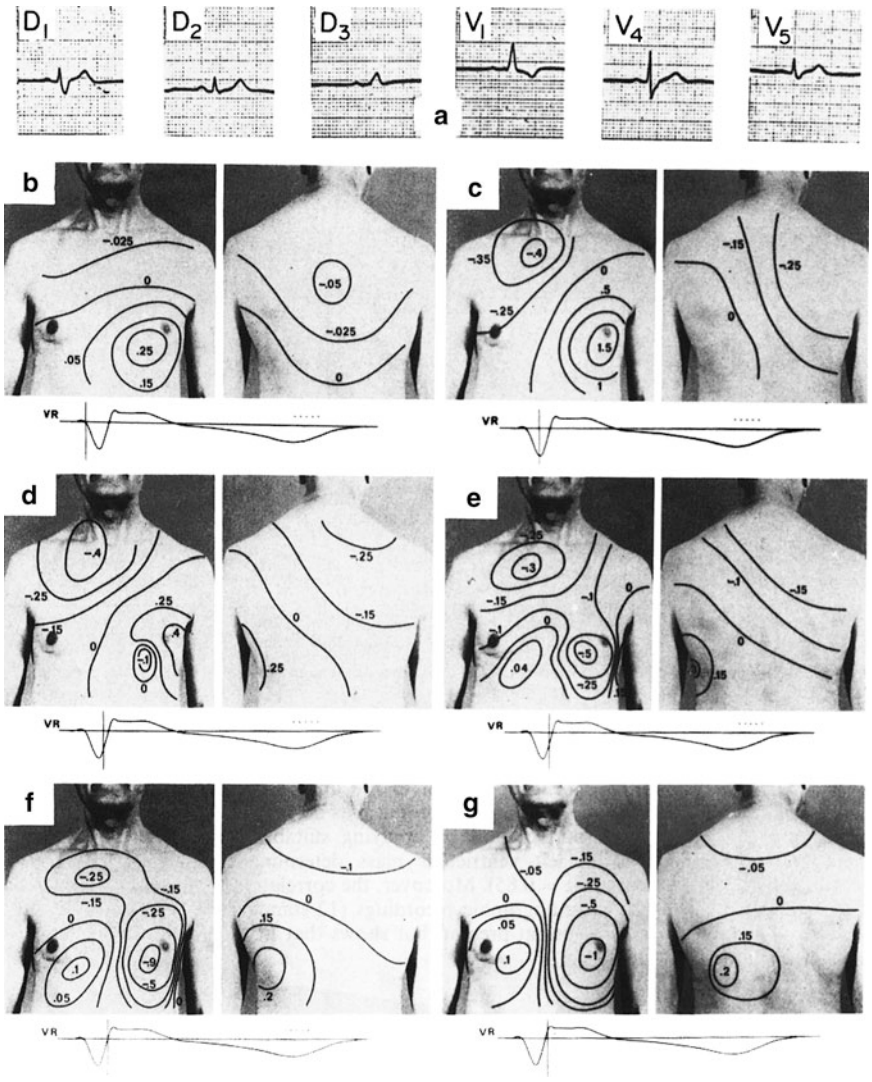

Figure 32.16

Subject with RBBB. (a) Standard ECG. (b–g) Each map refers to the instant of time indicated by the vertical line intersecting the reference ECG (VR). The values of equipotential lines are expressed in millivolts. (After Taccardi et al. [86]. © Churchill Livingstone, New York. Reproduced with permission.)

32.5.5 Left Bundle Branch Block

BSPMs have been described in uncomplicated left bundle branch block (LBBB), with or without left axis deviation [89–91] and in LBBB complicated by additional heart disease [90, 92].

In the uncomplicated LBBB studied by Musso et al. [90], at the onset of QRS (Fig. 32.18a), the potential maximum was consistently found in the sternal area. The minimum was generally located on the right chest, anteriorly or posteriorly. A few milliseconds later a new potential distribution developed, with a minimum in the presternal area and a maximum on the left mammary region. In some patients, the minimum migrated to the sternal area from its previous location. In other cases, an independent, secondary minimum appeared in this region and subsequently increased in magnitude, while the old minimum faded away. In both cases, the minimum settled in the sternal area earlier than in

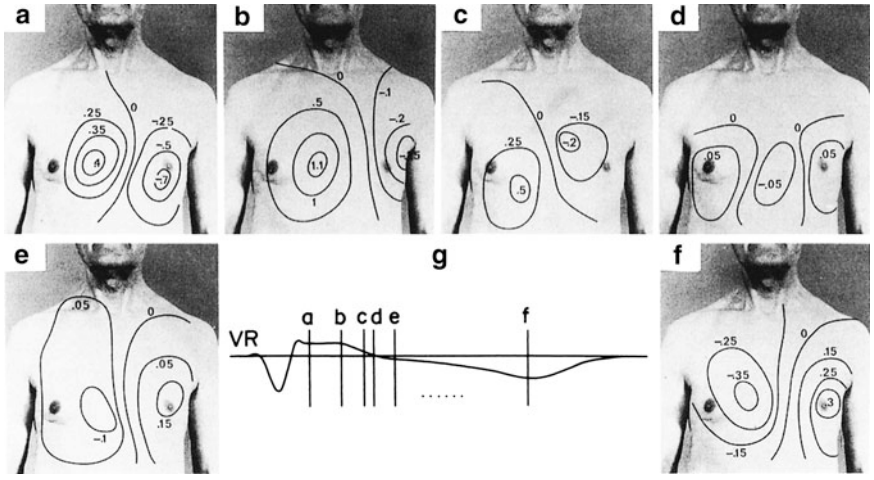

Figure 32.17

Same subject as in Fig. 32.16. BSPMs relating to second half of ventricular activation (a–d) and recovery (e, f). At instant d (end of QRS) recovery potentials are already present on the left side of the chest. (After Taccardi et al. [86]. © Churchill Livingstone, New York. Reproduced with permission.)

normal subjects. An early appearance of this minimum, which indicates right ventricular breakthrough, was also found by other investigators [91].

In LBBB, the initial phase of ventricular excitation differs from the normal sequence, in that the first electrical event occurring in the normal ventricles, that is, the excitation wavefront spreading through the septum from left to right and anteriorly, is missing. Therefore, ventricular excitation starts later than it would if the left bundle branch was functioning normally. As a consequence, the onset of ventricular activity as a whole is delayed in relation to His-bundle excitation.

The lack of left ventricular activity may explain the differences between the maps recorded in the early stages of QRS in LBBB patients and in normal subjects. The occurrence of the presternal minimum may be attributed, as in normal subjects, to the excitation wavefront reaching the right ventricular surface (right ventricular breakthrough). The shorter breakthrough time is not surprising since this time is calculated from the beginning of QRS, which is delayed in LBBB, as indicated above.

In the subsequent stages, the maximum moved to the left axilla, while the minimum persisted in the midsternal area. This distribution was a constant feature in the second half of QRS (Fig. 32.18b). In this interval, the potential maximum and minimum reached their peak value. However, the positive peak appeared later than the corresponding one in normal subjects. The surface patterns mentioned above can be related to the wide excitation wavefront, which, at these stages of the cardiac cycle, spreads through the septum from right to left and then invades the left ventricular walls.

In most cases of uncomplicated LBBB, 10–20 ms before the end of QRS a new maximum appeared in the upper sternal area (Fig. 32.18c). The maximum progressively increased in voltage and persisted throughout the ST-T interval. For this reason it was considered to be an early manifestation of the recovery process. The recovery minimum was located in the left axillary region (Fig. 32.18d), whence it generally moved toward the dorsal area at the end of the T wave. These events may be interpreted by inferring that (a) measurable repolarization potentials originate from the right ventricle before left ventricular depolarization is completed because the right ventricle is the first to depolarize and (b) the left ventricle behaves as a current sink during most of the recovery process, because of its delayed repolarization resulting from delayed activation.

Subjects with LBBB and left axis deviation described by Sohi et al. [91] differed from those with normal axes in that during the second half of the QRS interval, the maximum was generally located on the left shoulder and back. This pattern was attributed to a further selective slowing of depolarization in the anterobasal portions of the left ventricle.

BSPMs in complicated LBBB have been described by two groups of investigators [90, 92]. According to Preda et al. in LBBB associated with anterior MI, the middle third of the anterior chest wall remained negative during the final phases

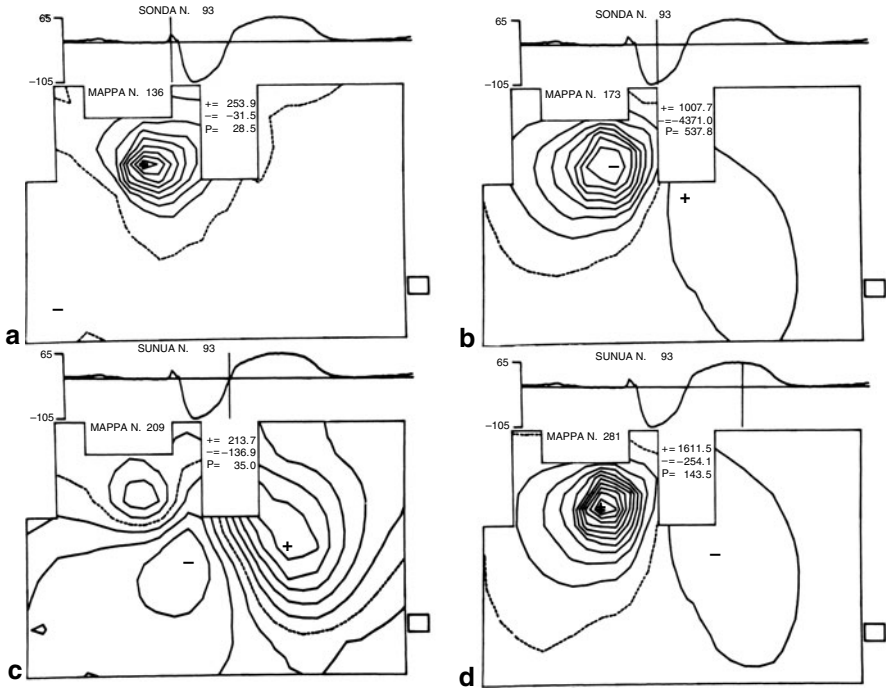

Figure 32.18

Patient with uncomplicated LBBB. BSPMs relating to four instants of time during ventricular excitation and recovery. The zero equipotential line is dashed. The plus and minus signs indicate the value of the positive and negative peaks (in microvolts). +P and −P indicate the step (in microvolts) between adjacent positive and negative equipotential lines.

of QRS. The authors attributed this finding to the lack of activation of the anterobasal region of the left ventricle, owing to the presence of the necrosis. In patients with infero-posterior MI, a persistent negativity was observed during the central portion of the QRS in the lower border of the chest, on the left lateral or posterior regions. Later, the negativity moved to the right side of the back. These findings were not confirmed by Musso et al. [90]. They studied LBBB complicated by anterior or inferior MI, LVH, myocardial ischemia, or a combination. By visually inspecting the maps, Musso et al. were unable to identify any potential pattern that could be uniquely found in a given LBBB group. However, several differences among groups were observed if the voltage values, rather than the potential patterns, were taken into account [90]. Generally, higher voltages were measured in patients with LVH and lower voltages were found in the MI groups as compared to uncomplicated cases of LBBB. These observations prompted Musso et al. to measure a set of voltage-related variables with a view to discriminating among different LBBB groups. The variables were derived by curves illustrating the behavior as a function of time during QRST of the highest instantaneous negative and positive potentials on the chest, the highest potential difference, the integral (extended to the entire chest surface) of the absolute value of the potential function, the size of the electropositive (or electronegative) thoracic areas, and so on. The statistical evaluation of the data (canonical variates analysis) permitted the classification of most complicated and uncomplicated patients into the correct group.

32.5.6 Left Anterior Fascicular Block

In left anterior fascicular block (LAFB), without MI or hypertrophy, one or more abnormal features could be detected in all patients. At the onset of QRS interval, in 8 out of 11 patients (unpublished data), the potential distribution was clearly abnormal in respect of (a) the location of the minimum, which was at a higher thoracic level with respect to the corresponding maximum, and/or (b) the anomalous position of the maximum (Fig. 32.19a). This potential pattern

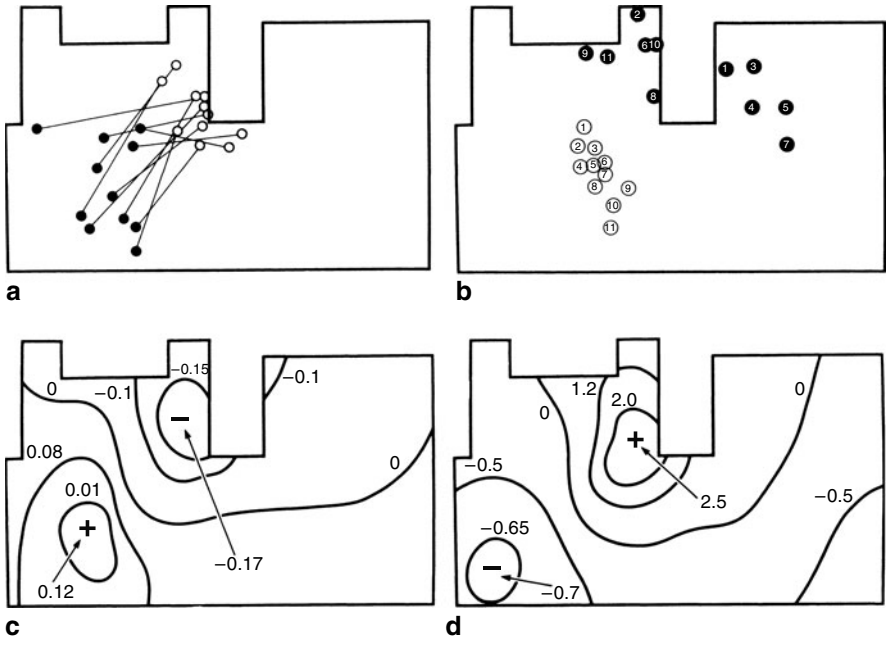

Figure 32.19

***Top*: Location of potential maxima (black circles) and minima (white circles) on the chest surface (a) at the onset of ventricular activation and (b) after 55 ms in 11 subjects with LAFB. The potential maximum and minimum relating to a given patient are indicated by the numbers inside the circles. *Bottom*: Subject with LAFB. Potential distribution at 10 ms (c) and at 46 ms (d) after the onset of ventricular activation. Potential values are expressed in millivolts.**

could be related to the direction of the activation wavefront, which spreads inferiorly and rightward. This anomalous direction is probably owing to the lack of early excitation of the anterosuperior portion of the left septal surface, as found in experimental studies [93].

During the mid- and late-QRS interval, a characteristic potential distribution was observed in all patients, by the authors and others [94]. After 28–30 ms from the onset of ventricular activation, the potential maximum was invariably located in the upper portion of the anterior or posterior chest surface, above the horizontal plane passing through the corresponding minimum (Fig. 32.19b). The minima clustered on the lower anterior chest wall (Fig. 32.19b) while the lower part of the chest was constantly electronegative. This potential distribution accounts for the left axis deviation in the standard ECG and can be attributed to the abnormal sequence of ventricular excitation in LAFB and particularly to the delayed activation of the anterosuperior part of the left ventricular wall.

The motion of the maximum to the upper thoracic areas occurred as follows. In 5 cases out of 11, the maximum did not migrate to the back, as in normal subjects, but moved directly from the left mammary region to the upper sternal or left clavicular areas. In the remaining six cases, it moved to the back and remained there (five cases) or reached the anterior left shoulder. It is suggested that in those patients where the maximum moved dorsally, a lesser degree of asynchronism existed between the activation of the posterior and anterior basal portions of the left ventricle. The variety of patterns observed may result from different degrees of delay in the anterior fascicle and/or from individual variations in the anatomical distribution of the peripheral conducting fibers.

32.5.7 Wolff–Parkinson–White Syndrome

It is well known that the Wolff–Parkinson–White (WPW) syndrome is a result of the early excitation of some portions of the ventricles through anomalous conduction pathways. These can be found at almost any location around the AV

ring, including the ventricular septum. Conventional ECGs and VCGs provide useful information on the orientation and direction of propagation of the pre-excitation wavefront, but they do not enable the location of the pre-excited area to be determined reliably. A number of investigations have shown that much more information on the location of the pre-excitation focus can be gained by measuring the instantaneous potential distribution on the entire chest surface [95–102].

Yamada et al. described three types of surface maps in 22 WPW patients on the basis of QRS potential distributions [95]. Type I potential patterns were ascribed to pre-excitation of the posterior aspect of the left ventricle, type II to pre-excitation of the basal part of the right ventricle, and type III to pre-excitation in the proximity of the posterior right AV groove close to the ventricular septum.

In a group of 42 WPW patients, De Ambroggi et al. [96] were able to recognize six types of maps, on the basis of the following considerations and criteria, derived mainly from previous studies on physical, mathematical, and physiological models [1, 103, 104].

At the onset of the delta wave, the pre-excitation wavefront is small and can be approximated by a single equivalent dipole, at least as far as surface potential patterns are concerned. When the two potential extrema on the body surface have nearly equal strength, the dipole is equidistant from the surface extrema and its depth in the chest is proportional to the distance between the extrema. When one extremum is stronger than the other, the dipole is closer to the stronger extremum. The direction of the dipole is approximated by a straight line joining the two extrema. After the delta wave, the body-surface potential patterns are not clearly related to the location of the pre-excitation wavefront. However, the appearance of a sternal minimum indicating a normal right ventricular breakthrough may suggest a left or posterior localization. On the basis of these simple rules, we proposed the following classification of the patients studied.

Type 1 (Figs. 32.20a, 32.21). During the delta wave, the maps of the 23 patients belonging to type 1 exhibited a potential maximum on the precordial area and a minimum on the back. It is suggested that the pre-excitation wave was located deep in the thorax, most likely in the posterobasal wall of the heart and spread in a postero-anterior direction. Between 40 and 90 ms after the onset of ventricular activation, a second minimum appeared on the sternal area in most patients, while the dorsal minimum reached the upper anterior chest wall. The second minimum was attributed to the right ventricular breakthrough. Its appearance suggested that the right anterior ventricular wall was excited through the normal pathways and was therefore not affected by pre-excitation.

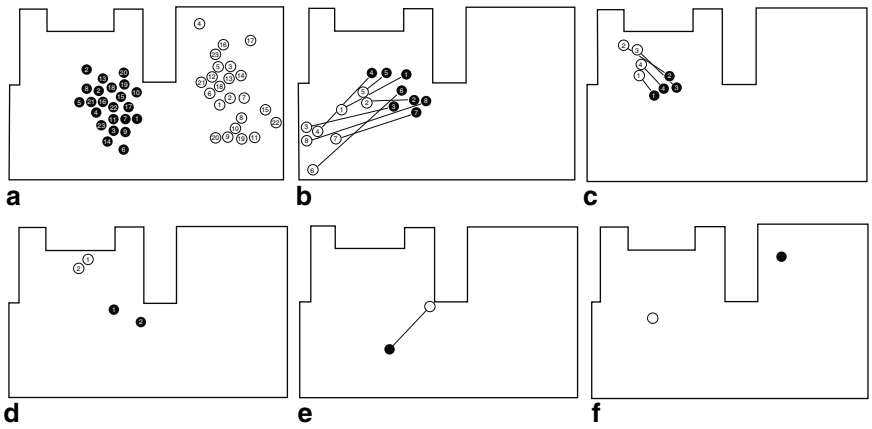

Figure 32.20

Location of potential maxima (black circles) and minima (white circles) on the chest surface during the delta wave in WPW patients belonging to type 1(a), 2(b), 3(c), 4(d), 5(e), and 6(f). The potential maximum and minimum relating to a given patient are indicated by the numbers inside the circles. (After De Ambroggi et al. [96]. © American Heart Association, Dallas, Texas. Reproduced with permission.)

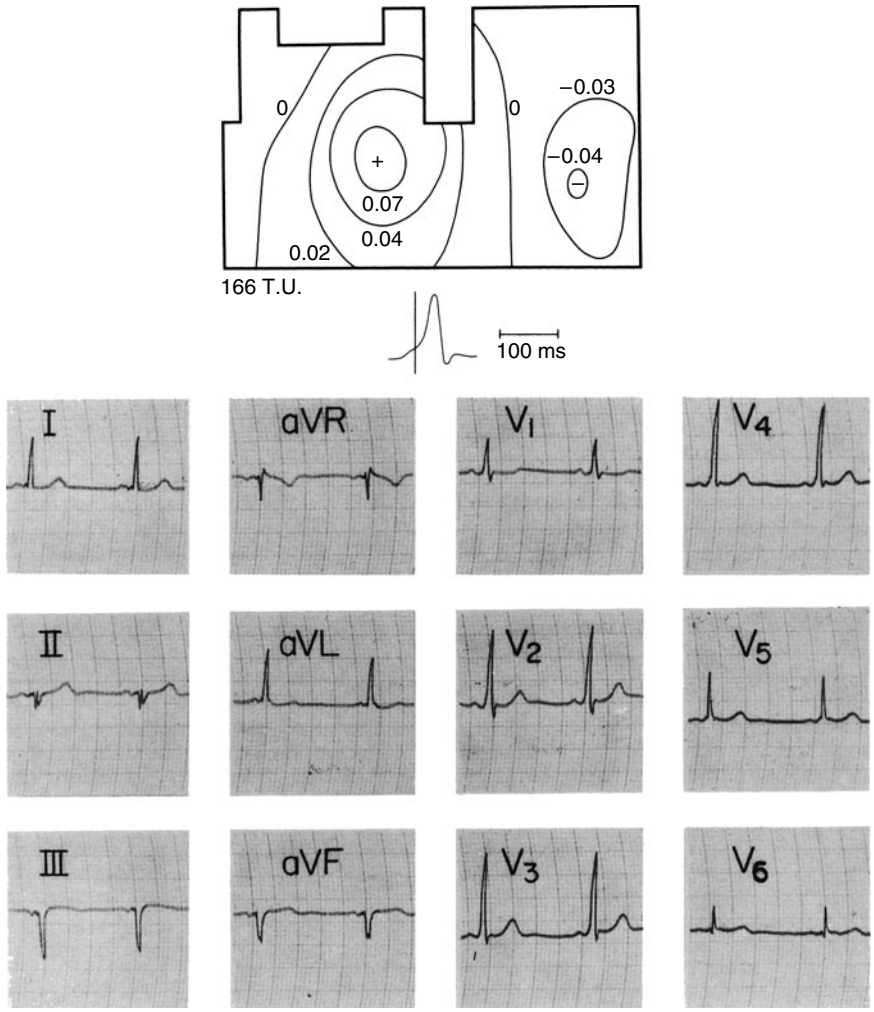

Figure 32.21

BSPM during the delta wave, at the instant indicated by the vertical line crossing the reference ECG in a WPW subject belonging to type 1. The 12-lead ECG shows a type A WPW pattern. (After De Ambroggi et al. [96]. © American Heart Association, Dallas, Texas. Reproduced with permission.)

Type 2 (Figs. 32.20b, 32.22). During the delta wave, in the eight patients belonging to type 2, the minimum was located on the inferior half of the right anterior chest wall and the maximum on the sternal or left mammary region. The location of the minimum and maximum suggests that the pre-excitation wave moved leftward and upward and probably spread from the lateral inferior portion of the AV groove through the right ventricular wall. In no patient of this group did a second minimum appear on the sternal area. This suggested that the right ventricular wall was not activated through the normal conducting pathways.

Type 3 (Figs. 32.20c, 32.23). During the delta wave in the four type-3 patients, the minimum was initially on the back and then moved to the right subclavicular area; the maximum was located in the mid-sternal area. This potential distribution suggested that an excitation wave was spreading through the anterior wall of the right ventricle from the upper part of the right AV groove, downwards and to the left. A second minimum did not appear in the sternal area in the patients of this group, suggesting that the right ventricular wall was not excited through the normal pathways.

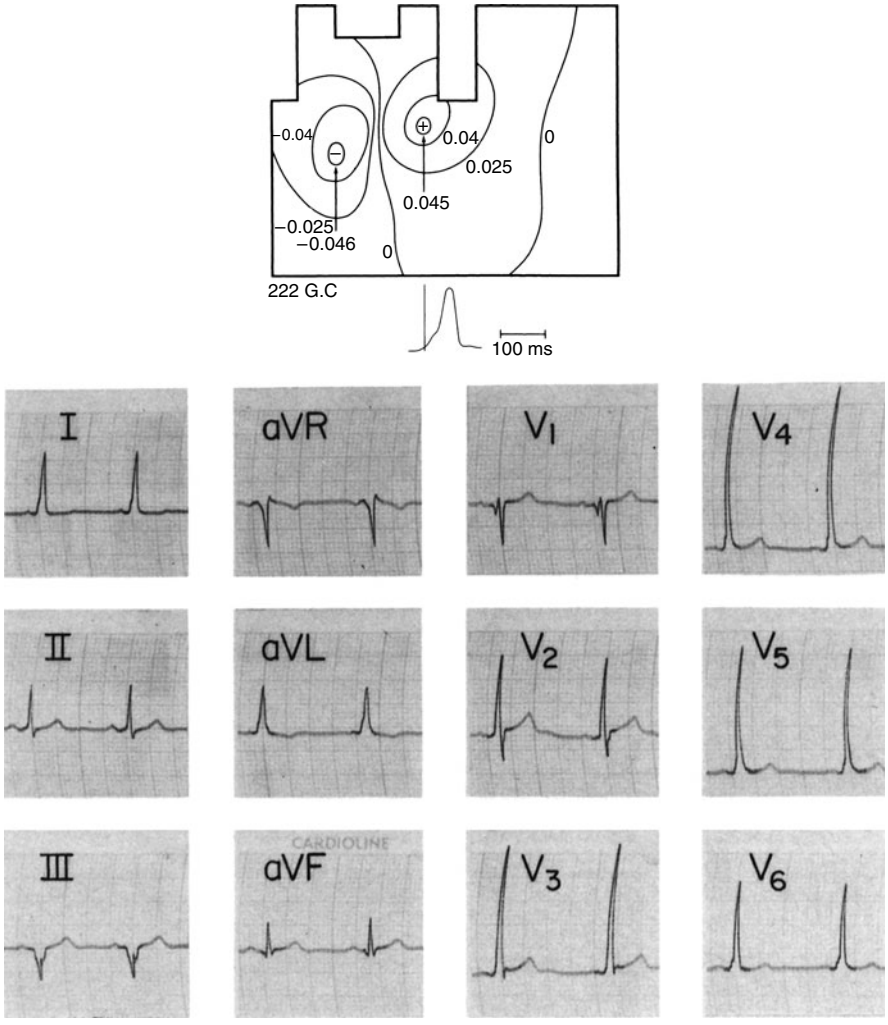

Figure 32.22

BSPM during the delta wave in a WPW patient belonging to type 2. The ECG shows a type B WPW pattern. (After De Ambroggi et al. [96]. © American Heart Association, Dallas, Texas. Reproduced with permission.)

Type 4 (Fig. 32.20d). Two patients were classified as type 4. During the delta wave, both the maximum and minimum were located on the left anterior chest wall, with the maximum being on the mammary region, and the minimum on the upper sternal area. This potential distribution suggested that pre-excitation probably started in the anterior portion of the left AV groove or in the anterior portion of the septal AV ring, spreading toward the apex of the left ventricle. A right-sided location was unlikely since neither extreme was on the right-chest surface. In agreement with this interpretation, a second minimum appeared on the sternal area in one patient. This minimum indicated a normal right ventricular breakthrough and showed that pre-excitation did not involve the anterior wall of the right ventricle. In the other patient, there was no second minimum; this patient, however, exhibited a sequence of surface potentials indicating right bundle branch block, which usually prevents the appearance of the sternal minimum.

Type 5 (Fig. 32.20e). Type 5 was represented by a single subject. The potential minimum was located in the left axillary region and the maximum on the inferior part of the left anterior chest wall. This potential distribution indicated

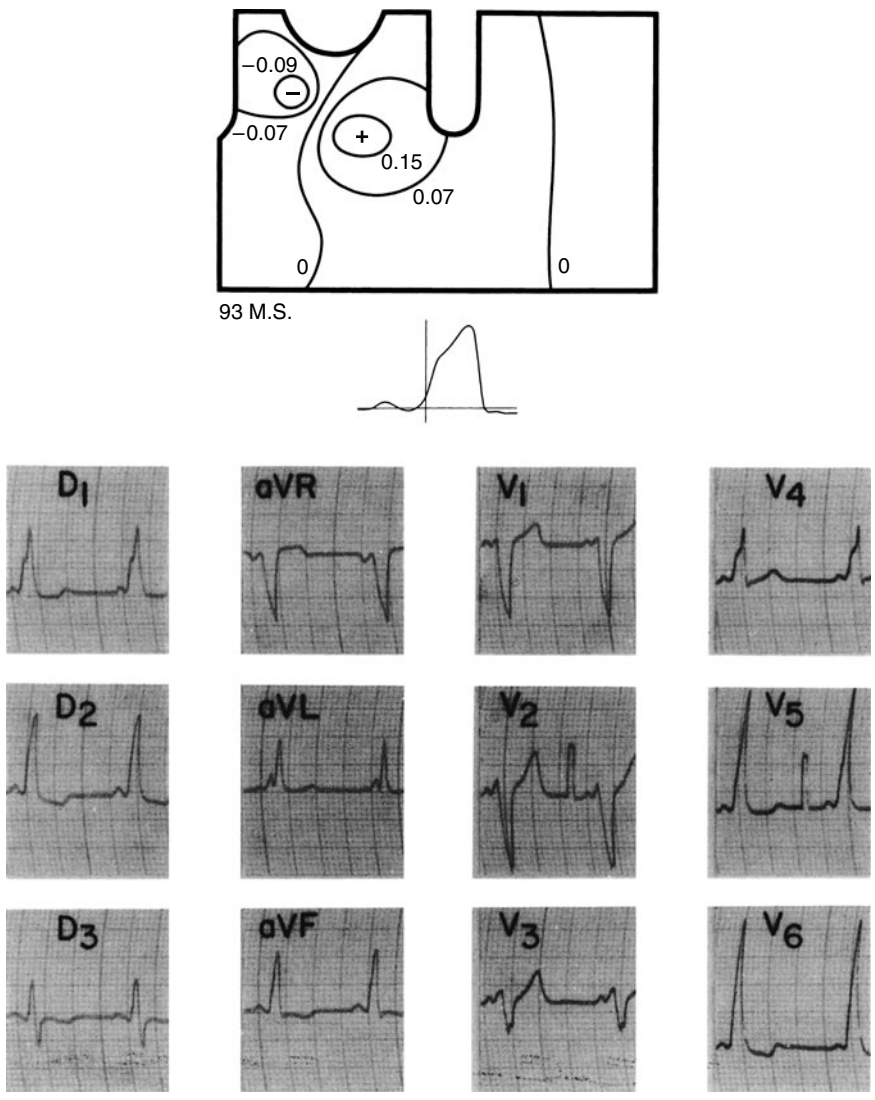

Figure 32.23

BSPM during the delta wave in a patient belonging to type 3. The ECG shows a type B WPW pattern. (After De Ambroggi et al. [96]. © American Heart Association, Dallas, Texas. Reproduced with permission.)

that pre-excitation most probably spreads through the left ventricular wall, starting from the anterolateral portion of the left AV groove and then moving downward and to the right.

Type 6 (Fig. 32.20f). Type 6 was also represented by a single patient. The ECG showed an unusual pattern of ventricular pre-excitation. A delta wave was not clearly detectable; a small Q wave was present in V1 and the QRS duration was within normal limits. Intracardiac recordings showed a short HV interval but during ajmaline administration, the Q wave in V1 disappeared and the HV interval rose from 15 to 40 ms. At the onset of ventricular excitation, the potential distribution was characterized by a minimum at the right lower sternal border and a maximum on the left scapular area. Twenty five minutes after the onset of ventricular activation, a normal sequence of potential patterns was observed. The initial location of the minimum and maximum indicated that an excitation wave was probably spreading in an antero-posterior direction, leftward and slightly superiorly. An acceptable location for such a wavefront might be in the right

side of the interventricular septum. The most likely mechanism for right septal pre-excitation would be through Mahaim fibers, stemming from the initial part of the right bundle branch.

In a number of patients belonging to types 1, 2, 3, 5, and 6, the site of pre-excitation as deduced from surface maps was in good agreement with that independently established using intracardiac recordings, epicardial maps, or surgical results [105].

Benson et al. [99] attempted to localize the site of pre-excitation in 49 WPW patients, where the location of the anomalous pathway was determined by intracardiac electrophysiological studies or surgical ablation. These authors were able to predict accurately at least seven pre-excitation sites on the basis of surface potential distribution during the QRS (at 40 ms after the onset of delta wave) and ST segment. Moreover, they found the potential distribution during early ST segment more useful than QRS maps for localizing the pre-excited area. Their classification was in reasonably good agreement with our classification previously presented.

Kamakura et al. [100] studied 41 WPW patients to determine the most reliable index for predicting the site of a single accessory pathway. They found that the location of the ventricular insertion of the accessory AV connection (determined at electrophysiological study or during surgery) is well estimated at the time the amplitude of the negative surface potential is −0.15 mV. On the basis of the chest position of the minimum with a potential of −0.15 mV, the location of the accessory AV connection was correctly predicted in 36 of 41 cases.

Liebman et al. [101] recorded BSPM in 34 patients with WPW syndrome in whom the site of ventricular insertion of the anomalous AV connection was localized by an electrophysiologic study and, in 18 cases, at surgery. Attempts were made to identify the 17 ventricular insertion sites along the AV grove described by Guiraudon et al. [106] mainly using QRS analysis (location of the initial minimum, occurrence of right ventricular breakthrough). The ventricular insertion sites determined by BSPM and EPS at surgery were identical or within one mapping site (i.e., 1.5 cm or less) in 14 of 18 cases; three of the four exceptions had more than one accessory AV connection, and the other had a very broad ventricular insertion. BSPM and EPS locations of accessory pathways correlated very well in the 34 cases despite the fact that BSPM determined the ventricular insertion and EPS the atrial insertion site of the accessory AV connection. BSPMs of QRS were very accurate in predicting the right ventricular versus left ventricular postero-septal AV connections, known to be particularly difficult at EPS in three of four surgical cases. Typical right ventricular breakthrough occurs in all patients with left ventricular free wall accessory connections, but was not observed in cases with right ventricular free wall or anteroseptal accessory AV connections.

In 1993, Dubuc et al. [102] reported on the use of BSPM to guide catheter ablation of accessory AV connection in 30 WPW patients. The catheter used for radiofrequency ablation was first placed in the vicinity of the ventricular pre-excitation site predicted by BSPMs previously recorded during the delta wave. BSPMs were then recorded during pacing with this catheter; the comparison between the pre-excited and paced BSPMs indicated whether the pacing site was too anterior or posterior with respect to the pre-excitation site, and the catheter was moved accordingly. This process was repeated until the pre-excited and paced BSPMs were almost identical, i.e., showed high correlation coefficient (>0.8) during the delta wave, and ablation was then attempted. In this way, it was possible to successfully ablate the accessory pathway in 93% of cases.

32.5.8 Arrhythmogenic Cardiopathies

32.5.8.1 Postinfarction Ventricular Tachycardias: Identification of Site of Origin of Ventricular Tachycardias

Extensive investigations were made by Sippens-Groenewegen et al. to assess the value of BSPMs in localizing the site of origin of ectopic ventricular activation in patients with a structurally normal heart and with myocardial infarction [107–109]. In patients with normal cardiac anatomy, the QRS maps allowed discrimination among 38 different LV and RV segments of ectopic endocardial impulse formation [107]. The use of 62 lead BSPMs instead of the 12-lead ECG during endocardial pace mapping technique enhanced the localization resolution of this technique and thus enabled more precise identification of the site of origin of postinfarction VT episodes [108].

In patients with previous anterior and inferior myocardial infarction, the same authors demonstrated that QRS integral maps enabled a precise localization of the origin of postinfarction ventricular tachycardia in 62% and regional

approximation (identification of a segment immediately adjacent to the actual endocardial segment of origin) in 30% of tachycardias [109].

More recently, McClelland et al [110] were able to compute epicardial potentials from BSPM (80 leads) using an inverse solution method. They were able to reconstruct in 5 patients epicardial isochronal maps demonstrating the exit site and the re-entry circuit of ventricular tachycardias.

32.5.8.2 Susceptibility to Ventricular Arrhythmias

Eigenvector analysis [111] was applied to QRST integral maps of two groups of patients with old myocardial infarction (11 patients with episodes of sustained ventricular tachycardia and 62 without arrhythmias) and in a control group of healthy subjects [112]. This method makes possible the detection and quantification of nondipolar components not evident on visual inspection of the integral maps. The cumulative contribution of the eigenvectors beyond the third to an individual map, expressed as percentage contribution of the total map content, has been considered a "nondipolar content" of that map. On average, the nondipolar content was significantly greater in patients with MI than in controls (8.3 ± 6.4% vs 4.1 ± 2.2%, $p < 0.001$) and, among patients, in those with ventricular tachycardia (7.2 ± 5.3% vs 16.6 ± 8.5%, $p < 0.001$). These findings were in agreement with those reported by Abildskov et al. [113]. Thus, the high nondipolar content of QRST maps in patients with ventricular tachycardia suggests the presence of local disparities of repolarization and it may be considered a useful marker of susceptibility to malignant arrhythmias.

Hubley-Kozey et al. [114] derived 16 eigenvectors from the total set of 204 QRST maps (102 patients with ventricular tachyarrhythmias and 102 patients without) but did not find a statistically significant difference in dipolar content between the two groups (13.1 ± 9.7 vs 12.9 ± 10.2%, $p > 0.05$). Because the nondipolar content did not perform well in their study population, the authors examined how individual eigenvector patterns contribute to QRST integral maps in each group of patients. Statistically significant differences were found between the values of Karhunen-Loeve coefficients in VT and non-VT groups for the 6th, 4th, 13th, 5th, 1st, 2nd, and 11th eigenvectors, in order of significance levels. Using stepwise discriminant analysis, they selected features subsets that best discriminated between the two groups. For an optimal set of eight spatial features, the sensitivity and specificity of the classifier for detecting patients with VT in 1,000 test sets were 90 ± 4% and 78 ± 6%, respectively. The authors concluded that the multiple body-surface ECGs contain valuable spatial features that can identify the presence of an arrhythmogenic substrate in the myocardium of patients at risk of ventricular arrhythmias.

Recently, Korhonen et al. [115] studied the complexity of T-wave morphology in BSPM of patients with recent myocardial infraction and cardiac dysfunction, by applying principal component analysis. They found that the 3rd principal component derived from BSPM was a significant predictor of arrhythmic events in this population.

32.5.8.3 BSPM and Ventricular Late Potentials

Vulnerability to arrhythmias has also been related to the existence of areas of delayed conduction at the end of the ventricular activation process. Ventricular late potentials recorded on signal-averaged ECG are the expression of this phenomenon. BSPM can be applied to detect these high-frequency, low-amplitude potentials [116, 117]. Maps not only made it possible to reveal the presence of late potentials, but also to determine the spatial distribution of late potentials in patients with ventricular tachycardia. Thus, BSPM may provide additional information about the thoracic location of ventricular late potentials, which can be related to the sites of conduction delay and possibly to the sites of origin of ventricular tachycardia.

32.5.8.4 Long QT Syndrome

BSPMs in patients with idiopathic long QT syndrome were described by De Ambroggi et al. [118]. No peculiar features were observed during the QRS interval, while the ventricular repolarization presented some abnormalities in addition to QT prolongation.

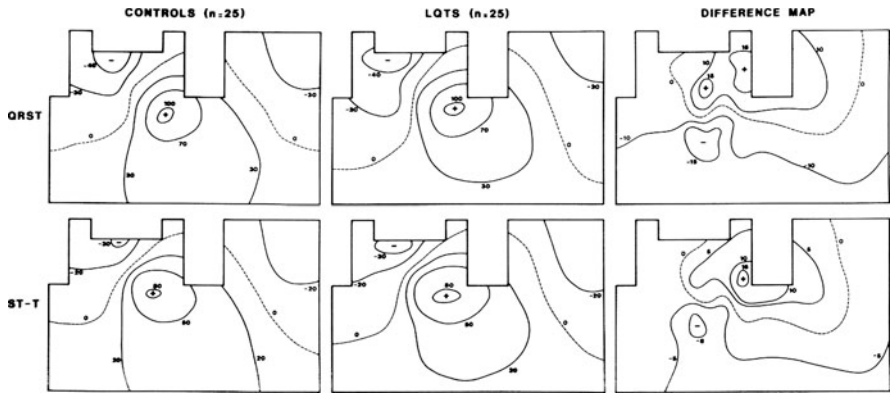

Figure 32.24

Mean integral maps of QRST and ST-T intervals in the control and LQTS groups. Difference maps are illustrated in the third column. Values are expressed in μVs. (After De Ambroggi et al. [118]. © American Heart Association, Dallas, Texas. Reproduced with permission.)

The visual inspection of instantaneous BSPMs revealed that the potential distributions were grossly abnormal (location of the potential extrema, presence of multiple peaks) in only a few cases. On the other hand, in most patients, BSPMs revealed less marked abnormalities in the instantaneous potential distribution. For instance, in several patients the negative potentials during the entire repolarization covered an area on the anterior thorax larger than in control subjects.

Differences between normals and LQTS patients were better quantified by analyzing ST-T and QRST integral maps. The mean integral map from the LQTS patients showed a potential distribution similar to that of the mean integral map from the control subjects. Nevertheless, the difference map (LQTS mean map minus control mean map) showed that LQTS patients had lower values on the inferior half of the trunk and on the right anterior thorax and higher values on the left anterior thorax compared with control subjects (Fig. 32.24). In 13 patients, the negative values covered almost entirely the right anterior thorax. In six patients, there was a multipeak distribution of the integral values. The prominent negative area on the anterior chest in LQTS patients could result from a delayed repolarization of the underlying anterior wall so that it remains electronegative longer than other cardiac regions. Moreover, the multipolar distribution may reflect local inequalities in recovery times. ST-T integral maps were substantially similar to QRST maps, but a multipolar distribution was observed in a few more patients.

Eigenvector analysis [111] was also applied to QRST and ST-T integral maps. As already mentioned, this method makes possible the detection and quantification of nondipolar components not evident on visual inspection of the integral maps. The percent contribution of nondipolar eigenvectors (all eigenvectors beyond the third) to maps was significantly higher in LQTS patients than in normals. Moreover, eight patients who had a high nondipolar content did not show a multipeak distribution on their integral maps. This demonstrates that eigenvector analysis can detect nondipolar components not evident on integral maps.

To identify markers of dispersion of the ventricular repolarization, in a subsequent investigation on 40 patients with LQTS [119], we applied principal component analysis to all the recorded ST-T waves in each subject studied. We defined the ratio between the information content of the first principal component and the total information of the original data as "similarity index." Actually, a high value of similarity index indicates a great similarity of all waveforms to one fundamental waveform, that is, a great similarity of all waves to each other. On the contrary, a low value of similarity index indicates a large variety of ST-T waves and is considered a marker of repolarization disparities. In the 40 patients affected by congenital LQTS [119], the mean value of the similarity index was significantly lower than in healthy control subjects (49 ± 10 vs $77 \pm 8\%$, $p < 0.0001$). A value lower than 61%, corresponding to two standard deviations below the mean value for controls, was found in 35 of 40 patients and in only one control subject (sensitivity 87%, specificity 96%). In our experience, the similarity index has proved to be a more sensitive marker than multipolar distribution of QRST integral maps in revealing electrical disparities of ventricular repolarization.

32.5.8.5 Arrhythmogenic Right Ventricular Cardiomyopathy

Characteristic features of BSPMs were described in patients with arrhythmogenic right ventricular cardiomyopathy (ARVC). De Ambroggi et al. studied 22 patients affected by ARVC, nine with episodes of sustained ventricular tachycardias (VT) and 13 without [120]. The QRST integral maps showed in most ARVC patients a larger than normal area of negative values on the right anterior thorax. This abnormal pattern could be explained by a delayed repolarization of the right ventricle. Nevertheless, it was not related to the occurrence of VT in our patient population. To detect minor heterogeneities of ventricular repolarization, the principal component analysis was applied to the 62 ST-T waves recorded in each subject. We assumed that a low value of the first or of the first three components (Co 1, 2, 3) indicates a greater than normal variety of the ST-T waves, a likely expression of a more complex recovery process. The mean values of the first three components were not significantly different in ARVC patients and in control subjects. Nevertheless, considering the two subsets of patients with and without VT, the values of Co 1, of Co 1 + 2, and of Co 1 + 2 + 3 were significantly lower in the group of ARVC patients with VT. Values of Co 1 < 69% (equal to one SD below the mean value for controls) were found in six of nine VT patients and in one patient without VT (sensitivity 67%, specificity 92%). A low value of Co 1 was the only variable significantly associated with the occurrence of VT.

QRST integral maps with an abnormal negative area on the anterior thorax were also observed by Peeters et al. [121] in eight out of eight patients with ARVC, but in only two of eight patients with idiopathic right ventricular tachycardia.

32.5.8.6 Brugada Syndrome

The Brugada syndrome is a familial, "primary" electrical disease of the heart due to gene mutations encoding for the sodium channel and is characterized by a delayed activation of the right ventricle, with a QRS complex resembling that of right bundle branch block in V1, early ST elevation (J wave) in the right precordial leads, normal QT duration, inducibility of ventricular tachycardia, and a high risk of sudden cardiac death [122].

ECG changes have been quantified by 120-lead BSPMs: the QRS integrals were higher over the upper-right precordium and lower than normal over the lower left precordium; steeper negative ST gradients compared to normal were present over the upper left precordium and more positive ST gradients compared to normal over the lower left precordium [123].

Early ST elevation ($\geqslant$0.2 mV) was observed on a variable area over the right precordium. If this area is larger than 50 cm^2, it has a 92% positive and a 62% negative predictive value for inducibility of ventricular tachycardia, but similar predictive power was found for ventricular late potentials in the same patients [124].

Amplitude of maximal ST elevation was also used to differentiate Brugada syndrome patients with inducible ventricular tachycardia from asymptomatic patients [125].

32.6 Conclusions

The most general advantage of BSPMs is the fact that they record cardiac potentials from broad areas of the chest, thus enabling the detection of significant physiologic and possibly diagnostic information outside the precordial regions usually explored. Moreover, BSPMs provide the spatial as well as the temporal and amplitude components of cardiac electrical activity, whereas the ECG scalar waveforms present only the voltage variation with time in a given site.

As reported in the previous pages, investigations by different authors so far published clearly demonstrated a higher diagnostic content of BSPMs, compared with conventional ECG, in various pathological conditions.

Nevertheless, a widespread or even limited clinical application beyond the research laboratories of BSPM has not occurred up to day for several reasons: (a) the recording and processing of large numbers of leads and the displaying of maps have been complex and time-consuming, (b) a completely automated instrumentation was not commercially available, (c) use of many lead systems in different laboratories, differing in the number and placement of leads, and (d) difficulty in interpreting BSPM. The last reason is probably the most important obstacle that hampers the clinical use of BSPM.

In recent years, some of these obstacles have been overcome. BSPM recording systems, even those not widely marketed, have been (and can) relatively easily be developed and produced by several laboratories. Today's computer facilities make the recording and the data analysis easier than in the past. The time for applying electrodes and for data acquisition and analysis has been reduced considerably. Procedures, which reduce the number of leads that are necessary for reconstructing surface maps without losing too much information, have also been proposed; among these, the 32-lead system of Lux is the most commonly used [126]. Moreover, methods for converting multilead ECGs from one lead system to another have been proposed and satisfactorily applied [10].

The problem of interpreting surface maps still remains; in general, it may be approached essentially in two ways. The first approach is based on statistical methods, that is, defining the normal variability range of a number of parameters derived from maps relating to healthy subjects of different age, sex, and body shape, and then comparing these parameters by means of multivariate statistical procedures with those recorded from patients. The second approach is "deterministic"; that is, it consists of establishing the relationships between the intracardiac current sources (i.e., number, shape, location, and motion of excitation wavefronts and sequence of repolarization) and surface potential distribution (i.e., number, location, and motion of potential maxima and minima). This can be made in different ways, by using physiological or mathematical models. For instance, the distribution of currents and potentials has been determined experimentally in conducting media surrounding isolated hearts [127] thus enabling epicardial potentials to be compared with potentials recorded at a distance from the heart. Intracardiac current sources of known location have been produced by simultaneously stimulating the heart at multiple sites [128]. This allowed surface potential patterns to be correlated with known distributions of generators. The relationships between epicardial and body-surface potentials during activation and recovery were studied in intact chimpanzees [129, 130] and mathematical procedures for solving the direct and inverse problem (i.e., calculating surface potentials from internal sources and vice versa) were proposed by different authors (see Chaps. 8 and 9).

In the intact dog, Spach et al. succeeded in calculating accurately body-surface potentials from epicardial potential distributions during activation and recovery [131]. As regards the inverse problem, epicardial potentials have been calculated from potential distributions at the body surface in dogs [132–137]. In this respect, particularly important are the studies of Rudy and coworkers. They demonstrated the ability to compute noninvasively epicardial potential distribution and epicardial activation sequences from measured surface potentials. They called this new electrocardiographic modality as "ECG imaging," which, of necessity, has to utilize BSPM recording. The ECG imaging has been successfully applied in humans [138–141], using geometrical information from computed tomography and a mathematical algorithm, in different situations including the normal heart, a heart with a conduction disorder (right bundle branch block), focal activation initiated by right or left ventricular pacing, focal atrial tachycardia and flutter. A simplified method of inverse solution, which adopts a general torso model in which the same anatomic data are used irrespective of the body habitus, was applied by McClelland et al [110]. Despite these limitations they were able to reconstruct epicardial potential or isochronal maps identifying the left ventricular pacing site or indicating the exit site and the re-entry circuit of ventricular tachycardias. Very recently improvements to the inverse solution method were made by A. van Oosterom and coworkers [142]. The required computation time and the quality of the results obtained should favour the applications of this inverse procedure in a clinical setting.

In addition to all the reasons discussed above, the lack of expansion in the clinical setting of BSPM, which indeed can be considered an "advanced electrocardiographic method," is partially due to the fact that electrocardiology in recent years has lost some of its importance compared with newer sophisticated imaging techniques. The anatomic and functional information on several heart conditions (e.g., hypertrophy, location and extension of myocardial infarction, and so on) that, in the past, was obtained with varying degrees of accuracy by means of electrocardiographic techniques, can be more precisely and directly obtained today by other techniques such as echocardiography, magnetic resonance, multislice computed tomography, and nuclear imaging. On the other hand, electrocardiology still has a unique, primary role in the field of arrhythmias and conduction disturbances, into which no other technique can provide relevant insights. In particular, ECG imaging, based on the solution of the "inverse problem," which is the final aim of electrocardiography, hopefully will be able in the near future to provide, noninvasively, information on the epicardial and intramural excitation and recovery processes. This could give the possibility of identifying, with sufficient accuracy, intramural heterogeneities, transmural re-entry and intramural focal arrhythmias, and of defining ischemic or necrotic areas within the myocardium. The future of body-surface potential maps should be in that direction.

References

1. Plonsey, R., *Bioelectric Phenomena*. New York: McGraw-Hill, 1969, pp. 202.
2. Colli Franzone, P., L. Guerri, C. Viganotti, et al., Potential fields generated by oblique dipole layers modeling excitation wavefronts in the anisotropic myocardium. Comparison with potential fields elicited by paced dog hearts in a volume conductor. *Circ. Res.*, 1982;**51**: 330–346.
3. Taccardi, B., E. Macchi, R.L. Lux, et al., Effect of myocardial fiber direction on epicardial potentials. *Circulation*, 1994;**90**: 3076–3090.
4. Yan, G.X. and C. Antzelevitch, Cellular basis for the normal T wave and the electrocardiographic manifestations of the long QT syndrome. *Circulation*, 1998;**98**: 1928–1936.
5. Antzelevitch, C., W. Shimitzu, G.X. Yan, et al., The M cells: its contribution to the ECG and to normal and abnormal electrical function of the heart. *J. Electrophysiol.*, 1999;**10**: 1124–1152.
6. Waller, A.D., On the electromotive changes connected with the beat of the mammalian heart and of the human heart in particular. *Philos. Trans. R. Soc. Lond. Ser. B*, 1889;**180**: 169–194.
7. Nahum, L.H., A. Mauro, H.M. Chernoff, and R.S. Sikand, Instantaneous equipotential distribution on surface of the human body for various instants in the cardiac cycle. *J. Appl. Physiol.*, 1951;**3**: 454–464.
8. Taccardi, B., Distribution of heart potentials on dog's thoracic surface. *Circ. Res.*, 1962;**11**: 862–869.
9. Taccardi, B., Distribution of heart potentials on the thoracic surface of normal human subjects. *Circ. Res.*, 1963;**12**: 341–352.
10. Hoekema, R., G.J.H Uijen, D. Stilli, and A. van Oosterom, Lead system transformation of body surface map data. *J. Electrocardiol.*, 1998;**31**: 71–82.
11. Abildskov, J.A., M.J. Burgess, P.M. Urie, R.L. Lux, and R.F. Wyatt, The unidentified information content of the electrocardiogram. *Circ. Res.*, 1977;**40**: 3–7.
12. Abildskov, J.A., M.J. Burgess, R.L. Lux, R.F. Wyatt, and G.M. Vincent, The expression of normal ventricular repolarization in the body surface distribution of T potentials. *Circulation*, 1976;**54**: 901–906.
13. Corlan, A.D., R.S. Macleod, and L. De Ambroggi, The effect of intrathoracic heart position on ECG autocorrelation maps. *J. Electrocardiol.*, 2005;**38**: 87–94.
14. Taccardi, B., Body surface distribution of equipotential lines during atrial depolarization and ventricular repolarization. *Circ. Res.*, 1966;**19**: 865–878.
15. Taccardi, B., L. De Ambroggi, and C. Viganotti, Body-surface mapping of heart potentials, in *The Theoretical Basis of Eleclrocardioiogy*, C.V. Nelson and D.B. Geselowitz, Editors. Oxford: Clarendon, 1976, pp. 436–466.
16. Mirvis, D.M., Body surface distribution of electrical potential during atrial depolarization and repolarization. *Circulation*, 1980;**62**: 167–173.
17. Spach, M.S., R.C. Ban, R. Warrcn, D.W. Benson, A. Walston, and S.H. Edwards, Isopotential body surface mapping in subjects of all ages: emphasis on low-level potentials with analysis of the method. *Circulation*, 1979: **59**: 805–821.
18. Spach, M.S., T.D. King, R.C., O.E. Barr Boaz, M.N. Morrow, and S. Hennan-Giddens, Electrical potential distribution surrounding the atria during depolarization and repolarization in the dog. *Circ. Res.*, 1969;**24**: 857–873.
19. Eddlemon, C.O., V.J. Rucsta, L.G. Horan, and D.A. Brody, Distribution of heart potentials on the body surface in five normal young men. *Am. J. Cardiol.*, 1968;**21**: 860–870.
20. Young, B.D., P.W. Macfarlane, and T.D.V. Lawrie, Normal thoracic surface potentials. *Cardiovasc. Res.*, 1974;**8**: 187–193.
21. Green, L.S., R.L. Lux, C.W. Haws, R.R. Williams, S.C. Hunt, and M.J. Burgess, Effects of age, sex, and body habitus on QRS and ST- T potential maps of 1100 normal subjects. *Circulation*, 1985;**71**: 244–253.
22. Spach, M.S., W.P. Silberberg, J.P. Boineau, et al., Body surface isopotential maps in normal children, ages 4 to 14 years. *Am. Heart. J.*, 1966;**72**: 640–652.
23. Liebman, J., C.W. Thomas, Y. Rudy, and R. Plonsey, Electrocardiographic body surface potential maps of the QRS of normal children. *J. Electrocardiol.*, 1981: **14**: 249–260.
24. Tazawa, H and C. Yoshimoto, Electrocardiographic potential distribution in newborn infants from 12 hours to 8 days after birth. *Am. Heart. J.*, 1969;**78**: 292–305.
25. Benson, D.W. Jr. and M.S. Spach, Evolution of QRS and ST-T-wave body surface potential distributions during the first year of life. *Circulation*, 1982;**65**: 1247–1258.
26. Durrer, D., R.Th van Dam, G.E. Freud, M.J. Janse, F.L. Meijler, and R.C. Arzbaecher, Total excitation of the isolated human heart. *Circulation*, 1970;**41**: 899–912.
27. Wyndham, C.R., M.K. Meeran, T. Smith, et al., Epicardial activation of the intact human heart without conduction defect. *Circulation*, 1979;**59**: 161–168.
28. Green, L.S., R.L. Lux, D. Stilli, C.W. Haws, and B. Taccardi, Fine details in body surface potential maps: accuracy of maps using a limited lead array and spatial and temporal data representation. *J. Eleclrocardiol.*, 1987;**20**: 21–26.
29. Hoekema, R., G.J. Uijen, and A. Van Oosterom, Geometrical aspects of the interindividual variability of multilead ECG recordings. *IEEE Trans. Biomed. Eng.*, 2001;**48**: 551–559.
30. Kozmann G, R.L. Lux, and L.S. Green, Sources of variability in normal body surface potential maps. *Circulation*, 1989;**79**: 1077–1083.
31. Montague, T.J., E.R. Smith, D.A. Cameron, et al., Isointegral analysis of body surface maps: surface distribution and temporal variability in normal subjects. *Circulation*, 1981;**63**: 1166–1172.
32. Flaherty, J.T., S.D. Blumenschein, A.W. Alexander, et al., Influence of respiration on recording cardiac potentials. Isopotential surface-mapping and vectorcardiographic study. *Am. J. Cardiol.*, 1967;**20**: 21–28.
33. Spach, M.S., R.C. Barr, D.W. Benson, A.H. Walston, R.B. Warren, and S.B. Edwards, Body surface low-level potentials during ventricular repolarization with analysis of the ST segment. Variability in normal subjects. *Circulation*, 1979;**59**: 822–36.
34. Corlan, A.D., P.W. Macfarlane, and L. De Ambroggi, Gender differences in stability of the instantaneous patterns of body surface potentials during ventricular repolarisation. *Med. Biol. Eng. Comput.*, 2003;**41**: 536–542.
35. Abildskov, J.A., A.K. Evans, R.L. Lux, and M.J. Burgess Ventricular recovery properties and QRST deflection area in cardiac electrograms. *Am. J. Physiol.*, 1981;**239**: H227–231.

36. Sano, T., Y. Sakamoto, M. Yamamoto, and F. Suzuki, The body surface U wave potentials, in *Progress in Electrocardiology*, P.W. Macfarlane, Editor. Tunbridge Wells: Pitman Medical, 1979, pp. 227–231.
37. L. De Ambroggi, E. Locati, T. Bertoni, E. Monza, and P.J. Schwartz, Body surface potentials during T-U interval in patients with the idiopathic long QT syndrome, in *Clinical Aspects of Ventricular Repolarization*, chapter 47, G.S. Butrous and P.J. Schwartz, Editors. London: Farrand Press, 1989, pp. 433–436.
38. L. De Ambroggi, M. Besozzi, and B. Taccardi, Aspetti qualitativi e quantitativi delle elettromappe cardiache nell'infarto miocardico anteriore e inferiore. *G. Ital. Cardiol.*, 1974;**4**: 540–553.
39. L. De Ambroggi, T. Bertoni, C. Rabbia, and M. Landolina, Body surface potential maps in old inferior myocardial infarction. Assessment of diagnostic criteria. *J. Electrocardiol.*, 1986;**19**: 225–234.
40. L. De Ambroggi, T. Bertoni, M.L. Breghi, M. Marconi, and M. Mosca, Diagnostic value of body surface potential mapping in old anterior non-Q myocardial infarction. *J. Electrocardiol.*, 1988;**21**: 321–329.
41. Flowers, N.C., L.G. Horan, and J.C. Johnson, Anterior infarctional changes occurring during mid and late ventricular activation detectable by surface mapping techniques. *Circulation*, 1976;**54**: 906–913.
42. Flowers, N.C., L.G. Horan, G.S. Sohi, R.C. Hand, and J.C. Johnson, New evidence for infero-posterior myocardial infarction on surface potential maps. *Am. J. Cardiol.*, 1976;**38**: 576–581.
43. Vincent, G.M., J.A. Abildskov, M.J. Burgess, K. Millar, R.L. Lux, and R.F. Wyatt, Diagnosis of old inferior myocardial infarction by body surface isopotential mapping. *Am. J. Cardiol.*, 1977;**39**: 510–515.
44. H. Pham-Huy, R.M. Gulrajani, F.A. Roberge, R.A. Nadeau, G.E. Mailloux, and P. Savard, A comparative evaluation of three different approaches for detecting body surface isopotential map abnormalities in patients with myocardial infarction. *J. Electrocardiol.*, 1981;**14**: 43–55.
45. Toyama, S., K. Suzuki, M. Koyama, K. Yoshino, and K. Fujimolo, The body surface isopotential mapping of the QRS wave in myocardial infarction: comparative study of the scintigram with thallium-201. *J. Electrocardiol.*, 1982;**15**: 241–247.
46. Ohta, T., A. Kinoshita, J. Ohsugi, et al., Correlation between body surface isopotential maps and left ventriculograms in patients with old inferoposterior myocardial infarction. *Am. Heart J.*, 1982;**104**: 1262–1270.
47. Osugi, J. T. Ohta, J. Toyama, F. Takatsu, T. Nagaya, and K. Yamada, Body surface isopotential maps in old inferior myocardial infarction undetectable by 12 lead electrocardiogram. *J. Electrocardiol.*, 1984;**17**: 55–62.
48. Hirai, M., T. Ohta, A. Kinoshita, J. Toyama, T. Nagaya, and K. Yamada, Body surface isopotential maps in old anterior myocardial infarction undetectable by 12-lead electrocardiograms. *Am. Heart J.*, 1984;**108**: 975–982.
49. Kubota, I., M. Yamaki, K Ikeda, I. Yamaguchi, I. Tonooka, K. Tsuiki, and S. Yasui, Abnormalities of early depolarization in patients with remote anterior myocardial infarction and ventricular septal hypoperfusion. Diagnosis of septal MI BSM. *J. Electrocardiol.*, 1990;**23**: 307–313.
50. Hayashi, H., M. Hirai, A. Suzuki, et al., Correlation between various parameters derived from body surface maps and ejection fraction in patients with anterior myocardial infarction. *J. Electrocardiol.*, 1993;**26**: 17–24.
51. Suzuki, A., M. Hirai., H. Hayashi, et al. The ability of QRST isointegral maps to detect myocardial infarction in the presence of simulated left bundle branch block. *Eur. Heart J.*, 1993;**14**: 1094–1101.
52. Medvegy, M., I. Preda, P. Savard, et al., A new body surface isopotential map evaluation method to detect minor potential losses in non-Q wave myocardial infarction. *Circulation*, 2000;**101**: 1115–1121.
53. Medvegy, M., P. Savard, A. Pinter, et al., Simple, quantitative body surface potential map parameters in the diagnosis of remote Q wave and non-Q wave myocardial infarction. *Can. J. Cardiol.*, 2004;**20**: 1109–1115.
54. Corlan, A.D. and L. De Ambroggi, New quantitative methods of ventricular repolarization analysis in patients with left ventricular hypertrophy. *Ital. Heart J.*, 2000;**1**: 542–548.
55. Corlan, A.D., B.M. Horacek, and L. De Ambroggi, Prognostic value for ventricular tachicardia of indices of ventricular repolarization in patients with and without myocardial infarction. 32nd Congress of International Society of Electrocardiology. *Folia Cardiol.*, 2005;12(Suppl C): 52.
56. Muller, J.E., P.R. Maroko, and E. Braunwald, Precordial electrocardiographic mapping. A technique to assess the efficacy of interventions designed to limit infarct size. *Circulation*, 1978;**57**: 1–18.
57. Maroko, P.R., P. Libby, J.W. Covell, B.E. So bel, J. Ross Jr, and E. Braunwald, Precordial S-T segment elevation mapping. An atraumatic method for assessing alterations in the extent of myocardial ischemic injury. *Am. J. Cardiol.*, 1972;**29**: 223–230.
58. Muller, J.E., P.R. Maroko, and E. Braunwald, Evaluation of precordial electrocardiographic mapping as a means of assessing changes in myocardial ischemic injury. *Circulation*, 1975;**52**: 16–27.
59. Holland, R.P. and H. Brooks, TQ-ST segment mapping: critical review and analysis of current concepts. *Am. J. Cardiol.*, 1977;**40** 110–129.
60. Surawicz, S., The disputed S-T segment mapping: is the technique ready for wide application in practice? *Am. J. Cardiol.*, 1977;**40**: 137–140.
61. Mirvis, D.M., Body surface distributions of repolarization forces during acute myocardial infarction. I. Isopotential and isoarea mapping. *Circulation*, 1980: **62**: 878–887.
62. Montague, T.J., E.R. Smith, C.A. Spencer, et al., Body surface electrocardiographic mapping in inferior myocardial infarction. Manifestation of left and right ventricular involvement. *Circulation*, 1983: **67**: 665–673.
63. Menown, I.B.A., J. Allen, J. McC Anderson, and A.A.J. Adgey, Early diagnosis of right ventricular or posterior infarction associated with inferior wall left ventricular acute myocardial infarction. *Am. J. Cardiol.*, 2000;**85**: 934–938.
64. McClelland, A.J.J., C.G. Owens, I.B. Menown, M. Lown, and A.A. Adgey, Comparison of 80-lead body surface map to physician and to 12-lead electrocardiogram in detection of acute myocardial infarction. *Am. J. Cardiol.*, 2003;**92**: 252–257.
65. Maynard, S.J., I.B. Menown, G. Manoharan, J. Allen, J. McC Anderson, and A.A. Adgey, Body surface mapping improves early diagnosis of acute myocardial infarction in patients with chest pain and left bundle branch block. *Heart*, 2003;**89**: 998–1002.

66. De Ambroggi, L., E. Macchi, B. Brusoni, and B. Taccardi, Electromaps during ventricular recovery in angina patients with normal resting ECG. *Adv. Cardiol*., 1977;**19**: 88–90.
67. Stilli, D., E. Musso, E. Macchi, et al., Body surface potential mapping in ischemic patients with normal resting ECG. *Can. J. Cardiol*., 1986;Suppl A: 107–112A.
68. Kornreich, F., P. Block P, and D. Brismee, The missing waveform information in the orthogonal electrocardiogram (Frank leads). Ill. Computer diagnosis of angina pectoris from "maximal" QRS surface waveform information at rest. *Circulation*, 1974;**49**: 1212–1222.
69. Spekhorst, H., A. Sippens-Groenewegen, G.K. David, M.J. Janse, and A.J. Dunning, Body surface mapping during percutaneous transluminal coronary angioplasty. QRS changes indicating regional myocardial conduction delay. *Circulation*, 1990;**81**: 840–849.
70. Shenasa, M., D. Hamel, J. Nasmith, et al., Body surface potential mapping of ST segment shift in patient undergoing percutaneous transluminal coronary angioplasty. *J. Electrocardiol*., 1993;**26**: 43–51.
71. Cahyadi, Y.H., N. Takekoshi, and S. Matsui, Clinical efficacy of PTCA and identification of restenosis: evaluation by serial body surface potential mapping. *Am. Heart J*., 1991;**121**: 1080–1087.
72. Fox, K.M., A.P. Selwyn, and J.P.A. Shillingford, method for precordial surface mapping of the exercise electrocardiogram. *Br. Heart J*., 1978: 40: 1339–1343.
73. Fox, K., A. Selwyn, and J. Shillingford, Precordial electrocardiographic mapping after exercise in the diagnosis of coronary artery disease. *Am. J. Cardiol*., 1979;**43**: 541–546.
74. Mirvis, D.M., F.W. Keller Jr., J.W. Cox Jr., D.G. Zetlergren, R.F. Dowdie, and R.E. Ideker, Left precordial isopotential mapping during supine exercise. *Circulation*, 1977;**56**: 245–252.
75. Mirvis, D.M., Body surface distribution of exercise-induced QRS changes in normal subjects. *Am. J. Cardiol*., 1980: **46** 988–996.
76. Miller, W.T. III, M.S. Spach, and R.B. Warren, Total body surface potential mapping during exercise: QRS- T-wave changes in normal young adults. *Circulation*, 1980;**62**: 632–645.
77. Simoons, M.L. and P. Block, Toward the optimal lead system and optimal criteria for exercise electrocardiography. *Am. J. Cardiol*., 1981;**47**: 1366–1374.
78. Wada, M., K. Kaneko, H. Teshigawara, et al., Exercise stress body surface isopotential map in patients with coronary artery disease: comparison with coronary angiographic and stress myocardial perfusion scintigraphic findings. *Jpn. Circ. J*., 1981;**45**: 1203–1207.
79. Yanowitz, F.G., G.M. Vincent, R.L. Lux, M. Merchant, L.S. Green, and J.A. Abildskov, Application of body surface mapping to exercise testing: S-T80 isoarea maps in patients with coronary artery disease. *Am. J. Cardiol*., 1982;**50**: 1109–1113.
80. Blumenschein, S.D., M.S. Spach, J.P. Boineau, et al., Genesis of body surface potentials in varying types of right ventricular hypertrophy. *Circulation*, 1968;**38**: 917–932.
81. Sohi, G.S., E.W. Green, N.C. Flowers, O.F. McMartin, and R.R. Masdcn, Body surface potential maps in patients with pulmonic valvular and aortic valvular stenosis of mild to moderate severity. *Circulation*, 1979;**59**: 1277–1283.
82. Holt, J.H. Jr, A.C.L. Barnard, and J.O. Kramer Jr., Multiple dipole electrocardiography: a comparison of electrically and angiographically determined left ventricular masses. *Circulation*, 1978;**57**: 1129–1133.
83. Yamaki, M., K. Ikeda, I. Kubota, K. Nakamura, K. Hanashima, K. Tsuiki, and S. Yasui, Improved diagnostic performance on the severity of left ventricular hypertrophy with body surface mapping. *Circulation*, 1989;**79**: 312–323.
84. Kornreich, F., T.J. Montague, P.M. Rautahariu, M. Kavadias, M.B. Horacek, and B. Taccardi, Diagnostic body surface potential map patterns in left ventricular hypertrophy during PQRST. *Am. J. Cardiol*., 1989;**63**: 610–617.
85. Hirai, M., H. Hayashi, Y. Ichihara, et al., Body surface distribution of abnormally low QRST areas in patients with left ventricular hypertrophy. An index of repolarization abnormalities. *Circulation*, 1991;**84**: 1505–1515.
86. Taccardi, B., L. De Ambroggi, and D. Riva, Chest maps of heart potentials in right bundle branch block. *J. Electrocardiol*., 1969;**2**: 109–116.
87. Sugenoya, J., S. Sugiyama, M. Wada, N. Niimi, H. Oguri, J. Toyama, and K. Yamada, Body surface potential distribution following the production of right bundle branch block in dogs: effects of breakthrough and right ventricular excitation on the body surface potentials. *Circulation*, 1977;**55**: 49–54.
88. Sugenoya, J., Interpretation of the body surface isopotential maps of patients with right bundle branch block. Determination of the region of the delayed activation within the right ventricle. *Jpn. Heart J*., 1978;**19**: 12–27.
89. Preda, I., I. Bukosza, G. Kozmann, Y.V. Shakin, A. Szèkely, and Z. Antalòczy, Surface potential distribution on the human thoracic surface in the left bundle branch block. *Jpn. Heart J*., 1979;**20**: 7–21.
90. Musso, E., D. Stilli, E. Macchi, et al., Body surface maps in left bundle branch block uncomplicated or complicated by myocardial infarction, left ventricular hypertrophy or myocardial ischemia. *J. Electrocardiol*., 1987;**20**: 1–20.
91. Sohi, G.S., N.C. Flowers, L.G. Boran, M.R. Sridharan, and J.C. Johnson, Comparison of total body surface map depolarization patterns of left bundle branch block and normal axis with left bundle branch block and left axis deviation. *Circulation*, 1983;**67**: 660–664.
92. Preda, I., Z. Antaloczy, I. Bukosza, G. Kozmann, and A. Szckely, New elcctrocardiological infarct criteria in the presence of left bundle branch block (surface mapping study), in *Progress in Electrocardiology*, P.W. Macfarlane, Editor. Tunbridge Wells: Pitman Medical, 1979, pp. 231–235.
93. Gallagher, J.J., A.R. Ticzon, A.G. Wallace, and J. Kasell, Activation studies following experimental hemiblock in the dog. *Circ. Res*., 1974;**35**: 752–763.
94. Sohi, G.S. and N.C. Flowers, Effects of left anterior fascicular block on the depolarization process as depicted by total body surface mapping. *J. Electrocardiol*., 1980: **13**: 143–152.
95. Yamada, K., J. Toyama, M. Wada, et al., Body surface isopotential mapping in Wolff-Parkinson-White syndrome. Noninvasive method to determine the location of the accessory atrioventricular pathway. *Am. Heart J*., 1975;**90**: 721–734.
96. De Ambroggi, L., B. Taccardi, and E. Macchi, Body-surface maps of heart potentials. Tentative localization of pre-excited areas in forty-two Wolff-Parkinson-White patients. *Circulation*, 1976;**54**: 251–263.
97. Spach, M.S., R.C. Ban, and C.F. Lanning, Experimental basis for QRS and T wave potentials in the WPW syndrome. The relation of epicardial to body surface potential distributions in the intact chimpanzee. *Circ. Res*., 1978;**42**: 103–118.

98. Iwa, T. and T. Magara, Correlation between localization of accessory conduction pathway and body surface maps in the Wolff-Parkinson. While syndrome. *Jpn. Circ. J.*, 1981;**45**: 1192–1198.
99. Benson, D.W. Jr., R. Sterba, J.J. Gallagher, A. Walston II, and M.S. Spach, Localization of the site of ventricular preexcitation with body surface maps in patients with Wolff-Parkinson-White: syndrome. *Circulation*, 1982;**65**: 1259–1268.
100. Kamakura, S., K. Shimomura, T. Ohe, M. Matsuhisa, and H. Yoyoshima, The role of initial minimum potential on body surface maps in predicting the site of accessory pathways in patients with Wolff-Parkinson-White syndrome. *Circulation*, 1986;**74**: 89–96.
101. Liebman, J., J.A. Zeno, B. Olshansky, et al., Electrocardiographic body surface potential mapping in the Wolff-Parkinson-White syndrome. Noninvasive determination of the ventricular insertion sites of accessory atrioventricular connections. *Circulation*, 1991;**83**: 886–901.
102. Dubuc, M., R. Nadeau, G. Tremblay, T. Kus, F. Molin, and P. Savard, Pace mapping using body surface potential maps to guide catheter ablation of accessory pathways in patients with Wolff-Parkinson-White syndrome. *Circulation*, 1993;**87**: 135–143.
103. Frank, E., Electric potential produced by two point current sources in a homogeneous conducting sphere. *J. Appl. Physiol.*, 1952;**23**: 1225–1228.
104. De Ambroggi, L. and B. Taccardi, Current and potential fields generated by two dipoles. *Circ. Res.*, 1970;**27**: 901–911.
105. Knippel, M., D. Pioselli, F. Rovelli, L. Campolo, E. Panzeri, and A. Pellegrini, Tachicardie ribelli nella sindrome da preeccitazione: trattamento chirurgico di cinque casi. *G. Ital. Cardiol.*, 1974;**4**: 657.
106. Guiraudon G.M., G.J. Klein, S. Gulamhusein, et al., Surgery for Wolff-Parkinson-White syndrome: further experience with epicardial approach. *Circulation*, 1986;**74**: 525–529.
107. Sippens-Groenewegen, A., H. Spekhorst, N.M. van Hemel, et al., Body surface mapping of ectopic left and right ventricular activation. QRS spectrum in patients without structural heart disease. *Circulation*, 1990;**82**: 879–896.
108. Sippens-Groenewegen, A., H. Spekhorst, N.M. van Hemel, et al., Localization of the site of origin of postinfarction ventricular tachycardia by endocardial pace mapping. Body surface mapping compared with the 12-lead electrocardiogram. *Circulation*, 1993;**88**: 2290–2306.
109. Sippens-Groenewegen, A, H. Spekhorst, N.M. van Hemel, et al., Value of body surface mapping in localizing the site of origin of ventricular tachycardia in patients with previous myocardial infarction. *J. Am. Coll. Cardiol.*, 1994;**24**: 1708–1724.
110. McClelland, A.J.J., C.G. Owens, C. Navarro, B. Smith, M.J.D. Roberts, J. Anderson, and A.A.J. Adgey, Usefulness of body surface maps to demonstrate ventricular activation patterns during left ventricular pacing and reentrant activation during ventricular tachycardia in men with coronary heart disease and left ventricular dysfunction. *Am J Cardiol* 2006;**98**: 591–596.
111. Lux, R.L., A.K. Evans, M.J. Burgess, R.F. Wyatt, and J.A. Abildskov, Redundancy reduction for improved display and analysis of body surface potential maps. I. Spatial compression. *Circ. Res.*, 1981;**49**: 186–196.
112. Bertoni, T., M.L. Breghi, M. Marconi, G. Bonifaccio, and L. De Ambroggi, Usefulness of the QRST integral maps to detect vulnerability to malignant arrhythmias in patients with old myocardial infarction, in *Electrocardiology '87*, E. Schubert, Editor. Berlin: Akademie-Verlag, 1988, pp. 247–250.
113. Abildskow, J.A., L.S. Green, and R.L. Lux, Detection of disparate ventricular repolarization by means of the body surface electrocardiogram, in*Cardiac Electrophysiology and Arrhythmias*, D.P. Zipes and J. Jalife, Editors. Orlando: Grune & Stratton, 1985, pp. 495–499.
114. Hubley-Kozey, C.L., B.L. Mitchell, M.J. Gardner, J.W. Warren, C.J. Penney, E.R. Smith, and B.M. Horacek, Spatial features in body-surface potential maps can identify patients with a history of sustained ventricular tachycardia. *Circulation*, 1995;**92**: 1825–1838.
115. Korhonen, P., T. Husa, T. Konttila, I. Tierala, M. Makijarvi, H. Vaananen, and L. Toivonen, Complex T-wave morphology in body surface mapping in prediction of arrhythmic events in patients with acute myocardial infarction and cardiac dysfunction. *Europace* 2009;**11**: 514–520.
116. Faugère, G., P. Savard, R.A. Nadeau, D. Derome, M. Shenasa, P.L. Page, and R. Guardo, Characterization of the spatial distribution of late ventricular potentials by body surface mapping in patients with ventricular tachycardia. *Circulation*, 1986;**74**: 1323–1333.
117. Shibata, T., I. Kubota, K. Ikeda, K. Tsuiki, and S. Yasui, Body surface mapping of high-frequency components in the terminal portion during QRS complex for the prediction of ventricular tachycardia in patients with previous myocardial infarction. *Circulation*, 1990;**82**: 2084–2092.
118. De Ambroggi, L., T. Bertoni, E. Locati, M. Stramba-Badiale, and P.J. Schwartz, Mapping of body surface potentials in patients with the idiopathic long QT syndrome. *Circulation*, 1986;**74**: 1334–1345.
119. De Ambroggi, L., M.S. Negroni, E. Monza, T. Bertoni, and P.J. Schwartz, Dispersion of ventricular repolarization in the long QT syndrome. *Am. J. Cardiol.*, 1991;**68**: 614–620.
120. De Ambroggi, L., E. Aimè, C. Ceriotti, M. Rovida, and S. Negroni, Mapping of ventricular repolarization potentials in patients with arrhythmogenic right ventricular dysplasia: principal component analysis of the ST-T waves. *Circulation*, 1997;**96**: 4314–4318.
121. Peeters, H.A., A. SippensGroenewegen, B.A. Schoonderwoerd, E.F. Wever, C.A. Grimbergen, R.N. Hauer, and E.O. Rohles de Medina, Body-surface QRST integral mapping. Arrhythmogenic right ventricular dysplasia versus idiopathic right ventricular tachycardia. *Circulation*, 1997;**95**: 2668–2676.
122. Antzelevitch, C., P. Brugada, M. Borggrefe, et al., Brugada syndrome: report of the second consensus conference. *Circulation*, 2005;**111**: 659–670.
123. Bruns, H.J., L. Eckardt, C. Vahlhaus, E. Schulze-Bahr, W. Haverkamp, M. Borggrefe, G. Breithardt, and T. Wichter, Body surface potential mapping in patients with Brugada syndrome: right precordial ST segment variations and reverse changes in left precordial leads. *Cardiovasc. Res.*, 2002;**54**: 58–66.
124. Eckardt, L., H.J. Bruns, M. Paul, P. Kirchhof, E. Schulze-Bahr, T. Wichter, G. Breithardt, M. Borggrefe, and W. Haverkamp, Body surface area of ST elevation and the presence of late potentials correlate to the inducibility of ventricular tachyarrhythmias in Brugada syndrome. *J. Cardiovasc. Electrophysiol.*, 2002;**13**: 742–749.
125. Hisamatsu, K., K.F. Kusano, H. Morita, S. Takenaka, S. Nagase, K. Nakamura, T. Emori, H. Matsubara, and T. Ohe, Usefulness of body surface mapping to differentiate patients with Brugada

syndrome from patients with asymptomatic Brugada syndrome. *Acta Med. Okayama*, 2004;**58**: 29–35.

126. Lux, R.L., C.R. Smith, R.F. Wyatt, and J.A. Abildskov, Limited lead selection for estimation of body surface potential maps in electrocardiography. *IEEE Trans. Biomed. Eng.*, 1978;**25**: 270–276.
127. Taccardi, B., C. Viganotti, E. Macchi, and L. De Ambroggi, Relationships between the current field surrounding an isolated dog heart and the potential distribution on the surface of the body. *Adv. Cardiol.*, 1976;**16**: 72–76.
128. Abildskov, J.A., M.J. Burgess, K. Millar, G.M. Vincent, R.F. Wyatt, and R.L. Lux, Distribution of body surface potentials with experimentally-induced multiple cardiac generators. *Adv. Cardiol.*, 1974;**10**: 69–76.
129. Spach, M.S., R.C. Barr, C.F. Lanning, and P.C. Tucek, Origin of body surface QRS and T wave potentials from epicardial potential distributions in the intact chimpanzee. *Circulation*, 1977;**55**: 268–278.
130. Spach, M.S., R.C. Barr, and C.F. Lanning, Experimental basis for QRS and T wave potentials in the WPW syndrome. The relation of epicardial to body surface potential distributions in the intact chimpanzee. *Circ. Res.*, 1978;**42**: 103–118.
131. Ramsey, M. III, R.C. Barr, and M.S. Spach, Comparison of measured torso potentials with those simulated from epicardial potentials for ventricular depolarization and repolarization in the intact dog. *Circ. Res.*, 1977;41: 660–672.
132. Barr, R.C. and M.S. Spach, Inverse calculation of QRS-T epicardial potentials from body surface potential distributions for normal and ectopic beats in the intact dog. *Circ. Res.*, 1978;**42**: 661–675.
133. Colli Franzone, P., L. Guerri, B. Taccardi, and C. Viganotti, A regularization method for inverse electrocardiology applied to data from an isolated dog heart experiment, in *Modern Electrocardiology*, Z. Antaloczy, Editor. Amsterdam: Excerpta Medica, 1978, pp. 75–80.
134. Oster, H.S., B. Taccardi, R.L. Lux, P.H. Ershler, and Y. Rudy, Noninvasive electrocardiographic imaging. Reconstruction of epicardial potentials, electrograms, and isochrones and localization of single and multiple electrocardiac events. *Circulation*, 1997;**96**: 1012–1024.
135. Burnes, J.E., B. Taccardi, and Y. Rudy, A Noninvasive electrocardiographic imaging modality for cardiac arrhythmias. *Circulation*, 2000;**102**: 2151–2158.
136. Burnes, J.E., B. Taccardi, P.H. Ershler, and Y. Rudy, Noninvasive electrocardiographic imaging of substrate and intramural ventricular tachycardia in infarcted hearts. *J. Am. Coll. Cardiol.*, 2001;**38**: 2071–2078.
137. Ghanem, R.N., J.E. Burnes, A.L. Waldo, and Y. Rudy, Imaging dispersion of myocardial repolarization, II. Noninvasive reconstruction of epicardial measures. *Circulation*, 2001;**104**: 1306–1312.
138. Ramanatham, C., R.N. Ghanem, P. Jia, K. Ryu, and Y. Rudy, Noninvasive electrocardiographic imaging for cardiac electrophysiology and arrhythmias. *Nat. Med.*, 2004;**10**: 422–428.
139. Ghanem, R.N., P. Jia, C. Ramanatham, K. Ryu, A. Markowitz, and Y. Rudy, Noninvasive electrocardiographic imaging (ECGI): comparison to intraoperative mapping in patients. *Heart Rhythm*, 2005;**2**: 339–354.
140. Intini, A., R.N. Goldstein, P. Jia, C. Ramanathan, K. Ryu, B. Giannattasio, R. Gilkeson, B.S. Stambler, P. Brugada, W.G. Stevenson, Y. Rudy, and A.L. Waldo, Electrocardiographic imaging (ECGI), a novel diagnostic modality used for mapping of focal left ventricular tachycardia in a young athlete. *Heart Rhythm*. 2005;**2**: 1250–1252.
141. Wang, Y., P.S. Cuculich, P.K. Woodard, B.D. Lindsay, and Y. Rudy, Focal atrial tachycardia after pulmonary vein isolation: Noninvasive mapping with electrocardiographic imaging (ECGI). *Heart Rhythm* 2007;**4**: 1081–1084.
142. Van Dam, P.M., T.F. Oostendorp, A.C. Linnenbank, and A. van Oosterom, Non-invasive imaging of cardiac activation and recovery. *Ann Biomed Eng* 2009;**37**: 1739–1756.

Section 8

Specialized Aspects of Electrocardiography Part 1

33 Ambulatory Electrocardiogram Monitoring

V. Hombach

P. W. Macfarlane, A. van Oosterom, O. Pahlm, P. Kligfield, M. Janse, J. Camm (eds.), *Comprehensive Electrocardiology*, DOI 10.1007/978-1-84882-046-3_33,

Abbreviations

AAD = Antiarrhythmic Drug
AECG = Ambulatory ECG
AF = Atrial Fibrillation
AFl = Atrial Flutter
AMI = Acute Myocardial Infarction
APB = Atrial Premature Beat
ARVCM = Arrhythmogenic Right Ventricular Cardiomyopathy
BRS = Baroreflex Sensitivity
CAD = Coronary Artery Disease
CHD = Coronary Heart Disease
CHF = Congestive Heart Failure
DCM = Dilatative Cardiomyopathy
EPS = Electrophysiological Study
HCM = Hypertrophic Cardiomyopathy
HOCM = Hypertrophic Obstructive Cardiomyopathy
HRV = Heart-Rate Variability
HRT = Heart-Rate Turbulence
ICD = Implantable Cardiac Defibrillator
LVEF = Left Ventricular Ejection Fraction
LVF = Left Ventricular Function
LVH = Left Ventricular Hypertrophy
MB = Megabyte
MI = Myocardial Infarction
NPV = Negative Predictive Value
PPV = Positive Predictive Value
PVC = Premature Ventricular Contraction (VPB)
PWD = P-Wave Duration
QTD = QT Dispersion
QTI = QT Interval
QTV = QT (Interval) Variability
SA-ECG = Signal-Averaged ECG
SCD = Sudden Cardiac Death
SI = Silent (Myocardial) Ischemia
SH = Systemic Hypertension
TO = Turbulence Onset
TS = Turbulence Slope
VEA = Ventricular Ectopic Activity
VF = Ventricular Fibrillation
VLP = Ventricular Late Potential
VPB = Ventricular Premature Beat
VT = Ventricular Tachycardia
nsVT = nonsustained Ventricular Tachycardia
sVT = sustained Ventricular Tachycardia

33.1 Introduction

Ambulatory electrocardiography (AECG) is a diagnostic procedure, which involves recording the electrical activity of the heart using a technique first described by Holter [1–5]. The method is therefore also known as Holter electrocardiography

or Holter (ECG) monitoring. The technique has been most commonly employed for the detection of arrhythmias and transient ST-T changes. However, due to increased use of multichannel, digitized, and telemetered signals, this traditional use has been expanded to the analysis of heart-rate variability (HRV), heart-rate turbulence (HRT), QT-dispersion (QTD) and variability (QTV), and signal averaging of long-term ECGs for retrieval of P-wave duration (PWD) and ventricular late potentials (VLP). Current AECG equipment consists of a recorder and an analysis system and provides the basis for the detection and analysis of the above-mentioned parameters. A complete set of recommendations for equipment standards was proposed in 1985 [6], and more recently the official ACC/AHA guidelines on technical aspects and clinical applications of AECG have been published [7].

33.2 Holter Monitoring Hardware and Software

33.2.1 Electrodes and Electrode Preparations

By convention, bipolar leads (see Chap. 11) are normally used to record a potential difference between two sites on the thorax. The electrodes most commonly employed are disposable electrodes that are pregelled and self-adhesive. They usually have a true silver/silver chloride sensing element mounted on a self-adhesive tape or foam material, which is nonirritating and hypoallergenic to skin (Fig. 33.1). It is the electrode adhesiveness and extent of skin irritation that generally affect the quality of the ambulatory electrocardiographic signal by producing baseline wander, a low signal-to-noise ratio, and a short duration of adequate performance. The coupling of the skin and electrode (the skin–electrode interface) acts as an additional circuit with a resistance and capacitance between the heart and the recorder (Fig. 33.2).

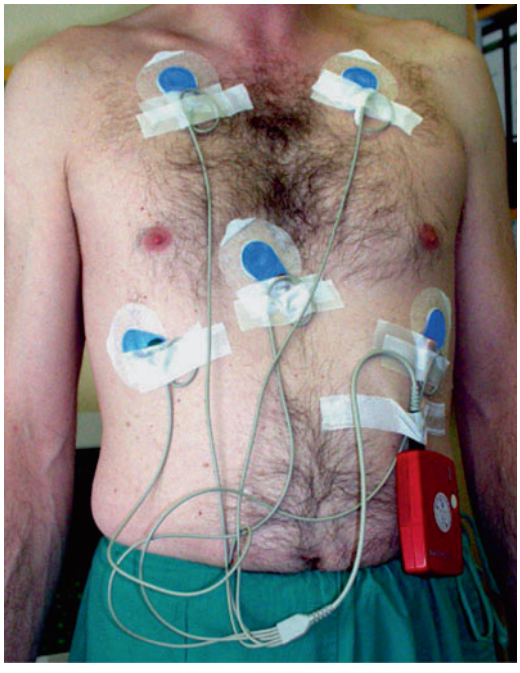

Figure 33.1
Electrode arrangement for three-channel AECG recording. Five pregelled disposable electrodes are used to record a CM_5 lead and a bipolar transthoracic lead. The fifth electrode is an indifferent electrode. The choice of these two bipolar leads provides high-amplitude ECG signals and the possibility of detecting the majority of changes in repolarization.

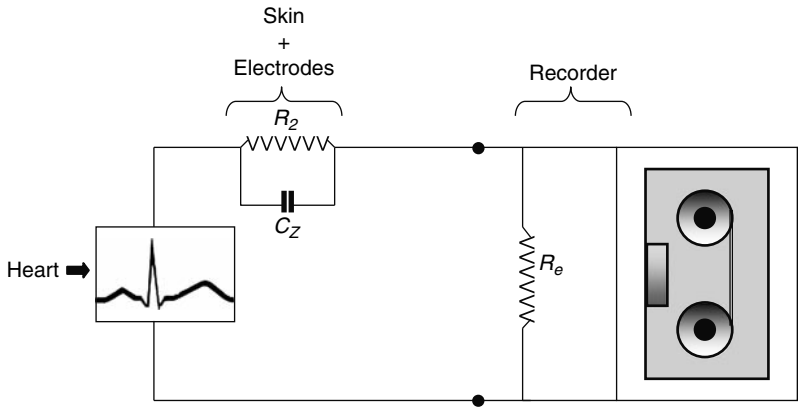

Figure 33.2

A model of the electrical circuit utilized in AECG recording. The coupling between skin and electrodes consists of a resistance and capacitance in parallel, which is responsible for diminishing the amplitude of the ECG signal if its impedance is high.

The total impedance of this circuit depends mainly on the preparation of the skin. The surface-skin oil and dirt should be removed prior to recording by cleaning the skin with gauze moistened with ether, making the skin slightly erythematous. If necessary, the skin over the electrode area should be shaved, gently abraded with emery tape, and thoroughly cleansed with an alcohol swab. One electrode can then be placed on each of the prepared skin-surface sites (Fig. 33.1), taking care to place the gelled pad firmly in contact with the abraded skin surface. The adequacy of the skin preparation for obtaining an optimum electrocardiographic signal can be checked by measuring the electrical impedance between the positive and negative poles of each bipolar lead. The measured resistance between electrodes should be $\leqslant 5\,k\Omega$, preferably $\leqslant 2\,k\Omega$. The impedance increases when the frequency of the signal decreases.

33.2.2 Selection of Lead Positions

Most AECG recorders utilize five or seven electrodes attached to the chest, which record two or three bipolar leads onto two or three channels [7–9], although systems employing multiple unipolar leads are now commercially available allowing a 12-lead ECG to be recorded. The first two channels may be used for arrhythmia and ischemia in the inferior myocardial wall. The lead positions recommended by the American Heart Association [6] are illustrated in Fig. 33.1, which provides an example of a three-bipolar lead/three-channel lead positioning. The practical advantages of multichannel Holter recording are increased reliability of the recorded ECG, improved recognition of ectopic cardiac beats, and enhanced detection of myocardial ischemia.

33.2.2.1 Leads for Recording Arrhythmias

A variety of bipolar lead configurations are used, the most common being a modified V_5 (CM_5), a modified V_3 (CM_3) or V_2 (CM_2), and a modified inferior lead (aVR, reverse Nehb I, Nehb D). No study has yet established the superiority of one lead over another; indeed, the choice of leads will differ according to the aim of the individual examination. A bipolar lead with positive electrode in the V_1 or V_2 position usually identifies atrial activity most clearly, showing the characteristic QRS patterns of right and left bundle branch block which help to distinguish supraventricular ectopic beats with aberrant conduction from ventricular ectopic beats. A bipolar lead with positive electrode in the V_5 position and the negative electrode in one of several other positions, such as the manubrium (lead CM_5), is the most sensitive single lead for the detection of ischemic ST-segment depression and provides a high-voltage ECG signal. However, with each of these two leads, some problems can occur in the presence of myocardial ischemia. One problem is that ST-segment depression

might exist in only one lead (usually V_5), while the second (V_1 or V_2) remains quite normal, as shown in Fig. 33.3. If, during the period of ischemia, the first lead becomes unsuitable due to artifacts, some false-positive diagnoses may be made. For example, in Fig. 33.3, the run of ventricular tachycardia (VT) might have been interpreted as not being a result of myocardial ischemia, so, for example, an antiarrhythmic drug (AAD) would have been prescribed instead of an antianginal drug. A second problem is that leads V_1 and V_5 may fail to record ST-segment elevation owing to spasm of the right coronary artery or circumflex coronary artery. In such a situation, an inferior lead is useful, and the most convenient one is probably a bipolar anteroposterior lead. In Fig. 33.4, lead V_5 shows ST-segment depression (mirror image), while the anteroposterior lead shows ST-segment elevation owing to spasm of the right coronary artery as was demonstrated by coronary angiography. Thus, where coronary artery disease (CAD) is concerned, a combination of a bipolar V_5-type lead and an anteroposterior or inferior lead is probably the best. With standard 12-lead ECG, a simultaneous recording of leads III or aVF or Nehb J together with V_3 can detect almost all cases of ST-segment elevation. With 3-lead Holter monitoring, a combination of two bipolar precordial leads together with an inferior lead is recommended for ST-segment elevation monitoring. In the absence of suspected CAD, the recording of V_1- or V_2-type (CM_2) and V_5-type (CM_5) leads (see Chap. 11) provides the best chance of obtaining an ECG tracing with sufficient details to make an accurate diagnosis of any cardiac arrhythmia.

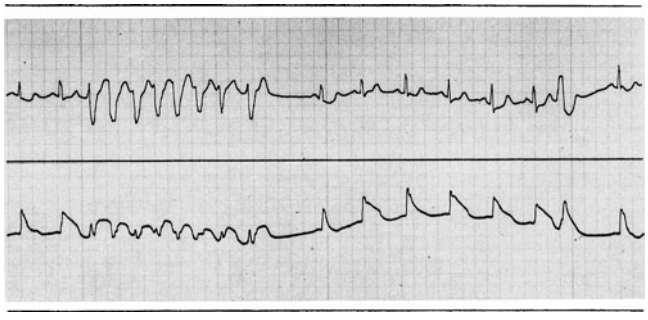

Figure 33.3

Sinus rhythm with a run of VT in a patient with variant angina. The two-channel recording confirms the diagnosis showing the characteristic marked ST elevation in the lower CM_5 lead. In the top channel (like V_1), only minor changes in repolarization occur. If the second lead had not been recorded, the variant angina would not have been detected and the VT would be considered as nonischemic in origin.

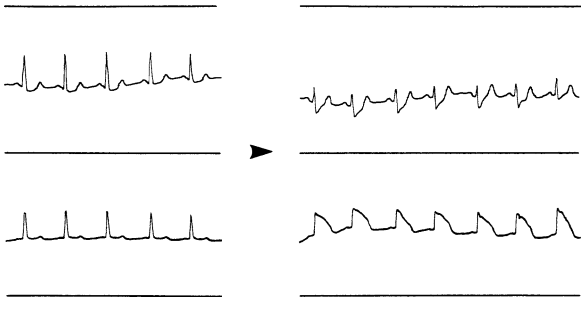

Figure 33.4

A two-channel recording in variant angina. The *left*-hand panel shows the baseline recordings while the *right*-hand panel shows the acute changes in the same patient. Note the characteristic marked ST elevation in the lower right CM_5 lead, whereas the mirror image in the other lead (like aVF) on its own might have led to a diagnosis of myocardial ischemia, but not of the variant form in the presence of chest pain.

33.2.2.2 Leads for Recording ST-Segment Depression (Myocardial Ischemia)

For the detection of ischemic ST-segment depression, specially adapted 3-lead Holter recordings are recommended. In a study of Lanza et al. [8] of simultaneous recordings of a 3-lead AECG and a conventional 12-lead ECG recording during an exercise test, CM_5 was the single lead with the highest sensitivity (89%) in detecting myocardial ischemia. The addition of CM_3 to CM_5 increased the sensitivity to 94%, particularly for improved detection of isolated inferior myocardial ischemia, and the combination of all 3 AECG leads had a sensitivity of 96% with only 2% more than the best combination of 2 AECG leads (CM_5 plus an inferior lead). Osterhues et al. [9] could detect myocardial ischemia in 23 out of 54 patients (43%) with single vessel disease using standard CM_2 and CM_5 Holter leads (total number of ischemic episodes = 372). When adding a bipolar Nehb D-like lead, the detection rate could be increased to 30 out of 54 patients (55%, total number of ischemic episodes = 1,048), and the Nehb D-like lead was most sensitive for the detection of inferior ischemia in patients with right CAD. Alternatively, the use of an inverse Nehb J lead, in which the positive electrode is placed on the left posterior axillary line, may enhance the sensitivity to detect ischemia, as well [10]. Thus, routine identification of ischemic ST-segment deviation may only require two leads, most favorably the combination of CM_5 with an inferior lead (aVF, inverse Nehb J, Nehb D) [11].

33.2.3 Electrode Leads and Cable

Electrode lead wires are individually insulated and have a silver contact (Fig. 33.1). The recorder cable is a shielded cable connected to the Holter recorder and is generally specific for each manufacturer's equipment. The electrode wires and the cable can both malfunction and be sources of artifacts.

33.2.4 Esophageal and Intracardiac Leads

One of the major problems in AECG with conventional electrode placements is the accurate detection of atrial depolarization. On account of various artifacts, P waves cannot always be recognized on a two- or three-channel recording, even during sinus rhythm. Moreover, during ectopic beats or tachycardia, the recognition of the P wave is often problematic. Therefore, the performance of ambulatory monitoring for the accurate diagnosis of arrhythmias remains doubtful compared to the more definitive results of an electrophysiological study (EPS). Several groups have attempted to record atrial activity during AECG using an esophageal bipolar lead [12, 13]. When the patient swallows the capsule, which contains a bipolar electrode, it is positioned so as to obtain an ECG signal with sufficient amplitude after the capsule has dissolved. The electrode wire should be fixed to the patient's cheek. However, difficulties experienced to date indicate that this technique cannot be easily used for the following reasons:

1. Difficulty is encountered in swallowing the capsule on account of its size (30 mm length).
2. The positioning of the electrode for recording an appropriate atrial ECG signal without significant ventricular depolarization is time consuming.

Nevertheless, the approach has been proved to be of considerable diagnostic value [13].

Some centers have preferred to use endoatrial leads to record atrial activity using a floating-catheter electrode. This technique permits a better atrial ECG signal to be obtained than does an esophageal lead. However, this procedure converts the AECG monitoring to an invasive examination [14]. The risk of local and general complications exists even if it appears relatively low. Thus, the use of intracardiac atrial leads remains confined to a few cases where an earlier attempt at recording the arrhythmia was unsuccessful and did not provide an exact diagnosis in patients in whom it is essential to determine the mechanism of the arrhythmia. In this case, AECG monitoring competes with an EPS because the benefits of the noninvasive technique disappear.

In practice, the interest of this technique remains confined to some cases where the knowledge of the exact mode of initiation of a tachycardia is useful for the management of the patient or in other patients in whom electrophysiological studies have been unable to provoke the arrhythmia.

33.2.5 Holter Recorders

Modern conventional AECG recorders are small, light-weight devices (110–320 g) that record two or three bipolar leads. They use a quartz digital clock and a separate recording track to keep time. The recorders are generally powered by a 9-V disposable alkaline battery (only rarely a rechargeable nickel–cadmium battery) and a calibration signal automatically inserted when the device is energized. In addition, a patient-activated event marker is conveniently placed on the device surface for the patient to note an event or indicate the presence of symptoms. The conventional format of the "first-generation" Holter recorders has been magnetic cassette-tape for directly recording the varying DC signals via the recording head onto the magnetic tape. Frequency-modulated (FM) systems are also available, although they are somewhat more prone to the generation of artifact. The tape-transport mechanism is driven by a hysteresis-synchronous motor assembly at speeds that are usually in the range of 1–2 mm/s; the speed is kept constant by an optical speed sensor on the flywheel and a crystal-controlled phase-locked loop.

33.2.5.1 Tape Recorders

Typically, such a unit records the ECG signal for between 24 and 48 h on a cassette or small magnetic tape, providing a permanent record of all electrical activity throughout the recording period and a playback as well as interrogation of the entire recording period (so-called "full disclosure"). Figure 33.5a shows the first Holter recorder developed by Avionics based on reel-to-reel magnetic-tape recording. This technology is adequate to detect abnormalities of conduction or rhythm, but it may be limited for recording low-frequency signals such as the ST segment. In some amplitude-modulated (AM) systems, an inadequate low-frequency response or a marked phase shift from the higher-frequency QRS signal may cause an artifactual distortion of the ST segment, which may be incorrectly interpreted as ischemic. It is usually claimed that only the FM type of recording system provides the necessary low-frequency response (down to 0.05 Hz) and less phase shift for accurate ST recording and reproduction, but this has to be counterbalanced against the higher costs, more baseline noise, and less clear display of such systems. This fact has been commented upon by Bragg-Remschell et al. [15]. More recent AM systems have been designed with improved low-frequency recording and playback characteristics and shown to record accurately ST-segment deviations [16, 17] and even T-wave alternans [18].

Caution should, therefore, be exercised with the older types of recorders in case ST-segment "depression" is a technical rather than a physiological phenomenon. One former development (Oxford Medical) has been the incorporation of a microprocessor inside the Holter recording unit itself so that signal analysis and classification can be carried out in real time. The ECG is also recorded on tape continuously because most cardiologists wish to have the acquired signal available for visual confirmation and assessment of any arrhythmia or ST-segment shift. Lastly, but not least, it should be noted

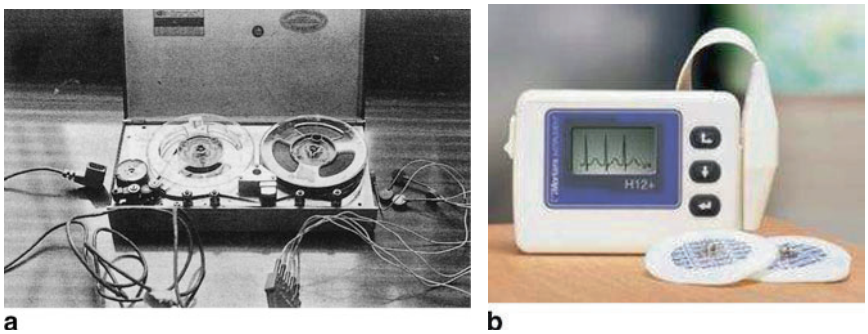

Figure 33.5
(a) Avionics 660 magnetic-tape recording system (one of the earliest systems used). (b) Mortara 12-lead Holter recorder (modern, solid-state recorder).

that regardless of whether AM or FM recording techniques are used, the tape itself may stretch and consequently distort the electrical signal.

33.2.5.2 Solid-State Recorders

Owing to the rapidly evolving technologies, nowadays direct recordings of the ECG signal in a digital format using solid-state recording devices are available ("second-generation" Holter recorders, Fig. 33.5b). Such direct digital recording avoids all of the biases introduced by the mechanical features of tape-recording devices and problems of analog recording formats that require analog-to-digital conversion before quantitative analysis. Digital ECG signals can be recorded up to 1,000 samples/s, which allow for the extremely accurate reproduction of the ECG signal necessary for highly sophisticated analysis methods like signal averaging or T-wave alternans measurements. Solid-state ECG recordings can be analyzed immediately and rapidly, and some recorders are equipped with microprocessors that can provide "on-line analysis" of the QRS complex and the ST segment and T waves as they are acquired. Also, the patient can be given feedback immediately in case of the detection of specific abnormalities, for example, ST-segment deviations. In addition, the solid-state format provides for ready electronic data transfer to a central analyzing unit. Limitations of this technology are the limited storage capacity of digital data, reliance on a computer algorithm in case of online analysis for identification of specific abnormalities, and the expense of the devices.

A full 24-h recording includes approximately 100,000 QRS-T complexes and requires about 20 megabytes (MB) of storage per channel. Therefore, compression of data is necessary, and at least two methods have been proposed, the "lossy" compression with very high compression ratios and the "loss-less" compression technique combined with an enhanced storage capacity. The problem with "lossy" compression is that the user is entirely dependent on the reliability of the microprocessor to distinguish important physiological abnormalities from artifact or wandering baseline, since, because of the lack of "full disclosure," confirmations of the decisions of the microcomputer cannot be made from the primary data, which are not recorded in their entirety and cannot be retrieved without error. Moreover, the accuracy of online interpretations may also be different for arrhythmia versus ischemia analyses [19]. However, it is essential for a physician using Holter monitoring that representative ECG tracings from all ischemic or arrhythmic episodes be confirmed by an experienced physician or technician, and thus, the lack of full disclosure may limit the reliability of the "lossy" compression method. The "loss-less" compression method in combination with enhanced storage capacity compresses ECG data by a factor of 3–5 by reducing the sampling rate from 256 to 64 or 16 Hz, respectively. Later, when the data are recalled, playback computer techniques recreate these abbreviated waveforms, whose sampling is often "weighted" about the R wave, to reproduce stored "full-disclosure" continuous electrocardiographic data. Some manufacturers have adopted the solid-state storage to their regular electrocardiographic instruments, whereby the recorder stores two channels of ECGs over 24 or 48 h on the recorder device, which subsequently is interfaced to the manufacturer's standard ECG cart or a data printer to provide 24 hourly continuous "full disclosure" printouts of all data recorded for visual interpretation.

Modern solid-state recorder devices provide special features such as an LCD display to control the quality of the ECG immediately after placement of the electrodes either by direct display (e.g., MT-101 from Schiller™, Lifecard from Delmar/Reynolds™, CardioMem from Getemed™), or by transfer via infrared to a Palm™ microcomputer (Medilog AR4 or AR12 from Oxford Instruments™). Some devices have a special loudspeaker incorporated for patient interaction, and most recorders provide pacemaker detection. Some provide recording of thoracic or respiratory activity as well (e.g., CardioMem from Getemed™, Medilog AR4 or AR12 from Oxford Instruments™). After the transfer of the full 24- or 48-h digital data, most analysis systems allow not only the analysis and presentation of normal and abnormal QRS complexes including bradycardias or tachycardias, but also the analysis of ST-segment deviations, HRV, QT duration and variability, and pacemaker function. Data transfer is usually completed within 2 min.

33.2.5.3 Storage Media

The storage media available are flash memory card or portable hard drive. Flash cards are about the size of a credit card, and have the capacity to store 20–40 MB of data (Fig. 33.14). After completion of the recording, the flash cards are removed from the recording device and are inserted directly into the analysis unit or into a separate device by which

the data can be transmitted electronically to another analyzing unit where the data can be played back and analyzed. Miniature hard drives can store more than 100 MB of data, and unlike flash cards, are not removed from the recorder, but the data are downloaded to another storage device or may be electronically transferred to a remote analysis unit.

33.2.5.4 Event Recorders

In contrast to the conventional 24-h Holter monitoring, both sampling and trans-telephonic devices record noncontinuous AECG data of an intermittent nature. There are two types of intermittent patient-worn recording devices (so-called event recorders), one that records and stores only a brief period of ECG activity, either by predefined criteria analyzed by the microcomputer (e.g., tachycardia, arrhythmia, bradycardia) or when activated by the patient in response to symptoms, and the other that records the ECG in a continuous manner but stores only brief periods of ECG recording (e.g., 5–300 s) in a memory when activated by the patient using the event marker at the time of a symptom (the so-called loop recorder). These event recorders can be used for prolonged periods of time, for example, many weeks, to identify infrequently occurring symptoms or arrhythmias that would not have been retrieved from a conventional 24-h AECG monitoring. A patient-activated event recorder needs rapid placement of electrodes, such as paddles connected to the recorder or a wrist bracelet, to record the ECG at the time of symptoms, whereas loop recorders use continuously worn electrodes. The recorded signal can be saved in memory and transferred at a later time to a central analysis unit or be transmitted to a receiving station by online transfer. Event recorders have the advantage of small size and light weight, their use is easy and they can be programmed to record many short episodes during an extended period of time (30 days to several weeks), and moreover, 1-, 2-, 3-, and mathematically reconstructed 12-lead formats are available.

A special type of event recorder is the implantable loop recorder (ILR), which may be used for identifying infrequent and transient symptoms of patients by long-term intermittent recordings. This device, of about the size of a pack of chewing gum is inserted under the skin at about the second rib on the left front of the chest and is activated by passing a special magnet over the device. It is capable of recording and storing up to 42 min of a single ECG channel, which can be partitioned for 1–7 episodes, with up to 20 min of preactivation ECG saved for subsequent downloading to a programming unit for analysis. The device can be configured to store patient-activated episodes, automatically activated recordings via, for example, low and high heart-rate limits, or a combination of both [20].

33.3 Artifacts in AECG Recording

An inherent problem with ambulatory monitoring is the almost inevitable occurrence of artifacts specific to this type of recording, resulting from a failure of one or more of the components of the system [4, 21–23]. Acknowledging these artifacts is of major importance because their misinterpretation can lead to erroneous clinical diagnoses and inappropriate therapeutic interventions. In addition, it is important to determine the cause of the artifact so that any fault in the equipment can be corrected. The major causes of artifact in Holter recordings are discussed in the following subsections. These essentially apply to recorders employing cassette tapes, as little experience has yet been gained with the newer solid-state technology (though problems with battery, electrodes, or cables are likely to be common to old and new systems).

33.3.1 Battery Failure

The most common artifact encountered during tape-based Holter monitoring is certainly the "pseudotachycardia" owing to the failure of the battery toward the end of the recording, as can be seen in Fig. 33.6, where a tachycardia characterized by a narrowing and lower voltage of the QRS complex occurs abruptly. The rhythm may be regular or irregular, simulating a paroxysmal supraventricular tachycardia (SVT). The replacement of the disposable or rechargeable batteries and, if necessary, the cassette or magnetic tape, could correct these artifacts. As a general rule, a new battery should be used with each recording, particularly in research studies where failure to record on a specific date can invalidate the whole study.

Figure 33.6
An illustration of one form of artifact encountered during AECG, where failure of the batteries toward the end of the recording has produced a "pseudotachycardia," with a decrease of P, QRS, and T-wave durations in particular making the diagnosis straightforward.

Figure 33.7
Cyclic slackening of the magnetic tape on account of mechanical difficulty within the recorder.

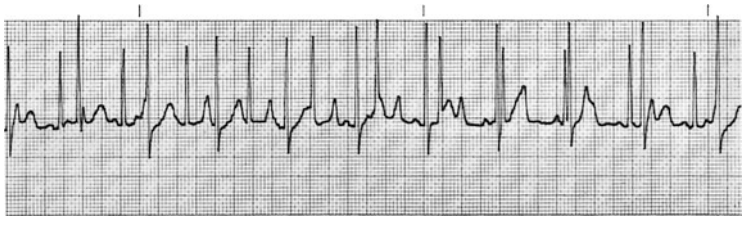

Figure 33.8
An illustration of artifact resulting from the use of magnetic tape, which has not been erased properly before being used a second time, resulting in the superposition of two ECG tracings.

33.3.2 Failure of the Magnetic-Tape Recording

Less frequently, a recording problem can occur intermittently, especially if some mechanical difficulty is present at each rotation of the cassette or magnetic tape. The characteristics of the artifact are the same as in battery failure, but they occur at periodic intervals (Fig. 33.7). The use of a cassette or tape, which has not been properly erased, during a subsequent recording, can lead to the superposition of two ECGs and make the interpretation of the new ECG signals impossible, as shown in Fig. 33.8. Therefore, as a rule, new cassette tapes should be used for each new patient AECG study in order to avoid these tape problems.

33.3.3 Failure of Electrodes, Lead Wires, or Patient Cable

Any dysfunction of electrodes, lead wires, or patient cable contributes to artifacts. Permanent failure, such as a break in the cable or loss of electrode contact, is easily identified, as a permanent defect occurs in one of the two recording

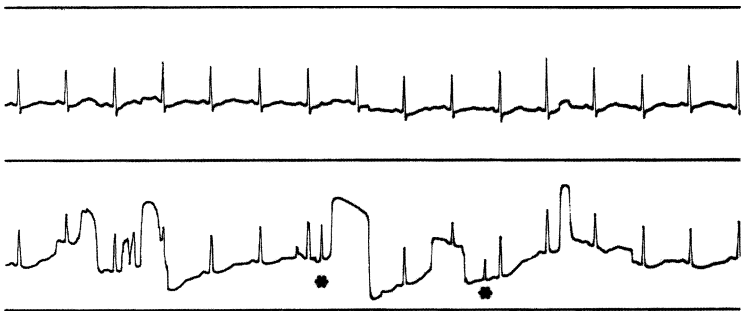

Figure 33.9

An example of the value of using two-channel recording during AECG. The lower channel shows artifact caused by intermittent failure of the ECG cable, with temporary loss of the ECG tracing and marked baseline shift producing "pseudo-QRS" waves marked by asterisks.

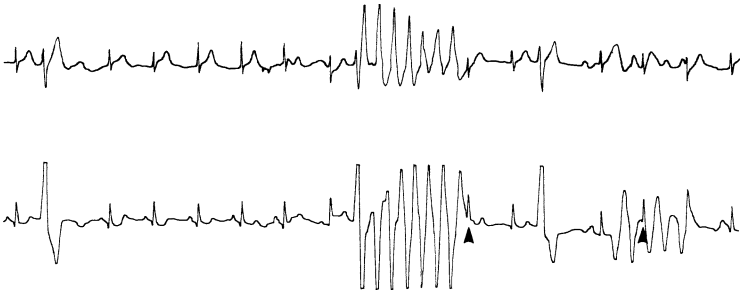

Figure 33.10

"Pseudo-VT " is produced by shaking the ECG cable during Holter recording. This artifact can be identified by the presence of normal QRS complexes, as marked by arrows within the runs of pseudo-VT.

leads. An intermittent failure, however, is more difficult to interpret. The use of at least two simultaneous leads in modern Holter recorders has considerably improved the detection of these artifacts. In a majority of cases, they occur only (or principally) in one lead as in Fig. 33.9. The intermittent loss of electrical contact in one of the two leads induces abrupt movements of the baseline without any recording of the ECG at that particular instant. However, in the other lead the normal ECG appearance easily permits the recognition of artifact. It should be noted that many analyzers, while displaying two channels, essentially analyze only one of the leads.

In some cases, the artifact can be present simultaneously in the two leads, particularly in the case of displacement of the patient's cable. In Fig. 33.10, the diagnosis of artifact is particularly difficult, because the presence of genuine VPBs can lead to an erroneous diagnosis of VT. Fortunately, two indices point to the diagnosis of artifact:

1. The second episode of pseudo-VT is not present in the upper tracing as it is in the lower tracing; and
2. The normal QRS rhythm can be observed within the artifact and coincides with the normal rhythm before and after the event.

As seen in the two preceding examples, the use of a second lead in the Holter recorder provides the most obvious means of identifying an artifact. In the absence of any displacement of the baseline, it is the only way to obtain an accurate diagnosis. In Fig. 33.11, for example, during a very short loss of electrical contact, only one PQRST complex disappears. In lead I, this is evidenced by a small undulation of the baseline. The presence of a normal QRS complex in lead II

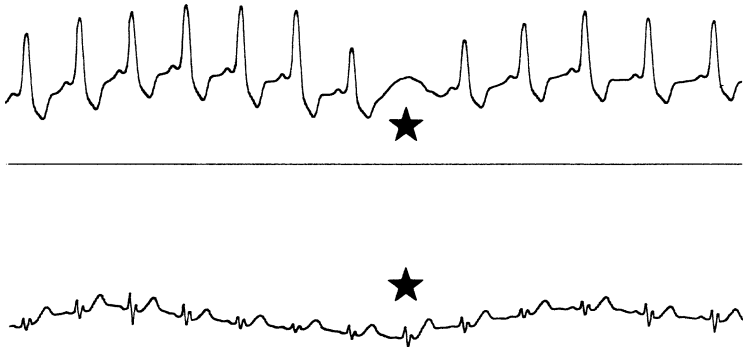

Figure 33.11
Transient loss of electrical contact in a lead wire or an electrode in the top channel producing the absence of one QRS complex (marked by a star). Its presence on the simultaneously recorded second channel permits its detection.

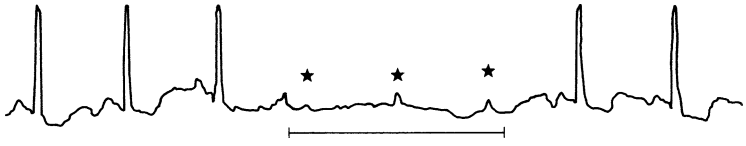

Figure 33.12
An example of an artifact during AECG recording producing pseudoatrioventricular block on account of a sudden decrease of QRS voltage owing to an increase of skin-electrode coupling impedance. The residual QRS complexes identified by stars may be wrongly identified as blocked P waves. The bar indicates the duration of the artifact.

makes it possible to exclude the diagnosis of a transient sinoatrial (SA) block. Figure 33.12 provides an example of pseudo-atrioventricular (AV) block due to a sudden decrease of QRS voltage.

33.4 Equipment for Analysis

33.4.1 Analog Holter Tape Recording

All methods of analysis require some form of playback system [4, 24–26] including those, which undertake real-time analysis of the AECG. All playback systems contain at least a magnetic-tape replay unit, while some older systems have an audio speaker and an ECG writer, which can provide samples. In addition, an oscilloscope or screen, an arrhythmia detector, a microprocessor-based analyzer (nowadays often a personal computer), an automatic ST-segment analysis system, and a fiber-optic or laser printer might form a part of such a system. Most current playback systems use generic computer hardware platforms and proprietary software protocols for data analysis and report generation. Signals recorded in analog format by magnetic tape are digitized at either a rate of 128 or 256 samples/s for subsequent analysis. The clock track on the tape can compensate for tape speed variations by a phase lock loop circuit. The resolution is usually at least eight bits and the sampling rate 128/s. The signal amplitude can be adjusted by the physician or technician based on the calibration signal recorded automatically at the beginning of each recording. Tape playback and scanning options include rapid playback with either superimposition of up to 1,000 times with or without audio-speaker control or page-type displays. Facsimile, modem, network, and internet integration allow for rapid distribution of AECG data and analyses throughout a hospital or larger health-care system.

The magnetic-tape unit, if required for playback, is a motor-driven assembly, which operates normally at 60 or 120 times the original recording speed, although more recently developed systems can function at 480 times the original recording speed. The magnetic heads detect and reproduce the original ECG signal for onward transmission to the

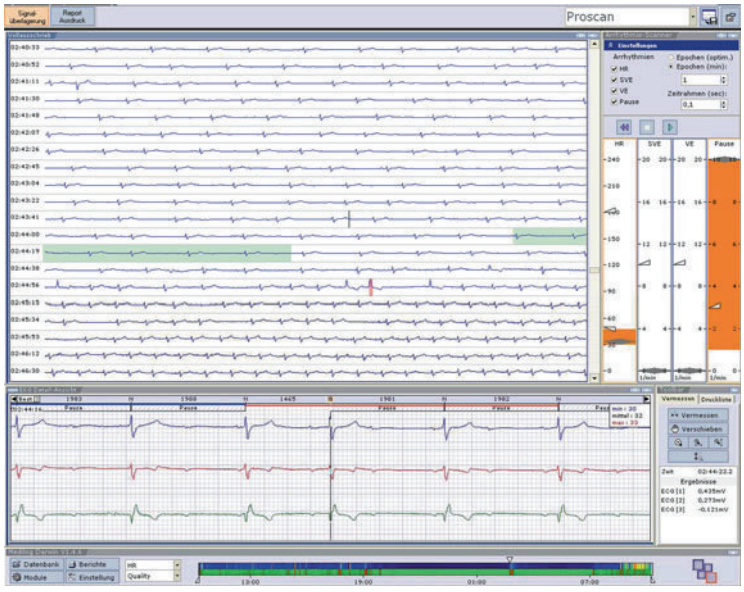

Figure 33.13

Full disclosure of long sequences of a single ECG lead for quick paging up or down (*top*) and an arrhythmia-scanning mode (*right*) for rapid detection of phases of arrhythmias, three-channel real time ECG (*bottom*) (Oxford MedilogDarwin system).

remainder of the system. In FM systems, it is necessary for the replay unit to demodulate the signal in order to retrieve the original waveforms. In most modern tape-recording systems, the analog signal from the tape is digitized for quick and convenient quantitative data analysis.

In every Holter system, an oscilloscope or flat panel screen is an essential part to control and guide the whole analysis procedure. Practically, all Holter analysis systems have the option of presenting data in a superimposed fashion at 30, 60, 120, 240, or 480 times the original recording speed, which when coupled with an audio speaker constitutes the AVSEP (audiovisual superimposition electrocardiographic pattern) display. In the majority of instruments, the use of a storage oscilloscope makes it possible to "freeze" the display of a real-time ECG for a period of 2–3 s up to 180 s if desired. Either one or both recorded leads may be displayed in this way. By using a technique for "jogging," it is possible to jump forward or backward for a variable time in order to inspect quickly a series of "frozen" ECG displays (Fig. 33.13). More recent systems sometimes use a graphics screen attached to a personal computer rather than a custom-engineered display (see Sect. 33.4.2).

In some older analog Holter systems, an audio speaker is incorporated that produces an audible sound, which is dependent on the detection of the R wave of the QRS complex. The tone can rise to a more shrill note in the presence of a fast heart rate or when an ectopic beat creates an isolated short R–R interval. On the contrary, with slow heart rates or longer R–R intervals, a low-pitched sound occurs. In some of the less-expensive units where there is no display, it is claimed that the ECG can be analyzed purely by listening to the audio signal produced by the replay unit.

The conventional form of a laser printer-ECG writer is incorporated into all Holter analysis systems and provides for up to three channels of ECG data to be written on standard (graphic) paper with an accompanying time printed on the edge track. It is evident that the production of specific examples of ECG abnormalities form a necessary part of the AECG report, providing essential material to enable the physician to interpret the 24-h recording. Moreover, graphic and tabulated AECG data, as well as a total 24-h ECG printout are provided by modern laser printers. Thus, this type of printout has supplanted the older fiber-optic printout system, which was able to print all or part of the ECG in a real-time format produced at high speed with a time reference frame. As previously mentioned, the display of the whole 24-h ECG on paper has become known as "full disclosure." This technique is very useful for giving information on the quality of the recording and for studying rare events, particularly when the major part of the Holter recording is normal. As can be

seen in Fig. 33.13, a second degree AV block is easily detected on a compressed ECG tracing. However, this technique requires that the technician or physician who must examine the complete 24-h ECG tracing spends some considerable time in doing so. The most recent AECG analyzing units provide abnormal sequences such as pauses, arrhythmias, etc. automatically for direct technician or physician review. Usually, one lead is printed, but if necessary the two leads could be printed separately. For time reasons, the use of full AECG disclosure is normally confined to quality control, verification of rare events, evaluation of AAD efficacy, and similar specialized functions and is not recommended for widespread routine use. The most modern solid-state Holter analyzing units provide abnormal episodes within the full disclosure ECG (e.g., pauses, arrhythmias, etc.) automatically, line-by-line for direct and quick control by the technician or physician.

33.4.2 Solid-State Holter Recording

The newer solid-state Holter systems consist of the digital recording (solid-state) device, the electronic interface to transfer the data from flashcard or hard drive to the personal computer, the flat panel screen, the alpha-numeric keyboard, the personal computer with the proprietary software protocols for data analysis and report generation, and a laser printer (Fig. 33.14). Some solid-state recorders are equipped with a microprocessor that provides "on-line analysis" of the QRS complex, the ST segment, as well as the T wave as they are acquired. Thus, a quick analysis and overview on the whole set of AECG data is immediately available at the technician's or physician's convenience, which facilitates and speeds up the interactive final analysis of the full 24h AECG. Details of the analysis workflow are given below.

33.5 Methods of Analysis

The approach to the analysis of 24-h ECG recordings varies from one manufacturer to another, and there are many systems commercially available worldwide. However, the different methods can be broken down into two very broad categories. Using discriminators, the hardware essentially differentiates between a normal (or dominant) QRS waveform and all others. The critical thresholds used to achieve the discrimination may (optionally) be adjusted by a technician. These are likely to be based on QRS width, amplitude or area, or some combination or derivative of these parameters. Various criteria based on the R–R interval, or the number of abnormal beats detected consecutively, can be set up to facilitate the detection and printout of arrhythmias. Using the method of a classifier, in microprocessor-based equipment the software automatically groups QRS complexes into a number of different categories ("templates"). This may be done in the recorder itself or in the laboratory-based analyzer. Thereafter, an operator may (optionally) adjust the classifications. Analysis of rhythm is then based on a study of the beat classifications, R–R intervals, and similar criteria. There are intermediate solutions where, for example, the second approach is used in the recorder to collect samples of arrhythmias

Figure 33.14
Modern type of solid-state recorder systems: digital AECG recorder of Medset (*top left*), digital AECG recorder (*bottom left*), and complete analysis system of OxfordDarwin (*right*) with personal computer, keyboard, flatpanel screen, and laser printer.

only, although details of heart rate over 24 h may also be stored. With some types of analyzers in either of the above categories, it is possible for the operator to view several minutes of an ECG on the screen in order to check visually for abnormalities or assess the quality of the recording.

33.5.1 Analog Tape Recordings

The first approach, that is, the use of the discriminator type, has the advantage that it can be used with a minimum of intervention by the operator and is thus suited to routine and automatic analysis of a large number of Holter recordings. On the other hand, experience shows that operator intervention can be valuable. The aim of using the discriminator approach in older Holter systems is not to provide an exact number of abnormal complexes (as is the case in the second approach), but to indicate their relative global frequency and, above all, to detect any arrhythmias. The principle of the technique is to use only a single pass of the tape (taking 12 or 24 min for 60 or 120 times real speed, respectively) in order to obtain data (e.g., trend plots) without intervention of the operator, or with minimal intervention such as an adjustment of the QRS width threshold, prior to the commencement of analysis, or to print any arrhythmias detected. This type of semiautomatic beat classification cannot provide the exact number of abnormal events because inevitably artifacts will be incorporated into QRS counts or because some normal QRS complexes will be considered abnormal or vice versa. However, if the original analog ECG signal is sufficiently high in amplitude without major artifacts, the QRS count is generally satisfactory with only a small percentage error. It is then possible to use such a system in order to obtain relatively quickly a large variety of presentations of the data contained on the recording.

33.5.2 Digital Solid-State Recordings

The most recent generation of automatic analyzers either undertakes the QRS analysis in real time using a microprocessor built into the recorder, or after replay using a similar technique whereby 64 or 128 different types of QRS complexes can be stored within the microprocessor memory. Each new QRS complex is compared with the different types already stored, and if it compares satisfactorily to one of these, the total count for that particular pattern is increased by one. If not, a new QRS morphology is then stored. At the end of the analysis, the various QRS morphologies can be displayed together with a count of beats in each group (Fig. 33.15a, b). In some systems, it is possible for the operator to decide that a certain group of complexes consists of artifacts and have them deleted from the analysis. Alternatively, if there are only subtle differences between different groups, they can be merged and finally a categorization of normal or abnormal premature ventricular complexes (PVCs), premature supraventricular complexes (PSVCs), and so on can be added to each group so that the various counts can be accurately produced. This approach is now the standard technique of practically all modern AECG monitoring systems. Real-time analysis using the above technique has the advantage that at the end of the recording, the results can be instantly printed out via the appropriate replay and print-out unit.

33.5.3 Arrhythmia Analysis

33.5.3.1 From Tape Recorders

By using the main criteria, the R–R interval, and the QRS width, it is possible to develop algorithms that are able to detect automatically many types of arrhythmias in Holter analog tape recordings [27–29]. Each beat is classified as normal, ventricular ectopic, supraventricular ectopic, paced, other, or unknown, and a template for each type of abnormality is created. Enlarged premature beats (premature ventricular contractions (PVCs) or atrial premature beats (APBs) with aberrant intraventricular conduction) and narrow premature beats (supraventricular premature beats or PVCs narrower than sinus beats) are the easiest arrhythmias to detect. The ease of detection of such abnormalities, as well as of couplets does not differ greatly compared to that of isolated extrasystoles. However, all these phenomena can be detected more confidently with the assistance of an experienced technician to run the analyzer. All users of Holter monitoring know that the first generation of PVC counters could be grossly inaccurate in analyzing the ECG tracings in the presence of artifact.

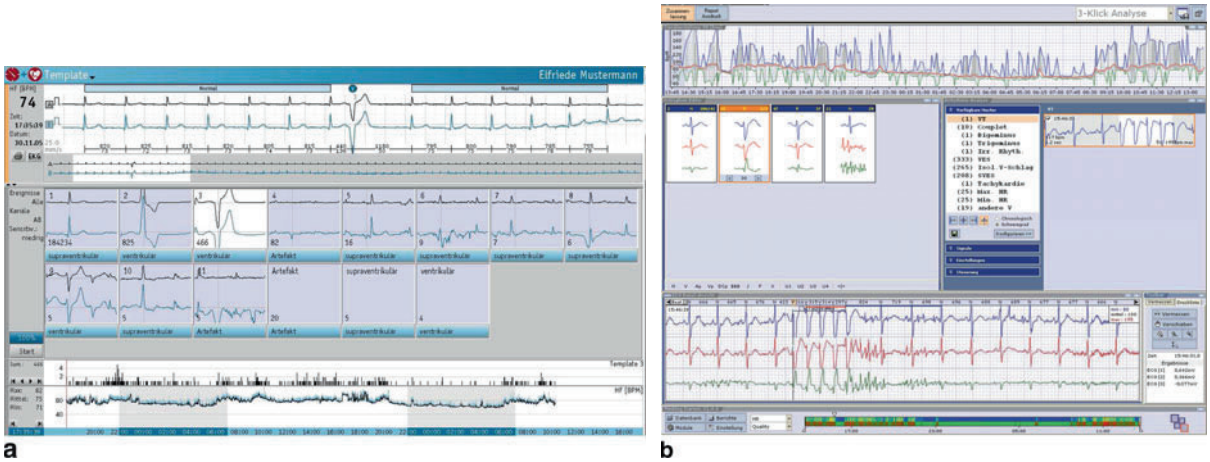

Figure 33.15

(a) Overview on the analysis forms of the computer program (Medset system) showing real time three-channel ECG (*top*), templates of QRS complexes (*center*), and summary of arrhythmias and heart-rate trend (*bottom*). (b) Overview on the analysis forms of the computer program (Oxford MedilogDarwin system) including heart-rate trend curve (*top*), QRS complex templates (*left*), types of available templates (*center*), selected single lead strips (*right*), and three-channel real-time ECG (*bottom*).

In this context, the superiority of human intervention compared to the use of an automatic detector is evident. However, automatic detectors can be used for other purposes with more complex algorithms. An example is the recognition of atrial fibrillation (AF) as opposed to sinus arrhythmia on the basis of studying only the irregularity of the R–R interval distribution. Another example of the utility of the automatic analysis of arrhythmias is the detection of ventricular pauses caused by SA or AV block. Visually, this search is very difficult and the automated approach provides higher sensitivity at the slight expense of a larger number of false-positive reports.

The interactive technique, which requires an operator, uses variable criteria for the recognition of arrhythmias, principally for ventricular or supraventricular extrasystoles. The simplest method is to use the classical criteria of recognition, but with the possibility of modifying the thresholds of prematurity and QRS width according to the characteristics of the particular ECG under study. However, more sophisticated detectors have appeared recently using different criteria in order to obtain an improved separation between "normal" and "abnormal" QRS; that is to say, different QRS patterns. These criteria can include the slope of the first component of the QRS complex, its derivative, the QRS area, or the morphological pattern calculated from the analog signal or from a digitized ECG. These criteria can be utilized separately or together in order to define the similarity between each QRS complex and the basic "normal QRS," which is usually learned by the machine with some prompting by the operator at the onset of the recording. With this operator-based approach to setting up criteria, which can be adjusted – if necessary – during the tape analysis, the separation between supraventricular and ventricular complexes is usually achieved satisfactorily. Table 33.1 summarizes some important causes of false positive and false negative findings in the analysis of arrhythmias from AECG.

33.5.3.2 From Solid-State Recorders

In solid-state digital AECG systems, the total number of QRS complexes is analyzed and classified in different templates, which can be interactively controlled and categorized into normal or abnormal premature ventricular complexes (PVCs) or PSVCs. Together with the R–R intervals, every type of bradyarrhythmia, tachyarrhythmia, supraventricular, or ventricular premature complexes can be quantified by the computer protocol. A comparative real-time ECG printout provides interactive control of the classification result of the computer (Figs. 33.15 and 33.16). In addition, most solid-state

Table 33.1

Some technical causes of false-positive and false-negative findings in arrhythmia detection and classification from the ambulatory electrocardiogram (AECG)

1. Battery failure with "pseudotachycardia"
2. Recorder malfunction with variable tape drive or inaccurate storage
3. Incomplete degaussing or erasure of data from previously used tapes or memory storage
4. Noise interference or lead-electrode baseline drift or artifact
5. Low-voltage recording
6. Physiologic variations in QRS form and voltage
7. Inadequate computer QRS detection and classification algorithms
8. Incorrect time stamping of AECG tracings
9. Inadequate or incorrect technician interpretation during analysis

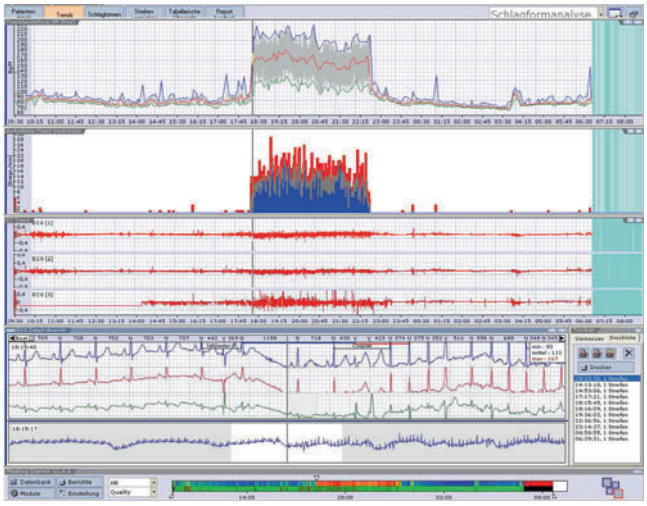

Figure 33.16

Trend analysis of heart rate (*top*), counts of ventricular ectopic beats (*second top row*), ST-segment trends (*third row*), and three-channel real-time ECG and single lead "full disclosure" ECG (*bottom*) (Oxford MedilogDarwin system).

systems provide a separate channel for pacemaker spike analysis, and software for analyzing HRV either in the time or frequency domain or both.

After replay and digitizing the analog ECG signals from Holter magnetic tapes or – in case of solid-state ambulatory Holter systems – following transfer of the digital AECG data from the recorder to the computer via an interface, subsequent analysis of all ECG data is relatively easy, quick, and convenient if an appropriate software program is available. With most solid-state systems, a primary computer-based automatic analysis is performed and these data are presented on the screen as simultaneous multiple trend curves of heart rate (maximum, minimum, mean), PSVCs, PVCs, ST-segment deviation, and QRS complex templates together with a strip of two or three channels of the original ECG (Figs. 33.15b and 33.17). Using the cursor at each time of the heart-rate trend or arrhythmia strip, a control and reclassification of QRS templates, arrhythmia classification, or ST-segment analysis can be made instantaneously. Moreover, further trend curves of pacemaker activity, HRV trends and instantaneous values at a given period of the 24 h recording, and respiratory activity may be displayed. Some modern systems also provide a 12-lead ECG, which is either recalculated mathematically from the 3-lead orthogonal X–Y–Z data using a transformation or an actual 12-lead ECG where the limb electrodes are placed on the chest (see Chap. 11). Alternatively, a full disclosure ECG may be presented first page by page and by

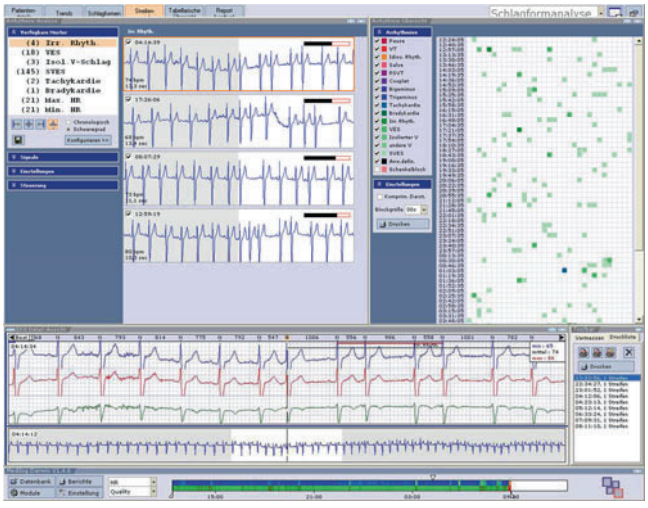

Figure 33.17

Arrhythmia overview including counts of single arrhythmic events (*left*), single lead arrhythmic episodes extracted from the overview on left side, survey on QRS templates over the full 24-h period with 30 s segments (*right*), and three-channel real-time ECG (*bottom*) (Oxford MedilogDarwin system).

quick paging up or down and reading all ECG sequences. Abnormal episodes such as bradycardias, pauses, PVCs, or tachycardias can easily be identified, marked by the mouse, presented in real-time, and finally confirmed or corrected if necessary.

33.5.4 ST-Segment Analysis for Myocardial Ischemia

33.5.4.1 Technical Aspects – Analysis of Ischemic Episodes

With respect to ST-segment analysis for detecting myocardial ischemia, some important technical, electrocardiographic, and clinical aspects have to be considered, for which the following recommendations have been given [7]. The QRS-T morphology must be carefully scrutinized to ensure that it is suitable for interpretation. Cardiac rhythm should be sinus rhythm, the baseline ST segment should have $\leqslant$0.1 mV deviation, and the ST segment ideally should be gently upsloping with an upright T wave. A flat ST segment associated with an inverted T wave may still be interpretable. However, downsloping or scooped ST-segment morphology should be avoided. The height of the R wave of the monitored lead should be $\geqslant$1.0 mV. The lead selected for ischemia monitoring should not have a Q wave $\geqslant$ 0.04 s or marked baseline ST-segment distortion. Patients with left-ventricular hypertrophy in the 12-lead ECG, left bundle branch block, nonspecific intraventricular conduction delay $\geqslant$100 ms, or pre-excitation are not suitable for monitoring myocardial ischemia in the AECG. Medication with digitalis or some antidepressant drugs may distort the ST segment and preclude accurate interpretation of ST-segment deviations. ST-segment deviation is tracked by the use of a cursor within the PR segment to define the isoelectric reference point, and another cursor at the J-point and/or 60–80 ms beyond the J point to identify the presence of ST-segment depression. Myocardial ischemia is diagnosed by a sequence of flat or downsloping ST-segment depression of $\geqslant$0.1 mV, with a gradual onset and offset that lasts for a minimum period of 1 min. Each episode of transient ischemia must be separated by a minimum duration of at least 1 min, during which the ST segment returns to baseline (the so-called 1 × 1 × 1 rule [30, 31]). Many investigators prefer a duration of at least 5 min between episodes, and the ACC/AHA Task Force also recommends a 5-min interval between episodes because the end of one episode and the onset of the next will take longer than 1 min to be physiologically distinct. Episodes of ST-segment deviation are characterized by identification of an onset and offset time, magnitude of deviation, and heart rate before and during the episode. Representative ECG strips at the time of ST-segment deviation in real time should be provided in the report format.

Table 33.2

Some causes of false-positive and false-negative findings in detection and interpretation of myocardial ischemia from the ambulatory electrocardiogram (AECG)

1. Inadequate lead system employed
2. Incorrect or lack of lead calibration
3. Inadequate recording fidelity
4. Recording signal processing that compresses or filters the data, altering the ST-segment characteristics
5. Height of R wave <1.0 mV and Q wave ⩾0.04 s
6. Downsloping or scooped ST-segment morphology
7. Positional changes on the ST-segment
8. Hyperventilation
9. Vasoregulatory or Valsalva-induced ST segment changes
10. Sudden excessive exercise-induced ST segment changes
11. Preexcitation (WPW-syndrome)
12. Intraventricular conduction disorders (LBBB, RBBB)
13. Undiagnosed or unappreciated left ventricular hypertrophy
14. ST segment changes secondary to tachyarrhythmias
15. False ST segment changes from atrial fibrillation or atrial flutter
16. ST segment changes secondary to electrolyte disturbance or drugs

Trend curves and/or a summary table of all ischemic episodes may be displayed in the final report. Alternatively, a miniaturized full-disclosure display can be printed out for all or part of the 24-h recording [7]. Table 33.2 summarizes some important causes of false positive and false negative findings regarding ST-segment analysis from the AECG.

One special problem is ST-segment elevation in variant angina, where the role of Holter monitoring is of considerable importance. During the playback analysis, the ST segment can be studied in two ways, either by visual examination or by automatic measurement, which can provide a trend of the ST amplitude. Some systems continuously monitor the ST amplitude, which is automatically compared to the baseline, defined by the onset of the accompanying QRS complex. In this case, the point of measurement can usually be placed by the operator at an appropriate distance from the J point in order to eliminate the detection of "physiological" ascent of the ST-segment depression. Other systems measure ST-segment depression automatically during the 24-h recording. This approach is subject to error in relating the ST measurement point to a fixed QRS trigger, which may vary with different QRS morphologies, that is, from patient to patient.

33.5.4.2 Beat-to-Beat Analysis

The most recent technical developments are fully automatic algorithms for beat-to-beat ST-segment amplitude measurements. Rather than identifying discrete sequential short episodes of ST-segment deviation, this approach utilizes frequency distributions of the ST-segment amplitude measurements for each 24-h recording (typically of 50,000–100,000 beats) in order to yield a better global perspective of ST-segment shifts that have occurred during the whole recording period [32, 33]. Following QRS detection and elimination of abnormal complexes, beat-by-beat isoelectric baseline estimation by cubic splines, and noise determination, the initial (R-ST1) and end point (R-ST2) of the regression line of the ST-slope is determined by the computer algorithm using the empiric formula for timing of the two points: $R\text{-}ST1 = 40 + K1\sqrt{RR}$ and $R\text{-}ST2 = 40 + K2\sqrt{RR}$. For a heart rate of 60 bpm, K1 was set to 70 ms and K2 to 110 ms, and the whole range of K1 and K2 was evaluated over a spectrum of heart rates up to R – R intervals of 1,600 ms. From the frequency distribution (histogram) of the average displacement of the ST-segment (AVD) time series over 24 h, several parameters indicative of transient myocardial ischemia were extracted. As expected, transient and ischemic episodes lasting only several minutes were shown to be skewed to the left and to be asymmetrically spread around an average deviation of

less than 0 mm, whereas nonischemic frequency distribution was narrow and symmetric with an average deviation close to 0 mm. Using several parameters like percentiles, spread measures, skewness, and clustering, the authors were able to distinguish between a normal cohort of 63 individuals and 37 patients with CAD by a cut-off point of 0.45 for the estimated probability of ischemia in ambulatory monitoring [32]. In a second study, the influence of the autonomic nervous system (ANS) on ST-segment variability was tested [33], using the same technique of computerized ST-segment analysis including a demodulator algorithm to compensate for respiratory baseline shifts. Nine healthy volunteers underwent the following experimental protocol: control period (breathing room air at 10 cycles/min = 0.17 Hz for 5 min), fast respiration period (breathing room air at 15 cycles/min = 0.25 Hz for another 5 min), metabolic period (breathing 100% oxygen at 10 cycles/min for about 8 min), and neurogenic period (after 10 min breathing pure air, administration of atropine iv. with breathing room air at 10 cycles/min for other 10 min). Analysis of power spectral densities of the AVD signal during the four different periods of the experimental protocol showed no effect of 100% oxygen inhalation, only a small effect of mechanical respiratory activity, but a significant decrease of both total variability and relative power with atropine intervention. The results were similar for HRV, and the conclusion of this study was that the ANS plays a significant role in the regulation of AVD time series. This is a new important physiological finding and should encourage further systematic studies by using the ST segment not only as a simple detector of myocardial ischemia, but rather as a target and component of comprehensive cardiovascular equilibrium [33].

33.5.5 Analysis of HRV

Twenty-four-hour Holter AECG recordings represent a near ideal source for both short- and long-term assessment of HRV. Analysis of HRV itself refers to beat-to-beat oscillations of the R – R interval, which in the absence of physical activity, postural changes, or emotional stimuli represents the balance between cardiac sympathetic and parasympathetic (vagal) efferent activity and in particular the autonomically mediated alterations of the sinus node discharge rate (R – R tachogram, Fig. 33.18). In general, two methods of HRV analysis have been described, namely, time domain and spectral analysis [34, 35]. The term "time domain" reflects the fact that the majority of methods used provide measures in units of time (e.g., milliseconds) and time domain parameters involve computing indexes that are not directly related to specific cycle lengths. This method offers a simple means of defining patients with decreased variability in the mean and standard deviations of the R – R intervals. In general, two methods of time domain analysis – statistical and geometric – are in use [34].

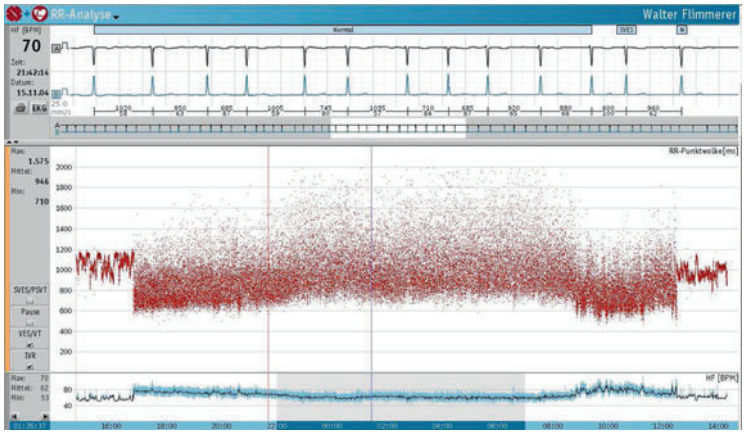

Figure 33.18

Trend of heart-rate tachogram (*center*) during sinus rhythm (*extreme left and extreme right*) and AF (*left* and *right center*) as a rough overview on HRV. Real time two-channel ECG (*top*) and heart-rate trend (*bottom*) are also included (Medset system).

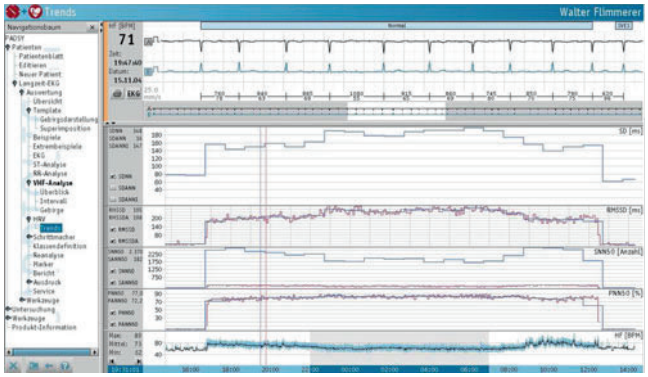

Figure 33.19

Trend curves of different time domain parameters of HRV (SDNN, rMSSD, SDNN50, and pNN50) and heart rate (*center* and *bottom*) together with a two-channel real-time ECG (*top*), same patient as in Fig. 33.18 (Medset system).

33.5.5.1 Statistical Methods for HRV Analysis

Among the statistical methods, time domain parameters analyzed include the mean R – R interval, the mean coupling interval between all normal beats, SDANN = standard deviation of the averaged normal sinus R – R intervals for all 5-min segments of the entire 24-h recording, SDNN = standard deviation of all normal sinus R – R intervals, SDNN index = mean of the standard deviations of all normal R – R intervals for all 5-min segments of the entire recording, NN50 = count of the number of pairs of adjacent R – R intervals differing by more than 50 ms in the entire recording, pNN50 = the percentage of adjacent R – R intervals that varied by more than 50 ms, and the rMSSD = root mean square of the difference between the coupling intervals of adjacent R – R intervals. Solid state recorders provide hour-to-hour trend analyses of different time-domain parameters (Fig. 33.19). rMSSD, NN50, and pNN50 correlate highly and are markers of high-frequency variations (vagal influence) in heart rate [34]. Of all parameters, rMSSD seems the most statistically stable (in standard clinical populations, the distribution of rMSSD data is more normal than that of pNN50 or NN50 values) and should be preferred, particularly since it correlates highly with others.

33.5.5.2 Geometric Measures for HRV Analysis

The main practical limitation of statistical methods is the time-consuming and extensive offline-manual editing of the ECG signals in order to ensure good quality R – R interval series. The use of filters to exclude outliers of R – R intervals, for example, perhaps those differing by more than 20% of the preceding R – R interval, is sometimes unsuccessful and may provide substantially inaccurate results. Therefore, a solution to eliminate incorrect R – R intervals is geometric measures, that is, the conversion of R – R interval data into a geometric pattern, such as the sample-density histogram of R – R interval duration, the sample-density histogram of the differences between successive R – R intervals (there exists little experience with this method), and the duration of each R – R interval against the immediately preceding R – R interval (so called Lorenz plots or Poincaré maps) (Fig. 33.20). Since the incorrect R – R intervals are usually substantially shorter (due to premature ectopic beats) or longer (due to sinus or compensatory pauses) than the population of correct R – R intervals, these incorrect R – R intervals fall outside the major peak of the distribution histogram and can easily be suppressed. Of the three geometric methods, the triangular index is the most important and most frequently used measure of HRV. It is calculated by dividing the total number of all R – R intervals by the height of the histogram of all R – R intervals measured on a discrete scale with bins of 7.8 ms, when using a sampling frequency of 128 Hz. A modification of the triangular index is the triangular interpolation of the R – R interval histogram (TINN), which is less dependent on the sampling frequency. This method interpolates the R – R interval histogram by a triangle, which has its base on the horizontal axis and its peak at the maximum point of the histogram, whereby the computation of the method identifies a triangle for which the square

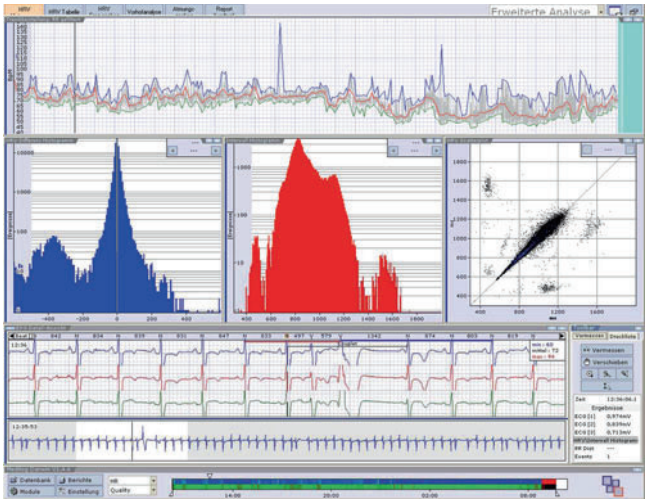

Figure 33.20

HRV histogram: Trend curve of heart rate (*top row*), histogram of the R–R interval differences (*center left*), R–R interval histogram (*center*), scatterplot with plotting the duration of each R–R interval against the immediately preceding R–R interval (so called Lorenz plots, *center right*), and three-channel real-time ECG (*bottom*) (Oxford MedilogDarwin system).

difference between the histogram and the triangle is the minimum among all possible triangles. The length of the base of such a triangle is used as the measure of HRV. Both the HRV triangular index and TINN, measured over 24 h, express overall HRV and are more influenced by lower than by higher frequencies [34].

Because many studies in the past have used different HRV parameters leading to a lack of standardization and given that many measures correlate closely, the ESC/NASPE Task Force developed guidelines [36] to standardize nomenclature and methods of measurement. They recommended four time-domain HRV parameters:

1. SDNN (as an estimate of the overall HRV)
2. HRV triangular index (as an estimate of overall HRV)
3. SDANN (as an estimate of long-term components of HRV), and
4. RMSSD (as an estimate of short-term components of HRV)

33.5.5.3 Frequency-Domain Analysis of HRV

The basic assumption underlying the technique of frequency-domain analysis is that every periodic signal such as systolic arterial pressure or heart rate (R – R intervals) may be decomposed into a series of oscillatory components with different frequency and amplitude. When considering short-term recordings (5–10 min), spectral analysis of HRV is characterized by three components:

1. A high-frequency (HF) band in the range of 0.15–0.40 Hz, which can be considered as a measure of the physiological respiratory sinus arrhythmia;
2. A low-frequency (LF) band in the range of 0.04–0.15 Hz that corresponds to the LF rhythmicity of systolic arterial pressure frequently observed in conditions of sympathetic activation; and
3. A very low-frequency (VLF) band in the range of 0.0033–0.04 Hz that often shows a progressive decrease of power instead of a discrete spectral peak [37].

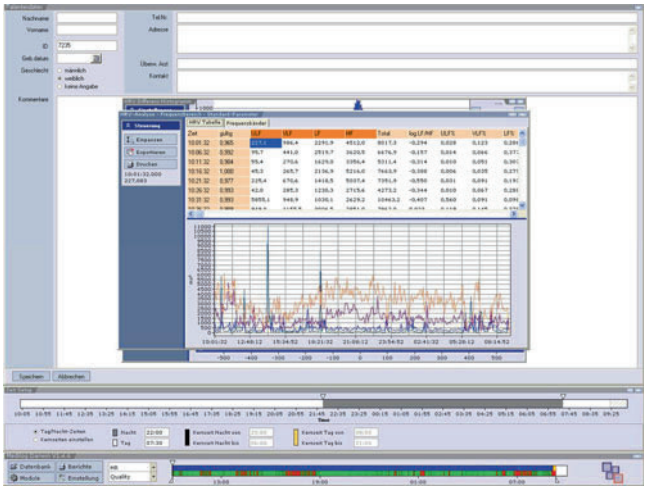

Figure 33.21

Trend curves of frequency-domain parameters of HRV (*bottom*) and numeric printout for the various parameters ULF, VLF, LF, and HF for every 5 min interval (*top*) (Oxford MedilogDarwin system).

Table 33.3

Correlation of the different time and frequency components of heart rate variability (HRV)

Spectral component	Time-domain correlates	Normal measures for 24 hours
HF	rMSSD pNN50	< 15 h < 0.75%
LF	SDNN index	< 30 ms
VLF	SDNN index	< 30 ms
ULF	SDNN SDANN HRV index	< 50 ms < 40 ms ...
TP	SDNN HRV index	< 50 ms ...

Abbreviations: VLF = very-low frequency; ULF = ultra-low frequency; TP = total power; SDNN index = mean of standard deviation of R-Rs; HRV index = integral of the total number of normal R-Rs divided by the maximum of the density distribution

In practical terms, parasympathetic tone is primarily reflected in the HF component, the LF component is influenced by both sympathetic and parasympathetic nervous systems, and the LF/HF ratio is considered a measure of sympathovagal balance, reflecting sympathetic modulations [37]. The spectral profile of long-term recordings is completely different from that of short-term recordings, because most of the energy (up to 90% of total power) is distributed within the ultra-low-frequency (ULF) range ($\leqslant$0.003 Hz) and the VLF range, whereas power of LF and HF accounts for only 10% of total power. Therefore, an alternative approach to the analysis of long-term recordings is to divide the entire 24-h period into a series of around 250 consecutive 5-min periods that are analyzed as short-term recordings [36, 37] (Fig. 33.21). In general, it should be stressed that the two analytical techniques of time and frequency-domain HRV are complementary in that they are different mathematical analyses of the same phenomenon, which explains why certain time and frequency-domain variables correlate strongly with each other, as shown in Table 33.3.

33.5.5.4 Pitfalls and Limitations of HRV Analysis

Some technical aspects and pitfalls of HRV analysis have to be borne in mind. HRV increases with increased periods of observations, and it is important to distinguish ranges on the basis of duration of recordings. In practice, long-term 24-h and short-term 5-min recordings are used. Frequency-domain methods are preferable for short-term, and time-domain methods are mainly used for 24-h recordings (e.g., using SDNN, SDANN, and HRV triangular index), but also for short-term recordings (e.g., using rMSSD). The recording period should last at least ten times the duration of the wavelength of the lowest frequency under investigation (for HF components at least 1 min, for LF components 2 min). Most systems contain and use computer-digitized data with a sampling rate of 128 Hz, which is suboptimal for some experimental short-term recordings, but useful for long-term recordings in adults. In such cases, template matching or interpolation algorithms should be used to optimize the temporal accuracy of R-wave peak identification. If an analog recorder is used, the digitization rate is not relevant, but magnetic tape data may introduce errors related to noise, motion-related artifacts with missing R waves or spuriously detected beats, or other errors in R-wave timing such as might be related to magnetic tape stretch. In addition, arrhythmias may introduce difficulties in the analysis of HRV, for example, persistent AF renders HRV analysis impossible. If more than 20% of the detected beats are ectopic, because the interval before and after each ectopic beat is usually eliminated from the analysis, numerical estimates of HRV will not be accurate. Two methods exist for handling abnormal heartbeats, namely interpolation of occasional abnormal beats [38] and limiting analysis to segments that are free of abnormal beats, respectively.

33.5.6 Analysis of Heart-Rate Turbulence (HRT)

33.5.6.1 Pathophysiological Background

The new parameter of heart-rate-turbulence (HRT) was initially described by Schmidt et al. in 1999 [39]. The concept depends on the influence of single ventricular ectopic beats on the post-extrasystolic oscillations of baroreflex activity. Heart rate is controlled by vagal nerve activity with its direct effect on sinus node depolarization rate and AV-nodal conduction, the latency time is very short (450–700 ms) and thus, the heart responds in a beat-to-beat manner to any changes in vagal nerve activity [40, 41]. Following a single VPB, an instant drop of systolic and diastolic blood pressure ensues with a compensatory pause both in normals and in patients with compromised cardiac function that unloads carotid and aortic baroreceptors with a subsequent decrease of tonic vagal nerve activity [40]. In healthy normals, the drop of blood pressure is prolonged for the first 2–4 post-VPBs together with a transient loss of vagal activity, which seems to be responsible for the acceleration of heart rate. There then follows a steady increase of blood pressure with subsequent baroreceptor loading and an increase of vagal activity leading to a final deceleration phase of cardiac rhythm. In patients with depressed LV function, there is a sudden increase of systolic and diastolic blood pressure in the first post-VPB beat due to post-extrasystolic potentiation that compensates for the drop of blood pressure and activates the baroreceptors. The ensuing increased vagal nerve activity limits the initiation of early acceleration phase and prevents late deceleration phase of cardiac rhythm, that is, HRT cannot be observed [40]. HRT is therefore considered as a parameter of baroreflex sensitivity (BRS) that can be measured much more easily than the classic and complicated baroreflex testing approach.

33.5.6.2 Parameters of Heart-Rate Turbulence

HRT can be quantified by two parameters: turbulence onset (TO) and turbulence slope (TS). TO quantifies the brief phase of early acceleration (usually lasting for 2–4 sinus cycles) and is defined as the difference between the mean duration of the first two sinus beats following a VPB and the mean duration of the last two sinus beats preceding the VPB, divided by the mean duration of the last two sinus beats preceding the VPB. TO is expressed as a percentage. TS describes the speed of the late heart-rate deceleration phase and is defined as the maximum positive slope of a regression line assessed over any sequence of five subsequent R − R intervals within the first 20 sinus rhythm intervals after a VPB. TS is expressed in ms/R − R interval. In patients at low risk for mortality, VPB triggers an early acceleration of heart rate followed by a late deceleration phase, whereas in high-risk patients, HRT is blunted. For prognostic use of HRT, it is important to have

appropriate cut-off values. TO and TS cut-off values were calculated by the group of Schmidt et al. [39, 42] with the use of a "training sample" composed of 100 patients with AMI. The log-rank test statistics for all possible cut-off points revealed optimal dichotomies of 0% for TO and 2.5 ms/R − R interval for TS.

33.5.6.3 Pitfalls and Limitations

It is important to note that Holter AECG data are very useful for evaluation of HRT, in case single VPBs are present in the entire recording, because different interesting time periods can be analyzed separately and, for example, diurnal variations of HRT in relation to clinical events can be detected. Some limitations of this method have to be mentioned. HRT analysis is limited to patients with dominant sinus rhythm. It cannot be used in patients with atrial flutter (AFl) or fibrillation, nor in those with second degree AV block or complete sinoatrial block. It cannot be used in patients with permanently firing cardiac pacemakers, while it is clear that the presence of VPBs in short- or long-term AECG recordings is essential for estimating HRT.

33.5.7 Analysis of QT Interval Variability (QTV)

33.5.7.1 Pathophysiological Background

QT interval (QTI) measurements, particularly in AECG recordings are of special interest, since prolonged ventricular repolarization with abnormal T-wave configuration and increased dispersion of QT-interval duration has been associated with increased risk of life-threatening ventricular arrhythmias both in congenital and in acquired conditions. In normal individuals, the QTI is modulated by multiple factors such as heart rate, circadian rhythm, and autonomic nervous-system activity. Acquired QT prolongation can be induced by myocardial ischemia, cardiac failure, electrolyte imbalances, diabetic neuropathy, and certain cardiac or non-cardiac drugs, while congenital QT prolongation and variability is caused by the abnormal function of cardiac ion channels following specific gene mutations. The main problems that limit the routine measurement of QTI are the absence of unequivocal criteria for determining T-wave offset, particularly in the presence of superimposed U waves, the absence of a general consensus on the best formula for adjusting the QTI to heart rate, and the diffusion of appropriate age- and gender-related normal values for corrected QTIs [43].

33.5.7.2 Technical Aspects

In 12-lead as well as in 3-lead Holter ECG recordings, the end of the T wave for assessing QTI may be determined either by the tangent method (drawing a tangent to the steepest point of downslope of T wave with T-wave offset being at the crossing of the tangent with the isoelectric line) [44], or visually by the return of the T wave to the TP baseline. In the case of U waves interrupting the T wave, the QT offset is measured at the nadir of the curve between T and U waves [45]. Finally, for AECG recordings analyzed by a computer-based technique, T-wave end may be automatically defined on a beat-to-beat basis by calculating the first derivative of the ECG signal and comparing it in the vicinity of expected T end with a threshold value [46].

The dynamic assessment of QTI during AECG monitoring requires computerized automatic measurements, with some technical problems due to low sampling rates, isoelectric baseline shifts, low signal-to-noise ratio, and difficult determination of the T-wave end at faster heart rates [43]. A low-noise ECG can be generated by averaging procedures that require the alignment of several consecutive beats over a given time interval with respect to R-wave peak (generally estimated by parabolic interpolation), and the averaged templates are then analyzed by specific algorithms that automatically detect QRS-T-wave features [47]. Averaging methods provide robust QTI measurements, but they lose the instantaneous variations in QT duration in the function of cycle length changes. Beat-to-beat analysis can explore instantaneous fluctuations of QT duration as a function of cycle length. However, this approach often requires the removal of large proportions of non-physiological data due to baseline noise. Therefore, beat-to-beat QTI measurements are best applied in short-term high-quality ECG recordings obtained under controlled conditions.

For evaluating long-term QTI dynamicity, two methods have been proposed, namely, the evaluation of the circadian excursion of the rate-corrected QTI (QTc), and the long-term evaluation of the QT/R–R relation, based on either beat-to-beat or averaging procedures. These two methods are increasingly implemented on modern commercial Holter systems and thus, are now available for routine clinical application.

33.5.8 Analysis of QT Dispersion (QTD)

33.5.8.1 Pathophysiological Background

The concept of measuring inter-lead variations of the QTI as a noninvasive parameter of QTD is based on observations made early in the 1950s, when Lepeschkin and Surawicz [44] reported QTI differences of 40 ms between leads I, II, and III, and of observations of Han and Moe, who demonstrated that nonuniform (asynchronous) recovery of excitability in the myocardium is an important factor for triggering ventricular tachyarrhythmias. They found meaningful differences in refractory periods even in adjacent (atrial and ventricular) myocardial fibers, for example, for ventricular refractory periods of 43 ms at a cycle length of 700 ms [48]. More recently, Antzelevich et al. showed important differences in refractory periods of myocardial slices due to the significantly longer depolarization and repolarization processes of the M cells in the midventricular myocardial wall compared to cells in the epicardial and endocardial layers [49]. QTD measured as the difference between the longest and shortest QTI within a 128-lead body surface mapping ECG, or a conventional 12-lead or a 3-lead Holter ECG is considered as a parameter of dispersion of ventricular repolarization and might be a prognostic marker of the propensity of a patient to life-threatening ventricular tachyarrhythmias.

33.5.8.2 Technical Aspects

Evaluation of repolarization duration in surface ECGs does not necessarily require a multi-lead system, as demonstrated by Sylvén et al. [50], who showed that the average QT duration computed from Frank's orthogonal leads highly correlates (r = .885, p < .001) with average QT duration obtained from 120-lead body-surface mapping. Zareba et al. [51] could show that in comparison to 12-lead ECGs, dispersion parameters calculated from 3 orthogonal-like leads (I, aVF, V_2) were equally effective in identifying patients who had arrhythmic cardiac death during follow-up. Thus, X, Y, and Z bipolar leads may be used for 24-h Holter AECG recordings to assess QTD at various time segments of the entire recording period.

33.5.8.3 Pitfalls and Limitations

There are several serious arguments against equating QTD with dispersion of ventricular repolarization that have been summarized by Rautaharju (2002) [52]. These arguments are as follows:

1. Measured QTD is determined primarily by dipolar components and does not represent dispersion of ventricular repolarization (the range of QTD in leads generated from strictly dipolar components is of the same order of magnitude as in the original 12-leads)
2. Inter-lead differences of QT duration are largely determined by T-wave "loop morphology" and by the projection of the terminal T-wave vector on individual leads (longest QT occurs in leads with the T-wave vector along the lead axis and shortest when near 90° angle)
3. Abnormal T-wave morphology has a strong influence on QTD (abnormal strictly dipolar morphological patterns can cause large inter-lead QT differences, which represent variability in amplitude/time domain rather than any physiologically meaningful intervals related to repolarization)

4. Overall technical variability of QTD measurement in the short- and long-range is too large to establish feasible thresholds and to separate normal from abnormal QTD (current consensus is that QTD values ⩾100 ms are considered abnormal, but such large variations are commonly occurring with grossly abnormal T-wave morphology)
5. Variations in T-wave amplitude, lead vector strength, and noise level cause additional QTD variation (most T_{offset} detection algorithms use fixed thresholds so that T-wave amplitude variations via projection of strictly dipolar components may cause large QTD variations)
6. The presence of non-dipolar components in body surface ECG during repolarization has not been demonstrated as yet (the presence of non-dipolar components is necessary for detection of the end of localized ventricular repolarization and localized dispersion from QT measurements).

Regarding the many positive as well as negative studies on the prognostic value of QTD measurements and these problematic technical and physiological arguments, it is rather unclear at present whether QTD measurements either from 12-lead or from 3-lead Holter AECG recordings should be further used for stratifying patients with structural heart disease prone to sudden cardiac death (SCD) from ventricular tachyarrhythmias [51–53].

33.5.9 Signal Averaging of the AECG

33.5.9.1 Pathophysiological Background and Parameters of VLP

The technique of signal averaging was developed in order to retrieve small electrical signals at the microvolt level that arise from areas of slow and inhomogeneous conduction in diseased ventricular myocardium. In the early 1980s, advanced techniques were introduced for refinement of filtering of the signals (bi-directional filtering), the selection of bipolar orthogonal X, Y, and Z leads, and their combination into a vector magnitude for maximal sensitivity. In addition, computer algorithms were developed to identify QRS offset and provide numerical values for signals in the terminal part of the QRS complex [54]. A task force of the ESC, AHA, and ACC [55] published standards for acquisition and analysis of VLP and provided clinical indications for a signal-averaged ECG (SA-ECG). Three common parameters for detecting the presence of VLP have been accepted, and suggested cut-off values were given for two conditions, namely, when noise levels <1 μV with 25 Hz high pass filtering or <0.7 μV with 40 Hz high pass filtering are obtained:

1. fQRS = filtered QRS duration; fQRS >114 ms is regarded as abnormal
2. LAS40 = duration of the low-amplitude fQRS signal <40 μV immediately prior to QRS offset; LAS40 >38 ms is regarded as abnormal, and
3. RMS40 = the root mean square voltage of the terminal 40 ms of the fQRS; RMS40 < 20 μV is regarded as abnormal.

33.5.9.2 Pitfalls and Limitations

From a theoretical point of view, signal averaging from Holter tapes may have some technical limitations such as those due to speed stability of the recording and playback processes, a possible increase of background noise due to the patient's activities or inadequate electrode contact, and a restricted frequency bandwidth of the tape recorder. Most of these shortcomings can now be avoided with modern solid-state digital recorders, which provide a wide frequency bandwidth for retrieving microvolt potentials and also have an appropriately high sampling rate (between 1,000 and 4,000 samples/s), thus enhancing the quality of SA-ECGs and allowing frequency analysis methods without the current frequency restrictions. Despite some technical differences between ambulatory and real-time signal averaging, both methodologies have examined orthogonal XYZ leads, but AECG signal averaging has shown that bipolar leads V1, V5, and aVF also correlate closely with orthogonal leads XYZ. In addition, despite appreciable differences between real time and AECG signal-averaging technologies for bandwidth sampling rate and bit resolution, clinical studies have found close correlation and percent agreement between the two methodologies [56, 57]. Finally, the ability to record and analyze signal-averaged high-resolution ECGs from Holter tapes or solid-state recorders offers clear advantages: easy handling of the recordings,

the option of several different recording periods during 24-h of registration, and the chance to assess arrhythmias, ST-segment changes, HRV, heart-rate turbulence, QTV, and late potentials from one data source and to correlate the results with each other.

33.5.10 Reports

There exists no established standard for an adequate AECG report. Most modern Holter recording systems provide composite trend curves for various parameters such as heart rate, arrhythmias, ST-segment deviations, and/or pacemaker activity, histograms of HRV or pacemaker stimulation, tabular summaries of various data, and ECG strips of relevant events either detected from the recordings or patient activated. Real-time ECG strips should provide samples of the ECG at times during which the patient has complained of symptoms, and present a variety of real-time ECG data including samples of each arrhythmia and any ST-segment changes. In many cases, the use of automated computer-based results together with a laser scanning printout of the ECG is useful, particularly for summarizing the data from a lengthy period of recording.

Twenty-four-hour heart-rate trend curves show a mean trend together with the maximum and minimum heart-rate trends calculated over brief time intervals. The difference between these two curves represents the HRV (Fig. 33.20). This visual representation is often useful in understanding the causes of events over a relatively long period of time and for comparison with other events, for example, supraventricular or ventricular arrhythmias or ST-segment depression. Combined with the enumeration of the QRS complexes, it provides some indices, which indicate the variation of the dominant heart rate (usually sinus rate) according to the influence of autonomic tone. In general terms, the difference between day time and night time heart-rate curves is a good index of the importance of sympathetic tone. Moreover, depending on the different special features of Holter systems, many manufacturers provide histograms of QT/R – R relation, HRV, pacemaker stimulatory activity (Figs. 33.22 and 33.23), or respiratory behavior of the patient.

Diagrams of premature beats are mainly used for displaying counts of PVCs. They express the variation of the number of abnormal events as a function of time and hence give an indication of the 24-h variation. The coupling interval of

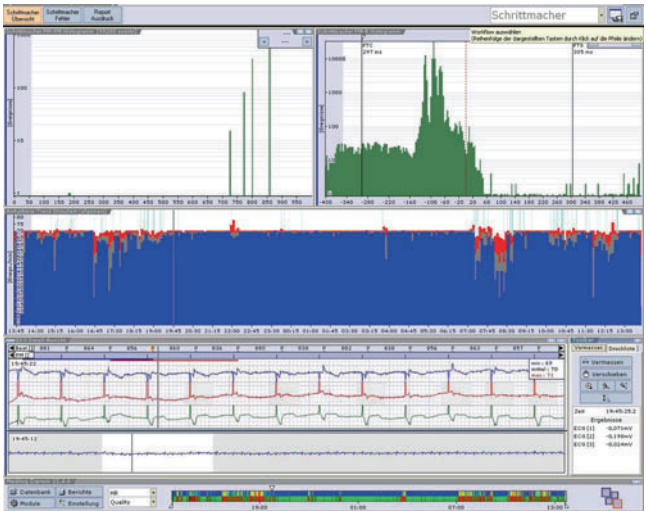

Figure 33.22

Pacemaker analysis: histogram of the intervals of successive pacemaker pulses (*top left*), histogram of the intervals of pacemaker pulses relative to the corresponding R waves (*top right*), trend diagram of pacemaker-induced ventricular stimulation in bpm over the whole monitoring period in a patient with predominant pacemaker activity (*second row*), and three-channel real-time ECG (*bottom*) (Oxford MedilogDarwin system).

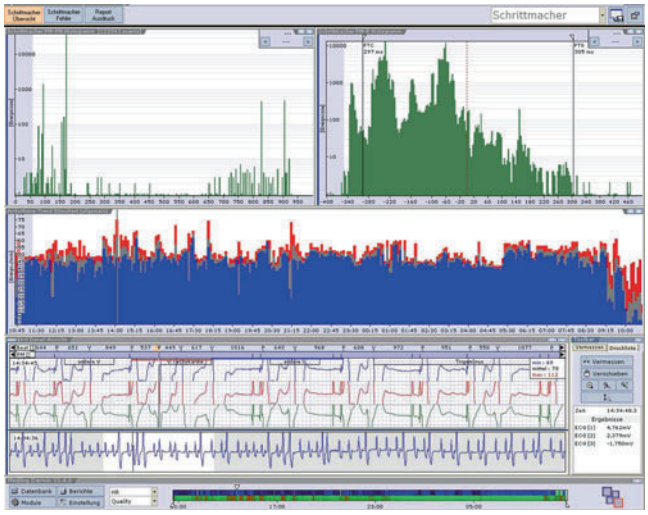

Figure 33.23

Pacemaker analysis: histogram of the intervals of successive pacemaker pulses (*top left*), histogram of the intervals of pacemaker pulses relative to the corresponding R waves (*top right*), trend diagram of pacemaker-induced ventricular stimulation in bpm over the whole monitoring period in a patient with intermittent pacemaker activity (*second row*), and three-channel real-time ECG (*bottom*) (Oxford MedilogDarwin system).

the premature beats can also be determined and displayed on a separate diagram. The comparison between the heart-rate trends and the PVC diagram is useful in presenting the relationship between heart rate and PVCs with their daily variations (Fig. 33.17).

R – R interval or pacemaker stimulation histograms (Figs. 33.22 and 33.23) are used by almost all manufacturers with some variations. A histogram of the R – R intervals presents all the QRS complexes arranged as a function of the preceding R – R interval. These R – R-interval histograms can be generated at fixed intervals during the 24 h of real time and superimposed to illustrate their progressive variation or the sudden appearance of an arrhythmia. Another type of graphic reporting is that of Lorenz or Poincaré plots, which summarize the data of HRV over a full AECG recording period. Recently, a novel application of these Lorenz plots has been developed for summarizing the full 24-h ECG data of AF (Fig. 33.24) together with hill-like trend curves (Fig. 33.25).

An essential part of a Holter AECG report is the presentation of a tabular summary of all relevant parameters on an hourly basis, for example, total number of QRS complexes, supraventricular and ventricular ectopic beats, couplets, triplets, or tachycardias, abnormal pauses of cardiac rhythm, HRV criteria both in the time and frequency domain, and pacemaker stimulation as well as pacemaker failures. In addition, full 24-h ECG disclosure – if desired – should be provided, as well as a variety of real-time ECG strips including samples of each arrhythmia or pauses of cardiac rhythm, any ST-segment changes and pacemaker dysfunction.

33.6 Incidence of Arrhythmias in Apparently Healthy Individuals

Before interpreting an AECG recording, the physician should be well acquainted with the findings in the apparently normal population. Some general points can be made from the literature [4, 26, 58–65] concerning the usual and unusual findings in apparently healthy persons.

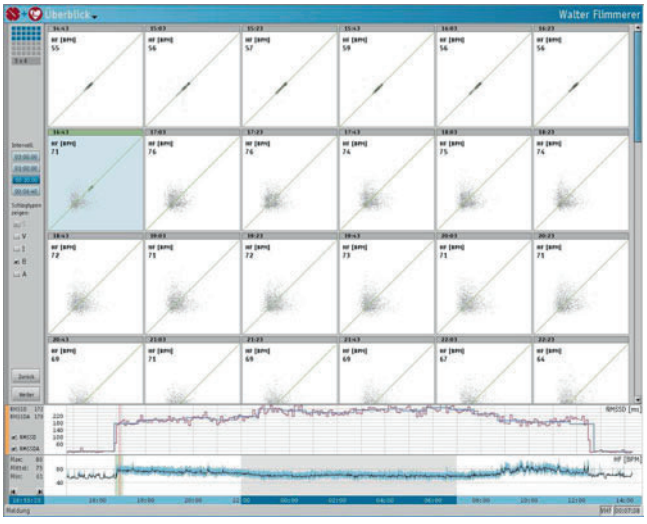

Figure 33.24
Lorenz plots in a patient with sinus rhythm (*top row*) and AF for 20 min intervals each (*middle row*) and trend of HRV time domain parameters together with heart-rate trend (*bottom*) (Medset system).

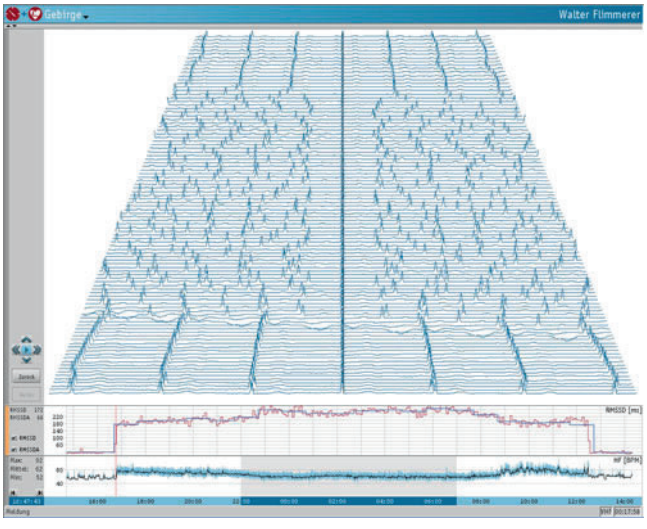

Figure 33.25
Hill-like plot of consecutive ECG complexes in a patient with sinus rhythm (*upper* and *lower segments*) and AF and trend of HRV time domain parameters together with heart-rate trend (*bottom*, Medset system).

33.6.1 Maximal and Minimal Heart Rate

In general, the sinus rate tends to diminish with age as judged by AECG monitoring [58]. This is particularly obvious for the maximum heart rate during daytime. In elderly persons, the heart rate does not usually exceed 130 bpm. On the other hand, in a young population, it is not uncommon for the sinus rate to exceed 180 bpm during waking hours. According to the literature, the mean heart rates for 24-h AECG monitoring are 76.3 ± 11.8 bpm, between 10 a.m. and

6 p.m. they are 79.2 ± 11.0 bpm, and between 1 a.m. and 5 a.m. 66.1 ± 10.8 bpm. Women have a significantly higher mean heart rate than men (5–10 bpm higher [59]). The usual definition of sinus bradycardia (less than 60 bpm) is inappropriate for 24-h Holter ECG reports, because in all "normal" populations, a sinus rate between 40 and 60 bpm is commonly registered during sleep. The minimal sinus rate usually occurs at the end of sleep, that is, between 5 am and 6 am in persons with a normal diurnal cycle. Diurnal and nocturnal variations of sinus rate can easily be appreciated by ambulatory monitoring.

33.6.2 Sinoatrial Pauses

In association with sinus arrhythmia and bradycardia, sinus pauses ranging from 1.2 to 2 s are commonly encountered in 24-h ECG. However, pauses greater than 2 s have been seen in less than 1% of the normal population, usually during sleep and in young subjects. These pauses are probably caused in part by an enhanced vagal tone. Such findings are common in athletes. Therefore, only sinus pauses in excess of 2 s can be considered as abnormal, and therefore require further attention in adult or elderly subjects.

33.6.3 AV Block

First-degree and second-degree AV block are occasionally noted during ambulatory monitoring in healthy individuals. These blocks most commonly occur during sleep and are accompanied by sinus bradyarrhythmia. Second-degree AV block is always of the Mobitz type I, even if in some cases it occurs abruptly, thus making the increase of PR-interval duration less obvious. These episodes, which occur during sleep in young subjects, are always asymptomatic. In some rare cases, more significant conduction disturbances can be recorded, as in the example of Fig. 33.26. The ECGs are from a 37-year-old man submitted to ambulatory monitoring because of atypical chest pain. The symptoms were subsequently found to be unrelated to CAD, which was confirmed by coronary angiography and vasospastic provocative tests. During sleep, two episodes of second-degree AV block occurred with two or three P waves blocked in succession. Another recording performed one week later revealed the same phenomenon. This patient remained free of syncope or dizziness after a 4-year follow-up. Table 33.4 summarizes the arrhythmias that should be considered "normal for age" according to the literature.

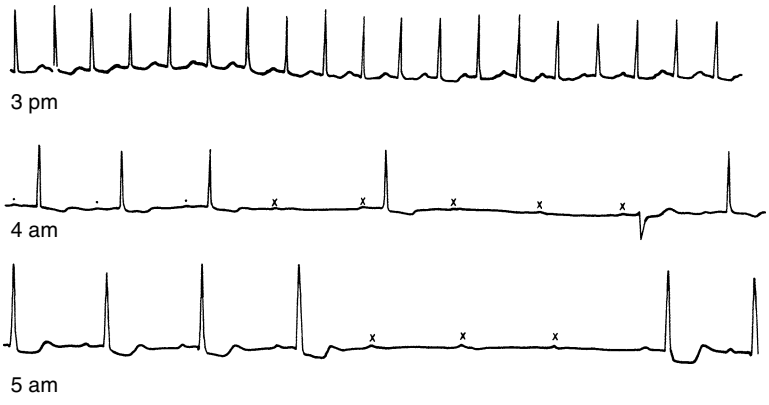

Figure 33.26
Paroxysmal AV block (blocked P waves are marked with crosses) occurring during the night in a young athletic man with no detectable heart disease. After four years of clinical follow up, this subject remained asymptomatic.

Table 33.4

Normal findings of heart rate and arrhythmias on 24-hour ambulatory ECG monitoring according to age

Arrhythmias	Age ⩽ 25 years	Age 25–65 years	Age > 65 years
Sinus pauses	⩽ 2500 ms	⩽ 2000 ms	⩽ 2000 ms
AV block	some occurring at night	none (except in case of regular physical training)	none
APCs	< 10 h^{-1}	< 10 h^{-1}	< 100 h^{-1}
Atrial tachycardia (3 or more APCs)	none	none < 50 years some > 50 years	some
PVCs	< 10 h^{-1}	< 10 h^{-1}	< 100 h^{-1}
Ventricular tachycardia (3 or more PVCs)	none	single < 10 QRS	single < 10 QRS

33.6.4 Atrial Arrhythmias

Atrial premature contractions (APCs) detected by AECG are reported to occur in 23–100% of normal persons studied [60–65]. The incidence of APCs increases significantly with age, being nearly absent in children (if it is distinguished from physiological sinus arrhythmia), but almost constantly present in healthy individuals of 65 years and more. Moreover, in these normal elderly patients, it is common to find frequent APCs (>1 min^{-1}) and/or episodes of paroxysmal atrial tachycardia (PAT). The incidence of PAT varies greatly from one report to another, but an awareness of the high incidence of PAT is of major importance for the interpretation of 24-h recordings in older patients complaining of symptoms. The discovery of a short isolated PAT in an 80-year-old subject does not imply any relationship with the symptom if it was not simultaneously felt during the recording.

33.6.5 Ventricular Arrhythmias

The occurrence of premature ventricular contractions (PVCs) in normal populations as detected by Holter recordings has been reported to range from 17% to 100% of individuals studied [60–65]. Depending on the variable length of ambulatory examination in these studies, one may conclude that the incidence of PVCs is approximately 50% in normal persons examined for 24 h and increases to approximately 75% in those studied for 48 h. Where various age groups have been studied, there is a clear relationship between age and the incidence of PVCs. Normally, healthy individuals have less than 100 PVCs per day without any runs of VT. In some healthy aged persons, however, numerous, perhaps multifocal, PVCs can occur and, more rarely, short runs of VT. In particular, accelerated idioventricular rhythm may occur during sleep.

According to these data, it is possible to consider as unusual the prevalence of frequent (>1 min^{-1}) or complex PVCs in individuals less than 65 years old. Such a prevalence and frequency of PVCs is not, of course, necessarily pathologic, but does require further examination to determine whether or not there is an underlying heart disease.

33.7 ST-Segment Changes in Apparently Healthy Persons

There are not many reports of ST-segment changes on 24-h ECGs in apparently healthy persons. However, three important studies have been published [66–68] involving 50, 120, and 182 volunteers, respectively.

In the first [66], ST-segment depression was defined as at least 0.1 mV horizontal or downsloping shift of the ST segment persisting 80 ms after the J point of the QRS complex. It occurred in 10–30% of the normal population in these

studies, with multiple episodes in the majority of these during a single 24-h ECG recording. These changes usually took place at the same time as daily exercise, with a cardiac rate of over 100 beats per minute. Isolated T-wave inversion was even more frequent.

The frequency of ST-segment elevation (>0.1 mV) at the J point in these healthy subjects is a matter of some debate, being absent in the study of Armstrong et al. [66] but present in 23% of the volunteers of Quyyumi et al. [67]. In this study, ST-segment elevation occurred preferentially in young men, with a simultaneous low heart rate. At the same time, T waves became upright and peaked. The mean duration was usually very long (several hours). The difference between the two studies is probably caused by a difference in the criteria of positivity, while the pattern of ST changes is different from that observed in spontaneous angina. In these latter patients, ST elevation includes the T wave, with an aspect of the monophasic action potential, and the R wave increases. These modifications are progressive and persist for a few minutes only. Some studies have emphasized the fact that ST-T changes are more frequently encountered in female volunteers than in male volunteers; for example, 18% versus 1% in the Bjerregaard study [68].

Many ST-T abnormalities may be caused by positional change of the subject during the course of 24 h, and every effort should be made to assess whether ST-T change is indeed a genuine phenomenon. It should also be noted that most analyzers available at the present time do not detect major T-wave changes including a complete reversal of T-wave polarity. This is a significant shortcoming of all systems, although the operator could in fact position the ST marker at a point in the early part of the T wave if a search for T-wave changes is particularly desired. According to the literature, ST-segment elevation $\leqslant$0.3 mV at night with T-wave increase upward or downward in individuals at ages below 40 years are considered normal, as is the case for ST-segment depression $\leqslant$0.2 mV during tachycardia with upward or downward sloping ST segment accompanied by all types of T-wave changes as well.

Despite its shortcomings, 24-h ECG examination represents a useful diagnostic procedure in patients with spontaneous chest pain. In subjects with exercise-related symptoms, an exercise test provides more precise data with a higher specificity.

33.8 Clinical Relevance of AECG Recording

33.8.1 Evaluation of Patient's Symptoms

Patients often complain of symptoms, which are transient but suggest a cardiac origin. Holter ECG is an essential examination in such cases. This noninvasive technique is able to provide an accurate diagnosis, especially if the symptom coincides with any ECG abnormality detected during the recording. The most widely accepted use of AECG is the determination of patient's transient symptoms to cardiac arrhythmias. Some symptoms such as palpitation, syncope, near syncope, or dizziness are commonly caused by transient arrhythmias, whereas other transient symptoms such as shortness of breath, chest discomfort, diaphoresis, weakness, or transient ischemic cerebral attacks are less commonly related to cardiac arrhythmias. In principle, four possible outcomes may be expected with AECG monitoring: (1) typical symptoms may occur with the simultaneous documentation of a cardiac arrhythmia, (2) symptoms may occur at periods with no cardiac arrhythmias seen in the AECG, (3) during cardiac arrhythmias the patient may remain asymptomatic, and (4) the patient may remain symptomatic during AECG recording, and no arrhythmias are documented. With regard to situations (1) and (2), such findings are useful for further management of the patient in that either the symptoms can be related to arrhythmias or arrhythmias are not the cause of symptoms. The finding in the third situation is equivocal and in the fourth situation not helpful for further clarification of the patient's complaints.

33.8.1.1 Palpitations

Many patients complain of a variety of symptoms grouped under the term palpitations [4, 69–71]. If these symptoms are frequent, for example, every day, 24-h Holter ambulatory monitoring is the optimum way for their evaluation. In many cases, an abnormality can be seen at the time of the symptoms, signifying that they are related to a cardiac arrhythmia. Sometimes, a sinus tachycardia represents the electrocardiographic basis for palpitations. In contrast, it is well known

that patients may have quite severe cardiac arrhythmias without being aware of them. This is particularly true for isolated PVCs, for frequent PVCs, and for short runs of VT. In any event, if palpitations are perceived during the recording, an accurate evaluation is easily provided by replaying the cassette tape or computer digitized ECG storage at the corresponding time. The problem is quite different in the absence of palpitations during ambulatory monitoring. In this case, the finding of one normal 24-h recording does not permit any conclusion to be drawn and the surveillance should be continued if symptoms have previously occurred with a reasonable frequency.

More difficult is the problem of the relevance of some arrhythmias recorded during ambulatory monitoring without simultaneous palpitations. Their significance depends on the incidence of the type of arrhythmia in the normal population. The occurrence of PVCs, even with some salvos, in an adult or aged patient, particularly if the patient suffers from coronary heart disease (CHD), is of little relevance; it is of limited importance to conclude that palpitations are caused by paroxysmal VT. Similarly, the discovery of short runs of atrial tachycardia in an elderly patient is irrelevant. However, if the arrhythmia observed is unusual according to the characteristics of the patient, it is probable that it may be the cause of the palpitations. This situation is variable according to the circumstances and the patient's activities. Nevertheless, the certainty of the diagnosis can only be assessed by an ECG recorded simultaneously with the symptom. For all these reasons, AECG monitoring is the preferred diagnostic method of examining such patients and is equally or more sensitive than other reported diagnostic techniques. The major exception is in relation to paroxysmal reciprocating junctional tachycardia where the attacks are very rare. The AECG recording is always normal between the attacks.

33.8.1.2 Dizziness or Syncope

Transient disturbances of consciousness producing dizziness or syncope are most commonly caused by a critical circulatory decrease in cerebral blood flow. Sinoatrial pauses or paroxysmal AV block may cause these symptoms, but modifications of heart rate alone may also cause disturbances of cerebral blood flow, mainly through tachycardia [4, 69–71]. It is now clear that healthy persons may tolerate a heart rate as low as 30 bpm and be asymptomatic, but ventricular rates higher than 150 bpm, particularly in elderly subjects or when underlying heart disease is present, often lead to a decrease in cerebral blood flow by causing inadequate ventricular diastolic filling and fall in cardiac output.

In several studies, a continuous ECG recording taken until symptoms have occurred shows that dizziness or loss of consciousness are, in the majority of cases, caused by a paroxysmal tachycardia (of atrial or ventricular origin) and not, as might be expected, by paroxysmal SA or AV blocks. Important inter-individual variations in the tolerance of arrhythmias are now well known. A normal young subject can tolerate an ectopic tachycardia with a heart rate in excess of 200 bpm or ventricular pauses of more than 3 s without producing symptoms of cerebral ischemia, whereas an older patient may faint after a few seconds of atrial tachycardia at 150 bpm. The state of the cerebral vessels, the presence or absence of cardiac disease, the body position and the duration of tachycardia or bradycardia are important considerations, and the occurrence or absence of symptoms depends on a combination of these factors.

Overall, the diagnostic yield of AECG monitoring for syncope or near syncope is relatively low. Seven to thirty-nine percent of patients with symptoms during AECG were reported to have no arrhythmia, and 1–26% to have arrhythmias. In patients without symptoms during AECG, 17–80% had no arrhythmia and 10–41% had episodes of arrhythmias [7]. In the study of Bass et al. [72], the value of three consecutive 24-h monitoring periods was evaluated. A major abnormality within the first 24-h recording was seen in 15% of patients, the additive yield was 11% on the second, and 4.2% in the third sequential recording. In this study, age, male sex, history of heart disease, and initial rhythm other than sinus were identified as factors that identified a useful recording [72].

33.8.1.3 Previous Ischemic Strokes

With the development of 24-h Holter recordings, previous ischemic cerebrovascular attacks become an important indication for this examination [73–76]. In most cases of this type of disease, the exact cause of the stroke remains unclear. Thus, the 24-h Holter examination is performed to search for a cardiac arrhythmia that might cause cerebral embolism.

Those arrhythmias able to induce a systemic embolism are almost always paroxysmal atrial arrhythmias and, in a few cases, VT, in the presence of left ventricular thrombus owing to previous myocardial infarction or cardiomyopathy. When an underlying cardiac disease is present, the diagnosis of systemic embolism is easier, but if clinical examination is completely normal, a 24-h AECG recording remains the best way of detecting a paroxysmal arrhythmia. However, the systematic use of this technique in all ischemic strokes is disappointing, since only a small proportion of patients with significant paroxysmal atrial arrhythmias may be identified. The great majority of these patients with previous stroke are over 60 years old and the relevance of these arrhythmias is unclear. As previously described, a significant proportion of "normal" elderly subjects can exhibit some short runs of atrial tachycardia. Therefore, the occurrence of such a disorder in a patient at risk of ischemic strokes does not prove by itself that the arrhythmia is the actual cause of the stroke. Only a sustained atrial tachycardia (lasting more than 10 min) should be considered as relevant in these elderly patients. As a result, the practical consequences (that is, the decision to begin anti-arrhythmic and/or anticoagulant therapy) are rarely directly related to the result of the 24-h AECG recording. In view of the economic and human costs of this technique, it is not recommended that it be performed systematically in all cases of stroke. It is preferable to reserve it for the younger patients (in which case an atrial arrhythmia is definitely relevant) or for cardiac patients, in whom there is the likelihood of a sustained arrhythmia.

33.8.1.4 Chest Pain

Transient unpredictable chest pain is a frequent symptom and may present a diagnostic problem for the clinician. Although exercise stress testing should be the first line of investigation, occasionally AECG may be a more practical and useful diagnostic test, particularly if the chest pain is unpredictable with respect to time of onset or cannot be provoked by exercise. Two- or three-channel AECG recording permits examination of anterior, inferior, and lateral myocardial leads for the detection of ischemic ST-segment changes during episodes of chest pain with or without cardiac arrhythmias [77–82].

Twenty-four-hour Holter ECG has emerged as a primary method of examination in patients with suspected variant angina in whom pain usually occurs unpredictably [78, 79]. The diagnostic value of this technique is demonstrated in the example of Fig. 33.27. In this case, considerable ST-segment elevation occurs during an episode of atypical chest pain, and there can be little doubt about the existence of variant angina probably caused by coronary artery spasm. The absence of ST-segment changes, however, appears to be of lesser value in reassuring the patient and the clinician that ischemic heart disease is absent because of the possibility of false-negative responses owing to inadequate lead positioning, short-lived ST-T changes, which are not detected during visual analysis of the replayed tape, as well as other factors. Finally, it should be stressed that only considerable deviation of the ST segment should be regarded as significant because of the frequency of minor abnormalities in normal persons during continuous ambulatory recordings.

33.8.2 Appraisal of the Mechanism of Arrhythmias

One of the major advantages of AECG is the facility to clarify the circumstances preceding the onset of arrhythmias. This technique enables the clinician to appreciate the many important characteristics concerning the mechanism of the arrhythmias, in particular the role of the autonomic nervous system (ANS) in more general terms, he/she can deduce the rhythmological explanation of the paroxysmal arrhythmia in question.

33.8.2.1 Sinoatrial Disorders

The main use of 24-h Holter ECG in this particular group of disorders [4, 83] is to indicate whether SA dysfunction is dependent on the daily cycle or on the sinus rate. This appears to be of importance in differentiating between "physiological" vagotonic SA pauses occurring in a young athletic subject during sleep or at rest and "pathological" SA block

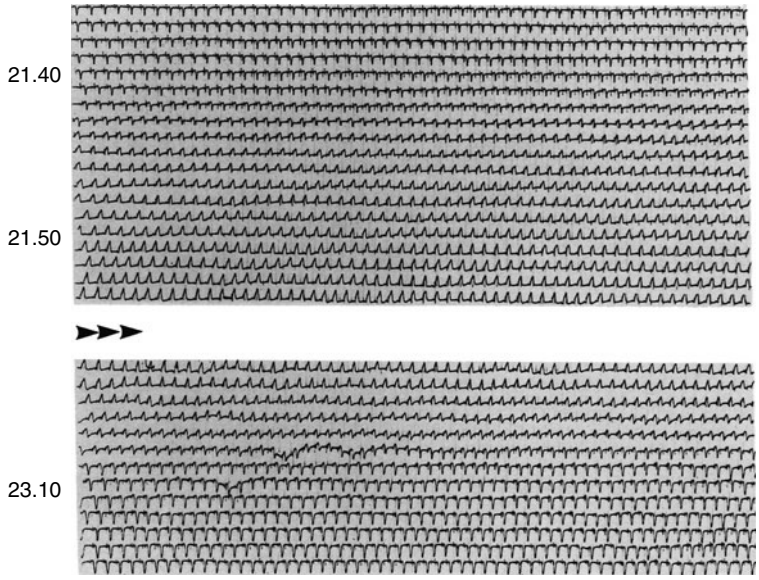

Figure 33.27

An example of an ECG recorded during an episode of variant angina. The ECG is produced as a fiber-optic printout where one line represents 1 min. The time of recording is indicated on the *left*. Note the alteration between deep negative T waves on the one hand (as at 21.40) and marked ST elevation on the other (as at 21.50).

occurring at any time of the day or night. Moreover, in some cases, Holter monitoring is able to indicate that SA dysfunction occurs specifically when the sinus rate increases. This is a strong argument for concluding that a phase III SA block exists, and not merely a transient interruption of sinus automaticity. In this type of conduction disorder, the abnormalities are usually detected during the first 24-h Holter recording. A completely normal AECG recording constitutes a strong argument for the elimination of SA block from the differential diagnosis.

33.8.2.2 AV Block and Intraventricular Disorders

AECG monitoring is sometimes able to determine the mechanism of AV or intraventricular conduction disorders. This technique may be able to distinguish between proximal and distal AV block (between Mobitz type I and II) and between physiological and pathological blocks. In general terms, if a nodal AV block exists, it is usually present on numerous occasions during a 24-h recording, while it is easy to differentiate the physiological nodal AV block occurring abruptly during sleep in a young athletic subject from the permanent pathological block (of varying degrees) in an elderly patient. It is much rarer to capture a distal AV block during a single 24-h examination. However, in this case it is sometimes possible to discern a peculiar mechanism such as modifications of sinus rate or occurrence of long or short R–R cycles. A typical pattern of paroxysmal AV block caused by sinus tachycardia (phase III block) is shown in Fig. 33.28. This kind of tachycardia-dependent AV block is characteristic of a distal localization (intra-Hisian or infra-Hisian).

In these examples, all the usual characteristics of the conduction disorder are detected by AECG monitoring and an EPS becomes unnecessary. In the same way, the mechanism of some intermittent intraventricular conduction disturbances can be elicited by 24-h monitoring (phase III or phase IV blocks, succession of long and short R–R cycles). The discovery of an intermittent bundle branch block may be important clinically. A paroxysmal AV block seems less probable in the presence of an isolated intermittent bundle branch block than in the presence of a permanent bundle branch block.

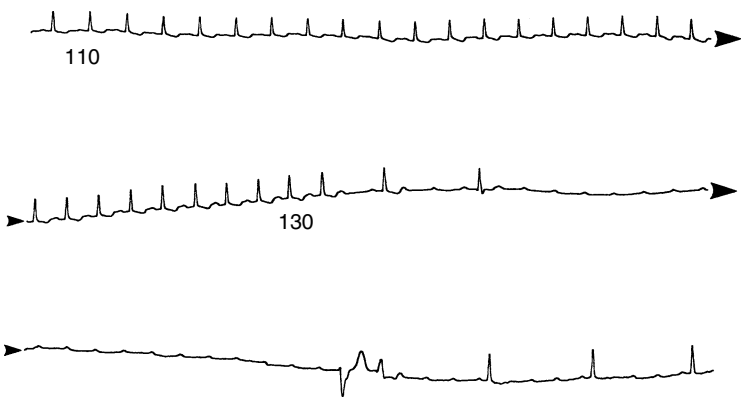

Figure 33.28
Paroxysmal AV block occurring during sinus tachycardia (phase III block) at 130 bpm (heart rate indicated on figure in bpm). A subsequent EPS showed intra-His bundle AV block reproduced by rapid atrial pacing.

33.8.2.3 Paroxysmal Atrial Arrhythmias

In a large number of patients, the reason for the occurrence of a paroxysmal atrial arrhythmia [84, 85] remains unclear, particularly when no morphologic changes of the atria can be found. AECG monitoring is often useful in such cases since on many occasions it demonstrates the importance of the ANS in the genesis of the arrhythmia. Two opposite forms of paroxysmal arrhythmias can then be described, namely, vagally induced arrhythmias and adrenergically induced arrhythmias. With respect to the former, the atrial arrhythmia is preceded by a progressive decrease of sinus rate either during night or at rest, as demonstrated by heart-rate trend curves (e.g., Fig. 33.29). Usually, this heart-rate threshold is not unduly low (50–60 bpm). Middle-aged patients may experience palpitations, and sometimes peripheral embolisms. The atrial arrhythmia remains in paroxysmal form for a long period, commonly more than 10 years. It becomes progressively more frequent, occurring either daily or several times a day, and appears resistant to conventional therapy. Beta blockers, digitalis, and verapamil usually aggravate the arrhythmia and class I drugs are also unsatisfactory. Only amiodarone may be helpful when taken alone in the initial stages of the disease and in the later stages when combined with a class I drug. In some instances, sinus bradycardia preceding the onset of the atrial arrhythmia occurs abruptly during a few R–R cycles, suggesting a sudden increase in vagal tone as shown in Fig. 33.30. In these cases, it is sometimes possible to find a gastrointestinal reason for this enhanced vagal tone. Treating this condition may suppress the arrhythmia simultaneously. In some cases, which are resistant to all combinations of drugs, rapid atrial pacing may improve the clinical situation.

The opposite form, the paroxysmal adrenergic atrial arrhythmia, appears less frequent in contrast to the high frequency of palpitations experienced during exercise, emotion, or other high-hyperadrenergic states, which are mainly caused by isolated sinus tachycardia without rhythm disturbances. This type of arrhythmia is preceded by a progressive increase of sinus rate during daytime, which is not necessarily related to physical exercise (Fig. 33.31). Except for some patients with an unsuspected hyperthyroidism, any organic cardiac disease may be present. Beta blockers are able to control the arrhythmia for some weeks or months, after which an escape phenomenon occurs, which requires additional class I drug therapy. Amiodarone or propafenone may be useful due to their noncompetitive inhibitive effect on the beta adrenoreceptors. The distinction between these two opposite forms of atrial paroxysmal arrhythmia often appears to be somewhat theoretical, because many patients cannot be easily classified into one or other type. On many occasions, however, ambulatory monitoring is of great value in these patients to provide a guideline for therapy.

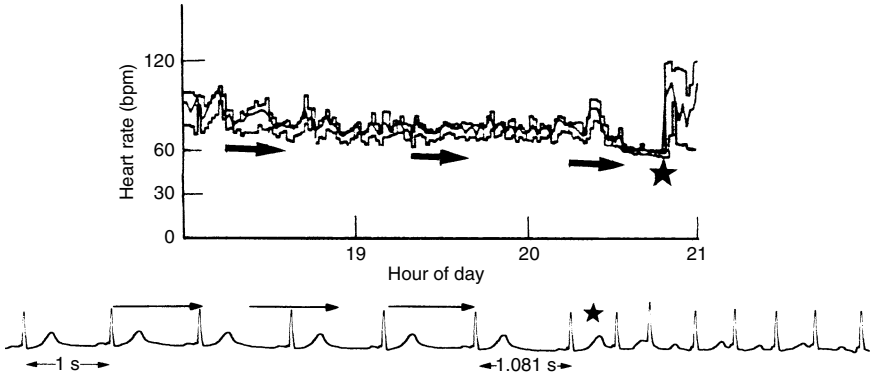

Figure 33.29

An example of a vagally induced atrial arrhythmia. A progressive sinus bradycardia with changes in atrial depolarization precedes the onset of AF. The change in rhythm marked by the star is also detected on the rate-trend curves.

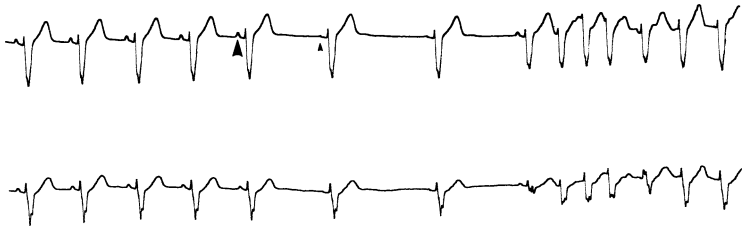

Figure 33.30

Another example of a vagally induced atrial arrhythmia. The onset of AF is preceded by a sudden sinus bradycardia.

33.8.2.4 Paroxysmal Junctional Reciprocating Tachycardias

Usually, Holter monitoring is unprofitable in paroxysmal junctional reciprocating tachycardias because of the rarity of the attacks and the normality of the ECG recording between attacks. However, in some patients with frequent episodes of this type of tachycardia, ambulatory monitoring is able to demonstrate the mechanism that triggers its onset. When combined with the data from an EPS detailing the reentry circuit, the knowledge of the triggering mechanism often constitutes a guideline for therapy, for patients incapacitated by their arrhythmia. The most frequent initiation mode of the reciprocating tachycardia appears to be premature atrial contractions (PACs). It is interesting that in some patients, PACs are able to trigger the arrhythmia only if they occur during sinus tachycardia, reflecting an increase in sympathetic tone. This predisposing role of the adrenergic system is well known. Clinicians use isoprenaline during electrophysiological studies to induce the tachycardia more easily by atrial premature stimulation; this is because of the facilitation of conduction through normal and/or accessory pathways. In some of these patients, beta-blocking drugs should be added to previous antiarrhythmic therapy in order to obtain a satisfactory result.

Less frequently, the triggering mechanism of the tachycardia is PVCs, and in some patients with numerous PVCs it is remarkable that the tachycardia occurs only with a couplet and never with isolated PVCs. In a similar manner, during electrophysiological studies, a single ventricular extrastimulus is frequently unable to induce the tachycardia, which occurs with two or more extrastimuli. The practical consequence in this case is that there is a good chance of success for class I or III AADs being able to suppress the repetitive phenomena of PVCs. The three other mechanisms of triggering, specific for accessory pathways, require individual recognition and treatment. Induction of reciprocating tachycardias by sinus tachycardia (owing to a phase III block in concealed anterograde conduction through the accessory pathway) should be treated by beta-blocking agents or by amiodarone. The reverse situation, that is, induction by junctional escape beats (preventing concealed or patent anterograde conduction through a Kent bundle) or sinus bradycardia (with a phase

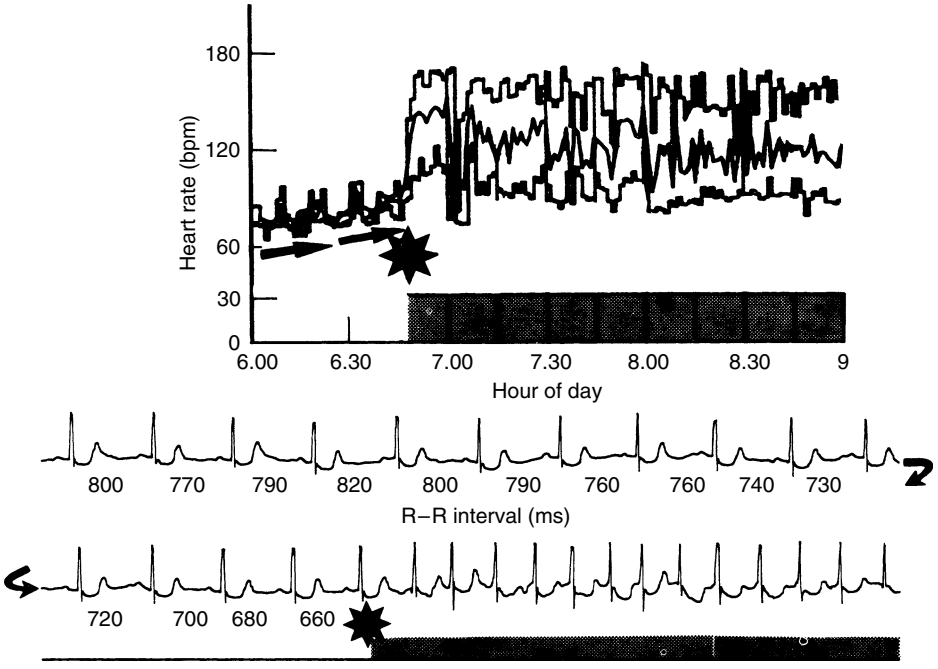

Figure 33.31

An example of an adrenergic atrial arrhythmia. Paroxysmal AF is preceded by a progressive sinus tachycardia. The change in rhythm labeled by the asterisk can also be seen on the heart-rate trend curves.

IV block in the Kent bundle) usually requires pacemaker implantation or catheter ablation. The most recent and highly effective mode of therapy is catheter ablation of the accessory pathway based on a detailed mapping procedure using multiple intracardiac catheter electrodes.

33.8.2.5 Ventricular Arrhythmias

AECG monitoring is normally less useful than electrophysiological studies in elucidating an electrophysiological mechanism of ventricular arrhythmias [86–88]. The EPS is superior in providing criteria that suggest reentry, for example. In contrast, 24-h Holter monitoring is the examination of choice in the case of parasystolic beats, providing most useful data for the study of these rhythm disturbances [89]. In general, recording the onset of VT often reveals important information on the intrinsic mechanisms of the arrhythmia. Some examples illustrating these findings and their practical consequences are now discussed.

Figure 33.32 shows a run of VT initiated by a compensatory pause following a single PVC with a morphological pattern different to those of the VT. This is a good demonstration of two different conditions necessary for the initiation of VT; that is, an isolated PVC as the trigger mechanism and a ventricular pause creating local conditions favorable to the sustaining mechanism of VT (focal or intraventricular reentry). In this situation, two therapeutic regimes can be proposed: suppression of the trigger mechanism or depression of the sustaining mechanism. Figure 33.33 is another example of a possible duality of the mechanisms involved in the genesis of a VT: an intraventricular reentry (as confirmed subsequently by EPS) triggered by APBs. In this case also, antiarrhythmic therapy may suppress the clinical VT in two different ways. The role of sympathetic tone, often important in the genesis of VT, is easily demonstrated by AECG monitoring, showing the relationship between VT and sinus tachycardia, which reflects an enhanced sympathetic activity. In the case presented in Fig. 33.34, paroxysmal VT occurs and persists during a period of sinus tachycardia owing

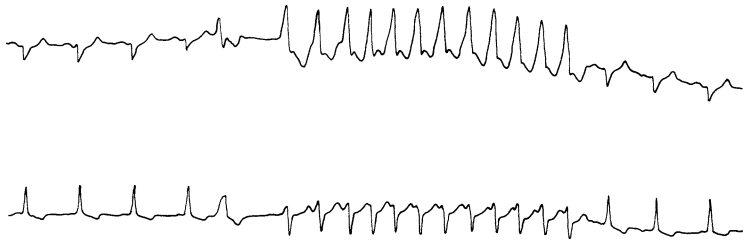

Figure 33.32

A two-channel Holter ECG showing a run of VT initiated by a PVC of different morphological patterns followed by a compensatory pause. This spontaneous mode of initiation is unusual in patients with reentrant VT, which is easily induced by electrophysiological means.

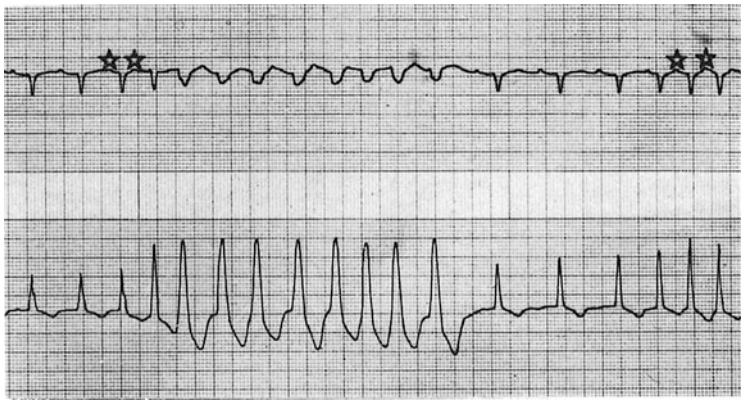

Figure 33.33

An example of bitachycardia (coexistence of atrial and VT) in a patient with cardiomyopathy. A run of VT is initiated by a couplet of APCs indicated by the first pair of stars. Two simultaneously recorded leads are shown. In this case, the VT could be triggered by extra stimulation and was probably caused by a reentrant mechanism.

to psychological stress, and disappears only when sinus tachycardia ceases. In the same manner, in some cases of sudden death, sinus tachycardia indicating an increased sympathetic tone seems to play an important role in the triggering mechanism of the fatal arrhythmia.

The understanding of the mechanism of sudden death in cardiac patients is probably the best recent example. As demonstrated by some important series [90–92], the role of myocardial ischemia is practically confined to asystoles, and the vast majority of sudden deaths caused by a ventricular tachyarrhythmia are not directly caused by ischemia. Iatrogenic (drug-induced) "torsades de pointes" may be responsible for sudden death in noncoronary patients. Ventricular fibrillation (VF) is the usual mode of sudden death in coronary patients without preceding ischemia. VF usually follows a sustained VT, which accelerates before its transformation into VF. The electrophysiological phenomena leading to VT/VF are a shortening of the coupling interval of PVCs, a long R–R cycle (postextrasystolic pause) in half of the cases, an atrial arrhythmia or, more generally, an increase of heart rate reflecting an increase of sympathetic tone. This latter represents the main determinant of VT/VF.

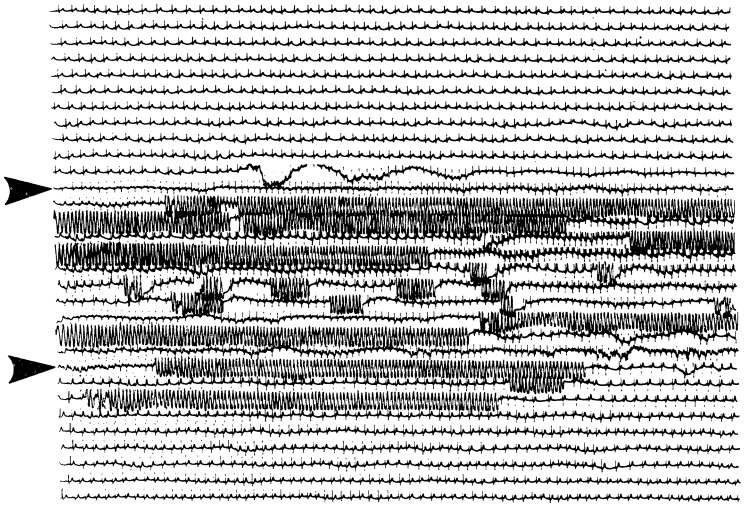

Figure 33.34

A fiber-optic printout showing clearly the catecholergic mechanism of a ventricular arrhythmia. The salvos of VT are preceded by a marked acceleration of the sinus rhythm (indicated by *arrows*) and disappear when the sinus rate decreases.

33.8.3 Monitoring for Myocardial Ischemia

33.8.3.1 General Considerations

In contrast to previous technical problems and limitations, with recent advancements of recorders with digital ECG and high-sampling rates, it is generally accepted that AECG monitoring provides accurate and clinically meaningful information about myocardial ischemia in patients with CAD [4, 90, 91]. After careful hook-up and testing for nonspecific ST-segment alterations due to hypoventilation or positional changes (testing in supine, prone, lateral, and sitting positions), the patients are asked to keep an accurate and complete diary of symptoms associated with specific events or activities, time of occurrence and disappearance of symptoms, and all other activities before the start of the recording. Upon return of the patient, a thorough review and confirmation of the diary entries has to be performed.

AECG provides a unique insight into the presence and severity of myocardial ischemia in patients with CAD. Unlike stress testing, AECG evaluates patients in their usual environment, allowing for assessment of ischemic jeopardy when the patient is exposed to the emotional or physical stress of daily life. Such insights concerning ischemia are fundamentally different from assessing ischemia in a supervised hospital or laboratory setting, where exercise stress testing is usually performed. The correlations between indices of ischemia during AECG monitoring and stress testing are quite weak [92]. An assessment of ischemic jeopardy by one technique is not a surrogate for ischemic jeopardy by the other technique [91, 93]. Most studies using AECG for ischemia assessment have been performed in patients with CAD, and there is a paucity of data regarding the role of AECG monitoring in asymptomatic individuals without known CAD or peripheral vascular disease. Thus, there is presently no evidence that AECG monitoring provides reliable information concerning ischemia in asymptomatic subjects without known CAD [93].

In addition to providing long-term monitoring for myocardial ischemia in an outpatient setting, AECG monitoring is also useful for detection of myocardial ischemia in preoperative risk stratification for patients who cannot exercise because of peripheral vascular disease, physical disability, or advanced lung disease. Moreover, it can be helpful for evaluation of patients with anginal episodes due to suspected variant angina, in whom an exercise test was negative. Finally, 24–48-h

AECG monitoring can provide information about the circadian pattern of myocardial ischemia and the pathophysiological mechanisms responsible for the ischemic episodes. It is particularly useful for detecting the extent of painless episodes of myocardial ischemia (so-called silent ischemia) that would otherwise remain undiagnosed, for example, by an exercise test.

33.8.3.2 Silent Myocardial Ischemia (SI)

The syndrome of painless myocardial ischemia was first described by Gettes in 1974 [94]. Since then, this syndrome, which is now usually referred to as SI, has attracted much attention, particularly its relation to sudden death [95–97]. The pathophysiology of painless (silent) ischemia in patients with stable CAD is not completely understood. Myocardial ischemia may occur either from episodic increase in myocardial oxygen demand, most conveniently identified by heart rate and blood pressure increase, or from an episodic decrease in myocardial oxygen supply related to either transient coronary artery vasoconstriction, transient platelet aggregation, or both. The actual identification of the presence of coronary vasoconstriction is deduced from heart-rate thresholds at which ischemia occurs: if heart-rate thresholds for ischemia vary in a given patient with stable CAD and ischemia occurs at lower heart-rate thresholds, it is likely that intermittent vasoconstriction is responsible, and when vasoconstriction is relieved, or vasodilation occurs, ischemia develops at higher heart-rate thresholds. If heart rate increases by $\geqslant$5 bpm prior to an ischemic episode, this may suggest an increase of myocardial oxygen demand as the cause of ischemia, whereas the absence of heart-rate increase favors a decrease of oxygen supply as the ischemia-producing mechanism [98]. The fact that ischemia can be seen on AECG during normal daily activities at heart-rate thresholds 10–20% lower than heart-rate thresholds for ischemia during an exercise test suggests that episodes of ischemia during normal activities may at least in part be related to intermittent coronary vasoconstriction [92, 99]. Understanding the pathophysiology of ischemia in patients with stable CAD is made more complicated by the fact that many routine daily activities both increase myocardial oxygen demand and provoke coronary vasoconstriction such as mental or physical stress, exposure to cold, or cigarette smoking. In addition, elevated serum cholesterol or estrogen deprivation may create or exacerbate endothelial dysfunction that is responsible for coronary vasoconstriction. These pathophysiological considerations are important, since pharmacological treatment is often quite different with regard to the culprit mechanism of ischemia, and these different treatment options may also have important implications for prognosis.

From the literature, it is quite clear that the vast majority of episodes of transient ST-segment deviation during AECG monitoring occur in the absence of symptoms. Episodes of asymptomatic ischemia occur in 20–50% of patients with all types of CAD, that is, stable angina, unstable angina, and AMI, and the asymptomatic episodes may outnumber the symptomatic episodes by more than 20-fold. Explanations for the fact that some episodes are painful and some produce no symptoms include the following:

1. Episodes of silent ischemia may be less "severe" than symptomatic episodes, so the anginal threshold is not reached [100].
2. Disorders of the peripheral autonomic nerves, for example, diabetic neuropathy, may blunt the nociceptive signal of ischemia [101].
h3. Increased beta-endorphin levels may decrease the central perception of myocardial pain [102, 103].
4. Abnormal central processing of afferent messages from the heart may occur due to non-myocardial factors and emotional or personality characteristics (so-called "gate theory": the cerebral cortex itself modulates the nociceptive signal that it receives) [104].

Cohn [96] has divided patients with SI into three groups:

1. Asymptomatic individuals who may suddenly die from CHD
2. Asymptomatic survivors of AMI; and
3. Anginal patients who have painless, as well as painful episodes

While detection of groups 1 and 2 relies on exercise testing, Holter monitoring is the most valuable method for detecting group 3. The clinical presentation of these 3 patient groups, as well as their prognosis, may be quite different. However,

myocardial ischemia by itself represents an independent risk factor for patients with all types of CAD, that is, stable angina pectoris as well as unstable coronary syndromes (NSTEMI, STEMI).

33.8.3.3 Prevalence and Prognostic Significance of Myocardial Ischemia

In patients with stable CAD and angina pectoris, the prevalence of myocardial ischemia in AECG monitoring ranges between 20% and 45%, and in patients with unstable angina or with a previous myocardial infarction, it is between 30% and 40% [7]. Between 60% and 80% of ischemic episodes detected by AECG monitoring are reported to be asymptomatic. As to the prognostic significance in AECG monitoring, silent as well as symptomatic myocardial ischemia identifies patients at a significantly higher risk of future cardiac events and cardiac death [105–116]. Table 33.5 shows the results of these studies: at a mean follow-up between 10 and 37 months, the event rate for death, cardiac death, myocardial infarction, unstable angina, or revascularization ranged from 3% to 42% in patients without ischemic episodes, compared to event rates from 23% to 56% in patients with documented episodes of myocardial ischemia. These differences were statistically significant for all studies cited. Moreover, some studies have shown that ischemia detected by AECG monitoring can provide prognostic information additional to that obtained from established parameters during exercise testing [93, 106, 111, 115].

In the past, AECG monitoring has also been used to define the risk of perioperative events in patients without clinical evidence of CAD undergoing surgery for peripheral vascular disease. These patients were reported to have evidence of myocardial ischemia in 10–40% of cases, and the perioperative event rates were between 1% and 16% in those with a negative test as compared to those with event rates of 4–15% with a positive test [7]. From a clinical point of view, it should be emphasized that an exercise test alone, eventually combined with an echo or other imaging study, should suffice for preoperative evaluation. Only in patients who cannot undertake an exercise test, AECG monitoring for ischemia can be used for further evaluation.

AECG monitoring has also been used for evaluation of anti-ischemic therapy in patients with CAD. In this respect, it should be stressed that due to the significant day-to-day variability of ischemic ST-segment alterations, prolonged monitoring periods of at least 48 h should be performed. A number of studies have shown that 48-h AECG recording performed at baseline and after initiation of antianginal therapy can provide reliable information about the anti-ischemic efficacy and the prognosis of the patients. Some randomized clinical trials have demonstrated that suppression of myocardial ischemia as evaluated by AECG monitoring may improve the outcome in patients with CAD (Table 33.6): the event rates in patients on antianginal drugs versus placebo, or for 100% responders versus non-100% responders, were significantly lower in patients with successful antianginal or anti-ischemic therapy [117–121]. Since data on this important application of AECG monitoring are relatively sparse, further large-scale prospective randomized clinical trials are needed to confirm these results, and to evaluate the definite role of AECG monitoring in the anti-anginal or anti-ischemic management of patients with CAD.

33.8.3.4 Limitations of Holter Monitoring for Myocardial Ischemia

When assessing patients with suspected myocardial ischemia, it is important to mention again that ST-segment changes and other repolarization abnormalities can occur for reasons other than myocardial ischemia, for example, LV hypertrophy, LV dysfunction, hyperventilation, systemic hypertension (SH), postural changes, conduction abnormalities, preexcitation, tachyarrhythmias, fluctuations of sympathetic tone, AADs, digitalis, psychotropic drugs, and electrolyte abnormalities. Moreover, the importance of proper electrode placement to retrieve myocardial ischemia from all parts of ventricular myocardium by using at least one anterior and one inferior lead has already been emphasized. A further potential limitation is the marked day-to-day variability in the frequency, degree and duration of ST-segment alterations, and ischemic episodes that makes the assessment of the effects of therapeutic interventions on ischemic indices very difficult. This problem may be overcome by prolonging the AECG recording period to 48 or 72 h and assessing similar physical and emotional activities of the patients during the serial monitoring sessions. Finally, in some patients, changes in T-wave polarity and morphology can be observed during Holter monitoring, but there are presently no data to suggest that such changes are specific for myocardial ischemia [7].

Table 33.5

Observational studies on the incidence and prognostic significance of daily life ischemia (modified according to Cohn PF 1998)

Authors, year	No. patients	Incidence of AECG ischemia (%)	End points	Mean follow-up (months)	Event rates (%)		*P*-value	Comments
					With AECG ischemia	Without ischemia		
Rocco (1988)	86	57	Death, MI, UA, revasc.	12.5	40	3	0.003	Patients monitored once off Rx
Tzivoni (1988)	118	33	Cardiac death, MI, UA, revasc.	28	51	20	< 0.001	All patients with previous MI
Hedblad (1989)	394	25	Cardiac death & nonfatal MI	43	15	3	< 0.001	
Deedwania and Carbajal (1990)	107	43	Cardiac death	23	24	8	0.02	Monitored on Rx
Raby (1990)	176	18	Cardiac death, nonfatal MI	20	38	7	< 0.0001	Patients with peripheral vascular disease
Yeung (1991)	138	59	Death, MI, revasc.	37	56	42	0.02	Monitored off Rx
Deedwania and Carbajal (1991)	86	45	Cardiac death	24	23	4	< 0.008	Monitored on Rx which controlled symptoms
Quyyumi (1993)	116	39	MI, UA, revasc.	29	13	15	NS	Very low-risk patients
Moss (1993)	936	5	Cardiac death, nonfatal MI, or UA	23	27	24	NS	Very low-risk patients
deMarchena (1994)	50	32	Cardiac death, MI, UA, revasc.	10	56	21	< 0.02	All patients monitored on Rx which controlled symptoms
Madjlessi-Simon (1996)	331	27	Death, MI, revasc., or worsening angina	21	33	17	0.004	All patients initially treated with a beta-blocker

Abbreviations: AECG = ambulatory ECG; MI = myocardial infarction; UA = unstable angina; revasc. = revascularization; Rx = anti-anginal medication

Table 33.6

Clinical trials regarding the effect of anti-ischemic therapies on the prognostic significance of daily life ischemia (modified according to Cohn PF 1998)

Authors, year	No. patients	End points	Follow-up	Event rate by treatment group	P
Pepine (1994)	306	Death, MI, UA, worsening angina, or revascularization	1 year	25% placebo 11% atenolol	0.001
Rogers (1995)	558	Death, MI, revascularization, hospital admission	1 year	32% angina-guided medical strategy 31% ischemia-guided medical strategy 18% revascularization strategy	0.003
Dargie (1996)	682	Cardiac death, nonfatal MI, and UA Revascularization, worsening angina	2 years	13% atenolol 11% nifedipine 8% combination 8% atenolol 9% nifedipine SR 3% combination	n.s. n.s.
von Armin (1996)	520	Death, MI, UA, or revascularization	1 year	32% for non-100% responders 18% for 100% responders 33% for nifedipine 22% for bisoprolol	0.008 0.03

Abbreviations: MI = myocardial infarction; UA = unstable angina

33.8.4 Assessment of Risk in Patients with Cardiac Disease

When trying to stratify survivors of AMI or patients with congestive heart failure (CHF) with respect to their risk of dying from an arrhythmic death, specific noninvasive risk-stratification methods like detecting the type and frequency of ventricular arrhythmias, signal-averaged ECG, HRV, heart-rate turbulence, QTV, QTD, and, last but not least, assessment of LV function (ejection fraction) are mainly used. From an epidemiologic as well as therapeutic interventional point of view, a risk-stratifying test should provide a high positive predictive accuracy (PPA) combined with a reasonably high sensitivity, so that as few patients as possible are unnecessarily exposed to treatment. Moreover, the current tests used should not only predict total mortality, but also specific causes of death, particularly death from life-threatening ventricular arrhythmias. Another practical prerequisite for using different tests is that they should be available not only in specialized referral centers, but also to physicians in all hospitals that take care of cardiac patients. The performance of each of the tests should be properly standardized.

33.8.4.1 Post Myocardial Infarction

Prevalence of Ventricular Arrhythmias

Due to the widespread use of thrombolytic agents, and more recently due to routine acute mechanical recanalization (PCI) of occluded coronary arteries as well as the routine use of aspirin, beta blockers, and ACE inhibitors, inhospital mortality of patients with AMI has substantially decreased from 16% to 20% in the late 1970s to 6–10% in the early 1990s, while the 1-year risk of developing a malignant arrhythmia in AMI survivors after hospital discharge is 5% or less [7]. Arrhythmogenic death accounts for approximately 40–50% of total mortality in the first year after AMI, and thereafter, the risk of dying from a malignant arrhythmia decreases significantly in the next 12–24 months to below approximately 10%. It should be mentioned that mortality rates reported from controlled randomized trials are lower than those derived from more unselected consecutive series of patients due to strict adherence to exclusion criteria resulting in exclusion of

higher risk patients such as older patients, those with recurrent MIs, MI after coronary bypass grafting, or ineligibility for thrombolysis or PCI.

Prognostic Significance of LV Function

For more than 20 years, depressed LV function assessed either by ejection fraction (EF) or by clinical signs of CHF represents the principal method of determining the risk of postinfarction patients. Numerous studies both in the pre- and post-thrombolysis, as well as the PCI era have demonstrated that depressed left ventricular ejection fraction (LVEF) < 35–40% is the most powerful predictor of total mortality in the first year after MI, while in patients with LVEF < 15–20% the vast majority of deaths are due to pump failure [7]. In a literature survey, Bailey et al. [121] have shown from 20 studies involving a total of 7,294 patients that sensitivity and PPA of impaired LV function was between 45% and 87% and between 9% and 33%, respectively, with a relative risk of 1.9–16.2 and an odds ratio of 2.0–21.6. It is quite clear that since the MADIT I and II trials in patients with an LVEF < 15–30% no further risk stratification is necessary and that these patients should receive an implantable cardiac defibrillator (ICD) [122]. In the remaining patients, at least in those with an LVEF ⩾ 35–40%, further tests for risk stratification have to be performed.

Prognostic Significance of Ventricular Arrhythmias

Since the 1970s, premature ventricular contractions (PVCs) are considered as the "traditional" risk markers after AMI [123]. Table 33.7 with results from 20 studies in more than 11,000 patients [124–142] shows that sensitivity and positive predictive value (PPV) of PVCs was between 16% and 82% and between 7% and 52%, respectively, with a relative risk of 1.9–16.2 and an odds ratio of 2.0–21.6. In general, frequent PVCs (e.g., ⩾10/h) and high-grade ventricular ectopy (e.g., repetitive PVCs, multiform PVCs, and non-sustained or sustained ventricular tachycardia (sVT)) have been associated with a higher mortality, but once the patients have at least 6 PVCs per hour, the risk of an arrhythmic event does not increase with more frequent PVCs [123]. The prognostic role of nonsustained VTs (nonsustained ventricular tachycardia [nsVT]) has received special interest. In contrast to previous findings, the GISSI investigators demonstrated that nsVT after AMI failed to predict arrhythmic death [123]. Similar results were reported by Hohnloser et al. [142], who could demonstrate that the prevalence of nsVT at the time of hospital discharge early after the index infarct was very low (95 of 325 consecutive infarct survivors) in a general postinfarction population of patients treated according to current therapeutic guidelines. During a mean follow-up of 30 months, the presence of nsVT was not an independent predictor of either arrhythmic or nonarrhythmic cardiac death. On multivariate stepwise regression analysis for the primary study endpoint of cardiac mortality and arrhythmic events, only the status of the infarct-related artery, HRV, and LV ejection fraction were found to be independent predictors.

In the MADIT I Trial, nsVTs were also used as a risk marker for inclusion of the patients into the study. In long-term survivors of MI with reduced LV function, it was shown that ICD implantation reduced the mortality rates by about 50% in MI survivors with reduced LVEF (⩽35%) and at least one symptomatic episode of nsVT, and in whom ventricular fibrillation or sustained VT was reproducibly induced during EPS and not suppressed by intravenous administration of procainamide [122]. At present, it is more or less accepted that in the thrombolysis or mechanical recanalization era (PCI in AMI patients), nsVT on its own is not a useful risk stratifier in patients after MI, but rather PVCs in general with a PPV between 5% and 15% should be combined with other risk markers such as impaired LV function, signal-averaged ECG (SAECG), parameters of HRV or of HRT to improve their prognostic impact.

Prognostic Significance of VLP

In the 1980s, the signal-averaged ECG (SAECG) was used to look for VLPs in patients after MI. VLPs were regarded as a sign of slow conduction in the peri-infarct zone that may facilitate the initiation of malignant ventricular tachyarrhythmias. Since then, numerous studies have been published on the prognostic significance of VLPs in survivors of MI before hospital discharge. In summary, the survey of Bailey et al. [121] on 22 studies in a total of 9,883 patients found that sensitivity and PPA of VLPs in the SAECG was between 35% and 83% and between 8% and 35%, respectively, with a relative risk of 1.8–31.5 and an odds ratio of 1.9–41.3. In this study, the SAECG was proposed as the first-step risk stratifier together with depressed LV function (see below). In a recent study on 1,800 consecutive survivors of MI in sinus rhythm and under 76 years, Bauer et al. [151] reported that the presence of VLPs before hospital discharge was not associated with the primary endpoint (SCD and serious arrhythmic events) in univariable and multivariable analysis after a follow-up

Table 33.7

Yield of ventricular arrhythmias within the AECG for predicting arrhythmic events after acute myocardial infarction (AMI)

Author (year)	No. of Patients	Criteria	End points	Sensitivity, %	Specificity, %	PPV, %	NPV, %
Ruberman (1981)	1739	Complex VPBs (multiform, R on T, nsVT)	total death, SCD	54	76	15	95
Olson (1984)	115	⩾ 10 PVCs/h or multiform or pair or VT	cardiac death	25	79	12	90
Mukharji (1984)	533	⩾ 10 PVCs/h	sudden death	10	93	8	95
Kostis (1987)	1640	⩾ 10 PVCs ⩾ 10 PVCs/h or PVC pair or VT ⩾ 10 PVCs/h or (PVC pair or VT) or multiform ⩾ 10 PVCs/h and (PVC pair or VT) and multiform	sudden death	25 43 67 16	88 75 61 94	6 8 8 11	96 96 97 96
Gomes (1989)	110	high grade VEA (couplets and nsVT)	arrhythmic event	81	57	25	94
Verzoni (1989)	208	PVCs-Lown grade 3–5	arrhythmic event	67	71	7	99
de Cock (1991)	99	⩾ 10 PVCs/h VT SVT	death or MI	44 26 41	83 100 97	52 100 86	78 75 80
Farrell (1991)	416	PVCs >10/h Repetitive PVCs	arrhythmic event	54 54	82 81	16 15	82 97
Richards (1991)	358	PVCs-Lown 3–5 PVCs-Lown 3–5	arrhythmic event cardiac death	82 75	40 76	6 16	98 98
Steinberg (1992)	182	high grade VEA	sustained VT, SCD	44	73	14	93
Bigger (1992)	715	high rate of PVCs (⩾ 3 per hour)	all cause mortality, cardiac death, SCD	48	75	24	89
Kuchar (1993)	206	high grade VEA (couplets and nsVT)	symptomatic VT, SCD	73	68	15	97
McClements (1993)	301	⩾ 10 PVCs/h or repetitive	arrhythmic event	38	74	6	96
Pedretti (1993)	305	⩾ 2 runs nsVT	arrhythmic event	42	91	25	96
Hohnloser (1994)	173	PVCs-Lown 4	arrhythmic event	22	78	5	95
Hermosillo (1995)	200	complex ventricular arrhythmias	sVT, SCD	38	92	36	92
El-Sherif (1995)	1158	⩾ 10 PVCs/h or VT	arrhythmic event	61	69	8	98
La Rovere (1998)	1170	complex ventricular arrhythmias	cardiac death	32	84	7	97
Hohnloser (1999)	325	nonsustained VT (nsVT)	cardiac death, sVT, resuscitated VF	16	85	8	92
Mäkikallio (2005)	2130	nonsustained VT, nsVT	sudden cardiac death	21	92	4.5	98

Abbreviations: NPV = negative predictive value; VT = ventricular tachycardia; SVT = supraventricular tachycardia; nsVT = nonsustained ventricular tachycardia; VEA = ventricular ectopic activity; PVC = premature ventricular complexes; SCD = sudden cardiac death; sVT = sustained Ventricular Tachycardia

period of median 34 months. In contrast, low LVEF (⩽30%) (hazard ratio 9.6, 95% CI 4.1–22.4), HRT turbulence category 1 (either TO or TS abnormal) (hazard ratio 5.1, 95% CI 1.9–14.4), and HRT category 2 (TO and TS abnormal) (hazard ratio 7.5, 95% CI 2.4–23.9) were significant predictors of the primary endpoint in both univariable and multivariable analysis.

Prognostic Significance of HRV

The sympatho–vagal balance and its regulatory activity on the circulatory system is disturbed in survivors of myocardial infarction, as can be determined from a decrease of HRV and BRS, as well as from a blunted heart-rate turbulence (HRT). The specific mechanism of decreased vagal modulation remains unknown. Pragmatically, HRV, BRS, and HRT decrease early after MI with a nadir of 2–3 weeks and then increase back to normal levels by 6–12 months. Decreased HRV and BRS as well as blunted HRT are independent predictors of increased mortality rates, including sudden death, in patients after MI (Table 33.8) [131, 134, 136, 142, 143–149]. The optimal time-domain parameters of HRV for analysis of risk are SDNN and HRV triangular index, and high-risk patients have either an SDANN < 70 ms, an HRV triangular index < 15, a BRS < 3 ms/mm Hg, or HRT parameters TO ⩾ 0% and TS ⩽ 2.5 ms/R − R. Overall, the PPV of HRV parameters, BRS and HRT criteria using the cut-off points mentioned is relatively low in the range of 8–13% at a sensitivity level of 40% [141].

Prognostic Significance of Heart-Rate Turbulence

Heart-rate turbulence (HRT) has also been shown to be of prognostic significance in survivors of MI [150, 151]. In the validation study of the PILP-cohort and the EMIAT placebo arm cohort, a strong and significant association of TO and TS with total mortality was observed [153]. Two recent studies on large cohorts of postinfarction patients (1,800 and 3,130 consecutive patients, respectively) have substantiated the prognostic power of HRT. In the first study [143], both TO and TS were predictive of death or SCD with hazard ratios of 5.3 and 7.5 in multivariable analysis, and in the second study [145], reduced post-ectopic TS (hazard ratio for SCD 5.9) and nsVT (hazard ratio 2.3) were also significant predictors. However, the general problem is that using these predictors alone PPV is too low (between 6% and 13%), and the PPV can be increased by a combination of several parameters (HRV plus VLPs plus HRT plus LVEF) at the cost of constantly lowering the sensitivity down to 10% [7].

Stepwise Risk Stratification

To overcome these practical problems, Bailey et al. [121] proposed a clinically applicable risk stratification procedure in three steps, based on the total number of 25,543 patients collected with a weighted overall estimated two-year major adverse event (MAE) incidence of 7.9%, which was used as a prior probability. Furthermore, to explore the implications of combining tests, the analysis was simplified by using only the composite weighted mean values for sensitivity and specificity. The *first step* was the combination of LVEF and SAECG. If the two tests were both negative or both positive (as would be true for 64.2% of the patients), further testing would not be done, as the two-year probability of a MAE would be as low as 2.2% in the former, and high enough (38.7%) in the latter situation to warrant consideration of ICD implantation. The *second step* would be the performance of a 24-h AECG in the 35.8% of patients who had only a low LVEF or a positive SAECG, resulting in an intermediate two-year risk of 10.6% for a MAE. If severe ventricular arrhythmia (SVA) and abnormal HRV were both present or absent (25% of patient population), no further testing would be needed, because in the former case the posterior probability is still below the original prior probability, despite having either a low LVEF or an abnormal SAECG, and in the latter situation, the posterior probability would again be high enough to warrant consideration of ICD implantation. The *third step* would refer to the remaining 10.8% of the original patients, who would have an intermediate two-year risk of 17.5%. They would undergo an EPS, and 2.6% of the original group would have a positive EPS, again with a two-year risk of 45.1%, which is high enough to justify consideration of ICD implantation. At the end of applying all three stages of risk stratification, there remains a small proportion (8.2%) of unstratified patients with essentially the same risk of 8.9% as the original prior probability of 7.9% [121]. It should be noted that with the exception of assessing LVEF (by echocardiography, left ventricular angiography or cardiac magnetic resonance imaging [MRI]), all other parameters of step one and two can be derived from one 24-h AECG recording using modern solid-state digital recorder devices, so that only two investigational tools are necessary to reach step three, if applicable, according to the results of the different test parameters described.

Table 33.8

Yield of heart rate variability (HRV) for predicting arrhythmic events after acute myocardial infarction (AMI)

Author (Reference)	No. of Patients	Criteria	End points	Sensitivity, %	Specificity, %	PPV, %	NPV, %
Kleiger (1987)	808	SDNN <50 ms*	all-cause death	34	88	34	88
Farrell (1991)	416	HRV triangular index <20† Mean R-R interval <750 ms	nonfatal VF	92 67	77 72	17 13	77 97
Odemuyiwa (1991)	385	HRV triangular index ⩽30†	nonfatal VF	75	76		
Bigger (1992)	715	ULF VLF ULF+VLF	all-cause death	28 30 20	93 92 96	41 39 48	
Pedretti (1993)	294	HRV triangular index ⩽29†	nonfatal VF	89	68	15	99
Zuanetti (1996)	567	SDNN, RMSSD, "NN50+"	total and CV mortality	42	87	24	93
Copie (1996)	551	24-h mean heart rate	cardiac death sudden death	46	88	16	97
Lanza (1998)	239	SDNN index, SDANN, VLF	sudden death	32	92	25	94
La Rovere (1998)	1170 1182	SDNN <70 ms* BRS <3.0 ms/mm Hg	nonfatal VF and cardiac death nonfatal VF and cardiac death	39 35	85 86	10 10	97 97
Hohnloser (1999)	325	SDNN <70ms	primary: cardiac death, sVT, resusciated VF Secondary: arrhythmic event	60	82	22	96
Katz (1999)	185	Difference <10 bpm between shortest and longest RR-interval on 6 deep respirations in 1 minute	cardiovascular mortality	90	68	46	99
Malik (2000)	451	SDNN ⩽50ms, HRV index ⩽20	all cause mortality	50	73	18	92

Abbreviations: NNP = negative predictive value, PPV = positive predictive value, VF = ventricular fibrillation, CV = cardiovascular

33.8.4.2 Chronic Heart Failure

Prognostic Significance of Ventricular Arrhythmias

The majority of patients with CHF suffer from advanced structural heart disease, either ischemic or idiopathic dilated cardiomyopathy (IDCM), with progressive symptoms. Death results mostly from VT or fibrillation, bradyarrhythmia or asystole, progressive pump failure, recurrent ischemia or infarction, electromechanical dissociation, stroke, pulmonary emboli, or renal complications. Ventricular arrhythmias are extremely common in patients with CHF [153]. Ambient ventricular ectopic beats can be detected in ⩾90% of these patients, frequent VPCs in 70–95% of DCM and heart failure, while many of these patients have complex and multiform PVCs and episodes of nsVT. In the Captopril–Digoxin Multicenter study of 295 patients with mild to moderate heart failure and reduced LVEF < 40%, the frequency of VPBs was significantly higher in older patients, in those with LVEF < 20%, or IDCM. In such high-risk group patients, 50% also had episodes of nsVT compared to 30% with nsVT in the overall study. By multivariate analysis, only nsVT frequency was an independent predictor of risk of sudden death. Patients with frequent occurrences of nsVT (>2/day) had an almost threefold increase in total mortality [154]. In the V-HeFT II study on 715 patients, ventricular couplets were seen in 98% of patients and 28% had one or more episodes of nsVT. The presence of nsVT and ventricular couplets identified a group of patients with increased mortality [155]. In the GESICA-Trial [156], 34% of 516 patients showed nsVT. These episodes of nsVT were more frequent in patients with advanced heart failure, higher heart rate, lower systolic blood pressure, increased creatinine, or with Chagas disease. During a three year follow-up, the presence of nsVT was associated with an increased risk of total mortality (relative risk 1.69, $p < .0002$) and an increased rate of SCD (relative risk 2.77, $p < .001$). It can be concluded from these three large studies that in patients with advanced heart failure, the presence of nsVT identifies a subgroup with an increased risk of overall cardiac mortality and SCD. However, despite identifying this population with an increased relative risk of an adverse event, AECG monitoring for analysis of ventricular arrhythmias is either not sensitive enough or reveals a PPV that is too low for patient management purposes.

Prognostic Significance of HRV

The prognostic significance of HRV in patients with CHF was unclear in the past. In one of the first studies in 40 patients with CHF, compared with normals and those with a history of nsVT and normal cardiac function, there was no significant difference in the HRV parameters despite a significantly lowered HRV in heart failure patients [157]. In a prospective study of 71 patients with IDCM and CHF, Hoffman et al. [158] studied HRV by time- and frequency-domain methods. After a follow-up period of 15 ± 5 months, no significant difference of time or frequency-domain indices of HRV among patients with arrhythmic events compared with those without major arrhythmic events was found. In a further study of 159 patients with IDCM and CHF, 30 patients died during follow-up. There was a significant correlation between LVEF, increased SDNN, and pNN50 with an increased risk of cardiac death. However, the risk of SCD correlated only with LVEF in contrast to an increased low-frequency power (LFP) and impairment of pNN50 that strongly correlated with an increased risk of death from progressive pump failure. Further, two studies showed that HRV was reduced in patients with CHF and there was a strong correlation between HRV and LV function and peak oxygen consumption [159, 160].

More recently, several studies on larger patient populations have been published that showed a positive prognostic power of HRV in patients with CHF (Table 33.9). Ponikowski et al. [161] studied 102 consecutive patients with CHF from ischemic or dilated cardiomyopathy, using AECG monitoring to assess all parameters of HRV both in the time and frequency domain. During follow-up of 584 ± 405 days, 19 patients died. In multivariate analysis, HRV parameters SDNN, SDANN, and LF were found to predict survival independently of NYHA functional class, EF, peak oxygen consumption, and the presence of VT within the AECG. The Kaplan–Meier survival curves revealed SDNN <100 ms to be a useful risk factor. Szabo et al. [162] investigated 159 patients with CHF due to ischemic or dilated cardiomyopathy, in whom both time and frequency-domain parameters were measured at entry to predict the endpoint of cardiac mortality. During a follow-up of 23 months (range 1–67), 30 of 159 patients died of cardiac causes. Both pNN50 < 2.0% and SDNN < 108 ms predicted cardiac death with a RR of 2.1 and 1.5 respectively, whereas pNN50 and LF power >14 ms^2 predicted death from pump failure with a RR of 5.4 and 6.8, respectively. Boveda et al. [163] reported on 190 patients with CHF and found the time-domain parameter SDNN < 67 ms to be significantly predictive for total death (RR 2.5, CI 1.5– 4.2). In the VA trial,

Table 33.9

Prognostic significance of heart rate variability (HRV) for predicting cardiovascular and total mortality in patients with congestive heart failure (CHF)

Author (Reference)	No. of patients	Criteria	End points	Adjusted RR (95% CI)
Szabo (1997)	159	pNN50 <2.00% SDNN <108ms	cardiac mortality	2.1 (1.4–3.3) 1.5 (1.0–2.4)
		pNN50 <2.00% LFP >14ms^2	death from pump failure	5.4 (1.7–17.5) 6.8 (2.2–20.9)
Boveda (2001)	190	SDNN <67ms	total death	2.5 (1.5–4.2)
Bilchick (2002)	127	SDNN <65.3ms (lowest quartile)	total death	3.7
			sudden death	2.4
La Rovere (2003)	242	LF $\leqslant$11ms^2 (8 min controlled breathing)	sudden death	3.0 (1.2–7.6)
		$\geqslant$ 83 VPB/hour	sudden death	3.7 (1.5–9.0)
Aronson (2004)	199	SDNN (lower tertile) SDANN Total power ULF	total mortality	2.2 (1.05–4.3) 2.1 (1.05–4.2) 2.2 (1.08–4.2) 2.6 (1.3–5.3)
Adamson (2004)	397	SDAAM <50ms (5′) (from implanted resynchronisation devices)	total death	3.2
			cardiovascular death	4.4
Guzzetti (2005)	330	VLF night $\leqslant$509 ms^2	progressive pump failure	2.3 (1.4–3.8)
		LF night $\leqslant$20 ms^2	sudden death	2.7 (1.3–5.6)
		HF night $\leqslant$60ms^2	sudden death	2.2 (1.0–4.6)

Abbreviations: RR = relative risk; CI = confidence interval; nsVT = nonsustained ventricular tachycardia; VT = ventricular tachycardia; VPB = ventricular premature beat

Bilchik et al. [164] reported on 179 patients with CHF, in whom the lowest quartile of patients were compared with the remaining, using SDNN as the sole HRV parameter. Among 127 patients meeting the inclusion criteria, SDNN < 65.3 ms (the lowest quartile) was the sole independent factor predictive of survival in a multivariate model (p = .0001). A Cox proportional-hazards model revealed that each increase of 10 ms in SDNN conferred a 20% decrease in risk of mortality (p = .0001). Furthermore, patients with SDNN < 65.3 ms had a significantly increased risk of sudden death (p = .016). Thus, in this study, HRV was the only independent predictor of overall mortality and was significantly associated with sudden death. Aronson et al. [165] measured time and frequency HRV parameters from 24-h Holter recordings in 199 patients with NYHA class III or IV hospitalized for decompensated CHF, and during a mean follow-up after discharge of 312 ± 150 days, 40 patients (21.1%) died. Kaplan–Meier analysis indicated that patients with decreased values of SDNN over a 24-h period, SDANN, total power, and ULF power in the lower tertile were at higher risk of death. In a multivariate Cox regression model, the same indexes in the lower tertile were independent predictors of mortality (RR from 2.2 to 2.6). The conclusion was that the severity of autonomic dysfunction during hospital admission for CHF decompensation, as reflected by measures of overall HRV, can predict survival after hospital discharge.

La-Rovere et al. [166] developed a multivariate survival model for the identification of sudden (presumably arrhythmic) death from data of 202 consecutive patients with moderate to severe CHF. Both time- and frequency-domain HRV parameters obtained from 8-min ECG recordings at baseline and during controlled breathing were challenged against clinical and functional parameters. This model was then validated in 242 consecutive patients referred for CHF as the validation sample. Sudden death was independently predicted by a model that included LFP of HRV during controlled breathing $\leqslant$13 ms^2 and left ventricular end-diastolic diameter $\geqslant$ 77 mm (RR 3.7, 95% CI 1.5–9.3 and RR 2.6, 95% CI 1.1–6.3,

respectively). LF $\leqslant$ 11 ms^2 during controlled breathing and $\geqslant$83 VPCs per hour on Holter monitoring were both independent predictors of sudden death (RR 3.0, 95% CI 1.2–7.6, and RR 3.7, 95% CI 1.5–9.0, respectively). The conclusion was that reduced short-term LFP during controlled breathing is a powerful and independent predictor of sudden death in patients with CHF. Similar results from the same group were reported by Guzzetti et al. [167], who studied 330 consecutive CHF patients. Using time, frequency, and fractal analyses, the risk of pump failure and of sudden death could be differentiated as follows: depressed power of night time HRV ($\leqslant$509 ms^2), VLP (<0.04 Hz), high-pulmonary wedge pressure ($\geqslant$18 mm Hg), and low left-ventricular EF ($\leqslant$24%) were independently related to pump failure, while reduction of LFP ($\leqslant$20 ms^2) and increased left ventricular end systolic diameter ($\geqslant$61 mm) were linked to sudden (arrhythmic) mortality. The dilemma, however, remains that there is no evidence that reducing the frequency of repetitive ventricular arrhythmias or increasing the HRV with medications can significantly reduce the incidence of total death or sudden death in patients with severe CHF.

From a technical point of view, it is interesting to note that HRV parameters may also be retrieved from the memory of implanted devices, as has been shown by Adamson et al. [168]. In 397 patients, continuous HRV was measured as the standard deviation of 5-min median atrial–atrial intervals (SDAAM) sensed by the biventricular pacing device. SDAAM < 50 ms, when averaged over 4 weeks, was associated with increased mortality risk (hazard ratio 3.2, p = .02), and SDAAM was persistently lower over the entire follow-up period in patients who required hospitalization or died. Automated detection of decreases in SDAAM was 70% sensitive in detecting cardiovascular hospitalizations, with 2.4 false-positives per patient-year follow-up.

Prognostic Significance of Heart-Rate Turbulence

Koyama et al. [169] measured heart-rate turbulence (HRT) in 50 patients with CHF, 34 with IDCM, and 16 with MI and compared this with 21 patients without obvious heart disease as a control group. HRT slope and HRT onset were measured by the original definition using digitized Holter ECG recordings, and cardiac pump function was assessed by echocardiography. The value of the HRT slope was significantly lower in CHF than in controls (3.7 ± 1.7 vs 16.4 ± 5.3, p < .01). The value of HRT onset in patients with CHF was significantly higher than in control patients (−1.1 ± 1.9 vs −3.6 ± 1.7, p < .05). The HRT slope and onset in CHF patients with VT were nearly identical to those without VT. It was concluded from this study that HRT slope appears to be a powerful prognostic marker that shows significant differences between CHF subgroups when divided by clinical events such as death or hospitalization from CHF. Kawasaki et al. [170] investigated 104 hypertrophic cardiomyopathy (HCM) patients, 44 MI patients, and 56 normal controls using HRT onset and slope. The latter parameters were abnormal in MI patients, but not in HCM patients as compared with normal control subjects. During a follow-up period of 27 ± 10 months, 7 HCM patients and 10 MI patients either died from cardiac death or were hospitalized for CHF. In MI patients, HRT onset was higher and the HRT slope was lower in patients with cardiac events than in patients without, whereas in HCM patients, the HRT onset or slope was similar between patients with and without cardiac events. It was concluded that, unlike MI patients, the HRT variables in selected HCM patients were not abnormal and failed to predict the clinical prognosis.

In the study of Grimm et al. [171] involving a cohort of 242 patients with IDCM, HRT analysis was performed in a blinded fashion. During 41 ± 23 months of follow-up, 54 patients (22%) died or underwent heart transplantation. On Cox univariate regression analysis, abnormal HRT onset, HRT slope, HRT onset combined with HRT slope, LV ejection, LV size, and NYHA functional class III showed a significant association with total mortality or the need for heart transplantation. On multivariable analysis, abnormal HRT onset identified patients without transplant-free survival, as did LV size and NYHA class III heart failure. Major arrhythmic events were observed in 42 patients (17%) during follow-up. On univariate analysis, abnormal HRT onset with HRT slope, male sex, NYHA class III, LV ejection fraction, and LV size were associated with a higher incidence of major arrhythmic events. On a multivariate analysis, only LV ejection fraction remained a significant arrhythmia risk predictor. It was concluded that in IDCM patients, HRT onset is a significant predictor of transplant-free survival, as well as LV size and NYHA class. For arrhythmia risk stratification, however, only LV ejection fraction remains a significant risk predictor. Again, the main problem is that, when using HRT parameters alone, their PPV is too low though sensitivity is reasonably high. In conclusion, at present there is not sufficient evidence to support routine use of AECG for HRT parameter analysis for therapeutic or prognostic purposes in patients with CHF.

33.8.4.3 Hypertrophic Cardiomyopathy (HCM)

The prevalence of ventricular arrhythmias detected from AECG monitoring is relatively high in patients with HCM [172, 176]. It is widely accepted that the presence and severity of ventricular arrhythmias in HCM are related to severe impairment of left ventricular function (LVF). Moreover, SCD and syncope are common among patients with HCM. There are studies showing that there is some association between ventricular arrhythmias and adverse events. However, they differ on the nature of this association [173–176]. Studies on HRV in patients with HCM are sparse and the results equivocal, for example, Counihan et al. [177] found no association between HRV indexes and adverse events in HCM. Reduced HRV on ambulatory monitor recordings appears to be less useful in risk stratification in patients with HCM, as compared to those after acute MI, and thus is not widely used in this patient population. The features that most reliably identify the 10–20% of HCM patients at high risk of sudden death include prior cardiac arrest or sVT, multiple and repetitive episodes of nsVT, young age < 30 years at diagnosis (especially in those with extreme left ventricular hypertrophy (LVH) and wall thickness $\geqslant$30 mm on echocardiography), a family history of HCM with sudden death, an abnormal blood pressure response to exercise especially in patients younger than 50 years, and genetic abnormalities associated with increased prevalence of sudden death [178]. In conclusion, the specific role of AECG monitoring to retrieve risk factors for prognostic reasons, such as ventricular (tachy-) arrhythmias, reduced HRV, or blunted HRT, remains unclear in the day-to-day treatment of HCM patients.

33.8.4.4 Valvular Heart Disease

The frequency of PVCs and the grade of arrhythmia (repetitive forms) are significantly correlated with LVF, but neither is related to the severity of valvular lesions (estimated valvular surface area or hemodynamically measured regurgitation). The occurrence of salvos of VT during an AECG recording in a patient with valvular disease (e.g., aortic stenosis or mitral regurgitation) is related in particular to a low LVEF and to an increased risk of sudden death [179]. Thus, the existence and severity of ventricular arrhythmias in valvular heart disease has an important prognostic value indicating poor myocardial performance, whatever the importance of the valvular lesion is.

A close relationship is now generally accepted between mitral valve prolapse and an increased frequency of ventricular arrhythmias during AECG monitoring compared to a normal population [180–183]. However, the prognostic significance of these findings remains unclear. Ventricular arrhythmias are unrelated to the severity of valvular disease. The prevalence of SVTs has been reported to be 5–10%. However, it includes usually only short runs of atrial beats and non-sustained tachycardias.

In conclusion, at present, the presence of mitral valve prolapse, chronic mitral regurgitation, aortic stenosis or regurgitation, or an aortic valve prosthesis without symptoms does not establish the need for AECG monitoring for analyzing the spectrum of ventricular arrhythmias, nor the parameters of HRV or HRT [7].

33.8.4.5 Systemic Hypertension (SH)

In most patients with SH, LVH is present. This is associated with an increased incidence of complex ventricular arrhythmias (VEA) and an increased risk of MI and sudden death [184, 185]. Because patients with SH and LVH with complex or frequent VEA have only a marginally significant risk of dying after adjusting for age, sex, and other clinical factors [186], AECG monitoring is of uncertain value in the management of asymptomatic patients with LVH. With respect to HRV, a few studies have shown an increase of low-frequency components of HRV in hypertensive patients compared to normals, with blunting of circadian patterns and reduced parasympathetic activity in hypertensives. In the Framingham Study, the predictive power of HRV parameters for the incidence of hypertension was tested and after adjustment for factors associated with hypertension, multiple regression analysis revealed that low-frequency components were associated with incident hypertension [187]. In the ARIC study of 2,061 normotensives, 64 participants developed hypertension during a 3-year follow-up, and a statistically significant inverse association between baseline HF band and the risk of incident hypertension was observed [188]. In a further study on dipper and non-dipper essential hypertensive individuals, both the LF and HF band were significantly lower in non-dipper hypertensives than in dipper hypertensive subjects throughout

the day. In dipper hypertensives, the LF band showed a nocturnal decrease and the HF band an increase, whereas these diurnal changes in LF and HF bands were significantly blunted in non-dipper subjects [189]. These data show that hypertensives, and particularly non-dipper hypertensives, are characterized by decreased physiological circadian fluctuations of the ANS. However, because of paucity of relevant clinical data, the true role of HRV in the diagnosis and treatment of patients with essential hypertension remains unclear. In conclusion, there is not sufficient evidence to support routine use of AECG for arrhythmia or HRV parameter analysis for therapeutic or prognostic purposes in patients with essential hypertension and LVH.

33.8.4.6 Miscellaneous

Diabetes is associated among other things with diffuse degeneration of sympathetic and parasympathetic small nerve fibers, and more than 50% of patients with symptomatic diabetic neuropathy will die within 5 years [190]. High-frequency components of HRV may detect small changes in autonomic function in diabetic patients [191, 192] and distinguish diabetic subjects with neuropathy from those without neuropathy [193]. The clinical utility of HRV analysis as a reliable test for cardiac parasympathetic function is limited in diabetics due to the fact that a large number of diabetic subjects have reduced HRV and that there is no evidence that early identification of subclinical neuropathy will lead to improved patient outcomes. Therefore, routine HRV testing in diabetic subjects is not indicated at this time [7].

Patients with chronic renal failure who are on chronic hemodialysis bear an increased risk of CAD and of dying from a cardiovascular event. They show an increase in ventricular ectopy during dialysis. Hemodialysis patients with known CAD or peripheral vascular disease display the highest risk of having an abnormal AECG recording [194]. Though patients with higher grade VEA have a decreased survival compared to those without this type of VEA, it is unclear at present, whether AECG monitoring should be routinely performed in these patients [7].

Regarding pre- and postoperative evaluation, no association has been found between preoperative VEA and postoperative events when AECG monitoring was used before surgery in high-risk patients without myocardial ischemia and depressed LV function, who underwent non-cardiac surgery [195]. In addition, no association has been found between the occurrence of complex VEA after coronary artery bypass surgery and death after controlling for other clinical factors [196]. Therefore, at present there is no general recommendation for the routine use of AECG monitoring for risk stratification in preoperative and postoperative patients [7].

33.8.5 Evaluation of Therapeutic Interventions

33.8.5.1 Pacemaker and ICD Function

Once a pacemaker or ICD is implanted, an AECG is useful in assessing postoperative device function and in guiding appropriate programming of enhanced features such as rate responsiveness and automatic mode switching. Sometimes, the AECG can be a useful adjunct to continuous telemetric observation or pacemaker/ICD-based monitoring in assessing device function, though the present generation of pacemaker/ICD has limited monitoring capacity that is not capable of entirely supplanting conventional AECG. Tabular data derived from complexes classified by the pacemaker algorithm according to whether or not they are preceded by atrial sensed or paced beats can be obtained from the pacemaker memory, which summarizes the number or percentage of atrial and ventricular events that were either sensed or paced, including a separate quantification of sensed ventricular events preceding atrial activity. Current pacemaker devices do not generally provide electrogram confirmation of the counts, so the accuracy provided by the devices depends on accurate sensing and pacing functions. These tabular data can be used to broadly determine the frequency of VPBs, but the resolution of the data does not allow for minute-to-minute counts or detailed characterization of repetitive ventricular ectopy (rate, duration, or morphology of VT). Therefore, there is an important role for AECG monitoring in evaluating patients' symptoms, despite pacemaker implantation, or in detecting details of pacemaker failure.

Syncope, dizziness, and palpitations may persist or sometimes reappear in up to 30% of patients after pacemaker implantation, and persistent symptoms are frequently due to various types of arrhythmia. Thus, indications for AECG

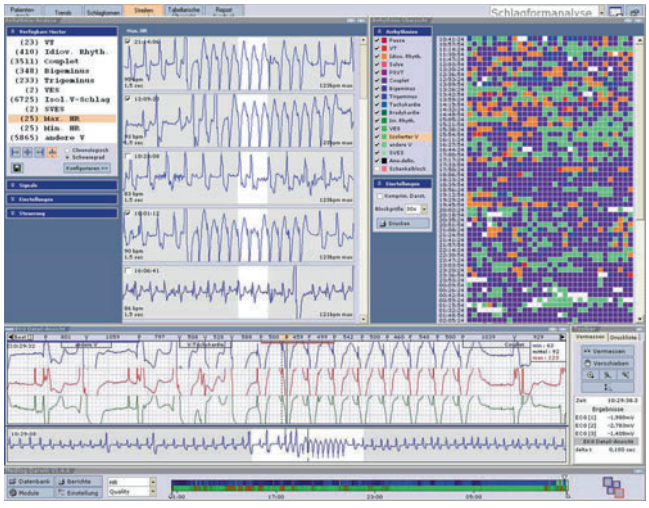

Figure 33.35

Arrhythmia overview in a patient with pacemaker-mediated tachycardia including counts of single arrhythmic events (*left*), single lead arrhythmic episodes extracted from the overview on left side, survey on QRS templates over the full 24-h period with 30 s segments (*right*), and three-channel real-time ECG and single lead "full disclosure" ECG (*bottom*) (Oxford MedilogDarwin system).

monitoring in patients with an implanted pacemaker include evaluation of frequent symptoms of palpitation, dizziness, syncope, or near syncope despite or due to pacemaker stimulation, for example, due to failure to sense, oversensing, failure to capture, or pacemaker pauses (myopotential inhibition) as well as due to pacemaker mediated tachycardia (endless loop tachycardia) (Fig. 33.35). Moreover, AECG monitoring may assist in the programming of simple (lower rate interval, AV interval, ventricular and postventricular refractory period, and upper rate response of DDD pacemakers) and of enhanced features like rate responsiveness and automatic mode switching. Evaluation of suspected component failure by AECG monitoring is particularly important in cases where device interrogation is not definitive in establishing a conclusive diagnosis. Pacemaker syndrome is another important symptomatic situation that needs AECG recording to exclude the presence of pacemaker malfunction and to detect the appropriateness of atrio-ventricular synchrony. Pacemaker syndrome as first described in patients with VVI pacemakers may also occur in dual-chamber pacing systems when the programmed AV delay does not allow enough time for the atria to contract against open atrio-ventricular valves. This phenomenon may be observed in the following conditions: (1) programmed prolonged AV delay, (2) DDI or DDDIR pacing modes, (3) pacemaker-mediated tachycardia, (4) sinus bradycardia below the lower limit in the VDD pacing mode, (5) pace mode switching from DDD(R) to VVI(R), and (6) rate smoothing or fallback during DDD pacing. In some cases, it may be difficult to differentiate severe pacemaker syndrome from vasovagal syncope, and in these patients head-up tilt-testing may help to clarify the situation. Finally, the efficacy of AADs to suppress concomitant intermittent tachycardias, for example, paroxysmal AF or frequent VPBs that interfere significantly with pacemaker function, can also be assessed by AECG monitoring.

Patients following ICD implantation for the management of ventricular tachyarrhythmias often have ICD shock therapy during follow-up. AECG monitoring can be a useful alternative or adjunct to continuous telemetric monitoring or interrogation of ICD memory in establishing the appropriateness of such therapy. Moreover, the rate of SVTs (sinus tachycardia or AF with high ventricular rates) that eventually interfere with the cut-off parameters of the ICD device, with the consequence of the delivery of inappropriate shocks, may be evaluated and the efficacy of adjunctive pharmacological therapy in suppressing spontaneous arrhythmias in an attempt to minimize the frequency of device activation can be assessed by the AECG, as well.

33.8.5.2 Antiarrhythmic Drugs (AADs)

AECG monitoring has been widely used in the past to assess the effects of antiarrhythmic therapy, because it is a non-invasive technique that provides quantitative ECG data and permits correlation of symptoms with ECG phenomena. However, there are important limitations of AECG as a therapeutic guide such as the significant day-to-day variability in the type and frequency of arrhythmias in many patients, a lack of correlation between arrhythmia suppression after an intervention and subsequent outcome, uncertain guidelines for the degree of suppression required to demonstrate an effect, either clinical or statistical, and an absence of quantifiable spontaneous asymptomatic arrhythmias between episodes in many patients with a documented history of life-threatening ventricular tachyarrhythmias [7, 197].

AECG monitoring with quantitative analysis has not been widely used to guide the therapy of supraventricular arrhythmias because of the limited day-to-day occurrence of these arrhythmias and the uncertain significance of asymptomatic non-sustained atrial ectopy. But for evaluating the effects of AADs in patients with supraventricular arrhythmias, particularly AF, intermittent monitoring to confirm the presence of an arrhythmic episode during symptoms and to document arrhythmia-free intervals has become more or less a standard approach. Moreover, the AECG may also be used to monitor the effects of AV nodal blocking agents on heart rate in patients with atrial arrhythmias (beta blockers, digitalis, calcium channel blockers), particularly in AF. Since short-term reproducibility of the frequency and type of arrhythmia, especially in ventricular arrhythmias, between repeat AECG recordings is rather poor, a large reduction between 60% and 90% in arrhythmia frequency is required to ensure that the change is due to an antiarrhythmic effect of any intervention [7].

The best way of assessing the efficacy of a drug is probably to select a group of patients with the same arrhythmia and to measure the spontaneous variability between a control and a placebo period. If the variability is small with a good correlation between the two periods, a drug trial appears possible. It is then feasible to compare the respective efficacy of two drugs in the same group of patients. The appropriate statistical method (such as that developed by Sami et al. [198, 199]) uses a one-tailed 95% confidence interval calculated between baseline and placebo PVC measurements. The appreciation of the antiarrhythmic effect is based on the comparison with the relation between drug and control (◉ Fig. 33.36). If a drug shifts a PVC value under the 95% confidence interval line, its effectiveness can most likely be assumed in that patient. If a drug A shifts more patients under the 95% confidence interval line than drug B, A is probably more effective than B in this selected arrhythmia. This method is largely used to compare a new drug with an established treatment chosen as reference. An important limitation is the necessity to observe several periods without treatment (control, placebo, follow-up). Patients with severe symptomatic arrhythmias cannot be included in these studies. Open studies are indicated in such patients.

The data from the CAST trial, in which a higher mortality rate during follow-up was observed in those patients who had suppression of spontaneous VPBs after a titration phase and then received chronic encainide or flecainide therapy as opposed to placebo, led to a revision of the former concept that suppression of PVCs by AADs would improve the prognosis of patients with structural heart disease. Indeed, the trial showed that antiarrhythmic therapy with encainide or flecainide may be harmful to patients. More or less similar inconsistent results have been obtained with the empiric use of amiodarone, since some studies such as the BASEL, CASCADE, or GESICA trials showed a benefit in patients with preserved or depressed LV function [200–203], while others like EMIAT or CAMIAT revealed no significant change in mortality rate [204–206]. In one trial, amiodarone produced a significant reduction in arrhythmia frequency but had no effect on mortality rate [206].

In contrast to supraventricular tachy(arrhythmias), placebo-controlled trials of antiarrhythmic interventions in patients with sustained life-threatening ventricular tachyarrhythmias are problematic. Although in the study of Lampert et al. [207] improvements in arrhythmia-free survival in CHD patients who met certain criteria for drug response during serial AECG were reported, it is not possible to estimate the effects of the "healthy responder" phenomenon [208] on these observations, which means that patients who responded to the AECG-guided drug therapy had a different (more favorable) prognosis than those who did not. With respect to the method of choice for monitoring the outcome of an antiarrhythmic intervention, AECG as well as EP testing may be used. The ESVEM study [209], which used both tests in a randomized fashion on patients with an entry criterion of inducibility of sVT on two occasions and $\geqslant$10 VPBs/h showed that there was no significant difference in predicting long-term success in either group, once a drug was determined to be effective (EPS: suppressing inducible VT, AECG: suppression of VPBs). However, AECG monitoring had the advantage in that it identified an AAD predicted to be effective more often than EPS in these patients. For practical reasons, despite

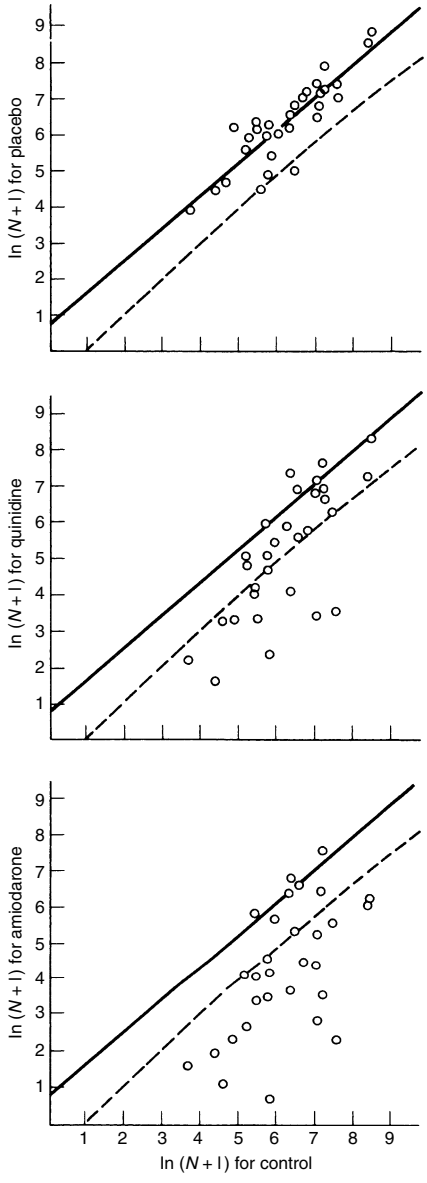

Figure 33.36

Results from a crossover comparative trial of quinidine (1 g day^{-1}) and amiodarone (400 mg day^{-1}) in 30 patients with frequent PVCs using the statistical methodology of Sami et al. [198, 199]. Each diagram shows a correlation line with a one-tailed 95% confidence interval indicated by the dashed line. In the top diagram, the control and placebo periods are compared with respect to the incidence of PVCs while similar comparisons are shown in the middle diagram for control versus quinidine and in the lower diagram for amiodarone versus control. The symbol *N* represents PVC frequency per hour. The effectiveness of the AAD therapy can be judged by the number of points beneath the 95% confidence interval line. In other words, the incidence of PVCs in patients on these drugs is lower than in control or placebo periods. It can also be seen that the antiarrhythmic efficacy is higher in patients with amiodarone than in those with quinidine.

the many criticisms of the ESVEM trial, it may be concluded that AECG monitoring may be used to assess AAD efficacy in patients with frequent VPBs, but not in those with spontaneous sustained VTs.

The same holds true for assessing the phenomenon of proarrhythmia, which is defined as the aggravation of an arrhythmia, particularly of VEA, for example, either the increase of the number or complexity of VEA or the new incidence of a given ventricular arrhythmia, as well as sinus node dysfunction, or new or worsened AV conduction abnormalities. Proarrhythmia may occur early or late during the course of therapy, and an increase of arrhythmia needed to differentiate proarrhythmia from day-to-day variability may be estimated statistically on the basis of baseline arrhythmia frequency [198, 199, 210, 211]. A particular type of proarrhythmia is the induction of torsades de pointes that may be induced by drugs that prolong the QTI (e.g., class III AADs, tricyclic antidepressants, antihistamines, antibiotics, etc.). In such cases, AECG monitoring may be useful for the evaluation of new markers of this type of proarrhythmia, such as alternating QTIs or T waves, or altered QT-interval adaptation to changes in heart rate.

33.8.5.3 Antianginal Drugs

Most antianginal drugs are commonly assessed by counting the frequency of anginal attacks, and the number of nitroglycerin tablets consumed. This kind of investigation relies entirely on subjective symptom appreciation. Changes in lifestyle, environmental conditions, or daily activity may deeply affect the results. ST-segment monitoring provides an objective technique, as does stress testing, which is now routinely performed to evaluate these therapies. Thus, physicians should use repetitive stress tests or continuous AECG monitoring in cases of exercise angina. Twenty-four-hour ECGs are more efficient for characterizing the pharmacological properties of the drug, such as delay and duration of effect. In the case of spontaneous (Prinzmetal's) angina, ambulatory monitoring is the optimum technique allowing an accurate evaluation of the drugs, which are used in this condition (calcium antagonists) [212]. The development of AECG has also revealed that all patients with spontaneous angina exhibit painless episodes of ST-segment elevation in addition to experiencing painful attacks. When an antianginal treatment such as a calcium antagonist is not completely effective, only painless episodes persist. Repeated 24-h ECGs are then necessary to assess the efficacy of treatment and the need for an increase in dosage or a change to another drug. Thus, suspected Prinzmetal's angina is obviously a good indication for ambulatory monitoring, which is useful both as a diagnostic procedure and for evaluation of therapy.

33.9 Pediatric Patients

Similar to adult patients, the purposes of AECG monitoring in pediatric patients include the evaluation of symptoms, risk assessment in patients with cardiovascular disease, with or without symptoms of an arrhythmia, and the evaluation of cardiac rhythm after an intervention like drug therapy or device implantation [7]. Selection of the method of monitoring, for example, continuous versus patient activated recording, is predicated on the frequency and symptoms of the arrhythmia. AECG monitoring may be useful for evaluation of symptoms in patients with known cardiovascular disease and for medical therapy and intervention. In children with asymptomatic congenital heart block, a yearly Holter monitor is recommended. The escape rate at resting conditions is used as one criterion for the need of pacemaker implantation. In general, a resting heart rate greater than 60 bpm in children under 2 years, greater than 50 bpm in children 2–10 years, and greater than 40 bpm in children over 10 years of age is considered to be an adequate escape rhythm. In addition, the mean heart rate, the slowest heart rate, and the longest pause on AECG monitoring can also be used as supportive data, and the presence of ventricular ectopy (as single escape beats) is another indication for pacemaker implantation.

33.9.1 Evaluation of Symptoms

AECG in pediatric patients may be used for the evaluation of symptoms including palpitations, dizziness, syncope or near syncope, and chest pain and their relation to an underlying arrhythmia. Because of the paroxysmal nature of palpitations, an event recorder is usually recommended to detect the cause of these symptoms. In 10–15% of young individuals, an arrhythmia, in most cases SVT, has been reported to correlate with symptoms (213–218), (Table 33.10), whereas ventricular ectopy or bradycardia was demonstrated in only other 2–5%. Interestingly, in about 50% of palpitations, sinus

Table 33.10

Yield of Holter monitoring for evaluation of palpitation in pediatric patients with no structural heart disease

Author (year)	No. of patients	Method	Mean no. of days of monitoring	Symptoms during monitoring, n(%)		No symptoms during monitoring, no arrhythmia, n (%)
				Arrhythmia	No arrhythmia	
Dick (1979)	6	TTM		2 (33)	4 (67)	0
Porter (1980)	25	TTM	1	3 (12)	9 (36)	13 (52)
Fyfe (1984)	41	HM	75	9 (22) (8 SVT)	12 (29)	20 (49)
Goldstein (1990)	48	TTM	14–90	10 (21) (7SVT)	15 (31)	23 (48)
Houyel (1992)[+]	201	TTM	85	24 (12) (23 SVT)	112 (56)	65 (32)
Karpawich (1993)	37	TTM	30	10 (27)	27 (73)	0
	45	HM	1	0	9 (20)	36 (80)
Total	403			58 (14)	188 (47)	157 (39)

Abbreviations: TTM = Trans Telephonic Monitoring, patient activated event recorder, HM = Holter Monitoring (24-h monitoring), [+]Includes 25 patients with heart disease

tachycardia was found, whereas 30–40% of young patients have no symptoms in AECG monitoring. Thus, one of the primary uses of AECG monitoring in pediatric patients is to exclude an arrhythmia as the cause of palpitations [7]. Recently, the value of transtelephonic monitoring (TTM) in the evaluation of symptoms in young persons has been clearly demonstrated by Saarel et al. [219] in a large cohort of 420 patients with palpitations, 43 with chest discomfort, and 32 with presyncope and syncope. Fifty-two percent ($n = 257$) of patients failed to transmit an ECG while experiencing symptoms. Of 238 symptomatic patients, 35 (15%) had SVT, and all patients with SVT had palpitations. The overall sensitivity of the TTM test was 83% (35 of 42) for detection of SVT, and the NPV was 99% in this patient population. The conclusion was that TTMs are useful for the evaluation of children and adolescents with palpitations but not with isolated chest pain, syncope, or presyncope.

Because of the intermittent nature of transient neurological symptoms such as dizziness, syncope, or near syncope in pediatric patients without structural heart disease, the efficacy of 24-h or 48-h AECG monitoring is low and thus, its ability to clarify patients' symptoms is limited. Therefore, prolonged AECG monitoring is only recommended in those individuals with known heart disease or with exertional symptoms, in whom the presence and significance of an arrhythmia may be increased [220, 221]. An alternative diagnostic tool may be the implanted loop recorder (ILR) in case conventional investigations have failed to identify the cause of syncope or palpitations. In a small series of 4 children with congenital heart disease, who suffered from presyncope ($n = 1$), syncope ($n = 2$), and palpitations ($n = 1$), an ILR was implanted. All patients experienced typical symptoms and activated the device appropriately at a median of 86 days (46–102) after implantation. In 2 of 4 cases, a likely cause for the symptoms was identified, with exclusion of more malignant arrhythmic diagnoses in all patients. The conclusion from this study was that an ILR can be implanted in young children without difficulty and that this device may prove to be very useful for excluding malignant arrhythmias as a cause of symptoms in patients at high risk [222]. Chest pain is a relatively rare symptom, and a cardiac cause is identified in only 5% or less of pediatric patients, so that the primary role of AECG monitoring in these patients may be to exclude rather than diagnose a cardiac cause [7].

33.9.2 Evaluation of Patients with Known Cardiovascular Disease

AECG monitoring may be particularly useful in pediatric patients after surgery for congenital heart disease, but the frequency of recording periods has to be based on the type of defect, ventricular function, and late postoperative arrhythmias. Uncomplicated repairs of simple defects such as atrial or ventricular septal defects or with aortic or pulmonary stenosis have a low incidence of late postoperative arrhythmias, whereas complex repairs or those with residual hemodynamic abnormalities display a high incidence of late postoperative arrhythmia. High grade ambulatory VEA associated

with ventricular dysfunction seems to identify patients at an increased risk of late sudden death [223–227]. Major atrial surgery such as Mustard's or Senning's operation for transposition of great arteries or Fontan's operation for functional single ventricle hearts is often associated with sinus node dysfunction and with unusual types of AFl (which is called incisional atrial re-entrant tachycardias = IART). Major ventricular surgeries such as tetralogy of Fallot repair, repair of double outlet right ventricle, etc. may predispose to serious ventricular tacharrhythmias in the long run. In the past, complex VEA or nsVT were considered as risk stratifiers in those patients. However, Cullen et al. [225] showed, at least in patients after repair of Fallot, that after a follow-up of 12 years, asymptomatic VPBs were common and the presence of complex VEA or non-sustained VT were not prognostically significant in this patient group. Nevertheless, if complex ventricular arrhythmias are detected with AECG monitoring in post-operative high-risk pediatric patients with depressed ventricular function, there is a need for further investigation, even in the absence of overt clinical signs or symptoms [228].

A second group of pediatric patients may benefit from periodic AECG monitoring, namely, those with hypertrophic or dilated cardiomyopathy as well as with the congenital long QT syndrome because of the tendency of progression of these diseases and the need to adjust medication doses with growth [7]. The rate of 9–15% of sudden death as a first symptom in young patients with these types of disease is significantly higher than in adults, and AECG monitoring is needed to identify occult arrhythmias that may indicate the need for reevaluation of therapy in asymptomatic patients, though the absence of an arrhythmia during one or several monitoring periods does not necessarily indicate a low risk of arrhythmic sudden death. There is no doubt that unexplained syncope or cardiovascular collapse in young patients with known cardiovascular disease generally requires in-hospital continuous ECG monitoring and sophisticated (e.g., by MRI) or invasive evaluation when the cause of the event is uncertain. But if a cause cannot be established by MRI or invasive methods, AECG monitoring may be used for subsequent surveillance to possibly detect both transient brady- and tachyarrhythmias [7].

33.9.3 Evaluation of Medical Therapy or Intervention

AECG monitoring may be helpful to evaluate both beneficial and potentially harmful effects of pharmacological therapy as well as to detect possible causes of symptoms in patients with pacemakers or after radiofrequency catheter ablation or cardiac surgery, particularly when complicated by transient AV block [229, 230]. Another important indication for AECG monitoring is the evaluation of cardiac rhythm after treatment of incessant tachyarrhythmias, which have been associated with progressive ventricular dysfunction [231]. In this context, the above mentioned technical aspects and limitations of AECG monitoring (e.g., day-to-day variability of arrhythmias, etc.) have to be taken into account.

33.10 Future Perspectives of Ambulatory Monitoring

Further advances in AECG monitoring analysis include better characterization of duration and dispersion of ventricular depolarization (QTI), the detection of T-wave alternans, the identification of different patterns of onset of arrhythmias (short–long–short sequence, tachycardia versus bradycardia dependence of arrhythmias), the computation of heart-rate turbulence indexes, and the evaluation of P wave and QRS-wave morphology including P-wave averaging and late potential analysis, from high-quality AECG signals [232]. By this means, old and new markers derived from AECG monitoring could be integrated to provide a comprehensive noninvasive AECG test, to fully characterize all three components of the triangle of risk factors (Fig. 33.37) that may lead to electrical instability and SCD: the electrophysiologic (arrhythmia) substrate, the triggers for malignant ventricular arrhythmias provoking SCD, and the modulation of the (background) sympatho–vagal balance of the ANS [233].

Thanks to the availability of larger storage capacities, in the near future long-term (weeks–months) continuous high-quality AECG monitoring may become available. Moreover, devices for long-term long-distance telemetric surveillance using transtelephonic transmission of ECG data for high-risk cardiac patients have already become a reality. Some modern digital recorders already have the capability for multichannel (8–12 channels) simultaneous ECG recordings, which

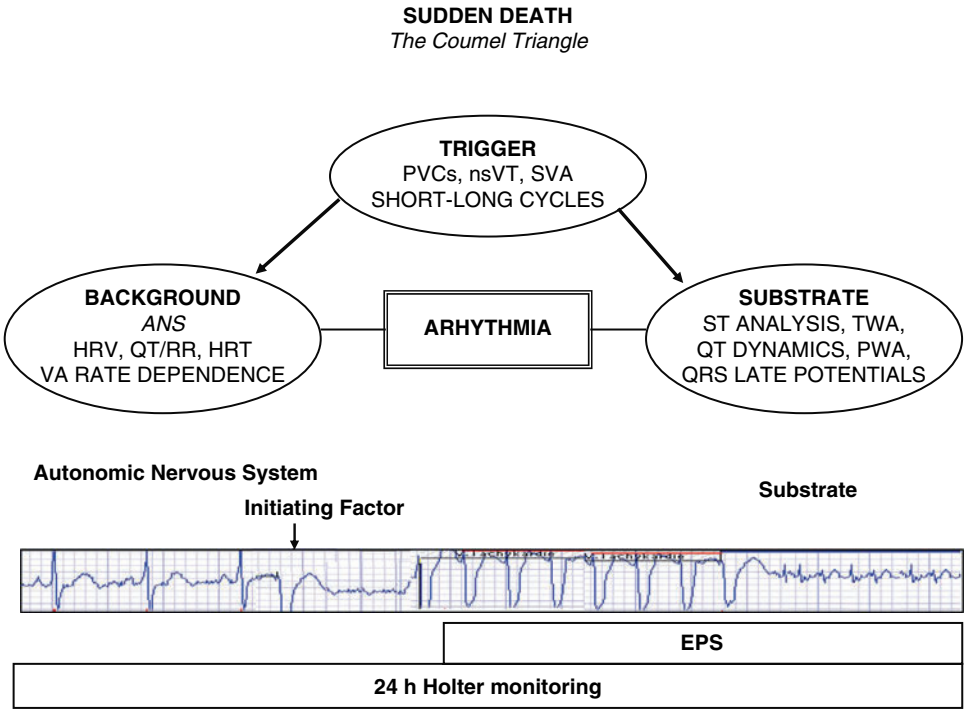

Figure 33.37

Schematic representation of the triangle of risk factors that may lead to electrical instability with subsequent ventricular fibrillation, including the different parameters that can be derived from AECG monitoring: the electrophysiologic substrate, the balance of the ANS, and the triggers of malignant ventricular arrhythmias that provoke SCD. Abbreviations: PVCs: premature ventricular contractions, nsVT: non-sustained VT, SVA: supraventricular arrhythmias, HRV: heart-rate variability, QT/R–R: QT/R–R interval relation, HRT: heart-rate turbulence, VA: ventricular arrhythmias, TWA: T-wave alternans, PWA: P-wave duration from averaged ECG (Modified from Coumel 1990).

might be interesting for ischemia monitoring. Finally, multichannel digital recordings will allow the retrieval of different biological signals by appropriate sensors, such as arterial pulse pressure, respiratory rate, peripheral oxygen tension, EEG, and others. This will transform AECG monitoring into ambulatory polycardiography that will allow the comprehensive evaluation of patients with complex disorders, such as CHF, cor pulmonale, or sleep apnea syndromes, and the detection and quantification of underlying interactive pathophysiological mechanisms [232].

References

1. Harrison, D.C., J.W. Fitzgerald, and R.A. Winkle, Ambulatory electrocardiography for diagnosis and treatment of cardiac arrhythmias. *N. Engl. J. Med.*, 1976;**294**: 373–380.
2. Hinkle, L.E., Jr., Equipment specifications and analytic techniques: clinical implications, in *Ambulatory Electrocardiographic Recording*, N.K. Wenger, M.B. Mock, and I. Ringqvist, Editors. Chicago, IL: Year Book Medical, 1981, pp. 33–57.
3. Holter, N.J., New method for heart studies: continuous electrocardiography of active subjects over long periods is now practical. *Science*, 1961;**134**: 1214–1220.
4. Kennedy, H.L., *Ambulatory Electrocardiography – Current Clinical Concepts*. Cardiol. Clin.; Philadelphia/London/Toronto/Montreal/Sydney/Tokyo: W.B. Saunders, 1992.
5. Van Keulen. G.J., J. Boter, C.A.A. Hakkenberg Van Gaasbeek, and G.E.P.M. Van Venrooij, *MFI Test "Holter Systems": Long-Term ECG Tape Recorder Systems*. Utrecht: Institute of Medical Physics TNO, 1980.
6. Sheffield, L.T., A. Berson, D. Bragg-Remschell, et al., Recommendations for standards of instrumentation and practice in the use of ambulatory electrocardiography. *Circulation*, 1985;**71**: 626A–636A.

7. Crawford, M.H., S.J. Bernstein, P.C. Deedwania, et al., ACC/AHA guidelines for ambulatory electrocardiography. A report of the American College of Cardiology/American Heart Association Task Force on Practical Guidelines (Commission to Revise the Guidelines for Ambulatory Electrocardiography). *J. Am. Coll. Cardiol*., 1999;**34**: 912–948.
8. Lanza, G.A., M. Mascellanti, M. Placentino, et al., Usefulness of a third Holter lead for detection of myocardial ischemia. *Am. J. Cardiol*., 1994;**74**: 1216–1219.
9. Osterhues, H.H., T. Eggeling, M. Kochs, and V. Hombach, Improved detection of transient myocardial ischemia by a new lead combination: value of bipolar lead Nehb D for Holter monitoring. *Am. Heart J*., 1994;**127**: 559–566.
10. Seeberger, M.D., J. Moerlen, K. Skarvan, et al., The inverse Nehb J lead increases the sensitivity of Holter electrocardiographic monitoring for detecting myocardial ischemia. *Am. J. Cardiol*., 1997;**80**: 1–5.
11. Cristal, N., M. Gueron, and R. Hoffman, VI-like and aVF-Iike leads for continuous electrocardiographic monitoring. *Br. Heart J*., 1972;**34**: 696–698.
12. Jenkins, J.M., D. Wu, and R.C. Arzbaecher, Computer diagnosis of supraventricular and ventricular arrhythmias. A new esophageal technique. *Circulation*, 1979;**60**: 977–985.
13. Schnittger, I., I.M. Rodriguez, and R.A.Winkle, Esophageal electrocardiography: A new technology revives an old technique. *Am. J. Cardiol*., 1986;**57**: 604–607.
14. Rosengarten, M.D., J.F. Leclercq, P. Attuel, and Ph. Coumel, Holter monitoring and cardiac rhythm, in *What's New in Electrocardiography*, H.J.J. Wellens and H.E. Kulbertus, Editors. The Hague: Nijhoff, 1981, pp. 344–365.
15. Bragg-Remschell, D.A., C.M. Anderson, and R.A. Winkle, Frequency response characteristics of ambulatory ECG monitoring systems and their implications for ST segment analysis. *Am. Heart J*., 1982;**103**: 20–31.
16. Nygards, M.-E., T. Ahren, I. Ringqvist, and A. Walker, Phase correction for accurate ST segment reproduction in ambulatory ECG recording, in *Computers in Cardiology, 1984*, K. Ripley, Editor. Silver Spring, MD: IEEE, 1984, pp. 33–38.
17. Shook, T.L., C.W. Balke, P.W. Kotilainen, et al., Comparison of amplitude-modulated (direct) and frequency-modulated ambulatory techniques for recording ischemic electrocardiographic changes. *Am. J. Cardiol*., 1987;**60**: 895–900.
18. Nearing, B.D., P.H. Stone, and R.L. Verrier, Frequency response characteristics required for detection of T-wave alternans during ambulatory ECH monitoring. *Ann. Noninvasive Electrocardiol*., 1996;**1**: 103–112.
19. Kennedy, H.L., S.C. Smith, J. Mizera, et al., Limitations of ambulatory ECG real-time analysis for ventricular and supraventricular arrhythmia accuracy detected by clinical evaluation. *Am. J. Noninvasive Cardiol*., 1992;**6**: 137–146.
20. Krahn, A.D., G.J. Klein, and V. Manda, The high cost of syncope: cost implications of a new insertable loop recorder in the investigation of recurrent syncope. *Am. Heart J*., 1999;**137**: 870–877.
21. Krasnow, A.Z. and D.K. Bloomfield, Artifacts in ambulatory ECG monitoring, in *Ambulatory ECG Monitoring*, S. Stern, Editor. Chicago, IL: Year Book Medical, 1978, pp. 171–189.
22. Leclercq, J.F., *L 'Enregistrement Holter en Rhythmologie*. Paris: Labaz, 1980.
23. Quiret, J.C., J.L. Rey, M. Lombaert, and P. Bernasconi. Les artefacts au cours de l'e:nregistrement electrocardiographique continu par la methode de Holter. *Arch. Mal. Coeur Vaiss*., 1979;**72**: 757–765.
24. Cashman, P.M.M., Methods for tape analysis II. *Postgrad. Med. J*., 1976;**52**(Suppl. 7): 19–23.
25. Crow, R.S. and R.J. Prineas, Quality control, in *Ambulatory Electrocardiographic Recording*, N.K. Wenger, N.I.B. Mock, and I. Ringqvist, Editors. Chicago, IL: Year Book Medical, 1981, pp. 19–64.
26. Palma Gamitz, J.L., *Electrocardiografia de Holter*. Madrid: Norma, 1983.
27. Corday, E. and T.-W. Lang, Accuracy of data reduction systems for diagnosis and quantification of arrhythmias. *Am. J. Cardiol*., 1975;**35**: 927–928.
28. Coumel, Ph., P. Attuel, J.F. Leclercq, and D. Flammang, Computerized quantitative evaluation of cardiac arrhythmias, in *Computers in Cardiology. (1977)*. New York: IEEE, 1977, pp. 571–577.
29. Weber, H.S., G. Joskowicz, D. Glogar, K.K. Steinbach, and F. Kaindl, Clinical importance of computer assisted long-term ECG analysis, in *Long-Term Ambulatory Electrocardiography*, J. Roelandt and P.G. Hugenholtz, Editors. The Hague: Nijhoff, 1982.
30. Stern, S. and D. Tzivoni, Early detection of silent ischaemic heart disease by 24-hour electrocardiographic monitoring of active subjects. *Br. Heart J*., 1974;**36**: 481–486.
31. Cohn, P.F. and W.B. Kannel, Recognition, pathogenesis, and management options in silent coronary artery disease. *Circulation*, 1987;75: II-1.
32. Benhorin, J., F. Badilini, A.J. Moss, et al., New approach to detection of ischemic-type ST segment depression, in *Noninvasive Electrocardiology – Clinical Aspects of Holter Monitoring*, A.J. Moss and S. Stern, Editors. London/Philadelphia/Toronto/Sydney/Tokyo: WB Saunders, 1996, pp. 345–355.
33. Badilini, F., W. Zareba, E.L. Titlebaum, and A.J. Moss, Analysis of ST segment variability in Holter recordings, in *Noninvasive Electrocardiology – Clinical Aspects of Holter Monitoring*, A.J. Moss and S. Stern, Editors. London/Philadelphia/Toronto/Sydney/Tokyo: WB Saunders, 1996, pp. 357–372.
34. Ghuran, A. and M. Malik, Time domain heart rate variability, in *Noninvasive Electrocardiology in Clinical Practice*, W. Zareba, P. Maison-Blanche, and E.H. Locati, Editors. Armonk/New York: Futura, 2001, pp. 145–162.
35. Lombardi, F., Frequency domain analysis of heart rate variability, in *Noninvasive Electrocardiology in Clinical Practice*, W. Zareba, P. Maison-Blanche, and E.H. Locati, Editors. Armonk/New York: Futura, 2001, pp. 163–180.
36. Task Force of the ESC and NASPE, Heart rate variability standards of measurement, physiological interpretation, and clinical use. *Circulation*, 1996;**93**: 1043–1065.
37. Malliani, A., M. Pagani, F. Lombardi, et al., Cardiovascular neural regulation explored in the frequency domain. *Circulation*, 1991;**84**: 482–492.
38. Saul, J.P., Y. Arai, R.D. Berger, et al., Assessment of autonomic regulation in chronic congestive heart failure by heart rate spectral analysis. *Am. J. Cardiol*., 1988;**61**: 1292–1299.
39. Schmidt, G., M. Malik, P. Barthel, et al., Heart-rate-turbulence after ventricular premature beats as a predictor of mortality after acute myocardial infarction. *Lancet*, 1999;**353**: 1390–1396.

40. Hainsworth, R., Physiology of the cardiac autonomic system, in *Clinical Guide to Cardiac Autonomic Tests*, chapter 1, M. Malik, Editor. London: Kluwer Academic, 1998, pp. 3–28.
41. Voss, A., V. Baier, A. Schymann, et al., Postextrasystolic regulation patterns of blood pressure and heart rate in idiopathic dilated cardiomyopathy. *J. Physiol. (London)*, 2002;**538**: 271–278.
42. Schneider, R., P. Barthel, G. Schmidt, Methods for the assessment of heart rate turbulence in Holter ECGs. *J. Am. Coll. Cardiol.*, 1999;**33**(Suppl. A): 351A.
43. Locati, E.H., QT interval duration and adaptation to heart rate, in *Noninvasive Electrocardiology in Clinical Practice*, W. Zareba, P. Maison-Blanche, and E.H. Locati, Editors. Armonk/New York: Futura, 2001, pp. 71–96.
44. Lepeschkin, E. and B. Surawicz, The measurement of the QT interval of the electrocardiogram. *Circulation*, 1952;**6**: 378–388.
45. Cowan, J.C., K. Yusoff, M. Moore, et al., Importance of lead selection in QT interval measurement. *Am. J. Cardiol.* 1988;**61**: 83–87.
46. Laguna, P., N.V. Thakor, P. Caminal, et al., New algorithm for QT analysis in 24-hour Holter ECG: performance and applications. *Med. Biol. Eng. Comput.*, 1990;**28**: 67–73.
47. Maison-Blanche, P., D. Catuli, J. Fayn, and P. Coumel, QT interval, heart rate and ventricular arrhythmias, in *Noninvasive Electrocardiology – Clinical Aspects of Holter Monitoring*, A.J. Moss and S. Stern, Editors. London/Philadelphia/Toronto/Sydney/Tokyo: WB Saunders, 1996, pp. 383–404.
48. Han, J. and G.K. Moe, Nonuniform recovery of excitability in ventricular muscle. *Circ. Res.*, 1964;**14**: 44–60.
49. Antzelevich, C., W. Shimizu, G.X. Yan, et al., The M cell: its contribution to the ECG and normal and abnormal electrical function of the heart. *J. Cardiovasc. Electrophysiol.*, 1999;**10**: 1124–1152.
50. Sylven, J.C., B.M. Horacek, C.A. Spencer, et al., QT interval variability on the body surface. *J. Electrocardiol.*, 1984;**17**: 179–188.
51. Zareba, W., A. Nomura, and J. Perkiömäki, Dispersion of repolarization: concept, methodology, and clinical experience, in *Noninvasive Electrocardiology in Clinical Practice*, W. Zareba, P. Maison-Blanche, and E.H. Locati, Editors. Armonk/New York: Futura, 2001, pp. 97–121.
52. Rautaharju, P.M., Why did QT dispersion die? *CEPR*, 2002;**6**: 295–301.
53. Malik, M., QT dispersion: time for an obituary? *Eur. Heart J.*, 2000;**21**: 955–957 (Editorial).
54. Simson, M.B., Use of signals in the terminal QRS complex to identify patients with ventricular tachycardia after myocardial infarction. *Circulation*, 1981;**64**: 235–241.
55. Breithardt, G., M. Cain, N. El-Sherif, et al., Standards for analysis of ventricular late potentials using high-resolution signal-averaged electrocardiography: a statement by a Task Force Committee of the European Society of Cardiology, the American Heart Association, and the American College of Cardiology. *J. Am. Coll. Cardiol.*, 1991;**17**: 999–1006.
56. Kelen, G., R. Henkin, M. Lannon, et al., Correlation between the signal-averaged electrocardiogram from Holter tapes and from real-time recordings. *Am. J. Cardiol.*, 1989;**63**: 1321–1325.
57. Leenhardt, A., P. Maison-Blanche, I. Denjoy, et al., Signal averaging of ventricular late potentials using Holter recordings. *Eur. Heart J.*, 1990;**11**: 402 (Abstract).
58. Kostis, J.B., A.E. Moreyra, M.T. Amendo, J. Di Pietro, N. Cosgrove, and P.T. Kuo, The effect of age on heart rate in subjects free of heart disease. Studies by ambulatory electrocardiography and maximal exercise stress test. *Circulation*, 1982;**65**: 141–145.
59. Bjerregaard, P., Mean 24 hour heart rate, minimal heart rate and pauses in healthy subjects 40–79 years of age. *Eur. Heart J.*, 1983;**4**: 44–51.
60. Bjerregaard, P., Prevalence and variability of cardiac arrhythmias in healthy subjects, in *Cardiac Arrhythmias in the Active Population. Prevalence, Significance and Management*, D.A. Chamberlain, H. Kulbertus, L. Mogensen, and M. Schlepper, Editors. Molndal Sweden: Hassle, 1980, p. 24.
61. Bjerregaard, P., Premature beats in healthy subjects 40–79 years of age. *Eur. Heart J.*, 1982;**3**: 493–503.
62. Djiane, P., A. Egre, M. Bory, B. Savin, S. Mostefa, and A. Serradimigni, L'enregistrement electrocardiographique chez les sujets normaux. *Arch. Mal. Coeur Vaiss.*, 1979;**72**: 655–661.
63. Goulding, L., Twenty-four hour ambulatory electrocardiography from normal urban and rural populations, in *ISAM 1977*, F.D. Stott, E.B. Raftery, P. Sleight, and L. Goulding, Editors. London: Academic, 1978, pp. 13–22.
64. Verbaan, C.J., J. Pool, and J. Van Wanrooy, Incidence of cardiac arrhythmias in a presumed healthy population, in *ISAM 1977*, F.D. Stott, E.B. Raftery, P. Sleight, and L. Goulding, Editors. London: Academic, 1978, pp. 1–5.
65. Brodsky, M., D. Wu, P. Denes, C. Kanakis, and K.M. Rosen, Arrhythmias documented by 24 hour continuous electrocardiographic monitoring in 50 male medical students without apparent heart disease. *Am. J. Cardiol.*, 1977;**39**: 390–395.
66. Armstrong, W.F., J.W. Jordan, S.N. Morris, and P.L. McHenry, Prevalence and magnitude of S-T segment and T wave abnormalities in normal men during continuous ambulatory electrocardiography. *Am. J. Cardiol.*, 1982;**49**: 1638–1642.
67. Quyyumi, A.A., C. Wright, and K. Fox, Ambulatory electrocardiographic ST segment changes in healthy volunteers. *Br. Heart J.*, 1983;**50**: 460–464.
68. Bjerregaard, P., Prevalence and magnitude of ST segment and T-wave abnormalities in healthy adult subjects during continuous ambulatory electrocardiography, in *Ambulatory Monitoring: Cardiovascular System and Allied Applications*, C. Marchesi, Editor. The Hague: Nijhoff, 1984, pp. 114–118.
69. Burckhardt, D., B.E. Luetold, M.V. Jost, and A. Hoffmann, Holter monitoring in the evaluation of palpitations, dizziness and syncope, in *Long-Term Ambulatory Electrocardiography*, J. Roelandt and P.G. Hugenholtz, Editors. The Hague: Nijhoff, 1982, pp. 29–39.
70. Krasnow, A.Z. and D.K. Bloomfield, The relationship between subjective symptomatology and objective findings from ambulatory ECG monitoring studies in a large unselected population, in *Ambulatory ECG Monitoring*, S. Stem, Editor. Chicago, IL: Year Book Medical, 1978, pp. 149–169.
71. Shenasa, M., P.V.L. Curry, and E. Sowton, The relationship between symptoms and arrhythmias during 24-hour ECG recording, in *ISAM 1979*, F.D. Stott, E.B. Raftery, and L. Goulding, Editors. London: Academic, 1980, pp. 39–49.
72. Bass, E.B., E.I. Curtiss, V.C. Arena, et al., The duration of Holter monitoring in patients with syncope: is 24 hours enough? *Arch. Intern. Med.*, 1990;**150**: 1073–1078.
73. Babalis, D., P. Maison-Blanche, J.F. Leclercq, and Ph. Coumel, Interet d'un electrocardiogramme de longue duree chez les patients ayant eu un accident cerebral ischemique. *Arch. Mal. Coeur Vaiss.*, 1984;**77**: 100–105.

74. Fisher, M., Holter monitoring in patients with transient focal cerebral ischemia. *Stroke*, 1978;**9**: 514–516.
75. Reed, R.L., R.G. Siekert, and J. Merideth, Rarity of transient focal cerebral ischemia in cardiac dysrhythmia. *J. Am. Med. Assoc.*, 1973;**223**: 893–895.
76. Tonet, J.L., R. Frank, A. Ducardonnet, et al., L'enregistrement de Holter dans les accidents ischemiques cerebraux. *Nouv. Presse Med.*, 1981;**10**: 2491–2494.
77. Allen, R.D., L.S. Gettes, C. Phalan, and M.D. Avington, Painless ST-segment depression in patients with angina pectoris. Correlation with daily activities and cigarette smoking. *Chest*, 1976;**69**: 467–473.
78. Araki, H., Y. Koiwaya, O. Nakagaki, and M. Nakamura, Diurnal distribution of ST-segment elevation and related arrhythmias in patients with variant angina: a study by ambulatory ECG monitoring. *Circulation*, 1983;**67**: 995–1000.
79. Biagini, A., M.G. Mazzei, C. Carpeggiani, et al., Vasospastic ischemic mechanism of frequent asymptomatic transient ST-T changes during continuous electrocardiographic monitoring in selected unstable angina patients. *Am. Heart J.*, 1982;**103**: 13–20.
80. Gettes, L.S. and S.R. Winternitz, The use of ambulatory ECG monitoring to detect "silent" ischemia, in *Ambulatory ECG Monitoring*, S. Stern, editor. Chicago, IL: Year Book Medical, 1978, pp. 93–105.
81. Sellier, P., F. Proust, P. Dellebarre, J.L. Guermonprez, P. Ourbak, and P. Maurice, l'enregistrement electrocardiographique continu dans l'insuffisance coronaire interet diagnostique. *Arch. Mal. Coeur Vaiss.*, 1978;**71**: 638–644.
82. Stern, S. and D. Tzivoni, Evaluation of ST-T alterations in the ECG by ambulatory monitoring, in *Ambulatory ECG Monitoring*, S. Stern, editor. Chicago, IL: Year Book Medical, 1978, pp. 85–91.
83. Coumel, Ph., D. Milosevic, M. Rosengarten, J.F. Leclercq, and P. Attuel, Interet theorique et pratique du monitoring de Holter dans le bloc sino-auriculaire. *Ann. Cardiol. Angeiol.* 1980;**29**: 19–22.
84. Coumel, Ph., J.-F. Leclercq, P. Attuel, J.-P. Lavalle, and D. Flammang, Autonomic influences in the genesis of atrial arrhythmias: atrial flutter and fibrillation of vagal origin, in *Cardiac Arrhythmias Electrophysiology, Diagnosis and Management*, O.S. Narula, Editor. Baltimore, MD: Williams and Wilkins, 1979, pp. 243–255.
85. Coumel, Ph., P. Attuel, J.F. Leclercq, and P. Friocourt, Arythmies auriculaires d'origine vagale ou catecholergique. Effets compares du traitement Beta-bloquant et phenomene d'echappement. *Arch. Mal. Coeur Vaiss.*, 1982;**75**: 373–387.
86. Anderson, G.J. and M. Greenspan, Ventricular ectopic beats with exit block: a retrospective Holter monitor study. *J. Electrocardiol.*, 1983;**16**: 133–140.
87. Coumel, Ph., J.-F. Leclercq, P. Attuel, J.-P. Lavallee, and D. Flammang, Autonomic influences: sympathetic drive and the genesis of ventricular arrhythmias, in *Cardiac Arrhythmias. Electrophysiology, Diagnosis and Management*, O.S. Narula, Editor. Baltimore, MD: Williams and Wilkins, 1979, pp. 457–473.
88. Lown, B., M. Tykocinski, A. Garfein, and P. Brooks, Sleep and ventricular premature beats. *Circulation*, 1973;**48**: 691–701.
89. Vellani, C.W. and A. Murray, The effect of sinus rhythm on the periodicity and coupling interval of ventricular parasystolic rhythm. *Eur. Heart J.*, 1981;**2**: 429–439.
90. Deedwania, P.C., Ischemia detected by Holter monitoring in coronary artery disease, in *Noninvasive Electrocardiology – Clinical Aspects of Holter Monitoring*, A.J. Moss and S. Stern, Editors. London/Philadelphia/Toronto/Sydney/Tokyo: WB Saunders, 1996, pp. 331–343.
91. Stone, P.H. and G. MacCallum, ST segment analysis in ambulatory ECG (Holter) monitoring, in *Noninvasive Electrocardiology in Clinical Practice*, W. Zareba, P. Maison-Blanche, and E.H. Locati, Editors. Armonk/New York: Futura, 2001, pp. 97–121.
92. Stone, P.H., B. Chaitman, R.P. McMahon, et al. for the ACIP Investigators, The relationship between exercise-induced and ambulatory ischemia in patients with stable coronary disease. *Circulation*, 1996;**94**: 1537–1544.
93. Tzivoni, D. and S. Stern, Complimentary role of ambulatory electrocardiographic monitoring and exercise testing in evaluation of myocardial ischemia. *Cardiol. Clin.*; in *Ambulatory Electrocardiography – Current Clinical Concepts*, H.L. Kennedy, Editor. Philadelphia/London/Toronto/Montreal/Sydney/Tokyo: W.B. Saunders, 1992, pp. 461–466.
94. Gettes, L.S., Painless myocardial ischemia. *Chest*, 1974;**66**: 612–613 (editorial).
95. Stern, S. and D. Tzivoni, Early detection of silent ischaemic heart disease by 24-hour electrocardiographic monitoring of active subjects. *Br. Heart J.*, 1974;**36**: 481–486.
96. Cohn, P.F., *Silent myocardial ischemia and infarction*. New York: Marcel Dekker, 1986.
97. Cohn, P.F., Silent myocardial ischemia: the early years, in *Silent Myocardial Ischemia*, S. Stern, Editor. London: Martin Dunitz, 1998, pp. 1–5.
98. Stone, P.H. and A.P. Selwyn, The prognostic significance of silent myocardial ischemia, in *Silent Myocardial Ischemia*, S Stern, Editor. London: Martin Dunitz, 1998, pp. 55–66.
99. Deanfield, J.E., A.P. Selwyn, S. Chierchia, et al., Myocardial ischemia during daily life in patients with stable angina: its relation to symptoms and heart rate changes. *Lancet*, 1983;**ii**: 753–758.
100. Chipkin, S.R., D. Frid, J.S. Alpert, et al., Frequency of painless myocardial ischemia during exercise tolerance testing in patients with and without diabetes mellitus. *Am. J. Cardiol.*, 1987;**50**: 61–65.
101. Marchant, B., V. Umachandran, R. Stevenson, et al., Silent myocardial ischemia: role of subclinical neuropathy in patients with and without diabetes. *J. Am. Coll. Cardiol.*, 1993;**22**: 1433–1437.
102. Droste, C. and H. Roskamm, Experimental pain measurement in patients with asymptomatic myocardial ischemia. *J. Am. Coll. Cardiol.*, 1983;**1**: 940–945.
103. Droste, C. and H. Roskamm, Pain perception and endogenous pain modulation in angina pectoris. *Adv. Cardiol.*, 1990;**37**: 142–149.
104. Rosen, S.D., E. Paulsen, P. Nihoyannopoulos, et al., Silent ischemia as a central problem: regional brain activation compared in silent and painful myocardial ischemia. *Ann. Intern. Med.*, 1996;**124**: 1006–1008.
105. Rocco, M.B., E.G. Nabel, S. Campbell, et al., Prognostic importance of myocardial ischemia detected by ambulatory monitoring in patients with stable coronary artery disease. *Circulation*, 1988;**78**: 877–884.
106. Tzivoni, D., A. Gavish, D. Zin, et al., Prognostic significance of ischemic episodes in patients with previous myocardial infarction. *Am. J. Cardiol.*, 1988;**62**: 661–664.
107. Hedblad, B., S. Juul-Möller, K. Swensson, et al., Increased mortality in men with ST segment depression during 24h ambulatory

long-term ECG recording. Results from prospective population study "Men born in 1914" from Malmo, Sweden. *Eur. Heart J.*, 1989;**10**: 149–158.

108. Deedwania, P.C. and E.V. Carbajal, Silent ischemia during daily life is an independent predictor of mortality in stable angina. *Circulation*, 1990;**81**: 748–756.
109. Raby, K.E., L. Goldman, E.F. Cook, et al., Long-term prognosis of myocardial ischemia detected by Holter monitoring in peripheral vascular disease. *Am. J. Cardiol.*, 1990;**66**: 1309–1313.
110. Yeung, A.C., J. Barry, J. Orav, et al., Effects of asymptomatic ischemia on long-term prognosis in chronic stable coronary disease. *Circulation*, 1991;**83**: 1598–1604.
111. Deedwania, P.C. and E.V. Carbajal, Usefulness of ambulatory silent myocardial ischemia added to the prognostic value of exercise test parameters in predicting risk of cardiac death in patients with stable angina pectoris and exercise-induced myocardial ischemia. *Am. J. Cardiol.*, 1991;**68**: 1279–1286.
112. Quyumi, A.A., J.A. Panza, J.G. Diodati, et al., Prognostic implications of myocardial ischemia during daily life in low risk patients with coronary artery disease. *J. Am. Coll. Cardiol.*, 1993;**21**: 700–708.
113. Moss, A.J., R.E. Goldstein, J. Hall, et al., Detection and significance of myocardial ischemia in stable patients after recovery from an acute coronary event. *JAMA*, 1993;**269**: 2379–2385.
114. de Marchena, E., J. Asch, J. Martinez, et al., Usefulness of persistent silent myocardial ischemia in predicting a high cardiac event rate in men with medically controlled, stable angina pectoris. *Am. J. Cardiol.*, 1994;**73**: 390–392.
115. Madjilessi-Simon, T., M. Mary-Krause, F. Fillette, et al., Persistent transient myocardial ischemia despite beta-adrenergic blockade predicts a higher risk of adverse cardiac events in patients with coronary artery disease. *J. Am. Coll. Cardiol.*, 1996;**27**: 1586–1591.
116. Gill, J.B., J.A. Cairns, R.S. Roberts, et al., Prognostic importance of myocardial ischemia detected by ambulatory monitoring early after acute myocardial infarction. *N. Engl. J. Med.*, 1996;**334**: 65–70.
117. Pepine, C.J., P.F. Cohn, P.C. Deedwania, et al., Effects of treatment on outcome in mildly symptomatic patients with ischemia during daily life: the Atenolol Silent Ischemia Study (ASIST). *Circulation*, 1994;**90**: 762–768.
118. Rogers, W.J., M.G. Bourassa, T.C. Andrews, et al., Asymptomatic Cardiac Ischemia Pilot (ACIP) study: outcome at 1 year for patients with asymptomatic cardiac ischemia randomized to medical therapy or revascularization: the ACIP Investigators. *J. Am. Coll. Cardiol.*, 1995;**26**: 594–605.
119. Dargie, H.J., I. Ford, and K.M. Fox, Total Ischaemic Burden European Trial (TIBET): effects of ischmaemia and treatment with atenolol, nifedipine SR and their combination on outcome in patients with chronic stable angina: the TIBET Study Group. *Eur. Heart J.*, 1996;**17**: 104–112.
120. von Arnim, Prognostic significance of transient ischemic episodes: response to treatment shows improved prognosis: results of the Total Ischemic Burden Bisoprolol Study (TIBBS) follow-up. *J. Am. Coll. Cardiol.*, 1996;**28**: 20–24.
121. Bailey, J.J., A. Berson, H. Handelsman, and M. Hodges, Utility of current risk stratification tests for predicting major arrhythmic events after myocardial infarction. *J. Am. Coll. Cardiol.*, 2001;**38**: 1902–1911.
122. Moss, A.J., W.J. Hall, D.S. Cannom, et al., Improved survival with an implanted defibrillator in patients with coronary disease at high risk for ventricular arrhythmia: Multicenter Automatic Defibrillator Implantation Trial Investigators. *N. Engl. J. Med.*, 1996;**335**: 1933–1940.
123. Denes, P., A.M. Gillis, Y. Pawitan, et al., Prevalence, characteristics and significance of ventricular premature complexes and ventricular tachycardia detected by 24-hour continuous electrocardiographic recording in the Cardiac Arrhythmia Suppression Trial. CAST Investigators. *Am. J. Cardiol.*, 1991;**68**: 887–896.
124. Ruberman, W., E. Weinblatt, J.D. Goldberg, et al., Ventricular premature complexes and sudden death after myocardial infarction. *Circulation*, 1981;**64**: 297–305.
125. Olson, H.G., K.P. Lyons, P. Troop, et al., The high-risk acute myocardial infarction patient at 1-year follow-up: identification at hospital discharge by ambulatory electrocardiography and radionuclide ventriculography. *Am. Heart J.*, 1984;**107**: 358–366.
126. Mukharji, J., R.E. Rude, W.K. Poole, et al., Risk factors for sudden death after myocardial infarction: two-year follow-up. *Am. J. Cardiol.*, 1984;**54**: 31–36.
127. Kostis, J.B., R. Byington, L.M. Friedman, et al., Prognostic significance of ventricular ectopic activity in survivors of acute myocardial infarction. *J. Am. Coll. Cardiol.*, 1987;**10**: 231–242.
128. Verzoni, A., S. Romano, L. Pozzoni, et al., Prognostic significance and evolution of late ventricular potentials in the first year after myocardial infarction: a prospective study. *Pacing Clin. Electrophysiol.*, 1989;**12**: 41–51.
129. Gomes, J.A., S.L. Winters, M. Martinson, et al., The prognostic significance of quantitative signal-averaged variables relative to clinical variables, site of myocardial infarction, ejection fraction and ventricular premature beats: a prospective study. *J. Am. Coll. Cardiol.*, 1989;**13**: 377–384.
130. Richards, D.A., K. Byth, D.L. Ross, et al., What is the best predictor of spontaneous ventricular tachycardia and sudden death after myocardial infarction? *Circulation*, 1991;**83**: 756–763.
131. Farrell, T.G., Y. Bashir, T. Cripps, et al., Risk stratification for arrhythmic events in postinfarction patients based on heart rate variability, ambulatory electrocardiographic variables and the signal-averaged electrocardiogram. *J. Am. Coll. Cardiol.*, 1991;**18**: 687–697.
132. de Cock, C.C., F.C. Visser, M.J. van Eenige, et al., Independent prognostic value of supraventricular arrhythmias on 24-h ambulatory monitoring following myocardial infarction. *Eur. Heart J.*, 1991;**12**: 1070–1075.
133. Steinberg, J.S., A. Regan, R.R. Sciacca, et al., Predicting arrhythmic events after acute myocardial infarction using the signal-averaged electrocardiogram. *Am. J. Cardiol.*, 1992;**69**: 13–21.
134. Bigger, J.T., Jr, J.L. Fleiss, R.C. Steinman, et al., Frequency domain measures of heart rate period variability and mortality after myocardial infarction. *Circulation*, 1992;**85**: 164–171.
135. Pedretti, R., M.D. Etro, A. Laporta, et al., Prediction of late arrhythmic events after acute myocardial infarction from combined use of noninvasive prognostic variables and inducibility of sustained monomorphic ventricular tachycardia. *Am. J. Cardiol.*, 1993;**71**: 1131–1141.
136. McClements, B.M. and A.A. Adgey, Value of signal-averaged electrocardiography, radionuclide ventriculography, Holter monitoring and clinical variables for prediction of arrhythmic events in survivors of acute myocardial infarction in the thrombolytic era. *J. Am. Coll. Cardiol.*, 1993;**21**: 1419–1427.

137. Kuchar, D.L., C.W. Thorburn, and N.L. Sammel, Prognostic implications of loss of late potentials following acute myocardial infarction. *Pacing Clin. Electrophysiol*., 1993;**16**: 2104–2111.
138. Hohnloser, S.H., P. Franck, T. Klingenleben, et al., Open infarct artery, late potentials, and other prognostic factors in patients after acute myocardial infarction in the thrombolytic era: a prospective trial. *Circulation*, 1994;**90**: 1747–1756.
139. Hermosillo, A.G., V. Araya, J.M. Casanova, et al., Risk stratification for malignant arrhythmic events in patients with an acute myocardial infarction: role of an open infarct-related artery and the signal-averaged ECG. *Coron. Artery Dis*., 1995;**6**: 973–983.
140. El-Sherif, N., P. Denes, R. Katz, et al., Definition of the best prediction criteria of the time domain signal-averaged electrocardiogram for serious arrhythmic events in the postinfarction period. *J. Am. Coll. Cardiol*., 1995;**25**: 908–914.
141. La Rovere, M.T., J.T. Bigger Jr, F.I. Marcus, et al., Baroreflex sensitivity and heart-rate variability in prediction of total cardiac mortality after myocardial infarction. ATRAMI (Autonomic Tone and Reflexes After Myocardial Infarction) Investigators. *Lancet*, 1998;**351**: 478–484.
142. Hohnloser, S.H., T.K. Klingenleben, M. Zabel, and O. Mauss, Prevalence, characteristics, and prognostic value during long-term follow-up of nonsustained ventricular tachycardia after myocardial infarction in the thrombolytic era. *J. Am. Coll. Cardiol*., 1999;**33**: 1895–1902.
143. Kleiger, R.E., J.P. Miller, J.T. Bigger, et al., Decreased heart rate variability and its association with increased mortality after acute myocardial infarction. *Am. J. Cardiol*., 1987;**59**: 256–262.
144. Odemuyiwa, O., M. Malik, T. Farrell, et al., Comparison of the predictive characteristics of heart rate variability index and left ventricular ejection fraction for all-cause mortality, arrhythmic events and sudden death after acute myocardial infarction. *Am. J. Cardiol*., 1991;**68**: 434–439.
145. Zuanetti, G., J.M. Neilson, R. Latini, et al., Prognostic significance of heart rate variability in post-myocardial infarction patients in the fibrinolytic era. The GISSI-2 results. Gruppo Italiano per lo Studio della Sopravvivenza nell'Infarto Miocardio. *Circulation*, 1996;**94**: 432–436.
146. Copie, X., K. Hnatkova, A. Staunton, et al., Predictive power of increased heart rate versus depressed left ventricular ejection fraction and heart rate variability for risk stratification after myocardial infarction. Results of a two-year follow-up study. *J. Am. Coll. Cardiol*., 1996;**27**: 270–276.
147. Lanza, G.A., V. Guido, M.M. Galeazzi, et al., Prognostic role of heart rate variability in patients with a recent acute myocardial infarction. *Am. J. Cardiol*., 1998;**82**: 1323–1328.
148. Katz, A., I.F. Liberty, A. Porath, et al., A simple bedside test of 1-minute heart rate variability during deep breathing as a prognostic index after myocardial infarction. *Am. Heart J*., 1999;**138**: 32–38.
149. Malik, M., A.J. Camm, M.J. Janse, et al., Depressed heart rate variability identifies postinfarction patients who might benefit from prophylactic treatment with amiodarone: a substudy of EMIAT (The European Myocardial Infarct Amiodarone Trial). *J. Am. Coll. Cardiol*., 2000;**35**: 1263–1275.
150. Mäkikallio, T.H., P. Barthel, R. Schneider, et al., Prediction of sudden cardiac death after acute myocardial infarction: role of Holter monitoring in the modern treatment era. *Eur. Heart J*., 2005;**26**: 762–769.
151. Bauer, A., P. Guzik, P. Barthel, et al., Reduced prognostic power of ventricular late potentials in post-infarction patients of the reperfusion era. *Eur. Heart J*., 2005;**26**: 755–761.
152. Schmidt, G. and Malik, M., Heart rate turbulence, in *Noninvasive Electrocardiology in Clinical Practice*, W. Zareba, P. Maison-Blanche, and E.H. Locati, Editors. Armonk/New York: Futura, 2001, pp. 207–215.
153. Kjekshus, J., Arrhythmias and mortality in congestive heart failure. *Am. J. Cardiol*., 1990;**65**: 421–428.
154. Gradman, A., P. Deedwania, R. Cody, B. Massie, M. Packer, B. Pitt, and S. Goldstein, Predictors of total mortality and sudden death in mild-to-moderate heart failure. Captopril-Digoxin Study Group. *J. Am. Coll. Cardiol*., 1989;**14**: 564–570.
155. Fletcher, R.D., G.B. Cintron, G. Johnson, J. Orndorff, P. Carson, and J. Cohn for the V-HeFT VA Cooperative Studies Group, Enalapril decreases prevalence of ventricular tachycardia in patients with chronic congestive heart failure. *Circulation*, 1993;**87**(Suppl.): VI-49–55.
156. Doval, H.C., D.R. Nul, H.O. Grancelli, et al., Nonsustained ventricular tachycardia in severe heart failure: independent marker of increased mortality due to sudden death. GESICA-GEMA Investigators. *Circulation*, 1996;**94**: 3198–3203.
157. Fei, L., P.J. Keeling, J.S. Gill, Y. Bashir, D.J. Statters, J. Poloniecki, W.J. McKenna, and A.J. Camm, Heart rate variability and its relation to ventricular arrhythmias in congestive heart failure. *Br. Heart J*., 1994;**71**: 322–328.
158. Hoffman, J., W. Grimm, V. Menz, and B. Maisch, Heart rate variability and major arrhythmias in patients with idiopathic dilated cardiomyopathy. *Pacing Clin. Electrophysiol*., 1996;**19**: 1841–1844.
159. Yi, G., J.H. Goldman, P.J. Keeling, M. Malik, and W.J. McKenna, Heart rate variability in idiopathic dilated cardiomyopathy: relation to disease severity and prognosis. *Heart* 1977;**77**: 108–114.
160. Fauchier, L., D. Babuty, P. Cosnay, M.L. Autret, and J.P. Fauchier, Heart rate variability in idiopathic dilated cardiomyopathy: characteristics and prognostic value. *J. Am. Coll. Cardiol*., 1997;**30**: 1009–1014.
161. Ponikowski, P., S.D. Anker, T.P. Chua, et al., Depressed heart rate variability as an independent predictor of death in chronic congestive heart failure secondary to ischemic or idiopathic dilated cardiomyopathy. *Am. J. Cardiol*., 1997;**79**: 1645–1650.
162. Szabo, B.M., D.J. van Veldhuisen, N. van der Veer, J. Brouwer, P.A. De Graeff, and H.J.G.M. Crijns, Prognostic value of HRV in chronic congestive heart failure secondary to idiopathic or ischemic dilated cardiomyopathy. *Am. J. Cardiol*., 1997;**79**: 978–980.
163. Boveda, S., M. Galinier, A. Pathak, et al., Prognostic value of heart rate variability in time domain in congestive heart failure. *J. Intervent. Card. Electrophysiol*., 2000;**5**: 181–187.
164. Bilchik, K.C., B. Fetics, R. Djoukeng, et al., Prognostic value of heart rate variability in chronic congestive heart failure (Veterans Affair's Survival Trial of Antiarrhythmic Therapy in Congestive Heart Failure). *Am. J. Cardiol*., 2002;**90**: 24–28.
165. Aronson, D., M.A. Mittleman, and A.J. Burger, Measures of heart period variability as predictors of mortality in hospitalized patients with decompensated congestive heart failure. *Am. J. Cardiol*., 2004;**93**: 59–63.
166. La-Rovere, M.T., G.D. Pinna, R. Maestri, et al., Short-term heart rate variability strongly predicts sudden cardiac death in chronic heart failure patients. *Circulation*, 2003;**107**: 565–570.

167. Guzzetti, S., M.T. La-Rovere, G.D. Pinna, et al., Different spectral components of 24 h heart rate variability are related to different modes of death in chronic heart failure. *Eur. Heart J.*, 2005;**26**: 357–362.
168. Adamson, P.B., A.L. Smith, W.T. Abraham, et al., Continuous autonomic assessment in patients with symptomatic heart failure: prognostic value of heart rate variability measured by an implanted cardiac resynchronization device. *Circulation*, 2004;**110**: 2389–2394.
169. Koyama, J., J. Watanabe, A. Yamada, et al., Evaluation of heart rate turbulence as a new prognostic marker in patients with chronic heart failure. *Circ. J.*, 2002;**66**: 902–907.
170. Kawasaki, T., A. Azuma, S. Asada, et al., Heart rate turbulence and clinical prognosis in hypertrophic cardiomyopathy and myocardial infarction. *Circ. J.*, 2003;**67**: 601–604.
171. Grimm, W., J. Sharkova, M. Christ, et al., Prognostic significance of heart rate turbulence following ventricular premature beats in patients with idiopathic dilated cardiomyopathy. *J. Cardiovasc. Electrophysiol.*, 2003;**14**: 819–824.
172. McKenna, W.J., S. Chetty, C.M. Oakley, et al., Arrhythmia in hypertrophic cardiomyopathy: exercise and 48 hour ambulatory electrocardiographic assessment with and without beta adrenergic blocking therapy. *Am. J. Cardiol.*, 1980;**45**: 1–5.
173. Maron, B.J., D.D. Savage, J.K. Wolfson, et al., Prognostic significance of 24 hour ambulatory electrocardiographic monitoring in patients with hypertrophic cardiomyopathy: a prospective study. *Am. J. Cardiol.*, 1981;**48**: 252–257.
174. McKenna, W.J., C.M. Oakley, D.M. Krikler, et al., Improved survival with amiodarone in patients with hypertrophic cardiomyopathy and ventricular tachycardia. *Br. Heart J.*, 1985;**53**: 412–416.
175. Fanapazir, L., A.C. Chang, S.E. Epstein, et al., Prognostic determinants in hypertrophic cardiomyopathy. *Circulation*, 1992;**86**: 730–740.
176. McKenna, W.J. and E.R. Behr, Hypertrophic cardiomyopathy: management, risk stratification, and prevention of sudden death. *Heart*, 2002;**87**: 169–178.
177. Counihan, P.J., L. Fei, Y. Bashir, et al., Assessment of heart rate variability in hypertrophic cardiomyopathy: association with clinical and prognostic features. *Circulation*, 1993;**88**: 1682–1690.
178. Elliott, P.M., J. Poloniecki, S. Dickie, et al., Sudden death in hypertrophic cardiomyopathy: identification of high risk patients. *J. Am. Coll. Cardiol.*, 2000;**36**: 2212–2220.
179. Von Olshausen, K., F. Schwarz, J. Apfelbach, N. Rohrig, B. Kriimer, and W. Kiibler, Determinants of the incidence and severity of ventricular arrhythmias in aortic valve disease. *Am. J. Cardiol.*, 1983;**51**: 1103–1109.
180. Chesler, E., R.A. King, and J.E. Edwards, The myxomatous mitral valve and sudden death. *Circulation*, 1983;**67**: 632–639.
181. Jeresaty, R.M., Sudden death in the mitral valve prolapse-click syndrome. *Am. J. Cardiol.*, 1976;**37**: 317–318.
182. Leclercq, J.F., M.C. Malergue, D. Milosevic, M.D. Rosengarten, P. Attuel, and Ph. Coumel, Troubles du rythme ventriculaires et prolapsus mitral. A propos de 35 observations. *Arch. Mal. Coeur Vaiss.*, 1980;**73**: 276–287.
183. Winkle, R.A., M.G. Lopes, R.L. Popp, and E.W. Hancock, Life-threatening arrhythmias in the mitral valve prolapse syndrome. *Am. J. Med.*, 1976;**60**: 961–967.
184. Kannel, W.B., A.L. Dannenberg, and D. Levy, Population implications of electrocardiographic left ventricular hypertrophy. *Am. J. Cardiol.*, 1987;**60**: 85I–93I.
185. Levy, D., K.M. Anderson, D.D. Savage, et al., Risk of ventricular arrhythmias in left ventricular hypertrophy: the Framingham Heart Study. *Am. J. Cardiol.*, 1987;**60**: 560–565.
186. Bikkina, M., M.G. Larson, and D. Levy, Asymptomatic ventricular arrhythmias and mortality risk in subjects with left ventricular hypertrophy. *J. Am. Coll. Cardiol.*, 1993;**22**: 1111–1116.
187. Singh, J.P., M.G. Larson, H. Tsuji, et al., Reduced heart rate variability and new-onset hypertension: insights into the pathogenesis of hypertension. *Hypertension*, 1998;**32**: 293–297.
188. Liao, D., J. Cai, R.W. Barnes, et al., Association of cardiac autonomic function and the development of hypertension: the ARIC Study. *Am. J. Hypertens.*, 1996;**9**: 1147–1156.
189. Kohara, K., W. Nishida, M. Maguchi, et al., Autonomic nervous function in nondipper essential hypertensive subjects: evaluation by power spectral analysis of heart rate variability. *Hypertension*, 1995;**26**: 808–814.
190. Ewing, D.J., I.W. Campbell, B.F. Clarke, et al., The natural history of diabetic autonomic neuropathy. *QJ Med.*, 1980;**49**: 95–108.
191. Malpas, S.C. and T.J. Maling, Heart rate variability and cardiac autonomic function in diabetes. *Diabetes*, 1990;**39**: 1177–1181.
192. Ewing, D.J., J.M. Neilson, C.M. Shapiro, et al., Twenty four hour heart rate variability: effects of posture, sleep, and time of day in healthy controls and comparison with bedside tests of autonomic function in diabetic patients. *Br. Heart J.*, 1991;**65**: 239–244.
193. Bellavere, F., I. Balzani, G. De Masi, et al., Power spectral analysis of heart-rate variations improves assessment of diabetic cardiac autonomic neuropathy. *Diabetes*, 1992;**41**: 633–640.
194. D'Elia, J.A., L.A. Weinrauch, R.E. Gleason, et al., Application of the ambulatory 24-hour electrocardiogram in the prediction of cardiac death in dialysis patients. *Arch. Intern. Med.* 1988;**148**: 2381–2385.
195. O'Kelly, B., W.S. Browner, B. Massie, et al., Ventricular arrhythmias in patients undergoing noncardiac surgery: the Study of Perioperative Ischemia Research Group. *JAMA*, 1992;**268**: 217–221.
196. Huikuri, H.V., S. Yli-Mayry, U.R. Korhonen, et al., Prevalence and prognostic significance of complex ventricular arrhythmias after coronary arterial bypass graft surgery. *Int. J. Cardiol.*, 1990;**27**: 333–339.
197. DiMarco, J.P. and J.T. Philbrick, Use of ambulatory electrocardiographic (Holter) monitoring. *Ann. Intern. Med.*, 1990;**113**: 53–68.
198. Sami, M., H. Kraemer, D.C. Harrison, N. Houston, C. Shimasaki, and R.I. De Busk, A new method for evaluating antiarrhythmic drug efficacy. *Circulation*, 1980;**62**: 1172–1179.
199. Sami, M., D.C. Harrison, H. Kraemer, N. Houston, C. Shimasaki, and R.F. De Busk, Antiarrhythmic efficacy of encainide and quinidine: validation of a model for drug assessment. *Am. J. Cardiol.*, 1981;**48**: 147–156.
200. Burkart, F., M. Pfisterer, W. Kiowski, et al., Effect of antiarrhythmic therapy on mortality in survivors of myocardial infarction with asymptomatic complex ventricular arrhythmias: Basel Antiarrhythmic Study of Infarct Survival (BASIS). *J. Am. Coll. Cardiol.*, 1990;**16**: 1711–1718.
201. Ceremuzynski, L., E. Kleczar, M. Krzeminska-Pakula, et al., Effect of amiodarone on mortality after myocardial infarction: a double-blind, placebo-controlled pilot study. *J. Am. Coll. Cardiol.*, 1992;**20**: 1056–1062.
202. Doval, H.C., D.R. Nul, H.O. Grancelli, et al., Randomised trial of low-dose amiodarone in severe congestive heart failure: Grupo

de Estudio de la Sobrevida en la Insufficiencia Cardiaca en Argentina (GESICA). *Lancet*, 1994;**344**: 493–498.
203. The CASCADE Investigators, Randomised drug therapy in survivors of cardiac arrest (the CASCADE Study). *Am. J. Cardiol*., 1993;**72**: 280–287.
204. Julian, D.G., A.J. Camm, G. Frangin, et al., Randomised trial of effect of amiodarone on mortality in patients with left-ventricular dysfunction after recent myocardial infarction: EMIAT, European Myocardial Infarct Amiodarone Trial Investigators. *Lancet*, 1997;**349**: 667–674.
205. Cairns, J.A., S.J. Conolly, R. Roberts, et al., Randomised trial of outcome after myocardial infarction in patients with frequent or repetitive ventricular premature depolarisations: CAMIAT, Canadian Amiodarone Myocardial Infarction Arrhythmia Trial Investigators. *Lancet*, 1997;**349**: 675–682.
206. Singh, S.N., R.D. Fletcher, S.G. Fisher, et al., Amiodarone in patients with congestive heart failure and asymptomatic ventricular arrhythmias: Survival Trial of Antiarrhythmic Therapy in Congestive Heart Failure. *N. Engl. J. Med*., 1995;**333**: 77–82.
207. Lampert, S., B. Lown, T.B. Graboys, et al., Determinants of survival in patients with malignant ventricular arrhythmia associated with coronary artery disease. *Am. J. Cardiol*., 1988;**61**: 791–797.
208. Hallstrom, A.P., H.L. Greene, and M.L. Huther, The healthy responder phenomenon in non-randomized clinical trial. CAST Investigators. *Stat. Med*., 1991;**10**: 1621–1631.
209. Mason, J.W., A comparison of electrophysiologic testing with Holter monitoring to predict antiarrhythmic-drug efficacy for ventricular tachyarrhythmias: Electrophysiologic Study Versus Electrocardiographic Monitoring Investigators. *N. Engl. J. Med*., 1993;**329**: 445–451.
210. Morganroth, J. and C.M. Pratt, Prevalence and characteristics of proarrhythmia from moricizine (ethmozine). *Am. J. Cardiol*., 1989;**63**: 172–176.
211. Kennedy, H.L., Late proarrhythmia and understanding the time of occurrence of proarrhythmia. *Am. J. Cardiol*., 1990;**66**: 1139–1143.
212. Balasubramanian, V., M.W. Millar Craig, A.B. Davies, and E.B. Raftery, Verapamil therapy in variant angina: assessment by high-fidelity frequency modulated ambulatory ECG. *Am. Heart J*., 1981;**101**: 849–850.
213. Dick, M., II, D. McFadden, D. Crowley, et al., Diagnosis and management of cardiac rhythm disorders by transtelephonic electrocardiography in infants and children. *J. Pediatr*., 1979;**94**: 612–615.
214. Porter, C.J., P.C. Gillette, and D.G. McNamara, Twenty-four-hour ambulatory ECGs in the detection and management of cardiac arrhythmias in infants and children. *Pediatr. Cardiol*., 1980;**1**: 203–208.
215. Fyfe, D.A., D.R. Holmes, S.A. Neubauer, et al., Transtelephonic monitoring in pediatric patients with clinically suspected arrhythmias. *Clin. Pediatr*., 1984;**23**: 139–143.
216. Goldstein, M.A., P. Hesslein, and A. Dunningan, Efficacy of trans-telephonic electrocardiographic monitoring in pediatric patients. *Am. J. Dis. Child*., 1990;**144**: 178–182.
217. Hoyel, L., A. Fournier, S. Centazzo, et al., Use of transtelephonic electrocardiographic monitoring in children with suspected arrhythmias. *Can. J. Cardiol*., 1992;**8**: 741–744.
218. Karpawich, P.P., D.L. Cavitt, and J.S. Sugalski, Ambulatory arrhythmia screening in symptomatic children and young adults: comparative effectiveness of Holter and telephone event recordings. *Pediatr. Cardiol*., 1993;**14**: 147–150.
219. Saarel, E.V., C.B. Stefanelli, P.S. Fischbach, et al., Transtelephonic electrocardiographic monitors for evaluation of children and adolescents with suspected arrhythmias. *Pediatrics*, 2004;**113**: 248–251.
220. Seliem, M.A., D.W. Benson, J.F. Strasburger, et al., Complex ventricular ectopic activity in patients less than 20 years of age with or without syncope, and the role of ventricular extrastimulus testing. *Am. J. Cardiol*., 1991;**68**: 745–750.
221. Driscoll, D.J., S.J. Jacobsen, C.J. Porter, et al., Syncope in children and adolescents. *J. Am. Coll. Cardiol*., 1997;**29**: 1039–1045.
222. Sanatani, S., A. Peirone, C. Chiu, et al., Use of an implantable loop recorder in the evaluation of children with congenital heart disease. *Am. Heart J*., 2002;**143**: 366–372.
223. Wolfe, R.R., D.J. Driscoll, W.M. Gersony, et al., Arrhythmias in patients with valvular aortic stenosis, valvular pulmonary stenosis, and ventricular septal defect: results of 24-hour ECG monitoring. *Circulation*, 1993;**87**(Suppl. I): I-89–I-101.
224. Garson, A., Jr, M. Bink-Boelkens, P.S. Heslein, et al., Atrial flutter in the young: a collaborative study of 380 cases. *J. Am. Coll. Cardiol*., 1985;**6**: 871–878.
225. Cullen, S., D.S. Celermajer, R.C. Franklin, et al., Prognostic significance of ventricular arrhythmia after repair of tetralogy of Fallot: a 12-year prospective study. *J. Am. Coll. Cardiol*., 1994;**23**: 1151–1155.
226. Chandar, J.S., G.S. Wolff, A. Garson, Jr, et al., Ventricular arrhythmias in postoperative tetralogy of Fallot. *Am. J. Cardiol*., 1990;**65**: 655–661.
227. Garson, A., Jr, Ventricular arrhythmias after repair of congenital heart disease: who needs treatment? *Cardiol. Young*, 1991;**1**: 177–181.
228. Paul, T., C. Marchal, and A. Garson, Jr, Ventricular couplets in the young: prognosis related to underlying substrate. *Am. Heart J*., 1990;**119**: 577–582.
229. Krongrad, E., Prognosis for patients with congenital heart disease and postoperative intraventricular conduction defects. *Circulation*, 1978;**57**: 867–870.
230. Fenelon, G., A. d'Avila, T. Malacky, et al., Prognostic significance of transient complete atrioventricular block during radiofrequency ablation of atrioventricular node reentrant tachycardia. *Am. J. Cardiol*., 1995;**75**: 698–702.
231. Packer, D.L., G.H. Bardy, S.J. Worley, et al., Tachycardia-induced cardiomyopathy: a reversible form of left ventricular dysfunction. *Am. J. Cardiol*., 1986;**57**: 563–570.
232. Locati, E.H., Advances in modern electrocardiographic equipment for long-term ambulatory monitoring. *Card. Electrophysiol. Rev*., 2002;**6**: 185–189.
233. Coumel, P., Noninvasive exploration of cardiac arrhythmias. *Ann. NY Acad. Sci*., 1990; 312–328.

34 The Pre-Hospital Electrocardiogram

Johan Herlitz · Leif Svensson · Per Johansson

P. W. Macfarlane, A. van Oosterom, O. Pahlm, P. Kligfield, M. Janse, J. Camm (eds.), *Comprehensive Electrocardiology*, DOI 10.1007/978-1-84882-046-3_34,

34.1 Background

34.1.1 Historical Background

The first mobile coronary care unit was reported by Frank Pantridge in 1967 [1]. He described 352 patients with presumed acute myocardial infarction who were treated prior to hospital admission. Ten of them were successfully resuscitated following an out-of-hospital cardiac arrest. In 1970, electrocardiographic telemetry from ambulances was first described [2]. At that stage, only rhythm strips were transmitted. However, in the 1980s, at the time of the introduction of fibrinolysis, many ambulance organizations started to routinely record a 12-lead electrocardiogram (ECG). This was originally done with the sole purpose of detecting ST-segment elevation, thereby starting treatment with fibrinolysis prior to hospital admission. However, when this research area was in its infancy, it was thought that all patients with an impending myocardial infarction could perhaps benefit from this treatment [3] and the need for a prehospital ECG was therefore not obvious [4].

In an important meta-analysis published in 1993 [5], it was clearly shown that patients who would benefit from fibrinolysis were those with ST-segment elevation or left bundle branch block and that the earlier the treatment started, the better it would be. This important finding put the 12-lead prehospital ECG in focus. However, in large screening studies, it was shown that only a minority of patients with acute chest pain, who were transported by ambulance, had these changes on their prehospital ECG [6]. At this early stage, it was shown that other ECG changes, such as ST depression, were also an alarming ECG sign, but the prehospital treatment for these changes was not established.

During the last few years, the use of the prehospital ECG has become more and more widespread, with the aim not only of starting prehospital fibrinolysis but also improving the prehospital triage of patients with acute chest pain. Parallel to this, research on out-of-hospital cardiac arrest has been going on for the past 3 decades. In this case, the prehospital ECG is the most important tool when it comes to advising optimal treatment. During the last decade, ECG research has focused on the opportunity to predict the outcome of defibrillation in ventricular fibrillation based on wave-form analysis.

34.1.2 Ideological Background

Two major pathophysiological considerations constitute the principal background for the need for a prehospital ECG when a heart attack is suspected: (1) "Time is saved myocardium" and (2) the occurrence of life-threatening arrhythmias in myocardial ischemia and myocardial infarction, which is most common in the very early phase.

1. The opportunity to limit myocardial damage with early medication was first described in dogs in 1971 [7]. These findings have been followed by a very large number of studies in humans, showing that early treatment with medical [8] or mechanical [9] reperfusion and with antiplatelet [10] and anti-ischemic agents [11] will improve the outcome in a threatening myocardial infarction.
   Although we lack absolute proof of the value of prehospital initiated aspirin versus aspirin started after hospital admission [12–14], for example, our current knowledge strongly indicates that the earlier the various interventions in acute coronary syndrome are started, the better it would be. The question of whether to start treatment prior to or after hospital admission is more a cost-benefit issue. Based on such thinking, the most optimal solution for every single patient with any suspicion of acute coronary syndrome should be that he or she has an ECG recorded prior to hospital admission.
2. The fact that life-threatening arrhythmias are most frequent in the early phase of acute coronary syndrome and nearly half the deaths from ischemic heart disease occur outside hospital (mostly as sudden deaths) underlines the importance of research in this area [15]. More knowledge on the information that is hidden in the electrocardiogram in this scenario might improve the outcome for these patients.
3. At present, we do not know whether a prehospital ECG might be of benefit in other clinical scenarios in the prehospital setting. Theoretically, there are conditions such as stroke [16].

34.1.3 Three Major Objectives

The three major objectives for a prehospital ECG are:

1. Detection of myocardial ischemia/infarction.
2. Detection of arrhythmias.
3. Remaining objectives, of which little is known, but heart rate variability and stroke are interesting aspects.

In what follows, these three objectives will be evaluated in more detail.

34.1.4 Symptoms that Indicate a Prehospital ECG

The indications for a prehospital ECG should be liberal, since a variety of symptoms might be caused by an acute coronary syndrome. These symptoms are listed in Table 34.1. Although the typical symptom in acute coronary syndrome is acute chest pain, the disease can present with pain in other locations and various other symptoms. The symptoms that are listed in the table often appear in combination.

34.1.5 Benefits

The principle behind the proposed benefit of using a prehospital ECG is shown in Table 34.2. The detection of the presence or absence of ECG abnormalities will improve the triage in patients in whom it is used. In selected patients, this will result in the earlier treatment of myocardial ischemia/infarction or arrhythmias, which are associated with hemodynamic consequences. It is to be hoped that this will then result in an improved outcome.

34.2 Detection of ECG Abnormalities

The various ECG abnormalities (excluding arrhythmias) that the ambulance crew or other health-care providers should look for in the prehospital setting are shown in Table 34.3. The percentage of patients with an abnormal or

Table 34.1
Symptoms that indicate a prehospital ECG

Suspicion of Ischemia/Infarction
Typical symptoms
Pain/oppression in chest
Atypical symptoms
Dyspnea
Pain in arms
Pain in back
Pain in stomach
Pain in neck
Unexplained tiredness
Nausea
Suspicion of arrhythmias
Palpitation
Syncope
Vertigo

Table 34.2

Aspects on mechanisms of how the introduction of a prehospital ECG might improve outcome in acute chest pain

1. Detection of electrical abnormalities
(a) Myocardial ischemia/infarction
(b) Arrhythmia
(c) Other (for example decreased heart rate variability)
2. Improved triage
(a) Direct transport to coronary care unit
(b) Direct transport to catheterization laboratory
(c) Direct transport to a remote hospital
3. Earlier start of treatment
(a) Earlier start of fibrinolysis
(I) Prior to hospital admission
(II) In hospital
(b) Earlier start of percutaneous coronary intervention (PCI)
(c) Earlier start of other antiplatelet agents
(d) Earlier start of other anti-ischemic agents
(e) Earlier start of antiarrhythmic treatment
4. Improved outcome
(a) Reduced mortality?
(b) Reduced morbidity?

Table 34.3

ECG abnormalities to look for when a prehospital ECG is recorded

Acute ischemia/infarction
ST elevation
ST depression
T-wave inversion
Q wave
Bundle branch block
Other abnormalities
Pacemaker ECG
Left ventricular hypertrophy
QRST signs indicating previous myocardial damage

pathological ECG depends on the study population. Reported studies have comprised patients who call for an ambulance due to acute chest pain or other symptoms raising suspicion of an acute coronary syndrome [17–19]. In these reports, a high percentage have an abnormal ECG (Fig. 34.1). It is important to stress that patients who call for an ambulance represent a population with high comorbidity and a high likelihood of underlying cardiac pathology as compared with other chest pain populations [20–22]. So, if a prehospital ECG was recorded among patients who visited a general practitioner because of acute chest pain, the percentage of patients with a pathological ECG could be expected to be lower, since these patients are less likely to have a cardiac pathology [23]. The most common ECG abnormalities in the prehospital ECG among patients with acute chest pain are those indicating myocardial ischemia/infarction and various rhythm abnormalities.

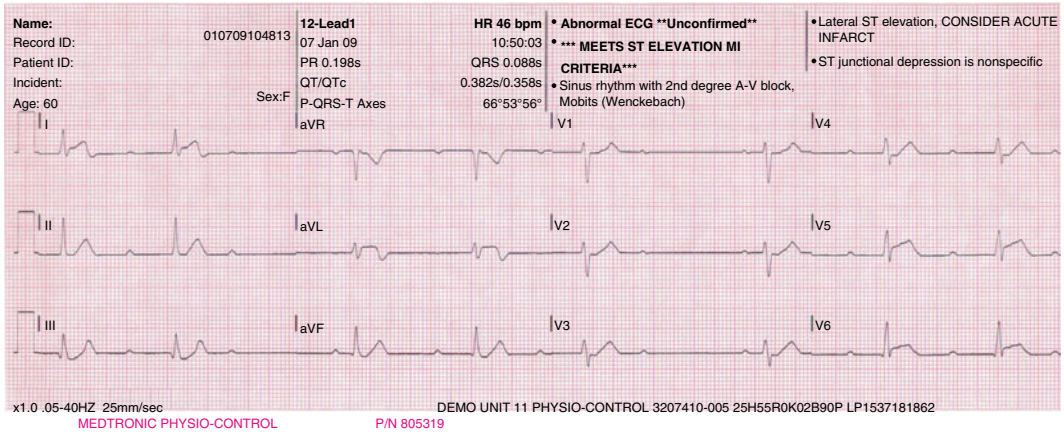

Figure 34.1

A 12-lead ECG report from a Lifepak15. This simulated example shows ST elevation that is correctly detected and highlighted.

34.2.1 Myocardial Ischemia/Infarction

Myocardial ischemia/infarction have been reported in about 50% of patients who called for an ambulance due to acute chest pain and in whom a prehospital ECG was recorded [17–19, 24]. Signs of myocardial ischemia/infarction include ST-segment deviation, Q waves and T-wave inversion. The relative importance of these changes will be described separately. In overall terms, when any of these are present in association with acute chest pain, the likelihood of a fresh myocardial infarction is high and the presence of any of them are mostly equivalent to an acute coronary syndrome. The presence of ECG changes indicating acute ischemia/infarction is also an alarming sign with regard to the risk of early death [25].

Difficulties in interpretation arise when a complete left bundle branch block is present. If this abnormality is new, it could indicate an extensive myocardial infarction and is therefore an indication for early reperfusion [5]. However, there are difficulties in the prehospital setting when it comes to determining whether the left bundle branch block is new or not, as no previous ECG is generally available for comparison. Similar difficulties might also arise for other ECG indicators of myocardial ischemia/infarction.

34.2.2 Arrhythmias

The rate of occurrence of various arrhythmias is entirely dependent on the study population. Among patients with acute chest pain who call for an ambulance, life-threatening arrhythmias leading to cardiac arrest are found, but only among a small percentage [19, 24]. On the other hand, among patients found in cardiac arrest and in whom resuscitation was attempted, about one third are found in ventricular fibrillation [26]. However, in such a study population, particularly if there is a cardiac etiology, a much higher percentage (about 80%) is thought to have ventricular fibrillation at the onset of cardiac arrest [26].

Supraventricular arrhythmias, such as atrial fibrillation, during ambulance transport have been reported to occur in about 10% of patients with acute chest pain [24] and in less than 10% of patients with ST-elevation acute myocardial infarction [27–29]. The occurrence of various arrhythmias during continuous ECG monitoring will be described later in this chapter.

34.2.3 Other

Other ECG abnormalities suggesting a cardiac pathology, including signs of a previous acute myocardial infarction, pacemaker ECG, and signs of left ventricular hypotrophy, are frequently seen in patients transported by ambulance with acute chest pain (between 10% and 20%) [18, 19]. It was recently reported that, among patients with trauma, the evaluation of heart rate variability in the prehospital setting might improve triage, if information on the Glasgow Coma Score (the degree of consciousness) was not available [30] and also independent of the Glasgow Coma Score [31].

34.3 Improved Triage

To date, the prehospital ECG has primarily resulted in the improved triage of patients with an acute coronary syndrome and patients with various arrhythmias. This improvement will have a number of consequences.

34.3.1 Direct Transport to Coronary Care Unit

Information on the percentage of patients with acute coronary syndrome or ST-elevation acute myocardial infarction, who are directly transported to a coronary care unit, bypassing the emergency department, is limited. In one previous study, it was reported that 67% of patients transported by ambulance fulfilled these criteria and that these patients had improved survival [32]. Experience from Sahlgrenska University Hospital in Göteborg, Sweden, indicates that among ambulance transported patients, 50% of patients with ST-elevation myocardial infarction have been directly transported to a coronary care unit and that this has been associated with a marked improvement in long-term survival [33].

34.3.2 Direct Transport to Catheterization Laboratory

Today in urban areas, there are single ambulance organizations which can transport the vast majority of patients with ST-elevation acute myocardial infarction directly to the catheterization laboratory with a median delay between the onset of symptoms and the start of percutaneous coronary intervention (PCI) of less than 2 h (unpublished observations). If the nearest hospital has facilities for PCI, effective collaboration can increase the opportunity for very early coronary intervention.

34.3.3 Direct Transport to Remote Hospital

Since primary coronary intervention is currently regarded as the preferred treatment strategy in ST-elevation acute myocardial infarction, it has been suggested that these patients should be transported to hospitals with these facilities, even if the transport time is prolonged [34]. It has been stated that patients admitted to noninterventional hospitals should be immediately transferred to interventional hospitals for primary coronary intervention, if the time from the first medical contact to balloon inflation is kept at less than 90 min [35–38]. Recent data indicate that an even longer delay might be acceptable [39].

In previous studies, patients have waited between 30 min and more than 1 h at local hospitals before being transferred to the intervention hospitals [37, 38, 40]. This local hospital delay may be reduced or even eliminated by prehospital diagnosis if a combined strategy of rerouting patients directly to an intervention hospital is implemented. However, limited evidence is available about the benefit, safety and feasibility of this kind of re-routing strategy. However, programs to further evaluate the possible benefits of such a procedure have been described [35].

34.4 Earlier Start of Treatment

34.4.1 Earlier Start of Fibrinolysis

34.4.1.1 Prior to Hospital Admission

A number of studies have shown that, if a 12-lead prehospital ECG is recorded and is followed by prehospital fibrinolysis, the potential time saved with regard to the start of fibrinolysis varies between 45 and 125 min [3, 6, 28, 29, 41–47]. In a national perspective (Sweden) it has been shown that treatment can start ⩽2 h after the onset of symptoms in half of patients [27]. However, such figures will vary between countries due to local facilities. It has been suggested that more patients can be treated at an early stage in urban areas compared with rural areas [48].

34.4.1.2 In Hospital

It has also been shown that a prehospital ECG reduces the in-hospital delay to the start of fibrinolysis (door-to-needle time) [49]. A systematic review in which 1,283 citations were identified and five studies met the inclusion criteria [50] indicated that the introduction of a 12-lead prehospital ECG and advanced emergency department notification reduced the mean door-to-needle time by 36 min (95% confidence limits 9–63 min).

In a national registry of acute myocardial infarction in the USA, the mean door to in-hospital drug time was reduced from 35 to 25 min with a prehospital ECG ($p < 0.0001$) [51]. A meta-analysis comprising four studies (99 patients) from an original 2,129 publications revealed a shortening of the in-hospital delay to reperfusion by 25 min (95% confidence limits 17–37 min) with the introduction of a prehospital ECG [52].

34.4.2 Earlier Start of Percutaneous Coronary Intervention (PCI)

A study from North Carolina revealed that prehospital wireless transmission of an ECG to a cardiologist's hand-held device reduced the median door-to-reperfusion time (PCI) by about 50 min [53]. In a national survey in Sweden, it was shown that, among patients who were transported by ambulance and had ST-elevation acute myocardial infarction, those who did not have a prehospital ECG had a delay between the onset of symptoms and reperfusion (PCI) of 240 min as compared with 181 min among patients with a prehospital ECG ($p < 0.0001$) (a time saving of 59 min) [54]. In the National Registry of Acute Myocardial Infarction in the USA, it was shown that, with a prehospital ECG, the in-hospital delay time to PCI was reduced from 1 h 49 min to 1 h 34 min [51]. A number of studies performed during the last few years have further confirmed these data, strongly suggesting a clear reduction in delay to PCI in ST-elevation acute myocardial infarction where a prehospital ECG is used and communicated to hospital appropriately [55–59].

34.4.3 Earlier Start of Antiplatelet and Antithrombotic Therapy

Various antiplatelet agents such as aspirin [60] and clopidogrel [61] and various antithrombotic agents such as heparin [62] have been shown to improve the prognosis in acute coronary syndrome. A prehospital ECG improved the opportunity to start this treatment prior to hospital admission. Aspirin treatment can then start as early as 1–2 h after the onset of symptoms. Similar findings have been reported for heparin and low molecular weight heparin [63].

34.4.4 Earlier Start of Anti-Ischemic Therapy

Beta-blockers have been shown to improve the prognosis in acute myocardial infarction [11], and intravenous treatment with beta-blockers, started prior to hospital admission, has been shown to relieve pain [24]. A prehospital ECG increases the opportunity to select the right patients for this treatment in the prehospital setting.

34.4.5 Earlier Start of Antiarrhythmic Therapy

Based on findings in the prehospital ECG, a number of antiarrhythmic drugs are of potential value in the prehospital setting when it comes to treating supraventricular and ventricular arrhythmias [64]. They include adenosine [65, 66], verapamil [67], diltiazem [68], and amiodarone [69].

34.5 Improved Outcome

34.5.1 Reduced Mortality

A systematic review found one study that revealed a nonsignificant reduction in all-cause mortality from 15.5% to 8.4% associated with the introduction of a prehospital ECG and advanced emergency department notification as compared with no such intervention [50].

In an observational study in Sweden on patients who had ST-elevation acute myocardial infarction, were transported by ambulance, and were treated with percutaneous coronary intervention, it was shown that a prehospital ECG was an independent predictor of reduced 30-day mortality [54]. Field triage of patients with ST-elevation acute myocardial infarction has also been shown to reduce mortality in Australia [70]. A similar trend was also found in the USA [71].

34.5.2 Reduced Morbidity

We are not aware of any study evaluating morbidity (various complications associated with the disease) changes associated with the introduction of a prehospital ECG. It can be assumed that there are subsets of patients in whom the duration of hospital stay (number of days in hospital) might be shortened. In a recent report, field triage with a prehospital electrocardiogram was associated with a preserved left ventricular function [70].

34.5.3 Health Economy

The use of health-economic analyses to assess the value of medical technologies is well established, but these analyses have been under-used in studies of ECG. One article [72] has outlined a general framework for the economic evaluation of the ECG and applied these methods to the development of an economic analysis protocol for assessing the economic attractiveness of the wireless transmission of ECG data to the cardiologist making the treatment decision.

34.6 Negative Consequences

There are two major negative consequences of the prehospital ECG.

34.6.1 Increase in Delay

The delay to arrival at hospital will increase, particularly among patients in whom the ECG does not show any pathological changes. However, it has been shown that the on-scene time is not dramatically prolonged by the recording of a 12-lead ECG [73, 74]. A systematic review revealed that the on-scene time increased by 1.2 min (95% confidence limits 0.8–3.2 min) [50].

34.6.2 False Information

The second major negative consequence is that ECG abnormalities may mimic myocardial infarction, but may in fact be caused by other conditions [75]. It has been reported that, among patients with chest pain and ST elevation in the prehospital setting [76] and at the emergency department [77], 85% and 51% respectively had diagnoses other than myocardial infarction. Conditions in which misinterpretation has occurred and in which fibrinolytic treatment can be detrimental include intracranial hemorrhage [75] and aortic dissection [78].

Negative consequences associated with technical problems will be dealt with in the implementation part of this chapter.

34.7 Implementation

34.7.1 Education and Training

There is currently a wide range of teaching techniques that can be used to train healthcare professionals in the use of 12-lead ECG-monitoring equipment and ECG interpretation.

The methods identified range from

1. Traditional teaching methods including (a) books, (b) lectures, (c) videos, (d) hospital placements (using patients), and (e) practical laboratory sessions (using volunteers) to
2. Advanced teaching methods including (a) PC-based ECG software packages (b) 12-lead ECG signal generators, and (c) advanced training mannequins (patient simulators) [79].

The traditional teaching methods have some disadvantages in terms of patient or volunteer consent and discomfort and also in terms of teaching effectiveness. The more advanced teaching methods make use of simulation which can be either screen based (computer software) or physical (realistic models or mannequins).

There are a number of ECG simulators on the market that can be connected to an ECG machine. Various models of ECG simulators that are connected to a mannequin are also available.

34.7.2 Technical Problems

The transmission of ECGs is the most common technical problem associated with the use of a prehospital ECG. With a few exceptions, the transmission of an ECG is associated with problems at the start. Most EMS systems experience a learning curve when a 12-lead ECG transmission technology is first implemented. One study reported a 33% failed transmission rate after initiating the system, but it had been reduced to 11% 6 months later [74].

34.7.3 Practical Implementation

Implementing a prehospital ECG program represents a significant investment in terms of time, effort, personnel and resources. The implementation has three phases: (1) phase I is a retrospective baseline analysis; (2) phase II is a feasibility and safety assessment; and (3) phase III involves the implementation of the accurate and routine prehospital identification of candidates for various aspects of treatment of an acute coronary syndrome, such as candidates for treatment with fibrinolysis or percutaneous coronary intervention [80]. Eligibility for fibrinolysis or percutaneous coronary intervention can be determined by means of a check list, the results of which can be sent to either the base or the receiving physician [81]. A written protocol including clinical algorithms for prehospital personnel should be established [80]. Finally, an effective quality assurance and improvement program should be initiated before implementing a prehospital ECG program [81].

Prehospital 12-lead ECG programs should be strongly considered by all EMS systems with advanced life support capability. Prehospital 12-lead ECG programs should be implemented through a systematic process that encompasses every facet of the EMS system [82].

34.7.4 Process Monitoring

One of the principal aims of the introduction of a prehospital ECG is to reduce the time to reperfusion in ST-elevation myocardial infarction. In order to evaluate the impact on this important end point, the delay from the first medical contact to the start of reperfusion either with fibrinolysis or with percutaneous coronary intervention must be continuously monitored. Although, as previously stated, the short-term impact on delay to reperfusion with a clear-cut reduction is impressive, the results in the long-term perspective are less well described. It is to be hoped that, in the long term, the teamwork between prehospital and in-hospital health-care providers will improve with a successive decline in the time to reperfusion over the years.

However, the results so far are disappointing. In a recent 10-year survey, it was shown that the delay from door to primary coronary intervention was not sustained [83]. In the first year of the intervention (including the implementation of the prehospital ECG), the time from hospital arrival to primary coronary intervention was 80 min. In years 2, 3, and 4, this delay was 93, 85, and 94 min, respectively. In 2003, 10 years after the intervention, the delay had increased to 113 min [83].

Experience from the Swedish registry on heart intensive care indicates that the time between admission to hospital and the start of reperfusion has remained unchanged during the last few years [84].

34.8 Interpretation

The category of health care professionals who interpret the prehospital ECG varies markedly. They include cardiologists, emergency physicians, anesthesiologists, general practitioners, nurses, semi-nurses (nursing assistants), paramedics, and emergency technicians. The educational levels of these various categories vary considerably. So, when discussing the problem of interpreting the prehospital ECG, each category of health-care professionals must be discussed separately, and separate educational programs should probably be implemented for these various groups.

There are different ways to interpret the prehospital ECG.

34.8.1 In-Field Interpretation

34.8.1.1 By Health-Care Providers

In-field interpretation by health-care providers without assistance requires a high educational level. This type of interpretation is most common when a physician is on board the ambulance or when a general practitioner sees the patient prior to the arrival of the ambulance. In several countries such as France, this is the most common way of interpreting the prehospital ECG. However, it has been suggested that highly trained paramedics in an urban EMS system can identify patients with ST-elevation acute myocardial infarction as accurately as blinded physician reviewers [85]. This has been supported by others [86] and it seems as though paramedics as well as CCU nurses can learn to conduct live reperfusion decision making in ST-elevation myocardial infarction [87].

34.8.1.2 With Computer Assistance

Computer algorithms for the diagnosis of ST-elevation myocardial infarction may also be considered [88, 89]. This strategy has, however, previously been restricted to the diagnosis of large ST-elevation myocardial infarctions with cumulative ST elevation above 600–1,000 μ V [90, 91]. Interpretation in the field with computer assistance has been reported to be a

relatively safe procedure [92]. Recently, a new acute coronary syndrome computer algorithm for interpreting prehospital ECGs was suggested [93]. The results demonstrated that, with the assistance of the new algorithm, the emergency physician and cardiologist improved their sensitivity when it came to interpreting acute myocardial infarction by 50% and 26% respectively, without any loss of specificity. The patients' age and gender were taken into consideration in the algorithm. However, it was recently suggested that a correction should be made to obtain optimal results in the automated analysis of ECGs [94].

34.9 Wireless Transmission

34.9.1 To Nearest Hospital

The in-field transmission of the prehospital ECG to the emergency department, coronary care unit, another hospital ward, or directly to the on-call cardiologist for interpretation by a more experienced health-care provider is common [53]. This mode of interpretation is more common when the ambulance is manned by a nurse and or a paramedic.

Studies have shown that cardiologists' diagnoses of cardiac abnormalities on a liquid crystal display are very similar to their interpretation of the same ECG displayed on paper [95, 96]. Furthermore, there was no significant difference with regard to cardiologists' decisions to initiate reperfusion therapy when interpreting study-displayed ECGs versus ECGs displayed on a liquid crystal display screen [97]. In many countries, this is a widespread means of communication between the prehospital and in-hospital health-care providers [27].

34.9.2 To Remote Hospital

Even in urban areas, up to 80% of ambulance-transported ST-elevation myocardial infarction patients can be diagnosed prehospitally using telemedicine [98]. In principle, a strategy of this kind could be adapted in any region covered by a mobile phone network and the health-care providers (mostly a physician) responsible for the diagnosis can be located at a central unit serving a large catchment area [34, 35, 98, 99]. It is possible to speculate that primarily low-risk patients (limited ST elevation) will be found to be eligible for prehospital referral directly to an intervention centre [98]. However, the opposite has been found, that is, patients transported directly to the intervention center were those with a more pronounced ST elevation [98]. It is most likely that there is a geographical border, at a certain distance or transport time from the intervention center, beyond which patients may obtain a beneficial effect from prehospital fibrinolysis or even in-hospital fibrinolysis.

An attractive way of solving the problem is to obtain an ECG on the scene for subsequent transmission to the intervention center. A physician on call will evaluate the ECG, phone the ambulance, possibly interview the patient who is in the ambulance and equipped with headphones, and thereby establish the prehospital diagnosis [34]. An ECG could also be sent to an attending cardiologists mobile telephone for rapid triage and transport to a primary PCI center [100].

34.9.3 Elsewhere

The in-field transmission of the ECG to an advanced mobile phone outside hospital was recently described [101]. This is an alternative when a helicopter is very far from the hospital, and an emergency medical service physician capable of interpreting the ECG is at a shorter distance, for example. He can then view the ECG on his advanced phone and give recommendations about fibrinolysis or other treatment alternatives. A novel approach is to use a cell phone with a camera feature. This method will allow transfer of ECG images to the local hospital and the PCI center [102].

34.10 ECG Indicators for Myocardial Ischemia/Infarction and Adverse Outcome

More than 10 years ago, it was shown that, in the prehospital setting, a pathological ECG was a strong predictor and was associated with a fourfold increase in the risk of a cardiac pathology as the etiology of acute chest pain [17]. It has also been shown that, if the patient has chest pain and/or other symptoms indicating acute coronary syndrome, signs of myocardial ischemia (including new ST-T wave changes or Q waves) are associated with a marked increase in 30-day and 1-year mortality, particularly if there is simultaneous elevation of biochemical markers prior to hospital admission [25].

34.10.1 ST Elevation

Among patients with chest pain and/or other symptoms of acute coronary syndrome, the presence of ST elevation in the prehospital ECG has been reported to increase the likelihood of acute myocardial infarction nearly 50 times when simultaneously considering other risk indicators including the elevation of biochemical markers [103].

34.10.2 ST Depression

It is important to stress that, from ECG studies in which the ECG was recorded directly after hospital admission, ST depression in the ECG among patients with symptoms indicating acute coronary syndrome has been reported to be associated with an adverse long-term prognosis [104, 105]. Among patients with chest pain or other symptoms of acute coronary syndrome, the presence of ST depression in the prehospital ECG has been reported to be associated with a fourfold increase in the risk of acute myocardial infarction [103].

Although by tradition patients with ST elevation or (presumed) new left bundle branch block have formed the group demanding urgent revascularisation in acute coronary syndrome, there are subsets among patients showing ST depression who also suffer from a critical coronary stenosis or occlusion and who therefore most likely would benefit from a similar treatment strategy. These include patients with marked ST depression in anterior leads and those with extensive ST depression where a large number of leads is involved.

A gender perspective has been found. If there are symptoms of acute coronary syndrome, the presence of ST depression in the prehospital ECG appears to be more strongly associated with acute myocardial infarction in men than in women [106].

34.10.3 T-Wave Inversion

Although the presence of T-wave inversion without simultaneous changes in the ST segment might indicate myocardial ischemia [107], these changes are less frequently associated with an ongoing acute myocardial infarction [103].

34.10.4 Other Changes

Needless to say, the presence of Q waves might also indicate acute myocardial infarction [103, 106]. However, as things stand, it is not possible in the prehospital setting to make comparisons with previous ECG findings and a Q wave in isolation without concomitant ST-T wave changes might therefore be a sign of an old myocardial infarction. Other ECG abnormalities found in the prehospital ECG, such as pacemaker ECG, bundle branch block, and signs of left ventricular hypertrophy, are less specific for acute myocardial infarction but are, on the other hand, often indicators of an adverse outcome in a long-term perspective [25].

34.11 Prehospital Continuous ECG Monitoring

34.11.1 Background

Little is known about the natural course of myocardial ischemia and the development of arrhythmias in the prehospital phase of acute coronary syndrome. Small pilot studies indicate a relatively high prevalence of tachyarrhythmias during prehospital ECG monitoring as compared with the first ECG recording in hospital [19]. Recent reports suggest that prehospital ECG monitoring should have the potential to detect myocardial ischemia in the prehospital phase much more frequently than a standard 12-lead ECG [108].

34.11.2 Method Development

This has been done in particular by Drew et al. [19]. A system was developed that: (1) synthesizes a 12-lead ECG from five electrodes, (2) measures ST amplitudes in all 12 leads every 30 s and (3) automatically transmits an ECG to the target emergency department if there is a change in ST amplitude of 200 μ V in one lead or more or 100 μ V in two contiguous leads or more lasting 2.5 min.

34.11.3 Occurrence of Arrhythmias

Among all the patients involved in the first part of a randomized clinical trial [19] (the ST SMART Study; n = 433), one third overall (33%) had some arrhythmias during continuous prehospital ECG monitoring as compared with 29%, according to the initial hospital ECG diagnosis among patients with chest pain – anginal equivalent ($p < 0.001$). The corresponding figure for patients with acute coronary syndrome was 30% versus 26% ($p < 0.001$). In overall terms, more tachyarrhythmias (sinus tachycardia, atrial fibrillation/flutter, supraventricular tachycardia of unknown mechanism and sustained ventricular tachycardia) were observed in continuous prehospital ECG monitoring, whereas more bradyarrhythmias (complete heart block, sinus arrest with junctional or ventricular escape rhythm) were observed in the first hospital ECG.

34.11.4 Wide QRS Complex

Among patients with acute coronary syndrome, 15% had a rhythm with a wide QRS complex and secondary repolarization abnormalities that confound the diagnosis of myocardial ischemia. These ECG confounders included left bundle branch block (6%), right bundle branch block (6%) and ventricular pacing rhythm (3%) [19].

34.11.5 Advantages of Continuous Prehospital ECG Monitoring

In the area of early reperfusion with percutaneous coronary intervention in acute coronary syndrome, a rerouting strategy may result in some patients being transported longer distances without any accompanying staff skilled in the diagnosis and treatment of malignant arrhythmias. Continuous real-time, one-lead ECG transmission from ambulance to hospital may then allow physicians to support ambulance personnel in the treatment of arrhythmias during this kind of transportation [98]. Furthermore, continuous prehospital ST monitoring indicates that patients with ST-elevation myocardial infarction are heterogeneous and various types of dynamic change in the prehospital setting might indicate a more favorable or a more adverse prognosis [109]. A pre-specified ST-monitoring classification may therefore be useful for stratifying patients at the time of percutaneous coronary intervention into groups with a low, intermediate, and high-risk profile [109].

34.11.6 Number of Electrodes for Detection of Myocardial Ischemia/Infarction

The optimal number of electrodes that should be used in the diagnosis of myocardial infarction/ischemia has been debated over the years [110]. An alternative to the 12-lead ECG, such as the five-electrode-derived EASI ECG, has been tested in the prehospital setting [111, 112]. It offers the advantages of using only five electrode positions (four active and one ground) over easy-to-locate, bony structures on the torso. The E electrode is therefore placed on the lower extreme of the sternum, the A and I electrodes in the left and right mid-axillary lines respectively and at the same transverse level as the E electrode, and the S electrode on the sternal manubrium.

The five-electrode-derived EASI ECG has been compared with the paramedic-acquired 12-lead ECG using Mason–Likar limb lead configuration in patients with chest pain [111, 112]. Both appear to produce a similar difference compared with standard ECGs in terms of wave forms. It has been suggested that either method can be used as a substitute for standard ECGs for monitoring, but neither should be regarded as being equivalent to the standard ECG for diagnostic purposes [111].

Parallel to this research, studies have been performed using 80-lead prehospital ECG mapping [113]. In these studies, the sensitivity has increased to 80% as compared with 57% for a 12-lead ECG [113]. The specificity remained unchanged (92%) for an 80-lead ECG versus 94% for a 12-lead ECG [113].

34.12 Different Technical Models

34.12.1 Medtronic Lifepak

The *Medtronic Lifepak15* (Fig. 34.2) is a traditional system transmitting a standard 12-lead ECG and is capable of defibrillation. The principle for this system is that it registers a snapshot ECG. This procedure can be repeated if the patient's symptoms change during transportation to hospital. One Lifepak version is able to transmit continuous ST monitoring while using a reduced number of electrodes [114].

Figure 34.2
The Lifepak15 in use. The ECG (cf Fig. 34.1) report is produced directly from the machine as shown.

Figure 34.3
The Ortivus Mobimed.

Table 34.4
Clinical determinants of patient instability

Altered mental status
Significant hypotension
Pulmonary edema
Ischemic chest pain
Ischemic electrocardiographic changes (or other evidence of significant hypoperfusion)

34.12.2 Ortivus Mobimed

Ortivus Mobimed (Fig. 34.3) is a prehospital concept presenting data in a Windows setup. This system is able to transmit a 12-lead ECG, continuous vector trends, or ST analysis and collect data such as patient files. This system requires a separate defibrillator.

34.12.3 Other

Several other manufacturers offer equipment for prehospital ECG recording and defibrillation. There are variations between countries in respect of choice of machine and a complete review is not appropriate here.

34.13 Various Types of Arrhythmia

The use of the prehospital ECG to detect various arrhythmias is particularly important when there are signs of clinical instability [64]. These signs are listed in Table 34.4.

34.13.1 No Cardiac Arrest

34.13.1.1 Bradyarrhythmias

Limited data are available on the occurrence of various bradyarrhythmias and the value of various treatments such as atropine and the use of pacemakers in these conditions. Continuous ECG monitoring among patients with chest pain indicated that 2% had sinus bradycardia (heart rate < 50 beats/min), 0.7% had heart block, and 0.7% had sinus arrest with ventricular escape rhythm during ambulance transport [19].

34.13.1.2 Tachyarrhythmias

Paroxysmal Supraventricular Tachycardia

Paroxysmal supraventricular tachycardia is usually a regular narrow-complex tachyarrhythmia caused by a reentry, which may or may not be accompanied by underlying cardiovascular disease. Many of these patients are clinically stable and in these patients a prehospital ECG will be a support for improved triage rather than improved treatment. Among patients with acute chest pain, supraventricular tachycardia (unknown mechanism) was reported to occur in 2% [19].

Atrial Fibrillation/Flutter

Because the disorder is not commonly seen by emergency medical system providers (the reported incidence among ambulance-transported patients ranges from only 0.2–0.7%) [58], there is no consensus on the optimal prehospital therapy. Among patients with acute chest pain, continuous ECG monitoring in the prehospital phase revealed atrial fibrillation flutter in 11% of cases [19]. Almost every patient with rapid atrial fibrillation has another underlying disease, such as heart failure, chronic obstructive pulmonary disease, or ischemic heart disease.

Perfusing Ventricular Tachycardia

Hemodynamically stable monomorphic ventricular tachycardia can be treated either pharmacologically or with synchronized cardioversion [58]. Cardioversion is the therapy of choice for unstable patients and for those with marginal blood pressure in whom there may not be enough time or stability to allow for drug infusion. Among patients with chest pain who underwent continuous ECG monitoring during transport, sustained ventricular tachycardia was reported to occur in 0.2% of cases [19].

34.13.2 Cardiac Arrest

Every year, between 40 and 50 patients per 100,000 inhabitants suffer an out-of-hospital cardiac arrest, and in such cases, it is regarded as meaningful to attempt resuscitation [115]. The prehospital ECG is used most importantly in order to distinguish patients with a shockable rhythm from those without. However, detection of ST elevation immediately after return of spontaneous circulation, has also been shown to reflect the presence of acute myocardial infarction as the underlying etiology behind cardiac arrest [116].

34.13.2.1 Ventricular Fibrillation

The percentage of patients found in ventricular fibrillation among cardiac arrest victims has been reported to have decreased during the last 2 decades [117, 118]. The mechanism behind this decrease is unclear. The earlier a prehospital ECG is recorded, the more likely is it to find the patients in a shockable rhythm. Out-of-hospital cardiac arrest has therefore been regarded by many as a community problem rather than an ambulance problem, as the ambulance frequently reaches the patient too late in the course of events. Over the years, a strong relationship has been reported between the delay from cardiac arrest and defibrillation, that is, the earlier the patient is defibrillated, the higher the likelihood of survival [26].

34.13.2.2 Pulseless Electrical Activity

The percentage of patients suffering an out-of-hospital cardiac arrest in whom resuscitation was attempted and who were found in pulseless electrical activity has been reported to be about 20% [119]. These patients have been reported to have a low chance of survival (1–2%). However, other studies have shown more encouraging results, indicating that some of these patients can be successfully resuscitated [120, 121]. The data do not indicate a strong relationship between the delay from cardiac arrest to the arrival of the rescue team and survival [119].

34.13.2.3 Asystole

The percentage of patients suffering an out-of-hospital cardiac arrest in whom resuscitation was attempted and who were found in asystole has been reported to be about 50% [122]. The longer the delay from cardiac arrest to ECG recording, the greater the likelihood of finding the patients in asystole. In one study, it was reported that, the earlier the mobile coronary care unit arrived at the patient's side, the greater the likelihood of survival [122].

34.14 Electrocardiographic Factors Associated with Outcome in Cardiac Arrest

34.14.1 Ventricular Fibrillation

34.14.1.1 Waveform Analysis

The determination of the optimal time for delivering a defibrillatory shock has focused on the ventricular fibrillation wave form in many studies [123–128]. It has been suggested that a characteristic pattern of median frequency could be used to estimate the duration of ventricular fibrillation [124, 125]. Eftestøl et al. described a combination of spectral features in the ventricular fibrillation wave form from which they developed a probability function for successful defibrillation in a study of ventricular fibrillation in cardiac arrest patients [129]. They were subsequently able to confirm their findings in an independent data set [130].

Following these findings, wavelet transform methods of ventricular fibrillation that could be useful in identifying patients for whom shocks would be ineffective were described [131, 132]. Further support for ECG analysis in order to predict outcome in ventricular fibrillation was given by Snyder et al. [133].

It was recently reported that the accuracy of shock outcome prediction could be further increased by using filtered ECG features from higher ECG subbands instead of features derived from the main ECG spectrum [134].

A new method, based on the roughness of the ventricular fibrillation waveform, called the logarithm of the absolute correlation, has been suggested to better predict the duration of ventricular fibrillation and thereby the chance of successful defibrillation [135].

By calculating the mean slope of the electrocardiogram it has been possible to estimate the association between the time without chest compression and the probability of return of spontaneous circulation [136].

By calculating the median slope of the electrocardiogram, a new indicator of a chest compression quality measurement has been developed [137]. The configuration of the waveform has also been shown to be helpful in the identification of acute myocardial infarction as the underlying etiology behind ventricular fibrillation [138].

It has been hypothesized that interventions with thrombolytic therapy in ventricular fibrillation will change the wave form with increased amplitude and thereby increase the chance of successful defibrillation [139].

34.14.2 Pulseless Electrical Activity

Previous ECG studies performed in animals and patients demonstrated a progression of ECG characteristics in pulseless electrical activity with the time from the onset of anoxia. In a retrospective study comprising 503 patients whose prehospital initial rhythm was pulseless electrical activity, Aufderheide et al. found that patients who were successfully

resuscitated had significantly higher initial heart rates, a higher incidence of p-values, and shorter average QRS and QT intervals than patients who did not respond to therapy [140]. It has been suggested that pulseless electrical activity often follows prolonged untreated ventricular fibrillation and that the characteristics of initial post-countershock pulseless electrical activity may predict the resuscitation outcome [141].

In animals, it has been shown that those with post-countershock pulseless electrical activity, which were converted to spontaneous circulation, had fewer shocks prior to the onset of initial post-countershock pulseless electrical activity, greater ventricular fibrillation wavelet amplitude prior to initial post-countershock pulseless electrical activity, and short QRS intervals and a higher heart rate [141]. It is therefore possible that various ECG characteristics among patients suffering from pulseless electrical activity might be used in order to predict outcome in these patients.

34.15 Use of a Prehospital Electrocardiogram in a Global Perspective

34.15.1 Use and Transmission of a Prehospital ECG

This information is based on rough estimations by leading authorities in the field. One exception is the USA, where data are collected from a reference [142]. The use of or response to a prehospital ECG is mainly dependent on the level of education among the EMS personnel who are in charge of the EMS vehicle. In cases where there is a physician in the ambulance (as in Spain and France), ECGs are usually interpreted on line by a doctor and there is usually no need for ECG transmission from the patient/ambulance to the hospital. However, in cases where a paramedic or a registered nurse (as is mostly the case in Scandinavia, Canada, and the USA) is in charge of the ambulance, the ECG must be transmitted to a nearby hospital. Printable copies of the ECG can be transmitted to the hospital emergency department, coronary care unit, or intensive care unit through a cellular phone or using the patient's regular phone. The doctor on call and the EMS personnel can then jointly discuss the ECG findings, patient symptoms, and risk profile. In some countries (like the Netherlands), an effective computerized algorithm is used to support the nurse when assessing the patient.

This estimation of the global use of prehospital ECG is unfortunately restricted to Europe and North America. In a large US survey among patients suffering from myocardial infarction 172,059 patients used the ambulance. Among them, only 6% had a prehospital ECG recorded. In a large database in the USA, it was recently shown that among 12,097 patients with ST-elevation myocardial infarction 59% used EMS and among them 27% had a prehospital ECG [71]. In contrast to these data, the 200-City survey in the USA previously reported that 67% of all emergency medicine service organizations do have a 12-lead ECG system (Table 34.5) [142]. Thus, with regard to the USA there is some uncertainty of the actual proportion of ambulance organizations using a prehospital ECG. The estimation indicates that, in overall terms, a prehospital ECG is implemented in the routine prehospital care of patients with a presumed acute coronary syndrome more frequently in Europe than in North America. However, the proportion of patients with presumed acute coronary syndrome in whom a prehospital ECG is recorded is not known.

34.15.2 Important Prehospital ECG Research Projects

Perhaps the most important ongoing clinical trial of the use of a prehospital ECG is the ST SMART trial in the USA [114]. This is an ongoing study which aims to evaluate the impact of implementing prehospital ST monitoring with the automatic mobile telephone transmission of ST events to the target hospital. It is a prospective, randomized trial using these ST data for real-time clinical decision-making. The first patient had been randomized by November 1, 2003 and randomization should continue for 5 years. All subjects calling 911 for chest pain or anginal equivalent symptoms receive prehospital, synthesized, 12-lead, ST-segment monitoring with the manual transmission of an initial ECG and the automatic transmission of subsequent ST-event ECGs to the target hospital. The experimental group of patients has incoming ECGs from the field conveyed to clinical staff at the hospital, heralded by an audible voice message and printed out at the emergency department. The control group of patients have no field ECGs printed out and the first ECG is recorded after hospital admission. It is to be hoped that this study will document the value of prehospital ECG monitoring in a presumed acute coronary syndrome.

Table 34.5

Use of prehospital ECG in a global perspective[a]

Country	Overall prehospital ECG use %	Transmission	Comments
Norway	> 90%	Yes	Mostly no physician – 1
Sweden	> 90%	Yes	No physician – 2
Denmark	> 90%	Yes	Mostly no physician – 3
Spain	> 90%	No	Physician operating – 4
Netherlands	> 90%	No/Yes	No physician but online computerized ECG – 5
France	> 90%	No	Physician operating – 6
Canada	25%	Yes	No physician – 7
USA	67%[b]	Yes	Williams D JEMS 2005;30:42–60

[a] Personal communication with: (1) Hans Morten Lossius, (2) Leif Svensson, (3) C Juhl Terkelsen, (4) Fernando Rosell, (5) Evert Lamfers, (6) Patrick Goldstein, and (7) Laurie Morrison.

[b] In ref [71], it was reported that only 27% of EMS transported patients with ST-elevation myocardial infarction received a prehospital ECG in 2007 in the USA.

34.16 Future Perspective

A number of important implementation and research issues remain to be addressed in the near future with regard to the prehospital ECG. The most important one is to implement a prehospital ECG in all EMS systems. The use of a prehospital ECG is probably the most important part of the prehospital care of patients suffering a heart attack. It seems as though the speed of this process varies in different parts of the world. It remains to be proved whether continuous ECG monitoring will improve the prehospital care in a presumed acute coronary syndrome as compared with a single 12-lead ECG recording on the arrival of the rescue team.

The optimal number of electrodes for use in the prehospital ECG has not been clarified. Should we use a 12-lead ECG or should we reduce or increase the number of electrodes? Wave-form analysis in ventricular fibrillation could perhaps be improved still further in order to optimize the timing of defibrillation. Finally, we need to decide whether there is hidden information in the ECG among patients suffering a cardiac arrest and pulseless electrical activity, which could guide us in the management of these patients.

But, most likely, the most important challenge for the future is to overcome barriers to the implementation and integration of the prehospital electrocardiogram into systems of care for acute coronary syndrome [143, 144].

References

1. Pantridge, J.F., Manning mobile intensive-care units. *Lancet*, 1967;**2**(7521): 888.
2. Uhley, H.N., Electrocardiographic telemetry from ambulances. A practical approach to mobile coronary care units. *Am. Heart J.*, 1970;**80**: 838–842.
3. Risenfors, M., G. Gustavsson, L. Ekström, M. Hartford, J. Herlitz, B.W. Karlson, R. Luepker, K. Swedberg, B. Wennerblom, and S. Holmberg, Prehospital throm-bolysis in suspected acute myocardial infarction: results from the TEAHAT Study. *J. Intern. Med.*, 1991;**229**(suppl 1): 3–10.
4. Herlitz, J., B.W. Karlson, T. Karlsson, M. Dellborg, M. Hartford, and R.V. Luepker, Diagnostic accuracy of physicians for identifying patients with acute myocardial infarction without an electrocardiogram. Experiences from the TEAHAT trial. *Cardiology*, 1995;**86**: 25–27.
5. Fibrinolytic Therapy Trialists' (FTT) Collaborative Group, Indications for fibrinolytic therapy in suspected acute myocardial infarction: collaborative overview of early mortality and major morbidity results from all randomised trials of more than 1000 patients. *Lancet*, 1994;**343**: 311–322.
6. Weaver, W.B., M.S. Eisenberg, J.S. Martin, et al., Myocardial infarction triage and intervention project – Phase I: Patient characteristics and feasibility of pre-hospital initiation of thrombolytic therapy. *J. Am. Coll. Cardiol.*, 1990;**15**: 925–931.

7. Maroko, P.R., J.K. Kjekshus, B.E. Sobel, T. Watanabe, J.W. Covell, J. Ross, and E. Braunwald, Factors influencing infarct size following experimental coronary artery occlusions. *Circulation*, 1971;**43**: 67–82.
8. Gruppo Italiano per lo Studio della Streptochinasi nell'Infarto Miocardico (GISSI), Effectiveness of intravenous thrombolytic treatment in acute myocardial infarction. *Lancet*, 1986;**1**: 397–401.
9. Grines, C.L., K.F. Browne, J. Marco, et al., A comparison of immediate angioplasty with thrombolytic therapy for acute myocardial infarction. *N. Engl. J. Med*., 1993;**328**: 673–679.
10. ISIS-2 (Second International Study of Infarct Survival) Collaborative Group, Randomised trial of intravenous streptokinase, oral aspirin, both or neither among 17.187 cases of suspected acute myocardial infarction: ISIS-2. *Lancet*, 1988;**2**: 349–360.
11. Hjalmarson, Å., D. Elmfeldt, J. Herlitz, S. Holmberg, I. Málek, G. Nyberg, L. Rydén, K. Swedberg, A. Vedin, F. Waagstein, A. Waldenström, J. Waldenström, H. Wedel, L. Wilhelmsen, and C. Wilhelmsson, Effect on mortality of metoprolol in acute myocardial infarction. A double-blind randomised trial. *Lancet*, 1981;**ii**: 823–827.
12. Freimark, D., S. Matetzky, J. Leor, V. Boyko, I.M. Barbash, S. Behar, et al., Timing of aspirin administration as a determinant of survival of patients with acute myocardial infarction treated with thrombolysis. *Am. J. Cardiol*., 2002;**89**: 381–385.
13. Barbash, I.M., D. Freimark, S. Gottlieb, H. Hod, Y. Hasin, A. Battler, et al., Outcome of myocardial infarction in patients treated with aspirin is enhanced by pre-hospital administration. *Cardiology*, 2002;**98**: 141–147.
14. Zijlstra, F., N. Ernst, M.J. deBoer, E. Nibbering, H. Suryaparanata, J.C.A. Hoorntje, et al., Influence of prehospital administration of aspirin and heparin on initial patency of the infarct-related artery in patients with acute ST elevation myocardial infarction. *JACC*, 2002;**39**: 1733–1737.
15. Chambless, L., U. Keil, A. Dobson, M. Mähönen, K. Kuulasma, A.M. Rajakangas, and H. Löwel, Tunstall-Pedoe H for the WHO MONICA project. Population versus clinical view of case fatility from acute coronary heart disease. Results from the WHO MONICA project 1985–1990. *Circulation*, 1997;**96**: 3849–3859.
16. Vingerhoets, F., J. Bogousslavsky, F. Regli, and G. Van Melle, Atrial fibrillation after acute stroke. *Stroke*, 1993;**24**: 26–30.
17. Grijseels, E.W.M., J.W. Deckers, A.W. Hoes, J.A.M. Hartman, E. Van der Does, E. Van Loenen, and M.L. Simoons, Pre-hospital triage of patients with suspected myo-cardial infarction. Evaluation of previously developed algorithms and new proposals. *Eur. Heart J*., 1995;**16**: 325–332.
18. Svensson, L., C. Axelsson, R. Nordlander, and J. Herlitz, Elevation of biochemical markers for myocardial damage prior to hospital admission in patients with acute chest pain or other symptoms raising suspicion of acute coronary syndrome. *J. Int. Med*., 2003;**253**: 311–319.
19. Drew, B.J., C.E. Sommargren, D.M. Schindler, J. Zegre, K. Benedict, and M.W. Krucoff, Novel electrocardiogram configurations and transmission procedures in the prehospital setting: effect on ischemia and arrhythmia determination. *J. Electrocardiol*., 2006;**39**: S157–S160.
20. Herlitz, J., Å. Hjalmarson, S. Holmberg, A. Richter, and B. Wennerblom, Mortality and morbidity in suspected acute myocardial infarction in relation to ambulance transport. *Eur. Heart J*., 1987;**8**: 503–509.
21. Herlitz, J., B.W. Karlson, A. Bång, and J. Lindqvist, Characteristics and outcome for patients with acute chest pain in relation to whether or not they were tran-sported by ambulance. *Eur. J. Emerg. Med*., 2000;**7**: 195–200.
22. Canto, J.G., R.J. Zalenski, J.P. Ornato, W.J. Rogers, C.I. Kiefe, D. Magid, et al., Use of emergency medical services in acute myocardial infarction and subsequent quality of care: observations from the National Registry of Myocardial Infarction 2. *Circulation*, 2002;**106**: 3018–3023.
23. Erhardt, L., J. Herlitz, L. Bossaert, M. Halinen, M. Keltai, R. Koster, C. Marcassa, T. Quinn, and H. van Weert, Task force report. Task force on the management of chest pain. *Eur. Heart J*., 2002;**23**(15): 1153–1176.
24. Gardtman, M., M. Dellborg, C.h. Brunnhage, J. Lindqvist, L. Waagstein, and J. Herlitz, Effect of intravenous metoprolol before hospital admission on chest pain in suspected acute myocardial infarction. *Am. Heart J*., 1999;**137**(5): 821–829.
25. Svensson, L., C. Axelsson, R. Nordlander, and J. Herlitz, Prognostic value of biochemi-cal markers, twelve lead ECG and patients characteristics among patients calling for an ambulance due to a suspected acute coronary syndrome. *JIM*, 2004;**255**: 469–477.
26. Holmberg, M., S. Holmberg, and J. Herlitz, Incidence, duration and survival of ventricular fibrillation in out-of-hospital cardiac arrest patients in Sweden. *Resuscitation*, 2000;**44**: 7–17.
27. Svensson, L., T. Karlsson, R. Nordlander, M. Wahlin, C. Zedigh, and J. Herlitz, Implementation of prehospital thrombolysis in Sweden. Components of delay until delivery of treatment and examination of treatment feasibility. *Int. J. Cardiol*., 2003;**88**: 247–256.
28. Weaver, W.D., M. Cerqueira, A.P. Hallstrom, P.E. Litwin, J.S. Martin, P.J. Kudenchuk, et al., Prehospital-initiated vs hospital-initiated thrombolytic therapy. The myocardial infarction triage and intervention trial. *JAMA*, 1993;**270**: 1211–1216.
29. The European Myocardial Infarction Project Group, Prehospital fibrinolytic therapy in patients with suspected acute myocardial infarction. *N. Engl. J. Med*., 1993;**329**: 383–389.
30. Cooke, W.H., J. Salinas, V.A. Convertino, D.A. Ludwig, D. Hinds, J.H. Duke, F.A. Moore, and J.B. Holcomb, Heart rate variability and its association with mortality in prehospital trauma patients. *J. Trauma*, 2006;**60**: 363–370.
31. Batchinsky, A.I., L.C. Cancio, J. Salinas, T. Kuusela, W.H. Cooke, J.J. Wang, M. Boehme, V.A. Convertino, and J.B. Holcomb, Prehospital loss of R-to-R interval complexity is associated with mortality in trauma patients. *Trauma*, 2007;**63**: 512–518.
32. Steg, P.G., J.P. Cambou, P. Goldstein, et al., Bypassing the emergency room reduces delays and mortality in ST-elevation myocardial infarction: the USIC 2000 registry. *Heart*, 2006;**92**: 1378–1383.
33. Bång, A., L. Grip, J. Herlitz, S. Kihlgren, T. Karlsson, K. Caidahl, and M. Hartford, Lower mortality after prehospital recognition and treatment followed by fast tracking to coronary care compared with admittance via emergency department in patients with ST-elevation myocardial infarction. *Int. J. Cardiol*., 2008;**129**: 325–332.
34. Terkelsen, C.J., B.L. Nørgaard J.F. Lassen J.C. Gerdes J.P. Ankersen, F. Rømer, T.T. Nielsen, and H.R. Andersen, Telemedicine used for remote prehospital diagnosing in patients suspected of acute myocardial infarction. *J. Intern. Med*., 2002;**252**: 412–420.

35. Terkelsen, C.J., B.L. Nørgaard, J.F. Lassen, and H.R. Andersen, Prehospital evaluation in ST-elevation myocardial infarction patients treated with primary percutaneous coronary intervention. *J. Electrocardiol*., 2005;**38**: 187–192.
36. Dalby, M., A. Bouzamondo, P. Lechat, and G. Montalescot, Transfer for primary angioplasty versus immediate thrombolysis in acute myocardial infarction: a meta-analysis. *Circulation*, 2003;**108**: 1809.
37. Andersen, H.R., T.T. Nielsen, K. Rasmussen, L. Thuesen, H. Kelbaek, P. Thayssen, et al., A comparison of coronary angioplasty with fibrinolytic therapy in acute myocardial infarction. *N. Engl. J. Med*., 2003;**349**: 733.
38. Widimsky, P., et al., on behalf of the PRAGUE Study Group Investigators, Multicentre randomized trial comparing transport to primary angioplasty vs immediate thrombolysis vs combined strategy for patients with acute myocardial infarction presenting to a community hospital without a catheterization laboratory. The PRAGUE study. *Eur. Heart J*., 2000;**21**: 823.
39. Stenestrand, U., J. Lindbäck, Wallentin L for the RIKS-HIA Registry, Long-term outcome of primary percutaneous coronary intervention vs prehospital and in-hospital thrombolysis for patients with ST-elevation myocardial infarction. *JAMA*, 2006;**296**: 1749–1756.
40. Grines, C.L., J. Westerhausen, L.L. Grines, J.T. Hanlon, T.L. Logemann, M. Niemela, et al., A randomized trial of transfer for primary angioplasty versus on-site thrombolysis in patients with high-risk myocardial infarction: the air primary angioplasty in myocardial infarction study. *J. Am. Coll. Cardiol*., 2002;**39**: 1713.
41. Aufderheide, T.P., D.J. Kereiakes, W.D. Weaver, W.B. Gibler, and M.L. Simoons, Planning, implementation and process monitoring for prehospital 12lead ECG Diagnostic programs. *Prehosp. Disaster Med*., 1996;**11**(3): 162–171.
42. Rawles J on Behalf of the GREAT Group, Halving of mortality at 1 year by domiciliary thrombolysis in the Grampian Region Early Anistreplase Trial (GREAT). *J. Am. Coll. Cardiol*., 1994;**23**: 1–5.
43. Aufderheide, T.P., M.H. Keelan, G.E. Hendley, et al., Milwaukee prehospital chest pain projekct – Phase I: Feasibility and accuracy of prehospital thrombolytic candidate selection. *Am. J. Cardiol*., 1992;**3**: 41–46.
44. Gibler, W.B., D.J. Kereiakes, E.N. Dean, et al., Prehospital diagnosis and treatment of acute myocardial infarction: north-south perspective. *Am. Heart J*., 1991;**121**: 1–11.
45. Castaigne, A., C. Herve, A. Duval-Moulin, et al., Prehospital use of APSAC: Results of a placebo-controlled study. *Am. J. Cardiol*., 1989;**64**: 30A–33A.
46. Schofer, J., J. Buttner, G. Geng, et al., Pre-hospital thrombolysis in acute myocardial infarction. *Am. J. Cardiol*., 1990;**66**: 1429–1433.
47. Aufderheide, T.P., W.C. Haselow, G.E. Hendley, et al., Feasibility of pre-hospital r-TPA therapy in chest pain patients. *Ann. Emerg. Med*., 1992;**21**: 379–383.
48. Svensson, L., T. Karlsson, R. Nordlander, M. Wahlin, C. Zedigh, and J. Herlitz, Safety and delay time in prehospital thrombolysis of acute myocardial infarction in urban and rural areas in Sweden. *Am. J. Emerg. Med*., 2003;**21**(4): 263–270.
49. Kereiakes, D.J., W.D. Weaver, J.C.L. Anderson, et al., Time delays in the diagnosis and treatment of acute myocardial infarction: A tale of eight cities. Report from the Prehospital Study Group and the Cincinnati Heart Project. *Am. Heart J*., 1990;**120**: 773–780.
50. Morrison, L.J., S. Brooks, B. Sawadsky, A. McDonald, and P.R. Verbeek, Prehospital 12-lead electrocardiography impact on acute myocardial infarction treatment times and mortality: A systematic review. *Acad. Emerg. Med*., 2006;**13**: 84–89.
51. Currtis, J.P., E.L. Portnay, Y. Wang, R.L. McNamara, J. Herrin, E.H. Bradley, D.J. Magid, M.E. Blaney, J.G. Canto, and H.M. Krumholz, The pre-hospital electrocardiogram and time to reperfusion in patients with acute myocardial infarction 2000–2002. *J. Am. Coll. Cardiol*., 2006;**47**: 1544–1552.
52. Brainard, A.H., W. Raynovich, D. Tandberg, and E.J. Bedrick, The prehospital 12-lead electrocardiogram's effect on time to initiation of reperfusion therapy: a systematic review and meta-analysis of existing literature. *Am. J. Emerg. Med*., 2005;**23**: 351–356.
53. Adams, G.L., P.T. Campbell, J.M. Adams, D.G. Strauss, K. Wall, J. Patterson, K.B. Shuping, C. Maynard, D. Young, C. Corey, A. Thompson, B.A. Lee, and G.S. Wagner, Effectiveness of prehospital wireless transmission of electrocardiograms to a cardiologist via hand-held device for patients with acute myocardial infarction (from the Timely Intervention in Myocardial Emergency, NorthEast Experience [TIME-NE]). *Am. J. Cardiol*., 2006;**98**: 1160–1164.
54. Björklund, E., U. Stenestrand, J. Lindbäck, L. Svensson, L. Wallentin, and B.A. Lindahl, Pre-hospital diagnostic strategy reduces time to treatment and mortality in real life patients with ST-elevation myocardial infarction treated with primary percutaneous coronary intervention. *JACC*, 2006;**47**(4) (Suppl A): 192A.
55. Brown, J.P., E. Mahmud, J.V. Dunford, and O. Ben-Yehuda, Effect of prehospital 12-lead electrocardiogram on activation of the cardiac catheterization laboratory and door-to-ballon time in ST-segment elevation acute myocardial infarction. *Am. J. Cardiol*., 2008;**101**: 158–161.
56. Sillesen, M., M. Sejersten, S. Strange, S. Loumann-Nielsen, F. Lippert, and P. Clemmensen, Referal of patients with ST-segment elevation acute myocardial infarction directly to the catheterization suite based on prehospital teletransmission of 12-lead electrocardiogram. *J. Electrocardiol*., 2008;**41**: 49–53.
57. Sejersten, M., M. Sillesen, P.R. Hansen, S. Loumann-Nielsen, H. Nielsen, S. Trautner, D. Hampton, G.S. Wagner, and P. Clemmensen, Effect on treatment delay of prehospital teletransmission of 12-lead electrocardiogram to a cardiologist for immediate triage and direct referral of patients with ST-segment elevation acute myocardial infarction to primary percutaneous coronary intervention. *Am. J. Cardiol*., 2008;**101**: 941–946.
58. Eckstein, M., W. Koenig, A. Kaji, and R. Tadeo, Implementation of speciality centers for patients with ST-segment elevation myocardial infarction. *Prehosp. Emerg. Care*, 2009;**13**: 215–222.
59. Eckstein, M., E. Cooper, T. Nguyen, and F.D. Pratt, Impact of paramedic transport with prehopsital 12-lead electrocardiography on door-to-balloon times for patients with ST-segment elevation myocardial infarction. *Prehosp. Emerg. Care*, 2009;**13**: 203–206.
60. Patrono, C., F. Bachmann, C. Baigent, C. Bode, et al., Expert consensus document on the use of antiplatelet agents. The task force on the use of antiplatelet agents in patients with atherosclerotic cardiovascular disease of the European society of cardiology. *Eur. Heart J*., 2004;**25**: 166–181.

61. Yusuf, S., F. Zhao, S.R. Mehta, S. Chrolavicius, G. Tognoni, and K.K. Fox, The Clopidogrel in unstable angina to prevent recurrent events trial investigators. Effects of Klopidogrel in addition to aspirin in patients with acute coronary syndromes without ST-segment elevation. *N. Engl. J. Med.*, 2001;**345**: 494–502.
62. Fragmin-During-Instability-In-Coronary-Artery-Disease-Study-Group, Low-molecular-weight heparin during instability in coronary artery disease. *Lancet*, 1996;**347**: 561–568.
63. Wallentin, L., P. Goldstein, P.W. Armstrong, C.B. Granger, et al., Efficacy and safety of tenecteplase in combination with the low-molecular-weight heparin enoxaparin or unfractionated heparin in the prehospital setting: the Assessment of the Safety and Efficacy of a New Thrombolytic Regimen (ASSENT)-3 PLUS randomized trial in acute myocardial infarction. *Circulation*, 2003;**108**: 135–142.
64. Slovis, C.M., P.J. Kudenchuk, M.A. Wayne, R. Aghababian, and E.J. Rivera-Rivera, Prehospital management of acute tachyarrhythmias. *Prehosp. Emerg. Care*, 2003;**7**: 2–12.
65. Lozano, M. Jr., B.A. McIntosh, and L.M. Giordano, Effect of adenosine on the management of supraventricular tachycardia by urban paramedics. *Ann. Emerg. Med.*, 1995;**26**: 691–696.
66. Gausche, M., D.E. Persse, T. Sugarman, et al., Adenosine for the prehospital treatment of paroxysmal supraventricular tachycardia. *Ann. Emerg. Med.*, 1994;**24**: 183–189.
67. Madsen, C.D., J.E. Pointer, and T.G. Lynch, A comparison of adenosine and verapamil for the treatment of supraventricular tachycardia in the prehospital setting. *Ann. Emerg. Med.*, 1995;**25**: 649–655.
68. Wang, H.E., R.E. O'Connor, R.E. Megargel, et al., The use of diltiazem for treating rapid atrial fibrillation in the out-of-hospital setting. *Ann. Emerg. Med.*, 2001;**37**: 38–45.
69. Kudenchuk, P.J., L.A. Cobb, M.K. Copass, et al., Amiodarone for resuscitation after out-of-hospital cardiac arrest due to ventricular fibrillation. *N. Engl. J. Med.*, 1999;**341**: 871–878.
70. Sivagangabalan, G., A.T.L. Ong, A. Narayan, N. Sadick, P.S. Hansen, G.C.I. Nelson, M. Flynn, D.L. Ross, S.C. Boyages, and P. Kovoor, Effect of prehospital triage on revascularization times, left ventricular function, and survival in patients with ST-elevation myocardial infarction. *Am. J. Cardiol.*, 2009;**103**: 907–912.
71. Diercks, D.B., M.C. Kontos, A.Y. Chen, C.V. Pollack, S.D. Wiviott, J.S. Rumsfeld, D.J. Magid, W.B. Gibler, C.P. Cannon, E.D. Peterson, and M.T. Roe, Utilization and impact of prehospital electrocardiograms for patients with acute ST-segment elevation myocardial infarction. *J. Am. Coll. Cardiol.*, 2009;**53**: 161–166.
72. Eisenstein, E.L., Conducting an economic analysis to assess the electrocardiogram's value. *J. Electrocardiol.*, 2006;**39**: 241–247.
73. Grim, P.S., T. Feldman, and R.W. Childers, Evaluation of patients for the need of thrombolytic therapy in the prehospital setting. *Ann. Emerg. Med.*, 1989;**18**: 483–488.
74. Aufderheide, T.P., G.E. Hendley, J. Woo, et al., A prospective evaluation of prehospital 12-lead ECG application in chest pain patients. *J. Electro-cardiol.*, 1992;**24**(suppl): 8.
75. Musuraca, G., F. Imperadore, C. Cemin, C. Terraneo, C. Vaccarini, P. Giuseppe De Girolamo, and G. Vergara, Electrocardiographic abnormalities mimicking myocardial infarction in a patient with intracranial haemorrhage: a possible pitfall for prehospital thrombolysis. *J. Cardiovasc. Med.*, 2006;**7**: 434–437.
76. Otto, L.A. and T.P. Aufterheide, Evaluation of ST-segment elevation criteria for the prehospital electrocardiographic diagnosis of acute myocardial infarction. *Ann. Emerg. Med.*, 1994;**23**: 17–24.
77. Brady, W.J., A. Perron, and E. Ullman, Errors in emergency physician interpretation of ST-segment elevation in emergency department chest pain patients. *Acad. Emerg. Med.*, 2000;**7**: 1256–1260.
78. Eriksen, U.H., H. Ölgaard, J. Ingerslev, and T.T. Nielsen, Fatal haemostatic complications due to thrombolytic therapy in patients falsely diagnosed as acute myocardial infarction. *Eur. Heart J.*, 1992;**13**: 840–843.
79. Alinier, G., R. Gordon, C. Harwood, and W.B. Hung, E.C.G. 12-lead, training: the way forward. *Nurse Educ. Today*, 2006;**26**: 87–92.
80. Aufderheide, T.P., Prehospital 12-lead electrocardiography and evaluation of the patient with chest pain, in *Emergency Cardiac Care*, W.B. Gibler and T.P. Aufterheide, Editors. St Louis, MO: Mosby Year Book, 1994, pp. 38–65.
81. Garvey, J.L., B.A. MacLeod, G. Sopko, and M.M. Hand, Prehospital 12.lead electrocardiography programs. A call for implementation by emergency medical services systems providing advanced life support – national heart attack alert program (NHAAP) coordinating committee; National Heart, Lung and Blood Institute (NHLBI); National Institutes of Health. *J. Am. Coll. Cardiol.*, 2006;**47**: 485–491.
82. Voluntary Guidelines for Out-of-Hospital Practices, A joint policy statement of PREP between the American College of Emergency Physicians, the National Association of Emergency Medical Services Physicians, and the National Association of State Emergency Medical Services Directors. June 2001. Policy # 400305.
83. Vaught, C., D.R. Young, S.J. Bell, C. Maynard, M. Gentry, S. Jacubowitz, P.N. Leibrandt, D. Munsey, M.R. Savona, T.C. Wall, and G.S. Wagner, The failure of years of experience with electrocardiographic transmission from paramedics to the hospital emergency department to reduce the delay from door to primary coronary intervention below the 90-minute threshold during acute myocardial infarction. *J. Electrocardiol.*, 2006;**39**: 136–141.
84. RIKS-HIA. www.ucr.uu.se/rikshia/
85. Feldman, J.A., K. Brinsfield, S. Bernard, D. White, and T. Maciejko, Real-time paramedic compared with blinded physician identification of ST-segment elevation myocardial infarction: results of an observational study. *Am. J. Emerg. Med.*, 2005;**23**: 443–448.
86. Trivedi, K., J.D. Schuur, and D.C. Cone, Can paramedics read ST-segment elevation myocardial infarction on prehospital 12-lead electrocardiograms? *Prehosp. Emerg. Care*, 2009;**13**: 207–214.
87. McLean, S., G. Egan, P. Connor, and A.D. Flapan, Collaborative decision-making between paramedics and CCU nurses based on 12-lead ECG telemetry expedites the delivery of thrombolysis in ST-elevation myocardial infarction. *Emerg. Med. J.*, 2008;**25**: 370–374.
88. Bouten, M.J.M., M.L. Simoons, J.A.M. Hartman, A.J.M. van Miltenburg, E. van der Does, and J. Pool, Prehospital thrombolysis with alteplase (rt-PA) in acute myocardial infarction. *Eur. Heart J.*, 1992;**13**: 925–931.
89. Lamfers, E.J.P., A. Schut, D.P. Hertzberger, T.E.H. Hooghoudt, P.W.J. Stolwijk E. Boersma, M.L. Simoons, and F.W.A. Verheught, Prehospital versus hospital fibrinolytic therapy using

automated versus cardiologist electrocardiographic diagnosis of myocardial infarction: abortion of myocardial infarction and unjustified fibrinolytic therapy. *Am. Heart J.*, 2004;**147**: 509–515.

90. Grijseels, E.W.M., M.J.M. Bouten, T. Lenderink, J.W. Deckers, A.W. Hoes, J.A.M. Hartman, E. van der Does, and M.L. Simoons. Prehospital thrombolytic therapy with either alteplace or streptokinase. Practical applications, complications and long-term results in 529 patients. *Eur. Heart J.*, 1995;**16**: 1833–1838.
91. Lamfers, E.J.P., A. Schut, T.E.H. Hooghoudt, D.P. Hertzberger, E. Boersma, M.L. Simoons, and F.W.A. Verheught, Prehospital thrombolysis with reteplase: the Nijmegen/Rotterdam study. *Am. Heart J.*, 2003;**146**: 479–483.
92. Kudenchuk, P.J., M.T. Ho, W.D. Weaver, P.E. Litwin, J.S. Martin, M.S. Eisenberg, A.P. Hallstrom, and L.A. Cobb, Kennedy JW for the MITI project investigators. Accuracy of computer-interpreted electrocardiography in selecting patients for thrombolytic therapy. *J. Am. Coll. Cardiol.*, 1991;**17**: 1486–1491.
93. Xue, J., T. Aufderheide, R.S. Wright, J. Klein, R. Farrell, I. Rowlandson, and B. Young, Added of new acute coronary syndrome computer algorithm for interpretation of prehospital electrocardiograms. *J. Electrocardiol.*, 2004;**37S**: 233 (Suppl).
94. Eskola, M.J., K.C. Nikus, L.M. Voipio-Pulkki, H. Huhtala, T. Parviainen, J. Lund, T. Ilva, and P. Porela, Comparative accuracy of manual versus computerized electrocardiographic measurement of J-, ST- and T-wave deviations in patients with acute coronary syndrome. *Am. J. Cardiol.*, 2005;**96**: 1584–1588.
95. Pettis, K.S., M.R. Savona, P.N. Leibrandt, C. Maynard, W.T. Lawson, K.B. Gates, and G.S. Wagner, Evaluation of the efficacy of hand-held computer screens for cardiologists' interpretations of 12.lead electrocardiograms. *Am. Heart J.*, 1999;**138**: 765–770.
96. Leibrandt, P.N., S.J. Bell, M.R. Savona, K.S. Pettis, R.H. Selvester, C. Maynard, R. Warner, and G.S. Wagner, Validation of cardiologist's decisions of initiate reper-fusion therapy for acute myocardial infarction using electrocardiograms viewed on liquid crystal displays of cellular telephones. *Am. Heart J.*, 2000;**140**: 747–752.
97. Nallamothu, B.K., Y. Wang, D. Magid, R.L. McNamara, J. Herrin, E.H. Bradley, E.R. Bates, C.V. Pollack, and H.M. Krumholz, Relation between hospital specialization with primary percutaneous coronary intervention and clinical outcomes in ST-segment elevation myocardial infarction. National Registry of Myocardial Infarction-4 Analysis. *Circulation*, 2006;**113**: 222–229.
98. Terkelsen, C.J., J.F. Lassen, B.L. Nørgaard, J.C. Gerdes, S.H. Poulsen, K. Bendix, J.P. Ankersen, L.B. Gøtzsche, F.K. Rømer, T.T. Nielsen, and H.R. Andersen, Reduction of treatment delay in patients with ST-elevation myocardial infarction: impact of pre-hospital diagnosis and direct referral to primary percutaneous coronary intervention. *Eur. Heart J.*, 2005;**26**: 770–777.
99. Rokos, I.C., D.M. Larson, T.D. Henry, W.J. Koenig, M. Eckstein, W.J. French, C.B. Granger, and M.T. Roe, Rationale for establishing regional ST-elevation myocardial infarction receiving center (SRC) networks. *Am. Heart J.*, 2006;**152**: 661–667.
100. Sejersten, M., M. Sillesen, P.R. Hansen, S. Loumann Nielsen, H. Nielsen, S. Trautner, D. Hampton, G.S. Wagner, and P. Clemmensen, Effect on treatment delay of prehospital teletransmission of 12-lead electrocardiogram to a cardiologist for immediate triage and direct referral of patients with ST-segment elevation acute myocardial infarction to primary percutaneous coronary intervention. *Am. J. Cardiol.*, 2008;**101**: 941–946.
101. Väisänen, O., M. Jäkijärvi, and T. Silfvast, Prehospital ECG transmission: comparison of advanced mobile phone and facsimile devices in an urban emergency service system. *Resuscitation*, 2003;**57**: 179–185.
102. Carmody, B.J., A novel approach to transmission of the out-of-hospital ECG in patients with ST segment elevation myocardial infarction. *Ann. Emerg. Med.*, 2008;**52**: 183–184.
103. Svensson, L., L. Isaksson, C. Axelsson, R. Nordlander, and J. Herlitz, Predictors of myocardial damage prior to hospital admission among patients with acute chest pain or other symptoms raising a suspicion of acute coronary syndrome. *Coron. Artery Dis.*, 2003;**14**(3): 225–231.
104. Lee, H.S., S.J. Cross, J.M. Rawles, and K.P. Jennings, Patients with suspected myocardial infarction who present with ST-depression. *Lancet*, 1993;**342**: 1204–1207.
105. Brady, W.J., A.D. Perron, S.A. Syverud, C. Beagle, R.J. Riviello, C.A. Ghaemmaghami, E.A. Ullman, B. Erling, A. Ripley, and C. Holstege, Reciprocal ST-segment depression: impact on the electrocardiographic diagnosis of ST-segment elevation acute myocardial infarction. *Am. J. Emerg. Med.*, 2002;**20**: 35–38.
106. Svensson, L., R. Nordlander, C. Axelsson, and J. Herlitz, Are predictors for myocardial infarction the same for women and men when evaluated prior to hospital admission? *Int. J. Cardiol.*, 2006;**109**: 241–247.
107. Karlson, B.W., J. Herlitz, O. Wiklund, A. Richter, and Å. Hjalmarson, Early prediction of acute myocardial infarction from clinical history, examination and electrocardiogram in the emergency room. *Am. J. Cardiol.*, 1991;**68**: 171–175.
108. Drew, B.J., M.M. Pelter, E. Lee, J. Zegre, D. Schindler, and E. Fleischmann, Designing prehospital E.C.G systems for acute coronary syndromes. Lessions learned from clinical trials involving 12-lead ST-segment monitoring. *J. Electrocardiol.*, 2005;**38**: 180–185.
109. Terkelsen, C.J., B.L. Nørgaard, J.F. Lassen, S.H. Poulsen, J.C. Gerdes, K. Bendix, J.P. Ankersen, L.B. Gøtzsche, F.K. Rømer, T.T. Nielsen, and H.R. Andersen, Reduction of treatment delay in patients with ST-elevation myocardial infarction: impact of pre-hospital diagnosis and direct referral to primary percutaneous coronary intervention. *Eur. Heart J.*, 2005;**26**: 770–777.
110. Herlitz, J., L. Sillfors, and Å. Hjalmarson, Experiences from the use of 24 precordial chest leads in suspected acute myocardial infarction. *J. Electrocardiol.*, 1986;**19**(4): 381–388.
111. Sejersten, M., O. Pahlm, J. Pettersson, S. Zhou, C. Maynard, C.L. Feldman, and G.S. Wagner, Comparison of EASI-derived 12-lead electrocardiograms versus paramedic-acquired 12-lead electrocardiograms using Mason-Likar limb lead configuration in patients with chest pain. *J. Electrocardiol.*, 2006;**39**: 13–21.
112. Feldman, C.L., S.Z. Milstein, D. Neubecker, B.K. Underhill, E. Moyer, S. Glumm, M. Womble, J. Auer, C. Maynard, R.K. Serra, and G.S. Wagner, Comparison of the five-electrode-derived EASI electrocardiogram to the Mason Likar electrocardiogram in the prehospital setting. *Am. J. Cardiol.*, 2005;**96**: 453–456.
113. Owens, C.G., A.J.J. McClelland, S.J. Walsh, B.A. Smith, A. Tomlin, J.W. Riddell, M. Stevenson, and A.A.J. Adgey, Prehospital 80-Lad mapping: does it add significantly to the diagnosis of acute coronary syndromes? *J. Electrocardiol.*, 2004;**37**: 223–232.

114. Drew, B.J., E.D. Dempsey, T.H. Joo, C.E. Sommargren, J.P. Glancy, K. Benedict, and M.W. Krucoff, Prehospital synthesized 12-lead ECG ischemia monitoring with transtelephonic transmission in acute coronary syndromes. *J. Electrocardiol.*, 2004;**37**(Suppl 1): 214–221.
115. Hollenberg, J., A. Bång, J. Lindqvist, J. Herlitz, R. Nordlander, L. Svensson, and M. Rosenqvist, Difference in survival after out of hospital cardiac arrest between the two largest cities in Sweden – a matter of time? *JIM*, 2005;**257**: 247–254.
116. Müller, D., L. Schnitzer, J. Brandt, and H.R. Arntz, The accuracy of an out-of-hospital 12-lead ECG for the detection of ST-elevation myocardial infarction immediately after resuscitation. *Ann. Emerg. Med.*, 2008;**52**: 658–664.
117. Kuisma, M., J. Repo, and A. Alaspää, The incidence of out of hospital ventricular fibrillation in Helsinki Finland from 1994 to 1999. *Lancet*, 2001;**358**: 473–474.
118. Herlitz, J., J. Engdahl, L. Svensson, M. Young, K.A. Ängquist, and S. Holmberg, Decrease in the occurrence of ventricular fibrillation as the initially observed arrhythmia after out-of-hospital cardiac arrest during 11 years in Sweden. *Resuscitation*, 2004;**60**: 283–290.
119. Engdahl, J., A. Bång, J. Lindqvist, and J. Herlitz, Factors affecting short and long-term prognosis among 1069 patients with out-of-hospital cardiac arrest and pulseless electrical activity. *Resuscitation*, 2001;**51**: 17–25.
120. Pepe, P.E., R.L. Levine, R.E. Fromm, P.A. Curka, P.S. Clark, and B.S. Zachariah, Cardiac arrest presenting with rhythms other than ventricular fibrillation: contribution of resuscitative efforts toward total survivorship. *Crit. Care Med.*, 1993;**21**: 1838–1843.
121. Stratton, S.J. and J.T. Niemann, Outcome from out-of-hospital cardiac arrest caused by nonventricular arrhythmias: contribution of successful resuscitation to overall survivorship supports the current practice of initiating out-of-hospital ACLS. *Ann. Emerg. Med.*, 1998;**32**: 448–453.
122. Engdahl, J., A. Bång, J. Lindqvist, and J. Herlitz, Can we define patients with no and those with some chance of survival when found in asystole out of hospital? *Am. J. Cardiol.*, 2000;**86**(6): 610–614.
123. Weaver, W.D., L.A. Cobb, D. Dennis, et al., Amplitude of ventricular fibrillation waveform and outcome after cardiac arrest. *Ann. Intern. Med.*, 1985;**102**: 53–55.
124. Brown, C.G., R. Dzwoncyk, and D.R. Martin, Physiologic measurement of the ventricular fibrillation ECG signal: esitimating the duration of ventricular fibrillation. *Ann. Emerg. Med.*, 1993;**22**: 70–74.
125. Brown, C.G. and R. Dzwoncyk, Signal analysis of the human electrocardiogram during ventricular fibrillation: frequency and amplitude parameters as predictors of successful countershock. *Ann. Emerg. Med.*, 1996;**27**: 184–188.
126. Noc, M., M.H. Weil, W. Tang, et al., Electrocardiographic prediction of the success of cardiac resuscitation. *Crit. Care Med.*, 1999;**27**: 708–714.
127. Strohmenger, H.U., T. Eftestol, K. Sunde, et al., The predictive value of ventricular fibrillation electrocardiogram signal frequency and amplitude variables in patients with out-of-hospital cardiac arrest. *Anesth. Analg.*, 2001;**93**: 1428–1433.
128. Ahmann, A., U. Achleitner, H. Antretter, et al., Analysing ventricular fibrillation ECG-signals and predicting defibrillation success during cardiopulmonary resuscitation employing N(alpha)-histograms. *Resuscitation*, 2001;**50**: 77–85.
129. Eftestøl, T., K. Sunde, S.O. Aase, et al., Probability of successful defibrillation as a monitor during CPR in out-of-hospital cardiac arrested patients. *Resuscitation*, 2001;**48**: 245–254.
130. Eftestøl, T., H. Losert, J. Kramer-Johansen, et al., Independent evaluation of a defibrillation outcome predictor for out-of-hospital cardiac arrested patients. *Resuscitation*, 2005;**67**: 55–61.
131. Watson, J.N., N. Uchaipichat, P.S. Addison, et al., Improved prediction of defibrillation success for out-of-hospital VF cardiac arrest using wavelet transform methods. *Resuscitation*, 2004;**63**: 269–275.
132. Watson, J.N., P.S. Addison, G.R. Clegg, et al., Practical issues in the evaluation of methods for the prediction of shock outcome success in out-of-hospital cardiac arrest patients. *Resuscitation*, 2006;**68**: 51–59.
133. Snyder, D.E., R.D. White, and D.B. Jorgenson, Outcome prediction for quidance of initial resuscitation protocol: Shock first or CPR first. *Resuscitation*, 2007;**72**: 45–51.
134. Neurauter, A., T. Eftestøl, J. Kramer-Johansen, B.S. Abella, V. Wenzel, K.H. Lindner, J. Eilevstjønn, H. Myklebust, P.A. Steen, F. Sterz, B. Jahn, and H.U. Strohmenger, Improving countershock success prediction during cardiopulmonary resuscitation using ventricular fibrillation features from higher ECG frequency bands. *Resuscitation*, 2008;**79**: 453–459.
135. Sherman, L.D., T.D. Rea, J.D. Waters, J.J. Menegazzi, and C.W. Callaway, Logarithm of the absolute correlations of the ECG waveform estimates duration of ventricular fibrillation and predicts successful defibrillation. *Resuscitation*, 2008;**78**: 346–354.
136. Gundersen, K., J.T. Kvaløy, J. Kramer-Johansen, P.A. Steen, and T. Eftestøl, Development of the probability of return of spontaneous circulation in intervals without chest compressions during out-of-hospital cardiac arrest: an observational study. *BMC Med.*, 2009;**7**: 6.
137. Gundersen, K., J. Nysaether, J.T. Kvaløy, J. Kramer-Johansen, and T. Eftestøl, Chest compression quality variables influencing the temporal development of ROSC-predictors calculated from the ECG during VF. *Resuscitation*, 2009;**80**: 177–182.
138. Olasveengen, T.M., T. Eftestøl, K. Gundersen, L. Wik, and K. Sunde, Acute ischemic heart disease alters ventricular fibrillation waveform characteristics in out-of hospital cardiac arrest. *Resuscitation*, 2009;**80**: 412–417.
139. Lederer, W., C.J. Schlimp, T. Niederklapfer, and A. Amann, Altered electrical activity of fibrillation process following thrombolytic therapy in out-of-hospital cardiac arrest patients with sustained ventricular fibrillation. *Med. Hypotheses*, 2006;**67**: 3313–335.
140. Aufderheide, T.P., R.K. Thakur, H.A. Stueven, et al., Electrocardiographic characteristics in EMD. *Resuscitation*, 1989;**17**: 183–193.
141. Fang, X., W. Tang, S. Sun, J. Wang, L. Huang, and M.H. Weil, The characteristics of post countershock pulseless electrical activity may indicate the outcome of CPR. *Resuscitation*, 2006;**69**: 303–309.
142. Williams, D. in collaboration with Fitch and associates, JEMS 200-City survey. *JEMS Feb.*, 2005;**30**: 42–60.
143. Ting, H.H., H.M. Krumholz, E.H. Bradley, D.C. Cone, J.P. Curtis, B.J. Drew, J.M. Field, W.J. French, W.B. Gibler, D.C. Goff,

A.K. Jacobs, B.K. Nallamothu, R.E. O'Connor, and J.D. Schuur. Implementation and integration of prehospital ECG:s into systems of care for acute coronary syndrome. *Circulation*, 2008;**118**: 1066–1079.

144. Frendl, D.M., S.T. Palmeri, J.R. Clapp, D. Hampton, M. Sejersten, D. Young, B. Drew, R. Farrell, J. Innes, J. Russell, G.I. Rowlandson, Y. Purim-Shem-Tov, B.K. Underhill, S. Zhou, and G.S. Wagner, Overcoming barriers to developing seamless ST-segment elevation myocardial infarction care systems in the United States: recommendations from a comprehensive prehospital 12-lead electrocardiogram working group. *J. Electrocardiol.*, 2009;**42**: 426–431.

35 Heart Rate Variability

Maciej Sosnowski

P. W. Macfarlane, A. van Oosterom, O. Pahlm, P. Kligfield, M. Janse, J. Camm (eds.), *Comprehensive Electrocardiology*, DOI 10.1007/978-1-84882-046-3_35,

Introduction

Changes of pulse rate and rhythm have attracted the attention of physicians since the earliest stages of medicine. Only recently, with the advance of computer techniques that allow for parsing heart rate variability (HRV) into components, which potentially yield information about the autonomic nervous control of cardiac activity, has there been an increased clinical interest. The technical advances, however, have not resulted in bedside application of HRV methods and evidence of their usefulness in real-world clinical practice is still limited. Moreover, from the point of view of the physician, complex approaches to HRV phenomena and the use of complicated mathematical formulae may have a rather limited implementation in everyday practice. In this chapter, several aspects of HRV are thoroughly reviewed giving priority to their physiological and pathophysiological meanings in order to render HRV more clinically useful. For that reason, technical descriptions are limited to providing only the necessary background information.

35.1 Historical Note

Fluctuations in heart rate were first recorded by ancient physicians. Disturbances of heart rate due to changes in psychoemotional state were revealed by Erastratos, an Alexandrian physician, in the third century B.C. [1]. Similarly, a description of pulse-shift in relation to emotion or illness is ascribed to Galen (129–199 A.D.) [1]. A decrease in heart rate variation was recognized by the Chinese physician Wang Shuhe (265–317 A.D.) as a sign which could predict the onset of death [2] (Fig. 35.1). Later, many physicians raised the examination of the pulse rate to the level of an art. An excellent example of this is given by Józef Struś, Polish physician to Zygmunt August, King of Poland, in his work "*Sphigmicae Artis*" (Basel 1555) [3].

The fundamentals of current knowledge are usually credited to the observations of Stephen Hales (1733) and Carl Ludwig (1847). Hales first found, in the horse, that the pattern of blood pressure was dependent on respiration [4, 5]. Ludwig, armed with the smoked kymograph, recorded a quickening of the pulse rate with inspiration and a slowing with expiration in the dog [5]. He is credited with the term *respiratory sinus arrhythmia (RSA)* [5, 6]. Two decades later, F.C. Donders (1868) followed up this research to describe the role of the vagus nerve in RSA. Traube (1865) advised on the importance of the medullary respiratory centers in modulating the brainstem nuclei controlling heart rate. Hering (1871) put forward an alternate explanation for RSA, namely the consequence of a reflex modulation of the central oscillator by pulmonary afferent feedback [5]. A few years later, Mayer (1877) established that longer-wave oscillation in blood pressure was due to vasomotor tone. Continuing these efforts, Hering (1910) first stated that the function of vagi could be quantified in humans by means of RSA [6]. Next, in 1920 Bainbridge reported on the effects of thoracic pressure changes with respiration and their association with RSA [6]. German psychiatrists Eppinger and Hess (1915) focused on the clinical application of RSA as a measure of vagal tone and first made observations on the effects of cholinergic agents [6]. This was further emphasized by the study of Samaan (1935) in which stimulation of a section of vagus nerve abolished RSA [7].

With the advent of electrocardiography (ECG), accurate and continuous recording of the electrical activity of the heart became possible. Not surprisingly, the first recording of RSA was made in the first decade of the twentieth century by Samojloff in 1909. Schlomka, in 1936, provided the first quantitative measures of RSA from short-term ECG tracings. He also reported on an age-dependency of RSA and the reduction of RSA in patients with advanced heart failure (After [8]).

The seminal works listed in Table 35.1 have provided a solid grounding for the current knowledge and application of HRV in cardiology. Interestingly, well before HRV analysis was appreciated in cardiology, its usefulness had been documented in obstetrics and psychology [5, 6, 10, 11].

35.2 Definitions, Synonyms, Abbreviations

Heart rate (HR) – frequency of the heart beating usually calculated as the average of four or more consecutive heartbeats, expressed in beats per minute (bpm).

Figure 35.1
HRV and an ancient medicine (From [2]).

Instantaneous heart rate (HRi) – heart rate confined to a given sinus cycle duration on a beat-to-beat manner (60/R–R interval).

Intrinsic heart rate (iHR) – heart rate after cessation of the autonomic influences (pharmacological or surgical denervation), i.e., in situ heart rate.

Heart period (HP) – the duration of a given cardiac cycle, usually calculated as a period between two consecutive R-waves or P-waves, expressed in seconds (s) or milliseconds (ms). Unless indicated otherwise, cardiac cycle is defined as a presumed sinus (in origin) cycle irrespective of the polarity of the P-waves. Sometimes, if the signal is acquired using a technique other than the ECG, heart period is referred to as a *pulse interval* or an *interbeat interval* (IBI).

R–R interval – description of heart period based on detection of the R-wave instead of the P-wave. The "R" labeling is used in short-term ECG recordings and assumes sinus origin of the heartbeat. However, in a few studies such a labeling indicates any depolarizations, irrespective of their origin (usually noted).

N-N interval – description of heart period for long-term ECG recordings, where sinus (supraventricular) origin of the heartbeat is assumed and labeled as normal (N).

Heart rate variability (HRV) – a variation in the duration of HP (which might not be consecutive). It can be quantified using various methods in the time, frequency, and nonlinear dynamics domains.

Heart period variability (HPV) – a term similar to HRV.

Time-domain analysis – an analytical approach to HRV quantification in which the sequence of heartbeats is generally ignored. It usually gives information about the magnitude of heart beat variation around its mean value.

Respiratory sinus arrhythmia (RSA) – heart period fluctuations due to breathing. RSA can be quantified preferably by using spectral analysis; however, time-domain analysis and other approaches are possible.

Table 35.1

Historical background of contemporary HRV analysis

Author[s]	Year	Issue discovered/solved	Ref.
Samaan A	1935	Various influence of separate and joined vagal-sympathetic stimulation upon heart rate	[7]
Anrep et al.	1936	First extensive and systematic study of RSA as a function of respiration	[9]
Lacey & Lacey	1958	RSA as a trait of behavioral response	[10]
Hon/Lee	1963	RR interval variation monitoring in prediction of a fetus death	[11]
Schneider/Costiloe	1965	Relationship of RSA to age and its prognostic significance in ischemic heart disease	[A34]
Wolf S	1967	Brain-heart link contribution to sudden cardiac death	[13]
Katona et al.	1970	Evaluation of the carotid baroreflex	[14]
Levy MN	1971	Description of the accentuated angiotensin	[15]
Hinkle et al.	1972	Association of chronotropic incompetence with adverse outcome in middle-aged man	[16]
Sayers	1973	First spectral analysis of HRV Detection of lower frequency components; association with vasomotor tone	[17]
Wheeler/Watkins	1973	Description of diabetic autonomic neuropathy	[18]
Wolf et al.	1978	First report on a prognostic significance of a reduced RSA in acute MI	[19]
Akselrod et al.	1981	Documentation of autonomic and humoral background of HRV	[20]
Kobayashi/Musha	1982	Nonlinear dynamics applied to HR data	[21]
Ewing et al.	1984	Usefulness of HRV for diagnosis of diabetic autonomic neuropathy	[22]
Pomeranz et al.	1985	Spectral analysis for physiological stimuli assessment in humans	[23]
Kleiger et al.	1987	Independent prognostic value of SDNN in AMI patients	[24]
Camm et al.	1998	First EBM-study that used HRV as the inclusion criterion	[25]

Spectral analysis – an analytical approach for decomposition of frequency components in a signal time series, which requires strict maintenance of R – R interval sequence. A graphical presentation is usually given as a plot of the amplitude of variation (cycle, bpm, s, or ms), variance or power ($cycle^2$, bpm^2, s^2, or ms^2), or power spectral density ($cycle^2$/beat, bpm^2/Hz, s^2/Hz, or ms^2/Hz) against various period or frequency ranges (beats/min, Hz).

High frequency component (HF) – part of the power spectrum that (in adult humans) is contained within the arbitrary frequency band between 0.15 and 0.40 Hz (or higher). The HF component represents short-term (2.5–6.0 s) heartbeat variation within the frequency of respiration. Its relative contribution to the total power decreases exponentially as duration of a time series is increasing; it is also cited as the RSA-related or vagally-related power.

Low frequency component (LF) – part of the power spectrum within the frequency band from 0.04 (0.05) to 0.15 Hz (*in humans*) and represents medium-term (6–25 s) heartbeat variation within the frequency of Mayer waves of blood pressure. Its relative contribution to the total power decreases exponentially as the duration of a time series is increasing.

Very low frequency component (VLF) – part of the power spectrum that (*in humans*) is contained within the frequency band between 0.003 and 0.04 Hz and represents long-term (> 25 s) heartbeat variation. Its relative contribution to the total power decreases as the duration of a time series is increasing.

Ultra low frequency component (ULF) – part of the power spectrum that (*in humans*) is contained within the frequencies below 0.003 Hz and represents very long-term (> 5 h) heartbeat variation. It cannot be reliably evaluated from a short time series. It constitutes the main contribution to the total power from a 24-h signal recording. Day–night difference is the most prominent oscillation within the ULF component.

Nonlinear dynamics – a field applying a variety of analytical approaches to the study of R – R interval variations that are not linearly related, and presumed not to be random. These approaches allow evaluating different properties of heartbeat variation in terms of its determinism, predictability, sequence, scale-invariant similarity, patterns, complexity, information flow, and other features.

Abbreviations related to HRV analysis

ACI–Acceleration change index
A_I–Asymmetry index
AIF–Autonomic information flow
ApEn–Approximate entropy
AR–Autoregressive modeling
BRS–Baroreflex sensitivity
CIPA–Cardiac index of parasympathetic activity
CE–Compressed entropy
CWA–Continuous wavelet analysis
CV–Coefficient of variation
CSI–Cardiac sympathetic index
CVI–Cardiac vagal index
DC–Deceleration capacity
DI–Deceleration index
$D_{iff}I$–Differential index
DFA–Detrended fluctuation analysis
EMD–Empirical mode decomposition
FFT–Fast Fourier transform
HR6%–Number of consecutive HRi periods that differ by > 6% from the preceding one
HRT–Heart rate turbulence
HRVF–Heart rate variability fraction (%)
HRVI–Heart rate variability index (St.George's index, absolute units)
HT–Hilbert transform
HHT–Huang-Hilbert transform
LLE–Largest Lyapunov exponent
MIF–Mutual information function
MSE–Multiscale entropy
MSSD–Mean sum of the squared difference between adjacent intervals
NL–Noise limit
(p)NN50–(percentage) Number of consecutive NN (RR) intervals that differ by > 50 ms
PLF–Prevalent low frequency
PLM–Power-law model
RQA–Recurrence quantification analysis
RLS–Recursive least-squares estimation
RMSSD–Root mean square of the successive difference between consecutive NN (RR) intervals
SampEn–Sample entropy
SD1–Standard deviation of interbeat intervals over minor axis of scatterplot
SD2–Standard deviation of interbeat intervals over major axis of scatterplot
SDNN (SDRR)–Standard deviation of the mean NN (RR) intervals
SDANN–Standard deviation of the averaged NN intervals over a pre-specified period (typically a 5-min period)
SDNNI–The average of the standard deviation of N – N intervals over a pre-specified period (typically a 5-min period)
SDyn–Symbolic dynamics
STFT–Short-term Fourier transform
TCA–Temporal cumulative approach
TINN–Triangular interpolation index
TO–Turbulence onset
TS–Turbulence slope
WVD–Wigner-Ville distribution

VR–Variation range, i.e., the difference between the longest and the shortest interval
%DET–Percent of determinism

Other abbreviations in the chapter

ACE–Angiotensin converting enzyme
ACEIs–ACE inhibitors
Ang–Angiotensin
ACh–Acetylcholine
AF–Atrial fibrillation
AFl–Atrial flutter
ANS–Autonomic nervous system
AVN–Atrio-ventricular node
ARBs–Angiotensin receptor blockers
BB–Beta-blockers (beta-adrenolytics)
BNP–Brain natriuretic peptide
BP–Blood pressure (*SBP* – systolic, *DBP* – diastolic, *MBP* – mean)
bpm–Beats per minute
CABG–Coronary artery by-pass grafting
CAD–Coronary artery disease (atherosclerotic)
CI–Confidence interval
CRT–Cardiac resynchronisation therapy
DAN–Diabetic autonomic neuropathy
dB–Decibel(s)
DM–Diabetes mellitus
DVN–Dorsal motor nucleus of the vagus nerve
E–Epinephrine
ECG–Electrocardiogram, electrocardiography, electrocardiographic (depending on a context)
HF–Heart failure (CHF – congestive heart failure)
Hz–Hertz
ICC–Intra-class coefficient
ICD–Implantable cardioverter-defibrillator
LOA–Limit of agreement
LVEF–Left ventricular ejection fraction
MI–Myocardial infarction
ms–Millisecond(s)
NA–Nucleus ambiguous
NE–Norepinephrine
NO–Nitric oxide
NYHA–New York Heart Association
OSAS–Obstructive sleep apnea syndrome
PEB(s)–Premature ectopic beat(s)
PNS–Parasympathetic nervous system
PSD–Power spectrum density
s–Second(s)
SAN–Sino-atrial node
SIDS–Sudden infant death syndrome
SCD–Sudden cardiac death
SNR–Signal-to-noise ratio
SNS–Sympathetic nervous system

SR–Sinus rhythm
VF–Ventricular fibrillation
VT–Ventricular tachycardia

35.3 Methods for HRV Assessment

Heart beat variation can be examined by replacing the complex waveform of an individual heartbeat recorded in the ECG with the time of occurrence of the contraction as a single number. Thus, the sequence of heartbeat duration can be expressed as a function of its duration (*tachogram*) (Time series derived from the occurrence time of the R-wave. The term is applicable also for cardiac events series, interval tachogram, interval function, instantaneous heart rate, heart timing signal, and low-pass filtered event series.). Sometimes, by interpolating and resampling the R – R sequence, the HRV signal can be presented as a function of time. Since the presence of sinus rhythm is formally defined as the onset of normally oriented P-waves, heartbeat variation assessment should ideally be based on a calculation of time-intervals between consecutive P-waves. Because the shape of the P-wave is unfavorable for its automated detection with currently used commercial equipment (difficulties in fiducial point determination, relatively low SNR), two important assumptions are made [26]. First, that the detection of the P-wave can be replaced by the detection of the R-wave, and second, that interbeat duration between consecutive R waves equals that of consecutive P waves. Since the variability of the P – R interval is approximately — two to three orders lower than that of the P–P or R–R intervals [27], it is assumed that the P–R interval variability does not influence the HRV measurements. Thus, in practice the QRS complex (R-wave) is commonly used to determine the time period between consecutive heartbeats.

35.3.1 Time Domain HRV Analysis

Techniques used in time-domain analysis provide the simplest measures of heartbeat variation over time. These measures are simple to calculate and relatively easy to understand. Time-domain methods describe the overall magnitude of R–R interval fluctuation around its mean value. One class is the statistical descriptors of beat-to-beat intervals (not necessarily consecutive) or of differences in the duration between adjacent heartbeats. Another class is the geometrical method (frequency distribution representations).

35.3.1.1 Statistical Methods

The earliest quantitative indices for HRV (RSA) have been described in studies by Schlomka et al. and Schäfers et al. (after [8]) in the 1930s, as the difference between the sum of the — three to four longest and — three to four shortest R–R intervals either as absolute values (*arrhythmia magnitude*) or as normalized data for the mean HR (percentage of the mean, *arrhythmia index*). Similar measures are still in use and referred to as the *variation range* (*VR, absolute*) and *coefficient of variation* (*CV, normalized*). Simple measures of cardiac vagal activity from standard ECG recordings have been described recently [28, 29].

The most widely used time-domain measure is the standard deviation (*SDNN or SDRR*) (Table 35.2), which is equal to the square root of the variance of all normal-to-normal or R–R intervals, respectively [30]. Depending on data-length and signal representation (HRi, HP) various SD-based measures are in use. This simple HRV measure can be drawn from a time series of any duration.

From 24-h ECG recordings, two other measures allow the quantification of the average N–N interval or SD changes over predefined periods, usually of 5-min duration (SDANN and SDNNI, respectively) [30]. If a permutation of SD is applied to the differences between consecutive N–N (R–R) intervals, a widely used and recommended index is derived, referred to as the *RMSSD* [30] (Table 35.2). The SD-based measures represent a coarse quantification of overall variation, while RMSSD represents a more accurate quantification of short-term beat-to-beat variation. More recently, a new index has been derived which is the ratio SD/RMSSD [31].

Table 35.2

Time-domain HRV measures from short- and long-term ECG recordings

Parameter	Units	Description
SDRR	ms	Standard deviation of all quantifiable R–R intervals over a period of recording
CV	%	Coefficient of variation, i.e., SDNN normalised for mean RRI
VR	ms	Variation range, i.e., difference between the longest and shortest RRI over a period of recording
DSCL	ms	Maximal difference between two consecutive R–R intervals (sinus cycles) over a period of recording
AAD	ms	Average absolute difference, i.e., the average of the differences between successive R–R intervals ignoring their sign
SDSD	ms	Standard deviation of differences between successive R–R intervals
RMSSD	ms	Root mean square of successive differences in R–R intervals, i.e., the square root of the mean squared differences of successive R–R intervals
CIPA	units	Cardiac index of parasympathetic activity
SDNN	ms	Standard deviation of all quantifiable N–N intervals
SDANN	ms	Standard deviation of the averages of N–N intervals in all quantifiable 5-min epochs of the entire recording
SDNNI	ms	Mean of the standard deviations of all N–N intervals for all quantifiable 5-min epochs of the entire recording
RMSSD	ms	The square root of the mean squared differences of successive N–N intervals
NN50 count		Absolute number of pairs of successive R–R intervals that differ by more than 50 ms; three variants are possible counting all such R–R interval pairs or only pairs in which the first or the second interval is longer
pNN50	%	Percentage of pairs of successive N–N intervals that differ by more than 50 ms, i.e., NN50 count divided by the total N–N intervals' number
HR6%	%	Number of consecutive heartbeats that differ in their instantaneous heart rate by more than 6%

A separate type of statistical analysis is based on counting of events defined as the occurrence of consecutive heartbeats that differs above a pre-selected (arbitrary) limit of values or bins (absolute or relative). The index NN50+ expresses the number ("counts") of consecutive heartbeats that differ by 50 ms or more [22, 30]. Conventionally 6% bpm (HR6%) or 50 ms difference (NN50 or pNN50) is used. However, those arbitrary cut-off values represent only one of a family of possible statistics (NNx) [32]. The unfavorable statistical properties of count-derived indices (Fig. 35.2) has led experts to advise against their use [4]. Logarithmic transformation of the pNN50 was proposed to improve count-derived index statistics and their reproducibility. A novel proposal that may help to overcome statistical limitations suggests the expression of the pNN50 after the logit transformation (logit50) [33]. The Logit50 = Ln [pNN50/(100-pNN50)] is the natural logarithm of the odds of the occurrence of preset R−R interval differences >50 ms (Fig. 35.2).

Statistical measures are the most commonly used method despite their sensitivity to extreme values (such as true or false) and which requires time-consuming review of the data-series to obtain reliable values [34]. Dependence on the duration of recording excludes comparisons of short-term and long-term data, even if they are closely correlated [4]. It might also influence the reproducibility of the statistical measures. As these indices provide only crude information, they do not allow different HRV patterns (or dynamics) to be distinguished. Moreover, various patterns of HRV with similar statistical properties can be erroneously gathered into one class of HRV [35].

35.3.1.2 Geometric Methods

Graphic representations of event distribution and their quantitative evaluation can be obtained by plotting the frequency of occurrence of values in selected ranges or bins. This is referred to as a *histogram*. Classic descriptors of such representation are skewness and kurtosis, which quantify symmetry and peakness, respectively. Such descriptors are frequently used in HRV studies [36].

A histogram of time series can be analyzed using the absolute or relative number of "frequencies" within bins [37]. The most frequent bin is termed the mode of the histogram and its "height" can be measured as the number of R−R

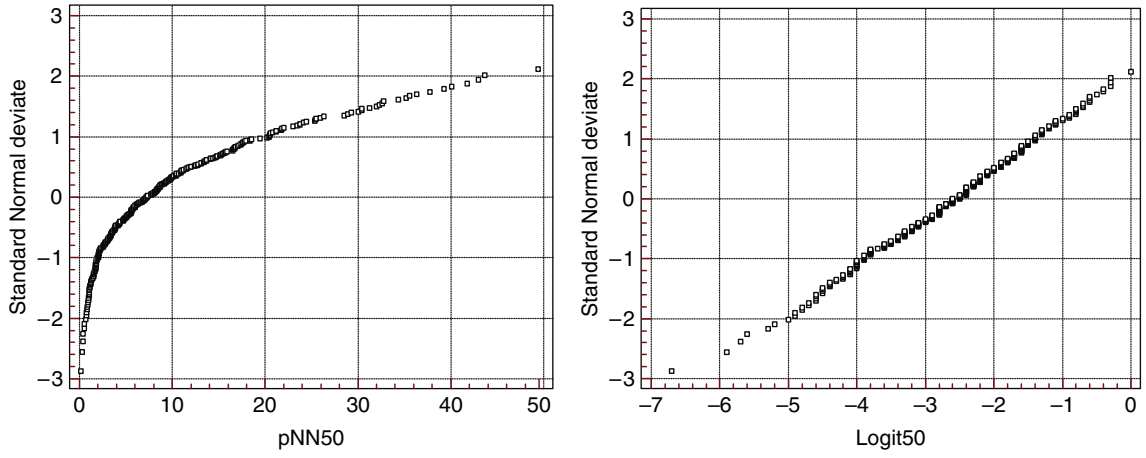

Figure 35.2

Unfavorable distribution of pNN50 (*left plot*) and its improvement if expressed as the Logit50 values. Data from 290 healthy subjects (author's data).

intervals with modal duration. The area of the histogram is equal to all R–R intervals. Assuming that the major peak of the histogram is a triangle, the simplest measure of any HRV geometric method can be derived. It is referred to as the *HRV Triangular index (HRVI)* [37, 38]. Here, if the number of intervals in the *i*th bin centered at t_i is represented as $b(t_i)$, then HRVI is defined as (35.1):

$$\mathrm{HRVI} = \frac{\sum_{i=1}^{Nb} b(t_i)}{\max_i b(t_i)} = \frac{N-1}{\max_i b(t_i)} \tag{35.1}$$

where N_b is the number of bins (Fig. 35.3). Usually, a constant bin is used with a width of $1/fs$ = 7.8125 ms, where *fs* is the sampling frequency. A selection of bin widths is critical for HRVI and other histogram-derived indices [39].

A modification of the HRVI, less dependent on the sampling frequency, is the *Triangular Interpolation Index* (TIRR or TINN depending on whether the selected intervals are R–R or N–N), which is the base of a triangle that approximates the highest peak of the sample density histogram by means of the minimum square difference interpolation [40] (Fig. 35.4). Generally, a uniform distribution representing large variability gives large values and a distribution with a single large peak provides small values.

The HRVI and TINN are dependent on the distribution of R–R intervals and are suitable for a reliable HRV estimation only if one dominant peak is present. Such a pattern is usual in a stable in-hospital environment. In ambulant patients and in normal subjects a bimodal distribution is more common, therefore, the HRVI or TINN underestimates the global HRV.

Similar approaches can be applied to data derived from the differences between successive heartbeats (*differential histogram*). Interestingly, a negative exponential interpolation of a differential histogram (specifically the slope of the interpolation curve) appears to be a robust method that is useful for the automatic assessment of HRV [41].

Another technique of differential histogram analysis referred to as a *sample asymmetry analysis* quantifying R–R interval deviations from the median (or mean) values has been proposed recently [42]. Two quantities representing the sum of the weighted deviation to the left (R1(α), HR accelerations) and to the right (R2(ß), HR decelerations) can be calculated, where α and β are parameters describing the degree of weighting from the median value (α = β = 2 are chosen). The ratio of R2/R2 represents the sample asymmetry. For a symmetric histogram, R1 and R2 are equal.

The *differential index* ($D_{iff}I$), obtained from a differential histogram, defined as the width of the base of a triangle constructed by using the width of the histogram at 10,000 R–R intervals and at 1,000 intervals, plotted on a semilogarithmic scale [43]. Data for healthy subjects and the prognostic value in subjects with angina pectoris have been obtained by using 16 ms bins [43, 44].

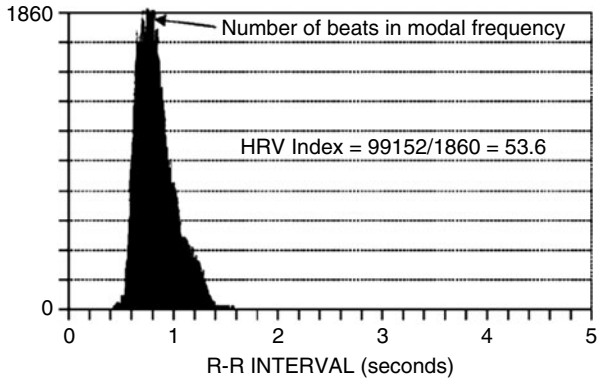

Figure 35.3
Calculation of the HRV triangular index (From [A30], Springer, with permission).

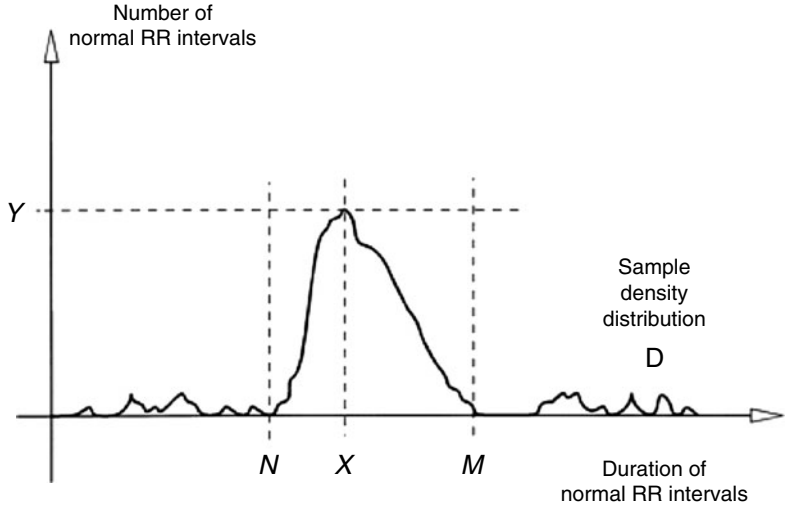

Figure 35.4
Calculation of the TINN index. For the computation of the TINN measure, the values *N* and *M* are established on the time axis and a multilinear function q constructed such that $q(t) = 0$ for $t \leqslant N$ and $t \geqslant M$ and $q(X) = Y$, and such that the integral $\int_0^{+\infty} (D(t) - q(t))^2 dt$ is the minimum among all selections of all values *N* and *M*. The TINN measure is expressed in milliseconds and given by the formula TINN = *M* − *N* (From [4]).

In general, histogram-based methods require a sufficient data length, so they are less applicable to a short data-series. They are also sensitive to the sampling frequency.

35.3.1.3 Return Map Evaluation

This geometric method is based on a *return map* (Plot of a time series as a function of the current and of the previous values. Known also as a Lorenz plot, scatterplot and less appropriately as a Poincaré plot.), which is a plot of each R–R interval (RR_n) (on the abscissa) against the following interval (RR_{n+1}) (on the ordinate) (Fig. 35.5). The first approaches

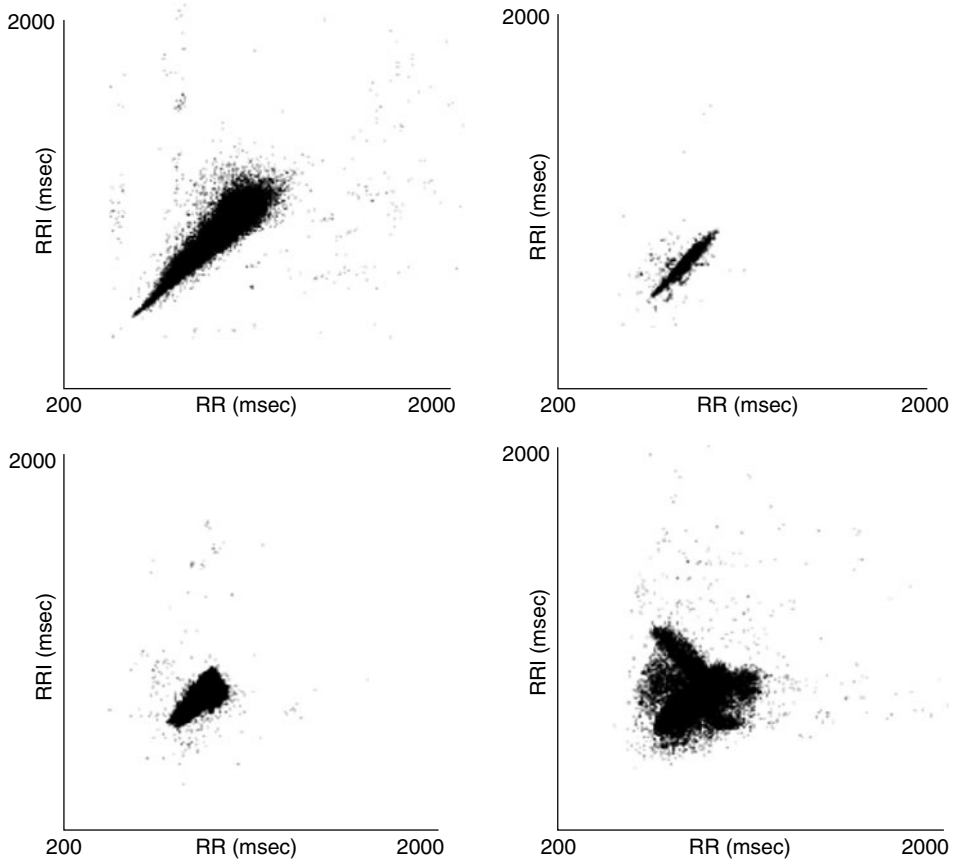

Figure 35.5

Examples of patterns of a return map. Upper panel, comet (left) and torpedo (right) pattern (usual in healthy subjects), lower panel, fan (left) and complex (right) pattern (usually abnormal) (From [47] with permission).

based on the return map for ventricular rhythm assessment in atrial fibrillation were reported by Arnoldi (1927) and Soderstrom (1950) [45]. Nakanishi et al. were the first to use this method for HRV analysis [46].

In this section, time-domain measures that can be drawn from the return map are described. Possible nonlinear approaches are discussed in a later section.

A qualitative evaluation of the return map is based on the overall shape of distribution (Fig. 35.5) [47]. The shape of the return map can be classified into several pattern-based categories, such as a comet or torpedo in healthy humans, while fan-like or more complex patterns may occur in patients with certain cardiovascular pathologies or after autonomic blockade. The use of qualitative evaluation is limited because of the subjective nature of evaluation and there is a probability of a misleading interpretation. However, a qualitative approach remains a unique and valid method for the assessment of the quality of the ECG recordings [4]. Recently, a subject-independent method for scatterplot pattern recognition has been proposed [47].

Several measures for return map quantification have been proposed. To be reliably calculated, longer ECG recordings are usually necessary. However, solutions for quantifying return maps from short-term recordings have been reported [46, 48–50].

The simplest measures can be derived from the regression line (slope, intercept, or correlation coefficient). The slope or the intercept of the regression line does not seem to have any advantage over simple max–min R–R interval difference or mean RRI itself. The Pearson correlation coefficient of the return map was shown to correlate with short-term variation

[50, 51]. Successive Pearson correlation coefficients calculated for each 1-min return map from long-term ECG recordings were proposed to reveal distinct patterns of sleep–wake states (Fig. 35.6) [52].

The most frequently used quantitative analysis of the return map includes calculation of its width- and length-derived parameters [53–60]. Schechtman et al. applied those parameters for HRV analysis in newborns with aborted SIDS [54–56]. They proposed calculating all following intervals for the given percentile value of the preceding R–R intervals, specifically at the 10th and 90th percentile [53]. Alternative methods were proposed by Kamen et al. [57] and Tulpo et al. [58] (Fig. 35.7). The derived indices *SD1* (standard deviation of intervals over the minor axis), *SD2* (standard deviation of intervals over the major axis), and their ratio *SD1/SD2*, all enable the approximate estimation of autonomic cardiac control [54–56]. Toichi et al. [59] calculated the length of the return map over transverse T and longitudinal L axes and derived two indices, referred to as the *Cardiac Vagal Index* ($\mathrm{CVI} = \log 10(L^{*}T)$) and the *Cardiac Sympathetic Index* ($\mathrm{CSI} = L/T$) (Fig. 35.8). They showed that only 100 R–R intervals (~2 min.) were necessary for a reliable calculation of those indices. Copie et al. [60] manually determined both L and T of the scatterplot in order to calculate the scatterplot area. Another variant of HRV partitioning has recently been proposed [61]. Unfortunately, in the presence of more complex patterns of the return map, width and length-related metrics cannot be used.

The introduction of a "z" coordinate as the next time lag (i.e., $\mathrm{R} - \mathrm{R}_{n+2(\mathrm{or}>)}$) was proposed for evaluating the return map in 3D space [62]. Such an approach gives a novel insight into the complexity of heartbeat dynamics, yet no clinically useful index has been proposed.

Another proposal is to represent the number of pairs ($\mathrm{RR_n}$, $\mathrm{RR_{n+1}}$) that lie within predefined bins, related to the percentiles [55], sampling interval (usually 7.8 ms) [63] or R–R ranges [64], equally spaced in "x" and "y" axes. In this way, a "z" axis represents a density function and a pseudo-3D graphic presentation can be obtained. In this proposal, for

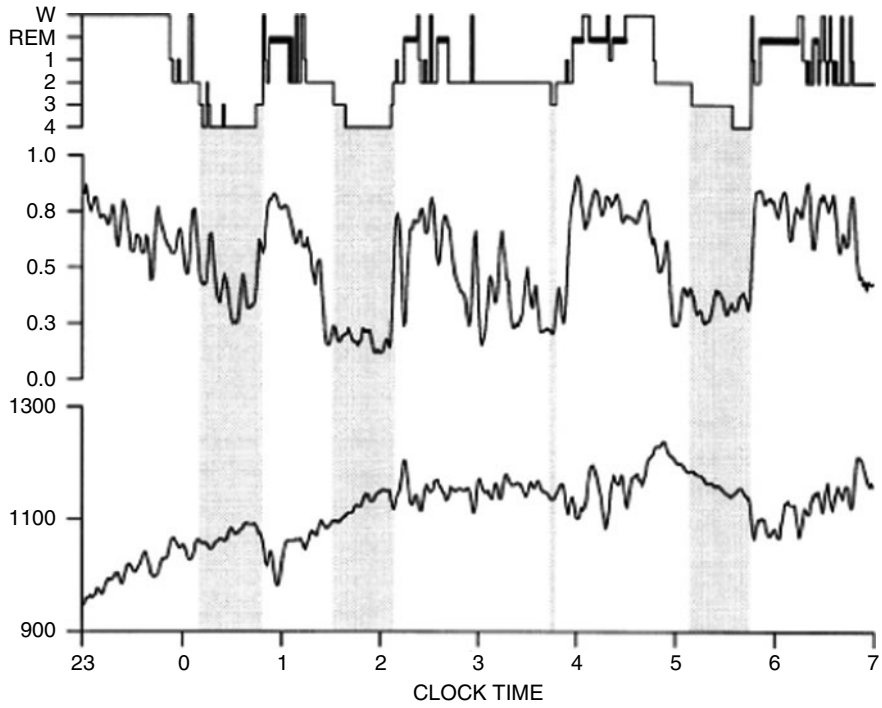

Figure 35.6

Return map coefficients use to follow transitory changes following various sleep stages. Profiles of 1-min interbeat autocorrelation coefficient rRR (*middle panel*) and of R – R interval (*lower panel*) together with sleep pattern (*upper panel*). Slow wave sleep (stage 3 and 4) lies in shaded areas. rRR and RR curves smoothed using the moving average method over a 5-point span (From [52]).

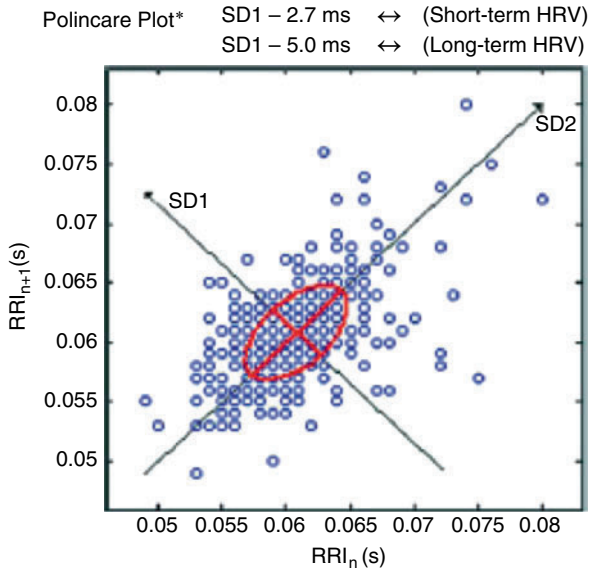

Figure 35.7

Example of quantification of a return map (from [A35], with permission).

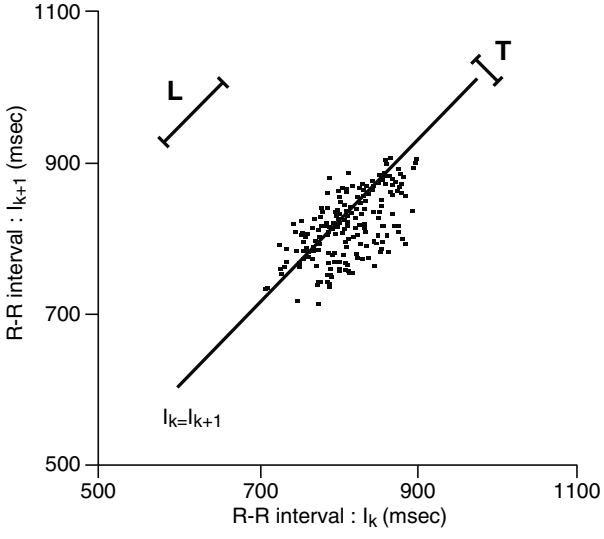

Figure 35.8

Quantitative assessment of the return map from short-term recordings. The lenght of the tansverse axis, *T*, and the length of the longitudinal axis, *L*, can be determined. The derived indices of vagal (CVI) and sympathetic (CSI) are proposed and can be calculated as simple product (decimal log) or ratio of the *L* and *T* (From [59]).

each rectangular area of the plot, the relative number of RR_n/RR_{n+1} samples is determined. Then, the maximum density of samples for each size of the area of the plot is calculated. Schechtman et al. found this approach useful for studying the changeable pattern over sleep–wake states in neonates [55]. Hnatkova et al. have proposed the logarithmic integral of the density function to express numerically the compactness of the plot in post-infarct patients (the *Compactness Index*) (Fig. 35.9) [63].

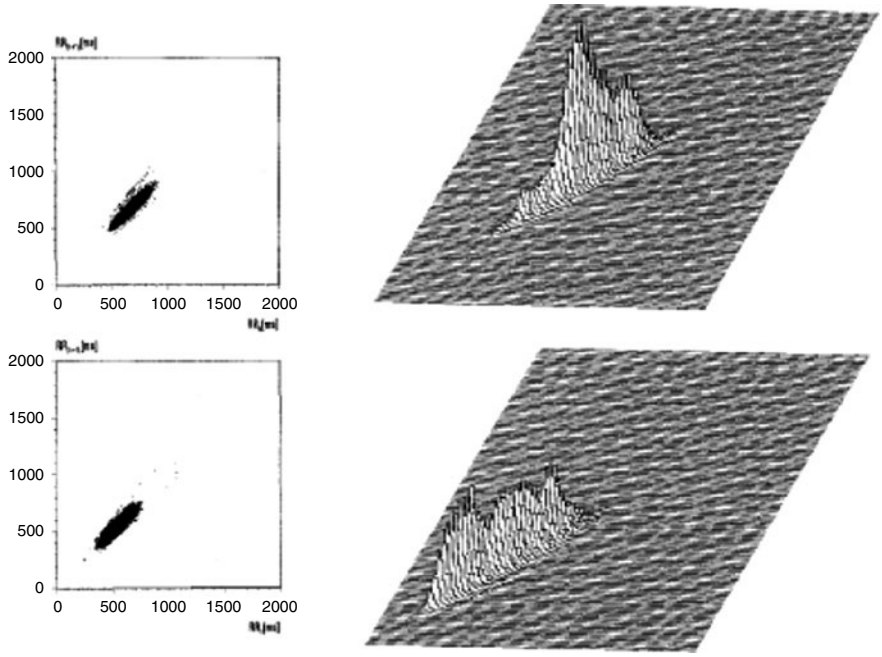

Figure 35.9

Three-dimensional representation of the return map from long-term ECG recordings. Two examples of 3-D return map (*right panel)* of low (*upper panel*) and high risk (*lower panel)* post-infarct patients clearly mark differences between both cases with nearly identical 2-D return map (*left panel*) (From [63]).

Sosnowski et al. proposed a simplified method for 3D return map evaluation [64, 65]. The distribution of pairs of neighboring heartbeats (counts) within R–R interval ranges with 100 ms resolution (bins) is presented (Fig. 35.10). Then, the density of counts in the two highest grid boxes (the area for each grid box being 0.01 s^2) can be determined by applying a 16 × 16 array to the scatterplot between 200 and 1,800 ms. Such a 3D view of the return map allows for an easy determination of the density function in normal subjects, patients with sinus rhythm (Fig. 35.11), with premature beats and atrial fibrillation. The derived index of HRV referred to as the *HRV Fraction (HRVF)* is calculated according to the following formula (35.2):

$$\mathrm{HRVF} = \left[1 - \frac{\mathrm{RR_1} + \mathrm{RR_2}}{\mathrm{RR} - \mathrm{RR50}}\right] * 100[\%] \tag{35.2}$$

where RR_1 and RR_2 represent two highest counts (from squares that are not necessarily adjacent), RR (total beat number) and RR50 (the number of intervals that differ from a succeeding interval by 50 ms or more).

The HRVF possesses unique properties that make it useful for HRV quantification irrespective of heart rhythm [65]. Actually, the HRVF is the only time-domain index allowing for HRV assessment in the presence of AF (Fig. 35.11). Significantly, a similar range of normal and abnormal HRV can be applied for subjects with sinus rhythm and atrial fibrillation [66]. The HRVF is normally distributed (as HR itself). This makes any statistical performance straightforward, contrary to most time-domain statistical measures, which frequently require transformation (usually logarithmic) before any statistical analysis (Fig. 35.12). In addition, its calculation is not affected by the distribution of data-points, so it can be applied to more complex patterns of the return maps. Physiological meaning of the HRVF as a global HRV index appears to be similar to that of other global HRV measures (i.e., SDNN). At present, only the author has evidence of the potential clinical utility of this method.

Moraes et al. have presented a somewhat different approach to return map construction [67]. A plot of RRI (on the *x* axis) against $RR_i - RR_{i+1}$ (on the y axis) and number of pairs within the bin of 7.2 ms duration (on the *z* axis) can be

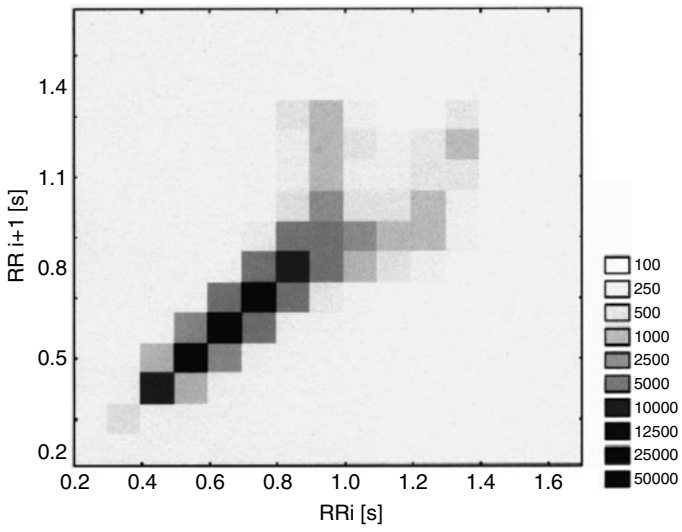

Figure 35.10

Simplified 2-D view of a return map of RR against RR_{I+1}. The boxes with two highest number of RR interval pairs is easily seen as black boxes lying between 0.6 and 0.8 s. These two numbers are RR1 and RR2 in the HRV Fraction equation. All heartbeats in the range of 0.2–1.8 s are included, irrespective of their origin (normal, supra-ventricular or ventricular) (From [64]).

obtained. The derived index MN is the product of parameters derived from the three axes (Fig. 35.13). Its clinical utility remains unknown.

35.3.1.4 Time-Domain Analysis for Parsing Frequency Components

Peak-to-valley ("*peak-to-trough*") statistics is the time-domain method introduced for distinguishing respiratory-related oscillation from nonrespiratory periodic components [5, 6, 49, 68]. Accordingly, the RSA is quantified as the average difference between the shortest sinus cycle associated with inspiration and longest sinus cycle within expiration. This method is vulnerable to artifacts associated with low frequencies. In addition, a separate measure of respiration is required. This method has become popular in psychological studies [5, 6, 68, 69].

The second time-domain method that allows for HRV distinction within specified frequency bands is the *moving polynominal method* [69]. By using this method, the statistical variance of the data within the respiratory frequency is obtained. However, it requires epochs of data points before and after the analytical time series to "prime" the polynominal filter. This method and other variants are extensively used in psychological studies [5, 6, 68–71].

Repeated calculations of the coefficient of return maps with increasing time-lag (RR_n vs. RR_{n+i}, i = 1–6) can reflect the RSA pattern from relatively short-term recordings (~2,000 heartbeats) [72]. Even shorter epochs (~70 heartbeats) are reported to be suitable for quantifying the pattern underlying RSA [73].

35.3.1.5 Time-Domain Analysis of the HR-HRV Relationship

Only a few attempts have been made to quantify the relationship between HR and HRV from long-term ECG recordings. The HRV Fraction is one example, as the probability of a certain value strongly depends on the mean RRI [65]. The most recent attempt is referred to as the *HRV Footprint*, which is a plot of heart rate against SDANN. This plot renders the likelihood (or density) of a particular HRV change occurring at each intrinsic HR over a 24-h period. The

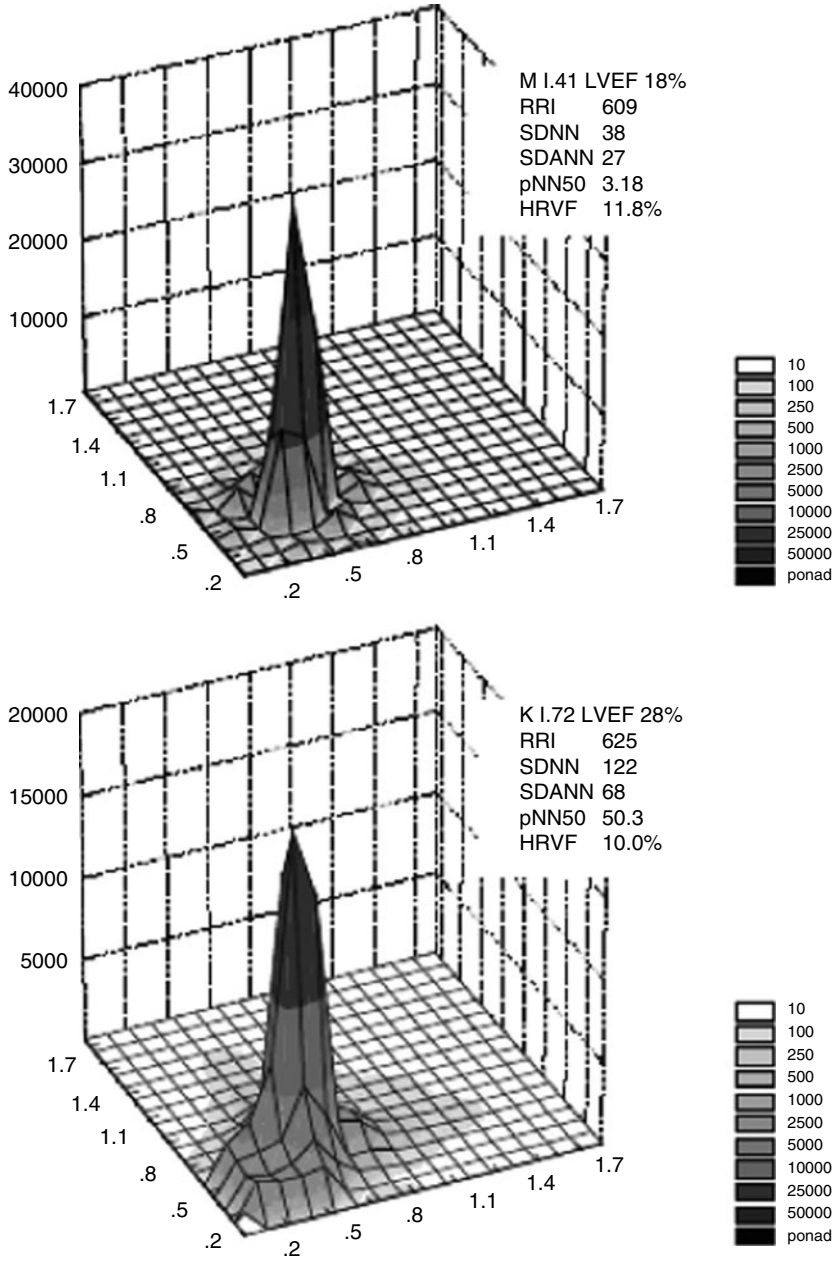

Figure 35.11

3D return map view in a patient with sinus rhythm and in a patient with atrial fibrillation. Two examples of R – R interval distribution in patients with depressed LV systolic function. Upper graph from a patient with sinus rhythm, lower – with AF. Values of HRV Fraction, as well as mean R – R interval are comparable, while SDNN was three times higher in AF-patient, reaching value far above the lower normal limit (Author's data).

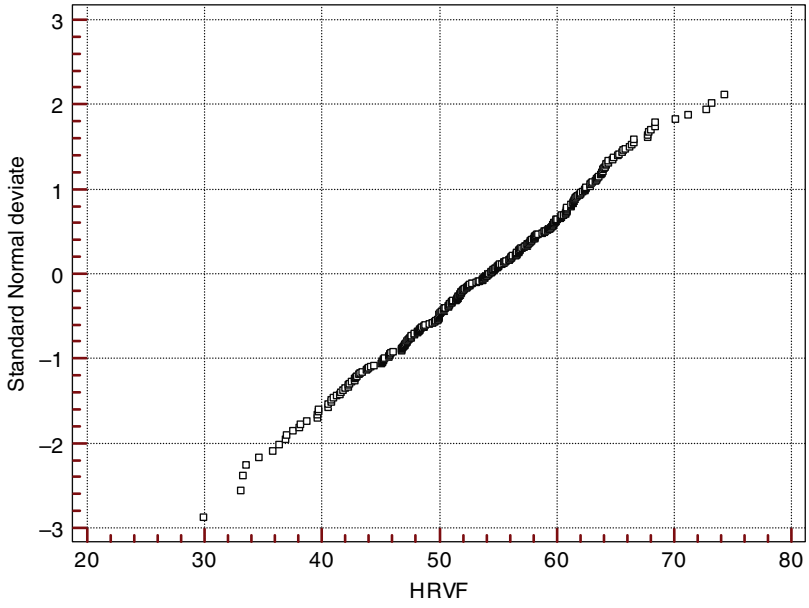

Figure 35.12
Plot of HRVF values distribution in healthy subjects against standard normal deviate (author's data).

footprint-area is calculated and expressed as a percentage. An example of the HRV Footprint in a patient with heart failure is shown in Fig. 35.14. [74]. Its usefulness has recently been documented in HF-patients with implantable cardiac resynchronization devices [74, 75].

35.3.2 Frequency-Domain Analysis

Time series collected from biological signals may be considered as a sum of oscillations (usually overlapping). Different mathematical analytical techniques used for the conversion of time series representation from time-domain to frequency-domain present the opportunity to quantify various amplitude and distinct frequencies that contribute to the underlying signal [4, 5, 17, 20, 23, 76–82].

Such a representation is termed *spectral analysis* and displays the distribution of the amplitude of each oscillation (usually a sine wave) as a function of its frequency. The squared contribution of each frequency is actually the *power* of that particular frequency contribution to the total power spectrum. The duration of the recording should be at least ten times the wavelength of the lowest frequency band of the investigated spectral component. According to *Parceval's theorem* (Parceval's theory states that the sum of squares measured among the time samples is equal to the sum of squares of the Fourier transform results, when frequency samples are included from zero to the sampling frequency (f_s).), the total power spectrum, defined as the area under the curve of the power spectrum, equals the variance irrespective of data length. For physiological and clinical information to be obtained, a post-processing of the power spectral density spectra is necessary.

The power spectrum of heartbeat variation in healthy humans consists of three or four major frequency peaks depending on the duration of data recordings (usually 5-min or 24-h period). Although they do not have fixed periods and the central frequencies may vary considerably, by convention [4, 5] these peaks lie within the following ranges: *high frequency* (HF) 0.15–0.4Hz (cycle length 2.5–6 s), *low frequency* (LF) 0.04–0.15 Hz (6–25 s), and *very low frequency* (VLF) <0.04 Hz (>25 s) (Fig. 35.15).

In 24-h recordings the VLF is subdivided into the VLF component 0.003–0.04 Hz (25 s–6 min) and the *ultra-low frequency* (ULF) component <0.003 Hz (cycle length > 5 h).

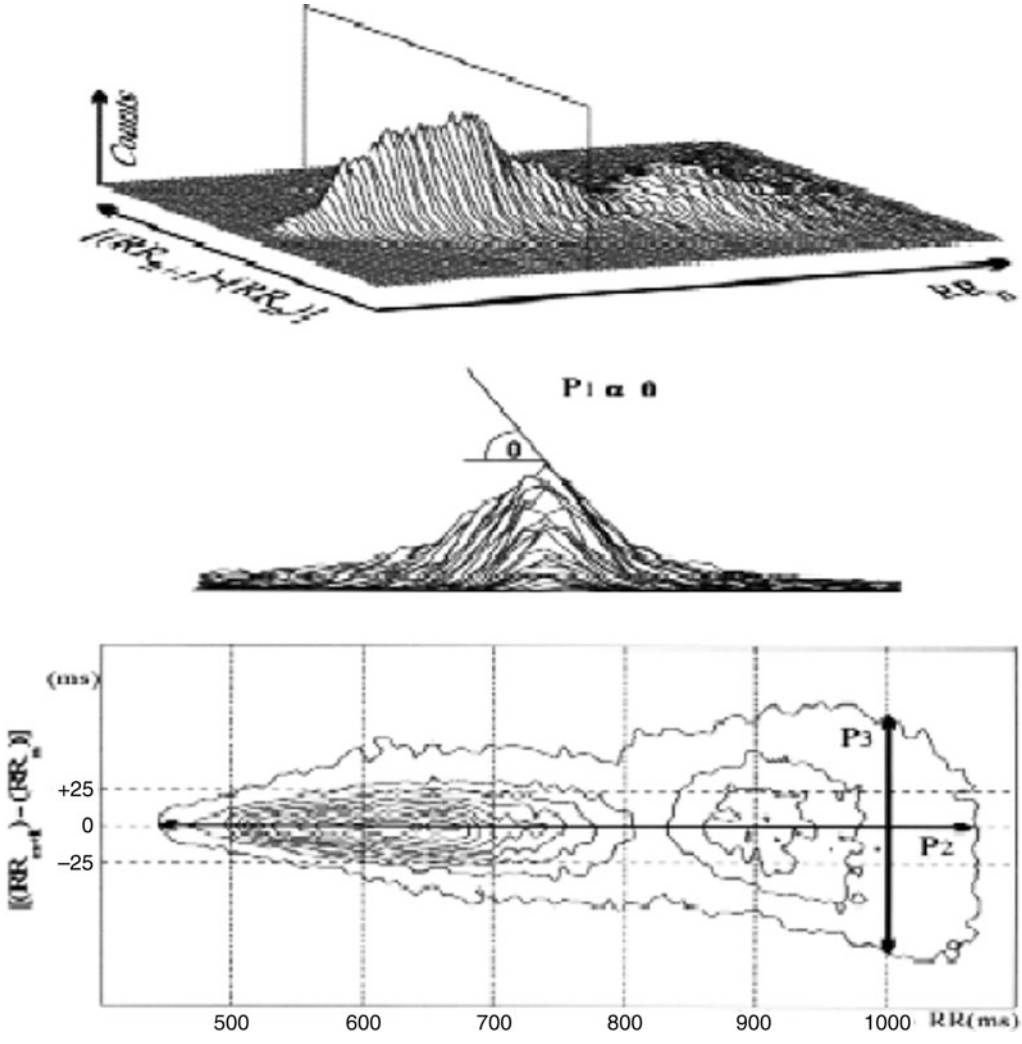

Figure 35.13

Presentation of 3-D distribution of RRI. The plane (*upper graph*) depicted intercept the distribution across maximum density (counts). The P1 (*middle graph*) is measured at maximum density taking into account the tangent of the angle. Other parameters (P2,P3, *lower graph*) are simply maximum longitudinal and transverse ranges. An MN index is a product of P1, P2 and P3 (x10^{-3}) (From [67]).

The power of an individual frequency component is the area under the proportion of the curve related to each component. The power of the ULF, VLF, LF, and HF components is usually expressed as square milliseconds and the PSD is expressed as milliseconds per Hertz. The ratio between LF and HF components (LF/HF ratio) is commonly calculated [4, 5, 79, 81]; however, it has not been resolved whether absolute or normalized values should be included for the LF/HF calculation.

The relative LF and HF power can be expressed in normalized units (or percentages) by dividing the power of the LF and HF components (in ms^2) by the total power from which the power <0.04 Hz is subtracted and multiplying by 100 [79–81]. The normalization procedure tends to minimize the effect of changes in total power on the HF and LF components. However, is seems important *to quote both the absolute and normalized values* in order to describe the distribution of power within the spectral components completely.

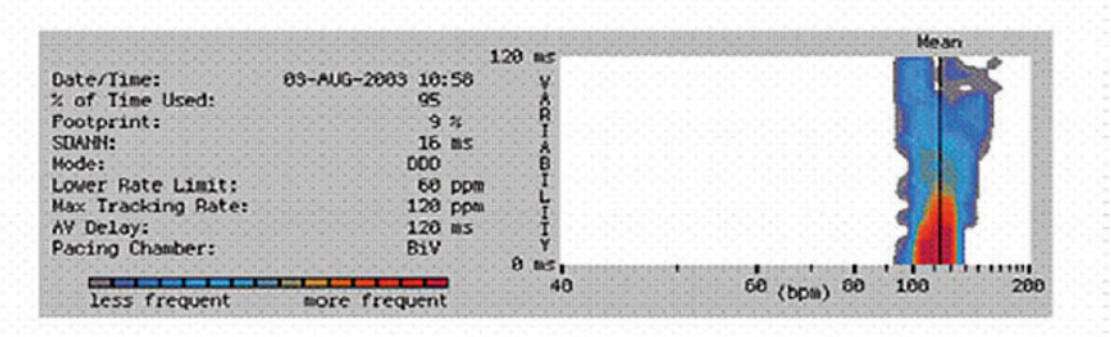

Figure 35.14

HRV footprint. A graphical representation of SDANN scatter occurring at each intrinsic sinus rate over a 24-h period. Colors indicate the frequency of HR and SDANN occurrence (third dimension, i.e., density) (From [75]).

Because of statistical properties, the absolute values of the total power spectrum (or PSD) and their components are usually reported after logarithmic conversion (either natural or decimal) [79].

The spectral measures of HRV are most widely applied in current clinical investigations. Their prognostic power is fully documented in a variety of populations [4, 5, 79–81].

A new index called *prevalent low frequency* (PLF, Hz) has been proposed by the St. George's Hospital Investigators Group [83]. Here, with 1/60 Hz resolution, the LF band contains seven power spectrum values at frequencies of 0.033, 0.050, 0.067, 0.083, 0.100, 0.117, and 0.133 Hz. In each spectrum, local peaks (spectral position with the PSD greater than both adjacent power spectral densities) are detected within the LF band, and the greatest powered peak is included in the PLF computation. Frequencies of all maximum peaks ($\leqslant$1 per each 5-min segment) are averaged over the entire Holter recording to obtain the single value of PLF. Detectable peaks in $\geqslant$10 segments are necessary for valid PLF calculation. At present, only the authors have found evidence of the potential clinical use of this method [83].

35.3.2.1 Nonparametric Spectral Analysis

Nonparametric methods are traditionally used for the evaluation of rhythmic events presented in a signal. The Fourier transform is the most common method for the decomposition of the signal. It provides an evaluation of the contribution of all frequencies, irrespective of whether its frequency components show specific spectral peaks or broadband powers. Thus, FFT techniques include all data independent of their deterministic or stochastic properties. These frequencies are multiples (harmonics) of the basic frequency, which is a reciprocal of time series data-length. For a reduction of the number of computations, the fast (a discrete) Fourier transform (FFT) is commonly employed [79, 84, 85]. The fast Fourier transform allows for obtaining the PSD of a signal directly from the time series by means of *periodogram* (Estimate of power spectral density on the basis of the modulus squared Fourier transform.) expression (see 35.4):

$$\mathrm{PSD}(f) = \left| \frac{1}{N\Delta t} \Delta t \sum_{k=0}^{N-1} y(k) \exp(-j2\pi k f \Delta t) \right|^2 = \frac{1}{N\Delta t} |Y(f)| \tag{35.3}$$

where Δt is the sampling period, N is the number of samples, and $Y(f)$ is the discrete Fourier transform of $y(k)$.

The FFT method uses a relatively simple algorithm with high-speed processing. It requires strict periodicity and stationarity (Property of a time series in which probability distributions involving values of the time series are independent of time translations.) of data. Also, the length of data for an FFT requires to be long enough (at least 256–512 consecutive heartbeats) for a reliable PSD estimation [79, 84].

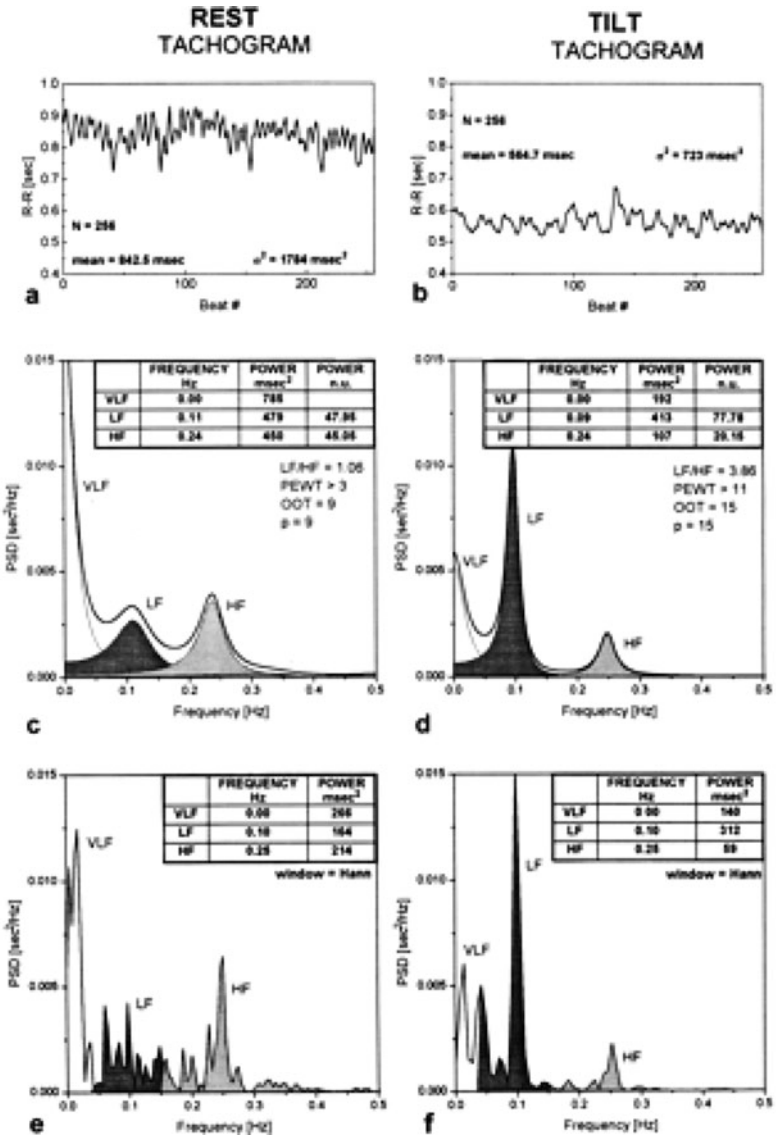

Figure 35.15

Interval tachogram of 256 consecutive RR values in a normal subject at supine rest (a) and after head-up tilt (b). The HRV spectra are shown, calculated by parametric autoregressive modeling (c and d) and by a fast Fourier transform-based non-parametric algorithm (e and f). Mean values (m), variances (s^2), and the number (N) of samples are indicated. For c and d, VLF, LF, and HF central frequency, power in absolute value and power in normalized units (n.u.) are also indicated together with the order p of the chosen model and minimal values of the prediction error whiteness test (PEWT) and optimal order test (OOT) that satisfy the tests. In e and f, the peak frequency and the power of VLF, LF, and HF were calculated by integrating the power spectral density (PSD) in the defined frequency bands. The window type is also specified. In c through f, the LF component is indicated by dark shaded areas and the HF component by light shaded areas (From [4]).

Since the FFT is theoretically defined on an infinite time series, its application to real data of finite length leads to unavoidable errors. The assumption of zero-value of the data outside the recording window is necessary and results in a *spectral leakage* (Spectral leakage is the effect whereby power is removed from the correct frequency and distributed in the neighboring frequencies. This is a case when periodicities are not precise factors of the epoch length.) in the PSD. Therefore, different window functions are used to connect the side samples to zero smoothly. The rectangular, triangular (Bartlett), cosine, Han, Hamming, Blackman-Harris, Lanczos, and Welch, window tapers are among the most popular. Spectra which are better formed are obtained at the expense of *frequency resolution* (Spectral resolution is related to the number of discrete harmonic components, each of which is separated in frequency by a given range (i.e., 0.0005 Hz). If the frequency difference between adjacent components is small, the power is distributed amongst more components, each of which must therefore be smaller.) [4, 79, 80].

A further reduction in the frequency resolution can be reached by smoothing the rapid oscillation of the spectrum [79, 80]. Different procedures of averaging and overlapping are used. One of the most popular methods is the Welch periodogram (Periodogram estimate is based on the splitting of the time series in overlapped segments multiplied by data windows, and on the ensemble average of periodograms computed in each data window.). In this method, data segments are allowed to overlap by 50% or 70%, and each data segment is weighted with a window function before calculating the periodogram. Sometimes it is necessary to approximate a periodogram more closely, which can be done by using the zero padding procedure [79, 85]. Zero padding actually interpolates the values of the measured spectrum at additional frequencies, producing a smoother spectrum.

Rüdiger et al. [86] proposed a new approach for the FFT use based on trigonometric regression. This method, similar to the cosinor method [87], creates the kth rhythmic part with amplitude a_k, frequency ω_k, and a phase shift φ_k as a regressively estimated function by using the method of least squares in the form (see 35.4):

$$u_k(t_i) = a_k * \sin(\omega_k t_i + \varphi_k) \tag{35.4}$$

This method provides a clear separation of rhythmic from nonrhythmic information. It is robust and does not require interpolation for artificial or missing segment deviations. Oscillations with a variance part ε <1% are stored as general residual variance. Estimation of the residual variance (nonrhythmic component) in four frequency bands from the FFT analysis showed that the total variance within each frequency band contains a substantial amount of the residual variance, especially in the VLF range (~13–17%) and in the HF range (~6–10%) [86]. The clinical usefulness of this method remains unknown (Fig. 35.15).

35.3.2.2 Parametric Spectral Analysis

Autoregressive modeling (AR) uses a raw signal to identify a best fitting model from which the spectrum is derived [78–81, 88–92]. AR modeling is based on the assumption that each value of the series depends on a weighted sum of the previous values of the same series with noise.

AR models are completely independent of the characteristics of the biological system, simply representing the "black-box" approach. The AR methods are suitable for identifying the central frequency driven by a fixed-rate oscillator. Thus, the AR method allows concentration on the most significant peaks, excluding noise-related frequencies. As a result, the AR analysis provides a better spectral resolution, where the components are smoother and easier for post-processing. AR enables spectral estimation from shorter time periods than the FFT approach [79, 89].

In the AR model, a priori choice of the structure and the order of the model are crucial. The order is usually empirically selected based on the investigator's expertise or by comparing the AR power spectra with those computed from other techniques. Too low a model order results in a low resolution power spectrum and too high a model order can generate false peaks in the spectrum [90].

Different criteria may help to determine the value of the order of the model (*Akaike, Rissanen, Parzen*) [79, 80, 90–92]. A correct identification of the model is required by using a posteriori tests of reliability. Changing the model order across different physiological conditions may introduce a new variable into the computation of the power spectrum. A fixed model order seems to be a practical rule for AR spectral estimation. This approach, although attractive in its

Table 35.3
Classification of time-frequency methods (After Cerutti et al. [78])

Linear decomposition of the signal	Short-time Fourier Transform Wavelet Transform
Quadratic energy distributions	Spectrogram Scalogram Wigner-Ville Transform Cohen's class of time-frequency distribution
Adaptive parametric models	Time-variant parametric models Adaptive filters

simplicity, is criticized as unrealistic as it assumes the same model for all subjects, independent of their clinical characteristics and physiological conditions, as well as of signal sampling rate and SNR [90]. Moreover, in contrast to the FFT-based estimation, the amplitude of AR peaks does not faithfully reflect the actual power of the associated spectral component [89].

Many algorithms are proposed for obtaining estimates of AR parameters, for example, methods based on estimation of the Yule-Walker autocorrelation sequence, the Burg algorithm, and the Kay-Marple least squares linear prediction algorithms (including the modified covariance method) [79, 80, 85, 92]. There are also adaptive algorithms such as mean or recursive least square (*RLS*) which permit updating the parameter estimates as a new data sample becomes available [91].

35.3.3 Time-Frequency Spectrum Analysis

An evaluation of the power spectral density for short time series when the stationarity is met and subsequent repetition through the entire recording allows changes in signal variation over time to be quantified in a continuous manner. Several time-varying spectral approaches have been proposed [93–105]. These methods are particularly suitable for evaluating power and frequency transient alterations over time in response to physiological (body movement, exercise, mental tasks, sleep), pathophysiological (ischemic episodes, cardiac arrhythmias), or treatment (drugs, interventions) stimuli. However, the patterns of signal variation that are present across the entire spectrum, including long-range control mechanisms, are hidden with time-variant spectral analysis. A classification of time-frequency methods is given in Table 35.3 [93]. Most of these methods use frequency bands corresponding to those arbitrarily chosen in the frequency domain analysis. Only those that have a clinical application are described below. More in-depth review of these methods is beyond the scope of this chapter (see references [93, 94, 98]).

35.3.3.1 Nonparametric Methods

Short-Time Fourier Transform

The short-time Fourier transform (STFT) is a linear time frequency representation of changes in the signal that vary with time. The Fourier transform does not explicitly show the time location of the frequency components, but some form of time location can be obtained by using a suitable pre-windowing *g(s)*. The STFT can be defined for $x(t)$ as a local spectrum of the signal *x(s)* around the analysis time as (see 35.5):

$$S_x^g(t,\omega) = \int x(s)g(s-t)e^{-j\omega s}ds \tag{35.5}$$

The time-frequency resolution of the STFT is limited by the time-frequency product, that is, having a small time resolution means poor frequency resolution, or vice versa. The resolution is also constant as a function of the frequency, which is due to the window chosen for the STFT. Also, it depends on the bandwidths of the analysis functions and the length of the window, which are unlikely to be optimally chosen [99–101].

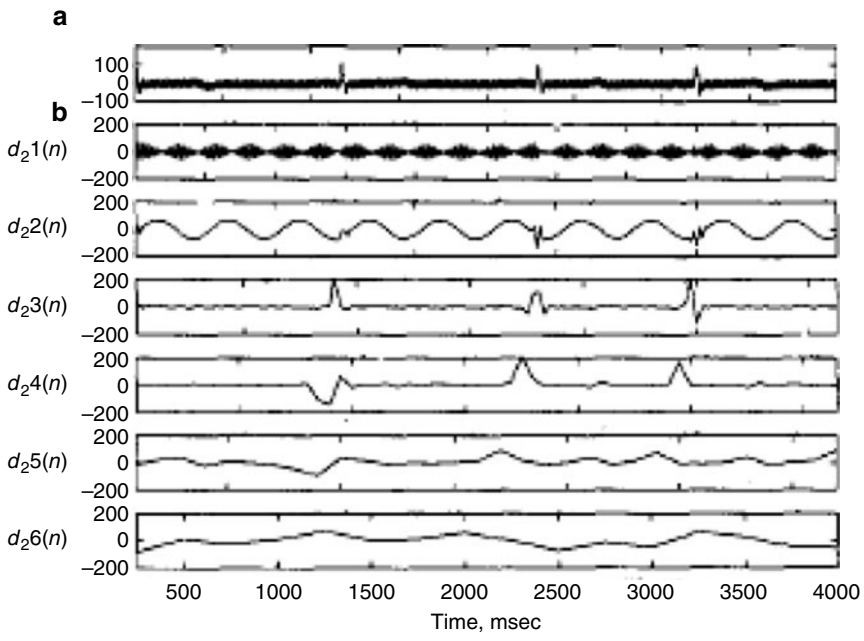

Figure 35.16

Wavelet analysis of HRV. (a) A theoretical example of wavelet analysis, (b) Wavelet analysis applied to HRV signal. For explanation see text and ref [103].

Wavelet Analysis

Continuous wavelet analysis (CWA) is another method that provides time–frequency decomposition of a continuous signal. This method is usually devoted to the analysis of non-stationary signals [98, 102, 103]. Conversely to STFT, CWA allows temporal evolution of the spectrum of frequencies contained in the signal to be followed.

A basic function of CWA is the wavelet (Wavelet – wave of finite duration and finite energy, which is correlated with the signal.) function, denoted as $m\psi(t)$. This function, used to decompose the analyzed signal in the time–frequency plane, is localized both in time and in frequency (and must have the spectral pattern of a band-pass filter). The initial function should be adequately regular and is the localized "mother" wavelet. There are a number of mother functions (Daubechies's fourth coefficient wavelet, Haar wavelet, Morlet wavelet). Starting from the mother wavelet, a family of wavelets is set by scaling (contracting or dilating) and shifting in time (Fig. 35.16). The resulting wavelets coefficients indicate the evolution of the correlation between the signal *x(t)* and the mother wavelet in different time-intervals and frequency-levels. Particular wavelets are defined as (35.6):

$$\psi_{k,j}(t) = a_0^{-\frac{1}{2}} \psi\left(a_0^{-j}\left(t - ka_0^j T\right)\right) \tag{35.6}$$

where a_0 is the dilation factor, j and k are integers that determine dilation (scale) and the time-position of the wavelet, respectively, and T is the sampling interval. The corresponding wavelet coefficients are (see 35.7):

$$C_{k,j} = \int x(t)\psi^*_{j,k}(t)\mathrm{d}t \tag{35.7}$$

By using CWA, the signal can be analyzed in different scale levels. Low scale levels (small j value) correspond to rapidly changing details (i.e., high frequency), whereas high scale levels (higher j values) correspond to slow changes (i.e., low frequency).

Wigner-Ville Technique

The energy distribution of the signal in the time and the frequency domain can be obtained simultaneously if the PSD of the signal is evaluated by Fourier transformation of the instantaneous autocorrelation function (central covariance function) [95, 97]. Obtaining the time–frequency distribution is known as the Wigner-Ville distribution (WVD) (see 35.8):

$$\mathrm{WVD}(t,f) = \int_{-\infty}^{+\infty} x\left(t - \frac{\tau}{2}\right) x * \left(t + \frac{\tau}{2}\right) e^{-j2\pi f\tau} \mathrm{d}t \tag{35.8}$$

It preserves the time t and frequency f shift of the signal. The time (of frequency) integral corresponds to the signal's instantaneous power (or power spectrum). The instantaneous frequency can also be estimated.

As the WVD introduces the cross-term interference due to nonlinearity of the transformation, the *kernel function* (Gaussian (known as Choi-Williams), Bessel, korn-shaped, and others) is used to remove this interference, obtaining the Cohen's class. The kernel performs a 2D filtering (in both domains) and determines the properties of the distribution. However, its choice influences the time and frequency resolution and optimal selection of the kernel requires knowledge about the signal. For the analysis of HRV data, the *smoothed pseudo-Wigner-Ville transform* (SPWV) has largely been used. It introduces time and frequency windows which determine SPWV resolution [97, 101].

Huang-Hilbert Transform

By using the *Huang-Hilbert transform* (HHT), an analyzed signal is represented in the time–frequency domain by combining the *empirical mode decomposition* (EMD) with the Hilbert transform (HT). The first step uses EMD [104]. This procedure decomposes the signal into so-called *intrinsic mode function* (IMF) (IMF defines an oscillating wave if the number of extrema and the number of zero crossings differ only by one and the local average is zero.). A finite number of IMFs can be obtained from a real data-series. The IMFs are produced sequentially with each subsequent IMF being derived from the residual (i.e., the portion of the initial signal not represented by a previous IMF) initial signal. The iterative algorithm is called *sifting*. The first IMF is defined as $c_1(t)$. Having separated $c_1(t)$ from $x(t)$, one has the residual signal $r_1(t) = x(t) - c_1(t)$. After several iterations (until the residual part becomes a monotonic function or a constant), the $x(t)$ can be expressed as the combination of $c_i(t)$ and $r_n(t)$ (35.9):

$$x(t) = \sum_{i=1}^{n} c_i(t) + r_n(t) \tag{35.9}$$

Then, the Hilbert transform (HT), given by (35.10),

$$H[x(t)] = y(t) = \frac{1}{\pi} \int_{-\infty}^{\infty} \frac{x(\tau)}{t - \tau} dt \tag{35.10}$$

is performed on the $c_i(t)$, and yields the instantaneous amplitude $a_i(t)$ and phase $\vartheta_i(t)$ (35.11):

$$a_i t = \sqrt{[c_i(t)]^2 + H[c_i(t)]^2}; \qquad \vartheta_i t = \tan^{-1}\left\{\frac{H[c_i(t)]}{c_i(t)}\right\} \tag{35.11}$$

The instantaneous frequency is given by (35.12).

$$\omega(t) = \frac{d\vartheta_i(t)}{d(t)}. \tag{35.12}$$

Thus, the Huang-Hilbert transform of $x(t)$, denoted as $\mathrm{HHT}(t,\omega)$, can be expressed as (35.13):

$$\mathrm{HHT}(t,\omega) = \sum_{i=1}^{n} a_i(t,\omega) \tag{35.13}$$

The HHT is adaptively data-driven and possesses higher time and frequency resolution than STFT, WVD, and CWA [102].

35.3.3.2 Parametric Methods

Recursive Autocorrelation

The recursive autocorrelation, also referred to as time-variant spectral estimation, is based on modeling of signal changes [93–97]. Spectral modification of a signal is realized by calculation of a new set of a model parameter *a(t)* from the preceding one *a(t − 1)* and from the prediction error (35.14):

$$a(t) = a(t-1) + K(t)[y(t) - \hat{y}(t)], \tag{35.14}$$

where $y(t) - \hat{y}(t)$ is the *prediction error* estimated by the model through the coefficients evaluated at time $t - 1$ and $K(t)$ is the *gain* of the algorithm. $K(t)$ contains a forgetting factor μ that exponentially weighs the past of the signal (the length of the past signal that really contributes to the change). Thus, the most recent terms contribute significantly to changes in a new sample, while the oldest one are progressively forgotten. The gain of the algorithm determines its adaptation and sensitivity to the signal changes. Many algorithms have been proposed for the $K(t)$ calculation (*RLS, smoothed Kalman filter, directional, Fortesque*). The sequence of spectra can be represented as a contor plot or a spectral array [93–97]. The recursive implementation of the AR models allows monitoring of the spectral components in real time. The advantage of this method is related to its possibility for multiple signal systems analyses for cross-correlation (*time and phase coherence*) evaluation.

Temporal Cumulative Approach (TCA)

This relatively simple approach uses a PSD calculation over the frequency range of interests within short-epochs and reconstruction of its cumulative plot against time. This method allows instability in PSD to be overcome from neighboring epochs and reduces the effects of noisy data. The temporal cumulative approach enables temporal changes of interesting spectral components to be tracked, especially those with a relatively undisputable physiological background, i.e., the HF component. The cumulative plot is constructed by summing the PSD of the HF component versus time. This plot is then analyzed by a stepwise linear regression procedure (least squares) that helps time segments with consistent parasympathetic tone to be isolated. The length of these segments is determined automatically in order to find a minimal number of segments that describes the cumulative plot. The intensity of parasympathetic tone at each time-segment is defined by the slope of power units per minute [106].

35.3.4 Nonlinear/Chaos-Derived Methods

The majority of biological systems exhibit nonlinear behavior (e.g., the baroreceptor reflex, Starling curve, hemoglobin dissociation, lung hysteresis on a pressure–volume curve, etc.). Attempting to explain such a behavior using linear models does not seem sufficient or even appropriate. Thus, it is not surprising that over the last decade many nonlinear methods have been developed and postulated for HRV evaluation [107–115]. They can be classified according to the main features that they evaluate (Table 35.4.) [107]. Overall, a valid and reliable assessment of HRV nonlinear behavior requires relatively long-term ECG recordings. Some mathematical formulae are provided below and physical meanings are only summarized as necessary. A more in-depth description of these methods does not seem to be of interest to clinicians. However, researchers with an interest are invited to explore more extensive reviews [107–112].

To become familiar with nonlinear methods knowledge and understanding of both the mathematical and physical background are required. Unfortunately, advanced mathematics and physics are areas of limited understanding for the vast majority of physicians. In addition, chaos-theory or nonlinear dynamics derived methods are actually far removed from a definite physiological explanation or interpretation. A statement such as "broken fractal" means little to a physician. Thus, despite being introduced into clinical studies, these methods still remain research tools, and will be unlikely to be commonly used at the bedside. Nevertheless, by providing insight into many aspects of cardiac (heart rate) behavior, their employment (despite being experimental) might widen our understanding of cardiovascular system control [116–120], and in some cases, these techniques might find a practical application [118]. In other words, some of the gaps between science and practice can be demonstrated with HRV analysis. Fortunately, mathematicians, physicists, and

Table 35.4

Nonlinear complexity mechanisms and phenomena in physiology: partial list of possible contenders (From [107]. With permission)

Abrupt changes • Bifurcations • Intermittent bursting • Bistability, multistability • Phase transitions	Scale-invariance • Fractal and multifractal scaling • Long-range correlations • Self-organized criticality • Diffusion limited aggregation
Hysteresis	Nonlinear waves: spirals; scrolls; solitons
Nonlinear oscillations • Limit cycles • Phase-resetting • Entrainment • Pacemaker annihilation	Complex periodic cycles and quasiperiodicities
Complex networks	Stochastic resonance and related noise-modulated mechanisms
Alternans phenomena	Time irreversibility
Deterministic chaos	Emergent properties

manufacturers have convinced physicians to employ these methods, albeit with their "black box" meaning remaining unresolved.

35.3.4.1 Scale Invariant/Fractal Analysis

The scale invariant self-similar nature is a property of *fractals* (Fractal, derived from the Latin word *fractus*, meaning broken or fragmented.), which are geometric structures that have no fixed length [21, 107, 113–115, 121–127]. Their length increases with increased precision (magnification) of measurement, a property that confers a non-integer dimension to all fractals (*fractal dimension* (Geometric dimension of an object which includes fractal objects (Hausdorff dimension D_H).)). With respect to time series, the pattern of variation appears to be the same at different scales (i.e., magnification of the pattern reveals the same pattern). The self-similar pattern can be recognized in either spatial or temporal aspects (Fig. 35.17).

Power-Law Behavior (1/f Fluctuation)

Kobayashi and Musha first reported the dependence of the spectral power on the frequency of the R–R interval fluctuations [21]. Further to this, different methods for a scale-invariant (self-similar) relationship between the magnitude of the effect and its frequency distribution (Fig. 35.18) have been developed [102–105, 118–120].

The power relationship is described by (35.15):

$$f = aE^{\beta}, \tag{35.15}$$

where E is the amount of variation (e.g., spectral power), f is the frequency of observations, and α and β are constants. Taking the logarithm of both sides the equation gives (35.16):

$$\log(f) = \log(\alpha) + \beta(\log(E)). \tag{35.16}$$

Plotting a graph of $\log(f)$ against $\log(E)$ reveals an almost straight line in the range of 10^{-2} to 10^{-4} Hz with β *as an exponent factor* (slope) and *log* (α) referred to as the intercept. The range of log–log representation is consistent with the size and duration of the system. Some authors also calculate the squared coefficient of correlation (r^2), referred to as the *coefficient of determination*.

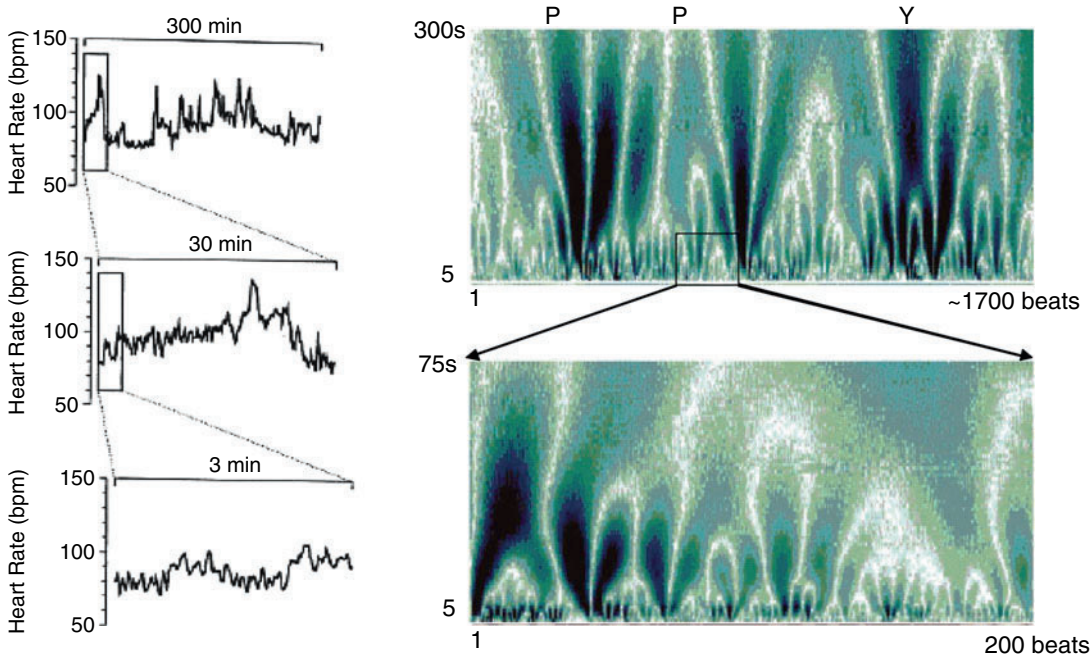

Figure 35.17

Fractal nature of heart rate variability. On the left graph heart rate variation appears to have no clear scale, as similar temporal pattern can be seen irrespective of time series data length. Right side graph shows distribution of wavelets in heartbeat series of different length. Pattern similarity is clearly seen between both epochs (From [107]).

The value of β *exponent* is around −1 in healthy subjects (Fig. 35.19). An altered β *exponent* was reported in patients after MI [126] and with CHF [127].

In contrast to a relatively stationary long time series (thousands of heartbeats) used for a reliable power-law behavior assessment, a model based on *HRi* calculation over a short time series (5 min) has been proposed [106]. Accordingly, the squared deviation from the mean heart rate is plotted on a 20-bin histogram with a bin size that equals 1/20 of the largest squared difference from the mean HR. A frequency distribution calculated from the histogram is plotted in the decimal log–log space. A regression line is fitted to the 20 data points and r^2, slope and intercept are derived. Although interesting results can been obtained in a selected population [128], this method is susceptible to the presence of non-stationarities or artifacts. In addition, a relatively long ECG recording is necessary for its reliable calculation.

Rescaled Range (R/S)

Fractal properties of data series can be measured by characterizing the divergence of data defined as the range (R) of the sum of deviations from the mean divided by sample standard deviation (S). For some processes that exhibit a long-range dependence (*persistence*), the R/S is proportional to a power of T (duration of the data sample) (see 35.17):

$$\frac{R}{S} = T^H. \tag{35.17}$$

The exponent H is called *Hurst exponent* [108, 109, 123, 124].

Given a time series $x(n)$, $n = 1, \ldots .N$, H can be estimated by taking the slope of the plot of (R/S) vs. n on a log–log scale. H is related to the fractal dimension $D_{(h)}$. For 1D signals, $H = 2D_{(h)}$ [123].

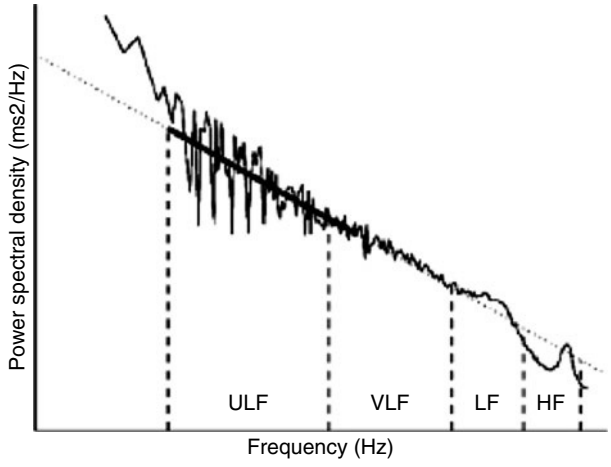

Figure 35.18

I/f scaling behavior of HRV spectrum. The slope of a plot of power against frequency is almost straight in the range of 10^{-2} and 10^{-4} Hz. Two measures can be taken from 1/f relationship: intercept and slope of this line (referred to as scaling index β) (From [A32]).

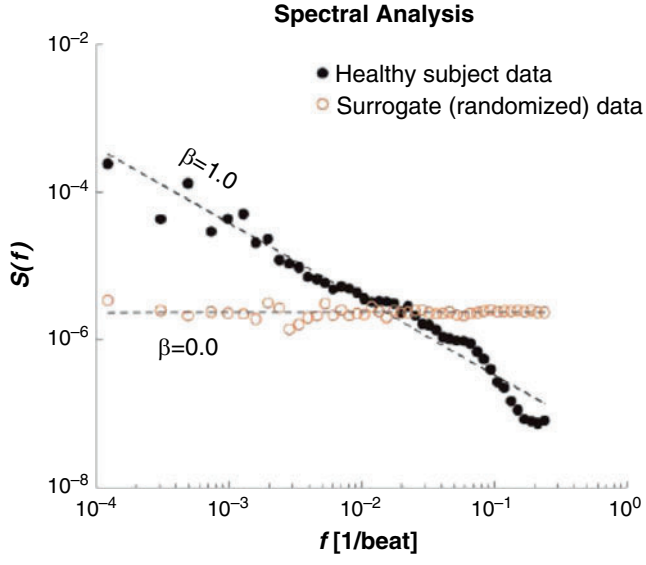

Figure 35.19

Scaling properties of power spectrum. Fractal scaling analyses for two 24-h inter-beat interval time series. The solid black circles represent data from a healthy subject, whereas the open red circles are for the artificial time series generated by randomizing the sequential order of data points in the original time series. Exponent β in healthy indicates for the presence of long-range correlation (1/f noise). Loss of correlation properties is consistent with uncorrelated random time series (white noise) and β -exponent equals zero (From [107]).

Detrended Fluctuation Analysis

A distinction between a local variation generated by external stimuli and intrinsic fluctuations from a complex system has been proposed to be feasible with *detrended fluctuation analysis (DFA)* [124]. These intrinsic fluctuations are presumed to exhibit a long-range scale-invariant (i.e., fractal) relationship. The DFA is a robust method for studying

fractal (or self-similar) behaviors of systems from which the originating signal exhibits an absence of characteristic temporal and/or spatial scale.

The calculation of DFA includes several steps. At first, heartbeat signals are represented as an integrated time series, following the equation (35.18):

$$y(k) = \sum_{i=1}^{N} (NN_i - NN_{ave}), \tag{35.18}$$

where $y(k)$ represents an evaluation of trends, NN_i is the difference between individual inter-beat intervals, and NN_{ave} is the average interval of the total number of heartbeats N. The trend function $y(k)$ is then separated into equal nonoverlapping boxes of length n, where $n = N/(\text{total number of boxes})$. In each box, the local trend $y_n(k)$ is calculated using the least square method (Fig. 35.20). By subtracting the local trend $y_n(k)$ from the trend function $y(k)$ ("detrending") for all possible length of boxes n, the function $F(n)$ is calculated as the root mean square of the integrated and detrended series (35.19):

$$F(n) = \sqrt{(1/N)\Sigma_{k=1}^{N}\left[y(k)^2 - y_n(k)^2\right]} \tag{35.19}$$

Graphic presentation of the relationship between $F(n)$ and n on a bi-logarithmic scale provides a regression line (Fig. 35.21). The slope of this line is termed the *scaling exponent* α. It may vary from 0.5 (uncorrelated random data or white noise) to 1.5 (random walk or Brownian noise). If the signal obeys the power-law behavior, that is, corresponds to the $1/f$ noise, the α exponent equals 1 (Fig. 35.16) [124]. The exponent α of this power relation defines

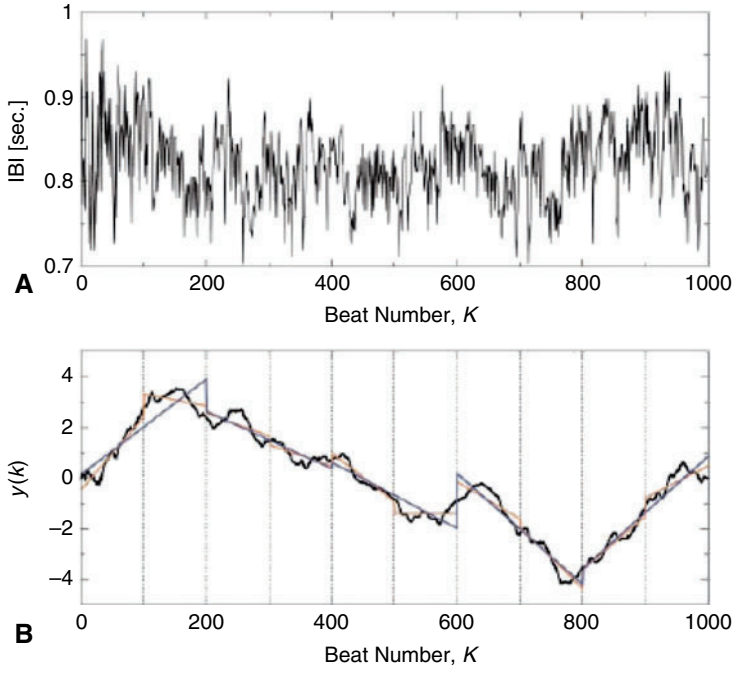

Figure 35.20

Illustration of the DFA algorithm to test for scale-invariance and long-range correlations. (a) Interbeat interval (IBI) time series from a healthy young adult. (b) The solid black curve is the integrated time series, *y(k)*. The vertical dotted lines indicate boxes of size *n* 100 beats. The red straight line segments represent the "trend" estimated in each box by a linear least squares fit. The blue straight line segments represent linear fits for box size *n* 200. Note that the typical deviation from the *y(k)* curve to the red lines is smaller than the deviation to the blue lines (From [107], Nat Acad Sci USA, with permission).

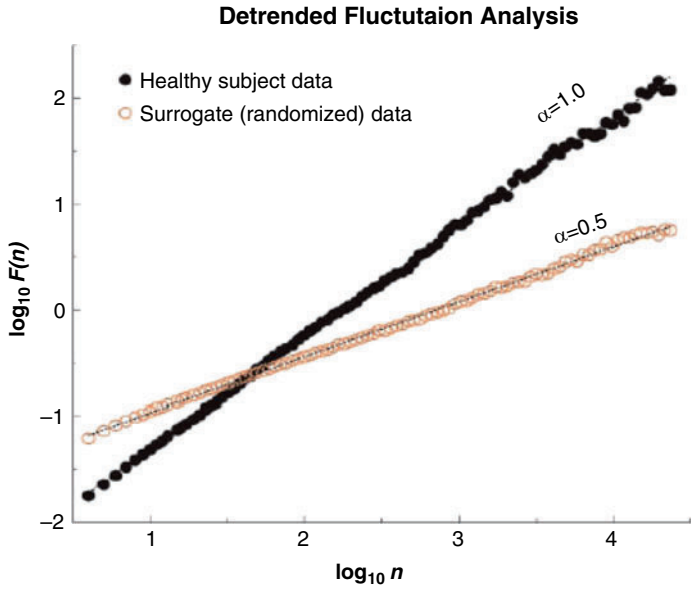

Figure 35.21

Bi-logarithmic presentation of the relationship between F(n) and n. The slope of the line is referred to as α-exponent and in healthy subjects varies around 1 (1/f noise). For white noise or uncorrelated random data α -exponent equals 0.5 (From [107]).

a pertinent parameter called the *self-similarity parameter* (when applicable it is related to the *Hurst exponent H* by $\alpha = H + 1$).

Applying this analysis to real-life data-series, the scaling exponent shows two distinct linear segments that depend on n values. Depending on a crossover phenomenon, arbitrary cutoffs for the n-values are initially proposed (n = 4–16 and n = 16–64) [122–127]. This yields two scaling exponents, α_1 and α_2, referred to as the short and intermediate-term exponents, respectively. However, in the most commonly applied variant of DFA, the n-values for α_1 and α_2 exponents range between 4–11 and 12–400, respectively [103, 110]. Thus, in contrast to $1/f$ scaling methods, the DFA allows the determination of a scale-invariant property over a relatively short data-series (~8,000 heartbeats). A loss of fractal-like HR dynamics has been shown to characterize patients with cardiovascular disease [112].

DFA is a mono-fractal technique, assuming that the scaling properties of the system are the same throughout the entire signal. In addition, only normal-to-normal heartbeats are included. As all of these assumptions may be flawed, another technique has been developed, namely multi-fractal analysis [129–132]. Multi-fractal DFA may help to detect changes of scaling behavior with time, providing the multiple scaling exponent $D(h)$ (Fig. 35.22).

Multi-fractality in heartbeat dynamics raises the possibility that many nonlinear control mechanisms are actually involved with coupled cascades of feedback loops in a system operating far from equilibrium. A loss of such dynamics was reported in patients with heart failure [132].

Correlation Dimension

Correlation dimension is an alternative procedure for the calculation of the fractal dimension (although it is not strictly the same) [133, 134]. It is also considered as a measure of degrees of freedom stimulated by a system, thus expressing the complexity of a system. From a defined data vector $(y_i,\ i = 1, \ldots, N)$ with N points, an m-dimensional phase-space of dimension p *(embedding dimension* (Number of axes of a return map sufficient to describe the properties of the corresponding phase space)) is constructed according to *Takens theorem* (A delay embedding theorem gives the

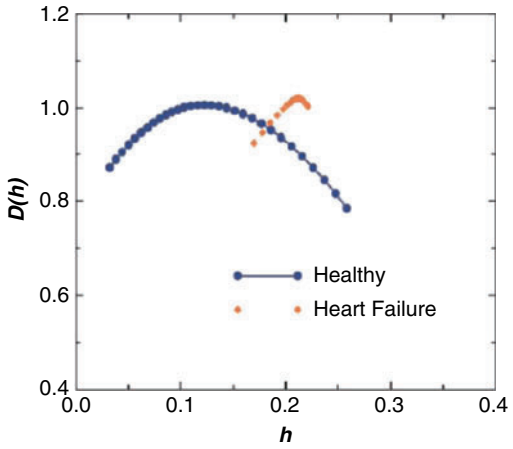

Figure 35.22
Multifractal properties of heartbeat variation (From [107]).

conditions under which a chaotic dynamic system can be reconstructed from a sequence of observations of the state of a dynamic system.) [113], obtaining (35.20):

$$\vec{x}_t \equiv (y_t, y_{t+\tau}, y_{t+2\tau}, \ldots, y_{t+(m-1_\tau)}, \tag{35.20}$$

for $t = 1, \ldots, N - (m-1)\tau$, where τ is the time delay or lag. Grassberger and Procaccia [136] have developed the basic algorithm which consists of computing the fraction of pairs of points in the *embedded space* that lie within a distance ε of each other with the dimension d (also referred to as D_2) (35.21):

$$d = \lim_{6 \to 0} \left[\frac{log_2(C_m(\varepsilon))}{log_2(\varepsilon)} \right], \tag{35.21}$$

where $C_m(\varepsilon)$ is the correlation integral which measures the number of points x_j that are correlated with each other in a sphere of radius ε around the points x_t. This algorithm is also known as *sphere (box) counting method*. Thus, in the phase-space, the correlation integral $C_m(\varepsilon)$ is defined (35.22):

$$C_m(\varepsilon) = \frac{1}{N \cdot (N-1)} \cdot \Sigma_{i \neq j} \theta \left(\varepsilon - |Z_i - Z_j| \right), \tag{35.22}$$

where $\Theta(z)$ is the Heaviside function: $\Theta(z) = 0$, if $z \leqslant 0$ and $\Theta(z) = 1$, if $z > 0$, and $|z_i - z_i|$ is the distance between a pair of points within the *attractor* (Attractor – an object to which the time series in a phase space is attracted.).

When $\log_2 C_m(\varepsilon)$ is plotted versus $\log_2(\varepsilon)$, the slope of the resulting straight line, determined by linear regression at lower ε, yields the dimension D_2. Several $C_m(\varepsilon)$ are computed for increasing values of the embedding dimensions m, and the slopes are determined from a *scaling region* of the log–log plot, as shown in Fig. 35.23a, obtaining a sequence of $d(m)$. As m is increased, $d(m)$ tends to a constant value of saturation (the D_2 value) shown in Fig. 35.23b [137]). The D_2 value is obtained by considering the points where $d(m)$ values remain constant (high values of m). A variance of the D_2 calculation, the point estimate of the heartbeat D_2, has also been proposed [138].

35.3.4.2 Entropy Analysis

Entropy H, as a physical term, is an energy that dissipates with time, as embodied by the Second Law of Thermodynamics. The concept of entropy was introduced into the theory of information by Shannon [139]. Applying entropy analysis to

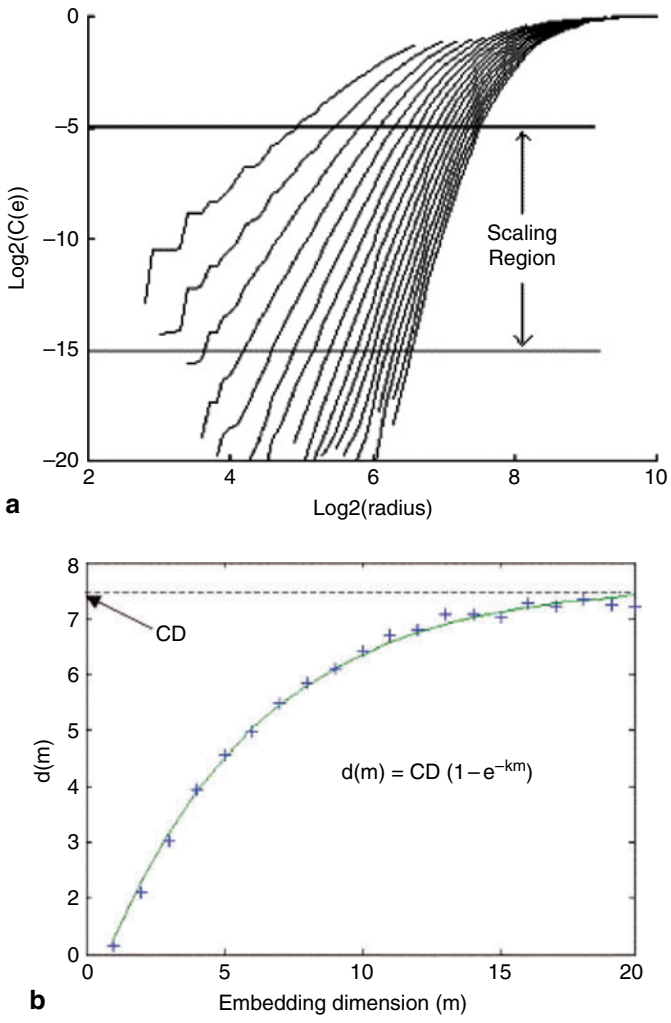

Figure 35.23

(a) Correlation integral as a function of the sphere radius (*r*) for each embedding dimension showing the scaling region. (b). Correlation dimension (D2, here CD) as a function of the embedding dimension *m* with a fitted exponential curve .

a real time series is based on its ability to measure order (regularity) and disorder (irregularity/randomness) and the probability p of these states.

Approximate Entropy (ApEn)

Approximate entropy analysis exhibits the rate of generation of new information within a biological signal (similar to the classic Kolmogorov-Sinai entropy).

To calculate *ApEn* [140], a data series is evaluated for the presence of recurrent patterns. First, a length m of data sequences is defined and the likelihood of similarity with other sequences of length m with a *tolerance* r is determined. Vector sequences $x(i)$ of consecutive data-points $u(i)_{(i=1,2,3\ldots N)}$ of length m are derived. Then, the distance $d(x(i), x(j))$ is defined, as the maximum difference between two vector components $x(i)$ and $x[j]$. If this difference is within tolerance r, the vectors are considered similar.

The frequency $(C_i^m(r))$ of occurrence of similar vectors *Nj* of sequences with length *m* and tolerance *r* throughout the data set is calculated (35.23):

$$C_i^m(r) = N_j \in d(x[i], x[j] \leqslant r)/(N - m - 1), \tag{35.23}$$

where $j \leqslant (N - m - 1)$. Then, the relative occurrence of repetitive patterns $\Phi_{m(r)}$ of length *m* within the tolerance *r* is obtained (35.24):

$$\Phi m(r) = \sum_i \ln C_i^m(r)(N - m - 1), \tag{35.24}$$

where Σ_i is a sum from $i = 1$ to $(N - m - 1)$. Finally, the approximate entropy ApEn is calculated, following the equation (35.25):

$$\mathrm{ApEn}(m, r, N) = \Phi_{m(r)} - \Phi_{m+1(r)}, \tag{35.25}$$

Thus, the ApEn(*m*, *r*, *N*) measures the logarithmic frequency (probability) that runs of patterns (within the tolerance *r*) of length *m* remain similar when the length *m* of the run is increased by 1. Small values of the ApEn indicate regularity, given that increasing the data sequence of a length *m* by 1 does not decrease the value of $\Phi m(r)$ significantly (i.e., regularity connotes that $\Phi_{m(r)} \approx \Phi_{m+1(r)}$). The value of ApEn (*m*, *r*, *N*) is expressed as a difference, but in essence it represents a ratio, as the $\Phi_{m(r)}$ is a logarithm of the averaged $C_i^m(r)$ and the ratio of logarithms is equivalent to their difference. Although the ApEn can be calculated from relatively short data-series, the length of ECG recordings influences the value of ApEn (similarly to the SDNN). In healthy subjects, the ApEn is found to be slightly over or around 1 [141]. In pathological conditions, ApEn was found to be higher [112, 142] indicating the existence of more unpredictable patterns.

As with many other HRV measures, the ApEn requires data to be stationary and noise-free (without artifacts). In addition, relatively long ECG recordings are required for the ApEn to be measured reliably. Also, ApEn includes a spurious contribution from "self-matching".

A variant of ApEn in which self-matching is not included, referred to as the *sample entropy (SampEn)* has been proposed [143]. SampEn describes the conditional probability that two sequences for *m* data points (with a tolerance *r*) remain within *r* of each other (similar) at the next point. The SampEn converges to a consistent value for a considerably lower *r* and *N* than the ApEn [143]. A reduced *SampEn* was described in neonates prior to the clinical diagnosis of sepsis [144] and before the onset of atrial fibrillation [145].

As biological systems are structured on multiple spatial-temporal scales, a description of their dynamics using the ApEn or SampEn, which evaluate regularity on one scale only, might provide conflicting results. Thus, the so-called *multi-scale entropy (MSE)* evaluation has been proposed in which the SampEn is calculated for the coarse-grained data for a range of scales (e.g., $\tau = 1$ to $\tau = 20$ [146]). The MSE is applicable to a data-series of finite length (~30,000). Increased regularity irrespective of variability (decreased or increased) was found to characterize pathological states. A reduced MSE, depending on the scale of reduction, distinguishes patients with CHF, AF, or diabetes from healthy subjects [146, 147].

Another variant is *compression entropy (CE)*. It quantifies the extent to which the data-series can be compressed, depending on the occurrence of repeated sequences [148]. CE reduction was documented in patients with CHF and malignant ventricular arrhythmia [149]. The reliability of this method depends on sampling rate, the window length, buffer size, and integer numbers [148].

Symbolic Dynamics

The absolute value of parameters is seldom of importance for diagnostic (classification) purposes, while the relative orders or qualitative values (above or below a threshold) are significant. In such instances, a great simplification in the form of *symbolic dynamics (SDyn)* can be applied [150–152]. SDyn is based on coarse graining and involves the transformation of the original time series into a series of a limited amount of discretized symbols that are processed to extract important information about the system generating the process.

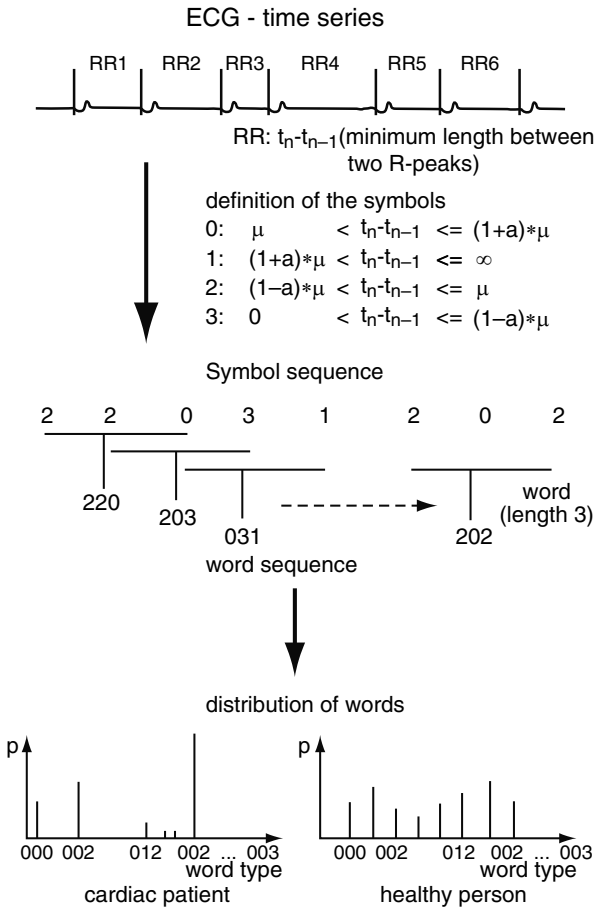

Figure 35.24

Illustration of symbolic analysis method. R – R interval series is uniformly spread on pre-determined levels. Each level is described by symbol (number) and 3-symbols patterns (words) are constructed (From [A37]).

A variant of the SDyn approach has been proposed to describe short-term HRV dynamics [151]. First, the data series is transformed into a sequence of symbols. These symbols are simply the alphabet A = (0,1,2,3. . .) and permit the classifying of various patterns and monitoring of their occurrence and changes with time (Fig. 35.24). At least three symbols (*strings*) are necessary to characterize short-time dynamics. The resulting data are expressed as the probability of distribution of each single word (3 symbols) within a word sequence. A modified procedure of SDyn that permits a shortened data series (~300 heartbeats) to be analyzed has been proposed [151]. This method naturally results in a considerable compression of the data with a subsequent loss of detailed information. It also improves the sensitivity to noise. However, the presence of artifact influences the symbol strings.

To quantify low-variability data epochs, a parameter called *POLVAR10* has been proposed [152]. It is calculated on the basis of the most simplified transformation of differences of 10 ms or more (symbol:1) or less (symbol:0) between successive heartbeats. Only words of six unique symbols (all 1 or all 0) are counted. The POLVAR10 represents the probability of occurrence of the word "000000," which indicates severely depressed variability [152].

The *acceleration change index (ACI)*, an index that can be obtained from the sign (1 for HR deceleration, 0 for acceleration) of the beat-to-beat difference, which characterizes the dynamics of zero-crossing, has been proposed [141].

A series of sign changes (SC) is generated. Then, the differentiation of SC (*DSC*) is calculated and the ACI is defined as (35.26):

$$\mathrm{ACI} = \frac{k}{M}, \tag{35.26}$$

where k is the number of times that the DSC time series equals 1, and M is the total number of samples in the DSC series. Therefore, the ACI is the proportion of times that a local maximum (or minimum) is followed immediately by a local minimum (or maximum) by the total number of local maxima and minima. Despite the method being simple and robust, the ACI quantifies similar changes of a different length (increase or decrease by 20 or 40 ms for example, and so on). Arif and Aziz have proposed the *threshold-based* (indicating the necessary change to be signed) *acceleration index* (TACI). The TACI allows better classification of patients with specific diseases [154]. However, its clinical applicability is not proven and the threshold value has to be chosen empirically.

Information Entropy

The entropy of a random variable is defined in terms of its probability distribution and can be considered as a good measure of randomness (or uncertainty). This is the basis of the so-called *Shannon entropy* (or *measure of uncertainty*) [155].

Consider a stationary time series $\{x(n)\}_{n=1}^{N}$ that is characterized by the discrete probability distribution $\{S_i\}_{i=1}^{K}$ with the marginal distribution $p_i = \sum_i S_i$. Then, for the discrete probability distribution $\{p_i\}$, the Shannon information measure is defined (35.27) as:

$$H_x = -\sum_i p_i \log_2 p_i \tag{35.27}$$

For HRV complexity measurements, the Shannon entropy can be applied for time series transformed into symbol sequences (see symbolic dynamics). Thus, having the W^k set of all words ω of length k, the H_k calculated from the distribution of probability of words $p(\omega)$ is given by (35.28):

$$H_k = -\sum_{\omega \mathrm{E} W^k, p(\omega)>0} p_\omega \log p_\omega \tag{35.28}$$

Larger values of *Shannon's entropy* H_k indicate a higher complexity. Among various "words" there are some that never or only seldom occur. These "words" are called "forbidden". Counting the forbidden words in the distribution of words (of length 3 symbols), regular or irregular behavior in the data series can be distinguished (with a high or low number, respectively).

If the data series contains negative values, one informative measure, which allows negative values in the distribution is *Renyi's entropy* described as (35.29):

$$H_\alpha = \frac{1}{1-\alpha} log_2 \left\{ \sum_{k=1}^{N} p_k^\alpha \right\} \tag{35.29}$$

where α is order ($\alpha > 0$, $\alpha \neq 1$). The result produced by this measure is expressed in *bits*: if one elementary signal yields zero bits of information, then two well-separated elementary singles will yield one bit of information, four well-separated elementary singles will yield two bits of information, and so on. Thus, for different cardiac signals, Renyi's entropy in the time–frequency domain is different [155].

Mutual information function (MIF) is an informative approach analogous to the cross-correlation or the auto-correlation function. For two stationary data series *x(n)* and *y(n)* the Shannon H_k can be calculated (H_x and H_y, respectively). Then, the MIF is given by (35.30):

$$MI_{xy} = H_x + H_y - H_{xy} = \sum_{ij} S_{ij} \log_2 \frac{S_{ij}}{p_i q_j} \tag{35.30}$$

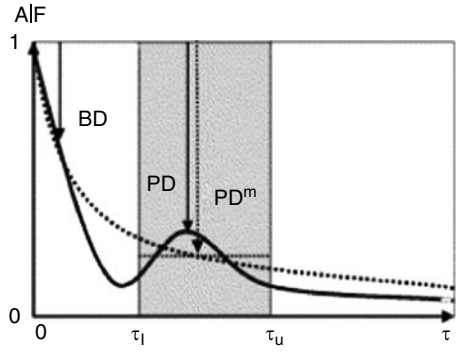

Figure 35.25

Scheme of Autonomic Information Flow (AIF) as function of the time scale τ. The AIF value at $\tau = 1$ heartbeat quantifies the information flow to the successive heartbeat. The respective loss of the signal inherent information (AIF normalised to 1 at $\tau = 0$) is quantified by the AIF decay measure BD (beat decay at $\tau = 1$ heart beat). Correspondingly, the loss of information over a longer time scale τ, such as the vagal or respiratory sinus arrhythmia rhythms, which can appear as peak in AIF (full line), can be assessed as PD (peak decay). In cases of nonappearing peaks, the decay with regard to the mean AIF of appropriate time scale range (PD^m, dashed lines) are used as robust measure. The lower boundary τ_l and the upper boundary τ_u of the time scale range is chosen according to the corresponding frequency band boundaries f by $\tau = 1/(2f)$ (From [A 36]).

The MIF measures the average information in $x(n)$ on $y(n)$ in units of "bit". MIF is symmetrical ($MI_{xy} = MI_{yx}$), non-negative, and bounded from above by min $\{H_x, H_y\}$. MIF vanishes if the time series are statistically independent. Thus, the $x(n)$ (almost surely) determines $y(n)$ only if $\mathrm{MI}_{xy} \geqslant H_y$.

On the basis of the MIF, the *autonomic information flow (AIF)* has been proposed by Hoyer et al. [156]. In this method, all statistical dependencies are considered as *information flow* within the time series. AIF is independent of signal amplitudes and allows the predictability and regularity of a signal to be quantified.

A typical AIF is sketched in Fig. 35.25. The amplitude at $\tau = 0$ (normalized to 1) represents the entire information of a time series. The decay of this function over a prediction time τ (which is considered as a time scale) represents the loss of information (here, over one heartbeat interval). In the case of a highly complex interval series, the next RRI is poorly predictable and consequently the decay of the AIF curve (information loss) is high (large BD, beat decay). In the opposite case of a confidently predictable heartbeat series, the AIF decay is low and consequently the BD is small. Predominant rhythms (such as vagal oscillations) can be assessed by the information loss over respective prediction time horizons (= time scales) corresponding to the well-known autonomic rhythms. The resulting measure is called *peak decay* [156]. Various time scales of AIF can improve prognostication in patients with multiple organ dysfunction syndrome and after cardiac arrest.

35.3.4.3 Methods for Chaos and Determinism Analysis

(Chaos – a property of a system that looks random being in fact deterministic (albeit irreversible and unpredictable). Determinism–this means that points close to each other in phase space at a time t will probably be close to each other at a time $t + \Delta t$. Thus, determinism implies that evolving from time t_0 to t_1, and then from t_1 to t_2, is the same as evolving from t_0 to t_2 *(known as Chapman-Kolmogorov law)*.)

Many biological phenomena which look like a random (stochastic) process (atrial fibrillation, ventricular fibrillation) are in fact related to many factors (the number of degrees of freedom (Mathematically, the number of degrees of freedom (or the dimension of state space) equals the number of first-order differential equations necessary to describe the system.), usually not known exactly) that determine their nonlinear dynamics (behavior) [108, 109, 111]. Dynamical

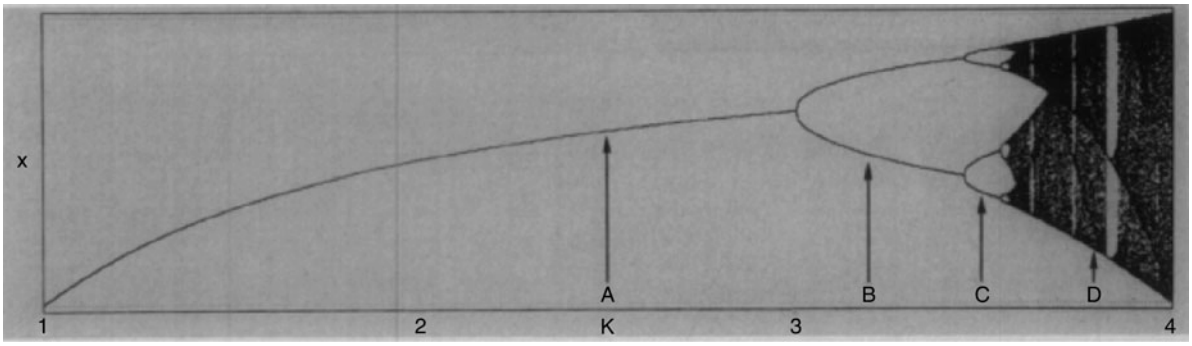

Figure 35.26
Bifurcation diagram of logistic map (From [108]).

(biological) systems (continuous) usually consist of phase space (M) and map (evolution, flow, F). Typically, there are at best *differential equations* (Differential equation is a mathematical equation for an unknown function of one or several variables that relates the values of the function itself and its derivatives of various orders.) to express the evolution of the system. For exploratory reasons, the continuous system behavior is evaluated after discretization (i.e., "time" is given as a set of points 1,2,3. . ...F). For a 1D system, a nonlinear behavior can be characterized by means of a so-called *logistic map* (Logistic map – a polynomial mapping of chaotic behavior can arise from very simple nonlinear dynamic equations.) (35.31):

$$x_{n+1} = ax_n\left(1 - x_n\right), \tag{35.31}$$

where x_{n+1} is the point (state) after time 1, x_n is the initial point (state), and a is the bifurcation parameter. When a increases, the system switches to higher periodicities (so-called *period-doubling bifurcations*) until at a certain value of a the system exhibits chaotic behavior (period-doubling route to chaos) (Fig. 35.26) [108, 109]. The transition from regular (periodic) to chaotic behavior takes place via a quasi-periodicity, sub-criticality, or intermittency. All possible dynamics have been observed with respect to cardiac arrhythmias (i.e., ventricular fibrillation [116–120]).

Consider two initial states of $x(t)$ and $y(t)$ at time $t = 0$. If the tendency is to diverge at an exponential rate with time ($\gamma > 0$), then the system exhibits chaotic dynamics (35.32)

$$|x(t) - y(t)| \approx |x(0) - y(0)|e^{\gamma t}, \tag{35.32}$$

which define a property of chaotic dynamics, that is, the sensitivity of the evolution of the system to the initial condition [157].

Largest Lyapunov Exponent

The Lyapunov exponent (λ) is a quantitative measure of the sensitive dependence on initial conditions [109, 157]. It defines the average rate of divergence of two neighboring trajectories. An exponential divergence of infinitesimally close trajectories in phase space, coupled with a folding of trajectories to ensure that the solutions will remain finite, is the general mechanism for generating deterministic randomness and unpredictability. A negative exponent implies that the orbits approach a common fixed point. A zero exponent means that the orbits maintain their relative positions – they are on a stable attractor. Finally, a positive λ implies that the orbits are on a chaotic attractor. Thus, Lyapunov exponents allow the discrimination between periodicity and chaotic dynamics. Amongst all possible λ, the largest Lyapunov exponent (LLE) is of particular interest. Its positivity is presumed to be a "gold standard" for chaos in "deterministic" time series.

Wolf et al. [158] have proposed the algorithm for LLE calculation from time series. For a given time series *x(t)* and the nearest to initial point *x(t0)*, the average exponential rate of divergence is characterized by (35.33):

$$\lambda = \frac{1}{t_M - t_o} \sum_{k=1}^{M} \log_2 \frac{L(t_k)}{L(t_{k+1})}, \tag{35.33}$$

where L indicates the distance between these two points. To calculate the LLE, the following set of parameters must be chosen: m – the embedding dimension, τ – the delay, evaluation time t_{k-1}, t_{k+1}, as well as separation points and maximum orientation error. For LLE calculation for ECG data series, an m between 5–20 and a time delay of 1 is indicated. However, a reliable calculation of LLE requires a relatively long and uncorrupted data series. In addition, it remains controversial whether LLE per se allows sufficient proof of chaos or provides a quantitative measure of chaos intensity.

Poincaré Sections

This is a way of obtaining a discrete $(n-1)$ dimensional dynamic from an n-dimensional continuous space-phase. For a 3D orbit, it is possible to intersect the orbit in a discrete set of points $x(t_k)$ with a suitably oriented plane *P (Poincaré section)*. Then, the points where the orbit intersects the plane from the same side (from behind) can be chosen. Therefore, a two-dimensional discrete dynamics $x_{k+1} = G(x_k)$ in the plane P can be determined [108, 116, 117].

Noise Limit Titration

The presence of noise in real (experimental) data series is the main factor that limits the reliability of various methods that are proposed for the detection of deterministic chaos. Poon and Barahona [159] have proposed an analytical technique called *noise titration*. Instead of removing or separating noise from the data, artificially generated random noise is added to the quantitatively titrate chaos. White (or linearly correlated) noise of increasing standard deviation (δ) is added to the data until its nonlinearity goes undetected by a particular *indicator* at a limiting value of δ = *noise limit (NL)* (noise ceiling of the signal) and at a limiting condition (equivalence point). An NL value > 0 indicates chaos, and its given value estimates its relative intensity. If NL = 0, the data-series can be considered either nonchaotic or the background noise (so-called noise floor) neutralizes the chaotic component. The power of the numerical titration technique depends critically on the choice of a suitable *nonlinear indicator*, which has to be specific (to nonlinear dynamics) and tolerant (to measurement noise). One verified method is the *Volterra-Wiener algorithm* [159]. The titration procedure is highly sensitive and specific to chaos, immune to noise, relatively simple and robust. Its ability to distinguish healthy young and elderly people from CHF-patients has recently been reported [160]. However, its clinical significance still remains unexplored.

35.3.4.4 Nonlinear Prediction (Forecasting)

A characteristic feature of a dynamic system with deterministic chaos is that the prediction of its behavior is possible with some degree of confidence only in the short term. Thus, with some knowledge about a part of system dynamics (so-called *library*), it is possible to try to predict its behavior several steps into the future. These assumptions provide a basis for the development of methods for HRV predictability (forecasting) [161, 162].

Correlation Coefficients

Sugihara and May [161] have arbitrarily proposed dividing a given time series into two equal parts, using the first half as a library, from which the behavior of the second half can be predicted. By constructing an m-dimensional vector (called *the predictee*) $X_t = (x_t, x_{t+1} \ldots . x_{t-(m-1)})$ from the first half of the time series, it is then possible to make a numerical prediction for the parts immediately following the elements of the predictee. Denoting these predicted values by $x_{t+p}^{\cdot}$ for $p = 1, 2, \ldots . p_{\max}$, it is then possible to plot the $x_{t+p}^{\cdot}$ against the values x_{t+p} actually occurring in the time series. By repeating this procedure for many m-dimensional vectors drawn from the second half of the series, it is feasible to compute the correlation coefficient ρ for the predicted and actual values as a function of p, the number of time-steps into the future.

S-map (Sequential Locally weighted Global Linear Maps)

A locally weighted map can provide a simple test for nonlinearity in a time series [156]. Suppose there is an embedding of the actual time series $X_t \in R^{m+1}$ where $X(t) \equiv 0$, and the time step Tp forward is $X_{t+Tp}(1)$, then the forecast at Tp is given by (35.34):

$$\widehat{Y}_t = \sum_{j=0}^{m} C_t(j) X_i(j). \tag{35.34}$$

35.3.4.5 Irreversibility/Asymmetry Analysis

Time irreversibility analysis is a nonlinear dynamics technique that produces temporal *asymmetries* in statistical properties that are different when the series are observed after time reversal. Thus, if a stationary time series is considered to be time reversible, then the probability of the vector $(z_n,..z_{n+k-1})$ is equal to the probability of the vector $(z_{n+k-1},..z_n)$ for all k and n [163]. *For* a time-reversible segment, it follows that the return map $R - R_{n+1}$ versus $R - R_n$ is symmetrical with respect to the line of identity. Thus, the irreversibility is defined by the asymmetry of the distribution of the difference of consecutive intervals with respect to zero. The simplest test statistic used for detection of deviations from time reversibility is the *skewness of the differences of R–R intervals* [163].

Costa et al. [164] have proposed a so-called multi-scale time asymmetry index A_I that is based on methods derived from basic physics assumptions. First, data-series are transformed into binary sequences of HR accelerations and decelerations. Then, a set of coarse-graining time series y_τ is constructed by taking the average inside the moving window with a different scale factor τ. The difference between the probability of energy distribution for HR accelerations and decelerations provides the estimator of time reversal asymmetry $\widehat{A}(\tau)$ (35.35):

$$\widehat{A}(\tau) = \frac{\Sigma_{y_\tau>0} P(y_\tau) \ln[P(y_\tau)]}{\Sigma_{y_\tau} P(y_\tau) \ln[P(y_\tau)]} - \frac{\Sigma_{y_\tau<0} P(y_\tau) \ln[P(y_\tau)]}{\Sigma_{y_\tau} P(y_\tau) \ln[P(y_\tau)]}, \tag{35.35}$$

where $P(y)$ denotes the probability of y_τ. For a range of time scales τ, the *multi-scale time asymmetry index* (A_I) is calculated as the summation of the asymmetry values $\widehat{A}(\tau)$ obtained for each time scale (35.36):

$$A_t = \sum_{\tau=1}^{L} \widehat{A}(\tau). \tag{35.36}$$

The A_I values are significantly higher for young healthy adults than for the elderly and subjects with CHF or AF. Interestingly, highly irregular time series of AF and less variable (compared to healthy subjects) time series of patients with CHF tend to be more symmetric [164]. Thus, A_I can be considered as a measure that can be applied irrespective of heart rhythm.

Many simple tests for time-irreversibility that are based on return map evaluation have been proposed by Ehlers et al. [165], Guzik et al. [166], and Porta et al. [167]. The distribution of R–R intervals (or differences) with respect to the main diagonal of the return map is quantified as the number of points (or distances) below or above the diagonal.

The clinical significance of time-irreversibility remains unresolved. However, evidence of a link between autonomic control and the asymmetry index has been found [168]. Recently, Porta et al. have described a method for distinguishing various types of nonlinearities over different temporal scales [169].

35.3.4.6 Phase-Rectified Signal Averaging Method

Periodicities in HR signals are usually contaminated by the presence of noise and artifacts, which may cause a reset of the periodicities (quasi-periodicities). These "new" quasi-periodicities can be determined by means of a phase-rectified

averaging method (Fig. 35.27) [170]. First, the so-called anchor points (Anchor points correspond to increases (or decreases) of the signal.) in the phase of deceleration or acceleration are determined (Fig. 35.27). The averages over anchor points are calculated within a segment (window) containing signals close to them (usually two intervals for each side). Differences in PRSA over increasing and decreasing parts of the signal indicate a loss of time-reversal symmetry. The derived index called *deceleration capacity* (DC) has been shown to be helpful in risk stratification in post-MI patients [171], especially in those with preserved left ventricular function [172].

35.3.4.7 Recurrence Quantification Analysis

Recurrence quantification analysis (*RCA*) is a method for quantification of determinism in a time series [173]. This method is especially useful for transient behavior far from equilibrium (RQA software (Webber & Zbilut), can be downloaded from the following URL: http://homepages.luc.edu/~cwebber/.). Basically, the difference in the embedding dimension $z_n - z_m$, which constitute the *recurrence matrix* $R_{n,m}$ can be calculated. Points of the recurrence matrix are designated "recurrent" if the difference between paired vectors is below a cut-off value. Recurrent points are plotted as darkened pixels at corresponding n, m coordinates (Fig. 35.28) [174]. If the signal is regular, its deterministic nature will show regular patterns. A quantitative description is given by the parameter percent of determinism (%DET) (among others proposed), which is about zero for the stochastic process and approximately 100 for a deterministic signal. %DET provides information about the intrinsic structure of the signal [174]. Although the RCA also allows for the determination of the LLE and Shannon entropy, this method has been found to be of limited clinical interest [175].

35.3.4.8 Stochastic Resonance

The presence of noise might not necessarily be considered harmful. In fact, under certain circumstances, an "extra dose" of noise can help the performance of the system [176]. The noise component can be calculated by means of several methods, with the most popular being the *signal-to-noise ratio (SNR)* [176]. The geometric mean of the average distribution values below and above the signal bandwidth has been proposed for its calculation. The SNR of the RRIs (SNR_{RRI}) can be calculated as a ratio of $(D_{S+N} - D_S)/D_N$, where D_{S+N} is a distribution of the recorded signal (signal *[s]* + noise *[n]*), and D_S is a distribution of the true signal over a prespecified bandwidth. For transient changes to be examined, a robust locally weighted regression can be used to smooth varying SNR temporally [177].

35.3.5 Methods for Qualifying and Quantifying HRV Relationship with Other Biological Signals

Important information provided by HRV analysis extracted from a single time series cannot enhance other time series. Therefore, the interaction between two (or more) physiological (sub)systems might be necessary. Sometimes, a single ECG time series can provide data regarding breathing rate though the respiratory function is not recorded [177, 178]. In addition, other ECG-derived parameters that might be related to heart rate control can be obtained, estimated, and correlated with the HRV signal [179].

Usually, simultaneously recorded time series for each system are required. Hence, many bivariate or multivariate techniques have been developed that aim to quantify the imprint of the physiological interaction between the two or more systems. Apart from the detection of interrelations, some of these techniques are designed to assess causal relationships between the signals.

35.3.5.1 Time-Domain Method

Time-domain approaches for quantifying a relationship between any two signals (HR and respiration or SBP or other) are based on the simultaneous measurement of changes of the two parameters and the calculation of the correlation of their

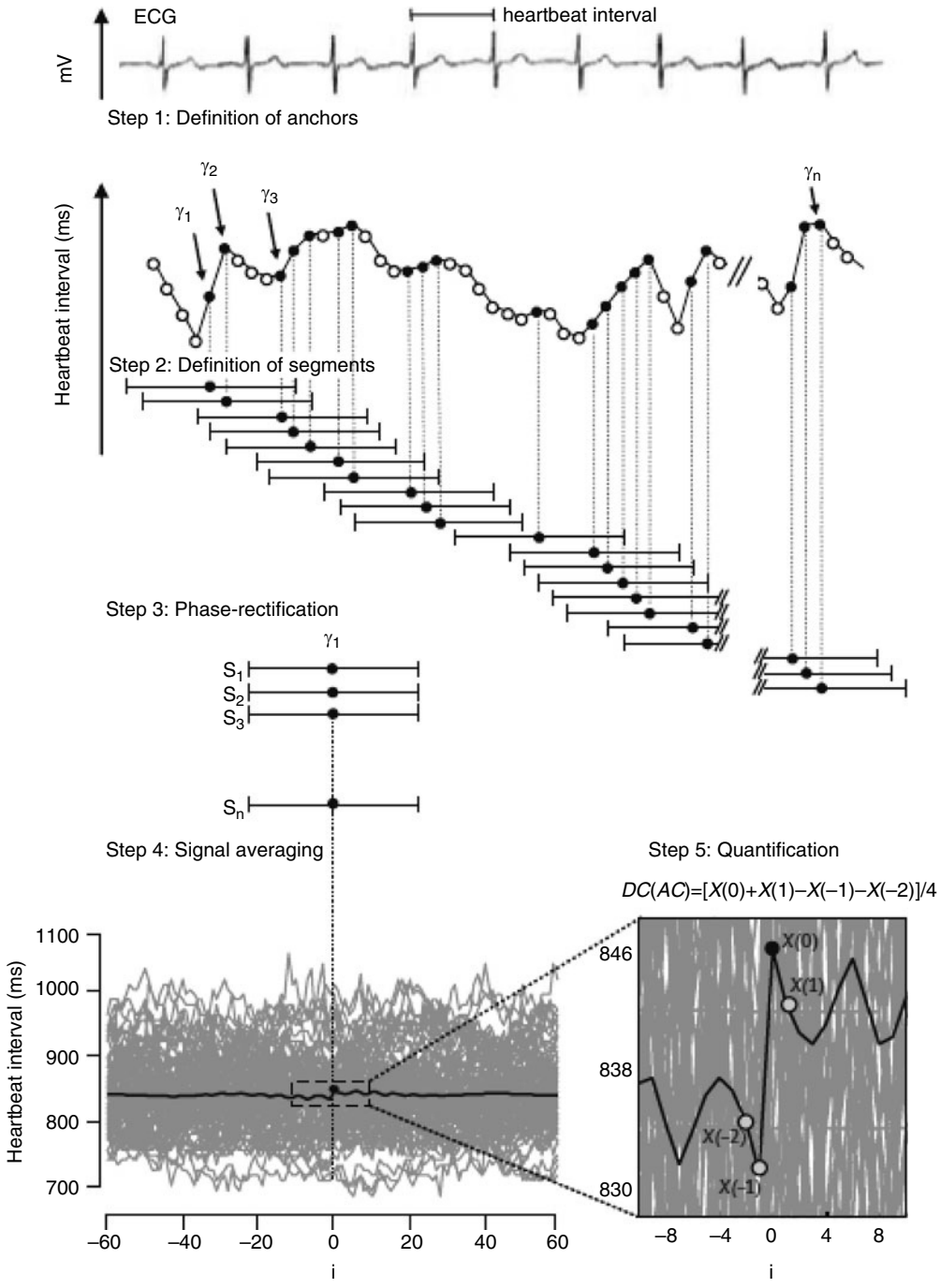

Figure 35.27

Calculation of Deceleration Capacity index by phase-rectified signal averaging. For explanation see [170, 171].

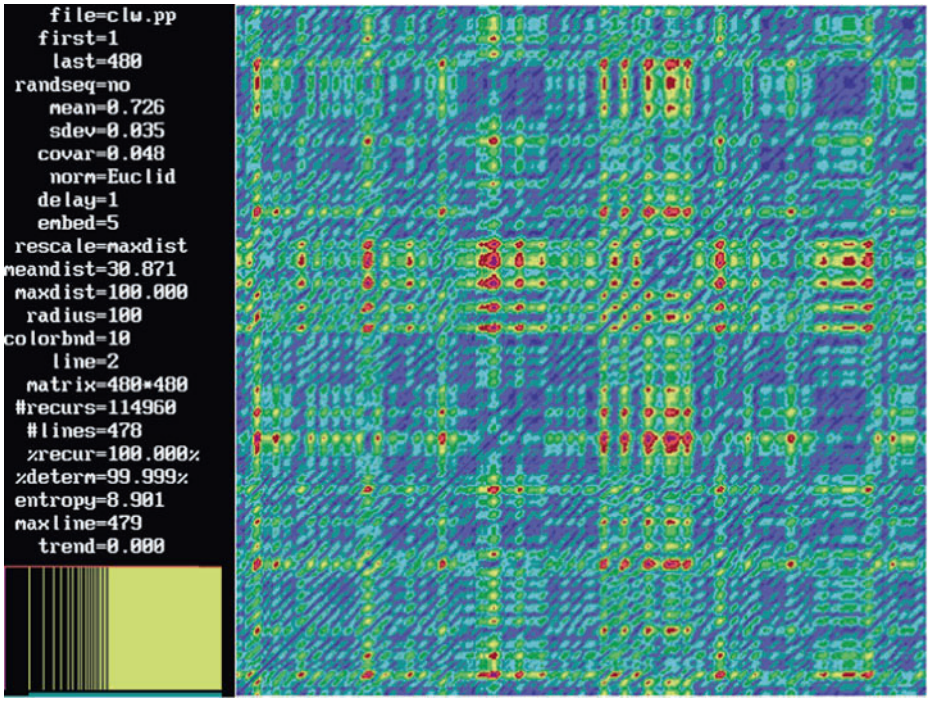

Figure 35.28

Recurrence plot. The various color s reflect different Euclidean distances between trajectories and are analogous to geographical relief maps. Five RQA variables are computed (%recurrence, %determinism, information entropy, maximum diagonal line length, state trend) which have relevancy as nonlinear markers of changes in dynamical systems and physiological states. If the signal is regular, its deterministic nature will show regular patterns (From http://homepages.luc.edu/~cwebber/with permission).

linear regression. Accordingly, the change of a signal $x(t) - x(t+i)$ is plotted against the change of a signal $y(t)$–$y(t+i)$. The slope of a linear regression describes the magnitude of the relation. This relatively simple approach forms the basis of some clinical tests, like the RSA deep breathing test, Valsalva or Muller test, tilt test, and BRS evaluation.

Time-dependent occurrence of the signal changes with another signal may help to investigate coordination and synchronization. The simplest example is the relation of the P-wave to the QRS complex. If the relation is given by the number 2, it simply indicates the presence of a II^{o} A-V block Mobitz I with a 2:1 pattern. A similar approach can be applied in studying coordination of HRV and respiration or blood pressure changes. In addition, nonlinear phenomena that can mimic AV block patterns (i.e., bifurcations) cycle-multiplying (i.e., periodicities including alternans) can also be examined.

35.3.5.2 Cross-Spectrum

The *coherence* is a complex function of the frequency and estimates a degree of linear correlation between two signals [180–187]. If $S_{xx}(f)$ and $S_{yy}(f)$ are spectra of *xx* and *yy* signals, and $S_{xy}(f)$ is a cross-spectrum of the signal $x(t)$ and $y(t)$, then the coherence $K(f)$ is given as:

$$K(f) = \frac{S_{xy}[f]}{\sqrt{S_{xx}[f] * S_{xyy}[f]}} \tag{35.37}$$

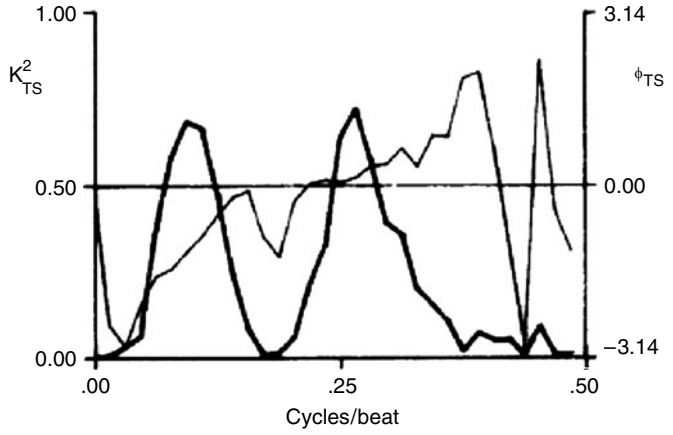

Figure 35.29

Bivariate analysis of BP-HR variation in a healthy subject. Thick line – squared coherence spectrum, thin line – phase spectrum (From [185]).

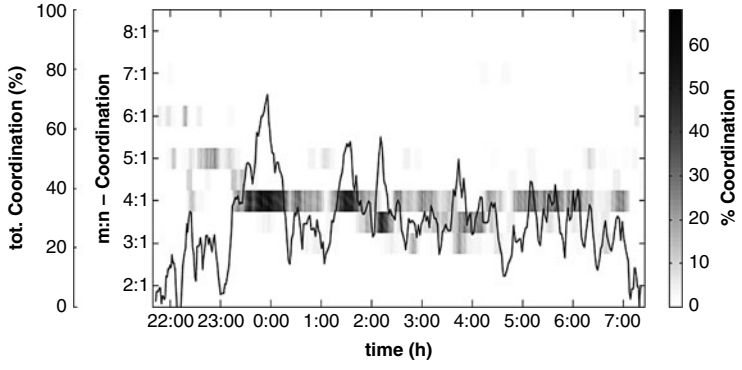

Figure 35.30

Example of a coordination diagram. The coordination diagram indicates changes in the relative number of coordinated R-peaks as a respective m:n ratio (see text). In this example the cardiorespiratory coordination is oscillating with the 4:1 pattern's predomination. The absolute maximum of 68% of coordinated R-peaks (left *y* axis) is reached at midnight. Amount of coordination regardless of m:n ratio is depicted by the line of the %coordination (right *y* axis) (From [195]).

The coherence is commonly represented as the squared modulus $K^2(f)$, which at any frequency band is an index between 0 and 1 of the amount of squared correlation. Values above 0.5 are considered significant (Fig. 35.29).

Availability of the cross-spectrum allows also the calculation of the phase relationship in the range of –180° and +180° or – ≠rad to + ≠rad, with a positive angle for a leading x(t), and a negative angle for a leading y(t). The phase relationship is commonly represented as the *phase spectrum* $(\varphi(f))$.

The relationship between two signals, which are the input and output of the system, can also be described by the *transfer function*, which is given as:

$$H(f) = \frac{S_{xy}[f]}{S_{xx}[f]} \tag{35.38}$$

The cross-spectrum can be calculated from spectra obtained by means of parametric or nonparametric methods, including the Fourier Transform, autoregressive modeling, wavelet transform and others [185, 186].

35.3.5.3 Nonlinear Methods

Phase Coordination and Synchronization

The term *coordination* means that there is some kind of temporal or phase incidence between HRV (the time of the R-wave) and another signal (e.g., onset of respiration, maximum blood pressure). The term *synchronization* means that there is a real physiological coupling between signals [187, 188].

In order to obtain coordination and synchronization indexes, signals (x, y) have to be recorded simultaneously and continuously and presented as time series $x(i)$ ($i = 1, \ldots..m(x)$) and $y(j)$ ($j = 1, \ldots..n(y)$). The absolute (t) or relative (φ) distance between the $y(j)$ and the preceding $x(i)$ or successive $x(i)$ can be calculated. This allows for presentation of the so-called synchrogram (or post-event time series) that illustrates variety in how the mth $x(t)$ corresponds with the nth $y(t)$ (i.e., *m:n coupling*) [187].

Hildebrandt et al. and Kenner et al. have provided the first description of methods for continuous measurement of the phase relation between HR and respiration [189, 190]. They found an intermittent coordination between the onset of inspiration and the preceding R-wave. In addition, the ratio of HR and respiratory rate has been suggested as a simple measure of cardiorespiratory coordination [191]. Many advanced approaches to cardio-respiratory coordination have been proposed (e.g., state-space correspondence, phase synchronization λ, phase recurrence, information flow, distribution) [192–194]. The performance of these methods depends on the time-window used. Cysarz and coworkers have recently shown (Fig. 35.30) that the largest number of coordinated R-peaks and coordinated sequences was detected by the phase recurrence approach [195]. As the clinical usefulness of these methods has not been thoroughly validated [196], all the proposed methods seem to be valid for research purposes only.

Nonlinear Prediction

Nonlinear predictability of one x(n) of two series given from samples of another series y(n) is used to define directional coupling. This approach is suitable for short and noisy data, frequently present in physiological series (artefacts, transitions etc.), which contains local constants, local linear parts and nonlinearities. The predictability can be quantified by using the cross-predictability and the predictability improvement calculation. The degree of predictability can be calculated as the squared coherence between the original and predicted values. Nonlinear prediction methods are especially useful for investigating HRV-BPV causal relationships in many clinical states [192].

Stochastic Resonance

The stochastic resonance analysis might be more helpful for the analysis of interactions between various systems (e.g., heart rate and blood pressure) [197]. Its analysis might open new possibilities for the understanding of physiological and pathological phenomena associated with HR control [198]. At present, data accumulated for its application is limited, being anecdotal for clinical use [199].

35.3.5.4 Baroreflex Sensitivity

Analysis of baroreflex sensitivity (BRS) enables the quantification of the reflex circulatory effects of arterial baroreceptor activation or deactivation at the sinus node level through changes in vagal and sympathetic activity [77, 82, 182, 183, 186, 200, 201]. It has to be borne in mind that HR changes are only a part of the complex circulatory response to short (sensitivity) and long-term (resetting) blood pressure fluctuations, in which the systemic vascular resistance control seems to be the main target. Various methods can be used for BRS assessment [202]. All of them are based on the measurement of the extent of R–R interval change (ms) per unit (mmHg) change in systolic blood pressure. Assuming that the relationship between SBP and R–R interval in response to a rapid BP change is linear, the quantitative measure of BRS is provided by the slope of the regression line fitting changes in SBP against the second succeeding R–R interval (one-beat delay) [186, 201]. Usually, a significant relationship is required to accept the BRS value obtained. However, the BRS value calculated on a linear fit with a lack of a significant correlation is allowed if an adequate increase in SBP (>20 mmHg) is obtained [186].

Invasive Approach (External Stimuli)

Vasoconstrictor agents are normally used to explore the vagal component of the baroreflex sensitivity. Phenylephrine, a pure α-adrenergic agonist, is administered intravenously during the continuous recording of ECG (R–R interval) and BP (beat-to-beat arterial pressure) [203]. The latter can be performed either invasively, mainly in experiments on animals, or noninvasively, by using the finger-cuff method, which provides overestimation of BP variability [204], largely within the lower frequency bands [205]. After a bolus dose of 1–2 ug/kg, incremental doses of 25–50 ug are given until a SBP increase of 20–30 mmHg is reached. In normal subjects, the average values of 15 ms/mmHg have been reported [186]. In certain clinical settings, the BRS values close to zero, or even a negative BRS, can be observed [206]. Vasodilating agents are normally used to explore the sympathetic component of the BRS [207]. Nitroglycerine, a direct vasodilator, is given via the injection of 100–200 μg to obtain a rapid and progressive fall in SBP of 20 mmHg. The BRS values after administration of vasodilators are lower, indicating that the use of both vasoactive agents allows for a more comprehensive assessment of BRS. Alongside, a "steady-state" method for estimating BRS has been proposed [208], in which either phenylephrine or nitroglycerine is administered in order to obtain the step-wise increase or reduction of blood pressure.

Methods that use vasoactive agents are criticized because of their nonselective actions leading to the introduction of changes that alter the baroreceptor reflex at various levels (e.g., central effects, direct action on sinus node). On the other hand, these methods allow the initiation of an integral response, irrespective of the mechanisms contributing to the reflex.

Mechanical maneuvers, like the neck chamber technique or lower body negative pressure, represent other approaches to studying BRS. In the neck chamber technique, either positive or negative pressure is applied to the neck region inducing a decrease or increase in SBP with corresponding changes in R–R intervals [209]. The negative pressure ranges from −7 to −40 mmHg and HR response is observed over three heartbeats following the maneuver. The BRS is defined as a slope of R–R interval over neck pressure. A modified method of the neck chamber method has been proposed that allows both for activation or for deactivation of carotid baroreceptors [210]. The lower body negative pressure that imitates a reduction in circulating blood volume can be helpful in an evaluation of sympathetic activation and HR response [211]. However, in contrast to direct carotid baroreceptor stimulation/inhibition, this method provides information regarding cardiopulmonary reflexes [211]. Methods based on mechanical manipulations should be used in a specifically designed research laboratory and for particular pathophysiological purposes [212, 213].

Noninvasive Approach (Internal Stimuli)

Noninvasive methods of BRS analysis represent alternatives to invasive techniques in that they use internal stimuli that can be simply induced (e.g., Valsalva or Muller maneuver, head-up, or downward tilt) or that they occur spontaneously (Fig. 35.26).

(a) The Valsalva maneuver

The Valsalva maneuver is a forced expiratory effort against a closed airway. The Muller maneuver is the reverse. There are four phases of these tests, and among them, phase IV is commonly used for the BRS assessment purposes. The BRS

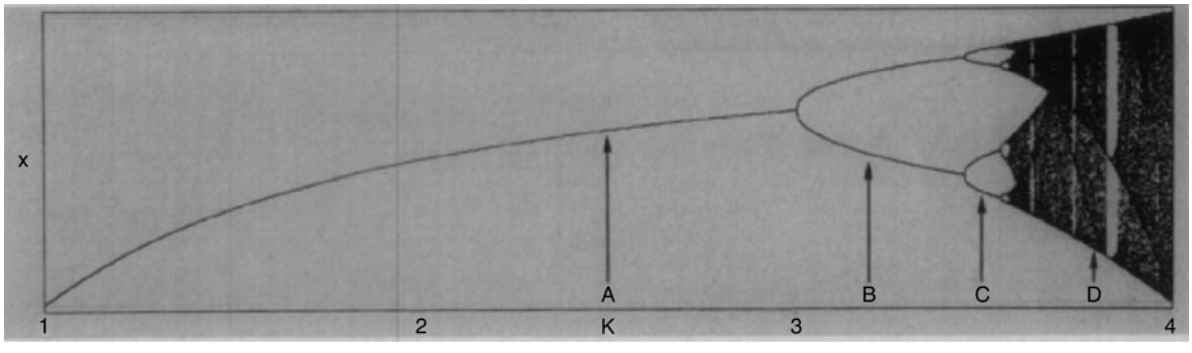

Figure 35.31

The relation between the changes in systolic blood pressure increase and corresponding RR interval lengthening during downward tilting (From [216], Elsevier, with permission).

is calculated using linear regression of instantaneous R–R intervals and corresponding SBP values. Kautzner et al. have proposed calculating the BRS index, which is the ratio of the differences between maximum and minimum R–R interval and SBP during the so-called overshoot period of the maneuver [214]. Unfortunately, reliable measurements cannot be obtained in a large proportion of normal and post-infarction patients [215]. In addition, the correlation coefficients with invasive methods vary between 0.27 and 0.91 [214].

(b) Tilt testing

A body movement introduces changes in blood pool compartments and venous return, with corresponding BP and HR changes. Takahashi et al. have proposed a method for BRS evaluation during a rapid downward tilting from an upright to a supine position, which provides values comparable to the phenylephrine test [216].

(c) Time-domain (sequence) method

The sequence method is based on the spontaneous presence of concurrent R–R interval and systolic blood pressure changes (increase or decrease) over at least three consecutive heartbeats (sequence) [217]. For each sequence, the linear correlation between R–R intervals and SBP values is fitted. The average of individual slopes of sequences that are significant ($r > 0.8$) and reach predefined minimum change (1 mmHg and 4–6 ms for SBP and interbeat duration respectively) is taken as the BRS measure. Usually, lower BRS values have been observed in comparison with the phenylephrine test [78]. Simplified variants of the sequence method have been proposed. Among them, the measurement of R–R interval variation over a 5-min period of controlled breathing at 0.1 Hz, that allows SBP changes to be ignored, has been documented as useful for distinguishing normal subjects (77 ms) from patients with heart failure (31 ms) [218].

(d) Spectral ratio (alpha-index)

Spectral ratio (gain, alpha-index) provides an estimate of the sensitivity of the baroreceptor-heart rate reflex based on frequency-domain analysis of the spontaneous variability of SBP and HR [77, 78, 82, 203]. The method is based on a high degree of linear correlation between systolic blood pressure and heart rate at the respiratory frequency and at 0.1 Hz in normal subjects, and on the assumption that that correlation is due to the baroreflex coupling [82].

First, the spectra of systolic blood pressure and RR-interval series, and their squared-coherence modulus, are computed. If the coherence at 0.1 Hz and at the respiratory frequency is sufficiently high (i.e., greater than a threshold usually set at 0.5), the spectra of systolic blood pressure and RR-interval are integrated over the 0.1 Hz peak, giving the SBP_{LF} and RR_{LF} powers, and over the respiratory peak, giving the SBP_{HF} and RR_{HF} powers. Then the square-root ratio of RR and SBP powers at low and high frequencies is computed:

$$\alpha_{LF} = \sqrt{\frac{RRI_{LF}}{SBP_{LF}}} \quad \text{and} \quad \alpha_{HF} = \sqrt{\frac{RRI_{HF}}{SBP_{HF}}} \tag{35.39}$$

A close correlation of α-coefficients with the phenylephrine methods has been reported in a small-number of initial studies. Larger studies have revealed a moderate linear association between the two techniques with a relatively high limit of agreement (~ 5 ms/mmHg in normal subjects and hypertensives and ~13 mmHg in post-infarct patients) [218–221]. These observations indicate limitations of the BRS assessment using frequency-domain methods. Despite these limitations, a noninvasive approach provides BRS estimation of a short-term liability coming from complex and redundant reflexes with no procedural (apart from laboratory conditions) requirements.

35.3.5.5 Heart Rate Turbulence

A short-term fluctuation in sinus cycle duration after a ventricular premature beat forms the basis for introducing another noninvasive method that is related to the baroreflex control of HR, and is referred to as heart rate turbulence (HRT) [222–226] for explanation see text and ref. [294] (Fig. 35.27). Interestingly, the description of this method has been forced by

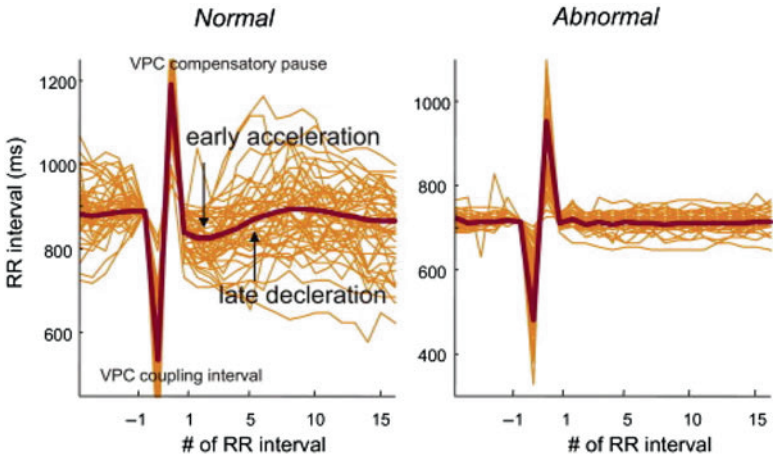

Figure 35.32

Normal (*left*) and abnormal (*right*) ventricular premature contractions tachograms used for the heart rate turbulence.

simultaneous evidence of its usefulness in risk stratification after myocardial infarction [222], while the pathophysiological background that might help to explain the strength of HRV as a risk stratifier [112, 222, 226, 227] using this method is not known.

The HRT is quantified by two measures termed turbulence onset (TO) and turbulence slope (TS). The turbulence onset is a measure of immediate initial R–R interval shortening following a ventricular premature beat and is calculated using the equation (35.40):

$$\mathrm{TO}\,[\%] = \frac{(RR_1 + RR_2) - (RR_{-2} + RR_{-1})}{(RR_{-2} + RR_{-1})} * 100 \tag{35.40}$$

where RR_{-2} and RR_{-1} are sinus cycles preceding a ventricular premature beat, and RR_1 and RR_2 are the two intervals following the compensatory pause. TO is calculated for each single premature beats and then averaged. TO > 0 means deceleration, TO < 0 means acceleration of the sinus rhythm.

The turbulence slope (ms/beat) is a measure of subsequent deceleration phase and is calculated as the maximum slope of a regression line assessed over any sequence of five subsequent sinus-rhythm RR intervals within the first 20 (15) sinus-rhythm intervals after a ventricular premature beat and is assessed in the average HRT tachogram.

HRT cannot be calculated in the presence of interpolated ventricular premature beats without compensatory pauses. Also, a minimum number of five premature beats is necessary to obtain a reliable pattern. However, a recommendation for TO and TS calculation in the presence of only a single premature beat can be found [226, 228]. The HRT measure depends on heart rate itself, and the coupling interval (prematurity) of ventricular beats [226, 229]. Considering HRT as a specific noninvasive measure of BRS, it is necessary to keep in mind that the sinus rate response to premature ventricular beats depends also on intact SAN function and the post-extrasystolic potentiation phenomenon [226, 230].

35.4 Methodological Considerations

35.4.1 Ideal HRV Method and Index

The complexity of heart rate fluctuation *a priori* excludes an ideal HRV method or index to be identified. However, such an attempt can be made for a particular purpose of HRV assessment. The requirements and characteristics of the index or method that can meet the purposes of an HRV study are presented in Table 35.5 and discussed below.

Criteria for an ideal HRV index that have to be met for the index to be applicable for the assessment of cardiac autonomic control in physiological and pathophysiological studies, proposed by Goldberger et al. [231], are listed as follows:

1. The ideal index should behave in a comparable manner in various subjects in response to stimulating or inhibiting maneuver s that lead to changes in cardiac autonomic balance or in its main components
2. Between-subject variability of the index at the same conditions should be minimal
3. The ideal HRV index should be explicable on the basis of physiological or pathopysiological mechanisms contributing to vagal-sympathetic interactions

For the reasons above, only short-term HRV analysis (and derived indices) seems to be applicable if cardiac autonomic control is to be explored (Table 35.6).

From a clinical point of view, an ideal HRV index should possess quite different features, while the association between HRV and cardiac autonomic control might not necessarily be so tight. Considering these issues, the criteria for a clinically useful HRV index might be proposed as follows:

1. The ideal HRV index should be an independent prognostic measure of the risk of death, especially if sudden (unexpected)
2. The ideal HRV index should have the potential to be applied in a wide population (without exception for cardiac rhythm disturbances)
3. Common applicability in clinical practice requires the ideal HRV index to be as simple as possible in order to be understandable to physicians
4. The ideal HRV method should be implemented in available analytical systems, allowing for its practical use in large populations
5. Normal limits defined as limits of agreement (LOA) should be established in a local (geographically or race-homogenous) population.

For these reasons, long-term HRV analysis (and derived indices) can be considered more suitable, as they cover most mechanisms related to the HRV phenomenon (Table 35.7). However, the interpretation of the meaning of these indices on the basis of cardiac autonomic control does not seem to be appropriate.

The common HRV measures also suffer from other limitations, including the non-normal distribution that requires mathematical transformation (usually natural logarithm), and a lack of standardization.

There is still a place for an ideal method and index from the mathematical, physical and technical point of view. The implementation of ideas that come from other areas or phenomena might prove to be fruitful. However, their physiological (Goldberger criteria) or clinical (clinical criteria) meaning should be tested each time. This requires close cooperation between inventors and clinicians. Otherwise, methods can proliferate without solving any important physiological or clinical issues, and simply add "scientific-like" noise.

35.4.2 Data Acquisition

35.4.2.1 Integration of the Signal

The basic cardiac signal, generally in the form of the electrocardiogram, is required to be digitized by a computer in order to obtain a series of R–R intervals. However, sometimes the R–R-interval series can be derived from analog systems. Also, a use of plethysmography or blood pressure recordings can provide the opportunity to derive pulse intervals.

Ideally, a raw ECG record should be preserved to check for the integrity of the signal, the presence of non-sinus beats and for editing artefacts [4, 5]. Accurate on- and off-line analysis depends primarily on the integrity of the signal. However, for HRV analysis purposes, the digitization rate (sampling frequency) is crucial for the detection of small variations of cardiac rhythm. Several types of errors and their solutions are presented in Table 35.8.

35.4.2.2 Errors Relating to Digitization Rate

A sampling frequency of 250–500 Hz has been recommended [4, 5]. However, in many studies the sampling frequency is not reported. Others considered a digitization rate of 500–1000 Hz, which would provide a basic resolution of 1–2 ms

Table 35.5

Characteristics of HRV index/method used in various kinds of studies (purpose-oriented)

Purpose/ Requirements	Index or method	Universality (no exclusions)	Availability (common)	Robustness (high)	Reproducibility	Inter-subjects variation	Physiological meaning	Diagnostic value
Epidemiological studies Fundamental requirements: HRV index calculable from short time series (routine ECG?) Controlled study conditions	Mean RRI (or HR)	Yes	Yes	Yes	High	Small	Sympatho-vagal balance	Prognostic value proven in many studies
	SDRR CV RMSSD CIPA	No	Yes	No	Relatively high	Large	Respiratory/ vagally related	Screening for DAN Screening for early atherosclerosis ? Outcome prediction
Physiological studies Fundamental requirements: HRV index calculable from short time series (1–5 min) Controlled study conditions Multi-signal recordings recommended	Mean RRI (or HR)	Yes	Yes	Yes	High	Small	Sympatho-vagal balance	Unspecific
	SDRR RMSSD	No	Yes	No	Relatively high	Large	Respiratory/ vagally related	Detection of sinus node dysfunction Screening for DAN ? Screening for early atherosclerosis ?
	Spectral/ cross-spectral analysis	No	Yes	No	Modest or unknown	Large	Ambiguous, (various in different frequency-band) Contradictory data	
	Time-variant spectral analysis					Large		
	Nonlinear methods	No	No	Various or unknown	Fair or unknown	Large or unknown	Unknown	
Clinical outcome studies Fundamental requirements: HRV index calculable from 24-h ECG recordings	SDNN	No	Yes	No	Relatively high	Large	Multifactorial Unexplainable	Prognostic value proven in many studies
	HRVI	No	Yes	Yes	High	Relatively small		
	HRVF	Yes	No	Yes	High	Relatively small		Prognostic value proven in one study
	DC	No	No	Yes	Unknown	Unknown		
	Nonlinear methods	No	No	Various or Unknown	Fair or unknown	Unknown		Prognostic value proven in many studies

Table 35.6

Short-term HR and HRV measures characteristics from an "ideal" HRV requirements view

Requirements	HR (RRI)	SDRR	SDSD	CV	VLF	LF	HF	Fractal measures	Others
Comparable (in direction) change in response to a defined stimulating or inhibiting maneuvers in various subjects	+++	+	+/–	+	+/–	+/–	+	+/–	NA
Minimal between-subjects variability	+++	+	+	+	+/–	+/–	+	+/–	NA
Explanation on basis of physiology and pathophysiology	+++	+	++	+	+/–	+/–	++	+/–	NA

+++ highly predictable/consistent data, ++ moderately predictable/exceptions reported, + marginally predictable/high variation, +/– unpredictable/conflicting data exists, NA - not assessed

Table 35.7

Long-term HR and HRV measures characteristics from an "ideal" HRV requirements view

Requirements	HR (NNI)	SDNN	SDANN	RMSSD	HRVI	HRVF	Fractal measures	HRT	BRS
Independent risk factor/marker of death/sudden death	+++	+	+/–	+/–	++	+	++	++	+++
Applicability to a wide range population	+++	+/–	++	+/–	+	++	+/–	+/–	–
Comprehensible for physician/bedside use	+++	+	+	+/–	+/–	+	–	+	+
Implementation on a commercial system	+++	+++	+++	+++	+/–	–	–	–	–
Normal limits with a LOA defined	+++	+	–	+	+/–	+/–	–	+/–	+/–

+++ well documented/consistent data, ++ moderately documented/consistent data, + moderately documented/inconsistent data, +/– less well documented/conflicting data exists, – undefined/lack of data/experimental tool as yet

[232–237]. A higher sampling frequency might be necessary to gain small variations in the amplitude of cardiac rhythm, especially in pre-term newborns and after heart transplantation. Most of the studies of HRV have gathered data using 24-h ECG systems with a nonoptimal sampling frequency of 128 Hz (~ 8 ms resolution), despite a resolution of at least 4 ms (250 Hz) suggested for adequate RSA quantification [4, 5, 235]. The noise introduced by an insufficient sampling rate can be overcome by the use of template matching or an interpolation algorithm. A digitization rate below 100 Hz is not considered acceptable [4, 5].

A low sampling frequency can cause a jitter in the determination of the fiducial points of the QRS complex, thus creating an error in the RR interval measurements [237]. The jitter-error is a source of additional high frequency content, and thereby affects the reliable determination of short-term variation.

Conventional Holter systems influence parameters estimating short-term, high frequency variation (RMSSD, NN50, pNN50). The R wave detection error using conventional systems can make spectral HRV analysis inaccurate and too low

Table 35.8

Errors in ECG data (unedited and edited)

Type of R–R interval distortion	QRS pattern	Mechanisms	Influence on HRV assessment	Solution	Limitation
True Premature ectopic beats (PEBs)	Supraventricular normal pattern	Abnormal automaticity or delayed potentials	Significant error in short-term statistical descriptors, spectral analysis unreliable	Rejection of epochs with beats which duration differ from neighbor by more than 20%	Inappropriate in the presence of long-coupled (late) PEBs
	Ventricular abnormal pattern			Rejection if frequent, interpolation procedures if sporadic	Ignores effects of PEBs on the autonomic milieu, introduces a sort of technical error
Parasystolic (allorhythmic) ectopic beats	Normal or abnormal	Constant coupling between repetitive PEBs	Presence of a separate oscillation	Unsolved, usually treated as PEBs	Introduces a sort of technical error
Normal sinus beats with abnormal connotation	Abnormal pattern	Abnormal intraventicular conduction (i.e., BBB)	"Jitter" error, may influence short-term spectral measures	Unsolved, usually treated and managed as ventricular PEBs	Introduces a sort of technical error
Spurious premature beats	Normal or abnormal	External noise, baseline shifting	None if recognised	Correct skin-electrode contact	Sometimes impossible due to sweating, body motion
		Low sampling rate		Appropriate sampling rate	Less possible in commercial long-term ECG recordings
		Large P- or T-wave amplitude		Appropriate threshold for QRS detection	Not always possible in commercial systems
Missed beats	None, RRI is doubled or a multiple of the preceding average	External noise, baseline shifting	Significant error in short-term statistical descriptors, spectral analysis unreliable	Correct skin-electrode contact, manual correction, splitting into equivalent R–R intervals, interpolation algorithms	Sometimes impossible due to sweating, body motion, introduces a sort of technical bias
		Low R-wave amplitude		Appropriate threshold for QRS detection, manual correction	Not always possible in commercial systems
Pauses	None, RRI is doubled or a multiple of the preceding average	Post-ectopic beats	Significant error in short-term statistical descriptors, spectral analysis unreliable	Rejection if frequent, interpolation algorithms if sporadic, splitting into equivalent R–R intervals	Ignores effects of or on the autonomic milieu, introduces a sort of technical bias
		Sinus arrest/high grade sino-atrial block			
		A-V block			

a sampling rate can influence high-frequency components irrespective of the spectral analysis methods used [236–238]. An error of up to 4% in the RMSSD and HF power has been reported when systems with conventional (8 ms) and high resolution (1 ms) timing accuracy have been compared [237]. These errors have been even greater in patients after MI, reaching 7.1% and 8%, respectively. A higher sampling rate leads to a reduction in the HF power. As a result, significant error is introduced with a sampling rate of 128 Hz not only to the HF power, but also to the LF/HF ratio with an error of up to 14%. Tapanainen et al. observed a large error in post-MI patients reaching 22.6% in those with low HRV and 17.5% in those with normal HRV. A 5% error of short-term components of the return map (SD1) has been shown to be due to a low sampling rate. Voss et al. reported a 2% error in the nonlinear symbolic RR interval dynamics in normal subjects, when a conventional system had been compared to a high resolution system with a sampling frequency of 2 kHz [235]. A similar range of error has been observed in the short-term scaling exponent α 1 (DFA) in subjects with normal HRV. However, the error increased to 5% in post-MI patients with a reduced HRV. A marked difference (11%) between low (~8 ms) and high (1 ms) resolution has been observed for the approximate entropy (ApEn). The error was more pronounced in post-MI patients with low HRV or faster HR (17.6% and 15.0%, respectively) [237]. The magnitude of all these differences grew proportionately when the overall heart HRV diminished. Thus, *the measurement of the nonlinear dynamics parameters should preferably be done with a sampling frequency higher than the conventional 128 Hz*.

The sampling frequency does not seem to affect long-term (RRI, SDNN, SDANN) or low-frequency HRV components (VLF, LF).

Sampling frequency is more important in the accurate detection of IBI short-term fluctuations if the RR interval series are shorter or smaller in amplitude [235]. Most prognostic studies on post-AMI patient populations, however, are based on the SDNN calculation. It is unlikely that the results of these studies would change with a higher sampling rate. However, *for experimental studies in physiology, psychophysiology and pathophysiology, the minimum sampling rate of 250 Hz should be mandatory*.

35.4.2.3 Errors Introduced by Noise

A rigorous recording method should be used in order to minimize noise, which usually interferes with the signal and results in an overlapping with the true R-wave amplitude [34, 239–242]. This can lead to *spurious R-wave* timing due to variation in peak amplitude and makes the use of simple maxima-based peak-finding algorithms unreliable. However, smoothing or filtering of the digitized signal, template or derivate matching and interpolation procedures can help to solve this problem. If the heartbeat signal is obtained from continuous BP recordings, where the fiducial point detection is more problematic due to a lack of clearly defined peaks, a template-matching approach is considered most appropriate.

Another consequence of noisy recordings is the identification of artifactual waves as *spurious R-waves*. Such erroneous R-waves might be harder to eliminate through the above mentioned algorithms. A careful visual investigation of a series of data is necessary. It is quite easy for short-term ECG recordings. However, for a 24-h recording it can be achieved through an automatic class (template) ascertainment of accuracy, by the visual checking of R–R interval (or differential) distribution histograms' tails, or step-by-step correction using a full disclosure option available in commercial systems. These procedures are time-consuming and may require up to 45 min for thorough analysis, labeling and editing.

35.4.2.4 Errors Related to the QRS-Wave Detectors

Another set of *spurious R-waves* results from an inappropriate threshold for R-wave detection. If the threshold is too low, an R–R interval would be subdivided into additional inter-event intervals due to the detection of T-waves (usually peaked with a relatively high amplitude, not infrequently in normal subjects), or more rarely, due to P-waves (usually when the amplitude of the R-waves is small, a frequent feature in patients with an advanced heart failure). If the threshold is set too high, R-waves of smaller amplitudes would be undetected and an exceptionally long IBI that merges two or more normal R–R interval would be recorded. These undetected beats are referred to as *missing beats* [239–242]. Their presence introduces sizeable and dramatic biases in estimates of HRV that can result in errors of up to 80% for SDNN, 25% for HF power and above 200% within lower frequencies [242].

Table 35.9

Steps to avoid non-stationarity in ECG recordings

1	Minimize non-stationarities in data through conditions control
2	Use filtering procedures for the removal of slow trends
3	Avoid unnecessarily long analytical epochs
4	Test for non-stationarities if appropriate
5	Omit (or remove) highly non-stationarity data segments
6	Use approaches explicitly designed for non-stationarity data evaluation

Another type of error is related to the identification of abnormal (either ectopic or artifactual) beats as normal. As the data-series containing abnormal heartbeats could be rejected from further analysis, leaving *mistakenly labeled R-waves* introducing a significant error especially in spectral estimates, particularly within the HF bands [34, 239–242].

Instabilities of the isoelectric line (baseline) with extreme upwards or downwards shifts due to a poor electrode-skin contact, and following rapid changes in impedance, would result in *missing beats* even if the technical requirements are fulfilled. Some aspects of these sources of errors are discussed in other chapters (Ambulatory ECG, Signal averaging etc.).

35.4.2.5 Errors Relating to the Presence of True Ectopic Beats

The presence of a few premature ectopic beats (PEBs) is a normal feature of long-term ECG recording in healthy subjects. The number of ectopic beats increases with age and in patients with CVD. In such cases, they can also appear in a short-time series. Irrespective of data length, their presence introduces an error that is related to a sudden shortening of the sinus fulfill cycle preceding the PEB (coupling interval) and a compensatory prolongation of the subsequent cycle (compensatory pause). As a result, a significant error in time-domain and especially in frequency domain measures is introduced [34, 238, 240–242]. In an excellent paper, Berntson and Stowell showed that the presence of only one ectopic PEB in a 2-min recording introduced an error in the SDNN of up to 50%, in the HF of around 10% and in the LF of approximately 80% [242]. Interpolation procedures for the replacement of PEBs with interpolation-derived heartbeats do not necessarily prevent these errors. The use of a filter function to interpolate for heartbeats preceding and following PEBs can help to solve this problem. However, it may lead to a disruption of the continuity of data.

35.4.2.6 Non-Stationarity as a Source of Errors

Stationarity is defined as the invariance of distributional characteristics of data-series in all moments over time. In a controlled laboratory setting, when short-time data series are subjected to evaluation, ECG signal non-stationarity might reflect the physiological properties of complex heart rate control. If long-term ECG recordings are used for HRV assessment, occurrence of sudden changes in sinus cycles related to internal or external stimuli is frequent. Also, sustained trends can reflect physiological control mechanisms. They may distort spectral frequencies and usually are subject to detrending procedures [243]. These procedures provide technically valid data-series, but at the cost of a loss of information. Another way to fit stationarity of data is the use of linear or polynominal trend removal or bandpass filters to isolate the periodicities of interests and minimize the effects of non-stationarities. For the stationarity of the time series to fit, the simplest way is to maintain test and subject conditions stable throughout the recording period and to minimize the length of recordings. If non-stationary epochs cannot be removed or extracted from prolonged data-series, multiple short-epochs, in which stationarity is satisfied, should be analyzed to examine the dynamics of the signal over time. Otherwise, *the analysis of relatively stable short-time series with appropriate methods (e.g., discrete FFT, time-frequency analysis) seems to be more advisable than the use of detrending algorithms*. Steps necessary to solve the stationarity issue are listed in Table 35.9.

35.4.2.7 Management with Errors Relating to the Presence of Ectopic, Spurious and Missed Beats

In acute studies, when the ECG signal recorded is of only a few minutes duration, continuous visual inspection is required. *Only data that does not contain any abnormal beats should be extracted for further analysis*. For short-term recordings, it seems advisable to acquire time series somewhat longer than the period assumed for further analysis as it increases the probability for taking undisturbed portions of a required length from the entire recordings. In any other cases, the studies have to be repeated or rejected [4, 5, 34, 242, 243].

Less strict approaches are proposed for 24-h ECG recordings [4, 5, 34, 242, 243]. For time-domain methods, data can be passed through various filters that eliminate annotated heartbeats other than the normal (dominant) beat. Additional logical conditions are imposed to eliminate the preceding and post-ectopic heartbeats. If the sequence of heartbeats is required to be sustained (e.g., for spectral analysis), various solutions are proposed. However, there are no specific recommendations regarding the cut-off of absolute or relative frequency of abnormal heartbeats. Many authors use different criteria.

If the number of abnormal heartbeats is considered insignificant, algorithms that allow the correction (substitute) of abnormal (usually ectopic) heartbeats could be applied. A variety of algorithms have been proposed and reviewed in depth elsewhere.

The duration of the compensatory pause depends in a complex manner on the coupling interval and the mean IBI before PEBs. Thus, PEBs can occur as interposed, compensated or phase-shifted extrasystoles, so simple replacement using interpolation procedures is not reliable. Also, the annotated PEBs may in fact represent either true physiological phenomena, especially in healthy young people, or true pathological phenomena related to SAN dysfunction. Most algorithms ignore the fact that ventricular PEB occurrence is associated with changes in the autonomic milieu.

All errors in QRS detection and IBI measurements are of special significance in individuals with low HRV, where the same level of error is associated with much greater influence upon a true signal. These errors are more likely to be found in persons with PEBs as well as intraventricular conduction disturbances. Guidelines indicate the necessity for a clear description of the specific procedures for interpolation or data rejection and for a discussion of their contribution to the results [4, 5, 242]. Even so, *if the data is corrupted, the analysis should be limited to more robust time domain statistics*.

35.4.3 Data Length

The duration of the R–R interval recording for HRV analysis is not a priori limited. However, for comparison between different studies, the data is required to be of similar length. The total variance of IBI increases with the length of recordings. From a physiological point of view, a fundamental issue is the duration of the cycle of a certain phenomenon (wavelength) considered for analysis, assuming a relative selectivity of various periodicities (spectral analysis). It is required that the R–R interval recording time be ten times longer than the wavelength of certain oscillatory phenomena. A recording of at least 1 min is necessary to assess reliably short-term vagally mediated respiratory-related HR variation, and of 2 min for longer-term variation attributed in part to sympathetic control. For cycles recognized as VLF (~0.0033 Hz), it is necessary to prolong recording time periods to approximately 1 h.

A standard recording period of 5 min is recommended for clinical purposes [4, 5]. However, it has been shown that very short ECG recordings of 8–10 s duration covering no more than two to three respiratory cycles, can efficiently estimate the vagal tone (i.e., CIPA) [28, 29]. In addition, for certain purposes (e.g., psychological, exercise studies), a 5-min period may be too long to meet stationarity requirements. It would be ideal to use time-frequency approaches if shorter data-length is required to be analyzed.

With the use of a nonlinear dynamics approach, nonlinearities in time series are apparently the true subject of analysis. For the calculation of nonlinear measures, more prolonged time series is advised. However, attempts have been made to calculate these measures from short-term recordings.

For long-term recording, it is necessary to present data regarding a true period of analysis since there are some methodical differences in data selection. These differences are related to the definition of prematurity of non-sinus heartbeats (>30% or >20% deviation from the previous heartbeat interval or >10% of an interpolated beat interval), pause detection (usually >125% of averaged local means or 120% of running time), minimum duration of recordings (from 12 h including 6 night hours, to 22 h) and at least 50–90% normal (sinus) heartbeats. Also, data substitution varies

with different equipment where non-sinus beats, together with the neighboring one to two heartbeats, are either eliminated or interpolated with a range of algorithms. The differences in these procedures influence time-domain HRV measurements by no more than 10%, while for spectral-measures, it can be expected to be even higher. However, this has not yet been calculated.

35.4.4 Data Presentation

Although IBI is usually employed for HRV analysis, heart rate and counts are also used as a basic metric in studies of cardiac rhythm. It is important, as a distinct relationship exists between vagal activation and HR or IBI, whereas the relationship between sympathetic activation and HR or IBI seems to be nonlinear. As the range of vagal control is considerably greater than that of the sympathetic branch and fundamentally influences the latter itself, IBI presentation has advantages over HR for the analysis of cardiac rhythms. However, if HR is employed on a beat-to-beat manner and referred to as an instantaneous HR (iHR), analyses based on iHR may not necessarily produce a similar pattern of results as for heart period analyses. Janssen et al. showed that various data presentations influenced the magnitude of HF power and LF/HF ratio, which could differ up to 37% depending on the method used [244]. Normalization procedure (dividing of observed values by their corresponding average values) has recently been proposed [245].

The HRV signal can be presented as a function of beat number. Such a presentation is referred to as the R–R *interval tachogram*. Interpolating and resampling the heartbeat series allow HRV to be expressed in a common time scale [4, 5, 77].

Successive R–R intervals are spaced unevenly in time. However, time series analyses require the data to be sampled at equal time intervals. Resampling procedures are necessary to derive the R–R series suitable for spectral analyses. Various methods have been proposed and discussed in the literature [4, 5, 77, 79].

As indicated by the guidelines, it is preferable to use a sampling approach in which the value at a given point represents a weighted average of the beats that fall within the sample interval [4, 5]. The resampling rate seems to be crucial in order to avoid aliasing. The sampling rate is recommended to be at least twice the lowest resolvable frequency. A sampling rate of 4 times the target frequency is considered most appropriate. Thus, the higher the mean heart rate, the higher is the sampling frequency required. For studies in adult humans, it is at least 2 Hz, whereas in children or individuals with higher heart rates it would be more prudent to use 4 Hz. For animal studies, a higher sampling frequency is needed [246].

35.4.5 Universality of HRV Analysis

Ideally, HRV measurement should be applied to all subjects. This requirement is referred to as *universality*. Current recommendations necessitate the presence of sinus rhythm in order to evaluate HRV qualitatively (high, normal, low or normal/abnormal pattern) and quantitatively. For this reason, heartbeats are labeled as normal (N) and IBIs as normal-to-normal (N-N or NN-intervals) [4, 5]. In fact, the American Heart Association/American College of Cardiology Task Force for Ambulatory Monitoring listed the presence of *sinus rhythm as an a priori inclusion criterion for standard HRV analysis* [247]. Such a statement excludes a substantial proportion of more severely diseased patients with a higher risk of an unfavorable outcome from studies on the clinical use of HRV, especially HF and older patients in whom the presence of frequent ectopic PEBs or atrial fibrillation is not uncommon.

A detailed analysis of the methodological descriptions of the most important studies indicates that standard HRV methods cannot be applied to 6–55% of study populations (Table 35.10). In addition, newer proposed measures based on spectral analysis or nonlinear techniques, including HRT, cannot be used in 17–35% of patients (Tables 35.10 and 35.11). The reasons for rejecting patients from HRV studies are varied and only rarely reported. In a small number of studies in which the reasons for exclusion are listed, the presence of artefact or insufficient data length accounts for 10–65% of exclusions, while the presence of cardiac arrhythmias/pacemakers is the reason for 10–100% of exclusions.

The clinical consequences of these assumptions and recommendations are critical in a high risk population with frequent ventricular premature beats and atrial flutter/fibrillation, in whom the opportunity for HRV analysis is abandoned (Table 35.10). Farrel et al. reported a significantly higher total mortality rate (19.7%) and arrhythmic events rate (12.3%) in acute MI patients excluded from the HRV study, compared to 11.3% and 5.7% in those who entered the study [248]. The clinical course of acute MI in the rejected group was worse, with higher Killip classes and a higher proportion of

Table 35.10

Applicability of HRV analysis in clinical outcome studies

Author/year	Population (included)	HRV measure (most prognostic)	% rejected[a]			Clinical significance/comments
			Overall	For the presence of artefacts	For the presence of cardiac arrhythmias	
Farrell et al. 1991 [40]	416 post AMI St George's Hospital	HRVI	14.6	NR	NR	Total mortality: rejected vs analyzed 19.7% vs 11.3%, arrhythmic events: 12.3% vs 5.7%
Cripps et al. 1991 [38]	177 post AMI St George's Hospital	HRVI	23	NR	NR	Total mortality: rejected vs analyzed 21% vs 6% Among rejected more frequently previous MIs, more common Killip >2
Odemuyiva et al. 1991 [A1]	385 post AMI St George's Hospital	HRVI	19.3	NR	NR	Not reported
Bigger et al. 1992 [A2]	715 post MI MPIP population	ULF power	8.8		2.6 (for AF)	Not reported
Bigger et al. 1993 [122]	331 post AMI MPIP population	SDANN	6.0	4.2	1.4	Similar characteristics, outcome not reported
Vainshav et al. [A3]	226 post AMI OCS[b]	SDNN	11.7	7.8	0.8	Not reported
Touboul et al. [A4]	383 post AMI OCS	SDNN	18.7	–	–	Not reported
Huikuri et al. [127]	446 post AMI	α_1–fractal index	31.9	–	–	Not reported
Tsuji et al. 1994 [A5]	1028 Framingham elderly cohort	Log LF 100s avgs	26.8	15.6	7.4	Similar outcome in excluded for arrhythmia/artefacts/medication use
Algra et al. 1993 [362]	245 SCD victims 268 controls	SDNNI SDANNI	19.6 14.1	– –	– –	90% survival rate in included 88% survival rate in excluded
Zuanetti et al. 1996 [346]	567 AMI GUSTO participants	NN50+	~50	NR	NR	Similar clinical characteristics Outcome not reported
Lanza et al. 1998 [348]	239 AMI OCS[b]	VLF	34	NR	NR	Not reported

Nollo et al. 2001 [A6]	324 AMI GISSI-3 participants	LF power	13.4	NR	13.4 (non-sinus rhythm)	Not reported
Bilchick et al. 2002 [360]	179 CHF-STAT participants	SDNN	29.1	2.7	19.6	Not reported
Carnethon et al. 2002 [249]	9267 ARIC participants	SDNN 2 min	13.3 25.6[d]	NR	NR	Rejected subjects older, more frequently females, obese. Worse outcome among rejected (higher MI and fatal CHD rate compared to included sample)
Forslund et al. 2002 [A7]	641 CAD APSIS participants		20.7	NR	NR	Not reported
Sosnowski et al. 2002 [64]	298 PMI patients OCS	HRVF	<1	0	<0.5[b]	[b]Implanted pacemaker and paroxysmal tachyarrhythmias among excluded
Sajadieh et al. 2003 [524]	643 Copenhagen Holter Study healthy	SDNN	17%	NR	NR	Technically best continuous period of 24 h selected from the 48-h Holter recordings
Abildstrom et al. 2003 [706]	366 BEAT Study screening phase participants	SDNN	23.9	NR	NR	Not reported
Lampert et al. 2003 [A8]	184 BHAT participants	HF pNN50	40.5	NR	NR	A significant proportion of patients excluded for insufficient data length
La Rovere et al. 2003 [A9]	202/242 CHF (derivation/ validation sample)	LF power (AR)	50.9	9.6	26 (AF or pace-maker)	15.3% clinically unstable patients among excluded
Jokinen V et al. 2003 [A10]	600 AMI/416 PMI MRFAT – OCS	α_1–fractal index	11.1	NR	NR	Not reported

Table 35.10 (Continued)

Author/year	Population (included)	HRV measure (most prognostic)	% rejected[a]			Clinical significance/comments
			Overall	For the presence of artefacts	For the presence of cardiac arrhythmias	
Schroeder EB et al. 2003 [A11]	6931 ARIC participants	RMSSD (2–6 min)	2.3	NR	NR	Not reported
Aronson et al. 2004 [361]	255 decompensated CHF, PRECEDENT participant	SDNN	22.0	NR	NR	Not reported
Stein Pk et al. 2004 [A12]	830 CAST participants		11.4		4.3	Not reported
Wichterle D et al. 2004 [83]	663 EMIAT participants	Time Spectral PLF	6.5 4.1 17.9	NR	NR	Not reported
Carpeggiani C et al. 2004 [A13]	413 AMI MCS[c]	LF power (AR)	9.2	NR	NR	Not reported
Jokinen V et al. 2005 [578]	41 elderly subjects longitudinal FU study		35.9		14 (AF)	Not reported
Rashba EJ et al. 2006 [250]	274 DEFINITE participants	SDNN	23.0	NR	16 (AF) 7 (frequent PEBs)	Worst outcome in patients excluded from the study ($p < 0.02$)
Casaleggi et al. 2007 [A14]	200 HF patients	SDNN	54.9	NR	23.9 (AF or pacemaker)	Not reported
Huikuri et al. 2009 [352]	312 CARISMA participants	SDNN HRT TWA	NR	NR	NR	HRV available in 252 (80.8%), HRT in 243 (77.9%), TWA in 215 (68.9%); outcome in those without HRV/HRT/TWA not reported

[a] Patients rejected due to exclusion criteria not included
[b] OCS – *one centre study*
[c] MCS – *multi-centre study*
[d] *in standing position* TM – *total (all-cause) mortality*, CVM – *cardio-vascular mortality*, AE – *arrhythmic events*, AMI – *acute myocardial infarction*, PMI – *previous myocardial infarction*, AF- *atrial firbirllation*, PEB– *premature ectopic beats*, NR- *not reported*

Table 35.11

Applicability of HRT, BRS or combined cardiac autonomic control measures in clinical outcome studies

Author/year	Population (included)	HRV measure (most prognostic)	% rejected[a]			Clinical significance/comments
			Overall	For the presence of artefacts	For the presence of cardiac arrhythmias	
Schmidt et al. 1999 [222]	577 MPIP 614 EMIAT	HRT (TS+TO)	19 [MPIP] 17.4 [EMIAT]	NR	NR	Outcome in excluded patients not reported AF among a priori criteria of exclusion
Ghuran et al. 2002 [226]	1212 ATRAMI	SDNN HRT BRS All 3	9.8 19.1 7.6 22.7	NR	NR	Similar survival in patients with and without HRT AF among a priori criteria of exclusion
Barthel et al. 2003 [A15]	1455 ISAR-HRT	HRVI HRT	NR	NR	NR	HRT calculation impossible in 29.1% Outcome in these patients as good as in patients with normal HRT
Bauer at al. 2006 [170]	608 EMIAT	HRT (TD)	58.8	NR	NR	Outcome in excluded patients not reported AF among a priori criteria of exclusion
Exner et al. 2007 [A16]	332 AMI REFINE	SDNN HRT BRS	49.0	NR	20 (for AF) 6 (ICD)	Outcome in excluded patients not reported
Stein PK et al. 2008 [365]	1197 CHS (>65 YOA)	DFA1 HRT	16.2	NR	6.1	Clinical characteristics of initial 1429 eligible subjects similar, outcome not reported AF among a priori criteria of exclusion
Mäkikallio et al. 2006 [A17]	2130 AMI FINGER	SDNN HRT (TS) DFA1	NR	NR	NR	NR AF among a priori criteria of exclusion
Klingenheben et al. 2008 [A18]	114 HF Frankfurt DCM	SDNN HRT BRS	2 10 25	NR	NR	23% with and ICD implanted AF among a priori criteria of exclusion

patients with previous MI. In an epidemiological study (The ARIC Study), excluded subjects were older, more frequently females and obese, and their outcome was worse with a higher MI/fatal CHD rate compared to HRV study participants [249]. Observations from the DEFINITE trial indicate that patients excluded due to the presence of frequent ventricular PEBs or atrial fibrillation have a lower survival rate than patients in whom HRV analysis is possible [250].

A new promising index of HRV, i.e., *deceleration capacity* (DC), has been shown to be applicable to almost all patients in sinus rhythm. However, the presence of atrial fibrillation still limits its applicability to the entire spectrum of patients [171].

The index that possesses the potential for HRV global description in patients either in sinus rhythm or in atrial fibrillation is the HRV Fraction [65]. A uniquely low exclusion rate (less than 1%) with HRVF use has been observed in the post-MI population [66]. Unfortunately, this index has not achieved wider interest. The HRVF can be applied extensively but not to ECG recordings with long periods of atrial flutter/tachycardia or very frequent PEBs (>25% of all heartbeats) or with a pacemaker-driven rhythm. Interestingly, the author's investigations indicate very similar properties for the SDANN (*unpublished*). However, systematic studies are necessary to justify its usefulness in nonselected populations of patients with and without arrhythmias. Nevertheless, documented data on risk prediction with the use of the SDANN, indicates its superiority compared to the SDNN [252–254], as does our own data. More intensive use of the SDANN in clinical outcome studies is awaited.

35.4.6 Robustness

Robustness is one of the most important properties of indices of HRV methods, mainly because the necessity for time-consuming manual editing of the data-series can be minimized [4, 5, 34]. Results of HRV analysis with the use of a robust index/method are similar irrespective of the presence of noisy data (artefacts, non-stationarities, PEBs, AF). The use of a less robust index/method requires noisy data to be eliminated. The latter procedure, however, might lead to a loss of significant information. From data provided in Table 35.10, it can be concluded that the standard time- and spectral HRV indices are sensitive to artefacts and sudden IBI changes of either physiological or pathological origins. The robustness of nonlinear indices is rather moderate and strongly depends on the method used. However, for most such indices, their robustness is unknown. The HRV index (St. George's index) was the first introduced to improve robustness. However, the HRVI is critically sensitive to the distribution of data and cannot be reliably determined in the presence of a bimodal distribution [38]. HRVF and DC are indices with high robustness, which are also independent of the distribution of IBIs [65, 171].

35.4.7 Biological Variations

Variation in HR reflects the adjustment to changeable metabolic demands of key vital organs in response to internal and external stimuli in a specific neuro-humoral milieu, and any of the HRV measures obtained at a given time varies accordingly. In a controlled environment (the same time of recording, mental and physical activity, drugs and so on), this variation is still present in an individual subject and between individuals. This variation is referred to as *biological variation*. The biological variation is always present as most of the factors (genetics, race, age, gender etc.) that determine HRV cannot be controlled in any way. Biological variation differs from other sources of HR variation which are related to investigator biases (intra- and inter-observer errors) and technical precision of measurements (Fig. 35.28). However, it has to be stressed that in an individual subject or a population sample, the biological variation can be much greater than reported as the average. The study population (healthy subjects, patients with certain diseases), conditions of examinations, like breathing (spontaneous, controlled, deep breathing, Valsalva maneuver), body position (supine, standing), exercise (treadmill, bicycle) or other testing (head-up or head-down tilting, mental stressing, cold pressor test, and so on) might be an important determinant of intra- and inter-individual reproducibility. Importantly, errors due to the foregoing might have a different contribution on the overall measurements in patients with an already reduced HRV. Lastly, use of various periods of ECG recordings (second, minutes, hours) or different algorithms for traditional spectral HRV measures (AR, FFT) might be in part responsible for differences in quantification of the degree of such errors. Thus, a purpose-specific use of different HRV methods requires the determination of predictable errors (possibly drawn from

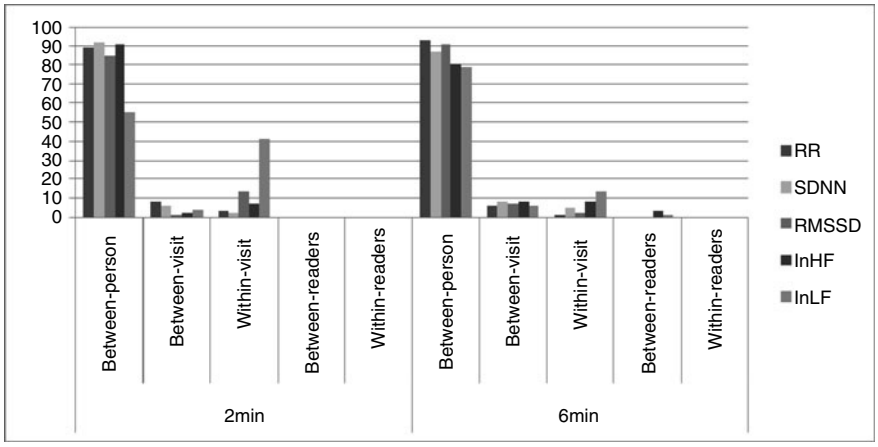

Figure 35.33

Measurement errors of common HRV measures: components by length of short-term recordings. The main source of HRV errors can attribute to inter-individual variation, except for spectral HRV measures, where between- and within-visit changes may play a significant role (i.e., lnLF, lnHF). Importantly, readers' errors are entirely negligible. However, there is a space for within-visit errors if spectral HRV is aimed to be measured (According to data provided by Schroder et al. [255]).

former validation studies) and a proper calculation of the sample in order to detect a significant change of a particular HRV measure [255].

35.4.7.1 Intra-Individual Variation

The determination of intra-individual variation of HRV indices requires the definition of their range in the setting of controlled conditions in the same subject. Within the same visit, variation attributed to intra-individual short-term variation accounted for 5–14% for SDRR, 2–7% for RMSSD, 8–28% for HF power and 14–41% for LF power [256]. The contribution of intra-individual variation decreases with prolongation of recording length (Table 35.12). Also, between-measurement period duration influences the contribution of intra-individual variation on the measurements (Table 35.12). If more repeated measurements on different visits are performed, the contribution of intra-individual variation between visits appears to be even lower. It accounted for 0.5–7% for SDRR, 2–7% for RMSSD, 3–8% for HF power and 4–6% for LF power [256]. In contrast, the contribution of intra-individual variation increases with prolongation of recording length and can reach 30% for a certain HRV measures. Intra-individual variations might be of importance for studies in which the effects of internal or external stimuli are to be examined. The intra-individual variation can be in part a source of measurement error of HRV indices calculated from long-term recordings. However, strict estimates of these errors have not yet been provided.

Intra-individual variation range provides limits beyond which HRV changes can be considered significant and interpreted as a true effect of interventions or changes in study conditions. It is of importance since intra-individual variation might be even greater than inter-individual variation [256].

35.4.7.2 Inter-Individual Variation

Inter-individual variation defines the range of HRV in a population. The determination of between-subject variation is necessary when population (or subpopulation) studies are going to be undertaken in order to detect effects of various interventions. Awareness of inter-individual variations is necessary with the interpretation of changes of the mean

Table 35.12

Intra-individual variability of HRV measures in healthy subjects (Coefficient of variation)

Author[s] Source/Year	Subjects	Condition[s]	RRI [or HR]	SDRR	RMSSD	LF	HF	Comments
Kanters et al. 1996 [A19]	12 healthy adults 6F, 6M Age 31 (25–38)	Supine Free breathing	3.7%	11.7%	NR	20.3%	*35.2%*	3 separate days 3 h FFT
Sinnreich et al. 1998 [269]	70 healthy adults 38F, 32M Age 49 (31–67)	Supine Free breathing	NR	6.0%	8.0%	11.5%	12.1%	2 months apart 5 min AR [16 order]
		Supine Metronome 15/min	NR	6.1%	7.4%	10.7%	10.5%	
Schroeder et al. 2004 [255]	63 healthy adults 31F, 32M Age 52 (45–64)	Supine Free breathing	8.6%	5.8%	6.7%	6.3%	8.0%	1–2 weeks apart 6 min FFT
Højgaard et al. 2005 [266]	14 healthy adults 5F, 9M Age 31 (22–38)	Supine Free breathing	6.0%	NR	NR	27%	28%	Day-to-day 1024 s (~17 min) FFT
		Head-up tilt of 60°	5.0%	NR	NR	26%	32%	
Zollei et al. 2007 [A20]	10 healthy adults 3F, 7M Age 25 ± 2	Supine Free breathing	7.1%	22.5%	*32.8%*	*61.8%*	*63.7%*	10 consecutive days 5 min, FFT
		Metronome 6/min	6.4%	17.3%	24.3%	*36.5%*	*50.4%*	
Kobayashi et al. 2007 [A21]	73 healthy males Age 20–61	Supine	5.0%[HR]	NR	NR	21.2%	19.5%	4–8 sessions 1 day 204.8 s (~3 min) FFT
		Standing	4.7%	NR	NR	23%	20.1%	

or median values. This is also an ultimate condition for the determination of normal limits and the definition of abnormal HRV.

Between-subject variation is the main source of measurement error. For time-domain HRV indices, it contributes 86 to 91% of the entire error and was shown to be independent of data length [256] (Table 35.13). For spectral HRV indices (HF and LF power), its contribution ranges from 69 to 81% and 55 to 79%, respectively, being greater for a longer data-length [256].

35.4.7.3 Intra and Inter-Observer Errors

Measurement errors define the range of subjective assessment of data-series. Intuitively, this depends on the robustness of the HRV method or index. If manual editing and visual inspection is necessary, the differences both between measurements performed by the same investigator (intra-observer error) and by two investigators within the same data-series (inter-observer error) can be assumed to be greater compared to a robust method/index, which is calculated automatically without any investigator's management of the data-series [34, 256].

Intra-observer errors for HRV short-term recordings have been shown to account for less than 0.1% of total measurements errors. Inter-observer errors for short-term HRV were estimated to account for less than 0.1% of the measurement error for time-domain indices and less than 3% for spectral indices [256]. In the ARIC study, the intra- and inter-observer variance of 2-min SDNN has been reported to reach 0.04 ms^2 (0.6%) and 3.24 ms^2 (5.3%) [258]. The inter-observer error relates also to the condition of analysis (manual, automatic, pre-defined fixed frequency) [259], being lower in the latter setting. The inter-observer error has been reported to be greater in a study on patients with chronic stable CAD, where the respective data for 5-min and 40-min recordings ranged between 0.2–6.0% and 0.1–1.2% [260] The longer the data-series analyze d, the greater the errors on the part of the observers. Kroll et al. noticed the inter-observer errors reaching 8% as a result of inaccurate labeling of heartbeats, especially PEBs, in intentionally selected patients with aortic regurgitation [261]. The SDANN index proved to be least sensitive to the inter-observer error [261, 262].

Only one study addressed this issue in children [263]. In the Bogalusa Heart Study, in which 20 children aged 10–16 years old had been included, the inter-observer errors in the estimation of time-domain and frequency-domain measures did not exceed 1% and 4%, respectively [263].

The intra- and inter-observer errors depend in part on technical characteristics of available instruments. The use of different devices influences the level of agreement for either short-time frequency-domain or long-term time-domain indices [257, 263, 264].

35.4.7.4 Reproducibility

Reproducibility characterizes the summarized effect of intra-individual, inter-individual, intra-observer and inter-observer errors, as well as precision accuracy, assuming similar length and conditions of HRV recordings. In addition, the use of different devices influences the comparisons of different interventions and their reproducibility. A high reproducibility can be defined by various measures, like the coefficient of variation (as being <10%), intra-class coefficient (>0.79), limits of agreement (LOA, 75–125%) and others [256]. Values of CV, ICC and LOA that indicate acceptable (minimum) reproducibility are <30% and >0.60 and 60–140%, respectively.

Tables 35.14 and 35.15 provide results of selected studies that addressed this issue in healthy subjects. The results of reproducibility in patients with specific CV diseases are presented in Tables 35.16 and 35.17.

Murray et al. showed a poor to moderate reproducibility of 5-min HRV measurements repeated 2–3 min apart with LOA between 61% and 157% for SDNN in a wide age-range sample (21–77 years) [265]. Similarly, minute-to-minute reproducibility of spectral HRV indices was found to be moderate in young subjects in a study of Højgaard et al. [266]. The CV was lowest for HF and LF/HF (27–28%), However, a great inter-individual variability range was noticed (2–75%). On the contrary, in middle-aged subjects, Pikkujämsä et al. found the SDNN very highly reproducible if evaluated by means of a CV of 2% [141].

Moderate or poor day-to-day reproducibility of short-term HRV measures has been reported for various spectral indices (mean CV between 27–39%) in young adults [266] and even poorer in children with a CV range of 35–97% [267].

Table 35.13

Inter-individual variability of HRV measures (Reliability coefficient)

Author[s] Year	Subjects	Condition[s]	RRI [or HR]	SDRR	RMSSD	LF	HF	Comments
Kanters et al. 1996 [A19]	12 healthy adults 6F, 6M Age 31 (25–38)	Supine Free breathing	0.96	0.86	NR	0.94 (AU)	0.89 (AU)	3 separate days 3 h FFT
Sinnreich et al. 1998 [268]	70 healthy adults 38F, 32M Age 49 (31–67)	Supine Free breathing	NR	0.77	0.75	0.68	0.76	2 months apart 5 min AR [16 order]
		Supine Metronome 15/min	NR	0.78	0.78	0.75	0.82	
Schroeder et al. 2004 [255]	63 healthy adults 31F, 32M Age 52 (45–64)	Supine Free breathing	0.93	0.87	0.91	0.79 (ln)	0.81 (ln)	1–2 weeks apart 6 min FFT

Table 35.14

Reproducibility of HRV measures from long-term ECG recordings in healthy subjects

Author[s]/ Source/Year	No of examined subjects	Between-measurement period	Parameter	Mean difference between recordings	Statistics	Results
Kleiger et al. 1991 [A22]	14 healthy adults	3–65 days	NNI SDNN SDNNI RMSSD pNN50 lnTP [*FFT*] lnLF lnHF	–	ICC (mean, ±3 SEM)	0.90, 297 ms 0.70, 54 ms 0.90, 24 ms 0.90, 24 ms 0.90, 12% 0.89, 4025 ms^2 0.91, 1042 ms^2 0.84, 1042 ms^2
Pitzalis et al. 1996 [296]	20 healthy adults Mean age 28 ± 2	Day-to-day 2 weeks and 7 months	NNI SDNN pNN50 RMSSD	NA	ICC	0.75 0.57 0.78 0.79
Nolan et al. 1996 [276]	19 healthy adults 44 ± 13 years	13 ± 9 days	pNN50	1.15%	ICC	0.97
Sosnowski M et al. 2005 [65]	165 healthy adults 49.5 ± 6 years	Day-to-day	RRI SDNN SDANN pNN50 HRVI HRVF	17.8 ms −2.8 ms −4.4 ms 0.78% −0.02 U −0.72%	LOA	−79 – 112.5 ms −41 – 35 ms −57 – 48 ms −4.79 – 6.35% −12.9 – 12.9U −13.4 – 11.9%
Huikuri et al. 1990 [284]	20 healthy males 20–40 years	7 days	SDNNI	–	CV (intraindividual) CV (interindividual)	7 ± 6% 24%
		Day-to-day (recalculated)	SDNNI	–	CV (intraindividual)	4.2 ± 2.9%

Table 35.14 (Continued)

Author[s]/ Source/Year	No of examined subjects	Between-measurement period	Parameter	Mean difference between recordings	Statistics	Results
Hohnloser et al. 1992 [281]	17 healthy adults Mean age 24±2.5 years	Day-to-day, 1 week and 1 month	SDNN pNN50 RMSSD	NA	CV	13.7 ± 6.8% 23.5 ± 14.6% 18.5 ± 12.6%
Ziegler D et al. 1997 [580]	17 healthy subjects 7M/10F 26–45 years	Median 29 weeks	SDNNI RMSSD pNN50 CV HRVI lnHF lnLF lnVLF CV-SA CV-LA	–	CV	6.8% 10.6% 14.8% 4.2% 1.9% 11.1% 11.9% 10.5% 7.9% 13.0%
Van Hoogenhuyze et al. 1991 [277]	33 healthy adults Mean age 34 years	Day-to-day	SDANN SDNNI SDNNI-CV	12.3 ± 11.7% 7.8 ± 6.9% 5.7 ± 4.3%	VR	0.2–46% 0.4–25.9% 0–16%

ICC (intraclass coefficient), ⩾0.6 acceptable, ⩾0.8 high, LOA (limit of agreement) 75–125% high, 60–140% acceptable, CV (coefficient of variation)=(SD_{within}/$mean_{between\ measurements}$)*100%, <30% acceptable, VR (variation range), <30% acceptable

Table 35.15

Reproducibility of HRV measures from short-term ECG recordings in healthy subjects

Author[s], Source/Year	Subjects	Duration of ECG recordings Between-measurements period	HRV measures	Statistics	Results
Intraclass coefficient (ICC, ⩾0.6 acceptable, ⩾0.8 high)					
Pitzalis et al. 1996 [296]	20 young adults 10F, 10M Aged 28 ± 2 SB / CB 16 breaths/min	10 min 2 weeks 7 months	RRI SDRR pNN50 RMSSD LF [FFT] HF LF/HF LF [AR12] HF LF/HF	ICC (mean) SB / CB	*0.37 / 0.35* *0.56 / 0.27* *0.40 / 0.43* *0.23 / 0.20* 0.77 / 0.60 0.48/0.65 *0.20 / 0.36* 0.70 / 0.60 0.15 / 0.70 *0.06 / 0.48*
Carrasco et al. 2003 [300]	11 healthy adults 6F, 5M Age 23.1± 1.3 SB / CB 12 breaths/min	5 min 3 sessions 5 day period	HR SDHR rMSSD [HR] CV [HR] HF [AR, order?] HF [N.U.] LF LF [N.U]. LF/HF	ICC (mean) SB / CB	0.82 / 0.81 0.93 / 0.94 0.92 / 0.94 0.91 / 0.94 0.86 / 0.93 0.77 / 0.88 0.86 / 0.92 0.79 / 0.88 0.85 / 0.88
Lobnig et al. 2003 [297]	7 healthy adults Age 20–28 CB 12 breaths/min	5 min 3 sessions (2 in supine position) 4 days	Ln LF [FFT] Ln HF	ICC (range of means)	0.66–0.69 0.76–0.81
Kowalewski, Urban 2004 [A23]	26 healthy males Age 22 ± 1 SB	10 min 3 pairs of tests, 3 days initially, 6 months, 24 months, Long-term (0', 6 and 24 months)	TP [FFT] LF HF LF/HF	ICC (95%CI)	0.73–0.89 0.66–0.85 0.72–0.89 0.54–0.75

Table 35.15 (Continued)

Author[s], Source/Year	Subjects	Duration of ECG recordings Between-measurements period	HRV measures	Statistics	Results
Schroeder et al. 2004 [255]	63 adults* 31F, 32M Age 45–64 SB	10 sec, 2 min, 6 min 1–2 weeks	RRI SDNN RMSSD HF [FFT] LF HF(N.U.) LF (N.U.).	ICC (95%CI)	0.78–0.96 0.22–0.92 0.30–0.95 0.79–0.93 0.65–0.89 0.48–0.85 0.48–0.85
Guijt et al. 2007 [302]	26 healthy adults 18F, age 28 ± 6 8M, age 34 ± 12 SB	7 min lying down, night 2nd and 4th 10 min light exercise (cycling)	SDNN RMSSD	ICC 95%CI	0.50–0.94 0.51–0.99
			SDNN RMSSD	SEM	12.35–13.95 2.01–10.37
Zollei et al. 2007 [A20]	10 healthy adults 3F, 7M Age 25 ± 2 SB / CB 6 breaths/min	5 min supine 10 consecutive days	RRI SDNN RMSSD LF (ms2)(FFT) HF	ICC (mean) SB / CB	0.961 / 0.961 0.967 / 0.979 0.968 / 0.977 0.873 / 0.974 0.964 / 0.970
Maestri et al. 2007 [268]	42 healthy adults 21F, 21M Age 38 (26–56)	5 min supine Day-to-day	RRI SampEn DFA HDF SD21 nCCE other nonlinear¶	ICC (mean, 95%CI)	0.76 (0.59–0.87) 0.54 (0.28–0.72) 0.68 (0.47–0.82) 0.69 (0.49–0.82) 0.78 (0.62–0.88) 0.67 (0.46–0.82) 0.18–0.72 (−0.13–0.84)

Murray et al. 2001 [265]	50 healthy adults 19F, 31M Age 21–77 SB	5 min 2–3 minutes apart	CIPA RMSSD SDNN ln HF ln LF	LOA	72–140% 68–*153%* 61–*157%* 76–133% 77–131%
Sandercock et al. 2004 [295]	29 healthy adults 9F, aged 29 ± 11 20M, aged 35 ± 13 SB / CB 12 breaths/min	5 min 7 ± 3 days apart	RRI SDNN RMSSD LF (FFT) HF	LOA For CB Absolute values	–147–147 –49.5–44.6 –73.8–63.9 –968–749 –1803–1670
Maestri et al. 2007 [268]	42 healthy adults 21F, 21M Age 38 (26–56) SB	5 min supine Day-to-day	RRI SampEn DFA HDF SD21 nCCE	LOA Absolute values	–162–162 –0.59–0.59 –0.45–0.45 –0.29–0.29 –1.48–1.48 –0.16–0.16
Coefficient of variation (CV, <30% acceptable)					
Kanters et al. 1996 [A19]	12 adults 6F, 6M Age range 25–38 SB	3 hour periods 3 separate days	RRI SDRR HF [a.u.][FFT] LF [a.u.] CorrDim	CV (mean)	3.7% 11.7% *35.3%* 20.3% 12.5%
Sinnreich et al. 1998 [269]	70 healthy adults 38F, 32M Age 31–67 SB / CB 15 breaths/min	5 min 2 month apart	Ln SDRR Ln RMSSD Ln TP [AR16] Ln LF LnHF	CV (mean)	6.0% /6.1% 8.0% / 7.4% 7.0%/ 6.7% 11.5% /10.7% 12.1% /10.5%
Lord et al. 2001 [271]	21 healthy adults Mean age 37 CB 10 breaths/min	5 min 3 sessions 3 separate days (one week apart)	lnLF [FFT]	CV (mean)	*45%*

Table 35.15 (Continued)

Author[s], Source/Year	Subjects	Duration of ECG recordings Between-measurements period	HRV measures	Statistics	Results
Pikkujämsa et al. 2001 [141]	50 healthy adults 25F, 25 M Age 40–59	5 min One session, two separate periods from 13 min recording	SDNN LF (ms^2) [AR20] HF (ms^2)	CV (recalculated, mean)	2% 10% 14%
Gerritsen J 2003 [599]	36 healthy adults Age 50–75	3 min 3 consecutive days 2 sessions one day	RRI SDNN HF LF LF/(LF+HF)	CV (mean)	8% 30% *71%* *76%* 22%
Winsley et al. 2003 [267]	12 healthy children Age 11–12 Controlled breathing 12 breath/min	5 min Day-to-day	SDNN RMSSD pNN50 HF (ms2) HF (N.U.) LF (ms2) LF (N.U.) LF/HF	CV (mean)	*31%* *37%* *81%* *84%* *35%* *97%* *38%* *83%*
Højgaard MV et al. 2005 [266]	14 healthy adults 5F, 9M Age 22–38 years	5 min Day-to-day 4 sessions	RRI TP [FFT] LF HF LF/HF	CV (mean, range)	4% (0–10) *36%* (9–93) *39%* (2–73) 27% (2–75) 28% (2–60)
		5 min, 17 min (1024 s) 2 weeks apart, 3 sessions	RRI TP (FFT) LF HF LF/HF	CV (mean, short/ long)	5 / 6% 25 / 24% 29 / 27% 31 / 28% 20 / 18%
Koskinen et al. 2009 [576]	43 healthy adults Age 24–39 CB 15 breaths/min	3 min supine 131 ± 4 days	SDNN RMSSD TP (FFT) LF HF LF/HF	CV	5.3% 7.1% 5.9% 8.1% 6.8% 11.5%

Table 35.16

Reproducibility of HRV measures from short-term ECG recordings in patients

Author[s], Source/Year	Subjects	Duration of ECG recordings Between-measurements period	HRV measures	Statistics	Results
Stein et al. 1995 [280]	15 CHF-patients Aged 52 ± 9 CB 6 breaths/min	30 s 2 weeks	RSA (peak-to trough, CB)	ICC	0.70
Ponikowski et al. 1996 [733]	16 CHF-patients Aged 60 ± 8	5-, 10-, 20 and 40 min from two 60-min recordings 25 days (mean)	RRI SDNN pNN50 Spectral *(FFT)*	CV (%)	*8%* *25.3–30.2%* *70–139%* *45–111%*
Freed et al. 1994 [274]	15 CHF-patients	2 adjacent 10-min Pre- and post-operative 2 periods	TP *(FFT)* LF HF	CV (%) Pre/Post	9/6 15/12 11/9
Salo TM et al. 1999 [270]	15 hypertensive patients with OSAS Aged 47 ± 10 SB/CB 6 breath/min	5 min/2 min > 3 weeks apart 4 recordings	HR RMSM (~SDNN) CV RMSSD HF (AR) HF [N.U.] LF LF [N.U.] LF/HF	CV_{SD} (mean)	9.3%/8.3% *33.9%/21.8%* *32.8%/21.4%* *56.7%/30.4%* *97.3%/56.3%* 13.9%/3.3% *92.7%/59.5%* 13.9%/3.3% *71.3%/48.6%*
Haas et al. 2000 [272]	158 AMI-patients 39F, 119M Aged 60 ± 12 SB (39) and CB (n=83) 10 breaths/min	5 min One session, 2 measurements (5 min in between) 1 week	SDRR [ms] VR [bpm]	Pearson's r	0.87/0.88 0.87/0.95
			SDRR [ms] VR [bpm]	LOA	−14.12 – 11.64 ms −8.87 – 7.98 bpm
Parati et al. 2001 [299]	8 hypertensive females Age 29–54 CB 18 breaths/min	15 min 1 month	PI (IBI) SD(PI) VLF *(FFT)* LF HF	VC (SB/CB)	5 ± 1/5 ± 4 19 ± 8/18 ± 15 6 ± 4/6 ± 5 5 ± 4/6 ± 9 12 ± 8/6 ± 8
Lord SW et al. 2001 [271]	21 HTX-patients Mean age 55 CB 10 breaths/min	5 min 3 sessions 3 separate days (1 week apart)	LF *(FFT)*	CV (%)	76

Table 35.16 (Continued)

Author[s], Source/Year	Subjects	Duration of ECG recordings Between-measurements period	HRV measures	Statistics	Results
Chemla et al. 2005 [275]	12 DM-patients Aged 49 ± 12	5 min 3 measurements 5 s apart (overlapping) Day-by-day	RRI SDRR TP (*FFT*) LF HF LF/HF TP (*AR*) LF HF LF/HF	CV (%) or bias error (%)*	2 ± 11* 17 ± 41* 8 ± 5 10 ± 6 5 ± 6 10 ± 5 7 ± 9 47 ± 55 6 ± 6 44 ± 55
Tarkiainen et al. 2005 [260]	89 stable CAD-patients 21F, 68M Aged 67 ± 8 (40–83) SB and CB (12 breaths/min)	5 min 3–4 months	RRI SDNN RMSSD lnLF *(FFT)* lnHF ln (LF/HF)	CV (%) (SB/CB)	6.1/6.0 29.9/37.1 *48.9/52.1* 11.3/16.5 14.7/14.9 11.5/16.1
	Spontaneous breathing + controlled breathing + exercise test + recovery period	40 min 3–4 months	NNI SDNN RMSSD lnVLF *(FFT)* lnLF lnHF ln(LF/HF)	CV (%) (all protocols)	5.1 16.7 31.1 4.9 8.6 11.0 7.3

The evidence for reproducibility of nonlinear HRV measures is sparse. In a study by Maestri et al. [268], only a ratio of SD1 to SD2 from a return map has been shown to be reproducible (Table 35.14). The DFA and SampEn were shown to be moderately reproducible. Reproducibility of other nonlinear HRV measures has been reported to be rather poor [268].

In several studies, measurement errors were quantified for a longer period between repeated investigations. It was found that the long-term reproducibility of short-term HRV indices appears better than that of the shorter term reproducibility. Sinnreich et al. found the CV values of logarithmically transformed HRV indices to be between 6–12.1% [269]. In their study, the SDNN, RMSSD, total and VLF power were highly reproducible while the HF and LF power were only moderately reproducible. Interestingly, controlled breathing did not improve their reproducibility. Reported ICC values for LF vary from 0.66 to 0.87 with FFT and 0.70–0.86 with AR. Similarly, for HF, the ICC values are between 0.48–0.96 (FFT) and 0.15–0.86 (AR). The largest differences of the ICC related to LF/HF with the worst reported being 0.06 (sic)(AR) and the best being 0.85 (AR). For very short registrations (10 s), the ICC values ranged between 0.41 and 0.57 [255]. Increasing the number of repeated measurements seems to improve reproducibility of short-term HRV measures (Table 35.14).

Thus, 5-min recordings provide most (moderate in fact) of the reproducible data for standard indices. However, in healthy subjects, their relative changes between examinations can reach 30% (overall), which should be considered as independent of biological and measurement variation.

Many studies have addressed the issue of reproducibility of HRV indices from 24-h ECGs in healthy subjects (Table 35.15). In the largest one, 165 healthy adults were included [65]. For the time-domain HRV indices the ICC was found to be good or high (>0.7) if compared from day-to-day. However, individual subjects showed a high range of variation explored by means of LOA. Thus, if significant changes of HRV indices are defined as lying beyond LOA, significant (independent from biological and measurement variation) changes of SDNN

Table 35.17

Reproducibility of HRV measures from long-term ECG recordings in patients

Author[s], Source/Year	Subjects	Between-measurements period	HRV measures	Statistics	Results
Bigger et al. 1992 [278]	40 PMI-patients (20 CAPS, 20 ESVEM participants)	Day-to-day	ULF (FFT) other spectral	ICC (CAPS/ESVEM)	0.79/0.89 > 0.85/ > 0.79
Van Hoogenhuyze et al. 1991 [277]	22 CHF-patients (CAD) NYHA II-III 4F, 18M Aged 59 ± 7	Day-to-day	RRI SDNNI SDANN	ICC (recalculated from data)	0.95 0.96 0.87
Stein et al. 1995 [280]	17 CHF-patients NYHA II-III, EF 12F, 5M Aged 52 ± 9	2 weeks	HR NNI SDNN SDANN SDNNI RMSSD pNN50 TP (ln) ULF (ln) VLF (ln) LF(ln) HF (ln)	ICC	0.95 0.88 0.91 0.88 0.87 0.49 0.23 0.91 0.90 0.91 0.88 0.86
Nolan et al. 1996 [276]	67 CAD-patients 58 ± 7	2–16 weeks	pNN50	ICC CR	0.94 *41%*
Anastasiou-Nana et al. 2001 [282]	14 CHF-patients NYHA II-IV, EF 13± 6% 2F, 12M Aged 52 ± 11 (25–65)	14 consecutive days > 18 h of analyzable data	SDNN SDANN SDNNI RMSSD pNN50 LF HF	ICC (mean ± SD)	0.87 ± 0.01 0.85 ± 0.02 0.82 ± 0.02 0.44 ± 0.05 0.31 ± 0.05 0.80 ± 0.02 0.66 ± 0.03
Kautzner J et al. 1995 [275]	33 AMI-patients 5F, 28M Aged 55 ± 11	Day-to-day (48-h recordings)	SDNN SDANN SDNNI RMSSD pNN50 HRVI TINN	Absolute relative errors (range)	1–27% 2–30% −2–23% −8–37% 0–90% 2–36% −1–38%
Weber et al. 1998 [283]	421 CAD-patients 45F, 376M Aged 56,6 (31–78)	Day-to-day	SDNN SDANN pNN50	Maximum value relative to base-line/Pearson's correlation coefficient	35.8/0.86 40.4/0.84 53.5/0.91
Burger et al. 1997 [A24]	23 DM1-type patients 8F, 15M Aged 37 ± 10	3, 6, 9, and 12 months	Time-domain Spectral-domain	Pearsons's correlation coefficient	0.35–0.98 0.47–0.93

would be considered if its value was reduced by 41 ms or increased by 35 ms (for the mean SDNN of 140 ms changes need to be less than 99 ms or greater than 175 ms) in an individual subject. This corresponds to a change of 25–30% from the initial value. Similarly, a change of at least 25% is necessary to consider significant difference for time-domain indices, including HRVI and HRVF. This finding is consistent with observations made by others for short-term recordings.

The reported CV of SDNN from 24-h ECG recordings in healthy subjects varies from 4.2 to 10.3% on a day-to-day basis, and 9.6% for a 6-month period between repeated measurements. Thus, *the difference of approximately 10% from the initial SDNN value can be considered statistically significant if the time-distance from repeated measurements is longer than 6 months*. The pNN50 was found to be least reproducible in some studies and highly reproducible in others (Table 35.15).

Reproducibility of the HRV indexes may play a greater role in patients with a reduced HRV, in whom a similar range of absolute differences between measurements makes the relative differences even greater. However, a simple comparison between data from healthy subjects and patients with certain diseases cannot be conclusive, as various data-length and reproducibility measures have been used.

Studies in which a comparison between normal subjects and patients has been performed are scarce. Short-term HRV reproducibility has been found to be poorer in hypertensive patients with OSAS in a study of Salo et al. [270] (Tables 35.14 and 35.16). In another study in patients after heart transplantation, the coefficient of variation of the LF component reached 76%, being greater than in healthy controls [45%] [271]. According to the dots-data (from the figure) provided in a report by Haas et al. in post-MI patients [272], the mean value of short-term (5-min) SDNN of around 20 ms was associated with the LOA of measurement being −14 to 12 ms, accounting for −70 to 160%, indicating rather a poor reproducibility. In a comparable study of Sinnreich et al. in healthy subjects, the recalculated mean value of 5-min SDNN of 37 ms has been associated with a 6% coefficient of variation (i.e., ± 17% range) [269].

A poor or moderate reproducibility of short-term HRV measures has been reported in patients with CHF (Table 35.16) with the CV range between 25 and 139% for time-domain, and 45–115% for frequency domain HRV indices in a study of Ponikowski et al. with a between-measurement period of 7–56 days [273]. In contrast, Freed et al. found a good short-term variability between two adjacent 10-min periods in CHF [274] with the CV range between 9–12% for LF and HF (FFT). Much better reproducibility of short-term HRV has been reported in the largest study in patients with stable CAD [260] with the CV range being between 11.3–29.9% for all measured indices, except for RMSSD with a CV value of 48.9%. Also in patients with diabetes mellitus, the day-to-day reproducibility has been moderate or high for SDNN (mean bias 17%) and moderate for FFT-derived spectral measures (mean bias 2–39%), while reproducibility for AR-derived spectral measures has been poor (27–102%) [275].

Thus, short-term HRV reproducibility seems to be lower in patients than in healthy subjects. Accordingly, a greater change of particular HRV measures is necessary to detect the true effect of interventions in patients with autonomic neuropathies or certain diseases. As yet, there are no indications from standards, statements or reviews. A magnitude of necessary change (absolute or relative) considered to be significant should be pre-defined taking into account the age of the population examined and the methods used.

There are independent studies in which normal subjects and patients with a certain disease have been compared simultaneously to evaluate reproducibility of 24-h HRV measures (Table 35.17). Nolan et al. analyzed the NN50+ index in 67 patients with CAD [276]. The ICC reached 0.94 (similar to 0.97 in healthy subjects). However, there was a much poorer CR (0.41) than in healthy subjects (0.21). In a sample of 87 diabetic patients in the same study, the ICC values have varied between 0.80–0.91 depending on between-measurement interval whereas the CR values were unacceptably large (0.61–0.98) [276]. Day-to-day variation of 24-h HRV has been found to be moderate in patients with CHF in a study of van Hoogenhuyze et al. [277]. The mean values of differences ranged from 8.5–13.8% (SDNNI and SDANN), However, individual variations have been observed of up to 50.6% and 28.2%, respectively [277]. Recalculated ICC values ranged from 0.87–0.95 (Table 35.17). Also, a high reproducibility for all 24-h spectral measures with an ICC>0.79 has been reported by Bigger's group [278] in post-AMI patients. Time-domain (SDNN, SDANN and SDNNI, geometric) measures have been found reproducible in a sample of post-AMI patients [279] and in HF studies [280–282]. However, reproducibility of the pNN50 has been shown to be poor in these studies (Table 35.17).

In the largest study on long-term HRV reproducibility in CAD patients, Weber et al. reported a maximum change of ~36 ms for SDNN in stable angina (~25% of the average) [283]. Comparing this value with the corresponding values reported by Hohnloser et al. [281] and Sosnowski et al. [65], the range of variation between examinations in cardiac patients appeared to be similar to that in healthy subjects (~30%).

Thus, whereas the reproducibility in patients with cardiac disease can be seen to be significantly lower with short-term HRV (~ twice than that in healthy subjects), in long-term recordings a similar reproducibility with long-term HRV examination can be assumed both in normal subjects and in patients with known cardio-vascular disease.

There is little data on the stability of diurnal variation of HRV measures. Huikuri et al. found the diurnal variation of HRV indices to be very stable in 20 normal persons on two consecutive days and then at 1-week intervals. However, neither results of rhythm analysis nor its reproducibility was reported [284]. A more detailed cosinor-based analysis [87] in patients with stable CAD has been provided by Hayano et al. [285], who repeated 48-h ECG recordings in 40 patients aged 58 years (38–72). The mesor (corresponding to the median values) of SDNN, LF (ms), HF (ms) and LF/HF were shown to be highly reproducible with ICC values ranging between 0.8–0.89. The values of the amplitude (the magnitude of change from the mesor) varied between 0.63–0.73, and of the acrophase (the time of maximum amplitude) varied between 0.76–0.95 [285]. These results may indicate that the use of a highly reproducible, understandable and robust cosinor-based circadian rhythm analysis may offer more than other statistical analyses to evaluate the effects of interventions. However, one has to bear in mind that the period of recording has to be longer than one day.

Noninvasive baroreflex sensitivity (BRS) reproducibility has been reported as being moderate to poor with a range of CVs of about 8–40% if the BRS is calculated using spontaneous approaches [266, 286–290]. However, some studies indicate a high reproducibility [291, 292]. The reproducibility of BRS is affected by the specific methodological features [289, 291, 293], age, health status, mean arterial pressure and period between measurements and the failure rate [287, 290, 291, 293]. The 95% limit of agreement varies between 1.7 ms/mmHg up to 10.6 ms/mmHg [287, 291] depending on the mean BRS value in the sample examined. Transfer function BRS and cross-spectral BRS appear to be applicable to most subjects, and calculated sample size to detect a change of 15% varies between 20 and 80 subjects [291, 292]. Within-subject variability seems to be responsible for a substantial proportion of reproducibility [287, 293]. The use of logarithmically-transformed HRV measures might improve the reproducibility [293]. However, the net results are similar. As pharmacologic and mechanical intervention-based methods are rarely used and restricted to highly specialized laboratory centres, the issue of the reproducibility of these methods is of marginal importance. However, in any laboratory study, the validity of the method of study still remains a fundamental requirement.

Heart rate turbulence (HRT) reproducibility (i.e., turbulence onset, turbulence slope, turbulence dynamics) has never been explored despite significant support in some investigators' teams for their superiority over traditional HRV measures (SDNN and HRVI only) [222, 226, 227]. A lack of reproducibility studies on HRT has been observed in recently published standards [294].

35.4.7.5 Reclassification Rate

Reproducibility of a specific HRV measure influences the categorization of its value as normal or abnormal depending on the cut-off values defined *a priori* (from the literature or guidelines) or *a posteriori* (from the distribution of values in the studied sample, i.e., mean or median, 10th, 25th, or 33rd percentile).

For the SDANN cut-off of 90 ms, the day-to-day variation in the SDANN calculation in data from van Hoogenhuyze et al. [277] caused a change in classification from normal to abnormal in 4 out of 22 CHF-patients (18%) and from abnormal to normal in 2 (9%). The overall reclassification rate achieved was 27% (6/22). Similar values for a cut-off of 100 ms resulted in a lower rate of reclassification (overall 2/22, 9%, from normal to abnormal 2/6, 30%), while with a cut-off value of 50 ms, only 1 out of 4 cases with SDANN<50 ms moved into the normal category (5% overall, 25% of abnormal). In 33 normal middle-aged (35 years) subjects, the reclassification rate from normal to abnormal (cut-off <100 ms) was 3 out of 29 (10%) and from abnormal to normal was 1 out of 4 (25%). Overall, there was a 6/33 (18%) rate of change in category for SDANN<120 ms, 4/33 (12%) for SDANN<100 ms and 3/33 (10%) for SDANN<90 ms.

From data of Haas et al. [272], the reclassification rate of 10.2% (4 out of 39 AMI-patients) can be calculated for 5-min SDRR with cut-off defined as values below 20 ms, and of 8 (9.6%) out of 83 for VR < 10 bpm. A detailed analysis of figures (1 and 2) from the paper of Stein et al. [280] on the stability of HRV indexes in CHF patients indicates that despite a high ICC of 24h-SDNN (= 0.91), the reclassification rate dichotomized at 70 ms regarding 6/17 patients (35%!), including 3 out of 5 with an abnormal value in the first recording and normal in the second visit. The SDANN categorization changes within two visits appeared similar (1 out of 3 (33%) changed from abnormal to normal).

Reclassification rate might be of importance in some clinical syndromes, which use an HRV analysis for their diagnosis, for example, diabetic autonomic neuropathy, sinus node dysfunction and obstructive sleep apnea syndrome. As yet, studies that address this issue are lacking.

35.4.8 Selection of Method for HRV Analysis

The choice of HRV method to be applied in a specific study is dictated by the purposes and conditions of the study. From a clinical point of view, it is important that the HRV measure is normally distributed (like LV ejection fraction), thereby providing results which can be easily expressed and understood as raw values rather than log-transformed measures (Fig. 35.34). If the distribution is not normal, data should be transformed for statistical calculation. However, the presentation of results requires re-transformation.

A fraction of abnormality, i.e., the proportion of abnormal range and total range, would also be informative (Fig. 35.35). Within a restricted limit of abnormality (98%CI) that is based on distribution of the results, there was nobody (neither healthy nor post-MI-patients) with the SDNN value <20 ms, whereas 13% of CAD patients were recognized on the basis of HRVF evaluation. For less restricted limits, there was still a significant difference in the proportion of CAD-patients with abnormal results (i.e., 5. % for SDNN vs 36.7%), albeit the cut-off points lay below the 2.5th percentile. This indicates that the definition of abnormal values is strongly affected by the normality of distribution of an HRV measure.

The duration of HRV recordings seems to play a crucial role in the applicability of HRV analysis. Studies on clinical outcome and risk factor association with HRV, in which HR had been used as an independent measure of the autonomic balance, were undertaken in tens of thousands of people. Meanwhile, in other studies in which short- or median-time HRV analysis was used, smaller populations, around a tenth of the size, were gathered. While 24-h HRV analysis was applied, the number of subjects studied was reduced by a further factor of 10 (Fig. 35.36).

If the HRV analysis is going to be performed in a large sample population, as in epidemiological studies and registries, the use of simple statistical methods from short-term recordings seems to be most appropriate (Fig. 35.37). HRV from routine ECG recordings lasting 8–10 s can be applied taking into account that each index derived from routine ECG strips (VR, SDRR, CIPA, CV) reflects vagally-mediated respiratory HR modulation. As short epochs are characterized by a relatively great biological variation, the reproducibility of individual measures should be assessed or simple HR used as an index of sympathovagal balance of greatest reproducibility. Otherwise, the duration of EGC recordings should last 5 min, because there is a relatively large experience with the use of HRV from 5-min epochs. However, as there is an inverse relationship between the statistical power of a study and the reliability of an HRV measure for a given sample size, it is necessary to calculate sample size on the basis of *a priori* defined change of an HRV index to be detected and of *a priori* or *a posterior* defined reproducibility [285].

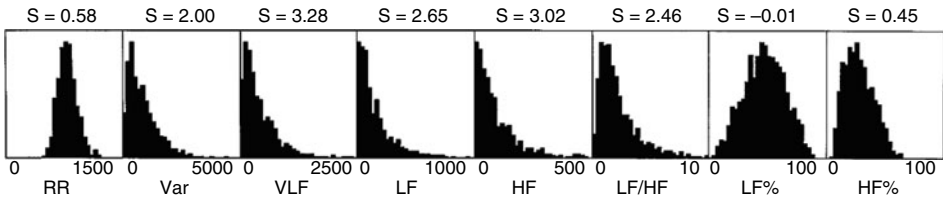

Figure 35.34

Frequency distribution and estimated skewness (S) of the commonly used HRV measures. Data from 1,070 healthy subjects. The SDNN (Var) and spectral HRV measures are characterized by a nonnormal distribution, so the logarithmic transformation is necessary. Normal distribution is present for the RRI, HF [N.U.] and LF [N.U.], however the latter two (HF, LF expressed as %) do not have an explanation on physiological or pathophysiological basis (From [324]).

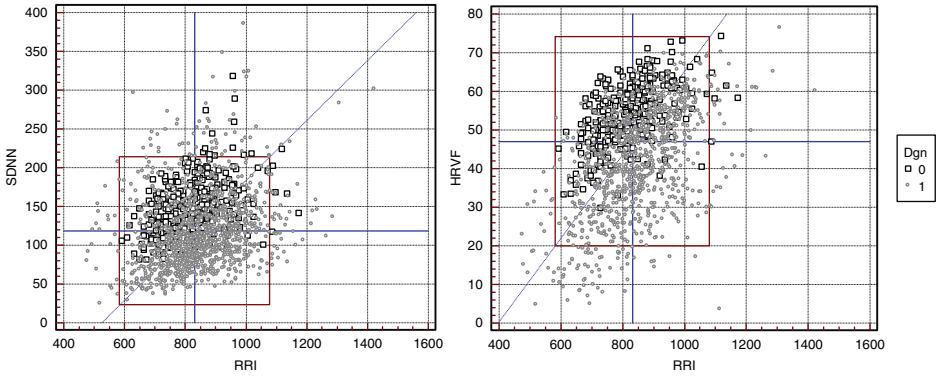

Figure 35.35

Comparison of the distribution of normal and abnormal SDNN and HRVF in respect to health status. Median values of the 24-h mean R – R interval (RRI = 830 ms), SDNN (119 ms) and HRVF (47%) in the entire cohort (805 subjects) are depicted by the vertical or horizontal lines (respectively). These values constitute approximately 30% and 60% of the total ranges, respectively. If one considers abnormally low HRV values on basis of a population distribution, only few normal subjects have SDNN and HRVF below the lower normal limit (here: 89 ms and 35%), however these values constitute various percentile of the total range (here: 23% and 46%). The open boxes indicate the 98% CI of prediction of the normal/abnormal result. Each value of RRI, SDNN and HRV that lies outside the boxes are definitively abnormal. Interestingly, there are none subjects (normal or post-MI) with SDNN<98%CI (22 ms), whereas 67 patients (13%) (exclusively from the postMI-cohort) had abnormal value (i.e., HRVF<20%). If we turn into established cut-off of SDNN (<50 ms) and HRVF (<30%), the respective proportions reach 27/515 (5.2%) for SDNN and 187/515 (36.7%) for HRVF again exclusively form the CAD cohort. Open squares indicate healthy subjects (n = 290) and circles indicate patients after myocardial infarction (with/without sinus rhythm, n = 515) (Author's data).

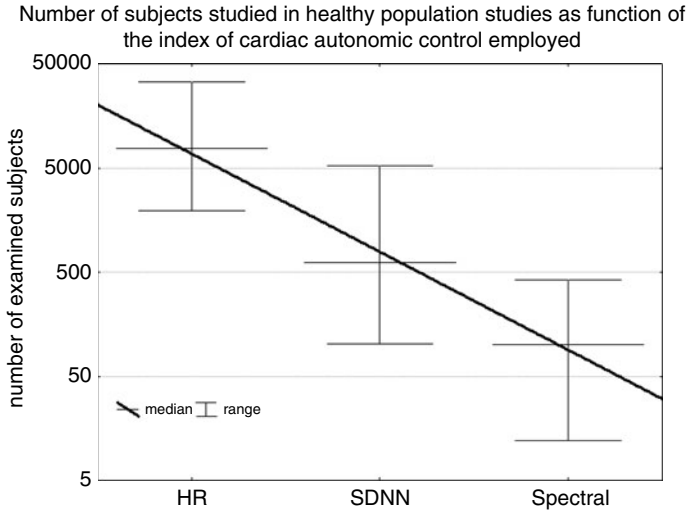

Figure 35.36

An exponential relationship between simplicity of available indices of cardiac autonomic tone and examined population. Data from 94 studies in normal population (either selectively healthy or random sample). A magnitude of 10 is a scaling factor for this relationship. Thus, HR as a crude sympathovagal balance index can be employed in largest population, whereas spectral analysis seems to be applicable to 100 times lower samples (Author's data).

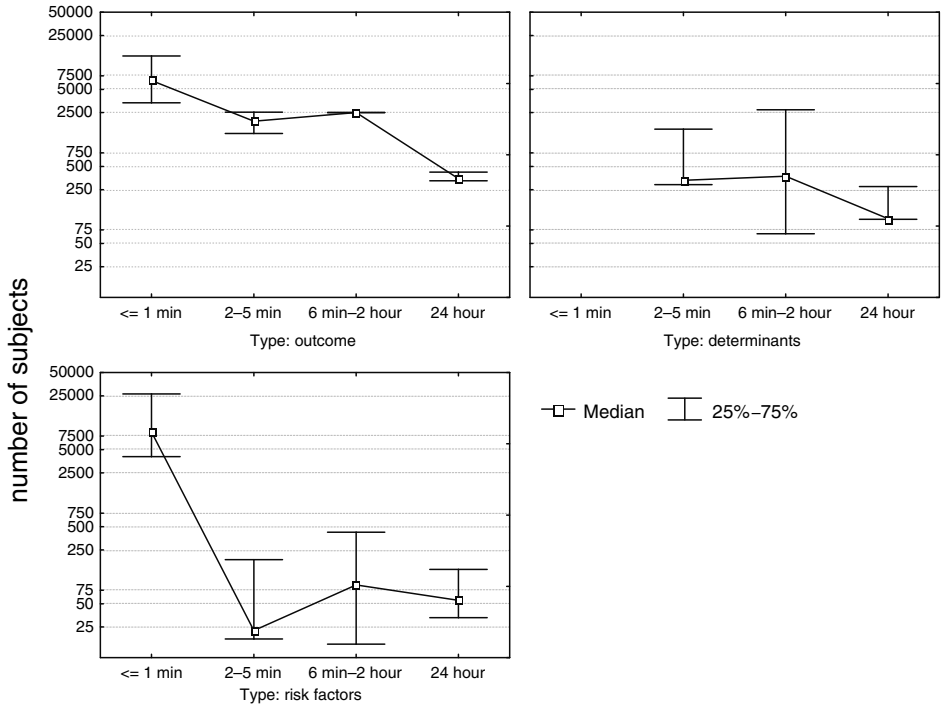

Figure 35.37

Reportable size of population samples as a function of HRV indices and length of ECG recordings chosen. Data from 94 studies that employed HR and/or different time- and spectral HRV measures for clinical outcomes, HR and HRV associations with risk factors and HRV determinants evaluation. (Author's data).

If HRV analysis is to be used for physiological, psychological, and pathophysiological reasons, either short-time or long-term time series could be appropriate. However, a prolongation of HRV recordings for these purposes reduces the number of factors that can be controlled during a study.

Cumulated experience indicates that long-term HRV analysis appears to be a useful tool for clinical outcome studies. It is necessary to be aware of the contribution of the autonomic control of HR to the entire HRV over a 24-h period, which is less than 10% of total variance [80]. Thus, in clinical outcome studies, it is not advisable to search for an association between clinical events and sympathetic and vagal activity as well as their balance. However, most global HRV measures certainly require the autonomic system to mediate their influences. The uses of various HRV methods/indices for different purposes are summarized in Table 35.18.

35.4.8.1 Reliability

Homogeneity in the evaluation of the effects of interventions and in agreement with other methods determines the reliability of various HRV indices as noninvasive measures of cardiac autonomic control. There are several methods that allow the determination of HRV reliability.

For short-term HRV reliability assessment, simple maneuvers are used (controlled breathing, body position change from supine to standing, head-up tilt, exercise, mental stress) for which changes in cardiac autonomic control are well established. Tables 35.19–35.21 summarize the results of selected studies that have addressed this issue.

The reproducibility of 5-min SDNN and spectral HRV indices in response to a head-up tilt has been shown to be poor or moderate [266, 295, 296]. Data are conflicting regarding the reproducibility of HRV in response to active standing.

Table 35.18

HRV methods used in population studies depending on their type and objectives

Authors, acronym of the study (if exists)	Year	Total sample (% men)	Age (range)	Length of recording	HRV method/ index	Specific purposes
Macfarlane et al. The WOSCOPS Study [A25]	2007	6596 (100%)	45–65 years	8–10 s	CIPA	Outcome prediction
Dekker et al. The Zutphen Study [A26]	1997	1763	40–85 years		SDRR	Outcome prediction (CHD mortality)
De Bruyne et al. The Rotterdam Study [650]	1999	5272 (40%)	⩾ 55 years	10 s	SDRR	Outcome prediction (Cardiac mortality)
Liao et al. The ARIC Study [248]	1995	1984 (46%)	45–64 years	2 min	LF, HF, LF/HF	Determinants of HRV
Liao et al. The ARIC Study [649]	1997	2252 (45%)			SDNN, LF, HF, LF/HF	
Dekker et al. The ARIC Study [258]	2000	856 (45%)			SDNN	Outcome prediction (CHD, mortality)
Carnethon et al. The ARIC Study [249]	2002	9267 (40.5%)			SDNN, LF, HF	
Kageyama et al. [817]	1997	282 (100%)	21–49 years	3 min	LF, HF	
Korkushko et al. Population-based [555/A27]	1991	354 (50%)	3 months to 89 years	4 min	LF, HF	Determinants of HRV in population
Sinnreich et al. Cross-sectional study [1998]	1998	294 (50%)	35–65 years	5 min	SDNN, LF, HF, LF/HF	
Kuo et al. Healthy volunteers [324]	1999	1070 (44%)	40–79 years		SDNN, LF, HF, LF/HF	
Agelink et al. [335]	2001	309 (49%)	18–77 years		LF, HF, LF/HF	
Kuch et al. [648]	2001	286 (52%)	56 years mean		LF, HF	
Ryan et al. [A28]	1994	67 (60%)	20–90 years	8 min	LF, HF, LF/HF	
Hotta et al. The LILAC Study [A29]	2005	298 (40%)	> 75 years	10 min	Nonlinear (a2, DFA)	Outcome prediction
Fagard et al. [654]	1999	424 (48%)	25–89 years	15 min	SDNN, LF, HF, LF/HF	
Huikuri et al. [323]	1996	374 (50%)	40–60 years	30 min	SDNN, LF, HF, LF/HF	
Tsuji et al. Framingham offspring [251]	1996	2722 (45%)	21–93 years	2 h	SDNN, LF, HF, LF/HF	Determinants of HRV in population, outcome study

Salo et al. [270] reported an unacceptably high CV for RMSSD and all spectral measures (42–83%), while Lobing et al. observed low ICC of LF and HF (0.57 and 0.33, respectively) using a very complicated protocol [297]. On the contrary, an excellent reproducibility has been reported by others (Table 35.19). In a study in children, Dietrich et al. observed good reproducibility of standing LF and HF (natural logarithms). However, differences in these measures have been found to be highly unpredictable (Table 35.19) [298].

In a head-to-head comparison of FFT and AR spectral HRV indices in analysis of controlled breathing, Pitzalis et al. showed a moderate ICC for the LF and HF, and a poor reproducibility (ICC<0.6) for TP and LF/HF in 20 young healthy subjects [296], while a moderate reproducibility was found for SDNN and RMSSD. Limitations of the reliability of spectral HRV measures for evaluation of the effect of controlled respiration have been confirmed in many studies (Table 35.20). On the other hand, positive studies confirming good reliability of HRV in the examination of the effects of respiration do exist (Table 35.20) [256, 269, 297, 299, 300]. Tarkiainen et al. reported that logarithmic transformation of the standard HRV measures (RMSSD, TP, LF, HF) improved the reliability of evaluation of HRV response to

Table 35.19

Reproducibility of HRV in response to body movement (active standing or head-up tilt (HUT))

Author	Intervention	Test for reproducibility	HR/RRI	SDRR	RMSSD	TP	LF	HF	LF/HF	Comments
Pitzalis 1996 [296]	Head-up tilt 70°	ICC > 0.6 accept.	0.44	0.30	0.30	0.59 0.57	0.65 0.65	0.59 052	0.36 (FFT) 0.09 (AR)	FFT, AR12 10 min
Salo 1999 Hypertensive [270]	Standing	CV_{SD} [%] < 30 accept.	6.6	26.3	41.7	83.2	75.3	56.3	75.1	FFT? 5 min
Sandercock 2004 [295]	Standing	ICC	0.87–0.93	0.67–0.85	0.86–0.91	–	0.77–0.94	0.79–0.92	0.71–0.82	3 different instruments, FFT, 5 min
Hojgaard 2005 [?]	Head-up tilt 60°	CV [%](intra) < 30 accept	5/5	–	–	33/25	28/26	33/32	18/23	FFT, 300s/1024s
Carrasco 2003 [300]	Standing	ICC	0.89	0.95	0.93	0.94	0.94	0.91	0.90	AR bpm2 5 min
Kowalewski Urban 2004 [A23]	Standing	ICC	–	–	–	0.73–0.91	0.69–0.86	0.71–0.89	0.68–0.85	FFT, 10 min 3 x 2 x 3periods
Lobnig 2003 [297]	Standing + CB 12/min	ICC	–	–	–	–	0.567	0.326	–	FFT (coarse-graining), ln values, 5 min 4 x 4–5 days
Kobayashi 2007 [A21]	Standing	Intra CV Inter CV	5 14.9	–	–	–	21.2 48.2	19.5 41.4	–	FFT bpm^2 204.8 s (~3′)
Dietrich A 2007 Children [298]	Standing Change from supine	CV	9.4 36.2	– –	– –	– –	6.2 315.3	7.7 44.6	– –	DFT 3 min

Table 35.20

Reproducibility of HRV in response to controlled breathing

Author	Controlled breathing	Test for reproducibility	HR/RRI	SDRR	RMSSD	TP	LF	HF	LF/HF	Comments
Pitzalis 1996, healthy [296]	16/min	ICC > 0.6 accept.	0.35	0.27	0.20	0.52 0.55	0.60 0.65	0.65 0.70	0.36 (FFT) 0.48 (AR)	FFT, AR12 10 min
Salo 1999, hypertensive [270]	6/min	CV_{SD} [%] < 30 accept.	8.3	21.8	30.4	58.2	59.5	56.3	48.6	FFT? 5 min
Sandercock 2004, healthy [295]	12/min	ICC	0.84–0.92	0.72–0.83	0.69–0.91	–	0.83–0.87	0.47–0.82	0.64–0.82	3 different instruments, FFT, 5 min
Sinnreich 1998 Healthy [530]	15/min	CV [%]	–	6.1	7.4	6.7	10.7	10.5	–	AR16 5 min
Parati 2001 Hypertensives [299]	18/min	CV [%]	5	18	–	–	6	6	–	FFT, 15 min
Jauregi-Renaud 2001, healthy [301]	12/min	CR < 30 accept.	6.33	–	–	–	–	40.8 (NU)	3.59	AR, 5 min
Carrasco 2003, healthy [300]	12/min	ICC	0.81	0.94	0.94	0.94	0.92	0.93	0.88	AR bpm^2 5 min
Lobnig 2003 Healthy [297]	12/min	ICC	–	–	–	–	0.66–0.69	0.71–0.81	–	FFT (coars-graining), ln values, 5 min, 4x4–5days
Tarkiainen 2005 CAD [260]	12/min	CV [%]	6 5.6 – –6.3	37.1 *35.0–39.5*	52.1 *49.1–55.4*	9.9 [ln] *9.3–10.5*	16.5 [ln] *15.5–17.5*	14.9 [ln] *14.0–15.8*	16.1 [ln] *15.2–17.2*	FFT 5 min
Lord 2001 Healthy [271]	10/min	CV [%]	–	–	–	–	–	0.45	–	FFT 5 min

Table 35.21

Reproducibility of HRV in response to other interventions

Author	Intervention	Test for reproducibility	HR/RRI	SDRR	RMSSD	TP	LF	HF	LF/HF	Comments
Salo 1999 Hypertensive [270]	Exercise Cold pressor test	CV_{SD} [%] < 30 accept	6.6 10.1	26.3 29.4	41.7 57.9	76.2 101.6	80.0 100.6	131.6 145.3	54.0 79.1	FFT? 5 min
Carrasco 2003 [300]	Exercise 80W	ICC	0.86	0.85	0.79	0.91	0.92	0.88	0.87	AR/ bpm^2 5 min
Jauregi-Renaud 2001 [301]	Cold pressor test+CB 12/m	CR	17.1	–	–	–	–	37.9 (NU)	2.87	AR, 2 min
Guijt 2007 [302]	Sleep	ICC	–	0.79/0.85 *0.54–0.94*	0.94/0.98 *0.86–0.99*	–	–	–	–	2 x 1 h
	Exercise 50W	ICC	–	0.85 *0.70–0.93*	0.84 *0.67–0.92*	–	–	–	–	15 min

controlled breathing [260]. The reliability of HRV in response to other maneuvers is shown in Table 35.21 [270, 300–302]. In general, the reliability of HRV measures in evaluating the effects of the aforementioned interventions seems to be unsatisfactory [256].

Other methods of reliability evaluation are related to the pharmacological action of agents that exert either direct or indirect stimulatory or inhibitory effects upon the vagus or sympathetic branch or both. Unfortunately, data on reliability of HRV analysis in such settings are extremely rare. Cloarec-Blanchard et al. examined the effects of nitroglycerin infusion on LF components in ten healthy volunteers 1 week apart and found it to be reproducible [303]. Moderate to good reproducibility (CV between 4 to 30%) of HRV has been reported by Piepoli et al. in heart failure patients under dobutamine infusion [304].

For long-term HRV reliability assessment, quite different approaches are in use. Physical training or body mass changes are assumed to be associated with HRV changes, but unfortunately, studies addressing HRV reliability in this area are lacking.

35.4.8.2 Explicitness

Ideally, the HRV index changes should be caused by a specific alteration in cardiac autonomic control. Effects of an intervention, like vagus nerve intersection, which results in almost total reduction of IBI variation [305], should be universally observed. Similar effects should be observed by a muscarinic receptor blockade in any examined subject [23]. Data from studies by the Goldberger group [231] indicates that cholinergic blockade with a high dose of atropine results in elimination of RSA and HRV in almost every subject examined. However, parasympathetic stimulation does not necessarily result in uniform HRV changes [231]. As indicated by an early study of Anrep et al. in dogs, blood pressure increment beyond a certain level (associated with a reflex parasympathetic excitement) results in a reduction of VR of HR [3]. A suppression of HRV (SDNN, LF and HF) as a result of the phenylephrine-induced activation of parasympathetic branch of the ANS has been found in normal humans [231]. However, changes of certain HRV spectral measures in response to parasympathetic baroreflex-related stimulation have been observed to depend on the initial level of HRV, because a reduction in those with a high basal HRV and an increase in those with a low basal HRV, despite slowing of HR, was found in each case [231]. A possible explanation for such a discrepancy is the phenomenon of saturation (see part 35.5), where the effects of inspiration and expiration-induced vagal activity can be rather diminished [231].

The situation is even more complicated if the effects of sympathetic inhibition or stimulation are considered. Alpha-adrenergic stimulation with phenylephrine in a setting of a so-called total autonomic blockade (atropine 0.04/kg + propranolol 0.2/kg [306]) has not been found to have an effect on either time or spectral HRV indices in healthy subjects, while a significant reduction of HRV has been observed in subjects with an intact activity of both branches of the ANS [231]. It indicates that inhibition of ß1-adrenergic and M1-muscarinic receptors prevents the effect of action of α-adrenergic-mediated stimulation, or that these effects are truly negligible [231].

The effects of beta-adrenergic stimulation or inhibition on HRV strongly relate to the choice of stimulus/inhibitor. For instance, a large increase of LF power in response to up-right body movement is accompanied by a significant reduction in total HRV [307]. Such an LF power increase has been observed to be lower in a setting of parasympathetic blockade [231]. In addition, the use of different sympathomimetics elicits various effects. Exogenous epinephrine has been shown to reduce HRV (SDNN) with variable changes (increase, no change or a decrease) in the LF power in healthy subjects, while isoproterenol infusion has exerted more of an inhibitory effect on LF power. Interestingly, the HF power has been simultaneously reduced with isoproterenol, in contrast to epinephrine [307].

Such experimental circumstances are rather unique in clinical settings. Changes in a specific physiologically explainable R–R variation (e.g., RSA, LF power) need not follow changes in the entire HRV [308]. Thus, *a reduction or an increase of heartbeat variation cannot definitively indicate its cause*.

For instance, in a patient with an acute MI, a reduction of HRV can be attributed to various mechanisms, which can depend on factors such as age of the MI, its location and size, LV function, drugs, interventions, coexisting diseases (e.g., diabetes, respiratory system disease, depression), and finally complications and adverse events such as malignant ventricular arrhythmia, stroke, cardiac tamponade, loss of blood, etc. In addition, the magnitude of HRV reduction is pre-determined by the pre-event level of cardiac autonomic control (age, sex, coexisting diseases).

For such a complex clinical entity, the detection of a specific alteration in the cardiac autonomic control is *a priori* impossible.

However, if an effect of a specific intervention with known patho-mechanism(s) contributing to a certain HRV measure is to be studied, a link between them can be explored. Again, the control of many factors is necessary to draw an explicit interpretation. The more sophisticated and mathematically complex the method used for HRV assessment, the less likely is its unequivocal explanation.

Actually, none of the currently used HRV measures can help to explain what specific alteration (in terms of level and location) is responsible for HRV changes in any physical condition or in cardiac and noncardiac diseases.

35.4.8.3 Redundancy and Inter-Changeability Among Different Methods and Measures

The variety of HRV measures determined in different domains has, in fact, a similar complex physiological and pathological background. Current guidelines indicate that some HRV measures are most useful, but actually only very few are commonly applied in clinical settings [309]. A plethora of methods and derived indices have been proposed for which the advantages over standard HRV measures have been justified in terms of a better description of underlying physiological and pathological processes and in prediction of hard end-points or their surrogates [310]. As a result, researchers and physicians are faced with a dilemma of choosing the most appropriate method and indices that would help to meet the purpose of their studies. From this point of view, it is important to know the meaning of particular HRV measures, but also their redundancy and inter-changeability, as well as differences between the methods used for obtaining their measurements. Simple comparisons of techniques for HRV analysis are given in Table 35.22 [after 310].

There are relationships between HRV indices from the same or different domains (time, spectral, nonlinear) that permit them to be used as a substitute for one another, or to interpret (within a limited credibility) simple time-domain or complex nonlinear measurements on the basis of the known background of spectral components. The higher the correlation between different indices, the higher is their inter-changeability. The most significant relationships among HRV indices in various domains are shown in Table 35.23. [4, 11, 311, 312].

Time-domain measures are least dependent on the algorithms used for their determination and the main differences between means are related to the duration of recording. However, spectral estimates are not necessarily similar if obtained using the two most popular methods, namely FFT and AR modeling.

In a comparative study of FFT and AR spectral techniques for LF and HF components of the HRV power spectrum, Pichon et al. found a significant bias between these two methods meaning that they are not interchangeable. For the 265 s ECG registrations, the bias calculated from FFT and AR [16th order] has been measured and reached −132 ms^2 for LF and −111 ms^2 for HF with the lower LOA of −1442 and −469 ms^2 for LF and HF respectively and the upper LOA of 1176 and 246 ms^2, respectively [313]. Even greater bias was found after body position movement, where LOA (lower and upper) lie far from the mean values [313]. Similar observations have been reported by Chemla et al. [275]. They found that the fast Fourier transform and AR analysis provided quite different estimates of spectral HRV in diabetic patients. Moreover, they stated that these methods are not interchangeable at all and in this specific patient population, the FFT method provided spectral estimates of TP, HF and LF in all patients contrary to the AR method which was unable to produce spectral peaks in almost half of the diabetic patients [275]! They observed that in subjects in whom spectral peaks could be detected by means of either method, spectral estimates within frequency bands were similar. Also, the FFT appeared less dependent on the minor changes (5%) in the timing of the onset of the analysis. In a former head-to-head study of Pitzalis et al., the power spectrum of LF and HF was 20–30% lower if assessed by means of AR [12th order] than that obtained by means of FFT [296]. Also, in a study of Sinnreich et al. in 398 healthy subjects [269], the AR [16th order] LF and HF spectral powers [mean of LF of 221 and HF of 151 ms^2 in males and 126 and 128 ms^2 in females, respectively] were clearly lower than those reported by Pikkujämsa et al. in 50 healthy subjects of similar age [mean LF of 520 and mean HF of 375 ms^2] calculated by using 5-min AR [20th order]. They were even lower than in diabetic patients (5-min) [275] and similar (with respect to LF components) to the mean 24-h value estimated in patients in the early phase of acute MI by means of AR [10th order] modeling (299 and 270 ms^2 respectively) [316]. A comparison of the corresponding means of AR-spectral indices

Table 35.22

Comparison of techniques of HRV analysis (Modified after [310] and [111])

HRV analysis	Description	Advantages	Limitations	Universality
Time-domain	Statistical	Simple, easy to calculate, proven clinical utility, gross distinction of high and low frequency variation	Sensitive to artefact; requires stationarity, fails to discriminate distinct signals	SDNN most widely used, SDANN most widely applicable (also in AF)
	Frequency distribution	Visual representation of data, can fit to normal or log-normal distribution	Lacks widespread clinical application, arbitrary number of bins	Undetermined
	Geometric	Visual representation of data, does not requires stationarity, relatively robust, can be also used for nonlinear analysis	Fails to discriminate distinct signals, requires relatively large datasets	HRVI most widely used HRVF most widely applicable (also in AF)
Frequency-domain	Frequency spectrum representation	Visual and quantitative representation of frequency contribution to waveform, useful to evaluate relationship to mechanisms, widespread HRV evaluation	Requires stationarity and periodicity for validity, sensitive to artifacts, altered by posture, sleep, activity	Only in subjects with sinus rhythm
Fractal analysis	Power law	Ubiquitous biologic application, characterization of signal with single linear relationship, enables prognostication	Requires stationarity and periodicity, requires large datasets, vulnerable to artifacts	1/f slope of power law most widely applicable (also in AF)
	Detrended fluctuation analysis	Indentifies intrinsic variations to system (versus external stimuli), does not required stationarity, enables prognostication	Requires large datasets (>8000 data points), dependence on artifacts	Undetermined (only in sinus rhythm?)
Entropy	Measures the degree of disorder (information or complexity)	Unique representation of data, requires fewest data points	Needs to be complemented by other techniques, stationarity is required	Undetermined (only in sinus rhythm?)

Abbreviations see Table 35.2 and Sect. 35.1

reported in a study of 50 age-comparable healthy subjects (LF of 520 ms^2 and HF of 375 ms^2) [141] and in those with diabetes (similar age range) (LF and HF of 222 ms^2 and 485 ms^2) in a study by Chemla et al. [275] might indicate that there is either a problem with the determination of a proper order for AR modeling or that it might not be [empirically] a reliable method for HRV spectral assessment.

There are also data indicating that the so-called sympatho-vagal balance, indicated by means of the LF/HF power ratio, is not interchangeable while using either FFT or AR for estimation. Apart from controversies regarding the rationale and background of the use of this index, the comparability of the LF/HF ratio is low either in normal subjects, namely 3.84 in AR[12] modeling in normal young subjects, 4.11 in AR[16] modeling in middle-aged subjects and around 5 in AR[20] modeling in a similar sample [269, 275, 313].

Table 35.23

Inter-changeability diagram of various HRV measures

Analytic method		Frequency-range			
		<0.033 Hz	**0.033-0.04 Hz**	**0.04-0.15 Hz**	**0.15-0.40 Hz**
	Time-domain	SDNN, SDANN	SDNNI		RMSSD, pNN50(20)
	geometric	HRVI, HRVF, SD2			SD1
	Frequency-domain	ULF	VLF	LF	HF
		TP (long-term)			TP*
	Non-linear dynamics	1/f slope			Symbolic dynamics ApEn*
			DFA α_2		
					DFA α_1*
				SampEn*	
	HRT		TS		
				TO	

Abbreviations as in Sect. 35.1. On basis of data provided by HRV Standards [4], Voss A et al. [111], Stein KM et al. [311], Cygankiewicz I et al. [312].
* short-term

The accumulated data also indicates that cut-off values of prognostic values of spectral HRV estimates stated in the Standards [4] should not be applied in studies in which AR modeling is to be applied. This might also imply that the use of the fast Fourier transform, despite its limitations [see 35.4], should be preferred for short-term HRV assessment in laboratory settings. If the AR modeling is to be used, referencing of previous studies should be limited and should include studies in which other methods (FFT in particular) had been applied.

35.4.9 Normal Limits and Abnormal HRV

The successful application of HRV analysis to clinical medicine is critically dependent on the definition of normal limits and abnormal values. Guidelines [4] provide standard HRV measurements in a healthy population. However, they might be useful only as a reference for comparison with population samples with known characteristics (e.g., prevalence of CAD, mean age, mean RRI, etc.). HRV analysis, like other diagnostic methods, should take into account the prevalence of the disease and its influence on the performance of a particular HRV index. As yet, in almost all studies, the positive predictive value of HRV indices has been reported ignoring the prevalence of a disease in a population (if normal persons had been comparators). The author's studies, confirmed by others, clearly indicates that examination of a sample of a population is necessary to determine normal limits and to define abnormal values [64, 65]. As there are significant age-, gender-, race-, HR-, respiration-, and distribution-related differences among various populations, normal limits as well as abnormal and risk-predictive values should therefore be determined in a sample of a "regional" population rather than be drawn from the literature [315, 316]. Also, even if they can be controlled for the constitutional factors, a skewed distribution of most standard HRV measures (Fig. 35.34) prevents use of their standard deviation value for setting normal limits. Thus, the use of data provided by the Standards [4] does not seem to be justified at present. It should be remembered that there have been specific technical limitations (>12 h with at least 6 night hours and >50% sinus heartbeats) for HRV analysis in the study of Bigger et al. [317] from which data cited in the Standards [4] have had been drawn. Currently, these data cannot be used further in terms of the same Standards, which indicates requirement for at least 18 h of acceptable data. Nevertheless, researchers might need to compare results of their studies to the corresponding data of others. Also, if population sample characteristics cannot be established accurately, the use of published normative values might be helpful.

Thus, reported values of traditional long-term and short-term HRV indices are provided (Tables 35.24 and 35.25). In addition, if nonlinear HRV measures are to be more commonly used, then reported values (not references) of either short-term or long-term HRV studies need to be provided as has been done (Table 35.26.). Strong dependence of HRV

Table 35.24

Reported values of 24-h HRV time-domain indices (average population ranges)

Author[s] Year	No sbs	Age (mean/range)	% males	Normal value		Normal ± 1,96SD or 95% CI* limits	Normal value		Normal ± 1,96SD or 95% CI* limits
				Mean/median	SD		Mean/median	SD	
				RRI (NNI) [ms] (only from papers on HRV)			**RMSSD [ms]**		
Standards 1996 [4] (Bigger 1995 [122])	274	40–63	73	–	–	–	27	12	NR
Mølgaard 1991 [318]	140	40–77	64	812	NR	645–1089*			
Ramaekers 1998 [319]	276	18–71	51	784	89	610–958			< 610
Pikkujämsa 1999 [320]	394	1–82	49	891	131	629–1153			
Grimm 2003 [366]	110	21–77	68	817	96	640–1055*	42/339	50	12–158
Bonnemeier 2003 [321]	166	20–70	51	789	86		32.6	16.9	NC
Sosnowski 2005 [65]	296	18–63	82	799	94	636–1005 (2–98%)/ 648–1024*	611–636		< 611
				SDNN [ms]			**HRVI [A.U]**		
Standards 1996 [4]	274	40–63	73	141	39	63–219	37	15	NR
Mølgaard 1991 [318]	140	40–77	64	139	NR	78–231			
Umetani 1998 [322]	167	30–79	50	131	29	76–211			
Raemaekers 1998 [319]	276	18–71	51	148	37	86			
Grimm 2003 [366]	110	21–77	68	154	44	83–272			
Bonnemeier 2003 [321]	196	20–70	51	149	40	NR	40.5	11.9	17.2–63.8
Sosnowski 2005 [65]	296	18–63	82	142	33	86–221 (2–98%)/ 89–220 (5–95%)	35.7	8.1	19.2–52.2 [2–98% CI]
				SDANN [ms]			**HRVF [%]**		
Standards 1996 [4]	274	40–63	73	127	35	58–196			
Raemaekers 1998 [319]	276	18–71	51	140	37	78–209 (5–95%)			
Pikkujämsa 1999 [320]	58	40–82	59	153	36	84–223			
Bonnemeier 2003 [321]	196	20–70	51	135	38				
Sosnowski 2005 [65]	296	18–63	82	135	39	74–230 (2–98%)/ 79–212 (5–95%)	53	9	35–70 [2–98% CI]

Abrreviations see Table 35.1 and Sect. 35.1

Table 35.25

Spectral HRV indices from a short-term ECG (supine) as reported in literature (average population ranges)

	Total power (ms^2) ln/raw			LF power (ms^2) ln/raw			HF power (ms^2) ln/raw			Method
Author[s], year number, age range	Mean/ *median*	SD	Normal limits	Mean /*median*	SD	Normal limits	Mean /*median*	SD	Normal limits	FFT/AR [order]
Standards 1996 [4]	8.15 3466	1018	NR	7.06 1170	416	NR	6.88 975	203	NR	NR
Mølgaard 1994 104, 40–77 [577]	–	–	–	6.18 484	–	3.99–7.60 56–2007	3.86 48	–	2.30–5.66 10–286	AR [?], 5min over 24h
Huikuri 1996 374, 40–60 [323]	–	–	–	6.42 613	526	NR	5.76 317	2.56 347	NR	AR [?], 512 heartbeats (~12′)
Sinnreich 1998 294, 35–65 [530]	6.57 713	–	5.95–7.29*	5.37 215	–	4.61–6.20*	4.79 120	–	4.04–4.99*	AR [16], 5min * [25–75%]
Kuo 1999 1070, 40–79 [324]	6.48 652	1.92	NR	4.60 99	1.92	NR	4.06 58		NR	FFT (288s, 2048 Datapoints)
Pikkujämsa 2001 389, 40–59 [320]	–	–	–	6.14 654	0.81 652	NR	5.41 383	1.00 580	NR	AR [20], 13min ECG
Pikkujämsa 2001 50, 40–59 [320]	–	–	–	6.23 512	396	NR	5.91 368	289	NR	AR [20], 5min ECG
Šlachta 2002 216, 12–70 [325]	7.46 1737	1.03	NR	6.08	1.14	NR	6.60	1.34	NR	FFT (300s, CGSA)
Laitinen 2004 63, 23–77 [326]	7.54 1888	441	NR	6.13 459	120	NR	6.62 752	280	NR	FFT (300s, triangular averaging)

Abbreviations see Table 35.2 and Sect. 35.1

Table 35.26

Reported data on nonlinear HRV measures

Author(s), year ECG duration	Age	N	1/f (ß)	DFA α1	DFA α2	ApEn	SD1/SD2
Pikkujämsa 1999 24-h ECG [320]	< 15	27	−1.15 ± 0.18	1.06 ± 0.11	0.98 ± 0.06	1.26 ± 0.12	–
	15–39	29	−1.12 ± 0.19	1.15 ± 0.16	1.00 ±0.08	1.21 ± 0.14	–
	40–60	29	−1.32 ± 0.14	1.19 ± 0.14	1.07 ± 0.07	1.01 ± 0.16	–
	> 60	29	−1.38 ± 0.17	1.19 ± 0.16	1.14 ± 0.07	0.88 ± 0.16	–
Acharya 2004 20-min ECG [327]	10 ± 5	25	–	2.01 ± 0.33	0.58 ± 0.35	1.90 ± 0.35	0.51 ± 0.19
	25 ± 10	50	–	1.83 ± 0.15	0.41 ± 0.20	2.07 ± 0.18	0.53 ± 0.24
	40 ± 15	40	–	1.67 ± 0.21	0.14 ± 0.21	1.88 ± 0.35	0.43 ± 0.19
	60 ± 5	35	–	1.71 ± 0.22	0.22 ± 0.32	1.68 ± 0.41	0.61 ± 0.29
				CD	LLE	ApEn	–
Kuo 2002 5-min ECG [328]	40–79	480	–	1.83 ±0.04	0.063 ± 0.003	0.303 ± 0.012	–

For abbreviations see Table 35.2 and Sect. 35.1

on age indicates that reference values require either age-adjustment or that age-related references need to be considered (Table 35.27). Separate data on HRV measures (not references) in children is presented in Table 35.28.

A multitude of factors influencing HRV prevents the determination of normal limits for short-term measures. Lower normal limits (2.5 percentile) of 5-min spectral indexes have been published (Table 35.29) [335]. However, these values can be considered as reference only if a similar method (FFT, 1 kHz sampling rate) is used. Thus, the use of other techniques or algorithms requires data from a control group with comparable characteristics and recordings made under similar examination conditions.

An apparently abnormal result from any HRV measurement has to be interpreted in the light of the known statistical performance (i.e., sensitivity, specificity, predictive value, likelihood etc.) of the measure. For HRV measures, a relative paucity of well defined normal limits excludes a wider use of values <2.5 percentile and >97.5 percentile in practice. Therefore, it is necessary to be aware of whether an apparently abnormal value is defined as population-driven or as an arbitrarily set cut-off value based on statistical performance (Table 35.30).

In fact, there are only a few studies in which the HRV value, thought to be abnormal on the basis of its distribution in a healthy sample, has been used in diagnosing patients with diabetic autonomic neuropathy (DAN) [336], sinus node dysfunction (SND) [337] or in risk-prognostication in patients after a myocardial infarction [64, 315]. By using a range of 2.5%–97.5% of the normal values, the specificity of the selected HRV index is 97.5% both for abnormally low and high results. The respective sensitivities of such a defined abnormal result have reached 88% [336], 70% [337] and 25% [64, 315]. Some authors have proposed defining three categories of results, i.e., abnormal, borderline, and normal for DAN detection [339–341] or in patients with diagnosed cardiovascular disease [342]. This message has already come from Standards [4], which have cited HRV values indicating severe (SDNN<50 ms, HRVI<15a.u.) and moderate (SDNN<100, HRVI<20s.u.) abnormality. It has also been proposed that for HRV indices with normal distributions, the values lower or higher than 2SD from the mean could be considered as pathologic, those between −1 SD and −2 SD or +1 SD and +2 SD as moderately changed and those within the mean ± 1 SD as normal [342]. For HRV indices with other than normal distribution, it has been suggested that the values lower than 2.3 percentile or higher than 97.7 percentile could be considered to be pathologic, those between 2.3–15.9 percentiles and 84.1–97.7 percentiles to be moderately changed and those between 15.9–84.1 percentiles to be normal [32]. An almost similar categorization of HRV data has been used in the ATRAMI study [343].

In another proposal, a categorical distinction of a low, moderate and high HRV has been made on the basis of a calculation of the mean and 1 SD value. Therefore, a low HRV is defined as < mean −1 SD, a high HRV as > mean +1 SD, and moderate HRV as a result in between [283]. In patients with stable angina pectoris, the corresponding 24-h SDNN values were <106 ms, >178 ms and 106–178 ms, for the SDANN, they were <94, >164 and 94–164 ms, and for RMSSD they were <15, >41 and 15–41 ms [283]. However, the use of standard deviation as a determinant of limits should be cautioned

Table 35.27

Reported normative data of 24-h HRV time-domain indices in respect to age

Author[s]/year	Age range	No of sbs.	SDNN		SDANN		RMSSD		HRVI	
			Mean ± SD	± 1.96 SD/ *95%CI*	Mean ± SD	± 1.96 SD/ *95%CI*	Mean ± SD	± 1.96 SD/ *95%CI*	Mean ± SD	± 1.96 SD/ *95%CI*
Bonnemeier 2003 [321]	20–29	47	177 ± 37	105–250	158 ± 37	85–231	46 ± 18	10.5–81.5	49 ± 11	27–71
	30–39	34	148 ± 34	81–214	133 ± 32	70–196	36 ± 15	6.5–65.5	41 ± 12	17–65
	40–49	28	141 ± 36	70–213	127 ± 33	62–192	26 ± 9	8.3–43.7	37 ± 11	15–59
	50–59	32	135 ± 34	68–202	130 ± 38	56–204	24 ± 11	2.3–45.7	35 ± 7	21–49
	60–70	25	118 ± 27	65–170	107 ± 26	56–156	19 ± 7	5.2–32.8	32 ± 7	18–46
Umetani 1998 [322]	10–19	30	176 ± 38	101 – 279	159 ± 35	85 – 261	53 ± 17	25–103		
	20–29	42	153 ± 44	93 – 257	137 ± 43	79 – 241	43 ± 19	21–87		
	30–39	39	143 ± 32	86 – 237	130 ± 33	73 – 223	35 ± 11	18–74		
	40–49	65	132 ± 30	79 – 219	116 ± 31	67 – 206	31 ± 11	15–63		
	50–59	22	121 ± 27	73 – 202	106 ± 27	63 – 190	25 ± 9	13–53		
	60–69	20	121 ± 32	68 – 186	111 ± 31	58 – 176	22 ± 6	11–45		
	70–79	21	124 ± 22	62 – 172	114 ± 20	53 – 163	24 ± 7	9–38		
	80–89	21	106 ± 23	*57–159/53–147**	95 ± 24	*49–151 (45–140)**	21 ± 6	8–32/7–28	**HRVF**	
Sosnowski 2002 [689]	18–34	31	189	115 – 289	161	96 – 260	–	–	55	50 – 72
	35–44	89	152	91 – 218	141	79 – 211	–	–	50	38 – 70
	45–54	122	143	89 – 216	133	79 – 213	–	–	47	26 – 65
	55–63	54	133	89 – 190	126	76 – 195	–	–	45	33 – 62

Table 35.28

Reported normative data of HRV time-domain indices in children in respect to age

Author[s], year	Age	No of sbs.	SDNN Mean ± SD *95%CI*	SDANN Mean ± SD *5–95%CI*	RMSSD Mean ± SD *5–95%CI*	HRVI Mean ± SD *5–95%CI*	ECG duration
Newborns	1–7 days						
Mehta 2002 , 2000 [329]		96	47 ± 12 30 – 75	35 ± 9 21 – 51	22 ± 6 14 – 33	14 ± 4 8 – 22	24-h
Longin 2005 [330]		80	50 ± 22 23 – 95	–	20 ± 15 8 – 62	–	10-min
Infants							
Massin 1998, 1997 [331]	2 week	Each data-group of 10 subjects	52 ± 13				24-h
	1 month		59 ± 15				
	3 month		74 ± 19				
	6 month		85 ± 22				
	1 year		97 ± 25				
Pre-school childhood	1–5 years						
Massin 1998, 1997 [331]			134 ± 34				
Silvetti 2001 [332]		23	102 ± 21	83 ± 18	53 ± 25		24-h
Young childhood	6–10						
Silvetti 2001 [332]		28	147 ± 33	115 ± 26	89 ± 60		24-h
Lenard 2004 [333]		34	64 ± 45	–	64 ± 68		10-min
Early-adolescence	11–14						
Silvetti 2001 [332]		37	169 ±	139 ± 40	74 ± 24		24-h
Faulkner 2003 [334]		43	174 ± 37	140 ± 37	55 ± 18	–	
Lenard 2004 [333]		37	61 ± 48	–	55 ± 60		10-min
Late-adolescence	15–17						
Silvetti 2001 [332]		15	194 ± 62	174 ± 30	71 ± 22		24-h
Faulkner 2003 [334]		15	150 ± 30	133 ± 29	50 ± 13		
Lenard 2004 [333]		35	81 ± 70		77 ± 93		10-min
Young adulthood	18–22						
Faulkner 2003 [334]		12	152 ± 37	127 ± 37	55 ± 16		24-h
Lenard 2004 [333]		31	72 ± 55		70 ± 76		10-min

Table 35.29

Lower normal limits of standard 5-min HRV spectral indices (2.5 percentile) in respect to age and gender

Index/age	15	20	25	30	35	40	45	50	55	60	65
Women (n = 158)											
LF	230	193	161	135	113	94	79	66	55	46	39
HF	194	154	122	97	77	62	49	39	31	25	20
Men (n = 151)											
LF	362	300	249	207	172	142	118	98	81	68	56
HF	236	185	145	113	89	69	54	42	33	26	20

Data from Agelink et al. 2001 [335]. Spectral analysis using a Fast Fourier Transform (5 min, 1,000 Hz, discrete signal of 1,024 datapoints)

as its value is influenced by outliers (from a statistical point of view) and by the age range of the sample (important for HRV indices). On the other hand, use of percentiles requires a relatively larger number of subjects in order to be reliably calculated. Also, a wide or narrow range of age may produce different 2.5 and 97.5 percentile values.

In most studies on HRV, the abnormal results indicating optimal statistical performance are drawn from the distribution of a particular index, with either median, tercile or quartile values defining a cut-off point. Such an attempt is commonly justified by the need to find the cut-off value of a particular index with the highest positive predictive power [338]. Actually, these values should not be considered "pure abnormal" since they do not necessarily correspond to an HRV index distribution in a population and might show a significant variation (Table 35.30). It might be suggested that the term "risk predictive value" (RPV) should be used.

It is necessary to be even more prudent when an index like the HRT-derived turbulence slope (TS) or onset (TO) is in use, as it is difficult (*a priori*) to determine normal limits and abnormal values in a sample of population since this requires either ventricular PEBs to be present or induced in persons without diagnosed cardiac disease. Even so, normal limits have been calculated in healthy volunteers with mean TO values ranging from −2.7% to −2.3% and mean TS from 11.0–19.2 ms/RRI [294]. Grimm et al. found the 95% percentile range for HRT slope to be 11.78–17.69 and HRT onset of −0.033 to −0.009 [366]. A bias regarding the presence of atrial PEBs conducted with intra-ventricular aberration should be noted, as many Holter systems detect abnormal ventricular PEBs only on the basis of the QRS duration [367].

In most clinical studies, TS<0% and TS>2.5 ms/RRI are considered normal. However, it should be noted that despite these values not being close to normal limits in normal persons cited above (of whatever calculation method), there is still a significant proportion of subjects with abnormal HRT results, especially for the HRT onset, reaching almost 20% [366]. Both descriptors of the HRT are in use for categorical classification, where an HRT category of 0 means that both TO and TS are normal, 1 means that either TO or TS is abnormal, while 2 is used if both TO and TS are abnormal. Importantly, those with no or too few suitable VES are considered to have an HRT category of 0 [294].

As the baroreflex sensitivity examination is limited to laboratory centers, normal and abnormal data are not provided, despite some efforts to define normal limits having been undertaken [368–371]. Various methods for the BRS (analogous to the frequency-domain HRV) exclude an indication of unified normal data. It would be helpful if definitive normal values could be agreed by the laboratories working in this field.

35.4.10 Physicians' Compliance with HRV Measures

The familiarity of physicians with HRV phenomena and currently available methods for its evaluation is generally poor. Such a statement seems to be justified by reviewing, in depth, the details from most of the so-called evidence-based studies in internal medicine and cardiology in particular. As a result, it can be stated that a fundamental clinical sign such as heart rate is frequently missed. Thus, it should not be expected that its variation (HRV) would attract greater attention. A simplified comparison of the proportion of real-life and scientific-life awareness of the importance of HRV and related phenomena (Table 35.31) indicates that the HRV contribution to knowledge regarding such important

Table 35.30

Risk predictive values (RPV) of HRV measures (abnormal values) in selected outcome studies

Author[s], year	HRV index	RPV	Choice of cut-off value	Method of verification
Acute myocardial infarction/Coronary artery disease				
Standards 1996 [4]	SDNN	50 ms	Statistical/arbitrary/post hoc	Highest statistical discrimination (Cox hazard)
	RMSSD	20 ms		
	HRVI	15 a.u.		
Kleiger et al. MPIP 1987 [24]	SDNN	50 ms	Arbitrary/post hoc	Mean – 1SD
Rich et al. 1988 symptomatic Emergency coronary angiography [344]	SDANN	50 ms	Arbitrary/post hoc	Univariate analysis
Farrell et al. 1991 [40]	SDNN	50 ms	Arbitrary/a priori	Mean – 1SD
	HRVI	16 a.u.		
Cripps et al. 1991 [38]	HRVI	25 a.u.	Statistical/post hoc	Highest statistical discrimination (ROC)
Odemuyiwa et al. 1994 [345]	HRVI	20 a.u.		Highest statistical discrimination (long-rank survival)
Zuanetti et al. GISSI-2 1996 [346]	SDNN	70		Highest statistical discrimination (ROC)
	RMSSD	17.5		
	NN50+	200		
Copie et al. 1996 [347]	HRVI	18 a.u.		
Lanza et al. 1998 [348]	SDNN	55		Highest statistical discrimination (Cox hazard)
	SDNNI	20		
	SDANN	50		
	RMSSD	23		
La Rovere et al. ATRAMI 1998 [343]	SDNN	70	Arbitrary/a priori	< 15th percentile (~1SD)
	BRS	3 ms*mmg		
Huikuri et al. DIAMOND 2000 [127]	SDNN	65	Statistical/post hoc	Highest statistical discrimination (long-rank survival) within 10–70 percentiles
	HRVI	16		
	DFA α1	0.75		
	ß (1/f)	–1.5		
Whang/Bigger MPIP 2003 [249]	SDNN	50		Highest statistical discrimination (ROC)
Balanescu et al. 2004 [350]	SDNN RMSSD	50 20	Arbitrary/ a priori	Reference-drawn
Stein PK et al. CAST 2005 [351]	SD1/SD2 SDNN	0.55 70	Statistical/post hoc Arbitrary/ a priori	Highest statistical discrimination (univariate Cox hazard) Reference-drawn

Table 35.30 (Continued)

Author[s], year	HRV index	RPV	Choice of cut-off value	Method of verification
Acute myocardial infarction/Coronary artery disease				
Huikuri et al. CARISMA 2009 [352]	SDNN	70	Arbitrary/a priori	Reference-drawn
	DFA α1	0.75		
	TS (HRT)	< 2.5 ms/RRI		
Heart Failure				
Stein KM et al. 1993 [353]	SDANN	decrease by 47ms	Arbitrary/a priori	mean-1SD
Szabó et al. 1995, 1997 [354]	SDNN	108	Arbitrary/post hoc	Median value
		50	Arbitrary a priori	Reference-drawn
Ponikowski et al. 1997 [355]	SDNN	100	Arbitrary/a priori (post hoc)	Median value (also a high association with cardiac death (Cox))
Nolan et al. UK-Heart Study 1998 [356]	SDNN	93	Arbitrary/a priori	Lower tercile
		117		Median value
		100	Arbitrary/ post hoc	Reference value
Fauchier et al. 1999 IDC [357]	SDNN	100	Arbitrary/a priori	
Galinier et al. 2000 [358]	SDNN	67 ms	Arbitrary/Lower tercile/ post hoc	Highest statistical discrimination (likelihood ratio)
Mäkikallio et al. DIAMOND-CHF 2001 [359]	SDNN	67	Statistical/post hoc	Highest log-rank survival estimate within 10–70 percentiles
	HRVI	22		
	DFA α1	0.9		
Bilchick et al. 2002 [360]	SDNN	65.3ms	Arbitrary/a priori	Lowest quartile
Aronson et al. 2004 Acute decompensated HF [361]	SDNN	44	Statistical/post hoc	Highest statistical discrimination (Cox hazard)
	SDANN	37		
Rashba et al. DEFINITE 2006 [250]	SDNN	81	Arbitrary/a priori	Lower tercile
General population				
Algra et al. 1993 Symptomatic patients with a 24-h ECG [362]	NN50+	3%	Arbitrary/a priori	Lower tercile
	SDNNI (1min)	25		
	SDANN (1min)	8		
Huikuri et al. 1998 Elderly subjects [363]	SDNN B (1/f)	120 −1.5	Statistical/post hoc	Highest statistical discrimination (Cox hazard)
Sajadieh et al. 2006 [364]	SDNN SDNNI pNN50	100 34 0.8%	Arbitrary/a priori	Lowest quartile
Stein PK et al. 2008 Elderly subjects CHS [365]	SDNN DFA α1 TS (HRT)	Continuous 1 < 3 ms/RRI	Arbitrary/a priori Arbitrary/a priori Arbitrary/post hoc	Highest statistical discrimination (Cox hazard)

Table 35.31

Proportion of studies on HRV/BRS or HRT use in myocardial infarction and heart failure as indicated by number of citations in various databases

Database	PubMed	CINAHL	Scopus	Cochrane	Google Scholar
Searched term[s]	N [%]	N [%]	N [%]	N [%]	N [%]
MI	154197 [100]	21112 [100]	167616 [100]	10672 [100]	~930, 000 [100]
MI + HRV	727 [0.47]	134 [0.63]	2368 [1.41]	98 [0.92]	~18, 900 [2.03]
MI + EF	7698 [4.99]	700 [3.31]	12917 [7.71]	1081 [10.13]	~91, 900 [9.88]
MI + HRV + EF	162 [0.11]	17 [0.08]	750 [0.45]	19 [0.18]	~6, 670 [0.72]
MI + BRS	165 [0.11]	25 [0.12]	681 [0.41]	20 [0.19]	~5, 290 [0.57]
MI + BRS + EF	43 [0.03]	4 [0.02]	276 [0.16]	3 [0.03]	~ 1, 900 [0.20]
MI + HRT	63 [0.04]	18 [0.09]	142 [0.08]	3 [0.03]	~839 [0.09]
MI + HRT + EF	26 [0.02]	11 [0.05]	80 [0.05]	3 [0.03]	~469 [0.05]
	N [%]	N [%]	N [%]	N [%]	N [%]
HF	102357 [100]	16452 [100]	147756 [100]	6857 [100]	~1, 460, 000 [100]
HF + HRV	600 [0.59]	97 [0.59]	2970 [2.01]	107 [1.56]	~17, 500 [1.20]
HF + EF	9612 [9.39]	1652 [10.0]	22234 [15.05]	1635 [23.84]	~109, 000 [7.47]
HF + HRV + EF	157 [0.15]	26 [0.16]	1141 [0.72]	35 [0.51]	~6, 730 [0.46]
HF + BRS	144 [0.14]	13 [0.08]	767 [0.52]	22 [0.32]	~5, 350 [0.36]
HF + BRS + EF	39 [0.04]	3 [0.02]	287 [0.18]	8 [0.12]	~1, 930 [0.13]
HF + HRT	30 [0.03]	12 [0.07]	118 [0.08]	3 [0.04]	~688 [0.05]
HF + HRT + EF	15 [0.015]	6 [0.04]	72 [0.05]	3 [0.04]	~424 [0.03]

MI – myocardial infarction, HF – heart failure, HRV – heart rate variability, EF – ejection fraction. Terms present in titles, abstracts or keywords. ? HRT

fields like myocardial infarction (past epidemic) or heart failure (future epidemic) is between 0.5–2.0%. Meanwhile, the contribution of studies, in which ventricular function is investigated, reaches 10% on average (range 5-~25%).

Some reasons for a such situation are related to the multiplicity of methods, variety of algorithms within the same method, different number of confounding factors, use of complicated measures sometimes (or commonly) completely unintelligible for physicians, and inconsistency of data.

It would greatly improve matters if members of the next Task Force setting new Standards could unequivocally establish a basic protocol for HRV analysis. In addition, recommendations for minimum requirements for investigation reports would be helpful.

Some methodological suggestions that present an opportunity for a wider use of HRV in clinical practice are listed in Table 35.32. As the investigators' and clinicians' interests might not appear to converge, a close cooperation between clinicians and technicians or physicists would seem to be mandatory.

35.5 Physiological Basis of Heart Rate Fluctuations

Changes in heart rate have to be considered in the context of changes in the entire cardiovascular system, as well as in extra-cardiac body compartments, mainly within key vital organs. Hence, the physiological and pathophysiological interpretation of HR variation cannot be restricted to HR control itself. For clinical use, it would be necessary to separate HR changes that are functional (reflex or compensatory) from those which are related to true neuropathies.

The primary assumption usually taken is that the function of the sino-atrial node (SAN) is intact. Really, this holds true mainly in physiological states. In certain settings, it might not be unusual that heartbeat formation is compromised. The common clinical syndrome of heart failure may serve as an example [306], according to the early observation of

Table 35.32

Methodological guide for clinical HRV studies

1	Use a method explicable to physicians not familiar with HRV phenomenon
2	For global HRV estimates it is required (not obligatory) to: 1. Calculate the number of subjects necessary to be examined on basis of reproducibility of the HRV measure going to be used 2. Look on data regarding reproducibility of chosen HRV measures in previous studies or provide results of a separate pilot-study 3. Be familiar with the prevalence of abnormal HRV within an examined sample (as it influences sensitivity of detection of abnormal HRV in a planned study) 4. Not rely on references' data that come from a limited (usually unsatisfactory) number of examined subjects 5. Be aware that there may be a substantial number of subjects (10–25%) with other than normal HRV indexes behavior 6. Do not rely on data obtained from a healthy population if the examined subjects suffer from any disease that is associated with HRV abnormality 7. Be sure that changes in HRV measures are really a result of an intervention and not contaminated by errors 8. Use devices with the lowest possible technical-related errors 9. Be familiar with the errors relating to characteristics of devices used 10. Balance gender proportion
3	For HRV estimates of certain [patho]physiological explanation (i.e., respiratory-related (=cardiac vagal tone), arterial pressure-related (= baroreflex (LF, HRT), vasomotor-tone related (VLF), day–night difference, activity (ULF, TP), baroreflex sensitivity, heart rate turbulence, it is required (not obligatory) to: 1. Be sure that chosen method truly complies with an examined phenomenon 2. Be aware of reproducibility of chosen method or provide coefficient of variation in a sample of examined population 3. Carefully observe conditions of study for all examined persons (i.e., the same time of study for short-term HRV, similar diurnal activity for long-term HRV) 4. Balance gender proportion or perform separate investigation in females and males 5. Perform investigation in a few groups of different ages instead of a single study in large age-range group 6. Use a control group (nested-study design) 7. Comprehensively check for outliers 8. Include individual data if a small number of subjects is examined 9. Use a reference method (if exists) if a new method or a modification of an established method is introduced 10. Provide data regarding other significant determinants of HRV phenomenon (age, gender, race, HR, BP, respiratory rate, usual physical activity) 11. Provide data regarding important clinical entities (for example in AMI-patients: time-to-reperfusion (successful or failed), door-to-balloon time, infarct extension (CKMB mass, cardiac troponins), functional status (Killip class), hemodynamic data LVEF), use of drugs that interfere with HRV, etc.) 12. Avoid inclusion of subjects with various ANS derangement (i.e., diabetics, post-CABG) or with other confounding factors into a single group with subjects with a presumed intact ANS (no neuropathy), instead perform an investigation in separate groups
4.	Carefully follow the HRV Standards or the other Statements' requirements (if applicable)

Wollenberger in 1939. In this syndrome, pacemaker function is compromised and the responsiveness of the SAN to sympathetic over-activity is attenuated (so-called *chronotropic incompetence* (A term indicating inadequacy between heart rate and requirements, i.e. impaired HR adjustment for functional needs (usually metabolic))) [372], despite the resting HR being accelerated and the HRV reduced. Moreover, changes in intrinsic SAN properties appear before the overt HF syndrome [306]. The importance of intrinsic SAN should also be considered in such syndromes like hyperthyroidism, inappropriate sinus tachycardia, postural orthostatic tachycardia, and also in subjects with a high-vagal tone (endurance athletes) [306, 373, 374]. Also, in the model of high renin systemic arterial hypertension, an increased intrinsic firing of the SAN has been observed [374].

One the other hand, SAN abnormalities may be responsible for the inadequate response to proper neural stimuli leading to pacemaker desynchronization and irregular heart rate fluctuation. This can be observed experimentally in transgenic knock-in mice without the expression of cardiac connexin $Cx40^{-/-}$ and in the clinical setting in patients with sinus node disease [375, 376].

The second assumption usually taken is that heart period changes reliably reflect changes in sinus node firing. As parallel changes are normally seen in physiology and pathophysiology, sporadically this assumption is false. Overdrive stimulation of the SAN may lead to the so-called exit block [377, 378]. In such settings, the surface ECG shows a prolongation of heart period, while a series of SAN depolarization can actually be recorded from intra-cardiac electrodes.

The examples mentioned are given to emphasize the fact that heart period variation should be interpreted with caution when making conclusions about cardiac autonomic control of SAN activity. In fact, significant progress in the understanding of mechanisms of heartbeat formation, briefly described below, makes a detailed evaluation of the contribution of the autonomic nervous system and other modulators to heart period variation even more difficult.

35.5.1 Ionic Mechanisms of Heart Beat Formation

The self-excitability of specialized cardiac cells is related to the function of ionic channels that carry ionic currents responsible for *spontaneous diastolic depolarization* (The fourth phase of action potential of specialised cardiac myocytes involved in the impulse propagation.). The most important currents in this phase of the action potential are inward calcium currents (I_{CaL}, I_{CaT}), outward potassium currents (I_{Kr},I_{Ks},$I_{K[ACh]}$, $I_{K[Ca]}$) and inward hyperpolarization-activated cyclic nucleotide-gated (HCN) current I_f (*funny current* (Funny current means a current having a combined property aimed at distinct ion transportation)) [379, 380]. The latter current plays a major role in the generation and control of pacemaker activity (*pacemaker current* (An ionic current specific to self-excitable cardiomyocytes, not present in other working myocardial cells)) [380]. The I_f activation range varies largely from cell to cell, being more negative at peripheral areas. The I_f channels are uniquely activated by a direct binding of cyclic AMP (cAMP) molecules to the intracellular aspect of the channels. This property means that a funny-channel can be voltage-gated, as well as being a cyclic-nucleotide-gated (CNG) channel – part of a superfamily of CNG channels of sensory neurons (for review see [380]). Four isoforms of molecular components of f-channels have been cloned forming a family of HCN channels. In the heart, HCN4 is the major component in the pacemaker region. Accumulated data suggests that HCN2 prevents the diastolic membrane potential from becoming too negative and HCN4 is the major channel mediating sympathetic stimulation of the pacemaker activity. Recent studies indicate that a manipulation in HCN components was able to modify the spontaneous rate of pacemaker cells, thus opening an area for a clinical application of the so-called "biological" pacemakers [380].

Experimental studies have shown that I_f is a common effector of muscarinic and β-adrenergic activation through an allosteric conformation of the α-subunit of G-protein, a trimer protein coupled with a membrane GTP-ase [380]. It is suggested that this interaction depends on a lipid composition of the P-cells plasma membrane [381]. Experimental data also indicates an involvement of the sodium channel in the generation of sinus arrhythmia. A low concentration of tetrodotoxine reduces sinus rate and increases its variability [382]. The accumulated experimental and clinical data strengthen the role of the I_f current in heartbeat formation and opens an area for the clinical use of drugs that inhibits I_f currents (so-called HR-lowering drugs) [383].

35.5.2 Cellular Mechanisms

35.5.2.1 Pacemaker Cells

Sinus beat formation is the result of a *synchronisation* (Forced rate by a dominant pacemaker over neighboring P-cells, which generate diverse rates of spontaneous depolarisation while uncoupled.) of a group of spontaneously depolarizing cells, referred to as pacemaker cells (P-cells, pale, pacemaker, primitive) [384]. The highest density of P cells is to be found in the central region. However, they are also sparsely scattered in the right atrium. Each isolated P-cell possesses a similar self-excitable property. However, the frequency of beating is varied, even among neighboring P-cells due to the stochastic nature of channels opening and closing. A synchronized rate of firing is possible thanks to the between-cell

communication related to the presence of gap junctions [384]. The common rate of a group of P-cells (synchronization) is based on a phenomenon called *phase resetting* (Changes in the frequency of depolarisation usually through recruitment of a new dominant pacemaker or alteration of the dominant pacemaker's rate.) due to mutual entrainment [385].

35.5.2.2 Sino-Atrial Node and Sino-Atrial Pacemaker Complex

That cardiac beats have their origin within the heart's own "substance" was initially proposed by Galen centuries ago. This "substance" had been discovered by Keith and Flack in 1907 as a fine subendocardial structure lying within the anterolateral part of the right atrium near the superior vena cava orifice (sino-atrial node, SAN). The proof of its role in heartbeat formation was provided by Lewis in 1910 [after 386]. However, electrophysiological studies in humans with the use of multisite mapping demonstrated that consecutive sinus beats of various lengths could appear in different sites that functionally might lie well beyond the anatomically defined SAN. This functional region, referred to as the *sino-atrial pacemaker complex*, spreads from the upper portion of the right atrium to the orifice of the inferior vena cava [387]. Pacemaker recruitment (a group of P-cells) with shortening cycle length appears more cranially, while when it moves caudally, a cycle length prolongation is observed due to the different sensitivity of P-cells to norepinephrine and acetylcholine depending on their location within the SAN and right atrium [388]. This phenomenon is referred to as *pacemaker shift* (A movement of a dominant pacemaker.) [381]. Apart from the different sensitivity of the P-cells to NA and ACh, a nonuniform autonomic innervation is thought to constitute an anatomical basis for the pacemaker shift, as evidenced by pharmacological interventions and SAN-specific autonomic nerve stimulation [389]. The pacemaker shift phenomenon is basically responsible for changeable sinus cycle length through variation in *sino-atrial conduction time* (Electrophysiological term (SACT, ms), indicates the time between the first depolarisation within the pacemaker complex (usually SAN) and the first depolarisation within atrial tissue (usually onset of the P-wave).). Changes in the chemical and physical environment could modulate this phenomenon, as happens with temperature changes, hypoxia, acidosis or hyperkalemia [390, 391].

35.5.3 Neuromediators and Hormones

35.5.3.1 Acethylcholine

Acethylcholine (ACh) is a key neurotransmitter of the parasympathetic branch of the autonomic nervous system [389]. ACh acts through the activation of ligand-gated ion channels (nicotinic receptors) or G-protein-coupled receptors (muscarinic receptors). With respect to heart rate autonomic control, nicotinic α-7 subunits mediate fast synaptic transmission in ganglia supplying the heart and muscarinic M_2 receptors mediate vagal stimulation in the SAN [389]. In addition, ACh modulates central pre-motor vagal activity [392].

ACh concentration at the SAN neuroeffector junction depends primarily on its kinetics. Tonic [DC] and phasic [AC] "net" vagal activity modulates ACh release from efferent cardiac vagal motorneurons endings [389]. In addition, ACh release is controlled by other mechanisms, including automodulation (pre-synaptic inhibition by ACh), transneuronal (pre-synaptic inhibition by NE through alfa1-adrenoceptor and NPY) and trans-synaptic (via prostaglandin PGE1 and adenosine) modulations [393]. Pre-synaptic automodulation is discussed as a possible mechanism involved in paradoxical HR slowing after low doses of atropine, an M_2-receptor antagonist [394].

The ionic mechanisms of ACh action depends on its local concentration. Small amounts of ACh inhibit I_f current, while larger (20-fold) amounts inhibit I_{CaL} and stimulates $I_{K[ACh]}$. The I_f inhibition is achieved through the stimulation of M_2-cholinergic receptor-coupled inhibitory G-protein G_i, that results in cAMP levels reduction and a negative shift of the I_f activation curve, thereby modulating its gating properties. It was also shown that a reduction of intracellular cAMP leads to a reduction of L-type Ca^{2+} current. The latter requires M_2-receptor coupling to $G_{\alpha 0}$ subunit and seems necessary to opposite effects of β-adrenergic stimulation [395].

Clearance properties depend on the rate of ACh hydrolysis by acethylcholinesterase. Its washout from the junction determines the actual local *effective concentration* of Ach [389]. Other factors, like the size of the release store terminal and diffusion to distant receptors, also influence the effective ACh concentration. ACh action on the P-cells is related

to the number of M_2-receptors and their *saturation* (Lack of changes in sinus cycle duration in response to a certain increment or reduction in stimulation frequency above or below breakpoints. In a clinical setting, saturation denotes a lack of changes in heart beat variation with alteration in heart period duration. Such a phenomenon may be observed either in an extreme heart period prolongation or shortening.). The binding of ACh to M_2-receptors is necessary for its inhibitory effect on P-cell activity. This action modulates the intrinsic diastolic depolarization rate and antagonizes simultaneous sympathetic effects. In an *in vitro* study on isolated rabbit pacemaker cells, a superperfusion with ACh increases cycle length and its variation exponentially and interdependently [396]. However, in earlier experiments with vagal stimulation, a linear relationship has been observed [397]. Within a physiological (and pathophysiological) range of sinus cycle length, a linear relationship with vagal stimulation can also be seen in studies that advocate nonlinear relationships (Fig. 35.38) [398]. Saturation at a longer sinus cycle length does not allow further prolongation to be linearly related, as an increase in stimulation frequency of the vagus does not result in a further substantial increase in ACh concentration (Fig. 35.38 inset) [398]. A clinical study supporting such experimental data has been published [399]. Thus, two parts of a relationship can be observed, one within the usual range of the sinus cycle, where such a relationship is linear and a second within prolonged sinus cycles, where such a relationship is also linear but flat. In an extreme case, further increase in the frequency of vagal stimulation would result in significant sinus cycle prolongation. However, nonlinearities in the SAN response to stimulation of the vagus may, sporadically, result in sudden cycle shortening [377, 378]. Experimental studies have shown that under normal physiological conditions maximal diastolic potential and threshold potential are actually not affected by neural activation. However, this may not hold true in a pathological setting [396].

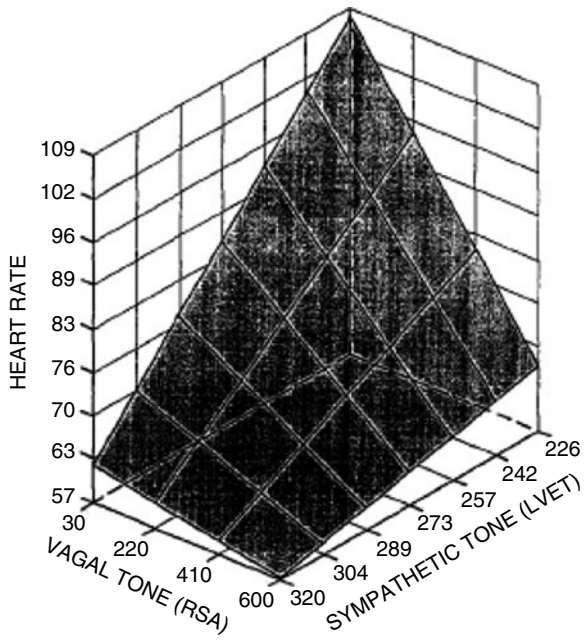

Figure 35.38

Dependency of pacemaker cycle length on the rate of vagal neural activity. Nonlinear relationship between the frequency of vagal stimulation and sinus cycle length in a rabbit pacemaker cells. Note, within physiological rate the relationship is linear. Inset: a plot of ACh concentration against the frequency of vagal stimulation indicating a phenomenon of saturation (From [396]).

35.5.3.2 Norepinephrine and Epinephrine

Norepinephrine (NE) is a catecholamine released from sympathetic nerve terminals, while epinephrine (Epi) is a circulating hormone synthesized in and released from the suprarenal medulla. These substances accelerate the spontaneous diastolic depolarization of the pacemaker cells via stimulation of the β-adrenergic receptors (βAR) coupled to the stimulatory G-protein G_s, with activation of adenylate cyclase and increase in cAMP levels [393, 398]. Subsequently, a shift of the I_f activation curve to a more positive voltage occurs and heart rate accelerates. In certain conditions, activation of I_{CA} and I_K channels mediates NE effects on pacemaker cells [400]. Although NE and Epi act mainly through activation of βAR, their effects depend on the specific properties and pathways of various types of βAR, as well as on the action on α-adrenergic receptors (αAR) [401, 402].

35.5.3.3 Neuropeptide Y

Neuropeptide Y (NPY) represents one of various neuropeptides that act in addition to the "classical" neurotransmitters. NPY coexists with NE in cardiac sympathetic nerve terminals. Dense population of NPY-immunoreactive nerves is found in the SAN region [403]. The NPY-nerves also form synapses on the soma and dendrites of vagal preganglionic neurons within NA [404]. Upon a direct sympathetic stimulation, NPY is co-released with NE within the α-adrenoceptor [404]. Some data suggests that NPY inhibits ACh release from pre- and postganglionic parasympathetic neurons, thereby attenuating cardiac vagal action [404–407].

35.5.3.4 Nitric Oxide

Nitric oxide (NO) is a signaling molecule that mediates vasomotor tone, ATP production and cardiac contractility. Recently, its role as a mediator of the peripheral autonomic control of the heart has been extensively studied [408–418]. The presence of endothelial NO synthase (eNOS) in human cardiomyocytes [413] and neuronal NO synthase (nNOS) in cholinergic and sympathetic nerve terminals, as well as NO-sensitive neurons in the stellate and intrinsic cardiac ganglia argues for a role for NO in heartbeat control [408, 409, 411, 412]. Neuronal NOS is present in the central nervous system nuclei contributing to vasomotor and cardiac control, like the solitary tract nucleus (STN), nucleus ambiguous, dorsal nucleus of vagus, ventrolateral zona reticularis in the medulla oblongata, and in the periphery in carotid bodies [409, 410].

NOS inhibition has been shown to block the negative chronotropic effects of cholinergic agonists and prevent cholinergic inhibition of I_{CaL} in sympathetically activated pacemaker cells *in vitro* [414]. In a study with a nNOS inhibitor, a dose-dependent profound bradycardia has been found in parallel with a large increase in heart rate variability and, at larger doses, vasoconstriction [415]. The effects of NO donors and inhibitors on HR control are thought to be indirect, consistent with a presynaptic modulation of vagal neurotransmission and ACh release during vagal activation. A significant post-synaptic action via ACh-M_2 receptor coupling to eNOS has also been reported. The post-synaptic action of NO (HR acceleration via I_f activation) has been shown to be opposite to that of pre-synaptic action (HR slowing via a facilitation of the ACh release). However, data are not consistent. The importance of NO action seems to be more pronounced with age and adrenergic activation [408, 410–412].

Nitric oxide can also interfere with β-adrenergic signaling. This action can be mediated through cAMP degradation (either via activation of phosphodiesterase activity or inhibition of Ca channels) and the inhibition of NE release (via NO-cGMP and, independently, K_{ATP}–channel mechanisms) [408]. Additionally, NO contributes to the metabolic breakdown of NE and provides a barrier for diffusion of the NE into the bloodstream. NO can also inhibit central sympathetic neurotransmission [411, 412]. The central part of NO contribution to CV control includes the modulation of aortic and carotid mechanoceptor reflexes, reduction in the sensitivity of cardiac baroreflex and augmentation of tonic vagal activity [410].

Recent studies indicate that NO action on the cardiac vagus might have a clinical perspective [416, 418]. In an experimental study, targeted nNOS gene transfer enhancing nNOS expression resulted in a rapid increase in parasympathetic

activity. In a study in patients with heart failure, those who were homozygous for the T/C polymorphism of the e-NOS promoter had a more advanced imbalance of the autonomic cardiac control [421] in spite of better left ventricular function.

As vagal stimulation is thought to be cardioprotective [419] and might increase the probability of survival after myocardial infarction [420], the importance of vagal modulation through NO donors [418] or NOS expression manipulations [416] awaits clinical verification.

35.5.3.5 Serotonin (5-Hydroxytryptamine)

All central brain nuclei that are involved in cardiovascular control are innervated by fibers containing serotonin and have direct or indirect synaptic contact with cardiac vagal preganglionic fibers that are likely to originate from within the brainstem [422]. Some vagal afferents also contain 5-HT. In addition, these regions express a wide range of 5-HT receptors. The blockade of 5-HT1A receptors attenuates the bradycardic response evoked by baroreceptor and cardiopulmonary receptor afferents stimulation. However, the number of 5-HT receptors and variable effects of their activation/inhibition limits understanding of their functional roles [422].

35.5.3.6 Neuregulins

Neuregulins are growth factors that are required for the maintenance of ACh receptor-inducing activity of nicotinic receptors. A recent observation in an experimental study in mice with neuregulin-1 gene deletion supports a role for neuregulins in maintaining normal parasympathetic modulation of excess β-adrenergic stimulation of the heart [423]. It might be of clinical importance in patients treated with cardiotoxic drugs that are known to suppress neuregulins signaling. Such drugs, i.e., doxorubicine, can lead to the development of cardiac impairment that is accompanied by a reduction in parasympathetic activity that may even precede the occurrence of overt heart failure [424].

35.5.4 Local Tissue Factors

Locally released mediators, mainly neuropeptides, may generally act as neurotransmitters, neuromodulators or neurohormones. Substances, like vasoactive intestinal peptide, somatostatin, substance P, neurotensin, phenyl-histidin-isoleucine, dynorphine or melatonin-stimulating hormone are released from neuronal endings within the SA node or from interconnecting neurons in peri-nodal ganglia. Peptides synthetized locally in the endothelium of coronary microcirculation or in the SA node, atrial or ventricular myocytes, can modulate sinus beat formation [425, 426]. Positive chronotropic action was observed after stimulation with adreno-medulline, angiotensin II (via AT1 receptor), atrial natriuretic peptide C and endothelin (via ET_A receptor), while a negative chronotropic effect was observed in response to bradykinin, somatostatin and endothelin (via ET_B receptor) [425, 426]. Other peptides (ANP, BNP, substance P) are considered as cardiac rhythm modulators. However, evidence for their direct actions are conflicting [427]. Cholinergic and sympathetic neuron activity can also be modulated by several amino acids, purine derivates, and free radicals [428]. A role for all of these local factors is probably limited in a normal physiological state.

35.5.5 Mechanical-Electrical Feedback

Active and passive changes in the mechanical load of the heart, either physiological or pathological, can influence the initiation and propagation of cardiac electrical excitation via pathways that are intrinsic to the heart itself. This cross-talk between mechanical and electrical activity is referred to as contraction-excitation or mechanical-electrical feedback (MEF) [429]. Processes involved in the MEF include stretch-activated ion channels in cardiomyocytes, changes in calcium handling, interaction with other mechano-sensitive non-myocyte cells, or stimulation of protein expression, local

peptides secretion, and biochemical changes [430, 431]. Mechanical factors are believed to be involved in heartbeat triggering during the early stages in embryogenesis [432]. The mechanical contribution to HRV can be observed in heart transplant patients, in whom a small (2–8% of normal) RSA has been recorded [433]. Similar findings have been reported in individuals after brain death [434].

35.5.6 Vascular Factors (Endothelium)

In general, the ANS and endothelium play opposite roles in controlling vascular tone through their action on the vascular smooth muscle layer, which lies between the two [435]. There is evidence that the ANS directly influences the endothelial cell function due to the presence of α_2- and β-adrenoceptors and muscarinic receptors. The activation of α_2-adrenergic and muscarinic receptors results in eNO release and subsequent vasodilation. In addition, sympathetic activation can stimulate the release of endothelium-derived contracting factors. The effect of ANS stimulation can be observed despite the presence of major conduit vessels that do not receive direct innervation. On the other hand, the endothelium may affect the extent of ANS-mediated vascular tone mainly through the changes in NO production and release [435]. The role of the endothelium in mediating ANS effects increases in clinical entities, in which endothelial dysfunction is a common feature (e.g., diabetes mellitus, hypertension).

35.5.7 Hormonal, Inflammatory and Other Humoral Factors

35.5.7.1 Renin–Angiotensin–Aldosterone System

The renin-angiotensin-aldosterone system (RAAS) interacts with the autonomic control of the heart at both central and peripheral levels [425]. Angiotensin II (AngII), a key hormone of RAAS, enhances central sympathetic tone and facilitates the NE release from sympathetic nerve terminals [436]. The net effect of RAAS activation is related to the entire circulatory response (circulating AngII level), cardiac local AngII action, and central local interaction within cardiovascular and respiratory centers [425, 437]. The magnitude of RAAS-ANS interactions depends on genetic variations (polymorphisms) within RAAS [438, 439]. In addition, the response of the RAAS blockade (with either ACEI or ARBs) varies, as different agents of these classes have been shown to exhibit divergent effects on autonomic function [440–442]. In addition, these effects depend on the initial status (before treatment) of the autonomic balance, with negligible changes in healthy persons or significant, albeit not uniform, changes in patients with hypertension or heart failure [440–442]. Sympathoexcitatory action of aldosterone (central or peripheral) both directly or via an inhibition of nitric oxide synthesis [443], together with the involvement of bradykinin, with its direct chronotropic effects [444, 445], further complicate explanation of the effects of RAAS activation or inhibition on cardiovascular autonomic control.

35.5.7.2 Hypothalamic–Pituitary–Adrenal System

Corticotropin-releasing hormone (CRH) is the principal regulatory neuropeptide that mediates stress-related biological responses as a physiologic regulator of adrenal epinephrine secretion [425, 446]. Neuroanatomical studies show a projection of CRH-fibers linked directly to autonomic regulatory nuclei in the brainstem [447, 448]. There is little experimental evidence of its sympathotonic effect. This action depends on a heterogeneous distribution of CRH-receptor subtypes between ANS brain centres and the heart and vasculature [447–449]. Recent studies have shown the presence of endogenous agonist for CRH2-receptor, referred to as urocortin, which mediates many actions previously attributed to CRH [450]. Interestingly, the results of a study in CRH2-receptor-deficient rodents suggest that CRH may act on a long time scale, i.e., h, thereby influencing the circadian rhythm of HR and its variation [451]. Adrenocorticotropin and cortisol actions are very complex and diverse, depending on the magnitude and length of stressful conditions [452]. Although they are involved in circadian and ultradian (12-h, 90-min) circulatory oscillations, short-term fluctuations (3-min) have been observed [453]. An increased vagal HR control has been reported in a clinical setting such as hypercortisolemia [454].

35.5.7.3 Insulin-Leptin-Adiponectin and Inflammatory Cytokines

Insulin leads to an acute hyperpolarization of the plasma membranes. With respect to excitable cardiac conduction tissue, this may result in an attenuation of the firing response to stimulation and desensitization of HRV during euglycemic hyperinsulinemia in subjects with intact autonomic control [455–459]. Insulin also affects the sensitivity of arterial baroreceptors. Insulin exerts its action indirectly through adrenergic activation that is expressed as a centrally-mediated stress reaction, an increase in the firing rate of adrenergic nerves and a shift in the sympathovagal balance in the HRV power spectrum [456–459]. These effects are age-dependent [460].

Insulin action, like other trophic factors (growth hormone, tumor necrosis factor α, transforming growth factor β), might be also related to the modification of M_2R expression via transcriptional regulation and M_2R downregulation. These changes may lead to parasympathetic withdrawal [459, 461]. Clinical studies suggest that parasympathetic modifications can occur early on in the development of obesity and diabetes and are concomitant with a greater variation in plasma insulin levels [460, 461] and insulin sensitivity or resistance [462, 463].

Leptin, the adipose tissue hormone, plays a crucial role in body weight control. A release of leptin is under tonic feedback control by the sympathetic nervous system. Adrenergic neurotransmitters exert an inhibitory effect on leptin release and synthesis [464]. Actually, leptin itself might influence the sympathetic neural drive and either acutely or chronically increase HR. This action can be completely reversed by a combined adrenergic blockade [465]. The significance of leptin-sympathetic activity in normal subjects is not clear, as a greater correlation with HR alone than with sympathetic nerve traffic has been reported. However, gender differences have been observed [466]. Recently, an association of leptin circadian and ultradian rhythms with a very-low oscillation of HR has been reported [467]. Also, the G/A polymorphism in the human leptin receptor gene influences sympathovagal balance.

Adiponectin is an adipocyte derived hormone which acts on the CNS to control autonomic function, energy and cardiovascular homeostasis [468, 469]. It acts as an insulin-sensitizing hormone and its circulating concentration is inversely related to adipose tissue mass [468]. Adiponectin receptors have been found in brain nuclei, playing a central role in the integration of cardiac autonomic control where it interacts with neuropeptide-Y neurons [470, 471]. Low serum adiponectin has been shown to negatively correlate with a sympathovagal index in patients with type-2 diabetes [472]. Hypoadiponectinemia has also been reported to be associated with sympathetic overactivity in obstructive sleep apnea syndrome [473].

Inflammatory cytokines are normally produced by the immune system. However, their excessive expression can in some circumstances lead to damage of various tissues, as they are involved in chronic inflammatory diseases, including atherosclerosis among others [474]. Experimental and clinical evidence indicates that stimulation of parasympathetic activity (via the nicotinic receptor) can result in anti-inflammatory action via inhibition of the production of some cytokines, like tumor necrosis factor α, interleukin-1, interleukin-6 and interleukin-8 [475]. Activated macrophages and lymphocytes also express specific receptors for other neurotransmitters released by the autonomic and central nervous system, including those mentioned above [475].

On the other hand, there are many clinical reports on the association of noninvasive measures of cardiac autonomic control (on the basis of HRV analysis) with the most commonly examined inflammatory substances, like C-reactive protein, interleukin-6 and TNF-α. However, negative observations also exist [370, 476, 477].

35.5.7.4 Gonadal Hormones

Accumulating evidence suggests that gonadal hormones, especially oestrogen, have significant effects on the brain, peripheral efferent nerves and signaling pathways of effector organ/cells that respond to neurotransmitters [478]. Gonadal hormone signals are mediated through binding of steroids to cytoplasmic/nuclear receptors (genomic actions) and membrane receptors (non-genomic actions). Nuclear oestrogen receptor and membrane binding sites for oestrogen, progestrone and testosterone have been identified in brain nuclei involved in the regulation of cardiovascular function [478].

The central action of oestrogen includes increased vagal tone via stimulation of choline uptake and ACh synthesis and suppressed sympathetic efferent activity via the stimulation of catalytic activity of catechol-0-methyltransferase and monamino oxidase. On the contrary, testosterone increases sympathetic activity via the stimulation of the synthesis of

NE and neuropeptide Y and the inhibition of NE clearance. Oestrogen increases the density and affinity of muscarinic receptors. In the periphery, the actions of gonadal hormones are similar to those acting centrally. Under experimental conditions, exogenous oestrogen and progesterone increases the density of β-adrenergic and muscarinic receptors in the heart, while testosterone stimulates choline uptake and thyrosine hydroxylase (catecholamine synthetase). Some effects of gonadal hormones are mediated through nitric oxide [478].

There are differences in the parasympathetic and sympathetic responsiveness in females and males - the parasympathetic response is greater in females and the sympathetic response greater in males. There is more pronounced bradycardia after vagal stimulation. Apart from experimental data, there are concordant data indicating the positive correlation between oestrogen level and cardiac vagal activity that can be observed during either the menstrual cycle or the menopausal period [479–482]. Some of these changes can be related to the action of endogenous progesterone-related steroids, which inhibits muscarinic receptors probably via their allosteric conformation and increases central NE release [478]. The attenuation of HRV has also been observed during progestogen-containing replacement therapy [483]. However, in a randomized trial on hormone replacement therapy in postmenopausal women, multiple 24-h HRV indices remained unchanged [484]. However, it has to be noted that the approach used in this trial is too crude to explore cardiac autonomic control.

35.5.8 Thermoregulation

Heart rate (or pulse rate) changes with hyper- or hypothermia are easy to detect. In some disease states (e.g., typhoid fever), a lack of heart rate acceleration, or even HR slowing in spite of increasing body temperature, has been considered to be an ominous sign by attending physicians.

Thermoregulation is a complex integrative process generating patterns of autonomic, motor, endocrine and behavioral changes in response to endogenous and environmental challenges. By considering the impact of thermoregulation on cardiac autonomic control, both circadian variation of body temperature balancing over a core temperature "set-point" and reactivity to cold or heat exposure can be investigated.

Circadian variation of body temperature is related to the central pacemaker located in suprachiasmatic nuclei, acting upon hypothalamic centres modulating the set point, and altering the thresholds for cutaneous vasodilatation and sweating [485, 486]. This circadian rhythm is involved in the regulation of the sleep–wake cycle together with pineal melatonin rhythm, and the responsiveness of the circadian pacemaker to light. From this point of view, thermoregulation is associated with the circardian rhythm of heart rate and its variation, being similar to sympathetic rhythm and opposite to cardiac vagal rhythm. There is neuroanatomical and neurochemical evidence linking central sympathetic activity with the sleep-wake clock and temperature rhythm [487].

The potentiation of cardiac vagal action in response to cold and vagal inhibitory effects during heat stress has been reported [488–490]. Also, thermogenic-related changes within cardiac autonomic control have been studied in response to various meals [491]. Variations in the frequency of the thermal component of HRV has been shown to arise from variations in the time delay in response to a periodic thermal stimulus and has been referred to as thermal entrainment [492].

35.5.9 Architecture of Cardiac Autonomic Control

35.5.9.1 Anatomical Basis for Cardiac Autonomic Control

Efferent Limb of Cardiac Vagal Control

Inhibitory vagal motorneurons originate in the dorsal vagal nucleus (DVN) and nucleus ambiguous (NA). The preganglionic motor neurons in the DVN and NA may exert preferential control over separate populations of neurons within the intrinsic cardiac ganglionated nervous system [493]. Their activity is characterized by tonic discharges modulated in phase with respiration. However, they are not able to generate spontaneous activity. Instead, their action potential generation rate follows the impulsation of glutaminergic neurones from the solitary tract nucleus (STN) in the dorsal medulla, where all afferent autonomic fibers are terminated. The importance of diverse cardiac vagal efferents may lie in

the fact that an intact DVN is not necessary for an efficient baroreceptor reflex, while other cardiopulmonary reflexes are critically-dependent on an intact DVN [494, 495].

Vagal efferent motorneurons sprouting to the mediastinum form the anterior and posterior cardiac plexus. Aside from presynaptic parasympathetic fibers, these plexi also contain presynaptic sympathetic fibers, intermediate purinergic neurons and autonomic ganglia [496]. Postsynaptic fibers of the vagi preferentially innervate SAN and AVN regions and atrial muscles [497]. Parasympathetic innervation of the ventricle is rather sparse and, accordingly, the ACh concentration in ventricular tissue is lower, achieving approximately $^1/_4$ of its concentration in the atria. Although a weak inhibitory action of parasympathetic stimulation on LV hemodynamics can be observed in experiments, especially when the sympathetic drive is augmented (*accentuated antagonism*), such an effect seems to be negligible in physiology [498].

The main effect of vagal stimulation is a reduction of sinus node rate. The magnitude of sinus cycle prolongation is greater after stimulation of the right vagus nerve, while the left vagus nerve exerts a stronger inhibitory action on the impulse conduction through the AV junction. A negative chronotropic action of vagal stimulation is phase and frequency-dependent. The SAN response to vagal stimulation is rapid, with a latency period less than 400 ms, and is sustained for less than 5 s after cessation of stimulation [396, 498]. Since the relationship between the frequency of vagal stimulation and slowing HR is nonlinear, changes in the heart period (sinus cycle) seem to be a better indicator of vagal influences [396]. However, it has to be remembered that the time-delay of the vagally-mediated response can vary significantly not only in healthy people, but even more so in patients with cardiac disease [499].

Efferent Limb of Cardiac Sympathetic Control

Pre-motor sympathetic neurons are located in clusters in four topographically defined nuclei in the intermediate gray matter on either side of the spinal cord (mainly intermediolateralis thoraco-lumbalis pars funiculus) [500]. Presynaptic sympathetic stimulating fibers spread like the sympathetic nerves into the thoracic sympathetic ganglia. Postsynaptic fibers from these ganglia travel by two pathways: firstly as sympathetic nerves directly to intrathoracic extra- and intra-cardiac plexi, further innervating atrial and myocardial muscle, and secondly, as sympathetic fibers of the stellate ganglions joining the vagi, traveling to specialized cardiac self-excitable and conducting tissue [500]. The sympathetic fibers traveling with the vagus nerve may contribute to the axo-axonal synapses that have been observed to lie between these nerves, providing a morphological basis for the observed vagal-sympathetic interaction [501].

Afferent Limb of Cardiac Autonomic Control

In general, cardiovascular afferent neurons are divided as those that are sensible to mechanical deformation in the region of their sensory endings (mechanosensors) and those that detect alteration in chemical milieu surrounding their sensory neurites (chemosensors) [397]. Anatomical and functional data indicate that most of afferent neurons can simultaneously transmit mechanical and chemical signals [502]. Also, the distribution of neural somata of different sensors is similar throughout nodose, dorsal root, intrathoracic and cardiac ganglia.

Mechanosensors localized in the right ventricular papillary muscle transmit RV loading or pressure in a linear and reciprocal manner. Those distributed throughout the outflow tract of the right and left ventricles sense development of chamber pressure, but their exponential activation patterns vary. Significant populations of mechanosensors along the adventitia of the inner arch of the thoracic aorta and the base of both venae cavae precisely detect phasic mechanical changes that are undergone during each systolic and diastolic event.

There is a limited population of chemosensors, which are activated when exposed to an altered concentration of a variety of local chemicals. Most local mechanical and chemical stimuli sensed by the neuronal endings are transmitted to adjacent neurons that form local circuit interconnections at cardiac and intrathoracic ganglia. These functional linkages are relevant to short-loop cardio-cardiac and vascular-cardiac reflexes. Sensory information arising from the heart and major vessels initiate central and peripheral reflexes that control the activity of extracardiac (long- and short-loop) and intrinsic cardiac motorneurons (ultra short-loop) [496, 503].

The direct measurement of vagal nerve activity is usually employed in experimental settings. However, the invasive nature, need for anesthesia and limited functional and behavioral contexts restrict the utility of the direct approach. Occasionally, direct recordings can be made from cervical vagal afferents and their stimulation can be applied to humans [504].

35.5.9.2 Local Cardiovascular-Cardiac Reflexes

Cardiac mechanosensory reflexes characterize short-tem latency due to a relatively short distance to the first synapse. The short-term scaling properties are responsible for the cardiac motorneurons' differential activation at any phases of the cardiac cycle [505]. Cardiac mechanosensitivity seems to be related to an expression of titin [506]. Some intrathoracic efferent neurons display activation reflecting initiation of the aortic and carotid baroreflex. In addition, the stretching of vena cava mechanosensors (which can be found with venous congestion) trigger intrathoracic reflexes.

Cardiac chemosensory reflexes modulate large numbers of cardiac motorneurons over longer timescales and multiple cardiac cycles. They also lead to the resetting of cardiac motorneuron activity for a period considered to be long enough to indicate the retention of information (*memory* (Biological phenomenon of determinism in which future events are causally set by past events)) [507].

35.5.9.3 Accentuated Antagonism

The nonlinear nature of autonomic interactions within the sino-atrial pacemaker complex is emphasized when both arms of autonomic cardiac control are activated. Levy et al. found that the cardiac pacemaker response to the vagus nerve stimulation is greater with a rise in sympathetic activity (*accentuation*) in spite of their opposite action (*antagonism*) [15, 498] (Fig. 35.39). Such a phenomenon, referred to as *accentuated antagonism*, can be seen in very fit humans. In older people, and in certain clinical pathophysiological settings, this phenomenon cannot be observed easily, as the vagal activity or inhibitory effects of its stimulation are usually depressed. Pyetan et al. [508] found an increase in power at respiratory frequency in a healthy young adult with a high level of cardiac vagal tone subjected to a relatively large

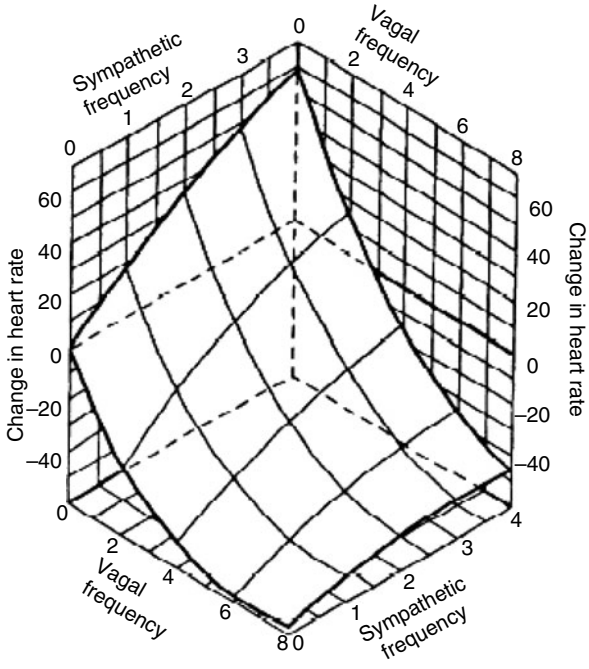

Figure 35.39

Sympathetic-parasympathetic accentuated antagonism. Changes in HR in response to various vagal and sympathetic stimulation. Vagal inhibition is greater when sympathetic activity increases, sympathetic stimulation is much less when vagi are active. The formed exemplifies synergism, the latter antagonism (From [A31]).

cumulative dose of atropine. They interpreted such a response as a feature of the reduction of sympathetic influence accompanying vagal effector inhibition.

35.5.10 Nonregulatory Reflexes Involving Co-Activation of ANS

Classic reciprocal action between sympathetic and parasympathetic outflows represents a highly simplified description of cardiac autonomic control. The presence of the accentuated antagonism between two branches of the ANS in physiologic and pathophysiologic settings can find further support in some protective reflexes that are accompanied by excitation of both autonomic outflows [509].

Among reflexes that are accompanied by the co-activation of both ANS branches, the peripheral chemoreflex, diving response, oculocardiac reflex, defense response, and somatic nociception response are considered [509]. The common functional significance of these reflexes/responses is considered to coordinate the relationship between ventricular contractility and heart rate with sympathetic and vagal activation targeting the ventricular myocardium and SAN, respectively. This may be of special importance during a prolonged and deep hypoxia (diving response), when the bradycardic response causes a substantial fall in ventricular function via a nonneural mechanism (So-called Bowdich effect.) and sympathetic co-activation may serve as a compensatory response to maintain stroke volume, as well as blood flow and oxygen delivery to the heart through action upon coronary arterioles via β-adrenoceptor stimulation. Another possible significance is related to vagally-mediated tachycardia, when both branches of the ANS act synergistically. It is suggested that this paradoxical feature is related to ACh release in the intrinsic cardiac ganglia neurons along with activation of chromafine cells to release catecholamines. Alternative explanations include the muscarinic receptor mediated release of neurotransmitters co-localizing cardiac vagal fibers, which may have the same effect as NE of increasing HR.

35.5.10.1 Peripheral Chemoreceptor Reflex

In experimental settings, activation of carotid body chemosensors resulted in the transient increase in cardiac vagal and sympathetic activity reflected by a profound bradycardic response. Co-activation of branches of the ANS can also be elicited by a mild prolonged hypercapnia and mild hypoxia, whereas a co-inhibition occurs in response to hypocapnia.

35.5.10.2 Diving Reflex

Vagally-mediated bradycardia is a major feature of the diving response in humans and other mammals. It is suggested that facial or nasopharyngeal stimulation is responsible for this reflex. Coincidence of sympathetic activation during the diving reflex is expressed as the occurrence of ventricular arrhythmias, including polymorphic VT, and shortening of the QT interval, that can be prevented by β-adrenoceptor blockade with propranolol.

35.5.10.3 Oculocardiac Reflex

The stimulation of trigeminal nerve endings triggers a reflex that produces vagally-mediated bradycardia and which in extreme cases may lead to cardiac arrest. Historically, this reflex has been used as a manual procedure for the termination of paroxysmal tachycardia (Aschner) by putting pressure on the ocular bulbs (more precisely on the corneal surface). A sympathetic component of this reflex is expressed as increased outflow to the ventricles and, subsequently the occurrence of ventricular ectopic beats.

35.5.10.4 Defence Responses

Experimental stimulation of different discrete hypothalamic areas evokes various possible patterns of ANS activation (sympathetic activation/vagal inhibition or co-activation or co-inhibition). In the case of centrally-mediated ANS co-activation, HR follows vagal changes. The defence-like response may also occur in the response to alerting-eliciting acoustic stimuli (startle reflex). Despite these stimuli provoking a small transient tachycardia, a pronounced negative chronotropic effect of sympathetic blockade suggests a role of vagal co-activation. Interestingly, the vagal response rapidly habituates with repeated stimuli, while sympathetic activation persists.

35.5.10.5 Somatic Nociception Response

Stimulation of somatic nociceptors typically leads to tachycardia, increase in blood pressure and hyperpnea in animals and humans. Direct cardiac vagal nerve recording has shown that the nociception response involves augmentation in the activity of cardiac vagal outputs. It is postulated that this complex response is centrally-mediated and modulated by central respiratory activity. Nociception-evoked tachycardia seems to be vagally-mediated and can be attenuated by atropine. However, a combined blockade is necessary to abolish this chronotropic response completely.

35.5.11 Brain–Heart Interactions

It is well recognized that sympathetic and parasympathetic neurons play a regulatory role in modulating cardiac dynamics. This regulatory role is achieved through a very complex structural and functional interplay between afferent neurons localized in different cardiac regions and within vascular beds (mainly intrathoracic and cervical) and efferent neurons localized in the cerebral cortex, brain stem nuclei, medulla oblongata, spinal cord, paravertebral cervical, and thoracic ganglia, as well as pericardial and intrinsic cardiac ganglia. Spatially overlapping afferent neurons differentially transduce regional cardiac and vascular events throughout each cardiac cycle directly or indirectly (via interconnecting neurons) allowing for temporally organized reflexes. All constitutive parts are redundant and stabilize the whole cardiac behavior [507].

In pathological settings, overactivity of the autonomic nervous system plays a critical role in myocardial damage and mortality [13, 510]. Therefore, abnormal cardiac rhythm oscillations can be seen in patients with stroke, subarachnoid hemorrhage, epilepsy, and head trauma [510–513]. Brain-heart interactions are also important in the pathogenesis of (a) sudden unexpected death in adults and infants, in specific circumstances (for example status asthmaticus, alcohol-withdrawal, drug abuse) [56, 510], and (b) cardiac dysfunction in tako-tsubo cardiomyopathy and phaeochromocytoma, in which altered fluctuations of heart rate can be detected [514–516].

35.6 Determinants of HRV

35.6.1 Genetic Factors

There is accumulating data confirming the role of genetic factors in HR and HRV control. Early data suggested that genetic variance can determine the arrhythmia index, the measure of RSA introduced by Schlomka, which has been reported by Fuller in 1951 in purebred dogs [517]. Kreutz et al. were the first group to identify HR-determining gene location on the rat chromosome 3 [518]. Since that time, other genes which contribute to heart rate have been described [519–523].

Martin et al. [519] performed the variance decomposition linkage analysis for genomic screening in 2209 individuals and found that the heritability of the resting HR was around 26%. In their study, HR linkage on chromosome 4 (4q28.2) was observed. Interestingly, in this region, linkages have also been found for insulin, blood pressure, abdominal subcutaneous fat, as well as for type 4 long QT syndrome, associated with bradycardia [after 519]. Similar heritability (24–27%), as well as HR linkage to chromosome 4 has been reported among hypertensives [520]. A heritability of 36% for HR and 20% for BP responses to exercise training has been found in another set of patients with high blood pressure [521] and

various candidate genes have been proposed [522]. A recent meta-analysis of genome wide scans indicates the location of a gene influencing HR on chromosome 5p13–14 [523].

The attempts that explore the HR genetic basis do not necessarily explain the genetic background of HRV. The results of the Copenhagen Holter Study indicate a significant association of a reduced HRV with the familial predisposition to premature heart attack [524]. Using a genome-wide scan in participants from the Framingham Heart Study, Singh et al. have provided evidence of linkage of the LF power to chromosome 2 and of the VLF power to chromosome 15, although the linkage odds scores have not exceeded the threshold for significant linkage on a genome-wide level [525]. Interestingly, around the region of interest (chromosome 2), a candidate gene for KCNJ3, a human gene encoding the G-protein activated inwardly rectifying potassium channel, known to be involved in HR regulation [526], has been identified. Also, candidate genes for human neuronal nicotinic cholinergic receptors have been reported on chromosome 15 [527].

The combined results of the Framingham Heart Study and Framingham Off-Spring Study (1151 subjects) indicate the presence of a significant correlation among standard HRV parameters in siblings (between 0.21 and 0.26), compared to spouses (0.01–0.19) [528]. Genetic factors seem to be responsible for substantial inter-individual variations in HRV that reached 23% in the Framingham cohort. However, after the adjustment for HR, this proportion is reduced to 9–22%, suggesting an involvement of similar genetic factors that determine both the HR and HRV [528]. Genes account for 13–23% of the variation among spectral HRV measures in this population [529]. Heritability estimates of 0.41–0.45 for SDNN and of 0.39–0.45 for RMSSD from 5-min ECG recordings have been reported to be independent of breathing mode (spontaneous vs controlled) [530].

Associations between HRV and genetics are frequently explored in twins [531–539]. In a small sample of twins, Piha et al. found that both ANS branches were strongly related to genetic factors independently of body mass [531]. In a larger sample of 160 twins, the RSA appeared to be determined by stable genetic factors and variable environmental components [532]. Snieder et al. have estimated a genetic contribution to RSA of 31% at rest and between 28% and 43% at four different stress task conditions [533], independently of respiratory rate. A genetic contribution to the mean ambulatory SDNN index (ranging from 35% to 47%) and the mean ambulatory RMSSD (ranging from 40% to 48%) has been reported [534]. Short-term vagally-related HRV measures (RMSSD and HV power) at rest and under stress have been found to be largely influenced by the same gene [535]. An association of reduced HRV and depression has been found to be genetically-predetermined [536]. Also, the dipper-pattern of the blood pressure has been found to be heritable [537]. Importantly, HRV-related familiarity can be detected already in newborns. However, environmental influences seem to play a greater role than genetic factors early in life [538].

In a recent study, an association of parasympathetic activity with the variation in the choline transporter, a component of ACh neurotransmission, has been reported. Subjects having any T-allele (TT or GT genotype) had greater HF power and lower LF power and LF/HF ratio, compared to subjects with GG genotype [539]. Studies that compared HRV in relation to known genetic polymorphisms (ACEI, angiotensinogen, uncoupling proteins) complement evidence for a genetic background of HRV [540, 541]. Furthermore, an experimental investigation has confirmed the importance of G-protein heritability for HR autonomic control [542].

35.6.2 Constitutional Factors

35.6.2.1 Age

Heart rate and its variation is critically dependent on age, especially if one considers the period of the entire lifespan [322]. Within the lifespan, two distinct phases are present with distinct HRV behavior. The first phase is a period of development and maturation, and the second starts early in adulthood and is related to aging and senescence. Therefore, in studies in which the age-range is limited (e.g., a young adult cohort or middle-aged subjects) the possibility of detection of significant HRV changes with age is *a priori* reduced. Also, data on the age-dependence of HRV is generally obtained from cross-sectional studies. To evaluate within-person age-related changes, longitudinal observations seem to be more appropriate.

Autonomic Control Changes During Development

Detectable variation in heart rate can already be observed in fetuses [543]. Mechanisms underlying these variations are largely unknown. An intrinsic rhythmicity of the SAN seems to determine HR changes early in gestation (9–15 weeks), albeit cholinesterase activity can be detected at the eighth gestational week. With the advance of gestation, parasympathetic effects become evident [543]. More data is available regarding maturation of cardiac autonomic control from infancy to adolescence. A dominating role of maturation of central parasympathetic signal processing has been suggested [544].

HRV Changes During Development

The main component of HRV is attributed to RSA, which is detectable at around 33 weeks gestational age, and remains a predominant component of HRV in neonates [330–332, 545]. An earlier occurrence of HR fluctuation in the LF range (<20 week of gestational age) has been documented. However, it seems to be secondary to maternal HR and BP variation [546]. A clear dependency of all time- and frequency domain measures on gestational age has been shown [547, 548]. It has to be pointed out that, in fetuses and neonates, the spectral HRV component may have different ranges, i.e., 0.025–0.07 Hz for VLF, 0.07–0.13 Hz for LF and 0.13–1.0 Hz for HF [549]. Global HRV changes from 3 h to 7 days of post-natal life have not been consistently observed [550]. It might also be difficult to assess spectral HRV indices in this period of life, since the influence of various factors may lead to misinterpretation of HRV data [551]. A significant increase in SDNN (+20%) and MSSD (+42%) between the first and third month, with a prominent increase in SDNN following awakening (+72%) in spite of a shortening of mean RR interval, has been reported [552]. In a study by Massin and von Bernuth in 210 healthy children aged 3 days to 14 years, 24-h SDNN values were found to have almost doubled between 1 month and 1 year, and tripled at 5–6 years (tab.35.28) [331]. Further increases of SDNN and SDANN from long-term ECG recordings with maxima at a late adolescence period have been reported [332, 334]. Meanwhile, RMSSD has been found to reach a maximum value already in early childhood [332]. This is in accordance with the findings of Finley and Nugent, who have observed maxima of both short- and long-term spectral HRV indices at about 5–6 year of age [553, 554]. The maxima of short-term HF and LF power have been observed at late adolescence in another study [555]. The difference between both studies might be as a result of different data presentation (instantaneous HR vs RR), length of ECG recordings and the use of different algorithms (FFT vs AR). The significance of data presentation and length as well as choice of algorithm for HRV power spectrum estimation is discussed in 35.4.

35.6.2.2 Cardiac Autonomic Control Changes Related to Aging

Aging is associated with complex and diverse changes in cardiovascular structure and changes [556]. The most important variations are listed in Table 35.33.

Some of these changes gain a special importance when HRV is considered. A reduced responsiveness of the SAN to adrenergic stimuli and an increased responsiveness to vagal stimulation is the most relevant [397, 556–560]. As intrinsic properties of the SAN are altered, leading to the partial uncoupling of P-cells [561], an increase in the level of sympathoexcitatory hormones is detected (increasing plasma NE) as well as central sympathetic discharge (increasing efferent sympathetic nerve activity in microneurographic studies) [562]. This is accompanied by a reduction in a high affinity state β_1-adrenergic receptor density, with changes in the proportion of β_1AR to β_2AR from 4:1 to 2.5:1, mimicking that observed in heart failure [558]. A 30% reduction in the amount of activated adenyl cyclase in response to G*s*-mediated β_2AR stimulation has been reported [557, 558]. As a net result, although aging is associated with sympathetic over-activity, HR and age has not been correlated in the majority of studies.

On the other hand, muscarinic receptor density is increased in older subjects in spite of a surprisingly increased responsiveness to vagal stimulation [556, 564]. This seems to indicate that a reduced central vagal outflow can play a greater role in tonic cardiac parasympathetic control changes with age than SAN responsiveness to ACh itself [556, 564]. However, these changes are not consistently observed, and even the opposite has been reported [557, 558]. In terms of M_2-R mRNA concentration and muscarinic/β-adrenergic mRNA proportion, the heart does not age as a unit: age-related changes are focused on the SA node area [564]. Among possible mechanisms leading to a reduced vagal tone in elderly people, a reduced baroreflex sensitivity mainly due to increased arterial wall thickening and stiffness, and a reduced arterial wall distensibility together with endothelial dysfunction (mainly a reduction in NO) are of greatest importance

Table 35.33

Factors affecting ANS control and HRV measures associated with aging (Modified after Ferrari et al. [550, 556])

Level of integration	Morphological changes	Functional changes	Consequences (regarding HRV)
Cellular/subcellular			
cardiomyocytes *non-muscle cells* *adrenergic receptors* *muscarinic receptors*	Increased dimension/number Increase in collagen cross-linking Altered β_1/β_2 density ratio Up-regulation	Reduced responsiveness to stimuli Increased responsiveness to stimuli	Altered SAN responsiveness
Cardiac tissue			
Sino-atrial node	Reduced P cells: all cells ratio P-cells uncoupling	Altered pacemaker shifting Reduced SAN-respiratory coupling	Altered SAN responsiveness
Organ			
Heart	Increase in heart weight, LV hypertrophy/ fibrosis Decreased sympathetic innervation	Reduced lusitropic properties/ diastolic function	Altered mechano-electrical coupling/reflexes
Circulation			
Endothelium	Reduced NO synthesis/release Reduced SOD activity VSMC migration	Endothelial dysfunction Increased oxidative stress Increased total peripheral resistance	Reduced baroreflex sensitivity
Arteries	Increased subendothelial collagen Increased intima-media thickness VSMC proliferation Reduced elastin Increased elastin fragmentation	Increased total peripheral resistance Decreased arterial distensibility Increased pulse wave velocity Reduced cardioacceleration after baroreceptor deactivation (delayed response)	Reduced baroreflex sensitivity
Hormones/ mediators	Increased level of vasoconstrictive peptides Increased ANP/BNP synthesis/release Increased inflammatory mediators level	Endothelial dysfunction Increased oxidative stress	Reduced baroreflex sensitivity
Brain			
ANS	Loss of neurons Pigments accumulation Neurotransmitters activity changes	Altered responsiveness to afferent inputs	Central control alteration

[556, 565]. Only a few studies systematically addressed the issue of cardiopulmonary reflexes in aging and the evidence is in favor of a blunting of the hemodynamic and humoral components of cardiopulmonary responses. However, evidence to the contrary does exist [556].

Consistently observed age-related reduction in vagal tone measures should not simply be interpreted as signs of vagal neuropathy or an impaired parasympathetic control. Instead, reduced afferent signals coming from peripheral sensors may lead to a reduced central vagal outflow, irrespective of an altered SAN responsiveness. Moreover, age related autonomic innervation changes can appear relatively early in adulthood (>35 years of age) [557] mainly as a reduction in sympathethic nerve endings [566]. Generally, aging is associated with alterations in cardiac autonomic control that, not surprisingly, lead to consistent observations on a reduction of HRV with age. However, other factors not necessarily directly connected to autonomic modulation, are also changed in ways that actually are associated with a reduced HRV, especially over a 24-h period.

HRV Changes Related to Aging

An age-dependent reduction in the RSA from short-term ECG tracings has been reported as early as 1940 by Schlomka et al. [after 8]. Further studies in adults consistently reported a reduction in time-domain HRV measures with aging

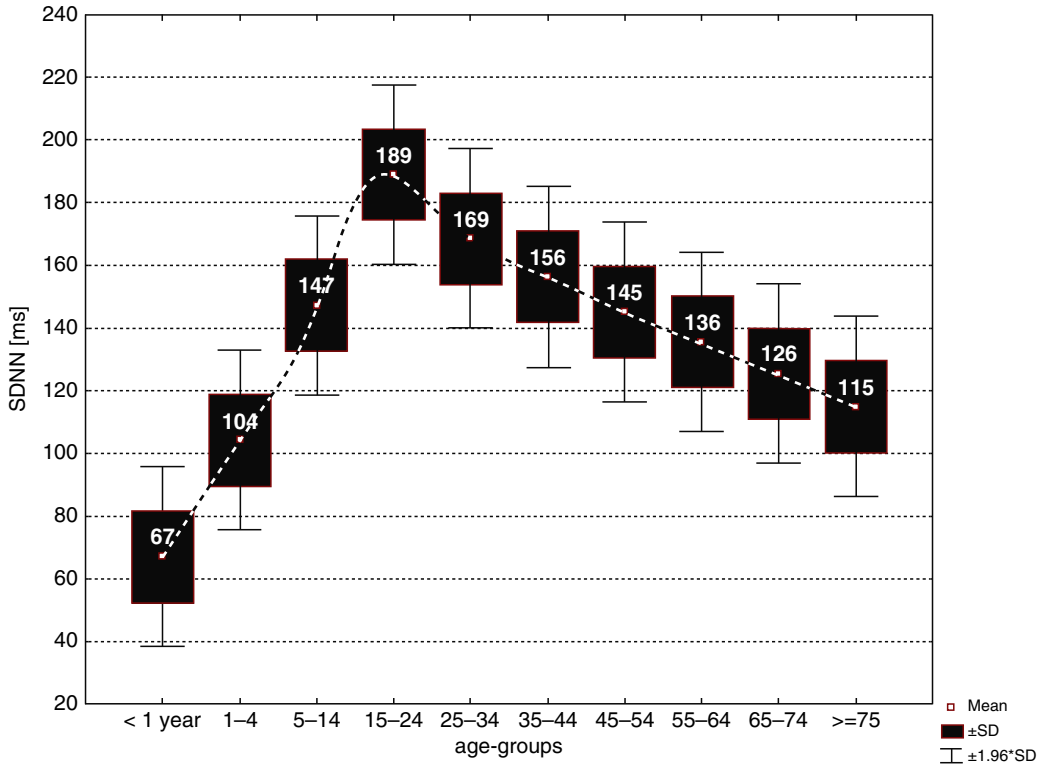

Figure 35.40

Age-dependence of the SDNN from 24-h ECG in healthy subjects. A combined data from 18 studies in children and adults. HRV reaches its maximum in late adolescence or early adulthood. Thereafter HRV reduces gradually. Confidence limits (1.96 SD) shown do not mean the normal limits (Author's data).

[567–570]. Interestingly, the RSA assessment over five heartbeats has originally been proposed to estimate "cardiac age" [570]. Similarly, the estimation of "cardiac age" has been proposed by others, though, by using a more sophisticated approach [571]. Actually, there is only one alternative method for "cardiac age" estimation, namely coronary artery calcium scoring on cardiac computed tomography [572].

The rates of HRV decline at different stages in the life course vary with different traditional HRV measures and the times of recordings. For the HRV indices that are acknowledged to strongly relate to vagal tone (RMSSD or pNN50 from 24-h recording and almost all statistical descriptors from short-term recordings) the decline is exponential and occurs early in adulthood, beginning usually well before the fourth decade of age [321, 322]. At the sixth decade of life, pNN50 and RMSSD reach values that are 25% and 50% of that observed in young adults. Over the following decades, these indices do not change significantly. In 4% to 12% of people after 65 years of age, these values can be as low as cut-off values indicating an increased risk of CV mortality [322].

The 24-h SDNN and SDANN decline more gradually. According to the accumulated data from 18 Holter-based studies, SDNN is reduced by approximately 25% in middle-aged persons (compared to young persons), and by ~40–50% in the elderly (>75 years of age) (Fig. 35.40) [64, 320–322]. There is still a small reduction of SDNN in senescence [322] (Table 35.27). Importantly, the lowest SDNN and SDANN values in subjects ⩾65 years old sporadically achieve the level indicating an increased risk for all-cause or CV death. Reported 24-h SDNNI values decline almost linearly from their maximum at 20–30 years of age achieving a 25% reduction in the elderly compared to young adults with a significant proportion (25%) below the cut-off value for being at risk [322].

Data from studies on HRV analysis from shorter ECG recordings show a similar trend. In the Framingham Heart Study in 2,722 subjects with an age range of 21–93 years, the 2-h SDNN has been reported to decline by 25% in

middle-aged persons and by 40% in subjects older than 70 years as compared to young persons [573]. In another cross-sectional study in subjects aged between 35 and 65 years, the reduction of the median values of 5-min SDRR and RMSSD has reached 17% to 25% from the fourth to fifth decade of age and 7% to 11% from fifth to sixth decade, respectively [269]. In another cross-sectional study in 373 healthy Japanese (16–67 years old), the rate of short-term SDRR decrease from the third to fifth decade was greater in females (−35%) than in males (−17%), and was similar from the fifth to sventh decade (17% and 15%, respectively) [574]. Agelink et al. reported a smaller rate of the 5-min RMSSD of 33% and 22% over 3 decades in men and women, respectively [335]. In a large prospective within-persons study (1,999 participants, 29% females, mean age 55.6 ± 6.0 years) over the 5-year follow-up period, the mean 5-min SDRR decrease of 2.3% after 55 years of age was observed only in males, in contrast to a mean increase of 3.9% in females [575].

The power of the HF component declines exponentially from the maximum value usually between the age of 16–20 with almost 50% reduction over next 2 decades [555]. In a longitudinal investigation of 1,780 young Finnish children re-examined at the ages of 24–39 years, the short-term (3 min) lower 2.5% reference limit of HF power decreased by more than 50% from young adulthood to middle-age consistently for three heart rate strata [576]. Thereafter, the 24 h-HF power reduced at a rate of 10–15% per decade [317, 577]. After 65 years of age, variations of HF power are smaller or insignificant [317, 577]. In a longitudinal within-persons study the power of 24-h HF was unchanged over 15 years in a small sample of elderly persons [578]. In another longitudinal study, a 6% reduction of the short-term HF power over 5 years of follow-up has been observed only in males [579]. At the same time, the lower normal limit of the 24-h HF power diminishes with age, being highest in subjects who are 20 years old, decreasing by 50% at 40 years of age, with a further reduction to 20% of the maximum values at 65 years of age [580].

The power of the LF component decreases more gradually from the maximum value at 20–30 years of age, with a rate of ~20% per decade [317, 320]. A similar rate of LF power decrease with age has been reported in a cross-sectional study on short-term HRV [335]. A steeper decline of ~30–35% per decade was found in the Framingham Heart Study population [573]. Biphasic changes with 50% reduction between the fourth and fifth decade and 10% between the fifth and sixth decade [269], as well as oppositely directed changes with a rate of 20% reduction between 35 and 55 and of ~50% from 55 to 65 years of age have been reported [574]. In a longitudinal study in young adults, the LF power diminished by 50% between 24- and 39-year-old persons [576], while in another longitudinal study in the elderly followed over 16 years, a continuous decrement of the LF power was noted [578]. A significant reduction of 11.3% in older males and an increase of 4.1% in older females has been reported over a 5-year period of follow-up [575]. There is also a report in which the LF power in subjects $\geqslant$ 60 years was comparable to that of younger people (<35 years old) despite a significant 40% reduction in cardiac NE turnover and peripheral MSNA over 2 decades [581].

The VLF and ULF power are almost linearly age-related. A rate of VLF power reduction of 12% per decade from the base value at age 40 years has been observed [317, 320]. A decrease of ULF power is less distinct and in persons $\geqslant$ 60 years of age, the ULF power represents ~ 90% of initial values [320].

Geometrical HRV measures are also age-dependent [64, 321, 580]. The highest value of HRVI is observed in young adults, and then it declines exponentially, reaching values of ~60% of maximum (overall 40% over 4 decades) in the seventh decade [321]. The mean HRVF decreases more gradually, from 55% at age 25 years to 45% at age 60 (overall decrease of 20% over 4 decades). Interestingly, there are distinct rates of reduction of the lower and the higher normal limits. They change from the third to sixth decade by 33% and 15%, respectively [64].

Results of investigations on age-dependence of nonlinear HRV measures are far from consistent. The DFA $\alpha 1$ index has been shown to increase with age in several studies [320, 584, 585], decrease [327, 583], or remain unchanged [582, 586]. However, in longitudinal studies in young and elderly persons, DFA $\alpha 1$ has been consistently found to decrease with age [578, 579]. In various reports, the DFA $\alpha 2$ index increases [320, 583, 584], decreases [327] or remains stable over various age ranges [582, 586]. The beta-coefficient (slope of 1/f power) becomes steeper with age [574, 578, 579], although in the elderly it remains stable [579]. Two distinct behaviors of the beta-coefficient have been reported depending on the frequency break-point [587]. There are other inconsistent data regarding other scale-invariant measures [583, 586].

Results of cross-sectional studies indicate a gradual decrease of the approximate entropy [320, 327, 583]. However, in a longitudinal observation, no change of ApEn has been seen [578]. Investigations on other entropy measures provide inconclusive data [582, 588]. In addition, aging -related alteration of the largest Lyapunov exponent has been found to differ in magnitude and direction in cross-sectional studies [327, 582, 583, 586, 588].

Multilevel influences of aging on cardiac autonomic control are reflected by changes in the baroreflex sensitivity (Table 35.33). An inverse effect of the aging process on BRS has been reported in several cross-sectional studies [589–594]. This age-association reduction has been confirmed in a number of investigations using various experimental techniques providing information on separate aspects of the BRS [595]. In a cross-sectional study, the BRS assessed by means of the Valsalva maneuver decreases by ~33% in middle-aged subjects (from 17.8 ± 1·8 to 11.9 ± 1·3 ms/mmHg), and by ~60% in older subjects (7.1 ± 0.6) [592]. A similar reduction has been found for the phenyleprhine method (19.5 ± 1.4, 10.7 ± 1.2 and 6.0 ± 0.6 ms/mmHg, respectively) [593].

The vagally-related arm of the BRS loop declines by a rate of 10% per decade, while sympathetic-related BRS reduces at a rate of 5% per decade [594]. The α-index of high- and low-frequency has been shown to reduce by ~33% and ~45% over 3 decades, respectively, as estimated by means of the spectral method and by 50% as estimated by means of the phenylephrine method [595]. Reduction in the BRS with age resulted in the occurrence of abnormal risk-predictive values in a significant proportion of elderly persons (30–50%). However, the proportion of abnormal BRS depends on the technique used for its assessment, with the mean BRS of 4.5 ms/mmHg with the Valsalva method (50% abnormal), 7.8 ms/mmHg with a vasopressor agent (phenylephrine, 37% abnormal) and 5.6 ms/mmHg with vasodilator (sodium nitroprusside, 30% abnormal) based techniques [596]. Cumulative data indicates that in subjects older than 50 years, it is almost impossible to differentiate whether the reduction of BRS is related to the aging process or the presence of other risk-factors, with systemic hypertension being amongst the most important [590, 597, 598]. However, spontaneous BRS during controlled breathing has been shown to linearly decrease from 50 to 75 years of age [599]. In one reported longitudinal study, the aging effect on spectral BRS has been evaluated in 205 men (36 ± 10 years at entry) over a mean 5-year period [600]. The rate of BRS decrease of 3.6% per year until 45 years of age has been observed. In the oldest group (46–50 years at baseline), no significant change over the 5-year follow-up was observed.

Age-associated changes of cardiac autonomic control are also reflected by the effect of age on heart rate turbulence. The TO increases with age, while the TS appears to remain stable [601]. These relationships strongly depend on the duration of the preceding sinus cycle at younger ages, and the influence of the basic HR attenuation as age increases [601]. On the contrary, in another study, an inverse relation of TS with age and no relation between age and TO has been reported [366]. In a study of healthy children, lower TS has been found in those with pre-pubertal status compared to those during puberty, while TO has been found to be age-independent [602]. Thus, conclusive statements on the age-relationship cannot be established as yet.

35.6.2.3 Gender

Gender differences in cardiac autonomic control are multi-factorial and originate not only from differences in hormonal status, but also from distinctive heart rate, blood pressure and respiratory control, constitutional and demographic factors, life-style and psycho- behavioral factors, as well as intrinsic central and peripheral nervous system features. Some of these factors with their possible influences upon HRV are presented in Table 35.34. Table 35.34. These factors may have a different role to play at various points throughout life, between women and men actually disappear.

Gender related differences in the time and frequency domain variables are the subject of diverse opinions. In most studies, some HRV measures are reported to be gender-related whereas others are not. Age and race (where applicable) are only rarely added as the covariate [248, 269, 315, 615, 616]. In a small number of studies, heart rate has been analyzed as a covariate or a separate analysis for various heart rate strata has been performed [319, 573, 576]. A combination of reported relationships between HRV and gender is schematically presented in Table 35.35. More detailed data from short-term and long-term HRV studies are shown in Tables 35.36 and 35.37.

Clearly, these results indicate that global HRV measures and LF power are either comparable or lower in females, while the respiratory-related HRV measures are either similar or higher. Interestingly, time-domain short-term variation measures (RMSSD, pNN50) from 24-h ECG recordings, which are known to be closely correlated with HF power, have been found to be either similar [65, 316, 319, 321, 332], higher [619], or lower [319, 322] in women. Some authors prefer using the relative powers of LF and HF for their superiority in detecting the effect of gender [323, 324]. However, these relative spectral indices have the least well defined or even no physiological background. Evidence for lower values of HRV measures in females might be of clinical importance, although in some instances, normal limits remain to be established. For example, Gerritsen et al. proposed separate reference values of 3-min LF power for women and men, while proposing HF power and SDRR normal limits for the entire population [599].

Table 35.34

Factors associated with gender differences in HRV. See Table 33.2 for list of abbreviations

Factor[s]	Difference	Mechanisms	Effect on HRV
Blood pressure	Lower	Baroreflex gain changes	Reduction
HR	Faster	Closer HRV-HR relationship	Reduction
Intrinsic HR	Faster	Intrinsic SAN properties	Reduction
Respiratory pattern	Thoracic	Greater intra-thoracic pressure changes	Increase (RSA)
Breathing frequency	Faster	Smaller intra-thoracic pressure changes	Reduction (RSA)
Physical fitness	Usually lower	Lower cardiac autonomic tone	Reduction
Smoking habits	Less frequent	Lower sympathetic activation	Reduction (LF)
Alcohol abuse	Less frequent	Greater cardiac vagal activity	Increase (RSA)
Psycho-behavioral factors	Multiple	Greater sympathetic activation, lower vagal sympatho-inhibitory actions	Reduction
Personality type	More complex	Multiple	Reduction
Nor/epinephrine level	Lower	Lower response to sympathetic activation Lower adrenal medullary content of Epi Higher epinephrine clearance rate Lower neuronal/extraneuronal uptakes	Reduction
Central control	Multiple	Less sensitive to excitatory stimuli and more sensitive to inhibitory stimuli, varies with oestral and menstrual cycles	Not studied
Noradrenergic neurotransmission	Higher	Increased presynaptic α_2-adrenoceptors number/activity varies with oestral and menstrual cycles	Not studied

Table 35.35

Patterns of HR and HRV differences in females (versus males) from short-term ECG recordings

HR	SDRR (or TP)	HF power	LF power
↑	↔	↔	↓
		↑	↓
	↓	↔	↓
↔	↔	↑	↔
			↓
		↔	↔
	↓	↔	↔

Variability in patterns depends on age, race, algorithms used, and statistical adjustment.

Differences between women and men have also been studied in terms of nonlinear dynamics. Gender differences of fractal dynamics measures vary depending on methods and duration of registration. In short-term HRV studies, the β-exponent has been found to be less steep in women than in men [481, 574], contrary to long-term study findings, where a steeper β-exponent or no difference has been observed in females [320, 583]. Short-term and long-term DFA α1 coefficients have been found to be lower in females, with no differences in DFA α2 [141, 320, 583]. Higher approximate entropy in women has been observed in some HRV studies [141, 328, 583], but not confirmed by others [320]. Other indices have only rarely been studied (Tables 35.36 and 35.37).

Actually, accumulated data indicates that gender-related differences should be taken into account or a proper statistical method should be applied for a valid interpretation to be drawn, irrespective of the duration of HRV recordings.

Table 35.36

Gender-differences in HRV measurements from short-term ECG recordings

Author, year	Sample	Parameter	Differences in women	Methodical issues
Korkushko et al. 1991 [555]	354 subjects 3 months – 89 years	LF HF	Higher/lower* Higher/lower ¶	4 min, FFT * > 40 years of age ¶ > 20 years of age
Ryan et al. 1994 [A28]	67 subjects 20–90 years	LF HF LF/HF	Lower Higher Higher	8 min FFT
Huikuri HV et al. 1996 [323]	374 subjects 40–60 years	HR* SDRR pNN50* HF (ms2)*/ HF (n.u.) LF (n.u.) LF/HF	Slower Lower Higher Higher Lower Lower	512 heartbeats AR 20 order * sitting posture
Tsuji H et al. 1996 [251]	2,722 subjects 21–93 years	SDNN* LF* HF*	Higher Lower Higher	2 h AECG 100s epochs, FFT * Ln transformed values Marginal effects of gender
Sosnowski et al. 1996 Author's data	228 healthy volunteers 8–67 years	RRI/ SDRR HF LF* LF/HF	No difference Higher Lower Lower	512 heartbeats FFT * standing position/no difference in supine
Liao et al. 1997 [649]	2252 subjects 45–64 years	SDNN LF HF LF/HF	Lower Lower Higher Higher	2 min FFT
Sinnreich R et al. 1998 [269]	294 subjects 35–65 years	SDRR*/ TP* RMSSD*/ HF* VLF*/ LF*/LF/HF*	No difference Higher Lower	5 min AR 16 order *age-adjusted
Fagard et al. 1998 [614]	424 subjects 25–89 years	SDNN LF HF LF/HF	Lower Lower No difference Lower/No difference*	15 min * in older subjects

Kuo TB et al. 1999 [324]	1070 healthy volunteers 40–79 years	RRI/ TP*/ VLF*/LF* LF% HF* HF% LF/HF*	No difference Lower Higher/No difference¶ Higher Lower/Higher¶	288 s FFT * Ln transformed spectral measures ¶> 60 years of age
Dishman et al. 2000 [611]	92 healthy volunteers 20–59 years	HR SDNN LF HF LF/HF	Faster Lower Lower No difference Lower	5 min FFT
Agelink et al. 2001 [335]	309 healthy volunteers 18–77 years	LF HF LF/HF	Lower No difference Lower	5 min FFT
Kuch B et al. 2001 [648]	286 subjects 45–65 year	TP* LF(ms^2, n.u.)* HF(ms^2, n.u.)*	No difference Lower Higher	5 min AR 16 order * age-adjusted
Pikkujämsä et al. 2001 [141]	392 subjects† 40–60 years	RRI SDNN HF (n.u.) LF (n.u.)* LF/HF* ApEN¶* fractal exponent $\alpha 1$ ¶	No difference Lower Higher Lower Lower Higher Lower	5 min AR 20 order * sitting posture/ no difference in supine ¶13 min † the same as in Huikuri 1996
Evans et al. 2001 [481]	20 volunteers 25 ± 1 year	All spectral parameters HF/total (VLF+LF)/HF β−slope	No difference Higher Higher Less rapid	20 min Welch periodogram, Coarse graining

Table 35.36 (Continued)

Author, year	Sample	Parameter	Differences in women	Methodical issues
Colhoun et al. 2001 [615]	163 healthy subjects 30–55 years	HR All spectral parameters*	No difference No difference	5 min AR * Age-adjusted
Kuo TB et al. 2002 [328]	480 healthy volunteers 40–79 years	RRI SDRR LLE† CD* ApEn¶	No difference No difference No difference Higher Higher	5 min † largest Lyapunov exponent *Correlation dimension ¶Approximate entropy
Gerritsen J et al. 2003 [599]	631 subjects 50–75 years	SDRR HF LF	No difference No difference Lower	3 min FFT
Laitinen T et al. 2004 [326]	63 HUT-negative subjects 23–77 years	All spectral parameters	No difference	5 min FFT
Neumann SA et al. 2005 [539]	378 subjects 30–54 years	LF HF LF/HF	Lower Higher Lower	5 min AR

Spectral parameters expressed as power (ms^2) either raw or log-transformed unless other metrics noted (i.e., normalized units, n.u.)

Table 35.37

Gender-differences in HRV measures from long-term ECG recordings

Author, year	Sample	Parameter	Differences in women	Methodological issues
Van Hoogenhuyze et al. 1991 [277]	33 subjects Mean age 33 years	SDANN/SDNNI SDNNI-CV	Lower No difference	
Mølgaard et al. 1991 [318]	140 subjects 40–77 years	SDNN*	Lower	* during night-time
Mølgaard et al. 1994 [577]	104 subjects 40–77 years	RRI/HF/HFsqrt power/ LF	No difference Lower	
Jensen-Urstad et al. 1997 [617]	101 subjects 20–69 years	SDNN LF/HF, HF LF/HF	Lower Lower Lower/higher*	* >40 years of age
Yamasaki et al. 1996 [618]	105 subjects 20–78 years	LF HF	No difference/higher* Lower	* > 50 years
Umetani et al. 1998 [322]	176 volunteers/outpatients 10–49 years	HR SDNN, SDANN/SDNNI RMSSD*, pNN50*	Faster Lower Lower	* difference only below 30 years of age
Ramaekers et al. 1998 [319]	276 healthy volunteers 18–71 years	HR SDNN/ SDANN/ TP RMSSD* pNN50/ HF LF, LF(n.u.), LF/HF HF (n.u.)	Faster Lower Lower No difference Lower Higher	TP 0.1–1.0Hz * difference disappeared after HR-adjustment
Silvetti et al. 2001 [332]	104 healthy children/adolescents 1–20 years	HR SDNN/SDANN SDNNI/ RMSSD/pNN50	Faster Lower* No difference	* higher in 16–20 years old females
Bonnemeier et al. 2003 [321]	166 healthy volunteers 20–70 year	HR SDNN/ SDANN/SDNNI NN50+/ RMSSD/HRVI	Faster Lower No difference	
Grimm et al. 2003 [366]	110 healthy volunteers 21–71 years	HR SDNN RMSSD/ pNN50	No difference Lower No difference	
Antelmi et al. 2004 [619]	653 subjects free of heart disease 14–82 years	SDNN/SDANN SDNNI/ LF, VLF, LF/HF RMSSD,pNN50/HF	No difference Lower Higher	
Sosnowski et al. 2005 [65]	210 healthy volunteers 50 ± 6 years	HR SDNN, SDANN, HRVI, HRVF pNN50	Faster Lower No difference	

The influence of gender on baroreceptor reflex control of heart rate in humans is controversial. Baroreceptor sensitivity has been found to be gender-related in some studies, being lower in women compared to men [323, 593, 621–624], whereas other studies have indicated similar BRS in females and males [625–627]. The discrepancy of BRS-dependence on gender is related to various methods used, age-difference, number of examined subjects (usually small, except for [323, 593, 623]) and training status. In a study of Adbel-Rahman et al. the gender-related differences in BRS were found to depend on the pattern of the rise in blood pressure, being significant with a brief increase (53% lower BRS in females) and undetectable with sustained BP [621]. Women have been found to exhibit greater inter-individual variation [593, 626], to have a shift of the BRS with lower blood pressure [626], and to require a lower infusion rate of phenyleprhine in order to increase SBP by 20 mmHg from baseline [625]. Also, the age-dependence of BRS has not been found in females in some studies [623, 627], while it has been observed in others [593]. Interestingly, many of these findings come from studies which had a negative result in assessing gender-BRS interaction [625, 626].

Effect of gender on heart rate turbulence is poorly recognized. Only one study aimed at examining HRT differences between women and men [601]. In women, a greater age-dependence of TO and a lower age-dependence of TS along with a weaker TS relationship with preceding R–R interval was found [601].

35.6.2.4 Ethnicity

Ethnic differences in heart rate response to heat were reported more than half of century ago [628]. Since then, epidemiological, physiological and clinical evidence has been accumulated confirming the importance of ethnicity in the mortality and morbidity from certain cardiovascular causes [629–631]. Ethnic-related variations in the resting ECG have been reported, but with negligible clinical relevance [632].

The evidence of ethnic differences in HRV is sparse and inconclusive. Lower long-term and similar short-term heart rate variations have been reported in the fetuses of African American or Caribbean women when compared to the fetuses of white women of European-ethnic origin [633]. A smaller post-stimulus deceleration of R–R interval and smaller acceleration following four cycles has already been found in black newborns compared to white newborns [634].

Deep-breathing RSA changes in response to atropine have been found to be similar in two ethnic groups [635]. Blunting sympathetic neural modulation as indicated by a lower 24-h LF normalized power and LF/HF ratio in Afro-Caribbean American hypertensives compared to CA hypertensives has been suggested [636]. In the same study, the 1/f power β-coefficient was found to be similar in both ethnic groups [636]. African Americans (AA) have been found to have a lower LF and higher HF compared to Caucasian Americans (CA) in an epidemiological study by Liao et al. [248]. Also, the I/D polymorphism of the ACE genotype may play a greater role in parasympathetic cardiac control in AA hypertensives [637]. In a study in American- and European American youth, a greater age- and HR-adjusted short-term RMSSD and HF power indicates an increased parasympathetic influence on the heart in blacks [638]. AA have around a 3.5 times greater probability of having depressed ULF power, compared to CA [639]. It has also been suggested that higher HRV may buffer AA from the deleterious effects of ethnic-related stress [640]. The HF power and BRS have been found to be lower in young AA males compared to age-matched non-AA males. However, the latter was a heterogeneous group (55% CA, 31% Asian, 15% Hispanic) [641]. In addition, spontaneous BRS assessed by means of sequence method has been found to be lower in AA than in non AA [641]. In another study, resting spontaneous BRS and its change in response to lower body negative pressure were comparable in AA and CA [642].

Results accumulated from cross-sectional comparisons suggest that there is a more parasympathetic predominance in young AA, a similar autonomic balance in middle-aged AA and CA, and greater sympathetic influences in older AA than CA.

Some ethnic HRV differences can result from environmental influences. Data from a study on Caucasian lowlanders and Himalayan Sherpas show higher values of respiratory-related indices (HF and VLF) in CA lowlanders, interpreted as a lower stability in breathing control in Caucasians compared to Sherpas [643].

In general, ethnicity should be taken into account if an HRV study is going to be undertaken in a multiethnic population.

35.6.2.5 Body Mass

There are no consistent data regarding the relationship or causality between body mass and HRV, despite a basic study indicating that dietary-induced weight gain is accompanied with a reduction in M_2-muscarinic gene expression, signaling modifications and density [644]. Moreover, the importance of circulating insulin, leptin and free fatty acids, known to interact with cardiac autonomic control in obesity, have been acknowledged [458, 462, 465–467, 645].

The differences in reported correlations are related to the various HRV measures used and the lack of adjustment for the variety of co-factors (age, gender, ethnics and others). Population size and characteristics examined vary in different studies (healthy volunteers, sample of general population, hypertensives, diabetics and others). Additionally, in a seminal study on HRV determinants, BMI was not included among potentially significant co-factors [573].

In a study of healthy children/adolescents, a significant correlation between BMI and age and gender adjusted 24-h pNN50 and RMSSD has been reported [332]. A similar observation has been reported in normotensive obese school children [646]. In healthy adolescents and young adults (15–31 years), neither BMI nor waist circumference was found to impact significantly on a statistical model of determinants of short-term HRV (30 sec) [647]. In a small sample of young women, BMI was graded as the second factor, after age, influencing overall HRV, but not pNN50 or RMSSD [608]. An approximate 5% contribution of BMI to the total HRV spectral power has recently been reported in a large sample of young adults [576].

In a population-based study, a significant correlation of BMI with age and HR adjusted short-term spectral HRV measures was found in middle-aged males, whereas a similar relationship was not present in females [648]. The contribution of BMI was found to be marginal (5% in males), although in certain conditions it clearly surpasses the effects of age and heart rate [315]. In the ARIC studies on a large cohort of middle-aged subjects, the BMI relationship with short-term HRV was not observed [649]. In a prospective HRV study in middle-aged adults, a higher BMI has been found to increase the probability of being at the worst quartile of age and gender adjusted 5-min HR and HRV over a 5-year follow-up period [575]. In contrast, in middle-aged normal persons, the BMI coefficient of determination relating to the age and gender adjusted total power of spectral HRV was found to be less than 5% [615].

There are conflicting data regarding the relationship of BMI with HRV in the elderly. The lowest short-term SDNN quartile has been found to be associated with a higher BMI in a large population-based cohort of the Rotterdam Study [650]. In a study across four European populations, a higher BMI was found to be associated with a lower HF and higher LF in one population, whereas no association was present in the other countries [651]. Also, in wide age range samples of population, insignificant or negligible contributions of BMI to HRV metrics were reported [580, 619, 652–655]. In the SAPALDIA study, the time and frequency domain HRV indices adjusted for many variables have been shown to correlate negatively with BMI in subjects >50 years old [609]. Also, in the CARLA study, the waist–hip ratio was inversely associated with HRV [655]. In contrast, observations from a longitudinal study in a small sample of the elderly did not produce evidence of a relationship between BMI change and standard HRV measures, while a significant correlation was found for the DFA $\alpha 1$ coefficient [578].

Despite the majority of data indicating that body mass contributes only marginally to HRV, in an individual case, the influence of weight gain or loss might be of importance as indicated by the more concordant data that come from studies in obesity. Both weight gain and its reduction have been found to be associated with a significant change of certain HRV indices [656–661]. Longitudinal studies also provide some evidence regarding the influence of body mass changes on HRV [647]. An impressive amount of data has come from a study in obese patients who were treated surgically for extreme obesity. In these patients with a mean weight loss of 32 kg (28%) over a 1-year follow-up, the mean NNI decreased by 8%, while SDANN and SDNNI increased by 5% and 24%, respectively [658]. Spectral HRV measures also increased by 21% (LF, HF), but a relative increase of 35% for LF and 43% for HF was observed only for daytime, with no changes during night-time. Data on changes in lower frequency components were not reported in that study [658]. In another study in a group of morbidly obese patients treated with bariatric surgery, the average 17% BMI reduction and 13.5 kg fat mass loss 3 months after surgery was associated with 39–49% increase of 24-h SDNN, RMSSD, HRVI and TINN, while the pNN50 values doubled. Further weight loss over the next 9 months (−33% BMI and −28.7 kg fat mass at 12 months after surgery) were not found to be associated with further increase in HRV. On the contrary, a small decrease of 5–16% (SDNN, HRVI, pNN50 and RMSSD) was observed, while the TINN remained unchanged [661]. Changes in HRV have been found to be independent of improvement in insulin resistance [661]. Even a small weight loss (~10%) after dietary restrictions has been found to result in an increase of 24-h HRV in the time and frequency domains [659]. Conversely, a 10% increase in body weight has been associated with HR acceleration and a reduction of short-term respiratory-related HR power [656].

A lower baroreflex sensitivity resulting from increasing body mass and visceral fat in resting conditions and under stress challenges [662–664] was reported to be related in part to sympathetic overactivity in obese subjects [657]. Body weight reduction was found to be associated with a restoration of BRS [665]. This effect has been observed both in young and old obese subjects [666].

In the only study that addresses HRT changes in obese normotensive subjects without co-morbidities, no difference was observed between normal and obese subjects. However, there were limitations in the methods, e.g., allowing calculation of HRT from one ventricular PEB [667].

In general, body mass influences HRV and BRS, but in large-sample studies, its contribution to measured indices is marginal, albeit sometimes significant, and can usually be neglected. However, in an individual, gain or loss in body mass contributes substantially to changes of heart rate and its variation that can surpass the effects of established factors (age, gender).

35.6.2.6 Heart Rate

Heart rate is one of the main factors that always has to be considered for the understanding and interpretation of HRV. Consequently, a lack of knowledge about HR (or RR interval) *a priori* excludes a reliable assessment of its variation. Although HR would be expected to be considered, this fundamental requirement has not necessarily been met in many clinical studies [e.g., 314, 343, 346, 350, 351, 352]

Coumel et al. listed reasons for which HR itself cannot be ignored: (1) HR is probably the best and simplest measure of the ANS balance, (2) HRV indices are influenced by HR itself, and (3) the HR and HRV relationship does have a physiological significance and this perfect harmony between HR and HRV should not be overlooked [668]. This harmony is related to the so called sympathovagal balance, and can be derived from the classical Rosenblueth-Simeone model, describing the net effect of combined vagal and sympathetic stimulation upon SAN [669]. In their model, an actual HR is a function of intrinsic HR and sympathetic and parasympathetic influence:

$$aHR = IHR^{*} m^{*} n, \tag{35.41}$$

where *aHR* is actual (resting) HR, *IHR* is an intrinsic HR, *m* is a sympathetic factor, and *n* is a parasympathetic factor [669]. This multiplicative relationship ($m^{*}n$) is in concordance with the phenomenon of accentuated antagonism [15]. The $m^{*}n$ product may be regarded as the sympatho-vagal balance [670]. Simply, $m^{*}n>1$ indicates a predominance of sympathetic activity (net HR acceleratory influence), while with $m^{*}n < 1$ there is vagal predominance (net inhibitory effect). Since IHR cannot be simply measured, and there is no HRV index that explicitly describes "m" or "n" factor, the measurement of actual HR remains still the most useful crude estimate of ANS balance. Corroborative observations can be found in a series of studies by investigators in Chicago [671–675], who proposed to replace the $m^{*}n$ product by the term VSE (vagal-sympathetic effect): VSE = RR interval/intrinsic RR interval [231] or simply aHR/IHR [676].

Intrinsic Heart Rate

A spontaneous firing of the cardiac pacemaker can be easily seen in the heart removed from a body of an experimental animal, when central and circulatory factors controlling heartbeat formation are disrupted. The rate of this spontaneous heartbeat activity is referred to as *intrinsic heart rate* (IHR) [677]. In humans, the IHR can be assessed after pharmacological denervation by means of a combined M_2 and β_1AR (double blockade), with the use of weight-adjusted doses of atropine (0.04 mg/kg) and propranolol (0.2 mg/kg) [677–679]. Despite some limitations owing to the use of a high dose of atropine (nicotine-receptor partial blockade with a subsequent inhibition of the NE release, antagonism with 5-HT and histamine) and propranolol (nonspecific membrane action, negative inotropic effects) and actually incomplete autonomic blockade (with no effects on α-adrenoceptor or humoral factors) [393, 676], this approach is the only one available in physiological and clinical studies.

In healthy subjects the mean IHR is approximately 80–125 bpm [306, 679, 680]. The mean IHR of 128 ± 24 bpm has been reported in seven healthy children [681]. The IHR does not seem to be dependent on gender [306, 680, 682]. The importance of IHR for understanding heartbeat variation is related to its age, ventricular function and autonomic tone dependencies. Age-dependence on IHR is recognized by the inclusion of age into the regression equation ($r^2 = 0.42$) proposed by Jose and Collison 4 decades ago [306]:

$$\text{IHR} = 118.1 - 0.56^{*}\,\text{age} \pm k \tag{35.42}$$

where the constant k is 14% for subjects aged <45 and 18% for subjects aged ⩾45 years.

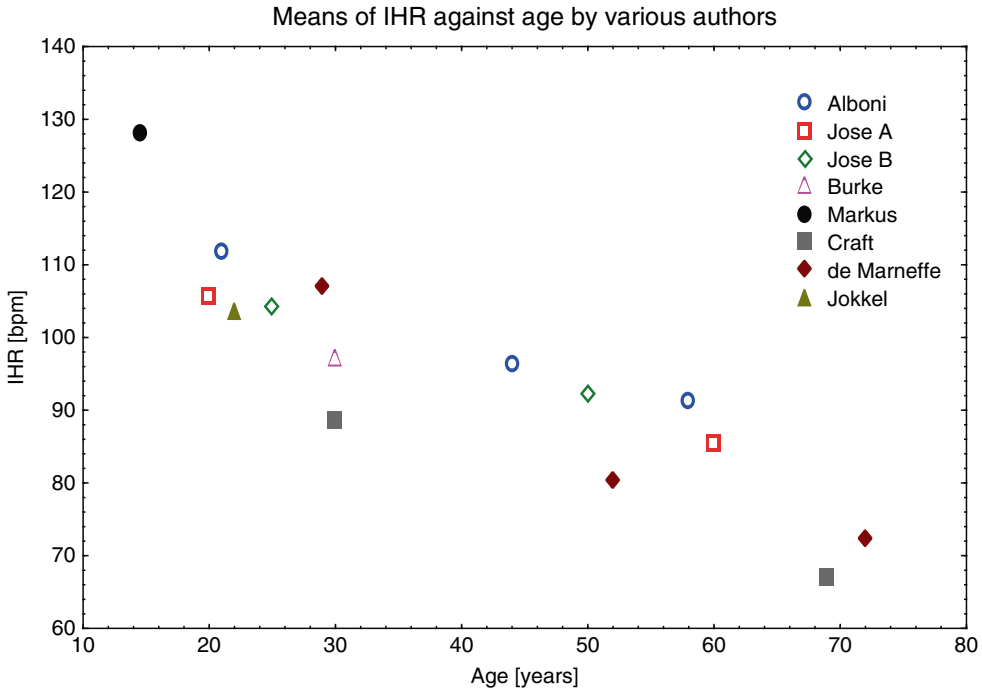

Figure 35.41

Scatterplot of reported means of the intrinsic heart rate against means of age of examined group in various studies. Data from studies in which IHR has been assessed by means of double autonomic blockade using muscarinic antagonist + beta2-adrenergic agents.

In a study of Alboni et al., the mean IHR of 103 ± 13 bpm in subjects 45 years of age or younger and of 93 ± 8 in subjects > 45 years was observed [680]. Their data indicate that IHR is additionally related to aHR (resting baseline). Thus, the recalculated equation ($r^2 = 0.61$) would be:

$$\text{IHR} = 90 - 0.57^{*}\text{age} + 0.41^{*}aHR \pm 7\,\text{bpm}. \tag{35.43}$$

Figure 35.37 shows a plot summarizing age-effect on the IHR in several studies that examined this relationship [306, 679–684].

A dependence of IHR on ventricular function was firstly reported by Wollenberger and Jehl in a model of cardiopulmonary function [685]. This relationship has been corroborated by others, indicating also that a reduction of IHR precedes the occurrence of overt heart failure [306, 678, 679]. An intact innervation of the SAN is a key factor for IHR, as indicated by experimental studies with extrinsic or SAN selective parasympathectomy and pericardial effusion [686, 687]. In clinical settings, it might play a role in patients after open heart surgery [688, 689], coronary artery by-pass surgery [690–692] pericarditis and myocarditis, including chronic Chagas' disease [693, 694], as well as after ablation procedures [695, 696]. In patients, following mitral valve replacement, a reduced HRV with an erratic spectrum can be detected [689], comparable to that seen in SAN dysfunction (Fig. 35.42) [697] and in patients after heart transplantation [433, 698]. An increase in IHR can be observed in patients with hyperthyroidism [306], inappropriate sinus tachycardia and postural orthostatic tachycardia [373]. There is also evidence that increased parasympathetic tone may result in a compensatory increase of IHR in renal hypertension [374]. In addition, temperature changes and atrial stretching might influence the intrinsic SAN firing [676, 699]. Thus, *the presence of changes in IHR in a number of settings indicates that RR interval may vary irrespective of cardiac autonomic tone.*

The change in mean RR interval (or ratio between the longest and shortest RRI) after parasympathetic blockade with atropine is used as an index of the relative basal vagal tone ($\tilde{V}$), while the difference in mean RR interval (or ratio between

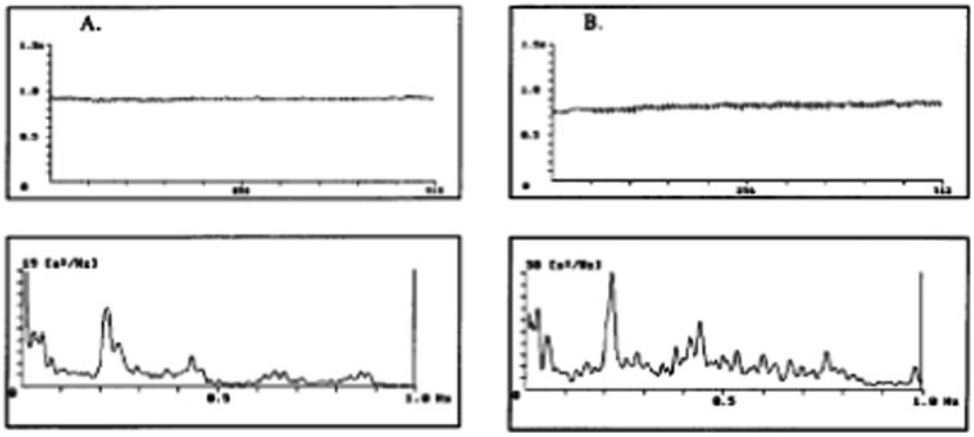

Figure 35.42

Patterns of abnormal HRV power spectra in patients with sinus node disease. Tachograms (*upper panel*) in two patients after double autonomic blockade (atropine+propranolol), power spectra (lower panel) show residual contents with abnormal distribution which are resemble harmonics or erratic variation over mean value (From [697]).

longest and shortest RRI) after sympathetic withdrawal and subsequent vagal blockade with atropine, can serve as an index of the absolute vagal tone [700, 701]. Similarly, an index of the relative and absolute sympathetic influences can be derived from RRI after adrenergic blockade and after atropine and subsequent propranolol administration, respectively. An alternative approach of autonomic control of the heart based on the analysis of HR recovery from exercise has been reported [702].

Actual Heart Rate (Resting)

Heart rate and HRV can be considered as factors that limit their ranges. Accordingly, at a certain actual HR, the HRV varies within some limits (depending mainly on age). However, a reverse relationship is possible, that is, ANS and other influences reflected by an actual HRV establishes HR limits. This can be easily seen when the circadian variation of heart rate and HRV is examined [284, 318, 321, 703]. Indices of short-term variation (RMSSD and pNN50) follow an RRI circadian pattern, while the index of long-term HRV (SDANN) behaves in a reciprocal manner [321]. Accordingly, circadian rhythm of 24-h HF power mimics the rhythm of RRI, while circadian rhythm of 24-h LF power shows the reciprocal reflection of RRI [703]. A significant negative correlation (r^2 = 0.74) of SDNN on day-night RRI difference described in healthy subjects emphasizes the importance of HR itself [318]. In older healthy subjects, similar relationships might not be observed because of a reduction of most time and frequency domain HRV indices, despite sustenance of circadian rhythm of RRI [321]. Interestingly, circadian rhythm of the SDANN index has been shown to be least affected by aging [321]. It has also been found that at in extreme conditions, both HRV decrease or increase cannot further follow changes in R – R interval (saturation areas) [399, 675]. In healthy persons, two distinct patterns of the HF power changes with RRI interval increment can be detected, i.e., saturated or linear [399]. Despite the authors having described a low-correlated pattern in their healthy subjects, detailed analysis of data provided indicates that these subjects had in fact been hypertensive [399].

In an experimental study on dogs with myocardial infarction, a low-correlated response to a beta-blockade with atenolol was observed in animals susceptible to sudden death, in contrast to resistant and sham-operated dogs, in which a parallel HR reduction and SDRR increase was found [704]. Actually, a close negative exponential relationship between HR and HRV (Fig. 35.43) and clearly VF-prone experimental dogs is characterized by a simultaneous reduction in HRV and acceleration of the HR, as expected from the HR-HRV relationship (Fig. 35.43 inset). Thus, the same data might bring different conclusions depending on the type of analysis adopted.

A significant relationship between RRI and HRVI on Holter recording has been found for risk prognostication after myocardial infarction [347]. For a wide range of statistical performance (sensitivity and positive predictive accuracy) results from the lower quartile of mean RRI and mean HRVI were comparable. All-cause mortality reached 24.3% and

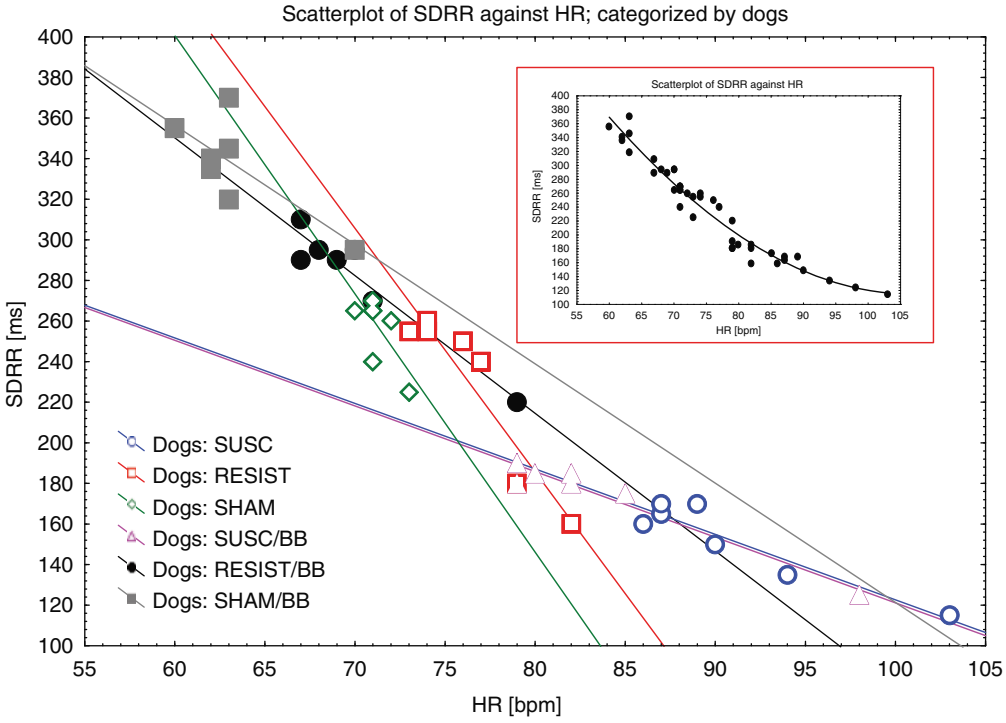

Figure 35.43

Relationship between HR and SDRR in experimental AMI in dogs. Distinct HR-SDRR relationship is shown in dogs with experimental AMI prone to sudden cardiac death (SUSC) before and after beta-blockade (SUSC-BB) as compared to dogs resistant (RESIST) and (RESIST-BB) or sham-operated (SHAM, SHAM-BB). However, an analysis on entire group (inset) indicate that susceptible dogs HR-HRV are simple representing reduced HRV in accordance with a reduced HRV. Plots on basis of data from Adamson et al. [704]).

22.2% over a mean 2-year follow-up, respectively. Post-AMI patients with simultaneous low HRVI (⩽20 U) and shorter RRI (⩽736 ms) had the highest all-cause mortality (28.7% over a mean 2-year follow-up). On the contrary, in those in the lowest quartile for HRVI and the highest for RRI, the survival rate was excellent (no deaths) [347]. However, the mortality rate in those with HRVI in the highest quartile and RRI in the lowest quartile was still substantial (16.7%). The impact of a beta-blockade (40% of patients) that might prolong RRI without significant alteration of HRVI was not discussed. It might also be speculated whether a good prognosis in patients with low HRVI and longer RRI overall reflects better survival in patients with sinus node disease [705]. Another outcome of a separate study in patients with acute MI has found evidence that HRV indices do not provide additional prognostic power over that of RRI itself, clearly because of the significant mutual relationship ($r^2 = 0.37$) [706].

The significance of basic RRI for HRV evaluation has been reflected in some investigations that addressed the issue of HRV normal limits [573, 576, 707]. In a recent study, the influence of RRI duration on HRV indices was underlined again [585]. In a short-term HRV study, the most common tests revealed a distinct behavior in RRI and HRV (Fig. 35.44) in healthy subjects and post-MI patients [708].

In certain pathological states (heart failure, sinus node dysfunction) the actual heart rate is different than expected from a concomitant HRV change [709]. As a reduced HRV represents parasympathetic withdrawal in HF patients (with/without sympathetic over-excitation) [710], an R – R interval shortening (faster HR) can be expected. In such cases, an impaired IHR prevents heart rate adjustment. Therefore, a relatively slow HR and a reduced HRV can be observed. The author referred to this feature as the *metronome-like bradycardia* (Metronome-like bradycardia – a specific feature of chronotropic impairment in which slow HR is associated with a significantly reduced HRV.) and found it to be a specific

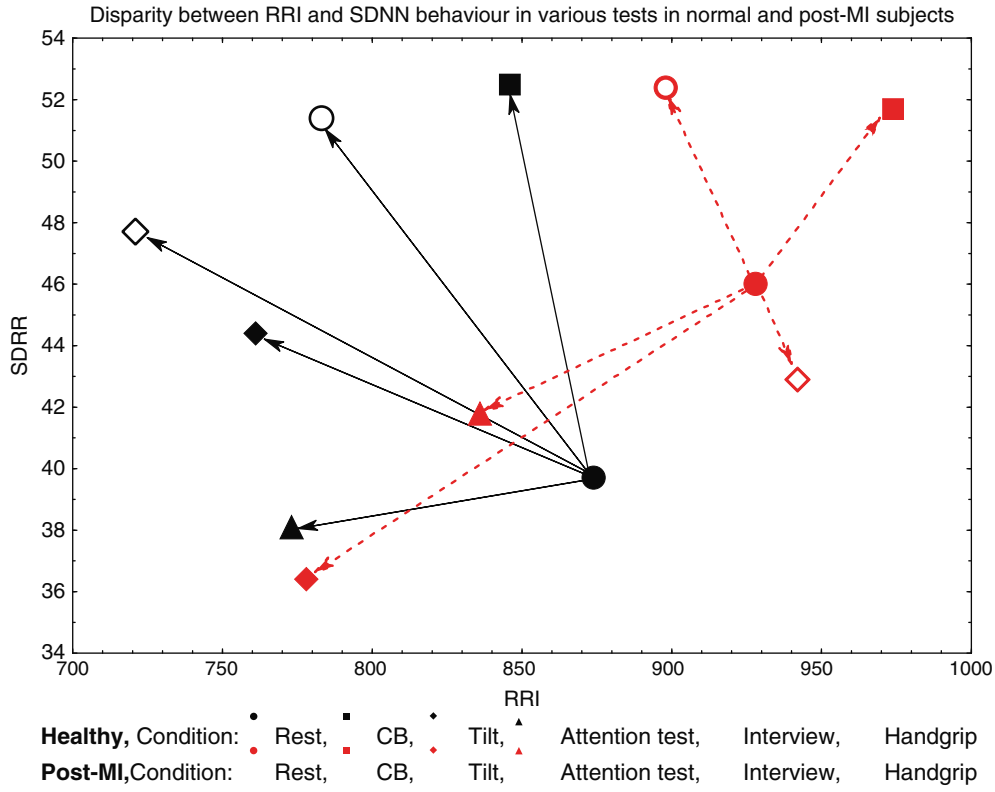

Figure 35.44

A distinct behavior of HR and HRV in response to various stimuli. Example shows that changes in HRV do not necessarily follow RRI alteration. Also, differences between healthy and post myocardial infarction patients are clearly seen (On basis of data from [708]).

sign of an organic sinus node impairment (in patients not treated with agents that may interfere with SAN function) [711]. In heart failure, circadian HRV measures have not been found to vary correspondingly to HR changes [712]. Also, in a third of post-AMI patients, a poorly correlated pattern of HF-RRI relationship has been reported [399]. Abnormal HR–HRV relationship can be ascribed to an increased HRV in spite of HR acceleration. Such behavior is seldom observed in heavily trained healthy subjects [709]. More commonly, such behavior can be seen in patients after heart transplantation and with obstructive sleep apnea syndrome [212, 433, 698, 713, 714]. Under these conditions, HRV may be increased due to the rising contribution of mechanical respiratory influences unrelated to cardiac autonomic tone (that is actually shifted towards a sympathetic predominance). A similar feature can be observed in patients with sinus node dysfunction after double autonomic blockade [697]. Therefore, an increase in short-term HRV in patients after heart transplantation cannot be simply interpreted as a sign of re-innervation or increased mechanical load unless sinus node function is reassessed [715, 716]. A higher HRV than expected from actual HR is a frequent feature of SAN dysfunction [337, 697, 711]. Interestingly, a prognostic value of increased HRV has recently been confirmed [53].

Baroreflex sensitivity does not seem to depend on heart rate. Despite a weak negative correlation ($r^2 = 0.06$) between BRS and HR having been found in healthy subjects, the significance of the relationship was lost in multivariate analysis [593]. The BRS–HR relationship was not found in persons $\geqslant$ 60 years old even in a univariate analysis [593]. Another study indicated that there might be a gender difference in BRS-HR correlation. However, the small number of subjects examined does not allow a conclusive opinion to be drawn [621]. A lack of correlation between HR and BRS has been reported in most studies in which the BRS had been estimated by means of various methods [595, 600, 627, 629].

Heart rate turbulence parameters are dependent on heart rate in healthy subjects. Turbulence onset and turbulence slope decreases with HR increase [601]. A need for adjustment of the turbulence slope for heart rate was concluded from

a study in patients with coronary heart disease [312]. However, the accumulated data is relatively sparse, so a general statement cannot be given.

In summary, heart rate is of the utmost importance in the analysis of HRV. Actually, an interpretation of HRV data without information regarding actual (or mean) HR or RR interval might be inappropriate, diminishing conclusions drawn from such an investigation. Even in a case of seemingly insignificant HR (RRI) differences in comparative studies, HRV measures should be adjusted not only for age, gender and ethnicity, but also for HR (RRI).

35.6.2.7 Respiration

Respiration is one of the most important determinants of short-term heartbeat variation, which is clearly evidenced by a phenomenon referred to as *respiratory sinus arrhythmia* (RSA, Carl Ludwig 1847) [1, 4–6, 9, 20, 23, 717–725]. During normal breathing, the raw (unadjusted) RSA contributes to 30–80% of the total short-term HRV. Respiratory-related short-term HR variation is frequently interpreted as an index of tonic cardiac vagal modulation of heart rate [68, 69, 700, 720, 721]. However, respiratory influences on HRV do extend beyond high frequencies, and in certain settings can affect HRV within low- and very-low frequencies (Fig. 35.45) [296, 717, 722].

The RSA magnitude is significantly related to respiratory parameters both in laboratory conditions and during daily life [6, 9, 718–720]. In an early investigation, Eckberg found that a 50% increase in tidal volume led to only a 15% increase of RSA estimated by means of the peak-valley method [720]. In a study of Grossman et al. with similarly determined RSA, the amount of variance accounted for by frequency of breathing and tidal volume has reached 64% (58–69%) [723]. By dividing RSA by tidal volume (RSA_{TF} [ms/ml]), the greater proportion of HR variance was explained. Additionally, a correction for breathing frequency has been shown to be unnecessary [723]. A need for additional adjustment for arterial partial pressure of CO_2 has also been pointed out, especially while central autonomic drive is affected, i.e., hyperventilation, sleep-related breathing disorders, heart failure [724]. The respiratory HR variation is accentuated during slow (~0.1 Hz) deep breathing [18, 718, 720]. This relationship constitutes the basis for a clinical test [18, 725]. Interestingly, an evolution of this method can still be seen [726].

Respiratory parameters should be obligatorily controlled for in laboratory studies [727]. In clinical settings, some information about respiration (breathing rate) might be extracted from the mean (or median) frequency of HF component of the short-term HRV power spectrum. Unfortunately, respiration parameters are only rarely taken into account in clinical studies both in normal subjects and those with various clinical entities. Meanwhile, the respiratory rate (defined as the frequency of maximum HF power) has been identified as a factor explaining HRV differences between CAD-patients

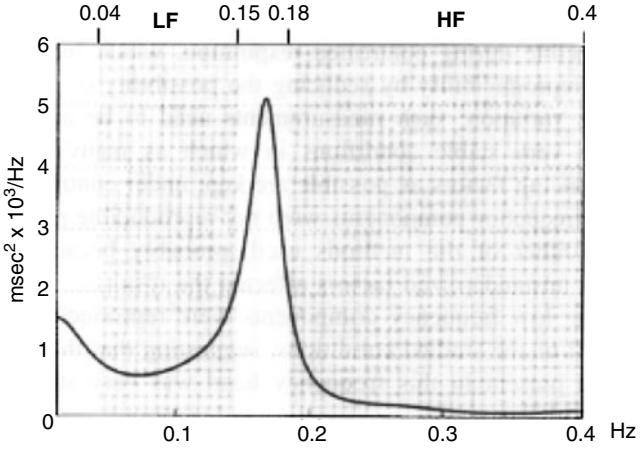

Figure 35.45

Spontaneous slow respiration effect on HRV spectral components. In an example, the power spectrum (AR) shows only one peak that cannot be considered either a LF or HF power (From [296], Oxford Univ Press, with permission).

with preserved and depressed LV systolic function [728]. As respiration influences frequencies lower than that of the HF component [184, 717, 722, 729], its contribution for VLF and LF components should also be considered. It could be of the utmost importance in patients with heart failure and sleep-related breathing disorders in whom chemoreceptor-reflex or centrally-driven changes contribute significantly to HRV [730–734]. Recently, it has been observed that the frequency of respiration influences fractal measures of HRV [735].

The contribution of nonneural influences to short-term HR variation due to lung volume oscillation is usually small under normal conditions (~3%). However, it can be responsible for up to 30% of the HF power in healthy middle-aged persons [730]. It has been shown that a slow deep breathing can provoke R – R interval oscillations of ~120 ms after complete autonomic blockade [717]. In addition, the proportion of nonneural components of RSA has been observed to increase during exercise [736]. The relative contribution of nonneural RSA mechanisms increases even in mild heart failure, and accounts for 15% of the HF power. Importantly, in an individual patient, this mechanical contribution can reach 77% of the HF component [730]. Abnormal breathing patterns that can occur in patients with heart failure during exercise influence lower frequencies [737].

Another form of respiratory contribution to HRV is related to so-called cardio-ventilatory coupling [188, 190, 193–196] and seems to be independent of cardiac autonomic tone, blood pressure variability, and baroreflex sensitivity [738]. The cardioventilatory coupling has been observed in two third of healthy subjects, being most apparent at low breathing rates and associated with high HRV [738]. As reduced cardiorespiratory interactions have been found in patients with a myocardial infarction [196] and is associated with low HRV [738], it might be another mechanism that should be taken into account while interpreting reduced HRV in a number of clinical conditions.

In general, respiratory parameters should be measured and reported in studies on HRV, especially in patients in whom breathing and related disorders play a significant role in pathophysiology and clinical presentation.

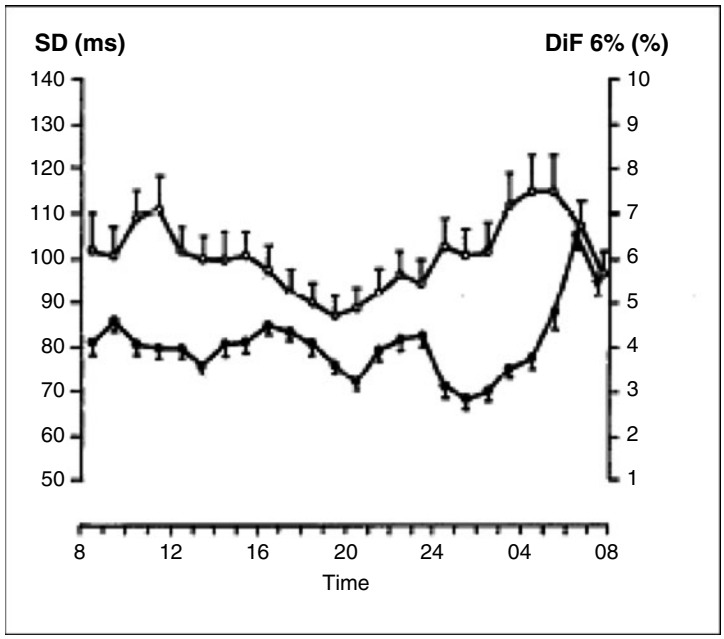

Figure 35.46

Examples of diurnal fluctuation of long-wave (SD) and short-term (dif 6%) measures of HRV in a healthy subject. (From [318], with permission).

35.6.2.8 Day–Night Rhythm

Diurnal variation of HR and HRV are well recognized [739]. They are related to the circadian rhythm of sleep and activity. Measurement of the global 24-h HRV indices (SDNN, SDANN, HRVI, or HRVF) provides a crude description of the level of circadian rhythm, since the sleep–wake cycle is the strongest determinant of overall HRV (Fig. 35.40). More detailed analysis requires a partitioning of 24-h recordings into day and night periods, or even hourly intervals. In healthy subjects, HRV measures of high frequency variation (pNN50, RMSSD, HF power) reach their maximum early in the morning before awakening (usually about 5 AM) independently of gender and activity [321, 618, 739, 740]. However, a lack of diurnal variation has been reported [318] as has attenuation of cardiac vagal modulation with age [321]. Sleep-related increase in HRV short-term indices has been confirmed in shift workers [741]. Also, cardiorespiratory coupling has been found to exhibit day–night differences [195]. Sleep deprivation has been shown to result in attenuation of parasympathetic and augmentation of sympathetic-related HRV indices [742]. Diminished LF/(LF+HF) ratio during non-REM sleep that mimics sleep deprivation has been found in subjects homozygous for the $PER3^{5/5}$ allele, in contrast to other polymorphisms in this gene encoding circadian clock [743]. Apart form the sleep–wake cycle, there is a role for light–dark rhythm intrinsically coupled with HRV changes over 24-h [744].

In a recent study, Hu et al. investigated intrinsic circadian cardiac dynamics in healthy subjects by adjusting the sleep–wake behavior cycle to 28 h [745]. They found significant circadian changes of DFA scaling exponent α with the average maximum value at ~9–11 am and the average minimum value at ~1 pm. The protocol used in this study forcing a lack of synchrony allowed the detection of the influence of the circadian pacemaker on cardiac dynamics independent of HR circadian rhythm [745].

Early HRV abnormalities can easily be detected in diabetic patients without autonomic test abnormalities and in patients with uncomplicated coronary artery disease in the form of a reduction of night-time (sleep) HF power, whereas daytime values can still be comparable [746, 747]. In diabetic patients with autonomic neuropathy, the HRV diurnal pattern is reduced or even lost, thereby making both daytime and night-time HF and LF power lower compared to healthy subjects [747]. Similar findings have been reported in heart failure patients [277]. Increased night-time SDNN, in spite of a smaller HF increase, has been observed in post acute MI patients [748]. Also, higher pNN50 values during sleep have been reported in hypertensive patients with left ventricular hypertrophy [749].The absence or reversal of circadian rhythm of a particular HRV measure has been shown to be of prognostic significance in post-MI patients and in survivors of sudden death [750–752]. Last, but not least, the pharmacodynamic effects of certain agents can be tracked by means of circadian HR and HRV analysis [753].

Baroreflex sensitivity also undergoes clear day-night rhythmicity with minimum values during the day [754].

In general, evaluation of HR and HRV circadian rhythms may add information beyond their mean values that may be useful in risk-prognostication. Additionally, diurnal changes of certain HRV measures indicate that measurements of short-term HRV should be performed at similar specific times in the day.

35.6.3 Behavioral Factors

35.6.3.1 Physical Activity

The autonomic nervous system is involved in the complex adjustment of circulatory control to altered demand in response to physical activity. Thus, the effects of short-term exercise or prolonged training can be easily recognized by means of HRV analysis. The autonomic response to exercise or training depends on the type of physical activity (tonic or phasic), its frequency, intensity, and duration. Also, initial physical status should be taken into account. On the contrary, spells of physical inactivity can be studied in the setting of prolonged bed rest.

Physical activity has been listed among the most important determinants of 24-h HRV [318]. Subjects with good fitness levels have a higher power of both HF and LF components [577]. However, conflicting data exists in general population studies. Vigorous self-reported physical activity has been found to be associated with short-term HRV in males. Those men in the highest category of vigorous activity had an 8% higher SDNN, 19% higher LF power, and 23% higher HF power than those men who reported no vigorous activity, after adjustment for age and for light and moderate activity [755]. Similar observations have been reported in healthy adolescents [756] and in middle-aged subjects [757].

Interestingly, in the latter study, moderate and vigorous physical activity has been associated with a higher LF power [757]. In the SAPALDIA study, each hour of heavy physical exercise has been associated with a 2.0% increase in SDNN, a 3.6% increase in the high frequency (HF) range power and a 4.2% increase in LF power [609]. A lower LF power but not HF power has been found in women with a sedentary lifestyle [758]. In contrast, in a large cross-sectional study in an elderly population, no association between physical activity and HRV measures has been reported [655]. In addition, in a cross-sectional study of Byrne et al., physical fitness has not been identified as an independent predictor of HRV, despite univariate associations having been observed [652]. Cumulated data indicate that preserved age-dependent HRV measures can be found in those humans who are physically active over years or decades [759, 760].

Basic physical fitness can be improved by various exercise protocols. However, the effects of training depend on its intensity and duration. Light or moderate physical training that can improve peak VO_2 does not necessarily alter HRV measures [761–763]. More vigorous training has been found to increase parasympathetically-mediated HRV indices irrespective of age [755, 759, 764–766]. Aerobic training at 50% of maximum VO_2 exerts evident influences on HRV in post-menopausal women [767, 768]. An extreme physical loading may exert harmful effects upon HRV [769]. A distinct effect of physical training on various measures of autonomic control (HRV, HR recovery, and HRT) has been discovered recently in patients with heart failure [770].

Increased HF power response to exercise and increased RMSSD during recovery have been associated with a worse prognosis in one study (mainly males) [771], whereas no evidence of prognostic value has been found in another [772]. Differences might result from exercise testing (treadmill test vs bicycle ergometer), gender-differences or intensity of workload. Heavy exercise above the ventilatory threshold has been shown to determine occurrence of increased HF power [773].

The effects of physical fitness and training on baroreflex function are more difficult to evaluate since exercise simultaneously exerts influence on central command, the exercise pressor reflex and the arterial baroreflex. Some harmony between these three components of an integrative response to exercise is required to produce a normal response to exercise [774]. The use of various methods for BRS assessment, different parameters for its description (usually only maximum gain), different intensity, protocols and duration of exercise or training is one reason for data inconsistency. Exercise capacity parameters, like maximum or peak VO_2, have been found not to correlate with BRS changes or their lack of change [593, 624].

Too short a period of physical training, as well as BRS examination by means of baroreceptor unloading, are more frequently reported in studies in which the BRS has been found reduced or unchanged [775–778]. Also, the use of semi-invasive maneuvers results in inconsistent observations, including those usually with unchanged BRS following exercise [779]. In studies with spontaneous BRS estimation, an increase of BRS in response to exercise can be observed more consistently [780–782]. More regular exercise of moderate intensity has been reported to attenuate age-related reduction in BRS [592]. Multi-phasic response to prolonged exercise training has been described with an initial BRS improvement after 3 months, which is sustained for the next few months and followed by a decline after a 1-year period despite markedly increased training [783]. This might be an effect of baroreceptor resetting. However, more detailed analysis of baroreflex function curve and its operative parameters would help to explain the changes described [774].

35.6.3.2 Mental Stress

Mental stressors (anger, mental arithmetic, presentation with/without audience participation, and others) are frequently used in acute psychophysiological studies in which short-term spectral HRV analysis is preferentially employed [5, 6, 10, 784, 785]. Others have investigated more chronic traits, like depression, anxiety disorders, panic disorder, personality types, hostility, mistrust, and work stress, as well as the white-coat effect and post-traumatic stress [785–790]. Also, the effects of anti-stressor behavior (mental distraction, yoga, relaxation training) have been investigated [791]. For the effects of chronic mental stress evaluation, either short-term or long-term HRV analysis is in use [785].

Cardiac vagal withdrawal is evoked by a wide range of stressful states [791]. However, acute stressors induce various effects on HRV sympathetic and parasympathetic-related components that are related to mutual influence on respiration [786]. Anger has been found to induce an increase in both LF and HF components, while anticipation of giving a presentation has been associated with an increase in LF power although HF power has remained unchanged [793, 794]. An increase of LF power and a shift of HF power towards higher frequencies in response to the reaction time task have been

associated with a shift of the respiratory spectrum in healthy subjects [784]. Meanwhile, a mental arithmetic test has been shown to induce a large increase in LF power with a reduction of HF power into almost undetectable values, broadening and flattening of the respiratory spectrum and a reduction of the alfa-index of BRS gain [784]. Unfortunately, the changes described have not been adjusted for accompanying HR acceleration and SBP increment. Delaney and Brodie found a shift of the HRV power spectrum towards low frequencies in response to defence-arousal reaction [795]. Decreases in HRV in response to random number generation have allowed the detection of anxiety and depression in apparently healthy subjects, even though basal HRV remained similar in all those in the study [796].

Anxiety traits and disorders are associated with changes in HRV [792]. In phobic disorder, decreased vagal and increased sympathetic cardiac function, have been revealed in a study of HRV by Yeragani et al. [797]. A phobic anxiety self-rating score has been inversely related with age-adjusted SDNN in the Normative Aging Study [798]. In a small case-control study, both 24-h HF and LF powers were found to be lower among subjects with panic disorder as compared to those without [799]. Also, a negative relationship between cardiac vagal indices and anxiety trait has been reported in many studies [see 792 for review], but contradictory data has appeared [800, 801]. Encouraging data on the potential of HRV analysis for evaluation of treatment of anxiety has been reported. These and other studies are reviewed elsewhere [785, 792]. Depression has been found to be another entity in which HRV can be seen as abnormal. Agelink et al. compared short-term HRV in depressive and normal subjects and found a faster HR in moderately and severely depressed subjects, while HF power was lower only in patients with a high Hamilton Depression Score [802].

Some difficulties in interpretation of the cumulated data arise from the lack of information about such fundamental physiological parameters as heart rate or respiration in the majority of studies. In the most frequently cited study of Carney et al., an association between depression and low 24-h HRV in patients with acute MI (the Enhancing Recovery in Coronary Heart Disease (ENRICHD) trial), the average HR in the groups compared has neither been adjusted for nor compared. In addition, more important clinical data have been missed [803]. Interestingly, in a few studies in which HR has been accounted for, the differences in HRV have not been seen. O'Connor et al. found significant differences in HR, but not in RSA, in bereaved and depressed subjects [804]. Similar results have been obtained by others [805]. A significant correlation of anxiety state with HR has been observed in a study by Watkins et al., while RSA and anxiety state were not found to be correlated [806]. These authors also reported that respiratory control did not change this relationship. However, in their multivariate analysis, they did not include heart rate and respiratory rate (despite being measured) into the final model [805]. In addition, respiratory rate and arterial pressure variability have been the most consistently changeable parameters among all those measured in an acute sleep deprivation study. However, conclusions have been drawn on the basis of unadjusted HRV parameters [807].

Generally, accumulated data document the role of mental stressors (acute and chronic) for cardiac autonomic control. However, the effects of heart rate and respiration are required to be considered or at least adjusted for in further investigations in order to draw clinically valid conclusions.

35.6.3.3 Smoking

Smoking is one of the most important determinants of HRV because of the direct effects of nicotine on the autonomic nervous system and the indirect consequences related to the role of smoking on the processes of atherosclerosis, thrombosis and chronic pulmonary diseases.

The association of smoking and increased heart rate is consistent across many reports. Gillum et al. quantified the HR increase of 2.9 bpm and 1.4 bpm in current male and female smokers, as compared to ex-smokers and those who had never smoked [808]. Acute nicotine administration increases HR by 10–25 bpm [809].

The acute effects of smoking in young persons was not reflected in the 5-min SDRR, although RSA was reduced [810]. Heavy chronic smoking (>25 cigarettes per day) can be associated with RSA being reduced to a level observed in sedentary nonsmoking subjects [810, 811]. However, in one study, differences in RSA were not detected in subjects older than 31 years of age [810]. In the ARIC study, a greater reduction of 2-min adjusted SDRR and HF power during active postural changes was noticed in smokers compared to nonsmokers [812]. Blunted changes of unadjusted short-term HRV measures in response to controlled breathing have also been reported [813]. Lower amplitudes of LF and HF components of 24-h HRV have been found in smokers [577]. A diverse influence upon circadian HRV measures has been described,

with significant differences between smokers and nonsmokers only within daytime HF power, while LF power has been reduced both during daytime and nighttime in smokers [577]. In another study, the 24-h SDNN and SDANN were found to be lower in smokers only during daytime, while RMSSD was comparable to that of nonsmokers over the whole ECG recording [814]. Also, tobacco use was found to be an independent determinant of global time-domain, but not short-term HRV measures in patients referred for coronary angiography [815].

There are also negative studies in which the relationship between smoking and HRV was not confirmed [816, 817]. The minimal significance of smoking as an HRV determinant has been observed as a lack of influence of smoking as a covariate on the predictive value of reduced SDNN in the Framingham Heart Study and in the ARIC Study [251, 649]. Also, in a study by Kuch et al., smoking was associated with short-term HF power only in women. However, the significance of association was weak and smoking as a determinant of HRV was rejected from the final multivariate models both for the resting state and controlled breathing [648]. The contribution of smoking to the total variance of HF and LF has been accounted for as approximately 3.5% [654]. In a number of studies, smoking habits have not been considered [141, 269, 322, 555, 583, 599]. Also, in the majority of clinical studies, smoking has not been listed among sample characteristics.

35.6.3.4 Other Factors

There are a plethora of reports accounting for the association between HRV and other factors, like anthropometrics (height), biochemical (lipids and glucose, insulin, leptin, adiponectin, uric acid, anemia), inflammatory measures (white blood cell counts, CPR, interleukins), habits (caffeine and alcohol consumption), social status and others [4–6, 521, 609, 655, 785, 816–821]. However, none of these factors has been evaluated reliably without taking into account contributions of all of the more important determinants. It is reasonable to consider the impact of a single factor that might influence HRV measures in certain circumstances. However, in general, the contribution of other factors to HRV seems to be negligible.

35.6.4 General Comments

In any subject, at a certain point of the life-course, HRV seems to be dependent on nonmodifiable determinants, such as heritability, age, gender and ethnicity. These factors should always be considered in any statistical analysis (if an examined population is heterogeneous). However, as indicated by studies in twins, these factors have accounted for less than 60% of explained variation in the HRV [521, 528, 533, 534, 638]. So, there is still a place for the role of other factors.

If short-term HRV examination is to be performed, the significance *of heart rate, respiration, body position and physical fitness* might be of importance, and so these determinants should be controlled apart from nonmodifiable factors. However, these factors have been found to account for no more than 8–15% of explained HRV variation.

If long-term HRV is to be examined, *median HR, day–night difference and sleep–wake cycle*, as well as *diurnal activity*, including work pattern, are of greater importance. Therefore, it seems necessary to check for these determinants in every study in addition to nonmodifiable factors.

Importantly, in longitudinal studies, a change in factor that is known to have only a marginal effect on HRV in the population might be of special interest, as changes in modifiable determinants can influence actual HRV by a factor of at least 10, as compared to their impact in population studies. Thus, if body mass influences HRV by 1–2%, an individual decrease of 10 kg affects HRV by at least 10%. Probably, a similar rule can influence changes in other factors, including physical training, smoking cessation, stress controlling approaches (i.e., yoga), and others. However, it is important to keep in mind that HRV error estimation is necessary to account for differences. As mentioned earlier, changes of at least 25–30% in HRV can be considered significant.

References

1. Hasset, J. and D. Danforth, An introduction to the cardiovascular system, in: *Perspectives in Cardiovascular Psychophysiology*, Cacioppo, J.T. and R.E. Petty, Editors. The Guilford Press: New York/London, 1982, pp. 4–18.
2. Cheng, T.O., Decreased heart rate variability as a predictor for sudden death was known in China in the third century A.D. *Eur. Heart. J.* 2000;**21**: 2081–2082.

3. Struthus, J., Sphygmicae artis tam mille ducentos annos perditae & desierate Libri V. Basel 1955 (Reprinted by the Polish Cardiac Society, Poznan 2004).
4. Task Force of the European Society of Cardiology and the North American Society of Pacing Electrophysiology, Heart rate variability, standards of measurement, physiological interpretation, and clinical use. *Eur. Heart. J.* 1996;**17**: 354–381.
5. Berntson, G.C., J.Tr. Bigger, D.L. Eckberg, P. Grossman, P.G. Kaufmann, M. Malik, H.N. Nagaraja, S.W. Porges, J.P. Saul, P.H. Stone, and M.W. van der Molen, Heart rate variability: origins, methods and interpretative caveats. *Psychophysiology* 1997;**34**: 623–648.
6. Porges, S.W., P.M. McCabe, and B.G. Younge, Respiratory-heart rate interactions: psychophysiological implications for pathophysiology and behavior, in: *Perspectives in Cardiovascular Psychophysiology*, Cacioppo, J.T. and R.E. Petty, Editors. The Guilford Press: New York/London, 1982, pp. 223–264.
7. Samaan, A., The antagonistic cardiac nerves and heart rate. *J. Physiol*. 1935;**83**: 332–340.
8. Holzmann, M., *Klinische Elektrokardiographie*. Georg Thieme Verlag: Stuttgart, 1961, pp. 554–561.
9. Anrep, G.V., W. Pascual, and R. Rössler, Respiratory variations of the heart rate. I. The reflex mechanism of the respiratory arrhythmia. *Proc. R. Soc. Lond. B. Biol. Sci.* 1936;**119B**: 191–217.
10. Lacey, J.I. and B.C. Lacey, Verification and extension of the principle of autonomic response-stereotypy. *Am. J. Psychol*., 1958;**71**: 50–73.
11. Hon, E.H. and S.T. Lee, Electronic evaluation of the fetal heart rate. *Am. J. Obstet. Gynecol*., 1963;**87**: 814–826.
12. Camm, A.J. and L. Fei, Clinical significance of heart rate variability, in *Noninvasive Electrocardiology. Clinical Aspects of Holter Monitoring*, Moss, A.J. and S. Stern S, Editors. W.B. Saunders: London, 1996, pp. 225–248.
13. Wolf, S., The end of the rope: the role of the brain in cardiac death. *Can. Med. Assoc. J*., 1967;**97**: 1022–1025.
14. Katona, P.G., J.W. Poitras, G.O. Barnett, and B.S. Terry, Cardiac vagal efferent activity and heart period in the carotid sinus reflex. *Am. J. Physiol*., 1970;**218**: 1030–1037.
15. Levy, M.N., Sympathetic-parasympathetic interactions in the heart. *Circ. Res*. 1971;**29**: 437–445.
16. Hinkle, L.E. Jr, S.T. Carver, and A. Plakun, Slow heart rates and increased risk of cardiac death in middle-aged men. *Arch. Intern. Med*., 1972;**129**: 732–748.
17. Sayers, B.M., Analysis of heart rate variability. *Ergonomics*, 1973;**16**: 17–32.
18. Wheeler, T. and P.J. Watkins, Cardiac denervation in diabetes. *Br. Med. J*., 1973;**8**: 584–586.
19. Wolf, M.M., G.A. Varigos, D. Hunt, and J.G. Sloman, Sinus arrhythmia in acute myocardial infarction. *Med. J. Aust*., 1978;**2**: 52–53.
20. Akselrod, S., D. Gordon, F.A. Ubel, D.C. Shannon, A.C. Berger, and R.J. Cohen, Power spectrum analysis of heart rate fluctuation: a quantitative probe of beat-to-beat cardiovascular control. *Science*, 1981;**213**: 220–222.
21. Kobayashi, M. and T. Musha, 1/f fluctuation of heart beat period. *IEEE. Trans. Biomed. Eng*., 1982;**29**: 456–457.
22. Ewing, D.J., J.M. Neilson, and P. Travis, New method for assessing cardiac parasympathetic activity using 24 hour electrocardiograms. *Br. Heart J*., 1984;**52**: 396–402.
23. Pomeranz, B., R.J. Macaulay, M.A. Caudill, I. Kutz, D. Adam, D. Gordon, K.M. Kilborn, A.C. Barger, D.C. Shannon, and R.J. Cohen, Assessment of autonomic function in humans by heart rate spectral analysis. *Am. J. Physiol. Heart Circ. Physiol*., 1985;**248** (1 Pt 2): H151–153.
24. Kleiger, R.E., J.P. Miller, J.T. Jr. Bigger, and A.J. Moss, Decreased heart rate variability and its association with increased mortality after acute myocardial infarction. *Am. J. Cardiol*., 1987;**59**: 256–262.
25. Camm, A.J., R. Karam, and C.M. Pratt, The azimilide post-infarct survival evaluation (ALIVE) trial. *Am. J. Cardiol*., 1998;**81**: 35D–39D.
26. Kors, J.A., J.H. Bemmel and C. Zywietz, Signal analysis for ECG interpretation. *Meth. Inf. Med*., 1990;**29**: 317–329.
27. Forester, J., H. Bo, J.W. Sleigh, and J.D. Henderson, Variability of R−R, P wave-to-R wave, and R wave-to-T wave intervals. *Am. J. Physiol. Heart Circ. Physiol*., 1997;**273**: H2857–2860.
28. Hamilton, R.M., P.S. Mckenzie, and P.W. Macfarlane, Can cardiac vagal tone be estimated from the 10-second ECG? *Int. J. Cardiol*., 2004;**95**: 109–115.
29. Teixeira, F.P., D.R. Ricardo, C.L.B. Castro, and C.G.S. Araújo, Evaluating cardiac vagal activity on a conventional electrocardiogram. *Arq. Bras. Cardiol*., 2007;**88**: 333–337.
30. Kleiger, E., P.K. Stein, M.S. Bosner, and J.N. Rottman, Time-domain measurements of heart rate variability, in *Heart Rate Variability*, Malik, M. and A.J. Camm, Editors. Futura Publishing: Armonk, NY, 1995, pp. 33–45.
31. Balocchi, R., F. Cantini, M. Varanini, G. Raimondi, J.M. Legramante, and A. Macerata, Revisiting the potential of time-domain indexes in short-term HRV analysis. *Biomed. Tech. (Berl)*., 2006;**51**: 190–193.
32. Mietus, J.E., C-K. Peng, I. Henry, R.L. Goldsmith, and A.L. Goldberger, The pNNx files: re-examining a widely used heart rate variability measure. *Heart*, 2002;**88**: 378–380.
33. Burr, R.L., S.A. Motzer, W. Chen, M.J. Cowan, and M.M. Heitkemper Logit50: a nonlinear transformation of pNN50 with improved statistical properties. *J. Electrocardiol*., 2003;**36**: 41–52.
34. Malik, M., Effect of electrocardiogram recognition artifact on time-domain measurement of heart rate variability, in *Heart Rate Variability*, Malik, M. and A.J. Camm, Editors. Futura Publishing Company, Inc.: Armonk, NY, 1995, pp. 99–118.
35. Kaplan, D.T., The analysis of variability. *J. Cardiovasc. Electrophysiol*., 1994;**5**: 16–19.
36. Griffin, M.P. and J.R. Moorman, Toward the early diagnosis of neonatal sepsis and sepsis-like illness using novel heart rate analysis. *Pediatrics*, 2001;**107**: 97–104.
37. Malik, M., T. Farrell, T. Cripps, and A.J. Camm, Heart rate variability in relation to prognosis after myocardial infarction: selection of optimal processing techniques. *Eur. Heart J*., 1989;**10**: 1060–1074.
38. Cripps, T.R., M. Malik, T.G. Farrell, and A.J. Camm, Prognostic value of reduced heart rate variability after myocardial infarction: clinical evaluation of a new analysis method. *Br. Heart J*., 1991;**65**: 14–19.
39. Scott, D.W., On optimal and data-based histograms. *Biometrika*, 1979;**66**: 605–610.
40. Farrell, T.G., Y. Basir, T. Cripps, M. Malik, J. Poloniecki, E.D. Bennett, D.E. Ward, and A.J. Camm, Risk stratification for arrhythmic events in postinfarction patients based on heart rate variability, ambulatory electrocardiographic variables and the

signal-averaged electrocardiogram. *J. Am. Coll. Cardiol.*, 1991;**18**: 687–697.

41. Scherer, P., J.P. Ohler, H. Hirche, and H.W. Höpp, Definition of a new beat-to-beat-parameter of heart rate variability. *PACE*, 1993;**16**: 939 (abs).
42. Kovatchev, B.P., L.S. Farhy, H. Cao, M.P. Griffin, D.E. Lake, and J.R. Moorman, Sample asymmetry analysis of heart rate characteristics with application to neonatal sepsis and systemic inflammatory response syndrome. *Pediatr. Res.*, 2003;**54**: 892–898.
43. Björkander, I., T. Kahan, M. Ericson, C. Held, L. Forslund, N. Rehnquist, and P. Hjemdahl, Differential index, a novel graphical method for measurements of heart rate varability. *Int. J. Cardiol.*, 2005;**98**: 493–499.
44. Björkander, I., L. Forslund, T. Kahan, M. Ericson, C. Held, P. Hjemdahl, and N. Rehnquist, Differential index: a simple time domain heart rate variability analysis with prognostic implications in stable angina pectoris. *Cardiology*, 2008;**111**: 126–133.
45. Soderstrom N., What is the reason for the ventricular arrhythmia in cases of auricular fibrillation? *Am. Heart J.*, 1950;**40**: 212–223.
46. Nakanishi, A., R. Tabata, and T. Kobayashi, Effect of aging and diseases to fluctuation of the ECG R-R intervals, in *Noise in Physical Systems and 1/f Fluctuations*, T. Musha, S. Sato, and M. Yamamoto, Editors. Ohmsha Ltd., Institute of Physics, 1991, pp. 669–702.
47. Woo, M.A., W.G. Stevenson, D.K. Moser, R.B. Trelease, and R.M. Harper, Patterns of beat-to-beat heart rate variability in advanced heart failure. *Am. Heart J.*, 1992;**123**: 704–710.
48. Esperer, H.D., D. Esperer, and R.J. Cohen, Cardiac arrhythmias imprint specific signatures on Lorenz plots. *Ann. Noninvasive Electrocardiol.*, 2008;**13**: 44–60.
49. Schechtman, V.L., K.A. Kluge,, and R.M. Harper, Time-domain system for assessing variation in heart rate. *Med. Biol. Eng. Comput.*, 1988;**26**: 367–373.
50. Kuo, C.D., G.Y. Chen, Y.Y. Wang, M.J. Hung, J.L. Yang, Characterization and quantification of the return map of RR intervals by Pearson coefficient in patients with acute myocardial infarction. *Auton. Neurosci.I*, 2003;**105**: 145–152.
51. Sosnowski, M., Z. Czyż, T. Petelenz, et al., Repeat return map distinguishes patients in the chronic phase after myocardial infarction with different risk for future cardiac events. *Comput. Cardiol.*, 1995; 285–288.
52. Otzenberger, H., C. Simon, C. Gronfier, and G. Brandenberger, Temporal relationship between dynamic heart rate variability and electroencephalographic activity during sleep in man. *Neurosci. Lett.*, 1997;**229**: 173–176.
53. Stein, P.K., P.P. Domitrovich, N. Hui, P. Rautaharju, and J. Gottdiener, Sometimes higher heart rate variability is not better heart rate variability: results of graphical and nonlinear analyses. *J. Cardiovasc. Electrophysiol.*, 2005;**16**: 954–959.
54. Schechtman, V.L., S.L. Raetz, R.K. Harper, A. Garfinkiel, A.J. Wilson, D.P. Southall, and R.M. Harper, Dynamic analysis of cardiac R-R intervals in normal infants and in infants who subsequently succumbed to the sudden infant death syndrome. *Ped. Res.*, 1992,**31**: 606–612.
55. Schechtman, V.L., R.K. Harper, and R.M. Harper, Development of heart rate dynamics during sleep-waking states in normal infants. *Pediatr. Res.*, 1993;**34**: 618–623.
56. Schechtman, V.L., M.Y. Lee, A.J. Wilson, and R.M. Harper, Dynamics of respiratory patterning in normal infants and infants who subsequently died of the sudden infant death syndrome. *Pediatr. Res.*, 1996;**40**: 571–577.
57. Kamen, P.W., H. Krum, and A.M. Tonkin, Poincare plot of heart rate variability allows quantitative display of parasympathetic nervous activity in humans. *Clin. Sci.*, 1996;**91**: 201–208.
58. Tulppo, M.P., T.H. Makikallio, T.E. Takala, T. Seppanen, and H.V. Huikuri, Quantitative beat-to-beat analysis of heart rate dynamics during exercise. *Am. J. Physiol. Heart Circ. Physiol.*, 1996;**271**: H244–252.
59. Toichi, M., T. Sugiura, T. Murai, and A. Sengoku, A new method of assessing cardiac autonomic function and its comparison with spectral analysis and coefficient of variation of R-R interval. *J. Auton. Nerv. Syst.*, 1997;**62**: 79–84.
60. Copie, X., J-Y. Le Heuzey, M-C. Iliou, R. Khouri, T. Lavergne, F. Pousset, and L.Guize, Correlation between time-domain measures of heart rate variability and scatterplots in postinfarction patients. *PACE*, 1996;**19**: 342–347.
61. Guzik, P., J. Piskorski, T. Krauze, A. Wykrętowicz, and H. Wysocki, Partitioning total heart rate variability. *Int. J. Cardiol.*, 2009, in press, doi:10.1016/j.ijcardiol 2008.12.151.
62. Schmidt, G. and G.E. Morfill, Nonlinear methods for heart rate variability assessment, in *Heart Rate Variability*, M. Malik and A.J. Camm., Editors. Armonk, NY: Futura Publishing, 1995, pp. 87–98.
63. Hnatkova, K., X. Copie, A. Staunton, and M. Malik, Numeric processing of Lorenz plots of R-R intervals from long-term ECS: comparisons with time-domain measures of heart rate variability for risk stratification after myocardial infarction. *J. Electrocardiol.*, 1995;**28**(Suppl.1): 74–80.
64. Sosnowski, M., P.W. MacFarlane, Z. Czyż, J. Skrzypek-Wańha, E. Boczkowska-Gaik, and M. Tendera, Age-adjustment of HRV measures and its prognostic value for risk assessment in patients late after myocardial infarction. *Int. J. Cardiol.*, 2002;**86**: 249–258.
65. Sosnowski, M., E. Clark, S. Latif, P.W. Macfarlane, and M. Tendera, Heart rate variability fraction—a new reportable measure of 24-hour R-R interval variation. *Ann. Noninvasive. Electrocardiol.*, 2005;**10**: 7–15.
66. Sosnowski, M., P.W. Macfarlane, R. Parma, J. Skrzypek-Wanha, and M. Tendera, Prognostic value of heart rate variability analysis in patients with depressed left ventricular function irrespective of cardiac rhythm. *Comp. Cardiol.*, 2006: 81–84.
67. Moraes, R.S., E.L. Ferlin, C.A. Polanczyk, L.E. Rohde, L. Zaslavski, J.L. Gross, and P. Ribeiro, Three-dimensional return map: a new tool for quantification of heart rate variability. *Autonom. Neurosci.*, 2000;**83**: 90–99.
68. Grossman, P., Respiratory and cardiac rhythms as windows to central and autonomic biobehavioral regulation: selection of window frames, keeping the panes clean and viewing the neural topography. *Biol. Psych.*, 1992;**34**: 131–161.
69. Porges, S.W., Respiratory sinus arrhythmia: an index of vagal tone, in *Psychophysiology of Cardiovascular Control: Models, Methods, and Data*, J.F. Orlebeke, G. Mulder, and L.J.P. Van Domen, Editors. New York: Plenum, 1985, pp. 437–450.
70. Allen, J.J.B., A.S. Chambers, and D.N. Towers, The many metrics of cardiac chronotropy: A pragmatic primer and a brief comparison of metrics. *Biol. Psych.*, 2007;**74**: 243–262.
71. Denver, J.W., S.F. Reed, and S.W. Porges, Methodological issues in the quantification of respiratory sinus arrhythmia. *Biol. Psych.*, 2007;**74**: 286–294.

72. Sosnowski, M., T. Petelenz, and J. Leski, Return maps: a nonlinear method for evaluation of respiratory sinus arrhythmia. *Comput. Cardiol*., 1994; 129–132.
73. Suder, K., F.R. Drepper, M. Schiek, H-H. Abel, One-dimensional, nonlinear determinism characterizes heart rate pattern during paced respiration. *Am. J. Physiol. Heart Circ. Physiol*., 1998; 275: H1092–1102.
74. Carlson, G., S. Girouard, M. Schlegl, and C. Butter, Three-dimensional heart rate variability diagnostic for monitoring heart failure through an implantable device. *J. Cardiovasc. Electrophysiol*., 2004;**15**: 506.
75. Gilliam, F.R. III[rd], J.P. Singh, C.M. Mullin, M. McGuire, and K.J. Chase, Prognostic value of heart rate variability footprint and standard deviation of average 5-minute intrinsic R-R intervals for mortality in cardiac resynchronization therapy patients. *J. Electrocardiol*., 2007;**40**: 336–342.
76. Penaz, J., J. Roukenz, and H.J. van der Waal, in *Spectral Analysis of Some Spontaneous Rhythms in the Circulation*, H. Drischel and N. Tiedt, Editors. Biokybernetik. Bd I, Karl Marx University, Leipzig, 1968, pp. 223–241.
77. DeBoer, R.W., J.M. Karemaker, and J. Strackee, Beat-to-beat variability of heart rate interval and blood pressure. *Automedica*., 1983;**4**: 217–222.
78. Parati, G., P. Castiglioni, M. Di Rienzo, S. Omboni, A. Pedotti, and G. Mancia, Sequential spectral analysis of 24-hour blood pressure and pulse interval in humans. *Hypertension*, 1990;**16**: 414–421.
79. Cerutti, S., A.M. Bianchi, and L.T. Mainardi, Spectral analysis of the heart rate variability signal, in *Heart Rate Variability*, M. Malik and A.J. Camm, Editors. Armonk, NY: Futura Publishing 1995, pp. 63–74.
80. Bigger, J.T. Jr., Heart rate variability: frequency domain, in *Non-invasive Electrocardiology. Clinical Aspects of Holter Monitoring*, Moss, A.J. and S. Stern, Ediotrs. London: W.B. Saunders, 1996: 175–198.
81. Malliani, A., M. Pagani, F. Lombardi, and S. Cerutti, Cardiovascular neural regulation explored in the frequency domain. *Circulation*, 1991;**84**: 482–492.
82. Pagani, M., F. Lombardi, S. Guzzetti, O. Rimoldi R. Furlan, P. Pizzinelli, G. Sandrone, G. Malfatto, S. Dell'Orto, and E. Piccaluga, Power spectral analysis of heart rate and arterial pressure variabilities as a marker of sympatho-vagal interaction in man and conscious dog. *Circ. Res*., 1986;**59**: 178–193.
83. Wichterle, D., J. Simek, M.T. La Rovere, P.J. Schwartz, A.J. Camm, and M. Malik, Prevalent low-frequency oscillation of heart rate: novel predictor of mortality after myocardial infarction. *Circulation*, 2004;**110**: 1183–1190.
84. Cooley, J.W. and J.W. Tukey, An algorithm for machine calculation of complex Fourier series. *Math. Comput*., 1965;**19**: 297–310.
85. Kay, S.M. and S.L. Marple, Spectrum analysis: a modern perspective. *Proc. IEEE*., 1981;**69**: 1380–1418.
86. Rüdiger, H., L. Klinghammer, and K. Scheuch, The trigonometric regressive spectral analysis—a method for mapping of beat-to-beat recorded cardiovascular parameters on to frequency domain in comparison with Fourier transformation. *Comput. Meth. Prog. Biomed*., 1999;**58**: 1–15.
87. Nelson, W., Y.L. Tong, J.K. Lee, and F. Halberg, Methods for cosinor-rhythmometry. *Chronobiologia*., 1979;**6**: 305–323.
88. Kitney, R.I., T. Fulton, A.H. McDonald, and D.A. Linkens, Transient interactions between blood pressure, respiration and heart rate in man. *J. Biomed. Eng*., 1985;**7**: 217–224.
89. Di Rienzo, M., P. Castiglioni, G. Mancia G. Parati, and A. Pedotti, 24 hour sequential analysis of arterial blood pressure and pulse interval in free moving subjects. *IEEE. Trans. Biomed. Eng*., 1989;**36**: 1066–1075.
90. Boardman, A., F.S. Schlindwein, A.P. Rocha, and A. Leite, A study on the optimum order of autoregressive models for heart rate variability. *Physiol. Meas*., 2002;**23**: 325–336.
91. Lacoss, R.T., Data adaptive spectral analysis methods. *Geophysics* 1971;**36**: 661–675.
92. Marple, S.L., A new autoregressive spectrum analysis algorithm. *IEEE Trans. Acoust., Speech, Signal Process*., 1980;**28**: 441–454.
93. Cohen, L., Time-frequency distribution. *A. Rev.. Proc. IEEE*., 1989;**177**: 941–981.
94. Cerutti, S., A.M. Bianchi, and L.T. Mainardi, Advanced spectral methods for detecting dynamic behaviour. *Auton. Neurosci*., 2001;**90**: 3–12.
95. Pinna, G.D., R. Maestri, and A. Di Cesare, Application of time series spectral analysis theory: analysis of cardiovascular variability signals. *Med. Biol. Eng. Comput*. 1996;**34**: 142–148.
96. Novak, P. and V. Novak, Time/frequency mapping of the heart rate, blood pressure and respiratory signals. *Med. Biol. Eng. Comput*., 1993;**31**: 103–110.
97. Bianchi, A.M., L.T. Mainardi, and S. Cerutti, Time-frequency analysis of biomedical signals. *Trans. Inst. Meas. Control*., 2000;**22**: 215–230.
98. Mainardi, L.T., On the quantification of heart rate variability spectral parameters using time-frequency and time-varying methods. *Phil. Trans. R. Soc. A*., 2009;**367**: 255–275.
99. Jason, S., C. Medique, P. Maison-Blanche, N. Montano, L. Meyer, C. Vermeiren, P. Mansier, P. Coumel, A. Malliani, and B. Swynghedaw, Instant power spectrum analysis of heart rate variability during orthostatic tilt using a time/frequency domain method. *Circulation*., 1997;**96**: 3521–3526.
100. Martinmäki, K., H. Rusko, S. Saalasti, and J. Kettunen, Ability of short-time Fourier transform method to detect transient changes in vagal effects on hearts: a pharmacological blocking study. *Am. J. Physiol. Heart Circ. Physiol*., 2006;**290**: H2582–2589.
101. Baillard, C., P. Gonçavales, L. Mangin, B. Swynghedauw, and P. Mansier, Use of time frequency analysis to follow transitory modulation of the cardiac autonomic system in clinical studies. *Autonom. Neurosci.: Basic. Clin*., 2001;**90**: 24–28.
102. Vigo, D.E., S.M. Guinjoan, M. Scaramal, L.N. Siri, and D.P. Cardinali, Wavelet transform shows age-related changes of heart rate variability within independent frequency components. *Autonom. Neurosci. Basic. Clin*., 2005;**123**: 94–100.
103. Pichot, V., J-M. Gaspoz, S. Molliex, A. Antoniadis, T. Busso, F. Roche, F. Costes, L. Quintin, J-R. Lacour, and J-C. Barthélémy, Wavelet transform to quantify heart rate variability and to assess its instantaneous changes. *J. Appl. Physiol*., 1999;**86**: 1081–1091.
104. Huang, N.E., Z. Shen, S.R. Long, M.L. Wu, H.H. Shih, Q. Zheng, N.C. Yen, C.C. Tung, and H.H. Liu, The empirical mode decomposition and Hilbert spectrum for nonlinear and nonstationary time series analysis. *Proc. Roy. Soc. London. A*., 1998;**454**: 903–995.

105. Li, M., X-K. Gu, and S-S. Yang, Hilbert-Huang transform based time-frequency distribution and comparison with other three. *Int. J. Circ. Syst. Signal. Proc.*, 2007;**2**: 155–160.
106. Perlstein, I. and A. Hoffman, Cumulative plot of heart rate variability spectrum assesses kinetics of action of cholinergic drugs in rats. *Am. J. Physiol. Heart. Circ. Physiol.*, 2000;**279**: H110–115.
107. Goldberger AL, L.A.N. Amaral, J.M. Hausdorff, P.C. Ivanov, C.K. Peng, and H.E. Stanley Fractal dynamics in physiology: alterations with disease and aging. *Proc. Natl. Acad. Sci. USA.*, 2002;**99**(Suppl 1): 2466–2472
108. Denton, T.A., G.A. Diamond, R.H. Helfant, S. Khan, and H. Karagueuzian, Fascinating rhythm: a prime on chaos theory and its application to cardiology. *Am. Heart. J.*, 1990;**120**: 1419–1440.
109. Elbert, T., W.J. Ray, W.J. Kowalik, K.E.G. Skinner, and N. Birbaumer, Chaos and physiology: Deterministic chaos in excitable cell assemblies. *Physiol. Rev.*, 1994;**74**: 1–47.
110. Goldberger, A.L., Non-linear dynamics for clinicians: chaos theory, fractals, and complexity at the bedside. *Lancet*, 1996;**347**: 1312–1314.
111. Voss, A., S. Schulz, R. Schreoder, M. Baumert, and P. Caminal, Methods derived from nonlinear dynamics for analysis heart rate variability. *Phil. Trans. Roy. Soc. London A.*, 2009;**367**: 277–296.
112. Huikuri, H.V., J.S. Perkiömaki, R. Maestri, and G.D. Pinna, Clinical impact of evaluation of cardiovascular control by novel methods of heart rate dynamics. *Phil. Trans. Roy. Soc. London A.*, 2009;**367**: 1223–1238.
113. Higuchi, T., Approach to an irregular time series on the basis of the fractal theory. *Physica. D.*, 1988;**31**: 277–283.
114. Katz, M., Fractals and the analysis of waveforms. *Comput. Biol. Med.*, 1988;**18**: 145–156.
115. Yamamoto, Y. and R.L. Hughson, Coarse-graining spectral analysis: new method for studying heart rate variability. *J. Appl. Physiol.*, 1991;**71**: 1143–1150.
116. Guevara, M.R. and L. Glass, Phase locking, period doubling bifurcations and chaos in a mathematical model of a periodically driven oscillator: a theory for the entrainment of biological oscillators and the generation of cardiac dysrhythmias. *J. Math. Biol.*, 1982;**14**: 1–23.
117. Chialvo, D.R. and J. Jalife, Non-linear dynamics of cardiac excitation and impulse propagation. *Nature.*, 1987;**330**: 749–752.
118. Garfinkel, A., M.L. Spano, W.L. Ditto, and J.N. Weiss, Controlling cardiac chaos. *Science.*, 1992;**57**: 1230–1235.
119. Weiss, J.N., A. Garfinkel, H.S. Karagueuzian, Z. Qu, and P.S. Chen, Chaos and the transition to ventricular fibrillation: a new approach to antiarrhythmic drug evaluation. *Circulation*, 1999;**99**: 2819–2826.
120. Sato, D., L.H. Xie, A.A. Sovari, D.X. Tran, N. Morita, F. Xie, H. Karagueuzian, A. Garfinkel, J.N. Weiss, and Z. Qu, Synchronization of chaotic early afterdepolarizations in the genesis of cardiac arrhythmias. *Proc. Natl. Acad. Sci. USA.*, 2009;**106**: 2983–2988.
121. Saul, J.P., P. Albrecht, R.D. Berger, and R.J. Cohen, Analysis of long-term heart rate variability: methods, 1/f scaling and implications. *Comput.Cardiol.*, 1987: 419–422. Silver Spring, MD: IEEE Computer Society Press.
122. Bigger, J.T. Jr., R.C. Steinman, L.M. Rolnitzky, J.L. Fleiss, P. Albrecht, and R.J. Cohen, Power law behavior of RR-interval variability in healthy middle-aged persons, patients with recent acute myocardial infarction, and patients with heart transplants. *Circulation*, 1996;**93**: 2142–2151.
123. Schepers, H.E., J.H.G.M. van Beek, and J.B. Bassingthwaighte, Four methods to estimate the fractal dimension from self-affine signals. *IEEE. Eng. Med. Biol.* 1992;**11**: 57–64.
124. Peng, C.K., S. Havlin, H.E. Stanley, and A.L. Goldberger, Quantification of scaling exponents and crossover phenomena in nonstationary heart beat time series. *Chaos*, 1995;**5**: 82–87.
125. Francis, D.P., K. Willson, P. Georgiadou, R. Wensel, L.C. Davies, A. Coats, and M. Piepoli, Physiological basis of fractal complexity properties of heart rate variability in man. *J. Physiol.*, 2002;**542**: 619–629.
126. Ho, K.K., G.B. Moody, C.K. Peng, J.E. Mietus, M.G. Larson, D. Levy, and A.L. Goldberger, Predicting survival in heart failure case and control subjects by use of fully automated methods for deriving nonlinear and conventional indices of heart rate dynamics. *Circulation*, 1997;**96**: 842–848.
127. Huikuri, H.V., T.H. Mäkikallio, C.K. Peng, A.L. Goldberger, U. Hintze, and M. Moller, Fractal correlation properties of R-R interval dynamics and mortality in patients with depressed left ventricular function after an acute myocardial infarction. *Circulation*, 2000;**101**: 47–53.
128. Tibby, S.M., H. Frndova, A. Durward, and P.H. Cox, Novel method to quantify loss of heart rate variability in pediatric multiple organ failure. *Crit. Care. Med.*, 2003;**31**: 2079–2080.
129. Ivanov, P.C., A.N. Amaral, A.L. Goldberger, S. Havlin, M.G. Rosenblum, Z.R. Struzik, and H.E. Stanley, Multifractality in human heart beat dynamics. *Nature*, 1999;**399**: 461–465.
130. Ching, E.S. and Y.K. Tsang, Multifractality and scale invariance in human heart beat dynamics. *Phys. Rev. E. Stat. Nonlin. Soft. Matter. Phys.*, 2007;**76** (4 Pt 1): 041910–04198.
131. Kiyono, K., Z.R. Struzik, N. Aoyagi,S. Sakata, J. Hayano, and Y. Yamamoto. Critical scale- invariance in healthy human heart rate. *Phys. Rev. Lett.*, 2004;**93**: 178103.
132. Kiyono, K., J. Hayano, E. Watanabe, Z.R. Struzik, and Y. Yamamoto, Non-Gaussian heart rate as an independent predictor of mortality in patients with chronic heart failure. *Heart Rhythm.*, 2008;**5**: 261–268.
133. Cerutti, S., D. Hoyer, A. Voss, Multiscale, multiorgan and multivariate complexity analysis of cardiovascular regulation. *Phi. Trans. Roy. Soc. London A.*, 2009;**367**: 1337–1358.
134. Batzel, J., G. Baselli, R. Mukkamala, and K.H. Chon, Modelling and disentangling physiological mechanisms: linear and nonlinear identification techniques for analysis of cardiovascular regulation. *Phil. Trans. Roy. Soc. London A.*, 2009;**367**: 1377–1391.
135. Takens, F., Detecting strange attractors in turbulence, in *Dynamical Systems and Turbulence*, *Lecture Notes in Mathematics*, vol. 898, D.A. Rand and L-S. Young, Editors. Berlin: Springer-Verlag, 1981; pp. 366–381.
136. Grassberger, P. and I. Procaccia, Measuring the strangeness of strange attractors. *Physica. D.*, 1983;**9**: 189–208.
137. Carjaval, R., N. Wessel, M. Vallverdu, P. Caminal, and A. Voss, Correlation dimension analysis of heart rate variability in patients with dilated cardiomyopathy. *Comput. Meth. Prog. Biomed.*, 2005;**78**: 133–140.
138. Skinner, J.E., C.M. Pratt,and T. Vybiral, A reduction in the correlation dimension of heart beat intervals precedes imminent ventricular fibrillation in human subjects. *Am. Heart. J.*, 1993;**125**: 731–734.

139. Shannon, C.E. and W. Weaver, *The Mathematical Theory of Information*. University of Illinois Press, 1949.
140. Pincus, S.M. and W.M. Huang, Approximate entropy: statistical properties and applications. *Commun. Stat. Theory. Meth*., 1992;**21**: 3061–3077.
141. Pikkujämsä, S.M., T.H. Mäkikallio, K.E. Airaksinen, and H.V. Huikuri, Determinants and interindividual variation of R-R interval dynamics in healthy middle-aged subjects. *Am. J. Physiol. Heart. Circ. Physiol*., 2001;**280**: H1400–1406.
142. Mäkikallio, T.H., T. Seppänen, N. Niemelä, K.E. Airaksinen, M. Tulpo, H.V. Huikuri, Abnormalities in beat to beat complexity of heart rate dynamics in patients with a previous myocardial infarction. *J. Am. Coll. Cardiol*., 1996;**28**: 1005–1011.
143. Richman, J.S. and J.R. Moorman,J.R Physiological time-series analysis using approximate entropy and sample entropy. *Am. J. Physiol. Heart. Circ. Physiol*., 2000;**278**: H2039–2049.
144. Lake, D.E., J.S. Richman, M.P. Griffin, and J.R. Moorman, Sample entropy analysis of neonatal heart rate variability. *Am. J. Physiol. Regul. Integr. Comp. Physiol*., 2002;**283**: R789–797.
145. Tuzcu, V., S. Nas, T. Borklu, and A. Ugur, Decrease in the heart rate complexity prior to the onset of atrial fibrillation. *Europace*., 2006;**8**: 398–402.
146. Costa, M., A.L. Goldberger, and C.K. Peng, Multiscale entropy analysis of complex physiological time series. *Phys. Rev. Lett*., 2002;**89**: 068–102.
147. Javorka, M., Z. Trunkvalterova, I. Tonhajzerova, J. Javorkova, K. Javorka, and M. Baumert Short-term heart rate complexity in reduced in patients with type 1 diabetes mellitus. *Clin. Neurophysiol*., 2008;**119**: 1071–1081.
148. Baumert, M., V. Baier, J. Hauesian, N. Wessel, U. Meyerfeldt, A. Schirdewan, and A. Voss, Forecasting of life threatening arrhythmias using the compression entropy of heart rate. *Meth. Inf. Med*., 2004;**43**: 202–206.
149. Treubner, S., I. Cygankiewicz, R. Schreoder, M. Baumenrt, M. Vallverdú, P. Caminal, R. Vazquez, A. Bayés de Luna, and A. Voss, Compression entropy contributes to risk stratification in patients with cardiomyopathy. *Biomed. Tech. (Berl.)* 2006;**51**: 77–82.
150. Bai-Lin, H., *Elementary Symbolic Dynamics and Chaos in Dissipative Systems*. Singapore: World Scientific, 1989.
151. Kurths, J., A. Voss, P. Saparin, A. Witt, H.J. Kleiner, and N. Wessel, Quantitative analysis of heart rate variability. *Chaos*, 1995;**5**: 88–94.
152. Wessel, N., C. Ziehmann, J. Kurths, U. Meyerfeldt, A. Schirdewan, and A. Voss, Short-term forecasting of life-threatening cardiac arrhythmias based on symbolic dynamics and finite-time growth rates. *Phys. Rev. E*., 2000;**61**: 733–739.
153. García-Gonzáles, M.A., J. Ramos-Castro, and M. Fernández-Chimeno, A new index for the analysis of heart rate variability dynamics: characterization and application. *Physiol. Meas*., 2003;**24**: 819–832.
154. Arif, M. and W. Aziz, Application of threshold-based acceleration change index (TACI) in heart rate variability analysis. *Physiol. Meas*., 2005;**26**: 653–665.
155. Porta, A., S. Guzzetti, N. Montano, R. Furlan, M. Pagani, A. Malliani, and S. Cerutti, Entropy, entropy rate and pattern classification as tools to typify complexity in short heart period variability series. *IEEE. Trans. Biomed. Eng*., 2001;**48**: 1282–1291.
156. Hoyer, D., H. Friedrich, U. Zwiener, B. Pompe, R. Baranowski, K. Werdan, U. Müller-Werdan, and H. Schmidt. Prognostic impact of autonomic information flow in multiple organ dysfunction syndrome patients. *Int. J. Cardiol*., 2006;**108**: 359–369
157. Eckmann, J.P. and D. Ruelle, Ergodic theory of chaos and strange attractors. *Rev. Mod. Phys*. 1985;**57**: 617–656.
158. Wolf, A., J.B. Swift, L.H. Swinney, J.A.Vastano, Determining Lyapunov exponent from a time series. *Physica. D*. 1985;**16**: 285–317.
159. Poon, C-S. and M. Barahona, Titration of chaos with added noise. *Proc. Natl. Acad. Sci. USA*. 2001;**98**: 7107–7112
160. Wu, G-Q., N.M. Arzeno, L-L. Shen, D-K. Tang, D-A. Zheng, N-Q. Zhao, D.L. Eckberg, and C-S. Poon, Chaotic signature of heart rate variability and its power spectrum in health, aging and heart failure. *PLoS. ONE*. 2009;**4**: e4323.
161. Sugihara, G. and R. May, Nonlinear forecasting as a way for distinguishing chaos from measurement error in a data series. *Nature* (London), 1990;**344**: 734–741.
162. Sugihara, G., Nonlinear forecasting for the classification of natural time series. *Phil. Trans. R. Soc. A*. 1994;**348**: 477–495.
163. Braun, C., P. Kowalik, A. Freking, D. Hadeler, K.D. Kniffi, and M. Messmann, Demonstration of non-linear components in heart rate variability of healthy persons. *Am. J. Physiol. Heart. Circ. Physiol*. 1998;**275**: H1577–H1584.
164. Costa, M., A.L. Goldberger, C-K. Peng, Broken asymmetry of the human heart beat: loss of time irreversibility in aging and disease. *Phys. Rev. Lett*. 2005;**95**: 198102.
165. Ehlers, C.L., J. Havstad, D. Prichard, and J. Theiler, Low doses of ethanol reduce evidence for nonlinear structure in brain activity. *J. Neurosci*. 1998;**18**: 7474–7486.
166. Guzik, P., J. Piskorski, T. Krauze, A. Wykrętowicz, and H. Wysocki, Heart rate asymmetry by Poincare' plots of RR intervals. *Biomed. Tech*. 2006;**51**: 272–275.
167. Porta, A., S. Guzzetti, N. Montano, T. Gnecchi-Ruscone, R. Furlan, and A. Malliani, Time reversibility in short-term heart period variability. *Comp. Cardiol*. 2006;**33**: 77–80.
168. Porta, A., K.R. Casali, A.G. Casali, T. Gnecchi-Ruscone, E. Tobaldini, N. Montano, S. Lange, D. Geue, D. Cysarz, and P. van Leeuwen, Temporal asymmetries of short-term heart period variability are linked to autonomic regulation. *Am. J. Physiol. Regulatory. Integrative. Comp. Physiol*. 2008;**295**(2): R550–557.
169. Porta, A., G. D'Addio, T. Bassani, R. Maestri, and G-D. Pinna, Assessment of cardiovascular regulation through irreversibility analysis of heart period variability: a 24 hours Holter study in healthy and chronic heart failure populations. *Phil. Trans. R. Soc. A*. 2009;**367**: 1359–1375.
170. Bauer A., J.W. Kantelhardt, A. Bunde, M. Malik, R. Schneider, and G. Schmidt Phase-rectified signal averaging detects quasi-periodicities in non-stationary data. *Physica. A*. 2006;**364**: 423–434.
171. Bauer, A., J.W. Kantelhardt, P. Barthel, R. Schneider, T. Mäkikallio, K. Ulm, K. Hnatkova, A. Schömig, H. Huikuri, A. Bunde, M. Malik, Schmidt G. Deceleration capacity of heart rate as a predictor of mortality after myocardial infarction: cohort study. *Lancet* 2006;**367**: 1674–1681.
172. Bauer, A., P. Barthel, R. Schneider, K. Ulm, A. Müller, A. Joeinig, R. Stich, A. Kiviniemi, K. Hnatkova, H. Huikuri, A. Schömig, M. Malik, G. Schmidt, Improved stratification of autonomic regulation for risk prediction in post-infarction patients with

preserved left ventricular function (ISAR-Risk). *Eur. Heart. J.* 2009;**30**: 576–583.
173. Eckmann, J.P., S.O. Kamphorst, and D. Ruelle, Recurrence plots of dynamical systems. *Europhys. Lett.* 1987;**4**: 973–977.
174. Webber, C.L. and J.P. Zbilut, Dynamical assessment of physiological systems and states using recurrence plot strategies. *J. Appl. Physiol.* 1994;**76**: 965–973.
175. Giuliani, A., G. Piccirillo, V. Marigliano, and A. Colosimo, A nonlinear explanation of aging-induced changes in heart beat dynamics. *Am. J. Physiol. Heart. Circ. Physiol.* 1998;**275**: H1455–1461.
176. Gammaitoni, L., P. Hänggi, P. Jung, and F. Marchesoni, Stochastic resonance. *Rev. Mod. Phys.* 1998;**70**: 223–287.
177. Moody, G.B., R.G. Mark, A. Zoccola, S. Mantero, J.T. Bigger, and J.L. Fleiss, Derivation of respiratory signals from multi-leads ECGs. *Comput. Cardiol.* 1985;**12**: 113–116.
178. Sosnowski, M., J. Skrzypek-Wańha, Z. Czyż, M. Petelenz, and M. Tendera, Importance of respiration for non-invasive assessment of cardiac autonomic control in patients with ischemic left ventricular dysfunction. *Wiad. Lek.*, 1999;**52**: 230–237.
179. Sosnowski, M., Z. Czyż, and M. Tendera, Scatterplots of RR and RT interval variability bring evidence for diverse non-linear dynamics of heart rate and ventricular repolarization duration in coronary heart disease. *Europace*, 2001;**3**: 39–45.
180. Challis, R.E. and R.I. Kitney, Biomedical signal processing (in four parts). Part 3 The power spectrum and coherence function. *Med. Biol. Eng. Comput.*, 1991;**29**: 225–241.
181. Porges, S.W., R.E. Bohrer, M.N. Cheung, F. Drasgow, P.M. McCabe, and G. Keren, New time-series statistic for detecting rhythmic co-occurrence in the frequency domain: the weighted coherence and its application to psychophysiological research. *Psychol. Bull.*, 1980;**88**: 580–587.
182. Kirchheim, H.R., Systemic arterial baroreceptor reflexes. *Physiol. Rev.*, 1976;**56**: 100–176.
183. Smyth, H.S., P. Sleight, and G.W. Pickering, Reflex regulation of arterial pressure during sleep in man. A quantitative method of assessing baroreflex sensitivity. *Circ. Res.*, 1969;**24**: 109–121.
184. Taylor, J.A. and D.L. Eckberg, Fundamental relations between short-term RR interval and arterial pressure oscillations in humans. *Circulation*, 1996;**93**: 1527–1532.
185. Baselli, G, S. Cerutti, S. Civardi, and D. Liberati. Spectral and cross-spectral analysis of heart rate and arterial blood pressure variability signals. *Comput. Biomed. Res.*, 1986;**19**: 520–553
186. La Rovere, M.T., A. Mortara, and P.J. Schwartz, Baroreflex sensitivity. *J. Cardiovasc. Electrophysiol.*, 1995;**6**: 761–774.
187. Bettermann, H., D. Amponsah, D. Cysarz, and P. Van Leeuwen, Musical rhythms in heart period dynamics – a cross-cultural and interdisciplinary approach to cardiac rhythms. *Am. J. Physiol.*, 1999;**277**: H1762–H1770.
188. Galletly, D.C. and P.D. Larsen, Cardioventilatory coupling in heart rate variability: methods for qualitative and quantitative determination. *Br. J. Anaesth.*, 2001;**87**: 827–833.
189. Engel, P., G. Hildebrandt and H.G. Scholz, Die Messung der Phasenkopplung zwischen Herzschlag und Atmung beim Menschen mit einem Koinzidenzmessgerät. *Pflugers. Arch.*, 1967;**298**: 259–270.
190. Kenner, T., H. Pessenhofer, and G. Schwaberger, Method for the analysis of the entrainment between heart rate and ventilation rate. *Pflugers. Arch.*, 1976;**363**: 263–265.
191. Hoyer, D., O. Hader, and U. Zwiener, Relative and intermittent cardiorespiratory coordination. *IEEE. Eng. Med. Biol. Mag.*, 1997;**16**: 97–104.
192. Nollo, G., L. Faes, R. Antolini, and A. Porta, Assessing causality in normal and impaired short-term cardiovascular regulation via nonlinear prediction methods. *Philos. Transact. A. Math. Phys. Eng. Sci.*, 2009;**367**: 1423–1440.
193. Schäfer, C., M.G. Rosenblum, J. Kurths, and H.H. Abel, Heart beat synchronized with ventilation. *Nature*, 1998;**392**: 239–240.
194. Seidel, H. and H. Herzel, Analyzing entrainment of heart beat and respiration with surrogates. *IEEE. Eng. Med. Biol. Mag.*, 1998;**17**: 54–57.
195. Cysarz, D., H. Bettermann, S. Lange, D. Geue, P. van Leeuwen. A quantitiative comparison of different methods to detect cardiorespiratory coordination during night-time sleep. *Biomed. Eng. OnLine*, 2004;**3**: 44
196. Cysarz, D., D. von Bonin, P. Brachmann, S. Buetler, F. Edelhäuser, K. LaederachHofmann, and P. Heusser, Day-to-night time differences in the relationship between cardiorespiratory coordination and heart rate variability. *Physiol. Meas.*, 2008;**29**: 1281–1291.
197. Hidaka, I., S-I. Ando, H. Shigematsu, K. Sakai, S. Setoguchi, T. Seto, Y. Hirooka, A. Takeshita, and Y. Yamamoto, Noise-enhanced heart rate and sympathetic nerve responses to oscillatory lower body negative pressure in humans. *J. Neurophysiol.*, 2001;**86**: 559–564.
198. Schmid, G., I. Goychuk, and P. Hänggi, Stochastic resonance as a collective property of ion channel assemblies. *Europhys. Lett.*, 2001;**56**: 22–28.
199. Chang, K.L., K.J. Monahan, P.M. Griffin, D. Lake, and J.R. Moorman, Comparison and clinical application of frequency domain methods in analysis of neonatal heart rate time series. *Ann. Biomed. Eng.*, 2001;**29**: 764–774.
200. Smyth, H.S., P. Sleight, and G.W. Pickering, Reflex regulation of arterial pressure during sleep in man: a quantitative method of assessing baroreflex sensitivity. *Circ. Res.*, 1969;**24**: 109–121.
201. DeBoer, R.W., J.M. Karemaker, and J. Strackee, Hemodynamic fluctuations and baroreflex sensitivity in humans: a beat-to-beat model. *Am. J. Physiol.*, **253** (Heart Circ Physiol) 1987;**22**: 680–689.
202. Laude, D., L-J. Elghozi, A. Girard, E. Bellard, M. Bouhaddi, P. Castiglioni, C. Cerutti, A. Cividjian, M. Di Rienzo, J-O. Fortrat, B. Janssen, J.M. Karemaker, G. Lefthériotis, G. Parati, P.B. Persson, A. Porta, L. Quintin, J. Regnerd, H. Rüdiger, and H.M. Strauss, Comparison of various techniques used to estimate spontaneous baroreflex sensitivity (the EuroBaVar study). *Am. J. Physiol. Regulatory. Integrative. Comp. Physiol.*, 2004;**286**: R226–231.
203. Robbe, H.W.J., L.J.M. Mulder, H. Rudel, W.A. Langewitz, J.B.P. Veldman, and G. Mulder, Assessment of baroreceptor reflex sensitivity by means of spectral analysis. *Hypertension*, 1987;**10**: 538–543.
204. Hartikainen, J.E., K.U.O. Tahvanainen, M.J. Mantysaari, P.E. Tikkanen, E.O. Lansimies, and K.E.J. Airaksinen, Simultaneous invasive and noninvasive evaluations of baroreflex sensitivity with bolus phenylephrine technique. *Am. Heart. J.*, 1995;**130**: 296–301.
205. Pinna, G.D., M.T. La Rovere, and R. Maestri, Estimation of arterial blood pressure variability by spectral analysis: comparison

between Finapres and invasive measurements. *Physiol. Meas.*, 1996;**17**: 147–169.

206. Mortara, A., M.T. La Rovere, G.D. Pinna, A. Prpa, R. Maestri, O. Febo, M. Pozzoli, C. Opasich, and L. Tavazzi, Arterial baroreflex modulation of heart rate in chronic heart failure: clinical and hemodynamic correlates and prognostic implications. *Circulation*, 1997;**96**: 3450–3458.
207. Osculati, G., G. Grassi, C. Giannattasio, G. Seravalle, F. Valagussa, A. Zanchetti, and G. Mancia, Early alterations of the baroreceptor control of heart rate in patients with acute myocardial infarction. *Circulation*, 1990;**81**: 939–934.
208. Korner, P.I., M.J. West, J. Shaw, and J.B. Uther, "Steady-state" properties of the baroreceptor-heart rate reflex in essential hypertension in man. *Clin. Exp. Pharmacol. Physiol.*, 1974;**1**: 65–76.
209. Eckberg, D.L., M.S. Cavanaugh, A.L. Mark, and F.M. Abboud, A simplified neck suction device for activation of carotid baroreceptors. *J. Lab. Clin. Med.*, 1975;**85**: 167–173.
210. Ludbrook, J., G. Mancia, A. Ferrari, and A. Zanchetti, The variable-pressure neck-chamber method for studying the carotid baroaflex in man. *Clin. Sci. Mol. Med.*, 1977;**53**: 165–171.
211. Sundlof, G. and B.G. Wallin, Effect of lower body negative pressure on human muscle sympathetic nerve activity. *J. Physiol.*, 1978;**278**: 525–532.
212. Bernardi, L., B. Bianchini, G. Spadacini, S. Leuzzi, F. Valle, E. Marchesi, C. Passino, A. Calciati, M. Viganó, M. Rinaldi, L. Martinelli, G. Finardi, and P. Sleight, Demonstrable cardiac reinnervation after human heart transplantation by carotid baroreflex modulation of RR interval. *Circulation*, 1995;**92**: 2895–2903.
213. Sleight, P., M.T. La Rovere, A. Mortara, G. Pinna, R. Maestri, S. Leuzzi, B. Bianchini, L. Tavazzi, and L. Bernardi, Physiology and pathophysiology of heart rate and blood pressure variability in humans: is power spectral analysis largely an index of baroreflex gain? *Clin. Sci.* (Colch), 1995;**88**: 103–109.
214. Kautzner, J., Noninvasive provocations of baroreflex sensitivity, in *Dynamic Electrocardiography*, M. Malik and A.J. Camm, Editors. London: Blackwell Futura Publishing, 2004, pp. 162–169.
215. Raczak, G., M.T. la Rovere, G.D. Pinna, R. Maestri, and G. Swiatecka, Assessment of baroreflex sensitivity in patients with preserved and impaired left ventricular function by means of the Valsalva manoeuvre and the phenylephrine test. *Clin. Sci.* (Lond)., 2001;**100**: 33–41.
216. Takaashi, N., M. Nakagawa, and T. Saikawa, Noninvasive assessment of the cardiac baroreflex response to downward tilting and comparison with the phenylephrine method. *J. Am. Coll. Cardiol.*, 1999;**34**: 211–215.
217. Di Rienzo, M., G. Bertinieri, G. Mancia, and A. Pedotti, A new method for evaluating the baroreflex role by a joint pattern analysis of pulse interval and systolic blood pressure series. *Med. Biol. Eng. Comput.*, 1985;**23**: 313–314.
218. Davies, L.C., H. Colhoun, A.J. Coats, M. Piepoli, and D.P. Francis, A noninvasive measure of baroreflex sensitivity without blood pressure measurements. *Am. Heart. J.*, 2002;**143**: 441–447.
219. James, M.A., R.B. Panerai, and J.E. Potter, Applicability of new techniques in the assessment of arterial baroreflex sensitivity in the elderly: a comparison with established pharmacological methods. *Clin. Sci.*, 1998;**94**: 245–253.
220. Maestri, R., G.D. Pinna, A. Mortara, M.T. La Rovere, and L. Tavazzi, Assessing baroreflex sensitivity in post-myocardial infarction patients: comparison of spectral and phenylephrine techniques. *J. Am. Coll. Cardiol.*, 1998;**31**: 344–351.
221. Pitzalis, M.V., F. Mastropasqua, A. Passantino, F. Massari, L. Ligurgo, C. Forleo, C. Balducci, F. Lombardi, and P. Rizzon, Comparison between noninvasive indices of baroreceptor sensitivity and the phenylephrine method in post-myocardial infarction patients. *Circulation*, 1998;**97**: 1362–1367.
222. Schmidt, G., M. Malik, P. Barthel, R. Schneider, K. Ulm, L. Rolnitzky, A.J. Camm, J.T. Jr Bigger, and A. Schomig, Heart-rate turbulence after ventricular premature beats as a predictor of mortality after acute myocardial infarction. *Lancet*, 1999;**353**: 1390–1396.
223. Mrowka, R., P.B. Persson, H. Theres, et al., Blunted arterial baroreflex causes "pathological" heart rate turbulence. *Am. J. Physiol. Regul. Integr. Comp. Physiol.*, 2000;**279**: R1171–1175.
224. Lin, L.Y., L.P. Lai, J.L. Lin, C.C. Du, W.Y. Shay, H.L. Chan, Y.Z. Tsend, S.K.S. Huang, Tight mechanism correlation between heart rate turbulence and baroreflex sensitivity: sequential autonomic blockade analysis. *J. Cardiovasc. Electrophysiol.*, 2002;**13**: 427–431.
225. Davies, L.C., D.P. Francis, P. Ponikowski, M.F. Piepoli, and A.J. Coats, Relation of heart rate and blood pressure turbulence following premature ventricular complexes to baroreflex sensitivity in chronic congestive heart failure. *Am. J. Cardiol.*, 2001;**87**: 737–742.
226. Ghuran, A., F. Reid, M.T. La Rovere, et al., Heart rate turbulence-based predictors of fatal and nonfatal cardiac arrest (the Autonomic Tone and Reflexes After Myocardial Infarction substudy). *Am. J. Cardiol.*, 2002;**89**: 184–190.
227. Cygankiewicz, I., W. Zareba, R. Vazquez, M. Vallverdu, J.R. Gonzalez-Juantey, M. Valdes, J. Almendral, J. Cinca, P. Caminal, A. Bayes de Luna and MUSIC Investigators, Heart rate turbulence predicts all-cause mortality and sudden death in congestive heart failure patients. *Heart. Rhythm.*, 2008;**5**: 1095–1102.
228. Schneider, R., P. Barther, and M. Watanabe, Heart rate turbulence on Holter, in *Dynamic Electrocardiography*, M. Malik and A.J. Camm, Editors. London: Blackwell Futura Publishing, 2004, pp. 190–193.
229. Watanabe, M.A., J.E. Marine, R. Sheldon, et al., Effects of ventricular premature stimulus coupling interval on blood pressure and heart rate turbulence. *Circulation*, 2002;**106**: 325–330.
230. Voss, A., V. Baier, J. Hopfe, et al., Heart rate and blood pressure turbulence– marker of the baroreflex sensitivity or consequence of postextrasystolic potentiation and pulsus alternans? *Am. J. Cardiol.*, 2002;**89**: 110–111.
231. Goldberger, J. and A.H. Kadish, Influence of sympathethic and parasympathetic maneuvers on heart rate variability, in: *Noninvasive Electrocardiology. Clinical Apects of Holter Monitoring*, A.J. Moss and S. Stern, Editors. London: WB Saunders, 1996, pp. 207–223.
232. Merri, M., D.C. Farden, J.G. Mottley, and E.L. Titlebaum, Sampling frequency of the electrocardiogram for spectral analysis of the heart rate variability. *IEEE. Trans. Biomed. Eng.*, 1990;**37**: 99–106.
233. Hilton, M.F., J.M. Beattie, M.J. Chappell, and R.A. Bates, Heart rate variability: measurement error or chaos. *Comp. Cardiol.*, 1997: 125–128.
234. Bianchi, A.M., L.T. Mainardi, E. Petrucci, M.G. Signorini, M. Mainardi, and S. Cerutti, Time-variant power spectrum analysis for the detection of transient episodes in HRV signal. *IEEE. Trans. Biomed. Eng.*, 1993;**40**: 136–144.

235. Voss, A., N. Wessel, A. Sander, H. Malberg, and R. Dietz, Requirements on sampling rate in Holter systems for analysis of heart rate variability. *Clin. Sci. (Lond).*, 1996;**91** (Suppl): 120–121.
236. Hejjel, L. and E. Roth, What is the adequate sampling interval of the ECG signal for heart rate variability analysis in the time domain? *Physiol. Meas.*, 2004;**25**: 1405–1411.
237. Tapanainen, J.M., T. Seppänen, R. Laukkanen, A. Loimaala, and H.V. Huikuri, Significance of the accuracy of RR interval detection for the analysis of new dynamic measures of heart rate variability. *Ann. Noninvas. Electrocardiol.*, 1999;**4**: 10–18.
238. Merri, M., D.C. Farden, J.G. Mottley, and E.L. Titlebaum, Sampling frequency of the electrocardiogram for spectral analysis of the heart rate variability. *IEEE. Trans. Biomed. Eng.*, 1990;**37**: 99–106.
239. Xia, R., O. Odemuyiwa, J. Gill, M. Malik, and A.J. Camm, Influence of recognition errors of computerised analysis of 24-hour electrocardiograms on the measurement of spectral components of heart rate variability. *Int. J. Biomed. Comput.*, 1993;**32**: 223–235.
240. Sapoznikov, D., M.H. Luria, Y. Mahler, and M.S. Gotsman, Computer processing of artifact and arrhythmias in heart rate variability analysis. *Comput. Methods. Progr. Biomed.*, 1992;**39**: 75–84.
241. Salo, M.A., H.V. Huikuri, and T. Seppänen, Ectopic beats in heart rate variability analysis: effects of editing on time and frequency domain measures. *Ann. Noninvasive. Electrocardiol.*, 2001;**6**: 5–17.
242. Berntson, G.G. and J.R. Stowell, ECG artifacts and heart period variability: don't miss a beat! *Psychophysiology*, 1998;**35**: 127–132.
243. Clifford, G.D., ECG statistics, noise, artifacts, and missing data, in *Advanced Methods for ECG Analysis*, G.D. Clifford, F. Azuaje, and P.E. McSharry, Editors. London: Artech House, 2006.
244. Janssen, M.J., C.A. Swenne, J. de Bie, O. Rompelman, and J.H. van Bemmel, Methods in heart rate variability analysis: which tachogram should we choose? *Comput. Meth. Prog. Biomed.*, 1993;**41**: 1–8.
245. Sacha, J. and W. Pluta, Different methods of heart rate variability analysis reveal different correlation of heart rate variability spectrum with average heart rate. *J. Electrocardiol.*, 2005;**38**: 47–53.
246. Borell von, E., J. Langbein, G. Després, S. Hansen, C. Leterrier, J. Marchant-Forde, R. Marchant-Forde, M. Minero, E. Mohr, A. Prunier, D. Valance, and I. Veissier, Heart rate variability as a measure of autonomic regulation of cardiac activity for assessing stress and welfare in farm animals — A review. *Physiol. Behav.*, 2007;**92**: 293–316.
247. Crawford, M.H., S.J. Bernstein, P.C. Deedwania, J.P. DiMarco, K.J. Ferrick, A. Jr. Garson, L.A. Green, H.L. Greene, M.J. Silka, P.H. Stone, C.M. Tracy, R.J. Gibbons, J.S. Alpert, K.A. Eagle, T.J. Gardner, G. Gregoratos, R.O. Russell, T.H. Ryan, S.C. Jr. Smith, ACC/AHA Guidelines for Ambulatory Electrocardiography. A report of the American College of Cardiology/American Heart Association Task Force on Practice Guidelines (Committee to Revise the Guidelines for Ambulatory Electrocardiography). Developed in collaboration with the North American Society for Pacing and Electrophysiology. *J. Am. Coll. Cardiol.*, 1999;**34**: 912–948.
248. Liao, D., R.W. Barnes, L.E. Chambless, R.J. Jr. Simpson, P. Sorlie, and G. Heiss, Age, race, and sex differences in autonomic cardiac function measured by spectral analysis of heart rate variability–the ARIC study. Atherosclerosis Risk in Communities. *Am. J. Cardiol.*, 1995;**76**: 906–912.
249. Carnethon, M.R., D. Liao, G.W. Evans, W.E. Cascio, L.E. Chambless, W.D. Rosamond, and G. Heiss, Does the cardiac autonomic response to postural change predict incident coronary heart disease and mortality? The Atherosclerosis Risk in Communities Study. *Am. J. Epidemiol.*, 2002;**155**: 48–56.
250. Rashba, E.J., N.A. Estes, P. Wang, A. Schaechter, A. Howard, W. Zareba, J.P. Couderc, J. Perkiomaki, J. Levine, and A. Kadish, for the Defibrillators in Non-Ischemic Cardiomyopathy Treatment Evaluation (DEFINITE) Investigators. Preserved heart rate variability identifies low-risk patients with nonischemic dilated cardiomyopathy: Results from the DEFINITE trial. *Heart. Rhythm.*, 2006;**3**: 281–286.
251. Tsuji, H., M.G. Larson, F.J. Jr. Venditti, E.S. Manders, J.C. Evans, C.L. Feldman, and D. Levy, Impact of reduced heart rate variability on risk for cardiac events: the Framingham heart study. *Circulation*, 1996;**94**: 2850–2855.
252. Bigger, J.T. Jr., J.L. Fleiss, R.C. Steinman, L.M. Rolnitzky, R.E. Kleiger, and J.N. Rottman. Correlations among time and frequency domain measures of heart period variability two weeks after myocardial infarction. *Am. J. Cardiol.*, 1992;**69**: 891–898.
253. Binder, T., B. Frey, G. Porenta, G. Heinz, M. Wutte, G. Kreiner, H. Gossinger, H. Schmidinger, R. Pacher, and H. Weber, Prognostic value of heart rate variability in patients awaiting cardiac transplantation. *PACE*, 1992;**15** (P.II): 2215–2220.
254. Frey, B., G. Heinz, T. Binder, M. Wutte, B. Schneider, H. Schmidinger, H. Weber, and R. Pacher, Diurnal variation of ventricular response to atrial fibrillation in patients with advanced heart failure. *Am. Heart. J.*, 1995;**129**: 58–65.
255. Schroeder, E.B., E.A. Whitsel, G.W. Evans, R.J. Prineas, L.E. Chambless, and G. Heiss, Repeatability of heart rate variability measures. *J. Electrocardiol.*, 2004;**37**: 163–172.
256. Sandercock, G., P. Bromley, and D. Brodie, The reliability of short-term measurements of heart rate variability. *Int. J. Cardiol.*, 2005;**103**: 238–247.
257. Radespiel-Tröger, M., R. Rauh, C. Mahlke, T. Gottschald, and M. Mück-Weymann, Agreement of two different methods for measurement of heart rate variability. *Clin. Auton. Res.*, 2003;**13**: 99–102.
258. Dekker, J.M., R.M. Crow, A.R. Folsom, P.J. Hannan, D. Liao, C.A. Sweene, and E.G. Schouten, Low heart rate variability in a 2-minute rhythm strip predicts risk of coronary heart disease and mortality from several causes. The ARIC study. *Circulation*, 2000;**102**: 1239–1244.
259. Van Schelven, L.J., P.L. Oey, I.H.I. Klein, M.G.W. Barnas, P. Blankstein, and G.H. Wieneke, Observer variations in short spectral analysis of heart period variability. *J. Auton. Nerv. Syst.*, 2000;**79**: 144–148.
260. Tarkiainen, T.H., K.L. Timonen, P. Tittanen, J.E.K. Hartikainen, J. Pekkanen, G. Hoek, A. Ibald-Mulli, and E.J. Vanninen, Stability over time of short-term heart rate variability. *Clin. Auton. Res.*, 2005;**15**: 394–399.
261. Kroll, D.J., L.A. Freed, K.M. Stein, J.S. Borer, and P. Kligfield, Rhythm annotation and interobserver reproducibility of measures of heart rate variability. *Am. J. Cardiol.*, 1996;**78**: 1055–1057.
262. Pardo, Y., C.N. Bairey Merz, P. Paul-Labrador, I. Velasquez, J.S. Gottdiener, W.J. Kop, D. Krantz, A. Rozanski, J. Klein, and T. Peter, Heart rate variability reproducibility and stability using commercially available equipment in coronary artery disease with daily life myocardial ischemia. *Am. J. Cardiol.*, 1996;**78**: 866–870.

263. Batten, L.A., E.M. Urbina, and G.S. Berenson, Interobserver reproducibility of heart rate variability in children (The Bogalusa Heart Study). *Am. J. Cardiol.*, 2000;**6**: 1264–1266.
264. Jung, J., A. Heisel, D. Tscholl, R. Fries, H. Schiefer, and C. Ozbek, Assessment of heart rate variability by using different commercially available systems. *Am. J. Cardiol.* 1996;**78**: 118–120.
265. Murray, P.G., R.M. Hamilton, P.W. Macfarlane, Reproducibility of a non-invasive real-time measure of cardiac parasympathetic acitivity. *Physiol. Meas.*, 2001;**22**: 661–667.
266. Højgaard, M.V., N-H.Holstein-Athlou, E. Agner, and J.K. Kanters, Reproducibility of heart rate variability and baroreceptor sensitivity during rest and head-up tilt. *Blood Pres. Monit.*, 2005;**10**: 19–24.
267. Winsley, R.J., N. Armstrong, K. Bywater, and S.G. Fawkner, Reliability of heart rate variability measures at rest and during light exercise in children. *Br. J. Sports. Med.*, 2003;**37**: 550–552.
268. Maestri, R., G.D. Pinna, A. Porta, R. Balocchi, R. Sassi, M.G. Signorini, M. Dudziak, and G. Raczak, Assesing nonlinear properties of heart rate variability from short-term recordings: are these measurements reliable? *Physiol. Meas.*, 2007;**28**: 1067–1077.
269. Sinnreich, R., J.D. Kark, Y. Friedelanger, D. Sapoznikov, and D. Luria, Five minute recordings of heart rate variability for population studies: repeatability and age-sex characteristics. *Heart*, 1998;**80**: 156–162.
270. Salo, T.M., L-M. Voipio, J.O. Jalonen, H. Helenius, J.S.A. Viikari, and I. Kantola, Reproduibility of abnormal heart rate variability indices: the case of hypertensive sleep apnoea syndrome. *Clin. Physiol.*, 1999;**19**: 258–268.
271. Lord, S.W., R.R. Senior, M. Das, A.M. Whittam, A. Murray, and J.M. McComb, Low-frequency heart rate variability: reproducibility in cardiac transplant recipients and normal subjects. *Clin. Sci.*, 2001;**100**: 43–46.
272. Haas, J., A. Liebich, E. Himmrich, and N. Treese, Kurzzeitmessung der Herzfrequenzvariabilitat bei Postinfarktpatienten – Methodik, Reproduzierbarkeit and Stellenwert im Rahmen den Postinfarktdiagnostik. *Hertzschr. Elektrophys.*, 2000;**111**: 102–109.
273. Ponikowski, P., M. Piepoli, A.A. Amadi, T.P. Chua, D. Harrington, M. Volterrani, R. Colombo, G. Mazzuero, A. Giordano, and A.J. Coats, Reproducibility of heart rate variability measures in patients with chronic heart failure. *Clin. Sci. (Lond).*, 1996;**91**: 391–398.
274. Freed, L.A., K. Stein, M. Gordon, M. Urban, and P. Kiligfield, Reproducibility of power spectral measures obtained from short-term sampling periods. *Am. J. Cardiol.*, 1994;**74**: 972–973.
275. Chemla, D., D. Young, F. Badilini, P. Maison-Blanche, H. Affres, Y. Lecarpetier, and P. Chanson, Comparison of fast Fourier transform and autoregressive spectral analysis for the study of heart rate variability in diabetic patients. *Int. J. Cardiol.*, 2005;**104**: 307–313.
276. Nolan, J., A.D. Flapan, N.E. Goodfield, R.J. Prescott, P. Bloomfield, and J.M. Neilson, Measurement of parasympathetic activity from 24-hour ambulatory electrocardiograms and its reproducibility and sensitivity in normal subjects, patient with symptomatic myocardial ischemia, and patients with diabetes mellitus. *Am. J. Cardiol.*, 1996;**77**: 154–158.
277. Van Hoogenhuyze, D., N. Weinstein, G.J. Martin, J.S. Weiss, J.W. Schaad, X.N. Sahyoni, D. Fintel, W.J. Remme, and D.J. Singer, Reproducibility and relation to mean heart rate of heart rate variability in normal subjects and in patients with congestive heart failure secondary to coronary heart disease. *Am. J. Cardiol.*, 1991;**68**: 1668–1676.
278. Bigger, J.T. Jr., J.L. Fleiss, L.M. Rolnitzky, and R.C. Steinman, Stability over time of heart period variability in patients with previous myocardial infarction and ventricular arrhythmias. The CAPS and ESVEM investigators. *Am. J. Cardiol.*, 1992;**69**: 718–723.
279. Kautzner, J., K. Hnatkova, A. Staunton, A.J. Camm, and M. Malik, Day-to-day reproducibility of time-domain measures of heart rate variability in survivors of acute myocardial infarction. *Am. J. Cardiol.*, 1995;**76**: 309–312.
280. Stein, P.K., M.W. Rich, J.N. Rottman, and R.E. Kleiger, Stability of index of heart rate variability in patients with congestive heart failure. *Am. Heart. J.*, 1995;**129**: 975–981.
281. Hohnloser, S.H., T. Klingenheben, M. Zabel, F. Schroder, and H. Just, Intraindividual reproducibility of heart rate variability. *Pacing. Clin. Electrophysiol.*, 1992;**15**: 2211–2214.
282. Anastasiou-Nana, M.I., L.A. Karagounis, J. Kanakakis, N.E. Kouvelas, A. Geramoutsos, K. Chalkis, J. Karelas, and N. Nanas, Correlation and stability of heart rate and ventricular ectopy variability in patients with heart failure. *Am. J. Cardiol.*, 2001;**88**: 175–179.
283. Weber, F., H. Schneider, T. von Arnim, and W. Urbaszek, for the TIBBS investigators group. Heart rate variability and ischemia in patients with coronary artery disease and stable angina pectoris; influence of drug therapy and prognostic value. *Eur. Heart. J.*, 1998;**19**: 38–50.
284. Huikuri, H.V., K.M. Kessler, E. Terracall, A. Castellanos, M.K. Linnaluoto, and R.J. Myerburg, Reproducibility and circadian rhythm of heart rate variability in healthy subjects. *Am. J. Cardiol.*, 1990;**65**: 391–393.
285. Hayano, J., W. Jiang, R. Waugh, C. O'Connor, D. Frid, and J.A. Blumenthal, Stability over time of circadian rhythm of variability of heart rate in patients with coronary artery disease. *Am. Heart. J.*, 1997;**134**: 411–418.
286. Dawson, S.L., T.G. Robinson, J.H. Youde, M.A. James, A. Martin, P. Weston, R. Panerai, and J.F. Potter, The reproducibility of cardiac baroreceptor activity assessed noninvasively by spectral techniques. *Clin. Auton. Res.*, 1997;**7**: 279–284.
287. Davies, L.C., D. Francis, P. Jurak, T. Kara, M. Piepoli, and A.J. Coats, Reproducibility of methods assessing baroreflex sensitivity in normal controls and in patients with chronic heart failure. *Clin. Sci. (Lond).*, 1999;**97**: 515–522.
288. Iellamo, F., J.M. Legramante, G. Raimondi, F. Gastrucci, M. Massaro, G. Perizzi, Evaluation of spontaneous baroreflex sensitivity at rest and during laboratory tests. *J. Hypertens.*, 1996;**14**: 1099–1104.
289. Laude, D., J-L. Elghozi, A. Girard, E. Bellard, M. Bouhaddi, P. Castiglioni, C. Cerutti, A. Cividjian, M. Di Rienzo, J-O. Fortrat, B. Janssen, J.M. Karemaker, G. Georges Lefthériotis, G. Gianfranco Parati, B. Pontus. P.B. Persson, A. Porta, L. Quintin, J. Regnard, H. Rüdiger, H.M. Stauss, Comparison of various techniques used to estimate spontaneous baroreflex sensitivity (the EuroBaVar study). *Am. J. Physiol. Regul. Integr. Comp. Physiol.*, 2004;**286**: R226–231.
290. Gao, S.A., M. Johansson, A. Hammaren, M. Nordberg, and P. Friberg, Reproducibility of methods assessing beroreflex sensitivity and temporal QT variability in end-stage renal disease and healthy subjects. *Clin. Auton. Res.*, 2005;**15**: 21–28.
291. Wichterle, D., V. Melenovsky, L. Necasova, J. Kautzner, and M. Malik, Stability of the noninvasive baroreflex sensitivity

assessment using cross-spectral analysis of heart rate and arterial blood pressure variabilities. *Clin. Cardiol.*, 2000;**23**: 201–204.
292. Herpin, D. and S. Ragot, Mid- and long-term reproducibility of noninvasive measurements of spontaneous arterial baroreflex sensitivity in healthy volunteers. *Am. J. Hypertens.*, 1997;**10**: 790–797.
293. Lord, S.D., R.H. Clayton, M.C.S. Hall, J.C. Gray, A. Murray, J.M. McComb, and R.A. Kenny, Reproducibility of three different methods of measuring baroreflex sensitivity in normal subjects. *Clin. Sci.*, 1998;**95**: 575–581.
294. Bauer, A., M. Malik, G. Schmidt, P. Barthel, H. Bonnemeier, I. Cygankiewicz, P. Guzik, F. Lombardi, A. Muller, A. Oto, R. Schneide, M. Watanabe, D. Wichterle, and W. Zareba, Heart rate turbulence: standards of measurements, physiological interpretation, and clinical use: International Society for Holter and Noninvasive Electrophysiology Consensus. *J. Am. Coll. Cardiol.*, 2008;**52**: 1353–1365.
295. Sandercock, G.R.H., P. Bromley, and D.A. Brodie, Reliability of three commercially available heart rate variability instruments using short-term (5-min) recordings. *Clin. Physiol. Funct. Imaging.*, 2004;**24**: 359–367.
296. Pitzalis, M.V., F. Mastropasqua, F. Massari, C. Foleo, M. Di Maggio, A. Passantino, R. Colombo, M. Di Biase, and P. Rizzon Short- and long-term reproducibility of time and frequency domain heart rate variability measurements in normal subjects. *Cardiovasc. Res.*, 1996;**32**: 226–233.
297. Lobnig, B.M., E. Maslowska-Wessel, and R. Bender, Repeatability of heart rate variability measured via spectral analysis in healthy subjects. *J. Clin. Basic. Cardiol.*, 2003;**6**: 29–33.
298. Dietrich, A., J.G.M. Rosmalen, A.M. van Roon, L.J.M. Mulder, A.J. Oldehinkel, and H. Riese, Short-term reproducibility of autonomic nervous system function measures in 10-to-13-year-old children, in PhD Thesis, Dietrich A. University Medical Center, Groningen, 2007.
299. Parati, G., S. Omboni, A. Villani, F. Glavina, P. Castiglioni, M. Di Rienzo, and G. Mancia. Reproducibility of beat-by-beat blood pressure and heart rate variability. *Blood Press. Monit.*, 2001;**6**: 217–220.
300. Carrasco, S., R. González, M.J. Gaitán, and O. Yáñez, Reproducibility of heart rate variability from short-term recordings during five manoeuvres in normal subjects. *J. Med. Eng. Technol.*, 2003;**27**: 241–248.
301. Jáuregui-Renaud, K., A.G. Hermosillo, M.F. Márquez, F. Ramos-Aguilar, M. Hernández-Goribar, and M. Cárdenas, Repeatability of heart rate variability during simple cardiovascular reflex tests on healthy subjects. *Arch. Med. Res.*, 2001;**32**: 21–26.
302. Guijt, A.M., J.K. Sluiter, M.H.W. Frings-Dresen, Test-retest reliability of heart rate variability and respiration rate at rest and during light physical activity in normal subjects. *Arch. Med. Res.*, 2007;**38**: 113–120.
303. Cloarec-Blanchard, L., C. F. Unck-Brentano, M. Lipski, P. Jaillon, and I. Macquin-Mavier, Repeatability of spectral components of short-term blood pressure and heart rate variability during acute sympathetic activation in healthy young male subjects. *Clin. Sci. (Lond).*, 1997;**93**: 21–28.
304. Piepoli, M., A. Radaelli, P. Ponikowski, S. Adamopoulos, L. Bernardi, P. Sleight, and A.J. Coats, Reproducibility of heart rate variability indices during exercise stress testing and inotrope infusion in chronic heart failure patients. *Clin. Sci. (Lond).*, 1996;**91** (Suppl): 87–88.
305. Randall, D., D. Brown, R. Raisch, J. Yinling, and W. Randall, SA nodal parasympathectomy delineates autonomic control of heart rate power spectrum. *Am. J. Physiol. Heart. Circ. Physiol.*, 1991;**29**: H985–988.
306. Jose, A.D. and D. Collison, The normal range and determinants of the intrinsic heart rate in man. *Cardiovasc. Res.*, 1970;**4**: 160–167.
307. Ahmed, M., A. Kadish, M. Paker, and J. Goldberger, Effect of physiologic and pharmacologic adrenergic stimulation on heart rate variability. *J. Am. Coll. Cardiol.*, 1994;**24**: 1082–1090.
308. Moser, M., M. Lehofer, A. Seminek, M. Lux, H-G. Zapotoczky, T. Kenner, and A. Noordergraaf, Heart rate variability as a prognostic tool in cardiology: a contribution to the problem from a theoretical point of view. *Circulation* 1994;**90**: 1078–1082.
309. Huikuri, H.V., T. Makikallio, K.E.J. Airaksinen, R. Mitrani, A. Castellanos, and R.J. Myerburg, Measurement of heart rate variability: a clinical tool or a research toy? *J. Am. Coll. Cardiol.*, 1999;**34**: 1878–1883.
310. Seely, A.L.E. and P.T. Macklem, Complex system and the technology of variability analysis. *Crit. Care.*, 2004;**8**: R367–384.
311. Stein, K.M., J.S. Borer, C. Hochreiter, P.M. Okin, E.M. Herrold, R.B. Cevereux, and P. Klgfield, Prognostic value and physiological correlates of heart rate variability in chronic severe mitral regurgitation. *Circulation*, 1993;**88**: 127–135.
312. Cygankiewicz, I., J.K. Wranicz, H. Bolinska, J. Zaslonka, and W. Zareba, Relationship between heart rate turbulence and heart rate, heart rate variability and number of premature beats in coronary patients. *J. Cardiovasc. Electrophysiol.*, 2004;**15**: 731–778.
313. Pichon, A., M. Roulaud, S. Antione-Jonville, C. de Bischop, and A. Denjean, Spectral analysis of heart rate variability: interchangeability between autoregressive analysis and fast Fourier transform. *J. Electrocardiol.*, 2006;**39**: 31–37.
314. Valkama, J.O., H.V. Huikuri, K.E.J. Airaksinen, M.L. Linnaluoto, and J.T. Takkunen, Determinants of frequency domain measures of heart rate variability in the acute and convalescent phases of myocardial infarction. *Cardiovasc. Res.*, 1994;**28**: 1273–1276.
315. Kuch, B., T. Parvanov, H.W. Hense, J. Axmann, and H.D. Bolte, Short-period heart rate variability in the general population as compared to patients with acute myocardial infarction from the same source population. *Ann. Noninvas. Electrocardiol.*, 2004;**9**: 113–120.
316. Grimm, W., J. Liedtke, and H-H. Muller, Prevalence of potential noninvasive arrhythmia risk predictors in healthy, middle-aged persons. *Ann. Nonivas. Electrocardiol.*, 2003;**8**: 37–46.
317. Bigger, J.R. Jr., J.L. Fleiss, R.C. Steinman, L.M. Rolnitzky, W.J. Schneider, and P.K. Stein, RR variability in healthy, middle-aged persons compared with patients with chronic coronary heart disease or recent acute myocardial infarction. *Circulation*, 1995;**91**: 1936–1943.
318. Mølgaard, H., K.E. Sørensen, and P. Bjerregaard, Circadian variation and influence of risk factors on heart rate variability in healthy subjects. *Am. J. Cardiol.*, 1991;**68**: 777–784.
319. Ramaekers, D., H. Ector, A.E. Aubert, A. Rubens, and F. van de Werf, Heart rate variability and heart rate in healthy volunteers. Is the female autonomic nervous system cardioprotective? *Eur. Heart. J.*, 1998;**19**: 1334–1341.

320. Pikkujämsä, S.M., T.H. Mäkikallio, L. Sourander, I.J. Räihä, P. Puuka, J. Skyttä, C-K. Peng, A.L. Goldberger, and H.V. Huikuri, Cardiac interbeat interval dynamics from childhood to senescence. Comparison of conventional and new measures based on fractals and chaos theory. *Circulation*, 1999;**100**: 393–399.
321. Bonnemeier, H., U.K.H. WIegand, A. Brandes, N. Kluge, H.A. Katus, G. Richardt, and J. Potratz, Circadian profile of cardiac autonomic nervous modulation in healthy subjects: differing effect of aging and gender on heart rate variability. *J. Cardiovasc. Electrophysiol.*, 2003;**14**: 791–799.
322. Umetani, K., D.H. Singer, R. McCraty, and M. Atkinson, Twenty-four hour time domain heart rate variability and heart rate: relations to age and gender over nine decades. *J. Am. Coll. Cardiol.*, 1998;**31**: 593–601.
323. Huikuri, H.V., S.M. Pikkujämsä, K.E.J. Airaksinen, M.J. Ikäheimo, A.O. Rantala, H. Kauma, M. Lilja, and Y.A. Kesäniemi, Sex-related differences in autonomic modulation of heart rate in middle-aged subjects. *Circulation*, 1996;**94**: 122–125.
324. Kuo, T.B., T. Lin, C.C.H. Yang, C-L. Li, C-F. Chen, and P. Chou, Effect of aging on gender differences in neural control of heart rate. *Am. J. Physiol. Heart. Circ. Physiol.*, 1999;**277**: H2233–2239.
325. Šlachta, R., P. Stejskal, M. Elfmark, J. Salinger, M. Kalina, and I. Rehova,. Age and spectral analysis of heart rate variability. *J. Auton. Nerv. Syst.*, 2002;**32**: 191–198.
326. Laitinen, T., L. Niskanen, G. Geelen, E. Lansimies, and J. Hartikainen, Age dependency of cardiovascular autonomic responses to head-up tilt in healthy subjects. *J. Appl. Physiol.*, 2004;**96**: 2333–2340.
327. Acharya, R.U., N. Kannanthal, O.W. Sing,L.Y. Ping, and T. Chua, Heart rate analysis in normal subjects of various age groups. *BioMed. Engineering. Online.*, 2004:**3**: 24.
328. Kuo, T.B.J. and C.C.H. Yang, Sexual dimorphism in the complexity of cardiac pacemaker activity. *Am. J. Physiol. Heart. Circ. Physiol.*, 2002;**283**: H1695–1702.
329. Mehta, S.K., D.M. Super, D. Connuck, A. Salvator, L. Singer, L.G. Fradley, R.A. Harcar-Sevcik, L. Kirchner, and E.S. Kaufman, Heart rate variability in healthy neonates. *Am. J. Cardiol.*, 2000;**89**: 50–53.
330. Longin, E., T. Schaible, T. Lenz, and S. König, Short term heart rate variability in healthy neonates: normative data and physiological observations. *Early. Hum. Develop.*, 2005;**81**: 663–671.
331. Massin, M. and G. von Bernuth, Normal ranges of heart rate variability during infancy and childhood. *Pediatr. Cardiol.*, 1997;**18**: 297–302.
332. Silvetti, M.S., F. Drago, and P. Ragonese, Heart rate variability in healthy children and adolescents is partially related to age and gender. *Int. J. Cardiol.*, 2001;**81**: 169–174.
333. Lenard, Z., P. Studinger, B. Merich, L. Kocsis, and M. Kollai, Maturation of cardiovagal autonomic function from childhood to young adult age. *Circulation*, 2004;**110**: 2307–2312.
334. Faulkner, M.S., D. Hathaway, and B. Tolley, Cardiovascular autonomic function in healthy adolescents. *Heart. Lung.*, 2003: **32**: 10–22.
335. Agelink, M.W., R. Malessa, B. Bauman, T. Majewski, F. Akila, T. Zeit, and D. Ziegler, Standardized tests of heart arte variability: normal ranges obtained from 309 healthy humans, and effects of ag, gender, and heart rate. *Clin. Auton. Res.*, 2001;**11**: 99–108.
336. Braune H- and U. Geisendörfer, Measurements of heart rate variations: influencing factors, normal values and diagnostic impact on diabetic autonomic neuropathy. *Diab. Res. Clin. Pract.*, 1995;**29**: 179–187.
337. Bergfeldt, L., M. Rosenquist, H. Vallin, R. Nordlander, and H. Astrom Screening for sinus node dysfunction by analysis of short-term sinus cycle variations on the surface electrocardiogram. *Am. Heart. J.*, 1995;**130**: 141–147.
338. Malik, M., K. Hnatkova, and A.J. Camm, Practicality of postinfarction risk assessment based on time-domain measurement of heart rate variability, in *Heart Rate Variability*, M. Malik and A.J. Camm, Editors. Armonk, NY: Futura Publishing, 1995, pp. 393–405.
339. Ewing, D.J., C.N. Martyn, R.J. Young, and B.F. Clarke, The value of cardiovascular autonomic function tests: 10 years experience in diabetes. *Diab. Care.*, 1985;**8**: 491–498.
340. O'Brien, I.A., J.P. O'Hare, and R.J.M. Corrall, Heart rate variability in healthy subjects: effects of age and the derivation of normal ranges for test of autonomic function. *Br. Heart. J.*, 1986;**55**: 348–354.
341. Howorka, K., J. Pumprla, A. Schabmann, Optimal parameters of short-term heart rate spectrogram for routine evaluation of diabetic cardiovascular autonomic neuropathy. *J. Auton. Nerv. Syst.*, 1998;**69**: 164–172.
342. Miličević, G., N. Lakušić, J. Szirovicza, D. Cerovec, M. Majsec, Different cut-off points of decreased heart rate variability for different groups of cardiac patients. *J. Cardiovasc. Risk.*, 2001;**8**: 93–102.
343. La Rovere, M.T., J.T. Jr. Bigger, F.I. Marcus, A. Mortara, and P.J. Schwartz for the ATRAMI (Autonomic Tone and Reflexes After Myocardial Infarction) Investigators, Baroreflex sensitivity and heart-rate variability in prediction of total cardiac mortality after myocardial infarction. *Lancet*, 1998;**351**: 478–484.
344. Rich, M.W., J.S. Saini, K.E. Kleiger, R.M. Carney, A. teVelde, and K.E. Freedland, Correlation of heart rate variability with clinical and angiographic variables and late mortality afer coronary angiography. *Am. J. Cardiol.*, 1988;**62**: 714–717.
345. Odemuyiwa, O., J. Poloniecki, M. Malik, T. Farrell, R. Xia, A. Staunton, P. Kulakowski, D. Ward, and J. Camm, Temporal influences on the prediction of postinfarction mortality by heart rate variability: a comparison with the left ventricular ejection fraction. *Br. Heart. J.*, 1994;**71**: 521–527.
346. Zuanetti, G., J.M. Neilson, R. Latini, E. Santoro, A.P. Maggioni, and D.J. Ewing, Prognostic significance of heart rate variability in post-myocardial infarction patients in the fibrinolytic era: The GISSI-2 results. *Circulation*, 1996;**94**: 432–436.
347. Copie, X., K. Hnatkova, A. Staunton, L. Fei, A.J. Camm, and M. Malik, Predictive power of increased heart rate versus depressed left ventricular ejection fraction and heart rate variability for risk stratification after myocardial infarction. Results of a two-year follow-up study. *J. Am. Coll. Cardiol.*, 1996;**27**: 270–276.
348. Lanza, G.A., V. Guido, M. Galeazzi, M. Mustilli, R. Natali, C. Ierardi, C. Milici, F. Burzotta, V. Pasceri, F. Tomassini, A. Lupi, and A. Maseri, Prognostic role of heart rate variability in patients with a recent acute myocardial infarction. *Am. J. Cardiol.* 1998;**82**: 1323–1328.
349. Whang, W. and J.T. Jr. Bigger, Comparison of the prognostic value of RR-interval variability after acute myocardial infarction in patients with versus those without diabetes mellitus. *Am. J. Cardiol.*, 2003;**92**: 247–252.
350. Balanescu, S., A.D. Corlan, M. DOrobantu, and L. Gherasim, Prognostic value of heart rate variability after acute myocardial infarction. *Med. Sci. Monit.*, 2004;**10**: CR307–315.

351. Stein, P.K., P.P. Domitrovich, H.V. Huikuri, and R.E. Kleiger for the CAST Investigators, Traditional and nonlinear heart rate variability. Are each independently associated with mortality after myocardial infarction. *J. Cardiovasc. Electrophysiol.*, 2005;**16**: 13–20.
352. Huikuri, H.V., P. Raatikainen, R. Moechr-Joergensen, J. Hartikainen, V. Virtanen, J. Boland, O. Anttonen, N. Hoest, L.V.A. Boersma, E.S. Platou, M.D. Messier, P-E. Bloch-Thomsen, for the Cardiac Arrhythmias and Risk Stratification after Acute Myocardial Infarction (CARISMA) study group, Prediction of fatal or near-fatal cardiac arrhythmia events in patients with depressed left ventricular function after an acute myocardial infarction. *Eur. Heart. J.*, 2009;**30**: 689–698.
353. Stein, K.M., J.S. Borer, C. Hochreiter, P.M. Okin, E.M. Herrold, R.B. Devereux, and P. Kligfield, Prognostic value and physiological correlated of heart rate variability in chronic severe mitral regurgitation. *Circulation*, 1993;**88**: 127–135.
354. Szabó, B.M., D.J. van Veldhuisen, N. van der Veer, J. Brouwer, P.A. De Graeff, H.J.G.M. Crijns, Prognostic value of heart rate variability in chronic congestive heart failure secondary to idiopathic or ischemic dilated cardiomyopathy. *Am. J. Cardiol.*, 1997;**79**: 978–980.
355. Ponikowski, P., S.D. Anker, T.P. Chua, R. Szelemej, M. Piepoli, S. Adamopoulos, K. Webb-Peploe, D. Harrington, A. Banasiak, K. Wrabec, and A.J.S. Coats, Depressed heart rate variability as an independent predictor of death in chronic congestive heart failure secondary to ischemic or idiopathic dilated cardiomyopathy. *Am. J. Cardiol.*, 1997;**79**: 1645–1650.
356. Nolan, J., P.D. Batin, R. Andrews, S.J. Lindsay, P. Brooksby, M. Mullen, W. Baig, A.D. Flapan, A. Cowley, R.J. Prescott, J.M. Neilson, and K.A. Fox, Prospective study of heart rate variability and mortality in chronic heart failure: results of the United Kingdom heart failure evaluation and assessment of risk trial (UK-heart). *Circulation*, 1998;**98**: 1510–1516.
357. Fauchier, L., D. Babuty, P. Cosnay, and J.P. Fauchier, Prognostic value of heart rate variability for sudden death and major arrhythmic events in patients with idiopathic dilated cardiomyopathy. *J. Am. Coll. Cardiol.*, 1999;**33**: 1203–1207.
358. Galinier, M., A. Pathak, J. Fourcade, C. Androdias, D. Curnier, S. Varnous, S. Boveda, P. Massabuau, M. Fauvel, J.M. Senard, and J.P. Bounhoure, Depressed low frequency power of heart rate variability as an independent predictor of sudden death in chronic heart failure. *Eur. Heart. J.*, 2000;**21**: 475–482.
359. Mäkikallio, T.H., H.V. Huikuri, U. Hintze, J. Videbaek, R.D. Mitrani, A. Castellanos, R.J. Myerburg, M. Møller, and DIAMOND Study Group (Danish Investigations of Arrhythmia and Mortality ON Dofetilide), Fractal analysis and time- and frequency-domain measures of heart rate variability as predictors of mortality in patients with heart failure. *Am. J. Cardiol.*, 2001;**87**: 178–182.
360. Bilchick, K.C., B. Fetics, R. Djoukeng, S.G. Fisher, R.D. Fletcher, S.N. Singh, E. Nevo, and R.D. Berger, Prognostic value of heart rate variability in chronic congestive heart failure (Veterans Affairs' Survival Trial of Antiarrhythmic Therapy in Congestive Heart Failure). *Am. J. Cardiol.*, 2002;**90**: 24–28.
361. Aronson, D., M.A. Mittleman, and A.J. Burger, Heasures of heart period variability as predictors of mortality in hospitalized patients with decompensated congestive heart failure. *Am. J. Cardiol.*, 2004;**93**: 59–63.
362. Algra, A., J.G.P. Tijssen, J.R.T.C. Roelandt, J. Pool, and J. Lubsen, Heart rate variability from 24-hour electrocardiography and the 2-year risk from sudden death. *Circulation*, 1993;**88**: 180–185.
363. Huikuri, H.V., T.H. Mäkikallio, K.E. Airaksinen, T. Seppänen, P. Puukka, I.J. Räihä, and L.B. Sourander, Power-law relationship of heart rate variability as a predictor of mortality in the elderly. *Circulation*, 1998;**97**: 2031–2036.
364. Sajadieh, A., O.W. Nielsen, V. Rasmussen, H.O. Hein, and J.F. Hansen, C-reactive protein, heart rate variability and prognosis in community subjects with no apparent heart disease. *J. Intern. Med.*, 2006;**260**: 377–387.
365. Stein, P.K., J.K. Barzilay, P.H.M. Chaves, S.Q. Mistretta, P.P. Domitrovich, J.S. Gottdiened, M.W. Rich, and R.E. Kleiger, Novel measures of heart rate variability predict cardiovascular mortality in older adults independent of traditional cardiovascular risk factors: The Cardiovascular Health Study (CHS). *J. Cardiovasc. Electropysiol.*, 2008;**19**: 1169–1174.
366. Grimm, W., J. Sharkova, M. Christ, R. Schneider, G. Schmidt, and B. Maisch, Heart rate turbulence following ventricular premature beats in healthy controls. *Ann. Noninvas. Electrocardiol.*, 2003;**8**: 127–131.
367. Lindgren, K.S., T.H. Mäkikallio, T. Seppänen, M.J.P. Ratikainen, A. Castellanos, R.J. Myerburg, and H.V. Huikuri, Heart rate turbulence after ventricular and atrial premature beats in subjects without structural heart disease, *J. Cardiovasc. Electrophysiol.*, 2003;**14**: 447–452.
368. Linden, D. and R.R. Diehl, Estimaton of baroreflex sensitivity using transfer function analysis: normal values and theoretical considerations. *Clin. Auton. Res.*, 1996;**6**: 157–161.
369. Madden, K.M., W.C. Levy, A. Jacobson, J.R. Stratton, The effect of aging on phenylephrine response in normal subjects. *J. Amer. Aging. Assoc.*, 2003;**26**: 3–10.
370. Wang, Y-P., Y-J. Cheng, and C-L. Huang, Spontaneous baroreflex measurement in the assessment of cardiac vagal control. *Clin. Auton. Res.*, 2004;**14**: 189–193.
371. Cooper, V.L,. M.W. Elliot, S.B. Pearson, C.M. Taylor, and R. Hainsworth, Daytime variability of carotic baroreflex function in healthy human subjects. *Clin. Auton. Res.*, 2007;**17**: 26–32.
372. Lauer, M.S., P.M. Okin, M.G. Larson, J.C. Evans, and D. Levy, Impaired heart rate response to graded exercise: prognostic implications of chronotropic incompetence in the Framingham Heart Study. *Circulation*, 1996;**93**: 1520–1526.
373. Morillo, C.A., D.L. Eckberg, K.A. Ellenbogen, L.A. Beightol, J.B. Hoag, K.U. Tahvanainen, T.A. Kuusela, and A.M. Diedrich, Vagal and sympathetic mechanisms in patients with orthostatic vasovagal syncope. *Circulation*, 1997;**96**: 2509–2513.
374. Machado, B.H. and M.J. Brody, Contribution of neurogenic mechanisms to control of intrinsic heart rate. *Am. J. Physiol.*, 1989;**256** (1 Pt 2): R231–235.
375. Hagendorff, A., B. Schumacher, S. Kirchhoff, B. Luderitz, and K. Willecke, Conduction disturbances and increased atrial vulnerability in connexin40-deficient mice analyzed by transesophageal stimulation. *Circulation*, 1999;**99**: 1508–1515.
376. Dobrzynski, H., M.R. Boyett, and R.H. Anderson, New insights into pacemaker activity: promoting understanding of sick sinus syndrome. *Circulation*, 2007;**115**: 1921–1932.
377. Asseman, P., B. Berzin, D. Desry, D. VIlarem, P. Durand, C. Delmotte, E.H. Sarkis, J. Lekieffre, and C. Thery, Persistent sinus nodal electrograms during abnormally prolonged postpacing atrial pauses in sick sinus syndrome in humans: sinoatrial block vs overdrive suppression. *Circulation*, 1983;**68**: 33–41.

378. Apfel, H. and M. Vassalle, Acetylcholine induces overdrive excitation in sheep Purkinje fibres. *Cardiovasc. Res.*, 1988;**22**: 425–438.
379. Satoh, H., Sino-atrial nodal cells of mammalian hearts: ionic currents and gene expression of pacemaker ionic channels. *J. Smooth. Muscle. Res.*, 2003;**39**: 175–193.
380. Barbuti, A. and D. DiFrancesco, Control of cardiac rate by "funny" channels in health and disease. *Ann. N. Y. Acad. Sci.*, 2008;**1123**: 213–223.
381. Braun, A.P., T.D. Phan, and P.V. Sulakhe, Muscarinic acetylcholine receptors in the sino-atrial node and right atrium of bovine heart. *Eur. J. Pharmacol.*, 1990;**189**: 201–215.
382. Maier, S.K., R.E. Westenbroek, T.T. Yamanushi, H. Dobrzynski, M.R. Boyett, W.A. Catterall, and T. Scheuer, An unexpected requirement for brain-type sodium channels for control of heart rate in the mouse sinoatrial node. *Proc. Natl. Acad. Sci. USA.*, 2003;**100**: 3507–3512.
383. Riccioni, G., Focus on ivabradine: a new heart rate-controlling drug. *Expert. Rev. Cardiovasc. Ther.*, 2009;**7**: 107–113.
384. Jalife, J., D.C. Michaels, and M. Delmar, Mechanisms of pacemaker synchronization in the sinus node. *Prog. Clin. Biol. Res.*, 1988;**275**: 67–91.
385. Guevara, M.R. and H.J. Jongsma, Phase resetting in a model of sinoatrial nodal membrane: ionic and topologic apects. *Am. J. Physiol.*, 1990;**258**: H734–747.
386. Fye, W.B., The origin of the heart beat: a tale of frogs, jelly-fish and turtles. *Circulation*, 1987;**76**: 493–500.
387. Boineau, J.P., R.B. Schuessler, T.E. Canavan, P.B. Corr, M.E. Cain, and J.L. Cox, The human atrial pacemaker complex. *J. Electrocardiol.*, 1989;**22** (Suppl): 189–197.
388. Schuessler, R.B., B.I. Bromberg, J.P. Boineau, Effect of neurotransmitters on the activation sequence of the isolated atrium. *Am. J. Physiol.*, 1990;**258**: H1632–1641.
389. Löffelholz, K. and A.J. Pappano, The parasympathetic neuroeffector junction of the heart. *Pharmacol. Rev.*, 1985;**37**: 1–24.
390. Miyazaki, T. and D.P. Zipes, Presynaptic modulation of efferent sympathetic and vagal neurotransmission in the canine heart by hypoxia, high K+, low pH, and adenosine. Possible relevance to ischemia-induced denervation. *Circ. Res.*, 1990;**66**: 289–301.
391. Boyett, M.R., H. Honjo, and I. Kodama, The sinoatrial node, a heterogeneous pacemaker structure. *Cardiovasc. Res.*, 2000;**47**: 658–687.
392. Jordan, D. and K.M. Spyer, Effects of acetylcholine on respiratory neurones in the nucleus ambiguus-retroambigualis complex of the cat. *J. Physiol.*, 1981;**320**: 103–111.
393. Rand, M.J., H. Majewski, and D.F. Story, Modulation of neuroeffector transmission, in *Cardiovascular Pharmacology*, M. Antonaccio, Editor. New York: Raven Press, 1990, pp. 229–292.
394. Bruck, H., A. Ulrich, S. Gerlach, J. Radke, and O.E. Brodde, Effects of atropine on human cardiac beta 1- and/or beta 2-adrenoceptor stimulation. *Naunyn. Schmiedebergs. Arch. Pharmacol.*, 2003;**367**: 572–577.
395. Valenzuela, D., X. Han, U. Mende, C. Fankhauser, H. Mashimo, P. Huang, J. Pfeffer, E.J. Neer, and M.C. Fishman, G alpha(o) is necessary for muscarinic regulation of Ca2+ channels in mouse heart. *Proc. Natl. Acad. Sci. USA.*, 1997;**94**: 1727–1732.
396. Zaza, A. and F. Lombardi, Autonomic indexes based on the analysis of heart rate variability: a view from the sinus node. *Cardiovasc. Res.*, 2001;**50**: 434–442.
397. Hainsworth, R., Physiological basis of heart rate variability, in *Dynamic Electrocardiography*, M. Malik and A.J. Camm, Editors. London: Blackwell Futura Publishing, 2004, pp. 3–12.
398. Warner, M.R., Time-course and frequency dependence of sympathetic stimulation-evoked inhibition of vagal effects at the sinus node. *J. Auton. Nerv. Syst.*, 1995;**52**: 23–33.
399. Kiviniemi, A.M., A.J. Hautala, T. Seppänen, T.H. Mäkikallio, H.V. Huikuri, and M.P. Tulppo, Saturation of high-frequency oscillations of R-R intervals in healthy subjects and patients after acute myocardial infarction during ambulatory conditions. *Am. J. Physiol. Heart. Circ. Physiol.*, 2004;**287**: H1921–1927.
400. Zhang, H.and M. Vassalle, Mechanisms of adrenergic control of sino-atrial node discharge. *J. Biomed. Sci.*, 2003;**10**: 179–192.
401. Ecker, P.M., .C-C. Lin, J. Powers, B.K. Kobilka, A.N. Dubin, and C. Bernstein, Effect of targeted deletions of β_1- and β_2-adrenrgic-receptor subtypes on heart rate variability. *Am. J. Physiol. Heart. Circ. Physiol.*, 2006;**290**: H192–199.
402. Brown, R.A. and R.G. Carpentier, Alpha-adrenoceptor-mediated effects of norepinephrine on the guinea pig sinus node. *J. Electrocardiol.*, 1988; 2**1**: 213–217.
403. Allen, J.M., P. Gjörstrup, J.A. Björkman, L. Ek, T. Abrahamsson, and S.R. Bloom, Studies on cardiac distribution and function of neuropeptide Y. *Acta. Physiol. Scand.* 1986;**126**: 405–411.
404. Gray, A.L., T.A. Johnson, J.M. Lauenstein, S.S. Newton, J.L. Ardell, and V.J. Massari, Parasympathetic control of the heart. III. Neuropeptide Y-immunoreactive nerve terminals synapse on three populations of negative chronotropic vagal preganglionic neurons. *J. Appl. Physiol.*, 2004;**96**: 2279–2287.
405. Kilborn, M.J., E.K. Potter, and D.I. McCloskey,. Neuromodulation of the cardiac vagus: comparison of neuropeptide Y and related peptides. *Regul. Pept.*, 1985;**12**: 155–161.
406. Revington, M.L. and D.I. McCloskey, Sympathetic-parasympathetic interactions at the heart, possibly involving neuropeptide Y, in anaesthetized dogs. *J. Physiol.*, 1990;**428**: 359–370.
407. Warner, M.and M.N. Levy, Neuropeptide Y as a putative modulator of the vagal effects on heart rate. *Circ. Res.*, 1989;**64**: 882–889.
408. Balligand, J.L., Regulation of cardiac beta-adrenergic response by nitric oxide. *Cardiovasc. Res.*, 1999;**43**: 607–620.
409. Chowdhary, S. and J.N. Townend, Role of nitric oxide in the regulation of cardiovascular autonomic control. *Clin. Sci. (Lond).*, 1999;**97**: 5–17.
410. Krukoff, T.L., Central actions of nitric oxide in regulation of autonomic functions. *Brain. Res. Rev.*, 1999;**30**: 52–65.
411. Zanzinger, J., Role of nitric oxide in the neural control of cardiovascular function. *Cardiovasc. Res.*, 1999;**43**: 639–649.
412. Sartori, C., M. Lepori, and U. Scherrer, Interactions between nitric oxide and the cholinergic and sympathetic nervous system in cardiovascular control in humans. *Pharmacol. Therap.*, 2005;**106**: 209–220.
413. Feron, O., C. Dessy, D.J. Opel, M.A. Arstall, R.A. Kelly, and T. Michel, Modulation of the endothelial nitric-oxide synthsecaeolin interaction in cardiac myocytes. Implications for the autonomic regulation of heart rate. *J. Biol. Chem.*, 1998;**273**: 30249–30254.
414. Herring, N., S. Golding, and D.J. Paterson, Pre-synaptic NO-cGMP pathway modulates vagal control of heart rate in isolated adult guinea pig atria. *J. Mol. Cell. Cardiol.*, 2000;**32**: 1795–1804.
415. Picker, O., T.W. Scheeren, and J.O. Arndt, Nitric oxide synthases in vagal neurons are crucial for the regulation of heart rate in awake dogs. *Basic. Res. Cardiol.*, 2001;**96**: 395–404.

416. Heaton, D.A., S. Golding, C.P. Bradley, T.A. Dawson, S. Cai, K.M. Channon, and D.J. Paterson, Targeted nNOS gene transfer into the cardiac vagus rapidly increases parasympathetic function in the pig. *J. Mol. Cell. Cardiol.*, 2005;**39**: 159–164.
417. Chowdhary, S., A.M. Marsh, J.H. Coote, and J.N. Townend, Nitric oxide and cardiac muscarinic control in humans. *Hypertension*, 2004;**43**: 1023–1028.
418. Chowdhary, S., S.L. Nuttall, J.H. Coote, and J.N. Townend, L-arginine augments cardiac vagal control in healthy human subjects. *Hypertension*, 2002;**39**: 51–56.
419. Vanoli, E., G.M. De Ferrari, M. Stramba-Badiale, S.S. Jr. Hull, R.D. Foreman, and P.J. Schwartz, Vagal stimulation and prevention of sudden death in conscious dogs with a healed myocardial infarction. *Circ. Res.*, 1991;**68**: 1471–1481.
420. Li, M., C. Zheng, T. Sato, T. Kawada, M. Sugimachi, and K. Sunagawa, Vagal nerve stimulation markedly improves long-term survival after chronic heart failure in rats. *Circulation*, 2004;**109**: 120–124.
421. Binkley, P.F., E. Nunziatta, Y. Liu-Stratton, and G. Cooke, A polymorphism of the endothelial nitric oxide synthase promoter is associated with an increase in autonomic imbalance in patients with congestive heart failure. *Am. Heart. J.*, 2005;**149**: 342–348.
422. Jordan, D., Vagal control of the heart: central serotonergic (5-HT) mechanisms. *Exp. Physiol.*, 2005;**90**: 175–181.
423. Okoshi, K., M. Nakayama, X. Yan, M.P. Okoshi, A.J. Schuldt, M.A. Marchionni, and B.H. Lorell, Neuregulins regulate cardiac parasympathetic activity: muscarinic modulation of beta-adrenergic activity in myocytes from mice with neuregulin-1 gene deletion. *Circulation*, 2004;**110**: 713–717.
424. Hrushesky, W.J., D.J. Fader, J.S. Berestka, M. Sommer, J. Hayes, and F.O. Cope, Diminishment of respiratory sinus arrhythmia foreshadows doxorubicin-induced cardiomyopathy. *Circulation*, 1991;**84**: 697–707.
425. Beaulieu, P. and C. Lambert, Peptidic regulation of heart rate and interactions with the autonomic nervous system *Cardiovasc. Res.*, 1998;**37**: 578–585.
426. Herring, N. and D.J. Paterson, Neuromodulators of peripheral cardiac sympatho-vagal balance. *Exp. Physiol.*, 2009;**94**: 46–53.
427. Woods, R.L., Cardioprotective functions of atrial natriuretic peptide and B-type natriuretic peptide: a brief review. *Clin. Exp. Pharmacol. Physiol.*, 2004;**31**: 791–794.
428. Anja, G., A.G. Teschemacher, and C.D. Johnson, Cotransmission in the autonomic nervous system. *Exp. Physiol.*, 2009;**94**:18–19.
429. Lab, M.J., Mechanosensitivity as an integrative system in heart: an audit. *Prog. Biophys. Mol. Biol.*, 1999;**71**: 7–27.
430. Kohl, P., P. Hunter, and D. Noble, Stretch-induced changes in heart rate and rhythm: clinical observations, experiments and mathematical models. *Prog. Biophys. Mol. Biol.*, 1999;**71**: 91–138.
431. Taggart, P. and P.M. Sutton, Cardiac mechano-electric feedback in man: clinical relevance. *Prog. Biophys. Mol. Biol.*, 1999;**71**: 139–154.
432. Rajala, G.M., J.H. Kalbfleisch, and S. Kaplan, Evidence that blood pressure controls heart rate in the chick embryo prior to neural control. *J. Embryol. Exp. Morphol.*, 1976;**36**: 685–695.
433. Bernardi, L., F. Keller, M. Sanders, P.S. Reddy, B. Griffith, F. Meno, and M.R. Pinsky, Respiratory sinus arrhythmia in the denervated human heart. *J. Appl. Physiol.*, 1989;**67**: 1447–1455.
434. Conci, F., M. Di Rienzo, and P. Castiglioni, Blood pressure and heart rate variability and baroreflex sensitivity before and after brain death. *J. Neurol. Neurosurg. Psychiatr.*, 2001;**71**: 621–631.
435. Harris, K.F. and K.A. Matthews, Interactions between autonomic nervous system activity and endothelial function: a model for the development of cardiovascular disease. *Psychosom. Med.*, 2004;**66**: 153–164.
436. Story, D.F. and J. Ziogas, Interaction of angiotensin with noradrenergic neuroeffector transmission. *Trends. Pharmacol. Sci.*, 1987;**8**: 269–271.
437. Zimmermann, B.G., E.J. Sybertz, and P.C. Wong, Interaction between sympathetic and renin-angiotensin system. *J. Hypertens.*, 1984;**2**: 581–587.
438. Thayer, J.F., M.M. Merrit, J.J. III Sollers, A.B. Zonderman, M.K. Evans, S. Yie, and D.R. Abernethy, Effect of angiotensin-converting enzyme insertion/deletion polymorphism DD genotype on high-frequency heart rate variability in African Americans. *Am. J. Cardiol.*, 2003;**92**: 1487–1490.
439. Ashley, E.A., A. Kardos, S.J. Jack, W. Habenbacher, M. Wheeler, M. Kim, J. Froning, J. Myers, G. Whyte, V. Froelicher, and P. Douglas, Angiotensin-converting enzyme genotype predicts cardiac and autonomic responses to prolonged exercise. *J. Am. Coll. Cardiol.*, 2006;**48**: 523–531.
440. Osterziel, K.J., R. Dietz, W. Schmid, K. Mikulaschek, J. Manthey, and W. Kubler, ACE inhibition improves vagal reactivity in patients with heart failure. *Am. Heart. J.*, 1990;**120**: 1120–1129.
441. Binkley, P.F., G.J. Haas, R.C. Starling, E. Nunziata, P.A. Hatton, C.V. Leier, and R.J. Cody, Sustained augmentation of parasympathetic tone with angiotensin-converting enzyme inhibition in patients with congestive heart failure. *J. Am. Coll. Cardiol.*, 1993;**21**: 655–661.
442. Heusser, K., J. Vitkovsky, R.E. Schmieder, and H.P. Schobel, AT1 antagonism by eprosartan lowers heart rate variability and baroreflex gain. *Auton. Neurosci.*, 2003;**107**: 45–51.
443. Schmidt, B.M., K. Horisberger, M. Feuring, A. Schultz, and M. Wehling, Aldosterone blunts human baroreflex sensitivity by a nongenomic mechanism. *Exp. Clin. Endocrinol. Diabetes.*, 2005;**113**: 252–256.
444. Nakashima, A., J.A. Angus, C.I. Johnston, Chronotropic effects of angiotensin I, angiotensin II, bradykinin and vasopressin in guinea pig atria. *Eur. J. Pharmcol.*, 1982;**81**: 479–485.
445. Tesfamariam, B., G.T. Allen, and J.R. Powell, Bradykinin β_2 receptor-mediated chronotropic effect of bradykinin in isolated guinea pig atria. *Eur. J. Pharmacol.*, 1995;**281**: 17–20.
446. Smagin, G.N., S.C. Heinrichs, and A.J. Dunn, The role of CRH in behavioral responses to stress. *Peptides*, 2001;**22**: 712–724.
447. Grammatopoulos, D.K. and G.P. Chrousos, Functional characteristics of CRH receptors and potential clinical applications of CRH-receptor antagonists. *Trends. Endocrinol. Metab.*, 2002;**13**: 436–444.
448. Nijsen, M.J.M.A., G. Croiset, R. Stam, A. Bruijnzeel, M. Diamant, D. de Wied, and V.M. Wiegant, The Role of the CRH Type 1 receptor in autonomic responses to corticotropin-releasing hormone in the rat. *Neuropsychopharmacology*, 2000;**22**: 388–399.
449. Arlt, J., H. Jahn, M. Kellner, A. Ströhle, A. Yassouridis, and K. Wiedemann, Modulation of sympathetic activity by corticotropin-releasing hormone and atrial natriuretic peptide. *Neuropeptides*, 2003;**37**: 362–368.
450. Parkes, D.G., R.S. Weisinger, and C.N. May, Cardiovascular actions of CRH and urocortin: an update. *Peptides*, **22**: 821–827.

451. Stiedl, O. and M. Meyer, Cardiac dynamics in corticotrophin-release factor receptor subtype-2 deficient mice. *Neuropeptides*, 2003;**37**: 3–16.
452. Schubert, C., M. Lambertz, R.A. Nelesen, W. Bardwell, J-B. Choi, J.E. Dimsdale, Effects of stress on heart rate complexity - a comparison between short-term and chronic stress. *Biol. Psychol.*, 2009;**80**: 325–332.
453. Benton, L.A. and F.E. Yates, Ultradian adrenocortical and circulatory oscillations in conscious dogs. *Am. J. Physiol. Regulatory. Integrative. Comp. Physiol.*, 1990;**258**: R578–590.
454. Fallo F, P. Maffei, A. Dalla Pozza, M. Carli, P. Della Mea, M. Lupia, F. Rabbia, and N. Sonino, Cardiovascular autonomic function in Cushing's syndrome. *J. Endocrinol. Invest.*, 2009;**32**: 41–45.
455. Muniyappa, R., M. Montagnani, K.K. Koh, and M.J. Quon, Cardiovascular actions of insulin. *Endocr. Rev.*, 2007;**28**: 463–491.
456. Muntzel, M.S., E.A. Anderson, A.K. Johnson, and A.L. Mark, Mechanisms of insulin action on sympathetic nerve activity. *Clin. Exp. Hypertens.*, 1995;**17**: 39–50.
457. Scherrer, U. and C. Sartori, Insulin as a vascular and sympathoexcitatory hormone: implications for blood pressure regulation, insulin sensitivity, and cardiovascular morbidity. *Circulation*, 1997;**96**: 4104–4113.
458. Van De Borne, P., M. Hausberg, R.P. Hoffman, A.L. Mark, and E.A. Anderson, Hyperinsulinemia produces cardiac vagal withdrawal and nonuniform sympathetic activation in normal subjects. *Am. J. Physiol. Regulatory. Integrative. Comp. Physiol.*, 1999;**276**(1): R178–183.
459. Hausberg, M., R.P. Hoffman, V.K. Somers, C.A. Sinkey, A.L.Mark, and E.A. Anderson, Contrasting autonomic and hemodynamic effects of insulin in healthy elderly versus young subjects. *Hypertension*, 1997;**29**: 700–705.
460. Paolisso, G., M. Varricchio, and F. D'Onofrio, Glucose intolerance in the elderly: an open debate. *Arch. Gerontol. Geriatr.*, 1990;**11**: 125–132.
461. Pathak, A., F. Smith, M. Galinier, P. Verwaerde, P. Rouet, P. Philip-Couderc, J.L. Monstastruc, and J.M. Senard, Insulin downregulated M2-muscarinic receptors in adult rat atrial cardiomyocytes: a link between obesity and cardiovascular complications. *Int. J. Obes.*, 2005;**29**: 176–182.
462. Bergholm, R., J. Westerbacka, S. Vehkavaara, A. Seppälä-Lindroos, T. Goto, and H. Yki-Järvinen, Insulin sensitivity regulates autonomic control of heart rate variation independent of body weight in normal subjects. *J. Clin. Endocrinol. Metab.*, 2001;**86**: 1403–1409.
463. Lindmark, S., U. Wiklund, P. Bjerle, and J.W. Eriksson, Does the autonomic nervous system play a role in the development of insulin resistance? A study on heart rate variability in first-degree relatives of Type 2 diabetes patients and control subjects. *Diabet. Med.*, 2003;**20**: 399–405.
464. Rayner, D.V. and P. Trayhurn, Regulation of leptin production: sympathetic nervous system interactions. *J. Mol. Med.*, 2001;**79**: 8–20.
465. Grassi, G., Leptin, sympathetic nervous sustem, and baroreflex function. *Curr. Hypert. Rep.*, 2004;**6**: 236–240.
466. Flanagan, D.E., J.C. Vaile, G.W. Petley, D.I. Phillips, I.F. Godsland, P. Owens, V.M. Moore, R.A. Cockington, and J.S. Robinson, Gender differences in the relationship between leptin, insulin resistance and the autonomic nervous system. *Regulat. Peptides.*, 2007;**140**: 37–42.
467. Takabatake, N., H. Nakamura, O. Minamihaba, M. Inage, S. Inoue, S. Kagaya, M. Yamaki, and H. Tomoile, A novel pathophysiologic phenomenon in cachexic patients with chronic obstructive pulmonary disease. The relationship between the circadian rhythm of circulating leptin and the very low frequency component of heart rate variability. *Am. J. Respir. Crit. Care. Med.*, 2001;**163**: 1314–1319.
468. Kadowaki, T. and T. Yamauchi, Adiponectin and adiponectin receptors. *Endocr. Rev.*, 2005 May;**26**(3): 439–451.
469. Katagiri, H., T. Yamada, and Y. Oka, Adiposity and cardiovascular disorders: disturbance of the regulatory system consisting of humoral and neuronal signals. *Circ. Res.*, 2007; 101: 27–39.
470. Hoyda, T.D., W.K. Samson, and A.V. Ferguson, Adiponectin depolarizes parvocellular paraventricular nucleus neurons controlling neuroendocrine and autonomic function. *Endocrinology*, 2009;**150**: 832–840.
471. Hoyda, T.D., P.M. Smith, and A.V. Ferguson, Adiponectin acts in the nucleus of the solitary tract to decrease blood pressure by modulating the excitability of neuropeptide Y neurons. *Brain. Res.*, 2009;**1256**: 76–84.
472. Wakabayashi, S. and Y. Aso, Adiponectin concentrations in sera from patients with type 2 diabetes are negatively associated with sympathovagal balance as evaluated by power spectral analysis of heart rate variation. *Diabetes. Care.*, 2004;**27**: 2392–2397.
473. Lam, J.C., A. Xu, S. Tam, P.I. Khong, T.J. Yao, D.C. Lam, A.Y. Lai, B. Lam, K.S. Lam, and S.M. Mary, Hypoadiponectinemia is related to sympathetic activation and severity of obstructive sleep apnea. *Sleep*, 2008;**31**: 1721–1727.
474. Sprague, A.H. and R.A. Khalil, Inflammatory cytokines in vascular dysfunction and vascular disease. *Biochem. Pharmacol.*, 2009;**78**: 539–552.
475. Reyes-García, M.G. and F. García-Tamayo, A neurotransmitter system that regulates macrophage proinflammatory functions. *J. Neuroimmunol.*, 2009;**216**: 20–31
476. Marsland, A.L., P.J. Gianaros, A.A. Prather, J.R. Jennings, S.A. Neumann, and S.B. Manuck, Stimulated production of proinflammatory cytokines covaries inversely with heart rate variability. *Psychosom. Med.*, 2007;**69**: 709–716.
477. Heansel, A., P.J. Mills, R.A. Nelesen, M.G. Ziegler, and J.E. Dimsdale, The relationship between heart rate variability and inflammatory markers in cardiovascular disease. *Psychoneuroendocrinol*, 2008;**33**: 1305–1312.
478. Dart, A.M., X-J. Du, and B.A. Kingwell, Gender, sex hormones and autonomic nervous control of the cardiovascular system. *Cardiovasc. Res.*, 2002;**53**: 678–687.
479. McCabe, P.M., S.W. Porges, and C.S. Carter, Heart period variability during estrogen exposure and withdrawal in female rats. *Physiol. Behav.*, 1981;**26**: 535–538.
480. Saeki, Y., F. Atogami, K. Takahashi, and T. Yoshizawa, Reflex control of autonomic function induced by posture change during the menstrual cycle. *J. Auton. Nerv. Syst.*, 1997;**66**: 69–74.
481. Evans, J.M., M.G. Ziegler, A.R. Patwardhan, J.B. Ott, C.S. Kim, F.M. Leonelli, and C.F. Knapp, Gender differences in autonomic cardiovascular regulation: spectral, hormonal, and hemodynamic indexes. *J. Appl. Physiol.*, 2001;**91**: 2611–2618.
482. Leicht, A.S., D.A. Hirning, and G.D. Allen, Heart rate variability and endogenous sex hormones during the menstrual cycle in young women. *Exp. Physiol.*, 2003;**88**: 441–446.
483. Christ, M., K. Seyffart, H-C. Tillmann, and M. Wehling, Hormone replacement in postmenoupasual women: impact of

progestogens on autonomic tone and blood pressure regulation. *Menopause*, 2002;**9**: 127–136.
484. Fernandes, E.O., R.S. Moraes, E.L. Ferlin, M.C.O. Wender, and J.P. Ribeiro, Hormone replacement therapy does not affect the 24-hour heart rate variability in ostmenopausal women: results of a randomized, placebo-controlled trial with two regimens. *Pacing Clin. Electrophysiol.*, 2005;**28**: S172–177.
485. Benarroch, E.E., Thermoregulation: recent concepts and remaining questions. *Neurology*, 2007;**69**: 1293–1297.
486. Kumar, V.M., R. Vetrivelan, and H.N. Mallick, Noradrenergic afferents and receptors in the medial preoptic area: neuroanatomical and neurochemical links between the regulation of sleep and body temperature. *Neurochem. Int.*, 2007;**50**: 783–790.
487. Weinert, D. and J. Waterhouse, The circadian rhythm of core temperature: effects of physical activity and aging. *Physiol. Behav.*, 2007;**90**: 246–256.
488. Potter, E.K., P. Parker, A.C. Caine, and E.R. Lumbers, Potentiation of cardiac vagal action by cold. *Clin. Sci. (Lond).*, 1985;**68**: 165–169.
489. Lee, K., D.N. Jackson, D.L. Cordero, T. Nishiyasu, J.K. Peters, and G.W. Mack, Change in spontaneous baroreflex control of pulse interval during heat stress in humans. *J. Appl. Physiol.*, 2003;**95**: 1789–1798.
490. Liu, W., Z. Lian, and Y. Liu, Heart rate variability at different thermal comfort levels. *Eur. J. Appl. Physiol.*, 2008;**103**:361–366.
491. Tentolouris, N., C. Tsigos, D. Perea, E. Koukou, D. Kyriaki, E. Kitsou, S. Daskas, Z. Daifotis, K. Makrilakis, S.A. Raptis, and N. Katsilambros, Differential effects of high-fat and high-carbohydrate isoenergetic meals on cardiac autonomic nervous system activity in lean and obese women. *Metabolism*, 2003;**52**: 1426–1432.
492. Kitney, R.I. and O. Rompelman, Thermal entrainment patterns in heart rate variability. *Proc. Physiol. Soc.*, 1977;**270**: 41–42.
493. Kawashima, T., The autonomic nervous system of the human heart with special reference to its origin, course, and peripheral distribution. *Anat. Embryol. (Berl).*, 2005. **209**: 425–438.
494. Wang, J., M. Irnaten, R.A. Neff, P. Venkatesan, C. Evans, A.D. Loewy, T.C. Mettenleiter, and D. Mendelowitz, Synaptic and neurotransmitter activation of cardiac vagal neurons in the nucleus ambiguus. *Ann. NY. Acad. Sci.*, 2001;**940**: 237–246.
495. Cheng, Z., H. Zhang, S.Z. Guo, R. Wurster, and D. Gozal,. Differential control over vagal efferent postganglionic neurons in rat intrinsic cardiac ganglia by neurons in the NA and the DmnX: anatomical evidence. *Am. J. Physiol. Regul. Integr. Comp. Physiol.*, 2004;**286**: R625–633.
496. Armour, J.A., D.A. Murphy, B.X. Yuan, S. Macdonald, and D.A. Hopkins, Gross and microscopic anatomy of the human intrinsic cardiac nervous system. *Anat. Rec.*, 1997;**247**: 289–298.
497. Hou, Y., B.J. Scherlag, J. Lin, Y. Zhang, Z. Lu, K. Truong, E. Patterson, R. Lazzara, W.M. Jackman, and S.S. Po, Ganglionated plexi modulate extrinsic cardiac autonomic nerve input: Effects on sinus rate, atrioventricular conduction, refractoriness, and inducibility of atrial fibrillation. *J. Am. Coll. Cardiol.*, 2007;**50**: 61–68.
498. Levy, M.N., Neural control of cardiac function. *Baillieres. Clin. Neurol.*, 1997;**6**: 227–244.
499. Keyl, C., A. Schneider, M. Dambacher, and L. Bernardi, Time delay of vagally mediated cardiac baroreflex response varies with autonomic cardiovascular control. *J. Appl. Physiol.*, 2001;**91**: 283–289.
500. Taylor, W.E., D. Jordan, and J.H. Coote, Central control of the cardiovascular and respiratory systems and the interactions in vertebrates. *Physiol. Rev.*, 1999;**79**: 855–916.
501. Bałkowiec, A. and P. Szulczyk, Properties of postganglionic sympathetic neurons with axons in the right thoracic vagus. *Neuroscience*, 1992;**48**: 159–167.
502. Fu, L.W. and J.C. Longhurst, Regulation of cardiac afferent excitability in ischemia. *Handb. Exp. Pharmacol.*, 2009;**194**: 185–225.
503. Arora, R.C., J.L. Ardell, and J.A. Armour, Cardiac denervation and cardac function. *Curr. Interven. Cardiol. Rep.*, 2000;**2**: 188–195.
504. Kamath, M.V., G. Tougas, D. Fitzpatrick, E.L. Fallen, R. Watteel, G. Shine, and A.R. Upton, Assessment of the visceral afferent and autonomic pathways in response to esophageal stimulation in control subjects and in patients with diabetes. *Clin. Invest. Med.*, 1998;**21**: 100–113.
505. Fahim, M., Cardiovascular sensory receptors and their regulatory mechanisms. *Indian. J. Physiol. Pharmacol.*, 2003;**47**: 124–146.
506. Granzier, H.L. and S. Labeit, The giant protein titin: a major player in myocardial mechanics, signaling, and disease. *Circ. Res.*, 2004;**94**: 284–295.
507. Armour, J.A., Cardiac neuronal hierarchy in health and disease. *Am. J. Physiol. Regul. Integr. Comp. Physiol.*, 2004;**287**: R262–271.
508. Pyetan, E., E. Toledo, O. Zoran, and S. Akselrod, Parametric description of cardiac vagal control. *Auton. Neurosci.*, 2003;**109**: 42–52.
509. Paton, J.F., P. Boscan, A.E. Pickering, and E. Nalivaiko, The yin and yang of cardiac autonomic control: vago-sympathetic interactions revisited. *Brain. Res. Brain. Res. Rev.*, 2005;**49**: 555–565.
510. Samuels, M.A., The brain-heart connection. *Circulation*, 2007;**116**: 77–84.
511. Baron, S.A., Z. Rogovski, and J. Hemli,. Autonomic consequences of cerebral hemisphere infarction. *Stroke*, 1994;**25**: 113–116.
512. Svigelj, V., A. Grad, and T. Kiauta, Heart rate variability, norepinephrine and ECG changes in subarachnoid hemorrhage patients. *Acta. Neurol. Scand.*, 1996;**94**: 120–126.
513. Tomson, T., M. Ericson, C. Ihrman, and L.E. Lindblad,. Heart rate variability in patients with epilepsy. *Epilepsy. Res.*, 1998;**30**: 77–83.
514. Ako, J., K. Sudhir, H.M. Farouque, Y. Honda, and P.J. Fitzgerald, Transient left ventricular dysfunction under severe stress: brain-heart relationship revisited. *Am. J. Med.*, 2006;**119**: 10–17.
515. Dabrowska, B., A. Dabrowski, P. Pruszczyk, A. Skrobowski, and B. Wocial, Heart rate variability before sudden blood pressure elevations or complex cardiac arrhythmias in phaeochromocytoma. *J. Hum. Hypertens.*, 1996;**10**: 43–50.
516. Nguyen, S.B., C. Cevik, M. Otahbachi, A. Kumar, L.A. Jenkins, and K. Nugent, Do comorbid psychiatric disorders contribute to the pathogenesis of tako-tsubo syndrome? A review of pathogenesis. *Congest. Heart. Fail.*, 2009;**15**: 31–34.
517. Fuler, J.L., Genetic variability in some physiological constants of dogs. *Am. J. Physiol.*, 1951;**166**: 20–24.
518. Kreutz, R., B. Struk, P. Stock, N. Hübner, D. Ganten, and K. Lindpaintner, Evidence for primary genetic determination of heart rate regulation: chromosomal mapping of a genetic locus in the rat. *Circulation*, 1997;**96**: 1078–1081.
519. Martin, L.J., A.G. Comuzzie, G.E. Sonnenberg, J. Myklebust, R. James, J. Marks, J. Blangero, and A.H. Kissebah, Major

quantitative trait locus for resting heart rate maps to a region on chromosome 4. *Hypertension*, 2004;**43**: 1146–1151.
520. Wilk, J.B., R.H. Myers, Y. Zhang, C.E. Lewis, L. Atwood, P.N. Hopkins, and R.C. Ellison. Evidence for a gene influencing heart rate on chromosome 4 among hypertensives. *Hum. Genet.*, 2002; 111: 207–213.
521. Rice, T., P. An, J. Gagnon, A.S. Leon, J.S. Skinner, J.H. Wilmore, C. Bouchard, and D.C. Rao, Heritability of HR and BP response to exercise training in the HERITAGE Family Study. *Med. Sci. Sports. Exerc.*, 2002; 34: 972–979.
522. Rice, T., T. Rankinen, Y.C. Chagnon, M.A. Province, L. Pérusse, A.S. Leon, J.S. Skinner, J.H. Wilmore, C. Bouchard, and D.C. Rao, Genomewide linkage scan of resting blood pressure: HERITAGE Family Study. Health, Risk Factors, Exercise Training, and Genetics. *Hypertension*, 2002;**39**: 1037–1043.
523. Laramie, J.M., J.B. Wilk, S.C. Hunt, R.C. Ellison, A. Chakravarti, E. Boerwinkle, and R.H. Myers, Evidence for a gene influencing heart rate on chromosome 5p13–14 in a meta-analysis of genome-wide scans from the NHLBI Family Blood Pressure Program. *BMC. Med. Genet.*, 2006;**7**: 17.
524. Sajadieh, A., V. Rasmussen, H.O. Hein, and J.F. Hansen, Familial predisposition to premature heart attack and reduced heart rate variability. *Am. J. Cardiol.*, 2003;**92**: 234–236.
525. Singh, J.P., M.G. Larson, C.J. O'Donnell, H. Tsuji, D. Corey, and D. Levy, Genome scan linkage results for heart rate variability (the Framingham Heart Study). *Am. J. Cardiol.*, 2002;**90**: 1290–1293.
526. Schoots, O., T. Voskoglou, and H.H. Van Tol, Genomic organization and promoter analysis of the human G-protein-coupled K+ channel Kir3.1 (KCNJ3/HGIRK1). *Genomics*, 1997;**39**: 279–288.
527. Rempel, N., S. Heyers, H. Engels, E. Sleegers, and O.K. Steinlein, The structures of the human neuronal nicotinic acetylcholine receptor beta2- and alpha3-subunit genes (CHRNB2 and CHRNA3). *Hum. Genet.*, 1998;**103**: 645–653.
528. Singh, J.P., M.G. Larson, C.J. O'Donnell, H. Tsuji, J.C. Evans, and D. Levy, Heritability of heart rate variability: the Framingham Heart Study. *Circulation*, 1999;**99**: 2251–2254.
529. Singh, J.P., M.G. Larson, C.J. O'Donnell, and D. Levy, Genetic factors contribute to the variance in frequency domain measures of heart rate variability. *Auton. Neurosci.*, 2001;**90**: 122–126.
530. Sinnreich, R., Y. Friedlander, D. Sapoznikov, and J.D. Kark, Familial aggregation of heart rate variability based on short recordings–the kibbutzim family study. *Hum. Genet.*, 1998;**103**: 34–40.
531. Piha, S.J., T. Rönnemaa, and M. Koskenvuo, Autonomic nervous system function in identical twins discordant for obesity. *Int. J. Obes. Relat. Metab. Disord.*, 1994;**18**: 547–550.
532. Boomsma, D.I., G.C. van Baal, and J.F. Orlebeke, Genetic influences on respiratory sinus arrhythmia across different task conditions. *Acta. Genet. Med. Gemellol. (Roma).*, 1990;**39**: 181–191.
533. Snieder, H., D.I. Boomsma, L.J. Van Doornen, and E.J. De Geus, Heritability of respiratory sinus arrhythmia: dependency on task and respiration rate. *Psychophysiology*, 1997;**34**: 317–328.
534. Kupper, N.H., G. Willemsen, M. van den Berg, D. de Boer, D. Posthuma, D.I/Boomsma, and E.J. de Geus, Heritability of ambulatory heart rate variability. *Circulation*, 2004;**110**: 2792–2796.
535. Wang, X., X. Ding, S. Su, Z. Li, H. Riese, J.F. Thayer, F. Treiber, and H. Snieder, Genetic influences on heart rate variability at rest and during stress. *Psychophysiology*, 2009;**46**: 458–465.
536. Vaccarino, V., R. Lampert, J.D. Bremner, F. Lee, S. Su, C. Maisano, N.V. Murrah, L. Jones, E. Jawed, N. Afzal, A. Ashraf, and J. Goldberg, Depressive symptoms and heart rate variability: evidence for a shared genetic substrate in a study of twins. *Psychosom. Med.*, 2008;**70**: 628–636.
537. Fava, C., P. Burri, P. Almgren, G. Arcaro, L. Groop, U. Lennart Hulthén, and O. Melander, Dipping and variability of blood pressure and heart rate at night are heritable traits. *Am. J. Hypertens.*, 2005;**18**: 1402–1407.
538. Dubreuil, E., B. Ditto, G. Dionne, R.O. Pihl, R.E. Tremblay, M. Boivin, D. Pérusse, Familiality of heart rate and cardiac-related autonomic activity in five-month-old twins: the Québec newborn twins study. *Psychophysiology*, 2003; 40: 849–862.
539. Neumann, S.A., E.C. Lawrence, J.R. Jennings, R.E. Ferrell, and S.B. Manuck, Heart rate variability is associated with polymorphic variation in the choline transporter gene. *Psychosom. Med.*, 2005;**67**: 168–171.
540. Busjahn, A, A. Voss, H. Knoblauch, M. Knoblauch, E. Jeschke, N. Wessel, J. Bohlender, J. McCarron, H.D. Faulhaber, H. Schuster, R. Dietz, and F.C. Luft, Angiotensin-converting enzyme and angiotensinogen gene polymorphisms and heart rate variability in twins. *Am. J. Cardiol.*, 1998;**81**: 755–760.
541. Matsunaga, T., N. Gu, H. Yamazaki, M. Tsuda, T. Adachi, K. Yasuda, T. Moritani, K. Tsuda, M. Nonaka, and T. Nishiyama, Association of UCP2 and UCP3 polymorphisms with heart rate variability in Japanese men. *J. Hypertens.*, 2009;**27**: 305–313.
542. Walther, T., N. Wessel, N. Kang, A. Sander, C. Tschöpe, H. Malberg, M. Bader, and A. Voss, Altered heart rate and blood pressure variability in mice lacking the Mas protooncogene. *Braz. J. Med. Biol. Res.*, 2000 Jan;**33**(1): 1–9.
543. Hirsh, M., J. Karin, and S. Akselrod, Heart rate variability in the fetus, in *Heart Rate Variability*, M. Malik and A.J. Camm, Editors. Armonk, NY: Futura Publishing, 1995, pp. 517–531.
544. Lenard, Z., P. Studinger, B. Mersich, L. Kocsis, and M. Kollai, Maturation of cardiovagal autonomic function from childhood to young adult age. *Circulation*, 2004;**110**: 2307–2312.
545. Thompson, C.R., J.S. Brown, H. Gee, and E.W. Taylor, Heart rate variability in healthy term newborns: the contribution of respiratory sinus arrhythmia. *Early. Hum. Dev.*, 1993;**31**: 217–228.
546. Struijk, P.C., N.T. Ursem, J. Mathews, E.B. Clark, B.B. Keller, and J.W. Wladimiroff, Power spectrum analysis of heart rate and blood flow velocity variability measured in the umbilical and uterine arteries in early pregnancy: a comparative study. *Ultrasound. Obstet. Gynecol.*, 2001;**17**: 316–321.
547. Van Leeuwen, P., D. Geue, S. Lange, W. Hatzmann, and D. Grönemeyer, Changes in the frequency power spectrum of fetal heart rate in the course of pregnancy. *Prenat. Diagn.*, 2003;**23**: 909–916.
548. Lange, S., P. Van Leeuwen, D. Geue, W. Hatzmann, and D. Grönemeyer, Influence of gestational age, heart rate, gender and time of day on fetal heart rate variability. *Med. Biol. Eng. Comput.*, 2005;**43**: 481–486.
549. Metsälä, T.H., J.P. Pirhonen, J.O. Jalonen, R.U. Erkkola, and I.A. Välimäki, Association of abnormal flow velocity waveforms in the uterine artery with frequency-specific fetal heart rate variability. *Early. Hum. Dev.*, 1993;**34**: 217–225.

550. Nagy, E., H. Orvos, G. Bárdos, and P. Molnár, Gender-related heart rate differences in human neonates. *Pediatr. Res.*, 2000;**47**: 778–780.
551. Witte, H. and M. Rother, High-frequency and low-frequency heart-rate fluctuation analysis in newborns: a review of possibilities and limitations 1992. *Basic. Res. Cardiol.*, 1992;**87**: 193–204.
552. Galland, B.C., R.M. Hayman, B.J. Taylor, D.P.G Bolotn, R.M. Sayers, and S.M. Williams. Factors affecting heart rate variability response to tilting in infants aged 1 and 3 months. *Pediatr. Res.*, 2000;**48**: 360–368.
553. Finley, J.P., S.T. Nugent, and W. Hellenbrand, Heart-rate variability in children. Spectral analysis of developmental changes between 5 and 24 years. *Can. J. Physiol. Pharmacol.*, 1987;**65**: 2048–2052.
554. Finley, J.P. and S.T. Nugent, Heart rate variability in infants, children and young adults. *J. Auton. Nerv. Syst.*, 1995;**51**: 103–108.
555. Korkushko, O.V. V.B. Shatilo, Yu.I. Plachinda, and T.V. Shatilo, Autonomic control of cardiac chronotropic function in man as a function of age: assessment by power spectral analysis of heart rate variability. *J. Auton. Nerv. Syst.*, 1991;**32**: 191–198.
556. Ferrari, A.U., A. Radaelli, and M. Centola, Invited review: aging and the cardiovascular system. *J. Appl. Physiol.*, 2003;**95**: 2591–2597.
557. Lakatta, E.G., Deficient neurondocrine regulation of the cardiovascular system with advancing age in healthy humans. *Circulation*, 1993;**87**: 631–636.
558. Brodde, O.E. and K. Leineweber, Autonomic receptor systems in the failing and aging human heart: similarities and differences. *Eur. J. Pharmacol.*, 2004;**500**: 167–176.
559. Kaye, D. and M. Esler, Autonomic control of the aging heart. *Neuromol. Med.*, 2008;**10**: 179–186.
560. Kelliher, G.J. and T.S. Conahan, Changes in vagal activity and response to muscarinic receptor agonists with age. *J. Gerontol.*, 1980;**35**: 842–849.
561. Bouman, L.N. and H.J. Jongsma, Structure and function of the sino-atrial node: a review. *Eur. Heart. J.*, 1986;**7**: 94–104.
562. Rodefeld, M.D., S.L. Beau, R.B. Schuessler, J.P. Boineau, J.E. Saffitz, β-Adrenergic and muscarinic cholinergic receptor densities in the human sinoatrial node: identification of a high β_2-adrenergic receptor density. *J. Cardiovasc. Electrophysiol.*, 1996;**7**: 1039–1049.
563. White, M., R. Roden, W. Minobe, F. Khan,P. Larrabee, M. Wollmering, D. Port, F. Anderson, D. Campbell, A.M. Feldman, and M.R. Bristow,. Age-related changes in β-adrenergic neuroeffector systems in the human heart. *Circulation*, 1994;**90**: 1225–1238.
564. Hardouin, S., F. Bourgeois, M. Toraasson, A. Oubenaissa, J.M. Elalouf, D. Fellmann, T. Dakhli, B. Swynghedauw, and J.M. Moalic, Beta-adrenergic and muscarinic receptor mRNA accumulation in the sinoatrial node area of adult and senescent rat hearts. *Mech. Age. Dev.*, 1998;**100**: 277–297.
565. Kaushal, P. and J.A. Taylor, Inter-relations amng declines in arterial distensibility, baroreflex function and respiratory sinus arrhythmia. *J. Am. Coll. Cardiol.*, 2002;**39**: 1524–1530.
566. Gill, J.S., G.J. Hunter, G. Gane, and A.J. Camm, Heterogeneity of the human myocardial sympathetic innervation: in vivo demonstration by iodine 123-labeled meta-iodobenzylguanidine scintigraphy. *Am. Heart. J.*, 1993;**126**: 390–398.
567. Jennett, S. and J.H. McKillop, Observations on the incidence and mechanism of sinus arrhythmia in man at rest. *J. Physiol.*, 1971;**213**: 58–59.
568. Jarisch, W.R., J.J. Ferguson, R.P. Shannon, J.Y. Wei, and A.L. Goldberger, Age-related disappearance of Mayer-like heart rate waves. *Experientia*, 1978;**43**: 1207–1209.
569. Waddington, J.L., M.J. MacCulloch, and J.E. Sambrooks, Resting heartrate variability in man declines with age. *Experientia*, 1979;**35**: 1197–1198.
570. Hrushesky, W.J.M., O. Schmitt, and V. Gilbertsen, The respiratory sinus arrhythmia: a measure of cardiac age. *Science*, 1984; 1001–1004.
571. Colosimo, A., A. Giuliani, A.M. Mancini, G. Piccirillo, and V. Marigliano, Estimating a cardiac age by means of heart rate variability. *Am. J. Physiol. Heart. Circ. Physiol.*, 1997;**273**: H1841–1847.
572. Nasir, K., C. Vasamreddy, R.S. Blumenthal, and J.A. Rumberger, Comprehensive coronary risk determination in primary prevention: an imaging and clinical based definition combining computed tomographic coronary artery calcium score and national cholesterol education program risk score. *Int. J. Cardiol.*, 2006;**110**: 129–136.
573. Tsuji, H., F.J. Venditti, E.S. Emnders, J.C. Evans, M.G. Larson, C.L. Feldman, and D. Levy, Determinants of heart rate variability. *J. Am. Coll. Cardiol.*, 1996;**28**: 1539–1546.
574. Fukusaki, C., K. Kawakubo, and Y. Yamamoto, Assessment of the primary effect of aging on heart rate variability in humans. *Clin. Auton. Res.*, 2000;**10**: 123–130.
575. Britton, A., M. Shipley, M. Malik, K. Hnatkova, H. Hemingway, and M. Marmot, Changes in heart rate and heart rate variability over time in middle-aged men and women in the general population (from the Whitehall II Cohort Study). *Am. J. Cardiol.*, 2007;**100**(3): 524–527.
576. Koskinen, T., M. Kahonen, A. Jula, T. Laitinen, L. Keltikandas-Jarvinen, J. Viikaris, I. Valimaki, and O.T. Raitakari, Short-term heart rate variability in healthy young adults. The Cardiovascular Risk in Young Finns study. *Auton. Neurosci.*, 2009;**145**: 81–88.
577. Mølgaard, H., K. Hermansen, and P. Bjerregaard, Spectral components of short-term RR interval variability in healthy subjects and effects of risk factors. *Eur. Heart. J.*, 1994;**15**: 1174–1183.
578. Jokinen, V., L.B. Sourander, H. Karanko, T.H. Mäkikallio, and K.V. Huikuri, Changes in cardiovascular autonomic regulation among elderly subjects: follow-up of sixteen years. *Ann. Med.*, 2005;**37**: 206–212.
579. Stein, P.K., J.I. Brzilay, P.H.M. Chaves, P.P. Domitrovich, and J.S. Gottdiener, Heart rate variability and its changes over 5 years in older adults. *Age. Ageing*, 2009;**38**: 212–218.
580. Ziegler, D., R. Piolot, K. Strasburger, H. Lambec, and K. Dannehl, Normal ranges and reproducibility of statistical, geometric, frequency domain, and non-linear measures of 24-hour heart rate variability. *Horm. Metab. Res.*, 1999 Dec;31(12):672–679.
581. Kingwell, B.A., J.M. Thompson, D.M. Kaye, G.A. McPherson, G.L. Jennings, M.D. Esler, Heart rate spectral analysis, cardiac norepinephrine spillover, and muscle sympathetic neve activity during human sympathetic activation and failure. *Circulation*, 1994;**90**: 234–240.
582. Vuksanovic, V. and V. Gal, Nonlinear and chaos characteristics of heart period time series: healthy aging and postural changes. *Auton. Neurosci:. Basic. Clin.*, 2005;**121**: 94–100.

583. Beckers, F., B. Verheyden, and A.E. Aubert, Aging and nonlinear heart rate control in a healthy population. *Am. J. Physiol. Heart. Circ. Physiol.*, 2006;**290**: H2560–2570.
584. Iyengar, N., C.K. Peng, R. Morin, A.L. Goldberger, and L.A. Lipsitz, Age-related alterations in the fractal scaling of cardiac interbeat interval dynamics. *Am. J. Physiol. Regul. Integr. Comp. Physiol.*, 1996;**271**: R1078–1084.
585. Platsia, M.M. and V. Gal, Dependence of heart rate variability on heart period in disease and aging. *Physiol. Meas.*, 2006;**27**: 989–998.
586. Schmitt, D.T. and P.Ch.Ivanov, Fractal scale-invariant and nonlinear properties of cardiac dynamics remain stable with advanced age: a new mechanistic picture of cardiac control in healthy elderly. *Am. J. Physiol. Regul. Integr. Comp. Physiol.*, 2007;**293**: R1923–1937.
587. Sakata, S., J. Hayano, S. Mukai, A. Okada, and T. Fujinami, Aging and spectral characteristics of the nonharmonic component of 24-hour heart rate variability. *Am. J. Physiol. Regul. Integr. Comp. Physiol.*, **276**: R1724–1731.
588. Giulliani, A., G. Piccirillo, V. Marigliano, and A. Coosimo, A nonlinear explanation of aging-induced changes in heart beat dynamics. *Am. J. Physiol. Heart. Circ. Physiol.*, 1998;**275**: H1455–1461.
589. Monahan, K.D., Effect of aging on baroreflex function in humans. *Am. J. Physiol. Regul. Integr. Comp. Physiol.*, 2007;**293**: R3–12.
590. Gribbin, B., T.G. Pickering, P. Sleight, and R. Peto, Effect of age and high blood pressure on baroreflex sensitivity in man. *Circ. Res.*, 1971;**29**: 424–431.
591. Jones, P.P., D.D. Christou, J. Jordan, and D.R. Seals, Baroreflex buffering is reduced with age in healthy men. *Circulation*, 2003;**107**: 1770–1774.
592. Monahan, K.D., F.A Dinenno, H. Tanaka, C.M. Clevenger, C.A. DeSouza, and D.R. Seals. Regular aerobic exercise modulates age-associated declines in cardiovagal baroreflex sensitivity in healthy men. *J. Physiol.*, 2000;**529**: 263–271.
593. Laitinen, T., J. Hartikainen, E. Vanninen, L. Niskanen, G. Geelen, and E. Länsimies, Age and gender dependency of baroreflex sensitivity in healthy subjects. *J. Appl. Physiol.*, 1998;**84**: 576–583.
594. Huang, C.C., P. Sandroni, D.M. Sletten, S.D. Weigand, and P.A. Low, Effect of age on adrenergic and vagal baroreflex sensitivity in normal subjects. *Muscle. Nerve.*, 2007;**36**: 637–642.
595. Piccirillo, G., V. Di Giuseppe, M. Nocco, M. Lionetti, A. Moisè, C. Naso, D. Tallarico, V. Marigliano, and M. Cacciafesta, Influence of aging and other cardiovascular risk factors on baroreflex sensitivity. *J. Am. Geriatr. Soc.*, 2001;**49**: 1059–1065.
596. Milic, M., P. Sun, F. Liu, C. Fainman, J. Dimsdale, P.J. Mills, and M.G. Ziegler, A comparison of pharmacologic and spontaneous baroreflex methods in aging and hypertension. *J. Hypertens.*, 2009;**27**: 1243–1251.
597. Kornet, L., A.P. Hoeks, B.J. Janssen, A.J. Houben, P.W. De Leeuw, and R.S. Reneman, Neural activity of the cardiac baroreflex decreases with age in normotensive and hypertensive subjects. *J. Hypertens.*, 2005;**23**: 815–823.
598. James, M.A., T.G. Robinson, R.B. Panerai, and J.F. Potter, Arterial baroreceptor-cardiac reflex sensitivity in the elderly. *Hypertension*, 1996;**28**: 953–960.
599. Gerritsen, J., B.J. TenVoorde, J.M. Dekker, R. Kingma, P.J. Kostense, L.M. Bouter, and R.M. Heethaar, Measures of cardiovascular autonomic nervous function: agreement, reproducibility, and reference values in middle age and elderly subjects. *Diabetologia*, 2003;**46**: 330–338.
600. Fauvel, J-P, C. Cerutti, I. Mpio, and M. Duchr, Aging process on spectrally determined spontanus baroreflex sensitivity. A 5-year prospective study. *Hypertension*, 2007;**50**: 543–546.
601. Schwab, J.O., G. Eichner, N. Shlevkov, J. Schrickel, A. Yang, O. Balta, T. Lewalter, B. Lüderitz, Impact of age and basic heart rate on heart rate turbulence in healthy persons. *Pacing. Clin. Electrophysiol.,* 2005;**28** (Suppl 1): S198–201.
602. Kowalewski, M., M. Alifier, D. Bochen, and M. Urban, Heart rate turbulence in children–age and heart rate relationships. *Pediatr. Res.*, 2007;**62**: 710–714.
603. Burke, J.H., J.J. Goldberger, F.A. Ehlert, J.T. Kruse, M.A. Parker, and A.H. Kadish, Gender differences in heart rate before and after autonomic blockade: evidence against an intrinsic gender effect. *Am. J. Med.*, 1996;**100** (5): 537–543.
604. Busha, B.F., E. Hage, and C. Hofmann, Gender and breathing route modulate cardio-respiratory variability in humans. *Respir. Physiol. Neurobiol.*, 2009;**166**: 87–94.
605. Aitken, M.L., J.L. Franklin, D.J. Pierson, and R.B. Schoene, Influence of body size and gender on control of ventilation. *J. Appl. Physiol.*, 1986;**60**: 1894–1899.
606. White, D.P., N.J. Douglas, C.K. Pickett, J.V. Weil, and C.W. Zwillich, Sexual influence on the control of breathing. *J. Appl. Physiol.*, 1983;**54**: 874–879.
607. Sato, N., S. Miyake, J. Akatsu, and M. Kumashiro, Power spectral analysis of heart rate variability in healthy young women during the normal menstrual cycle. *Psychosom. Med.,* 1995;**57**: 331–335.
608. Vallejo, M., M.F. Márquez, V.H. Borja-Aburto, M. Cárdenas, and A.G. Hermosillo, Age, body mass index, and menstrual cycle influence young women's heart rate variability –a multivariable analysis. *Clin. Auton. Res.*, 2005;**15**: 292–298.
609. Felber Dietrich, D., C. Schindler, J. Schwartz, J.C. Barthélémy, J.M. Tschopp, F. Roche, A. von Eckardstein, O. Brändli, P. Leuenberger, D.R. Gold, J.M. Gaspoz, U. Ackermann-Liebrich, and SAPALDIA Team, Heart rate variability in an ageing population and its association with lifestyle and cardiovascular risk factors: results of the SAPALDIA study. *Europace*, 2006;**8**: 521–529.
610. Grossman, P., F.H. Wilhelm, I. Kawachi, and D. Sparrow, Gender differences in psychophysiological responses to speech stress among older social phobics: congruence and incongruence between self-evaluative and cardiovascular reactions. *Psychosom. Med.*, 2001;**63**: 765–777.
611. Dishman, R.K., Y. Nakamura, M.E. Garcia, R.W. Thompson, A.L. Dunn, and S.N. Blair, Heart rate variability, trait anxiety, and perceived stress among physically fit men and women. *Int. J. Psychophysiol.*, 2000;**37**: 121–133.
612. Hinojosa-Laborde, C., I. Chapa, D. Lange, and J.R. Haywood, Gender differences in sympathetic nervous system regulation. *Clin. Exp. Pharmacol. Physiol.*, 1999;**26**: 122–126.
613. Insulander, P. and H. Vallin, Gender differences in electrophysiologic effects of mental stress and autonomic tone inhibition: a study in health individuals. *J. Cardiovasc. Electrophysiol.*, 2005;**16**: 59–63.
614. Fagard, R.H., K. Pardaens, J.A. Staessen, and L. Thijs, Power spectral analysis of heart rate variability by autoregressive modelling and fast Fourier transform: a comparative study. *Acta. Cardiol.*, 1998;**53**: 211–218.
615. Colhoun, H.M., D.P. Francis, M.B. Rubens, S.R. Underwood, and J.H. Fuller, The association of heart-rate variability with

cardiovascular risk factors and coronary artery calcification: a study in type 1 diabetic patients and the general population. *Diabetes. Care.*, 2001;**24**: 1108–1114.

616. Sloan, R.P., M.H. Huang, H. McCreath, S. Sidney, K. Liu, O. Dale Williams, T. Seeman, Cardiac autonomic control and the effects of age, race, and sex: the CARDIA study. *Auton. Neurosci.*, 2008;**139**: 78–85.
617. Jensen-Urstad, K., N. Storck, F. Bouvier, M. Ericson, L.E. Lindblad, and M. Jensen-Urstad Heart rate variability in healthy subjects is related to age and gender. *Acta. Physiol. Scand.*, 1997;**160**: 235–241.
618. Yamasaki, Y., M. Kodama, M. Matsuhisa, M. Kishimoto, H. Ozaki, A. Tani, N. Ueda, Y. Ishida, and T. Kamada, Diurnal heart rate variability in healthy subjects: effects of aging and sex difference. *Am. J. Physiol.*, 1996;**271**: H303–310.
619. Antelmi, I., R.S. de Paula, A.R. Shinzato, C.A. Peres, A.J. Mansur, and C.J. Grupi, Influence of age, gender, body mass index, and functional capacity on heart rate variability in a cohort of subjects without heart disease. *Am. J. Cardiol.*, 2004;**93**: 381–385.
620. Barantke, M., T. Krauss, J. Ortak, W. Lieb, M. Reppel, C. Burgdorf, P.P. Pramstaller, H. Schunkert, and H. Bonnemeier, Effects of gender and aging on diffeential autonomic responses to orthostatic maneuvers. *J. Cardiovasc. Electrophysiol.*, 2008;**19**: 1296–1303.
621. Abdel-Rahman, A.R., R.H. Merrill, and W.R. Wooles, Gender-related differences in the baroreceptor reflex control of heart rate in normotensive humans. *J. Appl. Physiol.*, 1994;**77**: 606–613.
622. Convertino, V.A., Gender differences in autonomic functions associated with blood pressure regulation. *Am. J. Physiol.*, 1998;**275**: R1909–1920.
623. Ylitalo, A., K.E. Airaksinen, A. Hautanen, M. Kupari, M. Carson, J. Virolainen, M. Savolainen, H. Kauma, Y.A. Kesäniemi, P.C. White, and H.V. Huikuri, Baroreflex sensitivity and variants of the renin angiotensin system genes. *J. Am. Coll. Cardiol.*, 2000;**35**: 194–200.
624. Beske, S.D., G.E. Alvarez, T.P. Ballard, and K.P. Davy, Gender difference in cardiovagal baroreflex gain in humans. *J. Appl. Physiol.*, 2001;**91**: 2088–2092.
625. Luzier, A.B., J.J. Nawarskas, J. Añonuevo, M.E. Wilson, and D.J. Kazierad, The effects of gender on adrenergic receptor responsiveness. *J. Clin. Pharmacol.*, 1998;**38**: 618–624.
626. Tank, J., A. Diedrich, E. Szczech, F.C. Luft, and J. Jordan, Baroreflex regulation of heart rate and sympathetic vasomotor tone in women and men. *Hypertension*, 2005;**45**: 1159–1164.
627. Sevre, K., J.D. Lefrandt, G. Nordby, I. Os, M. Mulder, R.O. Gans, M. Rostrup, and A.J. Smit, Autonomic function in hypertensive and normotensive subjects: the importance of gender. *Hypertension*, 2001;**37**: 1351–1356.
628. Wyndham, CHm., B. Metz, and A. Munro, Reactions to heat of Arabs and Caucasians. *J. Appl. Physiol.*, 1964;**19**: 1051–1054.
629. Cooper, R.S. and J.K. Ghali, Coronary heart disease: black-white differences. *Cardiovasc. Clin.*, 1991;**21**: 205–225.
630. Watson, K.E. and E.J. Topol, Pathobiology of atherosclerosis: are there racial and ethnic differences? *Rev. Cardiovasc. Med.*, 2004;**5** (Suppl 3): S14–21.
631. Saunders, E. and E. Ofili, Epidemiology of atherothrombotic disease and the effectiveness and risks of antiplatelet therapy: race and ethnicity considerations. *Cardiol. Rev.*, 2008;**16**: 82–88.
632. Macfarlane, P.W., S.C. McLaughlin, B. Devine, and T.F. Yang, Effects of age, sex, and race on ECG interval measurements. *J. Electrocardiol.*, 1994;**27** (Suppl): 14–19.
633. Ogueh, O. and P.J. Steer, Ethnicity and fetal heart rate variation. *Obstet. Gynecol.*, 1998;**91**: 324–328.
634. Schachter, J., J.L. Kerr, F.C. 3rd Wimberly, and JM 3rd Lachin, Phasic heart rate responses: different patterns in black and in white newborns. *Psychosom. Med.*, 1975;**37**: 326–332.
635. Du Plooy, W.J. and C.P. Venter, The effect of atropine on parasympathetic control of respiratory sinus arrhythmia in two ethnic groups. *J. Clin. Pharmacol.*, 1995;**35**: 244–249.
636. Guzzetti, S., J. Mayet, M. Shahi, S. Mezzetti, R.A. Foale, P.S. Sever, N.R. Poulter, A. Porta, A. Malliani, and S.A. Thom, Absence of sympathetic overactivity in Afro-Caribbean hypertensive subjects studied by heart rate variability. *J. Hum. Hypertens.*, 2000;**14**: 337–342.
637. Thayer, J.F., M.M. Merritt, JJ 3rd Sollers, A.B. Zonderman, M.K. Evans, S. Yie, and D.R. Abernethy, Effect of angiotensin-converting enzyme insertion/deletion polymorphism DD genotype on high-frequency heart rate variability in African Americans. *Am. J. Cardiol.*, 2003;**92**: 1487–1490.
638. Wang, X., J.F. Thayer, F. Treiber, and H. Snieder, Ethnic differences and heritability of heart rate variability in African- and European American youth. *Am. J. Cardiol.*, 2005;**96**: 1166–1172.
639. Lampert, R., J. Ickovics, R. Horwitz, and F. Lee, Depressed autonomic nervous system function in African Americans and individuals of lower social class: a potential mechanism of race- and class-related disparities in health outcomes. *Am. Heart. J.*, 2005;**150**: 153–160.
640. Utsey, S.O. and J.N. Hook, Heart rate variability as a physiological moderator of the relationship between race-related stress and psychological distress in African Americans. *Cultur. Divers. Ethnic. Minor. Psychol.*, 2007;**13**: 250–253.
641. Zion, A.S., V. Bond, R.G. Adams, D. Williams, R.E. Fullilove, R.P. Sloan, M.N. Bartels, J.A. Downey, and R.E. De Meersman, Low arterial compliance in young African-American males. *Am. J. Physiol. Heart. Circ. Physiol.*, 2003;**285**: H457–462.
642. Franke, W.D., K. Lee, D.B. Buchanan, and J.P. Hernandez, Blacks and whites differ in responses, but not tolerance, to orthostatic stress. *Clin. Auton. Res.*, 2004;**14**: 19–25.
643. Keyl, C., A. Schneider, R.E. Greene, C. Passino, G. Spadacini, G. Bandinelli, M. Bonfichi, L. Arcaini, L. Malcovati, and L. Bernardi, Effects of breathing control on cardiocirculatory modulation in Caucasian lowlanders and Himalayan Sherpas. *Eur. J. Appl. Physiol.*, 2000;**83**: 481–486.
644. Pelat, M., R. Verwaerde, C. Merial, J. Galitzky, M. Berlan, J.L. Montastruc, J.M. Senard, Impaired atrial M(2)-cholinoceptor function in obesity-related hypertension. *Hypertension*, 1999;**34**: 1066–1072.
645. Paolisso, G., D. Manzella, N. Montano, A. Gambardella, and M. Varricchio, Plasma leptin concentrations and cardiac autonomic nervous system in healthy subjects with different body weights. *J. Clin. Endocrinol. Metab.*, 2000;**85**: 1810–1814.
646. Martini, G., P. Riva, F. Rabbia, V. Molini, G.B. Ferrero, F. Cerutti, R. Carra, and F. Veglio. Heart rate variability in childhood obesity. *Clin. Auton. Res.*, 2001;**11**: 87–91.
647. Li, Z., H. Snieder, S. Su, X. Ding, J.F. Thayer, F.A. Treiber, and X. Wang, A longitudinal study in youth of heart rate variability at rest and in response to stress. *Int. J. Psychophysiol.*, 2009;**73**: 212–217.

648. Kuch, B., H.W. Hense, R. Sinnreich, J.D. Kark, A. von Eckardstein, D. Sapoznikov, and H.D. Bolte, Determinants of short-period heart rate variability in the general population. *Cardiology*, 2001;**95**: 131–138.
649. Liao, D., J. Cai, W.D. Rosamond, R.W. Barnes, R.G. Hutchinson, E.A. Whitsel, P. Rautaharju, and G. Heiss, Cardiac autonomic function and incident coronary heart disease: a population-based case-cohort study. The ARIC Study. Atherosclerosis Risk in Communities Study. *Am. J. Epidemiol.*, 1997;**145**: 696–706.
650. De Bruyne, M.C., J.A. Kors, A.W. Hoes, P. Klootwijk, J.M. Dekker, A. Hofman, J.H. van Bemmel, and D.E Grobbee, Both decreased and increased heart rate variability on the standard 10-second electrocardiogram predict cardiac mortality in the elderly: the Rotterdam Study. *Am. J. Epidemiol.*, 1999;**150**: 1282–1288.
651. Stolarz, K., J.A. Staessen, T. Kuznetsova, V. Tikhonoff, D. State, S. Babeanu, E. Casiglia, R.H. Fagard, K. Kawecka-Jaszcz, and Y. Nikitin, European Project on Genes in Hypertension (EPOGH) Investigators. Host and environmental determinants of heart rate and heart rate variability in four European populations. *J. Hypertens.*, 2003;**21**: 525–535.
652. Byrne, E.A., J.L. Fleg, P.V. Vaitkevicius, J. Wright, and S.W. Porges, Role of aerobic capacity and body mass index in the age-associated decline in heart rate variability. *J. Appl. Physiol.*, 1996;**81**: 743–750.
653. Ziegler, D., C. Zentai, S. Perz, W. Rathmann, B. Haastert, C. Meisinger, H. Löwel, and KORA Study Group, Selective contribution of diabetes and other cardiovascular risk factors to cardiac autonomic dysfunction in the general population. *Exp. Clin. Endocrinol. Diabetes.*, 2006;**114**: 153–159.
654. Fagard, R.H., K. Pardaens, and J.A. Staessen, Influence of demographic, anthropometric and lifestyle characteristics on heart rate and its variability in the population. *J. Hypertens.*, 1999;**17**: 1589–1599.
655. Greiser, K.H., A. Kluttig, B. Schumann, C.A. Swenne, J.A. Kors, O. Kuss, J. Haerting, H. Schmidt, J. Thiery, and K. Werdan, Cardiovascular diseases, risk factors and short-term heart rate variability in an elderly general population: the CARLA study 2002–2006. *Eur. J. Epidemiol.*, 2009;**24**: 123–142.
656. Hirsch, J., R.L. Leibel, R. Mackintosh, and A. Aguirre, Heart rate variability as a measure of autonomic function during weight change in humans. *Am. J. Physiol.*, 1991;**261**: R1418–1423.
657. Zahorska-Markiewicz, B., E. Kuagowska, C. Kucio, and M. Klin, Heart rate variability in obesity. *Int. J. Obes. Relat. Metab. Disord.*, 1993;**17**: 21–23.
658. Karason, K., H. Mølgaard, J. Wikstrand, and L. Sjöström, Heart rate variability in obesity and the effect of weight loss. *Am. J. Cardiol.*, 1999;**83**: 1242–1247.
659. Poirier, P., T. Hernandez, K. Weil, T. Shepard, and R. Eckel, Impact of diet-induced weight loss on the cardiac autonomic nervous system in severe obesity. *Obes. Res.*, 2003;**11**: 1040–1047.
660. Nault, I., E. Nadreau, C. Paquet, P. Brassard, P. Marceau, S. Marceau, S. Biron, F. Hould, S. Lebel, D. Richard, and P. Poirier, Impact of bariatric surgery–induced weight loss on heart rate variability. *Metabolism*, 2007;**56**: 1425–1430.
661. Bobbioni-Harsch, E., J. Sztajzel, V. Barthassat, V. Makoundou, G. Gastaldi, K. Sievert, G. Chassot, O. Huber, P. Morel, F. Assimacopoulos-Jeannet, and A. Golay, Independent evolution of heart autonomic function and insulin sensitivity during weight loss. *Obesity*, 2009;**17**: 247–253.
662. Skrapari, I., N. Tentolouris, D. Perrea, C. Bakoyiannis, A. Papazafiropoulou, and N. Katsilambros, Baroreflex sensitivity in obesity: relationship with cardiac autonomic nervous system activity. *Obesity*, 2007;**15**: 1685–1693.
663. Laederach-Hofmann, K., L. Mussgay, and H. Rúddel, Autonomic cardiovascular regulation in obesity. *J. Endocrinol.*, 2000;**164**: 59–66.
664. Beske, S.D., G.E. Alvarez, T.P. Ballard, and K.P. Davy, Reduced cardiovagal baroreflex gain in visceral obesity: implications for the metabolic syndrome. *Am. J. Physiol. Heart Circ. Physiol.*, 2002;**282**: H630–635.
665. Grassi, G., G. Seravalle, M. Colombo, G. Bolla, B.M. Cattaneo, F. Cavagnini, and G. Mancia, Body weight reduction, sympathetic nerve traffic, and arterial baroreflex in obese normotensive humans. *Circulation*, 1998;**97**: 2037–2042.
666. Alvarez, G.E., B.M. Davy, T.P. Ballard, S.D. Beske, and K.P. Davy, Weight loss increases cardiovagal baroreflex function in obese young and older men. *Am. J. Physiol. Endocrinol. Metab.*, 2005;**289**: E665–669.
667. Avsar, A., G. Acarturk, M. Melek, C. Kilit, A. Celik, and E. Onrat, Cardiac autonomic function evaluated by the heart rate turbulence method was not changed in obese patients without co-morbidities. *J. Korean. Med. Sci.*, 2007;**22**: 629–632.
668. Coumel, P., P. Maison-Blanche, and D. Catuli, Heart rate and heart rate variability in normal young adults. *J. Cardiovasc. Electrophysiol.*, 1994;**5**: 899–911.
669. Rosenblueth, A. and F.A. Simeone, The interrelations of vagal and accelerator effects on the cardiac rate. *Am. J. Physiol.*, 1934, **110**: 42–45.
670. Bootsma, M., C.A. Swenne, H.H. Van Bolhuis, P.C. Chang, V.M. Cats, A.V. Bruschke, Heart rate and heart rate variability as indexes of sympathovagal balance. *Am. J. Physiol. Heart. Cric. Physiol.*, 1994;**266**: H1565–1571.
671. Goldberger, J.J., M.W. Ahmed, M.A. Parker, and A.H. Kadish, Dissociation of heart rate variability from parasympathetic tone. *Am. J. Physiol. Heart. Circ. Physiol.*, 1994;**266**: H2152–2157.
672. Ahmed, M.W., A.H. Kadish, M.A. Parker, and J.J. Goldberger,. Effect of physiologic and pharmacologic adrenergic stimulation on heart rate variability. *J. Am. Coll. Cardiol.*, 1994;**24**: 1082–1090.
673. Goldberger, J.J., Y.H. Kim, M.W. Ahmed, and A.H. Kadish, Effect of graded increases in parasympathetic tone on heart rate variability. *J. Cardiovasc. Electrophysiol.*, 1996;**7**: 594–602.
674. Kim, Y.H., M.W. Ahmed, A.H. Kadish, and J.J. Goldberger, Characterization of the factors that determine the effect of sympathetic stimulation on heart rate variability. *Pacing. Clin. Electrophysiol.*, 1997;**20**: 1936–1946.
675. Goldberger, J.J., S. Challapalli, R. Tung, M.A. Parker, and A.H. Kadish, Relationship of heart rate variability to parasympathetic effect. *Circulation*, 2001;**103**: 1977–1983.
676. Opthof, T. and R. Coronel, The normal range and determinants of the intrinsic heart rate in man. *Cardiovasc. Res.*, 2000;**45**: 175–176.
677. Jose, A.D., Effect of combined sympathetic and parasympathetic blockade on heart rate and cardiac function in man. *Am. J. Cardiol.*, 1966;**18**: 476–478.
678. Frick, M.H., J. Heikkilä, and A. Kahanpää, Combined parasympathetic and beta-receptor blockade as a clinical test. *Acta. Med. Scand.*, 1967;**182**: 621–628.

679. Jose, A.D. and R.R. Taylor, Autonomic blockade by propranolol and atropine to study intrinsic myocardial function in man. *J. Clin. Invest.*, 1969;**48**: 2019–2031.
680. Alboni, P., C. Malacarne, P. Pedroni, A. Masoni, and O.S. Narula, Electrophysiology of normal sinus node with and without autonomic blockade. *Circulation*, 1982;**65**: 1236–1242.
681. Marcus, B., P.C. Gillette, and A. Garson, Intrinsic heart rate in children and young adults: an index of sinus node function isolated from autonomic control. *Am. Heart. J.*, 1990;**119**: 911–916.
682. Burke, J.H., J.J. Goldberger, F.A. Ehlert, J.T. Kruse, M.A. Parker, and A.H. Kadish, Gender differences in heart rate before and after autonomic blockade: evidence against an intrinsic gender effect. *Am. J. Med.*, 1996;**100**: 537–543.
683. Craft, N. and J.B. Schwartz, Effects of age on intrinsic heart rate, heart rate variability, and AV conduction in healthy humans. *Am. J. Physiol. Heart. Circ. Physiol.*, 1995;**268**: H1441–1452.
684. Jokkel, G., I. Bonyhay, and M. Kollai, Heart rate variability after complete autonomic blockade in man. *J. Auton. Nerv. Syst.*, 1995;**51**: 85–89.
685. Wollenberger, A. and J. Jehl, Influence of age on rate of respiration of sliced cardiac muscle. *Am. J. Physiol.*, 1952;**170**: 126–130.
686. Evans, J.M., D.C. Randall, J.N. Funk, and C.F. Knapp, Influence of cardiac innervations on intrinsic heart rate in dogs. *Am. J. Physiol. Heart. Circ. Physiol.*, 1990;**258**: H1132–1137.
687. Miyazaki, T., H.P. Pride, and D.P. Zipes, Prostaglandins in the pericardial fluid modulate neural regulation of cardiac electrophysiological properties. *Circ. Res.*, 1990;**66**: 163–175.
688. Marin-Neto, J.A., J.J. Carneiro, B.C. Maciel, A.L. Secches, L. Gallo Jr., J. Terra-Filho, J.C. Manço, E.C. Lima-Filho, W.V. Vicente, A.A. Sader, et al., Impairment of baroreflex control of the sinoatrial node after cardiac operations with extracorporeal circulation in man. *J. Thorac. Cardiovasc. Surg.*, 1983;**86**: 718–726.
689. Sosnowski, M., T. Petelenz, Z. Czyż, S. Woś, B. Białkowska, B. Grzybek, Noninvasive evaluation of autonomic control of heart rate in patients with mitral valvular disease treated surgically (authors' material, Petelenz T [Ed], Mitral valve disease: an old disease and modern medicine, Medical University of Silesia, 1992).
690. Niemelä, M.J., K.E. Airaksinen, K.U. Tahvanainen, M.K. Linnaluoto, and J.T. Takkunen, Effect of coronary artery bypass grafting on cardiac parasympathetic nervous function. *Eur. Heart. J.*, 1992;**13**: 932–935.
691. Petelenz, T., K. Singer, B. Gabrylewicz, T. Twardela, T. Pawłowski, S. Woś, M. Sosnowski, and Z. Nowak, Effect of aorto-coronary by-pass grafting on ventricular function assessed by means of noninvasive evalation in a 2-year follow-up. *Pol. Tyg. Lek.*, 1993;**48**: 681–685 (*in Polish*).
692. Tuinenburg, A.E., I.C. Van Gelder, M.P. Van Den Berg, J.G. Grandjean, R.G. Tieleman, A.J. Smit, R.C. Huet, J.M. Van Der Maaten, C.P. Volkers, T. Ebels, and H.J. Crijns, Sinus node function after cardiac surgery: is impairment specific for the maze procedure? *Int. J. Cardiol.*, 2004;**95**: 101–108.
693. Davila, D.F., C.F. Gottberg, J.H. Donis, A. Torres, A.J. Fuenmayor, and O. Rossell, Vagal stimulation and heart rate slowing in acute experimental chagasic myocarditis. *J. Auton. Nerv. Syst.*, 1988;**25**: 233–234.
694. Gao, X., L. Peng, Q. Zeng, and Z.K. Wu, Autonomic nervous function and arrhythmias in patients with acute viral myocarditis during a 6-month follow-up period. *Cardiology*, 2009;**113**: 66–71.
695. Jinbo, Y., Y. Kobayashi, A. Miyata, K. Chiyoda, H. Nakagawa, K. Tanno, K. Kurano, S. Kikushima, T. Baba, and T. Katagiri, Decreasing parasympathetic tone activity and proarrhythmic effect after radiofrequency catheter ablation–differences in ablation site. *Jpn. Circ. J.*, 1998;**62**: 733–740.
696. Miyanaga, S., T. Yamane, T. Date, M. Tokuda, Y. Aramaki, K. Inada, K. Shibayama, S. Matsuo, H. Miyazaki, K. Abe, K. Sugimoto, S. Mochizuki, and M. Yoshimura, Impact of pulmonary vein isolation on the autonomic modulation in patients with paroxysmal atrial fibrillation and prolonged sinus pauses. *Europace*, 2009;**11**: 576–581.
697. Sosnowski, M., T. Petelenz, and Z. Czyz, Patterns of non-linear heart rate behaviour in sinoatrial node dysfunction: effects of orthostatic test and autonomic blockade. *Comput. Cardiol.*, 1993: 5–8.
698. Bernardi, L., F. Valle, S. Leuzzi, M. Rinaldi, E. Marchesi, C. Falcone, L. Martinelli, M. Viganó, G. Finardi, and A. Radaelli, Non-respiratory components of heart rate variability in heart transplant recipients: evidence of autonomic reinnervation? *Clin. Sci.*, 1994;**86**: 537–545.
699. Jose, A.D., F. Stitt, and D. Collison, The effects of exercise and changes in body temperature on the intrinsic heart rate in man. *Am. Heart. J.*, 1970;**79**: 488–498.
700. Julu, P.O. and R.G. Hondo, Effects of atropine on autonomic indices based on electrocardiographic R-R intervals in healthy volunteers. *J. Neurol. Neurosurg. Psychiatr.*, 1992;**55**: 31–35.
701. Hayano, J., Y. Sakakibara, A. Yamada, M. Yamada, S. Mukai, T. Fujinami, K. Yokoyama, Y. Watanabe, and K. Takata, Accuracy of assessment of cardiac vagal tone by heart rate variability in normal subjects. *Am. J. Cardiol.*, 1991;**67**: 199–204.
702. Pierpont, G.L. and E.J. Voth, Assessing autonomic function by analysis of heart rate recovery from exercise in healthy subjects. *Am. J. Cardiol.*, 2004;**94**: 64–68.
703. Furlan, R., S. Guzzetti, W. Crivellaro, S. Dassi, M. Tinelli, G. Baselli, S. Cerutti, F. Lombardi, M. Pagani, and A. Malliani, Continuous 24-hour assessment of the neural regulation of systemic arterial pressure and RR variabilities in ambulant subjects. *Circulation*, 1990;**81**: 537–547.
704. Adamson, P.B., M.H. Huang, E. Vanoli, R.D. Foreman, P.J. Schwartz, and S.S. Jr.Hull, Unexpected interaction between beta-adrenergic blockade and heart rate variability before and after myocardial infarction. A longitudinal study in dogs at high and low risk for sudden death. *Circulation*, 1994;**90**: 976–982.
705. Rodriguez, R.D. and D.D. Schocken, Update on sick sinus syndrome, a cardiac disorder of aging. *Geriatrics*, 1990;**45**: 26–30, 33–6.
706. Abildstrom, S.Z., B.T. Jensen, E. Agner, C. Torp-Pedersen, O. Nyvad, K. Wachtell, M.M. Ottesen, J.K. Kanters and BEAT Study Group, Heart rate versus heart rate variability in risk prediction after myocardial infarction. *J. Cardiovasc. Electrophysiol.*, 2003;**14**: 168–173.
707. Goto, M., M. Nagashima, R. Baba, Y. Nagano, M. Yokota, K. Nishibata, and A. Tsuji, Analysis of heart rate variability demonstrates effects of development on vagal modulation of heart rate in healthy children. *J. Pediatr.*, 1997;**130**: 725–729.
708. Pagani, M., G. Mazzuero, A. Ferrari, D. Liberati, S. Cerutti, D. Vaitl, L. Tavazzi, and A. Malliani, Sympathovagal interaction

during mental stress. A study using spectral analysis of heart rate variability in healthy control subjects and patients with a prior myocardial infarction. *Circulation*, 1991;**83** (4 Suppl): II43–51.

709. Chiu, H.W., T.H. Wang, L.C. Huang, H.W. Tso, and T. Kao, The influence of mean heart rate on measures of heart rate variability as markers of autonomic function: a model study. *Med. Eng. Phys.*, 2003;**25**: 475–481.
710. Eaton, G.M., R.J. Cody, E. Nunziata, and P.F. Binkley, Early left ventricular dysfunction elicits activation of sympathetic drive and attenuation of parasympathetic tone in the paced canine model of congestive heart failure. *Circulation*, 1995;**92**: 555–561.
711. Sosnowski, M. and T. Petelenz, Heart rate variability. Is it influenced by disturbed sinoatrial node function? *J. Electrocardiol.*, 1995;**28**: 245–251.
712. Panina, G., U.N. Khot, E. Nunziata, R.J. Cody, and P.F. Binkley, Assessment of autonomic tone over a 24-hour period in patients with congestive heart failure: relation between mean heart rate and measures of heart rate variability. *Am. Heart. J.*, 1995;**129**: 748–753.
713. Vanninen, E., A. Tuunainen, M. Kansanen, M. Uusitupa, and E. Länsimies, Cardiac sympathovagal balance during sleep apnea episodes. *Clin. Physiol.*, 1996;**16**: 209–216.
714. Bauer, T., S. Ewig, H. Schäfer, E. Jelen, H. Omran, and B. Lüderitz, Heart rate variability in patients with sleep-related breathing disorders. *Cardiology*, 1996;**87**: 492–496.
715. Heinz, G., M. Hirschl, P. Buxbaum, G. Laufer, S. Gasic, and A. Laczkovics, Sinus node dysfunction after orthotopic cardiac transplantation: postoperative incidence and long-term implications. *Pacing. Clin. Electrophysiol.*, 1992;**15**: 731–737.
716. Scott, C.D., J.H. Dark, and J.M. McComb, Sinus node function after cardiac transplantation. *J. Am. Coll. Cardiol.*, 1994;**24**: 1334–1341.
717. Cohen, M.A. and J.A. Taylor, Short-term cardiovascular osllation in man: measuring and modeling the physiologies. *J. Physiol.*, 2002;**542**: 669–683.
718. Hirsch, J.A. and B. Bishop, Respiratory sinus arrhythmia in humans: how breathing pattern modulates heart rate. *Am. J. Physiol.*, 1981;**241**: H620–629.
719. Grossman, P. and M. Kollai, Respiratory sinus arrhythmia, cardiac vagal tone, and respiration: within- and between-individual relations. *Psychophysiology*, 1993;**30**: 486–495.
720. Eckberg, D.L., Human sinus arrhythmia as an index of vagal cardiac outflow. *J. Appl. Physiol.*, 1983;**54**: 961–966.
721. Hayano, J., Y. Sakakibara, A. Yamada, M. Yamada, S. Mukai, T. Fujinami, K. Yokoyama, Y. Watanabe, and K. Takata, Accuracy of assessment of cardiac vagal tone by heart rate variability in normal subjects. *Am. J. Cardiol.*, 1991;**67**: 199–204.
722. Malpas, S.C., Neural influences on cardiovascular variability: possibility and pitfalls. *Am. J. Physiol. Heart. Circ. Physiol.*, 2002;**282**: H6–20.
723. Grossman, P., F.H. Wilhelm, and M. Spoerle, Respiratory sinus arrhythmia, cardiac vagal control, and daily activity. *Am. J. Physiol. Heart. Circ. Physiol.*, 2004;**287**: H728–734.
724. Houtveen, J.H., S. Rietveld, and E.J. de Geus, Contribution of tonic vagal modulation of heart rate, central respiratory drive, respiratory depth, and respiratory frequency to respiratory sinus arrhythmia during mental stress and physical exercise. *Psychophysiology*, 2002;**39**: 427–436.
725. Ewing, D.J., D.Q. Borsey, F. Bellavere, and B.F. Clarke, Cardiac autonomic neuropathy in diabetes: comparison of measures of R-R interval variation. *Diabetologia*, 1981;**21**: 18–24.
726. Löllgen, D., M. Müeck-Weymann, and R.D. Beise, The deep breathing test: median-based expiration-inspiration difference is the measure of choice. *Muscle. Nerve.*, 2009;**39**: 536–544.
727. Grossman, P., J. Karemaker, and W. Wieling, Prediction of tonic parasympathetic cardiac control using respiratory sinus arrhythmia: the need for respiratory control. *Psychophysiology*, 1991;**28**: 201–216.
728. Sosnowski, M., J. Skrzypek-Wańha, Z. Czyż, B. Korzeniowska, and M. Tendera, Respiratory rate-heart rate interaction is responsible for reduced heart rate variability in patients with coronary heart disease and depressed left ventricular systolic function. *Eur. Heart. J.*, 1997;**18** (Suppl.): 575 (abstr).
729. Saul, J.P., R.D. Berger, M.H. Chen, and R.J. Cohen, Transfer function analysis of autonomic regulation. II. Respiratory sinus arrhythmia. *Am. J. Physiol.*, 1989;**256**: H153–161.
730. El-Omar, M., A. Kardos, and B. Casadei, Mechanisms of respiratory sinus arrhythmia in patients with mild heart failure. *Am. J. Physiol. Heart. Circ. Physiol.*, 2001;**280**: H125–131.
731. Mortara, A., P. Sleight, G.D. Pinna, R. Maestri, A. Prpa, M.T. La Rovere, F. Cobelli, and L. Tavazzi, Abnormal awake respiratory patterns are common in chronic heart failure and may prevent evaluation of autonomic tone by measures of heart rate variability. *Circulation*, 1997;**96**: 246–252.
732. Shiomi, T., C. Guilleminault, R. Sasanabe, I. Hirota, M. Maekawa, and T. Kobayashi, Augmented very low frequency component of heart rate variability during obstructive sleep apnea. *Sleep*, 1996;**19**: 370–377.
733. Ponikowski, P., T.P. Chua, A.A. Amadi, M. Piepoli, D. Harrington, M. Volterrani, R. Colombo, G. Mazzuero, A. Giordano, and A.J. Coats, Detection and significance of a discrete very low frequency rhythm in RR interval variability in chronic congestive heart failure. *Am. J. Cardiol.*, 1996;**77**: 1320–1326.
734. Tateishi, O., T. Shouda, Y. Honda, T. Sakai, S. Mochizuki, and K. Machida, Apnea-related heart rate variability and its clinical utility in congestive heart failure outpatients. *Ann. Noninvasive. Electrocardiol.*, 2002;**7**: 127–132.
735. Perakakis, P., M. Taylor, E. Martinez-Nieto, I. Revithi, and J. Vila, Breathing frequency bias in fractal analysis of heart rate variability. *Biol. Psychol.*, 2009;**82**: 82–88.
736. Casadei, B., J. Moon, A. Caiazza, and P. Sleight, Is respiratory sinus arrhythmia a good index of cardiac vagal activity during exercise? *J. Appl. Physiol.*, 1996;**81**: 556–564.
737. Ponikowski, P., T.P. Chua, M. Piepoli, W. Banasiak, S.D. Anker, R. Szelemej, W. Molenda, K. Wrabec, A. Capucci, and A.J. Coats, Ventilatory response to exercise correlates with impaired heart rate variability in patients with chronic congestive heart failure. *Am. J. Cardiol.*, 1998;**82**: 338–344.
738. Tzeng, Y.C., P.D. Larsen, and D.C. Galletly, Cardioventilatory coupling in resting human subjects. *Exp. Physiol.*, 2003;**88**: 775–782.
739. Fallen, E.L. and M.V. Kamath, Circadian rhythms of heart rate variability, in *Heart Rate Variability*, M. Malik and A.J. Camm, Editors. Armonk, NY: Futura Publishing, 1995, pp. 293–309.
740. Hartikainen, J., I. Tarkiainen, K. Tahvanainen, M. Mäntysaari, E. Länsimies, and K. Pyörälä, Circadian variation of cardiac autonomic regulation during 24-h bed rest. *Clin. Physiol.*, 1993;**13**: 185–196.
741. Freitas, J., P. Lago, J. Puig, M.J. Carvalho, O. Costa, and A.F. de Freitas, Circadian heart rate variability rhythm in shift workers. *J. Electrocardiol.*, 1997;**30**: 39–44.

742. Zhong, X., H.J. Hilton, G.J. Gates, S. Jelic, Y. Stern, M.N. Bartels, R.E. DeMeersman, and R.C. Basner, Increased sympathetic and decreased parasympathetic cardiovascular modulation in normal humans with acute sleep deprivation. *J. Appl. Physiol.*, 2005;**98**: 2024–2032.
743. Viola, A.U., L.M. James, S.N. Archer, and D.J. Dijk, PER3 polymorphism and cardiac autonomic control: effects of sleep debt and circadian phase. *Am. J. Physiol. Heart. Circ. Physiol.*, 2008;**295**: H2156–2163.
744. Vandewalle, G., B. Middleton, S.M. Rajaratnam, B.M. Stone, B. Thorleifsdottir, J. Arendt, and D.J. Dijk, Robust circadian rhythm in heart rate and its variability: influence of exogenous melatonin and photoperiod. *J. Sleep. Res.*, 2007;**16**: 148–155.
745. Hu, K., P.Ch. Ivanov, M.F. Hilton, Z. Chen, R.T. Ayers, H.E. Stanley, and S.A. Shea, Endogenous circadian rhythm in an index of cardiac vulnerability independent of changes in behavior. *Proc. Natl. Acad. Sci. U. S. A.*, 2004;**101**: 18223–18227.
746. Huikuri, H.V., M.J. Niemelä, S. Ojala, A. Rantala, M.J. Ikäheimo, and K.E. Airaksinen, Circadian rhythms of frequency domain measures of heart rate variability in healthy subjects and patients with coronary artery disease. Effects of arousal and upright posture. *Circulation*, 1994;**90**: 121–126.
747. Bernardi, L., L. Ricordi, P. Lazzari, P. Solda, A. Calciati, M.R. Ferrari, I.Vandea, G. Finardi, and P. Fratino, Impaired circadian modulation of sympathovagal activity in diabetes: a possible explanation for altered temporal onset of cardiovascular disease. *Circulation*, 1992;**86**: 1443–1452.
748. Lombardi, F., G. Sandrone, A. Mortara, M.T. La Rovere, E. Colombo, S. Guzzetti, and A. Malliani, Circadian variation of spectral indices of heart rate variability after myocardial infarction. *Am. Heart. J.*, 1992;**123**: 1521–1528.
749. Chakko, S., R.F. Mulingtapang, H.V. Huikuri, K.M. Kessler, B.J. Materson, and R.J. Myerburg, Alterations in heart rate variability and its circadian rhythm in hypertensive patients with left ventricular hypertrophy free of coronary artery disease. *Am. Heart. J.*, 1993;**126**: 1364–1372.
750. Malik, M., T. Farrell, and A.J. Camm, Circadian rhythm of heart rate variability after acute myocardial infarction and its influence on the prognostic value of heart rate variability. *Am. J. Cardiol.*, 1990;**66**: 1049–1054.
751. Burr, R., P. Hamilton, M. Cowan, A. Buzaitis, M.R. Strasser, A. Sulkhanova, and K. Pike, Nycthemeral profile of nonspectral heart rate variability measures in women and men. Description of a normal sample and two sudden cardiac arrest subsamples. *J. Electrocardiol.*, 1994;**27**(Suppl): 54–62.
752. Klingenheben, T., U. Rapp, and S.H. Hohnloser, Circadian variation of heart rate variability in postinfarction patients with and without life-threatening ventricular tachyarrhythmias. *J. Cardiovasc. Electrophysiol.*, 1995;**6**: 357–364.
753. Sarma, J.S., N. Singh, M.P. Schoenbaum, K. Venkataraman, and B.N. Singh, Circadian and power spectral changes of RR and QT intervals during treatment of patients with angina pectoris with nadolol providing evidence for differential autonomic modulation of heart rate and ventricular repolarization. *Am. J. Cardiol.*, 1994;**74**: 131–136.
754. Pagani, M., V. Somers, R. Furlan, S. Dell'Orto, J. Conway, G. Baselli, S. Ceruti, P. Sleight, and A. Malliani, Changes in autonomic regulation induced by physical training in mild hypertension. *Hypertension*, 1988;**12**: 600–610.
755. Seals, D.R. and P.B. Chase, Influence of physical training on heart rate variability and baroreflex circulatory control. *J. Appl. Physiol.*, 1989;**66**: 1886–1895.
756. Henje Blom, E., E.M. Olsson, E. Serlachius, M. Ericson, and M. Ingvar, Heart rate variability is related to self-reported physical activity in a healthy adolescent population. *Eur. J. Appl. Physiol.*, 2009;**106**: 877–883.
757. Rennie, K.L., H. Hemingway, M. Kumari, E. Brunner, M. Malik, and M. Marmot, Effects of moderate and vigorous physical activity on heart rate variability in a British study of civil servants. *Am. J. Epidemiol.*, 2003;**158**: 135–143.
758. Horsten, M., M. Ericson, A. Perski, S.P. Wamala, K. Schenck-Gustafsson, and K. Orth-Gomér, Psychosocial factors and heart rate variability in healthy women. *Psychosom. Med.*, 1999;**61**: 49–57.
759. De Meersman, R.E., Heart rate variability and aerobic fitness. *Am. Heart. J.*, 1993;**125**: 726–731.
760. Galetta, F., F. Franzoni, F.R. Femia, N. Roccella, F. Pentimone, and G. Santoro, Lifelong physical training prevents the age-related impairment of heart rate variability and exercise capacity in elderly people. *J. Sports. Med. Phys. Fitness.*, 2005;**45**: 217–221.
761. Boutcher, S.H. and P. Stein, Association between heart rate variability and training response in sedentary middle-aged men. *Eur. J. Appl. Physiol. Occup. Physiol.*, 1995;**70**: 75–80.
762. Davy, K.P., W.L. Willis, and D.R. Seals, Influence of exercise training on heart rate variability in post-menopausal women with elevated arterial blood pressure. *Clin. Physiol.*, 1997;**17**: 31–40.
763. Verheyden, B., B.O. Eijnde, F. Beckers, L. Vanhees, and A.E. Aubert, Low-dose exercise training does not influence cardiac autonomic control in healthy sedentary men aged 55–75 years. *J. Sports. Sci.*, 2006;**24**: 1137–1147.
764. Melanson, E.L. and P.S. Freedson, The effect of endurance training on resting heart rate variability in sedentary adult males. *Eur. J. Appl. Physiol.*, 2001;**85**: 442–449.
765. Soares-Miranda, L., G. Sandercock, H. Valente, S. Vale, R. Santos, and J. Mota, Vigorous physical activity and vagal modulation in young adults. *Eur. J. Cardiovasc. Prev. Rehabil.*, 2009 Sep 4. [Epub ahead of print].
766. Gamelin, F.X., G. Baquet, S. Berthoin, D. Thevenet, C. Nourry, S. Nottin, and L. Bosquet, Effect of high intensity intermittent training on heart rate variability in prepubescent children. *Eur. J. Appl. Physiol.*, 2009;**105**: 731–738.
767. Jurca, R., T.S. Church, G.M. Morss, A.N. Jordan, and C.P. Earnest, Eight weeks of moderate-intensity exercise training increases heart rate variability in sedentary postmenopausal women. *Am. Heart. J.*, 2004;**147**: e21.
768. Earnest, C.P., C.J. Lavie, S.N. Blair, and T.S. Church, Heart rate variability characteristics in sedentary postmenopausal women following six months of exercise training: the DREW study. *PLoS. One.*, 2008;**3**: e2288.
769. Melo, R.C., R.J. Quitério, A.C. Takahashi, E. Silva, L.E. Martins, and A.M. Catai. High eccentric strength training reduces heart rate variability in healthy older men. *Br. J. Sports. Med.*, 2008;**42**: 59–63.
770. Piotrowicz, E., R. Baranowski, M. Piotrowska, T. Zieliński, and R. Piotrowicz, Variable effects of physical training of heart rate variability, heart rate recovery, and heart rate turbulence in chronic heart failure. *Pacing. Clin. Electrophysiol.*, 2009;**32** (Suppl 1): S113–115.

771. Dewey, F.E., J.V. Freeman, G. Engel, R. Oviedo, N. Abrol, N. Ahmed, J. Myers, and V.F., Froelicher, Novel predictor of prognosis from exercise stress testing: heart rate variability response to the exercise treadmill test. *Am. Heart. J.*, 2007;**153**: 281–288.
772. Leino, J., M. Virtanen, M. Kähönen, K. Nikus, T. Lehtimäki, T. Kööbi, R. Lehtinen, V. Turjanmaa, J. Viik, and T. Nieminen, Exercise-test-related heart rate variability and mortality The Finnish cardiovascular study. *Int. J. Cardiol.*, 2009. [Epub ahead of print].
773. Cottin, F., C. Médigue, and Y. Papelier, Effect of heavy exercise on spectral baroreflex sensitivity, heart rate, and blood pressure variability in well-trained humans. *Am. J. Physiol. Heart. Circ. Physiol.*, 2008;**295**: H1150–1155.
774. Raven, P.B., P.J. Fadel, and S. Ogoh, Arterial baroreflex resetting during exercise: a current perspective. *Exp. Physiol.*, 2006;**91**: 37–49.
775. Raven, P.B., D. ROhm-Young, and C.G. Blomqvist, Physical fitness and cardiovascular response to lower body negative pressure. *J. Appl. Physiol.*, 1984;**56**: 138–144.
776. Mack, G.W., C.A. Thompson, D.F. Doerr, E.E. Nadel, and V.A. Conveertino, Diminished baroreflex control of forearm resistance following training. *Med. Sci. Sports. Exer.*, 1991;**23**: 1367–1374.
777. Lightfoot, J.T., R.P. Claytor, D.J. Torak, T.W. Journell, and S.W. Fortney, Ten weeks of aerobic training do not affect lower body negative pressure response. *J. Appl. Physiol.*, 1989;**67**: 894–901.
778. Bowman, A.J., R.H. Clayton, A. Murray, J.W. Reed, M.M. Subhan, and G.A. Ford, Effects of aerobic exercise training and yoga on the baroreflex in healthy elderly persons. *Eur. J. Clin. Invest.*, 1997;**27**: 443–449.
779. Smith, S.A., R.G. Querry, P.J. Fadel, R.M. Welch-O'Connor, A. Olivencia-Yurvati, X. Shi, and P.B. Raven, Differential baroreflex control of heart rate in sedentary and aerobically fit individuals. *Med. Sci. Sports. Exerc.*, 2000;**32**: 1419–1430.
780. O'Sullivan, S.E. and C. Bell, The effects of exercise and training on human cardiovascular reflex control. *J. Auton. Nerv. Syst.*, 2000;**81**: 16–24.
781. Ueno, L.M. and T. Moritani, Effects of long-term exercise training on cardiac autonomic nervous activities and baroreflex sensitivity. *Eur. J. Appl. Physiol.*, 2003;**89**: 109–114.
782. Pichot, V., F. Roche, C. Denis, M. Garet, D. Duverney, F. Costes, and J.C. Barthélémy, Interval training in elderly men increases both heart rate variability and baroreflex activity. *Clin. Auton. Res.*, 2005;**15**: 107–115.
783. Iwasaki, K., R. Zhang, J.H. Zuckerman, and B.D. Levine, Dose-response relationship of the cardiovascular adaptation to endurance training in healthy adults: how much training for what benefit? *J. Appl. Physiol.*, 2003;**95**: 1575–1583.
784. Pagani, M., D. Lucini, O. Rimoldi, R. Furlan, S. Piazza, and L. Biancardi, Effects of physical and mental stress of heart rate variability, in *Heart Rate Variability*, M. Malik and A.J. Camm, Editors. Armonk, NY: Futura Publishing, 1995, pp. 245–266.
785. Hemingway, H., M. Malik, and M. Marmot, Social and psychosocial influences on sudden cardiac death, ventricular arrhythmia and cardiac autonomic function. *Eur. Heart. J.*, 2001;**22**: 1082–1101.
786. Bernardi, L., J. Wdowczyk-Szulc, C. Valenti, S. Castoldi, C. Passino, G. Spadacini, and P. Sleight, Effects of controlled breathing, mental activity and mental stress with or without verbalization on heart rate variability. *J. Am. Coll. Cardiol.*, 2000;**35**: 1462–1469.
787. Lantelme, P., H. Milon, C. Gharib, C. Gayet, and J.O. Fortrat JO, White coat effect and reactivity to stress: cardiovascular and autonomic nervous system responses. *Hypertension*, 1998;**31**: 1021–1029.
788. Kageyama, T., N. Nishikido, T. Kobayashi, Y. Kurokawa, T. Kaneko, and M. Kabuto, Self-reported sleep quality, job stress, and daytime autonomic activities assessed in terms of short-term heart rate variability among male white-collar workers. *Ind. Health.*, 1998;**36**: 263–272.
789. Cohen, H., J. Benjamin, A.B. Geva, M.A. Matar, Z. Kaplan, and M. Kotler, Autonomic dysregulation in panic disorder and in post-traumatic stress disorder: application of power spectrum analysis of heart rate variability at rest and in response to recollection of trauma or panic attacks. *Psychiatry. Res.*, 2000;**96**: 1–13.
790. Cohen, H., M. Kotler, M. Matar, and Z. Kaplan, Normalization of heart rate variability in post-traumatic stress disorder patients following fluoxetine treatment: preliminary results. *Isr. Med. Assoc. J.*, 2000;**2**: 296–301.
791. Madden, K. and G.K. Savard, Effects of mental state on heart rate and blood pressure variability in men and women. *Clin. Physiol.*, 1995;**15**: 557–569.
792. Friedman, B.H., An autonomic flexibility–neurovisceral integration model of anxiety and cardiac vagal tone. *Biol. Psychol.*, 2007;**74**: 185–199.
793. McCraty, R., M. Atkinson, W.A. Tiller, G. Rein, and A.D. Watkins, The effects of emotions on short-term power spectrum analysis of heart rate variability. *Am. J. Cardiol.*, 1995;**76**: 1089–1093.
794. De Meersman, R.E., S. Reisman, M. Daum, and R. Zorowitz, Vagal withdrawal as a function of audience. *Am. J. Physiol. Heart. Circ. Physiol.*, 1996;**270**: H1381–1383.
795. Delaney, J.P. and D.A. Brodie, Effects of short-term psychological stress on the time and frequency domains of heart-rate variability. *Percept. Mot. Skills.*, 2000;**91**: 515–524.
796. Shinba, T., N. Kariya, Y. Matsui, N. Ozawa, Y. Matsuda, and K.Yamamoto, Decrease in heart rate variability response to task is related to anxiety and depressiveness in normal subjects. *Psychiatry. Clin. Neurosci.*, 2008;**62**: 603–609.
797. Yeragani, V.K., R.B. Pohl, R. Berger, R. Balon, C. Ramesh, D. Glitz, K. Srinivasan, and P. Weinberg, Decreased heart rate variability in panic disorder patients: a study of power spectral analysis of heart rate. *Psychiatr. Res.*, 1993;**46**: 89–103.
798. Kawachi, I., D. Sparrow, P.S. Vokonas, and S.T. Weiss, Decreased heart rate variability in men with phobic anxiety (data from the Normative Aging Study). *Am. J. Cardiol.*, 1995;**75**: 882–885.
799. McCraty, R., M. Atkinson, D. Tomasino, and W.P. Stuppy, Analysis of twenty-four hour heart rate variability in patients with panic disorder. *Biol. Psychol.*, 2001;**56**: 131–150.
800. Asmundson, G.J.G. and M.B. Stein, Vagal attenuation in panic disorder: an assessment of parasympathetic nervous system function and subjective reactivity to respiratory manipulations. *Psychosom. Med.*, 1994;**56**: 187–193.
801. Dishman, R.K., Y. Nakamura, M.E. Garcia, R.W. Thompson, A.L. Dunn, and S.N. Blair, Heart rate variability, trait anxiety, and perceived stress among physically fit men and women. *Int. J. Psychophysiol.*, 2000;**37**: 121–133.
802. Agelink, M.W., C. Boz, H. Ullrich, and J. Andrich, Relationship between major depression and heart rate variability. Clinical consequences and implications for antidepressive treatment. *Psychiatry. Res.*, 2002;**113**: 139–149.

803. Carney, R.M., J.A. Blumenthal, P.K. Stein, L. Watkins, D. Catellier, L.E. Berkman, S.M. Czajkowski, C. O'Connor, P.H. Stone, and K.E. Freedland, Depression, heart rate variability, and acute myocardial infarction. *Circulation*, 2001;**104**: 2024–2028.
804. O'Connor, M.F., J.J. Allen, and A.W. Kaszniak, Autonomic and emotion regulation in bereavement and depression. *J. Psychosom. Res.*, 2002;**52**: 183–185.
805. Moser, M., M. Lehofer, R. Hoehn-Saric, D.R. McLeod, G. Hildebrandt, B. Steinbrenner, M. Voica, P. Liebmann, and H.G. Zapotoczky, Increased heart rate in depressed subjects in spite of unchanged autonomic balance? *J. Affect. Disord.*, 1998;**48**: 115–124.
806. Watkins, L.L, P. Grossman, R. Krishnan, and J.A. Blumenthal, Anxiety reduces baroreflex cardiac control in older adults with major depression. *Psychosom. Med.*, 1999;**61**: 334–340.
807. Zhong, X., H.J. Hilton, G.J. Gates, S. Jelic, Y. Stern, M.N. Bartels, R.E. Demeersman, and R.C. Basner, Increased sympathetic and decreased parasympathetic cardiovascular modulation in normal humans with acute sleep deprivation. *J. Appl. Physiol.*, 2005;**98**: 2024–2032.
808. Gillum, R.F., Epidemiology of resting pulse rate of persons ages 25–74–data from NHANES 1971–74. *Public. Health. Rep.*, 1992;**107**: 193–201.
809. Robertson, D., C.J. Tseng, and M. Appalsamy, Smoking and mechanisms of cardiovascular control. *Am. Heart. J.*, 1988;**115**: 258–263.
810. Hayano, J., M. Yamada, Y. Sakakibara, T. Fujinami, K. Yokoyama, Y. Watanabe, and K. Takata, Short- and long-term effects of cigarette smoking on heart rate variability. *Am. J. Cardiol.*, 1990;**65**: 84–88.
811. Gallagher, D., T. Terenzi, and R. de Meersman, Heart rate variability in smokers, sedentary and aerobically fit individuals. *Clin. Auton. Res.*, 1992;**2**: 383–387.
812. Carnethon, M.R., D. Liao, G.W. Evans, W.E. Cascio, L.E. Chambless, and G. Heiss, Correlates of the shift in heart rate variability with an active postural change in a healthy population sample: the Atherosclerosis Risk In Communities study. *Am. Heart. J.*, 2002;**143**: 808–813.
813. Barutcu, I., A.M. Esen, D. Kaya, M. Turkmen, O. Karakaya, M. Melek, O.B. Esen, and Y. Basaran, Cigarette smoking and heart rate variability: dynamic influence of parasympathetic and sympathetic maneuvers. *Ann. Noninvas. Electrocardiol.*, 2005;**10**: 324–329.
814. Eryonucu, B., M. Bilge, N. Güler, K. Uzun, and M. Gencer, Effects of cigarette smoking on the circadian rhythm of heart rate variability. *Acta. Cardiol.*, 2000;**55**: 301–305.
815. Christensen, J.H., H.A. Skou, L. Fog, V. Hansen, T. Vesterlund, J. Dyerberg, E. Toft, and E.B. Schmidt, Marine n-3 fatty acids, wine intake, and heart rate variability in patients referred for coronary angiography. *Circulation*, 2001;**103**: 651–657.
816. Murata, K., P.J. Landrigan, and S. Araki, Effects of age, heart rate, gender, tobacco and alcohol ingestion on R-R interval variability in human ECG. *J. Auton. Nerv. Syst.*, 1991;**37**: 199–206.
817. Kageyama, T., N. Nishikido, Y. Honda, Y. Kurokawa, H. Imai, T. Kobayashi, T. Kaneko, and M. Kabuto, Effects of obesity, current smoking status, and alcohol consumption on heart rate variability in male white-collar workers. *Int. Arch. Occup. Environ. Health.*, 1997;**69**: 447–454.
818. Hamaad, A., M. Sosin, A.D. Blann, J. Patel, G.Y. Lip, and R.J. MacFadyen, Markers of inflammation in acute coronary syndromes: association with increased heart rate and reductions in heart rate variability. *Clin. Cardiol.*, 2005;**28**: 570–576.
819. Gehi, A., J. Ix, M. Shlipak, S.S. Pipkin, and M.A. Whooley, Relation of anemia to low heart rate variability in patients with coronary heart disease (from the Heart and Soul study). *Am. J. Cardiol.*, 2005;**95**: 1474–1477.
820. Stein, P.K., J.I. Barzilay, P.H. Chaves, J. Traber, P.P. Domitrovich, S.R. Heckbert, and J.S. Gottdiener, Higher levels of inflammation factors and greater insulin resistance are independently associated with higher heart rate and lower heart rate variability in normoglycemic older individuals: the Cardiovascular Health Study. *J. Am. Geriatr. Soc.*, 2008;**56**: 315–321.
821. Liao, D., J. Cai, F.L. Brancati, A. Folsom, R.W. Barnes, H.A. Tyroler, and G. Heiss, Association of vagal tone with serum insulin, glucose, and diabetes mellitus–The ARIC Study. *Diabetes. Res. Clin. Pract.*, 1995;**30**: 211–221.

Appendix 1
List of references cited only in tables and figures

A1. Odemuyiwa, O., M. Malik, T. Farrell, Y. Bashir, J. Poloniecki, and J. Camm, Comparison of the predictive characteristics of heart rate variability index and left ventricular ejection fraction for all-cause mortality, arrhythmic events and sudden death after acute myocardial infarction. *Am. J. Cardiol.*, 1991;**68**: 434–439.
A2. Bigger, J.T. Jr, J.L. Fleiss, R.C. Steinman, L.M. Rolnitzky, R.E. Kleiger, and J.N. Rottman, Frequency domain measures of heart period variability and mortality after myocardial infarction. *Circulation*, 1992;**85**: 164–171.
A3. Vaishnav, S., R. Stevenson, B. Marchant, K. Lagi, K. Ranjadayalan, and A.D. Timmis, Relation between heart rate variability early after acute myocardial infarction and long-term mortality. *Am. J. Cardiol.*, 1994;**73**: 653–657.
A4. Touboul, P., X. Andre-Fouët, A. Leizorovicz, R. Itti, M. Lopez, Y. Sayegh, H. Milon, and G. Kirkorian, Risk stratification after myocardial infarction. A reappraisal in the era of thrombolysis. The Groupe d'Etude du Pronostic de l'Infarctus du Myocarde (GREPI). *Eur. Heart. J.*, 1997;**18**: 99–107.
A5. Tsuji, H., F.J. Venditti Jr., E.S. Manders, J.C. Evans, M.G. Larson, C.L. Feldman, and D. Levy, Reduced heart rate variability and mortality risk in an elderly cohort. The Framingham Heart Study. *Circulation*, 1994;**90**: 878–883.
A6. Nollo, G., M. Del Greco, M. Disertori, E. Santoro, A.P. Maggioni, G.P.Sanna, and GISSI-3 Arrhythmias Substudy Investigators, Absence of slowest oscillations in short term heart rate variability of post-myocardial infarction patients. GISSI-3 arrhythmias

substudy. GISSI-3 Arrhythmias Substudy Investigators. *Auton. Neurosci.*, 2001;**90**: 127–131.

A7. Forslund, L., I. Björkander, M. Ericson, C. Held, T. Kahan, N. Rehnqvist, and P. Hjemdahl, Prognostic implications of autonomic function assessed by analyses of catecholamines and heart rate variability in stable angina pectoris. *Heart*, 2002;**87**: 415–422.

A8. Lampert, R., J.R. Ickovics, C.J. Viscoli, R.I. Horwitz, and F.A. Lee, Effects of propranolol on recovery of heart rate variability following acute myocardial infarction and relation to outcome in the Beta-Blocker Heart Attack Trial. *Am. J. Cardiol.*, 2003;**91**: 137–142.

A9. La Rovere, M.T., G.D. Pinna, R. Maestri, A. Mortara, S. Capomolla, O. Febo, R. Ferrari, M. Franchini, M. Gnemmi, C. Opasich, R.G. Riccardi, E. Traversi, and F. Cobelli, Short-term heart rate variability strongly predicts sudden cardiac death in chronic heart failure patients. *Circulation*, 2003;**107**: 565–570.

A10. Jokinen, V., J.M. Tapanainen, T. Seppänen, and H.V. Huikuri, Temporal changes and prognostic significance of measures of heart rate dynamics after acute myocardial infarction in the beta-blocking era. *Am. J. Cardiol.*, 2003;**92**: 907–912.

A11. Schroeder, E.B., D. Liao, L.E. Chambless, R.J. Prineas, G.W. Evans, and G. Heiss, Hypertension, blood pressure, and heart rate variability: the Atherosclerosis Risk in Communities (ARIC) study. *Hypertension*, 2003;**42**: 1106–1011.

A12. Stein, P.K., P.P. Domitrovich, R.E. Kleiger, and CAST Investigators, Including patients with diabetes mellitus or coronary artery bypass grafting decreases the association between heart rate variability and mortality after myocardial infarction. *Am. Heart. J.*, 2004;**147**: 309–316.

A13. Carpeggiani, C., A. L'Abbate, P. Landi, C. Michelassi, M. Raciti, A. Macerata, and M. Emdin, Early assessment of heart rate variability is predictive of in-hospital death and major complications after acute myocardial infarction. *Int. J. Cardiol.*, 2004;**96**: 361–368.

A14. Casaleggio, A., R. Maestri, M.T. La Rovere, P. Rossi, and G.D. Pinna, Prediction of sudden death in heart failure patients: a novel perspective from the assessment of the peak ectopy rate. *Europace*, 2007;**9**: 385–390.

A15. Barthel, P., R. Schneider, A. Bauer, K. Ulm, C. Schmitt, A. Schömig, and G. Schmidt. Risk stratification after acute myocardial infarction by heart rate turbulence. *Circulation*, 2003;**108**: 1221–1226.

A16. Exner, D.V., K.M. Kavanagh, M.P. Slawnych, L.B. Mitchell, D. Ramadan, S.G. Aggarwal, C. Noullett, A. Van Schaik, R.T. Mitchell, M.A. Shibata, S. Gulamhussein, J. McMeekin, W. Tymchak, G. Schnell, A.M. Gillis, R.S. Sheldon, G.H. Fick, H.J. Duff, and REFINE Investigators, Noninvasive risk assessment early after a myocardial infarction the REFINE study. *J. Am. Coll. Cardiol.*, 2007;**50**: 2275–2284.

A17. Mäkikallio, T.H., P. Barthel, R. Schneider, A. Bauer, J.M. Tapanainen, M.P. Tulppo, J.S. Perkiömäki, G. Schmidt, and H.V. Huikuri, Frequency of sudden cardiac death among acute myocardial infarction survivors with optimized medical and revascularization therapy. *Am. J. Cardiol.*, 2006;**97**: 480–484.

A18. Klingenheben, T., P. Ptaszynski, and S.H. Hohnloser, Heart rate turbulence and other autonomic risk markers for arrhythmia risk stratification in dilated cardiomyopathy. *J. Electrocardiol.*, 2008;**41**: 306–311.

A19. Kanters, J.K., M.V. Højgaard, E. Agner, and N.H. Holstein-Rathlou, Short- and long-term variations in nonlinear dynamics of heart rate variability. *Cardiovasc. Res.*, 1996;**31**: 400–409.

A20. Zöllei, E., A. Csillik, S. Rabi, Z. Gingl, and L. Rudas, Respiratory effects on the reproducibility of cardiovascular autonomic parameters. *Clin. Physiol. Funct. Imaging.*, 2007;**27**: 205–210.

A21. Kobayashi, H., Inter- and intra-individual variations of heart rate variability in Japanese males. *J. Physiol. Anthropol.*, 2007;**26**: 173–177.

A22. Kleiger, R.E., J.T. Bigger, M.S. Bosner, M.K. Chung, J.R. Cook, L.M. Rolnitzky, R. Steinman, and J.L. Fleiss, Stability over time of variables measuring heart rate variability in normal subjects. *Am. J. Cardiol.*, 1991;**68**: 626–630.

A23. Kowalewski, M.A. and M. Urban, Short- and long-term reproducibility of autonomic measures in supine and standing positions. *Clin. Sci. (Lond).*, 2004;**106**: 61–66.

A24. Burger, A.J., M. Charlamb, L.A. Weinrauch, and J.A. D'Elia, Short- and long-term reproducibility of heart rate variability in patients with long-standing type I diabetes mellitus. *Am. J. Cardiol.*, 1997;**80**: 1198–1202.

A25. Macfarlane, P.W., J. Norrie, and WOSCOPS Executive Committee, The value of the electrocardiogram in risk assessment in primary prevention: experience from the West of Scotland Coronary Prevention Study. *J. Electrocardiol.*, 2007;**40**: 101–109.

A26. Dekker, J.M., E.G. Schouten, P. Klootwijk, J. Pool, C.A. Swenne, and D. Kromhout, Heart rate variability from short electrocardiographic recordings predicts mortality from all causes in middle-aged and elderly men. The Zutphen Study. *Am. J. Epidemiol.*, 1997;**145**: 899–908.

A27. Korkushko, O.V., V.B. Shatilo, Yu.I. Plachinda, and T.V. Shatilo, Autonomic control of cardiac chronotropic function in man as a function of age: assessment by power spectral analysis of heart rate variability. *J. Auton. Nerv. Syst.*, 1991;**32**: 191–198.

A28. Ryan, S.M., A.L. Goldberger, S.M. Pincus, J. Mietus, and L.A. Lipsitz. Gender- and age-related differences in heart rate dynamics: are women more complex than men? *J. Am. Coll. Cardiol.*, 1994;**24**: 1700–1707.

A29. Hotta, N., K. Otsuka, S. Murakami, G. Yamanaka, Y. Kubo, O. Matsuoka, T. Yamanaka, M. Shinagawa, S. Nunoda, Y. Nishimura, K. Shibata, H. Saitoh, M. Nishinaga, M. Ishine, T. Wada, K. Okumiya, K. Matsubayashi, S. Yano, K. Ichihara, G. Cornélissen, and F. Halberg, Fractal analysis of heart rate variability and mortality in elderly community-dwelling people – Longitudinal Investigation for the Longevity and Aging in Hokkaido County (LILAC) study. *Biomed. Pharmacother.*, 2005;**59** (Suppl 1): S45–48.

A30. Stein, P.K., Assessing heart rate variability from real-world Holter reports. *Card. Electrophysiol. Rev.*, 2002;**6**: 239–244.

A31. Uijtdehaage, S.H.J., and J.F. Thayer. Accentuated antagonism in the control of human heart rate. *Clin. Autonom. Res.*, 2000; **10**: 107–110.

A32. Corino, V.D.A., M. Matteucci, L. Cravello, E. Ferrari, A.A. Ferrari, and L.T. Mainardi. Long-term heart rate variability as a predictor of patient age. *Comp. Meth. Prog. Biomed.*, 2006; **82**: 248–257.

A37. Voss, A., J. Kurths, H.J. Kleiner, A. Witt, N. Wessel, P. Saparin, K.J. Osterziel, R. Schurath, and R. Dietz, The application of methods of nonlinear dynamics for the improved and predictive recognition of patients threatened by sudden cardiac death. *Cardiovasc. Res.*, 1996;**31**: 419–433.

A34. Schneider, R.A. and J.P. Costiloe,. Relationship of sinus arrhythmia to age and its prognostic significance in ischemie heart disease (abstr). *Clin. Res.*, 1965;**13**: 219.

A35. Acharya U.R., K.P. Joseph, N. Kannathal, C.M. Lim, J.S. Suri. Heart rate variability: a review. *Med. Biol. Eng. Comput.*, 2006;**44**: 1031–1051.

A36. Hoyer D, Friedrich H, Zwiener U, Pompe B, Baranowski R, Werdan K, Müller-Werdan U, Schmidt H. Prognostic impact of autonomic information flow in multiple organ dysfunction syndrome patients. *Int J Cardiol.*, 2006;**108**: 359–369.

A37. Akay, M. Wavelets in biomedical engineering. *Ann. Biomed. Eng.*, 1995:**23**: 531–542.

Section 9

Specialized Aspects of Electrocardiography Part 2

36 Exercise Electrocardiography and Exercise Testing

K. Martijn Akkerhuis · Maarten L. Simoons

P. W. Macfarlane, A. van Oosterom, O. Pahlm, P. Kligfield, M. Janse, J. Camm (eds.), *Comprehensive Electrocardiology*, DOI 10.1007/978-1-84882-046-3_36,

36.1 Introduction

Exercise testing is a widely used method for diagnosis in patients with suspected ischemic heart disease and for functional evaluation of patients with known heart disease. Throughout the years, most attention has been given to the information obtained from the electrocardiogram during exercise. However, other information that can be obtained during the test is of equal importance. Such information, as listed in Table 36.1, can be obtained by observation of the patient, measurement of the heart rate and blood pressure responses, measurement or estimation of total body oxygen consumption, and from other noninvasive investigations such as myocardial-perfusion scintigraphy and evaluation of left ventricular function by radionuclide angiography or echocardiography. This chapter focuses on exercise electrocardiography.

Compared with the noninvasive stress imaging tests such as stress echocardiography and myocardial perfusion scintigraphy, exercise testing can be performed at a much lower cost. However, the noninvasive imaging modalities have been increasingly more used in the last decade and have been shown to outperform the standard exercise test in terms of diagnostic accuracy. This does not mean, however, that exercise electrocardiography should be replaced by these imaging modalities. The standard exercise test remains the initial test of choice in many clinical circumstances. However, new technical improvements in the field of the stress imaging tests are expected to further increase their performance and clinical use. Furthermore, new techniques are being developed that permit direct, noninvasive imaging of the coronary arteries (e.g., multislice computed tomography). These developments will require a continuous reassessment of the relative role of all commonly used diagnostic tests and procedures.

The report of an exercise test should contain a summary of the previous history of the patient, his present symptoms, medication, and an interpretation of the ECG at rest. The exercise protocol should be described with the expected performance of a normal subject of the same age, sex, and body size. The reasons for termination of the test should be stated and symptoms which occur during the test should be described, including the workload at which symptoms began, the type of symptoms, their severity, and the duration of the symptoms after exercise has ceased. Heart rate and blood pressure should be reported at rest, at the onset of symptoms, at peak exercise, and after approximately 6 min into the recovery period. A description of the ECG should contain any arrhythmias which may have occurred and changes in the QRS complex and ST segment. Finally, a conclusion should be drawn which answers the clinical questions that were posed before the test. The report should not be limited to words like "positive" or "negative."

36.2 Safety of Exercise Testing, Precautions, and Contraindications

Exercise testing is a well-established procedure that has been in widespread clinical use for many decades. Although exercise testing is generally a safe procedure, both myocardial infarction and death have been reported. A large survey reported

Table 36.1

Information obtained by exercise testing in patients with (suspected) heart disease

Information	Measurement
• Exercise tolerance	• Maximum workload • Heart rate response • Maximum oxygen consumption
• Limiting symptoms	• Symptoms during test
• Myocardial ischemia	• Angina pectoris • ST segment changes • Myocardial perfusion scintigraphy
• Left ventricular function	• Maximum workload • Blood pressure response • Echocardiography (Radionuclide angiography) (Left ventricular filling pressure)
• Arrhythmias	• Electrocardiogram

17 deaths among 712,285 patients tested in three German-speaking countries [1]. In addition, nonfatal ventricular fibrillation occurred at a rate of 1/7,000 tests and nonfatal myocardial infarction at a rate of 1/70,000 tests. Since these risks are not negligible, all stress testing should be done in a setting where emergencies can be treated efficiently and expeditiously. A defibrillator and an emergency kit of appropriate drugs should be immediately available, and the staff of the exercise laboratory should be trained in cardiopulmonary resuscitation [2]. In addition, exercise testing should be supervised by an appropriately trained physician, who should be in the immediate vicinity and available for emergencies [3]. However, the most important safety factors in stress testing are patient selection and good clinical judgment, deciding which patient should undergo exercise testing and knowing when not to start and when to stop a test are essential in reducing the risk of stress testing. Absolute and relative contraindications to exercise stress testing are listed in Table 36.2 [4].

36.3 Exercise Protocols

Exercise should be performed on a treadmill or a calibrated bicycle ergometer [5, 6]. Other modalities may be used in special situations; for example, in sports medicine a rowing ergometer or a canoe ergometer might be used. The various forms of step tests are outdated, since these do not permit quantification of the work performed. The choice between a bicycle ergometer and a treadmill can be made on the basis of personal preferences or local custom. In general, normal subjects can reach higher heart rates and a higher level of oxygen consumption on a treadmill [7]. Furthermore, virtually all subjects can be exercised on a treadmill, while riding a bicycle requires some skill. On the other hand, the body position is more stable on a bicycle ergometer, resulting in less motion artifacts on the ECG. For studies of left ventricular function during exercise or studies with indwelling catheters, only bicycles can be used, usually with the patient in the supine position. Guidelines for the design of a clinical exercise testing laboratory have been published by the American Heart Association [2].

Exercise should start at a low workload and increment stepwise or continuously, according to a fixed protocol. A large number of treadmill protocols has been described (Fig. 36.1). Probably the most widely used protocol has been described by Bruce [8]. In this protocol, both the grade (slope) of the treadmill and its speed are altered at the end of

Table 36.2

Contraindications to exercise testing (Adapted from ACC/AHA 2002 Guideline Update for Exercise Testing [4])

Absolute
• Acute myocardial infarction (within 2 days)
• High-risk unstable angina
• Symptomatic severe aortic stenosis
• Uncontrolled symptomatic heart failure
• Acute pulmonary embolus or pulmonary infarction
• Uncontrolled cardiac arrhythmias causing symptoms or hemodynamic compromise
• Acute myocarditis or pericarditis
• Acute aortic dissection
Relative
• Left main coronary stenosis
• Moderate stenotic valvular heart disease
• Electrolyte abnormalities
• Severe arterial hypertension[a]
• Tachyarrhythmias or bradyarrhythmias
• Hypertrophic (obstructive) cardiomyopathy and other forms of outflow tract obstruction
• Mental or physical impairment leading to inability to exercise adequately
• High-degree atrioventricular block

[a]Systolic blood pressure of >200 mmHg and/or diastolic blood pressure of >110 mmHg, as suggested by the ACC/AHA Committee on Exercise Testing

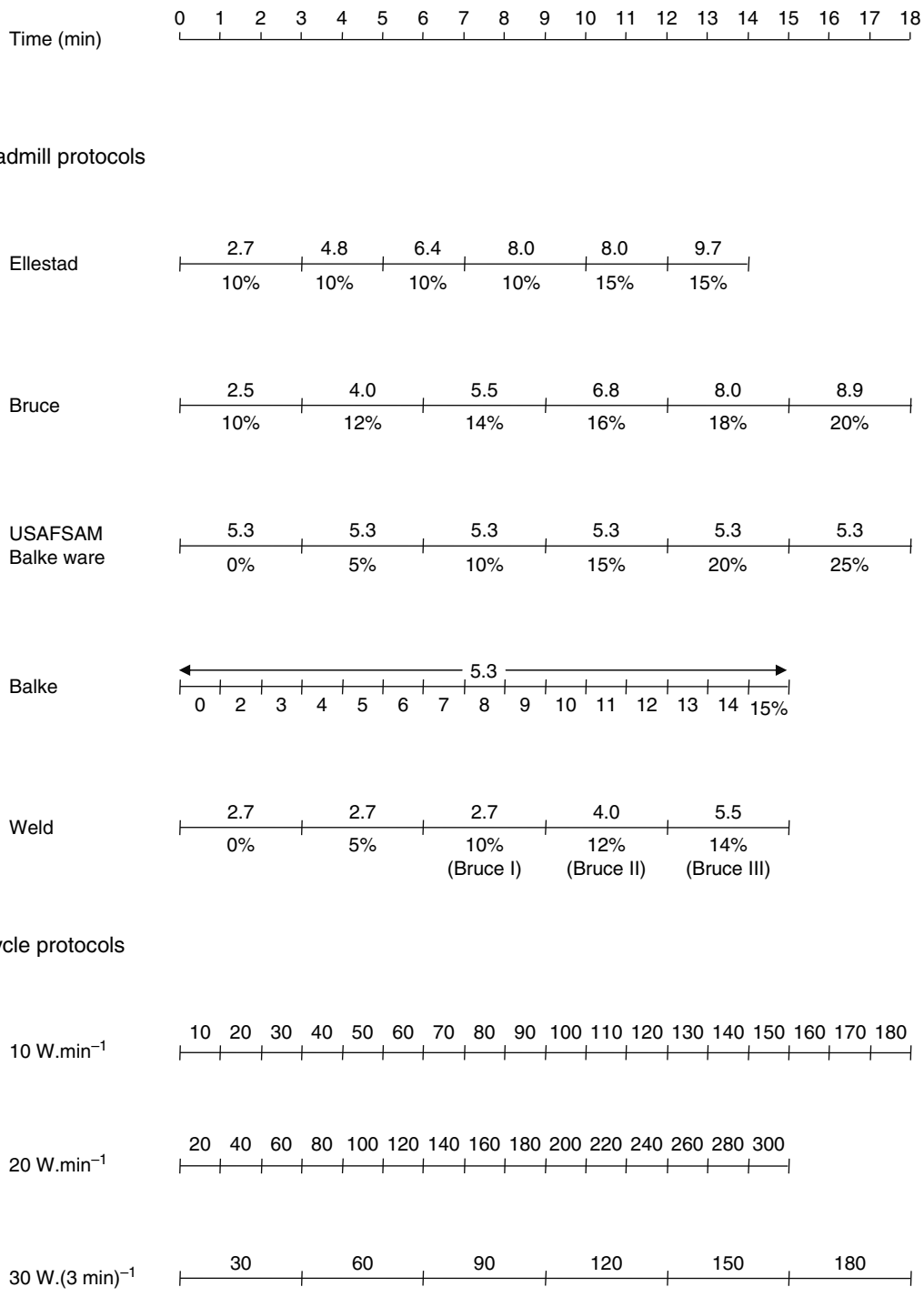

Figure 36.1

Summary of five treadmill protocols and three bicycle protocols. The figures above the lines of the treadmill protocols represent treadmill speed in kilometers per hour, and the figures below the lines represent the slope. Some treadmill protocols use steps of 3 min each (Bruce, USAFSAM, Weld), while others use steps of 1 min (Balke) or alternating steps of 3 and 2 min (Ellestad). The figures above the lines of the bicycle protocols correspond to workload in Watts. Either 1-min steps or steps of 3 min are used. The value of the divisions marked on these lines is indicated on the *left*.

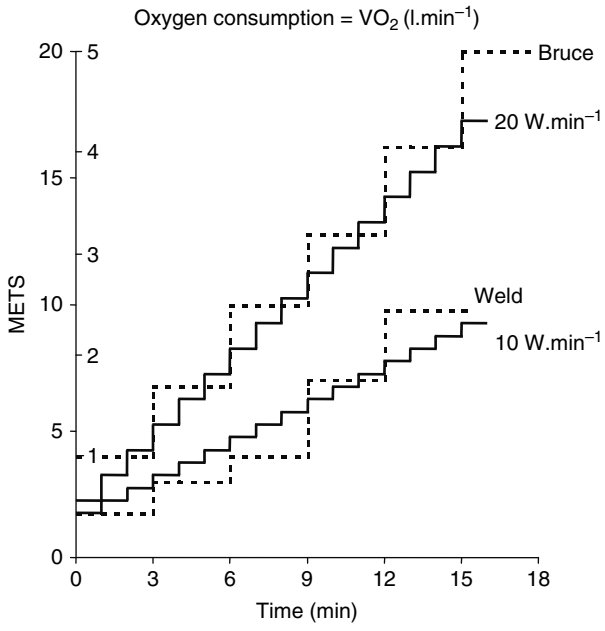

Figure 36.2

Comparison of oxygen requirements over time for two bicycle protocols (steps of 20 W/min or 10 W/min) and two treadmill protocols (Bruce and Weld) in a 75 kg male subject. The horizontal axis represents time in minutes and the vertical axis represents average oxygen uptake (l/min), which can be equated to metabolic equivalents (METS). It should be noted that the actual oxygen consumption of a given patient at a certain level of exercise varies widely and depends on their level of physical condition. Furthermore, oxygen consumption on the treadmill is dependent on body weight.

each 3-min stage. In the Ellestad protocol [9], the slope is constant during the first four stages, while the speed increases. At stage five, speed is kept constant while the slope is altered; for stage six, speed is again increased. The Balke protocol and its derivatives maintain a constant speed in the range of 4.8–6.4 km/h with changes of treadmill slope every minute or every 3 min [10]. Modifications of these protocols have been developed for the evaluation of patients prior to discharge from hospital after myocardial infarction. For example, the protocol used by Weld employs two stages with a low treadmill slope prior to the first stage of the Bruce protocol [11].

Workload on a treadmill is dependent on body weight. Accordingly, the workload performed using various protocols can be expressed as ml/kg/min oxygen consumption. In the literature, workload has frequently been expressed in metabolic equivalents (METS) [12, 13]. One MET equals 3.5 ml/kg/min oxygen consumption, which corresponds to the average resting oxygen consumption. In Fig. 36.2, mean oxygen consumption is given for various protocols and the corresponding METS have been indicated. Oxygen consumption rises more rapidly with the Bruce protocol or the Ellestad protocol than with the USAFSAM modification of the Balke protocol, which uses a speed of 5.3 km/h [14, 15]. The work on a bicycle ergometer is independent of body weight. Frequently used protocols on a bicycle ergometer in the sitting position increase the workload by 10 W/min or 20 W/min. For adult male subjects with average body weight, the metabolic requirement (total body oxygen consumption) of a protocol with 20 W/min workload increments is comparable to the Bruce protocol (Fig. 36.2). Similarly, a protocol with 10 W/min steps is comparable to the Weld protocol for submaximal predischarge tests after myocardial infarction. Predicted normal values for the peak workload for a protocol with steps of 20 W/min are presented in Table 36.3. In the supine position, lower workload increments are normally used; for example, 20 or 30 W every 3–5 min.

It should be realized that the hemodynamic response to exercise in the supine position differs considerably from the response in the sitting position. In patients with coronary artery disease (CAD), the peak level of exercise in the supine position is approximately 70% of the peak level in the sitting position. Peak heart rate and peak systolic blood pressure are

Table 36.3

Predicted normal exercise tolerance (in Watts) using a bicycle ergometer protocol for exercise testing

	Exercise tolerance in *women*					Exercise tolerance in *men*				
	Height (cm)					Height (cm)				
Age (years)	160	170	180	190	200	160	170	180	190	200
20	176	192	208	225	241	220	240	261	281	301
25	167	183	199	215	232	209	229	249	269	290
30	158	174	190	206	222	197	217	238	258	278
35	149	165	181	197	213	186	206	226	246	267
40	139	156	172	188	204	174	195	215	235	255
45	130	146	163	179	195	163	183	203	223	244
50	121	137	153	170	186	151	172	192	212	232
55	112	128	144	160	177	140	160	180	201	221
60	103	119	135	151	167	129	149	169	189	209
65	94	110	126	142	158	117	137	157	178	198
70	84	101	117	133	149	106	126	146	166	186

Predicted normal exercise tolerance (in Watts) for women (left) and men (right). These normal values are applicable when a protocol with steps of 20 W/min is used on a bicycle ergometer. The normal range is between 85% and 115% of these values. For example, a 45-year old man with a height of 190 cm has a predicted normal exercise tolerance of 223 W, ranging from 190 to 256 W.

approximately 10% lower. On the other hand, pulmonary capillary wedge pressure during exercise is higher in the supine position owing to the greater venous return [16–18]. In order to obtain reproducible results, each hospital and laboratory should select one or two protocols which can be applied to all subjects. Reference values for such protocols are readily available as shown in Fig. 36.3 and Table 36.3. Nevertheless, each laboratory should verify whether these values are indeed applicable to the local population. Measurement of oxygen consumption is not very useful in a laboratory for exercise electrocardiography. If necessary, oxygen consumption can be estimated from the workload as shown in Fig. 36.2. The standard deviation of this estimation is between 5% and 10%.

36.4 Exercise Endpoints

For most purposes, exercise can be continued until symptoms occur. It is a fallacy to terminate exercise at an arbitrary percentage (70 or 85%) of the age-adjusted maximum predicted heart rate for a number of reasons. First, the heart-rate response in normal subjects is highly variable [13]. The mean value at each age may be predicted as 220 minus age, or 200 minus age/2. These mean values apply both to men and women up to 70 years of age. However, the standard deviation is large, approximately 10 beats/min. Thus, the 95% confidence interval is between 20 beats below and 20 beats above the predicted mean value [12]. Second, the maximum heart rate reached by patients with severe disease is considerably lower than the heart rate reached by normal subjects. Thus, when heart rate is used as an endpoint for terminating exercise, patients with severe disease may be stressed beyond their limits, while other patients will be unnecessarily prevented from exercising to their true capacity. Finally, the target heart rate approach has additional limitations in patients with heart rate impairment, those with excessive heart rate response, and those receiving medication such as beta-blockers, some calcium antagonists, and specific sinus-node inhibitors [20–23].

Therefore, other endpoints for terminating exercise testing, as summarized in Table 36.4, are strongly preferred. It should be noted that ST segment elevation developing in leads (other than aVR or V_1) without diagnostic Q-waves of a previous myocardial infarction usually indicates transmural ischemia rather than just a subendocardial problem. It is almost always associated with a high-grade obstruction proximal in the respective coronary artery. If exercise continues, myocardial infarction may be imminent, so that it is necessary to terminate the test and direct the patient to immediate follow-up care including coronary angiography.

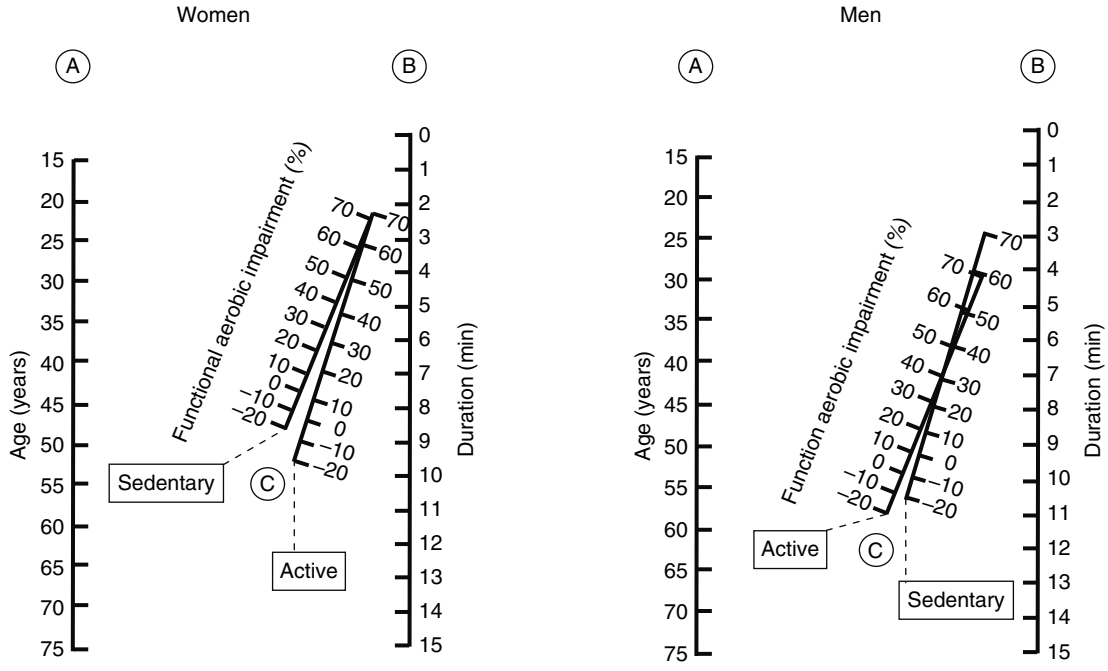

Figure 36.3

Nomogram for assessment of functional aerobic impairment of men and women according to age, duration of exercise by the Bruce multistage procedure, and habitual physical activity status. In order to find functional aerobic impairment (*C*), apply a straight-edge to age (*A*) and duration (*B*) and read intercepts of diagonal (Adapted from Bruce [19]).

It is advisable to express symptoms which occur during exercise on a semiquantitative scale, such as the Borg scale (Table 36.5) [24]. The use of rating of perceived exertion scales is often useful in assessment of patient fatigue. Symptom-limited testing with the Borg scale as an aid is very important when the test is used to assess functional capacity. It also permits a comparison of the degree of a patient's symptoms over time.

It has previously been recommended that all medication be stopped one or more days before an exercise test is done. Although this may be useful for some scientific applications, this principle is not generally followed in clinical practice. In patients with stable angina, a period of instability may develop if beta-blockers, nitrates, or calcium antagonists are withdrawn. If the interpretation of the test is significantly hampered by medication, for example, a normal response is obtained in a patient with angina using beta-blockers, the medication may be gradually withdrawn and the test repeated. However, most patients with angina will develop symptoms and ischemic ECG changes in spite of the use of antianginal drugs, albeit at a higher workload than without such drugs [21, 22, 25, 26]. Despite the effect of beta-blockers on maximal exercise heart rate, no differences in test performance were found in a consecutive group of men being evaluated for possible CAD when they were subgrouped according to beta-blocker administration initiated by their referring physician [4, 27]. Therefore, for routine exercise testing, it appears unnecessary for physicians to accept the risk of stopping beta-blockers before testing when a patient exhibits possible symptoms of myocardial ischemia.

36.5 Recording and Computer Processing of the Electrocardiogram

36.5.1 Recording of the Electrocardiogram

It is essential to record a high-quality ECG. Proper ECG quality can be achieved in virtually all patients if skin preparation is meticulous. The skin should be abraded with sandpaper or a special, commercially available, drill. Special electrodes

Table 36.4

Indications for terminating exercise testing (Adapted from ACC/AHA 2002 Guideline Update for Exercise Testing [4])

Sensations felt by *patient*	Observations made by *physician*
Absolute indications	
• Moderate to severe (progressive) angina • Increasing nervous system symptoms (e.g., ataxia,dizziness, or near-syncope) • Subject's desire to stop	• ST-elevation (≥1.0 mm) in leads without diagnostic Q-waves (other than V_1 or aVR) • Technical difficulties in monitoring ECG or systolic blood pressure • Sustained ventricular tachycardia • Drop in systolic BP of >10 mmHg from baseline despite an increase in workload, when accompanied by other evidence of ischemia • Signs of poor perfusion (cyanosis or pallor)
Relative indications	
• Fatigue, shortness of breath, wheezing, leg cramps, or claudication • Increasing chest pain	• Drop in systolic BP of >10 mmHg from baseline despite an increase in workload, in the absence of other evidence of ischemia • ST- or QRS-changes such as excessive ST-depression (>2 mm of horizontal or down-sloping ST segment depression, especially when the magnitude of the ST-depression is increasing rapidly at low workloads) or marked axis shift • Arrhythmias other than sustained ventricular tachycardia, including multifocal PVCs, triplets of PVCs, supraventricular tachycardia, heart block, or bradyarrhythmias • Development of bundle-branch block or IVCD that cannot be distinguished from ventricular tachycardia • Hypertensive response (systolic blood pressure of >250 mmHg and/or diastolic blood pressure of >115 mmHg)[a]

BP, blood pressure; ECG, electrocardiogram; PVCs, premature ventricular contractions; and IVCD, intraventricular conduction delay

[a] As suggested by the ACC/AHA Committee on Exercise Testing

should be used to prevent motion artifacts. Furthermore, the ECG cables should be of special design to prevent artifacts owing to cable motion. As stated, cycle ergometers produce less motion of the upper body resulting in less motion artifacts on the ECG. Finally, ECG amplifiers which meet the American Heart Association standards, and have high input impedance, should be used [2]. If a proper combination of skin preparation, electrodes, cables, and amplifiers is used, a stable baseline can be achieved throughout the test in most subjects.

36.5.2 Computer Processing of the Electrocardiogram

Computerized exercise stress test systems have become the method of choice in most stress testing laboratories. The principles of computer-assisted interpretation of exercise ECGs have been described [28–32] and a review of methods for computer-based resting electrocardiography is also presented elsewhere in this textbook (Chap. 37). A summary of methods for analysis of exercise ECGs is presented here in brief.

Table 36.5

Borg scale

Grade	Symptoms
0	Nothing at all
0.5	Extremely weak (just noticeable)
1	Very weak
2	Weak (light)
3	Moderate
4	Somewhat strong
5	Strong (heavy)
6	
7	Very strong
8	
9	Extremely strong (almost maximal)
10	Maximal

The Borg scale for rating of perceptual intensities constructed as a category scale with ratio properties [24]. This can be used for quantitative evaluation of symptoms, for example chest pain

Computer systems for exercise testing regulate the workload of the bicycle or treadmill ergometer according to one of several predefined protocols. The computer systems also maintain a record of time, heart rate, and workload, and display these data on a computer screen together with baseline ECG waveforms [33]. The continuous stream of ECG waveforms, data, and computer measurements are stored and processed online in the system. ECG waveforms are acquired by a process termed analog–digital conversion. Most current digital processing ECG and exercise test systems sample the analog waveforms at the rate of 250 samples/s. A representation of the original analog signal can be obtained by digital–analog reconstruction of the digitized waveform. The computer system subsequently processes the ECG waveforms online to minimize noise and artifactual effects. Especially, at the higher workloads and heart rates, the recorded basic ECG tracings may show so much noise and artifacts from exercising skeletal muscles and respiratory variability that measurements from the original ECG waveforms are unreliable.

The processing involves the steps of QRS-detection, temporal alignment, and signal averaging. The QRS complexes are detected with the aid of a combination of the derivatives of multiple ECG leads. Thus, the characteristic feature used for detection of the QRS complex is the large voltage changes that occur in all leads simultaneously during ventricular activation. The QRS complexes are then classified as normal or abnormal. Abnormal beats may be a result of premature ventricular or supraventricular complexes, or they may be normal beats distorted by excessive noise or baseline drift. The normal beats are then combined into a single representative complex by computation of an average (mean) or median beat. Signal averaging can be performed at preselected intervals, for example, during 20 s of each minute, or continuously. The latter is the method of choice because it permits continuous display of the updated ECG waveform. Since the averaging procedure might be subject to errors in some of the patients, the user should compare the shape of the averaged signal with the original ECG tracings.

From the representative complexes, measurements can be obtained. Since the noise level during exercise is rather high in comparison with resting ECGs, it is not appropriate to take measurements from individual beats as is the case in some resting ECG programs. In commercially available systems, the baseline and ST segment are defined at fixed intervals before and after a single fiducial point in the QRS complex. Therefore, it is necessary to define the proper onset and end of the QRS complex. Such precise definition of QRS-onset and end is only possible if a combination of multiple leads is used [29, 30]. Computerized algorithms for QRS-detection and time alignment are, therefore, more reliable and robust in multichannel recording. Additionally, algorithms are applied that reduce the effect of baseline drift during exercise caused by temperature changes, respiration, and body motion, especially at higher workloads and if there is poor skin–electrode contact.

The processed, online cleaned data allow more accurate measurements of the exercise ECG, especially the low-amplitude signals such as the P-wave, the PR-segment, the junction of the QRS complex and ST segment (J-point), and the ST segment itself [33]. The digital measurements are generally more accurate and reproducible than manual measurements. However, careful overreading to provide quality control for automated choice of onset–offset waveform fiducial markers on the signal-processed data is required to avoid error in interpretation resulting in false-positive test results [4, 33]. Therefore, ECG recordings of the raw, unprocessed ECG data should be available at each stage of the exercise protocol for comparison with the averages that the exercise test monitor generates. Recommendations and standards for the degree of filtering and processing of data have been published [2, 4].

36.5.3 Lead Systems for Exercise Electrocardiography

Various types of lead systems have been developed, studied, and used in the last decades. Bipolar precordial lead systems have been used for a number of years and have produced satisfactory results in patients with suspected CAD and a normal ECG at rest. The two optimal leads for detection of ST segment depression during exercise are the bipolar lead from the right infraclavicular region to the V5 position (CS5 bipolar lead system) and that from the manubrium of the sternum to the V5 position (CM5 bipolar lead system). They have been reported to detect up to 90% of all ST segment depression identified by multiple-lead systems [34–36]. In patients with a previous myocardial infarction, a single-lead system is inadequate and such patients should be tested with a multiple-lead system. Multiple-lead systems that have been evaluated include the pseudo-orthogonal lead system, the corrected orthogonal lead system (with computer-processed Frank leads), the precordial map, the conventional 12-lead ECG system, and systems using a combination of bipolar leads and the standard 12 leads [33–35, 38–41]. The arrival of powerful high-speed microcomputers has allowed the development of systems for continuous online recording and analysis of the standard 12 ECG leads, which has become the norm in most testing facilities today [33]. It should, however, be noted that lead V5 remains by far the most sensitive electrode position that outperforms the inferior leads and the combination of lead V5 with II, because the latter has a relatively high false-positive rate. Therefore, in patients without prior myocardial infarction and with normal resting ECGs, the precordial leads alone are a reliable marker for CAD, and monitoring of inferior limb leads adds little additional diagnostic information. In these patients, exercise-induced ST segment depression confined to the inferior leads is of little value for detection of CAD [4, 42].

36.5.3.1 Right-Sided Chest Leads

In a study of 245 patients, it was shown that the diagnostic accuracy of exercise testing was increased when right ventricular leads were added to the standard 12 ECG leads [43]. By using right-sided chest leads, the sensitivity for the detection of CAD by angiography was comparable to that of myocardial perfusion scintigraphy (92 versus 93%). However, it is important to realize that these data were obtained in a population with a very high prevalence of CAD and might well be less reliable if the prevalence of CAD were to be substantially lower. Therefore, routine clinical use of right-sided chest leads awaits confirmation of these results in differing populations [4].

36.6 Interpretation of the Electrocardiogram

36.6.1 Changes of the ECG During Exercise in Normal Subjects

Normal ECG changes during exercise have been studied in standard chest leads [44], in corrected orthogonal leads [45] and by body-surface mapping [46, 47]. It has been shown that such changes occur gradually in relation to heart-rate changes during stress.

The amplitude of the P-wave increases, without major changes in the waveform. At heart rates over approximately 120 beats/min, this is enhanced by the superposition of the T-wave and the P-wave. At peak exercise with heart rates over 160 beats/min, the P-wave amplitude is on average twice, but in some patients up to five times the amplitude at rest.

Obviously, the PQ-interval shortens, owing to increased sympathetic activity during stress. With the P-wave becoming taller and the Ta-wave (atrial repolarization) increasing, there is a downward displacement of the PQ-junction below the isoelectric line in the resting ECG. This point is considered to be the baseline for terms of measuring ST segment change [33]. Exaggerated atrial repolarization waves during exercise may extend into the ST segment and T-wave and can cause downsloping ST-depression in the absence of ischemia at high peak exercise heart rates [48, 49]. Patients with false-positive exercise tests based on this finding have a high peak exercise heart rate, absence of exercised-induced angina, and markedly downsloping PQ-segments in the inferior leads [4, 48, 49].

QRS-duration does not change significantly during exercise. In one specially designed study, a systematic reduction of QRS-duration of only a few milliseconds was observed [50]. Prolongation of QRS-duration, however, is certainly abnormal. Changes in QRS-morphology have been discussed extensively. At peak exercise, QRS-forces shift toward the right and superiorly. Accordingly, Q-waves in the left precordial leads deepen, R-waves in the left precordial leads decrease, and S-waves become wider and deeper. However, intra-individual variability is large. In standard precordial leads, R-wave amplitude increases frequently at intermediate workloads, with heart rates between 120 and 160 beats/min [44]. This is precisely the heart rate reached by most patients with CAD. At higher heart rates, R-wave amplitude decreases. The situation is even more complex when body-surface maps are analyzed [46, 51]. The position of the maximum amplitude on the chest wall during ventricular depolarization remains located in the left anterior region, but the precise location of the maximum shifted one electrode position or more in seven out of 25 normal subjects studied by Block [46]. No consistent pattern was observed in the changes of the maximum QRS-forces in body-surface maps in normal subjects exercised up to a heart rate of 150 beats/min during maximum exercise. The mechanism of the QRS-changes during exercise is still unclear. It has been claimed that these are related to reduction of end-diastolic volume, which would diminish the effect of the radially oriented depolarization fronts in the left ventricular wall traveling from endocardium to epicardium. However, no reduction in end-diastolic volume was seen in patients studied in the supine position with radionuclide ventriculography [52]. Furthermore, R-wave amplitude variations appeared not to be related to changes in left ventricular volume during experimental myocardial ischemia [53].

The QT-interval shortens during exercise, although it cannot be measured accurately when the T-wave and P-wave overlap at higher heart rates. Usually, there is depression of the J-point followed by an upsloping ST segment. However, the ST segment slope may vary considerably. The T-wave amplitude varies greatly during exercise but increases considerably in most normal subjects immediately after exercise. Generally, the ST segment amplitude 80 ms after the end of the QRS complex remains positive in normal subjects at heart rates around 140 beats/min in the left precordial area, while a minimum develops below the right clavicle. During exercise, depression of the J-point and ST segment are prominent in leads with a lateral and vertical orientation [54]. These changes are far less significant in anterior–posterior and transverse leads. This explains in part the relatively high incidence of so-called false-positive ST segment depressions in these leads. ECG changes in healthy female volunteers are similar to those in males, with the exception of ST segment measurements. Flat or even slightly negative ST segments are present in some of the females at rest. This contributes in part to the false-positive ST segment changes in females [55]. Accordingly, separate criteria were developed for quantitative interpretation of the ECG changes during exercise in females [56].

36.6.2 Changes of the ECG During Exercise in Patients with Coronary Artery Disease

The most prominent electrocardiographic findings associated with CAD are a depression or elevation of the ST segment in the left precordial leads.

36.6.2.1 ST Segment Depression

The probability that a given subject has CAD is higher if the ST segment depression adheres to the following pattern: it develops early during exercise at a low heart rate, is deeper and has a more horizontal, or even downsloping pattern. However, it should be appreciated that, in subjects with a normal ECG at rest, there remains a considerable overlap between ST segment measurements in normal subjects and in patients with CAD. Also, as mentioned, ST segment waveforms in females during exercise differ from males and show a greater tendency towards ST segment depression, particularly in

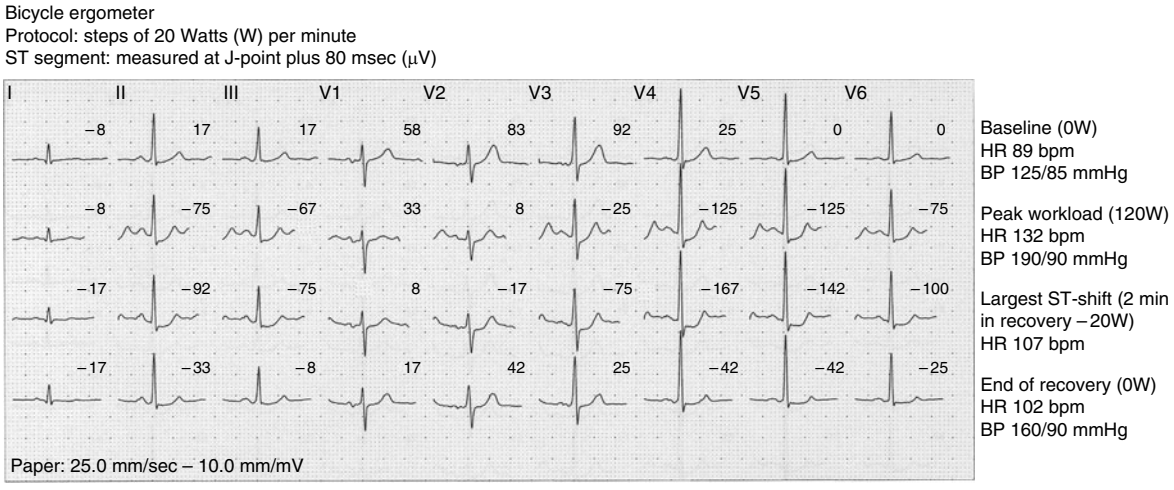

Figure 36.4

Bicycle exercise stress test in 56-year old male who underwent percutaneous coronary intervention of the left anterior descending artery 10 years earlier for stable angina. He was referred for screening before entering a fitness program. Upon request, he admitted that he had chest pain on exertion. The degree of functional impairment was difficult to assess because of an inactive lifestyle. The patient reached 120 W, whereas the predicted normal value for the peak workload was 174 W. He discontinued the test because of shortness of breath and chest pain. With increasing workload, there is a slow-upsloping ST segment depression up to 1 mm (0.1 mV) in the inferior and left precordial leads, evolving to a downsloping pattern in the recovery phase. The patient was referred for coronary angiography, which revealed a significant stenosis in the left circumflex artery that was subsequently treated by percutaneous coronary intervention.

the vertically-oriented leads [54]. In combination with the lower incidence of CAD in females, this results in an increased fraction of false-positive exercise test results in women, as reported in the literature [55, 57–59]. Nevertheless, exercise testing can be used in females when these factors are taken into account [57, 58]. Accordingly, the likelihood of CAD in females is lower than in males for most combinations of age, history, and ST segment depression, as will be discussed later.

Upsloping ST Segment Depression

The significance of upsloping ST segment depression has been studied extensively in the past decades and has generated much controversy. Clearly, downsloping ST segment depression is a stronger predictor of CAD than horizontal depression, and both are more predictive than upsloping depression. However, slowly-upsloping ST segment depression, for example, when the slope is less than 1 mV/s or when the degree of depression at 60–80 ms from the J-point is 1.5 mm (0.15 mV) or more below the baseline level of the PQ-junction, is associated with an increased probability of CAD (Figs. 36.4 and 36.5) [33, 60–62]. In a study of 70 patients with these ST segment changes, 57% had either two- or three-vessel CAD [33, 61]. On the other hand, junctional depression with a very steep upsloping ST segment is probably not pathological. From this it follows that, if slowly-upsloping ST-depression is considered an abnormal finding, sensitivity of exercise testing is increased, albeit at the cost of decreased specificity resulting in more false-positive test results. In the most recent ACC/AHA guidelines on exercise testing, the use of the more commonly-used definition for a positive test of ≥1 mm (0.1 mV) of horizontal or downsloping ST segment depression is favored [4].

Horizontal and Downsloping ST Segment Depression

The most commonly-used definition for visual interpretation of a positive exercise test result from an electrocardiographic standpoint is ≥1 mm (0.1 mV) of horizontal or downsloping ST segment depression for at least 60–80 ms after the end of the QRS complex (Fig. 36.6 (Continued)) [4]. As stated, downsloping ST segment depression is a stronger predictor of CAD than horizontal depression.

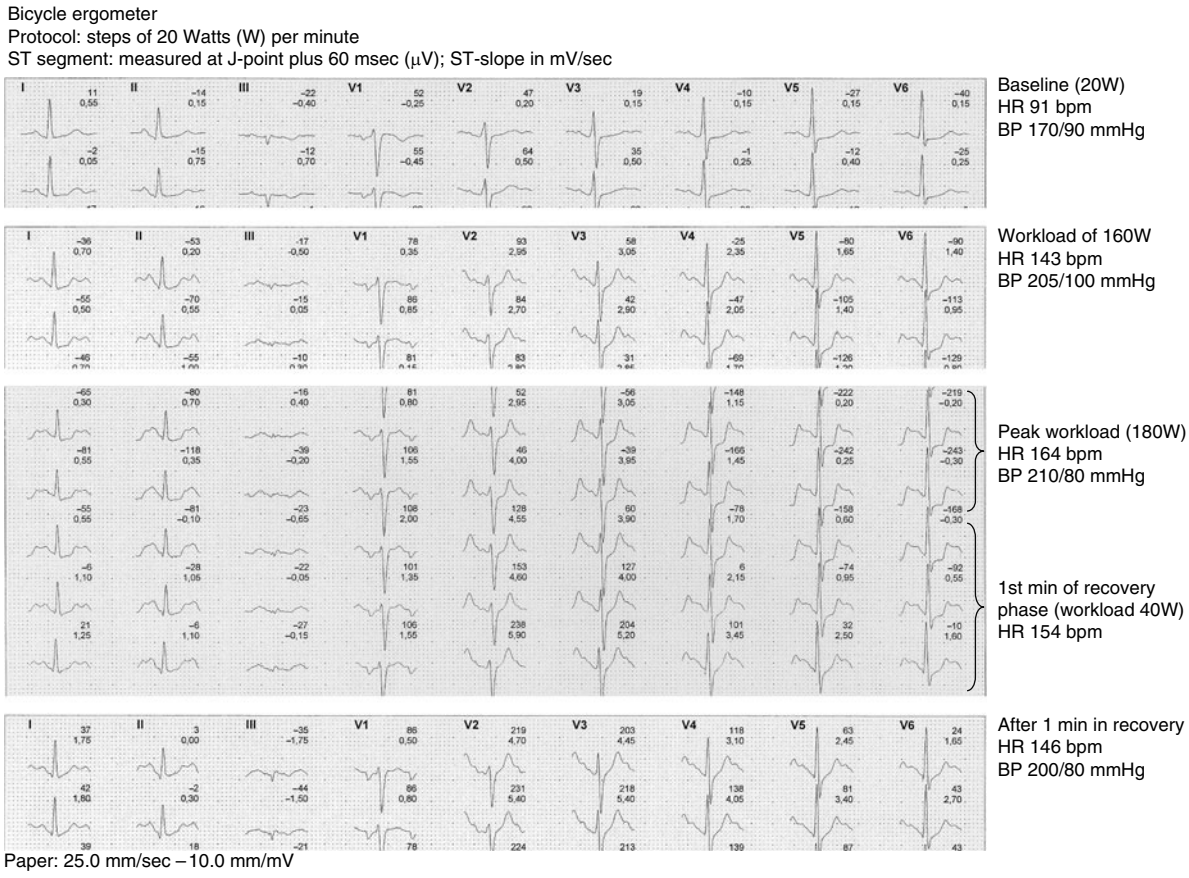

Figure 36.5

A 60-year old male treated for hypercholesterolemia by his general practitioner underwent exercise testing at the request of the specialist in allergy and immunology. He was suspected to have had a severe allergic reaction to the (rare) combination of wheat and exercise. Before planning an exercise test after ingestion of wheat to assess whether an allergic reaction could be provoked, a standard bicycle exercise test was performed as baseline. In daily life, the patient had a good exercise tolerance without any angina-like complaints. He reached 180 W (predicted peak workload 167 W) and discontinued because of fatigue. There were no angina-like symptoms or dyspnea. The baseline ECG was normal. Up to 160 W, there were no significant ST segment changes indicative of myocardial ischemia. From 160 W onward, minimal slow-upsloping ST segment depression developed in the left precordial leads, which got a more horizontal pattern and increased up to 2 mm (0.2 mV) at peak workload. The ST segment depression resolved directly following the discontinuation of exercise. This ECG pattern in which the ST segment becomes abnormal only at high workloads and returns to baseline in the immediate recovery phase may indicate a false-positive test in an asymptomatic subject. A nuclear perfusion scintigraphy using dipyridamole was subsequently performed which showed no signs of myocardial ischemia.

Magnitude of ST Segment Depression and Probability of Coronary Artery Disease

Table 36.6 summarizes data from various studies that related the magnitude of ST segment depression at peak exercise to the probability of CAD at coronary angiography [64–67]. It is evident that, for example, horizontal ST segment depression of ≥2 mm (0.2 mV) is highly specific (if only such results were considered abnormal, the specificity would be 99%), but occurs in the minority of patients with CAD (sensitivity would be only 28%). On the other hand, ST segment depression of 0.5 mm (0.05 mV) is nonspecific (sensitivity is 68%, but specificity only 80%), and should, therefore, not be used as a criterion for abnormality. A superior approach is to compute, from the data in Table 36.6, the ratio of

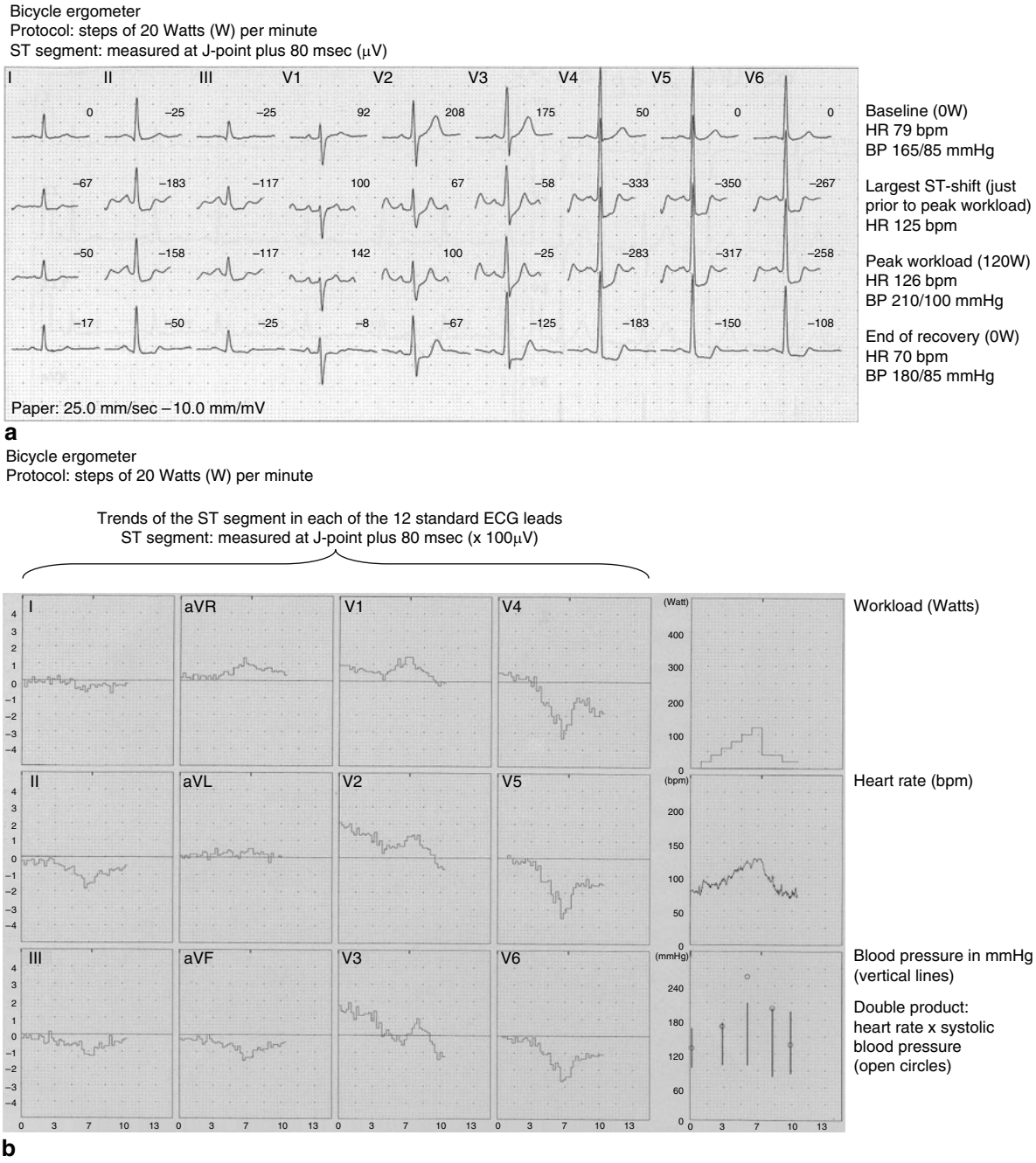

Figure 36.6

(a) Bicycle exercise stress test in 54-year old male with no history of cardiovascular disease who visited the outpatient clinic for angina-like chest pain complaints, class III according to the Canadian Cardiovascular Society [63]. The predicted maximum workload was 175 W. The patient discontinued the test at 120 W because of severe chest pain. Slow-upsloping to horizontal ST segment depression already developed at low workload (80 W) and increased to a maximum of 3.5 mm (0.35 mV) in the left precordial lead V_5 at maximal exertion. The ST segment depression evolved to a downsloping pattern in the recovery phase. Coronary angiography revealed a severe stenosis at the bifurcation of the left anterior descending artery and first diagonal branch, which was subsequently treated by percutaneous coronary intervention with bifurcation stenting according to the culotte technique. (b) Overview of ST segment trends and hemodynamic data of the same exercise test, showing the development of progressive ST segment depression in the inferior and precordial leads with increasing workload.

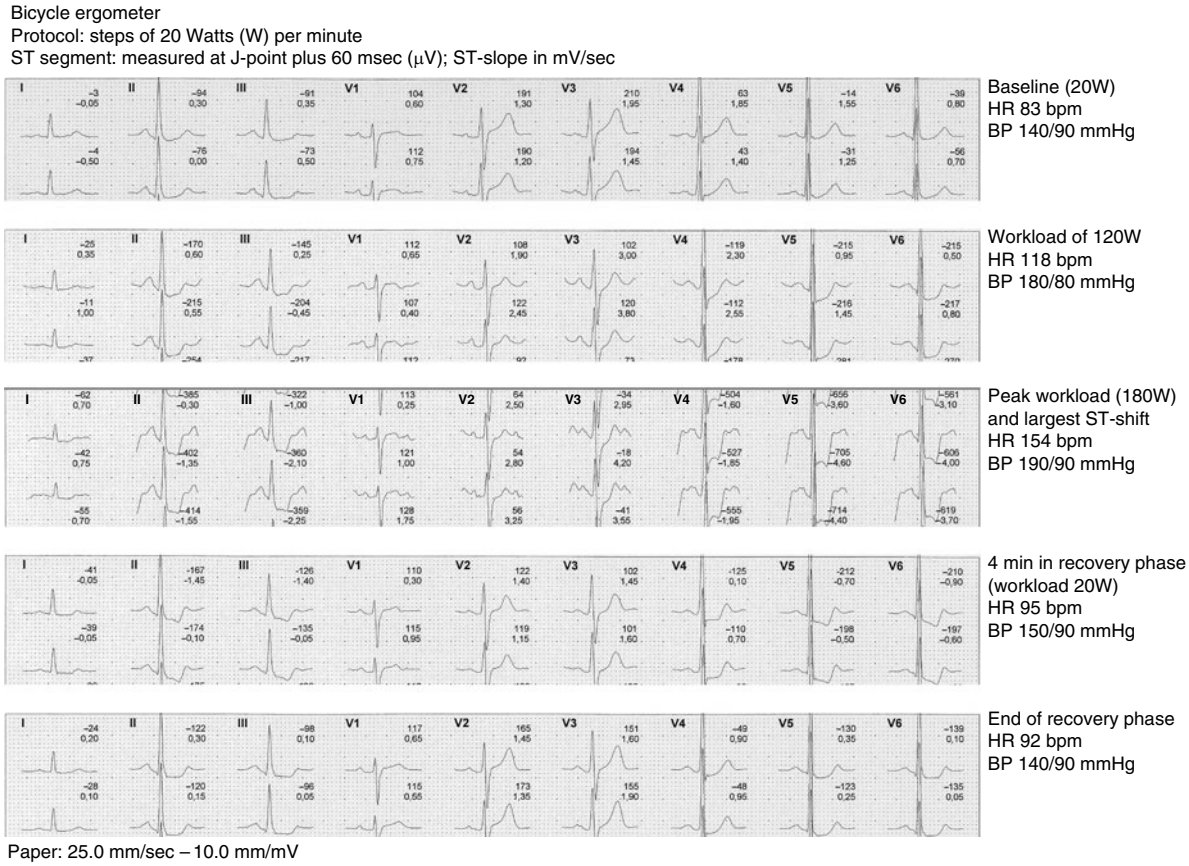

Figure 36.6 (Continued)

(c) The same patient visited the outpatient clinic approximately 1 year after the percutaneous coronary intervention. He indicated that he suffered again from chest pain similar to the complaints he had prior to the revascularization procedure. The only difference was that the chest pain now occurred with more strenuous exertion as compared to the complaints 1 year earlier (functional class II according to the Canadian Cardiovascular Society [63]). The patient reached the predicted workload of 171 W and discontinued the test because of tiredness and shortness of breath. The exercise electrocardiogram again showed marked ST segment depression up to 6 mm (0.6 mV) with a horizontal to downsloping pattern at maximal exertion. Coronary angiography revealed severe in-stent restenosis in the treated segments in the left anterior descending artery and first diagonal. The patient was subsequently successfully treated by repeat percutaneous coronary intervention.

the likelihood that a given range of ST segment depression is related to the presence or absence of CAD. This likelihood ratio is 0.4 for ST segment depression up to 0.9 mm (0.09 mV). Only ST segment depression greater than 1 mm (0.1 mV) is clearly associated with CAD. It is apparent that this likelihood increases when the ST segment depression is more pronounced.

Magnitude of ST Segment Depression and the Degree of Anatomical Coronary Artery Disease

Many investigators have attempted to correlate the magnitude of ST segment depression with the degree of anatomical CAD. Initial studies reported that an increased magnitude of ST-depression was associated with an increased degree of ischemia [33, 68]. Later studies have been unable to correlate the ischemia estimated from the magnitude of the ST segment depression in any lead or from the sum of the ST-changes in all leads with either the number of diseased coronary

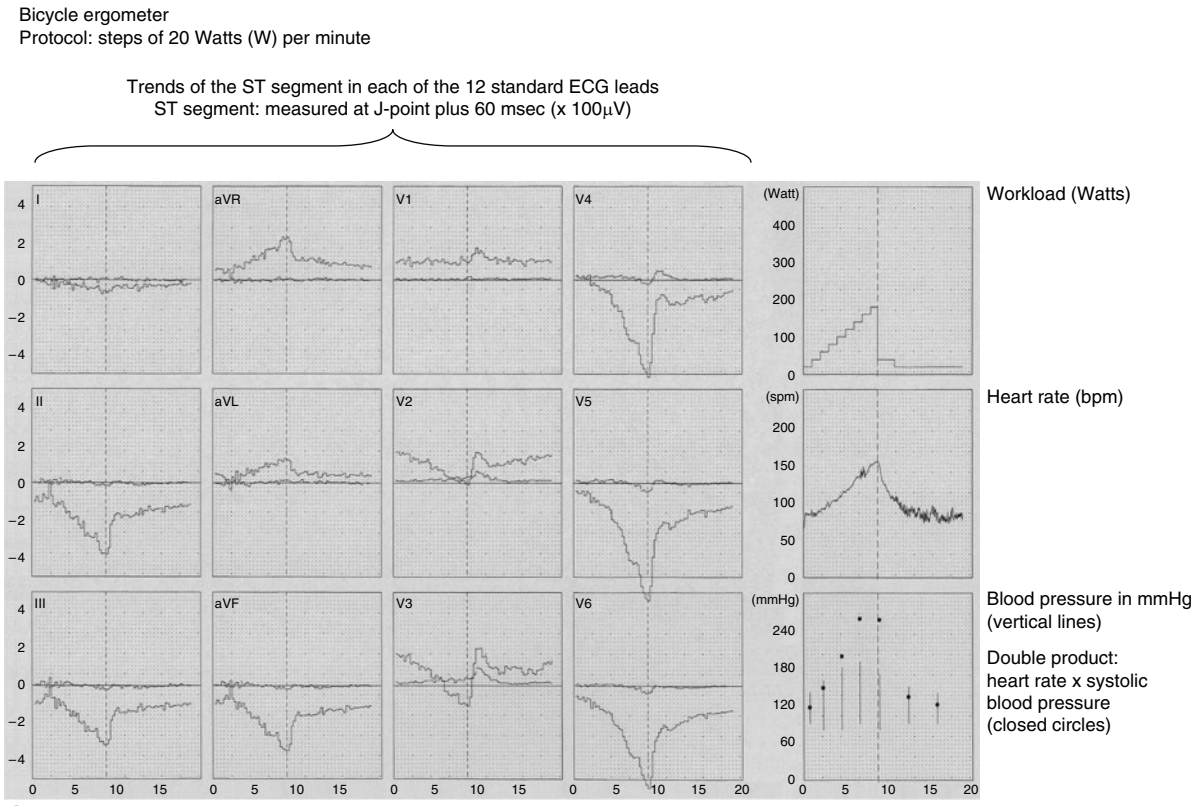

d

Figure 36.6 (Continued)

(d) The respective ST segment trends illustrate the marked ST segment depression, predominantly occurring in the inferior and left precordial leads.

Table 36.6

Probability of CAD in relation to degree of ST segment depression during exercise testing

ST-depression (mV)	Normal subjects (*n*=225)	Subjects with CAD (*n*=381)	Specificity (%)	Sensitivity (%)	Likelihood ratio for CAD
< 0.05	181	122			0.4
0.05–0.09	30	19	80	68	0.4
0.1–0.19	11	133	94	63	7.3
> 0.2	3	107	99	28	21.6

Pooled data from four studies [64–67] that provided information on the presence of coronary artery disease (CAD) in relation to the degree of ST segment depression during exercise stress testing. Seventeen patients with ST segment elevation have been excluded from reference 66.

arteries or the size of the area of reversible ischemia observed on myocardial perfusion scintigraphy [33, 69, 70]. As the development of ST segment depression as an electrophysiological phenomenon results from many influences, including those caused by electrolytes, hormones, and hemodynamic, metabolic, as well as anatomical changes, it is unlikely that the magnitude of ST segment depression would correlate well with the coronary anatomy in patients with CAD. Furthermore, the degree of ST-depression at higher workloads also depends on what is used as an indication to terminate exercise. For example, if patients with single vessel disease are encouraged to exercise strenuously or if they have some degree of left

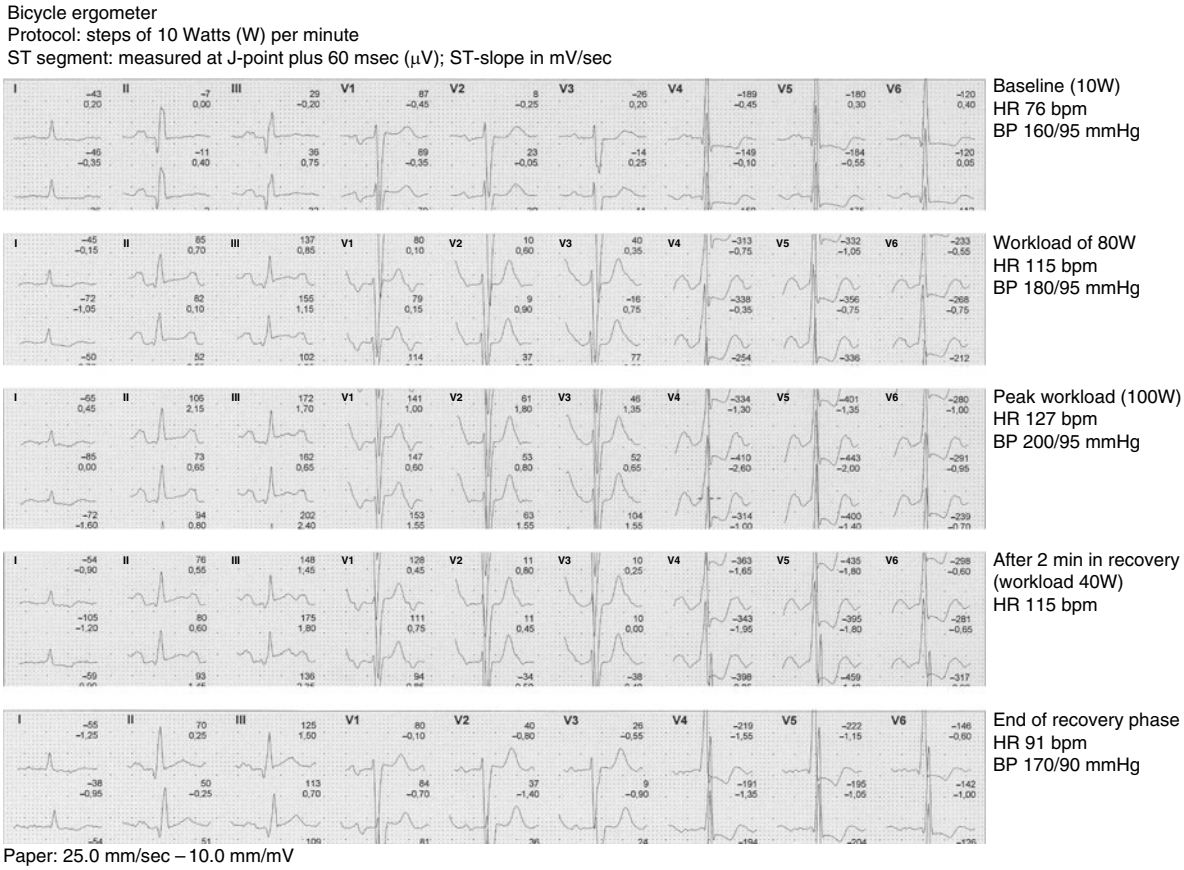

Figure 36.7

Bicycle exercise test (10 W/min protocol) in a 77-year old male with angina pectoris complaints, classified as II–III according to the Canadian Cardiovascular Society [63]. His medical history was unremarkable except for poorly controlled arterial hypertension. The resting ECG showed signs of an old inferior myocardial infarction (Q-waves in leads II, III, and aVF), as well as left ventricular hypertrophy with repolarization abnormalities in the left precordial leads (downsloping ST segment with inverted T-wave). With increasing workload, the preexistent ST segment depression increased progressively up to 4 mm (0.4 mV), persisting in the recovery period. Coronary angiography revealed three-vessel coronary artery disease and ventriculography showed a moderately impaired left ventricular systolic function. The patient subsequently underwent coronary artery bypass grafting.

ventricular hypertrophy, they may have severe ST-depression (see also Figs. 36.6 (Continued) and 36.7). Therefore, the magnitude of ST segment depression at maximum workload may not indicate the severity of CAD.

Time Course of ST Segment Depression

ST segment depression that comes on early during exercise at low workloads is associated with more severe disease and impaired prognosis [33, 68, 71–73]. In a study on the predictive value of the time course of ST segment depression during exercise testing in patients referred for coronary angiography, a direct relationship between the time of onset and offset of ST-depression and the number of diseased coronary arteries was demonstrated [33, 73]. Severe three-vessel CAD was found in 33% of patients with early onset and late offset of the ST-depression, while this increased up to 50% in those with resting ST-depression that increased with exercise [73]. Even ST segment depression occurring at high workloads and with

rapid resolution during recovery may be associated with significant CAD, although it may also indicate a false-positive response in an asymptomatic subject (Fig. 36.5).

Furthermore, although ST segment depression during exercise often persists into the recovery phase, it sometimes may not develop until exercise has been terminated (Fig. 36.4). Whereas this phenomenon is still not completely understood, several studies have demonstrated that ST segment depression occurring only during recovery has the same significance as exercise-induced ST-depression in predicting CAD [33, 74, 75].

Adjustment of ST Segment Depression

Subjects with tall R-waves exhibit a greater amount of ST segment depression than those with smaller R-wave amplitude [76]. Accordingly, when the R-wave in the lateral precordial leads is less than 10 mm, the sensitivity of ST-depression for the detection of CAD is low if 1 mm (0.1 mV) of ST-depression is required for a positive test result [77]. Correcting ST-depression for R-wave amplitude has been proposed by dividing the amount of ST segment depression by the R-wave height (both expressed in mm) [78]. The ST/R-ratio may then be used as an alternative to the amount of ST segment depression per se, with 0.1 as a cutoff value for an abnormal test result [33]. In studies, however, adjustment of the amount of ST segment depression by the R-wave height has not been shown to consistently improve the diagnostic value of exercise-induced ST-depression [4].

Several methods of heart rate adjustment have been proposed to increase the diagnostic accuracy of the exercise ECG. The first technique is to derive the maximal slope of the ST segment relative to heart rate (ST/HR slope). The second method, termed the ST/HR index, divides the difference between ST-depression at peak exercise by the delta heart rate (difference between resting and maximum heart rate) [4, 33, 79–82]. The value of ST/HR adjustment in improving diagnostic accuracy has been evaluated in several studies [4, 83–87]. Most studies, however, were limited by work-up bias and enrollment of relatively healthy patients, which presents a limited challenge to the ST/HR index [4, 85–87]. In a large multicenter study without these limitations, the ST/HR slope or index was not found to be more accurate than simple measurement of the ST segment depression [88]. The most recent guidelines on exercise testing take the perspective that the ST/HR adjustment approach in symptomatic patients has at least equivalent accuracy to the standard approach [4]. Although the ST/HR approach might be useful in assessing certain borderline or equivocal ST segment responses during exercise (e.g., ST segment depression associated with a very high exercise heart rate), further validation is required.

ST Segment Depression and the Location of Coronary Artery Disease

In several studies, an attempt has been made to relate the location of ST segment depression during exercise to coronary anatomy. As stated, extensive CAD (three-vessel disease) is more likely to be present in a patient who develops major ST segment depression in multiple leads at low workloads. However, even in patients with single-vessel disease, there is no clear separation between the leads in which ST segment depression develops when either the right coronary artery or the left anterior descending coronary artery is involved [67]. Studies using body-surface mapping indicate that the ST segment depression is most prominent in the precordium. The actual position where the largest ST segment depression occurs varies widely, from the level of the third intercostal space to the tenth intercostal space [46]. However, even analysis of precordial surface maps has not permitted an accurate prediction of the location of CAD [40, 89], although this has previously been claimed [40]. Furthermore, in another study, no relation was found between the spatial orientation of the ST segment vectors during exercise and the location of myocardial ischemia as detected by myocardial perfusion scintigraphy [90].

ST Segment Depression and/or Exercise-Induced Angina

The occurrence of chest pain during stress testing is of equal diagnostic value as the development of ST segment depression [91–93]. Symptoms that cannot be clearly understood during an outpatient clinic visit may be clarified if they occur during the actual exercise procedure and disappear rapidly in the recovery phase. In order to permit optimal comparison between the history of the patient and the observations during the stress test, it is recommended that either the test is performed by the patient's own physician, or that the physician supervising the test reports in detail all the complaints that occur during the test and notes whether these are similar to the complaints that led the patient to the outpatient clinic. In Fig. 36.8, the incidence of CAD and the number of diseased vessels are presented for ST segment depression with and without angina [92].

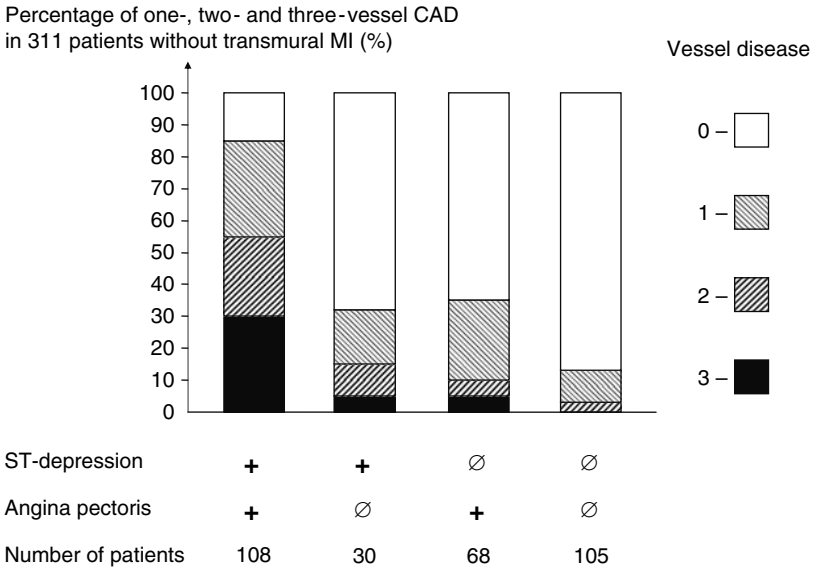

Figure 36.8

Incidence of normal coronary arteries (zero-) and one-, two-, or three-vessel disease in 311 patients without a history of transmural myocardial infarction. It should be noted that the incidence of CAD was similar in 30 patients with ST segment depression without symptoms (30%) and in 68 patients with exercise-induced angina without significant ECG changes (36%). ST-depression represents 0.1 mV or greater of ST segment depression in at least one precordial lead (Adapted from Roskamm [92]).

36.6.2.2 ST Segment Elevation

ST segment elevation during exercise is observed most frequently in leads with Q-waves in patients with a history of myocardial infarction (Fig. 36.9). The significance of ST segment elevation in areas of Q-waves of an old myocardial infarction is controversial. Some studies have suggested that this ST segment elevation is caused by an area with abnormal wall motion (ventricular akinesia or dyskinesia) [64, 94–97]. However, other studies have shown that in some patients such ST-elevation disappears after coronary bypass surgery, which suggests that the ST-elevation was a result of myocardial ischemia [98]. More recent studies using myocardial perfusion scintigraphy have found such ST-elevation to be a marker of residual viability in the infarcted area [99–101]. Therefore, it seems advisable to consider additional tests such as myocardial perfusion scintigraphy in patients with chest pain complaints after myocardial infarction and ST segment elevation during exercise stress testing.

Exercise-induced ST segment elevation in leads without Q-waves on a normal ECG (other than in aVR or V_1) is very rare and represents severe transmural myocardial ischemia (whereas ST segment depression represents subendocardial ischemia) [94, 102–109]. It is caused by a coronary artery spasm that completely obliterates antegrade flow through the epicardial artery, or a high-grade proximal stenosis in a coronary artery (Fig. 36.10). In patients with variant or Prinzmetal's angina, coronary spasm is most commonly seen at rest, but very occasionally it occurs with exercise, probably indicating the presence of hemodynamically significant coronary atherosclerosis [33, 110, 111]. In contrast to ST segment depression, exercise-induced ST segment elevation is very arrhythmogenic and localizes the ischemic area. When ST segment elevation occurs in leads V_2 through V_4, there is severe anterior wall ischemia with a high-grade stenosis in the proximal left anterior descending coronary artery (Fig. 36.10); in leads II, III, and aVF, there is severe inferior wall ischemia with involvement of a proximal stenosis in a large right coronary artery; and in the lateral leads, the left circumflex or diagonals are involved [4]. As stated previously, this rare finding warrants immediate discontinuation of the stress test and prompt referral for coronary angiography.

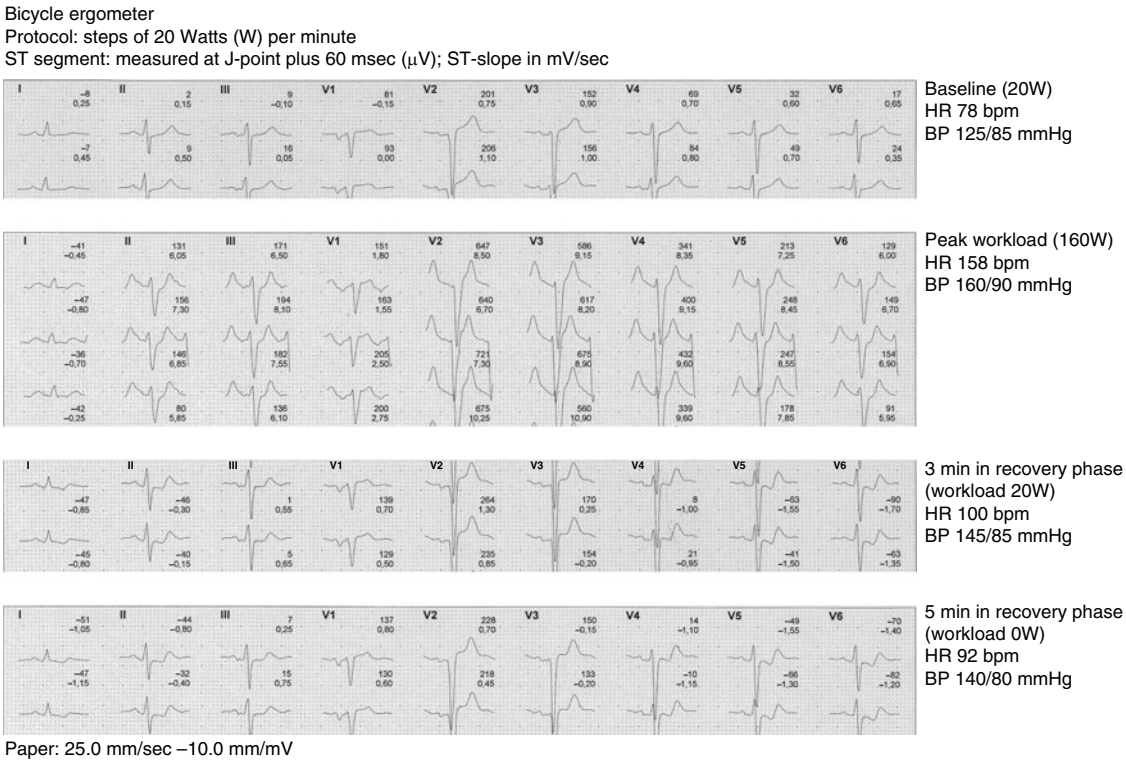

Figure 36.9

Bicycle exercise stress test in a 62-year-old male approximately 1 year after he underwent a primary coronary intervention with recanalization of the occluded left anterior descending coronary artery for an acute anterior myocardial infarction. The result of the intervention was suboptimal because there was no reflow in the infarct-related artery. No intervention was performed on a 50–70% stenosis in the left circumflex coronary artery. Echocardiography showed an impaired systolic left ventricular function with akinesia of the interventricular septum and hypokinesia of the anterior wall and apex. The baseline ECG showed sinus rhythm, a left anterior fascicular block, and a QRS-pattern compatible with an old antero-septal-apical myocardial infarction with QS-complexes in V_1 and V_2, a small R-wave in V_3, as well as a Q-wave in aVL. The patient reached 160 W and discontinued the test because of fatigue. The patient did not experience any anginal complaints or dyspnea during the test. With an increase in workload, there is an increasing level of ST segment elevation in the right precordial leads (V_1–V_3), representing either wall motion abnormalities or residual viability in the infarcted area. Furthermore, the duration of the QRS complex increased. In the recovery phase, minimal 0.5 mm (0.05 mV) downsloping ST segment depression developed in the inferior and left precordial leads.

36.6.2.3 Changes of the QRS Complex

R-Wave Amplitude

It has previously been reported that an increase in R-wave amplitude during exercise is a useful indicator of CAD [112]. The first reports on this phenomenon were based on an unusual series of patients with known false-positive or false-negative ST-changes during exercise. Although some studies supported these observations, others found that the R-wave amplitude changes were variable both in patients with CAD and in normal subjects [52–54, 113]. It is possible that the observed differences in R-waves between patients with CAD and normal subjects result in part from differences in heart rate, since most patients stop exercising at heart rates between 120 and 150 beats/min which is the rate at which normal subjects frequently exhibit increased R-wave amplitudes [44]. The mechanisms of these changes also remain unclear. In particular, the hypothesis that the increase in R-wave amplitude would be related to an increase in ventricular volume owing to

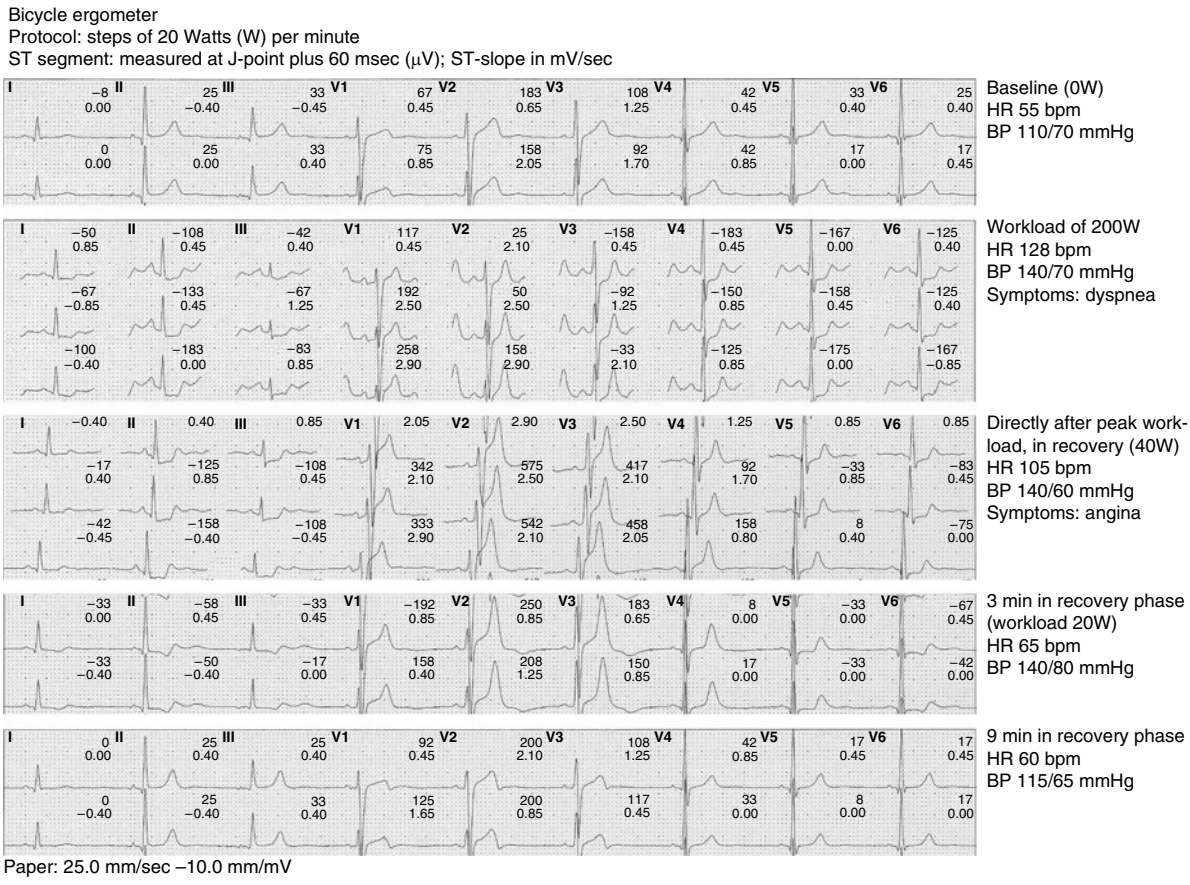

Figure 36.10

Bicycle exercise test in a 59-year-old male with no history of cardiovascular disease who underwent stress testing because of complaints of chest pain on exertion suspected for angina pectoris. The predicted maximum workload was 163 W. The test was discontinued at 200 W by the attending physician because of shortness of breath, as well as failure of the blood pressure to rise in the presence of ST segment depression. Starting at 180 W, up to 1.0–1.5 mm (0.1–0.15 mV) of slow-upsloping to horizontal ST segment depression developed in the inferior and left precordial leads, indicating subendocardial ischemia. Directly following discontinuation of exercise, the patient experienced angina-like chest pain. This was attended on the ECG by ST segment elevation and a marked increase in T-wave amplitude in the right precordial leads, suggesting transmural ischemia due to a high-grade stenosis in the proximal left anterior descending artery. Later on in the recovery phase, biphasic T-waves developed in the right precordial leads. At the end of the recovery period, the ECG had returned to normal. The patient was subsequently admitted to hospital. Coronary angiography was performed the same day and revealed, as expected, a severe stenosis in the proximal left anterior descending artery which was treated with stent implantation.

myocardial ischemia [114] was not supported by studies in which the volume changes were actually measured [52, 53, 115]. As exercise-induced changes in R-wave amplitude have provided very little, if any, discrimination for myocardial ischemia, the R-wave measurements are not routinely applied in clinical practice.

QRS-Duration

As stated, the duration of the QRS complex during exercise does not increase but may be reduced slightly because conduction velocity is increased by catecholamine release [50, 116]. Although a number of studies have shown that conduction

velocity is decreased by myocardial ischemia [61, 117], QRS-duration measurements are not routinely used for the diagnosis of CAD as studies on this phenomenon have had equivocal results [61]. Prolongation of the QRS-duration during exercise was found to be associated with CAD in 330 patients who underwent exercise testing and coronary angiography [118]. The greatest prolongation was found in patients with three-vessel disease. However, the observations could not be used in individual patients to determine the presence or absence of myocardial ischemia as the variations around the mean value were too large [118].

Bundle-Branch Block

Rate-dependent bundle-branch block may become apparent during exercise and the interpretation of such a finding is the same as in rate-dependent bundle-branch block occurring under other circumstances. Rate-dependent left bundle-branch block, right bundle-branch block or left anterior fascicular block may be related to CAD [33, 119]. However, they have also been observed in healthy subjects without myocardial or coronary pathology [33]. The isolated finding of a rate-dependent bundle-branch block should, therefore, not be used as a proof of significant heart disease. On the other hand, the occurrence of a bundle-branch block during exercise should be viewed in light of the other clinical findings in each patient in order to assess the probability that CAD is present. Leftward rotation of the frontal axis with development of a left anterior fascicular block during exercise in a patient *with* CAD usually signifies involvement of the proximal left anterior descending coronary artery or three-vessel CAD [120, 121]. The axis shift associated with left anterior fascicular block may mask the ischemic ST segment changes in the frontal plane and to a lesser extent in the precordial leads.

The significance of ST segment depression as a predictor of ischemia in the presence of right bundle-branch block has been the subject of debate. Exercise-induced ST-depression usually occurs with right bundle-branch block in the anterior chest leads V_1 through V_3, probably because of secondary repolarization changes, and is not associated with ischemia [4, 122]. However, ST segment depression in the left precordial leads (V_5 and V_6) or inferior leads (II and aVF) has the same significance in predicting CAD as exercise-induced ST-depression in a normal resting ECG [123, 124].

Exercise-induced ST-depression usually occurs with left bundle-branch block and has no association with ischemia [125]. Even up to 10 mm of ST-depression occurs in healthy subjects. There is no level of ST-depression that confers diagnostic significance in left bundle-branch block. Therefore, there is a consensus, as stated in the guidelines, that exercise-induced ischemia cannot be diagnosed from the ECG in patients with left bundle-branch block [4].

36.6.2.4 T-Wave Changes

As previously mentioned, the T-wave amplitude varies greatly during exercise but increases considerably in most normal subjects immediately after exercise as a result of an increased stroke volume, which makes up for the lingering metabolic debt after the heart rate has dropped very rapidly. Many patients with flat or inverted T-waves at rest will manifest upright T-waves at the time of exercise. This is particularly true in women. This phenomenon of normalization of inverted T-waves or pseudonormalization of the T-waves is not considered to indicate ischemia. In earlier studies, T-wave normalization was accompanied by significant ST segment depression in 90% of patients with CAD, but by a negative test result based on ST segment criteria in all patients without ischemic heart disease [33, 126]. Similarly, exercise-induced deep T-wave inversion is almost always accompanied by significant ST segment depression and is then associated with a more severe degree of CAD.

36.7 Exercise Testing to Diagnose Coronary Artery Disease

The vast majority of exercise testing is performed in adults with symptoms of known or suspected ischemic heart disease. There has been considerable discussion on the value and use of exercise testing for the diagnosis of CAD and the literature on this subject is extensive. Knowledge of terminology used in describing diagnostic test characteristics and test performance is required for understanding the exercise test literature (Table 36.7).

Table 36.7

Diagnostic test characteristics

True-positive test result (TP)	Abnormal test result in subject *with* disease
False-positive test result (FP)	Abnormal test result in subject *without* disease
True-negative test result (TN)	Normal test result in subject *without* disease
False-negative test result (FN)	Normal test result in subject *with* disease
Specificity	Percentage of subjects *without* disease who have a normal test result = TN/(TN + FP)
Sensitivity	Percentage of subjects *with* disease who have an abnormal test result = TP/(TP + FN)
Test accuracy	Percentage of true test results = (TP + TN)/total number of tests performed
Predictive value of a positive test result	Percentage of subjects with abnormal test who have the disease = TP/(TP + FP)
Predictive value of a negative test result	Percentage of subjects with normal test and without disease = TN/(TN + FN)
Formula for calculation of posttest probability (Bayes' theorem):	
Posttest odds (disease present) = pretest odds (disease present) × likelihood ratio (LR) where, odds = probability/(1 – probability) LR = sensitivity/(1 – specificity) in case of an abnormal test result = (1 – sensitivity)/specificity in case of a normal test result	
Posttest odds (disease absent) = pretest odds (disease absent) × likelihood ratio (LR) where, odds = probability/(1 – probability) LR = (1 – specificity)/sensitivity in case of an abnormal test result = specificity/(1 – sensitivity) in case of a normal test result	
The better (very high or very low) the likelihood ratio of the test (determined by sensitivity and specificity), the more discriminant the test is.	

Table 36.8

Pretest probability (%) of CAD in patients by age, sex, and chest pain characteristics (Adapted from Diamond and Forrester [127])

Age (years)	Sex	Non-anginal chest pain	Atypical angina	Typical angina
30–39	M	5.2 ± 0.8	21.8 ± 2.4	69.7 ± 3.2
	F	0.8 ± 0.3	4.2 ± 1.3	25.8 ± 6.6
40–49	M	14.1 ± 1.3	46.1 ± 1.8	87.3 ± 1.0
	F	2.8 ± 0.7	13.3 ± 2.9	55.2 ± 6.5
50–59	M	21.5 ± 1.7	58.9 ± 1.5	92.0 ± 0.6
	F	8.4 ± 1.2	32.4 ± 3.0	79.4 ± 2.4
60–69	M	28.1 ± 1.9	67.1 ± 1.3	94.3 ± 0.4
	F	18.6 ± 1.9	54.4 ± 2.4	90.6 ± 1.0

CAD denotes coronary artery disease

36.7.1 Pretest Probability

The pretest probability of obstructive CAD can be estimated from factors such as age, gender, risk factors, and chest pain characteristics [127–129]. The pretest probabilities described in this way by Diamond and Forrester in a series of over 60,000 patients are shown in Table 36.8 [127]. From this table, it is apparent that exercise testing is not very useful for establishing the diagnosis CAD in a 64-year-old man with typical or definite angina. The pretest probability of CAD

Table 36.9

Posttest probability (%) of coronary artery disease based on age, sex, symptom classification, and exercise test-induced electrocardiographic ST segment depression

		Typical angina		Atypical angina		Non-anginal chest pain		Asymptomatic	
Age	ST-depression (mV)	M	F	M	F	M	F	M	F
30–39	0.00–0.04	25	7	6	1	1	<1	<1	<1
	0.05–0.09	68	24	21	4	5	1	2	<1
	0.10–0.14	83	42	38	9	10	2	4	<1
	0.15–0.19	91	59	55	15	19	3	7	1
	0.20–0.24	96	79	76	33	39	8	18	3
	>0.25	99	93	92	63	68	24	43	11
40–49	0.00–0.04	61	22	16	3	4	1	1	<1
	0.05–0.09	86	53	44	12	13	3	5	1
	0.10–0.14	94	72	64	25	26	6	11	2
	0.15–0.19	97	84	78	39	41	11	20	4
	0.20–0.24	99	93	91	63	65	24	39	10
	>0.25	>99	98	97	86	87	53	69	28
50–59	0.00–0.04	73	47	25	10	6	2	2	1
	0.05–0.09	91	78	57	31	20	8	9	3
	0.10–0.14	96	89	75	50	37	16	19	7
	0.15–0.19	98	94	86	67	53	28	31	12
	0.20–0.24	99	98	94	84	75	50	54	27
	>0.25	>99	99	98	95	91	78	81	56
60–69	0.00–0.04	79	69	32	21	8	5	3	2
	0.05–0.09	94	90	65	52	26	17	11	7
	0.10–0.14	97	95	81	72	45	33	23	15
	0.15–0.19	99	98	89	83	62	49	37	25
	0.20–0.24	99	99	96	93	81	72	61	47
	>0.25	>99	>99	99	98	94	90	85	76

is so high that the test result does not substantially change this probability. As shown in Table 36.9, the likelihood of CAD is 79% if no ST segment depression occurs during the test, while it would be 99% if 2 mm (0.2 mV) of ST segment depression developed. However, the test may still be used to determine the functional impairment of that subject, to measure the blood-pressure and heart rate response, or to estimate the prognosis. Similarly, the diagnostic value of exercise electrocardiography is low in asymptomatic men and women (see also Fig. 36.11). The greatest diagnostic value of exercise testing is obtained in patients with an intermediate pretest probability of CAD, for example, between 20% and 80%, because the test result has the largest potential effect on diagnostic outcome. If the posttest likelihood is intermediate, another noninvasive (e.g., myocardial perfusion scintigraphy) or invasive test may be applied.

36.7.2 Diagnostic Characteristics and Test Performance

One of the problems with diagnostic tests for CAD is that there is a considerable overlap in the range of measurements for the normal population and those with CAD. Since the depth of exercise-induced ST segment depression and the extent of the myocardial ischemic response can be considered as continuous variables, a certain cutpoint or discriminant value (e.g., 1 mm (0.1 mV) of ST segment depression) cannot completely discriminate patients with CAD from those without

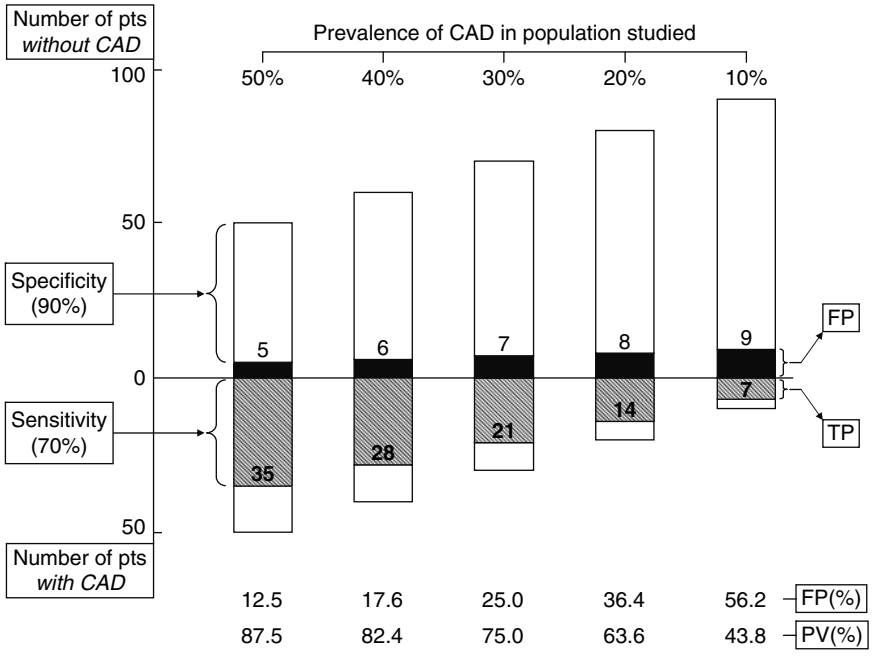

Figure 36.11

Illustration of the impact of the prevalence of CAD in the population studied on the fraction of false-positive test results and the predictive value of the exercise test. Each bar represents a population of 100 patients. In the left-most bar, 50 patients have CAD, while 50 do not have CAD. In the second bar, 40% has CAD, in the third 30%, in the fourth 20%, and in the right-most bar only 10%. In each theoretical example, the sensitivity for detection of CAD is 70%. Thus, 70% of patients with CAD do indeed have ischemic ST segment depression. On the other hand, the specificity is 90%. Thus, 10% of the patients without CAD exhibit false-positive ST segment depression (black area). In the population with a 50% prevalence of CAD (left-most bar), 40 abnormal tests are found, five of which are false-positive (12.5%). In the population with only a 10% prevalence of CAD (right-most bar), nine false-positive tests occur out of a total of 16 tests with ST segment depression (56.2%). In this latter population, which reflects the prevalence of CAD in many screening conditions, the number of false-positives is higher than the number of correct or true-positive test results. CAD, coronary artery disease; FP, false-positive; PV, predictive value; Pts, patients; and TP, true-positive.

disease. A higher discriminant value for ST segment depression improves specificity, but reduces the test's sensitivity. Therefore, sensitivity and specificity are inversely related and determined by the choice of a cutpoint or discriminant value. The positive predictive value (PPV) and negative predictive value (NPV) are also affected by the population tested. The PPV will be higher in a population with a higher prevalence of CAD. Accordingly, PPV is higher in patients with three-vessel CAD and lower in patients with one-vessel CAD. The NPV can be decreased if the test is used in patients in whom false-positive results are more likely such as those with ST segment depression on the resting ECG or left ventricular hypertrophy. Figure 36.11 illustrates these points.

36.7.3 Probability Analysis

The use of Bayes' theorem of conditional probability can assist in the interpretation of a test result and can also provide a meaningful estimate of the posttest probability in the individual patient. According to this theorem, posttest probability is a function of pretest probability, and the sensitivity and specificity (likelihood ratio) of the test [130].

Under the assumption of the independence of the exercise test result from the clinical (pretest) data, posttest probability can be calculated according to the formula listed in Table 36.7. Although this calculation is often made intuitively by the clinician, mathematical equations or scores have been developed from multivariate analysis of clinical and exercise test variables (including heart rate at peak exercise, ST segment response, the presence or absence of angina during the test, peak workload, and ST segment slope) that can provide a more accurate estimate of the probability that CAD is present, when compared with use of the ST segment measurements alone [4, 131–135]. However, the use of these statistical models remains limited. Nevertheless, they underline the importance of taking into account all relevant variables when estimating the probability of CAD in a given subject [136–138].

36.7.4 Diagnostic Accuracy of the Standard Exercise Test

A meta-analysis was performed on the diagnostic accuracy of the exercise test based on 147 consecutive published reports involving 24,074 patients who underwent both coronary angiography and exercise testing [139, 140]. There was a wide variability in the reported diagnostic accuracy of the standard exercise test among the studies (Table 36.10). The mean sensitivity was 68% (range 23–100%) and mean specificity was 77% (range 17–100%). This large variability results from the fact that most studies do not fulfill two major criteria that are important when evaluating diagnostic tests [4]. The first concerns the fact that the population studied does not represent the diagnostic dilemma group in clinical practice. In particular, inclusion of patients who most certainly have the disease (e.g., post-myocardial infarction patients) in the test group presents a limited challenge to the diagnostic test. The second cause concerns the presence of work-up bias which refers to the fact that most reported studies were affected to some degree by clinical practice wherein the results of the exercise test were used to decide who would undergo coronary angiography and be included in the study [4]. The reported meta-analysis provides, however, the best estimate of the diagnostic accuracy of the exercise test. When only studies that excluded patients with a previous myocardial infarction were considered, mean sensitivity was 67% and mean specificity 72% (Table 36.10). Only three studies avoided work-up bias and provide an estimate of the diagnostic accuracy of exercise testing in a more general population of patients presenting with chest pain [141–143]. The mean sensitivity and specificity in these studies were 50% and 90%, respectively (Table 36.10).

36.7.5 Electrocardiographic Factors Influencing Sensitivity and Specificity

The influence of left ventricular hypertrophy, resting ST segment depression and use of digoxin on the exercise test characteristics are summarized in Table 36.10. Left ventricular hypertrophy with repolarization abnormalities is associated

Table 36.10

Meta-analysis of diagnostic performance of exercise test (Adapted from ACC/AHA Practice Guidelines on Exercise Testing [4] and from [139, 140])

(Sub-)Groups	Number of studies	Total number of patients	Sensitivity (%)	Specificity (%)	Predictive accuracy (%)
Meta-analysis of standard exercise test	147	24,047	68	77	73
Meta-analysis *without* prior MI	58	11,691	67	72	69
Meta-analysis *without* work-up bias	3	>1,000	50	90	69
Meta-analysis *with* ST-depression	22	9,153	69	70	69
Meta-analysis *without* ST-depression	3	840	67	84	75
Meta-analysis *with* digoxin	15	6,338	68	74	71
Meta-analysis *without* digoxin	9	3,548	72	69	70
Meta-analysis *with* LVH	15	8,016	68	69	68
Meta-analysis *without* LVH	10	1,977	72	77	74

LVH, left ventricular hypertrophy; MI, myocardial infarction

with a decreased specificity, but sensitivity is unaffected. If the test result is negative, the probability of CAD is substantially reduced, but additional tests are indicated in patients with an abnormal test result (Fig. 36.7). Although not apparent from Table 36.10, studies have suggested that digoxin also lowers specificity by producing an abnormal ST segment response to exercise, which occurs in up to 40% of healthy individuals [144, 145]. Resting ST segment depression is associated with a higher prevalence of severe CAD and a higher incidence of adverse cardiac events [4, 146–151]. As shown in Table 36.10, resting ST-depression lowers specificity of the exercise test. The most recent guidelines on exercise testing state that, if the resting ST segment depression is less than 1 mm (0.1 mV), the standard exercise test may still be the first test because sensitivity is increased [4]. In a retrospective study of male patients with resting ST segment depression, but without prior myocardial infarction, undergoing exercise testing, 2 mm (0.2 mV) of additional exercise-induced ST segment depression, or downsloping ST segment depression of 1 mm (0.1 mV) or more in the recovery phase were found to be important markers for the diagnosis of CAD, with a sensitivity of 67%, a specificity of 80%, and a likelihood ratio of 3.4 [4, 151]. In patients with less than 1 mm (0.1 mV) of resting ST segment depression who are also taking digoxin or have left ventricular hypertrophy, as well as in those with more than 1 mm (0.1 mV) of resting ST segment depression (Fig. 36.7), the diagnostic merits of the standard exercise test may be insufficient and imaging tests such as myocardial perfusion scintigraphy or stress echocardiography are preferred [4].

Finally, as stated, specificity was lowered and sensitivity increased when upsloping ST segment depression was classified as abnormal. Furthermore, the presence of right bundle-branch block does not appear to reduce the diagnostic accuracy of the exercise test for the diagnosis of CAD. On the contrary, exercise testing should not be used for the diagnosis of CAD in patients with complete left bundle-branch block, or in those with pre-excitation (Wolff-Parkinson-White) syndrome, or electronically paced ventricular rhythm [4].

36.7.6 Exercise Electrocardiography Versus Noninvasive Stress Imaging Studies

Although it is beyond the scope of this chapter to include a complete discussion on the comparison of exercise electrocardiography with the noninvasive stress imaging tests for the diagnosis of CAD, some features are presented here in brief. Studies that compared the diagnostic performance between exercise electrocardiography and the noninvasive imaging modalities using pharmacological stress (e.g., stress echocardiography or stress single-photon emission computed tomography (SPECT) myocardial perfusion scintigraphy) indicate that the latter are both more sensitive and more specific for the detection of CAD [152–155]. Furthermore, myocardial perfusion scintigraphy and stress echocardiography permit, to a certain extent, separation of patients with single and multiple vessel CAD and detection of the location of significant coronary artery stenosis [152–156]. This does not mean that exercise electrocardiography should be replaced by these imaging modalities. In many patients, CAD can be effectively ruled out, or diagnosed, by conventional exercise testing. Noninvasive imaging tests may provide additional information if the diagnosis is uncertain after conventional exercise testing, for example, if there is a posttest likelihood of intermediate probability. This likelihood is then considered as the pretest likelihood for the stress imaging test, as shown in Table 36.11 for myocardial perfusion scintigraphy; a 50% likelihood will reduce to 15% if the scintigram is normal, or increase to 93% if a reversible perfusion defect occurs. Myocardial perfusion scintigraphy and stress echocardiography using pharmacological stress agents can also be a useful alternative to exercise stress protocols in patients who are unable to exercise because of neurological, orthopedic, or peripheral vascular disease, as well as in those patients in whom interpretation of the ECG is hampered [152–158]. For a more complete and detailed overview of the noninvasive imaging modalities and their usefulness in the evaluation of CAD, the reader is referred to the relevant literature and guidelines [152–158].

36.8 Exercise Testing in Patients with Coronary Artery Disease

The value of exercise testing for risk or prognostic stratification must be considered in the light of what is added to that which is already known about the patient's risk status. Most studies on risk assessment in patients with CAD using exercise testing have focused on the relation between test parameters and future survival. The strongest predictor of survival in patients with CAD is the function of the left ventricle. Other important prognostic factors include the anatomic extent

Table 36.11

Calculation of posttest probability of CAD after myocardial perfusion scintigraphy. The pretest probability (*after* exercise testing) can be obtained from the appropriate data in Table 36.9

	Posttest probability (after nuclear perfusion scintigraphy in %)		
Pretest probability (%)	No defect	Nonreversible defect	Reversible defect
10	2	14	56
20	4	26	74
30	7	38	83
40	10	49	89
50	15	59	92
60	21	68	95
70	29	77	96
80	41	85	98
90	61	93	99

CAD denotes coronary artery disease

and severity of CAD, evidence of a recent acute coronary syndrome resulting from a coronary plaque rupture, and the propensity for the development of ventricular arrhythmias.

36.8.1 Risk Stratification and Assessment of Prognosis with Exercise Testing

In patients with suspected or known CAD and symptoms suggestive of myocardial ischemia, exercise testing is the standard initial test in those with a normal ECG for identification of ischemia and risk assessment [4, 159–161]. In patients with a non-interpretable ECG, exercise testing may still provide useful prognostic information, but cannot be used to identify ischemia. Studies on the prognostic value of the exercise test in symptomatic patients with non-acute CAD identify the maximum exercise capacity to be the strongest and most consistent prognostic factor [4, 162–168]. Maximum exercise capacity can be expressed as maximum exercise duration, maximum workload or MET level achieved, maximum blood pressure, or double (rate-pressure) product and represents at least in part left ventricular function. Markers of exercise-induced ischemia (electrocardiographic and/or clinical) represent the second group of variables that bear adverse prognostic information. In particular, electrocardiographic evidence of myocardial ischemia in patients with a low maximum exercise capacity represents a high-risk population [4, 162, 169].

Using data of 2,842 patients with known or suspected CAD, without prior revascularization or recent myocardial infarction, who underwent exercise testing before coronary angiography, the Duke treadmill score was created [163, 170]. This score is calculated using multiple variables of prognostic importance from the exercise test and can subsequently be converted into an average annual mortality rate [163, 170]. Based on the individual scores, patients can be classified in a high-risk group with a high average annual cardiovascular mortality, an intermediate risk group, or a low-risk group. The Duke treadmill score was shown to independently add prognostic information to the standard clinical data plus the data resulting from cardiac catheterization. The score can also be applied in women, although women have a lower overall risk for any score value than men [171]. Comparable prognostic scores have been developed by other groups [164].

Recently, several studies have identified other parameters from the exercise test to bear important prognostic information. These include chronotropic incompetence, abnormal heart rate recovery, and delayed blood pressure response [172–179]. In one study of almost 10,000, mostly, asymptomatic patients, it was demonstrated that abnormal heart rate recovery and the Duke treadmill score were independent predictors of mortality [4, 177].

Exercise testing is a much stronger predictor of cardiovascular mortality than of nonfatal myocardial infarction. This may, in part, be a result of the fact that myocardial infarctions are mostly caused by rupture of relatively small, vulnerable atherosclerotic plaques that are difficult to detect by exercise testing because of their non-obstructive character, whereas exercise test results are correlated with the presence and severity of obstructive CAD [4, 163, 180].

36.8.2 Exercise Testing to Guide Patient Treatment

The results of exercise testing may be used to guide patient treatment. Patients with a low risk exercise test result and a low predicted average annual mortality rate can be treated medically, whereas patients at higher risk should be referred for additional testing or cardiac catheterization, especially in case of left ventricular dysfunction.

Patients with acute coronary syndromes without persistent ST segment elevation are stratified as low, intermediate, or high risk based on history, physical examination, 12-lead ECG, and cardiac markers of myocardial necrosis [181, 182]. High-risk patients will be scheduled to undergo coronary angiography and subsequent revascularization. In low or intermediate risk patients with unstable angina, exercise or pharmacologic stress testing plays an important part in risk stratification and identification of obstructive CAD. Exercise electrocardiography should be the standard mode of stress testing in patients with a normal resting ECG [4]. In general, stress testing can be performed as soon as the patient has stabilized clinically. Furthermore, studies have shown that exercise testing is safe when used in emergency department chest pain centers to provide risk stratification for chest pain patients believed to possibly have acute coronary disease [4, 183–185]. However, exercise testing in this setting should only be used in low, and intermediate risk patients on the basis of history, physical examination, 12-lead ECG, and markers of myocardial necrosis.

36.9 Exercise Testing after Acute Myocardial Infarction

Exercise testing after acute myocardial infarction can be used for patient management, risk stratification, and prognostic assessment. Treatment strategies for acute myocardial infarction have changed substantially over the past decades. In particular, the advent of reperfusion therapy involving the use of fibrinolytic agents or, more recently, direct or primary percutaneous coronary intervention has led to a marked improvement in the prognosis of patients after myocardial infarction. Contemporary medical treatment with beta-adrenergic blocking agents and angiotensin converting enzyme inhibitors has further improved prognosis. The patient population currently undergoing exercise testing after acute myocardial infarction is, therefore, far different from historical populations before the reperfusion era. The goals and basic principles of exercise testing have, however, not changed dramatically. Therefore, the role of exercise testing must be viewed in the context of the patients who present for exercise testing.

In patients following acute myocardial infarction, exercise testing is frequently performed before hospital discharge to establish the hemodynamic response and functional capacity for exercise prescriptions and cardiac rehabilitation, to detect serious ventricular arrhythmia, and to identify patients with inducible myocardial ischemia [186–191]. Furthermore, it is helpful in reestablishing patients' confidence in their ability to conduct their activities following discharge. Predischarge exercise testing in patients after acute myocardial infarction appears to be safe provided that the proper contraindications are observed [188, 192, 193]. Major contraindications in this patient population include manifest congestive heart failure and postinfarction angina. Predischarge exercise testing has historically been performed between 5 and 26 days following myocardial infarction [188, 192, 194, 196], although studies have suggested that exercise testing can also be performed safely within 3–4 days in patients with an uncomplicated myocardial infarction [196, 197]. Predischarge exercise testing following acute myocardial infarction has traditionally utilized a submaximal protocol that requires the patient to exercise until a target, predetermined workload (e.g., achievement of 5–6 METs or 70–80% of age-predicted maximum) has been reached [198]. However, it has been proposed that symptom-limited exercise testing prior to discharge may be safely performed in patients with an uncomplicated postinfarction course. As opposed to submaximal testing, performance of a symptom-limited test provides a better estimate of peak functional capacity and is associated with an increased detection rate of ischemic ST segment changes and angina pectoris [188, 193, 199].

36.9.1 Exercise Testing in Patient Management

Both in patients treated with thrombolysis and in those who have not received reperfusion therapy, a predischarge standard exercise test remains the test of choice to identify myocardial ischemia and select patients who might benefit from coronary angiography and revascularization. Imaging studies may be helpful for risk stratification and detection

of myocardial ischemia in patients who have physical limitations that prevent them from exercising to an adequate workload, or in those with ECG abnormalities that preclude an accurate interpretation of ST segment changes. As expected, patients treated with thrombolytic therapy exhibit exercise-induced angina and ST segment depression less frequently than patients who have not received reperfusion therapy. In patients treated with direct or primary percutaneous coronary intervention, the coronary anatomy is known. If, besides the infarct-related artery, one or more of the other coronary arteries also shows a significant and important coronary obstruction at the time of angiography, additional coronary revascularization may be warranted. If the other coronary lesions found at the time of angiography are of intermediate or equivocal severity and significance, exercise testing or noninvasive stress imaging studies can be used to provoke residual ischemia and select patients who might benefit from additional revascularization, as well as those who can be managed conservatively.

36.9.2 Risk Stratification and Prognostic Assessment

As stated, the prognosis among patients after myocardial infarction has improved significantly, particularly in those who have received thrombolytic therapy or revascularization during hospitalization. Consequently, the low subsequent cardiac event rate associated with this improved treatment and survival substantially reduces the predictive accuracy of early exercise testing. Parameters derived from the exercise test following acute myocardial infarction that are associated with an increased risk of future death or recurrent nonfatal myocardial infarction include inability to perform the submaximal predischarge exercise test, poor exercise capacity, inability to increase - or a decrease in - systolic blood pressure, the development and magnitude of ST segment depression, especially at low workloads, and the development of angina [186, 194, 200–206].

Patients who have not undergone coronary revascularization and are unable to undergo exercise testing have the highest cardiac event rate. This was demonstrated both in trials in the thrombolytic era and in earlier studies in patients not receiving thrombolytic agents [194, 200–204]. In patients who are able to perform the test, exercise capacity is an important predictor of adverse cardiac events [189, 194, 195, 200, 203, 206–209]. Similarly, the hemodynamic response during the exercise test is of prognostic importance. Failure to increase systolic blood pressure by 10–30 mmHg or a decrease in blood pressure during exercise have been shown to be independent predictors of adverse outcome in patients after myocardial infarction [191, 195, 200, 203, 206, 209–211]. In a study in the prethrombolytic era, the degree of blood pressure rise during the exercise test was reported to be the single best predictive measurement [210]. The exercise capacity and the change in systolic blood pressure are, in fact, measures of left ventricular function which is the most important prognostic determinant of mortality following acute myocardial infarction. However, it was demonstrated that the maximum exercise capacity achieved during exercise testing provided an incremental prognostic value in patients with a low (less than 35%) left ventricular ejection fraction by gated radionuclide scintigraphy 1 month after acute myocardial infarction [212].

Exercise-induced ischemic ST segment depression in patients after myocardial infarction is an independent predictor of death or nonfatal myocardial infarction, particularly if the ST segment depression is accompanied by angina, occurs at a low level of exercise or in patients with controlled congestive heart failure [189, 203, 205, 206, 213, 214]. The predictive value of exercise-induced ischemia for adverse outcome is, however, limited by the fact that many patients who have an abnormal test result undergo coronary revascularization, which may alter the natural history of the disease process [193, 194, 201, 208, 215].

Finally, exercise testing can be used for activity counseling after hospital discharge and is an important tool in exercise training as part of a comprehensive cardiac rehabilitation program [4, 198].

36.10 Exercise Testing after Revascularization

36.10.1 Exercise Testing after Coronary Artery Bypass Grafting

The conversion of a positive exercise test result performed before coronary artery bypass grafting (CABG) to a negative postoperative test result is associated with successful revascularization [4, 216]. In patients with recurrent chest pain after

CABG, exercise testing may be used to demonstrate myocardial ischemia, although the exercise ECG is limited in this group of patients by the relatively high frequency of resting ECG abnormalities and the inability to document the site and extent of ischemia, as compared to stress imaging tests [4, 217, 218].

Exercise testing may be used for guiding exercise training as part of cardiac rehabilitation. It has been demonstrated that exercise testing in an asymptomatic individual, who has undergone successful CABG, is not predictive of outcome when the test is performed within the first few years after CABG [219, 220]. Therefore, routine periodic monitoring of asymptomatic patients after CABG is not indicated [4].

36.10.2 Exercise Testing after Percutaneous Coronary Intervention

Several studies that evaluated the diagnostic accuracy of exercise testing for identification of restenosis after percutaneous coronary intervention have shown that the exercise ECG is an insensitive predictor of restenosis [221–226], especially in asymptomatic patients, with sensitivities ranging from 40% to 50%, significantly less than those obtained by stress imaging tests [227, 228]. The insensitivity may be caused by the failure of moderate one-vessel stenoses to lead to significant ischemia on the exercise ECG. Routine, periodic exercise testing of asymptomatic patients after percutaneous coronary intervention without specific indications is therefore not recommended, especially since the prognostic benefit of controlling silent ischemia needs to be proved [4].

36.11 Exercise Testing and Heart Rhythm Disorders

Heart rhythm disorders occur frequently with exercise. The prevalence increases steadily with age, both in patients with heart disease and in normal individuals [229–231]. Increased sympathetic tone with withdrawal of much of the vagal tone, as well as myocardial ischemia may all play a role in the development of cardiac arrhythmias.

36.11.1 Sinus Node Dysfunction

Exercise testing may distinguish subjects with resting bradycardia with a normal increase in heart rate with exercise from those with sinus node dysfunction with a low resting heart rate that fails to accelerate normally with exercise, which is also labeled as chronotropic incompetence [4]. The definition of chronotropic incompetence has varied, the most common definition being failure to achieve 85% of (i.e., more than two standard deviations below) age-predicted maximum heart rate [4, 232]. The mechanisms involved are complex and not yet completely understood [233]. However, studies have confirmed the adverse prognostic implications of chronotropic incompetence [172, 233, 234]. Furthermore, a normal exercise test result does not negate the possibility of sinus node dysfunction.

36.11.2 Supraventricular Arrhythmias

The incidence of any supraventricular arrhythmia during exercise testing varies from 4% to 18% and increases with age. Atrial premature beats regularly occur at lower workloads, disappear as exercise increases and may return in the recovery period. They are considered to be of little clinical significance.

The majority of patients with atrial fibrillation demonstrate an abnormal heart rate response to exercise, which comprises an initial reduction of heart rate followed by delayed acceleration at lower workloads and a subsequent exaggerated increase in heart rate with tachycardia often persisting for a long period of time in the recovery phase [4, 235]. In patients with atrial fibrillation, exercise testing may help to evaluate the efficacy of drug regimens aimed at ventricular rate control. The ST segment changes associated with myocardial ischemia in atrial fibrillation are similar to those observed with sinus rhythm. However, in patients with atrial fibrillation and a very high ventricular response, the very short diastolic intervals may produce subendocardial ischemia because of the inadequate perfusion time in the absence of CAD. Atrial fibrillation initiated by exercise can be associated with CAD, rheumatic heart disease, or cardiomyopathy. However, it is

also seen in subjects with no apparent cardiac abnormalities, in whom it may be a prelude to the development of sustained atrial fibrillation at a later stage [33].

Patients with Wolff-Parkinson-White syndrome may exhibit ST segment depression during exercise testing in the absence of CAD. In patients with Wolff-Parkinson-White syndrome, exercise testing may be used to help evaluate the risk of developing rapid ventricular response during atrial arrhythmias. When the pre-excitation disappears during exercise, the antegrade refractory period in the accessory pathway is longer than that in the atrioventricular node and it is unlikely that a rapid ventricular response will occur [4].

36.11.3 Ventricular Arrhythmias

In normal subjects, there is an increase in the incidence of resting premature ventricular contractions (PVCs) of 2–15% with age [236]. It has been demonstrated that, in the absence of overt heart disease, these resting PVCs are usually benign [237]. PVCs are often induced by exercise and the incidence in clinically normal, middle-aged or older subjects during maximum stress testing is about 35%–45%, usually at high workloads [238–240]. In general, exercise-induced ventricular arrhythmias in a large group of subjects without symptoms followed for 5–10 years were found to have no influence on subsequent morbidity and mortality, and appear to be benign [239, 241]. These data are generally believed to apply to all asymptomatic individuals although one study on a large cohort of asymptomatic men suggests that exercise-induced PVCs may have more adverse prognostic implications than previously reported [242].

In patients with CAD, the reported incidence of ventricular arrhythmias during exercise ranges from 40% to 65% [238, 243, 244]. In general, patients with CAD manifest arrhythmias at a lower heart rate than normal subjects. Despite the fact that PVCs are more easily evoked in patients with CAD than in normal subjects, there is too much overlap between those with and without ischemia to allow such arrhythmias to have diagnostic value. Accordingly, the appearance of PVCs, including multiform or repetitive PVCs, should not be interpreted as a sign of myocardial ischemia in diagnostic stress testing [245].

The appearance of frequent, multiform, or repetitive PVCs during exercise is associated with an increased risk of mortality in patients with a previous myocardial infarction, especially apparent in patients with an impaired left ventricular function [246–252]. Most studies suggest that exercise-induced PVCs are also associated with an impaired survival in patients with CAD without a previous myocardial infarction, especially in cases of multiform, repetitive PVCs or (non-sustained) ventricular tachycardia [238, 244, 253–256]. Some reports have disputed such an association, however, at least in low-risk patients with demonstrable stable CAD [245, 257, 258]. Significant multivessel disease is likely to be present in patients with angina and exercise-induced ventricular arrhythmias, especially if ischemic ST segment changes are also present [238, 244, 245, 255, 256]. Although the induction of PVCs by exercise is well recognized, ventricular ectopic activity may also be abolished by exercise in patients with CAD, just as it may be in normal subjects. Therefore, this finding does not exclude the presence of CAD [33, 238, 255].

In general, more arrhythmias are seen on recovery than during exercise. In the recovery period, the imbalance between oxygen supply and demand induced during exercise may be augmented in patients with CAD; peripheral dilatation induced by exercise combined with a reduced venous return caused by cessation of muscular activity may result in reduced cardiac output and coronary flow at a time when myocardial oxygen demand is still high owing to tachycardia. Furthermore, catecholamine levels are considerably elevated [259]. These changes can be minimized by a gradual cool down.

36.11.3.1 Exercise-Induced Sustained Ventricular Tachycardia

Sustained ventricular tachycardia during exercise testing is relatively rare and occurs most frequently in the group of patients with ventricular tachycardia or ventricular fibrillation as their primary complaint. As stated previously, because ventricular tachycardia can deteriorate into ventricular fibrillation, immediate termination of exercise is warranted. Sustained ventricular tachycardia or long runs of non-sustained ventricular tachycardia usually portray serious underlying diseases; either CAD with ischemia or some type of cardiomyopathy should be suspected. Ventricular tachycardia caused by ischemia almost never has a left bundle-branch block pattern.

36.11.3.2 Exercise Testing to Evaluate Spontaneous Ventricular Tachycardia

Exercise testing can play an important role in the workup of patients who survived sudden death, as well as in those with syncope and sustained ventricular tachycardia [4]. The usefulness of exercise-testing in patients with ventricular tachycardia is variable, according to the cause of the tachycardia. In patients with idiopathic right ventricular outflow tract tachycardia, the ventricular tachycardia can be reproducibly induced during stress testing as it is commonly provoked by exercise. During exercise testing, the patients also exhibit many PVCs and coupled PVCs. The ventricular tachycardia has a left bundle-branch block morphology and is more likely to be non-sustained [260].

In adrenergic-dependent ventricular tachycardia, including monomorphic ventricular tachycardia and polymorphic ventricular tachycardia related to long-QT syndromes, exercise testing may supply the circumstances necessary for induction of the ventricular tachycardia and is, therefore, a useful prelude to an electrophysiological study [4]. Furthermore, the occurrence and nature of exercise-induced ventricular ectopy is of prognostic value in these patients [4, 254, 261]. Even in patients at risk of ventricular tachycardia, maximal exercise testing can be conducted safely with the appropriate precautions [4, 262]. The main limitation of exercise testing in patients with ventricular arrhythmias is related to its limited reproducibility so that other testing modalities are also required in the evaluation of these patients [4, 263].

Exercise testing may also be used to unmask pro-arrhythmic responses with development of sustained ventricular tachycardia during exercise in patients receiving anti-arrhythmic therapy.

36.12 Exercise Testing in Valvular Heart Disease

The primary value of exercise testing in valvular heart disease is to objectively assess atypical symptoms, exercise tolerance, and extent of disability to guide decision making with regard to surgical treatment. This is particularly of importance when a patient is thought to be asymptomatic because of inactivity (e.g., as in the elderly) or when a discrepancy exists between the patient's symptom status and the echocardiographic severity of the valvular stenosis or regurgitation. Furthermore, exercise testing can be used in follow-up of asymptomatic patients with valvular heart disease to detect a reduction in exercise capacity over time [4]. Details regarding the uses of exercise testing in patients with valvular heart disease have also been described in the respective guideline for the management of patients with valvular heart disease [264].

36.12.1 Mitral Valve Stenosis and Regurgitation

Exercise testing in mitral valve stenosis is of most value when the patient's symptom status and mitral valve area show discrepancy. When exercise induces excessive heart rate responses to a relatively low level of exercise or hypotension as a sign of a reduction in cardiac output, a more aggressive therapeutic approach aimed at earlier surgery might be considered [264]. In a rare case, exercise may precipitate atrial fibrillation in a patient with mitral valve stenosis.

In patients with mitral valve regurgitation, exercise testing objectively determines the functional capacity of the patient. Patients with severe mitral valve regurgitation commonly demonstrate a reduction in exercise capacity and are usually limited by the development of dyspnea. In patients with moderately-severe mitral valve regurgitation, a combination of exercise testing and assessment of left ventricular function may be useful in documenting occult left ventricular dysfunction and provoking earlier surgery [4, 264, 265]. Furthermore, exercise testing can be used to monitor exercise tolerance over time in these patients.

36.12.2 Aortic Valve Stenosis and Regurgitation

Severe, symptomatic aortic valve stenosis is a contraindication to exercise testing. As aortic valve replacement is not indicated in asymptomatic patients [264], it is important to distinguish those who are truly asymptomatic from patients who are asymptomatic because they are inactive or have adjusted to their functional impairment. In these patients, exercise testing can be used to select a subpopulation of patients who are hemodynamically compromised by aortic valve

stenosis and in whom surgery should be considered. Studies in adults with moderate to severe aortic valve stenosis have demonstrated that, with the appropriate precautions, exercise testing can be safely performed in these patients [4, 264, 266, 267]. Adverse hemodynamic responses that advocate aortic valve replacement include profound functional limitation, hypotension during exercise or failure to augment systolic blood pressure with exercise, and a rapid increase in heart rate indicating a fixed stroke volume. In this way, exercise testing can be combined with echocardiography in the follow-up of patients with aortic valve stenosis to help in determining the time at which aortic valve replacement should be performed.

Exercise tolerance is preserved until late in the course of aortic valve regurgitation. Exercise testing is not routinely required to guide treatment as the decision to proceed to valve surgery in chronic aortic regurgitation is primarily based on symptom status, left ventricular systolic (dys)function, and left ventricular size [4, 268].

References

1. Kaltenbach, M., D. Scherer, and S. Dowinsky, Complications of exercise testing. A survey in three German-speaking countries. *Eur. Heart J.*, 1982;**3**: 199–202.
2. Pina, I.L., G.J. Balady, P. Hanson, et al., Guidelines for clinical exercise testing laboratories: A statement for healthcare professionals from the Committee on Exercise and Cardiac Rehabilitation, American Heart Association. *Circulation*, 1995;**91**: 912–921.
3. Schlant, R.C., G.C. Friesinger II, and J.J. Leonard, Clinical competence in exercise testing: A statement for physicians from the ACP/ACC/AHA Task Force on Clinical Privileges in Cardiology. *J. Am. Coll. Cardiol.*, 1990;**16**: 1061–1065.
4. Gibbons, R.J., G.J. Balady, J.T. Bricker, B.R. Chaitman, G.F. Fletcher, V.F. Froelicher, D.B. Mark, B.D. McCallister, A.N. Mooss, M.G. O'Reilly, and W.L. Winters Jr, ACC/AHA 2002 guideline update for exercise testing: A report of the American College of Cardiology/American Heart Association Task Force on Practice Guidelines (Committee on Exercise Testing). 2002.
5. Taylor, H.L., W. Haskell, S.M. Fox, et al., Exercise tests: A summary of procedures and concepts of stress testing for cardiovascular diagnosis and function evaluation, in *Measurement in Exercise Electrocardiography*, H. Blackburn, Editor. Springfield, IL: Thomas, 1969.
6. Sheffield, L.T. and D. Roitman, Stress testing methodology. *Prog. Cardiovasc. Dis.*, 1976;**19**: 33–49.
7. Niederberger, M., R.A. Bruce, F. Kusumi, et al., Disparities in ventilatory and circulatory responses to bicycle and treadmill exercise. *Br. Heart J.*, 1974;**36**: 377–382.
8. Bruce, R.A., Methods of exercise testing. Step test, bicycle, treadmill, isometrics. *Am. J. Cardiol.*, 1974;**33**: 715–720.
9. Ellestad, M.H., Memorial hospital protocol, in *Stress Testing. Principles and Practice*, M.H. Ellestad, Editor. Philadelphia, PA: Davis, 1975, pp. 67–84.
10. Balke, B. and R.W. Ware, An experimental study of physical fitness of Air Force personnel. *US Armed Forces Med. J.*, 1959;**10**: 675–688.
11. Weld, F.M., K.-L. Chu, J.T. Bigger Jr, et al., Risk stratification with low-level exercise testing 2 weeks after acute myocardial infarction. *Circulation*, 1981;**64**: 306–314.
12. Ellestad, M.H., C.G. Blomqvist, and J.P. Naughton, Standards for adult exercise testing laboratories. *Circulation*, 1979;**58**: 421A–430A.
13. Fox, S.M., III, J.P. Naughton, and W.L. Haskell, Physical activity and the prevention of coronary heart disease. *Ann. Clin. Res.*, 1971;**3**: 404–432.
14. Froelicher, V.F., Jr, A.J. Thompson Jr, I. Noguera, et al., Prediction of maximal oxygen consumption. Comparison of the Bruce and Balke treadmill protocols. *Chest*, 1975;**68**: 331–336.
15. Pollock, M.L., R.L. Bohannon, K.H. Cooper, et al., A comparative analysis of four protocols for maximal treadmill stress testing. *Am. Heart J.*, 1976;**92**: 39–46.
16. Lecerof, H., Influence of body position on exercise tolerance, heart rate, blood pressure, and respiration rate in coronary insufficiency. *Br. Heart J.*, 1971;**33**: 78–83.
17. Thadani, U., R.O. West, T.M. Mathew, et al., Hemodynamics at rest and during supine and sitting bicycle exercise in patients with coronary artery disease. *Am. J. Cardiol.*, 1977;**39**: 776–783.
18. Kramer, B., B. Massie, and N. Topic, Hemodynamic differences between supine and upright exercise in patients with congestive heart failure. *Circulation*, 1982;**66**: 820–825.
19. Bruce, R.A., Exercise testing of patients with coronary heart disease: Principles and normal standards for evaluation. *Ann. Clin. Res.*, 1971;**3**: 323–332.
20. Erikssen, J., E. Thaulow, R. Mundal, et al., Comparison of beta-adrenoceptor blockers under maximal exercise (Pindolol v Metoprolol v Atenolol). *Br. J. Clin. Pharmacol.*, 1982;**13**: 201S–209S.
21. Samek, L. and H. Roskamm, Antianginal and antiarrhythmic effects of pindolol in post-infarct patients. *Br. J. Clin. Pharmacol.*, 1982;**13**: 297S.
22. Simoons, M.L., M. Taams, J. Lubsen, et al., Treatment of stable angina pectoris with verapamil hydrochloride: A double blind cross-over study. *Eur. Heart J.*, 1980;**1**: 269–274.
23. Harron, D.W.G., J.G. Riddell, and R.G. Shanks. Alinidine reduces heart rate without blockade of beta-adrenoceptors. *Lancet*, 1981;**1**: 351–353.
24. Borg, G., A. Holmgren, and I. Lindblad, Quantitative evaluation of chest pain. *Acta Med. Scand.*, 1981;Suppl. 644: 43–45.
25. Simoons, M.L., J. Tumraers, H. van Meurs-van Woezik, et al., Alinidine, a new agent which lowers heart rate in patients with angina pectoris. *Eur. Heart J.*, 1982;**3**: 542–545.
26. Simoons, M.L. and K. Balakumaran, The effects of drugs on the exercise electrocardiogram. *Cardiology*, 1981;**68**(Suppl. 2): 124–132.

27. Herbert, W.G., P. Dubach, K.G. Lehmann, et al., Effect of beta-blockade on the interpretation of the exercise ECG: ST level versus delta ST/HR index. *Am. Heart J.*, 1991;**122**: 993–1000.
28. Simoons, M.L., P.G. Hugenholtz, C.A. Ascoop, et al., Quantitation of exercise electrocardiography. *Circulation*, 1981;**63**: 471–475.
29. Wolf, H.K., P.J. MacInnis, S. Stock, et al., Computer analysis of rest and exercise electrocardiograms. *Comput. Biomed. Res.*, 1972;**5**: 329–346.
30. Simoons, M.L., H.B.K. Boom, and E. Smallenburg, On-line processing of orthogonal exercise electrocardiograms. *Comput. Biomed. Res.*, 1975;**8**: 105–117.
31. Bhargava, V., K. Watanabe, and V.F. Froelicher, Progress in computer analysis of the exercise electrocardiogram. *Am. J. Cardiol.*, 1981;**47**: 1143–1151.
32. Pahlm, O. and L. Sornmo, Data processing of exercise ECGs. *IEEE Trans. Biomed. Eng.*, 1987;**34**: 158–165.
33. Ellestad, M.H., *Stress Testing: Principles and Practice*, 5th edn. New York, NY: Oxford University Press.
34. Simoons, M.L. and P. Block, Toward the optimal lead system and optimal criteria for exercise electrocardiography. *Am. J. Cardiol.*, 1981;**47**: 1366–1374.
35. Phibbs, B.P. and L.J. Buckets, Comparative yield of ECG leads in multistage stress testing. *Am. Heart J.*, 1975;**90**: 275–276.
36. Miller, T.D., K.B. Desser, and M. Lawson, How many electrocardiographic leads are required for exercise treadmill tests? *J. Electrocardiol.*, 1987;**20**: 131–137.
37. Simoons, M.L., Optimal measurements for detection of coronary artery disease by exercise electrocardiography. *Comput. Biomed. Res.*, 1977;**10**: 483–499.
38. Mason, R.E., I. Likar, R.O. Biern, et al., Multiple-lead exercise electrocardiography. Experience in 107 normal subjects and 67 patients with angina pectoris, and comparison with coronary cinearteriography in 84 patients. *Circulation*, 1967;**36**: 517–525.
39. Chaitman, B.R., M.G. Bourassa, P. Wagniart, et al., Improved efficiency of treadmill exercise testing using a multiple lead ECG system and basic hemodynamic exercise response. *Circulation*, 1978;**57**: 71–79.
40. Fox, K., A. Selwyn, and J. Shillingford, Precordial electrocardiographic mapping after exercise in the diagnosis of coronary artery disease. *Am. J. Cardiol.*, 1979;**43**: 541–546.
41. Fox, K.M., J. Deanfield, P. Ribero, et al., Projection of ST segment changes on the front of the chest. *Br. Heart J.*, 1982;**48**: 555–559.
42. Miranda, C.P., J. Liu, A. Kadar, et al., Usefulness of exercise-induced ST segment depression in the inferior leads during exercise-testing as a marker for coronary artery disease. *Am. J. Cardiol.*, 1992;**69**: 303–307.
43. Michaelides, A.P., Z.D. Psomadaki, P.E. Dilaveris, et al., Improved detection of coronary artery disease by exercise electrocardiography with the use of right precordial leads. *N. Engl. J. Med.*, 1999;**340**: 340–345.
44. Wolthuis, R.A., V.F. Froelicher, A. Hopkirk, et al., Normal electrocardiographic waveform characteristics during treadmill exercise testing. *Circulation*, 1979;**60**: 1028–1035.
45. Simoons, M.L. and P.G. Hugenholtz, Estimation of the probability of exercise-induced ischemia by quantitative ECG analysis. *Circulation*, 1977;**56**: 552–559.
46. Block, P., J. Tiberghien, I. Raadschelders, et al., Diagnostic value of surface mapping recordings registered at rest and during exercise, in *Computers in Cardiology 1977*, H.G. Ostrow and K.L. Ripley, Editors. New York, NY: IEEE, 1977.
47. Mirvis, D.M., F.W. Keller Jr, J.W. Cox Jr, et al., Left precordial isopotential mapping during supine exercise. *Circulation*, 1977;**56**: 245–252.
48. Sapin, P.M., M.B. Blauwet, G.G. Koch, et al., Exaggerated atrial repolarization waves as a predictor of false positive exercise tests in an unselected population. *J. Electrocardiol.*, 1995;**28**: 313–321.
49. Sapin, P.M., G. Koch, M.B. Blauwet, et al., Identification of false positive exercise tests with use of electrocardiographic criteria: A possible role for atrial repolarization waves. *J. Am. Coll. Cardiol.*, 1991;**18**: 127–135.
50. Bhargava, V. and A.L. Goldberger, New method for measuring QRS duration using high-frequency electrocardiography. *Am. J. Physiol.*, 1982;**242**: H507–H511.
51. Sketch, M.H., S.M. Mohiuddin, C.K. Nair, et al., Automated and nomographic analysis of exercise tests. *Am. Med. Assoc.*, 1980;**243**: 1052–1055.
52. Battler, A., V.F. Froelicher, R. Slutsky, et al., Relationship of QRS amplitude changes during exercise to left ventricular function and volumes and the diagnosis of coronary artery disease. *Circulation*, 1979;**60**: 1004–1013.
53. David, D., M. Naito, C.C. Chen, et al., R-wave amplitude variations during acute experimental myocardial ischemia: An inadequate index for changes in intracardiac volume. *Circulation*, 1981;**63**: 1364–1371.
54. Deckers, J.W., R.V. Vinke, J.R. Vos, et al., Changes in the electrocardiographic response to exercise in healthy women. *Br. Heart J.*, 1990;**64**: 376–380.
55. Cumming, G.R., C. Dufresne, L. Kich, et al., Exercise electrocardiogram patterns in normal women. *Br. Heart J.*, 1973;**35**: 1055–1061.
56. Deckers, J.W., B.J. Rensing, M.L. Simoons, et al., Diagnostic merits of exercise testing in females. *Eur. Heart J.*, 1989;**10**: 543–550.
57. Detry, J.M., B.M. Capita, J. Cosyns, et al., Diagnostic value of history and maximal exercise electrocardiography in men and women suspected of coronary heart disease. *Circulation*, 1977;**56**: 756–761.
58. Val, P.G., B.R. Chaitman, D.D. Waters, et al., Diagnostic accuracy of exercise ECG lead systems in clinical subsets of women. *Circulation*, 1982;**65**: 1465–1474.
59. Barolsky, S.M., C.A. Gilbert, A. Faruqui, et al., Differences in electrocardiographic response to exercise of women and men: A non-Bayesian factor. *Circulation*, 1979;**60**: 1021–1027.
60. Rijneke, R.D., C.A. Ascoop, and J.L. Talmon, Clinical significance of upsloping ST segments in exercise electrocardiography. *Circulation*, 1980;**61**: 671–678.
61. Stuart, R.J. and M.H. Ellestad, Upsloping ST segments in exercise stress testing: Six-year follow-up study of 438 patients and correlation with 248 angiograms. *Am. J. Cardiol.*, 1976;**37**: 19–22.
62. Kurita, A., B.R. Chaitman, and M.G. Bourassa, Significance of exercise-induced ST depression in evaluation of coronary artery disease. *Am. J. Cardiol.*, 1977;**40**: 492–497.
63. Campeau, L., Grading of angina pectoris. *Circulation*, 1975;**54**: 522–523.
64. Simoons, M.L., M. van den Brand, and P.G. Hugenholtz, Quantitative analysis of exercise electrocardiograms and left ventricular angiocardiograms in patients with abnormal QRS complexes at rest. *Circulation*, 1977;**55**: 55–60.
65. Piessens, J., W. van Mieghem, H. Kesteloot, et al., Diagnostic value of clinical history, exercise testing and atrial pacing in patients with chest pain. *Am. J. Cardiol.*, 1974;**33**: 351–356.

66. Bartel, A.G., V.S. Behar, R.H. Peter, et al., Graded exercise stress tests in angiographically documented coronary artery disease. *Circulation*, 1974;**49**: 348–356.
67. Ascoop, C.A., M.L. Simoons, W.G. Egmond, et al., Exercise test, history, and serum lipid levels in patients with chest pain and normal electrocardiograms at rest: Comparison to findings at coronary arteriography. *Am. Heart J.*, 1971;**82**: 609–617.
68. Bogaty, P., et al., Does more ST segment depression on the 12-lead exercise electrocardiogram signify more severe ischemic heart disease. *Circulation*, 1993;**88**(Suppl. 2): 1.
69. Taylor, A.J. and G.A. Beller, Patients with greater than 2 mm of ST depression do not have a greater ischemic burden by thallium-201 scintigraphy. *Circulation*, 1992;**86**(Suppl. II): 138.
70. Husted, R., et al., The failure of multilead ST depression to predict severity of ischemia. *Am. J. Noninvas. Cardiol.*, 1994;**8**: 386.
71. Barlow, J.B., The "false positive" exercise electrocardiogram: Value of time course patterns in assessment of depressed ST segments and inverted T waves. *Am. Heart J.*, 1985;**110**: 1328–1336.
72. Miranda, C.P., K.G. Lehmann, and V.F. Froelicher, Correlation between resting ST segment changes, exercise testing, coronary angiography, and long term prognosis. *Am. Heart J.*, 1991;**122**: 1617–1628.
73. Ellestad, M.H., L. Thomas, R. Ong, et al., The predictive value of the time course of ST depression during exercise testing in patients referred for angiograms. *Am. Heart J.*, 1992;**123**: 904–908.
74. Lachterman, B., K.G. Lehmann, R. Detrano, et al., Comparison of ST segment/heart rate index to standard ST criteria for analysis of exercise electrocardiogram. *Circulation*, 1990;**82**: 44–50.
75. Rywik, T.M., R.C. Zink, N.S. Gittings, et al., Independent prognostic significance of ischemic ST segment response limited to recovery from treadmill exercise in asymptomatic subjects. *Circulation*, 1998;**97**: 2117–2222.
76. Hollenberg, M., M. Go Jr, B.M. Massie, et al., Influence of R-wave amplitude on exercise induced ST depression: Need for a "gain factor" correction when interpreting stress electrocardiograms. *Am. J. Cardiol.*, 1985;**56**: 13–17.
77. Hakki, A.H., A.S. Iskandria, S. Kutalek, et al., R-wave amplitude: A new determinant of failure of patients with coronary heart disease to manifest ST depression during exercise. *J. Am. Coll. Cardiol.*, 1984;**3**: 1155–1160.
78. Ellestad, M.H., R. Crump, and M. Surber, The significance of lead strength on ST changes during treadmill stress tests. *J. Electrocardiol.*, 1992;**25**(Suppl.): 31–34.
79. Elamin, M.S., R. Boyle, M.M. Kardash, et al., Accurate detection of coronary heart disease by new exercise test. *Br. Heart J.*, 1982;**48**: 311–320.
80. Okin, P.M. and P. Kligfield, Computer-based implementation of the ST-segment/heart rate slope. *Am. J. Cardiol.*, 1989;**64**: 926–930.
81. Detrano, R., E. Salcedo, M. Passalacqua, et al., Exercise electrocardiographic variables: A critical appraisal. *J. Am. Coll. Cardiol.*, 1986;**8**: 836–847.
82. Kligfield, P., O. Ameisen, and P.M. Okin, Heart rate adjustment of ST segment depression for improved detection of coronary artery disease. *Circulation*, 1989;**79**: 245–255.
83. Okin, P.M. and P. Kligfield, Heart rate adjustment of ST segment depression and performance of the exercise electrocardiogram: A critical evaluation. *J. Am. Coll. Cardiol.*, 1995;**25**: 1726–1735.
84. Fletcher, G.F., T.R. Flipse, P. Kligfield, et al., Current status of ECG stress testing. *Curr. Probl. Cardiol.*, 1998;**23**: 353–423.
85. Morise, A.P., Accuracy of heart rate-adjusted ST segments in populations with and without posttest referral bias. *Am. Heart J.*, 1997;**134**: 647–655.
86. Okin, P.M., M.J. Roman, J.E. Schwartz, et al., Relation of exercise-induced myocardial ischemia to cardiac and carotid structure. *Hypertension*, 1997;**30**: 1382–1388.
87. Viik, J., R. Lehtinen, and J. Malmivuo, Detection of coronary artery disease using maximum value of ST/HR hysteresis over different number of leads. *J. Electrocardiol.*, 1999;**32**(Suppl.): 70–75.
88. Froelicher, V.F., K.G. Lehmann, R. Thomas, et al., The electrocardiographic exercise test in a population with reduced workup bias: Diagnostic performance, computerized interpretation, and multivariable prediction. Veterans Affairs Cooperative Study in Health Services #016 (QUEXTA) Study Group. Quantitative Exercise Testing and Angiography. *Ann. Intern. Med.*, 1998;**128**: 965–974.
89. Macfarlane, P.W., A. Tweddel, D. Macfariane, et al., Body surface ECG mapping on exercise. *Eur. Heart J.*, 1984;**5**(Suppl. 1): 279.
90. Simoons, M.L., A. Withagen, R. Vinke, et al., ST-vector orientation and location of myocardial perfusion defects during exercise. *Nuklearmedizin*, 1978;**17**: 154–156.
91. Samek, L., H. Roskamm, P. Rentrop, et al., Belastungsprufungen und koronarangiogramm im chronischen infarktstadium. *Z. Kardiol.*, 1975;**64**: 809–814.
92. Roskamm, H., L. Samek, K. Zweigle, et al., Die beziehungen zwischen den befunden der koronarangiographie und des belastungs-ekg bei patienten ohne transmuralen myokardinfarkt. *Z. Kardiol.*, 1977;**66**: 273–280.
93. Fisher, L.D., J.W. Kennedy, B.R. Chaitman, et al., Diagnostic quantification of CASS (Coronary Artery Surgery Study) clinical and exercise test results in determining presence and extent of coronary artery disease: A multivariate approach. *Circulation*, 1981;**63**: 987–1000.
94. De Feyter, P.J., P.A. Majid, M.J. van Eenige, et al., Clinical significance of exercise-induced ST segment elevation. Correlative angiographic study in patients with ischaemic heart disease. *Br. Heart J.*, 1981;**46**: 84–92.
95. Alijarde, M., J. Soler-Soler, J. Perez-Jabaloyes, et al., Significance of treadmill stress testing in transmural myocardial infarction. Correlation with coronary angiography. *Eur. Heart J.*, 1982;**3**: 353–361.
96. Manvi, K.N. and M.H. Ellestad, Elevated ST-segments with exercise in ventricular aneurysm. *J. Electrocardiol.*, 1972;**5**: 317–323.
97. Haines, D.E., G.A. Beller, D.D. Watson, et al., Exercise-induced ST segment elevation 2 weeks after uncomplicated myocardial infarction: Contributing factors and prognostic significance. *J. Am. Coll. Cardiol.*, 1987;**9**: 996–1003.
98. Fox, K.M., A. Jonathan, and A. Selwyn, Significance of exercise induced ST segment elevation in patients with previous myocardial infarction. *Br. Heart J.*, 1983;**49**: 15–19.
99. Margonato, A., C. Ballarotto, F. Bonetti, et al., Assessment of residual tissue viability by exercise testing in recent myocardial infarction: Comparison of the electrocardiogram and myocardial perfusion scintigraphy. *J. Am. Coll. Cardiol.*, 1992;**19**: 948–952.
100. Margonato, A., S.L. Chierchia, R.G. Xuereb, et al., Specificity and sensitivity of exercise-induced ST segment elevation for detection of residual viability: Comparison with fluorodeoxyglucose and positron emission tomography. *J. Am. Coll. Cardiol.*, 1995;**25**: 1032–1038.

101. Lombardo, A., F. Loperfido, F. Pennestri, et al., Significance of transient ST-T segment changes during dobutamine testing in Q wave myocardial infarction. *J. Am. Coll. Cardiol.*, 1996;**27**: 599–605.
102. Dunn, R.F., B. Freedman, D.T. Kelly, et al., Exercise-induced ST segment elevation in leads V_1 or aVL. A predictor of anterior myocardial ischemia and left anterior descending coronary artery disease. *Circulation*, 1981;**63**: 1357–1363.
103. Dunn, R.F., B. Freedman, I.K. Bailey, et al., Localization of coronary artery disease with exercise electrocardiography: Correlation with thallium-201 myocardial perfusion scanning. *Am. J. Cardiol.*, 1981;**48**: 837–843.
104. Waters, D.D., B.R. Chaitman, M.G. Bourassa, et al., Clinical and angiographic correlates of exercise-induced ST segment elevation. Increased detection with multiple ECG leads. *Circulation*, 1980;**61**: 286–296.
105. Waters, D.D., J. Szlachcic, M.G. Bourassa, et al., Exercise testing in patients with variant angina: Results, correlation with clinical and angiographic features and prognostic significance. *Circulation*, 1982;**65**: 265–274.
106. Hegge, F.N., N. Tuna, and H.B. Burchell, Coronary arteriographic findings in patients with axis shifts or ST segment elevations on exercise stress testing. *Am. Heart J.*, 1973;**86**: 603–615.
107. Chahine, R.A., A.E. Raizner, and T. Ishimori, The clinical significance of exercise induced ST segment elevation. *Circulation*, 1976;**54**: 209–213.
108. Longhurst, J.C. and W.L. Kraus, Exercise-induced ST elevation in patients without myocardial infarction. *Circulation*, 1979;**60**: 616–629.
109. Mark, D.B., M.A. Hlatky, K.L. Lee, et al., Localizing coronary artery obstructions with the exercise treadmill test. *Ann. Intern. Med.*, 1987;**106**: 53–55.
110. Prinzmetal, M., A. Ekmekci, R. Kennamer, et al., Variant form of angina pectoris, previously undelineated syndrome. *JAMA*, 1960;**174**: 1794–1800.
111. Detry, J.M., P. Mengeot, M.F. Rousseau, et al., Maximal exercise testing in patients with spontaneous angina pectoris associated with transient ST segment elevation. Risks and electrocardiographic findings. *Br. Heart J.*, 1975;**37**: 897–903.
112. Bonoris, P.E., P.S. Greenberg, M.J. Castellanet, et al., Significance of changes in R wave amplitude during treadmill stress testing: Angiographic correlation. *Am. J. Cardiol.*, 1978;**41**: 846–851.
113. Wagner, S., J.C. Cohn, and A. Selzer, Unreliability of exercise induced R wave changes as indexes of coronary artery disease. *Am. J. Cardiol.*, 1979;**44**: 1241–1246.
114. Brody, D.A., A theoretical analysis of intracavitary blood mass influence on the heart–lead relationship. *Circ. Res.*, 1956;**4**: 731–738.
115. Greenberg, P.S., M.H. Ellestad, R. Berge, et al., Radionuclide angiographic correlation of the R-wave, ejection fraction, and volume responses to upright bicycle exercise. *Chest*, 1981;**80**: 459–464.
116. Froelicher, V.F., Jr, R. Wolthuis, N. Keiser, et al., A comparison of two bipolar exercise ECG leads to V5. *Chest*, 1976;**70**: 611–616.
117. Froelicher, V.F. and J.N. Myers, *Exercise and the Heart*, 4th edn. Philadelphia, PA: W.B. Saunders.
118. Michaelides, A.P., H. Boudoulas, H. Antonakoudis, et al., Effect of number of coronary arteries significantly narrowed and status of intraventricular conduction on exercise-induced QRS prolongation in coronary artery disease. *Am. J. Cardiol.*, 1992;**70**: 1487–1489.
119. Wayne, V.S., et al., Exercise-induced bundle branch block. *Am. J. Cardiol.*, 1983;**52**: 283.
120. Levy, S., R. Gerard, A. Castellanos, et al., Transient left anterior hemiblock during angina pectoris: Coronarographic aspects and clinical significance. *Eur. J. Cardiol.*, 1979;**9**: 215–225.
121. Hegge, F.N., N. Tuna, and H.B. Burchell, Coronary arteriographic findings in patients with axis shifts or ST segment elevations on exercise stress testing. *Am. Heart J.*, 1973;**86**: 603–615.
122. Whinnery, J.E., V.F. Froelicher Jr, M.R. Longo Jr, et al., The electrocardiographic response to maximal treadmill exercise in asymptomatic men with right branch bundle block. *Chest*, 1977;**71**: 335–340.
123. Kattus, A.A., Exercise electrocardiography. Recognition of the ischemic response: False positive and negative patterns. *Am. J. Cardiol.*, 1974;**33**: 721–731.
124. Tanaka, T., M.J. Friedman, R.D. Okada, et al., Diagnostic value of exercise-induced ST segment depression in patients with RBBB. *Am. J. Cardiol.*, 1978;**41**: 670–673.
125. Whinnery, J.E., V.F. Froelicher, and A.J. Stuart, The electrocardiographic response to maximal treadmill exercise in asymptomatic men with left bundle branch block. *Am. Heart J.*, 1997;**94**: 316–324.
126. Aravindakshan, V., W. Surawicz, and R.D. Allen, Electrocardiographic exercise test in patients with abnormal T waves at rest. *Am. Heart J.*, 1977;**93**: 706–714.
127. Diamond, G.A. and J.S. Forrester, Analysis of probability as an aid in the clinical diagnosis of coronary artery disease. *N. Engl. J. Med.*, 1979;**300**: 1350–1358.
128. Fisher, L.D. J.W. Kennedy, B.R. Chaitman, et al., Diagnostic quantification of CASS (Coronary Artery Surgery Study) clinical and exercise test results in determining presence and extent of coronary artery disease. A multivariate approach. *Circulation*, 1981;**63**: 987–1000.
129. Morise, A.P., W.J. Haddad, and D. Beckner, Development and validation of a clinical score to estimate the probability of coronary artery disease in men and women presenting with suspected coronary disease. *Am. J. Med.*, 1997;**102**: 350–356.
130. Altman, X., *Practical Statistics for Medical Research*. London: Chapman and Hall, 1991, pp. 414–417.
131. Detry, J.M., A. Robert, R.R.J. Luwaert, et al., Diagnostic value of computerized exercise testing in men without previous myocardial infarction. A multivariate, compartmental and probabilistic approach. *Eur. Heart J.*, 1985;**6**: 227–238.
132. Pryor, D.B., F.E. Harrell Jr, K.L. Lee, et al., Estimating the likelihood of significant coronary artery disease. *Am. J. Med.*, 1983;**75**: 771–780.
133. Ellestad, M.H., S. Savitz, D. Bergdall, et al., The false positive stress test: Multivariate analysis of 215 subjects with hemodynamic, angiographic and clinical data. *Am. J. Cardiol.*, 1977;**40**: 681–685.
134. Yamada, H., D. Do, A. Morise, et al., Review of studies using multivariable analysis of clinical and exercise test data to predict angiographic coronary artery disease. *Prog. Cardiovasc. Dis.*, 1997;**39**: 457–481.
135. Shaw, L.J., E.D. Peterson, L.K. Shaw, et al., Use of a prognostic treadmill score in identifying diagnostic coronary disease subgroups. *Circulation*, 1998;**98**: 1622–1630.

136. Deckers, J.W., B.J. Rensing, J.G. Tijssen, et al., A comparison of methods of analysing exercise tests for diagnosis of coronary artery disease. *Br. Heart J.*, 1989;**62**: 438–444.
137. Lee, K.L., D.B. Pryor, F.E. Harrell Jr, et al., Predicting outcome in coronary disease: Statistical models versus expert clinicians. *Am. J. Med.*, 1986;**80**: 553–560.
138. Detrano, R., M. Bobbio, H. Olson, et al., Computer probability estimates of angiographic coronary artery disease: Transportability and comparison with cardiologists' estimates. *Comput. Biomed. Res.*, 1992;**25**: 468–485.
139. Gianrossi, R., R. Detrano, D. Mulvihill, et al., Exercise induced ST depression in the diagnosis of coronary artery disease: A meta analysis. *Circulation*, 1989;**80**: 87–98.
140. Detrano, R., R. Gianrossi, and V. Froelicher, The diagnostic accuracy of the exercise electrocardiogram: A meta analysis of 22 years of research. *Prog. Cardiovasc. Dis.*, 1989;**32**: 173–206.
141. Morise, A.P. and G.A. Diamond, Comparison of the sensitivity and specificity of exercise electrocardiography in biased and unbiased populations of men and women. *Am. Heart J.*, 1995;**130**: 741–747.
142. DelCampo, J., D. Do, T. Umann, et al., Comparison of computerized and standard visual criteria of exercise ECG for diagnosis of coronary artery disease. *Ann. Noninvasive Electrocardiogr.*, 1996;**1**: 430–442.
143. Froelicher, V.F., K.G. Lehmann, R. Thomas, et al., The electrocardiographic exercise test in a population with reduced workup bias: Diagnostic performance, computerized interpretation, and multivariable prediction. Veterans Affairs Cooperative Study in Health Services #016 (QUEXTA) Study Group. Quantitative Exercise Testing and Angiography. *Ann. Intern. Med.*, 1998;**128**: 965–974.
144. Sketch, M.H., A.N. Mooss, M.L. Butler, et al., Digoxin-induced positive exercise tests: Their clinical and prognostic significance. *Am. J. Cardiol.*, 1981;**48**: 655–659.
145. LeWinter, M.M., M.H. Crawford, R.A. O'Rourke, et al., The effects of oral propranolol, digoxin and combination therapy on the resting and exercise electrocardiogram. *Am. Heart J.*, 1977;**93**: 202–209.
146. Blackburn, H., Canadian colloquium on computer assisted interpretation of electrocardiograms, VI: importance of the electrocardiogram in populations outside the hospital. *Can. Med. Assoc. J.*, 1973;**108**: 1262–1265.
147. Cullen, K., N.S. Stenhouse, K.L. Wearne, et al., Electrocardiograms and 13-year cardiovascular mortality in Busselton study. *Br. Heart J.*, 1982;**47**: 209–212.
148. Aronow, W.S., Correlation of ischemic ST segment depression on the resting electrocardiogram with new cardiac events in 1,106 patients over 62 years of age. *Am. J. Cardiol.*, 1989;**64**: 232–233.
149. Califf, R.M., D.B. Mark, F.E. Harrell Jr, et al., Importance of clinical measures of ischemia in the prognosis of patients with documented coronary artery disease. *J. Am. Coll. Cardiol.*, 1988;**11**: 20–26.
150. Harris, P.J., F.E. Harrell Jr, K.L. Lee, et al., Survival in medically treated coronary artery disease. *Circulation*, 1979;**60**: 1259–1269.
151. Miranda, C.P., K.G. Lehmann, and V.F. Froelicher, Correlation between resting ST segment depression, exercise testing, coronary angiography, and long term prognosis. *Am. Heart J.*, 1991;**122**: 1617–1628.
152. Geleijnse, M.L., P.M. Fioretti, and J.R.T.C. Roelandt, Methodology, feasibility, safety and diagnostic accuracy of dobutamine stress echocardiography. *J. Am. Coll. Cardiol.*, 1997;**30**: 595–606.
153. Geleijnse, M.L., A. Salustri, T.H. Marwick, et al., Should the diagnosis of coronary artery disease be based on the evaluation of myocardial function or perfusion? *Eur. Heart J.*, 1997;**18**(Suppl. D): D68–D77.
154. Schinkel, A.F.L., J.J. Bax, M.L. Geleijnse, et al., Noninvasive evaluation of ischemic heart disease: Myocardial perfusion imaging or stress echocardiography? *Eur. Heart J.*, 2003;**24**: 789–800.
155. Geleijnse, M.L., A. Elhendy, and R.T. Van Domburg, Cardiac imaging for risk stratification with dobutamine–atropine stress testing in patients with chest pain. Echocardiography, perfusion scintigraphy, or both? *Circulation*, 1997;**96**: 137–147.
156. Rigo, P., I.K. Bailey, L.C. Griffith, et al., Value and limitations of segmental analysis of stress thallium myocardial imaging for localization of coronary artery disease. *Circulation*, 1980;**61**: 973–981.
157. Ritchie, J.L., T.M. Bateman, R.O. Bonow, et al., Guidelines for clinical use of cardiac radionuclide imaging: Report of the American College of Cardiology/American Heart Association Task Force on Assessment of Diagnostic and Therapeutic Cardiovascular Procedures (Committee on Radionuclide Imaging), developed in collaboration with the American Society of Nuclear Cardiology. *J. Am. Coll. Cardiol.*, 1995;**25**: 521–547.
158. Cheitlin, M.D., J.S. Alpert, W.F. Armstrong, et al., ACC/AHA guidelines for the clinical application of echocardiography: A report of the American College of Cardiology/American Heart Association Task Force on Practice Guidelines (Committee on Clinical Application of Echocardiography). Developed in collaboration with the American Society of Echocardiography. *Circulation*, 1997;**95**: 1686–1744.
159. Christian, T.F., T.D. Miller, K.R. Bailey, et al., Exercise tomographic thallium 201 imaging in patients with severe coronary artery disease and normal electrocardiograms. *Ann. Intern. Med.*, 1994;**121**: 825–832.
160. Gibbons, R.J., A.R. Zinsmeister, T.D. Miller, et al., Supine exercise electrocardiography compared with exercise radionuclide angiography in noninvasive identification of severe coronary artery disease. *Ann. Intern. Med.*, 1990;**112**: 743–749.
161. Ladenheim, M.L., T.S. Kotler, B.H. Pollock, et al., Incremental prognostic power of clinical history, exercise electrocardiography and myocardial perfusion scintigraphy in suspected coronary artery disease. *Am. J. Cardiol.*, 1987;**59**: 270–277.
162. Weiner, D.A., T.J. Ryan, C.H. McCabe, et al., Prognostic importance of a clinical profile and exercise test in medically treated patients with coronary artery disease. *J. Am. Coll. Cardiol.*, 1984;**3**: 772–779.
163. Mark, D.B., M.A. Hlatky, F.E. Harrell Jr, et al., Exercise treadmill score for predicting prognosis in coronary artery disease. *Ann. Intern. Med.*, 1987;**106**: 793–800.
164. Morrow, K., C.K. Morris, V.F. Froelicher, et al., Prediction of cardiovascular death in men undergoing noninvasive evaluation for coronary artery disease. *Ann. Intern. Med.*, 1993;**118**: 689–695.
165. Brunelli, C., R. Cristofani, and A. L'Abbate, Long term survival in medically treated patients with ischaemic heart disease and prognostic importance of clinical and electrocardiographic data (the Italian CNR Multicentre Prospective Study OD1). *Eur. Heart J.*, 1989;**10**: 292–303.
166. Luwaert, R.J., J.A. Melin, C.R. Brohet, et al., Non invasive data provide independent prognostic information in patients

with chest pain without previous myocardial infarction: Findings in male patients who have had cardiac catheterization. *Eur. Heart J.*, 1988;**9**: 418–426.
167. Gohlke, H., L. Samek, P. Betz, et al., Exercise testing provides additional prognostic information in angiographically defined subgroups of patients with coronary artery disease. *Circulation*, 1983;**68**: 979–985.
168. Hammermeister, K.E., T.A. DeRouen, and H.T. Dodge, Variables predictive of survival in patients with coronary disease: Selection by univariate and multivariate analyses from the clinical, electrocardiographic, exercise, arteriographic, and quantitative angiographic evaluations. *Circulation*, 1979;**59**: 421–430.
169. McNeer, J.F., J.R. Margolis, K.L. Lee, et al., The role of the exercise test in the evaluation of patients for ischemic heart disease. *Circulation*, 1978;**57**: 64–70.
170. Mark, D.B., L. Shaw, F.E. Harrell Jr, et al., Prognostic value of a treadmill exercise score in outpatients with suspected coronary artery disease. *N. Engl. J. Med.*, 1991;**325**: 849–853.
171. Alexander, K.P., L.J. Shaw, L.K. Shaw, et al., Value of exercise treadmill testing in women [published erratum appears in J Am Coll Cardiol 1999;33:289]. *J. Am. Coll. Cardiol.*, 1998;**32**: 1657–1664.
172. Lauer, M.S., G.S. Francis, P.M. Okin, et al., Impaired chronotropic response to exercise stress testing as a predictor of mortality. *JAMA*, 1999;**281**: 524–529.
173. Cole, C.R., E.H. Blackstone, F.J. Pashkow, et al., Heart-rate recovery immediately after exercise as a predictor of mortality. *N. Engl. J. Med.*, 1999;**341**: 1351–1357.
174. Cole, C.R., J.M. Foody, E.H. Blackstone, et al., Heart rate recovery after submaximal exercise testing as a predictor of mortality in a cardiovascularly healthy cohort. *Ann. Intern. Med.*, 2000;**132**: 552–555.
175. Diaz, L.A., R.C. Brunken, E.H. Blackstone, et al., Independent contribution of myocardial perfusion defects to exercise capacity and heart rate recovery for prediction of all-cause mortality in patients with known or suspected coronary heart disease. *J. Am. Coll. Cardiol.*, 2001;**37**: 1558–1564.
176. Watanabe, J., M. Thamilarasan, E.H. Blackstone, et al., Heart rate recovery immediately after treadmill exercise and left ventricular systolic dysfunction as predictors of mortality: The case of stress echocardiography. *Circulation*, 2001;**104**: 1911–1916.
177. Nishime, E.O., C.R. Cole, E.H. Blackstone, et al., Heart rate recovery and treadmill exercise score as predictors of mortality in patients referred for exercise ECG. *JAMA*, 2000;**284**: 1392–1398.
178. Shetler, K., R. Marcus, V.F. Froelicher, et al., Heart rate recovery: Validation and methodologic issues. *J. Am. Coll. Cardiol.*, 2001;**38**: 1980–1987.
179. McHam, S.A., T.H. Marwick, F.J. Pashkow, et al., Delayed systolic blood pressure recovery after graded exercise: An independent correlate of angiographic coronary disease. *J. Am. Coll. Cardiol.*, 1999;**34**: 754–759.
180. Bogaty, P., G.R. Dagenais, B. Cantin, et al., Prognosis in patients with a strongly positive exercise electrocardiogram. *Am. J. Cardiol.*, 1989;**64**: 1284–1288.
181. Bertrand, M.E., M.L. Simoons, K.A. Fox, et al.; Task Force on the Management of Acute Coronary Syndromes of the European Society of Cardiology, Management of acute coronary syndromes in patients presenting without persistent ST segment elevation. *Eur. Heart J.*, 2002;**23**: 1809–1840. Erratum in: *Eur. Heart J.*, 2003;**24**: 1174–1175. *Eur. Heart J.*, 2003;**24**: 485.
182. Boersma, E., K.S. Pieper, E.W. Steyerberg, et al., Predictors of outcome in patients with acute coronary syndromes without persistent ST segment elevation. Results from an international trial of 9461 patients. The PURSUIT Investigators. *Circulation*, 2000;**101**: 2557–2567.
183. Stein, R.A., B.R. Chaitman, G.J. Balady, et al., Safety and utility of exercise testing in emergency room chest pain centers: An advisory from the Committee on Exercise, Rehabilitation, and Prevention, Council on Clinical Cardiology, American Heart Association. *Circulation*, 2000;**102**: 1463–1467.
184. Gibler, W.B., J.P. Runyon, R.C. Levy, et al., A rapid diagnostic and treatment center for patients with chest pain in the emergency department. *Ann. Emerg. Med.*, 1995;**25**: 1–8.
185. Farkouh, M.E., P.A. Smars, G.S. Reeder, et al., A clinical trial of a chest-pain observation unit for patients with unstable angina. Chest Pain Evaluation in the Emergency Room (CHEER) Investigators. *N. Engl. J. Med.*, 1998;**339**: 1882–1888.
186. Froelicher, E.S., Usefulness of exercise testing shortly after acute myocardial infarction for predicting 10-year mortality. *Am. J. Cardiol.*, 1994;**74**: 318–323.
187. Mark, D.B. and V.F. Froelicher, Exercise treadmill testing and ambulatory monitoring, in *Acute Coronary Care*, R.M. Califf, D.B. Mark, and G.S. Wagner, Editors. St. Louis, Mosby-Year Book, 1995.
188. Juneau, M., P. Colles, P. Théroux, et al., Symptom limited versus low level exercise testing before hospital discharge after myocardial infarction. *J. Am. Coll. Cardiol.*, 1992;**20**: 927–933.
189. Stevenson, R., V. Umachandran, K. Ranjadayalan, et al., Reassessment of treadmill stress testing for risk stratification in patients with acute myocardial infarction treated by thrombolysis. *Br. Heart J.*, 1993;**70**: 415–420.
190. Moss, A.J., R.E. Goldstein, W.J. Hall, et al., Detection and significance of myocardial ischemia in stable patients after recovery from an acute coronary event: Multicenter Myocardial Ischemia Research Group. *JAMA*, 1993;**269**: 2379–2385.
191. Arnold, A.E., M.L. Simoons, J.M. Detry, et al., Prediction of mortality following hospital discharge after thrombolysis for acute myocardial infarction: Is there a need for coronary angiography? *Eur. Heart J.*, 1993;**14**: 306–315.
192. Hamm, L.F., R.S. Crow, G.A. Stull, et al., Safety and characteristics of exercise testing early after acute myocardial infarction. *Am. J. Cardiol.*, 1989;**63**: 1193–1197.
193. Jain, A., G.H. Myers, P.M. Sapin, et al., Comparison of symptom limited and low level exercise tolerance tests early after myocardial infarction. *J. Am. Coll. Cardiol.*, 1993;**22**: 1816–1820.
194. Krone, R.J., J.A. Gillespie, F.M. Weld, et al., Low level exercise testing after myocardial infarction: Usefulness in enhancing clinical risk stratification. *Circulation*, 1985;**71**: 80–89.
195. Nielsen, J.R., H. Mickley, E.M. Damsgaard, et al., Predischarge maximal exercise test identifies risk for cardiac death in patients with acute myocardial infarction. *Am. J. Cardiol.*, 1990;**65**: 149–153.
196. Topol, E.J., K. Burek, W.W. O'Neill, et al., A randomized controlled trial of hospital discharge three days after myocardial infarction in the era of reperfusion. *N. Engl. J. Med.*, 1988;**318**: 1083–1088.
197. Senaratne, M.P., G. Smith, and S.S. Gulamhusein, Feasibility and safety of early exercise testing using the Bruce protocol after acute myocardial infarction. *J. Am. Coll. Cardiol.*, 2000;**35**: 1212–1220.

198. Fletcher, G.F., G.J. Balady, E.A. Amsterdam, et al., Exercise standards for testing and training: A statement for healthcare professionals from the American Heart Association. *Circulation*, 2001;**104**: 1694–1740.
199. Vanhees, L., D. Schepers, and R. Fagard, Comparison of maximum versus submaximum exercise testing in providing prognostic information after acute myocardial infarction and/or coronary artery bypass grafting. *Am. J. Cardiol.*, 1997;**80**: 257–262.
200. Villella, A., A.P. Maggioni, M. Villella, et al., Prognostic significance of maximal exercise testing after myocardial infarction treated with thrombolytic agents: The GISSI 2 data base. Gruppo Italiano per lo Studio della Sopravvivenza Nell'Infarto. *Lancet*, 1995;**346**: 523–529.
201. Chaitman, B.R., R.P. McMahon, M. Terrin, et al., Impact of treatment strategy on predischarge exercise test in the Thrombolysis in Myocardial Infarction (TIMI) II Trial. *Am. J. Cardiol.*, 1993;**71**: 131–138.
202. Newby, L.K., R.M. Califf, A. Guerci, et al., Early discharge in the thrombolytic era: An analysis of criteria for uncomplicated infarction from the Global Utilization of Streptokinase and tPA for Occluded Coronary Arteries (GUSTO) trial. *J. Am. Coll. Cardiol.*, 1996;**27**: 625–632.
203. Froelicher, V.F., S. Perdue, W. Pewen, et al., Application of meta analysis using an electronic spread sheet for exercise testing in patients after myocardial infarction. *Am. J. Med.*, 1987;**83**: 1045–1054.
204. Maggioni, A.P., F.M. Turazza, and L. Tavazzi, Risk evaluation using exercise testing in elderly patients after acute myocardial infarction. *Cardiol. Elder.*, 1995;**3**: 88–93.
205. Théroux, P., D.D. Waters, C. Halphen, et al., Prognostic value of exercise testing soon after myocardial infarction. *N. Engl. J. Med.*, 1979;**301**: 341–345.
206. Shaw, L.J., E.D. Peterson, K. Kesler, et al., A meta analysis of predischarge risk stratification after acute myocardial infarction with stress electrocardiographic, myocardial perfusion, and ventricular function imaging. *Am. J. Cardiol.*, 1996;**78**: 1327–1337.
207. Volpi, A., C. de Vita, M.G. Franzosi, et al., Predictors of nonfatal reinfarction in survivors of myocardial infarction after thrombolysis: Results of the Gruppo Italiano per lo Studio della Sopravvivenza nell'Infarto Miocardico (GISSI 2) Data Base. *J. Am. Coll. Cardiol.*, 1994;**24**: 608–615.
208. Ciaroni, S., J. Delonca, and A. Righetti, Early exercise testing after acute myocardial infarction in the elderly: Clinical evaluation and prognostic significance. *Am. Heart J.*, 1993;**126**: 304–311.
209. Stone, P.H., Z.G. Turi, J.E. Muller, et al., Prognostic significance of the treadmill exercise test performance 6 months after myocardial infarction. *J. Am. Coll. Cardiol.*, 1986;**8**: 1007–1017.
210. Fioretti, P., R.W. Brower, M.L. Simoons, et al., Prediction of mortality in hospital survivors of myocardial infarction: Comparison of predischarge exercise testing and radionuclide ventriculography at rest. *Br. Heart J.*, 1984;**52**: 292–298.
211. Fioretti, P., R.W. Brower, M.L. Simoons, et al., Relative value of clinical variables, bicycle ergometry, rest radionuclide ventriculography and 24 hour ambulatory electrocardiographic monitoring at discharge to predict 1 year survival after myocardial infarction. *J. Am. Coll. Cardiol.*, 1986;**8**: 40–49.
212. Pilote, L., J. Silberberg, R. Lisbona, et al., Prognosis in patients with low left ventricular ejection fraction after myocardial infarction. *Circulation*, 1989;**80**: 1636–1641.
213. Krone, R.J., E.M. Dwyer, H. Greenberg, et al., Risk stratification in patients with first non Q wave infarction: Limited value of the early low level exercise test after uncomplicated infarcts: The Multicenter Post Infarction Research Group. *J. Am. Coll. Cardiol.*, 1989;**14**: 31–37.
214. DeBusk, R.F. and W. Haskell, Symptom limited vs heart rate limited exercise testing soon after myocardial infarction. *Circulation*, 1980;**61**: 738–743.
215. Abboud, L., J. Hir, I. Eisen, and W. Markiewicz, Angina pectoris and ST segment depression during exercise testing early following acute myocardial infarction. *Cardiology*, 1994;**84**: 268–273.
216. McConahay, D.R., M. Valdes, B.D. McCallister, et al., Accuracy of treadmill testing in assessment of direct myocardial revascularization. *Circulation*, 1977;**56**: 548–552.
217. Visser, F.C., L. van Campen, and P.J. de Feyter, Value and limitations of exercise stress testing to predict the functional results of coronary artery bypass grafting. *Int. J. Card. Imaging*, 1993;**9**(Suppl. 1): 41–47.
218. Kafka, H., A.J. Leach, and G.M. Fitzgibbon, Exercise echocardiography after coronary artery bypass surgery: Correlation with coronary angiography. *J. Am. Coll. Cardiol.*, 1995;**25**: 1019–1023.
219. Yli Mayry, S., H.V. Huikuri, K.E. Airaksinen, et al., Usefulness of a postoperative exercise test for predicting cardiac events after coronary artery bypass grafting. *Am. J. Cardiol.*, 1992;**70**: 56–59.
220. Krone, R.J., R.M. Hardison, B.R. Chaitman, et al., Risk stratification after successful coronary revascularization: The lack of a role for routine exercise testing. *J. Am. Coll. Cardiol.*, 2001;**38**: 136–142.
221. Kadel, C., T. Strecker, M. Kaltenbach, et al., Recognition of restenosis: Can patients be defined in whom the exercise ECG result makes angiographic restudy unnecessary? *Eur. Heart J.*, 1989;**10**(Suppl. G): 22–26.
222. Honan, M.B., J.R. Bengtson, D.B. Pryor, et al., Exercise treadmill testing is a poor predictor of anatomic restenosis after angioplasty for acute myocardial infarction. *Circulation*, 1989;**80**: 1585–1594.
223. Schroeder, E., B. Marchandise, P. DeCoster, et al., Detection of restenosis after coronary angioplasty for single vessel disease: How reliable are exercise electrocardiography and scintigraphy in asymptomatic patients? *Eur. Heart J.*, 1989;**10**: 18–21.
224. Laarman, G., H.E. Luijten, L.G. van Zeyl, et al., Assessment of silent restenosis and long-term follow-up after successful angioplasty in single vessel coronary artery disease: The value of quantitative exercise electrocardiography and quantitative coronary angiography. *J. Am. Coll. Cardiol.*, 1990;**16**: 578–585.
225. Desmet, W., I. De Scheerder, and J. Piessens, Limited value of exercise testing in the detection of silent restenosis after successful coronary angioplasty. *Am. Heart J.*, 1995;**129**: 452–459.
226. Vlay, S.C., J. Chernilas, W.E. Lawson, et al., Restenosis after angioplasty: Don't rely on the exercise test. *Am. Heart J.*, 1989;**117**: 980–986.
227. Echt, H.S., R.E. Shaw, H.L. Chin, et al., Silent ischemia after coronary angioplasty: Evaluation of restenosis and extent of ischemia in asymptomatic patients by tomographic thallium 201 exercise imaging and comparison with symptomatic patients. *J. Am. Coll. Cardiol.*, 1991;**17**: 670–677.
228. Hecht, H.S., L. DeBord, R. Shaw, et al., Usefulness of supine bicycle stress echocardiography for detection of restenosis after percutaneous transluminal coronary angioplasty. *Am. J. Cardiol.*, 1993;**71**: 293–296.

229. Bigger, J.T., Jr, F.J. Dresdale, R.H. Heissenbuttel, et al., Ventricular arrhythmias in ischemic heart disease: Mechanism, prevalence, significance and management. *Prog. Cardiovasc. Dis.*, 1977;**19**: 255–300.
230. Faris, J.V., P.L. McHenry, J.W. Jordan, et al., Prevalence and reproducibility of exercise-induced ventricular arrhythmias during maximal exercise testing in normal men. *Am. J. Cardiol.*, 1976;**37**: 617–622.
231. Busby, M.J., E.A. Shefrin, and J.L. Fleg, Prevalence and long-term significance of exercise-induced frequent or repetitive ventricular ectopic beats in apparently healthy volunteers. *J. Am. Coll. Cardiol.*, 1989;**14**: 1659–1665.
232. Ellestad, M.H. and M.K. Wan, Predictive implications of stress testing. Follow up of 2700 subjects after maximum treadmill stress testing. *Circulation*, 1975;**51**: 363–369.
233. Ellestad, M.H., Chronotropic incompetence: The implications of heart rate response to exercise (compensatory parasympathetic hyperactivity?). *Circulation*, 1996;**93**: 1485–1487.
234. Lauer, M.S., P.M. Okin, M.G. Larson, et al., Impaired heart rate response to graded exercise: Prognostic implications of chronotropic incompetence in the Framingham Heart Study. *Circulation*, 1996;**93**: 1520–1526.
235. Corbelli, R., M. Masterson, and B.L. Wilkoff, Chronotropic response to exercise in patients with atrial fibrillation. *Pacing Clin. Electrophysiol.*, 1990;**13**: 179–187.
236. Fisher, F.D. and H.A. Tyroler, Relationship between ventricular premature contractions in routine electrocardiograms and subsequent sudden death from coronary heart disease. *Circulation*, 1973;**47**: 712–719.
237. Buckingham, T.A., The clinical significance of ventricular arrhythmias in apparently healthy subjects. *Pract. Cardiol.*, 1983;**9**: 37.
238. McHenry, P.L., S.N. Morris, M. Kavalier, et al., Comparative study of exercise-induced ventricular arrhythmias in normal subjects and patients with documented coronary artery disease. *Am. J. Cardiol.*, 1976;**37**: 609–616.
239. Froelicher, V.F., M.M. Thomas, C. Pillow, et al., Epidemiologic study of asymptomatic men screened by maximal treadmill testing for latent coronary artery disease. *Am. J. Cardiol.*, 1974;**34**: 770–776.
240. Blackburn, H., H.L. Taylor, B. Hamrell, et al., Premature ventricular complexes induced by stress testing. Their frequency and response to physical conditioning. *Am. J. Cardiol.*, 1973;**31**: 441–449.
241. McHenry, P.L., S.N. Morris, and M. Kavalier, Exercise-induced arrhythmia: Recognition, classification and clinical significance. *Cardiovasc. Clin.*, 1974;**6**: 245–254.
242. Jouven, X., M. Zureik, M. Desnos, et al., Long-term outcome in asymptomatic men with exercise-induced premature ventricular depolarizations. *N. Engl. J. Med.*, 2000;**343**: 826–833.
243. Jelinek, M.V. and B. Lown, Exercise stress testing for exposure of cardiac arrhythmia. *Prog. Cardiovasc. Dis.*, 1974;**16**: 497–522.
244. Goldschlager, N., D. Cake, and K. Cohn, Exercise-induced ventricular arrhythmias in patients with coronary artery disease: Their relationship to angiographic findings. *Am. J. Cardiol.*, 1973;**31**: 434–440.
245. Surawicz, B. and T.K. Knilans, *Chou's Electrocardiography in Clinical Practice: Adult and Pediatric*, 5th edn. Philadelphia, PA: W.B. Saunders.
246. Kotler, M.N., B. Tabatznik, M.M. Mower, et al., Prognostic significance of ventricular ectopic beats with respect to sudden death in the late postinfarction period. *Circulation*, 1973;**47**: 959–966.
247. Chiang, B.N., L.V. Perlman, L.D. Ostrander Jr, et al., Relationship of premature systoles to coronary heart disease and sudden death in the Tecumseh epidemiologic study. *Ann. Intern. Med.*, 1969;**70**: 1159–1166.
248. Coronary Drug Project Research Group, Prognostic importance of premature beats following myocardial infarction. Experience in the Coronary Drug Project. *JAMA*, 1973;**223**: 1116–1124.
249. Henry, R.L., G.T. Kennedy, and M.H. Crawford, Prognostic value of exercise-induced ventricular ectopic activity for mortality after acute myocardial infarction. *Am. J. Cardiol.*, 1987;**59**: 1251–1215.
250. Krone, R.J., J.A. Gillespie, F.M. Weld, et al., Low-level exercise testing after myocardial infarction: Usefulness in enhancing clinical risk stratification. *Circulation*, 1985;**71**: 80–89.
251. Waters, D.D., X. Bosch, A. Bouchard, et al., Comparison of clinical variables and variables derived from a limited predischarge exercise test as predictors of early and late mortality after myocardial infarction. *J. Am. Coll. Cardiol.*, 1985;**5**: 1–8.
252. Margonato, A., A. Mailhac, F. Bonetti, et al., Exercise-induced ischemic arrhythmias in patients with previous myocardial infarction: Role of perfusion and tissue viability. *J. Am. Coll. Cardiol.*, 1996;**27**: 593–598.
253. Marieb, M.A., G.A. Beller, R.S. Gibson, et al., Clinical relevance of exercise-induced ventricular arrhythmias in suspected coronary artery disease. *Am. J. Cardiol.*, 1990;**66**: 172–178.
254. Califf, R.M., R.A. McKinnis, J.F. McNeer, et al., Prognostic value of ventricular arrhythmias associated with treadmill exercise testing in patients studied with cardiac catheterization for suspected ischemic heart disease. *J. Am. Coll. Cardiol.*, 1983;**2**: 1060–1067.
255. Helfant, R.H., R. Pine, V. Kabde, et al., Exercise-related ventricular premature complexes in coronary heart disease: Correlations with ischemia and angiographic severity. *Ann. Intern. Med.*, 1974;**80**: 589–592.
256. Udall, J.A. and M.H. Ellestad, Predictive implications of ventricular premature contractions associated with treadmill stress testing. *Circulation*, 1977;**56**: 985–989.
257. Sami, M., B. Chaitman, L. Fisher, et al., Significance of exercise-induced ventricular arrhythmia in stable coronary artery disease: A Coronary Artery Surgery Study project. *Am. J. Cardiol.*, 1984;**54**: 1182–1188.
258. Schweikert, R.A., F.J. Pashkow, C.E. Snader, et al., Association of exercise-induced ventricular ectopic activity with thallium myocardial perfusion and angiographic coronary artery disease in stable, low-risk populations. *Am. J. Cardiol.*, 1999;**83**: 530–534.
259. Dimsdale, J.E., W. Ruberman, R.A. Carleton, V. DeQuattro, E. Eaker, R.S. Eliot, C.D. Furberg, C.W. Irvin Jr, A.P. Shapiro, et al., Sudden cardiac death. Stress and cardiac arrhythmias. *Circulation*, 1987;**76**(1 Pt. 2): I198–I201.
260. Pinski, S.L., The right ventricular tachycardias. *J. Electrocardiol.*, 2000;**33**: 103–114.
261. Podrid, P.J. and T.B. Graboys, Exercise stress testing in the management of cardiac rhythm disorders. *Med. Clin. North Am.*, 1984;**68**: 1139–1152.
262. Young, D.Z., S. Lampert, T.B. Graboys, et al., Safety of maximal exercise testing in patients at high risk for ventricular arrhythmia. *Circulation*, 1984;**70**: 184–191.
263. Saini, V., T.B. Graboys, V. Towne, et al., Reproducibility of exercise-induced ventricular arrhythmia in patients undergoing

evaluation for malignant ventricular arrhythmia. *Am. J. Cardiol.*, 1989;**63**: 697–701.

264. ACC/AHA guidelines for the management of patients with valvular heart disease: A report of the American College of Cardiology/American Heart Association Task Force on Practice Guidelines (Committee on Management of Patients with Valvular Heart Disease). *J. Am. Coll. Cardiol.*, 1998;**32**: 1486–1588.
265. Hochreiter, C. and J.S. Borer, Exercise testing in patients with aortic and mitral valve disease: Current applications. *Cardiovasc. Clin.*, 1983;**13**: 291–300.
266. Chandramouli, B., D.A. Ehmke, and R.M. Lauer, Exercise induced electrocardiographic changes in children with congenital aortic stenosis. *J. Pediatr.*, 1975;**87**: 725–730.
267. James, F.W., D.C. Schwartz, S. Kaplan, et al., Exercise electrocardiogram, blood pressure, and working capacity in young patients with valvular or discrete subvalvular aortic stenosis. *Am. J. Cardiol.*, 1982;**50**: 769–775.
268. Bonow, R.O., Management of chronic aortic regurgitation. *N. Engl. J. Med.*, 1994;**331**: 736–737.

37 Computer Analysis of the Electrocardiogram

Jan A. Kors · Gerard van Herpen

P. W. Macfarlane, A. van Oosterom, O. Pahlm, P. Kligfield, M. Janse, J. Camm (eds.), *Comprehensive Electrocardiology*, DOI 10.1007/978-1-84882-046-3_37,

This chapter deals with the use of digital computers for the handling of the resting ECG. The reader is referred to other chapters of this book for a review of computer-assisted interpretation of the exercise electrocardiogram, for ambulatory monitoring, on-line arrhythmia detection in the coronary care unit, and for surface mapping and modeling applications.

37.1 Some History

It is a deep rooted fantasy of man, told in many stories, to be able to handicraft a creature in his own image and endow it with the breath of life: a "homunculus." More often than not, the endeavor is initially successful but ends in disenchantment. The advent of the computer seemed to make it possible to equip such a creation with human intelligence. Electrocardiography appeared to be a field where the computer could be expected to deploy its intelligent capabilities to the best advantage.

The ECG was an attractive object for computerization for a number of reasons: (1) it is an electrical signal, easily recorded and easily digestible for a computer; (2) it is a rather simple, orderly and repetitive signal; (3) it carries important information about which a vast corpus of knowledge has been amassed to prime the computer program; (4) ECGs are produced in enormous quantities all over the world which makes it worthwhile to let a computer reduce human workload.

ECG diagnosis by computer would be an instance of artificial intelligence which might ultimately challenge the specific human faculty of diagnosis. When is artificial intelligence really intelligent? Turing devised a thought experiment to answer this question [1]. Suppose that a computer and a human being are sitting in separate closed chambers and that an outside investigator is questioning them. If the investigator cannot decide from the answers whether they are given by the computer or by man, then the computer has attained full human intelligence. This implies that the computer's diagnosis of the ECG must exactly copy that of man in order to satisfy this requirement. Indeed, the agreement between computer classification and man-made diagnosis of the ECG has been extensively studied. But how intelligent is man? Disagreement between computer and man might even be due to a computer's superior diagnostic power! A second approach in testing a diagnostic ECG program, therefore, had to be to gauge it against reality, the clinical diagnosis, and to compare its performance with the skills of the human reader in this respect. The outcomes of both approaches will be discussed later.

The first attempts to automate ECG analysis by computer were made as early as the late 1950s, but it took considerably more time to develop operational computer programs than had originally been anticipated. At that time, the analog electric computer dominated the field. Analog computers were being used in basic electrocardiographic research [2], but their impact on clinical electrocardiography remained insignificant and they soon disappeared from the scene [3]. To have an analog signal processed by a digital computer, it must be broken down into digital samples. However, analog-to-digital (A-D) conversion systems (see Chap. 12) were not available as they are today and a special purpose A-D conversion system for ECGs had to be developed first [4].

A very crude computer program for the separation of normal from abnormal records became operational in 1959 [5]. It was based on angles and magnitude of spatial ventricular gradients, calculated from the time integrals over one PQRST cycle in the three orthogonal leads. Cycle recognition was still obtained through analog circuitry. The beginning and end of P, QRS, and T were not identified in this simple screening program. The first automatic wave-recognition program became available in 1961, opening the way for more detailed analysis of ECG records [6]. This original program, as well as its successors developed by Pipberger and coworkers [7, 8], was based on the Frank XYZ leads for the main reason that three leads laid less claim to computer capacity, still very limited both in speed and in memory space, than 12 leads. Through the pioneering work of Caceres et al. [9] the first program for conventional 12-lead ECG analysis became available in 1962. It was supported by the US Public Health Service and intended to make expert ECG analysis immediately available to all who needed it, using the telephone system. The 12 ECG leads were transmitted sequentially and, therefore, had to be analyzed individually. The loss of context between the leads, together with inherent cable noise, caused considerable waveform recognition errors and the program came to an untimely end.

User satisfaction, indeed, was not won by these early accomplishments and the initial state of excitement was to give way to one of dogged perseverance. Fresh investigators were, according to their state of awareness, attracted by the seeming easiness or the proven difficulties of the subject. Commercial suppliers started to be active in this market [10]. Gradually, a number of operational systems came into being in North America, Europe, and Japan. In the bigger hospitals, main frame computers were installed, which received the ECG signals on tape from mobile carts and could store them in databases.

For the less well-equipped customers, ECG diagnosis via telephone was offered by all kinds of entrepreneurial services, which did a thriving business in the 1970s and 1980s, sometimes handling millions of ECGs a year [11, 12]. The scene changed completely with the advent of the microprocessor [13]. Microprocessor-based systems have made it possible to distribute computerized ECG analysis outside hospital and laboratory to even the smallest hospitals, to screening clinics and to practitioners of every kind. While it took minutes to process a single ECG on a main frame computer in the early years, a present-day simple PC takes a fraction of a second to do the analysis. Most of these electrocardiographs are "stand-alone," that is, have a computer and printer on board. Some manufacturers offer separate front-end equipment (amplifiers and A-D converter) that can be interfaced with the computer standing in the doctor's office.

With a widening choice of systems on the market, the consumer may wish to know how intelligent the system being considered for purchase is. But where can the consumer turn for an objective intelligence test? It is clear that objective assessment of the quality of computerized ECG systems is needed. We will return to this subject in later sections of this chapter.

37.2 ECG-Processing Computer Systems

37.2.1 Advantages

Although diagnostic accuracy and reliability are greatly desirable characteristics of an interpretation system, the program's utility in a clinical environment is also determined by other factors. Reduction of the labor spent by the cardiological and clerical staff has been a key determinant in moving toward computer-aided processing systems in hospitals [11, 14]; improvement of overall process quality has been another. Rigorous operational control, as imposed by a computer system, can substantially add to the recording quality and thus the reliability of interpretation. The quality of reporting is also improved through the use of standard terminology and formats.

Computer analysis abolishes the well-known subjective differences arising in visual interpretation, and through a quantitative approach may enhance correct classification. Pipberger et al. [15] have, since the early 1960s, pointed to improved accuracy of interpretation as the primary objective of computer ECG processing. Automatic storage and retrieval, with the possibility of comparing the new ECG with its predecessors (serial analysis) is another asset of computerized ECG processing.

Computerized analysis of the resting ECG has also increased the feasibility of large-scale cardiovascular screening and epidemiological studies. "Minnesota coding" of the ECG can nowadays be performed by computer, quickly and reliably (see Chap. 40).

37.2.2 ECG Management Systems

An ECG management system can come in several forms and undertake multiple functions. In its simplest form, it effectively acts as a database for storage of ECGs and offers straightforward retrieval of ECGs for display or printing. It could be in the form of a small PC, to which an ECG machine might be directly attached as might be found in a small family medical practice.

At the other extreme, a large ECG management system could be used to centrally store all ECGs recorded within a large hospital or group of hospitals. Such systems generally have the capability to store multiple ECGs for a single patient and thereby facilitate serial comparison either through visual display of several ECGs on the same monitor screen or through automated techniques (see Sect. 37.16). The large systems offer the user the ability to measure wave amplitudes, durations, and standard time intervals on an averaged ECG waveform, generally using digital calipers.

One of the major benefits of the larger systems is to allow editing, sometimes known as over-reading, of the automated interpretations. Generally, manufacturers provide facilities to assist with editing such as through acronyms to represent standard interpretative statements. In many environments, a physician will handwrite comments onto an automated report and a member of the administrative staff with appropriate knowledge can edit the changes on the ECG management system. A problem then arises if serial comparison is available on the system. In such a case, the original electronic copy

of the automated interpretation also has to be edited so that any subsequent serial comparison is made with the corrected report. This is actually quite a complex issue and one which can inhibit automated serial comparison.

Clearly, the ECG management system offers the facility for the provision of statistics on throughput of ECGs, number of edits made by each cardiologist, and so on. Nowadays, there is a trend toward manufacturers providing multiple databases for ECGs, echocardiograms, x-rays, etc., on a single server, but flexibility of editing and retrieving ECGs easily on an ECG management system still remains of significant importance in many healthcare environments.

37.3 Information Content of Lead Systems; Lead Transformations

In the analysis of biological signals in general, an enormous flow of information is channeled through a limited number of transducers. The often still redundant transducer output stream is then reduced and transformed to a manageable number of parameters. These in turn are harnessed into decision machinery, which finally summarizes the input information in a few standardized "diagnostic" terms that carry significance for the user and are the basis for further action. The ECG is such a biological signal.

The electrical activity of the heart gives rise to a three-dimensional time-varying distribution of currents and potentials. To obtain a full picture of this process, it is necessary to measure the complete course of potential distributions in and on the body. Only the body surface signals are readily available for measurement and even then the amount of information generated by the heart is so large that it is necessary to curtail the information stream for practical purposes. For the recording of a body surface potential map (BSPM), grids of 64–192 electrodes are being used (see Chap. 31). In this way, in a single BSPM all ECG information of that moment may be considered to be present as to localization. However, in a sequence of BSPMs, it is not feasible to follow all these individual electrocardiograms in their time course. For practical reasons, global parameters like "isointegral maps" or "isochrone maps" have to be used, and for diagnostic purposes, "difference maps" and "departure maps" have also been used. All this manipulation of data has only become possible, thanks to the computer, but so far clinical acceptance of BSPM diagnostic systems has been poor.

The universally used standard 12-lead ECG system needs nine electrodes, the three original Einthoven electrodes and the six thoracic electrodes adapted from Wilson. With the use of nine electrodes, eight independent leads, as they are called, can be obtained. The four extra extremity leads, which complete the 12-lead system, are not independent as they are arithmetically derived from any two other extremity leads. Nine electrodes are a drastic reduction of the number of sampling sites used to create a BSPM; the diagnostic power retained in this reduced lead set is indeed amazing. The explanation lies in the large degree of redundancy present in the surface information. Even among the eight leads of the standard ECG there is much redundancy and the question arises how many leads are actually required to render all relevant information.

In the vectorcardiogram (VCG), all information is contained in only three orthogonal leads, the X, Y, and Z components of a single dipole vector that changes with time in direction and strength, but is assumed to be stationary in position. Clearly, the three leads of the VCG (composed from a set of selected primary leads by linear combination) carry less information than eight leads, but, in return, the vector depicts the temporal relation between leads, providing phase information that is largely neglected in the ECG. Vectorcardiography could properly be called "phase electrocardiography." This feature makes up for the restriction on information input so that the diagnostic performances of the ECG and VCG are comparable, as will be discussed later on. Thus, each choice of data input, whether it be BSPM, standard ECG, or VCG, incurs the sacrifice of some information aspect: time resolution, phase coherence, or localization.

Presently, all ECG computer programs which are in clinical use will handle the conventional 12-lead system. Systems processing only the VCG have been driven from the market. The advantage that the VCG offers a data reduction of 8:3 has become insignificant considering the power of present-day computers. The clinical acceptance of the VCG has been hampered by the variety of different lead systems (from which the Frank lead system [16] emerged as the most commonly embraced), by a lack of understanding by clinicians of the physical principles, by the requirement of dorsal electrodes found to be cumbersome to apply, and finally by the absence, at the time, of proper recording equipment [17].

The question remains: how many leads are actually required to render all relevant information? It is of more than anecdotal value that Dower [18] let his ECG service only take vectorcardiograms. The ECGs that were then delivered to the hospital were derived from these VCGs by means of a mathematical transformation – apparently for many years to everybody's satisfaction. The inverse transformation yields the VCG from the standard ECG [19, 20], or, for better

adjustment, from the standard ECG fitted out with some extra electrodes [21]. Kornreich [22, 23] demonstrated that the ECG and VCG leave some clinically useful spaces on the surface map not covered by their electrodes. With a set of electrodes also serving these areas, nine leads were determined that yielded better diagnostic classification (using multivariate analysis) than either the VCG or ECG [24, 25]. Kors et al. [26] proposed a system containing the standard electrodes of which two chest electrodes were moved to positions higher up and lower down on the chest. From the seven not-displaced electrodes (4 chest + 3 limb) the 12 leads could be reconstructed by linear transformation in very good approximation. In fact, it was possible to compose any set of ECG leads with electrode positions chosen for local information density and ease of placement, standard or nonstandard, and from these leads derive the standard ECG by a mathematical transformation [27]. Computer analysis of such a "derived" ECG should give all but the same result as that of its directly recorded counterpart. The nonstandard extra recorded leads might then be exploited for additional information – with the difficulty that no standard diagnostic criteria are available for such leads. Even an entire BSPM can be simulated from a limited number of measured ECG leads.

The EASI lead system designed by Dower uses only four electrodes to produce the 12 standard ECG leads by linear transformation [28]. Four electrodes will yield three independent leads; four was also the number of electrodes used originally by Burger to derive the three orthogonal vector components [29]. Linear transformations were also used to reduce signal noise [30] and to identify interchanged leads [31]. The first to use a linear transformation in electrocardiography were Burger et al. [32] to transform VCGs obtained from different lead systems into those from each other.

For practical purposes, this review will be further restricted to computer analysis of the resting standard 12-lead ECG with some reference to the orthogonal 3-lead ECG. Some ECG processing systems have an option to display and print vector loops, either directly recorded from the regular (Frank) electrode positions or computed through linear transformation from the ECG leads. The reader is referred to Chap. 11 in this book for a review of other lead systems.

37.4 Computer Processing of the ECG

In teaching electrocardiography, and in order to start the novice reader on a career in electrocardiography, it suffices to say: "This is a QRS complex, this little wiggle in front is a P, and the hump following QRS is a T." Some more detailed descriptions are absorbed with equal ease and the final touch is added by the recommendations and guidelines for nomenclature and measurements as issued by various committees and task forces [33–36]. Reading the electrocardiogram is in the first place a matter of visual observation, if necessary, aided by calipers and magnifying glass, and relies on the amazing deftness in pattern recognition of the human brain. The subsequent electrocardiographic diagnosis is a logic built on correct pattern recognition. The computer must do without human "eye balling" skills and needs to be instructed punctiliously about every detail of measurement down to the microvolt and millisecond level. Rules and definitions for visual ECG analysis may then appear imprecise and not consistent enough for computer application, and may even show gaps in their logic. New computer-compatible prescriptions for ECG signal measurements should, however, adhere as much as possible to accepted methods of visual measurement [34]. In the sections on waveform recognition (37.12) and parameter computation (37.13) we will go further into the matter.

As in visual ECG analysis, in an ECG data-processing system, the first of the two main parts that can be distinguished is that which contains program components to perform measurements. The second part includes the program components that derive the clinical significance of these measurements. This results in a final classification, or interpretation, of the ECG in terms familiar to the physician. The words "classification" or "interpretation" are preferred by some over "diagnosis," which is then the term reserved for the human interpretative activity.

The principal components of the ECG measurement section are as follows:

1. Data acquisition
2. Preprocessing and signal conditioning
3. Detection of QRS complexes and of P waves
4. Typing of QRS complexes
5. Forming a representative (P)-QRS-T complex
6. Boundary recognition, that is, detection of points of onset and offset of waves
7. Parameter extraction

The principal components of the ECG interpretative section are:

1. Rhythm analysis
2. Diagnostic classification
3. Serial comparison

These separate program components will be discussed in detail in the following paragraphs. Many ECG processing systems implement these different tasks in separate modules, each of which has well-defined objectives [37]. The advantage of such a structured setup is its easy implementation, evaluation, and maintenance [38]. In addition, systems for clinical use will have to offer an over-reading facility, which allows manual correction of the computer output. A fixed set of codes, most commonly acronyms, takes care of producing the required text elements, thereby ensuring consistency of terminology. In addition, entries in free text are admissible.

To inform the consumer about the quality of a computerized ECG system, it is necessary to have access to reference standards for objective evaluation. A paragraph on reference databases will therefore precede the discussion of the various parts of computer processing mentioned above, since it will often be necessary to refer to these standards.

37.5 Reference Databases for Program Evaluation

"How to test the intelligence of the computer" was the question raised in the introduction of this chapter. The simple precept is to compare the computer statements with the objective "truth" embodied in the ECG readings of the human expert or the clinical findings. How to carry this out will be shown to be no simple matter.

Two qualities are to be considered separately in the operations of the computer program, namely, waveform recognition skill and diagnostic competence, with correct waveform recognition being a sine qua non for reliable interpretation. As to the first quality, large measurement differences may become apparent between programs while analyzing identical ECGs [39, 40]. As to the second aspect, where is it possible to obtain the diagnostic truth? Initially, a number of program designers compared the computer output with their own ECG interpretation [41]. Diagnostic criteria were identical for both. As could be expected, agreement between computer and human readers was excellent. It is obvious that not diagnostic accuracy but reliability of the wave-recognition and measurement parts of the programs was tested in these studies. For example, in the study by Crevasse and Ariet [42] a computer accuracy rate of 98% was reported for LVH. Both the computer and the human readers used the Romhilt-Estes point score. When this criterion was tested by the originators of this scoring system in 150 autopsy cases with LVH, they found a true accuracy of only 60% [43]. This is therefore the closest to "truth" that the computer could ever get on the strength of this criterion [8]. In other studies, computer results were compared to interpretations of human readers who used their own, individual diagnostic rules [44–47]. As had to be expected, percentages of disagreement rose sharply, reaching almost 50% in one early study [48].

Comparisons with ECG-independent clinical evidence were also carried out in due course [8, 49–53]. These investigations were mostly limited to one or two programs only. Moreover, they are difficult to compare since they utilized different databases, most of them collected within a single institute. More and more the need was felt for common, objective, impartial reference standards to test and improve different ECG computer programs [14, 54–58]. For this purpose, well-established test libraries are indispensable, together with well-defined measurement rules and evaluation procedures. On several occasions, this necessity was stressed, as at the first IFIP Working Conference on Computerized ECG Analysis [54] or in the editorial of Pipberger and Cornfield [15]. Detailed guidelines for program testing were presented at the 1977 Bethesda Conference on Optimal Electrocardiography [14].

In 1979, a concerted European action was started to develop "Common Standards for Quantitative Electrocardiography" (abbreviated: CSE). The CSE Working Party consisted of investigators from 25 institutes in Europe with the participation of investigators from six North-American and one Japanese center.

The CSE project was divided into two 5-year periods, the first dealing with measurements, the second with diagnostic interpretation [59]. The main objectives of the first part of the CSE project were, firstly, to establish standards for computer-derived ECG measurements, which implied agreement on definitions of waves and amplitude reference levels, and, secondly, to compare the results of measurements from different programs.

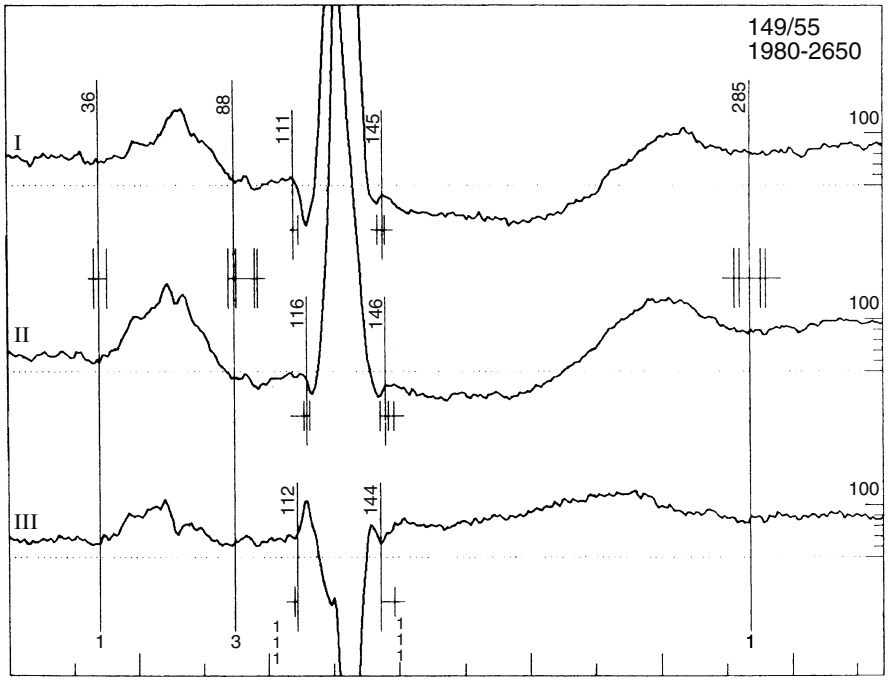

Figure 37.1

Example of wave boundary determination by five cardiologists (from Willems et al. [62]). The *short vertical lines* depict the individual, sometimes coinciding, referee estimates, the long ones the median results. The adjacent values denote the sample point locations relative to the onset of the recording window. The figures at the *bottom* of the *vertical lines* indicate the final reviewing round in which the estimates were obtained. Note that the onset of QRS in leads I and II is at a lower level than the onset of P, due to the presence of the atrial repolarization wave. In lead III the projection of this wave is isoelectric. Also, in lead III the T wave ends in an isoelectric segment. The observers disregarded this when they established T offset over the three leads simultaneously.

Thanks to this first CSE study, two reference databases came into being [60, 61]. They were composed of normal and a variety of abnormal cases. The first database [60] comprised 250 original and 310 so-called artificial ECGs. The recordings contain four lead groups of three simultaneously recorded leads each, as was common for most electrocardiographs at the time. From the original ECGs, companion artificial ECGs were constructed by concatenating one selected beat per lead group into strings of identical complexes. This artifice makes it possible to compare programs with different approaches for deriving a representative beat. To verify the effect of beat-to-beat variability, out of 30 original ECGs, two additional beats were selected to form an extra 60 artificial records. A group of five cardiologists determined the points of onset and offset of the various ECG waves (P, QRS, and T) on much enlarged tracings in an iterative, four-round, Delphi review process (Fig. 37.1).

The second database [61] comprised 250 original and 250 artificial ECGs in which all 15 leads – the 12 standard ECG leads plus the Frank XYZ leads – were recorded simultaneously. In view of the work load involved, the visual analysis strategy could not be repeated. Instead, the median wave-recognition results of 11 ECG and six VCG programs participating in the CSE study were taken as the reference. The cardiologists reviewed a random set of about 20% of the cases in a two-round process, and it was shown that the median of the program results was almost identical to the median results of the referees [61].

Both for the three-lead and multilead database, the original and corresponding artificial ECGs were divided over two sets. The waveform reference results of one set have been released [63, 64]; the results of the other set remain under lock and key at the CSE coordinating center for independent testing.

Differing mathematical algorithms may lead to similar solutions in pattern recognition [34]. For that reason, it was not seen as fitting to propose any specific algorithm as the exclusive standard for ECG wave recognition. At the same time, the CSE reference databases are strongly recommended as a bench mark for ECG measurement programs. Comparison with the standard involves two quality measures: a program should approach the reference as closely as possible, and the standard deviation of the differences of its results with respect to the reference should not exceed certain limits. These limits have been described in detail in a paper with recommendations for measurement standards in quantitative electrocardiography [34].

The second part of the CSE project aimed at the assessment of the diagnostic performance of ECG computer programs. This study commenced in 1985 and finished in 1990. A database consisting of 1,220 multilead recordings was collected, comprising seven diagnostic groups: normal (n = 382); left (n = 183), right (n = 55), and biventricular (n = 53) hypertrophy; and anterior (n = 170), inferior (n = 273), and combined (n = 73) myocardial infarction. Also some cases with both infarction and hypertrophy (n = 31) were included, but ECGs showing major intraventricular conduction defects were not. The clinical diagnosis was documented by ECG-independent evidence, such as cardiac catheterization, coronary arteriography, echocardiography, cardiac enzymes, and patient history [65]. The ECGs and VCGs were analyzed by 15 computer programs and by nine cardiologists, from seven European countries [66]. Evaluation results will be discussed later.

The CSE reference libraries have become an international standard for the evaluation and improvement of ECG and VCG computer programs. A comprehensive overview of the CSE project appeared in 1990 [59].

37.6 Data Acquisition

Before the ECG signals are transmitted to a computer system for analysis, the operator has to enter patient identification data. The patient's name, sex, and date of birth together with an identification code are essential for proper automatic handling of the ECG data. Data like weight, height, blood pressure, and medication might be useful – if they are not based on guess-work by a lackadaisical technician! The system will also store the time and date of the recording, as well as, mostly, a technician and location code. For programs that perform serial ECG analysis, the unique patient identification code is indispensable for record linking.

In order to achieve optimal performance of an ECG-processing system it is essential that the data used in the analysis are of good quality. In practice, ECG records can be disturbed by power line interference, baseline wander caused by electrode polarization, electromagnetic muscle artifacts, spikes, sudden baseline shifts due to electrode contact interruption, and amplitude saturation. Although automated systems can achieve a great deal of signal conditioning (see the following paragraphs), it devolves upon the operator to correctly apply the electrodes and to detect and remedy signal errors and disturbances before entering them in the system, according to the maxim "garbage in, garbage out." Power-line interference can be prevented or reduced by proper shielding and grounding, by appropriate skin preparation and electrode application. Muscle tremor can be reduced or removed by having the patient comfortable and relaxed, while respiratory baseline wander can be minimized by breath holding.

The front-end of an ECG processing system consists of analog amplifiers. Present-day technology even allows them to be incorporated in the electrodes and to transmit the signals by a local wireless system to the processing unit. The amplifiers must be of adequate bandwidth for a faithful rendering of the signals. For further technical details, the reader is referred to Chap. 12.

A digital computer can handle data only in numerical form, and therefore, the original continuous (or analog) voltage variations of ECG signals need to be converted into a series of numbers, corresponding to the voltage levels of the leads at any moment of time. General principles concerning analog-to-digital (A-D) conversion of the ECG have been reviewed by Berson et al. [67, 68]. The time and amplitude resolution of the A-D conversion is dependent on the sampling rate, the word size of the converter and the dynamic range of the analog input.

Sampling rates for ECG data in various programs originally varied from 250 to 500 samples per second. The American Heart Association [69] and the CSE Working Party [34] have recommended for clinical application a high-frequency cutoff of the analog amplifiers of 150 Hz and a sampling rate of 500 Hz for the A-D conversion. In the pediatric ECG, the waves, especially the QRS, are of shorter duration at often elevated voltage which results in high rates of acceleration and deceleration of the signal with corresponding high frequency content. This requires an extension of the minimal high-frequency cutoff to 250 Hz [70].

The more bits per word in an A-D converter, the greater the possible resolution. In addition, the dynamic range of the amplifiers must be wide enough to accept the largest possible excursion of the signal amplitude. Modern electrocardiographs have 16 or 18 bit converters, with quantization levels of 1.22 μV–4.88 μV for the least significant bit.

Until the introduction of "stand-alone," microprocessor-equipped systems for ECG analysis, ECG records needed to be transmitted to a central computing facility. This was possible by transferring magnetic tapes on which ECGs were recorded, or by sending the signals on-line over ordinary telephone lines. This involved frequency modulation and demodulation which noticeably contributed to recorder noise. In the present digital era, the total analysis of the ECG can be done on a stand-alone electrocardiograph. The central ECG management system is required for storage and retrieval, a necessary utility for serial analysis; as well as for providing a means of editing interpretations. Interchange with the central facility may occur through a local area network, possibly by wireless transmission, or the ECGs are conveyed on some digital storage medium.

In the acquisition device, all 12 leads are acquired simultaneously so that time coherence between the signals is preserved. In practice, eight independent leads are recorded (I, II, VI-V6) and the other four are reconstructed from leads I and II using the classical relations such as lead III = II − I. In some systems, additional leads may be entered simultaneously for the VCG or for other purposes. The signals are stored in memory and can be displayed for a visual quality check. The computer may interact with the operator and warn of excessive noise in a lead or indicate electrode reversal. Reversal between right and left arm is detected by most programs. Other forms of electrode interchange require more sophisticated approaches [31, 71]. After approval by the operator, the signals are processed.

While the electrodes may have been placed in the correct order, without interchange, they still may be ill-positioned, for example, one interspace too high or too low on the chest. These errors are almost refractory to detection and correction [72, 73].

Conventionally, 12-lead ECGs were presented on multichannel writers in four lead groups of 2.5 s, often with a 10.0 s rhythm strip, on one page. Sometimes 5.0 s was taken per lead group, requiring two pages, or 6-channel writers were used. With the entire ECG present in memory and the availability of a thermal writer or laser printer, a modern device will allow considerable flexibility of output format. The signals, in addition, are preprocessed by digital techniques in such a way that mains interference and baseline drift have been reduced to a minimum to produce a neat paper output.

37.7 Signal Preprocessing and Conditioning

ECG records may be disturbed by different types of artifacts as enumerated previously, namely, power-line interference, baseline wander, muscle noise, spikes, and amplitude saturation. The aim of the preprocessing stage is to detect and correct these artifacts as far as possible. In hopeless cases, rejection of a part or the whole of the recording may be inevitable. The problems of signal improvement have been a challenge to many capable technical minds and have resulted in an abundant literature on the subject. Some of the algorithms require that the locations of the QRS complexes are known, and thus are not properly part of the preprocessing stage. This will be mentioned when the case occurs. The evaluation of the performance of these algorithms applied to real ECGs is not straightforward since the undisturbed signals are unknown. This may in particular be an issue in treating baseline wander and muscle noise. A common approach to studying the problem is to add simulated noise to a clean, "noise free," ECG signal. This approach can be carried one step further by simulating both noise and signal. As with all simulations, the validity of the evaluation results will depend on how well the simulated signals mimic those that occur in practice.

37.7.1 Power-Line Interference

Power-line interference is a common problem and is characterized by its periodicity of 50 or 60 Hz (higher harmonics may also be observed). Different digital filters have been proposed for the removal of power-line interference [74, 75]. They can be categorized in three types:

1. Notch filters, which attenuate frequencies in a narrow frequency band around the interference frequency [76, 77].
2. Global filters, which make a single estimate of the interfering noise over the total duration of the signal and then subtract this estimate from the signal. Cramer et al. [75] describe two such global approaches. One is based on a least-squares error fit of the interference. The other approach requires the sampling rate to be an integer multiple of the power-line frequency, say n, and calculates an average amplitude for each of the n phase points in one period of the interference. Both approaches only perform well if the line frequency is stable within 0.02 Hz of the nominal frequency [75], which in practice may often not be the case. Also, these methods, by definition, cannot adjust to amplitude changes of the interference. Levkov et al. [78] proposed estimating the interference from each isoelectric or slowly changing part of the ECG signal, which allows tracking of interference amplitude changes. To ensure that the sampling rate was an integer multiple of the power-line frequency, they used a hardware-synchronized A-D converter. More recently, a software solution to adjust for interference frequency variation was proposed, involving estimation of the interference period and resampling of the ECG signal [79]. An extensive review of the method is given by Levkov et al. [80].
3. Adaptive filters, which use an auxiliary reference signal containing the interference alone [74, 81–83]. This reference is adaptively filtered to match the interfering sinusoid as closely as possible, and is then subtracted from the primary signal. An interesting variant of the classical adaptive filter approach is the "incremental estimation" filter proposed by Mortara [84] and further investigated by others [74, 85–87]. The filter generates a prediction of the power-line interference $v(n)$ contained in the signal $x(n)$, based on the noise estimate $w(n)$ at the previous two samples:

$$v(n) = 2\cos(2\pi f/f_s)\, w(n-1) - w(n-2),$$

with f the nominal frequency of the interference and f_s the sampling rate. If $v(n)$ is a good prediction, then the difference $x(n) - v(n)$ should be zero apart from a possible constant offset. Assuming a slowly changing signal, the difference $x(n-1) - w(n-1)$ is taken as an estimate of this offset, and the error

$$e(n) = (x(n) - v(n)) - (x(n-1) - w(n-1))$$

indicates how well $v(n)$ predicts the interference amplitude. A final estimate is then produced by incrementing or decrementing the value of $v(n)$ with a fixed amount δ, depending on the sign of $e(n)$:

$$w(n) = v(n) + \delta \mathrm{sgn}(e(n)).$$

Finally, the output $y(n)$ of the filter is

$$y(n) = x(n) - w(n).$$

The value of the increment δ is chosen heuristically. A value which is too small may cause sluggish adaptation to the interference amplitude and poor tracking of its changes. A value which is too large, on the other hand, may cause the estimate $w(n)$ to jitter around the power-line interference, introducing extra noise. Also, since the assumption of a slowly changing signal does not hold true for the QRS complex, large increments will result in ringing artifacts. An incremental value of 1.25 μV was proposed by Mortara [84]. Using a few simplifying assumptions, Talmon [85] analyzed the relationship between the amplitude of the sinusoidal disturbance, the increment, and the bandwidth of the filter. Glover [88] showed that the filter reduces to a standard notch filter if the nonlinear sign function in the update equation is replaced by a linear increment function.

A number of different filters, representative of the above filter types, were compared by McManus et al. [74]. They applied the filters both to artificial test signals simulating various forms of interference (including second and third harmonics of the nominal frequency), and to a small subset of real ECGs from one of the CSE databases. Tested against a list of 14 desiderata for an ideal interference filter, no single filter consistently performed better than the others for all requirements. Remarkably, the incremental estimation filter and the global filter were the only ones that did not produce a ringing effect at the end of the QRS as is the usual accompaniment of large-amplitude QRS complexes when filtered, as illustrated by Fig. 37.2. In another study [87], the incremental estimation filter was compared to a nonadaptive second order notch filter. The better transient behavior of the adaptive filter produced less distortion in the ST segment and removed the interference more effectively.

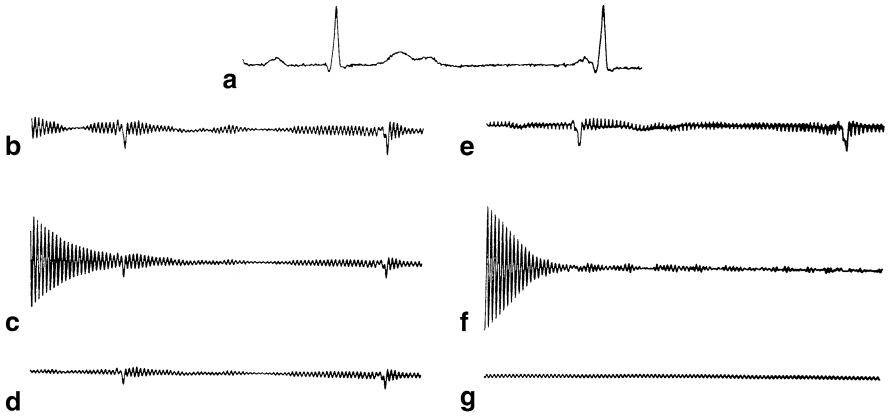

Figure 37.2

Effects of different interference removal filters on an ECG, which has no interference: (a) original ECG, and tenfold magnified differences between filter-input and output of two notch filter methods (b and c), three adaptive methods (d, e, and f; f is the incremental estimation filter), and a global method (g). Several filters can be seen to generate sizable differences during the QRS complex (From McManus et al. [74]. © Elsevier. Reproduced with permission).

37.7.2 Baseline Wander

Baseline wander is another annoyance. The source of low-frequency fluctuations of the baseline may be sought in changing electrode impedances, such as caused by respiratory movement. More abrupt changes may result from the patient being restless. The frequency content of baseline wander is typically less than 0.5 Hz. Baseline wander may severely disturb ECG beat morphology. A variety of techniques for estimating and removing baseline wander has, therefore, been developed.

In the 1975 recommendations of the American Heart Association (AHA) [89], for baseline wander removal a standard 0.05 Hz single pole high-pass filter was advised. While such a filter largely avoids the problem of phase nonlinearities, it does very little to suppress the baseline wander that can typically be observed in ECGs. In their 1990 recommendations, the AHA stipulated that a baseline removal filter should have a flat amplitude response within 0.5 dB from 1 to 30 Hz, with a −3 dB cutoff frequency of less than 0.67 Hz, and should adhere to certain test criteria based on triangular and rectangular wave impulse responses [69, 90].

A general problem in the evaluation of baseline correction methods is the difficulty in discriminating between baseline wander and the genuine ECG [85, 91]. Most studies only provide a qualitative assessment, showing ECGs before and after application of a correction algorithm. In a few studies, artificially generated baseline wander is added to "clean" ECGs constructed by concatenating identical beats [92, 93]. Since baseline correction may introduce new distortions, several algorithms try to identify periods with minimal or no baseline wander and skip these periods in the filtering [85, 93, 94].

Two main remedial approaches have been followed:

1. Interpolation.

Linear interpolation approximates the baseline by straight-line segments between isoelectric levels, usually estimated from the intervals preceding QRS onset [85, 94]. The estimated baseline is subsequently subtracted from the ECG signal. Boucheham et al. [95] proposed a piecewise linear correction based on "dominant" points as detected by a curve simplification algorithm [96]. An interesting feature of their algorithm is its capability to correct for sudden baseline shifts.

A more elaborate interpolation method estimates the baseline by a third-order polynomial, or cubic spline [97]. Each PR segment provides a "knot" through which the cubic spline must pass. Meyer [97] described an elegant and fast state-space approach for the computation of the cubic splines.

Talmon [85] compared the linear interpolation and cubic spline methods on a set of real ECGs, and concluded that both approaches performed similarly. Linear baseline correction, however, is to be favored because cubic spline correction is more difficult to apply in the presence of sudden baseline shifts.

Since all interpolation methods assume that reference points or knots can accurately be determined, they may break down if this assumption is not met, for example, in the case of a premature beat merging with the preceding T wave [98–100]. Performance may also degrade at lower heart rates as the knots become more separated.

2. High-pass filtering.

Infinite impulse response (IIR) filters are generally unacceptable due to their nonlinear phase response, which may induce distortions in particular in areas of the ECG where amplitudes change abruptly [90]. However, in off-line situations, or if some time delay between acquisition and processing of the signal is accepted, forward-backward or bidirectional filtering can be applied [100, 101], yielding overall linear-phase response [102]. Alternatively, De Pinto [103] proposed a linear-phase high-pass filter. He subtracted the output of a linear phase low-pass IIR filter from the original signal with a delay equal to the pass-band group delay of the low-pass filter. The filter was shown to adhere to the 1990 AHA recommendations.

Linear phase filtering is easily accomplished with finite impulse response (FIR) filters. However, these filters typically have very long impulse responses, resulting in many multiplications and long time delay [91, 104], which may be unacceptable for short-term resting ECG recordings. Van Alste et al. [104] proposed an FIR filter that combines removal of baseline wander with that of power line interference, and greatly saves on the number of computations. QRS complexes may heavily influence the baseline estimate. This may cause a shift of the assumed baseline with respect to the true one, resulting in measuring errors especially in diagnostically sensitive low-frequency segments such as the ST segment. Sörnmo et al. [92] described an approach in which the QRS complexes are removed prior to filtering the signal by one of a bank of linear low-pass filters with variable cut-off frequencies. The method was tested on ECGs with different types of simulated baseline wander and showed superior performance as compared to standard high-pass filtering or cubic spline interpolation (Fig. 37.3), especially when the baseline wander contained frequencies >0.5 Hz. It must be noted that the method requires that beat classification is performed prior to correction, to minimize the effects of ectopic beats.

A two-step method combining interpolation and filtering techniques was proposed by Shusterman [93]. First, the magnitude of baseline wander is determined and classified as small or large. If large baseline drift is present, the signals are filtered with a bidirectional high-pass filter with a cut-off that depends on the estimated frequency content of the baseline wander. In a second step, any residual, small baseline wander is removed by simple linear interpolation between PQ and TP segments.

A two-stage cascade filter was described by Jane et al. [105]. First, a high-pass notch filter is applied with a cut-off frequency at 0.3 Hz [83]. Any remaining baseline contamination at higher frequencies is then removed with an adaptive impulse correlated filter. The reference input consists of a sequence of unit impulses correlated with the QRS complexes. This filter was shown to be equivalent to an exponentially weighted average [106] and requires a QRS detector. It also removes other disturbances not correlated with the QRS complex, such as muscle noise or line interference. When tested on a few records of the MIT-BIH database [107], the filter was shown to perform better than cubic spline correction.

Park et al. [108] described a wavelet adaptive filter. The filter consists of two parts. A wavelet transform decomposes the ECG signal into seven frequency bands. The signal of the lowest frequency band (0–1.4 Hz) is then fed into an adaptive filter. The wavelet adaptive filter was compared with a "commercial standard filter" with a cutoff of 0.5 Hz and with a general adaptive filter. Using test data from the MIT-BIH and the European ST-T [109] databases, the wavelet filter was shown to perform better than the other two filters, especially with respect to distortion of the ST segment. When tested on a triangular wave, as recommended by the AHA, the wavelet filter showed negligible distortion of the ST segment, whereas the standard filter and the adaptive filter produced severe distortions.

Finally, nonlinear filtering methods for baseline correction have been proposed [110]. Sun et al. [111], building on earlier work of Chu and Delp [112], described an approach using morphological filtering, a technique widely used in the field of image processing [113]. Testing on simulated ECG signals, they compared their approach with the wavelet adaptive filter [108] and found morphological filtering to produce better results.

Figure 37.3

Example of baseline wander removal. (a) Original ECG, and resulting signal after baseline wander removal using (b) time-varying filter with beat subtraction, (c) time-varying filter without beat substraction, (d) time-invariant filter, and (e) cubic spline interpolation (from Sörnmo [92]. © Springer).

37.7.3 Muscle Noise

Muscle noise, another signal deformity, is caused by the electrical discharges of skeletal muscles. Common causes are patient restlessness, nervousness, cold shivers, and Parkinson tremor. Reduction of muscle noise is often effected by one of the other tasks in ECG signal processing as, for example, when the ECG signal is band-pass filtered for the purpose of QRS detection. Since most of the energy of the QRS complex is contained in the frequency band from 10 to 25 Hz, noise components outside the pass band can effectively be suppressed. For P-wave detection, even stronger noise reduction is possible because the frequency content of the P wave is lower. In these applications it is unnecessary to keep the original signal undistorted. For accurate amplitude and duration measurements, however, the requirement is to improve signal-to-noise ratio (SNR) without loss of signal information.

A common method to reduce muscle noise is coherent averaging. ECG complexes of one family are summed and the sum is divided by their number, giving an averaged ECG complex while uncorrelated noise averages out and disappears. Coherent averaging is one way of improving the SNR, as will be discussed later.

A number of other noise reduction techniques have been proposed. Adaptive filtering for muscle noise suppression was described by Thakor and Zhu [83]. To cancel the noise in a particular lead, they proposed employing, as a reference signal, another lead perpendicular to the first, in order to ensure that the noise in the two leads is uncorrelated.

Talmon et al. [114] describe an adaptive Gaussian filter, based on earlier work of Hodson [115]. The frequency characteristics of the filter are dependent on the estimated curvature of the signal to be filtered. A curvature estimate is obtained by fitting a polynomial function. The width of the filter is then adjusted according to the curvature, where low curvature (e.g., in the PR interval) implies a low-frequency cutoff, and a high curvature (e.g., in the QRS complex) a cutoff at higher

frequencies. A related approach is proposed by De Pinto [103], who describes a low-pass filter with time-varying bandwidth. The bandwidth is maximal during the QRS complex, and decreases in the interval between QRS complexes. The bandwidth is varied in increments by selecting one of six sets of coefficients, controlled by an estimate of the slope of the ECG signal.

Another approach, termed noise consistency filtering, was initially proposed by Mortara [30] and later investigated by Wei et al. [116]. This filter method requires the availability of multiple, simultaneously recorded leads, and exploits the redundancy in the ECG signals. Reconstruction coefficients are determined to synthesize each of the eight independent ECG leads from the remaining seven leads. The filter output is the original lead signal multiplied by a time-varying coherence measure with a value between 0 and 1, dependent on the correspondence between the predicted and the original signal. The lower the coherence, the stronger is the filtering, and vice versa. The filter was reported to reduce noise by a factor of 10, provided the noise in the leads is uncorrelated [30].

Wei et al. [116] proposed two modifications to the filter as it was described by Mortara. Firstly, to avoid problems with baseline wander, the signal is split into a low-frequency and a high-frequency part, and only the latter is filtered according to the source consistency method. Secondly, a modified coherence measure is used, to reduce unwanted filtering effects that were observed by the authors. The modified filter performance was verified on simulated and real ECG signals, and compared with the original source consistency filter and conventional low-pass filters. Results show more effective noise suppression and less distortion of the QRS complex with the modified filter.

More elaborate filtering methods, involving the discrete cosine transform and singular-value decomposition, have been described by several investigators [117–119]. These approaches are computationally demanding and were mainly developed for the suppression of excessive muscle noise during exercise testing.

Finally, several studies used morphological filtering for muscle noise suppression [110–112]. Morphological filtering was also employed to detect muscle noise, without attempting to suppress it [120].

37.7.4 Spikes

Spikes are sudden pulses of short duration and high amplitude. They may be due to an interfering electrical source in the environment or to an implanted artificial pacemaker.

Accurate pacemaker spike detection has become increasingly important with the growing population of patients with implanted pacemakers. Because of the small spike width, in the order of 0.2–0.5 ms, many electrocardiographs use high-bandwidth front end amplifiers and analog circuitry to detect pacemaker spikes before A-D conversion. To reduce the number of false detections that this approach may induce, it has been combined with software algorithms that must confirm the presence of the spikes in the diagnostic bandwidth (0.05–150 Hz) signals. Alternatively, signals have been sampled at very high frequency, of the order of several kHz, and then software is used to detect the spikes.

Only a few algorithms have been described that attempt to detect spikes in diagnostic bandwidth signals. As these signals have been sampled at no more than 500 Hz; one may wonder how it is possible to detect pulses that have a duration well below the sampling interval. The reason is that the anti-aliasing low-pass filtering broadens the spikes. However, this filter also greatly reduces the amplitude of the spikes, which makes detection more difficult. The presence of narrow QRS complexes mimicking spikes, high-frequency noise and other artifacts further complicates the detection task.

The Louvain VCG analysis program [121] used a simple spike detector: if the spatial velocity exceeds a fixed threshold, a spike is assumed to be present [122]. In the AVA program [123] a number of tests based on slope differences between four consecutive points (8 ms) in a single lead were performed to detect spikes or discontinuities in the input signals [122]. No evaluation of these methods has been given.

Talmon [85] described a spike detector that operates in two stages. First, signals are filtered with a parabolic filter and the root-mean-square (RMS) of the residuals is computed. If the residual at a certain time instant exceeds three times the RMS value in that signal, a potential spike is assumed to be present. In a second stage, an additional number of criteria, structured in a decision tree, are tested to verify whether a spike has truly been detected. The algorithm was tested on an independent test set of 1,908 ECGs and VCGs, showing a sensitivity of 90.9% and a positive predictive value of 95.4%.

Helfenbein et al. [124] proposed another pacemaker spike detector. The algorithm detects a spike if a steep slope exceeding a threshold is followed by an opposite polarity slope within a short time window. The threshold is adaptive and computed as a function of the maximum slope in a window preceding the spike. When tested on a set of 1,108 adult ECGs

containing a variety of pacemaker types and modes, excellent performance (sensitivity 99.7%, positive predictive value 99.5%) was obtained. On another set of 1,382 non-paced pediatric ECGs, only four false-positive QRS complexes were reported.

37.7.5 Amplitude Saturation and Sudden Baseline Shifts

No substantial literature is available dealing with the detection of amplitude saturation and sudden baseline shifts. In descriptions of various ECG processing systems, a statement is made that these artifacts are searched for, but the algorithms are not described.

37.8 Detection of QRS Complexes

The detection of QRS complexes is probably the most extensively studied problem in ECG signal analysis [86, 125–131]. A host of different algorithms has been proposed, most of them originating from applications in the fields of coronary care monitoring and Holter recording. Consequently, many of these QRS-detection algorithms were designed to operate on a single lead. In computerized resting ECG and VCG interpretation, three simultaneously recorded leads were used from early times. Now, multiple simultaneously recorded leads have also become increasingly common in the non-resting ECG.

Basically, a QRS detector consists of two stages [132]: a preprocessing stage, in which the signal is filtered and signal features are determined, and an identification stage, in which a decision is made about the presence and location of a QRS complex. Algorithms are commonly distinguished with respect to their preprocessing stages.

An extensive survey of single-lead QRS-detection algorithms is given by Kohler et al. [130]. The most common approaches are based on high-pass and band-pass digital filters, but many other approaches have been proposed, based on wavelet transforms [133, 134], artificial neural networks [127, 135], and genetic algorithms [136]. Some algorithms [137, 138] employ techniques from syntactic pattern recognition, but it has been difficult to demonstrate the practical utility of this approach [139].

In the multiple-lead algorithms, the simultaneous leads are transformed to a detection function. The transformation brings out the QRS complexes amongst the other parts of the signal, in order to increase the QRS detection rate. One of the most commonly used transformations is the computation of the spatial velocity of the VCG or of a similar derived function for the 12-lead ECG. The spatial velocity (SV) is defined as:

$$SV(n) = \sqrt{\sum_{k=1}^{3} (d_k(n))^2}$$

where $d_k(n)$ denotes the first derivatives of the VCG leads X, Y, and Z. Various difference equations have been proposed to approximate the derivatives [130]:

$$d(n) = x(n+1) - x(n-1);$$
$$d(n) = 2x(n+2) - x(n+1) - x(n-1) - 2x(n-2);$$
$$d(n) = x(n) - x(n-1).$$

In the case of the 12-lead ECG, the VCG leads can be reconstructed from the ECG leads by linear transformation, or approximated by a quasi-orthogonal set of ECG leads [140]. Alternatively, a pseudo-SV has been computed by combining the derivatives of all ECG leads.

The detection signal is then gauged against a threshold to detect the occurrence of a QRS complex. The threshold may be fixed, but more commonly is adaptive, changing with varying signal characteristics [140–142]. Some algorithms also require that the detected QRS complexes fulfill certain amplitude constraints. Other algorithms compute a second derivative,

$$d^2(n) = x(n+2) - 2x(n) + x(n-2),$$

and use a combination of first and second derivatives as the detection function. Balda et al. [143] used the sum of the absolute first and second derivatives over three simultaneous leads. This detection function was called the "waveform boundary indicator" as it also provided an estimate of the onset and the end of QRS complexes. A single-lead implementation of the method was given by Ahlstrom and Tompkins [86].

Once a potential QRS complex is detected, most of the algorithms apply further heuristic criteria to exclude false-positive detections, for example, by requiring a minimum time lag between adjacent QRS locations [140]. Laguna et al. [144] apply a single-lead detection algorithm to each of a set of simultaneously recorded leads, and then enter into a decision process comparing the detection positions over all leads to decide which detections are true or not.

An inventory of different methods used in seven VCG and eight ECG programs can be found in the second progress report of the CSE project [122]. However, only few developers of these ECG computer programs have published detailed evaluation results of their detection algorithms. On a set of 2,889 QRS complexes from the CSE multilead library, Kors et al. [140] found no false positive or false negative detections at all. Contrasting with the parsimonious communications on multilead QRS-detection algorithms, performance results for single-lead algorithms have been reported in fair abundance (see [130] for an overview). Many of these algorithms were evaluated on (part of) the MIT-BIH arrhythmia database, and achieved excellent results (>99% sensitivity and positive predictive value) [130]. A comparative study on noise sensitivity of nine single-lead QRS-detection algorithms for five different types of noise also indicated very good detection performance of most algorithms for all but the highest levels of noise [126]. In general, considering that the multiple leads of the standard 12-lead ECG offer redundancy of information and that noise levels in the resting situation are typically less troublesome than under monitoring conditions, it may be concluded that near-perfect QRS detection in the resting ECG is feasible.

37.9 Detection of P Waves

Detection of the P waves remains one of the most difficult tasks in automated ECG analysis. Failure of P-wave detection will jeopardize the rhythm interpretation program. Problems may arise owing to low amplitude, variable morphology and diverse timing of P waves. A P wave superimposed on a T wave, and even more so, a P wave that coincides with a QRS complex, are difficult to distinguish in surface ECGs (Fig. 37.4). Their probable location can only be extricated by considering the sequence of the preceding and following P waves and by recognizing small irregularities in the expected contour of QRS or T. This requires long and continuous recordings. Even then, problems remain in deciphering morphology and polarity. While P-wave detection on surface ECG leads may already pose problems to the eye of the cardiologist,

Figure 37.4
ECG showing an AV dissociation, with one P wave superimposed on a T wave and another P wave merging into a QRS complex.

more problems await the computer programmer working in this field [145]. The human ability to recognize even low-voltage P waves hidden in other waves and amidst noise and artifacts is indeed still far superior to the performance of all presently available ECG wave-recognition programs.

Different approaches with respect to automatic detection of P waves have been described in the literature. Stallman and Pipberger [6] applied a threshold approach to the smoothed spatial velocity curve. McManus [146] has worked further on this method. Bonner and Schwetman [147] used a piecewise approximation of the ECG, followed by tests on level crossings and slope changes. A two-stage detection method was introduced by Hengeveld and Van Bemmel [148], and later on refined by Talmon [85]. First, QRS-linked P waves are searched for, based on histograms of local signal extrema in the intervals preceding the QRS complexes. If they are not found, non-QRS-linked P waves are sought by cross-correlation of signal amplitudes with an empirical P-wave template. Schnyders and Jordan [149] applied an energy correlation technique on the 12-lead ECG with apparently good results. Martinez et al. [131] proposed a wavelet-based P-wave detector. Once the location of the QRS complex is found, local maxima in the wavelet transform of the higher scales (i.e., in the lower frequency bands) are sought in an RR-dependent search interval. If at least two local extrema exceed a certain threshold, a P wave is considered present. Gritzali et al. [150] used as a detection function the length transformation of a signal, which essentially is the length of the signal curve within a time window. The length transformation can be defined for more than one lead by adding the curve lengths of the individual leads. Simple thresholding of the transformation is used to detect the P waves, as well as their onsets and ends.

It can be very difficult to distinguish P waves from flutter waves. In the presence of 2:1 AV block it may be hard, even for a human observer, to choose between flutter and sinus tachycardia. In various programs, separate routines are applied to determine whether atrial flutter waves are present [37, 141]. Talmon et al. [151] described a method that detects the periodic components characteristic of flutter waves (Fig. 37.5). After appropriate filtering and removal of the QRS complexes, the resulting signal is autocorrelated. Flutter waves are assumed to be present if the autocorrelation function has a sufficiently large local maximum at a lag between 150 and 300 ms (corresponding with flutter rates between 200 and 400/min) and a second local maximum at twice the lag of the first maximum. A sensitivity of 86% and a specificity of 99.9% were reported. Taha et al. [152] employed a QRST subtraction technique and spectral methods to distinguish between atrial flutter, atrial fibrillation, and other rhythms. They obtained a sensitivity for flutter of 80%, at a specificity of 98.7%. Giraldo et al. [153] tried to detect the boundaries of atrial flutter and fibrillation waves, and used the coefficient of variation of the wave amplitudes to distinguish between flutter and fibrillation. They tested their approach on 40 short signal segments with flutter or fibrillation from the MIT-BIH database, but did not include segments with other heart rhythms in their analysis. Christov et al. [142] propose an atrial flutter-fibrillation parameter that is the mean value of the filtered and rectified signal, after subtraction of QRS-T complexes. On a test set, they obtained 76% sensitivity for flutter and fibrillation combined, at 97.9% specificity.

The detection rate of P waves varies according to the different algorithms that are applied. McManus [146] reported failures from 0–3%. For the 250 ECGs in the multilead CSE library [61], Kors et al. [140] obtained a sensitivity of 98.1% and a positive predictive value of 99.9%. Oversensitive methods cause difficulties in cases with atrial fibrillation. In the AVA program [123], as well as in several other programs, a P-wave search is only performed in an interval between the end of the T wave and the onset of QRS. In addition, only one P wave can be detected per QRS complex, which practically excludes the diagnosis of AV block or AV dissociation with an atrial rate higher than the ventricular rate. Programs that do attempt to detect more than one P wave per cycle have not reported detailed results [37, 141, 154], but judging from the results of arrhythmia detection (see section on rhythm interpretation), the success rate of these algorithms must be rather unsatisfying. A confounding factor is that P waves may alter their appearance in one recording, suddenly, from one beat to the other, or gradually, and that precisely this behavior is an element in rhythm diagnosis. To our knowledge, no work has been done on P-wave typing, that is, the distinction between different P-wave morphologies in one and the same recording.

37.10 QRS Typing

QRS typing is essentially a clustering task followed by a classification task, as the case requires. The clustering attempts to distinguish between different types, or families, of QRS complexes (if more than one). Within one family the complexes are similar in QRS morphology. If more than one type has been detected, the classification task is to determine which one

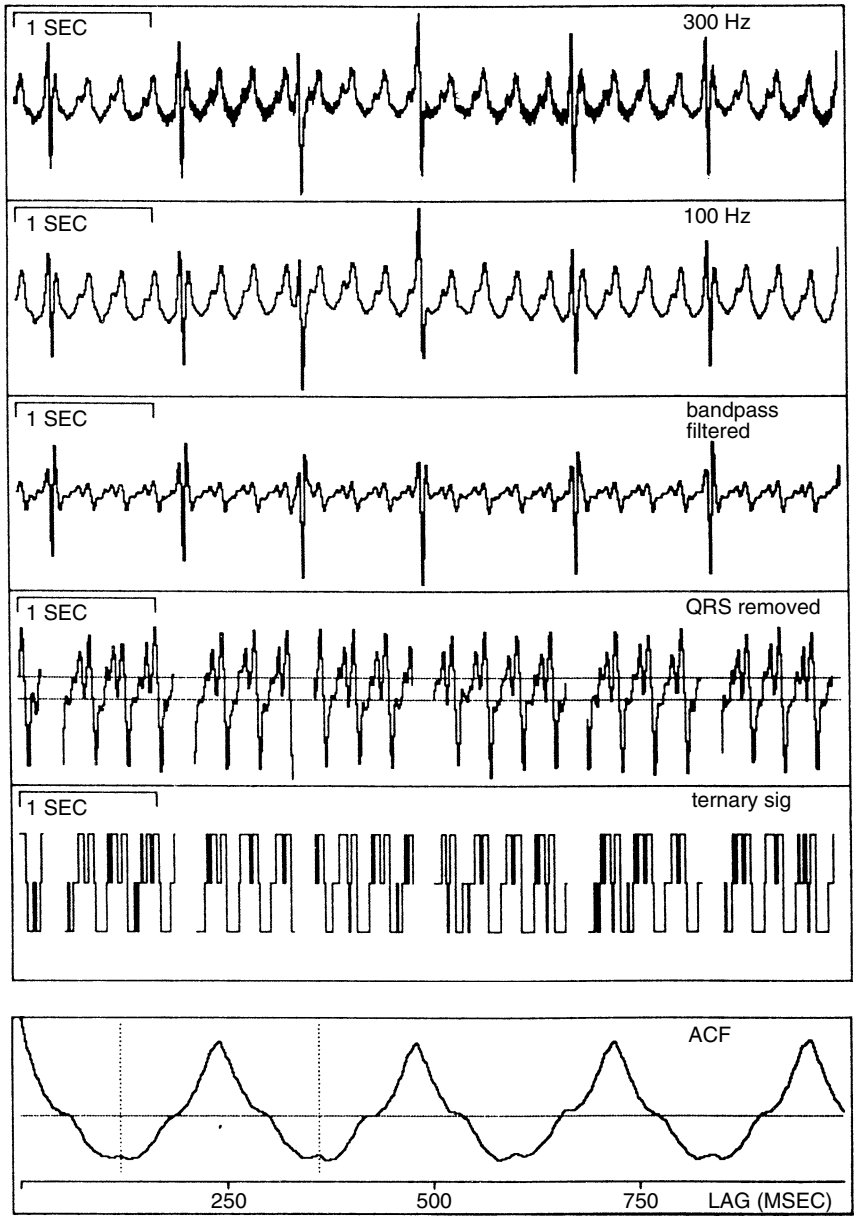

Figure 37.5

Example of the processing steps in a flutter wave detection algorithm (From Talmon et al. [151]). From *top* to *bottom*: original signal; signal after sampling rate reduction; signal after bandpass filtering; bandpass filtered signal after removal of QRS complexes; ternary signal; autocorrelation function.

is the dominant type. The term "dominant" is not synonymous with "most numerous." It may well be that in a recording the "dominant" sinus complexes are outnumbered by ectopics, for example. We define the term dominant as the indication for the family of complexes to be used for the morphological (or contour) diagnosis. The nondominant complexes may be further divided into several types, such as premature ventricular or supraventricular complexes (possibly from different foci) and escape beats. This makes it clear that correct QRS typing is indispensable for a reliable rhythm interpretation. Typing, however, is a less straightforward endeavor than one would wish. Commonly, the dominant complexes are sinus

beats, but they might also be of atrial or nodal, or even ventricular origin. What if the pacemaker site changes during the recording? And, quite annoyingly, complexes from the same origin may show sudden variation in QRS morphology, for example, in intermittent right bundle branch block. Which one will be labeled as the dominant morphology? Differentiating aberrantly conducted complexes from ectopic complexes is the next problem. Also, similar QRS complexes are not always followed by similar ST-T segments, a complication that inspired only a few investigators to take a closer look at ST-T typing [85, 155].

A variety of clustering methods and features for QRS typing has been proposed. All methods compute a similarity measure between a newly presenting complex and one or more of the complexes in each of the already existing clusters. The new complex is then assigned to the group with the complexes that are most similar to it, unless the similarity is below a certain threshold, in which case a new group is formed. Different similarity measures have been proposed, such as the area between the normalized spatial velocity curves of the two complexes [156], the difference in so-called arc lengths of the complexes [94], or the Mahalanobis distance using four morphological QRS features [157]. To determine whether two complexes were of similar type, Talmon [85] used a decision tree that involved two similarity measures, reflecting similarity in shape and in power. Lagerholm et al. [158] decomposed the QRS complexes into five orthogonal Hermite functions and used the resulting coefficients, together with RR-interval parameters, as features to cluster the complexes into 25 groups by means of a self-organizing map.

When more than one type of QRS complex has been found, it must be decided which is the dominant type. As mentioned above, this may not be so self-evident since the most frequent type is not necessarily the dominant one. More elaborate decision logic has been developed [85, 141], involving QRS duration, RR interval length preceding the complex, and the number of beats of each type.

Few quantitative results on QRS typing in the resting ECG have been published. Using the ECGs from the CSE multilead library, Kors et al. [140] found an error rate of 0.3% for their multilead ECG program in classifying four types of complexes. Lagerholm et al. [158], using the MIT-BIH database with 16 different beat types, report a chance of 1.5% that a beat ends up in the wrong cluster.

Several investigators have approached QRS typing primarily as a beat classification task [127, 159–162], rather than as a clustering task, possibly followed by a classification stage. They trained one or more classifiers based on a labeled set of beats of different morphology. For example, Hu et al. [127] applied artificial neural networks to distinguish between normal and abnormal beats (involving 12 different beat morphologies), using raw QRS samples from the MIT-BIH arrhythmia database as the input. They obtained a total accuracy of 90.6%, which compared favorably with the 73.0% accuracy of a simple nearest neighbor classifier, but this level of accuracy would not seem high enough for clinical application. This may not come as a surprise considering the large interindividual variability of QRS morphology. Only when the classifier was trained on patient-specific ECG data, were more acceptable results obtained [159]. Christov et al. [162] applied a nearest neighbor rule to 26 parameters derived from two ECG leads. Again, when tested on the MIT-BIH arrhythmia database, a general classifier performed poorly, but patient-specific classifiers showed good performance. However, the patient-specific approach to QRS typing requires initial human labeling of beats and, therefore, is of little value for computer programs that should analyze the short-duration resting ECG fully automatically.

37.11 Forming a Representative Complex

Most diagnostic ECG computer programs operate on a single "representative" P-QRS-T complex from the "dominant" family [37, 121, 122, 141, 163, 164]. From this representative complex, the measurements needed for the diagnostic interpretation stage are derived. Mostly, the representative complex (sometimes called a "template" complex) is obtained by the computation of an averaged beat or a median beat from as many complexes in the record as may qualify for the purpose. Such a procedure presupposes complexes of similar morphology, and thus requires that QRS typing has been performed. The following techniques are in use:

1. Coherent or ensemble averaging is a simple technique in which the average of the time-aligned complexes is calculated at each sample point. The technique has been shown to be equivalent to low-pass comb filtering and to yield optimal noise reduction for Gaussian distributed noise [165, 166]. Under this condition, the SNR improvement is equal to the

square root of the number of complexes being averaged. Since the average is vulnerable for outliers, it is imperative that complexes affected by sudden baseline shifts or other major disturbances are excluded from averaging.

2. Another approach is finding the median value for each sample point of the time-aligned complexes. The median beat is less sensitive to baseline shifts, but low-frequency baseline wander may introduce discontinuities in the median beat and result in reduced noise suppression [85, 167].
3. To reduce the effect of averaging widely differing amplitudes, Macfarlane et al. [94] compute a so-called modal beat. They assign weights to each sample of each QRS complex, with similar amplitudes across complexes having a high weight, the others having lower weights. The approach performed well [85], but was computationally expensive. In later versions of the Glasgow program, the technique was, therefore, abandoned in favor of simple averaging or, if any individual beat significantly deviated from the average, computation of a median cycle [141].
4. A hybrid approach, trying to combine the advantages of the averaging and median techniques, was proposed by Mertens and Mortara [167]. They first split the QRS complexes in three equally-sized groups and determine the averaged complex for each group. These three averaged complexes are then partitioned in their low- and high-frequency components with a simple moving average filter, and for both signals the median complex is determined. Finally, the two median complexes are added to form the representative complex.

For all these methods precise beat alignment is essential. In several programs [122, 163, 164], synchronization is performed by a cross-correlation method. In the MEANS program [37, 85], alignment is based on a reference point within the QRS complex, the position of an extremum in the band-pass filtered signal, whereas the Louvain program [121] uses the onset of individual QRS complexes. If complexes are not accurately aligned, beat-to-beat variations in the timing between peaks in the complexes may reduce the peak amplitudes [85]. To avoid this problem, some programs select only one "typical" complex for further analysis [168]. While this approach obviously does not need beat alignment, it does not help to improve the SNR.

The single complex approach is being taken a step further when wave recognition and measurements are done on each individual complex followed by computing an average or median of the measurements across the complexes [123, 143, 154, 169, 170].

There has been some discussion on the merits of signal averaging versus measurement averaging. Talmon [85] was not able to show any significant difference in QRS duration if wave recognition were performed on single complexes or on an averaged complex, after proper beat alignment [85]. The averaging method, however, offers the advantage of increasing the SNR. Based on results of extensive noise tests performed in the CSE project, a measurement strategy that uses selective averaging has been recommended for diagnostic ECG computer programs [171, 172].

37.12 Waveform Recognition

The goal of waveform or boundary recognition is to determine the inflectional points P onset, P end, QRS onset, QRS end, and T end, as much as possible in conformity with their visually determined counterparts (Fig. 37.6). No attempt is made in any ECG computer program to determine the end of the U wave, the orphan wave of electrocardiology. The CSE Working Party [34] stated that the inclusion or exclusion of isoelectric segments in the initial or terminal parts of a wave may lead to differences in wave duration of more than 10 ms between leads, and, therefore, urges that "the true onsets and offsets of P and QRS as well as the end of T should be determined using at least three simultaneously recorded leads." (cf. Fig. 37.1) The end of T deserves special attention in this respect. In 1990, Campbell and his group introduced the concept of QT dispersion (QTd) [173], defined as the difference between the longest and the shortest QT in any of the 12 surface ECG leads. QTd was supposed to reflect the dispersion of repolarization within the myocardium. The idea caused a tidal wave of papers but in due course became severely criticized [174–177]. Differences in QT duration will arise from differences in the projection of the spatial T vector onto the different leads, which in some leads may result in terminal isoelectric segments of various lengths and hence in shortened QT [174]. Also in QTd measurements, the U wave was regarded as a nuisance, obscuring the end of T. If it were too prominent, the lead was simply excluded from QTd determination. The U wave, however, might deserve more attention than this. Viewed in simultaneous leads, it may be seen in some as a separate wave, detached from the T; in other leads it may encroach on the T wave, and in still other leads it may blend in with the T wave. In fact, searching for the common end of the T wave is not pertinent if T and

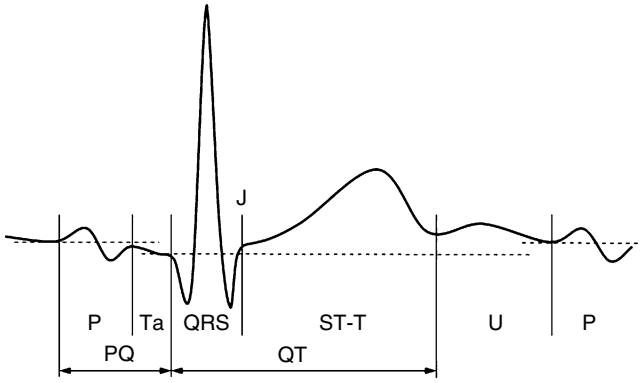

Figure 37.6

In the waveform recognition, onset and offset of P, QRS, and T are determined, as indicated by the *vertical bars*. QRS offset and J are identical points. A true 0-level cannot be identified: the onset of QRS is superimposed on the atrial repolarization wave (Ta), at the J point ventricular repolarization is already underway, and the end of T coalesces with the U wave, the end of which is hidden in the next P. As the operational 0-level for QRS and T the *horizontal line* through QRS onset is recommended, likewise for the P the horizontal through P onset. Amplitudes are measured with respect to these 0-levels.

U form a continuum as has been proposed [178], in the same way as it is impossible to ask for the common end of a Q wave in the QRS. Whatever the ultimate truth, it seems best for the time being and for practical purposes, for example, for QT duration measurement in drug safety testing, to let the computer determine T offset over multiple simultaneous leads.

As pointed out above, single lead, "one-dimensional" measurements systematically produce shorter measurements of wave duration than when, "multidimensionally," the first onset and latest offset in any lead are taken. Most ECG computer programs, therefore, use the spatial velocity or a similar multidimensional function as the detection function for waveform recognition (see Sect. 37.8). For single-lead recordings, other detection functions, such as the envelope of the ECG signal [179] or wavelet transforms [131, 133], have been applied. Basically, three different approaches of boundary recognition can be distinguished [180]. Each has to be trained and tested by human observers.

1. Thresholding

The most straightforward method is to apply a simple threshold to the detection function. For the onset, usually the maximum of the detection function is localized from where it is traced backward until where it first becomes smaller than an absolute or relative threshold. This point is considered to be the wave onset. The end of a wave is determined similarly.

According to an inventory of waveform-recognition methods used in various ECG computer programs in the CSE project [122], most programs applied threshold detectors. A number of different thresholding algorithms to detect the end of the T wave in single leads were described and compared by McLaughlin et al. [181, 182]. Using a threshold detector, Vila et al. [183] attempted to determine not only the end of the T but also the end of the U wave. They mathematically modeled the TU complex and used the modeled signal for detection. Laguna et al. [144] applied a single-lead threshold detector to each of the leads of multilead ECGs and then combined the wave boundaries in the individual leads to find overall onsets and offsets of P, QRS, and T.

2. Signal matching

A second approach is to search for the point where the weighted least-square difference between a reference waveform and the detection function is minimal [184]. The reference waveform is obtained from a learning set of detection functions with known wave boundaries, as indicated by one or more human observers. Rubel and Ayad [184] compared the

performance of a signal matching algorithm for different detection functions using the CSE database. They obtained the best results for QRS onset and offset detection with an unfiltered spatial area detection function.

3. Template matching

The template method takes into account information on the time-amplitude distribution of the detection function in a window around the inflectional point [185]. A template is constructed from a series of detection functions in which the wave boundaries have visually been assessed by a human observer. The boundary point in a new ECG is then located at that point where the cross-correlation between the template and the new detection function is maximal. Details of this approach and an efficient way of implementation have been described by Talmon [85].

A somewhat different approach, obviating the need for thresholding or matching, was proposed by Zhang et al. [186]. As a detection function, they took the output of a signal integrator in a window sliding over the T wave. With recourse to some simple assumptions, the maximum of the detection function was shown to coincide with the end of the T wave. A model-based approach to delineate single-lead QRS onset and offset was described by Sörnmo [187]. He statistically modeled the low-frequency segments (containing P and T waves) and high-frequency segments (QRS complex), and applied a maximum-likelihood procedure to estimate the points where a change occurred between low- and high-frequency segments.

Using the multilead CSE database, Willems et al. [61] evaluated the measurement performance of 11 ECG and 6 VCG computer programs (Fig. 37.7), incorporating a variety of wave boundary detection algorithms [122]. Onset of QRS showed overall the smallest deviations from the reference, with the narrowest confidence intervals. End of T showed the largest scatter. The median of the waveform recognition results of all programs coincided best with the median results of referee cardiologists, corroborating findings of the former 3-lead CSE study [60]. However, individual program results

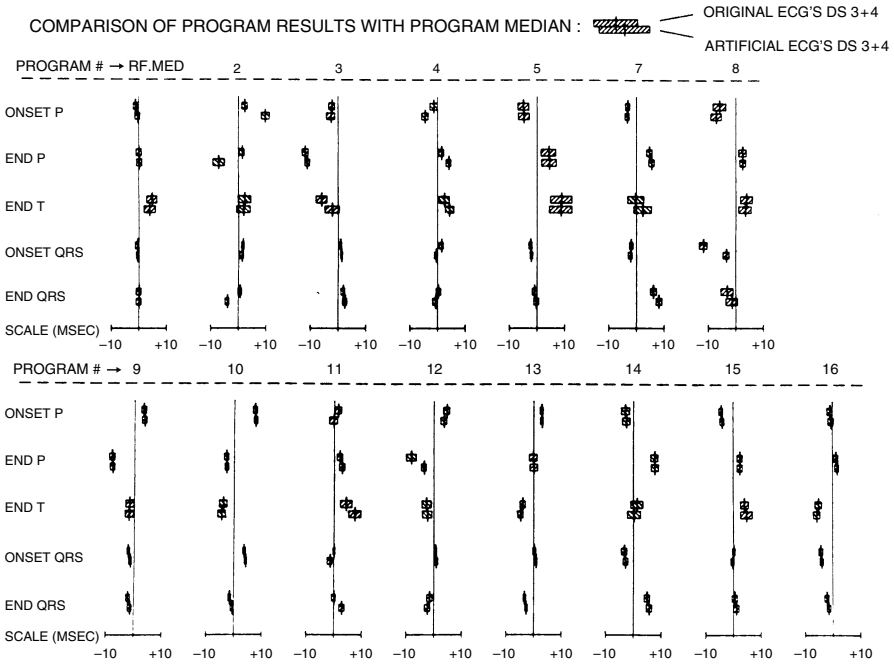

Figure 37.7

Comparison of individual program results (numbered 2–16) and median referee results (RF MED) with the median of all programs in the CSE multilead library. Mean differences and 99% confidence intervals are indicated by *small vertical lines* and *horizontal bars*, respectively (From Willems et al. [61]. © American College of Cardiology. Reproduced with permission).

were widely divergent. As a consequence, P, PR, QRS, and QT interval measurements also varied widely among the various programs.

Willems et al. [171] assessed the influence of noise on wave boundary recognition of eight ECG and six VCG programs. Seven different types of high- and low-frequency noise were added to each of ten recordings. Mains interference and baseline wander had no significant effect on boundary detection for the majority of programs, but increasing levels of high-frequency noise shifted the onsets and offsets of most programs outward. Programs which apply beat averaging techniques had more stable results than programs analyzing single beats, but it was noted that these results mainly occurred at high noise levels that reflect poor operational conditions and can be avoided by proper quality control [171]. In a second related study [172], the effect of noise on amplitude measurements was examined. Programs that showed the least variability in waveform onsets and offsets also exhibited the highest stability in waveform detection and amplitude measurements.

Laguna et al. [144] compared the waveform boundary results and interval measurements obtained by their own algorithm with the median program estimates and median referee estimates of the multilead CSE database. The standard deviations of the differences were shown to be within acceptable tolerance limits [34] for most of the measurements. Martinez et al. [131] used the same data set to evaluate their wavelet transform-based approach, but they obtained less favorable results for QRS end and T end.

An interesting method to assess and compare the results of various waveform recognition algorithms was proposed by Morlet et al. [188]. They use scatter graphs that picture the standard deviation of the differences between program results and reference when the largest differences are progressively removed. This information allows us to distinguish between the reliability of an algorithm, that is, its capacity to provide wave boundary estimates without flagrant errors, and its precision, that is, the standard deviation of the differences between its estimates and the references.

37.13 Parameter Computation

Once the onsets and offsets of the various ECG waveforms have been identified, parameter or feature extraction is the next step. Time intervals and wave durations follow directly from the established time points. The ambiguities around the QT interval have been pointed out in the previous section. For the amplitudes of the various deflections, a 0-line, or baseline, must be defined. It should be understood that there is no true 0-level anywhere in the ECG (Fig. 37.6). The T-P interval which has been recommended as such contains the U wave. The CSE Working Party defined baseline as "a horizontal reference line computed from a single base level" [34] and declared itself against the use of non-horizontal lines. For QRS and T combined, it recommended strongly the uniform use of a baseline through the onset of QRS in combination with a limited number of preceding sample points. For the P wave, the base level may be chosen at the onset of P. Voltage amplitudes are then simply determined with respect to the chosen baselines. A wave is defined as a discernible deviation from the baseline where at least two opposite slopes can be identified and where discernible means that both the amplitude and the duration of the deviation exceed certain minimum values [34]. Various amplitude ratios, such as Q/R and R/S, and also integrals and angles can be derived from these measurements. When simultaneously recorded orthogonal leads are available or are reconstructed from the 12-lead ECG [20, 189], spatial or planar vector magnitudes and directions, gradients and polar vectors can be obtained. The relative areas of the spatial QRS loop in each octant of the three-dimensional space are also measured in some systems [168].

Pipberger et al. [7, 8] applied the technique of time normalization of the QRS complex and the ST-T segment. Each was divided into eight equal time segments, regardless of their duration. In this way, measurements from QRS complexes with different durations can be compared one with another.

Advanced mathematical techniques, like Fourier analysis, polynomial fitting, or Karhunen–Loeve expansion, have been applied by some early investigators [190, 191]. It has been pointed out by Van Bemmel [180] that parameters derived from these techniques may allow an accurate reconstruction of the overall shape of the ECG, but are not necessarily the best discriminating features in ECG classification.

Computer processing systems frequently make 250–300 measurements per ECG. Ultimately, only a limited subset is used in the diagnostic classification stage and a still smaller number is printed out in the final computer report, which is submitted to the requesting physician. Most ECG processing systems will optionally display the averaged or median

beat, if desired with markings for wave onsets and offsets as determined by the program. The ECG reader, therewith, has a check on the correctness of the measurements underlying the computer diagnosis.

37.14 Diagnostic ECG Interpretation

37.14.1 Strategies for Diagnostic Classification

After the initial waveform-detection, pattern-recognition, and measurement algorithms have been applied, the diagnostic stage is entered in which the ECG is classified into one or more of the various possible diagnostic categories. Two basically different approaches to diagnostic classification have been developed since the early days of computer assisted electrocardiography [192]. In the first, the deterministic or heuristic approach, the cardiologist's method of interpreting ECGs is simulated. The majority of existing ECG computer programs follows this approach. In the second, a statistical or probabilistic approach is adopted whereby an attempt is made by mathematical means to establish the probability that a given ECG belongs to a particular diagnostic category.

More recently, other approaches to diagnostic ECG classification have been tried. Some investigators have applied fuzzy set theory [170, 193, 194], others the "expert system" approach [195, 196] and, finally, neural-network techniques have been used [197–201]. However, clinical application of the latter techniques on a larger scale is lacking.

37.14.2 Deterministic ECG Computer Programs

The analysis follows a logical path of questions regarding the presence or absence of certain predetermined criteria for every diagnostic category, to be answered with yes or no. The questions and answers can be arranged in a decision table or in a decision tree resulting in diagnostic statements [85]. Such decision schemes, often quite elaborate, are implemented in all programs using the deterministic approach. The likelihood of the resulting diagnostic statements may be indicated by modifiers like "definite," "probable," and "possible."

Deterministic programs have the advantage that the diagnostic criteria used are familiar to the cardiologist, and that the logic is easy to follow and comprehend [192]. Much experience with conventional ECG interpretation present in the brain of the developer or published in the literature can, theoretically at least, be incorporated in these programs. Decision-tree programs are organic and flexible in structure and remain open for modification. With advancing insight and experience diagnostic pathways can be improved. Criteria selection can be guided by deductive reasoning based on knowledge of electrophysiological processes, a design that is inherently excluded in the statistical diagnostic approach. Also, new diagnostic categories can be added quite easily without the need for recruiting new statistical data.

Emulation of the human reader brings advantages but has also its limitations. The criteria selection might tend to be arbitrary and based on impressions rather than founded on solid quantitative information. In some systems, criteria selection was the work of a single expert, in others the effort of a group [154]. The appreciation of ECG criteria may vary considerably between cardiologists, as demonstrated by many studies on intra- and inter-observer variability of ECG interpretation [202–204]. The set of criteria proposed by one cardiologist may be met with another cardiologist's disapproval. This lack of agreement on criteria and the dearth of reliable quantitative data on their sensitivity and specificity have resulted in a diversity of commercial systems, even in one where each user could incorporate his own preferences, if so desired [205].

Many studies on ECG criteria have demonstrated a considerable overlap between normal and abnormal populations with respect to almost all ECG parameters, notably of Q-wave durations and voltage measurements. This necessarily gives rise to a proportion of false-positive and false-negative statements. The addition of a new, independent criterion to an existing decision tree increases sensitivity, but is almost invariably accompanied by a loss in specificity. This practice led to intolerably high false-positive rates in some of the early programs that, as a result, were dismissed as unsuitable for clinical use [45, 206]. A weighty argument of the adherents of the probabilistic approach was that conventional ECG programs can never surpass an accuracy level of 54–60%, the level reached by eminent experts in Simonson's study [203], who read the ECGs and VCGs of patients whose diagnoses were known and documented by ECG-independent means. In the CSE

study, later to be discussed, the level of accuracy against the clinical "truth" was much higher, ranging between 73% and 81% [207].

Nowadays, however, decision-logic programs may also employ statistical tools. Computer programs are available that automatically generate decision-tree logic based on a given choice of features [208, 209]. Sensitivity and specificity of thresholds used in different criteria can be statistically optimized on population samples with well-defined disease entities. In a way, conventional ECG programs thereby move toward the statistical programs and, as we will see, vice versa.

37.14.3 Statistical ECG Computer Programs

The availability of the computer to perform voluminous mathematical computations for statistical purposes would seem to make the statistical approach the easy solution for diagnostic classification, but it will be shown that there are no easy solutions. For each diagnostic category, a population of ECGs has to be collected. The presence of normality or of the various types of abnormality (infarction, LVH, etc.) has preferably been established from clinical data, although ECG information does not have to be excluded. Next, the probabilities of occurrence of the various ECG measurements are determined for each diagnostic category. Having done this in a learning stage, any new ECG can be assigned to its presumed appropriate population in a test stage to evaluate the validity of the classification method. The measurements going into the statistical procedure are in principle just the amplitude values of samples in each lead of an ECG, in addition to certain duration measurements, not the values of the customary diagnostic ECG criteria, although, again in principle, there could be nothing against using them.

The main claim to preeminence of statistical over conventional programs is that diagnostic performance should be better and that mathematical objectivity takes the place of the personal idiosyncrasies of conventional program developers [192, 210]. Also, in the neighborhood of critical thresholds, minute changes in measurements may alter the interpretation in heuristic programs, but less so in statistical programs and certainly not when the probabilities for the diagnoses are above 70% [211, 212].

There are, however, distinct disadvantages [192]. First of all, large databases are needed for developing and testing. For each diagnostic category, a separate population of clinically documented records has to be collected. Case collection carries with it the problem of selection. The AVA program [123] has been developed almost exclusively on a database collected in a male and war veteran population. Statistical parameters may differ significantly in other populations that are more heterogeneous with respect to sex or to age and more homogeneous, on the other hand, with respect to race (see the Appendix on normal limits).

Furthermore, the diagnostic categories are mutually exclusive. A case may have a probability of 60% of belonging to the single category of, say, left ventricular hypertrophy (LVH), 30% of belonging to anterior myocardial infarction (AMI), and 10% of being normal. The individual probabilities add up to 100%. With this approach, it is not possible to have 100% probability of LVH and at the same time 100% probability of AMI. For this to be possible a separate collection of cases with LVH + AMI would have to be created and every other combination of diagnoses would again necessitate a different data base. In this way, the required number of cases soon increases out of control. Also, when one ECG presents an abnormality which does not belong to any of the existing categories, the probabilities will be spread over the existing categories [7]. To handle this problem, some diagnostic-tree type decisions were added in the AVA program in order to deal with some abnormalities not listed by the main AVA classification [123].

The common denominator of all the proposed statistical techniques is multivariate analysis. The first program using such methods dates back to 1961 and was described by Cady et al. [213]. They separated 23 normal tracings from 19 records with a typical pattern of LVH. Bayes' theorem was first applied to ECG diagnosis by Kimura et al. [214]. There were more early attempts to use multivariate analysis for ECG classification [215–218], but particularly Pipberger and coworkers have for many years persistently promoted the statistical method at numerous conferences and in many articles [7, 8, 41, 123, 219–222]. Following this lead, other investigators have applied statistical techniques for computer processing mainly to the VCG [163, 223]. Multivariate analysis has less frequently been applied to the standard 12-lead electrocardiogram [53, 163, 224].

The Bayes' formula is given by

$$P(i|\mathbf{x}) = \frac{f(\mathbf{x}|i) \cdot P(i)}{\sum_{j=1}^{m} f(\mathbf{x}|j) \cdot P(j)}$$

where $P(i|\mathbf{x})$ is the posterior or conditional probability that an ECG belongs to diagnostic category i (out of m possible categories) given the measurement vector $\mathbf{x}$; $f(\mathbf{x}|i)$ represents the conditional probability that the measurement vector $\mathbf{x}$ is produced in the cases belonging to category i; and $P(i)$ is the unconditional or prior probability for an ECG to belong to category i [7].

An essential feature of the classification strategy in the AVA program developed by Pipberger et al. [7, 8], as well as by some other investigators [223, 224], is the application of prior probabilities as expressed in the Bayes' formula. For this purpose, the relative frequencies of occurrence of various clinical diagnostic categories in the environment in question must be estimated. Thus, in Pipberger's approach, different prior probabilities were assigned to patients of different provenance (cardiological out-patient, general medicine, pulmonary disease) even to the extent of introducing "individual prior codes" [8]. This concept was argued to emulate the thought process of a physician who, when interpreting an ECG, weighs his diagnosis in the light of age, sex, and clinical condition of the patient, and the likelihood of occurrence of the disease in the specific population to which he happens to belong. The "proper prior code" for an individual is indicated on the ECG request form as one of several broad clinical categories, according to the tentative clinical diagnosis [8]. When entered with the patient's vital statistics, the prior probabilities are automatically set for computation of the posterior probabilities. The sensitivity and specificity for certain diagnostic categories of the AVA program can easily be adapted through manipulation of prior probabilities [8].

By including the prior probabilities of the various diagnostic categories, non-electrocardiographic information is introduced in a formalized way. In an extreme example, when a prior probability is set to zero or to one for a certain group, no case or every case will respectively be diagnosed in this disease category, no matter what the ECG appearance may be. These are the mathematical facts of this classification procedure [192]. Proponents of the use of prior probabilities argue that in a non-formalized way, prior knowledge and bias are applied by the clinician as well in routine ECG reading, in a justifiable and natural way. The opponents state that, by using clinical information, the role of the ECG is reduced to futility. They claim that evaluation of the ECG, in the larger framework of a final clinical diagnosis, should independently contribute to the diagnosis. In all these considerations, the element of "cost" cannot be neglected. The cost of missing the diagnosis of a single case of bubonic plague in a population hitherto thought to be free of the disease may be huge, as is the cost of overdiagnosing cervical cancer in a population where the disease is not uncommon. Prior probabilities should not be applied without discernment!

37.14.4 Methodology of ECG Computer Program Evaluation

The following paragraphs mainly address the topics of diagnostic accuracy and reliability of ECG computer programs. For other aspects such as utility, efficacy, and cost-benefit analysis, the reader is referred to some specific publications [12, 225–229].

It was pointed out earlier that comparison between computer and truth is a more cumbersome and problematic task than one would anticipate. To list the main complications:

1. There are ECG statements for which there is no clinical confirmation. Three types of statements can be made by human readers or computer programs [14], as follows:
   (a) Type A statements refer to an anatomic lesion or pathophysiologic state, such as myocardial infarction or hypertrophy, the presence of which can be confirmed by non-electrocardiographic evidence like cardiac catheterization, serum enzyme levels, ventriculograms, echocardiograms, scintigrams, and autopsy findings.
   (b) Type B statements apply to conditions which belong intrinsically to the realm of electrocardiography itself. They refer to electrophysiological processes such as arrhythmias and atrioventricular and intraventricular conduction disturbances. Sometimes these type B statements can be corroborated by the results of other diagnostic methods, such as scintigraphy in the case of a statement of ischemia based on a typical ST-T change. Most often, the physician's interpretation is the reference.
   (c) Type C statements refer to purely descriptive ECG features for which no substrate can be demonstrated by other means. Under this category, statements are subsumed like "nonspecific ST-T changes" or "axis deviation."

At the tenth Bethesda conference, Task force III [14] strongly recommended evaluation of type A statements by means of independent, clinical evidence. For type B and C statements, the human observer is the reference. A distinction was made between a constrained and a free observer, the constraint being a given set of measurements or criteria agreed upon before the evaluation. In fact, this again boils down to a test on the waveform recognition proficiency of the program. The free observer applies his own individual rules, or the majority opinion of a group of free observers may be obtained, but if these rules are formalized they can be put into computer logic and the observer is again constrained.

2. Collecting a type A database is a laborious and tedious task. In the early years, investigators were quite satisfied when they could single out one disease condition, say D, from a population composed of only D and normals. A simple 2 × 2 contingency table suffices to describe the diagnostic results, with sensitivity, specificity, positive predictive value, etc., as the indices of performance. This simple situation is already spoilt when non-D can be anything, not just normal. Non-normal conditions other than D may resemble D in some features and lead to false positive diagnoses of D and so degrade performance. In the real-life situation, the population contains all types of abnormality and the program is expected to classify each one correctly. This results in as many sensitivities and specificities as there are diagnostic conditions, and total performance cannot be expressed in a single, representative figure. The same "total accuracy" could be attained by one program scoring low on infarct recognition but high on LVH and a second one doing the reverse. Whatever the problems of assessing the agreement between computer and reference, it is mandatory that the database includes a spectrum of disease states, with different grades of severity and a representative number in each category, as well as combinations of different diseases. A database without any bias, however, is an illusion. Mostly, noisy recordings are excluded from the collection although noise is a fact of life (for testing purposes noise could be added afterward). Also, arrhythmias and conduction defects are sometimes excluded. Finally, databases differ in the populations they were drawn from, with respect to race, age, sex, social status, etc.
3. Output statements are not standardized and their meanings must be established first. What is to be understood by septal myocardial infarction? Does it mean the same thing as antero-septal myocardial infarction? What are the clinical grounds for diagnosing right ventricular hypertrophy (RVH)? Is RVH caused by pulmonary valve stenosis the same as RVH caused by an atrial septal defect? Such questions were addressed in the CSE study [65]. These considerations not only apply to type A statements, but to B and C as well. What is a nonspecific ST-T change? How will RBBB or LBBB be defined? Regarding the latter, a set of criteria for conduction disturbances and pre-excitation have previously been recommended [35].
4. Probability statements constitute another problem. A human observer may make a diagnosis of "probable inferior infarct." Does this mean "70% probability of IMI," but still a chance of 30% normal? Do the probabilities add up to 100%? In the case of "probable anterior infarct, possible LVH" does this mean 70% probability of AMI, 30% of LVH, and 0% normal, or must we understand that the case is probably abnormal (70%) with a preference for AMI (50%), a residual chance of 20% for LVH and leaving a 30% likelihood of normality? The problem is compounded by the tendency of ECG readers to cover all contingencies by statements like "posterior wall infarct not entirely excluded." It is, therefore, necessary that the reporting follows strictly prescribed rules. As an example, in the CSE study the number of categories was limited to seven. For each category, four certainty qualifiers were allowed: definite, probable, possible, and absent with numerical values of 3, 2, 1, and 0, respectively. The computer statements had to be transcribed into the same format by the program developers. As per diagnostic category, the scores were averaged over all readers or programs, and rounded. The category with highest score was taken to be the diagnosis of the "combined cardiologist" or "combined program." Additional rules were defined to handle some more complex situations [230].
5. Instability of interpretation is not restricted to man. Intra-observer variability is recognized to be sometimes considerable, but computer programs are generally viewed as robust against the diagnostically insignificant short-term variations that may occur between two successive ECGs of the same person. This is not entirely the case [231–233]. Even one and the same ECG may give rise to two different outcomes, as demonstrated by Bailey et al. [44, 45, 234, 235]. They processed two sets of digital samples, 1 ms apart, from the same recording, and, surprisingly, the separate results were by no means identical. The reproducibility of some of the older programs tested in this way proved to be unacceptably low. Spodick and Bishop [236] assessed the variability in the interpretations by an unspecified computer program of 92 unselected pairs of ECGs recorded 1 min apart. In 36 (39%) pairs, they found "grossly" different interpretations. The clinical significance of part of the differences, however, is debatable.

37.14.5 Comparison of Computer Interpretations with Physician's Interpretations

The 1,220 ECGs and VCGs from the CSE diagnostic library were read by nine cardiologists of whom four read ECGs and VCGs, four read only the ECGs and one read only the VCGs. For each recording, a combined result was derived in the above described manner. The results of nine ECG and six VCG computer programs were then compared with the "combined cardiologist." Different misclassification matrices, as well as sensitivity, specificity, predictive values of positive and negative test results, total accuracy, information content, and other measures of performance, were calculated [66, 207, 237]. The specificity of the ECG programs (median 87.7%, range 73.4–96.8%) was higher than that of the VCG program (median 75.5%, range 69.1–84.8%). Median sensitivities for LVH, RVH, AMI, and inferior myocardial infarction (IMI) were 71.6%, 58.6%, 81.0%, and 78.1%, respectively, but among the programs, sensitivities varied widely (Table 37.1). Total agreement between an individual program and the combined cardiologist varied between 68.1% and 80.3% for the ECG programs and between 69.2% and 78.1% for the VCG programs. The combined program agreed with the combined cardiologist in 87.9% of the cases, which was significantly higher than for any individual program. The figure may be compared with the intra-observer variability of the cardiologists, who interpreted 125 randomly selected cases a second time without their knowing. Reproducibility was then seen to vary between a low of 73.6% and 90.8% (median 82.4%) [66].

It should be noted that the cardiologists in the CSE study were experienced, highly-motivated electrocardiographers. In a study by Jakobsson et al. [238], the interpretations of 69 physicians (only four of them being cardiologists) were compared with those of a computer-based ECG recorder in routine clinical practice. The authors took their own judgment as the reference. The study population consisted of 474 routine ECGs taken in a general practice, a medical emergency department, and an out-patient department. No single physician interpreted more than 7% of the ECGs. A written physician's interpretation was lacking in 11% of the ECGs. The diagnostic sensitivity for myocardial infarction of the doctors was significantly lower than that of the program. The overall quality of the computer interpretations was judged as being satisfactory in 82% of the ECGs, whereas this was only 64% for the physicians' written interpretations. Most computer misinterpretations could be attributed to poor signal quality, and it was suggested that the nonexpert physician should team up with the computer to approach the performance of an experienced ECG reader.

The CSE study only dealt with type A diagnostic statements. Computer–physician comparison is the usual method for assessing type B and type C interpretative statements, for which the ECG itself is the reference. Although this may seem to be less essential than diagnostic type A accuracy, such comparison is important since agreement between computer and physician is a convincing argument for the clinical acceptability of an ECG computer program [46, 52, 239]. Further, physician review is mandatory for legal and other reasons [240].

37.14.6 Comparison of Computer Results with Clinical "Truth"

The results of the nine ECG and six VCG computer programs obtained in the same 1,220 clinically validated ECGs and VCGs in the CSE diagnostic library, as well as those from the nine readers, were now compared with the "clinical truth" [66, 207]. The classification accuracies of the different programs (Table 37.2), and to a lesser extent of the cardiologists

Table 37.1

Percentage agreement of nine ECG and six VCG computer programs and the combined program results with the combined cardiologists' interpretations on the 1,220 cases of the CSE diagnostic library (Adapted from Willems [66], p. 183)

Program	Normal	LVH	RVH	Anterior MI	Inferior MI	Total accuracy
ECG	87.7 (73.4–96.8)[a]	73.4 (63.2–90.7)	58.3 (25.0–66.7)	83.6 (65.1–89.3)	71.1 (44.6–87.5)	76.6 (68.1–80.3)
VCG	75.5 (69.1–84.8)	71.3 (47.9–77.8)	63.3 (21.7–85.0)	72.3 (50.9–82.1)	85.1 (74.4–91.9)	71.1 (69.2–78.1)
Combined program results						
ECG	95.6	88.2	66.7	87.7	81.0	85.4
VCG	85.3	80.3	78.3	83.0	93.4	82.1
ECG+VCG	95.2	87.9	75.0	88.7	91.0	87.9

[a]Median (range).

Table 37.2

Percentage correct classifications of nine ECG and six VCG computer programs and the combined program results against the clinical "truth" on the 1,220 cases of the CSE diagnostic library (Adapted from Willems [66], p. 181)

Program	Normal	LVH	RVH	Anterior MI	Inferior MI	Total accuracy
ECG	91.3 (86.3–97.1)[a]	56.6 (50.3–76.2)	31.8 (14.5–52.8)	77.1 (58.8–81.5)	58.8 (38.7–82.8)	69.7 (62.0–77.3)
VCG	80.9 (71.4–86.6)	55.4 (47.2–76.2)	35.9 (28.2–64.5)	68.0 (54.5–74.1)	74.1 (63.6–86.5)	68.3 (64.3–76.2)
Combined program results						
ECG	96.7	67.9	40.6	79.6	68.8	76.3
VCG	87.1	67.3	53.0	77.3	82.2	77.0
ECG+VCG	95.5	69.0	45.8	80.0	76.7	78.5

[a]Median (range).

Table 37.3

Percentage correct classifications of eight ECG readers and five VCG readers and the combined cardiologist results against the clinical "truth" on the 1,220 cases of the CSE diagnostic library (Adapted from Willems [66], p. 180)

Cardiologist	Normal	LVH	RVH	Anterior MI	Inferior MI	Total accuracy
ECG	96.1 (92.7–97.6)[a]	63.9 (54.8–69.3)	46.6 (40.6–51.5)	84.9 (79.0–87.5)	71.7 (59.2–84.1)	76.3 (72.6–81.0)
VCG	80.6 (73.8–87.2)	63.4 (48.4–68.5)	50.0 (45.5–56.4)	65.2 (62.4–79.4)	75.1 (69.8–82.1)	70.3 (67.5–74.4)
Combined cardiologist results						
ECG	97.1	65.8	47.6	87.3	75.1	79.2
VCG	84.7	64.7	53.0	74.1	78.6	74.8
ECG+VCG	96.5	68.2	50.3	85.7	78.3	80.3

[a]Median (range).

(Table 37.3), vary widely. The median specificity of the ECG programs was 91.3% (range 86.3–97.1%) against 80.9% (range 71.4–86.6%) for the VCG programs. Corresponding values for the cardiologists were 96.1% (range 92.7–97.6%) for the ECG and 80.6% (range 73.8–97.2%) for the VCG. The median sensitivities for LVH, RVH, AMI, and IMI were 55.7%, 32.7%, 74.1%, and 65.1%, respectively, for ECG and VCG computer programs together, versus 63.4%, 48.5%, 82.9%, and 73.3%, respectively, for all cardiologists. Total accuracy varied between 62.0% and 77.3% (median 69.7%) for the ECG programs, and between 64.3% and 76.2% (median 68.3%) for the VCG programs. Total accuracy of the cardiologists varied between 72.6% and 81.0% (median 76.3%) for the ECG, and between 67.5% and 74.4% (median 70.3%) for the VCG. However, the programs with the best performance reached almost equal levels as the best cardiologists.

The cardiologists obtained more accurate results for the ECG than for the VCG. The VCG readers had a lower specificity and, somewhat surprisingly, a lower sensitivity for anterior infarction, while sensitivities for RVH, inferior infarction, and combined infarction were slightly higher. These results largely corroborate those of other investigators demonstrating that the VCG is superior for most diagnostic categories as far as sensitivity is concerned, at the expense of specificity [241]. In another study [53], using 3,266 cases and the same statistical classification technique, the ECG and VCG were shown to have identical diagnostic information. One reason for the lower performance of the VCG readers in the CSE study may be, for some readers, an unusual display of the vector loops. It should be noted that the total accuracies of the combined ECG program (76.3%) and combined VCG program (77.0%) were almost identical.

Total accuracy of the four statistical programs was significantly higher (median 76.0%) than for the heuristic programs (median 67.4%). This may, at least in part, be explained by the fact that 87% of the database consisted of single-disease cases. The statistical programs were designed to classify a case into one of seven or eight disease categories, which is not the case for the open-ended heuristic programs. Thus, the composition of the database may have resulted in a bias favoring the statistical programs. Moreover, results of the AVA program may have been inflated thanks to its being fed with clinical information to adjust the prior probabilities on a case-by-case basis.

Combined results of programs and cardiologists were in almost all cases more accurate than those of the individual programs and cardiologists. This confirms previous findings on a subset of the CSE library [204].

The advantageous effect of combining programs was used in a study by Kors et al. [242] to improve the performance of their MEANS program. MEANS comprises two different classification programs, one for the ECG and one for the VCG. The interpretations of both programs in analyzing the ECGs and VCGs of the CSE diagnostic library were combined. The total accuracy of the combined program against clinical evidence was 74.2% (Fig. 37.8), significantly better than the total accuracy of each program separately (69.8% for the ECG, 70.2% for the VCG). Interestingly, to avoid the necessity of recording a VCG, in addition to the ECG, the VCGs were also reconstructed from the ECGs and then interpreted by the VCG classification program. The combined ECG and reconstructed VCG results (73.6%) were almost the same as those of the combined ECG and original VCG. Thus, the performance of an ECG computer program was improved by incorporating both ECG and VCG classificatory knowledge, drawing only on the ECG itself.

Another strategy, which takes into account possible beat-to-beat variations in the ECG was proposed by the same group [243]. In the first step, all individual complexes of the dominant type are analyzed and a classification is derived for each. In a second round, the individual classifications are combined in one final interpretation. When tested on the CSE diagnostic library, the total accuracy of MEANS against the clinical evidence significantly increased from 69.8% for the interpretations of the averaged complexes to 71.2% for the combined interpretations of the individual complexes.

Rather than combining the diagnostic outputs of an ECG and a VCG program, Andresen et al. [244, 245] integrated ECG and VCG criteria for acute and prior MI in one algorithm. VCG leads were synthesized using the "inverse Dower" transformation [19]. Using a database containing normals and patients with infarctions validated by ECG-independent means, the algorithm achieved sensitivity equal to that of three cardiologists and three primary care physicians, but had

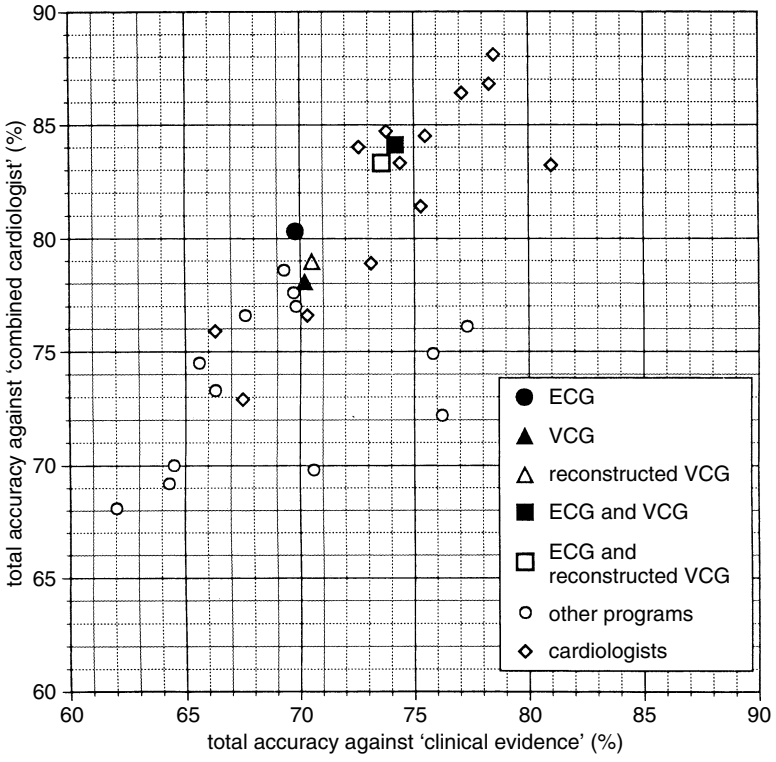

Figure 37.8

Total accuracies for the MEANS interpretation of the ECG, VCG, reconstructed VCG, and the combined interpretations. Also, the total accuracies of the other programs and of the cardiologists participating in the CSE study are shown (From Kors et al. [242]. © Elsevier. Reproduced with permission).

much higher specificity than the primary care physicians [246]. An improved version of the algorithm even outperformed the human readers [244], but these results might tend to be enhanced because the test database did not contain abnormalities other than infarctions.

The results of the CSE study showed that some ECG computer programs perform almost as well as the best cardiologists in classifying seven main diagnostic entities. However, it also became clear that some other programs were in need of considerable overhaul to meet reasonable standards.

37.14.7 Computer-Aided Physician's Interpretation of the ECG

Several studies evaluated the effect of computerized ECG interpretation on physicians' readings of ECGs. Milliken et al. [247] collected 180 ECGs from patients with various cardiac disorders known from ECG-independent data. Nine readers first read the ECG twice at an interval of several months without computer printouts. Months later, they reread the same ECGs, this time with the computer printout being available. The interpretations with several months intervening, but without computer output, resulted in an average change of 13.8% of the statements with 7.3% becoming correct and 6.5% becoming incorrect. When they reread the ECGs together with a computer output, the changes from incorrect to correct averaged 12% and from correct to incorrect 3%. From this study, it is apparent that the effect of priming the reader with computer results was in the direction of greater accuracy.

Hillson et al. [248] performed a randomized controlled trial to examine the effects of computer-assisted ECG interpretation on ECG reading time and agreement with the clinical diagnosis. Forty family physicians and general internists evaluated ten clinical vignettes accompanied by ECGs. Half of the physicians received the ECGs with computer-generated reports, the other half without. Those receiving the reports spent, on average, 25% less time in reading the ECGs. The first-listed diagnosis of those physicians who did not receive computer support agreed with the clinical diagnosis in only 15.3% of the cases, while the score rose to 30.1% in those who received support ($p = 0.004$). This effect could mainly be attributed to two cases with somewhat uncommon diagnoses (Wolff–Parkinson–White syndrome and pericarditis), which were correctly identified by the computer. However, in one of three cases that had erroneous computer reports, physicians who received the misleading reports were likely to adopt the diagnostic error. Another study [249] involved 22 cardiologists who each interpreted 80 ECGs, half of them with a computer report. Computer-assisted ECG interpretation gave an average reduction in reading time of 28% and significantly improved concordance of the cardiologists' interpretations with a gold standard established by a panel of five expert electrocardiographers.

In still another study, ten senior house officers were recruited in an emergency department [250]. They interpreted 50 ECGs and five of these junior doctors had access to the computer report. Their interpretations and the computer reports were compared with the consensus interpretation of two experienced clinicians. The computer made only two major errors. Access to the computer report improved the physicians' error rate (22.4% without report versus 18.4% with), but not significantly.

Tsai et al. [251] examined the effects of correct and incorrect computer advice. They performed a randomized controlled trial in which 30 internal medicine residents each interpreted 23 ECGs with a total of 54 findings. The gold standard was established by two cardiologists. Computer interpretations were correct in almost 60% of the findings. Overall, without computer report, the physicians' interpretations were correct in 48.9% of the findings. With the reports, they interpreted 55.4% correctly ($p < 0.0001$). For the subset in which the computer findings agreed with the gold standard, physicians without the computer report interpreted 53.1% correctly; when the computer report was included, accuracy increased to 68.1% ($p < 0.0001$). When computer advice that did not agree with the gold standard was not given to the physicians, accuracy was 56.7%. Accuracy dropped to 48.3% when the incorrect computer report was provided ($p = 0.13$). In the subset of findings in which the computer interpretation was incorrect, physicians agreed with the incorrect interpretation twice as often when they were prompted by the computer than when they were not (67.7% versus 34.6%, $p < 0.0001$).

Most studies have shown a clear improvement in ECG reading of physicians when they are provided with a computer-generated report. "Computerized electrocardiography – an adjunct to the physician" is the title of an editorial by Laks and Selvester [252] hailing the CSE report. Indeed, but there is a danger that nonexpert physicians let themselves be persuaded

by an incorrect computer interpretation. This underlines the need for well-validated ECG computer programs that should perform at the level of expert electrocardiographers.

37.15 Rhythm Analysis Programs

Automatic identification of various arrhythmias poses major problems in the routine resting ECG. The rhythm interpretation logic in all clinically used programs follows a deterministic approach, using measurements (RR intervals and PR intervals, results of QRS wave typing, morphology of P waves, etc.) derived by the measurement program. The quality of the rhythm section rests largely on the quality of the measurement algorithms. While QRS complexes can be detected quite reliably, serious problems persist in P-wave recognition, especially in noisy recordings. For this reason, in many programs the logic has been constructed so as to allow for a degree of wave-recognition failure and measurement error [145, 253]. The record length poses another major problem. With the current multichannel recorders, usually 10 s of data are analyzed. This is too short for reliable detection of parasystole, for example, or other complicated arrhythmias. Providentially, the shortcomings of routine rhythm analysis programs are generally not too apparent, thanks to the low incidence of complex arrhythmias in the general hospital environment [254, 255].

The first extensive program for rhythm analysis was developed by Bonner and Schwetman in 1968 [256]. In a second program [257], five sets of three simultaneously recorded leads were used as input. The basic rhythm was derived from each 5 s record and a "combining" program made a decision as to the final rhythm statement. The total number of rhythm statements was forty.

These statements were also implemented in the AVA program [145]. The arrhythmia logic was divided into four main sections dealing, respectively, with regular and irregular rhythms and single and multiple aberrant beats. In the regular rhythm section, three major branchings were made depending on the ratio of P waves to the number of QRS complexes found (P:QRS). If P:QRS $\leq$ 0.25, entry into the AV-junctional section was made. If P:QRS $\geq$ 0.75, sinus rhythm was considered, as was AV-junctional rhythm depending on the polarity of the P wave. If 0.25 < P:QRS < 0.75, further tests were made and in the case of inconclusive results, the statement "regular rhythm" was printed. In the irregular-rhythm section, P:QRS was also used as a major branching point.

The same ratio (P:QRS) was also used in the more elaborate rhythm program developed by Plokker [253]. He considered 13 different types of arrhythmias, each represented by and programmed according to a detailed flowchart. Instead of decision trees, Wartak et al. [258] used decision tables. The whole arrhythmia logic is subdivided into a set of tables, which are linked to each other.

A comparison of results published by different investigators is difficult and sometimes delusive. For rhythm program evaluation, there are no approved databases comparable to that of CSE. The ideal case collection would contain sufficient numbers of records in every rhythm category and evaluation should provide figures for sensitivity and specificity for each category. However, arrhythmia cases tend to be in short supply. Evaluation is then often restricted to the sensitivity and specificity of sinus rhythm diagnosis, in which specificity is calculated with respect to all non-sinus cases. The results are thus heavily influenced by the diagnostic difficulty of the cases in the non-sinus category.

The results of a number of programs were evaluated by several authors. Bailey et al. [44] analyzed results of the IBM-Bonner program, and reported a sensitivity for arrhythmias of 87.2% while specificity was 98.2%. Of the 31 false-negative arrhythmias, the statement "undetermined rhythm" was made in 18 cases, all found to be atrial fibrillation. Sensitivity for atrial fibrillation was 85.5%. Of eight cases with second-degree AV block, the program correctly identified two. The prevalence of complex arrhythmias was too low to derive any meaningful conclusions.

Similar detection rates of cardiac arrhythmias have been reported for other processing systems [52, 239, 253, 259]. For example, Bernard et al. [239] reported an overall correct detection rate of 86% in 240 arrhythmias by the Telemed program. They did not specify whether the missed arrhythmias were incorrectly called sinus rhythm or any other arrhythmia.

A comparative study of five computer programs in the diagnosis of various types of AV block was undertaken by Shirataka et al. [260], using an ECG signal generator. Although all systems correctly detected normal sinus rhythm and first-degree AV block, only one system recognized second-degree AV block with classic Wenckebach periodicity, and no system was able to classify atypical Wenckebach periods. Most systems performed reasonably well for Mobitz II AV block, third-degree AV block, and ventricular bigeminy and trigeminy.

Plokker [253] tested the rhythm analysis of an early version of the MEANS program. On a set of 2,769 ECGs, he found a sensitivity for sinus rhythm of 96.6% and a specificity of 98.0%. Using the HP program, Thomson et al. [261] reported a sensitivity for sinus rhythm of 96.6% and a specificity of 97.0% on a set of 5,110 ECGs.

Several reports [255, 262, 263] were devoted to the rhythm analysis program of GE Health Technologies (formerly Marquette). Farrell et al. [263] used 70,000 physician-confirmed ECGs from four teaching hospitals. Patients with pacemakers were excluded. Primary rhythm statements of a new and a previous program version were compared with the confirmed interpretations. Overall disagreement decreased from 6.9% for the older version to 4.1% for the new version. Increased sensitivities were observed for sinus rhythm (98.2%), atrial fibrillation (89.0%), and AV-junctional rhythms (63.1%), while specificity and positive predictive value improved for all arrhythmias. However, specificity for sinus rhythm was 85.5%, which means that as much as 14.5% of abnormal rhythms were called sinus. This would disqualify such a program for arrhythmia case-finding purposes.

Using a nearly identical software version as in Farrell's study, Poon et al. [255] assessed the performance of the GE program in 4,297 consecutive ECGs recorded in a university teaching hospital. Over-reading was performed by either one of two cardiologists. Overall, 13.1% of the ECGs required revision of the computer's rhythm interpretation, but about half of these ECGs involved patients with pacemakers. In the unpaced population, sensitivity for sinus rhythm was 98.7%, but specificity was again rather low at 90.1%. For atrial fibrillation, sensitivity was 90.8% and specificity 98.9%. Sensitivity for atrial flutter was 61.0%, whereas sensitivity for atrial tachycardia was only 2.8%. It was concluded that physician over-reading remains mandatory, in particular to confirm a computer statement of normal sinus rhythm, or rhythm statements in patients with pacemakers.

In another study involving the GE 12SL program, 2,072 ECGs collected in a tertiary care hospital were processed by the computer and then over-read by two cardiologists [264]. In 9.9% of the ECGs there were significant disagreements between the computer and the cardiologists; 86% of these related to arrhythmias, conduction disorders, and electronic pacemakers. Sensitivities for atrial fibrillation and atrial flutter were 76.1% and 65.9%, respectively, at specificities of more than 99.5%.

Sinus rhythm appears uniformly well recognized, but other results depend quite heavily on the material analyzed, not only with respect to the mix of various arrhythmias, but also to the noise content of the database.

37.16 Serial Comparison Programs

Comparison with previous records is a part of normal routine in ECG reading. It must, therefore, also be seen as a necessary adjunct to computerized ECG analysis. A prerequisite is an efficient database management system for storage and retrieval of results. In the past, restricted storage capacity limited the number of records and the type of data that could be kept on line. Pryor et al. [265] developed the first serial ECG comparison program but the comparison was essentially limited to the final diagnostic statements. Others compared measurements as well [266]. In some systems, raw data from one representative cycle for up to three records were stored [267], or the entire record could potentially be regenerated in case of arrhythmias [143, 268].

Nowadays, with vastly expanded storage capacity and transmission and processing speed boosted to previously unimagined heights, technical limitations hardly seem to be a consideration. Nevertheless, an operational difficulty remains. The modern stand-alone microprocessor-based electrocardiograph is able to perform a complete ECG analysis but does not contain the information of the central management system. If one wants serial analysis, a way of communication with the management system must be chosen from several options, the most advanced being instantaneous wireless transmission of data [269, 270].

The more fundamental problem of serial comparison is that of semantics: which meaning must be attached to a difference in measurements or in diagnostic statements between successive interpretations? As is well known, there is a certain variability in recordings from 1 day to the next or from 1 year to the next [271, 272]. This variability is caused by differences in electrode placement, variations in depth of respiration, alterations in posture, changes in body fat, and by other factors [273]. Measurement changes from one tracing to the next should be given attention only if they exceed the natural variability. As mentioned earlier, in deterministic programs, it is quite possible that small, insubstantial measurement fluctuations around a threshold value cause a material difference in diagnostic statements [234]. But which of the statements in this borderline situation is the correct one? Each serial analysis program deals with this problem in its own way.

Different checks are made to ascertain whether or not changes are the result of a borderline crossover of decision criteria. As an option, a graphic display of trends in measurements and diagnostic statements has been implemented in some processing systems [274–276]. Also, serial comparison summary statements, such as "no significant change" or "descriptive differences only," have been proposed as a means of taking into account normal ECG fluctuations [277]. Alternative methods for improving the consistency of serial ECG analysis are the use of smooth decision functions rather than binary thresholds [278, 279], or VCG loop alignment (if not available as such, the VCGs may be derived from the two ECGs to be compared by mathematical transformation) [280, 281].

On the other hand, as long as the measurements are essentially identical, a good program will produce the same diagnostic result which may mean persisting in making the same error. Meanwhile, the initial statement may have been corrected by a reviewer [282]. Only if the corresponding changes are made in the central ECG management system may a serial analysis program take them into account in the comparison with a subsequent ECG from the same patient [277].

Most programs for serial ECG analysis use decision rules to arrive at their diagnostic interpretation [141, 163, 267, 283]. Two studies investigated the use of artificial neural networks. Sunemark et al. [281] described a neural network to classify serial changes indicative of newly developed infarcts, taking the consensus opinion of three interpreters as the reference. The input data consisted of measurements from the ECG and the reconstructed VCG. At 90% specificity, the use of only ECG or VCG measurements gave a sensitivity of 63% and 60%, respectively, and increased to 69% when measurements were combined. Ohlsson et al. [284] also used neural networks to detect acute MI based on either the current ECG only, or on the combination of the previous and the current ECGs. Acute MI was diagnosed according to characteristic chest pain, elevated enzyme levels, or characteristic ECG changes. There was a small but significant improvement in the neural network performance when a previous ECG was used as an additional input. On the same set of ECGs, the neural network appeared to perform better than two physicians, an experienced cardiologist and an intern.

No independent evaluation studies of different systems for serial ECG analysis have been published.

37.17 Computer Analysis of Pediatric Electrocardiograms

The ECG in children differs considerably in signal characteristics from that of the adult. Small children usually have high heart rates, and the recordings are often much noisier and show more baseline wander than in adults. There is a fast and profound evolution of electrocardiographic patterns especially in the first days and weeks after birth, but changes continue up to adolescence [285, 286]. Consequently, normal limits of ECG and VCG parameters are heavily dependent on age, and for diagnostic criteria, especially in young children, it is necessary to rely on extensive tables of values for amplitudes, durations, and angles [287–292]. Here, obviously, the computer can be of assistance. Also, congenital heart diseases can be quite complex and can produce a variety of electrocardiographic patterns. In addition, qualified readers of pediatric ECGs are rare and mostly located in university centers [293]. Inter- and intra-observer variability in reading pediatric ECGs was shown to be substantial [294]. These were the main incentives for the development of pediatric ECG programs.

In the past, the Mayo computer system routinely processed pediatric VCGs for some time [295], and in the VA Research Center for Cardiovascular Data, a large cooperative study has been undertaken in this field [296]. Other programs have been developed for pediatric VCG [163, 223] and 12-lead ECG [297–300]. The combination of ECG and synthesized VCG measurements to discriminate between mild RVH with terminal conduction delay and partial RBBB in children was described by Zhou et al. [301].

Relatively few evaluation studies of pediatric ECG programs have been performed. In a study of 248 pediatric ECGs that were diagnosed by ECG-independent means, the HP pediatric program had a 70% sensitivity and 82% specificity for RVH and a 38% sensitivity and 93% specificity for LVH [302].

Based on a test set of 642 ECGs diagnosed by two pediatric cardiologists, Rijnbeek et al. [300] assessed the performance of the pediatric version of the MEANS program (Table 37.4). Sensitivities for RVH, LVH, RBBB, and LBBB were 74%, 79%, 84%, and 75%, respectively, at specificities of at least 95%. The program employs continuous age-dependent normal limits that in a separate study were shown to be considerably different from those commonly used in children [292].

In a study by Hamilton et al. [303], the diagnoses of RVH and LVH by the Glasgow program was compared with those of two pediatric cardiologists. When the cardiologists were not provided with clinical information, sensitivity of

Table 37.4

Performance of the computer program PEDMEANS on a training set (n = 1,076) and test set (n = 642) of pediatric ECGs (from Rijnbeek et al. [300])

Abnormality	Training set		Test set	
	Sensitivity (%)	Specificity (%)	Sensitivity (%)	Specificity (%)
LVH	71.7	97.1	74.3	96.5
RVH	80.0	95.0	79.4	95.6
LBBB	86.4	97.9	84.0	95.3
RBBB	62.5	99.3	75.0	99.7

the program for RVH was 73% at a specificity of 97%, but sensitivity for LVH was only 25% at 96% specificity though the sensitivity for LVH increased to 44% at the same specificity when the clinical information was provided. Interestingly, if the cardiologists had disagreed initially with each other, their consensus opinion was twice as likely to be in agreement with the program.

Finally, pediatric ECG interpretations by the Marquette 12 SL program were compared with those of emergency department physicians in a 12-month prospective study, taking the interpretation by a pediatric electrophysiologist as the reference [304]. The computer proved to be more accurate than the physicians for interpretations considered to be of minimal or indeterminate clinical significance, but both performed poorly in interpreting the few cases of definite clinical significance (prolonged QTc, acute MI, supraventricular tachycardia, and atrial fibrillation).

37.18 Conclusion

In 1989, the late Jos Willems, the author of this chapter on computerized electrocardiography in the first edition of this handbook, wrote: "Nowadays computerized ECG analysis is being utilized widely in many medical institutions" and "Microprocessor-equipped electrocardiographs are proliferating and are on the verge of widespread application in smaller hospitals, general practitioners' offices and the health-screening environment." Now, in 2010, it will be hard to find a non-microprocessor-based electrocardiograph outside a museum for medical instruments, where it may stand next to an Einthoven string-galvanometer-based electrocardiograph invented in 1902. Willems also wrote: "Since 1982, definite progress has been made in the development of reference standards aimed at the evaluation of ECG measurement programs. This has largely been the result of the cooperative study "Common Standards for Quantitative Electrocardiography" (CSE project). Much work still needs to be done in the objective assessment of the diagnostic performance of ECG-analysis computer programs. Many challenges are still ahead . . .."

In almost 20 years since the closure of the CSE project, certainly much work has been done, but many challenges remain. The volume per annum of publications on computerized ECG analysis has steadily decreased. It looks as if a certain amount of saturation has set in. The providers of "intelligent" ECG equipment seem to be less keen on improving their diagnostic programs: has not the CSE study shown that programs rival the cardiologists' intelligence in diagnosis? But the time has not arrived to sit back complacently. It must be remembered that the CSE study applies to an idealized breed of ECGs. In real life, ECGs are not selected for good appearance and straightforward character. They may be of unshapely physiognomy due to combinations of abnormalities and be disfigured by noise, arrhythmias, and conduction defects. Here, the computer's painstakingly taught tricks for detecting waves and inflectional points are eclipsed by man's innate talents for pattern recognition. Especially P-wave detection and, connected with it, rhythm analysis need improvement and it would help if electrocardiographs would routinely acquire records of at least 30 s for this purpose. On the other hand, man is unreliable and, except where waveform recognition is suddenly led astray – a weakness that still should be amended – computer measurements are much more consistent. Presently, computer measurement of the QT interval is widely used for drug safety testing. In general, computer diagnosis is very specific, that is, a statement of "normal" can be relied on almost blindly and computerized ECG analysis is, therefore, an adequate screening instrument. Also, population screening by Minnesota coding through computer is much more reliable, faster, and cheaper than by hand. For clinical purposes, an abnormal computer classification still requires over-reading by an expert. The confrontation of the

reader with the computer report was shown to improve quality and consistency of diagnosis. The huge advantages offered by a computerized system for automatic reporting, filing, and retrieval do not have to be emphasized. Finally, on the list-to-do in computerized electrocardiography, we should put the further development of serial analysis and perfection of the diagnosis of acute coronary syndromes. For this latter purpose, well-validated data bases are necessary.

The electrocardiograph with diagnostic facilities is often called "intelligent." Shannon once exclaimed: "Man is a machine, man can think, therefore some machines can think." The reader may speculate whether the third term of this syllogism will at some point apply to the computerized ECG machine.

References

1. Turing, A.M., Computing machinery and intelligence. *Mind*, 1950;**59**: 433–460.
2. Rijlant, P.B.L., L'analyse par un calculateur analogique des electrocardiogrammes scalaires et vectoriels. *Bull. Acad. Royal Med. Belgique*, 1962;**2**: 363.
3. Rautaharju, P.M., The impact of computers on electrocardiography. *Eur. J. Cardiol.*, 1978;**8**: 237–248.
4. Taback, L., E. Marden, H.L. Mason, and H. Pipberger, Digital recording of electrocardiographic data for analysis by means of a digital electronic computer. *IRE Trans. Med. Electron.*, 1959;**6**: 167–171.
5. Pipberger, H.V., R.J. Arms, and F.W. Stallmann, Automatic screening of normal and abnormal electrocardiograms by means of a digital electronic computer. *Proc. Soc. Exp. Biol. Med.*, 1961;**106**: 130–132.
6. Stallmann, F.W. and H.V. Pipberger, Automatic recognition of electrocardiographic waves by digital computer. *Circ. Res.*, 1961;**9**: 1138–1143.
7. Cornfield, J., R.A. Dunn, C.D. Batchlor, and H.V. Pipberger, Multigroup diagnosis of electrocardiograms. *Comput. Biomed. Res.*, 1973;**6**: 97–120.
8. Pipberger, H.V., D. McCaughan, D. Littmann, H.A. Pipberger, J. Cornfield, R.A. Dunn, et al., Clinical application of a second generation electrocardiographic computer program. *Am. J. Cardiol.*, 1975;**35**: 597–608.
9. Caceres, C.A., C.A. Steinberg, S. Abraham, J. CW, J.M. McBride, and W.E. Tolles, et al., Computer extraction of electrocardiographic parameters. *Circulation*, 1962;**25**: 356–362.
10. Rautaharju, P.M., The current state of computer ECG analysis: a critique, in *Trends in Computer-Processed Electrocardiograms*, J.H. van Bemmel and J.L. Willems, Editors. Amsterdam: North-Holland, 1976, pp. 117–124.
11. Drazen, E.L., Use of computer-assisted ECG interpretation in the United States, in *Computers in Cardiology 1979*, K.L. Ripley and H.G. Ostrow, Editors. Long Beach: IEEE Comp Soc. 1979, pp. 83–85.
12. Drazen, E.L., N. Mann, R. Borun, M. Laks, and A. Bersen, Survey of computer-assisted electrocardiography in the United States. *J. Electrocardiol.*, 1988;**21**(Suppl): S98–104.
13. Macfarlane, P.W., A brief history of computer-assisted electrocardiography. *Methods Inf. Med.*, 1990;**29**: 272–281.
14. Rautaharju, P.M., M. Ariet, T.A. Pryor, R.C. Arzbaecher, J.J. Bailey, R. Bonner, et al., The quest for optimal electrocardiography. Task force III: computers in diagnostic electrocardiography. *Am. J. Cardiol.*, 1978;**41**: 158–170.
15. Pipberger, H.V., J. Cornfield, What ECG computer program to choose for clinical application. The need for consumer protection. *Circulation*, 1973;**47**: 918–920.
16. Frank, E., An accurate, clinically practical system for spatial vectorcardiography. *Circulation*, 1956;**13**: 737–749.
17. Rautaharju, P.M., H.W. Blackburn, H.K. Wolf, and M. Horacek, Computers in clinical electrocardiology. Is vectorcardiography becoming obsolete? *Adv. Cardiol.*, 1976;**16**: 143–156.
18. Dower, G.E., H.B. Machado, and J.A. Osborne, On deriving the electrocardiogram from vectoradiographic leads. *Clin. Cardiol.*, 1980;**3**: 87–95.
19. Edenbrandt, L. and O. Pahlm, Vectorcardiogram synthesized from a 12-lead ECG: superiority of the inverse Dower matrix. *J. Electrocardiol.*, 1988;**21**: 361–367.
20. Rubel, P., I. Benhadid, and J. Fayn, Quantitative assessment of eight different methods for synthesizing Frank VCGs from simultaneously recorded standard ECG leads. *J. Electrocardiol.*, 1992;**24**(Suppl): 197–202.
21. Macfarlane, P.W., M.P. Watts, and T.D.V. Lawrie, Hybrid electrocardiography, in *Optimization of Computer ECG Processing*, H.K. Wolf and P.W. Macfarlane, Editors. Amsterdam: North-Holland, 1980, pp. 57–61.
22. Kornreich, F. and P.M. Rautaharju, The missing waveform and diagnostic information in the standard 12 lead electrocardiogram. *J. Electrocardiol.*, 1981;**14**: 341–350.
23. Kornreich, F., The missing waveform information in the orthogonal electrocardiogram (Frank leads). I. Where and how can this missing waveform information be retrieved? *Circulation*, 1973;**48**: 984–995.
24. Kornreich, F., P. Smets, and J. Kornreich, About challenging the uniqueness of a new, so-called "optimal", "total" or "maximal" 9-lead system, in *Trends in Computer-Processed Electrocardiograms*, J.H. van Bemmel and J.L. Willems, Editors. Amsterdam: North-Holland, 1977, pp. 293–301.
25. Kornreich, F., R.L. Lux, and R.S. MacLeod, Map representation and diagnostic performance of the standard 12-lead ECG. *J. Electrocardiol.*, 1995;**28**(Suppl): 121–123.
26. Kors, J.A. and G. van Herpen, How many electrodes and where? A "poldermodel" for electrocardiography. *J. Electrocardiol.*, 2002;**35**(Suppl): 7–12.
27. Nelwan, S.P., J.A. Kors, S.H. Meij, J.H. van Bemmel, and M.L. Simoons, Reconstruction of the 12-lead electrocardiogram from reduced lead sets. *J. Electrocardiol.*, 2004;**37**: 11–18.
28. Dower, G.E., A. Yakush, S.B. Nazzal, R.V. Jutzy, and C.E. Ruiz, Deriving the 12-lead electrocardiogram from four (EASI) electrodes. *J. Electrocardiol.*, 1988;**21**(Suppl): S182–S187.

29. Burger, H.C. and J.B. Van Milaan, Heart-vector and leads. *Brit. Heart J.*, 1946;**8**: 157–161.
30. Mortara, D.W., Source consistency filtering. Application to resting ECGs. *J. Electrocardiol.*, 1992;**25**(Suppl): 200–206.
31. Kors, J.A. and G. van Herpen, Accurate automatic detection of electrode interchange in the electrocardiogram. *Am. J. Cardiol.*, 2001;**88**: 396–399.
32. Burger, H.C., A. van Brummelen, and G. van Herpen, Compromise in vectorcardiography. II. Alterations of coefficients as a means of adapting one lead system to another. Subjective and mathematical comparison of four systems of VCG. *Am. Heart J.*, 1962;**64**: 666–678.
33. Surawicz, B., H. Uhley, R. Borun, M. Laks, L. Crevasse, K. Rosen, et al., The quest for optimal electrocardiography. Task force I: standardization of terminology and interpretation. *Am. J. Cardiol.*, 1978;**41**: 130–145.
34. The CSE Working Party, Recommendations for measurement standards in quantitative electrocardiography. *Eur. Heart J.*, 1985;**6**: 815–825.
35. Willems, J.L., E.O. Robles de Medina, R. Bernard, P. Coumel, C. Fisch, D. Krikler, et al., Criteria for intraventricular conduction disturbances and pre-excitation. World Health Organizational/International Society and Federation for Cardiology Task Force Ad Hoc. *J. Am. Coll. Cardiol.*, 1985;**5**: 1261–1275.
36. Kadish, A.H., A.E. Buxton, H.L. Kennedy, B.P. Knight, J.W. Mason, C.D. Schuger, et al., ACC/AHA clinical competence statement on electrocardiography and ambulatory electrocardiography: A report of the ACC/AHA/ACP-ASIM task force on clinical competence. *Circulation*, 2001;**104**: 3169–3178.
37. van Bemmel, J.H., J.A. Kors, and G. van Herpen, Methodology of the modular ECG analysis system MEANS. *Methods Inf. Med.*, 1990;**29**: 346–353.
38. Talmon, J.L. and J.H. van Bemmel, The advantage of modular software design in computerized ECG analysis. *Med. Inform.*, 1986;**11**: 117–128.
39. Willems, J.L. and J. Pardaens, Differences in measurement results obtained by four different ECG computer programs, in *Computers in Cardiology 1977*, H.G. Ostrow and K.L. Ripley, Editors. Long Beach: IEEE Comput Soc, 1977, pp. 115–121.
40. Willems, J.L., A plea for common standards in computer aided ECG analysis. *Comput. Biomed. Res.*, 1980;**13**: 120–131.
41. Pipberger, H.V., Comparative evaluation of electrocardiography computer programs, in *Computers in Cardiology 1976*, H.G. Ostrow and K.L. Ripley, Editors. Long Beach: IEEE Computer Society, 1976, pp. 85–88.
42. Crevasse, L. and M.A. Ariet, New scalar electrocardiographic computer program. Clinical evaluation. *JAMA*, 1973;**226**: 1089–1093.
43. Romhilt, D.W. and E.H. Estes, A point-score system for the ECG diagnosis of left ventricular hypertrophy. *Am. Heart J.*, 1968;**75**: 752–758.
44. Bailey, J.J., S.B. Itscoitz, J.W. Hirshfeld, L.E. Grauer, and M.R.A. Horton, Method for evaluating computer programs for electrocardiographic interpretation. I. Application to the experimental IBM program of 1971. *Circulation*, 1974;**50**: 73–79.
45. Bailey, J.J., S.B. Itscoitz, L.E. Grauer, J.W. Hirshfeld, and M.R.A. Horton, Method for evaluating computer programs for electrocardiographic interpretation. II. Application to version D of the PHS program and the Mayo clinic program of 1968. *Circulation*, 1974;**50**: 80–87.
46. Hodges, M., A clinical evaluation of the H-P ECG analysis program: program accuracy and value of adjustable criteria, in *Computers in Cardiology 1979*, K.L. Ripley and H.G. Ostrow, Editors. Long Beach: IEEE Comput Soc, 1979, pp. 167–170.
47. Garcia, R., G.M. Breneman, and S. Goldstein, Electrocardiogram computer analysis. Practical value of the IBM Bonner-2 (V2 MO) program. *J. Electrocardiol.*, 1981;**14**: 283–288.
48. Caceres, C.A. and H.M. Hochberg, Performance of the computer and physician in the analysis of the electrocardiogram. *Am. Heart J.*, 1970;**79**: 439–443.
49. Bourdillon, P.J. and D. Kilpatrick, Clinicians, the Mount Sinai program and the Veterans' Administration program evaluated against clinico-pathological data derived independently of the electrocardiogram. *Eur. J. Cardiol.*, 1978;**8**: 395–412.
50. Willems, J.L., H. Ector, J. Pardaens, J. Piessens, and H. de Geest, Computer and conventional ECG analysis: correlation with cineangiographic data. *Adv. Cardiol.*, 1978;**21**: 177–180.
51. Khadr, N.E., C.L. Bray, D.C. Beton, R.S. Croxson, M. Hughes, C. Jeffery, et al., Diagnosis of left ventricular hypertrophy and myocardial infarction by Bonner/IBM program verified by ECG-independent evidence, in *Computers in Cardiology*, K.L. Ripley and H.G. Ostrow, Editors. Long Beach: IEEE Comput Soc, 1979, pp. 93–97.
52. Macfarlane, P.W., D.I. Melville, M.R. Horton, and J.J. Bailey, Comparative evaluation of the IBM (12-lead) and Royal Infirmary (orthogonal three-lead) ECG computer programs. *Circulation*, 1981;**63**: 354–359.
53. Willems, J.L., E. Lesaffre, and J. Pardaens, Comparison of the classification ability of the electrocardiogram and vectorcardiogram. *Am. J. Cardiol.*, 1987;**59**: 119–124.
54. Zywietz, C. and B. Schneider, Editors. *Computer Application in ECG and VCG Analysis*. Amsterdam: North-Holland, 1973.
55. van Bemmel, J.H. and J.L. Willems, Editors. *Trends in Computer-Processed Electrocardiograms*. Amsterdam: North-Holland, 1977.
56. Wolf, H.K. and P.W. Macfarlane, Editors. *Optimization of Computer ECG Processing*. Amsterdam: North-Holland, 1980.
57. Willems, J.L., P. Arnaud, R. Degani, P.W. Macfarlane, J.H. van Bemmel, and C. Zywietz, *Protocol for the Concerted Action Project "Common Standards for Quantitative Electrocardiography"*. Leuven: ACCO, 1980.
58. The CSE European Working Party, An approach to measurement standards in computer ECG analysis, in *Optimization of Computer ECG Processing*, H.K. Wolf and P.W. Macfarlane, Editors. Amsterdam: North-Holland, 1980, pp. 135–137.
59. Willems, J.L., P. Arnaud, J.H. van Bemmel, R. Degani, P.W. Macfarlane, C. Zywietz, Common standards for quantitative electrocardiography: goals and main results. CSE Working Party. *Methods Inf. Med.*, 1990;**29**: 263–271.
60. Willems, J.L., P. Arnaud, J.H. van Bemmel, P.J. Bourdillon, R. Degani, B. Denis, et al., Establishment of a reference library for evaluating computer ECG measurement programs. *Comput. Biomed. Res.*, 1985;**18**: 439–457.
61. Willems, J.L., P. Arnaud, J.H. van Bemmel, P.J. Bourdillon, R. Degani, B. Denis, et al., A reference data base for multilead electrocardiographic computer measurement programs. *J. Am. Coll. Cardiol.*, 1987;**10**: 1313–1321.
62. Willems, J.L., P. Arnaud, J.H. van Bemmel, P.J. Bourdillon, C. Brohet, S. Dalla Volta, et al., Assessment of the performance of electrocardiographic computer programs with the use of a reference data base. *Circulation*, 1985;**71**: 523–534.

63. Willems, J.L., *Common Standards for Quantitative Electrocardiography. CSE Atlas*. Referee Results First Phase Library – Data Set 1. Leuven: ACCO, 1983.
64. Willems, J.L., *Common Standards for Quantitative Electrocardiography. CSE Multilead Atlas*. Measurement Results – Data Set 3. Leuven: ACCO, 1988.
65. Willems, J.L., *Common Standards for Quantitative Electrocardiography*, 4th Progress Report. Leuven: ACCO, 1984.
66. Willems, J.L., *Common Standards for Quantitative Electrocardiography*, 10th Progress Report. Leuven: ACCO, 1990.
67. Berson, A.S., Analog-to-digital conversion, in: *Computer Application on ECG and VCG Analysis*, C. Zywietz and R. Schneider, Editors. Amsterdam: North-Holland, 1973, pp. 57–72.
68. Berson, A.S., T.A. Ferguson, C.D. Batchlor, R.A. Dunn, and H.V. Pipberger, Filtering and sampling for electrocardiographic data processing. *Comput. Biomed. Res.*, 1977;**10**: 605–616.
69. Bailey, J.J., A.S. Berson, A. Garson, L.G. Horan, P.W. Macfarlane, D.W. Mortara, et al., Recommendations for standardization and specifications in automated electrocardiography: bandwidth and digital signal processing. A report for health professionals by an ad hoc writing group of the Committee on Electrocardiography and Cardiac Electrophysiology of the Council on Clinical Cardiology, American Heart Association. *Circulation*, 1990;**81**: 730–739.
70. Rijnbeek, P.R., J.A. Kors, and M. Witsenburg, Minimum bandwidth requirements for recording of pediatric electrocardiograms. *Circulation*, 2001;**104**: 3087–3090.
71. Hedén, B., M. Ohlsson, L. Edenbrandt, R. Rittner, O. Pahlm, and C. Peterson, Artificial neural networks for recognition of electrocardiographic lead reversal. *Am. J. Cardiol.*, 1995;**75**: 929–933.
72. Schijvenaars, R.J., J.A. Kors, G. van Herpen, and J.H. van Bemmel, A method to reduce the effect of electrode position variations on automated ECG interpretation. *J. Electrocardiol.*, 1995;**28**: 350–351.
73. Brodnick, D., A method to locate electrode placement. *J. Electrocardiol.*, 2000;**33**(Suppl): 211–218.
74. McManus, C.D., K.D. Neubert, and E. Cramer, Characterization and elimination of AC noise in electrocardiograms: a comparison of digital filtering methods. *Comput. Biomed. Res.*, 1993;**26**: 48–67.
75. Cramer, E., C.D. McManus, and D. Neubert, Estimation and removal of power line interference in the electrocardiogram: a comparison of digital approaches. *Comput. Biomed. Res.*, 1987;**20**: 12–28.
76. Lynn, P.A., Online digital filters for biological signals: some fast designs for a small computer. *Med. Biol. Eng. Comput.*, 1977;**15**: 534–540.
77. Weaver, C.S., J. von der Groeben, P.E. Mantey, J.G. Toole, C.A. Cole, J.W. Fitzgerald, et al., Digital filtering with applications to electrocardiogram processing. *IEEE Trans. Audio Electroacoust.*, 1968;**16**: 350–391.
78. Levkov, C., G. Michov, R. Ivanov, and I.K. Daskalov, Subtraction of 50 Hz interference from the electrocardiogram. *Med. Biol. Eng. Comput.*, 1984;**22**: 371–373.
79. Dotsinsky, I. and T. Stoyanov, Power-line interference cancellation in ECG signals. *Biomed. Instrum. Technol.*, 2005;**39**: 155–162.
80. Levkov, C., G. Mihov, R. Ivanov, I. Daskalov, I. Christov, and I. Dotsinsky, Removal of power-line interference from the ECG: a review of the subtraction procedure. *Biomed. Eng. Online*, 2005;**4**: 50.
81. Widrow, B., J.R. Glover, M. McCool, J. Kaunitz, C.S. Williams, R.H. Hearn, et al., Adaptive noise cancelling: principles and applications. *Proc. IEEE*, 1975;**63**: 1692–1716.
82. Glover, J.R., Adaptive noise canceling applied to sinusoidal interferences. *IEEE Trans. Acoust. Speech Signal Process.*, 1977;**25**: 484–491.
83. Thakor, N.V. and Y.S. Zhu, Applications of adaptive filtering to ECG analysis: noise cancellation and arrhythmia detection. *IEEE Trans. Biomed. Eng.*, 1991;**38**: 785–794.
84. Mortara, D.W., Digital filters for ECG signals, in *Computers in Cardiology 1977*, H.G. Ostrow and K.L. Ripley, Editors. New York: IEEE Comput Soc, 1977, pp. 511–514.
85. Talmon, J.L., *Pattern recognition of the ECG. A structured analysis*, dissertation. Amsterdam: Free University, 1983.
86. Ahlstrom, M.L. and W.J. Tompkins, Digital filters for real-time ECG signal processing using microprocessors. *IEEE Trans. Biomed. Eng.*, 1985;**32**: 708–713.
87. Hamilton, P.S., A comparison of adaptive and nonadaptive filters for reduction of power line interference in the ECG. *IEEE Trans. Biomed. Eng.*, 1996;**43**: 105–109.
88. Glover, J.R., Comments on "Digital filters for real-time ECG signal processing using microprocessors". *IEEE Trans. Biomed. Eng.*, 1987;**34**: 962–963.
89. Pipberger, H.V., R.C. Arzbaecher, A.S. Berson, S.A. Briller, D.A. Brody, N.C. Flowers, et al., Recommendations for standardization of leads and of specifications for instruments in electrocardiography and vectorcardiography: report of the Committee on Electrocardiography, American Heart Association. *Circulation*, 1975;**52**: 11–31.
90. Bailey, J.J., The triangular wave test for electrocardiographic devices: a historical perspective. *J. Electrocardiol.*, 2004;**37**(Suppl): 71–73.
91. van Alste, J.A., W. van Eck, and O.E. Herrmann, ECG baseline wander reduction using linear phase filters. *Comput. Biomed. Res.*, 1986;**19**: 417–427.
92. Sörnmo, L., Time-varying digital filtering of ECG baseline wander. *Med. Biol. Eng. Comput.*, 1993;**31**: 503–508.
93. Shusterman, V., S.I. Shah, A. Beigel, and K.P. Anderson, Enhancing the precision of ECG baseline correction: selective filtering and removal of residual error. *Comput Biomed Res* 2000; **33**:144–160.
94. Macfarlane, P.W., J. Peden, G. Lennox, M.P. Watts, and T.D.V. Lawrie, The Glasgow system, in *Trends in Computer-Processed Electrocardiograms*, J.H. van Bemmel and J.L. Willems, Editors. Amsterdam: North-Holland, 1977, pp. 143–150.
95. Boucheham, B., Y. Ferdi, and M.C. Batouche, Recursive versus sequential multiple error measures reduction: a curve simplification approach to ECG data compression. *Comput. Methods Programs Biomed.*, 2005;**78**: 1–10.
96. Douglas, D.H. and T.K. Peucker, Algorithms for the reduction of the number of points required to represent a digitized line or its caricature. *Can. Cartographer*, 1973;**10**: 112–122.
97. Meyer, C.R. and H.N. Keiser, Electrocardiogram baseline noise estimation and removal using cubic splines and state-space computation techniques. *Comput. Biomed. Res.*, 1977;**10**: 459–470.
98. Gradwohl, J.R., E.W. Pottala, M.R. Horton, and J.J. Bailey, Comparison of two methods for removing baseline wander in the ECG, in *Computers in Cardiology 1988*, K.L. Ripley, Editor. Los Angeles: IEEE Comput Soc, 1988, pp. 493–496.

99. Froning, J.N., M.D. Olson, and V.F. Froelicher, Problems and limitations of ECG baseline estimation and removal using a cubic spline technique during exercise ECG testing: recommendations for proper implementation. *J. Electrocardiol.*, 1988;**21**(Suppl): S149–157.
100. Pottala, E.W., J.J. Bailey, M.R. Horton, and J.R. Gradwohl, Suppression of baseline wander in the ECG using a bilinearly transformed, null-phase filter. *J. Electrocardiol.*, 1989;**22**(Suppl): 243–247.
101. Frankel, R.A., E.W. Pottala, R.W. Bowser, and J.J. Bailey, A filter to suppress ECG baseline wander and preserve ST-segment accuracy in a real-time environment. *J. Electrocardiol.*, 1991;**24**: 315–323.
102. Longini, R.L., J.P. Giolma, C. Wall, and R.F. Quick, Filtering without phase shift. *IEEE Trans. Biomed. Eng.*, 1975;**22**: 432–433.
103. de Pinto, V., Filters for the reduction of baseline wander and muscle artifact in the ECG. *J. Electrocardiol.*, 1992;**25**(Suppl): 40–48.
104. van Alste, J.A. and T.S. Schilder, Removal of base-line wander and power-line interference from the ECG by an efficient FIR filter with a reduced number of taps. *IEEE Trans. Biomed. Eng.*, 1985;**32**: 1052–1060.
105. Jane, R., P. Laguna, N.V. Thakor, and P. Caminal, Adaptive baseline wander removal in the ECG: comparative analysis with cubic spline technique, in *Computers in Cardiology 1992*, A. Murray and R.C. Arzbaecher, Editors. Los Alamitos: IEEE Comput Soc, 1992, pp. 143–146.
106. Laguna, P., R. Jane, O. Meste, P.W. Poon, P. Caminal, H. Rix, et al., Adaptive filter for event-related bioelectric signals using an impulse correlated reference input: comparison with signal averaging techniques. *IEEE Trans. Biomed. Eng.*, 1992;**39**: 1032–1044.
107. Moody, G.B. and R.G. Mark, The impact of the MIT-BIH arrhythmia database. *IEEE Eng. Med. Biol. Mag.*, 2001;**20**: 45–50.
108. Park, K.L., K.J. Lee, and H.R. Yoon, Application of a wavelet adaptive filter to minimise distortion of the ST-segment. *Med. Biol. Eng. Comput.*, 1998;**36**: 581–586.
109. Taddei, A., G. Distante, M. Emdin, P. Pisani, G.B. Moody, C. Zeelenberg, et al., The European ST-T database: standard for evaluating systems for the analysis of ST-T changes in ambulatory electrocardiography. *Eur. Heart J.*, 1992;**13**: 1164–1172.
110. Chu, C.H. and E.J. Delp, Nonlinear methods in electrocardiogram signal processing. *J. Electrocardiol.*, 1990;**23**(Suppl): 192–197.
111. Sun, Y., K. Chan, and S.M. Krishnan, ECG signal conditioning by morphological filtering. *Comput. Biol. Med.*, 2002;**32**: 465–479.
112. Chu, C.H. and E.J. Delp, Impulsive noise suppression and background normalization of electrocardiogram signals using morphological operators. *IEEE Trans. Biomed. Eng.*, 1989;**36**: 262–273.
113. Haralick, R.M., S.R. Sternberg, and X. Zhuang, Image analysis using mathematical morphology. *IEEE Trans. Pattern Anal. Mach. Intell.*, 1987;**9**: 532–550.
114. Talmon, J.L., J.A. Kors, and J.H. van Bemmel, Adaptive Gaussian filtering in routine ECG/VCG analysis. *IEEE Trans. Acoust. Speech Signal Process.*, 1986;**34**: 527–534.
115. Hodson, E.K., D.R. Thayer, and C. Franklin, Adaptive Gaussian filtering and local frequency estimates using local curvature analysis. *IEEE Trans. Acoust. Speech Signal Process.*, 1981;**29**: 854–859.
116. Wei, D., E. Harasawa, and H. Hosaka, A low-distortion filter method to reject muscle noise in multi-lead electrocardiogram systems. *Front Med. Biol. Eng.*, 1999;**9**: 315–330.
117. Acar, B. and H. Koymen, SVD-based on-line exercise ECG signal orthogonalization. *IEEE Trans. Biomed. Eng.*, 1999;**46**: 311–321.
118. Paul, J.S., M.R. Reddy, and V.J. Kumar, A transform domain SVD filter for suppression of muscle noise artefacts in exercise ECG's. *IEEE Trans. Biomed. Eng.*, 2000;**47**: 654–663.
119. Nikolaev, N., A. Gotchev, K. Egiazarian, and Z. Nikolov, Suppression of electromyogram interference on the electrocardiogram by transform domain denoising. *Med. Biol. Eng. Comput.*, 2001;**39**: 649–655.
120. Raphisak, P., S.C. Schuckers, and A. de Jongh Curry, An algorithm for EMG noise detection in large ECG data, in *Computers in Cardiology 2004*, A. Murray, Editor. Piscataway, NJ: IEEE Comput Soc, 2004, pp. 369–372.
121. Brohet, C.R., C. Derwael, A. Robert, and R. Fesler, Methodology of ECG interpretation in the Louvain program. *Methods Inf. Med.*, 1990;**29**: 403–409.
122. Willems, J.L., *Common Standards for Quantitative Electrocardiography*, 2nd CSE Progress Report. Leuven: ACCO, 1982.
123. Pipberger, H.V., C.D. McManus, and H.A. Pipberger, Methodology of ECG interpretation in the AVA program. *Methods Inf. Med.*, 1990;**29**: 337–340.
124. Helfenbein, E.D., J.M. Lindauer, S.H. Zhou, R.E. Gregg, and E.C. Herleikson, A software-based pacemaker pulse detection and paced rhythm classification algorithm. *J. Electrocardiol.*, 2002;**35**(Suppl): 95–103.
125. Hamilton, P.S. and W.J. Tompkins, Quantitative investigation of QRS detection rules using the MIT/BIH arrhythmia database. *IEEE Trans. Biomed. Eng.*, 1986;**33**: 1157–1165.
126. Friesen, G.M., T.C. Jannett, M.A. Jadallah, S.L. Yates, S.R. Quint, and H.T. Nagle, A comparison of the noise sensitivity of nine QRS detection algorithms. *IEEE Trans. Biomed. Eng.*, 1990;**37**: 85–98.
127. Hu, Y.H., W.J. Tompkins, J.L. Urrusti, and V.X. Afonso, Applications of artificial neural networks for ECG signal detection and classification. *J. Electrocardiol.*, 1993;**26**(Suppl): 66–73.
128. Suppappola, S. and Y. Sun, Nonlinear transforms of ECG signals for digital QRS detection: a quantitative analysis. *IEEE Trans. Biomed. Eng.*, 1994;**41**: 397–400.
129. Afonso, V.X., W.J. Tompkins, T.Q. Nguyen, and S. Luo, ECG beat detection using filter banks. *IEEE Trans. Biomed. Eng.*, 1999;**46**: 192–202.
130. Kohler, B.U., C. Hennig, and R. Orglmeister, The principles of software QRS detection. *IEEE Eng. Med. Biol. Mag.*, 2002;**21**: 42–57.
131. Martinez, J.P., R. Almeida, S. Olmos, A.P. Rocha, and P. Laguna, A wavelet-based ECG delineator: evaluation on standard databases. *IEEE Trans. Biomed. Eng.*, 2004;**51**: 570–581.
132. Pahlm, O. and L. Sörnmo, Software QRS detection in ambulatory monitoring—a review. *Med. Biol. Eng. Comput.*, 1984;**22**: 289–297.
133. Li, C., C. Zheng, and C. Tai, Detection of ECG characteristic points using wavelet transforms. *IEEE Trans. Biomed. Eng.*, 1995;**42**: 21–28.
134. Kadambe, S., R. Murray, and G.F. Boudreaux-Bartels, Wavelet transform-based QRS complex detector. *IEEE Trans. Biomed. Eng.*, 1999;**46**: 838–848.
135. Vijaya, G., V. Kumar, and H.K. Verma, ANN-based QRS-complex analysis of ECG. *J. Med. Eng. Technol.*, 1998;**22**: 160–167.

136. Poli, R., S. Cagnoni, and G. Valli, Genetic design of optimum linear and nonlinear QRS detectors. *IEEE Trans. Biomed. Eng.*, 1995;**42**: 1137–1141.
137. Belforte, G., R. De Mori, and F. Ferraris, A contribution to the automatic processing of electrocardiograms using syntactic methods. *IEEE Trans. Biomed. Eng.*, 1979;26: 125–136.
138. Papakonstantinou, G., E. Skordalakis, and F. Gritzali, An attribute grammar for QRS detection. *Pattern Recog.*, 1986;**19**: 297–303.
139. Skordalakis, E., Syntactic ECG processing: a review. *Pattern Recog.*, 1986;**19**: 305–313.
140. Kors, J.A., J.L. Talmon, and J.H. van Bemmel, Multilead ECG analysis. *Comput. Biomed. Res.*, 1986;**19**: 28–46.
141. Macfarlane, P.W., B. Devine, S. Latif, S. McLaughlin, D.B. Shoat, and M.P. Watts, Methodology of ECG interpretation in the Glasgow program. *Methods Inf. Med.*, 1990;**29**: 354–361.
142. Christov, I., G. Bortolan, and I. Daskalov, Automatic detection of atrial fibrillation and flutter by wave rectification method. *J. Med. Eng. Technol.*, 2001;**25**: 217–221.
143. Balda, R.A., G. Diller, E. Deardorff, J.C. Doue, and P. Hsieh, The HP ECG analysis program, in *Trends in Computer-Processed Electrocardiograms*, J.H. van Bemmel and J.L. Willems, Editors. Amsterdam: North-Holland, 1977, pp. 197–204.
144. Laguna, P., R. Jane, and P. Caminal, Automatic detection of wave boundaries in multilead ECG signals: validation with the CSE database. *Comput. Biomed. Res.*, 1994;**27**: 45–60.
145. Willems, J.L. and H.V. Pipberger, Arrhythmia detection by digital computer. *Comput. Biomed. Res.*, 1972;**5**: 273–278.
146. McManus, C.D., A re-examination of automatic P-wave recognition methods, in *Optimization of Computer ECG Processing*, H.K. Wolf and P.W. Macfarlane, Editors. Amsterdam: North-Holland, 1980, pp. 121–127.
147. Bonner, R.E. and H.D. Schwetman, Computer diagnosis of electrocardiograms. II. A computer program for EKG measurements. *Comput. Biomed. Res.*, 1968;**1**: 366–386.
148. Hengeveld, S.J. and J.H. Bemmel, Computer detection of P-waves. *Comput. Biomed. Res.*, 1976;**9**: 125–132.
149. Schnyders, H.C. and M. Jordan, Energy correlation technique for small P-wave detection in the presence of noise, in *Computers in Cardiology 1980*, K.L. Ripley and H.G. Ostrow, Editors. Los Angeles: IEEE Comput Soc, 1980, pp. 161–164.
150. Gritzali, F., G. Frangakis, and G. Papakonstantinou, Detection of the P and T waves in an ECG. *Comput. Biomed. Res.*, 1989;**22**: 83–91.
151. Talmon, J.L., J.A. Kors, and J.H. van Bemmel, Algorithms for the detection of events in electrocardiograms. *Comput. Methods Programs Biomed.*, 1986;**22**: 149–161.
152. Taha, B., S. Reddy, Q. Xue, and S. Swiryn, Automated discrimination between atrial fibrillation and atrial flutter in the resting 12-lead electrocardiogram. *J. Electrocardiol.*, 2000;**33**(Suppl): 123–125.
153. Giraldo, B.F., P. Laguna, R. Jane, and P. Caminal, Automatic detection of atrial fibrillation and flutter using the differentiated ECG signal, in *Computers in Cardiology 1995*, A. Murray and R.C. Arzbaecher, Editors. Piscataway, NJ: IEEE Comput Soc, 1995, pp. 369–372.
154. Bonner, R.E., L. Crevasse, M.I. Ferrer, and J.C. Greenfield, A new computer program for analysis of scalar electrocardiograms. *Comput. Biomed. Res.*, 1972;**5**: 629–653.
155. van Bemmel, J.H. and S.J. Hengeveld, Clustering algorithm for QRS and ST-T waveform typing. *Comput. Biomed. Res.*, 1973;**6**: 442–456.
156. Simoons, M.L., H.B. Boom, and E. Smallenburg, On-line processing of orthogonal exercise electrocardiograms. *Comput. Biomed. Res.*, 1975;**8**: 105–117.
157. Moraes, J.C.T.B., M.O. Seixas, F.N. Vilani, and E.V. Costa, A real time QRS complex classification method using Mahalanobis distance, in *Computers in Cardiology 2002*, A. Murray, Editor. Piscataway, NJ: IEEE Comput Soc, 2002, pp. 201–204.
158. Lagerholm, M., C. Peterson, G. Braccini, L. Edenbrandt, and L. Sörnmo, Clustering ECG complexes using hermite functions and self-organizing maps. *IEEE Trans. Biomed. Eng.*, 2000;**47**: 838–848.
159. Hu, Y.H., A patient-adaptable ECG beat classifier using a mixture of experts approach. *IEEE Trans. Biomed. Eng.*, 1997;**44**: 891–900.
160. Wieben, O., V.X. Afonso, and W.J. Tompkins, Classification of premature ventricular complexes using filter bank features, induction of decision trees and a fuzzy rule-based system. *Med. Biol. Eng. Comput.*, 1999;**37**: 560–565.
161. de Chazal, P., M. O'Dwyer, and R.B. Reilly, Automatic classification of heartbeats using ECG morphology and heartbeat interval features. *IEEE Trans. Biomed. Eng.*, 2004;**51**: 1196–1206.
162. Christov, I., I. Jekova, and G. Bortolan, Premature ventricular contraction classification by the Kth nearest-neighbours rule. *Physiol. Meas.*, 2005;**26**: 123–130.
163. Zywietz, C., D. Borovsky, G. Gotsch, and G. Joseph, Methodology of ECG interpretation in the Hannover program. *Methods Inf. Med.*, 1990;**29**: 375–385.
164. Rautaharju, P.M., P.J. MacInnis, J.W. Warren, H.K. Wolf, P.M. Rykers, and H.P. Calhoun, Methodology of ECG interpretation in the Dalhousie program; NOVACODE ECG classification procedures for clinical trials and population health surveys. *Methods Inf. Med.*, 1990;**29**: 362–374.
165. Rompelman, O. and H.H. Ros, Coherent averaging technique: a tutorial review. Part 1: Noise reduction and the equivalent filter. *J. Biomed. Eng.*, 1986;**8**: 24–29.
166. Rompelman, O. and H.H. Ros, Coherent averaging technique: a tutorial review. Part 2: Trigger jitter, overlapping responses and non-periodic stimulation. *J. Biomed. Eng.*, 1986;**8**: 30–35.
167. Mertens, J. and D.W. Mortara, A new algorithm for QRS averaging, in *Computers in Cardiology 1984*, K.L. Ripley, Editor. Long Beach: IEEE Comput Soc, 1984, pp. 367–369.
168. Arnaud, P., P. Rubel, D. Morlet, J. Fayn, and M.C. Forlini, Methodology of ECG interpretation in the Lyon program. *Methods Inf. Med.*, 1990;**29**: 393–402.
169. Goetowski, C.R., The Telemed system, in *Trends in Computer-Processed Electrocardiograms*, J.H. van Bemmel and J.L. Willems, Editors. Amsterdam: North-Holland, 1977, pp. 207–210.
170. Degani, R. and G. Bortolan, Methodology of ECG interpretation in the Padova program. *Methods Inf. Med.*, 1990;**29**: 386–392.
171. Willems, J.L., C. Zywietz, P. Arnaud, J.H. van Bemmel, R. Degani, and P.W. Macfarlane, Influence of noise on wave boundary recognition by ECG measurement programs. Recommendations for preprocessing. *Comput. Biomed. Res.*, 1987;**20**: 543–562.
172. Zywietz, C., J.L. Willems, P. Arnaud, J.H. van Bemmel, R. Degani, P.W. Macfarlane, et al., Stability of computer ECG amplitude

measurements in the presence of noise. *Comput. Biomed. Res.*, 1990;**23**: 10–31.
173. Day, C.P., J.M. McComb, and R.W. Campbell, QT dispersion: an indication of arrhythmia risk in patients with long QT intervals. *Br. Heart J.*, 1990;**63**: 342–344.
174. Kors, J.A., G. van Herpen, and J.H. van Bemmel, QT dispersion as an attribute of T-loop morphology. *Circulation*, 1999;**99**: 1458–1463.
175. Rautaharju, P.M., QT and dispersion of ventricular repolarization: the greatest fallacy in electrocardiography in the 1990s. *Circulation*, 1999;**99**: 2477–2478.
176. Malik, M., B. Acar, Y. Gang, Y.G. Yap, K. Hnatkova, and A.J. Camm, QT dispersion does not represent electrocardiographic interlead heterogeneity of ventricular repolarization. *J. Cardiovasc. Electrophysiol.*, 2000;**11**: 835–843.
177. van Herpen, G., H.J. Ritsema van Eck, and J.A. Kors, The evidence against QT dispersion. *Int. J. Bioelectromagn.*, 2003;**5**: 231–233.
178. Ritsema van Eck, H.J., J.A. Kors, and G. van Herpen, The U wave in the electrocardiogram: a solution for a 100-year-old riddle. *Cardiovasc. Res.*, 2005;**67**: 256–262.
179. Nygards, M.E. and L. Sörnmo, Delineation of the QRS complex using the envelope of the e.c.g. *Med. Biol. Eng. Comput.*, 1983;**21**: 538–547.
180. van Bemmel, J.H., C. Zywietz, and J.A. Kors, Signal analysis for ECG interpretation. *Methods Inf. Med.*, 1990;**29**: 317–329.
181. McLaughlin, N.B., R.W. Campbell, and A. Murray, Comparison of automatic QT measurement techniques in the normal 12 lead electrocardiogram. *Br. Heart J.*, 1995;**74**: 84–89.
182. McLaughlin, N.B., R.W. Campbell, and A. Murray, Accuracy of four automatic QT measurement techniques in cardiac patients and healthy subjects. *Heart*, 1996;**76**: 422–426.
183. Vila, J.A., Y. Gang, J.M. Rodriguez Presedo, M. Fernandez-Delgado, S. Barro, and M. Malik, A new approach for TU complex characterization. *IEEE Trans. Biomed. Eng.*, 2000;**47**: 764–772.
184. Rubel, P. and B. Ayad, The true boundary recognition power of multidimensional detection functions. An optimal comparison, in *Computer ECG Analysis: Towards Standardization*, J.L. Willems, J.H. van Bemmel, and C. Zywietz, Editors. Amsterdam: North-Holland, 1986, pp. 97–103.
185. van Bemmel, J.H., J.L. Talmon, J.S. Duisterhout, and S.J. Hengeveld, Template waveform recognition applied to ECG-VCG analysis. *Comput. Biomed. Res.*, 1973;**6**: 430–441.
186. Zhang, Q., A. Illanes Manriquez, C. Medigue, Y. Papelier, and M. Sorine, Robust and efficient location of T-wave ends in electrocardiogram, in *Computers in Cardiology*, A. Murray, Editor. Piscataway, NJ: IEEE Comput Soc, 2005, pp. 711–714.
187. Sörnmo, L., A model-based approach to QRS delineation. *Comput. Biomed. Res.*, 1987;**20**: 526–542.
188. Morlet, D., P. Rubel, P. Arnaud, and J.L. Willems, An improved method to evaluate the precision of computer ECG measurement programs. *Int. J. Biomed. Comput.*, 1988;**22**: 199–216.
189. Kors, J.A., G. van Herpen, A.C. Sittig, and J.H. van Bemmel, Reconstruction of the Frank vectorcardiogram from standard electrocardiographic leads: diagnostic comparison of different methods. *Eur. Heart J.*, 1990;**11**: 1083–1092.
190. Young, T.Y. and W.H. Huggins, Intrinsic component theory of electrocardiograms. *IEEE Trans. Biomed. Eng.*, 1963;**9**: 214–221.
191. Horan, L.G., N.C. Flowers, and D.A. Brody, Principal factor waveforms of the thoracic QRS complex. *Circ. Res.*, 1964;**15**: 131–145.
192. Willems, J.L., Introduction to multivariate and conventional computer ECG analysis: pro's and contra's, in *Trends in Computer-Processed Electrocardiograms*, J.H. van Bemmel and J.L. Willems, Editors. Amsterdam: North-Holland, 1977, pp. 213–220.
193. Smets, P., New quantified approach for diagnostic classification, in *Optimization of Computer ECG Processing*, H.K. Wolf and P.W. Macfarlane, Editors. Amsterdam: North-Holland, 1980, pp. 229–237.
194. Degani, R. and G. Bortolan, Combining measurement precision and fuzzy diagnostic criteria, in *Computer ECG Analysis: Towards Standardization*, J.L. Willems, J.H. van Bemmel, and C. Zywietz, Editors. Amsterdam: North-Holland, 1986, pp. 177–182.
195. Doue, J.C., The role of artificial intelligence in standardizing ECG criteria, in *Computer ECG Analysis: Towards Standardization*, J.L. Willems, J.H. van Bemmel, and C. Zywietz, Editors. Amsterdam: North-Holland, 1986, pp. 53–57.
196. Matthes, T., G. Götsch, and C. Zywietz, Interactive analysis of statistical ECG diagnosis on an intelligent electrocardiograph. An expert system approach, in *Computer ECG Analysis: Towards Standardization*, J.L. Willems, J.H. van Bemmel, and C. Zywietz, Editors. Amsterdam: North-Holland, 1986, pp. 215–220.
197. Edenbrandt, L., B. Devine, and P.W. Macfarlane, Neural networks for classification of ECG ST-T segments. *J. Electrocardiol.*, 1992;**25**: 167–173.
198. Yang, T.F., B. Devine, and P.W. Macfarlane, Use of artificial neural networks within deterministic logic for the computer ECG diagnosis of inferior myocardial infarction. *J. Electrocardiol.*, 1994;**27**(Suppl): 188–193.
199. Kennedy, R.L., A.M. Burton, and R.F. Harrison, Neural networks and early diagnosis of myocardial infarction. *Lancet*, 1996;**347**: 407.
200. Hedén, B., H. Ohlin, R. Rittner, and L. Edenbrandt, Acute myocardial infarction detected in the 12-lead ECG by artificial neural networks. *Circulation*, 1997;**96**: 1798–1802.
201. Olsson, S.E., M. Ohlsson, H. Ohlin, and L. Edenbrandt, Neural networks—a diagnostic tool in acute myocardial infarction with concomitant left bundle branch block. *Clin. Physiol. Funct. Imaging*, 2002;**22**: 295–299.
202. Segall, H.N., The electrocardiogram and its interpretation: a study of reports by 20 physicians on a set of 100 electrocardiograms. *Can. Med. Assoc. J.*, 1960;**82**: 847–850.
203. Simonson, E., N. Tuna, and N. Okamoto, Diagnostic accuracy of the vectorcardiogram and electrocardiogram. A cooperative study. *Am. J. Cardiol.*, 1966;**17**: 829–878.
204. Willems, J.L., C. Abreu-Lima, P. Arnaud, J.H. van Bemmel, C. Brohet, R. Degani, et al., Effect of combining electrocardiographic interpretation results on diagnostic accuracy. *Eur. Heart J.*, 1988;**9**: 1348–1355.
205. Balda, R.A., A.G. Vallance, J.M. Luszcz, F.J. Stahlin, and G. Diller, ECL—a medically oriented ECG criteria language and other clinical research tools, in *Computers in Cardiology 1977*, H.G. Ostrow and K.L. Ripley, Editors. New York: IEEE Comput Soc, 1977, pp. 481–495.
206. Bruce, R.A. and S.R. Yarnall, Reliability and normal variations of computer analysis of Frank electrocardiogram by Smith-Hyde program (1968 version). *Am. J. Cardiol.*, 1972;**29**: 389–396.

207. Willems, J.L., C. Abreu-Lima, P. Arnaud, J.H. van Bemmel, C. Brohet, R. Degani, et al., The diagnostic performance of computer programs for the interpretation of electrocardiograms. *N. Engl. J. Med.*, 1991;**325**: 1767–1773.
208. Breiman, L., J.H. Friedman, R.A. Olshen, and C.J. Stone, *Classification and Regression Trees*. Belmont, CA: Wadsworth, 1984.
209. Kors, J.A. and A.L. Hoffmann, Induction of decision rules that fulfill user-specified performance requirements. *Pattern Recognit. Lett.*, 1997;**18**: 1187–1195.
210. Pipberger, H.V., R.A. Dunn, and J. Cornfield, First and second generation computer programs for diagnostic ECG and VCG classification, in *XIIth International Colloquium Vectorcardiographicum*, P. Rijlant, Editor. Brussels: Presses Académiques Européennes, 1972, pp. 431–439.
211. Willems, J.L. and J. Pardaens, Reproducibility of diagnostic results by a multivariate computer ECG analysis program (AVA 3.5). *Eur. J. Cardiol.*, 1977;**6**: 229–243.
212. Dunn, R.A., R. Babuska, J.M. Wojick, and H.V. Pipberger, Variation in probability levels in electrocardiographic diagnosis. *Comput. Biomed. Res.*, 1978;**11**: 41–49.
213. Cady, L.D., M.A. Woodbury, L.J. Tick, and M.M.A. Gertler, Method for electrocardiogram wave pattern estimation. Example: left ventricular hypertrophy. *Circ. Res.*, 1961;**9**: 1078–1082.
214. Kimura, E., Y. Mibukura, and A. Miura, Statistical diagnosis of electrocardiogram by theorem of Bayes. A preliminary report. *Jpn. Heart J.*, 1963;**4**: 469–488.
215. Young, T.Y. and W.H. Huggins, Computer analysis of electrocardiograms using a linear regression technique. *IEEE Trans. Biomed. Eng.*, 1964;**11**: 60–67.
216. Stark, L., J.F. Dickson, G.H. Whipple, and H. Horibe, Remote real-time diagnosis of clinical electrocardiograms by a digital computer system. *Ann. N.Y. Acad. Sci.*, 1965;**126**: 851–872.
217. Specht, D.F., Vectorcardiographic diagnosis using the polynomial discriminant method of pattern recognition. *IEEE Trans. Biomed. Eng.*, 1967;**14**: 90–95.
218. Yasui, S., M. Yokoi, Y. Watanabe, K. Nishijima, and S. Azuma, Computer diagnosis of electrocardiograms by means of the joint probability. *Jpn. Circ. J.*, 1968;**32**: 517–523.
219. Goldman, M.J. and H.V. Pipberger, Analysis of the orthogonal electrocardiogram and vectorcardiogram in ventricular conduction defects with and without myocardial infarction. *Circulation*, 1969;**39**: 243–250.
220. Kerr, A., A. Adicoff, J.D. Klingeman, and H.V. Pipberger, Computer analysis of the orthogonal electrocardiogram in pulmonary emphysema. *Am. J. Cardiol.*, 1970;**25**: 34–45.
221. Eddleman, E.E. and H.V. Pipberger, Computer analysis of the orthogonal electrocardiogram and vectorcardiogram in 1,002 patients with myocardial infarction. *Am. Heart J.*, 1971;**81**: 608–621.
222. Pipberger, H.V., ECG computer analysis: past, present and future, in *Computer ECG Analysis: Towards Standardization*, J.L. Willems, J.H. van Bemmel, and C. Zywietz, Editors. Amsterdam: North-Holland, 1986, pp. 3–10.
223. Brohet, C.R., A. Robert, C. Derwael, R. Fesler, M. Stijns, A. Vliers, et al., Computer interpretation of pediatric orthogonal electrocardiograms: statistical and deterministic classification methods. *Circulation*, 1984;**70**: 255–262.
224. Willems, J.L., E. Lesaffre, J. Pardaens, and D. de Schreye, Multivariate logistic classification of the standard 12- and 3-lead ECG, in *Computer ECG Analysis: Towards Standardization*, J.L. Willems, J.H. van Bemmel, and C. Zywietz, Editors. Amsterdam: North-Holland, 1986, pp. 203–210.
225. Rios, J., F. Sandquist, D. Ramseth, R. Stratbucker, E. Drazen, and J. Hanmer, The quest for optimal electrocardiography. Tast force V: cost effectiveness of the electrocardiogram. *Am. J. Cardiol.*, 1978;**41**: 175–183.
226. Okajima, M., Current status and future optimization of computerized electrocardiography in Japan, in *Optimization of Computer ECG Processing*, H.K. Wolf and P.W. Macfarlane, Editors. Amsterdam: North-Holland, 1980, pp. 293–307.
227. Moorman, J.R., M.A. Hlatky, D.M. Eddy, and G.S. Wagner, The yield of the routine admission electrocardiogram. A study in a general medical service. *Ann. Intern. Med.*, 1985;**103**: 590–595.
228. Salerno, S.M., P.C. Alguire, and H.S. Waxman, Competency in interpretation of 12-lead electrocardiograms: a summary and appraisal of published evidence. *Ann. Intern. Med.*, 2003;**138**: 751–760.
229. Eisenstein, E.L., Conducting an economic analysis to assess the electrocardiogram's value. *J. Electrocardiol.*, 2006;**39**: 241–247.
230. Willems, J.L., C. Abreu-Lima, P. Arnaud, C.R. Brohet, B. Denis, J. Gehring, et al., Evaluation of ECG interpretation results obtained by computer and cardiologists. *Methods Inf. Med.*, 1990;**29**: 308–316.
231. Farb, A., R.B. Devereux, and P. Kligfield, Day-to-day variability of voltage measurements used in electrocardiographic criteria for left ventricular hypertrophy. *J. Am. Coll. Cardiol.*, 1990;**15**: 618–623.
232. van den Hoogen, J.P., W.H. Mol, A. Kowsoleea, J.W. van Ree, T. Thien, and C. van Weel, Reproducibility of electrocardiographic criteria for left ventricular hypertrophy in hypertensive patients in general practice. *Eur. Heart J.*, 1992;**13**: 1606–1610.
233. de Bruyne, M.C., J.A. Kors, S. Visentin, G. van Herpen, A.W. Hoes, D.E. Grobbee, et al., Reproducibility of computerized ECG measurements and coding in a nonhospitalized elderly population. *J. Electrocardiol.*, 1998;**31**: 189–195.
234. Bailey, J.J., M. Horton, S.B. Itscoitz, A method for evaluating computer programs for electrocardiographic interpretation. 3. Reproducibility testing and the sources of program errors. *Circulation*, 1974;**50**: 88–93.
235. Bailey, J.J., M. Horton, and S.B. Itscoitz, The importance of reproducibility testing of computer programs for electrocardiographic interpretation: application to the automatic vectorcardiographic analysis program (AVA 3.4). *Comput. Biomed. Res.*, 1976;**9**: 307–316.
236. Spodick, D.H. and R.L. Bishop, Computer treason: intraobserver variability of an electrocardiographic computer system. *Am. J. Cardiol.*, 1997;**80**: 102–103.
237. Michaelis, J., S. Wellek, and J.L. Willems, Reference standards for software evaluation. *Methods Inf. Med.*, 1990;**29**: 289–297.
238. Jakobsson, A., P. Ohlin, and O. Pahlm, Does a computer-based ECG-recorder interpret electrocardiograms more efficiently than physicians? *Clin. Physiol.*, 1985;**5**: 417–423.
239. Bernard, P., B.R. Chaitman, J.M. Scholl, P.G. Val, and M. Chabot, Comparative diagnostic performance of the Telemed computer ECG program. *J. Electrocardiol.*, 1983;**16**: 97–103.
240. Willems, J.L., Is human verification of computerized ECGs mandatory? *Adv. Cardiol.*, 1978;**21**: 193–194.
241. Chou, T.C., When is the vectorcardiogram superior to the scalar electrocardiogram? *J. Am. Coll. Cardiol.*, 1986;**8**: 791–799.
242. Kors, J.A., G. van Herpen, J.L. Willems, and J.H. van Bemmel, Improvement of automated electrocardiographic diagnosis by

combination of computer interpretations of the electrocardiogram and vectorcardiogram. *Am. J. Cardiol*., 1992;**70**: 96–99.
243. Kors, J.A., G. van Herpen, and J.H. van Bemmel, Variability in ECG computer interpretation. Analysis of individual complexes vs analysis of a representative complex. *J. Electrocardiol*., 1992;**25**: 263–271.
244. Andresen, A., J. Dobkin, C. Maynard, R. Myers, G.S. Wagner, R.A. Warner, et al., Validation of advanced ECG diagnostic software for the detection of prior myocardial infarction by using nuclear cardiac imaging. *J. Electrocardiol*., 2001;**34**(Suppl): 243–248.
245. Andresen, A., M.D. Gasperina, R. Myers, G.S. Wagner, R.A. Warner, and R.H. Selvester, An improved automated ECG algorithm for detecting acute and prior myocardial infarction. *J. Electrocardiol*., 2002;**35**(Suppl): 105–110.
246. Wagner, G.S., C. Maynard, A. Andresen, E. Anderson, R. Myers, R.A. Warner, et al., Evaluation of advanced electrocardiographic diagnostic software for detection of prior myocardial infarction. *Am. J. Cardiol*., 2002;**89**: 75–79.
247. Milliken, J.A., H. Pipberger, H.V. Pipberger, M.A. Araoye, R. Ari, G.W. Burggraf, et al., The impact of an ECG computer analysis program on the cardiologist's interpretation. A cooperative study. *J. Electrocardiol*., 1983;**16**: 141–149.
248. Hillson, S.D., D.P. Connelly, and Y. Liu, The effects of computer-assisted electrocardiographic interpretation on physicians' diagnostic decisions. *Med. Decis. Making*, 1995;**15**: 107–112.
249. Brailer, D.J., E. Kroch, and M.V. Pauly, The impact of computer-assisted test interpretation on physician decision making: the case of electrocardiograms. *Med. Decis. Making*, 1997;**17**: 80–86.
250. Goodacre, S., A. Webster, and F. Morris, Do computer generated ECG reports improve interpretation by accident and emergency senior house officers? *Postgrad. Med. J*., 2001;**77**: 455–457.
251. Tsai, T.L., D.B. Fridsma, and G. Gatti, Computer decision support as a source of interpretation error: the case of electrocardiograms. *J. Am. Med. Inform. Assoc*., 2003;**10**: 478–483.
252. Laks, M.M. and R.H. Selvester, Computerized electrocardiography – an adjunct to the physician. *N. Engl. J. Med*., 1991;**325**: 1803–1804.
253. Plokker, H.W.M., *Cardiac Rhythm Diagnosis by Digital Computer*, dissertation. Amsterdam: Free University, 1978.
254. Reddy, S., B. Young, Q. Xue, B. Taha, D. Brodnick, and J. Steinberg, Review of methods to predict and detect atrial fibrillation in post-cardiac surgery patients. *J. Electrocardiol*., 1999;**32**(Suppl): 23–28.
255. Poon, K., P.M. Okin, and P. Kligfield, Diagnostic performance of a computer-based ECG rhythm algorithm. *J. Electrocardiol*., 2005;**38**: 235–238.
256. Bonner, R.E. and H.D. Schwetman, Computer diagnosis of electrocardiograms. 3. A computer program for arrhythmia diagnosis. *Comput. Biomed. Res*., 1968;**1**: 387–407.
257. Bonner, R.E., IBM rhythm analysis program, in *Computer Application on ECG and VCG Analysis*, C. Zywietz and B. Schneider, Editors. Amsterdam: North-Holland, 1973, pp. 375–397.
258. Wartak, J., J.A. Milliken, and J. Karchmar, Computer program for diagnostic evaluation of electrocardiograms. *Comput. Biomed. Res*., 1971;**4**: 225–238.
259. Brohet, C., C. Derwael, R. Fesler, and L.A. Brasseur, Arrhythmia analysis by the Louvain VCG program, in *Computers in Cardiology*, K.L. Ripley, Editor. Los Angeles: IEEE Comput Soc, 1982, pp. 47–51.
260. Shirataka, M., H. Miyahara, N. Ikeda, A. Domae, and T. Sato, Evaluation of five computer programs in the diagnosis of second-degree AV block. *J. Electrocardiol*., 1992;**25**: 185–195.
261. Thomson, A., S. Mitchell, and P.J. Harris, Computerized electrocardiographic interpretation: an analysis of clinical utility in 5110 electrocardiograms. *Med. J. Aust*., 1989;**151**: 428–430.
262. Reddy, B.R., B. Taha, S. Swiryn, R. Silberman, and R. Childers, Prospective evaluation of a microprocessor-assisted cardiac rhythm algorithm: results from one clinical center. *J. Electrocardiol*., 1998;**30**(Suppl): 28–33.
263. Farrell, R.M., J.Q. Xue, and B.J. Young, Enhanced rhythm analysis for resting ECG using spectral and time-domain techniques, in *Computers in Cardiology*, A. Murray, Editor. Piscataway, NJ: IEEE Comput Soc, 2003, pp. 733–736.
264. Guglin, M.E. and D. Thatai, Common errors in computer electrocardiogram interpretation. *Int. J. Cardiol*., 2006;**106**: 232–237.
265. Pryor, T.A., A.E. Lindsay, and R.W. England, Computer analysis of serial electrocardiograms. *Comput. Biomed. Res*., 1972;**5**: 709–714.
266. Macfarlane, P.W., H.T. Cawood, and T.D. Lawrie, A basis for computer interpretation of interpretation of serial electrocardiograms. *Comput. Biomed. Res*., 1975;**8**: 189–200.
267. Bonner, R.E., L. Crevasse, M.I. Ferrer, and J.C. Greenfield, A new computer program for comparative analysis of serial scalar electrocardiograms: description and performance of the 1976 IBM program. *Comput. Biomed. Res*., 1978;**11**: 103–118.
268. Schnyders, H.C. and G.A. Kien, Computer-assisted serial comparison of ECGs: the Telemed version, in *Computer Application in Medical Care*, R.A. Dunn, Editor. New York: IEEE Comput Soc, 1979, pp. 652–659.
269. Rubel, P., J. Fayn, J.L. Willems, and C. Zywietz, New trends in serial ECG analysis. *J. Electrocardiol*., 1993;**26**(Suppl): 122–128.
270. Rubel, P., J. Fayn, G. Nollo, D. Assanelli, B. Li, L. Restier, et al, Toward personal eHealth in cardiology. Results from the EPI-MEDICS telemedicine project. *J. Electrocardiol*., 2005;**38**(Suppl): 100–106.
271. Willems, J.L., P.F. Poblete, and H.V. Pipberger, Day-to-day variation of the normal orthogonal electrocardiogram and vectorcardiogram. *Circulation*, 1972;**45**: 1057–1064.
272. de Bruyne, M.C., J.A. Kors, S. Visentin, G. van Herpen, A.W. Hoes, D.E. Grobbee, et al., Reproducibility of computerized ECG measurements and coding in a nonhospitalized elderly population. *J. Electrocardiol*., 1998;**31**: 189–195.
273. Schijvenaars, B.J., *Intra-individual Variability of the Electrocardiogram*, dissertation. Rotterdam: Erasmus University, 2000.
274. Pipberger, H.V., R.A. Dunn, and H.A. Pipberger, Automated comparison of serial electrocardiograms. *Adv. Cardiol*., 1976;**16**: 157–165.
275. Rubel, P., N. Saccal, J.L. Sourrouille, and M.C. Forlini, Multidimensional techniques for the optimal display of trends in sequential vectorcardiograms, in *Medinfo 1980*, D.A.B. Lindberg and S. Kaihara, Editors. Amsterdam: North-Holland, 1980, p. 274.
276. Zywietz, C., B. Widiger, and R. Fischer, A system for comprehensive comparison of serial ECG beats and serial ECG recordings, in *Computers in Cardiology*, A. Murray, Editor. Piscataway, NJ: IEEE Comput Soc, 2003, pp. 689–692.
277. Hedstrom, K. and P.W. Macfarlane, Development of a new approach to serial analysis. The manufacturer's viewpoint. *J. Electrocardiol*., 1996;**29**(Suppl): 35–40.

278. McLaughlin, S.C., T.C. Aitchison, and P.W. Macfarlane, Methods for improving the repeatability of automated ECG analysis. *Methods Inf. Med.*, 1995;**34**: 272–282.
279. McLaughlin, S.C., P. Chishti, T.C. Aitchison, and P.W. Macfarlane, Techniques for improving overall consistency of serial ECG analysis. *J. Electrocardiol.*, 1996;**29**(Suppl): 41–45.
280. Fayn, J. and P. Rubel, CAVIAR: a serial ECG processing system for the comparative analysis of VCGs and their interpretation with auto-reference to the patient. *J. Electrocardiol.*, 1988;**21**(Suppl): S173–S176.
281. Sunemark, M., L. Edenbrandt, H. Holst, and L. Sörnmo, Serial VCG/ECG analysis using neural networks. *Comput. Biomed. Res.*, 1998;**31**: 59–69.
282. Bonner, R.E., L. Crevasse, M.I. Ferrer, and J.C. Greenfield, The influence of editing on the performance of a computer program for serial comparison of electrocardiograms. *J. Electrocardiol.*, 1983;**16**: 181–189.
283. van Haelst, A.C., D.K. Donker, F.C. Visser, C.C. de Cock, A. Hasman, and J.L. Talmon, A computer program for the analysis of serial electrocardiograms from patients who suffered a myocardial infarction. *Int. J. Biomed. Comput.*, 1985;**17**: 273–284.
284. Ohlsson, M., H. Ohlin, S.M. Wallerstedt, and L. Edenbrandt, Usefulness of serial electrocardiograms for diagnosis of acute myocardial infarction. *Am. J. Cardiol.*, 2001;**88**: 478–481.
285. Schwartz, P.J., A. Garson, T. Paul, M. Stramba-Badiale, V.L. Vetter, and C. Wren, Guidelines for the interpretation of the neonatal electrocardiogram. A task force of the European Society of Cardiology. *Eur. Heart J.*, 2002;**23**: 1329–1344.
286. Dickinson, D.F., The normal ECG in childhood and adolescence. *Heart*, 2005;**91**: 1626–1630.
287. Davignon, A., P.M. Rautaharju, E. Boisselle, F. Soumis, M. Megelas, and A. Choguette, Normal ECG standards for infants and children. *Pediatr. Cardiol.*, 1979/80;**1**: 123–131.
288. Brohet, C.R., C. Hoeven, A. Robert, C. Derwael, R. Fesler, and L.A. Brasseur, The normal pediatric Frank orthogonal electrocardiogram: variations according to age and sex. *J. Electrocardiol.*, 1986;**19**: 1–13.
289. Perry, L.W., H.V. Pipberger, H.A. Pipberger, C.D. McManus, and L.P. Scott, Scalar, planar, and spatial measurements of the Frank vectorcardiogram in normal infants and children. *Am. Heart J.*, 1986;**111**: 721–730.
290. Macfarlane, P.W., E.N. Coleman, E.O. Pomphrey, S. McLaughlin, A. Houston, and T. Aitchison, Normal limits of the high-fidelity pediatric ECG. Preliminary observations. *J. Electrocardiol.*, 1989;**22**(Suppl): 162–168.
291. Macfarlane, P.W., S.C. McLaughlin, B. Devine, and T.F. Yang, Effects of age, sex, and race on ECG interval measurements. *J. Electrocardiol.*, 1994;**27**(Suppl): 14–19.
292. Rijnbeek, P.R., M. Witsenburg, E. Schrama, J. Hess, and J.A. Kors, New normal limits for the paediatric electrocardiogram. *Eur. Heart J.*, 2001;**22**: 702–711.
293. Horton, L.A., S. Mosee, and J. Brenner, Use of the electrocardiogram in a pediatric emergency department. *Arch. Pediatr. Adolesc. Med.*, 1994;**148**: 184–188.
294. Hamilton, R.M., K. McLeod, A.B. Houston, and P.W. Macfarlane, Inter- and intraobserver variability in LVH and RVH reporting in pediatric ECGs. *Ann. Noninvasive Electrocardiol.*, 2005;**10**: 330–333.
295. Guller, B., P.C. O'Brien, R.E. Smith, W.H. Weidman, and J.W. DuShane, Computer interpretation of Frank vectorcardiograms in normal infants: longitudinal and cross-sectional observations from birth to 2 years of age. *J. Electrocardiol.*, 1975;**8**: 201–208.
296. Guller, B., F.Y. Lau, R.A. Dunn, H.A. Pipberger, and H.V. Pipberger, Computer analysis of changes in Frank vectorcardiograms of 666 normal infants in the first 72 hours of life. *J. Electrocardiol.*, 1977;**10**: 19–26.
297. Francis, D.B., B.L. Miller, and D.W. Benson, A new computer program for the analysis of pediatric scalar electrocardiograms. *Comput. Biomed. Res.*, 1981;**14**: 63–77.
298. Laks, M.M., A computer program for interpretation of infant and children electrocardiograms, in *Computer ECG Analysis: Towards Standardization*, J.L. Willems, J.H. van Bemmel, and C. Zywietz, Editors. Amsterdam: North-Holland, 1986, pp. 59–65.
299. Macfarlane, P.W., E.N. Coleman, B. Devine, A. Houston, S. McLaughlin, T.C. Aitchison, et al., A new 12-lead pediatric ECG interpretation program. *J. Electrocardiol.*, 1990;**23**(Suppl): 76–81.
300. Rijnbeek, P.R., M. Witsenburg, A. Szatmari, J. Hess, and J.A. Kors, PEDMEANS: a computer program for the interpretation of pediatric electrocardiograms. *J. Electrocardiol.*, 2001;**34**(Suppl): 85–91.
301. Zhou, S.H., J. Liebman, A.M. Dubin, P.C. Gillette, R.E. Gregg, E.D. Helfenbein, et al., Using 12-lead ECG and synthesized VCG in detection of right ventricular hypertrophy with terminal right conduction delay versus partial right bundle branch block in the pediatric population. *J. Electrocardiol.*, 2001;**34**(Suppl): 249–257.
302. Guller, B., T. Jones, J. McCloskey, and S.P. Herndon, The Hewlett-Packard pediatric ECG computer program (HP-P3) and independent clinical information. *J. Electrocardiol.*, 1990;**23**(Suppl): 204.
303. Hamilton, R.M., A.B. Houston, K. McLeod, and P.W. Macfarlane, Evaluation of pediatric electrocardiogram diagnosis of ventricular hypertrophy by computer program compared with cardiologists. *Pediatr. Cardiol.*, 2005;**26**: 373–378.
304. Snyder, C.S., A.L. Fenrich, R.A. Friedman, C. Macias, K. O'Reilly, and N.J. Kertesz, The emergency department versus the computer: which is the better electrocardiographer? *Pediatr. Cardiol.*, 2003;**24**: 364–368.

38 Pacemaker Electrocardiography

Thomas Fåhraeus

P. W. Macfarlane, A. van Oosterom, O. Pahlm, P. Kligfield, M. Janse, J. Camm (eds.), *Comprehensive Electrocardiology*, DOI 10.1007/978-1-84882-046-3_38,

38.1 Introduction

When artificial cardiac stimulation was introduced in 1958 as a permanent treatment for bradycardia, the interpretation of pacemaker ECGs posed little difficulty. The indication for pacemaker implantation at that time was total atrioventricular block, and the available pacemaker systems provided fixed-rate ventricular stimulation (Fig. 38.1). Today multiprogrammable pacemaker devices are available with many different pacing modes, sophisticated functions, and diagnostic tools. Pacing during various arrhythmias creates ECG recordings which are sometimes rather difficult to analyze, and nowadays there are many methods for performing an evaluation of the pacemaker function other than looking at a standard surface ECG. To perform a comprehensive examination, an appropriate pacemaker programmer is sometimes necessary where the initial interrogation will allow retrieval of programmed settings and diagnostic data. The ECG (usually both surface ECG and intracardiac electrograms) monitoring capability simultaneously with telemetry event markers on the display facilitates the interpretation.

In this chapter, the basic principles of the interpretation of pacemaker ECGs will be presented, first concerning normal pacemaker function and thereafter concerning malfunction and pseudomalfunction. Most of the ECG recordings have been selected from the daily clinical work at the Skåne University Hospital, Lund, Sweden, and the intention is to provide a survey of the field of pacemaker ECG. Questions concerning the choice of the stimulation mode and clinical application have to be referred to text books dealing with pacemaker treatment.

The different pacing modes used are identified according to the recommendations of the 1987 NASPE and NASPE/BPEG codes. The original three-position letter code (since 1974) was revised to a five-position code in 1981, and has subsequently been expanded further in 2002 (Table 38.1). Usually, the first three letters are used, for example, VVI, DDD, AAI, VDD, etc., but today most pulse generators have a built-in sensor for rate modulation. When this function is activated, the code will be VVIR, DDDR, AAIR, and so on. The use of the letter code facilitates rapid acquisition of information about the programmed basic mode of the pacemaker and how it is pacing and sensing the heart.

38.2 Registration of Pacemaker Impulses

Pacemaker impulses should be clearly visible in the ECG tracings and are commonly called "spikes." An ECG recording of good quality facilitates correct interpretation of pacemaker performance. The typical standard pacemaker ECGs recorded when the lead tip is in the apex area of the right ventricle show broad QRS complexes with an LBBB pattern. New modes with different pacing sites have in some cases changed the QRS morphology. The print-out with data and ECG -markers from a programmer are very useful when difficult and problematic ECG's occur (Figs. 38.2 and 38.3).

The reproduction of the pacemaker spikes is influenced by many factors. One of the most important is the use of the interference filter of the ECG recorder (Fig. 38.4). While the amplitude of the spikes is huge in unipolar systems, much less stimulus artifact can be seen on the recording when a bipolar lead is used with anode and cathode only about a centimeter apart (Fig. 38.5). Furthermore, the spike amplitude is related to the actual pulse generator output as demonstrated by the example in Fig. 38.6, where the energy content of the pacemaker impulse is temporarily reduced to 10% for test purposes. The spike amplitude and vector orientation when dealing with unipolar systems are dependent on the choice of ECG lead and the position of the pulse generator (Fig. 38.7).

Digital ECG recorders are responsible for additional variation of the spike amplitude. If the sampling interval is 4 ms, ordinary pacemaker impulses of 0.2–0.5 ms duration may not be registered consistently, resulting in the changes of their reproduction (Fig. 38.8). The variation of the spike amplitude may easily be misinterpreted as a lead or stimulation problem. This can partly be circumvented by sampling the signal at a much higher rate; for example, every 0.25 ms.

38.3 Relationship Between the Stimulation Impulse and Cardiac Activity

In most transvenous ventricular pacing systems with only one electrode, the lead tip is usually positioned in the right ventricle, and during stimulation the ECG will show a left bundle branch block pattern. If the lead tip is located close to the ventricular septum or is positioned on the left ventricle with an epicardial technique, a right bundle branch block pattern will be produced (Fig. 38.9).

Figure 38.1

Continual asynchronous ventricular pacing at a rate of 60 bpm in the presence of complete AV block. A left bundle block pattern with wide QRS complexes appears due to stimulation first of the right ventricle and then the left.

Table 38.1

The revised NASPBE/BPEG generic code for antibradycardia, adaptive rate, and multisite pacing. Pace, 25(2), 260–264, February 2002

I What is stimulated?	II What is sensed?	III Reaction to sensing	IV Rate modulation	V Multisite pacing
0 = None	0 = None	0 = None	0 = None	0 = None
A = Atrium	A = Atrium	T = Triggered	R = Rate	A = Atrium
V = Ventricle	V = Ventricle	I = Inhibited	Modulation	V = Ventricle
D = Dual (A + V)	D = Dual (A + V)	D = Dual (T + I)		D = Dual (A + V)
S = Single	S = Single			
(A or V)	(A or V)			

The simultaneous occurrence of spontaneous cardiac activity and pacemaker impulses is not uncommon. When the endocardium close to the lead tip is already depolarized spontaneously, the pacemaker impulse will not affect the myocardium. However, the ECG will be distorted by the spike, a phenomenon referred to as a pseudofusion beat. If parts of the myocardium are depolarized by intrinsic activity while others are activated by the pacemaker impulse, fusion beats will occur. When the spontaneous heart rate and the basic stimulation rate are almost the same, fusion and pseudofusion beats are commonly seen (Fig. 38.10).

In atrial pacing, intermittent ventricular extrasystoles may result in a confusing ECG when the atrial spike is followed by a QRS complex, referred to as a pseudopseudofusion beat (Fig. 38.11). Tachycardia-terminating pacemakers provide additional variation to the relationship between spikes and the PQRS complexes; for example, during the termination of reentry tachycardias with rapid overdrive pacing with short sequences (bursts) of stimuli. In Sect. 38.10, there are more examples of tachycardia treatment (Fig. 38.12).

38.4 The ECG Appearance of Different Pacing Modes

One of the most commonly used modes is VVI pacing, which comprises ventricular stimulation and inhibition. A VVI pacemaker operates with two timing circuitries; the basic rate counter and the technical refractory period, both of which are initiated either by stimulation or sensing events. Possible ECG combinations are demonstrated in the timing diagram shown in Fig. 38.13. The basic rate interval in a VVI pulse generator is programmable. When the pulse generator detects ventricular depolarization within the basic interval, stimulation will be inhibited and a new basic interval will start (Fig. 38.14).

In the VVT mode, instead of inhibition, the pulse generator delivers an impulse triggered by the QRS complex during the refractory period, thereby leaving the spontaneous depolarization unaffected (Fig. 38.15). This pacing mode is very seldom used but can be useful when sensing problems occur (inhibition is avoided).

A sensing event followed by either inhibition (VVI) or triggering (VVT) occurs when the intracardiac signal reaches a certain amplitude at the site of the electrode. Sometimes the intrinsic deflection of this signal coincides with the beginning of the QRS complex in the surface ECG. Whether or not ectopic ventricular activity causes inhibition of a VVI pulse

Figure 38.2

Dual-chamber pacing and sensing (DDD) during second-degree AV block. The basic rate and intrinsic atrial rate are almost the same, which explains the additional variations of the QRS-T morphology.

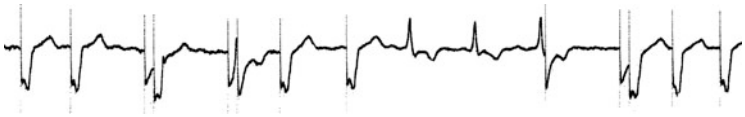

Figure 38.3

To interpret this ECG from a patient with a DDD pacemaker, a pacemaker programmer is very useful. Parameters such as rate, AV interval, and modes can be changed, diagnostic marker tools are available.

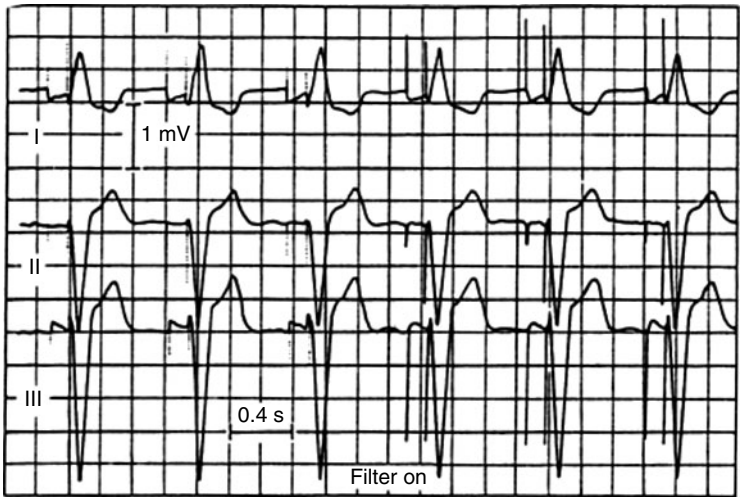

Figure 38.4

DDD pacing recorded without and with an interference filter. As the spike recording is more clearly seen with the low-pass filter switched on, it is recommended for routine use.

generator depends on the duration of the refractory period (Fig. 38.16). Multiprogrammable pulse generators offer a selection of different refractory periods.

Variation in the rate, because of different timing intervals, is provided in pulse generators where the hysteresis function has been activated. Without hysteresis, the automatic basic interval is equal to the escape interval. With hysteresis, the basic rate interval is constant during stimulation, but after an inhibition the escape interval is prolonged. Thus, a pulse generator with a fixed or programmable hysteresis function operates with an inhibition rate lower than the basic stimulation rate (Fig. 38.17).

Atrial pacing (AAIR) is achieved in a manner quite similar to ventricular pacing. Reliable AV conduction is, however, essential for the use of atrial pacing (Fig. 38.18). As the amplitude of the atrial signal is considerably lower than the corresponding QRS signal in ventricular sensing, the sensitivity of an AAI device must be high enough to allow correct sensing.

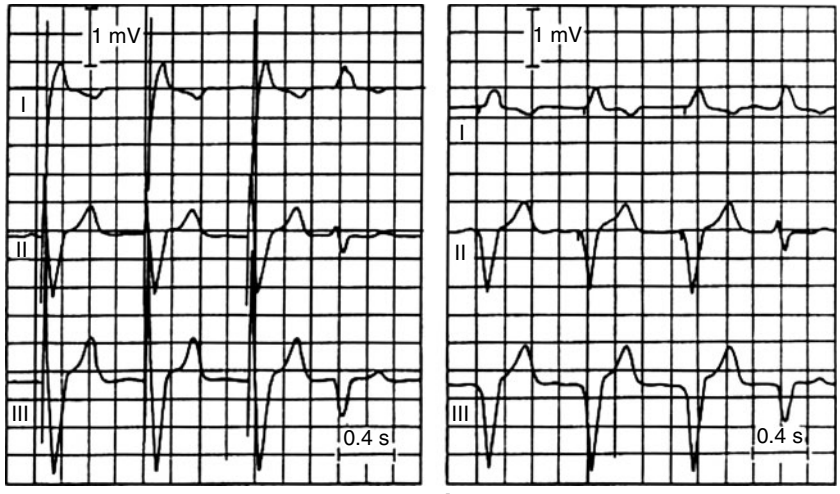

Figure 38.5

Unipolar pacing to the left (a) compared with bipolar (b) ventricular pacing through the same electrode system, which was achieved by means of a pulse generator with programmable polarity.

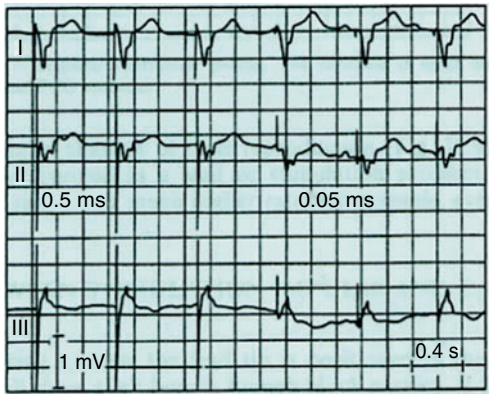

Figure 38.6

Unipolar ventricular pacing, during an automatic stimulation threshold test with reduction of impulse duration from 0.5 to 0.05 ms. Note the change of spike configuration. The output pulse corresponds to the spike on the ECG.

38.5 Dual-Chamber Pacing

The expression *dual-chamber pacing* is used to describe a pacing modality capable of delivering pacing stimuli to two chambers, usually the atrium and the ventricle (DOO, DDD, DDI, and DVI). During the last few years, the term *biventricular pacing* has been used to indicate cardiac resynchronization of the ventricles in heart failure. It is easy to be confused by the terms; resynchronization will be described later in this chapter. In the DVI mode, the stimulation of the atria is followed by ventricular pacing after a technical AV delay. As there is no sensing in the atria, a DVI pulse generator may only be inhibited by intrinsic ventricular activity. Atrial stimulation occurs at the programmed basic rate as long as the pulse generator is not inhibited by spontaneous ventricular beats (Fig. 38.19).

In the VDD mode, atrial sensing is followed by synchronous ventricular stimulation, but without the possibility of stimulating the atria during sinus bradycardia (Fig. 38.20). Ventricular inhibition is accomplished when spontaneous QRS complexes are sensed during the AV delay (Fig. 38.21). Ectopic beats sensed after the end of the technical refractory

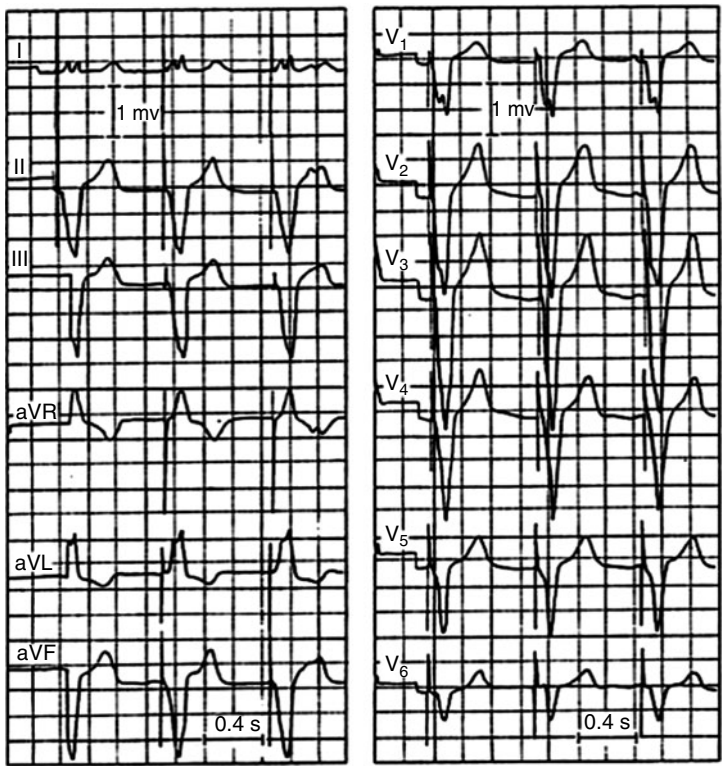

Figure 38.7

The vector orientation and amplitude of the spikes are depended on placement of the pulse generator and the ECG electrodes. The illustration is an example of unipolar right ventricular pacing with the pacemaker pocket located in the left pectoral region.

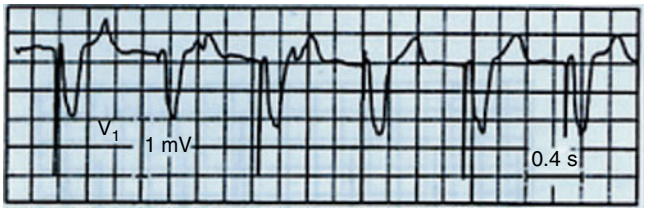

Figure 38.8

A digital ECG recording of unipolar ventricular pacing. The variation in the spike amplitude is caused by the digital sampling technique of this particular ECG recorder.

period may also cause inhibition and resetting of the basic rate interval. The disadvantages of only ventricular stimulation in the absence of spontaneous atrial activity make the VDD mode less attractive from a clinical point of view. The VDD mode is still available as a programmable mode in DDD pulse generators.

In the DDD mode, the pulse generator operates with sensing and stimulation of both the atrial and the ventricular chambers depending on the presence or absence of spontaneous cardiac activity and the programmed time intervals. Thus, it presents a functional combination of AAI, VAT, and VVI principles. The coincidence between dual-chamber

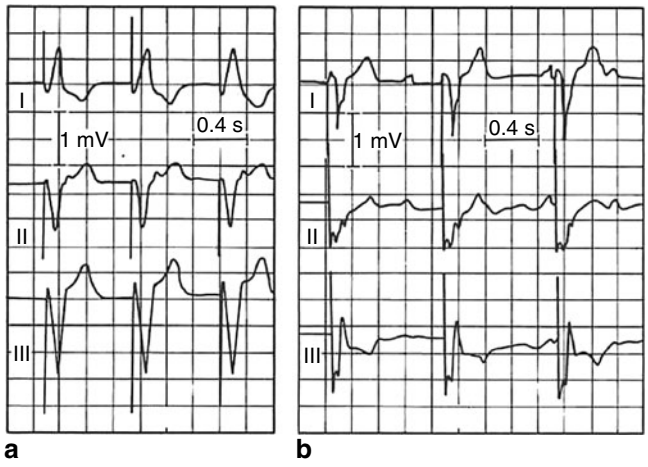

Figure 38.9

(a) Unipolar pacing through a transvenous right ventricular lead resembles a left bundle branch block (LBBB) pattern. (b) Left ventricular stimulation through a myocardial screw-in electrode produces a right bundle branch block (RBBB) pattern.

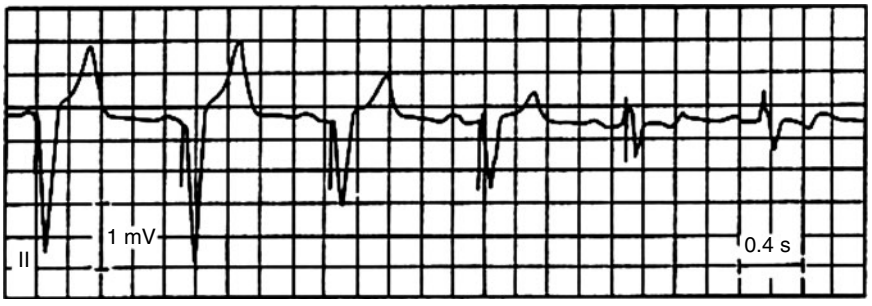

Figure 38.10

Unipolar ventricular-inhibited pacing demonstrating the difference between pacemaker-induced QRS complexes (QRS complexes #1 and #2) and different degrees of fusion beats (QRS complexes #3 and #4) caused by simultaneous depolarization via stimulation and normal AV conduction. The T-wave configuration in complex #5 indicates a spontaneously induced depolarization together with an ineffective pacemaker spike – a pseudofusion beat.

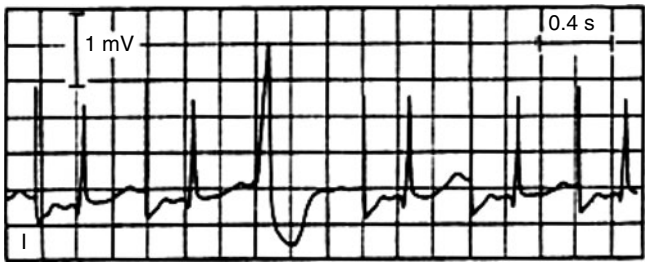

Figure 38.11

Atrial pacing at a rate of 100 min^{-1}. A ventricular ectopic beat (complex #3) coincides with an atrial spike producing a pseudopseudofusion beat.

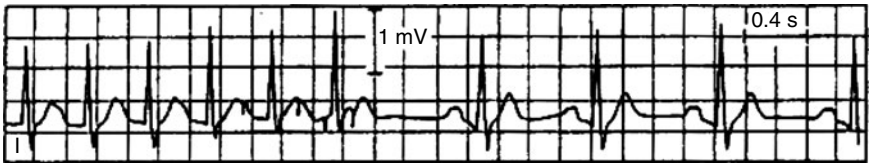

Figure 38.12
Atrial bipolar burst stimulation (300 min^{-1}) terminating a supraventricular tachycardia. The spikes in the burst sequence are clearly visible.

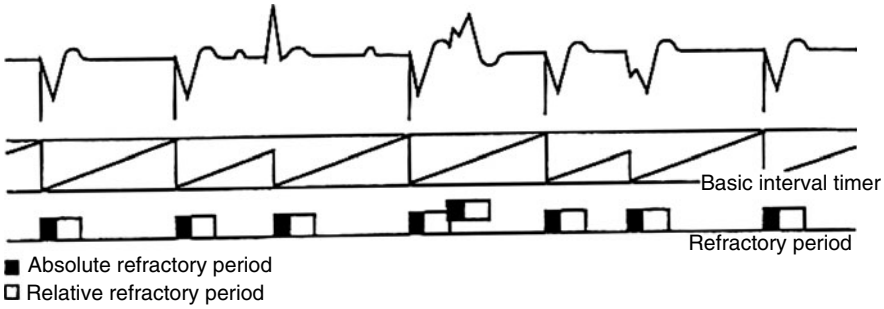

Figure 38.13
Schematic ECG illustration demonstrating the operation of the basic interval timer and the refractory period. In this example the refractory period is programmed to 312 ms. The absolute refractory period is 125 ms and the relative refractory period is thus 187 ms. A conducted ventricular complex which occurs during the relative refractory period (noise-sampling period) does not accomplish inhibition, that is, does not reset the basic interval timer, but restarts a new refractory period, as in the case of complex #5.

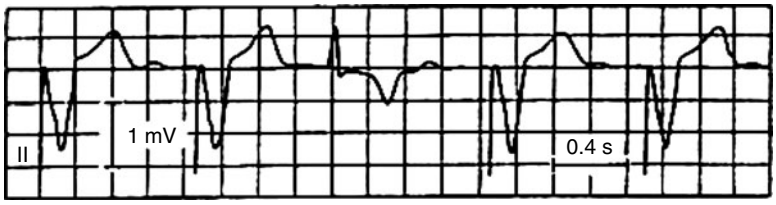

Figure 38.14
Ventricular-inhibited pacing (VVI mode) at a programmed rate of 70 min^{-1}. Inhibition will occur as soon as a spontaneous QRS complex at a higher rate occurs, as in this case.

pacing and the occurrence of spontaneous atrial and/or ventricular activity can cause many different ECG morphologies, including atrial and ventricular fusion or pseudofusion beats.

The resulting ECG appearance is even more confusing when spontaneous AV conduction varies intermittently (Fig. 38.22). Furthermore, the ECG appearance may be altered by different AV delay settings in the presence of AV conduction (Fig. 38.23). It is of clinical interest to have a long AV delay to support possible AV conduction and a normal activation of the ventricles. There are functions in pacemakers that automatically test the AV delay looking for intrinsic conduction and prolong the technical AV delay if the AV conduction is acceptable. During the last few years, the negative effects in some patients have been documented by long-term stimulation through the apex lead with an LBBB pattern. This electrical asynchrony can result in heart failure and in some cases a biventricular (Sect. 38.9) pacemaker system will be implanted.

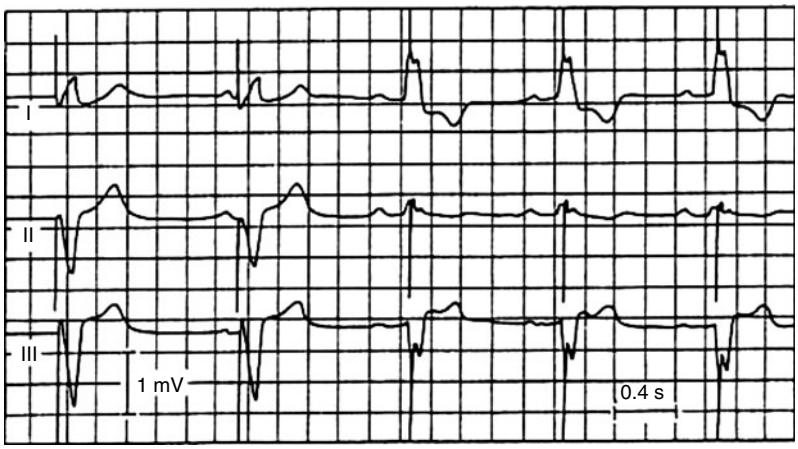

Figure 38.15

The ventricular-triggered pacing (VVT mode) at a basic rate of 50 min^{-1} followed by sinus rhythm at a higher rate (60 min^{-1}), and triggered ventricular spikes (pseudofusion beats).

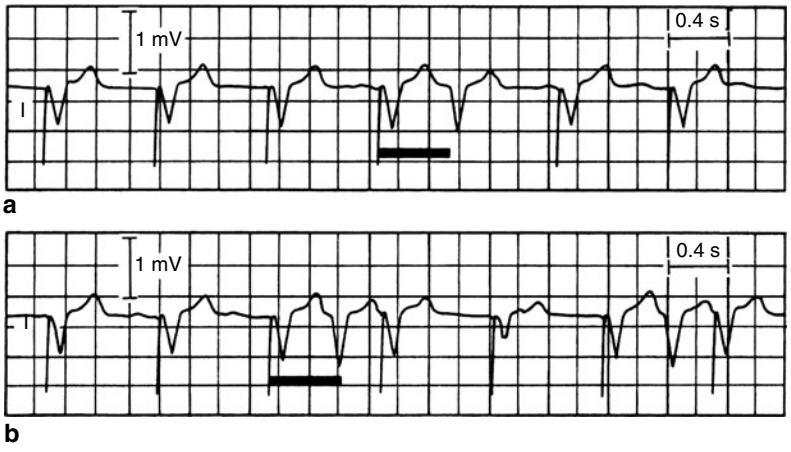

Figure 38.16

Ventricular pacing in the VVI mode at a rate of 80 min^{-1}. Ventricular ectopic beats accomplish inhibition as in (a) only if they occur after the end of the technical refractory period, denoted here by a horizontal bar. Early ectopic beats in (b) are ignored because the technical refractory period is 500 ms in this case.

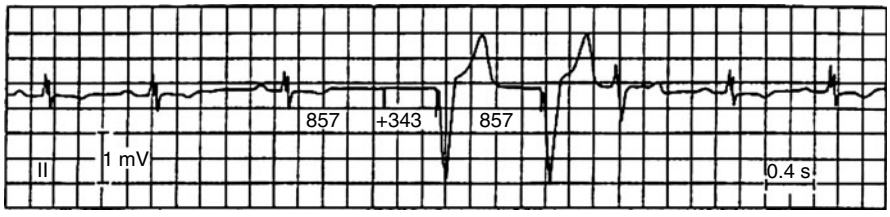

Figure 38.17

VVI pacing with a programmed basic rate of 70 min^{-1} and an activated hysteresis function. After an inhibition, a hysteresis delay of 343 ms is added to the basic rate interval of 857 ms thus permitting a slower intrinsic rhythm by consistent inhibition of the pulse generator. Lack of spontaneous rhythm is followed by stimulation at the programmed basic rate until a new inhibition occurs.

Figure 38.18
Atrial pacing at a programmed rate increased to 100 min^{-1} for test purposes. While consistent atrial capture can be seen, a blocked P wave indicates unreliable AV conduction.

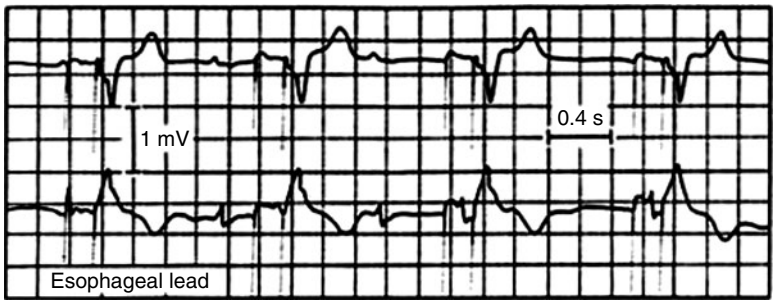

Figure 38.19
Dual-chamber stimulation (DVI mode) at a rate of 50 min^{-1} in the presence of AV block, and an intrinsic atrial rate of approximately 60 bpm. The esophageal ECG clearly indicates the asynchronous atrial stimulation owing to the lack of atrial sensing in a DVI pulse generator. Esophageal recordings are not used so often nowadays, due to availability of atrial electrograms.

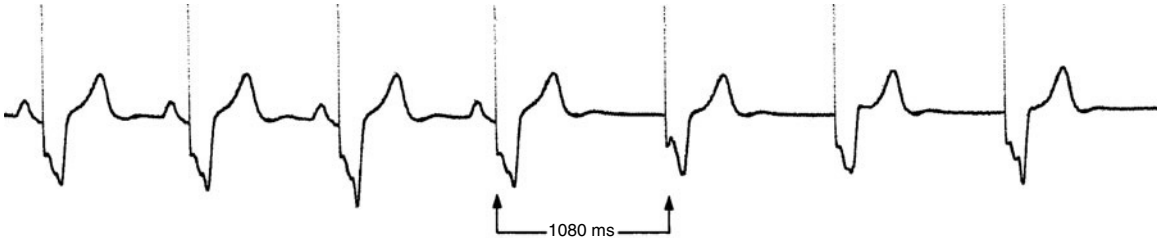

Figure 38.20
The basic function of a VDD pulse generator. In the absence of triggering P waves during sinus arrest or bradycardia, compensation by basic rate stimulation is achieved (The time interval is 1080 ms).

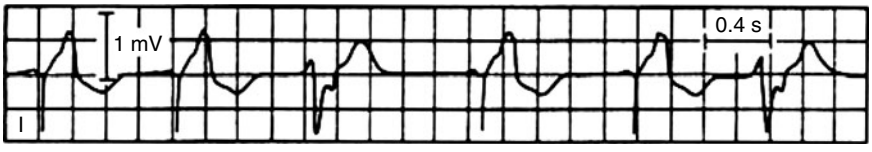

Figure 38.21
Atrial-triggered ventricular stimulation combined with ventricular inhibition (VDD mode). Every P wave is followed by ventricular pacing unless an ectopic beat inhibits the system. Hence, a spontaneous or retrograde P wave within the ectopic ventricular beat cannot initiate a new triggering.

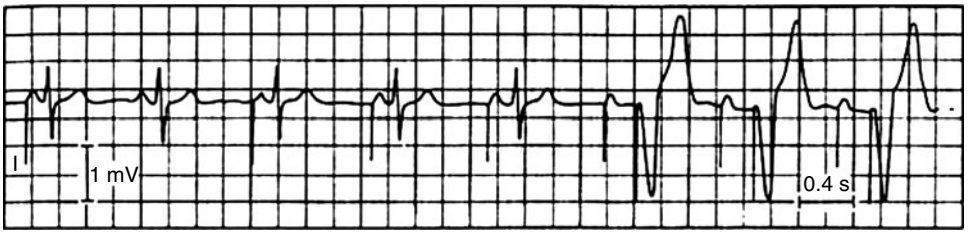

Figure 38.22

Dual-chamber pacing in the DDD mode at a basic rate of 70 min^{-1} alternating with sinus rhythm at a somewhat faster rate. As long as the AV conduction is normal, inhibition of the ventricular output is accomplished (complexes 1–5), but atrial activation is followed by ventricular pacing during impaired AV conduction (complexes 6–8).

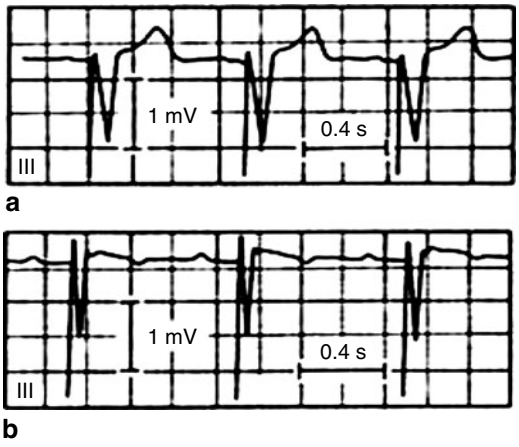

Figure 38.23

Atrial-triggered ventricular stimulation in the same patient as in Fig. 38.22, but with different technical AV delay settings. In the ECG shown in (a), the AV delay is 100 ms followed by typical pacemaker-induced ventricular complexes, while in the ECG in (b), a delay of 200 ms permits AV conduction resulting in pseudofusion beats.

Pathological atrial tachycardia or sensing interference may trigger DDD pulse generators to high rates. In order to avoid unacceptable fast-triggered ventricular pacing, different solutions for rate limitations have been introduced, for example, the technical Wenckebach behavior shown in Fig. 38.24. In atrial fibrillation, the amplitude and the configuration of the intrinsic fibrillation waves may intermittently be too low to be sensed by the atrial amplifier.

If too many high-frequency signals are detected, the pulse generator converts to basic rate stimulation (interference rate stimulation) as a protective countermeasure (Fig. 38.25).

It is therefore impossible to provide a complete survey of all conceivable ECG appearances regarding all different technical solutions, program settings, and changes in the intrinsic cardiac activity (Fig. 38.26).

38.6 Diagnostic Tools

Earlier, standard ECG registration remained the main tool for the evaluation of the pacemaker function. However, complete information about a particular pacemaker system and its function today requires the use of a pacemaker programmer.

Measures have to be taken for assessment of possible stimulation response. Most pulse generators can be converted to fixed-rate stimulation by the application of a magnet. Different manufacturers have chosen different features of the

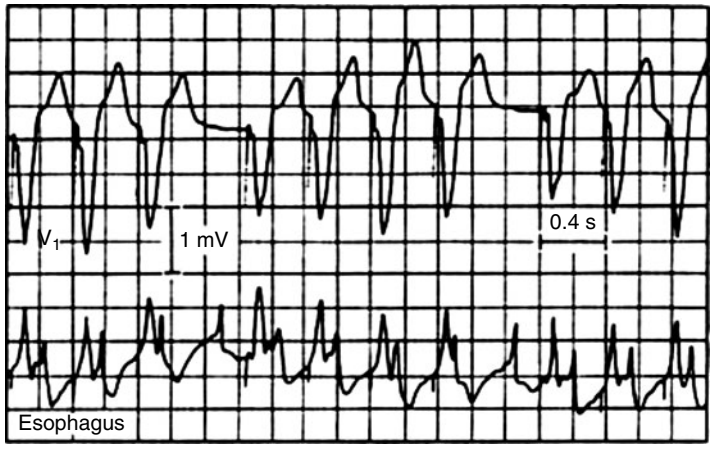

Figure 38.24

Atrial-triggered ventricular stimulation (DDD mode) at the highest synchronous rate. Esophageal registration discloses an atrial tachycardia, which runs at a rate of 175 bpm, while ventricular stimulation is running at 160 min^{-1} (the highest synchronous rate) resulting in repetitive Wenckebach block.

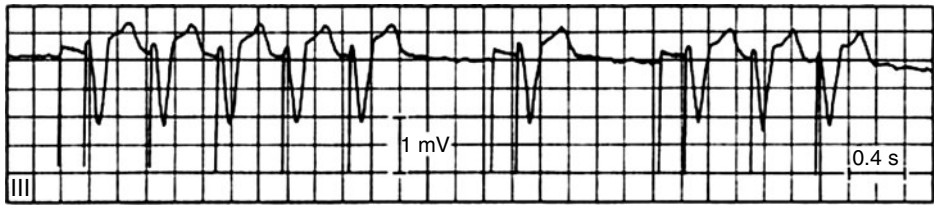

Figure 38.25

Atrial-triggered ventricular stimulation (DDD mode) running at different rates alternating with basic rate stimulation. This is a typical example of the impact of atrial fibrillation on a DDD pacemaker system without automatic mode switch when atrial fibrillation occurs.

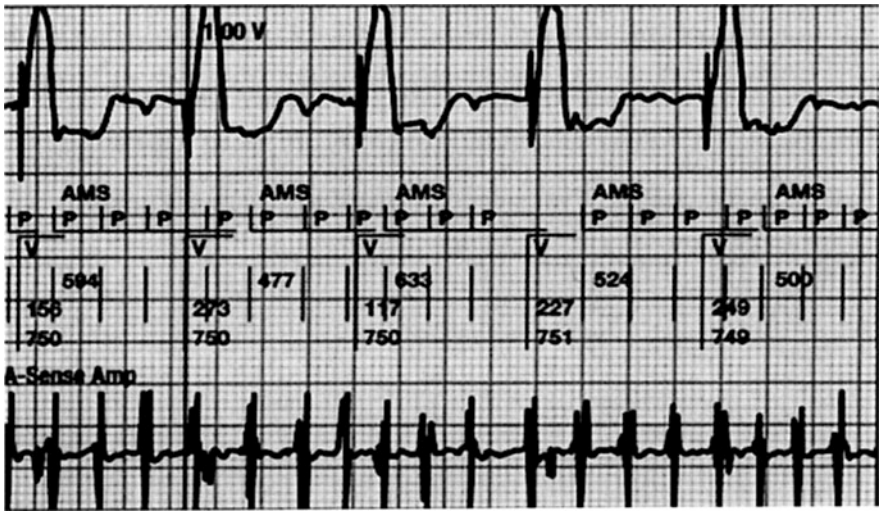

Figure 38.26

Print out from a pacemaker programmer with markers and intracardiac recordings. The intracardiac atrial ECG at the bottom reveals atrial fibrillation during DDDR pacing, but the rate of the ventricles is normal. The adequate sensing of the fibrillation waves results in an automatic mode shift (AMS) to DDIR pacing.

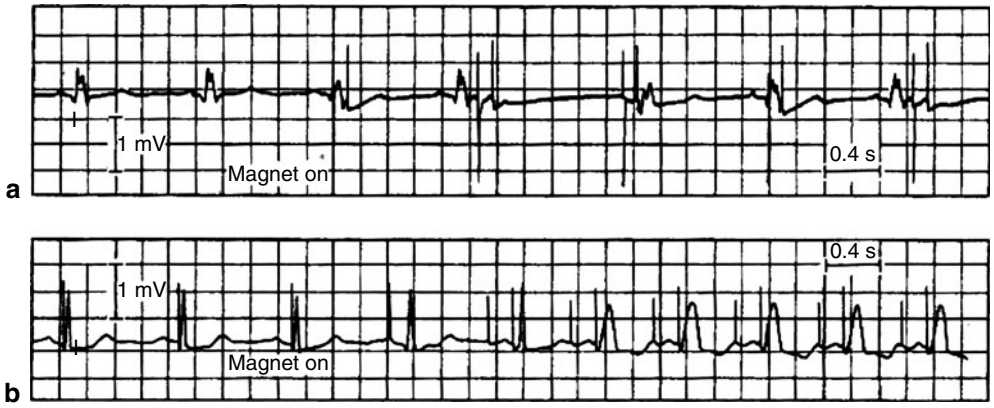

Figure 38.27

Two examples of DDD pacing in the presence of inhibiting atrial rates followed by normal AV conduction, which causes either inhibition of the ventricular output or pseudofusion beats. In (a), magnet application reverts the pulse generator to asynchronous stimulation (DOO) at the programmed basic rate. The interference between intrinsic activity and pacemaker stimulation produces pseudofusion beats without diagnostic information. In (b), the magnet test rate of 100 min^{-1} overdrives both spontaneous atrial activity and conducted ventricular beats thus providing information about atrial and ventricular capture.

magnet test response. The magnet test rate can be the same as the programmed basic rate (Fig. 38.27a). As long as interference between the intrinsic rhythm and pacemaker stimulation is followed by pseudofusion beats, no conclusion can be drawn about capture. Magnet tests running at higher rates facilitate the clinical investigation when overdrive suppression is accomplished (Fig. 38.27b).

Besides the assessment of stimulation response, the magnet test rate also reflects information about the battery condition. Today, telemetric data about the condition of the battery is a more reliable method of controlling the expected lifetime of the battery. Once more, it is necessary to emphasise the individual nature of the technical behavior of different pacemaker models and the need to obtain specific, relevant information before conclusions can be drawn.

The interpretation of a pacemaker ECG is easier when pulse generators with telemetric function are used. By means of corresponding programmers, marker pulses can be recorded indicating which chamber has been involved and whether sensing or stimulation is occurring (Fig. 38.28). In the new models, even the duration of the different refractory periods is displayed, together with the ongoing intracardiac ECG registration.

Besides marker pulses, intracardiac ECG recording can also be obtained via telemetry (Fig. 38.29).

The evaluation of atrial stimulation response in dual-chamber pacing is often difficult because of the distortion of the ECG registration by atrial impulses. It is not uncommon that standard ECG leads fail to permit any conclusion. Earlier, esophageal registration was therefore necessary to analyze atrial activity both concerning stimulation response and spontaneous ectopic beats if intracardiac atrial recording from the programmer is not available.

Nowadays, each patient should be equipped with a pacemaker "passport," including relevant data on the latest program setting. Pacemaker–ECG interpretation can be further facilitated when programmed parameters and information are printed out simultaneously on the ECG strip together with marker pulses.

38.7 Pacemaker Malfunction and Pseudomalfunction

When analyzing a "pathological" pacemaker ECG, it is necessary to differentiate between malfunction owing to lead or pulse generator disorders and pseudomalfunction caused by inappropriate program settings with regard to the underlying arrhythmia.

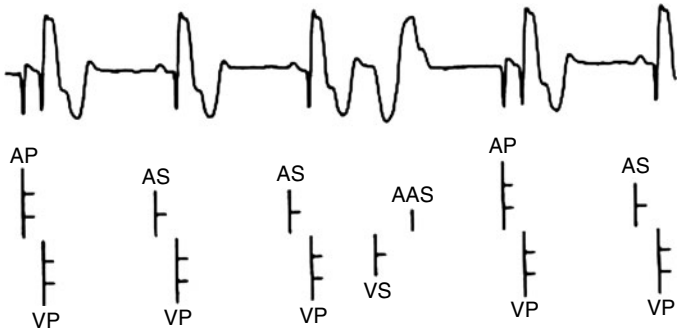

Figure 38.28

An early pacemaker example of the first markers of intracardiac ECG complexes. Dual-chamber pacing and simultaneous display of marker pulses indicating alternation between atrial pacing (AP), atrial sensing (AS), ventricular pacing (VP), ventricular sensing (VS), and abolished atrial sensing (AAS) after ventricular sensing of an ectopic beat.

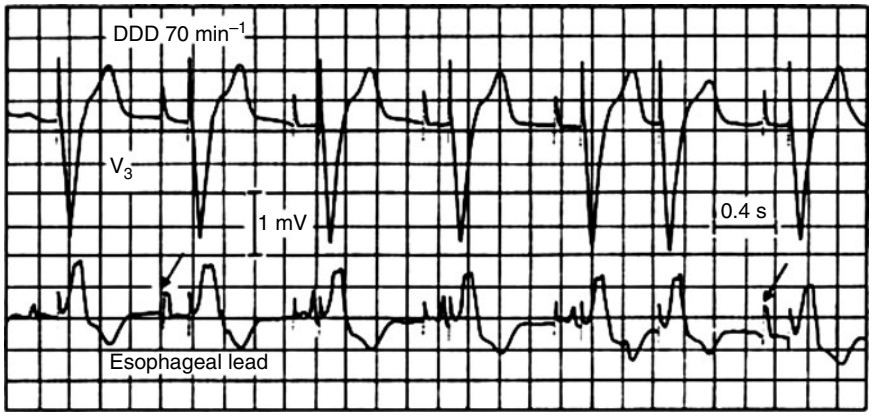

Figure 38.29

Esophageal-lead registration permits atrial activity to be visualized very clearly and discloses alternation between atrial fusion beats (*arrows*), normal atrial capture, and a supraventricular ectopic beat localized within the T wave of the preceding QRS complex. Today, intracardiac recordings and markers from the atrium make esophageal ECG recordings unnecessary.

Technical disorders of pacemaker systems are mainly related to lead problems, but other factors may also disturb the pacemaker operation. A collection of possible causes is given in Fig. 38.30. Some complications are accompanied by typical ECG patterns, and their diagnosis and assessment can be undertaken through the interpretation of standard ECG recordings. However, several malfunctions may cause the same ECG pattern, thereby creating difficulties in making a correct diagnosis and in deciding adequate countermeasures. The disclosure of intermittent and sporadic disorders sometimes requires a closer look at the diagnostic memory of the pacemaker or Holter monitoring.

The most important question regarding pacemaker function is whether there is adequate response (capture) to all pacemaker stimuli. A lack of capture is called *exit block*, a descriptive ECG term, which does not provide any information about the underlying cause. Hence, it is not possible to discriminate between lead dislodgment and pathological threshold rise with an unchanged lead-tip position (Fig. 38.31).

The presence of ventricular exit block is obvious in dual-chamber systems when there is AV block (Fig. 38.32). Sometimes, it is difficult to see if the exit block is from the atrial or the ventricular lead. However, it can be overlooked when spontaneous AV conduction occurs and initiates ventricular depolarization resulting in pseudofusion beats (Fig. 38.33).

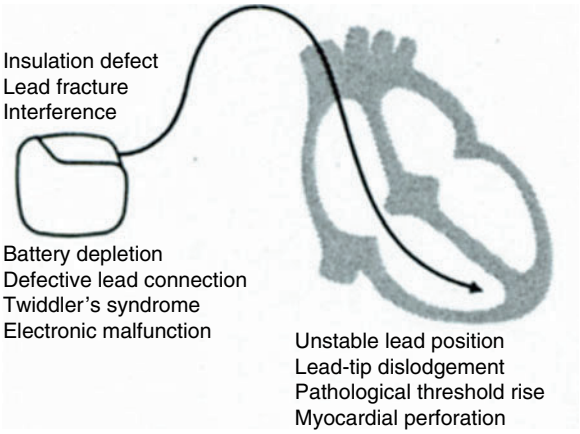

Figure 38.30

Different pacemaker malfunctions detailed concerning cause and location.

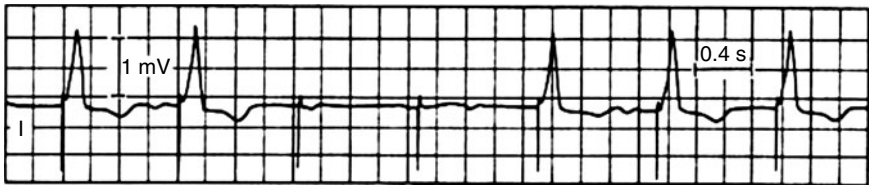

Figure 38.31

VVI pacing at a rate of 70 min^{-1} and intermittent exit block, but without any information about the cause of loss of capture.

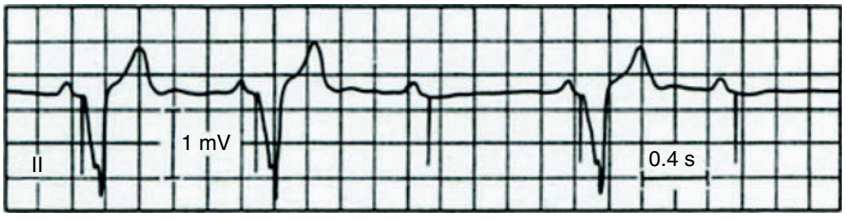

Figure 38.32

DDD mode. Atrial-triggered ventricular stimulation is followed by intermittent ventricular exit block.

Figure 38.33

Dual-chamber pacing at a rate of 70 min^{-1}. Two of the ventricular complexes differ in configuration and occur approximately 80 ms after the ventricular stimulus is delivered. This indicates the presence of an intermittent ventricular exit block "somewhat concealed" by the spontaneously conducted QRS complexes.

Figure 38.34

Dual-chamber pacing at a rate of 70 min^{-1}. Atrial depolarizations are clearly visible in this recording. The loss of atrial capture in complex #4 is followed by triggered ventricular stimulation, probably because of a spontaneous P wave hidden somewhere in the T wave of the preceding QRS complex.

Figure 38.35

VVI pacing at a rate of 80 min^{-1}. The first premature ectopic ventricular beat accomplishes inhibition indicated by the reset of the basic rate interval, while the second one differs in configuration and remains unsensed.

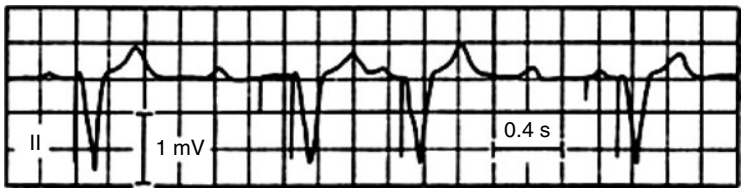

Figure 38.36

Dual-chamber pacing. Intermittent P wave undersensing is followed by atrial stimulation at a basic rate of 50 min^{-1}. Atrial capture can be obtained when the biological refractory period of the unsensed spontaneous P wave has passed.

As mentioned earlier, the assessment of atrial capture demands visualization of atrial activity (Fig. 38.34). If standard ECG leads do not provide sufficient information, intracardiac recording or reprogramming procedures may help to disclose possible atrial exit block.

The sensing function also has to be assessed in an ECG analysis. Ventricular ectopic activity may be sensed with different amplitudes and slew rates. The actual program setting may cover normal ventricular complexes, but not all ectopic beats (Fig. 38.35).

In dual-chamber pacing, one of the major concerns is consistent P-wave sensing. In the presence of AV block, P-wave undersensing is easily detected (Fig. 38.36). However, during normal AV conduction, P-wave undersensing may be overlooked when the pacemaker is correctly inhibited via the ventricular amplifier owing to sensing of spontaneous QRS complexes (Fig. 38.37).

Unfortunately, other signals may affect the pacemaker function; for example, myopotentials. In unipolar pacemaker systems, myopotentials near the pulse generator pocket may be sensed causing inhibition or interference rate pacing, the signals being perceived as cardiac activity. Inhibition by myopotentials is supposed to be a pseudomalfunction, as the pulse generator operates correctly according to the technical specifications (Fig. 38.38). Another example of pseudomalfunction is given in Fig. 38.39, which demonstrates far-field R wave oversensing in AAI pacing. In unipolar AAI pacing, sometimes rather large intra-atrial R waves can be seen resulting in sensing problems.

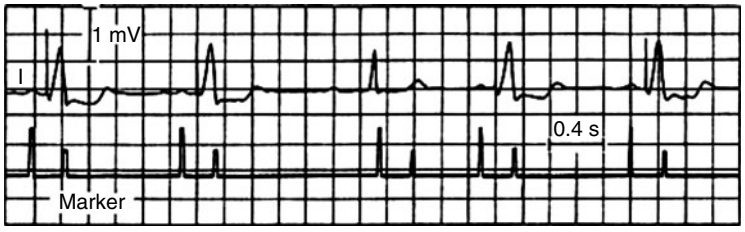

Figure 38.37
Dual-chamber pacing. One P wave (number 3) is not detected by the atrial amplifier. The following spontaneously conducted QRS complex is sensed by the ventricular amplifier as is clearly indicated by the simultaneous marker-pulse recording.

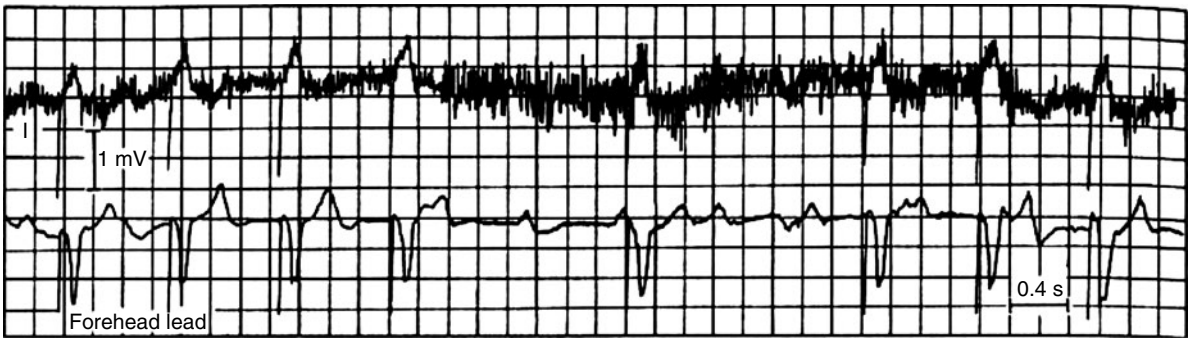

Figure 38.38
VVI pacing at a rate of 80 min^{-1}. The occurrence of myopotentials clearly seen in standard lead I causes intermittent inhibition. The lack of interference in the lower-lead recording is a result of the temporary placement of the ECG lead on the patient's forehead.

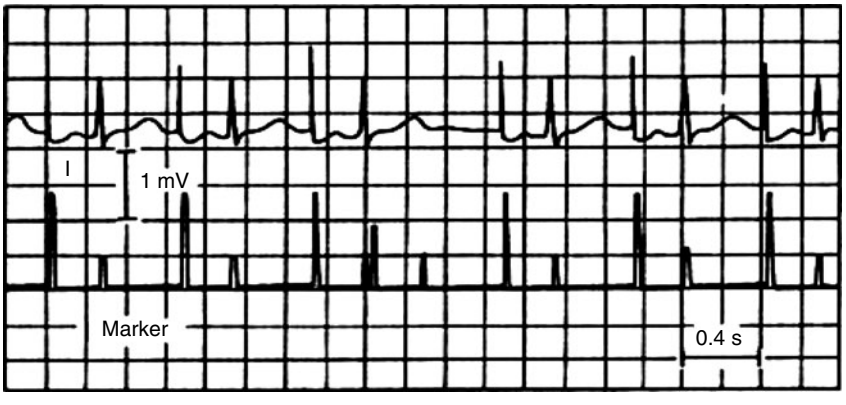

Figure 38.39
AAI pacing at a rate of 90 min^{-1} with an intermittent pause. Marker-pulse registration indicates a reset of the technical refractory period and the basic interval timer. The reset can be related to the QRS complex and the diagnosis is intermittent far-field R-wave oversensing; that is, the actual sensing program detects the "distant" ventricular activity.

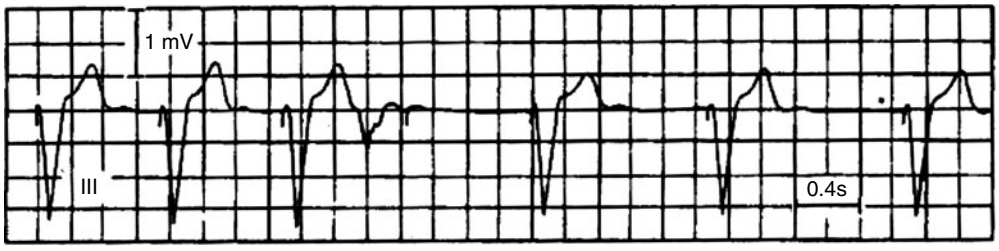

Figure 38.40

VVI pacing system with a programmed basic rate of 80 min^{-1}. A premature ventricular ectopic beat is not followed by inhibition. Intermittent and irregular variation of pacing intervals indicates inhibition owing to oversensing. Because there are neither signs of external electrical interference nor myopotentials, signals occurring within the lead system can be assumed to cause the intermittent inhibition or conversion to interference rate stimulation thus mimicking undersensing. In this particular patient, an insulation defect of the transvenous lead at the site of the tricuspid valve was found to be the reason for the pathological ECG.

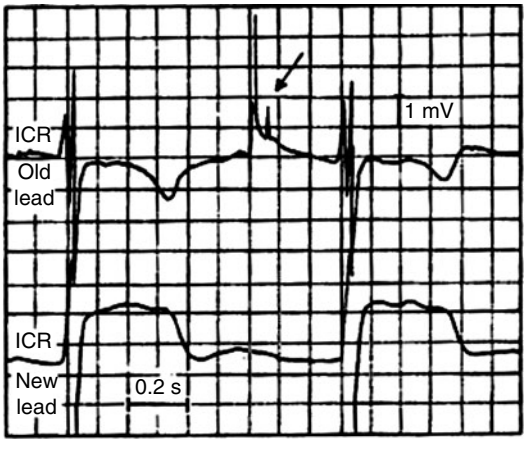

Figure 38.41

Intracardiac ECG recording (ICR) (paper speed 50 mm s^{-1}) obtained from the same patient as in Fig. 38.40 during lead replacement. Simultaneous registration discloses pathological signals with maximum amplitude of 5 mV from the old lead, but not from the newly implanted second ventricular lead.

Figure 38.42

DDD pacing system operating with irregular triggered ventricular stimulation, alternating with basic rate stimulation and occasionally P-wave undersensing. The reason for this confusion ECG turned out to be an insulation defect of the epicardial atrial lead a few centimeters from the lead tip.

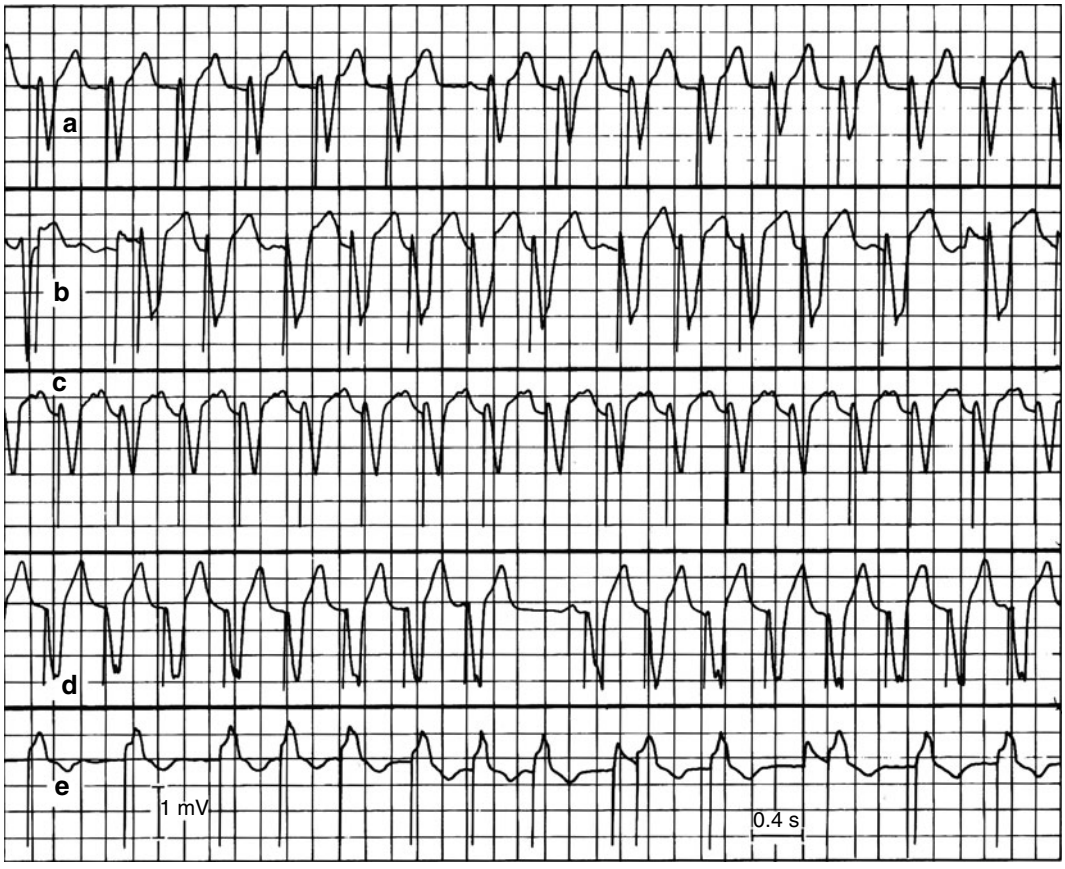

Figure 38.43

DDD-mode tachycardias. Recordings from five different patients, each with a different diagnosis. The recording taken from the patient shown in (a) illustrates sinus tachycardia at a rate slightly ahead of the programmed upper rate limit of 110 min^{-1} resulting in prolonged AV delay and a Wenckebach block type of behavior; (b) shows a patient with atrial fibrillation with irregular ventricular triggering limited by a programmed upper rate of 128 min^{-1}; (c) illustrates pacemaker-mediated reentrant tachycardia owing to sensing of retrograde P waves following ventricular stimulation; (d) shows repetitive far-field R-wave oversensing owing to inappropriate program setting with respect to the duration of the atrial refractory period and high atrial sensitivity; and (e) illustrates irregular triggered ventricular stimulation owing to "oversensing" of potentials generated by an insulation defect of the atrial lead.

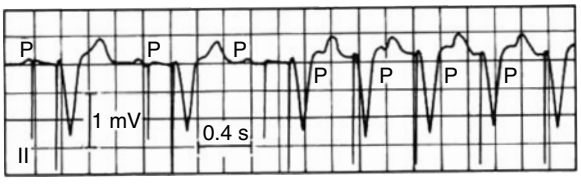

Figure 38.44

DDD pacing with good recording of atrial activity. After three unsensed P waves, ventricular stimulation is followed by a retrograde P wave, which is obviously sensed, subsequently triggering the next ventricular stimulation. Repetitive occurrence and consistent sensing of retrograde P waves maintain the running of an endless-loop reentrant tachycardia.

Rather confusing ECG patterns are obtained when a lead insulation defect appears (Fig. 38.40). Pathological inhibition alternating with interference rate stimulation resulting in pseudoundersensing may occur as intracardiac insulation defects giving rise to pathological potentials (Fig. 38.41). Another puzzling ECG is given in Fig. 38.42, where an insulation defect in an atrial lead is responsible for pathological triggering of ventricular stimulation.

Tachyarrhythmias in dual-chamber pacing pose challenging diagnostic problems as they may look alike despite different underlying mechanisms (Fig. 38.43). As mentioned earlier, a good ECG recording is necessary for the detection of P waves, which may help to disclose the cause of the arrhythmia (Fig. 38.44).

38.8 Functional Tests

The days when only a magnet was available as a test instrument have more or less disappeared. In multiprogrammable pacemakers, output can be reduced either by shortening the impulse duration or decreasing the amplitude with the programmer. Some manufacturers have chosen to provide an automatic stepwise decrease or a one-step change of the pacing threshold measurement (Fig. 38.45). This is a temporary programming, which necessitates access to the specific programmer and knowledge of how to handle this device. Episodes of asystole may occur during the stimulation tests (Figs. 38.46 and 38.47).

In dual-chamber pacing, the evaluation of the atrial stimulation threshold by the temporary reduction of voltage or impulse duration is facilitated when the atrial depolarization is clearly visible (Fig. 38.48). In some cases, it is difficult to see the P waves, but if the test is done with the programmer, markers and intracardiac ECG recordings are useful tools.

The clinical information obtained from only reading standard pacemaker ECG registration is limited. Even if the adequate pacemaker function can be assessed, it is advisable to evaluate safety margins for stimulation and sensing, as well as the battery condition during follow-up. Almost all programmers measure sensing automatically or semi-automatically (Fig. 38.48).

The assessment of atrial sensing threshold always requires a reprogramming procedure. P-wave sensing is subjected to changes in the postoperative course without correlation with the variation of stimulation thresholds. Additional provocation tests with ECG recordings in different postures and during maximal inspiration can expose intermittent undersensing (Fig. 38.49).

During the follow up of the AAI/R mode, special attention should be paid to the AV conduction. This can be done by reevaluation of the Wenckebach block by temporary incremental rate increase. Valsalva maneuvers and carotid massage can also provide useful information about the AV conduction properties (Fig. 38.50).

When normal AV conduction is present in the DDD mode, it is possible that – in the presence of long technical AV delay – the ventricular spikes will coincide with spontaneous QRS complexes or be inhibited depending on the critical timing. Hence, no information can be obtained about ventricular stimulation response unless the technical AV delay is reprogrammed to a very short value (Fig. 38.51). A possible exit block may thus be disclosed which is otherwise well-concealed by pseudofusion beats or inhibition.

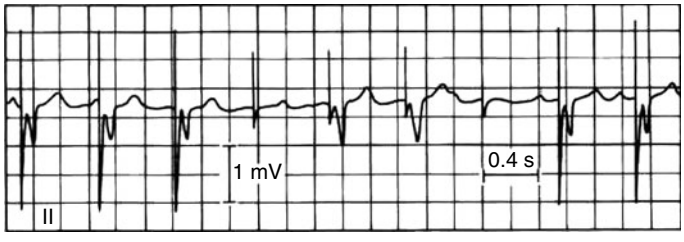

Figure 38.45

VVI pacing during a threshold test where the output of four stimuli is automatically reduced by a decrease in impulse duration from 0.5 to 0.07 ms. Intermittent loss of capture occurs.

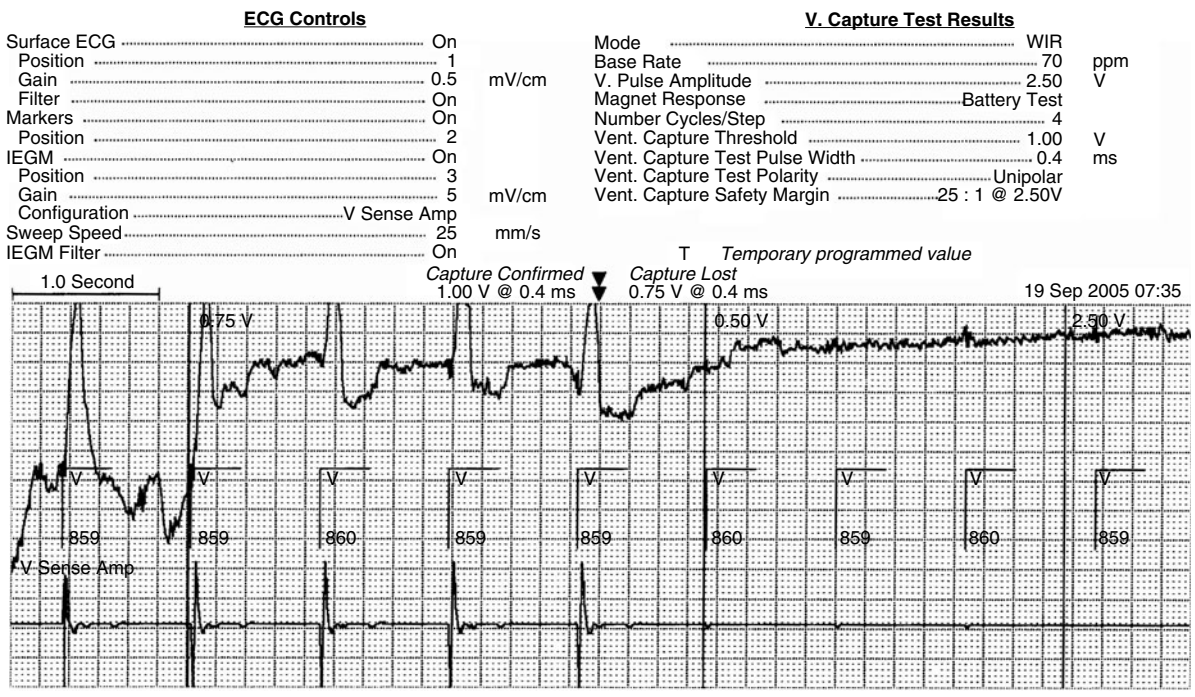

Figure 38.46

An automatic ventricular pacing threshold test with a printout from the programmer is done with reduction of the voltage of the pacing amplitude. The surface ECG has some muscle potential disturbances but loss of capture is clearly seen at 0.75 V. The markers line in the middle has a V sign indicating a ventricular output from the pacemaker. The bottom ECG is an intrinsic recording of the sensed amplitude, which, of course, disappears when capture is lost. No ventricular escape rhythm is detected.

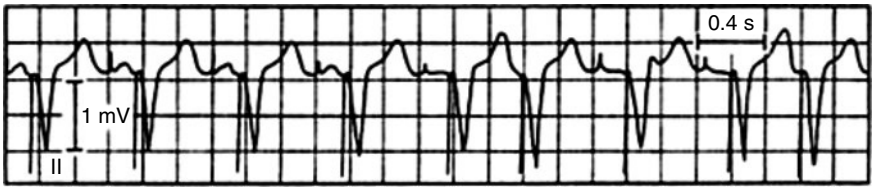

Figure 38.47

Automatic atrial stimulation threshold test of a DDD pacemaker. As the P waves are clearly visible it is simple to estimate when loss of capture occurs.

In unipolar pacing, sensing of myopotentials from muscles close to the pulse generator constitutes a well-known problem. To determine the extent to which an individual patient may experience myopotential inhibition, routine testing is recommended before a final decision on program setting is made. In the DDD pulse generators, both the atrial and the ventricular amplifier may be influenced by myopotentials depending on their amplitude and slew rate in relation to the sensitivity setting (Fig. 38.52).

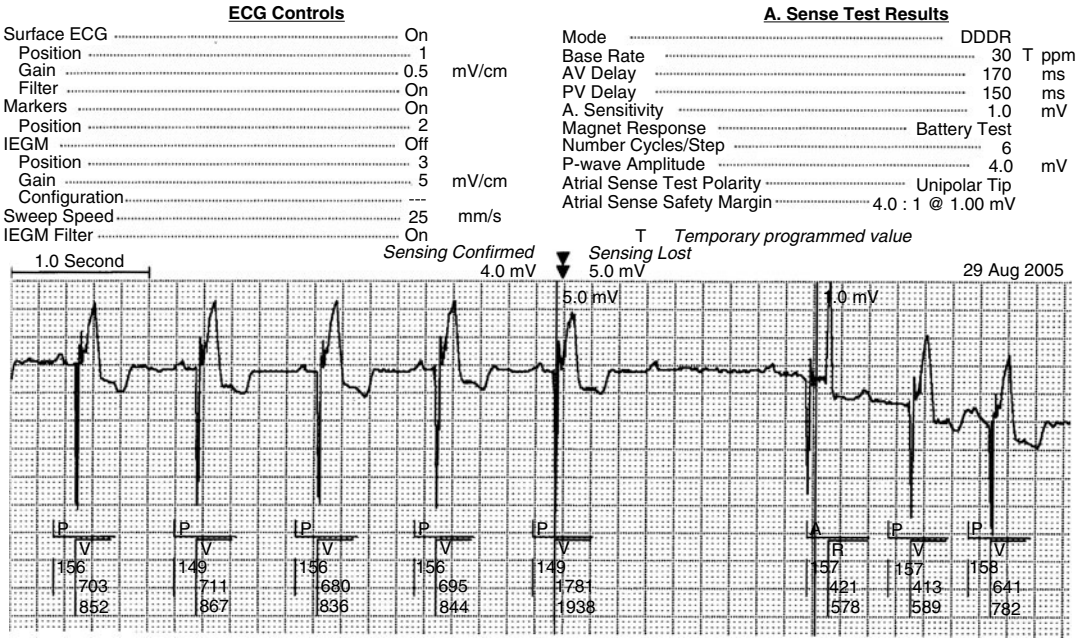

Figure 38.48

Here is an example of an automatic atrial-sensing test in a DDD system. Sensing of the P waves is lost at 5.0 mV, which the two arrows indicate. To simplify the test, the base rate is programmed to 30 bpm temporary.

***P* spontaneous P wave, *A* paced atrium, *V* paced ventricle, *R* spontaneous ventricular beat.**

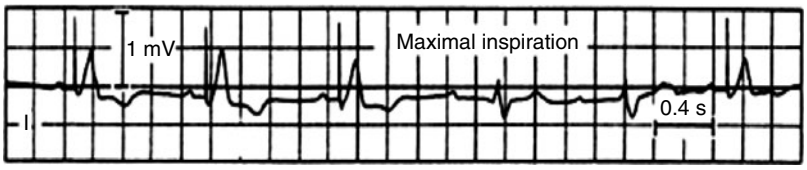

Figure 38.49

DDD pacing with obviously reliable atrial sensing. However, a test during deep inspiration discloses intermittent atrial undersensing.

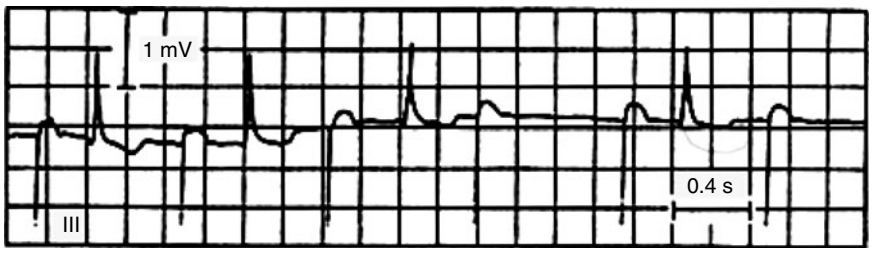

Figure 38.50

AV conduction test in an AAI system. When carotid sinus pressure is applied, intermittent second-degree AV block is exposed.

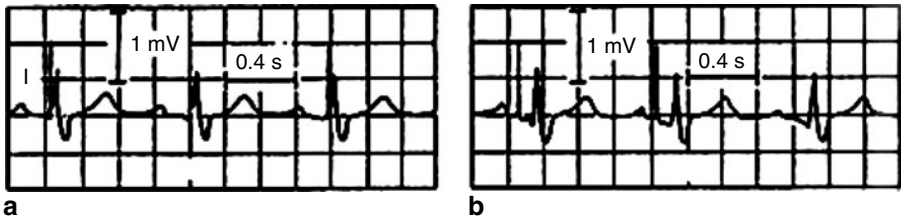

Figure 38.51

A DDD pacemaker with a technical AV delay programmed to 200 ms is shown in (a). Atrial triggered ventricular stimulation coincides with spontaneous conducted beats and the ECG could be interpreted as normal pacemaker function. However, reprogramming to a shorter AV delay of 120 ms discloses an underlying ventricular exit block, which is shown in (b).

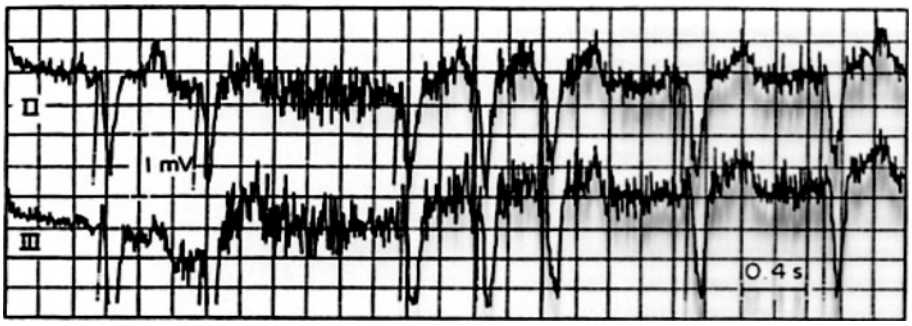

Figure 38.52

Myopotential provocation test. In DDD pacing, myopotentials sensed by the atrial amplifier will cause triggered ventricular stimulation, while sensing by the ventricular amplifier is followed by inhibition or conversion to interference rate stimulation. The type of reaction depends on the program setting and the amplitude of the myopotentials obtained.

38.9 Biventricular Pacing, Cardiac Resynchronization

During the last few years, there has been an enormous interest in treating patients with heart failure with pacing both ventricles at the same time or almost simultaneously by implanting an extra pacing lead on the left ventricle. This is possible by using branches of the coronary sinus vein and specially designed pacemaker leads for this purpose. It is not necessary that the patient has bradycardia; a major intraventricular electromechanical asynchrony with heart failure is the indication for CRT (cardiac resynchronization therapy). Instead of pacing only the right ventricle with bundle branch block as a result, stimulation of both ventricles at the same time is a more optimized treatment for each patient. If chronic atrial fibrillation does not exist, the patient will have three leads implanted: one in the right atrium, another in the right ventricle, and the third one in the coronary sinus (Fig. 38.53). In chronic atrial fibrillation, the atrial lead is skipped.

The ECGs from biventricular pacing can be very similar to the ordinary DDD ECGs, but during different tests it is easier to see how the system works. The pacing ventricular threshold tests can be done with a short AV delay or in the VVI modes for each ventricle (Fig. 38.54).

In the early stages of biventricular pacing, many different systems were available. For example, the ventricular ports were connected together to provide simultaneous pacing of both ventricles. The pacemaker senses RV and LV activity simultaneously. Today, the modern biventricular pulse generator usually has two independent ventricular ports and it is possible to program a short time delay between the LV and RV stimuli and optimize the therapy for each patient.

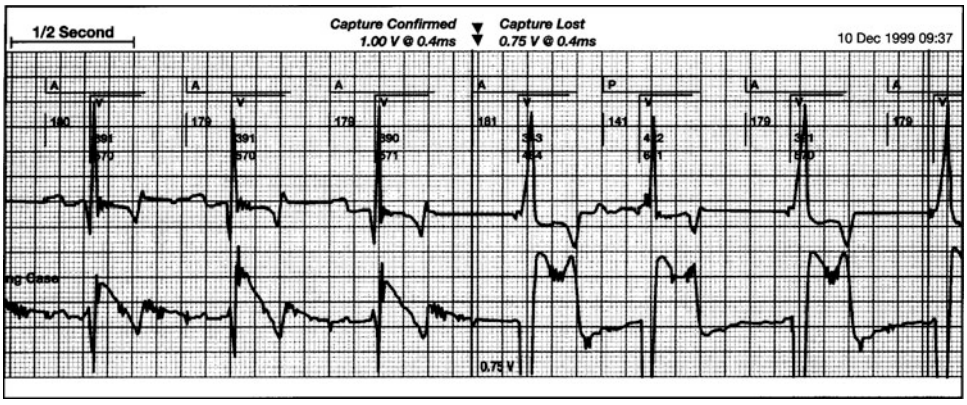

Figure 38.53

In the upper ECG lead, the three first QRS complexes are narrow due to biventricular stimulation. During an automatic threshold test, capture is lost at 0.75 V on one pacemaker channel resulting in a bundle branch block pattern visible both on the surface ECG and the intracardiac electrogram (EGM) in the lower part [7].

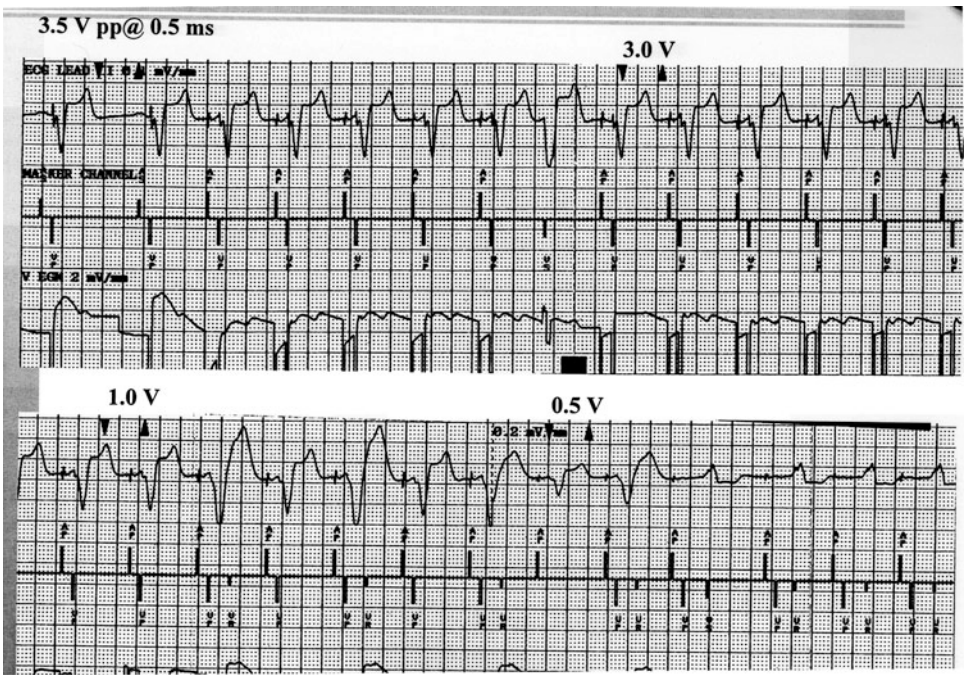

Figure 38.54

Another example of biventricular pacing. The first complexes are similar to ordinary DDD pacing. During the threshold test, bundle branch block occurs on one channel and at 0.5 V the spontaneous intrinsic QRS complex is seen.

38.10 Tachycardia and ICD

Many patients with a life-threatening tachycardia will receive an ICD. The ICD (implantable cardioverter defibrillator) has a built-in pacemaker, and depending on the lead configuration, the pulse generator can pace and sense in single or double chamber mode or even in biventricular configuration. Many patients need pacing just after termination of a tachycardia, when a short asystole can appear. During implantation, ventricular fibrillation is initiated in order to check that the shock therapy terminates the life-threatening tachycardia (Fig. 38.55).

Most implantable defibrillators have the opportunity to terminate a ventricular tachycardia by using a function called ATP (antitachycardia pacing). Instead of a painful shock therapy, a preprogrammed rapid overdrive (bursts) stimuli is automatically delivered with a low-pacing amplitude when the tachycardia starts (Fig. 38.56). If VF is initiated, shocks will be delivered.

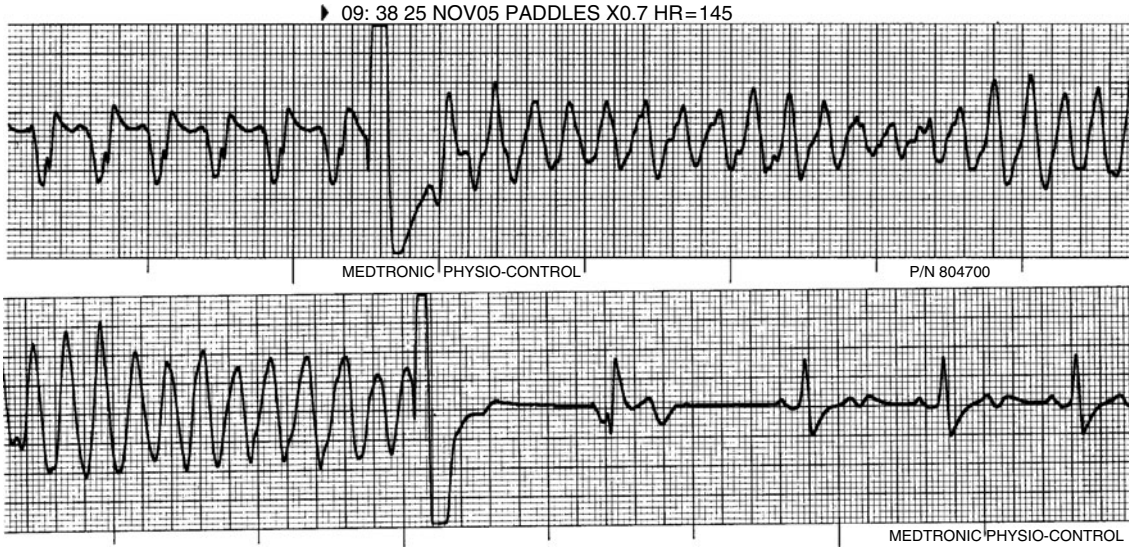

Figure 38.55

Initiation and automatic termination of VF in a test during an implantation of an ICD. The first six beats are overdrive pacing with a shock on the vulnerable phase of the T wave to start the VF. The bottom ECG has a pacemaker beat after the shock has been delivered and then sinus rhythm is established.

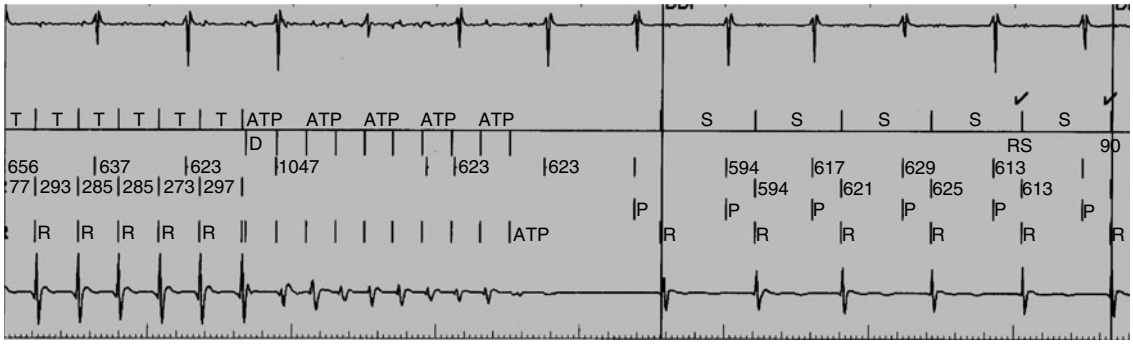

Figure 38.56

Print out from an ICD programmer with a stored ECG, EGM, and markers from an ICD device. The print out demonstrates a ventricular tachycardia and a burst of pacing stimuli is given (ATP) and the VT terminates to sinus rhythm (S). Markers of the P and R waves are also seen.

The pacemaker in the ICD device has a sensor which is very useful when antiarrhythmic drug therapy sometimes results in bradycardia.

The interpretation of stored ECGs in the ICD devices focuses a lot on the correct sensing of VT and VF. Unfortunately, many shocks are delivered due to false sensing (rapid atrial fibrillation, lead insulation defects, etc.). The pacing/sensing ventricular lead is tested in the same way as an ordinary pacing lead regarding thresholds.

References

1. Parsonnet, V., S. Furman, N.P.D. Smyth, and M. Bilitch, Optimal resources for implantable cardiac pacemakers. Pacemaker study group. *Circulation*, 1983;**68**: 227A–244A.
2. Barold, S.S, Editors. *Modern Cardiac Pacing*. Mount Kisco, New York: Futura, 1986.
3. Furman, S., D. Hayes, and D. Holmes, *A Practice of Cardiac Pacing*. Mount Kisco, New York: Futura, 1986.
4. Levine, P.A and R.C. Mace, *Pacing Therapy: A Guide to Cardiac Pacing for Optimum Hemodynamic Benefit*. Mount Kisco, New York: Futura, 1983.
5. Schüller, H. and T. Fåhraeus, *Pacemaker Electrocardiograms – An Introduction to Practical Analysis*. Solna, Sweden: Siemens-Elema, 1983.
6. Serge, B.X.S. Roland, and F.S. Alfons,*Cardiac Pacemakers Step by Step, an Illustrated Guide*. Futura: Blackwell, 2004.
7. Levine, P.A. *Guidelines to the Routine Evaluation, Programming and Follow-Up of the Patient with an Implanted Dual-Chamber Rate-Modulated Pacing System*. St Jude Medical, 2003.
8. Kenneth, E.A., K.G. Neal, and L.W. Bruce, *Clinical Cardiac Pacing*. W.B. Saunders, 1995.

39 The Signal-Averaged Electrocardiogram

Leif Sörnmo · Elin Trägårdh Johansson · Michael B. Simson

P. W. Macfarlane, A. van Oosterom, O. Pahlm, P. Kligfield, M. Janse, J. Camm (eds.), *Comprehensive Electrocardiology*, DOI 10.1007/978-1-84882-046-3_39,

39.1 Introduction

The signal averaging technique is applied to electrocardiographic recordings to reduce extraneous noise, which masks low-amplitude bioelectric signals from the heart. Although modern amplifier design and good recording techniques can minimize certain types of noise, other sources of noise, such as muscle activity, obscure low amplitude potentials. With signal averaging, the noise level can be reduced so that repetitive waveforms at the microvolt level can be reliably detected and analyzed. The noise level after averaging is, in most studies, below 1 μV, the equivalent of 1/100 of a millimeter at a standard ECG display scale.

This chapter discusses the methodology of signal averaging and its use in studying high-frequency components of the QRST complex, manifested either as ventricular late potentials (Sects. 39.3 through 39.7) or within the QRS complex (Sects. 39.8 and 39.9). Signal averaging is useful also in other ECG applications such as exercise testing (see Chap. 36), although the dynamic changes of the ST segment call for recursive signal averaging with a forgetting factor.

39.2 Methods of Signal Averaging

Signal averaging reduces the level of noise that contaminates a repetitive signal such as the ECG [1–3]. The most commonly used form is ensemble averaging in which multiple samples of a repetitive waveform are averaged with equal weights; random noise, which is not synchronized with the waveform of interest, is reduced. The process of averaging begins by measuring the voltage of an ECG fed through a high-gain (×1,000) amplifier with bandwidth ranging from 0.05 Hz to several 100 Hz. The analog signal is converted into digital form at a sampling rate of 1,000 Hz or more and stored. Once all beats of the ECG have been identified and aligned in time, the ensemble average is computed by first summing the samples at a particular instant within the beat and then dividing the sum by the total number of beats. This procedure is repeated for all the samples of the beat.

Several requirements must be met so that the signal averaging technique can reduce noise effectively [1, 3]. First, the waveform of interest must be repetitive so that multiple samples can be obtained to form an average waveform. Second, there must exist a unique feature in the ECG, which can be used as a reference time so that appropriate points of the repetitive signal can be averaged. The time of the maximum amplitude or maximum slope of the QRS complex may be used as reference time; however, such simplistic definitions are useful only when the noise level of the ECG is known to be low. A more robust approach is to cross-correlate each new waveform with a template waveform, determining the reference time as that point in time which corresponds to the highest cross-correlation value [4, 5]. If the algorithm for determining the reference time is inaccurate, that is, causing "trigger jitter," the averaged waveform becomes smoothed and the high-frequency components of the waveform are reduced. For example, it can be shown that a normally distributed jitter with a standard deviation of 1 ms causes the averaging operation to act as a linear, time-invariant low-pass filter with cut-off frequency at about 140 Hz [1]. Similarly, if the QRS complex is used as reference time, then the high-frequency components of an averaged P wave is smoothed because the PR interval varies slightly from beat to beat.

Third, the signal of interest must be uncorrelated with the contaminating noise. If so, the reduction of noise by signal averaging is proportional to the square root of the number of beats contained in the ensemble. For example, averaging of 100 beats will reduce the noise by a factor of 10 [1]. However, the noise must have certain properties to be reduced effectively by signal averaging: it should be random, uncorrelated with the beats, and characterized by an unchanging statistical distribution.

The noise that masks low-level electrical events of the heart has three primary origins:

1. Skeletal muscle noise, typically 5–20 μV even with a relaxed patient
2. Power line interference (50 or 60 Hz and related harmonics) and
3. Electronic and thermal noise from amplifiers and electrodes

Myoelectrical and electrode noise are the most troublesome ones in practice; modern isolation amplifiers have greatly reduced interference originating from power lines. Another noise source is the presence of ectopic beats. These complexes can be eliminated by their premature timing and through matching of a new beat against a template of the desired beat before averaging is performed [5–7].

39.3 Late Potentials and Time Domain Analysis

39.3.1 Introduction

One of the most frequent applications of signal averaging in electrocardiology has been the detection of ventricular late potentials, most often in patients with ventricular tachyarrhythmias. Late potentials are micro-volt level, high-frequency waveforms that are contiguous with the QRS complex and last a variable time into the ST segment. Such potentials are postulated to originate from small areas of delayed and fragmented ventricular depolarization, resulting primarily from myocardial infarction (MI).

39.3.2 Filtering and Time Domain Parameters

Characterization of late potentials is facilitated by linear, time-invariant high-pass filtering of the signal averaged ECG so as to reduce the influence of large-amplitude low-frequency content. Such filtering permits high-frequency components, that is, the late potentials, to pass without loss of amplitude, while low-frequency components are attenuated. High-pass filtering is used because depolarization of cells generates rapid changes in membrane voltage, fast movement of wave fronts of activation, and high frequencies on the body-surface ECG. The plateau or repolarization phases of the action potential generate more slowly changing membrane voltages and lower-frequency signals on the body surface [8]. Microvolt-level waveforms, arising from the late depolarization of small areas of myocardium, would be difficult to perceive if displayed at high gain without filtering. High-pass filters with a cut-off frequency ranging from 25 to 100 Hz have been employed in most studies.

The use of conventional linear, time-invariant high-pass filtering is, however, complicated by the fact that a transient event in the input signal, that is, the QRS complex, produces ringing in the output signal that is subsequent to the event (Fig. 39.1a) [5]. This property is most unfortunate because it impedes the detection of low-amplitude potentials occurring immediately after the QRS complex. While the ringing problem is inherent to linear, time-invariant high-pass filtering, its harm can be largely reduced by employing "bidirectional" filtering–a technique which is implemented in most systems for late potential analysis. The main idea behind this technique is to delay ringing by filtering the signal in different directions so that ringing occurs within the mid-QRS. Forward filtering starts at the P wave and continues until the mid-QRS is reached, whereas backward filtering starts at the T wave and ends at the mid-QRS (Fig. 39.1b) [5]. Evidently, bidirectional filtering suffers from the disadvantage of an undefined output at mid-QRS, and thus no measurements should be done from the bidirectionally filtered signal that involves the entire QRS complex.

Figures 39.2 and 39.3 show examples of recordings made with signal-averaging technique in patients with and without late potentials. The tracings at the top of each figure are signal-averaged bipolar X, Y, and Z leads (as used in most studies of late potentials) from about 150 beats. Each lead is then high-pass filtered with a bidirectional filter (cut-off frequency at 25 Hz) and combined into a vector magnitude ($\sqrt{(X^2 + Y^2 + Z^2)}$), a signal that combines the high-frequency information contained in all three leads. This signal, shown on the bottom of each figure, is here termed the "filtered QRS complex." In patients without late potentials, the filtered QRS complex exhibits an abrupt onset, a peak of high-frequency voltage 40–50 ms after QRS onset, and an abrupt decline to noise level at the end of the QRS complex (Fig. 39.2). There is no high-frequency signal above the noise level in the ST segment. The peak of the T wave is associated with a small amount of high-frequency content. In patients with late potentials (Fig. 39.3), the initial portion of the filtered QRS complex is similar to that in patients without late potentials, except that the voltage tends to be lower [9]. At the end of the filtered QRS complex, however, there is a "tail" of low-amplitude signal which is not present in recordings from patients without late potentials. The low-level signal, a late potential, is contiguous with the QRS complex and corresponds to low-amplitude activity which can be seen at the end of the QRS complex in the unfiltered leads when displayed at high gain. The amplitude of the late potential varies from 1 to 20 μV when 25 Hz filtering is used.

The accuracy of the endpoint of the filtered QRS complex is a crucial parameter in time domain analysis as all other parameters are computed with reference to this point. Poor accuracy of the endpoint definition obviously limits the overall accuracy of the analysis. Clearly, the presence of late potentials causes the transition from signal to noise to be much less clear-cut than when late potentials are absent. The endpoint may be found by a backward search in the vector magnitude for the first samples which exceed a certain threshold; the threshold value is related to the residual noise level

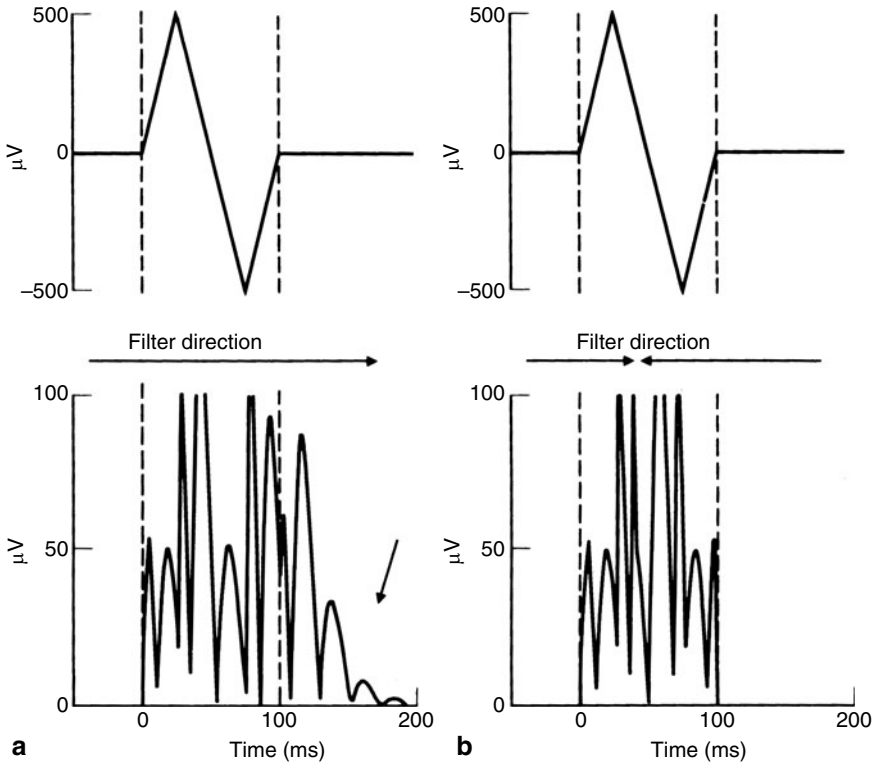

Figure 39.1

In (a), a test ECG signal is shown on top, while below the effect of a unidirectional filter with highpass (>25 Hz) characteristics is shown. Filtering starts at QRS onset and progresses, but it can be clearly seen that undesired signals (*ringing*, *arrowed*) have been introduced after the end of the QRS complex. In (b), however, the same filter is applied from QRS onset for 40 ms only and then applied from QRS end in the opposite direction, that is, toward QRS onset, again for 40 ms. This time no ringing outside the test ECG is apparent from the use of bidirectional filtering. (After Simson [5]. American Heart Association, Dallas, Texas. Reproduced with permission.)

of the averaged beat [5]; see also [10] for description of a more robust approach in individual leads. Several studies have required that the noise level of the averaged beat is reduced to a root mean square (RMS) level no more than 1 μV. However, it has been shown that the accuracy of the late potential endpoint, as well as the sensitivity and specificity of late potential analysis as such, can be further improved by extending the averaging period so that additional beats are included [11].

Time domain parameters are usually computed from the vector magnitude and include the RMS amplitude of the last 40 ms and the duration of the terminal filtered QRS amplitude <40 μV. These parameters are generally measured in commercially available equipment, as is the filtered QRS duration. The following, commonly used, diagnostic criteria for ventricular late potentials are based on filtering of the QRS complex with pass band 40–250 Hz:

1. RMS amplitude of last 40 ms of filtered QRS complex <20 μV (RMS40)
2. Duration of terminal low amplitude of filtered QRS complex below 40 μV < 38 ms (LAS40)
3. In the absence of a conduction defect, a filtered QRS duration >114 ms (FQRSd)

Using instead filtering with passband 25–250 Hz, the following criteria are commonly used: RMS40 <25μV, LAS40 >30 ms, and fQRSd >100 ms. At least two criteria should be met for late potentials to be considered present. A signal-averaged ECG with the three measurements (RMS40, LAS40, and FQRSd) is displayed in Fig. 39.4.

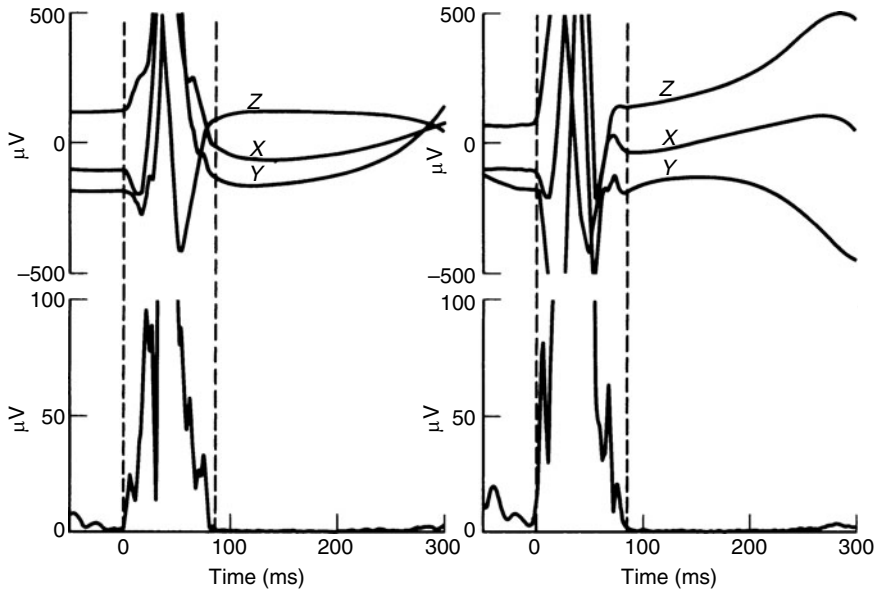

Figure 39.2

Recordings in patients without late potentials. These patients had anterior (*left*) and inferior (*right*) MI respectively. Bipolar signal-averaged leads are shown in high gain (*top*). On the bottom is the filtered signal-averaged QRS complex which is less than 100 ms in duration in both patients. There is a large RMS amplitude of signal in the last 40 ms of the filtered QRS complex (80 and 129 μV, respectively). The dashed vertical lines denote QRS onset and offset.

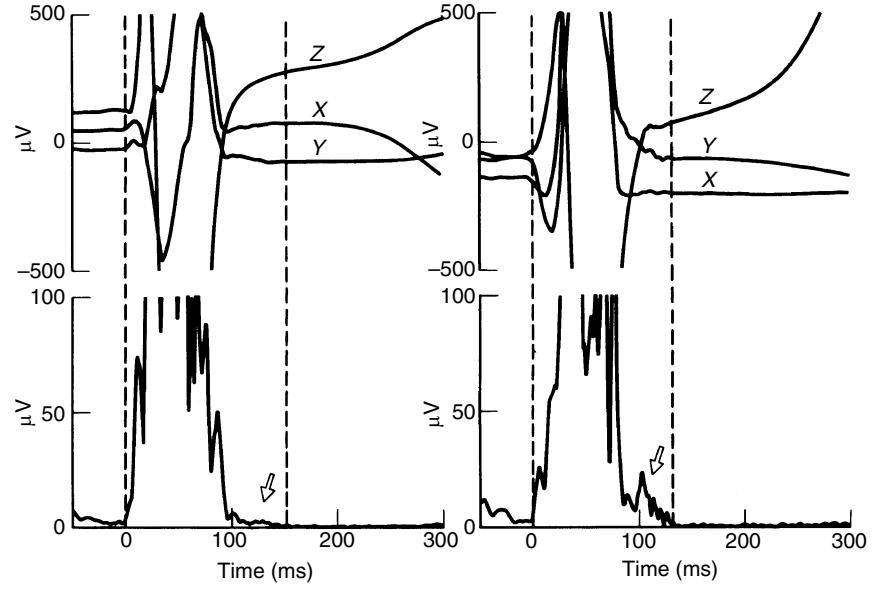

Figure 39.3

Signal processing in patients with VT and late potentials. The patient on the left had an anterior MI and the patient on the right had an inferior MI. The filtered QRS complex shows a longer duration in both patients and late potentials (*arrows*). The RMS voltages in the last 40 ms of the filtered QRS complex measured 2.0 and 11.2 μV, respectively. The *dashed vertical lines* denote QRS onset and offset.

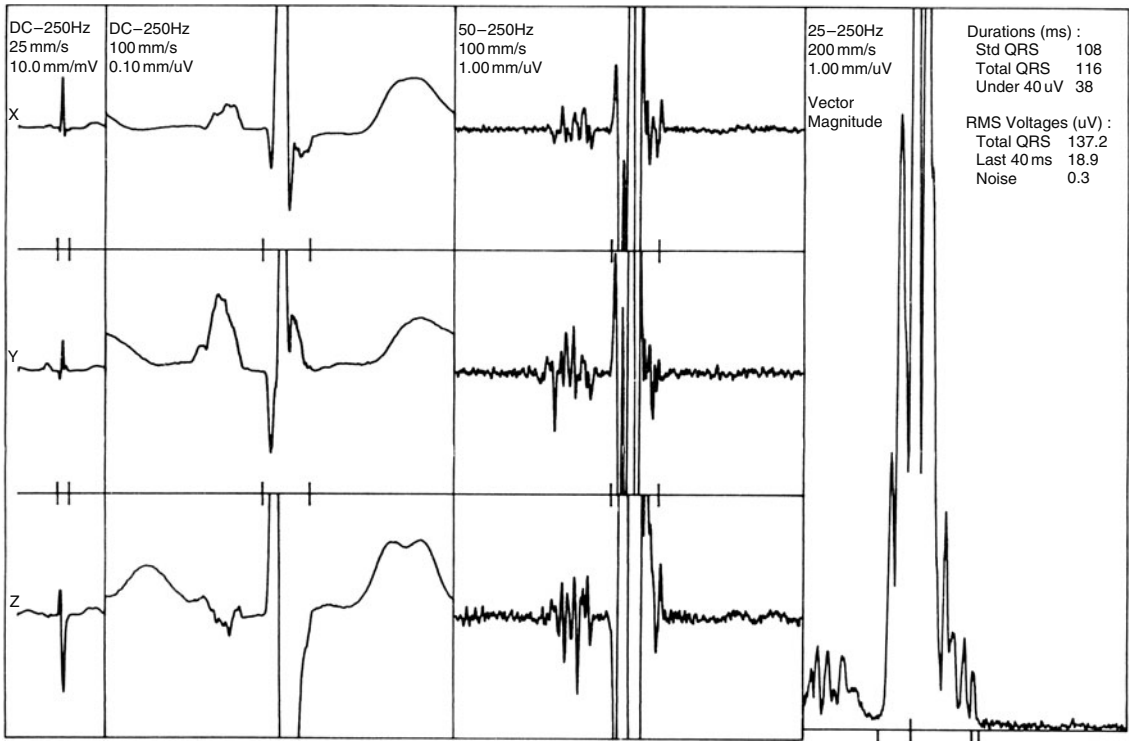

Figure 39.4

An example of the display of the signal-averaged ECG. The ECG is recorded from a 69-year old female with documented VT. The RMS voltage in the last 40 ms (RMS40) is abnormally low at 18.9 μV, the filtered QRS duration (fQRSd) is abnormally long at 116 ms, and the duration of late activity under 40 μV (LAS40) is also abnormally long at 38 ms.

39.3.3 Physiological Background

Late potentials are considered to originate from small areas of delayed ventricular depolarization. Disorganized and late ventricular activation has been recorded directly from infarcted and ischemic myocardium in animals and in humans [12–18]. Studies in animals with experimental infarcts have shown that the delayed ventricular activation can span diastole and that it relates to the occurrence of ventricular arrhythmias [12, 15, 16]. Josephson et al. demonstrated with endocardial recordings in man that fragmented electrical activity can outlast the surface QRS complex, and that the onset and maintenance of ventricular tachycardia (VT) depends on continuous diastolic activity [19]. When VT ceased, the continuous diastolic activity was no longer present. These studies provide evidence that VT after infarction has a reentrant mechanism and involves areas of abnormally slow and protected ventricular activation.

Several groups have reported examples of delayed epicardial ventricular activation in patients with late potentials [20–22]. To establish the time relationship between the body surface late potential and delayed ventricular activation, Simson et al. studied eight patients with signal-averaged ECGs and ventricular mapping [17]. The patients had medically intractable and inducible VT after infarction and underwent surgery for control of the arrhythmia. Twelve to 16 left ventricular endocardial sites were mapped with a catheter and 32–54 epicardial sites were directly recorded in the operating room at normal body temperature. Studies were performed during sinus rhythm. All patients showed evidence of fragmented and low-level electrograms which were prolonged (>60 ms) in duration. These electrograms were recorded from 6.6 ± 3.3 sites per patient; 88% of the fragmented electrograms began during the QRS complex and the latest fragmented electrogram for each patient ended a mean of 161 ms after QRS onset. Six patients with VT had late potentials and the late potentials on the body surface corresponded in time to fragmented and delayed electrogram activity. During the

last 40 ms of the filtered QRS complex, when the late potentials were recorded, 68% of the electrograms active showed fragmented activity. In contrast, in earlier segments of the QRS complex only 27% of the active electrograms showed fragmented activity. The mapping studies demonstrated that the late potentials correlated in time with fragmented electrogram activity, which begins during the normal QRS complex but which outlasts normal ventricular activation. The studies are in agreement with those performed in animals with experimental infarcts and late potentials [18, 23].

The mapping studies suggest that fragmented electrogram activity could be detected on the body surface as a low-level waveform only when it outlasted normal ventricular activation. Late potentials were not detected in a patient with left bundle branch block because the late epicardial activation occurred simultaneously with delayed and fragmented endocardial electrograms. When the fragmented electrograms were of brief duration and ended less than 90 ms after QRS onset, then no late potentials could be detected [17]. Because the duration of fragmented ventricular activation is prolonged with premature beats or at rapid heart rates, pacing the heart or inducing a premature beat may enhance the detection of late potentials [15, 16]. The frequency content of late potentials is similar to that of the entire QRS complex and it is unlikely that frequency analysis could detect small areas of fragmented ventricular activation occurring simultaneously with activation of a larger mass of normal myocardium.

39.4 Late Potentials and Time Domain Analysis in Clinical Applications

39.4.1 Recent Myocardial Infarction

Hundreds of articles have been published on clinical applications of analysis of late potentials. Most of these focus on patients after MI. It has been found that the prevalence of late potentials in patients with old MI varies between 71% and 90% in patients with sustained ventricular arrhythmias, compared to 26–34% in patients without ventricular arrhythmias [24–26]. The presence of late potentials after an MI has been associated with increased risk for VT in prospective studies [27, 28]. Breithardt et al. [28] studied 132 patients a mean of 22 days after acute MI. The prevalence of sustained VT on a mean follow-up of 15 months was 11.9% in patients with, and only 2.7% in patients without late potentials. The prevalence of VT increased with the duration of late potentials; VT occurred in 5% of those with late potential duration <40 ms, compared to 25% in whom the late potential lasted >40 ms.

Between 14% and 29% of the patients with late potentials have been shown to have sustained VT within the first year after MI, compared to only 0.8–4.5% of patients without late potentials [29]. The prevalence of late potentials is higher in patients with inferior MI (58%) compared to patients with anterior infarction (31%) [27], which is not surprising when considering the normal activation sequence of the ventricles, but the prognostic value for ventricular tachycardia is higher for anterior infarctions. Analysis of late potentials has higher prognostic value for ventricular tachycardia than offered by long-term ECG and left ventricular ejection fraction [27].

There is a correlation between the prevalence of late potentials and the degree of ventricular dysfunction. Breithardt et al. [25] found that in patients without a history of ventricular arrhythmia, late potentials were detected in only three of 32 patients (9%) with normal ventricular function, but were present in 32 of 69 patients (46%) who had ventricular akinesia or aneurysm. Hombach et al. [2] found a similar relation between the incidence of late potentials and increasing degrees of ventricular dysfunction. Regardless of the degree of ventricular dysfunction, however, late potentials were found more frequently and had a longer duration in patients with ventricular tachycardia or fibrillation [25]. A retrospective study compared the findings on a signal-averaged ECG, prolonged ECG monitoring and cardiac catheterization to determine which combination of findings best characterized patients with VT after MI [26]. A multivariate statistical analysis showed that the abnormalities on the signal-averaged ECG, including the late potentials, provided independent information useful in identifying patients with VT after MI. An abnormal signal-averaged ECG (presence of late potentials or a long-filtered QRS duration), a peak premature ventricular contraction rate >100 h^{-1} and the presence of a left ventricular aneurysm were the only three variables identified which provided significant information to characterize patients with VT. The study suggested that the abnormal signal-averaged ECG may be combined with other clinical information to provide a more specific identification of patients with VT.

The ACC expert consensus document from 1996 [30] concludes that a normal signal-averaged ECG indicates a low risk for developing life-threatening ventricular arrhythmias. The positive predictive accuracy of only 14–29%, however, is not high enough to justify interventions in individual patients with abnormal results.

39.4.2 Myocardial Reperfusion

Successful treatment of acute MI with thrombolytic agents has been shown to reduce the incidence of late potentials (range 5–24% in patients treated with thrombolytic agents compared to 18–43% in patients not treated) [31–40]. Maki et al. [41] investigated the relationship between the time required for reperfusion by percutaneous transluminal coronary angioplasty and the incidence of late potentials in 94 patients with acute MI. They found that the incidence of late potentials in patients undergoing primary angioplasty at ≤4, 4–6, 6–8, 8–10, and >10 h after infarction was 8%, 12%, 14%, 33%, and 43%, respectively. In the control group, consisting of 31 patients who were treated conventionally, the incidence of late potentials was 48%. The presence of late potentials has been shown to have a low positive predictive value in patients who undergo reperfusion after acute MI [42, 43]. The presence of late potentials has also been shown to be a poor predictor of sudden death after surgical revascularization [44]. Thus, signal-averaged ECG has limited value for risk stratification in an unselected postinfarction population, and is currently not recommended as a risk marker for increased mortality [45].

39.4.3 Sudden Death

The incidence of sudden death has been too infrequent in the studies to date to form a firm conclusion on the value of late potentials as a prognostic indicator for that event. Nevertheless, some prospective studies have been undertaken [46, 47] to evaluate whether the presence of late potentials is an independent risk factor for sudden death or serious ventricular arrhythmias after MI, and to establish the role of the signal-averaged ECG along with other noninvasive tests in identifying patients at high risk.

The combination of late potentials with a low left ventricular ejection fraction, as determined by radionuclide techniques, together with complex ventricular ectopy on Holter monitoring have been used to identify those patients at highest risk of sudden death or developing sustained VT from 6 months to 2 years following MI. Kuchar et al. [46] found that an abnormal signal-averaged ECG together with an ejection fraction <40% predicted arrhythmic events with 34% probability. On the other hand, if the patient had abnormal left ventricular function but a normal signal-averaged ECG, there was only 4% risk of the occurrence of an arrhythmia. The signal-averaged ECG, Holter monitoring, and ejection fraction were independently related to outcome, but a left ventricular ejection fraction <40% was the most powerful indicator.

In a similar study, Gomes et al. [47] also found that the presence of late potentials, an abnormal ejection fraction, and high-grade ectopic activity on Holter monitoring were the variables most significantly related to a future arrhythmic event. Their overall conclusion was that the combination of these abnormalities identified the group of patients at highest risk of VT, sudden death or both in the first year after MI.

39.4.4 Unexplained Syncope

The presence of late potentials in patients with unexplained syncope has been associated with high sensitivity and specificity for inducement of VT during electrophysiological studies. Kuchar et al. [48] evaluated 150 patients with syncope. Late potentials were detected in 29 patients, of whom 16 were found to have VT. In the patients with syncope due to other causes than VT, none of the patients had late potentials on signal-averaged ECG. In this study, the sensitivity was 73%, the specificity 55%, the positive predictive value 55%, and the negative predictive value 94%. Another study by Lacroix et al. [49] found that the positive predictive value of late potentials was 39% for predicting the inducibility of sustained VT. The clinical value of analysis of late potentials in patients with unexplained syncope is mainly in its negative predictive accuracy.

39.4.5 Success of Arrhythmia Surgery

Several investigators have reported that late potentials may disappear after a successful operation for VT [20, 22, 50–52]. The operation generally includes an aneurysmectomy and an additional procedure, such as endocardial excision,

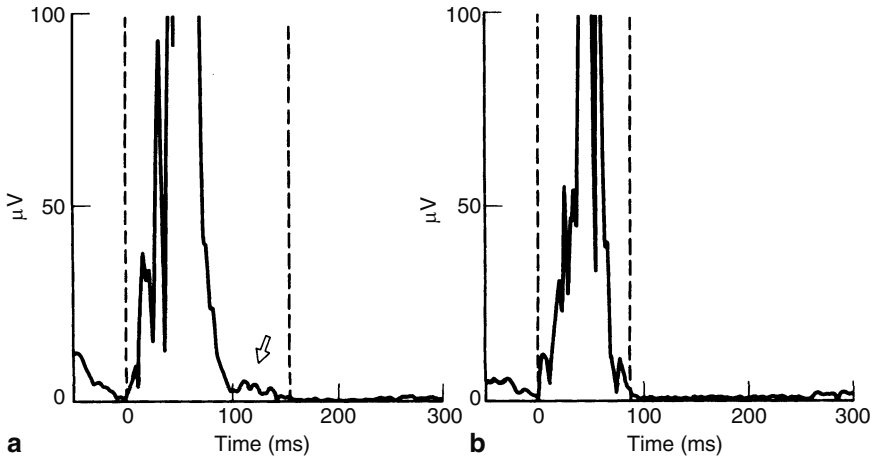

Figure 39.5

The filtered QRS complexes from a patient with VT who underwent aneurysmectomy and endocardial excision for control of the arrhythmia. In (a), before the operation, a 2.8 μV level of LP is present (*arrow*). In (b), after the operation, VT could not be induced and the LPs were no longer present.

to remove or isolate the apparent site of origin of VT. In one study, 24 patients in whom VT could not be induced after operation, the FQRSd decreased (from a mean of 137 to 121 ms) and the incidence of late potentials decreased (71–33%) [52] (Fig. 39.5). Eight patients continued to have late potentials, despite surgical control of the arrhythmias. The incidence of late potentials in the filtered QRS complex was not changed in 13 patients in whom VT could be induced after operation.

Experience indicates that a successful operation for control of VT may cause the late potentials to vanish, but they may persist despite successful control of the arrhythmia. This finding suggests that the operation need not remove all areas of delayed activation in order to control VT. In patients with persistent late potentials, despite surgical control of the arrhythmias, it is hypothesized that either the delayed activation does not outlast the refractoriness of the myocardium or that the interface between the slowly conducting tissue and normal myocardium is sufficiently disrupted so that reentry cannot occur.

39.4.6 Efficacy of Anti-Arrhythmic Drugs

Analysis of late potentials has not yet been established as a method for accurately assessing anti-arrhythmic drug efficacy. Class IA, IC, and II [53–58] anti-arrhythmic drugs have been shown to elicit changes in the late potentials, where especially class IC drugs are associated with a marked increase in FQRSd [58]. Only a few studies have examined the effects of class III drugs [59, 60]. In general, time domain analysis of the signal-averaged ECG has not shown a correlation between the changes induced during drug therapy and anti-arrhythmic drug efficacy [53, 54, 58]. A few studies have shown a correlation between the prolongation of the total FQRSd induced by class I drugs and prolongation of the cycle length of ventricular tachycardia [55–57].

Simson et al. [60] investigated the effect of anti-arrhythmic drug therapy on the signal-averaged ECG in 36 patients with VT after MI. Twenty-nine patients, or 81%, had late potentials on medications. The drugs evaluated, alone and in combination, were procainamide, quinidine, disopyramide, amiodarone, phenytoin, and mexiletine. Electrophysiological stimulation was used to evaluate the control of VT. The duration of the filtered QRS complex was increased by a mean of 8–13 ms by procainamide, quinidine, and amiodarone. Procainamide decreased the voltage in the last 40 ms of the

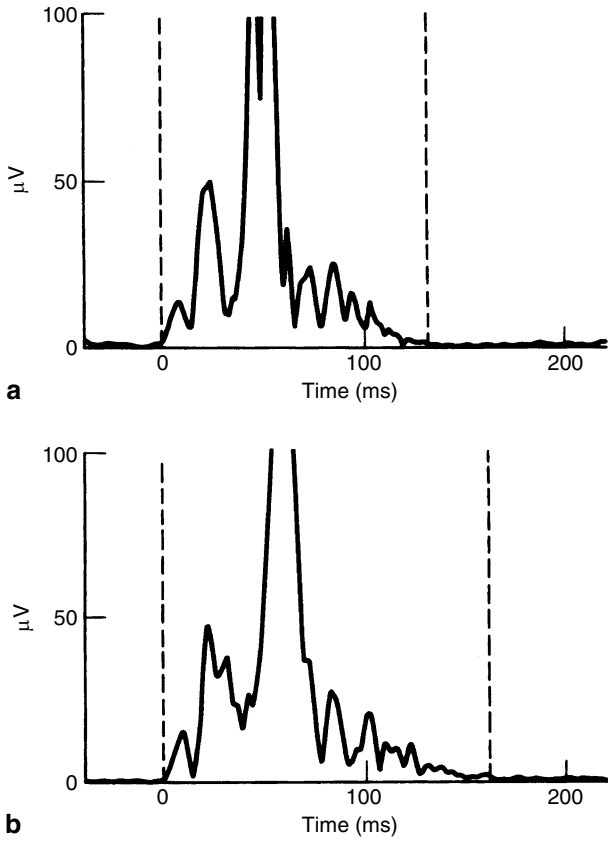

Figure 39.6

The effects of procainamide on the LPs in a patient with VT after MI. In (a), during the period without medication, the patient had a FQRSd of 129 ms and a 4.6 μV level LPs present at the end of the filtered QRS complex. In (b), when receiving the procainamide at a serum level of 16 μg/ml, the patient had a longer FQRSd (162 ms) but the LPs persisted. The VT remained inducible. (After Simson, (c) Saunders, Philadelphia, Pennsylvania. Reproduced with permission.)

filtered QRS complex by 4 μV; however, the incidence of late potentials with anti-arrhythmic drug therapy did not change (Fig. 39.6). Ventricular tachycardia was no longer inducible after anti-arrhythmic drug therapy in ten patients; nor was the late potentials abolished by any agent in these patients. There was no pattern of change in the filtered QRS complex that would indicate a successful response to anti-arrhythmic agents.

39.4.7 Cardiac Transplant

Several studies have investigated possible noninvasive methods for detection of cardiac transplant rejection. A few of them have examined the extent to which late potentials are a measure of heart transplant rejection [61–64]. One report showed a sensitivity of 65%, positive predictive accuracy of 92%, and negative predictive accuracy of 68% for acute rejection [61]. RMS values have also been shown to provide high sensitivity and specificity for rejection [62]. Thus, the potential of signal-averaged ECG analysis to detect acute rejection is promising, but more studies need to be done before the method can be used clinically.

39.4.8 Nonischemic Cardiomyopathy

The occurrence of late potentials in patients with nonischemic congestive cardiomyopathy has been investigated in a group of 41 patients and the findings compared with 55 normal controls [65]. It was found that the FQRSd was longer in patients with sustained ventricular arrhythmia than in those without (130.2 ± 19.5 ms as opposed to 105 ± 13.1 ms); a highly significant difference. The mean control value was 95.9 ms. The RMS voltage in the last 40 ms of the filtered QRS was lower in the group with arrhythmia than in those without (11.3 ± 9.3 as opposed to 53.5 ± 28.3 μV), again a highly significant difference. The corresponding normal group values were 53.7 ± 25.2 μV. Overall, 83% of patients in the group with sustained ventricular arrhythmia had both an abnormally long FQRSd and abnormally low late-potential amplitude; 14% of patients without an arrhythmia and 2% of controls had similar findings. Findings from other [66, 67], but not all [68–70] studies of patients with dilated nonischemic cardiomyopathy have shown similar results.

Arrhythmogenic right ventricular cardiomyopathy was one of the first pathologic entities in which late potentials were identified. Analysis of late potentials can be useful for screening purposes or detection of arrhythmogenic right ventricular cardiomyopathy in family members [71, 72]. Nava et al. [73] evaluated signal-averaged ECGs in 138 patients with arrhythmogenic right ventricular cardiomyopathy and compared the results with those of 146 healthy controls. Late potentials were found in 57% of the patients, and in 4% of the controls. They also found that there is a closer correlation between late potentials and the extent of the disease than with the presence of ventricular arrhythmias. Late potentials have also been found in a significant proportion of patients with the Brugada syndrome. Research suggests that late potentials might be helpful to identify patients at a higher risk of life-threatening arrhythmic events in this population, both in a retrospective [74] and a prospective [75] study, but the results need to be confirmed in larger studies.

39.5 Late Potentials and Frequency Analysis

As described above, late potentials are composed of frequencies which are higher than those of the ST segment, that is, higher than about 25 Hz. However, no specific information is available beforehand on their particular frequency content. By employing frequency analysis based on the discrete-time Fourier transform (and typically implemented by the fast Fourier transform, FFT), it would be possible to pinpoint the range of frequencies which is characteristic of late potentials. The main advantage of the frequency domain approach is that no prior knowledge is required on signal characteristics, whereas the time domain approach requires that the cut-off frequency of the high-pass filter is predetermined. However, this advantage comes at the sacrifice of temporal information as it is not possible to pinpoint the occurrence of late potentials as being late in the QRS complex or early in the ST segment. In practice, frequency analysis is also hampered by certain undesirable properties of the Fourier power spectrum related to frequency leakage and large variance [1, 76]. While these properties can be mitigated to a certain extent by various techniques, care should still be exercised when interpreting the outcome of frequency analysis.

In time domain analysis, a crucial signal processing step is to determine the endpoint of the high-pass filtered QRS complex in order to assure that the diagnostic measurements, that is, RMS amplitude, duration of low-amplitude signals, and filtered QRS duration are accurate. In frequency analysis, the corresponding crucial step is to determine the location and length of the signal segment to be processed. Since the segment begins in the terminal part of the QRS – a part of the heartbeat with drastic changes in amplitude – a displacement of its onset by just a few milliseconds can produce quite different spectra. The segment location should preferably be determined by an algorithmic procedure so as to avoid the subjectivity of manual delineation; one approach is to choose the segment onset as the point when the vector magnitude drops below 40 μV [77].

Different lengths of the segment are associated with different spectral resolution, implying that it is important to keep the length fixed from one patient to another in order to facilitate comparison of results. In the literature, lengths have ranged from 40 ms, thus only including the terminal part of the QRS, to about 200 ms so that a large part of the ST segment is included.

Prior to frequency analysis, it should be standard procedure to subtract the mean value of the ECG samples contained in the segment, that is, the DC component. Windowing is another common time domain operation with which samples at the boundaries of the segment are multiplied with weights smaller than those applied to samples in the middle of the segment, thus reducing the influence of abrupt changes which may occur at the segment boundaries. On the other

hand, windowing may have the undesirable effect of reducing the contribution of late potentials when these happen to be located at any of the segment boundaries.

Once the power spectrum has been computed, one or several parameters must be derived which condense its main features. The absolute power can be computed in frequency bands whose limits are determined by some prior knowledge. Alternatively, it may be more appropriate to compute relative power, defined as the ratio of the power in a single frequency band to either the total power or the power contained in certain bands. Relative power measurements are often preferred since the absolute power may be influenced by various nonphysiological factors.

It is sometimes convenient to display and analyze the power spectrum with a logarithmic magnitude scale since it allows detail to be displayed over a wider dynamic range. The scale is defined in units of $20 \cdot \log_{10}$, referred to as decibel (dB). With this scale, 0 dB corresponds to a magnitude equal to 1, −20 dB corresponds to a ten times smaller magnitude, −40 dB corresponds to a 100 times smaller magnitude, and so on. The magnitude function is normalized with respect to its maximum value, thus corresponding to 0 dB. It should be noted that although the power spectrum is commonly employed in the literature, that is, the squared magnitude of the FFT, the (unsquared) magnitude of the FFT is also sometimes employed.

As described earlier, the conventional time domain approach to handle multiple-lead recordings is to simply combine the filtered leads into a vector magnitude from which a set of descriptive parameters is derived. However, the vector magnitude does not lend itself to frequency analysis as this function may obscure the frequency content of the ECG. Instead, the power spectra of individual leads may be averaged into one spectrum from which a set of parameters is derived. Alternatively, parameters can be derived from each spectrum and combined with some suitable technique, for example, averaging of the resulting parameter values.

39.6 Late Potentials and Frequency Analysis in Clinical Applications

The first clinical study exploiting frequency analysis was presented by Cain et al. in 1984 for the purpose of distinguishing patients prone to sustained VT [78]. The analysis method was assessed in three groups of subjects, consisting of 16 patients with previous MI and sustained VT, 35 patients with previous MI but no sustained VT, and ten normal subjects, respectively. The ECG was recorded from the X, Y, and Z Frank leads, digitized, and subjected to signal averaging of 100 beats such that a noise level of 1.5 μV was reached.

In each lead, Fourier-based frequency analysis was performed on a manually delineated 40 ms segment at the terminal part of the QRS, windowed using the Blackman–Harris window. The power spectrum was characterized by two parameters derived from the logarithmic magnitude scale, the spectral value in decibels at 40 Hz and the area enclosed between the 0 and −60 dB level (Fig. 39.7). It should be noted that these two parameters are correlated since a large spectral value, in most cases, implies a large area.

The results for the three groups of subjects suggested that the area was considerably higher in patients with VT than in the other two groups, that is, the amplitude of the high-frequency components of the ECG in patients with VT was much greater than in those without. As one may expect, the spectral value in decibels at 40 Hz was larger in patients with VT than in the other two groups. Besides the terminal part of the QRS, frequency analysis was also performed on segments defined by the QRS complex, the ST segment, and the T wave; the ST segment was associated with results similar to those of the terminal part of the QRS, whereas the other two segments did not offer any discrimination between the VT group and non-VT groups.

In a subsequent study, Cain et al. modified their original way of deriving parameters from the spectrum by instead computing a ratio between the spectral areas defined by the intervals 20–50 Hz and 0–20 Hz [79]. Based on the findings of their previous study, the processed ECG segment was extended from the 40 ms at the terminal part of the QRS to also include the remaining part of the ST segment (though the segment was still manually delineated). The spectral area ratio was tested in 16 patients with a previous MI and sustained VT, 53 patients with a previous MI but without sustained VT, and 11 normal subjects. The results presented in Fig. 39.8 show that the VT patients have considerably larger ratios than the other two groups. However, the groups could not be discriminated when the 20–50 Hz interval was replaced by 70–120 Hz, a result which is somewhat surprising since the higher frequencies are important to the outcome of time domain analysis.

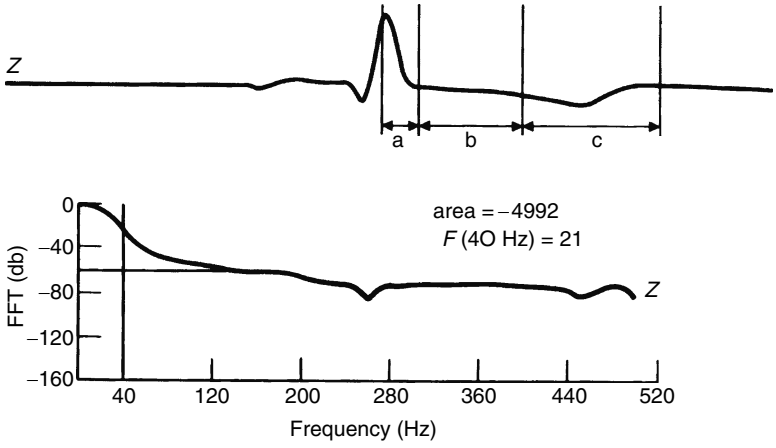

Figure 39.7

The logarithmic power spectrum characterized by the value in dBs at 40 Hz and the area enclosed between the 0 and −60 dB level. (Reprinted from Lindsay et al. [80] with permission.)

It should be noted that the spectral area ratio may account for signal properties unrelated to the presence of late potentials. Since the spectral area ratio involves frequencies in the interval 0–20 Hz, it is obvious that low-frequency components originating from, for example, baseline wander or a slowly changing ST segment will also influence the area ratio. In a later study, however, the lower limit was increased to 10 Hz so as to avoid this problem [80].

The studies by Cain and coworkers were followed by several studies from other groups who also employed frequency analysis to find out if late potentials present during sinus rhythm can be used as a marker for ventricular arrhythmias. The results presented in the literature have been most variable, ranging from "inability of frequency domain parameters to distinguish VT from non-VT patients" to "improved identification with frequency domain parameters." In the remaining part of this section, a number of studies are briefly summarized with variable outcomes. It should be noted that each of these studies has a slightly different approach to the implementation of frequency analysis, for example, the definitions of analyzed signal segment and frequency interval of interest.

In a study by Kelen et al., involving ten patients with spontaneous or inducible VT and ten normal subjects, it was shown that the spectral area ratio was markedly dependent on the length of the analyzed signal segment [81]. In fact, a change of as little as 3 ms in segment length changed the results across proposed boundaries of normalcy in normal subjects and in patients with VT. In contrast, the use of time domain analysis established that the patients had late potentials, whereas the normal subjects did not, using the standard diagnostic criteria.

Similar results were also obtained in a study by Machac et al. where the purpose was to determine whether time domain or frequency domain parameters were better in distinguishing patients with and without sustained VT [82, 83]. The two methods were tested in 26 patients with sustained VT, 18 control patients with organic heart disease but without sustained VT, and 11 normal volunteers. Frequency domain analysis was performed on three different segment lengths (the terminal 40 ms of the QRS complex, either alone or with 216 or 150 ms of the ST segment), and both power and power ratios were calculated in different frequency bands. At a fixed specificity of 78%, the best time domain sensitivity was 85%, whereas the best frequency domain sensitivity was 77%. It was thus concluded that frequency domain analysis did not offer any improvement over time domain analysis in distinguishing patients with VT from those without.

The study performed by Worley et al. was also designed to compare the value of time domain and frequency domain parameters [84]. However, they investigated the spectral area ratio, defined in the same way as in [79], not only for segments related to QRS end but also to QRS onset. Six different 140 ms segments started at 0, 40, 50, and 60 ms after QRS onset, two segments started at 40 and 50 ms before QRS end, and a variable-length segment started 40 ms before QRS end and extended to the T wave. The study included 36 patients with remote MI and sustained VT, 29 asymptomatic patients with remote MI, and 23 normal subjects. The results showed that the spectral area ratios from segments starting at 0, 40, and 60 ms after QRS onset were significantly different between infarct patients with and without VT; however,

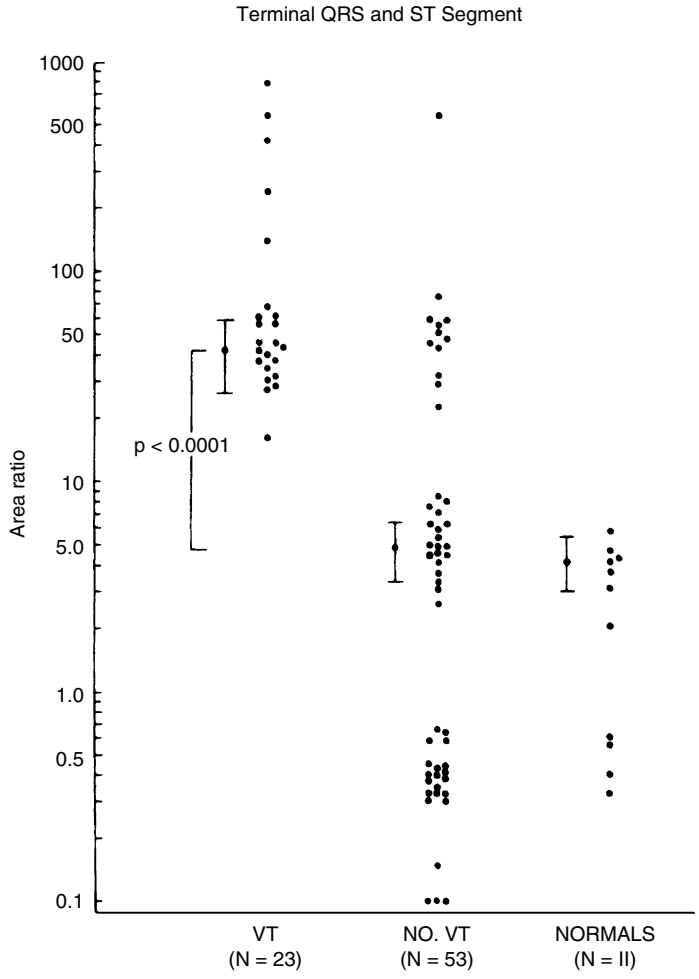

Figure 39.8

Comparison of the spectral area ratio for patients with sustained VT, without sustained VT, and normal subjects. The terminal QRS and the ST segment are analyzed. (Reprinted from Cain et al. [79] with permission.)

this finding did not apply to any of the segments related to QRS end. Thus, the results showed that the spectral content of the QRS complex is a marker to discriminate between the two patient groups. The time domain parameters studied were all found to be significantly different between the groups.

The idea to investigate the influence of the analyzed segment location was also pursued in a study by Buckingham et al. [85]. They used a data set consisting of 84 patients with VT and 150 patients without VT, all patients having had prior MI. All analyzed segments had a length of 140 ms and were located 0, 20, 40, 60, and 80 ms after QRS onset and 20, 40, 60, and 80 ms before QRS end. In each segment the spectral area ratio was computed using the same definition as the one given in [79]. Significant differences between the patient groups were only observed for ratios computed in segments 60 and 80 ms after QRS onset and 80 ms before QRS end.

The importance of higher-frequency components was investigated by Pierce et al. on a data set consisting of 24 patients with coronary artery disease and recurrent VT, 24 control patients with coronary artery disease, and 23 normal subjects [77]. The analyzed segment had its onset at the QRS end and a length of 120 ms. Unlike the studies by Cain et al., the frequency domain parameters involved considerably higher frequencies as contained in the interval 60–120 Hz; normalization was done with the entire interval 0–120 Hz. Quantifying performance in terms of the area under the receiver

operating characteristic, the frequency domain parameters were associated with larger areas than the time domain parameters. It was therefore concluded that the higher frequencies in late potentials better identified patients with coronary artery disease being prone to VT than did the time domain parameters.

39.7 Late Potentials and Time–Frequency Analysis

39.7.1 Spectrotemporal Mapping

Frequency analysis for identification of late potentials is, as indicated above, flawed by difficulties to accurately delimit the signal segment to be processed; small changes in segment position may lead to substantial changes in frequency domain parameters. The introduction of a sliding segment, whose initial position is located well before the end of the QRS complex and final position well into the T wave, has been suggested as a means to mitigate such difficulties; "sliding" means that the analysis segment is shifted by one or a few milliseconds at a time. For each segment, the power spectrum is computed so that, when the segment has reached its endpoint, a series of successive power spectra has been produced. Similar to frequency analysis, each segment is windowed and the DC level subtracted. This time-frequency approach is widely known as the short-term Fourier transform (STFT) and represents a standard signal processing tool for characterizing the time-varying spectral properties of a nonstationary signal. In the context of ventricular LPs, the STFT is commonly referred to as spectrotemporal mapping [86–89].

Figure 39.9a illustrates spectrotemporal mapping when implemented using an 80 ms segment whose position slides around the end of the QRS complex so that the presence of late potentials may be identified through spectral changes. In this particular case, the signal-averaged ECG contains low-amplitude activity at the end of the QRS complex, that is, late

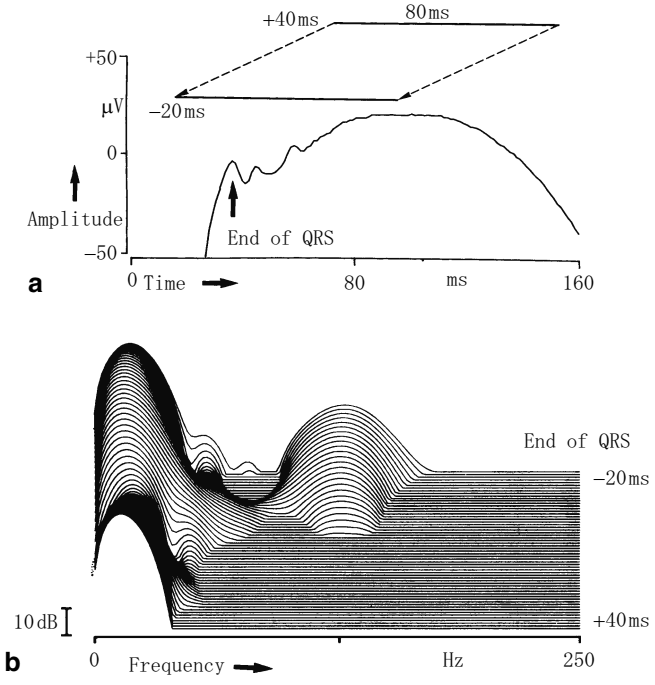

Figure 39.9

(a) Spectrotemporal mapping is created by computing successive Fourier transforms within a sliding window which, in this example, has 80-ms duration. (b) The spectrotemporal map of a patient with late potentials. (Reprinted from Haberl et al. [86] with permission.)

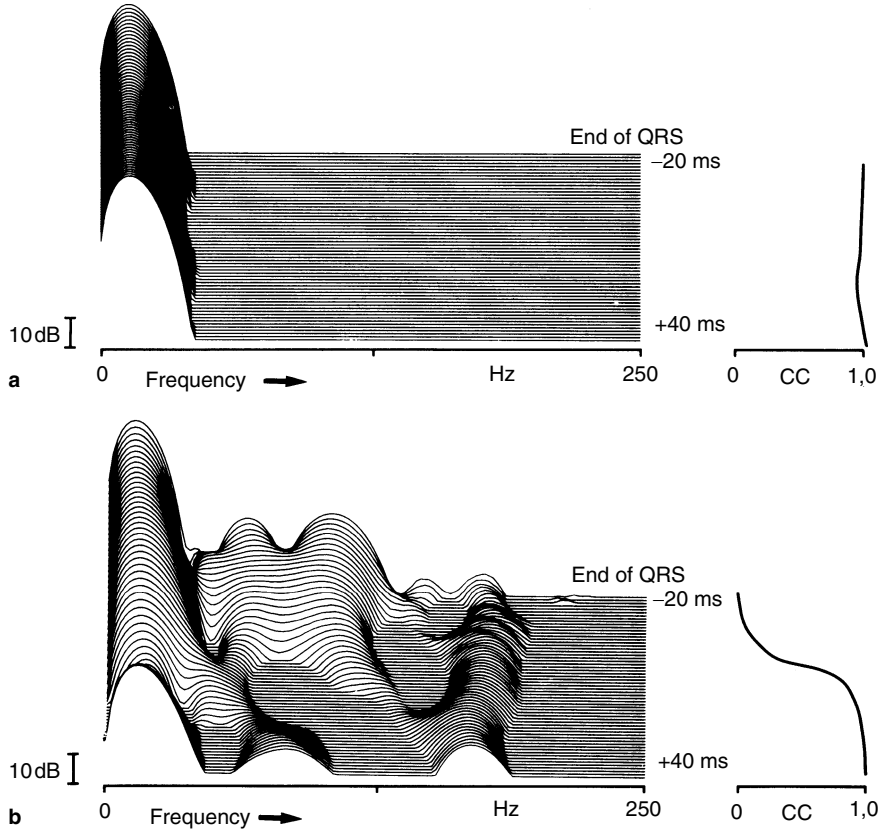

Figure 39.10

Spectrotemporal map for (a) a patient without late potentials, and (b) a patient with late potentials, manifested by a "landscape with ridges." The curve of cross-correlation coefficients is displayed to the right of each map. (Reprinted from Haberl et al. [86] with permission.)

potentials are considered to be present. The corresponding series of successive power spectra is displayed in Fig. 39.9b as a three-dimensional plot where the three axes of the diagram describe frequency, time, and spectral power, respectively. The plot shows that high-frequency components above 50 Hz, contained in segments at the QRS end, gradually vanish as the segment slides toward the T wave, that is, from top to bottom of the plot. The last few spectra are similar in that they do not contain any high-frequency components. In this case, the transition from late potentials to noise is clearly visible using spectrotemporal mapping since the signal-to-noise ratio of the signal-averaged ECG is high.

Although the parameters of frequency analysis can be applied to each individual power spectrum, parameters that exploit the time-dependent properties of spectrotemporal mapping can be expected to add information for identification of late potentials. An early approach to such characterization was the so-called normality factor which determines the similarity of successive spectra through the computation of a series of cross-correlation coefficients [87]; these coefficients have the property of being normalized to the interval [−1,1]. Each individual spectrum is correlated to a template spectrum being determined by averaging the last few spectra positioned at the end of the analysis interval. The curve of cross-correlation coefficients is illustrated for ECGs with and without late potentials in Fig. 39.10a and b, respectively. It is obvious from Fig. 39.10a that the correlation curve increases from almost 0 in segments where high-frequency components are present to a value well outside the QRS complex. On the other hand, Fig. 39.10b displays a correlation curve which remains close to one throughout all spectra, suggesting that late potentials are absent.

In the original work by Haberl et al. [87] an 80 ms segment was analyzed sliding in steps of 3 ms from a start time 23 ms before the QRS end until 52 ms after; the resulting 25 segments were indexed backward in time so that the last segment

had index 1. The normality factor was obtained as the ratio between the mean of the cross-correlation coefficients of segments 20–25, where late potentials were expected to occur, and the mean of the cross-correlation coefficients of the segments 1–5. The factor was then multiplied by 100 and interpreted as a percentage. Late potentials were considered to be present when the normality factor dropped below 30%.

The initial results obtained with spectrotemporal mapping surpassed those obtained by conventional time domain analysis when identifying patients prone to sustained VT in the presence of coronary artery disease [87]. Furthermore, most patients with bundle branch block were correctly classified with spectrotemporal mapping, while these patients had to be excluded in time domain analysis. Despite these promising initial results, this technique is not in widespread use, probably due to its poor reproducibility. In a study comparing spectrotemporal mapping to both time domain and frequency domain analysis, the reproducibility of spectrotemporal mapping was substantially lower than that of the other two types of analysis [89].

39.7.2 Spectral Turbulence Analysis

Spectral turbulence analysis defines another approach to time-frequency characterization of the signal-averaged ECG, originally developed to detect abnormal variations in frequency content during depolarization of the diseased myocardium [90]. The word "turbulence" signifies the transient spectral changes that were hypothesized to occur in the ECG as depolarization propagates throughout the ventricles around areas of abnormal conduction, thus resulting in a high degree of spectral turbulence. While spectral turbulence analysis has the short-term Fourier transform in common with spectrotemporal mapping, the analysis embraces the entire QRS complex and the ST segment and is not limited to an interval at the QRS end. Usually, the first segment starts 25 ms before QRS onset and ends 125 ms after QRS end, incremented in 2 ms steps. The resulting power spectra from all available leads are then normalized with respect to the spectrum with the highest magnitude; this magnitude is designated as 100% while the other magnitudes are smaller. A number of parameters are derived from the normalized spectra which describe the similarity between adjacent spectra expressed in terms of the above-mentioned cross-correlation coefficient. It was claimed that spectral turbulence analysis is applicable to patients irrespective of the QRS duration and the presence or absence of bundle branch block.

In the original study by Kelen et al. [90] both spectral turbulence analysis and conventional time domain late potential analysis (40–250 Hz) were employed for identifying patients with inducible sustained monomorphic VT. The signal-averaged ECG was obtained from 144 subjects using a recording configuration of three orthogonal bipolar leads. The data set contained 71 normal control subjects, 33 with both late potentials by time domain analysis and inducible sustained monomorphic VT, 28 with time domain late potentials but no evidence of spontaneous or inducible sustained monomorphic VT, and ten with inducible sustained monomorphic VT but absence of time domain late potentials. The total predictive accuracy for all groups was 94% with spectral turbulence analysis, whereas only 73% could be achieved with time domain analysis.

Spectral turbulence analysis has been employed in several subsequent studies with results that sometimes improve upon those obtained by conventional time domain analysis. In a study by Malik et al. [91], both techniques were considered for risk prediction after acute MI, using a material of 553 survivors of acute MI (bundle branch blocks and other conduction abnormalities were excluded); the patients were followed for at least 1 year. Spectral turbulence analysis provided significantly lower positive predictive accuracy than the time domain analysis for prediction of ventricular tachycardia/fibrillation during 1 year after infarction. On the other hand, it provided significantly higher positive predictive accuracy for the prediction of 1-year all-cause mortality. The study by Copie et al. [92] also made use of both time domain and spectral turbulence analysis for the prediction of cardiac death and arrhythmic events after acute MI in 603 patients (patients with bundle branch block and other conduction abnormalities were excluded). The results showed that spectral turbulence analysis was essentially equivalent to time domain analysis for the prediction of arrhythmic events after MI, but performed significantly better than time domain analysis for the prediction of cardiac death.

Although it was initially claimed that spectral turbulence analysis is equally suitable for patients with bundle branch block, the study by Englund et al. [93] came to the opposite conclusion, that is, spectral turbulence analysis is applicable only to patients without bundle branch block. Their results were based on a material of 169 patients of whom 120 had a QRS duration ≤120 ms; 47 patients had inducible sustained monomorphic VT and were compared to 122 control patients.

The total predictive accuracy for predicting inducible VT was as low as 47% when the whole material was analyzed, however, it increased to 73% when only patients with QRS duration <120 ms were included.

39.7.3 Combined Time Domain and Spectral Turbulence Analysis

The idea to combine time domain and spectral turbulence analysis has been investigated in a number of studies for the purpose of increasing the power of predicting serious arrhythmic events in post-infarction patients [94–96]. The results of these studies indicated that the combined approach may lead to a higher total predictive accuracy than can be achieved using each of the analysis techniques independently. Based on a material of 262 patients with acute MI, Ahuja et al. [89] obtained a total predictive accuracy of 92% when combined analysis was employed for predicting arrhythmic events. The corresponding performance figures for time domain analysis and spectral turbulence analysis were 87% and 78%, respectively.

Improved risk stratification was also found in a study by Mäkijärvi et al. [95] though the levels of predictive accuracy were considerably lower than those reported in [94]. The study comprised a prospective material of 778 males who survived the acute phase of MI. The most powerful prediction of arrhythmic events was achieved by combining time domain and spectral turbulence analysis, reaching a total predictive accuracy of 61% when one of the two techniques showed abnormality and a total predictive accuracy of 87% when both showed abnormality. Spectral turbulence analysis was clearly inferior to time domain analysis in predicting arrhythmic events when used separately.

In yet another study, Vazquez et al. [96] investigated the value of combined analysis on a material of 602 patients after acute MI (of which 38 patients had a major arrhythmic event during the 1-year follow-up period). The total predictive accuracy of combined analysis was 89.9%, significantly higher than achieved separately by time domain analysis (75%) and spectral turbulence analysis (78%).

39.8 High-Frequency QRS Components

39.8.1 Introduction

Frequency analysis of an ECG signal shows that the signal also includes frequencies above the standard frequency range [97]. These high-frequency components are mainly found within the QRS complex, having a low amplitude compared to the components of the standard ECG (μV compared to mV) (Fig. 39.11). Early attempts to visualize high-frequency ECG components employed signal amplification in combination with high paper speed. With this technique, "notches" and "slurs" could be observed within the QRS complex [98, 99]. Studies in the 1970s showed that patients with heart disease had an increased number of notches and slurs compared to healthy individuals. Later analysis of the ECG signal showed that the notches and slurs contained frequencies between 40 and 185 Hz [100].

The development of high-resolution recording techniques combined with digital filtering and signal averaging enabled better analysis of high-frequency components in the ECG signal. Several studies, both on humans and animals, have investigated whether high-frequency QRS components (HF-QRS) contain diagnostic information. Several heart diseases have been studied, such as acute myocardial ischemia [101–109], old MI [109–117] and left ventricular hypertrophy [118, 119]. It is still unknown, however, if the method is useful as a complement to standard ECG for the clinical diagnosis of different heart diseases.

The physiological mechanisms underlying HF-QRS are still not fully understood. One theory is that HF-QRS are related to the conduction velocity and the fragmentation of the depolarization wave in the myocardium. In a three-dimensional model of the ventricles with a fractal conduction system it was shown that high numbers of splitting branches are associated with HF-QRS. In this experiment, it was also shown that the changes seen in HF-QRS in patients with myocardial ischemia might be due to the slowing of the conduction velocity in the region of ischemia [120]. Further electrophysiological studies are needed, however, to better understand the underlying mechanisms of HF-QRS.

There is no standardized method for the recording and quantification of HF-QRS. Both orthogonal leads and all or some of the 12 standard leads have been used in different studies. Several frequency ranges (most commonly 150–250 Hz) and filters have been used as well. Different methods for quantification have also been used. The two most commonly used

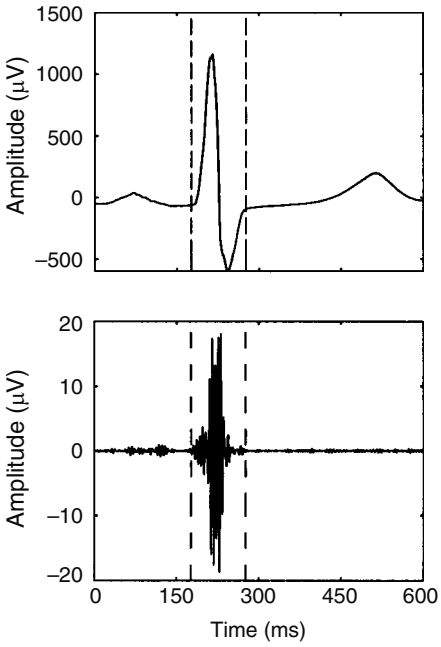

Figure 39.11

A signal-averaged ECG in the standard frequency range (*upper panel*) and the same ECG within the 150–250 Hz frequency range (*lower panel*). *Dashed lines* indicate the QRS duration determined from the standard frequency range. (Reprinted from Pettersson et al. [126] with permission.)

methods for quantification are RMS values during the entire QRS duration and "reduced amplitude zones" (RAZ), a way of describing zones in the filtered QRS complex with reduced amplitudes. Due to the low amplitude of the HF-QRS, noise reduction is necessary before analysis. In order to achieve this in a clinical environment, signal averaging is necessary.

39.8.2 Signal Recording and Analysis

To be able to extract HF-QRS it is important to use recording equipment with high resolution acquisition, both in time and amplitude. The sampling rate should be 1,000 Hz or higher [1], and the amplitude resolution at least 1 μV. Since the amplitudes of HF-QRS are in the microvolt range, a low noise level is required. For example, the influence of noise due to skeletal muscle can be reduced by moving the electrodes on the legs and arms to a more proximal position according to Mason and Likar [121]. More importantly, signal averaging must be performed in order to attain an acceptable noise level, sometimes requiring a recording time of several minutes. If the ECG morphology is subject to dynamic changes, for example, observed during percutaneous transluminal coronary angioplasty, recursive averaging with a forgetting factor must be used instead as conventional ensemble averaging is unsuitable.

The HF-QRS is extracted from the signal averaged beats through band pass filtering, often by employing a Butterworth filter [122]. This filter type has a nonlinear phase response which may distort temporal relationships of the various signal components. Linear phase filtering can be obtained, however, by first filtering the entire signal in a forward direction and then filtered signal once more but backward. Different studies have used different bandwidths when extracting HF-QRS, although the frequency range 150–250 Hz is the most common choice.

Several methods have been used for quantification of HF-QRS of which calculation of RMS values during the entire QRS duration is the most common one. For a correct RMS value it is necessary to correctly identify the onset and end of the QRS complex. It has been shown that the most correct delineation of the QRS complex is obtained when determining the QRS duration in the standard frequency range.

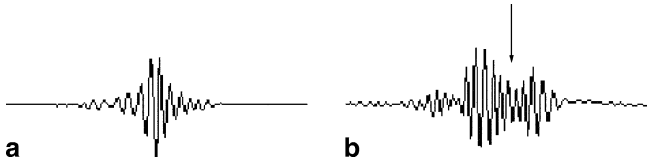

Figure 39.12
HF-QRS (150–250 Hz) from two individuals, with (a) and without (b) RAZ.

Another method for quantification of HF-QRS is calculation of reduced amplitude zones (RAZ). The RAZ measure is a morphological measure and is defined as an interval between two adjacent local maxima or two adjacent local minima in the HF-QRS, where a local maximum or minimum must have an absolute value higher than the three preceding and three following envelope points (Fig. 39.12). The method was first introduced by Abboud in the 1980s [103]. It was discovered that areas with lower amplitude were present in the high-frequency signal in dogs with myocardial ischemia but not in normal dogs. The method has been developed further, and a scoring system has been proposed [123, 124]. Other methods for quantification of HF-QRS include peak-to-peak amplitude and the integral of the signal.

A recent approach to HF-QRS quantification is to compute the upward and downward slopes of the QRS complex [125]. This technique was designed with the aim to reduce the leakage and smearing caused by linear band pass filtering of the QRS complex. It was shown that both slope coefficients are more sensitive to ischemic changes than is the RMS value obtained from the band pass filtered QRS complex.

The amplitude of HF-QRS differs among the 12 standard leads (Fig. 39.13). The largest amplitudes are usually found in the anterior-posterior-oriented leads V2–V4 and in the inferior-superior-oriented leads II, aVF, and III. The lowest amplitudes are found in the left-right-oriented leads aVL, I, -aVR, V1, V5, and V6 [126]. In the transverse plane, the leads V1 and V6 are located furthest away from the left ventricle, which is a possible explanation for the low amplitudes recorded in these leads. In the frontal plane, however, no leads are located close to the heart, but there is still a large difference in amplitude of HF-QRS between these leads.

The correlation between HF-QRS and the QRS amplitudes in standard ECG is generally low. Thus, factors other than the QRS amplitude in standard ECG seem to influence the size of HF-QRS. There is also a large variation in HF-QRS between individuals. During consecutive registrations on the same individual, however, only small variations in HF-QRS are registered [126]. When studying healthy individuals, no significant differences in HF-QRS regarding sex and age have been found [117].

39.9 HF-QRS in Heart Disease

39.9.1 Ischemic Heart Disease

Several studies have compared HF-QRS in patients with old MI to HF-QRS in normal subjects. The vast majority of these studies show reduced amplitudes after old MI. In the frequency range 80–300 Hz HF-QRS are significantly lower in leads V2 and V5 in patients with old anterior MI [112]. In patients with old inferior infarction, HF-QRS are reduced in leads II, aVF, and III [110, 112]. When recording with Frank leads (X, Y, and Z leads), reduced HF-QRS are found in patients with old anterior and/or inferior infarction [114]. There are some studies, however, that show higher HF-QRS in patients with old MI compared to normal individuals, measured with frequencies >90 Hz using Frank leads [115].

Studies on patients with angiographically documented ischemic heart disease, with and without signs of old MI on ECG, do not show any difference in HF-QRS between the two populations [116]. When comparing a healthy population with patients with ischemic heart disease, both with and without old MI, the healthy population shows higher HF-QRS than the patient group [117]. These results indicate that ischemic heart disease, with and without old MI, causes a reduction of HF-QRS. A possible explanation is that chronic ischemic heart disease leads to structural changes in the myocardial tissue. These changes may contribute to abnormal impulse propagation in the ischemic heart. This abnormal propagation might be the reason for the reduced high-frequency content in patients with ischemic heart disease.

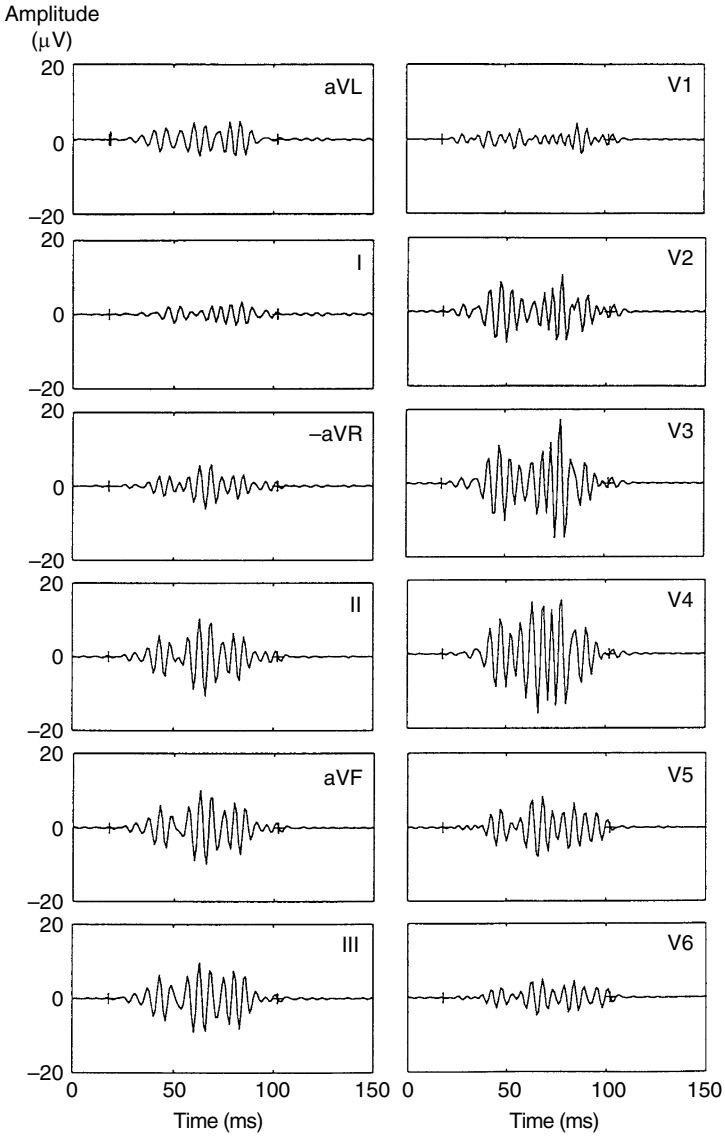

Figure 39.13

Filtered QRS complexes (150–250 Hz) in 12 standard leads from a patient with typical amplitude distribution among the leads. *Tick marks* indicate QRS onset and offset, determined from the standard frequency ECG. (Reprinted from Pettersson et al. [126] with permission.)

39.9.2 Acute Myocardial Ischemia

Several studies have reported lower HF-QRS during acute myocardial ischemia. In a study on dogs, ECG was recorded both from epicardial electrodes and from surface electrodes during occlusion of the left anterior descending coronary artery. HF-QRS recorded from the epicardium of the left ventricle were significantly reduced during the occlusion, while HF-QRS recorded from the nonischemic right ventricle remained unchanged. Reduced HF-QRS from the surface electrodes were also found [102]. Other animal studies have shown similar results [101, 104–106].

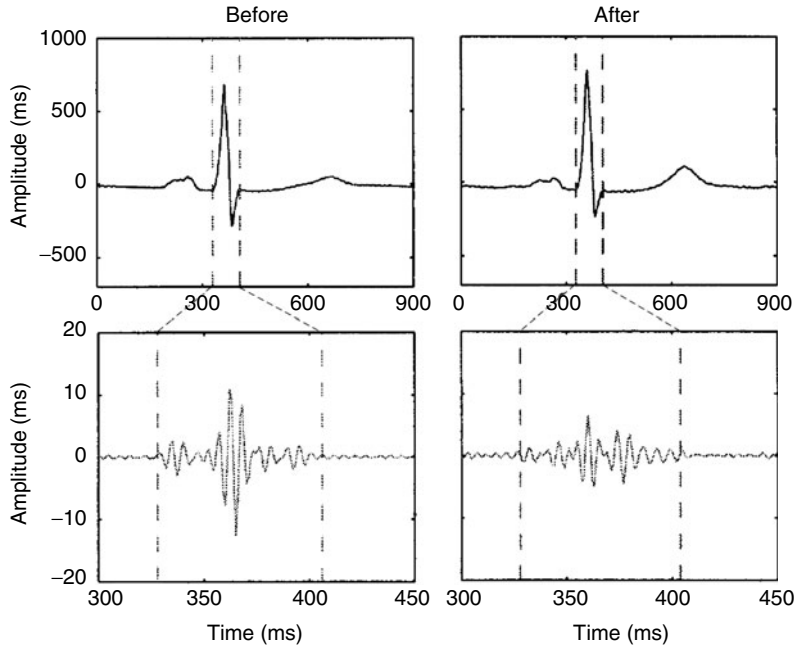

Figure 39.14

Lead V5. *Upper panel*: Pre-inflation and inflation ECGs in the standard frequency range. *Lower panel*: The same ECGs within the HF range (150–250 Hz). The *dashed lines* indicate the QRS duration, determined from the standard frequency ECG. (Reprinted from Pettersson et al. [109] with permission.)

In humans, the ECG has been recorded during percutaneous transluminal coronary angioplasty [108, 109]. The results from these studies show that ischemia leads to changes in HF-QRS in a majority of the patients. These changes can be observed even when no ST changes in standard ECG are seen (Fig. 39.14). The results indicate that acute myocardial ischemia can be detected with higher sensitivity with analysis of HF-QRS compared to conventional analysis with standard ECG. Analysis of HF-QRS might therefore serve as a complement to standard ECG in the detection of myocardial ischemia. The large inter-individual variation in HF-QRS, however, probably makes high-frequency analysis most applicable to monitoring situations when changes from baseline can be identified.

During occlusion of the left anterior descending coronary artery a reduction in HF-QRS is observed in many leads, most commonly in lead V3. During occlusion of other large coronary arteries a reduction in HF-QRS is seen in various leads. Thus, HF-QRS seem to be poorer than standard ECG in detecting the location of ischemia.

39.9.3 Reperfusion

To assess the resolution of ST segment elevation is the most commonly used method for detecting reperfusion during thrombolytic therapy for acute MI. A couple of studies have shown that successful reperfusion also results in a significant increase in HF-QRS (Fig. 39.15) [127, 128]. More and larger studies are needed, however, to determine if analysis of HF-QRS could be a useful method for monitoring patients during treatment of acute MI.

39.9.4 Stress-Induced Ischemia

Analysis of HF-QRS during exercise test has been suggested as a complement to assessment of the ST segment reaction for detection of exercise-induced ischemia. It has been shown that HF-QRS increase during exercise in healthy

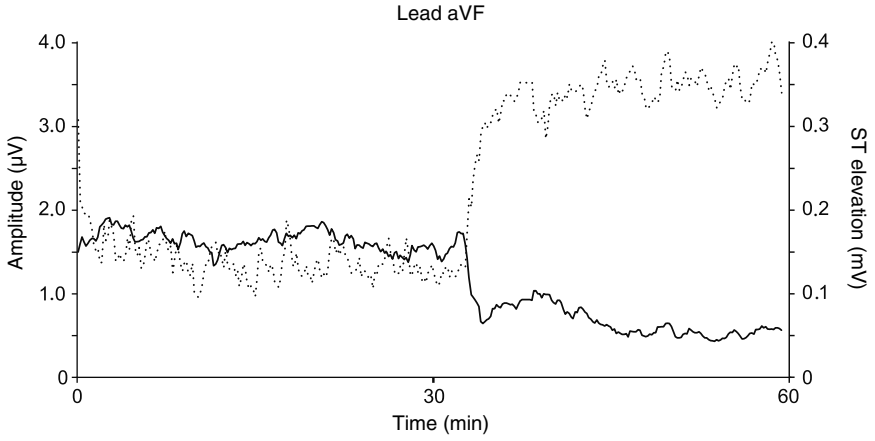

Figure 39.15

Dynamic changes in lead aVF in HF-QRS (*dashed line*) and ST segment (*solid line*) during reperfusion therapy for acute inferior MI. After 30 min of therapy, the ST elevation decreases and the HF-QRS simultaneously increases.

individuals [129]. In a study comparing healthy individuals to patients with ischemic heart disease, it was found that HF-QRS are significantly higher in the healthy population, both during and after exercise [130]. Two other studies have shown that a large relative change in HF-QRS during exercise is more sensitive for detecting ischemia in myocardial perfusion imaging test compared to conventional ST analysis [131, 132]. A recent study investigated changes in HF-QRS during adenosine myocardial perfusion imaging stress tests [133]. It was found that analysis of HF-QRS is highly sensitive and specific for detecting reversible perfusion defects, and significantly more sensitive than conventional ST segment analysis. Another study trying to reproduce these findings found, however, that analysis of HF-QRS was no better than tossing a coin for detecting reversible perfusion defects [134]. A problem with analysis of HF-QRS recorded during exercise is the high noise level generated by skeletal muscle.

39.9.5 Left Ventricular Hypertrophy

Standard ECG is one of the most common methods to detect left ventricular hypertrophy. Several different ECG-based criteria are used clinically. These methods, however, have low sensitivity when a high level of specificity is required. Studies on rabbits, with and without left ventricular hypertrophy, have shown that HF-QRS correlate well with left ventricular mass [119]. In the study, the vector magnitude from orthogonal leads in different frequency ranges was studied. High-pass filtering at 44 Hz showed the best correlation between left ventricular mass and HF-QRS ($r = 0.84$). A high correlation between left ventricular mass and HF-QRS was also found among the healthy rabbits alone.

Studies on humans have shown more diverging results. A study on 15 patients, both with normal and pathologic left ventricular mass, determined by echocardiography, showed that the sum of vectors in orthogonal leads in the 2–250 Hz range had approximately the same correlation with left ventricular mass as do established electrocardiographic criteria for left ventricular hypertrophy [118]. Another study on 60 healthy individuals, using magnetic resonance imaging as gold standard, found no correlation between HF-QRS and left ventricular mass [135]. Thus, it is not certain whether HF-QRS can be of value in the electrocardiographic diagnosis of left ventricular hypertrophy.

39.9.6 Conduction Abnormalities

In dogs, HF-QRS are reduced during slow conduction velocity in the heart [136]. By infusing sodium channel blockers (lidocaine, disopyramide) in the left anterior descending coronary artery at the same time as recording ECGs from the

entire ventricular surface, it has been shown that HF-QRS are significantly lower in the areas affected by the sodium channel blockers. These results indicate that HF-QRS is a potent indicator of disturbed local conduction.

39.9.7 Heart Transplantation and Heart Surgery

Allograft rejection is a major cause of morbidity and mortality in patients who have undergone heart transplant. There is no reliable method for detecting rejection except endomyocardial biopsy. Some studies have investigated whether HF-QRS could be used as a noninvasive marker for rejection [137, 138]. The results from the studies have in part showed diverging results, with both an increase and a decrease in HF-QRS at rejection.

In a study on patients after heart surgery, a reduction of HF-QRS correlating with the dysfunction of the heart has been found [139]. It is therefore suggested that HF-QRS could be used as a noninvasive marker of myocardial dysfunction after heart surgery. In children who have undergone heart surgery, the change in HF-QRS during aortic clamping has been investigated [140]. I was found that the recovery time of the HF-QRS significantly correlated with cardioplegic arrest time during surgery.

References

1. Sörnmo, L. and P. Laguna, *Bioelectrical Signal Processing in Cardiac and Neurological Applications*. Amsterdam: Elsevier (Academic Press), 2005.
2. Hombach, V., V. Braun, H.W. Hopp, et al., The applicability of the signal averaging technique in clinical cardiology. *Clin. Cardiol.*, 1982;**5**: 107–124.
3. Ros, H.H., A.S.M. Koeleman, and T.J. Akker, The technique of signal averaging and its practical application in the separation of atrial and His Purkinje activity, in *Signal Averaging Technique in Clinical Cardiology*, V. Hombach and H.H. Hilger, Editors. Stuttgart: Schattauer, 1981, p. 3.
4. Rompelman, O. and H.H. Ros, Coherent averaging technique: a tutorial review. Part 1: noise reduction and the equivalent filter. Part 2: trigger jitter, overlapping responses and nonperiodic stimulation. *J. Biomed. Eng.*, 1986;**8**: 24–35.
5. Laciar, E., R. Jané, and D.H. Brooks, Improved alignment method for noisy high-resolution ECG and Holter records using multiscale cross-correlation. *IEEE Trans. Biomed. Eng.*, 2003;50: 344–353.
6. Simson, M.B., Use of signals in the terminal QRS complex to identify patients with ventricular tachycardia after myocardial infarction. *Circulation*, 1981;**64**: 235–242.
7. Berbari, E.J. and P. Lander, Principles of noise reduction, in *High-Resolution Electrocardiography*, N. El-Sherif and G. Turitto, Editors. Armonk: Futura, 1992, pp. 51–66.
8. Plonsey, R., *Bioelectric Phenomena*. New York: McGraw-Hill, 1969, pp. 281–299.
9. Kienzle, M.G., R.A. Falcone, and M.B. Simson, Alterations in the initial portion of the signal averaged QRS complex in acute myocardial infarction with ventricular tachycardia. *Am. J. Cardiol.*, 1988;**61**: 91–103.
10. Atarius, R. and L. Sörnmo, Maximum likelihood analysis of cardiac late potentials. *IEEE Trans. Biomed. Eng.*, 2006;**43**: 60–68.
11. Steinberg, J.S. and J.T. Bigger, Importance of the endpoint of noise reduction in analysis of the signal-averaged electrocardiogram. *Am. J. Cardiol.*, 1989;**63**: 556–560.
12. Boineau, J.P. and J.L. Cox, Slow ventricular activation in acute myocardial infarction: A source of reentrant premature ventricular contraction. *Circulation*, 1973;**48**(4): 702–713.
13. Waldo, A.L. and G.A. Kaiser, A study of ventricular arrhythmias associated with acute myocardial infarction in the canine heart. *Circulation*, 1973;**47**(6): 1222–1228.
14. El-Sherif, N., B.J. Scherlag, and R. Lazzara, Electrode catheter recordings during malignant ventricular arrhythmias following experimental acute myocardial ischemia. *Circulation*, 1975;**51**(6): 1003–1014.
15. El-Sherif, N., B.J. Scherlag, R. Lazzara, and R.R. Hope, Reentrant ventricular arrhythmias in the late myocardial infarction period. 1. Conduction characteristics in the infarction zone. *Circulation*, 1977;**55**(5): 686–702.
16. El-Sherif, N., R.R. Hope, B.J. Scherlag, and R. Lazzara, Reentrant ventricular arrhythmias in the late myocardial infarction period. 2. Patterns of initiation and termination of re-entry. *Circulation*, 1977;**55**(5): 702–719.
17. Simson, M.B., W.J. Untereker, S.R. Spielman, L.N. Horowitz, N.H. Marcus, R.A. Falcone, et al., The relationship between late potentials on the body surface and directly recorded fragmented electrograms in patients with ventricular tachycardia. *Am. J. Cardiol.*, 1983;**51**(1): 105–112.
18. Berbari, E.J., B.J. Scherlag, R.R. Hope, and R. Lazzara, Recording from the body surface of arrhythmogenic ventricular activity during the S-T segment. *Am. J. Cardiol.*, 1978;**41**(4): 697–702.
19. Josephson, M.E., L.N. Horowitz, and A. Farshidi, Continuous local electrical activity. A mechanism of recurrent ventricular tachycardia. *Circulation*, 1978;**57**(4): 659–665.
20. Breithardt, G., R. Becker, L. Seipel, R.R. Abendroth, and J. Ostermeyer, Non-invasive detection of late potentials in man–a new marker for ventricular tachycardia. *Eur. Heart J.*, 1981;**2**(1): 1–11.
21. Fontaine, G., G. Guiraudon, R. Frank, et al., Stimulation studies and epicardial mapping in ventricular tachycardia. Study of mechanisms and selection for surgery, in *Reentrant Arrhythmias*, H. Kulbertus, Editor. Lancaster: MTP; 1977, p. 334.

22. Rozanski, J.J., D. Mortara, R.J. Myerburg, and A. Castellanos, Body surface detection of delayed depolarizations in patients with recurrent ventricular tachycardia and left ventricular aneurysm. *Circulation*, 1981;**63**(5): 1172–1178.
23. Simson, M.B., D. Euler, and E.L. Michelson, Detection of delayed ventricular activation on the body surface in dogs. *Am. J. Physiol.*, 1981;**241**(3): H363–H369.
24. Denniss, A.R., D.A. Richards, D.V. Cody, P.A. Russell, A.A. Young, D.L. Ross, et al., Correlation between signal-averaged electrocardiogram and programmed stimulation in patients with and without spontaneous ventricular tachyarrhythmias. *Am. J. Cardiol.*, 1987;**59**(6): 586–590.
25. Breithardt, G., M. Borggrefe, U. Karbenn, R.R. Abendroth, H.L. Yeh, and L. Seipel, Prevalence of late potentials in patients with and without ventricular tachycardia: correlation and angiographic findings. *Am. J. Cardiol.*, 1982;**49**(8): 1932.
26. Kanovsky, M.S., R.A. Falcone, C.A. Dresden, M.E. Josephson, and M.B. Simson, Identification of patients with ventricular tachycardia after myocardial infarction: signal-averaged electrocardiogram, Holter monitoring, and cardiac catherization. *Circulation*, 1984;**70**(2): 264–270.
27. Gomes, J.A., S.L. Winters, M. Martinson, J. Machac, D. Stewart, and A. Targonski, The prognostic significance of quantitative signal-averaged variables relative to clinical variables, site of myocardial infarction, ejection fraction and ventricular premature beats: a prospective study. *J. Am. Coll. Cardiol.*, 1989;**13**(2): 377–384.
28. Breithardt, G., M. Borggrefe, and K. Haerten, Role of programmed ventricular stimulation an noninvasive recording of ventricular late potentials for the identification of patients at risk of ventricular tachyarrhythmias after acute myocardial infarction, in *Cardiac Electrophysiology and Arrhythmias*, D.P. Zipes and J. Jalife, Editors. New York: Grune and Stratton, 1985, pp. 553–561.
29. Breithardt, G. and M. Borggrefe, Recent advances in the identification of patients at risk of ventricular tachyarrhythmias: role of ventricular late potentials. *Circulation*, 1987;**75**(6): 1091–1096.
30. Cain, M.E., J.L. Anderson, M.F. Arnsdorf, J.W. Mason, M.M. Scheinman, and A.L. Waldo, Signal-averaged electrocardiography. *J. Am. Coll. Cardiol.*, 1996;**27**(1): 238–249.
31. Gang, E.S., A.S. Lew, M. Hong, F.Z. Wang, C.A. Siebert, T. Peter, Decreased incidence of ventricular late potentials after successful thrombolytic therapy for acute myocardial infarction. *N. Engl. J. Med.*, 1989;**321**(11): 712–716.
32. Eldar, M., J. Leor, H. Hod, Z. Rotstein, S. Truman, E. Kaplinsky, et al., Effect of thrombolysis on the evolution of late potentials within 10 days of infarction. *Br. Heart J.*, 1990;**63**(5): 272–276.
33. Chew, E.W., P. Morton, J.G. Murtagh, M.E. Scott, and D.B. O'Keeffe, Intravenous streptokinase for acute myocardial infarction reduces the occurrence of ventricular late potentials. *Br. Heart J.*, 1990;**64**(1): 5–8.
34. Turitto, G., A.L. Risa, E. Zanchi, and P.L. Prati, The signal-averaged electrocardiogram and ventricular arrhythmias after thrombolysis for acute myocardial infarction. *J. Am. Coll. Cardiol.*, 1990;**15**(6): 1270–1276.
35. Tranchesi, B.J., M. Verstraete, F. van de Werf, C.P. de Albuquerque, B. Caramelli, O.C. Gebara, et al., Usefulness of high-frequency analysis of signal-averaged surface electrocardiograms in acute myocardial infarction before and after coronary thrombolysis for assessing coronary reperfusion. *Am. J. Cardiol.*, 1990;**66**(17): 1196–1198.
36. Aguirre, F.V., M.J. Kern, J. Hsia, H. Serota, D. Janosik, T. Greenwalt, et al., Importance of myocardial infarct artery patency on the prevalence of ventricular arrhythmias and late potentials after thrombolysis in acute myocardial infarction. *Am. J. Cardiol.*, 1991;**68**(15): 1410–1416.
37. Vatterott, P.J., S.C. Hammill, K.R. Bailey, C.M. Wiltgen, and B.J. Gersh, Late potentials on signal-averaged electrocardiograms and patency of the infarct-related artery in survivors of acute myocardial infarction. *J. Am. Coll. Cardiol.*, 1991;**17**(2): 330–337.
38. Santarelli, P., G.A. Lanza, F. Biscione, A. Natale, G. Corsini, C. Riccio, et al., Effects of thrombolysis and atenolol or metoprolol on the signal-averaged electrocardiogram after acute myocardial infarction. Late Potentials Italian Study (LAPIS). *Am. J. Cardiol.*, 1993;**72**(7): 525–531.
39. Moreno, F.L., L. Karagounis, H. Marshall, R.L. Menlove, S. Ipsen, and J.L. Anderson, Thrombolysis-related early patency reduces ECG late potentials after acute myocardial infarction. *Am. Heart J.*, 1992;**124**(3): 557–564.
40. de Chillou, C., N. Sadoul, S. Briancon, and E. Aliot, Factors determining the occurrence of late potentials on the signal-averaged electrocardiogram after a first myocardial infarction: a multivariate analysis. *J. Am. Coll. Cardiol.*, 1991;**18**(7): 1638–1642.
41. Maki, H., Y. Ozawa, N. Tanigawa, I. Watanabe, R. Kojima, S. Yakubo, et al., Effect of reperfusion by direct percutaneous transluminal coronary angioplasty on ventricular late potentials in cases of total coronary occlusion at initial coronary arteriography. *Jpn. Circ. J.* 1993;**57**(3): 183–188.
42. Kawalsky, D.L., K.N. Garratt, S.C. Hammill, K.R. Bailey, and B.J. Gersh, Effects of infarct-related artery patency and late potentials on late mortality after acute myocardial infarction. *Mayo Clin. Proc.*, 1997;**72**(5): 414–421.
43. Savard, P., J.L. Rouleau, J. Ferguson, N. Poitras, P. Morel, R.F. Davies, et al., Risk stratification after myocardial infarction using signal-averaged electrocardiographic criteria adjusted for sex, age, and myocardial infarction location. *Circulation*, 1997;**96**(1): 202–213.
44. Scharf, C., H. Redecker, F. Duru, R. Candinas, H.P. Brunner-La Rocca, A. Gerb, et al., Sudden cardiac death after coronary artery bypass grafting is not predicted by signal-averaged ECG. *Ann. Thorac. Surg.*, 2001;**72**(5): 1546–1551.
45. Bauer, A., P. Guzik, P. Barthel, R. Schneider, K. Ulm, M.A. Watanabe, et al., Reduced prognostic power of ventricular late potentials in post-infarction patients of the reperfusion era. *Eur. Heart J.*, 2005;**26**(8): 755–761.
46. Kuchar, D.L., C.W. Thorburn, and N.L. Sammel, Prediction of serious arrhythmic events after myocardial infarction: Signal-averaged electrocardiogram, Holter monitoring and radionuclide ventriculography. *J. Am. Coll. Cardiol.*, 1987;**9**(3): 531–538.
47. Gomes, J.A., S.L. Winters, D. Stewart, S. Horowitz, M. Milner, and P.A. Barreca, New noninvasive index to predict sustained ventricular tachycardia and sudden death in the first year after myocardial infarction: based on signal averaged electrocardiogram, radionuclide ejection fraction and Holter monitoring. *J. Am. Coll. Cardiol.*, 1987;**10**(2): 349–357.
48. Kuchar, D.L., C.W. Thorburn, and N.L. Sammel, Signal-averaged electrocardiogram for evaluation of recurrent syncope. *Am. J. Cardiol.*, 1986;**58**(10): 949–953.
49. Lacroix, D., M. Dubuc, T. Kus, P. Savard, M. Shenasa, and R. Nadeau, Evaluation of arrhythmic causes of syncope; correlation between Holter monitoring, electrophysiologic testing,

and body surface potential mapping. *Am. Heart J.*, 1991;**122**(5): 1346–1354.

50. Uther, J.B., C.J. Dennett, and A. Tan, The detection of delayed activation signals of low amplitude in the vectorcardiogram of patients with recurrent ventricular tachycardia by signal averaging, in *Management of Ventricular Tachycardia – Role of Mexiletine*, E. Sabndoe, D.J. Julian, and J.W. Bell, Editors. Amsterdam: Excerpta Medica, 1978, p. 80.
51. Breithardt, G., L. Seipel, J. Ostermeyer, U. Karbenn, R.R. Abendorth, M. Borggrefe, et al., Effects of anti-arrhythmic surgery on late ventricular potentials recorded by precordial signal averaging in patients with ventricular tachycardia. *Am. Heart J.*, 1982;**104**(5 Pt 1): 996–1003.
52. Marcus, N.H., R.A. Falcone, A.H. Harken, M.E. Josephson, and M.B. Simson, Body surface late potentials: Effects of endocardial resection in patients with ventricular tachycardia. *Circulation*, 1984;**70**(4): 632–637.
53. Denniss, A.R., A.J. Ross, D.A. Richards, D.V. Cody, P.A. Russell, A.A. Young, et al., Effect of anti-arrhythmic therapy on delayed potentials detected by the signal-averaged electrocardiogram in patients with ventricular tachycardia after acute myocardial infarction. *Am. J. Cardiol.*, 1986;**58**(3): 261–265.
54. Simson, M.B., E. Kindwall, A.E. Buxton, and M.E. Josephson, Signal averaging of the ECG in the management of patients with ventricular tachycardia: prediction of anti-arrhythmic drug efficacy, in *Cardiac Arrhythmias: Where to Go From Here?* P. Brugada and H.J. Wellens, Editors. Armonk, NY: Futura, 1987, p. 299.
55. Hopson, J.R., M.G. Kienzle, A.M. Aschoff, and D.R. Shirkey, Noninvasive prediction of efficacy of type IA anti-arrhythmic drugs by the signal-averaged electrocardiogram in patients with coronary artery disease and sustained ventricular tachycardia. *Am. J. Cardiol.*, 1993;**72**(3): 288–293.
56. Kulakowski, P., Y. Bashir, S. Heald, V. Paul, M.H. Anderson, S. Gibson, et al., Effects of procainamide on the signal-averaged electrocardiogram in relation to the results of programmed ventricular stimulation in patients with sustained monomorphic ventricular tacycardia. *J. Am. Coll. Cardiol.*, 1993;**21**(6): 1428–1439.
57. Freedman, R.A. and J.S. Steinberg, Electrophysiologic Study Versus Electrocardiographic Monitoring Trial (ESVEM) Investigators. Selective prolongation of QRS late potentials by sodium channel blocking anti-arrhythmic drugs: relation to slowing of ventricular tachycardia. *J. Am. Coll. Cardiol.*, 1991;**17**(5): 1017–1025.
58. Greenspon, A.J., G.A. Kidwell, M. DeCaro, and S. Hessen, The effects of type I anti-arrhythmic drugs on the signal-averaged electrocardiogram in patients with malignant ventricular arrhythmias. *Pacing Clin. Electrophysiol.*, 1992;**15**(10 Pt 1): 1445–1453.
59. Goedel-Meinen, L., M. Hofmann, G. Schmidt, W. Maier-Rudolph, P. Barthel, A. Schrag, et al., Amiodarone-efficacy and late potentials during long-term therapy. *Int. J. Clin. Pharm. Ther. Toxicol.*, 1990;**28**(11): 449–454.
60. Simson, M.B., H.L. Waxman, R. Falcone, N.H. Marcus, and M.E. Josephson, Effects of anti-arrhythmic drugs on noninvasively recorded late potentials, in *New Aspects in the Medical Treatment of Tachyarrhythmias*, G. Breithardt and F. Loogen, Editors. Munich: Urban and Schwarzenberg, 1983, pp. 80–86.
61. Keren, A., A.M. Gillis, R.A. Freedman, J.C. Baldwin, M.E. Billingham, E.B. Stinson, et al., Heart transplant rejection monitored by signal-averaged electrocardiography in patients receiving cyclosporine. *Circulation*, 1984;**70**(3 Pt 2): 1124–1129.
62. Lacroix, D., S. Kacet, P. Savard, F. Molin, J. Dagano, A. Pol, et al., Signal-averaged electrocardiography and detection of heart transplant rejection: comparison of time- and frequency-domain analyses. *J. Am. Coll. Cardiol.*, 1992;**19**(3): 553–558.
63. Haberl, R., M. Weber, H. Reichenspurner, B.M. Kemkes, G. Osterholzer, M. Anthuber, et al., Frequency analysis of the surface electrocardiogram for recognition of acute rejection after orthoptic cardiac transplantation in man. *Circulation*, 1987;**76**(1): 101–108.
64. Valentino, V.A., H.O. Ventura, F.M. Abi-Samra, C. van Meter, H.L. Price, The signal-averaged electrocardiogram in cardiac transplantation. *Transplantation*, 1992;**53**(1): 124–127.
65. Poll, D.S., F.E. Marchlinski, R.A. Falcone, M.E. Josephson, and M.B. Simson, Abnormal signal averaged electrocardiograms in patients with nonischemic congestive cardiomyopathy: relationship to sustained ventricular tachyarrhythmias. *Circulation*, 1985;**72**(6): 1308–1313.
66. Mancini, D., K.L. Wong, and M.B. Simson, Prognostic value of an abnormal signal-averaged electrocardiogram in patients with nonischemic congestive cardiomyopathy. *Circulation*, 1993;**87**(4): 1083–1092.
67. Ohnishi, Y., T. Inoue, and H. Fukuzaki, Value of the signal-averaged electrocardiogram as a predictor of sudden death in myocardial infarction and dilated cardiomyopathy. *Jpn. Circ. J.*, 1990;**54**(2): 127–136.
68. Middlekauff, H.R., W.G. Stevenson, M.A. Woo, D.K. Moser, and L.W. Stenvenson, Comparison of frequency of late potentials in idiopathic dilated cardiomyopathy and ischemic cardiomyopathy with advanced congestive heart failure and their usefulness in predicting sudden death. *Am. J. Cardiol.*, 1990;**66**(15): 1113–1117.
69. Denereaz, D., M. Zimmermann, and R. Ademec, Significance of ventricular late potentials in non-ischemic dilated cardiomyopathy. *Eur. Heart J.*, 1992;**13**(7): 895–901.
70. Keeling, P.J., P. Kulakowski, G. Yi, A.K. Slade, S.E. Bent, and W.J. McKenna, Usefulness of signal-averaged electrocardiogram in idiopathic dilated cardiomyopathy for identifying patients with ventricular arrhythmias. *Am. J. Cardiol.*, 1993;**72**(1):78–84.
71. Santangeli, P., F. Infusino, G.A. Sgueglia, A. Sestito, and G.A. Lanza, Ventricular late potentials: a critical overview and current applications. *J. Electrocardiol.*, 2008;**41**: 318–324.
72. Francés, R.J., Arrhythmogenic right ventricular dysplasia/cardiomyopathy. A review and update. *Int. J. Cardiol.*, 2006;**110**: 279–287.
73. Nava, A., A.F. Folino, B. Bauce, P. Turrini, G.F. Buja, L. Daliento, and G. Thiene, Signal-averaged electrocardiogram with arrhythmogenic right ventricular cardiomyopathy and ventricular arrhythmias. *Eur. Heart J.*, 2000;**21**: 58–65.
74. Ikeda, T., H. Sakurada, K. Sakabe, T. Sakata, M. Takami, N. Tezuka, T. Nakae, M. Noro, Y. Enjoji, T. Tejima, K. Sugi, and T. Yamaguchi, Assessment of noninvasive markers in identifying patients at risk in the Brugada syndrome: insight into risk stratification. *J. Am. Coll. Cardiol.*, 2001;**37**: 1628–1634.
75. Ikeda, T., M. Takami, K. Sugi, Y. Mizusawa, H. Sakurada, and H. Yoshino, Noninvasive risk stratification of subjects with a Brugada-type electrocardiogram and no history of cardiac arrest. *Ann. Noninvasive Electrocardiol.*, 2005;**10**: 396–403.
76. Marple, S.J., *Digital Spectral Analysis with Applications*. New Jersey: Prentice-Hall, 1987.

77. Pierce, D.L., A.R. Easley, J.R. Windle, and T.R. Engel, Fast Fourier transformation of the entire low amplitude late QRS potential to predict ventricular tachycardia. *J. Am. Coll. Cardiol.*, 1989;**14**: 1741–1743.
78. Cain, M.E., H.D. Ambos, F. Witkowski, and B.E. Sobel, Fast-Fourier transform analysis of signal-averaged electrocardiograms for identification of patients prone to sustained ventricular tachycardia. *Circulation*, 1984;**69**: 711–720.
79. Cain, M.E., H.D. Ambos, J. Markham, A.E. Fischer, and B.E. Sobel, Quantification of differences in frequency content of signal-averaged electrocardiograms in patients with compared to those without sustained ventricular tachycardia. *Am. J. Cardiol.*, 1985;**55**: 1500–1505.
80. Lindsay, B.D., J. Markham, K.B. Schechtman, H.D. Ambos, and M.E. Cain, Identification of patients with sustained ventricular tachycardia by frequency analysis of signal-averaged electrocardiograms despite the presence of bundle branch block. *Circulation*, 1988;**77**: 122–130.
81. Kelen, G.J., R. Henkin, J. Fontaine, and N. El-Sherif, Effects of analysed signal duration and phase on the results of fast fourier transform analysis of the surface electrocardiogram in subjects with and without late potentials. *Am. J. Cardiol.*, 1987;**60**: 1282–1289.
82. Machac, J., A. Weiss, S.L. Winters, P. Barecca, and J.A. Gomes, A comparative study of frequency domain and time domain analysis of signal averaged electrocardiograms in patients with ventricular tachycardia. *J. Am. Coll. Cardiol.*, 1988;**11**: 284–296.
83. Machac, J. and J.A. Gomes, Frequency domain analysis, in *Signal-Averaged Electrocardiography. Concepts, Methods and Applications*, chapter 6, J.A. Gomes, Editor. Boston, MA: Kluwer, 1993, pp. 81–123.
84. Worley, S.J., D.B. Mark, W.M. Smith, P. Wolf, R.M. Califf, H.C. Strauss, M.G. Manwaring, and R.E. Ideker, Comparison of time domain and frequency domain variables from the signal-averaged electrocardiogram: a multivariable analysis. *J. Am. Coll. Cardiol.*, 1988;**11**: 1041–1051.
85. Buckingham, T.A., C.M. Thessen, D. Hertweck, D.L. Janosik, and H.L. Kennedy, Signal-averaged electrocardiography in the time and frequency domains. *Am. J. Cardiol.*, 1989;**63**: 820–825.
86. Haberl, R., G. Jilge, R. Pulter, and G. Steinbeck, Comparison of frequency and time domain analysis of the signal-averaged electrocardiogram in patients with ventricular tachycardia and coronary artery disease: methodologic validation and clinical relevance. *J. Am. Coll. Cardiol.*, 1988;**12**: 150–158.
87. Haberl, R., G. Jilge, R. Pulter, and G. Steinbeck, Spectral mapping of the electrocardiogram with Fourier transform for identification of patients with sustained ventricular tachycardia and coronary artery disease. *Eur. Heart. J.*, 1989;**10**: 316–322.
88. Lander, P., D.E. Albert, and E.J. Berbari, Spectrotemporal analysis of ventricular late potentials. *J. Electrocardiol.*, 1990;**23**: 95–108.
89. Malik, M., P. Kulakowski, J. Poloniecki, A. Staunton, O. Odemuyiwa, T. Farrell, and J. Camm, Frequency versus time domain analysis of signal-averaged electrocardiograms. I. Reproducibility of the results. *J. Am. Coll. Cardiol.*, 1992;**20**: 127–134.
90. Kelen, G.J., R. Henkin, A.M. Starr, E.B. Caref, D. Bloomfield, and N. El-Sherif, Spectral turbulence analysis of the signal-averaged electrocardiogram and its predictive accuracy for inducible sustained monomorphic ventricular tachycardia. *Am. J. Cardiol.*, 1991;**67**: 965–975.
91. Malik, M., P. Kulakowski, K. Hnatkova, A. Staunton, and A.J. Camm, Spectral turbulence analysis versus time-domain analysis of the signal-averaged ECG in survivors of acute myocardial infarction. *J. Electrocardiol.*, 1994;**27**: S227–S232.
92. Copie, X., K. Hnatkova, A. Staunton, A.J. Camm, and M. Malik, Spectral turbulence versus time-domain analysis of signal-averaged ECG used for the prediction of different arrhythmic events in survivors of acute myocardial infarction. *J. Cardiovasc. Electrophysiol.*, 1996;**7**: 583–593.
93. Englund, A., M. Andersson, and L. Bergfeldt, Spectral turbulence analysis of the signal-averaged electrocardiogram for predicting inducible sustained monomorphic ventricular tachycardia in patients with and without bundle branch block. *Eur. Heart J.*, 1995;**16**: 1936–1942.
94. Ahuja, R.K., G. Turitto, B. Ibrahim, E.B. Caref, and N. El-Sherif, Combined time-domain and spectral turbulence analysis of the signal-averaged ECG improves its predictive accuracy in postinfarction patients. *J. Electrocardiol.*, 1994;**27**: S202–S206.
95. Mäkijärvi, M., T. Fetsch, L. Reinhardt, A. Martinez-Rubio, M. Shenasa, M. Borggrefe, and G. Breithardt, Comparison and combination of late potentials and spectral turbulence analysis to predict arrhythmic events after myocardial infarction in the Post-Infarction Late Potential (PILP) study. *Eur. Heart J.* 1995; **16**: 651–659.
96. Vazquez, R., E.B. Caref, F. Torres, M. Reina, A. Espina, and N. El-Sherif, Improved diagnostic value of combined time and frequency domain analysis of the signal-averaged electrocardiogram after myocardial infarction. *J. Am. Coll. Cardiol.*, 1999;**33**: 385–394.
97. Golden, D.P. Jr., R.A. Wolthuis, and G.W. Hoffler, A spectral analysis of the normal resting electrocardiogram. *IEEE Trans. Biomed. Eng.*, 1973;**20**: 366–372.
98. Reynolds, E.W., B.F. Muller, G.J. Anderson, and B.T. Muller, High frequency components in the electrocardiogram. A comparative study of normals and patients with myocardial disease. *Circulation*, 1967;**35**: 195–206.
99. Flowers, N.C., L.G. Horan, J.R. Thomas, and W.J. Tolleson, The anatomic basis for high-frequency components in the electrocardiogram. *Circulation*, 1969;**39**: 531–539.
100. Mor-Avi, V., S. Abboud, and S. Akselrod, Frequency content of the QRS notching in high-fidelity canine ECG. *Comput. Biomed. Res.*, 1989;**22**: 18–28.
101. Abboud, S., Subtle alterations in the high-frequency QRS potentials during myocardial ischemia in dogs. *Comput. Biomed. Res.*, 1987;**20**: 384–395.
102. Mor-Avi, V., B. Shargorodsky, S. Abboud, S. Laniado, and S. Akselrod, Effects of coronary occlusion on high-frequency components of the epicardial electrogram and body surface electrocardiogram. *Circulation*, 1987;**76**: 237–243.
103. Abboud, S., R.J. Cohen, A. Selwyn, P. Ganz, D. Sadeh, and P.L. Friedman, Detection of transient myocardial ischemia by computer analysis of standard and signal-averaged high-frequency electrocardiograms in patients undergoing percutaneous transluminal coronary angioplasty. *Circulation*, 1987;**76**: 585–596.
104. Abboud, S., J.M. Smith, B. Shargorodsky, S. Laniado, D. Sadeh, and R.J. Cohen, High frequency electrocardiography of three orthogonal leads in dogs during a coronary artery occlusion. *PACE*, 1989;**12**: 574–581.
105. Abboud, S., R.J. Cohen, and D. Sadeh, A spectral analysis of the high frequency QRS potentials observed during acute myocardial ischemia in dogs. *Int. J. Cardiol.*, 1990;**26**: 285–290.

106. Mor-Avi, V. and S. Akselrod, Spectral analysis of canine epicardial electrogram; short term variations in the frequency content induced by myocardial ischemia. *Circ. Res.*, 1990;**66**: 1681–1691.
107. Abboud, S., High-frequency electrocardiogram analysis of the entire QRS in the diagnosis and assessment of coronary artery disease. *Prog. Cardiovasc. Dis.*, 1993;**35**: 311–328.
108. Pettersson, J., P. Lander, O. Pahlm, L. Sörnmo, S.G. Warren, and G.S. Wagner, Electrocardiographic changes during prolonged coronary artery occlusion in man: comparison of standard and high-frequency recordings. *Clin. Physiol.*, 1998;**18**: 179–186.
109. Pettersson, J., O. Pahlm, E. Carro, L. Edenbrandt, M. Ringborn, L. Sörnmo, S.G. Warren, and G.S. Wagner, Changes in high-frequency QRS components are more sensitive than ST segment deviation for detecting acute coronary artery occlusion. *J. Am. Coll. Cardiol.*, 2000;**36**: 1827–1834.
110. Goldberger, A.L., V. Bhargava, V. Froelicher, J. Covell, and D. Mortara, Effect of myocardial infarction on the peak amplitude of high frequency QRS potentials. *J. Electrocardiol.*, 1980;**13**: 367–372.
111. Bhargava, V. and A. Goldberger, Myocardial infarction diminishes both low and high frequency QRS potentials: power spectrum analysis of lead II. *J. Electrocardiol.*, 1981;**14**: 57–60.
112. Goldberger, A.L., V. Bhargava, V. Froelicher, and J. Covell, Effect of myocardial infarction on high-frequency QRS potentials. *Circulation*, 1981;**64**: 34–42.
113. Talwar, K.K., G.S. Rao, U. Nayar, and M.L. Bhatia, Clinical significance of high frequency QRS potentials in myocardial infarction: analysis based on power spectrum of lead III. *Cardiovasc. Res.*, 1989;**23**: 60–63.
114. Berkalp, B., E. Baykal, N. Caglar, C. Erol, G. Akgün, and T. Gürel, Analysis of high frequency QRS potentials observed during acute myocardial infarction. *Int. J. Cardiol.*, 1993;**42**: 147–153.
115. Novak, P., L. Zhixing, V. Novak, and R. Hatala, Time-frequency mapping of the QRS complex in normal subjects and in postmyocardial infarction patients. *J. Electrocardiol.*, 1994;**27**: 49–60.
116. Ringborn, M., O. Pahlm, G.S. Wagner, S.G. Warren, and J. Pettersson, The absence of high-frequency QRS changes in the presence of standard electrocardiographic QRS changes of old myocardial infarction. *Am. Heart J.*, 2001;**36**: 1827–1834.
117. Trägårdh, E., O. Pahlm, G.S. Wagner, and J. Pettersson, Reduced high-frequency QRS components in patients with ischemic heart disease compared to normal subjects. *J. Electrocardiol.*, 2004;**37**: 157–162.
118. Vacek, J.L., D.B. Wilson, G.W. Botteron, and J. Dobbins, Techniques for the determination of left ventricular mass by signal-averaged electrocardiography. *Am. Heart J.*, 1990;**120**: 958–963.
119. Okin, P.M., T.M. Donnelly, T.S. Parker, D.C. Wallerson, N.M. Magid, and P. Kligfield, High-frequency analysis of the signal-averaged ECG. Correlation with left ventricular mass in rabbits. *J. Electrocardiol.*, 1992;**25**: 111–118.
120. Abboud, S., O. Berenfeld, and D. Sadeh, Simulation of high-resolution QRS complex using a ventricular model with a fractal conduction system. Effects of ischemia on high-frequency QRS potentials. *Circ. Res.*, 1991;**68**: 1751–1760.
121. Mason, R.E. and I. Likar, A new system of multiple-lead exercise electrocardiography. *Am. Heart J.*, 1966;**71**: 196–205.
122. Proakis, J.G. and D.G. Manolakis, *Digital Signal Processing – Principles, Algorithms, and Applications*. Upper Saddle River, NJ: Prentice-Hall, 1996.
123. Schlegel, T.T., W.B. Kulecz, J.L. DePalma, A.H. Feiveson, J.S. Wilson, M.A. Rahman, and M.W. Bungo, Real-time 12-lead high-frequency QRS electrocardiography for enhanced detection of myocardial ischemia and coronary artery disease. *Mayo Clin. Proc.* 2004;**79**: 339–350.
124. Schlegel, T.T., B. Arenare, V. Starc, E.C. Greco, G. Poulin, D.R. Moser, and R. Delgado, The best identifiers of cardiomyopathy in short duration ECG recordings: high frequency QRS reduced amplitude zone score, QT interval variability, low frequency RR interval power and heart rate turbulence slope. *Folia Cardiol.*, 2005;**12**(SupplC): 1–4.
125. Pueyo, E., E. Sörnmo, and P. Laguna, QRS slopes for early ischemia detection and characterization. *IEEE Trans. Biomed. Eng.*, 2008;**55**: 468–477.
126. Pettersson, J., E. Carro, L. Edenbrandt, C. Maynard, O. Pahlm, M. Ringborn, L. Sörnmo, S.G. Warren, and G.S. Wagner, Spatial, individual, and temporal variation of the high-frequency QRS amplitude in the 12 standard electrocardiographic leads. *Am. Heart J.*, 2000;**139**: 352–358.
127. Abboud, S., J. Leor, and M. Eldar, High frequency ECG during reperfusion therapy of acute myocardial infarction. *IEEE Comput. Soc. Comput. Cardiol.*, 1990; 351–353.
128. Aversano, T., B. Rudicoff, A. Washington, S. Traill, V. Coombs, and J. Raqueno, High frequency QRS electrocardiography in the detection of reperfusion following thrombolytic therapy. *Clin. Cardiol.*, 1994;**17**: 175–182.
129. Bhargava, V. and A.L. Goldberger, Effect of exercise in healthy men on QRS power spectrum. *Am. J. Physiol.*, 1982;**243**: H964–H969.
130. Beker, A., A. Pinchas, J. Erel, and S. Abboud, Analysis of high frequency QRS potential during exercise testing in patients with coronary artery disease and in healthy subjects. *PACE*, 1996;**19**: 2040–2050.
131. Lipton, J.A., S.G. Warren, M. Broce, S. Abboud, A. Beker, L. Sörnmo, D.R. Lilly, C. Maynard, B.D. Lucas Jr, and G.S. Wagner, High-frequency QRS electrocardiogram during exercise stress testing for detecting ischemia. *Int. J. Cardiol.*, 2008;**124**: 198–203.
132. Toledo, E., J.A. Lipton, S.G. Warren, S. Abboud, M. Broce, D.R. Lilly, C. Maynard, B.D. Lucas Jr, and G.S. Wagner, Detection of stress-induced myocardial ischemia from the depolarization phase of the cardiac cycle – a preliminary study. *J. Electrocardiol.*, 2009;**42**: 240–247.
133. Rahman, M.A., A. Gedevanishvili, Y. Birnbaum, L. Sarmiento, W. Sattam, W.B. Kulecz, and T.T. Schlegel, High-frequency QRS electrocardiogram predicts perfusion defects during myocardial perfusion imaging. *J. Electrocardiol.*, 2006;**39**: 73–81.
134. Trägårdh, E., T.T. Schlegel, M. Carlsson, J. Petterson, K. Nilsson, and O. Pahlm, High-frequency electrocardiogram analysis in the ability to predict reversible reperfusion defects during adenosine myocardial perfusion imaging. *J. Electrocardiol.*, 2007;**40**: 510–514.
135. Trägårdh, E., H. Arheden, J. Pettersson, G.S. Wagner, and O. Pahlm, High-frequency QRS components vs left ventricular mass in humans. *Folia Cardiol.*, 2005;**12**(suppl C): 68.
136. Watanabe, T., M. Yamaki, H. Tachibana, I. Kubota, and H. Tomoike, Decrease in the high-frequency QRS components depending on the local conduction delay. *Jpn. Circ. J.*, 1998;**62**: 844–848.
137. Valentino, V.A., H.O. Ventura, F.M. Abi-Samra, C.H. Van Meter, and H.L. Price, The signal-averaged electrocardiogram in cardiac transplantation. A non-invasive marker of acute allograft rejection. *Transplantation*, 1992;**53**: 124–127.

138. Graceffo, M.A. and R.A. O'Rourke, Cardiac transplant rejection is associated with a decrease in the high-frequency components of the high-resolution, signal-averaged electrocardiogram. *Am. Heart J.*, 1996;**132**: 820–826.
139. Matsushita, S., Y. Sakakibara, T. Imazuru, M. Noma, Y. Hiramatsu, O. Shigeta, T. Jikuya, and T. Mitsui, High-frequency QRS potentials as a marker of myocardial dysfunction after cardiac surgery. *Ann. Thorac. Surg.*, 2004;**77**: 1293–1297.
140. Abe, M., S. Matsushita, and T. Mitsui, Recovery of high-frequency QRS potentials following cardioplegic arrest in pediatric cardiac surgery. *Pediatr. Cardiol.*, 2001;**22**: 315–320.

40 Electrocardiography in Epidemiology

Pentti M. Rautaharju

P. W. Macfarlane, A. van Oosterom, O. Pahlm, P. Kligfield, M. Janse, J. Camm (eds.), *Comprehensive Electrocardiology*, DOI 10.1007/978-1-84882-046-3_40,

40.1 Introduction

Like other areas of electrocardiography, epidemiological electrocardiography has grown and evolved in content since the publication of the first edition of this book. The emphasis in epidemiological electrocardiography has shifted from primarily descriptive population studies to follow-up studies with risk evaluation. Electrocardiographic (ECG) recording technology has evolved, and computer electrocardiography has matured, developments that have greatly enhanced the feasibility of high-volume ECG acquisition and analysis with substantially enhanced precision and reproducibility.

At the time of the preparation of the material for the first volume of this book, computer electrocardiography in epidemiology was still a novelty that required special consideration. This is no longer necessary. The second area of epidemiological electrocardiography that has gone through a similar period of maturation and growth is the use of electrocardiography in clinical trials. This subject area has, in fact, grown so much that it is no longer feasible to cover it any more in the context of this chapter, with a few exceptions. Exercise electrocardiography and ambulatory electrocardiography are covered in separate chapters of this book.

The subject areas covered in this chapter belong in the realm of epidemiological electrocardiography that includes the following broad topics of ECG investigation:

- Estimation of the prevalence and incidence of ECG abnormalities in cross-sectional population studies.
- Determination of the normal limits for ECG intervals, amplitudes, and waveform patterns.
- Assessment of the evolution with age, significance of ECG findings in relation to physiological and anthropometric measurements, and coronary heart disease (CHD) risk factors and natural history of disease processes.
- Assessment of the risk of future adverse events, morbidity, and mortality associated with ECG abnormalities.

Each of these major application areas has certain special requirements which may be different from the needs of the traditional electrocardiographic practice in clinical diagnostic applications. Consideration of normal limits for ECG patterns is covered elsewhere in this book.

There is a scarcity of systematic reviews of epidemiological aspects of electrocardiography. One of the few, published since the first edition of Comprehensive Electrocardiography is the review from 2000 by Ashley et al. [1].

40.1.1 ECG Coding Schemes from Historical Perspective

Modern cardiovascular epidemiological studies were initiated in the USA, several European countries, and Japan during the 1950s when little was still known about the epidemiology of CHD and hypertensive heart disease (HHD). Many of these studies were inspired by the pioneering efforts of Ancel Keys at the Laboratory of Physiological Hygiene, School of Public Health of the University of Minnesota. Dr. Keys initiated a 15-year prospective study in 1947 of business and professional men from Minnesota [2], and in the 1950s, the classic Seven Countries study [3, 4]. These studies led to intensive electrocardiographic research and developmental work in this area of epidemiology. The Framingham study was initiated around 1948–1950 [5]. That study, as well as the studies in Albany, New York [6], Los Angeles [7], and Chicago [8, 9], are other milestones among modern cardiovascular epidemiology. However, the state-of-the-art of ECG coding in the 1950s was appalling. The only common guidelines for ECG wave definitions and measurements were those proposed by the Criteria Committee of the New York Heart Association [10]. Most wave definitions and classification criteria were largely qualitative descriptions and thus were too ambiguous for epidemiological applications. It was evident that the comparability of the reported prevalence of ECG abnormalities from these studies in the 1950s was questionable.

The Minnesota code (MC) was developed between 1956 and 1960. Its primary purpose was to improve the comparability of ECG classification and thus the consistency of the assessment of the coronary heart disease prevalence rates among the cohorts of the Seven Countries study. At that time, it was a formidable task to reach an agreement within any group of cardiologists on any set of ECG criteria, for instance for myocardial infarction (MI) or ventricular hypertrophies. The authors of the Minnesota code were cautious to avoid any reference to diagnostic classification. The code was described strictly as a scheme for objective reporting of morphological ECG wave measurements without prejudice to any interpretation. However, the classification criteria were based on clinical ECG criteria commonly used at that time,

many of which were developed during the late 1950s. Dr. Henry Blackburn was in charge of the Minnesota code development. One of the earliest field trials of the new code was carried out in Finland from 1956 to 1959 in epidemiological studies, which assessed the prevalence of arteriosclerotic and hypertensive heart disease among ostensibly healthy working populations [11]. The report concluded that with the aid of the Minnesota code, the ECG can be successfully used as an objective tool in the study of cardiovascular epidemiology. After the publication of the original Minnesota code in Circulation in 1960 [12], it rapidly gained widespread acceptance. The code was systematically used in the Seven Countries study and in a variety of other population studies such as the Tecumseh study of a total natural community in Michigan [13], the Tukisenta study in New Guinea [14], and the National Cooperative Pooling project including Tecumseh and four other longitudinal investigations in the USA [15].

A more recent development is the Novacode [16], which has been used in a variety of epidemiological studies sponsored by the National Institutes of Health. There are several other ECG coding schemes, which have been proposed for morphological description of ECG patterns or for diagnostic ECG classification [17–21]. However, most of these schemes are more suitable for clinical than for epidemiological applications.

40.1.2 Minnesota Code

The Minnesota code belongs to the group of classification systems called linguistic or syntactic. In general, these classifiers extract "morphs" or various feature patterns observed or measured and use a "grammar" to categorize the morphs into a given set of usually, but not necessarily, mutually exclusive diagnostic classes. In most instances, the grammar can be expressed as a branching tree of Boolean decisions. Boolean logic uses the presence or absence of various features in each decision node to determine which branch of the diagnostic decision tree to follow.

40.1.2.1 ECG Measurement Rules

The ECG measurement rules were left fairly ill defined and incomplete in the original version of the Minnesota code. These rules were defined a little more clearly in the 1968 version of the Minnesota code [22]. The Minnesota code ECG measurement rules are best described in the 1982 version of the code [23], which provides detailed illustrations of visual ECG wave measurement devices and procedures. The older hot stylus electrocardiographs, with ECGs recorded on thermosensitive paper produced a tracing that had a thick "baseline." This can considerably bias wave-duration measurements, depending on the writing characteristics of the stylus and the paper speed [24]. Proper measurement procedures can reduce but cannot eliminate these errors, which can have a significant impact on ECG coding.

It was recommended in the original version of the Minnesota code that the majority rule should be applied throughout without exception and a majority of codable complexes was required from each ECG lead coded. The measurement rules for the 1982 version of the Minnesota code specify several exceptions to the majority rule. For instance, an initial R wave exceeding 0.025 mV even in one complex in a given lead (except V_1) rules out codable Q and QS waves in that lead. For some other codes (for instance code 1.2.8), a given feature has to be present in all complexes in order to qualify as a codable item.

Three different reference or baseline points are used for amplitude measurements in the Minnesota code. All QRS-complex and ST-segment amplitude measurements are made with respect to the PR segment immediately preceding the onset of QRS. P-amplitude measurements are referred to the TP segment preceding the P-wave and T-amplitude measurements to the flattest part of the TP segment following the T wave. The amplitudes of positive deflections are measured from the upper margin of the tracing and negative deflections from the lower margin of the tracing at the baseline point.

40.1.2.2 Definition of Codable Waves

An attempt to give unambiguous definitions for codable ECG waves was one of the most important contributions of the Minnesota code. The logic for wave definitions is relatively simple as described in the following sequence:

- The first codable wave is the first deflection within the QRS complex ≥0.025 mV or ≤ −0.1 mV. The first codable wave is denoted as R wave if it is positive and a Q or QS wave if it is negative.
- The second codable wave is the first deflection following the first codable wave with an opposite polarity and an absolute amplitude ≥0.1 mV. The second wave is an R wave if it is positive and an S wave if it is negative.
- Subsequent codable waves within QRS, with alternating signs, are defined similarly with 0.1 mV amplitude thresholds. The third codable wave is an R′ wave if it is positive and S′ wave if it is negative. The fourth codable wave is an R′ wave if it positive and an S′ wave if it is negative.
- A Q wave is the first codable wave within QRS if it is negative and is followed by a codable R wave.
- A QS wave is the first codable wave if it is negative and is not followed by another codable wave within QRS.

The above definitions are adequate for describing objectively all possible combinations of QRS patterns of type R, RS, RSR′, RSR′S′, QR, QRS, QRSR′, and QS.

40.1.2.3 Coding Criteria for Serial ECG Changes

The basic problem with the initial set of the Minnesota code criteria for serial ECG changes was that trivial changes in ECG amplitudes or wave durations frequently induced artifactual new codable events in myocardial infarction (MI) classification. The coding scheme was vulnerable to considerable coding variation. A new classification scheme for coding of serial ECG changes [25] was developed for determining the incidence rate of reinfarction in the Coronary Drug Project [26], a large secondary prevention trial. This was done when it was noted that up to 27% of ECG changes, coded as significant worsening or reinfarction in the Coronary Drug project, were caused by coding variation alone. Similar problems were encountered in another large intervention study, the Multiple Risk Factor Intervention Trial (MRFIT) [27].

The serial change criteria for the Minnesota code are not based on changes in ECG measurements or simultaneous comparison of successively recorded ECGs acquired from periodic examinations. Instead, the coding scheme is based on changes in the severity level of the coding category of independently coded records. For major Q–QS changes, a jump over one severity level in code 1 is required (e.g., from 1.3 to 1.1). For minor Q–QS changes, a worsening by one severity level in code 1, plus a worsening by one severity level in code 5 (T waves) is needed (excluding code 5.4).

A significant worsening for ST changes requires a transition over one severity level (e.g., from 5.3 to 5.2). There are no serial change criteria for items related to ventricular hypertrophies.

The coding rules suitable for use in algorithms for classification of serial changes in Q–QS patterns are summarized in Table 40.1. There are additional rules for certain other items. For instance, a codable new left bundle branch block (LBBB) (7.1) requires a QRS-duration increase of 0.020 s or more from the baseline ECG.

Table 40.1

Serial change comparison rules for significant worsening of Minnesota Code (MC) Q and QS waves

Follow-up ECG Minnesota Code	Qualifying conditions for a significant change
1.1.6, 1.1.7, 1.2.3, 1.2.7, 1.3.2, 1.3.6, 1.1.1, 1.1.4, 1.1.5, 1.2.1, 1.2.2, 1.2.4	Initial R amplitude decrease ≥0.1 mV or Q:R amplitude ratio increase ≥50%
1.1.2	Initial R-amplitude decrease ≥0.15 mV and Q: R ratio increase ≥50%
1.1.3	Initial R-amplitude decrease ≥0.10 mV or Q: R ratio increase ≥75%
1.2.6	(Initial R-amplitude decrease >0.10 mV or Q: R ratio increase ≥75%) and appearance of a new codable Q wave in a VF
1.2.8	R-amplitude decrease in the "lead to the left" causing new code ≥0.10 mV

40.2 Prevalence of ECG Abnormalities

Most cardiovascular epidemiological studies have primarily focused on coronary heart disease (CHD) and hypertensive heart disease. ECG coding of Q waves and associated ST-T abnormalities has been considered as an index of old myocardial infarction (MI) in comparison with contrasting populations. Left ventricular hypertrophy (LVH) by ECG criteria (ECG-LVH), in turn, has been considered as an index of true anatomical LVH. Limited diagnostic accuracy of more moderate ECG-MI criteria and low prevalence of more strict ECG-MI criteria limits the utility of ECG-MI prevalence estimation in free-living populations. As will be shown later, similar or even more severe limitations are encountered with the application of ECG-LVH criteria. Prognostic evaluation in early epidemiological studies was done for broad categories of ECG abnormalities, in part because of limited sample size in categories considered disease specific.

40.2.1 Contrasting Prevalence and Age Trends of ECG Abnormalities in Middle-Aged Men and Women

The coronary heart disease study of the Social Insurance Institution of Finland is one of the best-documented recent prevalence surveys conducted in free-living male and female populations [28]. The study population of 5,738 men and 5,224 women consisted of whole or random samples of rural or semi-urban populations, with an overall participation rate of 90%.

Table 40.2 summarizes the prevalence of selected Minnesota code (MC) abnormalities for various age-groups of men and women ranging from 30 to 59 years. In Finnish men, the prevalence of major and minor Q waves (MC 1.1 to 1.3) was nearly four times higher than in Finnish women. These prevalence rates are nine times higher than in a 1965 report from Tecumseh population in the corresponding age range (30–59 years and less) [13]. The linear gradient in increase of the prevalence of Q waves with age was not significant in Finnish men and only of borderline significance in women. The prevalence of Q waves was higher in men than in women. However, the gender difference was no longer significant for the age-group 55–59 years.

In the Finnish study group, the prevalence of left axis deviation (MC 2.1) was 4.1% in men and 2.3% in women. The prevalence increased significantly with age in a fashion similar to that in the Tecumseh population and several others. Interestingly, such left axis trend with age was not present in men in a Polynesian community of Pukapuka [29]. Blood pressure levels in Pukapuka men have low mean values and show no rise with age and the prevalence of obesity is reportedly low.

Among the most intriguing observations in the study of Finnish communities was the contrasting age trend between men and women in the prevalence of high-amplitude R waves in leads V_5, V_6, or the frontal plane limb leads (MC 3.1). The prevalence was very high (25.9%) among Finnish men and showed no significant age trend. Evidently, the decrease of R-wave amplitudes with age observed among normotensive men is offset by R-wave amplitude increase with hypertension. The prevalence of high blood pressure (≥ 160 mm Hg systolic, or ≥95 mm Hg diastolic) among men increased from 12.9% in the age-group 30–39 years to 33.1% in the age-group 50–59 years.

The prevalence of high-amplitude QRS waves in Finnish women was substantially lower than in men, and particularly in women younger than 50 years. The gradient with age in women is significant. The striking sex differences in the prevalence indicate the inappropriateness of using identical criteria for men and women. These differences also reflect the influence on these voltage criteria of factors other than LVH associated with hypertension, such as physical activity level, age, sex, and other anthropometric extracardiac factors.

The inclusion of high-voltage criteria of Sokolow and Lyon (MC 3.1 and 3.3) causes a substantial increase in the LVH prevalence estimates. With these criteria, the prevalence was 41.9% in men and 19.5% in women. The prevalence of LVH according to the high-voltage criteria combined with ST-T changes is very low in most populations studied and these criteria are likely to be too insensitive to be used as an index for LVH in hypertension.

Abnormal ST depression in the resting ECG (MC 4.1, 4.2 or 4.3) was present significantly more often in women (4.3%) than in men (2.2%), and the prevalence increased markedly with age in both sex groups. The inclusion of the borderline abnormal ST category (J depression in excess of 0.1 mV with upsloping ST where the J point denotes the end of the QRS complex) added merely 0.8% to the prevalence in men and 1.4% in women. This reflects a deficiency in the hierarchical structure of abnormal ST codes regarding the severity of the ST abnormality, since prevalence would be expected to

Table 40.2

Prevalence (%) of Minnesota Codes among a Finnish cohort representing total or random samples of middle-aged rural or semi-urban community dwellers or factory employees by age and gender*

Age and Gender	MC Category N	Q, QS Waves 1.1–1.3	Left Axis 2.1	High R Waves 3.1	Abnormal ST 4.1–4.3	Abnormal T 5.1–5.3	PR Prolonged 6.3	LBBB 7.1	RBBB 7.2	*R′* Wave 7.3	Atrial Fibrillation 8.3	ST Elevation 9.2
30–34												
M	1,073	6.1	2.4	26.6	0.7	2.5	1.4	0.0	0.4	0.6	0.0	22.3
F	865	3.0	0.9	3.9	1.5	7.4	0.6	0.0	0.1	0.2	0.2	0.4
35–39												
M	1,076	5.7	3.0	25.1	0.9	3.2	1.3	0.1	0.2	0.5	0.1	18.8
F	889	4.6	1.2	5.0	1.1	8.2	0.0	0.1	0.1	0.3	0.0	0.3
40–44												
M	1,099	6.6	2.8	25.8	0.9	3.1	1.8	0.5	0.0	1.0	0.1	15.2
F	997	4.0	1.8	5.3	2.7	10.7	0.2	0.1	0.1	0.3	0.0	0.5
45–49												
M	906	5.7	5.0	23.1	1.6	6.2	1.9	0.3	0.6	0.9	0.2	14.6
F	927	3.8	3.0	7.7	3.9	13.1	0.5	0.1	0.2	0.5	0.0	0.4
50–54												
M	791	8.2	6.6	25.2	3.2	9.2	1.4	0.3	0.9	1.1	0.4	9.2
F	793	5.2	3.3	11.1	7.8	18.5	0.8	0.5	0.4	0.9	0.3	0.9
55–59												
M	793	8.1	5.8	29.5	6.3	13.1	1.3	1.0	1.3	0.8	1.0	10.6
F	753	6.9	3.9	16.1	9.7	24.0	1.3	0.9	0.4	0.5	0.4	0.9
All												
M	5,738	6.6	4.1	25.9	2.2	5.8	1.5	0.4	0.5	0.8	0.3	15.6
F	5,224	4.5	2.3	7.9	4.3	13.3	0.6	0.3	0.2	0.5	0.1	0.6

M = males; F = females; MC = Minnesota code. Data from the Finnish Social Insurance Institution's Coronary Heart Disease Study, Reunanen et al. [28], Acta Med Scand 1983;673 (suppl.):1–120.

increase with decreasing severity of the code. For instance, for men, the prevalences for codes 4.1 to 4.4 were 0.9%, 0.7%, 0.6%, and 0.8%, respectively.

Abnormal T waves (MC 5.1 to 5.3) were coded in 5.8% of men and 13.3% of women. The prevalence increased with age and was significantly higher in women. In women aged 55–59 years, the prevalence of abnormal T waves at rest was as high as 24%. Over 60% of abnormal T waves were flat or biphasic (MC 5.3).

The high prevalence of T-wave abnormalities in women observed in the Finnish populations, Tecumseh, and other studies, evidently indicates that repolarization abnormalities in women are often associated with factors not related to CHD. Similar relatively high prevalence rates have been reported in nonindustrialized native female populations relatively free from CHD. For instance, about one quarter of the women aged 40–59 years had T-wave abnormalities (MC 5.1 to 5.3) in a non-urbanized population of Tukisenta, New Guinea [14].

The prevalence of other coded ECG abnormalities in men and women was low, with the exception of ST elevation in men. Prolonged PR (MC 6.3) was present in 1.5% of men and in 0.6% of women, left bundle branch block in 0.4% of men and 0.3% of women, right bundle branch block (RBBB) in 0.5% of men and 0.2% of women, incomplete right bundle branch block in 0.8% of men and 0.5% of women, and atrial fibrillation in 0.3% of men and 0.1% of women.

One striking contrast between the prevalence rates of men and women was the high prevalence of ST elevation in Finnish men (15.6%). The corresponding prevalence in women was only 0.6%. The prevalence of ST elevation in men was seen to decrease significantly with age. An opposite, less-pronounced trend was observed in women. The high prevalence of ST elevation in men is apparently associated with tall T waves in the chest leads, which is a common finding especially in younger men. For other abnormalities of interest, the prevalence of Wolff–Parkinson–White syndrome (MC 6.4) was 0.2% in men and 0.1% in women. Frequent ventricular ectopic complexes (over 10% of QRS complexes) were present in 1.0% of men and 1.4% of women. Occasional ventricular ectopic complexes were observed in 1.2% of men and 1.4% of women. The prevalence of frequent supraventricular ectopic complexes (over 10%) was 0.5% in both sex groups, and the prevalence of occasional supraventricular complexes was 0.8% in men and 1.0% in women.

The reported prevalence of abnormal ECG findings in three major coding categories of the Minnesota code in five male and female population studies [13, 28, 30–32] is summarized in Table 40.3. The data confirm the uniform trend toward higher prevalence of ST depression and lower prevalence of significant Q waves in women. The prevalence of significant Q waves varies little between male populations, as a contrast to quite dramatic variations in the prevalence of high-amplitude QRS waves.

The prevalence of high-amplitude QRS waves in Finnish men is unusually high. Comparable prevalence rates have been reported only for black Jamaican males [33], with a reported prevalence of 29.9% for MC 3.1. Prevalence rates for code 3.1 as low as 0.6% have been reported for British men aged 50–59 years employed as civil servants [34]. However, this Whitehall study of Rose et al. was based on limb-lead ECGs only. As pointed out by Reunanen et al. [28], differences in occupational distributions may partly explain these differences in prevalence that, however, remain largely unresolved discrepancy.

Table 40.3

Contrasting prevalence (%) of major Q waves, high-amplitude R waves, and ST depression in five studies on male and female populations aged 50–59 years

Study/Ref.	No. Subjects		Major Q Waves MC 1.1, 1.2		High-Amplitude R Waves MC 3.1		ST Abnormalities MC 4.1–4.3	
	Male	Female	Male	Female	Male	Female	Male	Female
Tecumseh [13]	331	327	4.2	0.6	3.3	3.4	3.3	12.2
Framingham [30]	650	808	3.5	1.9	9.5	5.0	5.2	6.7
Busselton [31]	310	375	2.3	0	6.8	1.1	3.2	2.7
Copenhagen [32]	2,014	2,791	2.2	0.7	12.0	4.1	4.0	4.7
Finland's Soc. Ins. Inst. [28]	1,584	1,546	3.9	2.5	27.3	13.5	4.7	8.7

MC = Minnesota code.

As a contrast to the variability of the high R-wave amplitude prevalence, the ST-depression prevalence among male populations was relatively uniform.

40.2.2 Prevalence of ECG Abnormalities in Adult Male Populations

Table 40.4 summarizes prevalence data for ECG findings from the classic Seven Countries study of Keys et al. [3]. Twelve of these 17 cohorts of men aged 40–59 years represent total populations of males in each geographical area. Four occupational groups included in the study consisted of rail employees from the USA and Italy. One of the European populations (Zutphen) was drawn as a random (five out of nine) subsample.

The prevalence of any codable Q, QS waves, and related items ranged from 0.6% in the Japanese fishing village of Ushibuka to 6% among US railroad executives. An even larger range of variation was found in the prevalence of high-amplitude R waves (code 3.1): 1.2% among US railroad executives and 17.9% in Karelia, Finland. However, the prevalence of MI and LVH according to more stringent criteria, which gives a higher specificity, was very low. The total prevalence of diagnostic Q waves (code 1.1), lesser Q waves plus negative T waves (code 1.2 or 1.2 with code 5.1 or 5.2) or ventricular conduction defects (7.1, 7.2, or 7.4) ranged from 0.9% in Crete to 7.1% among non-sedentary US railroad clerks. The range for the prevalence of high-amplitude R waves combined with ST changes (code 3.1 and any of the codes 4.1 to 4.4) was from 0.13% for the Italian railwaymen to 1.98% in the farming village of Tanushimaru in Japan.

Rose et al. [35] compared prevalence rates for Minnesota code ECG abnormalities in six cohorts of middle-aged male clerical workers from five European countries (Belgium, Denmark, Italy, The Netherlands, and the USSR). The prevalence of Q, QS waves (MC 1.1 to 1.3) ranged from 3.4% to 5.5%, ST abnormalities (MC 4.1 to 4.3) from 2.6% to 3.6%,

Table 40.4

Prevalence (%) of Minnesota Code ECG abnormalities among 17 cohorts of adult male populations in the Seven Countries Study of Keys et al.[a]

MC Category/Cohort	N	Major Q 1.1	Any Q 1.1–1.3	Minor Q + Abn. T 1.3 + 5.1, 5.2	Major Abn. T 5.1	High R 3.1	High R + Abn. ST 3.1 + 4.1–4.4	Abn. ST, Isolated 4.1–4.4	Abn. T, Isolated 5.1–5.3	Ventricular Conduction 7.1, 7.2, 7.4
Crete, Greece	683	1 (0.2)	9 (1.3)	0 (0.0)	0 (0.0)	35 (5.1)	2 (0.3)	4 (0.6)	5 (0.7)	5 (0.7)
Corfu, Greece	529	3 (0.6)	17 (3.2)	0 (0.0)	1 (0.2)	40 (7.6)	5 (1.0)	6 (1.1)	3 (0.6)	11 (2.1)
Velikakrsna, Yugoslavia	510	5 (1.0)	14 (2.7)	0 (0.0)	0 (0.0)	62 (12.2)	6 (1.2)	1 (0.2)	0 (0.0)	6 (1.2)
Dalmatia, Yugoslavia	669	0 (0.0)	14 (2.1)	1 (0.2)	0 (0.0)	19 (2.8)	1 (0.2)	5 (0.8)	5 (0.8)	7 (1.1)
Slavonia, Yugoslavia	694	3 (0.4)	13 (1.9)	0 (0.0)	0 (0.0)	79 (11.4)	5 (0.7)	2 (0.3)	9 (1.3)	6 (0.9)
Finland, West	857	6 (0.7)	15 (1.8)	0 (0.0)	0 (0.0)	139 (16.2)	10 (1.2)	1 (0.1)	21 (2.5)	12 (1.4)
Finland, Karelia	814	7 (0.9)	18 (202)	4 (0.5)	0 (0.0)	146 (17.9)	12 (1.5)	2 (0.3)	25 (3.1)	5 (0.6)
Italy, Crevalcore	993	5 (0.5)	35 (3.5)	3 (0.3)	0 (0.0)	55 (5.5)	13 (1.3)	1 (0.1)	18 (1.8)	14 (1.4)
Italy, Montegiorgio	717	4 (0.6)	15 (2.1)	1 (0.1)	0 (0.0)	24 (3.6)	3 (0.4)	4 (0.6)	3 (0.4)	5 (0.7)
Rome, Railwaymen	766	4 (0.5)	22 (2.9)	0 (0.0)	0 (0.0)	26 (3.4)	1 (0.1)	4 (0.5)	13 (1.7)	9 (1.2)
Netherlands, Zuthen	877	8 (0.9)	33 (3.8)	0 (0.0)	0 (0.0)	38 (4.3)	8 (0.9)	2 (0.2)	5 (0.6)	21 (2.4)
Japan, Tanushimaru	504	3 (0.6)	11 (2.2)	0 (0.0)	0 (0.0)	38 (7.5)	10 (2.0)	38 (7.5)	4 (0.8)	4 (0.8)
Japan, Ushibuka,	484	2 (0.4)	3 (0.6)	0 (0.0)	0 (0.0)	71 (14.7)	7 (1.5)	32 (6.6)	2 (0.4)	6 (1.2)
USA, Switchmen	835	8 (1.0)	31 (3.7)	0 (0.0)	0 (0.0)	13 (1.6)	2 (0.2)	4 (0.5)	16 (1.9)	11 (1.3)
USA Clarks Sedentary	847	10 (1.2)	29 (3.5)	1 (0.1)	0 (0.0)	29 (3.4)	4 (0.5)	6 (0.7)	15 (1.8)	12 (1.4)
USA Clarks, Nonsedentary	155	2 (1.3)	8 (5.2)	2 (1.3)	0 (0.0)	10 (6.5)	1 (0.7)	2 (1.3)	1 (0.7)	7 (4.5)
USA, Executives	250	4 (1.6)	15 (6.0)	1 (0.4)	0 (0.0)	3 (1.2)	1 (0.4)	1 (0.4)	2 (0.8)	7 (2.8)
Totals	11184	75 (0.7)	302 (2.7)	13 (0.1)	1 (0.0)	827 (7.4)	91 (0.8)	115 (1.0)	147 (1.3)	148 (1.3)

[a] From Keys et al., Acta Medica Scand 1966; Suppl 460, pp 1–392, Tampereen Kirjapaino, Tampere, Finland.

and T-wave abnormalities from 3.4% to 5.9%. No significant heterogeneity was evident between the cohorts except for T-wave abnormalities in the younger age-group (40–49 years). Rose et al. also concluded that the codable ECG abnormalities did not directly reflect national CHD mortality except the prevalence of major Q, QS waves (MC 1.1, 1.2), and even this association may have been owing to the small number of men with these changes (1.6%).

The World Health Organization (WHO) European Collaborative Group [36] reported contrasting prevalence rates for major Q, QS waves, and ST-T segment abnormalities in industrial populations (mainly factories) in five countries (Belgium, Italy, Poland, Spain, and the UK). The prevalence estimates for the intervention group of this large multifactorial prevention trial (63,732 men aged 40–59 years, employed in 88 factories) varied significantly between centers in various countries. The prevalence of major Q, QS waves (MC 1.1 and 1.2) ranged from 0.74% in Italy to 1.34% in Poland.

There was no apparent parallelism between the prevalence of major Q, QS waves, and the mean CHD risk for each center estimated using multiple logistic coefficients derived from the Seven Countries study based on age, number of cigarettes smoked per day, systolic blood pressure, plasma or serum cholesterol, and body mass index (BMI). The prevalence of other ECG abnormalities considered to be related to suspect myocardial ischemia (ST depression, MC 4.1 to 4.3, T-wave abnormalities, MC 5.1 to 5.3 or complete bundle branch block, MC 7.1) also varied significantly between centers, with prevalence rates for the UK and Belgian centers more than double those of the Polish and Spanish centers. The authors of the report suggest that these independent variations in the prevalence of Q, QS, and ST-T changes may indicate that populations may differ in the type of CHD as well as the extent, possibly in relation to the severity, chronicity, or age at the onset of ischemia.

The determination of prevalence estimates for ECG abnormalities for clinically normal populations as well as the establishment of normal ECG standards based on unselected samples of the general population can be problematic because of difficulties in setting up criteria for "clinically normal." This is evident, for instance, by considering the problem of clinically unrecognized "silent" MI. On the other hand, results from studies in highly selected populations cannot easily be extrapolated to general populations as pointed out by Barrett et al. [37]. However, some of these studies in selected populations (e.g., aviators) have provided information regarding the significance of ECG abnormalities. This holds true particularly for the natural history studies on conduction defects and other evolutionary investigations. One key question is whether given ECG abnormalities are indicators of latent CHD in asymptomatic individuals such as healthy aviators.

The reported prevalence rates in various occupational groups vary widely, evidently dependent on the selection criteria and differences in ECG classification criteria. For instance, the prevalence of ST-segment abnormality in the resting ECG was 0.08% among 3,983 aviators with a mean age of 27 years [38]. In contrast, the prevalence of ST abnormalities (myocardial ischemia) was 11.7% in a large random sample of Israeli male permanent civil service employees aged 40 years or over [39]. It appears that in the latter study, the ischemic category included negative T waves (−0.1 mV or more negative) and incomplete left bundle branch block [40]. On the other hand, nearly 3% of the aviators in the former study had T-wave abnormalities (primary T-wave changes). Differences in classification criteria make it difficult to compare reported prevalence rates in different occupational groups.

There is increasing evidence that repolarization abnormalities in the resting ECG have significant association with latent CHD in asymptomatic men. For instance, Froelicher et al. have reported coronary angiographic findings in 58 asymptomatic aviators with repolarization abnormalities in their resting ECG [41]. Twenty six (45%) of these men had 50% or greater obstruction in one or more coronary arteries and 55% had some evidence of coronary lesions.

40.2.3 Prevalence of ECG Abnormalities in Ostensibly CHD-Free US Male Populations

The 1978 report of the Pooling Project Research group [15] provides detailed information on the prevalence of codable ECG abnormalities from three studies on samples of working male populations drawn from employment groups and from two studies based on community populations samples (Table 40.5). The report is limited to white males aged 40–59 years. Excluded were all men with definite, probable, or suspect MI, definite angina pectoris by history, or Minnesota code 1.1 or 1.2 Q or QS waves.

Table 40.5

Prevalence (percent) of major and minor ECG abnormalities in five adult populations of US males considered free from coronary heart disease at study baseline

Population	N	No Codable Abnormality	Minor Abnormality[a]	Major Abnormality[b]	Minor of Major Abnormality
Albany	1,765	90.4	7.1	2.5	9.6
Chicago Peoples Gas Co.	1,264	92.2	4.7	3.1	7.8
Chicago Western Electric Co.	1,981	86.4	11.1	2.5	13.6
Framingham	1,375	90.0	5.1	4.9	10.0
Tecumseh	691	73.0	20.7	6.4	27.1
Total	7,076	88.0	8.7	3.5	12.2

[a] Minnesota code 1.3; 4.3; 5.3; 6.3; 3.1; 9.1; 2.1, 2.2.
[b] Minnesota code 5.5, 5.2; 6.1, 6.2; 7.1, 7.2, 7.4; 8.1; 8.3.

The following Minnesota code items were coded as major abnormalities:

MC 4.1	Significant ST depression
MC 5.1 and 5.2	Negative T waves
MC 6.1 and 6.2	Complete and second-degree atrioventricular (AV) block
MC 7.1, 7.2 and 7.4	Complete left bundle branch block, complete right bundle branch block. and intraventricular (IV) block
MC 8.3	Atrial flutter or fibrillation and
MC 8.1	Frequent ventricular ectopic complexes

The prevalence of major ECG abnormalities ranged from 2.5% to 3.1% in the employee groups and 5.0% and 6.4% in the two community samples in Table 40.5. ST depression, T-wave inversion, and frequent premature ventricular complexes accounted for the majority of major abnormalities, each category having an individual prevalence of approximately 1%.

The wide prevalence difference of minor ECG abnormalities among these five male populations is of interest. The Framingham and Tecumseh study groups represent male populations of total communities. The 5.1% prevalence rate of minor ECG abnormalities in Framingham contrasts with 20.7% prevalence in Tecumseh. A closer examination of the data reported reveals that this highly significant difference in the prevalence is caused by left axis deviations and flat or biphasic T waves in Tecumseh in comparison with Framingham and other populations. The prevalence of code 5.3 (flat T waves) was 11.6% in Tecumseh and 4.2% in Framingham. The prevalence of left axis deviation (code 2.1) was 7.2% in Tecumseh and 0.9% in Framingham. The fact that the ECGs in Tecumseh were recorded during a glucose tolerance test may explain the higher prevalence of minor T-wave changes in that population. There is no obvious reason for the high prevalence of left axis deviation in Tecumseh. Perhaps systematic coding differences may at least in part be responsible.

40.3 Broad Abnormal ECG Categories and Mortality Risk

Early epidemiological studies commonly reported mortality risk for broad categories of ECG abnormalities, mainly because sample size and endpoint events were too low for a meaningful risk evaluation of disease-specific abnormalities.

40.3.1 ECG Abnormalities and Mortality Risk in General Male Populations

Blackburn et al. reported detailed analyses of the 5-year risk of incident CHD for various ECG findings by Minnesota code among men aged 40–59 years [42, 43] The groups compared for risk were matched for age, skinfold thickness, systolic blood pressure, serum cholesterol, smoking, and physical activity. Diagnostic Q waves (code 1.1), negative T waves (code 5.2), and atrial fibrillation (code 8.3) were all highly significant predictors of CHD death. The ratio of observed to expected number of deaths ranged from 10 to 15 for these three categories. Moderately large Q waves associated with T-wave inversion (1.2 and (5.1 or 5.2)) and bundle branch blocks (7.1, 7.2, 7.4) were not significant predictors of CHD death.

In prediction of all CHD events, both fatal and nonfatal, minor T-wave abnormalities (code 5.3), first-degree AV block (code 6.3), and frequent ventricular ectopic complexes (code 8.1) were significant predictors of subsequent clinical CHD in cohorts outside the USA but not in the US cohorts. Any level of ST depression (codes 4.1 to 4.3) carried a significant association with future CHD. Smaller Q waves (code 1.3) and high-amplitude R waves (code 3.1) were not significant independent predictors of CHD; nor was sinus tachycardia (heart rate >100).

Blackburn et al. also reported a more detailed breakdown of the association of ST depression with 5-year mortality from all causes in their pooled European populations (without any exclusion and irrespective of other ECG findings). The results are best summarized by expressing the risk ratio (RR), or the ratio of death rate in the subgroup with a certain ST code to the rate in the subgroup with no codable ST items. The ratios were 10.1, 4.3, 4.0 and 3.3 for codes 4.1, 4.2, 4.3 and 4.4, respectively.

Keys has subsequently reported 10-year follow-up data for a subgroup of the Seven Countries study populations [44]. This subgroup was considered CHD-free at the initial examination. However, nonspecific resting ECG abnormalities in the absence of clinical judgment of definite or possible heart disease did not qualify for exclusion, thus men with any of the following codes were included in the CHD-free subgroup: 1.2, 1.3, 4.1, 4.2, 5.1, 5.2, 6.1, 6.2, 7.1, 7.2, 7.4. and 8.3. The observed-to-expected ratio of the death rate from all causes among men with any of these nonspecific ECG abnormalities ranged from 1.0 to 2.7 in different populations, with the average value of 1.7. Adjusting for the age difference between men with and without ECG abnormalities reduced to the observed-to-expected ratio to 1.48. Thus, the all-causes 10-year death rate among men with nonspecific ECG abnormalities was 48% greater than that for the other men. High-amplitude criteria for LVH showed no predictive significance among the CHD-free cohorts of the Seven Countries study.

Risk of incident CHD for newly acquired ECG-LVH was reported by Kannel et al. in the 14-year follow-up of 5,127 men and women in the Framingham study [45]. Life-table analysis from that study showed that persons who acquired definite LVH by their ECG criteria at any time during the first seven biennial examinations, had a threefold increase in risk of clinical CHD after adjustment for coexisting hypertension. A twofold increase in risk of incident CHD was found among persons with possible LVH by ECG. However, the latter association was no longer significant after adjustment for hypertension.

Criteria for definite LVH in the above-mentioned Framingham study included primarily high voltage associated with ST-segment and T-wave changes or left axis deviation or increased left ventricular activation time. Criteria for possible LVH were based solely on QRS-amplitude criteria without ST-T changes. Thus, in both the Framingham study and the Seven Countries study, high-voltage criteria alone did not carry predictive information independently of other CHD risk factors, in contrast to criteria that included ST-T changes.

40.3.2 Major and Minor ECG Abnormalities and CHD Risk in Industrial Populations

Findings from three longitudinal studies on white, middle-aged, male populations screened from industrial companies and organizations in Chicago provide new information on the importance of major and minor ECG abnormalities for subsequent risk of death from CHD and other causes [46]. Excluded were men who had major Q waves (codes 1.1, 1.2) at the entry examination. Two of these studies, the Chicago Peoples Gas Company study and the Chicago Western Electric Company study are follow-up projects included in the Pooling project described earlier. The third major study reported is the Chicago Heart Association detection project in industry. The combined population of the three projects is 11,204 men aged 40–59 years at baseline, with 5–20 years of follow-up.

40.3.2.1 Major Abnormalities

The following Minnesota codes were included among the major abnormalities: ST depression (codes 4.1, 4.2), T-wave inversion (codes 5.1, 5.2), complete atrioventricular (AV) block (code 6.1), second-degree AV block (code 6.2), complete left bundle branch block (code 7.1), complete right bundle branch block (code 7.2), intraventricular (IV) block (code 7.4), frequent ectopic ventricular beats (code 8.1), and atrial flutter/fibrillation (code 8.3).

Major abnormalities were found in 11.2% among subgroups, which had a full 12-lead ECG recorded. The yield was significantly lower when only 5-lead or 6-lead ECGs were used. The risk ratio for CHD death for men with major ECG

abnormalities relative to men with normal ECG was 1.57 for the Chicago Peoples Gas Company, 2.85 for the Western Electric Company, and 6.89 for the men in the Chicago Heart Association detection project in industry. The corresponding risk ratios for death from all causes were 1.64, 1.79, and 3.85. Thus, the death rates for men with major ECG abnormalities were considerably higher than those among men with a normal ECG. ECG abnormalities retained a significant association with death rates when baseline age, diastolic blood pressure, serum cholesterol, relative weight, and number of cigarettes smoked per day were taken into consideration in multivariate analysis.

40.3.2.2 Minor ECG Abnormalities

The following items were included among minor ECG abnormalities: Borderline Q waves (code 1.3), borderline ST depression (code 4.3), flat or biphasic T waves (code 5.3), first-degree AV block (code 6.3), low-voltage QRS (code 9.1), high-amplitude R waves (code 3.1), left axis deviation (code 2.1), and right axis deviation (code 2.2). The risk ratio for CHD death for men with minor ECG abnormalities in relation to men with normal ECG was 1.04 for the Chicago Peoples Gas Company, 1.63 for the Chicago Western Electric Company, and 3.67 for the Chicago Heart Association detection project in industry. The corresponding risk ratios for death from all causes were 1.29, 1.35, and 2.42. Minor ECG abnormalities were shown to carry significant predictive information independently from CHD risk factors in the Chicago Western Electric Company study and the Chicago Heart Association study groups. The association with excess mortality and ECG abnormalities was demonstrated for deaths, which occurred within the first 10 years of follow-up as well as for deaths that occurred more than 10 years after entry.

The overall CHD death risk ratio for men with major or minor ECG abnormalities in relation to men with a normal ECG in the Chicago studies was 1.79 and the risk ratio for death from all causes was 1.57. These risk ratios are similar to those reported by Keys from the Seven Countries study (and the follow-up data from the pooling project [44]). The Pooling Project Research group reported an average risk ratio of 1.7 for a first major or minor ECG abnormality defined as in the Chicago study report summarized above.

40.3.3 Comparative Value of the ECG in Prediction of CHD Risk in Men and Women

The coronary heart disease study of the Finnish Social Insurance Institution [28] provides well-documented information on the relative risk of CHD death and total mortality within 5 years in men and women for various severity levels of Minnesota code abnormalities. The results of the study concerning prognostic value of ECG-MI are summarized later in the section 40.4.1. Gender comparison of more nonspecific categories is summarized here.

The Finnish study consisted of whole or random samples of rural or semi-urban dwellers. The reported relative risk for CHD death and total mortality within 5 years for a subgroup of 3,589 men and 3,470 women aged 40–59 years is of particular interest here. The relative risk was expressed as the age-adjusted risk ratio for subgroups with defined CHD-related abnormalities compared to those without such abnormalities. In judging the practical utility of risk ratios, it is important to consider what fraction of the total population has such abnormalities. It is possible to achieve, by strict classification criteria, very high-risk ratios in subgroups so small that they would be of limited value in screening and prevention because of an insufficient fraction of the total risk in a given population for a preventive effort with an adequate efficacy.

The combined category of other ischemic abnormalities (smaller Q, QS waves, ST changes, significant conduction defects, or atrial fibrillation) had a substantial increase in relative risk in men for CHD death (risk ratio 7.2) and death from all causes (risk ratio 3.1). Nonspecific T-wave changes (MC 5.3, flat or biphasic T) had over threefold excess risk for CHD death and nearly twofold risk ratio for death from all causes.

The results from the Finnish study illustrate the difficulties encountered in the evaluation of the prognostic significance of ECG abnormalities in female populations. Only 16 of the 3,470 women (0.46%) aged 40–59 years had ECG findings compatible with a probable old MI, and none of them died in 5 years of follow-up. The prevalence of ischemic findings in the resting ECG was quite high (12.8%) in women aged 40–59 years. Ten of these 445 women died within 5 years (risk ratio of 2.2 for death from all causes compared to women without CHD-related ECG abnormalities). There were only two CHD deaths in this group. Similarly, there was only one CHD death in the group of

509 women in this age range who had nonspecific T-wave changes. Thus, although there was some indication of a trend toward an increased risk ratio for death from all causes among women with increasing severity level of ECG abnormalities, the predictive power of such ECG changes for CHD deaths appears weak, and the low overall incidence of CHD deaths does not permit meaningful analysis of a possible association between ECG abnormalities and coronary mortality.

Similar problems were encountered in other studies in attempts to compose risk ratios for ECG abnormalities in men and women owing to the relatively low incidence of CHD death in women during the follow-up period involved. The report from the Framingham study [30] compared the risk of CHD (8-year incidence of CHD including angina pectoris, MI, and sudden death) in 2,336 men and 2,873 women with various combinations of Minnesota code ECG abnormalities. This cohort, aged 32–62 years at entry to the study, included only those persons who were considered CHD-free at the initial examination. The relative risk of CHD for a given category of ECG abnormalities was determined by calculating the ratio of the observed and expected number of cases with CHD. For both men and women without codable ECG abnormalities, the risk was 0.9. For 241 men with any Q waves (MC 1.1 to 1.3), ST or T abnormalities (MC 4.1 to 4.3, 5.1 to 5.3), the risk was 1.8, and for 375 women with any of these abnormalities, the risk was 1.1. Thus, there was a twofold risk for men with these abnormalities compared to men without codable abnormalities, and the risk ratio for women was 1.2.

The Copenhagen City heart study [32] evaluated the risk of death from all causes in a random sample of men and women for eight major categories of the Minnesota code. This prognostic evaluation was done for age-groups 50 years or older, and the association with mortality was assessed by comparing the ratio of the observed and expected number of deaths in a given coding category with the ratio in the group with a completely normal ECG. There was a total of 325 deaths among males and 135 among females during the variable follow-up period between February 1, 1976 and March 31, 1980. The log-rank test in the age-group 50–59 years indicated significant association with mortality in men for high-amplitude R waves, bundle branch blocks (MC 7.1, 7.4), and arrhythmias (MC 8.1 to 8.3). In women, aged 50–59 years the expected number of deaths in all these categories was too low to permit a meaningful evaluation of risk. In the older age-groups of women, there was a significant association with mortality for abnormal T waves in the age-group 70–79 years.

40.3.4 Contrasting Prognostic Significance of ECG Abnormalities in Symptomatic and Asymptomatic Men

Rose et al. reported on the 5-year incidence of CHD death according to the initial ECG findings in standard limb-lead ECGs among 18,403 male civil servants aged 60–64 years (Table 40.6) [34]. The men were divided into subgroups according to the presence or absence of symptomatic heart disease, defined at the initial examination as either a positive response to the chest-pain questionnaire (angina or history of possible MI) or being under medical care for heart disease or high blood pressure. Age-adjusted CHD mortality incidence rates were given in the report so that the outcome in men with and without given ECG abnormalities can be compared in spite of differences in age distribution.

Of interest is the overlap between predictive information from different sources. As expected, men who were under medical care, had a history of angina or possible MI and also had an ischemic ECG had the highest mortality (20%) but the prevalence was also low (0.6%), and this category contributed only 7% of all deaths. An ischemic ECG included the following abnormalities: any Q waves, any ST abnormality, negative or flat T waves, or left bundle branch block. The prevalence of an isolated ischemic ECG was 6.5%, and this category contributed 27 of the total of 274 deaths (9.9%), a relatively small fraction. The 5-year age-adjusted CHD mortality for men with ischemic ECG only was 3.3%, slightly higher than the mortality rate for men with chest pain only (2.5%).

For asymptomatic men, only three categories of Minnesota code abnormalities were associated with excess CHD deaths at ≤5% level of statistical significance (in a two-tailed test): Q, QS waves (MC 1.1 to 1.3), T-wave abnormalities (MC 1.1 to 1.3), and left bundle branch block (MC 7.1). The 5-year CHD mortality rate was in general low for asymptomatic men. It exceeded 5% only for men with prominent Q waves (MC 1.1 to 1.2) and atrial fibrillation (MC 8.3). For the total group of asymptomatic men, the 5-year CHD mortality was 1%. It was 2% for asymptomatic men with left axis deviation (MC 2.1) and 2% for men with ventricular conduction defects (MC 7.1, 7.3, 7.4). There was no excess CHD mortality among asymptomatic men with prolonged PR interval (MC 6.3).

Table 40.6

Five year coronary heart disease mortality among 18,228 men according to mutually exclusive combinations of baseline findings

Status Combinations	N (%)	Number of CHD Deaths	Age-adjusted Percentage
Chest pain[a] only	1,453 (8.0)	38	2.5
Ischemic ECG[b] only	791 (6.5)	27	3.3
Under medical care, no chest pain or ischemic ECG	313 (1.7)	16	4.5
Chest pain and under medical care, no ischemic ECG	201 (1.1)	17	6.0
Ischemic ECG and under medical care, no chest pain	98 (0.5)	11	7.6
Ischemic ECG and chest pain, not under medical care	147 (0.8)	22	10.2
Ischemic ECG and chest pain and under medical care	107 (0.6)	20	20.2
Remainder of men	15,118 (82.9)	123	0.84

[a]Positive response to questionnaire (angina or history of possible myocardial infarction.

[b]Minnesota codes 1.1–1.3; 4.1–4.4; 5.1–5.3; 7.1.

Recomposed from Fig. 40.2, Rose et al., Ref. [34], British Heart J 1978;40:636–643, © 1978 BMJ Publishing Group, amended with permission.

The Israel ischemic heart disease project [39, 40] introduced new information on the value of nonspecific ECG abnormalities in predicting future symptomatic and asymptomatic ischemic heart disease. The results were based on a 5-year follow-up of a random sample of 10,000 Israeli male permanent civil service employees aged 40 years and over in 1963.

Two categories of resting ECG abnormalities were associated with a significant increase in the 5-year incidence of angina pectoris: nonspecific T-wave abnormalities, and probable infarct by computer criteria when two electrocardiographers disagreed with the computer interpretation! The prevalence of these nonspecific T waves by computer was close to 6% of the Israeli study population chosen for the follow-up, and the prevalence of probable MI was 3.3%.

40.3.5 Contrasting Racial Differences in Prognostic Significance of ECG Abnormalities

Substantial differences have been reported in many studies in the prevalence of ECG abnormalities between black and white populations. The increased prevalence of ST-T abnormalities in black males compared to white males has been known a long time [33, 47, 48].

The Evans County study gave a comprehensive description of the rather drastic differences in the prevalence of Minnesota code ECG abnormalities in black and white males and females, and also differences in the prognostic significance of various ECG abnormalities [49]. The Evans County study population screened between 1960 and 1962 consisted of 3,009 persons 15 years or older who were considered free of evidence of past or present CHD at the time of the initial examination. Also excluded from the CHD incidence comparisons were individuals with diagnosed hypertensive heart disease in the initial examination. The reported age-adjusted prevalence of abnormal ECGs (any specified abnormality) was considerably higher in blacks than in whites. The excess prevalence of ECG abnormalities in black men and women was largely due to high prevalence of high-amplitude R waves and T-wave abnormalities (both major and minor).

In sharp contrast to the highly significant increased prevalence of ECG abnormalities in black men, the 1971 follow-up report showed a significantly lower CHD incidence associated with an abnormal ECG in black males. Small sizes of the subgroups and small number of CHD events does not permit a meaningful comparison in specific categories of abnormalities in men and particularly in women. The comparability of the prognostic significance of ECG abnormalities from this study is also limited by the age structure of the study population. Approximately 39% of the black makes, 22.2% of the white males, and about 43% of the black and white females were from the age-group 15–45 years.

A more recent 20-year mortality follow-up report from the Evans County heart study clarified the role of the racial differences regarding the prognostic value of ECG abnormalities in this cohort. That newer report was restricted to black and white men who were aged 40–64 years of age at entry. Men with major or moderate Q waves (MC 1.1, 1.2) and men with a history of angina pectoris or myocardial infarction at the initial examination were excluded.

Baseline ECG abnormalities were categorized into major and minor abnormalities using a similar grouping of the Minnesota codes as was done in the pooling project cited above [15]. The association between baseline ECG abnormalities and time to death was examined using the Cox proportional hazards model to adjust for standard CHD risk factors. Relative risks were estimated for CHD, cardiovascular disease (CVD), and all cause mortality. They were not significantly increased for black or for white men with respect to minor ECG abnormalities, which included minor Q waves (MC 1.3) and high-amplitude R waves (MC 3.1).

For major ECG abnormalities, the unadjusted relative risk of CHD, CVD, and all-cause mortality was significantly increased in both race groups. The relative risks of CVD and all-cause mortality remained significant in both races after adjustment for age at entry, systolic blood pressure, cholesterol, current and past smoking, and body mass index (BMI). The adjusted relative risk was over twofold for CVD mortality (2.3 for black men and 2.2 for white men, with 95% CI 1.1–4.5 and 1.2–4.2, respectively) and the relative risk of CHD mortality was nearly as high although no longer significant after adjustment for standard CHD risk factors. It thus appears that the adjusted relative risks of CVD mortality for major ECG abnormalities were of the same order of magnitude in black and white men.

40.4 ECG-MI and Mortality Risk

CHD prevalence is known to differ drastically in populations from different geographic locations, as was initially demonstrated by the Seven Countries study. The massive WHO MONICA project used carefully standardized procedures for data entered into population registers by MONICA centers selected for the study for documenting death rates in men and women aged 35–64 years [50]. The survey was conducted during the 1985–1987 period in 38 selected communities from 21 countries. The data revealed a 12-fold range in age-standardized annual event rates (coronary deaths and definite MI) in men and an 8.5-fold range in women. Event rates for men were highest in North Karelia, Finland (907/100,000) and lowest in Beijing, China (73/100,000). In women, event rates were highest in Glasgow, UK (241/100,000) and the rates were lowest in Toulouse, France (24/100,000) and Catalonia, Spain (25/100,000).

40.4.1 Mortality Risk in Q Wave Myocardial Infarction

Data from three well-documented studies reporting mortality risk for Q wave MI are listed in Table 40.7. In a CHD-free cohort of the Seven Countries study, there was a drastic, over 15-fold increase in short-term mortality risk (up to 5 years) for diagnostic Q waves (large Q waves or major Q waves with ST-T abnormalities) and an over fourfold increased risk for the combined category of any Q waves with or without ST-T abnormalities [51, 52]. The long-term (6–25 years) mortality risk was increased over threefold for diagnostic Q waves but was not significant for the combined category of any Q waves.

In Finland's Social Insurance Institute's study [28], the mortality risk was increased in men for diagnostic Q wave MI (defined similarly as in the Seven Countries study) for all mortality endpoints: RR was 19.5 for CHD mortality, 13.3 for CVD mortality, and 5.6 for all-cause mortality. There were too few events in women for risk evaluation in this ECG category. The risk for Minnesota code 1.1 large Q waves in men was 13.4, and for smaller Q waves in codes 1.2, 1.3 approximately threefold compared to men without significant Q waves. The prevalence of diagnostic Q wave myocardial infarction was quite low. The prevalence of the category labeled as "other ischemic abnormalities" was considerably higher, and also the risk of CHD, CVD, and all-cause mortality was markedly increased in all men, in men with an apparent silent MI, and also in women for CVD and all-cause mortality.

The Italian RIFLE Pooling project [53] reported mortality risk for large group of CHD-free men ($n = 12,180$) and women ($n = 10,373$) aged 30–69 years. CHD mortality risk for combined category of any Minnesota code Q waves was not significant in men or in women. There was a profound, over 17-fold increased risk of CHD mortality in men with major Q waves combined with major T waves. Again, there were too few events in women for risk evaluation.

As seen from Table 40.7, the low prevalence of diagnostic Q wave codes in all three of the populations is too low for population screening for preventive efforts, in spite of the extremely high mortality risk associated with them. However, when identified in any other connection, they warrant consideration for intensified secondary prevention. The Italian study suggests that the prevalence and the mortality risk for the combined category of ischemic abnormalities is at least potentially high enough for identification of subgroups for intervention.

Table 40.7

Three population studies with evaluation of the risk for ECG manifestations of an old myocardial infarction (MI)

Study/Ref.	Seven Countries Study [15, 16]	Finland's Social Insurance Institution's CHD study [17]	Italian Rifle Pooling Project [18]
Geographic Location	Finland, Greece, Italy, the Netherlands, former Yugoslavia, Japan, the USA	South-western, western, central, and eastern districts of the country	Eight regions in Italy.
Source population	12,763 men (11 cohorts from rural areas of Finland, Greece, Japan, and Yugoslavia; three other more diverse cohorts from Yugoslavia; the town of Zutphen, the Netherlands; and cohorts of railroad employees from the USA and Italy.	Men and women of the districts. Participation rate 90% (5,738 men and 5,224 women).	Reported four out of nine studies, 23 cohorts total. Participation rate 65–70%.
Baseline	1958–1964	1966–1972	1978–1987
Exclusions	Sampling goal: total male population from selected geographic areas. Participation rate ≥60%. For CHD-free sample, excluded 854 with prevalent CHD at baseline; no ECG exclusions.	All participants included; risk evaluated separately for subjects with ischemic ECG free from symptoms typical of MI.	History of angina pectoris by Rose questionnaire, hospitalization with discharge diagnosis of MI, history of other heart disease.
CHD-free sample	11,860		12,180 men, 10,373 women.
Age range	40–59 years	30–59 years	30–69 years.
Follow-up	Initial 5-years and subsequent 6–25 years	5 years	6 years
Q wave MI-related ECG findings evaluated for risk	1. Any Q wave codes, with or without other ECG abnormalities (MC 1.1–1.3) 2. Diagnostic Q wave MI (MC 1.1 OR (MC 1.2 and MC 5.1–5.2)).	1. Diagnostic Q wave MI (MC 1.1 OR (MC 1.2 and MC 5.1–5.2). 2. Other "ischemic" categories (MC 1.2–1.3, 4.1–4.3, 5.1–5.3, 6.1–6.2, 7.1, 7.2, 7.4, 8.3))	Any Q wave codes (MC 1.1–1.3) Any Q wave codes with any T wave codes (5.1–5.3) 3. Q codes 1.1–1.2 with T codes 5.1, 5.2

Table 40.7 (Continued)

Study/Ref.	Seven Countries Study [15, 16]	Finland's Social Insurance Institution's CHD study [17]	Italian Rifle Pooling Project [18]
Baseline prevalence	MC 1.1–1.3 (all men combined): 2.7% CHD-free men: 2.1%	1. Diagnostic Q wave MI Men 40–59 years: 1.3% Women 40–59 years: 0.5% Other "ischemic" ECG Men 40–59 years: 10.4% Women 40–59 years: 12.8%	Men Any Q codes 30–49 years: 0.6% 50–69 years: 1.1% Women Any Q codes 30–49 years: 0.5%; 50–59 years: 1.2%
Follow-up (Years)	25	5	6
Associated risk (hazard ratio HR)	Short-term (Years 0–5), Risk for CHD death (CHD-free men) Any Q: HR 4.1 (2.20, 7.61) Large Q or major Q with ST-T: HR 15.6 (7.2, 34.1) (not significant if large Q category excluded) Long-term (Years 6–25), Risk for CHD Death 1. Any Q: HR 1.2 (0.84, 1.58) 2. Large Q or major Q with ST-T: HR 3.4 (1.9, 6.2)	1. Diagnostic Q wave MI (5-year, age-standardized risk for age-group 40–49) Men: CHD mortality RR = 19.5 CVD mortality RR = 13.3 All-cause mortality RR = 5.6 Women: too few events for risk evaluation 2. "Other ischemic" ECG Men: CHD mortality RR = 7.2 CVD mortality RR = 6.4 All-cause mortality RR = 3.1 Women: CVD mortality RR = 3.0; All-cause mortality 2.2 Symptom-free men with "other ischemic" ECG CHD mortality, RR = 4.4 CVD mortality, RR = 3.9	CHD mortality Any Q waves: not significant in men or in women Any Q waves with any T waves: not significant for men or for women Major Q waves with major T waves: Men: RR 17.2 (1.54, 1.92) Women: Too few events for RR calculations

40.4.2 Other Studies with Mortality Risk Assessed for Major and Minor Q Waves

Mortality risk for various categories of Q waves has been evaluated in many other diverse populations. The Whitehall study on 18,403 male civil servants in the age-group 40–60 years conducted in early 1970s evaluated the 5-year CHD mortality risk for Q waves coded from limb-lead ECGs [34]. The study population contained a subgroup of 15,974 non-symptomatic men with no history of angina pectoris or MI and who were not under medical care for heart disease or hypertension. The prevalence of codes 1.1–1.3 was 2.0% in the whole group and 1.6% in the non-symptomatic group. Approximately two thirds of the Q waves were minor, Minnesota code 1.3. The age-adjusted CHD mortality ratio for men with any Q waves was 6.1 with all men in the study as the reference. In the non-symptomatic group, the mortality ratio was 4.0.

The Busselton study on 2,119 unselected subjects reported that the 13-year standardized CVD mortality rate was significantly higher in the pooled group of men and women with Minnesota code 1.1–1.3 Q waves than among those with a normal ECG [54].

The cross-sectional data from the Copenhagen City Heart Study involved a random sample of 9,384 men and 10,314 women aged 20 years and older [32]. In the age-group 60–69 years, 92 men (5.9%) and 38 women (2.4%) had Minnesota code 1.1–1.3 Q waves. Among 25 men who died, 21 had major Q waves (Minnesota code 1.1, 1.2), a highly significant difference between the observed and expected number of deaths compared to men without Q waves. There was only one death among women with Q waves.

40.4.3 Unrecognized Compared to Recognized Myocardial Infarction

Three studies listed in Table 40.8 evaluated mortality risk for recognized versus unrecognized MI: the Reykjavik study, the Framingham study, and the Honolulu study. Unrecognized MI was defined in these studies as either totally asymptomatic or associated with symptoms atypical for acute MI.

40.4.3.1 The Reykjavik Study

This study in a large male cohort (N = 9,141) was performed in five stages, 3–5 years apart, with the last stage conducted in 1983–1987 [55]. The overall prevalence of unrecognized MI at the first (0.5%) stage of the study increased sharply with age, from 0.5% at age 50 years to over 5% at age 75 years. The prevalence also increased at the later phases of the study, to 2.8% in 1987. About 30% of all MIs in the pooled data from all phases of the study were unrecognized. In logistic regression analysis, angina, age, smoking, serum cholesterol level, cardiomegaly, and diuretic therapy were associated with both types of MI. Impaired glucose tolerance and digoxin therapy were significantly associated only with recognized MI. Factors with predictive power for future unrecognized and recognized MI from Poisson regression included age, diastolic blood pressure, and hypertension medication. Digoxin therapy was significantly predictive for future unrecognized MI. Current smoking had a more consistent association with future recognized MI than with unrecognized MI.

Relative risk of CHD mortality for MI without angina pectoris was 4.6 (2.4, 8.6) for unrecognized MI and 6.3 (3.7, 10.6) for recognized MI. For all-cause mortality, the corresponding relative risks were 2.7 (1.5, 4.8) for unrecognized MI and 2.9 (1.8, 4.6) for recognized MI. The survival probabilities for both types of MI from life table analysis were relatively similar for subjects with and without MI in the first four stages of the study. Ten-year survival probabilities for unrecognized and recognized MI were 49% and 45%, respectively, and 15-year survival probabilities 62% and 48%, respectively.

40.4.3.2 Framingham Study

In a 1984 report from the Framingham study population, subjects with unrecognized MI were as likely as those with recognized MI to be at increased risk of death, heart failure, or strokes [56]. In subjects initially free from CHD, three successive 10-year periods since the start of the Framingham study in 1948 were used as the baseline for comparing the risk for the two types of MI. Of all baseline MIs in 5,127 subjects at the initial examination, 130 of 469 (27.7%) among

Table 40.8

Mortality risk for recognized versus unrecognized myocardial infarction

Study/Ref.	The Reykjavik Study [21]	Framingham [22]	Hawaii Heart Program [24]
Geographic Location	Reykjavik area, Iceland	Framingham, Massachusetts	Oahu Island, Hawaii
Source population	Male residents born between 1907 and 1934. Response rate 64–75%.	Town's representative adult population, 2,336 men, 2,873 women	Men of Japanese ancestry born between 1900 and 1919. Participation rate 73%.
Baseline	1967–1968	Onset of each of the three successive 10-year periods starting 1948	1965–1968
Selection criteria	Whole cohort included	Free from overt CHD at baseline, excluding from next follow-up subjects with MI during the preceding period	CHD-free at baseline, with at least one follow-up examination
Sample size	9,141	5,127 men and women	7,331
Age range	33–80 years	35–62 years	45–68 years
Follow-up period	4–24 years (in four stages, at 3–5 year intervals)	30 years	10 years from the examination where incident MI was detected
Definition of MI	1. Recognized MI: MONICA criteria (Patients with MC 1.1,1.2 Q waves, or with MI by enzymes, chest pain, borderline Q waves) 2. Unrecognized MI: MC 1.1, 1.2 with no history of MI	Appearance of pathologic (≥40 ms) Q waves or loss of initial R waves Unrecognized MI: Incident MI when neither the patient nor the attending physician had considered heart attack.	1. Serial ECG changes at follow-up considered diagnostic for old or age-undetermined MI; 2. Hospitalization with acute chest pain with evolving ECG changes and/or elevated enzymes 3. Serial ECG changes at hospital surveillance considered as old or age-undetermined MI
Prevalence/incidence of MI	Prevalence of unrecognized MI 0.5% at first stage, increased at later stages to 2.8% in 1980. Prevalence increased sharply with age, from 0.5% at age of 50 years to over 5% at age of 75 years. About 30% of all MI unrecognized (in pooled data from all phases).	Incidence of all MIs (during three 10-year periods): Increased in men from 7.1%, in women from 1.3% at age 45–54 years to 12.8% at age 75–84 years. Over one quarter of all MIs in men and over one third in women were unrecognized.	Average annual rate/1,000 of recognized MI (in category 1 above) 1.46, unrecognized MI 0.71, with significant age trend in both. Unrecognized MIs 32.6%.

Associated Risk	CHD death, MI without angina: RR = 4.6 (2.4, 8.6) for unrecognized MI, RR = 6.3 (3.7, 10.6) for recognized MI CHD death, MI with angina: RR = 16.9 (9.4, 30.3) for unrecognized MI, RR = 8.5 (5.8, 12.6) for recognized MI	Ten-year age-adjusted mortality risk ratio (unrecognized MI versus recognized MI) from proportional hazards model Men CHD death 1.0 CVD death 1.2 Sudden coronary death 0.6 All deaths 1.2 Women CHD death 0.6 CVD death 0.5 Sudden coronary death 0.8 All deaths 0.7	Ten-year CHD mortality 35% versus 25% (p = 0.107), CVD mortality 39% versus28% (p = 0.045), total mortality 45% versus 35% (p = 0.045), for unrecognized versus recognized MI, respectively.
Multivariate adjustment	Not clearly stated. Age, cholesterol level, antihypertensive medication, diastolic pressure, and smoking were associated with risk of unrecognized MI	Age-adjusted, controlling also for the effect of the loss of subjects to follow-up because of death from unrelated causes.	Unadjusted (age distribution similar in both groups).
Comments	Ten-year survival probabilities for CHD death: 49% for unrecognized MI, 62% for recognized MI; 15 years: 45% for unrecognized MI, 48% for symptomatic MI.	$p < 0.05$; not significant difference for other recognized versus non-recognized MI	

men and 83 of 239 (34.7%) among women were unrecognized, almost half without any symptoms. A similar proportion as mentioned above was unrecognized among incident MI during the three 10-year follow-up periods. Table 40.8 shows that the cause-specific mortality and all-cause mortality in men was similar for unrecognized and recognized MI. In women, the mortality was lower for unrecognized compared to recognized MI, and the difference was significant ($p < 0.05$) for CVD mortality.

A 1986 report from the Framingham study compared the relative 10-year risk of clinical CHD for unrecognized, asymptomatic ECG-MI and ECG-LVH [57]. The evaluation group was CHD-free at the baseline and new asymptomatic ECG-MI and ECG-LVH was detected as a 2-year incidence before the start of the follow-up. There was a profound two- to fourfold increase in CHD mortality, particularly sudden death, for both ECG abnormalities, with similar rates for both. Of interest was also the finding that ECG-LVH carried a significantly greater risk than ECG-MI for CHD death in women.

40.4.3.3 Honolulu Heart Program

The prognosis of recognized and unrecognized MI was also evaluated in the Honolulu Heart Program in a 10-year follow-up among 7,331 men who were CHD-free at baseline examination and who had serial ECG changes classified as incident Q-wave MI at the second or third examinations (2 and 6 years following the baseline) [58]. There was a total of 89 Q-wave MIs classified from serial ECG changes, 33% of them asymptomatic. Among men who were classified as MI from hospital surveillance of the study, the proportion of silent MIs among all nonfatal MIs was 22%. (The average annual incidence rate (per 1,000) for all nonfatal MIs was 3.29). The unrecognized MI group had a consistently higher (60–70%) total CVD and CHD mortality than the group with recognized MI. The number of events in groups compared in the Honolulu study was small and the difference in risk was not significant. However, consistent with the other studies mentioned above, the results suggest that the mortality risk for silent MI is at least as high as for recognized, symptomatic MI.

40.4.3.4 Other Studies Comparing Recognized Versus Unrecognized MI

A Finnish cohort of 697 men aged 65–84 years of the Seven Countries study, who had survived at the time of the 23-year follow-up examination, was followed up for the next 5-year period [59]. At the time of the beginning of the follow-up, 98 of the men (14.1%) had Minnesota code 1.1–1.3 Q waves. Q waves combined with ST depression (codes 4.1–4.3) or negative T waves (codes 5.1 or 5.2) were significantly associated with excess risk of fatal and nonfatal MI and total mortality. Isolated Q waves were not associated with independent risk with any of the endpoints.

The Bronx Aging Study assessed the prognosis of recognized and unrecognized MI in 390 elderly (75–85 years) community-based men and women in an 8-year prospective evaluation [60]. In this older group, baseline prevalence of MI was 18.5%, over one third (34.7%) of them unrecognized (completely silent MI and MI with atypical symptoms were included in this category). During the follow-up, the proportion of unrecognized MIs among all incident or recurrent MIs was 44%. The total mortality rate in subjects with recognized or unrecognized MI was 5.9/100 person–years compared with 3.9/100 person–years in the group without MI ($p = 0.059$). The sample size is small and the event rates in study subgroups are low, but the mortality rates were similar among those with recognized and unrecognized MI. The report reviewed other studies on unrecognized MI and noted that in newer reports (often from prospective studies) the average proportion of unrecognized MI was 30%.

In the older Israel ischemic heart disease project [61], the mortality follow-up was conducted 5 years from the initial examination in 1963. The second clinical examination took place in 1965 and the third in 1968. The occurrence of the MI was assumed to have taken place halfway between the two closest examinations before and after the abnormality developed. The average annual mortality rate in the group of men without any signs of MI during the follow-up period was 4.6/1,000.

There was a total of 170 men with clinically unrecognized MI during the follow-up and the annual mortality rate in this group of men was 17.3/1,000, or 3.8 times the mortality rate in men without any sign of MI. One half of all unrecognized MIs were silent and classified strictly on the basis of ECG findings in the 1965 or 1968 reexamination. The other half of clinically unrecognized MIs was not asymptomatic but their complaints were considered atypical for MI. The annual

mortality rate of 17.3/1,000 for men with unrecognized MI can be compared with the rate of 36.3/1,000 for the group of 120 men with clinically recognized MI.

The incident (or recurrent) MI rate, particularly that of unrecognized MI, was high among men with possible or probable MI at baseline according to computer criteria but who were considered as non-MI by electrocardiographers reviewing the computer interpretation. A sizable fraction of these men may have had latent CHD already at the onset of the study.

No serial ECG change classification criteria were evidently used in the study and it is possible that relatively minor changes from the baseline ECG were more likely to cause a classification as a new unrecognized MI in this subgroup. In any case, ECG signs of unrecognized MI seemed to be associated with excess mortality, with a prognosis perhaps half as serious as that for clinically recognized MI. It is noted that in the Israel study, 62% of the unrecognized MIs were categorized as possible old anterior MI, defined by the presence of a Q wave in V_2 or V_3 or R wave ≤100 mV in any two of the leads V_2–V_5. Multivariate analyses also indicated that the increased incidence of unrecognized MIs was associated with age, cigarette smoking, blood pressure (systolic and diastolic), left axis deviation, and LVH on the ECG. Poor progression of R waves in anterior chest leads is often seen in hypertensives with LVH, and it is possible that a significant proportion of these unrecognized MIs were false positives because of the limited specificity of the criteria used.

40.4.4 ECG Risk Predictors in Heart Attack Survivors

The Coronary Drug project was the first large-scale clinical trial that reported on systematic analyses of the prognostic value of ECG abnormalities among survivors from a first heart attack during a 3-year period of a longer follow-up [62]. Baseline ECGs, including the placebo group, were recorded at least 3 months after the acute phase.

ST depression had the strongest association of any ECG items with excess mortality. The risk ratio for major ST depression (>0.1 mV J depression with horizontal or downsloping ST segment) relative to normal ST was 4.0, and any degree of ST depression, except J-point depression with upsloping ST had a significant association with excess mortality. Actually, any degree of ST depression, except J-point depression with upsloping ST, was associated with a significant excess mortality. T waves more negative than −0.1 mV were also associated with over twofold excess mortality, and there was also a significant excess among men with minor T-wave abnormalities (flat or biphasic T waves).

Of particular importance was the observation that resting ECG ST depression was related to excess mortality also among men with no history of heart failure and among men not taking digitalis.

Extensive multivariate analyses were performed using Coronary Drug project data to elucidate possible independent prognostic value of ECG findings after simultaneous adjustment for all major known CHD risk factors and clinical risk indicators. Minnesota code items that contain independent prognostic information included the following categories: Q, QS waves (any code 1), ST depression (codes 4.1 to 4.4), ventricular conduction defects (e.g. codes 7.1 and 7.4) except complete right bundle branch block (code 7.2), atrial flutter/fibrillation (code 8.3), and any ventricular premature beats (code 8.2).

ST depression in the resting ECG turned out to be the strongest single ECG predictor of mortality and as strong an independent risk predictor as cardiac enlargement and functional class. This is clinically important because codable ST changes are common among survivors of a first heart attack (25% of men in the Coronary Drug project had codable ST changes) and a considerable proportion of all deaths occur among this subgroup.

40.4.5 Heart Attack Prevention Programs and Prognostic Value of Rest and Exercise ECG Abnormalities

Numerous studies cited in previous sections have demonstrated the adverse prognostic value of several resting ECG abnormalities. Relatively little is known, however, on how the presence of these abnormalities may influence heart attack prevention efforts, for instance, whether persons with defined ECG abnormalities might respond particularly favorably to intervention. The MRFIT project was designed to test the effect of a multifactor intervention program on mortality from CHD in 12,866 high-risk men aged 35–57 years. The two a priori ECG-based subgroup hypotheses were formulated with the expectation that intervention would be especially beneficial in men with a normal resting ECG and a normal exercise

ECG, respectively. No significant difference in CHD mortality was found between the special intervention and usual care (UC) groups of the trial [63]. The findings from the MRFIT study even brought up the possibility that hypertensive high-risk men with resting ECG abnormalities may have experienced increased CHD mortality in the special intervention group of the trial, an observation that created a great deal of interest because of its potential implications on diuretic therapy [64]. Similar adverse trends in coronary events were reported from the Oslo study trial on mild hypertension although the number of events involved was too low to reach nominal statistical significance [65].

The Hypertension Detection and Follow-up Program (HDFP) [66] compared CHD and total mortality in a subgroup of mild hypertensives (diastolic pressure 90–104 mm Hg) with resting ECG abnormalities similar to the MRFIT study population. CHD mortality for persons receiving systematic antihypertensive therapy in special program centers (stepped care group) was compared to that for persons referred to existing community medical care (referred care group.) The CHD mortality rate was slightly but not significantly higher in the stepped care group than in the referred care group in white men and black women, but not in black men. However, the rates for all-cause mortality were consistently lower in the stepped care group than in the referred care group. This 24% difference in favor of the stepped care group did not reach a nominal level of statistical significance because the subgroups with ECG abnormalities of HDFP cohort were small, again demonstrating problems in reaching adequate statistical power even in very large clinical trials.

In primary prevention trials, the emphasis is in demonstrating the effectiveness of risk-factor intervention in subgroups without ECG abnormalities. This is based on the assumption that intervention should be most beneficial in an early, asymptomatic phase of the disease process before end-organ damage develops.

As a contrast to the unexpected negative overall outcome of the intervention among men with a normal ECG response to exercise in MRFIT, men with an abnormal exercise ECG seemed to benefit substantially from risk-factor reduction [67]. There was a 57% lower rate of CHD deaths among men in the special intervention group with an abnormal ECG response to exercise compared with men in the usual care group (22.2 versus 51.8/1,000). Abnormal ECG response to exercise was defined as an ST-depression integral measured by a computer as 16 μVs or more in peak exercise or immediate recovery records in any of leads CS5, aVL, aVF, or V_5, with the ST-depression integral being less than 6 μVs in the above leads in the pre-exercise sitting record. These abnormal responses to a submaximal heart-rate-limited treadmill exercise test represented mainly early repolarization abnormalities with upsloping ST in lead CS5 during peak exercise. At the baseline of the study, 12.2% of the usual care men of the study had an abnormal exercise ECG. There was a nearly fourfold increase in 7-year coronary mortality among men with an abnormal response to exercise compared with men with a normal response [68].

Changing trends in CHD mortality can cause formidable problems for primary prevention trials. Unexpectedly, low CHD and total mortality particularly among subgroups or high-risk men selected on the basis of normal resting and exercise ECG can become problematic. In MRFIT, the CHD mortality rate was only about 2 per 1,000 per year in the large subgroup (61%) of these high-risk men with a normal resting and exercise ECG. It is difficult to demonstrate a significant reduction of CHD deaths below this level because a very large sample size is required for attaining adequate statistical power.

MRFIT mortality follow-up data were later extended to cover a 10.5-year follow-up period [69]. Ischemic response to exercise remained the only abnormality in the UC men with a significant association with CHD mortality, confirming the results from the initial 7-year mortality data. In the SI group, ST-T abnormalities at rest, absent or low-amplitude U waves and an abnormal cardiac infarction injury score (CIIS) [20] were all significantly associated with 10.5-year CHD mortality. However, absent or low-amplitude U waves were the only ECG abnormalities with a significant difference between the special intervention and usual care men in the relative risk estimates ($p = 0.004$).

In the Belgian heart disease prevention project [70], there was no significant difference in CHD incidence between intervention and control groups among men with a normal resting ECG. However, reduction of CHD risk factors among men with ischemic changes in their resting ECG by the Minnesota code criteria was associated with a significant reduction in 6-year CHD incidence and total mortality.

40.4.6 Time Trends: Are Risk Evaluation Data from Older Studies Still Valid?

To what extent are risk evaluation results from the older studies still valid in view of the reported decline in-hospital MI mortality rate? For instance, a survey of patients hospitalized for acute Q-wave MI in Worcester, Massachusetts,

metropolitan area hospitals, compared two periods 1 decade apart (1995–1997 versus 1986–1988) [71]. The in-hospital case fatality rate had declined from 19% to 14%. Controlled clinical trials have demonstrated reduced mortality with more common use of primary angioplasty and improved treatment of acute MI with more widespread use of coronary reperfusion and antiplatelet therapy.

It is apparent that the short-term risk of acute MI patients has improved at least in industrialized countries that have benefited from improved acute care. The question remains to what extent the long-term prognosis has improved. Already before the introduction of the major improvements in the care of CHD patients, factors other than ECG evidence of old MI seemed to determine the long-term outcome. Unrecognized MI may be less likely to benefit from improved care until a later phase of the evolution of the disease. The proportion of unrecognized MI has been approximately one third of all MIs in the studies cited above, including the Western Collaborative Group Study [72].

It takes a prolonged period of time and a large sample size to produce results from long-term studies, and by the time the results come in, the question of obsolescence often arises. The popularity of the traditional observational population studies has declined, in part because of funding problems and because clinical drug trials have taken a higher priority for funding as well as for the acceptance of manuscripts for publication in high-impact medical journals.

40.5 ECG-LVH: A Spectrum of Connotations

40.5.1 Age Trends and Ethnic Differences in ECG-LVH

The Copenhagen City Heart Study [32] conducted from 1976 to 1978, reported in 1981, combined Minnesota code 3.1, 3.3 prevalence data of 6,505 men and 7,713 women. The data showed the well-known drop in LVH prevalence in young adult men until age 40–49 years. There was little subsequent variation with age in men but in women, there is a steady increase in ECG-LVH prevalence by these criteria after age 40–49 years.

In US populations, there are rather striking differences in age trends of ECG-LVH by Cornell voltage and Sokolow–Lyon voltage criteria [73]. The Cornell voltage increases by age in men and in women (Figs. 40.1 and 40.2). Cornell voltage patterns are relatively similar in Hispanic and white men and women, and the amplitudes are drastically higher in African–American men and women. In contrast to Cornell voltage, Sokolow–Lyon voltage decreases with age in all three ethnic groups except African–American women (Figs. 40.3 and 40.4).

Many studies have reported a higher ECG-LVH prevalence in blacks compared to whites. In the Evans County study, LVH prevalence by Sokolow–Lyon criteria was threefold in blacks compared to whites, and also the ECG estimate of LV mass was significantly higher [49, 74, 75]. By Sokolow–Lyon criteria, LVH prevalence was over fourfold in the Charleston study [76]. In the Chicago Heart Study, LVH was defined by Minnesota code 3.1 criteria combined with repolarization abnormalities (MC 4.1–4.3 or MC 5.1–5.3) [77]. Although the overall LVH prevalence by this combination was substantially lower, the black and white differences were still pronounced in all age-groups from 20 to 64 years. ECG-LVH prevalence in Nigerian civil servants by Minnesota code 3.1–3.3 criteria was reported as 36.3% in men and 16.9% in women [78].

40.5.2 Time Trends in ECG-LVH Prevalence

A notable decline was found in ECG-LVH prevalence from 1950 to 1989 in the predominantly white combined original and offspring cohorts of the Framingham study [79]. ECG-LVH by combined high R and abnormal ST criteria had decreased from 4.5% to 2.5% in men and from 3.6 to 1.1% in women. The mean age-adjusted Cornell voltage amplitude had declined 80 μV per decade in men ($p = 0.03$) and 60 μV per decade in women ($p = 0.06$). Similar, profound decline has been observed in other US populations, including data from the National Health and Nutrition Surveys [80]. Although increasing use and improved effectiveness of antihypertensive medications parallel this decrease in ECG-LVH prevalence, questions remain about the reliability of ECG-LVH criteria in general and possible confounding factors.

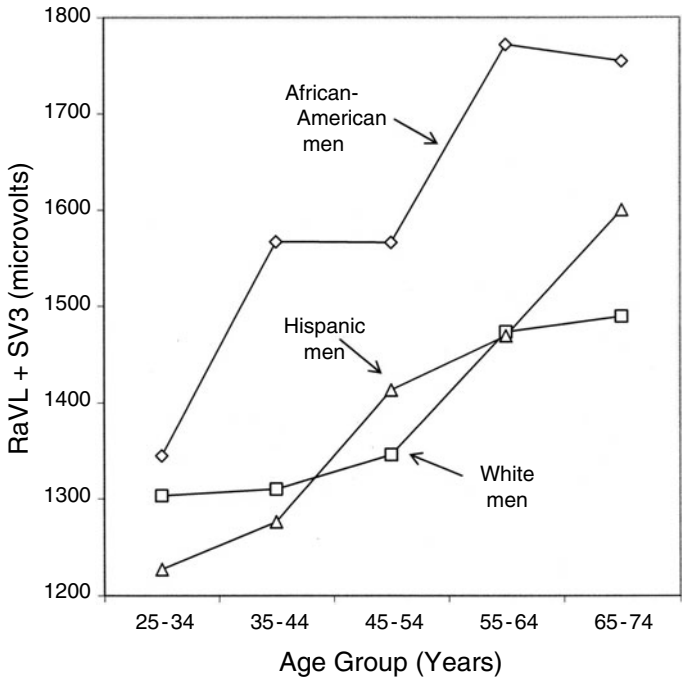

Figure 40.1

Cornell voltage (RaVL + SV3) by age in white (*squares*), Hispanic (*triangles*), and African–American men (*diamonds*). Note consistent increasing trend with age in all three ethnic groups and the substantially higher mean values in African–American compared to white and Hispanic men. Data modified from ref. [73], Rautaharju et al., J Electrocardiol 1994; 27(suppl): [20–30]. © 1994 Churchill Livingstone, reproduced with permission.

40.5.3 Echo-LVH Versus ECG-LVH: Gender and Racial Differences

In the Treatment of Mild Hypertension Study (TOMHS) [81], Echo-LVH (LV mass index ≥134 g/m^2 for men and ≥110 g/m^2 for women) was present in 13% of men and in 20% of women. ECG-LVH was reported to be "virtually absent" by Minnesota code 3.1 criteria combined with abnormal repolarization (Minnesota code 4.1–4.3 or 5.1–5.3).

Okin et al. concluded that gender differences in body size and LV mass do not completely account for gender differences in voltage measurements and QRS duration [82].

Although available echocardiographic data are limited, it has become evident that standard electrocardiographic criteria overestimate racial differences in LVH prevalence [83]. There was no notable difference in the echocardiographic LV mass between white and African–American men or women in CHD-free subgroups of the CHS population of men and women 65 years old and older [84]. In that report, relatively strict selection criteria were used to establish upper normal limits for LV mass (116 g/m^2 for men and 104 g/m^2 for women). LVH prevalence was 18.1% in white men, 15.5% in African–American men, 14.7% in white women, and 12.8% in African–American women. Thus, racial differences in Echo-LVH were relatively small. These relative differences are not overly dependent on the LV mass cut points chosen.

40.5.4 LVH and Overweight

The role of overweight and obesity in relation to ECG-LVH and Echo-LVH is a relatively complex issue, and space limitations do not permit presentation of any data here. Classification accuracy of ECG-LVH by Sokolow–Lyon criteria is limited in general, and in particular in the presence of obesity. Revaluation of the CHS data indicated that there is a

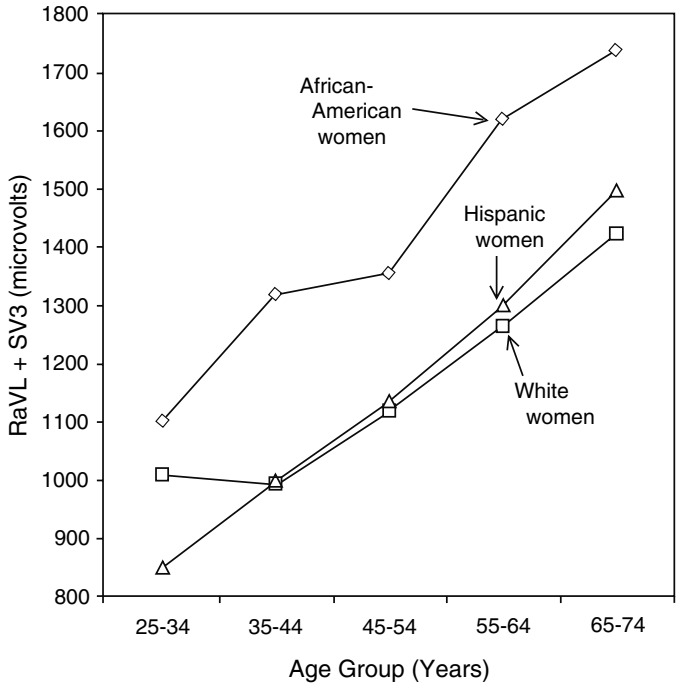

Figure 40.2

Cornell voltage (RaVL + SV3) by age in white (*squares*), Hispanic (*triangles*), and African–American women (*diamonds*). Note consistent increasing trend with age in all three ethnic groups and the substantially higher mean values in African–American compared to white and Hispanic men. Data modified from ref. [73], Rautaharju et al., J Electrocardiol 1994;27(suppl):20–30. © 1994 Churchill Livingstone, reproduced with permission.

substantial underestimate in ECG-LVH by the Cornell voltage criteria particularly in white men. In white and in African–American women, being overweight is associated with a notably higher Echo-LVH [85]. The overall LVH prevalence estimates by both methods may not differ substantially but the fraction of cases where both methods agree with the classification is relatively small.

Various studies have produced differing results about the role of overweight and LVH. The results differ depending on the method of indexing of LV mass to body size [82–86]. The availability of lean body weight data may be necessary to resolve the role of overweight in LVH.

40.5.5 ECG-LVH Prevalence in Hypertensive Cohorts

Higher ECG-LVH prevalence in blacks than in whites has also been reported in hypertensive cohorts. The Hypertension Detection and Follow-up Program (HDFP) evaluated ECGs of 10,940 hypertensive men and women with diastolic blood pressure (fifth phase) at the second screening visit of 90 mm Hg or above [54]. By Minnesota code 3.1, 3.3 plus 4.1–4.3, 5.1–5.3 criteria, the prevalences were 2.7% and 8.6% for white and black men, and 1.7% and 7.7% for white and black women, respectively. With high QRS amplitudes combined with ST-T abnormalities, the specificity of the criteria is very high, but the sensitivity is very low. The question of the need for improved LVH criteria arises again.

The Italian PIUMA study [87] reported Cornell voltage sensitivity as 16% and specificity as 97%. The authors reported that for the Perugia score for LVH [88], the sensitivity was 34% and specificity 93%. The operating points for various criteria can be expected to be quite different in hypertensive hospital populations compared to community-dwelling populations.

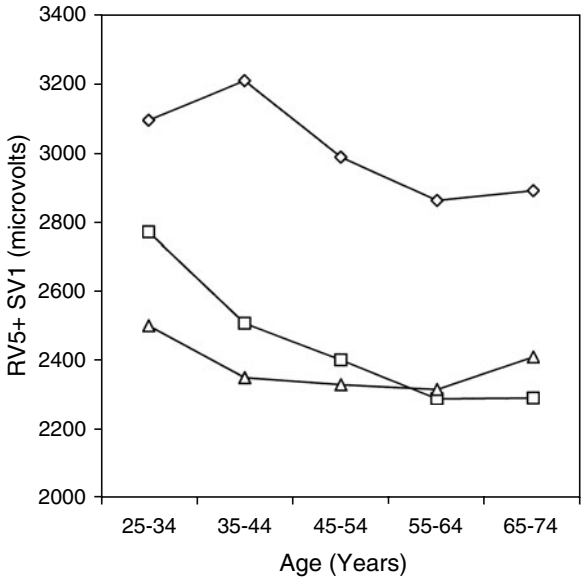

Figure 40.3

Sokolow–Lyon voltage (RV5 + SV1) by age in white (*squares*), Hispanic (*triangles*), and African–American men (*diamonds*). Note the opposite age trend in Sokolow–Lyon voltage in all three ethnic groups in comparison to the systematic increase in Cornell voltage with age in Fig. 40.1. The mean values of the Sokolow–Lyon voltage in African–American men are substantially higher compared to white and Hispanic men. Rautaharju, PM, unpublished data.

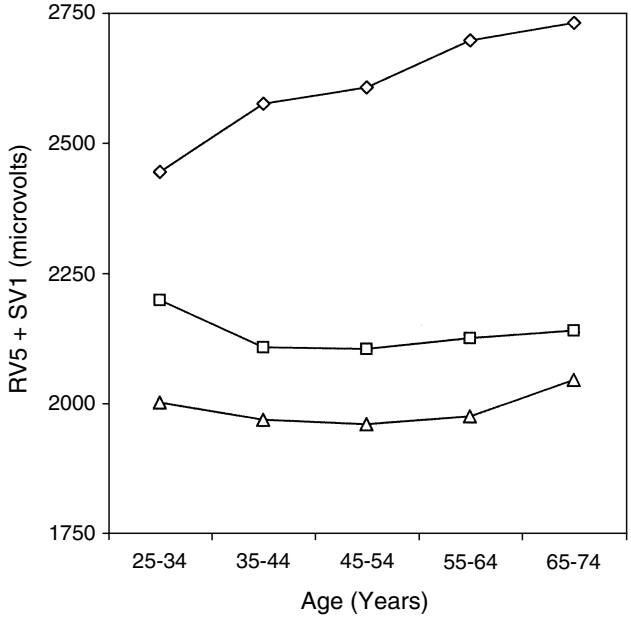

Figure 40.4

Sokolow–Lyon voltage (RV5 + SV1) by age in white (*squares*), Hispanic (*triangles*), and African–American women (*diamonds*). Increasing age trend in Sokolow–Lyon voltage is present only in African–American women and their mean values are substantially higher compared to white and Hispanic women. From NHANES 3 and HHANES ECG data, ref. [73], Rautaharju, PM, unpublished.

In summary, there are profound problems in using ECG-LVH criteria for estimating LVH prevalence in contrasting populations. LVH prevalence estimates by echocardiographic criteria will face similar, although not quite as severe, problems when some more accurate evaluation method will become available as an independent standard.

40.5.6 Visual Coding Errors as Source for Limited Sensitivity

The primary reason for visual coding errors is the complexity of the Minnesota code coding rules, particularly for serial comparison. All significant findings, particularly in code 1 category, are usually verified by an experienced supervisor in case there are any coding disagreements after duplicate reading by two coders (the procedure usually followed). Thus, false coding of significant abnormalities is actually rare. From experience in large clinical trials such as the Multiple Risk Factor Intervention Trial, the major problem in visual coding is the relatively frequent miss rate of truly codable items in spite of duplicate or even triplicate coding of each record. This miss rate can be 20% or even 30% when high volumes of records have to be coded. These error rates were found when visually coded items were verified with a computer program and all disagreements were again arbitrated.

Rautaharju et al. used a statistical model in an attempt to elucidate the reasons for the high miss rate with visual coding [89]. The authors concluded that a high miss rate in certain difficult categories of Code 1 will explain the high overall miss rate, and they also suggested that an initial screening by a computer and possible visual verification of selected items may substantially improve the accuracy and efficiency of ECG coding.

40.5.7 Prognostic Value of ECG-LVH in General Populations

Population characteristics and ECG-LVH criteria used differ from study to study, and the reported CVD mortality risk data differ considerably as seen from data derived from five diverse populations in Table 40.9. In the Framingham cohort, ECG-LVH by high QRS amplitude with LV strain was associated with a substantial excess of CVD, CHD, and all-cause mortality [51], and the mortality rates for ECG-LVH were similar as for MI by ECG, and in women they were always higher for ECG-LVH. Two-year age-adjusted incidence of ECG-LVH increased sharply both in men and in women with hypertensive status classified as mild and definite, compared with non-hypertensive groups.

LVH by Cornell voltage criteria was associated with an over threefold increased risk in black men and with an over twofold increased risk in white women in the NHANES one survey from the early 1970s. The risk was not significantly increased in any of the subgroups for Sokolow–Lyon criteria (PM Rautaharju, unpublished observations).

The Belgian Inter-University Research on Nutrition and Health (BIRNH) found a significantly increased age-adjusted and multivariately adjusted relative risk for ECG-LVH by high QRS amplitude criteria of the Minnesota code in men for CVD mortality but not for CHD mortality or total mortality [70]. The risk model included an adjustment for other major ECG abnormalities. The multivariately adjusted risk ratio for ECG-LVH was 3.14 (1.36–7.26). The risk was not significantly increased in women for any of the three major endpoints.

Data in Table 40.9 includes data from two elderly cohorts, namely an older Finnish cohort of men aged 65–84 years of the Seven Countries study [59] and the Bronx Longitudinal Aging Study that included men and women aged 75–85 years [90]. In the Finnish study with a 5-year follow-up of 697 survivors aged 65–85 years subsequent to the 25-year examination of the initial Finnish cohort of the Seven Countries study, the mortality risk for high-amplitude QRS waves and other Minnesota code items was evaluated, first separately for each abnormality and then according to a clearly defined hierarchic scheme. In the latter scenario, high QRS codes (MC 3.1, 3.3) without significant Q, ST, and T codes were entered into logistic regression models also adjusted for major CHD risk factors. High QRS amplitude codes entered without considering other coexisting codes were associated with a significant excess risk of all-cause mortality, and also with risk of fatal and nonfatal MI. The risk for isolated high R waves alone in the absence of ST-T abnormalities was not significant for any of the study endpoints. This finding again suggests that the inclusion of repolarization abnormalities with high-amplitude QRS variables is essential, not only for diagnostic applications but in particular for improved risk identification.

Table 40.9

ECG-LVH and CVD Mortality risk in general adult populations, including two old cohorts

Study/Baseline years	Age (years)	Follow-Up	Criteria	Endpoint	Gender/Race	RR (95% CI)	Comments
Framingham 1948	> 28	18 biennials	High QRS, ST Strain	CVD mortality	Men Women	3.4 ($p < 0.05$) 3.4 ($p < 0.05$)	RR = age-adjusted mortality rate versus general Framingham sample.
BIRNH 1981–1984	25–74	≥ 10 years	High R MC	CVD mortality	Men Women	3.14 (1.36–7.26) 2.20 (0.53–9.16)	CHD-free at baseline;
NHANES 1 1971–1975	35–74	7–13 years	High QRS + ST-T MC		White Men Black Men White Women Black Women	3.26 (1.91, 5.56) 4.29 (2.00, 9.18) 2.59 (1.29, 5.19) 1.90 (0.64, 5.65)	RR multivariately adjusted RR age-adjusted
RIFLE Pooling Project 1978–1987	30–69	6 years	High R MC High QRS + ST-T MC	CVD mortality CVD mortality	Men Women Men Women	1.86 (1.13, 3.07) 3.66 (0.96, 14.0) 6.33 (3.02, 13.3) 5.91 (0.70, 49.9)	Reference group free from LVH; multivariately adjusted, also for other ECG abnormalities
Bronx Longitudinal Aging Study 1980	75–85	10 years	High QRS, ST-T MC	CVD mortality All-cause mortality	Men and women Men and women	2.72 (0.53, 2.09) 2.18 (1.06, 4.45)	
Finnish cohort of the Seven Countries Study 1984	65–84	5 years	High QRS MC With or without Q, ST-T codes High QRS alone MC	All-cause mortality All-cause mortality	Men Men	1.27 ($p = 0.034$) 0.68 (0.22, 1.45)	p value from chi-square test adjusted for age and geographic area Reference group men with no major ECG abnormalities

In the Bronx Longitudinal Aging Study, ECG-LVH (MC 3.1, 3.3 with 4.1–4.3 or 5.1–5.3) had a significantly higher risk of CVD mortality than no ECG-LVH, with risk ratio 2.65 (1.58–4.41). In a multivariate model adjusting for common risk factors, CVD mortality risk was increased but not statistically significant.

One of the most informative reports from evaluation of the risk of LVH with various combinations of the relevant Minnesota codes comes from the Copenhagen City Heart Study [91]. In that report, ECG abnormalities for risk evaluation were classified as normal (reference group) together with five hierarchic, mutually exclusive abnormal categories: high-voltage QRS alone, negative T wave, ST depression with negative T wave, high-voltage QRS with negative T, and high-voltage QRS with ST depression and negative T. Each abnormality was an isolated finding, with no other abnormalities. Short-term (7-year) risk and long-term (21-year) risk were estimated for three endpoints: fatal and nonfatal MI, ischemic heart disease (ICD 8:410–414), and CVD mortality. The short-term risks for ischemic heart disease and CVD mortality are listed in Table 40.10, reproduced from Tables 4 and 5 of the Copenhagen study report. The study found no evidence of significant interaction between gender and ECG abnormalities in the Cox risk models when evaluated as individual categories or as a combined group.

The results confirm the findings from other studies that high QRS voltage alone is of little importance for risk identification, particularly when adjusted for blood pressure. Negative T waves and ST depression as isolated findings and not associated with high-voltage QRS were important predictors. The highest relative risk was found for high QRS voltage combined with negative T waves and high QRS voltage with ST depression was the strongest risk predictor of all five abnormal combinations. The report did not try to identify dominant predictors by entering all ECG abnormal categories simultaneously into the multivariately adjusted risk model. It is most likely, however, that such a model would have identified high-voltage QRS with ST depression and possibly also with negative T wave as dominant predictors among the abnormal categories.

Using ECG predictors as continuous variables will, in principle, improve the risk prediction power. An older ECG model for estimation of LV mass indexed to body surface area was used in an older study to evaluate mortality risk using NHANES1 data [92]. Comparing relative risk for an increment from 20th to 80th percentile, age-adjusted risks for CVD mortality were 1.39 (1.21, 1.60) for white men, 1.67 (1.21, 2.29) for black men, 1.62 (1.17, 2.24) for white women, and 2.08 (1.27, 3.42) for black women. With an additional adjustment for systolic blood pressure and history of heart attack, CVD mortality risk remained significant in white men (RR = 1.21 (1.03, 1.43)), white women (RR = 1.36 (1.08, 1.70)), and in black women (RR = 1.95 (1.44, 2.66)) but not for black men (RR = 1.26 (0.81, 1.96)). These data suggest that the risk is graded across a wide range of estimated LV mass values.

40.5.8 Incident ECG-LVH

The Framingham study is among the very few with adequate documentation of CHD risk in persons developing new ECG evidence of LVH during a long follow-up period [93]. It is of practical importance that the incidence of ECG-LVH is higher than anticipated from the cross-sectional prevalence data. In the Framingham population, one in ten people developed some evidence of ECG-LVH in the first 12 years of follow-up. In about 3% of the cohort, ECG findings were categorized as definitive new LVH (mostly high-amplitude R waves combined with repolarization abnormalities).

There was a pronounced increase in the risk of every manifestation of CHD in men and women with definite LVH, including stroke and heart failure. The incidence of angina, MI, and sudden death in this group was about as high as in persons surviving a first MI. Data from 20-year follow-up of the Framingham study indicate a risk ratio for the age-adjusted overall mortality of about five for both males and females with definitive LVH compared to those without ECG evidence of LVH. For men, this risk ratio was nearly six for CHD death and sudden death. For women, the risk ratio for total cardiovascular mortality was nearly ten. The excess mortality associated with definite LVH on ECG carried a greater risk of cardiovascular events than cardiac enlargement. The risk was three times the risk associated with hypertension alone. As a contrast, electrocardiographic LVH based on high-amplitude R-wave criteria alone carried a risk for CHD mortality, which was about half of the risk for definite LVH. Furthermore, this excess risk was no longer manifest when adjustment was made for the coexisting hypertension.

Table 40.10

Age-standardized incidence and relative risk of ischemic heart disease events and of cardiovascular disease mortality during 7 years of follow-up in relation to ECG findings among those without ischemic heart disease at baseline, for the age range 35–74 years in Copenhagen City Heart Study

	Ischemic Heart Disease Events			Cardiovascular Disease Mortality		
	N (Inc.)	Age-adjusted RR	Multivariately adjusted RR[a] (95% CI)	N (Inc.)	Age-adjusted RR	RR[a] (95% CI)
Normal ECG (n = 8,460)	345 (6.7)	1	1	223 (4.5)	1	1
Voltage-only LVH (n = 1,197)	66 (10.2)	1.16 (0.89–1.52)	1.15 (0.88–1.51)	45 (6.6)	1.23 (0.89–1.69)	1.28 (0.92–1.77)
T, n = 799	73 (11.6)	1.69 (1.31–2.18)*	1.56 (1.21–2.03)†	55 (8.5)	1.82 (1.35–2.45)*	1.61 (1.19–2.18)†
ST/T, n = 257	27 (14.1)	2.25 (1.52–3.34)*	2.07 (1.39–3.08)*	17 (9.1)	1.98(1.21–3.26)†	1.68 (1.02–2.77)†
LVH with neg. T (n = 137)	17 (16.2)	1.95 (1.20–3.19)†	1.89 (1.15–3.09)††	14 (13.4)	2.28 (1.32–3.92)†	2.16 (1.25–3.74)†
LVH with ST/T (n = 132)	32 (30.5)	4.27 (2.95–6.16)*	3.62 (2.47–5.30)*	22 (17.8)	3.75 (2.41–5.85)*	2.96 (1.87–4.68)*

CI = confidence interval; RR = relative risk; ECG = electrocardiographic; LVH = left ventricular hypertrophy; ST/T = LVH with ST depression and negative T wave; Inc. = age-standardized number of endpoint events per 1,000 years of follow-up.

[a] Adjusted for age, systolic and diastolic blood pressure, heart rate, body mass index, cholesterol, smoking, diabetes, alcohol, physical exercise, and family history of ischemic heart disease.

* $P < 0.001$.

† $P < 0.01$.

†† $P < 0.05$.

From Larsen et al., ref [90], Eur Heart J 2002;23:315–324. ©2001 the European Society of Cardiology, reproduced with permission.

40.6 Incident Bundle Branch Blocks: Prognostic Value

The Framingham study cited above has also reported on the prognostic significance of newly acquired left and right bundle branch block [93]. There were 55 individuals in the Framingham population who acquired a left bundle branch block and 70 who acquired a right bundle branch block during 18 years of follow-up. The CVD mortality in these two subgroups of men and women was compared to the mortality in a group of age-matched members of the Framingham population who were presumed free from bundle branch block. Within 10 years after the onset of the block, the cumulative cardiovascular disease mortality was more than four times greater in those with left bundle branch block and more than three times greater in those with right bundle branch block than in the age-matched group of the study population. The proportion of sudden deaths was similar in those with left and right bundle branch block. In women, there was no indication of a different trend in cardiovascular disease mortality rates for left and right bundle branch block.

The acquired bundle branch blocks were all associated with prospective cardiovascular abnormalities during the 18-year follow-up. In men with right bundle branch block and in women with either kind of block, the presence of a block did not contribute to the increased risk of death from cardiovascular disease independently from associated cardiovascular abnormalities, whereas the appearance of a new left bundle branch block in men contributed important independent predictive information.

The University of Manitoba follow-up study report on a 29-year follow-up of 3,983 young pilots included observations on 28 men who developed complete left bundle branch block [94]. Excluded were blocks associated with ischemic or valvular heart disease at the time of the occurrence of the conduction defect. The 5-year incidence of sudden death as the first manifestation of heart disease was at least ten times higher among men with acquired left bundle branch block than among the remainder of the men without left bundle branch block (and apparently also free from ischemic heart disease). However, this marked excess risk of sudden death was not manifest for men who were less than 45 years old at the occurrence of the left bundle branch block.

It is uncertain to what extent observations from these highly selected special occupational groups can be extrapolated to general populations. The low incidence of these incident abnormalities makes risk assessment for them difficult.

40.7 ADDENDUM

40.7.1 New Reports on Repolarization Abnormalities as Mortality Predictors from Large Population-Based Cohorts

Several new reports have been published since the preparation of the manuscript for this chapter five years ago. Some of these reports on large population-based cohorts have brought new information about the risk associated with repolarization abnormalities as mortality predictors. Summary tables describing most salient results from these studies can be found in a 2007 monograph Investigative Electrocardiography in Epidemiological Studies and Clinical Trials by Rautaharju and Rautaharju [80].

Of particular interest are the results from the Women's Health Initiative (WHI) involving nearly 40,000 women aged 50 years and older. One of the WHI reports evaluated the risk of CHD and all-cause mortality for ECG abnormalities and a second report the risk of incident CVD and congestive heart failure (CHF) [95, 96]. With all significant individual risk predictors entered simultaneously into a multivariably-adjusted CHD mortality risk model, QRS-T angle was associated with an over two-fold increase in risk, and the rate-adjusted QT interval also remained a significant predictor [95]. QRS nondipolar voltage, possibly reflecting fragmented excitation, was a dominant predictor in these women, together with an old ECG-MI. Wide QRS-T angle, ST V5 depression, high T V1 amplitude and prolonged QT were dominant predictors of incident CHF [96]. The investigators concluded that ventricular repolarization abnormalities are as important as an old ECG-MI as predictors of incident CHD, CHF and mortality.

CHF is one of the leading causes of mortality and morbidity in the USA, and the prevalence of diastolic dysfunction has been reported to be higher in women than in men [97, 98]. In the Cardiovascular Health Study (CHS), the prevalence of CHF was 8.8% and was associated with increased age, particularly for women [99]. In women with CHF, systolic ventricular function was normal significantly more often than in men (67% vs. 42%). Diagnosis of diastolic dysfunction

is presently done by clinical exclusion of other cardiac conditions. Potential importance of repolarization abnormalities as markers of CHS and for monitoring its evolution is obvious..

A report from CHS compared the relative risk of CHD and all-cause mortality during a 9-year follow-up in 4,912 men and in women aged 65 years old and older [100]. In men and in women, the relative risk of CHD mortality was increased 60% for wide QRS-T angle and there was a two-fold increase in risk of CHD mortality for ST depression. These risk levels were as high as for an old ECG-MI. Relative risk for left ventricular mass (LVM) from an ECG model with Cornell voltage and body weight as model covariates was significant in women only, as was QRS nondipolar voltage. These investigators concluded that the association of ECG abnormalities with mortality risk in women was consistently as strong as in men.

Acknowledgement

Dr. Farida Rautaharju has contributed to the contents and the preparation of this chapter.

References

1. Ashley, E.A., V.K. Raxwal, and V.F. Froelicher, The prevalence and prognostic significance of electrocardiographic abnormalities. *Curr. Probl. Cardiol*., 2000;**25**: 1–72.
2. Keys, A., H.L. Taylor, H. Blackurn, J. Brozek, J.T. Anderson, and E. Simonson, Coronary heart disease among the Minnesota business and professional men followed fifteen years. *Circulation*, 1965;**28**: 381–395.
3. Keys, A., C. Aravanis, H.W. Blackburn, et al., Epidemiological studies related to coronary heart disease: characteristics of men aged 40–59 in seven countries. *Acta Med. Scand*., 1967;**460**(Suppl): 1–392.
4. Keys, A., Editor. *Coronary Heart Disease in Seven Countries*. Heart Association Monograph Number 29. New York: American Heart Association, Inc., 1970.
5. Dawber, T.R., F.E. Moore, and G.V. Mann, Coronary heart disease in the Framingham study. *Am. J. Public Health*, 1957;**47**(Suppl. 1): 4–24.
6. Doyle, J.T., A.S. Heslin, H.E. Hilleboe, P.F. Formel, and R.F.A. Korns, prospective study of degenerative cardiovascular disease in Albany. Report of three years' experience –I. Ischemic heart disease. *Am. J. Public Health*, 1957;**47**(Suppl. I): 25–32.
7. Chapman, J.M., L.S. Goerke, W. Dixon, D.B. Loveland, and E. Phillips, The clinical status of a population group in Los Angeles under observation for two to three years. *Am. J. Public Health*, 1957;**47**(Suppl. 1): 33–42.
8. Stamler, J., H.A. Lindberg, D.M. Berkson, A. Shaffer, W. Miller, and A. Poindexter, Prevalence and incidence of coronary heart disease in strata of the labor force of a Chicago industrial corporation. *J. Chronic Dis*., 1960;**11**: 405–420.
9. Paul, O., M.H. Lepper, W.H. Phelan, et al., A longitudinal study of coronary heart disease. *Circulation*, 1963;**28**: 20–31.
10. New York Heart Association, Subcommittee on Electrocardiographic Criteria. *Nomenclature and Criteria for Diagnosis of Diseases of the Heart and Blood Vessels*, 5th edn. New York: New York Heart Association, 1953.
11. Rautaharju, P.M., M.J. Karvonen, and A. Keys, The frequency of arteriosclerotic and hypertensive heart disease among ostensibly health working populations in Finland. *J. Chronic Dis*., 1961;**13**: 426–438.
12. Blackburn, H., A. Keys, E. Simonson, P. Rautaharju, and S. Punsar, The electrocardiogram in population studies. A classification system. *Circulation*, 1960;**21**: 1160–1175.
13. Ostrander, L.D. Jr, R.L. Brandt, M.O. Kjelsberg, and F.H. Epstein, Electrocardiographic findings among the adult population of a total natural community, Tecumseh, Michigan. *Circulation*, 1965;**31**: 888–898.
14. Sinnett, P.F. and H.M. Whyte, Epidemiological studies in a total highland population. Tukisenta, New Guinea, Cardiovascular disease and relevant clinical, electrocardiographic, radiological and biochemical findings. *J. Chronic Dis*., 1973;**26**: 265–290.
15. The Pooling Project research Group, Relationship of blood pressure, serum cholesterol, smoking habit, relative weight and ECG abnormalities to incidence of major coronary events: Final report of the Pooling Project. *J. Chronic Dis*., 1978;**31**: 201–306.
16. Rautaharju, P.M., H.P. Calhoun, and B.R. Chaitman, Novacode serial ECG classification system for clinical trials and epidemiological studies. *J. Electrocardiol*., 1992;**24**: 179–187.
17. Burch, G.E. and T. Winsor, *A Primer of Electrocardiography*, 5th edn. Philadelphia, PA: Lea and Febiger, 1966.
18. Robles de Medina, E.O., *A New Coding System for Electrocardiography*. Assen: Royal van Gorcum, 1966.
19. Schamroth, L. and H.D. Friedberg, A coding system for cardiac arrhythmias. *J. Electrocardiol*., 1970;**3**: 169–172.
20. Rautaharju, P.M., J.W. Warren, U. Jain, H.K. Wolf, and C.L. Nielsen, Cardiac infarction injury score: an electrocardiographic coding scheme for ischemic heart disease. *Circulation*, 1981;**64**: 249–256.
21. Pipberger, H.V., E. Simonson, E.A. Lopez Jr, A. Araoye, and H.A. Pipberger, The electrocardiogram in epidemiologic investigations. A new classification system. *Circulation*, 1982;**65**: 1456–1464.
22. Rose, G.A. and H. Blackburn, *Cardiovascular Survey Methods*. Geneva: World Health Organization, 1968. Monograph Series, no. 56
23. Prineas, R.J., R.S. Crow, and H. Blackburn, *The Minnesota Code Manual of Electrocardiographic Findings. Standards and Procedures for Measurement and Classification*. Boston, MA/Bristol/London: John Wright PSG Inc, 1982.

24. Rautaharju, P.M., D. Seale, R. Prineas, H. Wolf, R. Crow, and J. Warren, Changing electrocardiographic recording technology and diagnostic accuracy of myocardial infarction criteria. Improved standards for evaluation of ECG measurement precision. *J. Electrocardiol.*, 1978;**11**: 321–230.
25. Crow, R., R.J. Prineas, D.R. Jacobs, and H. Blackburn, A new epidemiological classification system for interim myocardial infarction from serial electrocardiographic changes. *Am. J. Cardiol.*, 1989;**64**: 454–461.
26. The Coronary Drug Project Research group, The coronary drug project: design, methods, and baseline results. *Circulation*, 1973;**47**(Suppl. 1): 11–50.
27. Rautaharju, P.M., S.K. Broste, R.J. Prineas, W.J. Eifler, R.S. Crow, and C.D. Furberg, Quality control procedures for the resting electrocardiogram in the multiple risk factor intervention trial. *Controlled Clin. Trials*, 1986;**7**(Suppl. 3): 46S–65S.
28. Reunanen, A., A. Aromaa, K. Pyörälä, S. Punsar, J. Maatela, and P. Knekt, The Social Insurance Institution's Coronary Heart Disease Study. Baseline data and 5 year mortality experience. *Acta Med. Scand.*, 1983;**673**(Suppl): 1–120.
29. Evans, J.G., I.A.M. Prior, and W.M.G. Turnbridge, Age-associated change in QRS axis: intrinsic or extrinsic aging? *Gerontology*, 1982;**28**: 132–137.
30. Higgins, I.T.T., W.B. Kannel, and T.R. Dawber, The electrocardiogram in epidemiological studies: reproducibility, validity and international comparison. *Br. J. Prev. Soc. Med.*, 1965;**19**: 53–68.
31. Cullen, K.J., B.P. Murphy, and G.N. Cumpston, Electrocardiograms in the Busselton population. *Aust. N.Z. J. Med.*, 1974;**4**: 325–330.
32. Ostor, E., P. Schnohr, G. Jensen, J. Nybe, and A.T. Hansen, Electrocardiographic findings and their association with mortality in the Copenhagen city heart study. *Eur. Heart J.*, 1981;**2**: 317–328.
33. Miall, W.E., E. Campo, J. Fodor, et al., Longitudinal study of heart disease in a Jamaican rural population. 1. Prevalence, with special reference to ECG findings. *Bull. W.H.O.*, 1972;**46**: 429–441.
34. Rose, G., P.J. Baxter, D.D. Reid, and P. McCartney, Prevalence and prognosis of electrocardiographic findings in middle aged men. *Br. Heart J.*, 1989;**1**: 73–80.
35. Rose, G.A., M. Ahmeteli, L. Checcacci, et al., Ischemic heart disease in middle-aged men: Prevalence comparisons in Europe. *Bull. W.H.O.*, 1968;**38**: 885–895.
36. World Health Organization European Collaborative Group, Multifunctional trial in the prevention of coronary heart disease: 1. Recruitment and initial findings. *Eur. Heart J.*, 1980;**1**: 73–80.
37. Barrett, P.A., C.T. Peter, H.J.C. Swan, B.N. Singh, and W.J. Mandel, The frequency and prognostic significance of electrocardiographic abnormalities in clinically normal individuals. *Prog. Cardivasc. Dis.*, 1981;**23**: 299–319.
38. Mathewson, F.A.L. and G.S. Varnam, Abnormal electrocardiograms in apparently healthy people. I. Long term follow-up study. *Circulation*, 1960;**21**: 196–203.
39. Medalie, J.H., M. Snyder, J.J. Croen, H.N. Neufeld, U. Goldbourt, and E. Riss, Angina pectoris among 10,000 men: 5 year incidence and univariate analysis. *Am. J. Med.*, 1973;**55**: 583–594.
40. Medalie, J.H., H.A. Khan, H.N. Neufeld, et al., Myocardial infarction over a five-year period. I. Prevalence, incidence and mortality experience. *J. Chronic Dis.*, 1973;**26**: 63–84.
41. Froelicher, V.F. Jr, F.G. Yanowitz, A.J. Thomson, and M.C. Lancaster, The correlation of coronary arteriography and the electrocardiographic response to maximal treadmill testing in 76 asymptomatic men. *Circulation*, 1973;**48**: 597–604.
42. Blackburn, H., H.I. Taylor, and A. Keys, The electrocardiogram in prediction of five-year coronary heart disease incidence among men aged forty through fifty-nine. *Circulation*, 1979;41(Suppl. 1): 154–161.
43. Blackburn, H., The importance of electrocardiograms in populations outside the hospital. *Can. Med. Assoc. J.*, 1973;**108**: 1262–1265.
44. Keys, A., *Seven Countries. A Multivariate Analysis of Death and Coronary Heart Disease*. Cambridge, MA: Harvard University Press, 1960.
45. Kannel, W.B., T. Gordon, W.P. Castelli, and J.R. Margolis, Electrocardiographic left ventricular hypertrophy and risk of coronary heart disease. The Framingham study. *Ann. Int. Med.*, 1970;**72**: 813–822.
46. Cedres, B.L., K. Liu, J. Stamler, et al., Independent contribution of electrocardiographic abnormalities to risk of death from coronary heart disease, cardiovascular diseases and all causes. Findings of three Chicago epidemiological studies. *Circulation*, 1982;**65**: 146–153.
47. Walker, A.R.P. and B.F. Walker, The bearing of race, sex, age, and nutritional state on the precordial electrocardiograms of young South African Bantu and Caucasian subjects. *Am. Heart J.*, 1969;**77**: 441–459.
48. Gottschalk, C.W. and E. Craige, A comparison of the precordial S-T and T waves in the electrocardiograms of 600 healthy young negro and white adults. *South. Med. J.*, 1956;**49**: 453–457.
49. Beaglehole, R., H.A. Tyroler, J.C. Cassel, D.C. Deubner, A.G. Bartel, and C.G. Hames, An epidemiological study of left ventricular hypertrophy in the biracial population of Evans County, Georgia. *J. Chron. Dis.*, 1975;**28**: 549–559.
50. WHI MONICA Project, Myocardial infarction and coronary deaths in the World Health Organization MONICA Project. Registration procedures, event rates, and case-fatality rates in 38 populations from 21 countries in four continents. *Circulation*, 1994;**90**: 583–612.
51. Menotti, A. and H. Blackburn, Electrocardiographic predictors of coronary heart disease in the seven countries study, in *Prevention of Coronary Heart Disease. Diet, Lifestyle and Risk Factors in the Seven Countries Study*, D. Kromhout, A. Menotti, and H. Blackburn, Editors. Norwell, MA: Kluwer, 2002, pp. 199–211.
52. Menotti, A., H. Blackburn, D.R. Jacobs, et al., *The predictive value of resting electrocardiographic findings in cardiovascular disease-free men. Twenty-five-year follow-up in the Seven Countries Study*. Internal document, Division of Epidemiology, School of Public Health, University of Minnesota, 2001.
53. Menotti, A., F. Seccaraccia, and the RIFLE Research Group, Electrocardiographic Minnesota Code findings predicting short-term mortality in asymptomatic subjects. The Italian RIFLE Pooling Project (Risk Factors and Life Expectancy). *G. Ital. Cardiol.*, 1997;**27**: 40–49.
54. Cullen, K., N.S. Stenhouse, K.L. Wearne, and G.N. Cumpston, Electrocardiograms and 13 year cardiovascular mortality in Busselton study. *Br. Heart J.*, 1982;**47**: 209–212.
55. Sigurdson, E., M. Sigfusson, H. Sigvaldason, and G. Thorgeirsson, Silent ST-T changes in an epidemiologic cohort study – A marker of hypertension or coronary artery disease, or both: The Reykjavik study. *J. Am. Coll. Cardiol.*, 1996;**27**: 1140–1147.

56. Kannel, B.W. and R. Abbott, Incidence and prognosis of unrecognized myocardial infarction. An update on the Framingham study. *N. Engl. J. Med.*, 1984;**311**: 1144–1147.
57. Kannel, W.B. and R.A. Abbott, Prognostic comparison of asymptomatic left ventricular hypertrophy and unrecognized myocardial infarction: The Framingham Study. *Am. Heart J.*, 1986;**111**: 391–397.
58. Yano, K. and C.J. MacLean, The incidence and prognosis of unrecognized myocardial infarction in the Honolulu, Hawaii, Heart Program. *Arch. Intern. Med.*, 1989;**149**: 1526–1532.
59. Tervahauta, M., J. Pekkanen, S. Punsar, and A. Nissinen, Resting electrocardiographic abnormalities as predictors of coronary events and total mortality among elderly men. *Am. J. Med.*, 1996;**100**: 641–645.
60. Nadelmann, J., W.H. Frishman, W.L. Ooi, et al., Prevalence, incidence and prognosis of recognized and unrecognized myocardial infarction in persons aged 75 years or older: The Bronx Aging Study. *Am. J. Cardiol.*, 1990;**6**: 533–537.
61. Medalie, J.H. and U. Goldbourt, Unrecognized myocardial infarction: five-year incidence, mortality, and risk factors. *Ann. Intern. Med.*, 1976;**84**: 526–531.
62. The Coronary Drug Project Research Group, The prognostic importance of the electrocardiogram after myocardial infarction. Experience from the Coronary Drug Project. *Ann. Intern. Med.*, 1972;**77**: 677–679.
63. The MRFIT Research Group, Relationship between baseline risk factors and coronary heart disease and total mortality in the Multiple Risk Factor Intervention Trial. *Prev. Med.*, 1986;**15**: 254–273.
64. The Multiple Risk Factor Intervention Trial Research Group, Baseline rest electrocardiographic abnormalities, antihypertensive treatment and mortality in the Multiple Risk Factor Intervention Trial. *Am. J. Cardiol.*, 1985;**55**: 1–15.
65. Holme, I., A. Helgeland, I. Hjermann, P. Leren, and P.G. Lund-Larsen, Treatment of mild hypertensives with diuretics: the importance of ECG abnormalities in the Oslo Study and in MRFIT. *J. Am. Med. Assoc.*, 1984;**251**: 1298–1299.
66. The Hypertension Detection and Follow-up Program Cooperative Research Group, The effect of antihypertensive drug treatment on mortality in the presence of resting electrocardiographic abnormalities at baseline: the HDFP experience. *Circulation*, 1984;**70**: 996–1003.
67. The Multiple Risk Factor Intervention Trial Research Group, Exercise electrocardiogram and coronary heart disease mortality in the Multiple Risk Factor Intervention Trial. *Am. J. Cardiol.*, 1985;**55**: 16–24.
68. Rautaharju, P.M., R.J. Prineas, W.J. Eifler, C.D. Furberg, J.D. Neaton, R.S. Crow, J. Stamler, and J.A. Cutler for the Multiple Risk Factor Intervention Trial Research Group, Prognostic value of exercise ECG in men at high risk of future coronary heart disease. *J. Am. Coll. Cardiol.*, 1986;**8**(1): 1–10.
69. Rautaharju, P.M. and J.D. Neaton for, the MRFIT Research Group, Electrocardiographic abnormalities and coronary heart disease mortality among hypertensive men in the Multiple Risk Factor Intervention Trial. *Clin. Invest. Med.*, 1987;**10**: 606–615.
70. De Bacquer, D., G. De Backer, M. Kornitzer, and H. Blackburn, Prognostic value of ECG findings for total, cardiovascular disease, and coronary heart disease death in men and women. *Heart*, 1998;**80**: 570–577.
71. Dauerman, H.L., D. Lessard, J. Yarzebski, M.I. Furman, J.M. Gore, and R.J. Goldberg, Ten-year trends in the incidence, treatment, and outcome of Q-wave myocardial infarction. *Am. J. Cardiol.*, 2000;**86**: 730–735.
72. Rosenman, R.H., M. Friedman, C.D. Jenkins, R. Straus, M. Wurm, and R. Kosichek, Clinically unrecognized myocardial infarction in the Western Collaborative Group Study. *Am. J. Cardiol.*, 1967;**19**: 776–782.
73. Rautaharju, P.M., S.H. Zhou, and H.P. Calhoun, Ethnic differences in electrocardiographic amplitudes in North American white, black and hispanic men and women: effect of obesity and age. *J. Electrocardiol.*, 1994;**27**(Suppl): 20–30.
74. Strogatz, D.S., H.A. Tyroler, L.O. Watkins, and C.G. Hames, Electrocardiographic abnormalities and mortality among middle-aged black men and white men of Evans County, Georgia. *J. Chron. Dis.*, 1987;**40**: 149–155.
75. Arnett, D.K., D.S. Strogatz, S.A. Ephross, C.G. Hames, and H.A. Tyroler, Greater incidence of electrocardiographic left ventricular hypertrophy in black men than in white men in Evans County, Georgia. *Ethn. Dis.*, 1992;**2**: 10–17.
76. Arnett, D.K., P. Rautaharju, S. Sutherland, B. Usher, and J. Keil, Validity of electrocardiographic estimates of left ventricular hypertrophy and mass in African Americans (The Charlston Heart Study). *Am. J. Cardiol.*, 1997;**79**: 1289–1292.
77. Xie, X., K. Liu, J. Stamler, and R. Stamler, Ethnic differences in electrocardiographic left ventricular hypertrophy in young and middle-aged employed American men. *Am. J. Cardiol.*, 1994;**73**: 564–567.
78. Huston, S.L., C.H. Bunker, F.A.M. Ukoli, P.M. Rautaharju, and H.K. Lewis, Electrocardiographic left ventricular hypertrophy by five criteria among civil servants in Benin City, Nigeria: prevalence and correlates. *Int. J. Cardiol.*, 1999; **70**: 1–14.
79. Mosterd, A., R.B. D'Agostino, H. Silbershatz, P.A. Sytkowski, W.B. Kannel, D.E. Grobbee, and D. Levy, Trends in the prevalence of hypertension, antihypertensive therapy, and left ventricular hypertrophy from 1950 to 1989. *N. Engl. J. Med.*, 1999;**340**: 1221–1227.
80. Rautaharju P, Rautaharju F. *Investigative Electrocardiography in Epidemiological Studies and Clinical Trials*. Springer-Verlag London Limited, London, 2007, pp 1:289.
81. Liebson, P.R., G. Grandits, R. Prineas, S. Dianzumba, J.M. Flack, J.A. Cutler, R. Grimm, and J. Stamler, Echocardiographic correlates of left ventricular structure among 844 mildly hypertensive men and women in the Treatment of Mild Hypertension Study (TOMHS). *Circulation*, 1993;**87**: 476–486.
82. Okin, P.M., J. Sverker, R.B. Devereux, S.E. Kjeldsen, and B. Dahlof, Effect of obesity on electrocardiographic left ventricular hypertrophy in hypertensive patients: the Losartan Intervention for Endpoint (LIFE) Reduction in Hypertension Study. *Hypertension*, 2000;**35**: 13–18.
83. Lee, D.K., P.R. Marantz, R.B. Devereux, P. Kligfield, and M.H. Alderman, Left ventricular hypertrophy in black and white hypertensives. Standard electrocardiographic criteria overestimate racial differences in prevalence. *J.A.M.A.*, 1992;**267**: 3294–3299.
84. Rautaharju, P.M., L.P. Park, J.S. Gottdiener, D. Siscovick, R. Boineau, V. Smith, and N.R. Powe, Race-and sex-specific ECG models for left ventricular mass in older populations. Factors influencing overestimation of left ventricular hypertrophy prevalence by ECG criteria in African-Americans. *J. Electrocardiol.*, 2000;**33**: 205–218.

85. Rautaharju, P.M., T.A. Manolio, D. Siscovick, S.H. Zhou, J.M. Gardin, R. Kronmal, C.D. Furberg, N.O. Borhani, and A. Newman, for the Cardiovascular Health Study Collaborative Research Group. Utility of new electrocardiographic models for left ventricular mass in older adults. *Hypertension*, 1996;**28**: 8–15.
86. Levy, D., K.M. Anderson, D.D. Savage, W.B. Kannel, J.C. Christiansen, and W.P. Castelli, Echocardiographically detected left ventricular hypertrophy: prevalence and risk factors. The Framingham study. *Ann. Intern. Med.*, 1988;**108**: 7–13.
87. Verdecchia, P., G. Schillaci, C. Borgioni, A. Ciucci, R. Gattobigio, I. Zampi, G. Reboldi, and C. Porcellati, Prognostic significance of serial changes in left ventricular mass in essential hypertension. *Circulation*, 1998;**97**: 48–54.
88. Schillaci, G., P. Verdecchia, Borgioni, A. Ciucci, M. Guerrieri, I. Zampi, M. Battistelli, C. Bartoccini, and C. Porcellati, Improved electrocardiographic diagnosis of left ventricular hypertrophy. *Am. J. Cardiol.*, 1994;**74**: 714–719.
89. Rautaharju, P.M., J. Warren, R.J. Prineas, and P.h. Smets, Optimal coding of electrocardiograms for epidemiological studies. The performance of human coders – a statistical model. *J. Electrocardiol.*, 1979;**13**: 55–59.
90. Kahn, S., W.H. Frishman, S. Weissman, W.L. Ooi, and M. Aronson, Left ventricular hypertrophy on electrocardiogram: prognostic implications from a 10-year cohort study of older subjects: a report from the Bronx longitudinal aging study. *J. Am. Geriatr. Soc.*, 1996;**44**: 524–529.
91. Larsen, C.T., J. Dahlin, H. Blackburn, H. Scharling, M. Appleyard, B. Sigurd, and P. Schnohr, Prevalence and prognosis of electrocardiographic left ventricular hypertrophy, ST segment depression and negative T-wave. *Eur. Heart J.*, 2002;**23**: 315–324.
92. Rautaharju, P.M., A.Z. LaCroix, D.D. Savage, S. Haynes, J.H. Madans, H.K. Wolf, W. Hadden, J. Keller, and J. Cornoni-Huntly, Electrocardiographic estimate of left ventricular mass vs. Radiographic cardiac size and the risk of cardiovascular disease mortality in the epidemiologic follow-up study of the First National Health and Nutrition Examination Survey. *Am. J. Cardiol.*, 1988;**62**: 59–66.
93. Levy, D., M. Salomon, R.B. D'Agostino, A.J. Belanger, and W.B. Kannel, Prognostic implications of baseline electrocardiographic features and their serial changes in subjects with left ventricular hypertrophy. *Circulation*, 1994;**90**: 1786–1793.
94. Mathewson, F.A.L., J. Manfreda, R.B. Tate, and T. Cuddy, The University of Manitoba Follow-up Study-an investigation of cardiovascular disease with 35 years of follow-up (1948–1983). *Can. J. Cardiol.*, 1987;**3**: 378–382.
95. Rautaharju, P.M., C. Kooperberg, J.C. Larson, and A. LaCroix, Electrocardiographic abnormalities that predict coronary heart disease events and Mortality in Postmenopausal Women. The Women's Health Initiative. *Circulation*, 2006;**113**: 473–480.
96. Rautaharju, P.M., C. Kooperberg, J.C. Larson, and A. LaCroix, Electrocardiographic Predictors of Incident Congestive Heart Failure and All-cause Mortality in Postmenopausal Women. The Women's Health Initiative. *Circulation*, 2006;**113**: 481–489.
97. Zile, M.R. and D.L. Brutsaert, New concepts in diastolic dysfunction and diastolic heart failure: Part I: diagnosis, prognosis, and measurements of diastolic function. *Circulation*, 2002;**105**: 1387–1393.
98. Zile, M.R. and D.L. Brutsaert, New concepts in diastolic dysfunction and diastolic heart failure: Part II: causal mechanisms and treatment. *Circulation*, 2002;**105**: 1503–1508.
99. Kitzman, D.W., J.M. Gardin, J.S. Gottdiener, A. Arnold, R. Boineau, G. Aurigemma, E.K. Marino, M. Lyles, M. Cushman, and P.L. Enright, Importance of heart failure with preserved systolic function in patients ≥65 years of age. CHS Research Group. Cardiovascular Health Study. *Am. J. Cardiol.*, 2001;**87**: 413–419.
100. Rautaharju, P.M., S.G. Ge, J. Clark Nelson, E.K. Marino Larsen, B.M. Psaty, C.D. Furberg, Z.M. Zhang, J.A. Robbins, MD, MHS, J.S. Gottdiener, MD, and P. Chaves, Comparison of Mortality risk for Electrocardiographic Abnormalities in Men and Women With and Without Coronary Heart Disease (From the Cardiovascular Health Study). *Am. J. Cardiol.*, 2006;**97**: 309–315.

41 The Dog Electrocardiogram: A Critical Review

David K. Detweiler[†]

[†]For this 2nd Edition of "Comprehensive Electrocardiology," Dr. Sydney Moise has updated this 1st Edition chapter, which was originally written by the late Dr. Detweiler.

P. W. Macfarlane, A. van Oosterom, O. Pahlm, P. Kligfield, M. Janse, J. Camm (eds.), *Comprehensive Electrocardiology*, DOI 10.1007/978-1-84882-046-3_41,

41.1 History and Literature

Electrocardiographic studies in dogs date back to the pioneering investigations of Augustus Waller [1] with the capillary electrometer and Willem Einthoven's development of the string galvanometer electrocardiograph [2–4]. As late as 1914 [5], Waller considered electrocardiography (ECG) as an experimental method, useful to physiologists rather than as a clinical tool for physicians. However, clinical application in man had already started and advanced rapidly (Lewis, 1909–1925 [6]; Rothberger, 1912–1930 [7]; Winterberg, 1912–1930 [9]; Scherf, 1921–present [8]; Wenckebach, 1899–1930 [9]; and Wilson, 1919–1945 [10]). Clinical use in canine medicine was modest in those early days (Nörr, 1913–1931 [11]; Roos, 1925 [12]; Haupt, 1929 [13]; Ludwig, 1924 [14]; and Gyarmati, 1939 [15]) and subsequently, until Nils Lannek's systematic study and statistical analysis of clinical records from healthy and diseased dogs [16]. Lannek also introduced a precordial-lead system that is still in use. Scherf and Schott's encyclopedic monograph, *Extrasystoles and Allied Arrhythmias* [8], reviews much of the electrocardiographic literature on experimental cardiac arrhythmias and drug effects in dogs. Burch and DePasquale's *A History of Electrocardiography* [17], Sir Thomas Lewis's classical *The Mechanism and Graphic Registration of the Heart Beat* [6], and Wilson's collected works (edited by Johnston and Lepeschkin [10]) are rich sources of information on earlier canine studies.

Modern imaging of the heart with echocardiography, angiography, magnetic resonance imaging (MRI), endocardial mapping, computer-assisted tomography (CT) and other modalities potentially provides more valuable information of the structure, function, and electrical competency than the routine surface electrocardiogram. However, the ECG is the mainstay for the diagnosis of arrhythmias in all animals. In the complete diagnosis of disease, the ECG must be supplemented with other technologies. The ECG remains a cornerstone for the initial screening and recognition of disease. Moreover, in pharmacological studies, the dog remains a key animal of study for which the review of ECG changes for the treatment effect or toxicity involves routine examinations.

Besides the routine analysis of the ECG in the dog, more thorough approaches to the clues of the disease, drug effect, or toxicity that the ECG offers are in use today. These include 24-h ambulatory ECG monitoring (Holter monitoring), telemetry recordings via implantable recording devices, loop-recording devices to capture arrhythmias, and heart rate variability.

41.1.1 Canine Electrocardiography

An enormous amount of literature has been published on experimental electrocardiographic studies in dogs. Historical and useful reviews are found in textbooks and monographs on arrhythmias and conduction disorders such as Bellet [18, 19], Scherf and Schott [8], and Schamroth [20]. Normal values for dog ECGs have been summarized in several textbooks (Ettinger and Suter [21], Detweiler et al. [22], Bolton [23], and Tilley [24]). In early papers and textbooks, generalized statements were frequently made with regard to the interpretation of ECG measurements to heart size based on the amplitude and duration of a specific waveform. Today, we recognize that some of these conclusions were too specific because of breed, age, and body conformation. Some examples will be addressed in the following discussions on the ECG waveforms.

41.1.2 Beagle Electrocardiogram

The ECG of the beagle is of special interest because of its widespread use as a research animal [25]. The published normal values for the ECG waveforms with regard to time and amplitude serve as a guideline to the evaluation of the ECG for the beagle. Table 41.1 lists findings that are commonly found when evaluating the electrocardiogram of the research beagle.

Table 41.1

Electrocardiographic findings of the research beagle that are not within the usual normal range for dogs and that are not likely pathologic[a]

Number	Electrocardiographic finding	Comments	Level of concern for use of dog in cardiovascular studies
1	Deep (not wide) S waves in lead III (1.0 mV > S wave > 0.7 mV)	Common singular finding without known association to structural or electrical abnormality	Low
2	Deep (not wide) S waves in lead III (S wave ⩾ 1 mV) only	Less common than #1. May be an insignificant finding	Low-medium
3	Deep (not wide) S waves in leads II, III, and aVF (0.5 mV > S wave > 0.3 mV in lead II, 1 mV > S wave > 0.5 mV in lead III, and 1 mV ⩾ S wave > 0.5 mV in lead III)	Common cluster finding without known association to structural or electrical abnormality or may be associated with right ventricular enlargement, incomplete right bundle branch block, or left anterior fascicular block	Medium
4	Very deep (not wide) S waves in II, III, and aVF (S wave > 0.5 mV in lead II, S wave > 1 mV in lead III, and S wave > 1 mV in lead III)	Much less common cluster finding without known association to structural or electrical abnormality but more likely than #3 to be associated with right ventricular enlargement, incomplete right bundle branch block, or left anterior fascicular block	High
5	T_a wave (Tsub "a" wave)	Occasionally seen. A negative deflection immediately following the P wave. Indicates the T wave of the P wave (repolarization of the atria)	None unless associated with large P wave
6	Tall (not wide) R wave (3.5 mV > R wave > 3.0 mV)	Common. Mild elevation in the amplitude of the R wave is usually not associated with structural or functional abnormality, but could indicate left ventricular hypertrophy	Low
7	Very tall (not wide) R waves (R wave > 3.5 mV)	Less common than #6. Moderate elevation in the amplitude may still not be associated with structural or functional abnormality, but more likely to be associated with left ventricular hypertrophy than #6	Medium
8	Splintered or notched QRS complex	Occasionally seen. The appearance of this finding can be affected by the filter settings of the ECG recording device. Splintered R waves are associated with tricuspid dysplasia in the dog, but this congenital anomaly has not been reported in the beagle	Low, but if marked could affect ease of interpretation
9	Low amplitude QRS complex (QRS complex < 0.7 mV)	Occasionally seen. Although low R waves are reported for a variety of conditions (e.g., pericardial effusion, ascites, pleural effusion, obesity, hypothyroidism, pulmonary embolism) in the beagle this is seen with a normal heart	Low
10	Deep Q waves (Q wave > 1.2 mV)	Common. May be a singular finding or with a tall or very tall R wave. Can be a normal variation or indicative of septal hypertrophy or right ventricular hypertrophy	Low as a singular finding
11	Large T wave (>25% of the R wave)	Occasionally seen as a singular finding. May be present with tall and very tall R wave. In the latter situations the T wave is large as a negative deflection	Low as a singular finding

Table 41.1 (Continued)

Number	Electrocardiographic finding	Comments	Level of concern for use of dog in cardiovascular studies
12	Second-degree heart block (low grade with only single P waves not associated with QRS complex)	Occasionally seen in dogs more than 4 months of age. Common in dogs less than 2 months of age. In these situations usually not associated with disease, but with high vagal tone	Low as a singular finding, but most investigators do not want dogs with this finding[b]
13	Sinus bradycardia or long sinus pauses (heart rate < 60 bpm, PP interval > 1.5 s)	Occasionally seen. Dogs bred for calm personality tend to have slower heart rates due to higher vagal tone and less sympathetic tone. Many of these dogs have heart rates that approach the lower limit of 60 bpm	Low to medium depending on the degree of the bradycardia and the length of the sinus pause. Extreme bradycardia or pauses would have a high concern
14	Presence of a J wave. The J wave is a positive deflection at the very terminal point of the downstroke of the R wave. It may be a complete secondary positive deflection with amplitudes of 0.2 mV or just a widening of the R wave usually beginning at the amplitude of 0.1–0.2 mV	Common finding and is due to the current density of I_{to}. Seen in other breeds too	None, but in some cases can make the determination of the QRS duration problematic because the end of the QRS is difficult to determine Some include this wave in the duration of the QRS

[a]This table is not a listing of electrocardiographic abnormalities per se, but is a listing of findings often found in the beagles that usually are not associated with pathology. However, as described, the findings may be associated with an abnormality although frequently they are not
[b]In 2,232 beagles on which two 1-min recordings were taken was about 1% [26], while that in 11 resting dogs monitored for about 6 h by radiotelemetry was about 64%. This figure increased to 100% in 12 puppies, 8–11 weeks old [47]

41.2 Recording Techniques

41.2.1 Lead Systems

A variety of lead systems has been used for decades in the dog. Most commonly used is the six-lead limb system which includes leads I, II, III, aVR, aVL, and aVF. However, the addition of other leads may be beneficial for some studies.

Historically, Waller [1] initiated the limb-lead system of recording from dogs when he taught his pet bulldog "Jimmie" to stand in beakers filled with a conducting solution into each of which an electrode was fixed (Fig. 41.1). In Waller's earliest experiments, wires connected these electrodes to the capillary manometer (Fig. 41.2). This method of recording was also used with other species including humans and anticipated the technique that Einthoven adopted for his string galvanometer.

Because of the offset potentials generated at the metal–skin surface interface, nonpolarizable electrode systems were required with the capillary electrometer and the early string galvanometers of the Einthoven type. This was accomplished by immersing the limb in a bath containing a salt of the metal used in the electrode; for example, silver chloride solution with silver electrodes or zinc chloride with zinc or nickel silver (German silver, a silver white alloy of copper, zinc, and nickel) electrodes. Soon, the bath was replaced by cloth strips that were saturated with the solution and wrapped about the limb to form contact between the electrode and the skin. Later, the material was replaced by conducting electrolyte pastes and gels placed between the skin and the electrodes. In animals, a variety of needle and clip electrodes was used to fix the leads firmly in place despite inadvertent movement of the subjects.

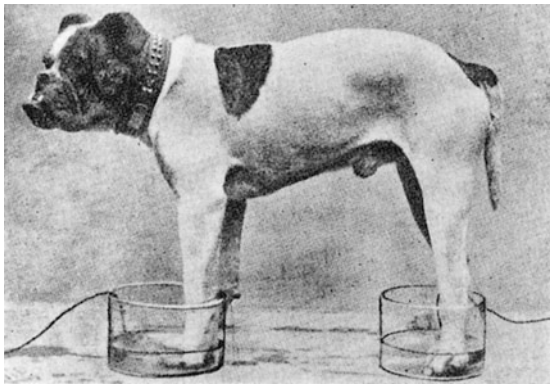

Figure 41.1

Waller's pet dog "Jimmie" patiently standing with his left foreleg and connected by wires to an electrometer. (A. Waller. *Physiology, the Servant*. London Press/Hodder & Stoughton, London, 1888. Reproduced with permission.)

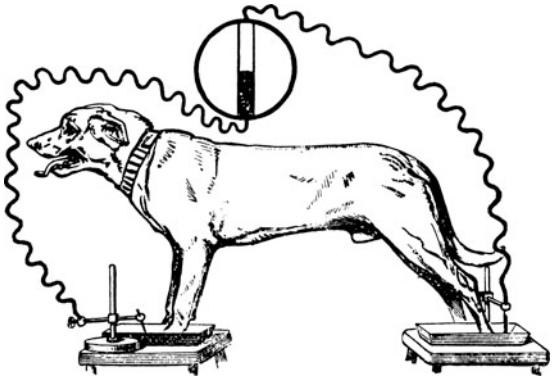

Figure 41.2

Probably the first picture of an ECG being recorded from a dog. The instrument is a capillary electrometer. The line drawing depicts a dog standing with the left foreleg and hindleg in pans of saline solution and wires leading from electrodes immersed in the solution to a schema of the electrometer. (Waller [1]. © British Medical Association, London. Reproduced with permission.)

The idea prevailed for some years [13, 26] that a bipolar lead along the imaginary anatomical longitudinal axis of the heart would be best for animals. A single lead with one electrode attached to the left precordium over the cardiac apex and the other electrode attached over the base of the heart at the junction of the neck and thorax, the scapular spine, or anterodorsal edge of the scapula on the right side, became popular. It was not realized that this was essentially a precordial lead with a neck or scapular electrode acting more or less as the indifferent electrode. A later modification of this was a three-lead triangular system similar to that of Nehb [27] with the three limb electrodes placed at the cardiac apex (left leg [LF] electrode), the base of the neck (anterodorsal edge of the scapula) on the right side (right arm [RA] electrode), and the sacral region (left arm [LA] electrode). The leads thus obtained are termed dorsal (RA to LA), axial (RA to LF), and inferior (LA to LF) [28]. This system never gained popularity in the dog, but has been used more often in large farm animals and the laboratory rat [29].

Lannek [16] developed a precordial-lead system that has been used in the dog. This system utilized anatomical criteria to position one electrode over the right ventricle and two electrodes over the left ventricle. In taking these precordial leads, he paired the exploring electrode with the right foreleg electrode and used the symbol CR for these chest leads.

Wilson's central terminal soon replaced the right leg as the indifferent electrode and by early 1960, Hamlin [30] initiated the use of a lead corresponding to V_{10} in man to the chest leads for the dog. V_{10} is uncommonly used today.

The original lead symbols introduced by Lannek were CR_5RL, CR_6LL, and CR_6LU. With the introduction of Wilson's central terminal, these symbols were changed to CV_5RL, CV_6LL, and CV_6LU. In 1977, the Committee of the American Academy of Veterinary Cardiology introduced new lead symbols [31] similar to those used for man. Although these electrode positions in the dog roughly approximate, they do not correspond, accurately, to the identically named lead positions in man. Both nomenclatures are given here. The electrode positions for each lead are as follows:

(a) V_2 (CV_6LL): sixth left intercostal space near the edge of the sternum at the most curved part of the costal cartilage
(b) V_4 (CV_6LU): sixth left intercostal space at the costochondral junction
(c) V_{10}: over the dorsal spinous process of the seventh thoracic vertebra (on the dorsal midline vertically above the V_4 position)
(d) rV_2 (CV_5RL): fifth right intercostal space near the edge of the sternum at the most rounded part of the costal cartilage

The abbreviations in the parentheses are the terms originally used by Lannek [16] to designate these electrode positions. The terminology and corresponding equivalent in humans has been questioned [32]. The conformation of the thorax of the dog is dissimilar to humans. Thus, the positioning of the leads at the same points on the thorax does not correspond exactly to that of the humans. Also, the location and effect of the diaphragm on cardiac position is different between the two species. Importantly, the morphology of the thorax varies greatly amongst different somatotypic breeds of dogs, such that even within the canine species, variability must be expected when trying to make anatomical comparisons to the location and direction of the electrical depolarization. Moreover, consistent positioning of these leads and additional precordial leads (V_1, $V_{2,}$, V_3, V_4, V_5, and V_6) is critical for an acceptable amount of variability between recordings.

Three-lead (X, Y, and Z)-corrected orthogonal systems such as those of McFee and Parungao [33] (Fig. 41.3) and Frank [34, 35] (Fig. 41.4) have been used historically for vectorcardiography. Vectorcardiography has been replaced by more sophisticated means of electrical mapping of the heart. Such systems are beyond the scope of this review. The X-, Y-, and Z-lead system has been used extensively in the Holter Laboratory of Cornell University, College of Veterinary Medicine. Such a system typically provides excellent recordings for analysis in the dog.

A more complex lead system is used in Japan [37]. Takahashi [38], on the basis of experimental studies in the dog, introduced an elaborate 12-lead precordial system with 6 leads on each side of the thorax as follows (Fig. 41.5): C_1, C_2, and C_3 at the left costochondral junction anterior to rib one and at the second and fifth intercostal space, respectively; C_4, C_5, and C_6 at the right costochondral junctions in the seventh, fifth, and third intercostal spaces, respectively; M_1, M_2 at the widest portion of the thorax in the third and sixth left intercostal spaces, respectively; M3 at the left of the xiphoid process; M_4 at the right of the xiphoid process; and M_5, M_6 at the widest portion of the thorax in the right seventh and third intercostal spaces, respectively.

In 1966, the Japanese Association of Animal Electrocardiography recommended a bipolar base-apex (termed A-B) lead similar to that recommended in 1929 by Haupt [13], one of Nörr's [11] pupils, for use in dogs. The positive electrode (A) is placed at the costochondral junction of the left sixth rib and the negative electrode at the right scapular spine (Japanese Association of Animal Electrocardiography, 1975) [36]. In addition, they recommend the use of the Takahashi precordial leads $C_1 - C_6$, M_1, and M_6.

In summary, although multiple lead systems have been proposed, the most common one used for the evaluation of the electrical activity of the dog is the six-lead limb system. Importantly, in modern times, a critical evaluation demanded in pharmacological studies is the evaluation of the QT interval. Most of time and amplitude measurements are done in lead II; however, in approximately 10–20% of the canine recordings, the clarity of the T wave and particularly the offset point is not clear in lead II or other limb leads. In such situations, other leads may be better suited to more definitively make the QT interval measurement (see below).

41.2.2 Position and Restraint

In quadrupeds, the magnitude and direction of electrocardiographic vectors determined from limb leads can be vastly altered by changes in the position of the muscular attachments of the shoulder girdle to the thorax (Fig. 41.6).

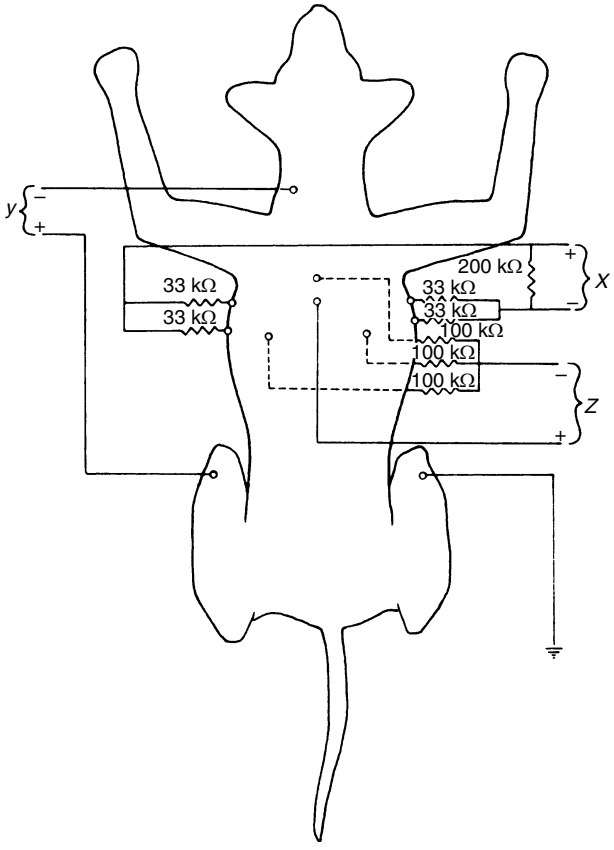

Figure 41.3

The corrected orthogonal-lead system designed for the canine thorax by McFee and Parungao [33]. Electrode placement for transverse (*X*), longitudinal (*Y*), and sagittal (*Z*) axis leads. Viewed from the dorsal aspect of the dog. Note that the Z+ electrode is on the back of the dog. (After Chastain et al. [83]. ©American Veterinary Medical Association, Schaumburg, Illinois. Reproduced with permission.)

Thus consistent positioning of the forelimbs, and especially the scapulae, is crucial to obtaining reproducible vectors in serial ECGs. This was not known until the early 1950s, while Lannek [16] reported that in dogs, the mean manifest QRS vector in the frontal plane could be highly variable. This finding was later confirmed independently by Cagan et al. [39, 40], Hulin and Rippa [41], and was studied systematically by Hill [42, 43]. The following technique is recommended: The dog is placed in right lateral recumbency. The head and neck are held flat on the table in line with the long axis of the trunk. The forelegs are positioned parallel to one another and perpendicular to the long axis of the body so that the point of the left shoulder (anterior aspect of the scapulohumeral joint) is vertically above the point of the right shoulder. The complexes in lead aVL are often those most sensitive to changes in foreleg position. Therefore, in serial records, complexes in lead aVL can be compared to verify the consistency in foreleg positioning.

To restrain the dogs on a table, the handler should face the right side of the standing animal with its head to his right side, reach over the animal's back, grasp the forelegs in his right hand and the hind legs in his left hand. The dog is then laid on its right side, the head and neck pressed flat against the table with the right forearm, and its back restrained against the handler's body. The technician operating the electrocardiograph then attaches the electrodes and arranges the forelimbs and head and neck as described. The handlers must avoid touching moist surfaces or electrodes in case AC interference is introduced.

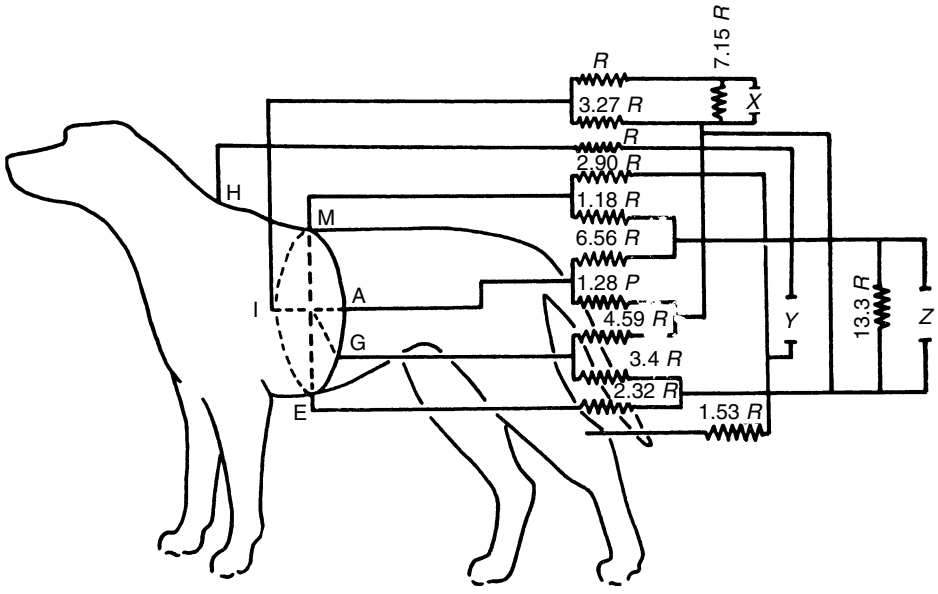

Figure 41.4

Frank's orthogonal-lead system applied to the dog. $R = 100,000\Omega$. (After Bojrab et al. [35]. © American Veterinary Medical Association, Schaumburg, Illinois. Reproduced with permission.)

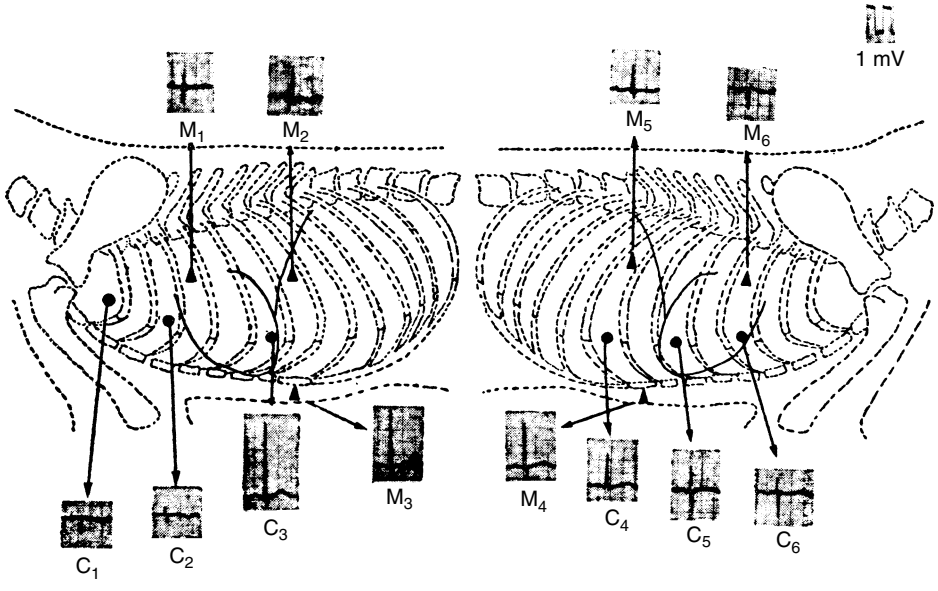

Figure 41.5

The precordial-lead system proposed by Takahashi for clinical use. (After Takahashi [38]. Society of Veterinary Science, Tokyo. Reproduced with permission.)

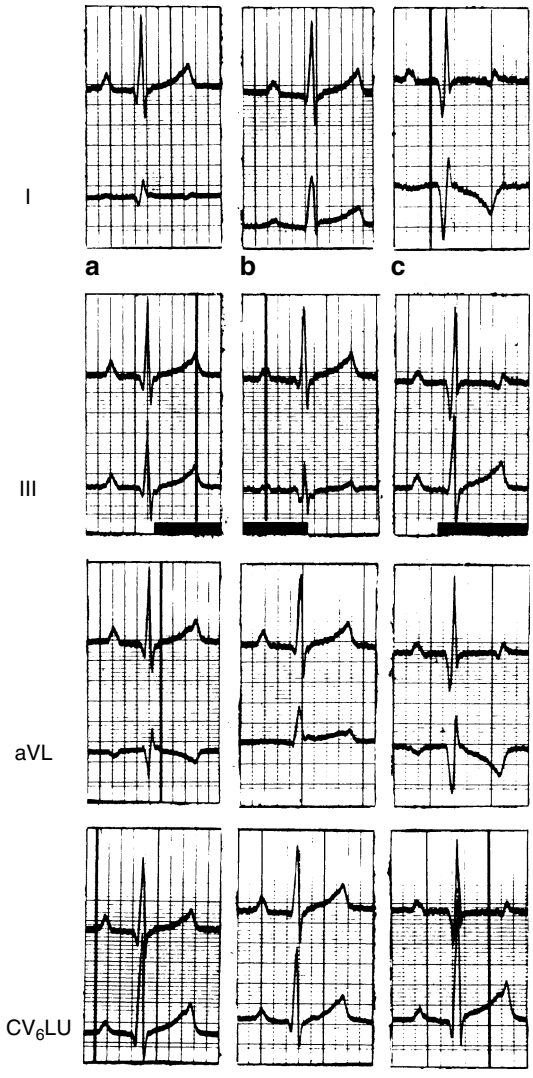

Figure 41.6

The effect of foreleg position on the ECG. The upper tracing in each recording is lead II. The dog was positioned in right lateral recumbency. In column (a) the forelegs are parallel and at right angles to the long axis of the body. In column (b) the right foreleg is pulled forward and the left foreleg pulled backward. In column (c) the right foreleg is pulled backward and the left forward. Note the dramatic alterations in the QRS complexes and T waves in leads I, III, and aVL that falsely suggest changes in ventricular excitation and recovery pathways. See also Table 41.5.

41.2.3 Electrodes

From the standpoint of their electrical characteristics, plate electrodes are superior to electronic alligator clips, while needle electrodes are unacceptable for use in conscious dogs [44]. Electronic alligator clips are recommended, however, because their somewhat inferior electrical characteristics compared to those of plate electrodes are offset by their convenience in application and their tendency to remain in place when dogs struggle. They must all be of the same metal (copper is preferred) to avoid offset voltages that can cause baseline instability. The serrations on the jaws should be flattened to reduce discomfort and maximize the area of contact with the skin. The contact area (including both jaws of the clip)

should be approximately 1.0 cm^2. The skin and hair under the electrodes are saturated with a conductive gel or solution. The site of foreleg attachment must be well below the ventral thoracic surface (e.g., halfway between the olecranon and carpus) to avoid the influence of precordial potentials.

41.2.4 Duration of Recording

It is generally possible to restrain untrained and unsedated dogs in the recommended recording position (right lateral recumbency) for about 1 min before struggling becomes excessive. Electronic ECG systems are available now that have enhanced the ability to keep recording until the dog is relaxed. Such systems also allow the electronic storage of the ECG. Because arrhythmias are sporadic events, if it is required to compare arrhythmia prevalence rates in groups such as in the chronic toxicity testing, the duration of recording should be the same in each individual dog and a standard recording time of 1 min has been proposed for such studies [26]. However, it must be emphasized that such a duration actually evaluates less than 0.1% of the QRS complexes that a dog has in 24 h. Most normal beagles have approximately 150,000–175,000 beats in 24 h, and realizing that a 1-min recording only documents approximately 75–100 of these beats gives a perspective for conclusions.

As is well known, for the comparison of the incidence of cardiac arrhythmias, 24-h monitoring of the ECG (Holter monitoring) is optimal [45–47]. In veterinary practice, Holter monitoring is commonly performed. Despite its common use clinically, an appreciation of the need for validation of the accuracy is lacking. When arrhythmias are infrequent, the accuracy of modern analyzing systems is acceptable. However, when complex, frequent, and rapid arrhythmias are present, the accuracy of the analysis suffers. Importantly, quality control and validation of the accuracy of the reports is required, yet few labs have such oversight for canine recordings. Consequently, if Holter monitoring is required for studies, confirmation of high standards in the evaluation of the recordings should be sought.

41.2.5 Artifacts

Since the occurrence of artifacts (see reference [26] for a description of common artifacts) is nearly universal in dog ECGs, they must be identified as such in screening for abnormalities. The most common artifacts that cause problems in diagnosis are:

(a) Skeletal muscle movements
(b) Baseline drift (including oscillations associated with normal breathing and with panting)
(c) Fifty- or 60-Hz electrical inference (Fig. 41.7)

Somatic muscle artifacts appear in most ECGs taken from unanesthetized dogs. Three general types may be recognized:

(a) *Somatic muscle tremor*. The frequency of skeletal muscle tremor artifact is irregular, ranging from about 15 to 35 Hz. Often a constant baseline "jiggle" is caused in long stretches of the record. Typically, such trembling intensifies on inspiration and diminishes on expiration so that it may wax and wane, or appear and disappear periodically.
(b) *Intermediate frequency somatic muscle artifacts*. These are caused by more sporadic muscle twitching that are discontinuous and occur at a frequency of about 1–15 Hz in tense subjects. Their amplitude is generally from 0.1 to 0.5 mV. These artifacts are likely to distort electrocardiographic complexes and may mimic the morphology of P waves.
(c) *Gross muscle movement artifact*. High-amplitude deflections with rapid voltage change (high Vmax) may resemble bizarre QRS complexes and mimic ventricular ectopic beats, or when rapid, paroxysmal ventricular tachycardia. Their amplitudes are often from 1.0 to 5.0 mV or greater and may exceed the excursion limit of the electrocardiographic stylus. Rhythmic tail wagging sometimes transmits movement to electrode–skin–surface interfaces, mimicking a run of ventricular tachycardia (VT), while panting can cause baseline oscillations with the frequency and amplitude of those seen in atrial flutter or atrial fibrillation.

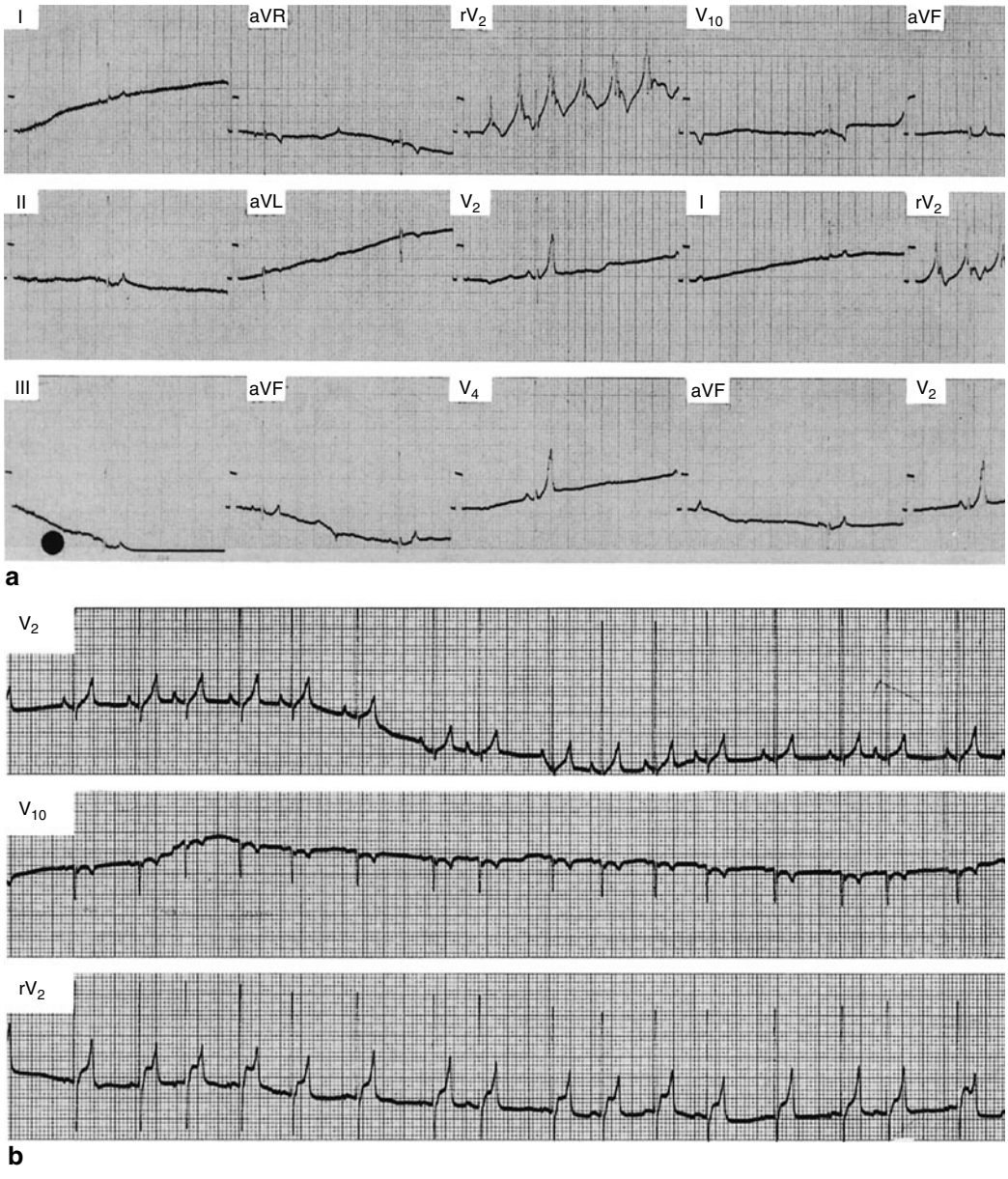

Figure 41.7

The ECG in (a) illustrates several artifacts caused by skeletal muscle movement in dogs. Five sets of three leads, each are recorded automatically in each of four 2.6-s panels. Baseline drift is present in all panels. Muscle tremor artifact at 30–35 Hz and intermediate frequency muscle movement artifact at a frequency of about 15 Hz are present in the limb leads. "Tail-wag" artifact simulates paroxysmal ventricular rhythm in lead rV_2; this is caused by the movement of the rV_2 electrode (which is situated between the right thorax wall and the table surface) as the chest is moved synchronously with the wagging tail. The R wave in lead V_2 in the third panel from the left is clipped. In (b), the rV_2 lead illustrates simulated ST-segment elevation caused by the apex beat artifact in which the thrust of the heart against the chest wall at the fifth right intercostal space moves the electrode. Note the variability in the ST-segment elevation and contour.

Artifacts present should be identified and the records examined more closely if they:

(a) Resemble electrocardiographic abnormalities
(b) Interfere with interval measurement
(c) Distort many complexes

41.3 The Normal Electrocardiogram

41.3.1 Values

The chief sources summarizing normal values are Lannek [16], Grauwiler [48], Hill [42, 43], Ettinger and Suter [21], Bolton [23], Hahn et al. [31], Tilley [24], and Detweiler [25]. A representative normal ECG is shown in Fig. 41.8. It should be emphasized that there is breed variability in the normal values for the dog. Most dogs "fit" within the "established normals"; however, some breeds have their own particular standard. For example, giant large-boned dogs with a somatotype similar to a Saint Bernard will have R waves of lower amplitude than dogs of similar weight such as a Great Dane. Also, dogs such as the Saint Bernard can have P waves with a duration that exceeds the "usual" standard in most breeds. Most research dogs are beagles; however, in recent years, pharmaceutical and device companies have requested larger mongrels. Obviously, this stresses the importance of pretrial electrocardiographic recordings for comparisons to be made.

Importantly, it should be stated that although most of the differences in the ECG discussed are the result of the conformation of the dog, there are likely differences in the current density of certain ion channels amongst breeds, particularly those of repolarization.

41.3.1.1 Amplitude

Because foreleg position affects limb-lead potentials, the limb-lead data from Hill [42], who standardized foreleg position, are given in Tables 41.2 and 41.3.

41.3.1.2 Intervals

Representative lead II time intervals are 0.03–0.06 s for P, 0.06–0.14 s for PR, 0.03–0.07 s for QRS, and 0.15–0.23 s for QT, all at heart rate 60–180 bpm [23, 26, 33]. In Table 41.4, the available regression formulae are given, and Table 41.5 relates PR and QT intervals and heart rate in beagles. The values represented by these three sources do not agree, probably because the authors used different criteria to determine where the time intervals begin and end.

Today the ECG measurement that garnishes the greatest attention is the QT interval. This duration measured from the first depolarization deflection to the end of the T wave must be considered in the context of heart rate. Thus, the QT interval is often corrected using formulas. The Bazett formula [49] has historically been the one most commonly used across species, although a variety of others have also been proposed [50–57]. However, the limitations and inaccuracies of this formula should be stressed. The Bazett formula was specifically developed by Bazett to correct for the influence of heart rate under specific conditions. Unfortunately, for decades, his original work was applied widely across species and conditions that were not in the original intent for heart rate correction of the QT interval. The majority of formulas either over or under correct the QT interval depending on the rate. This problem has been addressed with a proposal to specifically adjust the QT to the HR [50–57]. The latter is the only one of many proposals for the evaluation of the QT interval. Because the accurate interpretation of the QT interval is imperative to the evaluation of drugs, international conferences have been held to address the proper approach in the pharmacological evaluations of drugs.

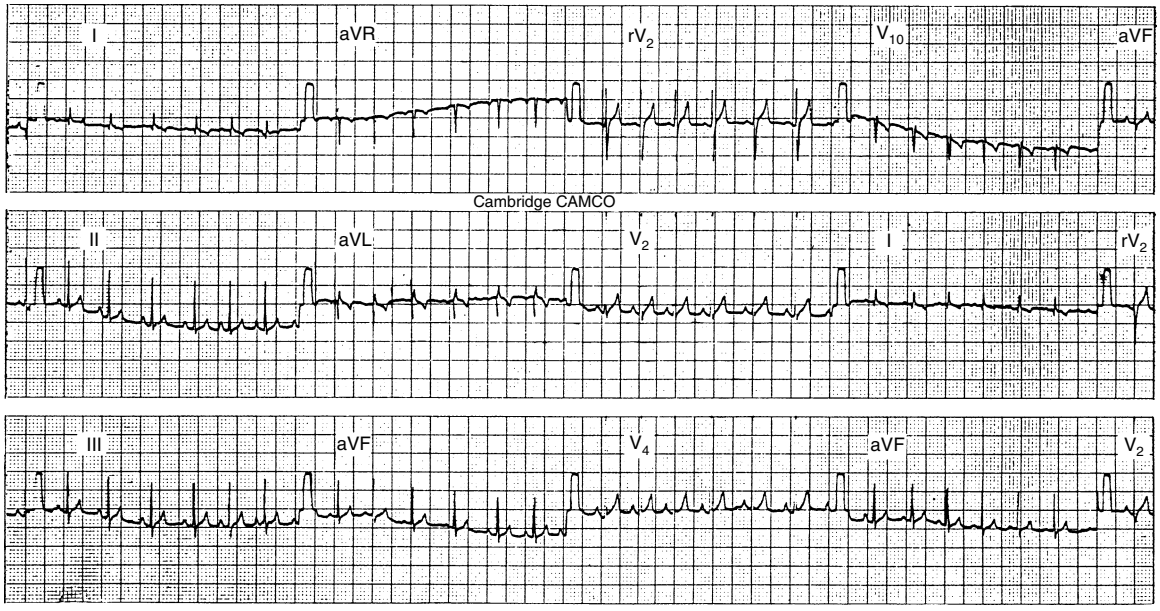

Figure 41.8

A ten-lead ECG from an 8-month-old male beagle recorded with the dog in right lateral recumbency with the forelegs held parallel and at a right angle to the long axis of the body. The recording format for each 2.8-s panel separated by 1.0 mV = 10 divisions sensitivity standardization signal is shown. Panel 5 is the beginning of a rhythm strip of 48-s duration to complete a standard (approximately) 1-min recording interval, which is the duration recommended for routine ECGs taken on groups of dogs in toxicological studies. Note that the R waves in leads V2 and V4 are clipped (by 0.2 mV for lead V2), because the true amplitude determined when the baseline was adjusted exceeds the maximum positive excursion of the stylus. Because such clipping often goes unnoticed, the true amplitude of R waves in these leads frequently present in young dogs (sometimes exceeding 6.0 mV) has been underestimated in the literature except by Lannek [16], who recorded at half sensitivity (10 divisions = 2.0 mV). The T-wave polarity in the dog changes with body position and age in addition to physiologic, pharmacologic, and pathaologic alterations. See also Fig. 35.7.

41.3.2 P-Wave Amplitude and Configuration

The form and amplitude of P waves are more variable in canines than in most other animals. The variability is generally far more pronounced in limb leads than in the conventional thoracic leads (rV_2, V_2, V_4, and V_{10}), where it may be minimal or absent. When the P wave varies in association with respiration (RR interval), it is referred to as a "wandering pacemaker." The P wave also may vary within a dog during serial recordings. The P-wave amplitude can change quickly with changes in heart rate. The faster the heart rate, the taller the P wave. The T wave also changes with heart rate. Both are related to the changes in parasympathetic/sympathetic tone.

41.3.2.1 Wandering Pacemaker

As the heart rate speeds and slows with respiratory sinus arrhythmia, there are cyclic P-wave changes, both in form and amplitude. These are most pronounced in the limb leads in which the P waves are usually of greatest amplitude (e.g., II, III, and aVF). Ordinarily, there is no change in the PR interval, except when the initial part of the P wave becomes isoelectric, or having been isoelectric, becomes positive or negative.

Table 41.2

The amplitude of positive and negative P and T waves (in millivolts) from 70 normal dogs with standardized body and limb positions [43]

	I	aVF	V_{10}	V_4	rV_2
Positive P waves					
Relative frequency	97.1	100.0	47.1	100.0	72.9
Range	0.05–0.15	0.05–0.25	0.05–0.10	0.05–0.25	0.05–0.15
Median	0.05	0.15	0.05	0.10	0.05
Mean	0.063	0.133	0.055	0.126	0.065
Variance	0.00084	0.0037	0.00023	0.0029	0.00073
Negative P waves					
Relative frequency			38.6		10.0
Range			0.05–0.10		0.05–0.10
Median			0.05		0.05
Mean			0.059		0.066
Variance			0.0004		
Positive T waves					
Relative frequency	44.3	45.7	8.6	65.7	98.5
Range	0.05–0.25	0.05–0.45	0.05–0.20	0.05–0.90	0.05–0.80
Median	0.05	0.20	0.05	0.25	0.30
Mean	0.071	0.186	0.075	0.320	0.346
Variance	0.002	0.012		0.048	0.037
Negative T waves					
Relative frequency	51.4	45.7	87.1	15.7	1.5
Range	0.05–0.25	0.05–0.60	0.05–0.40	0.05–0.35	0.15
Median	0.05	0.25	0.20	0.25	
Mean	0.095	0.236	0.211	0.236	
Variance	0.003	0.019	0.006		

The cause of these changes is currently attributed to shifting of the pacemaker within the sinoatrial node, induced by variations of vagal tone (wandering pacemaker within the sinoatrial node). As is well known, experimental vagal stimulation can move the apparent pacemaker site from the upper to the lower end of the sinoatrial node [58–60]. The effect of such vagally induced shifts in pacemaker location in experimental dogs has been confirmed and related to P-wave configurational changes in leads I, aVF, and V_{10} [61]. The pacemaker location was established by plotting wave-front vectors from two sets of bipolar electrodes located close to the sinoatrial node. The inspiration was accompanied by an increase in the heart rate and a shift in the pacemaker location toward the head of the sinoatrial node and the expiration (or electrical stimulation of the right vagus or carotid sinus pressure) by slowing of the heart rate and movement of the pacemaker location toward the tail of the sinoatrial node. The shift of the plotted pacemaker location amounted to about 1.4 cm. With slowing of the heart rate, P waves increase slightly in amplitude in leads I and V_{10} and decrease (often markedly) in lead aVF, frequently becoming notched or bifid in lead aVF. Rarely, P-wave polarity may reverse in leads III (becoming negative) and aVL (becoming positive) during expiration. When pacemaker locations were determined [61], the P-wave in lead aVF was:

(a) Peaked when the pacemaker was located in the head of the sinoatrial node
(b) Of lower amplitude and bifid when the pacemaker was located in the middle area of the sinoatrial node and a low amplitude
(c) Flat when the pacemaker was low in the tail of the sinoatrial node

Table 41.3

Amplitudes of the QRS complex (in millivolts) from 70 normal dogs with standardized body and limb positions

	I	II	III	aVR	aVL	aVF	V2	V4	V10	rV2
Q wave										
Relative frequency	90.0	98.6	87.1	1.5	37.1	97.1	40.0	81.5	100.0	None
Range	0.05–0.60	0.05–1.20	0.05–1.00	0.30	0.05–0.65	0.05–1.05	0.05–0.35	0.05–0.55	0.15–1.20	
Median	0.15	0.30	0.25		0.30	0.25	0.05	0.15	0.65	
Mean	0.22	0.38	0.27		0.30	0.31	0.09	0.17	0.65	
Variance[a]	0.022	0.075	0.046		0.0324	0.052	0.004	0.013	0.057	
R wave										
Relative frequency	100.0	100.0	100.0	100.0	100.0	100.0	100.0	100.0	98.6	100.0
Range	0.10–1.50	0.45–3.00	0.25–2.35	0.05–0.70	0.05–0.90	0.20–2.40	0.50–4.00	0.25–5.40	0.05–0.80	0.15–3.60
Median	0.60	1.60	1.10	0.25	0.15	1.35	1.90	1.90	0.30	1.00
Mean	0.64	1.61	1.12	0.27	0.23	1.37	1.96	1.97	0.31	1.11
Variance[a]	0.117	0.334	0.247	0.032	0.042	0.366	0.593	0.828	0.0286	0.449
S wave										
Relative frequency	8.6	32.9	34.3	100.0	64.3	35.7	80.0	54.3	None	100.0
Range	0.05	0.05–0.35	0.05–0.70	0.15–2.30	0.10–1.10	0.05–0.55	0.05–1.60	0.05–1.30		0.05–1.60
Median		0.15	0.20	1.10	0.40	0.10	0.30	0.20		0.60
Mean		0.16	0.22	1.09	0.42	0.16	0.39	0.28		0.67
Variance[a]		0.009	0.029	0.223	0.054	0.014	0.093	0.067		0.156

[a]Standard deviations are not listed because of the number of asymmetrical distributions found in this series

Table 41.4

Linear regression formulae for time intervals (R-R in milliseconds)

	Grauwiler [48]	Lannek [16]
PQ (ms)	82 + 0.023 (R-R) ± 30 (3SD)	
QT (ms)	136 + 0.084 (R-R) ± 10 (5SD)	160 + 0.03 (R-R) ± 38 (2SE)

It appeared that in each dog there were several specific locations in the sinoatrial node for pacemaker activity, and that a change in vagal tone caused a sudden shift in the location of pacemaker activity from one of these preferred sites to another. This is in accordance with the view that major changes in sinoatrial node discharge rate result from, say, suppression of a faster pacemaking cell and shift of pacemaking dominance to a slower discharging cell, rather than from a slowing in rate of the original pacemaker cell. Stellate ganglion stimulation or norepinephrine injection can also cause shifts in pacemaker site and alterations in P-wave morphology [62]. Mapping studies [63] have demonstrated three regions of origin of atrial depolarization located at anterior, middle, and posterior regions of the anterior vena cava-right atrial junction. The middle position was near the sinoatrial node. The anterior and posterior positions were 1–2 cm away from the sinoatrial node area. Changes in P-wave morphology resulted from abrupt shifts in the region of earliest activation among these three points, two of which were outside the sinoatrial node. The multiple points of origin of atrial activation might represent a trifocal, distributed pacemaker or the epicardial exits of three specialized pathways that rapidly conduct the impulse from a single focus. Higher heart rates and taller P waves in lead II were associated with the higher centers of early activation, while lower rates and lower-amplitude notched P waves were linked with the lower centers of early activation. Others have demonstrated that in the dog, the sinus node is long (4 cm in length), providing multiple areas for discharge that are influenced by autonomic tone and the affected spontaneous discharge rate. In summary, when ECGs

Table 41.5

Variation of PR and QT intervals with heart rate in the beagle ECG [165]

Group number	Heart rate (bpm)	Sex	Number of ECGs	Interval (s)	
				PR	QT
1	61–80	Male	16	0.105 ± 0.029	0.214 ± 0.037
		Female	16	0.100 ± 0.027	0.213 ± 0.041
2	80–100	Male	96	0.102 ± 0.028	0.206 ± 0.031
		Female	86	0.104 ± 0.032	0.203 ± 0.028
3	101–120	Male	210	0.096 ± 0.025	0.195 ± 0.030
4	121–140	Female	219	0.101 ± 0.028	0.192 ± 0.027
		Male	353	0.095 ± 0.020	0.183 ± 0.031
		Female	324	0.097 ± 0.028	0.182 ± 0.029
5	141–160	Male	295	0.092 ± 0.026	0.173 ± 0.028
		Female	326	0.095 ± 0.026	0.174 ± 0.028
6	161–180	Male	172	0.088 ± 0.020	0.167 ± 0.026
		Female	187	0.078 ± 0.020	0.165 ± 0.028
7	181–200	Male	51	0.086 ± 0.020	0.160 ± 0.020
		Female	47	0.083 ± 0.021	0.160 ± 0.023
Student's t for groups 1 vs 7		Male		3.366*	5.036**
		Female		3.198*	4.942*

Values for PR and QT intervals are the means and 95% range for the numbers of ECGs shown. The asterisks indicate the degree of significance associated with the differences between the values for the lowest and highest heart-rate groups

*$p < 0.001$; **$p < 0.01$

Table 41.6

QRS patterns in various leads. For each lead the patterns are given in the order of frequency of occurrence. Patterns that are encountered less often or rarely are placed in parentheses. Refer to Fig. 41.6 and note how these patterns are altered by changing forelimb position

Lead	Pattern	Lead	Pattern	Lead	Pattern
I	QR, qR, (qRS)	aVR	rS, rSr′, (qrS)	rV_2	RS, (Rs)
II	qR, zRs, Rs, (QrS)	aVL	Qr, QR, (qRs)	V_2	Rs, qRs, (qR)
III	qR, qR, Rs, (rS)	aVF	qR, Rs, (QrS)	V_4	Rs, qRs, (qR)
				V_{10}	Qr, rS, (qR, QR)

are monitored in the dog, the autonomic tone will alter the P wave, and thus, this parameter is not one which is likely to be reliable in detecting differences between recordings that have impact on a study.

Given the above discussion, if the P wave is measured, it has not to our knowledge been stated which P wave to measure on an ECG recording (e.g., tallest, shortest, average). This in itself is problematic. We have arbitrarily decided to always measure the tallest P wave. It should also be emphasized that in an evaluation, if the heart rate changes, the P-wave values are likely to change as a consequence of rate, and not because of pathology of the atria.

41.3.3 QRS Complex

Typical QRS patterns in the various leads are given symbolically in Table 41.6. The QR pattern in lead I corresponds to the high incidence of counterclockwise rotation of the QRS vector loops in dogs (see Sect. 41.5).

41.3.4 ST-T Wave

In dogs, the ST segment is seldom horizontal and often the onset of T is imperceptible. Except for leads rV_2 and V_{10}, the polarity of the T waves may be positive or negative. In Fig. 41.9, a series of ST-T patterns observed in lead II are depicted. ST segment or ST junction (STj) deviations, especially in leads II, aVF, V_2, and V_4 are common. These ST deviations seldom remain consistent in serial records, but vary or disappear entirely from record to record. Also, the degree of ST deviation often varies cyclically with the changing R ~ R intervals of respiratory sinus arrhythmia. In this case, the degree of deviation increases with shorter preceding R-R intervals. Recent work in serial recordings of beagles and mongrels studied at Cornell University has demonstrated further that the polarity of the T wave is dependent on the age of the dog. The younger the dog, the more likely the T wave is to be positive. The T wave does not "stabilize" in the dog until approximately 12 months of age. This is an important notation for long-term studies in the dog in which the evaluation of repolarization as assessed by the ECG is important. The T wave is changing during the first year of life, so if a study is begun when the dog is 3–6 months of age, changes at 12 months of age must be assessed in conjunction with the expected changes seen developmentally with a more negative T wave at the older age. Again, the importance of control dogs is obvious for all studies.

41.3.5 U Wave

When present, U waves are generally most prominent in leads rV2, V_2, and V_4. They may vary in amplitude or disappear in consecutive beats and are usually less than 0.05 mV in amplitude and concordant with positive T waves. The TU interval approximates 0.04 s and U-wave duration approximates 0.07–0.09 s. The electrophysiological genesis of U waves is controversial [64]. They have been attributed to:

(a) Purkinje cell repolarization potentials
(b) An afterpotential gradient from endocardium to epicardium created during ventricular relaxation [65]

Tall U waves appear in hypokalemia, and in humans, have been described in hypomagnesemia, and in patients receiving digoxin, phenothiazines or tricyclic antidepressants [64]. U-wave inversion in humans has been described in hypertension, valvular, pulmonary, congenital, and ischemic heart disease [64]. In dogs, U-wave amplitude exceeding 0.05 mV has been associated with hypertension and anemic heart disease, but this finding is not consistent and is therefore diagnostically unreliable. U-wave values of 0.08 ~ 0.15 mV may occur in otherwise normal dogs.

41.3.6 Evolution During the First 3 Months of Life

Consistent with the functional and morphological cardiovascular changes during the first few weeks after birth [66–68], the mean (sometimes termed modal) QRS vector moves from a rightward, cranial and ventral orientation to the leftward, caudal and ventral direction [69–71]. The principal cause of this change is that the two ventricles are of about equal mass at birth, and this 1:1 ratio of right to left ventricular mass changes to a ratio of 1:2 or 1:3 [67] depending on how the ventricles are separated.

The mean QRS axis (derived from leads I and aVF) in the frontal plane is directed toward the right and either cranially or caudally at birth. By the 12th week, the mean QRS axis is directed to the left and usually resides in the left caudal quadrant of the frontal plane. In the transverse plane (leads I and V_{10}), the mean QRS axis changes from the right ventral quadrant at birth to the left ventral quadrant at week 12. The shift in the sagittal plane is from a more cranial ventral direction to a more caudal ventral orientation.

The R/S ratio in the left precordial leads increases primarily between the first and second week. It is less than 1.0 at birth and exceeds 1.0 at the sixth week. Later, this ratio becomes larger and may reach infinity because the S wave disappears. There is little change in the R/S ratio in lead rV2. In the frontal plane, the mean QRS vector shift may be from the right cranial through the left cranial to the left caudal quadrant (i.e., clockwise), or from the right cranial through the right caudal to the left caudal quadrant (i.e., counterclockwise).

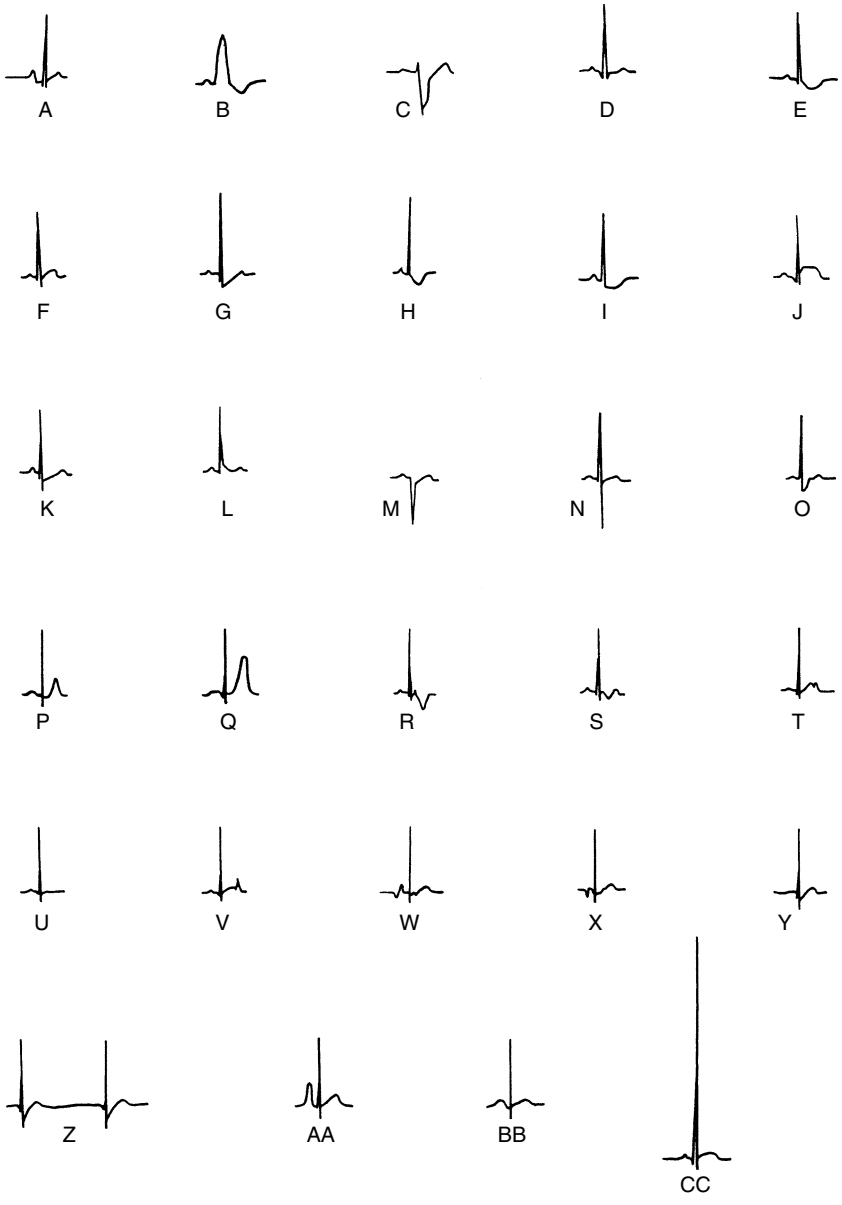

Figure 41.9

Pattern code: A, increased Ta amplitude; B, left bundle branch block like pattern (LBBB-like); C, right bundle branch block like pattern (RBBB-like); D, flat ST segment; E, coved ST segment; F, arched ST segment; G, ascending ST segment; H, descending ST segment; I, depressed ST segment; J, elevated ST segment; K, STj depressed; L, STj elevated; M, QS complex; N, deep S wave; 0, broad S wave; P, symmetrical T wave; Q, tall T wave; R, deep negative T wave; S, diphasic T wave: −/+ or +/−; T, notched T wave: − or −t; U, flat T wave; V, dome-dart ST-T complex; W, diphasic P wave: −/+ or +1/−; X, negative P wave; Y, flat P wave; Z, absent P waves; AA, tall P waves: >0.4 mV; BB, broad P waves: >60 ms; and CC, tall RV_2, V_4: >5.0 mV.

41.3.7 Classification

All canine ECGs fall into one of the following three general categories: normal, normal variant, or abnormal.

(a) *Normal ECGs*. These are ECGs in which all variables (heart rate, time intervals, amplitude and polarity of waves in all leads, and rhythm) fall within the specified ranges given in Tables 41.2–41.6.
(b) *Normal variant ECGs*. These ECGs have characteristics as described in Table 41.1 without pathology of the heart.
(c) *Abnormal ECGs*. These include any electrocardiographic feature that is outside normal limits and is definitely more prevalent in the presence of heart disease or cardiotoxicity.

41.3.8 Normal/Abnormal ECG Screening

Screening becomes necessary when records of large numbers of experimental dog ECGs are examined to eliminate any dogs with abnormal or questionable ECGs. Since the beagle is the breed normally used in such studies (e.g., chronic toxicity trials in preclinical drug testing), the criteria listed apply primarily to this breed, although they would apply equally well to most mongrels and other breeds of similar size and conformation.

Since over 95% of experimental beagle ECGs will ordinarily be within normal limits, the initial goal in examining pretest records is to identify the few abnormal records rapidly. This is done by quickly scanning the records for a series of features that establish normality. The criteria should be conservative so that borderline records will be scrutinized more closely.

41.3.8.1 Normal Criteria

The following criteria are customized from our experiences in the interpretation of the ECG recorded from the beagle. These criteria are not exactly the same as the normal published values for dogs in general.

(a) Intervals and rhythm
  (i) Heart rate: 60–190 bpm (R-R interval 316–1,000 ms)
  (ii) P interval: less than 50 ms
  (iii) PR interval: greater than 70 ms, less than 130 ms
  (iv) QRS interval: less than 60 ms
  (v) QT interval: less than 220 ms
  (vi) Sinus arrhythmia present
  (vii) No abnormal arrhythmias
(b) Wave amplitudes and patterns
  (i) T wave amplitude: 0.05–1.0 mV in any lead
  (Flat T waves are not necessarily abnormal especially in leads I, aVR, aVL, and V_{10})
  (ii) ST deviation: less than 0.20 mV in limb leads and less than 0.25 mV in chest leads
  (iii) ST-T complex: no dome-dart complexes
  (iv) R wave:
    - Less than 3.0 mV in limb leads rV_2 and V_{10}
    - Less than 5.0 mV in leads V_2 and V_4
    - More than 0.5 mV in II, III, and aVF
  (v) QRS axis in frontal plane: −20° to +110°
  (vi) P wave: less than 0.4 mV
  (vii) R/S amplitude ratio:
    - Greater than 0.5 in rV_2; and
    - Greater than 0.9 in V_2 and V_4

(viii) QRS: no rs, rS, Rs or RS patterns
(ix) S/QRS duration ratio: less than 50%

Records that do not meet these normal criteria require closer examination to determine if they are abnormal or normal variants.

41.3.9 Normal Variants

A large number of electrocardiographic characteristics are sufficiently rare or puzzling to attract attention in records from dogs not known to have cardiac disease. These are grouped together here as normal variants. They are based primarily on findings in young dogs (5–18 months old) of a single breed, the beagle [26].

41.3.9.1 QRS Complex

(a) *Variant frontal plane QRS vector loop*. This is also known as the "butterfly" QRS vector loop and requires a special mention. In a small number of beagles and in some other breeds as well, the mean QRS frontal plane axis is negative, ranging from −30° to −110° (Figs. 41.11 and 41.12). The QRS complexes in thoracic leads are within normal limits. In leads II, III, and aVF, the QRS pattern is characterized by having a small r wave (e.g., qrS or QrS pattern) or a W-shaped pattern in which the "r" wave fails to reach the isoelectric line. In lead I, there is usually a deep Q and pronounced R wave, the descending limb of which is slurred or notched as it approaches the isoelectric level. The QRS in lead aVL is usually markedly positive. If a frontal plane vector diagram is constructed from leads I and aVF, the early forces are directed counterclockwise to the right and craniad, then return close to their starting point before passing counterclockwise to the left and craniad. Thus, two connected vector loops are formed vaguely resembling butterfly wings, hence the name "butterfly" QRS vector loop (Figs. 41.10 and 41.11).

This variant has neither been studied systematically nor investigated electrophysiologically. Since the thoracic lead complexes are essentially normal with tall R waves in leads V_2 and V_4 and typical configuration in leads rV2 and V_{10}, there does not appear to be an electrophysiological abnormality. It is obvious, however, that the vector forces producing tall R waves in leads V_2 and V_4 do not do so in the limb leads. This pattern, when seen in 5–7-month-old dogs, may persist into adulthood, or within a few months or a year, tall R waves may appear in leads II, III, and aVF, while the chest lead complexes remain the same. The hearts are normal at necropsy.

The conclusion that can be drawn from the information at hand is that these low-amplitude R waves in leads II, III, and aVF and the "butterfly" QRS frontal plane vector loop result from the position of the heart in the thorax relative to the limbs, such that the major vector forces during the inscription of QRS are directed largely craniad and ventrad. As shown in Figs. 41.10 and 41.11, the two components of the QRS frontal plane-constructed vector loops may be more or less symmetrically disposed, with the initial part of the loop being directed toward the right arm and the final part of the loop directed toward the left arm.

(b) Other QRS complex variants (see Table 41.1 for most common variants):
(i) Circular frontal plane QRS vector loop
(ii) QRS slurring and notching
(iii) Delayed terminal forces causing broad SII, III, and aVF and broader RaVL; patterns variously (and often erroneously) described as incomplete RBBB, left anterior fascicular block
(iv) Rr' pattern in II, III, aVF, and rV_2 unaccompanied by broad S waves (see also (v))
(v) "Foot" or slur terminating QRS
(vi) Variable SrV_2 and V_2 amplitude

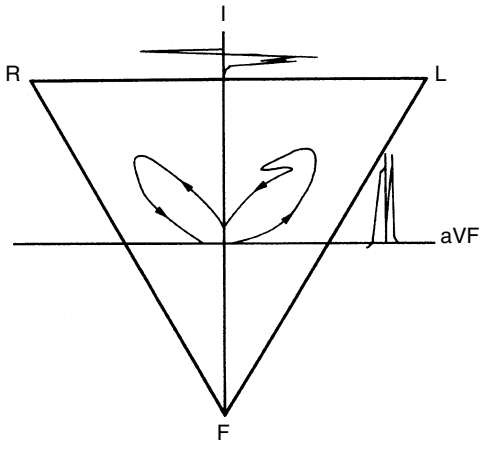

Figure 41.10

Butterfly QRS complex. A vector diagram constructed from QRS complexes of leads I and aVF. The QRS complexes are each traced on their respective zero potential lines, which intersect at zero potential in the center. The winged appearance of the vector diagrams of the variant QRS complexes gave rise to the term "butterfly" QRS complex. Note that the QRS complexes from leads I and aVF are drawn on their respective zero or isopotential lines which intersect at the middle of the triangle. To view lead aVF in its conventional orientation as recorded, the diagram must be rotated 90° counterclockwise. To view lead aVF in its conventional orientation, the diagram must be rotated 180° (i.e., lead aVF appears upside down here). The positive pole for lead I is toward L from its zero potential line and that for lead aVF is toward F, in the diagram.

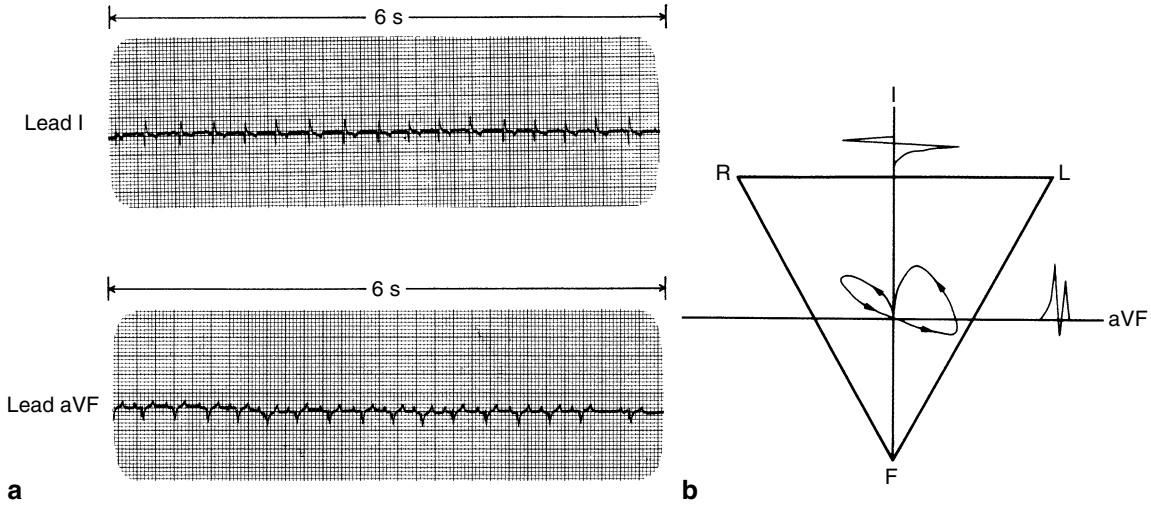

Figure 41.11

Butterfly QRS complex: (a) leads I and aVF and (b) vector diagram constructed from the QRS complex as in leads I and aVF. Note that the QRS complexes from leads I and aVF are drawn on their respective zero or isoelectric lines which intersect at the middle of the triangle. To view lead I in its conventional orientation as recorded, the diagram must be rotated 90° counterclockwise. To view lead aVF in its conventional orientation, the diagram must be rotated 180° (i.e., lead aVF appears upside down here). The positive pole for lead I is toward L from its zero potential line and that for lead aVF is toward F.

41.3.9.2 T wave and ST-T Complex: U Wave

(a) T wave in V_{10} flat, diphasic −/+ or positive
(b) T wave in rV_2 negative terminally or diphasic +/−
(c) Biphasic T waves in other leads
(d) T wave variable in amplitude and form (including polarity reversal) related to varying R-R intervals
(e) Tall-peaked T waves
(f) Dome-dart ST-T complex without QT prolongation
(g) Prominent U wave (>0.5 mV)
(h) TU fusion

41.3.9.3 P Wave and T_a Wave

(a) P-wave reversal in limb leads except lead I (wandering pacemaker within the sinoatrial node)
(b) Notched P waves
(c) High-amplitude (negative deflection) T_a waves (>0.05 mV; up to 0.15 mV in lead II)

41.3.9.4 Amplitude

(a) ST deviation (with accompanying ST-segment deviation or followed by rapid return of ST segment to baseline level) up to 0.20 mV in limb leads and 0.25 mV in chest leads. Variable deviation related to R-R-interval duration
(b) Amplitude variation of QRS and T waves with breathing cycle and R-R-interval duration
(c) Tall P wave in leads II and aVF (greater than 0.4 mV). Tall R wave in leads V_2 and V_4 (> 5.5 mV)

41.3.9.5 Rhythm and Rate

(a) Bradycardia (40–55 bpm)
(b) Tachycardia (rate > 200 bpm)
(c) First-degree AV block (PR > 0.14 s)
(d) Second-degree AV block

41.4 Normal Rhythm

41.4.1 Sinus Rhythm and Rate

In the denervated heart of the dog, the sinoatrial node discharges regularly at an intrinsic rate of about 90–120 bpm (see reference [72] for literature). Parasympathectomy alone results in a persistently rapid rate of 140–160 bpm. In intact, resting, and adult dogs, heart rates of 70–120 bpm are representative; with exercise, rates of 220–325 bpm are recorded; and in newborn and young puppies, the range is 140–275 bpm. In ECGs, the heart rates tend to be more rapid than in the resting dog owing to the effect of restraint. The ranges given in Sect. 41.3.1 and Table 41.5 are characteristic of those obtained from ECGs and show that the usual range in ECGs from beagles is 100–180 bpm. At the more rapid frequencies, respiratory sinus arrhythmia is decreased or abolished.

41.4.2 Respiratory Sinus Arrhythmia

In resting dogs, the heart rate decreases and increases with the breathing cycle, owing to a waxing and waning of vagal activity with respiration, although the primary reason is a central effect on the heart rate with variation in autonomic

tone. The usual pattern is acceleration with inspiration and deceleration with expiration, but this relationship is not absolute [73].

The control systems that interact to cause sinus arrhythmia include the radiation of respiratory center activity to medullary cardiovascular centers, the cardiac component of the Hering–Breuer reflex, the Bainbridge reflex (reflex cardioacceleration caused by increased stretch of the right atrium and great veins during inspiration), and the baroreceptor reflex (reflex cardiac slowing when the blood pressure rises during the accelerating phase of sinus arrhythmia). The degree of respiratory sinus arrhythmia decreases as vagal tone is decreased with exercise or excitement. The degree of sinus arrhythmia can be expressed as an index I [74]:

$$I = (\text{standard deviation of R-R} \times 100)/\text{mean R-R}.$$

This index is variable in serial records. For accuracy, 100 R-R intervals should be averaged for the calculation. Certain drugs can decrease this index or abolish sinus arrhythmia altogether at heart rates where it is ordinarily present. Other methods to evaluate heart rate variability have been studied extensively. These include time and frequency domains to assess the balance of autonomic tone [75].

In resting dogs, the rapid beats in respiratory sinus arrhythmias often occur in sets of two (bigeminy), three (trigeminy), or sets of three beats with a fourth beat during expiration [76]. Sets of four or five beats are rare. These cyclic changes in the R-R-interval duration are often accompanied by cyclic alterations in the amplitude of electrocardiographic complexes and, sometimes, in the form (and occasionally, polarity) of T waves. In puppies, Lange [77] found that respiratory sinus arrhythmia does not appear before 4 weeks of age.

Usually, the respiratory sinus arrhythmia tends to become more pronounced (i.e., the disparity between R-R intervals increases) as the heart rate slows. Rarely, this fails to occur and a slow heart rate with a relatively regular rhythm may be present. Certain drugs appear to depress the brain stem and ameliorate or abolish respiratory arrhythmia in dogs (see Sect. 41.10.1.3).

Over the years, the breeding of beagles for research purposes has led to some dogs being particularly calm with slow rates and more pronounced sinus arrhythmias.

41.5 Normal Vectorcardiogram

Starting in 1957 with the study of Horan et al. [78], vectorcardiography became a useful investigation tool in canine cardiology. Various lead systems have been employed: for example, the Wilson equilateral tetrahedral reference system [31, 78–82], the Frank corrected lead system [35, 37] (Fig. 41.4), and the orthogonal-lead system of McFee and Parungao [23, 34, 43, 82–84] (Fig. 41.3). Of these, the only lead system specifically corrected for the dog is that of McFee and Parungao [34]. Rarely is vectorcardiography performed today in clinical veterinary patients, in screening research dogs, or as a part of the evaluation of treatment. We continue a discussion of this method here because, although not performed, it is a valuable concept to grasp in the often two-dimensional representation of the frontal limb leads to which we are limited. In electrophysiology laboratories, extensive mapping has replaced the vectorcardiogram.

41.5.1 Normal Values

Vectorcardiographic data from 50 mongrel dogs using the axial-lead system of McFee and Parungao are given in Tables 41.7–41.9 [84]. In these tables, the term prevalent direction or θ expressed in degrees is used (see Chap. 13) rather than the mean of observed angular directions. This variable is an estimate of the average angle of the prevalent direction, and the range of distribution of the individual points is given in the tables for 5–95% of the grouping.

Table 41.7

Angles and magnitudes of P, QRS, and T maximal vectors [84]

	Maximal P vector	Maximal QRS vector	Maximal T vector
Frontal plane			
Amplitude (mV)[a]	0.42 ± 0.12	2.17 ± .0.44	0.28 ± 0.12
Prevalent direction $\hat{\theta}$ (°)	71	69	84
5–95% directional range (°)	44–85	38–95	−55 to −124
Horizontal plane			
Amplitude (mV)[a]	0.21 ± 0.11	1.72 ± 0.36	0.36 ± 0.19
Prevalent direction $\hat{\theta}$ (°)	9	71	87
5–95% directional range (°)	−55 to 72	−66 to 137	30 to −163
Left sagittal plane			
Amplitude (mV)[a]	0.41 ± 0.11	2.27 ± 0.43	0.42 ± 0.22
Prevalent direction $\hat{\theta}$ (°)	95	117	161
5–95% directional range (°)	70–125	47–153	119 to −104

[a]Mean ± standard deviation

Table 41.8

Maximal projections of QRS vectors on W, Y, and Z [84]

	Mean ± SD (mV)	5–95% range (mV)
X axis		
Initial right	−0.21 ± 0.30	0.0 to −0.60
Left	0.91 ± 0.43	0.20–0.160
Terminal right	−0.18 ± 0.28	0.00 to −0.80
Y axis		
Initial cranial	−0.04 ± 0.08	0.00 to −0.20
Caudad	1.9 ± 0.63	1.00–2.75
Terminal cranial	−0.21 ± 0.16	0.00 to −0.50
Z axis		
Sternal	−1.50 ± 0.54	−0.50 to −2.25
Vertebral	0.98 ± 0.44	0.20–1.80

Table 41.9

Spatial angles and magnitudes of instantaneous QRS vectors [84]

Time after onset of QRS (ms)	$\hat{\alpha}$[a] (°)	$\hat{\beta}$[b] (°)	Magnitude[c] (mV)	
			Mean ± SD	5–95% range
5	97	86	0.29 ± 0.17	0.12–0.46
15	81	128	1.81 ± .0.45	0.63–2.59
25	29	154	2.11 ± 0.53	1.03–2.89
35	292	128	1.28 ± 0.63	0.39–2.31
45	262	84	0.60 ± 0.48	0.08–1.62
55	257	97	0.27 ± 0.22	0.08–0.98

[a] $\hat{\alpha}$, longitude or angular deviation from the left in the horizontal plane (0°–360°) for the spatial prevalent direction
[b] $\hat{\beta}$, colatitude or angular deviation from the cranial (0°–180°) for the spatial prevalent direction
[c] Magnitude = $(X^2 + Y^2 + Z^2)^{1/2}$

41.5.2 P and T Vector Loops

With the lead system of McFee and Parungao, the P loop is a thin ellipse pointing sternally and to the left. The mean P-wave axis is within ±90° of the maximal QRS vector in 100% of the cases in the frontal plane, 82% in the horizontal plane, and 98% in the left sagittal plane [84]. With the McFee and Parungao lead system, the T loop is a moderately open ellipse with the mean axis within ±90° of the maximal QRS axis in 80% of the cases in the frontal plane, 77% in the horizontal plane, and 82% in the left sagittal plane. With the Frank system, the T vector loop is usually concordant with the QRS vector loop in the frontal (86%), transverse (90%), and sagittal (97%) planes [34]. Thus, the major T vector axis points either cranially or caudally in the frontal plane, ventrally in the horizontal plane, and sternocranially or sternocaudally in the left sagittal plane.

41.5.3 QRS Vector Loops

The incidence of counterclockwise rotation of QRS vector loops in frontal, left sagittal, and transverse ("horizontal") planes is very high with the three (Wilson tetrahedral, Frank, and McFee) lead systems. For example, with the McFee system, counterclockwise rotation of QRS in the frontal, transverse, and sagittal planes, respectively, was 52–60%, 80–98%, and 98–100% [43, 83, 84]. These percentages are similar to those reported for the frontal and left sagittal planes (85% and 100%) with the Wilson tetrahedron reference system and in all three planes with the Frank system (66%, 97%, and 100%, respectively) [35]. This predominance of counterclockwise QRS rotation in the dog frontal plane is in sharp contrast to the clockwise rotation more commonly found (65%) in the human VCG, which has a similar mean frontal axis. Since the spread of excitation through the heart in both species is similar, the difference must relate to the differing orientation of the heart within the thoracic cavity of man and dog.

Chest conformation has a distinct effect on the electrical axis of the heart such that narrow-chested breeds (e.g., Doberman pinschers, German shepherds) have more ventrally oriented QRS axes in the transverse plane and more caudally oriented QRS axes in the frontal plane than do broad-chested breeds (e.g., cocker spaniels and boxers) [83].

Vectorcardiographic appearances have been reported in dogs with a variety of spontaneous and experimental abnormal cardiac conditions such as right ventricular hypertrophy [23, 82, 85, 86], imperforate ventricular septal defect [87], congenital peritoneopericardial diaphragmatic hernia [88], patent ductus arteriosus [23, 89], idiopathic cardiomyopathy [23], coronary occlusion and other localized myocardial destruction [72, 73], ventricular ectopic beats [90], and bundle branch block patterns [23, 91–94].

41.5.4 The Vector Diagram

Despite the knowledge gained from these various investigations, vectorcardiography has been little used in the routine diagnostic cardiology in dogs. The vector diagram, however, derived from the limb-lead scalar ECG has a special usefulness in evaluating the QRS vector changes in the canine ECG [85] (Fig. 41.12). This is because the normal range of mean QRS axis values is broad and the normal limits for the various breeds have not been established statistically. For example, in right ventricular hypertrophy, the usual counterclockwise rotation of the constructed QRS vector loops in the frontal, transverse, and sagittal planes is reversed. In the frontal plane, early forces are usually directed cephalically or caudally toward the left and late forces toward the right and cranially. In left ventricular hypertrophy, in contrast, the QRS axis and loop are not usually altered in form or in direction of inscription.

41.5.5 Evolution During the First 3 Months of Life

With the Wilson tetrahedron system, the QRS loops shortly after birth are directed chiefly toward the right (frontal and transverse planes) and cranially (frontal and sagittal planes); at week 12, the major orientation is toward the left and caudally. The inscription of the QRS vector loops in all three planes changes from clockwise just after birth to a counterclockwise rotation at week 12 [69, 70].

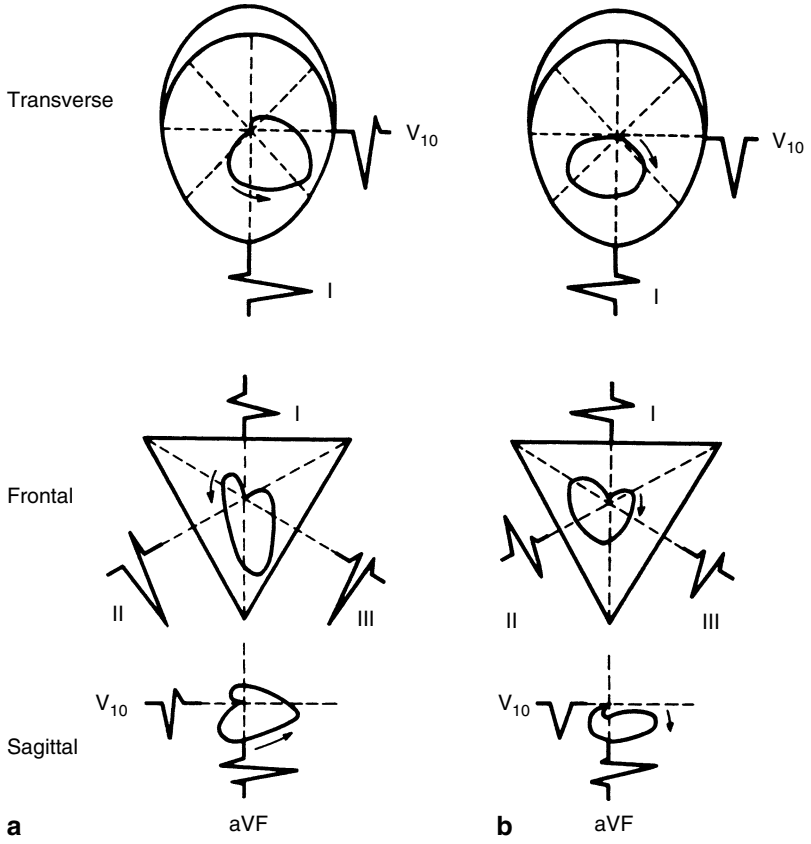

Figure 41.12

Vector diagrams in three planes constructed from limb-lead scalar ECGs (leads I, II, III, aVF, and V_{10}): (a) normal pattern and (b) right ventricular hypertrophy pattern. Note that the direction of rotation is counterclockwise in the normal record (a) and clockwise in right ventricular hypertrophy (b) in all three planes. (After Detweiler et al. [78]. © New York Academy of Sciences, New York. Reproduced with permission.)

The direction of the T-wave vector loop at birth in some dogs produces negative T waves in rV_2 and positive T waves in V_{10}. This changes with aging, so that by the fourth to the eighth week, the adult pattern (positive T wave in rV_2 and negative T wave in V_{10}) is present in most dogs. Positive T waves in V_{10} may persist in some dogs beyond the third month and become negative only between months 5 and 7. This T-wave polarity change from negative to positive in the right precordial lead (rV_2) is opposite to that observed in human infants, where the right precordial T waves are generally positive at birth and become negative after the first week after birth.

41.6 ECG Descriptors and Pattern Code

A number of electrocardiographic features that change spontaneously or are altered by drugs and disease are often described rather than quantified. Thus, wave contour, polarity, and amplitude characteristics require descriptive terms that are sufficiently specific to convey the intended meaning. Many terms in use are part of the jargon of electrocardiography, and few have found their way into medical dictionaries. Consequently, changes in meaning, elimination from use, or modification of terminology are continuing processes. The terms offered here have been found useful as descriptors for various recognizable characteristics of the dog ECG. Some are self explanatory while others require definition or examples. They are compiled here as an approach toward standardizing descriptive terms.

41.6.1 Descriptors Applicable to All Leads

(a) *Amplitude variable*. Amplitude variation of any of the electrocardiographic waves (P, Q, R, S, and T) from beat to beat. Example of use: P-wave amplitude variable from beat to beat in all limb leads.

(i) Related to previous R-R interval. The form and amplitude of P and T waves and the degree of deviation of the STj or ST segment may vary predictably with changes in the R-R interval during respiratory sinus arrhythmia. The P-wave changes have been discussed in previous sections. The changes in T waves and STj or segment deviations occur because the degree of recovery of conductivity in the heart is time dependent and less complete with shorter R-R intervals. When the R-R intervals are short enough, the conduction and recovery processes are somewhat aberrant and the form of the ST-T complex changes.

(ii) Electrical alternation. While this may occur in diseased hearts, minor variations (e.g., of the S wave in one of the chest leads) occurring in alternate beats are found in occasional records from the same dog and are not associated with any other abnormality.

(b) *Low amplitude*. Although all wave amplitudes vary in serial records, this term is used when the recorded potential is far below the average for a particular wave in a given lead. When cardiomyopathy is extensive, the entire QRST complex may be of reduced amplitude. The term is relative and the amplitudes may not be below the normal range when this term is applied. It is used primarily to describe P waves and R, R+S, or T waves. In the case of P and T waves, their polarity must be indicated as positive (+) or negative (−).

(c) *High amplitude*. The reverse of (b)

(d) *Polarity reversal*. The term is used when P and T waves change their polarity from beat to beat or from record to record in serial ECGs.

(e) *STj deviation*. The J (or junction) point is the sharp inflection marking the end of the QRS complex and the beginning of the ST segment. It deviates to some extent from the baseline in normal records. Increased STj deviation may accompany cardiac hypoxia, necrosis and epicardial inflammation. Depending on the polarity of the deviation, it is described as elevation or depression of the STj.

(f) *ST-segment deviation*. This term is used when the entire ST segment is elevated or depressed above or below the isoelectric line. The ST segments are seldom horizontal in dogs. They either ascend or descend from the STj to the T wave and a clear inflection point separating the ST segment from the beginning of T is often not present. Accordingly, it is necessary to measure the degree of ST deviation at some defined point in the ventricular complex. It is recommended that this point be located 0.04 ms after the J point.

(i) Variable ST-segment deviation (see (a) (i) above)

(g) *Coved ST segment*. Concave upward

(h) *Arched ST segment*. Convex upward

(i) *Ascending ST segment*

(j) *Descending ST segment*

(k) *Flat ST segment*

The terms (g)–(k) are used alone or together with items (e) and (f).

(l) *Dome-dart ST-T complex*. A relatively stereotyped drug effect (rarely also seen in control records) consists of ST-T complexes in which the ST segment and first limb of the T wave form a rounded arch. This terminates in a spike that peaks and is followed by the terminal limb of the T wave. These dome-dart T waves are positive in leads rV_2 and V_2, and negative in lead V_{10} (see Fig. 41.13).

(m) *Symmetrical T waves*. Ordinarily, the first limb of the T wave has a more gradual slope than the final limb. T waves that increase in amplitude may also become symmetrical (e.g., with excitement or during hyperkalemia).

(n) *Concordant T waves*. These have the same polarity as the predominant direction of the QRS complex and discordant T waves have the opposite polarity.

(o) *Prolonged terminal QRS forces*. Delays in intraventricular conduction or heritable patterns of ventricular excitation produce broad S waves.

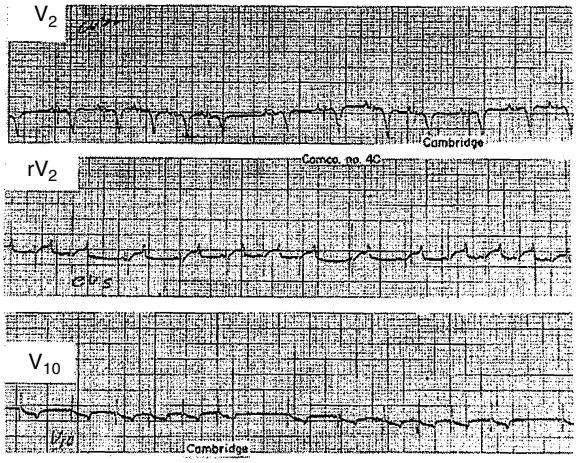

Figure 41.13

Dome-dart T waves in leads rV_2 and V_{10} accompanied by deep negative T waves in lead V_2 and QT prolongation (0.28 s). This beagle dog was receiving toxic doses of a tricyclic antidepressant neuroleptic drug with antihistaminic and local anesthetic properties. (After Detweiler [25]. ©CRC Press. With permission.)

(p) *Prominent U wave*. U waves are ordinarily absent or less than 0.05 mV in amplitude. They are regarded as prominent when their amplitude exceeds 0.05 mV.
(q) *R/S ratio*. This amplitude ratio is usually greater than 0.5 in rV2 and greater than 0.9 in V2 and V4. In disease (e.g., cardiomyopathy, focal cardiac hypertrophy), the ratio changes ordinarily by a reciprocal decrease in R and increase in S amplitudes.
(r) *High-amplitude Ta wave*. The Ta waves are usually absent or of low amplitude. A distinct increase may be apparent after certain drugs.
(s) *Afterpotential*. This is a distinct positive or negative potential change following the T wave that is of far greater amplitude and duration than the U wave.

41.6.2 Pattern Code for Various Types of PQRST Complexes

Various influences including autonomic and electrolyte changes, drugs, and disease affect the contour of the ECG. For descriptive purposes, frequently occurring patterns may be coded by capital letters as shown in Fig. 41.3.

41.7 Electrocardiographic Abnormalities: Diagnostic Criteria

The diagnostic criteria for specific cardiac lesions in dogs are far less reliable than those for humans for several reasons:

(a) The database for normal ranges is small.
(b) The great variation in body size and chest conformation among the various breeds of dogs increases the morphological extremes of electrocardiographic complexes in chest leads.
(c) The T waves are labile, change morphology spontaneously, and may reverse polarity in all conventional leads except rV_2 and V_{10}.
(d) ST-segment and STj-point deviation from isopotential is variable and in some normal dogs is large.
(e) Changes in the forelimb position produce marked swings in frontal plane vectors.
(f) Limb-lead P-wave morphology is normally extremely variable.

41.7.1 Hypertrophy

The electrocardiographic criteria for chamber enlargement are rather reliable for right ventricular hypertrophy (RVH), but unreliable for left ventricular hypertrophy (LVH) and for atrial enlargement.

41.7.1.1 Right Ventricular Hypertrophy

The 12 electrocardiographic criteria for the diagnosis of RVH are given in Table 41.10 [86]. Three or more of these criteria were present in 93% of dogs with RVH, the corresponding false-positive rate being about 1% [86]. An example is given in Fig. 41.14.

Table 41.10

Electrocardiographic criteria in order of relative frequency in which they occurred in 70 dogs with right ventricular hypertrophy and in 70 normal dogs matched by breed, age, and sex [85]. The first column lists the rank order of 12 diagnostic electrocardiographic criteria for right ventricular hypertrophy. Two of the 12 criteria have the same rank order of 1, since their relative frequencies (given in the fourth column) are the same. The numbers listed in the sixth column are totals representing the number of abnormal dogs out of 70 which had three or more of the electrocardiographic criteria listed by rank order *above* and row in which the number appears. Thus, for example, 57 dogs out of 70 had three or more of the six criteria listed under rank orders 1–5

Rank	Criteria	Lead	Relative frequency in dogs with right ventricular enlargement	Relative frequency in normal dogs [a]	Number of abnormal more dogs with three or ECG abnormalities	Relative frequency
1	S > 0.80 mV	V2	79.4	7.1		
1	Frontal plane QRS mean electric axis from +103° clockwise to 0°	I and aVF	79.4	0		
2	S > 0.70 mV	V4	78.8	2.9		
3	S > 0.05 mV	I	77.1	0		
4	R/S ratio < 0.87	V4	62.1	0		
5	Transverse plane QRS mean electric axis from +105° clockwise to −31°	I and V10	60.7	1.4		
6	QRS algebraic sum > −0.20 mV	I	55.7	0	57	81.4
7	S > 0.35 mV	II	50.0	0	60	85.7
8	Sagittal plane QRS mean electric axis from +91° clockwise to −12°	aVF and V10	32.8	0	61	87.1
9	A > 0.30 mV	aVR	29.4	0	62	88.6
10	Positive T > 0.25 mV	I	12.9	0	63	90.0
11	R′	II	11.4	0	64	91.5
					65	92.9

[a] None of the normal dogs had ECG abnormalities

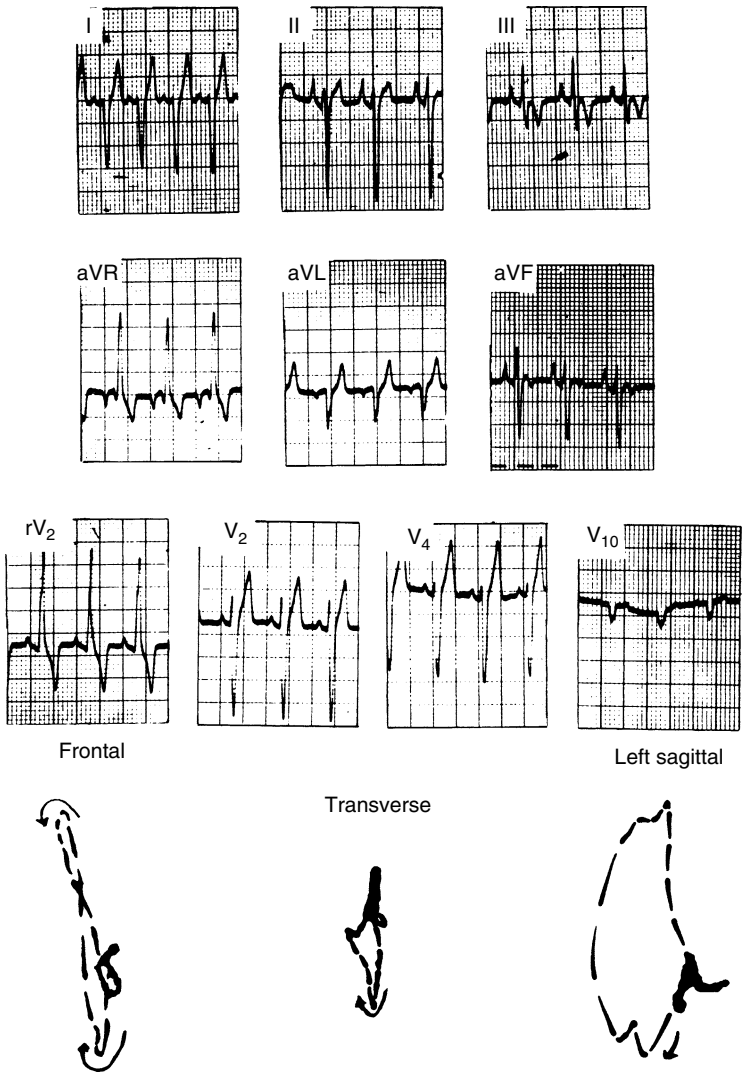

Figure 41.14

Right ventricular hypertrophy electrocardiographic patterns and VCGs from a 6-month-old Dalmatian with congenital pulmonic stenosis. The mean QRS axis is shifted far to the right (about −145 degrees), TrV_2 is negative, TV_{10} is positive and the vector loops rotate in a clockwise direction except for the final part of the figure-of-eight loop in the frontal plane (Wilson equilateral tetrahedron lead system). (Courtesy of D. F. Patterson.)

41.7.1.2 Left Ventricular Hypertrophy

Reliable criteria for the electrocardiographic diagnosis of LVH in dogs are not available. This is unfortunate since LVH secondary to mitral insufficiency is the most common form of chamber enlargement seen clinically in dogs [24].

The electrocardiographic findings compatible with LVH are tall R waves, wide QRS complexes, deep negative T waves in leads II, III, aVF, and V_{10} and a mean QRS axis in the frontal plane directed toward the left. The reason these findings are not diagnostic is that they may be present in normal dogs and absent in dogs with marked LVH [24]. The QRS axis and loop are usually not altered in dogs with confirmed LVH. Young dogs between 6 and 24 months of age are especially likely to have tall R waves, exceeding 3 mV in leads II, III, and aVF, and exceeding 4 mV in leads V_2 and V4. On the other

hand, such tall R waves in older dogs in the presence of QRS intervals greater than 0.07 s, a frontal mean QRS axis of less than 45°, deep negative T waves in leads I, II, III, and aVF, and the notching or slurring of the QRS complex are findings that indicate the possibility of LVH. In some cases of LVH, enormous R waves are present (e.g., 7.7 mV in lead III) [95]. On the other hand, in a series of 41 Newfoundlands with congenital subaortic stenosis, 31 had normal ECGs and the electrocardiographic features found in 10 cases with the most severe stenoses (atrial fibrillation in 4, ventricular extrasystoles in 3, RII greater than 2.5 mV in 3, and notching of QRS in 1) were not diagnostic of LVH [96].

41.7.1.3 Atrial Enlargement

Commonly in textbooks, a tall P wave is described as indicating right atrial enlargement and a wide P wave as indicating left atrial enlargement. However, these criteria are too often incorrect. It is likely better to just assume that if the P wave is either too tall or too wide that one of the atria is enlarged. Also, with atrial enlargement, the large P wave is sometimes accompanied by exaggerated T_a waves [23, 97]. Tall P waves are common in certain breeds (e.g., greyhounds) and P waves exceeding 0.4 mV are seen occasionally in young beagles as well as other breeds. Also, remember that a high sympathetic tone with fast rates results in tall P waves. This is also true if adrenergic drugs or parasympatholytic drugs are given.

41.7.2 Bundle Branch Block

The QRS interval is 0.08 s or longer in both right and left bundle branch block. In the right bundle branch block (RBBB) (Fig. 41.15), the widest part of the QRS complex is directed downward in leads I, II, III, aVF, the left precordial leads V_2 and V_4, and V_{10}, while it is upright in lead aVL, the right precordial lead rV_2, and in aVR. In the left bundle branch block (LBBB) this pattern is reversed. The widest part of the QRS complex is upright in the standard limb leads and aVF, as well as the left precordial leads V_2, V_4, and V_{10}. It is negative in the leads aVR, aVL, and rV_2.

The electrocardiographic pattern of RBBB can occur in the absence of organic heart disease in dogs [78, 95]. Complete RBBB (QRS complex > 0.08 s) or incomplete RBBB (same distribution of S waves but the QRS complex < 0.08 s) can exist (Fig. 41.15). When an S wave is identified in the anterior leads and left precordial leads, the following are potential reasons:

(a) Right bundle branch block (clinical and experimental)
(b) Left anterior hemiblock (experimental section of the left anterior fascicle of the left bundle branch [96])
(c) Localized hypertrophy of the free right ventricular wall at the outflow tract [94, 95]

Although the ECG criteria for bundle branch blocks are generally accepted amongst veterinary cardiologists, there is some descent as to their validity. Rosenbaum et al. [98] found that in experimental dogs, a section of the left anterior or the left posterior fascicles of the His bundle failed to produce characteristic changes in the limb-lead ECG when the heart was in the normal position, although this could be achieved by placing the heart in a more "horizontal" position by constructing a sling from the pericardium. Similarly, in a study by Okuma [99], the changes in the limb-lead and leads V_1 and V_5 of dogs caused by sectioning these fascicles were minor.

41.7.3 Bypass Conduction

(a) *Preexcitation*. Preexcitation occurs when the more distal heart is prematurely activated because supraventricular impulses travel via an accessory pathway to the distal AV node or the ventricles. This additional path of conduction is in addition to the normal conduction pathway. The accessory pathways are indeed anatomical structures [100]. In the dog, preexcitation is usually associated with a short PR interval. If this preexcitation has episodes of supraventricular tachycardia, the Wolff–Parkinson–White (WPW) syndrome is the most common diagnosis (Fig. 41.16). This conduction disorder is rare in dogs, occurring in approximately 1 in 2,000 experimental beagles [25] and in 1 in 3,000 clinic patients [101]. Bypass tachycardias can be concealed such that during normal heart rates, the premature activation is not identified by a short PR interval.

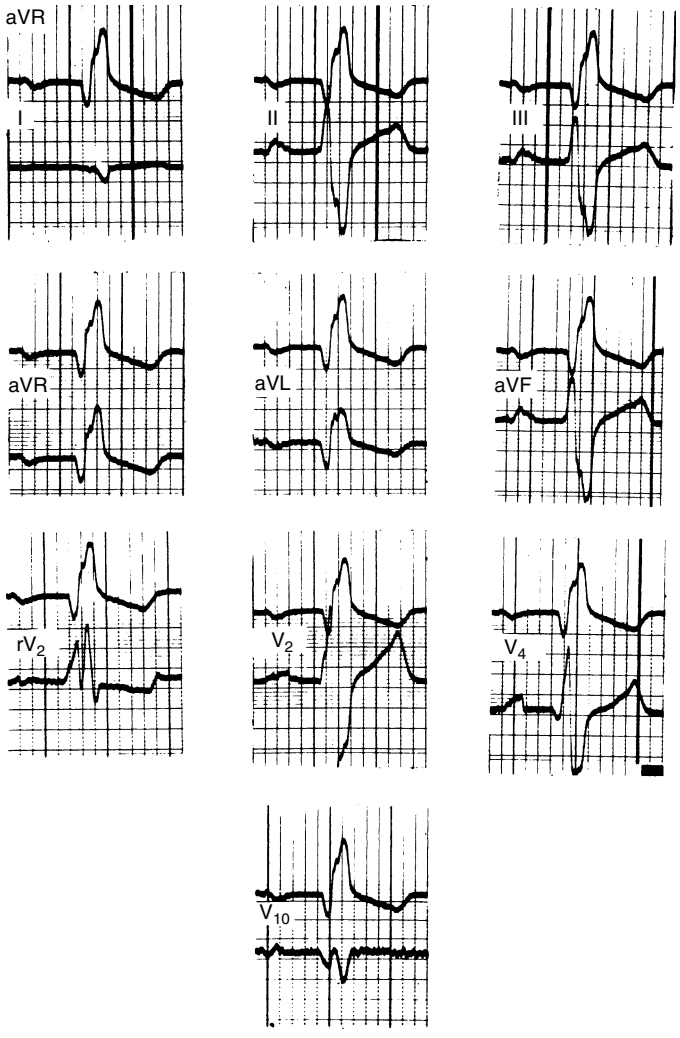

Figure 41.15

Right bundle branch block pattern from a 12-year-old male poodle with chronic mitral insufficiency, myocardial disease, and congestive heart failure. The upper trace is lead aVR in each record. Note the RR′ complex in lead rV_2; the wide part of the QRS complex is negative in leads I, II, III, aVR, V_2, V_4, and V_{10}, while it is positive in leads aVR and aVL. Paper speed is 75 mm s^{-1}.

41.8 Rhythm Abnormalities

41.8.1 Supraventricular Arrhythmias

41.8.1.1 Sinus Rhythms

The normal heart rate for dogs under clinical conditions is about 60–120 bpm. The heart rates given in data from dog ECGs [25] vary from 34 to 238 bpm. Such extremes would be abnormal if sustained, but when observed in a short ECG strip, are frequently not representative of the unperturbed heart rate. Heart rates determined from the ECG represent values obtained under some degree of duress. They must be interpreted with care.

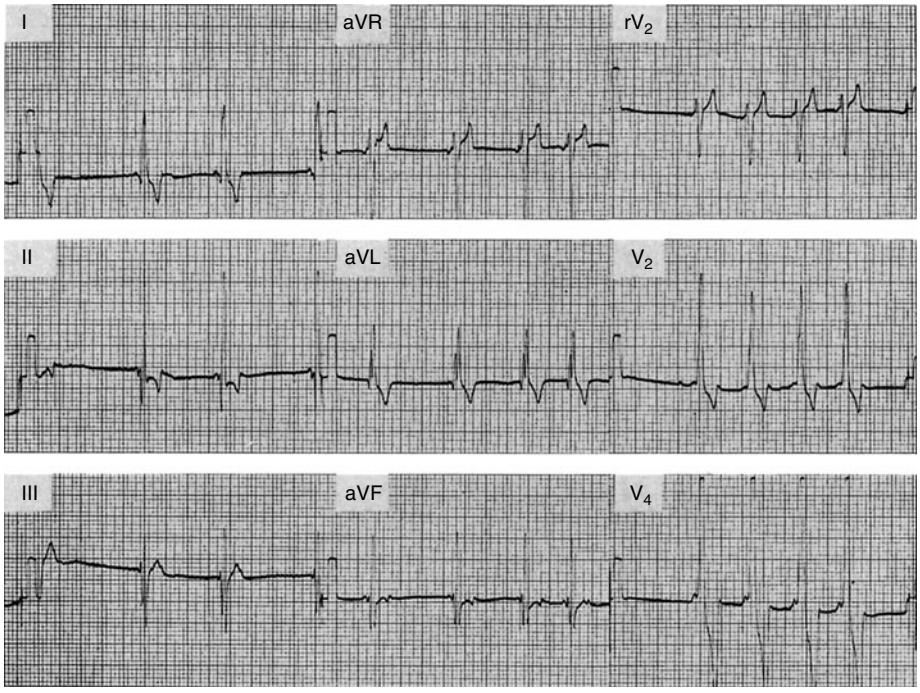

Figure 41.16

Wolff-Parkinson-White syndrome in a research beagle control record. The time intervals are: PR, 0.04; QRS, 0.08; and PJ, 0.12 s. The delta wave is positive in all three precordial leads.

Sinus bradycardia and tachycardia. Heart rates in individual ECGs below 60 and above 180 bpm may be arbitrarily designated bradycardia and tachycardia, respectively.

(a) *Sinus bradycardia. Sinus bradycardia* can be found occasionally in otherwise normal dogs. Long and associates [102, 103] demonstrated a substantial reduction in the average heart rate of groups of dogs (e.g., from a mean of 86 bpm upon first examination to 66 bpm for a group of 60 dogs) with restraint for 2 h in a quiet, isolated environment. Under these circumstances heart rates as low as 48 bpm were observed. Sick sinus syndrome is a disorder that is characterized by sinus bradycardia that often has long sinus pauses that can extend for more than 8 s and result in syncope. Moreover, some dogs are afflicted with episodes of supraventricular tachycardias in addition to the bradycardia and pauses. Sick sinus syndrome is most common in miniature schnauzers, cocker spaniels, dachshunds, and West Highland white terriers.

(b) *Sinus tachycardia*. It can be physiologic, in response to a pathologic condition or actually pathologic in and of itself. During the recording of an ECG in some dogs, the heart rate can be as high as 180 bpm, but rates exceeding 190–200 bpm are suspect. Based on Holter recordings, normal healthy dogs can obtain heart rates as high as 300 bpm for very brief times (<10 s) associated with excitement, fear, or acute pain. Kennel activities such as feeding time and the presence of strangers are likely to induce rapid heart rates in groups of dogs, even though the ECGs are taken at a distant location. Sinus tachycardia is expected in certain disease states; for example, anemia, fever, hemorrhage, shock, and congestive heart failure. As mentioned before, it has been found in toxicological studies that sustained (e.g., several hours daily over several days) sinus tachycardia exceeding 190–200 bpm results in myocardial damage with lesions (hemorrhage and necrosis, followed by fibrosis) in left ventricular subendocardium and papillary muscles.

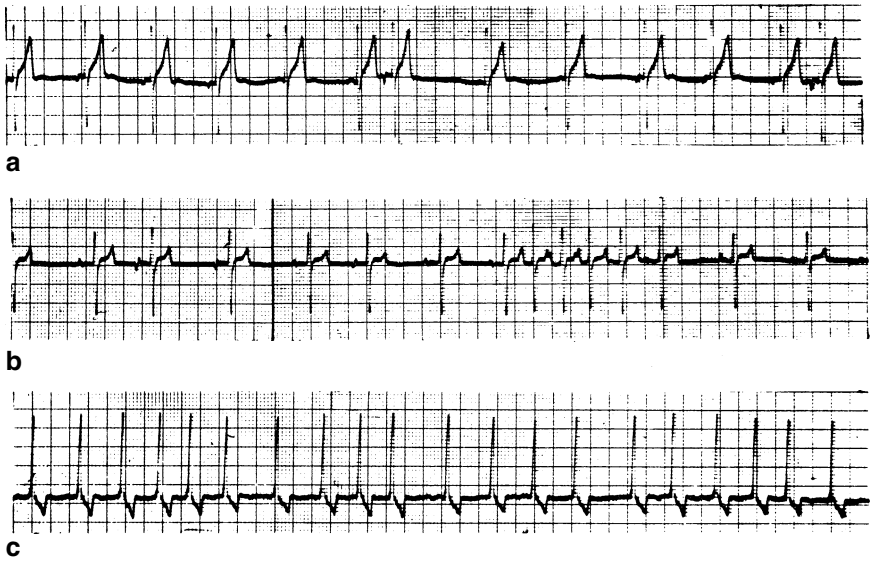

Figure 41.17

Atrial arrhythmias: (a) atrial premature beats. Two premature atrial beats with deeply inverted P waves are present, one in the middle and one at the end of the record (lead rV_2 of an eleven-year-old male cocker spaniel with mitral insufficiency). Part (b), a run of atrial tachycardia occurs after the seventh complex The P waves vary in shape from beat to beat, the PR interval is prolonged (0.16 s, first-degree AV block) and P waves are partially buried in the preceding T waves during the tachycardia (lead rV_2 of a nine-year-old male boxer with aortic body tumor infiltrating the right atrium). Part (c), atrial fibrillation. The ventricular rate has been slowed to 140 bpm with digoxin therapy (lead V_2 of a thirteen-year-o1d male Doberman pinscher with mitral insufficiency and congestive heart failure).

41.8.1.2 Atrial Rhythms

(a) *Atrial extrasystole* (see Fig. 41.17a). Premature atrial complexes are also known as atrial extrasystoles. They can originate from any location above the AV node. They may be singles, couplets, or triplets. If excessively premature, atrial extrasystoles can arrive at the AV node during the refractory period and not result in ventricular activation. In such cases, only a nonconducted P wave is identified.(b) *Atrial tachycardia* (see Fig. 41.17b). As with other atrial arrhythmias, the normally variable P waves complicate this diagnosis. Paroxysmal atrial tachycardia (PAT) with (AV) block occurs in digitalis intoxication in dogs especially when complicated by hypokalemia [98]. Such arrhythmias secondary to digitalis intoxication are far less common today because dosing (including the total dose used) is more cautious than in the past.

(c) *Atrial flutter*. It occurs at an atrial rate of usually 340–440 bpm in dogs. Although mechanistically the atrial flutter may vary from atrial tachycardia, difficulty can exist in clearly separating the two rhythms. Atrial flutter classically is characterized by undulating waves (F wave) that result in no baseline. There may be 2:1 AV block which results in a constant RR interval, although more commonly the conduction is varied and an irregular RR pattern prevails.

(d) *Atrial fibrillation*. It occurs at an atrial rate of 500–750 bpm in the dog. See Fig. 41.17c. The atrial rhythm results in fine undulations of the baseline identified as "f waves." Classically atrial fibrillation is a tachyarrhythmia in which the RR interval is very irregular.

41.8.1.3 Atrioventricular Junctional (Nodal) Rhythms

While studies in the rabbit [103] indicate that there are no pacemaker cells in the AV node, pacemaker cells have been found in the AV node of dogs [104]. Because of earlier findings in the rabbit, the term atrioventricular nodal rhythms

was changed to AV junctional rhythms or His-bundle rhythms since pacemaker cells are found in the region of the AV node, especially in the His bundle [105]. Because the precise origin of these ectopic beats cannot be determined in the ECG, the more general term, AV junction, is preferable. The AV junctional escape beats occur as a subsidiary pacemaker when the sinus rate falls below 60 bpm. The inherent escape rhythm rate of the AV junctional region is 40–60 bpm. Single escape complexes can occur after long sinus pauses or after AV nodal block. The AV junctional escaperhythms occur as a sustained rhythm to "rescue" the heart when the sinus node fails to fire sufficiently or the AV node is blocked.

41.8.2 Ventricular Rhythms

41.8.2.1 Ventricular Escape Rhythm

When the sinus node and AV junctional subsidiary pacemakers fail to fire, the heart is rescued by a ventricular escape beat or, if sustained for more than three complexes in a row, a ventricular escape rhythm. For most dogs, the rate of the secondary pacemakers from the Purkinje system in the ventricle is between 20 and 30 bpm. These can be seen on occasion during Holter recordings of normal dogs that are sleeping.

41.8.2.2 Ventricular Extrasystoles

Ectopic premature complexes originating from the ventricle are termed as: (1) ventricular extrasystoles, (2) ventricular premature complexes, or (3) premature ventricular complexes. Their prevalence in control records from beagles varies from 0.6% to 1.0% [25], which approximates to that reported in human ECGs [21]. Accordingly, the occurrence of ventricular extrasystoles in an occasional animal may not be related to drugs or disease. When ventricular extrasystoles alternate with normal complexes, the term to describe the pattern is ventricular bigeminy. See Fig. 41.18.

41.8.2.3 Ventricular Parasystole

For this and more complex arrhythmias, long recording times of the cardiac rhythm are required. Of the electrocardiographic criteria for parasystole, the most controversial is the mathematical relation of the interectopic intervals. As this type of ventricular rhythm has been studied, the initial "rules" to make this diagnosis have been altered as the complexity has been more fully understood. In the simplified understanding of ventricular parasystole, the ventricular ectopic pacemaker discharges with complete regularity, and the interectopic intervals (the intervals between two consecutive ectopic beats that are separated by intervening sinus beats) are nearly an exact multiple of the ectopic cycle length (the time interval between two consecutive ectopic beats without any intervening sinus beats). This is the case in humans with this arrhythmia [8], but is more difficult to identify in dogs. The ectopic cycle length can vary for a variety of reasons including:

(a) Changes in the fundamental discharge rate
(b) Delay in conduction from the ectopic focus to responsive myocardium

In dogs, the most likely cause of alterations in the ectopic cycle length is the presence of sinus arrhythmia associated with the parasystole. It has been demonstrated experimentally [106–108] that a parasystolic focus is protected, but not insulated by a surrounding area of depressed excitability, and can be modulated by electrical events in surrounding tissues; the ectopic cycle length can be lengthened or shortened by electrotonic influences [109]. In man, the parasystolic focus is seldom completely regular and can be altered by vagal reflexes (e.g., carotid sinus pressure), while the timing of normotopic beats during interectopic intervals [110] and the ectopic cycle length can change abruptly without intervention [111]. Also, in the intact heart, neurogenic, endocrine, and hemodynamic factors can change the discharge rate of parasystolic foci

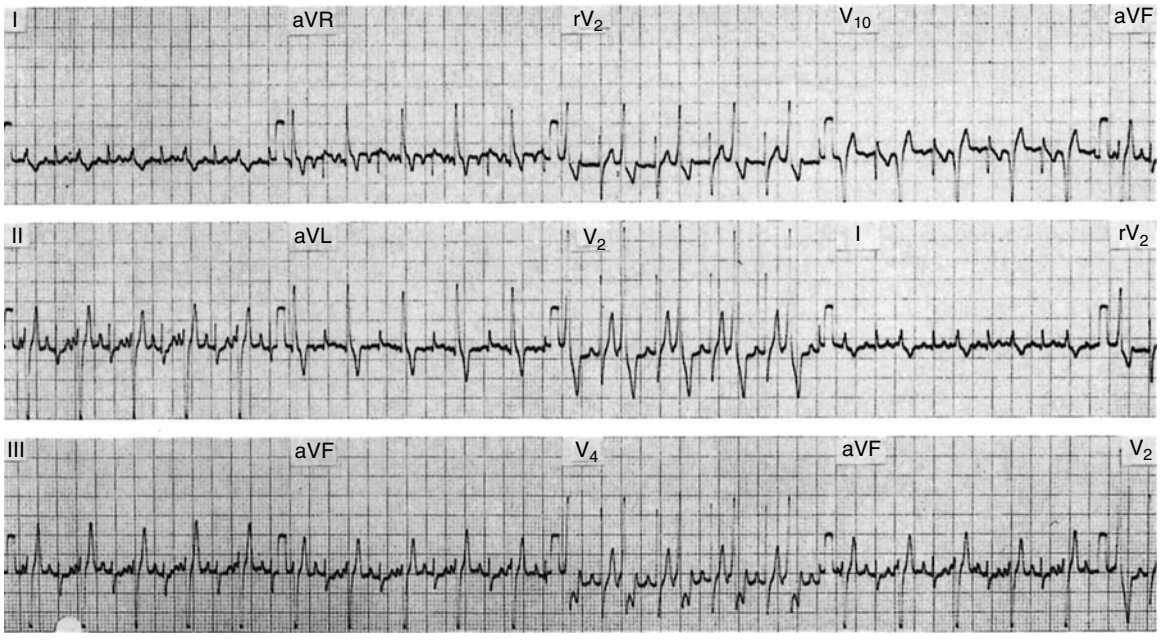

Figure 41.18

Ventricular bigeminy. This arrhythmia appeared in a control group beagle bitch in a routine ECG taken on day 1813 of a chronic drug trial. A record taken 16 days later was normal and no cardiac lesions were observed at necropsy 14 days later.

[110]. Further, the human heart can give rise to coupled ventricular extrasystoles and ventricular parasystole at different times from the same focus [111].

41.8.2.4 Ventricular Tachycardia

Ventricular tachycardia (VT) is a rapid succession of impulses originating from below the AV node. The rate of VT is one which is greater than the inherent rate of the Purkinje fibers in the ventricle which is approximately 30 bpm. In the dog, the usual rate of VT can be one that approximates a normal sinus rhythm (named idioventricular tachycardia) or be as rapid as 500 bpm. The latter rate usually can be maintained for less than a second.

The causes of VT in the dog are varied and include noncardiac and cardiac diseases. Noncardiac diseases include trauma both directly to the heart and indirectly such as to the cranium, gastric torsion, neoplasia, and varied causes of hemodynamic compromise. Several breeds have inherited ventricular arrhythmias that can cause sudden death [112–138]. Boxers are afflicted with arrhythmogenic right ventricular cardiomyopathy [112–118]. This disease results in a distinctive VT that is characterized by a positive QRS complex VT in the anterior (leads II, III, and aVF) leads since the arrhythmia originates from the right ventricle. Rate of the VT in the boxer is very high (frequently 250–300 bpm) and often results in syncope when it is sustained. Some boxers die suddenly while others do not, either due to treatment or chance, but do develop congestive heart failure as the disease progresses. German shepherds are afflicted with inherited ventricular arrhythmias that primarily are manifested in young dogs between the ages of 13 and 70 weeks. Sudden death can occur without prodromes that give evidence of the disease [119**?** –138]. Most commonly, the VT in the German shepherd is usually characterized as a nonsustained polymorphic rapid ventricular tachycardia. Ventricular tachycardia also is documented in Dobermans with dilated cardiomyopathy and other dogs with myocardial failure.

Figure 41.19
Multiform ventricular flutter (torsades de pointes). This arrhythmia was induced during a subchronic toxicity study with an experimental class I antiarrhythmic agent in an experimental beagle. The ventricular rate varies from 240 to 260 bpm.

Drugs can induce VT in dogs with structurally normal hearts, but more commonly when ischemia or other disorders are present. When drugs are screened, the development of VT is considered a marked adverse response to a drug.

(a) *Torsades des pointes*. Torsades des pointes is a specific type of VT that is characterized by a rapid polymorphic VT that shows the complexes changing polarity and morphology as though around a line similar to the twisting of a fence (thus the name). This particular arrhythmia has been the reason for extensive studies of many drugs, both cardiac and noncardiac to assure that the investigated drug does not induce torsades des pointes. This rhythm is induced most likely because of the drug's effects on repolarization currents that result in prolongation of the QT interval. Many drugs have been identified to induce prolongation of the QT and torsades des pointes, and an international registry exists for the logging of cases of prolonged QT (see www.qtdrugs.org). Examples of drugs known to prolong the QT interval include quinidine, disopyramide, lidocaine, procainamide, prenylamine, phenothiazines, and tricyclic antidepressants [139]. It can be induced experimentally by burst pacing hearts with coronary occlusion in dogs, given 30 mg kg^{-1} of quinidine [140] (Fig. 41.19).

41.8.2.5 Atrioventricular Dissociation

The term AV dissociation often should not be considered an "arrhythmia," but only the result of an arrhythmia [19]. AV dissociation occurs when the atria and ventricles are depolarizing independently. This general category includes arrhythmias such as the third-degree heart block and ventricular tachycardia. Isorhythmic dissociation (same rhythm rate but not associated) occurs when the rates of the sinus and ventricular discharge are almost exact (Fig. 41.20).

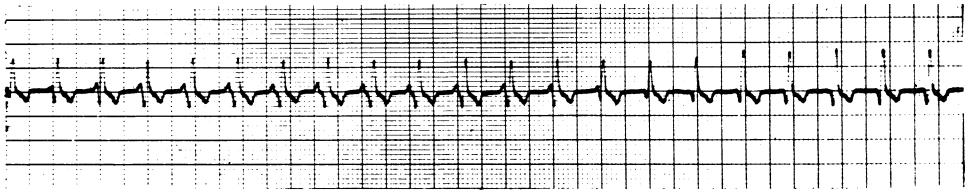

Figure 41.20

Isorhythmic atrioventricular dissociation: starting with the second complex, the p waves are seen to separate sequentially from the Q wave then move forward to fuse with the Q wave again, decreasing its amplitude for three beats, after which it moves further forward to fuse with the R wave, increasing its amplitude in the final five complexes (accrochage). Lead V_2 of a six-year-old male Labrador retriever with cor pulmonale caused by heartworm infestation and congestive heart failure is shown. The arrhythmia was caused by digoxin intoxication.

41.8.3 Atrial and Atrioventricular Conduction Disorders

41.8.3.1 Intra-atrial Conduction Disorders

(a) *Sinoatrial block*. Although this arrhythmia occurs spontaneously in dogs [23], the diagnosis of SA block usually cannot be made with certainty at resting heart rates because of the ubiquitous presence of sinus arrhythmia.

(b) *Sinus arrest, sinus standstill*. This electrocardiographic diagnosis indicates that the sinus P waves are absent for an interval that should have included several heartbeats. Such periods of pacemaker arrest are occasionally caused by reflex vagal effects (carotid sinus reflex, vasovagal reflex from the esophagus as induced by passing a stomach tube, etc.) or drug effects that increase baroreceptor sensitivity, and cause central vagal nucleus stimulation (e.g., digitalis, morphine, tranquilizers). In the clinic, it is observed sometimes in the presence of intracranial tumors, atrial disease, and as a hereditary abnormality in certain breeds [25].

(c) *Intra-atrial block*. This term is applied when there is evidence of a conduction delay in the atria causing widening and deformation of the P waves beyond normal limits of variation. As discussed before, the almost universal respiratory sinus arrhythmia is accompanied by marked P-wave variation in amplitude in certain limb leads. The duration of P waves, however, varies little. The notched P waves, in the absence of increased P-wave duration beyond 0.06 s, are not abnormal per se. Conduction defects are indicated when the P-wave duration increases beyond 0.06 s in limb leads. Drugs that slow myocardial conduction, such as type I antiarrhythmic agents, are likely to delay atrial depolarization. Hyperkalemia above 7.5 mEq l^{-1} will widen P waves and, at higher levels, abolish the P waves entirely. Widening of P waves sometimes accompanies atrial enlargement.

41.8.3.2 Atrioventricular Block

(a) *First-degree AV block*. In this case, the PR interval is prolonged beyond 0.13 s and rarely exceeds 0.20 s. The normal PR interval shortens with increasing heart rate (Table 41.5). When sinus tachycardia is present (i.e., at rates exceeding 150 bpm), the PR interval ordinarily is shortened to less than 0.12 s, so that PR intervals greater than this may be considered first-degree AV block at more rapid heart rates. Not infrequently, the PR interval varies in first-degree AV block, so that only some of the intervals exceed these upper limits.

(b) *Second-degree AV block*. The block may be sporadic or frequent, regular or irregular. It may be preceded by progressively increasing PR intervals, fixed PR intervals, or PR intervals that lengthen and then shorten. The ratio of blocked to conducted beats is only rarely constant in dogs, probably because of the superimposed respiratory sinus arrhythmia that is usually also present: Type I second-degree AV block (Wenckebach phenomenon or Mobitz type I) is more common in dogs than type II. Type II second-degree AV block (Mobitz type II) occurs in otherwise normal dogs only sporadically and often at fairly rapid heart rates. Although this conduction disorder (see Chap. 28) is reputed to occur in man only in the presence of organic heart disease [21], this is not true in dogs. Most likely, it occurs in

dogs as a more-or-less physiological phenomenon when, for some reason, there is a sudden, transient increase in vagal tone that blocks AV conduction for just a single cardiac cycle. When encountered, however, the presence of organic heart disease should be ruled out by further cardiac examination. In some dogs, type I second-degree AV block develops at slower sinus rates, when type II has occurred as an isolated event at a more rapid rate.

Except for type II (Mobitz) second-degree AV block in dogs, first-degree and second-degree AV blocks are generally simply normal physiological variants.

(c) *Third-degree AV block*. Third-degree AV block is a common bradyarrhythmia in the dog that demands the implantation of a permanent pacemaker. Although underlying myocardial disease that will eventually affect hemodynamic function exists, most dogs respond well to this treatment. Usually, the atrial rate is rapid (e.g., 105–145 bpm) and the ventricular rate is slow (e.g., 25–30 bpm). Syncope or weakness is a common clinical sign. If not treated, heart failure or sudden death will result in spontaneous cases [23].

In experimental AV block, following the crushing of the His bundle, ventricular rates were 49 ± 2 bpm after surgery and reached a plateau by day 31 at 44 ± 2 bpm [141]. This rate continued to the end of the 3-year observation period. One to 4 weeks after creating the AV block, other authors have reported similar rates, for example, Hurwitz [142] found an atrial rate of 120–200 bpm and a ventricular rate of 26–54 bpm; Reynolds and DiSalvo [143] found a ventricular rate of 55 ± 13 bpm; and Robinson et al. [144] gave an atrial rate of 125 ± 10 bpm and a ventricular rate of 37 ± 3 bpm.

41.8.4 Frequency of Arrhythmias in the Human and the Dog

The ideal way to evaluate the frequency of arrhythmias in any species is with a 24-h Holter. However, with a large number of subjects, an appreciation of the number of arrhythmias in a population can be gleaned. It must be understood that if the arrhythmia number is restricted to ECG recordings for a brief period, also in the situation whereby an animal is stressed by the procedure, the amount of arrhythmias will be different than in circumstances that do not provoke the autonomic nervous system as much. These latter conditions would include the 24-h Holter and telemetry recordings. Consequently, comparisons must be made with the same techniques. Also, the age of the animal has a bearing on the arrhythmia number.

Comparable electrocardiographic series in the dog and the human are not available. The most relevant data from the human that might be compared with data from young experimental beagles of both sexes are the findings among 67,375 asymptomatic young adult male air force officers from whom 12-lead records were taken [145]. The dog ECGs are from pretest records on 5,513 young (usually 5–7 months old) experimental beagles from which pretest records were taken before being used in toxicity trials. In about 90% of the beagles, two ten-lead ECGs taken several days apart were available. The overall arrhythmia prevalence rates in the two groups were similar (27.9 per thousand for the human against 25.6 per thousand for the dog). The prevalence of ventricular ectopic beats for the human (6.2 per thousand) was about the same as for the dog (8.0 per thousand). Note that the first-degree AV block is more common in the human than in the dog, while the reverse is true for the second-degree AV block. Ventricular parasystole may be more prevalent in beagles than in humans, as may be ventricular escape rhythms, and electrical alternans. Wolff–Parkinson–White syndrome and the bundle branch block may be more common in humans. However, because of the disparities between the data and their collection and analysis, comparison is, although interesting, of questionable validity.

41.9 Comparing Serial Electrocardiogram Records

Either in clinical heart disease or in experimental cardiotoxicity, serial ECGs may permit the recognition of electrophysiological changes that presage definite electrocardiographic abnormalities. This requires that the latest record from each dog should be compared with the previous records to detect subtle changes that are not necessarily outside normal limits. Ideally, adequate numbers of dogs are included in control and treated groups such that a statistical evaluation can be made; however, often studies are undertaken with very low numbers of animals (particularly pilot investigations), and this necessitates comparisons among dogs for treatment effects. Because of the variability in recording the ECG, however, enough of a difference must be documented in order to say that the change is less likely to be due to chance. The

following is a list of changes that, if exceeded, require further examination. Note that the following are suggested from experience and not based on the variability analysis. In toxicity trials, their significance is increased if several individuals in a dose group are similarly affected. It should be emphasized that these differences are based on testimonial experience of the author. Ideally, studies to document repeatability and variability between recordings for each study group are needed for precision. However, these can serve as a beginning for comparisons.

(a) Increases in time intervals
P wave + 20 ms
PR interval + 30 ms (when not rate related, see Table 41.5)
Second-degree AV block
QRS interval + 15 ms
QT + 40 ms (when not rate related, see Table 41.5)
(b) QRS frontal plane axis: change of 30°
(c) Increases in amplitude
R-wave amplitude increased by 0.7 mV
T-wave amplitude increased by 50%
ST-segment deviation greater than 0.15 mV
(d) Sinus arrhythmia index (I = 100 [R-R standard deviation/mean R-R]):
substantial decrease in the absence of a commensurate increase in heart rate
(e) Contour and polarity
P reversal in any limb lead
ST-segment slurring

Reversal of T-wave polarity (caution is advised when the evaluation involves a very young dog and also when a dog is close to 1 year of age)

41.10 Cardiotoxic and Drug Effects on the Electrocardiogram

An important sphere of canine electrocardiography is the detection of myocardial injury and of altered regulation of cardiac activity in drug trials, nutritional studies, immunopathological responses, and in the veterinary clinic. Although the injurious agents are legion, the types of electrophysiological changes possible are limited, so that the diagnosis of specific chemical or biological agent effects is not possible through electrocardiography. Certain classes of drugs and chemicals, however, produce characteristic constellations of electrophysiological changes, so that when the test agent is known or suspected, its presence may often be predicted from the electrocardiographic findings.

Reviews of cardiotoxicity and myocardial injury include those of Bohle [146], Wenzel [147], Selye [148], Chung and Dean [149], Davies and Gold [150], Bristow [151], Balazs [152], Van Stee [153], and Spitzer [154]. Reviews dealing principally with electrocardiological drug effects include those of Scherf and Schott [8], Bellet [18, 19], Surawicz and Lasseter [155], Surawicz [156, 157], Vaughan Williams [158], Singh et al. [159], Schamroth [20], Detweiler [26], Harrison [160], and Lazdunski and Renaud [161].

41.10.1 Drug Effects on Transmembrane Action Potentials and ECG Changes

The relationship between transmembrane action potential changes and electrocardiographic changes is known for a number of drugs and electrolytes. From simultaneous records of ventricular transmembrane potentials and ECGs, the influence of transmembrane potential (TMP) effects on the ECG can be shown [161].

(a) When the slope of phase 0 of the TMP is decreased, conduction velocity is slowed, and in the ECG the QRS increases in duration (e.g., quinidine and other type I antiarrhythmics).

(b) The duration of the TMP approaches that of the QT interval, so that shortening or lengthening of TMP duration has a directly corresponding effect on the QT interval (e.g., digitalis glycosides shorten and hypocalcemia lengthens the TMP).
(c) Lengthening of phase 2 of the TMP lengthens the ST segment of the ECG and shortening phase 2 has the opposite effect (e.g., hypocalcemia prolongs and digitalis shortens the ST segment).
(d) Increased velocity of repolarization during phase 2 of the TMP reduces or abolishes this plateau and the ST segment of the ECG is abbreviated (e.g., digitalis glycosides).
(e) A more acute transition from the slope of phase 2 to that of phase 3 of the TMP, together with increased slope of phase 3, produces symmetrical peaking of the T waves in the ECG (e.g., hyperkalemia).
(f) A less acute transition from the slope of phase 2 of the TMP to that of phase 3 such that the repolarization configuration approaches a straight line and causes reduction of the T-wave amplitude in the ECG (e.g., barbiturates).
(g) Prolongation and decreased slope of phase 3 of the TMP exaggerates the U wave of the ECG (e.g., hypokalemia).

41.10.1.1 Drug Effects on the ECG

There are some electrocardiographic alterations that are somewhat less well known [26, 162]. This consists of a characteristic configurational change in the form of the ST-T segments in lead rV_2 especially and sometimes also in leads V_2, V_4, and V_{10}. In the precordial leads (rV_2, V_2, and V_4), the ST segment and first portion of the T wave form a convex upward curve and the terminal portion of the T wave forms a positive spike, hence the descriptive term "dome-dart T waves." In lead V_{10}, the ST curve is concave upward and the terminal spike is negative; that is, more or less the reciprocal of the configuration in lead rV_2. This morphological change is usually accompanied by QT-interval prolongation. The duration of QT may vary, depending on the length of the preceding R-R interval in sinus arrhythmia (e.g., from 0.30 to 0.34 s, with the longer QT intervals following the shorter R-R intervals).

This combination of electrocardiographic effects has been observed in toxicological studies with tricyclic antidepressants, phenothiazine derivative and butyrophenone derivative antipsychotic agents, and certain antihistaminic compounds. When the various pharmacological properties of these test agents were known, they combined the central nervous system, antihistaminic, and local anesthetic actions. Often, however, only their central nervous system or antihistaminic effects had been identified at the time of the toxicity trial.

One of these experimental drugs, a butyrophenone derivative neuroleptic, in addition to dome-dart T waves and QT interval prolongation, produced cardiac slowing, first-degree and second-degree AV block, left and right bundle branch block (LBBB and RBBB), and ventricular ectopic beats. Marked sinus arrhythmia was present and the LBBB and RBBB appeared sporadically following short R-R intervals. Frequently, the PR intervals preceding these bizarre complexes were not prolonged beyond normal limits. Ventricular reentrant beats with RBBB configuration followed occasional RBBB beats, and LBBB reentrant beats followed occasional LBBB complexes. Since BBB occurred in the absence of prolonged PR intervals, sometimes it appears that the depression of conduction was relatively greater on the bundle branch Purkinje fibers than on the atrioventricular junctional tissues.

41.10.1.2 The QT Interval

The important thing about QT prolongation is not its possible relation to negative inotropy, but rather its relation to arrhythmia vulnerability. It is one manifestation of increased inhomogeneity of ventricular refractory periods. The long QT syndrome has been an extensive study and the measurement of the QT interval, the subject of thousands of papers. Moreover, the correct evaluation of the QT interval in the dog for toxicological studies is one for continued discussion [51–54], and drugs that prolong the QT interval are associated with sudden death [163]. Evaluation of the QT interval is a mainstay for drug studies; however, adjusting for the QT interval relative to heart rate remains problematic for studies

that involve small numbers of animals with brief recordings. The formulas derived for use in humans are not suitable for the dog [50, 51]. Full conferences have been held with this as the focus of attention. As this is a changing field of standards, it is advised to search via the Internet for the latest information at the time of design for studies in the dog for which the QT interval is an integral part of the examination.

41.10.1.3 ST-T and T-Wave Changes

The T waves in dog ECGs are markedly labile. They may be either positive or negative in most leads, and their polarity may change from record to record taken sequentially. The exceptions are lead rV_2 in which the T waves are almost always positive and lead V_{10} in which they are almost always negative. This characteristic of lead V_{10} applies only if the records are taken with the dogs in right lateral recumbency since, for example, V_{10} is frequently positive in beagles placed in the supine position.

The contour, slope, and deviation from the isopotential line of the ST segment in dog ECGs are also quite variable and change spontaneously from record to record taken at different times. Serum electrolyte alterations and cardioactive drugs often reveal their presence by changing the relative durations and contours of the ST segment and T wave. Depending on the magnitude of the change induced, such drug effects may merely alter the form of ST-T complexes in a characteristic way, but not produce a distinctly abnormal record. Thus, the complexes may be judged to be within normal limits of form and duration for the dog ECG, but because similar changes occur in several animals in a given dose group they can be attributed to drug action. For example, some drugs cause the ST-T complexes in several leads to assume a similar contour and polarity. Reversal of T waves in rV_2 and V_{10} is a reliable sign of left ventricular subendocardial and papillary muscle damage (e.g., ischemia, hemorrhage, necrosis) in the dog and, when present in toxicity trials, is accompanied by demonstrable histological lesions in myocardial tissue or small intramural coronary arteries in these regions in about 80% of the cases [164].

41.11 Interpretative Statements

When evaluating ECGs for drug studies, the interpretation is important not only to point out any relevant changes, but also to stress when the changes are unclear because of the vulnerability of the ECG. This is important when a small number of dogs are being studied. The interpretation should include an electrocardiographic diagnosis and relate this to possible electrophysiological mechanisms. It should not go beyond the scope of electrocardiography into possible cardiodynamic or hemodynamic consequences or effects on other organs and tissues. This correlative step can be made only after all the clinical or toxicological information has been assembled.

The interpretative statements should cover the following three areas:

(a) Electrophysiological characteristics detected by the ECG. This will include changes in conductivity and rhythmicity and speculations about the anatomical sites and possible effects on the transmembrane action potentials of the cardiac cell.
(b) Description of electrocardiographic features that may or may not be related to heart disease, cardiotoxicity, or physiological state. These may have a low order of significance in themselves, but may relate to other clinical or toxicological findings. Examples are nonspecific contour changes in ST segments and T waves in various leads.
(c) The likelihood that heart disease or a cardiotoxic effect is present because the physiological state of the heart has been sufficiently altered or because pathological myocardial lesions may be present.

Acknowledgement

Dr. Sydney Moise at Cornell University contributed updates to this chapter.

References

1. Waller, A., Introductory address on the electromotive properties of the human heart. *Br. Med. J.*, 1888;**2**: 751–754.
2. Einthoven, W., Enregistrement galvanométrique de l'électrocardiogramme humain et contrôle des résultats obtenus par l'emploi de l'électromètre capillaire en physiologie. *Arch. Néerland. Sci. Not.*, 1904;**11**(9): 202–209.
3. Einthoven, W., Weiteres über das Elektrokardiogramm. *Pfluegers Arch.*, 1908;**122**: 517–584.
4. Einthoven, W, G. Fahr, and A. de Waart, Über die Richtung und die manifeste Grösse **der** Potentialschwankungen immenschlichen Herzen und über den Einfluss der Herzlage auf die Form des Elektrokardiogramms. *Pfluegers Arch.*, 1913;**150**: 275–315.
5. Waller, A.D., *A Short Account of the Origin and Scope of Electrocardiography. The Harvey Lectures, 1913/14*. Philadelphia, PA: Lippincott, 1915, pp. 17–33.
6. Lewis, T., *The Mechanism and Graphic Registration of the Heart Beat*, 3rd edn. London: Shaw, 1925.
7. Rothberger, C.J., Normale und pathologische Physiologie der Rhythmik unct Koordination des Herzens. *Erg. Physiol.*, 1931;**32**: 472–820.
8. Scherf, D. and A. Schott, *Extrasysto/es and Allied Arrhythmias*, 2nd edn. Chicago, IL: Year Book Medical, 1973.
9. Wenckebach, K.F. and H. Winterberg, *Die unregelmässige-Herztätigket*. Leipzig: Engelman, 1927.
10. Wilson, F.N., F.D. Johnston, and E. Lepeschkin, Editors. *Selected Papers*. Ann Arbor, MI: Heart Station, University Hospital, 1954.
11. Nörr, J., Über Herzstromkurvenaufnahmen an Haustieren. Zur Einführung der Elektrokardiographie in die Veterinärmedizin. *Arch. Wiss. Prakt. Tierheilkd.*, 1922;**48**: 85–111.
12. Roos, J., Vorhofflimmern bei den Haustieren. *Arch. Wiss. Prakt. Tierheilkd.*, 1924;**51**: 280–293.
13. Haupt, K., *Die Aufnahmetechnik des Hundeelektrokardiogramms in der Veterinärklinik und ihre Ergebnisse*, dissertation. Giessen: University of Giessen, 1929.
14. Ludwig, K-H., *Die Elektrokardiographie beim gesunden Hund unter besonderer Berücksichtigung ihrer Anwendung in der Klinik*, dissertation. Leipzig: University of Leipzig, 1924.
15. Gyarmati, E., *Klinische elektrokardiographische Untersuchungen beim Hunde*, dissertation. Budapest: University of Budapest, 1939.
16. Lannek, N.A., *Clinical and Experimental Study on the Electrocardiogram in Dogs*, dissertation. Stockholm: Royal Veterinary College, 1949.
17. Burch, G.E. and N.P. DePasquale, *A History of Electrocardiography*. Chicago, IL: Year Book Medical, 1964.
18. Bellet, S., *Clinical Disorders of the Heart Beat*, 2nd edn. Philadelphia, PA: Lea & Febiger, 1963.
19. Bellet, S., *Essentials of Cardiac Arrhythmias: Diagnosis and Management*. Philadelphia, PA: Saunders, 1972.
20. Schamroth, L., *The Disorders of Cardiac Rhythm*, vols. 1, 2, 2nd edn. London: Blackwell Scientific, 1980.
21. Ettinger, S.J. and P.F. Suter, *Canine Cardiology*. Philadelphia, PA: Saunders, 1970.
22. Detweiler, D.K., D.F. Patterson, J.W. Buchanan, and D.N. Knight, The cardiovascular system, in *Canine Medicine*, vol. 2, 4th edn., E.J. Catcott, Editor. Santa Barbara, CA: American Veterinary, 1979, pp. 813–949.
23. Bolton, G.R., *Handbook of Canine Electrocardiography*. Philadelphia, PA: Saunders, 1975.
24. Tilley, L.P., *Essentials of Canine and Feline Electrocardiography*, 2nd edn. Philadelphia, PA: Lea & Febiger, 1985.
25. Detweiler, D.K., The use of electrocardiography in toxicological studies with Beagle dogs, in *Cardiac Toxicology*, vol. 3, T. Balazs, Editor. Boca Raton, FL: CRC Press, 1981, pp. 33–82.
26. Lautenschlager, O., *Grundlagen der Aufnahmetechnik des Elektrokardiogrammes von Pferd und Rind und ihre Ergebnisse*, dissertation. Giessen: University of Giessen, 1928.
27. Nehb, W., Zur Standardisierung der Brustwandableitungen des Elektrokardiogramms. *Klin. Wchnschr.*, 1938;**17**: 1807–1811. Cited by Lepeschkin, E., *Modern Electrocardiography*, vol. 1. Baltimore, MD: Williams & Wilkins, 1951.
28. Spörri, H., Der Einfluss der Tuberkulose auf das Elektrokardiogramm. (Untersuchungen an Meerschweinchen und Rindern.) *Arch. Wiss. Prakt. Tierheilkd.*, 1944;**79**: 1–57.
29. Detweiler, D.K., The use of electrocardiography in toxicological studies with rats, in *The Rat Electrocardiogram in Pharmacology and Toxicology*, R. Budden, D.K. Detweiler, and G. Zbinden, Editors. Oxford: Pergamon, 1981, pp. 83–115.
30. Hellerstein, H.K. and R. Hamlin, QRS component of the spatial vectorcardiogram and of the spatial magnitude and velocity electrocardiograms of the normal dog. *Am. J. Cardiol.*, 1960;**6**: 1049–1061.
31. Hahn, A.W., R.L. Hamlin, and D.F. Patterson, Standards for canine electrocardiography. *Academy of Veterinary Cardiology Committee Report*, 1977.
32. Kraus, M.S., N.S. Moise, M. Rishniw, et al. Morphology of ventricular arrhythmias in the boxer as measured by 12-lead electrocardiography with pace-mapping comparison. *J. Vet. Intern. Med.*, 2002;**16**(2): 153–158.
33. McFee, R. and A. Parungao, An orthogonal lead system for clinical electrocardiography. *Am. Heart J.*, 1961;**62**: 93–100.
34. Bloch, W.N. Jr., K.A. Busch, and T.R. Lewis, The Frank vectorcardiogram of the Beagle dog. *J. Electrocardiol.*, 1972;**5**: 119–125.
35. Bojrab, M.J., J.E. Breazile, and R.D. Morrison, Vectorcardiography in normal dogs using; the Frank lead system. *Am. J. Vet. Res.*, 1971;**32**: 925–934.
36. Morita, H., Electrocardiograms of conscious Beagle dogs by apex-base bipolar lead. *Adv. Anim. Cardiol.*, 1984;**17**: 19–23.
37. Sugano, S., Electrocardiographic studies in the beagle as an experimental dog. *Adv. Anim. Electrocardiography*, 1977;**10**: 45–50.
38. Takahashi, M., Experimental studies on the electrocardiogram of the dog. *Jpn. J. Vet. Sci.*, 1964;**24**: 191–210.
39. Cagan, S., Prespevok k elektrokardiogramu, psa. *Bratisl. Lek. Listy.*, 1959;**39**: 540–545.
40. Cagan, S. and E. Barta, Die Bedingungen des konstanten Elektrokardiogrammes beim Hund. *Z. Kreislaufforsch.*, 1959;**48**: 1101–1105.
41. Hulin, I. and S. Rippa, Why does the electrocardiogram of the dog change with a change in the foreleg position? *Am. Heart J.*, 1970;**79**: 143.
42. Hill, J.D., The significance of foreleg positions in the interpretation of electrocardiograms and vectorcardiograms from research animals. *Am. Heart J.*, 1968;**75**(4): 518–527.

43. Hill, J.D., The electrocardiogram in dogs with standardized body and limb positions. *J. Electrocardiol.*, 1968;**1**: 175–182.
44. Almasi, J.J., O.H. Schmitt, and E.F. Jankus,. Electrical characteristics of commonly used canine ECG electrodes. *Proc. Annu. Conf. Eng. Med. Biol.*, 1970;**12**: 190.
45. Rydén, L., A. Waldenström, and S. Holmberg, The reliability of intermittent ECG sampling in arrhythmia detection. *Circulation*, 1975;**52**: 540–545.
46. Morganroth, J., Ambulatory monitoring: the impact of spontaneous variability of simple and complex ventricular ectopy, in *Cardiac Arrhythmias*, D.G. Harrison, Editor. Boston, MA: Hall, 1981, pp. 479–492.
47. Moïse, N.S., Diagnosis and management of canine arrhythmias, in *Canine and Feline Cardiology*, 2nd edn., P.R. Fox, D.D. Sisson, N.S. Moïse, Editors. Philadelphia, PA: W. B. Saunders, 1999, pp. 331–385.
48. Grauwiler, J., *Herz und Kreislauf der Säugetiere: Vergleichend-Funktionelle Daten*. Batiel: Birkhäuser,1965.
49. Bazett, H.C., An analysis of the time relations of electrocardiograms. *Heart*, 1920;**7**: 353–370.
50. Chiang, A.Y., D.L. Holdsworth, and D.J. Leishman, A one-step approach to the analysis of the QT interval in conscious telemetrized dogs. *J. Pharmacol. Toxicol. Methods*, 2006 Mar 6; E-print.
51. Miyazaki, H., H. Watanabe, T. Kitayama, M. Nishida, Y. Nishi, K. Sekiya, H. Suganami, and K. Yamamoto, QT PRODACT: sensitivity and specificity of the canine telemetry assay for detecting drug-induced QT interval prolongation. *J. Pharmacol. Sci.*, 2005;**99**(5): 523–529.
52. Gauvin, D.V., L.P. Tilley, F.W. Smith Jr,, and T.J. Baird, Electrocardiogram, hemodynamics, and core body temperatures of the normal freely moving laboratory beagle dog by remote radiotelemetry. *J. Pharmacol. Toxicol. Methods*, 2006;**53**(2): 128–139.
53. Watanabe, H. and H. Miyazaki, A new approach to correct the QT interval for changes in heart rate using a nonparametric regression model in beagle dogs. *J. Pharmacol. Toxicol. Methods*, 2006;**53**(3): 234–241.
54. Camm, A.J., Clinical trial design to evaluate the effects of drugs on cardiac repolarization: current state of the art. *Heart Rhythm*, 2005;**2**(2 Suppl): S23–29. Review.
55. Harada, T., J. Abe, M. Shiotani, Y. Hamada, and I. Horii, Effect of autonomic nervous function on QT interval in dogs. *J. Toxicol. Sci.*, 2005;**30**(3): 229–237.
56. Batchivarov, V.N. and M. Makik, There is little sense in "common" QT correction methods. *J. Cardiovasc. Electrophysiol.*, 2005;**16**(7): 809.
57. Tattersall, M.L., M. Dymond, T. Hammond, and J.P. Valentin, Correction of QT values to allow for increases in heart rate in conscious Beagle dogs in toxicology assessment. *J. Pharmacol. Toxicol. Methods.*, 2006;**53**: 11–19.
58. Lewis, T., J. Meakins, P.D. White, The excitatory process in the dog's heart. Part I. The auricles. *Philos. Trans. R. Soc. Lond. Ser. B*, 1914;**205**: 375–420.
59. Meek, W.J. and J.A.E. Eyster, Experiments on the origin and propagation of the impulse in the heart. IV. The effect of vagal stimulation and of cooling on the location of the pacemaker within the sino-auricular node. *Am. J. Physiol.*, 1914;**34**: 368–383.
60. Hinds, M.H., D.R. Clark, J.D. McCrady, and L.A. Geddes, The relationship among pacemaker location, heart rate, and P-wave configuration in the dog. *J. Electrocardiol.*, 1972;**5**: 56–64.
61. Goldberg, J.M. and M.H. Lynn-Johnson, Changes in canine P wave morphology observed with shifts in intra-SA nodal pacemaker localization. *J. Electrocardiol.*, 1980;**13**: 209–217.
62. Boineau, J.P., R.B. Schuessler, and C.R. Mooney, et al., Multicentric origin of the atrial depolarization wave: the pacemaker complex. *Circulation*, 1978;**58**: 1036–1048.
63. Anonymous (editorial). U waves: unimportant undulations? *Lancet*, 1983;**2**: 776–777.
64. Watanabe, Y. and H. Toda, The U wave and aberrant intraventricular conduction. Further evidence for the Purkinje repolarization theory on genesis of the U wave. *Am. J. Cardiol.*, 1978;**41**: 23–31.
65. Kishida, H., J.S. Cole, and B. Surawicz, Negative U wave: A highly specific but poorly understood sign of heart disease. *Am. J. Cardiol.*, 1982;**49**: 2030–2036.
66. Rudolph, A.M., P.A.M. Auld, R.J. Golinko, and M.H. Paul, Pulmonary vascular adjustments in the neonatal period. *Pediatrics*, 1961;**28**: 28–34.
67. Averill, K.H., W.W. Wagner Jr., and J.H.K. Vogel, Correlation of right ventricular pressure with right ventricular weight. *Am. Heart J.*, 1963;**66**: 632–635.
68. Kirk, G.R., D.M. Smith, D.P. Hutcheson, and R. Kirby, Postnatal growth of the dog heart. *J. Anat.*, 1975;**119**: 461–469.
69. Trautvetter, E., *Untersuchungen zur EKG-Entwicklung an gesunden Welpen und Welpen mitangeborenen Pulmonalstenosen, Habilitationsschrift*. Berlin: Freie Universität Berlin, 1972.
70. Trautvetter, E., D.K. Detweiler, and D.F. Patterson, Evolution of the electrocardiogram in young dogs during the first 12 weeks of life. *J. Electrocardiol.*, 1981;**14**: 267–273.
71. Trautvetter, E., D.K. Detweiler, F.K. Bohn, and D.F. Patterson, Evolution of the electrocardiogram in young dogs with congenital heart disease leading to right ventricular hypertrophy. *J. Electrocardiol.*, 1981;**14**: 275–282.
72. Detweiler, D.K., The cardiovascular system, in *Duke's Physiology of Domestic Animals*, chaps. 5–12, 10th edn., M.J. Swenson, Editor Ithaca, NY: Cornell University Press, 1984, pp. 68–225.
73. Amend, J.F. and H.E. Hoff, Analysis of patterns and parameters of the respiratory heart rate response in the unanesthetized dog. *Southwest. Vet.*, 1970;**22**: 301–311.
74. Fuller, J.L., Genetic variability in some physiological constants of dogs. *Am. J. Physiol.*, 1951;**166**: 20–24.
75. Kleiger, R.E., P.K. Stein, and J.T. Bigger Jr., Heart rate variability: measurement and clinical utility. *Ann. Noninvasive Electrocardiol.*, 2005;**10**(1): 88–101. Review.
76. Werner, J., A. von Recum, E. Trautvetter, and H. Sklaschus, Über den Ruherhythmus des Herzens beim Hund. *Z. Kreislaufforsch.*, 1969;**58**: 593–600.
77. Lange, H., *Ober den Eintritt der Atmungsarrhythmie in der ersten Lebenszeit des Hundes*, dissertation. Munich: University of Munich, 1937.
78. Horan, L., G.E. Burch, and J.A. Cronvich, Spatial vectorcardiograms in normal dogs. *Circ. Res.*, 1957;**5**: 133–136.
79. Horan, L.G., G.E. Burch, and J.A. Cronvich, A study of the influence upon the spatial vectorcardiogram of localized destruction of the myocardium of dog. *Am. Heart J.*, 1957;**53**: 74–90.
80. Horan, L.G., G.E. Burch, and J.A. Cronvich, Spatial vectorcardiogram in dogs with chronic localized myocardial lesions. *J. Appl. Physiol.*, 1960;**15**: 624–628.

81. Hamlin, R.L., F.S. Pipers, and C.R. Smith, Computer methods for analysis of dipolar characteristics of the electrocardiogram. *Am. J. Vet. Res*., 1968;**29**: 1867–1881.
82. Boineau, J.P., J.D. Hill, M.S. Spach, and E.N. Moore, Basis of the electrocardiogram in right ventricular hypertrophy: relationship between ventricular depolarization and body surface potentials in dogs with spontaneous RVH-contrasted with normal dogs. *Am. Heart J*., 1968;**76**: 605–627.
83. Chastain, C.B., D.H. Riedesel, and P.T. Pearson, McFee and Parungao. Orthogonal lead vectorcardiography in normal dogs. *Am. J. Vet. Res*., 1974;**35**: 275–280.
84. Bruninx, P. and H.E. Kulbertus, The McFee-Parungao vectorcardiogram in normal dogs. *J. Electrocardiol*., 1974;**7**: 227–236.
85. Detweiler, D.K. and D.F. Patterson, The prevalence and types of cardiovascular disease in dogs. *Ann. N. Y. Acad. Sci*., 1965;**127**: 481–516.
86. Hill, J.D., Electrocardiographic diagnosis of right ventricular enlargement in dogs. *J. Electrocardiol*., 1971;**4**: 347–357.
87. Clark, D.R., J.G. Anderson, and C. Paterson, Imperforate cardiac septal defect in a dog. *J. Am. Vet. Med. Assoc*., 1970;**156**: 1020–1025.
88. Bolton, G.R., S. Ettinger, and J.C. Roush II, Congenital peritoneopericardial diaphragmatic hernia in a dog. *J. Am. Vet. Med. Assoc*., 1969;**155**: 723–730.
89. Patterson, D.F., Animal models of congenital heart disease (with special reference to patent ductus arteriosus in the dog), in *Animal Models for Biomedical Research*. Washington, DC: National Academy of Sciences Publication 1594, 1968, pp. 131–156.
90. Boineau, J.P., M.S. Spach, and J.S. Harris, Study of premature systoles of the canine heart by means of the spatial vectorcardiogram. *Am. Heart J*., 1960;**60**: 924–935.
91. Bolton, G.R. and S.J. Ettinger, Right bundle branch block in the dog. *J. Am. Vet. Med. Assoc*., 1972;**160**: 1104–1119.
92. Blake, D.F. and P. Kezdi, Vectorcardiography in uncomplicated canine bundle branch block. *Circulation*, 1961;**24**: 888–889.
93. De Micheli, A., G.A. Medrano, and D. Sodi-Pallares, Etude électro-vectocardiographique des blocs de branche chez le chien àla lumière du processus d'activation ventriculaire. *Acta Cardiol*., 1963;**18**: 483–514.
94. Moore, E.N., J.P. Boineau, and D.F. Patterson, Incomplete right bundle-branch block. An electrocardiographic enigma and possible misnomer. *Circulation*, 1971;**44**: 678–687.
95. Littlewort, M.C.G., Canine electrocardiography; some potentialities and limitations of thetechnique. *J. Small Anim. Pract*., 1967;**8**: 437–458.
96. Pyle, R.L., *A Study of Certain Clinical, Genetical, and Pathological Aspects of Congenital Fibrous Subaortic Stenosis in the Dog*, thesis. Philadelphia, PA: University of Pennsylvania, 1971.
97. Tilley, L.P., *Essentials of Canine and Feline Electrocardiography: Interpretation and Treatment*, 2nd edn. Philadelphia, PA: Lea & Febiger, 1985.
98. Rosenbaum, M.B., M.V. Elizari, and J.O. Lazzari, *The Hemiblocks*. Oldsmar, FL: Tampa Tracings, 1970.
99. Okuma, K., ECG and VCG changes in experimental hemiblock and bifascicular block. *Am. Heart J*., 1976;**92**: 473–480.
100. Glomset, D.J. and A.T.A. Glomset, A morphologic study of the cardiac conduction system in ungulates, dog, and man. I and II. *Am. Heart J*., 1940;**20**: 389–98, 677–701.
101. Patterson, D.F., D.K. Detweiler, K. Hubben, and R.P. Botts, Spontaneous abnormal cardiac arrhythmias and conduction disturbances in the dog. A clinical and pathologic study of 3,000 dogs. *Am. J. Vet Res*., 1961;**22**: 355–369.
102. Long, D.M., R.C. Truex, K.R. Friedmann, A.K. Olsen, and S.J. Phillips, Heart rate of the dog following autonomic denervation. *Anat. Rec*., 1958;**130**: 73–89.
103. Hoffman, B.F. and P.F. Cranefield, The physiological basis of cardiac arrhythmias. *Am. J. Med*., 1964;**37**: 670–684.
104. Tse, W.W., Evidence of presence of automatic fibers in the canine atrioventricular node. *Am. J. Physiol*., 1973;**225**: 716–723.
105. Damato, A.N. S.H. Lau, His bundle rhythm. *Circulation*, 1969;**40**: 527–534.
106. Jalife, J. and G.K. Moe, Effect of electrotonic potentials on pacemaker activity of canine Purkinje fibers in relation to parasystole. *Circ. Res*., 1976;**39**: 801–818.
107. Jalife, J. and G.K. Moe, A biologic model of parasystole. *Am. J. Cardiol*., 1979;**43**: 761–712.
108. Moe, G.K., J. Jalife, W.J. Mueller, and B. Moe, A mathematical model of parasystole and its application to clinical arrhythmias. *Circulation*, 1977;**56**: 968–979.
109. Furuse, A., G. Shindo, H. Makuuchi, et al. Apparent suppression of ventricular parasystole by cardiac pacing. *Jpn. Heart J*., 1979;**20**: 843–851.
110. Castellanos, A., E. Melgarejo, R. Dubois, and R.M. Luceri, Modulation of ventricular parasystole by extraneous depolarizations. *J. Electrocardiol*., 1984;**17**: 195–198.
111. Soloff, L.A., Parasystole, in *Cardiac Arrhythmias*, L.S. Dreifus and W. Likoff, Editors. New York: Grune & Stratton, 1973, pp. 409–415.
112. Meurs, K.M., Boxer dog cardiomyopathy: an update. *Vet. Clin. North Am. Small Anim. Pract*., 2004;**34**(5): 1235–1244.
113. Baumwart, R.D., K.M. Meurs, C.E. Atkins, et al., Clinical, echocardiographic, and electrocardiographic abnormalities in Boxers with cardiomyopathy and left ventricular systolic dysfunction: 48 cases (1985–2003). *J. Am. Vet. Med. Assoc*., 2005;**226**(7): 1102–1104.
114. Basso, C., P.R. Fox, K.M. Meurs, et al., Arrhythmogenic right ventricular cardiomyopathy causing sudden cardiac death in boxer dogs: a new animal model of human disease. *Circulation*, 2004;**109**(9): 1180–1185.
115. Kraus, M.S., N.S. Moise, M. Rishniw, et al., Morphology of ventricular arrhythmias in the boxer as measured by 12-lead electrocardiography with pace-mapping comparison. *J. Vet. Intern. Med*., 2002;**16**(2): 153–158.
116. Meurs, K.M., A.W. Spier, N.A. Wright, et al., Comparison of the effects of four antiarrhythmic treatments for familial ventricular arrhythmias in Boxers. *J. Am. Vet. Med. Assoc*., 2002;**221**(4): 522–527.
117. Moise, N.S., From cell to cageside: autonomic influences on cardiac rhythms in the dog. *J. Small Anim. Pract*., 1998;**39**(10): 460–468.
118. Harpster, N.K., Boxer cardiomyopathy. A review of the long-term benefits of antiarrhythmic therapy. *Vet. Clin. North Am. Small Anim. Pract*., 1991;**21**(5): 989–1004.
119. Moïse, N.S., V. Meyers-Wallen, W.J. Flahive, et al., Inherited ventricular arrhythmias and sudden death in German shepherd dogs. *J. Am. Coll. Cardiol*., 1994;**24**: 233–243.
120. Moïse, N.S., P.F. Moon, W.J. Flahive, et al., Phenylephrine induced ventricular arrhythmias in dogs with inherited sudden death. *J. Cardiovasc. Electrophysiol*., 1996;**7**: 217–230.

121. Gilmour, R.F. Jr. and N.S. Moïse, Triggered activity as a mechanism for inherited ventricular arrhythmias in German shepherd dogs. *J. Am. Coll. Cardiol*., 1996;**27**: 1526–1533.
122. Moïse, N.S. and R.F. Gilmour Jr., and M.L. Riccio, An animal model of sudden arrhythmic death. *J. Cardiovasc. Electrophysiol*., 1997;**8**: 98–103.
123. Moïse, N.S., D.A. Dugger, D. Brittain, et al., Relationship of ventricular tachycardia to sleep/wakefulness in a model of sudden cardiac death. *Ped. Res*., 1996;**40**: 344–350.
124. Moïse, N.S., R.F. Gilmour Jr., M.L. Riccio, et al., Diagnosis of inherited ventricular tachycardia in German shepherd dogs. *Am. J. Vet. Med. Assoc*., 1997;**210**: 403–410.
125. Freeman, L.C., L.M. Pacioretty, and N.S. Moïse, et al., Decreased density of I_{to} in left ventricular myocytes from German shepherd dogs with inherited arrhythmias. *J. Cardiovasc. Electrophysiol*., 1997;**8**: 872–883.
126. Dae, M., P. Ursell, R. Lee, C. Stilson, M. Chin, and N.S. Moïse, Heterogeneous sympathetic innervation in German shepherd dogs with inherited ventricular arrhythmias and sudden death. *Circulation*, 1997;**96**: 1337–1342.
127. Moïse, N.S., M.J. Riccio, W.J. Flahive, et al., Age dependent development of ventricular arrhythmias in a spontaneous animal model of sudden cardiac death. *Cardiovasc. Res*., 1997;**34**: 483–492.
128. Riccio, M.L., N.S. Moïse, N.F. Otani, et al., Vector quantization of T wave abnormalities associated with a predisposition to ventricular arrhythmias and sudden death. *Ann. Noninvasive Electrocardiol*., Jan 1998;**3**(1): 46–53.
129. Moïse, N.S., From cell to cageside cardiac rhythms in the dog: autonomic influence. *J. Small Anim. Pract*., 1998;**39**: 460–468.
130. Sosunov, E.A., E.P. Anyukhovsky, A. Shvilkin, M. Hara, S.F. Steinberg, P. Danilo Jr., M.R. Rosen, N.S. Moïse, et al., Abnormal cardiac repolarization and impulse initialization in German shepherd dogs with inherited ventricular analysis and sudden death. *Cardiovasc. Res*., 1999;**42**: 65–79.
131. Moïse, N.S., Inherited arrhythmias in the dog: potential experimental models of cardiac disease. *Cardiovasc. Res*., 1999;**44**: 37–46.
132. Merot, J., V. Probst, M. Debailleul, U. Gerlacin, N.S. Moïse, et al., Electropharmacological characterization of cardiac repolarization in German shepherd dogs with an inherited syndrome of sudden death. *J. Am. Coll. Cardiol*., 2000;**36**: 939–947.
133. Sosunov, E.A., R.Z. Gainullin, N.S. Moïse, et al., β_1 and β_2–Adrenergic receptor subtype effects in German shepherd dogs with inherited lethal ventricular arrhythmias. *Cardiovasc. Res*., 2000;**48**: 211–219.
134. Steinberg, S.F., S.A. Alcott, E. Pak, D.H. Hu, L. Protas, N.S. Moïse, et al., Beta-receptors increase in cAMP and include abnormal CAI cycling in the German shepherd sudden death model. *Am. J. Physiol. Heart Circ. Physiol*., 2002;**282**: H1181–H1188.
135. Obreztchikova, M.N., E.A. Sosunov, E.P. Anyukhovsky, N.S. Moïse, et al., Heterogeneous ventricular repolarization provides a substrate for arrhythmias in German shepherd model of spontaneous arrhythmic death. *Circulation*, 2003;**108**: 1389–1394.
136. Sosunov, E.A., M.N. Obreztchikova, E.P. Anyukhovsky, N.S. Moïse, et al., Mechanisms of alph adrenergic potentiation of ventricular arrhythmias in German shepherd dogs with inherited arrhythmic sudden death. *Cardiovasc. Res*., 2004;**61**: 715–723.
137. Protas, L., E.A. Sosunov, E.P. Anyukhovsky, N.S. Moïse, et al., Regional dispersion of L-type calcium current in ventricular myocytes of German shepherd dogs with lethal cardiac arrhythmias. *Heart Rhythm*, 2005;**2**: 172–176.
138. Gelzer, A.R.M., N.S. Mo¿se, and M.L. Koller, Defibrillation of German shepherds with inherited ventricular arrhythmias and sudden death. *J. Vet. Cardiol*., 2005;**7**(2): 97–107.
139. Wald, R.W., M.B. Waxman, and J.M. Colman, Torsade de pointes ventricular tachycardia: a complication of disopyramide shared with quinidine. *J. Electrocardiol*., 1981;**14**: 301–307.
140. Bardy, G.H., R.M. Ungerleider, W.M. Smith, and R.E. Ideker, A mechanism of Torsades de Pointes as observed in a dog model. *Circulation*, 1981;**64**(Suppl. 4): 218.
141. Boucher, M., C. Dubray, and P. Duchene-Marullaz, Long-term observation of atri, fl and ventricular rates in the unanesthetized dog with complete atrioventricular block. *Pfluegers Arch*., 1982;**395**: 341–343.
142. Hurwitz, R.A., Effect of glucagon on dogs with acute and chronic heart block. *Am. Heart J*., 1971;**81**: 644–649.
143. Reynolds, R.D. and J. Di Salvo, Effects of dl-propranolol on atrial and ventricular rates in unaesthetized atrioventricular blocked dogs. *J. Pharmacol. Exp. Ther*., 1978;**205**: 374–381.
144. Robinson, J.L., W.C. Farr, and G. Grupp, Atrial rate response to ventricular pacing in the unanesthetized A-V blocked dog. *Am. J. Physiol*., 1973;**224**: 40–45.
145. Averill, K.H. and L.E. Lamb, Electrocardiographic findings in 67,375 asymptomatic subjects. I. Incidence of abnormalities. *Am. J. Cardiol*., 1960;**6**: 76–83.
146. Böhle, E., Blutgefässe, in *Erkrankungen durch Arzneimittel*, R. Heinz, Editor. Stuttgart: Thieme, 1966, pp. 170–187.
147. Wenzel, D.G., Drug induced cardiomyopathies. *J. Pharm. Sci*., 1967;**56**: 1209–1224.
148. Selye, H., *Experimental Cardiovascular Diseases*, vols. 1, 2. Berlin: Springer, 1970.
149. Chung, E.K. and H.M. Dean, Diseases of the heart and vascular system due to drugs, in *Drug-Induced Diseases*, vol. 4, L. Meyler and H.M. Peck, Editors. Amsterdam: Excerpta Medica, 1972, pp. 345–381.
150. Davies, D.M. and R.G. Gold, Cardiac disorders, in *Textbook of Adverse Drug Reactions*, D.M. Davies, Editor. Oxford: Oxford University Press, 1977, pp. 81–102.
151. Bristow, M.R., Editor, *Drug-Induced Heart Disease*. Amsterdam: Elsevier, 1980.
152. Balazs, T., Editor, *Cardiac Toxicology*, vols. 1, 2, 3. Boca Raton, FL: CRC Press, 1981.
153. Van Stee, E.W., Editor, *Cardiovascular Toxicology*. New York: Raven, 1982.
154. Spitzer, J. J., Editor, Myocardial injury. *Adv. Exp. Med. Biol; Ser*., New York: Plenum, 1983;**161**: 421–443.
155. Surawicz, B. and K.C. Lasseter, Effect of drugs on the electrocardiogram. *Prog. Cardiovasc. Dis*., 1970;**13**: 26–55.
156. Surawicz, B., Relationship between electrocardiogram and electrolytes. *Am. Heart J*., 1967;**73**: 814–834.
157. Surawicz, B., The pathogenesis and clinical significance of primary T-wave abnormalities, in *Advances in Electrocardiography*, R.C. Schlant and J. Hurst, Editors. New York: Grune & Stratton, 1972, pp. 377–421.
158. Vaughan Williams, E.M., Classification of anti-arrhythmic drugs, in *Symposium of Cardiac Arrhythmias*, E. Sandøe, E. Flensted-Jensen, and K.H. Olesen, Editors. Södertälje, Sweden: Astra, 1970, pp. 449–468.

159. Singh, B.N., J.T. Collett, and C.Y. Chew, New perspectives in the pharmacologic therapy of cardiac arrhythmias. *Prog. Cardiovasc. Dis.*, 1980;**22**: 243–301.
160. Harrison, D.G., Editor, *Cardiac Arrhythmias: A Decade of Progress*. Boston, MA: Hall, 1981.
161. Lazdunski, M. and J.F. Renaud, The action of cardiotoxins on cardiac plasma membranes. *Annu. Rev. Physiol.*, 1982;**44**: 463–473.
162. Detweiler, D.K., Electrocardiographic monitoring in toxicological studies: principles and interpretations, in *Myocardial Injury*, J.J. Spitzer, Editor, *Adv. Exp. Med. Biol.*, 1983;**161**: 579–607.
163. Reynolds, E.W. and C.R. Vander Ark, Quinidine syncope and the delayed repolarization syndromes. *Mod. Concepts Cardiovasc. Dis.*, 1976;**45**: 117–122.
164. Detweiler, D.K., *Reversal of T Waves in Leads rV_2 and V_{10} in Toxicity Trials Indicates Left Ventricular Subendocardial and Papillary Muscle Ischemia or Damage*, Personal Observation. Philadelphia, PA: University of Pennsylvania, 1985.
165. Osborne, B.E. and B.D.H. Leach, The Beagle Electrocardiogram. *Food Cosmet. Toxicol.*, 1971;**9**: 857–864.

42 The Mammalian Electrocardiogram: Comparative Features

D.K. Detweiler[†]

[†]For this 2nd Edition of "Comprehensive Electrocardiology," Dr. Sydney Moise has updated this 1st Edition chapter, which was originally written by the late Dr. Detweiler.

P. W. Macfarlane, A. van Oosterom, O. Pahlm, P. Kligfield, M. Janse, J. Camm (eds.), *Comprehensive Electrocardiology*, DOI 10.1007/978-1-84882-046-3_42,

42.1 Introduction

The purpose of this chapter is to summarize the characteristics that distinguish electrocardiograms recorded from different mammalian species rather than reviewing the contributions of experimental animal research to cardiac electrophysiology.

In 1888, using the capillary electrometer, Waller [1] was the first to obtain electrocardiograms from mammals (human, horse, dog, cat, and rabbit). Since that time, aside from the enormous literature on animal experimentation, a modest literature has accumulated on applied mammalian electrocardiography, written by investigators interested in the comparative aspects of electrocardiography, the use of electrocardiography to record cardiac activity in various types of laboratory animal experiments, and the application of electrocardiography in veterinary medicine. While these investigations were generally not designed to add to the mainstream of basic electrocardiographic thought and concept, they have been useful in providing a database for the interpretation of animal electrocardiograms in veterinary medicine and in a large variety of animal research applications in which electrocardiograms are monitored to detect the effects of various experimental interventions on the heart. In more recent years, the mouse has emerged as a vital animal for investigation. Although the surface electrocardiogram is frequently assessed, more detailed electrophysiologic studies have been at the forefront.

Among prominent physician cardiologists, whose interests and work have given impetus to study in this field, are Tawara (anatomy of the conduction system [2]), Paul Dudley White (elephant [3] and whale [4] electrocardiograms), Rudolph Zuckermann (atlas of animal electrocardiograms [5]), Bruno Kisch (electrocardiographic and electrographic studies in animals [6]), Eugene Lepeschkin (literature survey and analysis [7, 8]), Pierre Rijlant (pacemaker function [9]), Thomas Lewis (atrial fibrillation in horses [10, 11]), Luisada (electrocardiograms and phonocardiograms of domestic animals [12]), and Jane Sands Robb (comparative anatomy, histology, embryology, and electrophysiology [13]).

Veterinary electrocardiography had its beginnings with studies in the horse. As a prelude to this, the first normal equine electrocardiogram published (1910) was a record, which von Tschermak obtained from Einthoven [14]. Shortly thereafter, Lewis (1911) published three abnormal records from a horse with atrial fibrillation [10]. In 1911, Kahn [15] published 26 records taken from six horses and in the same year, Waller [16, 17], in two short notes, briefly discussed the cardiac electrical axis of the horse and the relationship between the duration of mechanical systole and the electrocardiogram. Also in 1913, Norr published his inaugural dissertation on the electrocardiogram of the horse and a companion article in the *Zeitschrift fur Biologie* [18]. Norr was to become the leading figure in veterinary electrocardiography for the next 25 years [19–21], contributing by himself or through his students to the literature on animal electrocardiography and comparative pathophysiology of the circulation.

Following these beginnings, until the early 1940s, in addition to Norr and Kahn, only about 20 authors contributed articles on the electrocardiogram of the horse, recommending some five different lead systems [22]. During this period, only a handful of veterinary authors published articles on the canine electrocardiogram [23] and that of other domestic species [24].

During the 1940s, owing to World War II and its aftermath, scientific publication of all kinds diminished. Notable among the few publications that appeared were those of Sporri (ox, guinea pig [25, 26]) in Switzerland; Alfredson and Sykes (cattle [27]) in the United States; Charton, Minot, and Bressou (horse [28–30]) in France; Kelso (lamb [31]) in Australia; Krzywanek and Ruud (swine [32, 33]) in Germany; and Voskanyan and Filatov (horses, cattle [34, 35]) in Russia. Roshchevsky [36] credited Voskanyan with having developed the clinical use of electrocardiography in cattle in the Soviet Union in 1938–1939. This decade was followed by a 30-year period of ever increasing publications on applied electrocardiography in veterinary medicine, toxicological studies, and records from nondomesticated mammals. Modern day electrocardiography is becoming more "paper-free" with the advent of electronic electrocardiograph systems. These systems can store continuous recordings and post-process the leads shown, with adjustable filtering, speed, and gain on the display. Storage of recordings can be facilitated with electronic retrieval, and data bases are searchable by identification and diagnosis.

42.2 Literature Reviews

Today, internet searching for electrocardiographic data on numerous species is the standard. Wide searches can result in hits not only from published papers but also from other sources of information indexed on the web. Although such

means are the standard, some references may be missed from the past. From a historical perspective, the leading sources of references, listed chronologically, in comparative mammalian electrocardiography are the reviews written by Lepeschkin [7, 8], Grauwiler [37], and Roshchevsky [24, 38]. The following summarizes some of these early and important works.

Lepeschkin, in his book published in 1951 [8], covered publications on invertebrates, fish, amphibia, birds, and mammals, citing over 200 references published from 1934 to 1950 as well as publications prior to 1934 cited in his previous book [7]. Grauwiler [37] cites some 125 publications on mammalian electrocardiograms covering the period 1913–1962. Fourteen classes of mammals are represented from monotremes to primates with many illustrations of electrocardiograms and tables of electrocardiographic data for each of the 70 species.

Comparative electrocardiography was reviewed in the publications of Roshchevsky [24, 38]. His earliest effort [38] covers the entire animal kingdom and cites over 970 references. Electrocardiographic, anatomical, heart rate/body weight, and related data are reported. Roshchevsky's monograph [24] emphasizes the spread of ventricular excitation through analysis of intracardiac (endocardial), intramural, and epicardial electrograms, body-surface mapping, vectorcardiography, and the study of various electrocardiographic lead systems. This publication extended an earlier monograph published in 1958 [36]. Monographs on comparative electrocardiology edited by Roshchevsky include the *Physiological Basis of Animal EIectrocardiography* (1965) [39] and proceedings of the first (1979) [40] and second (1985) [41] International Symposia on Comparative Electrocardiology held in Syktyvkar, Komi Republic, USSR.

In 1952, Kisch and his coworkers [6] summarized their studies of electrograms recorded from vertebrate hearts, including those of the rabbit, cat, dog, calf, and human. Data are given on electrocardiographic time intervals, heart rate, and pattern of ventricular excitation from unipolar epicardial and endocardial ventricular electrocardiograms recorded from five mammalian species.

In 1959, Zuckermann, as part of the third edition of his textbook on electrocardiography [5], published an extensive atlas of animal electrocardiograms from arthropods, fish, amphibians, reptiles, birds, and mammals.

Other more recent review publications that contain extensive bibliographies and illustrations, which are not listed in the bibliographies of the works already cited, are on the following animals: horse [42], dog [43–45], monkey [46], and rat [47]. Table 42.1 lists some influential publications on mammalian electrocardiography that appeared between 1888 and 1970. Today, the internet serves as a means to identify electrocardiographic data for many species. Still, compared to the data for other commercial studies on animals, not much data are available to the public on animals used in nonacademic research.

42.3 Classification of Mammalian Electrocardiograms

42.3.1 Bases for Classification

Mammalian ECGs from different species can be classified in accordance with the following general characteristics:

1. Relative duration of QT interval and ST segment
2. QRS-vector direction and sense
3. Constancy of T-wave polarity (T-wave lability) [49, 50]

These differences, in turn, are determined by three electrophysiological properties that are genetically governed: the relative duration of the ventricular cell action potential as determined by the presence or absence of phase 2 (plateau); the pattern of spread of excitation throughout the ventricles; and constancy of the pattern of repolarization, that is, the constancy of the ventricular gradient.

42.3.2 QT Duration and ST Segment

Many species (rodents, insectivores, bats, and kangaroos) have short QT intervals relative to the duration of mechanical systole [51]. The ST segment is essentially absent. The QRST complex consists of rapid QRS deflections that merge with the slower T wave, and its duration is about half that of mechanical systole. The transmembrane action potentials of these

Table 42.1

Contributions important to the development of comparative mammalian electrocardiography

Year	Subject	Author	Reference
1988/9	First horse ECG (capillary electrometer).	Waller	[66]
1910	Einthoven provided horse ECG for veterinary textbook.	von Tschermak	[14]
1911	Visual proof that fibrillating atria produce f waves in ECG (from horses with atrial fibrillation)	Lewis	[10, 11]
1913	Veterinary clinical electrocardiography initiated.	Nörr	[18]
1921	Fetal electrocardiograms obtained from mares.	Nörr	[95]
1921	First elephant ECG	Forbes et al.	[216]
1924	Cardiac arrythmias in horses.	Nörr	[218]
1924	Atrial fibrillation in dogs and horses.	Roos	[219, 220]
1930	Electrocardiographic monitoring in chronic rat (nutritional) studies.	Agduhr, Drury et al.	[221, 222]
1935	Respiratory sinus arrhythmia in *canidae* (dog, fox).	Nörr	[223]
1942	Electrocardiography in dairy cattle.	Alfredson, Sykes	[27]
1949	Clinical chest leads for dogs (rV_2, V_2, V_4).	Lannek	[23]
1951	Survey of animal electrocardiography.	Lepeschkin	[8]
1952	Comparative electrocardiography in mammals.	Kisch et al.	[6]
1953	First whale ECG	King et al.	[4]
1953	First WPW in lower animals (cow).	Spörri	[161]
1953	His-bundle potentials recorded (dog).	Scher	[224]
1953	No ST segment and QT shorter than mechanical systole in adult mouse.	Richards et al.	[185]
1955	Ventricular activation pattern in the dog.	Scher	[225]
1956	QT shorter than mechanical systole and ST segment absent in adult Bennett Kangaroo but not in young in pouch.	Spörri	[186]
1957	Clinical electrocardiography in horse and cattle.	Brooijmans	[67]
1958	Right ventricular hypertrophy pattern in dog.	Detweiler	[226]
1958	Electrocardiography in cattle.	Roschchevsky	[36]
1959	Atlas of animal ECGs.	Zuckerman	[5]
1960	ECG finback whale.	Senft, Kanwischer	[181]
1960	Lead V_{10} introduced in dog.	Hamlin, Hellerstein	[84]
1965	Large atrial mass favors atrial fibrillation.	Moore et al.	[160]
1965	Survey of mammalian ECGs.	Grauwiler	[37]
1966	Monkey ECG.	Malinow	[80]
1967	Definitive criteria for right ventricular hypertrophy in the dog.	Hill	[228, 229]
1968	First journal of animal electrocardiography published (Japan).		[48]
1970	Accessory AV (Kent) bundle conduction identified in WPW syndrome (monkey, dog).	Boineau, Moore	[233]
1970	First monograph on canine cardiology.	Ettinger, Suter	[227]

species do not have a distinct plateau, which explains the absence of the ST segment (Fig. 42.1). This is in contrast to the QRST complex of the remainder of mammals that have an ST segment, a QT interval equivalent to mechanical systole, and an action potential with a distinct plateau. The reason for the differences in the QT interval, ST segment, and the T wave rests in the differences in the specific ion channels that are responsible for repolarization in these varied species. The differences in the ion channels are important not only to understand from the point of recognizing the different ECG

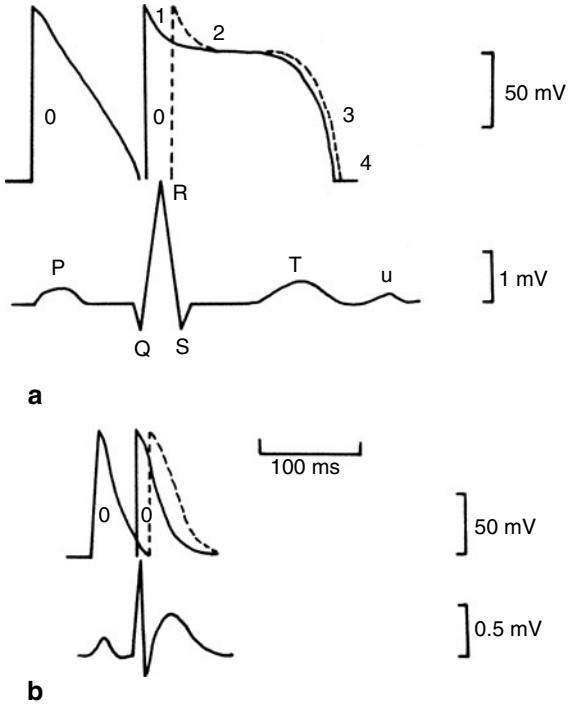

Figure 42.1

Schema of atrial and ventricular transmembrane action potentials (TMAP) and the ECG, drawn on the same time scale. In (a), the five phases of the dog TMAP are shown; 0, initial rapid depolarization or spike; 1, initial rapid repolarization; 2, slow repolarization or plateau; 3, final rapid repolarization; 4, resting or diastolic transmembrane potential. The rat TMAP is shown in (b). Note that the rat and dog atrial and the rat ventricular TMAPs have no plateaux. The TMAPs drawn with the *solid line* represent excitation of ventricular cells early during the QRS interval; those drawn with a *dashed line* represent excitation of ventricular cells later during the QRS. Note that in the dog the plateaux of the TMAPs overlap so that there is little difference in charge between groups of cells. This period of overlap coincides with the isopotential ST segment of the ECG. The T wave of the dog ECG is generated during the final rapid repolarization, phase 3, when at any given instant in time the charges of different masses of cells are not the same. In the rat, the ventricular TMAPs do not have a plateau and there is no period during repolarization when most cells are isopotential. Thus, no ST segment appears in the ECG.

patterns, but also for comparative medicine and the effects of drugs. The latter is vital in understanding the impact that ion channel type has on the response to a pharmacologic intervention that may have little or no effect in one species, yet have a profound consequence in another. This point is of particular importance with regard to the screening for QT prolongation [52].

42.3.3 Ventricular Activation Patterns

The ventricular activation patterns of various species fall into two general classes of QRS-vector direction and sense [24, 53] as follows:

1. Class A includes those animals with QRS vectors which, generally, are directed along the long axis of the body, caudally and ventrally, and produce a largely negative deflection in lead V_{10} and a positive deflection in lead aVF; for example, dogs, humans, monkeys, cats, and rats.

2. Class B includes those animals with QRS vectors which, generally, are directed from sternum toward the spine and which produce largely positive deflections in lead V_{10} and negative deflections in lead aVF; hoofed mammals and dolphins, for example.

These differences are associated with the distributive characteristics of the Purkinje network. In animals belonging to class A, it is primarily a subendocardial network. In class B animals, the Purkinje network is more elaborate and penetrates deeply into the ventricular myocardium.

42.3.4 T-Wave Lability

In humans, primates, and many hoofed mammals, T wave amplitude and polarity tend to be fairly constant in serial records. In dogs and especially in horses, T wave vectors are quite labile. The T waves vary in polarity and amplitude in limb leads and some thoracic leads in serial records, and sometimes change during the course of recording of a given lead. In the dog, there are two conventional thoracic leads in which the T wave polarity is remarkably consistent: the T wave is normally positive in lead rV_2 (this lead approximates that of V_1 in humans and negative in V_{10} in about 90% of individuals [54, 55]).

42.3.5 Effect of ECG Characteristics on Choice of Lead Systems and Terminology

For animals having QRS vector and sense of class A in Sect. 42.3.3, the conventional limb leads are oriented favorably for recording QRS potentials in the frontal plane projection. In animals with class B QRS vectors, on the other hand, the major QRS-vector forces are directed more-or-less perpendicular to the frontal plane and limb leads are not favorably disposed for recording these potentials. Hamlin and Smith's [53] use of lead V_{10} to compare species made this amply clear, but not until there had been a great deal of experimentation to find favorable lead systems, especially in large domestic animals (reviewed by Roshchevsky [24, 36]). Today the base-apex lead is the most common lead used in horses and cattle.

The discovery that another group of mammals has virtually no ST segment in the electrocardiogram caused another terminological dilemma, since ST-segment deviation is an important diagnostic term in classical electrocardiography. Actually, a flat or isopotential ST segment is abbreviated in limb leads in many mammals with the ST segment of class A (e.g., the dog) and is virtually absent in precordial leads of all species. The presence of a stable isoelectric ST segment depends on two factors: first, the occurrence of a distinct plateau and consequent long duration of the transmembrane action potential and second, in large hearts, the presence of a rapid conduction system that spreads the excitation quickly so that the plateaus of many ventricular cells overlap in time. Ventricular ectopic beats, for example, result in slowing of the depolarization throughout the ventricle such that synchrony of the plateau period in various parts of the heart is reduced and the ST segment is consequently abbreviated.

The terminological dilemma arises because the same perturbations that produce ST segment deviations in species with a distinct ST segment (for example, regional ischemia or hypoxia, "injury current") produce a similar shift of the slow-wave portion of the QRST complex in species with no ST segment (e.g., the rat). The phrase ST deviation is so ingrained in diagnostic electrocardiographic parlance as a term with definite diagnostic significance that it represents a concept. Therefore, it has been suggested that the term should be placed in quotation marks (e.g., "ST" segment elevation or depression) when used to indicate the effect of an injury potential on the immediate post-QRS portion of the ventricular complex in species lacking an ST segment [50].

Finally, for species with labile T waves in normal electrocardiograms (e.g., dog and horse), the significance of T-wave reversal in most leads in disease or cardiotoxicity cannot be evaluated. Fortunately, in the dog the T waves in leads rV_2 (V_1) and V_{10} are consistent in polarity and these leads can be used to detect T wave reversal associated with myocardial damage. No such leads have been established for the horse. Additionally, in dogs, rV_2 (V_1) may be a more reliable lead than lead II for the measurement of the QT interval because of the more consistent T wave morphology.

42.4 Technique

42.4.1 Electrocardiographs, Lead Lines, and Electrodes

Since the time of Einthoven, electrocardiographs have been designed primarily to record the cardiac potentials of humans. As the electrocardiograms of smaller mammals have frequency components that are higher than those of humans, electrocardiographs of an earlier era were found to have an inadequate frequency response for these small species [57, 58]. In the rat electrocardiogram, frequency components up to 400 Hz have been reported [59] but little distortion occurs when recording with equipment having a frequency response of 200 Hz [60]. Most modern electrocardiographs are reputed to approach an upper frequency response limit of 200 Hz. Electronic electrocardiographs now permit a longer recording time, as well as post-processing of rate, amplitude, filtering, and speed. The advantage for data storage and review is far superior performance compared to the use of paper recordings. However, these machines are often equipped with optional electronic filters that reduce response to well below that needed to record electrocardiograms of small mammals with fidelity [50]. Thus, to avoid distortion, an understanding of the filtering methods must be appreciated by the operator.

Lead lines connecting the animals to the electrocardiograph must be flexible, made of shielded cable and long enough to accommodate the size of the subject. Fine-wire extensions that are not shielded are satisfactory when dealing with very small species. The major problem to avoid is any tugging on the electrodes by swinging lead lines since this will shift the electrodes at the skin interface and cause baseline artifacts in the electrocardiogram at frequencies or harmonics of the lead-line motion that can vary from slow drift to rapid waves that mimic atrial flutter or fibrillation.

There has been considerable experimentation with electrodes in animal electrocardiography over the years but few studies of the electrical conductive properties of the various types recommended. One exception is the study of Almasi et al. [61]. Clip electrodes, such as electronic crocodile clips, are satisfactory if the total area of contact is ~1 cm^2. Clipping the fur and applying patches similar to the method used in humans is better for intermediate length recordings. The conductive properties of copper are superior to those of stainless steel. Importantly, the medal used for the different leads should not be mixed but uniform.

42.4.2 Restraint

42.4.2.1 Physical Restraint

For farm animals, the usual methods of tethering or use of stanchions are satisfactory. The main requirement is adequate control of foreleg position. For monkeys, flat restraint boards, V-boards or cradles (supine position), and monkey "chairs" (sitting position) are commonly used. Dogs and cats can generally be handled. The use of slings or support in a "begging position" [62] is not recommended. For small laboratory animals (rat, guinea pig, etc.) a variety of restraint devices have been used including the usual commercially available laboratory animal holders. Some investigators have constructed special holders for rats and guinea pigs, which confine the animal so that each limb dangles in separate beakers of saline [63] or each foot rests on electrodes covered with conducting paste [64]. A simple method is to attach the electrodes, cover the animal with a cloth to exclude light and visual stimuli, and hold by hand. For example, satisfactory records were obtained from moles by restraining by hand in a cloth, or by allowing freedom in a box containing earth under which they burrowed and became quiet [65]. For extended studies, implantable recorders are now possible for long-term recording of quality data in very small mammals.

42.4.2.2 Chemical Restraint

Whenever possible, anesthetics, narcotics, or tranquilizers should be avoided because all such agents affect heart rate, rhythm, and electrocardiographic time intervals while some are arrhythmogenic. On the other hand sedation may be required in order to obtain a quality recording. The final decision depends on the question to be answered.

42.4.3 Positioning

In all quadrupeds, it is necessary to control foreleg position to obtain consistent direction and magnitude of cardiac vectors from limb-lead scalar electrocardiograms. It must be emphasized that this precaution applies to large domestic animals as well as small laboratory species [50].

42.4.4 Leads and Lead Systems

42.4.4.1 Limb Leads

Since the time of Waller [1, 66] limb leads have been recorded in animals for scalar electrocardiograms and calculation of vector forces. They were used in Einthoven's laboratory for horses and dogs [67]. For years, some investigators rejected limb leads, considering them unsuitable for various quadrupeds. This was on the spurious ground that the heart is not in the center of an equilateral triangle as in man, not realizing that Einthoven's triangle concept relating the potentials of the three bipolar limb leads depends on Kirchhoff's second law of circuits rather than the geometry of the thorax or the location of limb attachment to the thorax.

Nörr [18] and Kahn [15], on the other hand, favored chest leads over limb leads for sounder reasons. Both investigators considered limb leads unsuitable for horses because the electrocardiographic waves were small and variable compared to those of man. For species belonging to the QRS vector and sense class A (primates, carnivores, certain rodents, etc.), the limb leads have always been considered satisfactory.

42.4.4.2 Chest Leads

In accordance with the aforementioned, Nörr [18] and Kahn [15] devised two similar bipolar electrode positions for the horse. Both placed one electrode on the ventral thoracic surface near the region of the ventricular apex. Nörr located the other electrode on the right anterior breast at the level of the scapulohumeral joint (point of the shoulder) while Kahn placed the other electrode on the right side of the base of the neck at the level of the middle of the anterior border of the scapula. The direction of the deflection was positive when the electrical vector was directed toward the anterior breast or neck electrode and vice versa. Nörr [19] later chose for cattle a location for the neck electrode similar to that used by Kahn for horses because of the more vertical anatomical axis of the ox heart.

Later, in 1928, Lautenschlager [69] investigated thoracic bipolar lead combinations systematically in horses and cattle by mapping a grid over the entire trunk, dividing the surface (right and left sides) into 106 squares measuring 15 × 15 cm. His essential conclusion was that electrode positions like those used by Kahn for horses and by Nörr for cattle were most suitable; that is, one electrode at the cardiac apex region on the left side of the chest at the level of the olecranon, and the other electrode on the right side at the base of the neck in the region of the right scapula. This bipolar thoracic lead, often referred to as a base-apex (or apex-base) lead because the electrodes are placed on the body surface where an extension of the anatomic longitudinal axis of the heart would meet the skin, has been used as a monitoring lead in hoofed mammals and is recommended by the Japanese Association of Animal Electrocardiography for use in dogs [70].

Since 1928, a large number of lead systems have been devised for domestic hoofed mammals in which the three limb-lead electrodes have been placed in some triangular configuration on the torso. These have all been detailed in Roshchevsky's book on hoofed mammal electrocardiography [24]. Sporri's [26] modification of these systems has had wide use in many species, including small animals such as the rat [50], since his 1944 publication. In this system, the Lautenschlager base-apex lead, that is, right arm electrode at the base of the neck (cervical) on the right side paired with the left leg electrode placed in the region of the cardiac apex (apical) on the left ventral chest wall at the level of the olecranon, is recorded when conventional electrocardiographs are switched to the lead II recording position. The left arm

electrode is placed on the back over the last thoracic vertebra. When lead I is recorded a longitudinal lead is recorded between the neck and the last thoracic vertebral electrodes and when lead III is recorded, the recording is between the cardiac apical and last thoracic vertebral electrodes. Sporri's designation for these leads is as follows:

1. Lead D for dorsal (neck to thoracic vertebral electrode, lead I electrodes)
2. Lead A for axial (neck to cardiac apical electrode, lead II electrodes) and
3. Lead J (or I) for inferior (sacral to cardiac apical electrode, lead III electrodes)

This D, A, J lead system, therefore, is equivalent to lead II (dorsal (0) lead) and two precordial leads with the different or "exploring" electrode at the cardiac apex region and the distant electrode at the base of the neck (axial (A) lead) or posterior thoracic region (inferior (1) lead). A variant of this system is to place the left arm electrode at the cardiac apex and the left leg electrode at the last thoracic vertebra (Sander [71]).

In 1954, Brooijmans [67, 72] proposed a thoracic unipolar lead system (employing Wilson's central terminal) in which nine (horse) or seven (cattle) equidistant chest leads encircle the chest vertically at the sixth (horse) or fifth (cattle) intercostal space and five (horse) or four (cattle) electrodes encircle the anterior chest in the horizontal plane. A more complicated thoracic lead system with 28 lead positions was studied by Sellers et al. [73] for dairy cattle. None of the more elaborate chest-lead systems has come into use.

Other triangular thoracic lead systems for large hoofed mammals have been proposed to represent the electrical forces of the cardiac cycle as projected on the frontal (F), transverse (T), and sagittal (S) planes. Roshchevsky [24, 36, 39] devised such a system for hoofed animals (cattle, reindeer, etc.) in which the frontal plane is defined by placing the right arm electrode at the right scapulohumeral (shoulder) joint, the left arm electrode at the left shoulder joint (lead IF), and the left leg electrode on the ventral abdominal midline at the level of the 13th (last thoracic) vertebra (leads I IF and IIIF). The sagittal plane is defined by placing the right arm electrode at the cranial end of the manubrium sterni, the left arm electrode on the withers at the fourth vertebra (lead IS), and the left electrode on the ventral abdomen at the same site as for the frontal plane (leads IIS and IIIS). The electrocardiograph is then switched to obtain six leads in each plane (that is, IF, IIF, IIIF, aVR_F, aVL_F, aVF_F, for the frontal plane and IS; IIS; IIIS, aVR_S, aVL_S, aVF_S, for the sagittal plane). Roshchevsky, from his detailed studies of the cardiac potential over the torso surface of ungulates, considered the sagittal lead system most suitable and it was adopted by [74], for clinical studies with cattle. Sugeno et al. [75] also adopted a three-lead triangular recording system with one lead at the cardiac apex for their earlier studies. Too et al. [76] investigated a three-bipolar-lead sagittal system in cattle (placing the right arm electrode at the cardiac apex, the left arm electrode at the scapulohumeral joint, and the left leg electrode at the withers) and a bipolar transverse three-lead system (placing the right arm electrode on the right olecranon, the left arm electrode on the left olecranon, and the left leg electrode at the withers). Kusachi and Sato [77] experimented with four bipolar systems in horses, finally recommending one in which three electrodes were placed on the right foreleg, left foreleg, and withers, respectively.

In horses, Lannek and Rutqvist [78] introduced a unipolar thoracic read system (employing Wilson's central terminal) patterned after the system Lannek had used in the dog [23]. This system, with the addition of leads V_{10} and CV_6RU, has been used in horses and cattle[42, 79]. These chest leads are as follows:

1. Lead CT_1 in which the exploring electrode was placed on the right side of the thorax 3–5 cm above a horizontal line through the highest point of the olecranon and behind the posterior edge of the triceps brachii muscle
2. Lead CT_2, where the exploring electrode was placed on the left side of the thorax at the same height as a horizontal line through the highest point of the olecranon and behind the triceps brachii muscle
3. Lead CT_3, where the exploring electrode was placed on the left side of the thorax about 8 cm above the CV_6LL (or CT_2) electrode

From this system the following thoracic unipolar leads evolved [79]:

1. Lead CV_6RU, with the electrode on the right side of the thorax at the sixth rib at the level of a horizontal line drawn through the point (scapulohumeral joint) of the shoulder
2. Lead CV_6RL, with the electrode on the right side of the thorax, just above the highest point of the olecranon, behind the triceps brachii muscle at the sixth rib

3. Lead CV_6LL, where the electrode is on the left side of the thorax at the same height as a horizontal line drawn through the highest point of the olecranon, behind the triceps brachii at the sixth rib
4. Lead CV_6LU, with the electrode on the left side of the thorax directly above CV_6LL at the level of a horizontal line drawn through the point of the shoulder
5. Lead V_{10}, where the electrode is placed over the vertebral column vertically above CV_6LL (at about the dorsal spinous process of the seventh thoracic vertebra)

In primates, two systems of thoracic leads have emerged. The most common practice is to use counterparts of the six precordial leads employed in humans [46, 80, 81]. Atta and Vanace [82] introduced a precordial three-lead system for the rhesus monkey (*Macaca mulatta*) with electrodes placed as follows: MV_1 fourth right intercostal space at the midclavicular line; MV_2, fourth left intercostal space at the midclavicular line; and MV_3, fifth left intercostal space at the left, midaxillary line. These leads correspond roughly to leads V_1, V_3, and V_5 in humans [80]. A thoracic lead system found satisfactory for squirrel monkeys (*Saimiri sciurcus*) was devised by Wolf et al. [83]. The precordial electrodes were placed as follows: V_6 over the third rib 1 cm to the right of the midline; V_4, over the ninth rib 1 cm to the left of the midline; and V_6 over the eighth rib at the midaxillary line.

In drug studies, lead V_{10} is often added to these precordial leads [49]. For cynomolgus monkeys (*Macaca fascicularis*) used in drug studies, the Atta and Vanace [82] system is often used [49]. Often however, for primates the system used for humans is used.

42.4.4.3 Orthogonal Leads and Cardiac Vectors

Hamlin and associates [53, 84] used leads I, aVF, and V_{10} as *X*, *Y*, and *Z* leads, respectively, to define three recording planes that could be considered somewhat orthogonal to one another: frontal, leads I and aVF (or *Z* and *Y*); sagittal, leads V_{10} and aVF (or *Y* and *Z*); and transverse, leads I and V_{10} (or *X* and *Z*). While arguably a nonorthogonal system in the true sense, this approach was useful and led to the current classification of mammalian electrocardiograms on the basis of QRS direction and sense [53].

Hamlin et al. later modified the orthogonal lead system of McFee and Parungao for dogs for use in studies with the horse [85] and miniature pig [86]. Roshchevsky [24] similarly employed an uncorrected lead system to obtain approximate orthogonality in cattle. The lead pairs for each axis were: *X*, right scapulohumeral joint to left scapulohumeral joint; *Y*, cranial end of the manubrium sterni to the ventral abdominal midline a handsbreadth in front of the navel; and *Z*, between the withers and the left foreleg.

Holmes et al. [87, 88] developed an orthogonal system as did Grauerholz [89] for vectorial evaluation of the horse electrocardiogram.

Grauerholz adopted the lead system of Baron [89]. The lead pairs for each axis were: *X*, right scapulohumeral joint to left scapulohumeral joint; *Z*, middle of the back, halfway between the forelimbs and hindlimbs to a point vertically under this on the abdominal midline; *Y*, determined trigonometrically from the Z-axis lead and a lead between the dorsal back electrode of lead Z and the right shoulder electrode of lead *X* on the right scapulohumeral joint.

42.4.4.4 Cardiac Electric Fields and Generation of Cardiac Potentials in Hoofed Mammals

In hoofed mammals (horses, cattle, sheep, swine) that are categorized by the QRS direction and sense into class A, reliable electrocardiographic criteria for the diagnosis of left and right ventricular hypertrophy and bundle branch block have not been established. It seems that the most likely reason for this is that the elaborate Purkinje conduction system is capable of maintaining an orderly spread of excitation despite considerable disruption of the ventricular myocardium by disease in these species.

42.4.4.5 Vectorcardiography

Vectorcardiography is not commonly used today. Mapping systems that evaluate the endocardial, epicardial, and even the transmural patterns of initiation and propagation of depolarization and repolarization are used in electrophysiological studies. Historically, the vectorcardiographic approach in mammalian electrocardiology was used primarily to determine the direction of electrical forces responsible for the form of the electrocardiogram in various species and for the study of appropriate lead systems [24, 85–93]. In the horse, for example, such vectorcardiographic investigations have used a Duchosal or similar cube system [79, 96], a form of tetrahedron [53], a triangulation of leads in the horizontal (frontal) and transverse planes [90], or some similar arrangement. Holmes et al. [87, 88] first experimented with an *XYZ* system in which the *X* lead consisted of five electrodes on the left and five on the right side of the chest, distributed over the shoulders and forelimbs so as to cover the heart area anatomically [87]. In a second study, these multiple electrodes were replaced with two malleable tin plates (0.6 mm thick) that could be molded to the body surface, covering an equivalent area [88]. The *Y* lead consisted of an electrode at the xyphoid and one at a point on the anterior chest on the midline between and on the level of the points of the shoulders (scapulohumeral joints). The Z lead consisted of two electrodes, one just to the left of the withers and the other on the upper left foreleg [90]. The resultant vector loops were displayed using an *XY* plotter [94].

42.4.4.6 Fetal Electrocardiography

Fetal electrocardiography has been practised in mares since 1921 [95]. In this species, the fetal QRS complexes may appear in limb leads II and III in advanced pregnancy (for instance, about 1 month before birth) and P and QRS complexes identified in abdominal leads [96]. In middle gestational stages (for example, 150 days or so), in both cows and mares, the fetal QRS complexes may be detected with appropriate abdominal and rectal leads [97].

In the mare the most favorable bipolar electrode positions are on the back at the midline in the midlumbar position and 6 in. (~15 cm) anterior to the udder on the midline of the ventral abdominal wall [96]. In the cow, favorable bipolar electrode positions are the right side of the lower abdomen or flank paired with an electrode located on the right side of the anterior abdomen or right paralumbar fossa region, or paired with a rectal or vaginal electrode [97]. The superiority of right-sided abdominal leads in cows has also been confirmed by other investigators (for example, Golikov and Vershinina [99]).

In pregnant ewes, fetal electrocardiograms from abdominal lead positions as used in cattle were obtained in only one of five animals tested [99].

As in other species, the heart rate of fetuses in cows and mares tends to decrease as pregnancy advances (for instance, in cows, fetal heart rate varies from about 140 beats per minute [bpm] at 160–191 days of pregnancy to about 120 bpm at days 251–281 of pregnancy and in mares, fetal heart rate varies from about 120 bpm in midstages of pregnancy to about 80 or 90 bpm toward the end of term) [96, 97, 99]. The fetal heart rate, however, is not stable and may vary from moment to moment independent of the maternal heart rate, possibly on account of fetal movement.

There has not been a great deal of clinical application of fetal electrocardiography in veterinary medicine although it is useful in cows and mares for monitoring fetal well-being, for making the diagnosis of fetal death after the midstage of gestation and, by identifying three spike rhythms (maternal and two fetal QRS complexes), for the diagnosis of twin pregnancies [96, 97]. In the case of twin pregnancy in cows, different bipolar lead positions were found best at different stages of pregnancy: at 5 months, vertical right-sided or longitudinal right-sided bipolar abdominal leads; at seven months bipolar leads between rectum or flank and midabdominal line on each side of lower abdomen; and at 9 months, bipolar leads from the right side to the left side of the lower abdomen [100].

Fetal electrocardiography has found another interesting application in teratological studies of toxins with rats [50, 101]. In this case, pregnant rats from the group used in a teratological study are selected and anesthetized. The fetuses are delivered surgically, and three-bipolar-lead electrocardiograms are recorded with intramuscular electrodes attached to both shoulders and one thigh of the fetus (leads I, II, III) while placental attachment is maintained. Since fetal and maternal rat electrocardiograms have different electrophysiological properties and sensitivity to such drugs as cardiac glycosides,

simultaneous recording of maternal as well as fetal electrocardiograms should have other applications in toxicology and pharmacology [50].

42.4.5 Types and Duration of Recording

42.4.5.1 Clinical Records

Electrocardiography for the diagnosis of disease in clinical medicine is commonly used in veterinary practice. Here, the selection of leads and duration of records will depend on the purpose being served. In the veterinary clinic the leads selected will depend on their usefulness in diagnosis for the species being examined; in dogs, for instance, the six- or 12-lead system can be used. If the detection or diagnosis of an arrhythmia is needed, the records may be quite long, depending on the tractability of the subject, the patience of the investigator, and the pertinence of the findings, such as for clinical diagnosis in a veterinary clinic. In an epidemiological study of 4,831 dogs from a clinic population, cardiac rate and rhythm were monitored over 5 min by auscultation, palpation of the precordium, palpation of the femoral pulse, and a short casual single-lead electrocardiogram [102]. This standardized examination procedure permitted an analysis of the incidence of abnormal arrhythmias in a clinical population of dogs under these circumstances [103]. It should be stressed that today 24-h ambulatory electrocardiographic monitoring is vital in the detection of arrhythmias and the management of treatment in these animals.

42.4.5.2 Serial Records

Repeated electrocardiograms taken at predetermined intervals are useful in following clinical cases and in monitoring experimental investigations such as chronic or subchronic toxicity studies [45, 49]. In the case of toxicological studies, one important question is whether the test animal has arrhythmogenic properties. Since arrhythmias are typically episodic or sporadic events, it is important that the duration of heart rhythm monitoring be standardized for groups and individuals within groups in such studies. Ideally, this would require continuous monitoring over 24 h.

42.4.6 Telemetry and Holter Monitoring

Electrocardiographic telemetry is almost as old as the electrocardiograph itself. Einthoven, in 1903, reported using the wires of the Leiden telephone system to transmit electrocardiographic signals from a hospital patient to his laboratory, a distance of about 1.6 km [104, 105]. From these early beginnings, remote recording of the electrocardiogram developed along two general lines: telemetry by telephone and radiotelemetry [106] and then, the early Holter monitors (24 h electrocardiographic monitoring) [107].

Extensive use of radiotelemetry for measuring biological variables began with the availability of transistors in 1954 [108] and a strong stimulus for work in this area was the telemetering of biological data from a dog in Sputnik II by the USSR in 1957 [109].

Radiotelemetry was soon applied to unrestrained domestic [110–117], wild [118] and laboratory [108, 119, 120] animals and veterinary patients [121]. With miniaturization and other technological advances, totally implantable biotelemetry systems are now available that record seven channels of physiological data and are small enough (for example, 2.5 × 2.5 ×1.0 cm) to insert into animals the size of infant bonnet monkeys [122–124].

Holter monitoring is commonly used in the clinical care of veterinary patients in order to diagnose arrhythmias, determine their frequency, and verify a successful treatment. In some studies, continuous 24 h ECG monitoring may be of value in determining whether arrhythmias develop as a result of a drug. It is not realistic to think that the brief rhythm strips of a routine ECG, whether it is a casual or serial ECG, could identify accurately the frequency of arrhythmias in response to a drug. Conversely, in the evaluation of the response to therapy for arrhythmias, it is essential that a 24-h Holter be used to most fully determine the benefits or proarrhythmic effects.

42.5 Interspecies Correlations

Electrocardiography is a routine examination undertaken as part of many investigations that seek to evaluate drugs for safety. Moreover, selected species are used in research of all types, including those specific to the cardiovascular system. The most common biomedical research animals today include the mouse [125], rabbit [126], dog [127], minipig [128], and nonhuman primates [129, 130].

42.5.1 Body Size, Heart Rate, and Time Intervals

Many biological variables are related to the size of animals and such allometric relations have been described for various measures of cardiac function including the electrocardiogram [131]. The resting heart rate is related to body size, which is in turn related to metabolic rate, while both heart rate and metabolic rate are regulated by autonomic balance and humoral agents. Broadly considered, the heart weight of mammals is nearly proportional to body mass (approximately 0.6% of body mass) and heart rate per minute is inversely related to both [130–133]. The relationship between heart rate and body weight can be expressed by equations, in which HR is heart rate per minute and W (in kg) is body weight. Two such equations proposed (see [133] and [131], respectively) are in essential agreement:

$$HR = 241 \times W^{-0.25}$$
$$HR = 360 \times W^{-0.26}$$

Individual species or strains may, however, differ substantially from such generalized relationships because of special physiological adaptations. For example, the resting heart rate of the horse ranges from 28 to 48 min^{-1} while that of dairy cattle is 48–84 min^{-1}; the heart rate of the domestic rabbit is 180–350 min^{-1} while that of the hare is 70–80 min^{-1} [132]. Likewise heart weight/body weight ratios may differ in species or strains of the same general size; the wild hare heart weight/body weight ratio is four times that of the Texas jackrabbit and 1.5 times that of the domestic rabbit [135, 136]; that of wild rats is twice the value of laboratory rats [135]; the adult greyhound heart weight/body weight ratio is about 1.3 times that of the mongrel [137]; and thoroughbred race horses have larger hearts than other breeds [135]. With these exceptions to allometric generalizations in mind, it is useful to examine such electrocardiographic relationships [130].

The nearly universal positive correlation between the R-R interval (heart rate) and PR, QRS, and QT durations observed with changes in heart rate in an individual is seen to be preserved in the intraspecies correlation, that is, as heart rates increase and heart sizes decrease, PQ, QRS, and QT intervals decrease linearly, although there are some species that do not fit the regression lines, for example, dolphin and draft horse for QT and draft horse for QRS. The ratio of QRS/QT duration is seen to be about the same among the different species at about 0.20–0.25 while that of PQ/QT is approximately 0.6.

42.5.2 Heart Rate Variability and Acceleration

Different species vary enormously in their respective degree of sinus arrhythmia and some species have a remarkable ability to increase heart rate over resting levels [130, 131].

There has been considerable recent interest in using changes in the degree of heart rate variability (HRV, sometimes termed HPV for heart period variability) as a measure of psychological stress in man and animals [137–139]. In man, HRV is suppressed during sustained attention and in certain psychiatric conditions. In drug testing, agents depressing the brain stem or the sinoatrial node (for instance, calcium-channel blockers) can decrease the degree of respiratory sinus arrhythmia [45] and this variable has been incorporated into a computer-assisted electrocardiographic analysis program for drug studies [140]. Among domestic and laboratory mammals, respiratory sinus arrhythmia is most pronounced in the dog. In this species the R-R intervals may vary as much as eightfold in a given record (that is, from 250 to 2,000 ms).

While sinus arrhythmia is known to be extreme in certain exotic animals, for example, the European mole [65] and the California ground squirrel [118], there is insufficient information on occurrence of this characteristic among the various mammalian species to make valid comparisons between species.

Table 42.2

Prevalence rates per thousand of common spontaneous arrhythmias and conduction disorders in pretest electrocardiograms for unanesthetized beagles (sample population *N* = 8,977), cynomolgus monkeys (*N* = 1,165) and albino rats (*N* = 442)

Arrhythmias or conduction disorders	Beagle	Cynomolgus monkey	Albino rat
Ventricular extrasystoles.	8.0	14.6	67.9
Second-degree AV block.	10.0	0.0	88.2
First-degree AV block.	1.9	0.0	2.3
Right bundle branch block.	0.0	42.1	0.1
Left bundle branch block.	0.0	1.7	2.3
Wolff–Parkinson–White Syndrome.	0.2	0.0	0.0
Any of the above.	20.1	38.6	160.6

With respect to cardiac acceleration, of the animals for which data are available, the horse has the greatest capacity to increase heart rate with exercise [137], for example, from 30 min^{-1} at rest to 240 min^{-1} with strenuous exercise, that is, about an eightfold increase. In man and dog the usual increase in heart rate with strenuous exercise is only about threefold although exceptional racing greyhounds may rival the horses' six to eightfold increase. There is both theoretical and experimental evidence (dog) that even at these high heart rates, continued increase in cardiac output with increase in rate prevails and that this positive relationship between increased heart rate and cardiac output is favored in thoroughbred horses and greyhounds because of their relatively larger hearts and stroke volumes [141].

42.5.3 Arrhythmias and Conduction Disorders

Table 42.2 compares the prevalence of cardiac arrhythmias in pretest (control) electrocardiograms from experimental beagles, cynomolgus monkeys, and albino rats. Respiratory sinus arrhythmia is not included in this table because it is ubiquitous in normal dogs at rest, although it is less frequent in restrained monkeys and rats. Except for Wolff–Parkinson–White (WPW) syndrome, the conduction disturbances are generally considered normal (see below).

In monkeys and rats (Table 42.2), and in pigs as well, ventricular extrasystoles appear to be induced by the excitement and struggling caused by restraint, because their prevalence decreases with training and because their appearance will occur in a few additional subjects during a study in which serial records are taken over a sustained period.

In minipigs, premature sinus beats with aberrant ventricular conduction may be fairly common in untrained groups of animals. In cats under halothane anesthesia, atrioventricular dissociation occurs frequently and may appear occasionally merely as the result of excitement [49].

42.5.4 Heart-Rate Dependence of Electrocardiographic Time Intervals PR, QRS, and QT

The change in PR, QRS, and QT intervals with change in R-R (that is, cycle length or heart rate) makes it necessary to correct these values when comparisons of time intervals are made at different heart rates. If this is not done, the effects of disease, drugs, or toxins, for example, on the QT interval (or on PR or QRS) may be masked by changes in the interval that are dependent on heart rate.

Various linear, cubic or square root, and logarithmic or exponential equations have been proposed to describe these relations [8, 144, 145]. Most of the adjustment formulae are flawed.

Probably the most useful approach at present is for each clinic or laboratory to develop its own database, as has been done for experimental beagles [146, 147]. Either a new formula that adequately describes the relations between the heart rates and time intervals over the entire data range, or a frequency distribution table of these values may be used (see Table 41.4). The practice of correcting the observed QT interval for heart rate by dividing it by the square root of the length of R-R interval serves very little purpose. With this formula, $QT_c = QT/(RR)^{1/2}$, the observed value of QT at a given heart rate over 60 is increased and, for a rate under 60 it is decreased, but the resultant QT_c does not necessarily

remain constant over the heart-rate range for the same animal. Hence, it does not increase the comparability of interval durations at different heart rates.

Since QRS is the shortest of these intervals, its absolute variation with heart-rate change is least and ordinarily is not considered, although the relationship is definitely present [8].

Determination of PR interval and QT interval change with R-R duration poses special problems with rapid heart rates in smaller species such as the rat [50]. There appear to be three reasons for this:

1. At high heart rates (475–600 min^{-1}) and paper speed of 50 mm s^{-1} or less, any changes in PR-interval and QT-interval duration with rate are small (that is, a few milliseconds) and therefore, difficult to measure accurately. This problem can be resolved with high-frequency sampling and electronic digital recordings that permit measurements at high speeds.
2. Also, at rapid rates (e.g., >450 min^{-1}) the succeeding P waves are superimposed on the descending limb of the previous T wave and the true QT interval cannot be determined accurately.
3. At lower heart rates (~250–350 min^{-1}) which occur frequently with anesthesia, these interval changes with rate are greater and easily measurable, but it is uncertain whether this is a rate effect or the result of anesthetic action on the myocardium.

The QT versus R-R relationship exhibits hysteresis; that is, with sudden changes in heart rate, the QT interval changes its duration gradually, requiring several heart beats at the same heart rate to attain a new steady state. Thus, with moderate variations in R-R intervals, as in respiratory sinus arrhythmia of the dog, the associated QT intervals do not undulate. This is also true with second-degree AV block in the dog in which the post-block PR interval is ordinarily shortened but the QT interval is little changed. Horses behave differently, however, because in this species both the PR and QT intervals are shortened in the post-block complex [148].

In premature ventricular extrasystoles, although the preceding R-R interval is shortened, the extrasystolic QT interval is usually longer because of the increase in QRS duration. Exceptionally, in premature ventricular extrasystoles, the QT interval may be shortened, perhaps because of the effect of the shortened R-R interval on conduction velocity and action-potential duration. This latter circumstance appears to be more common in standard swine and minipigs than in other species studied.

42.6 Normal Values

For each species, the lead II time intervals and amplitudes are presented. In these tables, only representative values (mean [above] and range [below]) for time intervals and amplitudes will be given for lead II. Unless otherwise stated, heart-rate and time-interval data are from unanesthetized and unsedated animals. Vectors (frontal plane unless otherwise designated), configuration, normal variants, and special features will be outlined in text.

Normal variants are electrocardiographic rhythm or conduction disturbances and uncharacteristic wave configurations, occurring with a sufficiently high incidence in otherwise healthy individuals of a given species that they cannot be considered abnormal [143]. Some examples are (Table 42.2): first-degree and second-degree atrioventricular block in dogs, horses, and rats; RBBB and (more rarely) LBBB in monkeys; rate-dependent LBBB in rats; premature sinus beats with aberrant ventricular conduction in minipigs; QRS complexes in limb leads only, with broad S waves and low-amplitude R waves, dome-dart ST-T complexes, exaggerated U waves, tall P waves (>0.4 mV), tall R waves (RV4 up to 6 mV), and P reversal in leads II, III, and a VF in dogs.

Special features mentioned include maximal heart rates with exercise, degree of sinus arrhythmia, and fetal or newborn versus adult electrocardiographic patterns when these facts are known.

42.6.1 Primates

The ECG classification and lead II time intervals and amplitudes for the primates discussed here, namely, the rhesus (Fig. 42.2), cynomolgus and squirrel monkeys (Fig. 42.3), the baboon, and the chimpanzee, are listed in Table 42.3.

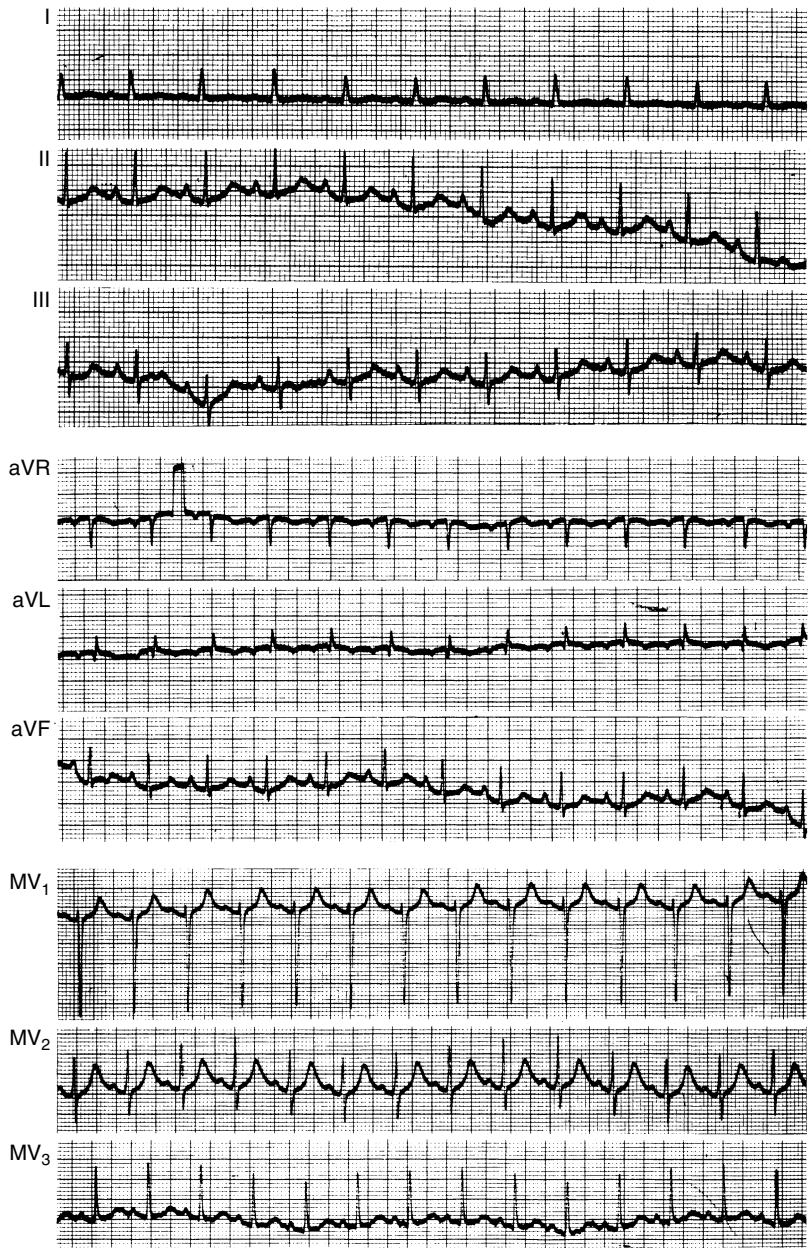

Figure 42.2

Electrocardiogram from an adult rhesus monkey (*Macaca mulatta*) restrained in a monkey chair: paper speed 50 div s^{-1}. The leads labeled MV_1, MV_2, and MV_3 are the thoracic leads recommended by Atta and Vanace [82]. MV_1 is located in the fourth right intercostals space, 4 cm from the midsternal line; MV_2 is on the left side symmetrical with MV_1; and MV_3 is registered at the left midaxillary line in the fifth intercostals space, approximately 1 cm below the level of MV_2. MV_1 is located over the right ventricle, MV_2 often records "transitional" type QRS potentials like those registered over the intraventricular septum and MV_3 is located over the left ventricle.

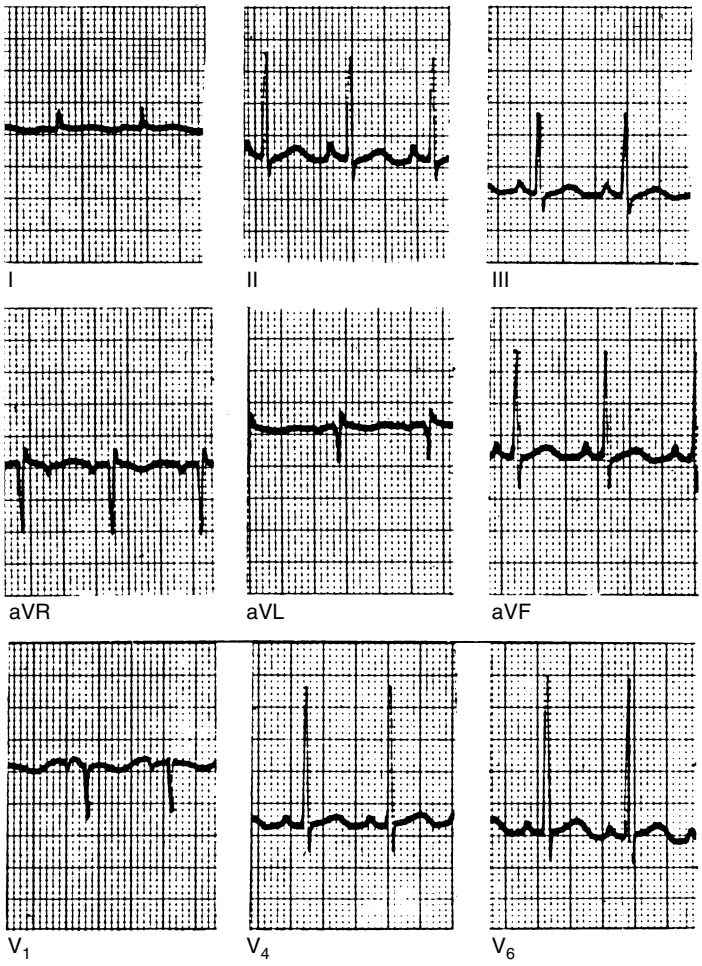

Figure 42.3

Electrocardiogram from a squirrel monkey (*Saimiri sciureus*) taken under sodium thiopental anesthesia in the supine position. Paper speed 50 div s^{-1}, standardization 0.1 mV div^{-1}. The lead positions are: V_1, third right rib 1 cm to the right of the midline; V_4, ninth left rib 1 cm to the left of the midline; V_6, eighth left rib at the midaxillary line. (After Wolf et al. [83]. @ American Physiological Society, Bethesda, Maryland. Reproduced with permission.)

The ECG configuration of the rhesus monkey commonly has peaked P waves in II, III, and aVF, and notchings in V_1 and V_3. The QRS complex is usually positive in standard limb leads and the ST segment is generally isoelectric in limb leads. The T wave is usually positive in standard and precordial leads.

Normal variants in the rhesus monkey include RBBB, which is present in about 1.4% and LBBB, which is present in about 0.8% [80]. QRS vectors suggesting incomplete RBBB occur in about 5% [80]. Negative T waves occur in bipolar limb leads in about 6% [80]. Negative T waves in thoracic leads are less common and, in serial electrocardiograms, reversal of T wave polarity may occur occasionally in limb or thoracic leads. Coupled ventricular extrasystoles may be expected in about 1.4%.

A special feature of the rhesus monkey is that the heart rates found in electrocardiograms are far more rapid than basal rates obtained by telemetry. In telemetered electrocardiograms from rhesus monkeys resting and isolated from man, the heart rates are 80–100 min^{-1} and sinus arrhythmia is pronounced. Electrocardiograms of the cynomolgus monkey (*Macaca fascicularis*) have an ECG configuration that is the same as that of the rhesus monkey. Normal variants

Table 42.3

ECG classification and normal parameters in primates

Common English name (*species name*)	ECG classification			Heart rate	Lead II time interval (s)				Lead II amplitude (mV)				
	QRS[a]	QT[b]	T[c]	(bpm)	P	PR	QRS	QT	P	Q	R	S	T
Rhesus monkey (*Macaca Mulatta*) [37, 38, 46, 78, 80]	A	A	A	257 160–350	0.05 0.03–0.06	0.07 0.05–0.10	0.03 0.02–0.05	0.14 0.11–0.19	0.25 0.12–0.37	0.10 0.00–0.50	0.90 0.00–2.04	0.15 0.00–0.40	0.10 −0.10–0.20
Cynomolgus monkey (*Macaca fascicularis*) [82, 130, 149]	A	A	A	180 120–220	0.03 0.02–0.05	0.08 0.06–0.11	0.03 0.03–0.05	0.19 0.16–0.25	0.07 0.04–0.26	0.06 0.00–0.30	0.30 0.10–0.95	0.09 0.00–0.46	0.07 0.00–0.50
Squirrel monkey (*Saimiri Sciureus*) [83]	A	A	A	248 160–340	0.03 0.025–0.035	0.05 0.042–0.058	0.03 0.023–0.037	0.15 0.11–0.20	0.18 0.05–0.30	0.05 0.0–0.1	0.90 0.10–1.70	0.20 0.00–0.50	0.05 −0.10–0.20
Baboon (*Papio spp*) [37, 81]	A	A	A	127 80–190	0.05 0.04–0.07	0.12 0.05–0.15	0.06 0.04–0.07	0.27 0.20–0.31	0.19 0.09–0.30	0.03 0.00–0.15	1.10 0.80–1.30	0.11 0.00–0.25	0.08 −0.10-0.25
Chimpanzee (*Pan Troglodytes*) [37]	A	A	A	159 100–249	0.071 0.04–0.10	0.11 0.07–0.15	0.045 0.03–0.07	0.233 0.18–0.32	0.17 0.05–0.40	0.06 0.20–1.70	0.82 0.20–1.70	0.25 0.05–0.90	0.04 −0.10–0.20

[a] QRS-vector and sense: A, along the long axis of the body, caudally and ventrally; B, from sternum toward spine.

[b] Relative QT-interval, ST-segment and action-potential duration: A, long; B, short.

[c] T-wave liability: A, constant; B, labile.

again include RBBB, which is present in about 4% of cases, and LBBB, which is present in about 0.2%. Coupled ventricular extrasystoles also occur with an incidence of 1.5%. Negative T waves may be present in bipolar limb leads and thoracic leads and reversal of previously positive T waves may occur spontaneously in serial records. An electrocardiogram (taken under sodium thiopental anesthesia in the supine position) of the squirrel monkey (Saimiri sciureus) as shown in Fig. 42.3 has a mean A QRS direction of 62° and A QRS range −60°–115°. The P wave of this species is usually positive in bipolar limb leads, occasionally tall and narrow (0.35 mV) in lead II, and sometimes its amplitude is variable in limb leads. The QRS is occasionally of low amplitude in limb leads. The ST segment is usually isoelectric but deviations of 0.1 mV are sometimes present. T is usually concordant and positive or diphasic in bipolar limb leads.

As in other monkeys, RBBB is not uncommon in its occurrence and is therefore considered a normal variant. A special feature concerning the squirrel monkey is that coupled ventricular extrasystoles occur occasionally in otherwise healthy subjects. Also, since two individuals with WPW syndrome have been found among a relatively small number of squirrel monkeys, a higher prevalence of Wolff–Parkinson–White syndrome may occur in this species than in others.

Electrocardiographic data have been obtained from several monkey species sedated with ketamine [149] including the three discussed above.

Two special features of the baboon should be mentioned. First, WPW syndrome was described among one group of 170 baboons and second, with telemetry the heart rate is 80–100 min^{-1} at rest.

ECGs from chimpanzees (Pan troglodytes) have a P wave that is usually positive in standard limb leads, but occasionally may be isoelectric in either lead I or III. The QRS complex is both of lower amplitude and lower duration than in humans and the T wave is usually concordant and positive in standard limb leads but may be isoelectric in about 30% and occasionally is discordant and negative.

Characteristics particular to the chimpanzee include sinus arrhythmia, which is frequent at heart rates below 125 min^{-1}. Also, wandering pacemaker from the SA node to the AV junction and premature atrial beats occur rarely.

42.6.2 Perissodactyla

The domestic horse (*Equus caballus*) (Fig. 42.4) is the only member of the Perissodactyla discussed here. Table 42.4 lists the ECG classifications and lead II time intervals and amplitudes. In the domestic horse, the area vector *A* QRS in the frontal plane lies between −64° and 102°. The range of its direction in the transverse plane is −32°–100° and in the left sagittal plane is −34°–173°. The P wave in bipolar leads is usually bifid, is most often positive, is sometimes diphasic and may change its form spontaneously (for instance, from bifid to single peak) for a series of beats. Such changes in form occur in about 30% of horses. Group B ventricular activation pattern results in major QRS vector forces being directed from the sternum toward the spine. Thus, maximal QRS deflections are rarely recorded in the frontal plane limb leads but rather in the thoracic leads, especially CV_6LL, V_{10}, Z, or the base apex bipolar lead. The ST segment is usually isoelectric in limb leads and is often arched or coved in chest leads. With regard to the T lability, amplitude may change and polarity reverses with changes in heart rate. In the post-block beat in second-degree AV block, the QT interval shortens, and there is reduction in T wave amplitude or change in form, for instance, from diphasic to positive.

Normal variants in the domestic horse include periodic changes in P-wave configuration (considered as wandering pacemaker in the sinoatrial node), sinoatrial block, first-degree and second-degree atrioventricular block, and nonrespiratory sinus arrhythmia, which all occur commonly in otherwise healthy horses. All these changes are considered to be largely the result of increases in vagal tone in this "vagotonic" species.

Atrial fibrillation is more common in horses and occurs with less-severe underlying heart disease (or with no evidence of heart disease) than in other domestic species. This arrhythmia is treated with quinidine sulfate. Electrical cardioversion is another successful means of treatment. This apparent increased susceptibility to atrial fibrillation in horses is considered to be related to two predisposing factors: large atrial mass and high vagal tone.

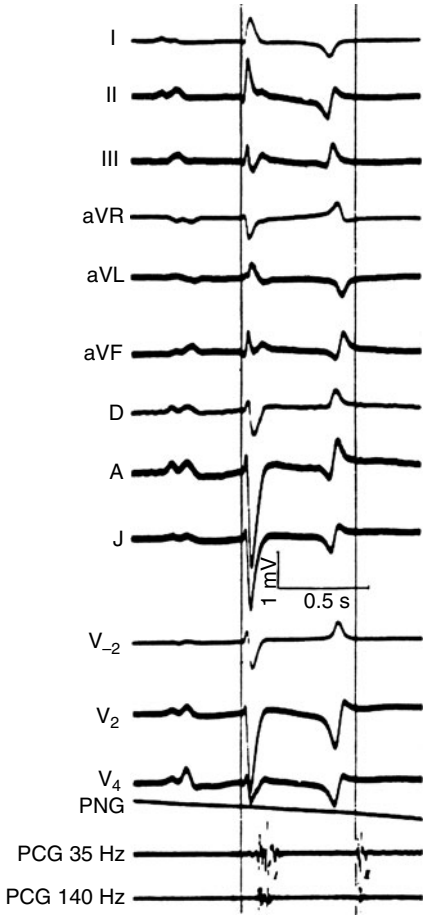

Figure 42.4

Electrocardiogram of a horse. Conventional bipolar and unipolar limb leads. D, A, and J leads after Sporri [26] as described in Sect. 42.4.4.2. The V leads are after Brooijmans [67, 72]: V_{-2} right sixth intercostal space at the junction of the lower and middle thirds of the vertical distance between the sternum and the level of the scapulohumeral joint; V_2, symmetrical with V_{-2} in the left sixth intercostal space; V_4 left sixth intercostal space at the level of the scapulohumeral joint. A pneumogram (PNG) and phonocardiograms (PCG) with cutoff filters set at two frequencies, 35 and 140 Hz, are shown at the bottom. The vertical lines are placed at the beginning of QRS and at the beginning of the second heart sound. (From Grauwiler [37]. © Birkhäuser, Basel. Reproduced with permission.)

42.6.3 Artiodactyla

The members of the Artiodactyla family discussed below are domestic cattle, sheep, goats, and pigs, giraffes, and camels. The ECG classifications, lead II time intervals and amplitudes, and references for further discussion are given in Table 42.4.

In domestic cattle (*Bos Taurus*), the mean *A* QRS is 70° with a range 30–90°. The P wave is usually positive in standard limb leads and may be bifid in left chest leads. QRS complexes are generally of low amplitude in the standard limb leads. T waves may be concordant or discordant in standard limb leads and are sometimes diphasic negative/positive.

P waves in the domestic pig (*Sus domesticus*) are usually upright in standard limb leads and may be bifid in V_{10} and the chest leads. The ST segment is isoelectric. T waves are often discordant in lead I and usually positive and sometimes diphasic in leads II and III.

Table 42.4

ECG classification and normal parameters in Perissodactyla and Artiodactyla

Common English name (*species name*)	ECG classification			Heart rate	Lead II time interval (s)				Lead II amplitude (mV)				
	QRS[a]	QT[b]	T[c]	(bpm)	P	PR	QRS	QT	P	Q	R	S	T
Perissodactyla Domestic horse (*Equus Caballus*) [37, 42, 65, 72, 75, 76, 83, 86–89, 159, 160]	B	A	B	35 26–50	0.14 0.08–0.20	0.33 0.22–0.56	0.13 0.08–0.17	0.51 0.32–0.64	0.28 0.1–0.5	0.12 0.025–0.35	1.13 0.2–2.5	0.15 0.025–0.45	0.20 −0.20-0.90
Artiodactyla Domestic cattle (*Bos Taurus*) [19, 24, 26, 27, 35–37, 53, 67–69, 71–76, 92, 93, 100, 161]	B	A	A	70 48–98	0.06 0.03–0.08	0.19 0.1–0.3	0.095 0.065–0.120	0.40 0.29–0.47	0.10 0.03–0.18	0.16 0.03–1.00	0.37 0.03–2.60	0.07 0.03–0.10	0.31 0.03–1.10
Domestic sheep (*Ovis aries*) [37, 162–168]	B	A	A	107 60–197	0.05 0.04–0.07	0.10 0.06–0.14	0.046 0.025–0.080	0.26 0.17–0.34	0.20 0.1–0.5	0.17 0.1–0.3	0.17 0.08–0.40	0.10 0.10	0.44 0.10–1.60
Domestic goat (*Capra hircus*) [37, 169–171]	B	A	A	96 70–120	0.04 0.02–0.06	0.12 0.08–0.16	0.045 0.03–0.06	0.30 0.24–0.36	0.08 0.02–0.15	0.48 0.07–0.95	0.19 0.02–0.50	0.08 0.02–0.25	0.20 0.05–0.50
Domestic pig (*Sus domesticus*) [37, 172–176]	B	A	A	135 100–180	0.04 0.03–0.05	0.09 0.08–0.12	0.04 0.03–0.06	0.24 0.21–0.26	0.13 0.05–0.30	0.09 0.00–0.14	0.61 0.40–0.78	0.39 0.14–0.50	0.38 −0.20–0.70
Giraffe (*Giraffa camelopardalis* reticulate) [177, 178]	B	A	A	70, 83	0.10, 0.08	0.18, 0.15	0.08, 0.10	0.45, 0.33	0.10, 0.08	0.00, 0.11	0.15, 0.70	0.00, 0.00	−0.30, −0.25
Camel (*Camelus dromedarius*) [179, 180]	B	A	A	30 24–49	0.10 0.08–0.10	0.25 0.24–0.26	0.09 0.04–0.09	0.50 0.48–0.52	0.10 0.06–0.20	0.00	0.40 0.20–1.20	0.45 0.40–0.50	−0.20 −0.40–0.10

[a] QRS-vector direction and sense; A, along the long axis of the body, caudally and ventrally; B, from sternum toward spine.
[b] Relative QT-interval, ST-segment and action-potential duration: A, long; B. short.
[c] T-wave lability: A, constant; B, labile.
[d] Two animals under etorphine (M99).

Ventricular extrasystoles are fairly frequent in excited pigs. In swine, the influence of body weight on electrocardiographic time intervals is separable from the influence of heart rate, as shown by holding the latter constant. When this is done, all electrocardiographic intervals can be shown to increase relatively with increasing body weight [150] (the effect of aging is not separable from that of increased body weight). When the influence of heart rate (R-R interval) alone on the electrocardiographic intervals was examined by holding the body weight constant, the R-R interval was found to have no effect on P-wave duration and a weak effect on PR and QRS intervals, but a strong effect on the QT interval [150]. Thus, both RR interval, that is, heart rate, as well as body weight *W* (in kg) serve to determine the expected QT interval. The following equations show these relations as calculated from data on 71 swine weighing 11–300 kg [150]:

$$P = 61 + 0.11W$$
$$PR = 107 + 0.17W$$
$$7QRS = 58.8 + 0.14W$$

and

$$QT = 159 + 0.15\,(R - R) + 0.26W$$

where P, PR, QRS, and QT are given in milliseconds.

In the ECGs of two giraffes, taken under etorphine, the QRS vectors were −25° and 95° (an example is shown in Fig. 42.5). The R wave was either positive or negative in leads I, II, and III. The QRS was positive in leads I and II in both animals and negative in lead III in one subject. The ST segment was isoelectric and the T waves were usually discordant.

Figure 42.6 shows the ECG of a dromedary camel (*Camelus droinedarius*) taken in the standing position and under no drugs. The mean *A* QRS is +250° (with a range between 90° and 280°). In standard limb leads, the P waves are positive, QRS complexes may be chiefly positive or negative and the ST segment is isoelectric. T waves are usually discordant. A special attribute of the camel is that sinus arrhythmia is present.

42.6.4 Cetacea

Table 42.5 lists the ECG classifications, lead II time intervals and amplitudes, and references of the finback, beluga and killer whales, and the dolphin. ECGs from bottle-nosed dolphins are shown in Fig. 42.7

The ECG of a finback whale (*Balaenoptera physalus*), beached 23 h before the recordings were made, has a broad P wave with low amplitude, a QRS complex which is chiefly negative in leads II and III and an ST segment which is isoelectric. T waves are discordant in most leads. In the beluga whale (*Delphinapterus leucas*), the bipolar lead between an electrode on the back at the pectoral girdle and one about the midportion of the back did not record the P wave distinctly. The QRS pattern was qR and the T wave was negative (discordant). In the killer whale (*Orcinus orca*), no P wave was recorded, the QRS had a qR configuration, and T was discordant.

42.6.5 Marsupialia

Table 42.5 lists the ECG classifications, lead II time intervals and amplitudes, and references of the Bennett's kangaroo and the opossum.

Electrocardiograms from the Bennett's kangaroo (*Macropus bennetti*) have P waves that are positive and sometimes bifid in standard limb and chest leads. In leads II, III, and in chest leads over the left ventricle, QRS complexes are somewhat similar with an RS configuration. The ST segment is absent in adults. T waves are positive, concordant in limb and chest leads, beginning immediately after QRS with no intervening ST segment.

Bennett's kangaroo was the first larger species in which it was shown that when the ST segment is absent and the QT, therefore, short, there is marked dissociation between the end of the T wave and the end of mechanical systole.

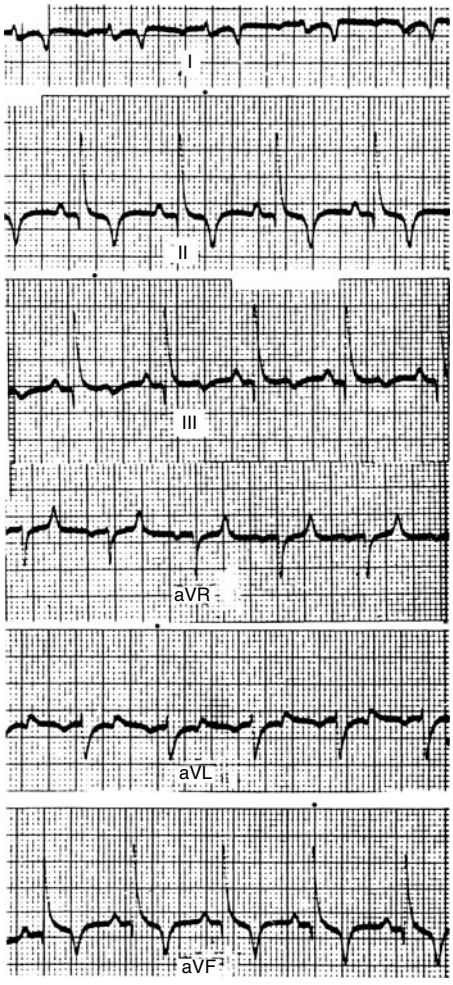

Figure 42.5

Electrocardiogram of a reticulated giraffe taken under etorphine HCl (M99) sedation in the right lateral recumbent position: paper speed 25 div s^{-1}; standardization 0.05 mV div^{-1}. (After Jefferson [154]. © American Veterinary Medical Association, Schaumburg, Illinois. Reproduced with permission.)

Correct interpretation of such fusion of QRS and T and mechanical and electrical dissociation in the mouse had been made a few years earlier in 1953 [151], The single record available from a wallaby (*Macropus walabatus*) had a short ST segment in limb leads and QT intervals of 0.16–0.18 s at a heart rate of l60 bpm. In another single record labeled "kangaroo" with no species designation, a short ST segment in limb leads was present and the QT interval was 0.23 s [5]. In 14 adult Australian rock kangaroos (*Macropus robustus*) under ketamine and pentobarbital anesthesia, the mean QT intervals of 0.214 s were far shorter than the mean mechanical systole of 0.393 s [152].

In the young Bennett's kangaroos still in the maternal pouch, the ST segment is present, as is true in the fetal or newborn rat [50] and mouse [151], and the duration of QT and mechanical systole are also similar. The adult conformation appears at the time the young kangaroos leave the pouch.

In the opossum (*Didelphis marsupialis*), the P waves are small and positive in standard limb leads. QRS complexes are chiefly positive in standard limb leads. Unlike the case of the adult Bennett's kangaroo, the ST segment is present. T waves are positive and concordant in standard limb leads.

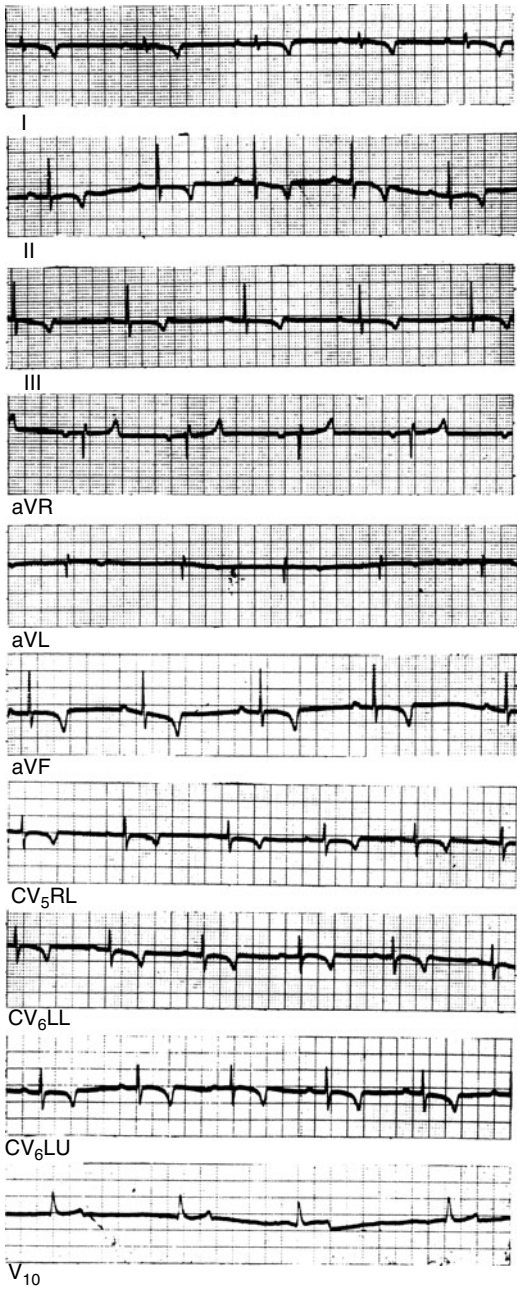

Figure 42.6

Electrocardiogram of a dromedary camel taken in the standing position. (Ind with no drugs: paper speed 25 div s^{-1}; standardization 0,1 mV div^{-1}) (See Sect. 42.4.4.2 for description of thoracic lead system) (After Jayasinghe et al. [158], © American Veterinary Medical Association, Schaumburg, Illinois, Reproduced with permission.)

Table 42.5

ECG classification and normal parameters in the Cetacea and Marsupialia

Common English name (*species name*)	ECG classification			Heart rate	Lead II time interval (s)				Lead II amplitude (mV)				
	QRS[a]	QT[b]	T[c]	(bpm)	P	PR	QRS	QT	P	Q	R	S	T
Cetacea Finback whale[d] (*Balaenoptera physalus*) [181]	B	A	A	27–32	0.40	0.68–0.73	0.32–0.34	0.96–1.08	0.10	0.30	0.00	0.00	0.50
Beluga whale (*Delphinapterus leucas*) [4]	B	A	A	16 12–24	not measurable	0.32	0.09–0.12	0.36–0.40	0.03	0.10	0.3–0.4	0.00	0.10–0.15
Killer whale (*Orcinus orca*) [182]	B	A	A	20–60	not visible P waves	not visible P waves	0.12	0.36	0.00	0.05	0.60	0.00	−0.30 0.10–0.25
Dolphin [183, 184]	B	A	A	100 60–137	0.82 0.06–0.10	0.178 0.120–0.210	0.065 0.05–0.08	0.257 0.05–0.320	0.03 0.03–0.20	0.03 0.00–0.15	0.30 0.20–0.40	0.20 0.03–0.40	0.15 0.10–0.25
Marsupialia Bennett's kangaroo (*Macropus bennetti*) [37, 186–231]	A	B	A	119 108–152	0.04 0.03–0.05	0.107 0.090–0.118	0.045 0.040–0.050	0.142 0.120–0.165	0.15	0.00	2.30	1.40	1.20
Opossum[e] (*Didelphis marsupialis*) [189]	A	A	A	200	not given	0.08	0.02–0.03	0.14	0.01	0.02	1.5	0.00	0.10

[a] QRS-vector direction and sense; A, along the long axis of the body, caudally and ventrally; B, from sternum toward spine.
[b] Relative QT-interval, ST-segment and action-potential duration: A, long; B, short.
[c] T-wave lability: A, constant; B, labile.
[d] Beached 23 h before recordings were made.
[e] Under pentobarbital sodium anesthesia.

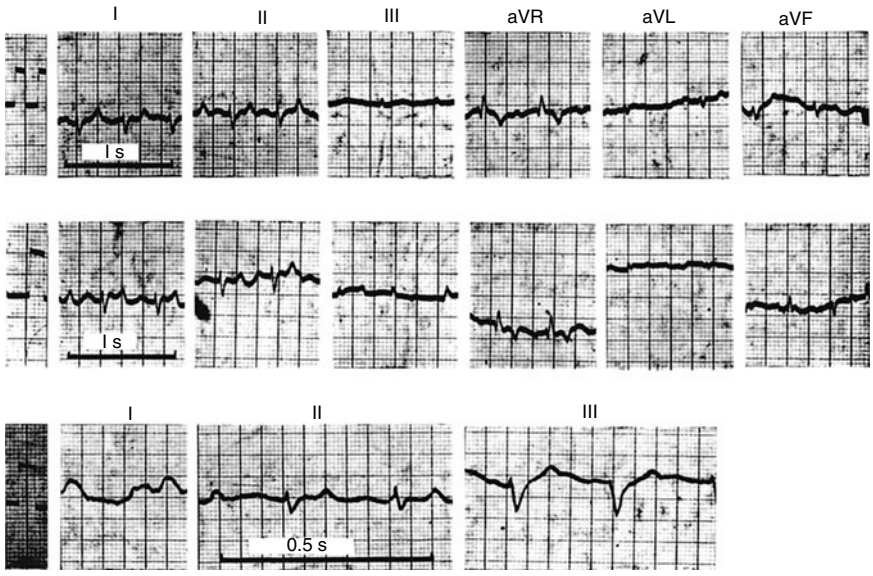

Figure 42.7

Electrocardiograms from a bottle-nosed dolphin: (a) ECG recorded immediately after loading on a truck at the port of Arari Bay: heart rate (HR) = 136.3 min^{-1}, interval times are R-R = 0.44 s, PQ = 0.16 s, QRS = 0.14 s, OT = 0.26 s, and T = 0.1 s. (b) ECG recorded after 4 h on the truck at Mishima: HR = 120 min^{-1}, interval times are R-R = 0.5 s, PQ = 0.2 s, QRS = 0.08 s, QT = 0.28 s, T = 0.14 s. (c) ECG recorded after 8 h on the truck at Enoshima: HR = 125 min^{-1}, R-R interval is 0.48 s. Needle electrodes or plate electrodes were placed at sites corresponding to the attachment of limbs in man. The pulses shown on the left of each panel indicate the scale of 1 mV. (After Tokita et al. [156]. © Geirui Kenkyosho, Tokyo, Japan. Reproduces with permission.)

42.6.6 Lagomorpha

The ECG classifications, lead II time intervals and amplitudes, and references of the rabbit (*Orytolagus cuniculus*) are given in Table 42.6.

The mean *A* QRS in the rabbit is 64° with a range of 0–180°. The P waves in rabbits are positive in standard limb leads and may be rather pointed in some strains. QRS complexes are generally positive, ST segments are usually isoelectric, and T waves are usually positive in standard limb leads. While a number of investigators have noted changes in T-wave polarity, especially in lead III and in chest leads, the amount of variability is only about the same as seen in nonhuman primates and is insufficient to classify this species as T labile or class B.

42.6.7 Rodentia

In recent years mice have been used extensively in genetic research. The expansion of this area of research, in addition to advances in the field of electrophysiology and the use of the mouse to match cardiac phenotype to genotype, has expanded the role of the mouse as a model. Despite this increase, criticism continues about the conclusions from the murine cardiac responses to that of other mammals and, importantly, humans [52]. The mouse has been evaluated by cardiac electrophysiological mapping studies, induction of particular arrhythmias, conduction abnormalities, infarction changes, and infectious responses by methods beyond the ECG.

The ECG classifications, lead II amplitudes and time intervals of the white laboratory rat and mouse and the guinea pig are listed in Table 42.6.

In the electrocardiograms of a white laboratory rat (*Rattus norvegicus*) for various foreleg positions the mean *A* QRS is 50° (with a range from −22° to 120°). There is some evidence that the *A* QRS shifts to the left with aging, but this has not

Table 42.6

ECG classification and normal parameters in Lagomorpha and Rodentia

Common English name (*species name*)	ECG classification			Heart rate	Lead II time interval (s)				Lead II amplitude (mV)				
	QRS[a]	QT[b]	T[c]	(bpm)	P	PR	QRS	QT	P	Q	R	S	T
Lagomorpha Rabbit (*Orytolagus cuniculus*) [37, 190–195]	A	A	A	240 190–300	0.30 0.25–0.40	0.70 0.5–0.8	0.35 0.10–0.15		0.10 0.05–0.20	0.00	0.40 0.30–0.80	0.15 0.05–0.30	0.15 0.05–0.30
Rodentia White laboratory rat (*Ratus norvegicus*) [37, 47, 50, 196–200]	A	B	A	460 228–600	0.013 0.010–0.016	0.040 0.033–0.050	0.017 0.012–0.026	0.066 0.038–0.080	0.11 0.02–0.20	0.00	1.06 0.22–1.50	0.20 0.00–0.05	0.15 0.05–0.30
White laboratory mouse (*Mus musculus*) [37, 185, 201–204]	A	B	A	632 500–750	0.010	0.038 0.028–0.50	0.010 0.006–0.020	0.035 –0.030-0.050	0.05 0.04–0.06	0.00	0.30 0.10–0.40	0.15 0.00–0.30	0.20 0.10–0.30
Guinea pig (*Cavia porcellus*) [26, 37]	A	A	A	226 200–300	0.036 0.022–0.048	0.061 0.046–0.077	0.023 0.020–0.030	0.146 0.110–0.185	0.17 0.10–0.22	0.02 0.00–0.11	1.65 0.82–2.63	0.19 0.00–0.58	0.21 0.08–0.38

[a] QRS-vector direction and sense; A, along the long axis of the body, caudally and ventrally; B, from sternum toward spine.
[b] Relative QT-interval, ST-segment and action-potential duration: A, along; B, short.
[c] T-wave lability: A, constant, B, labile.

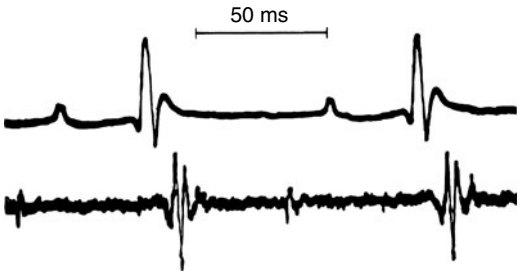

Figure 42.8

Electrocardiogram (*top*) and phonocardiogram (*bottom*) from a white laboratory mouse (*Mus musculus*), lead A (right arm electrode right side at base of neck, left leg electrode at cardiac apex). The second heart sound occurs 40 ms after the end of the T wave and no ST segment is present. (After Grauwiler [37]. © Birkhauser, Basel. Reproduced with permission.)

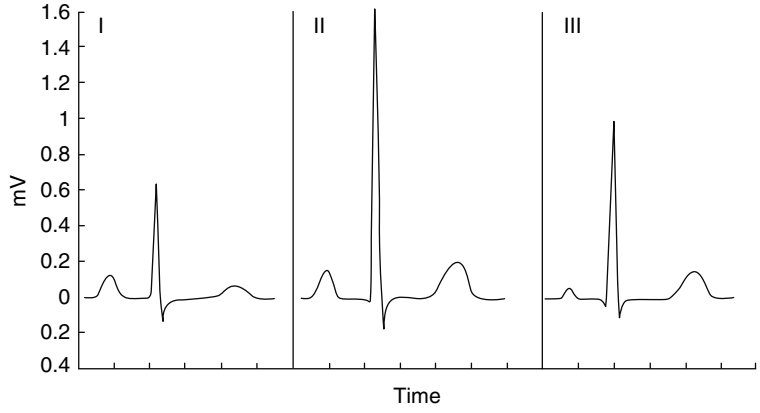

Figure 42.9

Limb leads I. II, III from a guinea pig (*Cavia parcellus*) (After Sporri H. *Habilitatiansschrift*. Zurich: University of Zurich, 1944 [26]. Reproduced with permission.)

been studied. In the white laboratory rat, the P wave is normally positive in leads I, II, III, and aVF, negative in aVR and flat or negative in aVL. Negative P waves are common in lead III. The Ta wave is usually discordant and appears to terminate or become isoelectric prior to the onset of the QRS complex. The Q of the QRS complex is usually absent in standard bipolar limb leads while R is prominent and S may be either prominent or absent. The ST segment is absent and the S-wave termination in bipolar leads is often difficult to separate from the onset of T. There is often no distinct isoelectric line during the electrocardiographic complex; that is, the points at which P, Ta, QRS, and T waves originate are often on different levels. This is especially true at more rapid heart rates when the P wave originates on the descending limb of the preceding T wave. The T wave is usually positive and concordant with QRS in leads II and III, but may be negative and discordant in lead I. Its ascending limb is typically steeper than its descending limb. The latter usually approaches the isoelectric line gradually, such that its termination is difficult to identify. At more rapid heart rates (450 bpm), the P wave interrupts the descent of the T wave. QT intervals are difficult to measure accurately on account of the gradual descent of T and because the succeeding P wave may interrupt the descent of T before it reaches the baseline. This has led to measuring the interval from the beginning of QRS to the apex of T (the QTa interval) instead of QT. Since the T apex can shift within the QT interval if the shape of T changes, this measurement is not a satisfactory determinant of the true QT interval.

Table 42.7

ECG classification and normal parameters in Carnivora and Proboscidea

Common English name (*species name*)	ECG classification			Heart rate rate	Lead II time interval (s)				Lead II amplitude (mV)				
	QRS[a]	QT[b]	T[c]	(bpm)	P	PR	QRS	QT	P	Q	R	S	T
Carnivora Domestic cat (*Felis catus*) [37, 205–212, 232]	A	A	A	190 110–300	0.03 0.02–0.05	0.07 0.05–0.10	0.03 0.015–0.04	0.15 0.1–0.2	0.16 0.00–0.20	0.15 0.00–0.30	0.50 0.00–1.05	0.27 0.00–0.70	0.18 −0.05–0.40
Proboscidea Indian elephant (*Elephas maximus*) [3, 37, 213–216]	B	A	A	38 30–46	0.16 0.12–0.30	0.44 0.36–0.48	0.16 0.12–0.18	0.64 0.60–0.70	0.05 0.03–0.10	0.05 0.03–0.10	0.70 0.60–0.80	0.15 0.10–0.20	0.10 0.05–0.20
African elephant (*Loxodonto Africana*) [37, 216, 217]	B	A	A	46 42–53	0.11 0.10–0.12	0.28 0.20–0.32	0.13 0.12–0.19	0.55 0.48–0.60	0.10	0.05	0.30	0.35	0.20

[a] QRS-vector direction and sense; A, along the long axis of the body, caudally and ventrally; B, from sternum toward spine.
[b] Relative QT-interval, ST-segment and action-potential duration: A, along; B, short.
[c] T-wave lability: A, constant, B, labile.

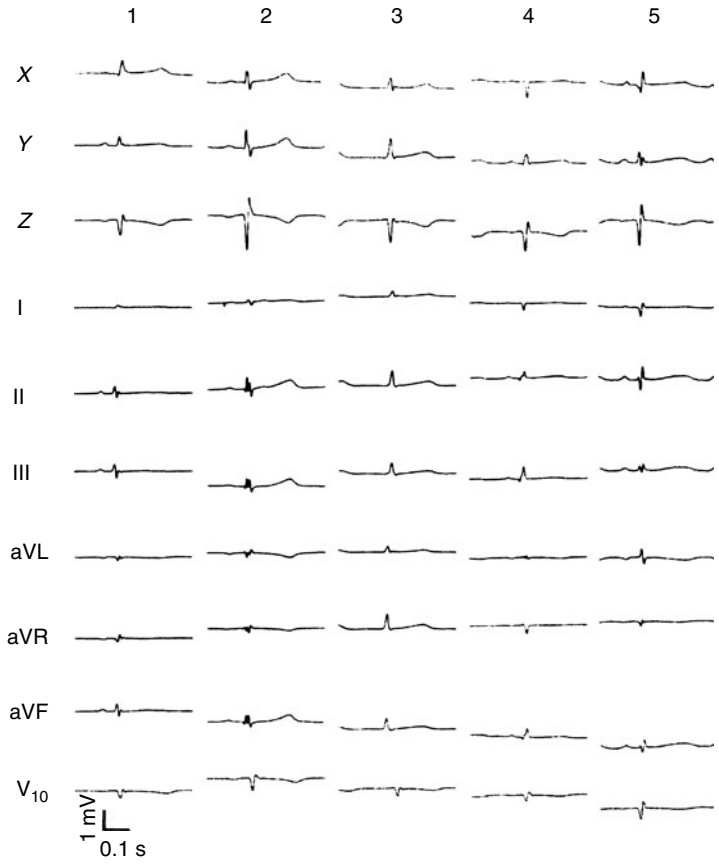

Figure 42.10

Electrocardiogram from five cats (1–5). *X, Y, Z* are the McFee leads described in Chap. 41 (for the dog). Note that the P waves are often small and difficult to identify, for example, as in ECG 3. (After Rogers and Bishop [157]. © Churchill Livingstone, New York. Reproduced with permission.)

As shown in Table 42.2, ventricular extrasystoles (about 7%) and second-degree atrioventricular block (about 8%) are sufficiently frequent in control electrocardiograms from rats to be considered normal variants. This is also true for sinus arrhythmia since in some series this has been present in over half the subjects.

A shift of *A* QRS in the frontal plane has been noted by some observers during the first 4 or 5 months of life. Others have found that the percentage of rats with a leftward QRS axis increased in older and postpartum groups of rats.

The maximum heart rate found in rat electrocardiograms is usually no higher than 600 bpm. In some individuals when rates exceed 600 bpm by a few beats (e.g., 620–635 bpm) an LBBB pattern appears in the electrocardiogram. Also, in a group of 75 rats entered in a drug study, LBBB appeared spontaneously in 32% after 1 year of age (week 65) unrelated to the test agent (that is, the distribution of the bundle branch block was the same in control and treated animals). This has not been seen in other studies and probably represents an inherited characteristic of this rat strain. As mentioned previously, the ST segment is present in newborn rats but disappears during the first three to four weeks of life.

An ECG and phonocardiogram of a white laboratory mouse (*Mus musculus*) is shown in Fig. 42.8. This species of rodent has a mean *A* QRS of 31° (with a range from −10° to 70°). P waves are usually positive in the standard limb leads. QRS complexes are chiefly positive in the standard limb leads with no Q wave and the S wave is absent or, if present, is usually small. The ST segment is absent and the T waves are concordant.

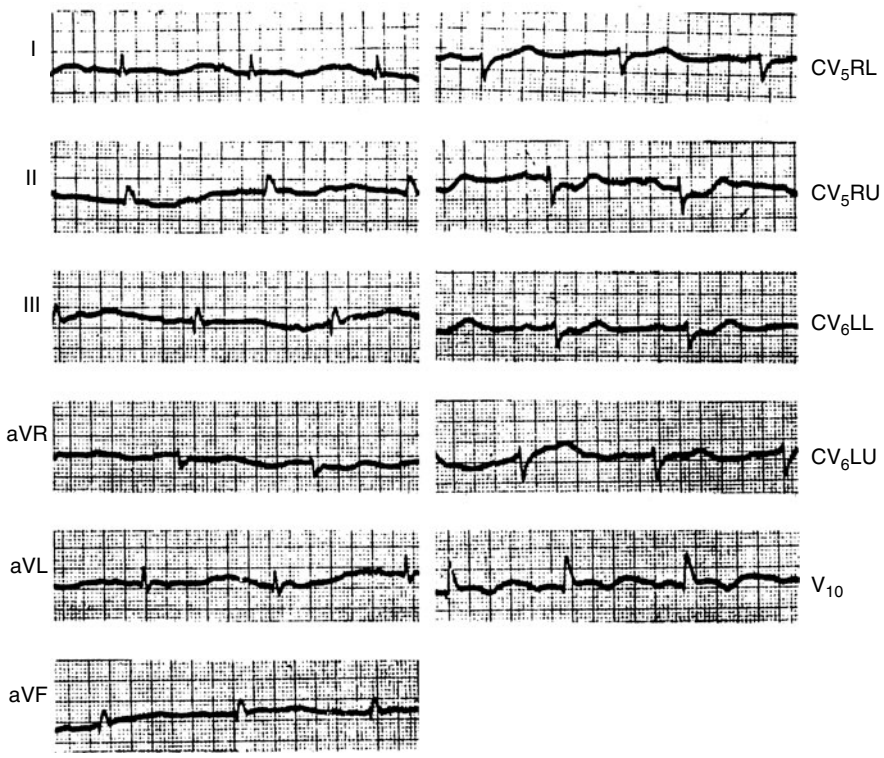

Figure 42.11

Electrocardiogram from the Indian elephant (*Elephas maximus*). The lead system is as described in Sect. 42.4.4.2. (After Jayasinghe et al. [158]. Bailliere Tindall, London. Reproduced with permission.)

In the ECG of the guinea pig (*Cavia porcellus*) (Fig. 42.9), the mean *A* QRS is 6° (range −20° to 60°). The ECG configuration has, in the standard limb leads, P waves which are positive and QRS complexes which generally have small q, large R and small S waves. The ST segment is present and usually isoelectric in limb leads. T waves are chiefly positive and concordant in the standard limb leads.

42.6.8 Carnivora

The domestic cat is the only member of the Carnivora discussed here. Table 42.7 lists the ECG classification lead II time intervals and amplitudes of the cat.

The ECG of the domestic cat (*Felis catus*) (Fig. 42.10) has a mean *A* QRS of 70° (the range is −20°–170°). P waves are usually positive in standard limb leads. When P waves are absent in limb leads, the recording should be inspected closely for signs of AV dissociation when P waves periodically become buried in the QRS. QRS complexes are dominated by R waves in standard limb leads. The ST segment is usually isoelectric and T waves are usually concordant and stable in limb leads.

Cardiomyopathy is a common disease seen in the cat. Such afflicted cats can have a normal ECG or evidence of left anterior fascicular block or left ventricular enlargement. The ECG in the kitten has also been studied from birth to 30 days [153].

42.6.9 Proboscidea

An example of the ECG of the Indian elephant (*Elephas maximus*) is shown in Fig. 42.11. Table 42.7 gives the ECG classification and lead II time intervals and amplitudes for the Indian elephant and the African elephant (*Loxodonto africana*).

Acknowledgements

This work was supported in part by the US National Institutes of Health Grant Number LM 01660 and by Smith, Kline and French Laboratories, Philadelphia, Pennsylvania. Dr. Sydney Moise at Cornell University contributed updates to this chapter.

References

1. Waller, A.D., Introductory address on the electromotive properties of the human heart. *Br. Med. J.*, 1888;**2**: 751–754.
2. Tawara, S., *Das Reizleitungssystem des Säugetierherzens*. Jena: Fischer, 1906.
3. White, P.D., J.L. Jenks Jr, and F.G. Benedict, The electrocardiogram of the elephant. *Am. Heart J.*, 1938;**16**: 744–750.
4. King, R.L., J.L. Jenks Jr, and P.D. White, The electrocardiogram of a Beluga whale. *Circulation*, 1953;**8**: 387–393.
5. Zuckermann, R., *Grundriss und Atlas der Elektrokardiographie*, 3rd edn. Leipzig: Thieme, 1959.
6. Kisch, B., F.M. Groedel, and P.R. Borchardt, *Comparative Direct Electrography of the Heart of Vertebrates*. New York: Fordham University Press, 1952.
7. Lepeschkin, E., *Das Elektrokardiogramm. Ein Handbuchfiir Theorie und Praxis*, 2nd edn. Dresden: Steinkopff, 1947.
8. Lepeschkin, E., *Modern Electrocardiography*. Baltimore, MD: Williams and Wilkins, 1951.
9. Rijlant, P.B., Origin of the heart beat in the mammalian heart (in Russian), in *Comparative Electrocardiology International Symposium* (in Russian), M.P. Roshchevsky, Editor. Leningrad: Akademiia Nauk SSSR, 1981, pp. 20–23.
10. Lewis, T., Irregularity of the heart's action in horses and its relationship to fibrillation of the auricles in experiment and to complete irregularity of the human heart. *Heart*, 1912;**3**: 161–171.
11. Lewis, T., *The Mechanism and Graphic Registration of the Heart Beat*, 3rd edn. London: Shaw, 1925.
12. Luisada, A. L. Weisz, and H.W. Hartman, A comparative study of electrocardiogram and heart sounds in common and domestic animals. *Cardiologia*, 1944;**8**: 63–84.
13. Robb, J.S., *Comparative Basic Cardiology*. New York: Grune and Stratton, 1965.
14. von Tschermak, A., Lehre von den bioelektrischen Strömen (Elektrophysiologie), in *Lehrbuch der Vergleichenden Physiologie der Haussäugetiere*, W. Ellenberger and A. Scheunert, Editors. Berlin: Parey, 1910, p. 520.
15. Kahn, R.H., Das Pferde-Ekg. *Pfluegers Arch. Gesamle Physiol. Menschen Tiere*, 1913;**154**: 1–15.
16. Waller, A.D., Electrocardiogram of horse. *J. Physiol.*, 1913;**47**(Proc. Physiol. Soc. London): xxxii–xxxiv.
17. Waller, A.D., A short account of the origin and scope of electrocardiography. *Harvey Lect.*, 1913–1914;**9**: 17–33. (*N. Y. Med. J.* 1914;97: 719).
18. Nörr, J., Das Elektrocardiogramm des Pferdes; seine Aufnahme und Form. *Z. BioI.*, 1913;**61**: 197–229.
19. Nörr, J., Elektrokardiogrammstudien am Rind. *Z. BioI.*, 1921;**73**: 129–140.
20. Nörr, J., Über Herzstromkurvenaufnahmen an Haustieren. Zur Einfiihrung der Elektrokardiographie in die Veteriniirmedizin. *Arch. Wiss. Prakl. Tierheilkd.*, 1922;**48**: 85–111.
21. GylstorffI. Prof. Dr. Nörr 85 Jahre. Berlin u. München. *Tieraerztl. Wochenschr.*, 1971;**4**: 240.
22. Lannek, N. and L. Rutqvist, Electrocardiography in horses. A historical review. *Nord. Veterinaermed*, 1951;**3**: 435–447.
23. Lannek, N., *A Clinical and Experimental Study on the Electrocardiogram in dogs*, Thesis. Stockholm, Sweden: Royal Veterinary College, 1949.
24. Roshchevsky, M.P., *Electrocardiology of Hoofed Animals* (in Russian). Leningrad: Nauka, 1978.
25. Spörri, H., Veränderungen der Systolendauer im Elektrokardiogramm von Rind und Meerschweinchen. *Arch. Wiss. Prakl. Tierheilkd.*, 1941;**76**: 236–247.
26. Spörri, H., Der Einfluss der Tuberkulose auf das Elektrokardiogramm. (Untersuchungen an Meerschweinchen und Rindern.) *Arch. Wiss. Prakl. Tierheilkd.*, 1944;**79**: 1–57.
27. Alfredson, B.V. and J.F. Sykes, Electrocardiographic studies in normal dairy cattle. *J. Agric.Res. (Washington D.C.)*, 1942;**65**: 61–87.
28. Charton, A. and G. Minot, Electrocardiogramme normal du cheval. *C. R. Seances Soc. Biol. Ses Fil.*, 1943;**137**: 150–152.
29. Charton, A., G. Minot, and M. Bressou, Electrocardiogramme normal du cheval. *Bull. Acad Vet. Fr.*, 1943;**16**: 141–148.
30. Bressou, M., *L 'Electrocardiogramme et le Phonocardiogramme du Cheval Normal*. Paris: Foulon, 1944.
31. Kelso, W.T., Electrocardiograms of young lambs. *Queensl. J. Agric. Sci.*, 1947;**4**: 60–71.
32. Krzywanek, F.W. and G. Ruud, Die Veränderungen des Elektrokardiogramms beim sogenannten Herztod des Schweines. *Tieraerztl. Umsch.*, 1944;**2**: 23–25.

33. Ruud, G., *Das Elektrokardiogramm des Schweines und die Veränderungen desselben beim sogenannten Herztod des Schweines*, Veterinary dissertation. Berlin, 1945.
34. Voskanyan, P.M., Electrocardiography of horses (in Russian). *Trudi XV Plenum Vet. Sektsii Vses. Akad. Moskva, Nauka* 1941; 250–256.
35. Filatov, P.B., Electrocardiography of cattle, in *Non-infectious Internal Diseases of Animals* (in Russian). *Sb. Rab. Voenno-Vel. Fakulteta Mosk. Vet. Akad. Moskva. Nauka* 1949;**6**: 207–222.
36. Roshchevsky, M.P., *Electrical Activity of the Heart and Methods of Recording Electrocardiograms from Large Livestock(Cattle)* (in Russian). Sverdlovsk: Uralskii Gosudarstvennyi Universitet, 1958.
37. Grauwiler, J., *Herz und Kreislauf der Säugetiere; Vergleichend-Funktionelle Daten*. Basel: Birkhäuser, 1965.
38. Roshchevsky, M.P., *Evolutional Electrocardiology* (in Russian). Leningrad: Nauka, 1972.
39. Roshchevsky, M.P., Editor. *Physiological Basis of Animal Electrocardiography*. Moscow: Nauka, 1965.
40. Roshchevsky, M.P., Editor. *Comparative Electrocardiology. Proceedings of the 1st International Symposium* (in Russian). Leningrad: Nauka, 1981.
41. Roshchevsky, M.P., Editor. *Comparative Electrocardiology. Proceedings of the 2nd International Symposium* (in Russian).
42. G.F. Fregin, The cardiovascular system, in *Equine Medicine and Surgery*, vol. 1, 3rd edn, RA Mansmann, ES McAllister, and PW Pratt, Editors. Santa Barbara: American Veterinary Publishing, 1982, pp. 645–704.
43. Edwards, N.J., *Bolton's Handbook of Canine and Feline Electrocardiography*, 2nd edn. Philadelphia, PA: Saunders, 1987.
44. Tilley, L.P., *Essentials of Canine and Feline Electrocardiography*, 2nd edn. Philadelphia, PA: Lea and Febiger, 1985.
45. Detweiler, D.K., The use of electrocardiography in toxicological studies with Beagle dogs, in *Cardiac Toxicology*, vol. 3, T. Balazs, Editor. Boca Raton, FL: CRC Press, 1981, pp. 33–82.
46. Malinow, M.R., The electrocardiogram (ECG) and vectorcardiogram (VCG) of the rhesus monkey, in *Anatomy and Physiology*, G.H. Bourne, Editor. New York: Academic Press, 1975, pp. 77–105. (*The Rhesus Monkey*; vol. 1.)
47. Budden, R., D.K. Detweiler, and G. Zbinden, Editors. *The Rat Electrocardiogram in Pharmacology and Toxicology*. Oxford: Pergamon, 1981.
48. Kachiku No Shindenzu *(Advances in Animal Electrocardiography)*. Tokyo: Japanese Association of Veterinary Cardiology. (Japanese language journals in existence since 1968. English translations of titles, legends, and summaries often included.)
49. Detweiler, D.K., Electrocardiographic monitoring in toxicological studies: Principles and interpretations, in *Myocardial Injury, Advances in Experimental Medicine and Biology*, vol. 161, J.J Spitzer, Editor. New York: Plenum, 1983, pp. 579–607.
50. Detweiler, D.K., The use of electrocardiography in toxicological studies with rats, in *The Rat Electrocardiogram in Pharmacology and Toxicology*, R. Budden, D.K. Detweiler, and G. Zbinden, Editors. Oxford: Pergamon, 1981, pp. 83–115.
51. Grauwiler, J. and H. Spörri, Fehlen der ST-Strecke im Elektrokardiogramm von verschiedenen Saugetierarten. *Helv. Physiol. Pharmacol. Acta.*, 1960;**C18**: 77–78.
52. Nerbonne, J.M., Studying cardiac arrhythmias in the mouse-a reasonable model for probing mechanisms? *Trends Cardiovasc. Med.*, 2004;**14**: 83–93.
53. Hamlin, R.L. and C.R. Smith, Categorization of common domestic mammals based upon their ventricular activation process. *Ann. N. Y. Acad. Sci.*, 1965;**127**: 195–203. (See also Hamlin, R.L., D.L. Smetzer, and C.R. Smith, Analysis of QRS complex recorded through a semiorthogonal lead system in the horse. *Am. J. Physiol.*, 1964;**207**: 325–333.)
54. Hill, J.D., The electrocardiogram in dogs with standardized body and limb positions. *J. Electrocardiol.*, 1968;**1**: 175–182.
55. Hill, J.D., The significance of foreleg positions in the interpretation of electrocardiograms and vectorcardiograms from research animals. *Am. Heart J.*, 1968;**75**: 518–527.
56. Detweiler, D.K., Electrophysiology of the heart, in *Dukes' Physiology of Domestic Animals*, 10th edn, M.J. Swenson, Editor. Ithaca, NY: Cornell University Press, 1984, pp. 103–130.
57. Rappaport, M.B. and I. Rappaport, Electrocardiographic considerations in small animal investigations. *Am. Heart J.*, 1943;**26**: 662–680.
58. Werth, G. and S. Wink, Das Elektrokardiogramm der normalen Ratte. *Arch. Kreislaufforsch.*, 1967;**54**: 272–308.
59. Angelakos, E.T. and P. Bernardini, Frequency components and positional changes in electrocardiogram of the adult rat. *J. Appl. Physiol.*, 1963;**18**: 261–263.
60. Godwin, K.O. and F.J. Fraser, Simultaneous recording of ECGs from disease-free rats, using a cathode ray oscilloscope and a direct writing instrument. *Q. J. Exp. Physiol.*, 1965;**50**: 277–281.
61. Almasi, J.J., O.H. Schmitt, and E.F. Jankus, Electrical characteristics of commonly used canine ECG electrodes. *Proc. Annu. Conf. Eng. Med. Biol.*, 1970;**12**: 190.
62. Osborne, B.E., A restraining device facilitating electrocardiogram recording in dogs. *Lab. Anim. Care*, 1970;**20**: 1142–1143.
63. Beinfield, W.H. and D. Lehr, Advantages of ventral position in recording electrocardiogram of rat. *J. Appl. Physiol.*, 1956;**9**: 153–156.
64. Richtarik, A., T.A. Woolsey, and E. Valdivia, Method for recording ECG's in unanesthetized guinea pigs. *J. Appl. Physiol.*, 1965;**20**: 1091–1093.
65. Detweiler, D.K. and H. Spörri, A note on the absence of auricular fibrillation in the European mole (Talpa europaea). *Cardiologia*, 1957;**30**: 372–375.
66. Waller, A.D., Ueber die den Pulsbegleitende elektrische Schwankung des Herzens (Ausserordentliche) Sitzung am 27. Dec. 1889. *Arch. Physiol. Physiologische Abtheilung des Arch. Anat. Physiol.*, 1890; 186–190.
67. Brooijmans, A.W.M., *Electrocardiography in Horses and Cattle: Theoretical and Clinical Aspects, Vet. Proefschrift Rijksuniversiteit*. Utrecht: Cantecleer, 1957.
68. Balbo, T. and U. Dotta, Gli effetti dell'eta sull'elettrocardiogramma del bovino. 1 and 2. *La Nuova Vet.*, 1966;**62**: 307–355 and Suppl. 6.
69. Lautenschlager, O., *Grundlagen der Aufnahmetechnik des Elektrokardiogrammes von Pferd und Rind und ihre Ergebnisse*, Veterinary dissertation. Giessen, 1928.
70. Morita, H., Electrocardiograms of conscious Beagle dogs by apex-base bipolar lead. *Adv. Anim. Cardiol.*, 1984;**17**: 19–23.
71. Sander, W., Das Elektrokardiogramm des Rindes. *Zentralbl. Veterinaermed.*, 1968;**15**: 587–634.
72. Brooijmans, A.W.M., Standardization of leads in veterinary clinical electrocardiography. *Tijdschr. Diergeneeskd.*, 1954;**79**: 801–811.

73. Sellers, A.F., A. Hemingway, E. Simonson, and W.E. Petersen, Unipolar and bipolar electrocardiographic studies in dairy cattle. *Am. J. Vet. Res.*, 1958;**19**: 620–624.
74. Junge, G., Über die Elektrokardiographie in der Veterinärmedizin unter besonderer Berücksichtigung der allgemeinen Elektrophysiologie und der Ableitung des Rinderelektrokardiogramms. *Arch. Exper. Veterinaermedizin*, 1967;**21**: 835–866.
75. Sugeno, H., Y. Yasuda, H. Nishikawa, and T. Takeya, Studies of the electrocardiogram of normal healthy cows. *J. Fac. Agr. Iwate Univ.*, 1956;**3**: 114–125.
76. Too, K., R. Nakamura, and K. Hirao, Studies on the applications of electrocardiogram in cattle. *Jpn. J. Vet. Res.*, 1958;**6**: 230–244.
77. Kusachi, R. and H. Sato, Fundamental studies on electrocardiograms of the horse. II. Bipolar lead. *Jpn. J. Vet. Res.*, 1955;**3**: 195–208.
78. Lannek, N. and L. Rutqvist, Normal area variation for the electrocardiogram of horses. *Nord. Veterinaermed.*, 1951;**3**: 1094–1117.
79. Detweiler, D.K. and D.F. Patterson, The cardiovascular system, in *Equine Medicine and Surgery*, 2nd edn, E.J. Catcott and J.F. Smithcors, Editors. Wheaton, IL: American Veterinary Publishing, 1972, pp. 277–347.
80. Malinow, M.R., An electrocardiographic study of *Macaca mulatta*. *Folia Primarol*, 1966;**4**: 51–65.
81. Herrmann, G.R. and A.H.W. Herrmann, The electrocardiographic patterns in 170 baboons in the domestic and African colonies at the primate center of the Southwest Foundation for Research and Education, in *The Baboon in Medical Research*, vol. I, H. Vagtborg, Editor. Austin, TX: University of Texas Press, 1965, pp. 251–264.
82. Atta, A.G. and P.W. Vanace, Electrocardiographic studies in the *Macaca mulatta* monkey. *Ann. N.Y. Acad. Sci.*, 1960;**85**: 811–818.
83. Wolf, R.H., N.D.M. Lehner, E.C. Miller, and T.B. Clarkson, Electrocardiogram of the squirrel monkey *(Saimiri sciureus)*. *J. Appl. Physiol.*, 1969;**26**: 346–351.
84. Hellerstein, H.K. and R. Hamlin, QRS component of the spatial vectorcardiogram and of the spatial magnitude and velocity electrocardiograms of the normal dog. *Am. J. Cardiol.*, 1960;**6**: 1049–1061.
85. Hamlin, R.L.,J.A. Himes, H. Guttridge, and W. Kirkham, P wave in the electrocardiogram of the horse. *Am. J. Vet. Res.*, 1970;**31**: 1027–1031.
86. Harolin, R.L., R.R. Burton, S.D. Leverett, andJ.W. Burns, The electrocardiogram from miniature swine recorded with the McFee-axial reference program. *J. Electrocardiol.*, 1974;**7**: 155–162.
87. Holmes, J.R. and P.G.G. Darke, Studies on the development of a new lead system for equine electrocardiography. *Equine Vel. J.*, 1970;**2**: 12–21.
88. Holmes, J.R. and R.W. Else, Further studies on a new lead system for equine electrocardiography. *Equine Vel J*, 1972;**4**: 81–87.
89. Grauerholz, G., Eine Methode zur vektoriellen Auswertung des Elektrokardiogramms beim Pferd. *Zentralbl. Velerinaermed. A*, 1974;**21**: 188–197. (This article cites: Baron M. Contribution a l'etude du vectorcardiogramme du cheval de sport. Applications dans l'examen preoperative, veterinary dissertation. Paris, 1970.)
90. Holmes, J.R. and B.J. Alps, Studies into equine electrocardiography and vectorcardiography. I. Cardiac electric forces and the dipole vector theory: II. Cardiac vector distribution in apparently healthy horses. III. Vector distribution in some cardiovascular disorders. IV. Vector distributions in some arrhythmias. *Can. J. Comp. Med. Vel. Sci.*, 1967;**31**: 92–102; 150–155; 207–212; 219–225.
91. Darke, P.G.G. and J.R. Holmes, Studies on the equine cardiac electric field. I. Body surface potentials. II. The integration of body surface potentials to derive resultant cardiac dipole moments. *J. Electrocardiol*, 1969;**2**: 229–234; 235–244.
92. Van Arsdel, W.C., III, *Lead Selection, Cardiac Axes, and the Interpretation of Electrocardiograms in Beef Cattle*. Corvallis, OR: Oregon State College, 1959.
93. Sugeno, H., Analytical study on bovine electrocardiogram. *Jpn. Circ. J.*, 1959;**23**: 1193–1203.
94. Holmes, J.R.A., Method of vectorcardiogram: loop portrayal. *Equine Vel. J.*, 1970;**2**: 27–34.
95. Nörr, J., Fötale Elektrokardiogramme von Pferd. *Z. Biol.*, 1921;**73**: 123–128.
96. Holmes, J.R. and P.G.G. Darke, Fetal electrocardiography in the mare. *Vel. Rec.*, 1968;**82**: 651–655.
97. Too, K., H. Kanagawa, and K. Kawata, Fetal electrocardiogram in dairy cattle. I. Fundamental Studies. III. Variations in fetal QRS pattern. *Jpn. J. Vel. Res.*, 1965;**13**: 71–83; 1966;**14**: 103–113.
98. Too, K., H. Kanagawa, K. Kawata, and H. Ono, Fetal electrocardiogram in dairy cattle. II. Diagnosis for twin pregnancies. *Jpn. J. Vet. Res.*, 1965;**13**: 111–119. Too, K., H. Kanagawa, K. Kawata, T. Inoue, T.F. Odajima, et al., Electrocardiogram in cattle. V. Findings at parturition. *Jpn. J. Vel. Res.* 1967;**15**: 21–30.
99. Golikov, A.N. and R.S. Vershinina, Electrocardiographic control of the stage of pregnancy in the cow (in Russian). *Velerinariya*, 1973;**2**: 87–88.
100. Larks, S.D., L.W. Holm, and H.R. Parker, A new technic for the demonstration of the fetal electrocardiogram in the large domestic animal (cattle, sheep, horse). *Cornell Vet*, 1960;**50**: 459–468.
101. Grabowski, C.T. and D.B. Payne, An electrocardiographic study of cardiovascular problems in Mirex-fed rat fetuses. *Teratology*, 1980;**22**: 167–177.
102. Detweiler, D.K. and D.F. Patterson, The prevalence and types of cardiovascular disease in dogs. *Ann. N.Y. Acad. Sci.*, 1965;**127**: 481–516.
103. Patterson, D.F., D.K. Detweiler, K. Hubben, and R.P. Botts, Spontaneous abnormal cardiac arrhythmias and conduction disturbances in the dog. A clinical and pathologic study of 3,000 dogs. *Am. J. Vet. Res.*, 1961;**22**: 355–369.
104. Einthoven, W., Die galvanometrische Registrierung des menschlichen Elektrokardiogramms. *Pfluegers Arch. Gesamte Physiol. Menschen Tiere.*, 1903;**99**: 472–480.
105. Einthoven, W., Le Télécardiogramme. *Arch. Int. Physiol.*, 1906;**4**: 132–164.
106. Caceres, C.A., Editor. *Biomedical Telemetry*. New York: Academic Press, 1965.
107. Holter, N.J., New method for heart studies. *Science*, 1961;**134**: 1214–1220.
108. Sandler, H., H.L. Stone, T.B. Fryer, and R.M. Westbrook, Use of implantable telemetry systems for study of cardiovascular phenomena. *Circ. Res.*, 1972;**31**(Suppl. II): 85–100.
109. Denton, D., Recording of physiological functions of a suitable experimental animal during protracted space flight. *Ausl. J. Sci.*, 1958;**20**: 202–207.
110. Benazet, P., R. Bordet, A. Brion, M. Fontaine, and J. Sevestre, Étude télémétrique de l'éléctrocardiogramme du cheval de sport. *Rect. Med. Vel.*, 1964;**140**: 449–459.

111. Nomura, S., Adaptation of radiotelemetry to equestrian games and horse racing. *Jpn. J. Vel. Sci.*, 1966;**28**: 191–203.
112. Fregin, G.F., Radioelectrocardiography in horses. *Pennsylvania Vel*, 1967;**9**: 6–10.
113. Banister, E.W. and A.D. Purvis, Exercise electrocardiography in the horse by radiotelemetry. *J. Am. Vet. Med. Assoc.*, 1968;**152**: 1004–1008.
114. Senta, T., D.L. Smetzer, and C.R. Smith, Effects of exercise on certain electrocardiographic parameters and cardiac arrhythmias in the horse. A radiotelemetric study. *Cornell Vet*, 1970;**60**: 552–569.
115. Börnert, D., H. Seidel, R. Maiwald, and G. Börnert, Drahtlos übertragene EKG-Ableitungen vom freibeweglichen Rind. *Arch. Exp. Velerinaermed.*, 1964;**18**: 701–712.
116. Dracy, A.E. and J.R. Jahn, Use of electrocardiographic radiotelemetry to determine heart rate in ruminants. *J. Dairy Sci.*, 1964;**47**: 561–563.
117. Fregin, G.F. and D.P. Thomas, Cardiovascular response to exercise in the horse: a review, in *Equine Exercise Physiology*, D.H. Snow, S.G.B. Persson, and R.J. Rose, Editors. Cambridge: Granta, 1983, pp. 76–90.
118. Adams, L., R.E. Wetmore, R.L. Limes, and H.J. Hauer, Automated analysis of heart rate in ground squirrels using radiotelemetry and computers. *BioScience*, 1971;**21**: 1040–1042.
119. Essler, W.O. and G.E. Folk Jr, Determination of physiological rhythms of unrestrained animals by radiotelemetry. *Nature*, 1961;**190**: 90–91.
120. Essler, W.O., *Radiolelemetry of Electrocardiograms and Body Temperatures from Surgically Implanled Transmitters*, State University of Iowa Studies in Natural History; vol. 20, no. 4. Iowa City, IA: State University of Iowa, 1961.
121. Branch, C.E., S.D. Beckett, and B.T. Robertson, Spontaneous syncopal attacks in dogs. A method of documentation. *I. Am. Anim. Hosp. Assoc.*, 1972;**13**: 673–679.
122. Reite, M., Implantable biotelemetry and social separation in monkeys, in *Animal Stress*, G.P. Moberg, Editor. Bethesda, MD: American Physiological Society, 1985, pp. 141–160.
123. Patiley, J.D. and M. Reite, A microminiature hybrid multichannel implantable biotelemetry system. *Biolelem. Patient Monit.*, 1981;**8**: 163–172.
124. Kimmich, H.P. and J.W. Knutti, Editors. Implantable telemetry systems based on integrated circuits. *Bioelem. Patient Monit.*, 1979;**6**: 91–170.
125. Mohler, P.J., I. Splawski, C. Napolitano, G. Bottelli, L. Sharpe, K. Timothy, S.G. Priori, M.T. Keating, and V. Bennett, A cardiac arrhythmia syndrome caused by loss of ankyrin-B function. *Proc. Natl. Acad. Sci. USA*, Jun 15; 2004;**101**(24): 9137–9142.
126. Farkas, A., A.J. Batey, and S.J. Coker, How to measure electrocardiographic QT interval in the anaesthetized rabbit. *J. Pharmacol. Toxicol. Methods*, 2004 Nov–Dec;**50**(3): 175–185.
127. Ryu, K., S.C. Shroff, J. Sahadevan, N.L. Martovitz, C.M. Khrestian, and B.S. Stambler, Mapping of atrial activation during sustained atrial fibrillation in dogs with rapid ventricular pacing induced heart failure: evidence for a role of driver regions. *J. Cardiovasc. Electrophysiol.*, Dec 2005;**16**(12): 1348–1361.
128. Kano, M., T. Toyoshi, S. Iwasaki, M. Kato, M. Shimizu, and T. Ota, QT PRODACT: usability of miniature pigs in safety pharmacology studies: assessment for drug-induced QT interval prolongation. *J. Pharmacol. Sci.*, 2005;**99**(5): 501–511.
129. Spach, M.S., R.C. Barr, C.F. Lanning, and P.C. Tucek, Origin of body surface QRS and T wave potentials form epicardial potential distributions in the intact chimpanzee. *Circulation*, Feb 1977;**55**(2): 268–278.
130. Gauvin, D.V., L.P. Tilley, F.W. Smith Jr, and T.J. Baird, Electrocardiogram, hemodynamics, and core body temperatures of the normal freely moving cynomolgus monkey by remote radiotelemetry. *J. Pharmacol. Toxicol. Methods*, Mar–Apr 2006;**53**(2): 140–151.
131. Sawazaki, H. and H. Hirose, Comparative electrocardiographical studies on the conduction time of heart in vertebrates. *Jpn. J. Vel. Sci.*, 1974;**36**: 421–426.
132. Detweiler, D.K., Regulation of the heart, in *Dukes' Physiology of Domestic Animals*, 10th edn, M.J. Swenson, Editor. Ithaca, NY: Cornell University Press, 1984, pp. 150–162.
133. Schmidt-Nielsen, K., *Animal Physiology: Adaptation and Environment*. London: Cambridge University Press, 1975.
134. Stahl, W.R., Scaling of respiratory variables in mammals. *J. Appl. Physiol.*, 1967;**22**: 453–460.
135. Schaible, T.F. and J. Scheuer, Response of the heart to exercise training, in *Growth of the Heart in Health and Disease*, R. Zak, Editor. New York: Raven, 1984, pp. 381–419.
136. Hermann, G.R., T.E. Vice, A.R. Rodriguez, and A.W. Herrmann, Heart weight to body weight, left to right ventricular weights, and ratios of baboon hearts, in *The Baboon in Medical Research*, vol. I, H. Vagtborg, Editor. Austin, TX: University of Texas Press, 1965, pp. 269–274.
137. Detweiler, D.K., Normal and pathological circulatory stresses, in *Dukes' Physiology of Domestic Animals*, 10th edn, M.J. Swenson, Editor. Ithaca, NY: Cornell University Press, 1984, pp. 207–225.
138. Porges, S.W., P.M. McCabe, and B.G. Yongue, Respiratory-heart-rate interactions: psychophysiological implications for pathophysiology and behavior, in *Perspectives in Cardiovascular Psychophysiology*, J. Cacioppo and R. Petty, Editors. New York: Guilford, 1982, pp. 223–264.
139. Porges, S.W., Spontaneous oscillations in heart rate; potential index of stress, in *Animal Stress*, G.P. Moberg, Editor. Bethesda, MD: American Physiological Society, 1985, pp. 97–111.
140. Kitney, R.I. and E. Rompelman, Editors. *The Study of Heart-Rate Variability*. Oxford: Clarendon Press, 1980.
141. Kwatny, E., D. Peltzman, and D.K. Detweiler, Automated analysis of Beagle electrocardiograms, in *Proceedingsof the 13th North England Bioengineering Conference*, K.R. Foster, Editor. New York: IEEE, 1987.
142. Melbin, J., D.K. Detweiler, R.A. Riffle, and A. Noordergraaf, Coherence of cardiac output with rate changes. *Am. J. Physiol.*, 1982;**243**: H499–H504.
143. Detweiler, D.K., Electrocardiographic detection of cardiotoxicity in preclinical studies, in *Safely Evaluation and Regulation of Chemicals*, vol. 3, F. Homburger, Editor. Basel: Karger, 1986, pp. 76–86.
144. Bauer, K. and O. Nehring, Betrachtungen zu den mathematischen Formuliertingen der Abhängigkeit der QT-Zeit von der Frequenz und die Deutung derselben. *Z. Kreislaufforsch*, 1968;**57**: 430–436.
145. Schoenwald, R.D. and V.E.Q.T. Isaacs, Corrected for heart rate: a new approach and its application. *Arch. Int. Pharmacodyn. Ther.*, 1974;**211**: 34–48.

146. Grauwiler, J., Das normale Elektrokardiogramm des Beagle-Hundes. *Naunyn-Schmiedebergs Arch. Pharmakol.*, 1970;**266**: 337.
147. Osborne, B.E. and G.D.H. Leach, The Beagle electrocardiogram. *Food Cosmet. Toxicol.*, 1971;**9**: 857–864.
148. Patterson, D.F., D.K. Detweiler, and S.A. Glendenning, Heart sounds and murmurs of the normal horse. *Ann. N.Y. Acad. Sci.*, 1965;**127**: 242–305.
149. Gonder, J.C., E.A. Gard, and N.E.I.I.I. Lott, Electrocardiograms of nine species of nonhuman primates. *Am. J. Vel. Res.*, 1980;**41**: 972–975.
150. von Mickwitz, G., *Herz- und Kreislaufuntersuchungen beim Schwein mit Berücksichtigung des Elektrokardiogramms und des Phonokardiogramms*. Hannover: Habilitationsschrift, 1967, pp. 1–246.
151. Richards, A.G., E. Simonson, and M.B. Visscher, Electrocardiogram and phonogram of adult and newborn mice in normal conditions and under the effect of cooling, hypoxia and potassium. *Am. J. Physiol.*, 1953;**174**: 293–298.
152. O'Rourke, M.F., A.P. Avolio, and W.W. Nichols, The kangaroo as a model for the study of hypertrophic cardiomyopathy in man. *Cardiovasc. Res.*, 1986;**20**: 398–402.
153. Lourenco, M.L. and H. Ferreira, Electrocardiographic evolution in cats from birth to 30 days of age. *Can. Vet. J.*, 2003 Nov;**44**(11): 914–917.
154. Jefferson, J.W., Electrocardiographic and phonocardiographic findings in a reticulated giraffe. *J. Am. Vet. Med. Assoc.*, 1971;**159**: 602–604.
155. Rossof, A.H., An electrocardiographic study of the giraffe. *Am. Heart J.*, 1972;**83**: 142–143.
156. Tokita, K., Electrocardiographical studies on bottle-nosed dolphin (Tursiops truncatus). *Sci. Rep. Whales Res. Inst.*, 1960;**15**: 159–165.
157. Rogers, W.A. and S.P. Bishop, Electrocardiographic parameters of the normal domestic cat: A comparison of standard limb leads and an orthogonal system. *I. Electrocardiol.*, 1971;**4**: 315–321.
158. Jayasinghe, J.B., S.D.A. Fernando, and L.A.P. Brito-Babapulle, The electrocardiographic patterns of *Elephas maxim us* – the elephant of Ceylon. *Br. Vel. I.*, 1963;**119**: 559–564.
159. Stewart, J.H., R.J. Rose, P.E. Davis, and K. Hoffman, A comparison of electrocardiographic findings in racehorses presented either for routine examination or poor racing performance, in *Equine Exercise Physiology* D.H. Snow, S.G.B. Persson, and R.J. Rose, Editors. Cambridge: Granta, 1983, pp. 135–143.
160. Moore, E.N., G. Fisher, D.K. Detweiler, and G.K. Moe, The importance of atrial mass in the maintenance of atrial fibrillation, in *International Symposium on Comparative Medicine*, R.J. Tashjian, Editor. Norwich, CT: Eaton Laboratory, 1965, pp. 229–238.
161. Spörri, H., Die ersten Fälle von sog. Wolff-Parkinson-White Syndrom, einer eigenartigen Herzanomalie, bei Tieren. *Schweiz Arch. Tierheilkd.*, 1953;**95**: 13–22.
162. Giuliano, G., G. Angrisani, P.P. Campa, M. Condorelli, and V. Pennetti, L'elettrocardiogram: na nella pecora. *Boll. Soc. Ital. Biol. Sper.*, 1958;**34**: 1785–1787.
163. Mullick, D.N., B.V. Alfredson, and E.P. Reineke, Influence of thyroid status on the electrocardiogram and certain blood constituents of the sheep. *Am. J. Physiol.*, 1948;**152**: 100–105.
164. Walper, F., *Elektrokardiographische und andere kardiographische Studien am Schaf*, Dissertation. Munich, 1932.
165. Unshelm, J., H.H. Thielscher, F. Haring, H. Hohns, U.E. Pfleiderer, and W. von Schutzbar, Elektrokardiographische Untersuchungen bei Schafen unter Berücksichtigung der Rasse, des Lebensalters und anderer Einflussfaktoren. *Zentralbl. Veterinaermed. A.*, 1974;**21**: 479–491.
166. Schultz, R.A., P.J. Pretorius, and M. Terblanche, An electrocardiographic study of normal sheep using a modified technique. *Onderstepoort J. Vet. Res.*, 1972;**39**: 97–106.
167. Rozanova, T.V., Electrocardiographic indicators of sheep of various constitutional types (in Russian). *Dokl. Skh. Akad. Sofia*, 1958;**32**: 369–377.
168. Roshchevsky, M.P., Vector- i elektrokardificheskie iccledovaniya cerdechnoi deyatel'nosti ovetz. *Skh. Biol.*, 1969;**4**: 594–600.
169. Szabuniewicz, M. and D.R. Clark, Analysis of the electrocardiograms of 100 normal goats. *Am. J. Vet. Res.*, 1967;**28**: 511–516.
170. Upadhyay, R.C. and S.C. Sud, Electrocardiogram of the goat. *Indian J. Exp. Biol.*, 1977;**15**: 359–362.
171. Senta, T., Experimental investigation of electrocardiogram in the goat. *Exp. Rep. Equme Health Lab.*, 1967;**4**: 37–72.
172. Dukes, T.W. and M. Szabuniewicz, The electrocardiogram of conventional and miniature swine (Sus scrofa). *Can. J. Comp. Med.*, 1969;**33**: 118–127.
173. Thielscher, H.H., Elektrokardiographische Untersuchungen an Deutschen veredelten Landschweinen der Landeszucht und der Herdbuchzucht. *Zentralbl. Veterinaermed. A.*, 1969;**16**: 370–383.
174. von Mickwitz, G., *Herz- und Kreislaufuntersuchungen beim Schwein mit Berücksichtigung des Elektrokardiogramms und des Phonokardiogramms*. Hannover: Habilitationsschrift, 1967, pp. 1–246.
175. Hausmann, W.O., *Das Elektrokardiogramm des Hausschweines*, Dissertation. München, 1934, pp. 1–28.
176. Cox, J.L., D.E. Becker, and A.H. Jensen, Electrocardiographic evaluation of potassium deficiency in young swine. *J. Anim. Sci.*, 1966;**25**: 203–206.
177. Jefferson, J.W., Electrocardiographic and phonocardiographic findings in a reticulated giraffe. *J. Am. Vet. Med. Assoc.*, 1971;**159**: 602–604.
178. Rossof, A.H., An electrocardiographic study of the giraffe. *Am. Heart J.*, 1972;**83**: 142–143.
179. Jayasinghe, J.B., D.A. Fernando, and L.A.P. Brito-Babapulle, The electrocardiogram of the camel. *Am. J. Vet. Res.*, 1963;**24**: 883–885.
180. Geddes, L.A., W.A. Tacker, J. Rosborough, A.G. Moore, and P. Cabler, The electrocardiogram of a dromedary camel. *J. Electrocardiol.*, 1973;**6**: 211–214.
181. Senft, A.W. and J.K. Kanwisher, Cardiographic observations on a fin-back whale. *Circ. Res.*, 1960;**8**: 961–964.
182. Spencer, M.P., T.A. Gornall III, and T.C. Poulter, Respiratory and cardiac activity of killer whales. *J. Appl. Physiol.*, 1967;**22**: 974–981.
183. Tokita, K., Electrocardiographical studies on bottle-nosed dolphin (Tursiops truncatus). *Sci. Rep. Whales Res. Inst.*, 1960;**15**: 159–165.
184. Hamlin, R.L., R.F. Jackson, J.A. Himes, F.S. Pipers, and A.C. Townsend, Electrocardiogram of bottle-nosed dolphin *(Tursiops truncatus)*. *Am. J. Vet. Res.*, 1970;**31**: 501–505.

185. Richards, A.G., E. Simonson, and M.B. Visscher, Electrocardiogram and phonogram of adult and newborn mice in normal conditions and under the effect of cooling, hypoxia and potassium. *Am. J. Physiol*., 1953;**174**: 293–298.
186. Spörri, H., Starke Dissoziation zwischen dem Ende der elektrischen und mechanischen Systolendauer bei Känguruhs. *Cardiologia*, 1956;**28**: 278–284.
187. Siegfried, J.P., *Elektrokardiographische Untersuchungen an ZOO-Tieren*, Dissertation. Zürich: University of Zurich, 1956, pp. 1–57.
188. Jayasinghe, J.B. and S.D.A. Fernando, Electrocardiograms of zoo animals, II. Leopard and Wallaby. *Ceylon Vet. J*., 1964;**12**: 21–22.
189. Wilbur, C.G., Electrocardiographic studies on the opossum. *J. Mammal., 1955*;**36**: 284–286.
190. Szabuniewicz, M., D. Hightower, and J.R. Kyzar, The electrocardiogram, vectorcardiogram, and spatiocardiogram in the rabbit. *Can. J. Comp. Med*., 1971;**35**: 107–114.
191. Levine, H.D., Spontaneous changes in the normal rabbit electrocardiogram. *Am. Heart J*., 1942;**24**: 209–214.
192. Massmann, W. and H. Opitz, Das normale Kaninchen-EKG. Z. *Gesamte Exp. Med*., 1954;**124**: 35–43.
193. Slapak, L. and P. Hermanek, Beobachtungen über das Elektrokardiogramm des Kaninchens. I: Das normale Extremitäten-Elektrokardiogramm des Kaninchens. *Z. Kreislaufforsch*., 1957;**46**: 136–142.
194. Slapak, L. and P. Hermanek, Beobachtungen uber des Elektrokardiogramm des Kaninchens. II: Das normale Brustwand-Elektrokardiogramm des Kaninchens. *Z. Kreislaufforsch*., 1957;**46**: 143–166.
195. Jacotot, B., L'electrocardiogramme du lapin. Analyse des tracés de 75 animaux sains. *Recl. Med. Vet*., 1965;**141**: 1095–1107.
196. Angelakos, E.T. and P. Bernardini, Frequency components and positional changes in electrocardiogram of the adult rat. *J. Appl. Physiol*., 1963;**18**: 261–263.
197. Beinfeld, W.H. and D. Lehr, QRS-T variations in the rat electrocardiogram. *Am. J. Physiol*., 1968;**214**: 197–204.
198. Beinfeld, W.H. and D. Lehr, P-R interval of the rat electrocardiogram. *Am. J. Physiol*., 1968;**214**: 205–211.
199. Werth, G. and S. Wink, Das Elektrokardiogramm der normalen Ratte. *Arch. Kreislaufforsch*., 1967;**54**: 272–308.
200. Langer, G.A., Interspecies variation in myocardial physiology: the anomalous rat. *Environ. Health Perspect*., 1978;**26**: 175–179.
201. O'Bryant, J.W., A. Packchanian, G.W. Reimer, and R.H. Vadheim, An apparatus for studying electrocardiographic changes in small animals. *Tex. Rep. Bioi. Med*., 1949;**7**: 661–670.
202. Lombard, E.A., Electrocardiograms of small mammals. *Am. J. Physiol*., 1952;**171**: 189–193.
203. Giordano, G. and G. Nigro, Caratteristiche dell' elettrocardiogramma normale del Mus musculus albus. *Sperimentale*, 1957;**107**: 63–68.
204. Goldbarg, A.N., H.K. Hellerstein, J.H. Bruell, and A.F. Daroczy, Electrocardiogram of the normal mouse, *Mus musculus*: general considerations and genetic aspects. *Cardiovasc. Res*., 1968;**2**: 93–99.
205. Callsen, A.D., *Elektrokardiographische Untersuchungen an wachen und anästhesierten Katzen mit einem System von zehn Standardableitungen*, Dissertation. Berlin: Freie University, 1983, Journal No.1130, pp. 1–105.
206. Tilley, L.P. and R.E. Gompf, Feline electrocardiography. *Vet. Clin. North Am*., 1977;**7**: 257–272.
207. Rogers, W.A. and S.P. Bishop, Electrocardiographic parameters of the normal domestic cat: a comparison of standard limb leads and an orthogonal system. *I. Electrocardiol*., 1971;**4**: 315–321.
208. Blok, J. and J.Th.F. Boeles, The electrocardiogram of the normal cat. *Acta Physiol. Pharmacol. Neerl*., 1957;**6**: 95–102, 209.
209. Massmann, W. and H. Opitz, Das Katzen-Ekg. *Cardiologia*, 1954;**24**: 54–64.
210. Rothlin, E. and E. Suter, Glykosidwirkung auf Elektrokardiogramm und Myokard. I Vergleichende elektrokardiographische Untersuchungen verschiedener herzwirksamer Glykoside an der Katze bei intravenöser Infusion. *Helv. Physiol. Pharmacol. Acta*, 1947;**5**: 298–321.
211. Purchase, I.F.H., The effect of halothane on the isolated cat heart. *Br. J. Anaesth*., 1966;**38**: 80–91.
212. Purchase, I.F.H., Cardiac arrhythmias occurring during halothane anaesthesia in cats. *Br. I. Anaeslh*., 1966;**38**: 13–22, 213.
213. Jayasinghe, J.B., S.D.A. Fernando, and L.A.P. Brito-Babapulle, The electrocardiograpic patterns of *Elephas maxim us* - the elephant of Ceylon. *Br. Vel. I*., 1963;**119**: 559–564.
214. Jayasinghe, J.B. and L.A.P. Brito-Babapulle, A report on an electrocardiogram of the Ceylon elephant. *Ceylon Vel. J*., 1961;**9**: 69–70.
215. Grauweiler, J., Beobachtungen am Elektrokardiogramm von nicht-domestizierten Säugetieren. *Schweiz. Arch. Tierheilkd*., 1961;**103**: 397–417.
216. Forbes, A. and S. Cobb, Cattell McK. An electrocardiogram and an electromyogram in an elephant. *Am. I. Physiol*., 1921;**55**: 385–389.
217. Siegfried, J.P., *Elektrokardiographische Untersuchungen an Zoo-Tieren*, Dissertation. Zürich: University of Zürich, 1956.
218. Nörr, J., Hundert klinische Fälle von Herz und Pulsarrhythmien beim Pferde. *Mh. Prakt. Tierheilkd. Slullgarl*, 1924;**34**: 177–232.
219. Roos, J., Vorhoffiimmern bei den Haustieren. *Arch. Wiss. Prakt. Tierheilkd*., 1924;**51**: 280–293.
220. Roos, J., Auricular fibrillation in the domestic animals. *Heart*, 1924;**11**: 1–7.
221. Agduhr, E. and N. Stenström, The appearance of the electrocardiogram in the heart lesions produced by cod liver oil treatment: electrocardiogram in rats treated with cod liver oil. *Acla Paediatr. (Uppsala)*, 1930;**9**: 280–306.
222. Drury, A.N., L.J. Harris, C. Maudsley, and B. Vitamin, deficiency in the rat. Bradycardia as a distinctive feature. *Biochem. J*., 1930;**24**: 1632–1649.
223. Nörr, J., Über Atmungsarrhythmie bei Caniden. *Verh. Dtsch. Ges. Kreislaufforsch*., 1935;**7**: 144–148.
224. Scher, A.M., Direct recording from the A-V conducting system in the dog and monkey. *Science*, 1955;**121**: 398–399.
225. Scher, A.M. and A.C. Young, The pathway of ventricular depolarization in the dog. *Circ. Res*., 1956;**4**: 461–469.
226. Detweiler, D.K., Perspectives in canine cardiology. *Univ. Pennsylvania Bull. Vet. Ext. Q*., 1958;**149**: 27–48.
227. Ettinger, S.J. and P.F. Suter, *Canine Cardiology*. Philadelphia, PA: Saunders, 1970.
228. Hill, J.D.A., *Correlative Study of Right Ventricular Conduction Disturbances in the Dog*, Veterinary thesis. Philadelphia, PA: University of Pennsylvania, 1967.

229. Hill, J.D., Electrocardiographic diagnosis of right ventricular enlargement in dogs. *J. Electrocardiol*., 1971;**4**: 347–357.
230. Pruitt, R.D., Electrocardiogram of bundle-branch block in the bovine heart. *Circ. Res*., 1962;**10**: 593–597.
231. O'Rourke, M.F., A.P. Avolio, and W.W. Nichols, The kangaroo as a model for the study of hypertrophic cardiomyopathy in man. *Cardiovasc. Res*., 1986;**20**: 398–402.
232. Gompf, R.E. and L.P. Tilley, Comparison of lateral and sternal recumbent positions for electrocardiography of the cat. *Am. J. Vet. Res*., 1979;**40**: 1483–1486.
233. Boineau, J.P., E.N. Moore, J.F. Spear, and W.C. Sealy, Basis of static and dynamic electrocardiographic variations in Wolff-Parkinson-White syndrome. *Am. J. Cardiol*, 1973;**32**: 32–45.

43 12 Lead Vectorcardiography

Peter W. Macfarlane · Olle Pahlm

P. W. Macfarlane, A. van Oosterom, O. Pahlm, P. Kligfield, M. Janse, J. Camm (eds.), *Comprehensive Electrocardiology*, DOI 10.1007/978-1-84882-046-3_43,

43.1 Vectorcardiography

43.1.1 What Is a Vector?

The term vector can have different meanings, but for the purposes of the study of vectorcardiography, the relevant definition states that a vector is an entity possessing a magnitude and a direction. For example, if a wind blows in an easterly direction at 10 km/h, it could be represented by the vector in Fig. 43.1a. On the other hand, if a light breeze blows at 5 km/h in a northeasterly direction, it would be represented using the same scheme by the vector of Fig. 43.1b. It can be seen that the length of the vector is proportional to the strength of the wind and the direction of the vector is that of the wind.

Of course, there can be many different forces that are represented by a vector. Within the context of electrocardiography (ECG), it is the cardiac electromotive force that is desired to be represented by a vector. It was Einthoven et al. [1] in their classic paper of 1913 who suggested that the electrical forces of heart could be summed and represented by a single vector.

43.1.2 Concept of Resultant Force

While a vector can be used to represent an individual force as shown in Fig. 43.1, a series of vectors can be used simultaneously to represent a variety of forces acting together or in opposition. It is possible to use some simple mathematical techniques to calculate the resultant effect of the different forces, and it is instructive to consider an example.

Imagine that a rower sets out to cross a river. He is able to row constantly at 4 km/h directly across the water but has to contend with a current that is flowing at a rate of 3 km/h. This is depicted in Fig. 43.2. It should be clear that if the rower consistently pulls directly across the river he will not reach the bank at a point directly opposite his starting point but will be carried some way downstream by the current. In fact, the distance can be calculated by what is known as the "Triangle of Forces," which shows that he would travel at a net speed of 5 km/h. The exact point at which the rower reaches the opposite bank, of course, depends on the width of the river but this can be calculated from the triangle. For example, if the river is 200 m wide, the boat should reach the opposite side 150 m downstream on the opposite side.

The combined velocity of the boat and the current produces a resultant velocity of 5 km/h depicted by the hypotenuse on the triangle. Conversely, it can be said that if there is a resultant velocity of 5 km/h, it has components of 3 and 4 km/h at right angles to each other in keeping with Fig. 43.2. Thus, there exists the concept that a resultant velocity has a component in a particular direction. The size of each component can be obtained by drawing a perpendicular from the tip of the resultant vector to a line indicating the direction in which it is desired to measure the component.

A similar concept applies in electrocardiography. Consider that in the frontal plane of the body, there is a resultant cardiac electromotive force of 2 mV acting at 45° to the horizontal, that is, approximately similar to the path of the rowing boat in Fig. 43.2. Figure 43.3 shows that there is a component of 1.41 mV in the direction of lead I. Similarly, it can be shown that there is a component of approximately 1.93 mV in the direction of lead II. This estimate assumes that the equilateral Einthoven triangle is a valid model, which in reality is not the case. However, the potential measured by lead I can be considered as the component of the resultant cardiac electromotive force acting in that direction in the frontal plane. It follows from Einthoven's Law (see Chap. 11) that the potential in lead III would be 0.52 mV at the same instant in the cardiac cycle.

43.1.3 Spatial Vector

Sections 43.1.1 and 43.1.2 have dealt with the two-dimensional situation of a vector or vectors acting effectively in a plane. A more realistic situation is a force or a vector having the ability to be directed at any point in space. Figure 43.4 illustrates the concept of a spatial vector drawn within a three-dimensional coordinate reference system with axes denoted

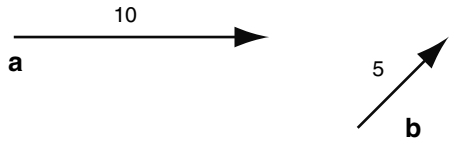

Figure 43.1
The direction and speed of the wind represented as a vector when the (a) wind blows in an easterly direction at 10 km/h (b) wind blows in a northeasterly direction at 5 km/h.

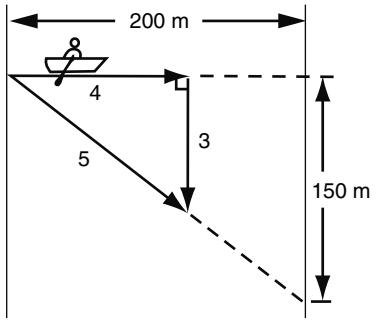

Figure 43.2
A rower crossing a river 200 m wide. For explanation, see text.

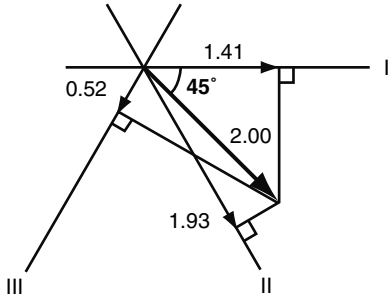

Figure 43.3
The cardiac electromotive force and its components in the direction of leads I, II, and III.

X, *Y*, and *Z*. It can be seen from the illustration that the magnitude of the vector can be calculated by using triangle OMA if the length of sides OA and AM can be determined.

However, from the Figure, it follows that:

$$OA^2 = x^2 + z^2$$

From right angled triangle OMA,

$$OM^2 = OA^2 + AM^2 = x^2 + y^2 + z^2$$

Thus, for a point M with coordinates *x*, *y*, *z* in three-dimensional space, the length of the vector OM is given by the above expression. By analogy with the two-dimensional situation, where it was shown that a vector lying in a plane could have

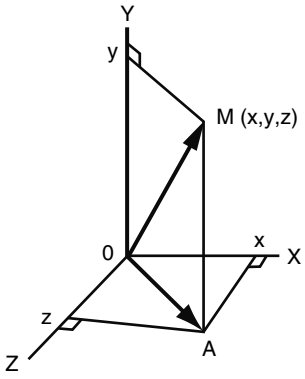

Figure 43.4
A spatial vector OM and its components *x, y, z* in a three-dimensional coordinate system.

components calculated in any particular direction by drawing a perpendicular to that line, it can also be shown that in the spatial situation, a vector, for example, OM, can have components in the three mutually perpendicular directions X, Y, Z. In the forward situation, if the components *x*, *y*, *z* can be measured at a particular instant in the cardiac cycle, then a resultant OM can be calculated. This is the basis of an orthogonal lead system.

43.1.4 Orthogonal Lead Systems

43.1.4.1 Theoretical Considerations

Section 43.1.3 suggests that if three leads can be designed to record components of a resultant cardiac electromotive force in three mutually perpendicular directions, then the problem of deriving the resultant cardiac electromotive force is solved. A considerable amount of research went into designing such lead systems over the past 50 years. The theory is detailed but a few simple concepts are worthy of discussion at this point. Further aspects are considered in Chap. 11, Sect. 11.5.

Assume that the potential measured by any electrocardiographic lead is represented by V. Then, assume that the resultant cardiac electromotive force is denoted by **H** or, as it is sometimes known, "The heart vector." Then from mathematical considerations, it can be shown that $V = \mathbf{H} \cdot \mathbf{L}$ where **L** is the vector representing the strength of the lead being used to measure the potential. In fact, it is one of the basic rules of vector mathematics that the dot product of two vectors is a scalar, that is, the potential or voltage does not have an associated direction but only a magnitude whereas the heart vector **H** and the lead vector **L** each has its own direction. This basic rule of vector mathematics can also be expanded to the following:

$$V = H_X L_X + H_Y L_Y + H_Z L_Z$$

where H_X, H_Y, H_Z are the three components of the heart vector and L_x, L_y, L_z are the three components of the lead vector. From this observation, it follows that if it is desired to measure the component of the heart vector in the X direction, then a lead should be designed that has components (L_X, 0, 0). In that case,

$$V_X = H_X L_X$$

If the strength L_X of the lead is known, then when the potential V_X is measured, H_X can be calculated.

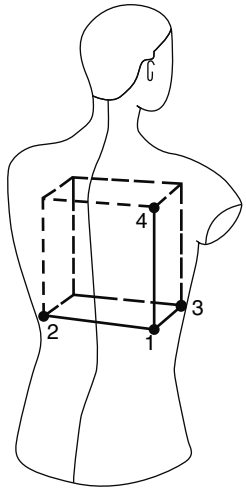

Figure 43.5
The cube lead system introduced by Grishman [2]. © American Heart Association, Dallas,Texas. Reproduced with permission.

43.1.4.2 Uncorrected Lead Systems

For historical reasons, it is worth noting that the earliest attempts at designing orthogonal lead systems were made on the basis of constructing leads such that lines joining the electrodes were essentially mutually perpendicular. This is most easily understood by considering the cube system introduced by Grishman [2] (Fig. 43.5). However, as experience was gained and mathematical modeling advanced, it was found that these lead systems did not accurately measure the required components.

43.1.4.3 Corrected Orthogonal Lead Systems

As a result of considerable modeling, both mathematical and physical, such as using model torsos filled with conducting solution, corrected orthogonal lead systems were gradually introduced.

The most notable and the one that is generally used wherever vectorcardiography is currently studied using an orthogonal lead system, is that of Frank [3]. This lead system is shown in Fig. 43.6. As can be seen, the lead positions are different from those of the 12-lead system, although the C and A electrodes are indeed close to the V_4 and V_6 positions, respectively.

Mathematical modeling showed that the following equations represent the derivation of the three potentials V_X, V_Y, V_Z:

$$V_X = 0.610V_A + 0.171V_C - 0.781V_I$$
$$V_Y = 0.655V_F + 0.345V_M - 1.0V_H$$
$$V_Z = 0.133V_A + 0.736V_M - 0.264V_I - 0.374V_E - 0.231V_C$$

These contributions to the individual leads from the different electrodes correspond to the resistor network also seen in Fig. 43.6. The major disadvantage of using this type of orthogonal lead system is the need to apply a completely different set of electrodes to the patient compared to that required for recording the conventional 12-lead ECG. There have been attempts to minimize the differences by doubling the C and A electrodes as V_4 and V_6, for example, and using a common left leg electrode but this still leaves four additional electrodes to be positioned on the thorax and neck.

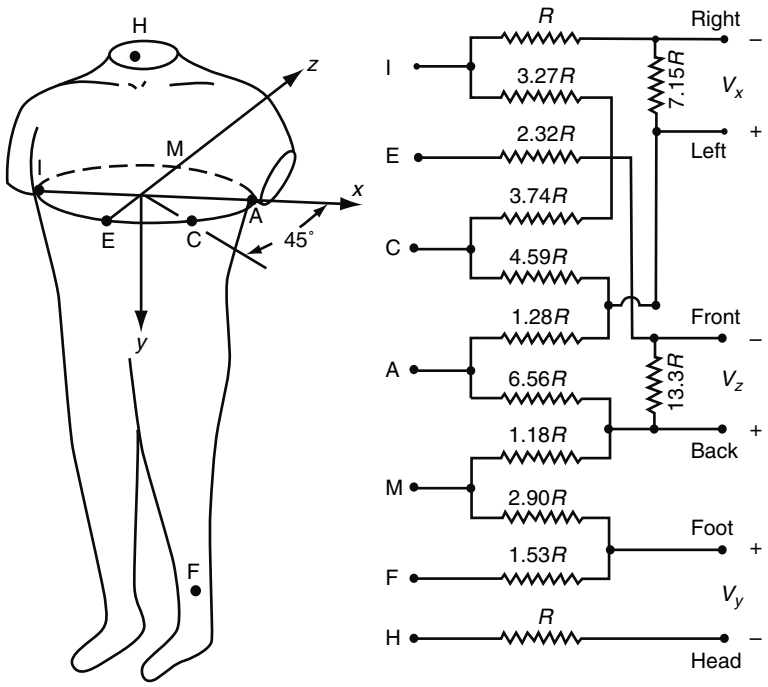

Figure 43.6
The Frank lead system (After Frank [3]). © American Heart Association, Dallas, Texas. Reproduced with permission.

43.1.5 Cardiac Activation

43.1.5.1 Vectorial Spread of Cardiac Activation

The concept of resultant cardiac electromotive force by now should be gaining hold. It is possible to consider the various resultant forces acting throughout ventricular depolarization, for example. Figure 43.7a shows a series of individual vectors each of which represents the resultant cardiac electromotive force at one particular instant during the process of ventricular depolarization. For example, the first small vector shows the initial septal activation from left to right. Note that all of these vectors are depicted in the two-dimensional situation, which in this case is the frontal plane of the body. Figure 43.7b indicates how each of these resultant vectors can be translated to a common origin and a loop drawn to connect the tips of the vectors. This loop is a form of vectorcardiogram. Indeed, the first form of planar vectorcardiogram was introduced by Mann in 1920 [4].

43.1.5.2 Spatial Vector Loop

The previous Sect. 43.1.5.1 showed a planar loop. However, the concept of spatial vector has been introduced in Sect. 43.1.3 and it follows that if a resultant vector varies in magnitude and direction throughout the cardiac cycle, then it can be imagined that the tip of this vector will trace out a three-dimensional path. This observation is illustrated in Fig. 43.8 for the case of ventricular depolarization, that is, a spatial QRS loop is shown. In addition, the projection of this loop onto three mutually perpendicular planes is also illustrated. The collection of three planar loop projections is known as the vectorcardiogram. While only the QRS loop is depicted here for clarity, it follows that P and T loops can also be derived.

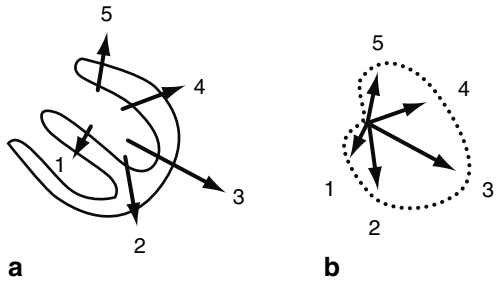

Figure 43.7
(a) Ventricular depolarization illustrated as a sequence of vectors, 1–5. (b) After translation of vectors to a common origin, a vectorcardiographic loop can be constructed.

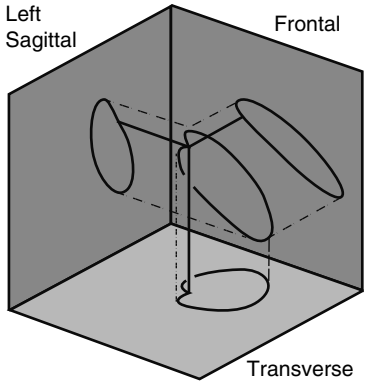

Figure 43.8
A vectorcardiographic loop in space projected onto the three orthogonal planes.

43.1.6 Vector Loop Presentation

43.1.6.1 Nomenclature

The American Heart Association committee on electrocardiography (1975) [5] published a set of recommendations for vectorcardiographic terminology. The committee recommended that the lead Z be directed positively to the posterior thorax, although this does mean that the scalar presentation of lead Z is essentially opposite to that of lead V_2. This recommendation certainly causes much confusion when describing scalar lead appearances and for this reason, in this chapter, lead Z is directed positively to the anterior to be similar to V_2. Thus, R_Z can be thought of in the same way as R_{V2}. Of more contention is the choice of whether to view the left or right sagittal planes, that is, the sagittal plane as viewed from the left or right. Figure 43.9 shows the left sagittal projection. The Committee did not make a particular recommendation, but for the purposes of illustrations in this book, the left sagittal view has been chosen in keeping with Fig. 43.9 so as to have a uniform collection of reference axes.

43.1.6.2 Display Techniques

About 20 years ago, the most common method of displaying the vectorcardiogram was via an oscilloscope. Pairs of leads such as X and Y were used to deflect the electron beam horizontally and vertically, respectively, and in this case, the

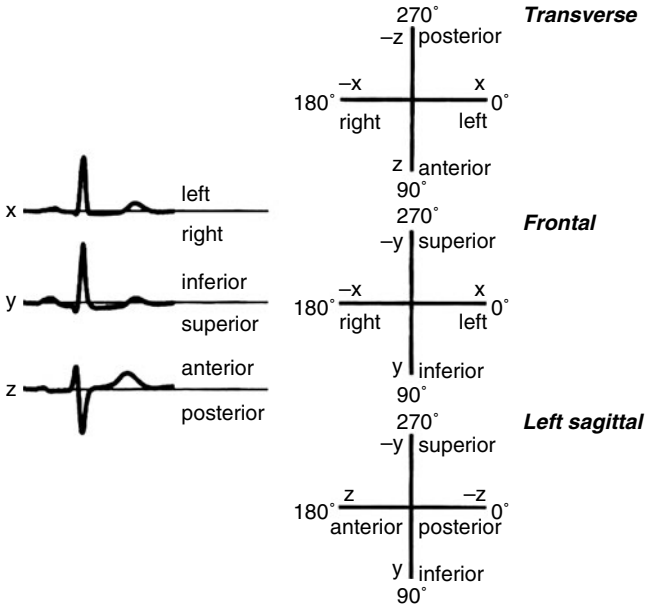

Figure 43.9

Polarity of leads X, Y, and Z and angular reference frame of the frontal, transverse, and left sagittal planes.

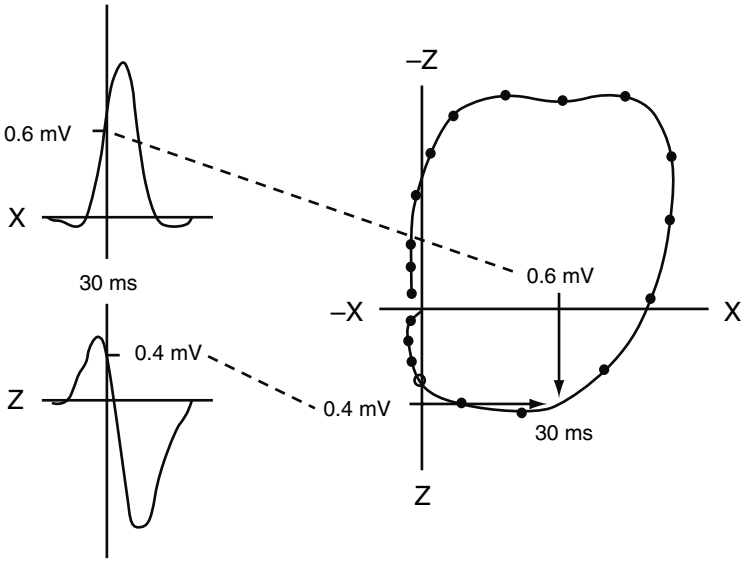

Figure 43.10

Derivation of transverse plane loop from leads X and Z. Dots are at 4 ms intervals and the 20 ms vector is indicated with an open circle.

frontal plane loop would be generated. Consider that leads X and Y are recorded simultaneously. At any instant in time, an amplitude for each lead is known, that is, an (*x*, *y*) coordinate pair of values is available. These values could be plotted simply on XY axes. If this is repeated throughout the cardiac cycle, then a complete frontal plane set of P, QRS, and T loops can be generated. Figure 43.10 shows the derivation of a QRS loop in the transverse plane.

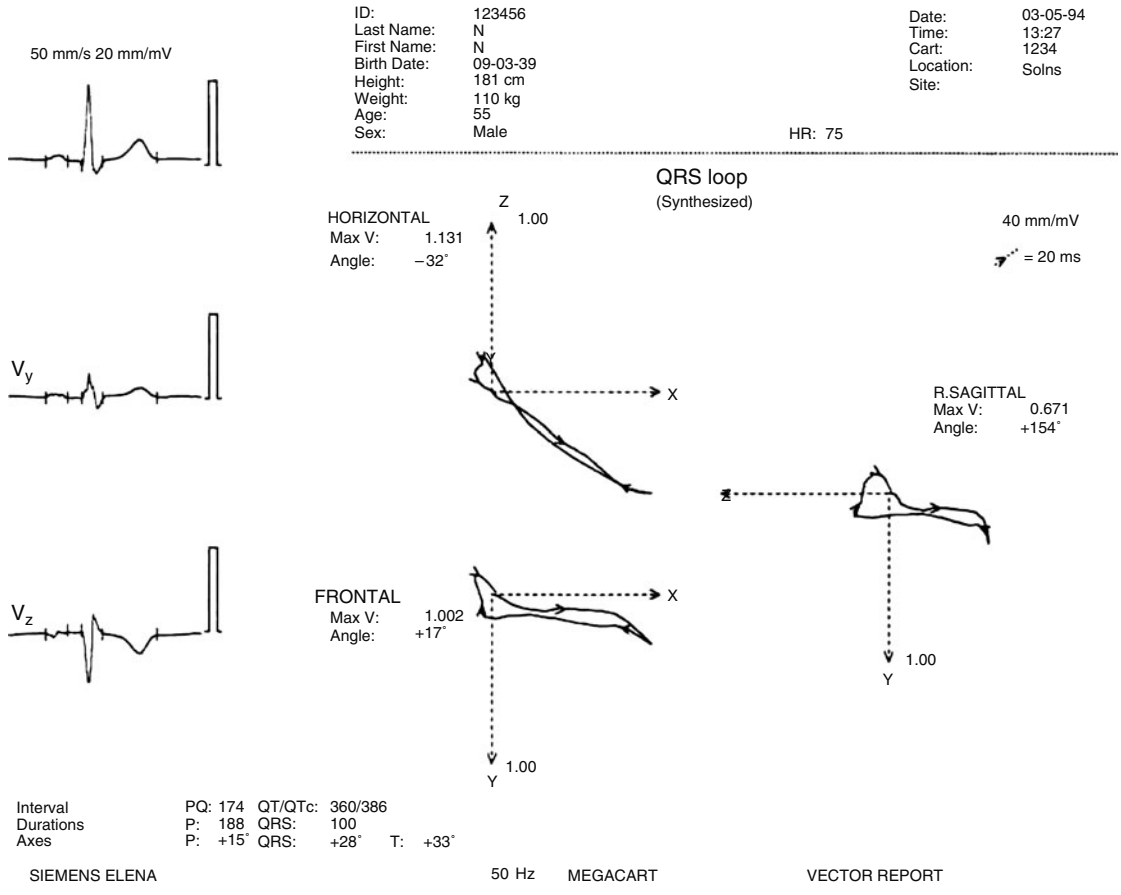

Figure 43.11

Vectorcardiogram printout from a commercially available electrocardiograph. Note that lead Z is inverted in comparison with other illustrations in this book.

If the leads X, Y, Z are considered in pairs, then by plotting leads XY, the frontal plane vectorcardiographic loop can be obtained. Similarly, XZ plots produce the transverse plane loop and ZY plots produce the sagittal plane vectorcardiographic loop. Nowadays, with the widespread availability of computer technology, these plots can be produced in a straightforward fashion. It is somewhat more complex to program a thermal writer to produce an XY display but nevertheless this is readily attainable. Thus, vectorcardiographic loops can now be produced even on small 4″ paper displays or on the larger A4 writers such as are common at the bedside. An illustration of a typical vectorcardiographic display from a computer-based electrocardiograph is shown in Fig. 43.11.

It is important that vectorcardiographic loops have some indication of the speed of inscription as this can contain diagnostic information. A number of methods have been used. Conventionally, the vectorcardiographic loop has been interrupted so that time intervals can actually be measured by counting the number of dots between two points. Generally, 2 or 4 ms intervals have been used. An alternative is to produce a continuous loop and mark a number such as 1, 2 indicating 10, 20 ms from the onset of the QRS complex. This is helpful but creates difficulties around the onset and termination of the QRS loop, which is often the most interesting part in terms of looking for conduction problems. Either way, the direction of inscription of the loop is also of vital clinical significance. Thus, if a numbering system is not used, some indication must be given to make it quite clear to the viewer in which direction the different planar loops are inscribed. With a knowledge of the theory of vectorcardiography, the experienced cardiologist can always determine the direction of inscription but it is certainly easier if this is made obvious in a good display.

In this book, loops are presented with an arrow indicating the direction of inscription. Further, black dots indicate 4 ms intervals and the 20 ms vector is indicated with an open circle.

43.2 Normal Ranges

43.2.1 Introduction

The aim of good diagnostic criteria is to separate normal from abnormal with the highest possible sensitivity and specificity. It may be superfluous to repeat well-known definitions but for the avoidance of doubt, the following apply:

$$\text{Specificity} = A/B$$
$$\text{Sensitivity} = C/D$$

where

A = number of normals correctly reported as normal
B = total number of normals
C = number of abnormals correctly reported as abnormal
D = total number of abnormals.

Figure 43.12 shows the distribution of Q wave duration in lead Y for normals and for a group of patients with inferior myocardial infarction. If a value of 20 ms is chosen as the upper limit of normal, it can be seen that the specificity of the

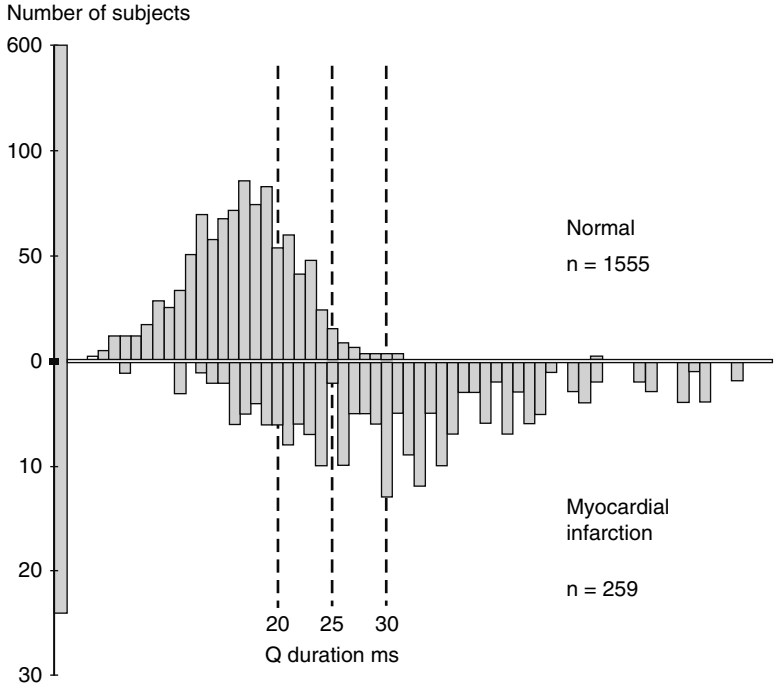

Figure 43.12
Shows distribution of Q duration in lead Y in a group of 1,555 normal subjects and in a group of 259 patients with inferior myocardial infarction. For explanation, see text.

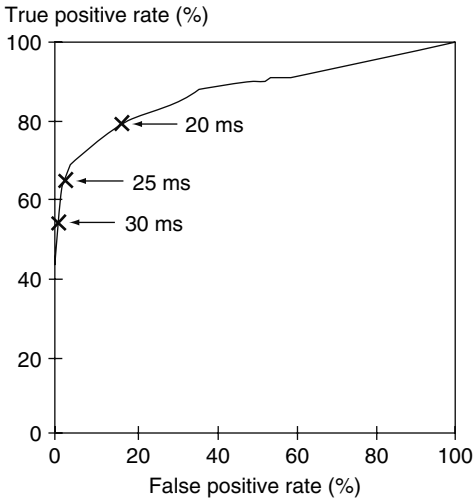

Figure 43.13

Receiver operating characteristic (ROC) curve showing the relationship between true positive rate (sensitivity) and false positive rate (100 – specificity) for different limits of Q duration in lead 1′: The curve is based on the data in Fig. 43.12.

criteria would be approximately 83%. The sensitivity for inferior infarction would be the order of 79%. However, some would argue that 83% specificity, that is, close to one in five normals reported as abnormal, is not high enough and might adjust the borderline value to 25 ms. In this case, the specificity would increase to 97% and the sensitivity for infarction would decrease to 65%. This process can be continued. For example, with a borderline of 30 ms, specificity is over 99% but sensitivity decreases to 54%.

It is possible to plot the relationship between sensitivity and specificity on what is known as a receiver operating characteristic (ROC) curve. This is shown in Fig. 43.13. The point on the curve, which approaches closest to 100% sensitivity and specificity, that is, the top left-hand corner, is often regarded as being optimum. In the case of electrocardiography, it is often preferable to choose a point on the curve with higher specificity (e.g., 25 ms point in Fig. 43.13).

While it is clear that ROC curves are dependent on the knowledge of measurements from a normal population and patients with a particular abnormality, it should also be noted that if a user decides that 95% specificity is the desired level, then the knowledge of the abnormal data are not required. This is perhaps an extreme view but it emphasizes the value of having well-defined normal data.

In Glasgow, every effort has been made over the past 25 years to gather a population of controls from birth upward, and of different ethnic origin, in order to meet the objectives outlined above. The remainder of this chapter will deal with the techniques involved and present the results obtained from the Caucasian cohort.

43.2.2 Data Acquisition

43.2.2.1 Techniques

Data have been gathered using two separate types of electrocardiographs each with a common factor of sampling electrocardiographic waveforms at 500 samples/s. All of the recordings made outside Glasgow Royal Infirmary, for example, on infants and children, were gathered using a Mingorec 4 from Siemens-Elema AB, Solna, Sweden. This acquires eight leads simultaneously, converts from analog to digital form at a rate of 500 samples/s for further analysis. More recent work has involved the use of the Burdick Atria 6100 electrocardiograph.

For ECGs recorded within Glasgow Royal Infirmary, an electrocardiograph designed and constructed within the Department of Medical Cardiology was used ([6], 1987). This device was connected by a broadband network from wards and clinics to the central computing facility within the Department.

The methods for analyzing the ECGs have been described in detail elsewhere [7] but are summarized very briefly here.

Up to 8 s of ECG with all leads sampled simultaneously, are processed initially to remove baseline wander, if present, and also any AC interference. Thereafter, QRS detection is undertaken. The same methods apply whether the ECG is recorded from a neonate or an adult. The QRS complexes so detected are then typed into different morphologies and logic selects one particular morphology for analysis. All PQRST cycles of that morphology are then averaged to form a single synthesized beat (with all 12 leads effectively recorded simultaneously). The derived leads X, Y, Z are then obtained using the methods outlined in detail in Chap. 11. In particular, the adult X, Y, Z leads were calculated using equation and the pediatric x, y, z leads were derived using equation. The wave measurement program then locates the onsets and terminations of the various P, QRS, and T components in order to measure amplitudes and durations.

Rhythm analysis is then undertaken. This uses some measurements from the average beat matrix but also three complete leads from the initial recording. Generally, these would be II, III, and V_1. When rhythm has been determined, diagnostic logic is then entered to interpret the measurements from the average beats. The program can output several hundred diagnostic statements. The same program can now be used for adults as well as for children [8]. In other words, the ability to interpret ECGs from children is not an optional add-on to the logic but is integral to the diagnostic criteria. Some details are presented elsewhere [9].

43.2.2.2 Sampling Methods

Different approaches to the selection of an apparently healthy population can be adopted. For example, age and sex registers can be used [10], but the technique adopted for adults in the Glasgow data was essentially to seek volunteers from the different departments of local government, for example, teaching, administration, and building. All individuals admitted to the normal group were seen by a physician who obtained a complete history and undertook a physical examination. The usual blood tests were performed and in the initial part of the study, chest x-rays were obtained. It was found that a positive yield from chest x-rays was essentially nil and latterly they were discontinued as part of the screening procedure.

For sampling from children, the procedure was different. Recordings were obtained from a maternity hospital with the full consent of parents. In preschool children, it was necessary to visit postnatal clinics, health centers, and play groups in order to obtain recordings from children, again with the permission of parents. Recordings were obtained from schoolchildren by installing the Siemens electrocardiograph for periods in different schools with the permission of the local health and education authority. Volunteers were sought subject to parental permission.

43.2.2.3 Population Data

A total number of 1,555 adults were entered into the normal database. The age and sex distribution is shown in Fig. 43.14. There tends to be a preponderance of males over 30 years of age, probably because of the predominance of male workers of that age group.

Figure 43.15 shows similar data for 1,782 healthy neonates, infants, and children whose ECGs were recorded. It should be pointed out that in this age group, lead V_{4R} was used in preference to lead V_3 as is the custom in many countries.

Actual numbers of males and females in the total group of 3,337 are given in Table 43.1.

In Taiwan, in collaboration with the Veterans' General Hospital in Taipei, it was possible to obtain 12-lead ECGs from 503 apparently healthy Chinese individuals [11]. From these, the 12-lead vectorcardiogram was obtained [12]. Essentially, methods used were similar to those for the collection of adult data in Caucasians although a higher percentage of individuals were in hospital with noncardiac problems.

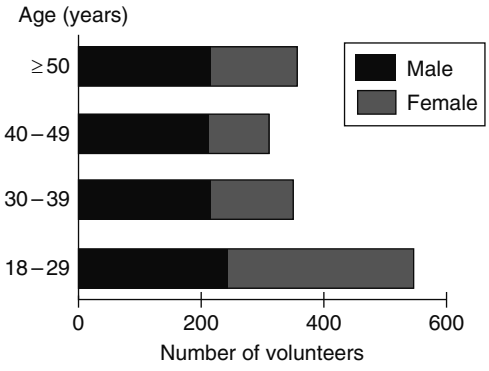

Figure 43.14
Age/sex distribution of the normal adult database. Further details are provided in Table 43.1.

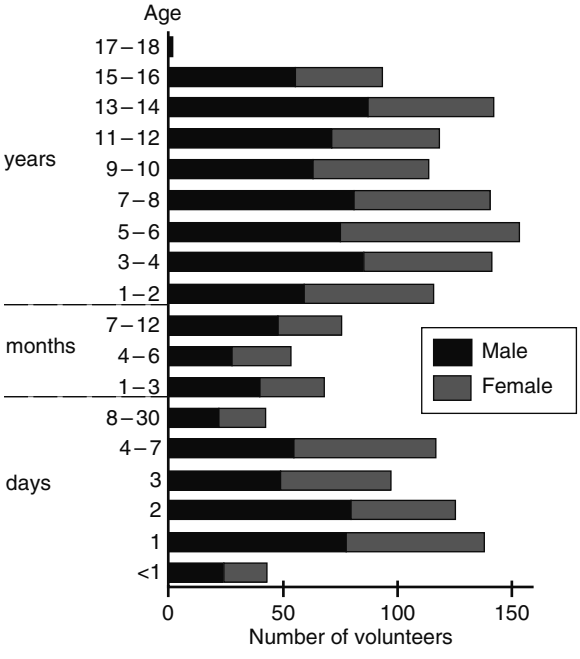

Figure 43.15
Age/sex distribution of the normal children's database. Further details are provided in Table 43.1.

43.2.2.4 Methods of Analysis

All measurements from each recording were stored on a computer file and added to a database. The adult and pediatric data were kept separate.

The BMDP suite of statistical programs was available for obtaining the basic data such as mean and standard deviation. The programs mainly used were P2D and P6D.

Table 43.1

Numbers of males and females in the total population group

Age	Male	Female	Total
⩽24 h	23	19	
1 day	77	61	
2 days	79	46	
3 days	48	49	
4–7 days	54	63	
⩽1 month	21	21	
⩽3 months	39	29	
⩽6 months	27	26	
⩽1 year	47	29	
1–2 years	59	57	
3–4 years	85	57	
5–6 years	75	79	
7–8 years	81	60	
9–10 years	63	51	
11–12 years	71	48	
13–14 years	87	56	
15–16 years	55	39	
17–18 years	0	1	
Children ∑	*991*	*791*	*1782*
18–29 years	242	304	
30–39 years	217	131	
40–49 years	210	97	
⩽50 years	215	139	
Adult ∑	*884*	*671*	*1555*
Total ∑	1875	1462	*3337*

43.2.2.5 Statistical Considerations

It has been known for many years that in general terms, ECG data are not normally distributed but tend to be skewed. An illustration is shown in Fig. 43.16. For this reason, normal ranges are best described not by using the mean ± twice the standard deviation but by 96 percentile ranges, that is, by excluding 2% of measurements at the top and bottom end of a particular set of measurements. Wherever possible this has been done in analyzing the data. Only in the case of small numbers such as, for example, healthy males with a Q wave in V_1, was it necessary to include the complete range because total numbers were too small. One other point that should be noted is that the calculation of the mean is based only on measurements that were present. In other words, if there were 100 patients in a particular group but only 40 had an S wave in a selected lead, then the mean amplitude was derived using only the 40 measurements and the 60 values of 0 mV for the remaining patients were excluded from the calculation of the mean.

With respect to angular data, care was taken to ensure that all measurements were in a meaningful range. In other words, the recommendations for measuring angles would suggest that the direction in the frontal plane of the *X*-axis would be labeled as 0°. If a vector measurement inferior to that was perhaps 20° and one superior to the *X*-axis was 340°, the mean value would certainly not be 180° but 0°. In other words, 340° would be converted to −20° before calculating the mean value. Alternative methods for dealing with angular data were elaborated many years ago by Downs et al. [13].

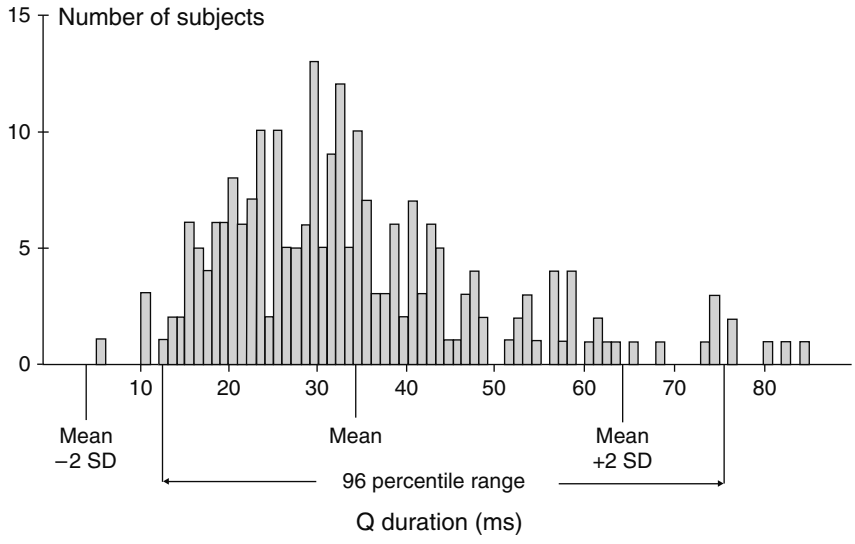

Figure 43.16

An example of a skewed distribution where there is a long tail of measurements at the upper end of the distribution. The figure shows a histogram of Q wave duration in lead Y in a group of 259 patients with proven inferior myocardial infarction. A total number of 24 patients with no Q waves in lead Y are excluded from the calculation of the mean.

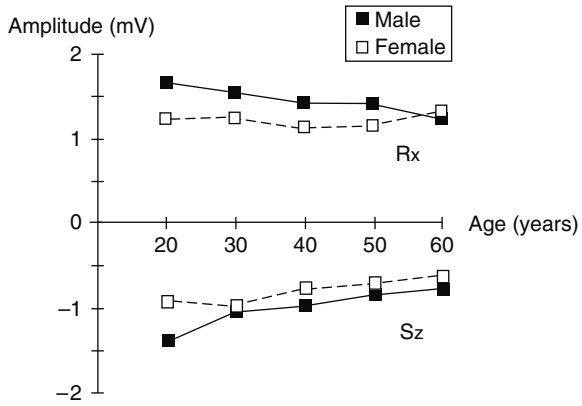

Figure 43.17

Effect of age and sex on mean R wave amplitude in lead X and mean S wave amplitude in lead Z.

43.2.3 Results: Scalar Data

43.2.3.1 Wave Amplitudes and Durations

The relevant tables of normal limits of PQRST amplitudes and durations in the derived leads X, Y, and Z are presented in Appendix 5A. Again, it can be confirmed that the effects of age and sex on the amplitudes of waveforms are significant. This can be seen in Fig. 43.17 where the mean S wave amplitude in lead Z is presented.

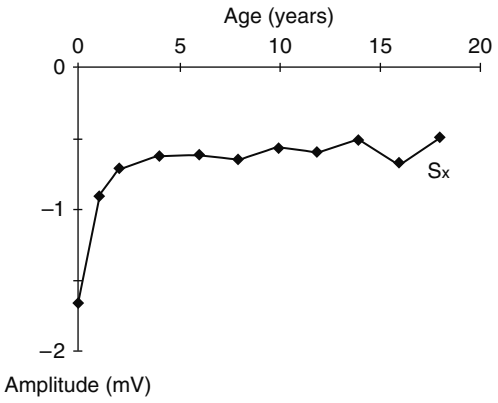

Figure 43.18
The upper limit of normal S_X amplitude in children from birth to adolescence.

Here the amplitude in young males is significantly higher than in young females, although the difference diminishes as age increases. These findings are similar to measurements of the S wave in V_2. The effect is not so marked for the mean R wave in lead X, which is also shown in the same figure.

In contrast, durations tended to show little difference between different age and sex groups with the exception of the QRS duration, which, as is well known, is approximately 7 ms longer in males than in females although strangely almost no cognizance is taken of this in any diagnostic criteria. This point is discussed in Chap. 13 (see Sect. 13.7.8).

43.2.3.2 Pediatric Data

It goes without saying that dramatic changes in pediatric measurements can be seen from birth onward. Again, appropriate tables are presented in Appendix 5B. As an example, the upper limit of normal S wave amplitude in lead X is shown in Fig. 43.18. There is a rapid decrease in S_X amplitude in the first year of life corresponding to a counterclockwise shift of the maximum frontal plane QRS vector.

43.2.3.3 Comparative Vectorcardiography

Yang and Macfarlane [14] reported on a comparison of the 12-lead vectorcardiogram in apparently healthy Caucasians and Chinese. To the database of 1,555 Caucasians, 503 Chinese were added giving a total of 2,058 individuals whose vectorcardiograms were derived from the conventional 12-lead ECG.

The trend of the influence of age and sex on the magnitude and direction of the derived QRS and T vectors was found to be similar in both cases. In the younger age groups, the magnitude of the maximal spatial vector was essentially greater in Caucasians than in Chinese while in the older age groups over 40, the reverse was the case. This was a somewhat surprising finding for which there is no clear explanation. Figures 43.19 and 43.20 show a comparison between the QRS and T vector magnitude in both races. It can be seen that it is essential to include the effect of age, sex, and race when interpreting 12-lead vectorcardiographic appearances.

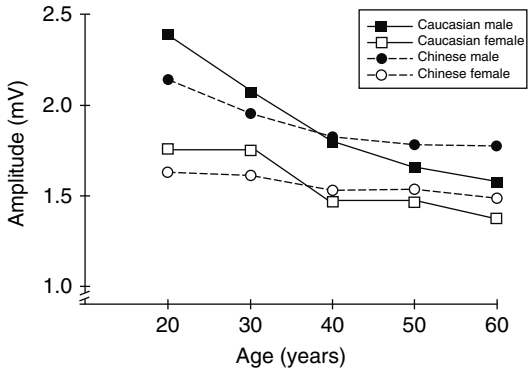

Figure 43.19
Mean magnitude of the maximal QRS vector amplitude in Caucasians and Chinese.

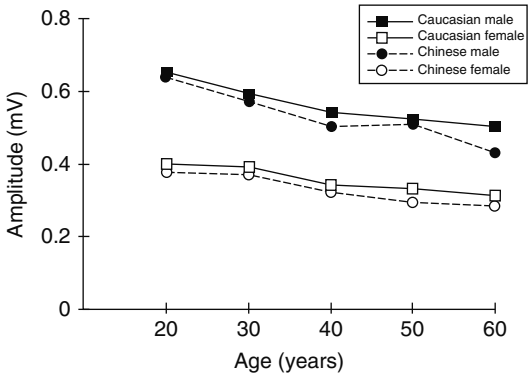

Figure 43.20
Mean magnitude of the maximal T vector amplitude in Caucasians and Chinese.

43.2.4 Results: Vector Data

43.2.4.1 P Loops

In the infant, the P loop tends to be directed vertically at birth but it soon rotates superiorly in the frontal plane and remains around 55°. In the transverse plane, the P loop in children at birth is approximately 20–25° and subsequently shifts a little toward the adult value of around 0°. Sex differences between the mean P wave vector in the transverse plane are significant with the mean direction for males being 349° and for females 14° (Draper et al. [15], Nemati et al. [16]). It should be noted that the results obtained by these authors were derived using the Frank system.

43.2.4.2 QRS Loops

There is, of course, a considerable change from birth to adulthood in the QRS loop in the 12-lead vectorcardiogram. Figure 43.21 shows a 12-lead QRS loop from a neonate where the maximum QRS vector is oriented around 150° in the frontal plane. On the other hand, in the normal adult QRS in the frontal plane, Fig. 43.22, the QRS loop is oriented at around 50°. In general terms, in the frontal plane, the QRS loop is in the vast majority of cases inscribed in a

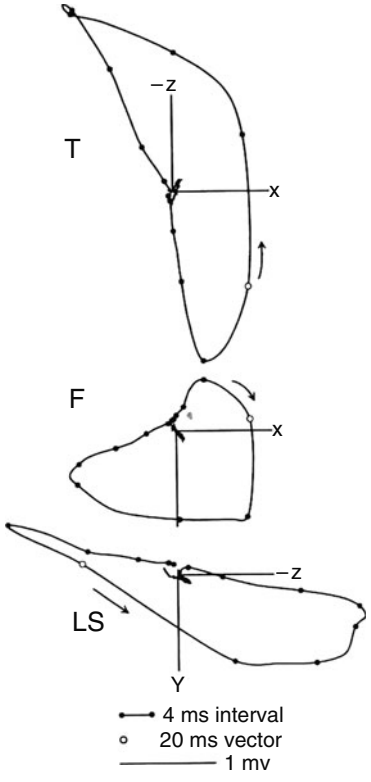

Figure 43.21
12-lead QRS and T loops from a healthy neonate.

clockwise direction in the infant. In the adult, the frontal plane loop can be inscribed either in a clockwise or counterclockwise direction, although the clockwise loop tends to predominate again. In the transverse plane, in the neonate, the inscription around birth is 43% clockwise and 45% counterclockwise but soon changes to being almost totally counterclockwise as it is in the normal adult. A figure-of-eight loop can be found in 20–40% of children up to 8 months of age using the Frank system [17] although our own 12-lead data suggest a lower incidence. Table 43.2 shows the results derived from the Glasgow data in respect of direction of inscription of the QRS loops in the frontal and transverse planes.

43.2.4.3 Left Axis Deviation

It may seem superfluous to consider a discussion on left axis deviation but the normal range of the maximum QRS vector in the frontal plane is, indeed, quite different in the 12-lead vectorcardiogram from that in the standard 12-lead ECG. A full list of ranges is given in Appendix 5.

It can be seen that in healthy females, for example, the maximum QRS vector is never superior to 0°. In males, this seems to occur in a few individuals in the 30–59 years age group but, by and large, the vast majority of individuals have a maximum QRS vector inferior to 0°. This observation suggests the following criteria:

Borderline/left axis deviation: $0^\circ \rightarrow -15^\circ \quad (360^\circ \rightarrow 345^\circ)$
Left axis deviation: $-15^\circ \rightarrow -90^\circ \quad (345^\circ \rightarrow 270^\circ)$

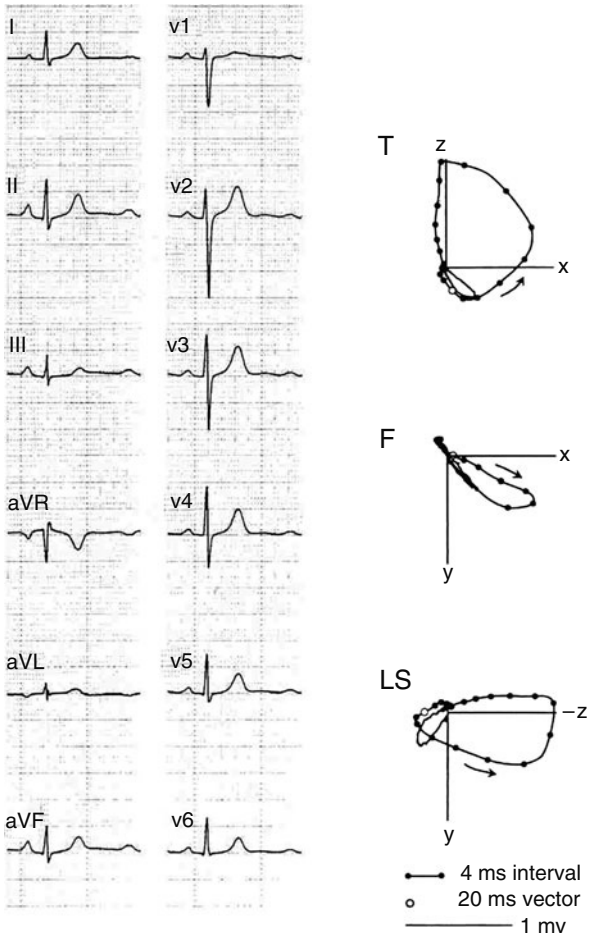

Figure 43.22

12-lead QRS and T loops from a healthy adult.

Table 43.2

Direction of inscription of the QRS vector loop in transverse and frontal planes expressed as a percentage from 1,555 adult Caucasian normals (CCW; Counterclockwise Rotation, CW; Clockwise Rotation)

Planes		CCW	Figure of 8	CW
Transverse	Male	98.1	0.9	1.0
	Female	97.9	1.2	0.9
Frontal	Male	22.9	19.1	58.0
	Female	21.8	25.3	52.9

43.2.4.4 Right Axis Deviation

The tables in Appendix 5 indicate that with the exception of young males <30 years of age, the normal maximum QRS vector in the frontal plane is always <65°. This indication is considerably different from the normal frontal plane vector calculated from the 12-lead ECG. It does suggest the use of the following criteria:

Borderline right axis deviation:
Females and (males > 30 years) 65° → 75°
Males < 30 years 90° → 100°

Right axis deviation:
Females and (males > 30 years) > 75°
Males < 30 years > 100°

43.2.4.5 T Loops

From Figs. 43.21 and 43.22 discussed above, the direction of the maximum T vector in the frontal and transverse planes can be seen for the average newborn and the average adult. It follows that there is a gradual change of T vector orientation from one position to another with increasing age. Details of some T vector measurements can be found in the Appendices.

43.3 Hypertrophy

43.3.1 Introduction

43.3.1.1 What is Hypertrophy?

Electrocardiographers tend to report the pattern of increased voltage in the lateral leads together with accompanying ST-T changes as left ventricular hypertrophy (LVH). The advent of echocardiography as well as cardiac catheterization has meant that the variety of pathologies, which constitute the generic term "hypertrophy" is now better known. In general terms, hypertrophy can be taken to mean an increase in mass. All four chambers of the heart can demonstrate hypertrophy or enlargement either in isolation or in combination. Enlargement is a term that is perhaps more associated with an increase in volume whereas hypertrophy strictly may relate to an increase in muscle mass.

The subdivision of different types of hypertrophy is essentially based around left ventricular geometry. Where there is an overall increase in mass with a dominant increase in muscle thickness without an increase in cavity volume, the term concentric hypertrophy is used. Where there is an increase in mass predominantly due to an increase in volume, the term eccentric hypertrophy is used.

Huwez, Pringle, and Macfarlane [18] have introduced a new classification for hypertrophy on the basis of mass and volume. The different types and the criteria are given in Table 43.3. A salutary lesson from that study was that a patient with apparently normal mass and volume could demonstrate the ECG changes of LVH described above. In addition, both concentric and eccentric hypertrophy could produce similar ECG changes or none at all.

Notwithstanding the above, the remainder of this chapter is generally concerned with the classical description of vectorcardiographic changes accompanying hypertrophy.

43.3.1.2 Effects of Age, Sex and Race

It will be apparent from the previous Sect. 43.2 on normal ranges, that QRS voltage in some leads such as X and Z increases with age until early adulthood and then decreases again. Likewise, it has also been shown that, in many cases,

Table 43.3
Left ventricular geometry classification

Left ventricular		Type
Mass	Volume	
Normal	Normal	Normal
Normal	Increased	Isolated left ventricular volume overload
Increased	Normal	Concentric LVH
Increased	Increased	Eccentric LVH

sex differences particularly with respect to voltage can be demonstrated in vectorcardiographic parameters. Similar effects can be seen within different races.

All these observations suggest that the criteria for ventricular hypertrophy have to be based on a knowledge of all of these three variables.

43.3.1.3 Value of Vectorcardiography

It goes without saying that the echocardiogram gives a detailed picture of left ventricular geometry. On the other hand, it is the ECG that may demonstrate secondary ST-T changes, which are well known to be associated with a poor prognosis [19, 20]. If a reasonable specificity of 95% is desired, then the best ECG criteria should have a sensitivity around 50%. Data such as these vary from one study to another depending on the gold standard, which may be postmortem weights, on the one hand, or echocardiographic measurements, on the other. The reader should therefore be aware, from the outset, that the vectorcardiographic diagnosis of LVH is somewhat insensitive.

43.3.2 Atrial Enlargement

In the normal 12-lead vectorcardiogram, the P wave may exhibit two distinct components, which probably result from asynchronous depolarization of the left and right atrium. In this event, the bifid nature of the P wave is best seen in the inferior lead Y. In view of the fact that normal atrial depolarization commences in the right atrium before spreading to the left atrium, it follows that the first component is due to right atrial excitation and the second due to left atrial excitation.

43.3.2.1 Right Atrial Enlargement

One of the manifestations of right atrial enlargement is a P wave in the inferior lead Y with an amplitude > 0.3 mV. As this abnormality not infrequently occurs in respiratory disorders, it is sometimes called P pulmonale (Fig. 43.23). Occasionally, P_Y may be of normal amplitude but there may be a prominent P_Z > 0.15 mV on account of right atrial enlargement.

Chou and Helm [21] have pointed out that the P-wave changes in the inferior lead Y occasionally resemble P pulmonale when there are no clinical findings to support such a diagnosis. The cause of the abnormal P wave may be left atrial hypertrophy and the term "pseudo P pulmonale" is used to describe such a phenomenon. Clearly, this diagnosis should be made on the basis of the clinical findings taken in conjunction with the ECG appearances. The normal ranges

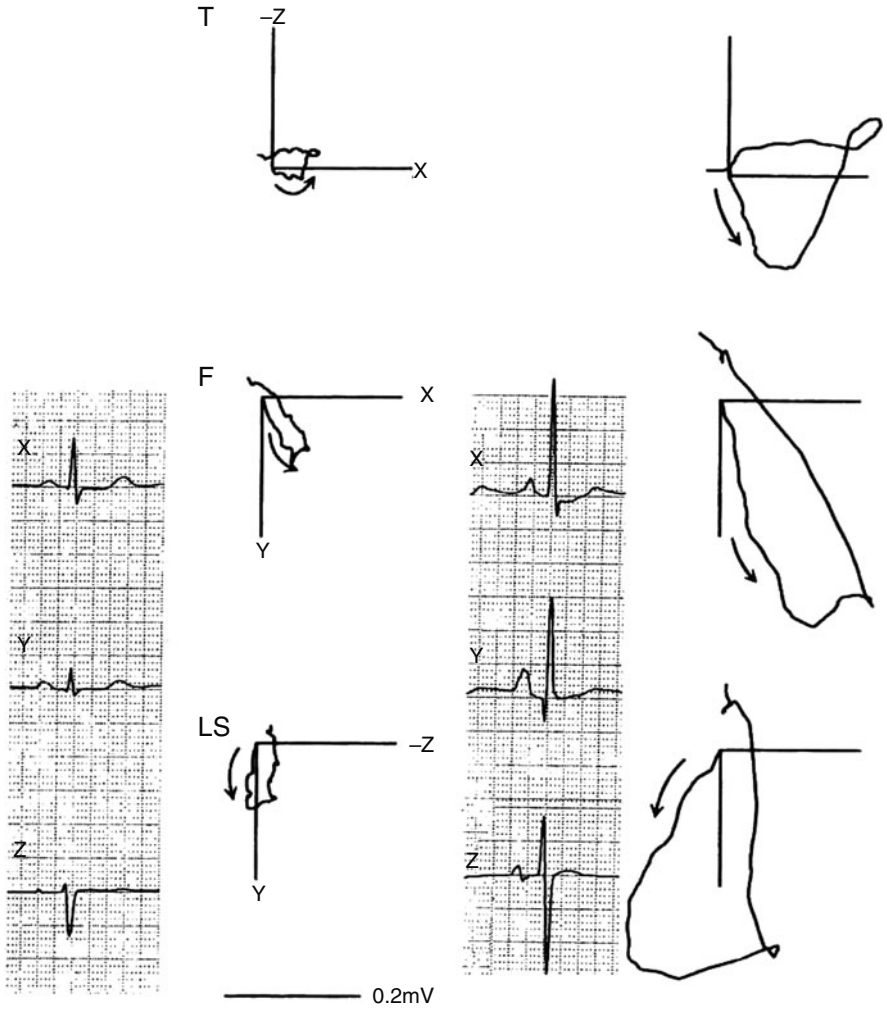

Figure 43.23
Normal P loops (*left*) and an example of combined atrial enlargement (*right*).

of the projections of the maximum P vector on to the three planes are so wide that little diagnostic advantage can be gained from a study of these parameters in respect of right atrial enlargement.

43.3.2.2 Left Atrial Enlargement

When left atrial enlargement occurs, several abnormalities may result. First, the P-wave duration may be increased beyond 120 ms. Second, bifid or M-shaped P waves of greater than normal duration may be found in the inferior lead Y and this pattern is often referred to as P mitrale because of its common association with mitral stenosis. From the vectorcardiographic point of view, enlargement of the left atrium may also cause an increase in the left atrial vectors, which in turn produce a rotation of the terminal portion of the P-wave vector posteriorly and to the left (Fig. 43.23). Thus, the terminal component of the scalar P wave in lead Z can be increased in negativity and in duration.

The maximum P vector amplitude may be increased but the normal range of P-vector orientation is so wide as to be of little value. On occasions, the maximum P-vector magnitude may exceed 0.3 mV when the individual scalar components are within normal. In this case, left atrial enlargement is the most likely cause.

43.3.2.3 Combined Atrial Enlargement

In general terms, a combination of the individual criteria for left and right atrial enlargement when present would be suggestive of combined atrial enlargement (Fig. 43.23).

43.3.3 Left Ventricular Hypertrophy

43.3.3.1 Diagnostic Criteria

When LVH or left ventricular enlargement produces alterations in QRS morphology, these relate generally to an increase in QRS vector amplitude. On occasions, the maximum QRS vector will be rotated posteriorly and this is seen best in the transverse plane where the resultant effect is to produce an increase in the amplitude of S_Z. Consideration of the basic principles of vectorcardiography indicates that if a vectorcardiographic loop rotates posteriorly increasing S_Z, then R_X would decrease simultaneously. Thus, one of the commonly used vectorcardiographic criteria is based on $R_X + S_Z$. The data from the 1,555 patients in the Glasgow database suggest that the upper limit of $R_X + S_Z = 3.95$ mV for males over 40 years of age. It is, however, possible to express the upper limit of normal for males as a continuous age dependent equation as follows:

$$R_X + S_Z = [72 : 81 - 0.02074\,\text{age (months)}]^2\ \mu\text{V}$$

Similar equations apply for women and for other races.

The typical vectorcardiographic appearances in LVH are shown in Fig. 43.24. In this case, there is increased magnitude of the QRS vector, which is more posteriorly oriented than the mean maximum QRS vector in normals in the transverse plane while the T loop is oppositely directed to the QRS loop. This is equivalent to the secondary ST-T pattern in the lateral leads.

It should be noted that the individual component amplitudes of the scalar leads may be normal while the resultant vector amplitude can be abnormal. For example, if the amplitude of R_X is 2.4 mV and, at the same instant, R_Y is 1.5 mV (although corresponding peak amplitudes might be a little higher), it follows that the amplitude of the maximum QRS vector would be

$$3.2\,\text{mV} = \sqrt{(2.4^2 + 1.5^2 + 1.5^2)}\,\text{mV}$$

Each of the scalar amplitudes is within the normal range for a 45-year-old male, but the vector magnitude is outside normal (see Appendix 5A).

Various types of QRS loop may be seen in the vectorcardiogram. These are best differentiated by appearances in the transverse plane. Type I may simply resemble a normal QRS loop but be of increased magnitude. In Type II, there is a rotation of the projection of the maximum QRS vector posteriorly beyond 310° in the transverse plane (Fig. 43.25), possibly with a normal QRS voltage.

It is not common, however, to find an abnormal orientation of the QRS vector loop in LVH without voltage evidence in addition. In Type III, where LVH is very marked, there may be a figure-of-eight loop in the transverse plane with the distal part of the loop inscribed in a clockwise direction (Fig. 43.26). In Type IV, there may be slightly increased QRS

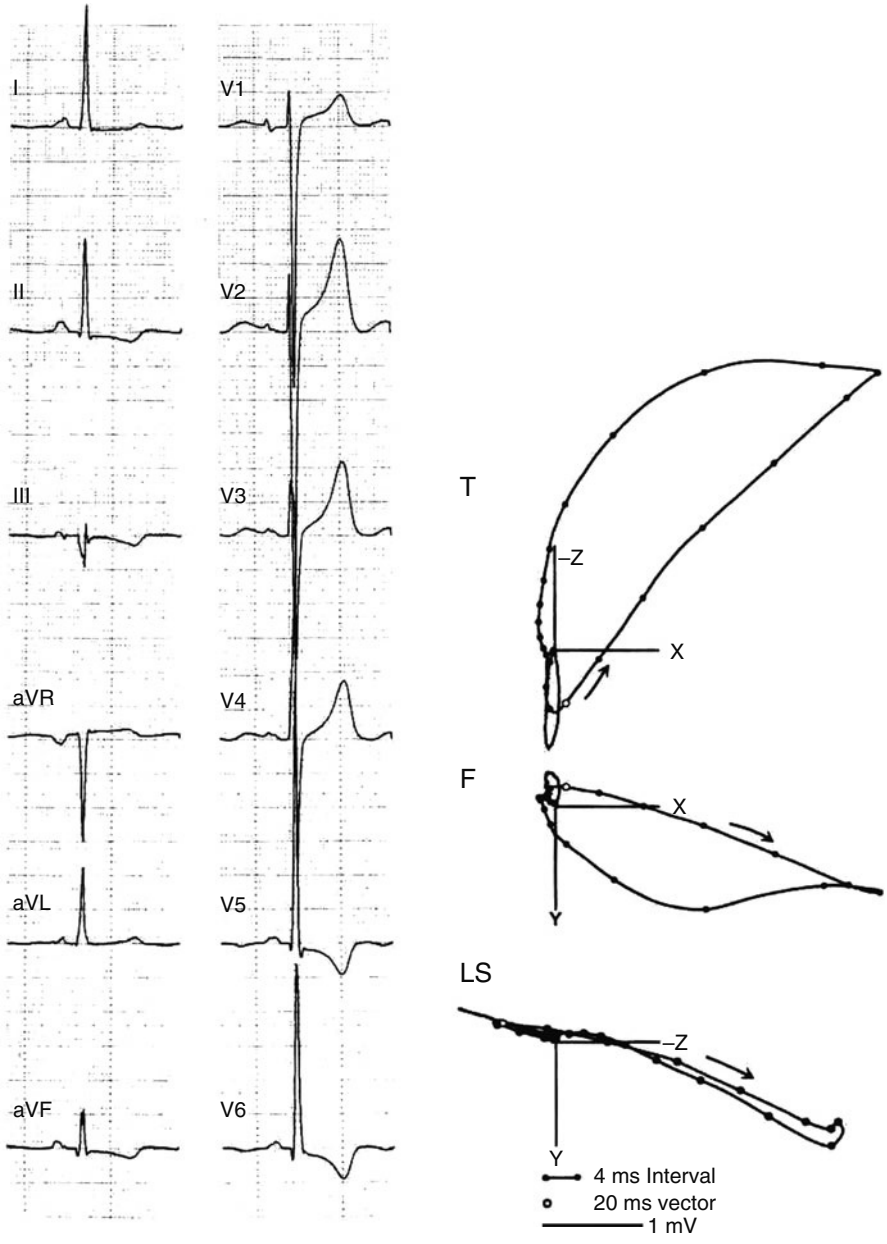

Figure 43.24

An example of left ventricular hypertrophy (LVH) Type I. Note the increased magnitude of the QRS loops best seen in the transverse plane where the T loop is essentially oppositely directed to the QRS loop.

duration, and an abnormally large QRS maximum vector, but the rate of inscription of the loop is slower than normal as manifested by the closeness of the dots. This pattern is sometimes called "incomplete left bundle branch block (LBBB)" that often accompanies LVH.

Reference has already been made to secondary STT changes (Fig. 43.24) sometimes called left ventricular strain or overload pattern. In a series of patients [22], it was found that this pattern of ST depression with asymmetric T wave

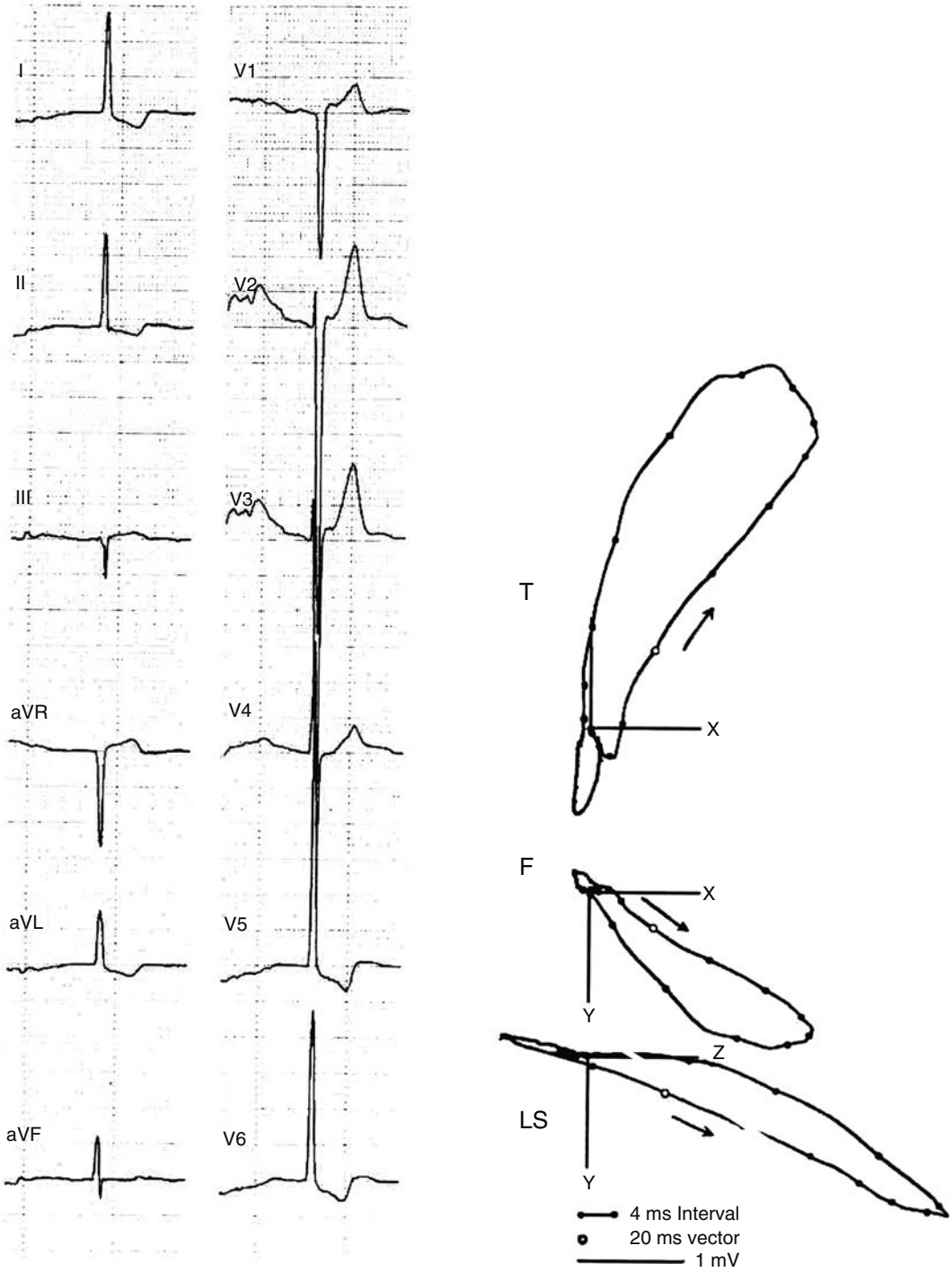

Figure 43.25

An example of LVH Type II. Note that the maximum QRS vector in the transverse plane is posterior to 310°.

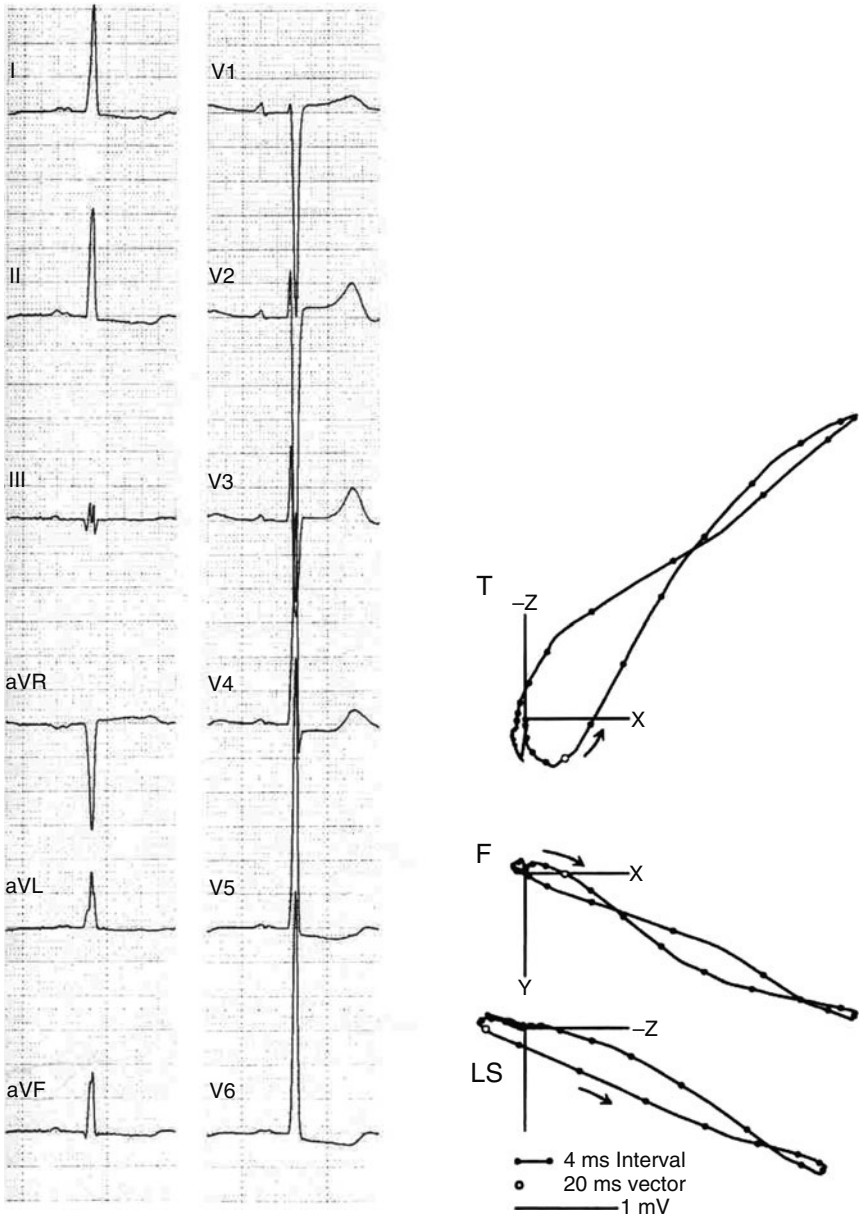

Figure 43.26

An example of LVH Type III. In this case, a figure-of-eight loop can be seen clearly in the transverse plane while the maximum QRS vector exceeds 4 mV.

inversion was 94% sensitive for LVH. Thus, even in the absence of high voltage, this ECG finding in the scalar lead X should be regarded as a pointer toward the diagnosis of LVH.

One further point can be made concerning the vectorcardiographic appearances in severe LVH. It can happen that the initial QRS vectors are directed posteriorly, that is, there is a Q wave in the anteroseptal lead Z or V_2. This makes the differential diagnosis of anteroseptal infarction from LVH difficult unless the clinical picture is relatively clear-cut. For example, Fig. 43.27 shows such a pattern in a 73-year-old male with hypertension and aortic stenosis and insufficiency.

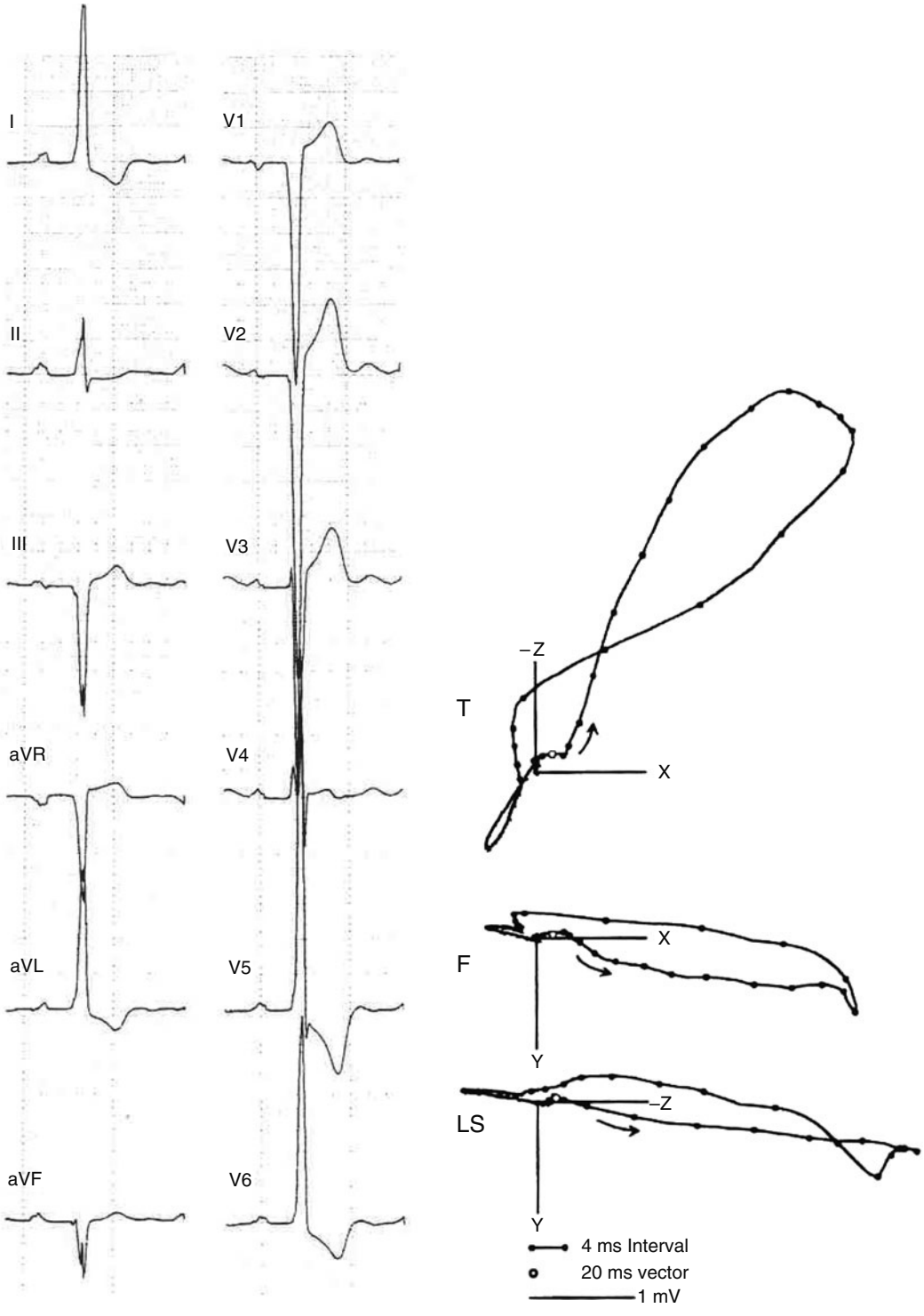

Figure 43.27

A 12-lead ECG and vectorcardiogram recorded from a 73-year-old male with hypertension and aortic stenosis and insufficiency. Note that the initial QRS vectors are directed posteriorly, that is, there is a Q wave in lead Z. Other typical features of LVH can also be seen.

The reasons for the presence of the Q wave are not fully understood although many hypotheses have been put forward. Possibly on account of there being three areas of initial activation in the left ventricle, the concept of the genesis of the Q wave may be revised. It could be postulated that the electrical activation of the area of the left ventricle adjacent to the posterior wall, which is among the first to be depolarized, predominates on account of left ventricular wall thickness, thereby leading to initial QRS forces oriented posteriorly producing a Q wave in the anteroseptal lead.

The other criteria that point to LVH include left axis deviation, which, in the vectorcardiogram, is a QRS axis superior to 0° in the frontal plane. Indeed, apart from the specific criteria of increased vector magnitude and posteriorly rotated maximum QRS vector orientation, other criteria mirror those for the conventional l2-lead ECG, for example, a delayed intrinsicoid deflection in lead X and increased P terminal force in lead Z.

43.3.3.2 Bundle Branch Block and LVH

The diagnosis of LVH from an ECG that shows bundle branch block is controversial. Some authors have claimed it is possible to make such a diagnosis while others have noted in various series that in the presence of LBBB, LVH is always found. Thus, no specific criteria for the diagnosis of LVH and LBBB are presented here. However, one or two points can be made.

As will be seen in Sect. 43.5, the vectorcardiographic appearances in LBBB are characteristic in having a narrow QRS loop in the transverse plane. If the scalar lead appears to have the LBBB pattern with a tall R_X but does not have the narrow bundle branch block loop, then LVH could be considered as a possible cause (incomplete LBBB/LVH pattern).

43.3.4 Right Ventricular Hypertrophy

Increased right ventricular excitation forces or increased right ventricular volume can produce varying ECG patterns depending on the time of the occurrence of the abnormal electrical activity compared to that of the left ventricle. Hypertrophy of the free wall of the right ventricle will produce abnormal anterior forces in early ventricular depolarization whereas basal hypertrophy will produce abnormal posterior forces late in ventricular depolarization. In the vectorcardiogram, there are essentially two presentations of right ventricular hypertrophy (RVH), namely, a prominent R wave in lead Z and a deep S wave in lead X. The presence of these abnormalities either singly or together produces four patterns of RVH or enlargement. These are as follows.

43.3.4.1 RVH: Type A

Type A RVH is manifested as an increase in the ratio of anterior/posterior forces in the transverse plane with counterclockwise inscription of the QRS loop (Fig. 43.28). Often the abnormal QRS loop may have a T loop directed posteriorly corresponding to the secondary ST–T abnormalities sometimes seen in V_1 and V_2.

One criterion of value in Type A is the projection of the maximum QRS vector onto the transverse plane >30°. Occasionally, this may be present when voltage and ratio measurements in the anteroseptal leads are normal.

43.3.4.2 RVH: Type B

One of the major advantages of the vectorcardiogram is preservation of the timing relationships between the different scalar leads. Thus, while two different scalar patterns may have similar appearances, the vectorcardiogram can be normal in one and abnormal in another. This is often apparent in Type B RVH. In this case, the QRS loop in the transverse plane

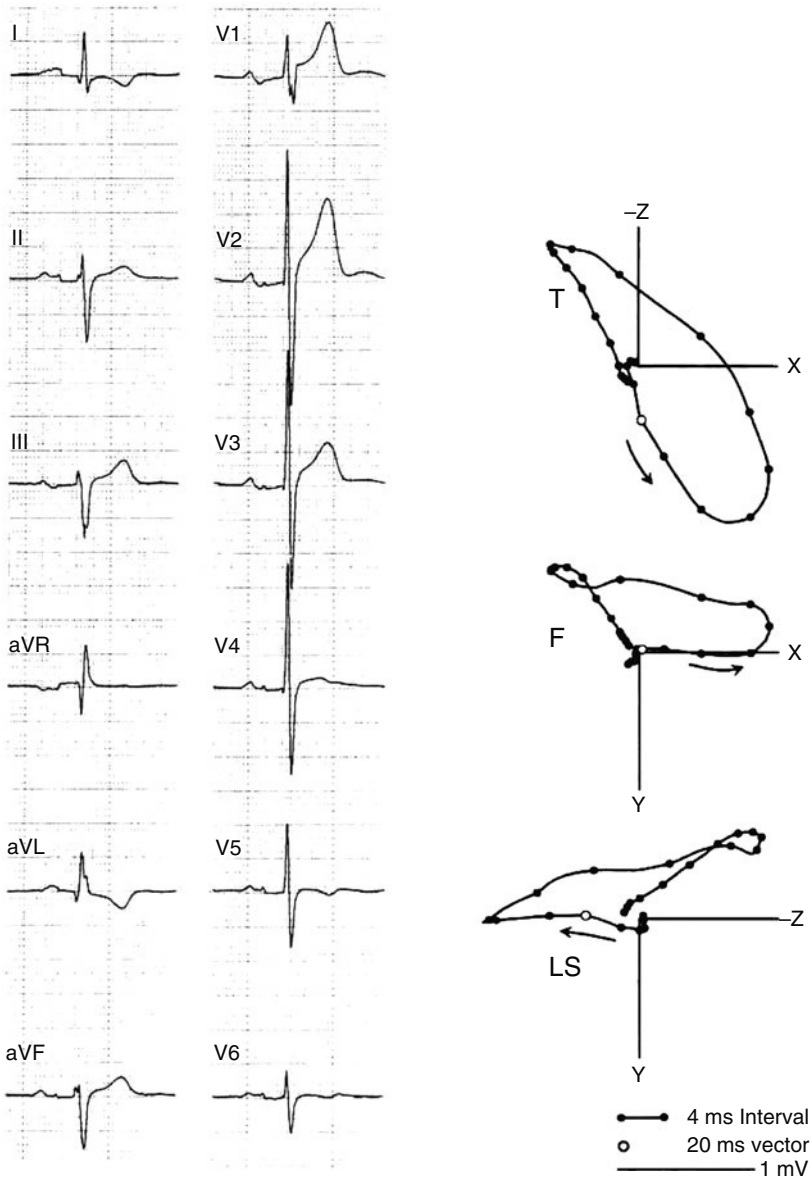

Figure 43.28
An example of right ventricular hypertrophy (RVH) Type A where there is a marked increase in anteriorly directed forces as seen in the transverse plane.

initially has normal counterclockwise inscription, but the second part of the loop is deviated anteriorly so that the net effect is to have a loop with clockwise or figure-of-eight inscription in the transverse plane (Fig. 43.29).

43.3.4.3 RVH: Type C

The third type of RVH is manifested as an abnormal transverse plane vectorcardiographic loop that is normally counterclockwise inscribed with the maximum QRS vector being oriented posteriorly and to the right (Fig. 43.30).

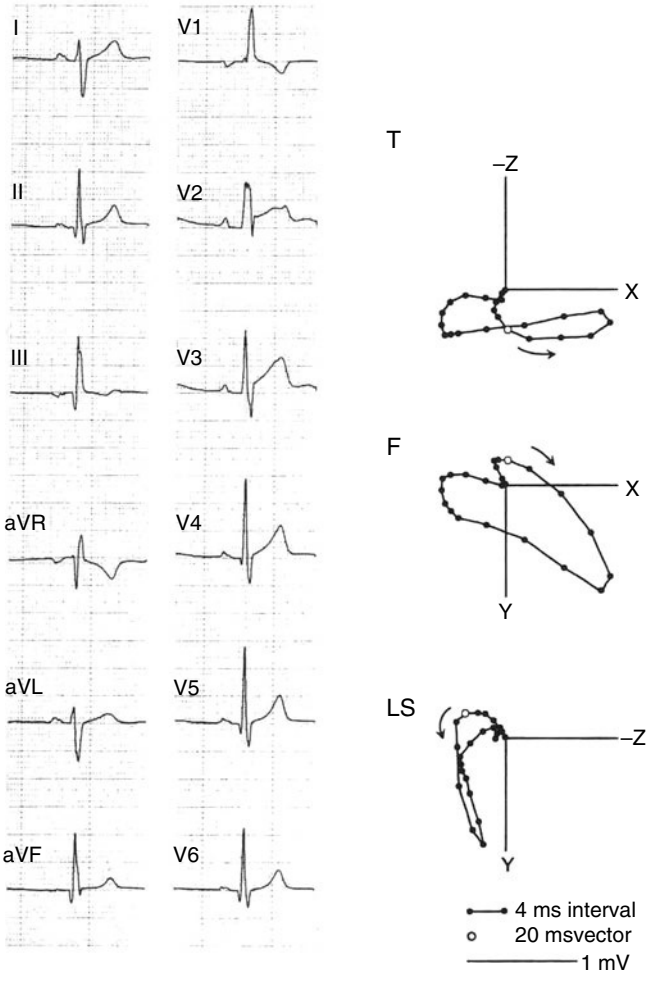

Figure 43.29

An example of RVH Type B where there is a figure-of-eight loop in the transverse plane in which all forces are seen to be anteriorly oriented. Note the late rightward-directed forces corresponding to the deep S wave in lead I.

This pattern is most often found in patients with chronic respiratory disease and therefore may be accompanied by P pulmonale. However, some patients with mitral stenosis also exhibit such findings. It is thought that the posterior rightward displacement of the QRS vector is due to hypertrophy of the basal portion of the right ventricle. Secondary ST-T changes can also be found in this pattern. The abnormal rightward forces also translate into right axis deviation in the frontal plane.

43.3.4.4 RVH: Type D

In the more severe forms of RVH, as may occur in certain forms of congenital heart disease the main QRS vector may be directed abnormally not only to the anterior but also to the right with clockwise inscription of QRS in the transverse plane (Fig. 43.31).

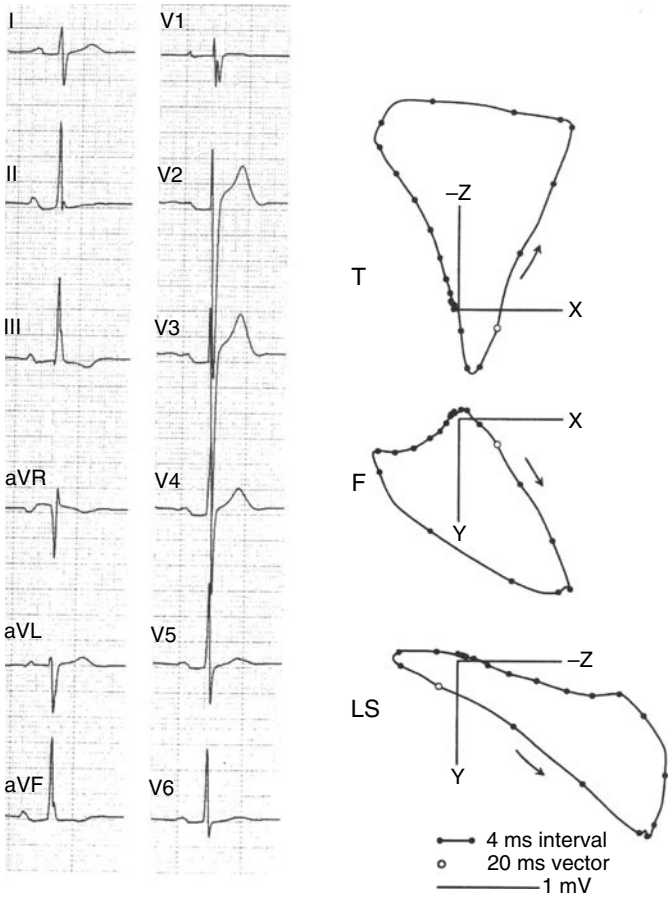

Figure 43.30
An example of RVH Type C. In this case, there is a large posterior and rightward-directed force in the later part of QRS.

43.3.5 Combined Ventricular Hypertrophy

It has been claimed that in most cases of LVH there is an accompanying RVH [23]. The vectorcardiographic diagnosis of biventricular hypertrophy is mainly based on finding features of both LVH and RVH separately. For example, if the transverse QRS loop is directed posteriorly and has an increased magnitude with the T loop oppositely directed, as in secondary changes of LVH, and the frontal QRS vector is oriented around 90°, then combined ventricular hypertrophy should be considered.

43.3.6 Pediatric Vectorcardiography

The various forms of congenital heart disease can produce a variety of vectorcardiographic patterns that can be extremely difficult to interpret. A few patterns are pathognomonic of rare forms of congenital heart disease but in any event, the report must remain an ECG interpretation. In other words, no attempt should be made to infer the anatomy of the congenital lesion in the majority of cases. Brohet [24] has reviewed the advantages of vectorcardiography in congenital heart disease.

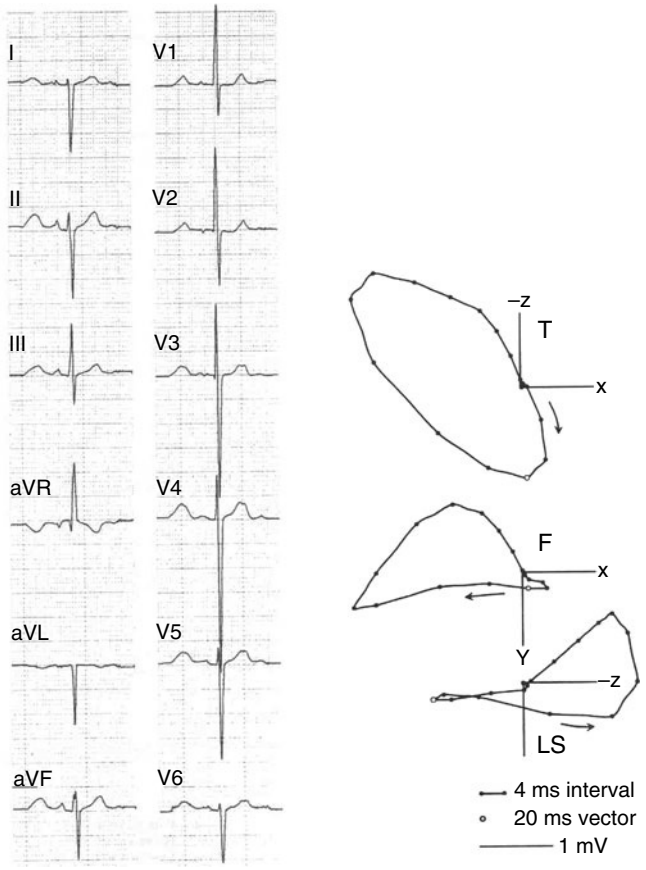

Figure 43.31

An example of RVH Type D where the QRS loop in the transverse plane is clearly abnormal, being inscribed in a clockwise direction and lying almost entirely to the right. Marked right axis deviation can also be seen in the frontal plane loop.

43.4 Myocardial Infarction

43.4.1 Introduction

43.4.1.1 Theoretical Considerations

A myocardial infarction is death of myocardial tissue as a result of insufficient blood supply, that is, due to a stenosis or occlusion of a coronary artery. An infarcted area is electrically inert and distorts the normal spread of excitation. The net effect is that the electrical forces, which are influenced by the "dead zone" or infarct vector, are directed away from the area of myocardial infarction. This is in contrast with hypertrophy that produces electrical forces directed toward the area of increased ventricular mass.

43.4.1.2 Anatomical Definitions

There is a lack of unanimity in describing myocardial infarction. In 1978, the American College of Cardiology Conference on Optimal Electrocardiography described myocardial infarction in terms of Q waves seen in the various leads of the

12-lead ECG [25]. This has resulted in terms such as septal, anteroseptal, and anterior infarction being used. However, there is still no consensus regarding the localization of an infarction among electrocardiographers.

Radiological or echocardiographic techniques can also be used to detect and localize a myocardial infarction. In coronary angiography, it is not the infarcted area per se that is detected but the stenosis or occlusion of the coronary artery that caused the myocardial infarction. An infarcted area causes abnormalities in the ventricular contraction pattern, which can usually be detected in a left ventriculogram or in an echocardiogram. The techniques described above show different aspects of the same disease. Differences in the position and orientation of the heart and a variation in the anatomy of the coronary arteries have varying influence on these techniques. Therefore, the correlations between electrocardiographic changes, abnormalities of ventricular contraction, and the degree of stenosis in relevant coronary arteries are not excellent. This should be borne in mind when comparing different techniques for the diagnosis of myocardial infarction.

Notwithstanding any of the above, in very general terms, occlusion of a left anterior descending coronary artery or a left main stem artery is likely to produce an infarct predominantly in the anterior (anteroseptal/anterosuperior) wall of the heart. An occlusion in the right coronary artery will generally produce an inferior myocardial infarction while occlusion of the left circumflex produces a lateral or posterolateral/inferior myocardial infarction.

43.4.2 The 12-Lead Vectorcardiogram in Myocardial Infarction

43.4.2.1 Anterior Infarction

In keeping with the concept of the dead zone or infarct vector, an anterior myocardial infarction will result in slightly increased posteriorly directed electromotive forces and a reduction, if not an absence, of anteriorly directed forces in the early part of ventricular depolarization. In 12-lead ECG terminology, this corresponds to a QS complex in V_2. The corresponding vectorcardiographic appearances are shown in Fig. 43.32. Here it can be seen that there is no electrical activity in the left anterior quadrant of the transverse plane vectorcardiogram. This type of clear-cut myocardial infarction, from an electrocardiographic point of view, is generally well delineated on the 12-lead ECG. Of more interest is the situation where the 12-lead ECG may be somewhat equivocal with low R waves in the anterior leads but the vectorcardiogram shows other features that are suggestive of myocardial infarction. In the transverse plane, common vectorcardiographic criteria for anterior myocardial infarction are listed in Table 43.4.

Figure 43.33 gives an example of a QRS loop where there are initial anteriorly directed forces but the 30 ms QRS vector is posterior to 300°. Figure 43.34 shows a different form of vectorcardiographic change where there is an initial counterclockwise inscription leading to a bite in the vectorcardiographic loop (see Sect. 43.4.2.8). Figure 43.35 illustrates a case of anterior myocardial infarction where the area of the QRS loop in the left anterior quadrant <1%.

43.4.2.2 Anterior Myocardial Infarction Versus LVH

In cases of severe LVH, the vectorcardiographic loop may also resemble anterior myocardial infarction. In many cases, the difference between the two can clearly be separated on non-electrocardiographic considerations, clearly including the clinical history. If the QRS loop and T loop are oppositely directed in the transverse plane with lack of QRS electrical activity anteriorly, the higher probability is that appearances are due to LVH (Fig. 43.27).

Of course, both abnormalities can be present simultaneously in an individual and this is more likely to be the case if the QRS–T angle is approximately 90°. A T vector directed posteriorly to the right suggests an ischemic component to the abnormality as isolated LVH would rarely produce a T vector so oriented.

43.4.2.3 Inferior Myocardial Infarction

The dead zone or infarct vector concept suggests that in inferior myocardial infarction there is an increase of electrical force superiorly. In turn, this produces a loss of inferiorly directed forces resulting in an initial superiorly directed vectorcardiographic loop in the frontal plane. However, as this is not altogether uncommon in normal individuals, the point

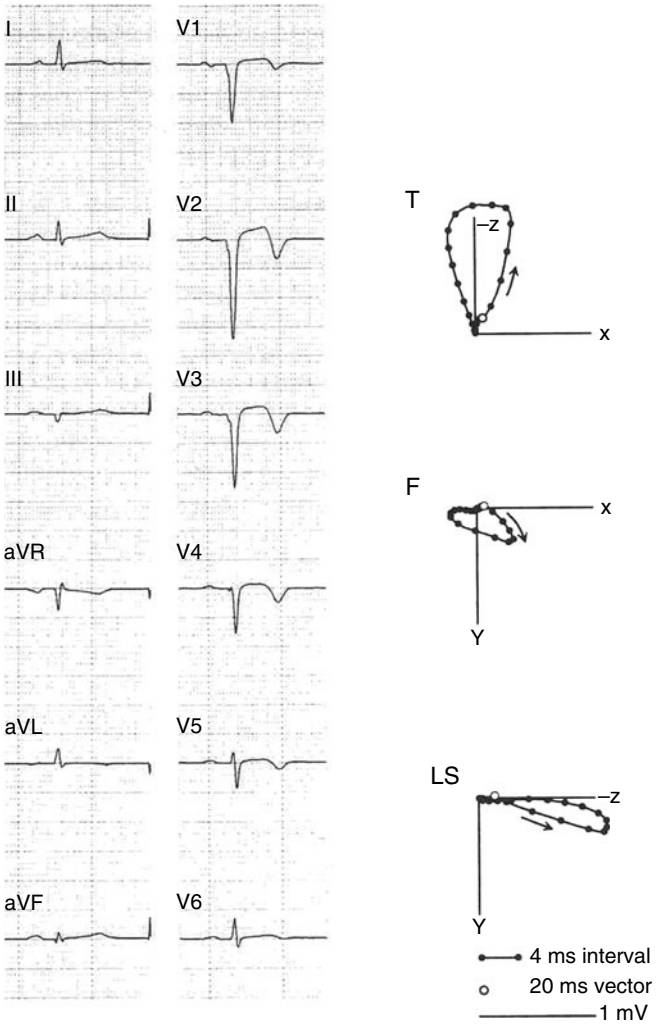

Figure 43.32

The classical features of anterior myocardial infarction with a complete absence of anteriorly directed QRS vectors. Note that the 30 ms vector is also posterior to 300° in the transverse plane.

Table 43.4

Criteria for anterior myocardial infarction

Any of the following in the transverse QRS loop
Direction of 30 ms vector 225–300°
Loop area in left anterior quadrant <1% of the total loop area
An early bite, that is, a clockwise inscription of the loop, with an amplitude >0.05 mV (see Sect. 43.4.2.8)

of importance is the length of time for which the loop persists in the superior quadrants and the ratio of superiorly to inferiorly directed forces. Common vectorcardiographic criteria for inferior myocardial infarction are presented in Table 43.5.

In addition to the superiorly directed forces having a duration >20 ms, the concept of *X*-intercept needs to be introduced. This is illustrated in Fig. 43.36. The *X*-intercept is the point at which a clockwise-inscribed frontal plane loop

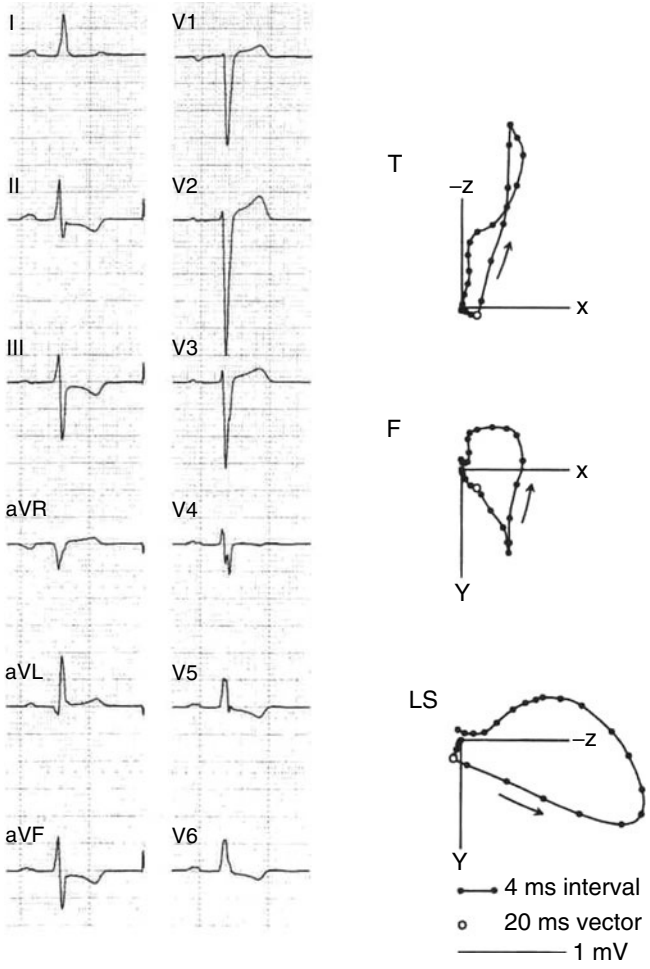

Figure 43.33

An example of anterior myocardial infarction where the initial QRS forces are anteriorly directed for a little over 20 ms but where the 30 ms vector is just posterior to 300°.

first crosses the *X*-axis. In a sense, it is clear that the longer the QRS loop remains superior to the *X*-axis, the greater the probability that the *X*-intercept will exceed 0.3 mV. Thus, in some ways, there is a correlation between this parameter and a superior duration >20 ms. Figure 43.37 gives an example of a vectorcardiographic frontal plane loop where all the criteria are met.

Analogous to the situation of low R waves in anterior leads consistent with myocardial infarction, it is possible that there can be very low amplitude R waves in the inferior lead Y in the presence of inferior infarction, that is, there is a very short inferiorly directed initial activation in the frontal plane. If the initial vector of activation is directed inferiorly and rightward followed by clockwise inscription, then the criteria of *X*-intercept >0.3 mV and a superior/inferior amplitude ratio >0.15 can often be met.

43.4.2.4 Inferior Myocardial Infarction Versus Left Anterior Fascicular Block

Often a common feature of the inferior myocardial infarction and left anterior fascicular block is the superior orientation of the frontal plane QRS vector loop. However, the left anterior fascicular block is always accompanied by a

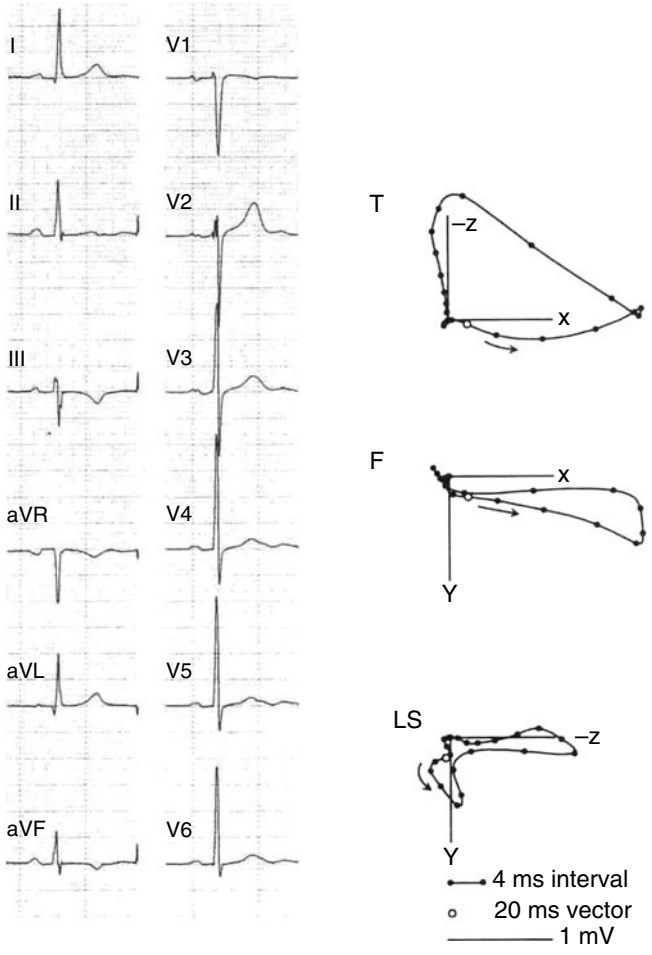

Figure 43.34

Anterior myocardial infarction proven by diagnostic cardiac catheterization in a 62-year-old male. Note the early bite in the QRS loop in the transverse plane.

counterclockwise inscription of the QRS loop whereas the inferior myocardial infarction invariably has a clockwise inscription of the QRS loop. A comparative example is shown in Fig. 43.38. It is also the case that in left anterior fascicular block, the QRS axis is generally more superiorly directed than in inferior myocardial infarction.

43.4.2.5 Posterior Myocardial Infarction

The theory of the dead zone or infarct vector applied to an infarction of the posterior wall of the heart indicates that there will be an increase in anteriorly directed electrical forces. The diagnosis of posterior myocardial infarction is again difficult, purely from an electrocardiographic standpoint. There may, of course, be other clinical factors that suggest a myocardial infarction which, taken together with the relevant vectorcardiographic changes, could point to infarction of the posterior wall.

The increase in anterior forces is reflected in an increased duration of the anteriorly directed forces in the transverse plane. In addition, the amplitude ratio of the anteriorly/posteriorly directed forces exceeds 1. Finally, the area

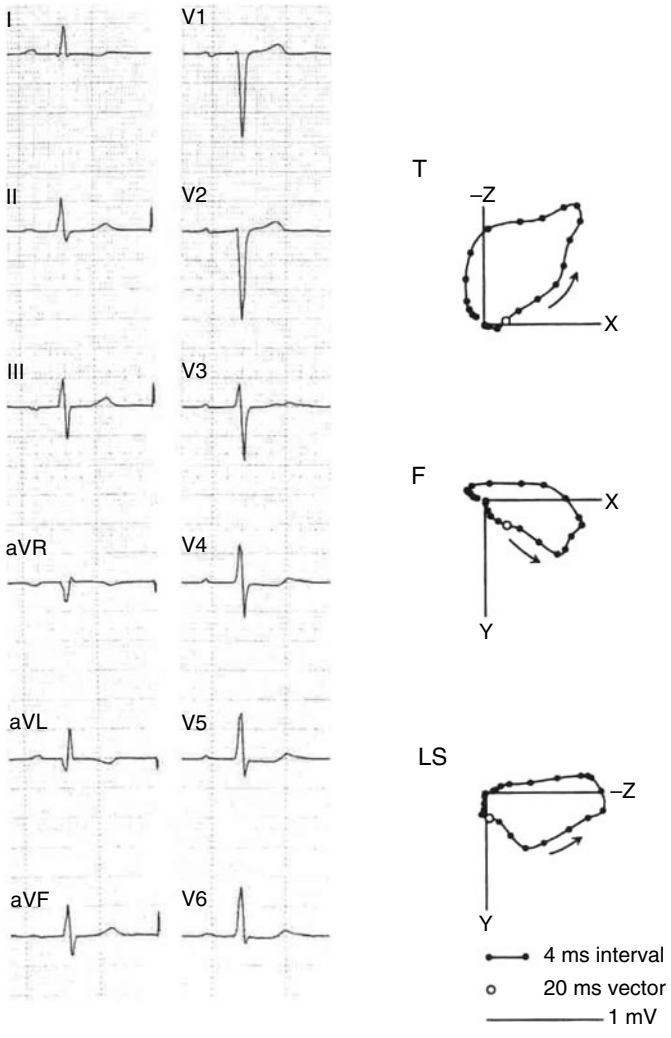

Figure 43.35

Anterior myocardial infarction proven by diagnostic cardiac catheterization in a 58-year-old male. Note the QRS loop area in the left anterior quadrant is almost 0% of the total QRS loop area.

Table 43.5

Criteria for inferior myocardial infarction

All of the following in the frontal QRS loop
An initial superior inscription >20 ms
A superior amplitude >0.1 mV
A superior/inferior amplitude ratio >0.15
An *X*-axis intercept >0.3 mV

in the left anterior quadrant of the transverse plane exceeds 50% of the total QRS loop area (Fig. 43.39). Common vectorcardiographic criteria for posterior myocardial infarction are presented in Table 43.6.

The other typical feature of posterior myocardial infarction is an increase in T vector amplitude. This may well correspond to a T vector oriented in the direction of 70–80° in the transverse plane.

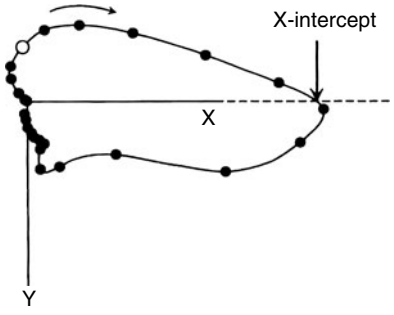

Figure 43.36
Frontal plane QRS loop showing the *X*-intercept.

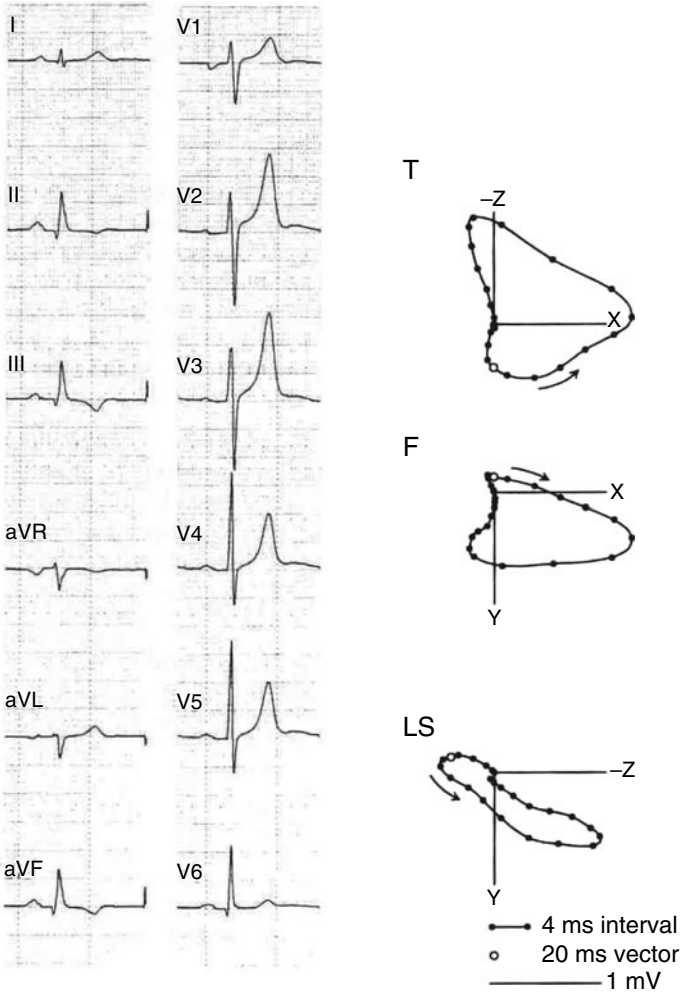

Figure 43.37
Vectorcardiogram of inferior myocardial infarction meeting the criteria of Table 43.5.

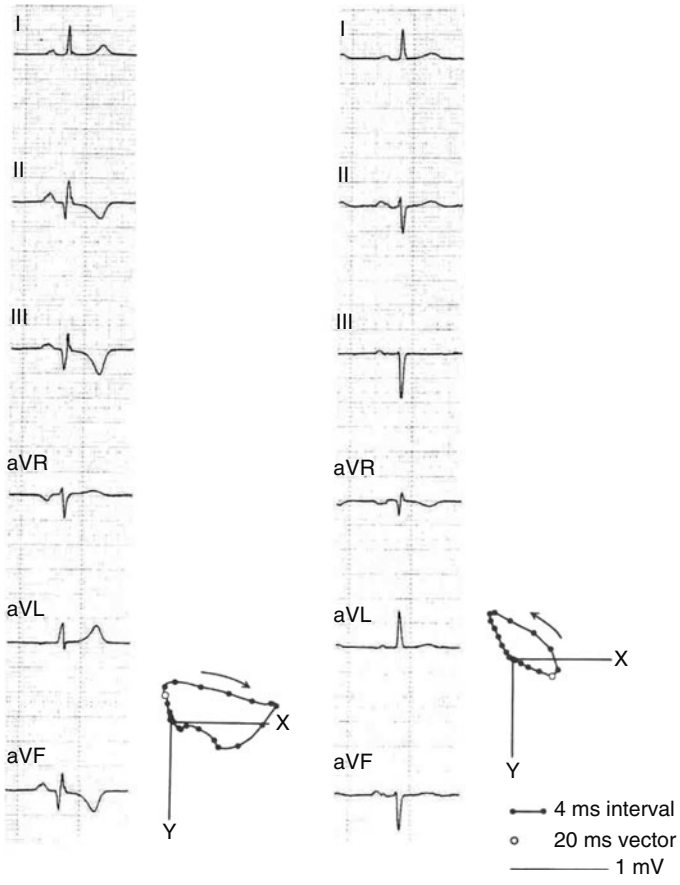

Figure 43.38
***Left* panel shows inferior myocardial infarction; *right* panel shows left anterior fascicular block.**

43.4.2.6 Posterior Myocardial Infarction Versus RVH

The features of RVH have been discussed in Sect. 43.3. The Type A vectorcardiographic loop is not too dissimilar from that of posterior myocardial infarction and therefore the differentiation between the two is difficult. However, the criteria of anteriorly directed forces exceeding 50 ms is more likely to be met in a case of posterior myocardial infarction than in RVH. Also, the T vector loop is more likely to be anteriorly directed in posterior infarction than in RVH.

Another factor that influences the situation is that an inferior or even lateral myocardial infarction, which extends toward the posterior wall of the heart, may produce, in addition, an increase in anteriorly directed forces. In that situation, a report of "increased anterior forces probably reflecting inferior/posterior myocardial infarction" is more likely to be correct than one which suggests that there is RVH in addition to inferior infarction, for example.

43.4.2.7 Anterolateral Myocardial Infarction

The effect of a lateral wall myocardial infarction is to produce an initial electrical force which is directed in the range 90–270° in the transverse plane. This is the principal requirement for the diagnosis of anterolateral myocardial infarction, an example of which is shown in Fig. 43.40. Isolated anterolateral infarction is uncommon and more often than not, the changes are associated with an anterior rather than a purely anterolateral myocardial infarction.

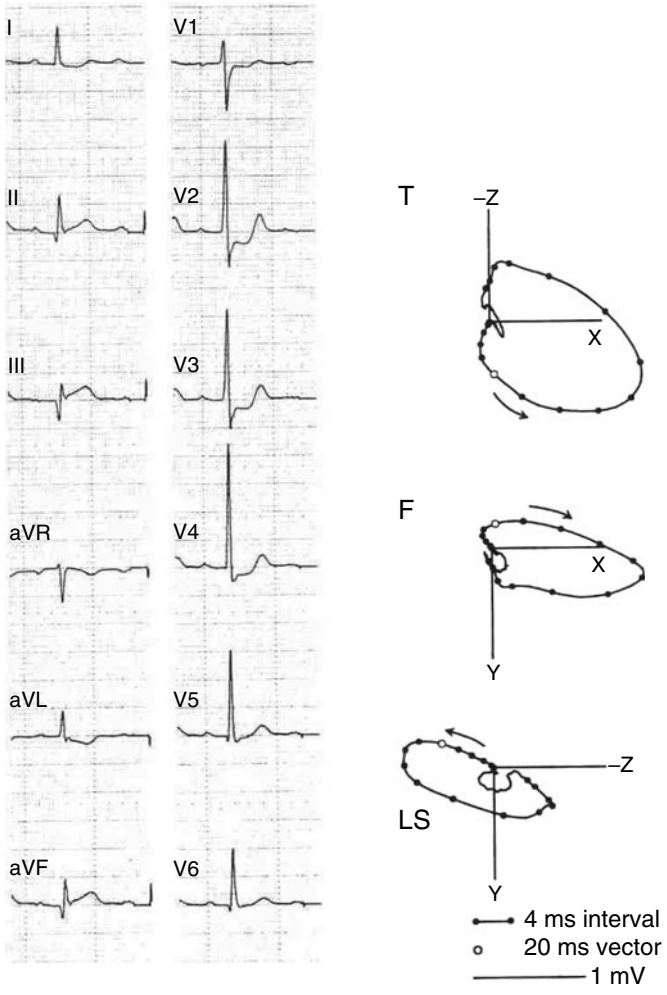

Figure 43.39

Inferior myocardial infarction with posterior wall involvement. Note that the area of the QRS loop in the left anterior quadrant exceeds 50% of the total QRS loop area. The *X*-intercept also greatly exceeds 0.3 mV.

Table 43.6

Criteria for posterior myocardial infarction

The QRS loop in the transverse plane shows:
an initial anteriorly directed loop >50 ms
an anterior/posterior amplitude ratio >1
a loop area in left anterior quadrant >50% of the total loop area

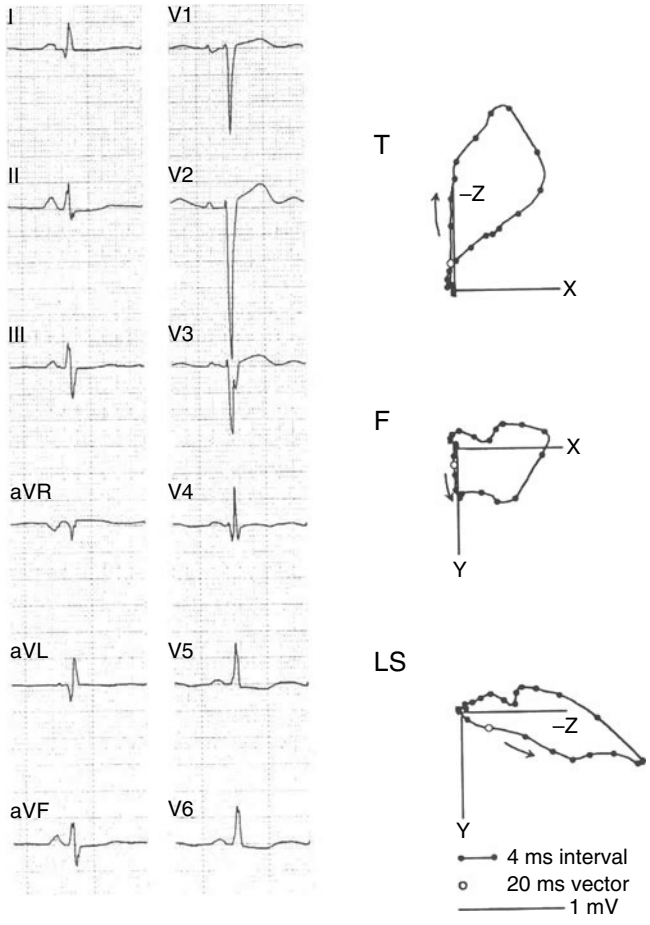

Figure 43.40

Vectorcardiographic example of anterolateral myocardial infarction. Note that in the transverse plane, the initial electrical forces are directed posteriorly to the right and that the inscription of the main body of this loop is clockwise. It should also be noted that there are no Q waves in the precordial leads of the 12-lead ECG.

43.4.2.8 Bites

The concept of a vectorcardiographic bite was mentioned earlier in this chapter. This is best explained by reference to Fig. 43.41, where a comparison is made between a normal transverse plane vectorcardiogram and one exhibiting a bite, that is, an indentation of the QRS loop, which often amounts to a reversal of the direction of inscription of the loop. For example, the normal QRS loop in the transverse plane has a constant counterclockwise inscription whereas the loop with a bite has an inscription that is initially counterclockwise, then changes to clockwise before returning to counterclockwise inscription. It is suggested that the amount of deviation of the bite from the normal loop gives an indication of the size of infarcted area. Considerable work was done in this area by Selvester and Sanmarco [26] with modeling studies and, indeed, a nomogram was produced, which linked the duration of the bite with the magnitude of the difference between the normal vectorcardiographic loop and the abnormal vectorcardiographic loop (Fig. 43.42). The nomogram allows calculation of an estimate of the percentage of myocardium that is damaged and in turn, an estimate of the ejection fraction of the left ventricle. Selvester et al. [27] also provided data on the occurrence of bites in diabetic patients. Edenbrandt et al. recently [28] developed a computer-assisted method for measuring the size of vectorcardiographic bites.

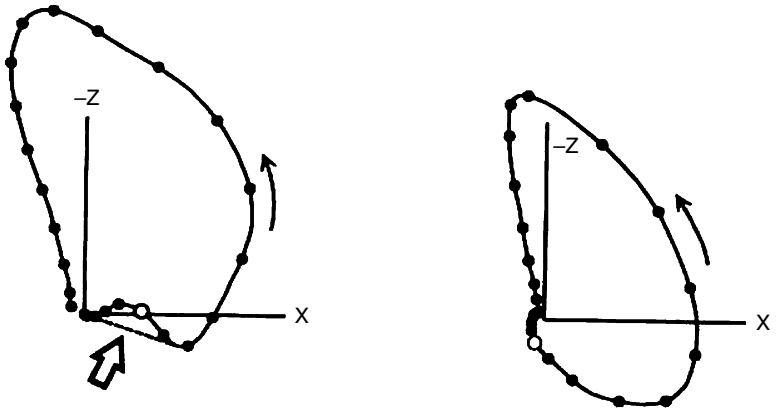

Figure 43.41

Vectorcardiographic loops in the transverse plane. The left loop shows an early bite whereas the right loop has a normal inscription.

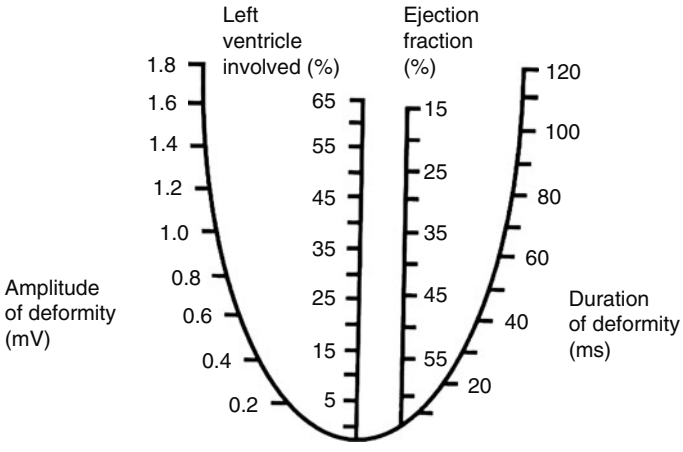

Figure 43.42

Nomogram for predicting infarct size from deformities in the Frank vectorcardiogram. The amplitude and duration of the deformity are transferred to the left side and right side of the nomogram, respectively. A line is then constructed through these two points and the points where it crosses the lines in the center are used to determine the angiographic percentage of left ventricle involved and the ejection fraction.

43.5 Conduction Defects

43.5.1 Introduction

It is certainly the case that conduction defects may be thought rather straightforward to diagnose from the 12-lead ECG. On the other hand, there are borderline situations where there can be doubt as to whether a QRS duration is prolonged. Indeed, it has gone almost unrecognized for many years that the normal mean QRS duration for males is almost 8 ms longer than for females in the 18–29 year age group (96.4 versus 87.7 ms) although as age increases the difference tends to

decrease (92.7 versus 87.1 ms at 50 years and over) [29]. Notwithstanding, there are few if any diagnostic criteria that take cognizance of this fact.

One of the advantages of vectorcardiography is that conduction defects can be seen on the vectorcardiographic loop display as a slowing of the inscription of the loop, that is, the loop markers appear closer together. There are other features sometimes pathognomonic of particular defects, as will be seen later in this chapter.

43.5.1.1 Conduction System

The heart muscle consists of three types of tissue – automatic, specialized conducting, and contractile tissue. The process of depolarization is common to all three tissues but only the automatic and specialized conducting tissues have the ability to depolarize spontaneously.

In the human heart (Fig. 43.43), the automatic tissue is concentrated mainly at the sinoatrial (SA) node. In the normal sequence of electrical events, an electrical impulse arising in the SA node, travels through the right atrium to the atrioventricular (AV) node and thereafter spreads into the ventricles via the specialized conducting tissue in the bundle of His.

Invasive recording of the signals in the atria and in particular in the area of the AV node has led to a much greater understanding of certain types of conduction defects but in particular, this approach has been of most value in the assessment of cardiac arrhythmias. On the other hand, this chapter is concerned more with abnormalities of conduction in the bundle of His and its various branches.

As seen in Fig. 43.43, the bundle of His divides at the base of the septum into the right bundle branch and the left bundle branch. The latter has been shown to divide into a variety of different forms, common to all of which are the left anterior and left posterior fascicles. Demoulin and Kulbertus [30] showed many years ago that there was often a third fascicle, which they called "the centroseptal fascicle."

Under normal circumstances, ventricular depolarization occurs first in the left ventricle, particularly on the left side of the septum, and then spreads to the free wall of the left ventricle. At the same time, shortly after left ventricular activation commences, the right ventricular excitation also starts. However, it is important to appreciate that the normal sequence of depolarization in the ventricles is from the left to the right side of the septum.

For completeness, it should be said that excitation in general terms spreads from the endocardium to the epicardium and from the apex to the base. In addition, ventricular repolarization takes place from the epicardium to the endocardium, giving rise to a normal upright T wave in the majority of precordial leads as well as most frontal plane leads with the exception of aVR. In the 12-lead vectorcardiogram, the T wave is normally upright in leads X, Y, and Z.

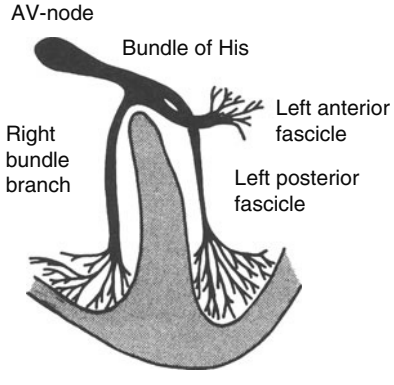

Figure 43.43
Conduction system of the human heart.

43.5.2 Bundle Branch Block

43.5.2.1 Left Bundle Branch Block

When the normal conduction to the left ventricle is prevented by a block in the left bundle branch, the excitation wavefront has to find an alternative pathway via normal cardiac muscle. A major consequence of this is naturally an increase in the time taken to depolarize the ventricles and hence, there is an increase in the QRS duration.

Because of the block in the left bundle branch above its division into the various fascicles, septal activation begins on the right side and progresses from the right to left. Thus, in the 12-lead vectorcardiogram in left bundle branch block (LBBB), there is frequently no primary R wave in lead Z and almost always, an absence of a Q wave in the anterolateral lead X. Right ventricular depolarization is virtually complete before the excitation waves later spread unopposed round both anterior and posterior walls of the left ventricle to meet at the lateral wall [31].

From a vectorcardiographic point of view, the initial QRS forces are therefore directed posteriorly and to the left. Commonly, the maximum QRS vector is also similarly directed posteriorly to the left and inferiorly. The vectorcardiographic appearances of LBBB are as shown in Fig. 43.44. These are quite distinctive with generally a long narrow QRS

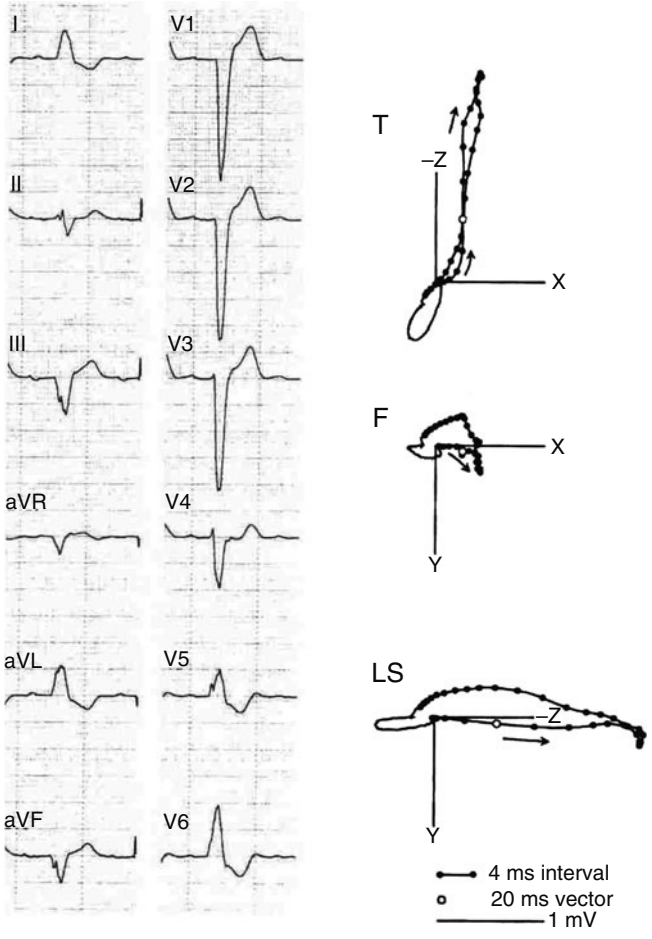

Figure 43.44

An example of left bundle branch block (LBBB). Note the closely spaced time-markers and the narrowness of the QRS loop particularly in the transverse plane. Also, it should be noted that the maximum QRS and T vectors are oppositely directed.

Table 43.7
Vectorcardiographic criteria for left bundle branch block (LBBB)

A maximum QRS vector directed oppositely to the T vector
An elongated or occasionally figure-of-eight loop in the transverse plane with minimal breadth
The main body of the loop is usually inscribed in a clockwise direction in the transverse plane
The timing markers are much closer together than in the normal vectorcardiographic loop

loop in the transverse plane with the T loop being oppositely directed. This corresponds to T wave inversion in lead X. It does also suggest that ventricular repolarization takes place in a sequence parallel to that of depolarization in view of the abnormally slow spread of the ventricular activation wave fronts. The characteristic vectorcardiographic features of LBBB are shown in Table 43.7.

43.5.2.2 Incomplete Left Bundle Branch Block

The concept of incomplete LBBB is perhaps more difficult to explain. It has been suggested that the progression of excitation via the left bundle branch is slower than normal although there is not a complete block. Initial septal activation will, therefore, be on the right side of the septum. From the vectorcardiographic point of view, the QRS loop is again elongated and narrow as in complete LBBB but the overall QRS duration is of the order of 120–140 ms. The remaining markers may also be a little closer than normal. An illustration is given in Fig. 43.45.

Often this pattern is associated with a slightly increased voltage and T wave abnormalities in the lateral leads, that is, a T vector loop almost oppositely directed to the QRS loop. This has given rise to the expression "incomplete LBBB/LVH pattern." It is possible that patients with hypertensive heart disease, for example, and LVH, exhibit fibrosis, which progresses to the extent that the conduction system becomes impaired resulting in the above described abnormalities.

43.5.2.3 Right Bundle Branch Block

In complete right bundle branch block (RBBB), there is a block in the conduction system in the right bundle branch below its junction with the bundle of His. Thus, left ventricular activation commences normally so that RBBB always manifests itself as an abnormality in the terminal part of the QRS complex. This allows other abnormalities such as myocardial infarction to be reported with reasonable confidence in the presence of RBBB.

Because of the normal left ventricular activation, appearances in RBBB show normal initial depolarization. After the greater part of the left ventricle has been depolarized, the delayed excitation wave has spread to the free wall of the right ventricle so that there is an electrically unopposed (but delayed) right ventricular depolarization. This action results in the terminal portion of the QRS complex exhibiting electrical forces oriented to the right, anteriorly. In addition, the QRS duration is abnormally prolonged beyond 120 ms. In the scalar presentation of lead Z there is a broad R′ wave.

The vectorcardiographic loop is shown in Fig. 43.46. It can be seen that the terminal portion of the QRS loop shows a marked slowing of the rate of inscription as evidenced by the closeness of the timing markers. The terminal loop is directed anteriorly, rightward, with quite characteristic features being demonstrated. The major part of the loop is inscribed in a counterclockwise direction.

43.5.2.4 Incomplete Right Bundle Branch Block

There can often be dispute as to whether on a scalar presentation there is, indeed, incomplete RBBB evidenced by the secondary r′ wave in V_1, V_2, or lead Z. It has been suggested that this late QRS activity is due to hypertrophy of the basal

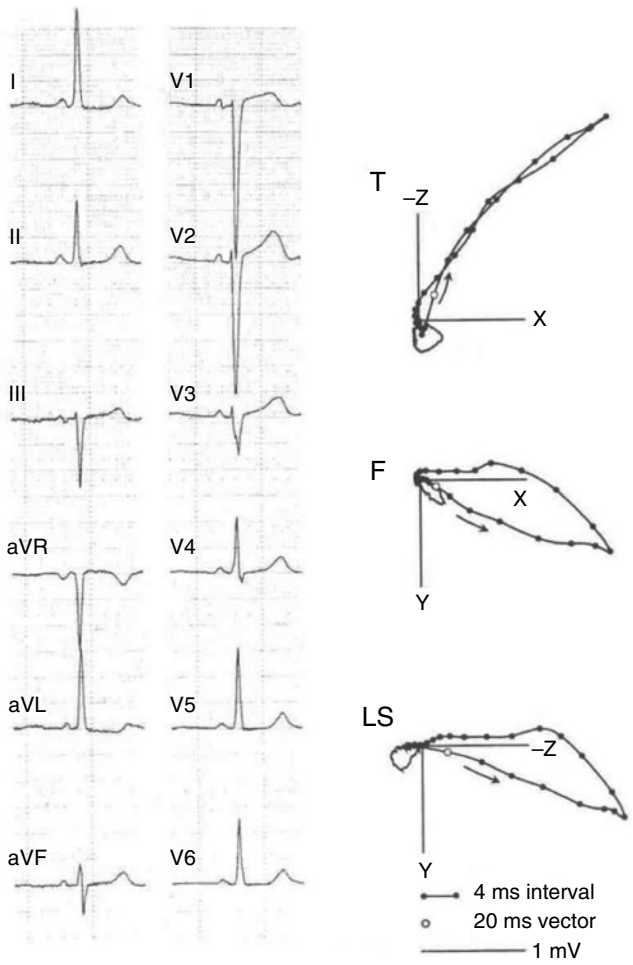

Figure 43.45

An example of incomplete LBBB where the QRS loop in the transverse plane is extremely narrow. The time-markers are also more closely spaced than normal.

portion of the right ventricle although, as it is often seen in younger individuals, it could indeed on occasions be considered a normal variant.

From the vectorcardiographic point of view, an incomplete RBBB is manifested as some slowing in the terminal inscription of the QRS loop seen best in the transverse plane. This portion of the loop will also be oriented anteriorly, rightward. In this situation, the presentation of a vectorcardiogram has an advantage over the scalar presentation in that terminal slowing can be seen.

It could be argued, since the normal QRS duration ranges from 60 to 110 ms, that an incomplete bundle branch block occurring in a patient who previously had a QRS duration of the order of 80 ms could well result in a relative prolongation of the QRS duration to 110 ms. Therefore, it should not be essential for conduction defects involving the right bundle branch in particular to be dependent on criteria which provide discrete time thresholds such as 110 ms for incomplete RBBB. On the other hand, it is unlikely in the adult that a QRS duration <90 ms would be consistent with even an incomplete RBBB. An illustration of the vectorcardiogram in incomplete RBBB is given in Fig. 43.47.

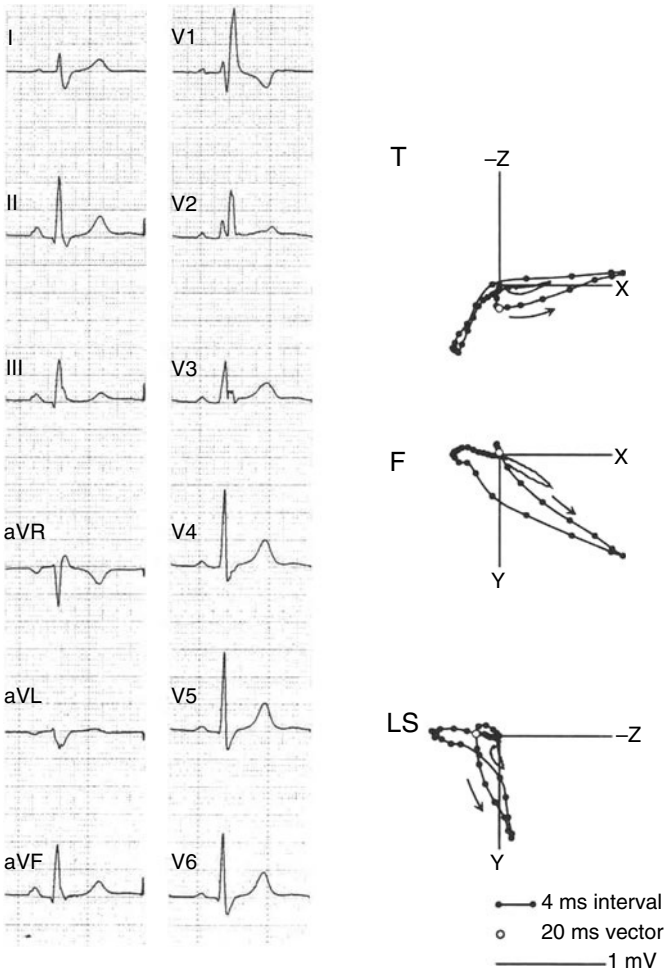

Figure 43.46

An example of right bundle branch block (RBBB) where the late QRS vectors are directed anteriorly to the right with very closely spaced time-markers in the loops corresponding to the slowed conduction. Note the terminal slowing of inscription of the QRS loop.

43.5.3 Fascicular Block

In 1966, Pryor and Blount [32] suggested that the pure left axis deviation might be due to a block in the superior division of the left bundle. They termed this abnormality the "Left Superior Intraventricular Block." They also suggested that right axis deviation could be caused by a block in the inferior division of the left bundle. It was surmised that the direction of the initial excitation depended on the nature of the lesion that produced the block, for example, fibrosis or necrosis. Subsequently, Rosenbaum [33] set out criteria for conduction defects arising from different parts of the conducting system. He postulated that localized abnormalities may occur in isolation, intermittently or in association with defects in other branches of the specialized conducting system. He also introduced the term "hemiblock" to replace "superior" and "inferior" intraventricular block but since there are often more than two specialized conducting fascicles in the left ventricle, the term is perhaps a misnomer. For this reason, it has been suggested [34] that the term "fascicular block" be used. This terminology will be used in the present discussion.

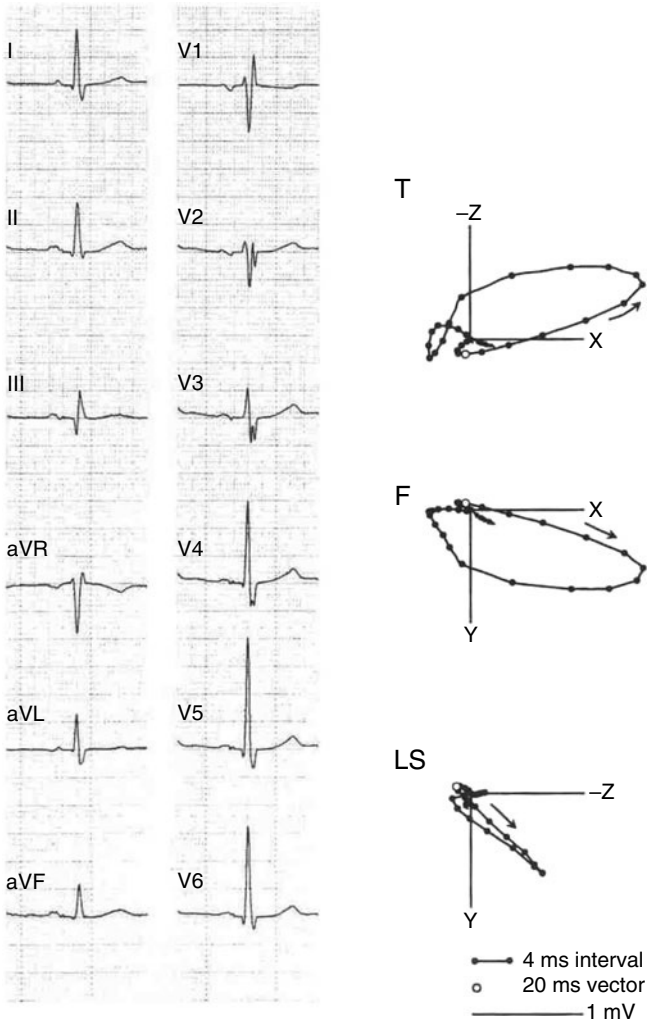

Figure 43.47
Example of incomplete RBBB.

43.5.3.1 Left Anterior Fascicular Block

In left anterior fascicular block, it is postulated that a block of the conduction of excitation arises in the anterior fascicle of the left bundle branch. In this case, ventricular depolarization probably takes place via the other intact fascicles. Excitation initially spreads inferiorly from the left posterior fascicle and it is feasible that there may also be some septal activation from another left-sided conducting fascicle such as the centroseptal fascicle. The net result is an initial, inferiorly directed and sometimes rightward spread of activation. Thereafter, the leftward upward spread of activation from the region of the left posterior fascicle becomes dominant, causing the ventricular resultant electrical force to be orientated posteriorly and superiorly producing a prominent S wave in lead Y.

The frontal plane vectorcardiographic loop shows left axis deviation in most cases, that is, the projection of the maximum QRS vector is superior to 0° and always has counterclockwise inscription [35]. This enables left anterior fascicular block to be differentiated from other forms of conduction abnormality such as due to inferior myocardial infarction.

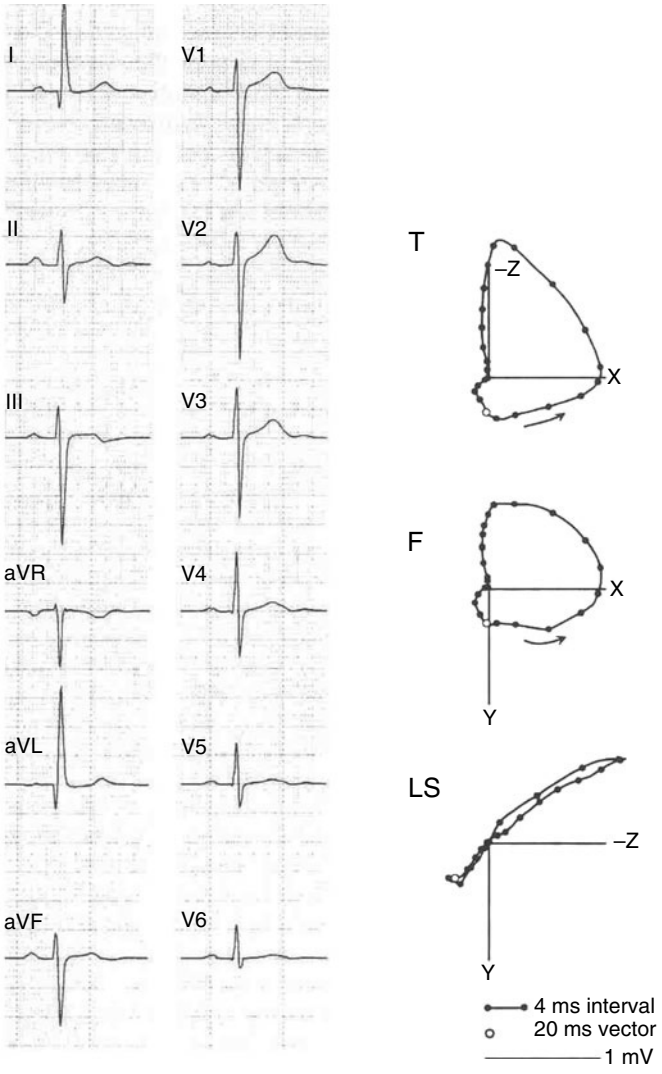

Figure 43.48

An example of left anterior fascicular block with counterclockwise inscription of the QRS loop in the frontal plane.

Table 43.8

Vectorcardiographic criteria for left anterior fascicular block

Initial QRS vectors directed inferiorly and rightward
Counterclockwise inscription in the frontal plane
QRS axis in the frontal plane superior to –30°

Figure 43.48 gives an example of left anterior fascicular block while Fig. 43.38 shows how inferior myocardial infarction can be separated from left anterior fascicular block by the fact that there is clockwise inscription in the frontal plane in the former. Lopes [36] has proposed that the vectorcardiographic criteria for left anterior fascicular block should include, those listed in Table 43.8.

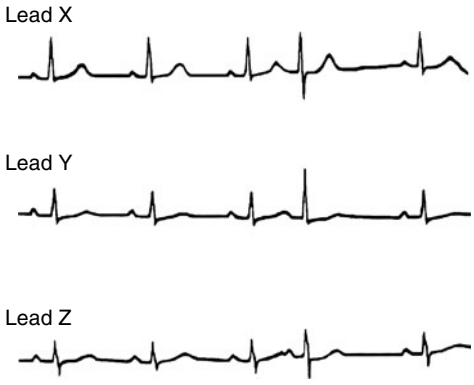

Figure 43.49
Example of intermittent left posterior fascicular block in the fourth beat.

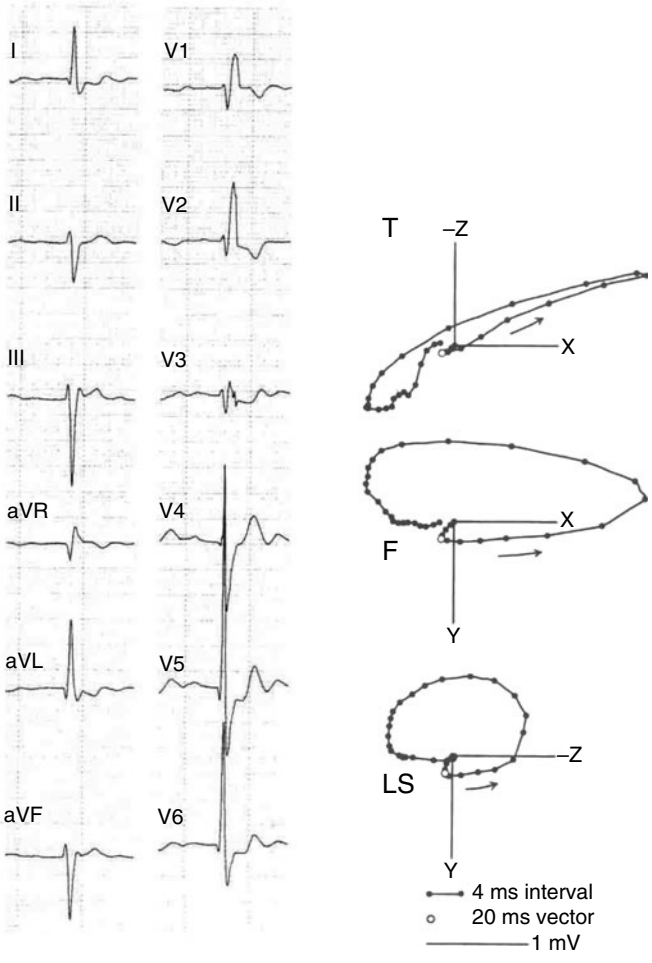

Figure 43.50
Example of RBBB + left anterior fascicular block.

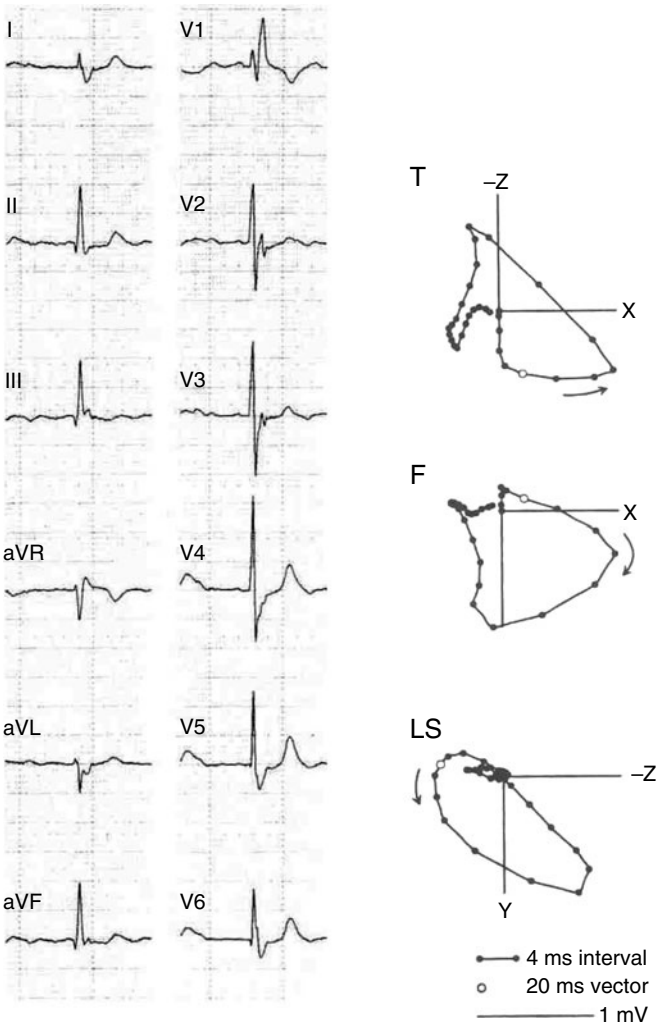

Figure 43.51

An example of RBBB plus left posterior fascicular block. Note that the QRS vector in the frontal plane exceeds 75° in this 39-year-old male.

Figure 43.52

Example of alternans where every second beat shows RBBB plus left posterior fascicular block.

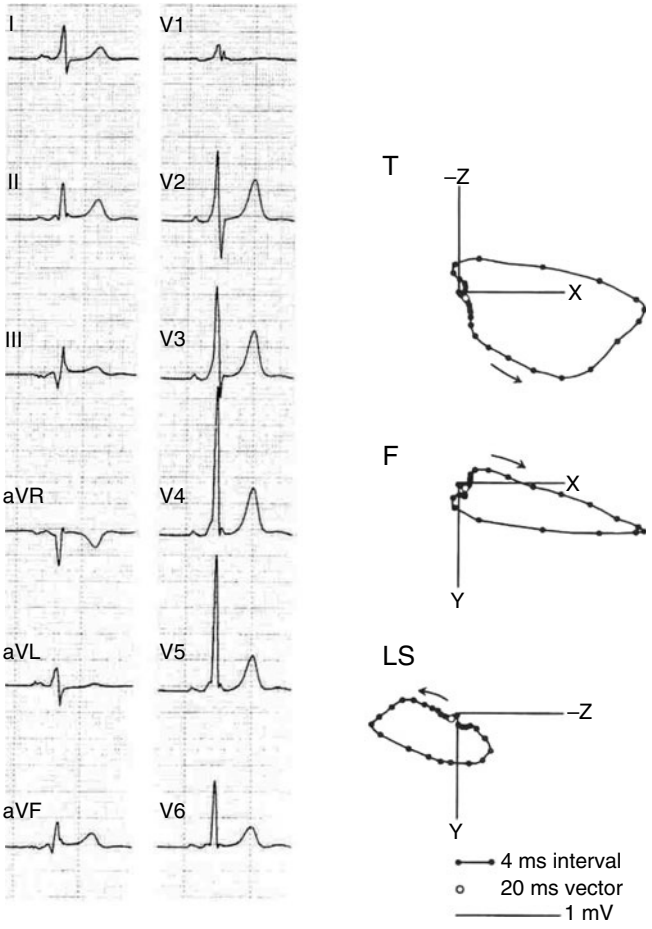

Figure 43.53

An example of Wolff–Parkinson–White (WPW) Type A with initial slowing of the inscription of the QRS loop and early QRS vectors directed anteriorly.

He also suggested that if the major axis of the QRS loop is not directed superiorly, but the late part of the loop lies in the left superior quadrant, possible left anterior fascicular block may be diagnosed.

43.5.3.2 Left Posterior Fascicular Block

It is postulated that if there is a block in the posterior fascicle of the left bundle branch, ventricular activation will proceed from the anterior wall of the left ventricle, spreading inferiorly. Right ventricular, and possibly septal activation are normal. However, the posterior wall of the left ventricle will be depolarized somewhat later than usual so that the excitation waves spreading anteriorly and inferiorly assume an increased importance in the development of ECG appearances. The QRS axis, therefore, shifts to the right, producing appearances suggestive of RVH. Often these appearances are best seen in an intermittent conduction defect in a rhythm strip, for example (Fig. 43.49). In this example, there is an atrial extrasystole that shows a change in QRS configuration compared to the dominant complex, namely, an increase in the amplitude of the R wave in the anteroseptal and inferior leads and a deepening of the S wave in the lateral lead. These appearances are in keeping with the concept of left posterior fascicular block, which, in this case, is intermittent, presumably being produced by a refractory left posterior fascicle at the time of the occurrence of the supraventricular extrasystole.

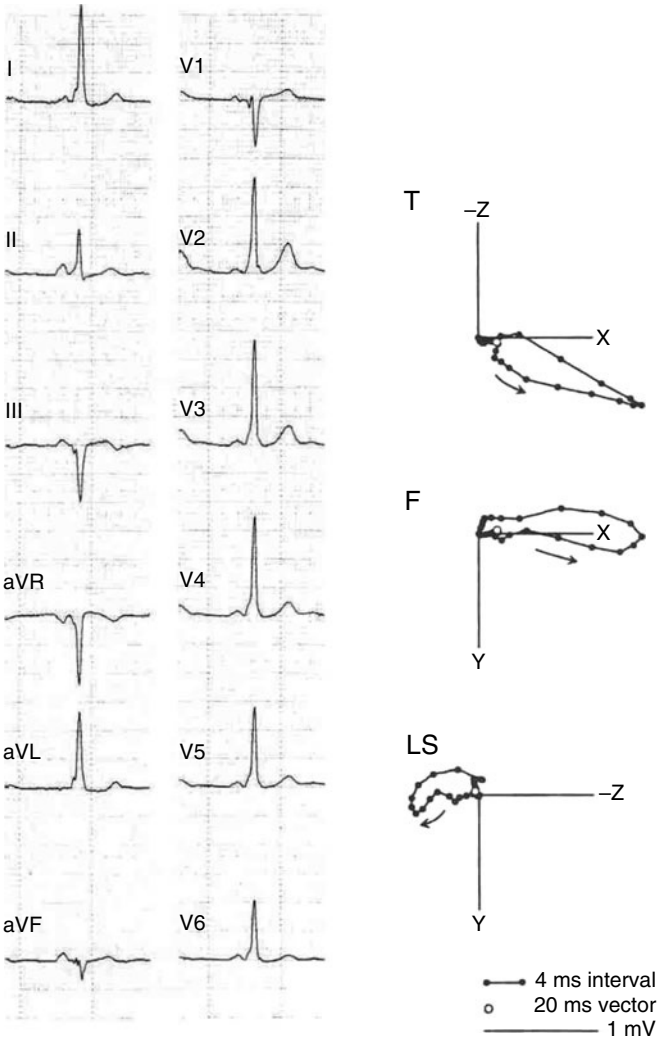

Figure 43.54

An example of WPW Type B where there is initial slowing of the early QRS vectors that are directed leftward for the first 20 ms.

The differentiation of pure left posterior fascicular block from RVH can be difficult. The former is best diagnosed only if there is a lack of clinical evidence to support RVH. It should be clear from Fig. 43.49 that the diagnosis of pure left posterior fascicular block from a single cardiac cycle is virtually impossible.

43.5.4 Bifascicular Block

Combinations of conduction abnormalities in the right bundle branch and different fascicles of the left bundle branch lead to bifascicular block. An example of bifascicular block is RBBB in association with left anterior fascicular block (Fig. 43.50). In this case, there is a marked superior displacement of the vectorcardiographic loop in the frontal plane while the terminal slowing of conduction is again apparent in the transverse plane where the terminal forces are directed anteriorly and to the right.

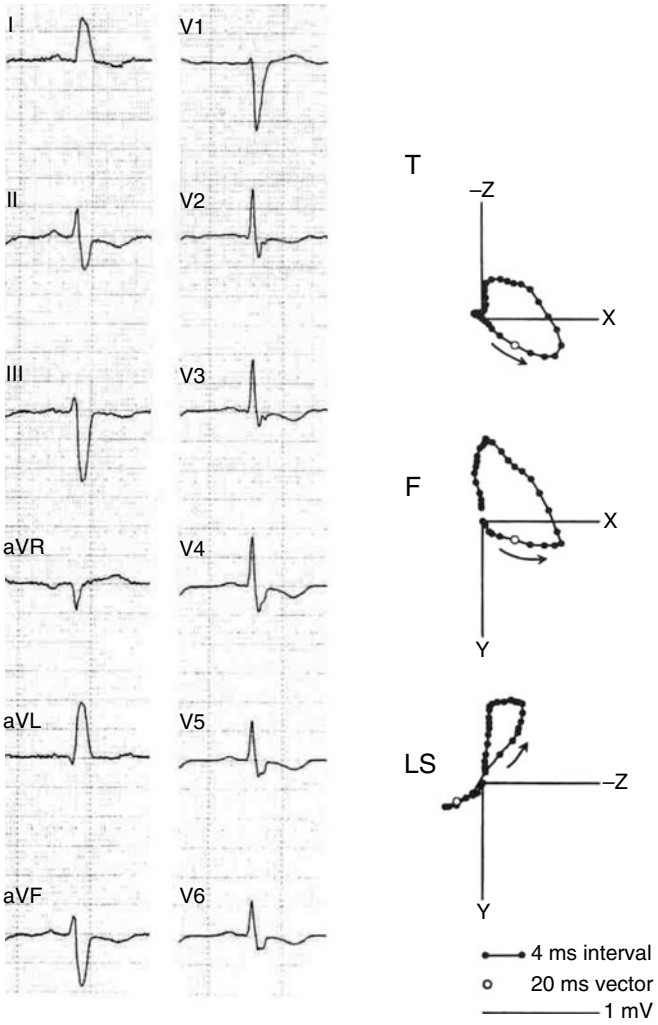

Figure 43.55

An intraventricular conduction defect exemplified by the closely spaced time-markers in all the QRS loops. The transverse loop is also open as opposed to being narrow in LBBB and does not have the late QRS vectors directed to the right as in RBBB.

On the other hand, RBBB with a left posterior fascicular block may be suspected when there is right axis deviation with other typical features of RBBB (Fig. 43.51). Again, the typical RBBB feature of terminal slowing of the QRS loop is apparent but the right axis deviation is abnormal. This feature can perhaps be seen more clearly in another rare example (Fig. 43.52) where there is electrical alternans. The narrow QRS complex suggests myocardial infarction with possible left posterior fascicular block while the alternate beats indicate RBBB in addition.

43.5.5 Wolff–Parkinson–White Pattern

The classical features of the Wolff–Parkinson–White (WPW) [37] pattern are those of an initial slurring of the QRS complex due to the spread of activation from atria to ventricles via an accessory pathway. Note that these features describe the WPW pattern, which, if associated with episodes of paroxysmal tachycardia, gives rise to the WPW syndrome. From the vectorcardiographic point of view, the main distinguishing feature is obviously the slowing of inscription in the initial

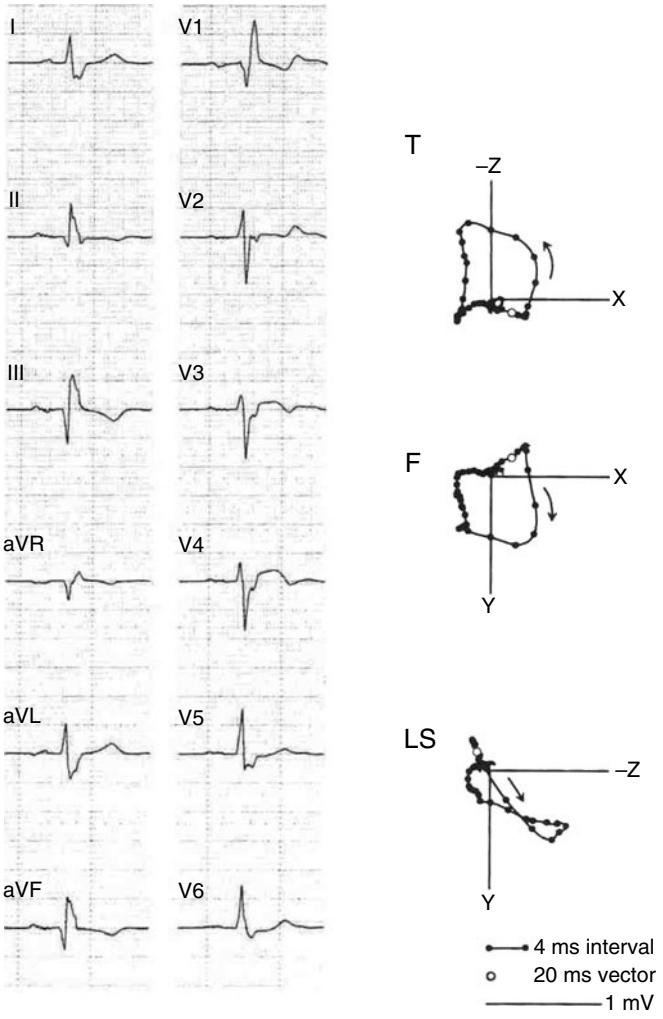

Figure 43.56
Example of RBBB and inferior myocardial infarction.

part of the vectorcardiographic loop. This may facilitate the diagnosis of WPW pattern in borderline cases where the initial slurring in the scalar presentation may be questioned as being technical in origin. There is a variety of accessory pathways such that there is no typical feature of the WPW pattern on the vectorcardiogram other than the initial slowing of inscription. In other words, initial vectors may be orientated in a whole spectrum of different directions depending on the location of the accessory pathway.

In broad terms, using the older classification of Type A and Type B, the initial vector orientation will be anterior in Type A and posterior/to the left in Type B. Figures 43.53 and 43.54 give examples of the vectorcardiographic loops in the WPW pattern.

43.5.6 Intraventricular Conduction Defects

There remains a class of conduction defects that does not fit any of the categories mentioned so far. In general terms, the QRS duration is prolonged in excess of 120 ms but the features of RBBB or LBBB are not apparent. On occasions,

such defects manifest themselves as an open loop in the transverse plane, which permits the diagnosis of intraventricular conduction defect as opposed to LBBB, for example, even when the QRS duration is the order of 140–160 ms (Fig. 43.55). This is another area where the vectorcardiographic loop can be of considerable diagnostic value.

43.5.7 Combined Conduction Defects and Myocardial Infarction

The diagnosis of myocardial infarction in the presence of RBBB is relatively straightforward. Because RBBB affects the terminal portion of the QRS complex and classical criteria for myocardial infarction affect the initial portion of the QRS complex, it is possible for myocardial infarction to be reported in the presence of RBBB. Figure 43.56 shows an example of inferior myocardial infarction and RBBB.

On the other hand, there is still controversy over the diagnosis of myocardial infarction in the presence of LBBB. In 1982, Havelda et al. suggested that inferior myocardial infarction could be diagnosed with 100% specificity in the presence of LBBB when there were QS complexes in the inferior leads [38]. Others have subsequently suggested that anterior infarction can be diagnosed in the presence of LBBB when, for example, there is a reversed R wave progression from V_3 to V_5 or there are Q waves in the lateral leads. On the other hand, left anterior fascicular block may mask or mimic inferior infarction [39].

43.5.8 ECG Versus 12-Lead Vectorcardiogram in Conduction Defects

This chapter has shown how there are certain situations where the vectorcardiographic display can exhibit the presence of conduction defects that may be less obvious on the scalar ECG. In particular, the slowing of timing marks on the vectorcardiogram is invariably an illustration of a conduction defect, whether it is at the beginning of the QRS complex as in the WPW pattern or at the end as in RBBB. If the slowing is throughout the QRS, then most likely the diagnosis is LBBB. It has also been shown how left anterior fascicular block and inferior infarction can be separated by the direction of inscription of the frontal plane vectorcardiographic loop. All of these points lend further weight to the conclusion that the vectorcardiogram has an important role to play in the diagnosis of ventricular conduction defects.

References

1. Einthoven, W., G. Fahr, and A. de Waart, Über die Richtung und die manifeste Grosse der Potentialschwankungen im menschlichen Herzen und über den Einfluss der Herzlage auf die Form des Elektrokardiogramms. *Pflügers Arch.*, 1913;**150**: 175–315. (Translation: Hoff, H.E. and P. Sekelj, *Am. Heart J.*, 1957;**40**: 163–194.)
2. Grishman, A. and L. Scherlis, *Spatial Vectorcardiography*, Philadelphia, PA: Saunders, 1952.
3. Frank, E., An accurate, clinically practical system for spatial vectorcardiography. *Circulation*, 1956;**13**: 737–749.
4. Mann, H., A method for analyzing the electrocardiogram. *Arch. Int. Med.*, 1920;**25**: 283–294.
5. American Heart Association Committee on Electrocardiography (Pipberger, H.V., R.C. Arzbaecher, and A.S. Berson, et al.), Recommendations for standardization of leads and of specifications for instruments in electrocardiography and vectorcardiography. *Circulation*, 1975;**52**(Suppl.): 11–31.
6. Watts, M.P. and D.B. Shoat, Trends in electrocardiograph design. *J. Inst. Electron. Radio Eng.*, 1987;**57**: 140–150.
7. Macfarlane, P.W., B. Devine, S. Latif, S. McLaughlin, D.B. Shoat, and M.P. Watts, Methodology of ECG interpretation in the Glasgow Program. *Meth. Inform. Med.*, 1990;**29**: 354–361.
8. Macfarlane, P.W., E.N. Coleman, B. Devine, et al., A new 12-lead pediatric ECG interpretation program. *J. Electrocardiol.*, 1990;**23**(Suppl.): 76–81.
9. Macfarlane, P.W., E.N. Coleman, E.O. Pomphrey, S. McLaughlin, and A. Houston, Normal limits of the high-fidelity pediatric ECG. *J. Electrocardiol.*, 1989;**22**(Suppl.): 162–168.
10. Lundh, B., On the normal scalar ECG. A new classification system considering age, sex and heart position. *Acta Med. Scand.*, 1984;691(Suppl.).
11. Chen, C.Y., B.N. Chiang, and P.W. Macfarlane, Normal limits of the electrocardiogram in a Chinese population. *J. Electrocardiol.*, 1989;**22**: 1–15.
12. Yang, T.F., C.Y. Chen, B.N. Chiang, and P.W. Macfarlane, Normal limits of derived vectorcardiogram in Chinese. *J. Electrocardiol.*, 1993;**26**: 97–106.
13. Downs, T.D., J. Liebman, R. Agusti, and H.C. Romberg, The statistical treatment of angular data in vectorcardiography, in

Proceedings of Long Island Jewish Hospital Symposium on Vectorcardiography, 1965, I. Hoffman and R.C. Traymore, Editors. Amsterdam: North Holland, 1966, pp. 272–278.
14. Yang, T.F. and P.W. Macfarlane, Comparison of the derived vectorcardiogram in apparently healthy Caucasians and Chinese. *Chest*, 1994;**106**: 1014–1020.
15. Draper, H.W., C.J. Peffer, F.W. Stallmann, D. Littmann, and H.V. Pipberger, The corrected orthogonal electrocardiogram and vectorcardiogram in 510 normal men (Frank lead system). *Circulation*, 1964;**30**: 853–864.
16. Nemati, M., J.T. Doyle, D. McCaughan, R.A. Dunn, and H.V. Pipberger, The orthogonal electrocardiogram in normal women. Implications of sex differences in diagnostic electrocardiography. *Am. Heart J.*, 1978;**95**: 12–21.
17. Namin, E.P., R.A. Arcilla, I.A. D'Cruz, and B.M. Gasul, Evaluation of the Frank vectorcardiogram in normal infants. *Am. J. Cardiol.*, 1964;**13**: 757.
18. Huwez, F.U., S.D. Pringle, and P.W. Macfarlane, A new classification of left ventricular geometry in patients with cardiac disease based on M-mode echocardiography. *Am. J. Cardiol.*, 1992;**70**: 681–688.
19. Kannel, W.B., Prevalence and natural history of electrocardiographic left ventricular hypertrophy. *Am. J. Med.*, 1983;**75**(Suppl. 3A): 4–11.
20. Macfarlane, P.W., British Regional Heart Study: The electrocardiogram and risk of myocardial infarction on follow-up. *J. Electrocardiol.*, 1987;**20**(Suppl.): 53–56.
21. Chou, T. and R.A. Helm, The pseudo P pulmonale. *Circulation*, 1965;**32**: 96–105.
22. Huwez, F.U., *Electrocardiography of the Left Ventricle in Coronary Artery Disease and Hypertrophy*, Ph.D. thesis. University of Glasgow, 1990.
23. Gottdiener, J.S., J.A. Gay, B.J. Maron, and R.D. Fletcher, Increased right ventricular wall thickness in left ventricular pressure overload: Echocardiographic determination of hypertrophic response of the 'non-stressed' ventricle. *J. Am. Coll. Cardiol.*, 1985;**6**: 550–555.
24. Brohet, C.R., Special value of the vectorcardiogram in pediatric cardiology. *J. Electrocardiol.*, 1990;**23**(Suppl.): 58–62.
25. American College of Cardiology, Tenth Bethesda conference report on optimal electrocardiology. *Am. J. Cardiol.*, 1978;**41**: 111–191.
26. Selvester, R.H. and M.E. Sanmarco, Infarct size in hi-gain hi-fidelity VCG's and serial ventriculograms in patients withproven coronary artery disease, in *Modern Electrocardiology*, Z Antoloczy, Editor. Amsterdam: Excerpta Medica, 1978, pp. 523–528.
27. Selvester, R.H., H.B. Rubin, J.A. Hamlin, and W.W. Pote, New quantitative vectorcardiographic criteria for the detection of unsuspected myocardial infarction in diabetics. *Am. Heart J.*, 1968;**75**: 335–348.
28. Edenbrandt, L., A. Ek, B. Lundh, and O. Pahlm, Vectorcardiographic bites. A method for detection and quantification applied on a normal material. *J. Electrocardiol.*, 1989;**22**: 325–331.
29. Macfarlane, P.W. and T.D.V. Lawrie, The normal electrocardiogram and vectorcardiogram, in *Comprehensive Electrocardiology*, Vol. 1, P.W. Macfarlane and T.D.V. Lawrie, Editors. Oxford: Pergamon Press, 1989, pp. 407–457.
30. Demoulin, J.C. and H.E. Kulbertus, Histopathological examination of the concept of left hemiblock. *Br. Heart J.*, 1972;**34**: 807–814.
31. van Dam, R.Th., Ventricular activation in human and canine bundle branch block, in *The Conduction System of the Heart*, H.J.J. Wellens, K.I. Lie, and M.J. Janse, Editors. Leiden: Stenfert Kroese, 1976, pp. 377–392.
32. Pryor, R. and S.G. Blount, The clinical significance of true left axis deviation. *Am. Heart J.*, 1966;**72**: 391–413.
33. Rosenbaum, B.M., The hemiblocks: Diagnostic criteria and clinical significance. *Mod. Concepts Cardiovasc. Dis.*, 1970;**39**: 141–146.
34. Pryor, R., Fascicular blocks and the bilateral bundle branch block syndrome. *Am. Heart J.*, 1972;**83**: 441.
35. Kulbertus, H.E., P. Collignon, and L. Humblet, Vectorcardiographic study of the QRS loop in patients with left anterior focal block. *Am. Heart J.*, 1970;**79**: 293–304.
36. Lopes, M.G., *Seminar in Vectorcardiography*, Stanford, CA: Stanford University Press, 1974.
37. Wolff, L., J. Parkinson, P.D. White, Bundle-branch block with short P–R interval in healthy young people prone to paroxysmal tachycardia. *Am. Heart J.*, 1930;**5**: 685–704.
38. Havelda, C.L.J., G.S. Sohi, N.C. Flowers, and L.G. Horan, The pathologic correlates of the electrocardiogram: Complete left bundle branch block. *Circulation*, 1982;**65**: 445–451.
39. Milliken, J.A., Isolated and complicated left anterior fascicular block: A review of suggested electrocardiographic criteria. *J. Electrocardiol.*, 1983;**16**: 199–211.

44 Magnetocardiography

Markku Mäkijärvi · Petri Korhonen · Raija Jurkko · Heikki Väänänen · Pentti Siltanen · Helena Hänninen

P. W. Macfarlane, A. van Oosterom, O. Pahlm, P. Kligfield, M. Janse, J. Camm (eds.), *Comprehensive Electrocardiology*, DOI 10.1007/978-1-84882-046-3_44,

44.1 Introduction

Although magnetocardiography (MCG) was first introduced in the early 1960s, it mainly remained as an experimental method practiced by engineers in research laboratories until the 1990s [1]. Today, it has developed into one of the new technologies in cardiology employed by medical doctors in several clinical laboratories. MCG still poses technical challenges, such as the instrumentation based on the use of liquid helium and the need for magnetically shielded rooms (MSR), but the clinical application of the method has significantly benefited from the availability of modern multichannel instrumentation in hospitals at the patient's bedside. In addition, the signal-to-noise ratio in routine MCG recordings is comparable to the best of electrical measurements. MCG studies provide online results quickly, and many groups are collecting libraries of reference data. Profound efforts in the direction of standardization and data comparability are also on the way.

There are several applications in which MCG has already provided clinically useful results. For example, an MCG can diagnose and localize acute myocardial infarction, separate myocardial infarction patients with and without susceptibility to malignant ventricular arrhythmias, detect ventricular hypertrophy and rejection after heart transplantation, localize the site of ventricular preexcitation and many types of cardiac arrhythmia, and can also reveal fetal arrhythmias and conduction disturbances [2].

In addition, several other clinical applications of MCG have recently been studied: detection and risk stratification of cardiomyopathies (dilated, hypertrophic, arrhythmogenic, and diabetic), risk stratification after idiopathic ventricular fibrillation, detection and localization of myocardial viability, and the follow-up of fetal growth and neural integrity. Some studies have clearly indicated that MCG is very sensitive to the changes of repolarization, for example, after myocardial infarction or in a hereditary long-QT syndrome [3].

In this review, we briefly overview the development in instrumentation, measurement techniques, data analysis, and the clinical aspects of MCG during the last few years and present a perspective for the near future.

44.2 Sources of MCG

44.2.1 Origin of Measured Magnetic Field

The biomagnetic fields are generated by the same bioelectric activity that generates electric potentials as discussed in Vol. 1. The ion pumps on the cell membrane and the diffusion gradients impress the flow of the charged ions (such as Na^+, K^+, and Ca^{2+}) in the myocardium. These ionic currents inside and in the vicinity of excited cells are called primary current density J_p [4]. The primary current causes changes of the electric potential ϕ, which in turn creates ohmic volume currents $J_V = -\sigma\nabla\phi$, where σ is the electric conductivity. The magnetic field of total current $J_T = J_p + J_V$ can then be solved by Maxwell's equations or in quasistatic approximation from the Biot–Savart law $dB = \frac{\mu_0}{4\pi}\frac{dJ\times r}{r^3}$, where the dB is the magnetic field from the differential current dJ in relative position r. By integrating the overall current density, we obtain the magnetic field B. The resulting magnetic field from all the cardiac activity is in the range of pT, below one millionth of the earth's magnetic field (30–60 μT).

44.2.2 Forward Problem

The calculation of the external magnetic field from the known cardiac currents, the *forward problem*, has similar properties to those of the forward problem in ECG. Analytically, the forward problem in a homogeneous volume conductor can be solved with only some simple geometry. Therefore, numerical methods are used in the calculations. In the boundary-element method (BEM), an analytical equation is discretized to linear matrix equations [5, 6], which can be extended to the torso models. In the finite element model (FEM), the anisotropic properties of the material can also be included in the calculations. As with the electric forward problem, realistic torso models are needed for accurate results. However, the magnetic field is not as sensitive for material properties of the torso as the electric potential, so the requirement for the model is not quite as strict. Interestingly, preliminary results for estimating the heart outline based only on MCG mapping have also been presented [7].

44.2.3 Inverse Problem

The biomagnetic inverse problem is ill-posed and has no unique solution even if the body surface potential mapping is combined with magnetic measurements. Therefore, different equivalent source models have to be used. The equivalent current dipole (ECD) is the most elementary source of magnetic fields and can be defined as $q = \int_V J_p(r)\mathrm{d}V$. Higher order equivalent generators, such as quadrupoles and octupoles, have also been presented by using multipole expansions [8]. Accuracies of 5–25 mm have been reported for best-fitting ECDs [9].

44.2.4 Inverse Problem with Distributed Source Model

To solve the inverse problem with a distributed source model like equivalent current density or uniform double-layer, a number of individual current dipoles are usually derived with the help of the lead field theory. The ill-posed problem of the lead field matrices requires the use of different regularization techniques for stabilizing the result. In addition to single-layer as well as double-layer sources, lead fields from each point on both the endocardial and epicardial surfaces, together with bidomain models for estimating the propagating wave front, are used [10, 11].

44.2.5 MCG vs ECG

Since the magnetocardiogram is generated by the same activity that generates the ECG, the signal waveforms corresponding to the P-, QRS-, and T-waves of the ECG are also seen in the magnetocardiogram. However, the differences in the information content between the MCG and ECG are still quite controversial; it can be shown that in an infinite and homogeneous volume conductor, J_V does not contribute to the magnetic field or electric potential which are independent of each other. In a homogeneous, semi-infinite volume conductor, all the magnetic field outside the conductor arises from the tangential current sources, while the ECG in general is more sensitive to the radial currents. In practice, due to torso inhomogeneities, conductivity differences, and anisotropy, the difference between the MCG and ECG is not that apparent. However, the sensitivity of MCG to the vortex currents seems also in practice to be remarkably different; an ideal vortex current does not produce any electric field outside the body [12]. The MCG has also been reported to be more sensitive to repolarization currents since it is not disturbed by electrode-skin potential, for example, distinguishing a real ST shift from an artifactual ST shift is possible [13]. As already discussed, the MCG is less affected by the torso inhomogeneities than the ECG, which is an advance, especially in inverse modeling. The measurement instrumentation where all the sensor localizations are always in the same relative positions to each other is also an advance, especially if the combination of measurement and torso coordinate systems is done correctly.

44.3 Measurement Technique and Instrumentation

44.3.1 History of MCG

The cardiac magnetic field was first measured by Baule and McFee [14] using a coil magnetometer. In 1970, D. Cohen et al. [15] introduced the superconducting quantum interference device (SQUID) for MCG, and 1 year after that, Zimmerman and Frederic [16] introduced a gradiometer that made MCG recording in an unshielded environment possible. In 1973 came the first modeling study [5]. Multichannel whole-thorax systems were introduced in the early 1990s, and high-Tc (high-temperature) superconductors appeared a few years later.

44.3.2 General

The DC-SQUID sensors offer the best sensitivity for MCG measurements. The strong environmental magnetic noise, unavoidable at urban hospitals and laboratories, makes the detection of biomagnetic signals impossible without special

techniques for environmental interference suppression: The environmental magnetic noise is reduced by MSRs, which typically consist of a combination of μ-metal and eddy current shields. In addition, gradiometer coils are used to diminish residual magnetic noise within the shields. Alternatively, high-order gradiometers can be utilized if no magnetic shielding is employed.

44.3.3 Measurement System – Torso Position

The position of the subject's thorax with respect to the sensor array can be determined, for example, by using special marker coils attached to the skin. The positions of these coils are determined by a 3D digitizer before the measurement (in torso coordinates), and from the MCG recordings (in device coordinates) when electric current is fed to the coils. A typical measurement setup is seen in Fig. 44.1.

44.3.4 Low-Temperature and High-Temperature Sensors

The SQUID sensors are commonly classified as low-temperature SQUID sensors (LTS), which operate at the temperature of liquid helium or as high-temperature SQUID sensors (HTS) operating at liquid nitrogen temperatures. LTS are more commonly used. They are easier to manufacture and have less noise. On the other hand, cooling with liquid nitrogen is much less expensive than with liquid helium, and the cryogenic dewars for HTS are easier to manufacture.

44.3.5 Different Systems: Sensors

Most of the MCG systems have planar sensor loops, which detect the Z-component of the magnetic field, that is, the component directed toward the measurement system. Instead of measuring the magnitude of the magnetic field, the axial and planar field gradients are measured in some systems. Magnetometer sensors have the highest sensitivity for nearby and far-field sources. Thus, selecting a gradiometer with proper distance between the SQUID sensors reduces the amount of unwanted external noise components. The gradients are realized with wire-wound or bonded two or three gradiometers or by electronically combining several reference coils to one measurement coil. Therefore, it should be noted

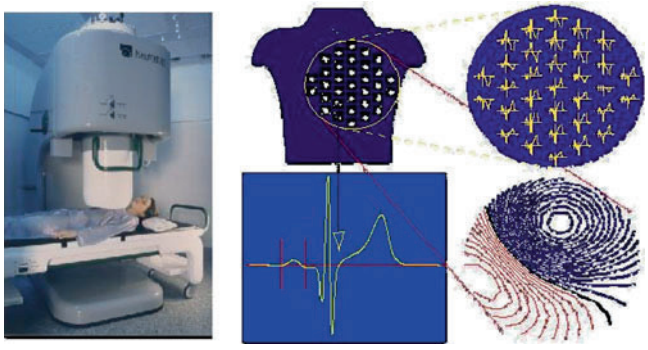

Figure 44.1

***Left*: MCG recording with 99-channel magnetocardiometer at 33- location (BioMag Laboratory, Helsinki, Finland). *Right*: The sensor arrangement in the cardiomagnetometer and an example of signal measured during 1 s and magnetic isofield integral map over atrial complex.**

that even one channel system may well contain nine SQUID sensors, and the 304-SQUID system may sample only at 57 sites. Hence, the measured number of channels does not necessarily tell everything about the effective dimension of the mapping. In some systems, gradients are also implemented with software from the separate magnetometer signals, and for multi-lead mappings also, many complex software noise cancellations are used (see below).

In addition to systems measuring only the Z-component of the field, there are also systems sensing only tangential fields or all three orthogonal vector component magnetometers. In quasistatic approximation ($\nabla \times B = 0$), it is directly seen that $\partial B_z/\partial x = \partial B_x/\partial z$, and so the tangential field gradients can be derived from the tangential gradients of the B_z.

44.3.6 Different Systems: Two Trends

Nowadays, the development of new MCG systems can be divided into two main trends: The "high-end," multichannel and high sensitivity systems mainly for research work and the "budget-priced" systems without MSRs for clinical use [17]. The lower cost systems bring MCG closer to the everyday clinical work. With efficient signal processing techniques, they can be used for single channel studies, but for mapping studies with these single or "quasi single" channel systems (seven or nine channel systems) several different measurements over certain sampling points are needed. Problems include the fact that scanning of the grid is very time-consuming, and the resulting measurement is not truly simultaneous although after averaging, signals should be time invariant. In high-end systems, more than 300 sensors are read simultaneously with a very high signal-to-noise ratio. Table 44.1 shows examples of different MCG systems with and without an MSR.

44.3.7 Different Systems: Need for Standardization

One of the problems with MCG studies is related to the number of systems with different sensor geometries, different sensor types, and different signal-to-noise ratios, which make multicenter studies difficult. In addition, the digital preprocessing of the measured signals varies. There are also problems with comparing the results obtained with different systems. Some standardization has been proposed several times including a proposal that was presented in the previous version of this book [1], but due to the huge variation of the systems in use, standardization has not been fully implemented.

Table 44.1
Examples of different MCG systems

Name	Type	Number of channels	Dewar diameter (cm)
Siemens Krenikon	Shielded, multichannel	37 axial gradiometers	19
Philips	Shielded, multichannel	2*31 axial gradiometers	13.5 + 13.5
PTB Berlin	Shielded, multichannel	63 electronical gradiometers + 20 reference	21
4-D Neuroimaging (Bti) Magnes	Shielded, multichannel	61 magnetometers	32.4
(Neuromag) VectorView	Shielded, multichannel	33 magnetometers, 66 planar gradiometers	30
AtB Argos	Shielded, multichannel	Vector-magnetometers	23
Hitachi	Shielded, multichannel	64 planar gradiometers	20
Cardiomag Imaging	Unshielded	9 + second-order axial gradiometers + three vectorial reference channels	
SQUID AG	Unshielded	4 + second-order axial gradiometers + 3 reference	
Jena (FSU)	HTS, unshielded	Two planar gradiometers	
Hitachi	HTS, open-ended shielding	16	

44.4 Digital Signal Processing

44.4.1 Preprocessing

44.4.1.1 Mapping Versus Multi-Lead Analysis

All signal processing meant for improving the signal quality, removing noise, and artifacts is hereinafter called "preprocessing." The preprocessing part, just as in the actual signal analysis and the calculation of the different measures, is further divided into mapping and multichannel methods. Mapping includes methods that utilize the spatial information on measurement channels, as the multichannel methods process one channel at a time and utilize the temporal information.

44.4.1.2 Order of Signal Processing

First, noise suppression preprocessing, can be divided into different phases. Selected map analysis may utilize methods like signal-space projection (SSP), signal-space separation (SSS), independent component analysis (ICA), filtering, baseline removal, and perhaps averaging. Sometimes filtering can be undertaken before the map-operator. The data conversion is usually made on the corrected signal. Then after possible conversion, the measures (markers) are calculated.

44.4.1.3 Signal-Space Projection

There are several different methods for noise suppression: The signal-space projection (SSP) method is based on defining a noise subspace from an empty room measurement and projecting the measured multichannel signal to the signal space orthogonal to the noise subspace [18]. A similar principle is also utilized in the "eigenvector-based spatial filtering of fetal biomagnetic signals," for example [19], where the fetal signal is extracted on the basis of projecting the data to the space that maximizes the fetal and maternal eigenvector ratio.

44.4.1.4 Signal-Space Separation

Signal-space separation (SSS) is based on mathematical separation of the signal sources to the cardiac sources that are inside a predefined subspace in normal space (a ball around the heart) and outside sources. After separating sources, the signal consisting only of cardiac activity can be formed. This method can also be used together with signal conversion to the different measurement geometry or for interpolating the poor quality channels [20].

44.4.1.5 Independent Component Analysis

Independent component analysis (ICA) is a method for the blind separation of linearly mixed signals. The assumptions in the method are that the number of mixed signals is, at a maximum, the number of measured signals. Mixed signals are non-Gaussian and linearly mixed, which in practice means that their sources are spatially separable. The most commonly used algorithm was presented by Hyvärinen [21]. The actual ICA algorithm is only a part of the solution as the algorithm separates the signals blindly, which means that the wanted and the unwanted signal components have to be somehow selected. The algorithm also loses the amplitude scaling of the signal, which has to be corrected afterwards. An automatic use of ICA for separating the fetal signal from the maternal signal was presented by Comani et al. [22].

44.4.1.6 One-Channel Digital Noise Suppression

In addition to signal processing in the mapping methods described above, preprocessing methods for individual MCG channels are used. The algorithms are similar to those used with ECG channels, where signals are band-pass filtered with finite (FIR) and infinite response filters (IIR). The 50 or 60 Hz powerline interference is filtered with different adaptive notch filters. Wavelet transforms are also used [23]. Low-frequency noise, such as baseline wander, is corrected with polynomial fits to the isofield (isopotential in ECG) intervals and signals are averaged. In fetal MCG, the maternal signal average is also used for separating the fetal and maternal signals.

44.4.1.7 Conversion Between Sensor Arrays

A separate part of preprocessing is the conversion between sensor arrays. There are several different MCG systems. Sensor locations and types vary. However, since there are many different systems, the comparison of the results is difficult. For that reason, different signal conversions based on multipole and minimum normal estimates have been proposed [24, 25]. In one of these studies [24], where the conversion from measurements was done with one multichannel MCG system to another, the reconstruction succeeded with 93–95% agreement. However, the overall accepted standard system for conversion is still missing.

44.5 Signal Analysis

44.5.1 MCG Morphology Analysis

Signal processing of individual MCG channels resembles that of an ECG lead. Often only scaling constants in algorithms for waveform detection are different. Markers derived from the MCG signal morphology are also very similar to those from the ECG, namely signal amplitudes (e.g., ST level), filtered signal amplitudes (e.g., late field/potential analysis), time intervals (e.g., QT interval), spectral characteristics (e.g., fragmentation index), etc.

44.5.2 MCG Mapping Analysis

The MCG mapping markers include mapping orientations (min-max, +−, centers of gravity, and maximum field gradient) of different time instants or time intervals of the signal (QT orientation, T-wave orientation, and ST orientation) and different markers representing spatial heterogeneity (nondipolar content of QRS, STT, QRST, QT-dispersion). Also, different spatiotemporal measures (ST, T-wave orientation, and heart rate dependency) and different source modeling parameterizations have been used.

44.5.3 Visualizations

Typically, the MCG data is visualized either as temporal time traces, like an ECG trace, from one or all the measurement channels, or with different isovalue maps from one time instant or from some defined marker (e.g., integral) from each channel (see Fig. 44.1). In these maps, the signal amplitude is displayed with color coding or with isocontours.

Another commonly used way for displaying the mapping information is the current arrow map, where pseudo current at each measurement location, derived from $dB_Z/dyx + dB_Z/dxy$ (**x** and **y** being unit vectors) is represented by a vector showing the amplitude (length of the arrow) and direction of the current at that location (Fig. 44.1). This current arrow map can also be projected onto a 3D model of the heart surface.

44.5.4 Experimental MCG

Experimental work utilizing MCG techniques began more than 30 years ago [26]. As a fully contactless method, MCG is ideal for noninvasive cardiac mapping of small experimental animals, for example.

MCG has also been used to detect reentry currents in cardiac flutter and fibrillation. The magnetic field produced by induced atrial flutter has been measured in isolated rabbit hearts. A moving dipole model was proposed to analyze the experimental data and to locate the reentry path [27].

In another newer study, acute myocardial infarction was induced by ligation of the left anterior descending coronary artery in a dog model. Magnetic field maps of early reperfused myocardium showed spatio-temporal field distributions consistent with anterior myocardial infarction. The use of super-paramagnetic contrast agents increased the sensitivity of standard MCG and may have an important implication for MCG in the assessment of regional myocardial ischemia, infarction, and perfusion [28].

A recent study was able to show that MCG mapping can detect age-related changes in cardiac intervals and in maps having significantly longer QTe, JTe, and T peak-Te intervals (Te = T end) in older Wistar rats. As compared to ECG recordings, MCG methodology simplified reproducible multisite noninvasive cardiac mapping of ventricular repolarization in an experimental setting [29].

44.6 Localization of Preexcitation and Cardiac Arrhythmias by Magnetocardiographic Mapping

The clinical accuracy of the MCG method has been tested by localizing the site of earliest ventricular activation during preexcitation in Wolff–Parkinson–White syndrome patients. The clinical reference has been obtained either during endocardial catheter mapping, or from successful catheter or surgical ablation of the accessory pathway. The results of the earlier studies showed that the MCG method was accurate enough for localization of cardiac electric sources for clinical purposes [30, 31]. The methodological localization accuracy of the MCG mapping has also been confirmed to be quite good [32].

In a newer study, 28 patients with Wolff–Parkinson–White syndrome were examined by MCG mapping and imaging techniques and with the five most recent accessory pathway localization ECG algorithms. ECD, effective magnetic dipole, and distributed-current imaging models were used for the inverse solution. MCG classification of preexcitation was found to be more accurate than that of ECG algorithms, and also provided additional information for the identification of paraseptal pathways and the existence of multiple accessory pathways [33].

By applying the completely noninvasive techniques of MCG and magnetic resonance imaging (MRI), it has been shown to be possible to define different origins of right ventricular ectopic beats in a complex heart model of nonischemic cardiomyopathy of 84 patients with surgically repaired Tetralogy of Fallot [34].

Postmyocardial infarction patients were investigated with cardiac MRI and signal-averaged 62-lead MCG. Three of six patients were suffering from sustained ventricular tachycardia (VT). A close matching of the low current density areas based on the QRS complexes and the high current density areas based on the late field signals were found. In three patients, the premature ventricular complexes morphologically resembling the clinical VT were localized close to the exit sites of these arrhythmias. The authors concluded that the MCG was useful in steering catheter ablation and coronary revascularization therapies [35].

An MCG was recorded pre- and post interventional therapy in three patients with atrial flutter and four patients with atrial fibrillation (AF), and in 20 healthy volunteers. The serial conduction pathway of the QRS segment was superimposed on a 3D heart outline generated by a magnetic field and verified by the silhouette on the magnetic resonance (MR) images. The MCG revealed a counterclockwise rotation of the atrial conduction in patients with atrial flutter, and random microreentry in the cases of AF [7]. An example of MCG localization in a patient suffering from continuous atrial tachycardia is presented in Fig. 44.2.

In conclusion, MCG has been used for localization of other sources of cardiac arrhythmias, such as the site of origin of tachycardias and extrasystoles, as well as for localization of a cardiac pacing catheter. The localization accuracies for a pacing catheter have been reported to be <1.0 cm, for extrasystoles 0.5–2.0 cm, and for tachycardias accuracy is more variable at 1.6–4.0 cm. In particular, the results in localizing a pacing catheter and the accessory pathway in preexcitation

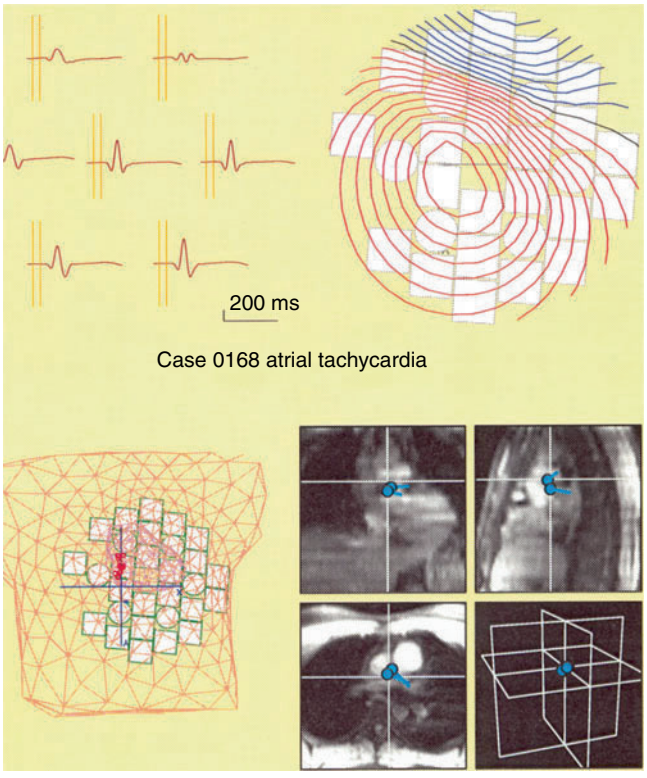

Figure 44.2

An example of MCG localization in a patient suffering from incessant atrial tachycardia. The integration of the MCG and MRI results was performed using electromagnetically localized MR positive fish-oil capsules. Invasive electrophysiologic study and successful catheter ablation confirmed the localization of the tachycardia focus in the intra-atrial septum. *Upper left panel*: time interval during the P-wave used for analysis. *Upper right panel*: magnetic field morphology relative to the sensors. *Lower left panel*: location of the tachycardia (*red dots*) relative to torso and sensors. *Lower right panel*: MCG localization of the tachycardia focus (*blue dots*) integrated to MR images.

confirm the good localization capability of the MCG method. The main obstacles in clinical cardiac source localization by MCG are the inherent problems concerning the clinical and imaging reference data integration.

44.7 Fetal Magnetocardiography

The fetal magnetocardiogram (FMCG) can be reliably recorded from approximately the 15th week of gestation onwards. The FMCG has the ability to accurately record cardiac time intervals, and to provide a real-time recording that reflects cardiac electrical activity. The FMCG has been demonstrated to be able to diagnose different types of atrioventricular conduction defects, paroxysmal supraventricular tachycardia, and repolarization abnormalities especially after 20 weeks of gestation. Standardization of the recording, signal processing, and measurement techniques has resulted in data that is reproducible, and when combined with normal values for different gestational ages, they can be of clinical value [36, 37].

In a study of 102 low-risk pregnant women, at the 20th to 42th gestational week, the fetal MCG provided a significant advantage via the technology available for recording the antenatal fetal heart. In the unaveraged recordings, the QRS complex was successfully detected in 68 cases (67%). Of those 68 traces, a P-wave was detected in 51 (77%) and a T-wave in 49 (72%) of the traces, using off-line signal-averaging techniques. Although good quality traces were obtained throughout the range of gestational ages, in general it was more difficult below 28 weeks. The QRS duration was found to increase

significantly with increasing gestation [38]. In another study, various parameters concerning the electrical excitation of the heart, such as AV conduction, repolarization period, and morphology of the QRS complex, could be determined, leading to a more profound analysis of fetal arrhythmias [39].

Distinct patterns of initiation and termination of paroxysmal SVT have been detected using the MCG [40] as well such phenomena as Wolff–Parkinson–White syndrome, QRS aberrancy, and multiple reentrant pathways. A strong association between fetal trunk movement and the initiation and termination of SVT, suggesting autonomic influences, was also found.

The ability of the FMCG to reveal conduction system disease was evaluated in 702 fetuses initially referred on account of an arrhythmia. Altogether 306 had an irregular rhythm confirmed using either FMCG or postnatal 12-lead ECG. Eight (2.6%) had intermittent first- or second-degree AV block confirmed by FMCG and/or postnatal 12-lead ECG. Cases with conduction block may benefit from transplacental therapy with dexamethasone [41]. This method provides additional information concerning the effect of congenital heart disease (CHD) on the cardiac conduction system. As in the neonate, the FMCG changes do not reflect the severity of CHD. Indeed, the FMCG cannot serve as a primary diagnostic tool in the case of CHD for which echocardiography is more helpful.

Repolarization abnormalities in fetal heart can also be detected with the MCG during gestation. In one study, two patients were evaluated because of sustained fetal bradycardia, the diagnosis of QT-prolongation was made at the 29th and at the 35th gestational week. In both newborns, the QT-prolongation was confirmed by the postpartal ECG [42].

In general, good agreement of the magnetocardiograms and cardiac findings in newborns has been documented in a study investigating 189 fetal MCGs in 63 pregnant women between the 13th and the 42th week of pregnancy. In 16 recordings before the 20th gestational week, the signal strength was too weak to permit evaluation. Brief episodes of bradycardia, isolated supraventricular and ventricular premature beats, bigeminy and trigeminy, sinoatrial block, and atrioventricular conduction delays were found [43].

It has been suggested that the MCG can be used for noninvasive evaluation of hypertrophy of the fetal heart. In uncomplicated pregnancies, the magnitude of the MCG current dipole correlates with the gestational age, whereas in fetuses with cardiomegaly, the magnitude of the current dipole has been higher, reflecting the increased myocardial mass confirmed by ultrasound [44].

FMCG has shown that fetal P-wave and QRS complex durations increase with gestational age, reflecting a change in the cardiac muscle mass. A total of 230 FMCGs were obtained in 47 healthy fetuses between the 15th and 42nd week of gestation. The authors concluded that, from approximately the 18th week to term, fetal cardiac time intervals, which quantify depolarization times, can be reliably determined using MCG. The P-wave and QRS complex duration show a high dependence on age which to a large part reflects fetal growth. Gender instead, plays a role in QRS complex duration in the third trimester. ECD strength reflected gestational age slightly more reliably (r^2 = 0.93) than signal amplitude values (mean, median, maximum: r^2 = 089, 0.88, 0.85, respectively). The overall correlation of the amplitude to gestational age compared favorably with that of QRS complex duration. Fetal development is thus in part reflected in the fetal MCG and may be useful in the identification of intrauterine growth retardation [45, 46].

In conclusion, FMCG allows an insight into the electrophysiological aspects of the fetal heart, is accurate in the classification of fetal arrhythmias, and shows potential as a tool in defining a population at risk of congenital heart defects. FMCG offers unique capabilities for assessment of fetal heart rate (FHR) and fetal behavior, which are fundamental aspects of neurodevelopment. FMCG actograms are specific for fetal trunk movements, which are thought to be more important than isolated extremity movements and other small fetal movements. The ability to assess FHR, FHRV, and fetal trunk movement simultaneously makes fMCG a valuable tool for neurodevelopment research. In clinical reality, fMCG devices are still rare and a fetal arrhythmia or a congenital heart defect is in general discovered during prenatal evaluation by ultrasonography.

44.8 Arrhythmia Risk Assessment

MCG is sensitive to cardiac electrical activity of a very small amplitude and has therefore made it an interesting tool in the assessment of the risk of serious ventricular arrhythmias. The rapid development in instrumentation from single to multichannel devices capable of mapping large precordial areas has made clinical risk assessment studies possible.

In almost any structural heart disease, abnormalities in both depolarization and repolarization periods may lead to ventricular arrhythmias and sudden cardiac death. MCG studies considering ventricular arrhythmia risk assessment are still relatively few in number, with most of the data coming from postinfarction populations.

Postmortem studies in patients with postinfarction VT have revealed thin layers of surviving myocardial tissue, which might show mostly tangential currents and thus be detectable more readily by MCG than by ECG [47]. Late potentials in ECGs have been shown to be markers of delayed conduction serving as a substrate for reentrant ventricular arrhythmias. Late fields in MCG comparable to late potentials in ECGs have also been described [48]. Subsequently, late fields have shown a capability similar to that of late potentials in the discrimination of patients with and without ventricular arrhythmias after myocardial infarction [49, 50]. A few studies have applied magnetic source imaging in localization of the sources of late fields, which might be of value prior to catheter ablation or arrhythmia surgery [35].

In addition to late fields that may be detected at the end of the QRS, the abnormal delayed depolarization displays increased fragmentation of the whole magnetocardiographic QRS. The intra-QRS fragmentation method is based on finding the number of signal extrema during filtered QRS (Fig. 44.3) and by computing the sum of the amplitude differences between neighboring extrema, thus yielding the intra-QRS fragmentation score (FRA) [51]. Recently, increased intra-QRS fragmentation in the MCG registered soon after acute MI has shown promise in the identification of patients at high risk of arrhythmic events in a prognostic study of 158 patients with acute MI and left ventricular ejection fraction (LVEF) < 50%. During follow-up of 50 +/− 15 months, 32 (20%) patients died and 18 (11%) had an arrhythmic event. Increased FRA in the MCG and LVEF < 30% yielded positive and negative predictive accuracies of 50 and 91% for arrhythmic events. The ECG predicted all-cause mortality ($P < 0.05$) but not arrhythmic events [52].

The dispersion of repolarization is increasingly recognized as a major factor in the genesis of malignant ventricular arrhythmias. Preliminary data from patients with hypertension and ischemic heart disease suggest that MCG might be especially sensitive to subtle changes in the repolarization period [53, 54]. Transmural repolarization in MCG, displayed as the terminal part of the T-wave, has been the subject of arrhythmia risk assessment studies in patients with ischemic

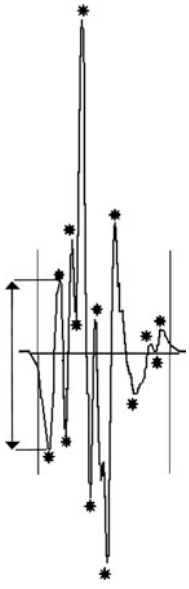

Figure 44.3

The principle of the intra-QRS fragmentation score analysis in MCG. After binomial filtering, the number of polarity changes or extrema () is computed. Next, the differences of each adjacent extrema are computed, and the differences are summed. As an example, the difference between the first and second extrema is shown with a thin arrow. Finally, the difference between the first and the last extrema is added to this sum, yielding the intra-QRS fragmentation score. The horizontal bars indicate the onset and offset of the filtered QRS.

heart disease and dilated cardiomyopathy. Patients with sustained ventricular arrhythmias showed prolonged T-wave peak to T-wave end interval as a sign of dispersion of transmural repolarization [55, 56]. In another study, nondipolar isointegral maps during the repolarization phase in postinfarction patients prone to ventricular arrhythmias were found [57]. It was suggested that the non-dipolarity might serve as a marker of increased repolarization heterogeneity.

Repolarization disparities related to idiopathic long-QT syndrome also seem to be detectable with MCG. Children with long-QT syndrome, both with and without symptoms were investigated [58]. All patients showed beat-to-beat variability in T-wave morphology. When the isofield maps during the T-wave were analyzed with eigenvectors for data reduction, the symptomatic patients displayed more disparity in their maps, suggesting more heterogeneous repolarization.

Modern multichannel devices seem to allow quick MCG registrations in the hospital environment thereby rendering it a potential tool in arrhythmia risk assessment. However, a few issues need more elucidation before the role of MCG in clinical decision making can be fully assessed. First, is there really essential information in MCG not available from the ECG? In order to evaluate this, we need risk assessment studies comparing MCG not to 12-lead ECGs but to signal-averaged ECGs (SAECGs) and body surface potential mapping equally covering large precordial areas. In addition, the MCG methodology needs to be subjected to well-designed large-scale prospective studies. Until this has been done, the role of the MCG in the assessment of the risk of ventricular arrhythmias and sudden cardiac death remains to be established.

44.8.1 AF

AF is the most prevalent clinically important rhythm disturbance. The initiating and perpetuating factors of AF may vary, and prolonged AF may lead to atrial electrical and mechanical remodeling [59–61]. The effective application of new treatments for AF calls for improved diagnostics and has also led to growing interest in noninvasive methods capable of detecting and characterizing abnormalities in atrial signals.

Subtle abnormalities in atrial electric and magnetic signals could serve as markers of foci or substrates for AF. The SAECG detects abnormalities in atrial signals in patients prone to AF. These include prolongation of atrial depolarization, abnormal frequency content, and increased spatial dispersion of atrial signal duration [62–64]. Recently, magnetocardiographic techniques have also been applied to the investigation of atrial electrophysiology and pathogenesis in AF.

44.8.1.1 Magnetocardiographic P-Wave in Patients with AF, Analyses of Non-Filter Signal and Application of High-Pass Filtering Techniques

Specific changes of the P-wave in MCG were found in a study in a total of 35 subjects, including 15 AF patients (50–70 years) with persistent AF converted to sinus rhythm and 20 healthy young men. The multichannel MCG over the anterior and posterior chest and 12-lead ECG were recorded simultaneously. Sum channels from all MCG channels and separately sums from anterior and posterior channels as well as ECG channels were created. The P-wave duration was manually measured in each sum channel. Also the homogeneity and fragmentation of MCG maps were evaluated. The P-wave was divided into four segments and the correlation between maps was calculated. All segments were compared with the first segment, and the average of these three correlations, the p-score, was used as the homogeneity factor. The fragmentation index of the P-wave was calculated as the sum of amplitude differences between two amplitude peaks multiplied by the total number of amplitude peaks in each sum channel. By MCG, the P-wave duration was longer and both correlation factor and fragmentation index were lower in patients compared to normals. Similar differences were not seen in the ECG. Differences were clearest in the sum channel of all MCG channels, for example, P-wave duration was 133 ms on average in patients versus 100 ms in controls [65].

High-pass filtering techniques have also been applied to the analysis of the atrial MCG signal. Multichannel MCG over the anterior chest and orthogonal three-lead ECGs were recorded in nine patients who had paroxysmal lone AF and in ten healthy subjects in duplicate at least 1 week apart. Data were averaged using an atrial wave template and high-pass filtered at 25, 40, and 60 Hz. Atrial signal duration with automatic detection of onset and offset and root mean square amplitudes

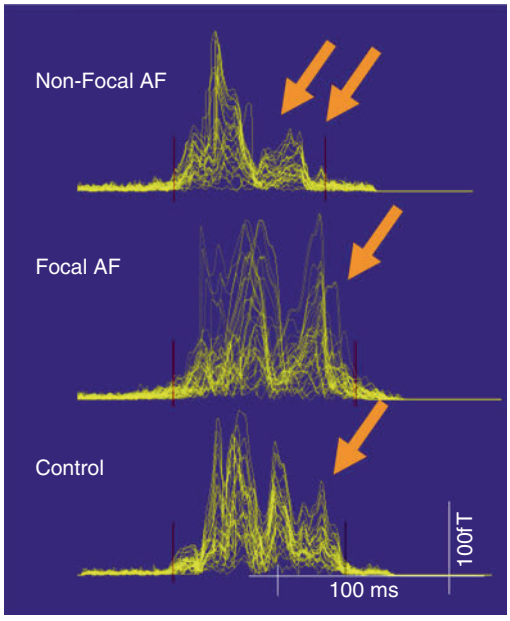

Figure 44.4

Examples of typical 40 Hz high-pass filtered atrial complex in a patient with non-focal AF, in a patient with focal AF and in a healthy subject. In the patients with focal AF, the atrial signal strength was normal also during late phase of atrial complex where the left atrium is depolarized, but in a patients not defined focal triggers late phase amplitudes were reduced. Data is expressed as superimposed display of 33 magnetometer channels.

(RMS) of the last portion of the atrial signal were determined. Reproducibility was best using a 40 Hz filter, somewhat better in MCG than in ECG and similar in patients and controls. For example, the difference between two measurements of atrial signal duration was 3.5 ms on average (coefficient of variation 3.3%) by MCG and 6.9 ms (coefficient of variation 6.1%) by ECG [66].

The atrial signal durations in MCG and SAECG were correlated, with $r = 0.64$ ($p < 0.01$). In addition, there was a correlation between RMS amplitudes of the first portion of the atrial complex in the MCG and the SAECG ($r = 0.49$, $p < 0.01$) but not in the last atrial portion ($r = 0.25$–0.30, p = NS).

In this small population comprising patients with lone paroxysmal AF, the atrial wave duration was not longer but RMS amplitudes of the last 40 ms of the atrial complex were lower in patients.

Lately, the methods have been applied in a study of 81 patients with paroxysmal lone AF and 81 matched controls. In this study, the atrial depolarization complex was slightly prolonged in patients, namely, 109 ms on average versus 106 ms. The late RMS amplitudes were reduced in a subgroup of patients with non-focal AF but were otherwise normal (Fig. 44.4). The findings are consistent with invasive measurements in focally triggered AF patients, in which only a minority of patients have shown conduction delay between or within the atria, or reduction in left atrial amplitude [67–69].

44.8.1.2 Spatial MCG Maps, Field Polarity, and Orientation during Atrial Activation and Application of Surface Gradient Methods

In another study, spatial MCG maps of 26 WPW patients were investigated [30]. Patients with AF attacks were found to have more dispersed atrial depolarization distributions compared to patients without AF. Altogether, 11/20 (55%) of the patients with AF problems were found to have more than two extrema in the atrial depolarization maps. On the other hand, 4/6 (67%) patients without AF had bipolar MCG maps. In an earlier study, multipolar MCG fields during the late

phase of atrial activation have related to left atrial overloading [70]. In a study comprising patients with lone paroxysmal AF, for example, with normal left atria, multipolarity in MCG maps (integral maps over last 20 and 50 ms) was related to lone AF [71].

Magnetic field patterns can be visualized and parameterized using pseudo-current (90 degrees rotated field gradient) amplitude and direction distributions. This method is applied in some ongoing studies focused on evaluating atrial signal propagation during sinus rhythm in patients with focally triggered paroxysmal AF and in healthy subjects [71, 72]. In a study comprising 28 patients with focally triggered paroxysmal AF and 23 controls, the magnetic field orientation during the early part of atrial depolarization was mainly to the left and downward, and was similar in patients and controls. On the other hand, during the late phase of depolarization, field orientation was more variable in both groups and differed between groups as illustrated in Fig. 44.5. The degree of maximum gradient rotation over the atrial wave was larger, and the upward orientation was more common in patients. Results showed diversity and inhomogeneity in the propagation of atrial signals especially at the late phase of activation when the left atrium was depolarizing. Findings were more pronounced in patients but some seemed to occur also in healthy atria. It was concluded that the altered depolarization front may represent a conduction defect in the left atrium, and that this may be a normal variant facilitating the manifestation of AF in the presence of focal triggers.

In another study, MCG field patterns derived by the pseudo-current method were compared to invasive electroanatomic activation maps (EAM) obtained from patients undergoing catheter ablation treatment with prior AF. The orientation of the magnetic fields during the first 30 ms of atrial depolarization representing RA activation, and during early (40-70 ms from P onset) and later part (last 50%) of LA depolarization was determined. The mean of the angles of the top 30% of the strongest pseudocurrents was used, zero angle direction pointing from subject's right to left and positive clockwise. Breakthrough of electrical activation to LA occurred through Bachmann bundle (BB) in 14, margin of fossa ovalis (FO) in 3, coronary sinus ostial region (CS) in 2, and their combinations in 10 cases by invasive reference in total of 29 different P-waves. The pseudocurrent direction in MCG maps over the first 30 ms of atrial complex was mostly leftward down, with a mean angle of 43° (CSD 28°). Over the time interval of 40–70 ms from the onset of the atrial complex, the mean angle was 39° (CSD 30°). Over the time interval of last 50% of atrial complex, the mean angle was 3° (CSD 51°).

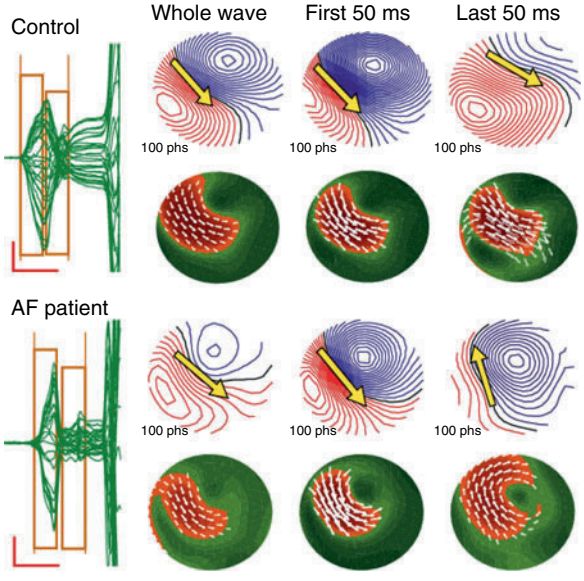

Figure 44.5

An example of orientation of magnetic fields during atrial depolarization from one healthy control (*upper rows*) and one patient with focally triggered lone AF (*lower rows*) performed as isofield integral maps (*rows 1 and 3*) and as pseudo-current maps (*rows 2 and 4*).

In the applied time interval the MCG pseudo-current angle corresponded the direction of propagation in EAM. When both the early and late LA MCG maps were viewed together, three types of combinations emerged: Type 1 with both maps showing pseudocurrent orientation leftward down, Type 2 with the map over the 40–70 ms orienting leftward down and the map over last 50% of atrial signal orienting leftward up, and Type 3 with both maps orienting leftward up. The three MCG atrial wave types correctly identified the LA breakthrough sites to BB, CS, FO, or their combinations in 27 of 29 (93%) cases [73].

Later on the method was applied in a population comprising 107 patients with lone paroxysmal AF (age 45 ± 12 years) and 94 controls. The Pd was longer in AF patients than in controls (112 ± 13 vs. 104 ± 13; $p < 0.001$), which was most obvious in Type 1 wave (109 ± 12 vs. 102 ± 11 ms, $p = 0.003$). The distribution of the atrial wave types differed between AF patients and controls: Type 1 occurred in 67% and Type 2 in 20% of controls whereas Type 1 occurred in 54% and Type 2 in 42% of AF patients, $p < 0.01$ for difference. Accordingly susceptibility to paroxysmal lone AF is associated with propagation of atrial signal to LA via margin of fossa ovalis or multiple pathways. When conduction occurs via Bachmann bundle, it is related with prolonged atrial activation. Thus altered and alternative conduction pathways may contribute to pathogenesis of lone AF [74].

44.8.1.3 Analyses of Atrial Signals during AF

The adaptation of QRS subtraction techniques and time frequency analysis has revealed the diagnosis of partial atrial standstill in an adult [75] and diagnosis of atrial flutter and AF in fetuses [76]. Now there are also ongoing studies designed to test the diagnostic performance of MCG mapping to separate clinical subgroups of AF, such as focal AF, by analyzing the atrial signal and its time domain as well as its spatial distribution during AF.

In conclusion, the effective application of new treatments for AF calls for improved diagnostics and has also led to a growing interest in noninvasive methods capable of detecting and characterizing abnormalities in atrial signals. The first applications of magnetocardiographic techniques to investigate atrial electrophysiology and pathogenesis in AF have presented extra dipoles in magnetic field maps during the last portion of the atrial depolarization signal in WPW patients with paroxysmal AF and in lone paroxysmal AF. Other abnormal features are altered field orientation during the late phase of atrial activation particularly in focally triggered lone AF, and reduced atrial signal amplitudes in AF patients without demonstrable focal triggers. In patients with persistent AF converted to sinus rhythm, prolongation and increased fragmentation of the atrial signal have been detected. Overall, abnormalities seem to be more pronounced in the late phase of the atrial complex corresponding to the depolarization of the left atrium. The diversity and inhomogeneity of propagation throughout the atrial signal seem to vary in different AF cohorts.

Currently, the patient series are still small, and further investigation is warranted before the real value of MCG in the clinical assessment of AF can be evaluated. However, MCG mapping techniques seem to be capable of noninvasively detecting abnormalities in the atrial activation sequences common in AF, even when the standard ECG is normal. It also seems that the MCG method may be applied to the study of pathophysiologic processes in AF and may identify subsets of patients with different underlying mechanisms for AF. Improved diagnostics could guide the selection of new treatment modalities, for example, catheter ablation or pharmacological treatment of AF.

44.9 Myocardial Ischemia and viability

One of the most interesting areas in clinical MCG is the detection and characterization of myocardial ischemia and viability. So far, few studies have been reported in this field, but the results are very encouraging. A new and accurate noninvasive method for recognition of acute and chronic ischemia could have important clinical applications, especially because therapeutic interventions for rapid and effective revascularization, such as percutaneous coronary interventions, are widely available.

It has been stated that some changes of the ST-segment could be explained by the ability of the MCG to detect DC currents, thus being more sensitive to ST changes than ECG or body surface mapping [53, 77–79]. In addition, the results of the equivalent dipole calculation during cardiac depolarization and repolarization has enabled the separation of patients with coronary artery disease from healthy controls [80].

The magnetic field orientation at rest has been proposed to separate coronary artery disease patients from healthy controls, with more prominent changes in the field orientation in severe disease. The magnetic field orientation is the angle between the line joining the field extrema and the right-left line of the torso [81]. In some studies, a semiautomatic surface gradient method helped to define the magnetic field orientation as the orientation of the maximum spatial field gradient, and this has been shown to separate both single-vessel and triple-vessel coronary artery disease patients from healthy controls during exercise-induced ischemia [82, 83]. Later, a method for heart rate adjustment of the magnetic field orientation during the recovery phase of exercise stress testing, which further improved ischemia detection, was developed [84].

The ST-segment depression and ST-segment slope, used in 12-lead ECG as ischemia parameters, can also detect ischemia in MCG. The ischemia-induced ST-depression takes place over the lower middle anterior thorax, and the reciprocal ST-elevation over the left anterior shoulder, locations orthogonal to those found in body surface potential mapping. The most prominent T-wave changes were found in patients with inferior ischemia and in patients with a history of myocardial infarction (Fig. 44.6) [83, 85]. The ratio of the ST-T and QRS isointegral maxima has been reported to be reduced in coronary artery disease patients compared to healthy controls [86].

A few smaller studies have been designed to test the diagnostic performance of MCG mapping in detecting and localizing areas of hibernating myocardium. The viability of the myocardium has been first confirmed by a full set of other diagnostic tests: exercise ECG, thallium stress test, dobutamine MRI, and positron emission tomography (PET). Preliminary results look promising, but there are still some problems concerning the modeling of chronic ischemia. Both the MCG and the ECG showed a significant elevation or depression of the ST-segment during exercise-induced ischemia when they were investigated using a nonmagnetic bicycle ergometer in a MSR. The injury currents were in most cases directed from the ischemic area to the nonischemic area. For example, anterior ischemia caused an injury current directed from the apex to the base of the heart. The injury currents induced by transient ischemia and infarction of the same anatomical region were found to flow in the opposite direction. This change of direction was reflected as either ST-depression or ST-elevation in morphological signals. The anatomical location of the injury currents was in topographical agreement with the results of the reference methods (coronary angiography and myocardial scintigraphy) [87].

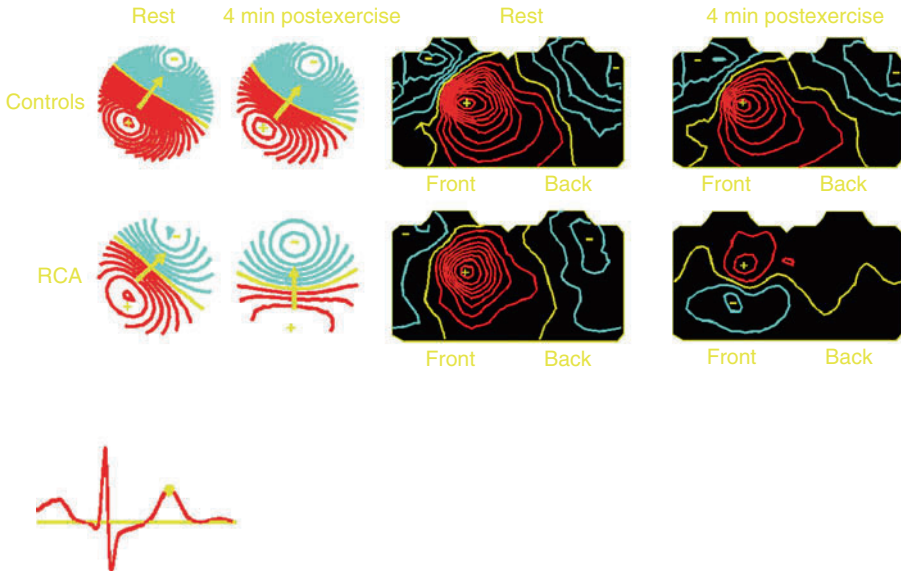

Figure 44.6

Exercise MCG in a coronary artery disease patient with a significant stenosis of the right coronary artery (RCA). The patient had the most extensive map rotation of the T-wave 4 min postexercise. Compared to the control group, the map rotation was more extensive (45 ± 39° vs 9 ± 8°, $p < 0.005$). Sensitivity for RCA was 75% at the specificity of 82% (Hänninen et al., 2000).

Corresponding to the absence of electrically active myocardial tissue, reduced current magnitudes were observed for the regions of infarcted myocardium (less than 1 $\mu A/mm^2$) in a series of 40 subjects, including normals and patients with a history of myocardial infarction. The current density distributions correlated well with other cardiological investigations (e.g., left ventricle catheterization, scintigraphy, echocardiography) [88]. Ischemia localization was attempted in a small study of four patients with single-vessel coronary artery disease with no previous myocardial infarction. Current density estimation (CDE) was focused on in the ischemic regions confirmed by positron emission tomography in all four patients and injury currents were restricted to the region of the stenosed coronary artery [89]. A recent large clinical study included 417 subjects: 177 patients with angiographically documented CAD (stenoses ≥ 50%), 123 symptomatic patients without hemodynamically relevant stenosis, and 117 healthy subjects [90]. Contrary to the ECG, unshielded MCG revealed significant differences between normals and symptomatic patients with and without relevant stenoses using current density reconstruction during repolarization at rest. The discrimination between normals and CAD patients was achieved with a sensitivity of 73.3%, and specificity of 70.1%. In another series of 50 patients with CAD (62 +/− 10 years; EF = 76 +/− 11%; registration: before, 24 h, and 1 month (n = 25) after PCI) and 57 normals (51 +/− 9 years), current density vector (CDV) maps were reconstructed within the ST-T interval and classified from category 0 (normal) to category 4 (grossly abnormal) [91]. Twenty-four hours after PCI, more maps were classified as category 2 ($P < 0.05$) and less as category 4 ($P < 0.005$). One month after PCI, the MCG results further improved: more maps were classified as category 1 ($P < 0.05$) and 2 ($P < 0.005$) and fewer maps as category 4 ($P < 0.0001$). The ECG remained unchanged in the course of PCI.

A few clinically interesting studies on acute myocardial ischemia in the emergency room setting have been published. A 6-min resting MCG scan has been shown to have sensitivity, specificity, positive and negative predictive values of 76.4, 74.3, 70.0, and 80.0%, respectively, for the detection of ischemia ($p < 0.0001$) in 125 patients with presumed ischemic chest pain [92]. In another new series of 264 acute chest pain patients without ST-elevation, T vector changes in the MCG were found to have a specificity and positive predictive value > 90% for angiographically confirmed diagnosis of significant coronary artery disease. It is noteable that 25% patients had to be excluded from the study for poor signal quality [93].

In conclusion, magnetocardiographic mapping seems to be an accurate method for ischemia and viability detection. Moreover, it is able to localize ischemic regions in the heart in a comparable fashion to other methods. Recent larger clinical series stress the potential of this noninvasive method for current clinical decision making. However, it is the task of future large-scale clinical studies to establish a clear mandate for the MCG method in every day patient work.

44.10 Discussion

The clinical application of any method means that it has to contribute at least in one of the following fields of clinical medicine: diagnosis, therapy, or prognosis. In particular, noninvasive methods improving the accuracy of diagnosis of a cardiac disease are valuable. However, most important new methods are able to deliver current palliative or curative therapy, either by improving the results of existing therapies or by providing new modes of therapy. Methods helping to assess better the prognosis of certain heart diseases in individual patients are also desired.

MCG has many advantages, and it may become a clinically accepted method. First of all, it is totally noninvasive. It is not necessary to attach electrodes or other sensors requiring direct contact to the patient to record an MCG. Currently operating multichannel magnetometers are feasible to use and enable fast MCG recordings. A full measurement can be carried out in few minutes. Such advantages of MCG recordings also mean high patient comfort. In addition, multiple temporal and spatial parameters can be extracted from a single heartbeat for complete electromagnetic characterization of the function of the patient's heart. The spatiotemporal resolution of MCG mapping is much higher than that of conventional ECG methods. Moreover, the MCG methods still have unexplored potential for extracting new physiological and pathophysiological information about the electrical activation in the myocardium.

However, the MCG has some disadvantages. The equipment is currently expensive, and requires the use of liquid helium and an MSR. Such technical demands so far exclude the wider applicability of MCG as a quick bedside test and during catheter interventions. The development of new supra-conducting materials, operating in higher temperatures achieved using liquid nitrogen, has not yet been able to solve this problem. Low-cost multichannel devices operating in an unshielded environment have recently been introduced with promising clinical results. This way of development might be one of the ways to bring this method closer to clinicians. One profound obstacle still remains: MCG systems are generally sensitive to moving magnetic objects, which excludes some patients from the studies.

44.11 Conclusions

From all magnetocardiographic studies published so far, it can be concluded that the diagnostic performance of the MCG is superior in several applications when compared to the conventional ECG or even body surface mapping. However, this advantage has not yet encouraged clinicians to widely accept and utilize the method, mostly because of the high cost, low availability, and lack of standardization. Nevertheless, clinical applications of MCG in the fields of therapy and prognosis are currently of growing interest. The localization of arrhythmias and the detection of arrhythmia risk are already established therapy-related applications. Non-pharmacologic antiarrhythmic and antirejection medical therapies guided by MCG have been proposed, but such suggestions need more comprehensive studies. The detection and localization of acute and chronic ischemia and assessment of myocardial viability would be applicable to a large number of cardiac patients, if the MCG method proves to be successful in larger patient series. Studies on the prognostic value of MCG after myocardial infarction, in long-QT syndrome, congenital heart disease, and cardiomyopathy, may offer new applications, taking into account the promising results of recent studies on the prophylactic use of implantable defibrillators in high-risk patient groups. The increasing availability of high-performance multichannel MCG systems in the clinical environment will strongly contribute to these efforts.

References

1. Siltanen, P.P., Magnetography, in *Comprehensive Eletrocardiology, Theory and Practice in Health and Disease*, vol. 2, M.W. Lawrie and T.D. Veitch, Editors. New York: Pergamon, 1989, pp. 1405–1438.
2. Stroink, G., W. Moshage, and S. Achenbach, Cardiomagnetism, in *Magnetism in* Medicine, W. Andrä and H. Nowak, Editors. Berlin: Wiley, 1998, pp. 136–189.
3. Mäkijärvi, M., K. Brockmeier, and U. Leder, et al.,, New trends in clinical magnetocardiography, in C. Aine*Biomag96: Proceedings of the 10th International Conference on Biomagnetism*, C. Aine, et al., Editors. New York: Springer, 2000, pp. 410–417.
4. Trip, J.H., Physical concepts and mathematical models, in *Biomagnetism: An Interdisciplinary Approach*, S.J. Williamson, Editor. New York: Plenum, 1982, pp. 101–149.
5. Horacek, B. M., Digital model for studies in magnetocardiography. *IEEE Trans. Magn.*, 1973;**9**: 440–444.
6. Nenonen, J., C. Purcell, B.M. Horacek, G. Stroink, et al.,, Magnetocardiographic functional localization using a current dipole in a realistic torso. *IEEE Trans. Biomed. Eng.*, 1991;**38**: 658–664.
7. Nakai, K., K. Kawazoe, H. Izumoto, J. Tsuboi, Y. Oshima, T. Oka, K. Yoshioka, M. Shozushima, A. Suwabe, M. Itoh, K. Kobayashi, T. Shimizu, and M. Yoshizawa, Construction of a three-dimensional outline of the heart and conduction pathway by means of a 64-channel magnetocardiogram in patients with atrial flutter and fibrillation. *Int. J. Cardiovasc. Imag.*, 2005;**21**: 555–561; discussion 563–564.
8. Katila, T. and P. Karp, Magnetocardiography: morphology and multipole presentations, in *Biomagnetism, An Interdisciplinary Approach*, S.J. Williamson, G.L. Romani, L. Kaufmann, and I. Modena, Editors. New York: Plenum, 1983, pp. 237–263.
9. Nenonen, J., Magnetocardiography, in *SQUID Handbook*, Vol. 2, Sect. 9.3, J. Clarke, and A. Braginski, Editors. Berlin: Wiley, 2005.
10. van Oosterom, A., T.F. Oostendorp, G.J. Huiskamp, and M. ter Brake, The magnetocardiogram as derived from electrocardiographic data. *Circ. Res.*, 1990;**67**: 1503–1509.
11. Sepulveda, N.G., B.J. Roth, and J. Wikswo Jr., Current injection into a two-dimensional anistropic bidomain. *Biophysical. J.*, 1989;**55**: 987–999.
12. Liehr, M., J. Haueisen, M. Goernig, P. Seidel, J. Nenonen, and T. Katila, Vortex shaped current sources in a physical torso phantom. *Ann. Biomed. Eng.*, 2005;**33**: 240–247.
13. Cohen, D. and L.A. Kaufman, Magnetic determination of the relationship between the S-T segment shift and the injury current produced by coronary artery occlusion. *Circ. Res.*, 1975;**36**: 414–424.
14. Baule, G. and R. McFee, Detection of the Magnetic Field of the Heart. *Am. Heart. J.*, 1963;**66**: 95–96.
15. Cohen, D. and E. Edelsack, J. Zimmerman, Magnetocardiograms taken inside a shielded room with a superconducting point-contact magnetometer *Appl. Phys. Lett.*, 1970;**16**: 278–280.
16. Zimmerman, J.E. and N.V. Frederick, Miniature ultrasensitive superconducting magnetic gradiometer and its use in cardiography and other applications. *Appl. Phys. Lett.*, 1971;**19**: 16–19.
17. Koch, H., Recent advances in magnetocardiography. *J. Electrocardiol.*, 2004;**37**: 117–122.
18. Uusitalo, M.A. and R.J. Ilmoniemi, Signal-space projection method for separating MEG or EEG into components. *Med. Biol. Eng. Comput.*, 1997;**35**: 135–140.
19. Chen, M. and R.T. Wakai, and B. Van Veen, Eigenvector based spatial filtering of fetal biomagnetic signals. *J. Perinat. Med.*, 2001;**29**(6): 486–496.
20. Taulu, S., M. Kajola, and J. Simola, Suppression of interference and artifacts by the signal space separation method. *Brain Topogr.*, 2004;**16**: 269–275.
21. Hyvärinen, A., Fast and robust fixed-point algorithms for independent component analysis. *IEEE Trans. Neural Networks*, 1999;**10**(3): 626–634.
22. Comani, S., D. Mantini, G. Alleva, S. Di Luzio, G.L.F. Romani, et al., Magnetocardiographic mapping using independent component analysis. *Physiol. Meas.*, 2004;**25**: 1459–1472.
23. Sternickel, K., A. Effern, K. Lehnertz, T. Schreiber, et al., Nonlinear noise reduction using reference data. *Phys. Rev.*, 2001;**E63**: 036209.
24. Burghoff, M., J. Nenonen, L. Trahms, and T. Katila, Conversion of magnetocardiographic recordings between two

different multichannel SQUID devices. *IEEE Trans. Biomed. Eng.*, 2000;**47**: 869–875.
25. Numminen, J., S. Ahlfors, R. Ilmoniemi, J. Montonen, et al., Transformation of multichannel magnetocardiographic signals to standard grid form. *IEEE Trans. Biomed. Eng.*, 1995;**42**: 72–78.
26. Cohen, D., Ferromagnetic contamination in the lungs and other organs of the human body. *Science*, 1973 May 18;**180**(87): 745–8.
27. Ribeiro, P.C., A.C. Bruno, P.L. Saboia e Silva, C.R. Barbosa, E.P. Ribeiro, E.C. Monteiro, and A.F. Costa, Detection of reentry currents in atrial flutter by magnetocardiography. *IEEE Trans. Biomed. Eng.*, 1999;**39**(8): 818–824.
28. Brazdeikis, A., C.W. Chu, P. Cherukuri, S. Litovsky, and M. Naghavi, Changes in magnetocardiogram patterns of infarcted-reperfused myocardium after injection of superparamagnetic contrast media. *Neurol. Clin. Neurophysiol.*, 2004;**30**: 16.
29. Brisinda, D., M.E. Caristo, and R. Fenici, Contactless magnetocardiographic mapping in anaesthetized Wistar rats: evidence of age-related changes of cardiac electrical activity. *Am. J. Physiol. Heart Circ. Physiol.*, 2005;Dec 22.
30. Mäkijärvi, M., J. Nenonen, L. Toivonen, J. Montonen, T. Katila, and P. Siltanen, Magnetocardiography: supraventricular arrhythmias and preexcitation syndromes. *Eur. Heart J.*, 1993;**14**(Suppl E): 46–52.
31. Moshage, W., S. Achenbach, K. Göhl, et al., Evaluation of the noninvasive localization accuracy of the cardiac arrhythmias attainable by multichannel magnetocardiography (MCG). *Int. J. Cardiac. Imag.*, 1996;**12**: 47–59.
32. Fenici, R., K. Pesola, P. Korhonen, M. Makijarvi, J. Nenonen, L. Toivonen, P. Fenici, and T. Katila, Magnetocardiographic pacemapping for nonfluoroscopic localization of intracardiac electrophysiology catheters. *PACE*, 1998,Nov;**21**(11 Pt 2): 2492–2499.
33. Fenici, R., D. Brisinda, J. Nenonen, and P. Fenici, Noninvasive study of ventricular preexcitation using multichannel magnetocardiography. *PACE*, 2003,Jan;**26**(1 Pt 2): 431–435.
34. Agren, P.L., H. Goranson, H. Jonsson, and L. Bergfeldt, Magnetocardiographic and magnetic resonance imaging for noninvasive localization of ventricular arrhythmia origin in a model of nonischemic cardiomyopathy. *PACE*, 2002,Feb;**25**(2): 161–166.
35. Leder, U., J. Haueisen, P. Pohl, R. Surber, J.P. Heyne, H. Nowak, H. R. Figulla, Localization of late potential sources in myocardial infarction. *Int. J. Cardiovasc. Imag.*, 2001,Aug;**17**(4): 315–325.
36. Grimm, B., J. Haueisen, M. Huotilainen, S. Lange, P. Van Leeuwen, T. Menendez, M. J. Peters, E. Schleussner, and U. Schneider, Recommended standards for fetal magnetocardiography. *PACE*, 2003 Nov;**26**(11): 2121–2126.
37. Stinstra, J., E. Golbach, P. van Leeuwen, S. Lange, T. Menendez, W. Moshage, E. Schleussner, C. Kaehler, H. Horigome, S. Shigemitsu, and M. J. Peters, Multicentre study of fetal cardiac time intervals using magnetocardiography. *BJOG*, 2002,Nov;**109**(11): 1235–1243.
38. Quinn, A., A. Weir, U. Shahani, et al., Antenatal fetal magnetocardiography: a new method for fetal surveillance? *Br. J. Obstet. Gynaecol.*, 1994;**101**: 866–870.
39. Menéndez, T., S. Achenbach, E. Beinder, et al., Usefulness of magnetocardiography for the investigation of fetal arrhythmias. *Am. J. Cardiol.*, 2001;**88**: 334–336.
40. Wakai, R. T., J. F. Strasburger, Z. Li, B. J. Deal, N. L. Gotteiner, Magnetocardiographic rhythm patterns at initiation and termination of fetal supraventricular tachycardia. *Circulation*, 2003 Jan 21;**107**(2): 307–12.
41. Cuneo, B.F., J.F. Strasburger, R.T. Wakai, and M. Ovadia, *Fetal Diagn. Ther.*, 2006;**21**(3): 307–313.
42. Menéndez, T., S. Achenbach, E. Beinder, et al., Prenatal diagnosis of QT prolongation by magnetocardiography. *PACE*, 2000;**23**: 1305–1307.
43. Van Leeuwen, P., B. Hailer, W. Bader, et al., Magnetocardiography in the diagnosis of fetal arrhythmia. *Br. J. Obstet. Gynaecol.*, 1999;**106**: 1200–1208.
44. Horigome, H., J. Shiono, S. Shigemitsu, et al., Detection of cardiac hypertrophy in the fetus by approximation of the current dipole using magnetocardiography. *Pediatr. Res.*, 2001;**50**: 242–245.
45. Van Leeuwen, P., S. Lange, A. Klein, D. Geue, and D.H. Gronemeyer, Dependency of magnetocardiographically determined fetal cardiac time intervals on gestational age, gender and postnatal biometrics in healthy pregnancies. *BMC Pregnancy Childbirth*, 2004,Apr 2;**4**(1): 6.
46. Van Leeuwen, P., Y. Beuvink, S. Lange, A. Klein, D. Geue, and D. Gronemeyer, Assessment of fetal growth on the basis of signal strength in fetal magnetocardiography. *Neurol. Clin. Neurophysiol.*, 2004, Nov 30;**47**(B).
47. Bolick, D.R., D.B. Hackel, K.A. Reimer, and R.E. Ideker, Quantitative analysis of myocardial infarct structure in patients with ventricular tachycardia. *Circulation,* 1986;**74**: 1266–1279.
48. Erne, S.N., R.R. Fenici, H.D. Hahlbom, W. Jaszczuk, H.P. Lehmann, and M. Masselli, High resolution magnetocardiographic recordings of the ST segment in patient with electrical late potentials. *Nuovo. Cimento.*, 1983;**2d**: 340–345.
49. Mäkijärvi, M., J. Montonen, L. Toivonen, P. Siltanen, M.S. Nieminen, M. Leiniö, and T. Katila, Identification of patients with ventricular tachycardia after myocardial infarction by high-resolution magnetocardography and electrocardiography. *J. Electrocardiol.*, 1993;**26**: 117–124.
50. Korhonen, P., J. Montonen, M. Mäkijärvi, T. Katila, M.S. Nieminen, and L. Toivonen, Late fields of the magnetocardiographic QRS complex as indicators of propensity to sustained ventricular tachycardia after myocardial infarction. *J. Cardiovasc. Electrophysiol.*, 2000;**11**: 413–420.
51. Müller, H.P., P. Gödde, K. Czerski, M. Oeff, R. Agrawal, P. Endt, W. Kruse, U. Steinhoff, and L. Trahms, Magnetocardiographic analysis of the two-dimensional distribution of intra-QRS fractionated activation. *Phys. Med. Biol.*, 1999;**44**: 105–120.
52. Korhonen, P., T. Husa, I. Tierala, H. Väänänen, M. Mäkijärvi, T. Katila, and L. Toivonen, Increased intra-QRS fragmentation in magnetocardiography as a predictor of arrhythmic events and mortality in patients with cardiac dysfunction after myocardial infarction. *J. Cardiovasc. Electrophysiol.*, 2006;**17**: 396–401.
53. Lant, J., G. Stroink, B. Ten Voorde, B. M. Horacek, and T. J. Montague, Complementary nature of electrocardiographic and magnetocardiographic data in patients with ischemic heart disease. *J. Electrocardiol.*, 1990;**23**: 315–322.
54. Nomura, M., K. Fujino, M. Katayama, A. Takeuchi, Y. Fukuda, M. Sumi, M. Murakami, Y. Nakaya, and H. Mori, Analysis of the T wave of the magnetocardiogram in patients with essential hypertensionby means of isomagnetic and vector array maps. *J. Electrocardiol.*, 1988;**21**: 174–182.
55. Oikarinen, L., M. Viitasalo, P. Korhonen, H. Väänänen, H. Hänninen, J. Montonen, M. Mäkijärvi, T. Katila, and L. Toivonen, Postmyocardial infarction patients susceptible to ventricular tachycardia show increased T wave dispersion independent

of delayed ventricular conduction. *J. Cardiovasc. Electrophysiol.*, 2001;**12**: 1115–1120.

56. Korhonen, P., H. Väänänen, M. Mäkijärvi, T. Katila, and L. Toivonen, Repolarization abnormalities detected by magnetocardiography in patients with dilated cardiomyopathy and ventricular arrhythmias. *J. Cardiovasc. Electrophysiol.*, 2001;**12**: 772–777.
57. Stroink, G., J. Lant, P. Elliot, P. Charlebois, and M.J. Gardner, Discrimination between myocardial infarct and ventricular tachycardia patients using magnetocardiographic trajectory plots and iso-integral maps. *J. Electrocardiol.*, 1992;**25**: 129–142.
58. Rovamo, L., M. Paavola, J. Montonen, M. Mäkijärvi, J. Nenonen, and T. Katila, Magnetocardioraphic repolarization maps in children with long QT syndrome, in *Biomagnetism: Fundamental Research and Clinical Applications*, C. Baumgartner, L. Deecke, G. Stroink, and S.J. Williamson, Editors. Amsterdam Oxford, Tokyo: IOS, 1995, pp. 615–618.
59. Haissaguerre, M., P. Jais, D. C. Shah, A. Takahashi, M. Hocini, G. Quiniou, S. Garrigue, A. Le Mouroux, P. Le Metayer, and J. Clementy, Spontaneous initiation of atrial fibrillation by ectopic beats originating in the pulmonary veins. *N. Engl. J. Med.*, 1998;**339**(10): 659–666.
60. Ausma, J., N. Litjens, M.H. Lenders, H. Duimel, F. Mast, L. Wouters, F. Ramaekers, M. Allessie, and M. Borgers, Time course of atrial fibrillation-induced cellular structural remodeling in atria of the goat. *J. Mol. Cell. Cardiol.*, 2001;**33**(12): 2083–2094.
61. Schotten, U., J. Ausma, C. Stellbrink, I. Sabatschus, M. Vogel, D. Frechen, F. Schoendube, P. Hanrath, and M.A. Allessie, Cellular mechanisms of depressed atrial contractility in patients with chronic atrial fibrillation. *Circulation*, 2001;**103**(5): 691–698.
62. Dilaveris, P.E., J.E. Gialafos, P-wave dispersion: a novel predictor of paroxysmal atrial fibrillation. *Ann. Noninvasive. Electrocardiol.*, 2001;**6**(2): 159–165.
63. Fukunami, M., T. Yamada, M. Ohmori, K. Kumagai, K. Umemoto, A. Sakai, N. Kondoh, T. Minamino, and N. Hoki, Detection of patients at risk for paroxysmal atrial fibrillation during sinus rhythm by P wave-triggered signal-averaged electrocardiogram. *Circulation*, 1991;**83**(1): 162–169.
64. Steinbigler, P. and R. Haberl B. Konig G. Steinbeck, P-wave signal averaging identifies patients prone to alcohol-induced paroxysmal atrial fibrillation. *Am J Cardiol*, 2003;**91**(4): 491–494.
65. Winklmaier, M., C. Pohle, S. Achenbach, M. Kaltenhauser, W. Moshage, and W.G. Daniel, P-wave analysis in MCG and ECG after conversion of atrial fibrillation. *Biomed. Tech. (Berl.)*, 1998;**43**(Suppl): 250–251.
66. Koskinen, R., M. Lehto, H. Vaananen, J. Rantonen, L.M. Voipio-Pulkki, M. Makijarvi, L. Lehtonen, J. Montonen, and L. Toivonen, Measurement and reproducibility of magnetocardiographic filtered atrial signal in patients with lone atrial fibrillation and in healthy subjects. *J. Electrocardiol.*, 2005;**38**(4): 330–336.
67. Hertervig, E., S. Yuan, S. Liu, O. Kongstad, J. Luo, S.B. Olsson, Electroanatomic mapping of transseptal conduction during coronary sinus pacing in patients with paroxysmal atrial fibrillation. *Scand. Cardiovasc. J.*, 2003;**37**(6): 340–343.
68. Markides, V. and R.J. Schilling, Atrial fibrillation: classification, pathophysiology, mechanisms and drug treatment. (Review) (5 refs) *Heart (British Cardiac. Soc.)*, 2003,Aug.; **89**(8): 939–943.
69. Verma, A., O.M. Wazni, N.F. Marrouche, D.O. Martin, F. Kilicaslan, S. Minor, R.A. Schweikert, W. Saliba, J. Cummings, J.D. Burkhardt, M. Bhargava, W.A. Belden, A. Abdul-Karim, and A. Natale, Pre-existent left atrial scarring in patients undergoing pulmonary vein antrum isolation: an independent predictor of procedural failure. *J. Am. Coll. Cardiol.*, 2005,Jan 18;**45**(2): 285–292.
70. Sumi, M., A. Takeuchi, M. Katayama, Y. Fukuda, M. Nomura, K. Fujino, M. Murakami, Y. Nakaya, H. Mori and P. Magnetocardiographic, Waves in normal subjects and patients with mitral stenosis. *Jpn. Heart J.*, 1986;**27**(5): 621–633.
71. Koskinen, R., H. Väänänen, V. Mäntynen, J. Montonen, J. Nenonen, L. Lehtonen, M. Mäkijärvi, and L. Toivonen, Field heterogeneity in magnetocardiographic atrial signals in patients with focally-triggered lone atrial fibrillation (abstract). *Heart Rhythm.*, 2004;**1**(1S): 226.
72. Kuusisto, J., R. Koskinen, V. Mäntynen, J. Nenonen, M. Mäkijärvi, J. Montonen, and L. Toivonen, Diversity in Activation of Healthy Atria by Magnetocardiographic Gradient Analysis (abstract), in *Proceedings of International Conference on Biomagnetism*, Boston, 2004: 407–408
73. Jurkko, R., V. Mäntynen, J. Tapanainen, J. Montonen, H. Väänänen, H. Parikka, L. Toivonen, Non-invasive detection of conduction pathways to left atrium using magnetocardiography: Validation by intracardiac electroanatomic mapping. *Europace* 2009;**11**: 169–177.
74. Jurkko, R., V. Mäntynen, M. Lehto, J.M. Tapanainen, J. Montonen, H. Parikka, L. Toivonen, Interatrial conduction in patients with paroxysmal atrial fibrillation and in healthy subjects. *Int. J. Cardiol.,* 2009, Jun 20.
75. Yamada, S., K. Tsukada, T. Miyashita, Y. Oyake, K. Kuga, I. Yamaguchi, Noninvasive diagnosis of partial atrial standstill using magnetocardiograms. *Circ. J.*, 2002;**66**(12): 1178–1180.
76. Kandori, A., T. Hosono, T. Kanagawa, S. Miyashita, Y. Chiba, M. Murakami, T. Miyashita, and K. Tsukada, Detection of atrial-flutter and atrial-fibrillation waveforms by fetal magnetocardiogram. *Med. Biol. Eng. Comput.*, 2002;**40**(2): 213–217.
77. Brockmeier, K., S. Comani, S. Erne, et al., Magnetocardiography and exercise testing. *J. Electrocardiol.*, 1994;**27**: 137–142.
78. Brockmeier, K., L. Schmitz, J.D. Bobadilla Chavez, et al., Magnetocardiography and 32-lead potential mapping: repolarization in normal subjects during pharmacologically induced stress. *J. Cardiovasc. Electrophysiol.*, 1997;**8**: 615–626.
79. Takala, P., H. Hänninen, J. Montonen, et al., Magnetocardiographic and electrocardiographic exercise mapping in healthy subjects. *Ann. Biomed. Eng.*, 2001;**46**: 975–982.
80. Van Leeuwen, P., B. Hailer, and M. Wehr, Changes in current dipole parameters in patients with coronary artery disease with and without myocardial infarction. *Biomed. Tech. (Berl.)*, 1997;**42**: 132–136.
81. Van Leeuwen, P., B. Hailer, S. Lange, et al., Spatial and temporal changes during the QT-interval in the magnetic field of patients with coronary artery disease. *Biomed. Tech. (Berl.)*, 1999;**44**: 139–142.
82. Hänninen, H., P. Takala, M. Mäkijärvi, et al., Detection of exercise induced myocardial ischemia by multichannel magnetocardiography in single vessel coronary artery disease. *Ann. Noninvas. Electrocardiol.*, 2000;**5**: 147–157.
83. Hänninen, H., P. Takala, P. Korhonen, et al., Features of ST segment and T-wave in exercise-induced myocardial ischemia evaluated with multichannel magnetocardiography. *Ann. Med.*, 2002;**34**: 1–10.
84. Takala, P., H. Hänninen, J. Montonen, et al., Heart rate adjustment of magnetic field map rotation in detection of myocardial

ischemia in exercise magnetocardiography. *Basic Res. Cardiol.*, 2002;**97**: 88–96.

85. Hänninen, H., P. Takala, M. Mäkijärvi, et al., Recording locations in multichannel magnetocardiography and body surface potential mapping sensitive for regional exercise-induced myocardial ischemia. *Basic Res. Cardiol.*, 2001;**96**: 405–414.
86. Tsukada, K., T. Miyashita, A. Kandori, et al., An iso-integral mapping technique using magnetocardiogram, and its possible use for diagnosis of ischemic heart disease. *Int. J. Card Imag.*, 2000;**16**: 55–66.
87. Seese, B., W. Moshage, S. Achenbach, et al., Magnetocardiographic (MCG) analysis of myocardial injury currents, in *Biomagnetism: Fundamental Research and Clinical Applications*, C. Baumgartner, et al., Editors. Amsterdam: Elsevier, 1995; 628–632.
88. Leder, U., H.P. Pohl, S. Michaelsen, et al., Non-invasive biomagnetic imaging in coronary artery disease based on individual current density. *Int. J. Cardiol.*, 1998;**64**: 83–92.
89. Pesola, K., H. Hänninen, K. Lauerma, J. Lötjönen, M. Mäkijärvi, J. Nenonen, P. Takala, L.M. Voipio-Pulkki, L. Toivonen, and T. Katila, Current densityestimation on the left ventricular epicardium: a potential method for ischemia localization. *Biomed. Tech. (Berl.)*, 1999b;**44**(suppl 2): 143–146.
90. Hailer, B., I. Chaikovsky, S. Auth-Eisernitz, H. Schafer, and P. Van Leeuwen, The value of magnetocardiography in patients with and without relevant stenoses of the coronary arteries using an unshielded system. *PACE*, 2005,Jan;**28**(1): 8–16.
91. Hailer, B., P. Van Leeuwen, I. Chaikovsky, S. Auth-Eisernitz, H. Schafer, and D. Gronemeyer, The value of magnetocardiography in the course of coronary intervention. *Ann. Noninvas. Electrocardiol.*, 2005,Apr;**10**(2): 188–196.
92. Tolstrup, K., B.E. Madsen, J.A. Ruiz, S.D. Greenwood, J. Camacho, R.J. Siegel, H.C. Gertzen, J.W. Park, and P.A. Smars, Non-invasive resting magnetocardiographic imaging for the rapid detection of ischemia in subjects presenting with chest pain. *Cardiology*, 2006;**106**(4): 270–276.
93. Park, J.W., P.M. Hill, N. Chung, P.G. Hugenholtz, and F. Jung, Magnetocardiography predicts coronary artery disease in patients with acute chest pain. *Ann. Noninvas. Electrocardiol.*, 2005,Jul;**10**(3): 312–323.

45 Polarcardiography

Gordon E. Dower

P. W. Macfarlane, A. van Oosterom, O. Pahlm, P. Kligfield, M. Janse, J. Camm (eds.), *Comprehensive Electrocardiology*, DOI 10.1007/978-1-84882-046-3_45,

45.1 Polarcardiography

Polarcardiography is a form of vectorcardiography. It provides a way of graphically representing the heart vector (Chap. 7), but instead of doing so in the form of vectorcardiographic loops, which show only one beat and lack a time scale, the polarcardiograph separately plots the magnitude and direction of the heart vector against time. These are its polar coordinates, which are obtained from its rectangular, or *xyz*, coordinates by a simple mathematical transformation. Their use in electrocardiography goes back to Einthoven's manifest potential difference and electrical axis of the heart; that is, the magnitude and direction of the maximal heart vector in the frontal plane [1].

The choice of coordinate system can greatly affect the simplicity of certain mathematical problems. The rectangular coordinates of the heart vector are given directly by vectorcardiographic lead systems because of their simple relationship with potential differences on the body surface. The ideal vectorcardiographic lead system, however, would yield *xyz* signals as if they came from orthogonally placed surface electrodes on the body (assuming the body were a relatively large homogeneous sphere with the heart at its center). With this concept of the heart and body, it is natural to employ a spherical (polar) coordinate system. The most familiar application of such a system is to the terrestrial sphere. If altitude (radius) is ignored, only two coordinates, latitude and longitude, are required to fix a position on the earth's surface, whereas three rectangular coordinates would be needed.

It seemed intuitively obvious to Einthoven, and subsequently to several people [2], that polar coordinates, either in a plane or with respect to a sphere, should be helpful in studying the heart vector. For example, an increase in the peak magnitude of the heart vector, such as occurs in left ventricular hypertrophy (LVH), is an expected consequence of increase in the muscle mass of the left ventricle and is not affected by the orientation of the heart. In contrast, different orientations can produce various combinations of increased voltage in limb and precordial leads of the ECG, giving rise to a plethora of ECG voltage criteria.

Intriguing though the prospect was, the application of polarcardiography had to await the development of a device for continuously transforming rectangular into polar coordinates. The first clinically practical polarcardiograph was an analog computer completed in 1961 [3]. The polarcardiograms obtained from it provided the basis for developing diagnostic criteria covering a wide range of electrocardiographic conditions. It is important to appreciate that the transformation of coordinates does not increase information content, but it may display information in a manner that makes certain diagnostic features more obvious or discernible. Some polar criteria can be translated back into ECG or VCG criteria that had not previously been recognized, but others may be very difficult to discern in either of those displays.

The equipment now employed in computerized electrocardiography can execute the necessary transformations so that dedicated polarcardiographs are no longer needed; however, polar criteria and the polar approach play a useful role in the development of diagnostic programs. At the Woodward ECG computer system in the Vancouver General Hospital, polar coordinates form the basis of the measurement and analysis programs. These give the cardiologist information additional to that obtained from reading the ECG. However, the 12-lead ECG derived from the *xyz* signals (see Chap. 11) remains the primary graphic output of the system, with VCGs being generated when polar criteria for infarction are satisfied (see Fig. 45.18 and Table 45.3). Polarcardiograms can also be generated from any current or stored data, on request, although they are not used routinely for the following reasons:

(a) They are not really necessary, since the polar criteria have been satisfactorily programmed into the computer
(b) They are relatively voluminous, being written out at five times the paper speed of the conventional ECG and
(c) Most cardiologists are not familiar with them

However, polarcardiograms are used in problem cases, in research, and in the development of new criteria.

45.2 Spherical Coordinates Applied to the Body

Figures 45.1 and 45.2 show how latitude and longitude are applied to the body to indicate the direction of the heart vector. The frontal plane of the body becomes the equatorial plane of the reference sphere. The angle in that plane α is the same as that used by Einthoven for the electrical axis of the heart. All points on a meridian of longitude have the same

angle α. The angle of the heart vector with respect to the equatorial frontal plane (that is, anterior or posterior to it) is ψ. All points on a parallel of latitude have the same angle ψ.

Aitoff's equal-area projection (Fig. 45.2) is a two-dimensional representation of the sphere that is useful in showing clustering of directions of corresponding heart vectors in groups of individuals (Fig. 45.3). The orientation of the body in the Aitoff projection has been chosen so that the North–South axis corresponds to the posteroanterior (−z) axis of the transverse plane vector loop. Hence, anterior vectors are depicted downward in this form of Aitoff plot.

Elevation and azimuth are electrocardiographic synonyms for latitude and longitude, but they are less familiar terms to the general reader and have difficult dictionary definitions. Strictly, they are not appropriate because they define a direction with respect to an observer on the earth's surface. The celestial coordinates, declination, and right ascension would be conceptually more applicable, though not more so than latitude and longitude.

Although the position of a point on the surface of a sphere is defined by latitude and longitude, in order to fix that point in space, the radius of the sphere (R in Fig. 45.1) must also be specified. In polarcardiography, this third coordinate is known as magnitude, because it represents the magnitude of the heart vector.

45.3 Spatial Magnitude

For reasons of clarity, the magnitude coordinate will be discussed first. The spatial magnitude of the heart vector, when plotted against time, yields the M tracing. Magnitudes in the frontal, transverse, and sagittal planes (i.e., the distances from the origin in the corresponding VCG loops) are denoted by m_f, m_t, and m_s, respectively. The relationships between the magnitude tracings and their parent xyz signals are as follows:

$$M = \left(x^2 + y^2 + z^2\right)^{1/2}, M \geqslant 0$$
$$m_f = \left(x^2 + y^2\right)^{1/2}, m_f \geqslant 0$$
$$m_t = \left(x^2 + z^2\right)^{1/2}, m_t \geqslant 0$$
$$m_s = \left(y^2 + z^2\right)^{1/2}, m_s \geqslant 0$$

In the polarcardiographic examples in this chapter, the xyz signals have been derived from the Frank system (Chap. 11).

At first sight, M tracings resemble ECGs and, so far as possible, they are similarly labeled. The P, QRS, and T events in the ECG have their counterparts in the M tracings (Fig. 45.4). However, by definition, there cannot be Q or S waves because magnitudes are never negative. Although small initial peaks (e.g., ″r in Fig. 45.4) in the M tracing correspond approximately to the Q wave in the ECG, the degree of correspondence is variable and indefinite. It is useful, however, to retain the letters Q and S to denote the onset and offset points of the QRS complex. This is logical because it makes the time between the Q and S points equal to the QRS duration – a term desirable to retain, along with QRS complex and QT interval. Because of the multiplicity of peaks sometimes seen in QRS complexes in M tracings and the inapplicability of the terms Q wave and S wave, it is preferable not to refer to an R wave but rather to the individual R peaks in the manner shown in Fig. 45.4.

In left and right bundle branch block (LBBB and RBBB, respectively), the M tracing is very distinctive, the QRS complex being smooth in the former and notched in the latter (Fig. 45.5). Nevertheless, angular data are included in the discrimination.

The M tracing is particularly valuable in determining QRS duration because of two useful properties. First, when the M tracing shows zero magnitude, all ECG leads must have zero signals, so problems relating to nonsimultaneity of the onset and offset of the QRS complex in various ECG leads (for example, an isoelectric Q wave) do not arise. Second, the M tracing returns, or almost returns, to the baseline to give a clear demarcation between QRS and ST events. (Exceptions to this are mentioned in Sect. 45.3.1.) The ECG does not give a good indication of this phenomenon and its QRS offset is often vague. The relative clarity of the Q and S points in the M tracing simplifies the programming of a computer to determine QRS duration [4]. This is a very important measurement in decision-tree logic leading to a diagnostic interpretation. Computer determinations of QRS durations based on the ECG show disappointing discrepancies from visual determinations. However, improving the agreement is difficult because visual determinations by different readers also

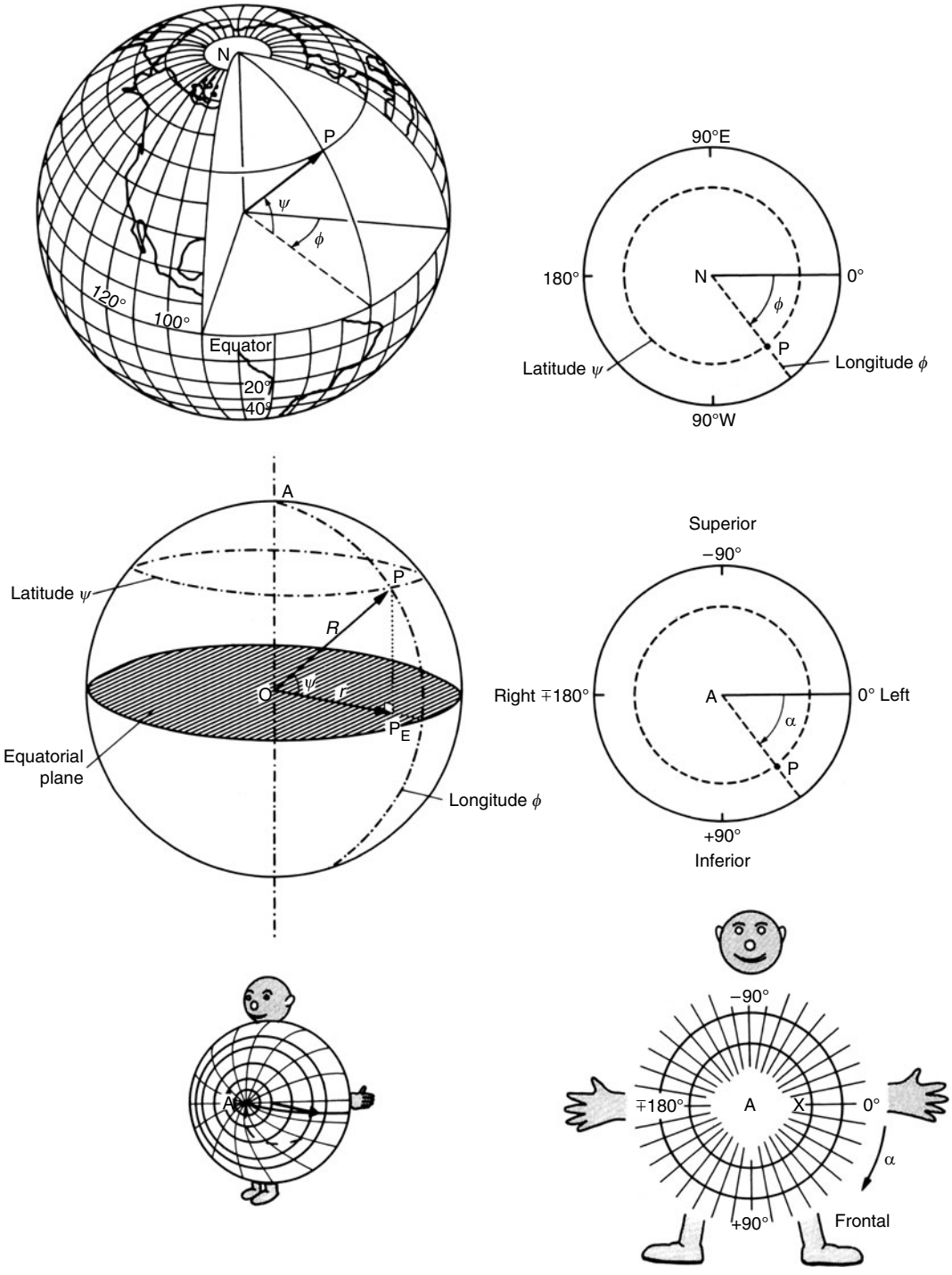

Figure 45.1

Definition of latitude and longitude. The vector from the center of the terrestrial sphere pierces the surface at P, the intersection of the meridian of longitude and the parallel of latitude. The angle Φ, between P meridian and reference (zero) meridian in the equatorial plane, is the longitude of P. The angle Ψ that the vector makes with respect to the equatorial plane is the latitude of P and is referred to as the posteroanterior (PA) latitude. Thus the latitude and longitude of P give spatial direction of the vector. The lower figures show spherical coordinates applied to the body: the North Pole becomes the anterior pole A, the equatorial plane becomes the frontal plane, and the angle Φ becomes α, following the tradition initiated by Einthoven.

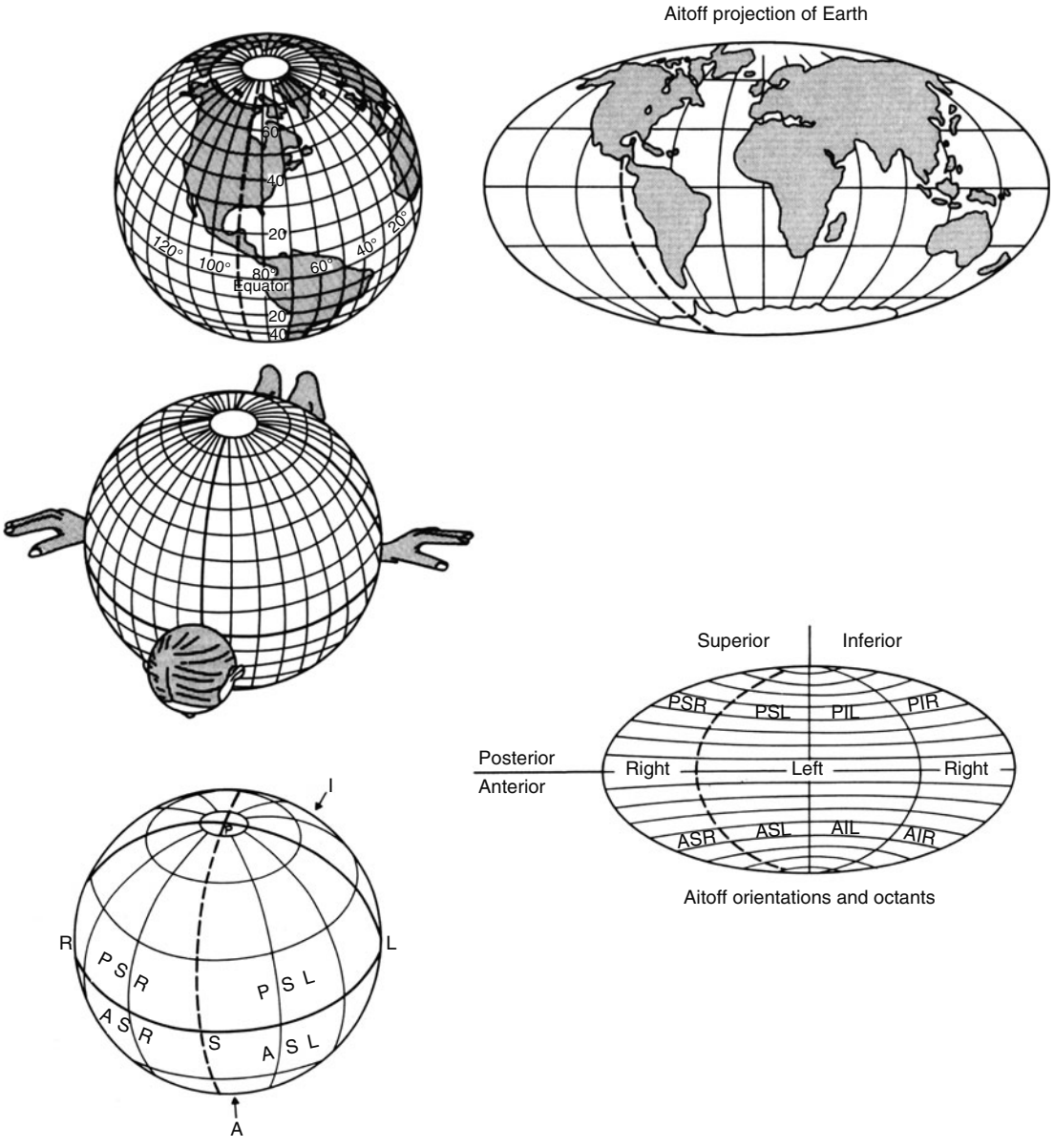

Figure 45.2

The orientation of Aitoff equal-area projection for two-dimensional display of vector direction. The distribution of points on the sphere is uniform in this projection. PSR, posterior superior right; ASR, anterior superior right; PSL, posterior superior left; ASL, anterior superior left; PIL, posterior inferior left; AIL, anterior inferior left; PIR, posterior inferior right; AIR, anterior inferior right.

vary a good deal. On the other hand, there is good agreement between computer and visual determinations of QRS duration using the spatial magnitude. The normal limits of QRS duration so determined are given in Tables 45.1 and 45.2 as diagnostic cut-off points used by the Woodward computers.

The ST segment is that part of the M tracing between S and T_i, the onset of the T wave. Sometimes, for example, in LBBB (Fig. 45.5), the ST segment initially rises steeply for a short distance then abruptly changes its slope to a more

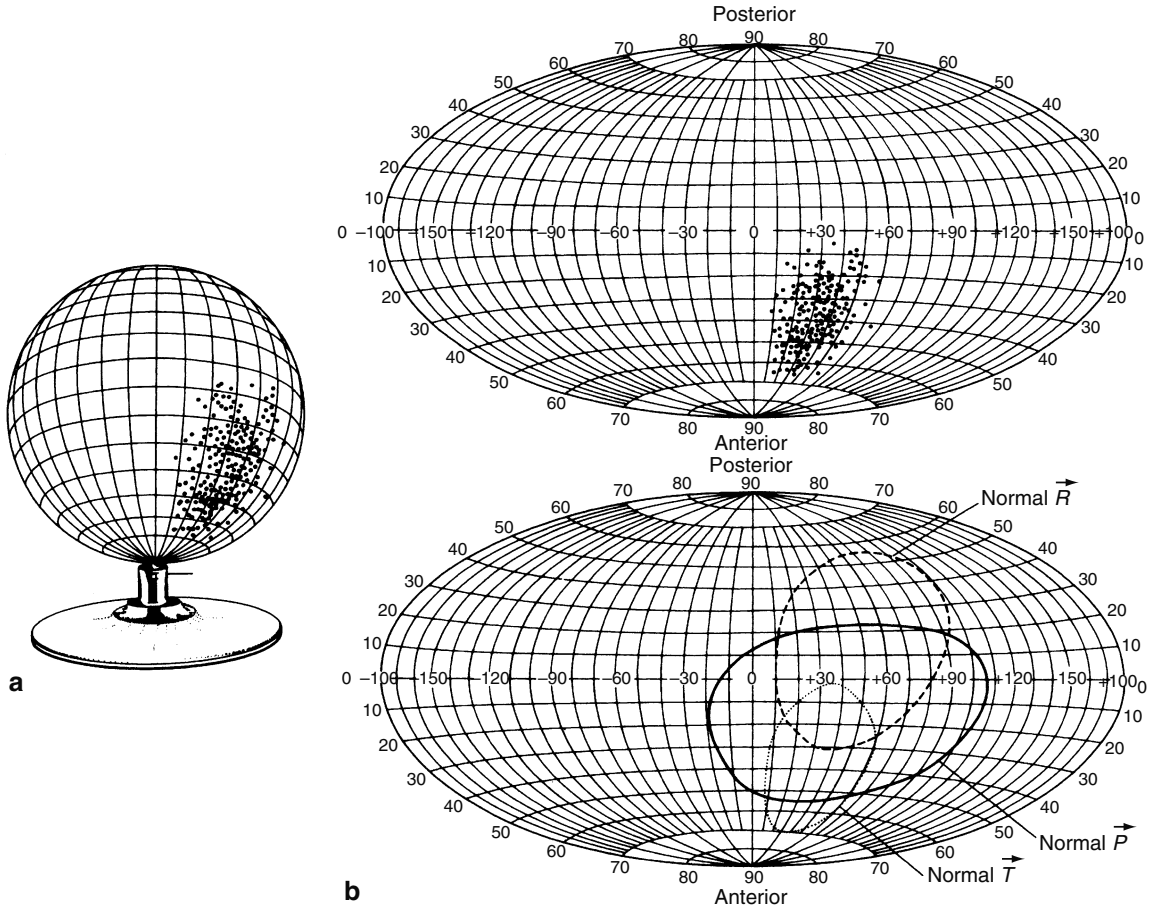

Figure 45.3

Direction of *T* in 195 young adults. Clustering in the sphere (a) is equally well shown in the Aitoff projection (*top* part of b). Normal "continents" of $\vec{P}$, $\vec{R}$, and $\vec{T}$ directions are thus defined (*bottom* part of b).

gradual one, forming a knee. This knee is labeled J because of its resemblance to the J point in the ECG (Fig. 45.4). Although, in the ECG, the J point is often used to mark the end of the QRS complex, the end of the QRS complex in the *M* tracing is defined as occurring at the S point because J is usually poorly defined.

M tracings reveal that there is not a clear-cut difference in identity between the ST segment and the T wave. However, it is useful to have some point in time that can be considered as representative of the ST segment so the ST point is taken as occurring midway between S and T, the peak of the T wave.

The points in the *M* tracing labeled P, R, ST, and T represent particular instants in time. A point U may often be identified also. These instants are not necessarily the same as those represented by similarly labeled points in the m_f, m_t, and m_s tracings. The vectors occurring at the points P, R, ST, and T in the *M* tracing are designated as $\vec{P}, \vec{R}, \vec{ST}$, and $\vec{T}$. The spatial magnitudes of these vectors are m_P, m_T, m_{ST}, and m_T: the heights of P, R, ST, and T above the baseline in the *M* tracing. By recording the *M*, m_f, m_t, and m_s tracings simultaneously, the magnitudes of these vectors in the frontal, transverse, and sagittal planes can be determined. These are designated as m_fP, m_tP, m_sP, and so on.

In vector loops, because of noise around the E point and lack of expansion on a time scale, the exact beginning of the QRS complex is difficult to determine, yet early QRS vectors, such as the 0.04 s vector, are often accorded considerable diagnostic importance. The timing of such vectors is clearly done more accurately from the *M* tracing. However, the greater detail afforded by the *M* tracing has disclosed that in many normal cases the development of early QRS vectors

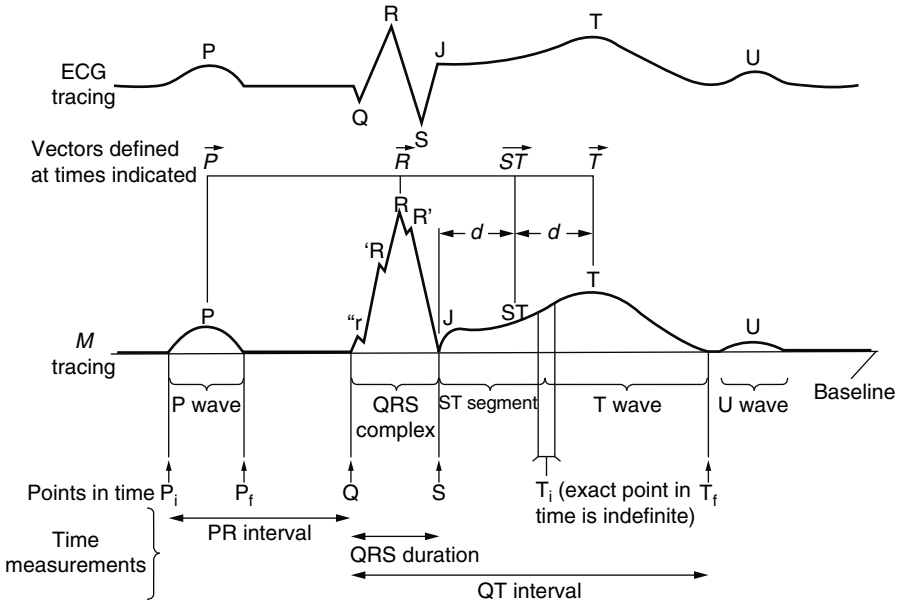

Figure 45.4

ECG and spatial vector magnitude (*M*) tracings are compared. All *M* deflections are above the baseline. The Q wave in the ECG corresponds to the so-called small foot ″r in the *M* tracing. Q and S points in the *M* tracing mark the beginning and end of the QRS complex to conform with terms PR and QT intervals, and QRS duration. The J point is not a useful time reference because it is often absent, whereas the nadir S is usually clear. P_i and P_f are P-wave onset and end, respectively; T_i and T_f are T-wave onset and end, respectively.

can be very gradual: a slight initial deflection, or foot (″r in Fig. 45.4) may be clearly discernible, conjectural, or absent from case to case (Fig. 45.5) and sometimes from beat to beat. The presence or absence of this feature can make a difference of about 0.01 s to the QRS onset. This is something to be borne in mind when the QRS onset point is used as a time reference for defining QRS vectors. Its variability, however, still allows the *M* tracing to give a more consistent basis for determining QRS duration by computer than the QRS complex in the ECG [4].

The value of the *M* tracing in measuring QRS durations extends also to the determination of PR and QT intervals (Table 45.3) for the same reason; namely, a zero value of the *M* tracing indicates that ECG signals are "zero," so that different ECG leads do not have to be compared.

45.3.1 Baseline Clamping

An interesting requirement of magnitude tracings, not obvious from the formulae for deriving them, is that the baselines preceding the QRS complex in the parent *xyz* signals should be clamped (that is, set to zero) before the transformation of coordinates is carried out. If this is not done, the apparent baseline of the magnitude tracing will ride above the zero level and there will appear to be negative deflections from that baseline, which may meet, but cannot cross that level. Negative magnitudes are of course impossible. The appearance of these pseudo negative deflections is obvious (Fig. 45.6) and the consequent distortion is therefore avoidable. In fact, since the computer program clamps automatically and virtually without fail, this is no longer a problem, but the solution is not simple or obvious and, because of its crucial importance to polarcardiography, a brief account of it is merited.

The clamp point is located shortly before the Q point, at a time when signals are negligible in relation to an estimate of noise made in a 30 ms window in the region of the clamp point. The method used by the Woodward computers has not required alteration for several years and produces satisfactory *M* tracings in almost every case although rarely, P waves

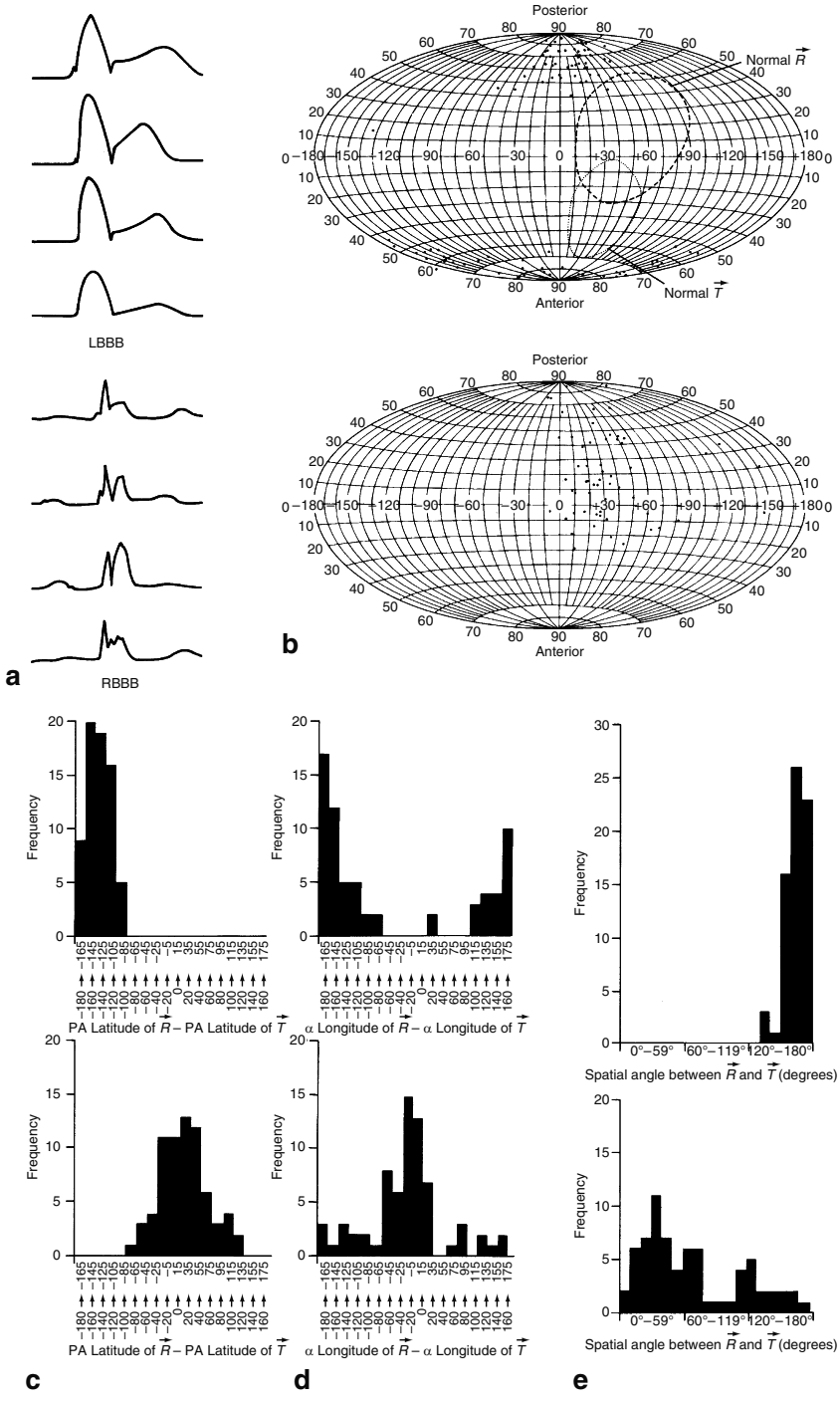

Figure 45.5

Left bundle branch block (LBBB) as compared to right bundle branch block (RBBB). *M* tracings in eight typical examples of LBBB and RBBB (a) show marked differences in the smoothness of QRS contour. Note the variability of the initial small deflection, or foot, in LBBB. Aitoff plots (b) show directions of $\vec{R}$ and $\vec{T}$ in 69 cases each of LBBB (*top*) and RBBB (*bottom*). In LBBB, these are at opposite poles. This difference is also shown in histograms of latitude differences (c), but less so in longitude differences (d) and spatial angles between $\vec{R}$ and $\vec{T}$ (e).

Table 45.1

Cutoff points for flagging interval measurements (ms): I, interpolate according to age; D, use default value

Interval	Flag	Default[a]	Age < 7	7 ⩽ age ⩽ 16	16 ⩽ age ⩽ 17
PR	>>	>210	> 180	I	>190 (rate > 100)
					>200 (rate ⩽ 100)
	<	<115	None	None	None
	<<	<106	<58	I	D
QRS	>>	>109	<88	I	D
	<<	<50	<46	I	D
QT_c	>>	>470	<473	I	D
	<<	<350	<300	I	D

[a]Age not otherwise specified

Table 45.2

Cutoff points for flagging vector magnitudes (mV), ratios, and ischemic index $(M_s\theta)$: I, interpolate; D, use default value

Vector	Flag	Default	Age < 5	5 ⩽ age ⩽ 16	Age ⩾ 16 Female	16 ⩽ age ⩽ 28 Male
P	>>	> 0.240	> 0.290	I	D	D
	>	> 0.200	> 0.240	I	D	D
R	>>	> 2.200	> 3.320	I	> 2.000	> 2.400
	>	> 2.100	> 2.840	I	D	None
	<	None	< 0.920	I	None	D
	<<	< 0.850	< 0.440	I	< 0.750	D
m_t	>>	> 2.150	> 2.340	I	> 1.850	> 1.700
	>	> 1.950	> 2.030	I	> 1.700	None
ST/R	>>	> 0.25	D	D	D	> 0.20[a]
T/R	>>	> 0.75	> 0.52	I	D	> 0.60[a]
	<<	< 0.10	< 0.01	I	D	D
$M_s\theta$	*	⩾ 5	D	D	D	D
	*	⩾ 10	D	D	D	D

[a]For 16 ⩽ age ⩽ 30

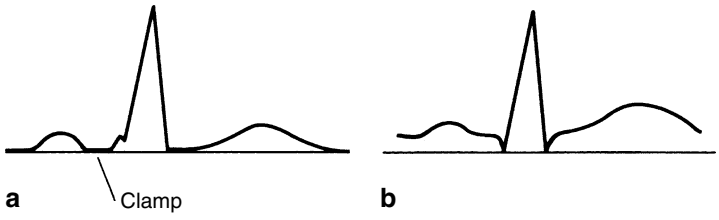

Figure 45.6

M **tracings from clamped *xyz* signals (a). If the baselines of *xyz* signals are not centered to zero (clamped) prior to transformation to polar coordinates, the magnitude tracing will show an upward displacement of the baseline and downward deflections (b).**

Table 45.3

Table of the information (with measurements made from polar coordinates) contained in computer outputs taken from a 99-year-old man with chest pain. Nine beats have been measured and analyzed. Measurements of time intervals are made from spatial magnitudes. Note the consistency of QRS durations, except for beat seven, which suggests aberrant conduction, probably owing to ectopy. P waves are not identified for every beat as they are rather small. R, ST, and T vectors all have abnormal longitudes $(^{**})$; $(M_s\theta)$ is increased $(^{**})$. The extreme right-hand column gives baseline drift in 10 μV units. Under "computer comments," beats are ranked in order of increasing drift. Rows of asterisks indicate beats to which the comments apply, thus providing an indication of consistency. Criteria for anterior myocardial infarction (AMI) and inferior myocardial infarction (IMI) are present in each beat and are identified by letters in parentheses: B, a; T, b; d, i; y, g; G, c; where the upper case indicates a stronger positive criterion and the second lettered component refers to the lettered criterion in the text. For example, G, c indicates criterion c based on gamma downslope. "EQ vectors" refer to spherocardiographic criteria. The transverse QRS-vector loop indicates anterior infarction by having a notch in the efferent limb

Beat	R-R	PR	QRS	QT	QT_c	*M*	Latitude	Longitude	*M*	Latitude	Longitude	*M*	Latitude	Longitude	M	Latitude	Longitude	m_tR	M_S	$M_S\theta$	Drift
1			82	382	409				1.80	29P	−5**	0.18	40A	−171**	0.32	40A	−171**	1.79	0.12	11**	12
2	874		82	385	412				1.83	27P	−5**	0.16	29A	−180**	0.31	31A	−171**	1.82	0.12	12**	3
3	863		82	383	410				1.83	27P	−5**	0.17	85A	−171**	0.31	31A	−171**	1.82	0.15	14**	8
4	868	160	83	368	394	0.10	36P	−14	1.81	29P	−5**	0.14	44A	−168*	0.32	34A	−167**	1.81	0.10	8*	8
5	845	161	84	398	426	0.06	45P	0	1.80	25P	−4**	0.22	33A	−180**	0.37	29A	−176**	1.80	0.12	11**	4
6	854		85	362	388				1.78	28P	−4**	0.13	38A	−143*	0.25	34A	−168**	1.78	0.06	5*	5
7	871	154	99	386	413	0.09	43P	−18	2.0	86A	−171**	0.20	36A	−180**	0.33	32A	−180**	2.10	0.14	13**	4
8	844		85	382	409				1.84	27P	−6**	0.13	38A	−168*	0.25	40A	−161**	1.83	0.10	9*	8
9	887	162	81	375	402	0.12	30P	−36**	1.78	29P	−7**	0.22	33A	−180**	0.38	31A	−176**	1.77	0.14	14**	

Computer comments

2 7 5 6 3 4 8 1 9 (valid for beats shown, in order or drift)

* Abnormally directed P vector

*** * * * ** Unusual R-vector direction

\+ LVH by voltage: possible *(+)/probable(*)

** * * * *** QRS suggests (+)/indicates (*) AMI, (BT BT BT BT BT BT BT BT BT)

*** + ***** QRS suggests (+)/indicates (*) IMI (dy dy dy dy dy dy dy dyG dy)

I I I I I I I I I EQ vectors suggest apical (A), lateral (L) or inferior (I) MI.

*** * * * ** Nonspecific T-wave abnormality

*** * ** Nonspecific ST abnormality

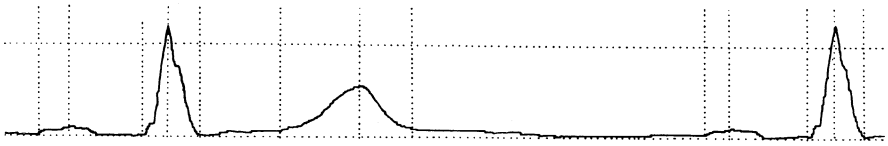

Figure 45.7

The normal spatial magnitude tracing in a computer-generated polarcardiogram. *Vertical dotted lines* show some computer-identified points in time. The time between dots horizontally is 10 ms. Note that the onset of each QRS in this *M* tracing is clamped to 0.

running into the QRS complex as is sometimes seen in the Wolff–Parkinson–White (WPW) syndrome, may give problems. The analysis program, however, bases its diagnosis of the WPW syndrome on the presence of delta waves in the ECG leads V_3–V_5, derived from the *xyz* signals. These signals are not distorted by clamping, since its effect is merely to straighten the baselines. Indeed, distortion resulting from drift tends to be reduced. The 12-lead ECGs derived from such clamped *xyz* signals (see Chap. 11) are free from baseline drift and are thereby much improved (Fig. 45.18b). A record of the drift between beats is printed out by the computer in its table of measurements (Table 45.3). The computer analyzes each beat separately and ranks its findings in order of increasing drift (Table 45.3). If beats show excessive drift they can be rejected by the program. Distortion might be expected from the so-called atrial T wave, occurring just before and during the QRS complex. This turns out not to be a problem, however, because atrial T waves are small and of low frequency, so they do not disturb early QRS vectors important in the diagnosis of infarction.

The designation of part of the ECG as baseline is arbitrary because the actual DC level (see Chap. 12) is not measurable with conventional equipment. Two possible choices for the baseline are the PR and TP segments. Early analog polarcardiographs used the TP segment, clamping being triggered by the preceding R wave, followed by a time delay adjusted by the operator. Fast heart rates and U waves gave problems, however. When tape-recorded *xyz* signals became available, the PR segment became the baseline of choice. Two reproducing heads allowed the R wave, detected through circuitry linked to the first head, to trigger clamping before the same QRS complex arrived at the second head; a short time delay allowed the clamp point to be positioned just before QRS onset. When baseline drift occurred between beats, clamping resulted in a step resetting the *M* tracing to zero (Fig. 45.8) prior to QRS onset. P vectors, preceding the clamp point, were thus affected by the total drift from the previous clamp. This problem was eliminated when digital signal-processing was adopted for polarcardiography, because baseline-drift removal could then be carried out forwards and backward between clamp points, so that drift corrections were linearly spread over the whole heart cycle. Digital processing, by allowing retrograde clamping, thus increased the accuracy of determinations of P-vector magnitudes and directions. It also permitted much refinement in the determination of the clamp points and eliminated operator adjustments.

It has been pointed out that no new information results from the transformation of rectangular to polar coordinates, although hidden features may be made obvious. It could be argued, however, that baseline clamping and straightening do add something to the tracings that is already known information but not contained in them, namely, that baseline wander or drift is non-cardiac in origin, and that the magnitude of the heart vector before the QRS complex may be taken as zero, to give a manifestly undistorted *M* tracing. The embodiment of this information in the polarcardiogram is, then, an addition. Clamping the *xyz* signals improves the quality and usefulness of the VCGs obtained from them because it provides accurate centering of the E point (Fig. 45.11). This often cannot be achieved with VCG loops, because the E point is a blurred spot resulting from the telescoping of noise and small signals around it.

45.3.2 Some Characteristics of Magnitude Tracings

45.3.2.1 P Waves

Generally, in magnitude (M) tracings P waves appear much as in the ECG, except that they are always positive. Sometimes there are two P-wave peaks, suggesting interatrial block. The so-called atrial T wave, sometimes seen in the ECG, will not

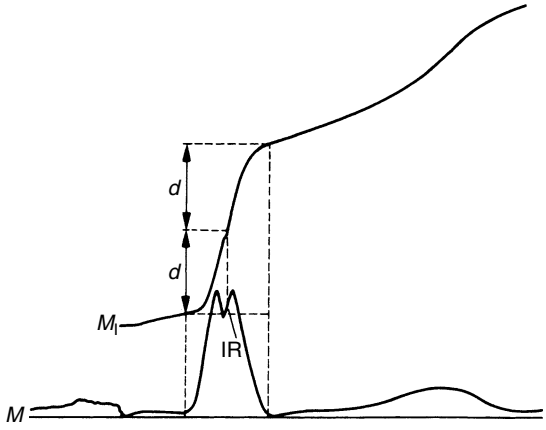

Figure 45.8

The definition of a representative QRS vector IR when there are two equal peaks in the *M* tracing. In these tracings, produced by an analog polarcardiograph, the *M* tracing is recorded together with its integral, *MI*. The height midway between Q and S points in the integral tracing defines the half-area point, IR. Note the step after P wave, caused by baseline clamping.

be observed directly in magnitude tracings because baselines are clamped during this period; however, its presence can be inferred because the baseline preceding the P wave will, in these cases, be displaced slightly upward. Atrial flutter and atrial fibrillation appear in magnitude tracings much as they do in the ECG. Large P waves in the M tracing, as in the ECG, suggest atrial hypertrophy. The cut-off point for the computer diagnosis of this condition is 0.22 mV.

45.3.2.2 QRS Complex

A typical normal QRS complex is shown in Fig. 45.7. It may begin with a decisive rise or show an initial foot. In myocardial infarction, the foot may be exaggerated and associated with diagnostic Q waves in the ECG. The foot may become diagnostic of infarction when it returns to the baseline before the main QRS deflection begins (Fig. 45.11). When this happens in the transverse magnitude, the criterion $m_t \rightarrow 0$ (see Sect. 45.5.1.1) is positive for anterior or anteroseptal infarction. In the VCG, $m_t \rightarrow 0$ may be discernible (Fig. 45.11 where the initial portion of the loop returns to the E point), but often it is lost in noise around the E point, in other parts of the QRS loop, or even in P and ST-T loops.

The peak of the QRS complex in the *M* tracing is usually distinct. The R vector whose magnitude is represented by this peak is then well defined. However, there may sometimes be two peaks of approximately equal magnitude and in this event the first or the second peak may alternately be the greater, from beat to beat. A useful definition of a characteristic QRS vector, in these cases, is the IR point, the point at which the area under the QRS complex is half its final value (Fig. 45.8). This is a more reliable time reference than the Q point, which can be displaced by the initial foot as described above. Such a foot would have little effect on the timing of IR.

Deep notching of the QRS complex in the *M* tracing is a feature of RBBB (Fig. 45.5); sometimes there appears to be a normal initial deflection followed by a delayed, slurred deflection, owing to the block. By contrast, in LBBB the QRS complex tends to be very smooth, but there is usually a small initial foot, corresponding to a small initial R wave in V_1 of the ECG. When magnitude and angle tracings are taken into account, the appearance of LBBB is so characteristic that myocardial infarction can sometimes be diagnosed in the presence of LBBB, which is much more difficult from the ECG (see also Chaps. 14 and 16). Fine notching of the *M* tracing near the peak is not normal and is associated with patchy fibrosis.

Delta waves in the *M* tracing are present in WPW syndrome, but they are not diagnostic. The computer program obtains better results from searching for delta waves in leads V 3–V 5 in the derived ECG. As would be expected, ventricular ectopy produces QRS complexes strikingly different from normally conducted beats, and various types may be classified.

45.3.2.3 ST Segment

Normally, the S point has a magnitude that is zero, or close to it. It is characteristically elevated in stress-induced ischemia (Fig. 45.9) and in injury currents from infarction or pericarditis. This provides a sensitive measure that is easy to quantify by computer. After the S point, the ST segment, normally, gradually slopes upward to become the T wave. In ischemia it may, however, be downsloping. In this case, the S point is at the junction between the steeply descending QRS and the gradually descending ST segment. Fortunately, this point is readily identified by the computer program. There is not, however, any readily identifiable point to be designated as a representative of the ST segment. Therefore, a point midway between the S and T points is used as mentioned in Sect. 45.1 (Fig. 45.4). Sometimes, in gross recent infarction, the ST segment may join with the QRS complex to form a monophasic pattern reminiscent of transmembrane potentials.

45.3.2.4 T Wave

In normal and most abnormal *M* tracings, the T wave is simple and smooth. Rarely, in recent infarction, double T-wave humps occur. Evolving inferior infarction often produces a marked increase in the amplitude of the T wave (Fig. 45.15). Myocardial ischemia usually reduces the relative amplitude of the T wave (Fig. 45.9). U waves, when they appear at all, are often attached to the terminal downslope of the T wave. T waves that are diphasic, or inverted, in the ECG arise from changes in vector direction, more than vector magnitude, and the corresponding abnormalities in the *M* tracing are often minimal though they are revealed by angle tracings.

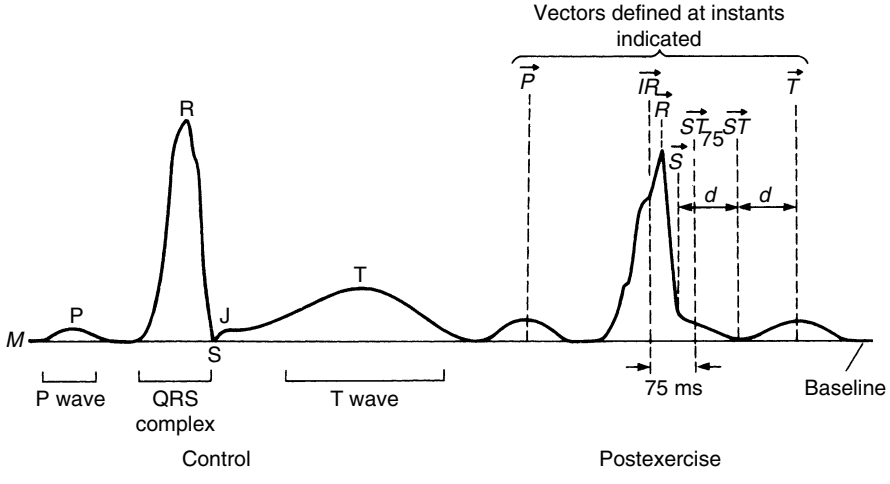

Figure 45.9

Spatial-magnitude changes in stress-induced ischemia, which causes the S-point to rise. The control *M* tracing is on the left and the post exercise *M* tracing on the right. The abnormal direction of ST_{75}, defined 75 ms after IR, is combined with the magnitude at S to give an ischemic index.

45.4 Angle Tracings

Directions of the heart vector in the frontal, transverse, and (left) sagittal planes of the VCG are denoted by angles α, β, and γ which, when plotted against time, give three of the angle tracings of the polarcardiogram (Fig. 45.10). The polarity chosen is such that positive angles appear in the lower half of the scale (Fig. 45.11) in conformity with the vectorcardiographic tradition initiated by Einthoven for describing the electrical axis. Consequently, upslopes in any of these angle tracings indicate counterclockwise rotations of the VCG loops about the E point. Just as the transverse QRS VCG loop in normal subjects consistently shows a counterclockwise rotation, the tracing shows an even upslope (Fig. 45.12). Downslopes in the tracing occur in anterior infarction (Figs. 45.11 and 45.18) and LBBB. There may be a reversal of direction, in normal individuals; that is, a small β downslope near the maximal radius of the loop which corresponds to the peak of the m_t tracing. Downslopes in the β tracing often appear as kinks in the VCG loop (Fig. 45.11). Though less consistent than the β tracing, the γ tracing is useful in revealing inferior infarction by downslopes occurring before the peak of the m_s tracing. However, there must be an initial Q wave in the y-signal tracing, while γ remains in the range $-175^\circ < \gamma < -45^\circ$. The α tracing, like the frontal loop, is much more variable in normal subjects and has not given rise to any polar criteria for infarction.

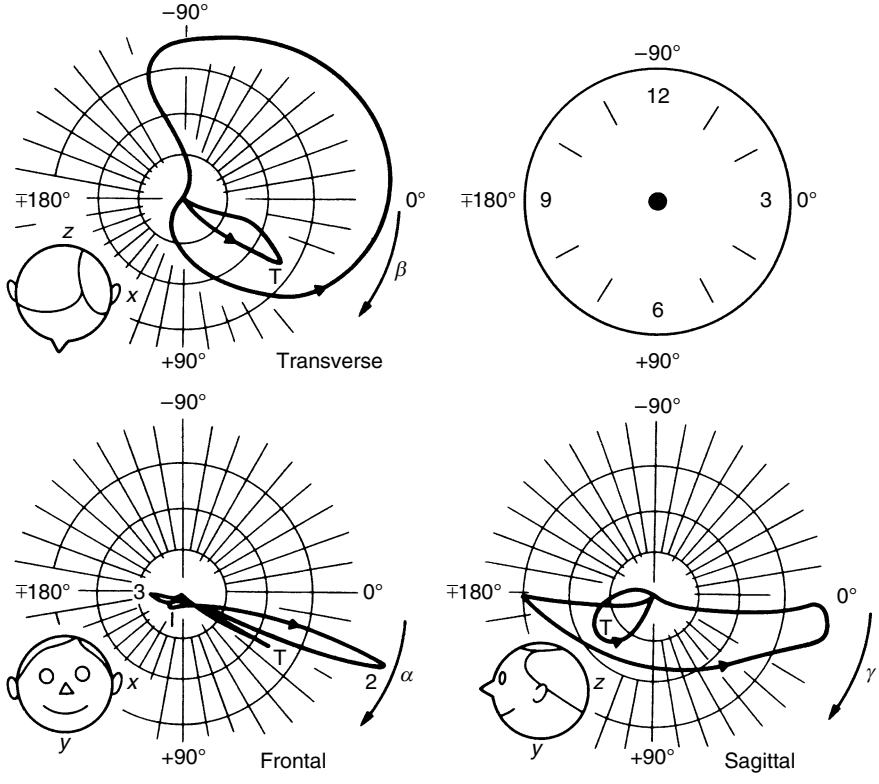

Figure 45.10

Using a clock face as reference for α, β, and γ angles in frontal, transverse, and left sagittal planes respectively, results in 0° at 3 o'clock, +90° at 6 o'clock, ±180° at 9 o'clock, and −90° at 12 o'clock.

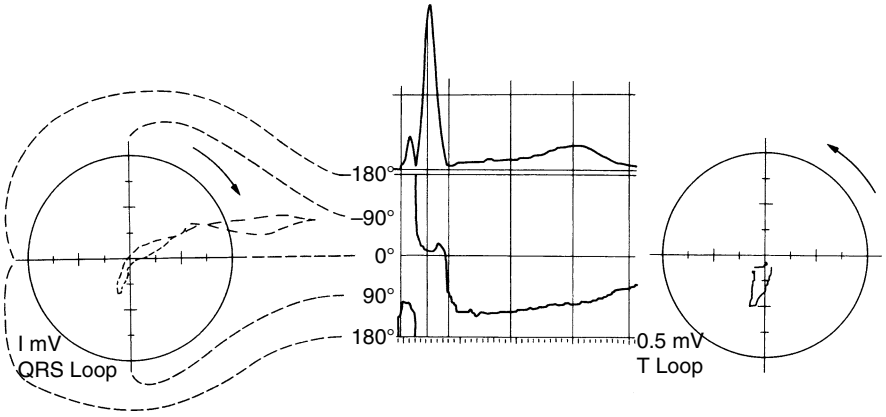

Figure 45.11

The relationship of the transverse QRS loop (*left*), T loop (*right*, amplification doubled), m_t magnitude, and angle tracings (*center*). Clockwise rotations of loops are associated with downsloping angle tracings. The example illustrates previous anterior infarction with $m_t \rightarrow 0$, indicated by the initial m_t deflection returning to the zero baseline and $\beta\downarrow$, indicated by the downsloping tracing, both of which criteria are present. That the initial lobe of the QRS loop returns exactly to the E point is indicated clearly by the m_t tracing; counterclockwise rotation of the T loop is indicated by the upsloping tracing opposite the T wave in the m_t tracing.

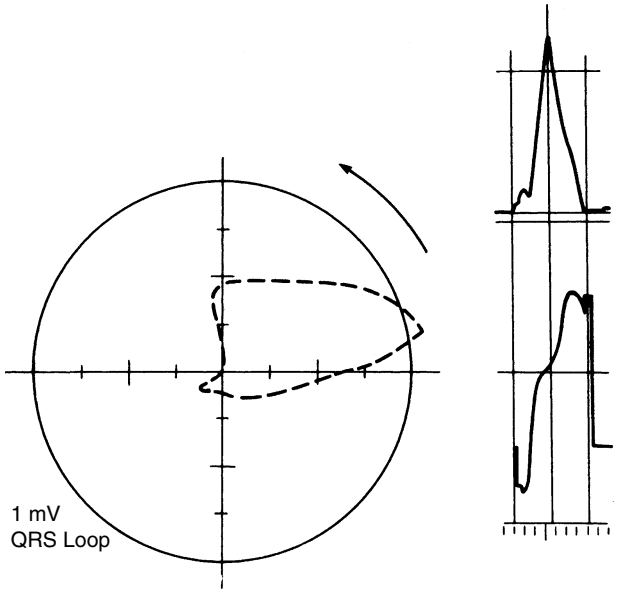

Figure 45.12

A normal transverse plane QRS loop with m_t and β tracings. Note the counterclockwise rotation of the loop and upsloping β tracing.

45.4.1 Latitudes and Longitudes

With the body conceptualized as a sphere, the frontal, transverse, and sagittal planes cut through the center to form equatorial planes of three different spherical polar coordinate systems. Each system has its respective polar axis: posteroanterior (PA), inferosuperior (IS), and right–left (RL). This polarity gives right-handed consistency of coordinates. The angles of the heart vector with respect to the planes give the PA-, IS- and RL-latitude tracings, respectively (Fig. 45.13). Latitudes are expressed in degrees followed by one of the six letters to indicate the direction with respect to

Figure 45.13

Polarcardiogram of the same patient as in Fig. 45.11 which shows the last of three beats displayed here. This beat had least baseline drift before clamping. Time marks occur every 10 ms. *XYZ* tracings (*bottom*) are of *xyz* signals which generate all other displays. *Vertical dotted lines* indicate computer-identified points (compare with Fig. 45.7) determined from the M tracing (second from *top*). Immediately below is the m_f tracing of frontal plane magnitude. Corresponding transverse and sagittal plane magnitudes appear lower down (m_t, m_s). Tracings of angles α, β, and γ appear below m_f, m_t, and m_s tracings, respectively. The remaining tracings are of angles anterior (A) and posterior (P) to the frontal plane, inferior (I) and superior (S) to the transverse plane, and right (R) and left (L) of the sagittal plane. Dots in vertical lines are 10° apart over angle ranges and 50 μV apart over magnitude ranges at standard recording sensitivity.

one of the three equatorial planes. The difference between the latitude of the *R* and *T* vectors differs distinctly in RBBB and LBBB – more so than the corresponding differences in longitudes or the spatial angle between these vectors (Fig. 45.5). Latitude tracings have been less productive of criteria than longitude tracings, although Bruce [5] has defined a criterion for apical infarction based on the RL-latitude tracing: a downslope from 45R or more within the initial 10 ms of QRS, crossing the zero-degree line after the first 10 ms, associated with a Q wave in the *x*-signal tracing and between −45° and −175°. It is, of course, doubly redundant to use six angle coordinates to describe spatial directions and, in fact, this is not done. The directions of *P, R, ST*, and *T*, printed out by the measurement program, are given in terms of α longitude and PA latitude (of angle ψ in Fig. 45.1). Justification for displaying all six angle tracings in the polarcardiogram would be

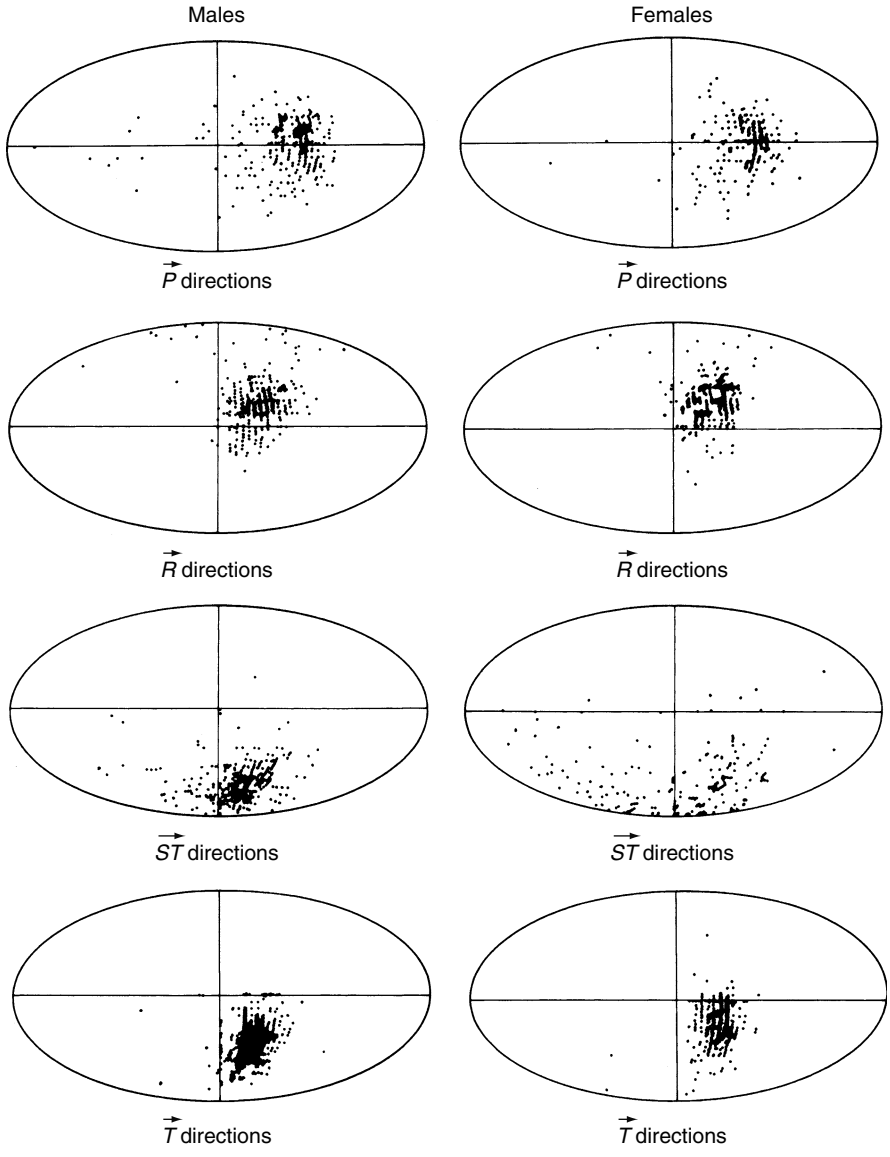

Figure 45.14

Directions of $\vec{P}$, $\vec{R}$, $\vec{ST}$ and $\vec{T}$ in 406 Cretan villagers. These findings should be compared with those of Fig. 45.3. Note that the T-vector distribution for women is slightly posterior to that for men.

the same as that for displaying six limb leads in the ECG or three VCG views when only two are sufficient: abnormalities may show better in some than in others.

45.4.2 Normal Directions of Representative Heart Vectors

The normal directions of $\vec{P}$, $\vec{R}$, and $\vec{T}$ are shown in Fig. 45.3 for 195 young adults, and in Fig. 45.14 for 406 Cretan villagers. Figure 45.14 also shows the directions of the ST vectors. As vector magnitudes decrease toward zero, angular

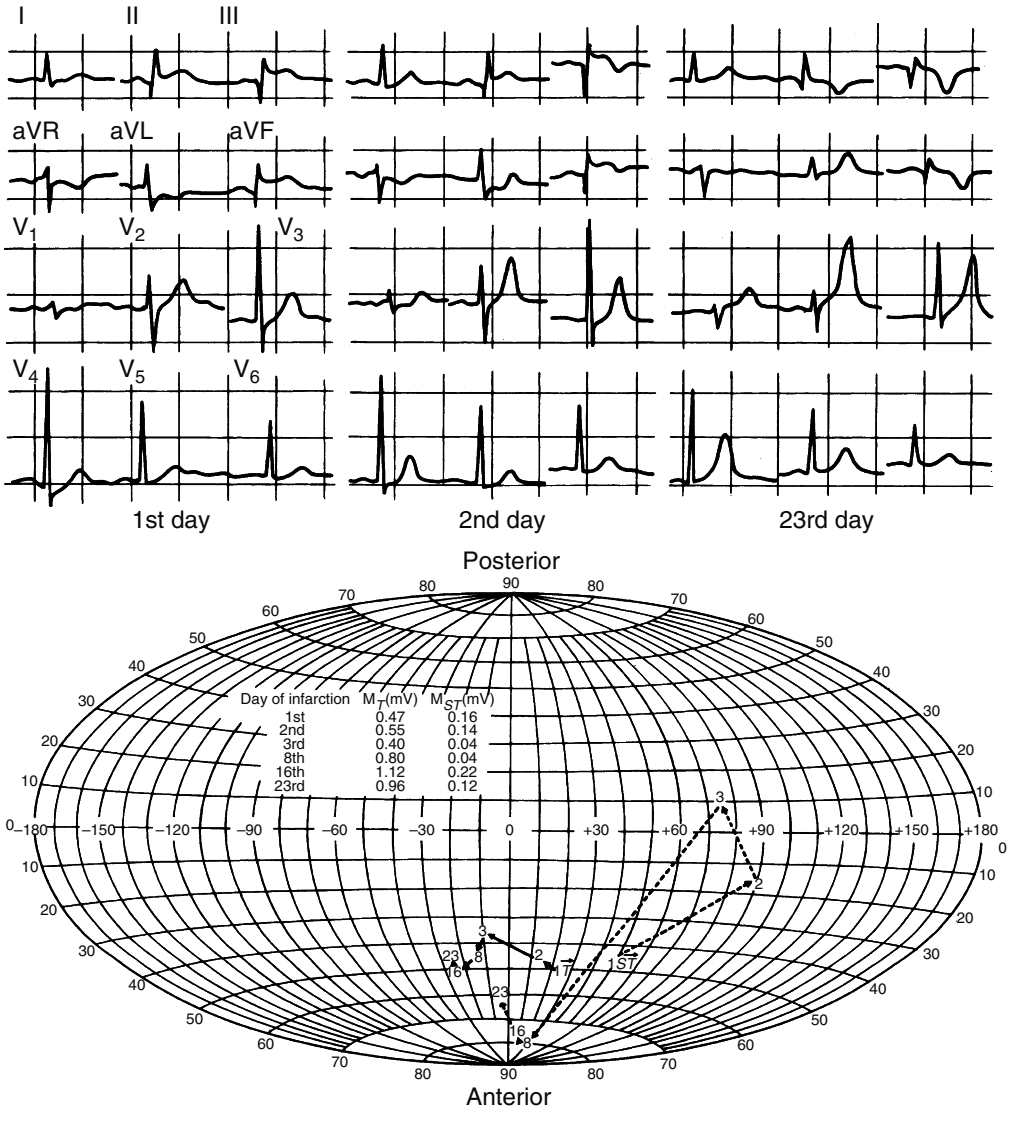

Figure 45.15

The typical migration of the T-wave vector in the Aitoff projection in evolving inferior infarction, with the movement toward "South America." The ST vector ultimately moves toward the same continent. ECGs (*above*) show evolving ST-T-wave changes. The spatial magnitudes of maximum $\vec{T}$ on first, second, third, eighth, 16th, and 23rd days are shown in the table (insert) together with the magnitudes of $\vec{ST}$. Note that on the 16th day, the magnitude of $\vec{T}$ is 2.4 times its initial value.

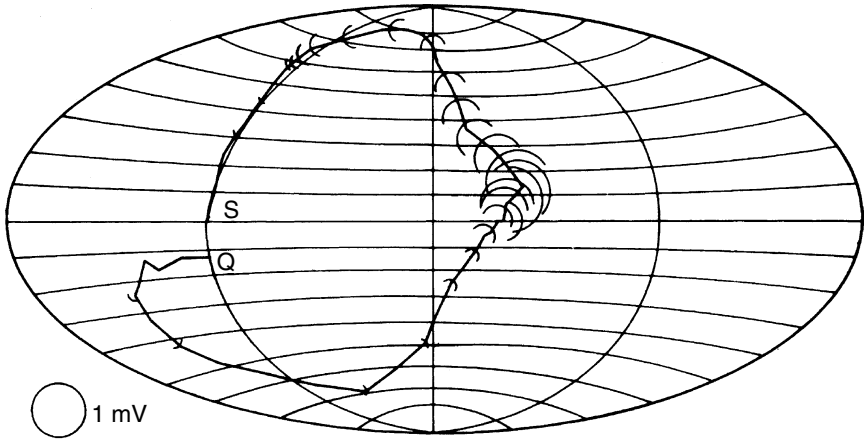

Figure 45.16

A normal spherocardiogram of the same subject as in Fig. 45.12. The snakelike pattern starts in the anterior (*lower*) hemisphere and crosses the equator "east" of the vertical, zero-degree meridian. The beginning and end of the snake are marked Q and S, respectively. Semicircles are drawn every 2 ms. Their diameters indicate spatial magnitude; the reference *circle* represents 1 mV.

directions have less resolution – at zero, directions are meaningless. This accounts for the wide scatter of $S\vec{T}$ directions among the women, whose $S\vec{T}$ magnitudes are often close to zero. In men, the $S\vec{T}$ tends to be larger and shows directions similar to those of the $\vec{T}$. The directions of $\vec{P}$ show considerable scatter, but it is the same in both sexes. $\vec{R}$ directions are well defined, but often change very quickly so that a few milliseconds difference in the timing of the R peak in the *M* tracing can result in a large difference in direction. This is responsible for some of the scatter seen for the $\vec{R}$ directions. $\vec{T}$, on the other hand, tends to change direction very gradually, if at all. It will be recalled that, in the VCG, the normal T loop is often a straight line. For this reason, and because magnitudes are large enough for accurate definition of direction, $\vec{T}$ directions show the least scatter. They form a well-defined "continent" that occupies only about 5% of the area of the globe (Fig. 45.3).

Abnormal $\vec{P}$ directions are useful in detecting abnormalities that, in the ECG, might be interpreted as a result of a low atrial focus. They have not, however, proven of much value in detecting atrial hypertrophy, which is more reliably done from the magnitude of $\vec{P}$.

Unusual $\vec{R}$ directions are helpful but tend to occur too frequently to justify calling them abnormal, if that is the only finding. It will now be appreciated by the reader that the longitude of $\vec{R}$ is a measure of Einthoven's electrical axis, which is not to be confused with the mean electrical axis (see Sect. 45.5.4).

The most useful vector direction is that of $\vec{T}$. Directions of $\vec{T}$ that fail to lie within the normal continent (Fig. 45.3) will give rise to abnormal T waves in the ECG. This efficient device for defining normality of T waves, presenting data in a way that immediately strikes the eye, should be compared with the prospect of defining T-wave normality on the basis of the 195 12-lead ECGs from the same subjects! It is an excellent example of the value of both the heart-vector concept and the use of spherical polar coordinates. It can also show subtle differences between populations. Figure 45.14 shows $\vec{T}$ distributions in male and female Cretan villagers: the center of the female distribution is slightly posterior to that of the male. A similar sex difference was observed in children aged 3–4 years [6] which is surprising in view of the similar body build at this age.

In evolving inferior infarction, there is a migration of $\vec{T}$ directions that is most characteristic (Fig. 45.15). If the normal T continent is analogous to the continent of Africa, $\vec{T}$ migrates westward to lie in South America. The concomitant ECG change is the development of inverted T waves in inferior leads.

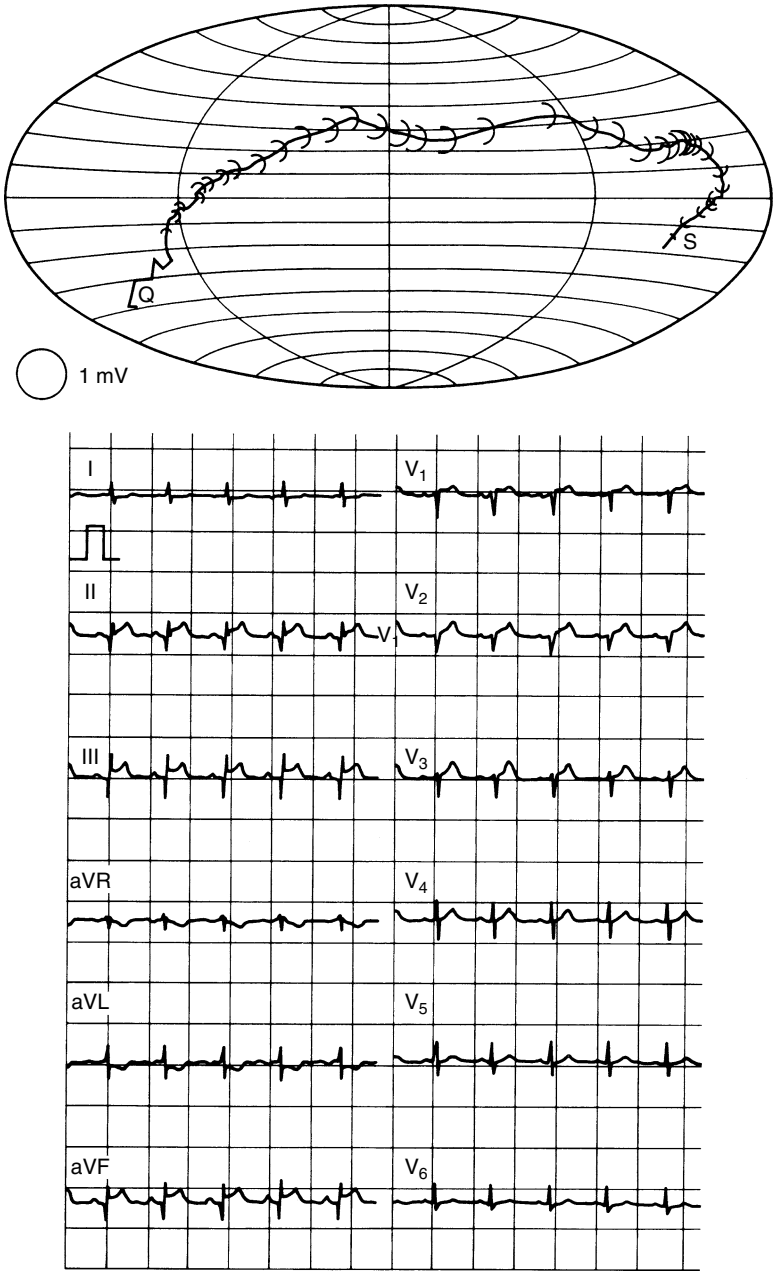

Figure 45.17

The spherocardiogram in inferior infarction. The "snake" begins in the anterior (*lower*) hemisphere and crosses the equator at longitude −80°. This should be compared with Fig. 45.16. The derived 12-1ead ECG below shows recent inferior infarction.

45.4.3 Spherocardiogram

Instead of plotting only a few vectors during the cardiac cycle, the Aitoff projection may be used to plot a full sequence of vectors, every 2 ms throughout the QRS complex (Fig. 45.16). The spherocardiogram [7] is such a display: vector magnitudes are represented by the radii of semicircles whose centers indicate direction and whose convexities indicate

the next plot in the sequence. The result resembles a snake which, for normal subjects, has the thickest part of its body in the region of the "continent" of the direction of the normal $\vec{R}$ (Fig. 45.3). The head of the snake lies in the "southern" hemisphere and its body crosses the equator slightly to the "east" of the zero meridian. Absent initial anterior forces, as in anteroseptal infarction, result in the head lying on the equator or in the "northern" hemisphere. When the body of the snake crosses the equator to the west, inferior infarction is indicated (Fig. 45.17). Although the spherocardiogram has been useful in developing computer criteria (see Sect. 45.5), like the polarcardiogram, it is not routinely generated. Despite being based on spherical polar coordinates, the spherocardiogram is more like a three-dimensional VCG: it suffers from the same shortcoming that phenomena are not displayed against a time coordinate.

45.5 Diagnostic Criteria

Rather than present the various criteria developed for visual interpretation of polarcardiograms, it is thought more useful to outline the criteria now used in the computer program for further analysis. These differ from the older analog criteria [8, 9] in several important ways: they are, of necessity, totally explicit; they are designed to give higher specificity, at the expense of some sensitivity; and they include some new criteria [10].

45.5.1 Criteria for Myocardial Infarction

45.5.1.1 Criteria Relating to the QRS Complex

(a) Polarcardiographic criteria

(i) $\beta\downarrow$: a downslope in the tracing of the angle in the transverse plane (Figs. 45.11 and 45.13), occurring 10 ms before the peak $m_t\boldsymbol{R}$ of the transverse plane magnitude tracing (downslopes in the first 20 ms may be discounted). This is a criterion of anteroseptal or anterior infarction and corresponds to a region of clockwise rotation in the transverse plane vector loop (Fig. 45.18a).

It must be noted that for the computer program, the definition of a downslope must be quite explicit. A downslope is an overall drop of 5° over a total downsloping time of at least 5 ms. A downslope begins at the onset of the first drop and ends at the beginning of the first rise following the fulfillment of its definition requirements of minimum time and overall drop. Small rises are allowed within a defined downslope provided that first, they are subtracted from the drop which has occurred up to that point and second, they do not thereby reduce the overall drop below 1°. Horizontal segments are also allowed, but neither they nor the segments containing rises contribute to the total downsloping time. Downslopes terminating with a net drop $\geqslant 10°$ are rated very marked, otherwise they are rated as significant. An upslope is similarly defined except that drops become rises.

(ii) $m_t \rightarrow 0$: a return to the baseline of the transverse magnitude tracing immediately following an initial deflection (Fig. 45.11). This is a criterion for anterior infarction that is often not apparent in the vector loop because of ambiguity of the E point. It may not be present in every beat (Fig. 45.13).

In the above criterion, "initial" means between 10 ms after the Q point and the time of the peak of the m_t tracing. Return to the baseline means falling to 0.01 mV or less, or to 0.02 mV if the estimate for baseline noise is at least 0.02 mY. Between Q and the return to the baseline there must be a deflection of the m_t tracing of more than 0.05 mV and this amount must be greater than twice the value of the noise estimate.

(iii) $\gamma\downarrow$: a downslope in the tracing of the angle in the left sagittal plane occurring 10 ms after the Q point and 10 ms before the peak m_sR of the sagittal plane magnitude tracing, provided that there is a Q wave in the Y tracing and longitude $< -45°$. This is a criterion of the inferior infarction; it corresponds to clockwise rotation in the initial anterosuperior segment of the left sagittal loop.

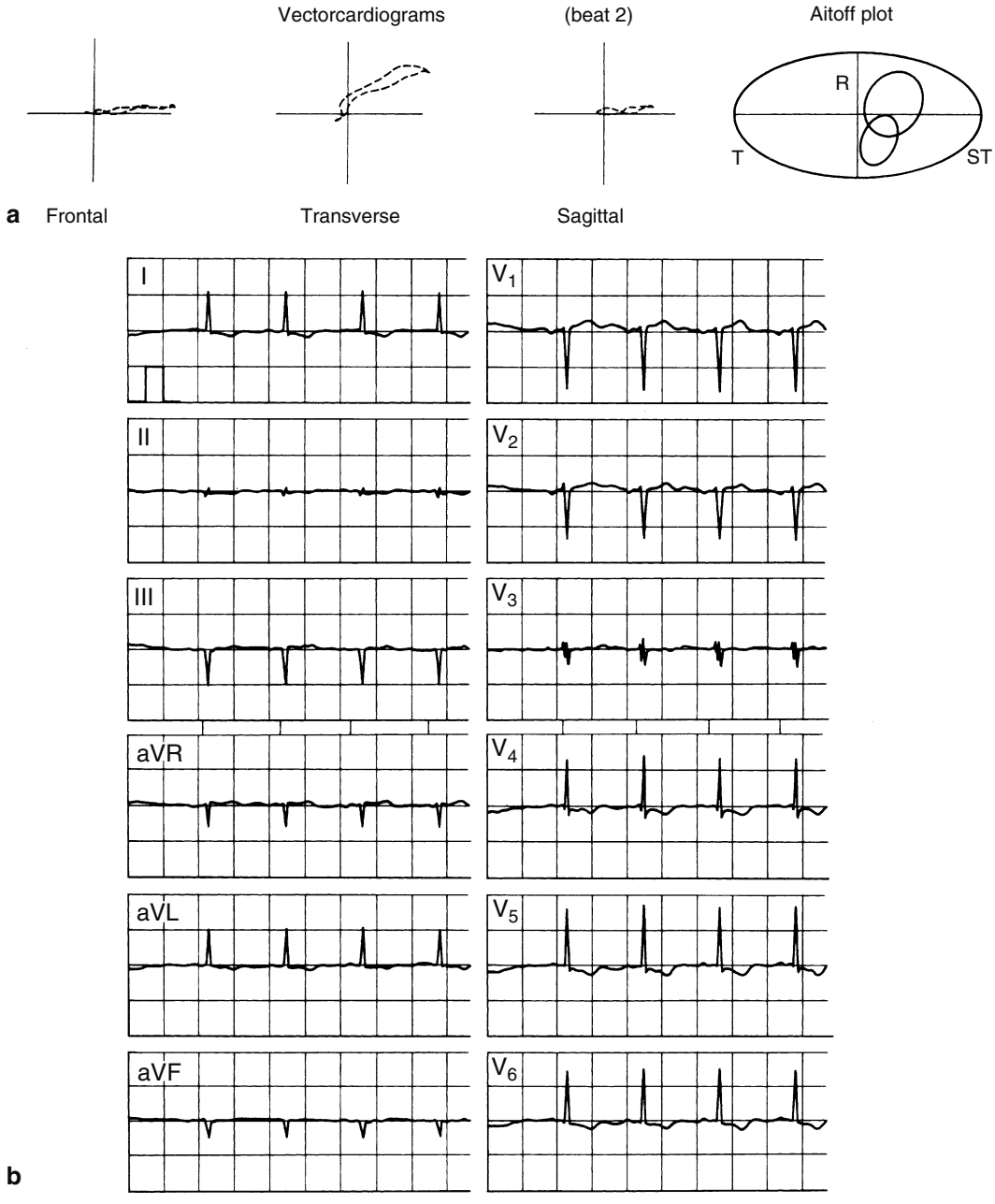

Figure 45.18

Part (a) shows VCGs and the Aitoff plot derived from the information for beat seven given in Table 45.3. The Aitoff plot illustrates that the directions of the R, ST, and T vectors are all outside the normal boundaries. Part (b) shows the ECG derived from three *xyz* signals of beats 1–4 (from Table 45.3); the ECG shows inferior infarction, but less-definite anterior infarction. Note the baseline drift prior to clamping of the first beat. Clamp points are indicated by short vertical lines between leads III and aVR, and V_3 and V_4.

(b) Quasi-electrocardiographic criteria

(iv) Absence of initial anterior forces, indicating by an initial Q wave in the Z tracing. This is a criterion of anteroseptal infarction; it corresponds to Q waves in V_1 and V_2 of the ECG.

(v) Initial anterior forces do not exceed 6% of posterior forces, as indicated in the Z tracing. This is a weaker criterion of anteroseptal infraction than (iv).

(vi) Posterior forces in the Z tracing do not exceed 9% of M_R, the maximum spatial QRS vector. This is a criterion of true posterior infarction; it is invalidated by complete or partial RBBB. It has no ECG equivalent but corresponds approximately to the finding of a small S wave in V_2.

(vii) Initial superior forces exceed 35% of inferior forces, indicated in the *Y* tracing. M_R is substituted for the inferior forces if these become less than 20% of M_R. This is a criterion of inferior infarction and corresponds to a relatively large Q wave in aVF.

(viii) Initial rightward forces exceed 23% of leftward forces, indicated in the *X* tracing. This suggests apical or lateral infarction; it corresponds to a relatively large Q wave in leads I, aVL or V_6.

(ix) Duration of the Q wave in the Y tracing exceeds 40% of the QRS complex in the spatial magnitude tracing. This criterion of inferior infarction roughly corresponds to a wide Q wave in aVF.

(c) Spherocardiographic criteria

(x) The locus of QRS directions on the sphere crosses the equator outside the normal longitude range of -15° to $+100^\circ$. This suggests inferior, lateral, or apical infarction (I, L, or A) according to the following ranges: $-130^\circ <$ longitude $< -15^\circ$ for inferior infarction; $+100^\circ <$ longitude $< +175^\circ$ for lateral infarction; and $+175^\circ <$ longitude $< -130^\circ$ for apical infarction (range passes through 180°). These criteria do not correspond to any ECG criteria.

Note that, near the crossing of the equator, the latitude must change from 5A to 5P within 10 ms. During this period, the vector magnitude must exceed 5% of M_R and the crossing must have occurred by 15 ms after the spatial magnitude tracing reaches its peak (M_R).

45.5.1.2 Non-QRS Criteria

(xi) $S\vec{T}$ suggests a current of injury if $M_S > 0.167M_R$, where M_S is the magnitude of the spatial vector at the end of QRS, that is, the S point. This criterion has no ECG counterpart. There are refinements of this criterion which indicate the region of the injury such as anteroseptal, lateral apical, according to the direction of $S\vec{T}$.

(xii) $\vec{T}$ suggests an evolving or old inferior infarction at first, $M_T > 0.2M_R$, where M_T is the spatial magnitude of the maximum $\vec{T}$; and second, this vector has a longitude between -10° and -60° and a latitude posterior to 70A and anterior to 20P.

(xiii) $\vec{T}$ suggests anterior injury if they have the following characteristics. First, $M_T > 0.2M_R$; second, the longitude of the maximum $\vec{T}$ is between -120° and $+165^\circ$; third, M_T has a latitude posterior to 20P, but lies outside a region defined between longitudes 0° and $+45^\circ$ and latitudes 19P and 45P; and finally, RBBB is not present. This corresponds to T-wave inversion in anterior precordial leads not of the type seen as a normal variant in women.

45.5.2 Evaluation of Performance of Infarction Criteria

The above criteria were evaluated with a test set of 369 subjects selected from a much larger population who were studied angiographically; 234 had 100% occlusion of a major coronary vessel and associated akinesia or dyskinesia (indicating infarction), and 135 had less than 50% occlusion, normal wall motion, normal hemodynamics, and no history of infarction [11]. The ECGs of the 369 subjects were separated into infarction and non-infarction groups by cardiologist ECG readers at two hospitals. A corresponding division was made by the computer using the above criteria. The computer's selection agreed slightly better with the angiographic evidence than the selections of the readers at the two hospitals: both its sensitivity and specificity were higher, though not significantly so. However, when the computer's selection of infarction cases was combined with the selections of either of the two groups of readers, the improvements in sensitivity were significant, while the corresponding reductions in specificity were not. This was satisfactory because the computer

Table 45.4

Apparent (worst case) specificity of polar computer program with respect to myocardial infarction (MI) tested on 473 presumed healthy Cretan villagers in various age-groups

	Men			Specificity
Age-group	Na	%	*MI + veb*	%
19–29	44	68	1	98
30–39	100	9	2	98
40–49	118	61	4	97
50–59	95	55	5	95
60–69	80	63	10	88
70–89	36	64	8	78
All	473	60	30	94

[a] Median ages for the men and women were both 46 years
[b] Positive diagnosis of previous infarction made by computer program

output was designed to be used as an aid to the cardiologist interpreting the ECG, rather than as an automated simulation of his interpretation. It is important to note, as an aside, that although the readers did not have VCGs for this evaluation, the computer generates these whenever it makes a diagnosis of infarction based on QRS evidence. This usually allows the reader to corroborate a positive diagnosis of infarction by the computer despite the lack of corroboration in the derived 12-lead ECG, that is, the ECGD (see Chap. 11). Sensitivity and specificity for the computer, alone, were 78% and 92%. However, the 92% specificity should be regarded as probably lower than it would be with a truly normal population because the 135 subjects who were negative angiographically could have had undetected lesions, since they all had sufficient chest pain to justify cardiac catheterization. When the computer criteria were applied to a test set of 118 Cretan villagers aged 40–49 years, the specificity was 97%. This is still probably lower than the true specificity because the Cretans were not examined – they were presumed healthy on the basis of the reported low prevalence of coronary artery disease among Cretan villagers [12]. Table 45.4 shows the specificity of the criteria in 473 Cretan villagers of various age-groups. Among the age-groups under 60 years, the specificity is 95% or better. There is a progressive decline in specificity with age, particularly after the age of 60 years. This decline is less than it appears, however, because 14 of the 30 positive cases had clear ECG evidence of previous myocardial infarction. Of course, it is possible to object that ECG evidence is inadmissible because it is not truly independent, but a cardiologist would find fault with failure of a computer program to detect "infarction" indicated by the ECG, so perhaps the program should not be faulted for those 14 cases. When this adjustment is made, the specificity for all subjects under 70% becomes 97%.

45.5.3 Criteria for Left Bundle Branch Block

This chapter would be unreasonably long if it contained every diagnostic criterion used by the polar analysis program. The myocardial infarction criteria have been given because of their importance and interest. The criteria for LBBB are also interesting and illustrate the polar approach when non-ECG evidence for a diagnosis is lacking.

Typical LBBB is recognized if:

(a) $\vec{R}$ is at least 70° posterior to $\vec{T}$
(b) The vector 30 ms before **IR** has transverse plane angle < 30°; that is, $\beta_{\mathrm{IR}} - 30\ \mathrm{ms} < 30°$
(c) The spatial angle between Rand $\vec{T}$ exceeds 120°
(d) β increases by less than 20° from **IR** to **IR** + 20 ms
(e) $\beta_{IR+10\ \mathrm{ms}} \leqslant \beta_{IR+10\ \mathrm{ms}} + 22$ and
(f) QRS duration is flagged in the table of measurements ">>" (see Table 45.1)

If condition (a) is false and $90^\circ \leqslant \vec{R} < -70^\circ$, or if $\vec{R}$ is posterior to 30P, then the LBBB is considered atypical.

If LBBB is otherwise typical but M_S exceeds 5% of M_R, there is the probability of injury or aneurysm.

Left ventricular hypertrophy is probably present in addition to LBBB if M_R exceeds 4 mV; it is also possible if M_R exceeds 3 mV.

45.5.3.1 Developing Criteria for LBBB

The marked differences between the above criteria for LBBB and those employed in conventional electrocardiography exemplify the polar approach used by the computer program. A view concerning the development of diagnostic criteria for computer analysis of the ECG that has enjoyed recent currency is that, to be valid, such criteria must be based on independent, that is, non-ECG disease classification. Independent means for selecting suitable populations are available for myocardial infarction and LVH (so-called type A diagnosis) but not for LBBB, a condition identified, and therefore defined by the ECG (a type B diagnosis [13]). Because no independent "gold standard" is available for LBBB, it might appear most reasonable to employ ECG criteria in the computer program. Instead of this, the ECG was used to select cases of LBBB whose polarcardiograms were then studied for clearly identifiable characteristics. Several polarcardiograms appeared that could not be simply stated in terms of the ECG. For example, striking differences in the contours of the *M* tracings separated LBBB from RBBB (Fig. 45.5). The $\vec{R}$ and $\vec{T}$ of these conditions show marked differences in latitudes (Fig. 45.5).

The approach followed in developing LBBB criteria was as follows:

(a) Identify, from ECGs, a population (training set) with well-recognized LBBB
(b) Compare polarcardiograms and vector loops of this population with those of a non-LBBB population and observe any clear-cut characteristics that separate the populations
(c) Organize these into an effective tool for identifying LBBB, and
(d) Observe how well this tool performs, in a separate test set, when the ECG is ambiguous, and whether it misidentifies LBBB in those cases where the ECG is definite as a gold standard

This approach can produce a better indicator even when there is no independent standard. It has historical parallels. Wenckebach's phenomenon, although nowadays an ECG diagnosis, was originally identified in polygraph tracings. Its description predated that of the electrocardiograph by 4 years. The polygraph, however, did not give satisfactory recordings in every case and was supplanted by the ECG as a gold standard for this condition.

An approach similar to the above was undertaken for RBBB and IV conduction delay. Once the various subtleties for discriminating these conditions had been programmed, approximately 100 examples of each were selected by the computer from stored data which was not used in developing the criteria, and the derived 12-lead ECGs were studied to check the accuracy of the computer identifications. There were no discrepancies beyond what would be considered acceptable differences of opinion. Since the ECG criteria for diagnosing LBBB have served so well over the years, it might be asked what the benefit is from introducing others, even if they seem less ambiguous. An example of the value of this is that the distinction between LBBB and LVH with IV conduction delay is sometimes difficult from a single ECG, whereas the computer tends not to confuse them. The ability of the program to identify injury or aneurysm in LBBB is particularly interesting: in LBBB, the S point in the *M* tracing returns to the baseline as it does in the normal subject. Departures from this are unusual and appear to connote injury or perhaps aneurysm. This feature cannot be detected from the ECG.

45.5.4 Left Anterior Fascicular Block

Like LBBB, left anterior fascicular block is an entity defined by the ECG but it seems to be less clearly defined. Its diagnosis hinges on the mean QRS axis being less than -45°. The mean QRS axis is defined from leads I and III using the Einthoven triangle, except that, instead of taking simultaneous points in time in each lead, the sums of the positive and negative deflections are normally used. Unfortunately, because simultaneity is abandoned, the triangle scheme no longer applies, since the "deflections" in lead II no longer fit the "vector" constructed from the other two leads. The result is not a vector

at all and lacks a physical basis. The mean QRS axis was introduced in order to determine some indication of axis *from* the nonsimultaneous data provided by the then-standard single-channel electrocardiograph. The α tracing is a continuous display of the electrical axis throughout the heart cycle with the improvement provided by a scientifically based lead system. With this available, there would seem to be little merit in persisting with a technically inferior and theoretically questionable measure, such as the mean QRS axis, as a diagnostic discriminator. However, with a continuous range of axes available, which should be selected as most representative of QRS events?

The polarcardiographic criteria for left anterior fascicular block are that the longitude of $I\vec{R}$ (Fig. 45.8) is between −110° and −45° with QRS duration <110 ms. The diagnosis is excluded if LBBB, RBBB, LVH, low voltage, inferior infarction, injury, current, or recent infarction are diagnosed. The use of $I\vec{R}$ rather than $\vec{R}$ gives a little more consistency in cases where there are two peaks in the M tracing. The directions of $I\vec{R}$ are generally the same as those of $\vec{R}$ but show slightly less scatter.

Polarcardiographic study of left anterior fascicular block has not revealed any clear-cut set of discriminators, such as those described for LBBB. Perhaps this gives support to the doubts expressed by some concerning the validity of left anterior fascicular block as a clinical entity [14]. Clearly, in this case, some independent "gold standard" would be useful.

Although the computer comment suggesting left anterior fascicular block tends to agree with the visual reading of the derived 12-lead ECG, occasional examples of disagreement should not be a surprise in the light of the foregoing. Of course, these examples could be reduced to zero by the expedient of adopting the mean QRS axis, despite its faults, as the discriminator. This could easily be done but it seems like a backward step.

45.5.5 Left Ventricular Hypertrophy

In the course of developing polarcardiographic criteria for LVH, electrocardiographic and autopsy criteria were closely examined. Problems were encountered with both. Nevertheless, some correlation exists between the mass of cardiac muscle and the strength of the electric field generated by the heart. This is exploited in the voltage criteria of the ECG, but amplitudes in several leads must be measured and correlated because individual variations in the orientation of the maximum heart vector produce maximal projections on different leads. This problem is solved in polarcardiography in which the *M* tracing gives a direct indication of field strength. Thus, one measurement, M_R, the spatial magnitude of the maximum QRS vector, $\vec{R}$, can replace measurements of several limbs and chest leads of the ECG. Another measurement, $m_t R$, the magnitude of the projection of $\vec{R}$ in the transverse plane, is also useful because there is a tendency for LVH to be associated with a 20° change in longitude of $\vec{R}$ toward the transverse plane, so that $m_t R$ is increased by these two effects. A study of 168 autopsied cases, comparing the ratio of heart weight to body length with M_R and $m_t R$ yielded correlation coefficients of 0.48 and 0.50, respectively [15]. These are not impressive, but fibrosis and scarring was present in many of the cases, and these tend to reduce voltage. (Pure LVH, observed in children, yielded much higher correlations [16].) Performance of ECG voltage criteria, if measurements are carefully made, on tracings obtained with good equipment turns out to be about the same, but not all cases of LVH recognized electrocardiographically meet polarcardiographic criteria for LVH, and vice versa.

An exact definition of LVH is difficult. Heart weights in normal subjects show such a wide variation that a patient's heart weight may undergo 50% hypertrophy, yet still not exceed the upper bounds *for* normal [17]. Taking body length into consideration reduces the spread somewhat but the coefficients of correlation are very low [17]. Body-surface area is commonly employed as a correlate of LVH diagnosed by echocardiography (see also Chap. 15). An echopolar study is overdue. Body build, athletic activity, and aging are normal factors that have a pronounced effect on body-surface voltages. If the effects of fibrosis, scarring, and myopathies are added to these, it is easy to appreciate that the diagnosis of LVH from body-surface potentials, whether these are studied as ECGs, VCGs, or vector magnitudes, is apt to be inexact. A further disquieting factor is that some patients show considerable day-to-day variations in voltage, beyond those attributable to differences in electrode placement or electrical activation.

The polarcardiographic criteria for LVH are indicated in Table 45.2. The appendix (Table Al.96) gives medians and upper 95 percentiles for 466 Cretan villagers for M_R and $m_t R$. Up to the age of 50 years, M_R is greater in males but gradually reduces with age in men, less clearly so in women. For the entire group, aged 19–82 years, for both sexes, the upper 95 percentiles for M_R and $m_t R$ are 2.25 mV and 2.05 mV, respectively.

Of the ECG criteria of LVH – hypervoltage, left axis deviation, increased ventricular activation, and ST-T changes – only the first, and to some extent the second, have polarcardiographic equivalents (M_R and $m_t R$). The ST-T changes were considered secondary and nonspecific. When abnormal, ST-T-vector directions, as shown on the Aitoff plot, resemble those seen in ischemia. Ventricular activation time is based on the concept of intrinsicoid deflection, which is untenable vectorcardiographically since precordial-lead tracings can be simulated from derivations of the *xyz* signals.

45.5.6 Right Ventricular Hypertrophy

"Probable" right ventricular hypertrophy (RVH) is stated by the computer program if $\vec{R}$ is directed to the right, that is, if the longitude of $\vec{R}$ is not in the range $-90^\circ <$ longitude of $R < +90^\circ$, provided that:

(a) The ratio of maximum anterior forces to maximal posterior forces, during the QRS complex, exceeds 4
(b) $M_P > 0.22$ mV
(c) T is not posterior to 50P, and
(d) RBBB is not diagnosed

It is also stated that if the direction of $\vec{R}$ is more than 10° outside the normal bounds, $I\vec{R}$ is not in the range $-I\ 10^\circ <$ longitude of $I\vec{R} < +120^\circ$, and the angle between $\vec{R}$ and the direction of the lead I lead vector (59A, + 100) is less than 90°.

45.5.7 Ischemia

In myocardial ischemia, the **T** tend to be distributed around the 180° meridian (see Table 45.3), that is, approximately 180° from the normal direction of the $\vec{T}$. This corresponds to T-wave inversions in the ECG in ischemia. When ST segments of the ECG are depressed in ischemia, the directions of **ST** tend to parallel those of $\vec{T}$. During exercise testing, ischemia produces characteristic polarcardiographic changes which have been incorporated into an index of ischemia, $M_S\theta$. In the *M* tracing, the S point, instead of lying on or close to the zero baseline, becomes elevated (Fig. 45.9); M_S increases. The magnitude of the T wave, M_T in the *M* tracing tends to diminish, while that of the ST segment midway between the points S and T is variable. However, the directional change of *ST* is characteristic. The optimal time selected for sampling the directional *ST* changes is 75 ms after IR (Fig. 45.9) [18]. The directional change from normal is given by the spatial angle θ between the ST_{75} vector so defined and the normal direction of that vector, which is taken as (50A, +20) (latitude and longitude) after exercise, or (50A, +30) at rest. The product of M_S and θ gives the ischemic index $M_S\theta$. Because directions become meaningless as magnitudes reduce to zero, θ is considered to be zero if M_{ST75}, the spatial magnitude of the ST_{75} vector, is $\leqslant$0.04 mV. For normal subjects, $M_S\theta < 7$ and the test is positive for ischemia if $M_S\theta$ exceeds 10.6; however, $M_S\theta$ may reach 60. Thus, ischemic changes seen in various leads of the ECG are reduced to a single number that has much more resolution than the microvolts of ST depression observed in various leads of the ECG. Furthermore, the ischemic index is easily programmed into the computer. It has shown statistically significant drug-induced changes that could not be demonstrated in the ECGs of the same patients [19].

45.6 Conclusion

The polar approach is but one of many means for studying and characterizing the electric field produced by the heart. Although it may strike the reader as strange, even alien, it often provides a relatively efficient means for categorizing abnormalities. In this regard, its very strangeness can be an asset since previously unrecognized features may be revealed. From a programming standpoint, the polar approach is attractive because it tends to be explicit.

References

1. Einthoven, W., G. Fahr, and A. De Waart, On the direction and manifest size of the variations of potential in the human heart and on the influence of the position of the heart on the form of the electrocardiogram. *Am. Heart J.*, 1950;**40**: 163–194.
2. Dower, G.E., *Polarcardiography*. Springfield, IL: Thomas, 1971, pp. 3–190.
3. Moore, A.D., P. Harding, and G.E. Dower, The polarcardiograph. An analogue computer that provides spherical coordinates of the heart vector. *Am. Heart J.*, 1962;**64**: 382–391.
4. Dower, G.E., D. Berghofer, and M. Kiely, Accuracy of computer measurements of QRS duration using spatial magnitude. Agreement with human readers. *Comput. Biomed. Res.*, 1983;**16**: 433–445.
5. Lerman, J., R.A. Bruce, and J.A. Murray, Correlation of polarcardiographic criteria for myocardial infarction with arteriographic and ventriculographic findings (substantiation of transmural and presentation of non-transmural criteria). *J. Electrocardiol.*, 1976;**9**: 219–226.
6. Niederberger, M., G.E. Dower, and H.B. Machado, Polarcardiographic and vectorcardiographic study of 70 normal children aged 3–4 years. *Clin. Cardiol.*, 1978;**1**: 142–151.
7. Niederberger, M. and G.A. Joskowicz, Global display of the heart vector (spherocardiogram). Applicability of vector and polarcardiographic infarct criteria. *J. Electrocardiol.*, 1977;**10**: 341–346.
8. Dower, G.E., H.E. Horn, and W.G. Ziegler, The polarcardiograph. Diagnosis of myocardial infarction. *Am. Heart J.*, 1965;**69**: 369–381.
9. Dower, G.E. and H.E. Horn, The polarcardiograph. Further studies of normal subjects, refinement of criteria for infarction, and a report on autopsied cases. *Am. Heart J.*, 1966;**72**: 451–462.
10. Dower, G.E., D. Berghofer, and M. Kiely, Polarcardiographic computer system vs cardiologists and derived ECG in diagnosis of infarction, in *Computers in Cardiology*, K.L. Ripley, Editor. New York: IEEE, 1982, pp. 75–80.
11. Dower, G.E., H. Bastos Machado, J.A. Osborne, D. Berghofer, and M. Kiely, Performance of computerized heart vector criteria in the diagnosis of myocardial infarction. *Rev. Port. Cardiol.*, 1984;**3**: 687–697.
12. Aravanis, C., A. Corcondilas, A.S. Dontas, D. Lekos, and A. Keys, IX The Greek islands of Crete and Corfu, in *Coronary Heart Disease in Seven Countries*, A. Keys, Editor. *Circulation*, 1910;**41**(Suppl I): 88–100.
13. Rautaharju, P.M., M. Ariet, T.A. Pryor, et al., Task Force III: computers in diagnostic electrocardiography. *Am. J. Cardiol.*, 1978;**41**: 158–170.
14. Rabkin, S.W., F.A.L. Mathewson, and R.B. Tate, Natural history of marked left axis deviation (left anterior hemiblock). *Am. J. Cardiol.*, 1979;**43**: 605–611.
15. Dower, G.E. and H.E. Horn, The polarcardiograph. Diagnosis of left ventricular hypertrophy. *Am. Heart J.*, 1967;**74**: 368–376.
16. Gamboa, R., P.G. Hugenholtz, and A.S. Nadas, Comparison of electrocardiograms and vectorcardiograms in congenital aortic stenosis. *Br. Heart J.*, 1965;**27**: 344–354.
17. Dower, G.E., H.E. Horn, and W.G. Ziegler, On electrocardiographic-autopsy correlations in left ventricular hypertrophy. A simple postmortem index of hypertrophy proposed. *Am. Heart J.*, 1967;**74**: 351–367.
18. Dower, G.E., R.A. Bruce, J. Pool, M.L. Simoons, M.W. Niederberger, and L.J. Meilink, Ischemic polarcardiographic changes induced by exercise: a new criterion. *Circulation*, 1973;**48**: 725–734.
19. Bruce, R.A., R. Alexander, Y.B. Li, et al., Electrocardiographic responses to maximal exercise in American and Chinese population samples, in *Measurement in Exercise Electrocardiography*, H. Blackburn, Editor. Springfield, IL: Thomas, 1969.

Appendix 1: Adult Normal Limits

P. W. Macfarlane, A. van Oosterom, O. Pahlm, P. Kligfield, M. Janse, J. Camm (eds.), *Comprehensive Electrocardiology*, DOI 10.1007/978-1-84882-046-3_A1

A1.1 Normal Limits of the 12-Lead ECG in White Caucasians

The data in the following tables have been derived from a study of over 1,450 apparently healthy Caucasians living in the west of Scotland. A few tables are based on smaller numbers. Further details can be found in Chap. 13. The results are presented as mean ± standard deviation together with the 96% range; that is, 2% of measurements have been excluded from each extreme of the range. P-, Q, S, T- wave amplitudes are presented as negative measurements (Tables A1.1–A1.31).

Table A1.1

Interval and duration of measurements (in milliseconds) from Caucasian normals

Age-group	Sex	PR interval	QRS duration	QT interval	QT_c interval Hodges[a]	QT_c interval Bazett[b]	P-wave duration	Heart rate (bpm)
18→29	Male	152.5 ± 23.0	96.4 ± 8.6	385.5 ± 28.9	403.6 ± 19.0	413.9 ± 23.1	103.0 ± 14.2	70 ± 12
		112→208	80→114	336→442	368→444	370→463	72→128	48→98
		n = 265	*n* = 265	*n* = 265	*n* = 265	*n* = 265	*n* = 266	*n* = 266
	Female	145.9 ± 19.7	87.7 ± 7.8	380.0 ± 27.8	411.6 ± 18.0	429.7 ± 22.9	99.0 ± 12.7	76 ± 12
		114→194	72→104	322→440	378→451	386→477	70→122	55→108
		n = 317	*n* = 317	*n* = 317	*n* = 317	*n* = 317	*n* = 318	*n* = 318
30→39	Male	155.7 ± 21.4	95.4 ± 9.8	385.5 ± 29.5	404.8 ± 19.4	416.0 ± 22.9	105.0 ± 12.3	71 ± 12
		116→206	78→114	326→448	366→448	375→468	78→130	52→99
		n = 218	*n* = 218	*n* = 218	*n* = 218	*n* = 218	*n* = 221	*n* = 221
	Female	145.7 ± 18.6	88.6 ± 7.3	386.6 ± 27.7	415.2 ± 16.9	432.6 ± 20.9	99.0 ± 11.6	77 ± 13
		114→184	76→106	330→438	384→445	395→473	72→122	57→105
		n = 115	*n* = 115	*n* = 115	*n* = 115	*n* = 115	*n* = 118	*n* = 118
40→49	Male	157.2 ± 21.8	94.4 ± 9.9	390.8 ± 29.3	409.2 ± 17.9	420.0 ± 21.9	106.0 ± 11.2	70 ± 12
		116→210	78→114	340→450	377→450	377→464	84→128	49→96
		n = 119	*n* = 119	*n* = 119	*n* = 119	*n* = 119	*n* = 119	*n* = 119
	Female	154.9 ± 20.4	89.4 ± 7.9	386.1 ± 27.0	415.2 ± 22.5	433.7 ± 28.4	104.0 ± 12.9	77 ± 12
		108→200	74→108	328→434	347→457	350→483	78→128	59→106
		n = 72	*n* = 72	*n* = 72	*n* = 72	*n* = 72	*n* = 73	*n* = 73
50+	Male	161.5 ± 18.9	92.7 ± 9.3	385.5 ± 26.0	407.4 ± 17.5	420.9 ± 22.7	110.0 ± 10.5	73 ± 12
		120→196	74→112	320→434	374→444	380→475	86→134	54→100
		n = 123	*n* = 123	*n* = 123	*n* = 123	*n* = 123	*n* = 125	*n* = 125
	Female	155.6 ± 6.9	87.1 ± 8.7	390.7 ± 31.5	419.5 ± 22.7	438.2 ± 24.8	106.0 ± 9.5	77 ± 11
		122→196	68→104	336→488	376→486	392→506	88→126	59→104
		n = 79	*n* = 79	*n* = 79	*n* = 79	*n* = 79	*n* = 80	*n* = 80

[a] QT_C = QT + 1.75 (rate – 60) – Ref. [107] in Chap. 13.
[b] QT_C = QT $(rate/60)^{1/2}$ – Ref. [106] in Chap. 13.

Table A1.2

Interval measurements (in milliseconds) from Caucasian normals versus heart rate

Heart rate (bpm)	PR interval	QT interval	QT_c interval Hodges[a]	QT_c interval Bazett[b]
<50	145.067 ± 18.19	443.6 ± 21.62	420.5 ± 20.49	391.537 ± 17.70
	116→176	396→482	376.75→459.25	357.864→426.6
	n = 15	*n* = 15	*n* = 15	*n* = 15
50→59	154.753 ± 25.81	417.425 ± 21.27	410.197 ± 21.08	402.633 ± 21.28
	110→220	378→468	370→458.5	358.078→454.235
	N = 146	*N* = 146	*n* = 146	*n* = 146

Table A1.2 (Continued)

Heart rate (bpm)	PR interval	QT interval	QT_c interval Hodges[a]	QT_c interval Bazett[b]
60→69	154.769 ± 22.62	399.339 ± 21.51	408.173 ± 20.54	415.549 ± 21.38
	116→208	354→444	368.75→450.25	372.64→462.2
	n = 372	*n* = 372	*n* = 372	*n* = 372
70→79	151.196 ± 20.28	382.44 ± 19.82	407.516 ± 19.18	425.481 ± 21.51
	114→196	344→426	372.25→452	388.32→477.234
	n = 408	*n* = 408	*n* = 408	*n* = 408
80→89	150.51 ± 20.19	367.522 ± 17.36	409.076 ± 16.93	434.074 ± 20.06
	114→194	332→406	376.5→444.5	395.044→474.053
	n = 247	*n* = 247	*n* = 247	*n* = 247
90→99	151.368 ± 17.52	356.842 ± 17.59	415.958 ± 17.34	446.019 ± 21.80
	114→182	320→388	383.5→449.25	405.54→488.23
	n = 114	*n* = 114	*n* = 114	*n* = 114
≥ 100	151.459 ± 14.14	328.108 ± 16.25	408.372 ± 18.63	435.705 ± 23.93
	130→180	298→352	377.25→439.5	395.685→476.246
	n = 37	*n* = 37	*n* = 37	*n* = 37

[a] $QT_c = QT + 1.75(\text{rate} - 60)$
[b] $QT_c = QT\ (\text{rate}/60)^{1/2}$.

Table A1.3

Durations (in milliseconds) in Caucasian adults: lead I

Age-group	Sex	Q duration	R duration	S duration
18→29	Male	16 ± 5	45 ± 11	29 ± 11
		9 → 28	27 → 76	9 → 52
		n = 126	*n* = 224	*n* = 168
	Female	15 ± 4	46 ± 10	26 ± 9
		7 23	29 → 70	12 → 47
		n = 127	*n* = 284	*n* = 155
30→39	Male	17 ± 4	47 ± 12	28 ± 11
		8 → 26	29 → 80	12 → 53
		n = 121	*n* = 212	*n* = 142
	Female	16 ± 4	47 ± 11	25 ± 9
		8 → 26	29 → 68	11 → 46
		n = *53*	*n* = 125	*n* = *61*
40→49	Male	17 ± 4	48 ± 12	28 ± 11
		9 → 26	30 → 77	7 → 51
		n = 115	*n* = 187	*n* = 110
	Female	15 ± 4	49 ± 10	26 ± 8
		8 → 22	*33 → 73*	*16 → 42*
		n = *52*	*n* = *82*	*n* = *31*
50+	Male	17 ± 4	50 ± 14	29 ± 10
		9 → 27	31 → 88	13 → 51
		n = 122	*n* = 197	*n* = *99*
	Female	15 ± 4	50 ± 12	23 ± 7
		7 → 27	27 → 74	12 → 42
		n = *74*	*n* = 124	*n* = *43*

Table A1.4

Durations (in milliseconds) in Caucasian adults: lead II

Age-group	Sex	Q duration	R duration	S duration
18–29	Male	17 ± 5	52 ± 14	26 ± 11
		8 → 26	35 → 84	6 → 49
		n = 162	*n* = 230	*n* = 148
	Female	15 ± 4	47 ± 11	25 ± 9
		8 → 26	30 → 74	9 → 44
		n = 182	*n* = 287	*n* = 175
30–39	Male	17 ± 5	55 ± 15	27 ± 13
		9 → 28	31 → 88	6 → 56
		n = 118	*n* = 207	*n* = 115
	Female	16 ± 4	48 ± 10	24 ± 10
		10 → 23	33 → 72	6 → 46
		n = *95*	*n* = 124	*n* = *65*
40–49	Male	16 ± 4	54 ± 15	29 ± 14
		7 → 24	33 → 90	9 → 57
		n = *94*	*n* = 182	*n* = *97*
	Female	15 ± 4	51 ± 13	25 ± 10
		7 → 24	33 → 78	10 → 45
		n = *45*	*n* = *80*	*n* = *40*
50+	Male	16 ± 4	53 ± 14	28 ± 13
		9 → 26	32 → 86	6 → 71
		n = *79*	*n* = 195	*n* = 122
	Female	15 ± 4	52 ± 13	26 ± 11
		8 → 24	32 → 76	8 → 56
		n = *64*	*n* = 129	*n* = *57*

Table A1.5

Durations (in milliseconds) in Caucasian adults: lead III

Age-group	Sex	Q duration	R duration	S duration
18–29	Male	23 ± 10	47 ± 20	30 ± 17
		10 → 50	11 → 87	6 → 84
		n = 128	*n* = 221	*n* = 116
	Female	22 ± 11	40 ± 16	29 ± 14
		9 → 80	10 → 74	7 → 68
		n = 166	*n* = 278	*n* = 160
30–39	Male	24 ± 12	42 ± 22	33 ± 20
		9 → 48	8 → 86	7 → 86
		n = 106	*n* = 205	*n* = 114
	Female	20 ± 7	41 ± 18	27 ± 16
		10 → 48	9 → 79	7 → 78
		n = *86*	*n* = 123	*n* = *64*

Table A1.5 (Continued)

Age-group	Sex	Q duration	R duration	S duration
40–49	Male	23 ± 11	39 ± 21	37 ± 20
		8 → 58	11 → 86	6 → 79
		n = 72	*n* = 181	*n* = 114
	Female	22 ± 12	35 ± 18	36 ± 17
		12 → 78	12 → 74	9 → 70
		n = 33	*n = 78*	*n = 48*
50+	Male	26 ± 15	35 ± 20	41 ± 21
		9 → 100	10 → 83	10 → 90
		n = 68	*n* = 195	*n* = 137
	Female	22 ± 11	34 ± 18	35 ± 18
		9 → 62	8 → 76	6 → 70
		n = 49	*n* = 123	*n = 82*

Table A1.6

Durations (in milliseconds) in Caucasian adults: lead aVR

Age-group	Sex	Q duration	R duration	S duration
18–29	Male	50 ± 13	19 ± 8	46 ± 11
		32 → 92	8 → 44	30 → 75
		n = 74	*n* = 208	*n* = 160
	Female	47 ± 9	18 ± 8	45 ± 9
		34 → 74	9 → 38	30 → 65
		n = 130	*n* = 248	*n* = 159
30–39	Male	51 ± 13	20 ± 10	50 ± 12
		34 → 84	9 → 50	32 → 78
		n = 91	*n* = 181	*n* = 125
	Female	46 ± 10	17 ± 6	45 ± 8
		36 → 78	8 → 39	34 → 65
		n = 41	*n* = 108	*n = 85*
40–49	Male	52 ± 12	20 ± 10	50 ± 12
		34 → 78	10 → 49	34 → 75
		n = 76	*n* = 157	*n* = 110
	Female	51 ± 13	17 ± 6	48 ± 9
		35 → 84	10 → 36	31 → 66
		n = 32	*n = 67*	*n = 51*
50+	Male	52 ± 13	20 ± 9	48 ± 13
		34 → 84	9 → 42	31 → 78
		n = 104	*n* = 159	*n = 95*
	Female	53 ± 13	18 ± 7	48 ± 12
		29 → 80	8 → 42	25 → 70
		n = 69	*n = 92*	*n = 61*

Table A1.7

Durations (in milliseconds) in Caucasian adults: lead aVL

Age-group	Sex	Q duration	R duration	S duration
18–29	Male	21 ± 13	35 ± 16	39 ± 18
		8 → 74	9 → 77	7 → 75
		n = 100	*n* = 219	*n* = 172
	Female	18 ± 6	38 ± 16	30 ± 14
		8 → 35	13 → 74	7 → 62
		n = 107	*n* = 284	*n* = 187
30–39	Male	20 ± 10	39 ± 17	37 ± 16
		9 → 68	11 → 79	7 → 71
		n = 114	*n* = 209	*n* = 158
	Female	18 ± 5	37 ± 16	33 ± 16
		9 → 29	10 → 76	8 → 66
		n = *40*	*n* = 125	*n* = *82*
40–49	Male	19 ± 7	41 ± 16	33 ± 15
		10 → 45	12 → 75	7 → 67
		n = 113	*n* = 186	*n* = 118
	Female	17 ± 4	45 ± 14	29 ± 13
		11 → 25	21 → 72	12 → 56
		n = *46*	*n* = *82*	*n* = *38*
50+	Male	20 ± 10	46 ± 17	34 ± 16
		10 → 52	19 → 89	10 → 72
		n = 125	*n* = 196	*n* = *98*
	Female	17 ± 6	45 ± 14	27 ± 13
		8 → 38	15 → 69	5 → 61
		n = *71*	*n* = 124	*n* = *56*

Table A1.8

Durations (in milliseconds) in Caucasian adults: lead aVF

Age-group	Sex	Q duration	R duration	S duration
18–29	Male	19 ± 5	53 ± 17	28 ± 13
		9 → 27	15 → 90	8 → 69
		n = 143	*n* = 231	*n* = 129
	Female	17 ± 5	47 ± 12	27 ± 9
		8 → 28	25 → 74	12 → 49
		n = 174	*n* = 288	*n* = 162
30–39	Male	18 ± 5	55 ± 17	31 ± 16
		8 → 32	23 → 90	7 → 74
		n = 110	*n* = 208	*n* = *95*
	Female	17 ± 4	47 ± 12	24 ± 10
		8 → 23	29 → 74	6 → 48
		n = *89*	*n* = 124	*n* = *66*

Table A1.8 (Continued)

Age-group	Sex	Q duration	R duration	S duration
40–49	Male	17 ± *5*	51 ± *19*	32 ± *18*
		9 → 28	13 → 92	6 → 80
		n = 76	*n* = 183	*n* = 102
	Female	16 ± 4	48 ± 14	27 ± 11
		9 → 24	20 → 76	11 → 53
		n = 36	*n* = 81	*n* = 43
50+	Male	18 ± 7	49 ± 18	33 ± 18
		9 → 52	15 → 88	8 → 79
		n = 73	*n* = 198	*n* = 125
	Female	16 ± 5	48 ± 15	31 ± 14
		8 → 28	18 → 78	9 → 69
		n = 55	*n* = 129	*n* = *62*

Table A1.9

Durations (in milliseconds) in Caucasian adults: lead V_1

Age-group	Sex	Q duration	R duration	S duration
18–29	Male	80	31 ± 6	55 ± 10
		80 → 80	20 → 46	30 → 76
		n = 1	*n* = 228	*n* = 229
	Female	57 ± 31	26 ± 5	54 ± 9
		3 → 78	14 → 37	32 → 71
		n = 5	*n* = 282	*n* = 282
30–39	Male	46 ± 31	28 ± 7	57 ± 9
		11 → 74	11 → 42	34 → 75
		n = 4	*n* = 210	*n* = 210
	Female		26 ± 5	55 ± 8
			16 → 36	37 → 68
			n = 126	*n* = 126
40–49	Male	68 ± 5	28 ± 7	57 ± 10
		58 → 72	15 → 45	29 → 75
		n = 6	*n* = 179	*n* = 179
	Female	60 ± 8	24 ± 5	57 ± 8
		54 → 66	12 → 32	45 → 78
		n = 2	*n* = *80*	*n* = *80*
50+	Male	38 ± 34	27 ± 6	56 ± 10
		14 → 62	15 → 45	34 → 79
		n = 2	*n* = 198	*n* = 198
	Female	9	24 ± 7	55 ± 9
		9 → 9	10 → 39	28 → 71
		n = 1	*n* = 125	*n* = 125

Table A1.10

Durations (in milliseconds) in Caucasian adults: lead V_2

Age-group	Sex	Q duration	R duration	S duration
18–29	Male	74	33 ± 7	52 ± 9
		74 → 74	21 → 48	36 → 72
		n = 1	*n* = 228	*n* = 228
	Female	9 ± 6	30 ± 7	52 ± 9
		5 → 13	17 → 44	31 → 70
		n = 2	*n* = 281	*n* = 280
30–39	Male	41 ± 35	33 ± 9	54 ± 10
		16 → 66	20 → 47	31 → 73
		n = 2	*n* = 208	*n* = 207
	Female		31 ± 6	52 ± 9
			19 → 45	29 → 67
			n = 126	*n* = 126
40–49	Male	72 ± 5	34 ± 8	51 ± 11
		66 → 76	19 → 52	31 → 75
		n = 3	*n* = 180	*n* = 180
	Female	36 ± 40	30 ± 7	51 ± 10
		8 → 64	18 → 47	29 → 71
		n = 2	*n* = *82*	*n* = *82*
50+	Male	30 ± 35	35 ± 8	49 ± 11
		8 → 82	20 → 55	26 → 73
		n = 4	*n* = 199	*n* = 199
	Female	44 ± 42	30 ± 7	50 ± 9
		14 → 74	16 → 45	27 → 67
		n = 2	*n* = 126	*n* = 126

Table A1.11

Durations (in milliseconds) in Caucasian adults: lead V_3

Age-group	Sex	Q duration	R duration	S duration
18–29	Male	12 ± 5	43 ± 10	40 ± 13
		8 → 17	25 → 62	16 → 63
		n = 3	*n* = 229	*n* = 227
	Female	23 ± 27	42 ± 9	37 ± 12
		5 → 62	23 → 59	12 → 60
		n = 4	*n* = 284	*n* = 275
30–39	Male	14 ± 4	43 ± 10	42 ± 12
		6 → 18	26 → 74	15 → 62
		n = 8	*n* = 208	*n* = 204
	Female		43 ± 10	38 ± 13
			23 → 74	15 → 63
			n = 124	*n* = 118

Table A1.11 (Continued)

Age-group	Sex	Q duration	R duration	S duration
40–49	Male	14 ± 4	43 ± 9	41 ± 13
		9 → 18	26 → 62	14 → 65
		n = 5	*n* = 185	*n* = 182
	Female	13 ± 2	41 ± 8	39 ± 11
		11 → 14	22 → 60	18 → 58
		n = 2	*n* = *81*	*n* = *79*
50+	Male	12 ± 5	43 ± 10	41 ± 13
		5 → 21	27 → 66	18 → 68
		n = 13	*n* = 192	*n* = 190
	Female	12 ± 5	40 ± 8	39 ± 11
		8 → 20	22 → 58	18 → 60
		n = 5	*n* = 128	*n* = 125

Table A1.12

Durations (in milliseconds) in Caucasian adults: lead V_4

Age-group	Sex	Q duration	R duration	S duration
18–29	Male	16 ± 6	46 ± 10	28 ± 11
		7 → 29	32 → 78	7 → 53
		n = 86	*n* = 227	*n* = 209
	Female	14 ± 4	44 ± 9	29 ± 9
		8 → 25	31 → 72	12 → 46
		n = 72	*n* = 284	*n* = 242
30–39	Male	14 ± 4	46 ± 10	32 ± 11
		8 → 27	33 → 86	11 → 57
		n = *62*	*n* = 210	*n* = 193
	Female	16 ± 4	45 ± 9	32 ± 10
		8 → 24	33 → 73	15 → 53
		n = *35*	*n* = 125	*n* = *97*
40–49	Male	13 ± 4	46 ± 9	33 ± 12
		7 → 25	34 → 76	12 → 61
		n = *49*	*n* = 184	*n* = 169
	Female	12 ± 4	44 ± 8	32 ± 11
		5 → 19	34 → 66	12 → 54
		n = *15*	*n* = *80*	*n* = *70*
50+	Male	14 ± 4	44 ± 9	35 ± 13
		8 → 24	31 → 72	12 → 57
		n = *54*	*n* = 199	*n* = 188
	Female	13 ± 4	42 ± 7	33 ± 10
		9 → 23	29 → 60	13 → 58
		n = *28*	*n* = 128	*n* = 122

Table A1.13

Durations (in milliseconds) in Caucasian adults: lead V_5

Age-group	Sex	Q duration	R duration	S duration
18–29	Male	17 ± 5	45 ± 12	27 ± 11
		9 → 27	30 → 80	6 → 49
		n = 171	*n* = 230	*n* = 181
	Female	14 ± 4	42 ± 9	27 ± 9
		8 → 24	29 → 69	10 → 46
		n = 148	*n* = 288	*n* = 214
30–39	Male	16 ± 5	46 ± 11	28 ± 12
		8 → 25	31 → 86	10 → 58
		n = 127	*n* = 211	*n* = 179
	Female	15 ± 5	43 ± 10	27 ± 9
		8 → 26	31 → 71	12 → 45
		n = *79*	*n* = 124	*n* = *88*
40–49	Male	15 ± 4	45 ± 10	29 ± 12
		7 → 24	33 → 79	8 → 55
		n = 103	*n* = 186	*n* = 149
	Female	13 ± 4	44 ± 9	29 ± 10
		8 → 20	33 → 67	12 → 51
		n = *35*	*n* = *81*	*n* = *64*
50+	Male	15 ± 4	45 ± 11	33 ± 12
		8 → 26	31 → 78	11 → 68
		n = 101	*n* = 198	*n* = 160
	Female	14 ± 4	43 ± 9	28 ± 10
		8 → 25	28 → 66	13 → 49
		n = *62*	*n* = 128	*n* = *98*

Table A1.14

Durations (in milliseconds) in Caucasian adults: lead V_6

Age group	Sex	Q duration	R duration	S duration
18–29	Male	18 ± 5	47 ± 12	25 ± 11
		10 → 28	31 → 76	6 → 46
		n = 202	*n* = 228	*n* = 137
	Female	16 ± 4	44 ± 9	24 ± 8
		9 → 25	30 → 70	12 → 42
		n = 215	*n* = 289	*n* = 161
30–39	Male	17 ± 4	49 ± 13	26 ± 12
		8 → 26	31 → 82	8 → 58
		n = 159	*n* = 208	*n* = 129
	Female	17 ± 5	45 ± 9	25 ± 8
		10 → 28	34 → 71	11 → 45
		n = 104	*n* = 124	*n = 59*
40–49	Male	16 ± 4	50 ± 11	29 ± 11
		8 → 24	34 → 76	12 → 52
		n = 139	*n* = 186	*n = 96*
	Female	15 ± 4	47 ± 10	26 ± 8
		8 → 23	33 → 68	14 → 42
		n = 51	*n = 82*	*n = 42*
50+	Male	16 ± 4	48 ± 12	30 ± 11
		9 → 25	31 → 78	12 → 57
		n = 130	*n* = 195	*n* = 124
	Female	15 ± 4	48 ± 11	25 ± 9
		8 → 23	30 → 72	12 → 47
		n = 80	*n* = 128	*n = 60*

Table A1.15

Amplitudes (in millivolts) in Caucasian adults: lead I

Age group	Sex	P+	P–	Q	R	S	STj	T+	T–
18–29	Male	0.099 ± 0.029	−0.020 ± 0.000	−0.074 ± 0.051	0.756 ± 0.333	−0.227 ± 0.139	0.031 ± 0.022	0.343 ± 0.116	
		0.055–0.174	−0.020–0.000	−0.238–0.000	0.202–1.624	−0.568–0.000	−0.006–0.077	0.116–0.641	
		n = 224	*n* = 1	*n* = 126	*n* = 224	*n* = 168	*n* = 224	*n* = 224	
	Female	0.101 ± 0.026	−0.058 ± 0.011	−0.070 ± 0.046	0.699 ± 0.283	−0.163 ± 0.096	0.011 ± 0.015	0.283 ± 0.093	
		0.056–0.161	−0.066–0.000	−0.225–0.000	0.226–1.411	−0.468–0.000	−0.022–0.038	0.112–0.506	
		n = 283	*n* = 2	*n* = 127	*n* = 284	*n* = 155	*n* = 284	*n* = 284	
30–39	Male	0.102 ± 0.027	−0.019 ± 0.001	−0.070 ± 0.046	0.807 ± 0.353	−0.189 ± 0.122	0.023 ± 0.019	0.300 ± 0.099	
		0.056–0.163	−0.019–0.000	−0.223–0.000	0.251–1.685	−0.536–0.000	−0.011–0.061	0.119–0.522	
		n = 212	*n* = 2	*n* = 121	*n* = 212	*n* = 142	*n* = 212	*n* = 212	
	Female	0.102 ± 0.032	−0.023 ± 0.000	−0.070 ± 0.044	0.666 ± 0.290	−0.145 ± 0.103	0.008 ± 0.017	0.257 ± 0.093	
		0.051–0.202	−0.023–0.000	−0.208–0.000	0.198–1.557	−0.622–0.000	−0.028–0.042	0.096–0.478	
		n = 124	*n* = 1	*n* = 52	*n* = 124	*n* =61	*n* = 124	*n* = 124	
40–49	Male	0.098 ± 0.032	−0.024 ± 0.016	−0.069 ± 0.041	0.791 ± 0.331	−0.159 ± 0.100	0.019 ± 0.020	0.271 ± 0.105	−0.087 ± 0.000
		0.045–0.184	−0.038–0.000	−0.173–0.000	0.286–1.509	−0.465–0.000	−0.017–0.074	0.105–0.547	−0.087–0.000
		n = 207	*n* = 4	*n* = 125	*n* = 207	*n* = 121	*n* = 207	*n* = 207	*n* =1
	Female	0.103 ± 0.026	−0.038 ± 0.000	−0.068 ± 0.042	0.773 ± 0.256	−0.129 ± 0.078	0.010 ± 0.018	0.245 ± 0.090	−0.021 ± 0.000
		0.055–0.184	−0.038–0.000	−0.191–0.000	0.374–1.414	−0.351–0.000	−0.027–0.046	0.095–0.461	−0.021–0.000
		n = 89	*n* = 1	*n* = 56	*n* = 89	*n* = 32	*n* = 89	*n* = 89	*n* = 1
50+	Male	0.097 ± 0.030	−0.019 ± 0.008	−0.072 ± 0.045	0.800 ± 0.272	−0.145 ± 0.087	0.015 ± 0.020	0.234 ± 0.097	
		0.043–0.166	−0.024–0.000	−0.195–0.000	0.292–1.416	−0.404–0.000	−0.028–0.060	0.079–0.502	
		n = 200	*n* = 2	*n* = 125	*n* = 200	*n* =99	*n* = 200	*n* = 200	
	Female	0.102 ± 0.029	−0.029 ± 0.000	−0.067 ± 0.043	0.807 ± 0.299	−0.119 ± 0.081	0.004 ± 0.018	0.218–0.098	−0.036 ± 0.036
		0.052–0.179	−0.029–0.000	−0.277–0.000	0.231–1.544	−0.339–0.000	−0.039–0.032	0.060–0.452	−0.087–0.000
		n = 125	*n* = 1	*n* = 54	*n* = 125	*n* = 44	*n* = 125	*n* = 124	*n* = 4

Table A1.16

Amplitudes (in millivolts) in Caucasian adults: lead II

Age group	Sex	P+	P−	Q	R	S	STj	T+	T−
18–29	Male	0.148 ± 0.057	−0.028–0.027	−0.089 ± 0.057	1.364 ± 0.428	0.212 ± 0.126	0.041 ± 0.033	0.419 ± 0.141	−0.022 ± 0.001
		0.040–0.294	−0.124–0.000	−0.251–0.000	0.566–2.357	−0.538–0.000	−0.015–0.117	0.150–0.780	−0.023–0.000
		n = 229	*n* = 16	*n* = 162	*n* = 230	*n* = 148	*n* = 230	*n* = 230	*n* = 2
	Female	0.149 ± 0.055	−0.029 ± 0.024	−0.075 ± 0.052	1.133 ± 0.340	−0.169 ± 0.097	0.012 ± 0.024	0.334 ± 0.110	
		0.052–0.305	−0.086–0.000	−0.202–0.000	0.523–1.828	−0.437–0.000	−0.037–0.058	0.147–0.617	
		n = 287	*n* = 8	*n* = 182	*n* = 287	*n* = 175	*n* = 287	*n* = 287	
30–39	Male	0.150 ± 0.052	−0.020 ± 0.004	−0.089 ± 0.061	1.118 ± 0.424	−0.198 ± 0.143	0.033 ± 0.029	0.363 ± 0.131	
		0.043–0.281	−0.025–0.000	−0.343–0.000	0.412–2.230	−0.617–0.000	−0.025–0.101	0.142–0.710	
		n = 207	*n* = 7	*n* = 118	*n* = 207	*n* = 115	*n* = 207	*n* = 207	
	Female	0.158 ± 0.056		−0.079 ± 0.044	1.080 ± 0.335	−0.158 ± 0.110	0.007 ± 0.027	0.302 ± 0.106	−0.064 ± 0.000
		0.055–0.274		−0.178–0.000	0.450–1.793	−0.579–0.000	−0.069–0.074	0.118–0.554	−0.064–0.000
		n = 123		*n* = 95	*n* = 123	*n* = 65	*n* = 123	*n* = 123	*n* = 1
40–49	Male	0.145 ± 0.047	−0.041 ± 0.013	−0.063 ± 0.039	0.911 ± 0.370	−0.197 ± 0.147	0.026 ± 0.030	0.336 ± 0.125	
		0.062–0.274	−0.052–0.000	−0.187–0.000	0.267–1.731	−0.731–0.000	−0.042–0.088	0.136–0.656	
		n = 200	*n* = 4	*n* = 103	*n* = 201	*n* = 108	*n* = 201	*n* = 201	
	Female	0.144 ± 0.051	−0.022 ± 0.008	−0.060 ± 0.037	0.886 ± 0.280	−0.159 ± 0.111	0.014 ± 0.022	0.282 ± 0.095	−0.027 ± 0.000
		0.058–0.258	−0.031–0.000	−0.192–0.000	0.491–1.438	−0.622–0.000	−0.029–0.053	0.100–0.523	−0.027–0.000
		n = 87	*n* = 3	*n* = 48	*n* = 87	*n* = 43	*n* = 87	*n* = 87	*n* = 1
50+	Male	0.144 ± 0.047	−0.018 ± 0.003	−0.072 ± 0.051	0.835 ± 0.368	−0.188 ± 0.156	0.022 ± 0.026	0.304 ± 0.115	−0.057 ± 0.000
		0.047–0.242	−0.023–0.000	−0.200–0.000	0.258–1.980	−0.719–0.000	−0.030–0.079	0.114–0.590	−0.057–0.000
		n = 198	*n* = 6	*n* = 79	*n* = 198	*n* = 124	*n* = 198	*n* = 198	*n* = 1
	Female	0.153 ± 0.054	−0.021 ± 0.013	−0.063 ± 0.037	0.865 ± 0.296	−0.179 ± 0.106	0.005 ± 0.025	0.270 ± 0.101	−0.067 ± 0.038
		0.066–0.270	−0.038–0.000	−0.187–0.000	0.401–1.534	−0.447–0.000	−0.066–0.053	0.079–0.498	−0.131–0.000
		n = 130	*n* = 5	*n* = 64	*n* = 130	*n* = 57	*n* = 130	*n* = 130	*n* = 7

Table A1.17

Amplitudes (in millivolts) in Caucasian adults: lead III

Age group	Sex	P+	P–	Q	R	S	STj	T+	T–
18–29	Male	0.086 ± 0.049	−0.049 ± 0.030	−0.134 ± 0.111	0.777 ± 0.562	−0.224 ± 0.230	0.009 ± 0.025	0.142 ± 0.095	−0.101 ± 0.081
		0.000–0.224	−0.165–0.000	−0.531–0.000	0.000–2.115	−1.140–0.000	−0.053–0.062	0.000–0.381	−0.304–0.000
		n = 197	*n* = 104	*n* = 128	*n* = 221	*n* = 116	*n* = 225	*n* = 187	*n* = 77
	Female	0.082 ± 0.048	−0.038 ± 0.024	−0.110 ± 0.091	0.560 ± 0.391	−0.209 ± 0.180	0.001 ± 0.019	0.093 ± 0.061	−0.058 ± 0.044
		0.000–0.220	−0.104–0.000	−0.562–0.000	0.000–1.475	−0.912–0.000	−0.034–0.039	0.000–0.276	−0.207–0.000
		n = 252	*n* = 125	*n* = 166	*n* = 278	*n* = 160	*n* = 282	*n* = 245	*n* = 109
30–39	Male	0.084 ± 0.045	−0.044 ± 0.021	−0.130 ± 0.095	0.524 ± 0.477	−0.328 ± 0.290	0.010 ± 0.021	0.123 ± 0.092	−0.076 ± 0.052
		0.000–0.206	−0.105–0.000	−0.429–0.000	0.000–1.813	−1.261–0.000	−0.031–0.055	0.000–0.399	−0.248–0.000
		n = 188	*n* = 90	*n* = 105	*n* = 205	*n* = 114	*n* = 206	*n* = 172	*n* =78
	Female	0.088 ± 0.050	−0.041 ± 0.022	−0.110 ± 0.085	0.542 ± 0.356	−0.204 ± 0.198	−0.001 ± 0.021	0.089 ± 0.061	−0.055 ± 0.043
		0.000–0.216	−0.109–0.000	−0.399–0.000	0.000–1.407	−1.002–0.000	−0.051–0.043	0.000–0.284	−0.175–0.000
		n = 113	*n* = 51	*n* = 86	*n* = 122	*n* = 63	*n* = 124	*n* = 106	*n* = 59
40–49	Male	0.082 ± 0.042	−0.044 ± 0.028	−0.116 ± 0.106	0.381 ± 0.307	−0.348 ± 0.307	0.007 ± 0.025	0.123 ± 0.091	−0.074 ± 0.057
		0.000–0.190	−0.134–0.000	−0.478–0.000	0.000–1.483	−1.120–0.000	−0.033–0.050	0.000–0.362	−0.228–0.000
		n = 189	*n* = 90	*n* = 81	*n* = 200	*n* = 129	*n* = 204	*n* = 164	*n* = 80
	Female	0.072 ± 0.041	−0.042 ± 0.024	−0.079 ± 0.058	0.295 ± 0.253	−0.292 ± 0.245	0.004 ± 0.016	0.080 ± 0.066	−0.056 ± 0.040
		0.000–0.187	−0.100–0.000	−0.319–0.000	0.000–1.033	0.000–1.269	−0.028–0.037	0.000–0.298	−0.161–0.000
		n = 80	*n* = 38	*n* = 35	*n* = 85	*n* = 54	*n* = 86	*n* = 73	*n* = 35
50+	Male	0.081 ± 0.043	−0.044 ± 0.023	−0.140 ± 0.143	0.322 ± 0.329	−0.382 ± 0.315	0.007 ± 0.022	0.117 ± 0.094	−0.068 ± 0.054
		0.000–0.184	−0.113–0.000	−0.847–0.000	0.000–1.422	−1.235–0.000	−0.038–0.064	0.000–0.423	−0.236–0.000
		n = 190	*n* = 90	*n* = 68	*n* = 198	*n* = 140	*n* = 200	*n* = 169	*n* = 72
	Female	0.083 ± 0.045	−0.039 ± 0.024	−0.103 ± 0.123	0.290 ± 0.249	−0.336 ± 0.272	0.001 ± 0.019	0.091 ± 0.063	−0.059 ± 0.050
		0.000–0.209	−0.126–0.000	−0.849–0.000	0.000–0.944	−1.080–0.000	−0.048–0.038	0.000–0.274	−0.196–0.000
		n = 120	*n* = 49	*n* = 50	*n* = 124	*n* = 83	*n* = 126	*n* = 109	*n* = 47

Table A1.18

Amplitudes (in millivolts) in Caucasian adults: lead aVR

Age group	Sex	P+	P–	Q	R	S	STj	T+	T–
18–29	Male	0.024 ± 0.012	−0.119 ± 0.034	−0.942 ± 0.237	0.093 ± 0.083	−1.060 ± 0.261	−0.036 ± 0.025		−0.379 ± 0.109
		0.000–0.041	−0.194 to −0.058	−1.408–0.000	0.000–0.360	−1.583–0.000	−0.086–0.011		−0.631 to −0.179
		n = 4	*n* = 231	*n* = 74	*n* = 208	*n* = 160	*n* = 231		*n* = 231
	Female	0.023 ± 0.008	−0.120 ± 0.033	−0.811 ± 0.226	0.085 ± 0.065	−0.959 ± 0.230	0.012 ± 0.017		−0.307 ± 0.092
		0.000–0.032	−0.205 to −0.059	−1.379–0.000	0.000–0.250	−1.443–0.000	−0.051–0.020		−0.504 to −0.153
		n = 3	*n* = 289	*n* = 130	*n* = 248	*n* = 160	*n* = 289		*n* = 289
30–39	Male		−0.121 ± 0.031	−0.871 ± 0.248	0.104 ± 0.093	−0.990 ± 0.275	−0.029 ± 0.022		−0.332 ± 0.098
			−0.197 to −0.062	−1.564–0.000	0.000–0.380	−1.557–0.000	−0.096–0.014		−0.573 to −0.140
			n = 215	*n* = 91	*n* = 181	*n* = 125	*n* = 215		*n* = 215
	Female		−0.127 ± 0.035	−0.723 ± 0.212	0.071 ± 0.052	−0.909 ± 0.242	−0.008 ± 0.020		−0.279 ± 0.090
			−0.220 to −0.063	−1.247–0.000	0.000–0.269	−1.447–0.000	−0.060–0.032		−0.497 to −0.121
			n = 124	*n* = 41	*n* = 107	*n* = 84	*n* = 124		*n* = 124
40–49	Male	0.032 ± 0.007	−0.115 ± 0.031	−0.764 ± 0.218	0.087 ± 0.084	−0.893 ± 0.233	−0.022 ± 0.022		−0.302 ± 0.098
		0.000–0.026	−0.196 to −0.060	−1.210–0.000	0.000–0.310	−1.403–0.000	−0.080–0.019		−0.539 to −0.146
		n = 3	*n* = 206	*n* = 86	*n* = 175	*n* = 120	*n* = 206		*n* = 206
	Female	0.033 ± 0.000	−0.121 ± 0.032	−0.719 ± 0.208	0.065 ± 0.043	−0.872 ± 0.203	−0.011 ± 0.019	0.024 ± 0.000	−0.263 ± 0.082
		0.000–0.033	−0.194 to −0.062	−1.357–0.000	0.000–0.239	−1.310–0.000	−0.049–0.024	0.000–0.024	−0.413 to −0.096
		n = 1	*n* = 90	*n* = 35	*n* = 74	*n* = 56	*n* = 90	*n* = 1	*n* = 90
50+	Male	0.025 ± 0.000	−0.115 ± 0.030	−0.748 ± 0.202	0.086 ± 0.074	−0.840 ± 0.246	−0.018 ± 0.020		−0.268 ± 0.088
		0.000–0.025	−0.176 to −0.057	−1.352–0.000	0.000–0.372	−1.404–0.000	−0.063–0.024		−0.468 to −0.115
		n = 1	*n* = 200	*n* = 104	*n* = 162	*n* = 98	*n* = 200		*n* = 200
	Female	0.034 ± 0.000	−0.122 ± 0.035	−0.766 ± 0.193	0.077 ± 0.056	−0.877 ± 0.252	−0.005 ± 0.019	0.041 ± 0.023	0.246 ± 0.086
		0.000–0.034	−0.195 to −0.061	−1.238–0.000	0.000–0.215	−1.407–0.000	−0.037–0.040	0.000–0.072	−0.452 to −0.092
		n = 1	*n* = 130	*n* = 70	*n* = 92	*n* = 61	*n* = 130	*n* = 5	*n* = 128

Table A1.19

Amplitudes (in millivolts) in Caucasian adults: lead aVL

Age group	Sex	P+	P−	Q	R	S	STj	T+	T−
18–29	Male	0.055 ± 0.028	−0.036 ± 0.021	−0.105 ± 0.113	0.311 ± 0.279	−0.387 ± 0.261	0.011 ± 0.017	0.154 ± 0.096	−0.043 ± 0.029
		0.000–0.120	−0.092–0.000	−0.492–0.000	0.027–1.254	−1.098–0.000	−0.019–0.045	0.020–0.412	−0.124–0.000
		n = 197	*n* = 106	*n* = 100	*n* = 219	*n* = 172	*n* = 225	*n* = 215	*n* = *28*
	Female	0.052 ± 0.023	−0.032 ± 0.023	−0.082 ± 0.053	0.283 ± 0.223	−0.253 ± 0.206	0.005 ± 0.012	0.124 ± 0.067	−0.023 ± 0.018
		0.000–0.111	−0.100–0.000	−0.254–0.000	0.040–0.980	−0.871–0.000	−0.021–0.030	0.014–0.284	−0.066–0.000
		n = 253	*n* = 132	*n* = 107	*n* = 284	*n* = 187	*n* = 285	*n* = 280	*n* = 22
30–39	Male	0.054 ± 0.024	−0.033 ± 0.018	−0.086 ± 0.059	0.414 ± 0.310	−0.288 ± 0.219	0.006 ± 0.013	0.136 ± 0.075	−0.051 ± 0.034
		0.000–0.114	−0.097–0.000	−0.287–0.000	0.040–1.199	−0.845–0.000	−0.021–0.034	0.022–0.334	−0.122–0.000
		n = 192	*n* = 108	*n* = 114	*n* = 209	*n* = 158	*n* = 212	*n* = 197	*n* = 24
	Female	0.053 ± 0.027	−0.035 ± 0.022	−0.077 ± 0.047	0.256 ± 0.241	−0.217 ± 0.147	0.005 ± 0.014	0.117 ± 0.068	−0.030 ± 0.020
		0.000–0.123	−0.106–0.000	−0.203–0.000	0.027–1.163	−0.614–0.000	−0.030–0.030	0.010–0.307	−0.071–0.000
		n = 103	*n* = 66	*n* =3 9	*n* = 124	*n* = 82	*n* = 124	*n* = 123	*n* = 12
40–49	Male	0.055 ± 0.028	−0.033 ± 0.017	−0.082–0.048	0.430 ± 0.326	−0.220 ± 0.166	0.006 ± 0.017	0.128 ± 0.081	−0.051 ± 0.034
		0.000–0.114	−0.083–0.000	−0.221–0.000	0.032–1.161	−0.799–0.000	−0.023–0.039	0.015–0.348	−0.155–0.000
		n = 176	*n* = 107	*n* = 123	*n* = 206	*n* = 130	*n* = 207	*n* = 186	*n* = 32
	Female	0.052 ± 0.024	−0.029 ± 0.017	−0.081 ± 0.055	0.397 ± 0.255	−0.173 ± 0.115	0.003 ± 0.013	0.114 ± 0.067	−0.031 ± 0.015
		0.000–0.113	−0.088–0.000	−0.298–0.000	0.040–1.070	−0.456–0.000	−0.022–0.023	0.017–0.285	−0.058–0.000
		n = 81	*n* = 40	*n* = 50	*n* = 89	*n* = 40	*n* = 89	*n* = 85	*n* = 9
50+	Male	0.055 ± 0.026	−0.034 ± 0.017	−0.093 ± 0.054	0.478 ± 0.298	−0.212 ± 0.156	0.004 ± 0.017	0.109 ± 0.077	−0.050 ± 0.039
		0.000–0.114	−0.085–0.000	−0.243–0.000	0.037–1.191	−0.648–0.000	−0.032–0.050	0.010–0.324	−0.181–0.000
		n = 171	*n* = 117	*n* = 128	*n* = 199	*n* = 98	*n* = 202	*n* = 179	*n* = 45
	Female	0.051 ± 0.024	−0.033 ± 0.018	−0.081 ± 0.052	0.441 ± 0.293	−0.159 ± 0.117	0.001 ± 0.013	0.096 ± 0.072	−0.035 ± 0.029
		0.000–0.121	−0.097–0.000	−0.302–0.000	0.028–1.209	−0.468–0.000	−0.027–0.025	0.011–0.316	−0.128–0.000
		n = 110	*n* = 65	*n* = 71	*n* = 125	*n* = 57	*n* = 126	*n* = 119	*n* = 26

Table A1.20

Amplitudes (in millivolts) in Caucasian adults: lead aVF

Age group	Sex	P+	P–	Q	R	S	STj	T+	T–
18–29	Male	0.111 ± 0.054	−0.034 ± 0.025	−0.095 ± 0.058	1.038 ± 0.510	−0.186 ± 0.121	0.025 ± 0.027	0.258 ± 0.122	−0.056 ± 0.052
		0.000–0.257	−0.144–0.000	−0.257–0.000	0.038–2.117	−0.489–0.000	−0.037–0.085	0.034–0.576	−0.164–0.000
		n = 226	*n* = 39	*n* = 143	*n* = 231	*n* = 129	*n* = 231	*n* = 229	*n* = 10
	Female	0.109 ± 0.052	−0.026 ± 0.022	−0.079 ± 0.049	0.822 ± 0.363	−0.163 ± 0.106	0.007 ± 0.020	0.198 ± 0.085	−0.041 ± 0.012
		0.000–0.237	−0.119–0.000	−0.203–0.000	0.174–1.652	−0.500–0.000	−0.037–0.045	0.055–0.411	−0.062–0.000
		n = 283	*n* = 30	*n* = 174	*n* = 288	*n* = 162	*n* = 288	*n* = 287	*n* = 9
30–39	Male	0.112 ± 0.047	−0.028 ± 0.014	−0.085 ± 0.059	0.772 ± 0.458	−0.217 ± 0.167	0.022 ± 0.023	0.222 ± 0.114	−0.029 ± 0.010
		0.000–0.237	−0.062–0.000	−0.320–0.000	0.072–2.015	−0.770–0.000	−0.023–0.070	0.033–0.546	−0.036–0.000
		n = 202	*n* = 26	*n* = 110	*n* = 208	*n* = 95	*n* = 208	*n* = 208	*n* = 6
	Female	0.118 ± 0.053	−0.021 ± 0.013	−0.078 ± 0.048	0.781 ± 0.348	−0.143 ± 0.104	0.003 ± 0.023	0.180 ± 0.083	−0.038 ± 0.024
		0.000–0.243	−0.052–0.000	−0.182–0.000	0.085–1.533	−0.532–0.000	−0.056–0.058	0.031–0.366	−0.069–0.000
		n = 121	*n* = 11	*n* = 89	*n* = 123	*n* = 66	*n* = 123	*n* = 123	*n* = 6
40–49	Male	0.107 ± 0.045	−0.033 ± 0.021	−0.065 ± 0.040	0.575 ± 0.383	−0.194 ± 0.171	0.016 ± 0.026	0.207 ± 0.109	−0.031 ± 0.013
		0.000–0.224	−0.075–0.000	−0.179–0.000	0.047–1.466	−0.955–0.000	−0.032–0.067	0.040–0.501	−0.047–0.000
		n = 201	*n* = 20	*n* = 85	*n* = 203	*n* = 115	*n* = 203	*n* = 202	*n* = 9
	Female	0.013 ± 0.046	−0.027 ± 0.011	−0.059 ± 0.031	0.529 ± 0.284	−0.174 ± 0.145	0.009 ± 0.017	0.164 ± 0.078	−0.028 ± 0.013
		0.000–0.223	−0.049–0.000	−0.147–0.000	0.093–1.231	−0.910–0.000	−0.029–0.047	0.055–0.404	−0.046–0.000
		n = 87	*n* = 10	*n* = 38	*n* = 88	*n* = 46	*n* = 88	*n* = 88	*n* = 4
50+	Male	0.108 ± 0.044	−0.026 ± 0.015	−0.072 ± 0.050	0.499 ± 0.373	−0.222 ± 0.205	0.014 ± 0.022	0.191 ± 0.105	−0.031 ± 0.021
		0.000–0.211	−0.069–0.000	−0.233–0.000	0.032–1.778	−0.977–0.000	−0.037–0.065	0.033–0.486	−0.062–0.000
		n = 200	*n* = 27	*n* = 73	*n* = 202	*n* = 127	*n* = 202	*n* = 202	*n* = 7
	Female	0.113 ± 0.050	−0.028 ± 0.015	−0.057 ± 0.029	0.509 ± 0.297	−0.216 ± 0.149	0.003 ± 0.021	0.165 ± 0.078	−0.049 ± 0.041
		0.000–0.238	−0.067–0.000	−0.154–0.000	0.100–1.198	−0.709–0.000	−0.058–0.042	0.040–0.339	−0.156–0.000
		n = 129	*n* = 14	*n* = 55	*n* = 130	*n* = 62	*n* = 130	*n* = 130	*n* = 13

Table A1.21

Amplitudes (in millivolts) in Caucasian adults: lead V_1

Age group	Sex	P+	P−	Q	R	S	STj	T+	T−
18–29	Male	0.073 ± 0.031	−0.039 ± 0.017	−1.317 ± 0.000	0.392 ± 0.200	−1.302 ± 0.455	0.055 ± 0.041	0.194 ± 0.147	−0.115 ± 0.082
		0.000–0.140	−0.091–0.000	−1.317–0.000	0.102–0.906	−2.246 to −0.503	−0.029–0.135	0.000–0.593	−0.290–0.000
		n = 229	*n* = 151	*n* = 1	*n* = 229	*n* = 229	*n* = 230	*n* = 201	*n* = 84
	Female	0.069 ± 0.030	−0.033 ± 0.017	−1.059 ± 0.672	0.262 ± 0.148	−1.075 ± 0.415	0.019 ± 0.028	0.086 ± 0.072	−0.102 ± 0.063
		0.000–0.135	−0.079–0.000	−1.544–0.000	0.050–0.648	−1.995 to −0.369	−0.076–0.070	0.000–0.321	−0.252–0.000
		n = 278	*n* = 155	*n* = 4	*n* = 282	*n* = 282	*n* = 285	*n* = 192	*n* = 193
30–39	Male	0.069 ± 0.028	−0.046 ± 0.020	−0.860 ± 0.848	0.295 ± 0.207	−1.158 ± 0.436	0.051 ± 0.033	0.179 ± 0.122	−0.095 ± 0.075
		0.000–0.143	−0.101–0.000	−1.594–0.000	0.040–1.030	−2.328 to −0.265	−0.023–0.119	0.000–0.519	−0.354–0.000
		n = 203	*n* = 162	*n* = 4	*n* = 211	*n* = 210	*n* = 213	*n* = 194	*n* = 54
	Female	0.064 ± 0.027	−0.038 ± 0.020		0.251 ± 0.146	−1.068 ± 0.384	0.020 ± 0.028	0.096 ± 0.073	−0.101 ± 0.068
		0.000–0.144	−0.095–0.000		0.039–0.629	−2.105 to −0.371	−0.076–0.056	0.000–0.316	−0.272–0.000
		n = 121	*n* = 80		*n* = 125	*n* = 125	*n* = 125	*n* = 88	*n* = 77
40–49	Male	0.061 ± 0.024	−0.046 ± 0.023	−1.208 ± 0.318	0.258 ± 0.163	−1.052 ± 0.408	0.045 ± 0.035	0.191 ± 0.123	−0.087 ± 0.068
		0.000–0.120	−0.117–0.000	−1.463–0.000	0.056–0.612	−2.110 to −0.364	−0.019–0.119	0.000–0.495	−0.305–0.000
		n = 194	*n* = 165	*n* = 6	*n* = 199	*n* = 199	*n* = 205	*n* = 192	*n* = 51
	Female	0.057 ± 0.022	−0.040 ± 0.019	−1.007 ± 0.188	0.214 ± 0.131	−0.951 ± 0.307	0.025 ± 0.018	0.079 ± 0.053	−0.073 ± 0.059
		0.000–0.104	−0.097–0.000	−1.140–0.000	0.029–0.634	−1.518 to −0.505	−0.010–0.067	0.000–0.255	−0.309–0.000
		n = 83	*n* = 73	*n* = 2	*n* = 87	*n* = 87	*n* = 89	*n* = 73	*n* = 50
50+	Male	0.057 ± 0.025	−0.046 ± 0.021	−0.443 ± 0.576	0.229 ± 0.123	−0.930 ± 0.365	0.047 ± 0.031	0.198 ± 0.117	−0.097 ± 0.083
		0.000–0.115	−0.110–0.000	−0.850–0.000	0.052–0.489	−1.904 to −0.319	−0.005–0.113	0.000–0.513	−0.337–0.000
		n = 193	*n* = 190	*n* = 2	*n* = 201	*n* = 201	*n* = 202	*n* = 187	*n* = 31
	Female	0.055 ± 0.024	−0.047 ± 0.021	−0.029	0.201 ± 0.130	−0.934 ± 0.340	0.030 ± 0.022	0.109 ± 0.065	−0.077 ± 0.058
		0.000–0.114	−0.105–0.000	−0.029–0.000	0.040–0.587	−1.630 to −0.349	−0.006–0.083	0.000–0.291	−0.319–0.000
		n = 116	*n* = 110	*n* = 1	*n* = 126	*n* = 126	*n* = 126	*n* = 108	*n* = 53

Table A1.22

Amplitudes (in millivolts) in Caucasian adults: lead V_2

Age group	Sex	P+	P−	Q	R	S	STj	T+	T−
18–29	Male	0.094 ± 0.033	−0.027 ± 0.011	−2.532 ± 0.000	0.833 ± 0.366	−2.164 ± 0.711	0.164 ± 0.077	0.887 ± 0.307	
		0.042–0.170	−0.064–0.000	−2.532–0.000	0.265–1.894	−3.562 to −0.826	0.016–0.320	0.342–1.634	
		n = 228	*n* = 39	*n* = 1	*n* = 228	*n* = 228	*n* = 229	*n* = 229	
	Female	0.090 ± 0.030	−0.021 ± 0.011	−0.026 ± 0.006	0.555 ± 0.259	−1.458 ± 0.554	0.055 ± 0.046	0.483 ± 0.213	−0.069 ± 0.041
		0.040–0.157	−0.050–0.000	−0.030–0.000	0.145–1.206	−2.889 to −0.550	−0.063–0.128	0.093–1.070	−0.116–0.000
		n = 281	*n* = 13	*n* = 2	*n* = 281	*n* = 280	*n* = 281	*n* = 281	*n* = 3
30–39	Male	0.089 ± 0.032	−0.030 ± 0.019	−0.969 ± 1.271	0.662 ± 0.355	−1.863 ± 0.671	0.136 ± 0.069	0.784 ± 0.276	−0.146 ± 0.110
		0.033–0.176	−0.118–0.000	−1.868–0.000	0.139–1.640	−3.518 to −0.664	−0.018–0.294	0.239–1.444	−0.267–0.000
		n = 209	*n* = 50	*n* = 2	*n* = 208	*n* = 207	*n* = 209	*n* = 208	*n* = 3
	Female	0.085 ± 0.033	−0.030 ± 0.019		0.505 ± 0.241	−1.375 ± 0.610	0.050 ± 0.045	0.462 ± 0.182	−0.146 ± 0.026
		0.027–0.169	−0.075–0.000		0.143–1.094	−3.126 to −0.485	−0.030–0.154	0.095–0.874	−0.174–0.000
		n = 125	*n* = 16		*n* = 125	*n* = 125	*n* = 125	*n* = 125	*n* = 3
40–49	Male	0.084 ± 0.032	−0.027 ± 0.014	−2.284 ± 0.215	0.604 ± 0.310	−1.502 ± 0.559	0.114 ± 0.061	0.708 ± 0.243	
		0.030–0.154	−0.094–0.000	−2.532–0.000	0.085–1.496	−2.724 to −0.548	−0.021–0.265	0.240–1.256	
		n = 201	*n* = 64	*n* = 3	*n* = 199	*n* = 199	*n* = 202	*n* = 202	
	Female	0.078 ± 0.028	−0.023 ± 0.008	−0.713 ± 0.969	0.430 ± 0.202	−1.175 ± 0.456	0.053 ± 0.030	0.418 ± 0.171	
		0.036–0.141	−0.043–0.000	−1.398–0.000	0.134–0.877	−2.470 to −0.390	−0.003 ± 0.110	0.161–0.823	
		n = 90	*n* = 15	*n* = 2	*n* = 89	*n* = 89	*n* = 90	*n* = 90	
50+	Male	0.079 ± 0.031	−0.025 ± 0.009	−0.428 ± 0.770	0.595 ± 0.331	−1.285 ± 0.528	0.103 ± 0.061	0.659 ± 0.249	−0.420 ± 0.000
		0.028–0.155	−0.047–0.000	−1.583–0.000	0.148–1.497	−2.425 to −0.271	−0.013–0.233	0.173–1.165	−0.420–0.000
		n = 203	*n* = 71	*n* = 4	*n* = 202	*n* = 202	*n* = 203	*n* = 202	*n* = 1
	Female	0.074 ± 0.027	−0.025 ± 0.012	−0.802 ± 1.076	0.453 ± 0.251	−1.126 ± 0.397	0.053 ± 0.036	0.383 ± 0.154	−0.066 ± 0.000
		0.019–0.134	−0.073–0.000	−1.563–0.000	0.148–1.081	−1.985 to −0.472	−0.033–0.132	0.073–0.672	−0.066–0.000
		n = 128	*n* = 48	*n* = 2	*n* = 127	*n* = 127	*n* = 128	*n* = 128	*n* = 1

Table A1.23

Amplitudes (in millivolts) in Caucasian adults: lead V_3

Age group	Sex	P+	P−	Q	R	S	STj	T+	T−
18–29	Male	0.093 ± 0.030	−0.024 ± 0.010	−0.061 ± 0.038	1.073 ± 0.506	−1.294 ± 0.655	0.151 ± 0.069	0.873 ± 0.280	
		0.038–0.160	−0.049–0.000	−0.103–0.000	0.326–2.344	−2.840 to −0.213	0.033–0.305	0.380–1.474	
		n = 228	*n* = 39	*n* = 3	*n* = 228	*n* = 227	*n* = 228	*n* = 228	
	Female	0.085 ± 0.027	−0.026 ± 0.036	−0.043 ± 0.037	0.761 ± 0.374	−0.753 ± 0.374	0.041 ± 0.036	0.517 ± 0.204	−0.130 ± 0.096
		0.043–0.151	−0.169–0.000	−0.086–0.000	0.177–1.800	−1.530 to −0.087	−0.019–0.108	0.160–1.012	−0.198–0.000
		n = 283	*n* = 18	*n* = 3	*n* = 284	*n* = 275	*n* = 284	*n* = 284	*n* = 2
30–39	Male	0.092 ± 0.028	−0.026 ± 0.011	−0.087 ± 0.068	0.983 ± 0.501	−1.188 ± 0.515	0.119 ± 0.065	0.779 ± 0.277	
		0.044–0.165	−0.067–0.000	−0.211–0.000	0.259–2.257	−2.338 to −0.186	0.004–0.269	0.253–1.472	
		n = 208	*n* = 29	*n* = 8	*n* = 208	*n* = 204	*n* = 208	*n* = 208	
	Female	0.086 ± 0.028	−0.028 ± 0.029		0.730 ± 0.367	−0.765 ± 0.439	0.038 ± 0.037	0.499 ± 0.200	−0.251 ± 0.208
		0.031–0.174	−0.116–0.000		0.180–2.174	−1.870 to −0.134	−0.035–0.132	0.135–0.987	−0.398–0.000
		n = 123	*n* = 12		*n* = 123	*n* = 117	*n* = 123	*n* = 122	*n* = 2
40–49	Male	0.088 ± 0.028	−0.022 ± 0.007	−0.066 ± 0.049	1.020 ± 0.506	−1.015 ± 0.490	0.096 ± 0.059	0.731 ± 0.257	
		0.039–0.152	−0.044–0.000	−0.150–0.000	0.250–2.221	−2.037 to −0.217	−0.014–0.203	0.311–1.322	
		n = 205	*n* = 33	*n* = 5	*n* = 205	*n* = 202	*n* = 205	*n* = 205	
	Female	0.082 ± 0.025	−0.022 ± 0.013	−0.062 ± 0.057	0.675 ± 0.329	−0.719 ± 0.366	0.033 ± 0.032	0.457 ± 0.184	
		0.038–0.139	−0.047–0.000	−0.128–0.000	0.187–1.633	−1.657 to −0.193	−0.035–0.099	0.132–0.917	
		n = 88	*n* = 10	*n* = 3	*n* = 88	*n* = 86	*n* = 88	*n* = 88	
50+	Male	0.088 ± 0.027	−0.023 ± 0.009	−0.066 ± 0.058	0.998 ± 0.506	−0.994 ± 0.494	0.086 ± 0.060	0.687 ± 0.270	
		0.040–0.167	−0.052–0.000	−0.219–0.000	0.200–2.235	−2.080 to −0.178	−0.017–0.230	0.229–1.307	
		n = 195	*n* = 23	*n* = 13	*n* = 195	*n* = 193	*n* = 195	*n* = 194	
	Female	0.084 ± 0.026	−0.021 ± 0.008	−0.051 ± 0.035	0.752 ± 0.409	−0.768 ± 0.372	0.030 ± 0.035	0.436 ± 0.169	−0.068 ± 0.059
		0.037–0.148	−0.039–0.000	−0.108–0.000	0.183–1.811	−1.696 to −0.214	−0.049–0.097	0.086–0.793	−0.110–0.000
		n = 128	*n* = 18	*n* = 5	*n* = 128	*n* = 126	*n* = 128	*n* = 128	*n* = 2

Table A1.24

Amplitudes (in millivolts) in Caucasian adults: lead V_4

Age group	Sex	P+	P–	Q	R	S	STj	T+	T–
18–29	Male	0.088 ± 0.028	−0.018 ± 0.005	−0.090 ± 0.075	1.973 ± 0.702	−0.584 ± 0.376	0.089 ± 0.054	0.705 ± 0.269	
		0.033–0.158	−0.025–0.000	−0.307–0.000	0.792–3.558	−1.660 to −0.074	−0.006–0.201	0.261–1.427	
		n = 227	*n* = 20	*n* = 85	*n* = 227	*n* = 209	*n* = 227	*n* = 227	
	Female	0.082 ± 0.027	−0.022 ± 0.020	−0.064 ± 0.049	1.247 ± 0.453	−0.372 ± 0.205	0.021 ± 0.027	0.413 ± 0.172	−0.060 ± 0.000
		0.038–0.150	−0.089–0.000	−0.271–0.000	0.452–2.264	−0.832 to −0.075	−0.037–0.088	0.141–0.847	−0.060–0.000
		n = 283	*n* = 14	*n* = 72	*n* = 284	*n* = 242	*n* = 284	*n* = 284	*n* = 1
30–39	Male	0.089 ± 0.027	−0.021 ± 0.009	−0.076 ± 0.063	1.717 ± 0.601	−0.627 ± 0.347	0.069 ± 0.050	0.625 ± 0.238	
		0.042–0.152	−0.041–0.000	−0.335–0.000	0.658–3.257	−1.571 to −0.113	−0.035–0.208	0.215–1.268	
		n = 208	*n* = 17	*n* = 62	*n* = 208	*n* = 193	*n* = 208	*n* = 208	
	Female	0.088 ± 0.028	−0.020 ± 0.011	−0.073 ± 0.039	1.277 ± 0.509	−0.433 ± 0.259	0.015 ± 0.031	0.418 ± 0.181	−0.030 ± 0.000
		0.032–0.155	−0.032–0.000	−0.197–0.000	0.285–2.705	−1.050 to −0.097	−0.056–0.095	0.081–0.961	−0.030–0.000
		n = 124	*n* = 3	*n* = 35	*n* = 124	*n* = 97	*n* = 124	*n* = 124	*n* = 1
40–49	Male	0.085 ± 0.024	−0.022 ± 0.008	−0.060 ± 0.047	1.620 ± 0.629	−0.571 ± 0.346	0.054 ± 0.046	0.593 ± 0.245	−0.077 ± 0.000
		0.044–0.142	−0.041–0.000	−0.306–0.000	0.516–3.222	−1.425 to −0.074	−0.017–0.166	0.213–1.185	−0.077–0.000
		n = 204	*n* = 18	*n* = 52	*n* = 204	*n* = 204	*n* = 204	*n* = 204	*n* = 1
	Female	0.085 ± 0.025	−0.021 ± 0.012	−0.058 ± 0.048	1.110 ± 0.454	−0.415 ± 0.257	0.010 ± 0.026	0.357 ± 0.159	
		0.035–0.142	−0.044–0.000	−0.175–0.000	0.384–2.200	−1.196 to −0.070	−0.046–0.075	0.094–0.787	
		n = 87	*n* = 6	*n* = 87	*n* = 87	*n* = 76	*n* = 87	*n* = 87	
50+	Male	0.086 ± 0.024	−0.018 ± 0.004	−0.079 ± 0.055	1.592 ± 0.546	−0.619 ± 0.377	0.045 ± 0.046	0.568 ± 0.248	−0.135 ± 0.000
		0.047–0.146	−0.025–0.000	−0.282–0.000	0.582–2.683	−1.500 to −0.099	−0.044–0.159	0.166–1.249	−0.135–0.000
		n = 202	*n* = 10	*n* = 54	*n* = 202	*n* = 191	*n* = 202	*n* = 201	*n* = 1
	Female	0.089 ± 0.027	−0.019 ± 0.009	−0.048 ± 0.030	1.150 ± 0.454	−0.444 ± 0.293	0.006 ± 0.030	0.352 ± 0.156	−0.080 ± 0.045
		0.041–0.151	−0.036–0.000	−0.148–0.000	0.435–2.326	−1.473 to −0.072	−0.075–0.074	0.074–0.690	−0.140–0.000
		n = 129	*n* = 12	*n* = 28	*n* = 129	*n* = 123	*n* = 129	*n* = 129	*n* = 4

Table A1.25

Amplitudes (in millivolts) in Caucasian adults: lead V_5

Age group	Sex	P+	P−	Q	R	S	STj	T+	T−
18–29	Male	0.082 ± 0.025	−0.020 ± 0.011	−0.101 ± 0.072	1.910 ± 0.598	−0.316 ± 0.228	0.051 ± 0.039	0.553 ± 0.226	
		0.028–0.136	−0.061–0.000	−0.324–0.000	0.958–3.530	−0.946 to −0.045	−0.010–0.155	0.194–1.152	
		n = 230	*n* = 20	*n* = 171	*n* = 230	*n* = 181	*n* = 230	*n* = 230	
	Female	0.079 ± 0.026	−0.016 ± 0.005	−0.070 ± 0.050	1.289 ± 0.383	−0.230 ± 0.131	0.013 ± 0.023	0.386 ± 0.141	
		0.037–0.143	−0.029–0.000	−0.233–0.000	0.574–2.112	−0.577 to −0.048	−0.032–0.061	0.149–0.720	
		n = 287	*n* = 14	*n* = 148	*n* = 288	*n* = 214	*n* = 287	*n* = 287	
30–39	Male	0.084 ± 0.023	−0.021 ± 0.008	−0.088 ± 0.069	1.761 ± 0.502	−0.330 ± 0.235	0.041 ± 0.039	0.497 ± 0.197	−0.370 ± 0.000
		0.035–0.135	−0.034–0.000	−0.283–0.000	0.756–3.012	−0.986 to −0.069	−0.029–0.154	0.181–1.028	−0.370–0.000
		n = 211	*n* = 11	*n* = 127	*n* = 211	*n* = 179	*n* = 211	*n* = 211	*n* = 1
40–49	Female	0.084 ± 0.026	−0.011 ± 0.005	−0.074 ± 0.048	1.299 ± 0.411	−0.239 ± 0.162	0.010 ± 0.027	0.369 ± 0.151	
		0.030–0.146	−0.014–0.000	−0.197–0.000	0.502–2.372	−0.689 to −0.057	−0.040–0.087	0.126–0.827	
		n = 123	*n* = 2	*n* = 78	*n* = 123	*n* = 88	*n* = 123	*n* = 123	
	Male	0.080 ± 0.022	−0.020 ± 0.010	−0.072 ± 0.049	1.576 ± 0.506	−0.306 ± 0.227	0.032 ± 0.034	0.458 ± 0.185	
		0.040–0.142	−0.044–0.000	−0.294–0.000	0.737–2.869	−0.952 to −0.049	−0.031–0.133	0.161–0.879	
		n = 206	*n* = 12	*n* = 111	*n* = 206	*n* = 165	*n* = 206	*n* = 206	
	Female	0.083 ± 0.026	−0.022 ± 0.012	−0.062 ± 0.046	1.190 v 0.393	−0.247 ± 0.190	0.004 ± 0.024	0.323 ± 0.128	−0.077 ± 0.000
		0.044–0.138	−0.043–0.000	−0.202–0.000	0.625–2.092	−1.034 to −0.046	−0.056–0.052	0.085–0.616	−0.077–0.000
		n = 88	*n* = 8	*n* = 39	*n* = 88	*n* = 68	*n* = 88	*n* = 87	*n* = 1
50+	Male	0.081 ± 0.022	−0.020 ± 0.011	−0.080 ± 0.054	1.581 ± 0.470	−0.366 ± 0.237	0.023 ± 0.036	0.427 ± 0.190	−0.067 ± 0.000
		0.043–0.134	−0.047–0.000	−0.241–0.000	0.745–2.488	−0.967 to −0.053	−0.047–0.104	0.114–0.916	−0.067–0.000
		n = 201	*n* = 8	*n* = 102	*n* = 201	*n* = 162	*n* = 201	*n* = 201	*n* = 1
	Female	0.084 ± 0.026	−0.016 ± 0.012	−0.063 ± 0.037	1.241 ± 0.379	−0.261 ± 0.189	−0.001 ± 0.025	0.310 ± 0.139	−0.098 ± 0.044
		0.029–0.145	−0.033–0.000	−0.229–0.000	0.570–2.295	−0.837 to −0.049	−0.050–0.052	0.088–0.636	−0.158–0.000
		n = 129	*n* = 5	*n* = 62	*n* = 129	*n* = 99	*n* = 129	*n* = 128	*n* = 4

Table A1.26

Amplitudes (in millivolts) in Caucasian adults: lead V_6

Age group	Sex	P+	P–	Q	R	S	STj	T+	T–
18–29	Male	0.075 ± 0.023	−0.011 ± 0.004	−0.106 ± 0.066	1.583 ± 0.463	−0.197 ± 0.142	0.032 ± 0.028	0.424 ± 0.166	
		0.032–0.125	−0.020–0.000	−0.262–0.000	0.766–2.806	−0.572 to −0.039	−0.017–0.091	0.153–0.897	
		n = 228	*n* = 11	*n* = 202	*n* = 228	*n* = 137	*n* = 228	*n* = 228	
	Female	0.074 ± 0.025	−0.020 ± 0.023	−0.076 ± 0.054	1.177 ± 0.319	−0.143 ± 0.083	0.009 ± 0.023	0.327 ± 0.109	−0.224 ± 0.168
		0.031–0.137	−0.075–0.000	−0.257–0.000	0.611–1.966	−0.359 to −0.046	−0.035–0.049	0.143–0.573	−0.343–0.000
		n = 289	*n* = 9	*n* = 215	*n* = 289	*n* = 161	*n* = 289	*n* = 289	*n* = 2
30–39	Male	0.077 ± 0.022	−0.019 ± 0.006	−0.090 ± 0.064	1.461 ± 0.456	−0.187 ± 0.141	0.026 ± 0.028	0.390 ± 0.150	
		0.040–0.131	−0.026–0.000	−0.271–0.000	0.623–2.540	−0.564 to −0.025	−0.026–0.088	0.149–0.782	
		n = 205	*n* = 5	*n* = 159	*n* = 207	*n* = 129	*n* = 207	*n* = 207	
	Female	0.079 ± 0.024	−0.013 ± 0.004	−0.083 ± 0.049	1.147 ± 0.323	−0.153 ± 0.125	0.006 ± 0.023	0.302 ± 0.119	
		0.032–0.140	−0.018–0.000	−0.229–0.000	0.605–1.978	−0.724 to −0.032	−0.043–0.074	0.081–0.649	
		n = 123	*n* =3	*n* = 102	*n* = 123	*n* = 59	*n* = 123	*n* = 123	
40–49	Male	0.075 ± 0.020	−0.024 ± 0.012	−0.071 ± 0.043	1.291 ± 0.399	−0.200 ± 0.137	0.021 ± 0.026	0.350 ± 0.140	
		0.040–0.132	−0.044–0.000	−0.202–0.000	0.664–2.290	−0.565 to −0.037	−0.031–0.094	0.137–0.680	
		n = 206	*n* = 8	*n* = 152	*n* = 206	*n* = 109	*n* = 206	*n* = 206	
	Female	0.079 ± 0.024	−0.036 ± 0.000	−0.065 ± 0.042	1.068 ± 0.315	−0.161 ± 0.127	0.004 ± 0.020	0.273 ± 0.104	−0.057 ± 0.000
		0.040–0.128	−0.036–0.000	−0.215–0.000	0.475–1.721	−0.728 to −0.025	−0.037–0.049	0.091–0.500	−0.057–0.000
		n = 89	*n* = 1	*n* = 55	*n* = 89	*n* = 45	*n* = 89	*n* = 88	*n* = 1
50+	Male	0.076 ± 0.020	−0.014 ± 0.004	−0.078 ± 0.050	1.304 ± 0.409	−0.200 ± 0.132	0.015 ± 0.029	0.318 ± 0.142	−0.049 ± 0.028
		0.038–0.117	−0.016–0.000	−0.233–0.000	0.649–2.287	−0.591 to −0.046	−0.045–0.067	0.102–0.680	−0.069–0.000
		n = 198	*n* = 2	*n* = 133	*n* = 198	*n* = 124	*n* = 198	*n* = 198	*n* = 2
	Female	0.080 ± 0.024	−0.015 ± 0.008	−0.067 ± 0.040	1.100 ± 0.335	−0.154 ± 0.084	−0.002 ± 0.021	0.259 ± 0.118	−0.063 ± 0.042
		0.033–0.137	−0.024–0.000	−0.185–0.000	0.523–1.859	−0.384 to −0.055	−0.051–0.037	0.078–0.561	−0.137–0.000
		n = 129	*n* = 6	*n* = 80	*n* = 129	*n* = 61	*n* = 129	*n* = 128	*n* = 6

Table A1.27

R/S ratio in Caucasians: leads $V_1 - V_6$

Age group	Sex	V_1	V_2	V_3	V_4	V_5	V_6
18–29	Male	0.333 ± 0.21	0.429 ± 0.25	1.345 ± 2.03	5.649 ± 7.15	10.327 ± 10.11	13.883 ± 12.47
		0.053–0.913	0.089–1.191	0.180–6.82	0.699–36.66	1.188–44.53	2.211–62.125
		n = 267	*n* = 267	*n* = 268	*n* = 243	*n* = 216	*n* = 169
	Female	0.289 ± 0.19	0.468 ± 0.31	1.548 ± 1.84	5.88 ± 8.07	7.879 ± 7.42	10.891 ± 8.81
		0.042–0.803	0.104–1.55	0.211–8.31	0.831–36.74	1.30–27.13	2.417–40.64
		n = 315	*n* = 318	*n* = 314	*n* = 284	*n* = 247	*n* = 188
30–39	Male	0.30 ± 0.25	0.420 ± 0.30	1.218 ± 1.62	4.623 ± 7.91	8.298 ± 7.87	13.093 ± 12.73
		0.050–0.940	0.090–1.214	0.194–4.04	0.63–19.14	1.33–23.07	2.305–62.07
		n = 214	*n* = 215	*n* = 214	*n* = 202	*n* = 181	*n* = 137
	Female	0.272 ± 0.17	0.480 ± 0.42	2.188 ± 6.17	4.482 ± 3.64	8.197 ± 6.07	13.757 ± 11.11
		0.035–0.62	0.102–1.728	0.241–11.48	0.781–14.684	1.104–25.228	1.916–47.47
		n = 116	*n* = 114	*n* = 113	*n* = 96	*n* = 88	*n* = 63
40–49	Male	0.269 ± 0.17	0.487 ± 0.48	1.478 ± 2.73	4.753 ± 6.47	8.818 ± 9.93	10.471 ± 9.22
		0.031–0.711	0.087–1.40	0.184–5.265	0.481–34.40	1.097–47.43	1.877–31.14
		n = 116	*n* = 115	*n* = 118	*n* = 114	*n* = 98	*n* = 68
	Female	0.239 ± 0.14	0.429 ± 0.26	1.354 ± 1.39	5.316 ± 7.79	7.99 ± 5.85	9.760 ± 6.18
		0.034–0.519	0.092–1.311	0.125–4.044	0.572–43.119	1.554–26.21	1.993–22.516
		n = 73	*n* = 73	*n* = 73	*n* = 71	*n* = 65	*n* = 48
50+	Male	0.263 ± 0.17	0.507 ± 0.35	1.340 ± 1.42	3.935 ± 3.71	7.29 ± 7.48	10.703 ± 10.62
		0.046–0.75	0.133–1.428	0.313–5.767	0.789–13.33	1.371–28.674	1.575–45.51
		n = 122	*n* = 121	*n* = 122	*n* = 117	*n* = 101	*n* = 80
	Female	0.227 ± 0.14	0.443 ± 0.28	1.369 ± 1.41	3.409 ± 3.07	8.274 ± 7.90	8.96 ± 6.93
		0.044–0.626	0.049–1.082	0.203–6.578	0.564–14.904	1.568–34.44	2.37–17.65
		n = 77	*n* = 79	*n* = 79	*n* = 77	*n* = 66	*n* = 40

Table A1.28

Q/R ratios (%) in Caucasians: leads I, II, III, aVL, aVF, V_5, V_6

Age group	Sex	I	II	III	aVL	aVF	V_5	V_6
18–29	Male	9.0 ± 5.5	6.0 ± 3.6	18 ± 51.8	37 ± 78.5	8.0 ± 6.6	5.0 ± 3.7	7.0 ± 4.1
		0.0–23.4	0.0–14.8	0.0–81.5	0.0–188	0.0–19.3	0.0–14.9	0.0–17.8
		n = 143	*n* = 189	*n* = 154	*n* = 119	*n* = 166	*n* = 199	*n* = 230
	Female	8.0 ± 4.5	6.0 ± 3.6	23 ± 38.9	27 ± 41.9	8.0 ± 4.8	5.0 ± 3.1	6.0 ± 3.7
		0.0–22.3	0.0–14.9	0.0–139	0.0–75.0	0.0–19.5	0.0–12.6	0.0–16.0
		n = 132	*n* = 204	*n* = 192	*n* = 115	*n* = 202	*n* = 168	*n* = 236
30–39	Male	8.0 ± 4.9	7.0 ± 4.0	35 ± 83.6	25 ± 33.6	9.0 ± 5.0	5.0 ± 3.2	6.0 ± 3.8
		0.0–21.6	0.0–19.3	0.0–236	0.0–138	0.0–22.2	*0.0–12.4*	0.0–14.7
		n = 122	*n* = 129	*n* = 115	*n* = 110	*n* = 120	*n* = 137	*n* = 171
	Female	9.0 ± 4.5	7.0 ± 3.3	21 ± 33.6	29 ± 25.2	9.0 ± 4.3	5.0 ± 3.1	7.0 ± 3.8
		0.0–18.9	0.0–14.6	0.0–85.3	0.0–92.0	0.0–17.5	0.0–12.2	0.0–15.0
		n = 54	*n* = 90	*n* = 76	*n* = 40	*n* = 83	*n* = 78	*n* = 99
40–49	Male	8.0 ± 3.6	6.0 ± 2.4	56 ± 11.0	24 ± 43.1	13 ± 24.2	4.0 ± 1.9	6.0 ± 2.6
		0.0–15.7	0.0–11.0	0.0–154	0.0–160	0.0–86.0	0.0–8.2	0.0–10.8
		n = 72	*n* = 65	*n* = 47	*n* = 69	*n* = 51	*n* = 70	*n* = 91
	Female	7.0 ± 4.7	6.0 ± 3.2	24 ± 31.5	19 ± 16.9	10 ± 8.60	5.0 ± 2.8	6.0 ± 3.0
		0.0–18.8	0.0–13.4	0.0–92.8	0.0–38.2	0.0–29.7	0.0–11.7	0.0–13.2
		n = 47	*n* = 41	*n* = 31	*n* = 44	*n* = 38	*n* = 38	*n* = 50
50+	Male	8.0 ± 5.5	7.0 ± 4.7	80 ± 192.7	26 ± 42.2	17 ± 31.2	5.0 ± 4.1	6.0 ± 4.6
		0.0–31.3	0.0–20.5	0.0–740	0.0–238	0.0–64.0	0.0–21.5	0.0–19.8
		n = 79	*n* = 52	*n* = 45	*n* = 79	*n* = 43	*n* = 69	*n* = 84
	Female	8.0 ± 4.3	7.0 ± 4.7	52 ± 109.4	14 ± 7.70	11 ± 8.90	5.0 ± 3.9	6.0 ± 4.8
		0.0–16.7	0.0–14.6	0.0–335	0.0–27.4	0.0–36.7	0.0–13.0	0.0–13.9
		n = 46	*n* = 39	*n* = 38	*n* = 43	*n* = 35	*n* = 39	*n* = 51

Table A1.29

Miscellaneous measures

Age group	Sex	QRS axis (°)	T axis (°)	QRS-T angle (frontal plane) (°)	Lewis index[a] (mV)	SV_1+RV_5 (mV)	SV_1+R V_6 (mV)	SV_1+ RV_6 (mV)
18–29	Male	57.5 ± 25.6	40.9 ± 16.7	16.6 ± 23.9	−0.117 ± 0.956	3.331 ± 0.881	3.905 ± 0.995	2.99 ± 0.79
		−10–91	2–69	−39–71	−1.831–2.048	1.685–5.252	2.049–6.372	1.59–4.85
		n = 265	*n* = 265	*n* = 265	*n* = 266	*n* = 264	*n* = 265	*n* = 265
	Female	51.2 ± 24.9	38.7 ± 15.0	12.5 ± 25.1	0.110 ± 0.736	2.442 ± 0.690	2.741 ± 0.727	2.32 ± 0.64
		−9–91	6–65	−46–59	−1.288–1.574	1.112–3.816	1.430–4.635	1.20–3.68
		n = 317	*n* = 317	*n* = 317	*n* = 317	*n* = 316	*n* = 317	*n* = 318
30–39	Male	46.5 ± 29.2	39.3 ± 17.2	7.2 ± 27.3	0.266 ± 0.899	3.007 ± 0.775	3.430 ± 0.875	2.69 ± 0.72
		−22–92	−1–70	−61–59	−1.476–1.962	1.549–4.680	1.846–5.257	1.31–4.14
		n = 220	*n* = 220	*n* = 220	*n* = 221	*n* = 220	*n* = 219	*n* = 220
	Female	49.6 ± 24.2	39.0 ± 15.4	10.6 ± 21.7	0.129 ± 0.626	2.454 ± 0.644	2.662 ± 0.834	2.29 ± 0.60
		−14–81	1–66	−47–61	−1.011–1.293	0.483–4.287	1.565–4.803	1.43–3.59
		n = 118	*n* = 118	*n* = 118	*n* = 118	*n* = 118	*n* = 115	*n* = 118
40–49	Male	37.7 ± 31.6	42.5 ± 17.3	−4.8 ± 26.3	0.491 ± 0.892	2.702 ± 0.763	2.842 ± 0.673	2.39 ± 0.69
		−37–85	5–71	−67–37	−1.060–2.395	1.420–4.227	1.634–4.170	1.22–3.77
		n = 117	*n* = 117	*n* = 117	*n* = 118	*n* = 118	*n* = 117	*n* = 118
	Female	36.2 ± 29.1	38.0 ± 15.7	−1.8 ± 27.9	0.521 ± 0.698	2.291 ± 0.634	2.418 ± 0.566	2.13 ± 0.57
		−53–85	5–67	−86–40	0.762–1.818	1.087–3.411	1.429–3.433	1.07–3.16
		n = 73	*n* = 73	*n* = 73	*n* = 73	*n* = 73	*n* = 73	*n* = 73
50+	Male	31.4 ± 30.6	44.4 ± 18.7	−13.0 ± 27.1	0.627 ± 0.742	2.709 ± 0.736	2.746 ± 0.703	2.35 ± 0.63
		−33–77	4–74	−82–40	0.703–2.120	1.612–4.558	1.546–4.144	1.34–3.78
		n = 125	*n* = 125	*n* = 125	*n* = 125	*n* = 125	*n* = 124	*n* = 125
	Female	26.9 ± 29.2	41.9 ± 15.9	−15.0 ± 27.8	0.714 ± 0.691	2.259 ± 0.567	2.316 ± 0.574	2.10 ± 0.55
		−36–73	4–72	−89-26	0.578–2.165	1.086–3.635	1.298–3.419	0.94–3.14
		n = 80	*n* = 80	*n* = 80	*n* = 80	*n* = 79	*n* = 80	*n* = 80

[a]Lewis index = (RI + SIII)–(SI + RIII).

Table A1.30

ST slope (°) in selected leads in Caucasians

Age group	Sex	I	aVF	V_2	V_5	V_6
18–29	Male	19 ± 7	12 ± 8	50 ± 12	28 ± 10	20 ± 8
		6–33	−2–31	21–69	11–51	6–38
		n = 265	*n* = 265	*n* = 265	*n* = 265	*n* = 265
	Female	12 ± 6	7 ± 5	31 ± 11	15 ± 7	11 ± 6
		3–24	−3–19	8–53	2–33	1–25
		n = 317	*n* = 318	*n* = 317	*n* = 318	*n* = 318
30–39	Male	17 ± 8	9 ± 7	46 ± 13	26 ± 10	18 ± 9
		3–36	−3–27	19–66	10–53	3–42
		n = 220	*n* = 220	*n* = 220	*n* = 220	*n* = 220
	Female	10 ± 5	6 ± 5	28 ± 10	14 ± 7	10 ± 6
		1–21	−4–16	10–50	0–33	0–25
		n = 118	*n* = 118	*n* = 116	*n* = 118	*n* = 117
40–49	Male	13 ± 6	9 ± 6	41 ± 13	22 ± 9	15 ± 7
		3–25	−1–22	13–63	7–43	2–31
		n = 118	*n* = 117	*n* = 117	*n* = 119	*n* = 119
	Female	10 ± 5	6 ± 6	25 ± 10	13 ± 7	10 ± 6
		2–20	−2–21	7–46	0–26	2–32
		n = 73	*n* = 73	*n* = 73	*n* = 73	*n* = 73
50+	Male	12 ± 7	9 ± 6	40 ± 12	21 ± 13	14 ± 8
		0–28	−1–24	15–61	2–43	0–31
		n = 125	*n* = 125	*n* = 125	*n* = 125	*n* = 124
	Female	7 ± 4	5 ± 5	24 ± 10	12 ± 7	7 ± 5
		0–14	−2–17	10–42	0–28	−1–19
		n = 80	*n* = 80	*n* = 80	*n* = 80	*n* = 80

Table A1.31

P terminal force in V_1, intrinsicoid deflection (ID) in V_5, V_6, and body-surface area (BSA) in the Caucasians studied as described in Chap. 13.

Age group	Sex	P terminal force in V_1 (mV ms)	ID V_5 (ms)	ID V_6 (ms)	BSA (m^2)
18–29	Male	1.09 ± 1.33	41 ± 13.4	41 ± 12.3	1.86 ± 0.15
		0.0–4.62	26–85	22–87	1.55–2.19
		n = 265	*n* = 265	*n* = 265	*n* = 257
	Female	0.75 ± 1.03	33 ± 8.40	35 ± 7.70	1.62 ± 0.14
		0.0–3.54	22–66	22–59	1.37–1.95
		n = 316	*n* = 318	*n* = 318	*n* = 315
30–39	Male	1.16 ± 1.21	37 ± 11.5	38 ± 10.7	1.89 ± 0.15
		0.0–3.94	22–79	22–84	1.60–2.26
		n = 219	*n* = 220	*n* = 220	*n* = 215
	Female	1.02 ± 1.25	35 ± 7.10	36 ± 6.90	1.62 ± 0.16
		0.0–4.29	22–48	24–47	1.38–2.07
		n = 118	*n* = 118	*n* = 117	*n* = 117
40–49	Male	1.49 ± 1.44	34 ± 9.40	35 ± 8.10	1.88 ± 0.17
		0.0–4.42	20–67	24–64	1.54–2.26
		n = 117	*n* = 119	*n* = 117	*n* = 115
	Female	1.57 ± 1.40	32 ± 6.70	33 ± 5.90	1.68 ± 0.16
		0.0–5.5	22–44	20–42	1.47–2.03
		n = 73	*n* = 73	*n* = 73	*n* = 69
50±	Male	1.47 ± 1.44	35 ± 10.7	33 ± 5.90	1.85 ± 0.14
		0.0–5.45	22–72	22–46	1.53–2.14
		n = 125	*n* = 175	*n* = 174	*n* = 121
	Female	1.42 ± 1.37	31 ± 6.30	32 ± 6.30	1.65 ± 0.11
		0.0–4.05	22–41	22–44	1.43–1.92
		n = 79	*n* = 80	*n* = 80	*n* = 79

A1.2 Normal Limits of the 12-Lead ECG in Chinese

The data in Tables A1.32–A1.38 were obtained from a study of 503 Chinese people with normal cardiovascular systems (see Chap. 13). There were 255 males and 248 females. The most significant differences with the Caucasian data presented in Sect. A1.1 were in the QRS amplitudes, and for this reason, only some amplitude data are tabulated here. Fuller details are available in: Chen C Y, Chiang B N, Macfarlane P W. Normal limits of the electrocardiogram in a Chinese population. *J. Electrocardiol*. 1989;**22**(1): 1–15. Most of these tables are reproduced from that article with the permission of Churchill Livingstone, New York. Data are presented as mean ± standard deviation together with 96% ranges; that is, 2% of the measurements have been excluded from each extreme of the range. Where numbers of subjects studied in a subgroup is small, the full range is given. P-, Q, S, T- wave amplitudes are presented as positive measurements.

A1.3 Normal Limits of the 12-Lead ECG in Japanese

The data in Tables A1.39–A1.43 are taken from a study of 1,329 normal Japanese individuals. The ECGs were recorded on paper and measurements made by hand. For this reason, only selected amplitudes are presented. These data have been reproduced from: The normal value of electrocardiogram in the Japanese. *Jpn. Heart J*. 1963; **4**: 141–172 with the permission of the University of Tokyo Press, Tokyo. Note that the maximum and minimum values are presented and not the 96% range. Q, S wave amplitudes are treated as positive values.

Table A1.32

Q-wave amplitude (millivolts) in normal Chinese in various age-groups: leads I-aVF

	18–29		30–39		40–49		50–59		60+	
	Male *n* = 56	Female *n* = 47	Male *n* = 50	Female *n* = 59	Male *n* = 50	Female *n* = 50	Male *n* = 50	Female *n* = 48	Male *n* = 49	Female *n* = 44
I	0.07 ± 0.04	0.04 ± 0.02	0.05 ± 0.03	0.06 ± 0.03	0.07 ± 0.05	0.05 ± 0.02	0.07 ± 0.04	0.06 ± 0.03	0.07 ± 0.04	0.06 ± 0.02
	0.00–0.15	0.00–0.07	0.00–0.10	0.00–0.10	0.00–0.10	0.00–0.10	0.00–0.11	0.00–0.12	0.00–0.14	0.00–0.08
	n = 23	*n* = 14	*n* = 15	*n* = 15	*n* = 15	*n* = 15	*n* = 21	*n* = 17	*n* = 22	*n* = 16
II	0.10 ± 0.05	0.07 ± 0.06	0.07 ± 0.06	0.08 ± 0.05	0.07 ± 0.05	0.06 ± 0.03	0.07 ± 0.05	0.07 ± 0.05	0.07 ± 0.04	0.07 ± 0.06
	0.00–0.17	0.00–0.20	0.00–0.22	0.00–0.15	0.00–0.15	0.00–0.10	0.00–0.11	0.00–0.11	0.00–0.15	0.00–0.10
	n = 23	*n* = 25	*n* = 29	*n* = 25	*n* = 19	*n* = 17	*n* = 18	*n* = 15	*n* = 23	*n* = 10
III	0.11 ± 0.06	0.12 ± 0.08	0.13 ± 0.10	0.10 ± 0.08	0.15 ± 0.13	0.11 ± 0.12	0.11 ± 0.09	0.10 ± 0.08	0.14 ± 0.12	0.17 ± 0.13
	0.00–0.20	0.00–0.27	0.00–0.28	0.00–0.21	0.00–0.25	0.00–0.43	0.00–0.27	0.00–0.19	0.00–0.34	0.00–0.37
	n = 23	*n* = 28	*n* = 32	*n* = 34	*n* = 23	*n* = 24	*n* = 17	*n* = 19	*n* = 25	*n* = 18
aVR	0.79 ± 0.22	0.73 ± 0.14	0.79 ± 0.17	0.76 ± 0.18	0.71 ± 0.18	0.70 ± 0.20	0.70 ± 0.20	0.68 ± 0.18	0.69 ± 0.20	0.69 ± 0.21
	0.00–1.22	0.00–0.95	0.00–1.12	0.00–1.05	0.00–0.95	0.00–1.28	0.00–1.03	0.00–1.04	0.00–0.88	0.00–1.05
	n = 33	*n* = 33	*n* = 31	*n* = 35	*n* = 35	*n* = 36	*n* = 29	*n* = 38	*n* = 30	*n* = 36
aVL	0.10 ± 0.07	0.09 ± 0.08	0.11 ± 0.09	0.13 ± 0.15	0.12 ± 0.12	0.07 ± 0.04	0.10 ± 0.07	0.07 ± 0.05	0.09 ± 0.05	0.10 ± 0.08
	0.00–0.19	0.00–0.23	0.00–0.27	0.00–0.44	0.00–0.27	0.00–0.10	0.00–0.23	0.00–0.18	0.00–0.21	0.00–0.21
	n = 27	*n* = 16	*n* = 17	*n* = 22	*n* = 22	*n* = 20	*n* = 29	*n* = 24	*n* = 25	*n* = 23
aVF	0.10 ± 0.05	0.09 ± 0.06	0.08 ± 0.06	0.08 ± 0.05	0.08 ± 0.05	0.06 ± 0.02	0.07 ± 0.06	0.07 ± 0.04	0.08 ± 0.05	0.08 ± 0.07
	0.00–0.18	0.00–0.19	0.00–0.23	0.00–0.17	0.00–0.15	0.00–0.10	0.00–0.14	0.00–0.14	0.00–0.16	0.00–0.12
	n = 22	*n* = 26	*n* = 29	*n* = 30	*n* = 20	*n* = 18	*n* = 18	*n* = 12	*n* = 24	*n* = 13

Table A1.33

Q-wave amplitude (millivolts) in normal Chinese in various age-groups: leads $V_1 - V_6$

	18–29		30–39		40–49		50–59		60+	
	Male $n = 56$	Female $n = 47$	Male $n = 50$	Female $n = 59$	Male $n = 50$	Female $n = 50$	Male $n = 50$	Female $n = 48$	Male $n = 49$	Female $n = 44$
V_1		1.08 ± 0.93			0.76 ± 0.81	0.98 ± 0.00	1.58 ± 0.00		0.33 ± 0.00	0.41 ± 0.01
		0.00–2.29			0.00–1.33	0.00–0.98	0.00–1.58		0.00–0.33	0.00–0.41
		$n = 4$			$n = 2$	$n = 1$	$n = 1$		$n = 1$	$n = 3$
V_2							0.04 ± 0.00		0.05 ± 0.00	0.04 ± 0.01
							0.00–0.04		0.00–0.05	0.00–0.04
							$n = 1$		$n = 1$	$n = 3$
V_3	0.07 ± 0.03	0.13 ± 0.06		0.03 ± 0.01			0.03 ± 0.00	0.23 ± 0.00	0.06 ± 0.01	0.06 ± 0.03
	0.00–0.09	0.00–0.18		0.00–0.04			0.00–0.03	0.00–0.23	0.00–0.07	0.00–0.10
	$n = 2$	$n = 2$		$n = 3$			$n = 1$	$n = 1$	$n = 2$	$n = 4$
V_4	0.11 ± 0.08	0.11 ± 0.10	0.07 ± 0.07	0.05 ± 0.02	0.09 ± 0.05	0.03 ± 0.01	0.07 ± 0.06	0.07 ± 0.07	0.09 ± 0.06	0.05 ± 0.04
	0.00–0.25	0.00–0.26	0.00–0.24	0.00–0.08	0.00–0.14	0.00–0.04	0.00–0.13	0.00–0.23	0.00–0.19	0.00–0.11
	$n = 18$	$n = 7$	$n = 9$	$n = 14$	$n = 5$	$n = 5$	$n = 12$	$n = 8$	$n = 7$	$n = 13$
V_5	0.11 ± 0.08	0.08 ± 0.07	0.09 ± 0.07	0.06 ± 0.03	0.08 ± 0.07	0.06 ± 0.02	0.08 ± 0.05	0.07 ± 0.05	0.07 ± 0.05	0.05 ± 0.03
	0.00–0.25	0.00–0.22	0.00–0.22	0.00–0.12	0.00–0.21	0.00–0.09	0.00–0.16	0.00–0.13	0.00–0.16	0.00–0.12
	$n = 31$	$n = 14$	$n = 24$	$n = 22$	$n = 15$	$n = 13$	$n = 23$	$n = 14$	$n = 23$	$n = 19$
V_6	0.11 ± 0.08	0.08 ± 0.06	0.09 ± 0.07	0.07 ± 0.03	0.08 ± 0.06	0.06 ± 0.03	0.08 ± 0.04	0.07 ± 0.04	0.07 ± 0.05	0.05 ± 0.03
	0.00–0.29	0.00–0.18	0.00–0.25	0.00–0.13	0.00–0.23	0.00–0.10	0.00–0.16	0.00–0.12	0.00–0.17	0.00–0.10
	$n = 37$	$n = 21$	$n = 32$	$n = 36$	$n = 23$	$n = 20$	$n = 29$	$n = 20$	$n = 33$	$n = 21$

Table A1.34

R-wave amplitude (millivolts) in normal Chinese in various age-groups: leads I-aVF

	18–29		30–39		40–49		50–59		60+	
	Male *n* = 56	Female *n* = 47	Male *n* = 50	Female *n* = 59	Male *n* = 50	Female *n* = 50	Male *n* = 50	Female *n* = 48	Male *n* = 49	Female *n* = 44
I	0.51 ± 0.23	0.41 ± 0.20	0.56 ± 0.25	0.50 ± 0.20	0.61 ± 0.30	0.60 ± 0.26	0.63 ± 0.30	0.61 ± 0.22	0.66 ± 0.29	0.66 ± 0.25
	0.13–1.00	0.08–0.86	0.22–1.14	0.17–0.87	0.17–1.27	0.25–1.21	0.17–1.27	0.30–1.07	0.23–1.37	0.19–1.11
	n = 56	*n* = 47	*n* = 50	*n* = 59	*n* = 50	*n* = 50	*n* = 50	*n* = 48	*n* = 49	*n* = 44
II	1.24 ± 0.42	1.19 ± 0.31	1.18 ± 0.40	1.09 ± 0.30	0.95 ± 0.41	0.93 ± 0.29	0.96 ± 0.41	0.81 ± 0.30	0.91 ± 0.45	0.78 ± 0.34
	0.49–2.17	0.68–1.65	0.58–2.21	0.53–1.70	0.21–1.60	0.51–1.47	0.25–1.97	0.39–1.37	0.30–1.90	0.35–1.49
	n = 56	*n* = 47	*n* = 50	*n* = 59	*n* = 50	*n* = 50	*n* = 50	*n* = 48	*n* = 49	*n* = 44
III	0.73 ± 0.49	0.90 ± 0.44	0.74 ± 0.51	0.72 ± 0.40	0.53 ± 0.42	0.46 ± 0.33	0.54 ± 0.50	0.39 ± 0.31	0.52 ± 0.48	0.35 ± 0.29
	0.02–1.71	0.21–1.85	0.04–2.08	0.06–1.46	0.04–1.38	0.04–1.10	0.05–1.94	0.05–1.36	0.05–1.63	0.04–1.16
	n = 56	*n* = 47	*n* = 50	*n* = 59	*n* = 49	*n* = 49	*n* = 50	*n* = 48	*n* = 49	*n* = 44
aVR	0.13 ± 0.12	0.11 ± 0.09	0.11 ± 0.09	0.08 ± 0.06	0.12 ± 0.09	0.09 ± 0.06	0.09 ± 0.08	0.11 ± 0.08	0.10 ± 0.06	0.11 ± 0.08
	0.00–0.43	0.00–0.32	0.00–0.37	0.00–0.23	0.00–0.31	0.00–0.24	0.00–0.23	0.00–0.24	0.00–0.26	0.00–0.28
	n = 51	*n* = 34	*n* = 43	*n* = 48	*n* = 41	*n* = 36	*n* = 39	*n* = 35	*n* = 40	*n* = 28
aVL	0.19 ± 0.16	0.16 ± 0.13	0.24 ± 0.19	0.18 ± 0.14	0.35 ± 0.27	0.27 ± 0.19	0.35 ± 0.31	0.32 ± 0.22	0.38 ± 0.32	0.38 ± 0.22
	0.04–0.59	0.04–0.52	0.04–0.59	0.00–0.54	0.00–0.98	0.04–0.69	0.05–1.07	0.07–0.83	0.04–1.07	0.06–0.83
	n = 56	*n* = 47	*n* = 49	*n* = 57	*n* = 48	*n* = 50	*n* = 49	*n* = 48	*n* = 49	*n* = 43
aVF	0.98 ± 0.48	1.04 ± 0.36	0.94 ± 0.46	0.90 ± 0.34	0.68 ± 0.44	0.68 ± 0.29	0.70 ± 0.48	0.55 ± 0.31	0.67 ± 0.49	0.49 ± 0.34
	0.09–2.07	0.48–1.81	0.13–2.13	0.28–1.56	0.07–1.50	0.13–1.34	0.04–1.92	0.03–1.27	0.09–1.73	0.03–1.24
	n = 56	*n* = 47	*n* = 50	*n* = 59	*n* = 50	*n* = 50	*n* = 50	*n* = 48	*n* = 49	*n* = 44

Table A1.35

R-wave amplitude (millivolts) in normal Chinese in various age groups: leads $V_1 - V_6$

	18–29		30–39		40–49		50–59		60+	
	Male $n = 56$	Female $n = 47$	Male $n = 50$	Female $n = 59$	Male $n = 50$	Female $n = 50$	Male $n = 50$	Female $n = 48$	Male $n = 49$	Female $n = 44$
V_1	0.43 ± 0.27	0.33 ± 0.28	0.33 ± 0.18	0.26 ± 0.12	0.27 ± 0.23	0.21 ± 0.13	0.27 ± 0.14	0.21 ± 0.15	0.27 ± 0.17	0.19 ± 0.12
	0.07–1.04	0.00–0.86	0.09–0.76	0.06–0.52	0.02–0.92	0.02–0.46	0.03–0.63	0.04–0.66	0.08–0.65	0.00–0.49
	$n = 56$	$n = 44$	$n = 50$	$n = 59$	$n = 49$	$n = 49$	$n = 50$	$n = 48$	$n = 49$	$n = 41$
V_2	0.92 ± 0.41	0.71 ± 0.41	0.85 ± 0.38	0.65 ± 0.25	0.72 ± 0.42	0.57 ± 0.28	0.73 ± 0.32	0.64 ± 0.30	0.76 ± 0.33	0.61 ± 0.35
	0.25–1.78	0.24–2.09	0.31–1.76	0.24–1.20	0.09–1.56	0.23–1.23	0.24–1.33	0.20–1.27	0.26–1.36	0.16–1.43
	$n = 56$	$n = 47$	$n = 50$	$n = 59$	$n = 50$	$n = 50$	$n = 50$	$n = 48$	$n = 49$	$n = 44$
V_3	1.21 ± 0.58	1.09 ± 0.47	1.21 ± 0.57	1.09 ± 0.48	0.99 ± 0.49	0.88 ± 0.39	1.19 ± 0.45	1.07 ± 0.50	1.30 ± 0.55	1.12 ± 0.46
	0.30–2.97	0.49–1.95	0.54–2.55	0.31–2.35	0.22–2.06	0.38–2.01	0.38–1.92	0.32–2.31	0.40–2.28	0.45–2.16
	$n = 56$	$n = 47$	$n = 50$	$n = 59$	$n = 50$	$n = 50$	$n = 50$	$n = 48$	$n = 49$	$n = 44$
V_4	2.06 ± 0.71	1.40 ± 0.45	1.83 ± 0.60	1.49 ± 0.48	1.76 ± 0.67	1.31 ± 0.40	1.85 ± 0.76	1.56 ± 0.48	1.97 ± 0.72	1.54 ± 0.48
	1.01–3.82	0.61–2.49	0.58–2.90	0.73–2.51	0.77–3.21	0.65–2.60	0.74–4.24	0.69–2.49	0.93–3.64	0.88–2.47
	$n = 56$	$n = 47$	$n = 50$	$n = 59$	$n = 50$	$n = 50$	$n = 50$	$n = 48$	$n = 49$	$n = 44$
V_5	1.84 ± 0.46	1.25 ± 0.38	1.83 ± 0.50	1.38 ± 0.35	1.83 ± 0.58	1.35 ± 0.39	1.82 ± 0.65	1.56 ± 0.45	1.89 ± 0.65	1.58 ± 0.47
	1.20–3.10	0.65–2.06	0.99–2.74	0.77–2.10	0.55–2.83	0.69–2.42	0.83–3.78	0.98–2.31	0.82–3.43	0.97–2.64
	$n = 56$	$n = 47$	$n = 50$	$n = 59$	$n = 50$	$n = 50$	$n = 50$	$n = 48$	$n = 49$	$n = 44$
V_6	1.43 ± 0.35	1.09 ± 0.32	1.50 ± 0.39	1.16 ± 0.26	1.47 ± 0.52	1.14 ± 0.34	1.48 ± 0.45	1.30 ± 0.41	1.47 ± 0.47	1.36 ± 0.43
	0.87–2.16	0.61–1.80	0.86–2.31	0.63–1.83	0.31–2.31	0.54–1.86	0.57–2.35	0.74–2.12	0.81–2.57	0.71–2.14
	$n = 56$	$n = 47$	$n = 50$	$n = 59$	$n = 50$	$n = 50$	$n = 50$	$n = 48$	$n = 49$	$n = 44$

Table A1.36

S-wave amplitude (millivolts) in normal Chinese in various age-groups: leads I-aVF

	18–29		30–39		40–49		50–59		60+	
	Male *n* = 56	Female *n* = 47	Male *n* = 50	Female *n* = 59	Male *n* = 50	Female *n* = 50	Male *n* = 50	Female *n* = 48	Male *n* = 49	Female *n* = 44
I	0.19 ± 0.13	0.18 ± 0.13	0.17 ± 0.09	0.14 ± 0.10	0.16 ± 0.11	0.13 ± 0.07	0.17 ± 0.11	0.16 ± 0.09	0.17 ± 0.09	0.14 ± 0.10
	0.00–0.49	0.00–0.44	0.00–0.33	0.00–0.40	0.00–0.44	0.00–0.29	0.00–0.41	0.00–0.36	0.00–0.30	0.00–0.34
	n = 47	*n* = 31	*n* = 42	*n* = 39	*n* = 40	*n* = 37	*n* = 30	*n* = 31	*n* = 39	*n* = 25
II	0.24 ± 0.16	0.17 ± 0.11	0.17 ± 0.13	0.17 ± 0.09	0.21 ± 0.12	0.15 ± 0.10	0.17 ± 0.13	0.20 ± 0.12	0.16 ± 0.07	0.18 ± 0.11
	0.00–0.63	0.00–0.43	0.00–0.48	0.00–0.48	0.00–0.48	0.00–0.33	0.00–0.35	0.00–0.44	0.00–0.26	0.00–0.37
	n = 39	*n* = 26	*n* = 28	*n* = 33	*n* = 34	*n* = 30	*n* = 30	*n* = 28	*n* = 31	*n* = 30
III	0.21 ± 0.16	0.17 ± 0.13	0.15 ± 0.14	0.15 ± 0.09	0.33 ± 0.28	0.17 ± 0.13	0.29 ± 0.36	0.27 ± 0.24	0.42 ± 0.31	0.32 ± 0.24
	0.00–0.55	0.00–0.42	0.00–0.48	0.00–0.33	0.00–0.90	0.00–0.41	0.00–1.36	0.00–0.79	0.00–0.91	0.00–0.81
	n = 43	*n* = 28	*n* = 27	*n* = 34	*n* = 33	*n* = 26	*n* = 36	*n* = 31	*n* = 26	*n* = 29
aVR	0.82 ± 0.36	0.80 ± 0.25	0.88 ± 0.30	0.76 ± 0.16	0.76 ± 0.40	0.85 ± 0.22	0.86 ± 0.18	0.62 ± 0.37	0.80 ± 0.29	0.70 ± 0.34
	0.00–1.43	0.00–1.33	0.00–1.39	0.00–1.16	0.00–1.72	0.00–1.19	0.00–1.22	0.00–1.07	0.00–1.30	0.00–1.15
	n = 26	*n* = 14	*n* = 20	*n* = 24	*n* = 17	*n* = 14	*n* = 21	*n* = 13	*n* = 21	*n* = 9
aVL	0.37 ± 0.21	0.41 ± 0.27	0.33 ± 0.24	0.32 ± 0.18	0.25 ± 0.16	0.20 ± 0.13	0.30 ± 0.28	0.22 ± 0.19	0.27 ± 0.24	0.17 ± 0.15
	0.00–0.89	0.00–0.98	0.00–0.92	0.00–0.72	0.00–0.55	0.00–0.45	0.00–0.99	0.00–0.75	0.00–0.71	0.00–0.52
	n = 50	*n* = 39	*n* = 45	*n* = 47	*n* = 38	*n* = 45	*n* = 34	*n* = 32	*n* = 41	*n* = 28
aVF	0.21 ± 0.14	0.15 ± 0.11	0.16 ± 0.10	0.16 ± 0.08	0.23 ± 0.16	0.14 ± 0.09	0.18 ± 0.23	0.19 ± 0.16	0.19 ± 0.14	0.18 ± 0.13
	0.00–0.51	0.00–0.34	0.00–0.32	0.00–0.31	0.00–0.54	0.00–0.33	0.00–0.98	0.00–0.44	0.00–0.49	0.00–0.39
	n = 40	*n* = 28	*n* = 22	*n* = 30	*n* = 34	*n* = 24	*n* = 31	*n* = 27	*n* = 30	*n* = 29

Table A1.37

S-wave amplitude (millivolts) in normal Chinese in various age-groups: leads V_1–V_6

	18–29		30–39		40–49		50–59		60+	
	Male $n = 56$	Female $n = 47$	Male $n = 50$	Female $n = 59$	Male $n = 50$	Female $n = 50$	Male $n = 50$	Female $n = 48$	Male $n = 49$	Female $n = 44$
V_1	1.05 ± 0.43	0.86 ± 0.35	0.90 ± 0.34	0.83 ± 0.35	0.84 ± 0.36	0.84 ± 0.37	0.83 ± 0.43	0.77 ± 0.36	0.76 ± 0.43	0.64 ± 0.28
	0.25–1.97	0.00–1.54	0.36–1.57	0.28–1.78	0.00–1.49	0.14–1.54	0.21–2.06	0.24–1.42	0.12–1.73	0.00–1.21
	$n = 56$	$n = 44$	$n = 50$	$n = 59$	$n = 48$	$n = 49$	$n = 49$	$n = 48$	$n = 49$	$n = 41$
V_2	2.07 ± 0.67	1.29 ± 0.55	1.68 ± 0.57	1.22 ± 0.46	1.49 ± 0.61	1.26 ± 0.48	1.26 ± 0.62	1.16 ± 0.45	1.25 ± 0.58	0.97 ± 0.39
	0.84–3.43	0.46–2.67	0.63–2.76	0.31–2.17	0.32–2.69	0.50–2.35	0.11–2.75	0.42–2.14	0.18–2.60	0.19–1.84
	$n = 56$	$n = 47$	$n = 49$	$n = 59$	$n = 50$	$n = 50$	$n = 50$	$n = 48$	$n = 49$	$n = 44$
V_3	1.14 ± 0.46	0.68 ± 0.41	1.04 ± 0.50	0.66 ± 0.32	1.04 ± 0.42	0.77 ± 0.32	0.98 ± 0.47	0.79 ± 0.37	1.05 ± 0.46	0.79 ± 0.36
	0.40–2.15	0.00–1.56	0.00–2.20	0.00–1.25	0.27–1.86	0.24–1.32	0.00–1.98	0.24–1.77	0.37–1.89	0.10–1.47
	$n = 56$	$n = 42$	$n = 48$	$n = 57$	$n = 50$	$n = 49$	$n = 47$	$n = 48$	$n = 49$	$n = 43$
V_4	0.61 ± 0.33	0.41 ± 0.29	0.61 ± 0.38	0.38 ± 0.21	0.63 ± 0.32	0.44 ± 0.24	0.59 ± 0.35	0.52 ± 0.28	0.74 ± 0.36	0.56 ± 0.27
	0.00–1.25	0.00–1.20	0.00–1.43	0.00–0.82	0.00–1.18	0.00–0.94	0.00–1.57	0.09–1.02	0.00–1.46	0.00–1.20
	$n = 50$	$n = 38$	$n = 41$	$n = 51$	$n = 48$	$n = 48$	$n = 45$	$n = 47$	$n = 46$	$n = 41$
V_5	0.38 ± 0.23	0.29 ± 0.20	0.40 ± 0.25	0.25 ± 0.16	0.43 ± 0.26	0.33 ± 0.17	0.37 ± 0.25	0.35 ± 0.21	0.49 ± 0.29	0.39 ± 0.21
	0.00–0.94	0.00–0.81	0.00–1.01	0.00–0.65	0.00–0.87	0.00–0.64	0.00–1.07	0.00–0.76	0.00–1.01	0.00–0.88
	$n = 45$	$n = 34$	$n = 38$	$n = 49$	$n = 46$	$n = 41$	$n = 44$	$n = 45$	$n = 46$	$n = 40$
V_6	0.22 ± 0.14	0.20 ± 0.13	0.21 ± 0.15	0.15 ± 0.11	0.26 ± 0.17	0.18 ± 0.10	0.21 ± 0.16	0.21 ± 0.16	0.26 ± 0.15	0.23 ± 0.14
	0.00–0.57	0.00–0.38	0.00–0.50	0.00–0.44	0.00–0.56	0.00–0.43	0.00–0.61	0.00–0.50	0.00–0.57	0.00–0.49
	$n = 45$	$n = 24$	$n = 36$	$n = 42$	$n = 42$	$n = 37$	$n = 39$	$n = 42$	$n = 42$	$n = 36$

Table A1.38

Maximal T-wave amplitude (millivolts) in normal Chinese in various age-groups

	18–29		30–39		40–49		50–59		60+	
	Male $n = 56$	Female $n = 47$	Male $n = 50$	Female $n = 59$	Male $n = 50$	Female $n = 50$	Male $n = 50$	Female $n = 48$	Male $n = 49$	Female $n = 44$
I	0.28 ± 0.08	0.21 ± 0.06	0.25 ± 0.10	0.22 ± 0.06	0.22 ± 0.09	0.20 ± 0.07	0.22 ± 0.09	0.18 ± 0.07	0.18 ± 0.08	0.17 ± 0.07
	0.12–0.44	0.11–0.29	0.10–0.47	0.11–0.33	0.08–0.41	0.10–0.33	0.08–0.41	0.07–0.29	0.08–0.35	0.06–0.33
II	0.37 ± 0.11	0.30 ± 0.12	0.35 ± 0.13	0.27 ± 0.10	0.28 ± 0.11	0.25 ± 0.08	0.29 ± 0.13	0.21 ± 0.09	0.27 ± 0.13	0.20 ± 0.10
	0.17–0.58	0.10–0.52	0.11–0.58	0.08–0.46	0.12–0.52	0.10–0.42	0.07–0.58	0.06–0.40	0.12–0.62	0.07–0.43
III	0.11 ± 0.13	0.11 ± 0.11	0.10 ± 0.14	0.06 ± 0.11	0.07 ± 0.13	0.06 ± 0.09	0.09 ± 0.14	0.03 ± 0.09	0.09 ± 0.15	0.04 ± 0.10
	−0.19–0.34	−0.14–0.33	−0.14–0.39	−0.12–0.26	−0.15–0.30	−0.10–0.23	−0.20–0.34	−0.11–0.18	−0.18–0.44	−0.14–0.17
aVR	−0.32 ± 0.08	−0.26 ± 0.07	−0.30 ± 0.09	−0.26 ± 0.07	−0.25 ± 0.08	−0.22 ± 0.07	−0.25 ± 0.09	−0.19 ± 0.07	−0.22 ± 0.08	−0.18 ± 0.07
	−0.50 to −0.20	−0.40 to −0.10	−0.46 to −0.10	−0.38 to −0.08	−0.42 to −0.12	−0.36 to −0.13	0.42 to −0.07	−0.35 to −0.07	−0.44 to −0.10	−0.35 to −0.08
aVL	0.09 ± 0.10	0.06 ± 0.08	0.08 ± 0.11	0.09 ± 0.07	0.08 ± 0.09	0.09 ± 0.06	0.07 ± 0.10	0.08 ± 0.06	0.05 ± 0.10	0.08 ± 0.07
	−0.08–0.26	−0.08–0.18	−0.10–0.30	−0.06–0.20	−0.07–0.27	−0.03–0.18	−0.10–0.27	−0.05–0.18	−0.15–0.27	−0.04–0.18
aVF	0.24 ± 0.11	0.20 ± 0.11	0.22 ± 0.12	0.17 ± 0.09	0.18 ± 0.10	0.15 ± 0.07	0.19 ± 0.12	0.12 ± 0.08	0.19 ± 0.12	0.12 ± 0.08
	0.04–0.45	−0.09–0.42	0.05–0.48	−0.05–0.37	0.03 ± 0.41	−0.03–0.29	−0.10–0.50	−0.06–0.26	0.04–0.51	−0.05–0.29
V_1	0.17 ± 0.15	−0.06 ± 0.14	0.12 ± 0.16	−0.05 ± 0.14	0.09 ± 0.15	−0.03 ± 0.09	0.12 ± 0.16	0.00 ± 0.11	0.09 ± 0.15	0.03 ± 0.09
	−0.14–0.50	−0.24–0.23	−0.25–0.35	−0.23–0.20	−0.18–0.36	−0.22–0.17	−0.21–0.39	−0.19–0.19	−0.15–0.33	0.18–0.10
V_2	0.82 ± 0.25	0.32 ± 0.21	0.79 ± 0.27	0.33 ± 0.22	0.62 ± 0.29	0.28 ± 0.19	0.63 ± 0.22	0.30 ± 0.16	0.51 ± 0.22	0.25 ± 0.17
	0.39–1.25	0.08–0.84	0.40–1.39	−0.12–0.71	0.09–1.18	−0.10–0.65	0.24–1.09	0.10–0.54	0.04–0.86	−0.11–0.55
V_3	0.90 ± 0.27	0.48 ± 0.20	0.81 ± 0.27	0.46 ± 0.25	0.68 ± 0.29	0.36 ± 0.23	0.69 ± 0.24	0.37 ± 0.20	0.55 ± 0.25	0.32 ± 0.13
	0.37–1.40	0.14–0.81	0.36–1.34	0.08–1.03	0.11–1.48	−0.13–0.83	0.27–1.18	0.10–0.83	−0.07–1.07	−0.04–0.80
V_4	0.77 ± 0.28	0.45 ± 0.16	0.69 ± 0.27	0.41 ± 0.21	0.60 ± 0.30	0.34 ± 0.19	0.60 ± 0.28	0.33 ± 0.20	0.50 ± 0.26	0.29 ± 0.19
	0.23–1.25	0.16–0.71	0.28–1.18	0.07–0.91	0.13–1.17	0.05–0.86	0.19–1.21	0.08–0.90	0.08–1.13	0.03–0.71
V_5	0.60 ± 0.20	0.41 ± 0.13	0.56 ± 0.23	0.38 ± 0.16	0.49 ± 0.20	0.33 ± 0.15	0.50 ± 0.26	0.31 ± 0.17	0.40 ± 0.21	0.28 ± 0.15
	0.22–0.93	0.20–0.65	0.16–1.08	0.09–0.73	0.14–1.01	0.06–0.59	0.09–0.92	0.07–0.71	−0.09–0.84	0.04–0.62
V_6	0.44 ± 0.14	0.34 ± 0.10	0.43 ± 0.17	0.32 ± 0.11	0.38 ± 0.15	0.29 ± 0.10	0.39 ± 0.20	0.26 ± 0.14	0.32 ± 0.14	0.25 ± 0.12
	0.18–0.72	0.19–0.57	0.13–0.80	0.10–0.57	0.14–0.74	0.12–0.47	0.08–0.75	0.07–0.52	0.08–0.59	0.05–0.50

Table A1.39

Amplitude of Q waves (in millimeters) in normal Japanese of various age-groups

		15–29		20–29		30–39		40–49		50–59		60–69		70+	
		Male *n* = 61	Female *n* = 39	Male *n* = 165	Female *n* = 109	Male *n* = 119	Female *n* = 94	Male *n* = 153	Female *n* = 82	Male *n* = 135	Female *n* = 102	Male *n* = 101	Female *n* = 79	Male *n* = 48	Female *n* = 42
I	Mn.	0.3	0.28	0.32	0.22	0.37	0.18	0.27	0.24	0.25	0.33	0.27	0.30	0.26	0.39
	Max.–Min.	1.9–0	1.5–0	1.4–0	1.5–0	2.47–0	1.8–0	2.1–0	2.0–0	1.7–0	2.0–0	2.3–0	2.3–0	2.0–0	1.7–0
II	Mn.	0.66	0.44	0.73	0.46	0.52	0.26	0.34	0.30	0.44	0.29	0.35	0.21	0.28	0.30
	Max.–Min.	3.2–0	2.5–0	9.2–0	2.7–0	3.2–0	1.9–0	2.4–0	2.1–0	5.6–0	1.1–0	2.0–0	1.7–0	1.1–0	1.7–0
III	Mn.	0.69	0.51	0.72	0.66	0.56	0.48	0.40	0.42	0.54	0.39	0.39	0.40	0.43	0.23
	Max.–Min.	3.0–0	3.2–0	8.8–0	3.2–0	2.9–0	2.11–0	2.9–0	5.6–0	11.0–0	4.4–0	2.0–0	2.3–0	2.6–0	2.9–0
aVR	Mn.	9.27	7.31	7.38	8.45	3.35	6.74	6.46	6.57	3.68	3.79	3.89	4.12	3.56	2.57
	Max.–Min.	2.0–0	10.1–5.5	13.5–0	14.3–2.8	12.9–0	11.5–0	18.2–0	14.5–0.8	14.0–0	10.9–0	12.9–0	9.9–0	16.9–0	1.39–0
		(30)[a]			(47)[a]										
aVL	Mn.	0.28	0.26	0.33	0.20	0.15	0.29	0.47	0.30	0.45	0.40	0.50	0.46	0.74	0.59
	Max.–Min.	2.0–0	2.1–0	4.0–0	3.0–0	3.2–0	4.4–0	5.2–0	1.8–0	3.8–0	2.6–0	4.1–0	4.1–0	5.3–0	3.2–0
aVF	Mn.	0.59	0.47	0.60	0.40	0.50	0.35	0.33	0.23	0.43	0.30	0.30	0.24	0.32	0.21
	Max.–Min.	3.8–0	2.4–0	5.8–0	2.5–0	3.0–0	3.4–0	3.1–0	2.2–0	5.3–0	2.6–0	2.0–0	1.7–0	1.1–0	1.4–0
V_4R	Mn.	0.3	0	0.15	0.03	0.11	0.01	0.15	0.18	0.23	0.09	0.07	0.18	0.01	0
	Max.–Min.	1.5–0	0	1.4–0	1.2–0	4.6–0	0.2–0	6.8–0	4.3–0	4.3–0	4.7–0	3.2–0	4.7–0	0.2–0	0
		(31)[a]		(117)[a]	(95)[a]		(75)[a]		(77)[a]	(96)[a]	(84)[a]	(74)[a]	(56)[a]	(23)[a]	
V_1	Mn.	0.03	0	0.01	0	0.01	0	0.11	0	0.09	0	0	0	0	0
	Max.–Min.	1.2–0	0	1.1–0	0	1.6–0	0	16.5–0	0	11.4–0	0	0	0.2–0	0	0.1–0
V_2	Mn.	0.04	0	0.01	0.01	0.01	0	0.10	0.01	0	0	0	0	0	0
	Max.–Min.	1.8–0	0	1.1–0	0.3–0	1.1–0		13.8–0	0.05–0	0	0.5–0	0.2–0	0	0.2–0	0.2–0
V_3	Mn.	0.03	0	0.01	0	0.01	0.01	0.04	0.02	0.02	0.01	0.03	0.01	0.04	0.04
	Max.–Min.	1.5–0	0	1.1–0	0	0.5–0	0.1–0	3.0–0	1.0–0	1.3–0	2.3–0	2.5–0	0.5–0	1.1–0	1.4–0
V_4	Mn.	0.35	0.16	0.31	0.13	0.4	0.01	0.27	0.70	0.24	0.25	0.26	0.23	0.35	0.50
	Max.–Min.	3.5–0	3.0–0	5.8–0	1.1–0	3.1–0	1.0–0	4.1–0	2.0–0	2.6–0	4.1–0	3.1–0	1.7–0	3.2–0	3.7–0
V_5	Mn.	1.01	0.39	0.87	0.33	0.70	0.04	0.52	0.39	0.51	0.34	0.53	0.34	0.36	0.59
	Max.–Min.	5.0–0	4.1–0	5.2–0	2.0–0	3.4–0	1.3–0	3.0–0	2.0–0	5.0–0	2.0–0	3.8–0	1.7–0	2.0–0	3.1–0
V_6	Mn.	0.95	0.56	0.92	0.45	0.58	0.39	0.59	0.48	0.31	0.49	0.52	0.36	0.45	0.52
	Max.–Min.	4.0–0	3.9–0	4.8–0	2.0–0	3.1–0	1.8–0	2.8–0	2.0–0	4.0–0	2.6–0	2.5–0	1.4–0	2.0–0	2.0–0

Mn., mean; Max., maximum; Min., minimum

[a]Number of cases in which measurement was made.

Table A1.40

Amplitude of R waves (in millimeters) in normal Japanese of various age-groups

		15–29		20–29		30–39		40–49		50–59		60–69		70+	
		Male *n* = 61	Female *n* =39	Male *n* = 165	Female *n* = 109	Male *n* = 119	Female *n* = 94	Male *n* = 153	Female *n* = 82	Male *n* = 135	Female *n* = 102	Male *n* = 101	Female *n* = 79	Male *n* = 48	Female *n* = 42
I	Mn., SD	5.68, 2.34	5.41, 2.13	5.14, 2.67	5.56, 2.59	5.46, 2.38	5.38, 2.38	5.56, 2.70	5.71, 2.87	5.30, 2.36	6.46, 2.75	5.27, 2.98	6.34, 25.1	5.05, 2.62	6.55, 3.18
	Max.–Min.	13.0–2.0	10.0–2.2	15.3–0.26	15.3–0.43	12.9–1.0	14.2–1.0	14.6–0.3	14.3–0	15.9–0	14.9–0.0	16.9–0	12.9–0	16.9–1.0	15.9–1.0
II	Mn., SD	14.25, 4.65	11.67, 2.99	13.73, 4.69	11.64, 3.97	12.99, 3.82	15.35, 3.16	10.74, 4.20	9.91, 3.66	10.78, 4.11	9.17, 3.24	9.35, 3.98	7.44, 4.06	7.89, 3.23	7.28, 2.98
	Max.–Min.	22.1–6.0	17.5–6.5	2.38–4.2	22.7–2.0	23.9–3.0	19.1–3.33	21.0–0.2	17.0–0	25.9–3.0	17.9–0.0	18.9–1.0	33.4–0	15.9–2.0	16,9–2.0
III	Mn., SD	10.0, 2.97	7.39, 3.95	9.44, 4.86	7.44, 4.26	8.15, 4.19	5.36, 3.34	6.24, 6.20	5.16, 4.15	6.53, 4.36	4.42, 3.15	5.51, 3.16	3.34, 2.66	6.62, 3.39	3.18, 2.41
	Max.–Min.	23.1–25	15.7–0.2	22.1–0.1	21.5–0	19.9–0	15.3–0.4	17.5–0.3	17.0–0.5	21.9–0.0	14.9–0.0	14.9–0	12.4–0	12.4–0	11.9–0.0
aVR	Mn., SD	0.48, 0.24	0.32, 0.73	0.49, 0.56	0.63, 0.74	0.45, 0.76	0.50, 0.72	0.74, 0.00	0.19, 0.00	0.36, 0.17	0.35, 0.54	0.37, 0.24	0.32, 0.43	0.30, 0.48	0.43, 0.48
	Max.–Min.	3.69–0.02	1.5–0	3.2–0	3.2–0	4.9–0	2.4–0	11.9–0	1.4–0	2.4–0	1.9–0.0	2.4–0	1.9–0	1.4–0	1.9–0.0
aVL	Mn., SD	1.62, 1.17	3.06, 1.69	1.93, 2.21	1.71, 2.09	1.89, 1.48	2.21, 2.01	2.37, 2.52	2.29, 2.09	2.16, 2.42	3.15, 2.02	2.53, 2.24	3.29, 2.28	3.22, 2.28	3.86, 0.63
	Max.–Min.	6.44–0.1	6.9–0	16.2–0	13.2–0	11.9–0	9.1–0	14.9–0.1	10.5–0.1	12.9–0	9.9–0	8.9–0	11.9–0	14.9–0	13.9–0.0
aVF	Mn., SD	11.80, 3.53	9.55, 3.70	11.07, 4.76	10.00, 3.88	9.57, 3.93	7.45, 4.71	8.01, 4.25	7.47, 4.71	8,19, 4.34	6.52, 3.36	6.84, 4.81	4.76, 2.68	5.97, 3.32	4.74, 2.30
	Max.–Min.	21.8–1.2	17.5–3.0	25.9–0.5	20.9–0.4	19.9–0	15.4–0.2	17.2–0.4	16.5–0.49	22.9–0.0	16.9–0.0	15.9–0	13.9–0	13.0–0	15.9–0.0
V_4R	Mn., SD	2.16, 3.26	1.43, 1.04	2.42, 1.65	1.51, 1.02	1.80, 1.05	0.98, 0.75	1.61, 0.00	5.50, 0.00	1.31, 0.74	1.04, 0.73	1.30, 0.96	1.09, 0.40	0.97	1.27, 0.85
	Max.–Min.	6.2–0.1	3.3–0	13.6–0	18.0–0	16.9–0	3.2–0.1	8.4–0.2	2.8–0.1	4.9–0	4.9–0.0	4.9–0	4.4–0	2.4–0	3.9–0.0
		(52)[a]	(34)[a]	(117)[a]	(97)[a]	(86)[a]	(76)[a]	(106)[a]	(76)[a]	(97)[a]	(80)[a]	(74)[a]			
V_1	Mn., SD	5.54, 2.56	3.95, 2.44	5.05, 3.19	3.53, 2.55	3.67, 2.06	2.81, 1.66	3.17, 3.64	2.44, 1.62	3.40, 2.28	2.59, 1.67	3.22, 2.57	2.35, 1.89	2.14, 1.57	2.57, 1.47
	Max.–Min.	15.5–1.6	10.8–0	15.8–0.54	10.0–0.23	10.9–0	7.5–0.2	13.9–0.2	6.1–0.3	13.9–0.0	8.9–0.0	13.9–0	9.9–0	8.9–0	8.9–0
V_2	Mn., SD	10.78, 4.16	7.32, 3.62	9.76, 4.69	7.10, 3.36	7.66, 3.95	6.48, 3.26	7.0, 4.12	5.52, 3.20	7,41, 4.27	5.95, 3.62	6.32, 3.38	6.38, 3.87	5.74, 3.87	6.28, 3.43
	Max.–Min.	15.7–3.5	18.0–0	22.4–0.8	23.7–1.0	17.9–0	12.5–1.2	18.6–1.0	17.2–0.7	21.9–0.0	15.9–0.0	17.9–0	23.9–0	14.4–0	13.9–0.0
V_3	Mn., SD	13.66, 5.80	9.05, 3.22	11.56, 5.73	9.83, 4.50	10.10, 5.37	4.04, 5.34	9.74, 5.38	9.33, 5.66	11.13, 3.25	9.95, 5.77	10.75, 5.69	11.65, 4.98	11.58, 7.40	13.43, 6.10
	Max.–Min.	33.3–3.1	18.5–0.2	3.70–1.17	24.6–3.5	29.9–0	26.1–0.4	24.3–0.6	27.0–1.3	29.9–0.0	35.9–0.0	27.9–0	21.9–0	35.9–0	31.9–2.0
V_4	Mn., SD	20.67, 7.05	13.49, 4.90	24.68, 7.53	14.60, 4.90	17.49, 7.35	14.65, 5.16	9.31, 6.51	15.86, 5.92	17.48, 6.04	15.99, 5.72	17.50, 8.41	17.29, 5.37	19.87, 7.94	21.09, 7.78
	Max.–Min.	35.8–2.3	24.8–6.8	53.2–5.0	30.6–2.87	41.9–2.0	34.0–7.1	33.8–3.4	26.8–5.5	35.9–0.0	37.9–0.0	49.9–2.0	37.4–2.0	37.9–0	39.9–6.0
V_5	Mn., SD	18.87, 5.31	13.51, 3.44	17.45, 5.84	13.4, 4.46	15.85, 6.29	14.10, 4.48	16.45, 6.09	15.50, 5.0	16.2, 5.52	15.20, 5.29	16.87, 8.23	14.43, 4.88	16.74, 5.81	17.33, 6.05
	Max.–Min.	55.0–8.0	24.0–9.0	43.0–3.98	27.4–2.01	33.9–2.0	26.4–1.7	35.2–1.8	28.5–5.6	35.9–2.0	35.9–0.0	55.9–4.0	24.4–0	24.4–0	35.9–6.0
V_6	Mn., SD	14.31, 4.31	11.56, 3.82	13.54, 5.11	11.07, 3.56	11.81, 4.54	11.65, 3.72	13.00, 5.06	11.88, 4.97	12.20, 4.27	11.85, 4.44	12.25, 5.99	10.30, 4.22	11.28, 4.05	10.0, 3.45
	Max.–Min.	28.2–7.0	21.8–7.0	29.0–2.4	23.7–1.2	23.9–2.0	24.9–1.1	24.7–0.9	26.1–1.7	25.9–2.0	23.9–0	37.9–2.0	23.9–0	23.9–20	17.9–4.0

Mn., mean; SD, standard deviation; Max., maximum; Min., minimum

[a]Number of cases in which measurement was made.

Table A1.41

Amplitude of S wave (in millimeters) in normal Japanese of various age-groups

		15–19		20–29		30–39		40–49		50–59		60–69		70+	
		Male *n* = 61	Female *n* =39	Male *n* = 165	Female *n* = 109	Male *n* = 119	Female *n* = 94	Male *n* = 153	Female *n* = 82	Male *n* = 135	Female *n* = 102	Male *n* = 101	Female *n* = 79	Male *n* = 48	Female *n* = 42
I	Mn.	1.40	0.54	1.19	0.10	0.86	0.63	0.79	0.40	0.76	0.66	0.56	0.54	0.68	0.56
	Max.–Min.	5.7–0	3.4–0	5.35–0	4.0–0	3.9–0	2.7–0	5.0–0	3.1–0	3.9–0	3.4–0	3.4–0	3.4–0	3.4–0	2.4–0
II	Mn.	2.02	0.76	1.31	0.66	1.30	0.65	1.14	0.48	1.14	0.64	1.37	1.07	1.18	1.04
	Max.–Min.	5.8–0	2.9–0	6.2–0	6.2–0	6.9–0	4.6–0	9.1–0	3.7–0	7.9–0	4.9–0	8.4–0	8.9–0	5.9–0.0	4.9–0
III	Mn.	1.8	0.76	0.94	0.53	1.22	0.77	1.42	0.83	1.28	1.52	1.91	2.08	2.37	2.18
	Max.–Min.	4.9–0	4.8–0	8.9–0	6.2–0	11.9–0	4.1–0	14.0–0	5.5–0	11.9–0	8.9–0	9.9–0	12.9–0	11.9–0.0	10.9–0
aVR	Mn.	9.60	8.83	9.05	8.92	5.87	7.36	7.62	0.80	4.50	4.52	4.06	3.67	2.70	4.66
	Max.–Min.	14.4–0	11.2–5.6	21.7–0.17	21.0–4.0	15.9–0	11.6–3.6	14.0–0.7	13.8–0.1	17.9–0	15.9–0	19.9–0	13.9–0	11.9–0	15.9–0
aVL	Mn.	3.27	1.82	2.98	2.12	2.39	1.43	2.44	1.26	1.83	1.50	1.76	1.21	1.12	0.88
	Max.–Min.	9.5–0	7.1–0	14.2–0	12.0–0	15.9–0	7.2–0	8.8–0	8.2–0	8.9–0	5.9–0	7.9–0	5.9–0	5.9–0.0	3.4–0
aVF	Mn.	1.42	0.62	1.20	0.53	1.27	0.53	1.04	0.54	1.03	0.90	1.66	1.45	1.70	1.35
	Max.–Min.	5.84–0	2.2–0	12.0–0	3.2–0	12.9–0	2.0–0	7.1–0	3.8–0	8.9–0	4.9–0	22.9–0	10.9–0	6.9–0.0	5.9–0
V_4R	Mn.	2.99	3.3	3.99	2.73	3.47	3.35	4.15	2.70	3.82	3.43	4.05	3.68	4.45	3.16
	Max.–Min.	8.05–0	8.4–0	11.0–0	14.0–0	8.9–0	10.2–0	18.6–0	9.4–0	13.9–0	10.9–0	10.9–0	20.9–0	9.9–0.0	6.9–0
		(49)[a]													
V_1	Mn.	10.85	9.2	9.7	9.59	9.71	8.90	9.42	9.62	9.58	9.07	8.83	8.46	8.87	8.47
	Max.–Min.	22.7–0	22.0–0	27.4–0	24.5–2.3	1.9–0	15.5–0	24.2–0	23.3–1.1	21.9–0	21.9–0	19.9–0	21.9–0	17.9–0	17.9–0
V_2	Mn.	18.04	15.8	20.05	14.06	15.37	13.38	13.97	12.26	14.14	13.25	12.55	13.08	13.03	12.38
	Max.–Min.	42.5–0	26.5–6.5	55.1–0	34.2–3.6	37.9–0	28.8–2.1	27.0–0	30.7–1.2	31.9–0	27.9–0	29.9–2.0	33.9–0	29.9–0.0	27.9–2.0
V_3	Mn.	13.37	8.8	12.62	7.71	10.26	7.42	11.31	8.24	11.40	9.03	10.35	10.85	11.95	12.05
	Max.–Min.	25.0–0	17.0–0	34.0–0	16.0–0	27.9–0	16.9–0	29.5–0	19.4–0	27.9–2.0	27.9–0	27.9–0	37.9–0	27.9–0	29.9–0
V_4	Mn.	7.22	4.5	6.46	6.42	5.54	4.00	6.43	3.91	6.82	5.85	7.01	6.36	7.66	7.38
	Max.–Min.	45.0–0	11.5–0	22.6–0	11.1–0	23.9–0	12.3–0	20.0–0	12.7–0	21.9–0	21.9–0	27.9–0	19.9–0	27.9–0	21.9–0
V_5	Mn.	2.92	2.7	2.28	1.86	2.02	1.73	2.46	1.46	2.53	2.06	2.75	2.80	2.26	2.50
	Max.–Min.	40.0–0	5.1–0	10.0–0	6.4–0	14.9–0	5.55–0	11.5–0	6.3–0	18.9–0	10.9–0	16.9–0	23.9–0	7.9–0	10.9–0
V_6	Mn.	1.32	0.62	0.99	0.54	0.85	0.51	0.64	0.39	0.91	0.72	0.99	0.94	0.80	0.84
	Max.–Min.	17.8–0	3.3–0	10.7–0	4.5–0	6.9–0	3.64–0	6.9–0	2.6–0.4	7.9–0	3.9–0	9.9–0	8.9–0	5.9–0	4.9–0

Mn., mean; Max., maximum; Min., minimum

[a]Number of cases in which measurement was made.

Table A1.42

ST segment "J" point (in millimeters) in normal Japanese of various age-groups

		15–29		20–29		30–39		40–49		50–59		60–69		70+	
		Male n = 60	Female n =39	Male n = 165	Female n = 109	Male n = 119	Female n = 94	Male n = 153	Female n = 82	Male n = 135	Female n = 102	Male n = 101	Female n = 79	Male n = 48	Female n = 42
I	Mn., SD	0.03, 0.21	0.1, 0.21	0.01, 0.25	−0.06, 0.23	0.08, 0.17	−0.01, 0.22	0.03, 0.17	0.08, 0.24	0.00, 0.22	−0.00, 0.18	0.06, 0.22	0.03, 0.10	0.00, 0.27	0.00, 0.09
	Max.–Min.	0.9 to −0.8	0.7 to −0.8	0.9 to −1.0	0.05 to −0.8	0.7 to −0.8	0.9 to −0.6	0.5 to −0.8	1.3 to −0.8	1.0 to −1.2	0.5 to −0.8	1.1 to −1.0	0.7 to −0.4	0.9 to −1.0	0.3 to −0.4
II	Mn., SD	0.02, 0.55	0.03, 0.45	0.13, 0.39	0.77, 0.42	0.16, 0.38	0.00, 0.23	0.03, 0.36	0.12, 0.46	0.07, 0.33	0.03, 0.26	0.05, 0.41	0.06, 0.08	0.00, 0.27	0.09, 0.41
	Max.–Min.	2.9 to −1.01	2.4 to −0.6	1.7 to −1.0	2.1 to −0.2	1.4 to −1.0	0.7 to −0.8	1.1 to −1.6	2.5 to −0.8	1.7 to −1.0	1.1 to −1.0	1.5 to −1.6	1.1 to −0.6	0.7 to −1.0	1.9 to −0.5
III	Mn., SD	0.05, 0.28	0.01, 0.30	0.07, 0.35	0.03, 0.40	0.15, 0.35	−0.01, 0.30	0.00, 0.41	0.07, 0.33	0.03, 0.28	0.06, 0.23	0.05, 0.38	0.09, 0.18	0.04, 0.17	0.03, 0.21
	Max.–Min.	1.1 to −1.2	1.5 to −0.6	1.9 to −0.8	1.3 to −0.8	1.9 to −0.8	1.3 to −1.0	1.1 to −1.2	1.1 to −1.0	1.0 to −1.1	0.9 to −1.0	1.1 to −2.0	1.1 to −0.6	0.5 to −0.4	1.9–0.5
aVR	Mn., SD	0.06, 0.41	−0.05, 0.20	0.00, 0.38	−0.05, 0.52	0.04, 0.34	0.01, 0.28	0.06, 0.29	0.04, 0.31	0.11, 0.28	0.04, 0.26	0.03, 0.29	0.04, 0.19	0.00, 0.23	−0.08, 0.19
	Max.–Min.	1.3 to −0.8	0.5 to −0.6	2.1 to −1.2	1.3 to −1.4	1.1 to −1.6	1.1 to −1.0	1.0 to −0.8	1.1 to −1.4	1.1 to −1.2	0.9 to −0.8	1.9 to −0.6	0.9 to −0.8	0.7 to −0.6	0.3 to −0.7
aVL	Mn., SD	−0.02, 0.23	0.03, 0.17	0.03, 0.31	0.20, 0.35	0.04, 0.19	−0.02, 0.27	0.06, 0.21	0.031, 0.22	−0.04, 0.21	0.05, 0.13	0.08, 0.17	0.02, 0.14	0.03, 0.13	0.02, 0.05
	Max.–Min.	0.9 to −0.8	0.5 to −0.6	1.3 to −1.2	1.5 to −0.6	0.9 to −2.0	1.0 to −1.8	1.1 to −1.0	0.7 to −1.2	0.7 to −1.0	0.7 to −0.6	1.3 to −0.6	0.3 to −0.6	0.3 to −0.6	0.2 to −1.0
aVF	Mn., SD	0.01, 0.35	0.3, 0.24	0.10, 0.41	0.53, 0.35	0.16, 0.35	0.00, 0.36	0.07, 0.37	0.09, 0.31	0.07, 0.33	0.04, 0.20	0.07, 0.37	0.09, 0.19	−0.03, 0.31	0.03, 0.30
	Max.–Min.	1.1 to −1.0	1.1 to −0.6	1.8 to −1.0	1.5 to −0.4	2.1 to −1.0	1.5 to −1.0	1.5 to −1.2	1.1 to −0.6	1.6 to −1.0	0.9 to −1.0	1.7 to −1.6	1.1 to −0.6	1.9 to −1.0	1.3 to −0.5
V_4R	Mn., SD	0.23, 0.36	0.00, 0.23	0.02, 0.24	0.17, 0.26	0.11, 0.10	−0.02, 0.21	0.08, 0.24	−0.02, 0.21	0.02, 0.19	0.07, 0.21	0.13, 0.14	0.09, 0.18	0.16, 0.10	0.08, 0.10
	Max.–Min.	1.1 to −0.5	1.1 to −0.6	1.1 to −0.6	1.1 to −0.6	0.9 to −0.2	1.1 to −0.6	1.1 to −1.4	0.9 to −0.8	1.7 to −0.8	1.1 to −1.0	0.9 to −0.4	0.9 to −2.0	0.7 to −0.4	0.9–0.1
		(32)[a]	(36)[a]	(114)[a]	(94)[a]	(87)[a]	(68)[a]	(107)[a]	(74)[a]	(93)[a]	(78)[a]	(74)[a]	(56)[a]	(23)[a]	(17)[a]
V_1	Mn., SD	0.28, 0.44	0.12, 0.35	0.44, 0.52	0.36, 0.29	0.38, 0.44	0.09, 0.25	0.39, 0.50	0.09, 0.38	0.39, 0.40	0.18, 0.25	0.08, 0.57	0.19, 0.30	0.46, 0.35	0.32, 0.39
	Max.–Min.	1.3 to −0.8	1.7 to −0.8	2.5 to −1.0	1.1 to −0.6	1.7 to −1.6	0.9 to −0.6	2.9 to −1.4	1.1 to −1.2	1.5 to −1.2	1.1 to −0.6	2.1 to −1.0	1.1 to −1.0	1.1 to −0.5	1.5 to −0.0
V_2	Mn., SD	0.94, 0.87	0.26, 0.48	0.93, 0.89	0.47, 0.31	0.70, 0.30	0.28, 0.47	0.88, 0.86	0.32, 0.50	0.69, 0.79	0.40, 0.47	0.75, 0.48	0.51, 0.54	0.83, 0.63	0.62, 0.43
	Max.–Min.	3.3–0	1.1 to −1.4	4.1 to −1.0	1.3 to −0.4	4.1 to −1.4	2.7 to −0.8	6.1 to −0.6	2.1 to −1.2	2.8 to −2.6	1.9 to −1.0	3.3 to −0.5	2.7 to −1.0	2.5 to −0.5	1.5 to −0.7
V_3	Mn., SD	1.00, 0.57	0.47, 0.57	0.87, 0.99	0.46, 0.29	0.67, 0.61	0.18, 0.44	0.76, 1.22	0.11, 0.93	0.56, 1.25	0.30, 0.62	0.60, 0.37	0.22, 0.40	0.59, 0.66	0.43, 0.57
	Max.–Min.	2.7 to −1.5	2.3 to −0.8	5.5 to −0.6	1.3 to −0.4	2.7 to −1.2	1.9 to −1.0	9.0 to −6.8	2.5 to −6.3	2.2 to −1.5	2.1 to −2.0	2.1 to −1.2	1.5 to −1.2	2.3 to −0.8	2.0 to −0.7
V_4	Mn., SD	0.51, 0.72	0.10, 0.47	0.57, 0.90	0.37, 0.23	0.59, 0.79	0.04, 0.44	0.37, 0.59	0.01, 0.38	0.23, 0.50	0.04, 0.51	0.29, 0.55	0.03, 0.43	0.09, 0.57	0.06, 0.46
	Max.–Min.	2.9 to −1.0	2.3 to −0.8	6.4 to −1.0	1.1 to −0.4	5.1 to −1.6	1.7 to −0.8	3.3 to −2.4	2.1 to −1.0	1.8 to −1.4	2.5 to −1.2	1.9 to −2.0	1.5 to −1.6	1.7 to −1.6	1.0 to −1.0
V_5	Mn., SD	0.35, 0.50	0.03, 0.31	0.26, 0.57	0.34, 0.22	0.25, 0.49	0.09, 0.33	0.19, 0.41	0.09, 0.54	0.05, 0.38	0.02, 0.35	0.09, 0.37	−0.02, 0.32	−0.02, 0.39	0.03, 0.25
	Max.–Min.	2.3 to −0.4	1.1 to −0.8	3.0 to −1.0	1.1 to −0.2	2.9 to −1.2	1.3 to −0.8	1.9 to −2.2	2.5 to −1.0	1.5 to −1.1	1.5 to −1.0	1.5 to −1.0	1.1 to −1.0	1.1 to −1.2	0.6 to −0.9
V_6	Mn., SD	0.24, 0.50	0.0, 0.14	0.24, 0.50	0.34, 0.25	0.21, 0.41	0.13, 0.37	0.14, 0.26	0.20, 0.54	0.10, 0.32	0.06, 0.26	0.09, 0.33	0.09, 0.19	0.15, 0.30	0.05, 0.27
	Max.–Min.	2.2–0.4	0.7 to −0.4	5.1 to −0.6	1.3 to −0.2	2.5 to −2.1	1.5 to −1.0	1.1 to −1.2	2.5 to −0.6	1.5 to −1.0	1.9 to −0.6	1.5 to −1.0	1.1 to −0.6	0.7 to −1.0	1.0 to −0.7

Mn., SD, standard deviation; Max., maximum; Min., minimum

[a]Number of cases in which measurement was made.

Table A1.43

Amplitude of T wave (in millimeters) in normal Japanese of various age-groups

		15–19		20–29		30–39		40–49		50–59		60–69		70+	
		Male n = 61	Female n =38	Male n = 165	Female n = 109	Male n = 119	Female n = 94	Male n = 153	Female n = 82	Male n = 135	Female n = 102	Male n = 101	Female n = 79	Male n = 48	Female n = 42
I	Mn., SD	3.21, 1.13	2.50, 0.88	2.80, 1.11	2.42, 0.98	2.42, 0.93	2.30, 0.79	2.42, 0.95	1.87, 0.89	2.23, 0.93	2.08, 0.81	2.07, 0.96	1.83, 0.96	1.54, 1.74	1.83, 0.78
	Max.–Min.	5.9–1.0	4.9–0.0	7.9–0.0	5.9–0.0	5.9–0.0	5.9 to –1.0	6.9–0.0	3.9–0.0	5.9–0.0	4.9–0.0	4.9–0.0	4.9–0.0	2.9 to –1.0	4.9 to –0.0
II	Mn., SD	4.65, 1.34	2.88, 1.04	4.26, 1.56	2.98, 1.40	3.79, 1.47	2.91, 1.15	3.63, 1.39	2.62, 1.02	3.40, 1.44	2.47, 1.22	3.18, 1.45	2.27, 1.02	2.56, 1.17	2.12, 0.87
	Max.–Min.	7.9–1.0	4.9–0.0	9.9–0.0	7.9 to –3.0	9.9–0.0	6.1–0.0	7.9–0.0	5.9–0.0	8.9 to –1.0	5.9 to –1.0	7.9 to –2.0	7.9–0.0	5.9–0.0	3.9–0.0
III	Mn., SD	1.93, 0.99	0.42, 0.95	1.78, 1.30	0.58, 1.10	1.65, 1.33	0.70, 0.76	1.45, 1.54	0.75, 0.99	1.40, 1.10	0.56, 0.90	1.46, 1.48	0.54, 1.07	1.33, 1.14	0.62, 0.78
	Max.–Min.	4.9 to –1.0	3.9 to –3.0	5.9 to –2.0	4.9 to –2.0	5.9 to –2.0	2.9 to –2.0	6.9 to –3.0	4.9 to –2.0	5.9 to –2.0	2.9 to –2.0	5.9 to –3.0	3.9 to –2.0	4.9 to –1.0	2.9 to –2.0
aVR	Mn., SD	–3.68, 1.58	2.42, 0.83	–2.37, 1.38	–0.3, 0.95	–2.74, 1.46	–2.50, 0.87	–2.00, 2.28	–1.55, 1.53	–2.31, 1.42	–1.88, 1.10	–2.16, 1.43	–1.58, 1.16	–0.16, 1.17	–1.12, 1.48
	Max.–Min.	–0.1 to –70	–0.1 to –5.0	–0.1 to –12.0	–0.1 to –5.0	3.9 to –7.6	–0.1 to –5.0	4.9 to –6	3.9 to –4.0	4.9 to –6.0	2.9 to –5.0	2.9 to –5.0	2.9 to –4.0	1.9 to –5.0	2.9 to –4.0
aVL	Mn., SD	1.05, 0.83	1.26, 0.83	0.89, 1.03	1.34, 1.02	0.70, 1.00	1.10, 0.72	0.87, 1.14	0.85, 0.66	0.73, 0.89	0.96, 0.72	0.52, 1.15	0.27, 0.84	0.52, 0.71	0.90, 0.85
	Max.–Min.	3.0 to –1.0	3.9 to –1.0	5.9 to –2.0	6.9 to –2.0	3.9 to –2.0	3.9 to –1.0	7.9 to –2.0	2.9 to –2.0	3.9 to –2.0	2.9 to –1.0	3.9 to –3.0	3.9 to –2.0	1.9 to –2.0	3.9 to –2.0
aVF	Mn., SD	3.18, 1.28	1.73, 0.95	2.98, 1.56	1.88, 1.20	2.62, 1.46	1.86, 0.93	2.45, 1.58	1.72, 0.90	2.21, 1.26	1.47–0.86	2.43, 1.37	1.41, 0.75	1.75, 1.23	1.23, 1.06
	Max.–Min.	5.9–0.0	4.9 to –1.0	7.9 to –6.0	6.9 to –2.0	6.9 to –4.0	4.9 to –1.0	12.0 to –1.0	4.9 to –0.2	6.9 to –2.0	4.9 to –1.0	6.9 to –2.0	3.9 to –1.0	4.9 to –1.0	3.9 to –4.0
V_4R	Mn., SD	–0.26, 1.10	–0.55, 0.78	0.17, 1.25	–0.68, 0.95	0.35, 1.02	0.67, 1.07	–0.01, 1.26	–0.49, 0.79	–0.02, 0.96	–0.42, 0.81	–0.26, 0.99	–0.55, 0.84	0.00, 1.16	–0.32, 0.57
	Max.–Min.	1.9 to –4.0	1.9 to –2.0	3.9 to –4.0	1.9 to –3.0	2.9 to –3.0	11.9 to –3.0	3.9 to –5.0	2.9 to –2.0	3.9 to –3.0	1.9 to –2.0	1.9 to –3.0	2.9 to –3.0	2.9 to –2.0	0.9 to –2.0
		(50)[a]	(37)[a]	(117)[a]	(96)[a]	(86)[a]	(67)[a]	(108)[a]	(74)[a]	(94)[a]	(78)[a]	(74)[a]	(56)[a]	(23)[a]	(17)[a]
V_1	Mn., SD	1.42, 2.55	–0.15, 1.38	1.99, 1.81	–0.45, 1.65	1.77, 2.02	–0.19, 1.34	1.52, 4.21	0.53, 1.28	1.35, 2.10	–0.13, 1.45	1.20, 1.95	0.08, 1.45	1.63, 1.67	0.29, 1.86
	Max.–Min.	7.9 to –5.0	2.9 to –4.0	6.9 to –3.0	4.9–4.0	8.9 to –2.0	2.9 to –3.0	10.9–5.0	2.9 to –4.0	7.9 to –5.0	4.9 to –4.0	5.9 to –3.0	4.9 to –3.0	5.9 to –3.0	6.9 to –4.0
V_2	Mn., SD	8.38, 3.67	3.20, 2.90	8.14, 3.65	2.96, 2.16	6.90, 3.57	3.17, 2.03	6.48, 3.04	2.78, 1.85	6.43, 3.01	3.35, 2.25	5.38, 2.90	3.08, 2.19	5.04, 2.80	3.24, 2.42
	Max.–Min.	19.9 to –1.0	10.9 to –3.0	23.9–0.0	8.9 to –4.0	18.9 to –2.0	8.9 to –2.0	13.9 to –1.0	7.9 to –2.0	13.9 to –3.0	9.9 to –3.0	11.9 to –5.0	10.9 to –2.0	11.9–0.0	9.9 to –3.0
V_3	Mn., SD	9.92, 3.52	4.50, 2.24	8.86, 3.63	4.05, 2.16	7.58, 3.37	4.21, 2.17	7.92, 3.03	3.78, 2.14	7.95, 2.97	4.43, 2.52	7.27, 2.98	4.36, 2.37	7.08, 2.98	4.62, 2.41
	Max.–Min.	20.9–0.0	10.9–0.0	22.9–2.0	9.9 to –0.0	20.9–1.0	10.9–0.0	16.9–0.0	9.9 to –2.0	18.9–2.0	12.9 to –3.0	15.9 to –2.0	11.9 to –1.0	14.9–2.0	8.9 to –1.0
V_4	Mn., SD	9.38, 3.75	5.15, 2.08	8,72, 3.93	4.80, 1.84	7.58, 3.89	4.87, 2.46	7.61, 3.35	4.36, 2.14	7.78, 2.93	4.32, 2.74	7.07, 3.27	4.22, 1.99	6.19, 2.63	4.33, 2.58
	Max.–Min.	16.9–1.0	10.9–0.0	24.9–1.0	10.9–0.0	40.9–1.0	13.0–0.0	26.9–1.0	11.9 to –1.0	15.9 to –2.0	13.9 to –2.0	17.4 to –5.0	12.9–0.0	13.9 to –4.0	11.9–0.0
V_5	Mn., SD	8.53, 3.58	4.45, 1.70	5.30, 2.82	4.25, 1.65	5.44, 2.86	4.45, 2.01	5.54, 2.43	4.03, 1.95	5.50, 2.43	3.11–1.66	5.48, 2.51	3.32, 1.77	4.42, 2.49	3.41, 1.66
	Max.–Min.	15.9–0.0	8.9–0.0	16.9–1.0	10.9 to –2.0	14.9–0.0	11.0–0.0	14.9–1.0	11.9–6	14.9 to –2.0	9.9–0.0	12.9–0.0	9.9–0.0	10.9 to –2.0	8.9–0.0
V_6	Mn., SD	4.96, 2.21	3.69, 1.37	4.48, 2.15	3.43, 2.41	3.80, 1.85	3.55, 1.45	3.87, 1.75	3.12, 1.42	3.27, 1.60	2.98, 1.33	3.96, 2.06	2.45, 1.00	2.92, 1.54	2.34, 1.11
	Max.–Min.	11.9–0.0	6.9–0.0	14.9–0.0	8.9–0.0	8.9–0.0	7.9–1.0	9.9–0.0	7.9–0.0	8.9 to –1.0	7.9–0.0	13.9–0.0	4.9–0.0	6.9 to –1.0	4.9–0.0
															(38)[a]

Mn., mean; SD, standard deviation; Max., maximum; Min., minimum

[a]Number of cases in which measurement was made.

A1.4 Normal Limits of Right-Sided Chest Leads in Caucasians

The tables in this section were derived from 109 subjects with no evidence of heart disease (Tables A1.44–A1.51b). The data is reproduced from: Andersen HR, Nielsen D, Hansen LG. The normal right chest electrocardiogram. *J. Electrocardiol.* 1987;**20**: 27–32 with the permission of Churchill Livingstone, New York.

Table A1.44

R-wave amplitudes (millimeters)

	Median	95% fractile values	Mean $\bar{x}$	Range	Number *n*
V_3R	1.5	0.4–3.9	1.7	0.1–4.3	107
V_4R	1.0	0.3–3.3	1.2	0.2–4.2	101
V_5R	1.0	0.3–2.4	1.0	0.2–5.0	79
V_6R	0.7	0.2–2.6	0.9	0.2–5.1	59
V_7R	0.5	0.3–3.6	1.0	0.3–5.6	37

Table A1.45

S-wave amplitudes (millimeters)

	Median	95% fractile values	Mean $\bar{x}$	Range	Number *n*
V_3R	5.1	1.7–11.4	5.7	0.9–13.5	108
V_4R	3.6	1.1–8.0	3.9	0.9–9.7	104
V_5R	3.6	1.0–7.7	3.5	0.5–8.8	89
V_6R	2.5	0.7–6.4	2.9	0.4–7.3	70
V_7R	2.7	0.8–5.4	2.8	0.7–6.8	45

Table A1.46

Secondary r-wave (qr, rSr′) amplitudes (millimeters)

	Median	95% fractile values	Mean $\bar{x}$	Range	Number *n*
V_3R	0.8	0.5–1.5	0.9	0.4–1.5	6
V_4R	0.7	0.2–1.8	0.8	0.2–1.8	11
V_5R	0.8	0.3–2.5	1.0	0.2–2.5	36
V_6R	0.9	0.3–3.6	1.3	0.2–4.2	50
V_7R	0.0	0.3–3.6	1.2	0.1–4.8	71

Table A1.47

Q-wave amplitudes (millimeters)

	Median	95% fractile values	Mean $\bar{x}$	Range	Number *n*
V_3R					2
V_4R	2.8	1.5–8.1	4.4	1.5–8.1	8
V_5R	2.5	0.8–5.3	2.7	0.7–5.9	30
V_6R	1.9	1.0–4.7	2.2	0.9–4.9	47
V_7R	1.8	0.9–3.9	2.0	0.6–4.1	71

Table A1.48

r + r′ amplitudes (millimeters)

	Median	95% fractile values	Mean $\bar{x}$	Range	Number *n*
V_3R	1.5	0.3–3.9	1.7	0.0–4.3	109
$\sum_{V_3R}^{V_4R} r + r'$	2.5	0.5–6.8	2.8	0.3–8.1	109
$\sum_{V_3R}^{V_5R} r + r'$	3.5	0.5–9.1	3.8	0.3–13.3	109
$\sum_{V_3R}^{V_6R} r + r'$	4.0	0.8–11.3	4.9	0.4–15.7	109
$\sum_{V_3R}^{V_7R} r + r'$	4.9	1.4–14.8	6.0	0.4–20.5	109

Table A1.49

J-point deviation (millimeters)

	Median	95% fractile values	Mean $\bar{x}$	Range	Number *n*
V_3R	−0.1	0.4 to −0.5	−0.1	−0.6 to +0.5	109
V_4R	−0.1	0.3 to −0.6	−0.1	−0.9 to +0.5	104
V_5R	0.0	0.3 to −0.7	−0.1	−0.8 to +0.5	107
V_6R	0.0	0.5 to −0.6	0.0	−0.8 to +0.5	108
V_7R	0.0	0.5 to −0.5	0.0	−0.9 to +0.6	103

Table A1.50

ST-segment deviation (millimeters) 40 ms after last QRS deflection

	Median	95% fractile values	Mean $\bar{x}$	Range	Number *n*
V_3R	0.1	0.6 to −0.5	0.1	−1.2 to +0.8	109
V_4R	0.1	0.5 to −0.4	0.0	−1.4 to +0.6	109
V_5R	0.1	0.5 to −0.4	0.1	−0.8 to +0.6	109
V_6R	0.0	0.5 to −0.3	0.1	−0.5 to +1.0	109
V_7R	0.1	0.4 to −0.4	0.1	−0.5 to +0.9	109

Table A1.51(a)

ST-segment deviation (millimeters) 80 ms after last QRS deflection

	Median	95% fractile values	Mean $\bar{x}$	Range	Number *n*
V_3R	0.3	0.9 to −0.3	0.3	−0.4 to +1.0	109
V_4R	0.2	0.6 to −0.3	0.2	−0.5 to +0.9	109
V_5R	0.1	0.5 to −0.3	0.1	−0.7 to +1.0	109
V_6R	0.0	0.5 to −0.3	0.0	−0.6 to +0.6	109
V_7R	0.0	0.4 to −0.3	0.0	−0.8 to +0.5	109

Table A1.51(b)

Q-wave duration (ms)

	Median	95% fractile values	Mean $\bar{x}$	Range	Number *n*
V_3R					2
V_4R	53	20–80	50	20–81	8
V_5R	34	20–64	40	17–108	30
V_6R	34	17–74	36	17–81	47
V_7R	34	17–58	34	14–64	71

A1.5 Normal Limits of the Three-Orthogonal-Lead ECG

A1.5.1 Normal Limits in Males

Some of the earliest work on the three-orthogonal-lead ECG was undertaken in the laboratory of Pipberger. His group studied 510 men, including whites and blacks, and with the use of computer methods, analyzed the ECGs automatically. Tables A1.52–A1.61 are reproduced from Draper H W et al. The corrected orthogonal electrocardiogram and vectorcardiogram in 510 normal men (Frank-lead system). *Circulation* 1964;**30**: 853–864 with the permission of the American Heart Association, Dallas, Texas.

Table A1.52

Measurements of P, QRS and T in scalar orthogonal leads *X*, *Y* and *Z*. The mean and standard deviation of each item is shown on the upper line. The second line indicates the limits of a 96 percentile range. A similar pattern is used for A1.52 to A1.61. Figures in parentheses in A1.52 show the actual number of measurements taken (e.g., Q waves in lead *X* were present in 306 cases only). Results not followed by a number in parentheses were obtained from the total series. All wave durations are based on the total QRS duration derived from the three leads. The earliest or last deflection in any one of the simultaneously recorded leads indicates onset or end of this complex

Item	*X*		*Y*		*Z*
P amplitude (mV)	0.06 ± 0.03		0.11 ± 0.07		0.03 ± 0.0
	0.03–0.12		0.05–0.23		−0.06–0.10
Q amplitude (mV)	0.10 ± 0.05	(306)	0.10 ± 0.07	(333)	0.41 ± 0.21
	0.03–0.25		0.01–0.29		0.09–0.93
Q duration (s)	0.019 ± 0.004	(306)	0.021 ± 0.005	(333)	0.033 ± 0.007
	0.012–0.028		0.008–0.032		0.020–0.048
R amplitude (mV)	1.17 ± 0.37		1.03 ± 0.41		0.93 ± 0.35
	0.51–1.97		0.35–1.95		0.36–1.79
R duration (s)	0.051 ± 0.016		0.061 ± 0.019		0.059 ± 0.010
	0.028–0.88		0.028–0.100		0.032–0.080
S amplitude (mV)	0.27 ± 0.15	(407)	0.18 ± 0.12	(274)	
	0.06–0.68		0.03–0.49		
S duration (s)	0.039 ± 0.008	(407)	0.035 ± 0.010	(274)	
	0.024–0.056		0.020–0.056		
T amplitude (mV)	0.27 ± 0.13		0.22 ± 0.13		−0.28± 0.13
	0.06–0.56		−0.11–0.48		−0.58 to −0.06
Q/R amplitude ratio	0.08 ± 0.04	(306)	0.10 ± 0.05	(333)	0.49 ± 0.35
	0.02–0.21		0.01–0.22		0.10–1.21
R/S amplitude ratio	5.74 ± 4.62	(407)	9.07 ± 9.39	(274)	
	1.40–19.25		1.11–38.51		
R/T amplitude ratio	5.44 ± 4.01		5.18 ± 3.25		4.02 ± 2.66
	1.63–20.16		1.67–13.79		1.12–12.42
Time from beginning of QRS to largest R peak (s)	0.037 ± 0.005		0.039 ± 0.005		0.049 ± 0.006
	0.028–0.048		0.028–0.052		0.036–0.064

Table A1.53

Time intervals obtained from three simultaneously recorded leads. The method of measurement is the same as indicated for Table A1.52

Item	Measurement (s)
P duration	0.102+0.016
	0.068–0.140
PR interval	0.153 ± 0.023
	0.112–0.204
PR segment	0.051 ± 0.019
	0.021–0.096
QRS duration	0.093 ± 0.009
	0.076–0.112
QT interval (uncorrected)	0.367 ± 0.034
	0.312–0.448

Table A1.54

Maximal P, QRS and T vectors in the frontal, sagittal and horizontal planes together with spatial amplitude and orientation. The vectors in the plane projections were obtained from *XY*, *YZ* and *XZ* leads, respectively, and do not therefore represent projections of the spatial maximal vectors onto these planes

Item	Maximal P vector	Maximal QRS vector	Maximal T vector
Frontal plane			
Amplitude (mV)	0.18 ± 0.06	1.57 ± 0.42	0.36 ± 0.14
	0.08–0.31	0.81–2.53	0.12–0.69
Direction (°)	67 ± 18	41 ± 14	40 ± 20
	22–91	14–71	4–74
Sagittal plane			
Amplitude (mV)	0.17 ± 0.06	1.32 ± 0.45	0.36 ± 0.13
	0.06–0.31	0.60–2.42	0.13–0.67
Direction (°)	87 ± 23	48 ± 30	142 ± 23
	54–129	343–114	93–180
Horizontal plane			
Amplitude (mV)	0.09 ± 0.03	1.39 ± 0.36	0.40 ± 0.14
	0.04–0.14	0.74–2.19	0.15–0.72
Direction (°)	349 ± 41	327 ± 34	46 ± 19
	285–91	245–29	8–83
Spatial amplitude (m)V	0.18 ± 0.06	1.73 ± 0.44	0.46 ± 0.16
	0.09–0.32	0.92–2.75	0.18–0.82
Spatial orientation			
Azimuth (°)	342 ± 38	331 ± 27	44 ± 19
	277–75	263–23	4–79
Elevation (°)	63 ± 17	35 ± 13	29 ± 13
	20–86	7–60	2–58

Table A1.55

Quantitative analysis of early QRS vectors. The upper row provides mean ±SD and the lower row gives a 96% range

Instantaneous vectors [a]	Scalar amplitude (mV)			Planar direction (°)			Spatial magnitude and orientation		
	X	*Y*	*Z*	Frontal	Sagittal	Horizontal	Amplitude (mV)	Azimuth (°)	Elevation (°)
0.01 s after	−0.04± 0.04	−0.03± 0.06	−0.11± 0.06	210 ± 61	189 ± 36	110 ± 34	0.14 ± 0.06	110 ± 34	−10± 27
QRS onset	−0.14–0.07	−0.13–0.08	−0.25–0.01	59–330	79–242	17–168	0.05–0.29	17–168	−59–58
0.02 s after	0.05 ± 0.14	−0.01± 0.12	−0.31± 0.15	325 ± 87	180 ± 25	81 ± 26	0.37 ± 0.15	81 ± 26	−1± 20
QRS onset	−0.19–0.38	−0.25–0.29	0.68 to −0.06	162–136	117–220	23–124	0.12–0.75	23–124	−39–42
0.03 s after	0.56 ± 0.27	0.35 ± 0.25	−0.20± 0.32	29 ± 23	120 ± 40	21 ± 30	0.79 ± 0.30	21 ± 30	26 ± 15
QRS onset	0.06–1.19	−0.06–0.97	−0.89–0.48	350–59	41–186	319–79	0.29–1.52	319–79	−6–53
0.04 s after	1.05 ± 0.37	0.86 ± 0.37	0.34 ± 0.46	40 ± 16	72 ± 27	343 ± 25	1.51 ± 0.42	343 ± 25	35 ± 11
QRS onset	0.33–1.79	−0.24–1.79	−0.59–1.26	14–66	28–139	294–35	0.78–2.53	294 ± 35	13–59
0.05 s after	0.65 ± 0.51	0.74 ± 0.47	0.77 ± 0.40	52 ± 36	42 ± 24	307 ± 28	1.40 ± 0.50	307 ± 28	31 ± 16
QRS onset	−0.27–1.76	−0.09–1.74	−0.01–1.67	343–147	351–89	248–1	0.56–2.57	248–1	−5–59

[a] Scalar components, plane projections, spatial magnitude and orientation of five initial instantaneous QRS vectors taken 0.01 s intervals after the onset of QRS. As in all other tables the beginning of QRS is taken at the earliest deflection in any one of the simultaneously recorded scalar leads. In this as in all consecutive tables the ranges for azimuth are to be followed in clockwise direction.

Table A1.56

Quantitative analysis of late QRS vectors. The upper row provides mean ±SD and the lower row gives a 96% range

Instantaneous vectors [a]	Scalar amplitude (mV)			Planar direction (°)			Spatial magnitude and orientation		
	X	*Y*	*Z*	Frontal	Sagittal	Horizontal	Amplitude (mV)	Azimuth (°)	Elevation (°)
End of QRS or J point	0.01 ± 0.03 −0.06–0.08	0.03 ± 0.04 −0.06–0.10	−0.07 ± 0.04 −0.17–0.00	79 ± 74 279–241	160 ± 30 95–227	83 ± 34 9–153	0.09 ± 0.04 0.03–0.19	83 ± 34 9–153	19 ± 27 −42–70
0.01 S before End of QRS	−0.01 ± 0.06 −0.13–0.10	0.01 ± 0.08 −0.13–0.15	0.01 ± 0.08 −0.15–0.16	156 ± 89 4–315	77 ± 97 267–250	197 ± 94 26–1	0.11 ± 0.05 0.03–0.24	197 ± 94 26–1	6 ± 45 −72–79
0.02 S before End of QRS	−0.09 ± 0.12 −0.36–0.12	0.00 ± 0.16 −0.30–0.33	0.24 ± 0.19 −0.10–0.67	173 ± 72 31–305	358 ± 53 242–122	247 ± 52 96–30	0.34 ± 0.17 0.07–0.74	247 ± 52 96–30	−2 ± 34 −74–63
0.03 S before End of QRS	−0.03 ± 0.32 −0.51–0.95	0.18 ± 0.33 −0.39–1.1	0.60 ± 0.28 0.05–1.14	128 ± 74 353–268	12 ± 32 290–68	263 ± 32 202–338	0.76 ± 0.31 0.25–1.51	263 ± 32 202–338	10 ± 26 −54–55
0.04 S before End of QRS	0.46 ± 0.59 −0.54–1.70	0.61 ± 0.49 −0.31–1.66	0.77 ± 0.37 −0.04–1.52	69 ± 55 341–214	35 ± 29 335–93	295 ± 36 230–1	1.30 ± 0.48 0.43–2.27	295 ± 36 230–1	26 ± 20 −26–58
0.05 S before End of QRS	0.87 ± 0.48 −0.28–1.75	0.81 ± 0.41 0.05–1.80	0.49 ± 0.50 0.47–1.56	46 ± 27 13–131	65 ± 32 7–148	331 ± 33 251–28	1.44 ± 0.48 0.57–2.53	331 ± 33 251–28	34 ± 13 2–58

[a] Scalar components, planar projections, spatial magnitude and orientation of five terminal instantaneous QRS vectors taken in retrograde fashion from the end of QRS at 0.01 s intervals.

Table A1.57

Quantitative analysis of ST segment. The upper row provides mean ±SD and the lower row gives a 96% range

Instantaneous vectors	Scalar amplitude (mV)			Spatial magnitude and orientation		
	X	*Y*	*Z*	Amplitude (mV)	Azimuth (°)	Elevation (°)
0.02 s after J point	0.01 ± 0.03 −0.06–0.08	0.02 ± 0.04 −0.06–0.10	−0.10 ± 0.04 −0.19 to −0.02	0.11 ± 0.04 0.04–0.21	82 ± 22 37–127	12 ± 20 −35–55
0.04 s after J point	0.03 ± 0.03 −0.04–0.10	0.03 ± 0.04 −0.06–0.11	−0.11 ± 0.05 −0.22–0.03	0.13 ± 0.05 0.05–0.24	77 ± 20 35–117	13 ± 19 −32–56
0.06 s after J point	0.04 ± 0.04 −0.03–0.13	0.04 ± 0.04 −0.05–0.14	−0.12 ± 0.05 −0.25 to −0.03	0.15 ± 0.06 0.05–0.29	72 ± 19 35–109	16 ± 17 −22–54

Table A1.58

Quantitative analysis of eight instantaneous QRS vectors

Instantaneous vectors [a]	Scalar amplitude (mV)			Spatial magnitude and orientation		
	X	*Y*	*Z*	Amplitude (mV)	Azimuth (°)	Elevation (°)
1/8 QRS	−0.04± 0.05	−0.03± 0.07	−0.14± 0.08	0.18 ± 0.07	108 ± 27	−10± 26
	−0.16–0.09	−0.18–0.10	−0.31–0.00	0.06–0.36	51–156	−59–58
2/8 QRS	0.17 ± 0.17	0.05 ± 0.13	−0.34± 0.19	0.44 ± 0.19	63 ± 27	7 ± 19
	−0.11–0.61	−0.21–0.34	−0.82–0.00	0.14–0.93	359–110	−30–50
3/8 QRS	0.87 ± 0.31	0.63 ± 0.30	0.03 ± 0.40	1.17 ± 0.37	359 ± 25	33 ± 11
	0.33–1.63	0.17–1.44	−0.74–0.90	0.59–2.19	308–47	12–55
4/8 QRS	0.89 ± 0.49	0.89 ± 0.44	0.70 ± 0.44	1.58 ± 0.48	320 ± 26	34 ± 14
	−0.15–1.84	0.02–1.85	−0.05–1.74	0.70–2.62	261–3	2–61
5/8 QRS	0.09 ± 0.40	0.34 ± 0.39	0.77 ± 0.29	1.00 ± 0.34	275 ± 30	18 ± 21
	−0.55–1.13	−0.36–1.28	0.10–1.38	0.39–1.73	224–341	−30–56
6/8 QRS	−0.13± 0.14	0.01 ± 0.19	0.34 ± 0.20	0.44 ± 0.18	248 ± 35	1 ± 29
	−0.41–0.17	−0.34–0.40	−0.04–0.76	0.12–0.89	153–328	−68–57
7/8 QRS	−0.02± 0.06	0.01 ± 0.09	0.02 ± 0.09	0.13 ± 0.05	288 ± 96	3 ± 45
	−0.15–0.11	−0.15–0.16	−0.15–0.20	0.04–0.27	116–101	−75–76
8/8 QRS (J point)	0.01 ± 0.03	0.03 ± 0.04	−0.07± 0.04	0.09 ± 0.04	83 ± 34	19 ± 27
	−0.06–0.08	−0.06–0.10	−0.17–0.00	0.03–0.19	9–153	−42–70

[a] Obtained after each eighth of the QRS duration.

Table A1.59

Quantitative analysis of ST and T vectors

Instantaneous vectors [a]	Scalar amplitude (mV)			Spatial magnitude and orientation		
	X	*Y*	*Z*	Amplitude (mV)	Azimuth (°)	Elevation (°)
1/8 (ST-T)	0.02 ± 0.02	0.00 ± 0.02	−0.04 ± 0.03	0.06 ± 0.02	67 ± 36	1 ± 29
	−0.02–0.06	−0.05–0.05	−0.10–0.02	0.02–0.10	317–133	−49–58
2/8 (ST-T)	0.04 ± 0.03	0.02 ± 0.03	−0.07 ± 0.04	0.10 ± 0.04	59 ± 23	11 ± 21
	−0.01–0.11	−0.04–0.08	−0.16–0.01	0.03–0.19	353–98	−33–52
3/8 (ST-T)	0.08 ± 0.05	0.05 ± 0.04	−0.12 ± 0.06	0.16 ± 0.07	55 ± 19	17 ± 15
	0.00–0.19	−0.03–0.15	−0.27 to −0.02	0.05–0.33	13–87	−16–48
4/8 (ST-T)	0.15 ± 0.08	0.10 ± 0.07	−0.19 ± 0.09	0.28 ± 0.11	52 ± 17	21 ± 12
	0.02–0.35	−0.01–0.29	−0.42 to −0.03	0.09–0.56	14–85	−3–47
5/8 (ST-T)	0.23 ± 0.11	0.18 ± 0.10	−0.25 ± 0.12	0.40 ± 0.15	46 ± 19	27 ± 12
	0.04–0.51	0.02–0.43	−0.51 to −0.02	0.14–0.73	6–81	5–55
6/8 (ST-T)	0.22 ± 0.12	0.20 ± 0.10	−0.17 ± 0.11	0.37 ± 0.14	37 ± 28	35 ± 15
	0.00–0.49	0.02–0.43	−0.38–0.02	0.06–0.68	352–81	8–68
7/8 (ST-T)	0.07 ± 0.05	0.08 ± 0.04	−0.04 ± 0.04	0.12 ± 0.06	28 ± 47	40 ± 22
	−0.02–0.17	−0.01–0.18	−0.11–0.03	0.02–0.24	244–163	−29–78

[a] Determined through time normalization of the ST-T segment.

Table A1.60

Time integrals of QRS and T derived from scalar leads *X*, *Y* and *Z*. Combinations of two scalar components lead to planar projections in the frontal, sagittal and horizontal planes. Spatial magnitude and orientation are obtained by vectorial addition of all three scalar components. Addition of the time integrals of QRS and T results in the ventricular gradient ($V\vec{G}$). The P wave was included in the QRS time integral as described in the text. The QRS-T angle is derived from the two vectors of the respective time integrals

	Planar direction (°)			Scalar amplitude (μVs)			Spatial magnitude, orientation and spatial angles		
Item	Frontal	Sagittal	Horizontal	*X*	*Y*	*Z*	Amplitude (μVs)	Azimuth (°)	Elevation (°)
SÂQRS	44 ± 23 351–85	53 ± 27 355–110	323 ± 25 274–14	22.20 ± 11.18 1.23–46.97	23.41 ± 13.36 −2.83–51.87	17.11 ± 12.35 −6.11–44.28	40.08 ± 13.51 15.16–71.32	323 ± 25 274–14	36 ± 17 −5–71
SÂT	33 ± 24 338–78	152 ± 21 106–197	52 ± 18 13–86	29.09 ± 15.78 2.33–64.86	20.12 ± 14.73 −6.86–56.06	−37.79 ± 17.50 −76.45 to −6.65	54.97 ± 20.72 20.29–106.33	52 ± 18 13–86	21 ± 14 −11–49
SV$\hat{G}$	40 ± 14 9–67	114 ± 23 71–159	21 ± 19 340–58	51.29 ± 20.79 15.30–102.55	43.54 ± 21.28 5.51–94.79	−20.67 ± 19.99 −66.46–13.35	74.35 ± 26.63 27.17–138.42	21 ± 19 340–58	36 ± 13 7–63
QRS-T angle	12 ± 33 0–88	97 ± 39 24–163	89 ± 31 23–148						78 ± 26 26–134

Table A1.61

Eigenvectors $\vec{A}$, $\vec{B}$ and $\vec{C}$ of the P, QRS, and T loops. The polar vector is identical with eigenvector $\vec{C}$. The ratios between eigenvectors give an estimate of the planarity of the loop and its configuration. The magnitude of the polar vector is based on the area of the loop in its 'broadside' projection. A multiplication constant was used for P and T because of their small magnitude

Item	P loop	QRS loop	T loop
Eigenvector $\vec{C}$ (polar vector)			
Azimuth (°)	35 ± 34	339 ± 30	337 ± 24
	304–95	285–46	292–36
Elevation (°)	−14 ± 15	−50 ± 12	−31 ± 17
	−50–11	−73 to −25	−63–8
Eigenvector $\vec{B}$			
Azimuth (°)	122 ± 31	65 ± 37	97 ± 33
	64–183	329–143	27–170
Elevation (°)	11 ± 15	3 ± 23	−37 ± 18
	−26–43	−45–49	−69–6
Eigenvector $\vec{A}$			
Azimuth (°)	352 ± 35	332 ± 42	39 ± 21
	293–79	244–56	354–79
Elevation (°)	62 ± 20	30 ± 15	31 ± 15
	0–84	−6–57	1–61
Eigenvector ratios			
C/B	0.20 ± 0.16	0.02 ± 0.04	0.05 ± 0.09
	0.00–0.65	0.00–0.10	0.00–0.38
B/A	0.21 ± 0.17	0.41 ± 0.20	0.17 ± 0.13
	0.00–0.67	0.06–0.85	0.01–0.51
C/A	0.03 ± 0.03	0.01 ± 0.01	0.01 ± 0.01
	0.00–0.14	0.00–0.03	0.00–0.03
Spatial amplitude of the Polar vector (area of "broadside" projection of the spatial loop) (mV^2)	$6.16 \pm 3.43 \times 10^{-3}$	1.62 ± 0.85	$5.03 \pm 3.48 \times 10^{-2}$
	$1.69–15.76 \times 10^{-3}$	0.45–3.89	$0.66–14.76 \times 10^{-2}$

A1.5.2 Normal Limits in Females

The group of Pipberger, in a later paper, published data on the normal limits of the Frank orthogonal-lead ECG in 450 women, including both whites and blacks. Tables A1.62–A1.68 are reproduced from Nemati M et al. The orthogonal electrocardiogram in normal women. Implications of sex differences in diagnostic electrocardiography. *Am. Heart J.* 1978;**95**: 12–21, with the permission of Mosby, St. Louis, Missouri.

Table A1.62

Measurements of P, QRS and T in orthogonal *X*, *Y* and *Z* leads

Item	*X*		*Y*		*Z*	
P amplitude[a]	0.05 ± 0.02[c]		0.09 ± 0.04		Positive component	
	0.02–0.09[d]		0.02–0.17		0.03 ± 0.02 0–0.08 Negative component −0.03 ± 0.02 −0.07–0	
Q amplitude	−0.08 ± 0.05	(237)[e]	−0.08 ± 0.05	(238)	−0.31 ± 0.17	(446)
	−0.22 to −0.01		−0.23 to −0.01		−0.77 to −0.07	
R amplitude	0.94 ± 0.35		0.81 ± 0.33		0.68 ± 0.25	
	0.35–1.75		0.27–1.55		0.22–1.25	
S amplitude	−0.17 ± 0.11	(319)	−0.17 ± 0.12	(252)	−0.19 ± 0.17	(9)
	−0.47 to −0.01		−0.52 to −0.01		−0.60 to −0.04	
T amplitude	0.22 ± 0.10		0.16 ± 0.09		−0.08 ± 0.10	
	0.05–0.44		−0.03–0.39		−0.31–0.10	
Q/R amplitude ratio	0.07 ± 0.04	(237)	0.09 ± 0.06	(238)	0.54 ± 0.42	(446)
	0.01–0.18		0.01–0.22		0.10–1.73	
R/S amplitude ratio	11.36 ± 18.00	(319)	9.20 ± 13.00	(252)	4.00 ± 3.30	(9)
	1.12–71.70		0.64–56.00		0.70–12.00	
Q duration[b]	0.016 ± 0.003	(237)	0.017 ± 0.004	(238)	0.030 ± 0.008	(446)
	0.010–0.024		0.009–0.028		0.014–0.047	
R duration	0.045 ± 0.012		0.050 ± 0.014		0.048 ± 0.010	
	0.028–0.071		0.028–0.081		0.028–0.069	
S duration	0.029 ± 0.009	(319)	0.028 ± 0.090	(252)	0.028 ± 0.009	(9)
	0.012–0.048		0.012–0.049		0.018–0.044	
R peak time	0.037 ± 0.005		0.039 ± 0.005		0.048 ± 0.006	
(instrinsicoid deflection)	0.028–0.048		0.027–0.050		0.036–0.062	
RX + RZ	1.60 ± 0.42					
	0.87–2.50					

[a]Amplitudes are in millivolts [b]Durations are in seconds [c]Mean ± standard deviation of each item [d]Limits of a 96 percentile range [e]Figures in parentheses show the actual number of observation: results not followed by a number in parentheses were obtained from total series.

A1.5.3 Effect of Age, Build and Race on the Orthogonal-Lead ECG

The correlation of various ECG parameters with age and race (black and white) was investigated by Pipberger *et al.* In general terms, voltages were higher in black men than in white men. Tables A1.69–A1.73 are reproduced from Pipberger HV et al. Correlations of the orthogonal electrocardiogram and vectorcardiogram with constitutional variables in 518 normal men. *Circulation* 1967;**35**: 536–551 with the permission of the American Heart Association, Dallas, Texas. Table A1.69 sets out the distribution of ages of subjects in Tables A1.70–A1.73.

Table A1.63

Measurements of initial, terminal and instantaneous vectors in orthogonal *X*, *Y* and *Z* leads

	X	*Y*	*Z*
Initial vectors from the onset of QRS			
0.01 s	−0.01 ± 0.05	−0.00 ± 0.06	−0.11 ± 0.06
	−0.11–0.10	−0.13–0.12	−0.23–0.01
0.02 s	0.16 ± 0.16	0.10 ± 0.14	−0.22 ± 0.16
	−0.13–0.56	−0.13–0.45	−0.51–0.14
0.03 s	0.62 ± 0.27	0.44 ± 0.26	−0.13 ± 0.31
	0.10–1.25	−0.01–1.07	−0.66–0.65
0.04 s	0.77 ± 0.41	0.63 ± 0.38	0.39 ± 0.36
	0.00–1.70	−0.08–1.46	−0.53–1.10
Terminal vectors from the end of QRS			
J point	0.00 ± 0.03	0.00 ± 0.03	0.01 ± 0.03
	−0.06–0.05	−0.06–0.06	−0.07–0.04
0.01 s	−0.01 ± 0.05	0.00 ± 0.08	0.09 ± 0.07
	−0.12–0.11	−0.15–0.14	−0.07–0.22
0.02 s	−0.03 ± 0.15	0.00 ± 0.17	0.31 ± 0.17
	−0.27–0.36	−0.28–0.38	−0.04–0.62
0.03 s	0.19 ± 0.38	0.21 ± 0.32	0.52 ± 0.26
	−0.29–1.18	−0.35–0.97	−0.05–1.04
0.04 s	0.61 ± 0.48	0.53 ± 0.40	0.44 ± 0.36
	−0.25–1.61	−0.29–1.32	−0.31–1.16
Instantaneous ST vectors			
0.02 s after J point	−0.02 ± 0.07	−0.03 ± 0.04	−0.01 ± 0.05
	−0.10–0.06	−0.12–0.07	−0.09–0.07
0.04 s after J point	−0.01 ± 0.07	−0.03 ± 0.05	−0.02 ± 0.04
	−0.09–0.07	−0.12–0.07	−0.09–0.05
0.06 s after J point	0.00 ± 0.08	−0.02 ± 0.07	−0.02 ± 0.04
	−0.08–0.07	−0.11–0.07	−0.10–0.05

Table A1.64

Measurements of P, PR, QRS and QT

Item	Measurement (s)
P duration	0.106 ± 0.019
	0.064–0.142
PR interval	0.154 ± 0.022
	0.112–0.208
PR segment	0.048 ± 0.018
	0.020–0.096
QRS duration	0.084 ± 0.008
	0.068–0.104
QT interval (uncorrected)	0.372 ± 0.026
	0.319–0.428

Table A1.65

Measurement of P, QRS and T vectors in frontal, left sagittal and horizontal plane

Item	Frontal		Left sagittal		Horizontal	
	Amplitude	Angle	Amplitude	Angle	Amplitude	Angle
Maximal P vector	0.01 ± 0.04[a]	61[b]	0.10 ± 0.04	96	0.06 ± 0.02	14
	0.04–0.19	0–93[b]	0.03–0.18	178–44	0.03–0.12	115 to −98
Maximal QRS vector	1.24 ± 0.38	41	1.00 ± 0.31	125	1.10 ± 0.32	29
	0.63–2.19	10–88	0.49–1.70	−156–48	0.55–1.84	114 to −35
Maximal T vector	0.28 ± 0.11	32	0.20 ± 0.08	62	0.25 ± 0.10	−17
	0.10–0.57	2–68	0.07–0.42	170 to −88	0.09–0.49	42 to −70
Half-area QRS vector	1.12 ± 0.45	42	0.93 ± 0.36	120	0.97 ± 0.33	29
	0.22–2.20	−1–82	0.24–1.71	−174–52	0.36–1.70	78 to −22
Initial QRS vectors						
0.01 s	0.07 ± 0.04	−137[c]	0.13 ± 0.05	−4	0.13 ± 0.05	−95
	0.01–0.18	20 to −10	0.03–0.24	80 to −58	0.03–0.24	−5 to −146
0.02 s	0.23 ± 0.17	28	0.29 ± 0.14	24	0.32 ± 0.14	−54
	0.02–0.69	−129–174	0.04–0.62	144 to −30	0.06–0.69	38 to −115
0.03 s	0.78 ± 0.32	34	0.53 ± 0.27	88	0.69 ± 0.27	−2
	0.17–1.51	1–64	0.04–1.16	156–10	0.12–1.32	54 to −57
0.04 s	1.06 ± 0.45	39	0.84 ± 0.35	124	0.96 ± 0.36	30
	0.10–2.00	−4–84	0.10–1.59	−168–42	0.20–1.75	88 to −26
Terminal QRS vectors						
0.01 s	0.08 ± 0.05	−150[c]	0.12 ± 0.06	−172	0.11 ± 0.06	96[c]
	0.01–0.20	16 to −18	0.01–0.24	−32–82	0.01–0.23	−98 to −36
0.02 s	0.18 ± 0.14	−169[c]	0.36 ± 0.16	−177	0.35 ± 0.17	99
	0.03–0.55	15 to −30	0.05–0.69	−82–108	0.03–0.72	−150–16
0.03 s	0.45 ± 0.35	63[c]	0.64 ± 0.27	163	0.66 ± 0.29	78
	0.04–1.44	−20 to −80	0.12–1.24	−124–84	0.13–1.34	150 to −5
0.04 s	0.90 ± 0.49	43	0.81 ± 0.34	132	0.89 ± 0.36	41
	0.06–2.00	−25 to −160	0.19–1.56	−140–54	0.18–1.75	122 to −26

[a] Amplitudes are in millivolts [b] Angles are in °. All angular ranges should be read in a clockwise sequence [c] Angles show no significant clustering as evidenced by wide 96 percentile ranges.

Table A1.66

Spatial magnitude and orientation of maximal P, QRS and T vectors

Item	Magnitude (mV)	Azimuth (°)	Elevation (°)
Maximal P*XYZ* vector	0.11 ± 0.04	14	48
	0.05–0.20	115 to −98[a]	−22–80
Maximal QRS*XYZ* vector	1.35 ± 0.36	29	34
	0.75–2.25	114 to −35	−5–61
Maximal T*XYZ* vector	0.33 ± 0.13	−17	31
	0.12–0.64	42 to −70	−50–64

[a] Angular ranges should be read in a clockwise sequence.

Table A1.67

Direction of inscription of QRS loops in the frontal, left sagittal and horizontal planes in 450 normal women: CW, clockwise; CW/CCW, figure-of-eight, clockwise then counterclockwise; CCW/CW, figure-of-eight, counterclockwise then clockwise; CCW, counterclockwise

	Frontal	Left sagittal	Horizontal
CW	230 (51%)	8 (2%)	0 (0%)
CW/CCW	37 (8%)	12 (3%)	0 (0%)
CCW/CW	61 (14%)	27 (6%)	8 (2%)
CCW	122 (27%)	403 (89%)	442 (98%)

Table A1.68

Sex-specific limits. Data are derived from records of 510 normal men and 450 normal women, unless indicated otherwise in parentheses ($p < 0.001$ for all measurements)

Item	Men		Women	
Scalar measurements				
QRS duration[a]	0.093 ± 0.009		0.084 ± 0.008	
	0.076–0.112		0.068–0.104	
QZ amplitude[b]	−0.41 ± 0.21		−0.31 ± 0.17	(446)
	−0.93 to −0.09		−0.77 to −0.07	
RX amplitude	1.17 ± 0.37		0.94 ± 0.35	
	0.51–1.97		0.35–1.75	
RY amplitude	1.03 ± 0.41		0.81 ± 0.33	
	0.35–1.95		0.27–1.55	
RZ amplitude	0.93 ± 0.35		0.68 ± 0.25	
	0.36–1.79		0.22–1.25	
SX amplitude	−0.27 ± 0.15	(407)	−0.17 ± 0.11	(319)
	−0.68 to −0.06		−0.47 to −0.01	
TZ amplitude	−0.28 ± 0.13		−0.08 ± 0.10	
	−0.58 to −06		−0.31–0.10	
Q/RZ amplitude ratio	0.50 ± 0.35		0.54 ± 0.42	(446)
	0.10–1.20		0.10–1.73	
RX + RZ amplitude	2.00 ± 0.52		1.60 ± 0.42	
	1.06–3.10		0.87–2.50	
J point in lead Z	−0.07 ± 0.04		−0.01 ± 0.03	
	−0.17–0.00		−0.07–0.04	

A1.6 Normal Limits of Polarcardiographic Data

The technique of polarcardiography is explained in Chap. 45. As an adjunct, some tables of normal limits derived from the work of Dower are presented in Tables A1.74 to A1.77. The terminology is also discussed in the chapter. In addition, data from exercise testing of normals is included.

Table A1.68 (Continued)

Item	Men		Women	
Planar measurements				
Max. QRS*XY* amplitude	1.57 ± 0.42		1.24 ± 0.38	
	0.81–2.53		0.63–2.19	
Max. QRS*ZY* amplitude	1.32 ± 0.45		1.00 ± 0.31	
	0.60–2.42		0.49–1.71	
Max. QRS*XZ* amplitude	1.39 ± 0.36		1.10 ± 0.31	
	0.74–2.19		0.55–1.83	
Max. T*ZY* amplitude	0.36 ± 0.13		0.20 ± 0.08	
	0.13–0.67		0.07–0.42	
Max. T*XZ* amplitude	0.40 ± 0.14		0.25 ± 0.10	
	0.15–0.72		0.09–0.49	
Max. T*ZY* angle[c]	38		62	
	87–0		170 to −88	
Max. T*XZ* angle	−46		−17	
	−8 to −83		42 to −70	
Spatial measurements				
Max. QRS*XYZ* magnitude	1,073 ± 0.44		1.35 ± 0.36	
	0.92–2,075		0.75–2.25	
Max. T*XYZ* magnitude	0.46 ± 0.16		0.30 ± 0.12	
	0.18–0.82		0.09–0.59	

[a]Duration are in seconds [b]Amplitudes are in millivolts [c]Angles are in degrees.

Table A1.69

Age distribution of subjects included in the study

Age-group	20–29	30–39	40–49	50–59	60–78	total
Number of cases	78	179	151	56	54	518

Note that in Table A1.74, the median values were obtained from grouped data. Prominent sex differences can be seen by comparing adjacent columns marked*. Progressive change with age can be seen by comparing corresponding columns at the same level; for example, systolic blood pressure (BP) increases from 120 to 145 mmHg for male and female (M + F) with increasing age.

With increasing age, the R vector decreases in magnitude and tends toward the transverse and frontal planes (longitude and latitude of R); the ST vector tends to be greater in the men than in the women; the longitude difference between the T and R vectors (long. T–long. R) also tends to decrease. Offered for comparative purposes the systolic blood pressure shows an increase with age, especially in the women.

With respect to sex differences the T vector is more anterior (latitude of T) in the men, and its magnitude is greater, especially in the 20–29 age-group. Relative to the R vector, the T vector is more strongly anterior (lat. T–lat. R) in the men, and of greater magnitude (M_T/M_R) (Tables A1.75–A1.79).

Table A1.70

Correlations between age-groups and ECG measurements. The means and standard deviations in this and the following tables are shown in the upper line of each measurement. The lower line indicates the limits of 96 percentile ranges. In the last column results of *t*-tests are given, comparing the youngest and oldest age-groups. Vector magnitude is denoted vc

	Correlation coefficient	Age-group (years)					*p* (youngest vs. oldest group)
		20–29	30–39	40–49	50–59	60–78	
Wave durations							
P duration (s)	0.223	0.096 ± 0.012	0.098 ± 0.012	0.099 ± 0.011	0.104 ± 0.011	0.104 ± 0.013	<0.01
		0.072–0.116	0.072–0.116	0.076–0.124	0.088–0.124	0.080–0.128	
Scalar QRS measurements							
RY (mV)	−0.338	1.25 ± 0.42	1.06 ± 0.39	1.02 ± 0.42	0.88 ± 0.38	0.72 ± 0.37	<0.001
		0.53–2.08	0.47–1.95	0.34–1.99	0.26–1.69	0.24–1.63	
RZ (mV)	−0.277	1.03 ± 0.37	0.98 ± 0.35	0.89 ± 0.31	0.78 ± 0.26	0.74 ± 0.33	<0.001
		(78)	(179)	(151)	(56)	(54)	
		0.51–1.71	0.42–1.76	0.38–1.54	0.33–1.24	0.28–1.74	
SX (mV)	−0.214	−0.27 ± 0.21	−0.26 ± 0.16	−0.25 ± 0.15	−0.24 ± 0.16	−0.15 ± 0.10	<0.01
		(37)	(100)	(86)	(42)	(41)	
		−0.04 to −0.79	−0.01 to −0.64	−0.03 to −0.57	−0.01 to −0.55	−0.01–0.34	
Initial 0.02 s lead *Z* (mV)	0.268	−0.30 ± 0.19	−0.26 ± 0.16	−0.24 ± 0.13	−0.18 ± 0.10	−0.17 ± 0.12	<0.001
		(78)	(179)	(151)	(56)	(54)	
		−0.63 to −0.13	−0.62 to −0.05	−0.63 to −0.03	−0.47 to −0.02	−0.45–0.03	
Initial 0.02 s lead *Z* (mV)	0.192	0.29 ± 0.47	0.34 ± 0.49	0.21 ± 0.41	0.15 ± 0.38	0.07 ± 0.42	<0.01
		−0.50–1.22	−0.51–1.23	−0.54–1.11	−0.61–0.77	−0.81–0.91	
Initial 0.05 s lead *Z* (mV)	−0.257	0.83 ± 0.44	0.76 ± 0.42	0.65 ± 0.39	0.53 ± 0.37	0.50 ± 0.40	<0.001
		0.10–1.56	−0.07–1.67	−0.12–1.38	−0.12–1.16	−0.26–1.43	
Planar QRS measurements							
Maximal vc. sagittal plane (mV)	−0.371	1.56 ± 0.46	1.37 ± 0.45	1.27 ± 0.41	1.12 ± 0.36	0.97 ± 0.42	<0.001
		0.73–2.46	0.72–2.39	0.59–2.25	0.43–2.00	0.48–2.03	
Maximal vc. direction, frontal plane (°)	−0.288	50 ± 15	41 ± 13	42 ± 15	38 ± 18	32 ± 16	<0.001
		17–77	17–66	13–73	6–74	3–56	
Maximal vc. direction, horizontal plane (°)	−0.217	312 ± 30	325 ± 32	326 ± 36	331 ± 36	340 ± 36	<0.001
		254–354	250–26	243–19	241–20	264–46	

Table A1.70 (Continued)

	Correlation coefficient	Age-group (years)					*p* (youngest vs. oldest group)
		20–29	30–39	40–49	50–59	60–78	
Spatial QRS measurements							
Maximal vc.	−0.367	1.88 ± 0.42	1.80 ± 0.43	1.65 ± 0.45	1.45 ± 0.33	1.36 ± 0.48	<0.001
(mV)		1.13–2.82	0.96–2.76	0.94–2.74	0.91–2.19	0.77–2.47	
Initial 0.02 s vc.	−0.269	0.36 ± 0.16	0.31 ± 0.17	0.27 ± 0.14	0.24 ± 0.11	0.22 ± 0.11	<0.001
(mV)		0.15–0.69	0.11–0.68	0.10–0.68	0.08–0.51	0.05–0.48	
Initial 0.05 s vc.	−0.359	1.65 ± 0.44	1.49 ± 0.47	1.36 ± 0.45	1.19 ± 0.41	1.07 ± 0.46	<0.001
(mV)		0.91–2.54	0.77–2.48	0.55–2.42	0.49–1.91	0.40–2.00	
Spatial ST-T measurements							
Maximal T vc.	−0.312	0.50 ± 0.17	0.45 ± 0.15	0.42 ± 0.14	0.40 ± 0.13	0.31 ± 0.12	<0.001
(mV)		0.26–0.82	0.20–0.80	0.16–0.75	0.20–0.71	0.10–0.61	
0.04 s ST-T vc.	−0.213	0.12 ± 0.05	0.11 ± 0.05	0.11 ± 0.04	0.09 ± 0.04	0.09 ± 0.04	<0.01
(mV)		0.02–0.22	0.04–0.23	0.03–0.20	0.02–0.17	0.03–0.20	
3/8 ST-T vc.	−0.361	0.19 ± 0.08	0.17 ± 0.07	0.15 ± 0.06	0.13 ± 0.06	0.10 ± 0.05	<0.001
(mV)		0.08–0.36	0.05–0.32	0.04–0.32	0.04–0.25	0.03–0.24	
4/8 ST-T vc.	−0.376	0.30 ± 0.11	0.26 ± 0.10	0.24 ± 0.10	0.21 ± 0.09	0.15 ± 0.07	<0.001
(mV)		0.11–0.54	0.10–0.48	0.06–0.46	0.09–0.42	0.05–0.32	
Time integrals							
SÂQRS	−0.243	42.0 ± 13.0	42.0 ± 14.5	39.5 ± 13.0	34.5 ± 11.4	32.4 ± 13.4	<0.001
(μVs)		18.7–65.6	15.0–72.1	18.9–74.0	16.9–56.2	12.3–62.7	
SÂT	−0.352	57.8 ± 22.8	52.8 ± 20.0	47.0 ± 17.7	44.0 ± 17.3	31.9 ± 14.9	<0.001
(μVs)		26.5–100.0	17.1–95.9	13.4–90.4	19.3–92.5	6.3–58.7	
SVĜ	−0.343	78.9 ± 27.5	73.3 ± 25.7	66.3 ± 24.4	59.4 ± 24.4	46.2 ± 20.8	<0.001
(μVs)		36.2–140.0	31.7–133.0	20.8–120.0	15.9–115.0	16.1–92.2	

Table A1.71

Correlations between subjects of the white and black race

	Correlation coefficient	Race				*p*
		White		Black		(W versus B)
Scalar QRS measurements						
QRS duration (s)	−0.320	0.098 ± 0.009		0.091 ± 0.009		<0.001
		0.080–0.116		0.076–0.108		
Q*X* duration (s)	−0.160	0.019 ± 0.006	(173)	0.017 ± 0.004	(96)	<0.02
		0.008–0.028		0.008–0.024		
Q*Y* duration (s)	−0.377	0.021 ± 0.007	(133)	0.015 ± 0.006	(72)	<0.001
		0.008–0.032		0.008–0.028		
Q*Y* (mV)	−0.267	0.09 ± 0.07	(133)	0.06 ± 0.05	(72)	<0.001
		0.01–0.27		0.01–0.23		
R*X* (mV)	0.264	1.06 ± 0.35		1.25 ± 0.36		<0.001
		0.49–1.84		0.63–1.94		
R*Y* (mV)	0.197	1.96 ± 0.42		1.13 ± 0.41		<0.001
		0.28–1.99		0.41–1.99		
R*Z* (mV)	0.275	1.84 ± 0.30		1.04 ± 0.37		<0.001
		0.33–1.53		0.44–1.98		
Q/R*X* ratio	−0.128	0.06 ± 0.05	(173)	0.05 ± 0.03	(96)	<0.05
		0.00–0.20		0.00–0.11		
Q/R*Y* ratio	−0.392	0.09 ± 0.06	(133)	0.05 ± 0.03	(72)	<0.001
		0.01–0.23		0.00–0.14		
Initial 0.04 s, lead *X* (mV)	0.280	1.88 ± 0.32		1.08 ± 0.38		<0.001
		0.31–1.59		0.44–1.79		
Initial 0.02 s, lead *Y* (mV)	0.279	−0.02± 0.09		0.04 ± 0.13		<0.001
		−0.22–0.15		−0.20–0.31		
Initial 0.03 s, lead *Y* (mV)	0.315	0.19 ± 0.20		0.33 ± 0.23		<0.001
		−0.09–0.73		−0.02–0.90		
Initial 0.04 s, lead *Y* (mV)	0.297	0.67 ± 0.36		0.91 ± 0.41		<0.001
		0.10–1.62		0.23–1.76		
Terminal 0.03 s, lead *Z* (mV)	0.284	0.51 ± 0.27		0.69 ± 0.30		<0.001
		0.06–1.12		0.13–1.37		
Planar QRS measurements						
Maximal vc. frontal (mV)	0.299	1.44 ± 0.41		1.70 ± 0.42		<0.001
		0.73–2.38		0.96–2.65		
Maximal vc. sagittal plane (mV)	0.238	1.22 ± 0.44		1.45 ± 0.46		<0.001
		0.52–2.12		0.73–2.46		
Maximal vc. horizontal plane (mV)	0.312	1.26 ± 0.34		1.49 ± 0.36		<0.001
		0.65–2.05		0.89–2.24		
Spatial QRS measurements						
Maximal vc. (mV)	0.305	1.58 ± 0.43		1.87 ± 0.45		<0.001
		0.83–2.52		1.06–2.94		
Initial 0.02 s vc., elevation angle (°)	0.256	−3 ± 22		9 ± 22		<0.001
		−44–47		−25–60		
Initial 0.03 s vc. (mV)	0.348	0.56 ± 0.25		0.77 ± 0.31		<0.001
		0.18–1.16		0.28–1.50		
Initial 0.04 s vc. (mV)	0.386	1.21 ± 0.40		1.58 ± 0.46		<0.001
		0.52–2.17		0.74–2.58		
Terminal 0.05 s vc., azimuth angle (°)	0.243	324 ± 37		342 ± 34		<0.001
		240–28		266–42		

Table A1.72

Correlations between chest configuration and ECG measurements. The ratio SD/TD was derived from sagittal and transverse chest diameters. Note the small increases of the mean Q/RY ratio accompanied by a marked increase of 136% of the upper limit of the 96 percentile range. Mean results failed frequently to reflect the magnitude of changes in range limits

	Correlation coefficient	Chest configuration				*p* (first versus fourth subgroup)
		0.69 (SD/TD)	0.70–0.74 (SD/TD)	0.75–0.79 (SD/TD)	0.80 (SD/TD)	
Scalar QRS measurements						
RY (mV)	−0.227	1.16 ± 0.45	1.09 ± 0.40	0.96 ± 0.42	0.91 ± 0.39	<0.001
		0.40–2.1	0.34–2.02	0.28–1.86	0.27–1.72	
RZ (mV)	−0.237	1.02 ± 0.33	0.94 ± 0.32	0.93 ± 0.36	0.80 ± 0.33	<0.001
		0.46–1.67	0.42–1.74	0.33–1.98	0.33–1.41	
Initial 0.04 s, lead *Y* (mV)	−0.220	0.85 ± 0.43	0.81 ± 0.39	0.72 ± 0.39	0.65 ± 0.36	<0.001
		0.23–1.85	0.20–1.71	0.08–1.75	0.03–1.40	
Initial 0.04 s, lead *Z* (mV)	−0.235	0.37 ± 0.49	0.29 ± 0.45	0.26 ± 0.47	0.10 ± 0.38	<0.001
		−0.50–1.23	−0.51–1.14	−0.55–1.27	−0.58–0.96	
Q/RY ratio	0.147	0.06 ± 0.04	0.07 ± 0.05	0.08 ± 0.06	0.09 ± 0.07	<0.05
		(38)	(67)	(41)	(59)	
		0.01–0.14	0.00–0.18	0.01–0.21	0.01–0.33	
Planar QRS measurements						
Maximal vc. direction, frontal	−0.218	46 ± 16	44 ± 14	40 ± 14	37 ± 17	<0.001
plane (°)		16–79	16–71	10–72	5–66	
Maximal vc. direction, horizontal	0.195	320 ± 32	320 ± 34	326 ± 34	335 ± 36	<0.001
plane (°)		252–13	239–19	247–24	248–36	
Spatial QRS measurements						
Maximal vc. (mV)	−0.200	1.81 ± 0.42	1.74 ± 0.44	1.64 ± 0.48	1.57 ± 0.46	<0.001
		1.01–2.69	0.94–2.76	0.84–2.81	0.81–2.64	
Initial 0.04 s vc., azimuth angle (°)	0.206	341 ± 28	345 ± 28	347 ± 25	355 ± 22	<0.001
		296–40	298–38	302–34	312–40	
Initial 0.04 s vc, elevation angle (°)	−0.190	37 ± 12	35 ± 12	33 ± 12	31 ± 14	<0.01
		15–60	14–58	5–55	2–54	
Spatial ST-T measurements						
0.04 s ST-T vc. (mV)	−0.196	0.12 ± 0.05	0.11 ± 0.04	0.10 ± 0.05	0.09 ± 0.04	<0.001
		0.05–0.23	0.03–0.19	0.03–0.26	0.03–0.19	

Table A1.73

Correlation between body weight and ECG measurements. When relative body weight or deviations from ideal weight were used instead of absolute weight, ECG items exhibiting significant relationships were almost identical but most correlation coefficients decreased noticeably

	Correlation coefficient	Weight				p (first versus fourth subgroup)
		≤134 (1b)	135–159 (1b)	160–184 (1b)	≥185 (1b)	
Scalar QRS measurements						
RZ (mV)	−0.171	0.99 ± 0.39	0.94 ± 0.35	0.89 ± 0.32	0.82 ± 0.29	<0.01
		0.41–1.94	0.36–1.74	0.41–1.65	0.38–1.44	
Initial 0.05 s, lead *X* (mV)	0.233	0.51 ± 0.49	0.70 ± 0.49	0.80 ± 0.50	0.86 ± 0.48	
		−0.35–1.49	−0.18–1.56	−0.28–1.77	−0.06–1.72	<0.001
Initial 0.04 s, lead *Z* (mV)	−0.316	0.43 ± 0.43	0.33 ± 0.45	0.16 ± 0.43	0.04 ± 0.41	
		−0.34–1.23	−0.44–1.22	−0.58–0.106	−0.61–0.95	<0.001
Initial 0.05 s, lead *Z* (mV)	−0.270	0.82 ± 0.41	0.75 ± 0.41	0.62 ± 0.40	0.52 ± 0.42	
		0.13–1.64	−0.10–1.67	−0.30–1.38	−0.34–1.29	
Planar QRS measurements						
Maximal vc. direction, frontal plane (°)	−0.262	47 ± 15	43 ± 15	40 ± 14	35 ± 17	<0.001
		19–74	13–69	11–70	6–73	
Maximal vc. Direction, horizontal plane (°)	0.261	310 ± 35	352 ± 34	326 ± 33	339 ± 32	<0.001
		243–4	248–32	248–19	263–38	
Spatial QRS measurements						
Maximal vc., azimuth angle (°)	0.232	318 ± 27	329 ± 24	330 ± 28	339 ± 30	<0.001
		265–5	271–15	252–18	274–24	
Initial 0.04 s vc., azimuth angle (°)	0.313	336 ± 26	344 ± 27	353 ± 25	358 ± 22	<0.001
		296–27	298–36	302–42	308–35	
Initial 0.04 s vc., elevation angle (°)	−0.263	38 ± 11	36 ± 12	32 ± 13	29 ± 12	<0.001
		17–52	13–58	9–53	6–56	
Initial 0.05 s vc., azimuth angle (°)	0.295	301 ± 29	310 ± 27	320 ± 29	325 ± 29	<0.001
		250–352	259–5	249–19	265–15	
Spatial ST-T measurements						
7/8 ST-T vc., elevation angle (°)	−0.190	42 ± 14	41 ± 14	37 ± 13	35 ± 14	<0.01
		13–68	16–71	9–66	6–58	
Polar vectors						
P, elevation angle (°)	−0.260	−5 ± 19	−9 ± 20	−13 ± 19	−21± 21	<0.001
		−41–29	−54–32	−62–20	−63–17	
QRS, elevation angle (°)	−0.229	−46 ± 12	−48 ± 12	−51± 12	−55 ± 13	<0.001
		−67 to −24	−75 to −25	−76 to −32	−81 to −28	
T, elevation angle (°)	−0.176	−27 ± 19	−29 ± 20	−35± 17	−36 ± 19	<0.01
		−58–5	−64–8	−70–5	−63–11	

Table A1.74

Polarcardiographic median normal values of Cretan villagers. See Chapter 45 for definitions

	M	F	M+F	M	F	M+F	M	F	M+F	M	F	M+F	M	F	M+F	M	F	M+F
Age-groups	20–82			20–29			30–39			40–49			50–59			60–82		
Number of cases	275	191	466	30	16	46	53	42	95	70	46	116	51	43	94	71	44	115
Median age (years)	46	48	48	26	26	26	36	36	36	44	46	44	54	54	54	68	68	68
Intervals (ms): PR	135	135	135	130	125	130	135	135	135	140	135	135	130	135	135	145	135	140
QRS	85	80	80	80	80	80	85	80	80	85	80	80	85	85	85	85	75	80
QT_c	370	360	370	350	360	360	370	360	360	360	370	360	370	360	360	390	370	380
Latitudes: P	10A	10A	10A	10A	10A	10A	10A	10A	10A	10A	10A	10A	10A	0	0	0	0	0
R	10P	20P	20P	20P	20P	20P	10P	20P	20P	10P	20P	20P	20P	10P	10P	10P	10P	10P
ST	60A	50A	60A	60A	60A	60A	60A	60A	60A	60A	60A	60A	60A	40A	60A	60A	50A	60A
T	40A*	20A	30A	40A	20A	30A	30A	30A	30A	40A	20A	30A	40A	10A	30A	30A	30A	30A
Lat. T–Lat. R	50	40	40	50	40	50	50	40	50	50	40	40	50	20	40	40	40	40
Longitudes: P	+60	+70	+70	+70	+70	+70	+70	+70	+70	+70	+70	+70	+70	+60	+70	+70	+60	+70
R	+30	+40	+30	+40	+50	+50	+40	+40	+40	+30	+30	+30	+30	+30	+30	+20	+30	+30
ST	+30	+50	+40	+50	−90	+40	+30	+50	+30	+30	+20	+30	+20	+70	+40	+50	+65	+50
T	+30	+40	+30	+30	+40	+40	+30	+40	+30	+30	+30	+30	+30	+40	+40	+30	+40	+30
Long. T–Long. R	−10	0	0	−10	−10	−10	0	−10	−10	0	−10	0	0	0	0	10	10	10
Magnitudes (mV): P	0.14	0.14	0.14	0.17	0.13	0.16	0.14	0.15	0.15	0.15	0.14	0.14	0.14	0.15	0.15	0.13	0.14	0.13
R	1.55	1.50	1.50	1.75	1.65	1.75	1.60	1.55	1.55	1.60	1.45	1.50	1.45	1.45	1.45	1.45	1.45	1.45
ST	0.14*	0.08	0.11	0.21	0.08	0.17	0.17	0.07	0.12	0.15	0.07	0.10	0.14	0.06	0.10	0.12	0.08	0.10
T	0.500*	0.350	0.450	0.625	0.400	0.575	0.525	0.400	0.475	0.500	0.325	0.450	0.500	0.325	0.400	0.475	0.350	0.425
m_1R	1.30	1.25	1.30	1.55	1.25	1.35	1.25	1.20	1.25	1.35	1.15	1.30	1.20	1.25	1.25	1.30	1.25	1.25
S	0.045	0.040	0.045	0.045	0.045	0.045	0.060	0.040	0.050	0.045	0.030	0.040	0.045	0.030	0.040	0.040	0.040	0.040
$M_{S.}\theta$	1	1	1	1	1	1	1	1	1	1	1	1	1	1	1	1	1	1
M_T/M_R	0.32*	0.24	0.30	0.36	0.24	0.30	0.34	0.28	0.30	0.30	0.26	0.28	0.34	0.22	0.30	0.32	0.22	0.30
$M_{P/}M_R$	0.08	0.10	0.08	0.08	0.08	0.08	0.10	0.10	0.10	0.08	0.10	0.10	0.10	0.12	0.10	0.08	0.10	0.08
Systolic BP (mmHg)	130	130	130	125	120	120	125	125	125	130	130	130	130	135	135	140	150	145

Table A1.75

Magnitudes in space (M_R) and transverse plane (m_tR) in Cretan villagers. Up to age 50, M_R is greater in males, but not m_tR. In males, M_R reduces with age, also in FEMALEs but only up to age 50. In females m_tR tends to increase with age, but not in males. No overall sex difference for M_R and m_tR, but younger males show greater M_R. Medians of M_R are always greater than m_tR, also 95 percentiles. 95 percentiles for R or T in either sex do not show change with age, but numbers are too small to draw a reliable conclusion

Age-group	Sex	*n*	M_R(mV) median	M_R (mV) upper 95%	m_t R (mV) median	m_t R (mV) upper 95%
20–82	M+F	466	1.50	2.25	1.30	2.05
	M	275	1.55	2.30	1.30	2.10
	F	191	1.50	2.10	1.25	1.85
20–29	M+F	46	1.75	2.50	1.35	2.15
	M	30	1.75	2.40	1.55	2.15
	F	16	1.65	2.20	1.25	1.50
30–39	M+F	95	1.55	2.15	1.25	1.75
	M	53	1.65	2.15	1.25	1.80
	F	42	1.50	2.10	1.20	1.75
40–49	M+F	116	1.50	2.30	1.30	1.95
	M	70	1.60	2.25	1.35	2.00
	F	46	1.45	1.95	1.15	1.65
50–59	M+F	94	1.45	2.10	1.25	1.95
	M	51	1.45	2.10	1.20	1.95
	F	43	1.45	2.05	1.25	1.90
60–82	M+F	115	1.40	2.35	1.25	2.10
	M	71	1.45	2.35	1.30	2.00
	F	44	1.40	2.10	1.25	2.05

Table A1.76

Normal lower and upper 2½ percentiles (After Dower G. Polarcardiography. 1961. © Thomas: Springfield, Illinois. Reproduced with permission)

	74 young women on university campus		121 young men on university campus		192 elderly men with normal ECGs	
	Lower	Upper	Lower	Upper	Lower	Upper
PR interval (s)	0.111	0.202	0.113	0.207	0.111	0.200
QRS duration (ms)	62.0	105.0	70.0	109.0	61.0	106.0
QT_C interval (s)	0.369	0.451	0.357	0.442		
QT interval (ms)					0.302	0.426
M_P (mV)	0.028	0.182	0.042	0.198		
M_R(Mv)	0.751	2.172	0.951	2.111	0.695	2.028
M_{ST}(mV)	0.042	0.193	0.088	0.332	0.000	0.222
M_T(mV)	0.209	0.654	0.300	0.875	0.193	0.742
M_{ST}/M_R	0.035	0.133	0.064	0.240	0.000	0.151
M_T/M_R	0.147	0.536	0.207	0.700	0.141	0.604
Latitude difference (°)	−78.0	−9.50	−105.0	−11.7		
Longitude difference (°)	−7.88	43.8	−18.7	73.3		
Angle between $\hat{R}$ and $\hat{T}$ (°)	14.7	80.9	14.9	114.5	18.2	149.6

Table A1.77

Lower 2½ percentiles, medians, and upper 2½ percentiles for various polarcardiographic quantities (measured by computer in apparently healthy hospital staff). M_P, spatial magnitude of maximum P vector, $\vec{P}$; M_R, spatial magnitude of maximum QRS vector, $\vec{R}$; M_T spatial magnitude of maximum T vector, $\vec{T}$; m_tR, magnitude of maximum transverse plane QRS vector; M_{ST}, spatial magnitude of vector $\vec{ST}$ occurring midway in time between end of QRS complex and $\vec{T}$; lat., latitude posterior or anterior to frontal plane; long., longitude, or angle α in the frontal plane (After Dower G E, Osborne JA. Polarcardiographic study of hospital staff-abnormalities found in smokers. *J. Electrocardiol*. 1972; 5: 273–80. © Churchill Livingstone, New York. Reproduced with permission)

	137 women, median age 47			117 men, median age 51		
	Lower 2½ percentile	Median	Upper 2½ percentile	Lower 2½ percentile	Median	Upper 2½ percentile
PR interval (s)	0.10 (0.11)[a]	0.14	0.19 (0.20)[a]	0.11 (0.11)	0.16	0.19 (0.21)[a]
QRS duration (ms)	60 (62)	80	100 (105)	70 (70)	80	100 (109)
QT_C interval (s)	0.36 (0.37)	0.41	0.45 (0.45)	0.35 (0.36)	0.40	0.44 (0.44)
M_P (mV)	0.06 (0.03)	0.14	0.26 (0.18)	0.06 (0.04)	0.14	0.24 (0.20)
			0.22 (0.17)[b]			0.22 (0.19)[b]
M_R (mV)	0.82 (0.75)	1.41	2.24 (2.17)	1.02 (0.95)	1.50	2.20 (2.11)
			1.98 (1.82)[b]			2.14 (1.90)[b]
m_tR (mV)	0.72 (0.56)	1.16	1.84 (1.40)	0.77 (0.77)	1.31	2.13 (1.68)
			1.71 (1.28)[b]			1.95 (1.59)[b]
M_{ST} (mV)	0.04 (0.04)	0.12	0.22 (0.19)	0.09 (0.09)	0.21	0.35 (0.33)
M_T (mV)	0.21 (0.21)	0.44	0.82 (0.65)	0.28 (0.30)	0.60	0.92 (0.88)
M_{ST}/M_R	0.02 (0.04)	0.08	0.20 (0.13)	0.06 (0.06)	0.13	0.27 (0.24)
M_T/M_R	0.13 (0.15)	0.31	0.68 (0.54)	0.19 (0.21)	0.39	0.68 (0.70)
Lat. difference between $\hat{R}$ and $\hat{T}$ (°)	−115 (−80)	−44	+3 (−10)	−109 (−105)	−47	−2 (−10)
Long. difference between $\hat{R}$ and $\hat{T}$ (°)	−41 (−10)	+5	+139 (+45)	−45 (−20)	0	157 (+75)
Angle between $\hat{R}$ and $\hat{T}$ (°)	9 (15)	46	134 (81)	11 (15)	50	125 (115)

[a] Corresponding values from 74 young women and 121 young men.
[b] Upper 5 percentiles.

A1.7 Linear and Directional Statistics

A1.7.1 Acknowledgment

The work in this section has been compiled by Dr. Jerome Liebman of the Rainbow Babies and Children's Hospital, Cleveland, Ohio.

A1.7.2 Linear Statistics

Linear statistics are utilized for all linear measurements such as durations and magnitudes. Standard statistical methods are readily available, although there are many issues which must be understood in order to ensure appropriate use.

First, most standard ECGs are recorded with a maximal frequency response of 100–125 Hz, as are some orthogonal ECGs. However, for most orthogonal ECGs, the frequency response has been at least 250 Hz, often 500 Hz. In the author's laboratory, for recording the standard ECG, an upper frequency response limit above 250 Hz is preferred while

Table A1.78

PCG variables, at rest and after maximal exercise, in 30 healthy middle-aged men and 32 healthy young men compared. (After Bruce R A, Li Y B, Dower G E, Nilson K. Polarcardiographic responses to maximal exercise and to changes in posture in healthy middle aged men. J. Electrocardiol. 1973; 6: 91–6. Churchill Livingstone, New York. Reproduced with permission)

	At rest					After exercise					
	Middle-aged		Young			Middle-aged		Young			Middle-aged rest versus exercise
Variables	$\bar{X}$	σ	$\bar{X}$	σ	*p*	$\bar{X}$	Σ	$\bar{X}$	σ	*p*	*p*
Heart rate (bmp)	67	11	72	13	NS	155	8	197	8	<0.001	<0.0001
PR interval (ms)	158	24	128	28	<0.001	121	15	110	15	<0.01	<0.0001
QRS duration (ms)	68	2	80	8	<0.05	75	6	79	8	<0.05	NS
RT interval (ms)	237	40				145	15				<0.0001
QT interval (ms)	360	30	341	40	<0.05	228	22	214	15	<0.01	<0.0001
$\hat{P}$: *M* (mV)	0.14	0.05	0.14	0.05	NS	0.20	0.05	0.27	0.08	< 0.001	<0.0001
α long. (°)	+45	28	+57	49	NS	+57	42	+63	41	NS	NS
PA lat. (°)	6P	23	2P	22	NS	7A	21	13A	23	NS	0.03
$\hat{R}$: *M* (mV)	1.48	0.36	1.76	0.46	NS	1.30	0.38	1.42	0.55	NS	NS
α long. (°)	+27	35	+42	15	<0.05	+38	57	+34	81	NS	NS
PA lat. (°)	26P	16	19P	22	NS	31P	28	43	20	NS	NS
$\hat{ST}$: *M* (mV)	0.15	0.05	0.20	0.06	<0.002	0.11	0.05	0.22	0.08	<0.001	<0.01
α long. (°)	+28	19	+33	18	NS	−8	94	+20	48	NS	NS
PA lat. (°)	41A	25	39A	24	NS	49A	26	43A	27	NS	NS
$\hat{T}$: *M* (mV)	0.56	0.17	0.59	0.18	NS	0.60	0.15	0.67	0.17	NS	NS
α long. (°)	+24	11	+33	12	<0.01	+26	20	+30	21	NS	NS
PA lat. (°)	29A	19	29A	16	NS	39A	20	35A	21	NS	

Table A1.79

Polarcardiographic responses in 72 apparently healthy middle-aged women and 40 young women before and after maximal exercise. M, spatial magnitude (After Bruce RA, Dower GE, Whitkanack S, Voigt AE. Polar-cardiographic responses to maximal exercise in middle-aged women. *J. Electrocardiol.* 1974; 7: J15–22. © Churchill Livingstone, New York. Reproduced with permission)

Variables	Before maximal exercise			After maximal exercise			Before versus after exercise middle aged *p*
	Young	(Mean ± SD) Middle-aged	*p*	Young	(Mean ± SD) Middle-aged	p	
Heart-rate (bpm)	81.0 ± 15.0	74.7 ± 10.6	0.01	192.2 ± 9.0	151.6 ± 17.1	0.00001	0.00001
PR interval (ms)	138 ± 26	141 ± 17	NS	108 ± 14	129 ± 16	0.00001	0.001
QRS duration (ms)	73 ± 6	77 ± 8	0.01	72 ± 10	76 ± 7	0.05	NS
QT interval (ms)	339 ± 43	351 ± 25	NS	215 ± 15	248 ± 23	0.00001	0.00001
$\hat{P}$: *M* (mV)	0.15 ± 0.07	0.14 ± 0.06	NS	0.22 ± 0.06	0.23 ± 0.09	NS	0.00001
α longitude (°)	62.0 ± 44.0	30.5 ± 38.4	0.001	69.0 ± 37.0	32.8 ± 48.0	0.0001	NS
PA latitude (°)	A4.6 ± 29.0	A1.5 ± 27.3	NS	A10.0 ± 31.0	A11.1 ± 31.1	NS	0.05
$\hat{R}$: *M* (mV)	1.40 ± 0.34	1.49 ± 0.37	NS	1.23 ± 34.0	1.32 ± 32.3	NS	NS
α longitude (°)	46.0 ± 20.0	32.7 ± 22.6	0.01	41.0 ± 50.0	39.2 ± 30.6	NS	NS
PA latitude (°)	P27.0 ± 18.0	P26.2 ± 22.7	NS	P40.0 ± 21.0	P32.9 ± 22.6	NS	NS
ST: *M* (mV)	0.10 ± 0.05	0.10 ± 0.04	NS	0.16 ± 0.07	0.10 ± 0.04	0.00001	NS
α longitude (°)	29.0 ± 34.0	8.7 ± 48.5	0.05	16.0 ± 60.0	−9.5± 72.4	NS	NS
PA latitude (°)	A36.0 ± 23.0	A57.7 ± 212	0.00001	A41.0 ± 30.0	A53.7 ± 29.2	0.05	NS
$\hat{T}$: *M* (mV)	0.37 ± 0.15	0.42 ± 0.14	NS	0.53 ± 0.16	0.45 ± 0.12	0.01	NS
α longitude (°)	33.0 ± 13.0	21.4 ± 13.7	0.0001	33.0 ± 20.0	17.9 ± 33.3	0.05	NS
PA latitude (°)	A15.0 ± 20.0	A27.0 ± 13.2	0.001	A35.0 ± 18.0	A40.0 ± 17.2	NS	0.00001

the machine which is regularly used has an upper limit listed at 700 Hz. Although it is not well known by most electrocardiographers, the higher-frequency response electrocardiograph allows detection of higher-frequency content in the ECG. It has been shown that in order to detect a frequency *content* of at least 100 Hz, it is necessary that the instrument have a frequency *response* of at least 200 Hz [1]. It should be appreciated that, in the *same patient*, with the electrodes attached and an appropriate electrocardiograph running, merely switching from the normal high-frequency response to the low-frequency response usually to avoid ac interference produces a significant decrease in QRS voltage. Therefore, separate tables of normal ranges should be available [2, 3] for both low-frequency response machines and high-frequency response machines. This is particularly true for the pediatric ECG. Manufacturers have a responsibility to produce equipment that meets the required standards. Nowadays, equipment has to meet strict standards but technical staff often opt for a low frequency setting to reduce noise, thereby running the risk of distorting the ECG.

A second issue is that from puberty, different age/sex groups have different normal voltage ranges. Pediatric cardiologists are aware that the voltages in pubescent females are lower than those of males. The same is true in virtually all age-groups through adulthood. In addition, for each decade throughout adulthood, total voltage decreases in both males and females, so that standards should be available for each, throughout the decades [4].

Prior to puberty, there is no difference in normal ECG ranges between males and females.

However, of great interest is the fact that the newborn baby has lower voltages than older infants and children, and these increase dramatically from the newborn period till about the age of 3 months. It is also striking that the prematurely-born infant has even lower voltages than does the full-term baby [5, 6]. Catch-up occurs at varying ages for each individual baby, and usually at about 3 months.

Racial differences are also important, but, again, probably not until puberty. Blacks may have much higher voltages than whites, and, occasionally, individual normal black teenagers may have extremely high voltages, with no available explanation. Unfortunately, separate large tables for normal blacks are not available.

A fourth major issue is that electrocardiographic amplitude data is skewed. The mean and the median are rarely the same, the distribution in the various age ranges not being Gaussian [2, 3]. Almost always the 50th percentile is below the mean, in addition to which the mean plus twice standard deviation may be higher than the maximal value recorded. Therefore, the use of means and standard deviations for magnitude is not appropriate, which is why the use of percentiles to describe the distribution is necessary (see Chap. 13). In describing the complete distribution, as is frequently done, a series of percentiles is optimal. In using the percentiles to describe low and high limits of the normal range, the $2^1/_2$ and $97^1/_2$ percentiles are recommended. However, because of known inaccuracies of measurement, the 5th and 95th percentiles denoted p_5 and p_{95} are considered as being satisfactory by the author.

A1.7.3 Directional Statistics

For directional (circular and spherical) data, linear statistics are not appropriate. The fallacies in employing linear methods for directional statistics are easily understood, although, because of the lack of available methodology, such incorrect measurements were almost invariably used [7]. For example, if two vectors, 1° and 359° are grouped, the mean of $360^\circ/2 = 180^\circ$ is obviously incorrect, since it is 180° away from the true average direction of 0°. Why not, therefore, change the terminology to +1° and −1°? The mean of $0^\circ/2 = 0^\circ$ would be correct. However, suppose two vectors at 179° and 181° were then averaged. According to the new terminology, the electrocardiographer would then have to average +179° and −179° in order to be consistent. The average of +179° and $-179^\circ = 0^\circ/2 = 0^\circ$, which is again 180° away from the true average direction of 180°. Some of these rotational adjustments have been reported [8], but in using linear statistics, the adjustments have a minimal error only when there is an intense clustering of the data. Every linear treatment of directional data has inherent error. Whether the angles are, measured from −180° to +180°, or from 0° to 360°, and so on, some of the observations (actually close together) *must inevitably be treated as being far apart*. Therefore, appropriate statistical analyses of planar data as well as spherical data were developed by Downs et al. [9, 10], based upon the Von Mises distribution [11–13]. This new set of statistics was termed the "center of gravity method." In linear analysis, there is an arithmetic mean. In circular analysis, there is a prevalent direction.

For details of the methods, the reader is referred to pertinent literature, including utilization with tabular data. However, some explanations and descriptions will be given here. Table A1.80 is a segment of a table from 50 premature infants where the ECG was recorded with the Frank system.

Table A1.80

Segment of a table from 50 premature infants where the ECG was recorded with the Frank-lead system. n_f, n_s, n_h are the number of angles under study; d_f, d_s, d_h are the distances to the center of gravity; $\hat{\alpha}_f$, $\hat{\alpha}_s$, $\hat{\alpha}_h$ are the prevalent directions of the vector. All parameters represent measurements taken in the frontal, sagittal and horizontal planes, respectively (denoted by the subscripts f, s, h)

Age (h)	Times vector (ms)	n_f	d_f	$\hat{\alpha}_f$	χ_f^2	n_s	d_s	$\hat{\alpha}_s$	χs^2	n_h	d_h	$\hat{\alpha}_h$	χ_h^2
24	10	50	0.41	7	16.4	50	0.95	178	90.6	50	0.96	83	91.6

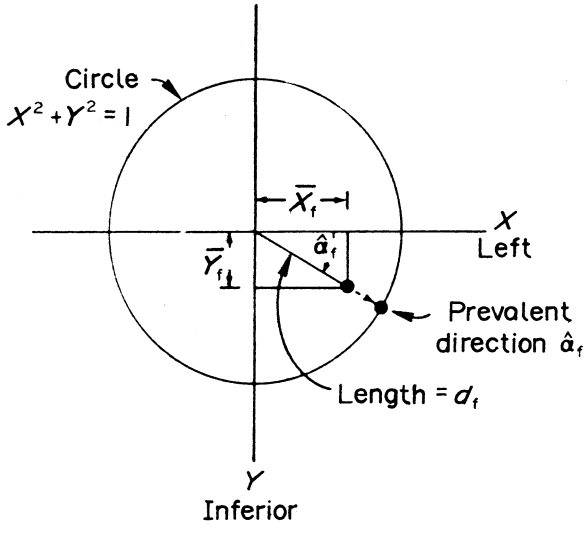

Figure A1.1

The center of gravity (X_f, Y_f) or, in polar coordinates (d_f, α_f) of points (x_f, y_f) on the circle $X^2 + Y^2 = 1$ in the frontal plane.

Imagine the data for the 10 ms vector of the 50 premature infants to be on a circular disk, balanced on a fulcrum at its center. If all the observations were in approximately the same direction, then they would all cluster together and the disk would tilt maximally. The direction of tilt would be toward the center of gravity of the points: this is termed the prevalent direction. If the points were scattered equally around the disk, there would be no tilt and there would be no prevalent direction.

In calculating the prevalent direction $\hat{\alpha}_f$ the "average" of the 50 10 ms angles (each α_f) in the frontal plane, reference is made to Fig. A1.1.

For each angle α_f, X_f and Y_f are computed as follows.

$$X_f = \cos \alpha_f, \qquad Y_f = \sin \alpha_f \tag{A1.1}$$

The means are then computed from:

$$\bar{X}_f = \sum X_f / n_f \qquad \bar{Y}_f = \sum Y_f / n_f \tag{A1.2}$$

where n_f is number of angles under study in the frontal plane.

The center of gravity corresponds to the point $(\bar{X}_f, \bar{Y}_f)$ and the distance d_f to the center of gravity is then

$$d_f = \left(\bar{X}_f + \bar{Y}_f\right) \tag{A1.3}$$

The direction α_f toward the center of gravity is calculated from

$$\cos \hat{\alpha}_f = \overline{X}_f / d_f \quad \text{or} \quad \sin \hat{\alpha}_f = \overline{Y}_f / d_f \tag{A1.4}$$

where d_f is termed the precision. If it is zero, then there is no prevalent direction. If it is 1.0, then *all* the individual measurements are the same. The higher the precision *d*, the more the clustering; the lower the precision d, the more the scatter.

In order to determine whether a calculated prevalent direction can be trusted, that is, whether a true prevalent direction actually exists, a χ^2 value can be calculated where:

$$\chi_f^2 = 2n_f d_f^2 \tag{A1.5}$$

Values of χ^2 greater than 5.99 are significant at the 5% level, and values of χ^2 greater than 9.21 are significant at the 1% level.

For Table A1.80, d_f is not high (0.41), so that there is little cluster of the $\hat{\alpha}_f$. However, the prevalent direction of 7° can be trusted, since the $\chi_f^2 = 16.4$. For the sagittal and horizontal planes, the values of χ^2 are extremely high at 90.6 and 91.6 so that the high precisions $d_s = 0.95$ and $d_b = 0.96$ (and thus high cluster) can be very reliably trusted. (To determine whether a particular measured angle α is likely to be within the accepted normal range, it is only necessary to determine whether the angle is between the p_5 and p_{95} for the normal population.)

For spatial data, a methodology has been developed similar to that of the above planar data. In this case, consider that there exists a sample of spatial vectors with coordinates (X, Y, Z) and that it is desired to determine an "average" spatial direction for n measurements. Imagine a sphere placed in the surface of a liquid. If the *n* measurements cluster about some direction, then the sphere will rotate in the liquid until the center of gravity of the *n* measurements points downward. This is the spatial prevalent direction (Fig. A1.2).

As before, the distance from the center of the sphere to the center of gravity $(\overline{X}, \overline{Y}, \overline{Z})$ is a measure of how much the observations cluster, and is called the *spatial precision*. The center of gravity $(\overline{X}, \overline{Y}, \overline{Z})$ can also be expressed in spherical coordinates $(d, \bar{\alpha}, \bar{\beta})$ where $\bar{\alpha}$ is the longitude or angular deviation from the left in the horizontal plane (0–360°) and $\bar{\beta}$ is the colatitude or angular deviation from the superior (0–180°). (The spherical α is identical to the planar α_h.) The spatial prevalent direction is $(\hat{\alpha}, \hat{\beta})$ and can be determined uniquely.

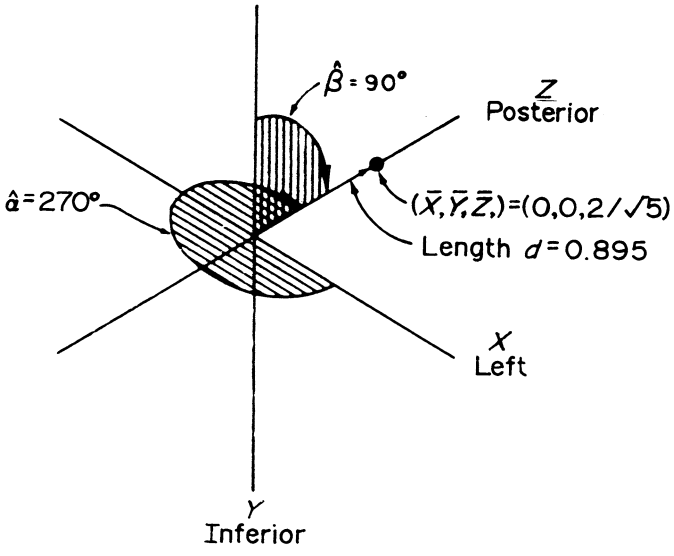

Figure A1.2

An example of the spatial prevalent direction expressed in spherical and Cartesian coordinates.

Table A1.81

Segment of spatial data for the same 50 premature babies tabulated in Table A1.80

Age (h)	Timed vector (ms)	X	Y	Z	d	$\widehat{\alpha}$ (°)	β (°)	χ^2	n
24	10	0.122	0.045	-0.910	0.920	82	93	127.1	50

A χ^2 can be calculated to test whether the clustering about the spatial prevalent direction can be trusted. Values of χ^2 greater than 7.81 are significant at the 5% level and values of χ^2 larger than 11.34 are significant at the 1% level. For further details and the methodology (with equations) for calculation of the above, the reader is referred to an original paper and a recent summary [14].

Table A1.81 is a segment of spatial data for the same 50 premature babies given in Table A1.80.

The d and χ^2 are both very high, consistent with the high d for the horizontal and sagittal planes, despite the low d for the frontal plane. The α of 82° is actually the $\tilde{\alpha}_h$. The $\widehat{\beta}$ of 93° has no corollary in the planar directions. However, from these spatial data, all the planar data can be calculated.

For detailed research (as well as descriptive) purposes, this methodology has been very satisfactory. As with linear statistics, for example, it is frequently necessary to determine whether two different samples of directional measurements are from the same or different populations. The necessary methodology is detailed in the appendix to [9].

References

1. Thomas, C., Electrocardiographic measurement system response, in *Pediatric Electrocardiography*, J. Liebman, R. Plonsey, and P. Gillette, Editors. Baltimore: Williams and Wilkins, 1982, Chap. 5, pp. 40–59.
2. Liebman, J. and R. Plonsey, Electrocardiography, in *Moss' Heart Disease in Infants, Children and Adolescents*, H. Adams and G.C. Emmanouillides, Editors. Baltimore: Williams and Wilkins, 1983, Chap. 3.
3. Liebman, J., Tables of normal standards, in *Pediatric Cardiology*, J. Liebman, R. Plonsey, and P. Gillette, Editors. Baltimore: Williams and Wilkins, 1982, Chap. 8, pp. 82–133.
4. Pipberger, H.V., M.J. Goldman, D. Littman, F.P. Murphy, J. Cosma, and J.R. Snyder, Correlations of the orthogonal electrocardiogram and vectorcardiogram with constitutional variables in 518 normal men. *Circulation*, 1967; **35**: 536.
5. Sreenivasan, V.V, B.J. Fisher, J. Liebman, and T.D. Downs, A longitudinal study of the standard electrocardiogram in the healthy premature infant during the first year of life. *Am. J. Cardiol.*, 1973;**31**: 57.
6. Liebman, J., H.C. Romberg, T.D. Downs, and R. Agusti, The Frank QRS vectorcardiogram in the premature infant, in *Vectorcardiography, 1965*, I. Hoffman and R.C. Taymore, Editors. Amsterdam: North-Holland, 1966.
7. Hugenholtz, P.C. and J. Liebman, The orthogonal electrocardiogram in 100 normal children (Frank system), with some comparative data recorded by the cube system. *Circulation*, 1962;**26**: 891.
8. Liebman, J., C. Doershuk, C. Rapp, and L. Matthews, The vectorcardiogram in cycstic fibrosis: diagnostic significance and correlation with pulmonary function tests. *Circulation*, 1967;**32**: 552.
9. Downs, T.D., J. Liebman, R. Agusti, and H.C. Romberg, The statistical treatment of angular data in vectocardiography, in *Vectorcardiography, 1965*, I. Hoffman and R.C. Traymore, Editors. Amsterdam: North-Holland, 1966, p. 272.
10. Downs, T.D. and J. Liebman, Statistical methods for vectorcardiographic directions. *IEEE Trans. Biomed. Eng.*, 1969;**16**: 87.
11. Stephens, M.A., *The Statistics of Directions. The Von Mises and Fisher Distributions*, PhD thesis. Tornto: University of Toronto, 1962.
12. Downs, T.D., *The Von Mises Distribution: Derived Distributions Regression Theory, and Some Applications to Meterological Problems*, PhD thesis. Ann Arbor: University of Michigan, 1965.
13. Downs, T.D., Some relationships amont the von Mises distributions of different dimensions. *Biometrika*, 1966;**53**: 269.
14. Liebman, J., Statistics related to electrocardiographic interpretation, in *Pediatric Electrocardiography*, J. Liebman, R. Plonsey, and P. Gillete, Editors. Baltimore: Williams and Wilkins, 1982, Chap. 7, pp. 76–81.

Appendix 2: Paediatric Normal Limits

P. W. Macfarlane, A. van Oosterom, O. Pahlm, P. Kligfield, M. Janse, J. Camm (eds.), *Comprehensive Electrocardiology*, DOI 10.1007/978-1-84882-046-3_A2

A2.1 Normal Limits of the Paediatric 12-Lead ECG

This appendix is based on a series of 1,784 ECGs collected from neonates, infants and children in Glasgow, Scotland in the late 1980s. Some outline information was previously published [1, 2] but the detailed normal limits as presented in this chapter have never previously been published. Lead V_{4R} has been recorded to the exclusion of lead V_3. Precordial leads are therefore presented in the sequence V_1, V_2, V_{4R}, V_4, V_5, V_6.

One of the significant aspects of this data is the availability of ECGs from over 500 neonates from birth to 7 days of life. Nowadays, new mothers tend to be discharged from hospital within 24–48 h and so the difficulty of collecting such a database is significantly increased.

The standard presentation of mean together with standard deviation and 96 percentile range has been used throughout. (Tables A2.1–A2.24) With small numbers in some groups this leads to an irregular upper limit of normal for some measures but in practice, continuous equations for normal limits can be developed (see Chap. 13).

Table A2.1

Durations (in milliseconds) in Caucasian children: lead I

Age-group	Q duration	S duration	R duration	R′ duration
<24 h	36 ± 17	16 ± 4	29 ± 4	
	6 → 62	10 → 23	22 → 40	
	n = 10	*n* = 35	*n* = 35	
<1 day	33 ± 15	17 ± 7	29 ± 4	
	9 → 52	6 → 25	22 → 40	
	n = 36	*n* = 112	*n* = 110	
<2 days	29 ± 17	17 ± 5	28 ± 5	24
	8 → 56	6 → 26	19 → 38	24 → 24
	n = 34	*n* = 99	*n* = 99	*n* = 1
<3 days	30 ± 16	17 ± 5	28 ± 5	30
	8 → 56	7 → 28	17 → 38	30 → 30
	n = 41	*n* = 80	*n* = 79	*n* = 1
<1 week	23 ± 17	16 ± 5	29 ± 6	17
	8 → 56	5 → 27	20 → 43	17 → 17
	n = 38	*n* = 104	*n* = 104	*n* = 1
<1 month	16 ± 15	18 ± 5	26 ± 6	
	5 → 52	11 → 32	17 → 43	
	n = 14	*n* = 43	*n* = 43	
<3 months	11 ± 5	22 ± 6	24 ± 6	24
	6 → 30	10 → 34	13 → 34	24 → 24
	n = 34	*n* = 66	*n* = 65	*n* = 1
<6 months	12 ± 4	24 ± 5	25 ± 6	
	5 → 18	17 → 41	14 → 35	
	n = 21	*n* = 50	*n* = 46	
<1 year	12 ± 3	24 ± 5	24 ± 7	33
	8 → 19	14 → 38	14 → 42	33 → 33
	n = 40	*n* = 73	*n* = 70	*n* = 1
1–2 years	13 ± 4	27 ± 7	24 ± 7	24 ± 2
	5 → 25	16 → 46	10 → 39	22 → 25
	n = 69	*n* = 111	*n* = 95	*n* = 2
3–4 years	14 ± 4	30 ± 7	28 ± 8	
	7 → 21	20 → 51	14 → 45	
	n = 77	*n* = 141	*n* = 109	

Table A2.1 (Continued)

Age-group	Q duration	S duration	R duration	R′ duration
5–6 years	14 ± 5	31 ± 6	27 ± 8	
	6 → 40	21 → 46	13 → 44	
	n = 71	*n* = 155	*n* = 136	
7–8 years	13 ± 5	32 ± 8	27 ± 8	10
	7 → 21	21 → 54	14 → 45	10 → 10
	n = 80	*n* = 141	*n* = 114	*n* = 1
9–10 years	13 ± 4	36 ± 9	27 ± 9	17 ± 5
	7 → 21	24 → 64	6 → 45	13 → 22
	n = 49	*n* = 115	*n* = 92	*n* = 3
11–12 years	14 ± 4	37 ± 7	29 ± 9	
	8 → 29	24 → 55	14 → 50	
	n = 62	*n* = 119	*n* = 90	
13–14 years	15 ± 4	39 ± 8	28 ± 10	23 ± 6
	7 → 27	27 → 63	12 → 55	19 → 27
	n = 62	*n* = 141	*n* = 113	*n* = 2
15–16 years	15 ± 5	39 ± 9	30 ± 11	
	8 → 29	27 → 63	11 → 61	
	n = 46	*n* = 92	*n* = 71	
17–18 years	32			
	32 → 32			
	n = 1			

Table A2.2

Durations (in milliseconds) in Caucasian children: lead II

Age-group	Q duration	S duration	R duration	R′ duration
<24 h	18 ± 11	21 ± 8	18 ± 5	
	9 → 68	9 → 39	12 → 35	
	n = 41	*n* = 41	*n* = 22	
<1 day	16 ± 5	21 ± 9	19 ± 6	19 ± 13
	7 → 24	7 → 41	10 → 39	5 → 38
	n = 132	*n* = 136	*n* = 71	*n* = 5
<2 days	16 ± 5	21 ± 9	19 ± 7	18 ± 9
	9 → 38	7 → 44	10 → 45	12 → 28
	n = 106	*n* = 116	*n* = 69	*n* = 3
<3 days	16 ± 6	22 ± 12	19 ± 6	23 ± 12
	10 → 38	7 → 43	7 → 32	12 → 36
	n = 102	*n* = 105	*n* = 56	*n* = 3
<1 week	17 ± 6	19 ± 6	20 ± 7	15 ± 0
	9 → 44	7 → 35	6 → 37	15 → 15
	n = 115	*n* = 114	*n* = 75	*n* = 2

Table A2.2 (Continued)

Age-group	Q duration	S duration	R duration	R′ duration
<1 month	16 ± 3	21 ± 6	19 ± 6	24
	11 → 23	9 → 39	12 → 32	24 → 24
	n = 41	*n* = 45	*n* = 28	*n* = 1
<3 months	16 ± 3	25 ± 7	17 ± 4	26 ± 0
	12 → 24	11 → 45	12 → 26	26 → 26
	n = 58	*n* = 67	*n* = 46	*n* = 2
<6 months	16 ± 5	27 ± 6	19 ± 6	19 ± 6
	6 → 24	19 → 38	13 → 34	15 → 23
	n = 40	*n* = 49	*n* = 32	*n* = 2
<1 year	14 ± 5	29 ± 7	21 ± 6	36
	6 → 26	18 → 54	12 → 34	36 → 36
	n = 54	*n* = 73	*n* = 52	*n* = 1
1–2 years	16 ± 4	32 ± 9	23 ± 7	21 ± 7
	8 → 26	21 → 56	12 → 37	13 → 26
	n = 79	*n* = 111	*n* = 74	*n* = 3
3–4 years	16 ± 4	34 ± 10	24 ± 9	17 ± 4
	7 → 23	23 → 57	8 → 41	14 → 21
	n = 106	*n* = 141	*n* = 98	*n* = 3
5–6 years	15 ± 4	36 ± 9	23 ± 8	24
	7 → 22	24 → 60	12 → 43	24 → 24
	n = 118	*n* = 155	*n* = 114	*n* = 1
7–8 years	15 ± 6	37 ± 8	25 ± 9	18
	7 → 24	26 → 61	13 → 46	18 → 18
	n = 94	*n* = 141	*n* = 115	*n* = 1
9–10 years	15 ± 4	40 ± 9	23 ± 10	17 ± 5
	7 → 21	26 → 64	7 → 47	14 → 23
	n = 86	*n* = 115	*n* = 84	*n* = 3
11–12 years	14 ± 5	43 ± 11	25 ± 9	17 ± 1
	7 → 26	29 → 78	7 → 45	16 → 18
	n = 83	*n* = 119	*n* = 87	*n* = 3
13–14 years	14 ± 4	43 ± 11	26 ± 10	13 ± 4
	7 → 25	30 → 75	9 → 50	7 → 17
	n = 100	*n* = 141	*n* = 111	*n* = 5
15–16 years	16 ± 6	45 ± 12	28 ± 11	16
	7 → 37	29 → 76	11 → 53	16 → 16
	n = 60	*n* = 92	*n* = 67	*n* = 1
17–18 years	15	22		
	15 → 15	22 → 22		
	n = 1	*n* = 1		

Table A2.3

Durations (in milliseconds) in Caucasian children: lead III

Age-group	Q duration	S duration	R duration	R′ duration
<24 h	17 ± 3	28 ± 7	18 ± 4	12
	12 → 23	15 → 41	12 → 21	12 → 12
	n = 41	*n* = 43	*n* = 4	*n* = 1
<1 day	18 ± 3	28 ± 8	15 ± 3	32 ± 6
	13 → 23	12 → 44	11 → 21	27 → 39
	n = 131	*n* = 138	*n* = 32	*n* = 3
<2 days	17 ± 3	27 ± 8	15 ± 5	16 ± 7
	9 → 24	7 → 44	7 → 32	9 → 25
	n = 110	*n* = 119	*n* = 32	*n* = 5
<3 days	17 ± 3	28 ± 12	15 ± 3	20 ± 3
	10 → 25	8 → 56	8 → 22	15 → 23
	n = 101	*n* = 106	*n* = 22	*n* = 6
<1 week	17 ± 3	27 ± 8	16 ± 4	14 ± 6
	10 → 24	8 → 43	12 → 31	9 → 20
	n = 115	*n* = 117	*n* = 32	*n* = 3
<1 month	19 ± 4	28 ± 9	15 ± 4	26 ± 7
	13 → 28	9 → 54	8 → 22	21 → 31
	n = 41	*n* = 45	*n* = 11	*n* = 2
<3 months	20 ± 3	27 ± 8	17 ± 5	24 ± 5
	13 → 28	8 → 43	10 → 32	18 → 30
	n = 59	*n* = 67	*n* = 17	*n* = 7
<6 months	22 ± 4	25 ± 9	17 ± 7	23 ± 5
	14 → 30	6 → 42	8 → 41	14 → 31
	n = 38	*n* = 50	*n* = 20	*n* = 9
<1 year	21 ± 4	23 ± 9	16 ± 6	22 ± 10
	14 → 30	5 → 38	8 → 39	5 → 53
	n = 47	*n* = 73	*n* = 35	*n* = 23
1–2 years	21 ± 6	25 ± 11	20 ± 11	20 ± 8
	9 → 54	7 → 54	8 → 63	8 → 39
	n = 68	*n* = 110	*n* = 63	*n* = 33
3–4 years	21 ± 6	31 ± 13	22 ± 12	24 ± 9
	6 → 32	6 → 64	6 → 58	9 → 44
	n = 94	*n* = 140	*n* = 79	*n* = 23
5–6 years	18 ± 5	33 ± 13	19 ± 10	26 ± 7
	5 → 27	6 → 60	6 → 49	13 → 43
	n = 106	*n* = 155	*n* = 84	*n* = 22
7–8 years	19 ± 6	35 ± 13	24 ± 11	28 ± 14
	8 → 28	7 → 62	7 → 53	8 → 48
	n = 82	*n* = 141	*n* = 94	*n* = 19
9–10 years	19 ± 4	39 ± 14	21 ± 11	23 ± 12
	9 → 28	13 → 72	5 → 60	5 → 47
	n = 78	*n* = 115	*n* = 70	*n* = 15

Table A2.3 (Continued)

Age-group	Q duration	S duration	R duration	R′ duration
11–12 years	18 ± 6	40 ± 16	24 ± 12	23 ± 12
	7 → 32	7 → 80	5 → 51	5 → 45
	n = 75	*n* = 119	*n* = 74	*n* = 14
13–14 years	19 ± 6	41 ± 17	26 ± 13	26 ± 17
	8 → 31	9 → 79	6 → 57	5 → 71
	n = 88	*n* = 141	*n* = 93	*n* = 21
15–16 years	19 ± 6	44 ± 17	28 ± 14	28 ± 14
	9 → 37	8 → 82	6 → 67	11 → 48
	n = 55	*n* = 92	*n* = 55	*n* = 8
17–18 years	14	17		
	14 → 14	17 → 17		
	n = 1	*n* = 1		

Table A2.4

Durations (in milliseconds) in Caucasian children: lead aVR

Age-group	Q duration	S duration	R duration	R′ duration
<24 h	17 ± 7	22 ± 13	16 ± 6	21 ± 7
	8 → 30	8 → 68	6 → 31	11 → 31
	n = 15	*n* = 42	*n* = 24	*n* = 15
<1 day	20 ± 6	22 ± 12	15 ± 7	19 ± 6
	8 → 35	8 → 50	6 → 40	0 → 33
	n = 46	*n* = 135	*n* = 73	*n* = 57
<2 days	21 ± 6	19 ± 10	14 ± 5	22 ± 6
	13 → 38	7 → 46	5 → 30	11 → 42
	n = 35	*n* = 117	*n* = 72	*n* = 62
<3 days	20 ± 6	20 ± 11	15 ± 6	20 ± 7
	8 → 33	7 → 48	6 → 35	11 → 32
	n = 26	*n* = 105	*n* = 67	*n* = 51
<1 week	18 ± 7	19 ± 11	14 ± 4	21 ± 5
	10 → 34	8 → 56	5 → 22	12 → 33
	n = 20	*n* = 116	*n* = 86	*n* = 80
<1 month	22 ± 3	15 ± 7	16 ± 4	21 ± 6
	17 → 27	8 → 42	8 → 26	13 → 37
	n = 8	*n* = 45	*n* = 36	*n* = 33
<3 months	26 ± 7	14 ± 5	21 ± 4	20 ± 5
	11 → 41	5 → 29	14 → 34	12 → 28
	n = 13	*n* = 67	*n* = 55	*n* = 48
<6 months	26 ± 4	16 ± 6	24 ± 3	21 ± 5
	18 → 31	6 → 33	20 → 34	13 → 32
	n = 16	*n* = 50	*n* = 34	*n* = 27
<1 year	28 ± 5	16 ± 8	26 ± 6	21 ± 6
	11 → 37	6 → 36	17 → 46	12 → 38
	n = 25	*n* = 72	*n* = 49	*n* = 37

Table A2.4 (Continued)

Age-group	Q duration	S duration	R duration	R′ duration
1–2 years	29 ± 7	17 ± 7	28 ± 6	22 ± 8
	11 → 46	7 → 35	19 → 45	8 → 38
	n = 33	*n* = 107	*n* = 80	*n* = 56
3–4 years	35 ± 8	17 ± 7	31 ± 6	24 ± 8
	24 → 72	8 → 38	21 → 51	12 → 43
	n = 39	*n* = 133	*n* = 102	*n* = 78
5–6 years	35 ± 7	17 ± 7	32 ± 5	23 ± 8
	27 → 68	7 → 36	24 → 48	12 → 44
	n = 52	*n* = 148	*n* = 103	*n* = 79
7–8 years	35 ± 4	18 ± 8	34 ± 7	25 ± 8
	29 → 46	8 → 44	24 → 51	12 → 40
	n = 45	*n* = 140	*n* = 96	*n* = 75
9–10 years	37 ± 5	17 ± 8	36 ± 7	23 ± 9
	29 → 48	7 → 41	27 → 62	7 → 49
	n = 43	*n* = 108	*n* = 72	*n* = 55
11–12 years	39 ± 7	19 ± 9	39 ± 8	25 ± 8
	28 → 60	8 → 46	28 → 67	13 → 44
	n = 48	*n* = 112	*n* = 71	*n* = 50
13–14 years	41 ± 8	19 ± 9	39 ± 7	25 ± 9
	33 → 74	8 → 43	29 → 62	12 → 52
	n = 59	*n* = 135	*n* = 83	*n* = 69
15–16 years	44 ± 9	22 ± 10	39 ± 6	27 ± 9
	33 → 68	9 → 48	30 → 60	15 → 50
	n = 41	*n* = 82	*n* = 50	*n* = 37
17–18 years		18	7	
		18 → 18	7 → 7	
		n = 1	*n* = 1	

Table A2.5

Durations (in milliseconds) in Caucasian children: lead aVL

Age-group	Q duration	S duration	R duration	R′ duration
<24 h	24 ± 17	16 ± 4	31 ± 4	
	9 → 40	10 → 22	23 → 42	
	n = 4	*n* = 41	*n* = 41	
<1 day	25 ± 18	17 ± 4	30 ± 5	13 ± 1
	7 → 54	11 → 23	21 → 41	0 → 13
	n = 8	*n* = 136	*n* = 134	*n* = 2
<2 days	23 ± 16	17 ± 4	30 ± 5	15 ± 4
	7 → 46	9 → 25	19 → 39	12 → 17
	n = 11	*n* = 116	*n* = 114	*n* = 2

Table A2.5 (Continued)

Age-group	Q duration	S duration	R duration	R′ duration
<3 days	20 ± 15	16 ± 4	30 ± 5	21 ± 7
	7 → 52	8 → 25	20 → 44	15 → 28
	n = 12	*n* =102	*n* = 102	*n* = 3
<1 week	16 ± 17	17 ± 4	30 ± 6	13 ± 5
	6 → 56	8 → 26	18 → 42	8 → 22
	n = 9	*n* = 115	*n* = 115	*n* = 6
<1 month	39 ± 27	19 ± 4	28 ± 6	12 ± 0
	9 → 62	11 → 29	16 → 47	12 → 12
	n = 5	*n* = 42	*n* = 42	*n* = 2
<3 months	12 ± 7	21 ± 4	27 ± 6	11 ± 2
	6 → 32	12 → 32	13 → 37	9 → 12
	n = 13	*n* = 66	*n* = 66	*n* = 2
<6 months	11 ± 4	24 ± 6	26 ± 6	20
	6 → 19	13 → 50	17 → 35	20 → 20
	n = 13	*n* = 50	*n* = 48	*n* = 1
<1 year	12 ± 5	22 ± 5	26 ± 7	25 ± 18
	6 → 26	12 → 37	13 → 41	12 → 37
	n = 30	*n* = 73	*n* = 71	*n* = 2
1–2 years	13 ± 5	24 ± 7	25 ± 8	17 ± 5
	6 → 28	14 → 52	8 → 43	13 → 26
	n = 54	*n* = 111	*n* = 98	*n* = 6
3–4 years	15 ± 8	25 ± 9	30 ± 10	19 ± 6
	6 → 40	10 → 49	6 → 48	6 → 33
	n = 60	*n* = 140	*n* = 118	*n* = 15
5–6 years	15 ± 10	23 ± 8	31 ± 11	18 ± 5
	5 → 62	8 → 44	9 → 51	12 → 28
	n = 58	*n* = 154	*n* = 140	*n* = 26
7–8 years	18 ± 10	25 ± 12	30 ± 12	21 ± 6
	6 → 54	10 → 60	6 → 53	12 → 35
	n = 71	*n* = 140	*n* = 115	*n* = 33
9–10 years	21 ± 17	25 ± 10	34 ± 12	21 ± 8
	7 → 76	10 → 57	10 → 60	9 → 44
	n = 37	*n* = 112	*n* = 99	*n* = 24
11–12 years	20 ± 10	27 ± 13	32 ± 14	23 ± 8
	10 → 57	6 → 66	7 → 59	7 → 39
	n = 49	*n* = 117	*n* = 100	*n* = 23
13–14 years	19 ± 11	29 ± 14	34 ± 16	22 ± 9
	6 → 74	9 → 69	6 → 72	7 → 42
	n = 55	*n* = 139	*n* = 118	*n* = 37
15–16 years	24 ± 17	30 ± 14	34 ± 14	22 ± 10
	8 → 78	10 → 63	6 → 65	7 → 45
	n = 41	*n* = 88	*n* = 70	*n* = 19
17–18 years		13	22	
		13 → 13	22 → 22	
		n = 1	*n* = 1	

Table A2.6

Durations (in milliseconds) in Caucasian children: lead aVF

Age-group	Q duration	S duration	R duration	R′ duration
<24 h	16 ± 4	24 ± 8	17 ± 8	
	11 → 24	10 → 41	6 → 37	
	n = 42	*n* = 43	*n* = 14	
<1 day	17 ± 4	25 ± 9	17 ± 5	21 ± 14
	10 → 24	11 → 45	11 → 36	9 → 37
	n = 133	*n* = 137	*n* = 44	*n* = 3
<2 days	17 ± 3	24 ± 8	17 ± 7	15 ± 3
	8 → 23	7 → 39	7 → 46	13 → 19
	n = 110	*n* = 119	*n* = 50	*n* = 3
<3 days	17 ± 4	25 ± 12	18 ± 5	22 ± 10
	10 → 27	5 → 51	10 → 31	15 → 29
	n = 101	*n* = 106	*n* = 36	*n* = 2
<1 week	17 ± 3	22 ± 7	18 ± 7	
	11 → 26	8 → 37	10 → 54	
	n = 116	*n* = 117	*n* = 56	
<1 month	17 ± 3	25 ± 7	17 ± 4	
	8 → 25	13 → 43	12 → 24	
	n = 43	*n* = 45	*n* = 19	
<3 months	17 ± 3	27 ± 8	15 ± 5	25 ± 8
	12 → 23	11 → 50	8 → 26	16 → 36
	n = 57	*n* = 67	*n* = 28	*n* = 6
<6 months	19 ± 4	26 ± 7	17 ± 7	20 ± 3
	11 → 27	8 → 42	8 → 38	16 → 24
	n = 40	*n* = 50	*n* = 26	*n* = 5
< 1 year	18 ± 4	28 ± 9	19 ± 7	26 ± 11
	11 → 28	5 → 58	7 → 36	5 → 36
	n = 50	*n* = 73	*n* = 40	*n* = 7
1–2 years	18 ± 5	30 ± 9	21 ± 9	23 ± 11
	8 → 27	9 → 52	5 → 46	5 → 38
	n = 73	*n* = 111	*n* = 66	*n* = 9
3–4 years	18 ± 4	35 ± 12	22 ± 10	23 ± 6
	11 → 26	8 → 62	6 → 41	10 → 31
	n = 95	*n* = 141	*n* = 85	*n* = 9
5–6 years	16 ± 4	36 ± 10	22 ± 8	29 ± 2
	7 → 24	13 → 62	12 → 43	27 → 31
	n = 114	*n* = 155	*n* = 99	*n* = 3
7–8 years	17 ± 6	38 ± 10	25 ± 10	18 ± 10
	7 → 24	24 → 68	7 → 47	6 → 33
	n = 87	*n* = 141	*n* = 97	*n* = 6
9–10 years	16 ± 4	42 ± 11	24 ± 10	16 ± 3
	7 → 22	25 → 72	9 → 53	13 → 19
	n = 79	*n* = 115	*n* = 74	*n* = 4
11–12 years	16 ± 5	44 ± 12	26 ± 10	10
	6 → 27	28 → 80	12 → 46	10 → 10
	n = 76	*n* = 119	*n* = 77	*n* = 1

Table A2.6 (Continued)

Age-group	Q duration	S duration	R duration	R′ duration
13–14 years	16 ± 5	44 ± 13	28 ± 10	19 ± 6
	8 → 26	29 → 80	9 → 48	13 → 27
	n = 94	*n* = 141	*n* = 96	*n* = 4
15–16 years	17 ± 6	45 ± 13	27 ± 12	44 ± 18
	6 → 38	24 → 76	6 → 53	24 → 57
	n = 57	*n* = 92	*n* = 63	*n* = 3
17–18 years	14	17		
	14 → 14	17 → 17		
	n = 1	*n* = 1		

Table A2.7

Durations (in milliseconds) in Caucasian children: lead V_1

Age-group	Q duration	S duration	R duration	R′ duration
<24 h		30 ± 7	23 ± 6	30
		19 → 44	14 → 36	30 → 30
		n = 43	*n* = 40	*n* = 1
<1 day	9 ± 1	32 ± 7	23 ± 6	
	8 → 10	21 → 52	12 → 35	
	n = 2	*n* = 137	*n* = 124	
<2 days	11 ± 8	33 ± 8	21 ± 6	
	5 → 17	20 → 54	13 → 37	
	n = 2	*n* = 117	*n* = 100	
<3 days	12 ± 6	32 ± 7	22 ± 10	11 ± 5
	8 → 16	20 → 48	12 → 42	7 → 17
	n = 2	*n* = 102	*n* = 93	*n* = 3
<1 week		35 ± 9	20 ± 5	
		23 → 60	12 → 34	
		n = 114	*n* = 99	
<1 month	10	35 ± 8	21 ± 6	
	10 → 10	24 → 62	13 → 36	
	n = 1	*n* = 41	*n* = 37	
<3 months	10 ± 3	33 ± 9	24 ± 8	7 ± 2
	8 → 12	20 → 56	7 → 55	6 → 10
	n = 2	*n* = 62	*n* = 56	*n* = 4
<6 months		31 ± 8	28 ± 9	12 ± 5
		20 → 60	9 → 43	9 → 19
		n = 49	*n* = 48	*n* = 4
<1 year		29 ± 8	29 ± 10	23 ± 11
		15 → 55	8 → 50	9 → 44
		n = 70	*n* = 69	*n* = 10
1–2 years	12 ± 6	28 ± 8	37 ± 9	14 ± 8
	8 → 16	14 → 58	12 → 51	6 → 32
	n = 2	*n* = 107	*n* = 103	*n* = 10
3–4 years	86	25 ± 5	39 ± 12	21 ± 9
	86 → 86	16 → 39	13 → 59	6 → 36
	n = 1	*n* = 135	*n* = 135	*n* = 27

Table A2.7 (Continued)

Age-group	Q duration	S duration	R duration	R′ duration
5–6 years	28 ± 28	25 ± 5	42 ± 11	18 ± 10
	8 → 48	13 → 40	15 → 55	4 → 43
	n = 2	*n* = 146	*n* = 146	*n* = 23
7–8 years		25 ± 4	43 ± 11	22 ± 9
		18 → 34	16 → 59	12 → 49
		n = 135	*n* = 135	*n* = 28
9–10 years		25 ± 4	42 ± 11	23 ± 11
		17 → 38	15 → 61	5 → 45
		n = 108	*n* = 108	*n* = 25
11–12 years		25 ± 5	44 ± 12	24 ± 9
		16 → 37	22 → 65	9 → 46
		n = 104	*n* = 104	*n* = 27
13–14 years	48 ± 36	25 ± 5	47 ± 13	23 ± 14
	8 → 76	13 → 36	18 → 82	6 → 59
	n = 3	*n* = 107	*n* = 107	*n* = 27
15–16 years	39 ± 38	26 ± 5	45 ± 13	28 ± 11
	12 → 66	15 → 37	11 → 67	11 → 49
	n = 2	*n* = 70	*n* = 70	*n* = 17
17–18 years		27	20	
		27 → 27	20 → 20	
		n = 1	*n* = 1	

Table A2.8

Durations (in milliseconds) in Caucasian children: lead V_2

Age-group	Q duration	S duration	R duration	R′ duration
<24 h		26 ± 5	29 ± 6	8!
		19 → 46	19 → 42	8 → 8
		n = 43	*n* = 42	*n* = 1
<1 day	13	26 ± 4	29 ± 5	10
	13 → 13	19 → 32	18 → 41	10 → 10
	n = 1	*n* = 137	*n* = 136	*n* = 1
<2 days	6	27 ± 5	28 ± 5	13
	6 → 6	19 → 45	19 → 48	13 → 13
	n = 1	*n* = 116	*n* = 114	*n* = 1
<3 days	10 ± 5	27 ± 5	27 ± 10	10 ± 4
	4 → 15	18 → 42	16 → 43	7 → 13
	n = 4	*n* = 104	*n* = 104	*n* = 2

Table A2.8 (Continued)

Age-group	Q duration	S duration	R duration	R′ duration
<1 week	10	29 ± 8	26 ± 5	10
	10 → 10	20 → 64	17 → 38	10 → 10
	n = 1	*n* = 114	*n* = 111	*n* = 1
<1 month	9	28 ± 6	26 ± 5	
	9 → 9	23 → 62	18 → 38	
	n = 1	*n* = 42	*n* = 41	
<3 months	8	30 ± 5	28 ± 5	
	8 → 8	22 → 46	19 → 50	
	n = 1	*n* = 63	*n* = 62	
<6 months	7 ± 1	29 ± 4	32 ± 5	
	6 → 8	22 → 42	23 → 40	
	n = 2	*n* = 48	*n* = 48	
<1 year	6	29 ± 6	35 ± 7	21 ± 8
	6 → 6	22 → 66	14 → 51	15 → 26
	n = 1	*n* = 73	*n* = 72	*n* = 2
1–2 years	11 ± 2	28 ± 6	39 ± 7	21 ± 16
	9 → 13	14 → 46	21 → 52	9 → 32
	n = 3	*n* = 106	*n* = 106	*n* = 2
3–4 years	21	27 ± 4	42 ± 8	21 ± 5
	21 → 21	19 → 39	19 → 59	14 → 30
	n = 1	*n* = 140	*n* = 140	*n* = 11
5–6 years	6 ± 3	26 ± 4	44 ± 7	17 ± 8
	4 → 8	18 → 36	26 → 57	5 → 29
	n = 2	*n* = 155	*n* = 155	*n* = 8
7–8 years		27 ± 4	45 ± 8	16 ± 6
		18 → 39	25 → 59	6 → 25
		n = 140	*n* = 140	*n* = 10
9–10 years		27 ± 4	46 ± 9	24 ± 9
		20 → 36	21 → 62	11 → 44
		n = 114	*n* = 114	*n* = 11
11–12 years	6	28 ± 6	47 ± 10	20 ± 10
	6 → 6	18 → 43	22 → 66	4 → 34
	n = 1	*n* = 119	*n* = 119	*n* = 10
13–14 years	43 ± 49	28 ± 6	46 ± 12	22 ± 9
	8 → 78	16 → 40	23 → 71	9 → 38
	n = 2	*n* = 138	*n* = 138	*n* = 29
15–16 years	9	29 ± 6	47 ± 11	23 ± 6
	9 → 9	17 → 40	28 → 69	12 → 34
	n = 1	*n* = 89	*n* = 89	*n* = 13
17–18 years		24	25	
		24 → 24	25 → 25	
		n = 1	*n* = 1	

Table A2.9

Durations (in milliseconds) in Caucasian children: lead V_{4R}

Age-group	Q duration	S duration	R duration	R′ duration
<24 h	11 ± 5	34 ± 6	17 ± 3	
	6 → 18	22 → 50	12 → 28	
	n = 7	*n* = 43	*n* = 29	
<1 day	13 ± 3	34 ± 7	18 ± 4	30
	9 → 18	21 → 50	12 → 29	0 → 30
	n = 14	*n* = 136	*n* = 93	*n* = 1
<2 days	10 ± 4	35 ± 7	17 ± 4	27
	6 → 20	23 → 52	12 → 30	27 → 27
	n = 19	*n* = 116	*n* = 72	*n* = 1
<3 days	10 ± 3	37 ± 8	16 ± 4	34
	6 → 15	24 → 56	12 → 28	34 → 34
	n = 15	*n* = 102	*n* = 52	*n* = 1
<1 week	10 ± 3	38 ± 8	16 ± 4	31
	6 → 16	23 → 56	12 → 35	31 → 31
	n = 15	*n* = 113	*n* = 62	*n* = 1
<1 month	12 ± 3	38 ± 8	17 ± 10	21 ± 3
	8 → 16	15 → 56	6 → 59	18 → 24
	n = 5	*n* = 44	*n* = 24	*n* = 3
<3 months	12 ± 8	36 ± 11	19 ± 7	19 ± 6
	5 → 25	14 → 66	5 → 52	9 → 27
	n = 5	*n* = 65	*n* = 47	*n* = 8
<6 months	18 ± 9	34 ± 11	19 ± 8	15 ± 6
	12 → 28	18 → 53	5 → 37	7 → 26
	n = 3	*n* = 49	*n* = 44	*n* = 9
<1 year	11 ± 3	30 ± 10	23 ± 11	18 ± 8
	6 → 14	16 → 70	6 → 44	7 → 45
	n = 4	*n* = 70	*n* = 66	*n* = 20
1–2 years	14 ± 9	27 ± 9	28 ± 13	15 ± 8
	8 → 33	13 → 54	5 → 53	6 → 34
	n = 7	*n* = 110	*n* = 106	*n* = 26
3–4 years	15 ± 12	25 ± 7	36 ± 13	17 ± 8
	8 → 40	14 → 44	9 → 54	4 → 35
	n = 6	*n* = 137	*n* = 136	*n* = 24
5–6 years	24 ± 28	25 ± 7	40 ± 12	14 ± 7
	5 → 56	15 → 48	11 → 54	5 → 28
	n = 3	*n* = 146	*n* = 145	*n* = 18
7–8 years	11	26 ± 6	43 ± 12	17 ± 10
	11 → 11	16 → 47	10 → 58	5 → 38
	n = 1	*n* = 136	*n* = 134	*n* = 13
9–10 years	12 ± 9	26 ± 8	43 ± 12	16 ± 10
	5 → 25	13 → 52	14 → 63	7 → 35
	n = 4	*n* = 109	*n* = 107	*n* = 10

Table A2.9 (Continued)

Age-group	Q duration	S duration	R duration	R′ duration
11–12 years	33 ± 27	25 ± 7	46 ± 11	21 ± 11
	7 → 64	13 → 43	20 → 64	7 → 40
	n = 5	*n* = 102	*n* = 102	*n* = 10
13–14 years	38 ± 31	26 ± 8	45 ± 14	21 ± 12
	10 → 72	13 → 59	8 → 66	4 → 44
	n = 4	*n* = 109	*n* = 107	*n* = 17
15–16 years	31 ± 33	27 ± 9	45 ± 14	19 ± 9
	7 → 54	12 → 64	9 → 68	5 → 32
	n = 2	*n* = 73	*n* = 71	*n* = 12
17–18 years		28	17	
		28 → 28	17 → 17	
		n = 1	*n* = 1	

Table A2.10

Durations (in milliseconds) in Caucasian children: lead V_4

Age-group	Q duration	S duration	R duration	R′ duration
<24 h	9 ± 2	26 ± 4	26 ± 5	
	6 → 11	18 → 34	18 → 43	
	n = 8	*n* = 43	*n* = 42	
<1 day	9 ± 3	25 ± 5	26 ± 5	
	4 → 13	16 → 35	16 → 38	
	n = 23	*n* = 138	*n* = 137	
<2 days	9 ± 3	26 ± 5	25 ± 6	
	4 → 15	14 → 36	13 → 38	
	n = 20	*n* = 119	*n* = 119	
<3 days	9 ± 3	25 ± 6	23 ± 6	22 ± 8
	5 → 15	13 → 37	8 → 34	17 → 32
	n = 25	*n* = 106	*n* = 104	*n* = 3
<1 week	10 ± 4	24 ± 6	23 ± 7	19
	4 → 33	13 → 39	12 → 40	19 → 19
	n = 57	*n* = 116	*n* = 115	*n* = 1
<1 month	10 ± 3	23 ± 5	24 ± 8	
	4 → 16	16 → 37	15 → 67	
	n = 20	*n* = 45	*n* = 45	
<3 months	11 ± 4	25 ± 7	24 ± 5	
	6 → 21	15 → 52	15 → 38	
	n = 35	*n* = 67	*n* = 65	
<6 months	12 ± 4	27 ± 6	26 ± 6	
	5 → 16	19 → 45	16 → 40	
	n = 20	*n* = 50	*n* = 50	

Table A2.10 (Continued)

Age-group	Q duration	S duration	R duration	R′ duration
<1 year	12 ± 4	27 ± 6	27 ± 8	22
	6 → 20	15 → 43	12 → 49	22 → 22
	n = 27	*n* = 72	*n* = 71	*n* = 1
1–2 years	13 ± 4	28 ± 7	27 ± 8	24 ± 6
	6 → 25	11 → 41	12 → 44	19 → 32
	n = 47	*n* = 110	*n* = 108	*n* = 4
3–4 years	13 ± 4	33 ± 7	28 ± 9	17 ± 5
	7 → 22	21 → 47	10 → 45	14 → 25
	n = 50	*n* = 141	*n* = 134	*n* = 4
5–6 years	12 ± 5	35 ± 7	28 ± 9	16 ± 7
	6 → 32	24 → 49	12 → 47	8 → 27
	n = 56	*n* = 155	*n* = 152	*n* = 5
7–8 years	13 ± 6	36 ± 7	30 ± 9	17 ± 7
	6 → 40	23 → 49	9 → 48	12 → 30
	n = 39	*n* = 141	*n* = 140	*n* = 5
9–10 years	11 ± 5	38 ± 6	29 ± 10	18 ± 7
	4 → 21	27 → 51	10 → 48	10 → 34
	n = 25	*n* = 115	*n* = 111	*n* = 7
11–12 years	13 ± 5	40 ± 8	31 ± 10	15 ± 2
	7 → 26	28 → 63	12 → 51	13 → 16
	n = 26	*n* = 119	*n* = 115	*n* = 2
13–14 years	12 ± 4	42 ± 7	32 ± 9	14
	6 → 18	31 → 52	14 → 54	14 → 14
	n = 26	*n* = 141	*n* = 138	*n* = 1
15–16 years	13 ± 6	42 ± 6	32 ± 11	
	6 → 25	30 → 57	10 → 56	
	n = 17	*n* = 91	*n* = 90	
17–18 years		25	22	
		25 → 25	22 → 22	
		n = 1	*n* = 1	
<24 h	11 ± 3	20 ± 5	24 ± 6	
	4 → 16	29 → 12	16 → 42	
	n = 22	*n* = 43	*n* = 41	
<1 day	11 ± 3	20 ± 6	23 ± 5	
	5 → 17	12 → 37	14 → 37	
	n = 77	*n* = 137	*n* = 134	
<2 days	12 ± 3	21 ± 6	24 ± 6	
	7 → 20	12 → 34	13 → 36	
	n = 59	*n* = 118	*n* = 116	

Table A2.11

Durations (in milliseconds) in Caucasian children: lead V_5

Age-group	Q duration	S duration	R duration	R′ duration
<3 days	11 ± 3	20 ± 6	22 ± 5	57 ± 24
	5 → 15	12 → 31	13 → 32	40 → 74
	n = 59	*n* = 106	*n* = 104	*n* = 2
<1 week	12 ± 4	18 ± 4	23 ± 7	
	6 → 18	11 → 35	12 → 39	
	n = 96	*n* = 116	*n* = 109	
<1 month	13 ± 3	19 ± 5	22 ± 6	30 ± 23
	8 → 23	14 → 38	13 → 40	14 → 46
	n = 36	*n* = 44	*n* = 42	*n* = 2
<3 months	13 ± 3	21 ± 5	22 ± 6	20
	5 → 23	14 → 36	12 → 33	20 → 20
	n = 56	*n* = 66	*n* = 65	*n* = 1
<6 months	14 ± 4	22 ± 4	23 ± 6	23
	8 → 24	15 → 31	12 → 38	23 → 23
	n = 38	*n* = 48	*n* = 46	*n* = 1
<1 year	14 ± 4	23 ± 6	24 ± 7	36 ± 18
	7 → 26	13 → 44	12 → 42	23 → 48
	n = 58	*n* = 73	*n* = 67	*n* = 2
1–2 years	15 ± 5	25 ± 7	24 ± 8	28 ± 15
	8 → 26	9 → 46	10 → 38	9 → 50
	n = 83	*n* = 111	*n* = 100	*n* = 5
3–4 years	15 ± 4	29 ± 7	25 ± 9	16 ± 2
	8 → 24	21 → 53	5 → 45	13 → 17
	n = 121	*n* = 140	*n* = 120	*n* = 4
5–6 years	14 ± 4	30 ± 6	25 ± 8	16 ± 9
	7 → 23	23 → 54	11 → 43	9 → 35
	n = 125	*n* = 155	*n* = 142	*n* = 7
7–8 years	15 ± 5	31 ± 6	27 ± 8	14 ± 3
	6 → 26	23 → 45	12 → 44	12 → 18
	n = 118	*n* = 141	*n* = 134	*n* = 3
9–10 years	15 ± 4	33 ± 8	25 ± 10	17 ± 5
	6 → 24	22 → 64	7 → 44	13 → 32
	n = 97	*n* = 115	*n* = 106	*n* = 10
11–12 years	15 ± 5	36 ± 8	26 ± 10	16 ± 2
	6 → 27	25 → 63	10 → 50	14 → 18
	n = 91	*n* = 118	*n* = 106	*n* = 4
13–14 years	16 ± 5	37 ± 7	28 ± 9	17 ± 6
	8 → 26	27 → 52	10 → 47	12 → 29
	n = 87	*n* = 140	*n* = 135	*n* = 6
15–16 years	16 ± 6	39 ± 8	29 ± 12	19 ± 4
	8 → 34	28 → 64	6 → 59	15 → 22
	n = 50	*n* = 92	*n* = 86	*n* = 3
17–18 years	12	15	17	
	12 → 12	15 → 15	17 → 17	
	n = 1	*n* = 1	*n* = 1	

Table A2.12

Durations (in milliseconds) in Caucasian children: lead V_6

Age-group	Q duration	S duration	R duration	R′ duration
<24 h	16 ± 10	18 ± 5	22 ± 8	
	8 → 60	12 → 31	12 → 45	
	n = 36	*n* = 40	*n* = 32	
<1 day	15 ± 8	18 ± 7	22 ± 6	18 ± 2
	6 → 50	7 → 39	9 → 40	0 → 19
	n = 100	*n* = 127	*n* = 104	*n* = 3
<2 days	14 ± 8	17 ± 6	22 ± 6	16 ± 4
	6 → 48	8 → 42	12 → 37	13 → 20
	n = 85	*n* = 111	*n* = 100	*n* = 3
<3 days	14 ± 8	18 ± 6	21 ± 6	21 ± 7
	6 → 48	9 → 34	10 → 32	14 → 27
	n = 81	*n* = 99	*n* = 79	*n* = 3
<1 week	15 ± 6	17 ± 5	21 ± 7	21 ± 4
	7 → 46	10 → 35	12 → 38	18 → 24
	n = 99	*n* = 110	*n* = 87	*n* = 2
<1 month	14 ± 3	18 ± 4	20 ± 6	22 ± 1
	9 → 23	10 → 27	12 → 37	21 → 22
	n = 38	*n* = 45	*n* = 40	*n* = 2
<3 months	14 ± 3	22 ± 5	20 ± 5	
	8 → 26	16 → 35	12 → 31	
	n = 61	*n* = 65	*n* = 53	
<6 months	15 ± 4	22 ± 4	20 ± 7	30 ± 1
	8 → 25	13 → 36	12 → 38	29 → 31
	n = 42	*n* = 49	*n* = 41	*n* = 2
<1 year	15 ± 4	24 ± 9	21 ± 7	24 ± 6
	7 → 23	8 → 64	10 → 38	18 → 33
	n = 59	*n* = 73	*n* = 60	*n* = 5
1–2 years	17 ± 5	27 ± 7	21 ± 7	30 ± 10
	7 → 27	11 → 50	11 → 34	18 → 43
	n = 91	*n* = 110	*n* = 76	*n* = 5
3–4 years	16 ± 4	29 ± 7	24 ± 8	29 ± 16
	8 → 25	19 → 52	12 → 44	16 → 48
	n = 131	*n* = 140	*n* = 99	*n* = 4
5–6 years	16 ± 4	31 ± 6	23 ± 7	13
	8 → 22	23 → 48	12 → 42	13 → 13
	n = 139	*n* = 154	*n* = 119	*n* = 1
7–8 years	16 ± 4	31 ± 6	24 ± 8	26 ± 16
	8 → 24	23 → 47	12 → 43	15 → 37
	n = 129	*n* = 140	*n* = 119	*n* = 2
9–10 years	16 ± 4	34 ± 8	23 ± 9	17 ± 1
	8 → 24	25 → 64	6 → 42	15 → 18
	n = 107	*n* = 115	*n* = 88	*n* = 4
11–12 years	16 ± 4	37 ± 8	25 ± 9	9 ± 2
	8 → 29	27 → 64	13 → 47	7 → 10
	n = 104	*n* = 117	*n* = 86	*n* = 2

Table A2.12 (Continued)

Age-group	Q duration	S duration	R duration	R′ duration
13–14 years	16 ± 5	37 ± 6	25 ± 9	15 ± 5
	8 → 29	29 → 58	5 → 44	12 → 21
	n = 124	*n* = 140	*n* = 122	*n* = 3
15–16 years	17 ± 5	40 ± 10	28 ± 10	38
	9 → 34	27 → 76	13 → 59	38 → 38
	n = 58	*n* = 88	*n* = 72	*n* = 1
17–18 years	15	16		
	15 → 15	16 → 16		
	n = 1	*n* = 1		

Table A2.13

Amplitudes (in μV) in Caucasian children: lead I

Age-group	P+	P−	Q	R	S	STj	T+	T−
<24 h	80 ± 27	−59 ± 0	−428 ± 311	208 ± 181	−742 ± 312	10 ± 18	84 ± 51	−70 ± 95
	37 → 136	−59 → −59	−903 → −36	30 → 906	−1,586 → −296	37 → −42	23 → 231	−378 → −12
	n = 43	*n* = 1	*n* = 10	*n* = 35	*n* = 35	*n* = 43	*n* = 41	*n* = 14
<1 day	81 ± 27	−42 ± 49	−427 ± 315	206 ± 161	−711 ± 227	18 ± 21	93 ± 50	−57 ± 38
	23 → 142	−137 → −11	−1,199 → −27	25 → 595	−1,392 → −347	−15 → 62	18 → 219	−158 → −12
	n = 138	*n* = 6	*n* = 36	*n* = 112	*n* = 110	*n* = 138	*n* = 133	*n* = 34
<2 days	79 ± 25	−26 ± 10	−333 ± 251	214 ± 145	−687 ± 202	22 ± 26	116 ± 57	−39 ± 25
	43 → 146	−37 → −17	−752 → −29	30 → 599	−1,171 → −335	−34 → 76	31 → 261	−95 → −12
	n = 119	*n* = 3	*n* = 34	*n* = 99	*n* = 99	*n* = 119	*n* = 119	*n* = 12
<3 days	82 ± 33	−22 ± 12	−303 ± 207	210 ± 141	−658 ± 239	28 ± 28	125 ± 54	−49 ± 30
	39 → 147	−41 → −8	−674 → −34	54 → 631	−1,193 → −240	−10 → 125	38 → 291	−101 → −7
	n = 106	*n* = 8	*n* = 41	*n* = 80	*n* = 79	*n* = 106	*n* = 106	*n* = 9
<1 week	83 ± 28	−25 ± 12	−244 ± 275	191 ± 138	−643 ± 198	37 ± 31	151 ± 58	−69 ± 49
	27 → 141	−43 → −10	−952 → −29	32 → 615	−1,185 → −351	−4 → 139	35 → 276	−138 → −22
	n = 116	*n* = 7	*n* = 38	*n* = 104	*n* = 104	*n* = 117	*n* = 117	*n* = 5
<1 month	89 ± 30	−37 ± 18	−141 ± 206	282 ± 199	−556 ± 197	37 ± 25	209 ± 76	−28 ± 3
	33 → 176	−48 → −16	−743 → −24	49 → 759	−1,043 → −215	−7 → 93	68 → 400	−30 → −26
	n = 45	*n* = 3	*n* = 14	*n* = 43	*n* = 43	*n* = 45	*n* = 45	*n* = 2
<3 months	96 ± 27		−78 ± 62	626 ± 291	−474 ± 185	28 ± 35	257 ± 89	−64 ± 47
	44 → 168		−350 → −23	56 → 1,270	−870 → −55	−98 → 101	64 → 457	−117 → −28
	n = 67		*n* = 34	*n* = 66	*n* = 65	*n* = 69	*n* = 66	*n* = 3
<6 months	102 ± 27	−23 ± 0	−107 ± 74	807 ± 230	−467 ± 206	34 ± 23	288 ± 85	
	48 → 197	−23 → −23	−336 → −22	321 → 1,307	−1,019 → −147	−12 → 85	159 → 539	
	n = 50	*n* = 1	*n* = 21	*n* = 50	*n* = 46	*n* = 50	*n* = 50	

Table A2.13 (Continued)

Age-group	P+	P–	Q	R	S	STj	T+	T–
<1 year	112 ± 31	−53 ± 24	−107 ± 71	870 ± 330	−374 ± 206	35 ± 31	310 ± 92	−47 ± 23
	41 → 188	−95 → −31	−334 → −33	339 → 1,714	−1, 054 → −94	−36 → 139	89→524	−63 → −31
	n = 73	*n* = 5	*n* = 40	*n* = 73	*n* = 70	*n* = 74	*n* = 73	*n* = 2
1–2 years	112 ± 28	−75 ± 49	−130 ± 96	821 ± 364	−311 ± 161	25 ± 33	330 ± 120	−50 ± 0
	61 → 197	−128 → −23	−501 → −22	238 → 1,838	−695 → −71	−25 → 146	112 → 680	−50 → −50
	n = 110	*n* = 5	*n* = 69	*n* = 111	*n* = 95	*n* = 116	*n* = 111	*n* = 1
3–4 years	99 ± 21	−28 ± 8	−103 ± 62	684 ± 261	−278 ± 141	14 ± 19	281 ± 87	−89 ± 50
	59 → 145	−34 → −19	−280 → −28	252 → 1,248	−614 → −67	−22 → 68	130 → 463	−136→−37
	n = 141	*n* = 3	*n* = 77	*n* = 141	*n* = 109	*n* = 141	*n* = 141	*n* = 3
5–6 years	97 ± 20	−59 ± 26	−89 ± 55	624 ± 238	−244 ± 127	11 ± 24	276 ± 86	−62 ± 40
	58 → 141	−77 → −40	−263 → −22	185 → 1,259	−581→−64	−60 →71	123 → 433	−94→−17
	n = 154	*n* = 2	*n* = 71	*n* = 155	*n* = 136	*n* = 155	*n* = 154	*n* = 3
7–8 years	95 ± 21	−45 ± 42	−80 ± 61	592 ± 278	−220 ± 140	11 ± 22	279 ± 88	−86 ± 64
	60 → 140	−74 → −15	−203 → −21	187 → 1,354	−781 → −62	−36 → 74	132 → 481	−131 → −40
	n = 140	*n* = 2	*n* = 80	*n* = 141	*n* = 114	*n* = 141	*n* = 141	*n* = 2
9–10 years	97 ± 26	−38 ± 0	−72 ± 53	541 ± 219	−202 ± 130	14 ± 24	285 ± 98	−57 ± 9
	50 → 162	−38 → −38	−259 → −21	190 → 1,042	−668 → −41	−19 → 73	103 → 519	−66 → −48
	n = 115	*n* = 1	*n* = 49	*n* = 115	*n* = 92	*n* = 115	*n* = 115	*n* = 3
11–12 years	101 ± 24	−102 ± 0	−80 ± 48	649 ± 245	−233 ± 121	10 ± 28	281 ± 86	−75 ± 42
	64 → 153	−102 → −102	−241 → −23	230 → 1,250	−563 → −70	−43 → 106	135 → 518	−135 → −41
	n = 118	*n* = 1	*n* = 62	*n* = 119	*n* = 90	*n* = 119	*n* = 119	*n* = 4
13–14 years	99 ± 25		−78 ± 57	630 ± 274	−221 ± 121	17 ± 32	297 ± 102	−146 ± 0
	58 → 153		−378 → −23	232 → 1,390	−491 → −46	−17 → 128	106 → 557	−146 → −146
	n = 141		*n* = 62	*n* = 141	*n* = 113	*n* = 141	*n* = 140	*n* = 1
15–16 years	92 ± 22	−37 ± 0	−71 ± 54	625 ± 308	−243 ± 153	13 ± 28	275 ± 107	−124 ± 40
	48 → 149	−37 → −37	−226 → −23	169 → 1,469	−761 → −46	−47 → 81	129 → 576	−152 → −95
	n = 92	*n* = 1	*n* = 46	*n* = 92	*n* = 71	*n* = 92	*n* = 91	*n* = 2
17–18 years	132 ± 0		−606 ± 0			24 ± 0	158 ± 0	
	132 → 132		−606 → −606			24 → 24	158 → 158	
	n = 1		*n* = 1			*n* = 1	*n* = 1	

Table A2.14

Amplitudes (in μV) in Caucasian children: lead II

Age-group	P+	P–	Q	R	S	STj	T+	T–
<24 h	146 ± 50		−208 ± 143	597 ± 303	−393 ± 197	46 ± 30	149 ± 65	−117 ± 81
	65 → 276		−722 → −47	111 → 1,398	−961 → −178	−3 → 131	55 → 314	−174 → −59
	n = 43		*n* = 41	*n* = 41	*n* = 22	*n* = 43	*n* = 42	*n* = 2
<1 day	157 ± 48	−16 ± 0	−208 ± 127	618 ± 365	−433 ± 193	48 ± 32	157 ± 65	−147 ± 204
	56 → 258	−16 → −16	−526 → −34	53 → 1,389	−966 → −55	1 → 115	51 → 299	−597 → −20
	n = 138	*n* = 1	*n* = 132	*n* = 136	*n* = 71	*n* = 138	*n* = 137	*n* = 7
<2 days	164 ± 53	−35 ± 19	−204 ± 107	579 ± 300	−460 ± 204	51 ± 31	182 ± 70	−99 ± 66
	68 → 298	−54 → −17	−510 → −44	116 → 1,348	−905 → −165	−9 → 121	47 → 404	−175 → −60
	n = 118	*n* = 3	*n* = 106	*n* = 116	*n* = 69	*n* = 119	*n* = 118	*n* = 3

Table A2.14 (Continued)

Age-group	P+	P–	Q	R	S	STj	T+	T–
<3 days	163 ± 61	−36 ± 24	−210 ± 126	542 ± 303	−425 ± 229	58 ± 35	199 ± 69	−32 ± 13
	60 → 322	−77 → −19	−609 → −42	86 → 1,399	−976 → −94	−9 → 169	70 → 394	−41 → −22
	n = 105	*n* = 5	*n* = 102	*n* = 105	*n* = 56	*n* = 106	*n* = 106	*n* = 2
<1 week	168 ± 53	−25 ± 0	−239 ± 107	662 ± 345	−453 ± 220	65 ± 37	222 ± 72	−58 ± 0
	73 → 305	−25 → −25	−542 → −27	104 → 1,485	−975 → −89	−14 → 173	100 → 398	−58 → −58
	n = 117	*n* = 1	*n* = 115	*n* = 114	*n* = 75	*n* = 117	*n* = 117	*n* = 1
<1 month	159 ± 46	−23 ± 8	−199 ± 103	695 ± 312	−308 ± 160	47 ± 43	260 ± 84	−29 ± 0
	88 → 250	−29 → −17	−567 → −70	86 → 1,392	−662 → −94	−1 → 274	135 → 607	−29 → −29
	n = 45	*n* = 2	*n* = 41	*n* = 45	*n* = 28	*n* = 45	*n* = 45	*n* = 1
<3 months	150 ± 32		−218 ± 108	1,029 ± 407	−226 ± 76	44 ± 35	287 ± 91	
	87 → 231		−470 → −43	99 → 2,177	−405 → −111	−23 → 162	123 → 568	
	n = 67		*n* = 58	*n* = 67	*n* = 46	*n* = 69	*n* = 67	
<6 months	150 ± 39		−209 ± 132	1,067 ± 360	−247 ± 129	47 ± 32	293 ± 84	
	72 → 274		−492 → −34	404 → 1,830	−732 → −108	−22 → 127	126 → 560	
	n = 50		*n* = 40	*n* = 49	*n* = 32	*n* = 50	*n* = 50	
<1 year	159 ± 35	−96 ± 23	−178 ± 137	1,112 ± 445	−260 ± 116	55 ± 35	327 ± 102	
	81 → 241	−113 → −70	−676 → −22	468 → 2,666	−510 → −87	−19 → 164	84 → 597	
	n = 73	*n* = 3	*n* = 54	*n* = 73	*n* = 52	*n* = 74	*n* = 73	
1–2 years	146 ± 43	−39 ± 44	−169 ± 123	1,068 ± 379	−257 ± 121	28 ± 35	299 ± 112	
	50 → 240	−100 → 0	−480 → −29	349 → 1,928	−561 → −43	−20 → 161	93 → 579	
	n = 111	*n* = 4	*n* = 79	*n* = 111	*n* = 74	*n* = 116	*n* = 111	
3–4 years	149 ± 42	−29 ± 16	−140 ± 87	1,252 ± 381	−233 ± 125	13 ± 27	361 ± 127	
	73 → 241	−40 → −18	−332 → −23	475 → 2,119	−507 → −52	−41 → 66	129 → 653	
	n = 140	*n* = 2	*n* = 106	*n* = 141	*n* = 98	*n* = 141	*n* = 141	
5–6 years	136 ± 53	−27 ± 11	−126 ± 87	1,342 ± 420	−236 ± 113	16 ± 30	370 ± 108	
	36 → 277	−47 → −12	−357 → −22	637 → 2,394	−531 → −58	−35 → 92	171 → 594	
	n = 155	*n* = 12	*n* = 118	*n* = 155	*n* = 114	*n* = 155	*n* = 155	
7–8 years	137 ± 49	−35 ± 26	−119 ± 96	1,317 ± 380	−249 ± 137	15 ± 30	398 ± 118	−57 ± 0
	45 → 242	−105 → −18	−329 → −22	708 → 2,205	−620 → −54	−29 → 93	196 → 685	−57 → −57
	n = 140	*n* = 10	*n* = 94	*n* = 141	*n* = 115	*n* = 141	*n* = 141	*n* = 1
9–10 years	129 ± 53	−22 ± 8	−109 ± 62	1,423 ± 378	−218 ± 120	21 ± 38	401 ± 134	
	38 → 253	−38 → −13	−260 → −24	619 → 2,180	−497 → −55	−39 → 200	173 → 705	
	n = 115	*n* = 8	*n* = 86	*n* = 115	*n* = 84	*n* = 115	*n* = 115	
11–12 years	137 ± 49	−23 ± 13	−89 ± 55	1,413 ± 379	−245 ± 137	16 ± 31	391 ± 125	−62 ± 9
	37 → 232	−45 → −10	−217 → −23	759 → 2,342	−617 → −54	−60 → 122	148 → 672	−68 → −55
	n = 119	*n* = 6	*n* = 83	*n* = 119	*n* = 87	*n* = 119	*n* = 119	*n* = 2
13–14 years	125 ± 61	−27 ± 12	−90 ± 64	1,368 ± 408	−271 ± 152	23 ± 45	393 ± 137	−231 ± 0
	21 → 250	−60 → −14	−303 → −23	584 → 2,387	−740 → −47	−33 → 139	172 → 736	−231 → −231
	n = 139	*n* = 16	*n* = 100	*n* = 141	*n* = 111	*n* = 141	*n* = 140	*n* = 1
15–16 years	141 ± 59	−36 ± 23	−94 ± 65	1,290 ± 407	−278 ± 183	16 ± 41	366 ± 123	−77 ± 9
	35 → 297	−82 → −18	−394 → −27	593 → 2,089	−732 → −54	−77 → 98	144 → 631	−87 → −67
	N = 91	*n* = 6	*n* = 60	*n* = 92	*n* = 67	*n* = 92	*n* = 92	*n* = 4
17–18 years	270 ± 0		−284 ± 0	792 ± 0		85 ± 0	246 ± 0	
	270 → 270		−284 → −284	792 → 792		85 → 85	246 → 246	
	n = 1		*n* = 1	*n* = 1		*n* = 1	*n* = 1	

Table A2.15

Amplitudes (in μV) in Caucasian children: lead III

Age-group	P+	P−	Q	R	S	STj	T+	T−
<24 h	83 ± 46	−26 ± 10	−289 ± 157	1,072 ± 443	−377 ± 244	35 ± 30	103 ± 72	−30 ± 15
	18 → 198	−41 → −6	−731 → −78	209 → 2,028	−725 → −162	−15 → 114	14 → 110	−55 → −16
	n = 41	*n* = 15	*n* = 41	*n* = 43	*n* = 4	*n* = 43	*n* = 43	*n* = 7
<1 day	89 ± 45	−26 ± 15	−311 ± 145	1,048 ± 419	−228 ± 95	30 ± 22	97 ± 56	−67 ± 131
	14 → 195	−64 → −12	−651 → −101	49 → 1,954	−428 → −108	−10 → 85	15 → 272	−612 → −7
	n = 135	*n* = 29	*n* = 131	*n* = 138	*n* = 32	*n* = 138	*n* = 135	*n* = 20
<2 days	101 ± 43	−42 ± 27	−290 ± 143	950 ± 413	−212 ± 121	28 ± 32	98 ± 51	−61 ± 43
	27 → 213	−104 → −15	−655 → −72	32 → 2,017	−497 → −74	−30 → 96	22 → 240	−174 → −14
	n = 112	*n* = 23	*n* = 110	*n* = 119	*n* = 32	*n* = 119	*n* = 109	*n* = 20
<3 days	98 ± 50	−39 ± 18	−271 ± 128	882 ± 374	−197 ± 107	30 ± 29	105 ± 57	−51 ± 27
	26 → 225	−86 → −16	−621 → −59	54 → 1,859	−445 → −52	−38 → 100	15-277	−108 → −13
	n = 99	*n* = 23	*n* = 101	*n* = 106	*n* = 22	*n* = 106	*n* = 97	*n* = 17
<1 week	102 ± 47	−28 ± 14	−304 ± 126	972 ± 412	−209 ± 105	27 ± 26	104 ± 57	−37 ± 23
	17 → 223	−69 → −5	−626 → −92	97 → 2,095	−506 → −91	−34 → 82	19-241	−102 → −10
	n = 113	*n* = 22	*n* = 115	*n* = 117	*n* = 32	*n* = 117	*n* = 112	*n* = 26
<1 month	86 ± 51	−29 ± 12	−263 ± 126	913 ± 375	−158 ± 69	9 ± 40	86 ± 55	−42 ± 26
	10 → 208	−44 → −13	−575 → −77	23 → 1,571	−277 → −57	−29 → 208	13 → 228	−88 → −11
	n = 44	*n* = 13	*n* = 41	*n* = 45	*n* = 11	*n* = 45	*n* = 37	*n* = 16
<3 months	73 ± 31	−30 ± 18	−348 ± 166	909 ± 456	−220 ± 163	15 ± 31	88 ± 64	−78 ± 51
	16 → 168	−78 → −12	−726 → −76	54 → 2,038	−704 → −77	−24 → 141	16 → 317	−210 → −16
	n = 65	*n* = 18	*n* = 59	*n* = 67	*n* = 17	*n* = 69	*n* = 57	*n* = 22
<6 months	64 ± 25	−24 ± 14	−372 ± 139	765 ± 450	−256 ± 203	11 ± 29	79 ± 52	−79 ± 67
	25 → 130	−67 → −10	−682 → −104	24 → 1,816	−876 → −72	−36 → 63	20 → 218	−315 → −21
	n = 50	*n* = 16	*n* = 38	*n* = 50	*n* = 20	*n* = 50	*n* = 36	*n* = 30
<1 year	66 ± 28	−38 ± 28	−373 ± 170	651 ± 482	−291 ± 206	19 ± 24	88 ± 58	−85 ± 45
	17 → 123	−162 → −16	−807 → −122	25 → 1,575	−824 → −60	−28 → 76	18 → 314	−230 → −29
	n = 70	*n* = 34	*n* = 47	*n* = 73	*n* = 35	*n* = 74	*n* = 57	*n* = 35
1–2 years	64 ± 36	−36 ± 22	−280 ± 140	563 ± 432	−289 ± 243	2 ± 19	69 ± 53	−98 ± 56
	12 → 158	−109 → −10	−751 → −61	25 → 1,739	−967 → −47	−35 → 39	13 → 262	−248 → −28
	n = 101	*n* = 56	*n* = 68	*n* = 110	*n* = 64	*n* = 116	*n* = 66	*n* = 77
3–4 years	76 ± 39	−34 ± 16	−232 ± 138	817 ± 524	−204 ± 147	−2 ± 22	131 ± 86	−73 ± 51
	15 → 177	−99 → −13	−648 → −27	35 → 1,893	−604 → −40	−37 → 43	14 → 352	−232 → −15
	n = 127	*n* = 57	*n* = 94	*n* = 140	*n* = 79	*n* = 141	*n* = 121	*n* = 46
5–6 years	74 ± 38	−41 ± 20	−191 ± 126	903 ± 550	−156 ± 112	4 ± 21	125 ± 78	−51 ± 30
	14 → 174	−91 → −13	−456 → −24	34 → 2,102	−335 → −41	−44 → 62	17 → 361	−153 → −14
	n = 126	*n* = 76	*n* = 106	*n* = 155	*n* = 84	*n* = 155	*n* = 146	*n* = 43
7–8 years	71 ± 37	−40 ± 23	−177 ± 118	882 ± 527	−217 ± 159	3 ± 23	140 ± 90	−45 ± 25
	16 → 169	−113 → −13	−528 → −25	28 → 1,972	−722 → −47	−33 → 96	26 → 366	−129 → −16
	n = 120	*n* = 72	*n* = 82	*n* = 141	*n* = 94	*n* = 141	*n* = 139	*n* = 31
9–10 years	67 ± 41	−44 ± 26	−162 ± 98	1,035 ± 518	−163 ± 110	6 ± 27	150 ± 96	−71 ± 58
	13 → 183	−132 → −9	−416 → −27	45 → 1,973	−589 → −36	−37 → 79	23 → 402	−265 → −16
	n = 92	*n* = 70	*n* = 78	*n* = 115	*n* = 70	*n* = 115	*n* = 107	*n* = 28
11–12 years	71 ± 35	−42 ± 20	−126 ± 78	908 ± 527	−193 ± 151	6 ± 22	142 ± 84	−62 ± 40
	14 → 149	−108 → −14	−2, 901 → −21	38 → 2,271	−808 → −28	−43 → 53	21 → 346	−163 → −13
	n = 100	*n* = 65	*n* = 75	*n* = 119	*n* = 74	*n* = 119	*n* = 111	*n* = 30

Table A2.15 (Continued)

Age-group	P+	P–	Q	R	S	STj	T+	T–
13–14 years	71 ± 44	−51 ± 25	−111 ± 66	878 ± 511	−227 ± 158	5 ± 26	133 ± 78	−63 ± 37
	13 → 220	−114 → −18	−303 → −24	34 → 1,985	−736 → −31	−46 → 71	21 → 341	−140 → −13
	n = 105	*n* = 90	*n* = 88	*n* = 141	*n* = 93	*n* = 141	*n* = 126	*n* = 35
15–16 years	82 ± 53	−38 ± 21	−123 ± 81	797 ± 482	−225 ± 158	3 ± 26	121 ± 78	−56 ± 28
	14 → 219	−137 → −14	−402 → −27	31 → 1,805	−751 → −41	−55 → 54	20 → 125	−156 → −23
	n = 77	*n* = 53	*n* = 55	*n* = 92	*n* = 55	*n* = 92	*n* = 89	*n* = 30
17–18 years	138 ± 0		−241 ± 0	1,399 ± 0		61 ± 0	95 ± 0	
	138 → 138		−241 → −241	1,399 → 1,399		61 → 61	95 → 95	
	n = 1		*n* = 1	*n* = 1		*n* = 1	*n* = 1	

Table A2.16

Amplitudes (in μV) in Caucasian children: lead aVR

Age-group	P+	P–	Q	R	S	STj	T+	T–
<24 h		−110 ± 32	−188 ± 180	273 ± 245	−228 ± 132	−28 ± 19	84 ± 87	−113 ± 49
		−181 → −60	−671 → −31	22 → 974	−533 → −64	−64 → 14	23 → 229	−231 → −46
		n = 43	*n* = 15	*n* = 42	*n* = 24	*n* = 43	*n* = 5	*n* = 42
<1 day	15 ± 2	−116 ± 32	−269 ± 155	283 ± 227	−263 ± 170	−32 ± 25	65 ± 72	−121 ± 50
	13 → 16	−181 → −46	−662 → −42	30 → 786	−778 → −46	−88 → 11	12 → 300	−237 → −42
	n = 2	*n* = 138	*n* = 46	*n* = 135	*n* = 73	*n* = 138	*n* = 18	*n* = 137
<2 days	9 ± 0	−118 ± 34	−286 ± 130	217 ± 197	−237 ± 141	−36 ± 24	51 ± 34	−147 ± 55
	9 → 9	−209 → −60	−571 → −42	22 → 809	−625 → −35	−96 → 11	14 → 114	−289 → −39
	n = 1	*n* = 119	*n* = 35	*n* = 117	*n* = 72	*n* = 119	*n* = 6	*n* = 117
<3 days	34 ± 33	−119 ± 42	−264 ± 124	218 ± 181	−248 ± 152	−43 ± 28	47 ± 22	−160 ± 51
	11 → 57	−203 → −42	−484 → −36	27 → 659	−723 → −42	−105 → 29	31 → 62	−289 → −68
	n = 2	*n* = 106	*n* = 26	*n* = 105	*n* = 67	*n* = 106	*n* = 2	*n* = 106
<1 week	22 ± 4	−122 ± 34	−240 ± 145	202 ± 183	−305 ± 173	−51 ± 31	59 ± 33	−183 ± 57
	19 → 24	−217 → −54	−638 → −77	29 → 892	−696 → −74	−130 → 0	36 → 97	−332 → −83
	n = 2	*n* = 117	*n* = 20	*n* = 116	*n* = 86	*n* = 117	*n* = 3	*n* = 117
<1 month	23 ± 10	−121 ± 29	−384 ± 121	151 ± 134	−389 ± 221	−42 ± 29	33 ± 8	−233 ± 69
	14 → 33	−193 → −62	−533 → −235	25 → 680	−1, 050 → −114	−84 → 11	27 → 39	−430 → −112
	n = 3	*n* = 45	*n* = 8	*n* = 45	*n* = 36	*n* = 45	*n* = 2	*n* = 45
<3 months		−119 ± 24	−609 ± 260	138 ± 105	−786 ± 272	−37 ± 32		−269 ± 79
		−190 → −78	−1, 017 → −74	24 → 465	−1, 262 to −309	−114 → 80		−511 → −92
		n = 67	*n* = 13	*n* = 67	*n* = 55	*n* = 69		*n* = 67
<6 months		−122 ± 32	−792 ± 259	188 ± 152	−906 ± 190	−41 ± 24		−288 ± 70
		−233 → −56	−1, 246 to −79	26 → 730	−1, 264 to −615	−92 → 11		−523 → −154
		n = 50	*n* = 16	*n* = 50	*n* = 34	*n* = 50		*n* = 50
<1 year	62 ± 36	−132 ± 29	−852 ± 299	179 ± 153	−980 ± 303	−45 ± 31		−316 ± 86
	27 → 99	−208 → −72	−1, 478 → −81	20 → 729	−2, 188 to −616	−94 → 51		−454 → −117
	n = 3	*n* = 73	*n* = 25	*n* = 72	*n* = 49	*n* = 74		*n* = 73
1–2 years	89 ± 34	−125 ± 29	−711 ± 231	174 ± 119	−983 ± 270	−26 ± 32		−313 ± 106
	65 → 113	−187 → −74	−1, 118 → −97	22 → 501	−1, 426 to −499	−87 → 24		−646 → −126
	n = 2	*n* = 110	*n* = 33	*n* = 107	*n* = 80	*n* = 116		*n* = 111
3–4 years		−120 ± 26	−797 ± 185	122 ± 89	−948 ± 221	−13 ± 20		−319 ± 93
		−177 → −69	−1, 362 → −457	23 → 392	−1, 405 to −466	−55 → 28		−552 → −149
		n = 141	*n* = 39	*n* = 133	*n* = 102	*n* = 141		*n* = 141

Table A2.16 (Continued)

Age-group	P+	P−	Q	R	S	STj	T+	T−
5–6 years	27 ± 18	−112 ± 31	−824 ± 166	125 ± 91	−975 ± 259	−13 ± 25	38 ± 0	−321 ± 87
	15 → 58	−184 → −54	−1, 288 → −553	23 → 363	−1, 568 → −607	−67 → 67	38 → 38	−495 → −148
	n = 5	*n* = 155	*n* = 52	*n* = 148	*n* = 103	*n* = 155	*n* = 1	*n* = 155
7–8 years	86 ± 0	−113 ± 28	−842 ± 251	114 ± 96	−924 ± 241	−13 ± 23	127 ± 0	−337 ± 91
	86 → 86	−184 → −65	−1, 451 → −463	21 → 384	−1, 459 → −535	−70 → 27	127 → 127	−562 → −183
	n = 1	*n* = 140	*n* = 45	*n* = 140	*n* = 96	*n* = 141	*n* = 1	*n* = 141
9–10 years	21 ± 0	−110 ± 30	−837 ± 194	103 ± 83	−977 ± 218	−17 ± 28	35 ± 0	−341 ± 102
	21 → 21	−182 → −57	−1, 240 → −521	22 → 364	−1, 578 → −585	−73 → 27	35 → 35	−560 → −166
	n = 1	*n* = 115	*n* = 43	*n* = 108	*n* = 72	*n* = 115	*n* = 1	*n* = 115
11–12 years	67 ± 0	−115 ± 30	−908 ± 177	122 ± 107	−1, 041 ± 223	−12 ± 27	58 ± 0	−334 ± 92
	67 → 67	−181 → −59	−1, 290 → −610	23 → 479	−1, 662 → −650	−77 → 81	58 → 58	−570 → −179
	n = 1	*n* = 118	*n* = 48	*n* = 112	*n* = 71	*n* = 119	*n* = 1	*n* = 119
13–14 years	14 ± 3	−107 ± 37	−826 ± 214	126 ± 107	−1, 036 ± 265	−20 ± 36	182 ± 0	−343 ± 110
	11 → 18	−176 → −41	−1, 414 → −465	21 → 401	−1, 573 → −522	−113 → 29	182 → 182	−600 → −145
	n = 4	*n* = 141	*n* = 59	*n* = 135	*n* = 83	*n* = 141	*n* = 1	*n* = 140
15–16 years	17 ± 10	−111 ± 33	−805 ± 277	139 ± 129	−1, 035 ± 241	−13 ± 32	84 ± 10	−317 ± 107
	9 → 31	−196 → −40	−1, 675 → −352	23 → 521	−1, 737 → −582	−63 → 75	77 → 91	−584 → −125
	n = 4	*n* = 92	*n* = 41	*n* = 82	*n* = 50	*n* = 92	*n* = 2	*n* = 92
17–18 years		−200 ± 0		166 ± 0	−108 ± 0	−54 ± 0		−199 ± 0
		−200 → −200		166 → 166	−108 → −108	−54 → −54		−199 → −199
		n = 1		*n* = 1	*n* = 1	*n* = 1		*n* = 1

Table A2.17

Amplitudes (in μV) in Caucasian children: lead aVL

Age-group	P+	P−	Q	R	S	STj	T+	T−
<24 h	34 ± 17	−29 ± 20	−295 ± 283	224 ± 160	−865 ± 322	−12 ± 19	47 ± 28	−62 ± 62
	9 → 65	−90 → −9	−681 → −47	34 → 731	−1, 654 → −394	−49 → 27	11 → 119	−369 → −15
	n = 31	*n* = 28	*n* = 4	*n* = 41	*n* = 41	*n* = 43	*n* = 22	*n* = 34
<1 day	31 ± 18	−30 ± 26	−291 ± 286	223 ± 140	−832 ± 251	−5 ± 15	51 ± 45	−57 ± 37
	7 → 76	−96 → −7	−759 → −36	46 → 546	−1, 518 → −465	−33 → 31	11 → 147	−165 → −12
	n = 104	*n* = 90	*n* = 8	*n* = 136	*n* = 134	*n* = 138	*n* = 79	*n* = 88
<2 days	24 ± 22	−32 ± 18	−264 ± 261	211 ± 131	−780 ± 250	−3 ± 25	57 ± 42	−40 ± 24
	0 → 92	−78 → −9	−609 → −24	42 → 582	−1, 563 → −354	−49 → 112	13 → 164	−113 → −9
	n = 119	*n* = 81	*n* = 11	*n* = 116	*n* = 114	*n* = 119	*n* = 82	*n* = 67
<3 days	33 ± 25	−31 ± 26	−177 ± 210	191 ± 118	−718 ± 230	−1 ± 22	53 ± 42	−45 ± 31
	6 → 86	−182 → −6	−548 → −24	32 → 535	−1, 318 → −308	−44 → 59	10 → 182	−159 → −6
	n = 75	*n* = 69	*n* = 12	*n* = 102	*n* = 102	*n* = 106	*n* = 78	*n* = 52
<1 week	29 ± 20	−31 ± 21	−158 ± 240	206 ± 111	−750 ± 248	5 ± 21	64 ± 38	−51 ± 31
	6 → 81	−101 → −5	−659 → −22	36 → 488	−1, 490 → −373	−41 → 47	11 → 139	−161 → −11
	n = 82	*n* = 90	*n* = 9	*n* = 115	*n* = 115	*n* = 117	*n* = 94	*n* = 44

Table A2.17 (Continued)

Age-group	P+	P–	Q	R	S	STj	T+	T–
<1 month	40 ± 22	–33 ± 24	–353 ± 396	225 ± 123	–703 ± 232	14 ± 25	98 ± 52	–56 ± 26
	9 → 93	–88 → –9	–912 → –26	65 → 625	–1, 147 → –243	–69 → 55	12 → 233	–93 → –17
	n = 34	*n* = 26	*n* = 5	*n* = 42	*n* = 42	*n* = 45	*n* = 40	*n* = 8
<3 months	40 ± 22	–22 ± 14	–76 ± 65	397 ± 199	–647 ± 246	7 ± 28	125 ± 69	–54 ± 59
	10 → 123	–76 → –6	–236 → –20	58 → 988	–1, 205 → –174	–110 → 59	25 → 322	–216 → –14
	n = 61	*n* = 38	*n* = 13	*n* = 66	*n* = 66	*n* = 69	*n* = 64	*n* = 11
<6 months	40 ± 19	–18 ± 10	–88 ± 46	480 ± 188	–598 ± 232	11 ± 19	154 ± 77	–30 ± 33
	14 → 83	–41 → –4	–163 → –25	110 → 1,092	–1, 159 → –208	–21 → 61	15 → 427	–78 → –4
	n = 50	*n* = 24	*n* = 13	*n* = 50	*n* = 48	*n* = 50	*n* = 49	*n* = 4
<1 year	52 ± 24	–23 ± 14	–103 ± 63	522 ± 238	–474 ± 224	8 ± 21	160 ± 70	–42 ± 24
	9 → 108	–73 → –9	–245 → –28	136 → 1,199	–1, 089 → –112	–32 → 57	32 → 331	–71 → –5
	n = 69	*n* = 33	*n* = 30	*n* = 73	*n* = 71	*n* = 74	*n* = 71	*n* = 8
1–2 years	56 ± 25	–30 ± 26	–117 ± 89	475 ± 275	–386 ± 207	11 ± 20	188 ± 90	–48 ± 17
	12 → 133	–132 → –9	–460 → –26	93 → 1,287	–1, 035 → –50	–22 → 68	27 → 410	–72 → –26
	n = 106	*n* = 38	*n* = 54	*n* = 111	*n* = 98	*n* = 116	*n* = 110	*n* = 5
3–4 years	48 ± 20	–27 ± 17	–106 ± 84	336 ± 185	–447 ± 272	8 ± 16	121 ± 65	–53 ± 38
	13 → 84	–88 → –9	–407 → –23	66 → 756	–10–74 → –48	–21 → 41	19 → 269	–159 → –7
	n = 127	*n* = 64	*n* = 60	*n* = 140	*n* = 118	*n* = 141	*n* = 132	*n* = 21
5–6 years	49 ± 22	–25 ± 13	–86 ± 69	255 ± 156	–454 ± 259	3 ± 17	109 ± 60	–46 ± 31
	10 → 94	–70 → –6	–410 → –22	38 → 719	–1, 114 → –59	–41 → 40	15 → 245	–136 → –10
	n = 146	*n* = 58	*n* = 58	*n* = 154	*n* = 140	*n* = 155	*n* = 145	*n* = 28
7–8 years	48 ± 23	–24 ± 13	–104 ± 77	248 ± 183	–440 ± 279	4 ± 17	102 ± 61	–43 ± 26
	11 → 98	–63 → –7	–483 → –23	43 → 768	–1, 176 → –46	–32 → 38	14 → 240	–107 → –8
	n = 129	*n* = 58	*n* = 71	*n* = 140	*n* = 115	*n* = 141	*n* = 130	*n* = 34
9–10 years	53 ± 28	–26 ± 15	–130 ± 129	197 ± 131	–484 ± 260	4 ± 16	110 ± 72	–51 ± 38
	11 → 127	–72 → –8	–473 → –23	41 → 558	–1, 104 → –63	–31 → 33	14 → 347	–169 → –13
	n = 105	*n* = 42	*n* = 37	*n* = 112	*n* = 99	*n* = 115	*n* = 107	*n* = 23
11–12 years	53 ± 23	–26 ± 17	–116 ± 97	232 ± 190	–415 ± 260	2 ± 19	109 ± 62	–52 ± 33
	13 → 104	–88 → –8	–595 → –28	38 → 867	–976 → –38	–44 → 51	20 → 262	–145 → –15
	n = 112	*n* = 47	*n* = 49	*n* = 117	*n* = 100	*n* = 119	*n* = 107	*n* = 18
13–14 years	60 ± 24	–29 ± 20	–110 ± 111	228 ± 196	–389 ± 235	7 ± 18	114 ± 67	–32 ± 20
	17 → 117	–96 → –9	–699 → –25	27 → 790	–945 → –43	–26 → 56	18 → 261	–81 → –7
	n = 134	*n* = 43	*n* = 55	*n* = 139	*n* = 118	*n* = 141	*n* = 136	*n* = 20
15–16 years	48 ± 23	–36 ± 18	–125 ± 124	231 ± 191	–373 ± 261	6 ± 19	111 ± 69	–55 ± 42
	11 → 103	–81 → –11	–537 → –21	46 → 884	–1, 050 → –56	–24 → 49	8 → 281	–169 → –16
	n = 85	*n* = 40	*n* = 41	*n* = 88	*n* = 70	*n* = 92	*n* = 85	*n* = 18
17–18 years		–16 ± 0		113 ± 0	–1, 002 ± 0	–18 ± 0	39 ± 0	
		–16 → –16		113 → 113	–1, 002 → –1,002	–18 → –18	39 → 39	
		n = 1		*n* = 1	*n* = 1	*n* = 1	*n* = 1	

Table A2.18

Amplitudes (in μV) in Caucasian children: lead aVF

Age-group	P+	P−	Q	R	S	STj	T+	T−
<24 h	111 ± 48	−16 ± 9	−226 ± 114	798 ± 360	−260 ± 184	40 ± 28	120 ± 58	−34 ± 38
	221 → 21	−25 → −7	−541 → −47	82 → 1,492	−703 → −70	−1 → 117	34 → 296	−78 → −11
	n = 43	*n* = 4	*n* = 42	*n* = 43	*n* = 14	*n* = 43	*n* = 43	*n* = 3
<1 day	121 ± 45	−22 ± 14	−251 ± 113	811 ± 380	−309 ± 131	39 ± 26	121 ± 55	−150 ± 253
	36 → 227	−40 → −8	−428 → −74	73 → 1,725	−691 → −106	0 → 98	29 → 260	−601 → −20
	n = 138	*n* = 5	*n* = 133	*n* = 137	*n* = 44	*n* = 138	*n* = 137	*n* = 5
<2 days	129 ± 50	−39 ± 23	−233 ± 112	723 ± 353	−316 ± 156	40 ± 28	135 ± 58	−42 ± 53
	21 → 247	−79 → −12	−555 → −36	38 → 1,462	−657 → −90	95 → −19	31 → 293	−150 → −13
	n = 118	*n* = 9	*n* = 110	*n* = 119	*n* = 50	*n* = 119	*n* = 117	*n* = 6
<3 days	128 ± 54	−29 ± 17	−232 ± 106	675 ± 337	−314 ± 141	44 ± 29	142 ± 63	−14 ± 0
	37 → 268	−58 → −11	−541 → −58	27 → 1,571	−622 → −141	−15 → 134	28 → 322	−14 → −14
	n = 104	*n* = 9	*n* = 101	*n* = 106	*n* = 36	*n* = 106	*n* = 106	*n* = 1
<1 week	132 ± 50	−15 ± 8	−264 ± 104	783 ± 373	−316 ± 149	46 ± 28	155 ± 61	−15 ± 0
	34 → 241	−22 → −6	−517 → −71	139 → 1,801	−785 → −65	−7 → 110	53 → 312	−15 → −15
	n = 117	*n* = 4	*n* = 116	*n* = 117	*n* = 56	*n* = 117	*n* = 117	*n* = 1
<1 month	120 ± 47	−21 ± 2	−212 ± 104	780 ± 300	−221 ± 101	27 ± 40	160 ± 72	
	44 → 225	−22 → −19	−571 → −62	276 → 1,377	−454 → −85	−14 → 241	72 → 480	
	n = 45	*n* = 2	*n* = 43	*n* = 45	*n* = 19	*n* = 45	*n* = 45	
<3 months	109 ± 30		−255 ± 126	880 ± 427	−154 ± 74	30 ± 28	172 ± 72	−42 ± 1
	55 → 176		−579 → −52	34 → 2,049	−351 → −66	−22 → 111	67 → 358	−43 → −41
	n = 67		*n* = 58	*n* = 67	*n* = 28	*n* = 69	*n* = 65	*n* = 2
<6 months	105 ± 30	−31 ± 0	−254 ± 114	831 ± 380	−158 ± 86	29 ± 28	158 ± 74	−60 ± 2
	53 → 185	−31 → −31	−459 → −62	46 → 1,671	−421 → −59	−26 → 92	30 → 316	−61 → −58
	n = 50	*n* = 1	*n* = 40	*n* = 50	*n* = 26	*n* = 50	*n* = 50	*n* = 2
<1 year	108 ± 30	−45 ± 43	−235 ± 136	788 ± 474	−160 ± 76	37 ± 26	185 ± 78	−69 ± 66
	35 → 171	−136 → −16	−628 → −53	26 → 1,819	−384 → −53	−6 → 94	72 → 454	−116 → −22
	n = 73	*n* = 7	*n* = 50	*n* = 73	*n* = 40	*n* = 74	*n* = 72	*n* = 2
1–2 years	100 ± 38	−28 ± 15	−183 ± 122	746 ± 405	−178 ± 87	15 ± 23	146 ± 78	−33 ± 20
	32 → 177	−52 → −12	−553 → −27	24 → 1,769	−353 → −49	69 → −24	17 → 329	−77 → −16
	n = 109	*n* = 10	*n* = 73	*n* = 111	*n* = 66	*n* = 116	*n* = 110	*n* = 10
3–4 years	107 ± 42	−24 ± 12	−165 ± 92	998 ± 469	−182 ± 106	6 ± 23	230 ± 107	−68 ± 33
	24 → 191	−57 → −11	−413 → −30	42 → 1,955	−512 → −45	44 → −42	25 → 466	−116 → −46
	n =140	*n* = 11	*n* = 95	*n* = 141	*n* = 85	*n* = 141	*n* = 139	*n* = 4
5–6 years	96 ± 49	−25 ± 13	−135 ± 100	1,113 ± 466	−183 ± 89	10 ± 23	237 ± 90	−35 ± 0
	14 → 228	−56 → −8	−366 → −21	111 → 2,245	−405 → −59	−34 → 73	87 → 452	−35 → −35
	n = 152	*n* = 34	*n* = 114	*n* = 155	*n* = 99	*n* = 155	*n* = 155	*n* = 1
7–8 years	99 ± 44	−31 ± 21	−133 ± 96	1,093 ± 426	−219 ± 133	9 ± 25	262 ± 100	−64 ± 20
	25 → 206	−74 → −11	−409 → −23	329 → 2,033	−551 → −48	−29 → 70	104 → 509	−78 → −50
	n = 136	*n* = 24	*n* = 87	*n* = 141	*n* = 97	*n* = 141	*n* = 141	*n* = 2
9–10 years	92 ± 48	−26 ± 15	−128 ± 76	1,237 ± 410	−189 ± 99	13 ± 30	263 ± 114	−52 ± 32
	15 → 216	−63 → −8	−304 → −29	414 → 2,072	−516 → −42	−41 → 137	43 → 539	−83 → −20
	n = 109	*n* = 25	*n* = 79	*n* = 115	*n* = 74	*n* = 115	*n* = 115	*n* = 3

Table A2.18 (Continued)

Age-group	P+	P–	Q	R	S	STj	T+	T–
11–12 years	98 ± 42	−24 ± 15	−97 ± 58	1,161 ± 428	−202 ± 111	11 ± 23	254 ± 107	−47 ± 28
	20 → 185	−68 → −5	−233 → −273	404 → 2,170	−477 → −52	−39 → 66	45 → 494	−91 → −17
	n = 115	*n* = 22	*n* = 76	*n* = 119	*n* = 77	*n* = 119	*n* = 119	*n* = 5
13–14 years	94 ± 51	−32 ± 18	−93 ± 62	1,117 ± 433	−249 ± 137	14 ± 33	250 ± 106	−54 ± 48
	13 → 211	−94 → −12	−287 → −24	309 → 2,144	−683 → −57	−35 → 89	77 → 484	−138 → −23
	n = 125	*n* = 47	*n* = 94	*n* = 141	*n* = 96	*n* = 141	*n* = 140	*n* = 5
15–16 years	104 ± 57	−26 ± 22	−98 ± 67	1,020 ± 434	−228 ± 157	9 ± 32	237 ± 90	−53 ± 21
	21 → 259	−105 → −10	−295 → −21	201 → 1,861	−605 → −275	−69 → 74	96 → 417	−80 → −15
	n = 89	*n* = 20	*n* = 57	*n* = 92	*n* = 63	*n* = 92	*n* = 91	*n* = 7
17–18 years	204 ± 0		−263 ± 0	1,095 ± 0		73 ± 0	171 ± 0	
	204 → 204		−263 → −263	1,095 → 1,095		73 → 73	171 → 171	
	n = 1		*n* = 1	*n* = 1		*n* = 1	*n* = 1	

Table A2.19

Amplitudes (in μV) in Caucasian children: lead V_1

Age-group	P+	P–	Q	R	S	STj	T+	T–
<24 h	93 ± 44	−40 ± 14		1,248 ± 547	−764 ± 458	−18 ± 31	175 ± 120	−121 ± 68
	28 → 186	−74 → −19		481 → 2,291	−1,780 → −141	−75 → 47	15 → 590	−254 → −39
	n = 40	*n* = 25		*n* = 43	*n* = 40	*n* = 43	*n* = 33	*n* = 22
<1 day	90 ± 52	−39 ± 16	−36 ± 7	1,169 ± 487	−786 ± 503	−24 ± 37	148 ± 102	−111 ± 57
	13 → 201	−83 → −13	−41 → −31	329 → 2,370	−2,176 → −74	−112 → 53	31 → 432	−281 → −24
	n = 132	*n* = 65	*n* = 2	*n* = 137	*n* = 124	*n* = 137	*n* = 12	*n* = 99
<2 days	83 ± 50	−49 ± 24	−69 ± 59	1,102 ± 524	−603 ± 379	−28 ± 40	124 ± 83	−145 ± 78
	25 → 244	−133 → −15	−110 → −27	404 → 2,592	−1,530 → −137	−110 → 64	18 → 320	−355 → −34
	n = 106	*n* = 58	*n* = 2	*n* = 117	*n* = 100	*n* = 117	*n* = 76	*n* = 102
<3 days	85 ± 43	−44 ± 26	−87 ± 70	1,102 ± 536	−615 ± 385	−37 ± 69	98 ± 52	−182 ± 104
	18 → 199	−121 → −15	−136 → −37	363 → 2,832	−1,718 → −145	−136 → 62	35 → 261	−621 → −47
	n = 97	*n* = 40	*n* = 2	*n* = 102	*n* = 93	*n* = 102	*n* = 57	*n* = 97
<1 week	86 ± 49	−44 ± 31		1,085 ± 445	−494 ± 326	−47 ± 42	102 ± 67	−211 ± 79
	17 → 249	−229 → −18		2,078 → 354	−1,530 → −103	−137 → 15	25 → 332	−428 → −70
	n = 109	*n* = 51		*n* = 114	*n* = 99	*n* = 114	*n* = 28	*n* = 110
<1 month	83 ± 49	−40 ± 20	−28 ± 0	873 ± 391	−463 ± 346	−32 ± 42	102 ± 68	−192 ± 102
	29 → 237	−81 → −10	−28 → −28	425 → 2,303	−1,529 → −102	−105 → 53	30 → 224	−467 → −58
	n = 38	*n* = 16	*n* = 1	*n* = 41	*n* = 37	*n* = 41	*n* = 16	*n* = 38
<3 months	65 ± 34	−45 ± 21	−134 ± 117	772 ± 345	−496 ± 337	−20 ± 60	102 ± 75	−251 ± 143
	17 → 144	−98 → −14	−217 → −51	194 → 1,656	−1,735 → −120	−137 → 336	38 → 314	−465 → 0
	n = 52	*n* = 40	*n* = 2	*n* = 63	*n* = 56	*n* = 65	*n* = 12	*n* = 65
<6 months	59 ± 28	−45 ± 28		829 ± 413	−511 ± 358	−19 ± 45	80 ± 46	−319 ± 99
	16 → 131	−127 → −18		298 → 2,222	−1,660 → −96	−92 → 192	40 → 156	−493 → −139
	n = 41	*n* = 32		*n* = 49	*n* = 48	*n* = 49	*n* = 5	*n* = 48
<1 year	68 ± 29	−53 ± 35		779 ± 420	−538 ± 330	−22 ± 27	160 ± 83	−343 ± 97
	21 → 142	−194 → −15		47 → 2,037	−1,562 → −95	−74 → 106	77 → 243	−577 → −204
	n = 59	*n* = 43		*n* = 70	*n* = 69	*n* = 71	*n* = 3	*n* = 69

Table A2.19 (Continued)

Age-group	P+	P−	Q	R	S	STj	T+	T−
1–2 years	91 ± 33	−57 ± 36	−114 ± 59	807 ± 382	−771 ± 385	−3 ± 31	126 ± 64	−317 ± 105
	26 → 152	−204 → −21	−155 → −72	99 → 1,804	−1,701 → −183	−86 → 65	46 → 224	−578 → −139
	n = 100	*n* = 46	*n* = 2	*n* = 107	*n* = 103	*n* = 112	*n* = 7	*n* = 105
3–4 years	95 ± 36	−56 ± 32	−526 ± 0	610 ± 244	−895 ± 394	13 ± 30	85 ± 37	−270 ± 92
	30 → 168	−153 → −16	−526 → −526	106 → 1,112	−1,893 → −205	−45 → 91	43 → 163	−467 → −88
	n = 129	*n* = 57	*n* = 1	*n* = 135	*n* = 135	*n* = 136	*n* = 25	*n* = 136
5–6 years	98 ± 35	−55 ± 25	−342 ± 409	509 ± 232	−1,008 ± 398	22 ± 28	77 ± 31	−249 ± 96
	33 → 182	−132 → −24	−631 → −53	84 → 1,020	−2,011 → −395	−28 → 88	40 → 155	−448 → −51
	n = 141	*n* = 62	*n* = 2	*n* = 146	*n* = 146	*n* = 147	*n* = 37	*n* = 145
7–8 years	88 ± 35	−54 ± 30		483 ± 283	−969 ± 426	25 ± 26	78 ± 37	−251 ± 98
	28 → 166	−180 → −17		142 → 1,388	−1,921 → −264	−37 → 78	38 → 185	−431 → −76
	n = 133	*n* = 69		*n* = 135	*n* = 135	*n* = 135	*n* = 34	*n* = 129
9–10 years	76 ± 32	−49 ± 25		403 ± 191	−1,090 ± 462	31 ± 31	111 ± 98	−218 ± 99
	21 → 150	−115 → −15		131-919	−2,213 → −214	−25 → 145	32 → 468	−436 → −43
	n = 104	*n* = 73		*n* = 108	*n* = 108	*n* = 108	*n* = 35	*n* = 102
11–12 years	75 ± 31	−57 ± 37		383 ± 225	−1,130 ± 451	30 ± 33	129 ± 121	−206 ± 99
	22 → 148	−228 → −16		66 → 1,090	−2,366 → −363	−33 → 109	34 → 573	−488 → −35
	n = 97	*n* = 70		*n* = 104	*n* = 104	*n* = 104	*n* = 39	*n* = 87
13–14 years	70 ± 30	−58 ± 32	−788 ± 692	329 ± 196	−1,097 ± 418	33 ± 36	91 ± 65	−176 ± 92
	25 → 136	−151 → −18	−1,364 → −20	52 → 912	−2,265 → −366	−26 → 164	31 → 342	−450 → −32
	n = 99	*n* = 81	*n* = 3	*n* = 107	*n* = 107	*n* = 109	*n* = 44	*n* = 96
15–16 years	72 ± 34	−54 ± 25	−115 ± 99	348 ± 211	−1,194 ± 529	38 ± 36	79 ± 114	−156 ± 93
	22 → 232	−110 → −19	−185 → −45	71 → 1,186	−2,303 → −98	−43 → 140	492 → 0	−420 → −37
	n = 65	*n* = 50	*n* = 2	*n* = 70	*n* = 70	*n* = 71	*n* = 71	*n* = 48
17–18 years	56 ± 0	−26 ± 0		1,028 ± 0	−466 ± 0	−17 ± 0		−139 ± 0
	56 → 56	−26 → −26		1,028 → 1,028	−466 → −466	−17 → −17		−139 → −139
	n = 1	*n* = 1		*n* = 1	*n* = 1	*n* = 1		*n* = 1

Table A2.20

Amplitudes (in μV) in Caucasian children: lead V_2

Age-group	P+	P−	Q	R	S	STj	T+	T−
<24 h	123 ± 55	−19 ± 8		1,642 ± 621	−1,758 ± 690	−17 ± 38	198 ± 151	−113 ± 57
	15 → 238	−33 → −13		709 → 3,673	−2,967 → −618	−77 → 77	21 → 487	−226 → −35
	n = 43	*n* = 5		*n* = 43	*n* = 42	*n* = 43	*n* = 35	*n* = 19
<1 day	114 ± 52	−51 ± 71	−36 ± 0	1,402 ± 500	−1,534 ± 674	−35 ± 48	169 ± 98	−133 ± 88
	36 → 229	−342 → −12	−36 → −36	494 → 2,393	−2,927 → −405	−119 → 70	25 → 417	−352 → −25
	n = 133	*n* = 21	*n* = 1	*n* = 137	*n* = 136	*n* = 137	*n* = 103	*n* = 91
<2 days	103 ± 47	−33 ± 17	−60 ± 0	1,402 ± 536	−1,346 ± 609	−27 ± 44	133 ± 91	−138 ± 75
	28 → 230	−65 → −8	−60 → −60	484 → 2,536	−2,887 → −414	−111 → 77	21 → 407	−313 → −28
	n = 116	*n* = 22	*n* = 1	*n* = 116	*n* = 114	*n* = 116	*n* = 84	*n* = 93
<3 days	111 ± 39	−33 ± 25	−83 ± 65	1,343 ± 504	−1,278 ± 556	−29 ± 72	125 ± 79	−179 ± 114
	32 → 192	−77 → −9	−166 → −21	501 → 2,689	−2,895 → −300	−161 → 76	26 → 376	−595 → −34
	n = 102	*n* = 9	*n* = 4	*n* = 104	*n* = 104	*n* = 104	*n* = 56	*n* = 89

Table A2.20 (Continued)

Age-group	P+	P–	Q	R	S	STj	T+	T–
<1 week	110 ± 53	−57 ± 55	−60 ± 0	1,332 ± 480	−1,130 ± 499	−35 ± 63	116 ± 75	−210 ± 128
	17 → 248	−219 → −21	−60 → −60	583 → 2,542	−2,070 → −238	−172 → 86	16 → 326	−574 → −37
	n = 112	*n* = 16	*n* = 1	*n* = 114	*n* = 111	*n* = 114	*n* = 43	*n* = 102
<1 month	108 ± 54	−36 ± 31	−52 ± 0	1,159 ± 519	−1,000 ± 494	0 ± 63	118 ± 78	−145 ± 110
	22 → 235	−87 → −10	−52 → −52	380 → 3,156	−2,431 → −276	−99 → 92	33 → 302	−500 → −20
	n = 42	*n* = 6	*n* = 1	*n* = 42	*n* = 41	*n* = 42	*n* = 32	*n* = 24
<3 months	102 ± 40	−49 ± 27	−56 ± 0	1,406 ± 411	−972 ± 433	11 ± 61	144 ± 94	−209 ± 134
	33 → 224	−96 → −20	−56 → −56	566 → 2,292	−2,306 → −307	−87 → 343	42 → 474	−554 → −50
	n = 63	*n* = 6	*n* = 1	*n* = 63	*n* = 62	*n* = 65	*n* = 35	*n* = 47
<6 months	96 ± 43	−32 ± 14	−33 ± 11	1,449 ± 464	−1,015 ± 489	0 ± 44	121 ± 91	−269 ± 142
	19 → 184	−56 → −5	−41 → −25	750 → 2,829	−2,142 → −344	−86 → 101	24 → 397	−638 → −48
	n = 48	*n* = 10	*n* = 2	*n* = 48	*n* = 48	*n* = 48	*n* = 18	*n* = 42
<1 year	104 ± 42	−44 ± 25	−134 ± 0	1,520 ± 463	−1,083 ± 466	1 ± 38	99 ± 40	−271 ± 132
	23 → 251	−82 → −15	−134 → −134	736 → 3,269	−2,650 → −378	−74 → 155	28 → 187	−671 → −58
	n = 73	*n* = 12	*n* = 1	*n* = 73	*n* = 72	*n* = 74	*n* = 24	*n* = 71
1–2 years	114 ± 37	−77 ± 63	−70 ± 24	1,473 ± 593	−1,478 ± 688	11 ± 46	134 ± 70	−307 ± 160
	31 → 193	−200 → −14	−84 → −43	275 → 2,720	−2,722 → −185	−108 → 124	51 → 380	−695 → −36
	n = 101	*n* = 13	*n* = 3	*n* = 106	*n* = 106	*n* = 111	*n* = 46	*n* = 89
3–4 years	110 ± 36	−48 ± 20	−362 ± 0	1,285 ± 442	−1,703 ± 613	38 ± 39	156 ± 83	−222 ± 112
	187 → 44	−95 → −21	−362 → −362	434 → 2,200	−3,188 → −572	−50 → 142	43 → 396	−486 → −50
	n = 140	*n* = 11	*n* = 1	*n* = 140	*n* = 140	*n* = 140	*n* = 107	*n* = 96
5–6 years	110 ± 32	−34 ± 9	−28 ± 10	1,090 ± 385	−1,819 ± 639	54 ± 46	184 ± 119	−154 ± 85
	60 → 214	−48 → −25	−35 → −21	399 → 2,004	−3,161 → −647	−28 → 175	46 → 478	−339 → −38
	n = 155	*n* = 8	*n* = 2	*n* = 155	*n* = 155	*n* = 155	*n* = 133	*n* = 85
7–8 years	106 ± 36	−29 ± 16		1,030 ± 444	−1,822 ± 638	58 ± 41	198 ± 128	−141 ± 93
	45→208	−57 → −15		353 → 2,050	−3,224 → −713	−23 → 184	47 → 547	−540 → −34
	n = 140	*n* = 13		*n* = 140	*n* = 140	*n* = 140	*n* = 131	*n* = 58
9–10 years	102 ± 34	−25 ± 13		870 ± 344	−1,891 ± 624	67 ± 46	280 ± 179	−129 ± 72
	41 → 211	−45 → −13		314 → 1,707	−3,635 → −744	−18 → 198	52 → 865	−259 → −27
	n = 113	*n* = 9		*n* = 114	*n* = 114	*n* = 114	*n* = 105	*n* = 32
11–12 years	94 ± 33	−44 ± 26	−21 ± 0	718 ± 295	−1,704 ± 590	69 ± 51	285 ± 184	−108 ± 61
	36 → 177	−109 → −18	−21 → −21	208 → 1,465	−3,335 → −644	−19 → 212	50 → 809	−237 → −32
	n = 118	*n* = 18	*n* = 1	*n* = 119	*n* = 119	*n* = 119	*n* = 117	*n* = 23
13–14 years	83 ± 34	−42 ± 27	−1,079±1,484	650 ± 336	−1,562 ± 611	66 ± 47	281 ± 186	−84 ± 54
	26 → 160	−125 → −12	−2,128 → −30	170 → 1,493	−2,910 → −387	−10 → 194	43 → 781	−244 → −21
	n = 134	*n* = 32	*n* = 2	*n* = 138	*n* = 138	*n* = 139	*n* = 134	*n* = 20
15–16 years	84 ± 29	−38 ± 17	−26 ± 0	632 ± 356	−1,603 ± 584	78 ± 59	367 ± 238	−117 ± 68
	34 → 152	−69 → −10	−26 → −26	183 → 2,034	−2,888 → −645	6-242	69 → 1,125	−228 → −49
	n = 86	*n* = 21	*n* = 1	*n* = 89	*n* = 89	*n* = 89	*n* = 87	*n* = 5
17–18 years	113 ± 0			1,481 ± 0	−1,599 ± 0	−43 ± 0	75 ± 0	−131 ± 0
	113 → 113			1,481 → 1,481	−1,599 → −1,599	−43 → −43	75-7-5	−131 → −131
	n = 1			*n* = 1	*n* = 1	*n* = 1	*n* = 1	*n* = 1

Table A2.21

Amplitudes (in μV) in Caucasian children: lead V_{4R}

Age-group	P+	P–	Q	R	S	STj	T+	T–
<24 h	75 ± 42	−40 ± 14	−64 ± 76	989 ± 365	−344 ± 169	−6 ± 27	116 ± 87	−82 ± 53
	17 → 178	−69 → −20	−225 → −22	307 → 1,747	−749 → −156	−55 → 74	17 → 440	−244 → −7
	n = 39	*n* = 24	*n* = 7	*n* = 43	*n* = 29	*n* = 43	*n* = 34	*n* = 23
<1 day	86 ± 43	−36 ± 20	−72 ± 31	992 ± 339	−359 ± 263	−13 ± 24	107 ± 71	−85 ± 49
	11 → 200	−142 → −13	−121 → −22	373 → 1,653	−1, 273 → −93	−66 → 36	22 → 292	−228 → −17
	n = 123	*n* = 69	*n* = 14	*n* = 136	*n* = 93	*n* = 136	*n* = 99	*n* = 103
<2 days	80 ± 39	−37 ± 22	−55 ± 34	980 ± 338	−298 ± 181	−15 ± 28	81 ± 52	−109 ± 65
	19 → 189	−149 → −12	−143 → −20	288 → 1,993	−804 → −36	−65 → 61	17 → 291	−285 → −24
	n = 110	*n* = 57	*n* = 19	*n* = 116	*n* = 72	*n* = 116	*n* = 70	*n* = 98
<3 days	74 ± 39	−35 ± 17	−39 ± 18	924 ± 321	−262 ± 161	−23 ± 48	67 ± 36	−129 ± 69
	16 → 166	−102 → −13	−73 → −20	405 → 1,713	−658 → −67	−84 → 30	25 → 199	−322 → −32
	n = 97	*n* = 47	*n* = 15	*n* = 102	*n* = 52	*n* = 102	*n* = 43	*n* = 99
<1 week	88 ± 44	−40 ± 30	−47 ± 22	962 ± 345	−299 ± 214	−34 ± 40	80 ± 59	−165 ± 62
	19 → 235	−169 → −12	−113 → −23	415 → 1,747	−1, 508 → −68	−170 → 29	26 → 328	−295 → −57
	n = 107	*n* = 34	*n* = 15	*n* = 113	*n* = 62	*n* = 113	*n* = 34	*n* = 109
<1 month	77 ± 44	−38 ± 22	−56 ± 57	758 ± 335	−242 ± 232	−28 ± 32	86 ± 43	−152 ± 71
	12 → 161	−110 → −9	−155 → −20	95 → 1,629	−1, 106 → −52	−91 → 82	13 → 167	−342 → −51
	n = 41	*n* = 20	*n* = 5	*n* = 44	*n* = 24	*n* = 44	*n* = 14	*n* = 42
<3 months	60 ± 26	−37 ± 25	−89 ± 91	551 ± 243	−241 ± 126	−26 ± 31	60 ± 46	−225 ± 88
	16 → 121	−105 → −11	−238 → −23	102 → 1,257	−553 → −65	−80 → 34	13 → 128	−464 → −51
	n = 60	*n* = 40	*n* = 5	*n* = 65	*n* = 47	*n* = 67	*n* = 7	*n* = 62
<6 months	53 ± 26	−35 ± 21	−232 ± 255	514 ± 237	−257 ± 210	−18 ± 26	56 ± 0	−236 ± 77
	15 → 144	−104 → −8	−526 → −76	110 → 1,189	−1, 088 → −54	−57 → 31	56 → 56	−466 → −110
	n = 46	*n* = 25	*n* = 3	*n* = 49	*n* = 44	*n* = 49	*n* = 1	*n* = 49
<1 year	58 ± 21	−35 ± 19	−38 ± 8	426 ± 221	−247 ± 148	−14 ± 28	61 ± 24	−234 ± 75
	22 → 123	−104 → −13	−47 → −29	95 → 1,248	−896 → −44	−79 → 116	48 → 97	−474 → −99
	n = 65	*n* = 38	*n* = 4	*n* = 70	*n* = 66	*n* = 71	*n* = 4	*n* = 69
1–2 years	63 ± 25	−36 ± 35	−92 ± 110	348 ± 173	−302 ± 201	−4 ± 37	83 ± 79	−192 ± 78
	16 → 131	−220 → −12	−341 → −35	89 → 835	−1, 026 → −42	−84 → 104	14 → 285	−407 → −52
	n = 102	*n* = 46	*n* = 7	*n* = 110	*n* = 106	*n* = 115	*n* = 10	*n* = 108
3–4 years	73 ± 31	−27 ± 12	−82 ± 68	349 ± 171	−419 ± 229	3 ± 24	46 ± 20	−175 ± 81
	22 → 135	−59 → −12	−202 → −29	77 → 745	−991 → −95	−40 → 62	18 → 100	−352 → −37
	n = 135	*n* = 41	*n* = 6	*n* = 137	*n* = 136	*n* = 137	*n* = 43	*n* = 136
5–6 years	68 ± 30	−28 ± 14	−117 ± 131	295 ± 140	−477 ± 236	10 ± 18	57 ± 60	−166 ± 75
	15 → 131	−75 → −10	−267 → −27	81 → 624	−1, 046 → −104	−24 → 45	26 → 419	−332 → 0
	n = 142	*n* = 65	*n* = 3	*n* = 146	*n* = 145	*n* = 147	*n* = 41	*n* = 147
7–8 years	66 ± 29	−28 ± 13	−70 ± 0	287 ± 151	−488 ± 249	11 ± 18	51 ± 29	−171 ± 74
	12 → 123	−63 → −10	−70 → −70	75 → 648	−1, 109 → −100	−36 → 49	20 → 164	−318 → −35
	n = 129	*n* = 63	*n* = 1	*n* = 136	*n* = 134	*n* = 136	*n* = 42	*n* = 128

Table A2.21 (Continued)

Age-group	P+	P–	Q	R	S	STj	T+	T–
9–10 years	59 ± 29	−31 ± 16	−27 ± 7	245 ± 122	−536 ± 304	13 ± 21	59 ± 39	−160 ± 75
	16 → 142	−115 → −12	−37 → −21	46 → 579	−1, 679 → −109	−42 → 63	26 → 204	−348 → −26
	n = 101	*n* = 67	*n* = 4	*n* = 109	*n* = 107	*n* = 109	*n* = 35	*n* = 104
11–12 years	59 ± 24	−32 ± 15	−270 ± 387	222 ± 131	−539 ± 287	9 ± 24	50 ± 26	−146 ± 80
	17 → 110	−93 → −11	−934 → −20	40 → 631	−1, 277 → −144	−57 → 47	21 → 172	−362 → −33
	n = 95	*n* = 71	*n* = 5	*n* = 102	*n* = 102	*n* = 104	*n* = 44	*n* = 95
13–14 years	46 ± 27	−34 ± 15	−282 ± 278	190 ± 115	−486 ± 274	13 ± 17	41 ± 22	−113 ± 63
	10 → 102	−76 → −12	−569 → −20	43 → 575	−1, 460 → −36	−26 → 51	13 → 94	−318 → −18
	n = 95	*n* = 90	*n* = 4	*n* = 109	*n* = 107	*n* = 111	*n* = 45	*n* = 103
15–16 years	51 ± 25	−29 ± 14	−166 ± 206	184 ± 135	−482 ± 320	13 ± 24	59 ± 49	−104 ± 66
	13 → 109	−76 → −11	−311 → −20	25 → 914	−1, 209 → −31	−36 → 83	15 → 219	−298 → −16
	n = 66	*n* = 46	*n* = 2	*n* = 73	*n* = 71	*n* = 74	*n* = 38	*n* = 55
17–18 years	24 ± 0	−48 ± 0		655 ± 0	−249 ± 0	−16 ± 0		−132 ± 0
	24 → 24	−48 → −48		655 → 655	−249 → −249	−16 → −16		−132 → −132
	n = 1	*n* = 1		*n* = 1	*n* = 1	*n* = 1		*n* = 1

Table A2.22

Amplitudes (in μV) in Caucasian children: lead V_4

Age-group	P+	P–	Q	R	S	STj	T+	T–
<24 h	139 ± 43	−78 ± 86	−83 ± 39	1,554 ± 484	−1, 573 ± 562	10 ± 51	187 ± 128	−92 ± 40
	66 → 250	−177 → −24	−156 → −32	700 → 2,427	−3, 213 → −592	−65 → 141	42 → 177	−175 → −51
	n = 42	*n* = 3	*n* = 8	*n* = 43	*n* = 42	*n* = 43	*n* = 38	*n* = 11
<1 day	141 ± 58	−104 ± 108	−72 ± 50	1,578 ± 483	−1, 565 ± 560	7 ± 53	178 ± 135	−134 ± 93
	57 → 279	−313 → −24	−233 → −20	2,513 → 536	−2, 834 → −530	−110 → 125	24 → 776	−446 → −24
	n = 138	*n* = 6	*n* = 23	*n* = 138	*n* = 137	*n* = 138	*n* = 113	*n* = 56
<2 days	134 ± 40	−62 ± 66	−107 ± 83	1,567 ± 510	−1, 439 ± 524	14 ± 52	144 ± 111	−115 ± 78
	62 → 236	−160 → −18	−367 → −30	540 → 3,072	−2, 608 → −424	−132 → 117	15 → 429	−350 → −250
	n = 119	*n* = 4	*n* = 20	*n* = 119	*n* = 119	*n* = 119	*n* = 89	*n* = 57
<3 days	144 ± 39	−39 ± 11	−91 ± 67	1,545 ± 534	−1, 254 ± 539	25 ± 69	139 ± 99	−166 ± 113
	69 → 229	−47 → −31	−218 → −20	67 → 2,847	−2, 502 → −132	−110 → 152	15 → 440	−580 → −43
	n = 106	*n* = 2	*n* = 25	*n* = 106	*n* = 104	*n* = 106	*n* = 75	*n* = 57
<1 week	143 ± 44	−71 ± 75	−116 ± 98	1,645 ± 542	−1, 173 ± 489	36 ± 63	178 ± 97	−187 ± 121
	56 → 251	−157 → −19	−481 → −20	695 → 3,126	−2, 392 → −261	−98 → 180	39 → 402	−644 → −54
	n = 116	*n* = 3	*n* = 57	*n* = 116	*n* = 115	*n* = 116	*n* = 79	*n* = 56
<1 month	142 ± 43	−72 ± 0	−140 ± 97	1,497 ± 463	−954 ± 369	32 ± 57	259 ± 127	−193 ± 129
	55 → 239	−72 → −72	−373 → −23	732 → 2,757	−2, 350 → −317	−76 → 157	41 → 561	−442 → −25
	n = 45	*n* = 1	*n* = 20	*n* = 45	*n* = 45	*n* = 45	*n* = 38	*n* = 11
<3 months	113 ± 37	−26 ± 8	−156 ± 123	1,983 ± 489	−863 ± 355	44 ± 61	273 ± 155	−162 ± 187
	48 → 208	−35 → −16	−540 → −26	1,094 → 3,084	−1, 649 → −150	−36 → 373	21 → 735	−647 → −40
	n = 67	*n* = 4	*n* = 35	*n* = 67	*n* = 65	*n* = 69	*n* = 63	*n* = 9
<6 months	104 ± 43	−29 ± 10	−185 ± 152	1,741 ± 549	−795 ± 331	48 ± 37	257 ± 180	−132 ± 65
	49 → 276	−38 → −18	−428 → −20	877 → 3,202	−1, 659 → −307	−11 → 162	58 → 910	−233 → −39
	n = 50	*n* = 3	*n* = 20	*n* = 50	*n* = 50	*n* = 50	*n* = 46	*n* = 11

Table A2.22 (Continued)

Age-group	P+	P–	Q	R	S	STj	T+	T–
<1 year	109 ± 40	−31 ± 19	−190 ± 184	1,792 ± 675	−794 ± 410	44 ± 48	270 ± 148	−223 ± 162
	49 → 257	−52 → −16	−777 → −25	541 → 3,768	−2, 462 → −222	−42 → 263	52 → 663	−713 → −63
	n = 72	*n* = 3	*n* = 27	*n* = 72	*n* = 71	*n* = 73	*n* = 63	*n* = 16
1–2 years	86 ± 27	−37 ± 28	−179 ± 129	1,668 ± 668	−741 ± 414	36 ± 33	282 ± 187	−147 ± 94
	25 → 155	−89 → −15	−549 → −25	50 → 3,095	−1, 995 → −165	−23 → 114	24 → 719	−348 → −27
	n = 109	*n* = 10	*n* = 47	*n* = 110	*n* = 108	*n* = 115	*n* = 98	*n* = 32
3–4 years	87 ± 27	−17 ± 5	−143 ± 113	2,125 ± 724	−861 ± 482	34 ± 33	433 ± 259	−113 ± 122
	41 → 150	−26 → −11	−523 → −22	886 → 3,760	−2, 083 → −145	−39 → 105	49 → 993	−443 → −31
	n = 141	*n* = 12	*n* = 50	*n* = 141	*n* = 134	*n* = 141	*n* = 140	*n* = 10
5–6 years	86 ± 25	−23 ± 12	−134 ± 118	2,263 ± 828	−963 ± 532	44 ± 41	523 ± 223	−206 ± 52
	43 → 154	−49 → −12	−613 → −21	929 → 4,305	−2, 694 → −200	−20 → 153	138 → 987	−261 → −158
	n = 155	*n* = 17	*n* = 56	*n* = 155	*n* = 152	*n* = 155	*n* = 153	*n* =3
7–8 years	84 ± 28	−25 ± 12	−110 ± 93	2,063 ± 793	−1, 037 ± 566	44 ± 42	571 ± 246	−129 ± 0
	47 → 159	−51 → −14	−459 → −24	911 → 3,804	−2, 307 → −114	−36 → 122	150 → 1,232	−129 → −129
	n = 141	*n* = 13	*n* = 39	*n* = 141	*n* = 140	*n* = 141	*n* = 141	*n* = 1
9–10 years	82 ± 24	−22 ± 6	−100 ± 80	1,955 ± 771	−972 ± 510	56 ± 51	652 ± 264	
	44 → 151	−37 → −14	−312 → −22	878 → 4,040	−2, 359 → −136	−19 → 198	168 → 1,328	
	n = 115	*n* = 12	*n* = 25	*n* = 115	*n* = 111	*n* = 115	*n* = 115	
11–12 years	87 ± 25	−25 ± 22	−102 ± 82	1,864 ± 686	−891 ± 495	45 ± 51	589 ± 251	
	43 → 145	−86 → −10	−292 → −22	713 → 3,400	−2, 475 → −149	−47 → 200	203 → 1,292	
	n = 118	*n* = 10	*n* = 26	*n* = 119	*n* = 115	*n* = 119	*n* = 119	
13–14 years	79 ± 28	−23 ± 12	−55 ± 32	1,632 ± 624	−1, 045 ± 547	68 ± 64	602 ± 251	−48 ± 0
	27 → 137	−47 → −7	−174 → −24	607 → 3,010	−2, 342 → −206	−21 → 253	168 → 1,176	−48 → −48
	n = 140	*n* = 22	*n* = 26	*n* = 141	*n* = 138	*n* = 141	*n* = 141	*n* = 1
15–16 years	83 ± 27	−19 ± 7	−85 ± 97	1,638 ± 735	−898 ± 554	60 ± 67	587 ± 289	−109 ± 58
	31 → 144	−38 → −10	−381 → −20	582 → 3,787	−2, 332 → −168	−38 → 229	188 → 1,314	−150 → −68
	n = 91	*n* = 11	*n* = 17	*n* = 91	*n* = 90	*n* = 91	*n* = 91	*n* = 2
17–18 years	199 ± 0			1,687 ± 0	−2, 201 ± 0	72 ± 0	143 ± 0	
	199 → 199			1,687 → 1,687	−2, 201 → −2,201	72 → 72	143 → 143	
	n = 1			*n* = 1	*n* = 1	*n* = 1	*n* = 1	

Table A2.23

Amplitudes (in μV) in Caucasian children: lead V_5

Age-group	P+	P–	Q	R	S	STj	T+	T–
<24 h	110 ± 40	−99 ± 109	−132 ± 102	924 ± 419	−893 ± 427	29 ± 41	161 ± 104	−55 ± 32
	45 → 218	−176 → −22	−381 → −22	292 → 1,890	−1, 848 → −148	−53 → 157	18 → 440	−98 → −11
	n = 42	*n* = 2	*n* = 22	*n* = 43	*n* = 41	*n* = 43	*n* = 43	*n* = 8
<1 day	112 ± 51	−60 ± 32	−104 ± 64	999 ± 434	−964 ± 470	29 ± 34	154 ± 88	−66 ± 39
	55 → 213	−102 → −13	−278 → −23	296 → 1,886	−1, 958 → −206	−37 → 106	29 → 385	−151 → −20
	n = 135	*n* = 7	*n* = 77	*n* = 137	*n* = 134	*n* = 137	*n* = 131	*n* = 33
<2 days	105 ± 33	−24 ± 10	−127 ± 100	941 ± 419	−924 ± 451	33 ± 38	173 ± 90	−64 ± 49
	43 → 205	−40 → −10	−543 → −27	221 → 1,840	−2, 171 → −210	−65 → 117	27 → 458	−204 → −11
	n = 116	*n* = 6	*n* = 59	*n* = 118	*n* = 116	*n* = 118	*n* = 110	*n* = 20

Table A2.23 (Continued)

Age-group	P+	P–	Q	R	S	STj	T+	T–
<3 days	115 ± 35	−34 ± 24	−124 ± 69	1,002 ± 427	−876 ± 477	52 ± 40	192 ± 91	−106 ± 65
	55 → 186	−51 → −17	−256 → −24	291 → 2,255	−2,343 → −225	−30 → 138	51 → 436	−278 → −22
	n = 106	*n* = 2	*n* = 59	*n* = 106	*n* = 104	*n* = 106	*n* = 97	*n* = 18
<1 week	114 ± 36	−26 ± 15	−172 ± 101	1,090 ± 473	−794 ± 385	59 ± 50	243 ± 114	−170 ± 167
	38 → 191	−40 → −11	−466 → −28	273 → 2,412	−1,685 → −154	−60 → 205	42 → 519	−510 → −18
	n = 116	*n* = 3	*n* = 96	*n* = 116	*n* = 109	*n* = 117	*n* = 109	*n* = 13
<1 month	119 ± 44	−45 ± 2	−184 ± 114	1,163 ± 538	−647 ± 375	42 ± 46	310 ± 150	−34 ± 16
	58 → 298	−46 → −43	−478 → −43	324 → 2,690	−1,767 → −112	−32 → 172	90 → 696	−45 → −22
	n = 43	*n* = 2	*n* = 36	*n* = 44	*n* = 42	*n* = 44	*n* = 43	*n* = 2
<3 months	101 ± 33	−24 ± 10	−228 ± 159	1,849 ± 630	−578 ± 272	47 ± 43	358 ± 130	−93 ± 0
	39 → 220	−38 → −17	−959 → −32	913 → 3,271	−1,367 → −177	−25 → 202	86 → 648	−93 → −93
	n = 66	*n* = 4	*n* = 56	*n* = 66	*n* = 65	*n* = 68	*n* = 66	*n* = 1
<6 months	96 ± 51	−31 ± 30	−195 ± 117	1,569 ± 563	−536 ± 329	60 ± 51	357 ± 202	−130 ± 0
	31 → 277	−75 → −9	−496 → −35	572 → 3,111	−1,368 → −157	−11 → 203	107 → 928	−130 → −130
	n = 48	*n* = 4	*n* = 38	*n* = 48	*n* = 46	*n* = 48	*n* = 47	*n* = 1
<1 year	94 ± 36	−29 ± 13	−218 ± 159	1,758 ± 667	−481 ± 272	53 ± 42	364 ± 148	−72 ± 18
	34 → 293	−52 → −18	−891 → −38	59 → 3,238	−1,277 → −95	−5 → 317	35 → 748	−88 → −45
	n = 73	*n* = 5	*n* = 58	*n* = 73	*n* = 67	*n* = 74	*n* = 73	*n* = 4
1–2 years	84 ± 48	−34 ± 27	−224 ± 155	1,569 ± 690	−379 ± 234	30 ± 48	333 ± 160	−109 ± 47
	29 → 391	−103 → −13	−626 → −35	35 → 3,080	−999 → −65	−25 → 120	63 → 724	−172 → −35
	n = 109	*n* = 13	*n* = 83	*n* = 111	*n* = 100	*n* = 116	*n* = 107	*n* = 6
3–4 years	78 ± 21	−18 ± 11	−189 ± 126	2,003 ± 661	−388 ± 234	15 ± 26	465 ± 204	−37 ± 26
	35 → 116	−45 → −6	−596 → −26	803 → 3,381	−1,047 → −56	−38 → 71	62 → 877	−76 → −21
	n = 140	*n* = 10	*n* = 121	*n* = 140	*n* = 120	*n* = 140	*n* = 140	*n* = 4
5–6 years	78 ± 22	−22 ± 16	−185 ± 130	2,443 ± 684	−493 ± 294	20 ± 33	578 ± 196	
	36 → 120	−85 → −12	−534 → −20	1,227 → 3,889	−1,475 → −105	−60 → 98	235 → 1,065	
	n = 155	*n* = 18	*n* = 125	*n* = 155	*n* = 142	*n* = 155	*n* = 155	
7–8 years	76 ± 21	−39 ± 62	−160 ± 114	2,392 ± 640	−488 ± 276	14 ± 32	627 ± 196	
	41 → 134	−267 → −11	−481 → −21	1,302 → 4,029	−1,159 → −109	−48 → 87	262 → 1,131	
	n = 139	*n* = 16	*n* = 118	*n* = 141	*n* = 134	*n* = 141	*n* = 141	
9–10 years	74 ± 21	−17 ± 4	−154 ± 108	2,373 ± 606	−424 ± 278	22 ± 34	676 ± 226	
	39 → 136	−23 → −12	−411 → −23	1,209 → 3,918	−1,200 → −86	−34 → 110	219 → 1,146	
	n = 115	*n* = 11	*n* = 97	*n* = 115	*n* = 106	*n* = 115	*n* = 115	
11–12 years	81 ± 23	−26 ± 29	−123 ± 91	2,317 ± 686	−430 ± 264	16 ± 41	604 ± 255	−110 ± 0
	43 → 153	−90 → −10	−346 → −20	933 → 3,796	−1,169 → −77	−58 → 152	200 → 1,286	−110 → −110
	n = 117	*n* = 7	*n* = 91	*n* = 118	*n* = 106	*n* = 118	*n* = 118	*n* = 1
13–14 years	74 ± 27	−19 ± 9	−123 ± 108	2,272 ± 795	−519 ± 309	29 ± 46	598 ± 240	−51 ± 0
	18 → 130	−43 → −5	−441 → −25	973 → 4,521	−1,213 → −126	−46 → 153	208 → 1,192	−51 → −51
	n = 138	*n* = 24	*n* = 87	*n* = 140	*n* = 135	*n* = 140	*n* = 139	*n* = 1
15–16 years	79 ± 24	−16 ± 4	−117 ± 94	1,901 ± 738	−508 ± 394	25 ± 39	515 ± 237	−101 ± 25
	35 → 150	−21 → −10	−383 → −23	665 → 3,687	−1,691 → −70	−23 → 105	186 → 1,089	−129 → −81
	n = 92	*n* = 8	*n* = 50	*n* = 92	*n* = 86	*n* = 92	*n* = 92	*n* = 3
17–18 years	146 ± 0		−125 ± 0	969 ± 0	−426 ± 0	69 ± 0	241 ± 0	
	146 → 146		−125 → −125	969 → 969	−426 → −426	69 → 69	241 → 241	
	n = 1		*n* = 1	*n* = 1	*n* = 1	*n* = 1	*n* = 1	

Table A2.24

Amplitudes (in μV) in Caucasian children: lead V_6

Age-group	P+	P−	Q	R	S	STj	T+	T−
<24 h	83 ± 30	−97 ± 91	−140 ± 92	521 ± 258	−372 ± 198	26 ± 37	162 ± 124	−40 ± 23
	42 → 166	−199 → −24	−412 → −26	83 → 1,118	−867 → −139	−29 → 200	36 → 604	−88 → −21
	n = 41	*n* = 3	*n* = 36	*n* = 40	*n* = 32	*n* = 42	*n* = 42	*n* = 8
<1 day	83 ± 31	−41 ± 28	−133 ± 84	563 ± 389	−467 ± 353	22 ± 28	131 ± 69	−54 ± 36
	29 → 136	−76 → −10	−328 → −22	67 → 1,705	−1,708 → −55	−32 → 81	28 → 323	−137 → −10
	n = 127	*n* = 11	*n* = 100	*n* = 127	*n* = 104	*n* = 132	*n* = 128	*n* = 16
<2 days	82 ± 30	−39 ± 29	−116 ± 83	488 ± 314	−438 ± 324	32 ± 42	159 ± 81	−75 ± 38
	38 → 161	−85 → −2	−380 → −22	38 → 1,328	−1,326 → −100	−24 → 130	37 → 464	−134 → −21
	n = 110	*n* = 7	*n* = 85	*n* = 111	*n* = 100	*n* = 115	*n* = 107	*n* = 10
<3 days	92 ± 34	−13 ± 4	−122 ± 82	545 ± 345	−493 ± 361	44 ± 38	173 ± 76	−83 ± 37
	30 → 177	−17 → −8	−377 → −24	68 → 1,562	−1,558 → −60	−21 → 171	51 → 391	−129 → −20
	n = 101	*n* = 4	*n* = 81	*n* = 99	*n* = 79	*n* = 103	*n* = 100	*n* = 9
<1 week	86 ± 33	−30 ± 22	−163 ± 99	574 ± 368	−407 ± 244	53 ± 65	203 ± 105	−55 ± 44
	29 → 177	−73 → −3	−388 → −27	69 → 1,814	−998 → −66	−38 → 301	25 → 493	−148 → −6
	n = 109	*n* = 8	*n* = 99	*n* = 110	*n* = 87	*n* = 112	*n* = 109	*n* = 9
<1 month	100 ± 39	−42 ± 33	−183 ± 93	743 ± 456	−339 ± 230	41 ± 50	267 ± 122	−7 ± 0
	40 → 225	−93 → −23	−346 → −49	43 → 1,867	−1,023 → −68	−12 → 237	90 → 666	−7 → −7
	n = 45	*n* = 4	*n* = 38	*n* = 45	*n* = 40	*n* = 45	*n* = 45	*n* = 1
<3 months	96 ± 30	−30 ± 21	−223 ± 127	1,359 ± 581	−361 ± 223	39 ± 36	330 ± 106	
	52 → 219	−55 → −17	−738 → −31	538 → 2,976	−1,087 → −60	−25 → 133	126 → 603	
	n = 64	*n* = 3	*n* = 61	*n* = 65	*n* = 53	*n* = 67	*n* = 65	
<6 months	88 ± 37	−33 ± 26	−200 ± 110	1,193 ± 472	−326 ± 212	52 ± 35	326 ± 143	−167 ± 0
	39 → 277	−73 → −11	−479 → −35	142 → 2,321	−820 → −64	−7 → 178	140 → 843	−167 → −167
	n = 48	*n* = 5	*n* = 42	*n* = 49	*n* = 41	*n* = 49	*n* = 48	*n* = 1
<1 year	91 ± 53	−31 ± 21	−223 ± 135	1,230 ± 561	−274 ± 223	51 ± 54	349 ± 113	−183 ± 0
	34 → 411	−57 → −6	−740 → −26	30 → 2,539	−1,600 → −42	−20 → 334	159 → 651	−183 → −183
	n = 72	*n* = 8	*n* = 59	*n* = 73	*n* = 60	*n* = 74	*n* = 72	*n* = 1
1–2 years	75 ± 29	−30 ± 22	−216 ± 134	1,196 ± 547	−227 ± 151	23 ± 30	282 ± 119	−55 ± 24
	28 → 146	−65 → −6	−539 → −23	54 → 2,324	−701 → −56	−25 → 120	54 → 550	−83 → −24
	n = 109	*n* = 9	*n* = 91	*n* = 110	*n* = 76	*n* = 115	*n* = 109	*n* = 4
3–4 years	74 ± 20	−28 ± 36	−179 ± 109	1,428 ± 511	−211 ± 109	7 ± 22	367 ± 135	−99 ± 104
	36 → 113	−135 → −6	−530 → −28	435 → 2,320	−442 → −66	−41 → 45	100 → 642	−255 → −37
	n = 138	*n* = 12	*n* = 131	*n* = 140	*n* = 99	*n* = 140	*n* = 137	*n* = 4
5–6 years	72 ± 21	−19 ± 8	−181 ± 112	1,747 ± 477	−240 ± 149	11 ± 29	434 ± 148	−63 ± 13
	26 → 115	−37 → −11	−511 → −25	803 → 2,974	−650 → −56	−51 → 85	168 → 801	−72 → −54
	n = 154	*n* = 10	*n* = 139	*n* = 154	*n* = 119	*n* = 154	*n* = 154	*n* = 2
7–8 years	72 ± 20	−27 ± 15	−162 ± 98	1,797 ± 538	−239 ± 153	9 ± 31	487 ± 150	
	40 → 120	−60 → −11	−417 → −35	968 → 3,137	−799 → −51	−51 → 110	234 → 908	
	n = 139	*n* = 13	*n* = 129	*n* = 140	*n* = 119	*n* = 140	*n* = 140	
9–10 years	70 ± 20	−14 ± 4	−153 ± 92	1,851 ± 453	−221 ± 140	13 ± 30	519 ± 173	
	30 → 125	−21 → −9	−404 → −28	1,030 → 3,135	−642 → −53	−37 → 136	193 → 946	
	n = 115	*n* = 12	*n* = 107	*n* = 115	*n* = 88	*n* = 115	*n* = 115	
11–12 years	76 ± 21	−22 ± 18	−130 ± 79	1,836 ± 478	−239 ± 134	7 ± 29	463 ± 173	
	42 → 121	−65 → −8	−306 → −23	907 → 3,022	−573 → −76	−55 → 121	892 → 163	
	n = 116	*n* = 9	*n* = 104	*n* = 117	*n* = 86	*n* = 117	*n* = 117	

Table A2.24 (Continued)

Age-group	P+	P–	Q	R	S	STj	T+	T–
13–14 years	70 ± 26	−21 ± 12	−117 ± 92	1,762 ± 515	−244 ± 139	15 ± 40	450 ± 177	−89 ± 49
	20 → 127	−45 → −6	−391 → −23	874 → 3,107	−384 → −36	−65 → 151	204 → 983	−124 → −54
	n = 136	*n* = 17	*n* = 124	*n* = 140	*n* = 122	*n* = 140	*n* = 139	*n* = 2
15–16 years	75 ± 23	−14 ± 6	−118 ± 74	1,574 ± 498	−267 ± 206	11 ± 29	395 ± 170	−127 ± 66
	28 → 144	−96 → −11	−377 → −26	656 → 2,691	−1, 075 → −62	−34 → 64	135 → 806	−226 → −89
	n = 87	*n* = 6	*n* = 58	*n* = 88	*n* = 72	*n* = 88	*n* = 87	*n* = 4
17–18 years	136 ± 0		−177 ± 0	595 ± 0		44 ± 0	153 ± 0	
	136 → 136		−177 → → 177	595 → 595		44 → 44	153 → 153	
	n = 1		*n* = 1	*n* = 1		*n* = 1	*n* = 1	

A2.2 Percentile Charts

The following percentile charts showing normal 12-lead ECG limits were obtained from a study of 2,141 white children between birth and 16 years. Data were derived from computer-assisted methods where the sampling rate was 333 samples per second so that there may be some underestimation of upper limits of normal. The charts are reproduced from: Davignon A *et al*. Normal ECG standards for infants and children. *Pediatr. Cardiol*. 1979/1980; **1**: 133–52 with the permission of Springer, New York. Note that V_3R was included while V_3 was omitted in this study (Figs. A2.1–A2.39).

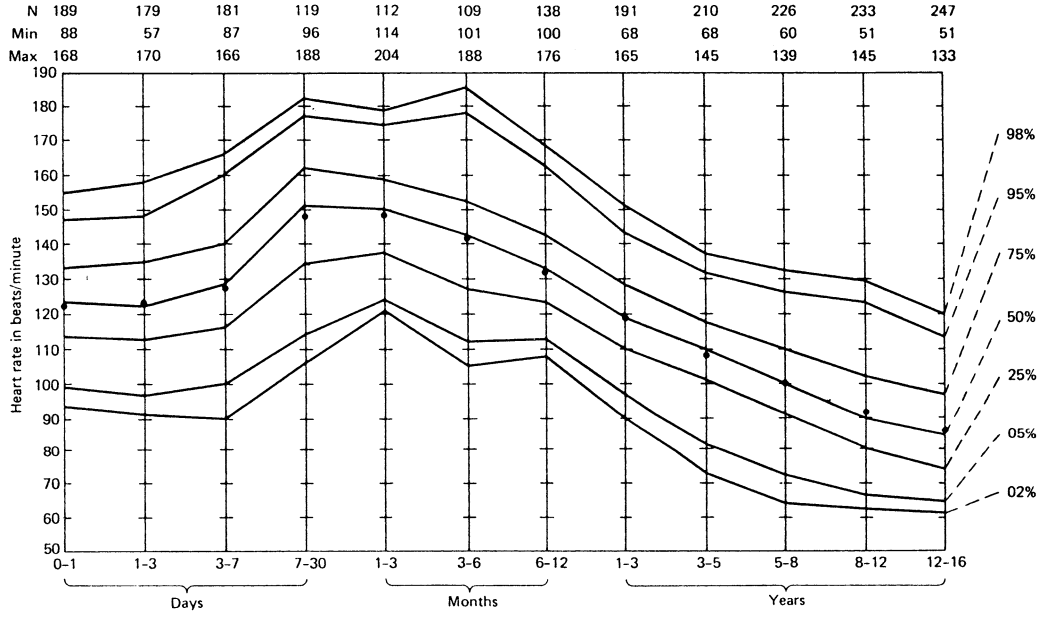

Figure A2.1
Heart rate versus age (•, mean).

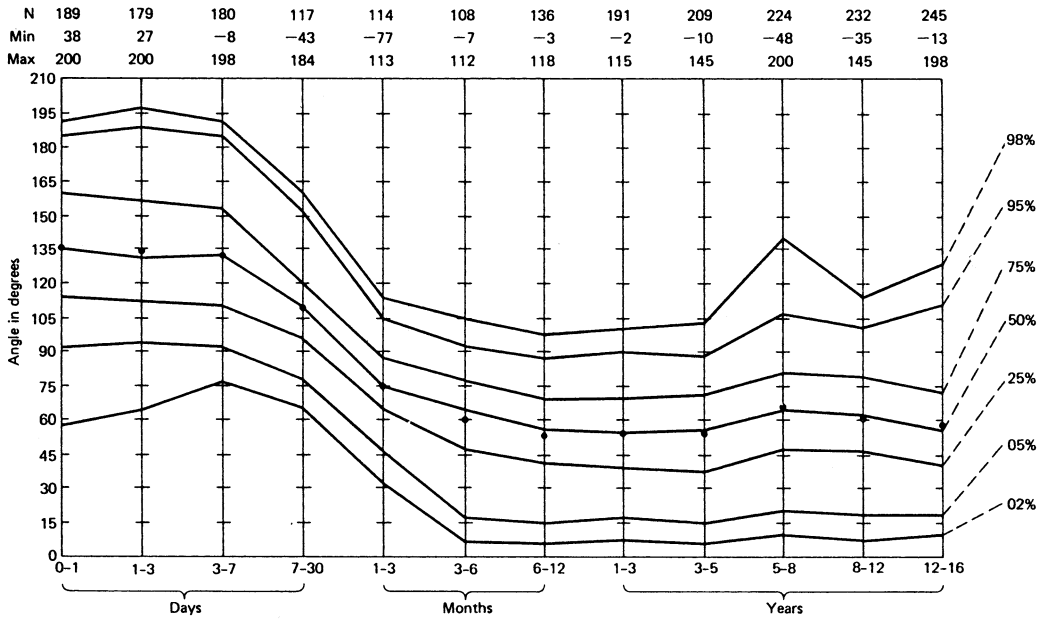

Figure A2.2

Frontal plane QRS angle versus age (•, mean).

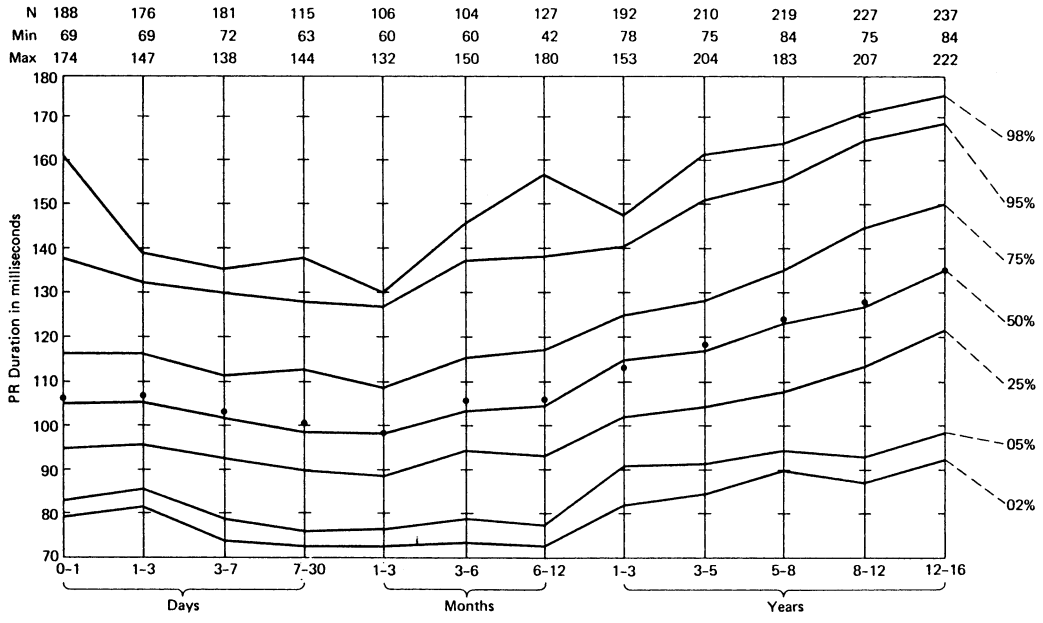

Figure A2.3

PR duration in lead II versus age (•, mean).

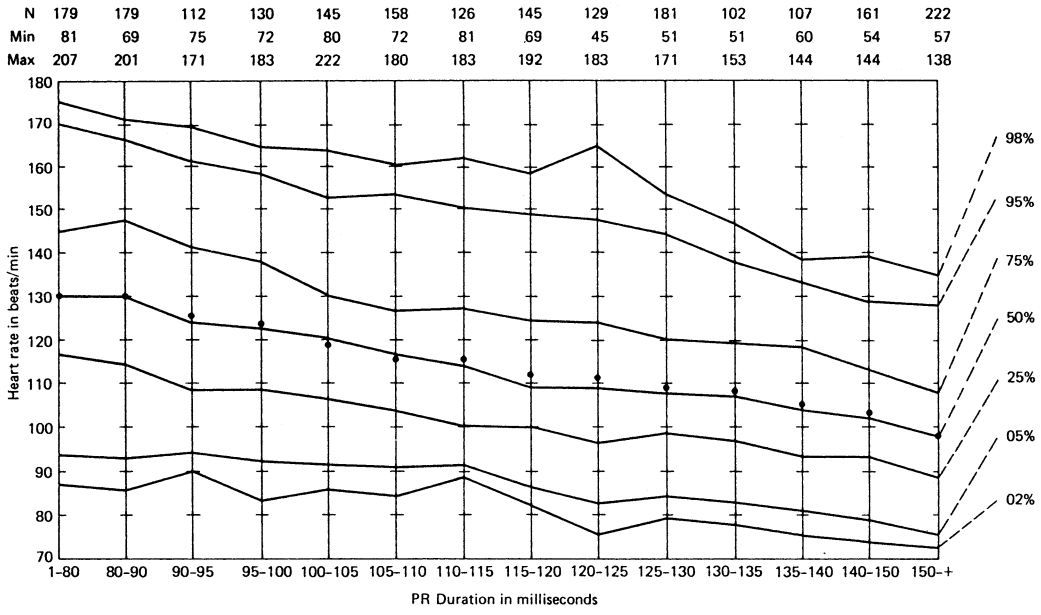

Figure A2.4

Heart rate versus PR duration in lead II (•, mean).

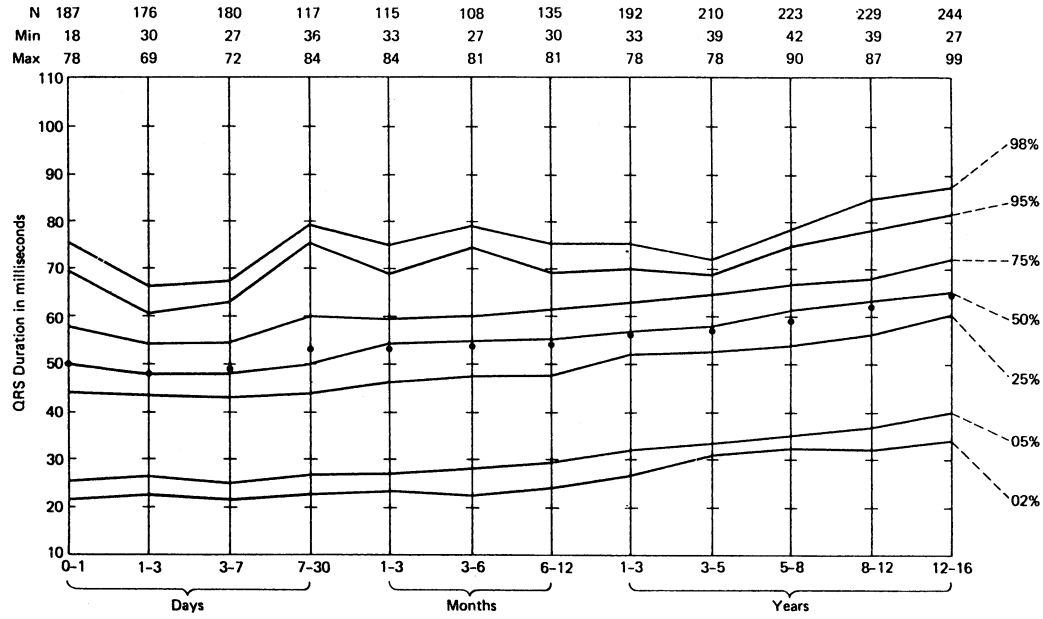

Figure A2.5

QRS duration in lead V_5 versus age (•, mean).

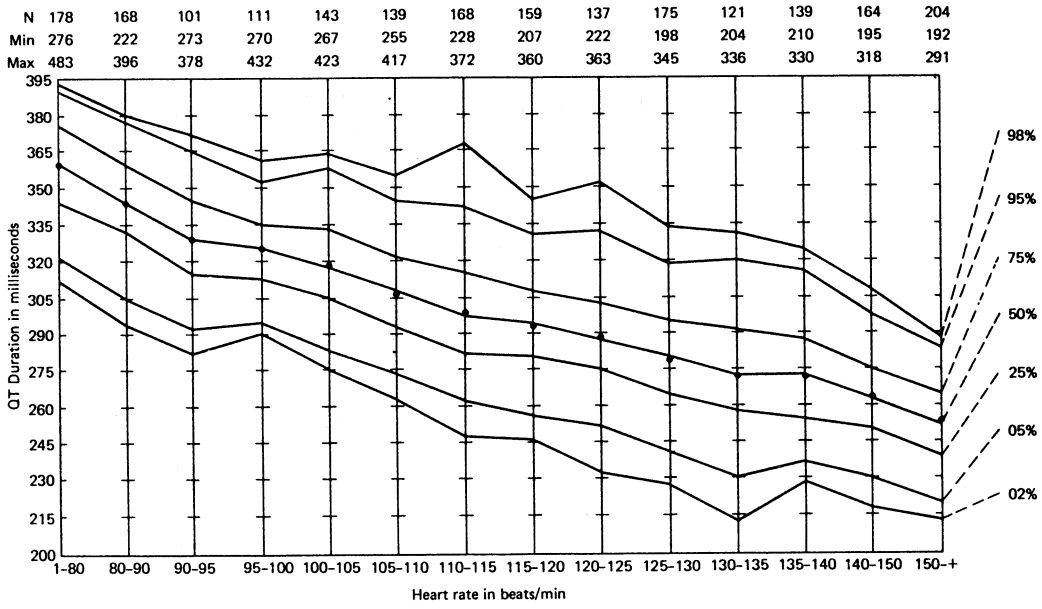

Figure A2.6

QT duration in lead V_5 versus heart rate (•, mean).

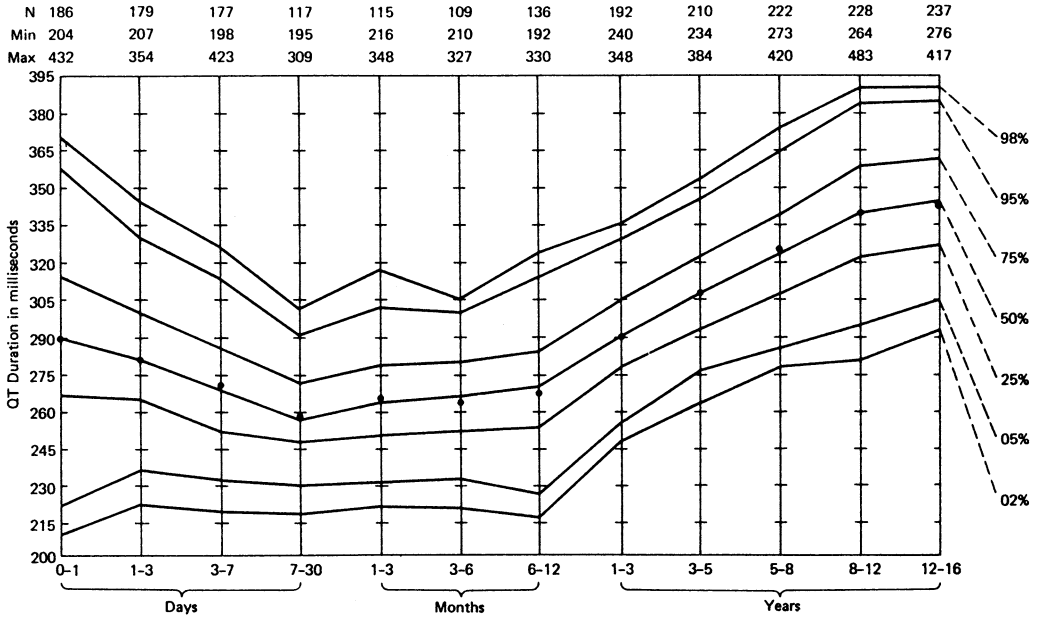

Figure A2.7

QT duration in lead V_5 versus age (•, mean).

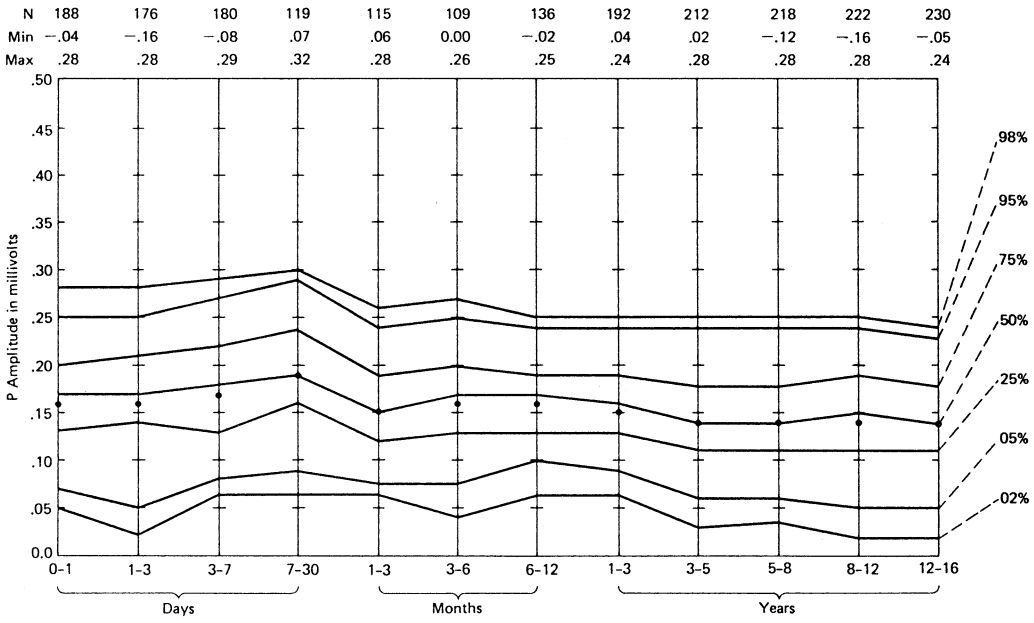

Figure A2.8

P amplitude in lead II versus age (•, mean).

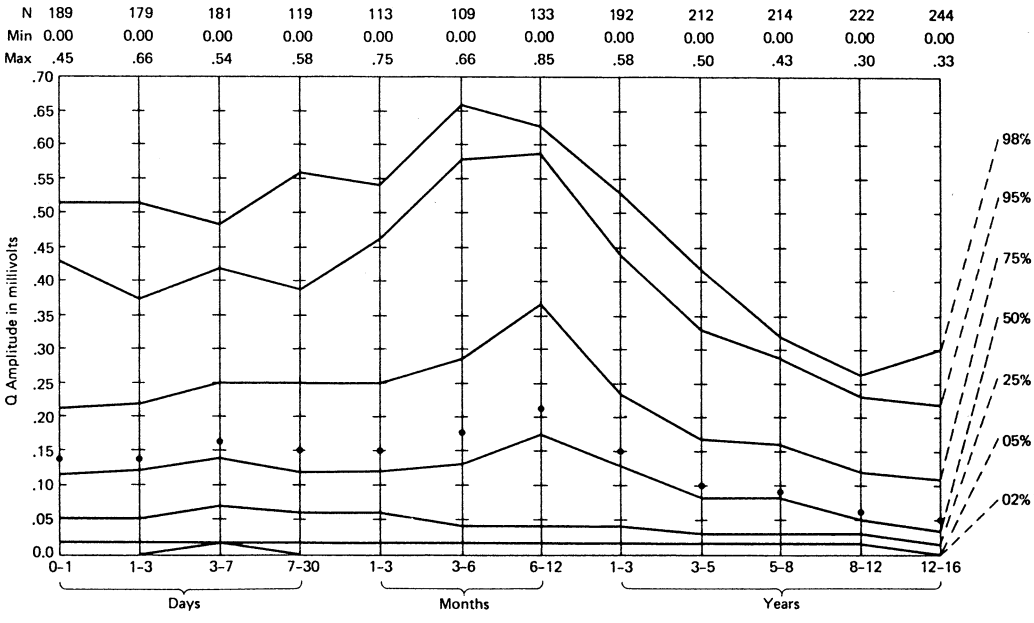

Figure A2.9

Q amplitude in lead III versus age (•, mean).

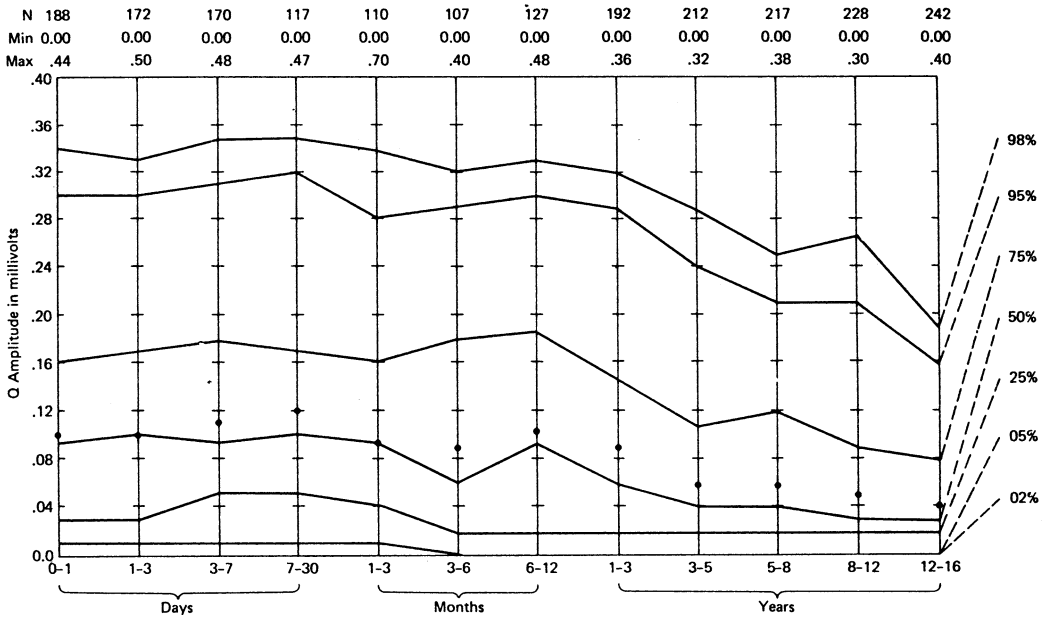

Figure A2.10

Q amplitude in lead a VF versus age (•, mean).

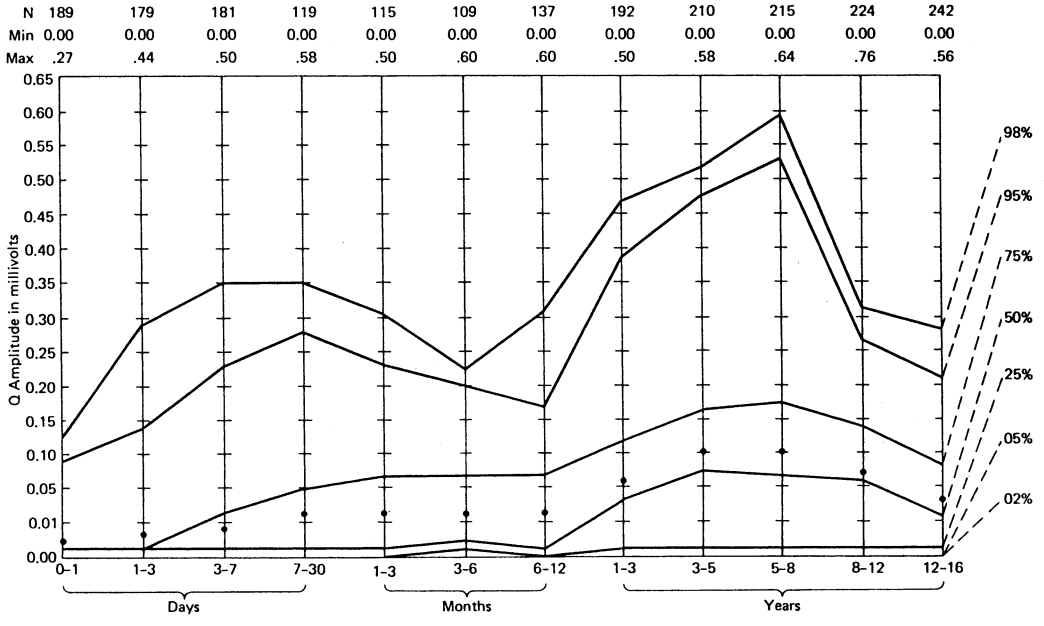

Figure A2.11

Q amplitude in lead V_5 versus age (•, mean).

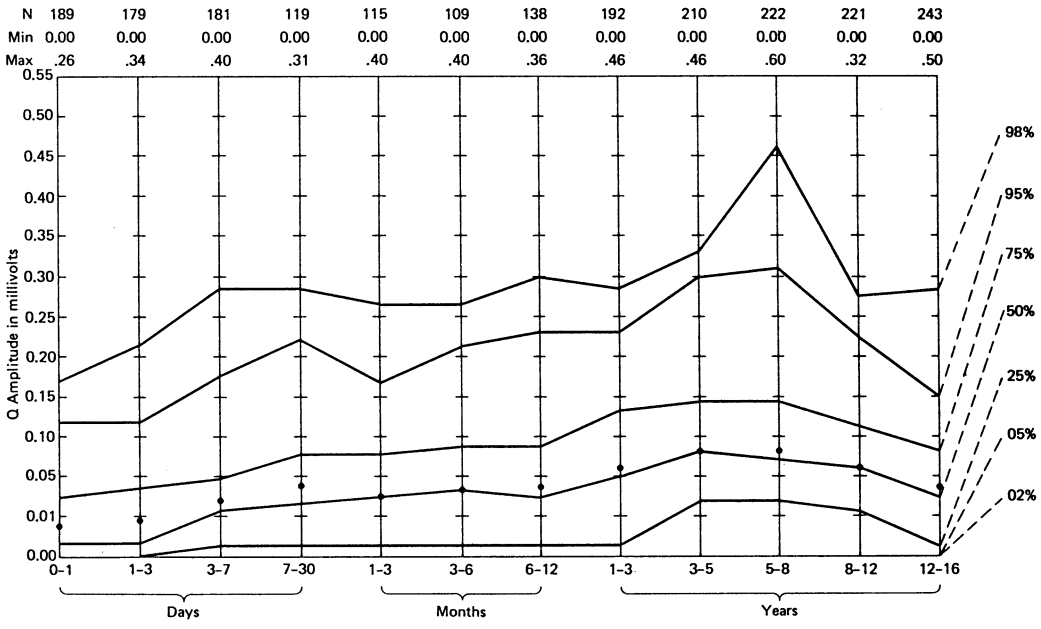

Figure A2.12

Q amplitude in lead V_6 versus age (•, mean).

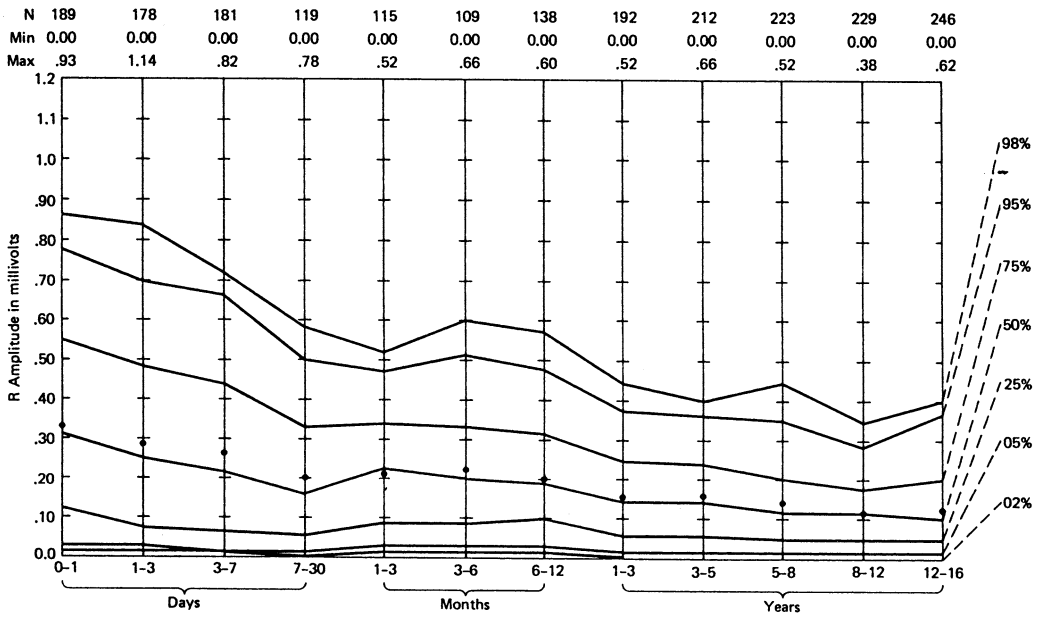

Figure A2.13

R amplitude in lead aVR versus age (•, mean).

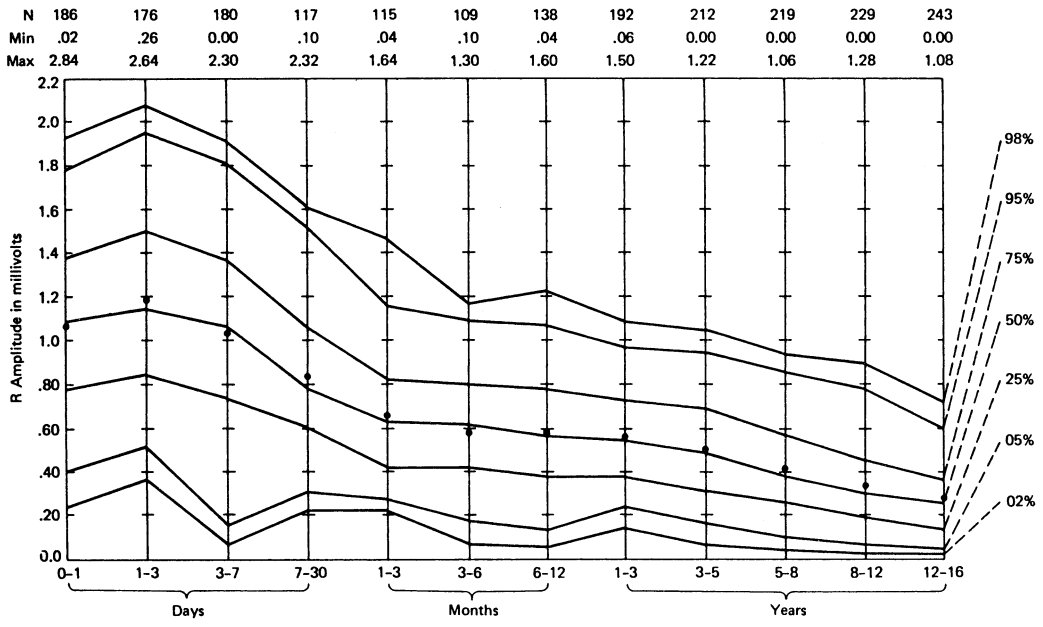

Figure A2.14

R amplitude in lead V_3R versus age (•, mean).

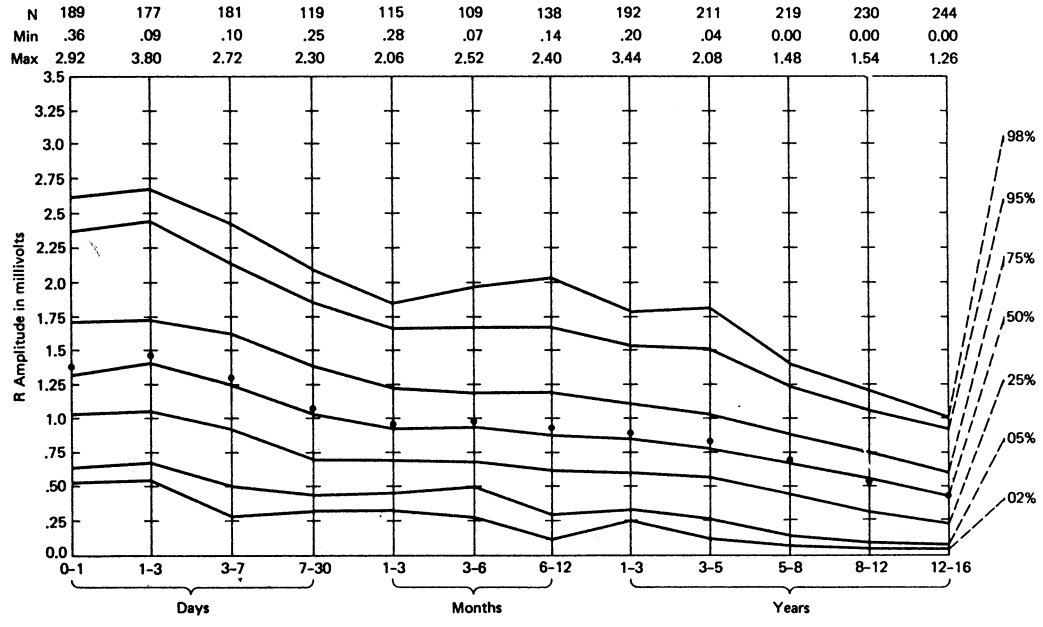

Figure A2.15

R amplitude in lead V_1 versus age (•, mean).

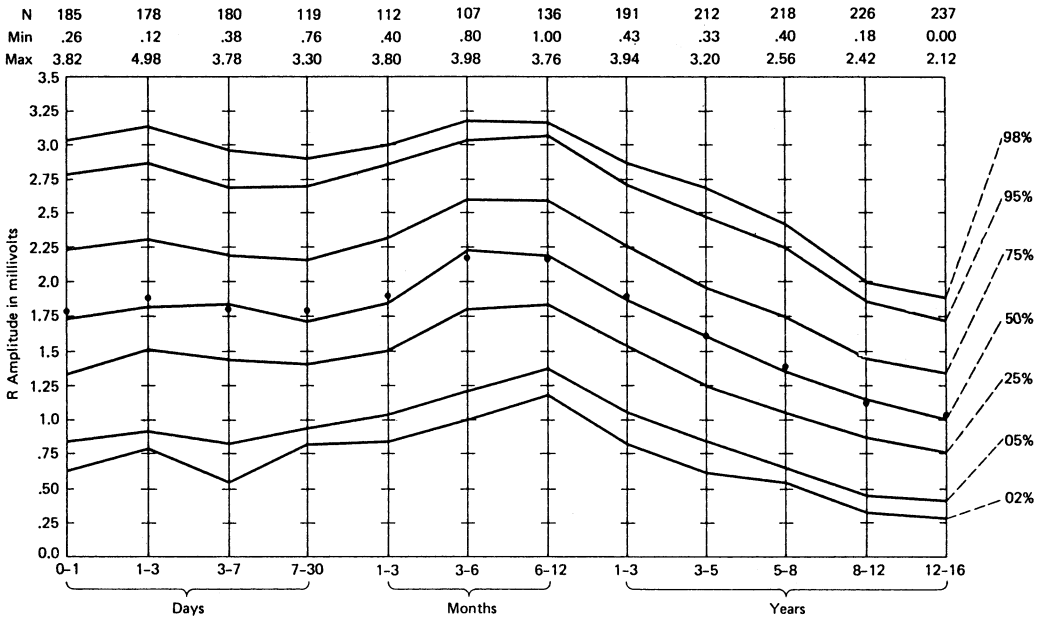

Figure A2.16

R amplitude in lead V_2 versus age (•, mean).

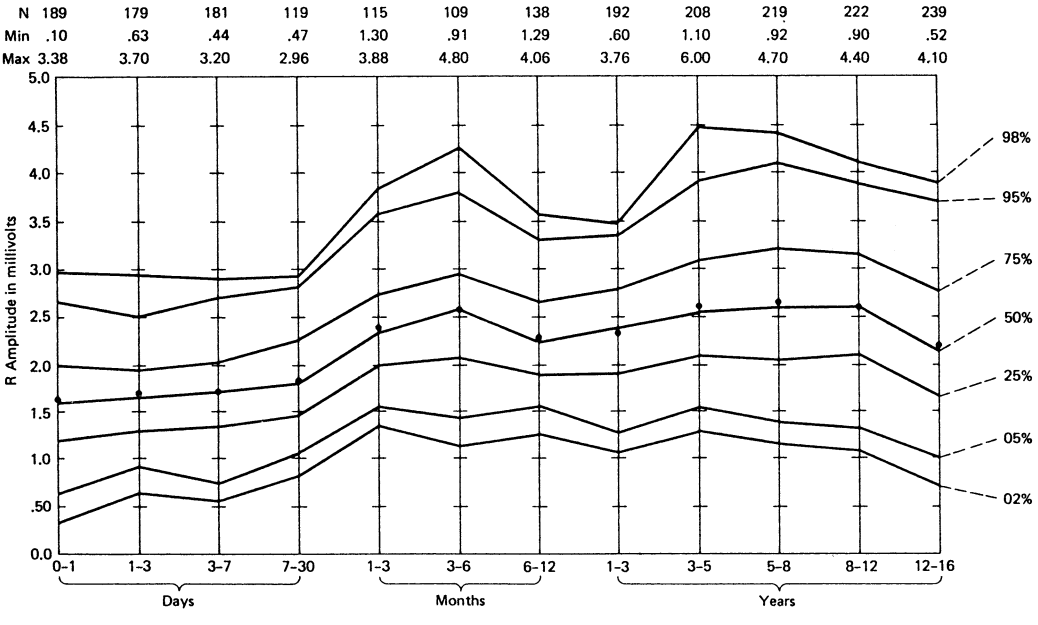

Figure A2.17

R amplitude in lead V_4 versus age (•, mean).

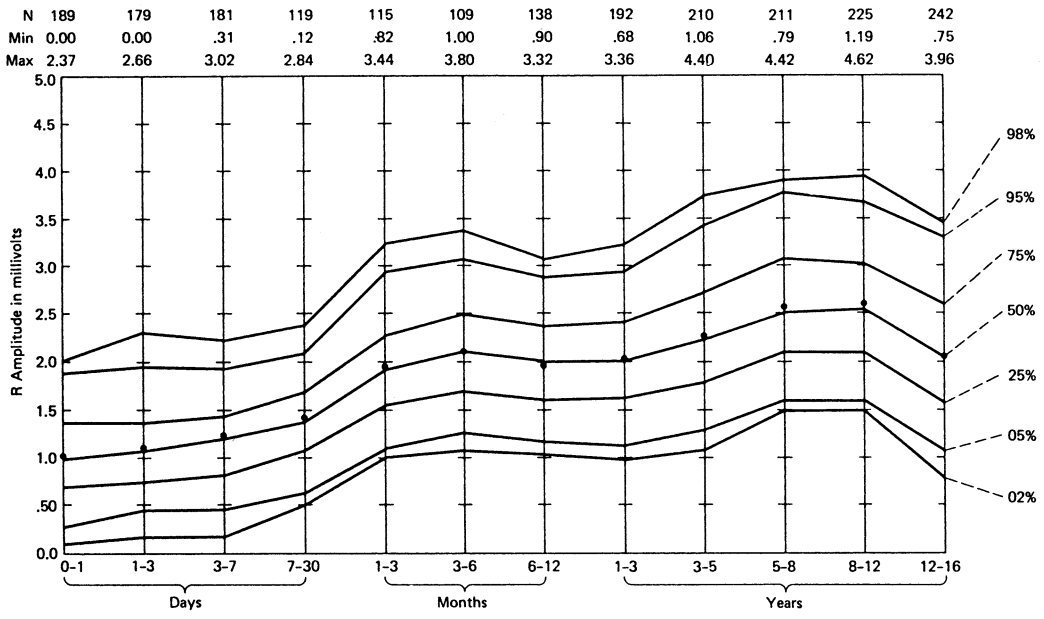

Figure A2.18

R amplitude in lead V_5 versus age (•, mean).

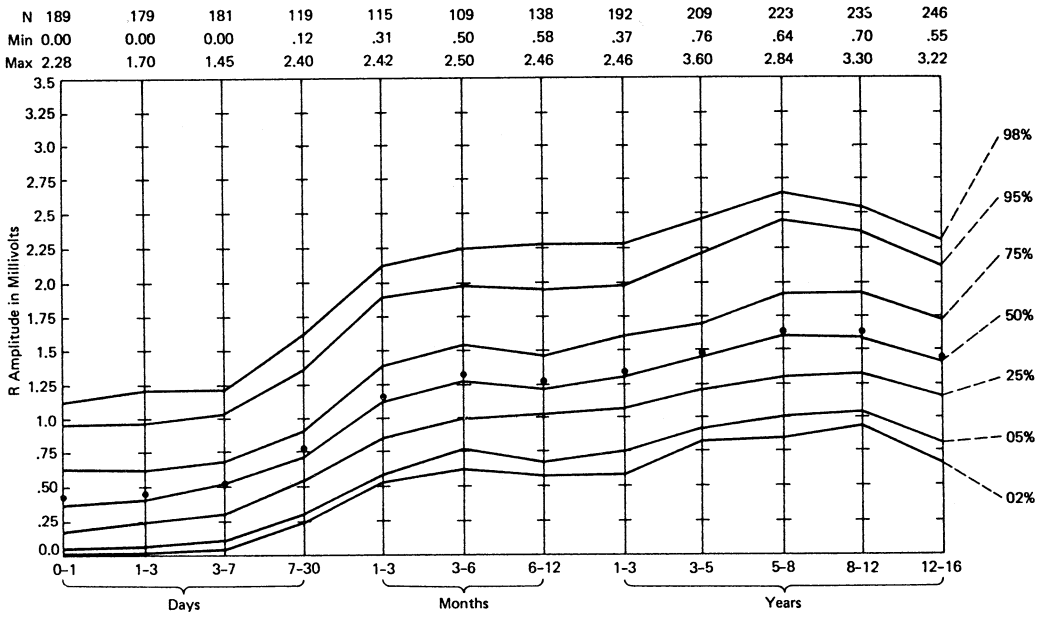

Figure A2.19

R amplitude in lead V_6 versus age (•, mean).

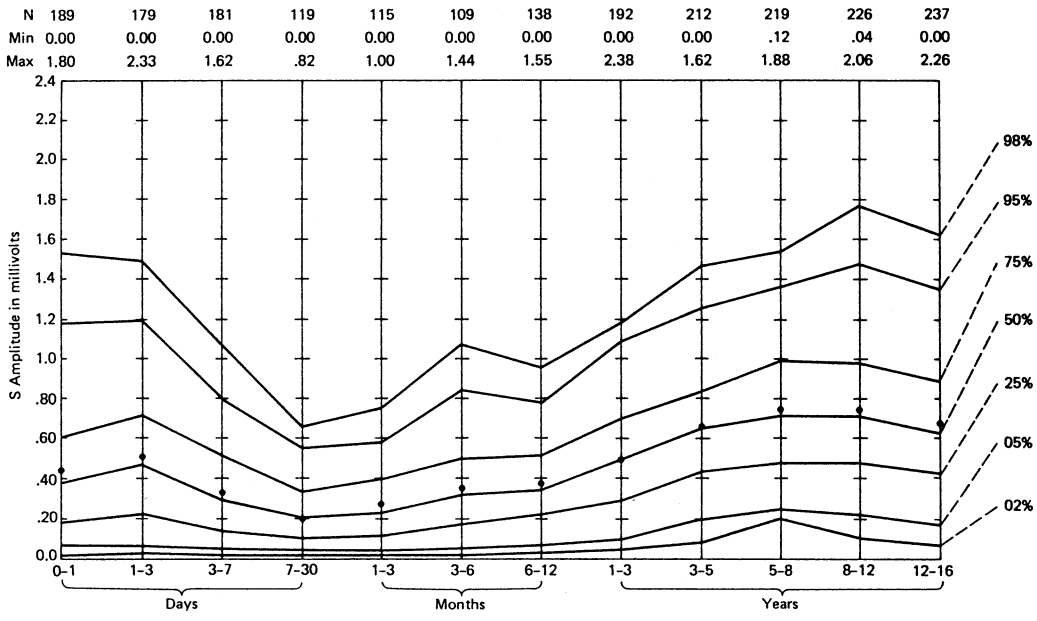

Figure A2.20
S amplitude in lead V_3R versus age (•, mean).

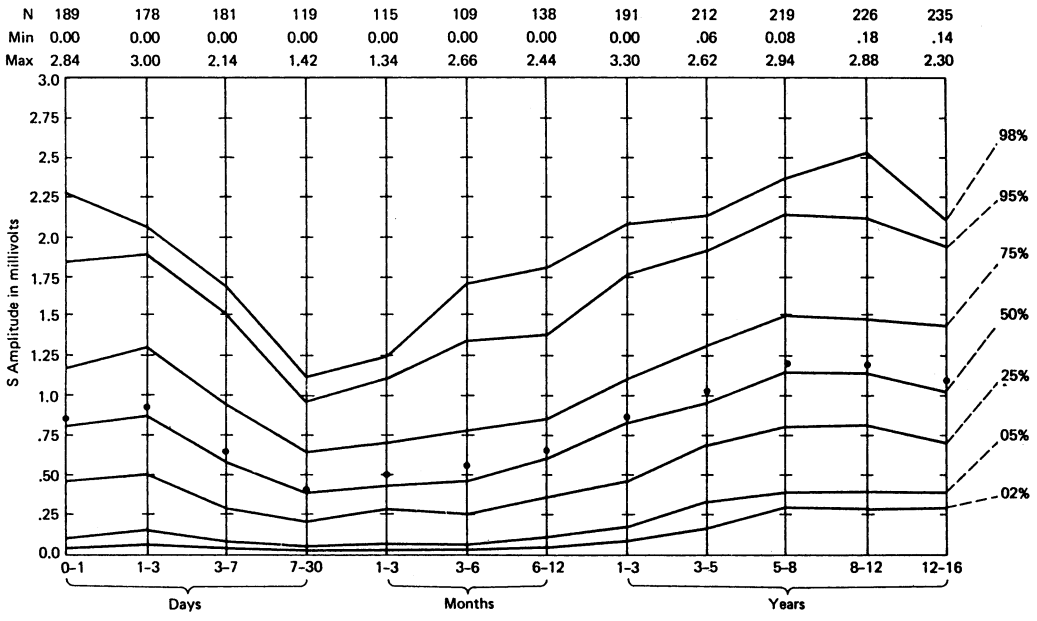

Figure A2.21
S amplitude in lead V_1 versus age (•, mean).

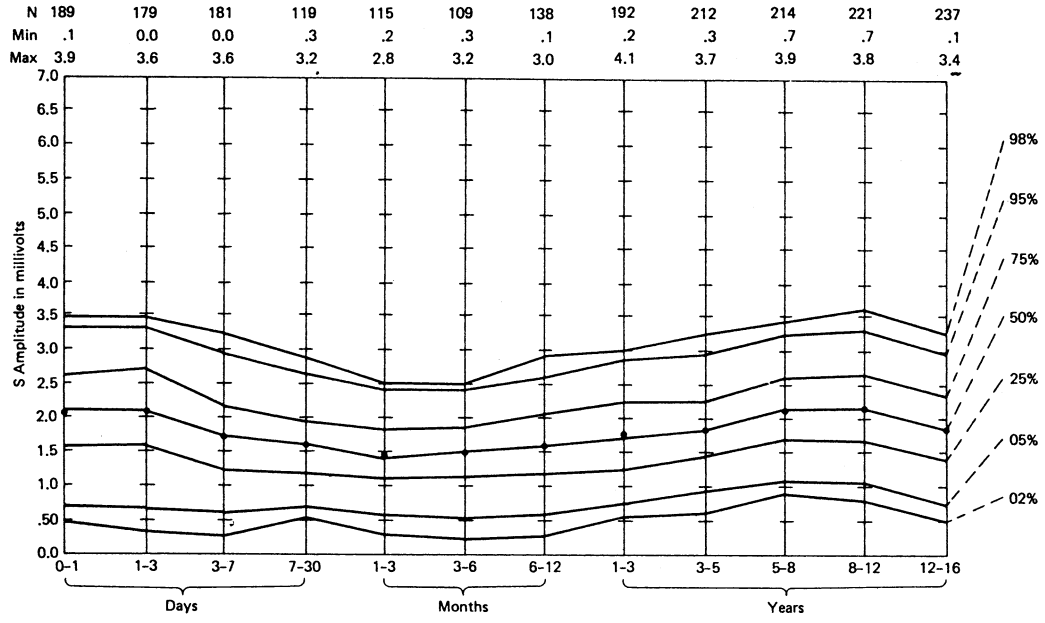

Figure A2.22

S amplitude in lead V_2 versus age (•, mean).

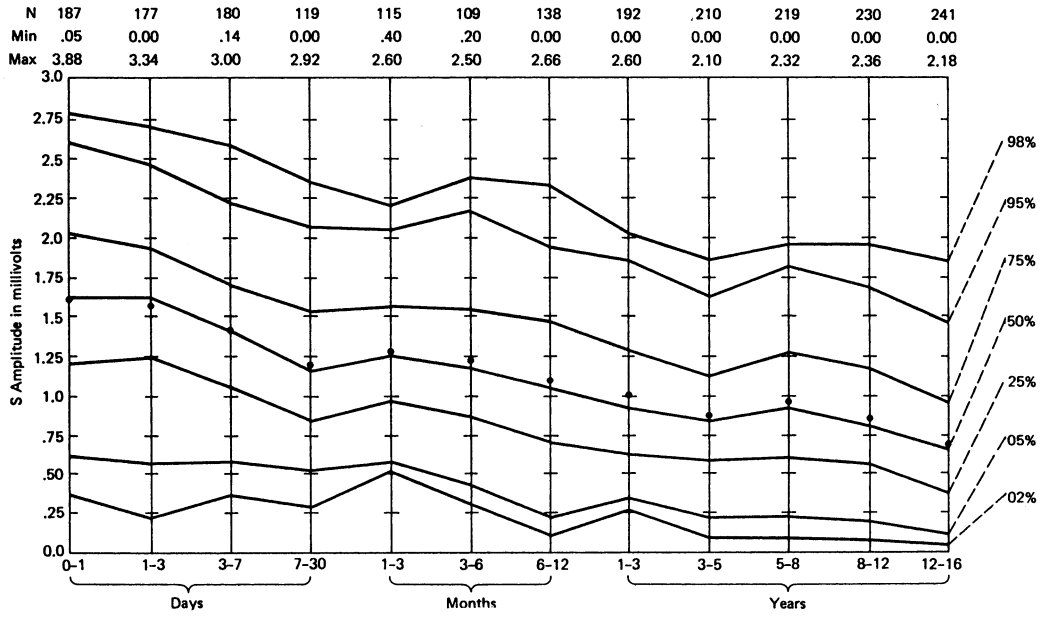

Figure A2.23

S amplitude in lead V_4 versus age (•, mean).

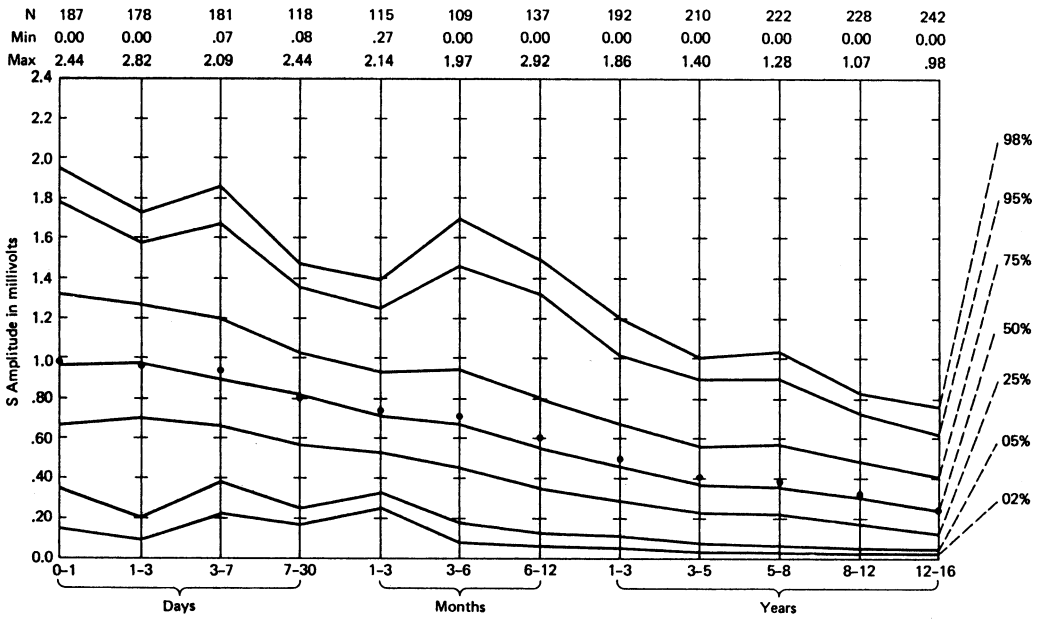

Figure A2.24

S amplitude in lead V_5 versus age (•, mean).

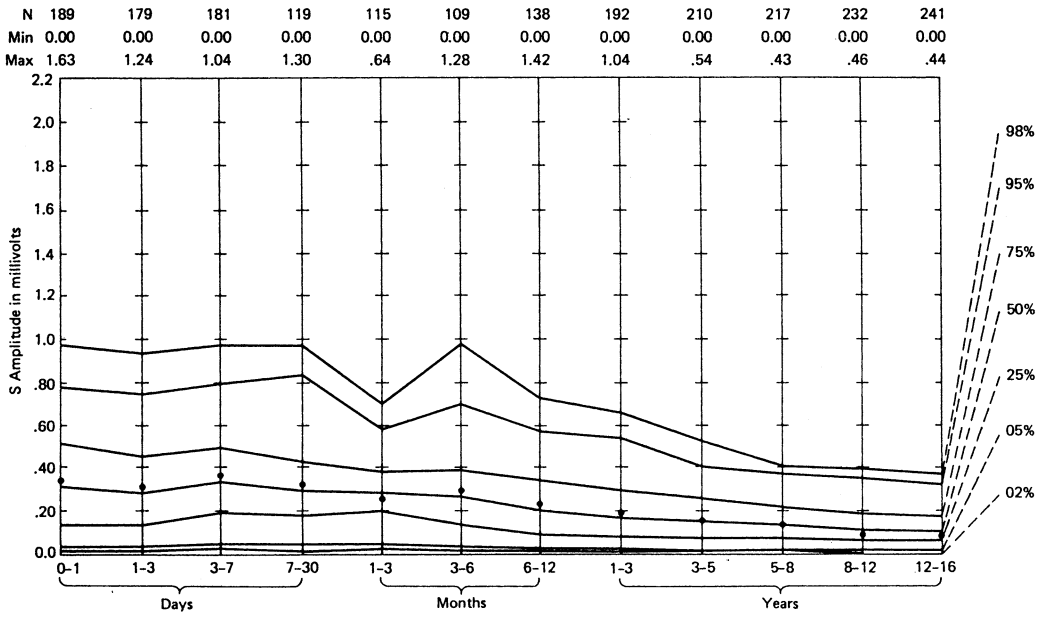

Figure A2.25

S amplitude in lead V_6 versus age (•, mean).

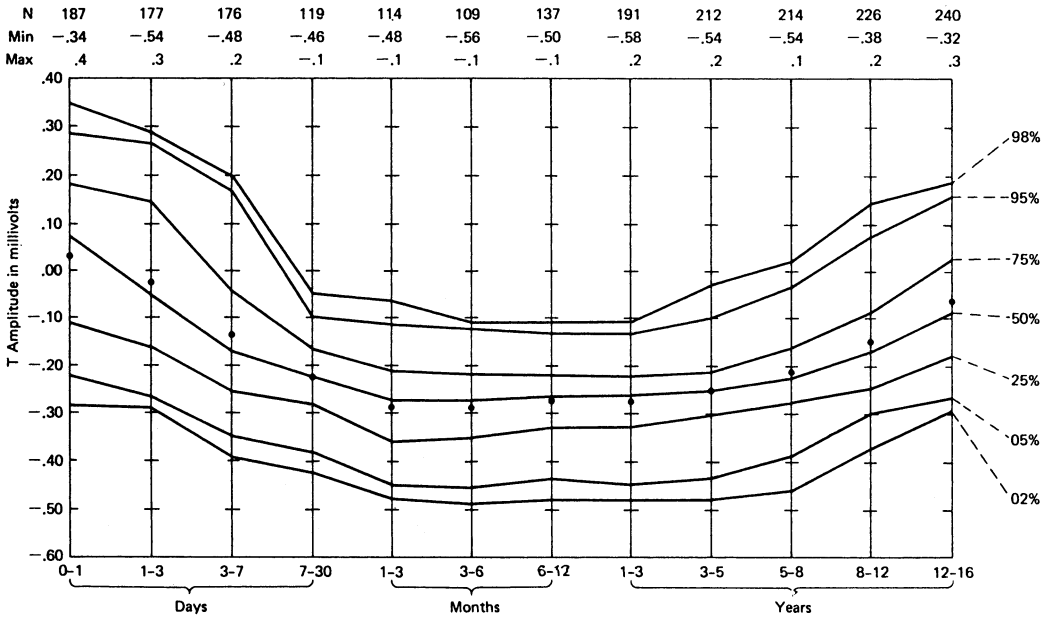

Figure A2.26
T amplitude in lead V_3R versus age (•, mean).

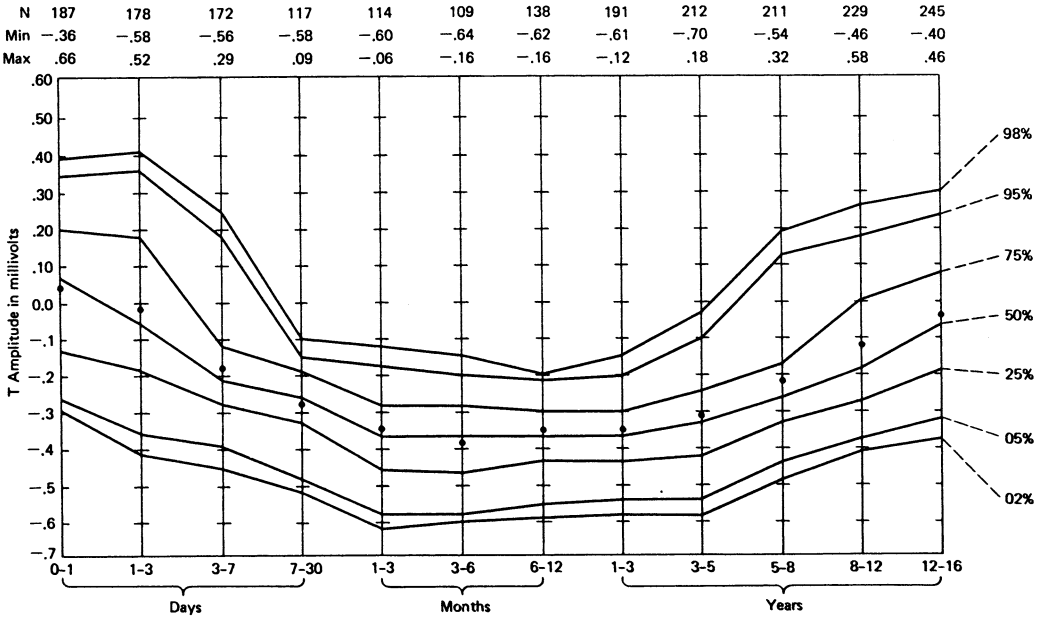

Figure A2.27
T amplitude in lead V_1 versus age (•, mean).

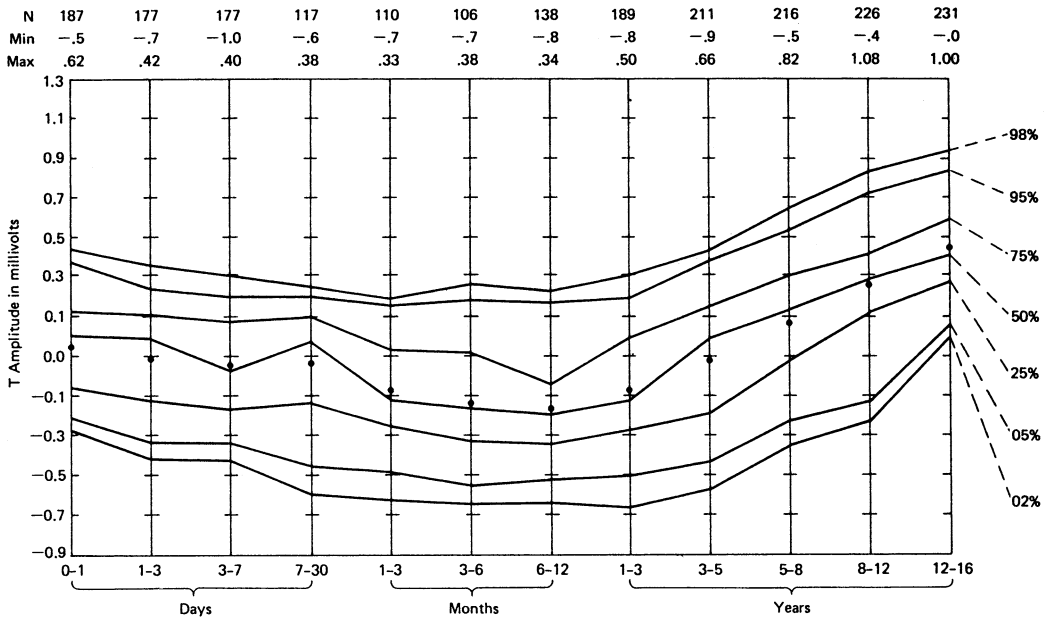

Figure A2.28

T amplitude in lead V_2 versus age (•, mean).

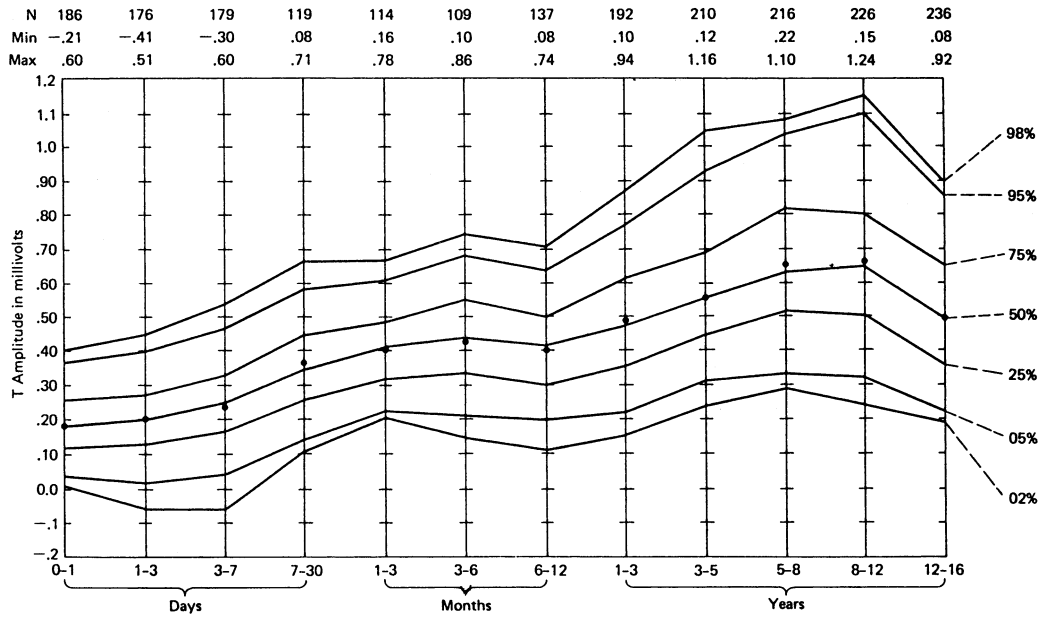

Figure A2.29

T amplitude in lead V_5 versus age (•, mean).

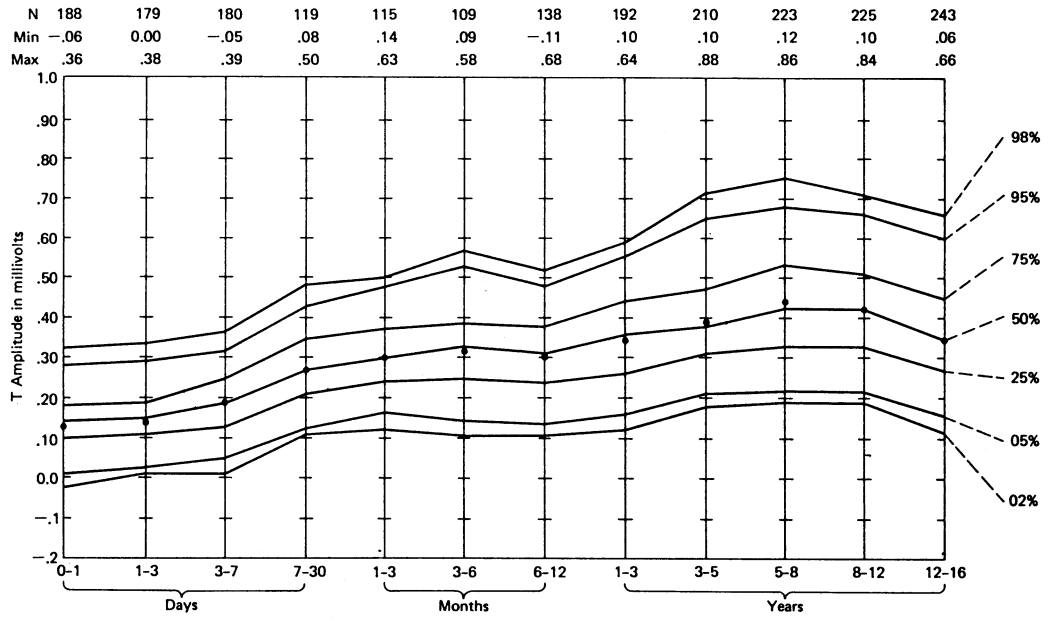

Figure A2.30

T amplitude in lead V_6 versus age (•, mean).

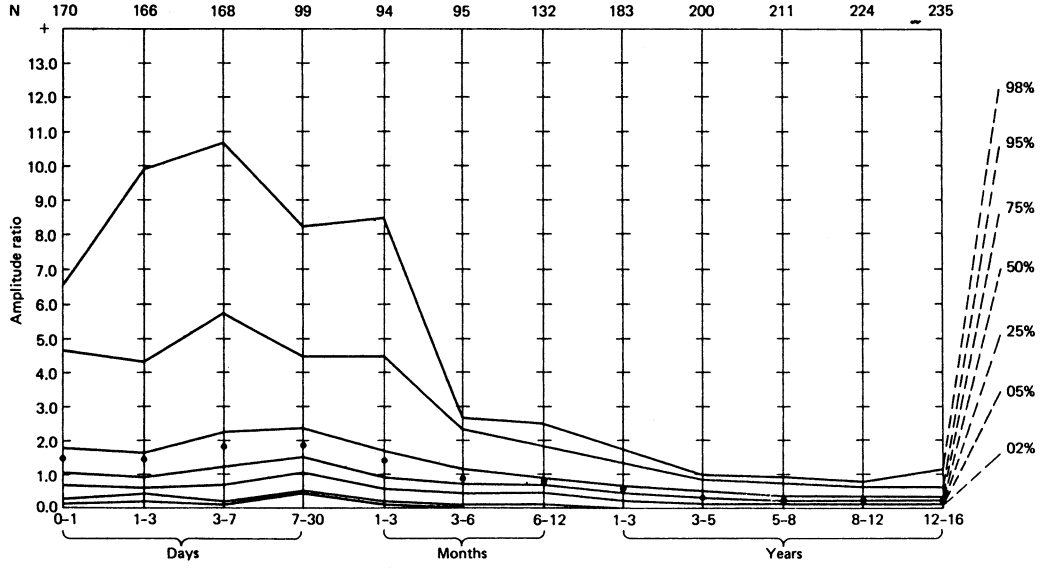

Figure A2.31

R/S amplitude ratio in lead V_3R versus age (•, mean).

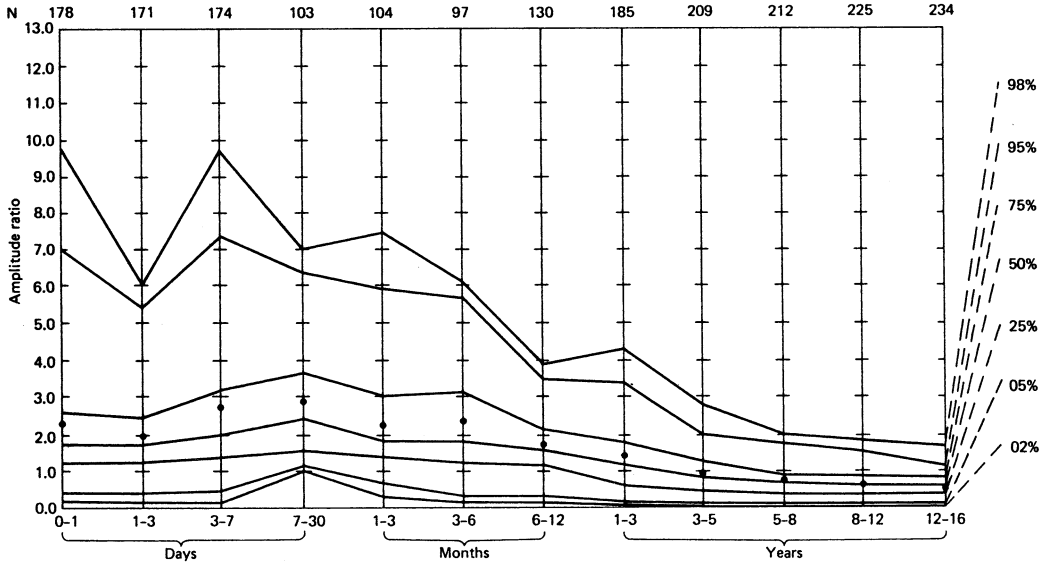

Figure A2.32

R/S amplitude ratio in lead V_1 versus age (•, mean).

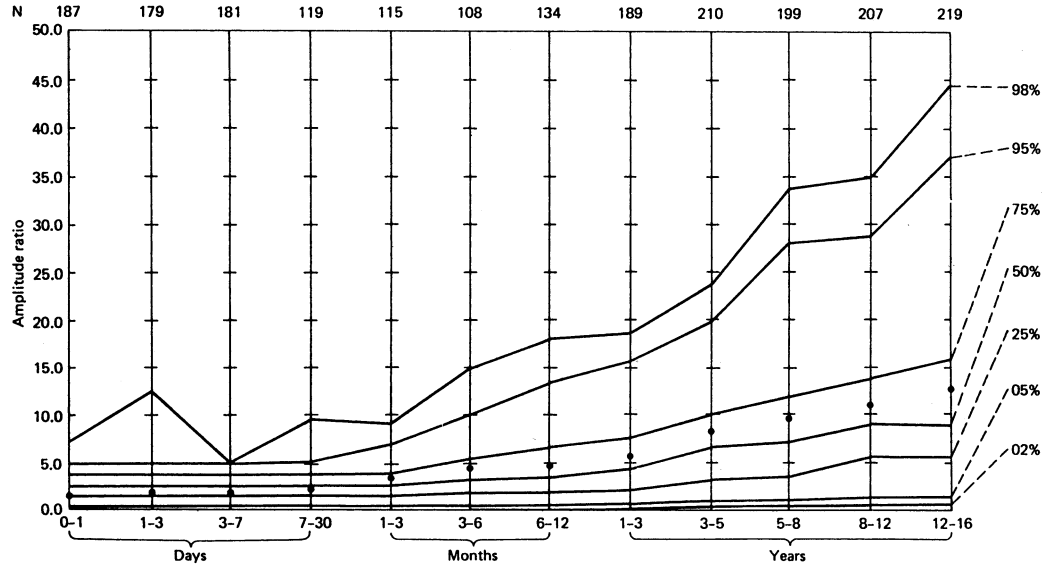

Figure A2.33

R/S amplitude ratio in lead V_5 versus age (•, mean).

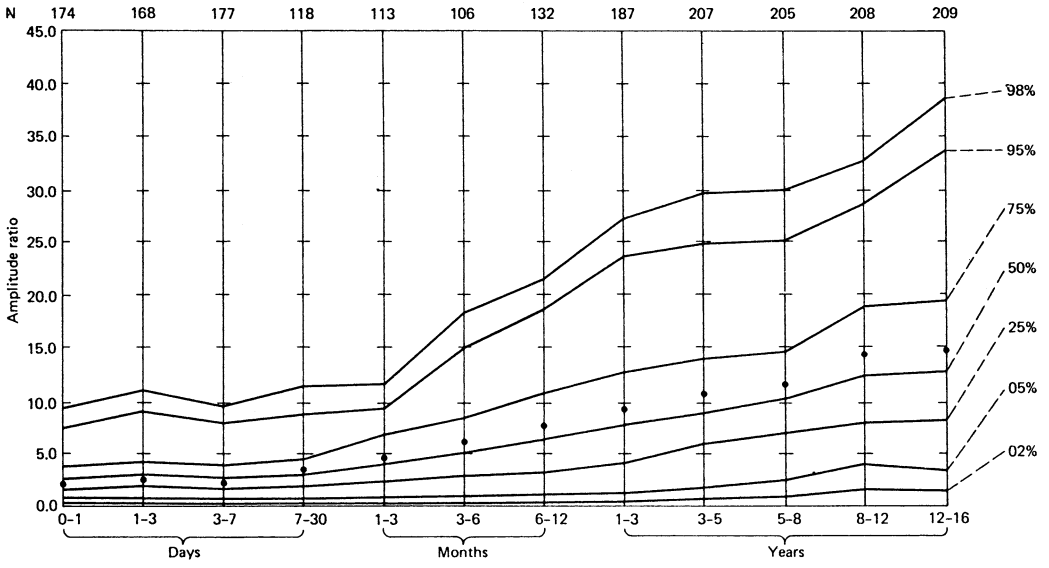

Figure A2.34

R/S amplitude ratio in lead V_6 versus age (•, mean).

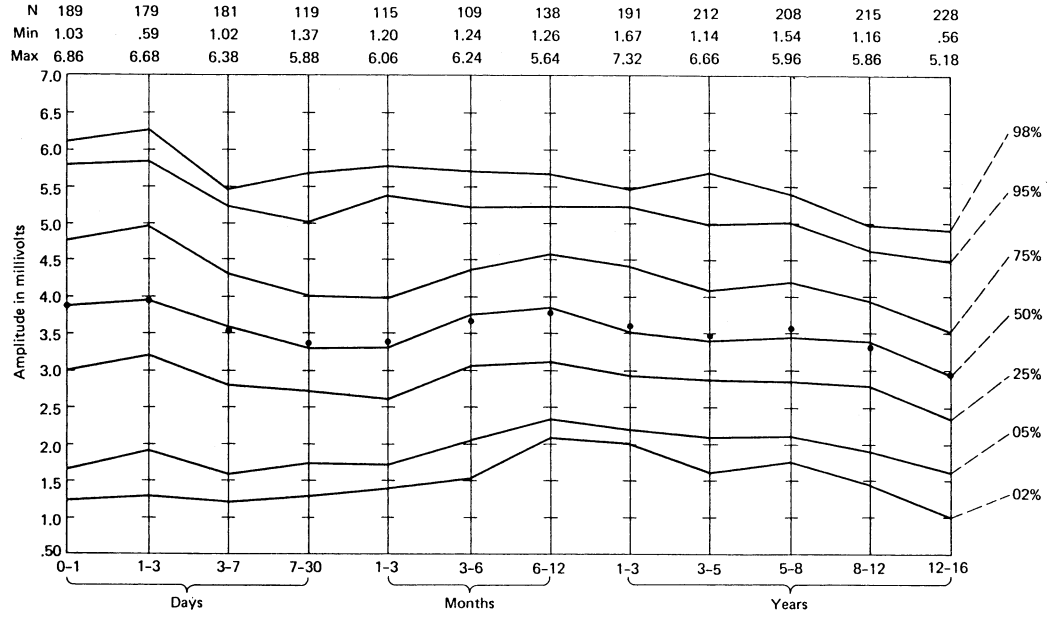

Figure A2.35

R + S amplitude in lead V_2 versus age (•, mean).

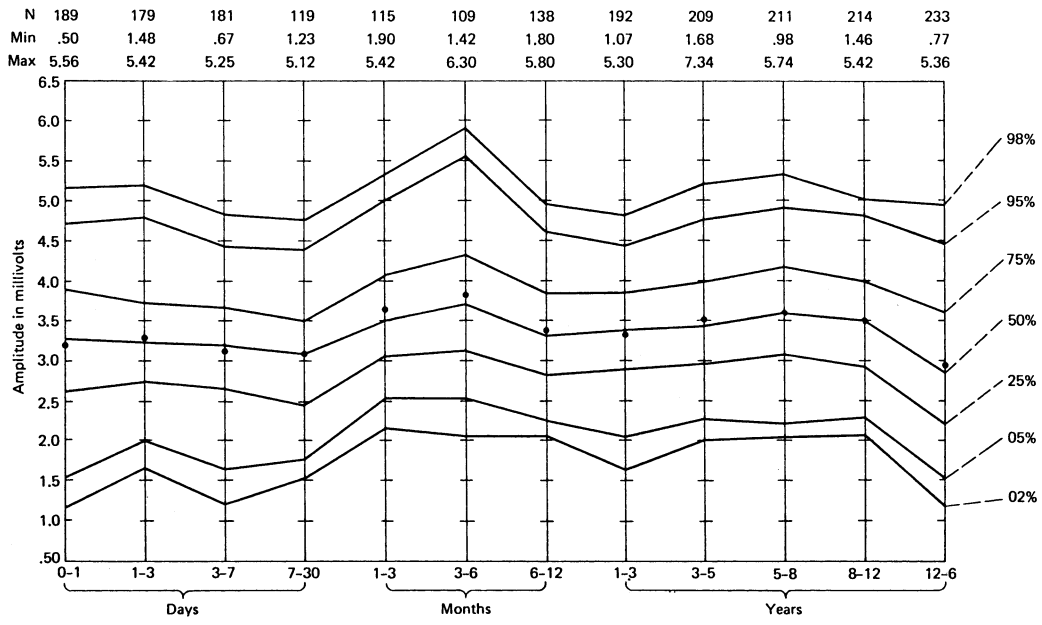

Figure A2.36

R + S amplitude in lead V_4 versus age (•, mean).

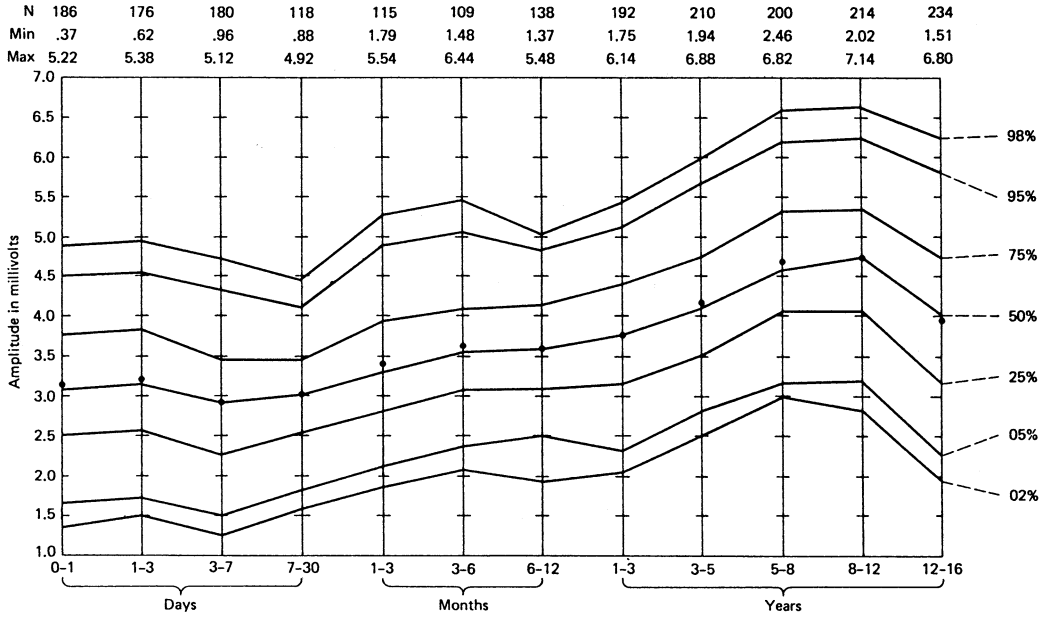

Figure A2.37

R amplitude in lead V_5 + S amplitude in lead V_2 versus age (•, mean).

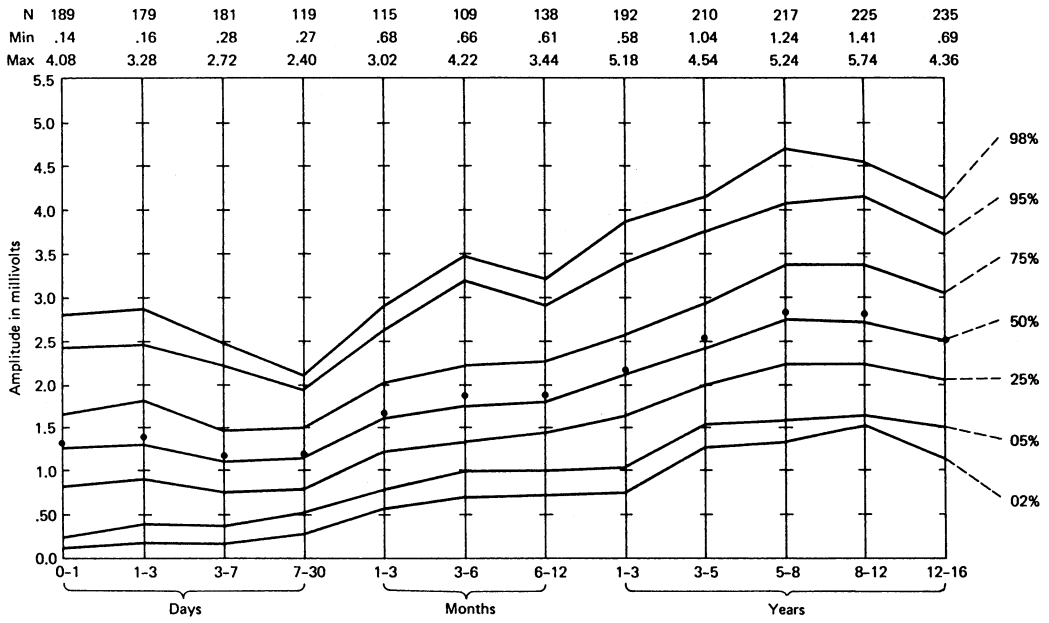

Figure A2.38

R amplitude in lead V_6 + S amplitude in lead V_1 versus age (•, mean).

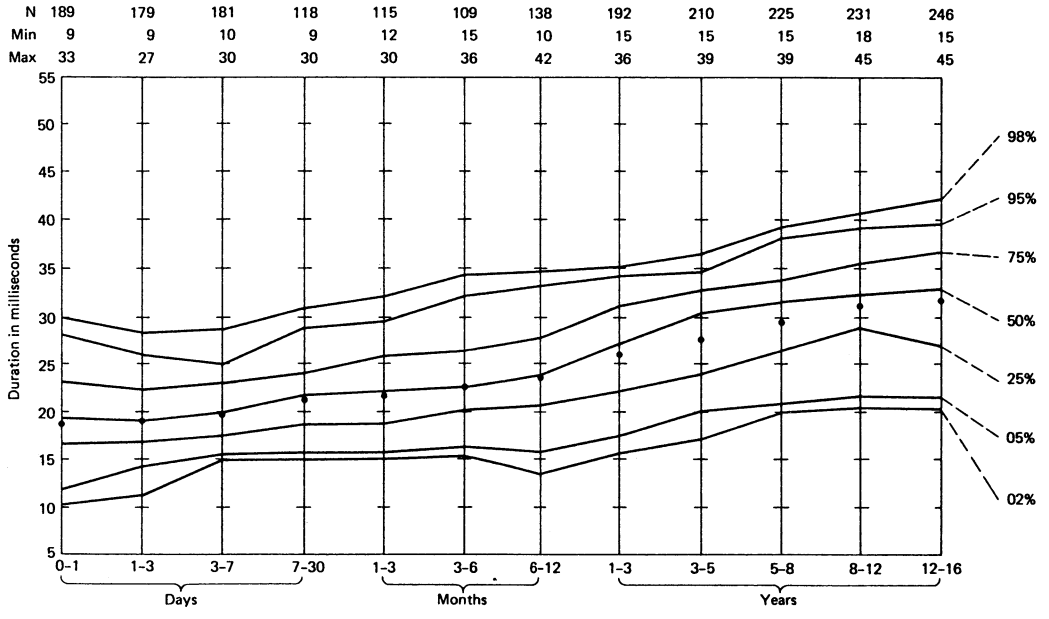

Figure A2.39

Ventricular activation time in lead V_5 versus age (•, mean).

A2.3 Additional 12-Lead Pediatric ECG Normal Limits

Liebman, who has contributed Chap. 21 as well as a short technical note on linear and directional statistics (see Appendix 1, Sect. A1.7), has published extensively on normal limits of the pediatric and adolescent ECG. He has stressed the difference between using equipment with high (adequate) and low (poor) frequency response. Some tables which are mostly complementary to Sect. A2.2 are reproduced from: Liebman J, Plonsey R, Gillette PC, eds. *Pediatric Cardiology*. 1982, with the permission of Williams and Wilkins, Baltimore, Maryland. These include a mixture of "high-" and "low-frequency data." The former are more correct for use with modern recording equipment (Tables A2.25–A2.30).

Table A2.25

High-frequency data

	Heart rate (bpm)						PR interval (s)					
Age	Min	5%	Mean	95%	Max.	SD	Min	5%	Mean	95%	Max.	SD
0–24 h	85	94	119	145	145	16.1	0.07	0.07	0.10	0.12	0.13	0.012
1–7 days	100	100	133	175	175	22.3	0.5	0.07	0.09	0.12	0.13	0.014
8–30 days	115	115	163	190	190	19.9	0.07	0.07	0.09	0.11	0.13	0.010
1–3 months	115	124	154	190	205	18.6	0.07	0.07	0.10	0.13	0.17	0.017
3–6 months	115	111	140	179	205	21.0	0.07	0.07	0.10	0.13	0.13	0.014
6–12 months	115	112	140	177	175	18.7	0.07	0.08	0.10	0.13	0.15	0.013
1–3 years	100	98	126	163	190	19.8	0.07	0.08	0.11	0.15	0.17	0.019
3–5 years	55	65	98	132	145	18.0	0.09	0.09	0.12	0.15	0.17	0.015
5–8 years	70	70	98	115	145	16.1	0.09	0.10	0.13	0.16	0.19	0.017
8–12 years	55	55	79	107	115	15.0	0.09	0.10	0.14	0.17	0.27	0.022
12–16 years	55	55	75	102	115	13.5	0.09	0.11	0.14	0.16	0.21	0.018
	P-wave duration (s)						QRS duration (s)					
0–24 h	0.040	0.040	0.051	0.065	0.075	0.066	0.05	0.05	0.065	0.084	0.09	0.010
1–7 days	0.035	0.038	0.046	0.061	0.065	0.066	0.04	0.04	0.056	0.079	0.08	0.010
8–30 days	0.040	0.040	0.048	0.057	0.065	0.064	0.04	0.04	0.057	0.073	0.08	0.009
1–3 months	0.040	0.040	0.046	0.058	0.065	0.063	0.05	0.05	0.062	0.080	0.08	0.007
3–6 months	0.040	0.040	0.049	0.065	0.065	0.072	0.06	0.06	0.068	0.080	0.08	0.008
6–12 months	0.040	0.046	0.058	0.068	0.075	0.058	0.05	0.05	0.065	0.080	0.08	0.008
1–3 years	0.045	0.053	0.065	0.082	0.085	0.090	0.05	0.05	0.064	0.080	0.08	0.008
3–5 years	0.040	0.051	0.069	0.087	0.095	0.108	0.06	0.06	0.072	0.084	0.09	0.009
5–8 years	0.050	0.059	0.070	0.084	0.095	0.095	0.05	0.05	0.067	0.080	0.08	0.017
8–12 years	0.050	0.061	0.075	0.092	0.105	0.098	0.05	0.05	0.073	0.084	0.09	0.008
12–16 years	0.060	0.064	0.081	0.095	0.105	0.095	0.04	0.04	0.068	0.080	0.10	0.010

Table A2.26

Heart rate and durations: adolescents

	Sex	Mean	SD	5%	50%	95%
Heart rate	Male	69	11	52	70	90
	Female	73	12	57	70	92
	Total	71	12	55	70	90
P-wave duration	Male	0.09	0.02	0.06	0.08	0.11
	Female	0.09	0.02	0.06	0.09	0.12
	Total	0.09	0.02	0.06	0.09	0.11
PR interval	Male	0.15	0.03	0.10	0.15	0.20
	Female	0.15	0.02	0.12	0.15	0.19
	Total	0.15	0.02	0.11	0.15	0.20
QRS duration	Male	0.08	0.01	0.06	0.08	0.10
	Female	0.08	0.01	0.05	0.08	0.09
	Total	0.08	0.01	0.06	0.08	0.10
QT interval	Male	0.38	0.04	0.32	0.38	0.42
	Female	0.37	0.03	0.32	0.38	0.42
	Total	0.37	0.04	0.32	0.38	0.43
T-wave duration	Male	0.21	0.06	0.16	0.20	0.35
	Female	0.19	0.04	0.15	0.18	0.28
	Total	0.20	0.05	0.15	0.20	0.31

Table A2.27

Heart rate (bpm): prematures

Infants		Mean	Percentile	
Age	Number	Heart rate	5th	95th
24 h	66	141	109	173
72 h	69	150	127	182
1 week	62	164	134	200
1 month	42	170	133	200
2 months	30	171	128	203
3 months	24	159	130	202
6 months	16	145		
1 year	18	142		

Table A2.28

P amplitude in lead II ×10 (mV): prematures

Infants		Mean	Percentile	
Age	Number	P amplitude	5th	95th
24 h	65	1.1	0.5	2.0
72 h	69	1.3	0.5	2.0
1 week	62	1.3	0.5	2.6
1 month	40	0.8	0.3	1.5
2 months	30	0.9	0.4	1.5
3 months	24	1.0	0.5	1.9
6 months	16	1.1		
1 year	18	1.2		

Table A2.29

Amplitudes in V_3(high-frequency data) ×10 (mV)

	R wave						S wave					
Age	Min.	5%	Mean	95%	Max.	SD	Min.	5%	Mean	95%	Max.	SD
0–24 h	12.0	12.7	18.8	26.7	28.0	4.12	10.0	12.0	25.0	32.0	38.0	6.05
1–7 days	4.0	8.8	18.1	30.0	40.0	6.55	0.0	2.	17.1	33.0	38.0	8.37
8–30 days	0.0	8.3	18.8	33.8	36.0	7.50	2.0	4.2	12.4	20.0	26.0	5.47
1–3 months	12.0	13.5	21.8	29.1	32.0	4.50	2.0	4.9	14.0	21.3	22.0	4.95
3–6 months	12.0	14.5	20.1	30.0	32.0	4.56	2.0	4.5	14.7	23.5	26.0	6.14
6–12 months	8.0	9.7	17.8	23.5	24.0	4.32	0.0	4.9	14.2	22.6	26.0	5.94
1–3 years	8.0	8.8	15.4	27.0	32.0	4.92	2.0	4.5	13.4	23.5	26.0	5.24
3–5 years	4.0	6.0	15.0	22.7	24.0	4.49	2.0	3.3	12.2	20.0	26.0	6.00
5–8 years	0.0	4.5	13.1	23.2	32.0	5.81	0.0	3.7	15.0	24.8	30.0	6.10
8–12 years	0.0	4.4	10.8	21.0	32.0	5.22	0.0	2.4	13.2	24.0	30.0	6.80
12–16 years	0.0	3.8	10.0	19.6	28.0	5.34	0.0	2.2	10.8	25.4	34.0	6.82

Table A2.30

Amplitude in lead V_4R (low-frequency data) ×10 (mV)

	R wave					S wave				
Age	Min.	5%	Mean	95%	Max.	Min.	5%	Mean	95%	Max.
30 h	3.5	4.0	8.6	14.2	15.0	0.0	0.2	3.8	13.0	12.0
1 month	3.0	3.3	6.3	8.5	12.0	0.0	0.8	1.8	4.6	9.0
2–3 months	0.5	1.1	5.1	10.1	15.0	0.0	0.0	3.4	9.3	15.0
4–5 months	2.0	2.4	5.2	7.5	9.0	1.0	0.3	3.5	6.7	9.0
6–8 months	2.0	1.3	4.4	7.1	7.0	0.0	0.2	3.9	11.7	10.0
9 months–2 years	1.0	0.2	4.0	6.6	8.0	0.0	0.8	4.9	8.1	10.5
2–5 years	1.0	1.6	3.4	7.4	8.0	1.0	1.2	4.8	9.5	12.0
6–13 years	0.2	0.6	2.5	5.7	7.0	0.5	0.9	5.8	12.5	20.0

A2.4 Normal Limits of the Pediatric Orthogonal-Lead ECG

A number of tables are included to provide an indication of the normal limits of the orthogonal-lead ECG in infants and children. The terminology is discussed in Chap. 21 and in addition, the concept of prevalent direction is described in Appendix 1, Sect. A1.7 by Liebman. Tables have been reproduced from Liebman J, Plonsey R, Gillette PC. *Pediatric Electrocardiography*. 1982, with the permission of Williams and Wilkins, Baltimore, Maryland. However, some of these tables are from earlier publications and the list at the end of the section relates to the identifying superscript in the legend to each table (Tables A2.31–A2.51). Figures A2.40 and A2.41 are reproduced from the work of Davignon and Rautaharju with the permission of Springer (See A2.2).

Table A2.31

Direction of inscription of the QRS complex: adolescents[a]

	Sex	Number	Clockwise		Figure-of-eight		Counterclockwise	
			No.	%	No.	%	No.	%
Frontal plane	male	67	42	62.6	2	2.9	23	34.3
	female	47	29	61.7	3	6.3	15	31.9
	total	114	71	62.2	5	4.3	38	33.3
Horizontal plane	male	67	0	0	1	1.4	66	98.5
	female	47	0	0	2	4.2	45	95.7
	total	114	0	0	3	2.6	111	97.3

Table A2.32

Direction of inscription of the QRS complex: prematures C, clockwise; CC, counterclockwise[b]

	Frontal plane		Horizontal plane			
Age of infants	C (%)	CC (%)	C (%)	CC (%)	Figure-of-eight initially CC (%)	Narrow[a] loop (%)
24 h	97	3	1.5	11	34	54
72 h	98.5	1.5	1.5	16.5	43.5	39
1 week	97	3		21.5	54	24.5
1 month	97.5	2.5	2.5	17	51	29.5
2 months	93.5	6.5	3.5	30	53.5	13.5
3 months	100		4.5	29	62.5	4
6 months	100		6	37.5	50	6
1 year	100		5.5	61	28	5.5

[a]Presence of a QRS loop so narrow that the specific direction of inscription has no significance.

Table A2.33

Evolution of the Frank vectorcardiogam in normal infants. In frontal plane, initial QRS to left 66.6% from birth to 30 days; initial QRS to left 55.5% from 1 to 2 months; initial QRS to left 10.5% from to 2 to 3 months; initial QRS to left 6.2% by 6–8 months[c]

	Frontal			Horizontal		
Groups	CW	Figure-of-eight	CCW	CW	Figure-of-eight	CCW
I (birth–30 h)	91.3	7.0	1.7	61.5	19.2	19.3
II (1 month)	88.9	11.1	0	18.5	40.7	40.8
III (2–3 months)	97.4	0	2.6	2.6	39.5	57.9
IV (4–5 months)	87.0	6.5	6.5	0	35.5	64.5
V (6–8 months)	87.6	6.2	6.2	0	21.9	78.1
VI (12–18 months)	83.3	10.0	6.7	0	6.6	93.4

Table A2.34

Prevalent direction of the QRS in the frontal plane: adolescents[a]

Prevalent direction							
Sex	Age	d	χ^2	$\hat{\alpha}_f$	5%	50%	95%
Male	11 → 15	0.94	51.2	65	10	70	90
Male	16 → 19	0.92	63.9	63	9	70	91
Female	11 → 15	0.97	48.5	62	38	60	87
Female	16 → 19	0.93	36.0	56	11	65	80
Male	11 → 19	0.93	115.0	64	10	70	90
Female	11 → 19	0.95	84.2	59	15	60	80
Total	11 → 19	0.93	198.9	62	14	65	90

Table A2.35

Prevalent direction of the QRS in the horizontal plane: adolescents[a]

Prevalent direction							
Sex	Age	d	$\chi 2$	$\hat{\alpha}_h$	5%	50%	95%
Male	11 → 15	0.94	51.6	330	292	335	8
Male	16 → 19	0.92	64.4	333	289	340	8
Female	11 → 15	0.96	48.0	334	290	340	354
Female	16 → 19	0.95	38.2	332	300	340	0
Male	11 → 19	0.93	116.0	332	292	340	5
Female	11 → 19	0.96	86.2	333	292	340	0
Total	11 → 19	0.94	202.1	332	293	340	0

Table A2.36

Prevalent direction of the T in the frontal plane: adolescents[a]

Prevalent direction							
Sex	Age	d	χ^2	$\hat{\alpha}_f$	5%	50%	95%
Male	11 → 15	0.96	53.8	42	15	45	60
Male	16 → 19	0.94	67.7	48	5	55	70
Female	11 → 15	0.98	49.6	42	17	45	60
Female	16 → 19	0.96	39.0	42	3	45	74
Male	11 → 19	0.95	121.2	45	7	45	70
Female	11 → 19	0.97	88.6	42	17	45	60
Total	11 → 19	0.96	209.6	44	10	45	63

Table A2.37

Prevalent direction of the T in the horizontal plane: adolescents[a]

Prevalent direction							
Sex	Age	d	$\chi 2$	$\hat{\alpha}_h$	5%	50%	95%
Male	11 → 15	0.90	47.5	15	310	15	60
Male	16 → 19	0.88	58.3	24	338	15	74
Female	11 → 15	0.96	48.4	12	335	15	38
Female	16 → 19	0.97	39.2	12	310	15	25
Male	11 → 19	0.89	105.1	20	334	15	60
Female	11 → 19	0.97	87.6	12	335	15	33
Total	11 → 19	0.92	191.4	17	335	15	60

Table A2.38

Frontal angular deviation of T from QRS: adolescents[a]

Prevalent direction							
Sex	Age	d	χ^2	$\hat{\alpha}_f$	5%	50%	95%
Male	11 → 15	0.90	46.9	337	285	335	40
Male	16 → 19	0.94	66.6	345	305	345	17
Female	11 → 15	0.97	48.8	340	302	340	0
Female	16 → 19	0.93	36.0	346	316	340	42
Male	11 → 19	0.92	113.0	342	299	340	34
Female	11 → 19	0.95	84.5	343	309	340	15
Total	11 → 19	0.93	197.5	342	305	340	18

Table A2.39

Horizontal angular deviation of T from QRS: adolescents[a]

Prevalent direction							
Sex	Age	d	$\chi 2$	$\hat{\alpha}_h$	5%	50%	95%
Male	11 → 15	0.85	41.8	45	330	35	98
Male	16 → 19	0.83	52.8	52	334	45	108
Female	11 → 15	0.95	46.4	39	4	35	80
Female	16 → 19	0.92	35.2	39	330	35	75
Male	11 → 19	0.84	94.3	49	339	45	103
Female	11 → 19	0.93	81.7	39	4	35	78
Total	11 → 19	0.87	174.3	45	356	40	93

Table A2.40

Prevalent direction of QRS: prematures[b]

Age of infants	Frontal plane				First horizontal vector				Second horizontal vector			
	No. of infants	Prevalent direction	5%	95%	No. of infants	Prevalent Direction	5%	95%	No. of Infants	Prevalent direction	5%	95%
24 h	60	127	75	194	58	74	338	340	16	239		
72 h	68	121	75	195	59	84	295	220	15	233		
1 week	61	117	75	165	54	69	332	216	21	231	9	332
1 month	42	80	17	171	35	58	340	115	13	232		
2 months	30	63	345	105	30	46	340	60	8	231		
3 months	24	59	352	105	23	51	346	108	2	223		
6 months	15	58			16	30			1	240		
1 year	18	46			18	12			2	253		

Table A2.41

Prevalent direction of T: prematures[b]

Age of infants	Frontal plane				Horizontal plane			
	No. of infants	Prevalent direction	5%	95%	No. of infants	Prevalent direction	5%	95%
24 h	52	41	319	84	56	314	240	111
72 h	65	28	315	60	61	318	241	101
1 week	60	31	345	75	59	335	290	15
1 month	42	53	30	75	36	346	281	52
2 months	30	43	353	67	30	334	259	15
3 months	24	47	19	74	24	335	295	14
6 months	14	41			15	333		
1 year	18	46			18	343		

Table A2.42

QRS magnitudes ×10 (mV): prematures[b]

Age of infants	No. of infants	R wave	5%	95%	No. of infants	S wave	5%	95%
Lead V_5 (*X* axis)								
24 h	64	6.5	2.0	12.6	61	6.8	0.06	17.6
72 h	65	7.4	2.6	14.9	64	6.5	1.00	16.0
1 week	61	8.7	3.8	16.8	56	6.8	0.00	15.0
1 month	38	13.0	6.2	21.6	38	6.2	1.20	14.0
2 months	30	18.3	12.1	31.5	29	7.0	0.96	15.0
3 months	24	21.0	14.6	31.5	24	6.7	1.30	21.4
6 months	16	20.3			16	6.8		
1 year	18	17.5			17	3.0		

Table A2.42 (Continued)

Age of infants	No. of infants	R wave	5%	95%	No. of infants	S wave	5%	95%
Lead aVF (*Y* axis)								
24 h	63	6.7	0.85	16.6	28	0.96	0.00	4.5
72 h	68	7.1	0.86	13.9	33	1.20	0.00	5.5
1 week	61	7.6	1.3	14.1	30	0.98	0.00	3.3
1 month	42	9.0	1.8	18.8	20	0.86	0.00	4.0
2 months	30	10.0	1.2	21.7	13	0.90	0.00	5.3
3 months	24	11.1	1.9	23.0	14	0.77	0.00	3.8
6 months	16	12.0			9	0.53		
1 year	18	9.1			9	0.56		
Lead V_2 (*Z* axis)								
24 h	65	11.4	3.5	21.3	65	15.0	2.5	26.5
72 h	66	11.9	5.0	20.8	66	13.5	2.6	26.0
1 week	60	12.3	4.0	20.5	60	14.0	3.0	25.0
1 month	41	15.0	8.3	21.0	41	14.0	5.1	26.3
2 months	30	19.0	8.6	32.0	30	17.1	8.0	34.5
3 months	23	20.1	13.3	30.0	23	16.1	6.0	37.6
6 months	16	20.6			16	18.5		
1 year	18	16.3			18	16.0		

Table A2.43

Spatial magnitude and orientation (MSVR in mV). M, male; F, female; T, total[d]

	n	$\hat{\alpha}$	β	D	χ^2	MSVR mean mag.	SD	$P_{2.5}$	P_5	P_{10}	P_{50}	P_{90}	P_{95}	$P_{97.5}$
Frank-lead system														
M 2-5	23	246	108	0.58	22.8	1.11	0.46		0.33	0.44	1.10	1.80	1.86	
M 6-10	60	254	107	0.73	96.6	1.11	0.41	0.45	0.49	0.59	1.02	1.78	1.99	214.
M 2-10	83	252	107	0.69	117.8	1.11	0.42	0.36	0.47	0.58	1.04	1.79	1.92	2.08
F 2-5	29	257	113	0.74	47.4	1.06	0.35		0.44	0.60	1.09	1.56	1.65	
F 6-10	63	253	109	0.69	90.3	1.01	0.39	0.20	0.34	0.51	0.95	1.46	1.80	2.05
F 2-10	92	254	111	0.71	137.5	1.02	0.38	0.25	0.39	0.56	0.95	1.52	1.67	1.97
T 2-5	52	252	111	0.66	68.6	1.08	0.40	0.33	0.34	0.58	1.10	1.69	1.80	1.85
T 6-10	123	254	108	0.71	186.7	1.06	0.40	0.33	0.47	0.56	0.99	1.62	1.91	2.08
T 2-10	175	253	109	0.70	254.9	1.07	0.40	0.33	0.46	0.58	1.02	1.65	1.81	2.02
T 2-19	341	252	112	0.63	406.5	0.94	0.43	0.22	0.30	0.40	0.92	1.51	1.71	1.94

Table A2.44

Spatial magnitude and orientation (MSVL). M, male; F, female; T, total[d]

	n		β	D	χ	MSVR mean mag.	SD	$P_{2.5}$	P_5	P_{10}	P_{50}	P_{90}	P_{95}	$P_{97.5}$
Frank-lead system														
M 2-5	23	347	129	0.85	50.2	1.73	0.60		0.83	0.87	1.80	2.59	2.74	
M 6-10	60	329	133	0.87	135.9	1.82	0.53	1.00	1.10	1.13	1.77	2.67	2.93	3.15
M 2-10	83	334	133	0.86	183.9	1.80	0.55	0.85	0.96	1.10	1.80	2.59	2.81	3.05
F 2-5	29	341	133	0.83	60.0	1.71	0.44		1.02	1.10	1.69	2.13	2.66	
F 6-10	63	340	138	0.93	162.5	1.77	0.44	1.03	1.10	1.13	1.76	2.36	2.60	2.80
F 2-10	92	340	136	0.90	221.7	1.75	0.44	1.02	1.09	1.13	1.75	2.31	2.58	2.81
T 2-5	52	344	131	0.84	109.9	1.72	0.51	0.93	0.88	1.01	1.76	2.40	2.70	2.97
T 6-10	123	334	136	0.90	296.5	1.80	0.49	1.05	1.10	1.13	1.76	2.43	2.77	2.93
T 2-10	175	337	135	0.88	404.5	1.77	0.49	0.95	1.05	1.12	1.76	2.42	2.75	2.89
T 2-19	341	336	136	0.88	801.1	1.71	0.48	0.88	1.00	1.11	1.69	2.31	2.59	2.82

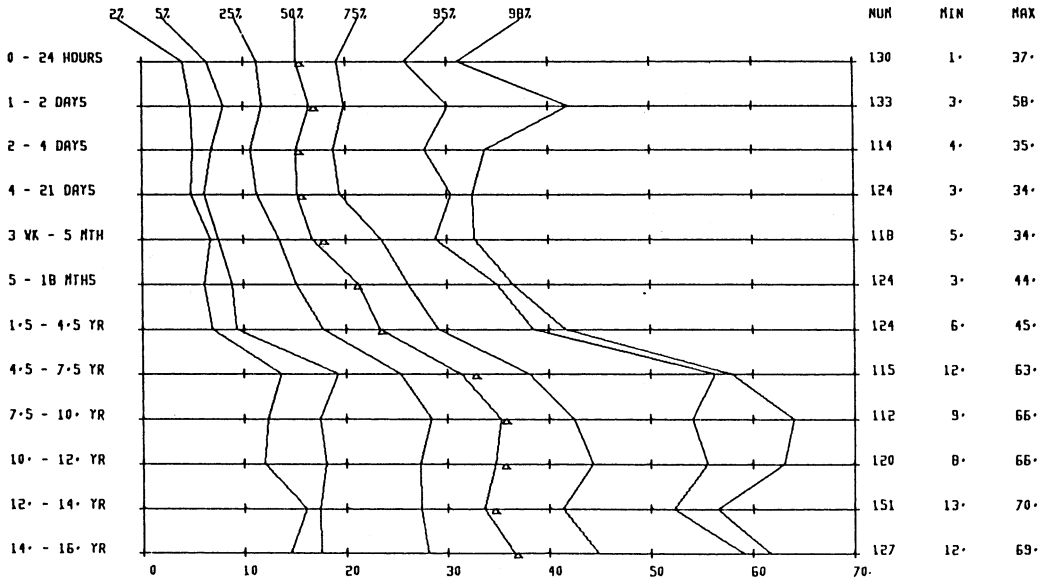

Figure A2.40

Percentile distributions for the spatial magnitude of the QRS integral sector in normal children from birth to aged 16 years.[g]

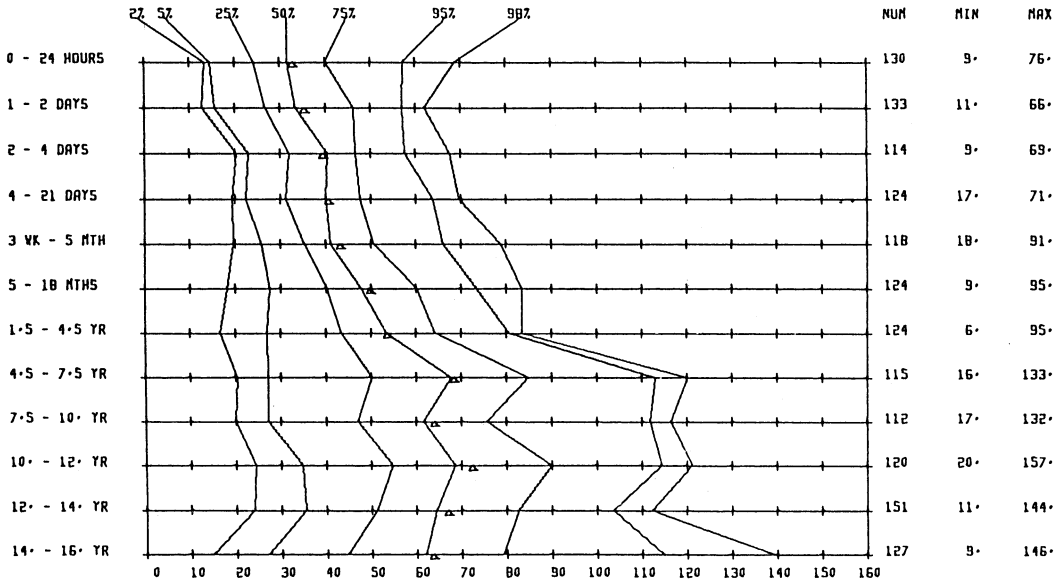

Figure A2.41

Percentile distribution for the spatial magnitude of the ST-T integral vector in normal children from birth to aged 16 years.[g]

Table A2.45

Maximal projections. M, male; F, female; T, total[d]: Magnitude is in mV

		Frank system								
	n	Mean mag.	SD	$p_{2.5}$	p_5	p_{10}	p_{50}	p_{90}	p_{95}	$p_{97.5}$
X initial right										
M 2-5	23	0.18	0.16		0.00	0.00	0.15	0.41	0.51	
M 6-10	60	0.12	0.12	0.00	0.00	0.00	0.09	0.28	0.36	0.48
M 2-10	83	0.14	0.14	0.00	0.00	0.00	0.11	0.33	0.36	0.55
F 2-5	29	0.11	0.09		0.00	0.00	0.11	0.24	0.26	
F 6-10	63	0.10	0.09	0.00	0.00	0.00	0.09	0.21	0.25	0.39
F 2-10	92	0.10	0.08	0.00	0.00	0.00	0.09	0.22	0.25	0.35
T 2-5	52	0.14	0.13	0.00	0.00	0.00	0.11	0.32	0.38	0.50
T 6-10	123	0.11	0.11	0.00	0.00	0.00	0.09	0.25	0.35	0.38
T 2-10	175	0.12	0.11	0.00	0.00	0.00	0.09	0.25	0.35	0.40
T 2-19	341	0.10	0.10	0.00	0.00	0.00	0.08	0.23	0.30	0.36

Table A2.45 (Continued)

		Frank system								
	n	Mean mag.	SD	$p_{2.5}$	p_5	p_{10}	p_{50}	p_{90}	p_{95}	$p_{97.5}$
X left										
M 2-5	23	1.23	0.52		0.49	0.55	1.22	2.02	2.22	
M 6-10	60	1.17	0.47	0.37	0.41	0.68	1.09	1.80	2.23	2.47
M 2-10	83	1.19	0.48	0.40	0.49	0.60	1.14	1.81	2.22	2.34
F 2-5	29	1.15	0.47		0.55	0.60	1.16	1.60	2.21	
F 6-10	63	1.08	0.36	0.18	0.46	0.65	1.08	1.55	1.66	1.89
F 2-10	92	1.10	0.40	0.28	0.52	0.60	1.10	1.55	1.64	2.03
T 2-5	52	1.19	0.49	0.49	0.53	0.59	1.18	1.79	2.15	2.62
T 6-10	123	1.13	0.42	0.34	0.46	0.68	1.08	1.66	1.82	2.25
T 2-10	175	1.14	0.44	0.40	0.52	0.61	1.10	1.68	1.90	2.25
T 2-19	341	1.06	0.44	0.35	0.46	0.56	1.04	1.60	1.80	1.99
X terminal right										
M 2-5	23	0.32	0.23		0.00	0.01	0.28	0.66	0.69	
M 6-10	60	0.29	0.20	0.00	0.00	0.03	0.30	0.52	0.58	0.84
M 2-10	83	0.30	0.21	0.00	0.00	0.02	0.30	0.55	0.65	0.70
F 2-5	29	0.30	0.21		0.00	0.06	0.25	0.62	0.75	
F 6-10	63	0.23	0.17	0.00	0.00	0.02	0.24	0.48	0.52	0.78
F 2-10	92	0.25	0.19	0.00	0.00	0.02	0.24	0.50	0.63	0.79
T 2-5	52	0.31	0.22	0.00	0.00	0.03	0.26	0.64	0.68	0.80
T 6-10	123	0.26	0.19	0.00	0.00	0.02	0.26	0.50	0.55	0.75
T 2-10	175	0.27	0.20	0.00	0.00	0.02	0.26	0.52	0.63	0.74
T 2-19	341	0.23	0.19	0.00	0.00	0.00	0.20	0.50	0.55	0.65

Table A2.46

Maximal projections. M, male; F, female; T total[d]: Magnitude is in mV

		Frank-lead system								
	n	Mean Mag.	SD	$p_{2.5}$	p_5	p_{10}	p_{50}	p_{90}	p_{95}	$p_{97.5}$
X initial superior										
M 2-5	23	0.12	0.12		0.00	0.00	0.10	0.28	0.46	
M 6-10	60	0.11	0.09	0.00	0.00	0.00	0.08	0.26	0.30	0.32
M 2-10	83	0.11	0.10	0.00	0.00	0.00	0.10	0.26	0.30	0.35
F 2-5	29	0.10	0.10		0.00	0.00	0.08	0.24	0.37	
F 6-10	63	0.10	0.09	0.00	0.00	0.00	0.08	0.21	0.30	0.37
F 2-10	92	0.10	0.09	0.00	0.00	0.00	0.08	0.22	0.31	0.38
T 2-5	52	0.11	0.11	0.00	0.00	0.00	0.10	0.25	0.36	0.47
T 6-10	123	0.10	0.09	0.00	0.00	0.00	0.08	0.22	0.30	0.35
T 2-10	175	0.10	0.10	0.00	0.00	0.00	0.08	0.24	0.30	0.35
T 2-19	341	0.10	0.08	0.00	0.00	0.00	0.08	0.20	0.25	0.30

Table A2.46 (Continued)

		Frank-lead system								
	n	Mean Mag.	SD	$p_{2.5}$	p_5	p_{10}	p_{50}	p_{90}	p_{95}	$p_{97.5}$
Y inferior										
M 2-5	23	1.02	0.45		0.39	0.45	1.00	1.78	1.98	
M 6-10	60	1.17	0.41	0.51	0.56	0.64	1.09	1.76	1.97	2.15
M 2-10	83	1.13	0.43	0.45	0.47	0.58	1.04	1.76	1.96	2.05
F 2-5	29	1.09	0.32		0.46	0.71	1.12	1.50	1.54	
F 6-10	63	1.27	0.40	0.64	0.68	0.72	1.30	1.82	2.00	2.24
F 2-10	92	1.22	0.39	0.58	0.67	0.72	1.21	1.64	1.97	2.07
T 2-5	52	1.06	0.38	0.36	0.42	0.50	1.06	1.51	1.71	1.97
T 6-10	123	1.22	0.41	0.56	0.63	0.70	1.20	1.77	2.00	2.10
T 2-10	175	1.17	0.41	0.46	0.56	0.66	1.16	1.69	1.96	2.03
T 2-19	341		0.40	0.47	0.58	0.65	1.12	1.70	1.88	2.02
Y terminal superior										
M 2-5	23	0.11	0.11		0.00	0.00	0.07	0.24	0.40	
M 6-10	60	0.13	0.11	0.00	0.00	0.00	0.15	0.28	0.32	0.38
M 2-10	83	0.12	0.11	0.00	0.00	0.00	0.10	0.27	0.32	0.43
F 2-5	29	0.08	0.10		0.00	0.00	0.06	0.23	0.35	
F 6-10	63	0.11	0.15	0.00	0.00	0.00	0.04	0.28	0.40	0.61
F 2-10	92	0.10	0.14	0.00	0.00	0.00	0.04	0.26	0.39	0.47
T 2-5	52	0.09	0.10	0.00	0.00	0.00	0.07	0.23	0.32	0.45
T 6-10	123	0.12	0.13	0.00	0.00	0.00	0.08	0.28	0.32	0.44
T 2-10	175	0.11	0.12	0.00	0.00	0.00	0.08	0.26	0.32	0.44
T 2-19	341	0.10	0.12	0.00	0.00	0.00	0.07	0.26	0.32	0.38

Table A2.47

Maximal projections. M, male; F, female; T total[d]: Magnitude is in mV

		Frank-lead system								
	n	Mean mag.	SD	$p_{2.5}$	p_5	p_{10}	p_{50}	p_{90}	p_{95}	$p_{97.5}$
Z anterior										
M 2-5	23	0.86	0.41		0.36	0.42	0.78	1.52	2.02	
M 6-10	60	0.64	0.27	0.23	0.28	0.31	0.60	1.00	1.18	1.37
M 2-10	83	0.70	0.32	0.25	0.30	0.36	0.62	1.09	1.25	1.68
F 2-5	29	0.72	0.30		0.26	0.34	0.70	1.10	1.35	
F 6-10	63	0.62	0.21	0.17	0.22	0.36	0.62	0.90	1.01	1.15
F 2-10	92	0.65	0.24	0.19	0.24	0.36	0.65	0.95	1.09	1.24
T 2-5	52	0.78	0.35	0.25	0.31	0.37	0.74	1.10	1.64	1.97
T 6-10	123	0.63	0.24	0.20	0.26	0.33	0.62	0.95	1.05	1.24
T 2-10	175	0.67	0.29	0.22	0.28	0.36	0.64	1.01	1.16	1.42
T 2-19	341	0.57	0.29	0.12	0.16	0.23	0.55	0.94	1.08	1.25

Table A2.47 (Continued)

	n	Frank-lead system								
		Mean mag.	SD	$p_{2.5}$	p_5	p_{10}	p_{50}	p_{90}	p_{95}	$p_{97.5}$
Z posterior										
M 2-5	23	1.02	0.44		0.29	0.45	1.04	1.70	1.72	
M 6-10	60	1.15	0.37	0.64	0.68	0.70	1.12	1.72	1.86	2.10
M 2-10	83	1.11	0.39	0.41	0.62	0.65	1.08	1.70	1.79	2.03
F 2-5	29	1.09	0.26		0.65	0.75	1.10	1.44	1.53	
F 6-10	63	0.97	0.39	0.18	0.23	0.56	0.94	1.41	1.87	2.01
F 2-10	92	1.01	0.35	0.22	0.42	0.61	0.99	1.42	1.63	1.93
T 2-5	52	1.06	0.35	0.31	0.48	0.63	1.08	1.54	1.70	1.71
T 6-10	123	1.06	0.39	0.23	0.56	0.66	1.00	1.65	1.85	2.04
T 2-10	175	1.06	0.38	0.26	0.55	0.65	1.02	1.58	1.75	1.93
T 2-19	341	0.97	0.40	0.22	0.32	0.48	0.94	1.45	1.70	1.90

Table A2.48

Ratios of maximal projections. M, male; F, female; T, total[d]: Magnitude is in mV

	X terminal right/*X* left						*Y* terminal superior/Y interior					*Z* anterior/*Z* posterior						
	n	Mean mag.	SD	P_{50}	P_{90}	P_{95}	Mean mag.	SD	P_{50}	P_{90}	P_{95}	n	Mean mag.	SD	P_5	P_{10}	P_{50}	P_{90}	P_{95}
Frank-lead system																			
M 11-15	62	0.23	0.21	0.18	0.63	0.75	0.10	0.12	0.06	0.28	0.42	62	0.57	0.28	0.21	0.24	0.52	0.94	1.11
M 16-19	30	0.29	0.46	0.15	0.53	1.55	0.14	0.13	0.11	0.30	0.43	29	0.54	0.24	0.21	0.25	0.50	0.92	0.97
M 11-19	92	0.25	0.31	0.17	0.55	0.75	0.11	0.12	0.08	0.28	0.28	91	0.56	0.27	0.21	0.26	0.50	0.94	1.04
F 11-15	42	0.26	0.40	0.13	0.71	0.83	0.08	0.13	0.02	0.21	0.46	42	0.85	1.44	0.15	0.17	0.56	1.35	1.98
F 16-19	32	0.23	0.25	0.12	0.65	0.88	0.12	0.13	0.09	0.29	0.28	32	0.63	0.50	0.13	0.16	0.49	1.47	1.95
F 11-19	74	0.25	0.34	0.13	0.69	0.84	0.10	0.13	0.03	0.26	0.43	74	0.76	1.13	0.14	0.17	0.50	1.33	1.94
F 11-15	104	0.24	0.30	0.15	0.67	0.75	0.09	0.12	0.04	0.26	0.43	104	0.68	0.94	0.18	0.22	0.53	1.10	1.36
T 16-19	62	0.26	0.37	0.13	0.55	0.85	0.13	0.13	0.11	0.29	0.32	61	0.59	0.40	0.15	0.21	0.50	1.11	1.53
Total	166	0.25	0.32	0.15	0.59	0.75	0.10	0.12	0.06	0.27	0.40	165	0.65	0.79	0.18	0.22	0.50	1.10	1.36

Table A2.49

Maximal spatial angles and magnitudes- QRS + T. M, male; F, female; T, total[d]: Magnitude is in mV

	n		β	D	χ	Mean Mag.	SD	$P_{2.5}$	P_5	P_{10}	P_{50}	P_{90}	P_{96}	$P_{97.5}$
Frank-lead system														
QRS														
M 2-5	23	347	129	0.85	49.5	1.73	0.60		0.83	1.87	1.81	2.59	2.74	
M 6-10	60	327	133	0.85	130.7	1.83	0.53	1.00	1.11	1.14	1.77	2.67	2.93	3.15
M 2-10	83	332	133	0.84	177.6	1.80	0.55	0.85	0.96	1.11	1.80	2.59	2.81	3.05
F 2-5	29	341	133	0.83	59.4	1.72	0.44		1.02	1.15	1.69	2.13	2.66	
F 6-10	63	336	138	0.90	152.1	1.79	0.43	1.08	1.12	1.15	1.76	2.36	2.60	2.80
F 2-10	92	338	136	0.87	210.9	1.76	0.43	1.07	1.11	1.15	1.76	2.31	2.58	2.81
T 2-5	52	344	131	0.83	108.6	1.72	0.51	0.83	0.88	1.01	1.76	2.40	2.70	2.97
T 6-10	123	331	136	0.87	281.3	1.81	0.48	1.07	1.11	1.15	1.76	2.43	2.77	2.93
T 2-10	175	335	135	0.86	387.5	1.78	0.49	0.95	1.06	1.13	1.76	2.42	2.75	2.89
T 2-19	341	334	136	0.87	772.9	1.71	0.48	0.91	1.02	1.12	1.69	2.31	2.59	2.82

Table A2.49 (Continued)

	n		β	D	χ	Mean Mag.	SD	$P_{2.5}$	P_5	P_{10}	P_{50}	P_{90}	P_{96}	$P_{97.5}$
T wave														
M 2-5	22	33	123	0.89	51.7	0.48	0.15		0.18	0.25	0.53	0.68	0.72	
M 6-10	58	360	128	0.93	149.2	0.54	0.18	0.22	0.27	0.32	0.49	0.79	0.83	1.00
M 2-10	80	352	127	0.90	195.3	0.52	0.17	0.20	0.25	0.31	0.51	0.76	0.79	0.92
F 2-5	29	341	121	0.91	72.3	0.51	0.18		0.25	0.28	0.51	0.81	0.90	
F 6-10	62	0	132	0.91	153.4	0.51	0.20	0.18	0.23	0.28	0.51	0.77	0.93	1.11
F 2-10	91	354	129	0.90	220.6	0.51	0.19	0.21	0.23	0.28	0.51	0.78	0.89	1.03
T 2-5	51	338	122	0.90	123.6	0.50	0.17	0.18	0.23	0.28	0.53	0.68	0.82	0.93
T 6-10	120	360	130	0.92	302.2	0.52	0.19	0.21	0.25	0.29	0.51	0.78	0.83	1.05
T 2-10	171	353	128	0.90	415.9	0.52	0.18	0.21	0.24	0.29	0.51	0.77	0.82	0.96
T 2-19	335	5	130	0.88	781.6	0.48	0.18	0.18	0.21	0.28	0.48	0.72	0.79	0.94

Table A2.50

Normal values – magnitudes – Frank scalars (atrial)[f]

Age	Median	*n*	Mean	SD	p_5	p_{10}	p_{50}	P_{90}	p_{96}
X left (μV)									
Birth–6 months	1.8 months	27	102	37	44	61	100	167	188
6 months–5 years	2.5 years	22	78	26	38	43	76	127	139
5–12 years	8.1 years	42	76	17	47	54	76	95	117
12–19 years	15.6 years	24	69	17	42	46	66	93	97
Entire group	6.6 years	115	81	27	45	51	76	117	134
Y interior (μV)									
Birth–6 months	1.8 months	27	114	43	45	62	112	175	189
6 months–5 years	2.5 years	22	134	41	25	64	135	175	191
5–12 years	8.1 years	42	118	47	43	55	114	187	202
12–19 years	15.6 years	24	137	45	55	69	150	171	189
Entire group	6.6 years	115	124	45	48	68	124	179	193
Z interior (μV)									
Birth–6 months	1.8 months	27	41	24	6	11	40	72	92
6 months–5 years	2.5 years	22	45	15	18	22	44	65	76
5–12 years	8.1 years	42	44	16	20	24	43	62	80
12–19 years	15.6 years	24	40	17	18	20	36	67	76
Entire group	6.6 years	115	43	18	18	20	41	65	77
Z posterior (μV)									
birth–6 months	1.8 months	27	40	24	0	18	42	76	85
6 months–5 years	2.5 years	22	32	19	1	14	30	64	67
5–12 years	8.1 years	42	30	16	1	18	27	54	57
12–19 years	15.6 years	24	26	18	1	9	20	57	61
Entire group	6.6 years	115	32	18	0	15	29	58	65

Table A2.50 (Continued)

Age	Median	*n*	Mean	SD	p_5	p_{10}	p_{50}	P_{90}	p_{96}
Spatial voltage anterior (μV)									
Birth–6 months	1.8 months	27	117	42	52	65	113	182	201
6 months–5 years	2.5 years	22	94	31	50	57	91	145	150
5–12 years	8.1 years	42	93	30	41	53	93	134	150
12–19 years	15.6 years	24	109	37	42	65	104	168	173
Entire group	6.6 years	115	102	36	50	60	99	151	167
Spatial voltage posterior (μV)									
Birth–6 months	1.8 months	27	109	58	0	0	110	189	196
6 months–5 years	2.5 years	22	113	58	3	23	115	195	213
5–12 years	8.1 years	42	85	38	2	35	82	126	157
12–19 years	15.6 years	24	84	44	7	39	68	160	179
Entire group	6.6 years	115	36	50	0	30	92	166	185

Table A2.51

Normal values (timing) – Frank scalars (atrial)[f]

Age	Median	*n*	Mean	SD	p_5	p_{10}	p_{50}	p_{90}	p_{96}
P duration (ms)									
Birth–6 months	1.8 months	27	63	12	44	48	65	85	89
6 months–5 years	2.5 years	22	77	9	58	64	78	90	92
5–12 years	8.1 years	42	85	8	67	77	84	95	102
12–19 years	15.6 years	24	91	10	75	77	91	103	114
Entire group	6.6 years	115	80	14	55	60	82	95	100
PR interval (ms)									
Birth–6 months	1.8 months	27	107	13	84	87	108	124	126
6 months–5 years	2.5 years	22	125	15	97	108	125	146	146
5–12 years	8.1 years	42	137	20	107	112	133	161	161
12–19 years	15.6 years	24	144	17	108	126	140	165	165
Entire group	6.6 years	115	120	21	91	101	130	160	160
Macruz index									
birth–6 months	1.8 months	27	1.58	0.61	0.82	0.91	1.41	2.72	3.23
6 months–5 years	2.5 years	22	1.80	0.80	1.10	1.13	1.56	3.46	3.99
5–12 years	8.1 years	42	1.81	0.58	0.89	1.08	1.75	2.76	2.89
12–19 years	15.6 years	24	1.93	0.77	0.92	1.19	1.85	2.68	4.18
Entire group	6.6 years	115	1.78	0.68	0.91	1.13	1.61	2.67	3.05

Table A2.51 (Continued)

Age	Median	*n*	Mean	SD	p_5	p_{10}	p_{50}	p_{90}	p_{96}
Time maximal anterior (%)									
Birth–6 months	1.8 months	27	39	11	19	23	40	52	64
6 months–5 years	2.5 years	22	34	17	20	25	35	43	45
5–12 years	8.1 years	42	38	9	27	28	37	51	56
12–19 years	15.6 years	24	37	7	26	27	37	48	51
Entire group	6.6 years	115	37	9	24	27	37	48	53
Time ant.-post. shift (%)									
Birth–6 months	1.8 months	27	59	14	32	42	54	76	96
6 months–5 years	2.5 years	22	57	13	40	42	57	83	87
5–12 years	8.1 years	42	61	10	44	48	59	85	91
12–19 years	15.6 years	24	62	14	44	48	59	85	91
Entire group	6.6 years	115	60	12	43	47	58	78	84

(a) Strong, W.B., T.F. Downs, J. Liebman, and R. Liebowitz, The normal adolescent electrocardiogram. *Am. Heart J.*, 1972;**83**: 115. The tables are reproduced with the permission of Mosby, St Louis, Missouri.

(b) Sreenivasan, V.V., B.J. Fisher, J. Liebman, and T.D. Downs, A longitudinal study of the standard electrocardiogram in the healthy premature infant during the first year of life. *Am. J. Cardiol.*, 1973;**31**: 57. The tables are reproduced with the permission of Yorke Medical Group, New York.

(c) Namin, E.P., R.A. Arcilla, I.A. D'Cruz, and B.M. Gasul, Evolution of the Frank vectorcardiogram in normal infants. *Am. J. Cardiol.*, 1964;**13**: 757. The tables are reproduced with the permission of Yorke Medical Group, New York.

(d) Kan, J.S., J. Liebman, M.H. Lee, and A. Whitney, Quantification of the normal Frank and McFee-Parungao orthogonal electrocardiogram at ages two to ten years. *Circulation*, 1977;**55**: 31. The tables are reproduced with the permission of the American Heart Association, Dallas, Texas.

(e) Liebman, J., M.H. Lee, P.S. Rao, and W. McKay, Quantification of the normal and Frank-McFee-Parungao orthogonal electrocardiogram in the adolescent. *Circulation*, 1973;**48**: 735. The tables are reproduced with the permission of the American Heart Association, Dallas, Texas.

(f) Ferrer, P.L. and R.C. Ellison, The Frank scalar atrial vectorcardiogram in normal children. *Am. Heart J.*, 1974;**88**: 467. The tables are reproduced with the permission of Mosby, St Louis, Missouri.

(g) Rautaharju, P.M., A. Davignon, F. Soumis, E. Boiselle, and C. Hoquette, Evolution of QRS- T relationship from birth to adolescence in Frank-lead orthogonal electrocardiograms of 1492 normal children. *Circulation*, 1979;**60**: 196–204. The tables are reproduced with the permission of the American Heart Association, Dallas, Texas.

References

1. Macfarlane, P.W., E.N. Coleman, E.O. Pomphrey, S. McLaughlin, A. Houston, and T. Aitchison, Normal limits of the high-fidelity pediatric ECG. *J. Electrocardiol.*, 1989;**22**(Suppl): 162–168.

2. Macfarlane, P.W., S.C. McLaughlin, and J.C. Rodger, Influence of lead selection and population on automated measurement of QT dispersion. *Circulation*, 1998;**98**: 2160–2167.

Appendix 3: Instrumentation Standards and Recommendations

P. W. Macfarlane, A. van Oosterom, O. Pahlm, P. Kligfield, M. Janse, J. Camm (eds.), *Comprehensive Electrocardiology*, DOI 10.1007/978-1-84882-046-3_A3,

A3.1 Introduction

All ECG instruments such as direct writing electrocardiographs, cardiac monitors, ambulatory monitoring electrocardiographic devices, stress ECG machines, fetal monitors and other ECG devices that process signals from galvanic biopotential sensors share the same design principles. Modern ECG equipment utilizes integrated digital signal processors (DSP) to perform signal amplification, analog-to-digital conversion, digital filtering, formatting and communication.

This section lists several of the available standards and recommendations related to the design of such instruments. The concepts discussed and their terminology are introduced in Sect. 12.4 (Vol. 1).

A3.2 General Design Considerations

Electrocardiographs have been optimized to best suit their particular application. The function of the analog processor is to form an ECG lead signal, amplify it, eliminate the common mode noise, and minimize the external interference.

The front-end, which is responsible for processing of the body surface potentials must be able to work with low voltage alternating current (AC) signals ranging from 0.01 to 5.0 mV, combined with a direct current (DC) common-mode component of up to ±300 mV resulting from the electrode–skin interface and a common-mode noise of up to 1.5 V AC.

The bandwidth of the electrocardiograph depends on the application and can range from 50 Hz for monitoring applications to 1 kHz for late-potential measurements. The bandwidth is of great importance in ECG diagnosis since many interpretation criteria are based on exact measurements of small notches and slurs. The faithful reproduction of the lower frequency regions, such as the ST segment, is essential since these have a critical diagnostic value. Many studies have been carried out for determining the frequency content of the adult and pediatric ECGs. The American Heart Association (AHA) recommends 150 Hz as minimum bandwidth and 500 Hz as minimum sampling rate for recording adult and pediatric ECGs. The report also states that it is unknown how far the bandwidth of systems may need to be extended, due to limitations of previous studies [1].

The analog ECG signal is then sampled and converted into digital data (Sect. 12.A). In modern electrocardiographs, the sampling rate is usually much higher than is required by the Nyquist criterion and may be as high as 50 kHz in some cases (Sect. 12.A.1.2). The advantage of sampling at such a high rate is the elimination of the need for using anti-aliasing filters at the front-end and to facilitate the reduction of noise in the input signal by computing running averages.

Rijnbeek et al. [2] reported on normal ECG features observed when using the higher sampling rate of 1,200 sps. On the basis of this study, a minimum bandwidth of 250 Hz for recording pediatric ECGs was recommended. He showed that with a bandwidth of 150 Hz, 38% of the cases in the study had an error >25 μV in the maximum positive deflection in lead V4. For leads V2 and V6, these percentages were 25% and 23%, respectively. Furthermore, 15% of the positive deflections and 7% of the negative deflections in V4 have amplitude errors >50 μV when a 150 Hz filter is used. The effect of age on the frequency content of the ECG signals was also addressed. It was found that the frequency content gradually decreases from infancy to adulthood. The data for children aged 12 to 16 years indicate that the system bandwidth should be 150 Hz to yield amplitude errors less than 25μV in 95% of the cases in this age group. This is close to the 125 Hz recommendation of the AHA for the adult ECG [3]. In vectorcardiographic leads, Berson et al. [4] found amplitude errors >50 μV in 8% of the R-wave amplitudes and 5% of the S-wave amplitudes when using a 150 Hz filter.

The differences between the results of the two studies may, in part, be explained by the difference in the sampling rates used (500 versus 1,200 sps) and by the use of different lead systems. Furthermore, the analyses by Berson et al. [4] were not performed on separate leads but on leads X, Y, and Z combined, which is likely to underestimate the effect of filtering on individual lead signals. More importantly, it was concluded that a threshold of 25 μV instead of 50 μV is preferable for measuring the effect of a reduced bandwidth on signal amplitudes.

Rijnbeek recommended using the minimum bandwidth of 250 Hz for the entire pediatric population. The higher bandwidth demands the sampling rate to be at least twice the bandwidth of the signal (Sect. 12.A.2). In order to facilitate a high quality data representation, the AHA recommends a sampling rate of at least two or three times this theoretical minimum. As a rule of thumb, the pediatric ECG should be sampled at least at 1,000 samples per second.

A3.2.1 FDA Performance Standards

All diagnostic pieces of ECG equipment are classified by the Federal Drug Administration as Class II devices. Hence their design is subject both to safety and performance standards. These standards have been developed by the American Association of Medical Instrumentation and adopted by the American National Standards Institute as ANSI/AAMI EC11:1991/(R)2001. The standards establish minimum safety and performance requirements for ECG systems with direct-writing devices that are intended for use under the operating conditions specified. Also included are standards for the analysis of rhythm and of detailed morphology of complex cardiac complexes. Subject to this standard are all parts of the ECG system necessary to (a) obtain the signal from the surface of the patient's body, (b) amplify this signal, and (c) display it in a form suitable for diagnosing the heart's electrical activity. Hence, this standard includes requirements for the entire electrocardiographic recording system, ranging from the input electrodes right up to the displayed output.

Included within the scope of this standard are:

1. Direct-writing electrocardiographs.
2. Electrocardiographs used in other medical devices (e.g., patient monitors, defibrillators, stress testing devices), when such devices are intended for use in obtaining diagnostic ECG signatures.
3. Electrocardiographs having a display that is remote from the patient (via cable, telephone, telemetry, or storage media), when such devices are intended for use in obtaining ECG signatures. These devices are subject to the functional performance requirements at the system output-input levels.

Excluded from the scope of this standard are:

1. Devices that collect ECG data from locations other than the external surface of the body
2. Devices for interpretation and pattern recognition (e.g., QRS detectors, alarm circuits, rate meters, diagnostic algorithms)
3. Fetal ECG monitors
4. Ambulatory monitoring electrocardiographic devices, including ECG recorders and associated scanning and read-out devices
5. Diagnostic electrocardiographic devices utilizing non-permanent displays
6. Vectorcardiographs, that is, a device for displaying loops derived from X,Y,Z leads (see Chap. 11)
7. Electrocardiographic devices intended for use under extreme or uncontrolled environmental conditions outside of a hospital environment or physician's office
8. Cardiac monitorsl

See FDA: http://www.fda.gov/cdrh/ode/ecgs.pdf for further details

A3.2.2 Guidance for Diagnostic ECG

The Industry Diagnostic ECG Guidance (including Non-Alarming ST Segment Measurement) was issued on November 5, 1998. This guidance applies to most of the diagnostic electrocardiographs covered by the ANSI/AAMI EC11-1991 standard for Electrocardiographs (EC-11 standard). Included in the EC-11 standard are ECG devices intended for diagnostic purposes.

The Guidance for Industry, Cardiac Monitors (including Cardiotachometer and Rate Alarm) was issued on: November 5, 1998. See

http://www.fda.gov/cdrh/ode/cmonitor.pdf

This guidance applies to most of the cardiac monitors covered by the ANSI/AAMI EC13-1992 standard for Cardiac Monitors, Heart Rate Meters, and Alarms (EC13 standard). Included in the EC13 standard are ECG devices intended for monitoring purposes.

A3.2.3 Typical Design Specifications for an Electrocardiograph

Sampling rate:

- Digital sampling rate: 4,000 sps/channel
- 10,000 samples/s/channel used for pacemaker spike detection
- ECG analysis frequency: 500 sps

Dynamic range:

- AC differential: ±10 mV DC offset: ±320 mV
- Resolution: 4.88 μV/LSB @ 500 sps
- Frequency response: −3 dB @ 0.01–150 Hz
- Common mode rejection: >140 dB (123 dB with AC filter disabled)
- Input impedance: >10 MΩ @ 10 Hz, defibrillator protected
- Patient leakage: <10 μA
- Pace detect: Orthogonal LA, LL and V6; 750 μV @ 50 μs

Communication:

- Modem and Fax transmission, WI-FI wireless 802.11X

Writers:

- Writer technology: Thermal dot array
- Writer speeds: 5, 12.5, 25 and 50 mm/s (same as displayed)
- Number of traces: 3, 6, 12 or 15, user selectable (same as displayed)
- Writer sensitivity/gain: 2.5, 5, 10, 20, 10/5 (split calibration) mm/mV (same as displayed)
- Writer speed accuracy: ±2%
- Writer amplitude accuracy: ±5%
- Writer resolution: Horizontal: 1,000 dpi @ 25 mm/s, Vertical: 200 dpi

Electrical power:

- Power supply: AC or battery operation
- Voltage: 100–240 VAC +10, −15%
- Current: 0.5A @ 115 VAC, 0.3 A @ 240 VAC, typical
- Mains Frequency: 50–60 Hz ± 10%
- Battery type: User replaceable, 18 V @ 3.5 AH ± 15%, rechargeable NiMH

A3.2.4 Typical Performance Requirements for Cardiac Monitors

Cardiac monitors, with or without heart rate meters and alarms, are intended primarily for detecting cardiac rhythm and are covered by the ANSI/AAMI standard for cardiac monitors, heart rate meters and alarms – ANSI/AAMI EC 13-2002. A separate AAMI standard EC 38-1998 covers the Ambulatory Electrocardiographs. The objective of these standards was to provide minimum labeling, performance, and safety requirements and to help ensure a reasonable level of clinical efficacy and patient safety in the use of cardiac monitors. With the few exceptions noted below, performance and disclosure requirements in that standard remain appropriate.

In one section, the standard defines performance requirements, specifying a minimum, a maximum or a range of values, as applicable, that must be met. A separate section lists several performance parameters without specifying values; the

requirement is for disclosure of the achieved value to the consumer in a standardized manner. For example, a minimum heart rate meter accuracy for irregular rhythms is not specified, but the accuracy of detecting several types of defined ECG complexes must be disclosed. Designation of specifications as either performance requirements or disclosures is appropriate. The reader is referred to standard-10 for further details, including test procedures and rationale. Below is a partial listing of some important parameters in each category:

1. Protection from overload: Protection should be adequate (no damage) for 1 V (peak to peak), 60 Hz, applied for 10 s to any electrode connection. The device should recover within 8 s after defibrillation shocks of up to at least 5,000 V, delivered with energies up to 360 J.
2. Isolated patient connection: The system should include isolated patient connections to meet standards defined in the publication: American National Standard for Safe Current Limits for Electromedical Apparatus: 11.

The American Heart Association has also published its own set of instrumentation and practice standards for electrocardiographic monitoring in coronary care units, intensive care units, telemetry units, surgical suites, emergency rooms, and all other areas in which ECG monitoring functions are performed. These were directed primarily at the cardiac monitors that detect and diagnose arrhythmias and also at those that detect ST segment changes that suggest myocardial ischemia. The AHA felt that specific guidelines for ECG monitors are required, even though much of the technology is similar to other forms of ECG measurement. The clinical environment, including severity and acuteness of illness and immediacy of treatment, combined with limited time for over-reading and editing, and initiation of urgent therapy by non-physicians mandate more critical evaluation of automated arrhythmia detection and diagnostic systems.

A3.2.5 Typical Specifications for the ECG Monitoring Devices

Frequency response	–3 dB @ 0.01–150 Hz
Sampling Frequency	500 samples per second (sps)
Dynamic range	AC differential: ±10 mV
	DC offset: ±320 mV
Resolution	4.88 μV/LSB @ 500 sps
Common mode rejection	>140 dB
Input impedance	>10MΩ@10 Hz, defibrillator protected
Patient leakage current	<10μA
Pace detect	750 μV @ 50 μs
Front-end circuits	See below

To ensure correct operation with typical electrode-skin impedances and typical interference sources, the front-end of an electrocardiograph should meet the following demands:

- Very high common mode input impedance (>100 MΩ at 50/60 Hz)
- High differential mode input impedance (>10 MΩ at 50/60 Hz)
- Equal common mode input impedances for all inputs
- High common mode rejection ratio (>80 dB at 50/60 Hz)

A3.3 Patient Safety Standards

Power-line–operated electromedical equipment, connected to patients for monitoring, may permit accidental flow (leakage) of weak alternating current (AC) through a patient's body to ground. An intracardiac catheter may provide a

low-resistance path to ground through the patient's heart and thereby place the patient at risk for electrically induced ventricular tachycardia (VT) or ventricular fibrillation (VF).

In addition to the performance standards, the Safe Current Limits for Electromedical Apparatus (ANSI/AAMI ES1-1993) standards apply to all electrocardiograph designs. It states that: "The electrocardiographic (ECG) or vectorcardiographic apparatus shall be designed so that no more than 50 μA root mean square, from direct current component to the tenth harmonic of the power line frequency shall flow through any patient-connected lead under either normal or single-fault conditions." This raised the limit from 10 to 50 μA [5], the value of the European standard since 1988 [6]. Both the 10-μA standard [7, 8] and the 50-μA standard were based on estimates of the risk of AC-induced VF. However, AC may cause cardiovascular collapse at levels that are below the VF threshold [9–13]. This adverse response to AC was not considered in the selection of either safety standard. Furthermore, safe levels of AC have not been determined in closed-chest humans.

The 10-μA standard was adopted in 1967 to ensure patient safety during cardiac catheterization [14] and pacemaker [15] procedures. The annual number of invasive cardiac procedures in the United States has increased from less than 60,000 when the 10-μA standard was adopted to more than 3 million today. The potential number of adverse outcomes from leakage current increased correspondingly.

Electromedical devices contain electrical isolation circuits and insulation to limit leakage current. Manufacturers continue to comply with the original 10-μA standard, but they may realize substantial cost savings by equipment designs that comply only with the newer 50-μA standard [16]. However, the American Heart Association continues to recommend the 10-μA standard [17–19].

A3.4 Recommendations for the Standardization and Interpretation of the Electrocardiogram

Around 2005, the American Heart Association, the American College of Cardiology Foundation and the Heart Rhythm Society agreed to collaborate on the establishment of a series of recommendations for the standardization and interpretation of the ECG. A number of working groups were set up and over the next few years, various publications emerged on the topic. These were all endorsed by the International Society for Computerized Electrocardiology. The six papers form an important contribution to the field and are recommended as essential reading for anyone interested in the development of diagnostic criteria, particularly for computer assisted interpretation of the ECG.

The titles of the different papers are self explanatory and there is no need to expand on the content. However, it is worth mentioning that the first paper [20] is wide ranging and includes many aspects of ECG recording through electrode positioning to requirements for digital filters. The other papers deal with terminology [21], intraventricular conduction disturbances [22], the ST Segment, T and U Waves, and the QT Interval [23], cardiac chamber hypertrophy [24] and acute ischemia/infarction [25].

It is also relevant to highlight again the guidelines published over 30 years ago in a paper [8] entitled "Recommendations for standardization of leads and their specifications for instruments in electrocardiography and vectorcardiography," which still contains many points that are of relevance in this area.

A3.5 Guidelines

A3.5.1 Heart Rate Variability

A Task Force of the European Society of Cardiology and the North American Society of Pacing and Electrophysiology produced a guideline paper relating to heart rate variability [26]. The paper dealt with standards of measurement, physiological interpretation and clinical use.

A3.5.2 Electrocardiographic Monitoring in Hospital Settings

A scientific statement for the American Heart Association Councils on Cardiovascular Nursing, Clinical Cardiology and Cardiovascular disease in the young, dealing with electrocardiographic monitoring in hospital settings was published in 2004 [27]. This sets out recommendations for the different types of monitoring that are necessary in the hospital environment, ranging from arrhythmia analysis through to ischemia monitoring and QT interval assessment. Different types of ECG lead systems for monitoring are described and recommendations relating to staffing, training and quality improvement are given.

A3.5.3 Recommendations for Ambulatory Electrocardiography

A paper on instrumentation and ambulatory electrocardiography published as a set of recommendations was published in 1985 [28]. Much of the information there is still of relevance although equipment is now predominantly based around digital recording techniques. A follow up paper was published in 1999 [29]. These more recent guidelines review equipment and also deal with assessment of symptoms that may be related to disturbances of rhythm and assessment of risk in patients without symptoms of arrhythmias.

A3.5.4 Exercise Testing

Guidelines for clinical exercise testing laboratories were published in 1995 [30]. These outlined the environment in which exercise testing should be undertaken and discussed equipment requirements, etc. Clinical guidelines were published in 1997 [31] and updated in 2002 [32]. These papers essentially deal with the conditions under which exercise testing is deemed to be appropriate.

A3.5.5 Clinical Competence

The ACC and AHA issued a statement on competence for reporting ECGs and ambulatory ECGs [33]. This publication outlines the diagnostic areas where physicians are expected to have a high degree of competence in reporting resting and ambulatory ECGs.

A3.5.6 Pacemakers/Electrophysiology Testing

One of the earliest guidelines on electrophysiology testing and pacemakers was published in 1984 [34]. This outlined the three position and the five position coding scheme for pacemakers. This was updated in 2002 [35]. A paper on guidelines for implantation of pacemakers, which was published in 2002 [36], contained earlier 1998 guidelines together with updated guidelines.

References

1. Kligfield, P., L.S. Gettes, J.J. Bailey, et al., Recommendations for the standardization and interpretation of the electrocardiogram: Part I: the electrocardiogram and its technology. A scientific statement from the American Heart Association Electrocardiography and Arrhythmias Committee, Council on Clinical Cardiology; the American College of Cardiology Foundation; and the Heart Rhythm Society Endorsed by the International Society for Computerized Electrocardiology. *Circulation*, 2007;**115**(10).
2. Rijnbeek, P.R., J.A. Kors, and M. Witsenburg, Minimum bandwidth requirements for recording of pediatric electrocardiograms. *Circulation*, 2001;**104**(25): 3087–3090.
3. Bailey, J.J., A.S. Berson, A. Garson, Jr., L.G. Horan, P.W. Macfarlane, D.W. Mortara, and C. Zywietz, Recommendations for standardization and specifications in automated electrocardiography: bandwidth and digital signal processing. *Circulation*, 1990;**81**: 730–739.

4. Berson, A.S., Y.K. Francis, B.A. Lau, J.M. Wojick, and H.V. Pipberger, Distortions in infant electrocardiograms caused by inadequate high-frequency response. *Am. Heart J.*, 1977;**93**: 730–734.
5. *Safe Current Limits for Electromedical Apparatus*. 1993, Association for the Advancement of Medical Instrumentation.
6. Medical Electrical Equipment- Part 1: General Requirements for Safety in Collateral Standard: Electromagnetic Compatibility – Requirements and Test. 1993.
7. Pipberger, H.V., R.C. Arzbaecher, A.S. Berson, et al., Amendment of recommendations for standardization of specifications for instruments in electrocardiography and vectorcardiography concerning safety and electrical shock hazards. 1972; Committee of Electrocardiography, American Heart Association. *Circulation*, 1972;**46**: 1–2.
8. Pipberger, H.V., R.C. Arzbaecher, A.S. Berson, et al., Recommendations for standardization of leads and of specifications for instruments in electrocardiography and vectorcardiography. 1975. Committee on Electrocardiography, American Heart Association. *Circulation*, 1975;**52**: 11–31.
9. Green, H., E.B. Raftery, and I.C. Gregory, Ventricular fibrillation threshold of healthy dogs to 50 Hz current in relation to earth leakage currents of electromedical equipment. *Biomed. Eng.*, 1972;**7**: 408–414.
10. Raftery, E., H. Green, and I. Gregory, Disturbances of heart rhythm produced by 50 Hz leakage currents in dogs. *Cardiovasc. Res.*, 1975;**9**: 256–262.
11. Raftery, E.B., H.L. Green, and M.H. Yacoub, Disturbances of heart rhythm produced by 50 Hz leakage currents in human subjects. *Cardiovasc. Res.*, 1975;**9**: 263–265.
12. Roy, O.Z., J.R. Scott, and G.C. Park, 60 Hz ventricular fibrillations and pump failure thresholds versus electrode area. *IEEE Eng. Med. Biol.*, 1976;**BME-23**: 45–48.
13. Graystone, P. and J. Ledsome, Microshock hazards in hospital: fibrillation thresholds: the wrong parameter, in *Digest of the 10th International Conference on Medical and Biologic Engineering*, Dresden, Germany, 1973.
14. Weinberg, D.I., J.L.D. Artley, R.E. Whalen, and H.D. Mcintosh, Electric shock hazards in cardiac catheterization. *Circ. Res.*, 1962;**11**: 1004–1009.
15. Whalen, R.E., C.F. Starmer, and H.D. McIntosh, Electrical hazards associated with cardiac pacemaking. *Ann. NY Acad. Sci.*, 1964;**111**: 922–931.
16. Bruner, J.M.R. and P.F. Leonard, Codes and standards: who makes the rules?, in *Electricity, Safety and the Patient*. Chicago: Year Book Medical Publishers, 1989, pp. 240–279.
17. Laks, M.M., R. Arzbaecher, D. Geselowitz, et al., Will relaxing safe current limits for electromedical equipment increase hazards to patients? *Circulation*, 2000;**102**: 823.
18. Laks, M.M., R. Arzbaecher, J.J. Bailey, et al., Recommendations for safe current limits for electrocardiographs: a statement for healthcare professionals from the Committee of Electrocardiography; American Heart Association. *Circulation*, 1996;**93**: 837–839.
19. Laks, M.M., R. Arzbaecher, J.J. Bailey, et al., Comments on "Special report: recommendations for safe current limits for electrocardiographs". *Circulation*, 1997;**95**: 277–278.
20. Kligfield, P., L.S. Gettes, J.J. Bailey, et al., AHA/ACC/HRS recommendations for the standardization and interpretation of the electrocardiogram. Part I: The electrocardiogram and its technology. A scientific statement From the American Heart Association Electrocardiography and Arrhythmias Committee, Council on Clinical Cardiology; the American College of Cardiology Foundation; and the Heart Rhythm Society (Endorsed by the International Society for Computerized Electrocardiology). *J. Am. Coll. Cardiol.*, 2007;49: 1109–1127, doi:10.1016/j.jacc.2007.01.024.
21. Mason, J.W., E.W. Hancock, and L.S. Gettes, AHA/ACC/HRS recommendations for the standardization and interpretation of the electrocardiogram. Part II: Electrocardiography diagnostic statement list. A scientific statement from the American Heart Association Electrocardiography and Arrhythmias Committee, Council on Clinical Cardiology; the American College of Cardiology Foundation; and the Heart Rhythm Society. (Endorsed by the International Society for Computerized Electrocardiology). *J. Am. Coll. Cardiol.*, 2007;**49**: 1128–1135, doi:10.1016/j.jacc.2007.01.025.
22. Surawicz, B., R. Childers, B.J. Deal, and L.S. Gettes, AHA/ACC/HRS recommendations for the standardization and interpretation of the electrocardiogram. Part III: Intraventricular conduction disturbances. A scientific statement from the American Heart Association Electrocardiography and Arrhythmias Committee, Council on Clinical Cardiology; the American College of Cardiology Foundation; and the Heart Rhythm Society. (Endorsed by the International Society for Computerized Electrocardiology). *J. Am. Coll. Cardiol.*, 2009;**53**: 976–981, doi:10.1016/j.jacc.2008.12.013.
23. Rautaharju, P.M., B. Surawicz, and L.S. Gettes, AHA/ACCF/HRS recommendations for the standardization and interpretation of the electrocardiogram. Part IV: The ST segment, T and U waves, and the QT interval. A scientific statement from the American Heart Association Electrocardiography and Arrhythmias Committee, Council on Clinical Cardiology; the American College of Cardiology Foundation; and the Heart Rhythm Society. (Endorsed by the International Society for Computerized Electrocardiology). *J. Am. Coll. Cardiol.*, 2009;**53**: 982–991, doi:10.1016/j.jacc.2008.12.014.
24. Hancock, E.W., B.J. Deal, D.M. Mirvis, et al., AHA/ACCF/HRS recommendations for the standardization and interpretation of the electrocardiogram. Part V: Electrocardiogram changes associated with cardiac chamber hypertrophy. A scientific statement from the American Heart Association Electrocardiography and Arrhythmias Committee, Council on Clinical Cardiology; the American College of Cardiology Foundation; and the Heart Rhythm Society. (Endorsed by the International Society for Computerized Electrocardiology). *J. Am. Coll. Cardiol.*, 2009;**53**: 992–1002, doi:10.1016/j.jacc.2008.12.015.
25. Wagner, G.S., P.W. Macfarlane, H. Wellens, et al., AHA/ACCF/HRS recommendations for the standardization and interpretation of the electrocardiogram. Part VI: Acute ischemia/infarction. A scientific statement from the American Heart Association Electrocardiography and Arrhythmias Committee, Council on Clinical Cardiology; the American College of Cardiology Foundation; and the Heart Rhythm Society Endorsed by the International Society for Computerized Electrocardiology. *J. Am. Coll. Cardiol.*, 2009;**53**: 1003–1011, doi:10.1016/j.jacc.2008.12.016.
26. Task Force of the European Society of Cardiology and the North American Society of Pacing Electrophysiology, Heart rate variability. Standards of measurement, physiological interpretation, and clinical use. *Circulation*, 1996;**93**: 1043–1065.

27. Drew, B., R.M. Califf, M. Funk, et al., AHA scientific statement. Practice standards for electrocardiographic monitoring in hospital settings. *Circulation*, 2004;**110**: 2721–2746.
28. Sheffield, L.T., A. Berson, and D. Bragg-Remschel, Recommendations for standards and instrumentation and practice in the use of ambulatory electrocardiography. The Task force of the Committee on Electrocardiography and Cardiac Electrophysiology of the Council on Clinical Cardiology. *Circulation*, 1985;**71**: 626A–636A.
29. Crawford, M.H., S.J. Bernstein, P.C. Deedwania, et al., ACC/AHA guidelines for ambulatory electrocardiography. Executive summary and recommendations: A report of the American College of Cardiology/American Heart Association Task Force on Practice Guidelines (Committee to Revise the Guidelines for Ambulatory Electrocardiography). *Circulation*, 1999;**100**: 886–893.
30. Pina, I.L., G.J. Balady, P. Hanson, A.J. Labovitz, D.W. Madonna, and J. Myers, Guidelines for clinical exercise testing laboratories. A statement for healthcare professionals from the Committee on Exercise and Cardiac Rehabilitation, American Heart Association. *Circulation*, 1995;**91**: 912–921.
31. Gibbons, R., G.J. Balady, J.W. Beasley, et al., ACC/AHA guidelines for exercise testing. A report of the American College of Cardiology/American Heart Association Task Force on Practice Guidelines (Committee on Exercise Testing). *J. Am. Coll. Cardiol.*, 1997;**30**: 260–311.
32. Gibbons, R., G.J. Balady, J.T. Bricker, et al., ACC/AHA 2002 guideline update for exercise testing: summary article. A report of the American College of Cardiology/American Heart Association Task Force on Practice Guidelines (Committee to Update the 1997 Exercise testing Guidelines). *Circulation*, 2002;**106**: 1883–1892.
33. Kadish, A.H., A.E. Buxton, H.L. Kennedy, B.P. Knight, C.D. Schuger, and C.M. Tracy, A report of the ACC/AHA/ACP-ASIM task force on clinical competence (ACC/AHA Committee to develop a clinical competence statement on electrocardiography and ambulatory electrocardiography). *Circulation*, 2001;**104**: 3169–3178.
34. Gettes, L.S., D.P. Zipes, P.C. Gillette, et al., Personnel and equipment required for electrophysiologic testing. Report of the committee on electrocardiography and cardiac electrophysiology, Council on Clinical Cardiology, the American Heart Association. *Circulation*, 1984;**69**: 1219A–1221A.
35. Bernstein, A.D., J.-C. Daubert, R.D. Fletcher, et al., The revised NASPE/BPEG generic code for antibradycardia, adaptive-rate, and multisite pacing. *PACE*, 2002;**25**: 260–264.
36. Gregoratis, G., J. Abrams, A.E. Epstein, et al., ACC/AHA/NASPE 2002 guideline update for implantation of cardiac pacemakers and antiarrhythmia devices: Summary article. A report of the American College of Cardiology/American Heart Association Task Force on Practice Guidelines (ACC/AHA/NASPE Committee to Update the 1998 Pacemaker Guidelines). *Circulation*, 2002;**106**: 2145–2161.

Appendix 4: Coding Schemes

P. W. Macfarlane, A. van Oosterom, O. Pahlm, P. Kligfield, M. Janse, J. Camm (eds.), *Comprehensive Electrocardiology*, DOI 10.1007/978-1-84882-046-3_A4,

A4.1 The Minnesota Code

The Minnesota code was initially developed and published in 1960 (see Ref. [20] in (Chap. 13). It remains the most widely used ECG coding scheme in epidemiological practice and has recently been revised and extended. The following section has been reprinted from: Prineas RJ, Crow RS, Zhang Z-M. The Minnesota Code Manual of Electrocardiographic Findings. 2009, with the permission of Springer, New York.

A4.1.1 Minnesota Code 2009

A4.1.1.1 Q and QS Patterns

(Do not code in the presence of Wolff-Parkinson-White (WPW) code 6-4-1), or artificial pacemaker code 6-8 or code 6-1, 8-2-1, 8-2-2, or 8-4-1 with a heart rate ≥ 140. To qualify as a Q wave, the deflection should be at least 0.1 mV (1 mm in amplitude).

Anterolateral site (leads I, aVL, V_6)

- 1-1-1 Q/R amplitude ratio ≥1/3, plus Q duration ≥0.03 s in lead I or V_6.
- 1-1-2 Q duration ≥0.04 s in lead I or V_6.
- 1-1-3 Q duration ≥0.04 s, plus R amplitude ≥3 mm in lead aVL.
- 1-2-1 Q/R amplitude ratio ≥1/3, plus Q duration ≥0.02 s and <0.03 s in lead I or V_6.
- 1-2-2 Q duration ≥0.03 s and <0.04 s in lead I or V_6.
- 1-2-3 QS pattern in lead I. Do not code in the presence of 7-1-1.
- 1-2-8 Initial R amplitude decreasing to 2 mm or less in every beat (and absence of codes 3-2, 7-1-1, 7-2-1 or 7-3) between V_5 and V_6. (All beats in lead V_5 must have an initial R >2 mm.)
- 1-3-1 Q/R amplitude ratio ≥1/5 and <1/3, plus Q duration ≥0.02 s and <0.03 s in lead I or V_6.
- 1-3-3 Q duration ≥0.03 s and <0.04 s, plus R amplitude ≥3 mm in lead aVL.
- 1-3-8[1] Initial R amplitude decreasing to 2 mm or less in every beat (and absence of codes 3-2, 7-1-1, 7-2-1, or 7-3) between V_5 and V_6 (All beats in lead V_5 must have an initial R > 2 mm.)

Posterior (inferior) site (leads II, III, aVF).

- 1-1-1 Q/R amplitude ratio ≥1/3, plus Q duration ≥0.03 s in lead II.
- 1-1-2 Q duration ≥0.04 s in lead II.
- 1-1-4 Q duration ≥0.05 s in lead III, plus a Q-wave amplitude ≥1.0 mm in the majority of beats in lead aVF.
- 1-1-5 Q duration ≥0.05 s in lead aVF.
- 1-2-1 Q/R amplitude ratio ≥1/3, plus Q duration ≥0.02 s and<0.03 s in lead II.
- 1-2-2 Q duration ≥0.03 s and <0.04 s in lead II.
- 1-2-3 QS pattern in lead II. Do not code in the presence of 7-1-1.
- 1-2-4 Q duration ≥0.04 s and <0.05 s in lead III, plus a Q wave ≥1.0 mm amplitude in the majority of beats in aVF.
- 1-2-5 Q duration ≥0.04 s and <0.05 s in lead aVF.
- 1-3-1 Q/R amplitude ratio ≥1/5 and <1/3, plus Q duration ≥0.02 s and <0.03 s in lead II.
- 1-3-4 Q duration ≥0.03 s and <0.04 s in lead III, plus a Q wave ≥1.0 mm amplitude in the majority of beats in lead aVF.
- 1-3-5 Q duration ≥0.03 s and <0.04 s in lead aVF.
- 1-3-6 QS pattern in each of leads III and aVF. (Do not code in the presence of 7-1-1.)
- 1-3-7[2] QS pattern in lead a aVF only. (Do not code in the presence of 7-1-1)

Anterior site (leads V_1, V_2, V_3, V_4, V_5)

- 1-1-1 Q/R amplitude ratio ≥1/3 plus Q duration ≥0.03 s in any of leads V_2, V_3,V_4,V_5.
- 1-1-2 Q duration ≥0.04 s in any of leads V_1, V_2, V_3, V_4, V_5.
- 1-1-6 QS pattern when initial R wave is present in adjacent lead to the right on the chest, in any of leads V_2, V_3, V_4, V_5, V_6.
- 1-1-7 QS pattern in all of leads V_1–V_4 or V_1–V_5.
- 1-2-1 Q/R amplitude ratio ≥1/3, plus Q duration ≥0.02 s and <0.03 s, in any leads V_2, V_3, V_4, V_5.
- 1-2-2 Q duration ≥0.03 s and <0.04 s in any leads V_2, V_3, V_4, V_5.
- 1-2-7 QS pattern in all of lead V_1, V_2, and V_3. (Do not code in the presence of 7-1-1.)
- 1-3-1 Q/R amplitude ratio ≥1/5 and <1/3 plus Q duration ≥0.02 s and <0.03 s in any of leads V_2, V_3, V_4, V_5.
- 1-3-2 QS pattern in lead V_1 and V_2. (Do not code in the presence of 3-1 or 7-1-1.)
- 1-3-8[1] Initial R amplitude decreasing to 2.0 mm or less in every beat (and absence of codes 3-2, 7-1-1, 7-2-1, or 7-3) between any of leads V_2 and V_3, V_3, and V_4, or V_4 and V_5. (All beats in the lead immediately to the right on the chest must have an initial R > 2 mm.)

A4.1.1.2 QRS Axis Deviation

(Do not code in presence of low-voltage QRS code 9-1, WPW 6-4-1, artificial pacemaker code 6-8, ventricular conduction defects 7-1-1, 7-2-1, 7-4 or 7-8.)

- 2-1 Left. QRS axis from −30° through −90° in leads I, II, III. (The algebraic sum of major positive and major negative QRS waves must be 0 or positive in I, negative in III, and 0 or negative in II).
- 2-2 Right. QRS axis from +120° through −150° in leads I, II, III. (The algebraic sum of major positive and major negative QRS waves must be negative in I, and zero or positive in III, and in I must be one half or more of that in III.)
- 2-3 Right (optional code when 2-2 is not present). QRS axis from +90° through +119°in leads I, II, III. (The algebraic sum of major positive and major negative QRS waves must be zero or negative in I and positive in II and III.)
- 2-4 Extreme axis deviation (usually S1, S2, S3 pattern). QRS axis from −90° through −149° in leads I, II and III. (The algebraic sum of major positive and major negative QRS waves must be negative in each of leads I, II and III.)
- 2-5 Indeterminate axis. QRS axis approximately 90° from the frontal plane. (The algebraic sum of major positive and major negative QRS waves is zero in each of leads I, II and III, or the information from these three leads is incongruous.)

A4.1.1.3 High-Amplitude R Waves

Do not code in the presence of codes 6-4-1, 6-8, 7-1-1, 7-2-1, 7-4, or 7-8.

- 3-1 Left: R amplitude >26 mm in either V_5 or V_6, or R amplitude >20.0 mm in any of leads I, II, III, aVF, or R amplitude >12.0 mm in lead aVL measured only on second to last complete normal beat.

- 3-2 Right: R amplitude ≥5.0 mm and R amplitude ≥S amplitude in the majority of beats in lead V_1, when S amplitude is >R amplitude somewhere to the left on the chest of V_1 (codes 7-3 and 3-2, if criteria for both are present).
- 3-3 Left (optional code when 3-1 is not present): R amplitude >15.0 mm but ≤20.0 mm in lead I, or R amplitude in V_5 or V_6, plus S amplitude in V_1 > 35.0 mm.
- 3-4 Criteria for 3-1 and 3-2 both present.

A4.1.1.4 ST Junction (J) and Segment Depression

(Do not code in the presence of codes 6-4-1, 6-8, 7-1-1, 7-2-1, 7-4, or 7-8. When 4-1, 4-2, or 4-3 is coded, then a 5-code most often must also be assigned except in lead V_1.)

Anterolateral site (leads I, aVL, V_6)

- 4-1-1 STJ depression ≥2.0 mm and ST segment horizontal or downward sloping in any of leads I, aVL, or V_6
- 4-1-2 STJ depression ≥1.0 mm but <2.0 mm, and ST segment horizontal or downward sloping in any of leads I, aVL, or V_6
- 4-2 STJ depression ≥0.5 mm and <1.0 mm and ST segment horizontal or downward sloping in any of leads I, aVL, or V_6
- 4-3 No STJ depression as much as 0.5 mm but ST segment downward sloping and segment or T-wave nadir ≥0.5 mm below P-R baseline, in any of leads I, aVL, or V_6
- 4-4 STJ depression ≥1.0 mm and ST segment upward sloping or U-shaped, in any of leads I, aVL, or V_6

Posterior (inferior) site (leads II, III, aVF)

- 4-1-1 STJ depression ≥2.0 mm and ST segment horizontal or downward sloping in lead II or aVF
- 4-1-2 STJ depression ≥1.0 mm but <2.0 mm and ST segment horizontal or downward sloping in lead II or aVF
- 4-2 STJ depression ≥0.5 mm and <1.0 mm and ST segment horizontal or downward sloping in lead II or aVF
- 4-3 No STJ depression as much as 0.5 mm, but ST segment downward sloping and segment or T-wave nadir ≥0.5 mm below P-R baseline in lead II
- 4-4 STJ depression ≥1.0 mm and ST segment upward sloping, or U shaped, in lead II

Anterior site (leads V_1, V_2, V_3, V_4, V_5)

- 4-1-1 STJ depression ≥2.0 mm and ST segment horizontal or downward sloping in any of leads V_1, V_2, V_3, V_4, V_5
- 4-1-2 STJ depression ≥1.0 mm but <2.0 mm and ST segment horizontal or downward sloping in any of leads V_1, V_2, V_3, V_4, V_5
- 4-2 STJ depression ≥0.5 mm and <1.0 mm and ST segment horizontal or downward sloping in any of leads V_1, V_2, V_3, V_4, V_5
- 4-3 No STJ depression as much as 0.5 mm, but ST segment downward sloping and segment or T-wave nadir ≥0.5 mm below P-R baseline in any of leads V_2, V_3, V_4, V_5
- 4-4 STJ depression ≥1.0 mm and ST segment upward sloping or U-shaped in any of leads V_1, V_2, V_3, V_4, V_5

A4.1.1.5 T-Wave Items

(Do not code in the presence of codes 6–4–1, 6-8, 7–1–1, 7–2–1, 7-4, or 7–8.)

Anterolateral site (leads I, aVL, V_6)

- 5-1 T amplitude negative 5.0 mm or more in either of leads I, V_6, or in lead aVL when R amplitude is ≥5.0 mm
- 5-2 T amplitude negative or diphasic (positive–negative or negative–positive type) with negative phase at least 1.0 mm but not as deep as 5.0 mm in lead I or V_6, or in lead aVL when R amplitude is ≥5.0 mm
- 5-3 T amplitude zero (flat), or negative, or diphasic (negative-positive type only) with less than 1.0 mm negative phase in lead I or V_6, or in lead aVL when R amplitude is ≥5.0 mm
- 5-4 T amplitude positive and T/R amplitude ratio <1/20 in any of leads I, aVL, V_6; R-wave amplitude must be ≥10.0 mm

Posterior (inferior) site (leads II, III, aVF)

- 5-1 T amplitude negative 5.0 mm or more in lead II, or in lead aVF when QRS is mainly upright
- 5-2 T amplitude negative or diphasic with negative phase (negative–positive or positive–negative type) at least 1.0 mm but not as deep as 5.0 mm in lead II, or in lead aVF when QRS is mainly upright
- 5-3 T amplitude zero (flat), or negative, or diphasic (negative-positive type only) with less than 1.0 mm negative phase in lead II; not coded in lead aVF
- 5-4 T amplitude positive and T/R amplitude ratio <1/20 in lead II; R-wave amplitude must be ≥10.0 mm

Anterior site (leads V_2, V_3, V_4, V_5)

- 5-1 T amplitude negative 5.0 mm or more in any of leads V_2, V_3, V_4, V_5
- 5-2 T amplitude negative (flat) n any codes, or diphasic (negative–positive or positive–negative type) with negative phase at least 1.0 mm but not as deep as 5.0 mm, in any of leads V_2, V_3, V_4, V_5
- 5-3 T amplitude zero (flat), or negative, or diphasic (negative–positive type only) with less than 1.0 mm negative phase, in any of leads V_3, V_4, V_5
- 5-4 T amplitude positive and T/R amplitude ratio <1/20 in any of leads V_3, V_4, V_5; R-wave amplitude must be ≥10.0 mm

A4.1.1.6 AV Conduction Defect in Codes

- 6-1 Complete (third degree) AV block (permanent or intermittent) in any lead. Atrial and ventricular complexes independent, and atrial rate faster than ventricular rate, with ventricular rate <60.
- 6-2-1 Mobitz type II (occurrence of P wave on time with dropped QRS and T).
- 6-2-2 Partial (second degree) AV block in any lead (2:1 or 3:1 block).
- 6-2-3 Wenckebach's phenomenon (PR interval increasing from beat to beat until QRS and T dropped).
- 6-3 PR(PQ) interval ≥0.22 s in the majority of beats in any of leads I, II, III, aVL, aVF.
- 6-4-1 Wolff-Parkinson-White pattern (WPW), persistent. Sinus P wave. PR interval <0.12 s, plus QRS duration ≥0.12 s, plus R peak duration ≥0.06 s, coexisting in the same beat and present in the majority of beats in any of leads I, II, aVL, V_4, V_5, V_6. (6-4-1 suppresses 1-2-3, 1-2-7, 1-3-2, 1-3-6, 1-3-8, all 3, 4, 5, 7, 9-2, 9-4, 9-5 codes.)

- 6-4-2 WPW pattern, intermittent. WPW pattern in ≤50% of beats in appropriate leads.
- 6-5 Short PR interval. PR interval <0.12 s in all beats of any two of leads I, II, III, aVL, aVF.
- 6-6 Intermittent aberrant atrioventricular conductions. PR > 0.12 s (except in presence of 6-5 or heart rate greater than 100); wide QRS complex >0.12 s; normal P wave when most beats are sinus rhythm. (Do not code in the presence of 6-4-2.)
- 6-8 Artificial pacemaker.

A4.1.1.7 Ventricular Conduction Defect in Codes

- 7-1-1 Complete left bundle branch block (LBBB). (Do not code in presence of 6-1, 6-4-1, 6-8, 8-2-1 or 8-2-2,) QRS duration ≥0.12 s in a majority of beats (of the same QRS pattern) in any of leads I, II, III, aVL, aVF, ***plus*** R peak duration ≥0.06 s in a majority of beats (of the same QRS pattern) in any of leads I, II aVL, V_5, V_6 (7-1-1 suppresses 1-2-3, 1-2-7, 1-2-8, 1-3-2, 1-3-6, all 2, 3, 4, 5, 9-2, 9-4, 9-5 codes. If any other codable Q wave coexists with the LBBB pattern, code the Q and diminish the 7-1-1 code to a 7-4 code.)
- 7-1-2 Intermittent LBBB. Same as 7-1-1 but with presence of normally conducted QRS complexes of different shape than the LBBB pattern.
- 7-2-1 Complete right bundle branch block (RBBB). (Do not code in the presence of 6-1, 6-4-1, 6-8, 8-2-1 or 8-2-2.) QRS duration ≥0.12 s in a majority of beats (of the same QRS pattern) in any of leads I, II, III, aVL, aVF, ***plus***: R′ > R in V_1 or QRS mainly upright, ***plus*** R peak duration ≥0.06 s in V_1 or V_2; or S duration > R duration in all beats in lead I or II. (Suppresses 1-2-8 + 1-3-8, all 2-, 3-, 4- and 5- codes, 9-2, 9-4, 9-5.)
- 7-2-2 Intermittent RBBB. Same as 7-2-1 but with presence of normally conducted QRS complexes of different shape than the RBBB pattern.
- 7-3 Incomplete right bundle branch block. QRS duration <0.12 s in each of leads I, II, III, aVL, aVF, and R′ > R in either of leads V_1, V_2. (Code as 3-2 in addition if those criteria are met. 7-3 suppresses code 1-2-8.)
- 7-4 Intraventricular block. QRS duration ≥0.12 s in a majority of beats in any of leads I, II, III, aVL. (7-4 suppresses all 2, 3, 4, 5, 9-2, 9-4, 9-5 codes.)
- 7-5 R-R′ pattern in either of leads V_1, V_2 with R′ amplitude ≤ R.
- 7-6 Incomplete LBBB. (Do not code in the presence of any codable Q or QS wave.) QRS duration ≥0.10 and <0.12 s in the majority of beats of each of leads I, aVL, and V_5 or V_6.
- 7-7 Left anterior hemiblock (LAH). QRS duration <0.12 s in the majority of beats in leads I, II, III, aVL, aVF, ***plus*** Q-wave amplitude ≥0.25 mm and <0.03 s duration in lead I, ***plus*** left axis deviation of −45° or more negative. (In presence of 7-2, code 7-8 if axis is <−45° and the Q wave in lead I meets the above criteria).
- 7-8 Combination of 7-7 and 7-2.
- 7-9-1[2] Type 1 Brugada pattern convex (coved) ST segment elevation ≥ 2 mm ***plus*** T-wave negative with little or no isoelectric (baseline) separation in at least 2 leads of $V_1 - V_3$.
- 7-9-2[2] Type 2 Brugada pattern ST segment elevation ≥ 2 mm ***plus*** T-wave positive or diphasic that results in a "saddle-back" shape in at least 2 leads of $V_1 - V_3$.
- 7-9-3[2] Type 3 Brugada pattern. 7-2-1 ***plus*** ST segment elevation ≥ 1 mm ***plus*** a "saddle-back" configuration in at least 2 leads of $V_1 - V_3$.
- 7-10[2] Fragmented QRS.

A4.1.1.8 Arrhythmias

- 8-1-1 Presence of frequent atrial or junctional premature beats (10% or more of recorded complexes).
- 8-1-2 Presence of frequent ventricular premature beats (10% or more of recorded complexes).

- 8-1-3 Presence of both atrial and/or junctional premature beats and ventricular premature beats (so that individual frequencies are <10% but *combined* premature beats are ≥10% of complexes).
- 8-1-4 Wandering atrial pacemaker.
- 8-1-5 Presence of 8-1-2 and 8-1-4.
- 8-2-1 Ventricular fibrillation or ventricular asystole.
- 8-2-2 Persistent ventricular (idioventricular) rhythm.
- 8-2-3 Intermittent ventricular tachycardia. Three or more consecutive ventricular premature beats occurring at a rate ≥100. This includes more persistent ventricular tachycardia.
- 8-2-4 Ventricular parasystole (should not be coded in presence of 8-3-1).
- 8-3-1 Atrial fibrillation (persistent).
- 8-3-2 Atrial flutter (persistent).
- 8-3-3 Intermittent atrial fibrillation (code if 3 or more clear-cut, consecutive sinus beats are present in any lead).
- 8-3-4 Intermittent atrial flutter (code if 3 or more clear-cut, consecutive sinus beats are present in any lead).
- 8-4-1 Supraventricular rhythm persistent. QRS duration <0.12 s; and absent P waves or presence of abnormal P waves (inverted or flat in aVF); and regular rhythm.
- 8-4-2 Supraventricular tachycardia intermittent. Three consecutive atrial or junctional premature beats occurring at a rate ≥100 min^{-1}.
- 8-5-1 Sinoatrial arrest. Unexpected absence of P, QRS and T, plus a R-R interval at a fixed multiple of the normal interval, ±10%.
- 8-5-2 Sinoatrial block. Unexpected absence of P, QRS and T, preceded by progressive shortening of P-P intervals, (R-R interval at a fixed multiple of the normal interval, ±10%).
- 8-6-1 AV dissociation with ventricular pacemaker (without capture). Requires: P-P and R-R to occur at variable rates with ventricular rate as fast as or faster than the atrial rate plus variable PR intervals, plus no capture beats.
- 8-6-2 AV dissociation with ventricular pacemaker (with capture).
- 8-6-3 AV dissociation with atrial pacemaker (without capture).
- 8-6-4 AV dissociation with atrial pacemaker (with capture).
- 8-7 Sinus tachycardia (≥ 100 min^{-1}).
- 8-8 Sinus bradycardia (≤ 50 min^{-1}).
- 8-9 Other arrhythmias. Heart rate may be recorded as a continuous variable.

A4.1.1.9 ST-Segment Elevation

Do not code in the presence of codes 6-4-1, 6-8, 7-1-1, 7-2-1, 7-4, or 7-8.

Anterolateral site (leads I, aVL, V_6)

- 9-2 ST-segment elevation ≥1.0 mm in any of leads I, aVL, V_6.

Posterior (inferior) site (leads II, III, aVF)

- 9-2 ST-segment elevation ≥1.0 mm in any of leads II, III, aVF.

Anterior site (leads V_1, V_2, V_3, V_4, V_5)

- 9-2 ST-segment elevation ≥1.0 mm in lead V_5 or ST-segment elevation ≥2.0 mm in any of leads V_1, V_2, V_3, V_4.

A4.1.1.10 Miscellaneous Items

- 9-1 Low QRS amplitude. QRS peak-to-peak amplitude <5 mm in all beats in each of leads I, II, III, or <10 mm in all beats in each of leads V_1, V_2, V_3, V_4, V_5, V_6. (Check calibration before coding).
- 9-3 P-wave amplitude ≥2.5 mm in any of leads II, III, aVF, in a majority of beats.
- 9-4-1 QRS transition zone at V_3 or to the right of V_3 on the chest. (Do not code in the presence of 6-4-1, 6-8, 7-1-1, 7-2-1, 7-4, or 7-8.)
- 9-4-2 QRS transition zone at V_4 or to the left of V_4 on the chest. (Do not code in the presence of 6-4-1, 6-8, 7-1-1, 7-2-1, 7-4, or 7-8.)
- 9-5 T-Wave amplitude >12 mm in any of leads I, II, III, aVL, aVF, V_1, V_2, V_3, V_4, V_5, V_6. (Do not code in the presence of 6-4-1, 6-8, 7-1-1, 7-2-1, 7-4, or 7-8.
- 9-6[2] Notched and widened P wave (duration ≥ 0.12 s) in frontal plane (usually lead II), and/or deep negative component to the P wave in lead V_1 duration ≥ 0.04 s and depth ≥ 1 mm.
- 9-7-1[2] Definite Early Repolarization. STJ elevation ≥ 1 mm in the majority of beats, T wave amplitude ≥ 5 mm prominent J point, upward concavity of the ST segment, and a distinct notch or slur on the down-stroke of the R wave in any of $V_3 - V_6$, OR STJ elevation ≥ 2 mm in the majority of beats and T wave amplitude ≥ 5 mm prominent J point, and upward concavity of the ST segment in any of $V_3 - V_6$.
- 9-7-2[2] Probable Early Repolarization. STJ elevation ≥ 1 mm in the majority of beats, prominent J point, and upward concavity of the ST segment in any of $V_3 - V_6$ and T wave amplitude ≥ 8 mm in any of the leads $V_3 - V_6$.
- 9-8-1[2] Uncorrectable lead reversal.
- 9-8-2[3] Poor Quality/Technical problems which interfere with coding.
- 9-8-3[2] Correctable lead reversal.
  i. Correctable limb lead connection error.
  ii. Correctable chest lead connection error in $V_1 - V_3$.
  iii. Correctable chest lead connection error in $V_4 - V_6$.
  iv. Correctable other chest lead connection error.
- 9-8-4[3] Technical problems that do not interfere with coding.

A4.1.1.11 Incompatible Codes

Table A4.1 gives a list of incompatible codes. The codes in the left-hand column suppress the codes in the right-hand column.

A4.1.1.12 ECG Criteria for Significant Serial ECG Change

A detailed explanation of criteria for serial change can be found in Chapter 15 of the recently published Minnesota Code Manual of Electrocardiographic Findings (RJ Prineas, RS Crow, Z-M Zhang, Springer, 2009). An extract is given here.

Evolving Q-wave

Q1. No Q-code in reference ECG followed by a record with a diagnostic Q-code (MC 1-1-1 through 1-2-7) ***OR*** an Equivocal Q-code (1-3-x) in reference ECG followed by record with any code 1-1-x Q-code.

[1] 1-3-8 was previously 1-2-8

[2] New code from first edition

[3] 9-8-2 in the first edition was 9-8-1, and 9-8-4 was 9-8-2 in the first edition.

Table A4.1

Incompatible codes

Code	Suppresses this code(s)
All Q, QS codes	7-6
Q ≥ 0.03 in Lead I	7-7
3-1	1-3-2
3-2	1-3-8, 7-3
6-1	All other codes except 8-2
6-4-1	All other codes
6-8	All other codes
7-1-1	1-2-3, 1-2-7, 1-3-2, 1-3-6, 1-3-7, 1-3-8, all 2-, 3-, 4-, and 5-codes, 7-7, 7-8, 7-9, 7-10, 9-2, 9-4, 9-5, 9-7-1, 9-7-2
7-2-1	1-3-8, all 2-, 3-, 4-, and 5-codes, 9-2, 9-4, 9-5, 9-7-1, 9-7-2
7-3	1-3-8
7-4	All 2-, 3-, 4-, and 5-codes, 9-2, 9-4, 9-5
7-8	1-3-8, all 2-, 3-, 4-, and 5-codes, 9-2, 9-4, 9-5, 9-7-1, 9-7-2
8-1-2	8-2-4
8-1-4	8-1-1, 9-3
8-2-1	All other codes
8-2-2	All other codes
8-2-3	8-1-2
8-3-1	8-1-1, 8-1-2
8-3-2	6-2-2, 8-1-1, 8-1-2
8-3-3	8-1-1, 8-1-2
8-3-4	6-2-2
8-4-1	6-5
8-4-1 + heart rate ≥140 bpm	All other codes except 7-4 or 6-2
Heart rate >100 bpm	6-5
8-4-2	8-1-1
9-1	All 2-codes

Q2. An Equivocal Q-code (any MC 1-3 x code) and no major ST-segment depression (MC 4-0, 4-4, 4-3) in reference ECG followed by a record with a diagnostic Q-code (MC 1-2-1 – 1-2-7) ***Plus*** a major ST-segment depression (MC 4-1-x or 4-2).

Q3. An Equivocal Q-code (any MC 1-3-x) and no major T-wave inversion (MC 5–4, 5-3 or 5-0) in reference ECG followed by a record with a diagnostic Q-code (MC1-2-1 through 1-2-7) ***Plus*** a major T-wave inversion (MC 5-1 or 5-2).

Q4. An Equivocal Q-code (any MC 1-3-x) and Q-code (MC 1-2-1 through 1-2-7) ***Plus*** and ST-segment elevation (MC 9-2).

Q5. No Q-code and no MC 4-1-x or 4-2 in reference ECG followed by a record with an Equivocal Q-code (any MC 1-3-x) ***Plus*** MC 4-1-x or 4-2.

Q6. No Q-code and no MC 5-1 or 5-2 in reference ECG followed by a record with an Equivocal Q-code (any MC 1-3-x) ***Plus*** a MC 5-1 or 5-2.

Q7. No Q-code and no MC 9-2 in reference ECG followed by a record with an Equivocal Q-code (any MC 1-3-x) ***Plus*** a MC 9-2.

Evolving ST-Elevation

STE-1	MC 9-0 in reference ECG followed by a record with MC 9-2 in at least 2 leads and > 100% increase ST elevation in both leads.
STE-2	MC 9-2 in reference ECG followed by a record with MC 9-2 in at least 2 leads and > 100% increase in ST elevation in both leads.
STE-3	MC 9-2 and no MC 5-1 or 5-2 in reference ECG followed by a record appearance of MC 5-1 or 5-2 with 100% increase in T wave inversion in at least 2 leads.
STE-4	Reversal of evolving STE-1 (within the hospital ECG only).
STE-5	Reversal of evolving STE-2 (within the hospital ECG only).

Evolving ST-Depression/T Wave Inversion

ST-T1	Either MC 4-0 (no 4-code), 4–4 or 4–3 in reference ECG followed by a record with MC 4–2 or 4–1-2 or 4-1-1 and > 100% increase in ST segment depression.
ST-T2	Either MC 4-2 4–1–2 in reference ECG followed by a record with MC 4–1–1 and > 100% increase in ST segment depression.
ST-T3	Either MC 5-0, 5-4 or 5-3 in reference ECG followed by a record with MC 5-2 or 5-1 and > 100% increase in T-wave inversion.
ST-T4	MC 5-2 in reference ECG followed by a record with MC 5-1 and > 100% in T-wave inversion.
ST-T5	MC 4–1-1 in reference ECG followed by a record with MC 4–1–1 and > 100% increase in ST depression.
ST-T6	MC 5-1 in reference ECG followed by a record with MC 5-1 and > 100% increase in T-wave inversion
ST-T7	MC 5-2 in reference ECG followed by a record with MC 5-2 and > 100% increase in T-wave inversion.
ST-T1R	Reverse of ST-T1[4]
ST-T2R	Reverse of ST-T2[4]
ST-T3R	Reverse of ST-T3[4]
ST-T4R	Reverse of ST-T4[4]
ST-T5R	Reverse of ST-T5[4]
ST-T6R	Reverse of ST-T6[4]
ST-T7R	Reverse of ST-T7[4]

Evolving Bundle Branch Block

E-BBB1	No MC 7-1 in the reference ECG followed by an ECG with MC 7-1-1 in follow-up ECG ***and*** QRS duration increase by > 0.02 s.
E-BBB2	No MC 7-2 in the reference ECG followed by an ECG with MC 7-2-1 in follow-up ECG ***and*** QRS duration increase by > 0.02 s.
E-BBB3	No MC 7-4 in the reference ECG followed by an ECG with MC 7–4 in follow-up ECG ***and*** QRS duration increase by > 0.02 s.

Evolving ECG – LVH

E-LVH 1	MC 3-0 in reference ECG flowed by an ECG with a MC 3-1 in the follow-up ECG, confirmed as a significant increase.

[4]Requires > 100% decrease in ST depression or T-wave inversion of follow-up record compared to reference ECG, and code changes must occur in the same lead groups.

E-LVH 2 MC 3-0 in reference ECG flowed by an ECG with a MC 3-3 in the follow-up ECG, confirmed as a significant increase.
E-LVH 3 MC 3-1 in reference ECG flowed by an ECG with a MC 3-0 in the follow-up ECG, confirmed as a significant decrease.
E-LVH 4 MC 3-3 in reference ECG flowed by an ECG with a MC 3-0 in the follow-up ECG, confirmed as a significant decrease.
E-LVH 5 MC 3-1 in reference ECG flowed by an ECG with a MC 3-1 in the follow-up ECG, confirmed by a significant increase or a significant decrease.
E-LVH 6 MC 3-3 in reference ECG flowed by an ECG with a MC 3-3 in the follow-up ECG, confirmed by a significant increase or a significant decrease.

A4.2 The Punsar Code

One of the authors of the original publication of the Minnesota code, Punsar, developed an alternative scheme, in collaboration with others, for classifying the ST-T segment. The code is described simply in Table A4.2 and Fig. A4.1 which is reproduced from: Punsar S, Pyorala K, Siltanen P. Classification of electrocardiographic ST segment changes in epidemiological studies of coronary heart disease. Ann. Med. Intern. Fenn. 1968; **57**:53–63, with the permission of Annales Medicinae Internae Fenniae, Helsinki.
The authors tested their code in a 5-year follow-up of 1,534 men aged 40–59. The incidence of events including death or myocardial infarction was highest in the ischemic group and decreased in the remaining groups in a progressive fashion. It was also noted that with each group, the prognosis varied according to the amount of ST depression present.

Table A4.2
Correspondence of the items in the new, modified code to those in the Minnesota code

Modified code		Minnesota code			
		At rest		Postexercise[a]	
I	1	IV	1	XI	1
	2		1		1
	3		2		2
	4		3		3
	5				
S	1	IV	4	XI	4
	2		4		4
	3				
	4				
R	1	IV	4		4
	2		4	XI	4
	3				

[a]The original 1960 Minnesota code had postexercise classifications, coded X to XVI

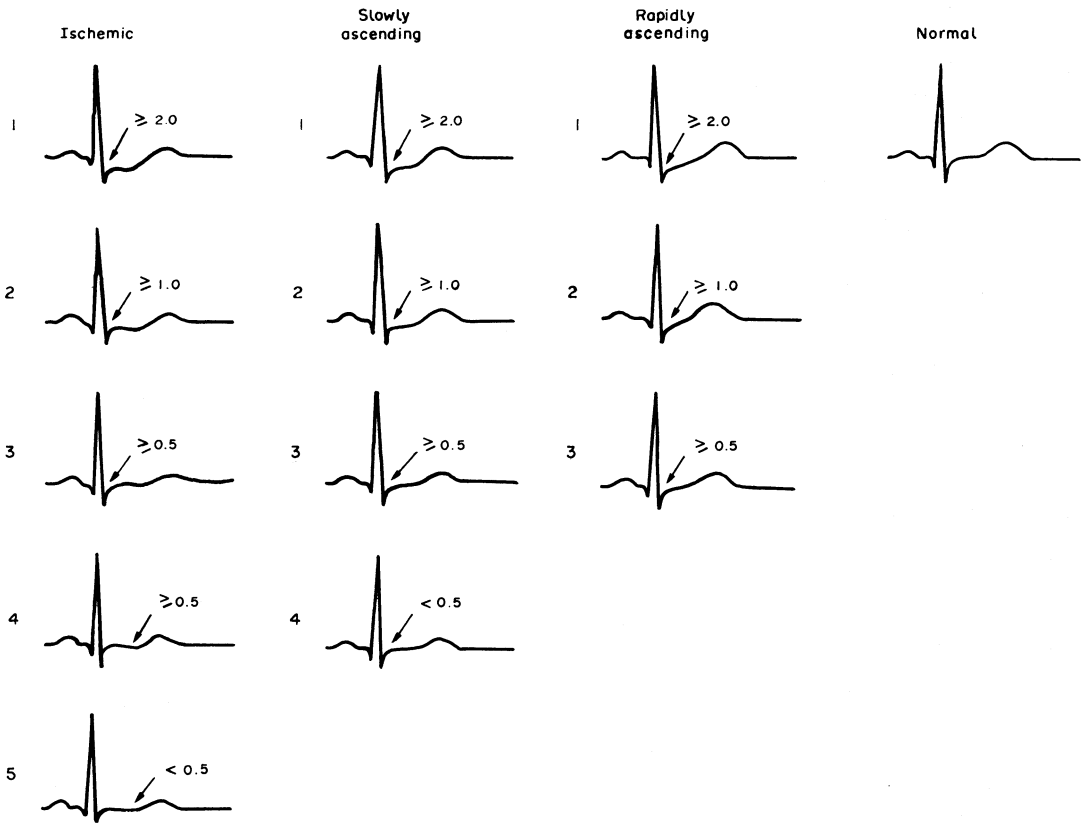

Figure A4.1

Categories of ST-segment changes in the new, modified classification (the Punsar code). Note that the figures beside each arrow indicate the amount of ST depression in millimeters.

Appendix 5: Normal Limits of the 12 Lead Vectorcardiogram

P. W. Macfarlane, A. van Oosterom, O. Pahlm, P. Kligfield, M. Janse, J. Camm (eds.), *Comprehensive Electrocardiology*, DOI 10.1007/978-1-84882-046-3_A5

Appendix 5A Normal Limits of Adult 12-Lead Vectorcardiogram

The tables of amplitudes and durations in this Appendix have been obtained from the X, Y, Z leads derived from the 12-lead ECG according to the methods described in Chap. 11, Sect. 11.6 and using the coefficients presented in Table 11.6. Data have been derived from 1,555 adult ECGs whose age distribution is shown in the lower part of Table 43.1. The 215 males over 50 have been subdivided, with 38 men being aged 60 and over, while similarly 139 females include 19 aged 60 and over.

Data are expressed as mean ± standard deviation below which is given the 96 percentile ranges, i.e., 2% of values are excluded at either end of the distribution except in the case of the groups aged 60 and over where the 100% range is presented. Angular data are presented with respect to the reference frames illustrated in Figure 43.9.

A5.1 Scalar Measurements from the Leads X, Y, and Z

A5.1.1 P Wave Amplitude and Duration

Table A5.1

P wave amplitudes (mV) in males

Age (years)	X	Y	Z
18–29	0.07 ± 0.02	0.11 ± 0.05	0.05 ± 0.02
	0.03 → 0.12	0.02 → 0.25	0.02 → 0.10
30–39	0.07 ± 0.02	0.11 ± 0.04	0.04 ± 0.02
	0.03 → 0.12	0.01 → 0.22	0.01 → 0.11
40–49	0.07 ± 0.02	0.11 ± 0.04	0.04 ± 0.02
	0.03 → 0.14	0.03 → 0.22	0.00 → 0.09
50–59	0.07 ± 0.02	0.11 ± 0.04	0.04 ± 0.02
	0.04 → 0.13	0.04 → 0.20	0.01 → 0.08
60–	0.07 ± 0.03	0.11 ± 0.04	0.04 ± 0.03
	0.03 → 0.11	0.04 → 0.18	0.00 → 0.08

Table A5.2

P wave amplitudes (mV) in females

Age (years)	X	Y	Z
18–29	0.07 ± 0.02	0.11 ± 0.05	0.04 ± 0.02
	0.03 → 0.13	0.02 → 0.26	0.01 → 0.08
30–39	0.08 ± 0.02	0.12 ± 0.05	0.04 ± 0.02
	0.04 → 0.13	0.03 → 0.24	0.01 → 0.09
40–49	0.08 ± 0.02	0.11 ± 0.04	0.04 ± 0.02
	0.04 → 0.12	0.03 → 0.24	0.01 → 0.08
50–59	0.08 ± 0.02	0.11 ± 0.04	0.04 ± 0.02
	0.04 → 0.13	0.03 → 0.22	0.00 → 0.07
60–	0.08 ± 0.03	0.12 ± 0.06	0.04 ± 0.01
	0.03 → 0.14	0.03 → 0.23	0.01 → 0.06

Table A5.3

P wave durations (ms) in males

Age (years)	X	Y	Z
18–29	93 ± 14	98 ± 14	98 ± 14
	66 → 122	66 → 122	66 → 122
30–39	103 ± 11	103 ± 11	103 ± 11
	78 → 124	78 → 124	78 → 124
40–49	107 ± 11	107 ± 11	107 ± 11
	86 → 128	86 → 128	86 → 128
50–59	108 ± 11	108 ± 11	108 ± 11
	80 → 128	80 → 128	80 → 128
60–	110 ± 12	110 ± 12	110 ± 12
	90 → 130	90 → 130	90 → 130

Table A5.4

P wave durations (ms) in females

Age (years)	X	Y	Z
18–29	97 ± 11	97 ± 11	97 ± 11
	72 → 116	72 → 116	72 → 116
30–39	100 ± 10	100 ± 10	100 ± 10
	78 → 116	78 → 116	78 → 116
40–49	104 ± 10	104 ± 10	104 ± 10
	82 → 124	82 → 124	82 → 124
50–59	104 ± 13	104 ± 13	104 ± 13
	64 → 128	64 → 128	64 → 128
60–	104 ± 12	104 ± 12	104 ± 12
	88 → 130	88 → 130	88 → 130

A5.1.2 Q Wave Amplitude and Duration

Table A5.5

Q wave amplitude (mV) in males

Age (years)	X	Y
18–29	−0.11 ± 0.09	−0.10 ± 0.06
	−0.37 → −0.02	−0.29 → −0.02
30–39	−0.09 ± 0.08	−0.10 ± 0.06
	−0.33 → −0.02	−0.30 → −0.02
40–49	−0.08 ± 0.05	−0.07 ± 0.04
	−0.21 → −0.02	−0.17 → −0.02
50–59	−0.09 ± 0.06	−0.07 ± 0.05
	−0.26 → −0.02	−0.21 → −0.02
60–	−0.07 ± 0.04	−0.08 ± 0.05
	−0.14 → −0.02	−0.21 → −0.02

Table A5.6

Q wave amplitude (mV) in females

Age (years)	X	Y
18–29	−0.08 ± 0.06	−0.10 ± 0.06
	−0.25 → −0.02	−0.29 → −0.02
30–39	−0.09 ± 0.06	−0.08 ± 0.05
	−0.26 → −0.02	−0.20 → −0.02
40–49	−0.07 ± 0.05	−0.06 ± 0.03
	−0.22 → −0.02	−0.13 → −0.02
50–59	−0.06 ± 0.04	−0.06 ± 0.03
	−0.17 → −0.02	−0.16 → −0.02
60–	−0.07 ± 0.04	−0.05 ± 0.03
	−0.14 → −0.02	−0.10 → −0.03

Table A5.7

Q wave durations (ms) in males

Age (years)	X	Y
18–29	17 ± 5	19 ± 7
	8 → 28	8 → 27
30–39	16 ± 6	19 ± 5
	8 → 27	7 → 31
40–49	16 ± 4	17 ± 5
	7 → 23	6 → 25
50–59	16 ± 4	18 ± 5
	10 → 24	6 → 27
60–	15 ± 3	19 ± 5
	10 → 23	5 → 29

Table A5.8

Q wave durations (ms) in females

Age (years)	X	Y
18–29	15 ± 4	17 ± 5
	7 → 25	7 → 26
30–39	16 ± 4	16 ± 4
	7 → 24	6 → 24
40–49	15 ± 3	14 ± 4
	9 → 21	8 → 24
50–59	14 ± 4	16 ± 4
	7 → 22	8 → 24
60–	15 ± 4	13 ± 6
	9 → 24	5 → 21

A5.1.3 R Wave Amplitude and Duration

Table A5.9

R wave amplitudes (mV) in males

Age (years)	X	Y	Z
18–29	1.66 ± 0.46	1.16 ± 0.46	0.52 ± 0.23
	0.08 → 2.86	0.31 → 2.23	0.13 → 1.02
30–39	1.53 ± 0.43	0.91 ± 0.46	0.42 ± 0.24
	0.69 → 2.44	0.14 → 2.13	0.09 → 1.07
40–49	1.40 ± 43	0.69 ± 0.39	0.37 ± 0.19
	0.66 → 2.41	0.04 → 1.51	0.04 → 0.87
50–59	1.38 ± 0.38	0.58 ± 0.34	0.36 ± 0.17
	0.72 → 2.01	0.11 → 1.46	0.10 → 0.76
60–	1.20 ± 0.36	0.65 ± 0.39	0.30 ± 0.19
	0.75 → 1.93	0.08 → 1.50	0.05 → 0.67

Table A5.10

R wave amplitudes (mV) in females

Age (years)	X	Y	Z
18–29	1.23 ± 0.34	0.91 ± 0.34	0.33 ± 0.15
	0.56 → 1.96	0.32 → 1.75	0.07 → 0.70
30–39	1.23 ± 0.37	0.87 ± 0.32	0.32 ± 0.15
	0.58 → 1.97	0.29 → 1.48	0.10 → 0.67
40–49	1.11 ± 0.32	0.66 ± 0.26	0.25 ± 0.12
	0.62 → 1.75	0.24 → 1.16	0.04 → 0.49
50–59	1.11 ± 0.29	0.61 ± 0.31	0.26 ± 0.14
	0.60 → 1.76	0.14 → 1.31	0.04 → 0.73
60–	1.28 ± 0.46	0.55 ± 0.21	0.32 ± 0.14
	0.54 → 2.23	0.25 → 1.16	0.04 → 0.56

Table A5.11

R wave durations (ms) in males

Age (years)	X	Y	Z
18–29	45 ± 15	55 ± 17	32 ±9
	27 → 79	28 → 86	20 → 45
30–39	46 ± 14	57 ± 16	31 ± 9
	28 → 84	26 → 86	17 → 44
40–49	47 ± 14	55 ± 18	32 ± 8
	31 → 82	15 → 90	15 → 48
50–59	46 ± 14	55 ± 17	33 ± 8
	30 → 79	22 → 90	21 → 52
60–	43 ± 11	54 ± 15	29 ± 8
	29 → 62	34 → 86	14 → 40

Table A5.12

R wave durations (ms) in females

Age (years)	X	Y	Z
18–29	44 ± 12	47 ± 13	28 ± 6
	27 → 76	24 → 78	15 → 41
30–39	44 ± 12	48 ± 12	28 ± 5
	31 → 67	31 → 72	17 → 38
40–49	45 ± 11	52 ± 14	27 ± 7
	31 → 71	28 → 86	10 → 41
50–59	44 ± 11	52 ± 15	27 ± 7
	26 → 86	20 → 77	11 → 43
60–	44 ± 11	51 ± 13	32 ± 5
	28 → 64	33 → 72	24 → 46

A5.1.4 S Wave Amplitude and Duration

Table A5.13

S wave amplitudes (mV) in males

Age (years)	X	Y	Z
18–29	−0.27 ± 0.18	−0.16 ± 0.09	−1.38 ± 0.47
	−0.68 → −0.05	−0.41 → −0.03	−2.50 → −0.59
30–39	−0.26 ± 0.20	−0.18 ± 0.16	−1.05 ± 0.37
	−0.71 → −0.05	−0.44 → −0.04	−1.70 → −0.49
40–49	−0.29 ± 0.18	−0.17 ± 0.13	0.37 ± 0.19
	−0.73 → −0.06	−0.44 → −0.03	0.04 → 0.87
50–59	−0.25 ± 0.17	−0.17 ± 0.16	0.36 ± 0.17
	−0.68 → 0.04	−0.60 → −0.05	0.10 → 0.76
60–	−0.35 ± 0.18	−0.18 ± 0.14	−0.81 ± 0.31
	−0.54 → −0.17	−0.28 → −0.06	−1.04 → −0.48

Table A5.14

S wave amplitudes (mV) in females

Age (years)	X	Y	Z
18–29	−0.17 ± 0.10	−0.15 ± 0.09	−0.92 ± 0.34
	−0.52 → −0.05	0.42 → 0.04	−1.65 → −0.35
30–39	−0.20 ± 0.11	−0.14 ± 0.12	−0.92 ± 0.33
	−0.39 → −0.06	−0.36 → −0.05	−1.65 → −0.35
40–49	−0.18 ± 0.14	−0.14 ± 0.11	−0.99 ± 0.39
	−0.34 → −0.04	−0.25 → −0.04	−1.54 → −0.46
50–59	−0.20 ± 0.14	−0.16 ± 0.09	−0.74 ± 0.30
	−0.42 → −0.06	−0.29 → −0.06	−1.32 → 0.34
60–	−0.16 ± 0.10	0.18 ± 0.10	−0.66 ± 0.25
	−0.19 → −0.11	−0.17 → −0.12	−0.79 → −0.50

Table A5.15

S wave durations (ms) in males

Age (years)	X	Y	Z
18–29	26 ± 12	26 ± 10	53 ± 8
	6 → 48	7 → 48	35 → 71
30–39	28 ± 13	29 ± 14	54 ± 10
	7 → 57	8 → 60	31 → 71
40–49	31 ± 12	32 ± 15	52 ± 11
	10 → 55	7 → 68	25 → 70
50–59	32 ± 12	30 ± 15	50 ± 11
	11 → 53	8 → 67	27 → 73
60–	33 ± 12	28 ± 11	53 ± 9
	12 → 56	11 → 50	31 → 67

Table A5.16

S wave durations (ms) in females

Age (years)	X	Y	Z
18–29	24 ± 9	25 ± 9	51 ±9
	7 → 41	10 → 45	30 → 67
30–39	28 ± 9	23 ± 10	52 ± 8
	8 → 43	8 → 43	35 → 64
40–49	26 ± 10	26 ± 10	52 ± 8
	12 → 41	12 → 50	27 → 75
50–59	27 ± 10	27 ± 11	51 ± 9
	12 → 47	11 → 58	30 → 64
60–	29 ± 11	33 ± 15	47 ± 10
	13 → 53	12 → 50	20 → 59

A5.1.5 T Wave Amplitude

Table A5.17

T wave amplitudes (mV) in males

Age (years)	X	Y	Z
18–29	0.46 ± 0.19	0.25 ± 0.11	0.47 ± 0.18
	0.10 → 0.95	0.02 → 0.55	0.14 → 0.86
30–39	0.42 ± 0.16	0.21 ± 0.10	0.42 ± 0.16
	0.12 → 0.80	0.03 → 0.48	0.08 → 0.80
40–49	0.38 ± 0.17	0.19 ± 0.10	0.39 ± 0.15
	0.08 → 0.82	0.03 → 0.43	0.12 → 0.72
50–59	0.35 ± 0.16	0.17 ± 0.08	0.38 ± 0.16
	0.09 → 0.72	0.04 → 0.38	0.07 → 0.74
60–	0.36 ± 0.18	0.21 ± 0.12	0.33 ± 0.17
	0.06 → 0.66	0.08 → 0.38	0.12 → 0.73

Table A5.18

T wave amplitudes (mV) in females

Age (years)	X	Y	Z
18–29	0.34 ± 0.12	0.20 ± 0.08	0.23 ± 0.11
	0.14 → 0.60	0.04 → 0.46	0.04 → 0.56
30–39	0.33 ± 0.13	0.18 ± 0.08	0.22 ± 0.11
	0.12 → 0.64	0.05 → 0.37	0.02 → 0.43
40–49	0.28 ± 0.11	0.16 ± 0.07	0.20 ± 0.09
	0.05 → 0.51	0.05 → 0.33	0.06 → 0.43
50–59	0.27 ± 0.11	0.17 ± 0.07	0.20 ± 0.09
	0.07 → 0.56	0.03 → 0.32	0.03 → 0.36
60–	0.26 ± 0.14	0.17 ± 0.08	0.21 ± 0.08
	0.03 → 0.62	0.10 → 0.30	0.04 → 0.37

A5.2 Planar and Spatial Measurements

A5.2.1 Direction of Inscription in the QRS Vector Loop

Table A5.19

Direction of inscription of the QRS vector loop in males (%)

	Frontal	Left sagittal	Transverse
Counterclockwise	22.9	88.0	98.1
Figure of 8	19.1	8.4	0.9
Clockwise	58.0	3.6	1.0

Table A5.20

Direction of inscription of the QRS vector loop in females (%)

	Frontal	Left sagittal	Transverse
Counterclockwise	21.8	94.5	97.9
Figure of 8	25.3	3.9	1.2
Clockwise	52.9	1.6	0.9

A5.2.2 Magnitude of Maximal Spatial QRS Vector

Table A5.21

Magnitude of maximal spatial QRS vector (mV)

Age (years)	Males	Females
18–29	2.39 ± 0.62	1.76 ± 0.47
	1.07 → 3.97	0.75 → 3.06
30–39	2.07 ± 0.58	1.74 ± 0.46
	1.00 → 3.61	0.92 → 2.77

Table A5.21 (Continued)

Age (years)	Males	Females
40–49	1.79 ± 0.49	1.46 ± 0.41
	0.85 → 2.94	0.79 → 2.26
50–59	1.65 ± 0.45	1.46 ± 0.37
	0.86 → 2.91	0.78 → 2.22
60–	1.57 ± 0.42	1.37 ± 0.51
	0.99 → 2.20	1.00 → 1.90

A5.2.3 Magnitude of Maximal Planar QRS Vector

Table A5.22

Magnitude of the maximal QRS vector in frontal, sagittal, and transverse planes (mV) in males

Age (years)	Frontal	Sagittal	Transverse
18–29	2.04 ± 0.52	1.75 ± 0.60	2.09 ± 0.52
	0.99 → 3.26	0.70 → 3.41	1.02 → 3.39
30–39	1.80 ± 0.49	1.48 ± 0.58	1.85 ± 0.48
	0.82 → 3.03	0.52 → 3.11	0.92 → 2.95
40–49	1.59 ± 0.46	1.23 ± 0.45	1.64 ± 0.43
	0.69 → 2.82	0.45 → 2.26	0.83 → 2.78
50–59	1.50 ± 0.42	1.07 ± 0.40	1.54 ± 0.39
	0.77 → 2.70	0.44 → 2.05	0.84 → 2.76
60–	1.40 ± 0.37	1.12 ± 0.41	1.42 ± 0.36
	0.92 → 2.03	0.64 → 1.91	0.89 → 2.08

Table A5.23

Magnitude of the maximal QRS vector in frontal, sagittal, and transverse planes (mV) in females

Age (years)	Frontal	Sagittal	Transverse
18–29	1.54 ± 0.40	1.28 ± 0.44	1.51 ± 0.39
	0.67 → 2.56	0.49 → 2.48	0.67 → 2.58
30–39	1.51 ± 0.42	1.25 ± 0.43	1.50 ± 0.40
	0.62 → 2.42	0.60 → 2.25	0.88 → 2.51
40–49	1.29 ± 0.33	1.02 ± 0.35	1.31 ± 0.36
	0.68 → 1.96	0.40 → 1.78	0.84 → 2.76
50–59	1.29 ± 0.33	1.02 ± 0.36	1.31 ± 0.31
	0.68 → 1.96	0.42 → 1.86	0.69 → 2.01
60–	1.27 ± 0.52	0.82 ± 0.30	1.27 ± 0.48
	0.99 → 1.88	0.60 → 1.18	0.93 → 1.77

A5.2.4 Maximal Planar QRS Vector Angle

Table A5.24

96-Percentile ranges of maximal QRS vector angle (degrees) in males

Age (years)	Frontal	Sagittal	Transverse
18–29	34 ± 14	40 ± 24	−37 ± 26
	12 → 62	0 → 96	−105 → 14
30–39	28 ± 14	38 ± 36	−32 ± 28
	3 → 54	−12 → 144	−99 → 19
40–49	23 ± 19	33 ± 34	−28 ± 31
	−2 → 53	−13 → 140	−103 → 27
50–59	20 ± 13	31 ± 41	−25 ± 36
	−5 → 43	−23 → 150	−117 → 25
60–	22 ± 35	32 ± 33	−32 ± 0.35
	0 → 58	0 → 84	−103 → 25

Table A5.25

96-Percentile ranges of maximal QRS vector angle (degrees) in females

Age (years)	Frontal	Sagittal	Transverse
18–29	34 ± 15	40 ± 22	−35 ± 19
	13 → 59	−9 → 89	−85 → 3
30–39	35 ± 11	44 ± 20	−36 ± 22
	14 → 55	−13 → 79	−97 → −2
40–49	27 ± 19	37 ± 31	−33 ± 25
	6 → 48	−20 → 99	−109 → 9
50–59	27 ± 12	34 ± 28	−31 ± 27
	6 → 23	−15 → 142	−108 → 16
60–	21 ± 10	42 ± 54	−16 ± 31
	0 → 47	−41 → 180	−107 → 27

A5.2.5 Maximal T Vector Angle

Table A5.26

96-Percentile ranges of maximal T vector angle (degrees) in males

Age (years)	Frontal	Sagittal	Transverse
18–29	28 ± 15	154 ± 18	45 ± 17
	−6 → 60	110 → 184	13 → 81
30–39	25 ± 17	154 ± 21	44 ± 17
	6 → 48	96 → 180	5 → 78
40–49	27 ± 16	155 ± 18	46 ± 17
	5 → 56	113 → 180	9 → 76
50–59	25 ± 14	156 ± 21	46 ± 20
	3 → 51	98 → 181	2 → 78
60–	32 ± 18	147 ± 26	38 ± 25
	10 → 81	95 → 176	2 → 65

Table A5.27

96-Percentile ranges of maximal T vector angle (degrees) in females

Age (years)	Frontal	Sagittal	Transverse
18–29	30 ± 19	134 ± 26	28 ± 18
	8 → 50	61 → 178	−15 → 62
30–39	29 ± 10	137 ± 26	−30 ± 19
	9 → 48	80 → 183	−15 → 68
40–49	30 ± 16	140 ± 21	34 ± 17
	9 → 56	98 → 185	10 → 77
50–59	29 ± 26	140 ± 26	33 ± 29
	8 → 53	82 → 187	−13 → 76
60–	38 ± 30	144 ± 22	40 ± 24
	0 → 153	78 → 180	−6 → 105

Appendix 5B Normal Limits of Paediatric 12-Lead Vectorcardiogram

The vector data presented in this Appendix have been obtained from X, Y, Z leads derived from the 12-lead ECG according to the methods described in 11.6 and using the coefficients presented in Table 11.9. Data have been derived from 1,782 neonates, infants, and children, whose age distribution is shown in the upper part of Table 43.1.

Data are expressed as mean ± standard deviation below which is given the 96 percentile ranges, i.e., 2% of values are excluded at either end of the distribution except when the total number in the age group is small, in which case the 100% range is presented. Angular data are presented with respect to the reference frames illustrated in Figure 43.9.

B5.1 Scalar Measurements from the Leads X, Y and Z

Table B5.1

Maximal spatial P, QRS, and T magnitudes (mV)

Age	Max P	Max QRS	Max T
< 24 h	0.16 ± 0.05	1.83 ± 0.48	0.25 ± 0.08
	0.09 → 0.25	0.95 → 2.76	0.08 → 0.41
1 day	0.17 ± 0.05	1.71 ± 0.43	0.23 ± 0.07
	0.09 → 0.25	1.03 → 2.48	0.11 → 0.38
2 days	0.17 ± 0.05	1.62 ± 0.41	0.25 ± 0.08
	0.10 → 0.27	0.93 → 2.51	0.12 → 0.43
3 days	0.17 ± 0.04	1.60 ± 0.41	0.28 ± 0.08
	0.10 → 0.25	1.00 → 2.48	0.14 → 0.43
≤ 1 week	0.18 ± 0.05	1.53 ± 0.35	0.34 ± 0.10
	0.10 → 0.31	0.99 → 2.36	0.16 → 0.55
≤ 1 month	0.18 ± 0.06	1.38 ± 0.40	0.37 ± 0.10
	0.08 → 0.26	0.76 → 2.04	0.19 → 0.60
≤ 3 months	0.16 ± 0.04	1.87 ± 0.45	0.43 ± 0.09
	0.07 → 0.24	1.17 → 2.95	0.28 → 0.60
≤ 6 months	0.15 ± 0.04	1.70 ± 0.38	0.44 ± 0.12
	0.09 → 0.27	1.02 → 2.35	0.27 → 0.67

Table B5.1 (Continued)

Age	Max P	Max QRS	Max T
≤ 1 year	0.17 ± 0.05	1.81 ± 0.48	0.49 ± 0.11
	0.11 → 0.25	1.09 → 2.80	0.30 → 0.69
1–2 years	0.15 ± 0.04	1.86 ± 0.49	0.47 ± 0.14
	0.09 → 0.24	1.03 → 2.82	0.22 → 0.70
3–4 years	0.15 ± 0.04	2.20 ± 0.53	0.53 ± 0.15
	0.09 → 0.24	1.25 → 3.21	0.21 → 0.84
5–6 years	0.14 ± 0.04	2.46 ± 0.55	0.58 ± 0.15
	0.08 → 0.24	1.56 → 3.61	0.31 → 0.87
7–8 years	0.14 ± 0.04	2.43 ± 0.48	0.61 ± 0.15
	0.08 → 0.23	1.56 → 3.38	0.36 → 0.90
9–10 years	0.14 ± 0.04	2.51 ± 0.53	0.65 ± 0.18
	0.07 → 0.23	1.55 → 3.33	0.34 → 1.00
11–12 years	0.14 ± 0.05	2.43 ± 0.52	0.60 ± 0.19
	0.07 → 0.24	1.45 → 3.51	0.30 → 0.92
13–14 years	0.14 ± 0.05	2.29 ± 0.59	0.58 ± 0.20
	0.06 → 0.25	1.25 → 3.60	0.26 → 1.00
15–16 years	0.14 ± 0.05	2.17 ± 0.61	0.55 ± 0.20
	0.07 → 0.27	1.20 → 3.23	0.24 → 0.95

Table B5.2

Maximal P, QRS, and T vector angles in transverse plane (degrees)

Age	Max P	Max QRS	Max T
< 24 h	22 ± 38	−6 ± 108	23 ± 69
	−42 → 70	−131 → 181	−76 → 136
1 day	28 ± 35	−10 ± 113	−4 ± 68
	−47 → 78	−139 → 216	−105 → 132
2 days	25 ± 35	26 ± 111	−32 ± 49
	−49 → 83	−135 → 217	−92 → 92
3 days	26 ± 31	10 ± 99	−43 ± 42
	−45 → 73	−138 → 206	−100 → 66
≤ 1 week	24 ± 33	34 ± 88	−44 ± 31
	−46 → 73	−130 → 210	−92 → 20
≤ 1 month	15 ± 36	29 ± 89	−25 ± 33
	−63 → 66	−126 → 185	−80 → 10
≤ 3 months	8 ± 37	14 ± 37	−31 ± 26
	−67 → 62	−111 → 62	−93 → 31
≤ 6 months	6 ± 33	10 ± 44	−38 ± 22
	−41 → 59	−107 → 74	−72 → 14
≤ 1 year	11 ± 34	13 ± 38	−45 ± 19
	−62 → 67	−45 → 83	−87 → −13
1–2 years	23 ± 36	−19 ± 50	−38 ± 25
	−50 → 69	−110 → 89	−83 → 5
3–4 years	20 ± 36	−28 ± 28	−22 ± 21
	−48 → 76	−109 → 27	−64 → 16
5–6 years	28 ± 37	−29 ± 21	−10 ± 17
	−43 → 87	−96 → 7	−45 → −23

Table B5.2 (Continued)

Age	Max P	Max QRS	Max T
7–8 years	19 ± 39	−30 ± 21	−4 ± 17
	−46 → 82	−63 → 16	−40 → 35
9–10 years	17 ± 37	−31 ± 30	3 ± 18
	−50 → 87	62 → 10	−31 → 43
11–12 years	14 ± 39	−33 ± 19	9 ± 17
	−53 → 82	−78 → 4	−21 → 51
13–14 years	10 ± 44	−32 ± 27	9 ± 17
	−62 → 90	−71 → 9	−20 → 41
15–16 years	4 ± 43	−29 ± 50	20 ± 20
	−57 → 81	−93 → 204	−19 → 56

Table B5.3

Maximal P, QRS, and T vector angles in frontal plane (degrees)

Age	Max P	Max QRS	Max T
< 24 h	54 ± 14	79 ± 87	76 ± 69
	27 → 74	−90 → 208	25 → 151
1 day	58 ± 16	88 ± 80	67 ± 39
	18 → 78	−106 → 190	18 → 135
2 days	58 ± 21	77 ± 81	62 ± 43
	12 → 83	−71 → 191	23 → 102
3 days	52 ± 23	67 ± 79	54 ± 22
	−41 → 72	−68 → 194	16 → 106
≤ 1 week	57 ± 14	62 ± 65	51 ± 22
	22 → 77	−46 → 186	19 → 94
≤ 1 month	54 ± 14	61 ± 68	42 ± 19
	30 → 81	−19 → 190	18 → 82
≤ 3 months	56 ± 12	36 ± 25	38 ± 22
	25 → 79	4 → 135	18 → 94
≤ 6 months	56 ± 13	35 ± 27	36 ± 13
	26 → 77	−7 → 105	13 → 56
≤ 1 year	56 ± 14	31 ± 35	41 ± 16
	18 → 76	−18 → 97	21 → 75
1–2 years	57 ± 14	41 ± 38	38 ± 17
	5 → 73	−73 → 151	16 → 72
3–4 years	58 ± 16	39 ± 23	34 ± 10
	23 → 82	12 → 127	18 → 55
5–6 years	52 ± 28	37 ± 20	29 ± 9
	−36 → 82	13 → 101	11 → 46
7–8 years	54 ± 22	38 ± 18	29 ± 8
	3 → 75	13 → 63	12 → 46
9–10 years	50 ± 25	41 ± 19	26 ± 8
	−21 → 80	15 → 65	12 → 45
11–12 years	53 ± 22	39 ± 17	28 ± 8
	−26 → 85	15 → 72	9 → 42
13–14 years	44 ± 41	41 ± 17	28 ± 8
	−91 → 81	13 → 74	12 → 46
15–16 years	50 ± 34	47 ± 32	28 ± 9
	−90 → 82	11 → 181	11 → 47

Index

Note: The page numbers that appear in bold type indicates a substantive discussion of the topic.

D

E

F

M

N

Q

R

S

T

U

V

W